WORLD ENVIRONMENTAL AND WATER RESOURCES CONGRESS 2009

GREAT RIVERS

PROCEEDINGS OF THE CONGRESS

May 17–21, 2009
Kansas City, Missouri

SPONSORED BY
Environmental and Water Resources Institute (EWRI)
of the American Society of Civil Engineers

EDITED BY
Steve Starrett, Ph.D., P.E., D.WRE

Published by the American Society of Civil Engineers

WORLD ENVIRONMENTAL AND WATER RESOURCES CONGRESS 2009

GREAT RIVERS

PROCEEDINGS OF THE CONGRESS

May 17–21, 2009
Kansas City, Missouri

SPONSORED BY
Environmental and Water Resources Institute (EWRI)
of the American Society of Civil Engineers

EDITED BY
Steve Starrett, Ph.D., P.E., D.WRE

Published by the American Society of Civil Engineers

Copyright and Disclaimer

ISBN: 978-0-7844-1036-3

Any statements expressed in these materials are those of the individual authors and do not necessarily represent the views of ASCE, which takes no responsibility for any statement made herein. No reference made in this publication to any specific method, product, process or service constitutes or implies an endorsement, recommendation, or warranty thereof by ASCE. The materials are for general information only and do not represent a standard of ASCE, nor are they intended as a reference in purchase specifications, contracts, regulations, statutes, or any other legal document.

ASCE makes no representation or warranty of any kind, whether express or implied, concerning the accuracy, completeness, suitability, or utility of any information, apparatus, product, or process discussed in this publication, and assumes no liability therefore. This information should not be used without first securing competent advice with respect to its suitability for any general or specific application. Anyone utilizing this information assumes all liability arising from such use, including but not limited to infringement of any patent or patents.

Copyright © 2009 by the American Society of Civil Engineers.
All Rights Reserved.

ASCE and American Society of Civil Engineers—Registered in U.S. Patent and Trademark Office.

American Society of Civil Engineers
ASCE International Headquarters
1801 Alexander Bell Drive
Reston, VA 20191-4400 USA

Call Toll-Free in the U.S.: 1-800-548-2723 (ASCE)
Call from anywhere in the world: 1-703-295-6300
Internet: http://www.pubs.asce.org

This product was produced for the American Society of Civil Engineers by Omnipress.

Duplication of this product and its content in print or digital form for the purpose of sharing with others is prohibited without permission from the American Society of Civil Engineers.

Photocopies and reprints.

You can obtain instant permission to photocopy ASCE publications by using ASCE's online permission service (www.pubs.asce.org/authors/RightslinkWelcomePage.html). Requests for 100 copies or more should be submitted to the Reprints Department, Publications Division, ASCE, (address above); email: permissions@asce.org. A reprint order form can be found at www.pubs.asce.org/authors/reprints.html.

In no event will ASCE, Omnipress or its suppliers be liable for any consequential or incidental damages to your hardware or other software resulting from the installation and/or use of this product.

No part of the product navigation and "Help" files may be reproduced or used without written permission from Omnipress.
© 2009 Omnipress - All rights reserved.

Table of Contents

11th Water Distribution Systems Analysis Symposium (WDSA 09)

Asset Management

Bursts Identification in Water Distribution Systems

I. Borovik, B. Ulanicki, and P. Skworcow

Damage Detection of Operating Transmission Mains with Measured Boundary Conditions

Aaron C. Zecchin, Martin F. Lambert, and Angus R. Simpson

Evaluating Risk of Multi-Segment Pipes for Prioritizing Pipe Rehabilitation

M. Poulton, I. Kropp, and A. Vanrenterghem-Raven

Water Distribution Systems Corrective Maintenance Supported by Real-Time Use of Hydraulic Models

Juan G. Saldarriaga, Susana Ochoa, César A. Niño, and Oscar J. Cortés

Water Price Forecasting Method Based on Marginal-Cost Theory: A Case Study in China

Cui-Mei Li and Sui-qing Liu

Field Work

Assessing the Impact of Climate Change on Drinking Water Treatment Plant Design and Operation

Zhiwei Li, Robert M. Clark, Steven G. Buchberger, and Y. Jeffrey Yang

Axial Dispersion Coefficients for Laminar Flows in Water Distribution Systems

P. Romero-Gomez, Z. Li, C. Y. Choi, and S. G. Buchberger

Case Study: Homeowner's Preference Trade-Offs toward Plumbing Systems in Pipe Failure Prone Area

Juneseok Lee, Darrell Bosch, Ewa Kleczyk, Eftila Tanellari, Andrea M. Dietrich, and Vinod K. Lohani

Field-Scale Assessment of a Multispecies Water Quality System: A Chloramination Study

Matthew T. Alexander, Dominic L. Boccelli, and Margaret J. Kupferle

Pressure vs. Flow Relationship for Pipe Leaks

Thomas Walski, Brian Whitman, Mary Baron, and Fred Gerloff

Seoul (Korea) Online Water Quality Monitoring of Drinking Water

P. S. Shin, Y. R. Song, Y. J. Choi, and Y. S. Park

Hydraulic Transients and Biofilms

Air/Vacuum Valve Breakage Caused by Pressure Surges – Analysis and Solution

Guohua Li, Christopher C. Baggett, and Roberto A. Rosario

The Impact of Biofilm Development on Pipe Roughness and Velocity Profile

Martin Francis Lambert, Ryan Wilson John Edwards, Sean James Howie, Benjamin Bernard De Gilio, and Shane Pearse Quinn

In-Line Partially Closed Valves: How to Detect by Transient Tests

S. Meniconi, B. Brunone, and M. Ferrante

Simple Model of Attachment and Detachment of Pathogens in Water Distribution System Biofilms

I. Schrottenbaum, J. Uber, N. Ashbolt, R. Murray, R. Janke, J. Szabo, and D. Boccelli

Network Modeling 1

Impact of Storage Tanks on Energy Consumption in Municipal Water Distribution Systems

Santosh R. Ghimire and Brian D. Barkdoll

Hydraulic Analysis of Water Distribution Network Using Harmony Search

Zong Woo Geem

Integrated Hydraulic Analysis and Data Management Tool for Water Supply Systems in Developing Countries

Philipp Klingel and Nicolai Guth

The Impacts of Demand Variability on Distribution System Hydraulics and Transport

Xueyao Yang and Dominic L. Boccelli

Network Modeling 2

Augmented Gradient Method for Head Dependent Modelling of Water Distribution Networks

Calvin Siew and Tiku T. Tanyimboh

Enhanced Global Gradient Algorithm: A General Formulation

L. Berardi, O. Giustolisi, and E. Todini

Enhanced WDN Analysis: Representation of Actual Pipe Connections

O. Giustolisi

Identification of the Hydraulic Model from Operational Measurements for Supervisory Pressure Control

Ping Li, Ian Postlethwaite, Emmanuel Prempain, Bogumil Ulanicki, and Ridwan Patel

Network Modeling 3

An Operative Approach to Water Distribution System Rehabilitation

L. Berardi, O. Giustolisi, and D. Savic

Calibration of Water Distribution Network Models as a Tool for Detecting Missing and Erroneous Cadastral and Hydraulic Information

Juan G. Saldarriaga, Susana Ochoa, Daniel Rodríguez, and César M. Jurado

Integrated Planning for Dual Distribution Systems

Nabin Khanal, Vanessa Speight, Venkatraman Radhakrishnan, Tim Francis, Laurel Passantino, and James Swanson

Reliability Analysis of Water Distribution Systems Using Graph Decomposition

Jochen Deuerlein, Andreas Wolters, Dietmar Roetsch, and Angus R. Simpson

Network Modeling 4

A Framework for Alternative Formulations of the Pipe Network Equations

Angus R. Simpson and Sylvan Elhay

Inexpensive Modeling of Intermittent Service Water Distribution Networks

J. A. Cabrera-Bejar and V. G. Tzatchkov

Operational Perspective of the Impact of Failures in Water Distribution Systems

J. Bicik, Z. Kapelan, and D. A. Savi•

Network Monitoring and Sampling

New Concepts for Meter Placement in Water Distribution Systems for Demand Estimation

Doo Sun Kang and Kevin Lansey

Online Hydraulic State Prediction for Water Distribution Systems

Ami Preis, Andrew Whittle, and Avi Ostfeld

Sampling of Residential Water Use for Leak Control via Water Budgets

C. Arena, A. Criminisi, A. Fortunato, and M. R. Mazzola

Smart Pipe—Nanosensors for Monitoring Water Quantity and Quality in Public Water Systems

Yu-Feng Lin, Chang Liu, and Jordan Whisler

Network Optimization 1

An Approach for Integrated Optimization of Wastewater, Recycled, and Potable Water Networks

Graeme Dandy, Alana Duncker, Joel Wilson, and Xavier Pedeux

Application of Optimization Technology to Water Distribution System Master Planning

C. K. Rogers, M. Randall-Smith, E. Keedwell, and R. Diduch

Industrial Distribution System Simulation for Optimal Water Resource Assignment Using Probabilistic Tabu Search

S. H. H. Nourzad and M. H. Afshar

Optimal Pump Scheduling by Linear Programming

M. F. K. Pasha and K. Lansey

Network Optimization 2

An Integrated Approach for Distribution System Hydraulic Criticality and Emergency Response

Laura Jacobsen, Sri Kamojjala, and Brian Bowler

Decision Making under Information Constraints

Jianhua Xu, Jeanne M. VanBriesen, Mitchell J. Small, and Paul S. Fischbeck

Optimal Distribution of Pressure Measurement Points in Water Distribution Networks

Hui Zhang and Tinglin Huang

Scalable Parallel Computing Framework for Pump Scheduling Optimization

Zheng Yi Wu and Qi Zhu

Network Security 1

A Multi-Objective Evolutionary Computation Approach to Hazards Mitigation Design for Water Distribution Systems

Lufthansa Kanta, Kelly Brumbelow, and Emily Zechman

Multi-Objective Sensor Placements with Improved Water Quality Models in a Network with Multiple Junctions

R. G. Austin, C. Y. Choi, A. Preis, A. Ostfeld, and K. Lansey

Robust Sensor Placement for Detecting Adversarial Contaminations in Water Distribution Systems

Andreas Krause and Carlos Guestrin

Sensor Network Design and Performance in Water Systems Dominated by Multi-Story Buildings

Robert Janke, Terra Baranowski Haxton, Walter Grayman, Rakesh Bahadur, Regan Murray, William Samuels, and Tom Taxon

Network Security 2

Comparative Evaluation of Two Algorithms for Locating Contaminant Ingress Points

Hailiang Shen, Edward McBean, and Mirnader Ghazali

Comparison of Pressures Simulated Using Transient Analysis with Field Data from a Full-Scale Distribution System

G. Ebacher, M.-C. Besner, J. Lavoie, B. S. Jung, B. W. Karney, and M. Prévost

Effects of Redesign of Water Systems for Security and Water Quality Factors

Walter M. Grayman, Regan Murray, and Dragan A. Savic

Propagation of Chlorine Demand Signals Induced by Microbial Contaminants in a Drinking Water Distribution System

D. E. Helbling and J. M. VanBriesen

Network Security 3

A Markov Chain Monte Carlo Implementation of Bayesian Contaminant Source Characterization in Water Distribution Systems under Stochastic Demands

Kenneth W. Harrison and Hui Wang

Conditioned Backward Probability Modeling to Identify Contamination Sources in a Water Distribution System

R. M. Neupauer and M. K. Records

Real-Time Implementation of Contamination Source Identification Method for Water Distribution Systems

Annamaria E. De Sanctis, Sam Hachett, James G. Uber, Dominic L. Boccelli, and Feng Shang

Threat Perceptions and Risk Management in Urban Water Supply Schemes

Mitthan Lal Kansal and Aditya Tyagi

Network Security 4

Getting More from Your Investment Using Water Security Monitoring Technology for Everyday Operations

Dan Kroll

Modeling a Hydraulic Response to a Contamination Event

Terranna Baranowski Haxton and Thomas M. Walski

Novel, Rapid Molecular-Based Technique for Detecting Contamination in Drinking Water Distribution Systems

Stacia L. Thompson and Jeanne M. VanBriesen

Trajectory Clustering Approach for Reducing Water Quality Event False Alarms

Eric Vugrin, Sean A. McKenna, and David Hart

Network Water Quality Analysis 1

Comparing Single- and Multi-Species Water Quality Modeling Approaches for Assessing Contamination Exposure in Drinking Water Distribution Systems

Stephen Klosterman, Sam Hatchett, Regan Murray, James Uber, and Dominic Boccelli

Real-Time Valve Operation for Water Quality Improvement in Water Distribution Systems

Doo Sun Kang and Kevin Lansey

Simulation of Particle Transport in Drinking Water Distribution Systems

Klaus Ripl and Wolfgang Uhl

WDS Water Quality Parameter Estimation and Uncertainty

M. F. K. Pasha and K. Lansey

Network Water Quality Analysis 2

A Hybrid Heuristic Search Approach for Contaminant Source Characterization

Li Liu, E. Downey Brill, G. (Kumar) Mahinthakumar, and S. Ranji Ranjithan

Analysis of Model Sensitivity and Uncertainty for Chlorine Transport and Decay in a Water

Distribution System

W. J. Dawsey, B. S. Minsker, and A. Ostfeld

Characterizing Reactive Contaminant Sources in a Water Distribution System

Jitendra Kumar, E. Downey Brill, G. Mahinthakumar, and Ranji Ranjithan

Low Pressure Propagation at Service Lines

Juneseok Lee, Vinod K. Lohani, Andrea M. Dietrich, and G. V. Loganathan

North American Drinking Water Infrastructure Assessment

Drinking Water Infrastructure Assessment: The National Research Council of Canada Perspective

Yehuda Kleiner, Balvant Rajani and Rehan Sadiq

National Mains Failure Database Project

Neil S. Grigg

Needs and Trends of the Nation's Water Infrastructure—The Utility Perspective

Steven Buchberger, Robert Clark, Walter Grayman, Zhiwei Li, Matthew McCutcheon and Jeff Yang

Water Usage

Combined Energy and Pressure Management in Water Distribution Systems

P. Skworcow, H. AbdelMeguid, B. Ulanicki, P. Bounds, and R. Patel

Design of Dual Water Supply Systems

R. Chee, D. S. Kang, K. Lansey, and C. Y. Choi

Modeling Domestic Water Demand on a Suburb Level

M. L. Griffioen, J. E. van Zyl, and A. S. le Roux

Preliminary Spatial-Temporal Statistical Analysis of Hourly Water Demand at Household Level

Ernesto Arandia-Perez, James G. Uber, Feng Shang, Dominic L. Boccelli, Robert Janke, David Hartman, and Yeongho Lee

6th Urban Watershed Management Symposium

10,000 Rain Gardens, One Green Region

Tom Jacobs

A Level Spreader—Vegetated Buffer System for Urban Stormwater Management

Ryan J. Winston and William F. Hunt

A New Methodology to Evaluate Pollutant Removal of Gross Solids Separation Devices

D. P. Smith

A Simplified Model of Combined Sewer Overflows to Estimate Event Driven Enteric Pathogen Concentrations in Drinking Water Sources

Rishab Mahajan, James Uber, and Joseph Eisenberg

Source Control: The Solution to Stormwater Pollution

Michael A. Ports

A Student-Led Effort to Assess the Effect of Urban Runoff on Potter Lake

England Porter, John Kenny, Edward Peltier, and C. Bryan Young

A Tool for the Performance Assessment of Hydrodynamic Separators

Omid Mohseni, Janna M. Kieffer, and Jennifer A. Koehler

Accurate Sampling of Suspended Solids

Gregory P. DeGroot, John S. Gulliver, and Omid Mohseni

An Evaluation of Stormwater Wetlands in Series

J. M. Hathaway and W. F. Hunt

An Innovative Approach for Modeling Large Urban Hydrologic Systems

J. P. Cantone and A. R. Schmidt

Analysis of Bioretention Media Specifications and Relationships to Overall Performance

Sean W. O'Neill and Allen P. Davis

Analyzing the Impacts of a Retrofit Detention Basin Flow Control Strategy on Biodiversity in an Urban Stream System

Natalie A. Postel, Christine A. Pomeroy, Tom A. Jacobs, and Elangovan Karuppasamy

Are Rational C Values Too Low?

C. B. Young, B. M. McEnroe, and A. C. Rome

Assessing Hydrodynamic Separators under High Water Flow Conditions

David Saddoris, Omid Mohseni, and John Gulliver

Assessment of Standard Sumps for Stormwater Treatment

Adam Howard, Omid Mohseni, John Gulliver, and Heinz Stefan

Bayesian Load Duration Curves for Bacterial Total Maximum Daily Loads: Urban Case Study

Mary Schoen, Mitchell Small, and Jeanne VanBriesen

Bioretention/Bioinfiltration Performance in the Mid-Atlantic

R. A. Brown, W. F. Hunt, A. P. Davis, R. G. Traver, and J. M. Olszewski

Breaking Down the Barriers to Low Impact Development in Colorado

Andrew Earles, Derek Rapp, Jane Clary, and Janice Lopitz

Challenges in Attaining Recreational Stream Standards for Bacteria: Setting Realistic Expectations for Management Policies and BMPs

Jane Clary, Jonathan Jones, and Ben Urbonas

Characterizing Water Inputs to Catchments in the Santa Monica Mountains with δ180 and δD

W. Hu, B. Hibbs, and R. Bugarin

Clark County Regional Flood Control District Arc Hydro (CCRFCD Arc Hydro): Toward Ongoing Stormwater Master Planning

Stephen Bourne, Kevin Eubanks, Harshal Desai, and Brian Rowley

Codorus Creek Restoration—A Case Study for the Chesapeake Bay

Matthew P. Hoch, Christina Y. S. Siu, Shirley E. Clark, and Katherine H. Baker

Combining GIS, BMP Performance, and Strategic Planning to Support Water Quality Implementation Planning

Ken Susilo, Marc Leisenring, and Eric Strecker

Considerations, Opportunities, and Strategies for Infiltration Stormwater BMPs

Ken Susilo, Neven Matasovic, and Ronald S. Johnson

Construction and Performance of Bioretention Cells

G. O. Brown, R. A. Chavez, D. E. Storm, and M. D. Smolen

Cost Estimating Tools for Low-Impact Development Best Management Practices

C. Dasch Houdeshel, Christine A. Pomeroy, Lisa Hair, and Robert Goo

Data Reporting Guidelines for Certification of Manufactured Stormwater BMPs: Part II

Robert M. Roseen, Ernie Carrasco, Yuan Cheng, Bill Hunt, Charlene Johnston, Jim Mailloux, Walt Stein, and Tim Williams

Design of Integrated Bioinfiltration-Detention Urban Retrofits with Continuous Simulation Methods

William C. Lucas

Design Optimization of Hydrodynamic Separators

James H. Lenhart, Joanna B. Ogintz, and Scott A. de Ridder

Developing a Water Budget for a Constructed Stormwater Wetland

Kristen Mogavero, Gerrad Jones, and Bridget Wadzuk

Effects of Media Depth on Bioretention Performance in the Upper Coastal Plain of North Carolina and Bioretention Construction Impacts Study

R. A. Brown and W. F. Hunt

Engineered Waste Materials as Amendments to Prevent Erosion and to Stabilize Contaminated Sites

S. P. Kakuturu, M. Xiao, and L. N. Reddi

Enhancing Rain Garden Design to Promote Nitrate Removal

Emilie K. Stander, Michael Borst, Thomas P. O'Connor, and Amy A. Rowe

EPA Aging Water Infrastructure Research Program: State of the Technology for the Condition

Assessment and Rehabilitation of Wastewater Collection Systems

Daniel J. Murray, Jr.

Evaluation and Optimization of Distributed Stormwater Controls in Spreadsheet

Joong Gwang Lee and Scott Struck

Evaluation of Atriplx Shrubs Growth in Semi Arid Area

Mehemed A. Razzaghi

Evolutionary Optimization of Combined Sewer Overflow Control

Andrea Zimmer, David Hill, Barbara Minsker, Avi Ostfeld, and Arthur Schmidt

Examination of Pervious Concrete and Porous Asphalt Pavements Performance for Stormwater Management in Northern Climates

Kristopher M. Houle, Robert M. Roseen, Thomas P. Ballestero, Joshua F. Briggs, and James J. Houle

Field Evaluation of Indicator Bacteria Removal by Stormwater BMPs in North Carolina

J. M. Hathaway, W. F. Hunt, J. D. Wright, and S. J. Jadlocki

Field Testing Guidelines for Certification of Manufactured Stormwater BMPs: Part II

John Sansalone, Jeff Benty, Ernie Carrasco, John Gulliver, Jon Hathaway, Bill Hunt, Masoud Kayhanian, Uday Khambhammettu, Robert M. Roseen, Betty Rushton, and Tim Williams

From Grey to Green: Strategies and Concepts for Implementing Green CSO and Wet Weather Solutions

James C. Schlaman, Bryce Lawrence, and Scott Schulte

Generalized Storage-Reliability-Yield Equations for Rainwater Harvesting Systems

Lars S. Hanson, Richard M. Vogel, Paul Kirshen, and Peter Shanahan

How the Heart of America is *Goin' Green* to Solve Water and Sewer Issues

Lynn Hinkle and Michael Ports

Graywater Irrigation as a Means to Meet Water Demands in Arid Regions

Sybil Sharvelle, Masoud N. Azar, Mary Stromberger, and Larry Roesner

HCFCD M3 System: Maximizing and Maintaining Local Investments in Floodplain Modeling

Karl McArthur, Stephen Bourne, Yu-Chun Su, and Jacob Spenn

Hydrologic Footprint Residence: A New Metric to Assess Hydrological Alterations Due to Urbanization

M. H. Giacomoni and E. M. Zechman

Hypothesis-Based Flow Monitoring for Green Solutions

Deb O'Bannon and Erich Schmitz

Impact of Wet-Weather Peak Flow Blending on Disinfection Performance

Mary K. Stinson, Richard Field, and R. Boris Rukovets

Improving Hydrologic Sustainability of Texas A&M University Campus

Prakash Khedun, Chandana Damodaram, Marcio Giacomoni, Andrea Ryan, Hillary Holmes, Ross Klein, William Saour, Michelle Hollingsworth, Troy Berthold, Meg Davis, Philip Bullock, Neetha Ravikumar, Emily Zechman, Georgianne Moore, Bryan Boulanger, and Radu Stoleru

An Investigation of Infiltration in a Constructed Stormwater Wetland and Implications for Groundwater Quality

Gerrad Jones, Kristen Mogavero, and Bridget M. Wadzuk

Integration of Low Impact Development Studies into the International Stormwater BMP Database

Jane Clary, Marcus Quigley, Andrew Earles, Marc Leisenring, Eric Strecker, and Jonathan Jones

Kansas City—Balancing Green Infrastructure with Traditional Approaches for CSO Control

Scott D. Struck, Tom Jacobs, Ginny Moore, Robert Pitt, Michael A. Ports, Deborah O'Bannon, Erich Schmitz, and Richard Field

Kansas City, Missouri Overflow Control Plan Summary

Terry Leeds and Scott Struck

Kansas City's Stream Setback Ordinance: A Case Study on the Benefits of Stream Buffers in Urban Areas

Laurie Brown, Scott Schulte, and Bryce Lawrence

KC-One: Comprehensive City-Wide Management Plan Creates Leading Stormwater Management Program

J. W. Henson and R. Gaskin

Laboratory Testing Guidelines for Certification of Manufactured Stormwater BMPs

Roger Bannerman, Hans de Bruijn, Shohreh Karimipour, Masoud Kayhanian, Jim Mailloux, Jon McDonald, Mark Miller, Omid Mohseni, Kwabena Osei, and Scott Perry

Land Use and Runoff Uncertainty

Celina Bochis and Robert E. Pitt

Linking Environmental Assessment and Solutions

L. Gosselink, C. Herrington, and R. H. Glick

Long-Term Effectiveness of a Bioretention System Treating Road Runoff in Northeastern Kansas

Edward Peltier, Xiaolu Chen, Kelly Kindscher, and C. Bryan Young

Looking Upstream and into the Watershed for the Big Picture of Stream Health

Christina Y. S. Siu, Shirley E. Clark, Ruth A. Sitler, and Katherine H. Baker

LID-SWM Practices as a Means of Resilience to Climate Change and Its Effects on Groundwater Recharge

Iulia A. Barbu, Thomas P. Ballestero, and Robert M. Roseen

Maintenance of Stormwater BMPs

Andrew J. Erickson, Joo-Hyon Kang, Peter T. Weiss, C. Bruce Wilson, and John S. Gulliver

Modeling Performances of Detention Basins with Uncertainty Analysis

Daeryong Park and Larry A. Roesner

Monitoring the Hydrologic Effects of an Extensive Green Roof

Nathaniel Hanna Holloway, Charles J. Werth, and Arthur R. Schmidt

Multiple Watershed Scales Approach for Placement of Best Management Practices in *SUSTAIN*

Fu-hsiung Lai, Jenny Zhen, John Riverson, Khalid Alvi, and Leslie Shoemaker

Nexus Projects in Kansas City's Suburban Watersheds

Brian Rast

Non-Point Source Nutrient Loading in an Urban Watershed

Eric Gurr and Fidelia (Ola) Nnadi

Pervious Pavement System Evaluation

Amy A. Rowe, Michael Borst, Thomas P. O'Connor, and Emilie K. Stander

Planning for Sustainable Growth and Water Resources in the Chesapeake Bay Watershed

Thomas E. Dumm

Pollutant Transport within the Vadose Zone: Interactions of Soil Horizon Chemistry on Water Quality

Daniel P. Treese, Shirley E. Clark, J. Bradley Mikula, and Katherine H. Baker

Potential Data Analysis Methodology to Evaluate the Performance of Manufactured BMPs

Masoud Kayhanian, Robert M. Roseen, James H. Lenhart, and Greg Williams

Proposed Scaling Relations for Manufactured Stormwater BMPs

John S. Gulliver, Qizhong Guo, John J. Sansalone, Gregory Williams, and J. S. Wu

Rainwater Harvesting for Non-Potable Use in Gardens: A Comparison of Runoff Water Quality from Green vs. Traditional Roofs

Natasha Nicholson, Shirley E. Clark, Brett V. Long, Julia Spicher, and Kelly A. Steele

Redesigning Constructed Stormwater Wetlands: An Integrated Modeling Approach to Optimize Form and Function

G. D. Jones, K. A. Mogavero, and B. M. Wadzuk

Research of Hydrologic and Water Quality Performance of Four Linear Wetlands in Eastern North Carolina

J. D. Wright and W. F. Hunt

Reservoir Sedimentation Estimation Using Genetic Programming Technique

Vaibhav Garg and V. Jothiprakash

Sediment Monitoring Bias by Autosampler in Comparison with Whole Volume Sampling for

Parking Lot Runoff

George D. Fowler, Robert M. Roseen, Thomas P. Ballestero, Qizhong Guo, and James Houle

Selecting Optimal Water Supply Options—A Regional Water Supply Case Study in the Upper Kissimmee Basin, FL

Aditya Tyagi, Mitchell Griffin, Richard Nevulis, and Chris Sweazy

Simplified Solution for Groundwater Mounding under Round Stormwater Infiltration Facilities

Kaveh Zomorodi

South Lake Park Bioretention Gardens

J. J. Dremsa and T. A. Hartsig

State of the Practice of Wet Weather Flow Analysis

Mitchell Heineman

The Application of Environmental Site Design Processes to Design a Residential Subdivision

Steven D. Trinkaus

Effect of Bioretention on Runoff Temperature in Trout Sensitive Regions

Matthew Jones and William F. Hunt

The Lawrence Technological University Greenroof Performance Evaluation Project

Donald D. Carpenter and Preethi Kaluvakolanu

The Road to LID Plan Approval in Coastal North Carolina: Development of a Spreadsheet Modeling Tool for LID Based Designs

Hunter Freeman

The Runoff Reduction Method

Kelly A. Collins, Dave Hirschman, Greg Hoffmann, and Tom Schueler

Unit Process Modeling of Stormwater Flow and Pollutant Sorption in a Bioretention Cell

Zhuangxiang He and Allen P. Davis

Use of the Basin Development Factor to Evaluate Urban Watershed Response

Shiva Sunder, Theodore G. Cleveland, and David B. Thompson

Water Quality and Hydraulic Properties of the Permeable Friction Course

Michael Barrett, Brandon Klenzendorf, Brad Eck, and Randall Charbeneau

Water Quality Design Storms for Stormwater Hydrodynamic Separators

Victoria Julia Fernandez-Martinez and Qizhong Guo

Water Sustainability Index: Application of CWSI for Ahwaz County

J. Attari and S. A. Mojahedi

Development of Watershed Management Modeling System: The Los Angeles County Flood Control

District's Watershed Based Approach for Urban Runoff and Stormwater Quality

Youn Sim

7th Symposium on Groundwater, Hydrology, Quality, and Management

Aquifer Characterization and Protection

Implementing Source Water Protection Programs in Texas

Camille W. Sowells, Christina Petersen, Gordon McCurry, Alexandria Doody, and Sean Ables

Lithostratigraphy of Nigeria—An Overview

Kazeem Akorede Shitta

Specific Problems Related to Partially Penetrating Wells in Confined Aquifers

Ahmad Wagdy, Hany G. Radwan, and Sherif M. El-Didy

Tool for Estimation of Additional Drawdown Due to Partially Penetrating Wells in Confined and Semi-Confined Aquifers

Ahmad Wagdy, Hany G. Radwan, and Sherif M. El-Didy

Groundwater Characterization and Monitoring

A Novel Approach to Groundwater Model Development

Thomas D. Krom and Richard Lane

Groundwater Mixing Using Pulsed Dipole Injection/Extraction Wells

C. R. Radabaugh, D. C. Mays, and R. M. Neupauer

Groundwater Management and Its Uncertainty

A Critical Realization Identification Method Based on Pareto Dominance Analysis

J. Wang, J. Guan, and M. M. Aral

Combining Rule-Based Fuzzy Model with GIS to Predict Groundwater Vulnerability to Contamination

Dhundi R. Pathak, Akira Hiratsuka, Isao Awata, and Luonan Chen

Evaluation of Alternative Geospatial Models Using Image Ranking and Machine Learning: An Application in Shallow Groundwater Recharge and Discharge

Yu-Feng Lin, Peter Bajcsy, Alex Yahja, and Chulyun Kim

Implementation of the Sustainable Development Concept in the Field of Groundwater Management

C. Schöpfer

Projecting Future Groundwater Availability for Power Generation Plant Licensing

G. A. Day and C. Krambis, Jr.

Simulation of Subsurface Water Flow by Galerkin Finite Element Method in Dhaka City Aquifer

Shikha Rahman and Mohammad A. Bhuiyan

Groundwater Quality and Human Health

A Methodology to Reconstruct Groundwater Contamination History with Limited Field Data

Jiabao Guan, Morris L. Maslia, and Mustafa M. Aral

A Tale of Two Cities—Source Water Protection Case Studies for Systems in Rural Settings

Tina Petersen, Camille W. Sowells, Gordon McCurry, Alexandra Doody, Claudia Krug, and Sean Ables

Quantifying the Spread of Arsenic Contamination in Groundwater of the Brahmaputra Floodplains, Assam, India: A Threat to Public Health of the Region

C. Mahanta, N. Pathak, R. Choudhury, P. Borah, and W. Alam

Vadose Zone Transport of Nitrate in the Sierra Pelona Groundwater Basin, Agua Dulce, California

Claudia T. Krug and Zbigniew Kabala

Groundwater Quality Modeling—Solute Transport and Reactive Transport

Exploring the Potential of Nonlinear and Non-Equilibrium Alcohol Partitioning for Assessment of DNAPL Source Zone Architecture

Rhiannon E. Ervin and C. Andrew Ramsburg

Solute Flux Rate Uncertainty Evaluation at a Monitored Boundary

David E. Langseth

An Analytical Solute Transport Model for In Situ Estimation of Retardation

Gustavious Paul Williams and David Tomasko

Assessing Postulated Accidental Releases of Radioactive Liquid Effluents from Nuclear Power Plants

S. W. Taylor, G. A. Day, A. N. Findikakis, G. A. McLane, and L. E. Young

Modeling of Chlorinated VOCs Transport under Dual Bioreactions

Wonyong Jang and Mustafa M. Aral

Reaction Rates in a Transport System with Both Kinetic and Equilibrium Reactions

Gour-Tsyh (George) Yeh and Yilin Fang

Impacts of Urbanization on Groundwater Quality and Quantity

Comparative Study of Two Standard Septic Tank Drain Fields Using Different Sand with Recirculation for Nutrient Removal

Ni-Bin Chang, Marty Wanielista, Fahim Hossian, Zhemin Xuan, and Ammarin Daranpob

Environmental Impacts on Surface Water and Groundwater for Expanding Urban Water Supply Capacity Using Stone Quarries

Xing Fang, Ni-Bin Chang, Ming-Kuo Lee, and Lorraine Wolf

Groundwater Baseflow Sourced from Miocene Rocks and Residuals Carries Elevated Selenium into Southern California

Barry Hibbs, Mercedes Merino, Rachel Andrus, Wynee Hu, and Anna Doro-on

Investigating the Temperature Effects on Nutrient Removal in Green Sorption Media

Ni-Bin Chang, Marty Wanielista, Devan Henderson, and Ammarin Daranpob

Nutrient and Pathogen Removal with an Innovative Passive Underground Drainfield for On-Site Wastewater Treatment

Ni-Bin Chang, Marty Wanielista, Ammarin Daranpob, Fahim Hossian, and Zhemin Xuan

Selection and Prioritization of Best Management Practices for Potential Sources of Contamination in a Wellhead Protection Area

Tina Petersen, Camille W. Sowells, Gordon McCurry, Alexandria Doody, and Sean Ables

Interaction of Stream and Groundwater and Integrated Management

Controlling Saltwater Intrusion to Environmental Sensitive Areas Due to the Construction of the Rio Anton Ruiz Flood Control Project

David Weston and Rafael Velez

Estimating Groundwater Seepages to St. Lucie Estuary

Gour-Tsyh Yeh, Jae-Young Lee, Gordon Hu, and Detong Sun

Analytical-Numerical Solution for Seepage along an Earth Canal Disconnected from the Shallow Aquifer

Yi Liu and Zhuping Sheng

Hydrogeologic Investigation for New Water Supply for Water District No. 1 of Johnson County, Kansas

J. W. Henson, T. Schrempp, M. B. Horsley, and K. L. Hahn

Probabilistic Methods for Aquifer Parameter Estimation and Groundwater Modeling and Inverse Modeling

A Heuristic Algorithm for Optimal Alignment and Matching of Borehole Stratigraphy

Gustavious P. Williams, Norman Jones, and Jeffrey Handy

Composite Analysis of Test-Well and Observation-Well Data during Constant-Head Test

Yen-Ju Chen and Hund-Der Yeh

Wavelet Analysis of Characteristic Length Scales of Permeability in Stationary and Non-Stationary Porous Media

X. Qi and R. M. Neupauer

Education and Research

Framing the Design Process in an Undergraduate Environmental Engineering Class

Deb O'Bannon and Tom Kimes

Integrating Design Heuristics in an Environmental Engineering Course

Kathleen M. Leonard

Non-Traditional University Research Partners That Facilitate Service Learning and Graduate Research for Sustainable Development

M. A. Trotz, H. E. Muga, L. D. Phillips, D. Yeh, A. Stuart, and J. R. Mihelcic

Emerging and Innovative Technology

EIT Posters

A Decision Support System for Beneficial Use of National Dam Water Resources in Swaziland

J. I. Matondo and K. M. Msibi

Assessment of Combined Hydroseeding and Coconet Reinforcement to Control Soil Erosion

Mervin M. Cereno

Designing Effective Rainfall Harvesting Systems in Developing Areas of Sub-Saharan Africa

Emmanuel U. Nzewi

Innovative Design at Lake Lenexa

Scott R. Brand and Tom A. Jacobs

Production of Drinking Water from Lake Water Sources with a Nanofilter Membrane to Prevent the Formation of Disinfection Byproducts

Rajib Sinha, Anita Anderson, Craig Patterson, and David Pearson

Rainwater Harvesting Experiences in the Humid Southeast USA

Matthew Jones, William F. Hunt, and Jason Wright

Emerging and Innovative Technology in Wastewater Treatment

Deployable Decentralized Biofilm System to Degrade Organic Carbon, Nutrients and Benzene from Wastewater

Dong Chen, Che-Jen Lin, R. Gavin Jones, Sehul Patel, Rachelle Smith, Thomas G. Chasteen, Micheal Radi, Sabin Holland, Scott A. Waisner, and Jeffery L. Davis

Development of Slow-Release Chemical Oxidation Methods for Environmental Remediation

Stephanie Luster-Teasley and Patrick Onochie

Peracetic Acid as an Alternative Disinfection Technology for Wet Weather Sewer Overflows

E. Coyle and L. Ormsbee

Recycling of Multiple Waste Streams for Transportation Fuel Production via Algae Cultivation at Wastewater Treatment Plants

Patrick J. Dunlap and Andrew R. Shaw

Emerging and Innovative Technology in Water Treatment

Development of a Community Water Security Filtration System Using Composite Cartridges

Nur Muhammad, Rajib Sinha, E. Radha Krishnan, Craig L. Patterson, Roy C. Haught, Harold H. Harms, and

Rick Seville

Evaluation of a UV/Ozone Treatment Process for Removal of MTBE in Groundwater Supplies in New Mexico

Craig Patterson, Fernando Cadena, Rajib Sinha, Dzung Kim Ngo-Kidd, Abbas Ghassemi, and E. Radha Krishnan

Removal of Waterborne Particles by Electrofiltration

J. Murphy, Y. Li, R. Ehrhard, K. Carns, C. Patterson, R. Krishnan, and R. Sinha

Water Distribution Optimization: Taking SCADA One Step Forward

Chuck Weber and Simon Bunn

Environmental Cyber-Sensing and Modeling I

ARC Population and Employment Allocation Disaggregator—A Simple GIS-Based Tool for Parcel-Scale Population Projection

Stephen Bourne, Mike Alexander, and Wei Wang

How to Build a Broadly Useable GIS Toolset for Estuary Analysis

Stephen Bourne, Sandra Fox, and Palmer Kinser

Predicting CSOs for Real Time Decision Support

D. J. Hill, B. Minsker, and A. Schmidt

Protocol Considerations to Improve the Reliability of Data Collection in a Radio Telemetry System

Daniel Lasorso, Patrick Garrett, and Craig L. Patterson

Visualizing Hydrologic Drought Information on the Web Using State-of-the-Art Geospatial Mapping Technology

Jae Ryu, Mark Svoboda, and Jane Okalebo

Environmental Cyber-Sensing and Modeling II

“Let It Rain”—Gage-Adjusted Radar Rainfall (GARR) Data for Peachtree Creek Sewer Basin Modeling

Alberto Bechara, Jim Moffitt, Vahe Kokorian, and Rasheed Ahmad

Adaptive Long-Term Monitoring at BP Environmental Restoration Sites

Matthew Zavislak, John Dustman, and Dennis Beckmann

Application of Radio Frequency Tracers to Individual and Group Particle Displacement within a Laboratory

T. J. Lauth and A. N. Papanicolaou

Cost-Effective Automated Water Quality Monitoring Systems Providing High-Resolution Data in Near Real-Time

Rob Ellison and Mike Cook

South Florida Water Control System Tracker: Real-Time Water Budgeting for Pragmatic Water Control Operations

Leslie Gowdish, Stephen Bourne, Lakin Flowers, Ken Stewart, and Jack Hampson

Interdisciplinary Education Programs

Coordinating and Implementing a Graduate Course on Interdisciplinary Modeling for Water-Related Issues

Laurel Saito

Experiences Teaching a Multi-Disciplinary Course

Daniel P. Loucks

Rural Water Supply Systems in Developing Countries

Water Resources in Sudan: Enhancing Rainfall Harvesting Methods for Water Supply

S. Mohamed-Ali, S. Luster-Teasley, and E. Nzewi

Water Resources and Environmental Vision 2050

Environment and Water Resources in 2050: The Challenge for Engineering Education

Jeff R. Wright

Environmental and Developmental Risks and Stressors Impacting a 2050 Vision

Walter M. Grayman

Flood Risk Management circa 2050

Gerald Galloway

Urban Stormwater Management in 2050

James P. Heaney and John J. Sansalone

Urban Water and Wastewater Management in 2050

Glen T. Daigger

Water Resources Disasters Waiting to Happen

Challenges of Managing California's Sacramento—San Joaquin Delta

Jay R. Lund, Ellen Hanak, William E. Fleenor, William A. Bennett, Richard E. Howitt, Jeffrey F. Mount, and Peter B. Moyle

Characterization of Water Resources and Environmental Disasters

Walter M. Grayman

How Reliable is New York City's Water Supply?

Daniel P. Loucks

Environmental

Environmental Modeling

Assessing Pollutant Loads and Evaluation of Treatment Systems to Achieve Water Quality Goals for Land Development Projects

Steven D. Trinkaus

Characterization of a Perchlorate Contaminated Site

Yacoub Najjar and Sam Mryyan

Numerical Modeling of Ozonation of Organic Chemicals in Surface Water

Tingting Zhu, Yafei Jia, Ajit Sadana, and Sam S. Y. Wang

Simulation of Tehran Air Pollution Using Artificial Neural Networks

Ali Yazdanpanahrostami and Kabir Rasouli

Environmental Permitting

Distributed Power Generation at State Facilities: Economic Analysis of Savings and Carbon Credits

Joel G. Burken, A. Curt Elmore, Mariesa Crow, Will Granich, and Trenton Blair

Drive for Zero Net Carbon Impact

Jessica Lamb, Ashlynn Horras, Luke Fencl, Courtney Warren, and Sebastian Medina

Permitting of Confined Animal Feeding Operations: Issues and Challenges

William F. Ritter and S. Rao Chitikela

Environmental Sustainability

A Comparative Study of Water Quality Indices for Karun River

S. Ali Mojahedi and J. Attari

Beyond Compliance and toward Sustainability: Advantages of Systems Environmental Engineering

Oral Saulters, Blase Leven, Larry Erickson, John Pickrell, Leslie Jamka, and Ryan Green

Environmental Impact of Coffee Processing Effluent on the Ecological Integrity of Rivers Found in Gomma Woreda of Jimma Zone, Ethiopia

Y. K. Kebede, F. Assefa, and A. Amsalu

How to Save the Second Aral Sea?

Rysbekov Yusup Khai

Environmental Track Poster Session

Air-Borne Heavy Metal Contamination to River Ganga (India)

J. Pandey, K. Shubhashish, and Richa Pandey

The Effect of Sewage Pollutant of Bandar Imam Petrochemical Company on Benthic Macofauna Community Using Biodiversity Indices and Bioindicators

Taybeh Tabatabaie, Fazel Amiri, M. B. Nabavi, M. Sh. Fazeli, and M. Afkhami

Landfills and Waste Treatment

Enzymatic Treatment of a Modified Food Processing Wastewater

Anastasia E. M. Chirnside

The Effect of Municipal Landfill Leachate on the Characterization of Fluid Flow through Clay

S. Merayyan and A. Hope

Time Series Analysis of Performance Data from Closed Landfills to Forecast Post Closure Monitoring Needs

Banu Sizirici and Berrin Tansel

Using Tracers to Derive Sediment Provenance after the Occurrence of a 500-Year Flood in a Midwestern Stream

Kevin D. Denn, A. N. (Thanos) Papanicolaou, and Christopher G. Wilson

Nutrients in the Environment

Nitrification Inhibition by UVA Photocatalytic TiO2 Nanoparticles: The Role of Reactive Oxygen Species on Nanotoxicity

Okkyoung Choi and Zhiqiang Hu

The Economic and Environmental Significance of Nonpoint Source Abatement in Large Watersheds

Jamie Lefkowitz, Kirk Westphal, Jeffrey Walker, and Gary Mercer

The Nitrogen Budget of DRW in Northeastern China

Chengwei Han and Shiguo Xu

Wastewater Utilities: Are You Ready for Kansas' Nutrient Removal Policy?

Heather Phillips and Katie Funderburk

Soil and Subsurface Remediation 1

Application of Biopile System for the Remediation of Petroleum-Hydrocarbon Contaminated Soils

C. M. Kao, H. Y. Chien, Rao Y. Surampalli, and W. P. Sung

Peroxidase-Mediated Stabilization of 2,4-Dichlorophenol in a Model Humin-Mineral Geomaterial

Mónica Palomo and Alok Bhandari

pH Variation and Its Effect on Metal Concentration during Electrokinetics

Ming Xiao, Ashleigh D. Love, and Zheng Teng

Pore-Scale Characterization of Residual Non-Aqueous Phase Liquids (NAPLs) in Fractional Wettability Porous Media

Riyadh I. Al-Raoush

Soil and Subsurface Remediation 2

Addressing Contaminated Groundwater and Promoting Environmental Stewardship in Wichita, Kansas—The Gilbert and Mosley Project Story

Paul Anderson, Shawn Maloney, and Roger Olsen

Use of In-Planta Solid Phase Sampling Devices to Delineate VOC Plumes

Joel Burken, Kendra Waltermire, and Emily Sheehan

Soil and Subsurface Remediation 3

Application of a Mass Balance-Based Subsurface Contaminant Transport Model

Benjamin W. Johnson, Andrew Curtis Elmore, and Jeffrey D. Cawlfield

Association of PAHs with Size Fractionated Sediment Particles

Jejal Reddy Bathi, Robert Pitt, and Shirley E. Clark

Sorption and Desorption of Testosterone in Agricultural Soils

Rui Ma and Tian C. Zhang

Wetland Mitigation and Water Management

A Study on Spatial Distribution of Water Quality and the Behavior of Do Concentration in Tidal Area of Urban Rivers

M. Okabe, M. Kawamura, T. Kato, and T. Yamada

Development of an Amphibian Biotic Index to Evaluate Wetland Health in Northern Missouri

C. D. Shulse, R. D. Semlitsch, and K. M. Trauth

GIS-Based Landscape Parameters for Wetland Evaluation Related to Amphibian Health

Miriam Romero, Kathleen M. Trauth, Yingkui Li, Raymond Semlitsch, and Christopher D. Shulse

The Rush Creek Detention Facility: Planning a Permanent BMP in the Real World

William Yord, Joe Ennett, and Jerry Richardson

Hydraulics and Waterways

Bridge Scour

General Hydraulic Characteristics of an Open Channel with Narrow Path

M. S. Quimpo and T. Yamada

Mathematical Modeling of Bed—Topography Changes at Bridge Abutments

Omer Kose and A. Melih Yanmaz

Predicting Rock Scour in an Alluvial River with a One-Dimensional Model

Blair P. Greimann, Yong G. Lai, and Kuowei Wu

Predicting Rock Scour in an Alluvial River with a Two-Dimensional Model

Yong G. Lai, Blair P. Greimann, and Kuowei Wu

Computational Hydraulics and Hydrodynamics I

3D Numerical Modeling of John Day Lock Tainter Valves

E. Allen Hammack and Richard L. Stockstill

A Three-Dimensional Numerical Model for Flow in a Lock Filling System

Richard L. Stockstill and R. Charlie Berger

Challenges on Three-Dimensional Simulations of Free Surface Flow

Jinwei Qiu and Xing Fang

Comparison of the Princeton Ocean Model and the Regional Ocean Modeling System Hindcasts in the Delaware River and Bay

Richard A. Schmalz, Jr.

Computational Hydraulics and Hydrodynamics II

A Process-Based Unsteady Model for Wave-Current-Morphodynamic Changes in Two-Dimensions

S. N. Kuiry, Yan Ding, and Sam S. Y. Wang

Simulation of Multilayer Shallow Water Fluid Flow Using Lattice Boltzmann Modeling and High Performance Computing

K. R. Tubbs and F. T.-C. Tsai

Two Dimensional Hydraulic Modeling of the Lower Skokomish River

Cassie Klumpp

Using Computational Model ADH to Evaluate Relationship of Water Surface Elevation to Wing Dikes

Renjie Xia

Computational Hydraulics and Hydrodynamics III

ADH = Fast and Stable 2D Finite Element Model

Thomas Gambucci

Evaluation of Methods to Reduce Backflows from the Chicago Waterway System to Lake Michigan

Charles S. Melching and Emre Alp

Modeling the Evolution of Incised Streams in Hammar Mesopotamian Marsh with Emphasis on the Contribution of Tidal Flow in the Filling Requirements

A. H. Alkaabi, A. Ramamurthy, H. A. Al-Thamiry, and A. A. Ali

Numerical Simulations of Coastal Floods and Morphological Changes Due to Sea Level Rise and Hazardous Storm

Yan Ding, Moustafa Elgohry, and Sam S. Y. Wang

Computational Hydraulics and Hydrodynamics IV

Comparison of HEC-RAS and InfoWorks RS: A Case Study in Grand Prairie, Texas

Thomas W. Mountz and Joshua Crowley

Diversion of S-4 Basin Drainage from Lake Okeechobee: Hydraulic Modeling of Alternatives Using

HEC-RAS

Stephanie C. Otis and Gene L. Foster

New Floodplain Delineation Capabilities in HEC-RAS

Cameron T. Ackerman, Mark R. Jensen, and Gary W. Brunner

Transitioning NWS Operational Hydraulics Models from FLDWAV to HEC-RAS

Fekadu Moreda, Angelica Gutierrez, Seann Reed, and Cecile Aschwanden

Computational Hydraulics and Hydrodynamics V

Numerical Simulation of Dissolved Oxygen Concentration in the Downstream of Three Gorges Dam

Xiangju Cheng, Xuewei Chen, and Yongcan Chen

On a Two-Dimensional Temperature Model: Development and Verification

Yong G. Lai and David Mooney

Simulations of Aquaculture Dissolved Waste Transport and Mixing in Near-Coastal Waters

S. K. Venayagamoorthy, O. B. Fringer, J. R. Koseff, and R. L. Naylor

The Importance of In-Stream Hydraulics in River Water Quality Models: Lessons from the Blackstone River

Jeffrey D. Walker, Paula Sturdevant Rees, and Thomas K. Walsh

Computational Hydraulics and Hydrodynamics VI

Inundation Mapping Using Hydraulic Models and GIS: Case Studies of Steady and Unsteady Models on the Tar River, NC

Cécile Aschwanden, Seann Reed, and Keren Cepero

Performance Evaluation of Articulated Concrete Matting (ACM) Spillway at Lake Odessa, Iowa

Thomas Gambucci

The Development of a Neural-Based Biomarker Forecasting Tool for Classifying Recreational Water Quality

Srinivas Motamarri and Dominic L. Boccelli

Use of Hydraulic Modeling to Develop a Small Dam for the Geum River Reach in Sejong City

Sangman Jeong, Christabel Jane Rubio, Joo-Heon Lee, Leehyung Kim, and Kwangseob Shin

Computational Hydraulics and Hydrodynamics VII

An Efficient Solution for Water Supply Networks

S. Engin Mendi

Comparison of Mean Flow and Turbulence around Experimental Spur Dike

Jennifer G. Duan and Li He

Measuring Discharge with ADCPs: Inferences from Synthetic Velocity Profiles

Chris R. Rehmann, David S. Mueller, and Kevin A. Oberg

Statistical Analysis of Water Distribution Networks Design Using Harmony Search

Daniel Mora, Pedro L. Iglesias, F. Javier Martinez, and Vicente S. Fuertes

Dam Operation, Management, and Safety I

Alternatives Study of Willwood Diversion Dam Siltation Removal in Wyoming, USA

Hui-Ming Shih, Chih Ted Yang, Patrick F. Horn, and Lynn C. Stutzman

Managing Reservoir Discharge through Accurate Flow Measurement

Bryan J. Heiner and Steven L. Barfuss

Numerical Modeling of Flushing Process in Dez Dam Reservoir by HR Wallingford Method

Ali Khosronejad, Afshin Ashrafzadeh, and Majid Vazifedoust

Simulation Study for Minimizing Diurnal Variation of Flow in a Hydroelectric Project to Reduce Downstream Impact

Maya R. Ray and Arup Kr. Sarma

Dam Operation, Management, and Safety II

Optimal Design and Operation of Fuse-Gates Considering Water Loss Due to Gates Tilting

Abbas Afshar and Zeinab Takbiri

The Effect of Step Height on Energy Dissipation in Stepped Spillways

S. L. Hunt and K. C. Kadavy

The Geneva Dam, IL, Hydraulic Roller Problem: Design of a Temporary Steep Riprap Ramp

Yu-Chun Su, Loren Wobig, Brad Winters, Xin He, and David T. Williams

Eco-hydraulics

Fish Passage and Abundance around Grade Control Structures on Incised Streams

J. T. Thomas, A. N. Papanicolaou, C. L. Pierce, D. C. Dermisis, M. E. Litvan, and C. J. Larson

Fish Passage Can Be Improved by Introducing Hydraulic Refuge: Can the Effects Be Quantified?

Matthew D. Hays, Suzanne K. Monk, Trevor P. Hawkes, Joseph R. Webb, Rollin H. Hotchkiss, Mark Belk, and Russell Rader

Hydraulic Model Study of Canoe Chute and Fish Passage for the Chicago River North Branch Dam

Jorge D. Abad, Andy Waratuke, Cristiana Barnas, and Marcelo H. Garcia

Some Findings on Effective Discharge Determination for Gravel Bed Rivers

Carmen E. Bernedo

Eco-hydraulics Modeling

Expanded Method for Filtering Submerged Objects in Echosounder Data

Tim D. Osting

Numerical Simulation of Chemical Spills Using CCHE2D Model and Chemical Property Database

Xiaobo Chao, Tingting Zhu, Munther Hammouri, and Yafei Jia

One-Dimensional Modeling of Water Quality and Aquatic Ecosystems in Streams

Podjanee Inthasaro, Weiming Wu, and Sam S. Y. Wang

Use of Artificial Neural Networks for Habitat Unit Composition Modeling

Jian-Ping Suen

Eco-hydrology

Considering River-Scale Ecological Improvements within Flood Management Planning: The Lower Menomonee River Watercourse Status Report

Michael Schwar and Tom Chapman

Developing Linkages between Biological Impairment and Stream Siltation: A Case Study in the Northern Great Plains Ecoregion

John S. Schwartz, Andrew Simon, and Lauren Klimetz

The Effect of Natural Hydrological Disturbances (Defined from HSPF Simulated Hydrographs) on Trout Populations in Ungaged Streams of the Great Smoky Mountains National Park

Keil J. Neff, Joseph Parker, John Schwartz, Matt Kulp, Steve Moore, and Meijun Cai

Upper Mississippi River Basin Envirohydrologic Observatory

Jeremy Bril, J. V. Loperfido, Craig Just, and Nathan Young

Hydraulic Structure

A Comparison of Formed Suction Inlets for Flood Control Applications

David Werth, Mark Allen, and Brent W. Nicholas

Case Study: Impact of Varying Mitered Suction Elbows on Large Wastewater Pumps

David Werth and Ted Stolinski

In-Stream Structures for Habitat Restoration

Culvert Retrofit and Fish Passage: An Update

Joseph R. Webb and Rollin H. Hotchkiss

Field Evaluation of Engineered Large Woody Debris for Structure Performance and Habitat Value

Kendra Russell and Elaina Holburn

Numerical Analysis of the Performance of Rock Weirs: Effects of Structure Configuration on Local Hydraulics

Christopher L. Holmquist-Johnson

Quantitative Evaluation of Rock Weir Field Performance

David Varyu, Kendra Russell, and Elaina Holburn

Large River Habitats

A Digital Floc Camera for Nonintrusive Measurement of Floc Parameters

Remya G. Kumar, Ariel Ruiz, and Kyle B. Strom

Multi-Criteria Assessment of Pallid Sturgeon Habitat Restoration for the Missouri River

John Stansbury, Jennifer Gitt, and Istvan Bogardi

River Bed Sediment Classification Using ADCP

F. Douglas Shields, Jr.

Large River Restoration

Environmental Aspects of Dredging: What About Air Quality?

Mark J. Anderson and Brian D. Barkdoll

Integrating Fluvial Geomorphology and Two-Dimensional Hydraulic and Sediment Transport Modeling to Support Sustainable Design of Large River and Floodplain Improvements: The Trinity River Corridor Project, Dallas, Texas, USA

Mark R. Tompkins, Greg Ajemian, Gregory Welch, Anthony Falzone, Kyle Winslow, Paul Frank, Beatriz Dongell, and Denny Mengel

Rehabilitation of the Middle Rio Grande near Bernalillo, New Mexico

Drew C. Baird and Carolyn Donnelly

USACE River Ecosystem Restoration Planning: Lessons Learned from the Illinois River Study

Michael Schwar

Modeling Dam Breach

A Depth-Averaged 2-D Model of Non-Cohesive Dam/Levee Breach Processes

Weiming Wu, Zhiguo He, and Sam S. Y. Wang

A Lattice Boltzmann Model for Dam Break Flows

H. Liu, J. G. Zhou, R. Burrows, and Y. Peng

Comparison of Dam Breach Parameter Estimators

D. Michael Gee

Representation of Linear Terrain Features in a 2D Flood Model with Regular Cartesian Mesh

Mustafa Altinakar, Marcus McGrath, Yavuz Ozeren, and Edie Miglio

Risk Uncertainty

Flood Risk Assessment of Complex Riverine Systems

Christopher N. Dunn and Michael K. Deering

Optimal Design of Water Diversion System: A Case Study

Mohammad Karamouz, Siyamak Doroudi, Azadeh Ahmadi, and Ali Moridi

River Stabilization

Kansas River Bank Stabilization and Post-Project Conditions

John Blancett and Pete Jarchow

Adverse Effects of Flood Flow at Skewed Railroad Crossings

William Yord, Jerry R. Richarson, and Vincent J. Zink

Physical Modeling of River Spanning Rock Structures: Evaluating Interstitial Flow, Local Hydraulics, Downstream Scour Development, and Structure Stability

Kent L. Collins, Christopher I. Thornton, Brent Mefford, and Christopher L. Holmquist-Johnson

Redesign and Rehabilitation of Railroad Bridges with Advanced Adverse Lateral Migration

William Yord, Jerry R. Richardson, and Vincent J. Zink

Sediment Transport Modeling I

A Direct Method for Determining Riprap Size for Erosion Protection in Rivers

Yongliang Jin and Brian D. Barkdoll

Modeling of Sediment Particle Deposition and Resuspension Processes Using a Stochastic Jump Diffusion Particle Tracking Model

Jungsun Oh and Christina W. Tsai

Numerical Model of Channel Meandering in the Middle Sacramento River

Jianchun Huang, David R. Varyu, and Blair P. Greimann

One- and Two-Dimensional Modeling of Deep Gravel Mining in the Rio Salado

Dong Chen and Mingfa Liu

Sediment Transport Modeling II

Effects of Gas Ebullition on Cohesive Sediment Resuspension and Cap Stability

Pinar Cakir Kavcar and Steven J. Wright

Empirical Equation for Abrasion of Stilling Basin Caused by Impact of Sediment

M. E. Banihabib and M. Elahi

Investigation of Land-Use Change and Hydrologic Forcing upon Streambank Erosion and In-Stream Sediment Processes Using a Watershed Model and Sediment Tracers

J. P. Russo, J. F. Fox, and D. Martin

Retrofitting Stormwater BMPs in a Supercritical Flow Regime: A Hydraulic Perspective

I. J. Tye

Sedimentation I

Numerical Simulation of Sediment Transport and Morphological Change of JiJi Weir Reservoir

Yaoxin Zhang, Yafei Jia, Keh-Chia Yeh, Chung-Ta Liao, and Sam S. Y. Wang

One-Dimensional Modeling of Sedimentation Processes on the Puyallup River

Brian G. Wardman, Brad R. Hall, and Casey M. Kramer

Physical Experimentation and CFD Modeling to Evaluate Sediment Scour in Catchbasin Sumps

Humberto Avila and Robert Pitt

Sedimentation Characteristics of the Lower Nakdong River Upstream of the Nakdong River Estuary Barrage

Sang-Kil Park, Un Ji, Byungdal Kim, and Dohoon Kim

Sedimentation II

Experimental Results on the Stability of Non-Cohesive Sediment Beds Subject to Vertical Pore Water Flux

Pinar Cakir Kavcar and Steven J. Wright

Suspended Sediment Concentration Measurements of Muddy Sediments with an ADV

M. Salehi and K. B. Strom

The Connectivity of Upland and Instream Processes

Athanasios (Thanos) N. Papanicolaou and Philip Ellis

Upstream Intrusion Effect of CSO Event in Bubbly Creek, IL

Xiaofeng Liu, Sumit Sinha, Davide Motta, and Marcelo H. Garcia

Stream Restoration I

A Simple Analytical Design Method for Small Alluvial Channels

Bruce M. McEnroe, John E. Shelley, and C. Bryan Young

Bankfull Discharge for Kansas Natural Alluvial Channel Design

J. Shelley, C. B. Young, and B. McEnroe

Sediment Load Based Single Thread Alluvial Channel Classification

Gregory Wilkerson and Gary Parker

Using Watershed Scale Geomorphic Assessment to Improve Urban Stream Restoration Design

Sue L. Niezgoda

Stream Restoration II

Habitat Restoration on the Middle Fork John Day River

E. R. Holburn, T. Turner, L. Piety, and R. E. Klinger

Hungry Canyons Alliance: Streambed Stabilization in Western Iowa

J. T. Thomas

Rehabilitation of Mine Impaired Creek in Idaho

Brian Murphy, Moosub Eom, Bill Adams, and Jeff Johnson

The Value of Protecting Ozark Streams: An Economic Evaluation of Stream Bank Stability for Phosphorus Reduction

E. Dove, K. Rodgers, and M. Keener

Stream Restoration III

Developing Probability of Failure Estimates for Stream Restoration Design Components

Timothy M. Sliwinski, Sue L. Niezgoda, and Michael DeVasher

Bedload Composition and Development of 2D Stream Sediment Model for Stream Restoration Design Applications in Urbanizing Watersheds

William R. Cantrell, John S. Schwartz, and William K. Barry

Two-Dimensional BOD and DO Water Quality Model for Engineering Applications: The Case of Bubbly Creek in Chicago, Illinois

Davide Motta, Jorge D. Abad, Xiaofeng Liu, and Marcelo H. García

Using HEC-RAS Hydraulic Design Functions for Geomorphic Channel Design and Analysis

John Shelley and A. David Parr

Stream Restoration IV

A Monitoring and Assessment Framework to Evaluate Stream Restoration Needs in Urbanizing Watersheds

John S. Schwartz, Sue L. Niezgoda, Louise O. Slate, Donald D. Carpenter, William K. Annable, Tess M. Wynn, Christine Pomeroy, and Munsell McPhillips

Post Project Appraisal of Riparian, Wetland, and Aquatic Habitat Restoration at Best Slough, Beale Air Force Base, Marysville, CA

M. R. Tompkins, D. Mengel, and T. Hamaker

Predicting Streambank Seepage Flows: Sensitivity to Soil Properties and Layering

D. M. Heeren, G. A. Fox, M. L. Chu-Agor, and G. V. Wilson

A Seepage Erosion Sediment Transport Function and Geometric Headcut Relationships for Predicting Seepage Erosion Undercutting

M. L. Chu-Agor, G. A. Fox, and G. V. Wilson

International

Improving Hydrologic Prediction in Developing Countries

A Blueprint for Advancing Hydrologic Predictability in Developing Countries: A Case Study for the Nile River Basin

M. Gebremichael

Distributed Hydrologic Model for Flood Prevention in the Yuna River Water shed, Dominican Republic

H. J. Robinson, Z. Fang, and P. B. Bedient

Evaluation of Land Use Land Cover Changes in Palleru (K-11) Sub Basin of River Krishna Using GIS and NDVI

M. V. S. S. Giridhar and G. K. Viswanadh

On the Local-Scale Spatial Variability of Daily Rainfall in the Highlands of the Blue Nile: Observational Evidence

Menberu M. Bitew, M. Gebremichael, F. A. Hirpa, Y. Michael, Y. Seleshi, and Y. Girma

International Water Resources Planning and Management

Characteristics of Integrated Water Resource Management in the Zambezi River and Great Lakes Basins: A Comparison of Two Approaches

Jonathan W. Bulkley, Imasiku Nyambe, and Christine J. Kirchhoff

Determining the Causes of Declining Upper Great Lakes Levels—Phase I of the International Upper Great Lakes Study by the St. Clair River Task Team

Anthony J. Eberhardt and Syed M. A. Moin

Economic Sustainability Evaluation of an Inter-Basin Water Transfer Project Using GWP Statement

Mohammad Karamouz, S. Ali Mojahedi, Asghar Elyasi, and Vahid Askarinejad

Recent Developments in Water Policy in the Americas

Mark W. Killgore

The Memorandum of Understanding (MOU) between the University of Zambia and the University of Michigan: Conception and Subsequent Implementation Goals

Jonathan W. Bulkley, Imaskiu Nyambe, and Christine J. Kirchhoff

Rural Water Supply Systems in Developing Countries

Environmental and Water Resources in Developing Countries: Development of Micro Irrigation Facility at Parsoda Village

P. K. Agale, N. N.Wankhede, P. B. Bhave, and S. Y. Mhaske

Feasibility Study for Implementing Renewable Energy to Power a Groundwater Pump in Rural Guatemala

Will Granich and Andrew Curtis Elmore

Drinking Water Field Analyses for the Detection and Enumeration of Coliform Bacteria in Rural Guatemalan Highlands

Jenna Tune and Andrew Curtis Elmore

Sustainability of Rural Water Supply Projects in Nicaragua

Jairo Hernandez Alvarado

Transboundary Water Issues

Framework for Improving Water Security in the Middle East

John A. Kliem

A War for Water

Jonah-Jong M. Lee

Water Resources in Jordan: Challenges and Accomplishments

S. Merayyan, S. Mrayyan, and M. Mihyar

Water Quality and Aquatic Ecosystems in Developing Countries

Impacts of Mining in the Upper Zambezi River Basin: An Overview of the Zambian Copperbelt

Imasiku A. Nyambe

Improving the Water Quality of One of the World's Great Lakes: Tai Lake Case Study of Environmental Responsibility in the Developing World

D. P. Albers

Investigating Aquatic Ecosystems of Small Lakes in Khorezm , Uzbekistan

Laurel Saito, Julian Scott, Michael Rosen, Bakhriddin Nishonov, Sudeep Chandra, John P. A. Lamers, Dilorom Fayzieva, and Margaret Shanafield

Prediction of Thermal Stratification in Proposed Bakhtyari Reservoir with CE-QUAL-W2

Mehrdad Nazariha, Erfan Danaei, Seyyed Hosein Hashemi, and Amir Hosein Izad Doustdar

Irrigation and Drainage

Crop Production and Water Balance

Physiological and Yield Response of Green Bell Pepper to Soil Moisture Sensor Controlled Drip Irrigation

Lincoln Zotarelli and Michael D. Dukes

Water Production Functions for High Plains Crops

Thomas Trout, Gerald Buchleiter, and Walter Bausch

Water Retention and Hydraulic Conductivity of Different Media Used for Containerized Agriculture Systems

Vivek Kumar, M. Reza Savabi, Felipe M. Guerrero, and Berrin Tansel

Water Use and Evapotranspiration Coefficients for Camelina Sativa

D. J. Hunsaker, A. N. French, T. R. Clarke, and D. M. El-Sheikha

Current Irrigation Scheduling Advisory Systems 1

Irrigation Scheduling for Deficit Irrigation

Norman L. Klocke, Loyd R. Stone, and Dale A. Bolton

The Arkansas Irrigation Scheduler

Earl Vories, Phil Tacker, and Steve Hall

The Next Generation of Irrigation Management Programs

P. M. Robinson

Woodruff Irrigation Charts

J. C. Henggeler

Current Irrigation Scheduling Advisory Systems 2

A Web-Based Advisory Service for Optimum Irrigation Management

Charles Hillyer, Marshall English, Carole Abourached, Chadi Sayde, Kent Hutchinson, and John Busch

Estimating Crop Coefficients from Fraction of Ground Cover and Height

Richard G. Allen and Luis S. Pereira

Manure Application to Soybeans in the Chesapeake Bay Watershed

William F. Ritter

On-Line Irrigation Scheduling within the Belle Fourche Irrigation District

Jared K. Oswald and Hal D. Werner

Drainage Infrastructure and Nonpoint Sources

Agricultural Drainage Management Systems Task Force (ADMSTF)

James L. Fouss and Michael Sullivan

Denitrifying Bioreactors for Treatment of Tile Drainage

Laura E. Christianson, Alok Bhandari, Matthew H. Helmers, and Martin St. Clair

Drainage Main Rehabilitation in Iowa

M. J. Helmers, S. Melvin, and D. Lemke

ET in Water Rights and Water Transfers 1

Alfalfa Reference ET from a Weighing Lysimeter and Estimates from the ASCE Standardized Reference ET Equation in the Arkansas Valley of Colorado

Allan Andales, Dale Straw, Thomas Ley, and Abdel Berrada

ASCE Standardized Penman-Monteith Alfalfa Reference ET and Crop ET Estimates for Arkansas River Compact Compliance in Colorado

Thomas W. Ley, Dale E. Straw, and Robert W. Hill

Interstate Collaboration in the Arkansas River Compact Compliance Process: The “Nuts and Bolts” of Developing PET for Canal Service Areas for Input to the H-I Model

Mary Kay Brengosz

Overview of Development and Use of Crop ET Estimates with Hydrological Models for Interstate Compacts

Dale E. Book and Mary Kay Brengosz

ET in Water Rights and Water Transfers 2

Adjusting Wind Speed Measured over Variable Height Alfalfa for Use in the ASCE Standardized Penman-Monteith Equation

Thomas W. Ley, Richard G. Allen, and Marvin E. Jensen

Estimation of Evaporation and Evapotranspiration during Nongrowing Seasons Using a Dual Crop Coefficient

Richard G. Allen and James L. Wright

Evapotranspiration and Net Irrigation Water Requirements for Nevada

J. L. Huntington and R. G. Allen

Integrated Water Management in an Ancestral Water Scheme in a Mountainous Area of Southern Spain

G. Vivas, E. Gómez-Landesa, L. Mateos, and J. V. Giráldez

ET Measurement and Calculation

Comparison of Sensible Heat Flux Measurements by a Large Aperture Scintillometer and Eddy Correlation Methods

Xinhua Jia, Xiaodong Zhang, and Dean D. Steele

Mid-Summer Deficit Irrigation of Alfalfa as a Strategy for Saving Water

B. R. Hanson, K. M. Bali, S. B. Orloff, B. L. Sanden, and D. Putnam

Recursive and Explicit Combination Methods for Calculating Reference Evapotranspiration

C. H. Hay and S. Irmak

Some Results of Evapotranspiration Measured by Three Weighing Lysimeters in La Mancha, Spain

R. López-Urrea, A. Montoro, P. López-Fuster, and F. Martín de Santa Olalla

Irrigation and Drainage Issues

Application of SIRMOD to Evaluate Potential Tailwater Reduction from Improved Irrigation Management

Byron Clark, Lindsay Hall, Grant Davids, Wynn Walker, and John Eckhardt

Evaluation of Magnetic Meters for Irrigation Pipeline Measurement

Stuart W. Styles and Bryan Busch

Increasing Field Work Productivity in Irrigation Evaluation Processes through the Use of Combined Irrigation Models

Sergio Lecina, Christopher M. U. Neale, Gary P. Merkley, and Carlos A. C. dos Santos

Neighborhood Channel is Redefined with Boulder Armoring

Ted Niemann and John Loechle

Landscape Irrigation Scheduling and Water Management

Evaluation of Irrigation Scheduling Efficiency and Adequacy by Various Control Technologies Compared to Theoretical Irrigation Requirement

Mary McCready and Michael D. Dukes

Irrigation Rain Sensors Accuracy

B. Cardenas-Lailhacar, M. D. Dukes, and L. Meaks

Preliminary Results for Bench Testing of Evapotranspiration-Based Irrigation Controllers in Florida

Stacia L. Davis and Michael D. Dukes

The Use of Soil-Water Sensors in Turf Irrigation Control—How Effective Are They?

Garry L. Grabow, Michael Dukes, and Bir Thapa

Evapotranspiration

Application of SVMs Algorithms for Prediction of Evaporation in Reservoirs

Arun Goel

Controlled Drainage Effects on Crop Yield and Water Use Efficiency under Semi-Arid Conditions of Iran

Negar Sharifi Mood, Masoud Parsinejad, and Farhad Mirzaei

Estimation of Regional Reference Evapotranspiration from Land Surface Temperature and Co-Kriging Method at Tehran Province, Iran

Mahdi Shahabifar, Maryam Chaichi, and Mahdi Kouchakzadeh

Remote Sensing of ET 1

Comparison of Evapotranspiration Estimates from Remote Sensing (SEBAL), Water Balance, and Crop Coefficient Approaches

Bryan Thoreson, Byron Clark, Richard Soppe, Andy Keller, Wim Bastiaanssen, and John Eckhardt

Independent Comparisons among Calibration and Output of Energy Balance Components Estimated by the METRIC Procedure

J. H. Kjaersgaard, P. H. Gowda, R. G. Allen, and T. A. Howell

Measuring Soil Moisture in a Heterogeneous Field

Chadi Sayde, John Selker, and Marshall English

Performance Evaluation of Soil Heat Flux Models in Great Plains

R. K. Singh, A. Irmak, E. A. Walter-Shea, and S. B. Verma

Remote Sensing of ET 2

Application of Remote Sensing Based Tillage Mapping Technique to Evaluate Water Quality Impacts of Tillage Management Decisions in Upper White River Basin

Shashank Singh, Indrajeet Chaubey, and Prasanna H. Gowda

Automated Selection of Anchor Pixels for Landsat Based Evapotranspiration Estimation

J. H. Kjaersgaard, R. G. Allen, M. Garcia, W. Kramber, and R. Trezza

Mapping ET at High Resolution in an Advective Semi-Arid Environment with Airborne Multispectral Imagery

J. L. Chávez, P. H. Gowda, T. A. Howell, L. A. Garcia, and K. S. Copeland

Local Issues—Kansas City Regional Topics

Brentwood Stream Restoration Project – Lenexa, Kansas

Anthony Hall and Tom A. Jacobs

Golden Eagle—Brown County, Kansas: Emergency Streambank Stabilization

James M. Alexander

Hutchinson, KS—4th and Carey Groundwater Remediation and Reverse Osmosis Water Treatment Facility Project

Danita S. Boettner, Don Koci, Darren L. Brown, and Bruce Allman

Hutchinson, KS—4th and Carey Site Groundwater and Source Control Measures at Two Grain Elevators

Darren L. Brown, Danita S. Boettner, and Don Koci

Impacts of Biota on Bioretention Cell Performance during Establishment in the Midwest

A. M. Greene, S. L. Hutchinson, R. Christianson, and T. L. Moore

Importance of Levees in the Kansas City Area

David W. Renetzky and John Grothaus

Kansas City, Missouri Wet Weather Solutions Program: A Twelve Step Program

Erin Ollig and Sheila Shockey

Kansas City, MO Overflow Control Program: Line Creek/Rock Creek Sanitary Sewer Study

Jeffrey W. Davies

Lake Winnebago Dam Relocation Project

Jonathan L. Polak and Shannon W. Tyree

Zona Rosa and Rush Creek Conservation Area—Applied Ecology in a Mixed-Use Development

J. J. Dremsa and D. M. Mensing

Modeling Impacts of Conventional and Low Impact Stormwater Controls on Receiving Streams

Elise Ibendahl and Dan Medina

Potable Water from a Superfund Site?

Marc Schlebusch

Riveside-Quindaro Bend Levee (L-385) on the Missouri River: The Essential Role of O&M and

Documentation

Gary W. Creason

Protecting Infrastructure: Emergency Streambank Stabilization

John Grothaus, Ken Markwell, Pete Jarchow, and John Blancett

The Impact of Smaller Detention Basins on Flood Hazard Areas in Lenexa, Kansas

Elangovan Karuppasamy, Natalie Postel, Christine A. Pomeroy, and Tom A. Jacobs

Water Quality of Streams in Johnson County, Kansas, 2002-07

T. J. Rasmussen

Water-Quality Assessment of the Largely Urban Blue River Basin, Metropolitan Kansas City, USA, 1998 to 2007

Donald H. Wilkison, Daniel J. Armstrong, and Sarah A. Hampton

Planning and Management

A Bayesian Framework for Cost Effective Management of Sediment Reduction in the Minnesota River Basin

Sarah K. Jacobi, Pearl Zheng, Benjamin F. Hobbs, and Peter R. Wilcock

A Decentralized Optimization Algorithm for Multi-Agent System Based Watershed Management

Yi-Chen E. Yang, Ximing Cai, and Dušan M. Stipanovi•

A Decision Support System for Water Resources Planning and Management for the North Slope of Alaska

Amy C. Tidwell, Kelly Brumbelow, Stephen F. Bourne, and William E. Schnabel

A Framework for Determining the Possible Impacts of a Changing Climate on Water Supply

Mark Summerton and Roland Schulze

A GIS-Based Decision-Making Methodology for Evaluation of Environmental Justice Impacts of Community Infrastructure Projects

James S. Cole, Kathleen M. Trauth, and Yingkui Li

A Pragmatic Cycle for Ongoing Water Resources Research and Management

Thomas L. Singleton, Stephen Bourne, and Jack Hampson

A Spatio-Temporal Drought Analysis for the Midwestern US

Shih-Chieh Kao, Rao S. Govindaraju, and Dev Niyogi

Agent Based Models for Simulation of Watersharing in a River Basin

S. Mohan and K. Santhosh Kumar

Analysis on Effect to EVW from Policy Intervention

Ben-qing Ruan, Chun-ling Zhang, Cheng-li Wang, and Feng-ran Xu

Application of Genetic Algorithms for Estimation of Flood Routing Model Parameters

S. Mohan

Application of Multi-Objective Differential Evolution Algorithm (MDEA) to Irrigation Planning

Josiah Adeyemo and Fred Otieno

Assessing Potential Implications of Climate Change for Long-Term Water Resources Planning in the Lower Colorado River Basin

Susan Butler, Armin Munevar, Ron Anderson, and Joseph Rippole

Asymptotic Variance of Regional Growth Curve for Generalized Logistic Distribution

Hongjoon Shin, Woosung Nam, Younghun Jung, and Jun-Haeng Heo

Balancing the Budget: A Limited Detail Approach to Flood Studies

Andrew J. Bonner

Climate Flow Forecast Model for the Brazilian Hydropower System

Mario T. L. Barros, João E. G. Lopes, Renato C. Zambon, Alberto L. Francato, Paulo S. F. Barbosa, and Fabio R. Zanfelice

Collaborative Groundwater Model Development

David W. Barfield

Communicating Drought Severity and Re-Evaluating Firm Yield—Cumberland County, Tennessee As a Case Study

Lars Hanson and Stuart Stein

Computer-Aided System for Managing, Controlling, and Analyzing Data from Hydroelectric Plants

Ieda G. Hidalgo, Darrell G. Fontane, Secundino Soares Filho, and Marcelo Augusto Cicogna

Copula Approach for Reducing Uncertainty in Design Flood Estimates in Insufficient Data Situations

Hemant Chowdhary and Vijay P. Singh

Deriving Rule Curve for Hydropower Reservoirs: Seymareh Experience

F. Sharifi, M. R. Jalali, and R. Afzali

Detection of Streamflow Trends and Variability in Karun River, Iran as Parts of Climate Change and Climate Variability

Alireza Farrokhi and Ahmad Abrishamchi

Developing Artificial Neural Networks to Represent Salinity Intrusions in the Delta

Francis I. Chung and Sanjaya A. Seneviratne

Developing Best Practices for Computer Aided Dispute Resolution

S. Langsdale and L. Bourget

Development of a Fuzzy Based Pipe Condition Assessment Model Using PROMETHEE

Yi Zhou, Kala Vairavamoorthy, and Frank Grimshaw

Development of Regression Models to Estimate Flow Duration Statistics at Ungaged Streams in Oklahoma Using a Regional Approach

Rachel A. Esralew

Development of Sustainable Water Supply Scheme in Reservoir Operation: Case Study

M. Karamouz, S. Nazif, and S. Mohammadi

Developments on Stochastic Analysis, Modeling, and Simulation (SAMS 2009)

J. D. Salas, O. Sveinsson, T. S. Lee, W. Lane, and D. Frevert

Does Collaborative Modeling Lead to Better Management of Our Water Resources?

S. Langsdale and W. Michaud

Flow Augmentation for Dissolved Oxygen Improvement in Chicago Waterways

Emre Alp, Charles S. Melching, and Richard Lanyon

Examining the Flow Regime Alteration and Its Potential Impacts to Freshwater Ecosystems under Changing Climate Conditions

Jian-Ping Suen

FEMA Flood Map Accuracy

David R. Maidment

Generating Different Scenarios of BMP Designs in a Watershed Scale by Combining NSGA-II with SWAT

P. Kaini, K. Artita, and J. W. Nicklow

Hardening a Great and Growing City's Water Supply

Scott Knight

High Resolution Radar Precipitation Evaluation

Dennis Miller, Shaorong Wu, David Kitzmiller, and Feng Ding

Hydrologic Modeling for Assessing Climate Change Impacts on the Water Resources of the Rio Conchos Basin

Eusebio Ingol-Blanco and Daene C. McKinney

Hydrological Feasibility of Environmental Flows in the Rio Grande/Bravo Basin

Samuel Sandoval-Solis and Daene C. McKinney

Impacts of the Upstream Storage Reservoirs on Itaipu Hydropower Plant Operation

Mario T. L. Barros, Renato C. Zambon, João Eduardo G. Lopes, Paulo S. F. Barbosa, Alberto L. Francato, and William W.-G. Yeh

Inflow Forecasting for Real-Time Reservoir Operation Using Artificial Neural Network

Taesoon Kim, Gian Choi, and Jun-Haeng Heo

Integrated Management of a Finite Water Supply in the Desert

Daniel Wendell, Steve Shultz, and Aditya Tyagi

Long-Lead Forecasting of Monthly Rainfall Using Large Scale Climate Signals and Statistical Disaggregation Models

Azadeh Ahmadi, Mohammad Karamouz, Sara Nazif, and Navideh Noori

Looking for a Solution—Joint Front Range Climate Change Vulnerability Study

Alfredo Rodriguez and Laurna Kaatz

Managing Salinity in the Upper Santa Clara River System of California

Nathan Brown, Brian Louie, Frank Guerrero, Terry Foreman, Sorab Panday, Vivek Bedekar, and Jagjit Kaur

Modeling Techniques to Incorporate Low Impact Development Features into Detention Analyses

Kristin White and Jennifer J. Walker

MOPSO in Multipurpose Operation of Single-Reservoir System

E. Fallah-Mehdipour, O. Bozorg Haddad, and M. A. Mariño

Multi-Criteria Decision Making under Uncertainty in Rainfall-Runoff Calibration: A Fuzzy Compromise Programming Approach Based on Alpha Level Sets

M. Shafii and F. De Smedt

Multiobjective Differential Evolution and Differential Evolution for Irrigation Planning

Piyush Gupta, A. Vasan, and K. Srinivasa Raju

Multireservoir Simulation Using Multipurpose Constraints and Object-Oriented Software Design

Marcelo A. Cicogna, Darrell G. Fontane, Ieda G. Hidalgo, and João E. Lopes

Nonlinear Dependence in Hydrologic Time Series

H. S. Kim, B. Sivakumar, and E. T. Lee

Paleo Pacific Ocean Sea Surface Temperature Variability and Upper Colorado River Basin Streamflow

Oubeidillah A. Aziz and Glenn A. Tootle

Planning for Climate Change

John A. Kliem

Probabilistic Streamflow Forecasts Based on Hydrologic Persistence in Central Texas

Wenge Wei and David W. Watkins, Jr.

Providing a Physical Basis for Statistical Homogeneity in Regional Frequency Analyses

Fredline Ilorme and Veronica W. Griffis

Reducing Uncertainty of Continuous Streamflow Predictions in Ungauged Basins (PUB) Using Regional Constraints: Using Regional Constraints for PUB

T. Wagener

San Joaquin River Restoration Program Monitoring and Management Plans

J. Payne and D. Mooney

Selection of Overflow Control Strategies for the Austin Clean Water Program

Joseph D. Smith and Eric D. Loucks

Spatial Evolutionary Algorithms for Characterizing Large-Scale Spatial Groundwater-Vegetation Dynamics in Arid Region

Jihua Wang, Ximing Cai, and Albert J. Valocchi

Study on the Water Value Conversion between Economy and Ecology and Countermeasures of Water Resources Distribution for Coordinated Development of Economy and Ecology

Hongzhen Ni, Hao Wang, Bo Zhao, and Dangxian Wang

The Implications of Discretizing Continuous Random Variables: An Example Using the U.S. Geological Survey Reporting Standards for Streamflow Data

Stacey A. Archfield and Richard M. Vogel

Uncertainty Analysis: You Need to Know What You Don't Know

David T. Williams and Joseph D. Countryman

Uncertainty and Sensitivity Analysis for Models with Calibrated Parameters

Seung Uk Lee and Jery R. Stedinger

Vulnerability of the Hydraulic Resources of the River Basin of the San Juan-Brave River with the Global Climatic Change

Rodríguez García José Luis and Cardoso Landa Guillermo

Water Demand Forecasting for the City of the Future against the Uncertainties and the Global Change Pressures: Case of Birmingham

K. B. Khatri and K. Vairavamoorthy

Water Quality Effects of Varying Crop, Fertilizer, and Carbon Prices

T. L. Ng, J. W. Eheart, and X. Cai

Water Resources Planning under Non-Stationary Hydroclimate in a Snow Dominant Watershed

Francis I. Chung, Tariq N. Kadir, and Jefferey K. Galef

Water Supply and Energy Generation

L. K. Lampe, L. M. Adams, and D. G. Jensen

Watershed Management in the Indian Himalayan Region: Issues and Challenges

Samagra Rana and Vaibhav Gupta

Whatever It Takes: From Water Availability Model to Cost of Water

Alfredo Rodriguez

Student and New Professionals

Student Author Competition Winners

Current Water Management Practices and the Effects of Climate Change on the Colorado River Basin

J. Brandon Klenzendorf

Does Polymer Have an Effect on Bacterial Regrowth in Anaerobically Digested Biosolids?

Jean M. Ryan

Effect of Acid Mine Drainage on Aluminum Release from Clay Minerals

Oscar Vazquez

Sensitivity Analysis of HEC-HMS Hydrologic Model to the Number of Sub-Basins: Case Study

Osama Z. Al-Hamdan

Study of Low Dosage Pre-Ozonation on Sand Filtration Efficiency

Walter Lee Ellenburg

The Dubai Palms: Construction and Environmental Consequences

Ethan Poole

Water, Wastewater, and Stormwater

Retrofitting Stormwater BMPs

Developing Green Streets Prototypes to Reduce Combined Sewer Overflows for Cincinnati, Ohio

Brian Marengo, Thomas Cahill, Daniel Wible, Courtney Marm, and Ralph Johnstone

Implementation and Performance of Stormwater Best Management Practice Retrofits in Wilmington, NC

J. D. Wright, W. F. Hunt, M. R. Burchell II, C. A. Perrin, and E. R. McCoy

Modeling Stormwater Basins for Potential Retrofit Designs

R. R. Headley and J. R. Wyrick

Stormwater Infiltration Retrofits: Experience Gained through Long Term Monitoring

R. G. Traver

Stormwater Research I

A Tool for Determining Effectiveness and Whole Life Costs of BMPs

C. C. Olson, L. A. Roesner, and B. R. Urbonas

Controlled Full-Scale Field Testing of an Up-Flow Filtration Device

Noboru Togawa and Robert Pitt

The Observed Effects of Stormwater Infiltration on Groundwater

M. D. Machusick and R. G. Traver

Water Quality Assessed by Benthic Macro-Invertebrates: Proposing the WQABI Method

J. K. McNett and W. F. Hunt

Stormwater Research II

A Robust and Fast Model for Simulating Street Flooding

Arturo S. León, Leonardo S. Nanía, Arthur Schmidt, and Marcelo H. García

Evaluating the Mixing Mechanism of Outfall Discharges from Municipal Separate Storm Sewer Systems

Michael H. Woo

Physical Processes Resulting in Geyser Formation in Rapidly Filling Stormwater Tunnels

Steven J. Wright, James W. Lewis, and Jose G. Vasconcelos

The "Silver Bullet": Proprietary BMPs and Metropolitan St. Louis Sewer District's Stormwater Program

J. S. Hoskins and M. T. Buechter

Security Enhancements in Water and Wastewater Utilities 1

Survey of Water and Wastewater Utility Security Standards

Dale Gabel, Yakir J. Hasit, and Yaron Ben Ari

Security Enhancements in Water and Wastewater Utilities 2

Advances in Data Validation, Event Detection, and Communications Structures for a CWS: Case Study—Glendale, Arizona

Kenneth A. Thompson, Rick Scott, Raja Kadiyala, Andreas Weingartner, and Joep van den Broeke

Implementing a Contamination Warning System at a Department of Defense Facility: Case Study—Port Hueneme, California

Kenneth A. Thompson, Steve Fann, Raja Kadiyala, Yakir J. Hasit, and Gary Jacobson

Concentrate Management in Desalination I

Concentrate Management and Disposal Practices in Australia

James H. Jensen

Desalination of Brackish Groundwater and Deep Well Injection of Concentrate in El Paso, Texas

William R. Hutchinson

Membrane Treatment of Rio Grande Water for Municipal Water Production during the Non-Irrigation Season

Anthony J. Tarquin, Michael P. Fahy, and John E. Balliew

Synopsis of National Research Council's Report on Desalination

Sandeep Sethi

Concentrate Management in Desalination 2

Cost Comparison of Membrane Treatment and Concentrate Management Practices at Drinking

Water Treatment Plants in Florida

Berrin Tansel and Irina Sosnikhina

Desalination Concentrate: Bay vs. Ocean

Patrick Treanor and Val S. Frenkel

Future Water Supply Desalination Technology: Forward Osmosis Co-Located with Power Generation

Tina Coop and Les Lampe

New Strategies for Managing Desalination Concentrate with Zero Liquid Discharge from Two WRF Research Projects

Rick Bond and Srinivas Veerapaneni

Water. Wastewater, and Stormwater Topics

A Mobile Emergency Drinking Water System Powered by Renewable Energy

Matthew Vitello, Andrew Curtis Elmore, and Mariesa Crow

Adding Value to Sanitary Sewers—An Important Asset of Municipalities

V. Firat Sever and Barton Bradshaw

Ecosystem Services Approach to Public Facility Planning

A. Yap, G. Honan, and M. Kealy

An Evaluation of Graywater Reuse Utilizing a Constructed Wetland Treatment System

A. W. Jokerst, L. A. Roesner, and S. E. Sharvelle

Application of Enhanced Methods of Phosphorous and Nitrogen Removal from Wastewater

Mohammad Reza Fallahpour, Mojtaba Fazeli, and Seyed Ahmad Mirbagheri

Bench-Scale Ozonation of Raw Industrial and Municipal Wastewater

Richard O. Mines, Jr., Cary M. Oglesby, and Laura W. Lackey

Biological Nutrient Removal from On-Site Wastewater Treatment Systems Using a Membrane Aerated Bioreactor

Zhihua Liang and Zhiqiang Hu

Boundary Conditions for Simulating Complex Storm-Sewer Systems in Free Surface, Pressurized, and Mixed Flow Conditions

Arturo S. León, Xiaofeng Liu, Mohamed S. Ghidaoui, Arthur R. Schmidt, and Marcelo H. García

City of St. Louis Permeable Pavement Alley Pilot Study

Dave Yates and Marjorie Melton

Competing Risks and the Development of Adaptive Management Plans for Water Resources: Field Reconnaissance Investigation of Risks to Fishes and Other Aquatic Biota Exposed to Endocrine Disrupting Chemicals (EDCs) in Lake Mead, Nevada, USA

Greg Linder and Edward E. Little

Construction of a Low-Flow Channel in Barber Creek: Case Study in the Powder River Basin, Wyoming

Robert W. Thoman and J. J. Brown

Decentralized Anaerobic Treatment of Blackwater: A Sustainable Development Technology Concept for Urban Water Management

N. T. Gallagher and S. Sharvelle

Development of a National GIS Database for Municipal Water and Wastewater Pipe Infrastructure System

Sunil Sinha, Randy Dymond, Rahul Vemulapally, Thomas Dickerson, and Seth Perry

Engineering Natural Filtration Systems to Remove Selenium, Nitrate, and Bacteria from Impaired Surface Waters—Foundational Studies

Ken Susilo, Eric Strecker, and Randy Sundberg

Extension of an LA-QUAL Model for Evaluating a Proposed Wastewater Discharge to Realistic Receiving Water Temperature and Flow Conditions

Chris Herrington

Gray Water and Treated Effluent Reuse

Steven Roznowski, Kristofer Bruun, and Larry Roesner

Green Alternatives to Channel Stabilization

Richard E. Besancon

Hydraulic Modeling and Engineering Evaluation of Fort Myers Beach's Water Distribution System

Jinsheng Huo, Robert Garland, Doug Eckmann, Jack Green, and Cathie Lewis

Innovative Strategies Alleviate Water Stress in South East Queensland, Australia

Hua Jiang, Scott Freeman, and Jonathan Bates

Multi-Objective Design of Transient Network Models

Bong Seog Jung, Misgana Muleta, and Paul F. Boulos

Municipal Water Systems in the Columbia River Basin: A Portfolio Management Approach for Multiple Benefits

Mark A. Anderson

Reliability Based Design of Water Distribution Network (WDN) Considering the Reliability of Nodal Pressures

N. Ghajarnia, O. Bozorg Haddad, and M. A. Mariño

Removal of Selenium and Nitrate from Surface Waters Using a Subsurface Microbial Filter

Stephen Lyon, Scott Lynch, Imad Feghali, and Randy Sundberg

Research and Application of Activated Sludge Models

Jinsheng Huo, Min Ji, and Yan Jiang

Risk Assessment to the Environment Due to Anionic Surfactants in Treated Sewages and Dried Sludges

Arvind Kumar Mungray and Pradeep Kumar

Riverbank Filtration for Water Supply: Indian Experience

Pradeep Kumar and Indu Mehrotra

Sustainable Design and Construction of Earthen-Dam Reservoirs for Water Produced in Association with Coalbed Natural Gas in the Powder River Basin, Wyoming

J. J. Brown and Robert W. Thoman.

Sustainable Development of Agriculture: Urban Waste Water a Viable Mean for Irrigation

Chhedi Lal and Vaibhav Gupta

Treatment Performance of Wastewater Lagoons in South Yungas Province of Bolivia

Helen E. Muga, James R. Mihelcic, Nathan W. Reents, Santiago Morales, Gabriela Gemio, Meredith Ballard, Valerie J. Fuchs, Cara M. Hanson, Esther M. Johnson, and Alison M. Hoyt

Understanding and Controlling Fouling in Membrane Bioreactors

Roger Babcock, Jr.

Using Media Filters in a Distributed Wastewater System Serving an Ecotourism-Oriented Development

Kevin M. Sherman

Water Treatment Industry Course Correction

John A. Kliem

Watershed

Debris Flow Hazard Analysis and Modeling

Associated Disasters to the Debris Flows

Guillermo Cardoso-Landa

Experimental Analyses of Sedimentation in the Slit Dam Reservoir

Mohammad Ebrahim Banihabib and Ehsan Bahram

Great Rivers of the World

Geochemistry of Yukon and Copper River Tributaries, Alaska

Melissa Carney, Andre Ellis, Thomas Bullen, and Jeff Langman

The Hydrology of the Congo River Basin: A GIS-Based Hydrological Water Balance Model

J. Bahati Chishugi and B. F. Alemaw

Preliminary Assessment of Planform Change at Low Flows with Vegetation Expansion: Platte River, Nebraska

Lisa M. Fotherby

Sediment Management for Shallow Water Habitat Creation on the Missouri River

Michael Gossenauer

Hydrologic Monitoring Network

Design of Solar Radiation Sensor Network Using Geo-Statistical Methods

Chandra S. Pathak, John R. Mecikalski, Ramesh S. Teegavarapu, and Jayanthi Srikishen

EPM Approach for Erosion Modeling by Using RS and GIS

Fazel Amiri and T. Tabatabaie

Evaluation of Improvised Spatial Interpolation Methods for Infilling Missing Precipitation Records

Alaa Aly, Chandra Pathak, Ramesh S. V. Teegavarapu, Jon Ahlquist, and Henry Fuelberg

Quantifying Uncertainty in Discharge Measurements: A New Approach

J. E. Kiang, T. A. Cohn, and R. R. Mason, Jr.

Land Use/Cover Changes and Water Quality/Quantity

Assessment of Lumped, Quasi-Distributed and Distributed Hydrologic Models of the US Army Corps of Engineers

Murari Paudel, E. James Nelson, and Charles W. Downer

Change in Surface Hydrology Due to Land Use Change in a Midwestern Watershed

A. Spencer, B. Walker, M. Arabi, J. Frankenburger, and R. S. Govindaraju

Do Upland Soil Conservation Measures Reduce Watershed Sediment Yield?

Jurgen D. Garbrecht and Patrick J. Starks

Human Impact on the Mobilization of a Naturally-Occurring Source of Selenium in an Urbanizing Catchment

Rachel Andrus, Barry Hibbs, and Andre Ellis

Long Term Effect of a Stream Restoration Plan on Water Quality

Yuan Cheng

Measurement of Velocity and Discharge of a Stream Using a New Floating Rod Equipped with a GPS Receiver

W. Kim and C. Lee

Prediction of Nitrate Concentration in Stream Water Based on Watershed Land Use and Stream Flow Rate

Jingjie Teng, Mira Olson, Patrick Gurian, Anna Sofranko, Janet Herman, and Aaron Mills

Studying the Impact of Land Use/Cover Changes on the Water Quality of Weeks Bay, AL: Model

vs. Regression

Harsh Vardhan Singh, Latif Kalin, and Graeme Lockaby

Mississippi River Basin

Modeling the Hydrology and Hydraulics of the Cache River System

Misganaw Demissie, Laura Keefer, Yanqing Lian, Feng Yue, and Elias Bekele

The Mississippi River: A National Resource

Nancy G. Bhowmik

The Nature Conservancy's Mississippi River Program: Sustainable Conservation of a Working River that Works

C. Stephen Haase and K. Douglas Blodgett

Modeling Hydroclimate

Historical Reconstruction of Hydroclimatic Data Based on the Control Runs of GCMs over Sabah and Sarawak, Malaysia

Noriaki Ohara, M. Levent Kavvas, ZhiQiang Chen, and Ahmad Jamalluddin bin Shaaban

Statistical Characteristics of Land Surface Properties for the Regional Hydroclimate Model

S. Kure, S. Jang, N. Ohara, and M. L. Kavvas

Modeling Hydroclimate—Statistical Approaches

Modeling the Kinematic Wave Parameters with Regression Methods

I. Haltas

On the Use of Data Uncertainty in Hydro-Climatic Modeling: A Bayesian Approach

Shivam Tripathi and Rao S. Govindaraju

NEXRAD Data Analysis

Adjustment of the Z-R Relationship in Real-Time for Use in South Florida

Amy Henschke, Emad Habib, and Chandra S. Pathak

Radar-Rainfall Analysis for Extreme August Storm in Sacramento

David C. Curtis

Use of Lightning and Storms Life Cycle Information in Radar Rainfall Estimation

Emmanouil N. Anagnostou, Chandra S. Pathak, and C. A. Morales

Use of NEXRAD Rainfall Data to Develop Climatologically Homogenous Rain Areas for Central and South Florida

Chandra S. Pathak, Matthew Onderlinde, and Henry E. Fuelberg

NEXRAD Data Analysis and Application

Impacts of Different Rainfall Estimates on Hydrological Simulation and Satellite Rainfall Retrieval

Error Propagation

Tadesse Meskele and Hamid Moradkhani

NEXRAD Data Application to Hydrologic Modeling

Application of NEXRAD for Freshwater Inflow Estimates to Texas Bays and Estuaries

Ruben S. Solis and Qingguang Lu

Distributed Hydrologic Modeling: From Research to Operational Forecasting

Michael Smith, Victor Koren, Ziya Zhang, and Zhengtao Cui

Flash Flood Forecasting for Ungauged Locations with NEXRAD Precipitation Data, Threshold Frequencies, and a Distributed Hydrologic Model

Brian A. Cosgrove, Seann Reed, Feng Ding, Yu Zhang, Zhengtao Cui, and Ziya Zhang

Gauge-Based Adjustment of Historical Multi-Sensor Quantitative Precipitation Fields and Resulting Effects on Hydrologic Simulations

Yu Zhang, Seann Reed, David Kitzmiller, and Daniel Brewer

Prediction Tools in Watershed Management

Estimating Probability of Extreme Events

Jeff Harris, Gary Brunner, and D. Michael Gee

Prediction of Changes in Soil Moisture Due to Rainfall, Infiltration, and Evapotranspiration Using a Physically-Based Model

Zhiguo He, Weiming Wu, and Sam S. Y. Wang

Reining in Log-Pearson Type III Flow-Frequency Estimates—Applying a Reasonable Bound through the Skew Parameter

Ben Tustison and Joseph D. Countryman

Understanding Water Quality Responses to Long-Term Acidic Deposition in a High-Elevation Southern Appalachian Watershed: A Focus on Soil Watershed Processes

Meijun Cai, John S. Schwartz, R. Bruce Robinson, Steve E. Moore, and Matt A. Kulp

Probabilistic Approaches for Watershed Processes 1

Estimation of TMDLs and Margin of Safety under Conditions of Uncertainty

Mohamed M. Hantush

Probable Maximum Precipitation for 24 Hour Duration over Four Central Provinces in Iran

M. Naseri Moghaddam, S. Ghazanfari, B. Ghahraman, and K. Davari

Regional Regression Analysis and the Rational Method

C. B. Young, B. M. McEnroe, and A. C. Rome

Stochastic Non-Equilibrium Bedload Transport Model

Ken Z. Kuai and Christina W. Tsai

Probabilistic Approaches for Watershed Processes 2

Parameter Uncertainty Estimation of Hydrologic Models Using Bootstrap Resampling

Mohammad Ebtehaj and Hamid Moradkhani

Optimization of Regional Stormwater Quality Control Systems Using Genetic Algorithms

Pradeep K. Behera and Ramesh S. V. Teegavarapu

Statistical Seasonal Streamflow Forecasting: An Intercomparison and Evaluation of Current Forecasting Procedures

Matthew Meier and Hamid Moradkhani

Watershed Management 1

Analysis of Water Quality Trends and Pollutant Loading for Cypress Creek Watershed

A. Teague, H. Robinson, and P. Bedient

Assessment of the Capability of Hydrologic and Artificial Neural Network Models for Flood Warning System in Land Use Change Condition

M. E. Banihabib and A. Arabi

Estimating Groundwater Pumping and Return Flow Based on Hydrologic Recession Analysis

Dingbao Wang and Ximing Cai

Historical Changes in the Streamflow in Kansas Streams: Variation, Causes, and Implications

Jonathan P. Aguilar, James K. Koelliker, and Nicole Marie Dick

Modeling Water Quality Impacts in Delaware's Coastal Bays with AGNPS

William F. Ritter, Bret A. Icenogle, and Monika N. Meckley

Parameterization of Seasonal Freshets for the Study of Effects of Freshwater Inflows on Galveston Bay

Tony L. Smith, George H. Ward, Jr., William H. Espey, Jr., and Richard Browning

Runoffs of the Xiangride and Qaidum Rivers in the Arid Qaidum Basin, Northwest China

S. Jia, S. Lin, Z. Sheng, R. Li, D. Liu, H. Yan, and N. Feng

Watershed Management 2

Design and Implementation of Optimized Hydrologic Unit Watersheds for Rainfall-Runoff Modeling

Ivan Rivas and Larry A. Roesner

Effects of Rainfall-Runoff on Soil Surface Roughness and Erosion Processes

D. C. Dermisis and A. N. (Thanos) Papanicolaou

Hydrologic Modeling and Flood Frequency Analysis of the Sonora River Watershed in Sonora, Northwest Mexico

Maureen L. Habarth and Brian D. Barkdoll

Integrated Watershed Protection Plan and Management Strategy for the Calleguas Creek Watershed in Ventura County

Kathleen Higgins, E. Zia Hosseinipour, and Jeff Friesen

McCormick Place West Hall Conference Center Stormwater Reclamation Tunnel and "Green Roof" Helps Advance Chicago's Clean Water Agenda

W. J. Weaver

Spatial Variation of Sediment Oxygen Demand in Athabasca River: Influence of Water Column Pollutants

Kusumakar Sharma, Preston McEachern, Mark Spafford, David Zhu, and Tong Yu

Watershed Management 3

A Comparison of a SWAT Model for the Cannonsville Watershed with and without Variable Source Area Hydrology

Josh Woodbury, Christine A. Shoemaker, Dillon Cowan, and Zach Easton

Effective Management of Natural Resources under Dry Land Farming through Watershed Basis

Murukannappa and N. Indrakumar

Evaluation of Uncertainties in the Simulation of Watershed Nutrient Load: A Case Study

M. Karamouz, M. Taheriyoun, M. Seyedabadi, and S. Behboodian

Modeling Framework for Establishing Water Quality Trading Units near Pacific, Missouri

Yee-Sook Shin and Kathleen M. Trauth

Statistical Evaluation of BMP Effectiveness in Reducing Nutrient Impairment in Mermentau and Vermilion-Teche River Basins

Z.-Q. Deng and H. Chowdhary

Using "Big Data" to Optimally Model Hydrology and Water Quality across Expansive Regions

Edwin A. Roehl, Jr., John B. Cook, and Paul A. Conrads

Watershed Modeling 1

Application of Northeast Regional Climate Center Research Results for the Purpose of Evaluating and Updating Intensity-Duration-Frequency (IDF) Curves –Case Study: Rochester, New York

S. B. Wolcott, M. Mroz, and J. Basile

Assessment of Flood Risk Due to Storm Surge in Coastal Bayous Using Dynamic Hydraulic Modeling

T. Ray, Z. Feng, and P. B. Bedient

Effects of Freezing and Thawing Processes on Bank Stability

Fabienne Bertrand and A. N. (Thanos) Papanicolaou

Integrated Surface Water and Groundwater Modeling of Orange River Basin in Southwest Florida for Flood Mitigation / Ecosystem Restoration

E. Zia Hosseinipour

Spatially Distributed Modeling of Soil Erosion and Sediment Transport at Watershed Scale

H. Zeinivand and F. De Smedt

The Role of the Clast Layer of Desert Pavement in Rainfall-Runoff Processes

Li Chen, Jun Yin, Julianne Miller, and Michael Young

Watershed Models for Storm Water Management: Comparing Hydrologic and Hydraulic Procedures

Deva K. Borah, Jamie H. Weist, Jack D. Wall, and David N. Powell

Water Subdivision for Modeling

Theodore G. Cleveland, Thuy Luong, and David B. Thompson

Wetlands

Integrated Watershed Modeling

Gour-Tsyh (George) Yeh, Guobiao Huang, and Hsin-Chi (Jerry) Lin

Understanding Uncertainties in Water Budget for Large Constructed Wetlands

R. Scott Huebner, Chandra S. Pathak, and Ramesh S. Teegavarapu

Preface

The **2009 World Environmental & Water Resources Congress** held in Kansas City, Missouri, May 17-21, 2009, consisted of over 700 presentations, special sessions and workshops. The theme of the Congress was **Great Rivers** with about 190 sessions that ranged from asset management to low-impact development to watershed modeling to hazardous waste management to large river habitat to groundwater quality to green infrastructure to urban hydrology topics. This year's technical program focused the engineering challenges of balancing environmental and development issues while achieving a sustainable future. It is imperative that those working on the front lines – at the environmental/water engineering nexus – share insights from research and practical experience in the field to generate best solutions for the future on issues such as river system management, environmental challenges, watershed management and restoration, dam safety, hydraulic structures, and so much more.

I greatly enjoyed and appreciated all the help from the about 100 volunteers and staff members that poured a lot of energy into the 2009 EWRI Congress. Everyone was a critical component to the Congress being a success.

The 2009 World Environmental & Water Resources Congress Committee was:

General Congress Chair
William H. Espey, Ph.D., P.E., D.WRE, M.ASCE
Espey Consultants, Inc., Austin, TX
wespey@espeyconsultants.com

General Congress Co-Chair
Karen C. Kabbes, P.E., D.WRE, M.ASCE
Kabbes Engineering, Inc., Barrington, IL
KCKabbes@KabbesEngineering.com

Technical Program Chair
Steve Starrett, Ph.D., P.E., D.WRE, M.ASCE
Kansas State University, Manhattan, KS
stevestarrett@gmail.com

Technical Program Co-Chair
Roger W. Babcock Jr., Ph.D., P.E., M.ASCE
University of Hawaii at Manoa, Honolulu, HI
rbabcock@hawaii.edu

Local Arrangements Chair
Dave Renetzky, P.E., M.ASCE
HNTB Federal Services Corporation,
Kansas City, MO
drenetzky@hntb.com

Technical & Social Tour Chair
Sam Mryyan, Ph.D., REM
Adjutant General's Department, Topeka, KS
Sam.mryyan@us.army.mil

Partners, Exhibits & Sponsorship Chair
Donald W. Baker, P.E., M.ASCE
Water Resources Solutions, LLC
wrs@kc.surewest.net

Young Professionals & Student Activities Chair
Leon Staab, P.E., M.ASCE
Burns & McDonnell Engineering Company, Kansas City, MO
lstaab@burnsmcd.com

EWRI Director
Brian Parsons, P.E., M.ASCE
EWRI of ASCE, Reston, VA
bparsons@asce.org

Conference Manager
Stacey Ann P. Gardiner, CMP
301-934-8589 Phone
413-473-0324 Fax
stacey.gardiner@tggroup.com

The key 2009 Track Chairs follow, they certain had a lot of help from colleagues.

11th Water Distribution System Analysis Symposium - **Avi Osfeld**
Water Resources Planning and Management Track - **Eric Loucks**
Water, Wastewater & Stormwater Track, **Rob Traver, Richard Tsang**
6th Urban Watershed Management Symposium - **Scott Struck; Richard Field**
Emerging & Innovative Technologies – **Lily Anne Baldwin**
Engineering History & Heritage – **Jerry Rogers**
Education - **Cassie Klumpp**
Environmental Engineering & Public Health – **Alok Bhandari, Zhiqiang Hu**
7th Groundwater Hydrology, Quality, and Management Symposium - **Zhuping Sheng**
Hydraulics and waterways– **Jennifer Duan, Weiming Wu, George Constantinescu**
Watersheds – **Sharon Jean-Baptiste**
International Issues – **David Watkins**
Irrigation & Drainage – **Richard Allen**
Student Track – **Karen Kabbes**
Local Issues - **Sarah Fjell**

BURSTS IDENTIFICATION IN WATER DISTRIBUTION SYSTEMS

I. Borovik[1] , B. Ulanicki[2] and P. Skworcow[2]

[1]Bauman MSTU, 2-nd Baumanskaya, 5, 105005, Moscow, Russia; email: irencha11@rambler.ru
[2]De Montfort University, Process Control - Water Software Systems, De Montfort University, The Gateway, Leicester, LE1 9BH, UK; email: bul@dmu.ac.uk,

ABSTRACT

The leakage reduction problem as a whole is complex and requires co-ordinated actions in different areas of water network management, such as: direct detection and repair of existing bursts, general pipe rehabilitation programmes and operational pressure control. Water companies undertake a mixture of these complimentary actions. General pipe rehabilitation is the most costly and long term action, but is undertaken to improve a number of different factors including leakage and water quality. Operational pressure control is a cost-effective action for reducing leakage over whole sub-networks, and for reducing the risk of further leaks by smoothing pressure variations and is the subject of ongoing research. Detection and repair actions are targeted at sub-networks where bursts are present. Benefits of quick burst repair include reduced water losses, reduced disruption to traffic, reduced consequent losses (e.g. from flooding), and also reduced disruption to customers' supplies, which is an important water industry performance measure. The existing methods typically use passive identification approach whilst the presented approach is based on the active identification procedure.

The proposed burst location algorithm is based on comparing data by means of statistical analysis from a simple field experiment with results of water network simulation. An extended network hydraulic simulator is used to model pressure dependent leakage terms. The presence of a burst changes the flow pattern and also pressure at network nodes, which may be used to estimate the burst size and its location. The influence of such random factors as demand flows and background leakage on the process of burst detection is also considered. The field experiment is an extended fixed and variable orifice (e-FAVOR) test. During this test inlet pressure is being stepped up and down and the following variables are measured: inlet flow, inlet pressure (head) and pressure at a number of selected sensitive nodes. The method consists of three stages and uses two different models; one is inlet flow model (IFM) to represent the total inlet flow and another is the extended hydraulic model to simulate different burst locations. Initially the presence of a potential burst is investigated. If this is confirmed values of the demand, background leakage flow and burst flow in IFM are subsequently estimated. These are used to identify the burst site at the third stage of the method. The approach has been validated by solving a practical case study with correct diagnosis of the existing problems.

INTRODUCTION

The UK water industry is addressing the major challenge of reducing leakage in water distribution systems (WDS). Especially, unreported bursts are cause for concern with significant water losses and potential damage to urban infrastructure. Water distribution systems are complicated entities with thousands of interconnected pipes and other components. There is a need for developing efficient methods for identifying unreported bursts which remain invisible with the water draining away and never reaching the surface. Benefits of quick burst repair will also result in reduced disruption to customers, which is an important water industry performance measure.

Recently the UK water companies have heavily invested into restructuring water networks into smaller sub-networks known as District Metering Areas (DMAs). A DMA is a sub-network where the boundary flow is monitored in order to assess leakage. Its boundary is closed except for a low number of inputs and outputs with flow and pressure meters. This facilitates leakage management in terms of pressure control and bursts detection. When a new burst occurs it causes a noticeable increase in the minimum night flow (MNF) – and subsequently a burst location method can be applied. This research proposes such a method by exploiting different behaviour of background leakage and bursts under varying pressure (May 1994). John May proposed a pressure stepping experiment (FAVOR test) during which the inlet flow and inlet pressure were monitored. The authors of this paper observed that monitoring only the inlet variables is not sufficient even to estimate the size of the burst. Therefore, the test was extended to include additional measurements at a number of internal nodes in a DMA and is termed the extended FAVOR test (e-FAVOR test). The method comprises three steps: first performing the e-FAVOR test, subsequently estimating the size of the burst and finally identifying the burst location.

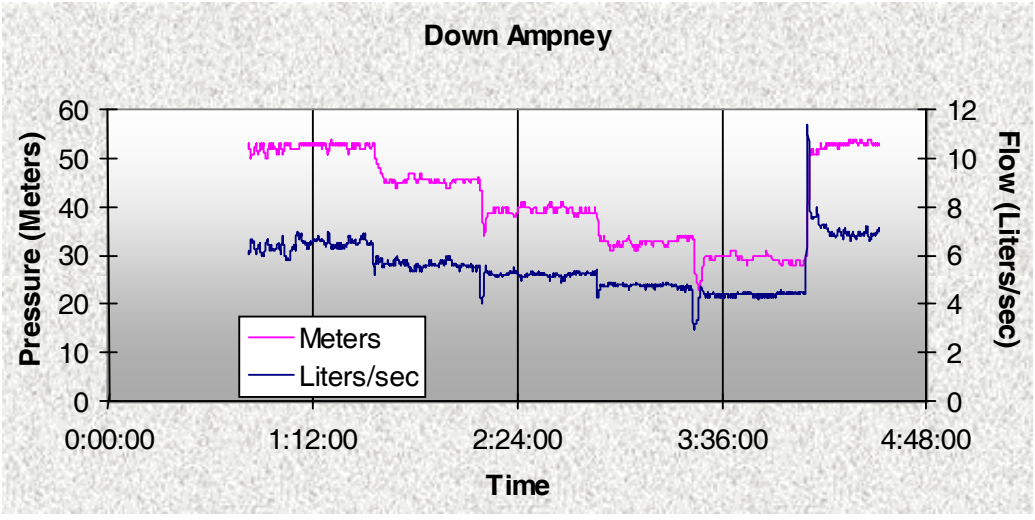

Figure 1. Typical results of the e-FAVOR Test – inlet flow and pressure

E-FAVOUR TEST

A typical e-FAVOR test is carried out during a night between 1 am and 5 am. The inlet pressure is changed stepwise over a typical range of values at 20-minute intervals during this period. Typical scenario of the inlet pressure and flow are depicted in Figure 1. It can be observed in Figure 1 that when the inlet pressure is changed stepwise, the flow changes in a similar manner. Note that only the steady-state data is considered and the data from the transient phase between steady states should be ignored.

It is not practical to measure internal pressure at all nodes in a DMA and therefore a small number of representative nodes (sensitive nodes) is selected for monitoring. The potential measurement points are hydrants and typically a water company is prepared to put 20 loggers for the experiment. The method of determining sensitive nodes has been developed by Prescott and Ulanicki (2006) and is related to that proposed by Bush and Uber (1998). The method uses the sensitivity matrix of the hydraulic model (Jacobian matrix) to determine how the pressure at each potential measurement node is affected by a burst at any node across the network. This matrix has dimension $m \times n$, where m is the number of potential pressure measurement points and n is the number of nodes in the network (possible burst location). The sensitivity matrix can be calculated from the network equations or extracted directly from a hydraulic simulator used in the method.

ESTIMATING THE BURST COEFFICIENT

The inlet flow can be represented by a three term inlet flow model (IFM):

$$q = d + c_1 p_i^{0.5} + c_2 p_{AZNP}^{1.5} \tag{1}$$

where d is an average total demand, p_i is pressure at a burst node, c_1 is the burst coefficient (related to the burst area), p_{AZNP} is average zonal night pressure and c_2 is the background leakage coefficient (related to the total area of the background leakage). The coefficients of the IMF can be estimated using least square method (LSM) from the available measurements for an assumed location of the burst.

It is assumed that the demand flow does not depend on pressure variations in a DMA and the average value of demand is constant over the considered period between 1 am – 5 am. The total background leakage flow represents the sum of all separate background leaks in a network and it is possible to use a single (common) coefficient of the background leakage c_2 and the Average Zonal Night Pressure p_{AZNP}.

The procedure is to assume the burst at a sensitive node and evaluate IFM model; this is carried out for each sensitive node using LSM. It is feasible because pressure p_i in model (1) is known from the e-FAVOR measurements. Note that number of obtained IFM models corresponds to number of sensitive nodes. Subsequently, the goodness of fit for each IFM model is tested using chi-square (χ^2) criterion and the best IMF model is selected to represent the burst flow and also the

demand and the background leakage flow. In order to verify the hypothesis, i.e. the compliance of the measured and calculated values of the inlet flow, the following measure is used:

$$\chi^2 = \sum_{k \in time\_steps} \frac{\left(q'_k - q_k\right)^2}{q'_k} \tag{2}$$

where q'_k = model flow, q_k = measured flow.

The algorithm of burst size estimation in a DMA has been implemented in the MATLAB package and progresses through the following steps:

1. Read Excel files containing the experimental data.
2. Prepare the matrix of pressures at the sensitive nodes and calculate the values of the Average Zonal Night Pressure.
3. In a case of a network with many inlets, add all inlet flows together to form a total inlet flow.
4. Solve the least squares problem for each sensitive node $i \in S$ where S is a set of sensitive nodes.
5. Choose the solution which corresponds to the minimum value of the chi-squared criterion.

The outputs of the algorithm are values of the IFM coefficients and the resulting theoretical inlet flows and the vector of the χ^2 criterion values.

IDENTIFICATION OF BURST LOCATION

It was important to find a sensitive indicator of a burst location and the gradient of a pressure line was a very good candidate. A pressure line is a functional relationship between the inlet pressure and the pressure at a chosen node. In absence of leakage it is a straight line with gradient equal to 1. In the presence of a burst the gradient becomes smaller than 1 and the minimum value of the gradient is attained for the burst node. If a small background leakage is added the general rule does not change and the order in the gradient values is preserved with the smallest gradient for the burst node and the biggest gradient for the inlet node as depicted in Figure 2.

The gradients can be found by the least squares method to minimise deviations of the approximating straight line from the experimental data. The following information should be available for the burst location identification:

- inlet pressure which is stepped during the field experiment
- pressure measurements at the sensitive nodes
- gradients of the regression pressure lines for the sensitive nodes
- the IMF model estimated at the previous stage
- hydraulic model of the network

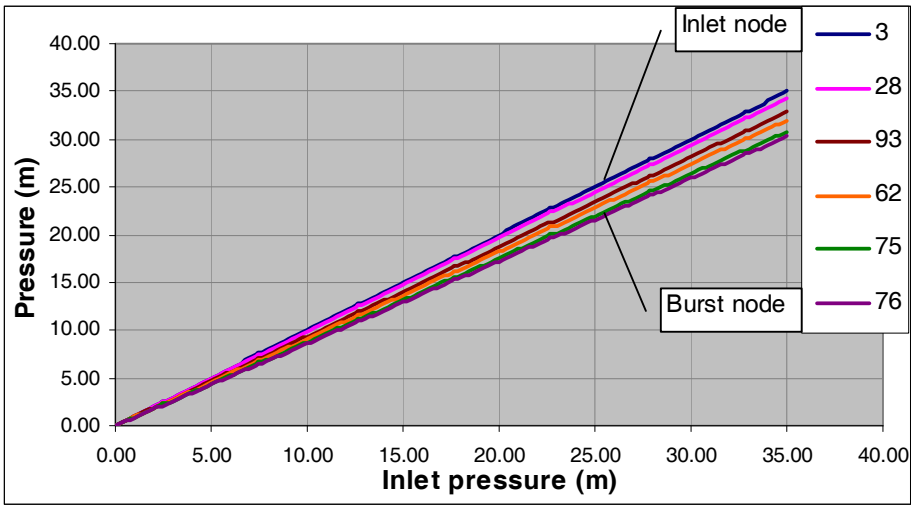

Figure 2. Pressure lines for a DMA nodes

The field measurements from the e-FAVOR test are used to estimate gradients of the measured pressure lines for sensitive nodes. A numerical experiments equivalent the e-FAVOR test is performed on the simulation model. The burst coefficient (calculated at the previous stage) is allocated to different nodes of the simulation model and the theoretical gradients of the pressure lines at the sensitive node are evaluated. For each burst location the value of the chi-squared criterion is calculated as:

$$\chi^2 = \sum_{i \in S} \frac{\left(b'_i - b_i\right)^2}{b'_i} \tag{3}$$

where b'_i = gradient estimated from measurements, b_i =gradient estimated from simulations. The allocation which gives the minimum value of the χ^2 criterion corresponds to the burst node.

SHENSTONE CASE STUDY

Shenstone DMA (illustrated in Figure 3) is fed through two PRV inlets and supplies 1008 consumers (917 domestic and 91 commercial). There are two 4 inch PRVs at inlet 1 and inlet 2, respectively, as shown in Figure 3. The recorded data from the e-FAVOR test are depicted in Figure 4.

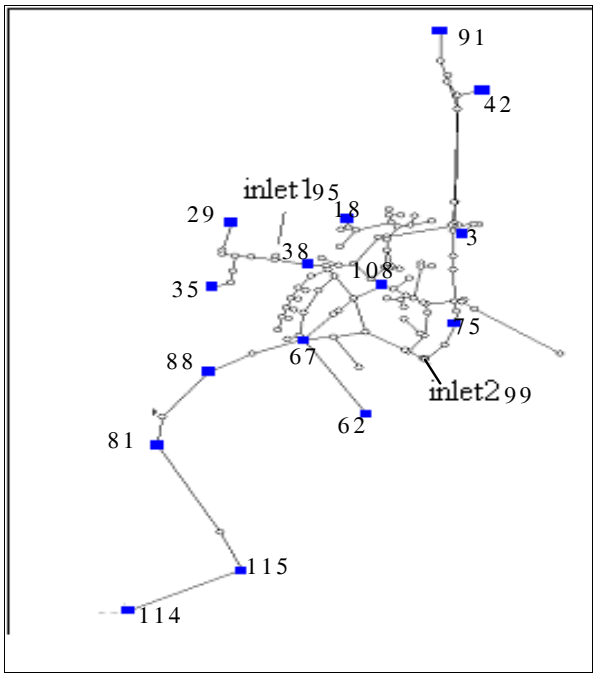

Figure 3. Shenstone DMA. Blue squares denote selected sensitive nodes.

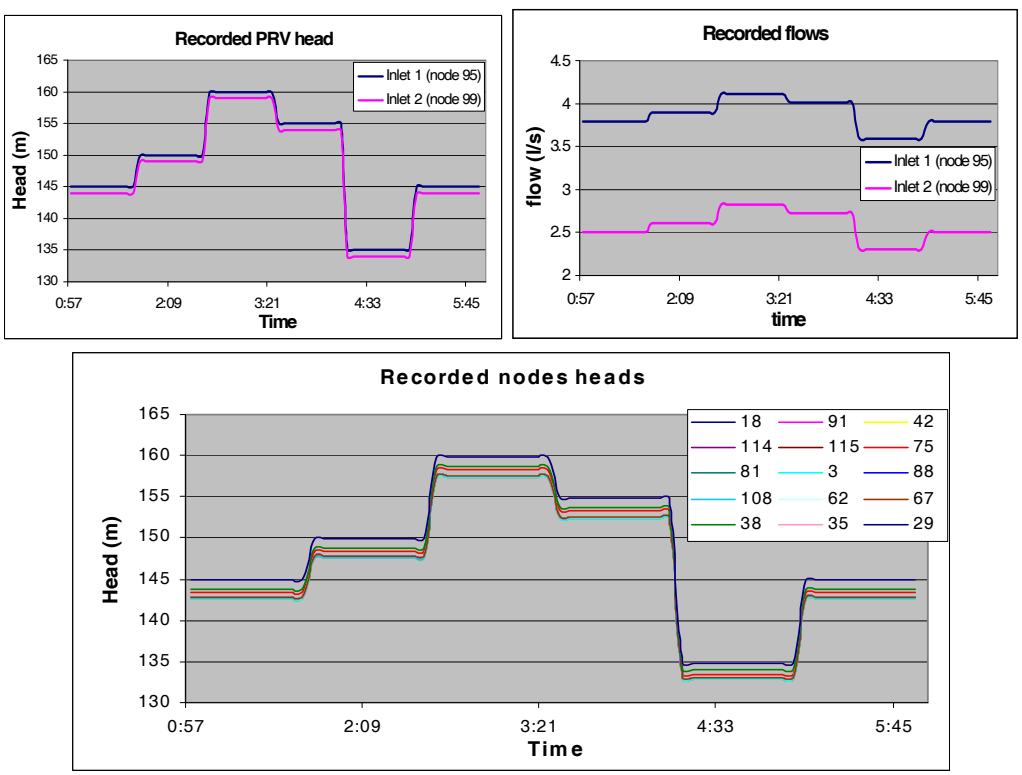

Figure 4. Recorded data

IFM models have been estimated by allocating a burst to different sensitive nodes. For each allocation a corresponding IFM model and the corresponding value of χ^2 have been calculated and are shown in Table 1. The IFM model corresponding to $\chi^2 = 9.31\times10^{-10}$ has been selected for estimating the size of the burst, therefore the coefficients of the model are $d = 4.0334$, $c_1 = 0.2429$ and $c_2 = 0.00227$.

Table 1.

Sensitive node	A demand factor (l/s)	A coefficient of the burst	A coefficient of the total background leakage	A value of χ^2 (the difference between calculated and recorded inlet flows)
The burst exponent = 0.512104				
95	3.643539	0.284718	0.002128	4.99E-08
99	4.033422	0.242887	0.002276	9.31E-10
18	3.709304	0.279806	0.002165	3.93E-08
91	3.876389	0.261679	0.002224	5.94E-08
42	3.873712	0.262168	0.002225	1.79E-08
3	3.55773	0.294989	0.002115	7.11E-08
114	4.333455	0.208249	0.002425	7.74E-08
115	4.305799	0.211826	0.00241	6.26E-08
81	4.032276	0.244776	0.002283	2.08E-08
88	4.117065	0.234884	0.00232	1.54E-08
108	4.360773	0.204427	0.002443	1.16E-07
62	3.922307	0.257142	0.002238	6.8E-08
67	3.950318	0.253477	0.002255	1.01E-08
38	3.803718	0.269449	0.002187	1.4E-07
75	3.972916	0.250807	0.002251	1.81E-08
35	3.766198	0.271833	0.002176	1.6E-08
29	3.735147	0.275068	0.002165	1.97E-08

The final stage was to find the burst location. The estimated burst coefficient $c_1 = 0.2429$ was allocated to each node of the hydraulic model one by one, simulated for each allocation and subsequently the model pressure regression lines were compared with the measured ones using χ^2 criterion. The best three allocation are shown in Table 2. The obtained results indicate a high degree of probability of the burst presence at node 80. The value of the total demand flow is 4 l/s, the value of the coefficient of the fixed area leakage (burst) is 0.2429. This finding was later confirmed by the water company following inspection of the area indicated by the proposed method.

Table 2.

Burst node	A value of χ^2 (reflects an error in prediction of burst location)
80	3.2E-06
69	1.44E-05
33	1.67E-05

CONCLUSIONS

The paper proposed a method for estimating burst flow and a burst location in a DMA. The method is based on an active identification procedure called e-FAVOR test which is carried out at night between 1 am and 5 am. The test requires deployment of pressure loggers to monitor pressure at sensitive nodes. The burst flow is estimated by comparing inlet measured flow and flow from the IFM model. The burst location is identified by comparing gradient of pressure lines from measurements and from hydraulic simulations. The method was formulated assuming presence of a single burst in a DMA, but can easily be generalised by application of genetic algorithms to search for the best flow and pressure line models. Findings were later confirmed by the water company following inspection of the area indicated by the proposed method. Another case study is currently under investigation.

REFERENCES:

Borovik, I., (2009). "Bursts identification in water distribution system", *PhD thesis,* De Montfort University, PC-WSS group, Leicester, UK.

May, J. (1994), "Pressure-dependent Leakage" *World Water and Environmental Engineering*, October.

Prescott, S., and Ulanicki, B. (2006), "Reduction of water losses and energy consumption using an effective process for burst detection", *Sustainable Technologies Initiative EPSRC (GR/S25715) & DTI, Final Project Report*.

Bush, C.A. and Uber, J.G. (1998), "Sampling Design Methods for Water Distribution Model Calibration." *Journal of Water Resources Planning and Management*, Vol. 124, No. 6.

Damage Detection of Operating Transmission Mains With Measured Boundary Conditions

Aaron C. Zecchin[1,2], Martin F. Lambert[1,3], and Angus, R. Simpson[1,4]

[1]The School of Civil, Environmental and Mining Engineering, The University of Adelaide, North Terrace, Adelaide Campus, S.A. 5005, Australia, [2]email: azecchin@civeng.adelaide.edu.au, ph: +61 8 8303 4323, [3]email: mlambert@civeng.adelaide.edu.au, ph: +61 8 8303 5135, [4]email: asimpson@civeng.adelaide.edu.au, ph: +61 8 8303 5874

ABSTRACT

Transmission mains are a pivotal component in water distribution systems. As such, regular testing of these mains, for the purpose of identifying regions of damage and deterioration, is an important aspect of responsible infrastructure management. Much research has been done on the use of hydraulic transient methods to aid in the assessment of pipelines. These methods typically require the isolation of the pipeline from the system to create the ideal conditions under which testing can be performed. In many cases, it is not practical to isolate the transmission mains and take them off line for testing. However, testing in an operating environment can serve to confuse existing transient assessment methods, as these methods require known boundary conditions, such as valves or reservoirs. This paper proposes a method that does not require knowledge of a pipelines boundary conditions, but uses a special arrangement of pressure sensors to facilitate the assessment of desired sections of the pipeline. The approach is based on the use of a frequency-domain model to analyze the pressure measurements and identify regions of damage and deterioration within the pipeline.

INTRODUCTION

Pipeline infrastructure represents some of the largest and most expensive infrastructure in the world. Fundamental to all industrial civilizations is the reliable transport of potable water through large transmission mains. These mains, typically a mild steel cement mortar lined composite, suffer deterioration with age whether it be internal spalling of the concrete, internal corrosion, development of blockages or leaks, or external weathering or damage (*Furness and Reet*, 1998). As such, regular testing of these mains, for the purpose of identifying regions of significant deterioration, is an important aspect of responsible infrastructure management.

Much research has been done on the use of hydraulic transient methods to aid in the assessment of pipelines, with a particular emphasis on leak detection (*Liggett and Chen*, 1994; *Vítkovský et al.*, 2000; *Wang et al.*, 2002; *Lee et al.*, 2005). The basic philosophy of hydraulic transient methods is that changes in the pipe condition will impact the nature of transient wave propagation within a pipeline, which is in turn observable from measurements of the fluid variables of the system (*Ferrante and Brunone*, 2003). Typically time-domain methods have been adopted (*e.g.* the inverse transient method (*Liggett and Chen*, 1994)), but there has been growing interest in

the use of frequency-domain methods (*Ferrante and Brunone*, 2003; *Lee et al.*, 2005; *Zecchin et al.*, 2005).

These methods require the isolation of the pipeline from the system to create the ideal conditions under which testing can be performed. In many cases, it is not practical to isolate the transmission mains and take them off line for testing. However, testing in an operating environment can serve to confuse existing transient assessment methods, as these methods require known boundary conditions, such as valves or reservoirs (*Wang et al.*, 2002; *Ferrante and Brunone*, 2003), known inputs (*Lee et al.*, 2005), or clean signals without any underlying transients (*Brunone*, 1999).

This paper proposes a method that does not require knowledge of a pipelines boundary conditions or measured inputs, but uses a special arrangement of pressure sensors to facilitate the assessment of desired sections of the pipeline. The approach is based on the use of a frequency-domain model to analyze the pressure measurements and identify regions of damage and deterioration within the pipeline. Advantages of the use of a frequency-domain model include (i) frequency-domain models are very efficient, (ii) the use of steady-oscillatory signals with frequency-domain identification makes the method robust to underlying transients, (iii) as frequency-domain models do not require discretization, spatial variables and wavespeeds can be easily estimated.

This paper is structured as follows. The next section presents the fundamental time- and Laplace-domain pipeline equations, where the admittance matrix expression for a pipeline with and without a damaged section is derived. This section is followed by an outline of the frequency-domain identification methodology where an expression for the system's feasible data space is used to derive a *goodness of fit* error function, the minimizer of which is the parameter estimate. After which a numerical example is presented, followed by the conclusions.

PIPELINE UNSTEADY FLOW EQUATIONS

Basic Partial Differential Equations

Unsteady pipe flow is governed by a system of two nonlinear hyperbolic partial differential equations. Under the standard assumptions (*Wylie and Streeter*, 1993), the equations governing the transient state variables of pressure and flow within a pipeline are the mass and momentum equations

$$\frac{\partial q}{\partial x} = -\frac{A_o^2}{\rho_o c_o^2}\left(\frac{\partial p}{\partial t} + \mathcal{C}\left[p\right]\right) \tag{1}$$

$$\frac{\partial p}{\partial x} = -\frac{\rho_o}{A_o^2}\left(\frac{\partial q}{\partial t} + \mathcal{R}\left[v\right]\right) \tag{2}$$

where $p = p(x,t)$, $q = q(x,t)$ are the state variables of pressure and flow continuous on the spatial and temporal coordinates x and t, A_o, ρ, and c_o the nominal cross-sectional area, density and wavespeed, respectively, and $\mathcal{C}$ and $\mathcal{R}$ are compliance and resistance operators, which are known to act on p and q respectively (*Zielke*, 1968; *Rieutord and Blanchard*, 1979). Intuitively, $\mathcal{C}$ describes how the cross-sectional inelastic storage

changes with pressure fluctuations, and $\mathcal{R}$ describes how the shear stresses within the fluid body change with the axial flow. An example of $\mathcal{C}$ is the Kelvin-Voigt viscoelastic model (*Rieutord and Blanchard*, 1979), and examples of $\mathcal{R}$ are the standard steady-state friction models (*Wylie and Streeter*, 1993), the laminar unsteady friction model (*Zielke*, 1968), and the unsteady turbulent friction model (*Vardy and Brown*, 2007).

Transform Representation of Fluid Equations

The Laplace transform is a useful tool in dealing with partial differential equations as it removes the time-dependency of the variables and yields a simpler ordinary differential equation (*Kreyszig*, 1999). Via the Laplace transform, the function $p(x,t)$ becomes the complex Laplace-domain function $P(x,s)$, where s is the complex Laplace variable. An important property of the Laplace transform is that the frequency-domain behavior of a function is given when the value of the Laplace-domain variable is restricted to the positive imaginary axis, that is $s = i\omega$ where i is the imaginary unit, and ω is the radial frequency (*Franklin et al.*, 2001).

The Laplace-domain representation of the pipeline equations (1)-(2) requires two simplifications, (i) the linearization of both equations, and (ii) homogeneous initial conditions. The standard approach to satisfy both these requirements is to linearize the system (1)-(2) about the initial conditions (*Wylie and Streeter*, 1993) and consider the transient fluctuations in p, q about these values. This is adequate for most applications as the initial conditions are typically the steady state conditions. The Laplace transformed solution to the linearized system (1)-(2) is

$$\begin{bmatrix} P(x,s) \\ Q(x,s) \end{bmatrix} = A(s)e^{-\tilde{\Gamma}(s)x} \begin{bmatrix} 1 \\ Z_c^{-1}(s) \end{bmatrix} + B(s)e^{\tilde{\Gamma}(s)x} \begin{bmatrix} 1 \\ -Z_c^{-1}(s) \end{bmatrix}, \tag{3}$$

where P and Q are the transformed pressure and flow, A and B are arbitrary functions dependent on the boundary conditions of the pipe, and $\tilde{\Gamma}$ and Z_c are the propagation operator and the characteristic impedance, respectively, and are given by

$$\tilde{\Gamma}(s) = \frac{1}{c_o}\sqrt{\left[s + \overline{\mathcal{R}}(s)\right]\left[s + \overline{\mathcal{C}}(s)\right]}, \quad Z_c(s) = \frac{c_o \rho_o}{A_o}\sqrt{\frac{s + \overline{\mathcal{R}}(s)}{s + \overline{\mathcal{C}}(s)}}$$

where $\overline{\mathcal{R}}(s)$ and $\overline{\mathcal{C}}(s)$ are the Laplace transforms of the linear approximations of the operators $\mathcal{R}$ and $\mathcal{C}$ respectively. Typically the only term requiring linearization is the steady-state quadratic term in $\mathcal{R}$, as for turbulent flow, $\mathcal{R}[q] = \overline{\mathcal{R}}[q] + O\left\{(q - q_o)^2\right\}$ where q_o is a reference flow rate (*Wylie and Streeter*, 1993; *Vardy and Brown*, 2007). However, the viscoelastic models (*Rieutord and Blanchard*, 1979) and unsteady friction models (*Zielke*, 1968; *Vardy and Brown*, 2007) are described by convolution operators, and hence are conveniently and exactly described by the Laplace transform.

A typical organization of (3) is the transfer matrix method (*Wylie and Streeter*, 1993). This method solves for A and B based on specifications of either pressure or flow at either end of a pipeline. Within this paper, the admittance form is of primary

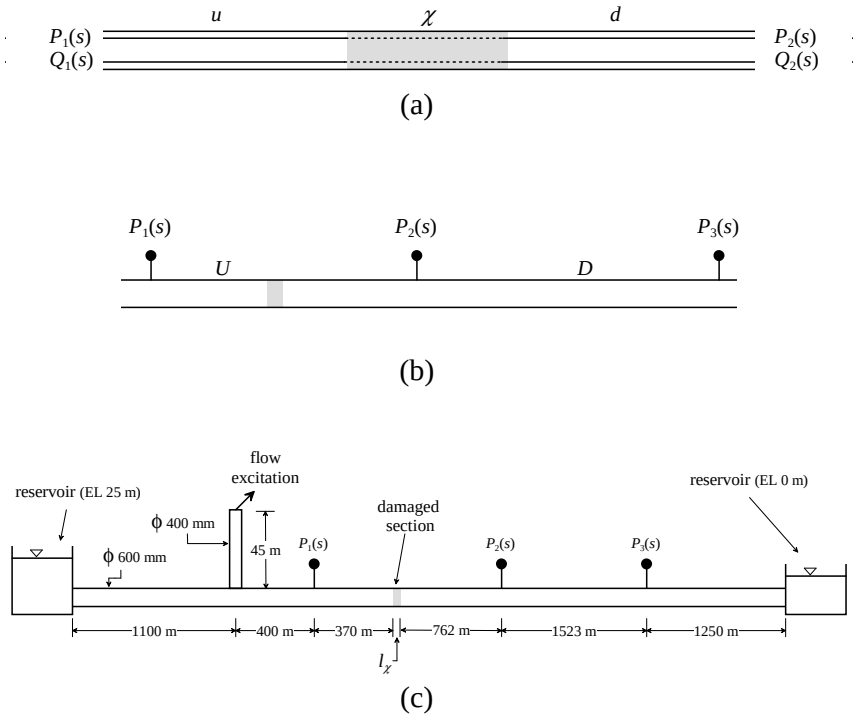

Figure 1: (a) Pipeline with damaged section χ. (b) Pipeline testing setup: a pipeline section bounded by two pressure sensors with a pressure sensor in between. (c) Network used in numerical examples (total length is 5405 + l_χ km).

interest, and, for a pipe of length l, is given as

$$Z_c^{-1}(s) \begin{bmatrix} \coth \Gamma(s) & -\operatorname{csch} \Gamma(s) \\ -\operatorname{csch} \Gamma(s) & \coth \Gamma(s) \end{bmatrix} \begin{bmatrix} P(0,s) \\ P(l,s) \end{bmatrix} = \begin{bmatrix} Q(0,s) \\ -Q(l,s) \end{bmatrix} \tag{4}$$

where $\Gamma(s) = l\tilde{\Gamma}(s)$. Equation (4) is termed an admittance map, as it describes the pipe end flows that are *admitted* from the pipe end pressures.

Admittance matrix of pipeline with damage

Consider the pipeline in Figure 1(a) consisting of undamaged sections u and d bracketing a damaged section χ. The admittance expression of this system takes the form

$$\boldsymbol{Y}_{u\chi d}(s) \begin{bmatrix} P_1(s) \\ P_2(s) \end{bmatrix} = \begin{bmatrix} Q_1(s) \\ -Q_2(s) \end{bmatrix} \tag{5}$$

where $\boldsymbol{Y}_{u\chi d}$ is the admittance transfer matrix for the system. By way of the transfer matrix rules in *Wylie and Streeter* (1993), or using the equation (4) expression for the

dynamics in sections u and d, by equating the end to end pressures and flows of each of the three sections, the following expression for $\boldsymbol{Y}_{u\chi d}$ can be derived

$$\begin{aligned}\boldsymbol{Y}_{u\chi d}(s) =& \frac{1}{Z_c(s)}\begin{bmatrix}\coth\Gamma_u(s) & 0\\ 0 & \coth\Gamma_d(s)\end{bmatrix} \\ &- \frac{1}{Z_c^2(s)}\begin{bmatrix}\operatorname{csch}\Gamma_u(s) & 0\\ 0 & \operatorname{csch}\Gamma_d(s)\end{bmatrix}\boldsymbol{Y}_{\tilde{\chi}}(s)^{-1}\begin{bmatrix}\operatorname{csch}\Gamma_u(s) & 0\\ 0 & \operatorname{csch}\Gamma_d(s)\end{bmatrix}\end{aligned} \tag{6}$$

where Γ_u and Γ_d are the propagation operators for sections u and d, Z_c is the characteristic impedance for these sections, and

$$\boldsymbol{Y}_{\tilde{\chi}}(s) = \boldsymbol{Y}_{\chi}(s) + \frac{1}{Z_c(s)}\begin{bmatrix}\coth\Gamma_u(s) & 0\\ 0 & \coth\Gamma_d(s)\end{bmatrix} \tag{7}$$

where $\boldsymbol{Y}_{\chi}$ is the transfer matrix admittance expression for the damaged section χ. By way of comparison, within the given notation, the admittance matrix for the case where section χ is undamaged (the pipeline is uniform) is given by (4) with

$$\Gamma(s) = \Gamma_u(s) + l_\chi\widetilde{\Gamma}(s) + \Gamma_d(s)$$

where l_χ is the length of section χ.

PIPELINE DAMAGE IDENTIFICATION METHODOLOGY

The objective of this paper is to develop a detection and identification methodology for the condition assessment of a single pipeline bounded by measurement stations. The approach involves estimating the parameters of the pipeline sections by minimizing a measure of the *goodness of fit* of the model to the data. As there are no defined inputs to this system, standard prediction error approaches (*Ljung*, 1999) cannot be used. Instead, the measure of the *goodness of fit* must be derived from analytic relationships between the measured system states. Mathematically, the analytic relationships between the states of the model are used to define the vector space that the model state lie within (*i.e.* a feasible data space, that is dependent on the model parameters), and the *goodness of fit* is defined as some measure of the distance of the measurements from this feasible data space.

Using the pipeline admittance matrices presented in the previous section, an expression of the models feasible data space is determined, from which a *goodness of fit* error function is derived.

Data space for pipeline model

Consider the segment of pipeline depicted in Figure 1(b) bounded by measurement stations 1 and 3 with a third station (station 2) in between. For pipes reach U and D between the three measurement stations, there are the following admittance relationships for the model states

$$\boldsymbol{Y}_U(s)\begin{bmatrix}P_1(s)\\ P_2(s)\end{bmatrix} = \begin{bmatrix}Q_1(s)\\ -Q_2(s)\end{bmatrix}, \quad \boldsymbol{Y}_D(s)\begin{bmatrix}P_2(s)\\ P_3(s)\end{bmatrix} = \begin{bmatrix}Q_2(s)\\ -Q_3(s)\end{bmatrix}, \tag{8}$$

where the admittance matrices $\boldsymbol{Y}_U$ and $\boldsymbol{Y}_D$ are of the form of (4) or (6) depending on whether they were damaged or not. From these expressions between the variables the feasible data space for the states $\boldsymbol{P} = [P_1\, P_2\, P_3]^T$ can be determined. Combining the expressions in (8) yields

$$\begin{bmatrix} Y_{U11}(s) & Y_{U12}(s) & 0 \\ Y_{U21}(s) & Y_{U22}(s) + Y_{D11}(s) & Y_{D12}(s) \\ 0 & Y_{D21}(s) & Y_{D22}(s) \end{bmatrix} \begin{bmatrix} P_1(s) \\ P_2(s) \\ P_3(s) \end{bmatrix} = \begin{bmatrix} Q_1(s) \\ 0 \\ -Q_3(s) \end{bmatrix} \tag{9}$$

where the elements of $\boldsymbol{Y}_U$ and $\boldsymbol{Y}_D$ are expanded out as Y_{Uij} and Y_{Dij} respectively. As Q_1 and Q_3 are unknown, only the second row can be used to define the feasible data space. That is, the only information about $\boldsymbol{P}$ that can be determined from (9) is that $\boldsymbol{y}^H \boldsymbol{P} = 0$ on $s \in \mathbb{C}$ where $\mathbb{C}$ is the space of complex numbers and

$$\boldsymbol{y}(s) = \begin{bmatrix} Y_{U21}(s) & Y_{U22}(s) + Y_{D11}(s) & Y_{D12}(s) \end{bmatrix}^H$$

where H is the Hermitian (conjugate transpose) operator. Omitting formal technical considerations, this implies that, for a given model, a feasible state vector $\boldsymbol{P}$ must be an element of the vector function space

$$\left\{ \boldsymbol{P}(s) : \mathbb{C} \mapsto \mathbb{C}^3 | \boldsymbol{P}(s) \perp \boldsymbol{y}(s) \text{ for all } s \in \mathbb{C} \right\}. \tag{10}$$

Geometrically this has the interpretation that, at each point $s \in \mathbb{C}$, $\boldsymbol{P}$ lies in a 2-D complex plane that is orthogonal to $\boldsymbol{y}$.

Parameter identification methodology

The vector function $\boldsymbol{y} = \boldsymbol{y}(\boldsymbol{\theta}, s)$ is a function of the system parameters $\boldsymbol{\theta}$ (*i.e.* roughness, wavespeed, *etc.*) and hence, so is the space (10). Given (10), a natural measure of the distance of the measurements $\boldsymbol{P_m}$ of the states $\boldsymbol{P}$ from this space is

$$\boldsymbol{P_m}^H(s) \left[\boldsymbol{y}(\boldsymbol{\theta}, s) \boldsymbol{y}^H(\boldsymbol{\theta}, s) \right] \boldsymbol{P_m}(s) \tag{11}$$

which is clearly only zero when $\boldsymbol{P_m}$ is in the set (10) and is greater than zero otherwise. From a parameter identification perspective, if $\boldsymbol{P_m} = \boldsymbol{P}$ (*i.e.* it is a perfect measurement), then (11) will be zero when $\boldsymbol{\theta}$ is the true value of the model from which $\boldsymbol{P_m}$ was measured.

The frequency-domain data consists of measurements $\boldsymbol{P_m}$ at discrete frequencies (*i.e.* as would arises from the discrete Fourier transform). That is, the data consists of $\boldsymbol{P_m}_n = \boldsymbol{P_m}(i\omega_n), n = 1, \ldots, N$ where ω_n are the measured frequencies (or Fourier frequencies). Motivated by (11), the *goodness of fit* error function for the model is

$$E(\boldsymbol{\theta}) = \sum_{n=1}^{N} \boldsymbol{P_m}_n^H \left[\boldsymbol{y}^H(\boldsymbol{\theta}, i\omega_n) \boldsymbol{y}(\boldsymbol{\theta}, i\omega_n) \right] \boldsymbol{P_m}_n \tag{12}$$

and the associated optimal parameter estimate is

$$\widehat{\boldsymbol{\theta}} = \arg \min_{\boldsymbol{\theta} \in \boldsymbol{\Theta}} E(\boldsymbol{\theta}). \tag{13}$$

where $\boldsymbol{\Theta}$ is the set of feasible values for $\boldsymbol{\theta}$.

EXAMPLES

Two numerical examples are presented below to demonstrate the utility of the proposed method. The example system is depicted in Figure 1(c), where the test section to be identified is between stations 1 and 3.

Preliminaries

The nominal pipeline properties for Figure 1(c) are: wavespeed c_o = 1000 m/s and relative roughness $(\epsilon/D)_o$ = 0.001. The damaged section, taken as a corroded section with a spalling of the internal m=cement mortar lining, was modeled as having a slightly increased diameter D_χ = 610 mm, a reduced wavespeed c_χ = 850 m/s and an increased relative roughness $(\epsilon/D)_\chi$ = 0.02. Two cases were considered, case 1 which involved a nominal size damage of length l_χ = 6.8 m, and case 2 which involved a small damage of length l_χ = 0.85 m.

All pipelines were modeled as unsteady turbulent pipes using the model of *Vardy and Brown* (2007). The transient generation was taken as the time varying flow excitation located as the end of the 45 m branch. This was modeled as a constant base demand superimposed with a time varying multisine outflow taking frequencies from 0 to 30 Hz (the resultant flow took values on the interval [0.198,0.202] m^3/s). The time-domain data was generated by a method of characteristics hydraulic solver, where a time step of 0.001 seconds was used and the computational grid was generated so as to ensure a Courant number of 1 in all reaches. The simulations were performed until the system was approximately in a steady-oscillatory state. To model the inaccuracies in the measurements, the time-domain data was contaminated by independent Gaussian $\mathcal{N}(0, 0.01)$ variates (in meters of head). The frequency-domain data used by the identification methodology was generated by a discrete Fourier transform of the contaminated time-domain data.

The variable set to be estimated was comprised of[1], the damaged section parameters (location x_χ, l_χ, c_χ, D_χ, relative roughness $(\epsilon/D)_\chi$, and the steady-state Reynolds number $\mathbb{R}_{e_\chi}$) and the nominal undamaged pipeline parameters (c_o, $(\epsilon/D)_o$, $\mathbb{R}_{e_o}$) This created a total of 9 parameters in $\boldsymbol{\theta}$. The estimate $\widehat{\boldsymbol{\theta}}$ in (13) was computed using an evolutionary approach by way of the particle swarm optimization (PSO) algorithm[2] (*M. Clerc*, 2002).

Results and discussion

Statistics for the parameter estimates $\widehat{\boldsymbol{\theta}}$, based on 10 trials (each with a different noise sequence), are given in Figure 2(a) for case 1 and Figure 2(b) for case 2. For case 1, the majority of the parameter estimates are highly accurate with very little error

[1]The Reynolds number required estimation as it is a parameter of the *Vardy and Brown* (2007) model. Note that $\log_{10} \epsilon/D$ and $\log_{10} \mathbb{R}_e$ were estimated as they yielded a better paramterization for the computation of (13).

[2]A toroidal grid neighborhood structure was used with 81 particles and a termination criteria of 1000 iterations.

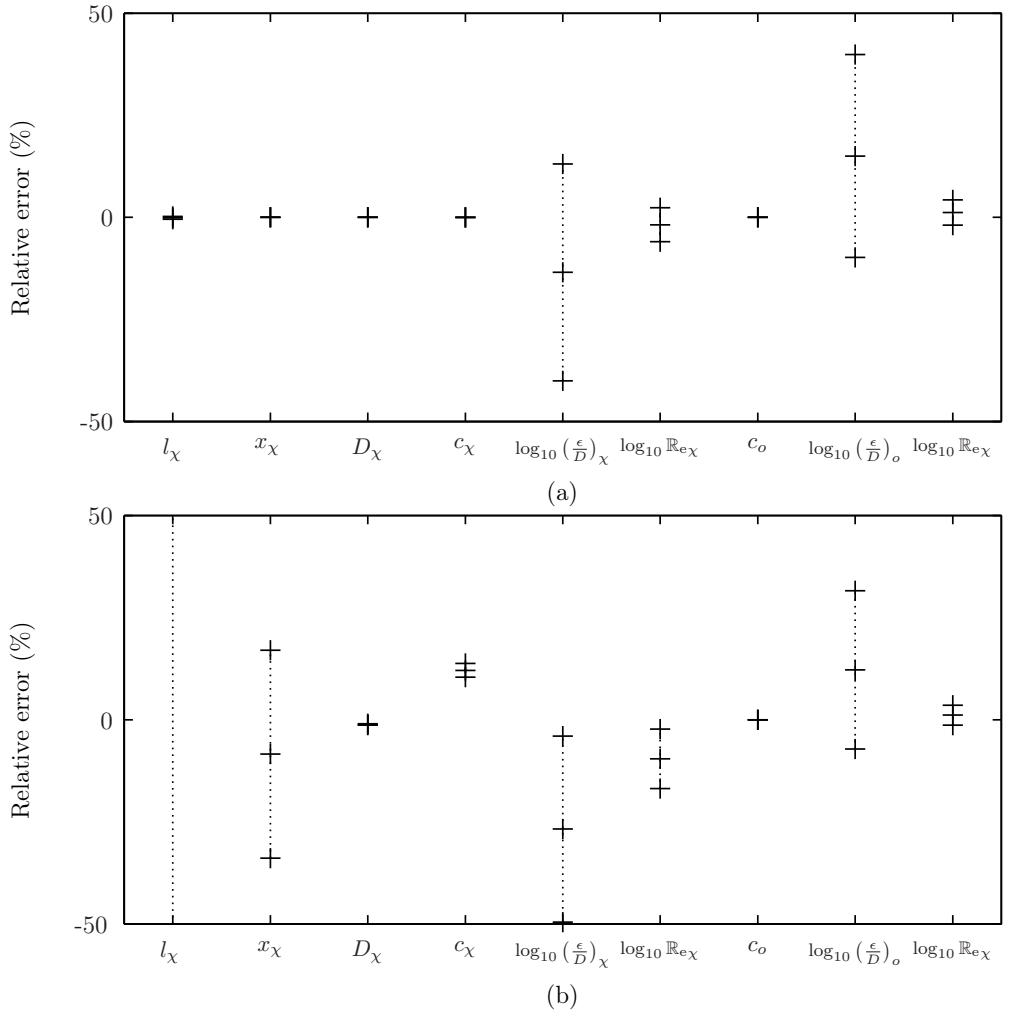

Figure 2: Relative errors of the parameter estimates for (a) case 1 with damaged section length l_χ = 6.8 m, and (b) case 2 with l_χ = 0.85 m. The relative errors are defined as $(\widehat{\theta} - \theta)/\theta\%$. The results are based on 10 trials (each with a different noise sequence) and are presented as the mean (centre bar) $\pm$ the standard deviation (upper and lower bars). The relative error statistics for l_χ in case 2 is 4.16$\pm$6.22.

and variance. This is particularly the case for the important parameters that locate the damage (x_χ), provide indications of its extent (l_χ) and degree of severity (D_χ and c_χ). The actual values for these estimates are given in Table 1, where the consistent high accuracy of the estimates is clear.

The $\mathbb{R}_e$, and to a greater extent, ϵ/D, parameters were not estimated with the accuracy of the other parameters. The $\mathbb{R}_e$ estimates were only slightly biased with a moderate variance, but the ϵ/D parameters were biased (with means 13% to 15% rela-

Table 1: Estimate statistics for important damage parameters. Statistics are based on 10 trials, each with a different noise sequence.

case	parameter	unit	actual value	estimate statistics	
				mean	standard deviation
1	l_χ	(m)	6.80	6.79	0.02
	x_χ	(m)	370.00	370.00	0.01
	D_χ	(mm)	610.00	609.94	$O\{10^{-5}\}$
	c_χ	(m/s)	850.00	849.74	0.42
2	l_χ	(m)	0.85	4.39	5.29
	x_χ	(m)	370.00	434.27	193.92
	D_χ	(mm)	610.00	602.79	$O\{10^{-3}\}$
	c_χ	(m/s)	850.00	952.69	14.32

tive error). Experience has shown that the error function (12) is typically less sensitive to these parameters. However, from a detection perspective, the accurate estimation of these parameters is secondary to the estimation of the damaged section parameters.

The performance of the nominal pipeline parameter estimates are similar for case 2 as with case 1, but the damage section parameter estimates are very different for l_χ, x_χ, and c_χ, as demonatrated in Figure 2(b) and Table 1. A positive error is seen in the estimates for wavespeed c_χ and, to a greater extent, the damage length[3] l_χ. Despite the large relative error for l_χ, the sample mean estimate was within a few meters of the actual damage length. The location estimate possesses an error of about -8 % (64.3 m), but the actual x_χ value is well within a standard deviation of the estimate, implying the promising result that, with a greater number of trials, the sample mean of estimates could yield a more accurate approximation of the true value.

The performance of any identification methodology is fundamentally dependent on the excitation of the system possessing a sufficiently broad spectrum. For pipeline systems, the impact of a damage is known to have a greater influence on the high frequency behavior of the system. Therefore, the lower performance of the small damage case 2 could be attributed to the fact that the system was only excited up to 30 Hz, meaning an excitation containing higher frequencies could yield an improved identification performance.

As a final comparison, the fit of the true damage location model was compared to the alternative models. The true model is the *damage in upstream section* model, and the two incorrect models are the *damage in downstream*, and the *no damage* models. Note that these models refer to the forms of the admittance matrices in (8). To undertake this comparison, the incorrect models were fitted to the perfect data to determine the smallest possible E value they could achieve. Table 2 presents the results of this

[3]These parameters are, to some extent, correlated in their influence on E as a larger damage length requires a higher wavespeed for the frequency response harmonics of the model to be more aligned with that of the measured system.

Table 2: Comparison of minimum error values for the three models . The upstream model values are the mean±standard deviation from 10 trials on noisy data, whereas the values for the other models are based on noise free data.

case	l_χ	damage model errors		
		upstream section	downstream section	no damage
1	6.80	0.0034 ± 0.0001	0.0610	0.0647
2	0.85	0.0041 ± 0.0021	0.0089	0.0098

comparison. For both cases, the true model fitted to the noisy data yielded a better fit than the incorrect models fitted to perfect data. This is a very promising result meaning that, even in the instance of inaccurate parameter estimates as with case 2, the true model can be detected as it yields a lower error value.

CONCLUSION

This paper has presented a frequency-domain methodology for the the identification of damage parameters within a section of pipeline bounded by pressure sensors. The methodology involved computing the minimizer of an error function derived from analytic relationships between the pressure sensors. Case studies involving a section of pipe over 2.6 km in length were presented where a damaged section 6.8 m long was identified with high accuracy, but a shorter damaged section (0.85 m) was not able to be identified as accurately (a explanation for this could be that the excitation was not sufficiently broad spectrum). This methodology shows great potential for future development and application.

ACKNOWLEDGEMENT

This research was supported by the Australian Research Council, discovery project grant number DP0450788.

REFERENCES

Brunone, B. (1999), Transient test-based technique for leak detection in outfall pipes, *Journal of Water Resources Planning and Management, ASCE*, *125*(5, September/October), 302–306.

Ferrante, M., and B. Brunone (2003), Pipe system diagnosis and leak detection by unsteady-state tests 1. Harmonic Analysis, *Advances in Water Resources*, *26*, 95–105.

Franklin, G. F., J. D. Powell, and A. Emami-Naeini (2001), *Feedback control of dynamic systems*, 4th ed., Prentice Hall PTR, Upper Saddle River, N.J. London.

Furness, R. A., and J. D. Reet (1998), Pipe line leak detection techniques, in *Pipe Line Rules of Thumb Handbook*, edited by E. W. McAllister, 4 ed., pp. 476–484, Gulf Publishing Company, Houston, Texas.

Kreyszig, E. (1999), *Advanced engineering mathematics*, 8th ed., John Wiley, New York.

Lee, P. J., J. P. Vítkovský, M. F. Lambert, A. R. Simpson, and J. A. Liggett (2005), Leak location using the pattern of the frequency response diagram in pipelines: a numerical study, *Journal of Sound and Vibration*, *284*(3-5), 1051–1073.

Liggett, J., and L.-C. Chen (1994), Inverse transient analysis in pipe networks, *Journal of Hydraulic Engineering, ASCE*, *120*(8), 934–955.

Ljung, L. (1999), *System Identification: Theory for the User*, 2 ed., Prentice Hall PTR, Upper Saddle River, New Jersey.

M. Clerc, J. K. (2002), The particle swarm: explosion, stability, and convergence in a multidimensional complex space, *IEEE Trans. Evolut. Comput,*, *6*, 58–73.

Rieutord, E., and A. Blanchard (1979), Pulsating viscoelastic pipe flow - water-hammer, *Journal of Hydraulic Research, IAHR*, *17*(3), 217–229, in French.

Vardy, A. E., and J. M. B. Brown (2007), Approximation of turbulent wall shear stresses in highly transient pipe flows, *Journal of Hydraulic Engineering-ASCE*, *133*(11), 1219–1228.

Vítkovský, J., M. Lambert, A. Simpson, and A. Bergant (2000), Advances in unsteady friction modelling in transient pipe flow, in *Safe Design and Operation of Industrial Pipe Systems: 8th International Conference on Pressure Surges*, pp. 471–482, BHR Group, The Hague, The Netherlands.

Wang, X.-J., M. Lambert, A. Simpson, J. Liggett, and J. Vítkovský (2002), Leak detection in pipeline systems using the damping of fluid transients, *Journal of Hydraulic Engineering, ASCE*, *128*(7, July), 697–711.

Wylie, E., and V. Streeter (1993), *Fluid Transients in Systems*, Prentice-Hall Inc., Englewood Cliffs, New Jersey, USA.

Zecchin, A. C., L. B. White, M. F. Lambert, and A. R. Simpson (2005), Frequency-domain hypothesis testing approach to leak detection in a single fluid line, in *CCWI2005, Water Management for the 21st Century*, vol. 2, edited by D. Savic, G. Walters, R. King, and S.-T. Khu, pp. 149–154, Exeter, UK.

Zielke, W. (1968), Frequency-dependent friction in transient pipe flow, *Journal of Basic Engineering, ASME*, *90*(1), 109–115.

Evaluating risk of multi-segment pipes for prioritizing pipe rehabilitation

Dr M. Poulton [1], I. Kropp [2] and Dr A. Vanrenterghem-Raven [3]

1 WTSim SARL, 15 impasse Fauré, 33000, Bordeaux, France
Tel/Fax: +33 540-212-408; E-mail: matthew.poulton@wtsim.com
Internet: http://www.wtsim.com/english
2 Ingenieurbüro Baur + Kropp, Nieritzstr. 5, 01097, Dresden, Germany
Tel: +49 351-482-4531; Fax: +49 351-482-4550; E-mail: info@baur-kropp.de
Internet: http://www.baur-kropp.com/en/index.html
3 Polytechnic Institute of NYU, Metrotech Center 6, Brooklyn, NY 11201
Tel: +1 212-243-8656; Fax: +1 718-260-3433; E-mail: avanraven@poly.edu

ABSTRACT

The evaluation of risk at the individual pipe level can play an important role in the rehabilitation planning of water distribution systems. Yet pipe segments are generally arbitrarily defined in GIS or other databases and individual sections rarely make suitable rehabilitation entities on their own. In reality, groups of pipes need to be considered together for viable projects. The ability to group neighboring segments either prior to or subsequent to risk analysis has the potential to facilitate analysis and/or the actual practical rehabilitation. This paper looks briefly at the assessment of risk at pipe level before discussing how individual segments of pipe can be grouped into meaningful entities before or after such analysis. The objective is to maximize the benefit, in terms of risk avoidance, whilst minimizing the number of multi-segment pipes proposed for rehabilitation. Data from case studies are used to illustrate any advantages or shortcomings of the methods proposed.

INTRODUCTION

Rehabilitation of drinking water mains provides water companies with a great technical and strategic challenge, as well as a huge financial burden. For this reason, effective and pro-active asset management has taken on a very important role in recent years. During the last decade or so, tools and strategies have been developed to aid water companies, such as *CARE-W* (Saegrov) in Europe, *PARMS* in Australia and *WARP* in Canada. These have led to applications and implementations all over the world, including the USA. These tools and the models behind them continue to evolve. However, it is important to put them into context too, and ensure that they are optimized for practical use.

The key word that links these approaches is **risk**, defined as the probability of a failure multiplied by its impact (consequences). Risk can be considered at both the macro level (i.e. groups of pipes with similar characteristics) and the micro level (individual pipes). This distinction ultimately affects the final choice of

rehabilitation candidates. Working at the macro level allows an overall strategy to be realized, but the varying performance of pipes of a seemingly similar nature means that rehabilitation might not be fully optimized. On the other hand, considering each pipe in turn may not be conducive to effective practical rehabilitation. Of particular relevance here, is the spatial aspect – replacing a mile of connected pipes in one zone is likely to be more desirable than replacing the equivalent length, comprised of 6m sections, all over the city. The challenge is to combine the macro and micro approaches and define rehabilitation projects that are optimized in terms of both risk reduction and spatial proximity. In order to do this individual pipes have to be grouped with one or more neighboring pipes to form new multi-segment entities. Whether this should be done before or after risk analysis and evaluation is the subject of this paper.

DATA AND GIS

Data is crucial to rehabilitation planning and establishing a transparent and well-maintained database should be the first priority for any utility wishing to improve their asset management. Perhaps the biggest single aid to data management has been the introduction of Geographical Information Systems. GIS now forms the backbone of most utilities' data management systems. The ability to view spatial data has considerable advantages in rehabilitation planning. Knowing which pipes are physically connected or in close proximity carries far more significance than "anonymous" identification numbers in a conventional database. Although GIS is widely used for visual purposes, spatial attributes are not yet incorporated into many models, meaning that there is still untapped potential in this information.

There is though, a fundamental question which needs to be asked: "*What constitutes a pipe in a GIS or other form of rehabilitation database?*" Typically, this definition is left to the whim of the water company and the reason they created their database in the first place. While this may be adequate for day-to-day operation of the network, it is unlikely that the majority of pipes in the original database will be of a length suited to rehabilitation planning (i.e. neither too short, nor too long).

Another problem that rehabilitation planners face is the inherent dynamic nature of databases. Old pipes get removed, replaced or patched up; new pipes get added and so forth. So in time, the network can change significantly in appearance, yet break prediction models have to use consistent definitions for each pipe. There are though, some golden rules that help maintain clarity and form part of good database management practice:

- Never reuse ID numbers
- Always keep a track of all changes to pipes, in particular the date of these changes
- Make sure maintenance records always reference the pipe ID
- Never delete data for pipes no longer in service

RISK

There are several drivers of risk, most notably structural failure (breaks and leaks) but also hydraulic performance and water quality. Models such as *PHM* (Eisenbeis) and *Leyp* – Linear Extended Yule Process (Le Gat) use physical and environmental attribute data and previous break history to predict the future break rate of any pipe at any time. These failure prediction models also helps establish the relative impact of the different risk factors (such as diameter, material type, soil type or traffic loading). If structural integrity is the driving force behind the rehabilitation program, then such a model can help establish a priority list of candidates. However, a high break rate pipe in a low population-density area might be considered less of a risk than a pipe that is likely to break less often but is in the middle of downtown, for example. For this reason, sorting the pipes by predicted break number (or rate) might not tell the whole story. What it does do though, is provide a method for the validation of the model and also the theoretical evolution of the overall break rate.

Model Validation

Given adequate historic data (generally seven or more years of break and rehabilitation information), the model can be calibrated over a shorter period and actual breaks compared to predicted breaks during the remaining years. The following steps are taken:

- Sort pipes by descending **predicted break number** (favors longer pipes) or descending **predicted break rate** (favors shorter pipes)
- Calculate the cumulative length of pipe
- Calculate the cumulative number of breaks observed (this can be considered as the maximum number of breaks that could have been avoided if the current pipe and all those above it had been rehabilitated)
- Calculate the cumulative number of breaks predicted
- Calculate the relative cumulative length of pipe
- Calculate the relative cumulative number of breaks observed
- Calculate the relative cumulative number of breaks predicted

Figure 1 shows an example of a validation curve (also referred to as the benefit index). The bottom left hand corner is the most useful part as this relates to the pipes that would be replaced first if this ranked list was the sole method for choosing rehabilitation candidates. Replacing 0.5% of pipes in a year would require 200 years to replace the whole network. If pipes were replaced randomly, this would correspond to 0.5% of the breaks too. Several case studies have shown the ability of the *Leyp* model to provide good break rate estimations (hence the proximity of the actual and predicted graphs). However, it is the ranking ability that provides the most use – particularly for pipes that have no recorded breaks yet.

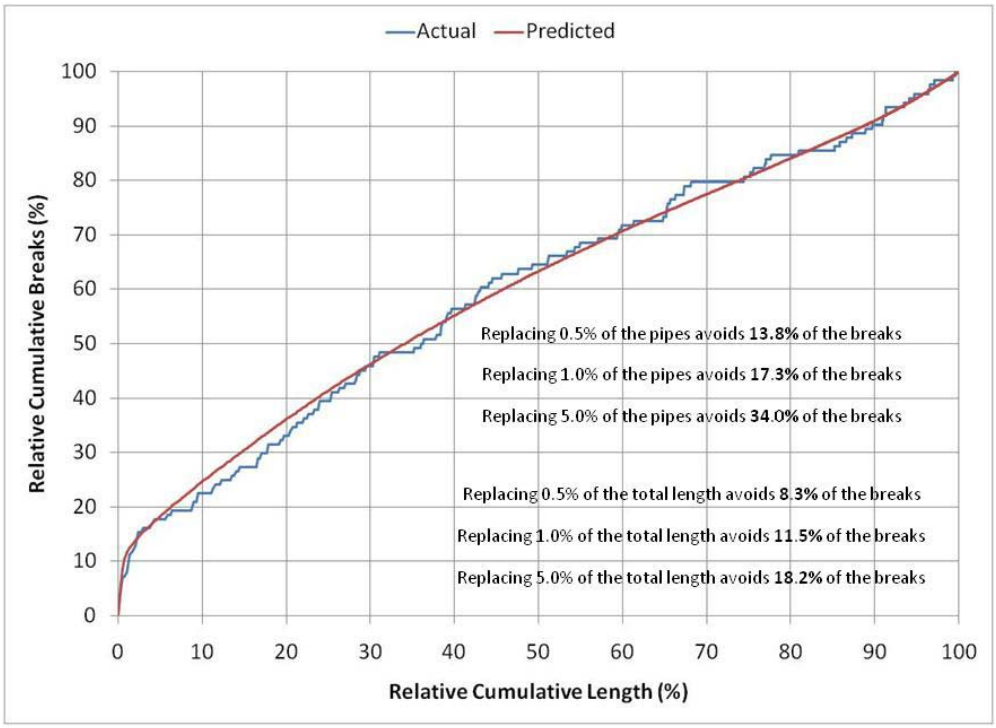

Figure 1: Validation curve based on results from the Leyp model and pipes ranked by decreasing predicted failure rate

Theoretical break rate evolution

By again making the assumption that pipes are replaced one-by-one according to their predicted break number/rate, it is possible to study the likely evolution of the break rate if different rehabilitation strategies (i.e. pipe mileages) are followed. In this case, the following steps are taken:

- Use *Leyp* to make break predictions for the next 20-25 years
- Sort pipes by descending predicted break number (favors longer pipes) or descending predicted break rate (favors shorter pipes) for the next year
- Calculate the cumulative length of pipe
- Sum the predicted breaks for each year
- By making the assumption that rehabilitated pipes inherit a negligible break rate for the rest of the study period (not necessarily the case), repeat the summation for each strategy but subtract the breaks corresponding to pipes that would be rehabilitated. For example, assuming rehabilitation of five km per year, in year one, the top five km will have zero predicted breaks and in year two, the top 10 km and so forth.

Figure 2 shows an example of such a break evolution.

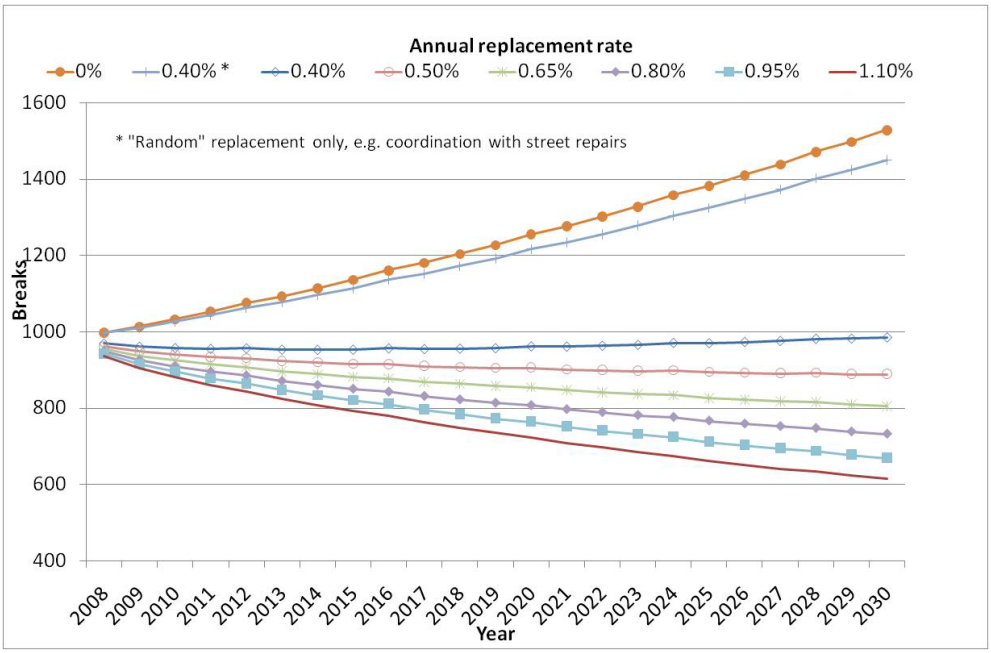

Figure 2: Example of break rate evolution according to different rehabilitation strategies

It is worth remembering that this is the maximum achievable benefit – inclusion of any lower ranked pipes as part of the rehabilitation total would lower the effectiveness. So, in effect this can be used as a benchmark for the maximum theoretical benefit. The reliability of predicted break rates so far in the future is less certain but in reality, break predictions can be updated on a yearly basis with new break data. It is certainly useful to establish the approximate rehabilitation rates that are required to stabilize or decrease the annual break rate.

GROUPING OF PIPES

In order to assess to what extent pipe definition affects break prediction results and to determine the optimal configuration, one must be able to manipulate the database, either by grouping or dividing pipes. This is best illustrated with a couple of examples:

In *figure 3(a)*, pipes A, B and C each have one recorded break. If the pipes are treated separately then the only two clues to the break frequency are:

1. The time between the start of break observations and the break
2. The time between the break and the end of the break observations.

In *figure 3(b)*, there is now a single pipe (D) with three breaks. Now there are four pieces of useful information:

1. The time between when break observations began and the first break
2. The time between the first and second breaks
3. The time between the second and third breaks
4. The time between the third break and the end of the break observations.

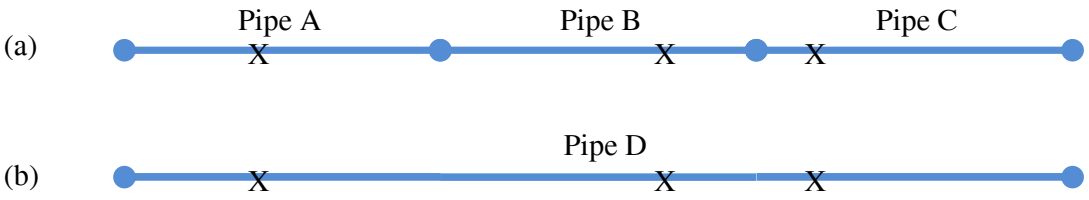

Figure 3: Grouping pipes

Although this paper focuses on pipe grouping, there are cases where the opposite is needed. In *figure 4(a)*, pipe E is very long and has three breaks in close proximity. Replacing the whole pipe may be expensive and unnecessary. Hence, it may be better to divide the pipe into two (F and G) as per *figure 4(b)*.

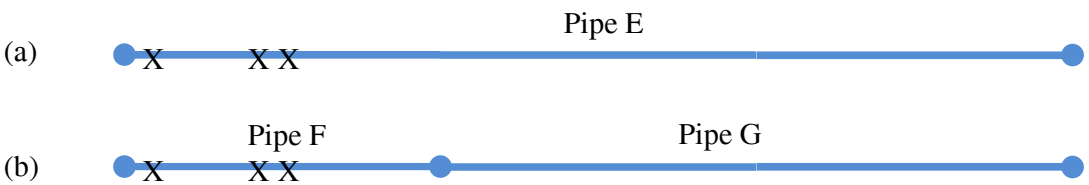

Figure 4: Dividing pipes

Having established that grouping pipes into multi-segments might be beneficial, the question remains at which point to carry out this aggregation. Pre-analysis grouping has the potential to facilitate analysis; post-analysis grouping has the potential to facilitate practical planning or rehabilitation projects.

Pre-analysis grouping

The grouping of pipes prior to any analysis means that the pipe attributes have to be considered. Obviously, grouping a 100 year old cast iron pipe with a brand new PVC one is pointless, as only one set of physical attributes could be used in any subsequent model. So it makes sense to create a list of rules for grouping pipes, for example:

- Pipes must be of the same material
- Pipes must be of the same diameter (or within a certain tolerance)
- Pipes must be of the same age (or within a certain tolerance)
- Total length of grouped pipes must be no longer than a predetermined threshold

Applying strict rules (i.e. no tolerances) has strong merits as pipes laid at the same time are likely to have the same "hidden attributes" (e.g. from the same batch from the same manufacturer). Often pipes from a particular period and sometimes a particular diameter show higher break tendencies than other pipes that would

otherwise appear to be fairly similar in characteristics. It is worth looking at the descriptive statistics of the data set (break rates for different attribute values) to establish if there are any trends that could influence the choice of grouping rules.

There are several methods for the actual grouping of pipes, ranging from advanced graph theory to simplified connectivity algorithms using common pipe nodes. Hydraulic modeling also relies on simplified versions of networks, so there are parallels to be made here. A reasonable degree of localized homogeneity is to be expected because of the way networks are originally designed. This could potentially lead to very long multi-segmented pipes, hence the reason for establishing a maximum length. For the purpose of this research, a single chain of grouped pipes was preferred to a group consisting of many "antennae". Two suggestions are made to achieve this:

1. Only consider grouping pipes that have a single neighboring pipe at each node
2. If a pipe has several neighboring pipes eligible for grouping, choose the longest

Additionally, many networks contain similar pipes separated by a short section of pipe that has been added after a break. These too can be grouped into a single pipe with the attributes of the longer segments being preserved. The following steps should therefore be implemented for pre-analysis grouping of pipes:

- Define the rules for grouping
- Eliminate sandwiched pipes as necessary
- Begin with any pipe (preferably with a single neighboring pipe) and test whether the two pipes can be grouped according to the rules
- Create two lists – one with the old (ungrouped IDs) and the new ID and one with the new IDs and all the IDs of the old pipes it regroups
- Continue, if appropriate with the next neighboring pipe or restart with another pipe
- Make sure that each pipe is only included in one new pipe group.

Post-analysis grouping: The grouping of pipes after any analysis means that the pipe attributes are less relevant (other than with respect to potential rehabilitation techniques maybe). This means that the 100 year old cast iron pipe **can** be grouped with the brand new PVC one if both are considered at risk. Nonetheless, rules can be used to limit the grouping options such as:

- Pipes must be of the same diameter
- Pipes must be in the same street

Grouping should be based on minimizing the overall risk. So far, only the break rate of grouped pipes has been used in this optimization. However, as previously stated, the ideal scenario is to use a score or categorization based on all the calculated risks and indeed opportunities (such as coordination with street repairs).

The following steps characterize a typical post-analysis grouping of pipes:

- Define a minimum threshold length for the grouped pipes e.g. 100m
- Define a maximum threshold length for the grouped pipes e.g. 500m
- Rank the pipes by the optimization parameter (e.g. predicted break rate for the following year)
- Start with the highest risk pipe and assuming it is less than the maximum threshold length find all its neighboring pipes
- Group with the neighboring pipe that together maximizes the optimization parameter
- Create two lists – one with the old (ungrouped IDs) and the new ID and one with the new IDs and all the IDs of the old pipes it regroups
- Stop if combined length now exceeds the maximum threshold length and begin with next pipe in the list that is not already part of a new group
- Continue regrouping if combined length is less than the minimum threshold length
- If the combined length is between the thresholds, only continue if adding another pipe increases the overall risk
- Make sure that each pipe is only included in one new pipe group.
- Rank the new multi-segment pipe groups

So at the end of the exercise, several viable rehabilitation projects have been created. Obviously these can be "fine tuned" using GIS to consider other pipes in the vicinity. As a useful indicator of efficiency, it is possible to refer back to the benefit index and see how replacing the new groups of pipes compares to spot replacement of individual pipes at risk.

CASE STUDY RESULTS AND DISCUSSION

Several pipe grouping studies have been carried out on European networks as part of larger break prediction and rehabilitation planning studies. Earlier research has concentrated on the grouping of pipes prior to running the *Leyp* model (Poulton). Interestingly, the study showed a slight decrease in performance using grouped pipes as opposed to the original configuration. Grouping not only results in fewer entities overall, but also fewer entities with one or more breaks. The apparent consequence of this was to decrease the effect of previous breaks and dampen the model's parameters, so as to weaken its ability to discriminate the break risk. It should be noted that only one dataset was used in the study and further studies are needed to confirm whether this is always the case.

From a practical perspective, pre-analysis grouping is very subjective because of the choice of rules and the chosen algorithm for regrouping. It is always recommended to first carry out the analysis with the original dataset. Should this produce satisfactory results (in reference to the model validation), then pre-grouping might be avoided altogether. In cases where the network is very fragmented though, it might be worth experimenting with grouping pipes.

Using the same original dataset, post-analysis grouping was proposed. Six separate simulations were performed with the following characteristics:

- Minimum "path" (i.e. chain of grouped pipes) length = approx. 150m
- Maximum path length = approx. 400m
- Pipes sorted by predicted break number (PBN) or predicted break rate (PBR)
- Paths restricted to same street? (yes or no)
- Diameter restrictions (all pipes can be grouped or only those <=300mm)
- Number of paths created
- Number of streets
- Number of pipes included in a path (total pipes = 216524)
- Total length of paths (total pipes = 8250km)

Table 1 summarizes the simulations and *table 2* summarizes the distribution of the number of pipes per path. Each simulation was able to create new multi-segment paths totaling more than half of the total network length, albeit that a large number of pipes already fell between the two threshold lengths and can already be considered as rehabilitation entities on their own. The remaining "orphaned" pipes were less than the minimum threshold length. Many of these could be added to rehabilitation projects during "fine tuning" if required, especially considering originally, 13% of the pipe segments had a length less than 5m and 38% less than 10m.

Table 1: Summary of grouping simulations

Sim. No.	Pipes sorted by	Same street	Diam	No. paths	No. streets	No. pipes	Length (km)
1	PBN 2008	Yes	All	24200	24200	76990	4980.0
2	PBN 2008	No	All	29665	48523	115821	6135.5
3	PBN 2008	No	<=300	26892	44782	105632	5452.9
4	PBR 2008	Yes	All	28675	28675	97999	6304.5
5	PBR 2008	No	All	31796	54899	136359	7069.6
6	PBR 2008	No	<=300	28356	50027	121838	6125.8

Table 2: Distribution of number of pipes per path

Sim. No.	1 pipe	2 pipes	3 pipes	4 pipes	5 pipes	6-8 pipes	9-11 pipes	12-14 pipes	15+ pipes
1	10281	2126	2758	2624	2108	3219	845	181	58
2	10243	1879	3025	3331	3121	5747	1774	421	124
3	8757	1778	2872	3185	2953	5378	1571	315	83
4	9412	4817	3537	2935	2312	3933	1311	321	97
5	9559	3748	2733	2983	2707	6118	2729	876	343
6	8124	3430	2494	2749	2512	5648	2434	723	242

To evaluate the benefit of post-analysis grouping, it is useful to make comparisons with results from individual pipe risk evaluations. Table 3 shows the following information:

- 4 rehabilitation strategies (15, 20, 25 and 30 km per year)
- For each simulation 1 to 6, paths are sorted by decreasing break rate
- PBN 2008 = original pipes sorted by descending predicted break number
- PBR 2008 = original pipes sorted by descending predicted break rate
- Number of paths, streets and pipes for the corresponding rehabilitation length
- Breaks 2008 = total breaks on groups of pipes comprising the corresponding rehabilitation length
- % PBR 2008 = percentage of maximum breaks (achieved by sorting by PBR)

Table 3: Comparison of break predictions for grouped pipes

Rehab Km	15	15	15	15	15	20	20	20	20	20
Sim. No.	No. paths	No. streets	No. pipes	Brks 2008	%PBR 2008	No. paths	No. streets	No. pipes	Brks 2008	%PBR 2008
1	67	67	111	22.8	78.7	93	93	145	28.5	79.2
2	70	89	135	23.7	81.7	97	123	186	29.4	81.8
3	78	101	157	21.6	74.5	104	132	201	27.1	75.3
4	70	70	158	21.3	73.3	91	91	218	26.4	73.5
5	71	101	191	22.4	77.3	96	138	259	28.1	78.0
6	77	116	214	21.4	73.7	99	144	266	26.6	74.0
PBN 2008	-	-	43	19.5	67.2	-	-	62	24.7	68.6
PBR 2008	-	-	462	29.0	100.0	-	-	604	36.0	100.0
Rehab Km	25	25	25	25	25	30	30	30	30	30
Sim. No.	No. paths	No. streets	No. pipes	Brks 2008	%PBR 2008	No. paths	No. streets	No. pipes	Brks 2008	%PBR 2008
1	115	115	191	33.6	78.6	136	136	224	38.4	78.1
2	119	148	223	34.5	80.5	141	177	272	39.5	80.3
3	126	161	245	32.1	74.9	151	197	317	36.9	75.1
4	115	115	278	31.7	74.0	140	140	344	36.5	74.2
5	119	172	323	33.5	78.2	144	211	410	38.5	78.3
6	123	180	336	32.0	74.7	149	225	426	36.8	74.9
PBN 2008	-	-	84	30.1	70.4	-	-	101	34.1	69.4
PBR 2008	-	-	745	42.8	100.0	-	-	944	49.2	100.0

The number of predicted breaks belonging to the paths selected for each rehabilitation strategy lies between the values obtained if sorting individual pipes by predicted break number (fewer pipes for any given rehabilitation length but also

fewer breaks "avoided") or predicted break rate (maximized "avoided" breaks but far more pipes). The grouping of pipes has a dramatic effect on the number of discrete rehabilitation projects that would be required and this is seen as a major benefit. The best way of grouping pipes, in terms of break avoidance potential, would appear to be using pipes with a high predicted break number (longer pipes) as starting points and building multi-segments from there irrespective of diameter or whether they lie on the same road.

CONCLUSIONS

The following conclusions can be drawn from this study:

- Spatial grouping of pipes has an impact on practical rehabilitation planning. The aim is to produce the most benefit in terms or risk prevention from the fewest separate physical interventions.
- Grouping prior to risk analysis is possible but the benefit remains inconclusive. In some cases this may improve or facilitate the analysis, while in others, the predictive capability of the risk model may be adversely affected.
- Grouping after risk analysis has clear advantages over treating each individual pipe as a separate rehabilitation project. In terms of likely break avoidance, this results in a slight decrease whilst dramatically reducing the number of rehabilitation entities.
- Further research should focus on optimizing all risk factors rather than just breaks.

REFERENCES

Eisenbeis P (1994), "Modélisation statistique de la prevision des défaillances sur les conduits d'eau potable",. *PhD thesis*, Université Louis Pasteur Strasbourg, 1994.

Le Gat Y (2009), "Etude du Processus de Yule Non Homogène – Application à la modélisation du risque de casses en réseau d'AEP", *PhD thesis*, ENGREF Paris, 2009 (in preparation).

Poulton M, Le Gat Y and Brémond B (2007), "The impact of pipe segment length on break prediction in water distribution systems", *Proceedings of Lesam 2007*, Lisbon, Portugal.

Saegrov *et al* (2003), "Computer-aided rehabilitation of water networks CARE-W", *Water Supply*, Vol 3, no1-2, pp 19-27.

Water Distribution Systems Corrective Maintenance Supported by Real-time Use of Hydraulic Models

Juan G. Saldarriaga[1], Susana Ochoa[2], César A. Niño[2] and Oscar J. Cortés[2]

[1] Professor, Civil and Environmental Engineering Department, Universidad de los Andes. Director, Water Distribution and Sewer Systems Research Center – CIACUA. Carrera 1 este No. 19 A – 40, Bogotá – Colombia; PH: (57 1) 339 49 49; email: jsaldarr@uniandes.edu.co

[2] Researcher, Water Distribution and Sewer Systems Research Center – CIACUA. Civil and Environmental Engineering Department, Universidad de los Andes, Carrera 1 este No. 19 A – 40, Bogotá – Colombia; PH: (57 1) 339 49 49; email: s.ochoa24@uniandes.edu.co, ce-nino@uniandes.edu.co, oj.cortes43@egresados.uniandes.edu.co

Abstract

This article presents a new tool that supports real-time corrective maintenance of water distribution systems (WDS). This tool integrates Geographic Information Systems (GIS) with hydraulic modeling of WDS, providing a graphic interface in which, in the case of a failure, the operator can select the damaged pipe (usually a burst pipe), obtaining the following information from the support tool: (1) the exact valves that need to be closed to isolate and repair the burst pipe; (2) the amount and cost of water that is lost while the damage is not fixed; (3) the users that are left without service when closing the valves identified in (1); (4) the amount and cost of water required by users but not supplied to them because of the damage. In the developed tool, the identification of the valves that must be closed to isolate the burst pipe is carried out by means of a Recursive Iterative Algorithm (RIA). On the other hand, for the loading and display of information in the GIS, binary search and a fast ordering technique, known as Quick Sort, are used. The developed tool was applied to the WDS of Sector Estadio (250,000 inhabitants), which is a complex area of the city of Bucaramanga (Colombia); it proved to be a valuable operational tool which could also be useful for prioritizing damage repair.

1. Introduction

In water distribution networks (WDN), corrective maintenance consists of the actions taken by the WDN operator to fix bursts or other damages that can occur in pipes or other elements of the network, in order to restore the system to operational status. These damages are usually caused by material wear, extremely high pressures, changes on the operation of the system, construction works close to the pipes, soil displacement, among others, and its occurrence is usually reported to the WDN operator by neighbors and passers-by.

Unlike preventive maintenance, in corrective maintenance the repair works are undertaken only after the damage has occurred; therefore, the WDN operator must always have

personnel, vehicles and materials available to repair any damage and should do it as soon and efficiently as possible. Besides, given that a regular supply of potable water is a vital necessity for any community, when service disruption is unavoidable it should not take place without giving prior notice to the users and without previously making sure that the valves that are closed to carry out the maintenance work are those which affect the least amount of users as possible. Because of this, for corrective maintenance purposes it is necessary to have computational tools that can rapidly give precise answers and information to help the personnel at the office make timely, clear and efficient decisions regarding the repair works that must be carried out. Furthermore, complete topological information of the WDN, including the location and state of all closing valves and the position of the consumption node to which each subscriber is connected, is also required for corrective maintenance purposes.

Knowing the importance of having a tool capable of optimizing repair and maintenance works and supporting decision making in water supply companies, the University of los Andes suggested to the Metropolitan Aqueduct of Bucaramanga (company which is in charge of the operation of the WDN of the city of Bucaramanga, Colombia) to take advantage of the recent and available knowledge on WDN modeling and on geographic information systems (GIS). The idea was to create and implement an innovative software which allowed to determine, in real time, the valves that need to be closed in order to isolate the area where a damage (usually a burst) has occurred and to identify the exact users or subscribers that would be affected by this situation. As will be explained, the developed software not only carries out the mentioned tasks (i. e. identification of closing valves and affected users), but goes a step further, since it also provides essential information for the prioritization of damage repair, which is critical for the integral management of WDN.

It is worth mentioning that, as any other tool which serves as a support for corrective maintenance, the developed software incorporates as its functional core a hydraulic model of the WDN, since it allows running algorithms that seek to model and predict the behavior of the network when a change is made to its operational scheme. Thus, if the characteristics and state of each of the components of the system are not well known and if the hydraulic model is not calibrated (i. e. if it does not represent the performance of the real system), it is not possible to make appropriate decisions in order to optimize the operation and maintenance of the WDN and the support tool would be worthless. For corrective maintenance purposes, it is essential to know precisely the location, characteristics and state of each of the valves of the network, given that these elements have a great impact on the hydraulic behavior of any WDN and allow isolating the burst pipe which must be repaired. Moreover, the calibration of the model which will be used in the developed software must be complemented by a complete database of users' information, containing their geo-location and current water demand; with this information, it is not only possible to make a proper allocation of water consumption along the model, but also to determine the impact and the area affected by a burst.

2. Case study description

As is common for any WDN operator, the Metropolitan Aqueduct of Bucaramanga (AMB for its initials in Spanish) has to deal with unpredictable damages that occur along the network, which must be repaired by the company to fulfill the good quality and continuous service standard inherent to all water supply activities.

In the city of Bucaramanga (located in the northeast area of Colombia, with a population of 1.1 million), the process begins with the detection of the damage: once the water reaches the surface, it is reported by passersby, neighbors or, in some cases, by company employees. To report the damage, the person who saw it communicates with the company's Call Center, where an operator is in charge of identifying, through a series of simple questions, the location and extent of the damage. When the person who witnesses the damage is a company employee, he/she reports it directly to the unit responsible for repair works, which is known as Maintenance Section.

This report is stored in a SAP (*Systeme, Anwendungen und Produkte*) tool, which is used by the company to allow Maintenance Section to have access to this information, since they are located elsewhere in the city. Then, according to the location of the damage, each report is assigned to one of the subareas into which the city is divided; lastly, the order in which each damage will be repaired is determined subjectively (based on the description of the damage and on the knowledge and skills of each repair team).

Once the repair works have been assigned, maintenance teams are sent to each subarea with the materials and tools necessary to repair the majority of the damages. One of the first tasks they must complete after verifying the existence of the damage is to determine, based on their experiences, knowledge of the network, and some physical maps (which contain the network layout), how the burst pipe is connected to the rest of the system and which are the valves that should be closed in order to isolate it.

Since mistakes are inherent to most human activities, letting maintenance personnel decide which valves to close in order to carry out the repair works might involve some error. It is even possible that, when subjectively closing valves in the attempt of isolating a burst pipe, new nearby bursts are created by maintenance personnel. This is why it is crucial to take as much advantage as possible from the benefits that are provided by the new information technologies in terms of calculation, storage and display capacity, all of which could facilitate the identification of the valves that must be closed in order to isolate a certain pipe or area of the system. It is worth mentioning that hydraulic modeling must always be present in this process, since it indicates the possible paths through which water can reach the area of interest.

The solution presented herein to the problems associated with corrective maintenance puts together computational tools, which carry out the hydraulic modeling of a WDN, with geographic information systems (GIS), which can store georeferenced information of each component of the system. The combination of these two tools allows for the implementation of algorithms that can give a solution to the problem stated above and that

can also display the answer in a graphic interface, making it easier to understand and analyze.

3. Algorithm

I0t is important to emphasize that without knowing the hydraulics of the WDN and the location, characteristics and state of each of its elements, it is not possible to determine how to operate it in order to solve the problems stated above regarding corrective maintenance. The performance of the hydraulic model of the WDN must match the behavior of the real system; this is why it is essential to have a calibrated hydraulic model before applying the algorithm that will be next described.

In order to identify the valves that need to be closed to isolate a burst pipe, it is first selected and the node through which the water is entering the pipe is identified. From this node, a Recursive Iterative Algorithm (RIA) is used to travel across the network in the upstream direction looking for the valves that close the pathways through which the water flows into the burst pipe. In general, it is not likely to have a closing valve just before the entrance node of the damaged pipe; the common situation is to have one or more pipes connected to the entrance node and to many other nodes upstream from them. Thus, the mentioned algorithm must "recall itself" as many times as necessary until all pathways through which the water is coming into the burst pipe are identified and closed; this is the main characteristic of a recursive algorithms.

This type of solution searching strategy is known as Backtracking: with this technique, a directed entity (in this case, the hydraulic network with a specific flow direction in each of its nodes) is traversed through in order to find a solution or set of solutions that satisfy the objective of the search. In the specific case that is being described in this paper, as a valve is found when looking through a certain pathway in the upstream direction, its state is changed to "closed" and the search in that specific pathway of the network finishes. Subsequently, the algorithm starts traveling back (i. e. in the downstream direction) through the same pathway that led to the valve that has been just closed; in its trajectory, it looks for nodes which are connected to pipes that have not been traversed through by the algorithm before. When a node like this is found, a new search process begins.

Any time a valve is closed, the hydraulics of the network must be calculated again to determine the new pathways through which the water is flowing into the burst pipe. This process is carried out iteratively until the damaged pipe is completely isolated and the initial group of valves that must be closed to achieve it is identified.

An exceptional situation found during the design of the algorithm was that, in some rare cases, even after traversing through the entire network it was not possible to isolate the burst pipe. When this happens, the algorithm throws an exception and informs the user about this situation.

Once the initial group of valves that must be closed to isolate the damaged pipe is identified, an additional algorithm which evaluates "valve redundancy" is executed. Valve

redundancy takes place when some valves of the initial group can stay open while the burst pipe still remains isolated. Therefore, it is required to identify which valves must be closed and which other valves can remain open; in this way, the least amount of valves is closed and no time and resources (both human and material) are wasted in closing unnecessary valves. The concept of valve redundancy is illustrated in the following figures.

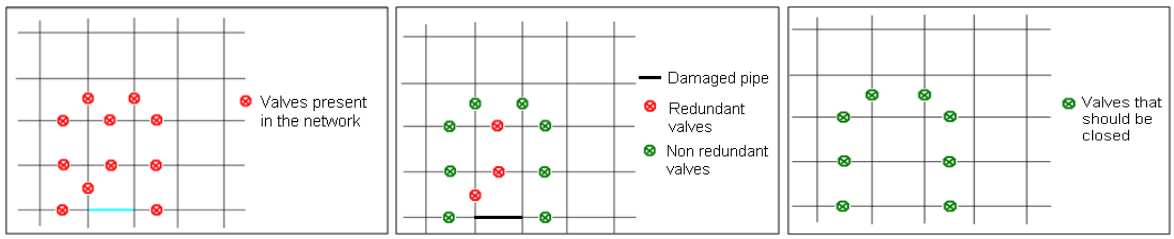

Figure 1. Valve redundancy: (a) initial group of valves of the system; (b) identification of redundant valves; (c) final group of valves which must be closed to isolate the burst pipe.

4. New software: CIERRES

CIERRES (which is the Spanish word for closure) is a computational tool implemented under the programming language *Visual Basic for Applications*, which was developed to be executed inside the program ArcGIS 9.1. Besides identifying the valves that must be closed to isolate a certain area of the WDN, *CIERRES* can also detect which users are affected by the service disruption and estimates the discharge that these users stop consuming while the damage is not fixed (i. e. the amount of water that is not sold during this time). Moreover, the program has a module which, based on the geometric characteristics and pressure regime of the system, can calculate the discharge that is lost because of the burst.

In order to obtain the required results, *CIERRES* is supported by a hydraulic modeling tool developed at the University of los Andes (i. e. hydraulic simulation software called REDES – see CIACUA, 2007b) which carries out the hydraulic calculations of the WDN and also runs the algorithm for the search and verification of the valves that must be closed to isolate the damaged pipe.

To test the program, a hydraulic model from a subarea of Bucaramanga's network was used. This subarea is known as "Distrito Estadio" and represents 25% of the city's network, supplying water for 27,000 house and commercial connections, with 5324 pipes (equivalent to a total pipe length of 1800 km) and 1772 valves.

Figure 2 shows an aerophotography of Distrito Estadio, as well as its hydraulic model.

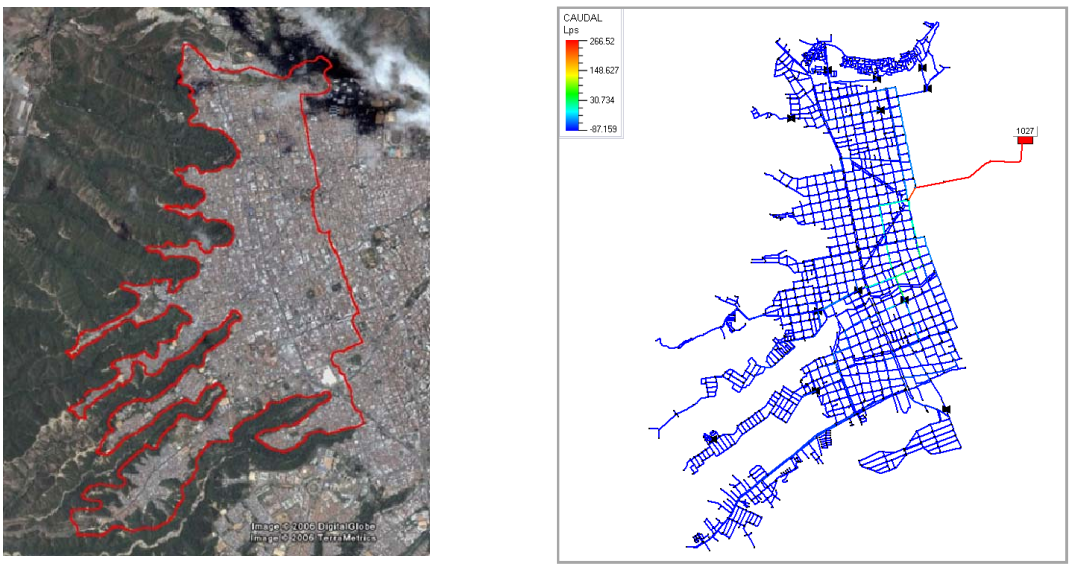

(a) **(b)**

Figure 2. Distrito Estadio: (a) aerophotography; (b) hydraulic model.

Since *CIERRES* is connected to ArcGIS, all the geographic information is displayed graphically to facilitate its understanding and allow the georeferenced location of the users that are left unattended while repair works are carried out and of the valves that must be closed to isolate the burst pipe.

4.1. Design of CIERRES

In the design of any computational tool, it is necessary to define the architecture that it will use; it determines the functional and non-functional requirements and the constraints of the final program.

Through components and layers, the architecture seeks to define the tasks of each component, the interactions between them and their physical location. For example, in a *distributed system* its architecture is split up into components that run simultaneously on multiple computers; some of these components run from a central server and have specific security, persistence, processing and concurrence responsibilities, among others. On the other hand, in *standalone* applications the responsibilities are different; in this case, no communication is necessary between multiple computers, there are not concurrence problems, security is managed differently, among other aspects which make this type of architecture more appropriate for the requirements of the software that is being developed.

During the design of *CIERRES*, a three layer (i. e. Interface - Logic - Persistence) architecture was chosen. This structure allows for the clear division and definition of the tasks, in order to improve the understanding of the program during its implementation as well as in the case of maintenance or further improvements to the tool. Figure 3 shows the three layers that make up the new program. Within the first layer -GUI (Graphic User Interface)- are the classes related with the graphic interface, which are in charge of

interacting with the user, requesting and receiving information from him/her and transmitting it to the "Logic of the business" layer.

The "Logic of the business" is in charge of receiving the user's requests in order to represent each of the components of the network and communicate with *REDES* (a hydraulic simulation software) to calculate the hydraulics of the model, run the valve searching algorithm and extract from it the information that is required for the prioritization of corrective maintenance.

The last layer is "Persistence": it contains the classes that are in charge of extracting information from plain files and files related with the GIS used by *CIERRES*.

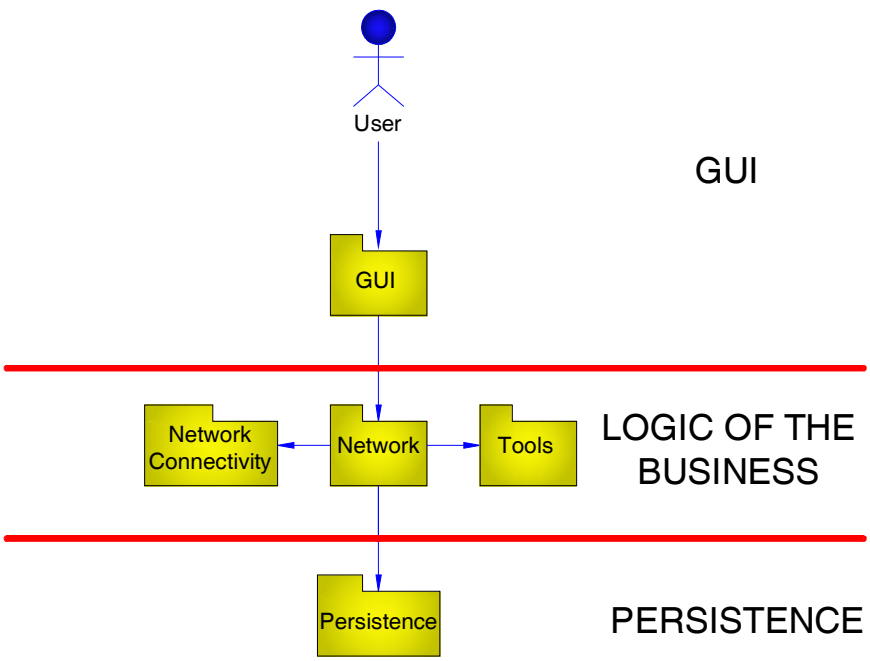

Figure 3. Three layer architecture of the program *CIERRES*.

With respect to the architecture of the program, it is important to highlight that the final application software is a *standalone* program, which means that all its components are installed and can be executed in only one computer, without requiring any connection with another computer.

4.2. Files used by CIERRES

The identification of the valves that must be closed to isolate a specific area of a WDN depends mainly on the hydraulics of the system, whose determination requires a hydraulic model of it. This model must have some special characteristics to allow *CIERRES* establishing the location of the valves that need to be closed to isolate a certain pipe.

The hydraulic models of the WDN that will be evaluated through *CIERRES* must be *.INP files, which corresponds to the type of file used in the hydraulic modeling of water distribution systems. Furthermore, when modeling WDN, there is usually not an element

exclusively aimed at simulating closing valves; thus, what is commonly done to model these elements is using short pipes whose state is changed from "open" to "closed" (as the closing valve open or closes).

For the program to identify the location and state of the closing valves, these must be represented by short pipes whose identifier starts with the letter "V". When the program detects a pipe with this characteristic (i. e. letter "V" at the beginning of its ID), it reads its state; if it is "closed", the program will know that it is a valve which is permanently closed, otherwise, it will know that it is an open valve which could be used to isolate a certain area.

Another important aspect related with the input information that must be given to the program is that associated to the spatial location of the users, its water consumption and consumption nodes to which they are connected. The information about water consumption must be provided through a plain file, which contains each user's identifier, geographic coordinates (X, Y, Z) and water consumption. The consumption node to which each subscriber is assigned is determined from the output file of the program *ASIGNA*. This program was also developed at the University of los Andes; it connects the water consumption of each subscriber to the closest node of the system.

4.3. Using CIERRES

The initial window of *CIERRES* (see Figure 4) is displayed inside the ArcMap environment of ArcGIS. In this window, the user must provide the location of the file with the calibrated hydraulic model; the location of *REDES*, which is executed underneath; and the location of the files that contain the users' geographic coordinates, demands and nodes to which they are assigned.



Figure 4. Initial window of CIERRES – options to generate shapefiles.

Figure 5 shows the graphical display of the shapefiles that were created; in this display, the yellow crosses represent the users, the nodes are shown by black dots, the blue lines

correspond to pipes, the closing valves whose state is “open” are shown by green lines, and the red lines show the valves that are permanently closed.

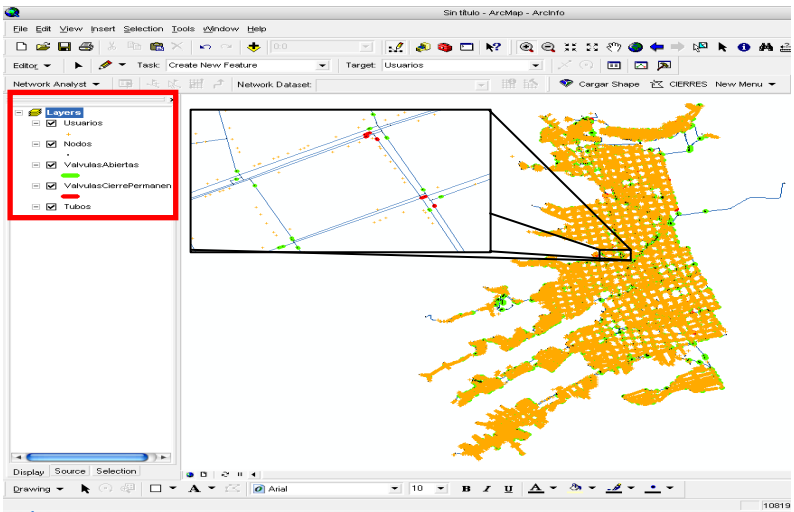

Figure 5. Graphical display of the shapefiles.

Once the input files have been processed and the shapefiles have been created, the next step is to indicate the burst pipe, so that the program can determine the area of the WDN which will be affected by the repair or maintenance works. To do this, the user must use the object selection button (see Figure 6) in order to point out the damaged pipe.

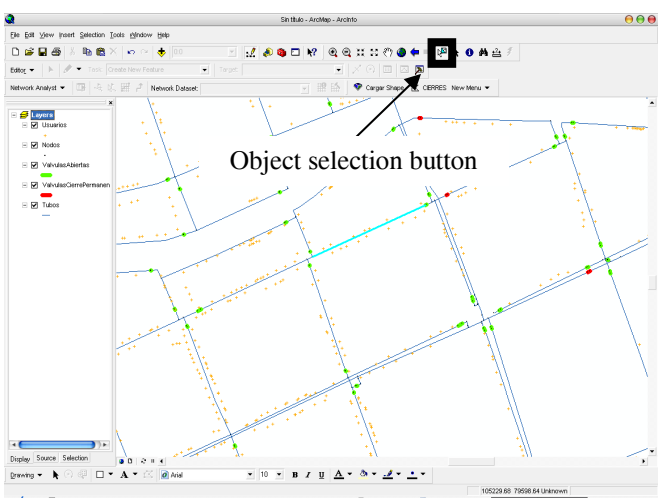

Figure 6. Selection of the burst pipe.

After the running *CIERRES*, the results are displayed in a window (see Figure 7) that shows the following items: the valves that must be closed to carry out the repair works, the users that are left unconnected (represented by black dots), and the pipe that will be repaired. In addition to this graphical display of the results, a plain file is generated which contains a report of the valves and users identifiers, as well as relevant information for the repair works.

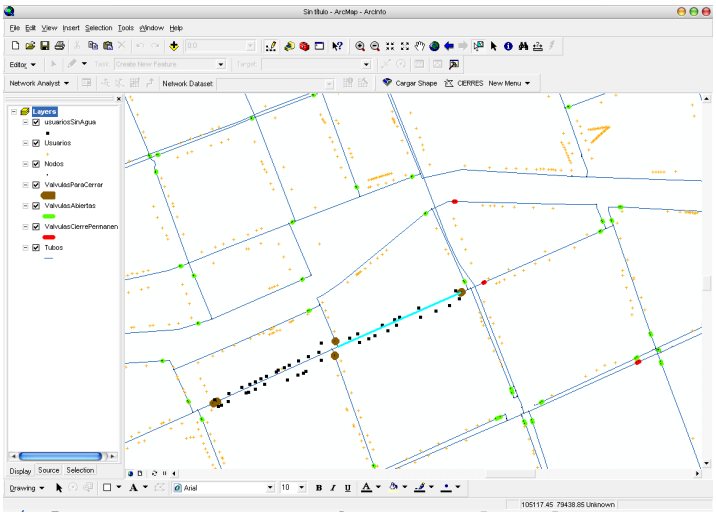

Figure 7. CIERRES response.

4.4. CIERRES as a Decision Support System (DSS)

The technologic and globalization level to which the modern world has come forces everyone to be more competitive, efficient and resourceful in order to generate good quality solution in as little time as possible. For this reason, it is important to have tools such as *CIERRES* which support the WDN operator in the decision making process, thus becoming a DSS (Decision Support System) tool.

The DSS are computational tools which help the people in charge during the decision making process, without substituting their expert knowledge. These systems use data and underlying models and are created based on the knowledge and rules provided by the experts; they facilitate the learning process of the user and put together the human knowledge with the processing capacity of the computers in order to improve the quality of the decisions and reduce the time that it takes to make them. Furthermore, the DSS are interactive, easy to use and user-friendly programs.

In the case of the Metropolitan Aqueduct of Bucaramanga, *CIERRES* was conceived as a system to support real-time decision making. Since it uses hydraulic modeling and GIS to tell the user which valves must be closed in order to isolate a certain pipe, *CIERRES* avoids letting the maintenance personnel decided it, which, as was stated before, might involve great errors and might also lead to an inefficient use of the available resources.

Furthermore, *CIERRES* allows for a continuous feedback between the model and the real distribution system; by identifying valves that are not working properly or areas whose isolation requires the closing of a great amount of valves, which leaves many users unconnected, the WDN operator can make decisions regarding the need for new valves or the need for a better division of the network into independent hydraulic sectors.

5. Conclusions

- Corrective maintenance should leave aside the empirical knowledge of maintenance crew members, which involves subjectivity and error, and should use computational tools in order to become an optimized process.

- In order to have adequate work tools that can aid WDN operators in the decision process, it is important to have a calibrated hydraulic model, which implies acquiring information of excellent quality, such as: topology, topography, users' census, registry of their historical demands, and flow and pressure measurements along the network, among others.

- Geographic information systems and advanced methodologies of programming must be combined with calibrated hydraulic models to develop support systems that enable companies to take actions on their networks, in order to improve the service, reduce the response time, and optimize repair maintenance works whenever a damage occurs.

- Reducing costs and improving service quality are issues that are generated by the use of such tools.

- When testing the developed software *CIERRES*, which combines geographic information systems with hydraulic modeling of water distribution networks, it proved to be a valuable operational tool that supports real-time corrective maintenance, making it more efficient and optimizing the use of resources required for repair works; besides, this software proved to be helpful for supporting decision making at the water supply company.

6. References

CIACUA. (2007a). *Final Report of the Optimum Pressure Surface Project – Water Distribution Network of Sector Estadio, Bucaramanga*. Universidad de los Andes – Acueducto Metropolitano de Bucaramanga, Colombia.

CIACUA. (2007b). *Redes 2007 - Manual de Usuario*. Bogotá, Colombia: Universidad de los Andes.

Jurado, C. M. and Saldarriaga, J. G. (2007). Water Distribution Networks Calibration under Leaks Environment - Study Cases. *Proceedings of the World Environmental & Water Resources Congress 2007*, Tampa, USA.

Saldarriaga, J. G. (2007). *Hidráulica de Tuberías: abastecimiento de agua, redes, riegos*. Bogotá, Colombia: Editorial Alfaomega.

Water Price Forecasting Method Based on Marginal-cost Theory: a case study in China

LI Cui-mei[1,2], LIU Sui-qing[1]

[1] College of Environmental Science and Engineering, Tongji University, Shanghai City, 200092, P. R. China, PH(FAX)(0086)02165895869, email: cuimeili@163.com; Depart. Of Environmental Science and Engineering, Science and Technology University of Suzhou, Suzhou 215011, P. R. China

[2] College of Environmental Science and Engineering, Tongji University, Shanghai City, 200092, P. R. China, PH(FAX)(0086)02165895869, email: liusuiqing@mail.tongji.edu.cn

Abstract:

The purpose of this paper is to evaluate the pricing of China water utilities according to past twenty year's data. An econometric model describing both water supply and demand is specified and estimated on utilities located in the east area of China. Based on the estimated technology and demand parameters, a new method of forecasting water price is presented. It used the marginal-cost theory that is close to the historical data to establish the water price forecasting function, and according to the process of marginal-cost function to build the forecasting model. We derive the estimated parameters and discuss estimates of returns to scale and elasticity of water demand, analyzing the current pricing of water utilities by comparing marginal costs and marginal prices. In a case study of Shanghai, these estimates are then used to simulate first-best optimal pricing by solving a supply-demand system in prices and quantities. Finally, we find that the marginal cost price is the optimal pricing scheme, which is much better than fixed charge price and average cost price.

Key words: water pricing; forecast; marginal-cost theory; water utility; Simulation

INTRODUCTION

Water is an important natural resource, and a basic necessity for human survival. Due to rapid industrial development and accelerating urbanization, the number of cities in China has increased dramatically, from 180 to 666, since the 1980s. As a result, the urban population and water demands have also increased rapidly, thus causing severe water shortages in urban areas. At the same time, the increasingly serious water pollution caused by urban development not only does great damage to human health but also intensifies the shortage of water resources.

Up to the end of 2004 in China, the total urban water supply production capability per day is about 247.5302 million m^3, compared with 142.203 million m^3 in 1990, it was increased 74%; service population is 30.33968 million persons, increased 94% contrast to 156.0010 million persons in 1990.

The capacity of public water supply increased fleetly, there are now about 3000 water treatment plants, of which the total production capacity is 167.9213 million m^3

per day. Increased 185% compared with 58.8590 million m^3 per day in 1990; service population is 266.1603 million people, compared with 112.0740 million persons in 1990, it increased about 137%; the urban public water supply capacity account for more than 68% of the total social water supply capacity, increased 27%; the ratio of urban water supply and demand increased 0.44, now reached 1.38.

In 2004 the total urban water supply is 49.03 billion m^3, in which industrial water consumption is 21.14 billion m^3 accounted for 43%; domestic consumption (included public service water consumption, housing water consumption, fire water consumption and etc.) reached 27.89 billion m^3 occupied 57%. Compared with 1990, the proportion of industrial water decreased 29%, whilst the proportion of domestic usage increased 29%.

Financial balance of water supply enterprises is very important for the safe supply of which guaranteed quality. Due to events in the past， the price of water in China is still too low to meet the operating and maintenance needs of basic water supply facilities. The price does not reflect the real usage value of water, thus resulting in over consumption. Hence, we must implement water price reform and establish a water price management system, and regulate the price through cost control. Only in that way can we recover investments, get a reasonable profit, and ensure normal operations and sustainable development.

In summary, price adjustment should be based on the following principles: cost compensation, reasonable profit, improved water saving, and equal contribution. Firstly, the price should be such that it would help to save water, and make the cost of water account for a specific portion of inhabitants' income and of industrial expenditure. At the same time, consumers' saving consciousness would be promoted, and they would stand to gain by saving water. Secondly, a reasonable charge should be levied for water resource and wastewater treatment, and a reasonable water price should be set. Thirdly, consumers' acceptance level should be considered. There should be a difference in water prices, and the price should be introduced step by step. A system of reward and punishment can be can be applied when necessary so as to save water and ensure that it is used reasonably. Finally, water should be publicized as a consumer good. A scientific water price measure and flexible price policy are also needed. The important point in price reform is to establish a proper price forming and operating system, to set up a price management system adapted to a market economy in order to let the price act in resource distribution, saving and efficient usage and, ultimately, to realize the sustainable development of water resources.

During last 10 years, water price in China have been average increased 2~10 times, especially in some well developed area. Figure 1 provides the average water consumption (liters /cap. d) and average Water Price (fen RMB/m^3) from 1980 to 2004 in China. Figure 2 depicts the water price of each province in 1999. By analyzing the water price variety with economic method, we can conclude appropriate water price. With water resources becoming more and more deficient,

how to save water usage has become an important problem in China. As one problem of water resources management, water price policy has economic lever effect and an effectively measure. Some previous studies evaluating water price efficiency have already been published, such as marginal-cost pricing(MCP)(FANG, 2004), average cost pricing(ACP)(SHI, 2003), shadow price(SP)(SHI, 2002), elastic water price(EWP)(DU, 2003). But to our knowledge, none of them use appropriate methods.

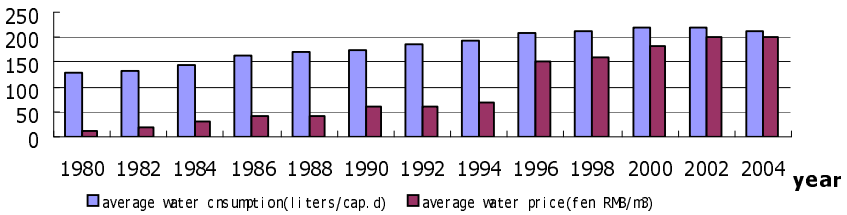

Figure. 1 water consumption and water price in China

The efficiency of water pricing is also an important concern in most developed countries. In England and Wales, the economic regulator (OFWAT) requires companies to publish their long run marginal costs. In Portugal, the 1994 Decree-Law also requires newly privatized water services to price water at a charge equivalent to the long run marginal cost. But if there is now a consensus on the importance of efficiency criteria in water pricing determination, it is surprising to note that only a few recent studies have evaluated the pricing of water utilities (WUies hereafter). See Kim(1995) and Renzetti(1999) for water pricing analysis in North America. See, for example, Mithchell(1978)for the telecommunication industry and Dimopoulos(1981) and Protti and McRae(1980) for the electric power industry.

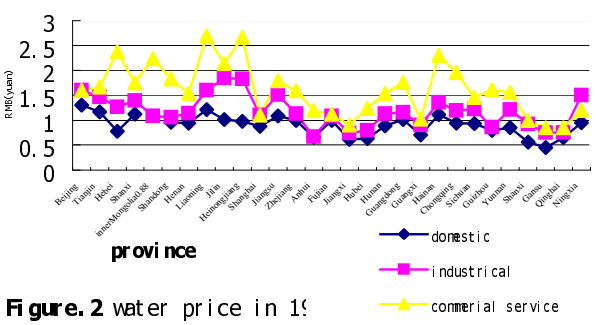

Figure. 2 water price in 19

It is also interesting to see that, while the economics literature is quite consistent in its criticisms of water pricing by WUies, only few studies have estimated the magnitude of the gains to be expected from moving to efficient prices. Moreover, estimates of welfare gains vary from one study to another. Swallow and Marin (1988) show that moving toward efficient prices will result in an increase of welfare within 2% of the

actual surplus. But Renzetti (1992) finds that a move to seasonally differentiated pricing raises the aggregated surplus by approximately 4%. This situation contrasts strongly with the exhaustive analysis of the potential welfare gains to be achieved from reforming the pricing practices of other types of public utilities.

Marginal-cost theory(MCP)

Marginal cost （MC）as a term, has been around for nearly 20 years, e. g. Mann (1982) with respect to water service and the provision of infrastructure. Marginal cost is the additional cost of producing or selling a single incremental unit, thus marginal cost of water service is the cost or saving incurred in providing more or less water service. Marginal cost has two components－short-run marginal cost, defined as the change in operating costs by changing the rate of utilization of existing capacity, and long-run marginal cost , defined as the cost of expanding capacity as well as the operating costs associated with increased capacity. In contrast to average cost, which uses embedded or historic accounting costs, marginal cost calculation involves projecting future operating and capacity costs for a specified time span by using cost changes that occur because of long-run incremental cost are concepts similar to marginal cost. Marginal cost refers to multi-unit changes. For practical purposes, incremental and marginal cost concepts are interchangeable.

Application of MCP to water price forecasting

Designing efficient water price is a crucial issue for water utilities and local communities. The first objective of a water utility pricing scheme is to generate revenues covering costs. But any pricing rate must also have two other functions: a pricing rate allocates costs between users and it has to provide incentives for efficient use and water conservation. Applying these criteria to determine the best rate structure is not an easy task. First, some of the criteria may directly conflict and require making tradeoffs among them. The balance between revenue stability and efficiency of price is an example of such tradeoff. Moreover, as water services involve high capital investments, a lot of expenses are fixed costs, which do not vary with the quantity of water consumed. This makes the allocation of costs among users more difficult to achieve.

The theoretical literature on public sector pricing prescribes the form of efficient prices for a variety of circumstances. In the simplest formulation, maximizing social welfare leads a public utility to use marginal-cost pricing (MCP). Maximizing aggregate net surplus leads to the well-known price equal to social marginal-cost rule:

$$P = \frac{\partial C(Q)}{\partial Q} + \lambda \qquad (1)$$

where Q is the volume produced by the water utility, C(Q), with $C' > 0$ and $C'' > 0$, its cost function, and λ is the marginal shadow price of water. This shadow price is positive when water is scarce or when water withdrawals have environmental impacts. If the price does not reflect the social marginal-cost, consumers do not receive an appropriate information about the societal cost of a marginal increase of demand.

Notice that the list of assumptions required for using this result is quite impressive. Among others, the demand for output must be stable, known with certainty and it must depend on no other price but its own. Furthermore, the public utility must be indifferent to the distributional consequences of its decisions and also to the possibility that its pricing may not be financially self-sustaining. MCP deserves a certain number of criticisms and gives rise to a certain number of practical difficulties. Firstly, the absence of a budget constraint may provide managers with inappropriate incentives for cost reduction. This is one of the reasons why average cost pricing (ACP) has been imposed on many regulated industries. Secondly, MCP does not reveal whether it is worth incurring the fixed costs, Coase (1946) Calviou et.al. (1993). MCP requires that the public authority decides for consumers whether they are ready or not to pay for covering total costs. Unfortunately, in many cases, the public authority may lack information to correctly implement this decision. Thirdly, MCP implies that the public utility runs a deficit if it operates under increasing returns to scale. One of the earliest criticisms of MCP is related to the distortion implied by this deficit. In the absence of lump-sum transfers, the benevolent authority must resort to distortionary taxes. Therefore, optimal pricing in the presence of a cost of public funds requires the price to diverge from the marginal-cost. An alternative solution is to use two-part tariffs with a marginal price corresponding to the marginal-cost and a fixed charge allowing to recover the deficit. Last, implementation of MCP can also generate considerable administrative costs which may counter-balance the efficiency gains. For example, MCP requires the installation of sophisticated meters capable of determining not only the total consumption level of each water user but also the time at which water consumption takes place.

Hunt & Shuttleworth (1993) discussed several advantages of a marginal costing approach, the main of which consists of encouraging investment and operation in the right direction from an efficiency point of view.

Case study in China

Shanghai is situated at 31'14' north latitude and 121'29' east longitude. Bordering on Jiangsu and Zhejiang Provinces on the west, Shanghai is washed by the East China Sea on the east and Hangzhou Bay on the south. North of the city, the Yangtze River pours into the East China Sea. Thanks to its advantageous geographic location, Shanghai has today become an excellent sea and river port, boasting easy accesses to a vast hinterland. With a pleasant northern subtropical maritime monsoon climate, Shanghai enjoys four distinct seasons, generous sunshine and abundant rainfall every year. Its spring and autumn are relatively short comparing with the summer and winter. In 2002, the average annual temperature was 17.8 degrees Celsius. The city had a total sunshine time of 1,686.5 hours in 2002 and received an annual rainfall of 1,427.9 millimeters. However, about 60% of the precipitation came during the May-September flood season, which is divided into three rainy periods, namely, the Spring Rain, the Plum Rain and the Autumn Rain.

The city had a total area of 6,340.5 square kilometers at the end of 2002, 0.06% of China's total territory. Shanghai extends about 120 kilometers in north and south and

nearly 100 kilometers in east and west. The city's 19 districts cover a total area of 5,299.29 square kilometers and its only county has an area of 1,041.21 square kilometers. The city has three islands -- Chongming, Changxing and Hengsha -- under its jurisdiction and Chongming Island is the third largest island in China, covering an area of 1,041.21 square kilometers. By the end of 2004, Shanghai's population of residents with permanent resident certificates had grown to 13.5239 million, representing 1% of China's total population. Since 1990 and particularly since the beginning of this century, Shanghai has been striving to build itself into an international economic, financial, trade and transportation center. Since 1992, the city has maintained a double- digit GDP growth rate for 13 consecutive years. In 2004, its GDP reached 745.027 billion yuan, 13.6% higher than the previous year in terms of comparable prices, representing the highest growth rate since 1996. The figure was 3.9 times that of 1990 and the average annual growth rate during the 1990-2004 period stood at 12%.

Residential affordability analysis in Shanghai

Since the beginning of reform and opening, Shanghai's economy has been developed rapidly. If dollars，Shanghai's per capita GDP was 4,172 U.S. $ to 4,515 U.S. $ from 2000 to 2001，then increased to 4,909 U.S. $ in 2002, and then to 5,642 U.S. $ per capita in 2003, Four years of aggregate growth is 35.23% per capita GDP, with a average annual growth rate of 10.59%.

Shanghai residents water consumption increased from the 682 million m^3 in 2000 to 743 million m^3 in 2003, while residents water consumption expanded 8.94%, total residents water consumption for the annual growth rate is 2.9%. Annual residents water consumption around 51.6~55.4 m^3 per capita. Per capita water consumption is between 141L/d~152L/d. During four years the residents water consumption elasticity coefficient is 2.9%÷10.59%=0.2738. Resident water consumption is about 0.27% growth each 1% growth of per capita GDP. Table 1 shows per capita GDP and per capita water consumption variety from 1990 to 2003 in Shanghai.

According to the “Shanghai Statistical Yearbook” (1990～2003), Average annual disposable income have increased from￥2,182 to￥14,867 from 1990 to 2003. Water expenditures accounted for less than 1% of per capita consumption expenditure, much lower proportion of the total disposable income, 2003 to 0.54%. The downward trend in the last three years, water expenditures is only ￥80 per capita. To further investigate the affordability of residents for water charges, the research group conducted a random sample survey, questionnaire that covers almost Shanghai. The survey shows: Shanghai residents have affordability to the adjustments of water price. The results of the survey are as following:

（1）64% of households drink barrel water that the residents have a higher water consumption；If water consumption can be directly, urban residents will account for 4% of the purchase barrels of water，88% will not buy，Improving water quality of drinking water for residents will cause a greatly cost reduced。

（2）According to questionnaire of the family’s attitude toward water expenditures monthly, it is not a burden for 30%; and only a small burden for 38%.

（3）If water quality agreed with the EU standards, water price would increase reasonable 80%.

（4）The families think that acceptable water expenditures account for less than 1% of the total household income is about for 37%; and the proportion of 1~2% is 30%; the proportion of 2~3% is 26%.

（5）The families accept three-part water price is 61%.

Enterprise affordability analysis

First, take water consumption and the proportion of the total cost as evaluation indicators. The bigger water consumption and bigger water costs proportion as major focus of investigation. Through comparing several cities industrial water price, we drew an conclusion that industrial water price in Shanghai is lower. With huge capital investments and water quality improved，water price increases are inevitable. In recent 20 years in Shanghai, water consumption per thousand yuan industrial value is decreased year after year, which indicates that water price effect is increased. Table 2 shows the tend of recent 20 years shanghai water consumption variety and industrial water consumption decreased per thousand yuan of industrial output.

Table 2 urban water construction variety in Shanghai unit: billion m^3, billion yuan

year	total	industrial	domestic	Industrial proportion	Industrial value	Consumption($m^3/10^3$RMB yuan)
1985	1.051	0.626	0.413	60%	32.563	1922
1986	1.054	0.607	0.436	58%	33.602	1806
1987	1.097	0.614	0.477	56%	36.438	1685
1988	1.159	0.622	0.526	54%	43.305	1436
1989	1.181	0.598	0.558	51%	46.618	1283
1990	1.225	0.59	0.611	48%	48.268	1222
1991	1.241	0.581	0.628	47%	55.134	1054
1992	1.29	0.602	0.656	47%	67.739	889
1993	1.351	0.596	0.714	44%	90.033	662
1994	1.418	0.547	0.778	39%	114.32	4478
1995	1.904	0.74	1.028	39%	140.985	525
1996	1.979	0.708	1.077	36%	158.25	447
1997	1.981	0.674	1.124	34%	175.439	384
1998	2.008	0.619	1.155	31%	184.72	335
1999	1.933	0.55	1.145	28%	195.398	281
2000	1.975	0.549	1.188	28%	216.368	254
2001	2.027	0.514	1.226	25%	235.553	218
2002	2.026	0.531	1.189	26%	256.469	207
2003	2.079	0.566	1.26	27%	313.072	181

Table 1 Average GDP and average domestic water consumption per capita

year	1990	1991	1992	1993	1994	1995	1996	1997	1998	1999	2000	2001	2002	2003
Population(10^4)	1283.35	1287.20	1289.37	1294.74	1298.81	1301.37	1304.43	1305.46	1306.58	1313.12	1321.63	1327.14	1334.23	1341.77
GDP(billion RMB yuan)	75.645	89.377	111.432	151.161	197.192	246.257	290.22	336.221	368.82	403.496	455.115	495.084	540.676	620.581
Domestic water consumption(billion m^3)	0.611	0.628	0.656	0.714	0.778	1.028	1.077	1.124	1.155	1.145	1.188	1.226	1.189	1.26
Average water consumption per cap(m^3)	47.61	48.79	50.88	55.15	59.90	78.99	82.56	86.10	88.40	87.20	89.89	92.38	89.12	93.91
Average GDP(yuan)	5910	6955	8652	11700	15204	18942	22275	25275	28240	30805	34547	37382	40646	46718
Convert to USA dollar(1:8.28)											4172	4515	4909	5642
Domestic water consumption(billion m^3)											0.682	0.709	0.692	0.743
Average domestic water consumption(m^3)											51.60	53.42	51.87	55.37

Shanghai Statistic Yearbook (2004)

Water price forecasting in Shanghai

By comparing water supply costs, evaluation residents affordability and assessing enterprise affordability, we can draw the conclusion that residents and enterprise are able to afford for the water price increase, and it will help to save water all over the society. Forecasting of Shanghai water price is based on the following principia:

First, green belt sprinkling, fire demand, street flushing demand and other municipal water must be paid. Second, cost control should be enhanced to restrain water price adjustment. Thirdly, it suggests that supply different water quality to different enterprise, to satisfy different industrial water requirement and to save industrial water cost. Last, there should be some special policy to protect the poor for water demand and

provide them basic water usage welfare. But the welfare is limitative, table 3 analyzes the basic per household water demand per month in shanghai. Base on the analysis we know that household basic water demand is about 15m^3 per month, two suggestions are given as follow. One is that under the 15m^3 per month, water price is an welfare and very low, a charge will be made whose water consumption exceed the specified limit. The current charge per excess cube meters is about ￥2.21(not include charge for wastewater discharge).

According to these principia, marginal cost theory and 20 years water demand and consumption data, we can forecast Shanghai water price in the future 5 years. The conclusion can be seen in table 4.

Table 3 Domestic water consumption investigation in Shanghai

Domestic average water consumption(m^3/ month)	2001		2002		2003	
	houses	Percentage	houses	Percentage	houses	Percentage
＜15	872651	58.56%	1012191	64.29%	1025952	60.80%
16～25	275094	18.46%	249947	15.88%	302809	17.94%
26～35	134271	9.01%	121270	7.70%	146499	8.68%
36～45	63151	4.24%	55874	3.55%	67223	3.98%
＞45	100955	6.77%	89884	5.71%	103153	6.11%
else	44080	2.96%	45138	2.87%	41842	2.48%
total	1490202	100.00%	1574304	100.00%	1687478	100.00%

Note: The consumer proportion from 2001 to 2003 monthly average water consumption below 10m^3 account for total is 47.82%, 46.17%.

Table 4 Three-part water price in shanghai (not include wastewater discharge cost) unit: RMB yuan

Water price (Yuan)	Water consumption(m^3/month)	2006	2007	2008	2009	2010
Basic water price	＜15	1.38	1.74	1.74	1.74	2.08
Second part water price	16~25	1.79	2.26	2.26	2.26	2.7
Third part water price	＞25	2.21	2.78	2.78	2.78	3.33

Conclusions

According to the Shanghai Statistic Yearbook (SSY)(1990~2003), household average water consumption is 13m^3 per month. For 58.56% of the households, the figure is below 15m^3 per month, while for other 18.46%, it is between 16-25m^3 per month. As the total of these two parts is 78%, this explains that carry out three-part water price is feasible and reasonable.

Artificially low water price in Shanghai leads to water over consumption and large quantity of wastewater discharge, which result in high pressure on the water environment. In order to develop and utilize water resources sustainable, justifying water pricing in Shanghai is necessary and pressing. It is proposed that water pricing could be justified in a marginal cost method and eventually towards the full cost

pricing. The assessment of impacts on water resources by raising water pricing shows that water pricing could be an effective tool for more sustainable water consumption.

Acknowledgements

The authors would like to thank the Shanghai Comprehensive Water Quality Improvement Act 2004-2010(SCWQIA 2004-2010) and National Nature Science Foundation of China (50409016) for funding.

References

Liu Suiqing, Tao Tao and Li Shuping, Approaches to Urban Sustainable Water Resources Management in China, Proceedings SUSDEV-CHINA Symposium, China, 2005, 130-139.

Fang Hong-yuan, Wang Yin-tang, Application of marginal cost analysis to water resources development, Advances in water science. J. 15(2) 243-248.

Shi Xican, Determination of shadow prices of commercial water and electric energy, Journal of hydro electric engineering. J. 77(2) 1-8.

Du Rong-jiang, Chen Hao, Chui Guang-bai, Case study on elastic water price and bearing capacity of water users, Journal of Hohai University (Natural Science). J. 31(4)475-478.

Kim, Y., 1995. Marginal-cost and second-best pricing for water. Review of Industrial Organization 10, 323–338.

Renzetti, S., 1999. Municipal water supply and sewage treatment. costs, prices and distorsions. Canadian Journal
of Economics 32, 688–704.

Mitchell, B., 1978. Optimal pricing of local telephone service. American Economic Review 68, 517–537.

Dimopoulos, D., 1981. Pricing schemes for regulated enterprises and their welfare implications in the case of electricity. Bell Journal of Economics and Management Science 12, 185–200.

Protti, G., McRae, R., 1980. The impact of rate structure change on electricity demand: a case study of Calgary Power Limited. Discussion paper, Canadian Research Institute.

Swallow, S., Marin, C., 1988. Long-run price inflexibility and efficiency loss for municipal water supply, Journal of Environmental Economics and Management 15, 233–247.

Renzetti, S., 1992. Evaluating the welfare effects of reforming municipal water prices. Journal of Environmental Economics and Management 22, 147–192.

Patrick C. Mann and Donald L. Schlenger, Marginal cost and seasonal pricing of water service, Journal AWWA, J.74 (1) 6-11

M.C. Calviou, R.M. Dunnett, P.H. Plumptre, Charging for useof a transmission system by marginal cost methods, Eleventh Power System Computation Conference, Avignon, France, 1993.

Assessing the Impact of Climate Change on Drinking Water Treatment Plant Design and Operation

Zhiwei Li[1], Robert M. Clark[2], Steven G. Buchberger[1] and Y. Jeffrey Yang[3]

[1]Department of Civil and Environmental Engineering, University of Cincinnati, Cincinnati, OH 45221-0071; PH (513) 675-5988, (513) 556-3681; email: zhiwei.li@uc.edu, steven.buchberger@uc.edu
[2]Environmental Engineering and Public Health Consultant, 9627 Lansford Drive, Cincinnati, OH 45242; PH (513) 891-1641; FAX (513) 891-2753; email: rmclark@fuse.net
[3]US Environmental Protection Agency, ORD/NRMRL/WSWRD, 26 W. Martin Luther King Drive, Cincinnati, OH 45268; PH (513) 569-7655; FAX (513) 569-7185; email: Yang.Jeff@epa.gov

ABSTRACT

This paper applied a water treatment plant (WTP) simulation model developed by the USEPA to evaluate effects of climate change on a WTP design and operation. The simulation model was validated using the Greater Cincinnati Water Works' Richard Miller WTP based on data collected for the Information Collection Rule (ICR) database. As part of the validation process, individual influent water quality parameters were "perturbed" and processed through the simulated Miller WTP to identify key influent water quality factors that significantly affect regulated contaminants in the treated water. TOC and ammonia were identified as key water quality parameters. After the validation process was completed, the simulation model for the Miller WTP was used to examine the impact on regulated contaminants of a set of influent water quality scenarios that might result from climate change. Results of the case study scenarios indicated that the existing Miller WTP operation might not be able to meet Safe Drinking Water Act MCL requirements. Therefore design and operational changes may be required to meet these climate change induced changes in source water quality.

BACKGROUND

Climate change may adversely affect water quality in streams and other raw water sources in the United States and therefore impact the design and operation of existing and future drinking water treatment. Climate change may affect both surface water and ground water quality. Increases in precipitation and resulting increases in flows can result in problematic turbidity levels, increased levels of organic matter, high levels of pathogens and increased levels of pesticides in lakes, rivers and streams. Although some areas may experience increases in run-off, some areas may experience droughts resulting in elevated levels of potentially toxic algae, and high concentrations of

organic matter, bacteria, etc (Interlandi *et al*. 2003, Jacobs *et al.*, 2001). Some of these changes may have an adverse impact on the ability of water treatment plants to meet Safe Drinking Water Act regulations. Climate change coupled with increasing population in urban areas will therefore impact existing and future drinking water treatment infrastructure. Water utilities are concerned about the effect of global climate changes on future water demands, influent water quality and the consequent quality of finished water. Therefore, it is important to assess how WTP effluents will respond to changes in influent water quality (pH, TOC, ammonia, UVA, turbidity, bromide, etc.) under possible future climate change conditions. This knowledge will help water utilities identify the water quality parameters that can affect regulated water quality parameters such as disinfectant residual, pH, and total trihalomethanes (TTHMs), and to seek effective treatment alternatives to control these key factors.

A tool that can assist in these efforts is the EPA Water Treatment Plant Model (EWTPM). The EWTPM primarily uses empirical correlations to predict central tendencies of natural organic matter removal, disinfection, and DBP formation in a treatment plant. The relationship between various water quality parameters, such as trihalomethane species, and the variables that influence their formation, such as pH, temperature, chlorine dosage, TOC and bromide can often be described using a nonlinear function. Changes in water quality parameters are caused by chemical addition and/or by unit treatment processes simulated in the EWTPM (USEPA, 2005). It can be useful to (1) assist utilities in identifying and screening new treatment technologies that can assist in meeting both the required levels of disinfection and DBPs regulated under USEPA's various microbial/DBP rules, (2) assist utilities in evaluating the possible effects of source water or treatment process operations on DBP formation, and (3) assist regulatory agencies in assessing the potential impact of new regulations on treatment requirements over a large group of plants. The EWTPM is utilized in this study to simulate the effect of climate induced influent water quality change on regulated parameters associated with the Safe Drinking Water Act.

An important step in applying the EWTPM is to validate the model based on known data inputs and outputs. Data from USEPA's Information Collection Rule (ICR) were utilized for this purpose, specifically data collected for the Greater Cincinnati Water Works' Richard Miller WTP. The ICR was designed to obtain water quality, water treatment, and occurrence information needed for development of Safe Drinking Water Act regulations (Obolensky and Singer, 2005; Obolensky et al, 2007). ICR data sources include detailed information about treatment, plant design and operations from all large public water systems in the United States serving populations of 100,000 or more for 18 monthly monitoring periods from July 1997 through December 1998.

This paper applies the EWTPM to evaluate the performance at the Miller WTP. First, the EWTPM is validated using the simulation of the Miller WTP to confirm that the EWTPM provides reasonable results. As part of the validation process, individual influent water quality parameters were "perturbed" and processed through the simulated Miller WTP to identify key influent water quality factors that significantly affect finished water quality. Next, the EWTPM is applied to a case study at the

Miller WTP to examine WTP performance under future assumed climate change scenarios. Finally, suggestions are made for the adaptation of current water treatment processes and associated infrastructure to meet the future needs.

VALIDATION OF THE EWTPM

Inputs to the EWTPM

Input requirements for the EWTPM, Miller plant simulation can be extracted from the ICR database including unit process design parameters, influent water quality, flow rate and chemical feed rates. The ICR database also provides water quality parameter values at various sampling locations along the treatment train and in the distribution system. These data can be compared against the output from the EWTPM. In this study, the data utilized for validating the Richard Miller WTP are based on sample period 10 (April 1998) in the ICR because of completeness of available data during this period. The unit process treatment train for the Miller WTP is shown in Figure 1.

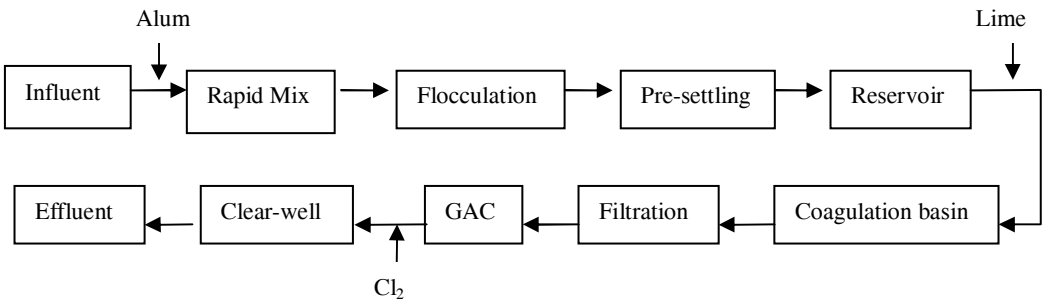

Figure 1 Unit Process Treatment Train for the Miller Plant

Design parameters are listed in Table 1. Chemical feed concentrations are: aluminum - 0.865 mg/L (before Rapid Mix); $Ca(OH)_2$ - 6.732 mg/L (before settling); Chlorine-3 mg/L (before clear well). During sample period 10, the influent flow rate was 4.41 m^3/s. The ICR water quality values at various sampling points are listed in Table 2.

Table 1 Miller WTP Unit Process Design Parameters

Unit Process	Volume, m^3	T10, min	T50, min
Rapid mixing	31.8	2	0.12
Flocculation basin	7342.9	14	27.77
Pre-settling	8440.6	14	31.92
Reservoir settling	1411805.0	1,728	5,339.20
Coagulation basin	98410.0	144	339.75
Filtration	9352.0	4	32.29
GAC	9311.1	--	33.55
Clear-well	107115.5	77	385.91

--: data not available

Table 2 ICR Water Quality Values for Sample Period 10 (April 1998) at Miller WTP

Location	pH --	ALK mg/L	TURB Ntu	TEMP ◦C	CA_HARD mg/L	T_HARD mg/L	TOC mg/L	UV_254 cm^{-1}	TTHMs µg/L	Free Cl_2 mg/L
Influent	7.7	56	22	11.2	89	113	1.8	0.0685	--	--
Coag. Basin	8.7	59	1.7	11.1	110	128	1.5	0.0275	--	--
Filtration	8.6	58	0.07	11.1	108	120	1.4	0.024	--	--
GAC	8	58	0.08	12.2	83	119	1	0.012	--	--
Finished water	8.5	58	0.07	12.2	100	120	1	0.0095	--	1.0
AVG1*	8.6	60	0.07	15	85	121	--	--	23.7	0.9
AVG3**	8.6	60	0.07	13.3	66	115	--	--	28.8	0.7

*AVG1 refers to average retention time, 1 day.

**AVG3 refers to the maximum retention time, 3 days

--: data not available

Validation of the EWTPM Using Miller WTP Data

Results from the EWTPM and the ICR database are compared in Table 3. They show reasonable agreement for pH, alkalinity (ALK), hardness, TOC, UVA_{254}, free chlorine residual and TTHMs. Simulated pH and alkalinity are slightly higher than sampled pH and alkalinity after lime is added. Sampled Calcium hardness and total hardness agree well with the corresponding simulated results. The sampled and modeled TOC results were in reasonable agreement in the finished water. The ICR data show that UVA_{254} is removed through coagulation and GAC in the Miller plant but most of the UVA_{254} is removed by GAC in the EWTPM. The simulated effluent UVA_{254} agrees well in the finished water. The simulated chlorine residuals are higher than the sampled results which imply that the initial simulated chlorine concentration in the model is probably higher than needed. For DBP TTHMs, good agreement was found between the simulated and the sampled results at the average tap (AVG1) and end of system (AVG3) points. It was concluded that the EWTPM adequately simulates the operations of the Miller Plant.

Table 3 Comparison of sampling and modeling water quality at Miller WTP

Water quality parameter	Unit	Data type	Influent	Coag. Basin	Filtration	GAC	Finished water	AVG1 *	AVG3 **
pH	--	Sampled	7.7	8.7	8.6	8.0	8.5	8.6	8.6
		Modeled	7.7	9.4	9.4	9.4	8.9	8.9	9.0
Alkalinity	mg/L	Sampled	56	59	58	58	58	60	60
		Modeled	56	64	64	64	60	61	61
Calcium hardness	mg/L	Sampled	89	110	108	83	100	85	66
		Modeled	89	98	98	98	98	98	98
Total hardness	mg/L	Sampled	113	128	120	119	120	121	115
		Modeled	113	122	122	122	122	122	122
TOC	mg/L	Sampled	1.8	1.5	1.4	1.0	1.0	--	--
		Modeled	1.8	1.8	1.8	1.0	1.0	1.0	1.0
UVA_{254}	cm^{-1}	Sampled	0.069	0.028	0.024	0.012	0.010	--	--
		Modeled	0.069	0.061	0.061	0.012	0.009	0.009	0.009
Free chlorine residual	mg/L	Sampled	--	--	--	--	1.0	0.9	0.7
		Modeled	0.0	0.0	0.0	0.0	1.7	1.4	1.1
TTHMs	µg/L	Sampled	--	--	--	--	--	23.7	28.8
		Modeled	0.0	0.0	0.0	0.0	12	21	30

*AVG1 refers to average retention time 1 day.

**AVG3 refers to the maximum retention time, 3 days.

--: data not available.

Effect of Perturbation of influent water quality

For the perturbation analysis, the operating conditions and most of the influent water quality levels in the Miller plant are assumed as constant, based on ICR sample period 10. One influent water quality parameter at a time is increased to 150% and then 200% of the existing value for subsequent runs of the EWTPM. Thus, the effect of perturbation on individual influent water quality were studied for the following water quality parameters: TOC (MCL 2mg/L), Chlorine residual (MCL 4mg/L), and TTHMs (MCL 80 µg/L). Table 4 summarizes the results at three observation points: effluent, average tap (1 day residence time) and end of system (3 days residence time). In Table 4, columns labeled with "100%" represent the results of the unperturbed influent. It can be seen that influent TOC has a significant effect on effluent TOC, chlorine residual and TTHMs at all three observation points. It can also be seen that increasing ammonia has no effect on effluent TOC levels but does decrease chlorine residuals and TTHMs. Bromide and alkalinity had no effect on effluent TOC and free chlorine residual but increases in bromide and alkalinity increased TTHMs slightly. UVA_{254}, hardness and turbidity had no effect on TOC, TTHMs or chlorine residual. Therefore, TOC and ammonia were identified as the key parameters affecting free chlorine residuals and TTHM formation.

Table 4 EWTPM response to a change of individual influent water quality parameter

Varied parameter	Input value	Regulated contaminant	Effluent			AVG1			AVG3		
			100%	150%	200%	100%	150%	200%	100%	150%	200%
TOC	1.8 mg/L	TOC, mg/L	1.0	1.6	2.2	1.0	1.6	2.2	1.0	1.6	2.2
		Free Cl_2,mg/L	1.7	1.6	1.4	1.4	1.0	0.8	1.1	0.7	0.4
		TTHMs,µg/L	12	21	37	21	36	56	30	51	71
UVA_{254}	0.069cm^{-1}	TOC, mg/L	1.0	1.0	1.0	1.0	1.0	1.0	1.0	1.0	1.0
		Free Cl_2,mg/L	1.7	1.7	1.7	1.4	1.4	1.4	1.1	1.1	1.1
		TTHMs, µg/L	12	12	12	21	21	21	30	30	30
Calcium Hardness	89 mg/L	TOC, mg/L	1.0	1.0	1.0	1.0	1.0	1.0	1.0	1.0	1.0
		Free Cl_2,mg/L	1.7	1.7	1.7	1.4	1.4	1.4	1.1	1.1	1.1
		TTHMs ,µg/L	12	12	12	21	21	21	30	30	30
Ammonia	0.1 mg/L	TOC, mg/L	1.0	1.0	1.0	1.0	1.0	1.0	1.0	1.0	1.0
		Free Cl_2,mg/L	1.7	1.4	1.1	1.4	1.1	0.8	1.1	0.8	0.5
		TTHMs, µg/L	12	11	11	21	20	19	30	28	27
Bromide	0.046mg/L	TOC, mg/L	1.0	1.0	1.0	1.0	1.0	1.0	1.0	1.0	1.0
		Free Cl_2,mg/L	1.7	1.7	1.7	1.4	1.4	1.4	1.1	1.1	1.1
		TTHMs,µg/L	12	13	14	21	23	25	30	33	35
Alkalinity	56 mg/L	TOC, mg/L	1.0	1.0	1.0	1.0	1.0	1.0	1.0	1.0	1.0
		Free Cl_2,mg/L	1.7	1.7	1.7	1.4	1.4	1.4	1.1	1.1	1.1
		TTHMs,µg/L	12	11	10	21	19	17	30	26	25
Turbidity	22 NTU	TOC, mg/L	1.0	1.0	1.0	1.0	1.0	1.0	1.0	1.0	1.0
		Free Cl_2,mg/L	1.7	1.7	1.7	1.4	1.4	1.4	1.1	1.1	1.1
		TTHMs,µg/L	12	12	12	21	21	21	30	30	30

IMPACT OF CLIMATE INDUCED WATER QUALITY CHANGES

In order to assess the impact of climate change, three specific scenarios were assumed. The performance of the Miller plant was evaluated and a determination made as to whether the current plant could meet the requirements associated with these scenarios and what modifications should be considered to account for these changes. These scenarios and assumptions are discussed in the following paragraphs.

Future scenarios at the Miller WTP

An average treated water flow during the 18 month ICR sampling period (July 1997-December 1998) at the Miller Plant, of 5.35 m^3/s. The raw water quality for the simulated plant is assumed to be the average of the influent water quality at the

following plants that use the Ohio River: Neville Island WTP in Pittsburgh of Pennsylvania, Richard Miller WTP in Cincinnati of Ohio, Evansville WTP in Indiana, Be Payne WTP in Louisville of Kentucky, Crescent Hill Filter WTP in Louisville of Kentucky and Fort Thomas WTP in Kentucky. These base-line data are shown in Table 5. Two future scenarios were assumed that increase the base-line average of the key water quality parameter TOC (2.56 mg/L) by 25% and 50%, which are 3.20 mg/L and 3.83 mg/L for scenario 1 and 2. It was assumed that the other water quality parameters remain constant.

Table 5 Base-line influent water quality parameters for the Miller WTP

Water quality parameter	pH --	ALK mg/L	TURB NTU	Ca_H mg/L	T_HARD mg/L	TOC mg/L	UV_{254} cm^{-1}	BROMIDE mg/L	NH3_N mg/L
Base-line value	7.76	71.8	26.6	77.4	141.0	2.56	0.096	0.069	0.21
Stan Deviation	0.20	23.3	41.5	32.9	34.0	0.54	0.049	0.040	0.19
Sample size	107	107	107	107	107	93	86	86	82

Performance of the Miller WTP subject to future changes

The performance of the Miller WTP is evaluated for TOC concentration and TTHM concentration in the finished water. The existing WTP processing train shown in Figure 1 and settings listed in Table 1 are assumed. Figure 2 and 3 shows the results of this analysis. It can be seen that TOC is stable after entering the distribution system but increases with increased influent TOC under scenarios 1 and 2. TOC meets the MCL (2.0mg/L) for the base-line condition but violates the MCL for scenarios 1 and 2. Figure 3 compares the formation of TTHMs for the three conditions. It can be seen that TTHMs increase with both the retention time in distribution system and the influent TOC concentration (represented by scenarios 1 and 2). TTHMs violate the MCL (80 ppb) at a retention time of 3 days for scenario 1 and at a retention time of 2 days for scenario 2.

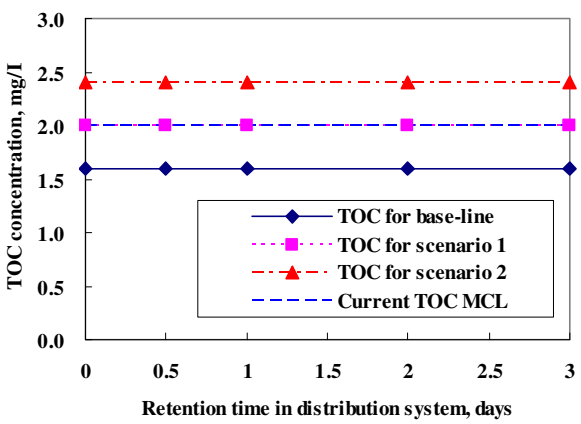

Figure 2 Remaining TOC in distribution system

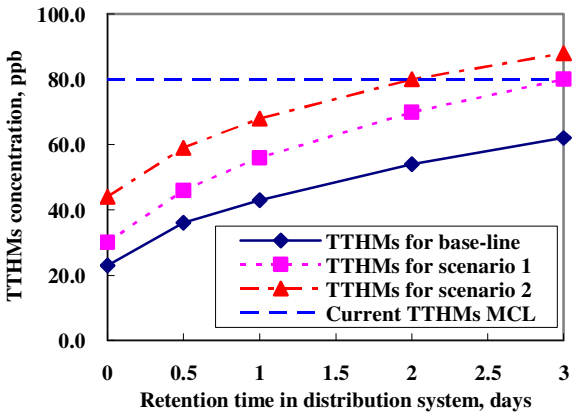

Figure 3 TTHMs formation in distribution system

Adaptation of the Miller WTP to future changes

Results in previous section shows the existing operation at the Miller WTP can not meet the MCL requirements for TOC and TTHMs under the assumed climate change scenarios. Therefore, the current design or operation needs to be modified to meet these requirements. Reducing the GAC reactivation period from 365 days can increase TOC removal.

It was found that the effluent TOC could be reduced to 1.8mg/L (lower than the MCL 2.0mg/L) when the GAC reactivation period is changed from 365 days to 180 days for scenario 1 and to 90 days for scenario 2. Figure 4 compares the formation of TTHMs for base-line conditions and for scenarios 1 and 2 against the change in reactivation rates. It is interesting to note that the TTHM formation curves are the same for both scenario 1 and 2 assuming the respective changes in reactivation rate. Clearly these adaptations to the existing operation in the Miller WTP, allow both TOC and TTHMs to meet their respective MCLs. However there is an increasing cost associated with each level of performance.

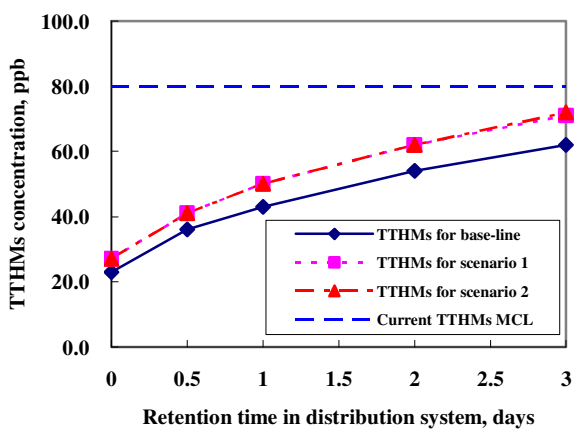

Figure 4 TTHMs formation after GAC reactivation period was changed

SUMMARY

The EWTPM was applied using the assumed conditions that currently prevail at the Richard Miller WTP to evaluate the effect of deteriorating water quality due to climate change. The results show that the EWTPM provides a reasonable replication of the existing WTP performance. A perturbation analysis using the EWTPM identified TOC and ammonia as key water quality parameters, which have significant effects on regulated contaminants.

The results of the analysis show that existing treatment operations can not meet the TOC and TTHM MCLs when influent TOC was increased by 25% (scenario 1) and 50% (scenario 2). Therefore, existing WTP operations were modified. When the GAC reactivation period is reduced to 180 days for scenario 1 and to 90 days for scenario 2, both MCL requirements can be met. The findings of this investigation will lead to identification of the key factors in water quality changes that can significantly affect the finished water quality, and provide an example to demonstrate how to adapt water infrastructure to future water resource changes.

ACKNOWLEDGMENT

This study is part of Water Resources Adaptation Program (WRAP)-Infrastructure supported by USEPA under project/contract EP-C-05-056 but has not been subject to review by USEPA.

REFERENCES

Interlandi, S. J., and Crockett C. S. (2003). "Recent water quality trends in the Schuylkill River, Pennsylvania. USA: a preliminary assessment of the relative influences of climate, river discharge and suburban development." *Water Resources,* 37, 1737-1748.

Jacobs, K., Adams, D. B., and Gleick, P. (2001). "Chapter 14, Potential Consequences of Climate Variability and Change for the Water Resources of the United States", in *Climate Change Impacts On the United States –the Potential Consequences of Climate Variability and Change* edited by Jerry Meilillo, Anthony Janetos and Thomas Karl, Cambridge University Press, New York.

Obolensky, A., and Singer, P. C. (2005). "Halogen Substitiution Patterns among Disinfection Byproducts in the Information Collection Rule Database." *Envi ron. Sci. Technol.* 39, 2719-2730

Obolensky, A., Singer, P. S., and Shukairy. H.(2007). "Information Collection Rule Data Evaluation and Analysis to Support Impacts on Disinfection By-Product Formation." *Journal of Environmental Engoneering (ASCE)*. 133(1), 53-63.

USEPA (2005). *Water Treatment Plant Model Version 2.2 User's Manual.* Office of Ground Water and Drinking Water, United States Environmental Protection Agency, Cincinnati, Ohio.

Axial Dispersion Coefficients for Laminar Flows in Water Distribution Systems

P. Romero-Gomez[1], Z. Li[2], C.Y. Choi[1], and S.G. Buchberger[2]

[1]Department of Agricultural and Biosystems Engineering
The University of Arizona, Tucson, Arizona 85721, U.S.A.
[2]Department of Civil and Environmental Engineering
The University of Cincinnati, Cincinnati, Ohio 45221, U.S.A.

A dispersive transport component has recently been incorporated into the constituent transport equation used for modeling water quality in pressurized distribution systems. Among the various issues that arose from this major development, dispersion coefficients (E) relevant to water distribution systems still remain unknown. In order to quantify E values, researchers have considered the long-established Taylor's theory (E) and time-dependent functions. However, discrepancies between theoretical and experimental approaches still exist because the former does not consider the transient nature of dispersion whereas the latter derives from the analytical relations that overestimate dispersion rates. The present study quantifies dispersion coefficients in pressurized pipes under laminar conditions by using Computational Fluid Dynamics (CFD). Assumptions made with CFD are few and mostly related to the velocity field in pipe flows. Consequently, the mass transports are obtained by solving the species equation over an axi-symmetric domain. Next, the resulting spatial-temporal constituent concentrations are used to estimate dispersion coefficient values determined by the method of moments (MOM) at equally-spaced locations along the length of the pipe. With the aim of building a quasi-analytical relation of* $E/E^* = \beta\, f_E = f(\mathrm{Re}, T, Sc)$*, transient simulations at a series of Reynolds numbers for laminar flows (Re < 2,100) were carried out in consideration of constituents with different molecular diffusivity in water. Among the various challenges that this study confronts, two are thoroughly described here: (i) the pre-analysis needed to obtain a solution that is independent of the numerical setup and (ii) the CFD benchmarking solution required under conditions when Taylor's theory applies (T > 0.30).*

1. INTRODUCTION

The dispersive transport of solutes has progressively been taken into consideration to better describe the water quality behavior of pressurized water systems. The fundamental aim is to expand the one-dimensional Advection-Reaction model (1D-AR) currently in use and turn it into a 1D-Advection-Dispersion-Reaction (1D-ADR) equation that predicts quality parameters with higher accuracy. The numerous research efforts in this field can be categorized into *(i)* those that seek a more efficient, accurate and applicable numerical solution to the expanded equation, and *(ii)* those that seek to determine the dispersion coefficients that better represent the solute transport. To the best of our knowledge, Sir Geoffrey Taylor (1953) was the first to quantify steady-state dispersion rates (*E**) via analytical solutions and corresponding experimental validations. Furthermore, he stated that "… the effect of molecular diffusion [D_{AB}] is negligible" before the steady-state conditions are reached, and that his formula for dispersion rates

only applies when the time of flow is greater than $\tau = a^2/(3.8^2 D_{AB})$. Such groundbreaking findings unfolded other investigations aimed at determining dispersion rates before τ is reached, a condition that most likely occurs in pipes of sizes and flows of a magnitude typically found in municipal water distribution systems.

Gill and Sankarasubramanian (G-S, 1970) derived a complex method for finding dispersion rates for an instantaneous injection of solute in a long pipe under steady laminar flows. They demonstrated that the dispersion rate increases with time as the solute travels downstream and asymptotically approaches the value calculated with Taylor's formula, E^*. However, the process of implementing the derived model into the 1D-ADR equation is complex and not feasible. In order to overcome this drawback, Lee (2004) provided simplified forms of G-S's equation (1970), versions that can actually be integrated into the 1D-ADR model. Romero-Gomez et al. (2008) used Computational Fluid Dynamics (CFD) to compute dispersion coefficients at various Reynolds numbers, thus covering the laminar, transitional and turbulent flow regimes. Because they found the CFD approach to be an expedient tool in quantifying dispersion rates in multiple flow and water quality scenarios, the objective of the present study is to thoroughly examine the effect of three parameters: *(i)* Reynolds number (Re) to account for flow characteristics, geometry dimensions, and solvent (water) properties, *(ii)* Schmidt number (Sc) to include the properties of dissolved substances, and *(ii)* dimensionless time (T) in order to define the extent to which the dispersion coefficient has elapsed before reaching steady-state conditions. These coefficients are defined as follows

$$Re = \frac{U_0 d}{\nu}; \qquad Sc = \frac{\nu}{D_{AB}}; \qquad T = \frac{4 D_{AB} t}{d^2}$$

2. COMPUTATIONAL FLUID DYNAMICS

Computational Fluid Dynamics (CFD) consists of discretizing a set of conservation equations and calculating their numerical solution under prescribed initial/boundary conditions. In order to perform CFD simulations of the species transport in a long pipe, three steps were carried out.

(i) The computational domain over which the conservation equations are solved was defined as a 2D axi-symetric rectangle with height (H) equal to the pipe radius and width (W) equal to the pipe length. A quadrilateral mesh was applied to all the simulated cases. In all instances, approximately 30% of the total number of cells (N) pertained to the boundary layer zone defined near the pipe walls. Characteristics of the mesh specific to each simulated geometry are provided in subsequent sections. The following boundary types were set at the domain edges: velocity inlet (left), outflow (right), wall (top), and axis (bottom).

(ii) All the simulations were two-dimensional, axi-symmetric, unsteady-state, and solved with a laminar viscous model. The mixture material was composed of water (ρ= 997 kg m^{-3}, *molecular weight* = 18.01) and the dissolved substance (sodium chloride, potassium permanganate or a theoretical material the properties of which were provided for each instance in the succeeding sections). The composite properties of this mixture were μ = 1.003 x 10^{-3} kg m^{-1} s^{-1} and D_{AB} of the solute. The hydrodynamic Boundary Condition (BC) at the inlet was the fully-developed velocity profile, whereas the species BC was the time-varying inlet concentration profile specific to the simulated scenario. The velocity field was assumed to be fully-

developed through the entire domain, thus reducing the numerical effort to solving only the uncoupled species transport equation with the following transient form

$$\frac{\partial}{\partial t}(\rho C_i) + \nabla \cdot \left(\rho \bar{u} C_i\right) = \nabla \cdot (\rho D_{AB}) \nabla C_i \tag{1}$$

(iii) The simulations provided the radial distribution of solute at the set time and space intervals by executing a prescribed command that saved the data into text files. Based on such data, the post-processing work involved the construction of either concentration vs. time curves, $C = C(t)$, at different locations, or concentration vs location curves, $C = C(x)$, at different times.

3. DISPERSION COEFFICIENTS

Lee (2004) provided a simple but accurate approximation for the exact but cumbersome expression developed by Gill and Sankarasubramanian (1970) describing the unsteady instantaneous rate of dispersion for a mass transported in a steady laminar flow through a pipe. The corresponding expression for the time-averaged rate of dispersion in a steady laminar flow during the period $[0, t]$ is given by

$$\overline{E(t)} = E^* \beta(T) \tag{2}$$

where, E^* is the steady-state dispersion rate by Taylor (1953), given by, $E^* = \frac{a^2 U_0^2}{48 D_{AB}}$ and $\beta(T)$ is a dimensionless factor defined by

$$\beta(T) = \left[1 - \left(\frac{1 - \exp(-16T)}{16T}\right)\right] \tag{3}.$$

Note that $\overline{E(t)}$ is a function of time, even in steady flow. Hence, in pipe network applications it is necessary to define a representative time in order to characterize the average rate of dispersion expected along a pipe link. Li (2006) found that this representative or "evolution" time of dispersion for a pipe link of length L is given by the nominal travel time, $t = L/U_0$. However, some recent preliminary studies suggest that time-averaged dispersion coefficients based on the nominal travel time in steady a laminar flow may be over-estimated (Romero-Gomez et al, 2008). Thus, Equation 2 may need correcting.

One way to correct Equation 2 is to apply a correction factor, f_E, to the right-hand-side,

$$\overline{E(t)} = E^* \beta(T) f_E \tag{2a}$$

f_E may be defined by,

$$f_E = \frac{\overline{E_m}}{E^* \beta(T)} = \frac{192\left(\overline{E_m}/\nu\right)}{Re^2\ Sc\ \beta(T)} \tag{4}$$

Herein, $\overline{E_m}$ is a time-averaged dispersion rate computed using the method of moments (MOM) based on a time history of the outflow concentration measured at end of a pipe.

According to Fischer *et al.* (1979), a numerical time-averaged axial dispersion rate during the period $[0, t]$ can be given by

$$\overline{E_m} = \frac{U_0^2\left(\sigma_t^2 - \sigma_0^2\right)}{2m(t)} \tag{5}$$

Where, σ_0^2 and σ_t^2 are the variance of tracer cloud at the upstream and downstream locations, given by, $\sigma_t^2 = m(t^2) - [m(t)]^2$; *m(t) and m(t²)* are the first-order and second-order concentration weighted moments for time *t*, given by, $m(t) = \frac{\sum_{i=1}^{n} t_i C_i \Delta t}{\sum_{i=1}^{n} C_i \Delta t}$ and $m(t^2) = \frac{\sum_{i=1}^{n} t_i^2 C_i \Delta t}{\sum_{i=1}^{n} C_i \Delta t}$; C_i is the solute or microbial concentration measured at t_i; Δt is the time interval between readings; and n is sample size.

4. CFD PRE-ANALYSIS

The aim of CFD pre-analysis is to determine the mesh size, discretization scheme and time step that have no effect on the CFD-simulated solution for axial dispersion. Conventionally, an increasing mesh size enhances the accuracy of results, though beyond a certain mesh refinement numerical errors begin to prevail and worsen the overall solution. The discretization scheme refers to how the continuous conservation equations are transformed into a discrete algebraic system of equations. In time-dependent modeling of phenomena, the time step setting determines the frequency with which a numerical solution is provided. The following mesh sizes (*N*) for the entire computational domain were tested: 1600, 3200, 4800, and 12000. Three discretization schemes were tested: 1st order upwind, 2nd order upwind and QUICK. Considering the typical time spans for the analyzed phenomenon, the following time steps (*Δt*, in seconds) were examined: 0.5, 0.1, 0.02, and 0.01.

The CFD-simulated conditions were as follows: d = 0.016 m, U_0 = 0.1128 m s^{-1}, (Re = 897), D_{AB} = 1.5 x 10^{-9} m^2 s^{-1}, (Sc = 670), ρ = 2,170 kg m^{-3}, MW = 58.45 kg $kgmol^{-1}$ (properties for NaCl), t = 100 s (T = 0.0023), H = 0.008 m, W = 1.6 m. The inlet concentration was a transient profile with background concentration equal to zero and a rectangular-shaped pulse of 10 s (starts at 5 s, ends at 15 s) with C_0 = 1 g L^{-1}. Such conditions result in a bell-shaped downstream concentration profile with respect to time.

The ratio of the downstream peak concentration (C_{MaxOut}) to C_0 is used for quantitatively assessing the effect of the settings on the solution. Figure 1a depicts the increase in C_{MaxOut}/C_0 that occurs with progressively increasing mesh sizes over the range of tested time steps, until a value of N = 4,800. A finer mesh (*N = 12,000*) overproduced numerical errors that consequently decreased the simulated downstream peak concentration. Thus, a mesh of *N = 4,800* was selected to further examine the discretization schemes, results of which are shown in Figure 1b. Whereas the 1st order upwind scheme largely lowers C_{MaxOut}/C_0 at all Δt's, the 2nd order upwind and QUICK schemes produce similar outcomes, although the latter slightly underestimates values as compared to the former. Because a simpler scheme was preferred for succeeding simulations, the 2nd order upwind was selected. In terms of the time step, Δt = 0.02 s produces values of C_{MaxOut}/C_0 that are slightly lower than Δt = 0.01 s; however, the latter significantly prolongs the computational time at the expense of less than 1% of improvement with respect to the former. Thus, Δt equal to 0.02 s was used in succeeding simulated scenarios.

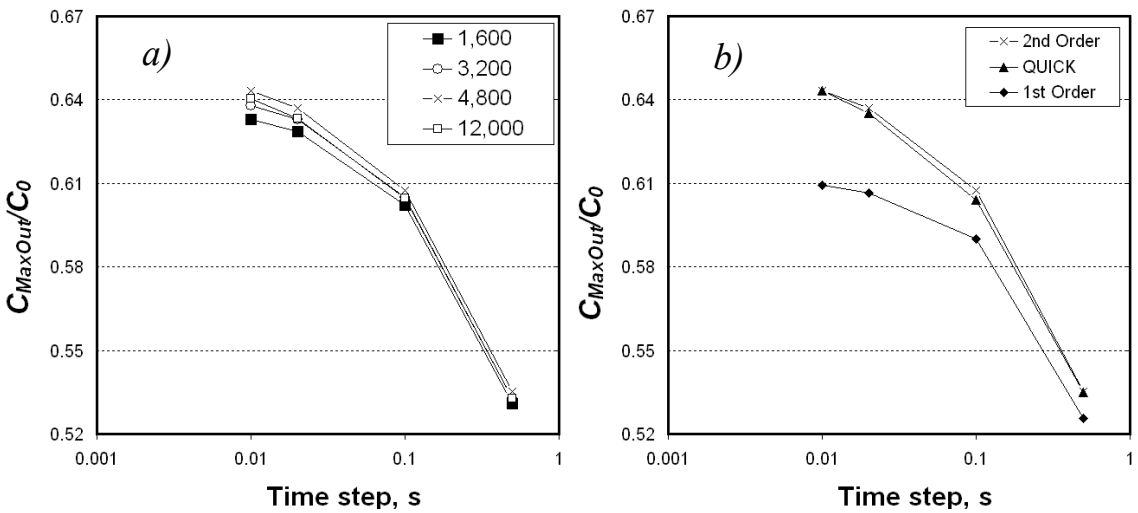

Figure 1. Maximum concentration related to inlet concentration at different CFD settings indicate that a mesh of size 24x200, 2nd order discretization scheme, and Δt = 0.02 s must be used to further carry out simulations

5. BENCHMARKING THE CFD SETUP

Although all CFD commercial programs or in-house codes are carefully tailored to fulfill the intended modeling purposes, benchmarking the CFD setup is advised in order to minimize the possibility of wrong settings or erroneous assumptions. In this work, the numerical setup and the simulated results were benchmarked against the experiments by Taylor (1953) in which a uniform concentration C_0 is allowed to enter the pipe at uniform rate at $x = 0$. Initially the pipe is filled with water, only ($C = 0$). Taylor (1953) called this configuration the special case B2, and thus demonstrated the applicability of his analytical solution to the problem of quantifying dispersion rates (E^*) when long times have elapsed, $t > \tau,\ \tau = a^2/(3.8^2 D_{AB})$. The CFD-simulated scenario was based on experimental conditions and results reported by Taylor (1953). Those results are as follows: d = 0.000504 m, U_0 = 0.00524 m s^{-1}, (Re = 2.627), D_{AB} = 6 x 10^{-10} m^2 s^{-1}, (Sc =

Table 1. Taylor's (1953) experimental results of type B2, for $t = 240\ s$, and continuous upstream injection of $Co = 10\ g\ L^{-1}$ (dissolved substance was potassium permanganate, $KMnO_4$, see Table 2 in Taylor, 1953 for more details).

x	C/C_0
0.450	0.90
0.537	0.80
0.580	0.70
0.605	0.60
0.638	0.50
0.667	0.40
0.680	0.30
0.711	0.20
0.740	0.10
0.750	0.08
0.760	0.06
0.770	0.04
0.795	0.02
0.804	0.01

1,675), ρ = 2,703 kg m^{-3}, MW = 158.04 kg $kgmol^{-1}$ (properties for $KMnO_4$), t = 240 s (T = 2.267), H = 0.000252 m, W = 1 m, N = 230,400, and C_0 = 10 g L^{-1}. The experimental results of the distribution of solute concentration as a function of distance from the pipe inlet are presented in Table 2. Note that the solute concentration is given with respect to the inlet concentration (C/C_0).

Figures 2a – 2f depict the concentration vs. distance curves at different times (and the corresponding T-value). Short simulation times (t ≤ 20 s, Figures 2a, 2b and 2c) show that the concentration drop from 1 to 0 in fact occurred within short distances (consider the x-axis range to be 0 - 0.12 m). Only Figure 2a (t = 5 s) corresponds to the case in which Taylor's theory assumes no effect of molecular diffusivity on the distribution of C/C_0, at $t < \tau$. At longer time spans (Figure 2d, 2e and 2f) the concentration drop took place within increasing distances, due to a stronger effect produced by axial dispersion. The experimental results in Table 2 and corresponding CFD-simulated concentrations are plotted in Figure 2f and show an excellent agreement between them; however, small overestimations of the modeling approach at $x < 0.55\ m$ are present. Taylor's analytical solution also overestimated the concentration values within this range of x-values, an outcome that suggests the possibility of slight experimental errors. Furthermore, the CFD-based dispersion rate (with Equation 5) is E = 1.48 x 10^{-5} m^2 s^{-1}, as compared to Taylor's coefficient E* = 1.52 x 10^{-5} m^2 s^{-1}. The error percentile of E with respect to E^*, $|E - E^*|/E^*$, is 2.7%, which confirms the suitability of using the CFD approach to further examine axial dispersion in other instances and scenarios.

Taylor's theory has been revisited and complemented in order to account for the transient phase of the dispersion rate before a steady-state condition is reached (at τ = 7.33 s, for this benchmarking case). The present research efforts aim to develop a coefficient that relates the transient dispersion rate to Taylor's dispersion coefficient (f_E, Eq. 4). At prescribed simulation times, transient coefficients can be calculated based on the concentration distribution along the pipe, $C(x)$, by using the MOM equation (Eq. 5). Therefore, an E-value exists for each considered dimensionless time T, for which the relation $E_i = E(T_i)$ can be plotted as shown in Figure 3. When the quasi-theoretical function indicated in Eq. 2 is also considered and plotted in Figure 3, an excellent agreement between both approaches is observed. However, there is evidence that such theoretical dispersion rates can be further generalized for applications to scenarios that most commonly occur in real water distribution systems (Tzatchkov *et al* 2002 and Li 2006). Therefore, the CFD tool could potentially be used for constructing a relation of dispersion rates (E) as a function of other relevant parameters that account for the solute properties (Sc) and flow/geometry characteristics (Re).

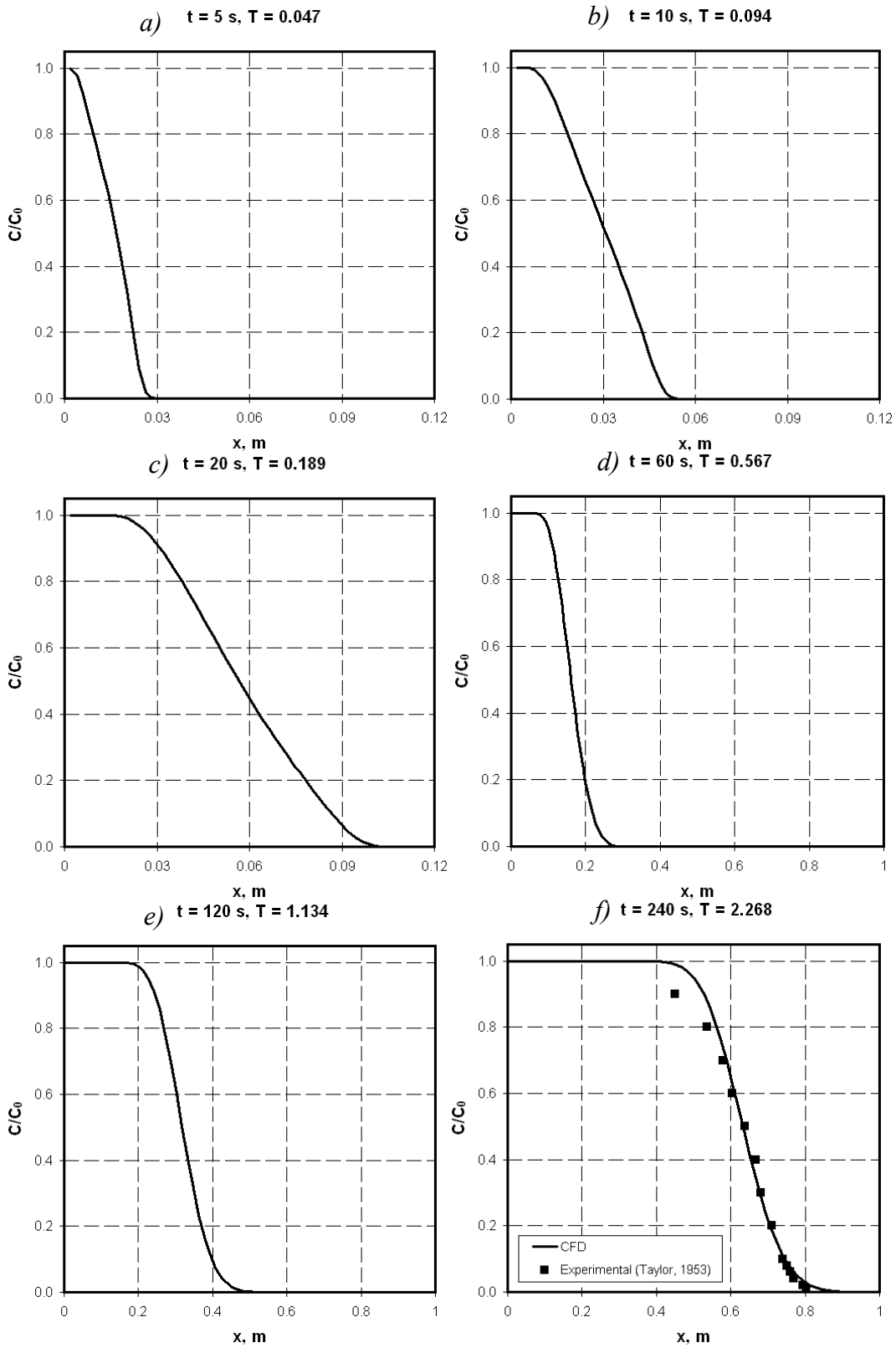

Figure 2. Concentration vs. distance at different simulation times. *x*-axis range is 0.00-0.12 m for (a), (b) and (c); x-axis range is 0-1 m for (d), (e), and (f).

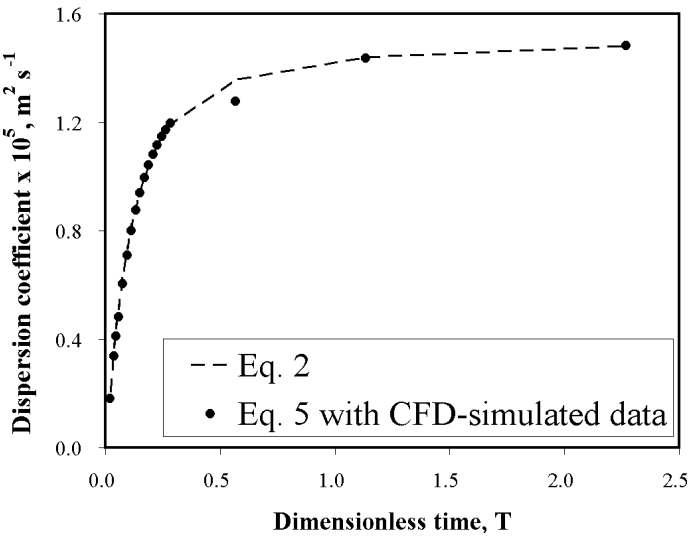

Figure 3. Comparison of unsteady-state dispersion coefficients between analytical and CFD-based MOM calculations.

6. PARAMETRIC STUDY (Re, Sc, T)

The parametric study consisted of examining the effect of Re, Sc and T on the unsteady-state dispersion rates. The characteristics of the numerical setup that remained the same for all the simulated scenarios were as follows: d = 0.016 m, H = 0.008 m, W changed as a function of the simulated scenario, N = 230,400, and C_0 = 1 g L^{-1} at a constant injection rate at the pipe inlet. The following values of mean flow velocities (U_0 in m s^{-1}) were examined: 0.0126, 0.0251, and 0.0503, which lead to Reynolds numbers of 200, 400 and 800, respectively.

The species molecular diffusion for material A was of the same order of magnitude as NaCl, D_{AB} = 1.5 x 10^{-9} m^2 s^{-1}, whereas material B was theoretical with a value of D_{AB} ten times as large as material A (1.5 x 10^{-8} m^2 s^{-1}). Such values led to Schmidt numbers equal to 670 and 67, respectively. The simulation times were calculated so that the resulting dimensionless time T had the following values: 25, 50, and 100 (all values multiplied by 10^{-4}).

The results shown in Table 2 as a function of multiple parameters demonstrate that the β-coefficient, as calculated with CFD-simulated data, is neither sensitive to the Reynolds number nor to the Schmidt number, but solely a function of the dimensionless time, T, as the analytical equation (Eq. 3) originally suggests. Nevertheless, there exists a consistent overestimation of analytical β (from Eq. 3) with respect to the CFD-based value for all the scenarios tested. Such overestimation may empirically be corrected by the coefficient f_E (Eq. 4) that ranged from 0.70 to 0.75 as a function of the parameter T. The trend of results in Table 2, as well as those presented in Figure 3, suggests that the value of f_E will continue to increase to a longer dimensionless time until it reaches an asymptotic value of 1. They can be quantified by performing simulations at other T-ranges and validated by means of experimental runs in short pipes at relatively small time spans. The conditions that produce small values of T give rise to large concentration gradients in the radial direction, which in turn may result in a lower accuracy for Eq. 5 to quantify the actual values of dispersion rates at different time spans. This claim, however, needs further studies.

7. CONCLUSIONS AND FURTHER RESEARCH

The present study provided an analysis of dispersion rates via Computational Fluid Dynamics (CFD) simulations as a function of the multiple parameters that characterize the flow, the fluid, the dissolved substance and the evolution of dispersion. First, the pre-analysis of the CFD setup determined the values of mesh size, time step and discretization scheme that have virtually no effect on the numerical solution. Next, the setup was benchmarked against the long-established experimental results obtained by Taylor (1953) for steady-state dispersion rates. The excellent agreement between both the experimental and CFD-simulated data proved the validity of the CFD approach to examining dispersive transport of solutes at multiple scenarios of flow and water quality. Thus, a parametric study with Reynolds number (Re) and Schmidt number (Sc) at small dimensionless times ($T \leq 0.01$) quantified the overestimation of the dispersion rates produced by the existing analytical equations. Such discrepancies may be corrected by means of either a correction factor or a redefinition of the dispersion coefficients (by using the method of moments), when short dimensionless times have elapsed. This investigation is relevant to water quality modeling in pressurized systems because solutes in drinking water travel along the pipes at relatively short T-values, too. In such conditions, large gradients of radial concentrations may well lead to an inadequate quantification of dispersion rates via the method of moments (MOM) that assumes uniform cross-sectional concentrations. This issue, as well as the experimental validation of CFD simulations, is the subject of ongoing research.

Table 2. Values of the coefficient β as a function of Reynolds number (Re), Schmidt number (Sc) and dimensionless time (T).

Parameters			Resulting Coefficients		
Re	**Sc**	**$Tx10^4$**	**β - CFD**	**β - Eq. 3**	**f_E - Eq. 4**
200	670	25	0.0139	0.0200	0.70
		50	0.0283	0.0394	0.72
		100	0.0577	0.0768	0.75
	67	25	0.0142	0.0200	0.71
		50	0.0285	0.0394	0.72
		100	0.0579	0.0768	0.75
400	670	25	0.0139	0.0200	0.70
		50	0.0283	0.0394	0.72
		100	0.0577	0.0768	0.75
	67	25	0.0141	0.0200	0.71
		50	0.0285	0.0394	0.72
		100	0.0579	0.0768	0.75
800	670	25	0.0139	0.0200	0.70
		50	0.0283	0.0394	0.72
		100	0.0577	0.0768	0.75
	67	25	0.0141	0.0200	0.71
		50	0.0285	0.0394	0.72
		100	0.0579	0.0768	0.75

8. REFERENCES

Fisher, H.B., E.J. List, R.C.Y. Koh, J. Imberger, N.H. Brooks (1979). Mixing in inland and coastal waters. *Academic Press*, San Diego, California, 483 pg.

Gill, W. N. and Sankarasubramanian, R. (1970). Exact analysis of unsteady convective diffusion. *Proceedings of the Royal Society of London Series A*, 316: 341-350.

Lee, Y. (2004). Mass Dispersion in Intermittent Laminar Flow. *PhD Dissertation,* University of Cincinnati, Cincinnati, Ohio.

Li, Z. (2006). Network Water Quality Modeling with Stochastic Water Demands and Mass Dispersion. *PhD Dissertation,* University of Cincinnati, Cincinnati, Ohio.

Romero-Gomez, P., Z. Li, C. Y. Choi, S.G. Buchberger, K.E. Lansey, and V.T. Tzatchkov. (2008). "Axial dispersion in pressurized pipes under various flow conditions." *10th Annual Water Distribution Systems Analysis Symposium*, Kruger National Park, South Africa.

Taylor, G. (1953). "Dispersion of soluble matter in solvent flowing slowly through a tube." *Proceedings of the Royal Society of London. Series A, Mathematical and Physical Sciences*, 219, 186-203.

Tzatchkov, V.G., A.A. Aldama, F.I. Arreguin, (2002) Advection-Dispersion-Reaction modeling in water distribution networks, *ASCE Journal Water Resources Planning and Management*, 128(5):334-342.

9. NOTATION

a = pipe radius, m
C_0 = inlet concentration
C_i = solute concentration at i-*th* cell
d = pipe diameter, m
D_{AB} = molecular diffusivity, $m^2\ s^{-1}$
E = transient dispersion coefficient, $m^2\ s^{-1}$
E^* = steady-state dispersion coefficient (Taylor's coefficient), $m^2\ s^{-1}$
H = height of computational domain, m
N = number of computational cells
t = time, s
T = dimensionless time
U_0 = mean flow velocity, $m\ s^{-1}$
W = width of computational domain, m
β = transient dispersion rate / Taylor's coefficient
ρ = fluid density, $kg\ m^{-3}$
τ = time of the flow, s
ν = fluid kinematic viscosity, $m^2\ s^{-1}$
μ = fluid dynamic viscosity, $kg\ m^{-1}\ s^{-1}$

ACKNOWLEDGMENTS

This study was supported by the Center for Advancing Microbial Risk Assessment (CAMRA) funded by the U. S. Environmental Protection Agency Science to Achieve Results and the U. S. Department of Homeland Security University Programs grant number R3236201.

Case Study: Homeowner's Preference Trade-Offs Towards Pluming Systems in Pipe Failure Prone Area

Juneseok Lee[1], Darrell Bosch[2], Ewa Kleczyk[3], Eftila Tanellari[4], Andrea M. Dietrich[5], and Vinod K. Lohani[6]

[1]Assistant Professor, Department of Civil and Environmental Engineering, San Jose State University, San Jose, CA 95112; email: Juneseok.Lee@sjsu.edu
[2]Professor, Department of Agricultural and Economics, Virginia Tech, Blacksburg, VA 24061; email: bosch@vt.edu
[3]Sr. Econometrician, New Product Development, TargetRx, 220 Gibraltar Rd. 2nd Floor, Horsham, PA. 19044; ekleczyk@targetrx.com
[4]Ph.D. Candidate, Department of Agricultural and Economics, Virginia Tech, Blacksburg, VA 24061; email: etanella@vt.edu
[5]Professor, Department of Civil and Environmental Engineering, Virginia Tech, Blacksburg, VA 24061; email: andread@vt.edu
[6]Associate Professor, Department of Engineering Education, Virginia Tech, Blacksburg, VA 24061; email; vlohani@vt.edu

ABSTRACT

Pinhole leaks in copper plumbing pipes have become a nationwide concern because these leaks cause property damage, lower property values, and result in possibility of adversely affecting homeowners' insurance coverage. Multiple attributes of a plumbing system including cost, taste and odor impacts, potential for corrosion, health effects, warranty, convenience of installation, and proven performance in the market are considered when choosing an alternative plumbing material. Two phase surveys are conducted with selected homeowners in pinhole leak prone area in southeastern US community to observe their revealed and stated preferences. Health effects, taste and odor of water turned out to be the most important factors from the survey. In real life, however, homeowners were not well aware of these safety issues related with plumbing materials. It is recommended that water professionals should work on bridging the gap between public perception and research results.

INTRODUCTION

Recently, increased pinhole leaks in domestic copper plumbing pipes have been observed (Lee, 2006). When there is a leak incident in a house, the homeowners cover the repair/replacement cost of a home plumbing system as it is private property. The homeowners are typically faced with the following issues when a leak occurs: water damage and repair cost, service disruption, possible lowering of home value, and potential health consequences resulting from brown mold growth on the surface of walls, floors, and ceilings. Home plumbing decisions that may affect drinking water risks include choice of when to repair or replace as well as the type of material

to use in replacement. When informed about the attributes of each plumbing material alternative, consumers can decide on the alternative most preferable to them based on the preference tradeoffs among plumbing materials' attributes. The decision of choosing an appropriate plumbing material can be based on various attributes of materials such as cost (material cost plus labor and installation cost), health effects, corrosion susceptibility, strength, property real estate values, and behavior in the case of a fire, taste and odor of the water, longevity of the pipe system, warranty, proven performance in the market, and convenience of installation or replacement.

According to Marshutz' survey (2001), copper accounts for 90% of plumbing installed in new homes, followed by PEX (cross linked polyethylene) at 7%, and CPVC (chlorinated polyvinyl chloride) at 2%. A telephone survey (Lee, 2008) observed that the share of plastic pipe in plumbing industry is increasing due to ease in installation and lower material cost. Woodson (1999), an author with extensive plumbing experience, selected consumers' plumbing material alternatives as copper, CPVC, and PEX. It is noted that copper pipes generally performed well in plumbing except where there are major pinhole leak problems.

In this study, we developed a mail survey for selected homeowners in a southeastern community in USA which had experienced unusually high rate of pinhole leak incidents. Two phase survey approach was taken to systematically understand homeowner's attitudes and experiences regarding home plumbing system. Phase I focused on the revealed preferences; to gather information about the costs in addressing the problems and their experiences in dealing with the problems. Phase II is eliciting homeowner's preferences towards home drinking water plumbing attributes and materials (stated preferences) under the framework of Analytic Hierarchy Processes (Saaty, 1980).

HOMEOWNER SURVEY OF PINHOLE LEAK PRONE AREA

The southeastern community A was founded in 1980's and approximately 4,700 acres in size and is close to a river. There are about 3,300 homes including condos and apartments; and a total of 6,600 residents. Most of the residents are retired people. Water quality changes turned out to be the culprit for high rates of leaks. Even 6 year-old houses have suffered leaks. Ninety-five percent of the leaks were in cold water pipes and builders used copper pipes from the same suppliers.

In year 2006, there was a switch from Utility 1 to Utility 2. The switch caused problems mainly because of the differences in water qualities such as chlorine level, hardness, and pH. Contrary to affected home plumbing systems, utilities' major system did not have a leak problem because they are using different piping materials (mainly iron pipes). According to the recommendations from water quality experts from Virginia Tech, Utility 2 added corrosion inhibitor (phosphate) to water treating process (after April of 2006); and the number of newly reported leaks has decreased so far (Martin, 2007).

The affected homeowners in this community had three alternatives i) repairing the leak, ii) doing a complete replacement of existing plumbing system, and iii) coating the existing pipe system with epoxy. When they make a decision, they had to balance the risk of possible future leaks that might cause another damages to homes and personal belongings vs. the cost of a replumb or relining. So, their information sources were from other homeowners or plumbers who have had leaks recently and experienced repair, epoxy coating, or replumbed with other alternatives (PEX, CPVC). As mentioned, utilities took actions by adding corrosion inhibitors to reduce the leaks at home. If a certain period of warranty from replumbing or epoxy coating is guaranteed, their decision was based on the *cost* in addition to the repair of collateral damages to the home and furnishings due to replumb or relining operations.

Some community residents have been taking several additional actions such as i) *preventive replumbing*, which was even done by those who did not experience any leaks in their houses (after seeing what happened to their neighbors), ii) applied epoxy coating with or without leak experiences, iii) inline injection of phosphate (corrosion inhibitor) into home water systems, and iv) water softener or water conditioning systems.

Methodology and Survey Design

A two-phase survey approach was used to understand homeowner's concerns, attitudes, and experiences in pinhole leak prone area regarding drinking water and home plumbing system. In phase I, the survey instrument was designed to gather a wide variety of information about the nature of pinhole leaks, costs in addressing the problems, and their experiences in dealing with the problems. Socioeconomic data were included at the end of the survey. Specifically, 1st phase survey module includes items such as pipe materials, failed locations, whether they repair/replaced the systems, what alternatives they chose after a leak incident, and any preventive actions (if they had taken any). Time spent to deal with these issues, level of stress, level of concern for future possible leaks were also included in the module.

In phase II, AHP is adopted; a multiattribute preference elicitation tool that allows for examining tradeoffs among the available attributes. The decision making processes (replacing plumbing systems) of residents' coping with leak incidents (stated preferences from phase II) are compared with real decisions (revealed preferences) from Phase I survey. The surveys themselves could be administered in a mail format. In addition, this survey module was pre-tested with 135 Civil Engineering students in Virginia Tech, committee members of a property owner association in the affected community, and 3 faculty members from Civil Engineering in Virginia Tech who have extensive knowledge and experiences on these issues.

<u>Revealed Preference Survey (Phase I)</u>

A mail survey was implemented to the community residents in July 2007. Selected total sample size that we could contact by regular mail was 1,600. We followed the standard mail survey techniques (Dillman, 2000). The basic steps are; s*tep i)* questionnaire survey is included in the mail with postage-paid return envelope, s*tep ii)* send a reminder card, and *step iii)* for those who had not responded to the first

survey, send a second copy of the survey. We received total of 1,047 responses (65% response rate). Usual successful response rate in survey is known to be around 20-25% (Boyle, 2007). This unusually high response rate shows that community residents are interested and serious regarding these issues.

Stated Preference Survey (Phase II)

In the second phase of the survey, AHP was applied to those who were willing to be contacted again. From Phase I, we received 1,047 respondents and 400 respondents were willing to be contacted again for further questionnaire. Using the similar steps (Dillman, 2000), we sent 400 surveys and received 250 surveys back (63%). In this phase, we wanted to understand homeowner's decision making process in the choices of home drinking water plumbing systems and materials. After personal communications with the homeowner association committees and pinhole leak experts, we developed the most important and relevant criteria; corrosion, taste and odor of drinking water, health effects, convenience of installation, proven performance in the market, cost (labor + material), and manufacture warranty. Also we considered materials copper, PEX, and Epoxy Coating which corresponds to their existing real alternatives. For complete survey modules, refer to Lee (2008).

RESULTS

Revealed Preferences for Community Residents

In this section, important aspects of survey results relevant to the scope of this study are included. For complete survey results, refer to Bosch et al. (2008). Out of 1,047 respondents, 212 respondents (20%) reported incidents of pinhole leaks in their potable plumbing systems; 780 respondents (74%) reported no experience of leak incidents in their houses; and 32 respondents (3.2%) reported do not know. One hundred and twenty eight respondents (60%) of the respondents with leaks had experienced 1 or 2 leaks; 47 respondents (22%) had 3 or 4 leaks; and 33 respondents (15%) reported more than 5 leak incidents.

Seventy-seven respondents repaired the leak using a clamp (Table 1). It is likely that a clamp was used initially before leaking sections were replaced or replumbed for the whole house. One hundred thirty-three respondents repaired the leak by replacing the leaking pipe section. Copper was most often used. Fifty respondents repaired the leak by *replumbing the entire house*. PEX was most often used (32 respondents) for replumbing followed by Epoxy coating (9 respondents). Five respondents replumbed with copper (same or thicker pipes) and 4 respondents did replumb with CPVC.

Table 2 lists the cost of repairing pinhole leaks. Twenty-nine percent of respondents with leaks reported that the expense of repairing pinhole leaks was less than $100; while 30% reported expenses between $100 and $500; and 37% reported more than $500 in expenses for pinhole leak repairs. Seven respondents reported more than $10,000 in costs of repairs. This figure possibly includes replumbing the whole house. Property damage cost due to pinhole leaks are shown in Table 3. Ninety-two percent of respondents with leaks reported having to repair property damage caused by leaks in addition to the expense of repairing leaks. Forty percent of respondents with

damage reported less than $100 of damage while 49% had over $100 in damage. Twelve respondents had over $5,000 in property damage**.**

Table 1 Method of Leak Repair

Repair method	Number of observations	Percent[a]
Clamp over leak	77	7
Replaced leaking pipe section with copper	75	35
Replaced leaking pipe section with CPVC	5	2
Replaced leaking pipe section with PEX	7	3
Replaced leaking pipe section-material not specified	46	22
Applied coating of Epoxy to all plumbing	9	4
Replumbed with copper	5	2
Replumbed with CPVC	4	2
Replumbed with PEX	32	15
Replumbed-material not specified	9	4
Other	7	1
Don't know	3	1
Total	279	129
[a]Multiple choices per respondent were accepted. Percent = number reported divided by the total number of respondents with leaks (212).		

Table 2 Costs of Repairing Pinhole Leaks

Amount	Number of observations	Percent[a]
Less than $100	61	29
$100 to $500	64	30
$501 to $1,000	14	7
$1,001 to $3,000	11	5
$3,001 to $5,000	20	9
$5,001 to $10,000	28	13
$10,001 to $20,000	6	3
More than $20,000	1	0
Do not know	3	1
Missing/not reported	4	2
Total	212	99

Table 3 Costs of Repairing Property Damage from Pinhole Leaks

Amount	Number of observations	Percent[a]
Less than $100	85	40
$100 to $500	47	22
$501 to $1,000	16	8
$1,001 to $3,000	18	8
$3,001 to $5,000	10	5
$5,001 to $10,000	12	6
More than $10,000	0	0
Do not know	8	4
No property damage	16	8
Total	212	101
[a]Totals do not sum to 100 due to rounding.		

Stated Preferences for Community Residents

Among 250 surveys received, 133 respondents' data turned out to be reliable. Mean attribute results for 133 respondents show that health effect and taste/ odor are the two important factors in deciding on the plumbing materials. Corrosion resistance and proven performance in the market constitute the next set of important attributes. Cost and convenience of installation seems to be the least important factor. It is interesting to see that cost is not highly dominant factor for homeowners. This is partly due to the similar cost ranges listed in the given information. In real life, cost figure may become major factors if there is a large difference among alternatives.

To see the preference difference between those who have leak experiences and no experiences, 133 respondents' are broken down into two groups; with leaks (28 respondents) and without leak experiences (105 respondents). There is little difference in between each group and majority of respondents regarded health and taste of odor as their major decision factors.

Comparison between Revealed Preferences and Stated Preferences

To compare revealed and stated preferences, we link 133 respondents' AHP results with revealed preferences surveys. As mentioned, 28 households had experienced pinhole leak incidents. Hundred and five households had not experienced any leak incidents in their plumbing system. For 28 households who had experienced leak incidents, their original pipe materials were all copper before they had any leaks.

Among 28 homeowners, 7 households did replumb their whole plumbing systems and 21 households repaired the failed section. Table 4 shows the real actions and AHP results for those who replumbed after leak incidents. For example, respondent # 1,310 replumbed with Epoxy coating in real life; and AHP result (revealed preferences; 3rd column in Table 4) is Epoxy coating. Their real actions are corresponding to the AHP's decision results. Likewise, respondent1,301's real replumb choice was PEX and AHP decision result are matching. However, 1,322's AHP results are Epoxy; real actions were with thicker copper pipes.

Table 4 Preference of those who replumbed after leak incidents

Respondent Number	Revealed preferences (Real actions)	Stated preferences (AHP)
1,301*	PEX	PEX
1,310	Epoxy coating	Epoxy coating
1,314	Epoxy coating	Epoxy coating
1,322	Thicker copper	Epoxy coating
1,295	Copper	PEX
1,127	PEX	Epoxy coating
1,730	PEX	Epoxy coating

*highlighted part indicates indivdiduals who had the same revealed and stated preferences

CONCLUSIONS

Selecting alternative plumbing material is subjective to homeowners' perception and preferences. According to AHP results, health effects and taste and odor of water turned out to be the dominant factors for homeowners. Some homeowners showed preference for one material, but they chose another option in real life. It is highly likely that their decisions are influenced by the amount information they could access. For example, southeastern community A residents seem to think corrosion resistance as the only criteria when choosing an alternative plumbing material. Even though safety issues (health, taste and odor) turned out to be the most important in the stated preferences, homeowners were not well aware of these issues related with plumbing materials in real life. Due to limitations in the number of attributes in AHP, we could only include the most important 7 attributes in the survey. There should be other attributes that will affect consumer's decisions such as attractive marketing strategies, special discount offers or purchase incentives and advise from others (plumbers, consultants, architects, neighbors etc). In addition, higher number of sample size will show better comparison between revealed and stated preferences.

Through this research, homeowners will be able to make better informed decisions in selecting alternative plumbing materials. Water professionals, policy makers, water utilities should work on bridging the gap between public perception and research results. The results of these surveys can help fill the information gap about pinhole leaks among policy experts and water utilities who are dealing with this problem. This information will be helpful for advising policy experts and utility companies on ways to deal with pinhole leaks.

ACKNOWLEDGEMENTS

This material is based upon work supported by the National Science Foundation under Grant No. 0329474.

REFERENCES

Bosch, D., Kleczyk, E., Lee, J., and Tanellari, E. (2008). Southeastern community A Survey Report

Boyle, K. (2007). Personal communication

Dillman, Don A. (2000). *Mail and Internet Surveys : The Tailored Design Method* New York: J. Wiley.

Lee, J., Loganathan, G.V., Bosch, D., Dwyer, S., and Kleczyk, E. (2006). "Consumer concerns and preference tradeoffs in home plumbing systems." *8th Annual International Symposium on Water Distribution Systems Analysis*. Cincinnati, Ohio. August 27-30, 2006

Lee, J. (2008). Ph.D. Dissertation. *Two Issues in Premise Plumbing: Contamination Intrusion at Service Lines and Choosing an Alternative Plumbing Material*. Virginia Tech.

Marshutz, S. (2001). "Hooked on copper: A comparison shows the gap is narrowing with PEX gaining popularity as a preferred material in new construction and repiping work." Reeves Journal. Available online at: http://www.accessmylibrary.com/coms2/summary_0286-7338309_ITM

Martin, D. (2007). Personal communications.

Saaty, T.L. (1980). *The Analytic Hierarchy Process*. McGraw-Hill. New York.

Woodson, R.D. (1999). *Plumber's Standard Handbook*. McGraw-Hill. New York.

Field-Scale Assessment of a Multispecies Water Quality System: A Chloramination Study

Matthew T. Alexander†, Dominic L. Boccelli‡, and Margaret J. Kupferle*

Department of Civil and Environmental Engineering, University of Cincinnati, P.O. Box 210071, Cincinnati, OH 45221-0071; FAX (513) 556-2599

†PH (937) 217-0626; email: alexanmt@email.uc.edu
‡PH (513) 375-6901; email: dominic.boccelli@uc.edu
*PH (513) 556-3329; email: margaret.kupferle@uc.edu

Abstract

Water distribution system network models are used to simulate both hydraulic and water quality characteristics in water distribution systems. These models primarily focus on modeling hydraulics and are unable to model more than one water quality parameter. EPANET-MSX (Multi-Species eXtension), a recently developed multi-species water quality version of EPANET, has the ability to model complex multi-species systems of water quality species. This study proposes to provide the first comprehensive evaluation of integrated models associated with chloramine dynamics, by-product formation, and nitrification through the use of field-scale measurements and distribution system network modeling. Hydraulic and multi-species water quality simulations will be performed using EPANET-MSX. This investigation will gauge the accuracy of EPANET-MSX through comparison with a comprehensive set of field-data. Successful implementation of such a model could change the way water distribution maintenance and operation is approached in the future.

1 Introduction

Water distribution systems are designed to transport a sufficient quantity of treated water from a treatment facility to consumers without compromising the water quality. In reality, this is not always achieved. At the time when many water distribution systems were designed, the primary objective was to provide adequate pressure throughout the system. As a result, networks were frequently over designed in anticipation of satisfying increasing demands. In such cases, the excessive hydraulic residence times make maintaining adequate disinfection residuals difficult. Providing too much disinfection encourages the formation of hazardous disinfection by-products, while providing too little disinfection encourages the formation of biological contaminants. Operating such a system can be challenging, especially when strict water quality regulations must be satisfied.

In recent years, water distribution system network models have generally been utilized to remedy quantity related issues. From a water quality perspective, these

models have generally been limited to representing a single water quality species, with first-order dynamics, derived from a single source. EPANET-MSX (Multi-Species eXtension), a recently developed multi-species water quality version of EPANET, allows for the simulation of more complex water quality behavior from multiple sources. However, little research has been performed to confirm the results of the integrated models that evaluate both hydraulics and a multi-species water quality model within an actual distribution system. Verification of such models could facilitate the use of modeling software in troubleshooting and maintaining water quality issues in the future.

This study intends to provide a comprehensive water quality analysis that integrates chloramine decay, by-product formation, and nitrification into a single model in conjunction with system-wide field-scale measurements. This model will also be the first field-verified evaluation of EPANET-MSX, which will focus only on chemical and biological components within the bulk phase, not the pipe surface. Additionally, this comprehensive analysis will assess the accuracy of EPANET-MSX and identify any disparities between advanced water quality simulations and actual distribution system performance. Successful verification of such a comprehensive model would demonstrate that water quality models can be used in the decision making processes related to water quality maintenance of distribution systems.

2 Materials and Methods

Hydraulic and water quality simulations will be performed using EPANET-MSX, a recently developed extension of EPANET that provides a general environment for performing multispecies water quality modeling. An existing hydraulic model was provided by our partner utility (*see Section 2.1*). Model hydraulics will be modified in anticipation of simulating observed conditions in the actual system (*see Section 2.2*). Existing kinetic models and nonlinear equilibrium relationships associated with chloramine dynamics, by-product formation, nitrification, and other chemical and biological species will be incorporated to approximate the interaction of various species within the bulk fluid (*see Section 2.3*). Bench-scale studies will be performed on water samples from the system to estimate the necessary parameters related to kinetic models (*see Section 2.4*). After kinetic parameters are estimated, a comprehensive field study will be performed to assess the performance of the model and to determine if any knowledge gaps exist (*see Section 2.5*).

2.1 *Network Characteristics*

This study is being conducted in collaboration with our partner utility and focuses on a portion of their distribution system. The system serves 19.2 MGD of water to predominately residential customers (*see Figure 1*). The system contains no storage tanks and is supplied by three different water sources (surface water,

ground water, and a combination of surface, ground and desalinated water). As seen in Figure 1, the system is divided into three regions, where each region is supplied by a different type of source water. Region 1 is supplied by ground water, Region 2 by surface water, and Region 3 by a combination of surface, ground, and desalinated water. The dashed lines in Figure 1 approximate the service boundaries of the three source waters. Blended source waters are expected in the areas near these regional boundaries.

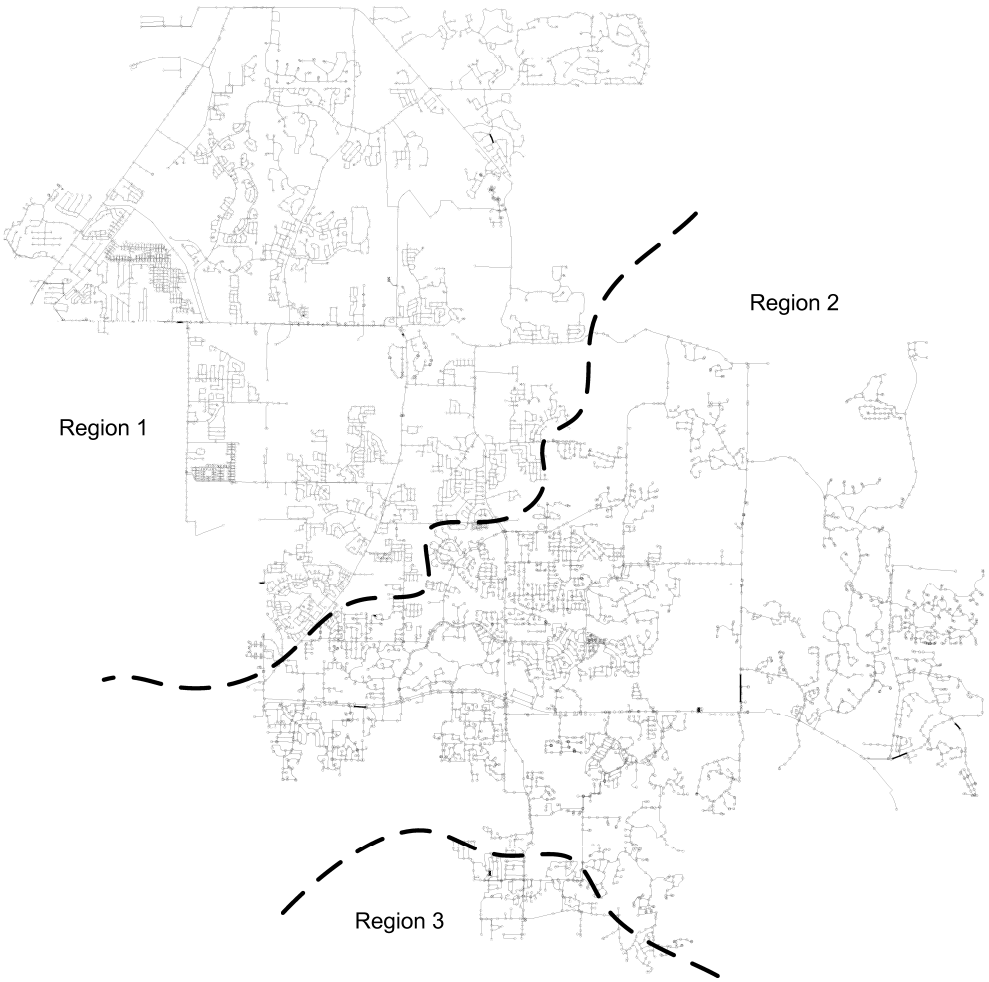

Figure 1: Partner Utility Network Model

2.2 *Hydraulic Simulations*

In order to achieve an accurate representation of water quality parameters, the hydraulics of the model network will likely need to be modified to characterize the conditions in the actual system. With the cooperation of our partner utility, pump operations and flow rates, in-line system flow rates and pressures, and other

significant data will be provided through their SCADA system. This data will be used to update the hydraulic model for representing the conditions observed during the field-study time period.

In such a system, with three different water sources, accurate representation of the hydraulics is important. Therefore, the demand pattern multiplier will be adjusted to ensure that the system is hydraulically balanced (i.e., the total volume of water entering the system will balance the water demanded by the system). In addition to adjusting the demand pattern, background levels of sulfate, each varying by approximately one order of magnitude, may be used to identify the water source throughout the system.

2.3 *Water Quality Simulations*

Chloramine System: Monochloramine (NH_2Cl) and dichloramine ($NHCl_2$) kinetics are modeled based on an existing auto-decomposition model developed by Vikesland et al. (2001) (*see Table 1*). This model incorporates hydrolysis reactions involving chlorine with ammonia or chloramines (*reactions 1 through 4*), disproportionation reactions of the chloramine species (*reactions 5 and 6*), redox reactions that occur at low levels of free chlorine (*reactions 7 through 10*), reaction pathways of monochloramine in the presence of natural organic matter (*reactions 11 and 12*), and acid/base equilibrium reactions of chlorine, ammonia, and carbonates (*reactions 13 through 16*) (Duirk et al., 2005; Vikesland et al., 2001). This model will require the estimation of the dissolved organic carbon (DOC) reactive site fractions, represented by DOC_1 and DOC_2 with monochloramine and free chlorine, respectively. Other parameters that will be measured include pH, temperature, dissolved organic carbon (DOC), alkalinity, free chlorine, ammonia, monochloramine, and dichloramine. These measurements will be used to determine the initial conditions of the multi-species model.

Disinfectant By-Product Formation: Two disinfectant by-products, N-nitrosodimethylamine (NDMA) and trihalomethanes (THM), are simulated using existing kinetic models (*see Table 2*). The NDMA model was developed by Chen and Valentine (2006), which provides a linear relationship between NDMA formation and reaction pathways of monochloramine and chlorine with natural organic matter (*reactions 13 and 14*). The THM model was developed by Boccelli et al. (2003), which presents a linear relationship between total trihalomethanes (TTHM) and total chlorine demand, or amount of natural organic matter that is oxidized. The rate of chloramine loss, and both linear parameters, θ and ϕ, will be estimated through bench-scale kinetic studies (*see Section 2.4*). These site-specific parameters will measured at various locations throughout the system.

Nitrification: Historically, nitrification has occurred in distribution systems with chloramine disinfection (Fleming et al., 2005; Liu et al., 2005). Ammonia loss within a distribution system may be attributed to assimilative growth and biochemical nitrification by ammonia oxidizing bacteria (AOB) and nitrite oxidizing

Table 1: Chloramine Loss – various pathways of decay (Duirk et al., 2005; Vikesland et al., 2001).

	Reaction Stoichiometry	Rate Coefficients & Equilibrium Constants
1	$HOCl + NH_3 \rightarrow NH_2Cl + H_2O$	$k_1 = 1.5 \times 10^{10}$
2	$NH_2Cl + H_2O \rightarrow HOCl + NH_3$	$k_2 = 7.6 \times 10^{-2}$
3	$HOCl + NH_2Cl \rightarrow NHCl_2 + H_2O$	$k_3 = 1.0 \times 10^{6}$
4	$NHCl_2 + H_2O \rightarrow HOCl + NH_2Cl$	$k_4 = 2.3 \times 10^{-3}$
5	$NH_2Cl + NH_2Cl \rightarrow NHCl_2 + NH_3$	$k_5 = 2.5 \times 10^{7}[H^+]$ $+4.0 \times 10^{4}[H_2CO_3]$ $+8.0 \times 10^{2}[HCO_3^-]$
6	$NHCl_2 + NH_3 \rightarrow NH_2Cl + NH_2Cl$	$k_6 = 2.2 \times 10^{8}$
7	$NHCl_2 + H_2O \rightarrow I$	$k_7 = 4.0 \times 10^{5}$
8	$I + NHCl_2 \rightarrow HOCl + Products$	$k_8 = 1.0 \times 10^{8}$
9	$I + NH_2Cl \rightarrow Products$	$k_9 = 3.0 \times 10^{7}$
10	$NH_2Cl + NHCl_2 \rightarrow Products$	$k_{10} = 55.0$
11	$NH_2Cl + DOC_1 \rightarrow Products$	$k_{11} = 3.0 \times 10^{4}$
12	$HOCl + DOC_2 \rightarrow Products$	$k_{12} = 6.5 \times 10^{5}$
13	$HOCl \rightarrow H^+ + OCl^-$	$pK_a = 7.5$
14	$NH_4^+ \rightarrow NH_3 + H^+$	$pK_a = 9.3$
15	$H_2CO_3 \rightarrow HCO_3^- + H^+$	$pK_a = 6.3$
16	$HCO_3^- \rightarrow CO_3^{2-} + H^+$	$pK_a = 10.3$

Rate coefficients and equilibrium constants are given at 25°C.

The term I is an unknown reactive intermediate.

Table 2: DBP Formation – various pathways of formation (Boccelli et al., 2003; Chen and Valentine, 2006; Clark, 1998).

	Reaction Expression	Parameter
13	$\text{NDMA}(t) = \theta\left(k_{11}[\text{NH}_2\text{Cl}][\text{DOC}_1] + k_{12}[\text{HOCl}][\text{DOC}_2]\right)$	$^a\theta = 2.58 \times 10^{-5}$
14	$\text{TTHM}(t) = \phi\left(^b k_{13}([\text{HOCl}] + [\text{OCl}^-])[\text{DOC}_{total}]\right)$	$^c\phi = 42.5$

[a]Estimated mass ratio of NDMA produced to NOM oxidized
[b]First-order chlorine decay coefficient
[c]Estimated unit of TTHM formation per unit of chlorine demand

bacteria (NOB) (*see Table 3*). The individual growth rates of AOB and NOB were modeled by Liu et al. (2005). This model utilizes Monod kinetics to express biomass concentration and considers the inhibition effect of monochloramine and the rate limiting effect of dissolved oxygen (Liu et al., 2005). This model can be found in *Table* 3 where $\mu_{1\ max}$ ($0.4\ day^{-1}$) is the maximum specific growth rate of AOB, $\mu_{2\ max}$ ($0.55\ day^{-1}$) is the maximum specific growth rate of NOB, K_1 ($2.0 \times 10^{-4}\ mg/cm^3$ as Cl_2) is the ammonia concentration yielding half of the AOB maximum rate, K_2 ($1.2 \times 10^{-3}\ mg/cm^3$ as N) is the nitrite concentration yielding half of the NOB maximum rate, K_3 ($4.0 \times 10^{-4}\ mg/cm^3$) is the estimated oxygen concentration giving half of the AOB and NOB maximum rate, and K_4 ($5.0 \times 10^{-4}\ mg/cm^3$ as Cl_2) is the inhibition concentration of monochloramine.

Microbial: Previous studies have suggested that chlorine to ammonia concentration ratios, or nitrification potential curves, may be used to indicate that conditions are favorable for nitrification to occur (Fleming et al., 2005). This theory is based on growth and inactivation kinetics of AOB in the presence of chlorine and ammonia. This strategy of predicting regions of greater nitrification potential, based on a straightforward ratio, will be implemented to assist in determining the water quality sampling locations. If nitrification occurs where measured ratios indicate, further validation would be provided that nitrification may be predicted by a simple chlorine to ammonia ratio.

Analysis of the biological species will take place only at 24 hour intervals. Collections of biomass, for the analysis of biological species, will be collected from the bulk water and concentrated. DNA will be extracted from the concentrated biomass with a commercially produced extraction kit. The *presence* of AOB and NOB will be determined by using polymerase chain reaction (PCR) of extracted nucleic acids using an available ABI real-time instrument (Hermansson and Lindgren, 2001; Rotthauwe et al., 1997; Schmid et al., 2003). Gel electrophoresis and Southern Blot hybridization will be used to validate the identity of each target

sequence. This procedure should be adequate in qualitatively predicting the *presence* or *absence* of AOB and/or NOB.

Table 3: Nitrification Modeling – various pathways of ammonia disappearance (Liu et al., 2005).

	Reaction Expression
15	$\mathrm{AOB}(t) = \left(\frac{\mu_{1\ max} * [\mathrm{NH_3}]}{\mathrm{K_1} + [\mathrm{NH_3}]}\right) \times \left(\frac{[\mathrm{DO}]}{\mathrm{K_3} + [\mathrm{DO}]}\right) \times \left(1 + \frac{[\mathrm{NH_2Cl}]}{\mathrm{K_4}}\right)^{-1}$
16	$\mathrm{NOB}(t) = \left(\frac{\mu_{2\ max} * [\mathrm{NO_2}]}{\mathrm{K_2} + [\mathrm{NO_2}]}\right) \times \left(\frac{[\mathrm{DO}]}{\mathrm{K_3} + [\mathrm{DO}]}\right) \times \left(1 + \frac{[\mathrm{NH_2Cl}]}{\mathrm{K_4}}\right)^{-1}$

For parameter definitions see Section 2.3

2.4 *Bench-Scale Assessment*

Parameter estimation studies will be performed prior to field-scale data collection. These studies will be performed to assess the kinetics associated with reactions of chloramine ($\mathrm{DOC_1}$) and chlorine ($\mathrm{DOC_2}$) with natural organic matter and the formation of NDMA (θ) and TTHM (ϕ). A sample of non-chloraminated treated water has been obtained from the utility for use in parameter estimation studies. Water quality species discussed in Section 2.3 will be measured prior to disinfection of the sample. These measurements will be used to provide initial background concentrations of the respective species in the model. The provided sample will be divided into smaller samples. One sample will be *chloraminated* at a standard 5:1 ratio of chlorine to ammonia-N. The other sample will be *chlorinated* at a low dosage to evaluate the kinetic behavior of reactions under such conditions (*see Table 1*)

After both samples have been treated with disinfectant, two groups of several disinfectant demand-free bottles will be filled (Summers et al., 1996). One group will be filled with the chlorinated sample and the other with the chloraminated sample. Both groups of samples will be stored in a dark temperature controlled environment. Sample bottles from both groups will be removed and necessary water quality parameters will be analyzed after 5 min, 15 min, 30 min, 1 hr, 2 hr, 4 hr, 8 hr, 24 hr, 48 hr, 72 hr, 96 hr, and 120 hr. Species concentration at various time intervals will be used to estimate kinetic parameters by using a Levenberg-Marquardt approach to minimize the sum-of-the-squared errors between observed and expected values.

In addition to parameter estimation studies, bench-scale measurements of nitrite ($\mathrm{NO_2^-}$) and nitrate ($\mathrm{NO_3^-}$) will be performed to gauge the accuracy of the nitrification model.

2.4.1 *Water Quality Measurements*

Chlorine and chloramines will be measured using *Hach Method 8167* (Hach Company, 2000), an adaptation of the DPD Colorimetric Method [4500-Cl G] (Eaton et al., 2005). This method uses *N,N*-diethyl-*p*-phenylenediamine (DPD) reagent packets as an indicator with a colorimeter to measure concentrations of free chlorine, monochloramine, and dichloramine (Eaton et al., 2005). A *Hach DR/850 Colorimeter* (Hach Company, 2000) will be used to make both bench-scale and field-scale measurements. Ammonia will be measured according to the Ammonia-Selective Electrode Method [4500-NH_3 D] (Eaton et al., 2005), which incorporates the use of an electrode to measure aqueous ammonia levels in acidified solutions, that converts NH_3 to NH_4^+.

Nitrate will be gauged by means of *Hach Method 8039* (Hach Company, 2000), an adaptation of the Cadmium Reduction Method [4500-$N0_3^-$ E] (Eaton et al., 2005). This is another colorimetric method, which uses cadmium treated with $CuSO_4$, to reduce nitrate to nitrite. The nitrite is then treated with an agent to form a red color, which is then measured with a colorimeter. Nitrite concentration will be quantified by *Hach Method 8507* (Hach Company, 2000), another adaptation of the Colorimetric Method [4500-$N0_2^-$ B] (Eaton et al., 2005), which is the same procedure as the Cadmium Reduction Method [4500-$N0_3^-$ E], excluding the reduction of nitrate to nitrite with cadmium. Nitrite and nitrate samples will be taken at time intervals no less than one hour, due to the time required to conduct their analysis.

Organic carbon measurements will be assessed using a *Shimadzu TOC analyzer*, which utilizes the combustion catalytic oxidation/NDIR to quantify a full array of organic compounds. The pH of various samples will be determined by using a glass membrane pH electrode, which is described in detail by the Electrometric Method [4500-H^+ B] (Eaton et al., 2005). Sulfate concentration will also be measured by *Hach Method 8051* (Hach Company, 2000), a colorimetric procedure adapted from the Turbidimetric Method [4500-SO_4^{2-} E] (Eaton et al., 2005) that utilizes a barium chloride ($BaCl_2$) reagent.

Disinfectant by-products, NDMA and TTHM, will be evaluated by using a gas chromatography/mass spectrometer (GC/MS). *N*-nitrosodimethylamine will be gauged by isolating contaminants with solid-phase extraction (SPE) followed by analysis with a GC/MS with selective-ion monitoring (SIM) (Choi and Valentine, 2002). Total trihalomethanes will be measured according to the Purge and Trap Capillary-Column Gas Chromatographic Method [6200 C] (Eaton et al., 2005), which is a commonly used procedure to measure a variety of halocarbons and aromatic organic compounds.

2.5 *Field-Scale Assessment*

Field-scale activites will consist of both water quality and hydraulic data collection activities performed over a two week time period in the Winter/Spring of 2009. Due to temporal and spatial challenges the field-scale assessment will focus on only a portion of the system. Once all kinetic parameters are estimated and initial background concentrations of various species are quantified, the field-scale data collection may begin. These parameters and concentrations will be used to conduct a preliminary simulation. This simulation will be used to determine areas in the system where nitrification, or loss of disinfection residual, are expected to occur. This is expected to occur in areas where source waters are mixed (*see the dashed source boundary lines in Figure 1*). Sampling locations will be determined using a modified version of TEVA-SPOT (Boccelli and Hart, 2007; Hart et al., 2007), which assists in the placement of sampling locations. This will ensure that field-scale measurements accurately represent the entire system through adequate spatial coverage and a distribution of hydraulic residence times. In addition to the sampling locations determined by the software, samples will be collected at system sources and areas where source blending occurs.

Water quality samples will be taken from either fire hydrants or dedicated water quality sampling taps. Sampling sites will be visited two to four times daily, depending on spatial location and sampling time. All water quality measurements (*see Section 2.4.1*) will be performed in the field with the *Hach DR/850 Colorimeter* (Hach Company, 2000), excluding DBPs and biological species, which will be preserved and returned to the laboratory for analysis. Biological samples will be taken only once at each sampling location, unless nitrification conditions are suspected.

In addition to water quality sampling, hydraulic conditions will also be monitored throughout the system. As mentioned in Section 2.2, pump operations and flow rates, in-line system flow rates and pressures, and other significant data will be provided by our partner utility, through their SCADA system. This data will be used to update the distribution system demand estimates for the system model.

3 Preliminary Analysis

When selecting potential sampling locations, a few criteria must be considered. The locations must be spatially diverse and represent a broad range of hydraulic behavior (Boccelli and Hart, 2007). In this study, we would also like to capture areas with elevated nitrification potential (Fleming et al., 2005). This criteria may be satisfied by examining water age, chloramine residual, and/or Cl:NH_3 ratios. As mentioned in Section 2.5, the field-scale activities will be limited by temporal and spatial constraints. Therefore, sampling will likely be limited to a portion of a system that represents typical hydraulic and water quality conditions. This section illustrates the proposed approach of selecting sampling locations.

A provisional analysis of the partner utility network was performed to assist in identifying potential sampling locations. This preliminary model only considers chloramine decomposition to ammonia in the presence of natural organic matter (NOM), which is based on the model previously implemented by Shang et al. (Duirk et al., 2005; Shang et al., 2008a,b; Vikesland et al., 2001). An illustration of the spatial distribution in chloramine residual after a period of 72 hours may be seen in Figure 2. The initial conditions for this simulation were set at a pH of 7.55, 4.12 mg/L (80 μmole/L) of monochloramine, 200 mg/L of alkalinity (as $CaCO_3$), and 3.00 mg/L of TOC, with slow and fast reaction sites of 0.02 and 0.50, respectively. This figure depicts a small portion of the network model that borders a source water boundary (shown by a dashed line). In this system, the disinfection residuals were typically lower near extremities of the network and source water boundaries, where the age of the water is expected to be the greatest.

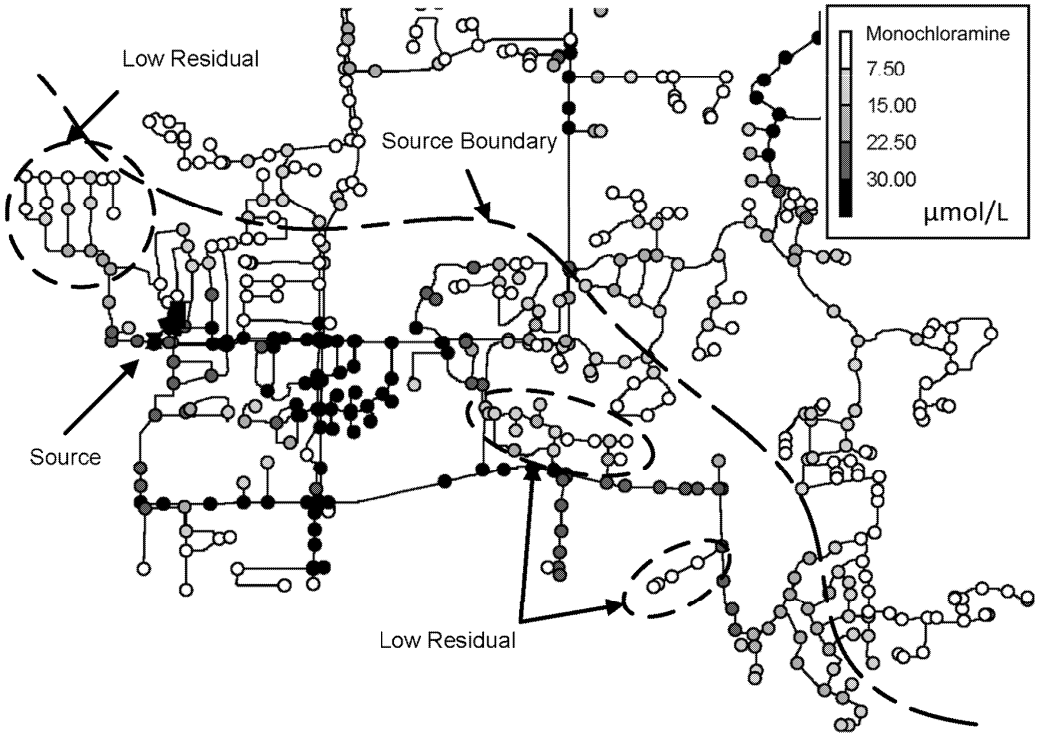

Figure 2: Preliminary Model of Monochloramine Residual in Portion of Network at 72 Hours

The preliminary simulations will be used to identify sampling locations that represent the overall distribution of water quality parameters to be measured. Figure 3 shows the empirical cumulative distribution function (cdf) of the monochloramine residual shown in Figure 2. The cdf represents the distribution system information that could be generated if sampling could occur at every location. In reality,

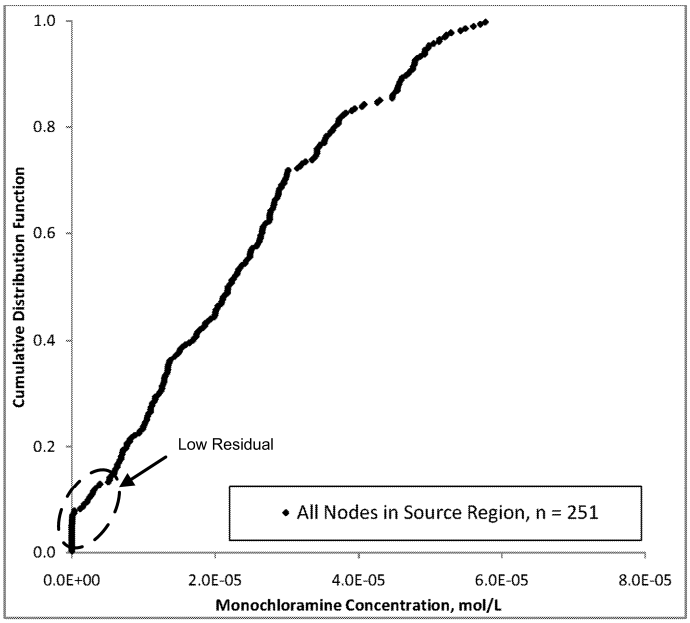

Figure 3: Illustration of the Distribution of Monochloramine Residual in Portion of Network at 72 Hours

only a subset of locations can be sampled. This subset of locations should be selected to represent the overall distribution to ensure adequate representation of all conditions within the distribution system. In addition to representing the overall distribution, the subset of sampling locations must also be spatially diverse. As an illustrative example, if the only interest were in representing the low monochloramine concentration range of the overall distribution, this objective could be satisfied by sampling entirely in the south east region of the system. However, the more preferable approach would be to more evenly distribute the sampling locations between the southeast and northwest area, both of which have low residuals. Such a design satisfies both the overall distribution and achieves spatial distribution of the measurements.

4 Summary/Future Work

This study intends to provide the first comprehensive evaluation of integrated water quality and hydraulic models, which places particular emphasis on the ability of EPANET-MSX to represent the multi-species water quality system. Successful verification of this comprehensive model could demonstrate that water quality models similar to this could be used in decision making processes related to water quality maintenance of distribution systems in the future.

The framework of this study has been established and parameter estimation studies will be completed over the next month with water supplied by the utility.

After the parameter values specific to the study water system are established, the model will be updated and actual sampling locations will determined. Once the sampling locations are determined, a two week field-scale assessment will follow. After data is collected and analyzed, the observed hydraulic and water quality data will be compared to the predicted model results, focusing on the ability of the model to represent both the hydraulics and water quality.

5 Acknowledgements

This research is based on funding by the Water Research Foundation, formerly known as the American Water Works Association Research Foundation. Their support is greatly appreciated. We would also like to thank Dr. Dan Oerther and his research assistant Mau-Yi Wu for their time and guidance particularly associated with the PCR analysis.

References

Boccelli, D. L. and W. E. Hart (2007). Optimal monitoring location selection for water quality issues. In *9th Annual Symposium on Water Distribution System Analysis. Proceedings of the World Water and Environmental Resources Conference*, Tampa, FL,.

Boccelli, D. L., M. E. Tryby, J. G. Uber, and R. S. Summers (2003). A reactive species model for chlorine decay and THM formation under rechlorination conditions. *Water Research 37*(11), 2654–2666.

Chen, Z. and R. L. Valentine (2006). Modeling the formation of N-nitrosodimethylamine (NDMA) from the reaction of natural organic matter (NOM) with monochloramine. *Environmental Science and Technology 40*(23), 7290–7297.

Choi, J. and R. Valentine (2002). A kinetic model of N-nitrosodimethylamine (NDMA) formation during water chlorination/chloramination. *Water Science and Technology 46*(3), 65–71.

Clark, R. M. (1998). Chlorine demand and TTHM formation kinetics: A second-order model. *Journal of Environmental Engineering 124*(1), 16–24.

Duirk, S. E., B. Gombert, J.-P. Croue, and R. L. Valentine (2005). Modeling monochloramine loss in the presence of natural organic matter. *Water Research 39*(14), 3418–3431.

Eaton, A. D., L. S. Clesceri, E. W. Rice, and A. E. Greenberg (2005). *Standard Methods for the Examination of Water & Wastewater* (21st ed. ed.). American Public Health Association, American Water Works Association, & Water Environment Federation.

Fleming, K. K., G. W. Harrington, and D. R. Noguera (2005). Nitrification potential curves: A new strategy for nitrification prevention. *Journal of the American Water Works Association 97*(8), 90–99.

Hach Company (2000). *DR/850 Datalogging Colorimeter Handbook* (2nd ed. ed.). Loveland, CO.

Hart, W. E., J. W. Berry, R. Murray, C. A. Phillips, L. A. Riesen, and J.-P. Watson (2007). SPOT: A sensor placement optimization toolkit for drinking water contamination warning system design. In *9th Annual Symposium on Water Distribution System Analysis. Proceedings of the World Water and Environmental Resources Conference*, Tampa, FL,.

Hermansson, A. and P.-E. Lindgren (2001). Quantification of ammonia-oxidizing bacteria in arable soil by real-time PCR. *Applied and Environmental Biology 67*(2), 972–976.

Liu, S., J. S. Taylor, A. Randall, and J. D. Dietz (2005). Nitrification modeling in chloraminated distribution systems. *Journal of the American Water Works Association 97*(10), 98–108.

Rotthauwe, J.-H., K.-P. Witzel, and W. Liesack (1997). The ammonia monooxygenase structural gene amoA as a functional marker: Molecular fine-scale analysis of natural ammonia-oxidizing populations. *Applied Environmental Microbiology 63*(12), 4704–4712.

Schmid, M., K. Walsh, R. Webb, W. I. C. Rijpstra, K. van de Pas-Schoonen, M. J. Verbruggen, T. Hill, B. Moffett, J. Fuerst, S. Schouten, J. S. S. Damst, J. Harris, P. Shaw, M. Jetten, and M. Strous (2003). *Candidatus* scalindua brodae, sp. nov., *Candidatus* scalindua wagneri, sp. nov., two new species of anaerobic ammonium oxidizing bacteria. *Systematic and Applied Microbiology 26*(4), 529–538.

Shang, F., J. G. Uber, and L. A. Rossman (2008a). *EPANET Multi-Species Extension User's Manual*. Cincinnati, OH: National Risk Management Research Laboratory and National Homeland Security Research Center, U. S. Environmental Protection Agency.

Shang, F., J. G. Uber, and L. A. Rossman (2008b). Modeling reaction and transport of multiple species in water distribution systems. *Environmental Science and Technology 42*(3), 808–814.

Summers, R. S., S. M. Hooper, H. M. Shukairy, G. Solarik, and D. Owen (1996). Assessing DBP yield: Uniform formation conditions. *Journal of the American Water Works Association 88*(6), 80–93.

Vikesland, P. J., K. Ozekin, and R. L. Valentine (2001). Monochloramine decay in model and distribution system waters. *Water Research 35*(7), 1766–1776.

Pressure vs. Flow Relationship for Pipe Leaks

Thomas Walski, Bentley Systems
Brian Whitman, Wilkes University
Mary Baron, Wilkes University
Fred Gerloff, Wilkes University

Abstract

Leakage can be reduced by reducing pressure in a water distribution system. The magnitude of that reduction depends on the equation used to predict leakage. A common equation is to use a power function where the flow is estimated from the pressure terms raised to an exponent. There are a wide range of values reported in the literature for that exponent. Laboratory experiments were performed in which flow and pressure were measured for a wide range of leak shapes and sizes. The median value of the exponent was 0.54 which is lower than most reported but close to the theoretical value for an orifice. The high values in the literature can be explained in some cases as due to the method for estimating leak reduction. This is illustrated using a model of a small zone.

Background

Water loss through leakage has been identified as a problem in virtually all water distribution systems. Leakage is inevitable in all water systems. It is estimated that roughly 32 billion cubic meters of water is lost annually from water distribution systems by way of leakage (Kingdom, Limberger and Marin, 2006). Thornton (2002) estimated that the worldwide value of this lost was on the order of $81 billion per year.

Because the rate of leakage depends on the pressure within the pipe, one method of reducing leakage is pressure management. Reducing pressure has been shown to be effective in reducing leakage. Predicting the reduction in leakage due to pressure reduction is not exact. Most investigators agree that a power function of the form below should explain the pressure vs. leak relationship.

$$Q_f = Q_i\left(\frac{P_f}{P_i}\right)^n \qquad (1)$$

Where Q_f = final leak rate, Q_i = initial leak rate, P_f = final pressure, P_i = initial pressure, n = exponent

There have been a wide range of values reported to the exponent n (referred to as N1 in some papers). This paper will describe the literature regarding this problem, present the results of some experiments to determine n and discuss some issues with determining n in existing systems with an example using a water distribution model.

Theoretically, leaks should behave as orifices which implies that the value of n should be roughly 0.5. However, values reported in the literature show considerable range as summarized in Table 1.

Table 1. Reported Values of Leak Power

Reference	Values	Conditions
Ogura (1979)	1.39-1.72	Slits
Hikki (1981)	0.5	Drilled holes
May (1994)	0.5 fixed area 1.5 size = f(P) 2.5 long	Fixed area Size = f(Pressure) Longitudinal
Lambert (2001)	0.52-2.79	Literature
Farley and Throw (2003)	0.70-1.68 0.63-2.12 0.52-2.79	UK (1977) Japan (1979) Brazil (1999)
Thornton and Lambert (2005)	0.5-1.6	Function of ILI
Walski et al. (2006)	0.66-0.76	Drilled holes
Greyvenstein and VanZyl (2007)	0.52 1.38-1.85 0.79-1.04 0.41-0.53 0.67-2.3	Round Hole Longitudinal PVC Longitudinal AC Circumferential Corrosion steel
Noack and Ullanicki (2007)	0.5 – 1.0	f(soil permeability)

The prevailing hypothesis for the leak flow vs. pressure relationship is referred to as the FAVAD (Fixed and Variable Area Discharge) theory. It proposes that for circular leaks, the orifice equation adequately describes flow and an exponent of 0.5 is accurate. However, as the pressure increases, the pressure can actually expand the orifice size such that the apparent exponent is significantly greater than 1.

This has been further modified by correlating n with the ILI (Infrastructure Leakage Index) which is a ratio of current annual real losses divided by unavoidable annual real losses (Farley and Throw, 2003). A value of 1 would indicate a system that has only unavoidable losses while higher values indicate the presence of more losses that can be corrected. For plastic piping an n value of 1.5 is indicated while for metal pipes the values should range from 1.2 for an ILI of 1 to 0.5 for systems with a high ILI.

Walski et al. (2006), Noack and Ullanicki (2007) and Van Zyl and Clayton (2007) studied the effect of the surrounding soil on leak rate. In general, the nature and size of the orifice has a much greater effect on leakage rate that the porous media flow through the soil. Walski et al. (2006) described the conditions necessary for the soil to be limiting flow based on a dimensionless number and in general these conditions are not met for typical leaks. The remainder of this paper describes some experiments to determine n and how those values affect leakage estimates in large systems.

Test Apparatus Design

To effectively model leakage through various pipe materials and holes, an apparatus was constructed in a controlled laboratory environment where flow and pressure could be accurately controlled and measured. The test apparatus included one tank containing clean water, which housed the test sections of pipe. The water supply was directly connected to pressurized water pipe and was controlled via a pressure regulator. A calibrated pressure gauge was located after the regulator and placed at the same height as the water surface inside the tank (see Figure 1).



Figure 1. Picture of Experimental Apparatus

Each test section was secured within the tank using a union connector that easily allowed the removal and replacement of test sections. Schedule 40 PVC test sections ranged in size from 25 to 150 mm (1 – 6 inch) including either a circular, longitudinal (crack running parallel to direction of flow), or circumferential (crack running perpendicular to direction of flow) break.

The test sections with circular holes of varying size were used to verify previous research and confirm that the test apparatus was functioning properly. The circular holes were created using two drill bits which were sized at 2.7 mm and 5.6 mm (7/64 and 7/32 inches).

Longitudinal slits cut into the pipes to simulate a crack ranged from 25 to 50 mm (1 to 2 in) in length. These slits were constructed by using a heat gun and heated razor blade, similar to that of a small electric soldering tool. The desired area where the pipe was to be cut was gently heated with the heat gun as to not burn or seriously deform the pipe material. Upon sufficient heating, the hot razorblade was used to slowly cut the slit in the pipe to the desired length. Additional razor blades similar to that of the one doing the cutting (same thickness) were immediately inserted to the freshly cut slit to ensure that the PVC would not adhere back together while cooling. All razor blades were pulled out from the slit after cooling and examined for any areas or burs that might later obstruct flow. This slit construction method helped to assure some degree of consistency when simulating the same slit among different pipe test sections. Any large variation between two constructed slits, holes or circumferential breaks has the potential to adversely affect the measured discharge.

The half-circumferential breaks were constructed by use of a thin bladed band saw. The band saw was used to make cuts exactly half-way through the pipe, perpendicular to its length. The burs and other pipe shaving were then thoroughly removed from the area.

To compare different pipe materials, a 31 mm (1.25 inch) diameter copper pipe test section was tested. The 1 inch slit in the cooper pipe was created using a small cutting wheel (1.59mm (1/16) inch thick) attached to a pneumatic grinder. The two ends of the slit in the copper piping were cleaned using a small file of similar thickness.

The flow emitted though the break created in each test section will discharge though a hole in the side wall of the tank. The volume of water collected for a specific time interval was collected and measured to determine the system's flow rate. This method was used to measure all flows and was compared to the reading from the digital flow meter installed on the apparatus for quality assurance. Prior to any experimental tests, the flow meter was calibrated to ensure accurate readings and positioned between the pressure regulator and the bleeder valve. The bleeder valve is use to remove any of the air bubbles in the system that occur when changing system pressure. This calibrated pressure gauge served to monitor experimental pressures within the system.

Experimental Techniques and Methods

Values of both pressure and flow were measured for each of the experimental breaks constructed in the numerous test sections. The range of pressure readings selected was from 68.9 kPa (10 psi) to 483 kPa (70 psi) in increments of roughly 68.9 kPa (10 psi). There are three types of test sections used for the experiment, one for each type of break. Due to the cost of pipe materials, the tests sections were used to run multiple tests, starting with the smallest hole or slit.

The first set of tests consisted of the test sections with the circular hole. In the test section a circular 2.7 mm hole (7/64 inch) was first drilled into each of the test sections. The experiment first began starting at the lowest pressure. Once the flows through the orifice have been measured, the pressure increased incrementally to the maximum pressure; the

flow measurements were again calculated for each pressure. A minimum of six measurements were obtained over 15 second intervals for each pressure. When all of the readings were taken for the smallest hole, a bigger hole was then drilled overtop the existing hole and subjected to the exact testing procedure.

The experiments for the longitudinal slits and circumferential breaks were conducted using the same procedure. The longitudinal slits began with a slit 25 mm (1 in) long and were then increased to a 50 mm (2 in) slit. The half-circumferential breaks only needed to be cut once.

Data Analysis

The data collected demonstrated the water loss through the breaks at variable pressures. The measured flow rates and pressures were used to determine values of the coefficients a and n in equation (2).

The plots of pressure vs. flow are shown in Figures 2 for each type of leak. All of the results were fit to a power function of the form

$$Q = aP^n \qquad (2)$$

Where Q = flow, L/s, P = pressure, m, a and n are coefficients.

The index of determination for virtually all the graphs was on the order of 0.99. The values plotted as straight lines on log – log graphs.

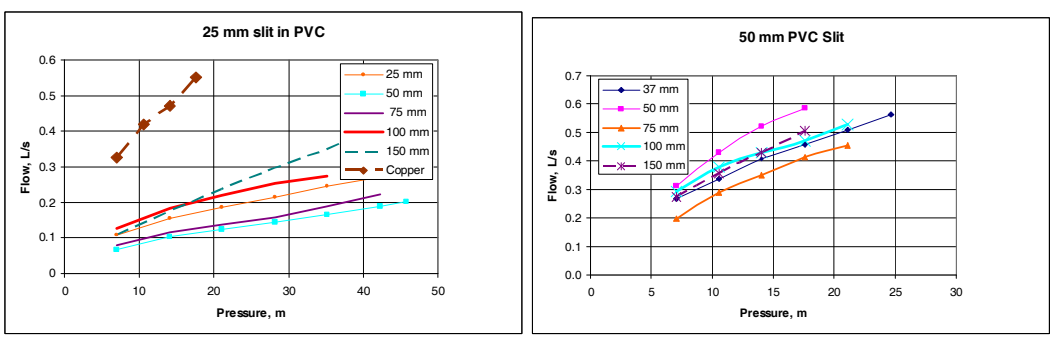

Figure 2a. Leak flow vs. Pressure for 25 mm slit in PVC Pipe (and one copper pipe)
Figure 2b. Leak flow vs. Pressure for 50 mm slit in PVC Pipe
(Values in the legend refer to the nominal pipe diameter)

Table 2 shows that the mean value of n is 0.58 and the median value is 0.54. It is difficult to reconcile these values with the values in excess of 1 as found in the literature. The following section provides an explanation for apparent n values larger than those found in this study.

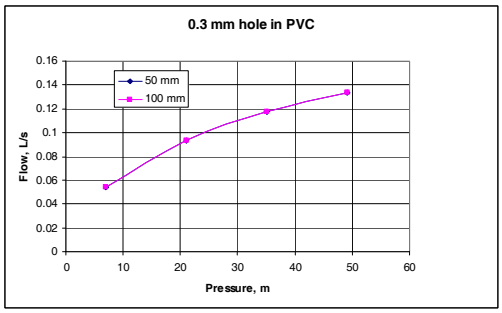

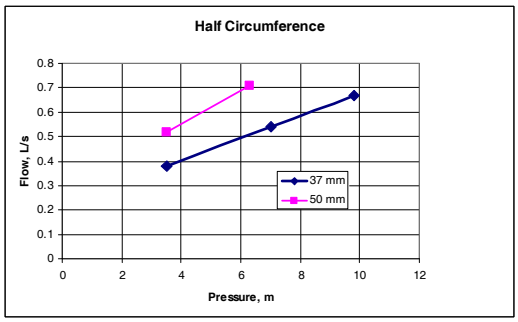

Figure 2c. Leak flow vs. Pressure for Circular Holes
Figure 2d. Leak flow vs. Pressure for Circumferential Slit of Half Circumference
(Values in the legend refer to the nominal pipe diameter)

Table 2. Results of Experimental Runs

Type	a	n	Length, mm	Pipe Diameter, mm
Slit	0.040	0.51	25	25
Slit	0.022	0.58	25	50
Slit	0.028	0.54	25	75
Slit	0.051	0.48	25	100
Slit	0.025	0.74	25	150
Slit	0.085	0.59	25	25
Slit	0.082	0.69	50	50
Slit	0.046	0.76	50	75
Slit	0.107	0.52	50	100
Slit	0.073	0.67	50	150
Copper Slit	0.11	0.55	25	25
Hole	0.022	0.47	0.3	50
Hole	0.022	0.47	0.3	100
Half Circ	0.19	0.54	58	37
Half Circ	0.27	0.53	78	50

All pipe is PVC except for Copper Slit
Half Circ = half of a circumferential break

System Wide Exponent for Leak Reduction due to Pressure Control

The water produced at a source can be delivered to customers to meet fixed demands, pressure dependent demands or leaks.

$$Q_s = Q_f + Q_p + Q_L \qquad (3)$$

Where Q is flow and the subscripts on flow refer to supply (s), fixed (f), pressure dependent (p) and leakage (L), where leakage refers to leakage on the utility's side of the customer meters.

Both pressure dependent demand and leaks can be represented by an orifice equation of the general form:

$$Q = KP^n \qquad (4)$$

Where K is an orifice coefficient, P is pressure and n is an exponent which should be roughly 0.5. Substituting gives

$$Q_s = Q_f + K_p P^n + K_L P^n \qquad (5)$$

Where K_p and K_L are the orifice coefficients for pressure dependent demands and leaks.

The question becomes one of how to determine the exponent n to analyze the effect of pressure changes. Some investigators assume that pressure dependent demand is essentially zero such that given the water production before and after pressure reduction, the leakage after reduction can be determined as

$$Q_L(f) = Q_s(f) - Q_f(f) \qquad (6a)$$

or

$$Q_L(f) = Q_L(i) - [Q_s(i) - Q_s(f)] \qquad (6b)$$

Equation (6b) can overestimate the loss because it also includes reduction in pressure dependent demand. Ignoring the pressure dependent demand term and solving for n yields

$$n(apparent) = \frac{\log(Q_L(i)/Q_L(f))}{\log(P(i)/P(f))} \qquad (7)$$

Where i refers to initial (before pressure reduction) and f refers to final (after pressure reduction.

However, this equation tends to overestimate n (and the impact of pressure reduction) because it does not account for the fact that some of the reduction in source production is really due to reduction in metered water use (pressure dependent demand), not reduction in leakage.

This can best be illustrated by a numerical example. Given

Q_f = 20 ML/day (5.3 MGD)
P(i) = 400 kPa (59 psi)

$K_p = 0.4$
$K_L = 0.2$
$n = 0.5$

The initial flow into the area is given by

$$Q_s(i) = 20 + 0.4\ (400)^{0.5} + 0.2(400)^{0.5} = 20 + 8 + 4 = 32 \text{ ML/day (8.5 MGD)} \quad (8)$$

Next the pressure is reduced to 350 kPa (51.5 psi)

$$Q_s(f) = 20 + 0.4(350)^{05} + 0.2(350)^{0.5} = 20 + 7.48 + 3.74 = 31.2 \text{ ML/day (8.3 MD)} \quad (9)$$

The value of n should be calculated as

$$n(actual) = \frac{\log(4/3.74)}{\log(400/350)} = 0.5 \quad (10)$$

However, looking at source production numbers it is difficult to distinguish between pressure dependent demand and leakage so that the reduction in leakage (which should be 0.26) includes the reduction in pressure dependent demand (of 0.52). Hence n is calculated as

$$n(apparent) = \frac{\log(4/(4-0.78))}{\log(400/350)} = 1.67 \quad (11)$$

This results in overestimating leakage reduction due to pressure reduction. The value of n(actual) is the appropriate n for estimating the reduction in leakage, while the value of n(apparent) can be used to estimate the reduction in water source production as a result of pressure reduction.

System-wide Analysis of Leak Reduction by Pressure Control

As shown in the previous section, leak rates are dependent on pressure and the exponent for individual leaks is roughly 0.5. However, leaks are not the only pressure dependent demand on a water system and reducing pressure not only reduces leaks but also reduces other pressure dependent demands (PDD). In the following section, a model of a typical demand management area (DMA) is presented and the effects on a system are analyzed.

The area under consideration is a zone with 92 junction nodes and 120 pipes. Most pipes are nominal 150 mm (6 in.) although there are some 100 and 200 mm (4 and 8 in.) pipes. There is one source in the southwest corner through which the flow is metered and the pressure can be controlled. The average day demand is 37.8 L/s (600 gpm).

Leakage in the system is 20% of initial average day demand. The pressure head at the source is 90 m (295 ft) which results in average pressures of roughly 700 kPa (100 psi)

through the system depending on elevation. In this study, the pressure head is reduced in turn to 80, 70 and 60 m (262, 230 and 197 ft) and the leaks are assigned an orifice coefficient of 0.5.

As the pressure is reduced, the water use due to leakage and pressure dependent demand is also reduced. (The calculations were done with the WaterCAD program (Bentley Systems, 2008).) When all demand is considered to be fixed, there is no reduction in supply when the pressure is reduced. When only leakage is considered (and other demand is fixed), the use is reduced according to the orifice equation. When all PDD is considered (equation 6b), the apparent reduction in leakage is much larger.

When only leak flows are inserted into the formula for determining n (equation 10), then the values for n are 0.5 but when reduction in other PDD is included with leakage, higher values of n are found. This is shown in Table 3.

Table 3. Values of n calculated when pressure dependent uses are included and are not include in flow reduction determining n

Pressure reduction, m	Leak Only	Leak + PDD
10	0.5	1.4
20	0.5	1.5
30	0.5	1.7

Implications

The key implication of these calculations is that, if one is determining the expected reduction in leakage as a function of pressure, it is very important to understand what fraction of system demand is pressure dependent. Without knowing this it is not possible to accurately predict the reduction in leakage due to pressure reduction, especially if one is attempting to use a global n value to adjust demands in anticipation of pressure reduction.

Without knowing the fraction of demand that is pressure dependent, it is necessary to determine leak reduction by way of pressure control only by performing long term comparisons of source inflow vs. metered demand, not by using the drop in source production immediately upon reduction.

Conclusion

The results of the experiments reported in this paper indicate that the exponent (n) should not vary much from the orifice exponent of 0.5 for the set of leaks test in this study. Depending on the way in which reduction in leak flows are determined in calculating n, it is possible to calculate a value much higher than 0.5.

References.

Bentley Systems, 2008, WaterCAD, Bentley Systems, Inc., Exton, PA.

Farley, M. and Throw, S. 2003. *Losses in Water Distribution Networks,* IWA Publishing, London, UK.

Greyvenstein, B. and Van Zyl J., 2007, "An Experimental Investigation into the Pressure-Leakage Relationship of some Failed Water Pipes," *Journal of Water Supply Research and Technology – AQUA,* 56 (2), 117..

Hikki, S, 1981, "Relationship Between Leakage and Pressure," *Journal Japanese Waterworks Association*, May, p. 50-54.

Kingdom, W.D.; Limberger, R.and Marin, P., 2006, "The Challenge of Reducing NRW in Developing Countries." *WSS Sector Board Discussion Paper* No.8, World Bank

Lambert, A. 2001, "What Do We Know about Pressure-Leakage Relationships in Distribution Systems?", IWA Conference System Approach to Leakage Control and Water Distribution Systems Management, Brno, Czech Republic.

May, J. 1994. Leakage, Pressure and Control. BICS International Conference on Leakage Control, London.

Noack C. and Ullanicki, B., 2007, "Modeling of Soil Diffusibility on Leakage Characteristics of Buried Pipe," 8th Annual Water Distribution Systems Analysis Symposium Cincinnati, OH.

Ogura (1979) Japan Water Works Association Journal, June.

Thornton, J. 2002. *Water Loss Control Management,* McGraw-Hill, New York.

Thornton, J. and Lambert, A. (2005) "Progress in practical prediction of pressure: leakage, pressure: burst frequency and pressure: consumption relationships," Proceedings of Leakage, London.

Van Zyl, J. and Clayton, C., 2007, "The Effect of Pressure on Leakage in Water Distribution Systems, *Water Management,*160 (WM2), 109.

Walski, T., Bezts, W., Posluszny, E., Weir, M. and Whitman, B., 2006, "Modeling Leakage Reduction through Pressure Control," *J AWWA,* 94:4, p. 147, April.

Seoul(Korea) online water quality monitoring of drinking water

P. S. Shin[1], Y. R. Song[2], Y.J. Choi[3], Y.S. Park[4]

[1- 4] Seoul Metropolitan Waterworks Research Institute, 130-1 Kuui 2 dong Gwangin Gu Seoul , Korea, PH(822) 3146-1845; FAX(822) 3146-1728; email : sps119@seoul.go.kr

ABSTRACT

In the Metropolis of Seoul, Republic of Korea, more than 10.42million citizens are supplied with potable water by the waterworks Seoul metropolitan government. Seoul's waterworks now has a total of 6 treatment plants with a total daily production capacity of 5.10million m^3 (2007). An average daily production of 3.34million m^3 (2006) is guaranteed. This water is transmitted via a supply network consisting of more than 14,106Km of mains covering nearly 1.96 mil. taps. The distribution system includes 109 reservoirs (total storage volume: 2.35 million m^3) that provide emergency storage, balance water demands, and equalize pressure. The Seoul Metropolitan Government has various policies aimed at providing our citizens with safe and tasty tap water. We have a real time monitoring system to thoroughly manage the production and supply processes from the water supply sources to every household. The automatic water quality monitoring system was completed in July, 2006 according to a Seoul Water-Now Plan (Feb. 2001).

The water quality is monitored for 24 hours from the water source supply to the tap to secure safety of water, and the data is positively used to raw water monitoring, optimum water purification treatment and safe water distribution control. The real-time monitoring data is opened to the public through the homepage from 2008 March 21. Web site' address is http://water.seoul.go.kr/waternow/RealDataFullScale.php. 13 items are monitored including turbidity, residual chlorine, water temperature, etc. and 72 places consisting of 6 intakes, 6 water purifying plants and 60 supply places are monitored. It is planned to enlarge to 145 places to be monitored until 2010. As a result of running the system, The online monitoring system were contributed to maintain the safety of water quality from the source water to the tap water

Keywords: on-line**,** water quality monitoring, early warning system, SCADA

BACKGROUND

In the Metropolis of Seoul, Republic of Korea, more than 10.42million citizens are supplied with potable water by the waterworks Seoul metropolitan government.

Seoul's waterworks now has a total of 6 treatment plants with a total daily production capacity of 5.10million m^3 (2007). An average daily production of 3.34million m^3 (2006) is guaranteed. This water is transmitted via a supply network consisting of more than 14,106Km of mains covering nearly 1.96 mil. taps. The distribution system includes 109 reservoirs (total storage volume: 2.35 million m^3) that provide emergency storage, balance water demands, and equalize pressure.

There have been many changes along the 100-year history of Seoul's Waterworks. In the 1960's when the city's population was booming, the citizens had to suffer from lack of drinking water. After the 1990's, there is a growing demand for high-quality tap water among the citizens of Seoul. The Seoul Metropolitan Government has various policies aimed at providing our citizens with safe and tasty tap water. So, We have a real time monitoring system to thoroughly manage the production and supply processes from the water supply sources to every household. According to a Seoul Water-Now Plan (Feb. 2001), The automatic water quality monitoring system was completed in July, 2006.

PURPOSE OF ONLINE MONITORING

Seoul Water - Now system consist of early warning system, inner information system, opening to the public system. Each system has one's own purpose for system management.

The purpose of early warning system is as follow.

- The " source" monitoring purpose are oriented toward early warning systems that detect problems and signal the utility with a water intake on the source so they can take some action, such as shutting down the intake or changing the treatment to account for the unusual condition.
- The" treatment process" monitoring purpose are optimizing the amount of flocculants and disinfectants (free chlorine).
- The" distribution systems" monitoring purpose are supporting the operators and managers of small waterworks for early detection.

The purpose of opening to the public system is the increase of consumer confidence in drinking water quality

DESCRIPTION OF MONITORING EQUIPMENT

The water quality is monitored for 24 hours from the water source supply to the tap to secure safety of water, and the data is positively used to raw water monitoring, optimum water purification treatment and safe water distribution control.

Figure 1 shows the locations of the analyzers and sensors at Seoul Water Now (Korea) Several monitoring devices that measure different basic parameters are in place at the site. The chemical and physical, biological monitors were chosen on the basis of their reliability (see Table 1)

Site	Intake	Treatment Process					Distribution System		
	Pump station	Arrival bassin	Mixing & Flocculation	Sedimentation	Filtration	Clean water well	Pump Station	Reservoir	Household
Monitoring Items	Temp. pH Turbidity Ammonia TOC Cyanide phneols DaphnidTest Algae Flow	Temp. pH Turbidity R.C Alkalinity Flow	pH Turbidity R.C Alkalinity	pH Turbidity R.C Alkalinity	Turbidity	pH, temp., turb., R.C, Cond Flow	pH, temp., turb., R.C, Cond	pH, temp., turb., R.C, Cond	pH, temp., turb., R.C, Cond

Figure 1. Sensors and analyzers installed at Seoul Water Now (Korea)

Table 1. Measurement methods of online monitoring system at Seoul Water Now

Parameter	Measuring Method
Temperature	Thermo-resistive measurement technique
pH	Electrochemical
Conductivity	Probe equipped with two steel electrodes
Turbidity	Surface scattering using to detect the reflected luminance
Ammonia, Cyanide, Phenols	Ion-Selective Electrode
Residual chlorine	DPD method or electrodes
TOC	Chemical oxidation, catalyzed by UV radiation
Alkalinity	Titration- pH end point
VOCs	Purge-and-trap systems/ GC(ECD)
Toxicity	Daphnid Test
Algae	Fluorometry

As shown in Figure 2, 72 places consisting of 6 intakes, 6 water purifying plants and 60 supply places are monitored.

Namely, To block the infusion of hazardous pollutants and maintain the safety of the source water, automatic monitoring is in operation around the clock at 6 intake pumping stations involving 10 monitored items.(Phenols, Cyanide, turbidity, NH3-N, TOC, Temp, pH, Daphnid Test, Algae, etc.) To monitor the treatment process and provide safer and better-quality water, automatic monitoring is in operation around the clock at 6 water treatment plants involving 6 monitored items (Turbidity, Temp, pH, Alkalinity, Conductivity, R.C) To maintain the same water quality from at the time of departure from the purification plants to the time of arrival at the faucets, automatic monitoring is in operation around the clock at 65sites involving 5 monitored items. (pH, temp., turb., R.C, Cond.) It is planned to enlarge to 145 places to be monitored until 2010.

Each selected station employing remote water quality monitoring was equipped with sample taps, sample drains, controller. Except for turbidity measurements. All system require that suspended solids levels be reduced for proper performance. Therefore, a system for inline filtering of particles larger than 100um has been installed.

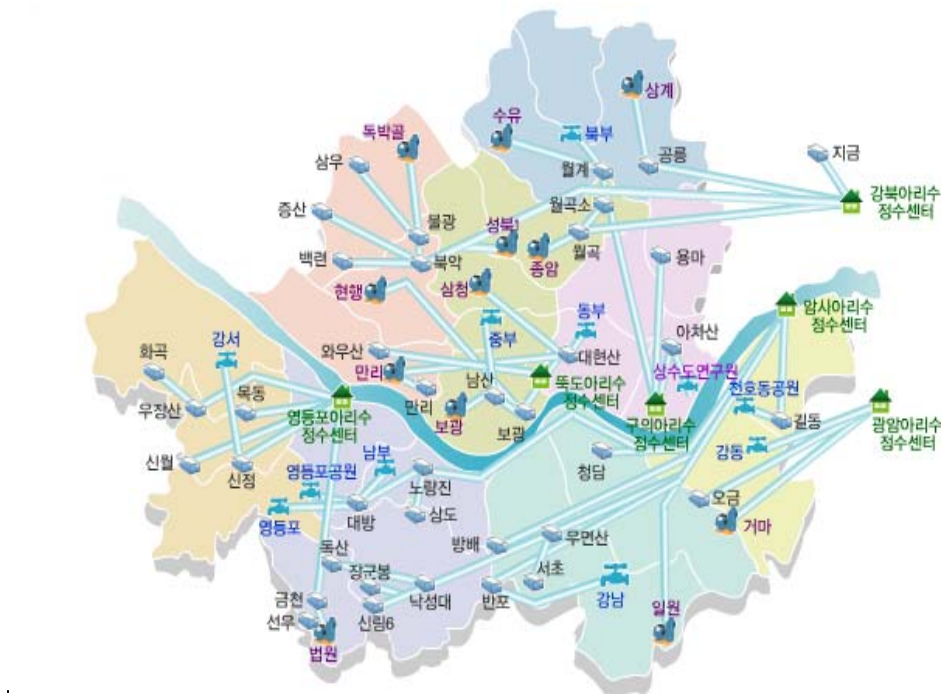

Figure 2. Locations of automatic online monitoring site in Seoul Water Now

DATA ACCESSIBILITY AND USE

As shown in the SWN system architecture scheme(see Figure 3), the acquired data are collected at the site, viewed through a user interface, and stored in a process database. Hourly data and daily average data, monthly average data, yearly average data are stored in a historical database.

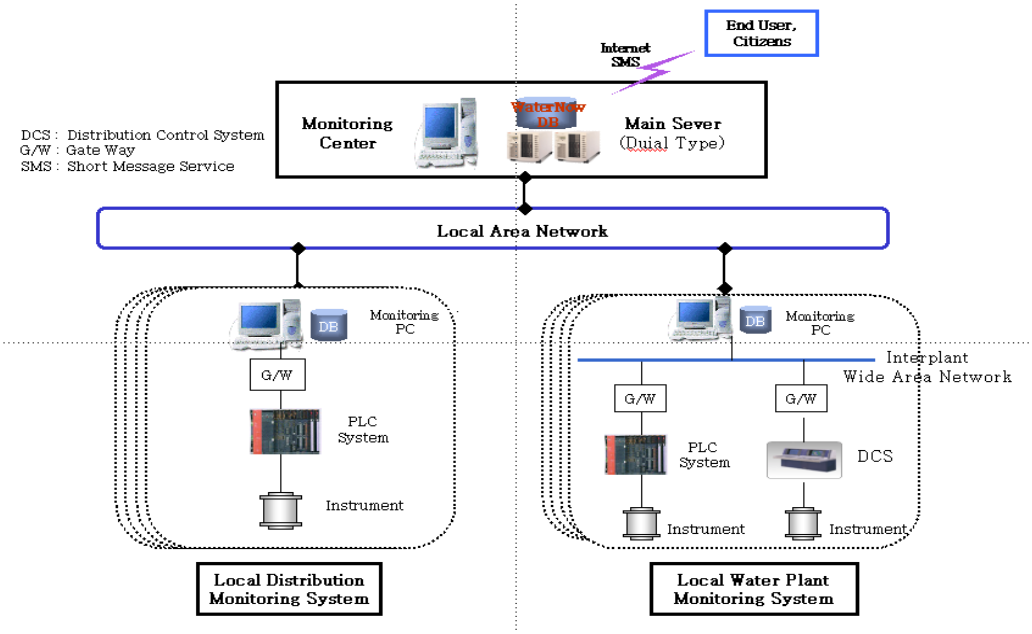

Figure 3. SWN system architecture scheme

The SWN system architecture is characterized by a client-server platform that includes RTUs, modems, LAN, and leased (point-to-point continuous link), and switched telephone lines.

Signals are collected by local RTUs, which are linked to the SWN system through a leased line. The same kind of link is used as a communication line between the facility site(14station) and master monitor station. End users view and data through a software interface developed in the framework of the SWN system. (Figure 4, 5, 6)

Data are used by treatment plant operators for process management , and control. Because the system is considered an integral part in water quality monitoring, the regional authority has electronic access to the data as well.

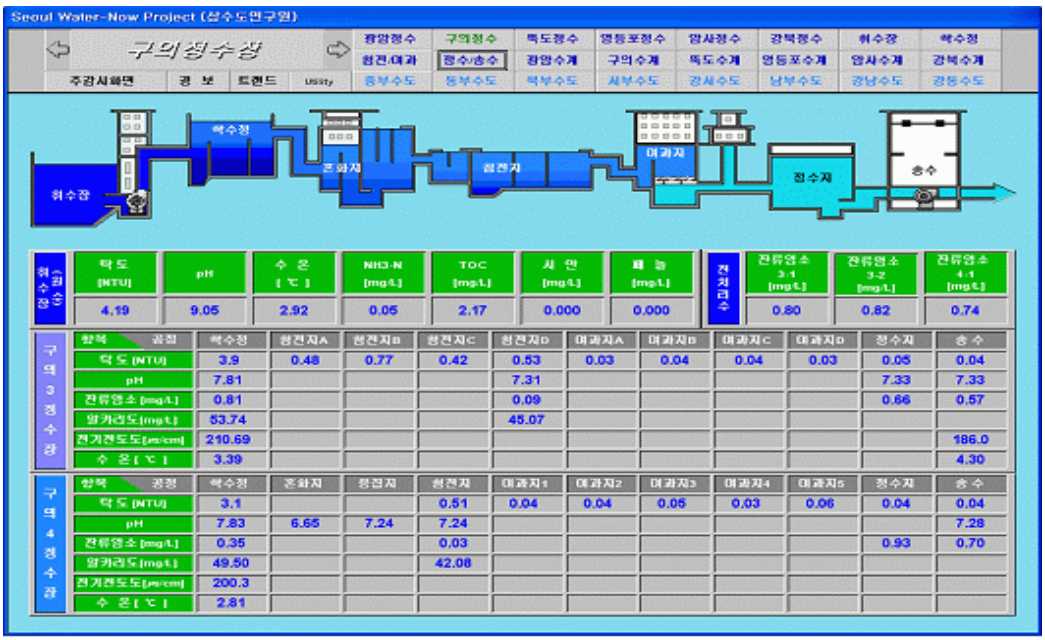

Figure 4. HMI system user interface of showing Source & Treatment process

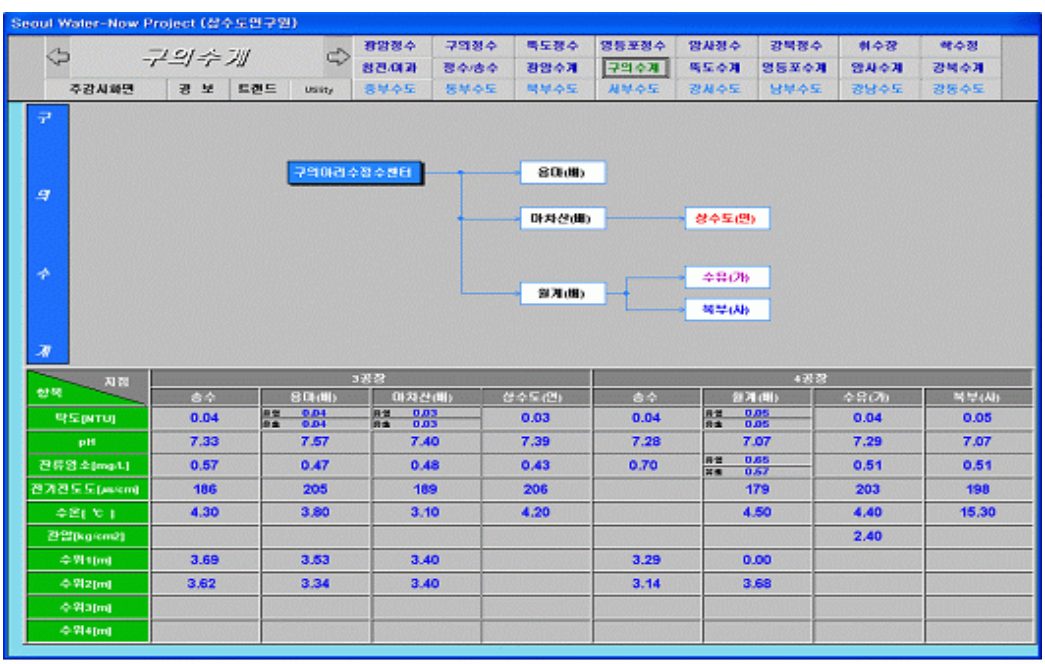

Figure 5. HMI system user interface of showing distribution water quality

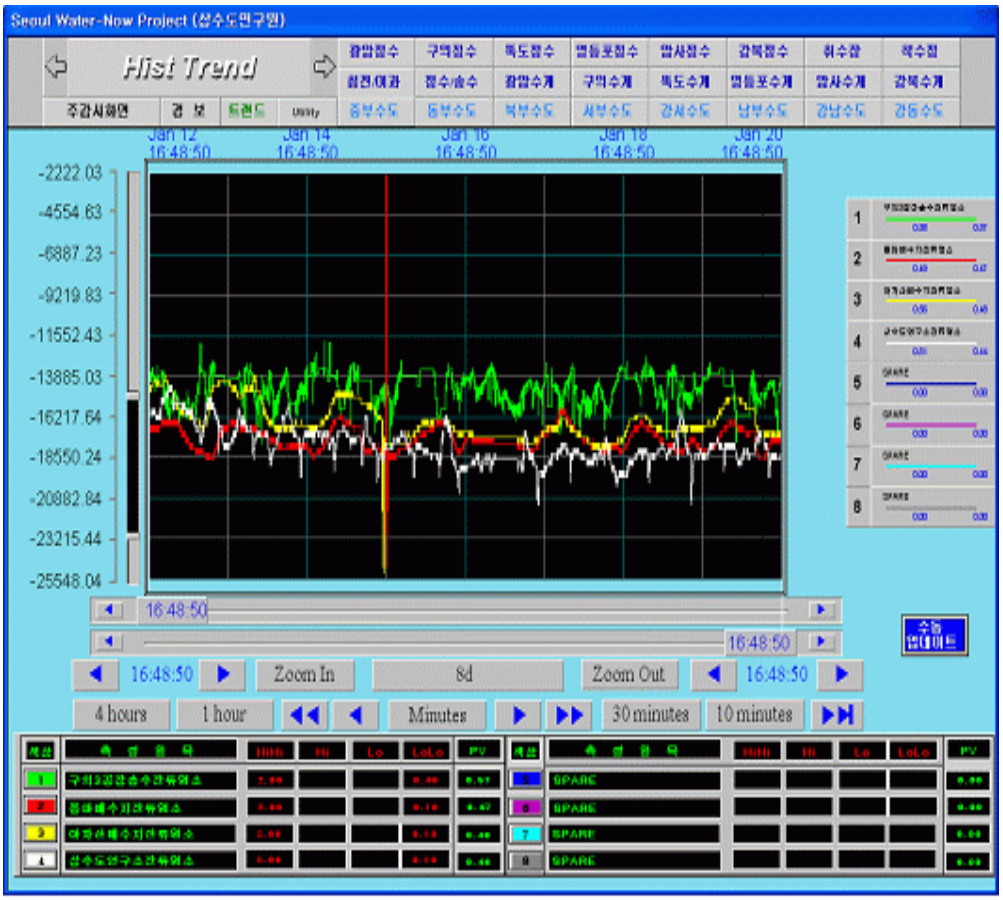

Figure 6. HMI system user interface of showing chlorine trends (distribution, weekly)

The SWN system provides for alarms and diagnosis of the analyzers functionality (e.g., alarms in terms of thresholds, low levels in process tanks, electrodes to be changed, etc.) Once abnormal water quality is monitored, the warning is informed through alarms & SMS to the operators and directors. Quickly, The operators conduct according to the accident treatment guidance

Seoul citizens can also obtain real time data by looking at a Web site, established by the Seoul waterworks Authority.

Web site' address is http://water.seoul.go.kr/waternow/RealDataFullScale.php

As shown in Figure 7, 3 items are opened including turbidity, residual chlorine, pH .

Opens to the public an hour average data and the calculation of an hour mean data is an mean value which excepts the max and min data in 5 minute data

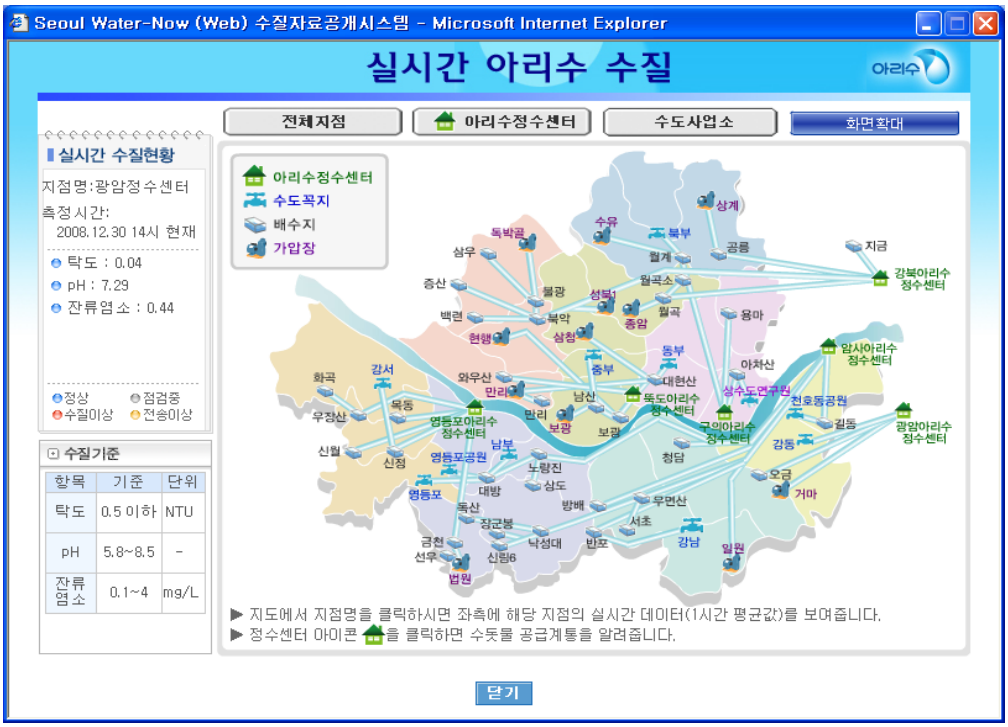

Figure 7. Web site user interface available through Seoul Water work Authority

QUALITY ASSURANCE

The online monitoring system is maintained by operators who have knowledge of the system processes as well as the sensors. Each week, a technician visits Sites to conduct maintenance, calibration, and verification of sensor reading. The on-line monitor results are checked by collecting grab samples and analyzing for free chlorine, pH, specific conductivity,

There have been occasions where faulty instrument readings were suspected and later verified by manual grab samples.

EVALUATION OF SUCCESSES

There have been several instances in which online monitoring result have alerted department staff of potentially harmful water quality situations in the treatment process and distribution system.

In one case, elevated turbidity values resulting from altering flow in the distribution system were tracked via online monitors, giving the operators a chance to address the

issue prior to any customer complaints. In another case, online monitoring allowed operators to respond quickly to a low chlorine residual front moving through the distribution system. Finally, recent online monitoring at locations previously monitored manually revealed that valve operation in part of the distribution system altered flow and created a temporal dead end.

CONCLUSION

The Seoul Water work is confirming to its customers that the drinking water it supplies is healthy, highly controlled, and of the best quality. According to a Seoul Water-Now Plan (Feb. 2001), The automatic water quality monitoring system was completed in July, 2006. SWN system were contributed to maintain the safety of water quality from the source water to the tap water. One of the most successful element of online system is unique display of information on the internet. Public accessibility to continuous water quality information has increased consumer confidence in drinking water quality as well as in water utility operations.

REFERENCES

Erica Hargesheimer (2002) "Online Monitoring for Drinking Water Utilities.", AWWA Research Foundation, Denver, 313-405.

Larry W. Mays (2003) " Section 8: Developing an early warning system for drinking water security and safety." *Water Supply Systems Security*, Mc Grw-Hill N.Y., 8.1-8.9

Seoul International Symposium on Water Policy & Waterworks Technology (2008), *Water Quality Management of Seoul Waterworks,* Han Sun hee, 304-326

U.S. EPA(2005) " Section 5: Monitoring Distribution System Water Quality" *A Reference Guide for Utilities*, EPA/600/R-06/028, 5.1-5.16

Air/Vacuum Valve Breakage Caused by Pressure Surges – Analysis and Solution

Guohua Li, Ph.D. (gli@jonesedmunds.com)
Christopher C. Baggett, P.E. (cbaggett@jonesedmunds.com)
Roberto A. Rosario, E.I. (rrosario@jonesedmunds.com)

Jones Edmunds & Associates, Inc., 730 NE Waldo Road, Gainesville, Florida 32641; PH (352) 377-5821; FAX (352) 377-3166

ABSTRACT

An improperly designed air/vacuum valve could generate excessive pressure surges in the valve caused by the instant valve closure and the rapid expulsion of air. This study characterized dynamics of the air valve and other air valves. Simulation results in a case study showed that large pressure spikes could be generated in the air valve. An air accumulator could reduce the surge pressures. Theoretical analysis demonstrated the feasibility of an air-throttling orifice and the mechanism of an anti-slam device in reducing pressure spike values. The study also illustrated that the excessive pressure surges generated in the valve tend to be damped out in the pipe main and the valve connections tend to experience higher pressure surges for potential breakages.

INTRODUCTION

An air/vacuum valve is usually installed in a water/wastewater pipeline system for vacuum prevention and surge suppression during hydraulic transients. Hydraulic transients could be introduced into the system through active changes such as pump shutdown/startup and reactive changes such as air valve opening/closing in response to the pump operations. Low-pressure waves caused by pump shutdown could result in air being drown in the air/vacuum valve and in the system. High-pressure waves due to operating pumps or pump startup tend to expel the air out of the valve. The rapid air release and the instant valve closure could lead to high pressure spikes at the valve. In some pipeline systems where hydraulic transients occur frequently, the repeated high pressure spikes might cause the air valve to break because of cyclic fatigue failure.

Li et al. (2009) described air valve breakages in a portion of Pinellas County's wastewater force main system due to significant and repeated pressure spikes. Field-recorded pressures at two air valves were even above 3.45 MPa. A transient model for the system has been developed to investigate the excessive pressure surges. Solutions have been proposed to dampen pressure surges and to prevent air valve breakages.

Lingireddy et al. (2004) described the pressure surges due to the rapid release of air through an air valve and stated that using smaller outflow orifices could decrease the pressure surges in the valve by two example applications.

AIR/VACUUM VALVE STRUCTURE

A typical air/vacuum valve is shown in Figure 1. The air/vacuum valve includes an inlet, an outlet, a chamber, a float, a valve disk, and a valve seat. The disk and the float are usually integrated as a single moving component. The valve seat often forms an orifice. The orifice might have dual-orifice sizes, a larger inflow orifice and a smaller outflow orifice. When the pressure inside the valve is lower than the atmospheric pressure, the float drops away from the orifice, and the valve will open and allow air to enter the valve and/or the pipe main. When the pressure inside the valve is larger than the atmospheric pressure, the air in the valve and in the pipeline system is exhausted from the valve and the system. Liquid will enter the valve and lift the float to close the valve.

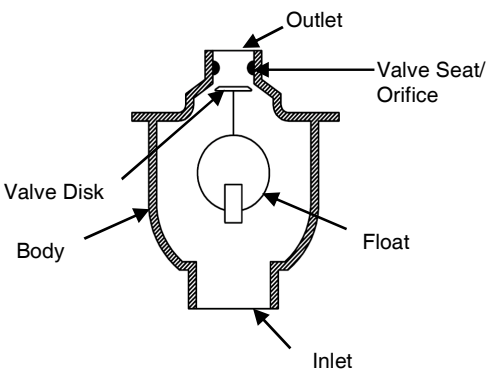

Figure 1. A Typical Air/Vacuum Valve Structure

Air/Vacuum Valve Modeling

The schematic of an installed air/vacuum valve is shown in Figure 2. The air/vacuum valve is connected with a water/wastewater pipe main through a connecting pipe and/or an isolation valve. The installed air valve could be characterized by using the following hydraulic components: the orifice, the air valve chamber, the connecting pipe, as well as the pipe main with a junction.

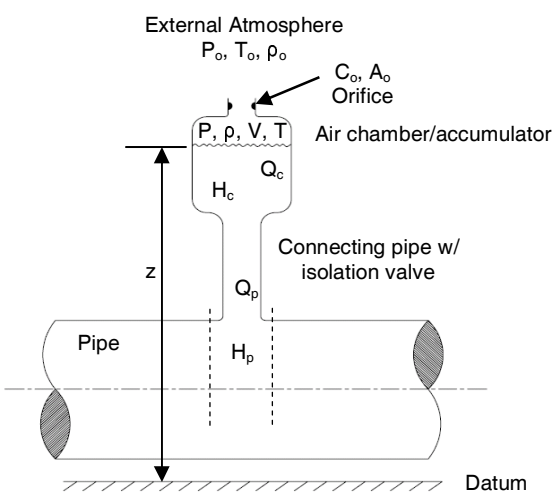

Figure 2. Schematic of an Installed Air/Vacuum Valve for

The orifice. The mass flows of air entering and exiting the valve are determined by the orifice. The mass

flow rates of air exiting the air valve under reversible polytropic flow conditions are given by (Lingireddy et al., 2004, Wylie and Streeter, 1993)

$$m = C_o A_o \sqrt{2p\rho\left(\frac{n}{n-1}\right)\left[\left(\frac{p_o}{p}\right)^{\frac{2}{n}} - \left(\frac{p_o}{p}\right)^{\frac{n-1}{n}}\right]} \qquad \text{for subsonic flow} \qquad (1)$$

$$m = C_o A_o \sqrt{p\rho n\left(\frac{2}{n+1}\right)^{\frac{n+1}{n-1}}} \qquad \text{for critical flow} \qquad (2)$$

$$\rho = \rho(p, T) \qquad (3)$$

In which m is outflow mass flow rate, C_o is coefficient of discharge for the outflow orifice, A_o is flow area for the outflow orifice, p is absolute pressure of air in the air valve, ρ is density of air in the valve, p_0 is atmospheric absolute pressure, T is absolute temperature of air in the air valve, and n is a polytropic index defining the thermodynamic process. A polytropic index of 1.0 implies an isothermal process for an ideal gas; 1.4 implies an isentropic process for small chambers with fast response times. Often an average value of 1.2 is used in design calculations.

The air valve chamber. The air inside the air valve chamber is assumed to follow the reversible polytropic relation

$$pV^n = C_A \qquad (4)$$

In which V is the volume of air in the valve chamber and C_A is a constant.

The pressure in the valve chamber is assumed to be the same throughout the volume at any instant. The compressibility of the liquid in the chamber is considered negligible compared with air compressibility. Inertia and friction are neglected. The integrated continuity equation is

$$\frac{dV}{dt} = -Q_c \qquad (5)$$

In which Q_c is volumetric liquid flow rate in the valve chamber.

Using the absolute liquid head in the valve chamber, the reversible polytropic equation is transformed into

$$\left(H_c' + H_o - z\right)\left[V - \Delta t\left(\frac{Q_c' + Q_c}{2}\right)\right]^n = C_A \qquad (6)$$

In which H_c' is the gauge liquid head in the valve chamber at the current time increment, H_o is barometric pressure head, z is liquid elevation head relative to the datum, V is the volume of air in the valve chamber at the previous time increment,

Δt is the time step, and $Q_c^{'}$ *and* Q_c are the volumetric liquid flow rates in the valve chamber at the current time increment and at the previous time increment.

The connecting pipe. For a short connecting pipe, the short connector may be considered to be inelastic and to contain an incompressible liquid. The equation of motion applied to the short connector is represented by (Wylie and Streeter, 1993)

$$H_p^{'} - H_c^{'} = C_1 + C_2 Q_p^{'} \tag{7}$$

In which $H_p^{'}$ is the gauge liquid head in the pipe main at the current time increment, $Q_p^{'}$ is the volumetric liquid flow rate in the connector at the current time increment, and C_1 and C_2 are constants that depend on length, diameter, and area of the connector as well as the head and flow rate at the previous time increment.

For a long connecting pipe, the compatibility equations could be used.

The pipe main with junction. The compatibility equations as well as a continuity equation at the junction are used.

Surge Pressures in Air/Vacuum Valve

Assume that at the instant the air is fully expelled, the air valve is instantaneously closed and liquid will be rapidly decelerated to zero from an initial velocity. The initial liquid velocity is approximately equal to the air velocity that is determined by the mass flow of air through an orifice. The rapid liquid deceleration produces a pressure surge which could be represented by the basic equation of water hammer:

$$\Delta H = -\frac{a\Delta V}{g} = -\frac{aV_o}{g} \tag{8}$$

In which ΔH is increment of pressure head change, a is wave speed, V_o is the initial air velocity through the orifice or the liquid flow velocity at the valve seat just before the valve closure, and g is acceleration of gravity.

The mass flow of air through the orifice could be expressed under standard atmospheric pressure and temperature conditions

$$m = \rho_o V_o A_o \tag{9}$$

$$\rho_o = \rho_o(p_o, T_o) \tag{10}$$

In which ρ_o is the density of atmospheric air and T_o is absolute temperature outside the air valve.

The initial air velocity through the orifice or the liquid flow velocity at the valve seat just before the valve closure could be expressed by

$$V_o = \frac{C_o}{\rho_o}\sqrt{2p\rho\left(\frac{n}{n-1}\right)\left[\left(\frac{p_o}{p}\right)^{\frac{2}{n}} - \left(\frac{p_o}{p}\right)^{\frac{n-1}{n}}\right]} \qquad \text{for subsonic flow} \qquad (11)$$

$$V_o = \frac{C_o}{\rho_o}\sqrt{p\rho n\left(\frac{2}{n+1}\right)^{\frac{n+1}{n-1}}} \qquad \text{for critical flow} \qquad (12)$$

From the above equations, the initial air velocity through the orifice just before the valve closure depends on the values of atmospheric absolute p_o and absolute temperature T_o outside the valve, as well as the absolute temperature T and pressure p in the air valve chamber. Since the air mass in the valve chamber is small and large areas of pipe and liquid surface provide heat capacity to the air mass, the air temperature in the valve chamber is close to the liquid temperature. The three parameters, the absolute atmospheric pressure, the absolute atmospheric temperature, and the air temperature in the valve chamber, are considered constant. Thus, the initial air velocity depends on the absolute pressure and the air density in the valve chamber. Under the same absolute pressure and the air density in the valve chamber, the initial air velocities are the same for different orifice sizes.

Surge Pressures in Pipe Main

The pressure surge generated at the valve disk/seat will propagate towards the valve chamber, the connector, and the pipe main. When a pressure pulse propagates from one pipe to another pipe or other pipes, the pressure pulse might be unchanged, increased, or decreased. To determine the fate of the pressure pulse, the characteristic impedance of each connected pipe must be considered. The characteristic impedance is $a/(gA)$, where A is the pipe area. The characteristic impedance of a pipe impacts the incident pressure waves. The higher a pipe's impedance, the more severe the pressure pulse is affected. When a pressure pulse propagates from a lower impedance pipe section to a higher impedance pipe section, the pressure pulse is increased. When the impedances of adjacent pipe sections are equivalent, the pressure pulse is unchanged. When a pressure pulse propagates from a higher impedance pipe section to a lower impedance pipe section, the pressure pulse is decreased.

Mathematically, an incident pressure pulse, H_w, by wave transmission, is related to the pressure pulse, H_n, at the nth step change of pipe section areas, A, by the following relationship (Wylie and Streeter, 1993):

$$\frac{H_n - H_0}{H_w - H_0} = \frac{\Delta H_n}{\Delta H_w} = 2^n \prod_{j=1}^{n} \frac{1}{1 + a_{j+1}A_j / a_j A_{j+1}} \qquad (13)$$

Since the pipe main has low impedance, the pressure surges generated in the valve tend to be dissipated in the pipe main**.** The air valve inlet and outlet tend to have high impedances because of small area and thick wall. The pressure surges generated in the valve might be amplified at the locations. Thus, the inlet and outlet

of the valve might experience higher pressure surges and the air valve tends to break here.

Reducing Surge Pressures in Air Valve

Using a smaller outlet orifice. Lingireddy et al. (2004) attempted to reduce pressure spikes caused by air valve closure by using smaller outlet orifices. As described above, the initial air velocity just before the valve closure has no direct link to the orifice size. The method could not be verified in this paper.

Using an air-throttling orifice. An air-throttling orifice could be installed at the air valve outlet to reduce the pressure spikes generated by the air valve closure. Usually, the air-throttling orifice is much smaller than the valve seat opening. The air flow through the air valve will be dominated by the air-throttling orifice.

Considering the short distance between the orifice and the valve seat, the air density in the valve outlet pipe could be assumed to be the same. The air flow velocity at the valve seat is given by

$$V = \frac{A_o V_o}{A} = \frac{D_o{}^2 V_o}{D^2} \tag{14}$$

In which D_o is the orifice diameter and D is the diameter of valve seat opening. The velocity of air flow at the valve seat is related to the air velocity through the orifice and the ratio of the orifice area over the valve seat opening. If the orifice diameter is a half of the valve seat opening diameter, the velocity of air flow at the valve seat is one quarter of the velocity through the orifice. Using an air-throttling orifice will decrease potential surge spikes generated by the valve closure.

Using an anti-slam valve. An anti-slam device is integrated with an air/vacuum valve to prevent valve slam shut. Figure 3 shows an example of such valves. Air passes unrestricted through the anti-slam device. When liquid rushes into the device, a disc closes and reduces the rate of liquid flow into the valve by throttling orifices.

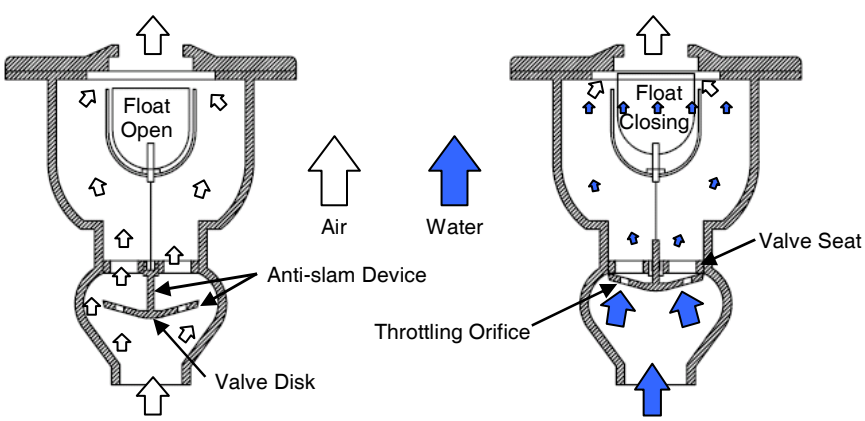

Figure 3. Schematic of an Anti-Slam Valve

Forming an air chamber/accumulator in the valve. At the instant the air valve is closed and air is not fully expelled out, an air pocket could be trapped in the air valve chamber. The air pocket functions as a surge-arresting device. The air pocket volume shall be large enough to absorb liquid momentum and to reduce the deceleration of the liquid in the air chamber/accumulator.

Structurally, an air/vacuum valve could form an air accumulator by having a longer body, a larger float, and a distance between the float and the valve disk/seat. Figure 4 shows the schematic of the air/vacuum valve.

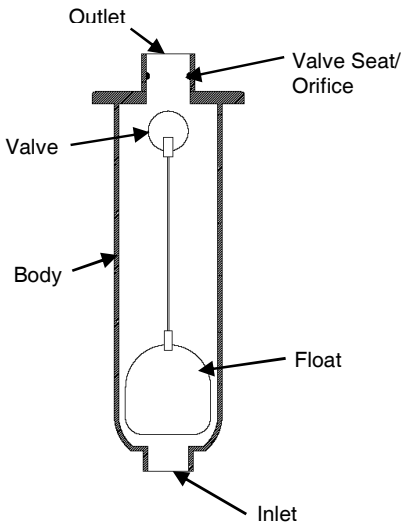

Figure 4. An Air/Vacuum Valve with an Air Accumulator

A Case Study

A portion of Pinellas County's wastewater force main system is shown in Figure 5.

The system includes Pump Station 95 (PS 95), Indian Rocks Beach Pump Station (IRB PS), McKay Booster Pump Station (McKay PS), and two associated force mains: Belleair Beach force main (Belleair Beach FM) between PS 95 and IRB PS and Indian Rocks Beach force main (IRB FM) between IRB PS and McKay PS.

PS 95 and IRB PS are lift stations with submersible pumps. McKay PS is an inline booster pump station with constant suction pressure control. Belleair Beach FM has a length of about 4150 meters with 0.254-meter PVC and 0.305-meter HDPE pipes. The IRB FM has a length of about 1370 meters and 0.406-meter HDPE pipe. Twelve .051-meter air/vacuum valves are installed in Belleair Beach FM and their locations and elevations are shown in the pipeline profile (Figure 6).

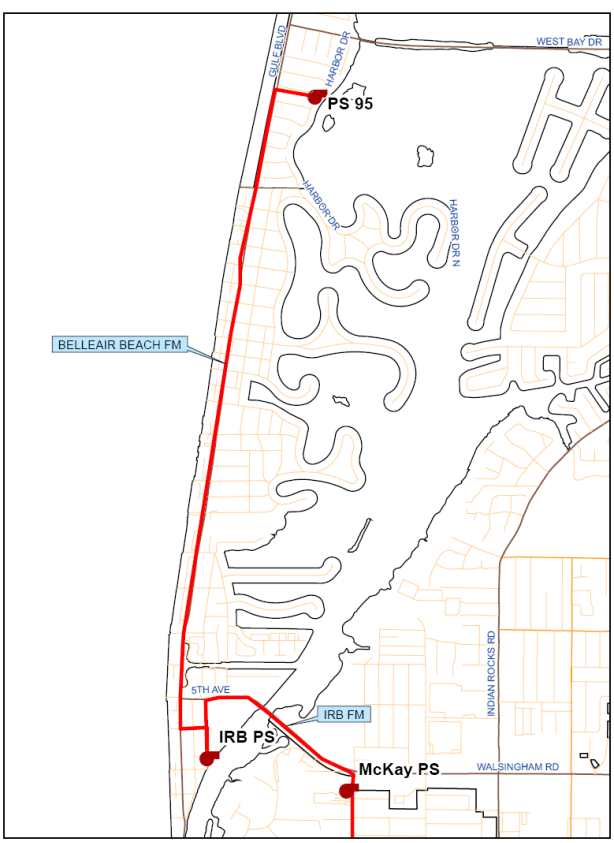

Figure 5. A Portion of Pinellas County's Wastewater Force Main System

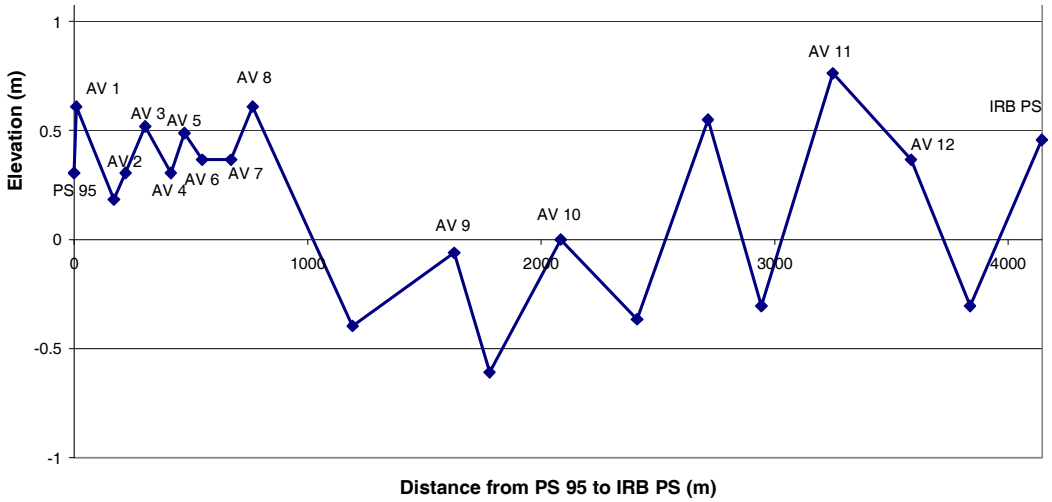

Figure 6. Pipeline Profile of Belleair Beach FM with Air/Vacuum Locations and Elevations

A transient model has been developed for the system using HAMMER V8 XM (Bentley Systems, Incorporated). The model has been described and calibrated in the paper (Li et al, 2009).

In the following simulations, IRB PS runs at full speed during the simulation period. PS 95 runs at the following time schedules. From 0~5 seconds, PS 95 runs at full speed; PS 95 shuts down at 5 seconds and its speed spins down to zero in 3 seconds; PS 95 starts up at 300 seconds and its speed ramps up to full speed in 5 seconds. The total simulation time is 400 seconds.

The air/vacuum valves have 0.038-meter diameters in their inlet orifices and outlet orifices. Three volumes (zero liter, 3.8 liter, and 7.6 liter) of the air chamber/accumulator have been simulated to investigate the effects of the air chamber sizes on the pressure surges in the valve. Figure 7 shows the simulated heads at Air Valve 1 under three accumulator volumes.

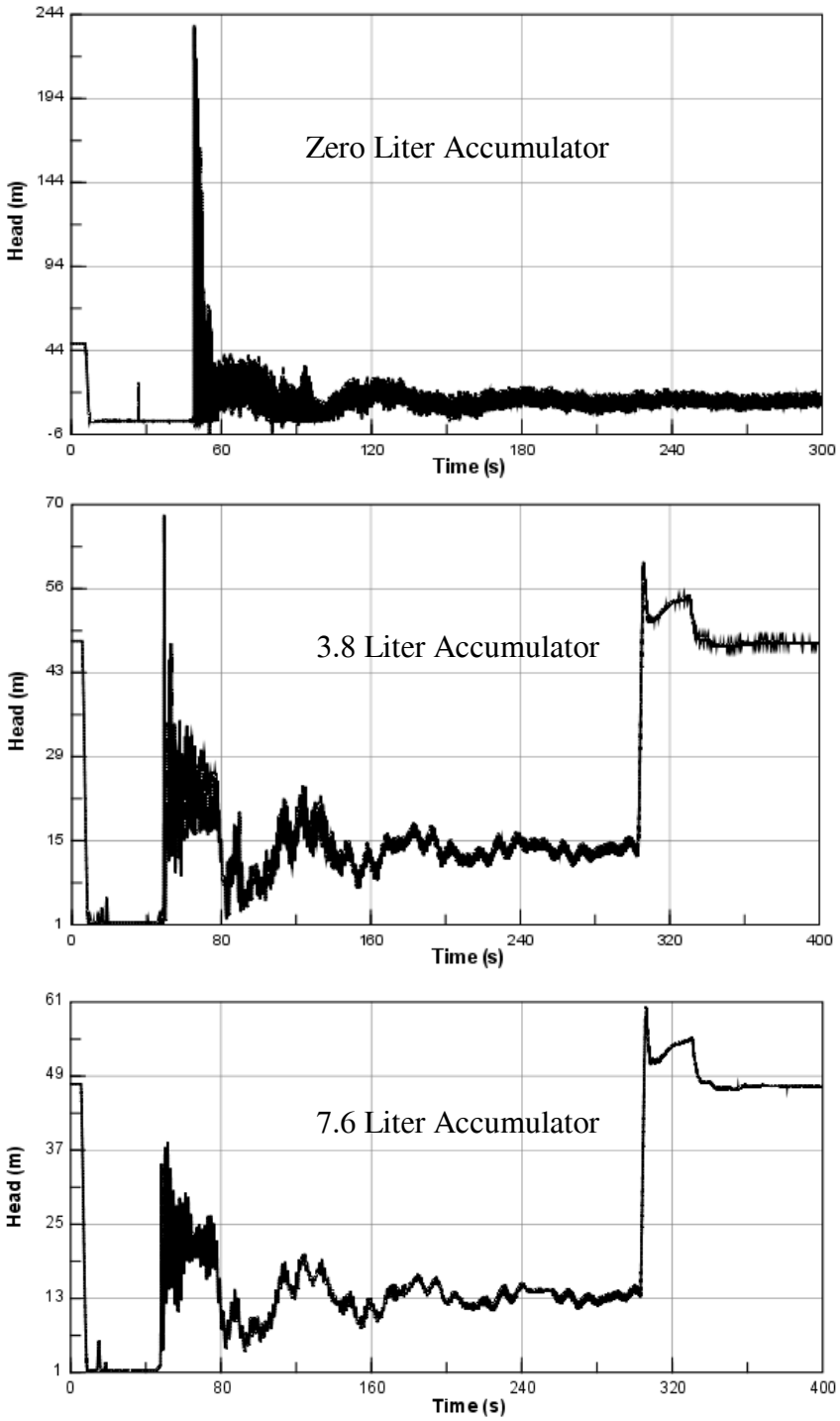

Figure 7. Simulated Heads with Three Accumulator Sizes at Air Valve 1

Simulation results show that the maximum pressures surge pressures are about 240 meters and 65 meters for accumulator sizes of zero and 3.8 liters. The pressure surges have been suppressed completely for accumulator size of 7.6 liter.

CONCLUSIONS

The rapid air release and the instant air/vacuum valve closure could result in detrimental pressure surges in the valve. The repeated high pressure spikes could cause the air valve breakage in its inlet and/or outlet connection. Fortunately, the pressure surges generated in the valve tend to be dissipated in the pipe main.

The pressure surges could be reduced by using an air/vacuum valve that forms an air chamber/accumulator. An air pocket formed in the valve just before the valve closure has significant impact to decrease the pressure spikes and even to suppress the pressure surges completely based on our case study in a portion of Pinellas County's wastewater force main system.

Installing an air-throttling orifice in the outlet of the valve could reduce the pressure surges in the valve. Using an anti-slam valve could prevent the valve slam and dampen the pressure surges.

REFERENCES

Lingireddy, S., Wood, D. J., and Zloczower, N. (2004). "Pressure Surge in Pipeline Systems Resulting from Air Release." *Journal AWWA*, Vol. 113, pp. 643-647.

Li, G., Baggett, C. C., and Horvath, J. H., (2009). "Solutions for Air Valve Breakage Caused by Hydraulic Transients in Pinellas County's Wastewater Force Main System." To be presented at 2009 WEF Collection Systems Specialty Conference, April 19-22, Louisville, Kentucky.

Wylie, E.B. and Streeter, V.L., (1993). *Fluid Transient in Systems*, Prentice, Englewood Cliffs, New Jersey.

The Impact of Biofilm Devlopment on Pipe Roughness and Velocity Profile

Martin Francis Lambert[1], Ryan Wilson John Edwards[2], Sean James Howie[2], Benjamin Bernard De Gilio[2] and Shane Pearse Quinn[2]
[1]Professor, School of Civil, Environmental and Mining Engineering, University of Adelaide, SA 5005, Australia, mlambert@civeng.adelaide.edu.au
[2]Honours Research Student, School of Civil, Environmental and Mining Engineering, University of Adelaide, SA 5005

ABSTRACT

The unpredictable impact of biofilms on friction in pipes causes difficulty in accurately designing for pipe roughness in biofouled pipes. The effects of biofilm growth on pipe roughness were experimentally investigated with the variation of growth conditions of velocity, diameter and water source. The results showed that differences in the growth velocity and source water altered the equivalent sand grain roughness of the biofouled pipes. The variation of the friction factor with Reynolds number in these biofouled pipes was not as expected for a rough surface and did not follow the traditional pipe friction equations. In addition, the change to the pipe velocity profile once biofilm had developed was analysed. One of the most important findings was that the Von Karman constant was significantly lower than normal in the biofouled pipes and that it varied with velocity. This enabled a modified version of the Colebrook-White equation to be created to describe the friction factor variation with Reynolds number in biofouled pipes. This research provides a basis for a method to predict the impact of biofilm development on pipe roughness.

INTRODUCTION

Water is the single most important resource for human civilisation and water pipelines are important in industrialised society for the transportation and distribution of water. For efficient pipeline design the energy lost within a pipe, which is mainly due to friction resistance at the pipe wall, must be accurately known. Recent studies have found that given the right conditions biological growth within pipelines can increase friction headloss dramatically Barton (2007), Picologlou et al. (1980) and (Sharp, 1954). This increase is not included in current design practice and as such results in a reduction in pipeline flow capacity, inefficient pump operation and ultimately greater cost. It has also been shown that these increases cannot be explained by the traditional equations such as the Colebrook-White equation (Eq.1).

$$\frac{1}{\sqrt{f}} = -0.86 \ln\left(\frac{\varepsilon}{3.7D} + \frac{2.51}{\mathrm{Re}\sqrt{f}}\right) \quad (1)$$

The most common form of biological growth within pipelines is biofilms. Biofilms are aggregations of microorganisms bound by a polymeric matrix which form on

surfaces in contact with water, shown in Fig. 1. Biofilms occur predominantly in systems which pump water containing a high amount of nutrients, in particular dissolved organic carbon (DOC). Most raw and recycled water is high in DOC and therefore biofilms present a problem for these pipelines, which are becoming more prevalent. Recycled water, in particular, is being used increasingly around the world.

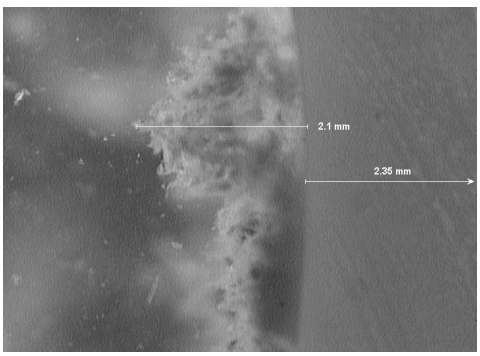

Figure 1. Biofilm inside a pipe

Several studies have found that biofilms have a significant impact on headloss in pipelines. Sharp (1954) found that friction had increased significantly in a 90km raw water rising main reducing its capacity by 22% in the eight years since its construction, increasing pumping costs by 13%. Upon inspection of the pipeline the source of the increased friction was found to be biofilm up to 9.4 mm thick coating the inside of the pipe. More recently, Barton (2007) found that biofouling had increased headloss by up to 25% in a Tasmanian hydroelectricity pipeline and decreased hydroelectric electricity output by 4%. Researchers have also consistently found that the headloss caused by biofilms is greater than their physical thickness would suggest and does not follow the conventional relations of pipe friction such as the Colebrook-White equation (Eq.1) and the Moody diagram. Picologlou et al. (1980) proposed the headloss due to biofilm development was mainly caused by two physical mechanisms; filaments that increase the roughness of biofilms and oscillate in the flow which increases drag, and the biofilm viscoelastic properties which allow them to deform and absorb energy.

A major issue preventing engineers from developing an allowance for friction caused by biofilms is the fact that their physical characteristics, and therefore the headloss they produce in pipes, are highly variable. Biofilm growth models have shown that the structure (and therefore surface roughness), density, growth rate, thickness and viscoelasticity of biofilms all vary depending upon the conditions in which they grow. These conditions include pipe velocity, nutrient availability and specific species of bacteria making up the biofilm (Picioreanu et al 2000).

The objectives of the study were to further understand the effect of biofilms on headloss in pipes. Two separate areas of investigation were pursued; the first was the variable physical characteristics and friction due to biofilms grown in varying velocity, diameter and initial inoculum conditions and second the effect of biofilms

on the velocity profile observed within of pipes. To achieve these aims, experimental work was required to grow biofilms under controlled conditions and measure their effects on the flow.

EXPERIMENTAL METHODS

To achieve the objectives of the study, two identical water recirculation systems were constructed in the Robin Hydraulics laboratory at the University of Adelaide to grow biofilms in both raw Myponga Reservoir water and River Murray water (collected from the Mannum-Adelaide pipeline at Millbrook Reservoir). The system was designed so that the desired growth variables could be compared and contrasted. Two systems were constructed to test biofilm grown in water from two different sources. Each system consisted of three pipes of the same diameter to identify the effect of velocity on the growth of the biofilm and a fourth pipe of a larger diameter was used to determine the influence of diameter on the growth of the biofilm and also enabled velocity profiles to be measured within it.

Experimental System

A diagram of the experimental setup can be seen in Fig. 2. The experiments involved a water recirculation system such that steady water flow could pass through four smooth plastic pipes, three 25 mm in diameter and one 50 mm diameter. Transparent pipes were used for the biofilm pipes so that biofilm growth within them could be observed with opaque plastic sheeting covered these pipes throughout the experiments so that biofilm growth was not affected by light. All other pipes including the delivery and overflow pipes were opaque uPVC material.

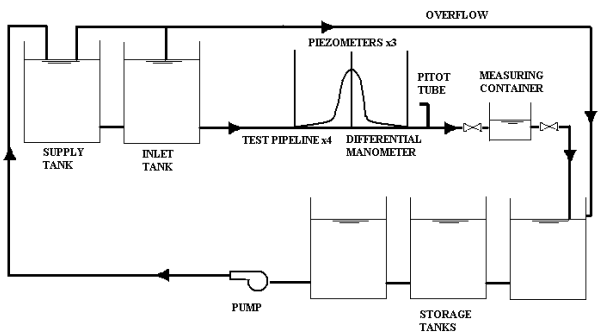

Figure 2. Experimental diagram

All eight pipelines over the two systems used valves to control the velocity. These were placed at the downstream end of the pipeline, after the test section. The overflow pipes for each system maintained a constant head level in the supply tanks to ensure constant velocity. To take headloss measurements differential manometers were attached to each test pipe to measure headloss over a 5 m length of the biofilm pipe. Piezometers were also included as a check to ensure accuracy. 50 litre measuring containers were used for volumetric flow measurements. A Pitot tube was

incorporated into the experimental design to measure the velocity profile within the 50 mm diameter biofilm pipe on the River Murray system.

Once constructed, initial testing was undertaken and confirmed that test pipes were hydraulically smooth. Smooth pipe velocity profiles were also measured. Following this, the biofilm was grown with the addition of the raw waters and excess nutrients in the form of dried River Red Gum leaves, *Eucalyptus camaldulensis*. Measurements were taken over the growth phase of the biofilm and final testing after 600 hours of growth.

At the conclusion of the experiments, microscopic photographs were taken of the biofouled pipe cross sections with the use of a dissecting microscope. This enabled biofilm thickness to be estimated. A viable count test was also conducted at the conclusion of the experiment on the biofilm grown in both the River Murray water and Myponga water. This was to provide a measure of the bacteria type and density in the biofilms grown from both source waters to determine if there was a difference.

The recorded volumetric flow rates and manometer headloss measurements were used to calculate friction factor by the use of the Darcy-Weisbach equation (Eq. 2) to find the friction factor of the biofouled pipe.

$$f = h_f \frac{D}{L}\frac{2g}{V^2} \tag{2}$$

where h_f = head loss (m), f = friction factor (dimensionless), L = length of pipe (m), D = pipe diameter (m), V = mean velocity (m/s) and g = 9.81 m/s^2.

The Swamee-Jain equation is equivalent to the Colebrook-White equation and can be rearranged to determine the equivalent sand grain roughness of a pipe (Eq.3). This represents the diameter of sand grains uniformly covering the inside of the pipe to produce the same friction factor.

$$\varepsilon = 3.7D\left[\exp^{-\left(\frac{1.325}{f}\right)^{0.5}} - \frac{5.74}{\mathrm{Re}^{0.9}}\right] \tag{3}$$

By the use of Eq. 1, 2, 3 and frequent regular measurements of headloss and flow rate, the friction factor and roughness of the pipes were recorded throughout the growth of the biofilm.

Experimental Approach

The two replicate water recirculation systems contained different source water and therefore different initial inoculums for biofilm growth. All other growth conditions were identical between the two systems so that initial inoculum was isolated as the only factor varying between the two systems. Biofilms were grown at three different velocities in each of the 25 mm diameter biofilm pipes in each replicate system. The selected velocities were 0.3 m/s, 0.7 m/s and 1.0 m/s so that the only growth factor varying between the pipes was velocity. The 50 mm diameter pipe was set at 0.3 m/s so a comparison could be made between different diameters with the same velocity. Following completion of the biofilm growth stage, the velocity (and therefore

Reynolds number) was varied through each pipe over the full range possible and the corresponding headloss was measured. This enabled a Moody-type diagram to be plotted relating Reynolds number to friction factor for each pipe. Velocity profile was measured for three different mean pipe velocities. It was measured prior to biofilm development and at the end of the experiment so that a comparison between smooth pipe conditions and biofouled conditions could be made.

EFFECT OF INOCULUM ON BIOFILM GROWTH AND FRICTION

The bacteriological tests of biofilms showed that the biofilms grown in each system were clearly composed of different types of bacteria and had different bacterial densities. The experimental results showed that this produced no clear trend to which initial inoculum produce rougher pipes. There were, however, clear growth patterns for each water source. The biofilm in the Myponga system grew at a relatively faster rate initially before reaching a plateau at 350 hours. The biofilm in the River Murray system on the other hand grew at a relatively constant rate throughout the experiment (Fig. 4). Initial inoculum is the only variable growth factor between the two systems and is therefore the cause of the different bacterial communities and growth patterns.

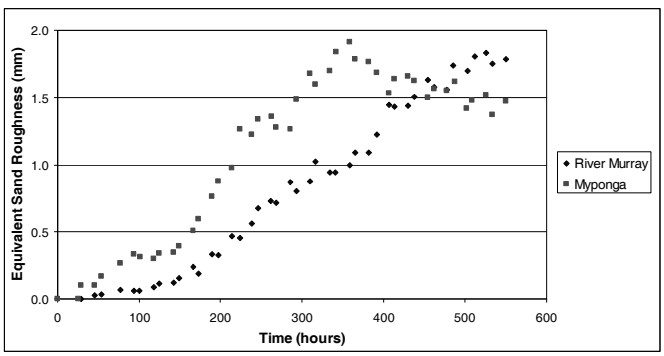

Figure 4. Equivalent roughness with time in the 25 mm diameter pipes at 0.3 m/s for both systems

The photographs of the biofouled pipes showed that there is great variation in biofilm thickness and structure both between different pipes and even in the same pipe. Despite this, the Myponga system biofilms were generally more clustered and the River Murray system more filamentous (Fig. 5). This is supported by observations of the biofilm pipes during the experiments in which the River Murray pipes appeared to have longer filaments vibrating in the flow than the Myponga pipes. These differences are due to the different bacterial communities present in each system.

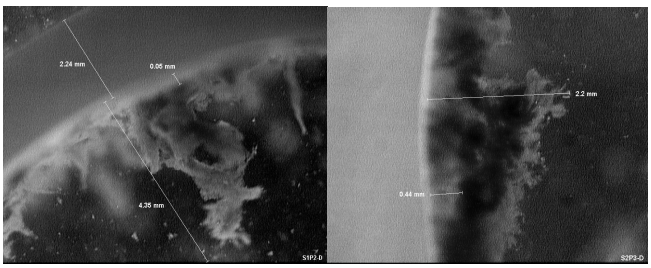

Figure 5. Biofilm in 25 mm diameter 0.3 m/s pipe in River Murray system (left) and Myponga (right)

EFFECT OF PIPE VELOCITY ON BIOFILM GROWTH AND FRICTION

It was discovered in both systems that biofilms grown under higher velocities were less rough than those grown under lower velocities. Fig. 6 shows the results from the 25 mm diameter pipes in the Myponga system.

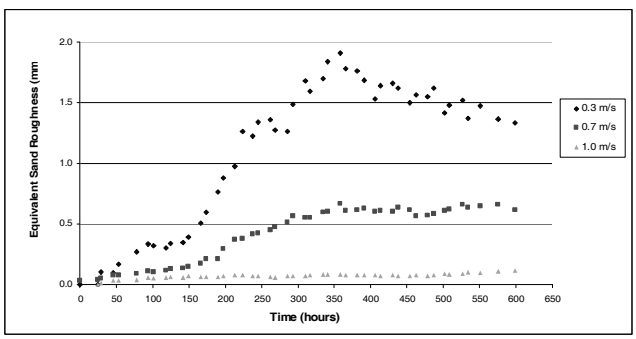

Figure 6. Equivalent roughness for 25 mm diameter pipes with varying velocity in Myponga system

When comparing the equivalent roughness of the 50 mm diameter pipes at 0.3 m/s and the 25 mm diameter pipes at 0.3 m/s in their respective systems, they produced very similar equivalent roughness values. This is shown for the River Murray system in Fig. 7. This implies biofilm growth is relatively independent of pipe diameter and highly dependent on pipe velocity. This may allow scale tests to be used to predict the biofilm roughness that will grow in any particular pipe.

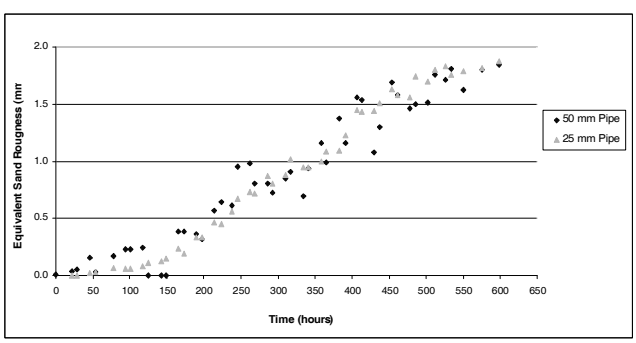

Figure 7. Equivalent roughness in Murray system with growth velocity of 0.3 m/s

VARIATION OF FRICTION FACTOR WITH REYNOLDS NUMBER

The results show that the biofouled pipes yield a different variation in friction factor with Reynolds number to that predicted for clean pipes by the Colebrook-White equation. Fig. 8 shows the observed trends for each different growth velocity in the Myponga system, with the predicted Colebrook-White curves for each pipe. With a lower growth velocity, friction factor was higher, supporting the previous results. The shapes of the observed curves also change with growth velocity, with the rate of increase of friction factor with Reynolds number increasing. It is clear that with more biofilm growth in a pipe, the more its variation with friction factor deviates from the predicted Colebrook-White curves. The curves for the River Murray system were similar shape for each growth velocity, indicating that velocity has a greater impact on friction variation than the initial inoculum.

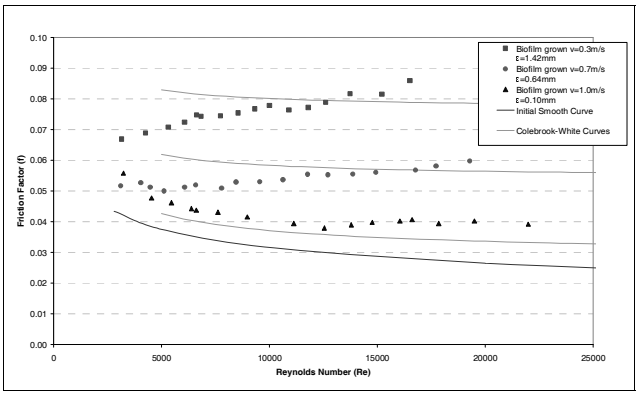

Figure 8. Friction factor variation for the Myponga system 25 mm diameter pipes

Another distinct observation was made in the 0.3 m/s growth velocity biofouled curves for the River Murray system (Fig.9) where a sudden and large drop in friction factor was observed at higher Reynolds numbers.

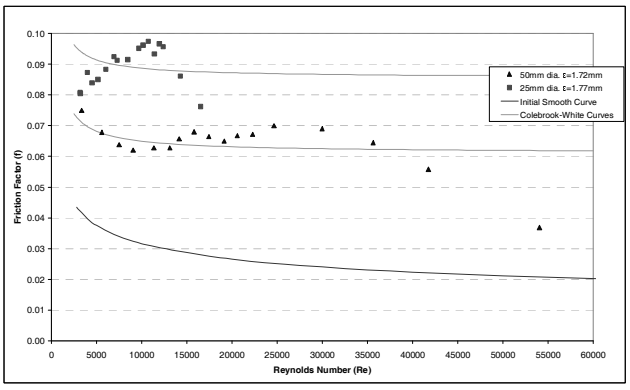

Figure 9. Friction factor variation for River Murray system 0.3 m/s pipes

The observed drop was due to the biofilm being sheared and washed from the pipe wall at these higher velocities. Only the biofilms grown at 0.3 m/s were sheared off at the range of velocities tested, suggesting these biofilms had lower strength than those grown at higher velocities. Although the biofilms sheared off at different velocities in the two 0.3 m/s growth velocity pipes, the pipe wall shear stresses at which this occurred were calculated to be nearly identical, at 3.0 N/m^2. This again shows that the physical and friction characteristics of biofilms are closely related to the growth velocity and independent of pipe diameter. Revisiting Fig. 8, it can be seen that the Myponga biofilms did not shear off at any pipe velocity. The Myponga biofilms were stronger, which can only be due to the different initial inoculum of each biofilm. Therefore, although it appears that the initial inoculum does not play a large role in determining the friction variation profile, it does determine biofilm strength and the shear stress at which it is sheared. This is an important finding for management of biofouled pipes.

EFFECT OF BIOFILM GROWTH ON PIPE VELOCITY PROFILE

Measured velocity profiles were compared with the theoretical velocity profiles for each bulk velocity. Theoretical profiles were determined using theory from Streeter and Wylie (1997). The velocity distribution within hydraulically smooth pipes is described by the following equation:

$$\frac{u}{u_*} = \frac{1}{\kappa} \ln \frac{y u_*}{\nu} + A \qquad (4)$$

where u is the point velocity at a distance y from the pipe wall, ν is the kinematic viscosity of the water, κ is the Von Karman constant where κ = 0.40 as shown in Nikuradse's (1932) experiments and A = 5.5, also shown by Nikuradse. u_* is the friction or shear velocity as described in the following equations:

$$u_* = \sqrt{\frac{\tau_o}{\rho}} \qquad (5) \qquad\qquad \tau_o = \gamma h_f \frac{D}{4\delta L} \qquad (6)$$

where ρ is the density of water at a certain temperature and τ_o is the shear stress at the pipe wall where γ is the specific weight of water, h_f is the headloss, D is pipe diameter and δL is the length of pipe over which the headloss is measured.

The theoretical velocity profiles were calculated using Eq.4 and are shown in Fig.10 with the measured velocity profiles. The velocity profiles are shown as vertical slices through the centre of the pipe. The measured smooth velocity profiles match the theoretical profiles well. There is a small upward skew in the 0.89 m/s and 0.93 m/s profiles but this did not change the average velocity of the profiles.

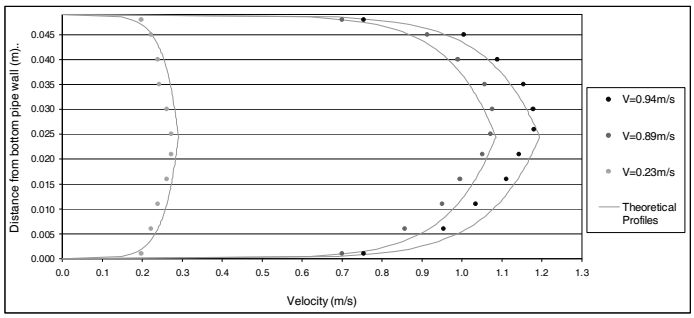

Figure 10. Observed and theoretical velocity profile in smooth pipe conditions

Velocity Profile in Biofouled Pipes

Given that biofouled pipes will not be hydraulically smooth, it was appropriate to model them as a fully rough velocity profile, described by the following equation from Streeter and Wylie (1997):

$$\frac{u}{u_*} = \frac{1}{\kappa} \ln \frac{y}{\varepsilon} + B \tag{7}$$

where all terms are as in Eq. 4, ε is the equivalent sand grain roughness and B = 8.48, shown by Nikuradse (1932) for rough pipes.

At the time of testing, biofilm had been growing in the pipes for almost 600 hours. Equivalent sand roughness calculated by the Colebrook-White equation (Eq.1) was 1.725 mm. This estimate is flawed given that the Colebrook-White equation has been shown to be inadequate for biofilms. It was used, however, given the lack of a more accurate estimate. The theoretical rough profile did not match the observed velocity profiles in the biofouled pipe (Fig.11). Repeated attempts using different values of ε also failed to match the observed profiles. Therefore to fit each profile, a different value of ε was required for each bulk velocity. It is impractical, however, to vary roughness heights with velocity while designing for biofouled pipes.

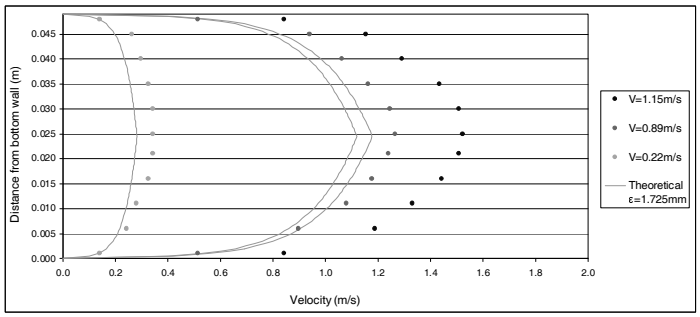

Figure 11. Theoretical rough profiles assuming ε = 1.725 mm

On closer inspection of the theoretical profiles it can be seen that the profile shapes do not match, with the theoretical velocities too low near the centre of the pipe and too high near the pipe walls. A sharper theoretical profile is required. To change the shape of the velocity profile the Von Karman constant, κ, must be altered. To determine the best fit for each of the observed profiles in the biofouled pipe, linear

regression was used to determine the κ and B values. The theoretical rough profile equation (Eq.7) was used in the following manner to achieve this:

$$\text{let} \qquad y = \frac{u}{u_*} \text{ and } x = \ln \frac{y}{\varepsilon}$$

$$\text{is in the form} \qquad y = mx + c$$

$$\text{where} \qquad m = \frac{1}{\kappa} \text{ and } c = B$$

Linear regression was used to determine the best fit slope (m) and y-intercept (c) for each profile. The values of κ and B found from each profile are shown in Table 1.

Table 1. Values of κ and B for observed velocity profiles of varying bulk velocity

Bulk Velocity of Profile (m/s)	κ	B
1.15	0.3569	12.25
0.89	0.3106	8.85
0.22	0.2821	9.60

These results show that Von Karman constant is significantly lower in the biofouled pipe than the 0.40 generally accepted for pipes. There is also a trend of decreasing κ with decreasing velocity. This is a significant result and suggests the equations used to calculate and predict headloss in pipes such as the Colebrook-White (Eq.1), which assume κ = 0.40, are not valid for biofouled pipes. Fig.12 shows the theoretical profiles found by linear regression which closely fit the observed velocity profiles.

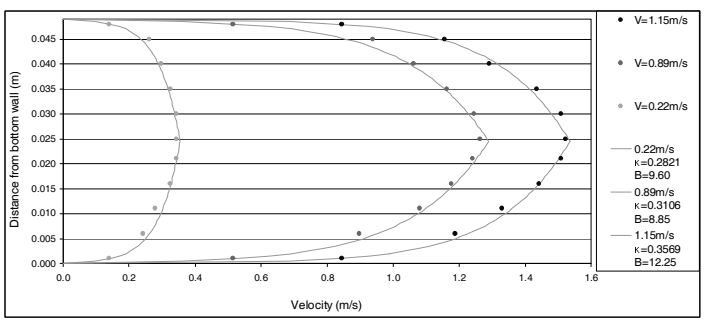

Figure 12. Observed and theoretical velocity profiles using κ, B found by linear regression

Given that the velocity profiles were experimentally derived there could be some error in the calculated values for κ and B. The same process of linear regression was performed on the observed smooth pipe profiles to determine κ. This found that κ was 0.4002 in the smooth pipe. This gives confidence in the values of κ calculated.

Modification of Colebrook-White Equation

The Colebrook-White equation (Eq. 1) was derived from the logarithmic velocity profile equation (Matthew, 1990). It assumes that κ = 0.40 in all pipes and this term was integrated in the –0.86 multiplier on the right hand side of the equation. By expressing the –0.86 multiplier in its true form, κ becomes a variable:

$$\frac{1}{\sqrt{f}} = -\frac{1}{\sqrt{8}\kappa}\ln\left(\frac{\varepsilon}{3.7D} + \frac{2.51}{\mathrm{Re}\sqrt{f}}\right) \tag{8}$$

This expression of the Colebrook-White equation may now be applied using a lower value of κ to test whether it better explains friction in biofouled pipes. A linear best fit equation for the calculated values of κ (Table 1) was used to express κ as a function of Reynolds number. It was found initially that although the equivalent roughness relationship for the biofouled pipes held in Eq.8, the absolute roughness values were predicted to be too high. Eq.8 was therefore modified further to correct this. This was achieved by changing the dimensionless constant multiplier for D in the equation to 0.85. The final modified Colebrook-White equation is consequently:

$$\frac{1}{\sqrt{f}} = -\frac{1}{\sqrt{8}\kappa}\ln\left(\frac{\varepsilon}{0.85D} + \frac{2.51}{\mathrm{Re}\sqrt{f}}\right) \tag{9}$$

The modified Colebrook-White curves are shown in Fig.13 with observed data from the River Murray 50 mm and also the 25 mm diameter pipe at 0.3 m/s. Both pipes were grown at the same velocity and should be expected to produce a similar trend in κ.

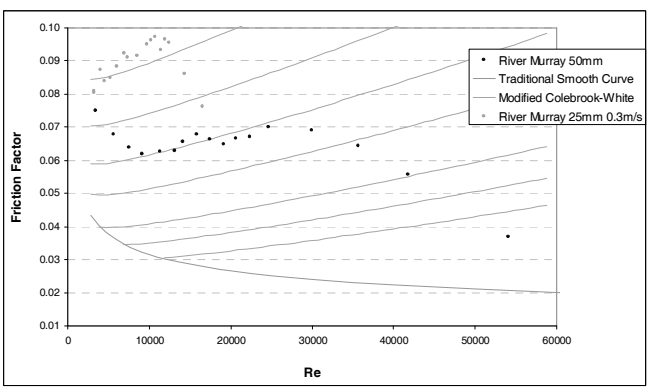

Figure 13. Modified Colebrook-White curves with observed data from River Murray system

The modified Colebrook-White equation goes someway to explaining the observed variation of friction factor with Reynolds number in the 0.3 m/s pipes from the River Murray system reasonably well. There is a departure from the predicted line at low Reynolds numbers for the 50 mm diameter pipe. There is also a departure at higher Reynolds number in both pipes due to the shearing and loss of biofilm. Both the relative roughness and equivalent roughness relationships are approximately that which should be expected, therefore Eq. 9 is a reasonably good description for the friction of the biofilms grown at 0.3 m/s in the River Murray system.

The observed data from the corresponding pipes in the Myponga system were plotted on the same modified Colebrook-White equation lines (Eq. 9) and shown in Fig.14. The Myponga pipes also match the modified Colebrook-White lines reasonably well.

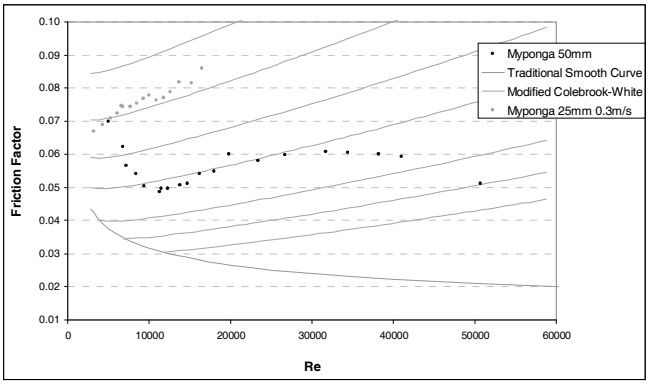

Figure 14. Modified Colebrook-White curves with observed data from Myponga system

On the limited evidence, Eq. 9 may be a start at understanding how biofilms grown under the same velocity behave when the flow conditions are varied. More research will be required to measure velocity profiles in biofouled pipes with various source waters, diameters, and velocities, to determine if a common trend in κ holds between them.

SUMMARY AND CONCLUSIONS

Investigation into the conditions that govern biofilm growth illustrated that biofilms grown from different initial inoculum had different growth patterns and different strengths. Velocity was shown to be the dominant factor in determining the roughness of biofilms and their resistance to fluid shear, however. Significantly, it was shown that Von Karman constant is much lower than the normal 0.40 in biofouled pipes and that it varies with velocity. A modified Colebrook-White equation accounting for this variation in κ was able to explain the variation in friction factor with Reynolds number in a biofouled pipe, which may provide a path to develop an accurate biofilm prediction equation.

REFERENCES

Barton, A. 2007, 'Friction, Rougness and Boundary Layer Characteristics of Freshwater Biofilms in Hydraulic Conduits', PhD Thesis, University of Tasmania.

Matthew, G.D. 1990, 'The Colebrook-White equation – an oft sited result but neglected derivation?', *Proceedings of the Institution of Civil Engineers*, vol. 89, pp 39-45.

Nikuradse, G. 1932, 'Gesetzmassigkeiten der turbulenten Stomung in glatten Rohren', *Ver. Dtsch. Ing. Forschungsh*, vol. 3.

Picioreanu, C., van Loosdrecht, M., Heijnen, J. 2000, 'Effect of Diffusive and Covective Substrate Transport on Biofilm Structure Formation: A Two-Dimensional Modeling Study', *Biotechnology and Bioengineering*, vol. 69, no. 5, pp. 504-15.

Picologlou, B., Zelver, N., Characklis, W. 1980, 'Biofilm Growth and Hydraulic Performance', *Journal of the Hydraulics Division*, vol. 106, no. 5, pp. 733-46.

Sharp B.B., 1954 *Examination of the Friction in the Morgan-Whyalla Pipeline*, SA Water, Australia.

Streeter, V.L., Wylie, E.B., Bedford, K. 1997, *Fluid Mechanics*, 9th edition, McGraw Hill, Boston.

In-line partially closed valves: how to detect by transient tests

S. Meniconi, B. Brunone and M. Ferrante

Dipartimento di Ingegneria Civile ed Ambientale, DICA, Università degli Studi di Perugia, via G. Duranti 93, 06125 Perugia, Italy; e-mail: silvia.meniconi@unipg.it

ABSTRACT

Reliable and quick techniques are needed to locate and estimate the asset of in-line partially closed valves in pressurised pipes. The methodology considered in this paper is based on the analysis of transient tests. As a matter of fact, singularities (e.g., junctions, partial blockages, partially closed in-line valves, leaks) give rise to reflected waves whose arrival time and amplitude – recorded in one or more sections of the pipe – allow their detection. Transients are generated by means of a total and fast closure of an end valve and the pressure time-history – referred to as pressure signal – is measured at a section immediately upstream the end valve. In the paper, first some numerical simulated signals show that this kind of analysis can be useful for locating the valve and determining its asset, also by means of two simplified numerical models. Then some results of an extensive laboratory campaign carried out at the Water Engineering Laboratory (*WEL*) of the University of Perugia, Italy, are reported.

INTRODUCTION

In recent years it was proposed to detect both blockage and partially closed in-line valves by means of transient tests. Such technique is convenient since the duration of tests is short and costs are noticeably lower than those of other methods (e.g., acoustic or steady-state tests), since it requests only the analysis of the time-history of the piezometric head (hereafter, the "pressure signal"). There are different approaches that follow this methodology and can be distinguished on the basis of the duration of the period of analysis. In the short period analysis approach (e.g., *Adewumi at al.*, 2000; *Misiunas et al.*, 2005; *Arbon et al.*, 2008), the analysis is limited to the first characteristic time of the pipe; whereas in the long period analysis approach it is studied the blockage-induced damping (*Wang et al.*, 2005) or the blockage-induced oscillations of the pressure response (*Mohapatra et al.* 2006a; 2006b; *Lee et al.*, 2008; *Sattar et al.*, 2008).

This paper follows the short period analysis approach, analysing the pressure signal during the first characteristic period of the pipe. In the first part, the results of numerical experiments are reported with regard to transients in a pipe with an in-line partially closed ball valve. By means of the numerical model proposed by *Wylie and Streeter* (1993) and *Contractor* (1965), it is pointed out that the asset of the device can be evaluated by means of the first pressure wave reflected back. Then the paper shows some results of an experimental campaign carried out at the Water Engineering Laboratory (WEL) of the University of Perugia, Italy.

NUMERICAL MODEL

In the numerical experiments, transients are generated in a single pipe system (i.e., supply reservoir, pipe, end valve) by the total instantaneous closure of an end valve. A numerical model based on the integration of the governing equations of transient flow by the classical Method of Characteristics (MOC) has been used for this purpose (*Wylie and Streeter*, 1993). The schematised pipe has a length of 164.93 m, an inner diameter, D, equal to 93.3 mm and a wave speed a = 371 ms^{-1}. The upstream reservoir has an invariable level, while the end valve discharges in the air. The presence of an in-line ball valve (Figure 1) has been considered at a distance L_{il} = 75.97 m from the end valve.
According to Figure 1, at the in-line valve, the following equations can be written:

$$\begin{cases} Q_{il} = Q_{1,n+1} = Q_{2,1} \\ h_{2,1} = C_N + B_N Q_{il} \\ h_{1,n+1} = C_P - B_P Q_{il} \\ \zeta = h_{1,n+1} - h_{2,1} = \chi \dfrac{Q_{il}\left|Q_{il}\right|}{2gA^2} \end{cases} \tag{1}$$

where $B_P = B+R_1|Q_{1,n}|$, $C_P = h_{1,n}+BQ_{1,n}$, $B_N = B+R_2|Q_{2,2}|$, $C_N = h_{2,2}-BQ_{2,2}$, B = characteristic impedance = a/gA, $R = f\Delta s/(2gDA^2)$, Q = discharge, h = piezometric head (= pressure signal), g = gravity acceleration, A = pipe area, f = friction factor, Δs = spatial-step size and χ = in-line valve head loss coefficient. In equations (1) the discharges and the piezometric heads are relative to time t, whereas B_P, C_P, B_N and C_N are calculated at t-Δt, with Δt = time-step size; moreover the first subscript refers to the pipe (1 = upstream the in-line valve; 2 = downstream), whereas the second one refers to the node (n + 1 = number of nodes of the pipe 1). The last equation of the system (1) gives the local head loss, ζ, across the in-line valve and it is assumed valid also in the unsteady-state. According to usual flow conditions in real pipe systems, numerical and experimental tests concern wholly turbulent flow. Subsequently the value of χ is constant for any given degree of throttling, δ.
To evaluate directly the pressure wave reflected by the in-line valve, $\Delta h_{R,WS}$, by neglecting friction losses, *Wylie and Streeter* (1993) proposed the following equation:

$$\Delta h_{R,WS} = \left(\frac{\chi g}{2a^2}\Delta h_I - \left(1+\frac{\zeta_0}{Q_0 B}\right) + \sqrt{\left(1+\frac{\zeta_0}{Q_0 B}\right)^2 - 2\frac{\chi g}{2a^2}\Delta h_I} \right) \Bigg/ \frac{\chi g}{2a^2} \tag{2}$$

where Δh_I = incident wave and the subscript "0" is relative to steady-state. When an instantaneous closure of the manoeuvre valve occurs, equation (2) reduces to the expression:

$$\Delta h_{R,WS} = \left(-1 + \sqrt{1 + \zeta_0 \frac{\chi g}{2a^2}} \right) \Big/ \frac{\chi g}{2a^2} \tag{3}$$

If the following condition is fulfilled:

$$\chi < \chi_{\lim} = 2aA/Q_0 \tag{4}$$

equation (3) can be written as (*Contractor*, 1965):

$$\Delta h_{R,C} = \zeta_0 / 2 \tag{5}$$

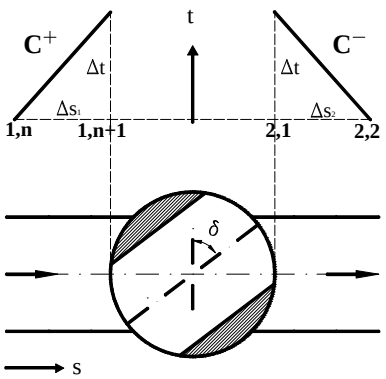

Figure 1. In-line valve numerical scheme.

NUMERICAL EXPERIMENTS

As an example, Figure 2 shows numerical pressure signals, h_M, at the measurement section immediately upstream the end valve, hereafter indicated as section M; h_M is calculated with respect to the value $h_{M,0}$ at the beginning of the transient. For a given steady-state discharge (Q_0 = 2.6 l/s), different values of χ (= 3118.3, 2000.0, 916.6, 399.2, 164.1, 109.4, 0.0) are considered. The total instantaneous closure of the end valve causes a sharp increase of the signal at t_v = 0.00 s. When the in-line valve is partially closed, it is also observed that the pressure rises at $t_{il,1}$ = 0.41 s and $t_{il,2}$ = 0.82 s, as a result of the arrival of the first and second pressure wave reflected by the in-line valve. At t_r = 0.89, the wave reflected by the upstream reservoir reaches the measurement section. It has to be noted that the larger the head loss coefficient – i.e. the smaller the degree of throttling – the larger the increase of the pressure signal, Δh_M, at $t_{il,1}$ (*Brunone et al.*, 2008), with Δh_M = 0 in the case of fully opened valve (χ = 0). Furthermore Δh_M is about the double with respect to the wave reflected back by the in-line valve that reaches the section M, $\Delta h_{R,M}$, because of the particular choice of the measurement section immediately upstream the manoeuvre valve.

In Figure 3 the reflection coefficient, C_R, i.e., the ratio between the in-line valve reflected wave and the incident wave, is plotted for different values of the relative roughness, ε/D (with ε = Colebrook-White roughness), and χ.

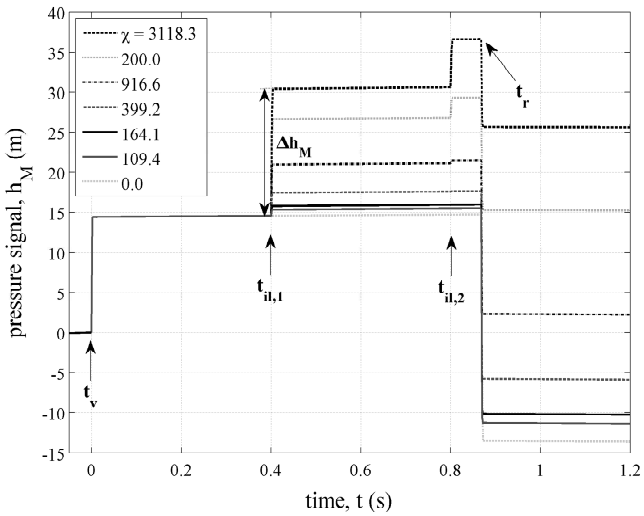

Figure 2. Numerical pressure signals (Q_0 = 2.6 l/s).

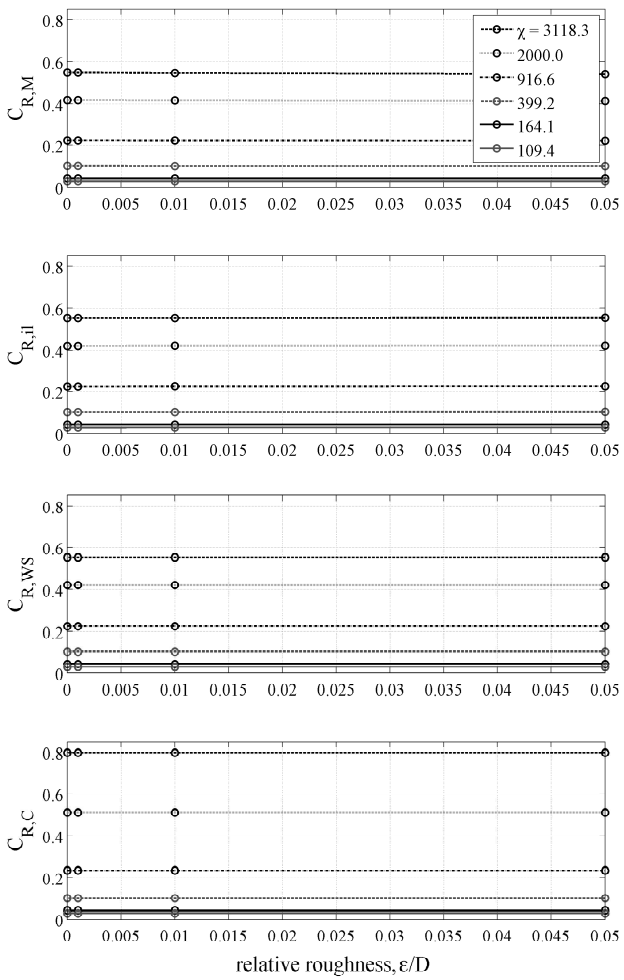

Figure 3. Numerical reflection coefficient by: a) MOC at section M, b) MOC at section 2, c) equation (3); d) equation (5).

In particular, in Figure 3a and 3b $C_{R,M}$ and C_R, are calculated by MOC at section M and at the section immediately downstream the in-line valve, respectively. In Figure 3c and 3d reflection coefficients $C_{R,WS}$ and $C_{R,C}$ are obtained as the ratio between the reflected wave of equations (3) and (5), respectively, and the incident wave. It can be noted that, given χ, all the coefficients are about constant with ε/D: the increase of the friction losses has no effect on the first reflection by the in-line valve. This is also demonstrated by the fact that $C_{R,M}$, $C_{R,il}$ and $C_{R,WS}$ are approximately coincident, given ε/D. There is also a good agreement between $C_{R,WS}$ and $C_{R,C}$: the only two discrepancies, shown in such a figure, can be ascribed to the failure of condition (4).
In Figure 4 the dependence of the limit value of χ, χ_{lim}, on the steady-state discharge and the wave speed is reported. The smaller Q_0, the larger the value of χ_{lim}, given a; furthermore, the smaller the pipe stiffness (i.e. a), the smaller the value of χ_{lim}. In such a figure it is evident the value of χ_{lim} for signals of Figure 2: this value is 1940.61, and subsequently the values of $C_{R,C}$ for χ = 2000.0 and 3118.3 are incorrect (Figure 3d).

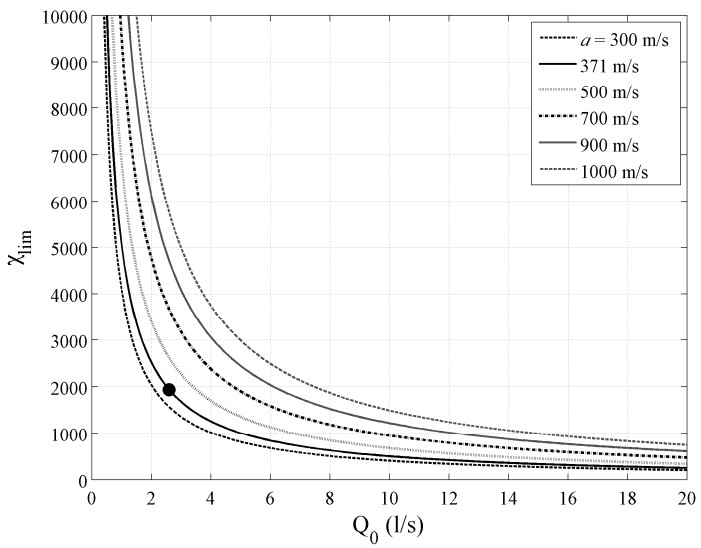

Figure 4. The value of χ_{lim} of equation (4) versus Q_0 for different values of a.

EXPERIMENTAL TESTS

Experimental tests were carried out at WEL in a high-density polyethylene pipe, with the same characteristics of that considered in the numerical simulation. The set-up is shown in Figure 5: the in-line valve is a ball valve with a nominal diameter DN90. All transient tests are generated by the fast and complete closure of the downstream end ball valve DN50.
In order to determine the hydraulic behaviour of the in-line valve, steady-state tests were carried out: the local head loss across the device, ζ_0, was measured by a variable reluctance differential pressure transducer, varying the discharge Q_0 and the degree of throttling, δ. In Table 1 the experimental mean values of χ and δ are reported.

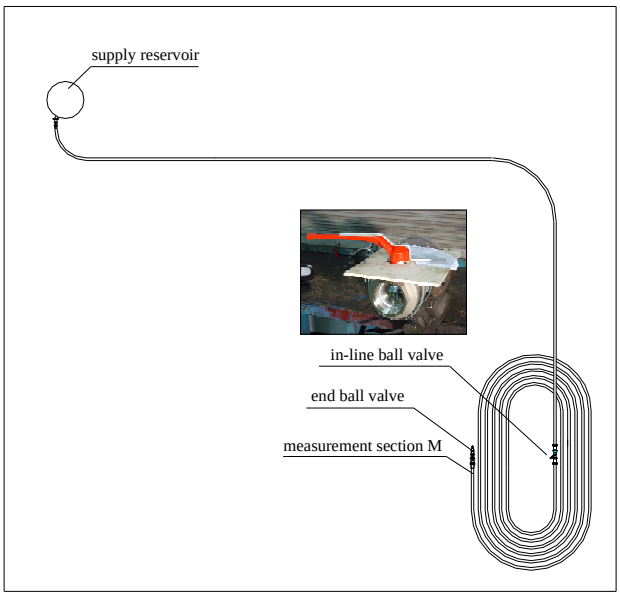

Figure 5. Experimental set up.

δ	90°	60°	50°	40°	35°	30°	25°	20°
χ	0	11.3	35.3	109.4	164.1	399.2	916.6	3118.3

Table 1. Experimental values of δ and χ for wholly turbolent flow.

As an example, Figure 6 shows the pressure signals, h_M, acquired with a frequency equal to 1024 Hz, with the same values of the steady-state discharge and χ of some signals reported in Figure 4; also in this case the occurrence χ = 0, corresponding to fully opened valve, is included as useful reference. The behaviour of experimental pressure signals is on the whole in good agreement with that given by MOC.
For all cases portrayed in Figures 4 and 6, the location of the in-line valve can be evaluated using the relationship:

$$L_{il} = \left(t_{il,1} - t_v\right) L / t_r \tag{6}$$

which connects the distances from the measurement section to the in-line valve, L_{il}, and the reservoir, L, to times t_v, $t_{il,1}$ and t_r. It is worthy noting that, according to equation (6), location of singularities coincides with the evaluation of the times at which pressure waves pass through the measurement section and then it is not necessary to estimating pressure wave speed.
Detection of these times can be properly and precisely done by means of wavelet analysis that is a powerful tool for edge detection that improves the precision of the procedure, with respect to time domain analysis (*Stoianov et al.*, 2001; *Al-Shidhani et al.*, 2003; *Ferrante and Brunone*, 2003b; *Ferrante et al.*, 2007). The wavelet transform of a discontinuous signal, sampled at constant frequency for a limited

number of time increments N ($s(i\Delta t)$, $i = 0 \ldots N\text{-}1$, with Δt = sampling period) can be defined as:

$$Ws(i\Delta t) = \frac{1}{2^j}\sum_{k=0}^{N-1} s(k\Delta t)\psi\left(\frac{(k-i)\Delta t}{2^j}\right) \quad j = 1,2,\mathrm{K}\ J \tag{7}$$

where 2^j is the scale parameter, with $J<\log_2 N$ and $\psi(t)$ is defined by the following expression:

$$\psi(t) = \begin{cases} 0 & 1 \le |t| \\ \psi(-t) & 0 \le t < 1 \\ -24t^2 - 16t & -0.5 \le t < 0 \\ 8(t+1)^2 & -1 < t < -0.5 \end{cases} \tag{8}$$

which is an approximation of the first derivative of the Gaussian function (*Mallat and Zhong*, 1992).

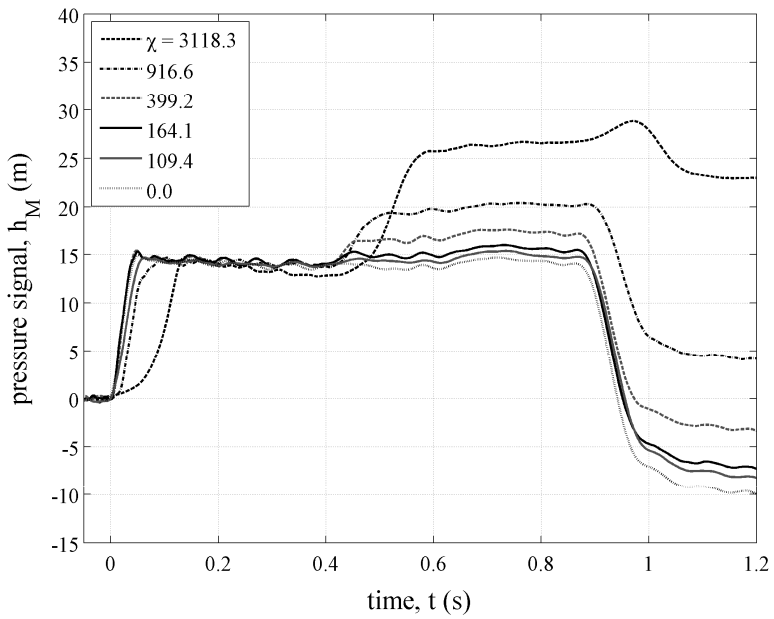

Figure 6. Experimental pressure signals (Q_0 = 2.6 l/s).

In correspondence to singularities, i.e. to the passage of waves through section M, the wavelet transform is marked by maximum local moduli that organize themselves into "chains", indicated by dotted lines in Figure 7, even in case of a modest fluctuation in pressure. An example of performance of wavelet analysis is given in Figure 7, where even if the time domain analysis (Figure 6) of the signal with χ = 109.4 does not reveal any evident singularities at $t_{il,1}$, the wavelet properly points out at $t_{il,1}$ = 0.41 s the presence of a very small step variation due to the passage of the

wave reflected back by the valve. Scrutiny of Figure 7 reveals of course also the singularities occurring at t_v = 0 s, and at t_r = 0.89 s. Then the distance L_{il} from equation (6) is equal to 75.73 m, with a relative error equal to 0.32%.

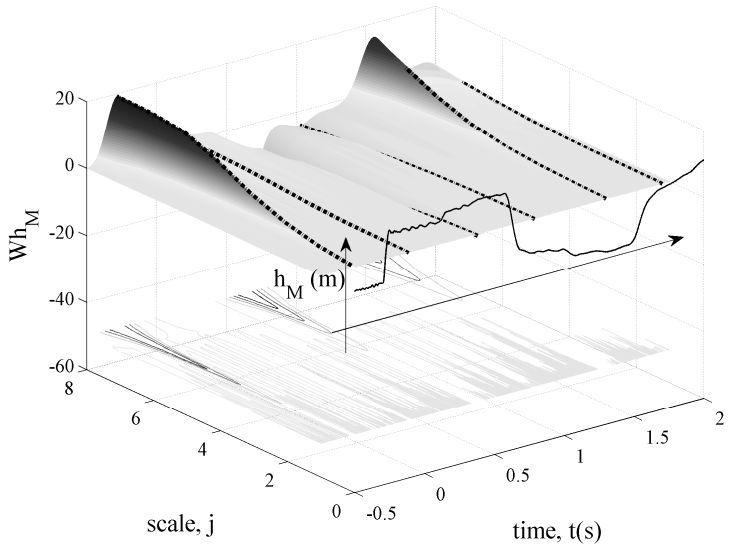

Figure 7. Wavelet transform, Wh_M, of the signal of Figure 6 with χ = 109.4.

Since the numerical simulation shows that friction losses have negligible effects on the first wave reflected by the in-line valve, in experimental tests the degree of throttling is estimated on the basis of the value of the first wave reflected by the in-line valve and registered at section M, Δh_M. Considering that such a value is approximately double with respect of $\Delta h_{R,M}$ and taking into account equation (3), the value of the head loss coefficient, χ_{WS}, may be derived. In Figure 8 the experimental value of the in-line valve head loss coefficient, χ, is compared with χ_{WS}: it can be noted that the error increases when the valve is very closed.

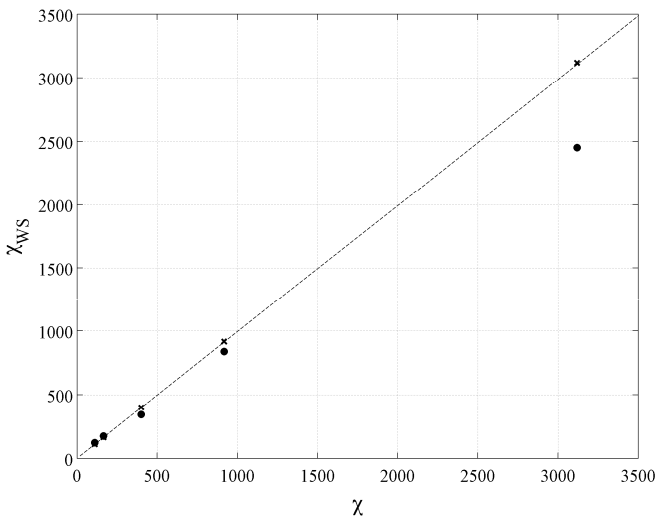

Figure 8. Comparison between of experimental head loss coefficient, χ, and χ_{WS}.

CONCLUSIONS

Numerical experiments carried out by MOC show that an in-line valve can be detected by analysing the pressure signal during the first characteristic time, i.e. within short period analysis approach. Moreover both the location of measurement section and friction losses have negligible effects on the value of the reflection coefficient of the in-line valve.
Laboratory tests carried out at WEL confirm on the whole the behaviour of numerical pressure signals. The good prediction of the in-line valve location by wavelet analysis – even for large degree of throttling – confirms the reliability of such a technique. A more extensive experimental campaign is needed to properly analyse the mechanism of interaction between in-line valves and incident pressure waves.

ACKNOWLEDGMENTS

This research has been jointly supported by the Italian Ministry of Education, University and Research (MIUR) under the Project of Relevant National Interest "Innovative criteria for the sustainable management of water resources in the water distribution systems", and by Fondazione Cassa Risparmio Perugia. The support of M. E. Castori is greatly acknowledged.

REFERENCES

Adewumi, M. A., Eltohami, E. S., and Ahmed, W. H. (2000). "Pressure transients across constrictions." *J. Energy Resour. Technol.*, 122, 34-41.

Al-Shidhani, I., Beck, S. B. M., and Staszewsky, W. J. (2003). "Leak monitoring in pipeline networks using wavelet analysis." *Key Eng. Materials*, 245-246, 51-58.

Arbon, N. S., Stephens, M., Lambert, M. F., Simpson, A. R., and Lucas, B. (2008). "Field validation of transient analysis for in-line valve condition assessment." *10th Int. Conf. on Pressure Surges, entitled "Surge Analysis - System Design, Simulation, Monitoring and Control"*, BHR Group, Edinburgh, 169-179.

Brunone, B., Ferrante, M., and Meniconi, S. (2008). "Discussion of "Detection of Partial Blockage in Single Pipelines" by P. K., Mohapatra, M. H., Chaudhry, A. A., Kassem, and J., Moloo." *J. Hydraul. Eng.*, 134, 872-874

Contractor, D. N. (1965). "The reflection of waterhammer pressure waves from minor losses." *J. Basic Eng.*, 445-451.

Ferrante, M., and Brunone, B., (2003). "Pipe system diagnosis and leak detection by unsteady-state tests. 2. Wavelet analysis." *Adv. Water Resour*, 26, 107-116.

Ferrante, M., Brunone, B., and Meniconi, S., (2007), "Wavelets for the analysis of transient pressure signals for leak detection." *J. Hydraul. Eng.*, 133, 1274-1282.

Lee, P. J., Vítkovský, J. P., Lambert, M. F., Simpson, A. R., and Liggett, J. A. (2008). "Discrete blockage detection in pipelines using the frequency response diagram: numerical study." *J. Hydraul. Eng.*, 134, 658-663.

Mallat, S. G., and Zhong, S. (1992). "Characterization of signals from multiscale

edges." *IEEE Trans. on Pattern Analysis and Machine Intelligence*, 14, 710-732.

Misiunas, D., Simpson, A., Lambert, M., and Olsson G. (2005). "Hydraulic transients for diagnosis of inline valves water transmission pipelines." *Int. Conf. on Computing and Control for the Water Industry*, Exeter, 293-298.

Mohapatra, P. K., Chaudhry, M. H., Kassem, A. A., and Moloo, J. (2006a). "Detection of a partial blockage in single pipelines." *J. Hydraul. Eng.*, 132, 200-206.

Mohapatra, P. K., Chaudhry, M. H., Kassem, A. A., and Moloo, J. (2006b). "Detection of a partial blockages in a branched piping system by the frequency responce method." *J. Fluids Eng.*, 128, 1106-1114.

Sattar, A. M., Chaudhry, M. H., and Kassem, A. A. (2008). "Partial blockage detection in pipelines by frequency response method." *J. Hydraul. Eng.*, 134, 76-89.

Stoianov, I., Karney, B. W., Covas, D., Maksimovic, C., and Graham, N. (2001). "Wavelet processing of transient signals for pipeline leak location and quantification." *Int. Conf. on Computing and Control for the Water Industry*, 65-76.

Wylie, E. B., and Streeter, V. L. (1993). *Fluid transients in systems*, Prentice-Hall Inc., Englewood Cliffs, NJ.j

Simple model of attachment and detachment of pathogens in water distribution system biofilms

Schrottenbaum, I.[1], Uber, J.[1], Ashbolt, N.[2], Murray, R.[2], Janke, R.[2], Szabo, J.[2], Boccelli, D. [1]

[1]Department of Civil and Environmental Engineering, University of Cincinnati,Cincinnati, OH, 45220; email:schrotis@email.uc.edu, jim.uber@uc.edu.
[2] Research Scientist, U.S. Environmental Protection Agency, Cincinnati OH 45268

Abstract

The influence of wall biofilms on the transport of pathogens through a water pipe is mathematically described using an attachment - detachment model. The process coefficients of attachment and detachment are estimated from experimental data. A biofilm annular reactor model is presented and model predictions are compared to experimentally derived bulk phase and biofilm-sorbed pathogen data. The resulting pair of parameters, through minimizing the weighted root mean square error, are used in a single pipe model, and the results are discussed.

INTRODUCTION

Biofilms (BF) are ubiquitous and a common matrix for microbial growth and environmental persistence. While the majority of a biofilm is water, its other major constituents are microorganisms and various extracellular polymeric substances (carbohydrates, proteins, nucleic acids) interspersed with colloidal detritus (e.g. iron oxides) and water channels. Biofilms are beneficial in nature and in engineered systems where conversion of organic and inorganic substrates is desirable (i.e. wastewater treatment). However, in water distribution systems (WDS), microbial activity within the biofilm can deteriorate water quality in terms of aesthetics and public health (LeChevallier et al. (1987); Characklis and Marshall (1990)). Of particular concern for this paper is the potential role biofilm may play in modifying the temporal signature of human exposure to pathogens, and, as a result, potential disease risk. Pathogens introduced into the WDS may attach and accumulate in the biofilm matrix, then subsequently detach in higher densities either randomly or because of the changes in hydraulic conditions.

Early biofilm models were limited to linking substrate flux to the mechanisms of mass transport and substrate utilization (Rittmann and McCarrty (1980); LaMotta (1976)).

These models were further extended to multispecies models for 1-D biofilms by Rittmann (1992) and Wanner and Gujer (1986). Subsequent modeling attempts were expanded in two directions, a discrete versus a continuum approach. Examples of discrete descriptions of a heterogeneous multidimensional biofilm morphology are grid based Cellular Automata (CA) models (e.g. Noguera et al. (2004); Pizarro et al. (2001); Hermanowicz (2001)) and individual particle based models (IbM) (e.g. Kreft et al. (2001); Kreft and Wimpenny (2001); Piciorenau et al. (2004); Xavier et al. (2005)). Continuum models describe transport phenomena assuming that concentration is expressed by a density field that follows conservation laws, (i.e.conservation of mass and momentum), resulting in a system of differential equations. Newer continuum models describing multispecies interactions often are based on the model developed by Wanner and Gujer (1986), representing dissolved components in a diffusion reaction equation. Eberl et al. (2001), for example, describes a system of advection diffusion equations for the liquid phase and diffusion reaction equations for the biofilm, while others have focused on redistribution mechanisms using viscous fluid models (Dockery and Klapper (2001) and Cogan and Keener (2004)). Due to computational demands, models of biofilm processes appropriate for WDS scale would require a continuum approach. Early models by Dukan et al. (1996) and Servais and Prvost (1994) describing biofilm growth processes, were modified by Munavalli and Kumar (2004) and Zhang et al. (2004) to reduce complexity and allow application to hydraulic networks.

Whereas these and other WDS scale biofilm models have focused on biomass processes such as growth and accumulation on pipe surfaces, we are interested in the effect of established biofilm on pathogen transport in water distribution pipes. Experimental studies in biofilm reactors (e.g.Storey (2002)) and pilot scale systems (e.g.Quignon et al. (1997)) indicate that microorganisms transported in bulk flow can be incorporated into biofilm. Different surrogates have been investigated on different surfaces. Szabo (2006) for instance observed accumulation and persistence of *Klebsiella pneumoniae* (KP) on corroding biofilm coupons in annular reactors (AR).

In this paper we will present a modeling approach that includes the influence of the biofilm interactions on the transport of pathogens. Measurements of KP concentrations in the bulk and on the coupons in the dechlorinated AR system from Szabo (2006) will be used for the estimation of attachment and detachment model coefficients. First, pathogen pipe wall interaction (attachment - detachment) will be presented. Then, a comparable AR model will be established to support the estimation of the model parameters (attachment and detachment coefficient). Finally the model and estimated parameters will be applied to a simple WDS network of a single pipe.

MODEL DESCRIPTION

The modeling domain is divided into three compartments: the bulk phase, the concentration boundary layer, and the biofilm itself (see Figure.1). The pathogen concentration in the bulk (P_b), at the biofilm surface (P_s), in the biofilm (P_f) and in the detached

biofilm material (P_d) are predicted within their compartment. Note that the bulk phase concentrations are stated per volume, the biofilm concentration has units per area.

Model Assumptions

The one dimensional model describes the change in pathogen concentration over time. Advectional transport is solved with a Lagrangian scheme within the WDS network application used to interpret the temporal patterns of pathogen exposure. Biofilm is assumed to be a homogenous fixed layer at steady state, covering the inner pipe wall entirely. The nonmotile pathogenic matter attaches to the biofilm via transport to the biofilm and adsorption to the biofilm surface. It is assumed that there are unlimited sorption sites, and particulates, once attached, are assumed to be uniformly distributed within the biofilm. The pathogens colonizing the biofilm do not grow and natural mortality and inactivation are not included. This is also true for the bulk phase. It is assumed that the detached biofilm with incorporated pathogens does not reattach.

Attachment Process Description

Attachment processes are described as a combination of particle transport from the bulk liquid to the wall and the adsorption of those particles to the surface. Convectional transfer is due to superposition of diffusion and advection, and occurs between a fluid in motion and a surface. If the concentration at the surface (C_s) differs from that in the bulk (C_b) (cross sectional mean) a concentration gradient is developed by establishing an equilibrium between adjacent layers of the bulk phase. Figure 1 shows the concentration profile for turbulent flow as a dashed line. Although the transition is gradual, the flux over the concentration boundary layer, perpendicular to the surface, is approximately linear as illustrated in Figure 1 with a blue line. The change of pathogen concentration in the bulk due to transport of matter to the wall in order to achieve equilibrium, yields:

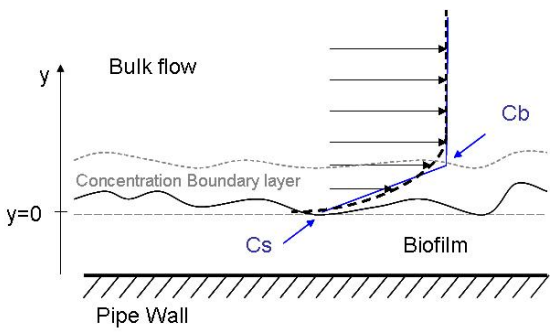

Figure 1: Concentration profile

$$V_b \frac{dP_b}{dt} = -h_m A(P_b - P_s) \tag{1}$$

where V_b is the bulk volume, A is the surface of the pipe and h_m is the mass transfer coefficient.

The boundary layer theory states that the transfer coefficient ($h_m = Sh\frac{D}{d}$) is proportional to the Sherwood number (Sh) and the diffusion coefficient (D) over the pipe diameter (d) derived after normalization of transfer equations. Chilton-Colburn's anal-

ogy, which is most accurate in the turbulent region, relates the Sherwood number to the D'Arcy Weisbach friction factor (f), the Reynolds number (Re) and the Schmidt number ($Sc = \frac{\nu}{D}$), thus providing a tool to estimate $Sh = \frac{f}{8} ReSc^{1/3}$, and the mass transfer coefficient.

Adsorption depends on particle surface properties and biofilm sorption sites. The rate of incorporation of particles that are situated close to the wall in the boundary layer into the biofilm is assumed to be first order. Therefore the change of wall pathogen concentration due to transport to the wall and adsorption to the biofilm is expressed as

$$V_b \frac{dP_s}{dt} = h_m A(P_b - P_s) - A_f k_a P_s \tag{2}$$

where A_f is the biofilm surface area and k_a is the attachment coefficient.

Detachment Process Description

The dominant detachment mechanism under the given hydrodynamic condition is assumed to be erosion, however, biofilm sloughing is the more important event. Continuous loss of biofilm particles will be a function of biofilm density and shear stress on the biofilm surface (τ). The detachment rate expression ($r_d = k_d A_f \tau P_f$) proposed in similar form by Bakke et al. (1990) depends on the concentration of pathogens within the biofilm. Thus, the pathogen concentration change in the biofilm, increasing with attachment of particles and decreasing due to detachment, can be written as:

$$A_f \frac{dP_f}{dt} = k_a A_f P_s - k_d A_f \tau P_f \tag{3}$$

where k_d is the detachment coefficient. The concentration of detached pathogens is tracked separately from the bulk matter in order to ensure no reattachment in the model. The change in detached concentration is expressed through the detachment rate.

$$V_b \frac{dP_d}{dt} = k_d \tau A_f P_f \tag{4}$$

Model Summary

Equations (1), (2), (3) and (4) simplify to the system of differential equations of first order:

$$\begin{aligned}
\frac{dP_b}{dt} &= -\frac{1}{r_h} h_m (P_b - P_s) \\
\frac{dP_s}{dt} &= \frac{1}{r_h} h_m (P_b - P_s) - \frac{A_f}{V_b} k_a P_s \\
\frac{dP_f}{dt} &= k_a P_s - k_d \tau P_f \\
\frac{dP_d}{dt} &= \frac{A_f}{V_b} k_d \tau P_f
\end{aligned}$$

where we introduce the hydraulic radius (r_h) as the cross sectional area of flow per wetted perimeter.

PARAMETER ESTIMATION

Pathogen persistence experiments conducted by Szabo (2006) simulated wall shear stress in a pipe with a diameter $d = 0.102\ m$ and a flow velocity of $v = 0.305\ m/s$, using an annular reactor (AR) with a motor speed of $100\ rpm$, a volume of one liter, and a residence time (θ) of two hours. Three iron foil coupons per slide were inserted in the AR and biofilm and corrosion were established through continuous contact with dechlorinated Cincinnati tap water for three to four weeks before KP was spiked into the system. Five different experiment with different initial KP concentrations and cultivating broth strength were performed in two reactor duplicates. Bulk and coupon concentrations were measured 30 minutes after inoculation and each day thereafter until KP was not detected in either phase.

Annular Reactor Model for Parameter Estimation

To allow estimation of detachment and attachment parameters, the pathogen transport model was adjusted to the geometry of an annular reactor. We assume that the shear stress at the AR wall imitates the shear stress at a pipe wall, and therefore that the velocity gradient over the boundary layer at the AR wall is equal to that at the pipe wall. Then the shear stress (τ) and the mass transfer coefficient (h_m) describing the transport of particles towards the biofilm surface are calculated for pipe flow, and used in the AR model to estimate the attachment and detachment coefficient k_a and k_d, respectively. The bulk concentration (P_b) in the AR case includes detached matter (P_d). Therefore the AR model is given as,

$$\begin{aligned}
\frac{dP_b}{dt} &= -\frac{1}{\theta}P_b - h_m\frac{A_{AR}}{V_{AR}}(P_b - P_s) + \frac{A_{AR}}{V_{AR}}k_d\tau P_f \\
\frac{dP_s}{dt} &= h_m\frac{A_{AR}}{V_{AR}}(P_b - P_s) - \frac{A_{AR}}{V_{AR}}k_a P_s \\
\frac{dP_f}{dt} &= k_a P_s - k_d\tau P_f
\end{aligned}$$

where V_{AR} is the AR volume, A_{AR} is the AR biofilm surface area and θ is the mean residence time. Note this is a linear system as θ, h_m, A_{fAR}, V_{AR}, k_d, k_a and τ are constant.

With the characteristic quantities $P_b^* = P_{b0}$, $P_s^* = P_{b0}$, $P_f^* = rP_{b0}$, $t^* = \theta$, where $1/r = A_{AR}/V_{AR}$, the AR biofilm model is nondimensionalized by substituting $P_b' = P_b/P_b^*$, $P_s' = P_s/P_s^*$, $P_f' = P_f/P_f^*$ and $t' = t/t^*$.

$$\begin{aligned}
\frac{dP'_b}{dt'} &= -P'_b - \alpha(P'_b - P'_s) + \beta P'_f \\
\frac{dP'_s}{dt'} &= \alpha(P'_b - P'_s) - \gamma P'_s \\
\frac{dP'_f}{dt'} &= \gamma P'_s - \beta P'_f
\end{aligned}$$

With the dimensionless parameter groups $\alpha = \frac{\theta h_m}{r}$, $\beta = k_d \tau \theta$, and $\gamma = \frac{k_a \theta}{r}$. α, β and γ can be regarded as the dimensionless mass transfer, detachment and attachment coefficients, respectively. By nondimensionalizing the AR experimental data in the same way we have previously, a consistent basis is created for combining field data to model predictions for estimation of β and γ (note that α is calculated). This nondimensionalization also imposes the natural scaling of the problem with benefits for numerical computation.

Estimation of Attachment and Detachment Coefficients

The AR measurements of bulk and biofilm KP concentrations by Szabo (2006) are used to estimate the attachment and detachment coefficients γ and β for the non-dimensional AR biofilm model. A grid search is implemented over a plausible parameter space (γ, β) and the minimum weighted root mean squared error is

$$J = \sqrt{\frac{1}{N}\left(\delta \times \sum(\widehat{P}_b - P'_b)^2 + (1-\delta) \times \sum(\widehat{P}_f - P'_f)^2\right)} \tag{5}$$

where $\delta = 0.4$ was selected using judgment, N is the number of measurements, P'_b and P'_f are the nondimensional concentrations predicted by the model and $\widehat{P}_b$ and $\widehat{P}_f$ are the nondimensionalized measured bulk and coupon biofilm concentrations of KP measures from the five experiments.

RESULTS AND CONCLUSION

Parameter Estimation

Calculated bulk and biofilm KP concentrations from the nondimensional AR model are compared to the measured data over the parameter space (γ, β). The response surface (J), defined by Eq. 5, is presented in Figure 2, using a 10×10 grid. The minimum of J occurs at the grid point $(\gamma, \beta) = (32080, 1.32)$ where $J = 0.86694$. The parameter pair at this minimum is assumed to best represent the experimental data. The results clearly show, however, that the estimate of γ is highly uncertain due to the experimental conditions and sampling intervals used, which were not designed for model parameter estimation.

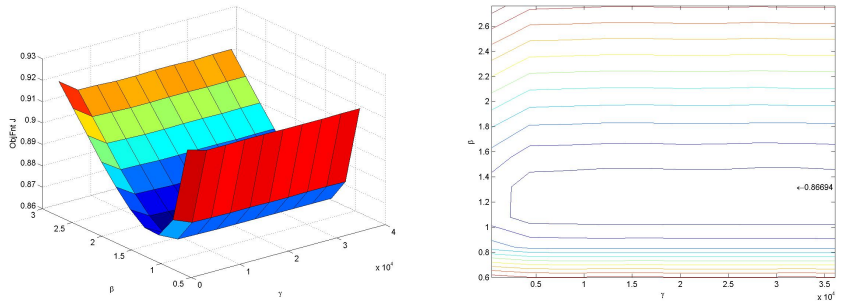

Figure 2: Response surface (left) and contours (right) of the weighted root mean squared error over the parameter space

The complete set of parameters for the AR model application is listed in Table 1. The nondimensional mass transfer coefficient used in the nondimesional AR model is determined to be $\alpha = 7.1715$. The estimated coefficients γ and β in dimensional form give, for the attachment coefficient $k_a = \frac{\gamma r}{\theta} = 0.022057$, and the detachment coefficient $k_d = \frac{\beta}{\tau\theta} = 6.6179 \times 10^{-7}$. The AR model with nondimensional model coefficients computes bulk and biofilm KP concentrations over time as presented in Figure 3 and Figure 4 respectively (black line). The two figures also show the nondimensional ex-

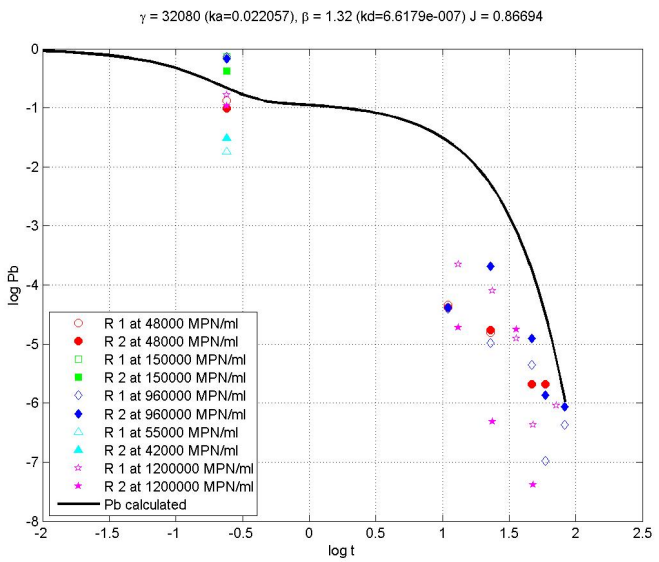

Figure 3: Dimensionless logarithmic KP concentration in the AR bulk phase versus dimensionless log time (where $(log(t) = log(\theta))$. The nondimensional experimental data are shown for duplicated reactors and five different experiments (the legend indicate the initial concentration of each experiment). Concentration over time estimated by the AR model is indicated by the solid black line.

perimental data for five different experiments (each conducted in duplicate (R1 and R2)) with varying initial KP concentration. The model prediction underestimates the experimental biofilm concentrations. This results from mass transfer limitations, as the

larger attachment coefficient γ does not decrease the error . This phenomena could be due to a variety of reasons. The calculated mass transfer coefficient could be too small, due to the friction factor (f) calculation using the Blasius formula for pipe flow. The mass transfer coefficient also depends on the diffusion coefficient (D), and the diffusion coefficient of KP could be too small (it is assumed equal to the value for *Escherichia coli* reported by Berg (1993)). Finally, the assumption of a similarity between the concentration gradient adjacent to the wall in pipe flow, and in an annular reactor could be inaccurate. Experiments, using smaller sampling steps, would be more suitable for attachment investigation and varying rotational AR speed, would help to understand the influence of the shear stress induced detachment.

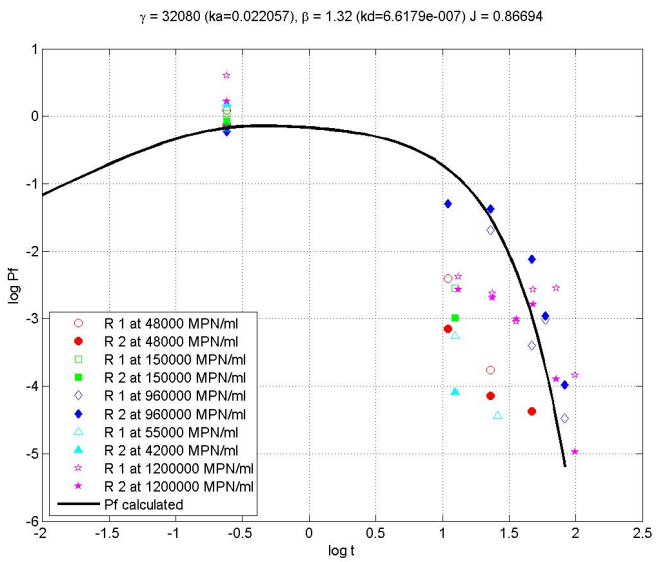

Figure 4: Dimensionless logarithmic KP concentration in the AR biofilm phase versus dimensionless log time (where $log(t) = log(\theta)$). The nondimensional experimental data are shown for duplicated reactors and five different experiments (the legend indicate the initial concentration of each experiment). Concentration over time estimated by the AR model is indicated by the solid black line.

WDS System Application of the Pathogen Transport Model

The set of parameters $(k_a, k_d) = (0.022057, 6.6179 \times 10^{-7})$ estimated by minimizing the weighted root mean squared error over an appropriate parameter space were applied to the attachment-detachment model for a pipe. The predictions are presented for a single pipe advection model application. A single pipe of 21km length with a residence time of 20 hours for given flow (v) and pipe diameter (d) describes the hydraulics for the model. The model was executed with a initial pathogen concentration ($P_{b0} = 4.8 \times 10^{10}\ MPN/m^3$) introduced in the system for the initial 20 hours, and run for a simulation time of 200 hours. The resulting pathogen concentration pattern for

bulk, surface, biofilm and detached material can be observed in Figure 5. The bulk concentration and the concentration of detached material at the end of the pipe are shown in Figure 6. The results predict a fast washout of the system, so the system is nearly cleaned out after twice the residence time. This behavior is likely a result of the discussed shortcoming of the parameter prediction. The model is under-predicting biofilm concentration in the AR, thus the washout rate would also be higher than expected.

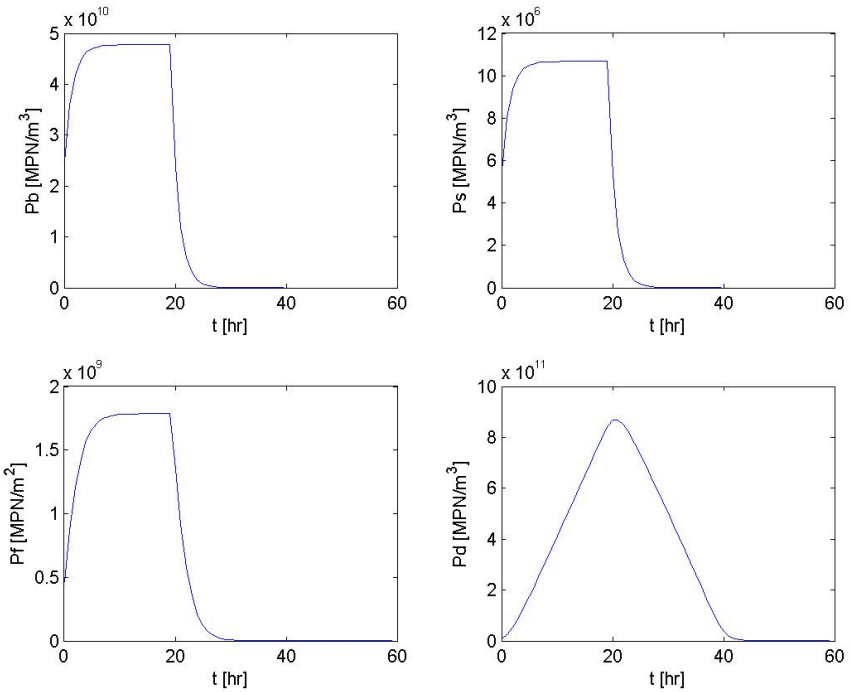

Figure 5: Average concentration for bulk (upper left), the surface (upper right), in the biofilm (lower left) and detached material (lower right) over time.

Conclusion

A simple linear pathogen attachment-detachment model was developed for applications to pipe flow, where advection would be incorporated by a Lagrangian scheme. The unknown coefficients of attachment and detachment are estimated with a least square search over the plausible parameter space using experimental data collected in annular reactors. The results suggest limitations from mass transfer assumptions, which require further investigation. Nevertheless, a first application of the transport model is presented, for a hydraulic pipe model with the set of fitted parameters. This results indicate that future work should be directed towards a more sound prediction of the unknown model parameters. The form of the mass transfer model should also be investigated. In addition to improvements in pathogen measurement frequency, investigation of the

influence of the AR mass transfer and the impact of the shear stress on detachment will improve the pathogen transport model predictions.

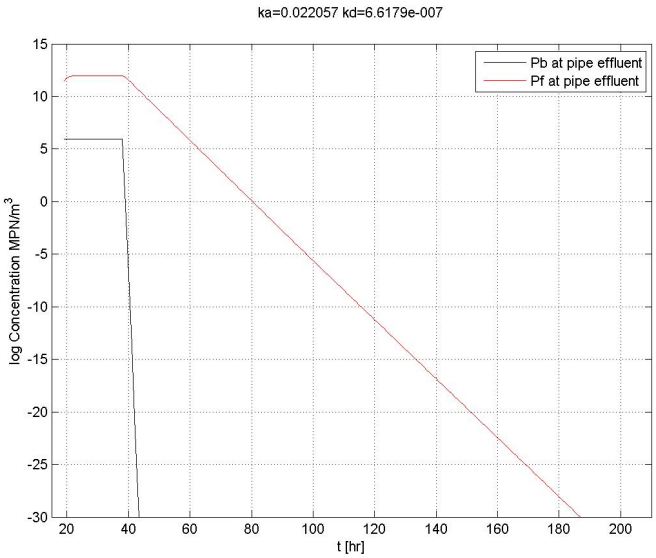

Figure 6: Logarithmic concentration at the effluent of the pipe of bulk material (left) and detached material (right) over time.

Acknowledgements

The U.S. Environmental Protection Agency through the Office of Research and Development funded, managed, and participated in the research described here under a contract with the University of Cincinnati. The views expressed in this paper are those of the authors and do not necessarily reflect the views or policies of the USEPA. Mention of trade names or commercial products does not constitute endorsement or recommendation for use. Work at the University of Cincinnati was sponsored by the USEPA under the Pegasus Contract, Contract Number EP-C-05-056, Work Assignment WA 3-06.

α	7.1715	non-dimensional mass transfer coefficient
β	1.32	non-dimensional detachment coefficient
γ	32080	non-dimensional adsorption coefficient
k_d	6.6179×10^{-7}	$[ms/g]$ detachment coefficient
k_a	0.022057	$[m/s]$ adsorption coefficient
D	4.000000×10^{-10}	$[m^2/s]$ diffusion coefficient
v	0.305	$[m/s]$ mean velocity
d	0.102	$[m]$ diameter
θ	2	$[hr]$ mean residence time of AR
$1/r$	202	$[1/m]$ surface area per volume in the AR
r_h	2.550000×10^{-2}	$[m]$ hydraulic radius for fully filled smooth pipe
A_f	351.8458	$[m^2]$ biofilm surface area in pipe equals pipe surface area
f	2.382382×10^{-2}	friction factor
Re	31110	Reynolds number pipe
τ	$2.770264 \times 10^{+2}$	$[g/ms^2]$ wall shear stress
Sc	2500	Schmidt number
Sh	$1.257385 \times 10^{+3}$	Sherwood number
h_m	4.930920×10^{-6}	$[m/s]$ mass transfer coefficient
ν	1.0×10^{-6}	$[m^2/s]$ kinematic viscosity of water
ρ	$1.0 \times 10^{+6}$	$[g/m^3]$ density of water

Table 1: Model Parameters

References

Bakke, R., W. Characklis, M. Turakhia, and A. Yeh (1990). *Biofilms*, Chapter 13 Modeling a monopopulation biofilm system: Pseudomonas Aeruginosa, pp. 487–522. New York: Wiley.

Berg, H. (1993). *Random Walks in Biology*. Princeton University Press.

Characklis, W. and K. Marshall (1990). *Biofilms*. John Wiley and Sons.

Cogan, N. and J. Keener (2004). The role of the biofilm matrix in structural development. *Mathematical Medicine and Biology 24*(2), 147–166.

Dockery, J. and I. Klapper (2001). Finger formation in biofilm layers. *Math.Med and Biol. 62*(3), 853–869.

Dukan, S., Y. Levi, P. Piriou, F. Guyon, and P. Villon (1996). Dynamic modelling of bacterial growth in drinking water networks. *Water Research 30*(9), 1991–2002.

Eberl, H., D. Parker, and M. Loosdrecht (2001). A new deterministic spatio-temporal continuum model for biofilm development. *J. Theor. Med. 3*, 161–175.

Hermanowicz (2001). A simple 2D biofilm model yields a variety of morphological features. *Mathematical Biosciences 169*, 1–14.

Kreft, J., C. Picioreanu, J. Wimpenny, and M. van Loosdrecht (2001). Individual-based modelling of biofilms. *Microbiology* (147), 2897–2912.

Kreft, J. and J. Wimpenny (2001). Effect of EPS on biofilm structure and function as revealed by an individual-based model of biofilm growth. *Water Science and Technology 43*(6), 13514.

LaMotta, E. (1976). Internal diffusion and reaction in biological films. *Environmental Science and Technology 10*(8), 765769.

LeChevallier, M., T. Babcock, and R. Lee (1987, December). Examination and characterization of distribution system biofilms. *Applied and Environmental Microbiology 53*(12), 27142724.

Munavalli, G. and M. Kumar (2004). Dynamic simulation of multicomponent reaction transport in water distribution systems. *Water Research 38*, 1971–1988.

Noguera, D., G. Pizarro, D. A. Stahl, and B. E. Rittman (2004). Simulation of multispecies biofilm development in three dimensions. *Water Science and Technology 39*, 123–130.

Piciorenau, C., J. Kreft, and L. M. (2004). Particle-based multidimensional multispecies biofilm model. *Appl. Environmental Microbiology 70*(5), 3024–3040.

Pizarro, G., D. Griffeath, and D. Noguera (2001). Quantitative cellular automaton model for biofilms. *Journal of Environmental Engineering 127*(9), 782–789.

Quignon, F., L. Kiene, Y. Levi, M. Sardin, and L. Schwartzbrod (1997). Virus behaviour within a distribution system. *Water science and technology. 35*(11-12), 311–318.

Rittmann, B. and P. McCarrty (1980). Model of steady-state-biofilm kinetics. *Biotechnology and Bioengineering 22*, 2343–2357.

Rittmann, B.E., M. L. (1992). Development and experimental evaluation of a steady-state, multispecies biofilm model. *Biotechnology and Bioengineering 39*, 914–922.

Servais, P., L. P. G. D. and M. Prvost (1994). Modeling bacterial dynamics in distribution systems. *AWWA Water Quality Technology Conference Procedures.*.

Storey, M. (2002, April). *The ecology of enteric viruses within distribution pipe biofilms*. Ph. D. thesis, School of Civil and Environmental Engineering the University of new South Wales Sydney, Austalia.

Szabo, J. (2006, August). *Persistence of microbiological agents on corroding biofilm in a model drinking water system following intentional contamination*. Ph. D. thesis, Civil and Environmental Engineering the University of Cincinnati, USA.

Wanner, O. and W. Gujer (1986). A multispecies biofilm model. *Biotechnology and Bioengineering 28*, 314–328.

Xavier, J., C. Picioreanu, and M. Loosdrecht (2005). A general description of detachment for multidimentional modelling of biofilms. *Biotechnology and Bioengineering 91*(6), 651–669.

Zhang, W., C. Miller, and F. DiGiano (2004, September). Bacterial regrowth model for water distribution systems incorporating alternating split-operator solution technique. *J. of Environmental Engineering 130*(9), 932–941.

Impact of Storage Tanks on Energy Consumption in Municipal Water Distribution Systems

Santosh R. Ghimire, S.M. ASCE [1] and Brian D. Barkdoll, F. ASCE[2]

[1]Civil & Environmental Engineering Dept., Michigan Technological University, Houghton, MI 49931, PH: (906) 487-3494, FAX: (906) 487-2943, email: sghimire@mtu.edu
[2]Civil & Environmental Engineering Dept., Michigan Technological University, Houghton, MI 49931, PH: (906) 487-1981, FAX: (906) 487-2943, email: barkdoll@mtu.edu

ABSTRACT: Municipal water distribution systems (MWDS) use a significant amount of electrical energy for the pumping of water from low elevations to higher ones. The use of electrical energy has an effect on pollution emissions and, therefore, potential global climate change as well. There are many aspects of MWDSs that affect energy usage. The properties of the storage tank(s), namely diameter and tank maximum water level, are singled out here for analysis. Various values of these tank parameters are modeled on seven MWDSs of various sizes using a system solver and the energy usage recorded. It was found that when averaged over all seven systems analyzed (1) a reduction of tank diameter of 20% results in approximately a 4% energy savings, and (2) the reduction of maximum tank water level by 20% results in approximately a 1% energy reduction.

INTRODUCTION

The use of electrical energy for pumping in municipal drinking water distribution systems (MDWS) has contributed to air pollution emissions and perhaps to global climate change. There is a need to incorporate water conservation, environmental impacts, energy consumption, and social aspects in addition to the system flows and pressures (Ellis 1978). There are several factors that influence energy consumption of pumping, such as scheduling (Brion and Mays 1991, Farmani et al. 2004, Pezeshk and Helweg 1996, Tarquin and Dowdy 1989) and pump configuration (Walski 2001). Storage tank capacity and minimum normal operational level have an affect on cost and the system hydraulics (Vamvakeridou-Lyroudia et al. 2007) but their affect on energy consumption is unclear.

The present paper presents an analysis of the effect of altering the tank diameter and maximum water level on energy consumption. The method is demonstrated in seven municipal water systems of varying size and complexity.

System Modeling

To examine the effect of varying storage tank parameters on MWDS energy consumption, seven systems were modeled using the system solver EPANET 2.0 (EPA 2000). Extended period simulations of ninety-six hours were modeled with a varying diurnal demand pattern based on data from Lineweaver 1963. This time period of simulation was chosen to ensure a long enough time for initial conditions to be insignificant.

SYSTEMS STUDIED

Seven MWDSs were used in the analysis (summarized in Table 1). It can be seen that there are a wide variety of system sizes, number of pumps, tanks and complexity, thereby providing a wide variety sample for the analysis. After simulations were performed on all seven systems, results were analyzed treating the systems together in a statistical approach.

ENERGY USAGE WITH VARYING TANK DIAMETER

Tank parameters that are somewhat under the MWDS utility's control are tank diameter and maximum water level. Each of these was systematically altered and the energy usage calculated.

Table 2.1 Summary of system characteristics (After Ghimire and Barkdoll, 2008)

System	Junctions (#)	Pipes (#)	Pumps (#)	Reservoirs (#)	Tanks (#)	Valves (#)	Δz_{max} (m)
S1	6	8	1	1	1	0	39.6
S2	44	62	1	1	1	0	33.7
S3	126	168	2	1	2	8	217
S4	126	144	6	2	2	4	93.0
S5	347	394	8	1	2	1	100.3
S6	873	958	3	1	1[#]	6	27.4
S7	12,525	14,824	6	2	4	5	73.7

Tank Diameter

Altering the tank diameter changed the hydraulics of the system for some cases and, therefore, it was necessary to alter the pump characteristics (head versus discharge) in order to ensure adequate pressure at all junctions at all times (Ghimire 2008). The normalized tank diameter, D' was defined as follows:

$$D' = \frac{D}{D_o} \tag{1}$$

where D is the diameter modeled, and D_o is the original tank diameter. Similarly, the normalized consumed energy, E' during the simulation period was as:

$$E^* = \frac{E}{E_o} \tag{2}$$

where E is the energy consumed by the system pumps with the modeled tank diameter and E_o is the energy consumed with tank(s) unaltered.

The results are plotted below in Figure 1. It can be seen that the energy utilization of 9 of the tanks is less sensitive to the variation of tank diameter than the remaining five tanks (S2, S3T1, S3T2, S4T1 and S4T2).

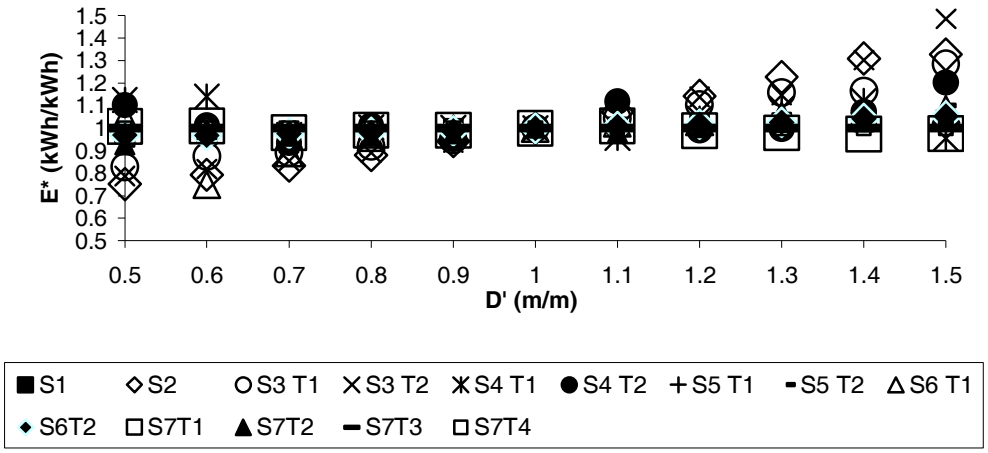

Figure 1. The sensitivity of energy consumption to the tank diameter of seven systems: 'S' represents 'System' and 'T' represents 'Tank'.

A closer-look at the diameter-sensitive tanks reveals that the high energy use was caused by an oversized pump(s) for those systems. Adjustment of pump curves was made to have the smallest pump that satisfied minimum pressures. After adjusting the pump curves thusly, the energy usage declined (Fig. 2). This agrees with the fact that pumps are more efficient at near-maximum discharge values. Figure 2 shows that the normalized energy can be altered by as much as 10% for a 50% change in normalized tank diameter, or have almost no effect, depending on the system and if the pumps are operating at peak efficiency.

Analyzing all seven systems en mass by taking the E* value averaged over D' reveals that (Fig. 3) an equation of energy utilization for the variation of diameter is given by an equation

$$E^* = 0.12D^* + 0.87 \quad (3)$$

with an R^2 value of 0.9480 and the error bars denoting ± 1 of standard deviation. The curve of the coefficient of variation (COV) exhibits wider variation between the system energy consumption values at values further away from D' = 1.0 and a maximum value of 0.087.

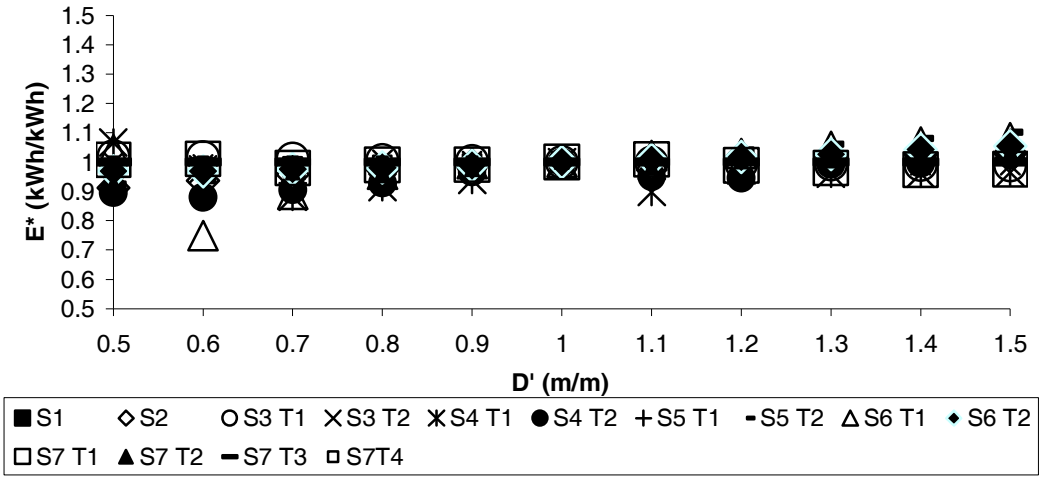

Figure 2. The sensitivity of energy consumption to the tank diameter of seven systems: After redesigning pumps of 3 systems S2, S3 and S4. 'S' represents 'System' and 'T' represents 'Tank'

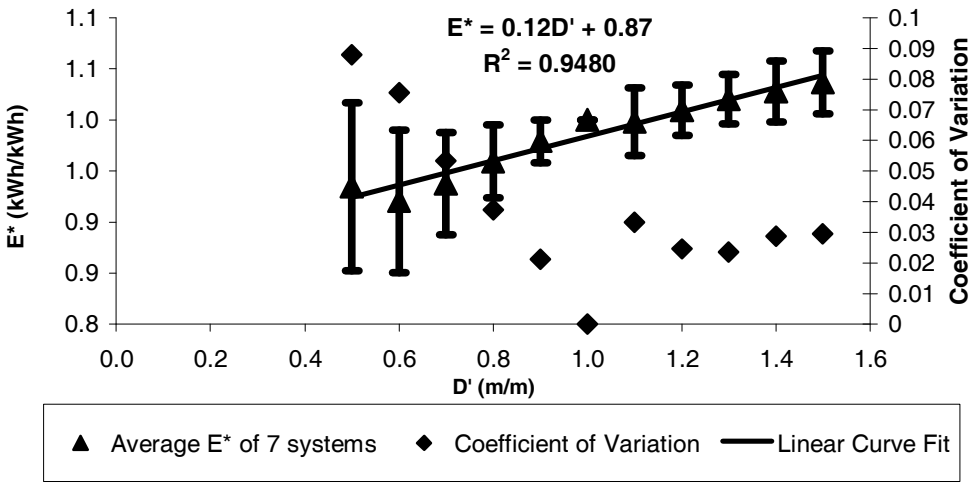

Figure 3: Average E* of seven systems for tank diameter variation for pumps sized correctly. Error bars denote ± 1 standard deviation (Ghimire 2008).

Energy Usage with Varying Maximum Tank Water Level

In addition to tank diameter, the maximum tank water level set point was varied in each tank one by one and the energy usage recorded. Each simulation was begun with the analyzed tank empty. The initial tank water level values of the remaining tanks were unaltered. During certain simulations, the pumps had to be altered to ensure adequate system pressures.

The maximum tank level was normalized (Eq. (3)).

$$H^* = \frac{H}{H_o} \tag{4}$$

where H^* is the normalized water height, H is the simulated maximum water height above the minimum value, and H_o is the original range in water levels between minimum and maximum water levels. The normalized energy is defined as above in Eq (2). For all values of H simulated see Ghimire (2008).

The results (Fig. 4) show that the energy usage is system specific, with some tanks exhibiting proportional, and others inversely proportional, behavior. The most sensitive tank resulted in a 30% reduction and/or increase in energy consumption and the least sensitive tank had a negligible change in energy use.

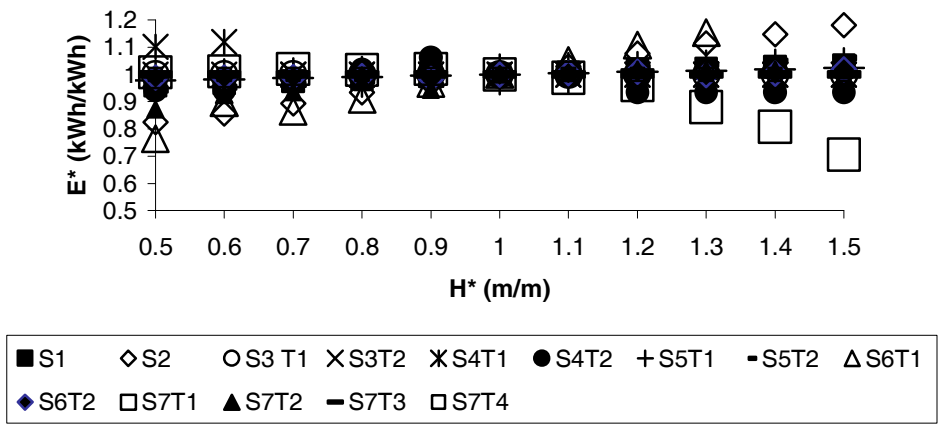

Figure 4: The sensitivity of energy consumption of seven systems to their tank maximum level before redesigning the pumps

The pump sizes were analyzed next to determine if pump over-sizing had an influence. It was found that the pumps were overly sized for systems exhibiting a high sensitivity to tank water level (S2 and S6T1) and non-monotonic behavior (S4T1, S4T2, and S7T1).

After redesigning the pump sizes, separate results were obtained and presented below in Figure 5. Eliminating pump over-sizing resulted in little energy sensitivity in all but S1, the simplest system.

When E* is averaged over all seven systems (Figure 6) it can be seen that the system-averaged E* values are linear (Eq. (5)) with an R^2 value of 0.9345 and a coefficient of variation ranging from 0 to 0.024.

$$E^* = 0.04H^* + 0.96 \tag{5}$$

CONCLUSIONS

From the results of current study, it is found that the variation of tank diameter has a greater impact in energy consumption than the tank water height, as evidenced by

the fact that a 20% reduction in tank diameter results in a 3.44% energy use reduction, while the same percentage reduction in maximum tank water level results in a mere 0.8% reduction, on average for the seven systems examined.

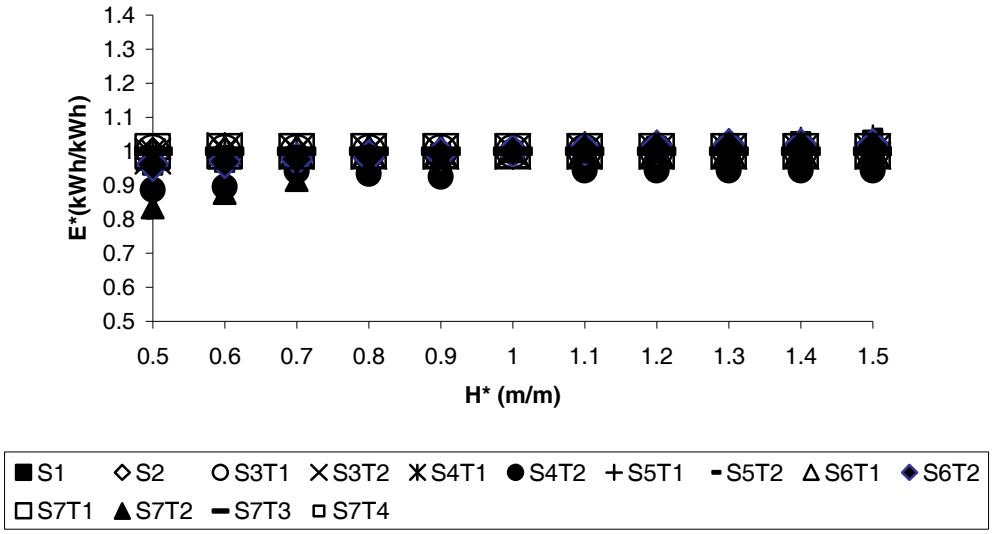

Figure 5: The sensitivity of seven systems and their tanks maximum level for energy consumption after redesigning the pumps

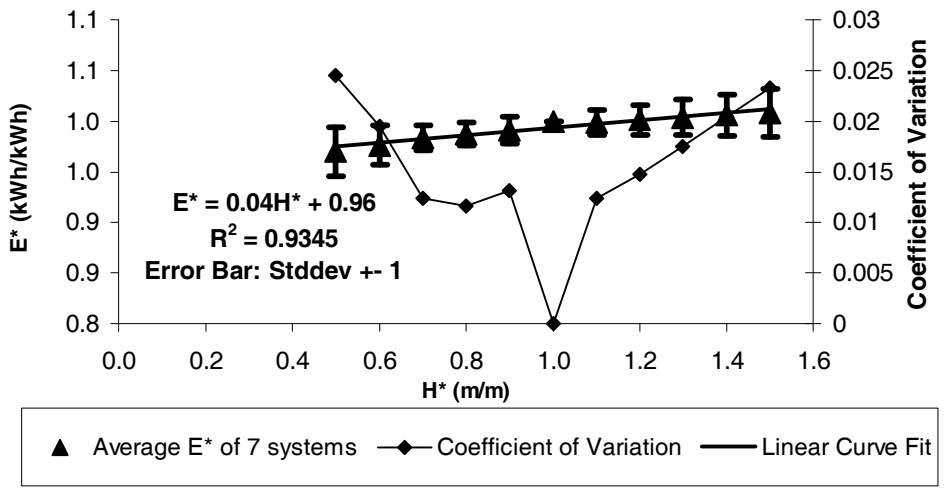

Figure 6: Average E* of seven systems for tank height variation after pump redesign. Error bars denote ± 1 standard deviation (Ghimire 2008).

ACKNOWLEDGEMENTS

The authors gratefully acknowledge support from the Sustainable Futures *Integrative Graduate Education and Research Traineeship* (IGERT) project sponsored by the National Science Foundation (NSF) (under Grant No. DGE 0333401). The research outcomes are the views of the authors and not those of the NSF.

REFERENCES

Brion, L.M. and Mays, L.W. (1991) "Methodology for optimal operation of pumping stations in water distribution systems" *J. Hydraulic Engng*, v 117, n 11, Nov, 1991, p 1551-1569.

Ellis, R. H. (1978) "New Considerations for Municipal Water System Planning" *Water Resources Bulletin,* v 14 n 3, June 1978, p 542-553.

EPA (2000), *EPANET 2, Users Manual,* by Lewis A. Rossman, Water Supply and Water Resources Division National Risk Management Research Laboratory Cincinnati, OH.

Farmani, R., Savic, D.A., and Walters, G.A. (2004) "The simultaneous multi-objective optimization of anytown pipe rehabilitation, tank sizing, tank siting and pump operation schedules" *Proceedings of the 2004 World Water and Environmental Resources Congress: Critical Transitions in Water and Environmental Resources Management*, Salt Lake City, UT, 2004, p 4663-4672.

Ghimire, S.R. (2008) *The Effect of Demand, Tank Parameters, and Pumping Stations on Energy Use in Municipal Drinking Water Distribution Systems*, PhD dissertation, Michigan Technological University, Houghton, MI.

Ghimire, S.R. and Barkdoll, B.D. (2008) "Effect of Demand on Energy Use in Municipal Water Distribution Systems, *Proceedings of The World Environmental & Water Resources Congress*, May 12-16, 2008, Honolulu, Hawai'i; pp. 1-5.

Linaweaver, F. P., Jr. (1963) *Report on Phase One, Residential Water Use Research Project,* The Johns Hopkins University, Department of Sanitary Engineering, Baltimore, October, 1963.

Vamvakeridou-Lyroudia, L. S., Savic, D. A., and Walters G. A. (2007), "Tank Simulation for the Optimization of Water Distribution Systems" *J. Hydr. Engrg.,* v 133, Issue 6, June 2007, p. 625-636.

Pezeshk, S. and Helweg, O.J. (1996) "Adaptive search optimization in reducing pump operating costs" ASCE *Journal of Water Resources Planning and Management*, v 122, n 1, Jan-Feb, 1996, p 57-63.

Tarquin, A. J. and Dowdy, J. (1989) "Optimal pump operation in water distribution" ASCE *Journal of Hydraulic Engineering*, v 115, n 2, Feb, 1989, p 158-168.

Walski, T.M. (2001) "Don't forget Energy Cost When Selecting Pumps" *American Water Works Association Annual Conference Proceedings*, pp. 1-16.

Hydraulic Analysis of Water Distribution Network Using Harmony Search

Zong Woo Geem

Environmental Planning and Management Program, Johns Hopkins University, 11833 Skylark Road, Clarksburg, Maryland 20871; email: zwgeem@gmail.com

ABSTRACT

So far, water distribution networks have been hydraulically analyzed by using various techniques such as Hardy Cross method, Newton-Raphson method, linear theory, and Todini algorithm. This study proposes a novel technique for the analysis of water distribution networks using a phenomenon-mimicking optimization algorithm, harmony search (HS). The HS algorithm mimics the behaviors of musicians in improvisation process, where they play musical notes based upon randomness, experience, or variation of experience. In order to use the HS optimization algorithm, the network analysis is formulated as an optimization problem where energy conservation equation is incorporated in an objective function and mass conservation equations are incorporated in constraints. The proposed HS model is successfully applied to two example networks.

INTRODUCTION

Since 1936 when Hardy Cross first presented a systematic method from an idea in moment distribution method (Cross, 1936), various methods such as Newton-Raphson (Epp and Fowler, 1970), linear theory (Wood and Charles, 1972), and Todini algorithm (Todini and Pilati, 1987) have been proposed for water distribution network analysis.

The Hardy-Cross method initially estimates flows that satisfy the mass conservation at each node, and then updates flows in order to satisfy energy conservation in each loop. Because it updates a group of flows in each loop at a time, the convergence of the method is relatively slow. The Newton-Raphson method is a similar approach to Hardy-Cross method. However, it updates the flows by considering all loops simultaneously, which quickens the convergence. Linear theory initially estimates flows, and then iteratively updates the flows using a matrix of successively-linearized energy conservation equations. The Todini algorithm is a hybrid one between calculus-based optimization technique and Newton-Raphson method.

Meanwhile, there is still a chance to develop a new method for water distribution network analysis. The goal of this study is to provide a novel approach to hydraulic analysis of water distribution networks using a phenomenon-mimicking algorithm named harmony search (HS). The proposed HS algorithm (Geem et al., 2001), which mimics music improvisation, has been successfully applied to various

water engineering optimization problems such as pipe size design (Geem, 2006), ground water modeling (Ayvaz, 2007), multiple dam operation (Geem, 2007), and hydrologic parameter calibration (Kim et al., 2001). From the success demonstrated in previous applications, the HS algorithm is applied to the analysis of water distribution networks in this study.

EXISTING HYDRAULIC ANALYSIS TECHNIQUES

A steady-state flow of incompressible water through a pipe network is governed by two fundamental equations: a mass conservation equation and an energy conservation equation (Huddleston et al., 2004).

A mass conservation equation at each node can be expressed as

$$\sum Q_{in} - \sum Q_{out} = d_j \tag{1}$$

where Q_{in} denotes pipe flow into the node j; Q_{out} denotes pipe flow out of the node j; and d_j denotes nodal demand at the node j (positive sign of the nodal demand stands for outflow).

If there is no energy gain in any loop, the energy conservation equation at each loop can be expressed as

$$\sum_i h_f = 0, \quad i \in k \tag{2}$$

where h_f denotes head loss along the pipe i which forms loop k.

While mass conservation equations are linear as in Equation 1, energy conservation equations are nonlinear because the head loss equation has the following form:

$$h_f = K_i Q_i^n \tag{3}$$

where K_i denotes a friction coefficient for pipe i; Q_i denotes a flow through pipe i; and n denotes a flow exponent.

Normally, the following Hazen-Williams equation is used for head loss calculation in water distribution networks (Rossman, 2000):

$$h_f = 10.667 C_i^{-1.852} D_i^{-4.871} L_i \, Q_i^{1.852} \tag{4}$$

where C_i denotes the Hazen-Williams roughness coefficient; D_i denotes the pipe diameter (m); and L_i denotes the pipe length (m).

Another popular equation is Darcy's one (Mott, 2006) as follows:

$$h_f = f_i \times \frac{L_i}{D_i} \times \frac{v_i^2}{2g} = \frac{8 f_i L_i}{\pi^2 g D_i^5} Q_i^2 \tag{5}$$

where f_i denotes friction factor (dimensionless); v_i denotes average velocity of flow (m/s); g denotes the acceleration due to gravity (9.81 m/s^2); and π denotes the ratio of a circle's circumference to its diameter.

The Hardy-Cross method for analyzing the flow in water distribution networks follows the next procedure:

Step 1: Represent the head loss in each pipe in the form of $h_f = K_i Q_i^n$ as in Equation 3.

Step 2: Assign a flow rate for each pipe such that total flow into each node equals total flow out of the node plus nodal demand as in Equation 1.

Step 3: For each loop, the adjustment ΔQ is calculated as follows:

$$\Delta Q = \frac{-\sum h_f}{\sum \left| K_i \; n \; Q_i^{n-1} \right|} \tag{6}$$

where, if the flow is clockwise, the sign for Q_i (and h_f) is positive. Otherwise, the sign for Q_i (and h_f) is negative.

Step 4: Calculate a new estimate for Q_i by adding the adjustment ΔQ.

$$Q_i^{New} = Q_i^{Old} + \Delta Q \tag{7}$$

Step 5: Repeat Steps 3 and 4 until the adjustment ΔQ becomes negligibly small.

Other popular techniques in hydraulic network analysis, such as Newton-Raphson method, linear theory, and Todini algorithm use matrix operation in order to simultaneously analyze the network, but they also analyze it iteratively.

PROBLEM FORMULATION

For the hydraulic analysis, this study introduces the HS algorithm. Because the algorithm was originally developed for solving optimization problems, the hydraulic network analysis is transformed into an optimization problem. The energy conservation equation in Equation 2 can become an objective function in this optimization problem as follows:

$$\min \quad Z = \sum_k \left| \sum_i sd_i \; K_i \left| Q_i^{n-1} \right| Q_i \right|, \quad i \in k \tag{8}$$

where, in order to consider flow direction, the sign of flow direction sd (clock-wise is plus) and the expression $\left| Q^{n-1} \right| Q$ are used.

The approach shown in the above function intends to find a solution with a minimal sum of the error in each loop. Actually, Hardy-Cross method previously mentioned has the same objective of minimizing the error. But, while the latter minimizes it by adding the adjustment ΔQ to all pipe flows, the former minimizes it by selecting better flow rate Q_i for only certain pipes at each iteration.

Variables to be decided in this optimization are flows in all pipes. However, because some flows are dependent on other flows, the number of decision variables is actually reduced. For example in Figure 1, where there are four pipes and one loop, if we optimally update only one flow (say, Q_1 in pipe 1), we can deterministically

calculate the other three flows (Q_2 , Q_4 , and Q_3) using the mass conservation equation as in Equation 1.

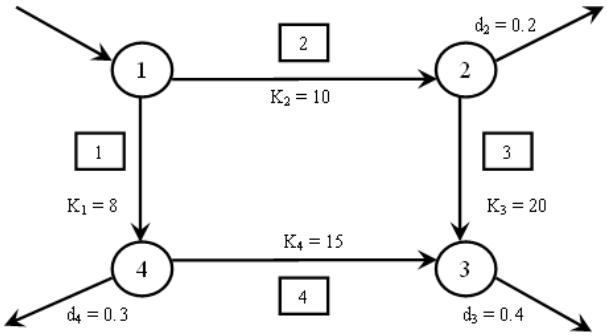

Figure 1. Schematic of One-Loop Network

The value range of the decision variable Q_1 in Figure 1 can be as follows:

$$0 \le Q_1 \le S \tag{9}$$

$$S = -d_1 = d_2 + d_3 + d_4 \tag{10}$$

The other flows in Figure 1 are specified as the following constraints:

$$Q_2 = S - Q_1 \tag{11}$$

$$Q_4 = Q_1 - d_4 \tag{12}$$

$$Q_3 = Q_2 - d_2 \tag{13}$$

In summary, the HS optimization model is to determine the values of certain independent decision variables (e.g., Q_1 in Figure 1) after incorporating energy conservation equations in the objective function and mass conservation equations in the constraints in order to minimize the error of energy loss.

HARMONY SEARCH OPTIMIZATION ALGORITHM

The proposed optimization model in the previous section is solved by using a phenomenon-mimicking optimization algorithm, harmony search (Geem et al., 2001). The HS algorithm uses an analogy between music improvisation and the optimization process. In music improvisation, musicians are playing musical pitches out of possible ranges of musical instruments in order to search for better harmonies. Likewise in the optimization process, algorithms are assigning variable values out of a possible range of decision variables in order to search for better solution vectors. Thus, a musical instrument corresponds to a decision variable; its pitch range corresponds to a value range; and harmony corresponds to a solution vector.

In the HS algorithm, a musician plays a pitch based upon one of three factors such as randomness, experience, or variation of experience. This mechanism becomes a novel stochastic derivative, rather than a calculus-based gradient derivative, for the optimization problem with discrete variables (Geem, 2008).

For the analysis of water distribution networks, the HS algorithm starts with an array named harmony memory (HM) which contains initial solution vectors randomly generated out of a possible value range:

$$\left[\begin{array}{cccc|c} Q_1^1 & Q_2^1 & \cdots & Q_n^1 & Z^1 \\ Q_1^2 & Q_2^2 & \cdots & Q_n^2 & Z^2 \\ \vdots & \vdots & \vdots & \vdots & \vdots \\ Q_1^{HMS} & Q_2^{HMS} & \cdots & Q_n^{HMS} & Z^{HMS} \end{array}\right] \tag{14}$$

where $(Q_1, Q_2, \ldots, Q_n)$ denotes a solution vector; Z denotes a corresponding objective function value; and HMS denotes the number of solution vectors stored in HM.

Based on the above-mentioned initial HM, a new solution vector $(Q_1^{New}, Q_2^{New}, \ldots, Q_n^{New})$ is generated. Variable Q_i^{New} can have one value as follows:

$$Q_i^{New} \leftarrow \begin{cases} Q_i & where \quad 0 \le Q_i \le S & w.p. \quad P_{Random} \\ Q_i & where \quad Q_i \in \{Q_i^1, Q_i^2, \ldots, Q_i^{HMS}\} & w.p. \quad P_{Memory} \\ Q_i + \Delta & where \quad Q_i \in \{Q_i^1, Q_i^2, \ldots, Q_i^{HMS}\} & w.p. \quad P_{Adjust} \end{cases} \tag{15}$$

where P_{Random} denotes a probability of random selection (randomness); P_{Memory} denotes a probability of memory consideration (experience); Δ denotes the amount of pitch adjustment; and P_{Adjust} denotes a probability of pitch adjustment (variant of experience). The amount of pitch adjustment, Δ, can have the following value:

$$\Delta = bw \times u(-1, 1) \times S \tag{16}$$

where bw denotes a bandwidth which is a tiny segment of total range; and $u(-1, 1)$ denotes a value generated by a uniform distribution between -1 and 1.

If a newly generated vector $(Q_1^{New}, Q_2^{New}, \ldots, Q_n^{New})$ is better than the worst vector stored in HM in terms of the objective function, those two vectors are swapped. Then, another new solution vector is generated using Equation 15 until a terminating criterion is satisfied.

EXAMPLE 1: ONE-LOOP NETWORK

The HS model was applied to a simple network, which has one loop, one supply node, three demand nodes and fours pipes, as shown in Figure 1 (Bhave and Gupta, 2006). Problem specifications are as follows: Type of Head Loss Function $h_f = K_i Q_i^2$; Friction Coefficients K_1 = 8, K_2 = 10, K_3 = 20, and K_4 = 15; Water Demands d_2 = 0.2 m^3/s, d_3 = 0.4 m^3/s, and d_4 = 0.3 m^3/s; Harmony Memory Size HMS = 10; Probability of Random Selection P_{Random} = 0.3; Probability of Memory Consideration P_{Memory} = 0.49; Probability of Pitch Adjustment P_{Adjust} = 0.21; Bandwidth bw = 0.1; and Tolerance (terminating criterion) $Z \le 0.01\,m$.

With the above values, HS found a solution vector (Q_1=0.4931, Q_2=0.4069, Q_3=0.2069, Q_4=0.1931) as shown in Figure 2. Table 1 shows the history of the best solution vectors HS found.

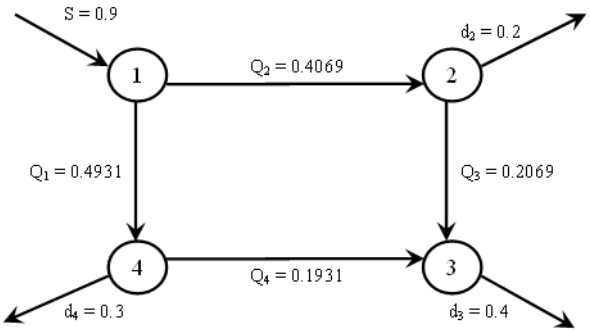

Figure 2. Final Solution for One-Loop Network

Table 1. History of Solution Vectors for One-Loop Network

Iterations	Z (m)	Q_1 (m^3/s)	Q_2 (m^3/s)	Q_3 (m^3/s)	Q_4 (m^3/s)
17	0.3446	0.5048	0.3952	0.1952	0.2048
26	0.2526	0.4850	0.4150	0.2150	0.1850
36	0.1116	0.4896	0.4104	0.2104	0.1896
53	0.0901	0.4904	0.4096	0.2096	0.1904
224	0.0309	0.4944	0.4056	0.2056	0.1944
380	0.0059	0.4931	0.4069	0.2069	0.1931

As previously mentioned, because the expression $\left|Q^{n-1}\right|Q$, instead of Q^n, was used, the HS model calculated flows correctly under the wrong assumption of flow direction. The flow Q_4 became -0.1931 m^3/s when the direction of Q_4 was assumed reversely (from node 3 to node 4; $sd_4 = +1$) and the constraint in Equation 12 was substituted with the following constraint:

$$Q_4 = Q_3 - d_3 \tag{17}$$

If Equation 12 was not substituted, a wrong solution vector (0.5639, 0.3361, 0.1361, 0.2639) was obtained as shown in Figure 3.

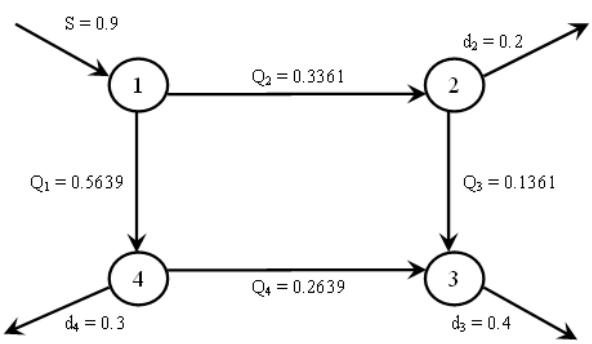

Figure 3. Wrong Direction Solution for One-Loop Network

Although the solution satisfies the mass conservation constraint of Equation 12, and also the energy conservation objective of Equation 8 (Table 2), the actual value of the

objective function becomes 2.0884 because Q_4 is -0.2639 under the constraint of Equation 12 (Table 3). Meanwhile, if the sign of flow direction was not properly considered ($sd_4 = -1$) with Equation 17, similar wrong solution vector (0.5639, 0.3361, 0.1361, -0.2639) was obtained.

Table 2. Objective Function Calculation with Incorrect Flow Direction

Pipe	K	Sign	Flow Rate	Head Loss
1	8	-1	0.5639	-2.5439
2	10	1	0.3361	1.1296
3	20	1	0.1361	0.3705
4	15	1	0.2639	1.0446
∑				0.0009

Table 3. Objective Function Calculation with Corrected Flow Direction

Pipe	K	Sign	Flow Rate	Head Loss
1	8	-1	0.5639	-2.5439
2	10	1	0.3361	1.1296
3	20	1	0.1361	0.3705
4	15	1	-0.2639	-1.0446
∑				2.0884

EXAMPLE 2: TWO-LOOP NETWORK

The HS model was further applied to another network, which has two loops, one supply node, three demand nodes and seven pipes, as shown in Figure 4 (Bradley, 2005).

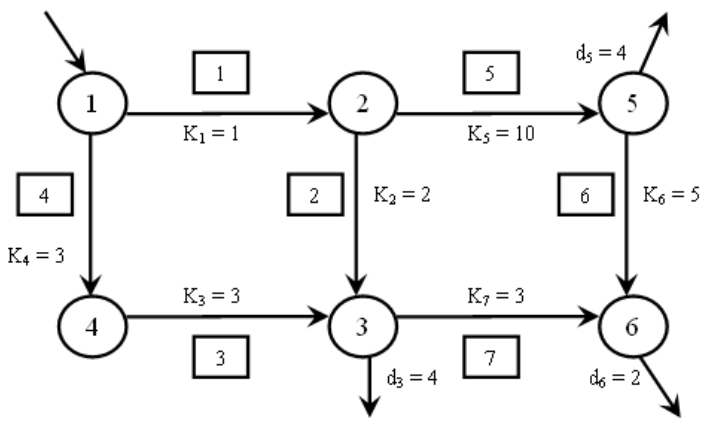

Figure 4. Schematic of Two-Loop Network

Problem specifications for two-loop network are as follows: Type of Head Loss Function $h_f = K_i Q_i^2$; Friction Coefficients K_1 = 1, K_2 = 2, K_3 = 3, K_4 = 3, K_5 = 10, K_6 = 5, and K_7 = 3; Water Demands $d_3 = 4$ m^3/s, $d_5 = 4$ m^3/s, and $d_6 = 2$ m^3/s; Harmony Memory Size HMS = 30; Probability of Random Selection P_{Random} =

0.3; Probability of Memory Consideration P_{Memory} = 0.49; Probability of Pitch Adjustment P_{Adjust} = 0.21; Bandwidth bw = 0.1; Tolerance (terminating criterion) $Z \le 0.5\,m$.

It should be noted that the number of decision variables for the two-loop network is only two such as Q_1 and Q_5. If Q_1 is assigned, Q_4 and Q_3 are successively determined, and if Q_5 is assigned, Q_2, Q_7, and Q_6 are successively determined. Thus, the number of decision variables in the HS model is equivalent to the number of loops in the problem network.

The mass conservation constraints for the two-loop network are as follows:

$$0 \le Q_1 \le \sum_{i=3,5,6} d_i \tag{18}$$

$$Q_4 = \sum_{i=3,5,6} d_i - Q_1 \tag{19}$$

$$Q_3 = Q_4 \tag{20}$$

$$0 \le Q_5 \le \sum_{i=3,5,6} d_i \tag{21}$$

$$Q_2 = Q_1 - Q_5 \tag{22}$$

$$Q_6 = Q_5 - d_5 \tag{23}$$

$$Q_7 = Q_2 + Q_3 - d_3 \tag{24}$$

After the HS model started with a solution vector (7.7160, 4.7343, 2.2840, 2.2840, 2.9817, -1.0183, 3.0183) with $Z = 84.62$, it reached a solution vector (6.5274, 3.8489, 3.4726, 3.4726, 2.6785, -1.3215, 3.3215) with $Z = 0.40$, as shown in Figure 5.

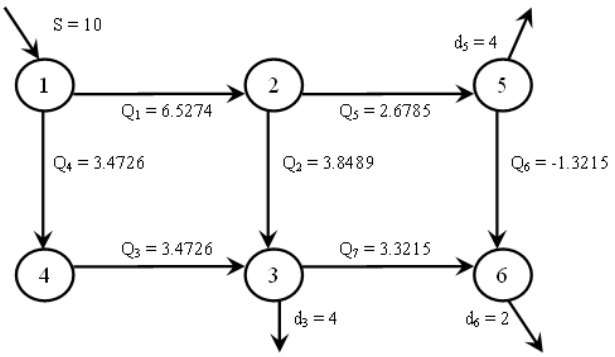

Figure 5. Final Solution for Two-Loop Network

CONCLUSIONS

This study proposed a new approach to the hydraulic analysis of water distribution networks using harmony search. The analysis was formulated as an optimization problem which has an objective function of energy conservation, constraints of mass conservation, and decision variables whose size is equal to the number of loops. The HS model successfully found pipe flows for two sample networks.

One advantage of the HS model is the fact that it does not require an initial solution vector which is sometimes critical to the convergence. Also, the HS model does not require any complicated mathematical expression and operation.

Based upon this fundamental study, further research should consider how to reduce the number of computing iterations and how to automatically generate energy conservation objective function and mass conservation constraints. Also, future research should cover more complex and realistic networks containing various hydraulic appurtenances such as pumps, valves, and multiple reservoirs.

REFERENCES

Ayvaz, M. T. (2007). "Simultaneous Determination of Aquifer Parameters and Zone Structures with Fuzzy C-Means Clustering and Meta-Heuristic Harmony Search Algorithm." *Advances in Water Resources*, 30(11), 2326-2338.

Bhave, P. R. and Gupta, R. (2006) *Analysis of Water Distribution Networks*, Alpha Science International Ltd, Oxford, U.K.

Bradley, A. (2005) *Hydraulics and Hydrology*, http://www.icaen.uiowa.edu/~water/ >(Jan. 9, 2009).

Cross, H. (1936) *Analysis of Flow in Networks of Conduits or Conductors*, Bulletin No. 286, University of Illinois, Urbana, IL.

Geem, Z. W. (2006). "Optimal Cost Design of Water Distribution Networks Using Harmony Search." *Engineering Optimization*, 38(3), 259-280.

Geem, Z. W. (2007). "Optimal Scheduling of Multiple Dam System Using Harmony Search Algorithm." *Lecture Notes in Computer Science*, 4507, 316-323.

Geem, Z. W. (2008). "Novel Derivative of Harmony Search Algorithm for Discrete Design Variables." *Applied Mathematics and Computation*, 199(1), 223-230.

Geem, Z. W., Kim, J. H., and Loganathan, G. V. (2001). "A New Heuristic Optimization Algorithm: Harmony Search." *Simulation*, 76(2), 60-68.

Epp, R. and Fowler, A. G. (1970). "Efficient Code for Steady State Flows in Networks." *Journal of the Hydraulics Division*, ASCE, 96, 43-56.

Huddleston, D. H., Alarcon, V. J., and Chen, W. (2004). "Water Distribution Network Analysis Using Excel." *Journal of Hydraulic Engineering*, 130(10), 1033-1035.

Kim, J. H., Geem, Z. W., and Kim, E. S. (2001). "Parameter Estimation of the Nonlinear Muskingum Model Using Harmony Search." *Journal of the American Water Resources Association*, 37(5), 1131-1138.

Mott, R. L. (2006). *Applied Fluid Mechanics*, Pearson Prentice Hall, Upper Saddle River, NJ.

Rossman, L. A. (2000). *EPANET2 Users Manual*, US Environmental Protection Agency, Cincinnati, OH.

Todini, E. and Pilati, S. (1987). "A Gradient Method for the Analysis of Pipe Networks." *Proceedings of the International Conference on Computer Applications for Water Supply and Distribution*, Leicester Polytechnic, UK.

Wood, D. J. and Charles C. O. A. (1972). "Hydraulic Network Analysis Using Linear Theory." *Journal of the Hydraulics Division*, ASCE, 98, 1157-1170.

Integrated Hydraulic Analysis and Data Management Tool for Water Supply Systems in Developing Countries

Philipp Klingel[1] and Nicolai Guth[1]

[1]University of Karlsruhe, Institute for Water and River Basin Management, Water Supply Section, 76137 Karlsruhe, Germany; PH +49 (0)721 608 4561; FAX +49 (0)721 608 4608; email: klingel@iwg.uka.de

ABSTRACT

In developing countries hydraulic models of water distribution systems are rarely used efficiently. The lack of appropriate know-how is one reason. Further, water distribution networks are dynamic technical systems changing rapidly due to maintenance works and network extensions. Therefore, the foundation for all technical tasks to assure a sustainable water supply is the deep going knowledge of the system. In developing countries the available system data is usually not up to date and of poor quality due to missing appropriate data management concepts. Integrating the data management and the hydraulic model as well as adapting the resulting tool to local constraints remedies the challenges resulting from the situation described above. Furthermore, linking the necessary work-flow of data collection to the tool eases the model implementation as well as the subsequent database update. In this paper a novel integrated data management and hydraulic analysis tool for water supply networks and linked work-flows specifically tailored towards its application in developing countries is presented. Based on a project of the German-Algerian technical cooperation in Béni Abbès the application of the tool is demonstrated.

1. INTRODUCTION

In developed countries hydraulic models and geo-information systems (GISs) are commonly applied to successfully analyze, design and operate centralized water distribution systems (Trifunović and Vairavamoorthy, 2008; Cornell and Dunphy, 2005). On the contrary, these sophisticated tools and models are rarely used efficiently in developing countries. Various reasons for the inefficient application or the absence of such tools and models exist. First, the benefits of hydraulic models and GISs are often simply not known or not seen. If those models and tools are known, the expectations regarding the possible results are usually high, while the necessary foundations to interpret the results achieved by model based calculations are often not present (Farley and Liemberger, 2005). Consequently, the lack of appropriate know-how is the second major reason for inefficient and inappropriate application and implementation of those tools. Third, the hydraulic model, the GIS and sometimes a digital or hardcopy network register are usually implemented, managed and updated separately consequently leading to redundancies and inaccuracies in the data bases and complex data transfer processes. Often a network

register does not even exist resulting in a poor and non-trustable data base quality and consequently in a poor model quality (Farley and Liemberger, 2005; Kumar, 1997, 1998). Integrating the network register, the GIS and the hydraulic model as well as adapting the resulting tool to local constraints remedies the challenges resulting from the situation described above. Furthermore, linking the necessary extended data collection process to the integrated tool eases the model implementation as well as the subsequent data base update.

This paper presents a hydraulic analysis and data management tool for water distribution systems specifically tailored towards its application in developing countries. The tool integrates the hydraulic model, the GIS and the network register and provides additional applications such as a graph decomposition module, automatic demand allocation and automatic topology generation. The system data as well as general spatial data are stored in a single central geo-database. All applications are integrated into the graphical user interface of the GIS as a toolbar. The common GIS functionalities together with the adapted network register tools allow data management and data analysis. Steady state and time extended simulation is supported. The graph decomposition module enables advanced topology analysis. The integrated tool is described in Section 2. Common work-flows, such as data collection, characterization of defects and model update are simplified by linking standardized processes with the novel user interface (see Section 3). Given a trained expert coordinates the overall process these simplified work flows can be delegated to non-experts. In Section 4, the advantages of the developed tool are demonstrated based on its application in the integrated water resources management (IWRM) project of the German-Algerian technical cooperation in the oasis Béni Abbès, Algeria (GTZ, 2008).

2. THE HYDRAULIC ANALYSIS AND DATA MANAGEMENT TOOL

Program architecture

In this subsection the components of the integrated tool and the interfaces of the components are presented. The functionalities and the realization of the integration of the components are described more detailed in the following subsections.

The tool consists of a geo-database, the hydraulic analysis and graph decomposition model KANET and the data management software package ArcGIS by ESRI. Further, an interface to an enhanced version of the hydraulic simulation program EPANET is implemented. The ArcGIS component ArcMap is used for visualization and spatial data analysis. For editing the system data of a water distribution network a toolbar is integrated into the graphical user interface (GUI) of ArcMap. Additionally, the toolbar consists of further tools for hydraulic modeling and analysis. The program codes of the components are integrated as Dynamically Linked Libraries (DLLs). All functions of the components are accessible through an ActiveX Dynamically Linked Library written in Visual Basic. Furthermore, it connects the KANET DLL on demand to perform simulation calculations or graph decomposition. If calculation is to be performed by EPANET, the data is transferred

through the KANET DLL to the EPANET DLL. The functions are implemented as commands and use the ArcGIS library ArcObjects to communicate with the host application. Therefore, ArcObjects acts as an interface between the database, ArcMap and the DLLs. Figure 1 gives an overview of the program architecture.

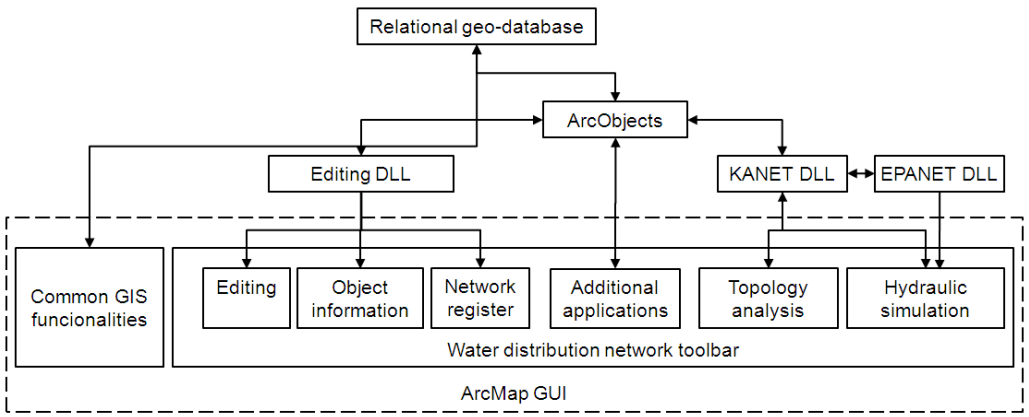

Figure 1: Components and program architecture of the integrated tool

The GIS model ESRI ArcGIS

ArcGIS is a software suite to manage and alter geo-spatial data and related attributes developed and distributed by the company ESRI (Ormsby et al., 2004). Geo-spatial data can be point features, line features or polygon features stored in feature classes. Attributes are data without a spatial reference stored in tables. Attributes are mostly related to a feature class. The data are stored in a relational geo-database or shape-files. ArcSDE offers the opportunity to connect ArcGIS to a centrally located Relational Database Management Systems (RDMS). The main components of ArcGIS are ArcMap and ArcCatalog. ArcMap allows all data analysis and modification regarded crucial for a GIS. Furthermore, ArcMap consists of applications and a GUI for user defined visualization of the geo-spatial data and the related attributes. ArcCatalog provides a GUI and functionalities to create data classes and manage data storage. ArcObjects is a Component Object Model (COM) library containing functions to develop GIS applications. ArcObjects allows the communication with the GUI of ArcGIS and the access to object data stored in feature classes and tables. Thereby the data access is independent from the physical representations of the data (for example shape-files, a personal geo-database or an ArcSDE connection). ArcObjects is applicable through the ArcGIS developer kit.

Database

The database contains all geo-spatial and object related data. The database may be a personal geo-database (for example MS Access) or an ArcSDE connection to a centrally located RDMS. The system data of water distribution networks are stored in a given database structure. A line feature class with the link information and a point

feature class with the node information of the network graph are the core of the structure. The feature classes consist of the geo-spatial shape information and additional attributes of the links and the nodes. Further necessary system data are stored in hierarchical organized tables. The data sets (objects) are connected through unique identifications (IDs). The shape information of the links and nodes allow geo-spatial visualization in the GUI of ArcMap. The interface of the hydraulic model KANET demands human readable data. Therefore the necessary data to build the network graph are saved as common object related attributes. Additional geo-spatial data can be freely organized in the same or other databases.

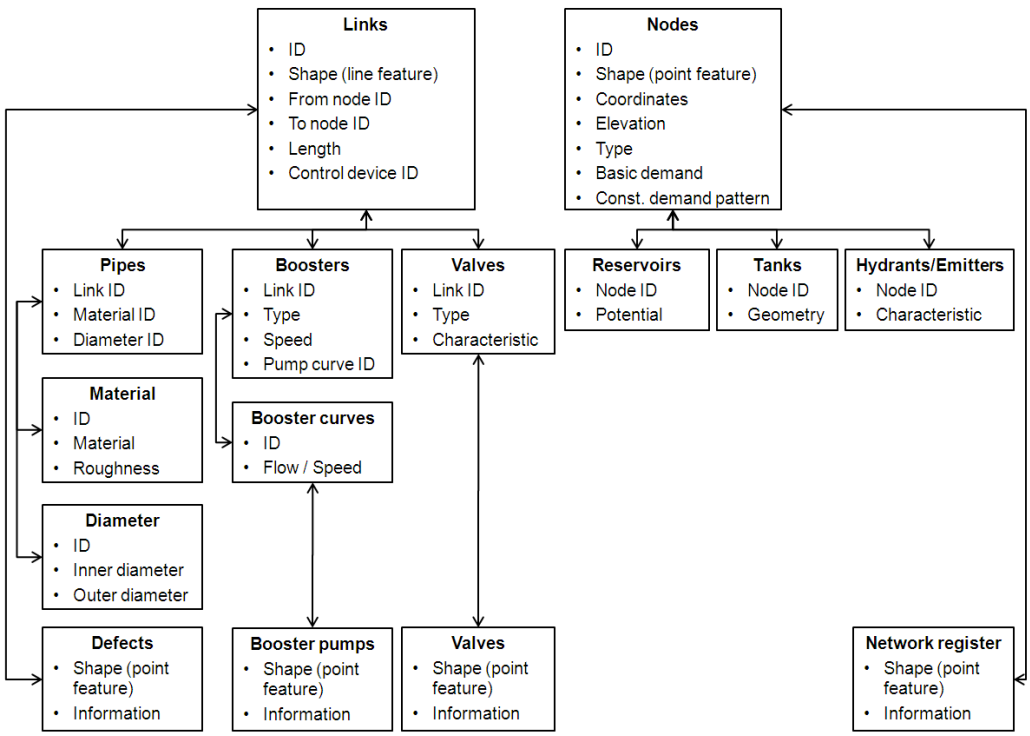

Figure 2: Schematic overview of the database structure for steady-state calculations

The link information is limited to the information needed to build the graph. The physical attributes of the pipes are organized in a separate pipe table. The KANET-algorithm for cost-optimal network design uses the link information as parameters and the pipe information as variables. For simulation calculations both the link and the pipe information are given parameters. Control devices like booster pumps and various types of control valves are related to links due to the modeling of their hydraulic behavior. In reality, control devices are elements with rather punctual then longish shape and location. For the visualization with real-world coordinates the true geo-spatial positions of control devices are additionally saved as point features. Accordingly, data concerning the network register are stored in a separate point feature class connected to the nodes point feature class. Defect data are stored in a

point feature class. The defect data is connected to the links line feature class to allow link related statistics.

Figure 2 gives a simplified schematic overview of the database structure for steady-state calculations. For time extended calculations patterns for control device settings, pump speeds, input node potentials and demands add to the structure. Further, the table with general parameters for the calculation algorithm is not shown.

The data management and network register tool

The data management and network register tool is a single library which contains all subsequent tools for manipulation and visualizing the water distribution system data. The functions are linked to the ArcObjects environment as a DLL (Editing DLL, Figure 1). The functionalities of the DLL are integrated into the GUI of ArcMap as part of the Water distribution network toolbar. The corresponding tools are described in the following.

Being exclusively responsible for editing and storing the data concerning the water distribution system the editing tool guarantees the consistency of the above described database structure. Tools for digitizing and modifying network elements and their attributes are implemented. Editing the network elements the accordant shape information of the link and node features are created and stored in the database. Additionally, the necessary attributes to build a network graph are generated automatically. References to relevant objects are made to check missing information. Dialogs to enter missing data are generated automatically. Further, the common attributes of the network elements can be edited. In addition to the shape information of the network graph the node coordinates are stored in the database as numbers. Therefore, the GUI of the stand-alone version of the hydraulic analysis model KANET can still be used. A database of the stand-alone version of KANET can be automatically converted to a geo-database compatible with ArcGIS. The spatial reference can be adjusted during the conversion process.

The information tool displays properties of the network elements. After a hydraulic simulation has been performed, the information dialog contains an additional diagram displaying the calculation results. Further, altering object related data and adding additional information of network elements in form of text or pictures is possible. Besides the visualization and manipulation of object related data the information tool allows the registration of defects. Thereby, the defects are characterized following given categories which can be adapted to the local constraints. Multiple defects can be related to one link. The real world location is stored in a separate point feature class (see accordant subsection further down). The relation of defects to links allows significant user defined reports and statistics.

Nodes of the network graph mark points of changes of the physical attributes of the system. Therefore, to achieve a complete information picture of the network the data at every node must be correct. According to this principle the later described work-flow to implement and update a consistent data base was developed. The network register tool supports the update of the network register with data collected in the field. In the GUI of the integrated tool surveyed nodes are labeled with a special symbol to get an overview of the progress. Further, an ID of the survey point

is generated automatically. The ID connects the node and the questionnaire for the data collection in the field. The completed questionnaire can be node related stored as an image. Therefore a scanner is connected to the integrated tool. The image is stored in a subfolder of the database´s path.

Additional data management and modeling applications

To support the conditioning of existing data (preprocessing) during the modeling process of the integrated tool several applications are implemented (Additional applications, Figure 1). The applications are written in Visual Basic and directly integrated into ArcGIS through the ArcObjects environment.

A tool provides functionalities to automatically and semi-automatically treat data without sufficient consistency to build a proper network graph. Not existing nodes at the ends of links are created. End points of links are adjusted to existing nodes if they are in distinct surroundings of the existing nodes. If a node is on a continuous link, the link is split. That can be either applied automatically or user controlled. The topology (the references of a link to its "start node" and "end node") of the modified elements is created automatically.

Further, functionalities for allocating a given population distribution to the demand nodes are implemented. The population expanses are divided into Thiessen polygons (Voronoi diagram) against the demand nodes. Thus, to each demand node a certain polygon with a related area and population density can be allocated.

The hydraulic analysis tool KANET

KANET is a hydraulic analysis tool developed by the Institute for Water and River Basin Management (IWG) of the University of Karlsruhe. The program consists of a graph model and algorithms for steady state and time extended hydraulic simulation and for graph decomposition. The hydraulic balance of a looped network with control devices is formulated as a set of optimization problems influencing one another. The problem can be solved by formulating it as a Nash Equilibrium with guaranteed convergence (Deuerlein et al., 2005). The components of the network graph can be identified according to their connectivity properties (Deuerlein, 2008). The application allows advanced topology analysis and data management. Supply areas, bottle necks, branched and looped network partitions are determined straightforward considering the state of the control devices. Accordingly, the graph decomposition can be used to calculate the hydraulic state of single components independently resulting in faster calculation times.

To enable data exchange with the Editing DLL and ArcMap a special DLL version of Kanet has been developed. KANET and the Editing DLL use the same data structure. Therefore, KANET only needs to gain access to the current database state. This is attained by handing over the ArcMap workspace of the database including all data needed. KANET uses ArcObjects to read the workspace data. Thus, it does not matter whether the data is stored in any kind of a local geo-database or a geo-database located on a server and connected via ArcSDE.

After KANET has knowledge of the data specific requests and functions can be performed. To proceed the requests and functions tools are integrated into the Water distribution network toolbar (see Figure 1). The results are returned either value by value or all values of a feature in a single request. The data exchange is performed by using the unique IDs of the features stored in the internal data structure of KANET. The results of calculation related functions are handled in three different ways. First, graph position information is stored into the respective feature class feature by feature. Second, calculated hydraulic analysis results are returned by the KANET DLL on demand as single values. Third, all calculated results are saved to a temporary Scratch Workspace provided by ArcObjects to allow the visualization of the hydraulic state of the network at each time-step. The time-step can be chosen in a drop down menu of the Water distribution network toolbar. Further, editing and simultaneously perform and display graph decomposition is possible. The KANET DLL is triggered to build the graph and perform the graph decomposition once an editing operation is executed. An editing operation may be the removal or modifying of a network element or the change of a valve state.

The hydraulic simulation tool EPANET

The hydraulic simulation software package EPANET is developed by the U.S. Environmental Protection Agency EPA (Rossmann, 2000). The software and the source code can be freely copied and distributed. EPANET allows steady state and time extended simulation calculations of the hydraulic state of a given looped pipe network including control devices. EPANET uses the Gradient Method by Todini and Pilati (1987) to solve the hydraulic state. The node-orientated approach treats control valves with certain heuristics.

In some circumstances such as less complex mainly branched networks the EPANET solver is faster than the KANET solver. Therefore, the main reason for integrating EPANET was the possibility of using its calculation algorithm. It is thought to combine the two algorithms in order to optimize calculation speed. EPANET could be used to solve the branched parts of the network while KANET solves the core of the network. Anyhow, as mentioned above, KANET guarantees the convergence, which EPANET in certain cases does not (Simpson, 1999; Deuerlein, Simpson and Gross, 2008). For connecting EPANET directly to the KANET DLL and ArcMap the DLL version of EPANET has been enhanced. The data for hydraulic calculations with EPANET is provided by the KANET DLL. The data is transferred by DLL-calls. Next, KANET triggers EPANET to calculate the hydraulic state of a time-step. After receiving the calculation results KANET triggers EPANET to calculate the next time-step. This procedure is continued until all time-steps of the simulation period have been calculated. Finally, KANET signals to the calling tool in ArcMap that the calculation is finished. The results can be displayed. Hence, there is no need for exporting and importing the data to a separate file. It is possible to load data into EPANET without creating an EPANET input file (*.inp). But the EPANET input file can be written by the enhanced EPANET DLL. Thus, EPANET itself is the export function to EPANET files.

User interface with integrated Water distribution network toolbar

ArcMap serves as the GUI of the integrated tool. The functionalities of all applications to edit, manage or analyze data concerning the modeled water distribution system are integrated into ArcMap as a toolbar (Water distribution toolbar, Figure 1). Geo-spatial data and the related attributes not concerning the distribution system can be edited, managed and analyzed using the common GIS-functionalities of ArcGIS. Figure 3 shows the GUI of ArcMAP and the integrated French version of the Water distribution network toolbar. Further, dialogs of the editing and information tools are shown.

An alternative for editing the water distribution system data and for hydraulic analysis calculations is the GUI of the stand-alone version of KANET. It accesses the same database as ArcMap and features read and write capability of ArcMap shape information. Therefore, import or export functions are not needed. The data is consistent and displayed equally in both user interfaces.

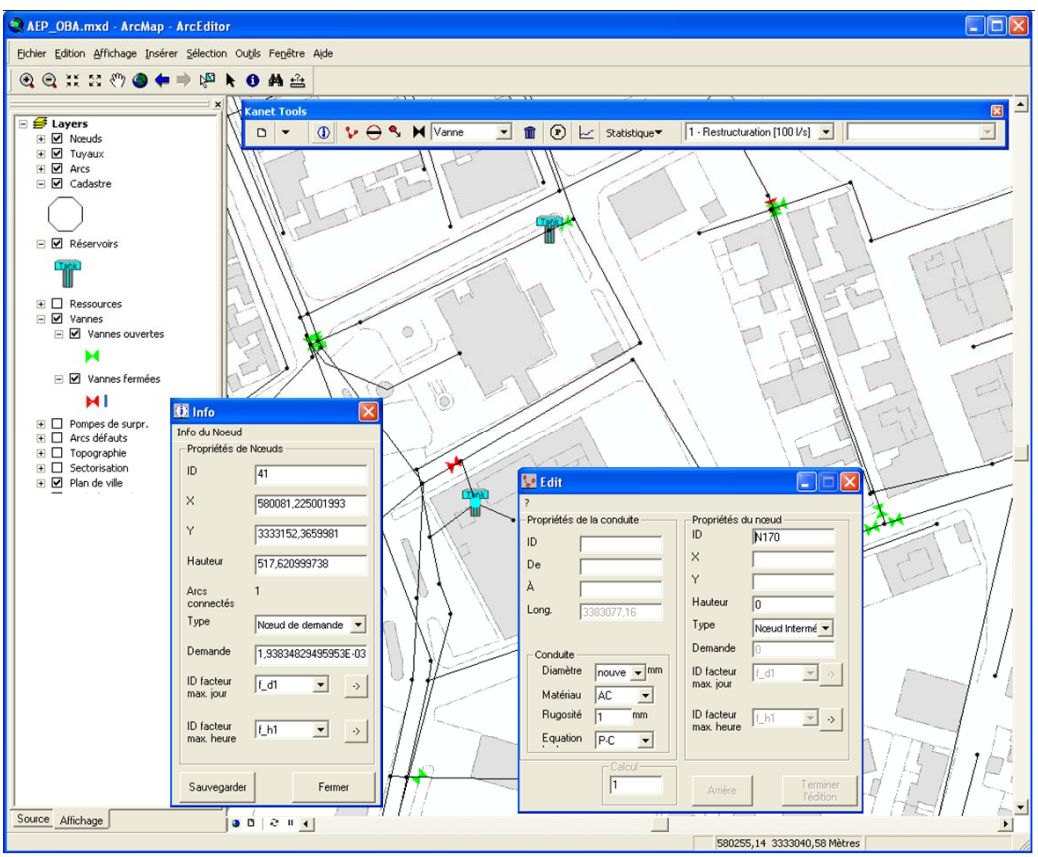

Figure 3: GUI of the integrated hydraulic analysis and data management tool

3. LINKED STANDARDIZED PROCESSES

Water distribution networks are dynamic technical systems changing rapidly due to maintenance works and network extensions (Roscher, 2006). Therefore, the foundation for all technical tasks to assure a sustainable water supply is the deep going knowledge of the system. This paper presents a novel integrated data management and hydraulic analysis tool for water supply networks and linked work-flows specially tailored towards its application in developing countries. The tool is described in Section 2. In this section, the standardization and linking of the work-flows to update the network register and to characterize defects are presented.

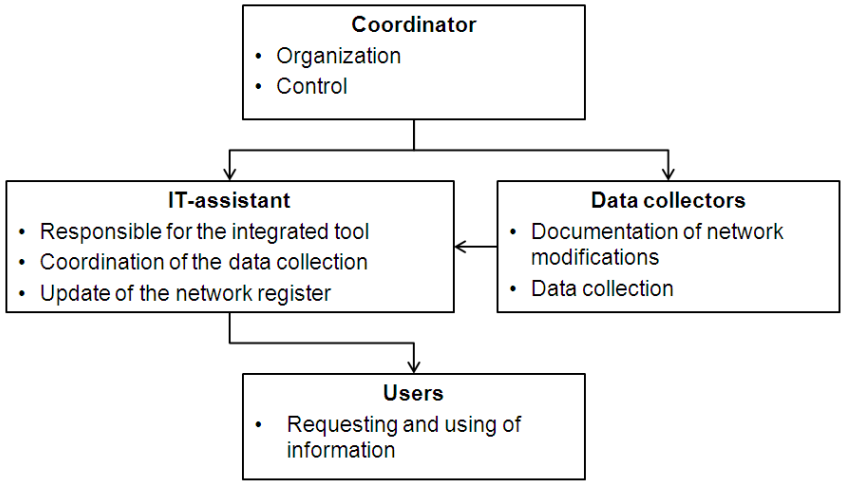

Figure 4: Organization of the data collection and network register update

To update the network register of the integrated tool a process with a questionnaire was developed (see Figure 4). A trained expert coordinates the overall process and controls the quality of the work. The IT-assistant exclusively works with the integrated tool. The assistant initializes a data collection at certain points in the network. Therefore, a questionnaire with a unique ID generated automatically in the network register is handed to the Data collectors. The Data collectors are favourably technicians of the maintenance sections of the water utility. The collectors document the physical attributes of the surveyed pipe section in the questionnaire following a given catalogue. Further, the location of the pipe section is documented referring to existing buildings etc. since the lack of knowledge is often a major problem. Hence, the pipe section can be detected even though the real-world coordinates of the section are still not known. The network register is updated by the assistant based on the documentation. The questionnaires are scanned and object based saved in the network register. The progress of the update and data collection can be visualized spatially. Additionally, the collectors document modifications of the network during their daily work. The corresponding questionnaires are handed over to the assistant to update the network register.

A second standardized process has the objective to characterize and document defects and its repairs. Therefore, a second questionnaire has been developed. In the questionnaire all necessary steps from the announcement, the survey of the defect to the repair of the defect are documented. The process is integrated into the organization of the process to update the network register (see Figure 4). The data is saved object based in the network register. Related reports and statistics are generated automatically.

4. APPLICATION IN BÉNI ABBÈS, ALGERIA

Initial situation and given data base

The oasis city Béni Abbès with approximately 13.500 inhabitants is located in the north-western part of the Algerian Sahara desert. The water supply is deficient in terms of water quality and water quantity distributed to the customers. The main deficiencies concerning the network are the complex topology with no pressure zones, the bad state of the infrastructure and the intermittent and intuitive operation. The lack of knowledge of the network results in unplanned network extensions, the impossibility of a proper maintenance and the intuitive system operation.

Within an integrated water resources management project of the German-Algerian technical cooperation the deficient water supply of the city will be rehabilitated (Klingel and Deuerlein, 2008). Amongst other topics, in the subproject *drinking water supply* a network register and a hydraulic model was set up. Therefore the IWG has developed and implemented the adapted integrated hydraulic analysis and data management tool.

Two public institutions are responsible for the water supply. In none of the two institutions exists a network register or some kind of data management. The only existing data of the infrastructure of the water distribution network are hardcopy plans made by an Algerian consultant. Verifications in the field have shown that the available data is unreliable to a high grade. Therefore the knowledge of the system is limited to the personal knowledge of a few employees. The risk of losing information or not having it available when needed is obvious.

Implementation of the network model

First, the available hardcopy plans of the system were digitized in order to implement a basic network register. A topographical survey delivered the necessary data to develop a digital land model. The elevations of the model nodes were generated automatically by merging the land model data and the nodes of the basic system graph. To clarify the most important topological aspects additional data were collected in the field. Accordingly, the existing data were verified in the field to plan the successive update of the network register.

By using the toolbar of the integrated tool the topology of the hydraulic model is generated automatically. This eased the modeling process resulting in immense time savings. Thus, together with the basic network register a basic hydraulic model

was set up. To complete the basic model further parameters had to be input. Consumption data was determined based on the population distribution. The demand data was allocated using the Thiessen-application of the integrated tool. The consumption behavior assuming a continuous supply was determined in a field study. Further, the tank geometries and pump characteristics were collected.

Process of data collection and model update

The data model of the integrated tool was implemented and updated by the IWG to an accuracy which allowed the planning of the restructuring of the network in order to introduce and establish a continuous water supply. The necessary further update of false information and the never ending process of updating the network register due to the dynamic nature of a distribution network were initialized by the IWG and will be carried out by the local staff of the water utilities. Therefore the above described (see Section 3) method for systematic update of the network register was developed. System elements are characterized and measured during data collection campaigns or maintenance works. The data is recorded in standardized questionnaires. Afterwards, the data is digitized in the network register. The employees are participating in ongoing trainings. The trainings are mostly on-the-job to consolidate the processes within the daily work. In near future the employees should be in the position to work and update the integrated tool independently.

Application of the tool for the planning of the restructuring

Based on a deficiency analysis, a concept for the rehabilitation and restructuring of the network was developed. The superior concept divides the network into pressure zones supplied by tanks by gravity. The pressure zones can be divided in subzones to allow water balances, leak detection and the successive introduction of continuous supply. The network restructuring with the necessary exchange, shut down and implementation of pipes was planned in an iterative process. The current topology was analyzed and the pressure zones were designed using the graph decomposition application. Simulation calculations were used within sensitivity studies to dimension the pipes and design the operation. During the planning, additional punctual surveys were made to update the network register successively. Two test periods in a pilot subzone were accomplished to proof the feasibility of a continuous supply and to sensitize the customers. The network data of the subzone will be updated completely within trainings of the local operators. The data collection campaigns have already started and will be finished before the final introduction of continuous supply. Klingel and Deuerlein (2008) detailed describe the network restructuring and the introduction of continuous water supply in Béni Abbès.

5. SUMMARY AND CONCLUSION

In developing countries the available system data of water distribution networks are often not up-to-date and of poor quality. The data are kept in hardcopy network

registers or single maps. Accordingly, hydraulic models are rarely applied successfully. One reason is the lack of adequate data. In this article a hydraulic analysis and data management tool for water distribution networks specially tailored towards its application in developing countries has been presented. By integrating the applications for data management, data preprocessing for hydraulic modeling and hydraulic analysis a data exchange between the applications is no longer necessary. Database consistency is achieved and the subsequent database update is simplified. Further, the work-flow for data collection is linked to the tool to ease the organization and to promote transparency. The application of the tool within the IWRM project in the oasis Béni Abbès was demonstrated. It is thought to transfer the developed IWRM concept to neighboring oases. The tool will be available for application along with manuals and concepts for the implementation.

6. ACKNOWLEDGMENTS

The project *IWRM for oases* in Béni Abbès, Algeria is part of the *Integrated Water Management Programme* of the *Deutsche Gesellschaft für Technische Zusammenarbeit (GTZ) GmbH* and financed by the *German Federal Ministry for Economic Cooperation and Development (BMZ)*. The authors would like to thank for financial support.

7. REFERENCES

Cornell R. and Dunphy, J. (2005). "Water Distribution System Asset Management - Needs and Nice to Have." *Journal of the American Water Works Association*. http://www.hatchmott.com/documents/adobe/Cornell%20-%20Water%20Distribution%20System%20Asset%20Management.pdf (Jan. 26, 2009).

Deuerlein, J., Cembrowicz, R. G. and Dempe, S. (2005). "Hydraulic simulation of water supply networks under control." *Proceedings of the World Water and Environmental Resources Congress EWRI05, 7th Annual Symposium on Water Distribution Systems Analysis*, ASCE Conf. Proc., 173, 24.

Deuerlein, J. (2008). "Decomposition Model of a General Network Graph." *Journal of Hydraulic Engineering*, ASCE, 134, 822-832.

Deuerlein, J., Simpson, A. R. and Gross, E. (2008) "The never-ending story of modeling control-devices in hydraulic systems analysis." *Proceedings of the 10th International Water Distribution System Analysis conference*, 832-843.

Farley, M. and Liemberger, R. (2005). "Developing a non-revenue water reduction strategy: planning and implementing the strategy." *Water Science and Technology: Water Supply*, 5(1), 41-50.

GTZ (2008). "Integrated water management programme." Deutsche Gesellschaft für Technische Zusammenarbeit (GTZ) GmbH, http://www.eau-algerie.org/index.php?id=7&L=2> (Dec. 9, 2008).

Kumar, A. (1997). "Leakage control in intermittent water supplies." *Water Supply*, 15(1), 55-58.

Kumar, A. (1998). "Technologies to improve efficiency in distribution system with intermittent supplies." *Water Supply* 16(1/2), 576-579.

Klingel, P. and Deuerlein, J. (2008). "Rehabilitation Strategy for Water supply Systems in Developing Countries - Case Study IWRM Oasis Béni Abbès, Algeria." *Proceedings of the 10th International Water Distribution System Analysis conference*, 150-162.

Ormsby, T., Napoleon, E. and Burke, R. (2004). *Getting to know ArcGIS desktop*, Environmental Systems Research Institute, 2. edition.

Roscher, H. (2000). *Sanierung städtischer Wasserversorgungssysteme*, Verlag Bauwesen, Berlin, 1. Auflage.

Rossmann, L. A. (2000). "Epanet 2 Users Manual." *EPA/600/R-00/057*, Water Supply and Water Resources Division, National Risk Management Research Laboratory, Environmental Protection Agency, Cincinnati, OH.

Simpson, A. R. (1999) "Modeling of Pressure Regulating Devices - A Major Problem Yet to be Saitsfactorily Solved in Hydraulic Simulation." *Proceedings of the Water Distribution System Analysis Conference*, Tempe, Arizona.

Todini, E. and Pilati, S. (1987). "A gradient method for the analysis of pipe networks." *Proceedings of the International Conference on Computer Applications for Water Supply and Distribution*, Leicester.

Trifunović, N. and Vairamoorthy, K. (2008). "Use of demand-driven models for reliability assessment of distribution networks in developing countries." *Proceedings of the 10th Annual Water Distribution Systems Analysis Conference*, 129-141.

The Impacts of Demand Variability on Distribution System Hydraulics and Transport

Xueyao Yang* and Dominic L. Boccelli†

Department of Civil and Environmental Engineering
University of Cincinnati, P.O. Box 210071, Cincinnati, OH 45221

*PH: 513-378-9651, email: yangxueyao@gmail.com
†PH: 513-375-6901, email: dominic.boccelli@uc.edu

Abstract

A stochastic water demand generator (PRPsym) and a well known distribution system network solver (EPANET) were linked together to analyze the impact of water demand variability on the underlying hydraulics and transport in a distribution system. The modified EPANET example 2 network model was used as a template and test network model for both hydraulic and water quality simulations at three different temporal aggregations (1-hour, 10-minute, and 1-minute). The mean, standard deviation and coefficient of variation at each hour for both hydraulic and water quality parameters were calculated for all nodes or links. Results showed that decreasing temporal aggregation of the water demands leads to increased flow rate variability. The increase in flow rate variability is related to the increased demand variability and the localized flow reversals that alter the travel path. The increase in flow rate variability was more evident in the links located at edges of the system rather than the main trunk lines. In addition to the hydraulics, water age simulations – used as a water quality surrogate – indicate that increased demand variability can significantly impact water quality simulations by altering residence times and travel paths. These preliminary results suggest that there are likely portions of a distribution system where typical modeling assumptions do not adequately represent localized water quality conditions.

1 Introduction and Objectives

Drinking water distribution systems are important and efficient devices for conveying water to consumers. However, operators face significant challenges in understanding and managing these systems since water quality in the distribution system deteriorates between the treatment plant and the consumers' tap. This issue has led to an increase in the modeling of transport and transformation of water quality constituents through drinking water distribution systems. In recent years, distribution system network models have become increasingly utilized for water quality analysis and advanced technical management, such as optimal sensor placement (Berry et al., 2006; Propato, 2006) and monitoring site selection for

the initial distribution system evaluation associated with the Stage 2 Disinfectants and Disinfection Byproduct Rule (USEPA, 2006). All of these require accurate representation of contaminant transport and water quality dynamics. Thus, accurate water demands – the factor primarily responsible for driving distribution system hydraulics and most influences the overall response of water distribution networks (Garcia et al., 2004) – are vital for adequately representing transport as well as performing network calibration, validation, and simulation.

Demands are inherently variable (e.g., daily and seasonal) and impact the underlying hydraulics and transport. Typical network modeling assumes deterministic demands (i.e., known and constant for short time periods) with temporal changes perfectly correlated in space. These deterministic assumptions generally focus on understanding the average hydraulic conditions without considering the impact that the intrinsic demand variability might impart on system dynamics. For a highly skeletonized system, these assumptions might be appropriate as the spatial aggregation of plentiful consumptive demands would likely reduce the overall impact of demand variability (due to averaging). However, as the industry moves towards "all-pipes" models, the loss of demand variability information through the use of deterministic demands may no longer adequately represent transport through the system. For example, when considering a residential area, the duration of any demand event is generally much shorter than a 1-hour time frame (Buchberger and Wells, 1996). The short demands can be quite variable during any 1-hour time frame and may include significant time fractions where the demands are zero. Therefore, the "smoothing" of the demands using typical network modeling approaches may not realistically represent the transport associated with these demands, which ultimately impacts the water quality description.

Overall, the objective of this study intends to investigate the potential impacts of demand variability over a range of spatial and temporal scales for representing transport through a distribution system. The current research is focused on analyzing the impacts of demand variability at three different levels of temporal demand aggregation (e.g., 1 hour, 10-minute, and 1-minute) on the underlying hydraulics and transport.

2 Methodology

Recognizing the natural randomness of network water demands, Buchberger and Wu (1995) proposed a non-homogeneous Poisson Rectangular Pulse (PRP) model to characterize the stochastic nature of residential water demands. The PRP model is the basis for PRPsym, a C-code developed for generating random water demands via Monte Carlo simulation. PRPsym assumes that the average network demands are known on an hourly basis and represents those hourly water demands through a sequence of rectangular pulses that represent individual water uses. The occurrence of each pulse is governed by a Poisson process; the intensity and duration of the demands are represented by log-normal distributions and

the resulting series of pulses are compiled by PRPsym into second-by-second demands for the simulation duration. Finally, the PRPsym produces time-averaged demands from the second-by-second data for any user defined time scale (Li and Buchberger, 2005). The ability of the PRPsym algorithm to generate demands at varying time aggregation allows the impacts of demand variability on distribution system hydraulics and transport dynamics to be evaluated.

3 Test Network and Simulation Experiments

3.1 Test Network

Figure 1 shows the test network – the modified EPANET Example 2 distribution system – including the node and pipe identification numbers. The system consists of 35 nodes, 40 pipes, 1 tank, and a pump station that operates based on the level of the tank. The pump station and the tank operate in a cyclical manner and alternatively serve as the supply source for the water demands in the system. When the pump is on, the tank is generally receiving water flowing up from the south along the main trunk line. When the pump is off, the tank acts as a source to transmit the water to both the south and the north. All of the nodes in the model are represented by the same, singular demand pattern.

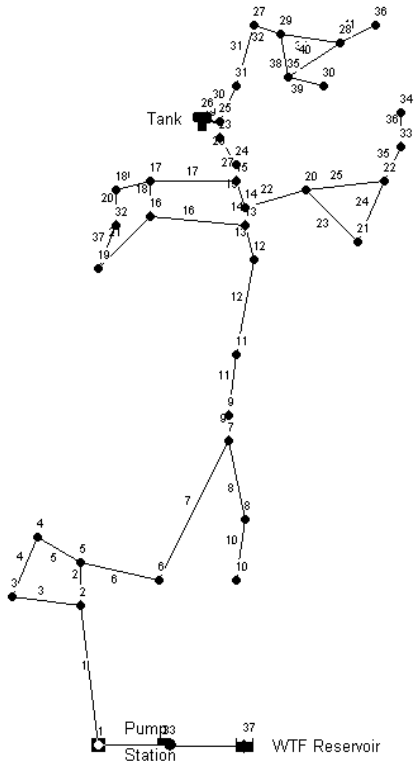

Figure 1: The modified EPANET Example 2 distribution system.

3.2 Simulation experiments

The EPANET toolkit (Rossman, 2000) was linked with PRPsym to perform the hydraulic and water quality simulation. PRPsym is used to generate a series of new EPANET input files with each node receiving its own unique 24 hour demand multiplier with respect to the three different time aggregation intervals (1 hour, 10-minute, 1-minute). From the simulations, parameters regarding both the hydraulics (demand, pressure, and flow rate) and water quality (water age as a surrogate) were collected at the three different levels of temporal aggregation (1-hour, 10-minute, 1-minute). The hydraulic simulations were performed with a 24 hour duration while the duration for water quality simulations was 720 hours. The lengthy water quality simulations were required to overcome the initial conditions in the network model, and allowed the system to achieve approximate stationarity. The 1-hour temporal aggregation was used as the benchmark deterministic case (equivalent to "typical" modeling approaches) and the deterministic results compared with the information from the other two temporal aggregations. Statistical measurements from the 10-minute and 1-minute temporal aggregations used in the comparison include the weighted average, standard deviation, and coefficient of variation (COV) calculated for both the 10-minute and 1-minute time aggregation intervals over each 1-hour time period. The coefficient of variation, defined as the ratio of the standard deviation to the mean, was used as a metric to show the relative variability on the metrics of interest for the temporal aggregation steps.

4 Results

The following sections present preliminary results associated with the impacts of temporal aggregation on consumptive demands with respect to pressure, flow rate, and water age (a rough surrogate for water quality). All of the results are based on a single realization of demands for a simple distribution system model. Additional effort will be placed on assessing the impacts from a more complete Monte Carlo ensemble as well as tested on a large, all-pipe network model.

4.1 Water demand variability

PRPsym provides the capability to maintain the same average hourly demands as the benchmark scenario (constant, 1-hour demands) for the 10-minute and 1-minute time aggregations. The functionality to maintain the same average demands for each temporal aggregation scenario ensures that the only difference between the cases is the demand variability at smaller time aggregations. In general, PRP theory indicates that demand variability will increase with decreasing time scale, and this relationship has been observed from measured demand data (Moughton et al., 2006).

Results from all 35 nodes illustrate this theory, and the demands from Node 10 have been selected as an example to represent the time series demands under the three different temporal aggregations. Figure 2 shows that as the temporal aggre-

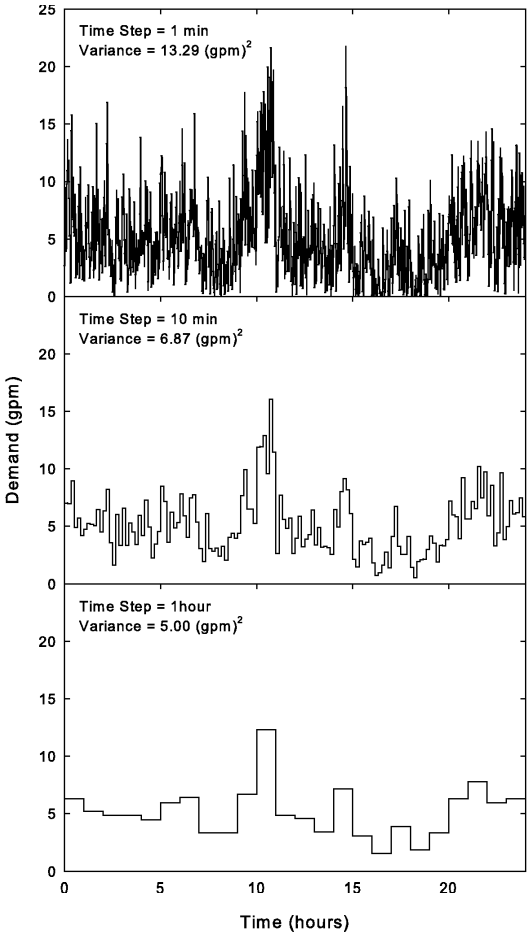

Figure 2: Time series of demands for node 10 for temporal aggregation scales at 1-minute, 10-minute and 1-hour.

gation increases, the average demands are "smoothed" with the demand variance decreasing from 13.25 $(\text{gpm})^2$ to 5 $(\text{gpm})^2$. The increasing temporal aggregation not only reduced the large peak demands, but also removed any instances of zero demands. While demand variability can be shown to increase with decreasing temporal aggregation, the remaining data needs to be evaluated to assess the impact that demand variability has on the underlying hydraulic and transport characteristics.

4.2 Pressure

Recognizing that demand variability will result in hydraulic and transport variability associated with the scale of temporal aggregation, pressure was selected as an initial parameter to evaluate the possible influence of demand variability on system hydraulics. Node 10 is selected as representative of the simulation results for all 35 nodes. Figure 3 shows that the mean and COV of the simulated pressure at node 10 at each hour for the 10-minute and 1-minute time aggregation simu-

lations. These results show there is little variability in the pressure data during the simulation period. Results from the other nodes are similar suggesting that demand variability has little influence on the pressure of this system.

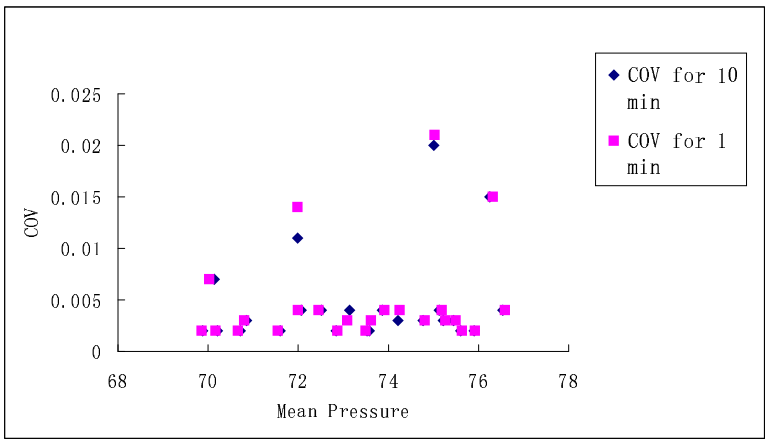

Figure 3: The COV value for pressure at node 10 for temporal aggregation of demands at 10-minute and 1-minute.

4.3 Flow rate

The influence of demand variability on flow rate provided an analysis challenge. As mentioned in section 3.1, the pump and tank alternate as sources to the system, which results in significant flow reversals throughout the system. Within EPANET, the directional component of flow rates are designated with a '+' or '-' coefficient. Therefore, during the 1-hour intervals where a flow reversal occurs, the estimated variance is much higher than at other times (due to the incorporation of both "positive" and "negative" flows). In order to eliminate the influence of the flow reversal conditions, and perform a better analysis of the flow rate variability by time aggregation, the simulations were separated into two scenarios: pump on and pump off. Results from one realization of the 10-minute and 1-minute aggregation scenarios showed that, for almost every link at all times, flow rates from the 1-minute temporal aggregation have higher COV values compared to those of the 10-minute temporal aggregation. There are only a few singular cases where the results were reversed, and were associated with flow reversals due to random changes in nodal demands, which will be further investigated at a later time.

To illustrate flow rate variability, a subset of pipes were selected to represent the spatial differences of variability in the system. These links include some in the main trunk line (link 2 and link 7), some associated with dead ends (link 10, 36, 39, 41), and others at branches (link 24). Figure 4 and Figure 5 compare the hourly flow rate COV values for the 10-minute time aggregation against the 1-minute time aggregation for "pump on" and "pump off" status, respectively. From

the two figures, two generalizations can be made associated with the temporally aggregated values for this system. First, all of the flow rate COV for the 1-minute aggregation step are greater than the 10-minute aggregation step (i.e., all data are above the "y=x" line, which is provided as the solid line in the figures). This data illustrates that the general concept of the PRP model (i.e., increased variability at smaller time aggregations) holds even for an interconnected distribution system. Second, the dead end and branch pipes have much greater COV values for both 10-minute and 1-minute time aggregation steps than the main trunk line pipes. The COV values for the main trunk lines are very small and appear to be located at the (0,0) point on both figures. As for the branch pipe (link 24), the COV is generally higher than the dead end pipes as a result of flow reversals that occur within the pipe (as before, the directional component needs to be accounted for in the analysis). This result confirms the (probable) intuitive insight that the stochastic nature of demands would have more of an observed impact at the edges of the distribution system than in the main trunk lines.

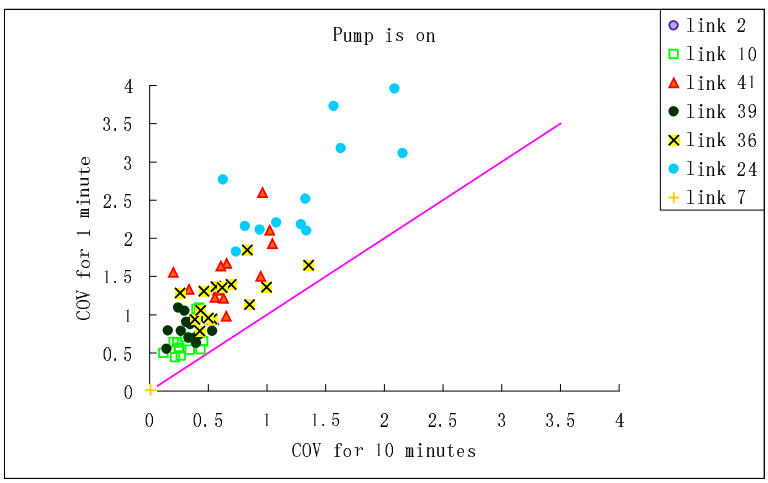

Figure 4: Flow rate COV comparison of the 10-minute and 1-minute temporal aggregations for selected links when the pump is on.

To further illustrate overall network response to time aggregation, the average COV for each pipe over the 24 hour simulation duration was computed for both the 10-minute and 1-minute cases and the differences between them calculated. These differences were projected onto the EPANET map to illustrate the spatial impacts of temporal aggregation on the flow rate variability over the entire network. Figure 6 shows the differences in flow rate COV due to the temporal aggregation (COV_{1-min} minus COV_{10-min}). This map illustrates that in the main trunk line, since the flow rate is relatively high, the COV value changes are relatively low between the two time aggregation steps, which is consistent with the data in Figures 4 and 5. At the edges of the system, where the links have

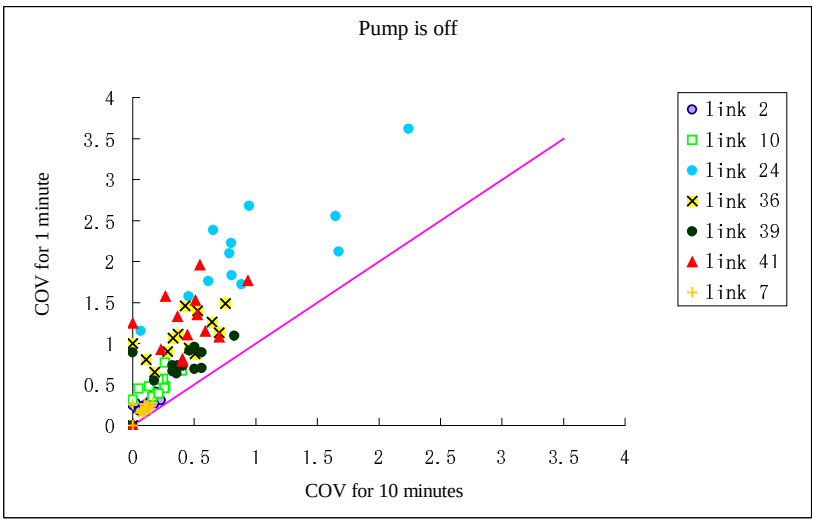

Figure 5: Flow rate COV comparison of the 10-minute and 1-minute temporal aggregations for selected links when the pump is off.

much smaller flow rates, the change in COV values is much greater. All of these results demonstrate the temporal aggregation of water demands leads to greater influence on flow rate variability at the system edge than in the main trunk line. However, while these results indicate that flow rate variability is impacted by the temporal aggregation (and ultimately transport), to truly understand the impacts associated with transport additional water quality simulations must be performed.

4.4 Water quality

Hydraulic residence time (water age) was used as a surrogate for water quality analysis for two reasons: 1) water quality, in general, is negatively impacted by longer residence times, and 2) significant differences in travel paths should result in observable differences in the simulated water age. Figure 7 shows the simulated water age data of node 29 from the last 24 hours of a 720-hour duration water quality simulation using the 1-minute, 10-minute, and 1-hour time aggregation steps. From Figure 7 there are two noticeable observations. First, there is a clear distinction regarding when the water is coming from the reservoir (water age $\leq$ 20 hours) or tank (water age $\geq$ 100 hours). Second, the short time aggregation steps indicate larger variability (although not very significant) in water age when the water is being fed from the reservoir. When the tank is feeding node 29 the increase in age continues to increase almost uniformly. However, by moving just a short distance downstream to node 30 the difference in water age results at the three time aggregations are significantly different. Figure 8 presents the simulated water age of node 30 from the last 24 hours of a 720-hour simulation. While the shapes of the water age data are generally the same for all three time aggregations, the shorter duration simulations show much greater variability than

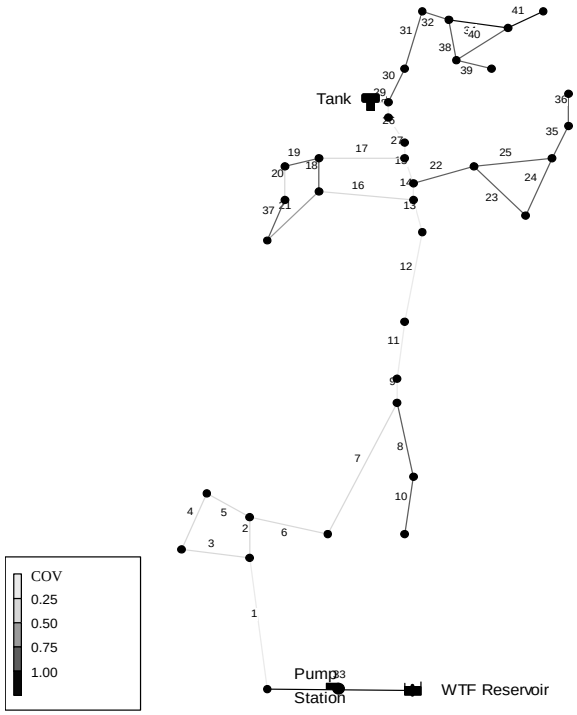

Figure 6: The overall network response to the change of time scale .

the 1-hour simulations. The increased variability results primarily from the flow reversals that occur between nodes 28 and 35. This indicates that a dynamic water quality parameter might exhibit significant variation at some points in the distribution system where the stochastic nature of the demands can impact travel paths. Ultimately, the influence of water demand variability on water quality may be much more complex and challenging than it appears to be for this simple network. Additional studies will be performed to further investigate the possible water quality implications for ubiquitous chemicals (e.g., disinfectant residuals) and for short-term contamination events

5 Summary and Future Work

In general, residential consumptive demands have been represented by a stochastic process model. As the drinking water industry moves towards more "all-pipe" network models and water quality applications where transport characteristics are more important, the role of stochastic demands may be significant in understanding and modeling distribution systems. The objective of this study was to perform a preliminary analysis by simulating the impacts of stochastic demands at multiple temporal aggregations on factors that impact hydraulics and transport characteristics.

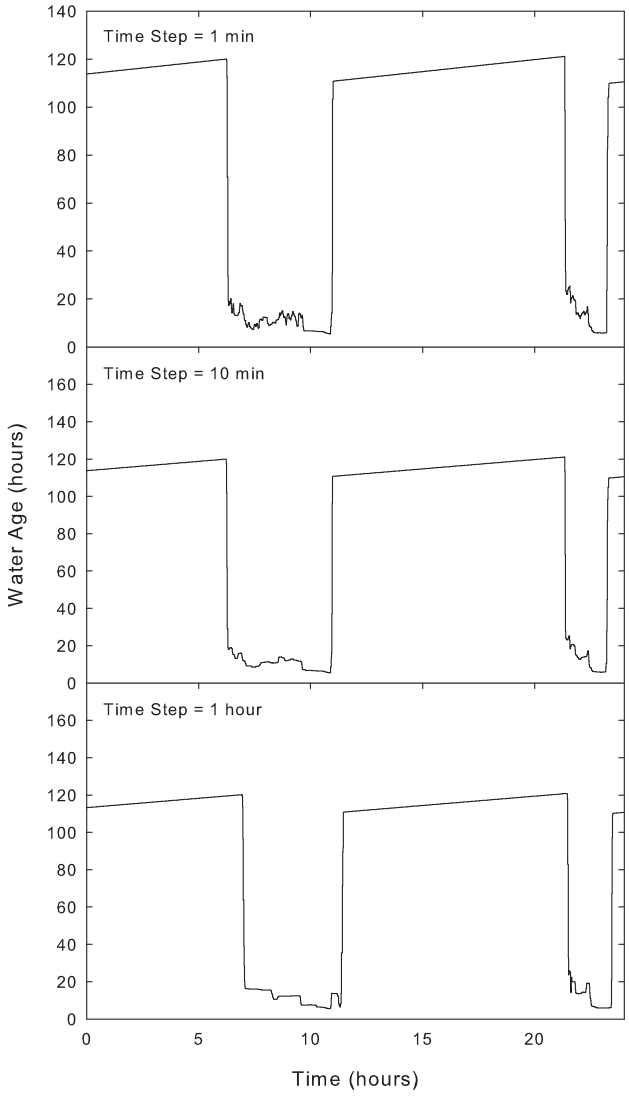

Figure 7: Time series of water age for node 29 for temporal aggregation scales at 1-minute, 10-minute and 1-hour.

From the preliminary analysis performed in this study, demand variability had an influence on this small network that varied with respect to the metric considered. From a hydraulic standpoint, the demand variability had very little impact on pressure, but did result in flow rate variability in parts of the system. For the main trunk lines, the demand variability had virtually no effect on the flow rates. However, as the branch and dead-end pipes were analyzed, there was an increase in flow rate variability that also correlated to decreasing temporal aggregation. As the industry moves towards more "all pipes" models, the impact of demand variability on flow rates may play a more important role. With respect to transport aspects, the water age analysis also illustrated that decreasing temporal aggregation increased variability, but a more significant impact on the water age

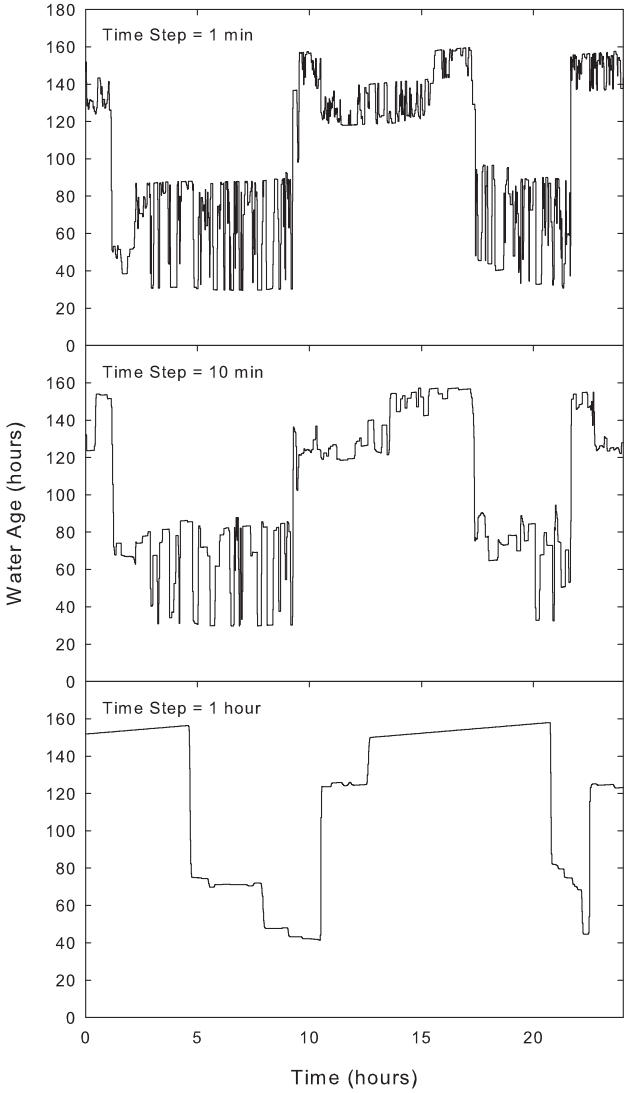

Figure 8: Time series of water age for node 30 for temporal aggregation scales at 1-minute, 10-minute and 1-hour.

variability was observed when the demand variability impacted the resulting flow path.

While the current study suggests that demand variability can have an impact on distribution system hydraulics and transport, these results are preliminary and performed with a single realization of demands on a relatively small network model. Future studies associated with temporal aggregation will consider: 1) a larger Monte Carlo ensemble of demand pattern realizations; 2) two additional water quality cases that consider a ubiquitous parameter (e.g., a disinfectant) and a short-duration event; and 3) extend the analysis to an "all-pipes" network model that consists of approximately 10,000 nodes. The objectives of these studies will

be to better understand the characteristics of distribution systems and problem types that are significantly impacted by demand variability.

6 Acknowledgement

The authors sincerely appreciate the help of Dr. Zhiwei Li, who helped in the understanding and utilization of the PRPsym code for generating EPANET input files.

References

Berry, J., W. E. Hart, C. A. Phillips, J. G. Uber, and J.-P. Watson (2006). Sensor placement in municipal water networks with temporal integer programming models. *Journal of Water Resources Planning and Management 132*(4), 218–224.

Buchberger, S. G. and G. J. Wells (1996). Intensity, duration, and frequency of residential water demands. *Journal of Water Resources Planning and Management 122*(1), 11–19.

Buchberger, S. G. and L. Wu (1995). Model for instantaneous residential water demands. *Journal of Hydraulic Engineering 121*(3), 232–246.

Garcia, V. J., R. Garcia-Bartual, E. Cabrera, F. Arregui, and J. Garcia-Serra (2004). Stochastic model to evaluate residential water demands. *Journal of water resources planning and management 130*(5), 386–394.

Li, Z. and S. G. Buchberger (2005). *PRPsym User's Manual*. Cincinnati, OH: University of Cincinnati.

Moughton, L. J., S. G. Buchberger, D. L. Boccelli, Y. R. Filion, and B. W. Karney (2006). Effect of time step and data aggregation on cross correlation of residential demands. In *Proceedings of the Water Distribution System Analysis Symposium*, Cincinnati, OH.

Propato (2006). Contamination warning in water networks: General mixed-integer linear models for sensor location design. *Journal of Water Resources Planning and Management 132*(4), 225–233.

Rossman, L. A. (2000). *EPANET2 User's Manual*. Cincinnati, OH: Risk Reduction Engineering Laboratory, U. S. Environmental Protection Agency.

USEPA (2006). *Initial Distribution System Evaluation Guidance Manual*. Washington, D.C.: Office of Water, U. S. Environmental Protection Agency. EPA 815-B-06-002.

Augmented Gradient Method for Head Dependent Modelling of Water Distribution Networks

Calvin Siew and Tiku T. Tanyimboh
Department of Civil Engineering, University of Strathclyde, Glasgow G4 0NG, UK
Email: calvin.siew@strath.ac.uk, tiku.tanyimboh@strath.ac.uk

Abstract

When analysing a pressure deficient network, it is crucial that the pressure dependent nature of nodal outflows be taken into account. The head dependent analysis (HDA) produces an accurate representation of the nodal outflows and network hydraulic performance. This is essential when modelling pipe leakages, network redundancy and reliability. These are vital aspects often considered in the optimization of a water distribution system (WDS). This paper describes an approach for head dependent analysis in which an embedded function for the head-outflow relationship is incorporated in the Gradient Method (GM). The procedure is capable of simulating both normal and deficient network operating conditions effectively. Results based on networks from the literature show that the proposed method is robust and converges smoothly and rapidly.

Keywords: demand-driven analysis, evolutionary computing, head-dependant modelling, head-outflow relationship, nodal outflow function, optimization, water distribution systems, augmented gradient method.

Introduction

Most of the available hydraulic simulation models for water distribution systems (WDSs) are based on demand-driven analysis (DDA). DDA assumes that all nodal demands are satisfied at all times, disregarding the fact that nodal outflows are pressure dependent. Hence, this method is only sufficient for analysing a network under normal operating conditions. The DDA becomes inadequate when considering pressure deficient scenarios such as major mechanical and hydraulic failures, fire-fighting flows etc, as it is prone to yield very low or even negative pressure values at some nodes. A solution to this problem is the head dependent analysis (HDA) method which considers the relationship between pressure and outflow. By applying this method, one would be able to identify the problematic nodes along with the exact magnitude of deficiency in terms of nodal pressure and outflow.

There are several head-outflow relationships, for instance Tanyimboh and Templeman (2004), Wagner et al. (1988), Fujiwara and Ganesharajah (1993), Germanopoulos (1985) are but a few. This paper introduces an algorithm which

incorporates the Tanyimboh and Templeman (2004) function within the Gradient Method (GM) (Todini and Pilati 1987). This proposed simulation model will be referred to as the head dependent GM (HDGM). Ultimately, the goal is to embed this pressure-outflow relationship within EPANET 2, converting it from a DDA to a HDA hydraulic network solver. This would be advantageous as HDA can then be explicitly applied to the extended period simulation and water quality analysis. After presenting a brief introduction of the Tanyimboh and Templeman (2004) function and GM, the HDGM is demonstrated. For reasons of simplicity, elements such as pumps, valves and other dissipation devices have not been included in the simulation model.

Head Outflow Relationship

Previous work shows that the Tanyimboh and Templeman (2004) function is computationally efficient. Compared to other head-outflow relationships, this function is unique in that it has no discontinuities in its function and/ or derivatives. This allows a smooth transition between zero and partial nodal outflow and between partial and full demand satisfaction, avoiding convergence difficulties in the computational solution of the system of constitutive equations. The Tanyimboh and Templeman (2004) function can be described as:

$$Qn_i(Hn_i) = Qn_i^{req} \frac{\exp(\alpha_i + \beta_i Hn_i)}{1 + \exp(\alpha_i + \beta_i Hn_i)} \tag{1}$$

where Qn_i and Hn_i are the outflow and head, respectively, at the demand node i. Qn_i^{req} is the required supply at node i. Both α_i and β_i are parameters to be calibrated with relevant field data. Figure 1 clearly depicts the basic form of the function. Further details of this function can be found in Tanyimboh and Templeman (2004).

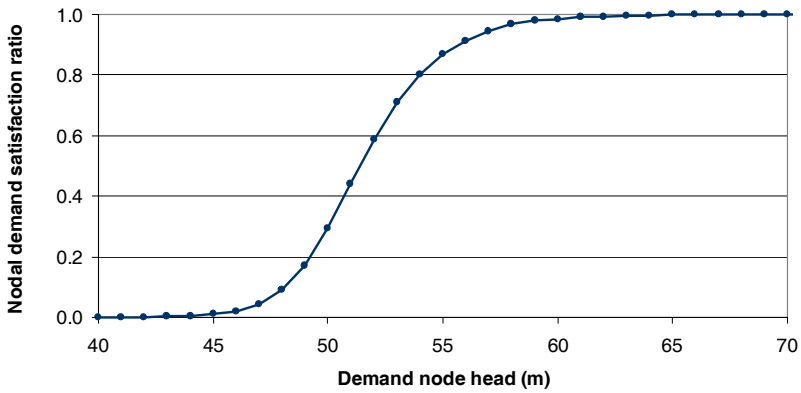

Figure 1. Tanyimboh and Templeman function (elevation= 45m, desired head= 60m)

Pressure Dependent Demand Simulation Model

A network hydraulics model is defined through a set of equations corresponding to two conservation laws, namely mass balance at nodes and energy conservation along hydraulic links. These equations can be solved simultaneously using a unified formulation such as the GM as described below:

$$\begin{bmatrix} A_{11} & \vdots & A_{12} \\ \cdots & \cdots & \cdots \\ A_{21} & \vdots & A_{22} \end{bmatrix} \begin{bmatrix} Qp \\ \cdots \\ Hn \end{bmatrix} = \begin{bmatrix} -A_{10}H_0 \\ \cdots \\ 0 \end{bmatrix} \tag{2}$$

where A_{11} represents the diagonal matrix whose elements are the $K_j(Qp_j)^{n-1}$. K_j and n are the pipe resistance coefficient and flow exponent in the head loss formula respectively. Qp_j is the flow rate in pipe j. The overall incidence matrix relating the pipes to nodes with unknown and known heads is represented by A_{12} and A_{10} respectively. A_{21} is the transpose of A_{12}. Qp denotes the column vector of unknown pipe flow rates. Hn and H_0 are column vectors for unknown and known nodal heads respectively. In the original GM where nodal demands are assumed to be fully satisfied, the elements of diagonal matrix A_{22} are Qn_i^{req} / Hn_i. To solve for pressure dependent demand, the elements of A_{22} are redefined as $Qn_i(Hn_i)/Hn_i$ where $Qn_i(Hn_i)$ represents the pressure dependent nodal outflow. Equations (2) are differentiated with respect to the pipe discharges and nodal heads to give:

$$\begin{bmatrix} D_{11} & \vdots & A_{12} \\ \cdots & \cdots & \cdots \\ A_{21} & \vdots & D_{22} \end{bmatrix} \begin{bmatrix} dQp \\ \cdots \\ dHn \end{bmatrix} = \begin{bmatrix} dE \\ \cdots \\ dq \end{bmatrix} \tag{3}$$

where D_{11} and D_{22} are derivatives of A_{11} and A_{22} respectively. dE and dq represent the pipe head loss and flow conservation at each node respectively and from Equations (2) can be rewritten as:

$$\begin{aligned} dE &= A_{11}Qp + A_{12}Hn + A_{10}H_0 \\ dq &= A_{21}Qp + A_{22}Hn \end{aligned} \tag{4}$$

By substituting equations (4) into equation (3), the iterative formulation of the HDGM can be described as:

$$Hn_i^{k+1} = (A_{21}D_{11}^{-1}A_{12} - A_{22})^{-1}\left[A_{21}Qp^k + Qn_i(Hn_i^k) - A_{22}Hn^k - A_{21}D_{11}^{-1}A_{11}Qp^k - A_{21}D_{11}^{-1}A_{10}H_0\right]$$

$$Qp_j^{k+1} = Qp_j^k - D_{11}^{-1}(A_{11}Qp^k + A_{12}Hn^{k+1} + A_{10}H_0) \quad (5)$$

where *k* represents the iteration number. Hence the algorithm first solves the equation for Hn_i before solving for Qp_j. More details regarding matrices A_{11}, A_{12}, A_{21} and A_{10} can be found in Rossman (2002) and Salgado et al. (1993).

Examples, Results and Discussion

The examples below are presented with the objective of demonstrating the effectiveness of the HDGM in the context of small and large networks. A FORTRAN 90 implementation of the above algorithm has been developed. To ensure convergence, a line search procedure has been incorporated into the program to facilitate the selection of a relaxation coefficient for each iterative solution. All the results herein were generated using the above-mentioned FORTRAN 90 HDGM program.

Example 1

The first example shown in Figure 2 is based on a simple network taken from the literature (Fujiwara and Ganesharajah 1993; and Tanyimboh and Templeman 2004). This single source network consists of 8 pipes of length 1000m and 6 demand nodes with the desired pressure heads of 60m. The HDGM was carried out with a variation of source heads from 40m to 80m. Performance of the network and each node are illustrated in Figure 3 and Figure 4 respectively.

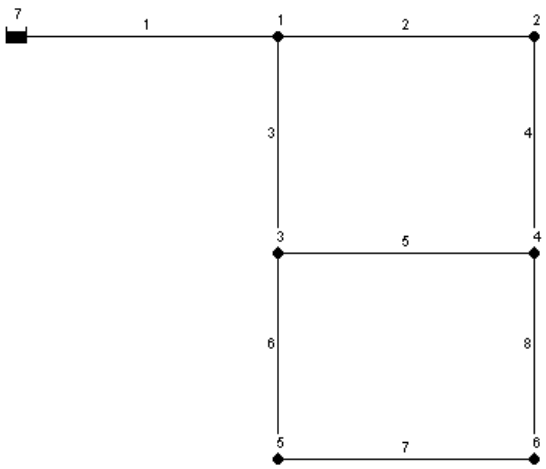

Node	Elevation (m)	Demand (m^3/s)
1	50	0.0417
2	50	0.0417
3	45	0.0778
4	45	0.0417
5	55	0.0556
6	55	0.0889

Pipe	Diameter (mm)	HW roughness
1	500	140
2	400	140
3	400	140
4	400	140
5	250	140
6	250	140
7	250	140
8	250	140

Figure 2. Example 1

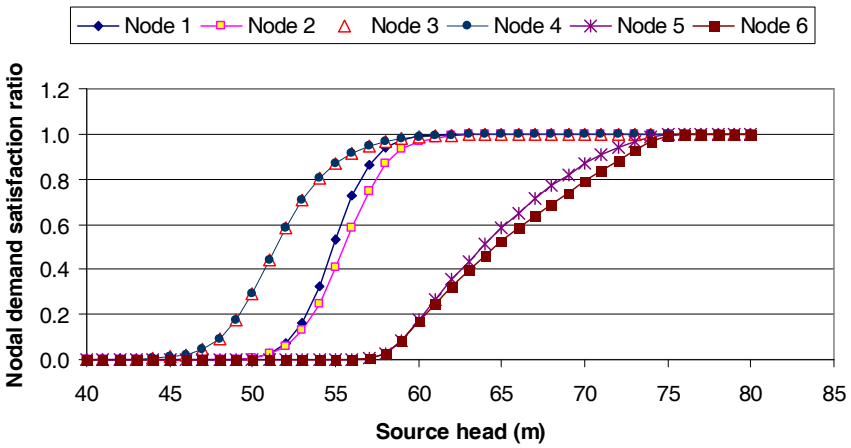

Figure 3. Nodal performance of Example 1

The demand nodes each have a unique head-outflow curve depending on their elevations, demands and relative distances from the source. The curves vividly show the magnitude of each nodal outflow at various source heads. For example, at source head 70m, the demand satisfaction ratio (DSR) of nodes 5 and 6 are 0.87 and 0.79 respectively whereas demands at nodes 1 to 4 are fully satisfied. In addition, the sequence of each node being fully satisfied (with the increment of source head) and the required source head for all demands to be satisfied can be easily deduced. In this case, node 3 and 4 are satisfied simultaneously followed by nodes 1, 2, 5 and 6. A source head above 76m is required for all demand nodes to be fully satisfied. It is worth noticing that the curves depict a smooth transition from no outflow at minimum head to a full outflow stage, exhibiting no discontinuities. The network performance is illustrated in Figure 4.

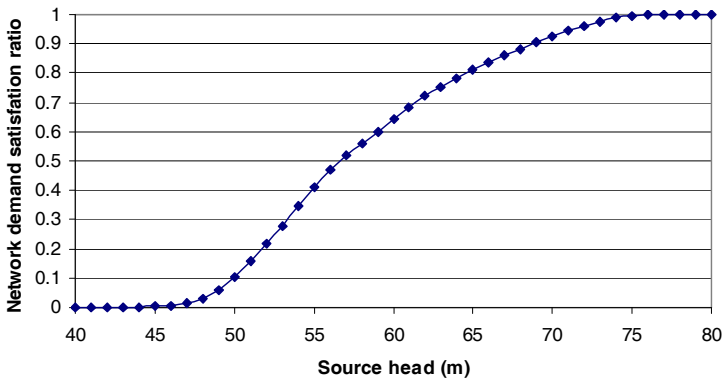

Figure 4. Network performance of Example 1

Result verification was carried out using the hydraulic feasibility test (Ackley et al. 2001) where the nodal outflows obtained from the HDGM are applied in EPANET 2 as nodal demands. Simulations for source heads ranging from 40m to 80m were performed. Nodal heads generated by EPANET 2 were then compared with those of

the proposed algorithm. Figure 5 shows a correlation of $R^2 = 0.9999995$ or $1 - R^2 = 5 \times 10^{-7}$ between the heads produced by both methods. This clearly confirms that the HDGM is producing results which are accurate and reliable.

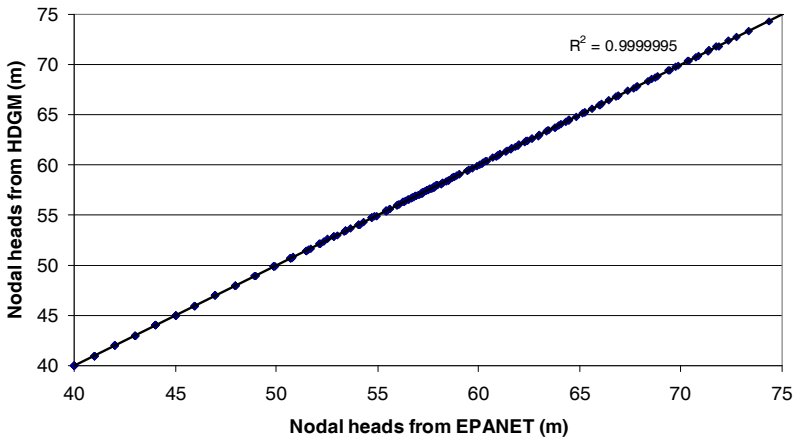

Figure 5. Hydraulic feasibility test for Example 1 for source heads between 40m and 80m

Example 2

The network in Example 2 consists of 48 nodes, 74 pipes and 2 reservoirs (Nodes 47 and 48) as shown in Figure 6. Data for the nodes and pipes can be found in Shan (2004). Both source heads were varied at the same rate within a range of 100m.

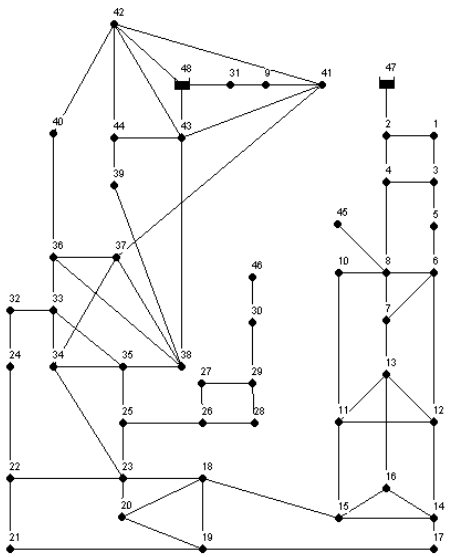

Figure 6. Example 2

Figure 7 shows the network performance of Example 2 for the full range of DSRs. The fact that results were obtained without convergence problems suggests the HDGM is robust. The network head outflow curve consists of two steps. All 13 demand nodes have elevation of 100m and desired head of 115m where demands are satisfied in full. The first step corresponds to the scenario where demand nodes 1, 14 and 17 have been fully satisfied with the head of source 47 and 48 rising above 115m and 65m respectively as shown in Figure 8. The remaining demand nodes only experienced a negligible increase in outflows. As soon as the head of sources 47 and 48 exceeded 150m and 100m respectively, outflows of demand nodes 9, 10, 21, 25, 30, 31, 32, 37, 45 and 46 began to increase significantly. This time, it is ten demand nodes achieving a DSR of 1.0 and hence the network experiences a leap in performance. This clearly explains why the latter step is steeper than the former.

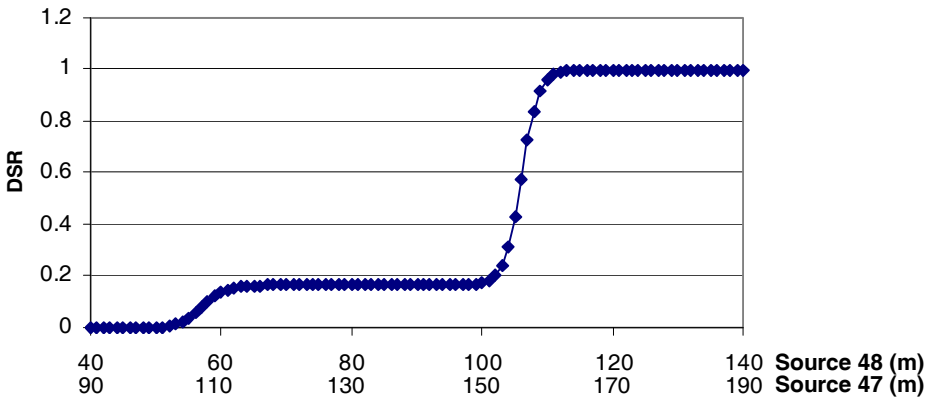

Figure 7. Network performance of Example 2

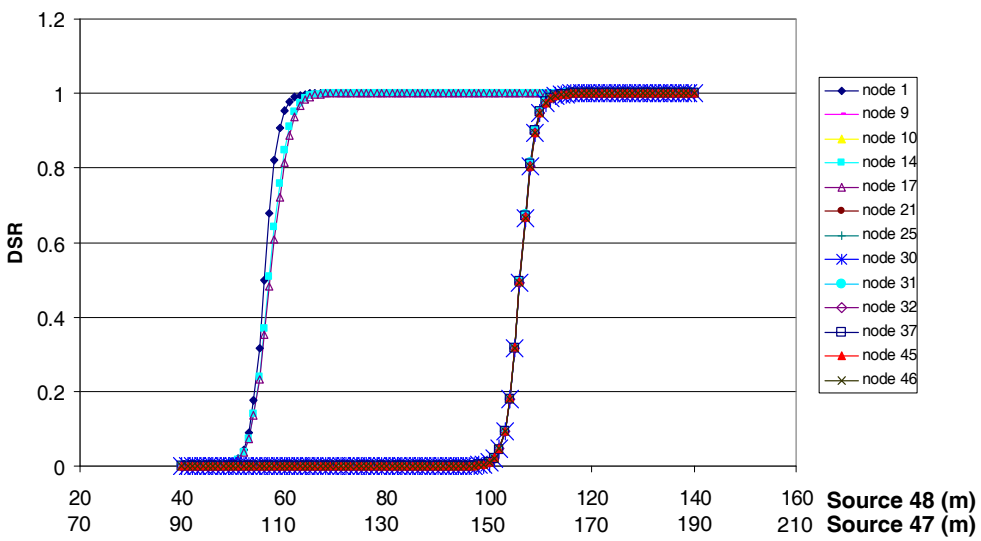

Figure 8. Nodal performance of Example 2

Figure 9 shows the number of iterations needed to achieve convergence. An average convergence rate of 8.68 iterations for this relatively large network suggests the HDGM converges rapidly and is efficient in simulating both normal and deficient operating conditions. A good method of ensuring that the algorithm does not converge falsely is to evaluate the norm of the right hand side of Equation 3. At solution, the norm should approach a value of 0 as an indication of the progress and accuracy of the algorithm. Figure 10 shows a consistent decrease of the norm value for several network operating conditions. The hydraulic feasibility test described above gave a correlation coefficient of $R^2 = 0.9997$ which confirms the accuracy of the HDGM. This verification was further strengthened by the identical results produced from the modelling of this network using PRAAWDS (Tanyimboh 2008).

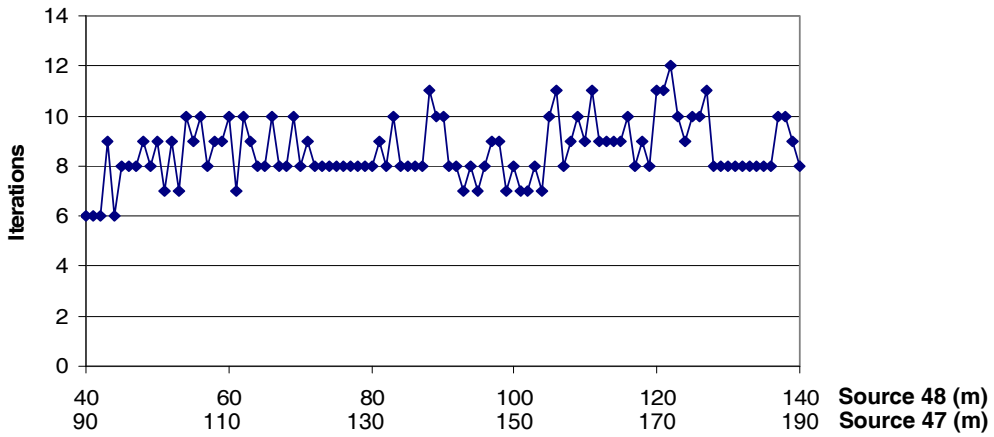

Figure 9. Iterations required to achieve convergence for Example 2

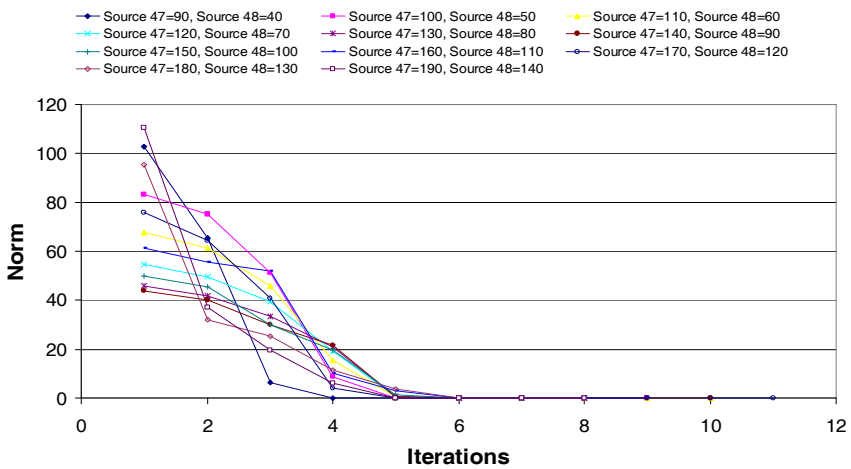

Figure 10. Value of norm at each iteration for Example 2

Conclusions

An augmented gradient method (HDGM) for the hydraulic analysis of water distribution networks has been presented. The proposed model is based on the Tanyimboh and Templeman (2004) head-outflow function and is shown to be capable of simulating both normal and pressure deficient conditions of a water distribution network. Result verification using the hydraulic feasibility test of Ackley et al. (2001) shows that the algorithm generates results that are reliable and accurate. Furthermore, the networks were also modelled using PRAAWDS which gave identical results. The algorithm is demonstrated to be efficient and robust as it converged rapidly and without problems for the analysis of a relatively large network over the full range of DSRs from 0 to 1.0. Hence, the goal of embedding this head-dependent demand model into EPANET 2 seems highly achievable.

The mentioned application would be the first phase of a project on long term optimal rehabilitation and upgrading of water distribution networks based on evolutionary computing (EC). DDA, which is liable to exaggerate the network deficiency, may produce unreliable results in terms of nodal outflows and heads and consequently mislead the EC search. Conversely, with the HDA, evaluation of candidate solutions will be precise, guiding the EC in a much enhanced way.

Reference

Ackley, J.R.L., Tanyimboh, T.T, Tahar, B. and Templeman, A.B. (2001) "Head-driven analysis of water distribution systems." *Water Software Systems: Theory and Applications, Vol. 1*, Ulanicki, B., Coulbeck, B. and Rance, J. (eds.), Research Studies Press Ltd, England, ISBN 0863802745, Chapter 3:183-192.

Fujiwara, O. and Ganesharajah, T. (1993) "Reliability assessment of water supply systems with storage and distribution networks." *Water Resource Research*, 29(8), 2917-2924.

Germanopoulos, G. (1985) "A technical note on the inclusion of pressure dependent demand and leakage terms in water supply network models", *Civil Engineering Systems*, 2, 171-179.

Rossman, L. A. (2002) *EPANET 2 User's Manual*, Water Supply and Water Resources Division, National Risk Management Research Laboratory, Cincinnati, OH45268.

Salgado, R., Rojo, J., Zepeda, S. (1993) "Extended gradient method for fully non-linear head and flow analysis in pipe networks." *Integrated Computer Applications in Water Supply-- Methods and Procedures for Systems Simulation and Control*, 1, pp. 49-60.

Shan, N. (2004) "Head dependent modelling of water distribution network." MSc Dissertation, University of Liverpool, UK.

Tanyimboh, T.T. (2008) "Robust algorithm for head-dependent analysis of water distribution systems." *Proceedings of the 10th Annual Water Distribution Systems*

Analysis Conference WDSA2008, Van Zyl, J.E., Ilemobade, A.A., Jacobs, H.E. (eds.), August 17-20, 2008, Kruger National Park, South Africa.

Tanyimboh, T.T. and Templeman, A.B. (2004) "A new nodal outflow function for water distribution networks." *Proceedings of the 4th International Conf. on Eng. Computational Technology*, Topping, B.H.V. and Mota Soares, C.A. (eds.), Civil-Comp Press, Stirling, UK, ISBN 0-948749-98-9, Paper 64, pp. 12, CD-ROM.

Todini, E. and Pilati, S. (1987) "A gradient method for the analysis of pipe networks". *International Conference on Computer Application for Water Supply and Distribution*, Leicester Polytechnic, UK, September 8-10.

Wagner, J.M., Shamir, U. and Marks, D.H. (1988) "Water distribution reliability: simulation methods." *Journal of Water Resources Planning and Management*, 114(3), 276-294.

Enhanced Global Gradient Algorithm: a general formulation

L. Berardi[1], O. Giustolisi[2] and E. Todini[3]

[1] Technical University of Bari, Engineering Faculty of Taranto, Department of Civil and Environmental Engineering, viale del Turismo 8, Taranto, Italy; e-mail: l.berardi@poliba.it
[2] Technical University of Bari, Engineering Faculty of Taranto, Department of Civil and Environmental Engineering, viale del Turismo 8, Taranto, Italy; e-mail: o.giustolisi@poliba.it
[3] Department of Earth and Geo-Environmental Sciences, University of Bologna, Via Zamboni, 67, Bologna, Italy; e-mail: ezio.todini@unibo.it

ABSTRACT

The behaviour of a looped water distribution network, operating under pressure in steady flow conditions, can be modelled by imposing mass and momentum conservation. When distributed demands along the pipes are present, they tend to be represented as lumped withdrawals at the pipes ending nodes. Although such simplification preserves mass balance, it might cause significant head loss errors which may lead to inconsistent results. Giustolisi and Todini (2008) recently proposed a correction scheme within a modified Global Gradient Algorithm (GGA) under the common assumptions of Darcy-Weisbach head loss formula and pipe friction factors independent from the flow regime.
This paper provides an extension of the mentioned approach to any generic monomial head loss formula, so it can be easily incorporated into existing commercial water distribution network simulators.

INTRODUCTION

The problem of identifying the hydraulic status of a looped pressurized water distribution network (WDN) consists in determining pipe discharges and nodal heads once network topology, pipe geometry, water demands and head value of at least one node are assigned. In steady flow condition, solution of such a problem should obey flow continuity (conservation of mass) at any point of the network and conservation of momentum along any path. Although mass conservation is represented by linear equations, usually referred to flow entering and exiting from each node, momentum conservation law depends on head loss along a given path (at least one link in the network) which is non-linear in flow.

On this premise, literature works on WDN hydraulic analysis follow two distinct approaches, namely the direct solution of the resulting non-linear system of equations or the use of optimization techniques. The first approach was introduced by H. Cross (1936) is based on iterative solution of linear approximations of the

original equations with respect to closed loops. This method was extended to simultaneously account for all the loops by using Newton-Raphson methods (Epp and Forley, 1970; Kesavan and Chandrashekar, 1972). The Newton-Raphson method was also used to calculate heads at nodes after non-linear transformation of pipe discharges (Martin and Peters (1963), Shamir and Howard (1968); Mignosa, 1987). Wood and Charles (1972) introduced the Linear Theory to provide the direct solution of the original equations by calculating pipe discharges, after a linear transformation of nodal heads. The second approach, based on optimization was introduced by Collins at al. (1978) and is centred on the minimization of the "content" and "co-content" models. Such a minimisation is performed by means of a network linear programming (NLP) code. Despite the NPL was tested to be less efficient than the GGA (Berghout and Kuczera, 1997), the optimization approach deserves attention as it is based on the convexity of the "content" functional which is fundamental to demonstrate the existence and uniqueness of the solution. Such a result is of crucial importance for successive development of gradient methods proposed by Todini (1979) and Todini and Pilati (1988). They used Collins et al. (1978) results to demonstrate that the solution of the system of non linear equations obtained from the minimization of a convex function (the Collins "content") under linear constraints is unique. On these grounds, they applied a Newton-Raphson gradient technique to solve, both in terms of pipe discharges and nodal heads, the system of non-linear equations, resulting from the minimization of the content. The resulting Global Gradient Algorithm (GGA) has been recognised to be the most robust and fast method for WDN analysis and it is considered to be a benchmark for any new WDN hydraulic solver. Moreover, GGA is embedded in several commercial software packages (e.g. EPANET2)

Irrespectively to the approach followed, a common assumption of all abovementioned methods is the representation of pipe distributed demand as equal lumped withdrawals at end nodes. It mainly descends from the poor knowledge of actual pipe connection but is useful to reduce problem unknowns by simultaneously preserving mass conservation at nodes. Recently, Giustolisi and Todini (2008) demonstrated that such a simplification results in significant errors in momentum balance which eventually impair correctness of the analyses performed for calibration, system design, real-time operations, rehabilitation strategies, optimal operation studies, reliability analyses, etc. They proved it considering the simple assumption of uniformly distributed demands along the pipes by means of a uniform function. In order to take advantage from the classical GGA they still assumed a symmetric partition of pipe distributed demand as nodal withdrawals and introduced a correction term of the hydraulic resistance coefficient. At the same time, they provided similar corrections for all matrices involved in the classical GGA. The mathematical development reported in that introductory work was based on Darcy-Weisbach formula and did not account for other monomial head loss formulas widely used by practitioners (e.g. Hazen-Williams).

This work is primarily aimed at filling in this gap by providing and extended formulation of the enhanced GGA, to be easily implemented into the existing algorithms or software packages.

HEAD LOSS CONSIDERING UNIFORMLY DISTRIBUTED DEMAND

When a liquid flows through a pipeline, shear stresses develop between the liquid and the pipe wall. This shear stress is a result of friction and its magnitude depends upon the properties of the fluid that is passing through the pipe, the speed at which it is moving, the pipe internal roughness, length and diameter. Under steady flow conditions, the head losses slope J due to fiction along a pipe is described by the Darcy-Weisbach formula (1) which is derived from the governing equations of the physical phenomenon at hand.

$$J = -\frac{dH}{dx} = \frac{8 f\left(\mathrm{Re}, \mathrm{Ke}\right)}{g\pi^2 D^5} Q|Q| = K\left(\mathrm{Re}, \mathrm{Ke}, D\right) Q|Q| \tag{1}$$

x is a linear coordinate whose origin is at the beginning of the pipe (see Figure 1), Q is the water discharge passing through the pipe with length L and diameter D, and f is the pipe friction factor which depends on equivalent roughness Ke and flow regime (i.e. Reynolds Number, Re); g is the gravitational acceleration constant and K is the pipe unit hydraulic resistance. In Eq.(1) the minus sign underlines the fact that the head always decreases in the direction of the flow (which can be either opposite or in agreement with the assumed positive direction of coordinate x).

The Darcy-Weisbach formula can be potentially used to find the head losses through pipe for any Newtonian fluid under any flow regime. However, in technical practice, there are other empirical formulations of the head losses in pressurized water pipeline that can be condensed into the generic monomial expression (2), where K_∞ usually does not depend on Re (i.e. fully turbulent flow is assumed)

$$J = -\frac{dH}{dx} = K_\infty\left(\mathrm{Ke}, D\right) Q|Q|^{n-1} \tag{2}$$

n=2 is predominant in Europe while n=1.852 it represents the Hazen-Williams expression, which nowadays is the most popular in the U.S. (Walski et al., 2001).
The empirical formulations have been developed from experimental data recorded under fully turbulent flow regime, which is assumed to be the most common in water distribution system. From a modelling point of view, the great advantage of using such expressions descends from computing pipe unit hydraulic resistance K_∞ only once during the simulation, by assuming that the only existing flow regime is fully turbulent irrespectively of the actual flow conditions.

Traditionally, actual demand is assumed to be uniformly distributed along the pipe. Such a simplification usually accounts for the inaccurate knowledge of actual connections.
In order to mathematically compute the head losses through a generic pipe connecting nodes i and j in the network a positive direction for the pipe discharge Q is assumed in the direction of coordinate x. Under the hypothesis of pressure independent demand (generally assumed in "demand-driven" simulation models as that originally discussed in Giustolisi and Todini (2008)) the functioning of such pipe is represented in Figure 1, where Q_i and Q_j represent the flow at nodes i and j respectively. Without loss of generality (considering the symmetry of the problem), in both cases the flow Q_i is assumed positive (in the same direction as abscissa x) and

the total uniformly distributed demand is designated as $P=qL$, with q, and consequently P, non-negative quantities. The first figure (top-left) entails the case of flow passing through the pipe in one direction (i.e. $Q_i \geq Q_j$), meaning that inlet flow entirely meet the distributed demand; the second drawing (top-right) refers to the opposite condition, where water flow is entering from both nodes and a flow inversion point (y) occurs within the pipe.

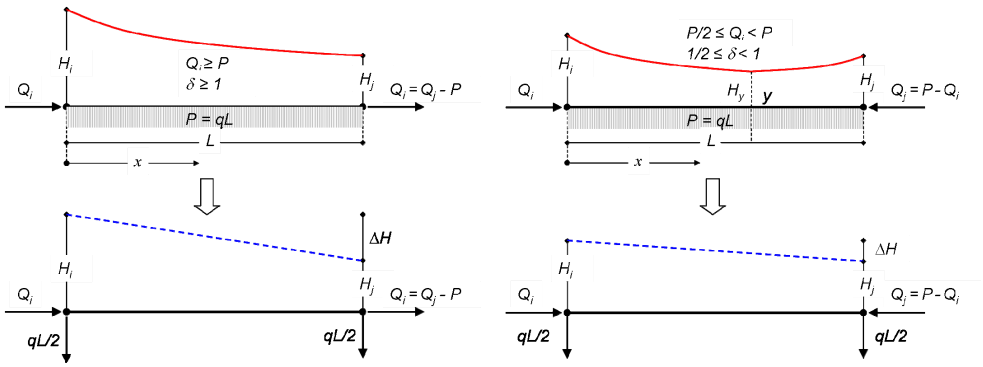

Figure 1. Uniformly distributed demand and its schematization in WDN model

It can be easily proved that the following equality holds irrespectively of the sign of actual flows Q_i and Q_j (with respect to the assumed positive sign)

$$Q_i - Q_j = P \tag{3}$$

Unfortunately, the existence of a uniformly distributed demand and variable discharge along the pipe prevent from using straightway the generic head loss formulation (2) unless it is referred to the head loss slope J_x occurring into each infinitesimal pipe element of length dx, carrying flow Q_x at distance x from the origin of the axis.

$$J_x = -\frac{dH}{dx} = K_\infty \left(\mathrm{Ke}, D\right) Q_x \left|Q_x\right|^{n-1} \tag{4}$$

Furthermore, the mass balance equation (3) written for section x (i.e. $Q_x = Q_i - qx$) allows deriving the linear variation Q_x with x (again independent on actual flow direction): $dQ_x/dx = -q$. Such a result is used to analytically compute the actual head loss through the pipe in the case of no flow inversion (Case (A) of Figure 1).

$$\begin{aligned} \left(H_i - H_j\right)_{actual} &= \int_0^L J_x dx = \int_0^L K_\infty Q_x \left|Q_x\right|^{n-1} dx = \int_0^L \frac{K_\infty}{-q} Q_x \left|Q_x\right|^{n-1} \frac{dQ_x}{dx} dx = \\ &= -\frac{K_\infty}{q} \int_{Q_i}^{Q_j} \left|Q_x\right|^n d\left|Q_x\right| = K_\infty \left[\frac{\left|Q_x\right|^{n+1}}{n+1}\right]_{Q_j}^{Q_i} \frac{L}{P} = K_\infty \frac{\left|Q_i\right|^{n+1} - \left|Q_j\right|^{n+1}}{n+1} \frac{L}{P} \end{aligned} \tag{5}$$

It can be easily demonstrated that Equation (5), obtained for one-direction flow, holds irrespectively on the sign of flows Q_i and Q_j as well as in the case of flow

inversion. In fact, the existence of inversion point *y* factually divides pipe into two sub-portions connecting nodes *i* and *j* to the fictitious node *y* (with $Q_y=0$) having the same positive direction assumed for pipe discharges. Head loss between nodes *i* and *j* can be computed by summing the head losses though the two sub-portions 0 – *y* and *y* – *L* (from 0 to *y* and from *y* to *L*) respectively by using Eq.(5).

In order to take advantage from the original formulation of the problem proposed by Giustolisi and Todini (2008), let's introduce the dimensionless quantity δ, which is the ratio between the inlet flow *Q* and the total distributed discharge *P*.

$$\delta = \frac{Q}{P}; \qquad Q_i = P + Q_j \Rightarrow \frac{Q_j}{P} = \delta - 1 \tag{6}$$

The head loss can be re-written accordingly.

$$\left(H_i - H_j\right)_{actual} = K_\infty \frac{\left|\delta\right|^{n+1} - \left|\delta - 1\right|^{n+1}}{n+1} P^n L \tag{7}$$

Thus, under fully turbulent flow and uniformly distributed demand Equation (7) represents the actual pipe head loss.

ENHANCED WDN SIMULATION MODEL

Usually, WDS simulation models represent distributed demands as two equal lumped demands at the terminal nodes. The two figures at the bottom of Figure 1 represent the effect of schematization in the two opposite cases considered, where the discharge through the modelled *k*-th pipe is constant ($Q_k=Q_i - P_k/2$) and head loss is computed by using Eq. (2).

$$\left(H_i - H_j\right)_{simulation\ model} = K_\infty \left(\delta - \frac{1}{2}\right)\left|\delta - \frac{1}{2}\right|^{n-1} P_k^{\,n} L \tag{8}$$

It is clearly different from the head loss in the original demand configuration (7). Giustolisi and Todini (2008) proposed to use a correction of hydraulic resistance *R* (=*KL*) to compensate the error of momentum balance due to schematisation, while preserving the symmetrical partition of distributed demand into the two end nodes.

In order to introduce such a correction into the existing algorithms, both Equations (7) and (8) are re-written in terms of the dimensionless parameter $\delta_k = Q_k/P_k = \delta - 1/2$ as follows.

$$\begin{aligned}\left(H_i - H_j\right)_{actual} &= K_{k,\infty} \frac{\left|\delta_k + \frac{1}{2}\right|^{n+1} - \left|\delta_k - \frac{1}{2}\right|^{n+1}}{n+1} P_k^{\,n} L \\ \left(H_i - H_j\right)_{simulation\ model} &= K_{k,\infty} \delta_k \left|\delta_k\right|^{n-1} P_k^{\,n} L\end{aligned} \tag{9}$$

Thus, the correction ε_k of pipe hydraulic resistance is obtained by equating the two head loss expressions in Equation (9)

$$K_{k,\infty}\left(1+\varepsilon_k\right)\delta_k\left|\delta_k\right|^{n-1}P_k{}^nL = K_{k,\infty}\frac{\left|\delta_k+\frac{1}{2}\right|^{n+1}-\left|\delta_k-\frac{1}{2}\right|^{n+1}}{n+1}P^nL \;\Rightarrow$$
$$\Rightarrow \qquad \varepsilon_k = \frac{\left|\delta_k+\frac{1}{2}\right|^{n+1}-\left|\delta_k-\frac{1}{2}\right|^{n+1}}{\left(n+1\right)\delta_k\left|\delta_k\right|^{n-1}}-1 \tag{10}$$

It is worth noting that Eq. (10) always returns a positive correction for both negative and positive δ_k as shown in Figure 2, which represents ε_k for three significant values of n. It is also noteworthy that the correction is null when the exponent n equals 1, as happens for laminar flow regime.

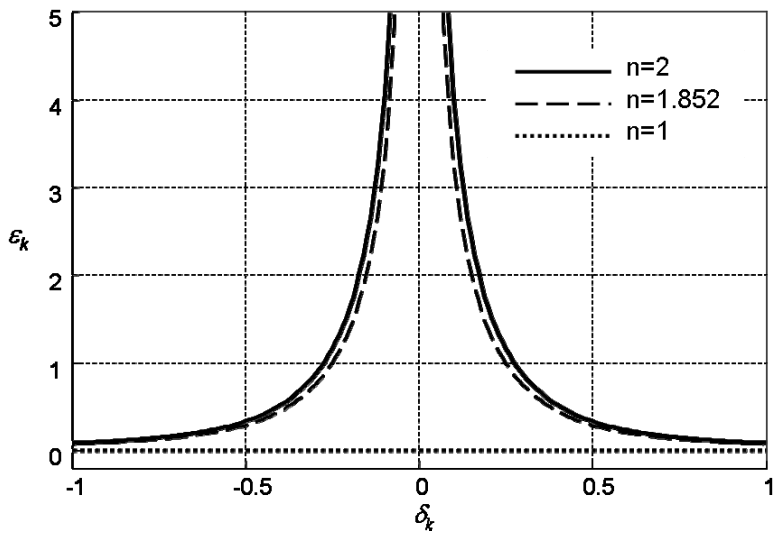

Figure 2. Representation of ε_k as a function of ratio δ_k for different values of n

The correct head loss term is the sum of the head loss resulting from the schematization plus the correction $E_k{}^{\varepsilon}$ introduced to take into account the "actual" uniformly distributed demand.

$$E_k^{\varepsilon} = \varepsilon_k R_{k,\infty}Q_k\left|Q_k\right|^{n-1} = \varepsilon_k R_{k,\infty}\delta_k\left|\delta_k\right|^{n-1}P_k^n = z_k R_{k,\infty}P_k^n$$
$$z_k = \varepsilon_k\delta_k\left|\delta_k\right|^{n-1} = \frac{\left|\delta_k+\frac{1}{2}\right|^{n+1}-\left|\delta_k-\frac{1}{2}\right|^{n+1}}{n+1}-\delta_k\left|\delta_k\right|^{n-1} \tag{11}$$

where $R_{k,\infty}$ (=$L_kK_{k,\infty}$) is k-th pipe hydraulic resistance. The dimensionless parameter z_k is instrumental to introduce the correction into the existing WDN simulation algorithms by using the same schematization of distributed demand as concentrated withdrawals at end nodes. Figure 3 plots the parameter z_k as a function of δ_k for different n values. As reported in the same figure, the head loss correction $E_k{}^{\varepsilon}$

numerically coincides with z_k under the hypothesis of P_k=1m^{3}s^{-1} and $R_{k,\infty}$ =1s^{n}m^{1-3n} (Giustolisi and Todini, 2008).

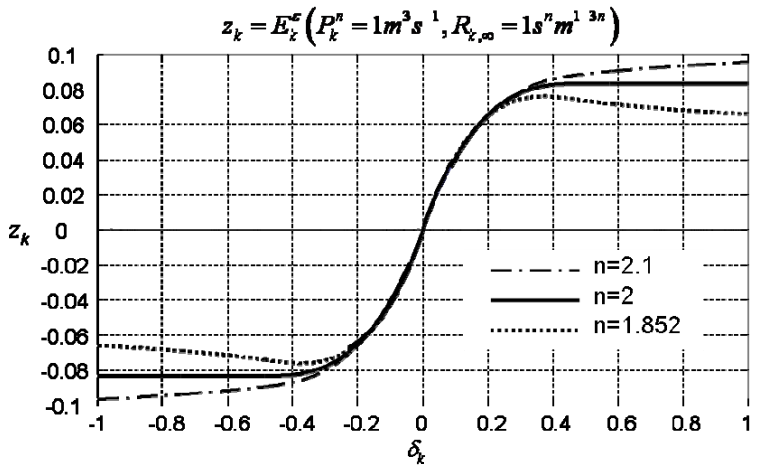

Figure 3. Representation of z_k for different values of exponent n.

In particular for exponent n=1 the correction is always null as the scenarios of both distributed and concentrated demands are equivalent in terms of head loss (due to the model linearity). In the case of n=2, the correction term increases up to the value 1/12 until pipe discharge is half of the distributed demand (δ_k = 0.5), from this point on it remains constant (Giustolisi and Todini, 2008). When other head loss monomial formulations are used, with n<2 (e.g. Hazen-Williams expression - n=1.852), the correction parameter z_k reaches a maximum value (lower than 1/12) for $\delta_k \leq 0.5$.

Finally, the z_k curves obtained for n>2 (i.e. n=2.1) shows that the error due to the schematization increases with δ_k towards infinity. This suggests that, apart from its physical meaning, the exponent n=2 leads to the maximum finite value of correction needed and should be considered as an upper bound of n to ensure the convergence of automatic algorithms.

GENERAL FORMULATION OF ENHANCED GGA

When the functioning of a WDN comprised of n_p unknown discharges (i.e. pipes), n_n unknown heads (i.e. internal nodes) and n_0 known heads (e.g. water tanks) is simulated following a demand-driven approach mass and momentum balance equations (12) must be simultaneously satisfied.

$$\begin{aligned} \mathbf{A}_{pp}\mathbf{Q} + \mathbf{A}_{pn}\mathbf{H} &= -\mathbf{A}_{p0}\mathbf{H}_0 \\ \mathbf{A}_{np}\mathbf{Q} &= \mathbf{d} \end{aligned} \tag{13}$$

Where matrix $\mathbf{A}_{pn}$=$\mathbf{A}^T_{np}$ and $\mathbf{A}_{p0}$ are the topological incidence sub-matrices of size [n_p, n_n] and [n_p, n_0], respectively, derived from the general topological matrix $\bar{\mathbf{A}}_{pn}$=[$\mathbf{A}_{pn}$ ¦ $\mathbf{A}_{p0}$] of size [n_p, n_n+ n_0], as defined in Todini and Pilati (1988); **d** is the column vector of pipe demands lumped at nodes; **Q** and **H** are the vectors of pipe discharges and nodal heads respectively.

The generic iteration (*iter*) of the Global Gradient Algorithm, as described in Giustolisi and Todini (2008), provides an approximated solution of the non-linear system of equations (12)

$$\begin{aligned}
&\mathbf{B}_{pp}^{iter} = \left(\mathbf{D}_{pp}^{iter}\right)^{-1}\mathbf{A}_{pp}^{iter}\\
&\mathbf{F}^{iter} = \mathbf{A}_{np}\left(\mathbf{Q}^{iter} - \mathbf{B}^{iter}\mathbf{Q}^{iter}\right) - \mathbf{d} - \mathbf{A}_{np}\left(\mathbf{D}_{pp}^{iter}\right)^{-1}\left(\mathbf{A}_{p0}\mathbf{H}_0\right)\\
&\mathbf{H}^{iter+1} = \left(\mathbf{A}_{np}\left(\mathbf{D}_{pp}^{iter}\right)^{-1}\mathbf{A}_{pn}\right)^{-1}\mathbf{F}^{iter}\\
&\mathbf{Q}^{iter+1} = \left(\mathbf{Q}^{iter} - \mathbf{B}^{iter}\mathbf{Q}^{iter}\right) - \left(\mathbf{D}_{pp}^{iter}\right)^{-1}\left(\mathbf{A}_{p0}\mathbf{H}_0 + \mathbf{A}_{pn}\mathbf{H}^{iter+1}\right)
\end{aligned} \tag{13}$$

To solve the system of equations (13) it is necessary to compute the diagonal matrices $\mathbf{D}_{pp}$ (containing the derivatives of the head losses with respect of the *k*-th pipe discharge Q_k) and $\mathbf{A}_{pp}$ together with their product $\mathbf{B}_{pp} = \mathbf{A}_{pp}(\mathbf{D}_{pp})^{-1}$.
Equation (14) reports the expression of the dimensionless parameter zD_k for any *n* and discharge condition (δ_k). zD_k is represented in Figure 6. In particular, the negative values zD_k are due to the existence of a maximum value of z_k for $n<2$.

$$\begin{aligned}
&D_{pp}(k,k) = \frac{d\left[R_{k,\infty}\left(Q_k\left|Q_k\right|^{n-1} + z_k P_k^n\right)\right]}{dQ_k} = R_{k,\infty}\left(n\left|Q_k\right|^{n-1} + \frac{dz_k}{d\delta_k}P_k^{n-1}\right) =\\
&= R_{k,\infty}\left(n\left|\delta_k\right|^{n-1} + zD_k\right)P_k^{n-1}\\
&zD_k = \frac{dz_k}{d\delta_k} = \left(\delta_k + \frac{1}{2}\right)\left|\delta_k + \frac{1}{2}\right|^{n-1} - \left(\delta_k - \frac{1}{2}\right)\left|\delta_k - \frac{1}{2}\right|^{n-1} - n\left|\delta_k\right|^{n-1}
\end{aligned} \tag{14}$$

From a numeric point of view, it is important to note that for δ_k approaching zero, $zD_k>0$. This fact assures robustness of the developed GGA.
Equation (15) reports the elements of the diagonal matrix $\mathbf{A}_{pp}$ which are the ratio between pipe head losses and relevant discharges; their expression is a function of the dimensionless parameter zA_k.

$$\begin{aligned}
&A_{pp}(k,k) = \frac{R_{k,\infty}\left(Q_k\left|Q_k\right|^{n-1} + z_k P_k^n\right)}{Q_k} = R_{k,\infty}\left(\left|Q_k\right|^{n-1} + \frac{z_k P_k^n}{Q_k}\right) =\\
&= R_{k,\infty}\left(\left|\delta_k\right|^{n-1} + \frac{z_k}{\delta_k}\right)P_k^{n-1} = R_{k,\infty}\left(\left|\delta_k\right|^{n-1} + zA_k\right)P_k^{n-1}\\
&zA_k = \frac{z_k}{\delta_k} = \frac{\left|\delta_k + \frac{1}{2}\right|^{n+1} - \left|\delta_k - \frac{1}{2}\right|^{n+1}}{(n+1)\delta_k} - \left|\delta_k\right|^{n-1}
\end{aligned} \tag{15}$$

Finally, the elements of the diagonal matrix representing the term $\mathbf{B}_{pp}$ are reported in Equation (16).

$$\frac{A_{pp}(k,k)}{D_{pp}(k,k)} = \frac{|\delta_k|^{n-1} + zA_k}{n|\delta_k|^{n-1} + zD_k} = zB_k \tag{16}$$

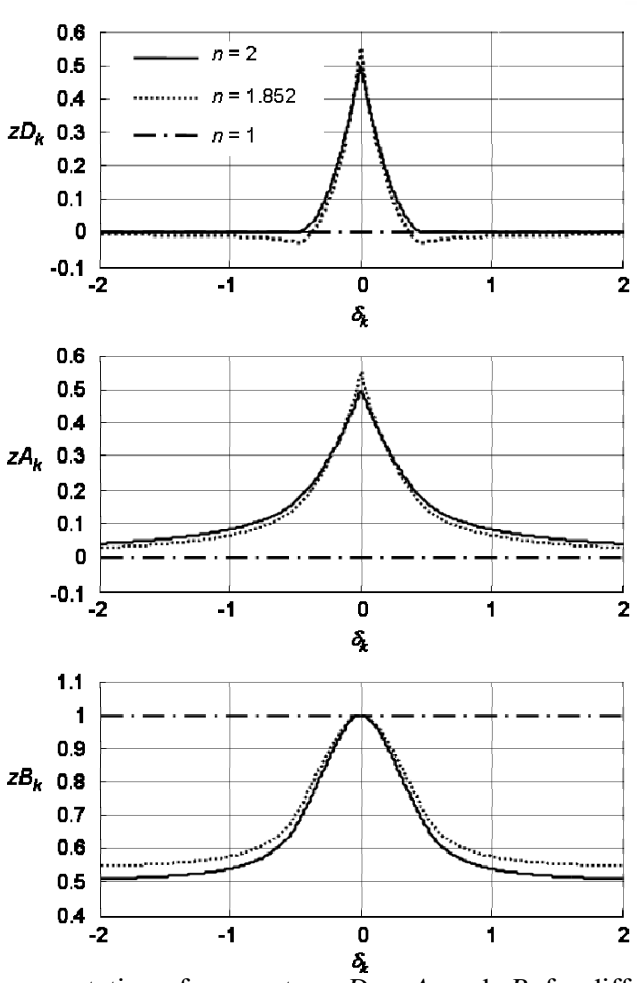

Figure 4: Representation of parameters zD_k , zA_k and zB_k for different exponents n

CONCLUSIONS

Giustolisi and Todini (2008) introduced an enhanced Global Gradient Algorithm which allows for correcting head loss error due to representation of uniformly distributed demands as nodal concentrated withdrawals. This paper provides an extension of the enhanced Global Gradient Algorithm aimed at using any empirical monomial formulation for describing pipe head loss. The resulting formulation represents a valuable basis for further investigations on WDN functioning by using the existing simulation algorithms.

REFERENCES

Berghout B.L., and Kuczera G. (1997) "Network linear programming as pipe network hydraulic analysis tool", *J.of Hydraulic Engineering*, ASCE, 123(6), 549-559.

Collins, M., Cooper, L., Helgason, R., Kenningston, J. and LeBlanc, L. (1978) "Solving the pipe network analysis problem using optimization techniques", *Management Science*, 24 (7), 747-760.

Cross H. (1936) "Analysis of flow in networks of conduits or conductors", Bulletin no.286, University of Illinois Engineering Experimental Station, Urbana Illinois, USA, 1-29.

Epp, R. and Fowler, A.G. (1970) "Efficient Code for steady-state flows in networks", *J. of Hydr. Div.*, ASCE, 96 (11), 3-56.

Giustolisi, O., and Todini, E. (2008) "Pipe hydraulic resistance correction in WDN analysis", Special Issue on *WDS Model Calibration, Urban Water Journal,* Taylor & Francis, UK, No. 4, Vo. 5.

Kesavan, H.K. and Chandrashekar, M. (1972) "Graph-theoretic models for pipe network analysis", *J. of Hydr. Div.*, ASCE, 98 (2), 345-364.

Martin, D.W. and Peters, G. (1963) "The application of Newton's method to network analysis by digital computers", *J. Inst. of Water Engrs.*, (17). 115-129.

Mignosa, P. (1987) "Sui problemi di verifica delle reti di distribuzione idrica complesse", *Idrotecnica*, (6), 257-273 (in Italian).

Shamir, U. and Howard, C.D.D. (1968) "Water distribution network analysis", *J. of Hydr. Div.*, ASCE, 94 (1), 219-234.

Todini, E. (1979). Un metodo del gradiente per la verifica delle reti idrauliche. Bollettino degli Ingegneri della Toscana, 11, 11–14 (in Italian).

Todini, E. and Pilati, S. (1988) "A gradient method for the solution of looped pipe networks", *Computer Applications in Water Supply*, John Wiley & Sons, Vo.1, 1-20.

Walski, T.M., Chase, D.V. and Savic, D.A. (2001) *Water Distribution Modeling,* Haestad Methods, Inc.

Wood, D.J. and Charles, C.O.A. (1972) "Hydraulic network analysis using linear theory", *J. of Hydr. Div.*, ASCE, 98 (7), 1157-1170.

Enhanced WDN Analysis: Representation of Actual Pipe Connections

O. Giustolisi[1]

[1] Technical University of Bari, Engineering Faculty of Taranto, Dept. of Civil and Environmental Engineering, via Turismo, 8, 74100, Taranto, Italy, phone +39 80 5964214, fax: +39 80 5963719, email: o.giustolisi@poliba.it

ABSTRACT

The classical assumption of representing the total demand along a pipe as two lumped withdrawals at its terminal nodes is hitherto common. It is a simplification of the network topology which is useful in order to drastically reduce the number of nodes during network simulation. Conversely, this simplification does not preserve pipes' energy balance equation and, for this reason, it is a wrong approximation that could generate large head loss errors. This paper presents an extension of the Global Gradient Algorithm (GGA) which entails a modified GGA permitting the effective introduction of the lumped nodal demands, and without forfeiting a correct pipe head loss, by means of a pipe hydraulic resistance correction.

INTRODUCTION

The application of local linearization methods (Cross, 1936) and the global linearization techniques characterized by the simultaneous solution of all the equations of the network analysis problem (Collins et al., 1978) are the two main key moments of the search for the most efficient network simulation algorithm in terms of rapid convergence and robustness (reduced number of cases in which the search for the solution fails). The most comprehensive approach to global linearization techniques was set out by *Collins et al.* (1978) who defined the "content" and "co-content" models.

Different approaches to global linearization technique are treated in the literature: the Newton-Raphson Global Gradient Algorithm (Todini, 1979; Todini and Pilati, 1988); two similar approaches named Hybrid Method (Hamam and Brameller, 1971; Carpentier et al., 1985) and Newton Loop-Node Method (Osiadacz, 1987); the Linear Theory Algorithm (Wood and Charles, 1972; Isaacs and Mills, 1980; Wood and Rayes, 1981); the Newton-Raphson Loop Algorithm (an extension of the Cross method where all the loops are considered at the same time) (Epp and Fowler, 1970; Kesavan and Chandrashekar, 1972) and; the Newton-Raphson Head Algorithm (Martin and Peters, 1963; Shamir and Howard, 1968).

These algorithms share the common characteristic of requiring the solution of a system of linear equations several times in order to iteratively reach (i.e., by means

of successive approximations) the solution of the original system of partly linear and partly non-linear equations. However, the size of the linear system to be solved, and the information that has to be provided to formulate it or to identify a first-attempt solution required to initiate the iterative process, vary according to the method chosen.

The Global Gradient Algorithm (GGA) (Todini, 1979; Todini and Pilati, 1988) was used to develop EPANET2 (Rossman, 2000), which has probably become the de facto most widely used network simulation model in the world and which is also embedded in several commercial software packages.

Nevertheless, in all the previously discussed and available methods, water demands are uniquely represented as nodal withdrawals, although they are inevitably distributed along the pipes throughout connections to the properties. Such a simplification of the demand distribution was mainly due to the lack of detailed and reliable knowledge about the position and number of actual connections. However, information, data and maps needed to analyse the water distribution networks are today available and the use of information technology and geographical information system (GIS) is becoming common in water industry in order to map systems and support management. In particular, the improved description of both network topology (number and position of the connections to the properties along the mains of the water distribution networks) and its boundary conditions (demands) permit a more detailed system analysis for simulation purposes. The inclusion of such new information could be potentially achieved by adding one node for each connection point, but this would drastically increase the complexity of network analysis. Thus, the simplification of real demands as two lumped withdrawals at pipe end nodes is vital for maintaining acceptable computational times. Unfortunately, the assumption of two equal lumped withdrawals (each one half of the pipe demand) does not preserve pipes' energy balance equation. Thus, it could generate large head loss errors.

In fact, *Giustolisi and Todini* (2008) recently demonstrated that the assumption of uniformly distributed demands along the pipes, an expedient used when there is poor knowledge about the actual connections and demands, can generate large errors in energy balance when uniform demand is lumped into the two end nodes of a pipe in order to exclusively conserve mass balance. It is worth noting that the results obtained in this classical "average" assumption are conceptually valid also for different shapes of distributed demands along a pipe (Hamberg and Shamir, 1988), considering that in more general cases the error could be higher than that related to the uniform distribution assumption, as will be demonstrated later on in the paper. Furthermore, even when the actual pipe connections and demands are known, coarse simplifications focusing solely on mass balance conservation can produce significant errors in the energy balance, which cannot be assured without considering the actual network status (i.e., topological and mass balance considerations).

Thus, this paper will presents an extension of the GGA permitting the effective introduction of the lumped nodal demands, and without forfeiting a correct pipe head loss, by means of a pipe hydraulic resistance correction. It is worth noting that the standard hydraulic commercial software (e.g., a specific numerical minimisations of

the Content energy function (Carpentier et al., 1985; Piller 1995)), that relies on other algorithms can benefit from the improvement here presented as well.
Finally, the simplification here reported should not be confused with network skeletonization in the sense of model simplification (Anderson and Al-Jamal, 1995) through linearization around a given working point eliminating all redundant nodes by means of the Gauss-Jordan elimination technique (Ulanicki et al., 1996).
In fact, it is here reported a way to account for general shapes of demand distribution along pipes as reported in Hamberg and Shamir (1988) considering the adjustment of the network simulation model (GGA for example) in order to continue using the schematization of the demands as two concentrated water withdrawal at the end of pipes while preserving both energy and mass balance equations in the network model.

WDN SIMULATION MODEL AND HEAD LOSS FORMULATION

The demand-driven simulation of a network of n_p pipes with unknown discharges, n_n nodes with unknown heads (internal nodes) and n_0 nodes with known heads (tank levels, for example) can be described in matrix figure and formulated in the following non-linear system of equations based on energy and mass balance equations

$$\begin{aligned} \mathbf{A}_{pp}\mathbf{Q} + \mathbf{A}_{pn}\mathbf{H} &= -\mathbf{A}_{p0}\mathbf{H}_0 \\ \mathbf{A}_{np}\mathbf{Q} &= \mathbf{d} \end{aligned} \tag{1}$$

where $\mathbf{Q}$ is the $[n_p,1]$ column vector of unknown pipe flow rates, $\mathbf{H}$ is the $[n_n,1]$ column vector of unknown nodal heads, $\mathbf{H}_0$ is the $[n_0,1]$ column vector of known nodal heads, $\mathbf{d}$ is the $[n_n,1]$ column vector of demands lumped in the nodes driving the simulation, $\mathbf{A}_{pn}=\mathbf{A}^T_{np}$ and $\mathbf{A}_{p0}$ are topological incidence sub-matrices of size $[n_p,n_n]$ and $[n_p,n_0]$, respectively, derived from the general topological matrix $\bar{\mathbf{A}}_{pn}=[\mathbf{A}_{pn} \mid \mathbf{A}_{p0}]$ of size $[n_p,n_n+n_0]$, as defined in Todini and Pilati (1988). Furthermore, in the first equation of the system (1) $\mathbf{A}_{pp}\mathbf{Q}$ is the $[n_p,1]$ column vector of pipe head loss whose elements are:

$$E_k = \frac{8f\left(\mathrm{Re},\mathrm{Ke}\right)}{g\pi^2 D_k^5} Q_k \left|Q_k\right| L_k = R_k\left(\mathrm{Re},\mathrm{Ke},D,L\right) Q_k \left|Q_k\right| \tag{2}$$

where k = pipe index; f = Darcy-Weisbach friction factor dependent on the Re = Reynolds number and Ke = equivalent roughness; D_k = internal diameter, g = gravitational acceleration constant, Q_k = pipe flow rate and L_k = pipe length. Thus, R_k = pipe hydraulic resistance that is a function of Re (i.e. Q), Ke, D and L. Eq. (2) holds for laminar, rough turbulent and rough fully turbulent flow regimes.
In technical practice Eq. (2) is very often substituted by

$$E_k = R_k\left(\mathrm{Ke},D,L\right) Q_k \left|Q_k\right|^{n-1} = R_{k,\infty} Q_k \left|Q_k\right|^{n-1} \tag{3}$$

where $R_{k,\infty}$ is not dependent on flow regime (i.e. Q) and, therefore, constant during network simulations, while n is an exponent dependent on the head loss relationship used (1.852 for the Hazen-Williams and 2 for the Darcy-Weisbach rough fully

turbulent flow). The water demands are commonly lumped into the nodes, becoming the elements of the column vector **d**, although in reality they are distributed along the pipes converging at such nodes.

ERROR DUE TO INCORRECT DEMAND APPROXIMATION

Giustolisi and Todini (2008) have recently demonstrated that the above approximation is wrong because it generates head loss errors which may be significant when network analysis is performed for calibration, system design, real-time operations, rehabilitation strategies, optimal operation studies, reliability analyses, etc. They proved it considering the simple assumption of uniformly distributed demands along the pipes by means of a uniform function.
Therefore, Eq. (3) must be re-written to account for error in energy balance by means a correction ε_k in order to consider actual demand distribution in pipes,

$$\begin{aligned} E_k &= R_{k,\infty}\left(1+\varepsilon_k\right)Q_k\left|Q_k\right|^{n-1} = R_{k,\infty}\left(\left|Q_k\right|^{n-1}+\varepsilon_k\left|\delta_k\right|^{n-1}P_k^{n-1}\right)Q_k = \\ &= R_{k,\infty}\left(\left|Q_k\right|^{n-1}+\frac{z_k}{\delta_k}P_k^{n-1}\right)Q_k = R_{k,\infty}\left(\left|Q_k\right|^{n-1}+zA_kP_k^{n-1}\right)Q_k = A_{pp}\left(k,k\right)Q_k \end{aligned} \tag{5}$$

Hence,

$$\begin{aligned} &z_k = \varepsilon_k\delta_k\left|\delta_k\right|^{n-1}; \quad zA_k = \frac{z_k}{\delta_k} = \varepsilon_k\left|\delta_k\right|^{n-1} \\ &E_k^{\varepsilon} = R_{k,\infty}\varepsilon_k\delta_k\left|\delta_k\right|^{n-1}P_k^n = R_{k,\infty}z_kP_k^n \\ &A_{pp}\left(k,k\right) = R_{k,\infty}\left(\left|\delta_k\right|^{n-1}+zA_k\right)P_k^{n-1} = R_{k,\infty}\left(\left|Q_k\right|^{n-1}+zA_kP_k^{n-1}\right) \end{aligned} \tag{6}$$

where $A_{pp}(k,k)$ = elements of the new description of the diagonal matrix $\mathbf{A}_{pp}$ of Eq. (1), E_k^{ε}= head loss error due to incorrectness of demand representation, ε_k, z_k and zA_k = pipe dimensionless parameters useful in order to account for actual demand distribution along the pipes which are depend $\delta_k=Q_k/P_k$ = dimensionless parameter.
Furthermore, it is worth noting that the assumption $R_{k,\infty}$ (i.e. a constant pipe hydraulic resistance) in Eq. (5) implies that the correction ε_k accounts for the error due to the use of f(Ke) instead of f(Re,Ke) as will be demonstrated in the remainder of the text.
Assuming a uniformly distributed demand P_k and n=2 (corresponding to Darcy-Weisbach relationship for rough fully turbulent flow), *Giustolisi and Todini* (2008) have recently demonstrated that hydraulic resistances are underestimated in the model and, thus, overestimated during calibration in order to compensate this error.
This fact is particularly significant for pipes whose discharges (transferred water) are low with respect to the distributed demand outflow (δ_k tending to zero).
Considering now the well-known solution of the system (1) (Todini and Pilati, 1988):

$$\begin{aligned}
&\mathbf{B}_{pp}^{iter} = \left(\mathbf{D}_{pp}^{iter}\right)^{-1} \mathbf{A}_{pp}^{iter} \\
&\mathbf{F}^{iter} = \mathbf{A}_{np}\left(\mathbf{Q}^{iter} - \mathbf{B}^{iter}\mathbf{Q}^{iter}\right) - \mathbf{d} - \mathbf{A}_{np}\left(\mathbf{D}_{pp}^{iter}\right)^{-1}\left(\mathbf{A}_{p0}\mathbf{H}_0\right) \\
&\mathbf{H}^{iter+1} = \left(\mathbf{A}_{np}\left(\mathbf{D}_{pp}^{iter}\right)^{-1}\mathbf{A}_{pn}\right)^{-1}\mathbf{F}^{iter} \\
&\mathbf{Q}^{iter+1} = \left(\mathbf{Q}^{iter} - \mathbf{B}^{iter}\mathbf{Q}^{iter}\right) - \left(\mathbf{D}_{pp}^{iter}\right)^{-1}\left(\mathbf{A}_{p0}\mathbf{H}_0 + \mathbf{A}_{pn}\mathbf{H}^{iter+1}\right)
\end{aligned} \tag{7}$$

where *iter* = counter used during the iterative solution, it is necessary to achieve the diagonal elements of the matrix $\mathbf{D}_{pp}$ considering that they are the derivatives of the column vector $\mathbf{A}_{pp}\mathbf{Q}$ with respect to Q_k. Hence,

$$\begin{aligned}
&D_{pp}(k,k) = \frac{d\left(A_{pp}(k,k)Q_k\right)}{dQ_k} = \frac{d\left[R_{k,\infty}\left(Q_k\left|Q_k\right|^{n-1} + z_k P_k^n\right)\right]}{dQ_k} = \\
&= R_{k,\infty}\left(n\left|Q_k\right|^{n-1} + \frac{dz_k}{d\delta_k}P_k^{n-1}\right) = R_{k,\infty}\left(n\left|\delta_k\right|^{n-1} + zD_k\right)P_k^{n-1}
\end{aligned} \tag{8}$$

zD_k together with zA_k are useful in order to build the diagonal of $\mathbf{B}_{pp}$ in Eqs. (7),

$$\frac{A_{pp}(k,k)}{D_{pp}(k,k)} = \frac{\left|Q_k\right|^{n-1} + zA_k P_k^{n-1}}{n\left|Q_k\right|^{n-1} + zD_k P_k^{n-1}} = \frac{\left|\delta_k\right|^{n-1} + zA_k}{n\left|\delta_k\right|^{n-1} + zD_k} = zB_k \tag{9}$$

It is important to note that zD_k and zA_k tend to zero when δ_k tends to infinity (i.e. P_k is close or equal to zero) and the element zB_k of the diagonal matrix $\mathbf{B}_{pp}$ becomes equal to $1/n$ (i.e. 0.5 for n=2) and, consequently, GGA results unmodified for the k-th pipe. Furthermore, considering the case of P_k=0 (i.e. infinitesimal from a mathematical point of view), R_k(Re,Ke,D,L) and n=2 (i.e. the pipe head loss computed using the general Darcy-Weisbach formulation and without any distributed demand), the correction becomes

$$\varepsilon_k = \frac{R(\mathrm{Re},\mathrm{Ke},D,L)}{R_{k,\infty}} - 1 \Rightarrow E_k = R(\mathrm{Re},\mathrm{Ke},D,L)Q_k\left|Q_k\right| \tag{10}$$

Then, in this simple case, it is possible to obtain z_k, zA_k, zD_k and $\mathbf{D}_{pp}$,

$$\begin{aligned}
&z_k = \varepsilon_k\delta_k\left|\delta_k\right| = \frac{R_k}{R_{k,\infty}}\delta_k\left|\delta_k\right| - \delta_k\left|\delta_k\right| \Rightarrow E_k^{\varepsilon} = R_{k,\infty}\left(\frac{R_k}{R_{k,\infty}}\delta_k\left|\delta_k\right| - \delta_k\left|\delta_k\right|\right)P_k^2 = R_kQ_k\left|Q_k\right| - R_{k,\infty}Q_k\left|Q_k\right| \\
&zA_k = \frac{z_k}{\delta_k} = \frac{R_k}{R_{k,\infty}}\left|\delta_k\right| - \left|\delta_k\right| \Rightarrow A_{pp}(k,k) = R_{k,\infty}\left(\left|\delta_k\right| + \frac{R_k}{R_{k,\infty}}\left|\delta_k\right| - \left|\delta_k\right|\right)P_k = R_k\left|Q_k\right| \\
&zD_k = \frac{dz_k}{d\delta_k} = 2\left(\frac{R_k}{R_{k,\infty}}\left|\delta_k\right| - \left|\delta_k\right|\right) + \frac{P_k}{R_{k,\infty}}\frac{dR_k}{dQ_k}\delta_k\left|\delta_k\right| \Rightarrow \\
&\Rightarrow D_{pp}(k,k) = R_{k,\infty}\left(2\left|\delta_k\right| + 2\left(\frac{R_k}{R_{k,\infty}}\left|\delta_k\right| - \left|\delta_k\right|\right) + \frac{P_k}{R_{k,\infty}}\frac{dR_k}{dQ_k}\delta_k\left|\delta_k\right|\right)P_k = 2R_k\left|Q_k\right| + \frac{dR_k}{dQ_k}Q_k\left|Q_k\right|
\end{aligned} \tag{11}$$

ACTUAL DEMAND DISTRIBUTION IN WDN SIMULATION MODEL

The aim of this article is to improve the head loss error correction strategy by extending the results to the general case of *m* connections along the each *k*-th pipe delivering the demands $q_{k,j,}$ as reported in Figure 1.

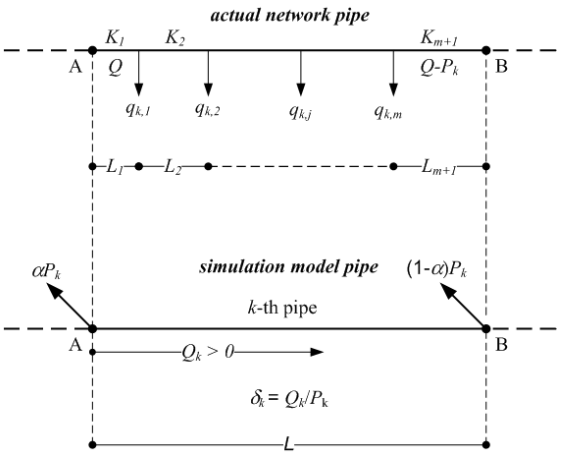

Figure 1. Actual pipe connections and schematic representation in WDN model

In fact, the improvement of the information technologies allows to describe better and better the network topology and the detail of the single connection are already available into the GIS systems. Thus, extending the demand-driven simulation model in order to consider this information without drastically increasing the number of nodes and pipes of the simulation model is an effective way to improve water network analysis avoiding course errors due to the wrong approximation of lumped demands into the nodes. Referring to Figure n.1, the general formulation for total pipe head loss considering *m* connections along the *k*-th pipe A-B is

$$\left(H_A - H_B\right)_{actual} = K_1 Q\left|Q\right|^{n-1} L_1 + \\ + \sum_{i=1}^{m-1} K_{i+1}\left(Q - \sum_{j=1}^{i} q_{k,j}\right)\left|Q - \sum_{j=1}^{i} q_{k,j}\right|^{n-1} L_{i+1} + K_{m+1}\left(Q - P_k\right)\left|Q - P_k\right|^{n-1} L_{m+1} \qquad (12)$$

$$K_1 = K_1\left(Q\right); \quad K_{i+1} = K_{i+1}\left(Q - \sum_{j=1}^{i} q_{k,j}\right); \quad K_{m+1} = K_{m+1}\left(Q - P_k\right)$$

where Q = flow rate entering or exiting from pipe depending on its sign, $q_{k,j}$ = demands of the *m* connections, L_i = *m*+1 lengths between two connections or one connection and ending nodes of the pipe and the related K_i = *m*+1 unitary hydraulic resistances which may depend on flow rates.
Assuming the dimensionless parameters,

$$\kappa_i = \frac{K_i}{K_{k,\infty}}; \quad \lambda_i = \frac{L_i}{L_k}; \quad \delta = \frac{Q}{P_k}; \quad \pi_i = \frac{\sum_{j=1}^{i} q_{k,j}}{P_k}; \tag{13}$$

where $K_{k,\infty}$ (=$R_{k,\infty}/L_k$) = unitary hydraulic resistance of the k-th pipe depending on the equivalent roughness only as in rough turbulent flow regime. Thus, Eq. (12) becomes

$$\begin{aligned}\left(H_A - H_B\right)_{actual} = &\left(\kappa_1 \delta \left|\delta\right|^{n-1} \lambda_1 + \right. \\ &\left. + \sum_{i=1}^{m-1} \kappa_{i+1} \left(\delta - \pi_i\right) \left|\delta - \pi_i\right|^{n-1} \lambda_{i+1} + \kappa_{m+1} \left(\delta - 1\right) \left|\delta - 1\right|^{n-1} \lambda_{m+1} \right) K_{k,\infty} P_k^n L_k\end{aligned} \tag{14}$$

It is important to note that the demand distribution along the k-th pipe is not symmetric with respect to flow direction and, therefore, Eq. (14) is written considering the positive flow direction (i.e. considering Q in A and the positive flow from A to B) and in particular π_i are related to the assumed positive flow versus.
Referring again to Figure 1, the pipe head loss in the simulation model (assuming the pipe resistance correction strategy) is given by,

$$\left(H_A - H_B\right)_{simulation\ model} = K_{k,\infty} \left(1 + \varepsilon_k\right) Q_k \left|Q_k\right|^{n-1} L_k = K_{k,\infty} \left(1 + \varepsilon_k\right) \delta_k \left|\delta_k\right|^{n-1} P_k^n L_k \tag{15}$$

where Q_k (=$Q - \alpha P_k$) = flow rate of the k-th pipe in the simulation model and $\delta_k = Q_k/P_k$, therefore $\delta_k = \delta - \alpha$. Thus, substituting $\delta = \delta_k + \alpha$ in Eq. (14) and equating ($H_A - H_B)_{actual}$ with ($H_A - H_B)_{simulation\ model}$ in order to achieve the conservation of energy balance, it is possible to obtain the correction,

$$\begin{aligned}\varepsilon_k = &\frac{\kappa_1 \left(\delta_k + \alpha\right) \left|\delta_k + \alpha\right|^{n-1} \lambda_1}{\delta_k \left|\delta_k\right|^{n-1}} + \\ &+ \frac{\sum_{i=1}^{m-1} \kappa_{i+1} \left(\delta_k + \alpha - \pi_i\right) \left|\delta_k + \alpha - \pi_i\right|^{n-1} \lambda_{i+1}}{\delta_k \left|\delta_k\right|^{n-1}} + \\ &+ \frac{\kappa_{m+1} \left(\delta_k + \alpha - 1\right) \left|\delta_k + \alpha - 1\right|^{n-1} \lambda_{m+1}}{\delta_k \left|\delta_k\right|^{n-1}} - 1\end{aligned} \tag{16}$$

It is worth noting that ε_k (i.e. z_k, zD_k and zA_k) is generally dependent on δ_k, as found in *Giustolisi and Todini* (2008) for the uniform function used as surrogate of the uniform distributed demand, but also on λ_i and π_i, which are parameters related to connection and demand distribution, κ_i and n, which are parameters related to flow regime, and α which is the parameter related to the way the total pipe demand is lumped into the two nodes A and B.
Furthermore, it is worth noting that for m=0, P_k=0, R_k(Re,Ke,D,L) and n=2 the corrections becomes equal to that of Eq. (10),

$$\varepsilon_k = \frac{\kappa_1 \left(\delta_k + \alpha\right) \left|\delta_k + \alpha\right|}{\delta_k \left|\delta_k\right|} - 1 = \frac{\kappa_1 \left(Q_k + \alpha P_k\right) \left|Q_k + \alpha P_k\right|}{Q_k \left|Q_k\right|} - 1 = \kappa_1 - 1 \tag{17}$$

CONCLUSIONS

An extension of the Global Gradient Algorithm (GGA) allowing the effective introduction of the lumped nodal demands without forfeiting the correct pipe head loss has been presented. A pipe hydraulic resistance correction (Giustolisi and Todini, 2008) has been used in order to modify the classical GGA.

The formulation of the pipe hydraulic resistance correction for any pipe demand pattern due to pipe connections has been achieved. Consequently, some dimensionless parameters have been gained in order to account for any pipe demand pattern in classical GGA.

The new formulation of the GGA can be easily implemented in all simulation packages based on GGA, such as for instance EPANET 2, and it can serve as a guide for other network simulation model strategies. Furthermore, it is envisaged that the new simulation model is essential for network model calibration purposes and also for other network analyses such as that of pressure-driven leakage and demand simulation model (Giustolisi et al., 2008).

REFERENCES

Anderson, E.J. & Al-Jamal, K.H. Hydraulic Network Simplification. *J. of Water Res. Plan. and Manage.*, ASCE, 121 (3), pp. 235-240, 1995.

Carpentier, P., Cohen, G. & Hamam, Y. Water Network Equilibrium, Variational Formulation and Comparison of Numerical Algorithms, EURO VII, Bologna, Italy, 1985.

Collins, M., Cooper, L., Helgason, R., Kenningston, J. & LeBlanc, L. Solving the pipe network analysis problem using optimization techniques, *Management Science*, 24 (7), 747-760, 1978.

Cross H. Analysis of flow in networks of conduits or conductors, Bulletin no.286, University of Illinois Engineering Experimental Station, Urbana Illinois, USA, 1-29, 1936.

Epp, R. & Fowler, A.G. Efficient Code for steady-state flows in networks, *J. of Hydr. Div.*, ASCE, 96 (11), 3-56, 1970.

Giustolisi, O., Savic, D.A. & Kapelan, Z. Pressure-driven demand and leakage simulation for water distribution networks, *J. of Hydr. Eng.*, ASCE, 134 (5), 626-635, 2008.

Giustolisi, O., & Todini, E. Pipe hydraulic resistance correction in wdn analysis, Special Issue on *WDS Model Calibration, Urban Water Journal,* Taylor & Francis, UK, No. 4, Vo. 5, 2008. DOI: 10.1080/15730620802541623

Hamam, Y.M. & Brammeler, A. Hybrid method for the solution of piping networks, *Proc. IEE*, 118 (11), 1607-1612, 1971

Hamberg, D. & Shamir, U. Schematic Models for Distribution Systems Design: I Combination Concept, *J. of Water Res. Plan. and Manage.*, ASCE, 114 (2), 129-140, 1988.

Kesavan, H.K. & Chandrashekar, M. Graph-theoretic models for pipe net-work analysis, *J. of Hydr. Div.*, ASCE, 98 (2), 345-364, 1972.

Isaacs, L.T. & Mills, K.G. Linear Theory Method for Pipe Network Analysis. *J. of Hydr. Div.*, ASCE, 106 (7), 1191-120, 1980.

Martin, D.W. & Peters, G. The application of Newton's method to network analysis by digital computers, *J. Inst. of Water Engrs.*, (17). 115-129, 1963.

Osiadacz, A.J. 1987. Simulation and Analysis of Gas Networks. E. & F.N. Spon, London.

Piller, O. Modeling the behavior of a network - Hydraulic analysis and a sampling procedure for estimating the parameters, PhD thesis from the University of Bordeaux I, defended on, 288 pages, Bordeaux, 1995.

Rossman, L.A. Epanet2 Users Manual, US EPA, 2000.

Shamir, U. & Howard, C.D.D. Water distribution network analysis, *J. of Hydr. Div.*, ASCE, 94 (1), 219-234, 1968.

Ulanicki, B., Zehnpfund, A. & Martínez, F. Simplification Of Water Distribution Network Models. *Hydroinformatics '96*, Rotterdam, pp. 493-500, 1996.

Todini, E. Un metodo del gradiente per la verifica delle reti idrauliche, Bollettino degli Ingegneri della Toscana, No.11, 11-14, 1979 (in Italian).

Todini, E. & Pilati, S. A gradient method for the solution of looped pipe networks, Computer Applications in Water Supply, John Wiley & Sons, Vo.1, 1-20, 1988.

Wood, D.J. & Charles, C.O.A. Hydraulic network analysis using linear theory, *J. of Hydr. Div.*, ASCE, 98 (7), 1157-1170, 1972.

Wood, D.J. & Rayes, A.G. Reliability of algorithms for pipe network analysis, *J. of Hydr. Div.*, ASCE, 107 (10), 1145-1161, 1981.

Identification of the hydraulic model from operational measurements for supervisory pressure control

Ping Li, Ian Postlethwaite*, Emmanuel Prempain*,*
Bogumil Ulanicki† and Ridwan Patel‡
*Department of Engineering, University of Leicester, Leicester, UK
emails: pl62@le.ac.uk, ixp@le.ac.uk, ep26@le.ac.uk
†Process Control - Water Software Systems, De Montfort University, Leicester, UK
emails: bul@dmu.ac.uk
‡Yorkshire Water Services, Bradford, UK
emails: ridwan.patel@yorkshirewater.co.uk

Abstract

The operational pressure control is a cost-effective way to leakage reduction and many pressure control methods and algorithms have been developed. Whilst the pressure control algorithm is model-based, the hydraulic model of the considered distribution network is not always available. Therefore, this paper will focus on the development of an aggregated hydraulic model of the network considered, in particular, identification of a leakage enhanced model using the operational measurements or the available historical data. This will enable a pressure optimisation algorithm to calculate the optimal pressure schedules for the implementation of a pressure control scheme. The identification problem is formulated as a parameter estimation problem in this paper and a least-square based method is derived for estimating the parameters in the model. A case study provided by a UK water company is performed to illustrate the use of the method and the identification results from real operational data are presented.

Introduction

Leakage from water distribution networks is a source of major concern for water companies worldwide and leakage reduction is a key factor of water distribution network management. It is well known that water leakage in a distribution network is directly related to the system service pressure, hence pressure control is an effective way to reduce background leakage and various methods and algorithms have been developed for optimising the operational pressure so as to minimize background leakage and, at the same time, to satisfy pressure requirements at critical points (see e.g. Jowitt and Xu (1990), Ulanicki et al (2000, 2008) and references therein). Before implementing a pressure control scheme, it is necessary to perform planning studies to investigate the economical aspects of such a scheme. Such studies are usually based on the knowledge about the particular network considered and a convenient form of such knowledge

is a hydraulic model of the network. However, it is often the case that such a hydraulic model is not available from the water company and has to be obtained by some identification procedures using measurements or historical operational data.

This paper focuses on the development of an aggregated hydraulic model of the network considered, in particular, identification of a leakage enhanced model using the operational measurements or the available historical data for the implementation of supervisory pressure control. The rest of the paper is organized as follows. Next section gives the problem statement, which is followed by the derivation of a least-square based method for estimating the parameters in both pipe element model and leakage model of the network. A case study provided by a UK water company is then performed to illustrate the use of the method and the identification results from real operational data are presented. The conclusions are given in the last section.

Problem statement

To facilitate monitoring and control activities, it is common practice for water companies to split the water distribution network into district metered areas (DMAs) that are typically small areas and are isolated apart from designated inlets and outlets through which flows are monitored. Pressure reducing valves (PRVs) are used to maintain a specified pressure to the inlets of a DMA against the fluctuations in PRV inlet pressure and the changes of demand from the DMA. This structure also facilitates application of a pressure control scheme.

A prerequisite for pressure control design is an appropriate model of the network to be controlled, but such a model is not always available in practice, therefore some kind of identification procedure is needed so as to estimate an equivalence model from the available measurements or historical data. The equivalence hydraulic model will contain only boundary nodes, target (critical) nodes and fictitious pipes with which these nodes are connected (Ulanicki et al 2000). The data available for model identification are boundary heads and flows, target heads and flows, and the aim of the identification is to obtain a leakage enhanced network model for pressure control. More specifically, the parameters to be identified are the resistance/conductance of the fictitious pipes, the leakage coefficients and leakage exponent.

Hydraulic model identification

The aforementioned equivalence network structure can be conveniently represented by a node-branch incidence matrix $\mathbf{\Lambda}$ (see e.g. Ulanicki et al 2000). The matrix has a row for each node and a column for each branch. A row contains information about which branches are connected to a particular node. The elements of $\mathbf{\Lambda}$ take one of the three values -1, 0 and $+1$. The value -1 indicates that the flow of the branch is oriented towards the node, the value $+1$ indicates the flow of the branch is leaving the node and value 0 indicates that a branch is not connected to the node. Therefore, each column of $\mathbf{\Lambda}$ contains only two non-zero entries, $+1$ for the branch origin node and -1 for the branch destination node. Let N_{node} denote the total number of the (boundary and target) nodes in the equivalence network, in the most general case, the total number of branches (fictitious pipes) will be $N_{pipe} = \frac{1}{2}(N_{node} - 1)N_{node}$ and $\mathbf{\Lambda}$

will be a $N_{node} \times \frac{1}{2}(N_{node}-1)N_{node}$ matrix.

Pipe model parameter estimation

The main components in the aforementioned equivalence network are the (fictitious) pipes which can be described by many different formulae. In this paper, the head-flow relationship for the jth pipe element is expressed by Hazen-Williams formula (see e.g. Walski *et al* 2003):

$$\Delta h_j = h_{j,o} - h_{j,d} = R_j q_j |q_j|^{0.852} \tag{1}$$

where $h_{j,o}$ and $h_{j,d}$ are heads in [m] at origin and destination nodes of the jth pipe element respectively; R_j is the resistance of the jth pipe element; q_j is the flow in [l/s] through the element.

Let $\mathbf{\Lambda}_i$ denote the ith row of $\mathbf{\Lambda}$; $\mathbf{\Lambda}_j^T$ denote the jth column of $\mathbf{\Lambda}$; the heads at each node and the flows in each branch are collected in the nodal head vector $\mathbf{h}$ and the branch flow vector $\mathbf{q}$ respectively, i.e. $\mathbf{h} = [h_1, h_2, \cdots, h_{N_{node}}]^T$, $\mathbf{q} = [q_1, q_2, \cdots, q_{N_{pipe}}]^T$. The head-flow relationship for the pipe elements in the network can then be written as follows:

$$\mathbf{\Lambda}_j^T \mathbf{h} = R_j q_j |q_j|^{0.852} \quad j = 1, 2, \cdots, N_{pipe} \tag{2}$$

The mass balance equations at nodes can be written as:

$$\mathbf{\Lambda}_i \mathbf{q} = -q_{t,i} + q_{b,i} \quad i = 1, 2, \cdots, N_{node} \tag{3}$$

where $q_{t,i}$ is the total target flow (i.e. demand and leakage) for node i, $q_{b,i}$ is the boundary flow ($q_{b,i} = 0$ for non-boundary node) for node i. The above mass balance equations at nodes can be written in a compact form:

$$\mathbf{\Lambda q} = \underbrace{\begin{bmatrix} -q_{t,1} + q_{b,1} \\ -q_{t,2} + q_{b,2} \\ \vdots \\ -q_{t,N_{node}} + q_{b,N_{node}} \end{bmatrix}}_{\mathbf{q}_{t,b}} \tag{4}$$

To estimate the pipe resistance R_j, the pipe model (1) is rewritten in a reverse form:

$$q_j = G_j \Delta h_j |\Delta h_j|^{-0.46} \quad j = 1, 2, \cdots, N_{pipe} \tag{5}$$

where $G_j = 1/R_j^{0.54}$ is the conductance of the jth pipe in the network. The pipe equations (5) can be assembled in a vector form as follows:

$$\mathbf{q} = \begin{bmatrix} q_1 \\ q_2 \\ \vdots \\ q_{N_{pipe}} \end{bmatrix} = \underbrace{\begin{bmatrix} \Delta h_1 |\Delta h_1|^{-0.46} & 0 & \cdots & 0 \\ 0 & \Delta h_2 |\Delta h_2|^{-0.46} & \cdots & 0 \\ \vdots & \vdots & \ddots & \vdots \\ 0 & 0 & \cdots & \Delta h_{N_{pipe}} |\Delta h_{N_{pipe}}|^{-0.46} \end{bmatrix}}_{\mathbf{\Delta H}} \underbrace{\begin{bmatrix} G_1 \\ G_2 \\ \vdots \\ G_{N_{pipe}} \end{bmatrix}}_{\mathbf{G}} \tag{6}$$

Substituting (6) into (4), the following compact network model can be derived:

$$\mathbf{\Lambda \Delta H G} = \mathbf{q}_{t,b} \tag{7}$$

Since all heads, target flows and boundary flows are measured or available from historical data, the model equation (7) is linear with respect to the parameter vector $\mathbf{G}$ (from which the resistance $R_j, j = 1, 2, \cdots, N_{pipe}$ can be derived). Assume that a time history measurement data set of length K (i.e. $\{\Delta h_j(k), q_{t,i}(k), q_{b,i}(k)\}_{k=1}^{K}$ for $j = 1, 2, \cdots, N_{pipe}$ and $i = 1, 2, \cdots, N_{node}$) is selected, the parameter estimation can then be formulated as a least-square problem. For the model defined by (7), it is straightforward to write the explicit linear regression form in terms of the parameter vector $\mathbf{G}$ to be estimated:

$$\underbrace{\begin{bmatrix} \mathbf{q}_{t,b}(1) \\ \mathbf{q}_{t,b}(2) \\ \vdots \\ \mathbf{q}_{t,b}(K) \end{bmatrix}}_{\mathbf{Q}_{t,b}} = \underbrace{\begin{bmatrix} \mathbf{\Lambda}\Delta\mathbf{H}(1) \\ \mathbf{\Lambda}\Delta\mathbf{H}(2) \\ \vdots \\ \mathbf{\Lambda}\Delta\mathbf{H}(K) \end{bmatrix}}_{\mathbf{\Phi}} \mathbf{G} \tag{8}$$

where, for $k = 1, 2, \cdots, K$

$$\mathbf{q}_{t,b}(k) = \begin{bmatrix} -q_{t,1}(k) + q_{b,1}(k) \\ -q_{t,2}(k) + q_{b,2}(k) \\ \vdots \\ -q_{t,N_{node}}(k) + q_{b,N_{node}}(k) \end{bmatrix} \tag{9}$$

and

$$\Delta\mathbf{H}(k) = \begin{bmatrix} \Delta h_1(k)|\Delta h_1(k)|^{-0.46} & 0 & \cdots & 0 \\ 0 & \Delta h_2(k)|\Delta h_2(k)|^{-0.46} & \cdots & 0 \\ \vdots & \vdots & \ddots & \vdots \\ 0 & 0 & \cdots & \Delta h_{N_{pipe}}(k)|\Delta h_{N_{pipe}}(k)|^{-0.46} \end{bmatrix} \tag{10}$$

$\mathbf{G}$ can then be estimated by solving the above linear regression problem with the LS method as follows:

$$\hat{\mathbf{G}} = \mathbf{\Phi}^{+}\mathbf{Q}_{t,b} \tag{11}$$

where $\mathbf{\Phi}^{+}$ is the pseudo-inverse of $\mathbf{\Phi}$. From equations (8), (9) and (10), it is clear that the matrices $\mathbf{Q}_{t,b}$ and $\mathbf{\Phi}$ in equation (11) are formed entirely using the available measurement data $\{\Delta h_j(k), q_{t,i}(k), q_{b,i}(k)\}_{k=1}^{K}$ for $j = 1, 2, \cdots, N_{pipe}$ and $i = 1, 2, \cdots, N_{node}$.

Equations (8)$\sim$(11) provide a method for identifying an equivalence network model in the general case. If, however, the mass balance equation (4) can be solved, hence branch flows $q_j, j = 1, 2, \cdots, N_{pipe}$ are available; the identification algorithm can be greatly simplified. Since q_j is available, it is straightforward to write the explicit linear regression form in terms of the R_j from equation (1) for each pipe:

$$\underbrace{\begin{bmatrix} \Delta h_j(1) \\ \Delta h_j(2) \\ \vdots \\ \Delta h_j(K) \end{bmatrix}}_{\Delta\mathbf{H}_j} = \underbrace{\begin{bmatrix} q_j(1)|q_j(1)|^{0.852} \\ q_j(2)|q_j(2)|^{0.852} \\ \vdots \\ q_j(K)|q_j(K)|^{0.852} \end{bmatrix}}_{\mathbf{Q}_j} R_j \quad j = 1, 2, \cdots, N_{pipe} \tag{12}$$

Similar to (11), the resistance R_j can then be estimated as follows:

$$\hat{R}_j = \mathbf{Q}_j^{+} \Delta \mathbf{H}_j \quad j = 1, 2, \cdots, N_{pipe} \tag{13}$$

Assume that the measurement errors are independent, identically distributed (i.i.d.), the estimation error, i.e. the standard deviation of the estimate $\hat{R}_j$ can also be evaluated, this is given by:

$$\sigma(\hat{R}_j) = \sqrt{\frac{S}{K-1}(\mathbf{Q}_j^T \mathbf{Q}_j)^{-1}} \tag{14}$$

where S is the sum of squared residuals defined as follows:

$$S = \sum_{k=1}^{K} (\Delta h_j(k) - q_j(k)|q_j(k)|^{0.852} \hat{R}_j)^2 \tag{15}$$

Leakage model parameter estimation

The pressure management for leakage reduction requires an enhanced hydraulic model, which incorporate pressure dependent leakage terms. Several mathematical models relating the leakage and the operating pressure based on experimental results have been proposed. The leakage-pressure relationship as shown in equation (16) (Ulanicki *et al* 2008) is assumed in this paper:

$$l_i = k_i p_i^{\alpha_i} = k_i (h_i - H_i)^{\alpha_i} \tag{16}$$

where k_i is the leakage coefficient; α_i is the leakage exponent, h_i is the head of node i and H_i is the elevation of node i. The leakage exponent α_i ranges from 0.5 to 2.5 depending on many factors described in the literature. In this paper, the leakage exponent will be estimated along with the leakage coefficient k_i using the leakage measurement data $\{h_i(k), H_i, l_i(k)\}_{k=1}^{K}$. In practice, the leakage $l_i, i = 1, 2, \cdots, N_{node}$ may not be available, some kinds of estimation or approximation have to be used. The minimum night flow (MNF) will be used in the following case study to approximate the leakage.

The linear least-square method can not directly be used for estimating the parameters k_i and α_i in leakage model (16) as the model is not linear in terms of α_i. However, the problem can be resolved by taking logarithms of equation (16):

$$\ln l_i = \ln k_i + \alpha_i \ln p_i \tag{17}$$

For the given data set $\{h_i(k), H_i, l_i(k)\}_{k=1}^{K}$ of size K, the following standard linear regression form in terms of the transformed variables $\boldsymbol{\theta} = \begin{bmatrix} \ln k_i & \alpha_i \end{bmatrix}^T$ can readily be derived from equation (17):

$$\underbrace{\begin{bmatrix} \ln l_i(1) \\ \ln l_i(2) \\ \vdots \\ \ln l_i(K) \end{bmatrix}}_{\mathbf{L}} = \underbrace{\begin{bmatrix} 1 & \ln p_i(1) \\ 1 & \ln p_i(2) \\ \vdots & \vdots \\ 1 & \ln p_i(K) \end{bmatrix}}_{\mathbf{\Phi}} \boldsymbol{\theta} \tag{18}$$

The LS estimates of k_i and α_i is then given by:

$$\hat{\boldsymbol{\theta}} = \begin{bmatrix} \ln \hat{k}_i \\ \hat{\alpha}_i \end{bmatrix} = \boldsymbol{\Phi}^{+}\mathbf{L} \quad \text{and} \quad \hat{k}_i = e^{\ln \hat{k}_i} \tag{19}$$

The variance-covariance matrix of the estimate $\hat{\boldsymbol{\theta}}$ is given by:

$$\boldsymbol{\sigma}(\hat{\theta}) = \frac{S_T}{K-2}(\boldsymbol{\Phi}^T\boldsymbol{\Phi})^{-1} \tag{20}$$

where S_T is the sum of squared transformed residuals defined as follows:

$$S_T = \sum_{k=1}^{K}(\ln l_i(k) - \ln \hat{k}_i - \hat{\alpha}_i \ln(p_i(k)))^2 \tag{21}$$

The standard deviations of the model parameter estimates is then given by (see e.g. Bevington and Robinson 2003):

$$\sigma(\hat{k}_i) = \boldsymbol{\sigma}(\hat{\theta})_{11} / \frac{d(\ln \hat{k}_i)}{d\hat{k}_i} = \hat{k}_i \boldsymbol{\sigma}(\hat{\theta})_{11} \quad \text{and} \quad \sigma(\hat{\alpha}_i) = \boldsymbol{\sigma}(\hat{\theta})_{22} \tag{22}$$

where $\boldsymbol{\sigma}(\hat{\theta})_{ii}(i = 1, 2)$ is the main diagonal element of the matrix $\boldsymbol{\sigma}(\hat{\theta})$ defined by (20).

Case study

Pressure management in UK water industry has been an ongoing process for a period of time and an event-driven pressure management trial was recently carried out at a UK water company. As a part of the UK Engineering & Physical Science Research Council (EPSRC)-funded project NEPTUNE, a supervisory pressure control scheme covering wide areas and the associated implementation through the hardware used in the aforementioned trial are proposed for minimizing leakage and customer interruptions. However, the water company does not have a hydraulic model for the area considered. Without a model it is also difficult to estimate how much savings would result from the implementation of the proposed pressure control scheme.

In this section, an aggregated hydraulic model for the area considered will be developed using the available measurements for the implementation of the proposed supervisory pressure control scheme. The network extracted from the schematics of the considered area is shown in Figure 1. It has one boundary node (PRV in the figure) which is connected to six target (critical) nodes (DMAs in the figure). As there is no connections between target (DMA) nodes, the mass balance equation (4) can be solved and the branch flows $q_j, j = 1, 2, \cdots, 6$ will be available, which are equal to the measured target flows in this case. The PRV node is the common origin for all the pipe elements in the network, and the destination nodes are the associated DMAs. The total leakage for each target (DMA) node will be approximated by its MNF for estimation of parameters in leakage model (16).

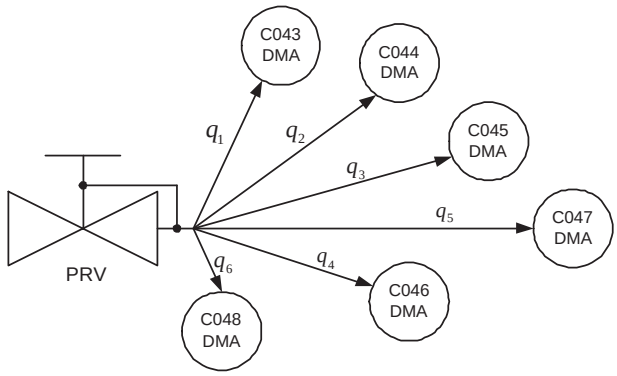

Figure 1: Schematic structure of the considered network

Historical data for parameter estimation

The available historical data files associated with the considered area are provided by a UK water company and they are summarized in Table 1. As can been seen, from this table, the data is not complete. Figure 2 shows the typical plots of the daily PRV outlet head and a DMA node flow over a week.

Table 1: Available data for identification

Nodes	DG2 pressure data	DG2 elevation	Flow data
C043	04/05/07∼04/08/08	130[m]	12/06/08 (Thur)
C044	01/04/07∼04/08/08	140[m]	01/04/07∼13/06/08
C045	01/04/07∼04/08/08	148.6[m]	01/04/07∼07/07/08
C046	01/04/04∼19/06/08	148.55[m]	01/04/07∼07/07/08
C047	01/04/07∼04/08/08	141.38[m]	01/04/07∼31/07/08
C048	09/07/08∼18/07/08	141.9[m]	09/07/08∼18/07/08
PRV	25/09/07∼12/02/08	149[m]	01/01/06∼10/10/07

It can be seen that the flow and head plots on weekdays approximately follow the same pattern which are obvious different from the plots on weekends. The minimum night flow occurs between 2:00am and 3:00am and there are two peaks in a daily flow plot. The first peak occurs around 6:45am in weekdays and two hours later on the weekends, the second peak occurs around 6:00pm.

The data collected between 11/01/2008 and 06/02/2008 are selected for modelling because this is the latest period of time over which the measurements for the PRV and most of the DMAs are available as shown in Table 1.

Identification results

Since there is no overlap between the PRV outlet head data and the C043, C048 head data as shown in Table 1, it would not be possible to estimate the resistances

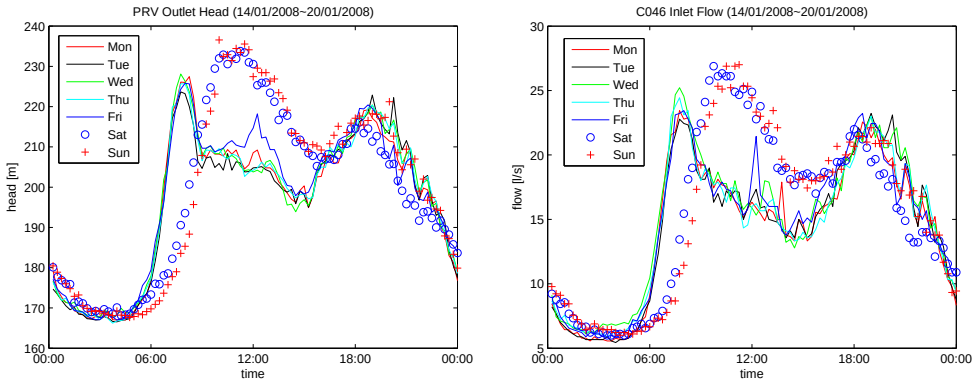

Figure 2: Daily PRV outlet head and DMA flow over a week

between PRV and C043, C048 DMAs. However, as shown in Figure 2, the PRV outlet heads on the weekdays approximately follow the same pattern, the PRV outlet heads taken in the different dates will be used as the replacement data for estimating the resistances between PRV and C043, C048 DMAs. Having removed all the outliers detected in the original data sets, model identification is performed and the results of parameter estimation are summarized in Table 2.

Table 2: Results of parameter estimation with the outliers being removed

DMA	R_j	$\sigma(R_j)$	k_j	$\sigma(k_j)$	α_j	$\sigma(\alpha_j)$
C043	0.7739	4.0945×10^{-2}	3.4763×10^{-2}		1.1	
C044	2.7862	1.8876×10^{-2}	9.6198×10^{-5}	1.0191×10^{-3}	2.5111	3.0285
C045	1.3865	1.4331×10^{-2}	2.2914×10^{-2}		1.1	
C046	0.1495	5.4148×10^{-4}	1.9783×10^{-1}	7.1931×10^{-1}	1.0091	1.0915
C047	0.4480	3.2228×10^{-3}	5.3411×10^{-2}	7.2589×10^{-1}	0.9741	3.8450
C048	0.3971	1.5554×10^{-2}	4.7983×10^{-2}		1.1	

The R_js in the table are estimated with equation (13) with the associated standard deviations $\sigma(R_j)$ being estimated with equation (14). Figure 3 shows the results of data fitting for C046 and C047 using their R_j estimates. The k_js and α_js of the leakage model in Table 2 are estimated by equation (19) with the associated standard deviations being evaluated with equations (20)$\sim$(22), where the leakage measurements are approximated by their MNFs.

However, the estimate of leakage exponent for C045 takes negative value ($\hat{\alpha}_j = -3.4095 \times 10^{-1}$). To investigate the problem, the results of leakage data fitting for C045 DMA with the outlier being removed is plotted in Figure 4 and it shows, in overall, a slightly negative correlation between the MNF and pressure. This may indicate that the MNF is not a good estimate of the leakage for C045 DMA. As a remedy, the minimum MNF over the dates between 11/01/2008 and 06/02/2008 (excluding the outlier) is used as the estimate of leakage for C045 DMA and α_j takes the value of 1.1. k_j is then

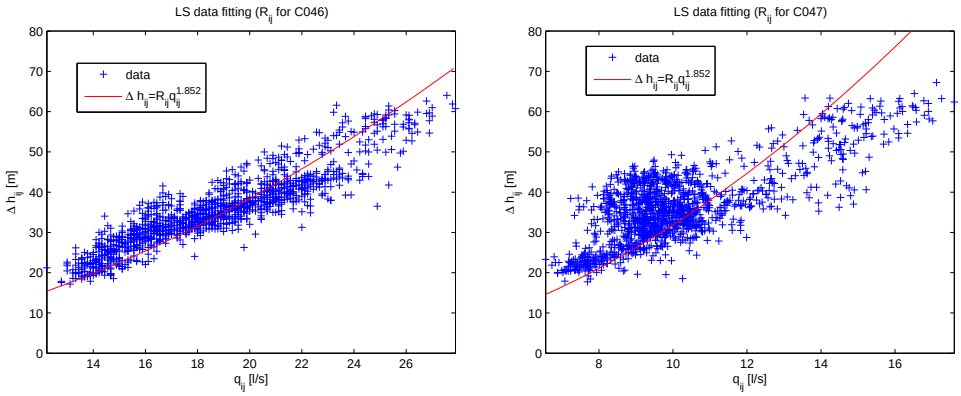

Figure 3: Results of R_j data fitting for C046 and C047 with outliers being removed

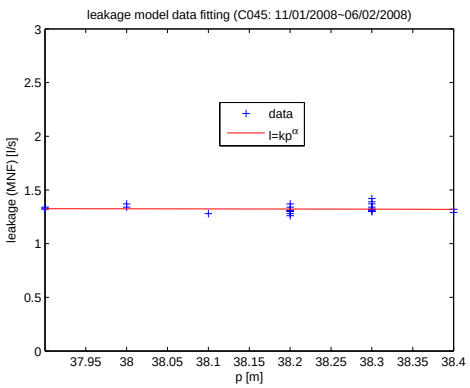

Figure 4: C045 MNF-pressure plot with outlier being removed

obtained as:

$$k_j = \frac{\text{minimum MNF}}{p_{minMNF}^{1.1}} \tag{23}$$

and this result is shown in Table 2.

The α_js for C043 and C048 are also assumed to be 1.1 as shown in Table 2 and the corresponding k_js are estimated with equation (23). This is because: (i) only one-day flow data (i.e. only one MNF) is available for C043 DMA; (ii) there are many missing data in flow and DG2 files for C048, therefore the averages of MNFs and the associated pressures over 09/07/2008-18/07/2008 are used for estimating k_j for C048 DMA with equation (23).

It needs to be pointed out that the estimation errors (standard deviations) of leakage model parameters k_j and α_j evaluated with equations (20)$\sim$(22) are quite large in comparison with the values of the corresponding parameter estimates as shown in Table 2. This is because the matrix $\mathbf{\Phi}^T\mathbf{\Phi}$ in (20) is ill-conditioned. This occurs when the measurements have only a marginal effect on the estimated parameters. In our case study, this is because we do not have the leakage measurements over a sufficient range

of pressure points. The MNFs have to be used in this study to approximate the leakage measurements for parameter estimation and the corresponding pressure range is very small (the pressure variations are not more than 1m at the most). This results in a nearly rank-deficient $\mathbf{\Phi}$ matrix defined in (18) which implies that the measurements are not "informative" enough and the identified leakage model will not be reliable when the pressure is outside the range of the measured pressure data used for identification.

Conclusions

A method for identifying a steady-state leakage enhanced hydraulic model of a water distribution network from measurements or historical operational data is presented in this paper. Only the head and flow data of the considered nodes are required by the method for identification. The method has been applied for a case study where a model of a real water distribution network provided by a UK water company has been identified from the available historical operational data. The case study also shows that the MNF alone is not "informative" enough for identifying a reliable leakage model and, sometimes, it is even not a good approximate to the leakage.

Further work is being carried out to validate and refine the identified model and to use the identified model for supervisory pressure control. The research is also being performed to develop the appropriate method for pre-processing the raw data, for example, to detect outliers and to deal with missing data etc, so as to facilitate the practical application of the method.

References

Jowitt, P. W., and Xu, C. (1990), "Optimal valve control in water distribution networks", *Journal of Water Resources Planning and Management*, 116(4), pp445-462.

Ulanicki, B., Bounds P.L.M., Rance J.P., and Reynolds, L. (2000). "Open Loop and Closed Loop Pressure Control for Leakage Reduction", *Urban Water Journal*, Elsevier Science, Vol.2, No.2

Ulanicki, B., AbdelMeguid, H., Bounds P., and Patel, R. (2008), "Pressure Control in District Metering Areas with Boundary and Internal Pressure Reducing Valves". *The 10th International Water Distribution System Analysis Conference*, 17-20 August, 2008, Kruger National Park, South Africa.

Walski, T. M., Chase, D. V., Savic, D. A., Grayman, W., Beckwith, S. and Koelle, E. (2003), "Advanced Water Distribution Modelling and Management". Haestead Press. First Edition.

Bevington, P. R. and Robinson, D. K. (2003), "Data reduction and error analysis for the physical sciences", McGraw-Hill, New York. Third Edition.

An operative approach to water distribution system rehabilitation

L. Berardi[1], O. Giustolisi[2] and D. Savic[3]

[1] Technical University of Bari, Engineering Faculty of Taranto, Department of Civil and Environmental Engineering, viale del Turismo 8, Taranto, Italy; e-mail: l.berardi@poliba.it
[2] Technical University of Bari, Engineering Faculty of Taranto, Department of Civil and Environmental Engineering, viale del Turismo 8, Taranto, Italy; e-mail: o.giustolisi@poliba.it
[3] Centre for Water Systems, School of Engineering, Computing and Mathematics, University of Exeter, North Park Road, Exeter, EX4 4QF, England, UK; e-mail: d.savic@exeter.ac.uk

ABSTRACT

The selection of the most effective course of action for pipe rehabilitation is crucial to avoid the uncontrolled deterioration of water distribution systems (WDS). Moreover, it provides a rare opportunity to modify some elements of the existing infrastructure in order to meet the present service requirements. For instance, a rehabilitation plan could be aimed at simultaneously improving system reliability, pressure levels and/or leakage reduction. In this work WDS rehabilitation is formulated as a multi-objective optimization problem where decision variables for each pipe are "do-nothing" or "replace" by selecting from a set of commercial pipe diameters. It is shown that the solutions returned by a multi-objective genetic algorithm (MOGA) in such a complex decision scenario although good, could not be easily used to support decision making. A prioritization strategy is developed and presented which is based on MOGA solutions and provides an effective tool for both analysts and decision makers.

INTRODUCTION

There are several factors which make planning rehabilitation of municipal water distribution systems (WDS) a complex task. Some of these are the shortage of funds available, the large size of real networks, the choice of the right rehabilitation options among all available alternatives and the appealing opportunity of improving network performances by renewing infrastructure elements. The development of fast and robust tools for water distribution network analyses as well as computationally effective search and optimization methodologies has provided technicians and researchers with a wide range of tools aimed at constructing effective decision support systems (DSS). Decision makers are now asked to choose the most appropriate solution from the technically optimal alternatives returned by the DSS according to their own management criteria.

The review of literature dealing with the development of DSS for WDS rehabilitation clearly shows how the formulation of the problem moved from a single-objective to a multi-objective approach. In particular, the earliest works by Shamir and Howard, (1979), Walski and Pelliccia (1982) and Male et al. (1990) provided general guidelines for evaluating whether a pipe should be replaced/rehabilitated during a given planning horizon according to mainly economic criteria. Later on other criteria have been considered such as those aimed at reducing pressure deficiencies (Walski, 1985), improving water quality and system flexibility (Halhal et al., 1997) and reducing pumping costs (Kim and Mays, 1994).

Another crucial rationale included in some work, is the maximization of network reliability (Quimpo and Shamsi, 1991; Todini, 2000; Dandy and Engelhardt, 2006), although the common definition of WDS "reliability" has not been agreed upon. In a recent paper, Berardi et al. (2008) also demonstrated the effectiveness of accounting for leakage reduction and actual valve deployment while selecting pipes to be replaced.

The problem of selecting the most effective rehabilitation intervention is discrete, because of the limited commercial rehabilitation alternatives, and combinatorial, as it is aimed at pointing out a subset of pipes within the network. In recent years, the problem of selecting optimal rehabilitation action has been solved by using multi objective genetic algorithms (MOGA) (Goldberg, 1989; Savic 2002). They represent heuristic search-and-optimization techniques particularly suited for discrete and combinatorial problems. MOGA are usually able to return good approximations of the so-called theoretical "Pareto optimal set", which consists of the best set of trade-offs between all (conflicting) objectives. The interest of the scientific community in the use of MOGA in such a context is documented in many papers (e.g. Halhal et al., 1997; Cheung et al., 2003, Dandy and Engelhardt, 2006). Nonetheless, most literature only focuses on refining some objective functions or comparing the performance of different GAs. It is quite unusual to look at the decision process; this is usually left to decision makers without considering how complex this process could be for them starting from MOGA solutions. In fact, the number of technically optimal alternatives increases with the amount of objective functions and rehabilitation options involved in the optimization. Moreover, solutions which are economically comparable involve the selection of different interventions for the same pipes (i.e. solutions are not *contiguous*) (Giustolisi et al., 2006). Such evidence could potentially leave the decision maker in a quandary over the selection from MOGA solutions.

Recently, Berardi et al. (2008) demonstrated the effectiveness of assigning priority to each pipe when the problem is to select pipes for replacement (without changing their diameter) on a real WDS and optimizing 5 objective functions. That procedure was used to create a new set of *contiguous* interventions by adding pipes according to their priority up to the monetary budget available. Such a procedure differs from other existing "priority" models (for example Quimpo and Shamsi, 1991) as it explicitly accounts for the expected behaviour of the rehabilitated system as a whole.

This work enlarges the discussion reported in Berardi et al., (2008) by considering a wider range of rehabilitation alternatives rather than a binary decision

variable. Without loss of generality, the decision variables reported here refer to the options of "do-nothing" or "replace by selecting pipe diameter". For each pipe to be replaced the new diameter is selected from a set of commercial sizes. In spite of the fact that other rehabilitation options (i.e. different from replacement) are still not explicitly considered here, it can be argued that changing a pipe's diameter means to change its carrying capacity which produces a similar effect to that expected from other techniques (i.e. relining). On the other hand, it allows a simpler cost analysis to be included in this work and the implicit assumption of improving pipe structural condition. Furthermore, the main aim of the paper is not to show how specific rehabilitation technologies could be introduced for developing a DSS, but rather to discuss the use of the prioritization strategy (Giustolisi et al., 2006a, Berardi et al., 2008) in a more complex decision scenario.

MULTI-OBJECTIVE WDS REHABILITATION PROBLEM

The brief literature review reported above clearly shows that the selection of the best course of action for WDS rehabilitation is a multi-objective problem where each criterion should be represented by a specific objective function. The main advantages of adopting a multi-objective (MO) approach instead of a single-objective (SO) approach are: (1) defining the objective functions independently from each other and with simple mathematical formulations, (2) searching for several optimal solutions instead of just one "best" solution (as in SO optimization), (3) obtaining a set of "optimal" solutions which represent the final decision support (Savic, 2002). The evaluation of solutions in a MO optimization context is based on the so-called Pareto domination concept (Pareto, 1896-7). Each solution of the "Pareto optimal set" is *not dominated* by any other solution, i.e. in going from one solution to another, it is not possible to improve on one objective (e.g. reduce the risk of future failure) without making at least one of the other objectives worse (e.g. increase cost). Unlike in SO approaches (Halhal et al., 1997), the Pareto domination criterion allows immeasurable objectives to be considered without merging them into a weighted function.

In this work six objective functions are considered in order to emphasize the MO nature of a realistic decision context. They are listed below.

f_1: minimization of the investment required;
f_2: minimization of the expected cost of pipe breaks in one year time horizon;
f_3: fulfilment of preferential selection of some pipes;
f_4: maximization of system reliability;
f_5: optimal work allocation based on existing deployment of isolation valves;
f_6: maximization of expected leakage reduction.

The next sub-sections briefly report the mathematical formulation of each objective function; for further details the reader is referred to Berardi et al. (2008).

The possible decisions for each pipe are to "do-nothing" or "replace with a new diameter". It is evident that such an optimization problem differs conceptually from the previous one as the selection of a new diameter for replaced pipes affects the performance of the whole existing network. This means that two equally advisable solutions (i.e. similar objective function values) could refer to completely

different rehabilitation decision (i.e. different deployments of diameters) and network expected performance.

Investment (f_1). It represents the sum of all direct costs of pipe replacement and its formulation is reported in Eq. (1)

$$f_1 = \underset{R}{Min}\left(\sum_{p \in R} C_{repl} \cdot L_p \right) \tag{1}$$

C_{repl} represents the cost of replacement per unit length and is presumed to change according to pipe diameter; L_p is pipe length and R stands for the set of pipes selected for replacement.

Expected cost of pipe breaks (f_2). This objective function is based on a pipe failure prediction model. In literature several models have been proposed to predict pipe failures ranging from physically based to statistical approaches (Kleiner and Rajani, 2001), the latter being best suited for studying small distribution pipes. Irrespective of the model adopted, the objective function f_2 is reported in Eq. (2)

$$f_2 = \underset{R}{Min}\left(\frac{\sum_{p \in NR} D_p \cdot C_{repair} \cdot BR_p}{\sum_{p \in Net} D_p \cdot C_{repair} \cdot BR_p} \right) \tag{2}$$

where BR_p is the number of pipe breaks predicted in a one year time horizon; D_p is a "damage and other cost multiplier" which accounts for both direct and indirect costs of pipe breaks (Walski and Pelliccia, 1982; Dandy and Engelhardt, 2006); *NR* is the set of pipes not replaced; *Net* designates the whole set of pipes in the network. The choice of an annual time horizon allows urgent short-term intervention to be determined, avoiding the hypothesis of a discount rate and minimizing the uncertainties on future demand and pipe deterioration (Berardi et al., 2008). Eq.(3) returns values between 0 and 1 representing complete network replacement and do-nothing scenarios, respectively.

Preferential pipe selection (f_3). This objective allows preferences on the selection of certain pipes to be introduced into the MO decision context for WDS rehabilitation. For instance, such a selection criterion could be linked to company-specific needs for warehouse management or to policies aimed at removing/leaving undisturbed some materials (e.g. avoid removing asbestos cement pipes). Preferences on pipe selection are introduced in terms of weights w_p ranging between 0 and 1 and relevant objective function is reported in Eq.(3).

$$f_3 = \underset{R}{Min}\left(\frac{\sum_{p \in NR} w_p}{|NR|} \right) \tag{3}$$

$|NR|$ is the number of non-replaced pipes. Objective function f_3 should be minimized in order to push towards an earlier replacement of pipes with the highest preference.

System reliability (f_4). In literature there are many different definitions of water distribution system reliability (Walski and Gessler, 1999; Todini, 2000; Prasad and Park, 2004). In this work reliability analysis is based on network topology modifications resulting from the isolation of a failed pipe. In fact, when a pipe breaks, the emergency intervention requires the closure of the entire segment of the pipe concerned by shutting down the existing isolation valves. Due to the fact that real isolation valves are usually fewer than pipes, this operation could either result in unintentionally isolating other portions of the network or severe pressure drops, which could be below acceptable values. The measure of reliability adopted herein is similar to that proposed by Dandy and Engelhardt (2006) and is formulated in Eq.(4)

$$f_4 = \frac{\sum_{p \in NR} \left[\left(D \cdot Pr \right)_i + \left(D \cdot Pr \right)_d \right]_p \cdot BR_p}{\sum_{p \in Net} \left[\left(D \cdot Pr \right)_i + \left(D \cdot Pr \right)_d \right]_p \cdot BR_p} \tag{4}$$

Subscripts i and d denote the properties *isolated* (i.e. intentionally and unintentionally forced out of service) and *deficiently* supplied due to isolation of the segment containing the (failed) pipe p, respectively. Pr is the number of properties affected by segment closure; without loss of generality D is the same cost multiplier as in f_2; BR_p is the number of pipe breaks predicted over the planning time horizon. Computing f_4 requires the topological analysis of the network resulting from the isolation of each pipe segment (i.e. dependent on actual valve deployment) and the "pressure-driven" hydraulic simulation under the peak-hour demand scenario, which is the most critical in terms of pressure drops. Eq. (4) encompasses the realistic case of multiple emergency interventions within the same pipe segment and returns values between 0 and 1.

Optimal work allocation (f_5). An optimal rehabilitation plan should both minimize emergency service interruptions and avoid multiple planned works within the same area. In this paper such a selection criterion is based on the reasonable assumption that each pipe segment coincides with a service area. Hence, minimising the number of pipe segments affected by planned interventions would result in minimizing multiple service interruption for the same customers.

$$f_5 = \frac{|S_R|}{|S_{Net}|} \tag{5}$$

$|S_R|$ is the number of isolated segments and $|S_{Net}|$ is the number of all segments in the network.

Expected leakage reduction (f_6). Irrespective of the rehabilitation options included among decision variables, the selection of a pipe for intervention is assumed to coincide with (at least) its inspection and repair of possible detected leakages from joints and fittings. Accordingly, there is an opportunity of gaining the quickest

leakage reduction by means of rehabilitation interventions. Eq. (6) is assumed here to describe leakage reduction objectives. It slightly differs from that used in Berardi et al. (2008) because in the present decision problem, pipe diameters resulting from complete network replacements are still unknown. This fact prevents an upper bound of leakage reduction from being defined, thus f_6 is not scaled in [0, 1].

$$f_6 = Q_R^L \tag{6}$$

$Q_R{}^L$ is the total leak flow through pipes during the minimum demand hour, which is the most critical from a leakage perspective because pressure tends to be at a maximum. Such an objective requires network simulation for each rehabilitation solution evaluated during the optimization run.

All the hydraulic simulations in this work have been consistently performed by using the "pressure-driven" hydraulic simulator proposed by Giustolisi et al. (2008a, 2008b) It incorporates the pressure-leakage relationship of Germanopoulos and Jowitt (1989) where the k-th pipe leakage flow is $q_k=\beta_k L_k P_k{}^{\alpha}$, with L_k pipe length and P_k pipe average pressure. The effects of the k-th pipe rehabilitation are modelled by assuming a new leakage coefficient β_N (less than the present value β_0) and a reduced internal roughness in pipes. The automatic detection of network topological changes is performed here by using a recently developed algorithm (Giustolisi and Savic, 2008c) which shares the same matrix representation of network topology as that adopted into the hydraulic simulator, thus making their integration easier.

CASE STUDY

The network analyzed in this work is named "Apulian_1" and has been presented in several previous studies (for example Giustolisi et al., 2008b). Its layout is reported in Figure 1 where the existing valves are also depicted in order to visualize the pipe segments to be isolated when an intervention (either planned or emergency) is required. The main network data are reported in Table 1. Due to the lack of both recorded failures and age information, values of BR_p are obtained by assuming that all pipes are 30 years old and that 27 pipe breaks have been recorded in 14 years of monitoring. The failure prediction model used herein is reported in Eq. (7) (Giustolisi and Berardi (2007) and is based on the Evolutionary polynomial regression (Giustolisi and Savic, 2006) technique.

$$BR = a \cdot \frac{Ae^{1.5} Lt}{De} \tag{7}$$

It has been proved to be reasonably accurate for describing the total number of pipe bursts expected for homogeneous pipe classes with the same age (Ae) and diameter (De) for 48 different WDS. Lt stands for the total length of pipes in the class while a is a regression parameter which depends on the particular system analyzed (a= $1.24 \cdot 10^{-3}$ in this case). Without additional information on individual pipe history, the number of individual pipe failures BR_p is assumed to be proportional to its length. It

is worth noting that values of BR_p<1 should be interpreted as a propensity to future pipe breaks.

Table 1. Node and pipe data of "Apulian_1"

Node	Demand q_{design} [l/s]	Elevation [m]	Minimum pressure [m]	Pipe	Length [m]	Diameter [mm]	*Pr*	BR_p
1	10.863	6.4	10	1	348.5	327	36	0.0172
2	17.034	7	10	2	955.7	290	97	0.0473
3	14.947	6	10	3	483	100	49	0.0721
4	14.280	8.4	10	4	400.7	290	41	0.0198
5	10.133	7.4	10	5	791.9	100	80	0.1183
6	15.35	9	10	6	404.4	368	41	0.0200
7	9.114	9.1	10	7	390.6	327	39	0.0193
8	10.510	9.5	10	**8**	482.3	100	49	0.0720
9	12.182	8.4	10	9	934.4	100	95	0.1396
10	14.579	10.5	10	10	431.3	184	44	0.0350
11	9.0072	9.6	10	11	513.1	100	52	0.0766
12	7.5745	11.7	10	12	428.4	184	44	0.0348
13	15.200	12.3	10	13	419	100	42	0.0626
14	13.550	10.6	10	14	1023.1	100	104	0.1528
15	9.226	10.1	10	15	455.1	164	46	0.0415
16	11.200	9.5	10	16	182.6	290	19	0.0090
17	11.469	10.2	10	17	221.3	290	22	0.0110
18	10.818	9.6	10	18	583.9	164	59	0.0533
19	14.675	9.1	10	19	452	229	46	0.0295
20	13.318	13.9	10	20	794.7	100	80	0.1187
21	14.631	11.1	10	21	717.7	100	73	0.1072
22	12.012	11.4	10	22	655.6	258	67	0.0325
23	10.326	10	10	23	165.5	100	17	0.0247
24		**H24**=36.4		24	252.1	100	26	0.0377
				25	331.5	100	34	0.0495
				26	500	204	51	0.0365
				27	579.9	164	59	0.0529
				28	842.8	100	85	0.1259
				29	792.6	100	80	0.1184
				30	846.3	184	86	0.0687
				31	164	258	17	0.0081
				32	427.9	100	44	0.0639
				33	379.2	100	39	0.0566
				34	158.2	368	0	0.0078

In Figure 1 pipes 8, 25, 27 and 30 are put into a box because they are assumed to be *preferred* for selection. Note that their choice does not follow any specific strategy, but rather provides an example of including any type of preference into the DSS. The preferences are deliberately set w_p=0.5 for these pipes and w_p=0 for the others.
Figure 2 depicts the demand fluctuation assumed for "Apulian_1" with respect to the peak hour demand, as described in the second column of Table 1. It is evident that the two extreme demand scenarios are 8.00 a.m. (peak demand) and 1.00 a.m. (lowest demand and peak average system pressure). The former scenario is used for assessing system reliability (f_4) and the latter for estimating the leakage level (f_6).

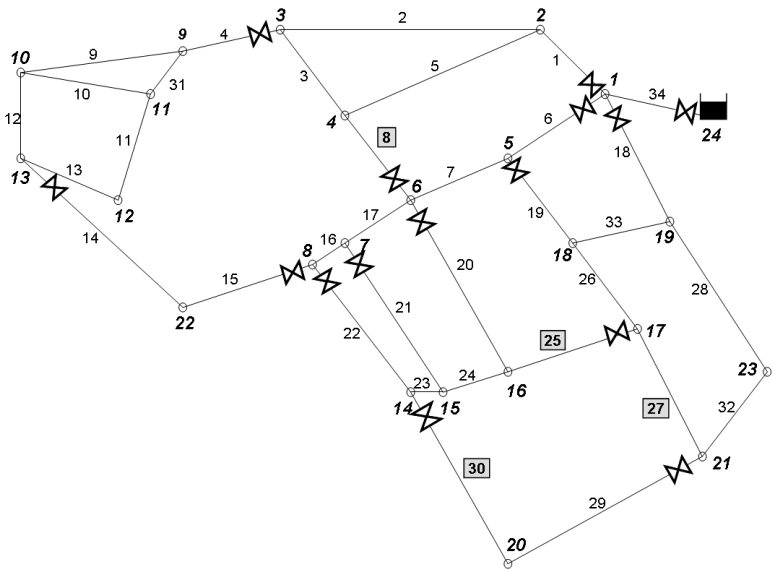

Figure 1. Layout of the network "Apulian_1"

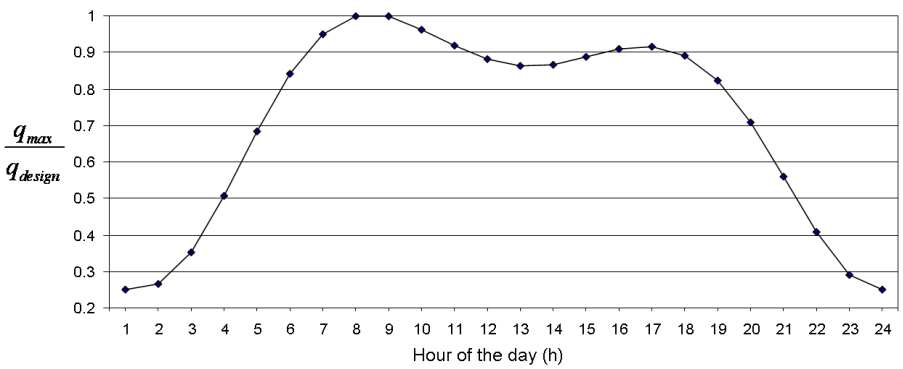

Figure 2. Daily demand pattern

Table 2. Repair and replacement cost

Index	Diameter [mm]	Repair cost [$/break]	Replacement costs [$/m]
1	100	572.00	62.00
2	164	637.42	73.20
3	184	654.56	80.71
4	204	671.96	88.21
5	229	694.10	97.21
6	258	726.07	107.41
7	290	782.49	118.23
8	327	886.58	125.70
9	368	977.47	137.89

Repair and replacement costs are reported in Table 2; the cost multiplier Dp = 1.5 for all pipes means that all properties are assumed to be domestic (Berardi et al., 2008).

A leakage coefficient $\beta_0 = 2.35 \cdot 10^{-7}$ is assumed for all pipes in the network due to the assumption that present water loss equals 25% of the peak hour demand; the leakage coefficient for replaced pipes is $\beta_N = 2.71 \cdot 10^{-8}$ as estimated from the realistic assumption of a residual water loss of 5% in the peak hour. $\alpha = 1.2$ in both cases. Furthermore, new pipes are assumed to have a Bazin's roughness coefficient $\gamma_N = 0.10 m^{1/2}$, lower than $\gamma_N = 0.20 m^{1/2}$ of old pipes.

FROM MOGA SOLUTIONS TO OPERATIONAL DSS

The MO problem is solved by using a Multi-Objective Genetic Algorithm called OPTIMOGA (Giustolisi et al., 2004). Each solution (individual) is comprised of 34 genes (i.e. decision variables) whose values (alleles) range between 0 and 9: 0 signify leaving the pipe undisturbed, while values 1-9 indicate the new diameter of the replaced pipe according to Table 2. The size of the resulting search space is 10^{34}. Although the search space could be significantly resized by reducing the range of diameters allowed for each pipe (e.g. according to technical expertise on WDS design), the present analysis aims to perform a global exploration of the search space without including additional information.

One single OPTIMOGA run (500 generations) returned about 5,000 solutions. As in other literature case studies, there are considerable differences between the rehabilitation options of equally expensive solutions. This makes it difficult to outline the best course of action without any additional selection strategy.
The prioritization strategy proposed here exploits MOGA solutions to retrieve information about the most advisable interventions. Pipes are initially sorted according to their frequency of selection for replacement (i.e. alleles values from 1 to 9) among MOGA optimal solutions. This first ranking helps point out the most critical pipes in the network (i.e. whose replacement could effectively improve system performance). Based on this additional information, analysts could proceed with a new optimization targeted at those pipes only. This "step-by-step" procedure would allow for a smaller search space to be investigated in the next optimization run and a less complex set of solutions to be provided to decision maker.
Alternatively, a second further sorting could be applied. This would be based on the distribution of diameters selected for each pipe and is aimed at getting the most advisable course of action starting from the original MOGA solutions. This strategy requires that each pipe is replaced by using the most frequently selected diameter. The set of interventions to be planned is then obtained by progressively adding replacement solutions up to the complete renewal of the network. The histograms in Figure 3 refer to the pipes of "Apulian_1" sorted according to their priority for replacement (pipe indices are in brackets). The "do-nothing" option is designated with "N" while diameter indices are 1-9. It shows that 3 out of 4 preferred pipes are selected for replacement within the first 9 interventions (i.e. pipes 8, 25, 27). Moreover, pipe 34 connecting the water tank to the rest of the network is one of the less important for replacement (it is the 29th most advisable intervention). This is consistent with the complete system isolation needed for its planned replacement. Nonetheless, the risk of its future failures and emergency system isolation make it preferable over pipes 16, 31, 17, 15 and 22.

Each sub-plot reports in black and white the diameter of the present network configuration (as reported in Table 1), and in solid black the percentages of selection among all MOGA solutions. For some pipes (e.g. #8, #5 and #28) there is only one predominant diameter which coincides with the original one. For other pipes (e.g. #1, #6 and #27) the most frequently selected diameter is very different from the original one, and it is usually smaller than the existing one.

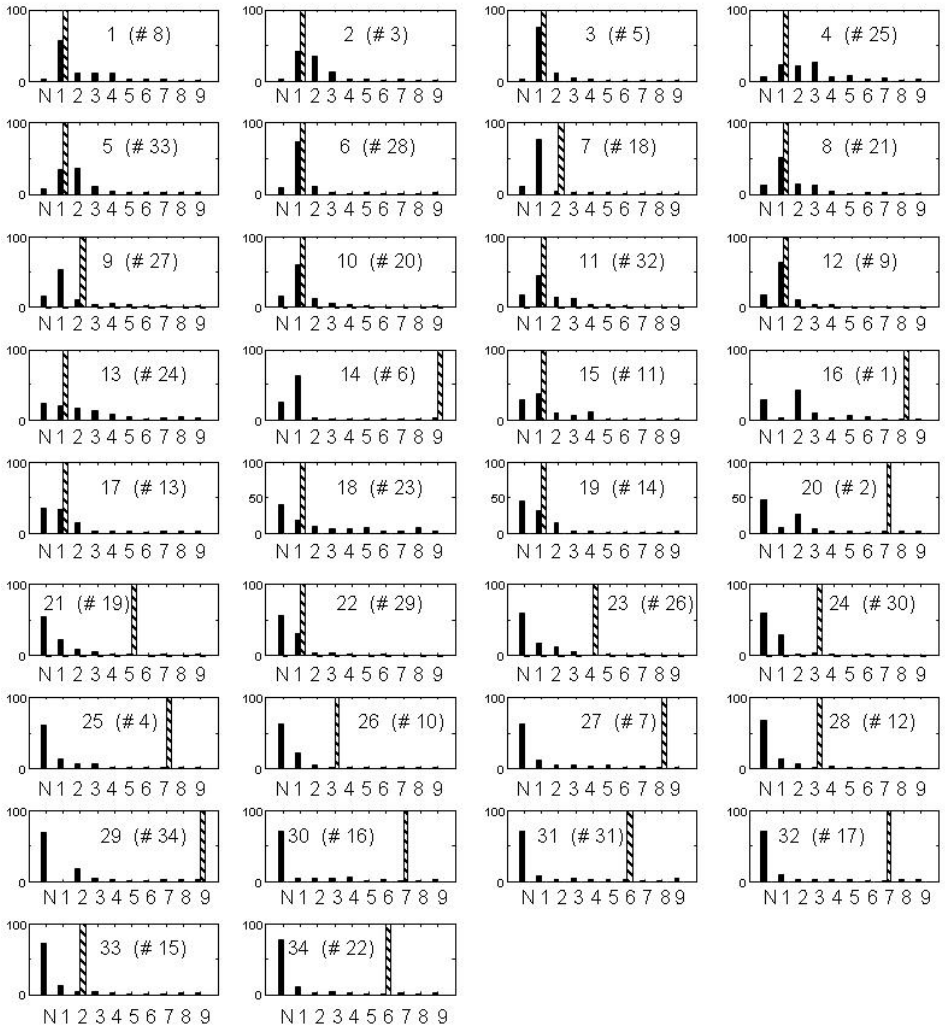

Figure 3. Statistics of pipe diameters in MOGA solutions

An operational DSS for planning interventions is obtained here by selecting pipes according to the priority shown in Figure 3. Relevant diameters are the most frequently selected. A set of 34 hypothetical new solutions is obtained by progressively adding such replacement works. However, differently from previous results (Berardi et al., 2008), not every solution is acceptable. In fact, after replacing the 27th pipe (i.e. #7 in Figure 1) with diameter 100mm instead of 327mm, the resulting network configuration no longer meets the minimum pressure required

during the peak demand hour (i.e. 10m). Nonetheless, the first 26 interventions (more than 76% of the complete network replacement) are still Pareto optimal if compared with MOGA solutions and with each of the other new solutions. The following Table 3 reports the incremental variation of each objective function achievable by replacing any individual pipe, up to the 26th intervention. Δf_1 is pipe replacement cost; Δf_2 is the reduction of breakage risk; Δf_3 is the fulfillment of preferential selection (it decreases for preferential pipes only); Δf_4 is the reduction of system unreliability; Δf_5 is 1 when a new pipe segment is isolated; Δf_6 is the percent reduction of leakage flow with respect of the do-nothing option at the peak-pressure hour (i.e. 1.00 a.m.).

Table 3. Incremental variations of objective function values.

Pipe	Δf_1 [$]	Δf_2 [$]	Δf_3	Δf_4	Δf_5	Δf_6 [%]
8	29903	-62	-0.0134	-81.04	1	-1.54
3	29946	-62	0.0014	-81.16	0	-1.87
5	49098	-101	0.0015	-133.06	0	-3.78
25	20553	-42	-0.0151	-48.35	1	-0.74
33	23510	-49	0.0011	-58.88	1	-1.54
28	52254	-108	0.0012	-130.85	0	-2.33
18	42744	-51	0.0013	-55.41	0	-4.39
21	44497	-92	0.0014	-104.68	0	-2.56
27	42451	-51	-0.0185	-55.03	0	-2.23
20	49271	-102	0.0008	-115.91	0	-3.52
32	26530	-55	0.0009	-66.44	0	-1.17
9	57933	-120	0.0010	-91.90	1	-3.11
24	15630	-32	0.0011	-36.77	0	-1.08
6	55763	-29	0.0012	-41.25	1	-38.38
11	31812	-66	0.0013	-50.47	0	-1.37
1	43806	-23	0.0015	-19.41	0	-16.86
13	25978	-54	0.0016	-41.21	0	-0.30
23	10261	-21	0.0018	-24.14	0	-0.03
14	63432	-131	0.0021	-97.88	1	-0.58
2	112994	-56	0.0024	-53.22	0	-5.80
19	43941	-31	0.0027	-30.65	0	-0.23
29	49141	-102	0.0032	-62.86	1	-0.02
26	44105	-37	0.0038	-37.98	0	-0.09
30	68307	-67	-0.0455	-36.48	0	0.03
4	47376	-23	0.0000	-13.06	0	-1.23
10	34811	-34	0.0000	-23.05	0	-0.11

CONCLUSIONS

In this paper the planning of WDS rehabilitation works is formulated as a multi objective problem with six objective functions and multiple intervention alternatives. The solution returned by applying a multi-objective genetic algorithm is analysed from a decision maker's perspective. The adoption of a prioritization strategy is discussed in order to overcome the ambiguities stemming from MOGA solutions and to plan effective courses of action. In this case study the rehabilitation

strategy obtained is Pareto optimal up to the replacement of the 76% of the network. Although different "off-line" prioritization strategies could be adopted, future works should investigate the effects of including a prioritization strategy during the MOGA run ("on-line" prioritization) in order to obtain contiguous and Pareto-optimal solutions to be easily analysed by decision makers.

REFERENCES

Berardi L., Colombo A. and Giustolisi O., (2008), "Optimal pipe replacement accounting for leakage reduction and isolation valves", *Proc. of 10th Water Distribution Systems Analysis*, Kruger National Park, (CDROM).

Clark R.M., Stafford C.L. and Goorich J.A., 1982, "Water distribution systems: a spatial and cost evaluation", *J. Water Resour. Plan. and Manage.*, **108**(3), pp. 243-256.

Cheung P.B., Reis L. F. R., Formiga K.T.M., Chaundhry F.H. and Ticona W.C. (2003) "Multiobjective Evolutionary Algorithms applied to the rehabilitation of a water distribution system: a comparative study", Proc. of Evolutionary Multi-Criterion Optimization: Second International Conference, Faro, Springer Berlin/Heidelberg publisher, 2632, pp. 662-676.

Dandy, G.C. and Engelhardt, M.O. (2006) "Multi-Objective Trade-Offs between Cost and Reliability in the Replacement of Water Mains." *Journal of Water Resources Planning and Management*, **132**(2), 79-88.

Germanopoulos, G., and Jowitt, P.W. (1989) "Leakage reduction by excessive pressure minimization in a water supply network." *Proc. Instn. Civ. Engrs.*, Part 2, 87, pp, 195-214.

Giustolisi O., Laucelli D., and Savic D.A., (2006), "Development of rehabilitation plans for water mains replacement considering risk and cost-benefit assessment", *Civil Eng. and Env. Syst. J.*, **23**(3), pp. 175-190.

Giustolisi, O., Savic, D.A., and Kapelan, Z. (2008a) "Pressure-driven demand and leakage simulation for water distribution networks." *Journal of Hydr. Eng.*, **134**(5), 626-635.

Giustolisi, O., Kapelan, Z., and Savic, D.A. (2008b) "Extended Period Simulation Analysis Considering Valve Shutdowns." *Journal Water Resour. Plan. and Manage.*, accepted for publication.

Giustolisi, O., Kapelan, Z., and Savic, D.A. (2008c) "An algorithm for automatic detection of topological changes in water distribution networks." *Journal of Hydr. Eng.*, **134** (4) , 435-446.

Giustolisi, O., Doglioni, A., Savic, D.A., and Laucelli, D. (2004) "A proposal for an effective multi-objective non-dominated genetic algorithm: the OPTimised Multi-Objective Genetic Algorithm: OPTIMOGA." *Report 2004/07*, School of Engineering, Computer Science and Mathematics, Centre for Water Systems, University of Exeter, UK.

Giustolisi, O., and Savic, D.A. (2006) "A Symbolic Data-driven Technique Based on Evolutionary Polynomial Regression." *Journal of Hydroinformatics*, IWA-IAHR Publishing, UK, **8**(3), 207-222.

Giustolisi, O., and Berardi, L. (2007) "Pipe level burst prediction using EPR and MCS-EPR." *Proceedings of Water Management Challenges in Global Change, CCWI2007 and SUWM2007 Conference*, De Montfort University, Leicester, UK, 3-5 September.

Goldberg, D.E. (1989) "Genetic Algorithms in Search, Optimization and Machine Learning." Addison-Wesley, Reading, Massachusetts.

Halhal, D., Walters, G.A., Ouzar, D., and Savic, D.A. (1997) "Water network rehabilitation with a structured messy genetic algorithm." *Journal of Water Resources Planning and Management*, **123**(3), 137-146.

Kim, J.H., and Mays, L.W. (1994) "Optimal rehabilitation model for water distribution systems." *Journal of Water Resources Planning and Management*, **120**(5), 674-692.

Kleiner, Y., and Rajani, B.B., (2001), "Comprehensive review of structural deterioration of water mains: Statistical models". *Urban Water*, **3**(3), pp. 121-150.

Lei J. and Saegrov S., 1998, *Statistical approach for describing failures and lifetime of water mains*, «Water Science and Technology», **38**(6), pp. 209-217.

Male, J.W., Walski, T.M., and Slutsky, A.H. (1990) "Analyzing water main replacement policies." *Journal of Water Resources Planning and Management*, **116**(3), 362-374.

Pareto V., (1896-7), Cours d'économie politique professé à l'Université de Lausanne, 2 vols. Losanna.

Prasad, T.D., and Park, N.S. (2004). "Multiobjective Genetic Algorithms for Design of Water Distribution Networks." *J. Water Resour. Plan. and Manage.*, **130**(1), 73-82.

Quimpo R. G. and Shamsi U. M., 1991, "Reliability based distribution system maintenance", J. Water Resour. Plan. and Manage., **117**(3), pp. 321- 339.

Savic, D.A. (2002) "Single-objective vs. multiobjective optimisation for integrated decision support." *First Biennial Meeting of the International Environmental Modelling and Software Society*, Lugano, Switzerland.

Shamir, U., and Howard, C.D.D. (1979) "An analytic approach to scheduling pipe replacement." *Journal American Water Works Association*, **117**(5), 248-258.

Skipworth, P., Engelhardt, M., Cashman, A., Savic, D.A., Saul, A.J., and Walters, G.A. (2002) "Whole life costing for Water Distribution Network Management." Thomas Telford ltd, London, UK.

Todini, E., (2000). "Looped water distribution networks design using a resilience index based heuristic approach." *Urban Water*, **2**, 115-122.

Walski, T.M.,and Pelliccia, A. (1982) "Economic analysis of water main brakes." *Journal American Water Works Association*, **74**(3), 140-147.

Walski, T. M. (1985). "Cleaning and lining versus parallel mains." *J. of Water Resources Planning and Management Division*, ASCE, **111**(1), 43-53.

Walski, T.M., and Gessler, J. (1999). "Discussion on "Improved design of 'Anytown' distribution network using structured messy genetic algorithms by G.A. Walters, D. Halhal, D.A. Savic, and D. Ouzar." Urban Water, 12, 265-268.

Calibration of Water Distribution Network Models as a Tool for Detecting Missing and Erroneous Cadastral and Hydraulic Information

Juan G. Saldarriaga[1], Susana Ochoa[2], Daniel Rodríguez[2] and César M. Jurado[2]

[1] Professor, Civil and Environmental Engineering Department, Universidad de los Andes. Director, Water Distribution and Sewer Systems Research Center – CIACUA. Carrera 1 este No. 19 A – 40, Bogotá – Colombia; PH: (57 1) 339 49 49; email: jsaldarr@uniandes.edu.co

[2] Researcher, Water Distribution and Sewer Systems Research Center – CIACUA. Civil and Environmental Engineering Department, Universidad de los Andes, Carrera 1 este No. 19 A – 40, Bogotá – Colombia; PH: (57 1) 339 49 49; email: s.ochoa24@uniandes.edu.co, d.rodriguez49@egresados.uniandes.edu.co c-jurado@uniandes.edu.co.

Abstract

In the first place, this paper presents an examination of the effects of missing cadastral information on the modeling and calibration of water distribution networks (WDN). For this purpose, cadastral errors were artificially introduced to the hydraulic models of the WDN of three cities of the province of Valle del Cauca (Colombia), with population in the range of 15,000-30,000 inhabitants. The cadastral errors were introduced by eliminating some pipes from the unaltered models using the resilience index as selection criterion. From this examination, typical responses observed during the calibration process were associated to specific topological and hydraulic errors and it was also noted that there is a direct relation between the resilience index and the effect of the removal of a certain pipe on the hydraulic performance of the model. In the second place, after identifying the effects of missing and erroneous cadastral and hydraulic information on the calibration of WDN models, the inverse procedure was carried out: the calibration process was used as a tool for detecting missing and erroneous cadastral and hydraulic information. This methodology was successfully applied to the WDN of Sector Estadio (250,000 inhabitants), which is a complex area of the city of Bucaramanga (Colombia); through the calibration of this WDN, errors such as failing water meters, pipes and valves that existed in the real system but were not in the model, significant errors in pipe diameters in the model, among others, were identified.

1. Introduction

In order to optimize the operation of water distribution networks (WDN) and make effective decisions regarding their maintenance, rehabilitation, and enlargement, among other issues, good-quality calibrated models are necessary. The calibration of a WDN model consists of adjusting the model input parameters in such a way that model performance matches the measured system performance over a wide range of operating conditions (Walski et al, 2001).

To carry out the calibration of a WDN, complete cadastral information, as well as measurements of discharge at the entrance of the system, of water consumption and pressure at demand nodes are required. These measurements must cover a rather long time period, so that the system performance over a representative range of operating conditions is known. During the calibration process, several scenarios in which different values are given to each input parameter are created and, for each scenario, extended period hydraulic simulations are carried out; the calibration process finishes when a scenario whose performance reasonably agrees with measured system performance is found.

Although it may sound like a simple procedure, in many cases, especially in developing countries, the cadastral information is incomplete or erroneous, making the calibration process complicated and impeding the achievement of a good-quality hydraulic model. This is the reason why it is necessary to have a tool, within the calibration process, with which cadastral misinformation can be detected. In view of this necessity, this paper presents an analysis of the effects of missing and erroneous cadastral information on the hydraulic simulation and calibration of WDN models. Furthermore, from the results obtained in this analysis, a methodology is proposed which uses the calibration of WDN as a tool for detecting missing and erroneous cadastral and hydraulic information.

2. Theoretical background

2.1. Calibration methodology (Jurado and Saldarriaga, 2007)

As mentioned before, the calibration of a WDN model consists in adjusting the parameters that rule its hydraulic behavior. The calibration parameters taken into account by the methodology developed by the authors (Water Distribution and Sewer Systems Research Center – CIACUA) can be divided into hydraulic and topological ones. Among the hydraulic parameters are the unknown demands and node's emitters (i. e. emitters' coefficients and exponents), whereas among the topological ones are the pipes' internal diameters, absolute roughness, and minor losses. The calibration methodology is summarized in Figure 1.

In Figure 1, *Initial Model* corresponds to the first hydraulic-digital model which is obtained after processing and digitalizing all the topological and consumption information provided by the WDN operator. It contains nominal diameters, theoretical roughness coefficients, and does not take into account minor losses and Non-Revenue Water (NRW) records; thus, the hydraulic simulations carried out with this *Initial Model* do not match the pressure and discharge field measurements.

Base Line 1 is obtained by assigning the real internal diameters (according to the manufacturer's catalogues) to all pipes and also by assigning minor losses per meter of pipeline to each pipe of the model (for this purpose, typical values of minor losses per meter that have been found in previous calibrations are used). The minor losses To carry out the next steps of the methodology, the WDN must be first divided into groups or sectors with similar hydraulic, topologic and socioeconomic characteristics.

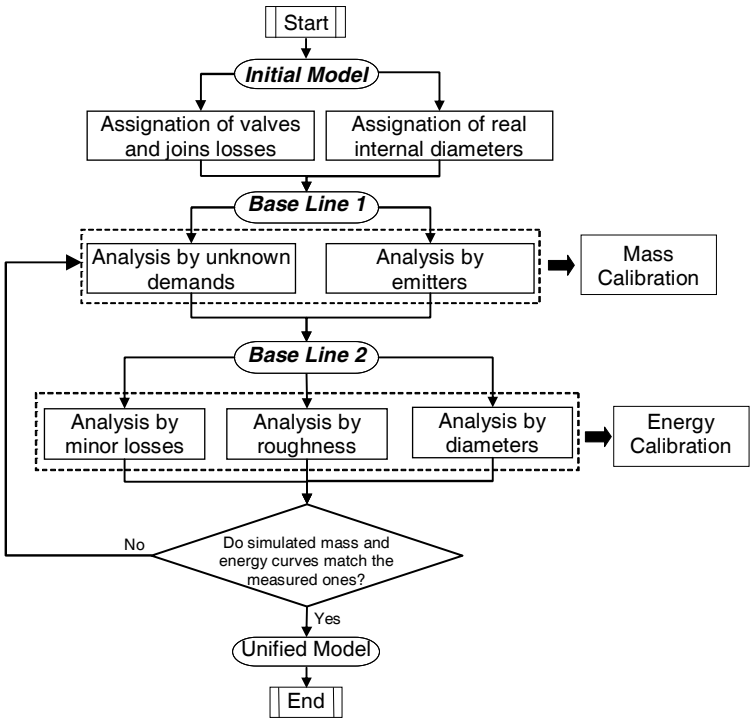

Figure 1. Calibration algorithm (CIACUA)

The *Analysis by unknown demands* is performed by creating several scenarios in which different multiplying factors are applied to the base demand of each group of nodes; this is done with the purpose of calibrating the system's mass (i. e. to balance the mass that goes into the system and the mass that goes out of it). With this analysis, it is possible to detect areas with high commercial losses (unaccounted demands, unknown demands, and/or illegal connections). In the *Analysis by emitters*, scenarios are created in which different values of the emitter's coefficient are assigned to the nodes of each group or sector; this analysis intends to simulate the technical losses that take place in the real system and to adjust the discharges and pressures of the WDN model to the measured ones. *Base Line 2* is obtained after compiling the results achieved from the two previous independent analyses (i. e. *Analysis by unknown demands* and *Analysis by emitters*). In *Base Line 2* the mass curves of the model must coincide with the measured ones and a good approximation to the measured pressure or energy curves must be achieved. Afterwards, a sensibility analysis of the hydraulic variables (i. e. pipe's internal diameters, absolute roughness, and minor losses coefficients) is carried out: scenarios in which different values of these variables are assigned to the pipes of each group or sector are created. The *Analysis by minor losses* evaluates the effect of fittings and other accessories, which generate minor energy losses, on the hydraulic behavior of the system. In the *Analysis by roughness* and in the *Analysis by diameters*, slight variations of the pipes' absolute roughness and internal diameter are carried out taking into account the pipes' material and medium flow velocity; the effects of such variations on the hydraulic behavior of the system are analyzed. Lastly, the *Unified Model* is created by compiling and iteratively adjusting the results obtained from the previous analyses: given that the adjustments made in the analyses by minor losses, roughness and diameters may

affect the mass curves that had been previously calibrated through the analyses by unknown demands and emitters, an iterative process in which small adjustments are made to all these variables (i. e. unknown demands, emitter's coefficients, minor losses per meter, absolute roughness, and pipes' internal diameters) must be carried out until the simulated curves of discharge and pressure coincide with the measured ones. Thus, the *Unified Model* corresponds to the calibrated model.

2.2. Resilience index (I_r)

The concept of network *resilience* was introduced by Ezio Todini in 2000; he defined it as "… the capability in the system to allow to overcome local failures and to guarantee the distribution of water to users…". The resilience index (I_r) is an indicator of the network *resilience*; it is a measurement of the system vulnerability of letting some nodes without service in the occurrence of a failure (Saldarriaga et al., 2007). In order to describe the concept of network *resilience*, Tondini introduced the concept of power: the total power of a WDN (P_{tot}) is defined as the sum of the power that is supplied by reservoirs and the power that is supplied by pumps:

$$P_{tot} = \gamma \sum_{i=1}^{n_r} Q_i H_i^* + \sum_{i=1}^{n_p} P_{pi}$$

where Q_i and H_i^* correspond to the flow and piezometric pressure of each of the n_r entrance reservoirs and P_{pi} is the power supplied by each of the n_p pumps. The total power of the system can also be expressed as the sum of the power that is dissipated by means of friction and because of the existence of leaks (P_{dis}), plus the power that is delivered at demand nodes (P_{out}), as shown in the following equation:

$$P_{tot} = P_{dis} + P_{out} \tag{1}$$

The power that is delivered at consumption nodes (P_{out}) can be classified in two ways: as the objective delivered power (P_{out}^{obj}), which is generated when all consumption nodes have the minimum service pressure; and as the real delivered power (P_{out}^{real}), which takes place under real service pressure conditions. P_{out}^{obj} and P_{out}^{real} are estimated as shown:

$$P_{out}^{obj} = \gamma \sum_{i=1}^{n_n} q_i h_{i,\min}^* \qquad\qquad P_{out}^{real} = \gamma \sum_{i=1}^{n_n} q_i h_i^*$$

where q_i, h_i^* and $h_{i,\min}^*$ correspond to the flow, real piezometric pressure, and minimum required piezometric pressure in each of the n_n consumption nodes of the system. From equation 1: $P_{dis} = P_{tot} - P_{out}$. From this equation and given P_{out}^{obj} and P_{out}^{real}, it is possible to define mathematical expressions to estimate the optimum and real dissipated power:

$$P_{dis}^{obj} = P_{tot} - P_{out}^{obj} \qquad P_{dis}^{real} = P_{tot} - P_{out}^{real}$$

The I_r of a WDN is defined as a function of the relationship between the objective dissipated power (P_{dis}^{obj}) and the real dissipated power (P_{dis}^{real}):

$$I_r = 1 - \frac{P_{dis}^{real}}{P_{dis}^{obj}}$$

When substituting in this equation the terms previously described, a general equation for the I_r is obtained:

$$I_r = \frac{\sum_{i=1}^{n_n} q_i \left(h_i^* - h_{i,\min}^* \right)}{\left[\sum_{i=1}^{n_r} Q_i H_i^* + \sum_{i=1}^{n_p} P_{pi} \right] - \sum_{i=1}^{n_n} q_i h_{i,\min}^*}$$

3. *Resilience Index vs. impact of the removal of a certain pipe on the hydraulic behavior of the WDN model*

As mentioned above, with the aim of evaluating the effects of missing cadastral information on the modeling and calibration of WDN, cadastral errors were artificially introduced to the hydraulic models of the WDN of three cities of the province of Valle del Cauca (Colombia). The cadastral errors were introduced by eliminating some pipes from the unaltered models using the resilience index (I_r) as selection criterion. In order to use the I_r as indicator or selection criterion, an analysis was first conducted to determine the relationship between the effect of the removal of a certain pipe on the I_r and on the hydraulic behavior of the system. The first step of this analysis was to calculate the hydraulics of the system without cadastral errors, to estimate its I_r, and to identify the pipes that could be removed without letting any consumption node disconnected. From now on, these pipes will be referred to as "removable pipes". Subsequently, one at a time, each of the removable pipes was removed from the unaltered model; for each of the models without a certain removable pipe, the system hydraulics and the I_r were calculated. With this information, the difference between the I_r of the unaltered model and the I_r of the model without one removable pipe was calculated; this difference will be referred to as ΔI_r. Besides, the pressure curves of the models without one removable pipe were estimated and compared against those of the unaltered model or prototype. Thus, it was possible to analyze the relationship between the change on the resilience index (ΔI_r) and the capacity of the model without one removable pipe to adequately reproduce the hydraulics of the prototype. This analysis was carried out for the WDN of three cities of the province of Valle del Cauca (Colombia): La Cumbre, Andalucía and Candelaria, which have varied topography and a population in the range of 15,000-30,000 inhabitants. For the three case studies, similar results were obtained. Next, the results found for the WDN of Andalucía are presented. In this network, 190

of the total of 360 pipes were identified as removable ones. Thus, 190 models were created in which one single pipe was removed. For each of these models, the pressure time series (i. e. values of pressure at different times of the day) at each of its nodes were compared to those of the nodes of the prototype; for every value of pressure at a certain node and time, a relative error was estimated as follows:

$$Relative\ Error\ in\ Pressure_{ij} = \frac{\left|P_{ij\ unaltered} - P_{ij\ mod\ ified}\right|}{P_{ij\ unaltered}} * 100\%$$

where *i* corresponds to the time of the day and *j* to the node of the system for which the relative error in pressure is calculated; the subindex "*unaltered"* refers to the pressure in the prototype or complete model and the subindex "*modified"* refers to the model without one removable pipe. In this case, the pressure at each node was calculated every 15 minutes. After estimating the relative error for each node at each time of the day, the average relative error was calculated. Figure 2 illustrates the relationship between the ΔI_r caused by the removal of a certain pipe and the average relative error in pressure observed in the model without that pipe.

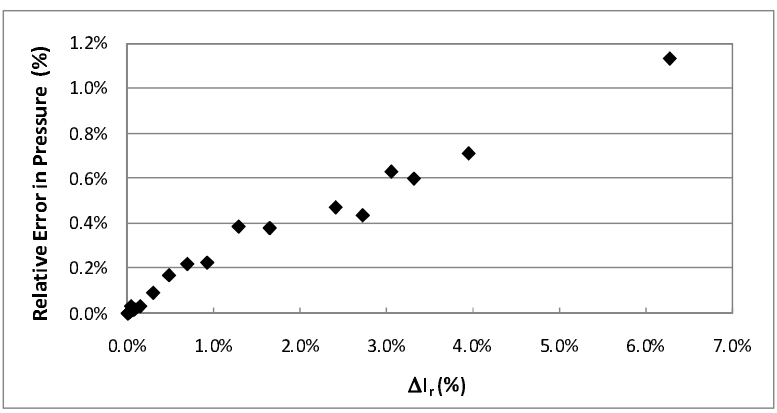

Figure 2. Change on the resilience index (ΔI_r) vs. relative error in pressure caused by the removal of a certain pipe from the model.

It can be noted that, in general, as the ΔI_r increases, the relative error in pressure also increases; it means that, when the removal of a pipe generates a great change on the resilience index of the network, the model without that pipe cannot accurately reproduce the hydraulic behavior of the prototype. Likewise, if a pipe that has a little impact on the resilience index of the network is removed, it does not affect in a significant manner its hydraulic behavior and the reduced model can adequately reproduce the hydraulics of the prototype.

4. Effects of cadastral misinformation on the calibration of WDN models

Normally, in the application of the calibration methodology described above (see Figure 1), a complete knowledge of the WDN topology is assumed. Therefore, the range of variation of the pipes' internal diameters during the calibration process is very narrow: in this process, the magnitude of the internal diameters is slightly varied

with the purpose of accounting only for pipe wall erosion or for biofilm growth. Nonetheless, as will be next explained, the only way in which a model with major cadastral errors can be calibrated is by significantly increasing the diameters of the pipes which are close to the missing element or cadastral error; this increase in the diameters gets to compensate the greater energy losses caused by the higher velocities that take place in adjacent pipes when the cadastral error is introduced. For this reason, the calibration algorithm was modified in such a way that greater variations in pipes' internal diameters were allowed during the calibration process.

Case Study: La Cumbre's WDN model (CIACUA, 2006)

To illustrate the effects of cadastral misinformation on the calibration of WDN models, the results obtained for the calibration of a hydraulic model of La Cumbre's WDN in which an important cadastral error was introduced are presented. In this model, the pipe with the highest impact on the system's I_r was removed (the ΔI_r caused by its removal is 13.09%), causing the greatest effect on the hydraulic behavior of the WDN model. It is worth mentioning that similar results were obtained for the calibration of Candelaria's and Andalucía's WDN models.

Initial Model and Base Line 1: These models were set up by digitalizing the existing topological and consumption information and by assigning real internal diameters and minor losses coefficients according to the manufacturer's catalogues and existing statistical information; these actions correspond to the first Scenario of Table 1. Moreover, in this phase, the mentioned cadastral error was artificially introduced and the network was divided into 6 groups according to the hydraulic, topologic and socioeconomic characteristics of each area of the WDN.

Base Line 2: In order to obtain the *Base Line 2* model, 13 scenarios were analyzed in which different multiplying factors were applied to the base demands of each group of nodes and different values of the emitter's coefficient were assigned. By doing this, it was possible to evaluate the sensibility of the WDN to the presence of leaks and unknown demands. The 13 scenarios that were analyzed and the first scenario, in which real internal diameters and minor losses were assigned, are shown in Table 1. From the creation and analysis of these scenarios, a model was achieved in which the discharge or mass curves coincide almost perfectly with the measured curves. Besides, the obtained model (*Base Line 2*) can reproduce, with an acceptable degree of accuracy, the pressure or energy curves at one of the pressure measuring points (Element 20); in the other measuring points (e. g. Element 204), the cadastral error (i. e. the removed pipe) has a sever effect on their energetic behavior and the simulated curve is below the measured one. These results are illustrated in Figure 3.

Subsequently, in order to calibrate the energy of the WDN and adjust the simulated pressure curves to the measured ones, the *Analysis by diameters* is performed.

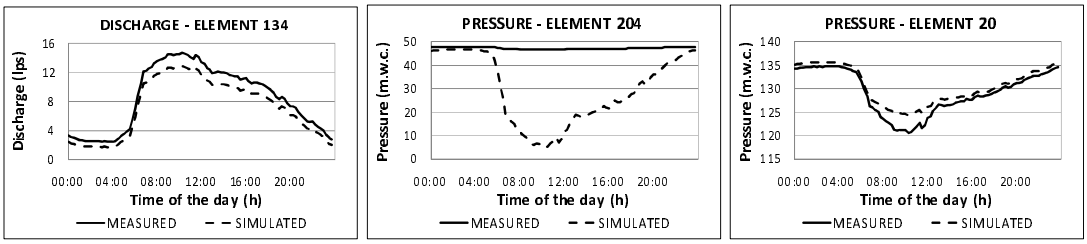

Figure 3. Discharge and pressure curves - Scenarios 1-14, *Base Line 2*, La Cumbre

Table 1. Scenarios 1-14. *Base Line 2*, La Cumbre

Scenario	Actions or variations
Scenario 1	PVC Pipes - k_m of 0.04 per meter
	AC Pipes - k_m of 0.05 per meter
	Real Internal Diameter PVC and Steel
	Assignation of k_m to known valves
	Assignation of k_m of 0.2 to each valve
Scenario 2	Nodes SEL 1 - Demand*1.2
	Nodes Group 1 - Demand *0.8
	Nodes Group 2 - Demand *3.6
	Nodes Group 3 - Demand *1.1
	Nodes Group 4 - Demand *1.2
Scenario 3	Nodes Group 3 SEL 1 -- Demand *2.3
	Nodes Group 6 SEL 1 - Demand *0.7
Scenario 4	High Pressure - Emitter Coefficient = 0.0002
	Medium Pressure - Emitter Coefficient = 0.0001
	Low Pressure - Emitter Coefficient = 0.000001
Scenario 5	SEL 1 - Emitter Coefficient *1.25
	Steel Pipes - Emitter Coefficient *1.25
	Very high pressure - Emitter Coefficient *5
Scenario 6	Nodes Group 1 - Demand *0.5
Scenario 7	Nodes Group 2 - Demand *1
Scenario 8	Nodes Group 3 - Demand *0.8
Scenario 9	Nodes Group 4 - Demand *0.8
Scenario 10	Nodes Group 4 - Demand *1
Scenario 11	Nodes Group 4 - Demand *1.1
Scenario 12	Nodes Group 4 - Demand *1.05
Scenario 13	Nodes Group 3 - Demand *1.3
Scenario 14	Nodes Group 3 - Demand *1.35

SEL = Socioeconomic Level

Analysis by diameters: In this analysis, 5 scenarios were created in which different multiplying factors were applied to the internal diameters of the pipes of each group; these scenarios are shown in Table 2. Such variations in the internal diameters were performed with the purpose of calibrating the pressure curves, without modifying the behavior of the discharge curve, which was already calibrated in *Base Line 2*. This analysis showed that the increase of the internal diameters of the pipes of groups 2 and 5, which are the closest ones to the error, was the only action capable of raising the simulated pressure curves and bringing them close to the measured ones. Besides, it was found that the simulated discharge curves would remain close to the measured ones after applying the mentioned multiplying factors to the internal diameters.

Table 2. Scenarios 15-19. *Analysis by diameters*, La Cumbre.

Scenarios	Actions or variations
Scenario 15	Group 1 - Diameters*2
Scenario 16	Group 2 - Diameters *2
Scenario 17	Group 3 - Diameters *2
Scenario 18	Group 4 - Diameters *2
Scenario 19	Group 5 - Diameters *2

Unified model: After determining that the simulated pressure curves were sensitive to the increase of the internal diameters in groups 2 and 5, more scenarios in which different multiplying factors were applied to the internal diameters of the pipes of these two groups were created in order to complete the calibration process. These scenarios are shown in Table 3.

Table 3. Scenario 20-25, Unified model. La Cumbre.

Scenario	Actions or Variation
Scenario 20	Group 5 - Diameters*2.2
Scenario 21	Group 5 - Diameters *2.4
Scenario 22	Group 5 - Diameters *2.7
Scenario 23	Group 2 - Diameters *0.9 Group 5 - Diameters *2.7
Scenario 24	Group 2 - Diameters *0.95 Group 5 - Diameters *2.7
Scenario 25	Group 2 - Diameters *0.933 Group 5 - Diameters *2.7

It was found that the 25th scenario, in which the diameters of group 2 were multiplied by 0.933 and the diameters of group 5 (where the error was located) were multiplied by 2.7, generated a model that represents in a very precise way the hydraulic behavior (i. e. mass and energy curves) of the unaltered system. These results are shown in Figure 4.

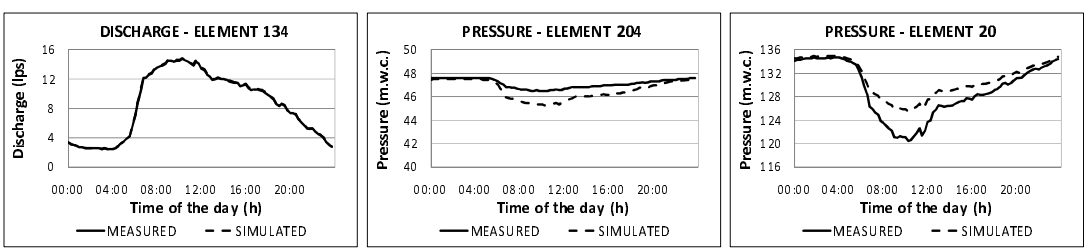

Figure 4. Discharge and pressure curves - Scenarios 20-25, *Unified Model*, La Cumbre.

It can be seen that with these adjustments, it was possible to generate a calibrated model with the presence of a significant cadastral error. Besides, it can be noted that the calibration methodology assigns greater diameters in the area where the error is located. This can be explained by the fact that, when there is an important cadastral error, such as a missing relevant pipe, the water has to flow greater distances to supply the demands throughout the network, which generates greater energy losses; the higher energy losses caused by larger distances of flow are compensated by assigning greater diameters to the pipes around the cadastral error, which reduces the

friction losses and makes it possible to calibrate the energy in the WDN model. Knowing that greater diameters are assigned to the pipes that are close to the error, it is possible to identify the areas with significant cadastral errors through the calibration process.

5. Calibration as a tool for detecting missing and erroneous cadastral and hydraulic information

5.1. Case study: Sector Estadio (CIACUA, 2007)

Sector Estadio is a hydraulic zone of the city of Bucaramanga (Colombia); it has 250,000 inhabitants and 27,000 subscribers from different socioeconomic levels. The WDN of Sector Estadio is made up of 190 km of pipeline with diameters ranging from 25 mm (1") to 600 mm (24") and pipes made of different materials, like PVC, steel, galvanized iron, among others. For this WDN, 4 discharge meters were used in order to monitor the system's hydraulic behavior and obtain the discharge curves that are required for the calibration process. One of the discharge meters was located at the entrance of the WDN, right after the supply tank; two other ones were placed each at one end of the hydraulic sector, at points where water is supplied to two other sectors of the city (sectors Bienestar and Regadero); and the other one was located at a strategic point of the network called Glorieta de San Francisco. The location of the discharge measuring stations is shown in Figure 5. On the other hand, pressure was measured at 21 measuring stations spread all over the hydraulic sector. Besides, water consumption of each subscriber was also monitored.

5.2. Division of the hydraulic model into groups

Before carrying out the calibration process, Sector Estadio's WDN model was divided into 23 groups according to the hydraulic, topologic and socioeconomic characteristics of each area of the WDN. This division is shown in Figure 6.

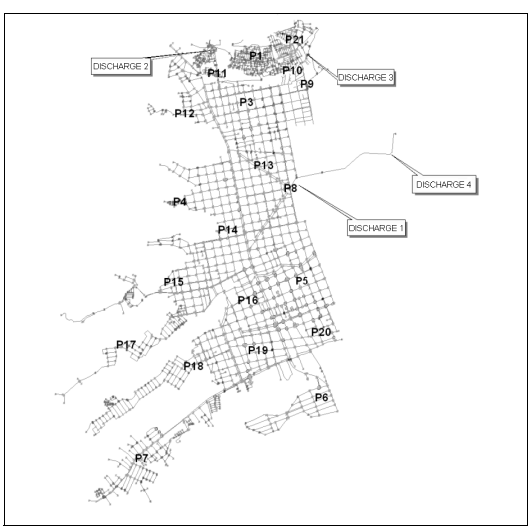

Figure 5. Location of discharge measuring stations, Sector Estadio.



Figure 6. Division of Sector Estadio's WDN model into groups.

5.3. Calibration Results

During the calibration process, several scenarios were analyzed. Table 4 shows the multiplying factors and values that were applied to the base demands, emitter coefficients and minor losses coefficients of each of the groups into which the network had been previously divided in order to obtain a calibrated model.

Table 4. Multiplying factors and values of base demands, emitter coefficients and minor losses coefficients.

Multiplying Factors of Base Demands		Emitter Coefficients		Minor Losses Coefficients	
Sector	Value	Sector	Value	Sector	Value
Group 11 (G11)	1.5	Group 7 (G7)	0.017	Group 1 (G1)	2
Group 11 (G11)	1.5	Group 1 (G1)	0.009	Group 4 (G4)	15
Group 12 (G12)	3	Bienestar	0.1	Group 5 (G5)	1
Group 15 (G15)	1.6	Regadero	0.1	Group 6 (G6)	40
Group 15 (G15)	2			Group 7 (G7)	20
Group 17 (G17)	2.5			Group 9 (G9)	10
Group 20 (G20)	1.5			Group 12 (G12)	15
Group 10 (G10)	7			Group 14 (G14)	1
Group 4 (G4)	1.5			Group 15 (G15)	1
Bienestar	1.2			Group 16 (G16)	1
Regadero	1.2			Group 17 (G17)	5
				Group 18 (G18)	1
				Group 19 (G19)	1

During the analysis by diameters, different multiplying factors were applied to each internal diameter depending on the pipe material and flow velocity. However, the multiplying factors with which a calibrated model was obtained were very small, which indicated that there were no important pipes missing in the model and that there were not significant errors in pipes' diameters either.

The calibration of this WDN model was conducted with data corresponding to high pressure regime; after the model had been calibrated, its performance was validated against data collected during medium and low pressure regimes. The performance of the calibrated model under the three pressure regimes is shown in Figure 7.

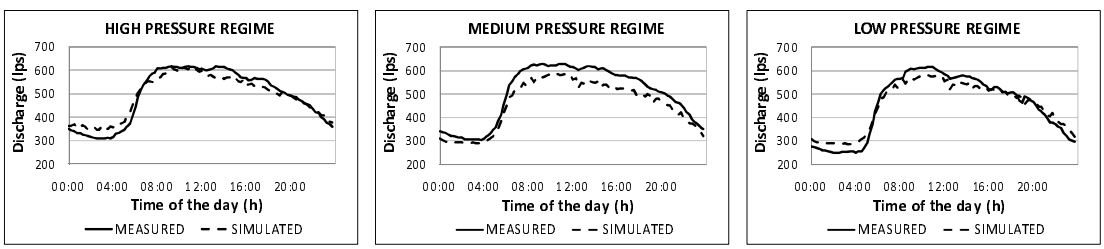

Figure 7. Performance of the Sector Estadio's calibrated model under high, medium and low pressure regimes.

5.4. Cadastral and hydraulic errors detected through the calibration process

Through the calibration process of Sector Estadio's WDN model, two important errors were found: an uncalibrated discharge meter at the entrance of the system and the existence of an unknown connection between two neighborhoods. Next, the way in which these errors were detected is described.

Uncalibrated discharge meter at the entrance of the system

During the calibration of the hydraulic model, it was found that the only way in which it was possible to adjust the simulated discharge curves (i. e. mass curves) to the measured ones was by applying an extremely high multiplying factor to the base demands of the nodes of Group 10: the multiplying factor with which the mass curves could be calibrated was 7.0 (see Table 4), which is a value outside of the normal range of variation of these multiplying factors. This abnormality suggested that there was an error close to Group 10; knowing this, an exhaustive search (both in the field and in the mathematical model) was conducted. From the field inspections, it was found that the cause of the problem was that the discharge meter located at the entrance of the system (at the exit of the supplying tank) was uncalibrated; this measuring device was overestimating the water discharges in approximately 45 l/s. The way in which the calibration process managed to balance the mass even with this error in discharge measurements, which caused an excess of water to enter the system, was by taking the water surplus out of the network in the area which was closest to the entrance (i. e. Group 10). After calibrating the discharge meter and producing new measured discharge curves, it was possible to eliminate the enormous multiplying factor that had been previously assigned to the base demands of the nodes of Group 10.

Existence of an unknown connection between two neighborhoods: Bosque Norte Alto and Villa Mercedes

When the calibrated model was being validated using data from the medium pressure regime, it was found that the model performance did not agree with the measured system performance. As shown in Figure 8, pressure measurements taken at measuring station F23, only match the simulated pressure between 6 a.m. and 6 p.m. After a detailed analysis, it was found that the only fact that could explain the measured behavior of the pressure at measuring station F23 was the existence of an unreported connection between the networks of Villa Mercedes and Bosque Norte neighborhood. In order to prove this hypothesis, the WDN operator conducted a campaign to look for the unreported connection in the field, finding the connection shown in Figure 9.

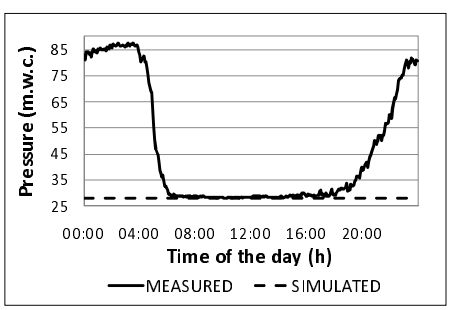

Figure 8. Simulated vs. Measured pressure at measuring station F23.

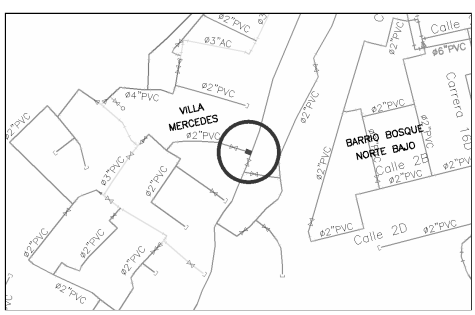

Figure 9. Unreported connection between Villa Mercedes and Bosque Bajo neighborhoods.

6. Conclusions

- The change generated by the removal of a certain pipe on the resilience index of a WDN (ΔI_r) has an inverse relationship with the capability of the reduced model (i. e. model without that pipe) to accurately simulate the hydraulic behavior of the unaltered system.
- The calibration methodology proposed herein allows to obtain a calibrated model even when there is a significant cadastral or hydraulic error in it and also makes it possible to identify the area where the error is located.
- When a relevant pipe is missing on the hydraulic model of a WDN, the calibration methodology gets to compensate the greater energy losses generated by the absence of the pipe by assigning greater diameters to the pipes that are close to the missing one; knowing this, it is possible to use the calibration methodology as a tool for detecting significant cadastral errors as like this one.
- In the same way, when there is an uncalibrated or failing discharge measuring device, the calibration methodology compensates this error in the mass of the system by applying extremely high multiplying factors to the base demands of the nodes which are close to the failing device. Thus, the calibration methodology constitutes a tool for detecting this kind of hydraulic errors.
- After identifying the effects of missing and erroneous cadastral and hydraulic information on the calibration of WDN models, the inverse procedure could be carried out: the calibration methodology proved to be an effective tool for detecting missing and erroneous cadastral and hydraulic information in WDN models.

7. References

CIACUA. (2006). *Design and Implementation of a Strategic Management Plan for the Water Distribution Networks of the Cities of Andalucía, Ansermanuevo, Bolívar, Bugalagrande, Candelaria, Ginebra, Guacarí, La Cumbre y Toro*. Universidad de Los Andes - ACUAVALLE, Colombia.

CIACUA. (2007). *Final Report of the Optimum Pressure Surface Project – Water Distribution Network of Sector Estadio, Bucaramanga*. Universidad de los Andes – Acueducto Metropolitano de Bucaramanga, Colombia.

Jurado, C. M. and Saldarriaga, J. G. (2007). Water Distribution Networks Calibration under Leaks Environment - Study Cases. *Proceedings of the World Environmental & Water Resources Congress 2007*, Tampa, USA.

Saldarriaga, J., Moreno, M., Romero, N., and Cortés, O. (2008). Prioritized rehabilitation of water distribution networks using dissipated power concept to reduce non-revenue water. *Proceedings of the World Environmental & Water Resources Congress 2008*, Honolulu, USA.

Todini, E. (2000). Looped water distribution networks design using a resilience index based heuristic approach. *Urban Water*, 2(3), 115-122.

Walski, T. M., Chase, D. V, and Savic, D. A. (2001). *Water Distribution Modeling*. Waterbury, USA: Haestad.

Integrated Planning for Dual Distribution Systems

Nabin Khanal[1], Vanessa Speight[2], Venkatraman Radhakrishnan[3], Tim Francis[4], Laurel Passantino[5], and James Swanson[6]

[1]Project Engineer, Malcolm Pirnie Inc., 4646 E Van Buren St., Ste 400, Phoenix, AZ 85008, Ph: (602)-797-4675, Fax: 602-231-0131, nkhanal@pirnie.com

[2]Associate, Malcolm Pirnie Inc., 3101 Wilson Blvd., Ste 550, Arlington, VA 22201, Ph: (703)-842-5620, Fax: 703-351-1305, vspeight@pirnie.com

[3]Engineer, Malcolm Pirnie Inc., 4646 E Van Buren St., Ste 400, Phoenix, AZ 85008

[4]Sr. Associate, Malcolm Pirnie Inc., 4646 E Van Buren St., Ste 400, Phoenix, AZ 85008

[5]Sr. Project Engineer, Malcolm Pirnie Inc., 4646 E Van Buren St., Ste 400, Phoenix, AZ 85008

[6]City of Surprise, 12425 W. Bell Road, Suite C-305, Surprise, AZ 85374

Abstract

The southwest region of the US is facing problems with limited water resources and population growth. Some water utilities in the region are taking a proactive approach to planning that incorporates acquiring water resources in the future. Reusing treated wastewater effluent (reclaimed water) is one of the most viable solutions to expand water resources under conditions of fresh water scarcity.

Reclaimed water can be used primarily to fulfill the outdoor demands such as landscape irrigation and other non-potable water use. The possibility of treating the reclaimed water to the standards of potable water and using the same distribution system to supply the water is generally not considered to be a viable option. However, cities are studying options to provide dual distribution systems, with separate potable water and reclaimed water systems.

Traditional water master plans analyze potable water distribution systems, however with the limitations in water resources, new master plans have started to include consideration of reclaimed water infrastructure. This integrated approach to master planning will help utilities to understand the dynamics of their water sources and utilize the resources effectively. Medium-sized utilities such as the City of Surprise in Arizona have taken the initiative to implement such integrated water master planning to evaluate the feasibility of dual distribution systems.

The City of Surprise, AZ, with a planning area of nearly 300 square miles, is projected to grow from a current population of 100,000 to over 700,000 at build-out. The City is developing an Integrated Water Master Plan to provide guidance for the orderly improvement and growth of the City's water supply portfolio. The integrated

master plan consists of five components: water resources, groundwater recharge, drinking water infrastructure, wastewater infrastructure, and reclaimed water infrastructure. The three infrastructure components were studied using hydraulic models to evaluate the functionality and applicability of a dual distribution system for the growing city. The reclaimed water system was primarily evaluated to fulfill the landscape demand.

This paper summarizes the preliminary results of an integrated master planning for the City of Surprise, AZ with focus on benefits of simultaneous infrastructure master planning.

Introduction

Communities in arid areas of the country are facing problems with limited water resources. Reusing treated wastewater effluent (reclaimed water) is one of the most viable solutions to expand water resources under conditions of fresh water scarcity. The use of reclaimed water for landscaping and non-potable water uses can significantly reduce the burden on the potable water system.

Dual Distribution Systems

Dual distribution systems use separate pipe networks and facilities to supply potable and non-potable water. Rather than providing a single distribution system that provides potable water to serve all water demands, separate reclaimed water distribution systems can provide water for landscape irrigation and non-potable water uses. A reclaimed water system can be designed as a system totally separate from the potable water system or planned as a part of dual distribution system that provides reclaimed and potable water to the service area (Asano et al., 2007).

Most of the dual distribution systems in operation today consist of reclaimed water mains installed along with existing potable water pipes. Since reclaimed water can be used for non-potable water uses, smaller quantities of water would need to be treated to high potable water standards, resulting in cost saving at the treatment plant. However, a separate system necessitates the additional cost of facilities and operations. New communities, where no facilities currently exist, are in a position to optimize their systems because both reclaimed and potable systems could be built simultaneously (NRC, 2007). The cost savings realized from the reduction in potable water treatment could offset the costs of constructing two systems to some extent. Cities can adopt integrated water master plans for new developments that incorporate dual distribution systems to minimize their costs.

Sizing of most potable water systems is driven by fire flow requirements, resulting in large facilities. If non-potable water demand and fire flow could be served by a reclaimed water system, then sizing of the potable water system facilities could be reduced. The cities with current dual distribution systems are adopting partial dual distribution system where reclaimed water is used for landscape and non-potable water use and in some cases fire protection is provided from both the potable and reclaimed water lines (NRC, 2007). Utilities using partial dual distribution systems

include Irvine Ranch Water District, CA, City of Tucson, AZ, St. Petersburg, FL, and Colorado Springs, CO.

Some southwest water utilities are taking a proactive approach to planning that incorporates acquiring water resources in the future and studying options to provide dual distribution systems, with separate potable water and reclaimed water systems. The integrated approach to master planning will help utilities to understand the dynamics of their water sources and proper planning for their future infrastructure.

This paper summarizes the preliminary results of an integrated master planning approach for the City of Surprise, Arizona. Three infrastructure components (potable water, reclaimed water, and wastewater) were simultaneously studied using hydraulic models to plan and evaluate the functionality and applicability of optimized infrastructure for the growing city.

Integrated Master Planning for City of Surprise

Traditional water master plans analyze potable water distribution systems; however, with the limitations in water resources, new master plans have started to include consideration of reclaimed water infrastructure. Integrated planning, design, and construction of dual systems offer advantages in both water resource management and cost savings (Asano et al., 2007). The City of Surprise integrated master plan has five major components: water resources, groundwater recharge, drinking water infrastructure, wastewater infrastructure, and reclaimed water infrastructure.

The City of Surprise, AZ has undertaken a project to develop and implement an integrated water master plan. The integrated water master plan will provide guidance to the City for the orderly improvement and growth of the City's water supply portfolio and drinking water, wastewater, reclaimed water, and groundwater recharge infrastructure. The master plan was divided in two components: Water Resources and Water Infrastructure.

The Water Resources component of the integrated water master plan identified the projected water demands as the City continues to grow and develop, along with a water supply and reuse strategy that will meet the demands in a cost-effective and sustainable manner. The Water Infrastructure component of the integrated master plan developed comprehensive plans and infrastructure improvements that will allow the City to meet its growing demand in a cost-effective and sustainable manner.

Located in the greater Phoenix area, the City's 300 square-mile planning area is currently less than 20 percent developed. There is a great deal of uncertainty as to how and when the planning area will develop. The City is expecting to grow from a 2007 population of 104,895 to over 400,000 by 2030, and ultimately to 700,000 by build-out. The City would like to plan for new development by evaluating how investment in reclaimed water infrastructure can decrease the need for large-scale drinking water infrastructure. A key feature of this study was the desire to co-locate potable water and reclaimed water facilities to reduce the land requirements. The

tradeoffs between serving the new demands from fewer central facilities versus many distributed facilities were also examined.

Study Area

The study area for this project, shown in Figure 1, includes all of the City's Municipal Planning Area (MPA). The MPA has been divided into six Special Planning Areas (SPA) to maintain consistency with the City's previous master plan efforts and for convenience of wastewater and reclaimed water planning; i.e., the SPAs comprise logical drainage areas for existing, planned, and potential water reclamation facilities.

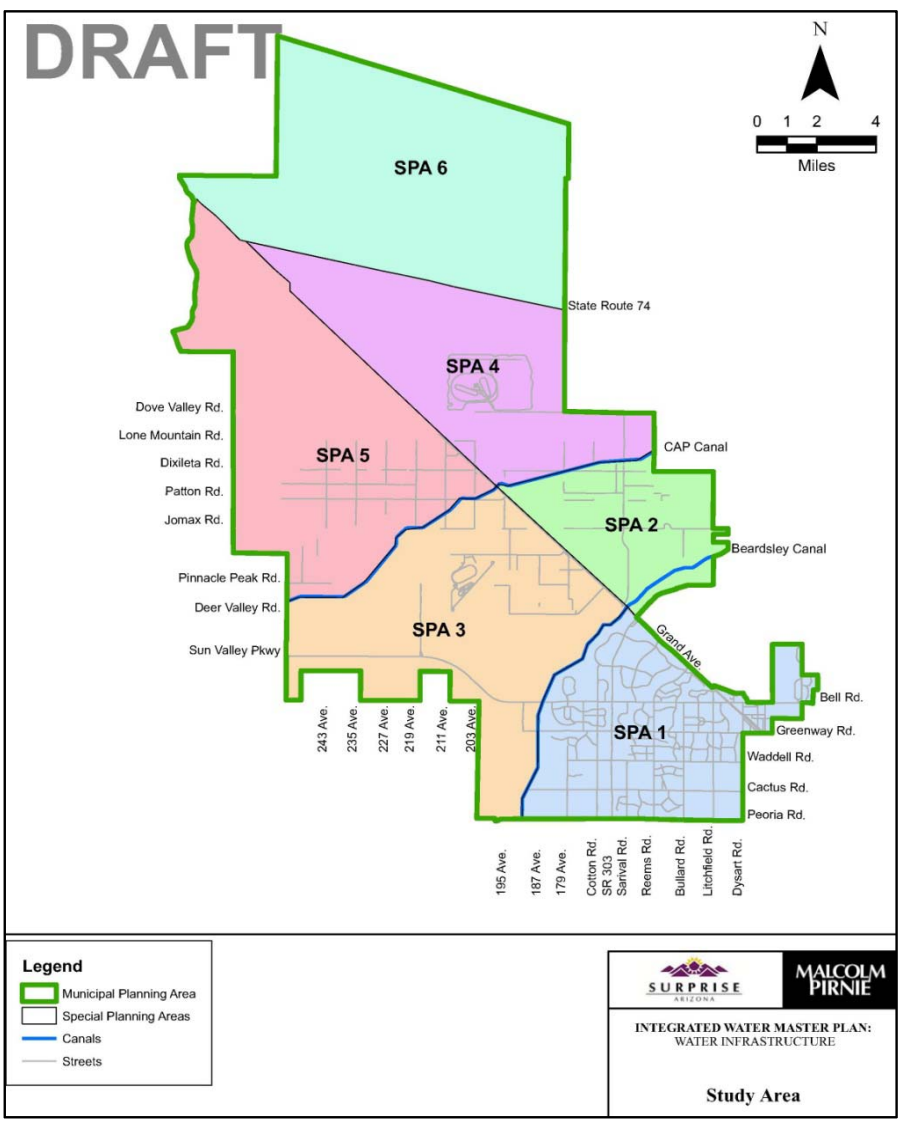

Figure 1: City of Surprise Study Area

Methodology

The City's drinking and reclaimed water distribution system was modeled under steady-state conditions using Bentley WaterCAD® V8 XM edition. Different infrastructure alternatives for potable water, wastewater, and reclaimed water were evaluated against system performance criteria and City's design guidelines.

A Demand Module tool was created as a part of the Water Resources component of the master plan to dynamically simulate water resource needs from GIS-based land use data, residential densities, and demand and flow factors. The tool combined the GIS data with indoor, outdoor, and landscape demand factors for the City and was used to allocate demand in the drinking water and reclaimed water hydraulic models. The drinking water system model was evaluated to supply indoor and outdoor demand while the reclaimed water system was evaluated to fulfill landscape demand, which represents the largest reclaimed water customers.

All infrastructure alternatives were developed using a common set of guidelines and assumptions relating to water demands, the reclaimed water management strategy, and system layouts and configurations:

- Piping networks followed the road alignments in the City's transportation element of the General Plan. No pipes were located in areas that were known to be undevelopable, such as mountainous regions.
- The piping networks for the future system were skeletonized models of the drinking water and reclaimed water transmission systems to an approximate one square-mile grid.
- Drinking water and reclaimed water pressure zones were delineated with 120-foot intervals of ground elevation in the planning area (12 pressure zones total).
- The Water Service Facilities (WSFs) i.e. storage tanks and pump stations for the drinking water system were centrally located within future service areas to minimize pumping requirements. Reclaimed water WSFs (storage tanks and pump stations) were co-located with the drinking water WSFs.
- The reclaimed water system was divided into distribution and transmission components. The distribution system supplied water from the reclaimed WSFs to customer locations while the transmission system supplied water from Water Reclamation Facilities (WRFs) to reclaimed WSFs.
- Reclaimed water distribution system pipes were laid alongside but not connected with the drinking water distribution pipes to minimize construction costs.
- Excess reclaimed water beyond the landscape irrigation demands was diverted to recharge facilities. These recharge facilities were located in areas where the depth to groundwater was high and away from potential interferences such as the landfill, the airport, and other regional recharge projects.

Summary of Results

Because of the close interrelation between wastewater, reclaimed water, and recharge infrastructure, the three systems were evaluated simultaneously to identify the most cost effective solution for the City. Alternatives for wastewater treatment, and corresponding generation of reclaimed water, were developed to serve the 6 SPAs using one of the following layouts:

- *Construct and Operate 6 WRFs* - Under this alternative, the City will design and construct a WRF in each SPA. Reclaimed water will be pumped from the WRF to storage and booster facilities that are co-located with WSFs. All surplus reclaimed water will be recharged.
- *Construct and Operate 4 WRFs* - Under this alternative, the City will design and construct four WRFs: one each in SPAs 1, 2, 3, and 5. The SPA 1, 2, and 3 WRFs will receive flows from their respective SPA. The SPA 5 WRF will receive wastewater flows from SPAs 4, 5, and 6. Reclaimed water storage, distribution, and recharge will be similar to the first alternative; however, reclaimed transmission mains and booster pumping will change slightly.
- *Construct and Operate 3 WRFs* - Under this alternative, the City will design and construct 3 WRFs: one each in SPAs 1, 2, and 3. Collection system flows from SPA 5 will be routed to the WRF in SPA 3. Flows from SPAs 4 and 6 will flow into the WRF in SPA 2. Reclaimed water storage, distribution, and recharge will be similar to the first two alternatives, but reclaimed water transmission and booster pumping will change.

Using the different locations for WRF sites, the wastewater collection system was laid out and sized to evaluate the tradeoffs between treatment costs and conveyance infrastructure costs. All three alternatives shared the same WSF setup used for the water distribution system. There were total 16 WSFs each serving particular service area in the drinking water system. Since the potable WSF and the reclaimed WSF were co-located for each service area in a pressure zone, cost for alternatives were affected by the choice of sites for WRFs. The location of the WRFs affected the total cost for all infrastructures through the need to pump reclaimed water produced at the WRF to the reclaimed WSFs, thus requiring different pump and transmission mains capacities for different alternatives.

The total 20-year present worth costs for the three alternatives were essentially the same at this level of planning with less than 1.5 percent difference between the highest and lowest total present worth costs. The cost savings from building fewer WRFs was offset by the larger collection system piping needed to convey wastewater from the northern areas to the WRFs and by the additional pumping of reclaimed water back to the northern areas. The 6 WRFs alternative had the lowest capital costs, but the highest annual O&M (primarily due to operating 6 WRFs). The 3 WRFs alternative had higher capital costs but the lowest annual O&M costs (due to lower WRF O&M and lift station pumping costs). The 3 WRFs alternative did have a slight 20-year present worth cost advantage over the other alternatives. However, the main disadvantage of 3 WRFs was the need for larger reclaimed water transmission

piping and pumping to return reclaimed water to the northern areas; this disadvantage was exacerbated by the fact that there were substantial elevation differences that would have to be overcome by pumping. The large wastewater and reclaimed water piping could also be less accommodating to developments that occur at remote locations early on as they would have to build the larger and longer piping to receive wastewater and reclaimed water service. This could again be mitigated to some extent by installing smaller, parallel piping, but at additional cost.

The analysis indicated that there were no appreciable differences in the long-term costs of all alternatives evaluated, but the alternative with 6 WRFs provided the following benefits:

- By placing the WRFs closer to the WSFs, this alternative reduced the need for larger conveyance and transmission piping and also reduced pumping requirements for the reclaimed water.
- This alternative with a larger number of WRFs could be more accommodating to development as it provides more flexibility in phasing the WRFs and infrastructure as development occurs within each WRF service area.

Performing simultaneous master planning allowed for the evaluation of a tradeoff between treatment costs & infrastructure costs (as well as for a tradeoff between costs for water, wastewater and reclaimed water) to arrive at an optimal solution. Refinements were made to further optimize the selected alternative. Figure 2 illustrates the reclaimed water distribution and transmission system at build-out. A cost comparison between a single potable water system and a dual potable-reclaimed water system was not made as part of this project because reclaimed water is an integral part of the City's water supply portfolio in the future. The results presented in this paper are preliminary, subject to approval by the City of Surprise and full adoption of the integrated master plan.

References

Asano, T., Burton. F.L., Leverenz, H.L., Tsuchihashi, R., and Tchobanoglous, G. (2007). Chapter 14: Distribution and Storage of Reclaimed Water In: Water Reuse Issues, Technologies, and Applications, 1st ed., McGraw Hill. 829-847.

National Research Council (NRC). (2007). Drinking Water Distribution Systems: Assessing and Reducing Risks. Committee on Public Water Supply Distribution Systems: Accessing and Reducing Risks, National Academic Press, Washington, DC. 27-30.

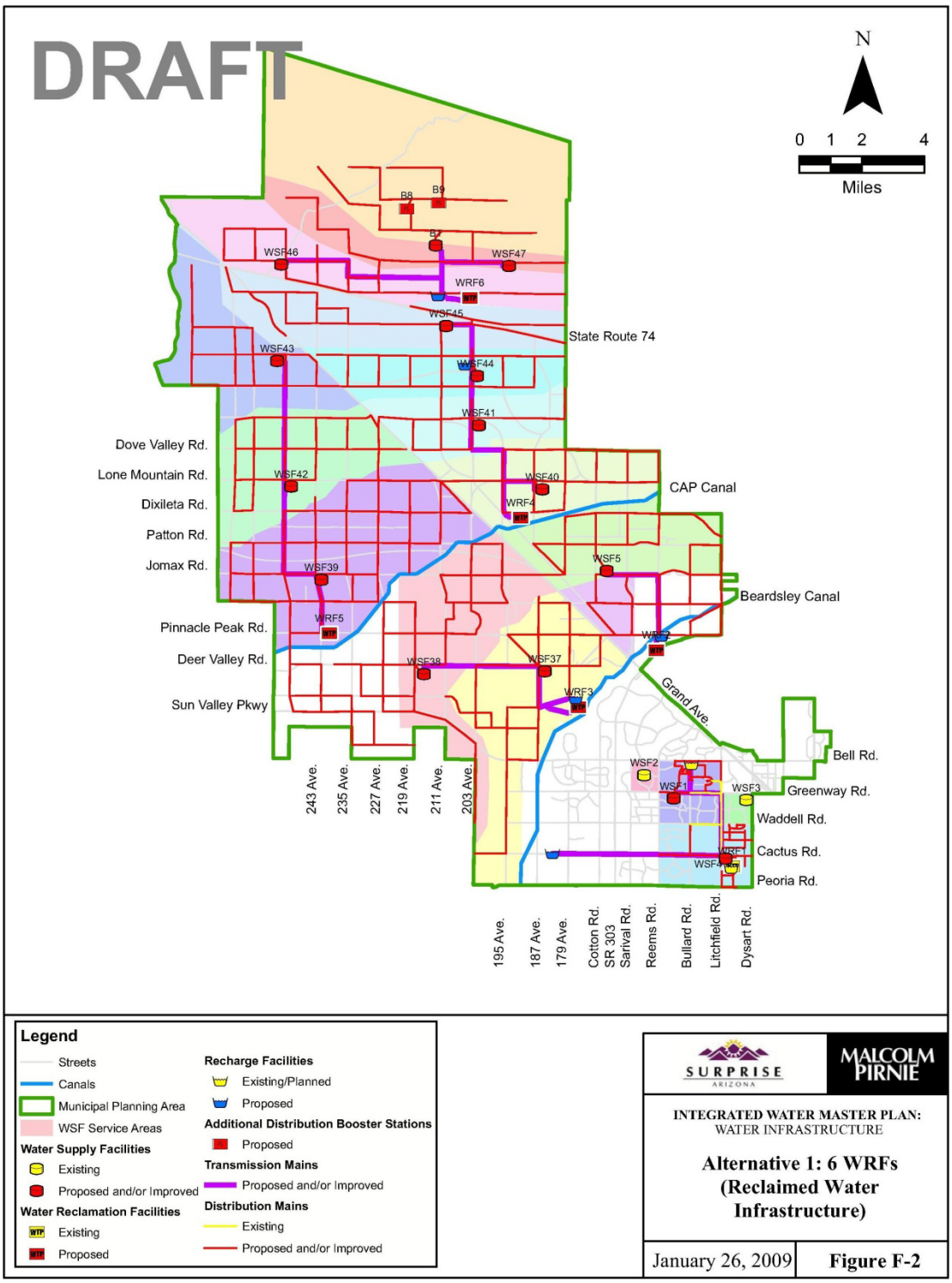

Figure 2: Build-out reclaimed water distribution and transmission system

Reliability Analysis of Water Distribution Systems Using Graph Decomposition

Jochen Deuerlein*, Andreas Wolters*, Dietmar Roetsch** and Angus R. Simpson***

* 3S Consult GmbH, 30827 Garbsen, Germany,
** Energietechnik & Ingenieursoftware, 06844 Dessau, Germany
*** School of Civil, Environmental and Mining Engineering, University of Adelaide, Adelaide SA 5005,Australia.

Abstract

Water supply utilities are increasingly being confronted with growing maintenance requirements in order to provide a reliable and cost efficient operation of the water distribution system in order to deliver high standard drinking water. One specific challenge is to find a satisfactory compromise between the contradictory objectives of saving investment cost and meeting the increasing expectations of customers. A valuable tool for the planner is reliability analysis of the system that for instance provides information about the importance of each particular pipe in determining the total reliability of the system. This information can be used to decide which pipes should be replaced next or potentially duplicated to reduce the risk of system isolation. Since structural (topological) reliability only considers the connectivity of the network a new approach for the calculation of structural hydraulic reliability is presented in this paper. The algorithmic implementation is based on a decomposition method of the network graph that greatly enhances both the calculation of pure structural reliability as well as structural hydraulic reliability.

INTRODUCTION

The calculation or estimation of the reliability of a system is a very important issue in all fields of engineering. Reliability and associated key performance parameters are becoming more and more the driving forces for decision making in water distribution network planning and management. There exist different concepts for the definition and calculation of water supply network reliability (Ostfeld, 2004). Xu and Goulter (1998, 1999) use a probabilistic hydraulic simulation model where the nodal demands, tank levels and pipe roughness values are stochastic parameters. The reliability of the system is defined as its capability of satisfying the customer's demands with sufficient pressure availability. Tolson et. al. (2001) distinguished between mechanical and hydraulic failures as well as reliability. Mechanical failures are caused by the components of the system such as pipes and pumps whereas hydraulic failures are the consequence of insufficient pressure conditions.

In this paper the mechanical reliability is called component reliability. It is defined as the probability that a particular component will satisfactorily perform a required function under predefined conditions for a specified period of time. In water supply systems analysis the reliability of the pipelines, pumping stations, control devices such as regulating valves and water treatment plants is of special interest. The reliability of pipes having similar age, material and diameters can be derived for example from defect statistics of such a pipe group. Different stochastic approaches are

used for transferring the statistical data into a probability of failure. For a more detailed explanation of the calculation of component reliability the reader is referred to literature (e.g. Mays and Ozger, 2004).

In contrast to the component reliability that is a particular characteristic of a component in the water distribution system, the structural network reliability is a property of the topological composition of the entire distribution system and the reliability of its components. Theoretical network reliability models may be used for the estimation of the probability that the total system performs well under given conditions for a certain period of time. Basically, three types of structural reliability may be distinguished: The *k-out-of-n-reliability* and their special cases for $k = n$ and $k = 2$. The *2-out-of-n-reliability* is also known as source – sink reliability and if $k = n$ the *n-out-of-n-reliability* is called all terminal reliability. Different methods exist for both the exact calculation of the structural (topological) reliability as well as simulation methods. Exact methods include for example full enumeration, minimum-path and minimum-cut-methods, inclusion – exclusion and factorization. A few of these methods will be outlined in this paper. A good overview of different methods can be found in Lucet and Manouvrier (1997) and Kuo (2002).

In the analysis of a hydraulic system like a water distribution network, the structural reliability is applicable only to a limited extent because the connectivity of a system does not guarantee that all customers can be supplied with sufficient pressure. On the other hand hydraulic reliability (sufficient pressures under different load cases) does not consider the topology of the system sufficiently. Consequently in this paper a new concept of structural hydraulic reliability is introduced that is based on the hydraulic supply reliability of the demand nodes. The computationally expensive calculations of structural reliability are simplified by use of decomposition of the network graph. In a general water supply network serial and parallel subsystems can be distinguished from so called complex subsystems. Subsystems are identified by application of a graph decomposition approach that subdivides the total system graph into 1-connected (trees and bridges) components and 2-connected (blocks) components. The structural property of the system describing the interconnectivity of its serial and parallel components is modelled by the so called block graph tree (Deuerlein 2008). Since real water distribution systems usually consist of different components such as main transmission lines (often bridge components), supply and pressure zones (often blocks) and secondary distribution pipes including house connections the calculation time can be dramatically reduced by application of the graph decomposition method.

First, the calculation of structural network reliability is explained using a simple example and the application of graph decomposition is also presented. So far hydraulic issues have not been considered in the analysis. This is done in the second part of the paper where the hydraulic reliability analysis is presented. The nodal supply reliability is introduced followed by an explanation of the so called (*m-0*)-analysis and (*m-1*)-analysis. In the former, the reliability is calculated assuming that all pipes are available. With the latter the so called importance of each pipe of the network can be calculated as the difference between the reliability of the configuration including the particular link and the reliability without that link. In contrast to the definition of

hydraulic reliability based on random demands using Monte-Carlo Simulation techniques, the structural hydraulic reliability is calculated for one particular load case.

THEORETICAL FORMULATION OF NETWORK RELIABILITY

General Concepts

The term reliability denotes the probability that a system performs a certain operation at a certain time under predefined conditions. A system usually is composed of several components. Consequently, the reliability of the system is a function of the reliability of its components. There are different kinds of physical systems that can be distinguished by the configuration of their components. There exist parallel and serial systems as well as so called complex systems. The configuration of the components highly affects the complexity of the calculation of system reliability.

Water distribution networks are an example for such complex systems. In terms of reliability modeling the water distribution system is represented by a so called stochastic graph. In a particular state the configuration of the graph depends on the current state of its components. Let us assume that the components have exactly two functioning states and thus failure may be expressed by the Boolean variable x_i with $x_i = 1$, if component i is functioning and $x_i = 0$ if it is not functioning. Let us further assume that only the links of the graph representing connecting components of the network such as pumps, pipes and valves are subject to failure and that the nodes are perfect. Then each state k of the stochastic network graph can be expressed by the vector $\mathbf{x}_k$ of its entire link set. Furthermore let p_j be the probability that a link j is functioning and $q_j = 1 - p_j$ the probability that it is not. The probability of a state k of the graph G can then be calculated (Lucet and Manouvrier, 1997) by

$$\Pr(G_k) = \prod_{j=1}^{m} \left[[\mathbf{x}_k]_j \, p_j + \left(1 - [\mathbf{x}_k]_j\right) q_j \right] \tag{1}$$

The reliability of the system is the probability that it fulfills a certain expectation. In general three kinds of network reliability are distinguished: The *2-out-of-n-reliability*, the *k-out-of-n-reliability* and the *n-out-of-n-reliability*. The *2-out-of-n-reliability* is also known as source-sink-problem and for the calculation of the all terminal reliability, the system is classified as functioning if there exists at least one spanning tree of the network graph. The different reliabilities can be calculated as the sum of the probabilities of system states where the network graph meets its specific requirements (J: set of all those states):

$$R(G) = \sum_{k \in J} \Pr\left(G_k\right) \tag{2}$$

Theoretically, the exact calculation of network reliability could be carried out by full enumeration of all possible states of the system. However, in reality, full enumeration is impractical for real existing systems with hundreds of thousands of links due to the extremely large number of combinations that would need to be enumerated. The total number of possible states of the system is 2^m. For only 100 network links this number is 1.2677e+30. The network reliability problem belongs to the class of NP-hard problems (see for example Ramesh et. al. 1987).

Serial Systems

Since a serial system functions only if all its components are functioning, its reliability depends heavily on the reliability of its weakest component. Consequently, a serial system in total is always only as good as its weakest component. The calculation of the reliability of the serial system *S* can be derived from Eq. (1) and Eq. (2) and results in the simple expression:

$$R(S) = \prod_{j=1}^{m} p_j \tag{3}$$

Parallel Systems

In contrast to serial systems, a parallel system is intact if at least one of its components works properly. In other words, a parallel system only fails if all its components fail. The reliability of a parallel system *P* is 1 minus the probability that the system fails. Using again equations (1) and (2) the formula for the calculation of the reliability of the parallel system is:

$$R(P) = 1 - \prod_{j=1}^{m} q_j = 1 - \prod_{i=j}^{m} \left(1 - p_j\right) \tag{4}$$

Complex Systems

Systems that do not fall under the category of serial or parallel systems are denoted as complex systems. As mentioned above the reliability of those systems theoretically can be calculated by a full enumeration as the sum of probabilities of all feasible states (see Eq. (1) and Eq. (2)). Due to the great amount of calculation time required by this method the reliability of complex networks is usually determined by other approaches. Methods include path enumeration where all possible paths between the terminals are investigated and the cut enumeration where all minimal cuts leading to an infeasible system state are considered.

Theoretical Concepts of Component Importance

The importance of a network component is a measure for the change in structural reliability of a general system (graph *G*) if the component either is removed or fails. There exist qualitative and quantitative methods. One example is the so called reliability or Birnbaum importance $I_{B,j}$ (B-importance) which is defined by the equation

$$I_{B,j} = \frac{\partial R(G)}{\partial p_j} \tag{5}$$

The B-Importance is a measure for the change of system reliability as a result of a change of reliability of component *j* (Kuo, 2002). In general the analytical solution of Eq. (5) is very difficult for large systems. Another method of estimating the component importance is derived from the so called (*m*-1)-analysis. The reliability calculation as described above is called (*m*-0)-reliability since all network links are considered. Accordingly, the (*m*-1)-reliability is the reliability of the reduced system where one link is removed. The (*m*-1)-reliability of the reduced system can be calculated for each link with the same methods. Using the results of the (*m*-0)- and (*m*-1)-analysis the reliability importance $I_{B,j}$ of the network link *j* of graph *G* can be simp-

ly approximated by the difference of the two reliabilities for the system with and without component *j*:

$$I_{B,j} = R(G)_{(m-0)} - R(G)_{(m-1)_j} \tag{6}$$

A complete (*m*-1)-reliability analysis requires the calculation of *m* system configurations and is very time consuming. After the example in the following section the application of the decomposition of a general network graph as described in Appendix I to a more efficient calculation of structural network reliability will be outlined.

Example

Figure 1 shows the graphs of two simple networks. Network a) consists of four links, four nodes and one loop. In network b) the nodes *b* and *c* are connected by an additional link 5. The assumed pipe reliabilities range from 0.6 for link 4 to 0.9 for link 1.

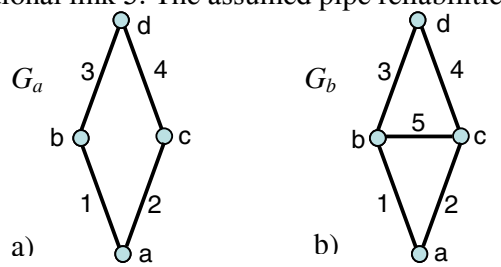

Link	p
1	0.9
2	0.8
3	0.7
4	0.6
5	0.85

Figure 1: Example networks: a) rhombus, b) bridge system

The two-terminal reliability of the network is to be calculated. Node *a* is the source node and node *d* is the sink node. From the section above it follows that in case a) the network can be divided into serial and parallel components. The paths a-1-b-3-d and a-2-c-4-d are alternative paths from node *a* (source) to node *d* (sink). The two paths consist each of a serial system of two links. Consequently, the two-terminal-reliability of the system can be calculated using Eq. (3) and Eq. (4):

$$R(G_a) = 1 - (1 - p_1 p_3)(1 - p_2 p_4) = 1 - (1 - 0.63)(1 - 0.48) = 0.8076$$

The same result is obtained by use of the general formulations of Eq. (1) and Eq. (2).

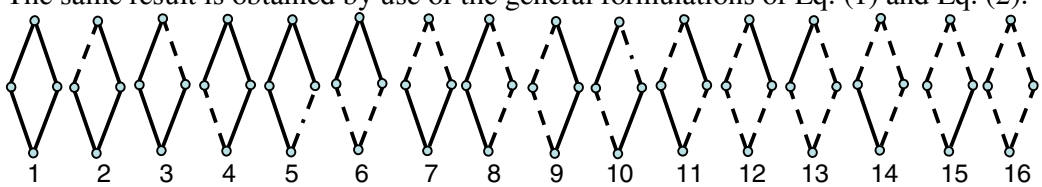

Figure 2: Full enumeration of possible system states of network G_a

A full enumeration of feasible states of the system (see Figure 2) shows that only the states 1, 2, 3, 4, 5, 8, 9 are feasible since in all other cases node *a* and node *d* are disconnected. Let $J=\{1, 2, 3, 4, 5, 8, 9\}$ be the set of feasible states. The reliability calculation using Eq. (1) and Eq. (2) can then be written as

$$R(G_a) = \sum_{i \in J} \prod_{j=1}^{m} \left[[\mathbf{x}_i]_j \, p_j + \left(1 - [\mathbf{x}_i]_j\right) q_j \right] = p_1 p_2 p_3 p_4 + p_1 p_2 q_3 p_4 + p_1 p_2 p_3 q_4 +$$

$$q_1 p_2 p_3 p_4 + p_1 q_2 p_3 p_4 + p_1 q_2 p_3 q_4 + q_1 p_2 q_3 p_4 = 0.8076,$$

which agrees with the value computed previously. Now let us consider system b) with the additional link 5. In this case the system can not be broken down into serial and parallel components. The number of possible system states is $2^5 = 32$, twice the number as in case a. Its two-terminal-reliability can be calculated for example by a full enumeration (result: $R(G_b) = 0.85418$).

Calculation of structural reliability using graph decomposition

It has been shown before that the calculation of structural reliability of serial and parallel systems is straight forward in contrast to that of complex systems. A serial representation of a complex system is its block graph tree (see Appendix I). From the right system in Figure 4 in Appendix I it is clear that if the reliabilities of the virtual block links or the connection nodes were known then the supply reliabilities of the block graph tree nodes could be calculated easily. For example if we know the reliability of the root node of tree 1 the supply reliability of the tree can be calculated as the product of the root node reliability and all tree link reliabilities. However, in general the blocks are complex systems that can not be reduced to combinations of serial and parallel systems and other methods need to be used.

Block reduction

The advantages of the application of the graph decomposition can be demonstrated by the comparison of the number of system states that have to be considered using a full enumeration of possible states of the system in Figure 4. Without application of the graph decomposition the total number of possible states is: 2^{19}= 524,288. Using the knowledge of the block graph tree structure the calculation of the reliability by full enumeration is only required for the complex systems of block 1 and block 2. Following the example of Figure 1b) the number of system states to be calculated is 32+32=64. However for real networks the number of pipes within a block often prevents the application of a full enumeration even for separate blocks.

Path element reduction

For the simplification of the block reliability calculation the nodes of the block are distinguished according to their nodal degree (number of connected links). A node with degree two is called an inner path node, a node with degree greater or equal three is denoted as path node. The link sequences without bifurcation between two path nodes are called path elements. Figure 3 shows a looped block subgraph and its path representation. The reliability calculation of a path element can be performed using the formula for serial systems. In the original system the full enumeration of the remaining complex system consists of 2^{17}=131,072 different states whereas in the reduced system only 2^{11}= 2048 states have to be calculated.

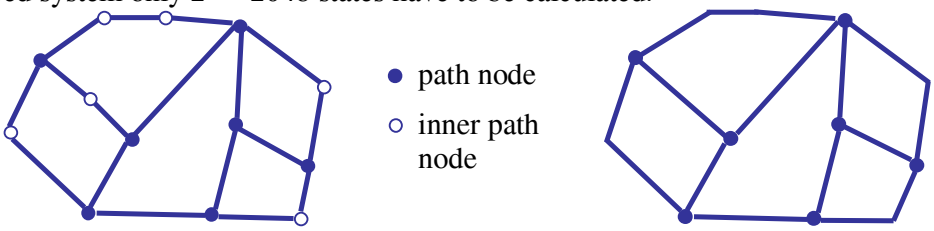

Figure 3: Path reduction of a looped block.

RELIABILITY CALCULATION OF WATER SUPPLY NETWORKS

General assumptions

The structural reliability calculation as explained above is suitable only to a limited extent for hydraulic systems analysis. In order to supply the customers with a sufficient amount of water it is not only sufficient that all nodes of the system are connected to a water source (topological criterion). In addition, the pressure heads at all demand nodes must be above a certain minimum allowable pressure. A full enumeration approach of hydraulic systems reliability would include the consideration of all 2^m possible states of the network similar to the structural reliability calculation above followed by hydraulic steady-state calculations or even extended period simulations of topologically feasible system states for different loading conditions. Since an exact calculation that considers all the different aspects is not possible for real existing water distribution systems assumptions and simplifications of the problem are needed.

In this paper a new concept for the supply reliability of a water distribution system is introduced that combines a hydraulic steady-state calculation with structural reliability analysis. In order to get an idea about the importance of each pipe of the system a so called (m-1)-analysis is carried out. Each (m-1) case includes the calculation of the hydraulic steady-state of the system followed by a topological (or structural) analysis of the system based on the particular flow distribution (as a result of the (m-1)-topology and the particular load case). In particular the (m-1)-calculations require the consideration of pressure dependency of nodal demands.

The calculation of the reliability of water supply networks in this paper is based on the following assumptions.

1.) For the definition of the stochastic network graph only the pipe states are subject to uncertainty. The nodes are assumed to be perfect and also pipe failures are assumed to be stochastically independent.
2.) The probability of failure of water treatment plants and storage tanks is considered as the reliability of the virtual links.
3.) It is assumed that both structural as well as hydraulic reliability of the virtual ground nodes is 1.

In the following measures for the reliability of the system and the supply reliability of a network node are introduced.

Nodal supply reliability

A very important piece of information in hydraulic systems analysis is the probability that a certain node is supplied with adequate amount of water under sufficient pressure conditions. This probability is denoted as nodal supply reliability $NSR_i \in [0;1]$. Its corresponding value is the probability of insufficient supply $NFP_i = 1 - NSR_i$. It can be visualized as the time fraction for which the node is not sufficiently supplied (e. g. a value of 0.00228311 means 20 hours/year). The nodal supply reliability $NSR_{i,(m-0)}$ of node i of the full system is distinguished from $NSR_{i,(m-1)}$ of the reduced system which is called (m-1)-nodal supply reliability (with $R_{s,i}$: structural 2-out-of-n-reliability, D_i, (Q_i): demand, (withdrawal) of node i):

$$a) \quad NSR_{i,(m-0)} = R_{s,i}\frac{Q_i}{D_i} \qquad b) \quad NSR_{i,(m-1)} = \frac{1}{m}\sum_{j=1}^{m} R_{s,i,(m-1)_j}\frac{Q_{i,j}}{D_i} \tag{7}$$

Network reliability definition

The definition of network reliability in this paper is a combination of both hydraulic as well as structural reliability (Index HS) based on nodal supply reliabilities. The reliability of the system is defined as the mean value of all nodal supply reliabilities.

$$a) \quad R_{HS,(m-0)}(G) = \frac{1}{n}\sum_{i=1}^{n} NSR_{i,(m-0)} \quad and \quad b) \quad R_{HS,(m-1)}(G) = \frac{1}{n}\sum_{I=1}^{n} NSR_{i,(m-1)} \tag{8}$$

The information that can be gained from this reliability formulation is more significant to hydraulic systems analysis than the pure structural reliability since it takes also into account the hydraulic properties of the system. An additional benefit is that the nodal supply reliabilities can be weighted, for example, by the demand and further scale factors for important customers like hospitals, etc.

Hydraulic pipe importance

The definition of the hydraulic importance of a network pipe is based on the (*m*-1)-hydraulic steady-state calculation with pressure dependent demands.

$$I_{H,j} = 1 - \frac{\mathrm{Q}_{total}(n-1)_j}{\mathrm{Q}_{\mathrm{total}}(n-0)} \tag{9}$$

$\mathrm{Q}_{total}(n-0)$ denotes the total withdrawal of the system in the (*m*-0) case and $\mathrm{Q}_{total}(n-1)_j$ is the maximal withdrawal with respect to the pressure dependency of the nodal demands for the network without pipe *j*. The hydraulic importance of a pipe can take values between 0 and 1. If as a result of the (*m*-1)-calculation all nodes of the system can be supplied with sufficient pressure then the value for the hydraulic importance of the corresponding pipe is zero. In contrary, if all the nodes of the system are disconnected by a pipe break, for example of a transmission line, then the hydraulic importance of this pipe is one. The hydraulic simulation algorithm used for the hydraulic importance calculations must be capable of simulating the pressure dependent behavior of the nodal demands realistically.

Algorithmic calculation of nodal supply reliability

As explained before the (*m*-1)-analysis consists of the calculation of structural reliability for a particular load case with one link removed from the network graph. A full (*m*-1)-reliability calculation including the calculation of the hydraulic importance of all pipes of the network requires the number of pipes independent steady-state calculations. Since nowadays the usage of 1:1 network models has become more and more common practice in hydraulic system analysis the number of network pipes can often exceed 100,000. Even with respect to the increasing speed of modern computers a full (*m*-1)-analysis would result in unacceptable calculation time. Therefore it is very important to use as much topological information as possible for simplifications of the water distribution system. In particular the (*m*-1)-calculations can take advantage of the knowledge of the different network components and their interconnectivity.

For the sake of simplicity it is assumed in the following description that under normal (m-0) - conditions all demands at the network nodes can be satisfied with sufficient pressure.

Algorithmic steps:

1.) (m-0)-calculation of hydraulic steady-state and nodal supply reliabilities of the total system using graph decomposition as described above and in Deuerlein (2008). Calculation of system reliability by Equation (8 a).

2.) (m-j)-calculations of hydraulic steady-state and nodal supply reliabilities for all pipes $j = 1,\ldots,m$ by using the following subdivision of cases:
Case 1: Pipe j is part of the 1-connected subgraph (Serial systems bridges and trees):
The network graph is subdivided into two separate components $C_{1,j}$ and $C_{2,j}$. The component $C_{2,j}$ that is not connected to the source node is disconnected from any supply node. In this case the hydraulic importance (see Eq. (9)) of the corresponding pipe can be stated simply as the ratio of the sum of demands of the disconnected components to the total network demand, without the need for a hydraulic steady-state calculation. In this case the nodal supply reliabilities of the disconnected nodes are zero as well as the topological all terminal reliability. The decrease of the total system demand has no effect on the reliabilities of the nodes of the supplied component since it was assumed that in the (m-0) case all nodes are fully supplied and the decrease in demand results in higher pressures in component $C_{i,j}$.
Case 2: Pipe j is part of the 2-connected subgraph (complex system block):
The (m-1)-calculation is carried out only for the block that pipe j belongs to. After the calculation it is checked if all the demand nodes of the block and all subsequent components (other blocks, bridges or tress) are above the minimum allowable pressure. If not, a pressure driven calculation of these components is carried out. The preliminary blocks are not negatively affected (only a rise of pressure is possible there). The topological reliabilities of the preliminary blocks are not affected at all; the ones of subsequent blocks can be easily updated by multiplication with the new cut node reliabilities. The reliability calculation within the block takes advantage of the path elimination (Figure 3). The algorithm processes only path elements and path nodes. The path reliabilities can be easily calculated from the pipe reliabilities by using the formula for serial systems. However, for real existing distribution networks with a large number of pipes and nodes this process may be still a very time consuming task.

3.) Calculation of the (m-1)-nodal supply reliabilities and (m-1)-system reliability: After all the $(m\text{-}1)_j$-cases are calculated the (m-1)-nodal supply reliability and the (m-1)-reliability of the total system follow from Eq. (7b) and Eq. (8b), respectively.

SUMMARY AND CONCLUSION

A new approach for the estimation of the water distribution system reliability has been presented in this paper. The main difference in comparison to other methods is

that it is based upon both structural reliability as well as network hydraulics. The consideration of pressure dependent demands requires a hydraulic solver that is capable of performing correct pressure driven analysis in hydraulic steady-state calculations. Although the graph decomposition approach is a promising tool for simplification of the analysis the structural reliability calculations are still a very time consuming task for large distribution networks having multiple redundancies. The graph decomposition supports the enhancement of the algorithm, yet more research needs to be done for the development of more sophisticated methods for a simplified and approximate calculation of the block reliability.

APPENDIX I: Graph Decomposition

In Deuerlein (2008) the decomposition of a general water supply network graph is described. An example is given in Figure 4. Firstly, a virtual ground node (node "r" in Figure 4) is introduced that is connected with all input nodes such as reservoirs and tanks (nodes "m", "n") by so called virtual links (links "16", "17"). The first step of the graph decomposition consists of the identification of connected components that are further subdivided into 1-connected and 2-connected components. The 2-connected subgraph includes the looped blocks of the network graph. The 1-connected subgraph can be further subdivided into bridge components (link "4") and the forest that is composed of several trees. Whereas the link sets of the graph components are distinct, the nodal sets are overlapping in the so called connection nodes.

Three different types of connection nodes are distinguished: The root nodes connecting a tree with a block (nodes "k", "e") or a bridge, the bridge terminal nodes that a bridge and the 2-connected blocks have in common (nodes "c", "d") and the articulation nodes that directly connect two looped blocks (node "l"). A very useful simplification of the network graph is the block graph tree where all looped blocks are substituted by a single block node that is connected with all cut nodes of the block. The application of the decomposition of the network graph and the block graph tree representation will be used for a more efficient calculation of network reliability of water supply networks. Figure 4 shows the decomposition of a simple network with three blocks B_1, B_2, B_3, one bridge and two Trees T_1 and T_2.

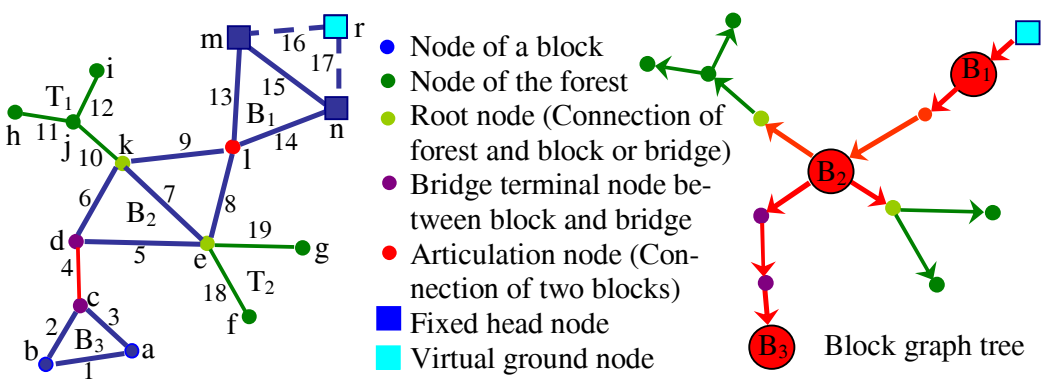

Figure 4: Graph Decomposition of an example network and its block graph tree

APPENDIX II: Notation and Abbreviations

n:	Number of nodes
m:	Number of pipes
D_i:	Demand at node i
Q_i:	Calculated outflow at node i
$NSR_{i,(m-0)}$ (or NSR_i):	(m-0)-reliability of node i (total system including all pipes)
$NSR_{i,(m-1)}$:	(m-j)-reliability of node i for the system without pipe j
$NSR_{i,(m-1)_j}$:	(m-1)-reliability of node i: mean value of all $NSR_{i,(m-j)}$
$R(G)_{(m-k)}$	(m-k)-structural reliability of G (k=0, 1)
$R_{HS}(G)_{(m-k)}$	(m-k)-$h$ydraulic supply reliability *of* G (k=0, 1)
$I_{B,j}$:	Reliability (Birnbaum) importance of pipe j
$I_{H,j}$:	Hydraulic importance of pipe j

REFERENCES

Deuerlein, J. (2008): "Decomposition model of a general water supply network graph". *Journal of Hydraulic Engineering*, 134(6), 822-832.

Kuo, W. (2002). *Optimal reliability modeling : Principles and applications*. Hoboken, NJ, John Wiley & Sons, Inc.

Lucet, C. and J. Manouvrier (1997). *Exact methods to compute network reliability*. In MMR'97, 1st International Conference on Mathematical Methods in Reliability, Bucharest, Romania.

Mays, L. and Ozger, S. (2004): "*Optimal location of isolation valves in water distribution systems: A reliability/optimization approach*." URL: http://www. public.asu.edu/~lwmays/Ch07_Mays_144381-9.pdf (January, 16th, 2009).

Ostfeld, A. (2004): "Reliability analysis of water distribution systems." *Journal of Hydroinformatics*, 6(4), 281 – 294.

Ramesh, A.; Ball, M. O.; Colbourn, C. J. (1987): Bounds for all terminal-reliability in planar networks. *Annals of Discrete Mathematics*, 33, 261-273.

Tolson, B. A.; Maier, H. R.; Simpson, A. R.: (2001) : **"***Water distribution network reliability estimation using the First-Order Reliability Method.*" World Water and Environmental Resources Congress 2001 Don Phelps, Gerald Sehlke, Editors Orlando, Florida, USA, May 20–24.

Xu, C and Goulter, I. C (1998): "Probabilistic model for water distribution reliability." *Journal of Water Resources Planning and Management*, 124(4), 218–228.

Xu, C and Goulter, I. C (1999): "Reliability-based optimal design of water distribution networks." *Journal of Water Resources Planning and Management*, 125(6), 352–362.

A FRAMEWORK FOR ALTERNATIVE FORMULATIONS OF THE PIPE NETWORK EQUATIONS

Angus R. Simpson[1] and Sylvan Elhay[2]

[1]School of Civil, Environmental and Mining Engineering, University of Adelaide, Adelaide SA 5005, Australia. email: asimpson@civeng.adelaide.edu.au
[2]School of Computer Science, University of Adelaide, Adelaide SA 5005, Australia. email: elhay@cs.adelaide.edu.au

Abstract

Since the late 1960s and early 1970s numerous papers have been written on the formulations and methods for solving the governing equations for flows and heads in water distribution systems. Many different names have been given to the various formulations and methods for solution used including the linear theory method, Newton's method, the Todini and Pilati method etc. The underlying equations are the flow continuity equations at nodes in the network, the head loss-flow relationships for individual pipes and finally the head losses around closed loops or for paths between fixed head nodes in the network. The set of equations is nonlinear and hence requires an iterative solution process.

The aim of this paper is to revisit the formulations of the equations for flows and heads in water distribution systems and provide clarity for a logical presentation of a framework for the different formulations. Five formulations are described including 1) flow equations where the equations are formulated only in terms of the unknown flows in a network 2) head equations 3) loop flow equations 4) flow and head equations and 5) the Todini and Pilati flow and head formulation. Graph theory is used to show how many unknowns are required to be solved for in each of the five formulations. A Newton solution method is derived for the flow formulation and the Todini and Pilati formulation.

INTRODUCTION

Pipes, pumps, tanks and valves are connected to form a water distribution system, often in a complex manner. A network for a city, small town or new subdivision is an example. Many or several loops or circuits are usually present in the network. There are usually entry points to the network (for example–tanks, storages and reservoirs) and also many withdrawal points (for example–homes, industries, parks and gardens, commercial buildings, etc.).

Nodes are defined as the end points of links in the network (pipes, pumps or valves) and are identified as either junction nodes with a variable head or fixed head nodes (for example–reservoirs). Flow may enter or leave the network at junction nodes.

There are a number of alternative formulations of the equations describing a water distribution system (Wood and Rayes (1981)–for the first three formulations; Todini and Pilati (1988) for the fifth formulation). Five formulations that are presented in detail in the paper include:

1. flow equations or *Q–equations* formulation in terms of unknown flows (*Q*s) in each link
2. head equations or *H–equations* formulation in terms of unknown heads or HGLs (*H*s) at each node
3. loop flow equations formulation or *LF–equations* in terms of unknown loop flows (*LF*s)
4. flow and head equations or *Q–H equations* formulation in terms of both the unknown flows and unknown heads

5. *Todini and Pilati Q–H equations* formulation in terms of unknown flows and unknown heads (Todini and Pilati 1988)

The objective of this paper is to provide clarity in the presentation of the five different possible formulations of the equations governing flow and head in a water distribution system network. The structure of the paper is as follows. Graph theory is briefly introduced to define the number of variables to be solved for in each formulation. The vectors and matrices required are then defined. Finally, details of the five formulations are given.

GRAPH THEORY FOR NETWORKS

Consider a network in the most general terms (based on the nomenclature of both Wood and Rayes 1981 and Boulos and Altman 1991). From graph theory it is shown that the above variables are related as follows (Boulos and Altman 1991)

$$NP = NJ + NL + (NF - NC) \quad (1)$$

where

- NP = number of links (including pipes, pumps and valves) in the network
- NJ = number of nodes in the network (excluding reservoirs or fixed head nodes))
- NL = number of closed simple loops in the network (loops that have no interior crossing links—also called non–overlapping or natural or primary loops)
- NF = number of reservoirs or fixed head nodes in the network
- NC = number of separate disconnected subnetworks. Usually $NC = 1$ but if a link closes in a network that results in separated parts it is possible to have $NC > 1$.

For networks containing two or more reservoirs (or other form of fixed head source), it is necessary to consider NF-NC required independent paths between nodes of fixed head in the analysis of a network. A path is defined as a non–intersecting series of links between any two fixed head nodes (e.g. reservoirs) that does not contain a closed simple loop. Consider an example network that is fully connected such that NC=1. For two reservoirs (NF=2) there is only one path between the two reservoirs (thus NF-NC= 2-1=1). For three reservoirs (NF=3) there are three possible paths between the reservoirs, however, there are only two independent paths required (NF-NC=3-1=2). It does not matter which of the two paths between the reservoirs are selected in the three reservoir case, as one path between two of the reservoirs is redundant and is not required.

Based on Eq. 1, it generally holds that there are more links NP in the network than nodes NJ such that

$$NP > NJ.$$

In addition there are usually more links NP or nodes NJ than closed simple loops NL plus required independent paths in the network (NF-NC) such that

$$NP > NL + (NF\text{-}NC).$$

Finally, for networks with at least one closed simple loop the number of nodes (NJ) exceeds the number of closed simple loops plus required independent paths

$$NJ > NL + (NF\text{-}NC).$$

As a result, the ordering from the minimum number of variables to the maximum to be solved for is shown in Table 1. A ten pipe example network is shown in Figure 1.

Table 1. Number of variables to be solved for each formulation

FORMULATION	NUMBER OF VARIABLES	NUMBER FOR TEN-PIPE NETWORK
Loop flows	$NL + (NF - NC)$	3
Heads	NJ	7
Flows	NP	10
Todini Q+H	$NP + NJ^*$	17/10
Flows+Heads	$NP + NJ$	17

*however, only a matrix solution of size NJ is required to solve for the heads (see later on in the paper)

Thus in summary, for networks that contain loops, the number of unknown loop flows (*LF*s) is always less than or equal to the number of unknown heads (*H*s) that in turn is always less than the number of unknown link flows (*Q*s).

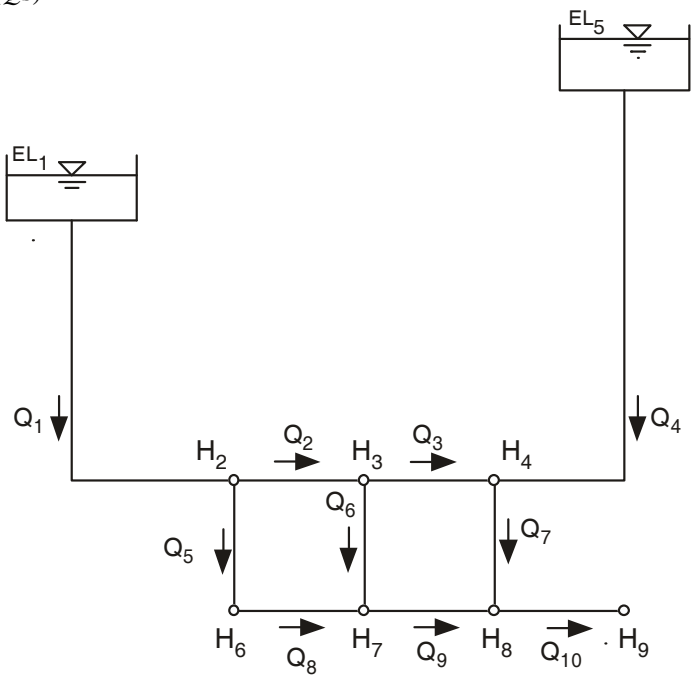

Figure 1. The unknown flows and heads in a ten-pipe network

VECTORS OF UNKNOWNS AND KNOWNS

Consider a water distribution network of pipes and junctions or nodes in which the system has *NP* pipes, *NJ* variable-head nodes, *NF* fixed-head nodes and *NL* closed loops. The number of required independent paths is (*NF-NC*). Assume the network is completely connected (thus *NC*=1). The general column vector of flows for *NP* pipes or links (expressed as the transpose of a row vector) for a water distribution system is

$$\mathbf{q} = [Q_1, Q_2, \ldots, Q_{NP}]^{\mathbf{T}}$$

The general column vector of heads for *NJ* nodes is

$$\mathbf{h} = [H_1, H_2, \ldots, H_{NJ}]^{\mathbf{T}}$$

The ten pipe network shown in Figure 1 has 10-unknown flows and 7-unknown heads.

The known column vector of demands for *NJ* nodes in a general network is

$$\mathbf{dm} = [DM_1, DM_2, \ldots, DM_{NJ}]^{\mathbf{T}}$$

In the third formulation of the equations for a water distribution system unknown loop flows will be solved for. A vector of unknowns is defined as

$$\mathbf{u} = [LF_1, LF_2, \ldots, LF_{NTL}]^{\mathbf{T}}$$

where the number of closed loops and required independent paths is $NTL = NL + (NF - NC)$.

TOPOLOGY MATRICES FOR NETWORKS

Two matrices are useful for describing the topology of a network (Todini and Pilati 1988) including:

- The unknown head node matrix = **A1** (the size of the matrix is *NP* x *NJ*). If a link (in row *j* of **A1**) enters the node *i* in the designated flow direction (in column *i* of the **A1** matrix) then the a_{ji} element is -1. If it leaves the node it is +1. If the node and link are not connected it is 0 (zero).
- The fixed head node matrix = **A2** (the size of matrix is *NP* x *NF*). If a link (in row *j* of matrix **A2**) enters the fixed head node *f* in the designated flow direction (in column *f* of matrix **A2**) then the a_{jf} element is -1. If it leaves the fixed head node it is +1. If the fixed head node and link are not connected it is 0 (zero).

THE BASIC NODE AND PIPE GOVERNING EQUATIONS

There are two types of governing equations for flow and head (HGL or pressure) in a network of pipes. These include

- continuity of flow at each node
- head loss–flow relationship for each individual pipe

The continuity equation at each of the variable-head nodes in the network is given by:

$$\sum_{j=1}^{NP} \langle a_{ij} Q_j \rangle + DM_i = 0 \ldots\ldots\ldots \text{for } i = 1, 2, \ldots, NJ \qquad (2)$$

where the a_{ij} elements (a zero, -1 or +1 value) are from the $\mathbf{A1}^{\mathbf{T}}$ matrix. Typically only 2 to 4 a_{ij} elements of a row of the $\mathbf{A1}^{\mathbf{T}}$ matrix will be non-zero. Thus only non-zero values of a_{ij} will contribute to the continuity equation for the pipes attached to node *i*. Note that flows out of the node will be positive while flows into the node will be negative.

The head loss equation (or energy equation) for the pipe p_j in the network connecting node *i* and node *k* is given by:

$$H_i - H_k = r_j Q_j |Q_j| \ldots\ldots\ldots \text{ for } j = 1, 2, \ldots, NP \qquad (3)$$

where r_j = resistance factor assuming say the Darcy Weisbach head loss equation based on the Darcy-Weisbach friction factor *f* is used (that is dependent on the Reynolds number and the relative roughness for the pipe). The modulus sign in Eq. 3 ensures that the sign of the flow matches the sign of the head difference on the left hand side of the equation. The resistance factor is given by:

$$r_j = \frac{8 f_j L_j}{\pi^2 g D_j^5} \text{ …… for } j = 1, 2, \ldots, NP \quad (4)$$

where L_j = pipe length, g = gravitational acceleration, D_j = pipe internal diameter. The friction factor may be estimated by the Swamee and Jain (1976) equation as:

$$f_j = \frac{1.325}{\left[\ln\left(\frac{\varepsilon_j}{3.7 D_j} + \frac{5.74}{\mathbf{Re}^{0.9}}\right)\right]^2} \text{ …… for } j = 1, 2, \ldots, NP \quad (5)$$

where ε_j = roughness height, **Re** = Reynolds number for the flow in the pipe. A Hazen-Williams head loss equation could easily be also used to replace Eq. 4. The vector of pipe resistance factors is $\mathbf{r} = (r_1, r_2, \ldots, r_{NP})^T$.

FORMULATION 1: FLOW EQUATIONS OR THE Q–EQUATIONS FOR A NETWORK

The unknown flows Q_js are labeled on Figure 1 for the ten-pipe network. The direction of flow in each pipe has been selected based on an expected flow pattern in the network. The direction may have been selected incorrectly in some pipes but this does not matter. In the final solution, if a pipe flow turns out to be negative, then that flow was assumed to be in the wrong direction initially.

The flow equations are formed from both the continuity equations at each of the nodes (a total of *NJ* equations) and the energy equations for simple closed loops and required independent paths in the network (a total of *NL+NF-NC* equations). To implement this formulation the loops need to be defined via the loop matrix (Todini and Pilati 1988). In addition, required independent paths between nodes of fixed head also have to be defined.

For the Q-equations formulation, the set of continuity equations are given by Eq. 2.

Now consider the energy equations around closed simple loops or between fixed head nodes along required independent paths in a network. These equations are nonlinear. A direction (usually positive for clockwise) for each of the loops must be assumed. Upon traversing a closed simple loop in the network the sum of head loss around the loop must be zero. This is expressed as

$$\sum_{j \in S_k} r_j Q_j \left| Q_j \right| = 0 \text{ ……for } k = 1, \ldots, NL \quad (6)$$

for each closed simple loop in the network where S_k = {indices of the pipes in loop k}.

In addition to closed simple loop energy equations, (*NF-NC*) required independent paths between reservoirs or fixed head nodes in the network must also be considered. Consider a series of pipes between two reservoirs designated as reservoir m and reservoir q. The head loss in the pipes between two reservoirs must be equal to the difference in elevation or HGL between the 2 reservoirs (EL_m and EL_q). Each path should be traversed in the same direction as the loop flow direction (usually clockwise). This may be expressed as

$$\sum_{j \in S_k} r_j Q_j \left| Q_j \right| - (EL_m - EL_q) = 0 \ldots\ldots\ldots \text{for } k = 1,..., NF\text{-}NC \qquad (7)$$

where S_k = {indices of the pipes in path k}. Note that application of Eq. 7 may be a little tricky. It is best to traverse the loop in the direction of the loop flow arrow between the reservoirs–then make the right–hand side equal to the head loss difference between the reservoirs or fixed head nodes. Finally, move the right–hand side term to the left–hand side of the equation so that the function is then equal to zero. The same sign convention regarding the sign of the assumed head loss and the assumed flow direction in the pipe is assumed for required independent path energy equations as for closed simple loop energy equations. It is clear that the equations in Eq. 2 are linear while Eqs. 6 and 7 are non-linear.

Solving this set of non-linear equations for the flow equations formulation can be carried out by using a Newton iterative solution which requires computation of the Jacobian matrix. This approach provides a linearizing approximation that is amenable to an iterative solution process (details of the Newton solution process are given in Formulation 5). Newton's method is equally applicable to all formulations presented here. The characteristics of the Jacobian (for example- symmetry, positive definiteness, Stieltjes type) and the use of sparse solution methods, where applicable, will significantly affect the computational cost and hence the speed of the Newton solution technique for each of the formulations. The formulation with the minimum number of variables to be solved for does not necessarily lead to the most effective method in terms of speed of convergence. A detailed comparison of the numerical and convergence properties of the various formulations is beyond the scope of this paper.

FORMULATION 2: HEAD EQUATIONS OR THE H–EQUATIONS

The unknown heads H_is are labeled on Figure 1 for the ten-pipe network. The head equations are formed from the continuity equations (Eq. 2) and the link flow equations (Eq. 3) by eliminating the flow terms in Eq. 2 between both sets of equations. Solving for the flow from Eq. 3 gives for pipe p_j linking nodes i and k:

$$Q_j = \frac{(H_i - H_k)\left|H_i - H_k\right|^{(1/n)-1}}{r_j^{1/n}} \ldots\ldots\ldots \text{for } j = 1,2,\ldots, NP \qquad (8)$$

The H-equations formulation thus becomes by substituting Eq. 8 into Eq. 2.

$$\sum_{i=1}^{NP} a_{ij} \frac{(H_i - H_k)\left|H_i - H_k\right|^{(1/n)-1}}{r_j^{1/n}} + DM_i = 0 \ldots\ldots\ldots \text{for } i = 1,2,\ldots, NJ \qquad (9)$$

where the a_{ij} elements (a zero, -1 or +1 value) are from the $\mathbf{A1}^{\mathbf{T}}$ matrix. If the node connected to node i for a particular pipe is a fixed head node then the H_k value is replaced by EL_m. Note that all equations in Eq. 9 are non-linear in contrast to the Q-equations formulation where the continuity equations (Eq. 2) are linear equations. The H-equations formulation is easy to implement in a computer code. It is not necessary to define the loops for this formulation (in contrast to the Q-equations formulation) and this is a huge advantage of the technique. Only the link connectivity information is needed including the node numbers at the end of each link, the length, diameter and roughness of each pipe and the properties of each node (elevation and demand) (Todini and Pilati 1988).

FORMULATION 3: LOOP FLOW OR LF–EQUATIONS

The loop flow or LF–equations are obtained by writing the energy equations (similar to Eq. 6 and 7) for the closed simple loops and all required independent paths in the network by incorporating appropriate loop flows or *LF* values. The LF values for the ten-pipe network are shown in Figure 2. As each closed simple loop is traversed the head loss along each link is added (or subtracted) according to the sign convention used. Flow directions must be assumed for each pipe. A direction (usually positive for clockwise) for each of the loop flow *LF*s must also be assumed.

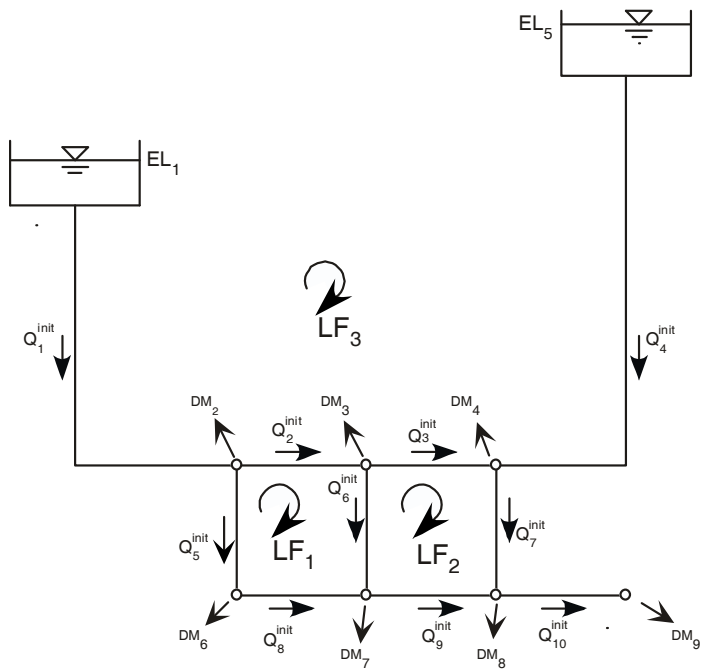

Figure 2. Unknown loop flows for the LF-equations formulation

A column vector of initial flows in the network must be chosen such that they satisfy continuity at each node as follows

$$\mathbf{q} = [Q_1^{init}, Q_2^{init}, ..., Q_{NP}^{init}]^{\mathbf{T}}. \tag{10}$$

Thus as shown in Figure 2, flow directions in each pipe must be chosen for each Q_j^{init} in each pipe. In Eq. 10, the Q_j^{init} values that satisfy continuity at each node in the network remain unchanged for all iterations. Note that this is quite different from the loop flow corrections formulation for the manual Hardy Cross method (1936) where the initially selected flows are updated in the loop immediately after the computation of each loop flow correction.

From Eq. 6, the energy equations in the LF-equations formulation for each of the *NL* closed loops in the network are

$$\sum_{j \in S_k} \left\langle r_j \left[Q_j^{init} + \sum_{s \in L_j} LF_s \right] \middle| Q_j^{init} + \sum_{s \in L_j} LF_s \middle| \right\rangle = 0 \ldots \text{for } k = 1, ..., NL \tag{11}$$

where S_k = {indices of the pipes in closed loop s} and L_j = {indices of the loops associated with pipe j}.

From Eq. 7, the energy equations in the LF-equations formulation for each of the (*NF-NC*) required independent paths in the network are

$$\sum_{j \in S_k} \left\langle r_j \left[Q_j^{init} + \sum_{s \in L_j} LF_s \right] \left| Q_j^{init} + \sum_{s \in L_j} LF_s \right| \right\rangle - (EL_m - EL_q) = 0 \ldots \text{for } k = 1,..., (NF\text{-}NC) \quad (12)$$

where S_k = {indices of the pipes in closed loop k} and L_j = {indices of the loops associated with pipe j}. If the direction of the loop flow *LF* is in the same direction as the assumed link flow, the *LF* value is added to the initial flow assumed for the pipe or link. To the contrary, if the *LF* direction for the closed simple loop being considered is opposite to the assumed flow direction in the link, the *LF* value is subtracted from the pipe flow. The initial link flow is adjusted by the final converged value of *LF*s computed for each closed simple loop s of which the link is a member.

As seen in Table 1, the minimum number of equations results for the LF–equations formulation where the *NL* closed simple loop equations and the (*NF-NC*) required independent path equations are formulated in terms of a loop flows in each simple loop and path. All of the equations in the LF–equations formulation are nonlinear. In the LF-equations formulation, as for the Q–equations formulation, all loops and required independent paths need to be identified.

The continuity equations do not form part of the set of the LF–equations as long as the initial flow in each link satisfies the continuity at each node in the network.

The LF–equations in terms of the unknown loop flows in the network have in the past been recommended as the preferred formulation of the equations for a network due to the smaller size of the number of variables to be solved for in the equation formulation (Epp and Fowler 1970, Wood and Rayes 1981, Nielsen 1989). Ellis and Simpson (1998) indicated that the process for determining the preferred formulation is not straightforward. It not only depends on the number of equations but also the initial set up time prior to the equations being iteratively solved for (e.g. in determining a set of link flows that satisfy continuity) and also is quite dependent on the starting vector for the set of unknowns that is selected to commence the iterative solution process.

FORMULATION 4: THE Q-H EQUATIONS FORMULATION

The flow and head equations are formed from both the continuity equations (from Eq. 2) at each of the nodes and the head loss equations for each pipe expressed in terms of nodal heads at each end of the pipe (from Eq. 3). Thus there are a total of $NP + NJ$ unknowns to be solved for in the Q-H equation formulation.

The column vector of unknown flows and heads in the network is

$$\mathbf{m} = [Q_1, Q_2, \ldots Q_{NP}, H_1, H_2, \ldots H_{NJ}]^{\mathrm{T}}.$$

Thus the Q-H equation formulation is made up of the continuity equations from Eq. 2 as:

$$\sum_{j=1}^{NP} \langle a_{ij} Q_j \rangle + DM_i = 0 \ldots\ldots \text{ for } i = 1, 2,\ldots, NJ \quad (13)$$

where the a_{ij} elements (a zero, -1 or +1 value) are from the $\mathbf{A1^T}$ matrix and the pipe head loss equations from Eq. 3 which are

$$H_i - H_k - r_j Q_j \left|Q_j\right| = 0 \qquad \text{for } j = 1,2,\ldots, NP \tag{14}$$

where the *i* and *k* indices refer to the node numbers at the end of each pipe *j*.

The number of equations in this formulation is clearly larger than the number of equations for the Q-equations formulation or the H-equations formulation. Thus the size of the matrices that need to be dealt with in the iterative solution process will consequently be larger. However, the form of the governing equations is simpler and computation of the Jacobian elements is considerably easier. In addition, it is not necessary to determine the loops in the network as for the Q-equation formulation.

FORMULATION 5: THE TODINI AND PILATI Q-H EQUATIONS FORMULATION

The Todini and Pilati (1988) formulation is effectively a type of Q–H equation formulation. The description below is based on material from Simpson and Elhay (2008). The formulation is based on two sets of equations solving for all unknown heads and flows simultaneously in a sequential iterative manner. The method has an extremely efficient approach to the inversion of the Jacobian matrix by partitioning the governing equations in a smart way. The advantage of the Todini and Pilati formulation is that the Jacobian matrices are symmetric. The Todini and Pilati (1988) formulation is used in EPANET (Rossman 1994) and a number of other commercially available hydraulic software packages for the simulation of water distribution systems.

Based on Eq. 2 the continuity equations for all the pipes in the network and the topology matrices introduced earlier in the paper, the following matrix form can be written:

$$\mathbf{A}\,1^{\mathbf{T}}\,\mathbf{q} + \mathbf{dm} = 0 = \mathbf{f}_2(\mathbf{q}, \mathbf{h}) \tag{15}$$

where the left-hand-side of Eq. 15 is denoted by the function $\mathbf{f}_2(\mathbf{q}, \mathbf{h})$. Now for the head loss equations for each pipe p_j connecting nodes *i* and *k* then Eq. 3 can be re-written as:

$$r_j Q_j \left|Q_j\right| - \left(H_i - H_k\right) = 0\,. \tag{16}$$

This can also be written in matrix form, but first a diagonal matrix **G** of size *NP* x *NP* is introduced where:

$$\mathbf{G} = \begin{pmatrix} r_1\left|Q_1\right| & 1 & \ldots & \ldots & 0 & 0 \\ 0 & r_2\left|Q_2\right| & \ldots & \ldots & 0 & 0 \\ \ldots & \ldots & \ldots & \ldots & \ldots & \ldots \\ \ldots & \ldots & \ldots & \ldots & \ldots & \ldots \\ 0 & 0 & \ldots & \ldots & r_{NP-1}\left|Q_{NP-1}\right| & 0 \\ 0 & 0 & \ldots & \ldots & 0 & r_{NP}\left|Q_{NP}\right| \end{pmatrix} \tag{17}$$

The non-linearity in the system arises because the matrix **G** depends on the unknown flows in **q**. The matrix form of Eq. 16 can be written as follows (taking into account that some nodes are fixed head nodes):

$$\mathbf{Gq} - \mathbf{A}1\mathbf{h} - \mathbf{A}2[\mathbf{el}] = 0 = \mathbf{f}_1(\mathbf{q}, \mathbf{h}) \tag{18}$$

where **[el]** is a vector of the reservoir or fixed node heads. Note that Eq. 18 is denoted by the vector function $\mathbf{f}_1(\mathbf{q}, \mathbf{h})$. The two sets of matrix equations in Eq. 15 and Eq. 18 may be written in the following block matrix form as:

$$\mathbf{f}(\mathbf{q}, \mathbf{h}) = \begin{pmatrix} \mathbf{G} & | & -\mathbf{A}1 \\ -- & - & -- \\ -\mathbf{A}1^{\mathbf{T}} & | & 0 \end{pmatrix} \begin{pmatrix} \mathbf{q} \\ -- \\ \mathbf{h} \end{pmatrix} - \begin{pmatrix} \mathbf{A}2[\mathbf{el}] \\ -- \\ \mathbf{dm} \end{pmatrix} = 0 \tag{19}$$

This system is really the set of equations for Formulation 4 – the Q-H equations, however, the partitioning in Eq. 19 will be exploited below to develop a much more efficient solution scheme. The first matrix on the left hand side of Eq. 19 shows the partitioning of a (*NP* + *NJ*)–square matrix into 2 block rows and 2 block columns. Note that the first block matrix on the left had hand side of Eq. 19 has a special structure that may be exploited because it is symmetric. In addition the only non-constant values in this matrix are the diagonal elements of **G**. A Newton iterative solution to the set of non-linear equations in Eq. 19 can be formulated in terms of Taylor's series expansion and linearization as:

$$\mathbf{J}(\mathbf{q}^{(k)}, \mathbf{h}^{(k)}) \begin{pmatrix} \delta\mathbf{q}^{(k+1)} \\ -- \\ \delta\mathbf{h}^{(k+1)} \end{pmatrix} = \begin{pmatrix} -\mathbf{f}_1^{(k)} \\ -- \\ -\mathbf{f}_2^{(k)} \end{pmatrix} \tag{20}$$

for the k+1st iteration where k = 0, 1, 2, etc. Decomposition methods that avoid the need for solving for the inverse of the Jacobian are applied to solve Eq. 20. An initial set of guesses of initial flows (Eq. 10) are required. A value corresponding to a velocity of 1.0 fps is often selected.

The Todini and Pilati (1988) method solves the equations describing the flows and nodal heads in a water distribution network by a reformulation of Eq. 19 which exploits the diagonal nature of **G** and which uses an explicit block-form of the inverse as shown below. This leads to a simplification and hence a significant improvement in the speed of the solution algorithm.

Now consider the derivative of the first matrix on the left side hand multiplied by the vector $(\mathbf{q}^{\mathbf{T}}, \mathbf{h}^{\mathbf{T}})^{\mathbf{T}}$ of Eq. 19 so that we can form the Jacobian as shown in Eq. 20. The diagonal nature of **G** can be exploited with only the diagonal elements of the **Gq** matrix changing upon differentiation so computation of the Jacobian is very straightforward. Rewrite Eq. 19 as:

$$\mathbf{f}(\mathbf{q}, \mathbf{h}) = \begin{pmatrix} \mathbf{Gq} & | & -\mathbf{A}1\mathbf{h} \\ -- & - & -- \\ -\mathbf{A}1^{\mathbf{T}}\mathbf{q} & | & 0 \end{pmatrix} - \begin{pmatrix} \mathbf{A}2[\mathbf{el}] \\ -- \\ \mathbf{dm} \end{pmatrix} = 0 \,. \tag{21}$$

The derivatives of the diagonal elements of **Gq** assuming that *r* is constant (despite the fact that friction factors *f* actually depend on flow: the friction factors may be updated at the end of each iteration) are:

$$\frac{d}{dQ_j}\left(r_j Q_j \left|Q_j\right|^{n-1} \right) = r_j n \left|Q_j\right|^{n-1} \qquad \text{for } Q_j \neq 0 . \tag{22}$$

The terms in the second matrix (with **A2** etc.) on the left hand side of Eq. 21 do not depend on **q** and **h**. The Jacobian matrix for the system of equations in Eq. 22 becomes:

$$\mathbf{J} = \begin{pmatrix} n\mathbf{G} & | & -\mathbf{A}1 \\ -- & - & -- \\ -\mathbf{A}1^{\mathbf{T}} & | & 0 \end{pmatrix} \tag{23}$$

This matrix has some very nice properties of symmetry and sparseness. Todini and Pilati (1988) show an analytic expression for the block-form of the inverse of **J** where we denote the inverse of **G** to be **D** temporarily. This inverse is easy to compute for a diagonal matrix and is tractable as long as all flows Q_j are not zero. It has terms $1/(nr_j|Q_j|)$ at each location along the diagonal. Assume that the head loss exponent *n* is the same for each pipe. The Jacobian becomes:

$$\mathbf{J}^{-1} = \begin{pmatrix} \frac{1}{n}\mathbf{D} - \frac{1}{n}\mathbf{DA}1(\mathbf{A}1^{\mathbf{T}}\mathbf{DA}1)^{-1}\mathbf{A}1^{\mathbf{T}}\mathbf{D} & | & -\mathbf{DA}1(\mathbf{A}1^{\mathbf{T}}\mathbf{DA}1)^{-1} \\ ---------- & - & ---------- \\ -(\mathbf{A}1^{\mathbf{T}}\mathbf{DA}1)^{-1}\mathbf{A}1^{\mathbf{T}}\mathbf{D} & | & -n(\mathbf{A}1^{\mathbf{T}}\mathbf{DA}1)^{-1} \end{pmatrix} \tag{24}$$

The reformulation allows the solution process for each iteration to be done in two stages: one for the flows and another for the heads. Substituting Eq. 24, Eq. 15 and Eq. 18 into Eq. 20 and simplifying gives the two-step Todini and Pilati algorithm for solving successively at each iteration for the heads and discharges as follows:

$$\mathbf{h}^{(k+1)} = (\mathbf{A}1^{\mathbf{T}}\mathbf{G}^{-1}\mathbf{A}1)^{-1}\left[\mathbf{A}1^{\mathbf{T}}\left\langle (1-n)\,\mathbf{q}^{(k)} - \mathbf{G}^{-1}\mathbf{A}2[\mathbf{el}]\right\rangle - n\,\mathbf{dm}\right] \tag{25}$$

and

$$\mathbf{q}^{(k+1)} = (1-\frac{1}{n})\,\mathbf{q}^{(k)} + \frac{1}{n}\mathbf{G}^{-1}(\mathbf{A}1\mathbf{h}^{(k+1)} + \mathbf{A}2[\mathbf{el}]) \tag{26}$$

where $n = 2.0$ for the Darcy Weisbach head loss formula or $n = 1.852$ for the Hazen-Williams head loss equation. Note that in the pair of equations above the only matrix inverse that is not trivial to compute occurs in Eq. 25 and involves the *Schur Complement* term of $\mathbf{A}1^{\mathbf{T}}\mathbf{G}^{-1}\mathbf{A}1$ which is the size of *NJ* by *NJ* (the number of nodes in the network). Thus although we are dealing with a total of (*NP* + *NJ*) unknowns the use of an analytical inverse of the Jacobian has reduced the matrix to be solved down to the size of *NJ*.

CONCLUSIONS

The objective of this paper has been to provide clarity in the presentation of the five different possible formulations of the equations governing flow and head is a water distribution system network. A set of

non-linear equations arises for each of the formulations. These include: 1) flow equations 2) head equations 3) loop flow equations 4) flow and head equations and 5) the Todini and Pilati flow and head equations formulation. Details of each of these formulations have been presented in this paper. Graph theory has been used to show the relationship between the numbers of variables in each formulation.

The order of size of problem ranked from minimum to maximum number of variables for the five different formulations is: 1) loop flows 2) heads 3) Todini and Pilati Q-Hs 4) flows 5) flows and heads. The size of the problem does not necessarily determine which is the most effective formulation. Currently the Todini and Pilati Q-H equations formulation is commonly used in many commercial and Government hydraulic simulation packages. The main part of the iterative solution process in the Todini and Pilati algorithm has been reduced to same size of problem as the head equations formulation. This has been achieved by a smart reorganisation of the governing equations using an analytic expression for the inverse of the Jacobian using partitioning of the matrix. Further work is required to evaluate if the loop flow equations formulation can be competitive with the Todini and Pilati method is terms of computational speed.

REFERENCES

Boulos, P.F. and T. Altman (1991). "A graph-theoretic approach to explicit nonlinear pipe network optimization." *Applied Mathematical Modelling*, Vol. 15(September): pp. 459-466.

Collins, M., L. Cooper, R. Helgason, J. Kennington and L. LeBlanc (1978). "Solving the Pipe Network Analysis Problem Using Optimization Techniques." *Management Science,* 24(7): pp. 747-760.

Cross, H. (1936). Analysis of flow in networks of conduits or conductors. *Bulletin No. 286,* Urbana, Illinois, University of Illinois Engineering Experimental Station.

Ellis, D.J. and Simpson, A.R. (1998). "Improving water distribution systems design and operating methodologies using fast steady state network solvers." *Hydrastorm Conference*, The Institution of Engineers, Australia, Adelaide, South Australia, September, 317–322.

Epp, R. and A. G. Fowler (1970). "Efficient Code for Steady-State Flows in Networks." *Journal of the Hydraulics Division*, Proceedings of the ASCE, January, Vol. 96, No. HY1: 43-56.

Nielsen, H. B. (1989). "Methods for Analyzing Pipe Networks." *Journal of Hydraulic Engineering,* Vol. 115, No. 2, February: 139-157.

Rossman, L. A. (1994). EPANET Users Manual. Washington, DC, U.S. Environmental Protection Agency.

Salgado, R., Todini, E., and O'Connell, P. E. (1988). "Extending the gradient method to include pressure regulating valves in pipe networks." Proc. Inter. Symposium on Computer Modeling of Water Distribution Systems, (also in Computer Applications in Water Supply: Vol. I., Systems Analysis and Simulation, Coulbeck, B, and Orr, C.H., editor, Research Studies Press.), University of Kentucky, pp. 157-180.

Simpson, A.R. and Elhay, S. (2008). "Formulating the water distribution system equations in terms of heads and velocity." *10th Annual Symposium on Water Distribution Systems Analysis*, American Society of Civil Engineers, Kruger National Park, South Africa, 17-20 August.

Swamee, P.K., and Jain, A.K. (1976). "Explicit equations for pipe-flow problems." *Journal of the Hydraulics Division,* 102(5): 657-664.

Todini, E., Pilati, S. (1988). A gradient algorithm for the analysis of pipe networks. In: *Computer Applications in Water Supply*, Research Studies Press, Letchworth, Hertfordshire, UK.

Wood, D.J. and A.G. Rayes (1981). "Reliability of Algorithms for Pipe Network Analysis." *Journal of the Hydraulic Division* . Vol. 107, No. HY10, October: 1145-1161.

Inexpensive Modeling of Intermittent Service Water Distribution Networks

J. A. Cabrera-Bejar[1] and V. G. Tzatchkov[2]

[1]Department of Hydraulics, Faculty of Engineering, National Autonomous University of Mexico; Edif. B, México, D.F.; PH (52)5556223279; FAX (52)5556223279; email: antoncabejar@yahoo.com.mx
[2]Urban Hydraulics Department, Mexican Institute of Water Technology, Paseo Cuauhnahuac 8532, Jiutepec, Morelos, CP 62550, Mexico; PH (52)7773293678; FAX: (52)7773293678; email: velitchk@tlaloc.imta.mx

ABSTRACT

Intermittent supply is prevalent among developing countries. Inequitable water distribution, possible water contamination, wasting water, coping costs of consumers and water providers, meter malfunctioning and inconvenience to consumers are some of its consequences. There are two major views on how this problem should be considered. The first view looks at a transfer to the 24-hour supply by reducing water loss and adding new supply sources, while the other accepts intermittent supply as a reality and looks for appropriate design and operation methods that can minimize its negative impacts. Important differences between intermittent and continuous service water distribution networks operation should be considered in the second case, such as initial network charging, pressure-dependent water demand, and design pressure. In this paper, the use of known free public domain network models, such as SWMM for modeling initial pipe network charging and EPANET for modeling the network intermittent operation, is proposed and exemplified.

INTRODUCTION

Intermittent supply is prevalent among developing countries in Latin America, Asia and Africa (Totsuka et al. 2004; Lee and Schwab, 2005). Inequitable water distribution, possible water contamination, wasting water, coping costs of consumers and water providers, meter malfunctioning and inconvenience to consumers are some of its consequences (Totsuka et al. 2004; Lee and Schwab, 2005). Quite frequently tap water is not pure enough for drinking or water with no good flavor. For these reasons users have to buy expensive purified water. To overcome the inconveniences of being with no tap water, users are encouraged to have a water tank on the house roof, cistern, or other permanent deposit at home. This house addition provides families a water reservoir in case of supply breaks. Its need varies considerably from one neighborhood to another and from one city to another. Figure 1-(a) and 1-(b) show the roof tank arrangements used in Mexico. The first of them, shown in Figure 1-(a), comprises a larger tank (cistern) at ground level and a pump to fill the roof

tank, and is employed when more water storage is needed or when water pressure in the supplying network main during service hours is very low. The second one, shown in Figure 1-(b) is used when water pressure is not so low so that that the roof tank can be filled directly from the network main.

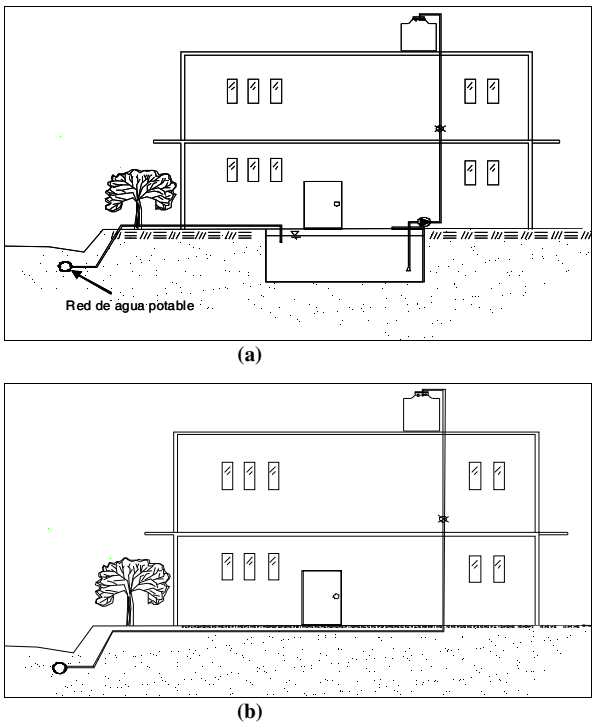

Figure 1 Roof tank arrangements used in Mexico: (a) Ground level cistern, water pump and roof tank, (b) Roof tank alone

A study carried out by the Mexican Institute of Water Technology during 2005-2006 defined country specific water utility performance indicators (Bourguett-Ortiz and Tzatchkov 2007). The appropriateness for Mexico of existing performance indicator systems was assessed first, e.g. the IWA Manual for Performance Indicators (Alegre et al., 2000), the World Bank (Yepes and Dianderas, 1996) and the Asian Development Bank indicator directives (McIntosh and Yniguez, 1997). Most of them turn out not to be practical for the conditions of Mexico, mainly because of the long lists of indicators they manage and the related large amount of data needed, some of which are difficult to obtain. Then, instead of adopting one of those systems, the following 12 specific indicators were defined: per capita water produced, updating of water user database, source water metering, customer water metering, updating of infrastructure asset information, service connections with continuous water service, water production cost, urban wastewater treated, customer complaints, customers that pay on time for the water service, number of water utility employees per every 1,000 service connections, and number of water utility employees dedicated to leak reduction and control.

A free access Internet Web site (http://www.pigoo.gob.mx/) was created in order to make the described performance indicator information transparent and easily accessible for different institutions in the country and for the public in general. The

Internet Web site is in Spanish and displays the evolution of the indicators for the participating water utilities. The information can be consulted by city or grouped by states, administrative regions according to the Mexican National Water Commission, or city size. Sixty three Mexican cities with more than 50,000 inhabitants participate providing information to this study. These cities cover all the Mexican states and the different climatic zones existing in the country, that vary from dry desert and semi desert regions in Northern Mexico to humid subtropical regions in South Mexico. Figure 2 shows the evolution of the indicator Service connections with continuous 24 hours a day drinking water service, expressed by the relation of the number of service connections with continuous service to the total number of service connections in the city.

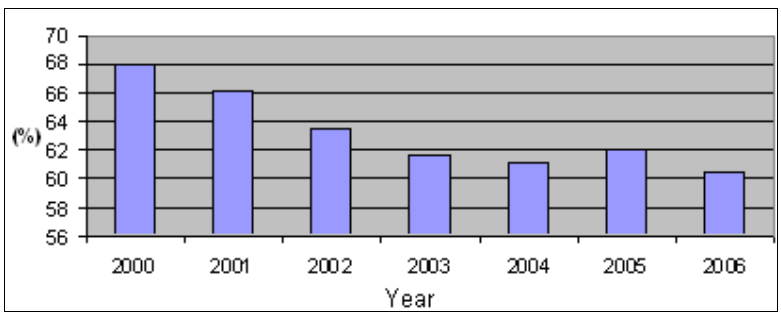

Figure 2. Evolution of the indicator Service connections with continuous 24-hours a day drinking water service (http://www.pigoo.gob.mx/)

This indicator shows a low percentage of continuous 24 hours a day supply, that decreased from 68% of connected households in 2000 to about 60% in 2006.

There are two major views on how intermittent water supply problems should be considered (Totsuka et al. 2004). The first one looks at a transfer to the 24-hour supply by reducing water loss and/or adding new supply sources, while the other accepts intermittent supply as a reality and therefore advocates the necessity of providing appropriate design and operation methods that can minimize its negative impacts. Water distribution network models can be very useful tools in developing such methods. Important differences between modeling and design of intermittent and continuous service water distribution networks should be considered in the models, however, such as pressure-water demand relation, hourly demand variation, peak demand factors, minimum design pressure and initial pipe network charging (Batish 2003, Tzatchkov and Cabrera-Bejar 2008).

Up to the knowledge of the authors of this paper, K. Vairavamoorthy and coworkers (Vairavamoorthy and Lumbers 1994; Vairavamoorthy and Elango 2002; Vairavamoorthy et al. 2000; Vairavamoorthy 2001) are the only authors that have developed models specific for intermittent supply distribution networks. Although in some of their papers they say their models would be available, at present they are not. Besides that, from the brief explanation given in the papers, their models seem to be more academic than practical. Ease of use and low cost (or no cost) of a model are fundamental for models to be used in developing countries where economic resources are generally limited. Fortunately, free public domain computer sewer and water

network models, such as SWMM and EPANET, can be used to model intermittent supply distribution networks, as proposed in this paper.

MODELING INTERMITTENT SERVICE WATER DISTRIBUTION NETWORKS

Water distribution network models originated from developed countries where water service is continuous and the water demand is satisfied all the time. When a user needs water, he or she opens the tap and receives the water he or she needs. Because of that such models are normally "demand-driven models", i.e., water demand is fixed and the model obtains the pressure in the network for the given demand. Most known water distribution network models, such as Epanet (Rossman, 2002), Infoworks WS, and others, are of that kind. On the contrary, intermittent service water distribution networks operate for a limited time, only when supplied with water, the amount of water each user is able to collect depends on the available pressure at his connection and the duration of the service, and not always the user demand is fully satisfied, i.e., these networks are "supply-driven" and "pressure-driven" or "pressure-dependent demand", and should be modeled this way. A common error is to model a pressure-driven network as a demand-driven. Hydraulic behavior obtained from a supply-driven and pressure-dependent demand network model is very different from that of a demand-driven model, however (Batish 2003, Tzatchkov and Cabrera-Bejar 2008).

On the other hand, continuous service distribution networks are always full with water, and intermittent services ones are filled with water every time service is resumed. Initial water charging of the networks obviously cannot be modeled with known demand-driven network models, so that special models have to be developed. Such a model would give the time a network needs to start the service, the volume of water that is needed to fill it, which of the users would receive the service first, and which last; and which would have deficient service.

MODELING INITIAL NETWORK CHARGING WITH SWMM

The Storm Water Management Model (SWMM) is a dynamic rainfall-runoff simulation model used for runoff quantity and quality that transports this runoff through a system of pipes, channels, storage/treatment devices, pumps, and regulators. Produced by the Water Supply and Water Resources Division of the U.S. Environmental Protection Agency's National Risk Management Research Laboratory, it can be freely downloaded from the following Internet site: http://www.epa.gov/ednnrmrl/models/swmm/index.htm. Being capable of modeling the transition from free surface to pressurized flow in the network pipes, it could be used to model, to some extent, the initial water distribution network charging. The following process can be used (explained in SWMM terms):

1. No subcatchment areas are introduced
2. The water source or tank is represented by a storage with the real dimensions of the tank and an inflow pattern corresponding to the given supply schedule is introduced into it.

3. A large value (say 100 m) is assigned to the Surcharge depth at each network junction. This way surface flooding at the node is avoided and pressure flow in the pipes can be modeled.
4. Every roof tank (or group of roof tanks) is represented as a Storage with its dimensions.
5. The water demand, taken from the roof tanks, is represented as an Inflow curve with negative values applied to each Storage.
6. "Dynamic wave" routing method is activated in the SWMM simulation options.
7. Under dynamic wave routing SWMM requires there must be at least one outfall node in the network. Since there are no such nodes in water distribution networks, a fictitious node is added somewhere and connected with a fictitious pipe to the nearest real network junction. The diameter of this fictitious pipe is assigned with a very small value, say 0.001 m, so that it does not influence the simulation results.
8. SWMM is run obtaining the evolution of the flow in the network pipes, the evolution of roof tanks filling, and so on.

Figure 3 shows a small size water distribution network located in the city of Guadalajara, Mexico modeled in SWMM for a period of 3 days with intermittent water supply, 5 hours of water supply daily. The corresponding supply itinerary, applied at the water source, is shown in Figure 4. The model comprises 3 cycles of network charging, five hours of water service, and network emptying. The service area has 462 parcels and 2310 inhabitants, corresponding to a maximum hourly design flow of 17.40 L/s according to the Mexican design standards. The total length of the pipes in the network is 4,090 m, with diameters for 50 to 150 mm. The supply source is a tank. Figure 5 shows the instantaneous water surface profile during network charging, obtained by SWMM for a series of three 10 cm diameter pipes from this network. Figure 5 shows the water level evolution in one of the roof tanks (the closest to the supply source) obtained by SWMM for a period of 3 days. The rising reaches correspond to water service hours, and the falling ones to water demand during non-service hours.

A slightly different approach would be to model with SWMM only the initial network charging, and after that to model the charged network operation with EPANET, as explained in the next section, in order to make use of more modeling options included in EPANET, that are specific for water distribution networks.

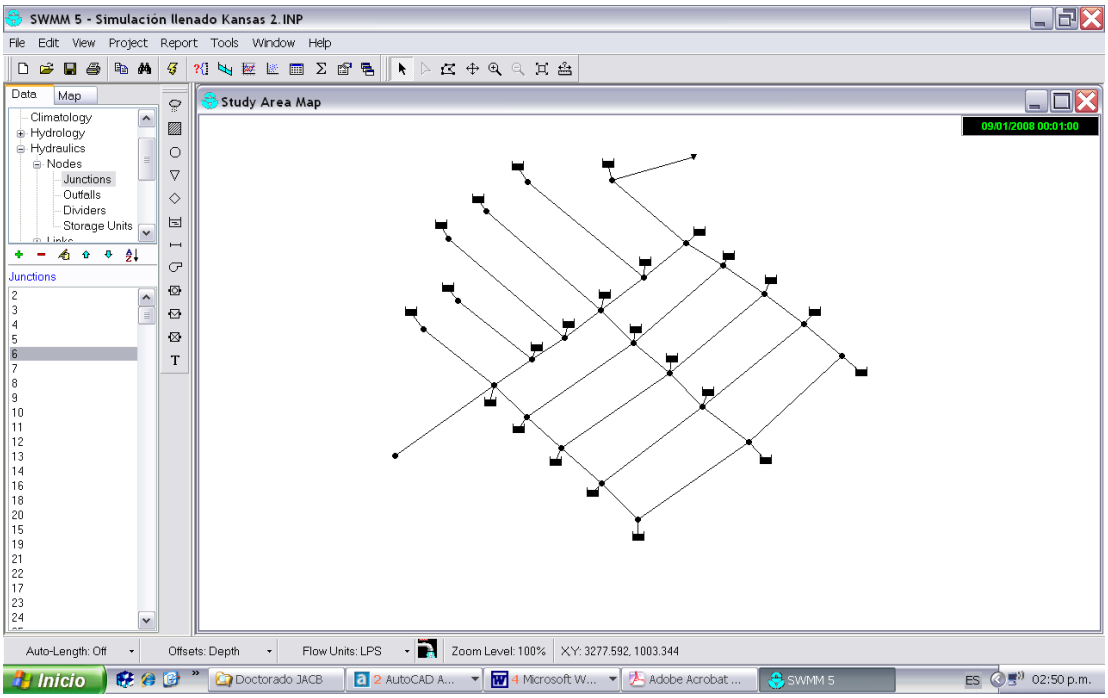

Figure 3. A small water distribution network modeled for initial charging in SWMM

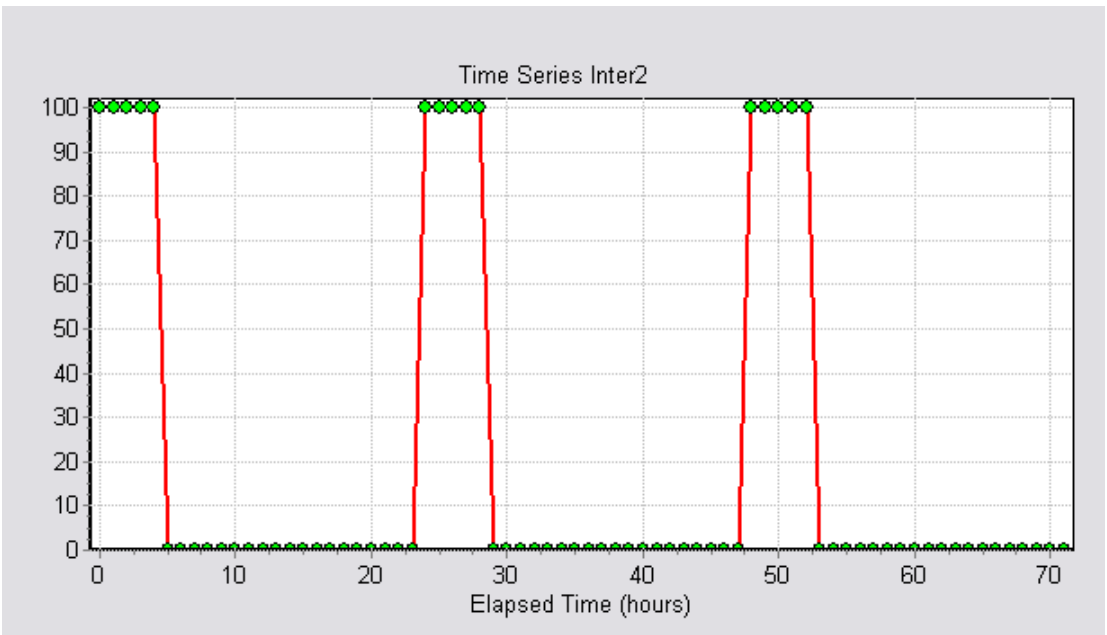

Figure 4. Water supply itinerary applied at the source tank of the network shown in Figure 3.

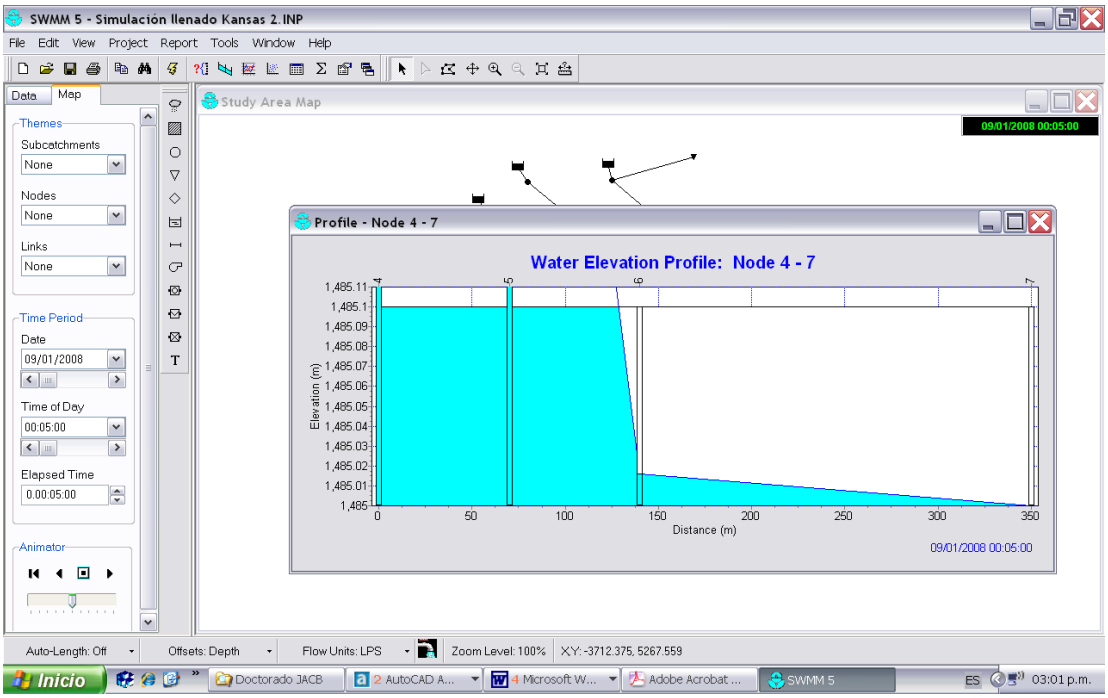

Figure 5. Instantaneous water surface profile during network charging, obtained by SWMM for a series of three 10 cm diameter pipes from the network shown in Figure 3.

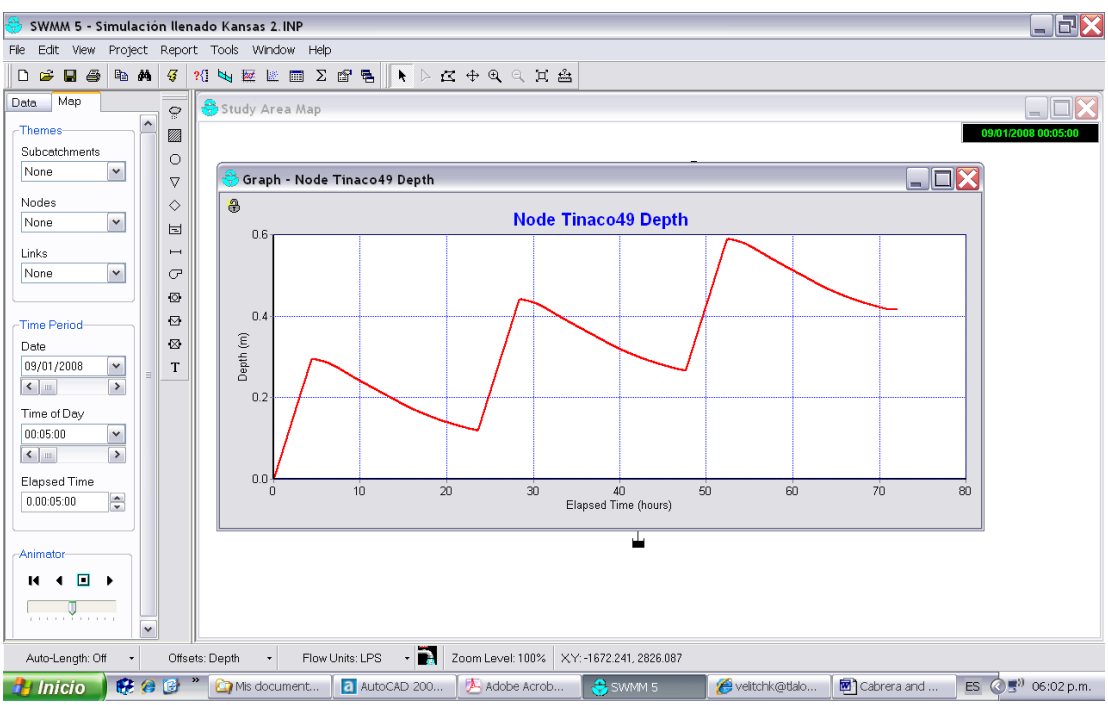

Figure 6. Water level evolution in one of the roof tanks of the network shown in Figure 3, modeled by SWMM

MODELING WATER DISTRIBUTION NETWORKS WITH ROOF TANKS WITH EPANET

Developed by of the U.S. Environmental Protection Agency's Water Supply and Water Resources Division, EPANET is software that models water distribution piping systems. It can be freely downloaded from the following Internet site: http://www.epa.gov/nrmrl/wswrd/dw/epanet.html. Although it is based mainly on a demand-driven model, it has a node component named *emitter* that can be used to represent pressure-dependant demand. EPANET can be used to model intermittent water service, after the initial water charging, in one of the following two ways:

1. In principle, every roof tank could be modeled in EPANET as a tank connected to the network. Given the extremely large number of service connections in a water distribution network, this approach obviously is impractical, but could be used with equivalent tanks, each of them representing a group of roof tanks, the same way as water demand for a group of service connections is concentrated in network nodes in conventional water distribution network models. Figure 7 shows the network from Figure 3 modeled in EPANET by this approach. Figure 8 is a zoom to one of the equivalent tank. The pipe leaving the tank is used to represent water use inside the houses.
2. Representing each demand node as emitter. This approach is simpler and may be more appropriate for large networks.

More details and examples are presented by Tzatchkov and Cabrera-Bejar (2008).

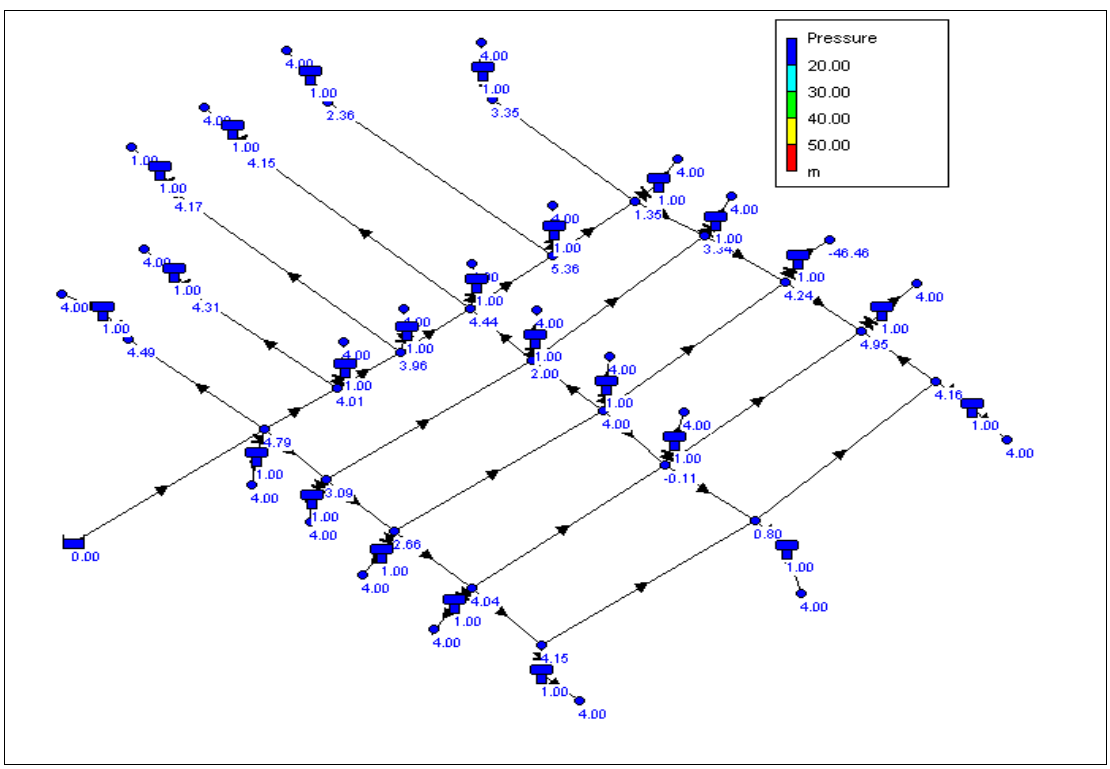

Figure 7. Network with roof tanks modeled in EPANET.

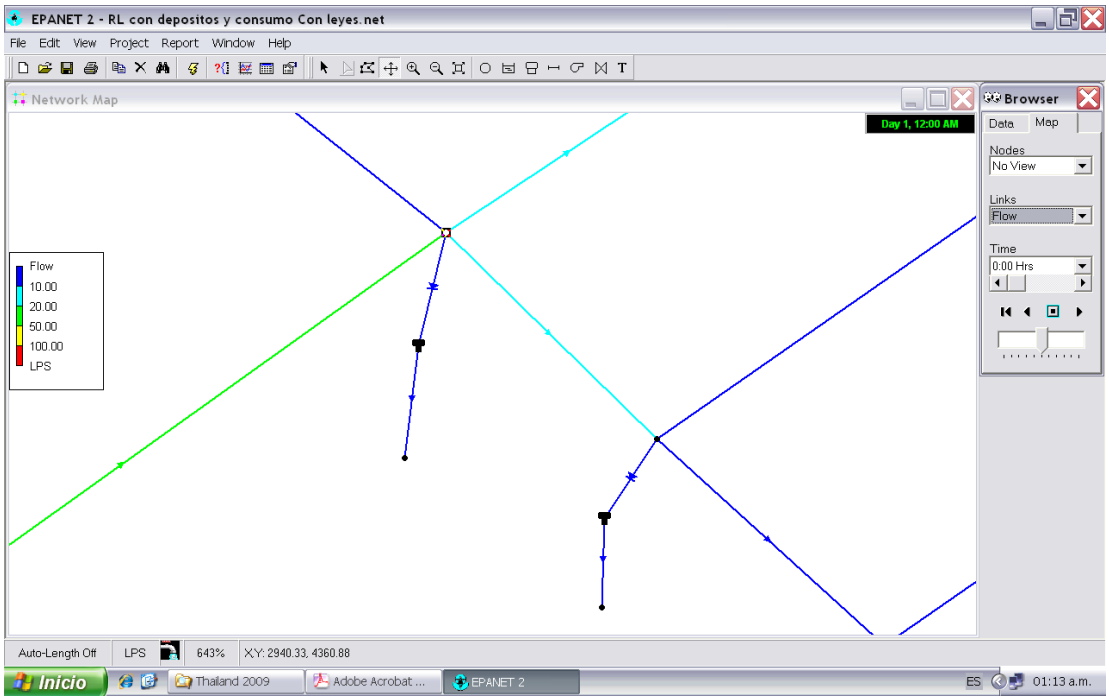

Figure 8. Network with roof tanks modeled in EPANET: zooming to a roof tank.

CONCLUSIONS

Intermittent water service is undesirable, but present in many cities in developing countries. A transfer to continuous 24-hours is possible by non-revenue water reduction and other technical means, provided sufficient water is available at sources, but it may take many years to be accomplished. Meanwhile, intermittent water service specific models could be used to better understand the hydraulic behavior of intermittent service water distribution networks and improve their design and operation. Most known water distribution network models are demand-driven and not appropriate for intermittent water service networks that are supply and pressure driven. Inexpensive software models, such as SWMM and EPANET can be used to model initial network charging and roof tanks, typical for intermittent service water distribution networks.

REFERENCES

Alegre, H., Hirner, W., Baptista, J. and Parena, R. (2000). *Manual of Best Practice. Performance Indicators for Water Supply Services*. IWA Publishing.

Batish R. (2003). "A New Approach to the Design of Intermittent Water Supply Networks", *Proc. ASCE EWRI World Water and Environmental Congress in Filadelfia*, EUA. ASCE, Reston, Va., 1-11.

Bourguett-Ortiz, V. J. and Tzatchkov, V. "Water utility performance indicators of Mexican cities", *Proc. 4th IWA Specialist Conference on Efficient Use and Management of Urban Water Supply, Jeju, Korea, 2007*, 1-8.

Lee, E. J. and Schwab, K. J. (2005) "Deficiencies in drinking water distribution systems in developing countries." *Journal of Water and Health*, 3.2, 109-127.

McIntosh A. C. and Yniguez C. (1997). *Second Water Utilities Data Book: Asian and Pacific Region,* Asian Development Bank, Manila.

Rossman L. (2002) *EPANET2, Users Manual*, Water Supply and Water Resources Division, United States Environmental Protection Agency. http://www.epa.gov/nrmrl/wswrd/dw/epanet.html

Rossman L. (2008) *Storm Water Management Model, User's Manual, Version 5.0*, Water Supply and Water Resources Division National Risk Management Research Laboratory Cincinnati, OH 45268, http://www.epa.gov/ednnrmrl/models/swmm/index.htm.

Totsuka, N.; Trifunovic N.; Vairavamoorthy K. (2004) "Intermittent urban water supply under water starving situations" *Proc. 30th WEDC International Conference, Vientiane, Lao PDR.*

Tzatchkov V. G. and A. Cabrera-Bejar (2008) "Una forma de modelar el suministro intermitente de una red de distribución de agua potable", *Proc VIII Seminario Ibero-americano SEREA* (in Spanish), Lisbon, Portugal.

Vairavamoorthy, K and Elango, K. (2002) *Guidelines for the design and control of intermittent water distribution systems*, International J. Appropriate Technologies for Water Supply and Sanitation- Waterlines, ITDG, 21(1):19-21.

Vairavamoorthy, K., Ali, M., and Lin, Z. (2000). "An Appropriate Design Tool For Intermittent Water Supply Systems", *Proceedings of the International Conference on Intermittent Drinking Water Supply system Management, Mumbai*

Vairavamoorthy, K. and Lumbers, J.P. (1994). "New perspectives on the design and operation of sustainable water supply systems in developing countries", Paper presented at CIWEM Symposium, Dec. 1994.

Vairavamoorthy, K. (2001). "Launch of new I*nternational guidelines for design of water networks in developing countries*", Paper presented at CIWEM Metropolitan Branch Jan.

Yepes, G. and Dianderas, A. (1996). *Water and Wastewater Utilities: Indicators, 2nd Edition*. Water and Sanitation Division. The World Bank, Washington, D.C.

Operational Perspective of the Impact of Failures in Water Distribution Systems

J. Bicik, Z. Kapelan and D. A. Savić

Centre for Water Systems, School of Engineering, Computing and Mathematics,
University of Exeter, North Park Road, Exeter, Devon, EX4 4QF, United Kingdom,
Tel: +44 (0)1392 26{3730, 4054, 3637}, Fax: +44 (0)1392 217965,
Email: {j.bicik, z.kapelan, d.savic}@exeter.ac.uk

ABSTRACT

Failures in water distribution systems (WDS) occur on daily basis, requiring the fast response from WDS operators. This paper presents an impact model which investigates the adverse effects of failures from an operational rather than strategic perspective in order to provide a better insight into their development over a given impact horizon. The performance indicators (PI) currently in place have been found inadequate and a set of new operational PI considering the magnitude, duration and sensitivity of customers has been introduced. The proposed operational impact model has been applied on a case study where a pressure-driven hydraulic model has been coupled with a geographic information system (GIS) and a discolouration model in order to provide a comprehensive overview of the failure to allow WDS operators to make more informed decisions.

INTRODUCTION

Failures in water distribution systems (WDS) occur on daily basis, primarily due to ageing infrastructure or equipment failure, but often also due to damage caused by third parties. The magnitude and scale of the impact typically depends on a number of factors among which the geographic location and topology of the WDS play an important role. Generally, three types of failures in WDS can be recognised: mechanic, hydraulic and water quality failures (Filion et al., 2007). Many researchers over the years have tried to estimate the impact of failures in WDS on its stakeholders. However, this is a complex problem, in particular because of its social aspects. The work done so far has focused primarily on impacts from pipe bursts, as part of strategic management and long term asset management plans (e.g. Skipworth et al., 2002). In the UK the high standard of the delivery of potable water is monitored by the Water Services Regulation Authority (OFWAT) using several performance indicators (PI), which amongst other focus on long term pressure adequacy (e.g. Pressure of water mains - DG2) and continuity of water supply (e.g. Supply interruptions - DG3) (OFWAT, 2008). It is believed that these indicators do not sufficiently reflect the impact of a failure on customers since the measures used ignore their type and vulnerability to service disruptions. Most of the research dealing with failures in WDS uses the fraction of delivered demand (FDD) and its similar forms as a PI to assess the level of service (e.g. Gupta and Bhave, 1994; Ostfeld et al., 2002; Kapelan et al., 2006). Although being an effective measure on a large scale, FDD does not consider the sensitivity of individual customers to a reduced level of service. Mansoor et al. (2005) defined several performance measures including

"adequacy" which was again based on the amount of delivered demand, but furthermore distinguished the importance of customers by applying different severity weightings.

Modelling of failures in WDS is prone to many errors and uncertainties due to the stochastic nature of water consumption and also because the hydraulic models typically available are not calibrated for simulating such conditions. Bhave (1981) was probably the first to stress the importance of using a pressure driven analysis when modelling WDS under failure conditions in order to capture the dependence of nodal outflows on available pressure. Since then various pressure-driven models were developed and are being used more frequently. In this work, a pressure driven modification of EPANET (Rossman, 2000), based on the method proposed by Ang and Jowitt (2006), was used in order to model the behaviour of WDS under failure conditions.

With the current improvements in monitoring technologies and wider availability of near real-time data, there is a need to investigate the impacts of various failures from an operational of view, in order to better prioritize work of WDS operators and field technicians. Giustolisi et al. (2008) have already proposed several operational PIs based on the amount of unsupplied demand over 24 hours, however, the sensitivity of customers has not been taken into account. This might be seen as a disadvantage for current customer-oriented water utilities. It is argued that the currently available PIs are not fully suitable to support these new requirements and a comprehensive impact model needs to be established to enable quantification of operational impacts of failures and their effect on various stakeholders (e.g. the customers and the water utility). This paper provides a brief overview of such an impact model, tailored specifically to assessment of failures from operational perspective.

METHODOLOGY

As suggested earlier by Bicik et al. (2008), it is important to consider different stakeholders (e.g. water utility, its customers, etc.) when assessing the impact of failures in WDS. The approach, initially based on a value tree (Michaud and Apostolakis, 2006) has been revised because different impact factors affect multiple stakeholders (e.g. low pressure, supply interruption, etc.), however in a different way. Hence, it is proposed to represent the effects of the impacts in a tabular rather than a tree like structure. The main impact factors caused by a failure (e.g. pipe burst, pump failure, etc.) currently envisaged and their different effects on the interested parties are listed in Table 1. The various effects included in Table 1 have been further classified into three categories: economic, environmental and social, denoted as [EC], [EN] and [S] respectively.

Table 1. Impact factors and their economic, environmental and social effects on stakeholders

Impact Factor	Effect	
	Water Utility	Customer
Lost Water	Cost of lost water [EC] Carbon Footprint of extraction and treatment [EN]	Lost Revenue [EC]

Low Pressure	Regulatory penalties [EC] Customer Complaints [EC] Undelivered water - revenue loss [EC] Water quality problems [EC]	Contaminant intrusion [S] Inconvenience & danger [S] Lost Revenue [EC]
Interruption to Supply	Regulatory penalties [EC] Customer Complaints [EC] Undelivered water - revenue loss [EC] Water quality problems [EC] Regulatory penalties [EC]	Contaminant intrusion [S] Inconvenience & danger [S] Lost Revenue [EC]
Discolouration	Customer Complaints [EC] Interventions (flushing) [EC] Water quality problems DWI [EC]	Discolouration [S]
Damage to third parties	Compensations [EC]	Flooding [S] Transport disruption [S]
Energy Losses	Cost of energy [EC] Energy required to clean & pump water [EN]	

From the table above, it can be seen that failures generally have greater economic impacts on water utilities whereas customers are more concerned about the social aspects. Since social impacts are difficult to quantify (Rahman et al., (2005) several surrogate measures are proposed here. These measures are based on the amount of undelivered water as well as the failure duration and increase in discolouration potential. Due to the complexity and the fact that there are no existing models for some of the effects in Table 1 (e.g. contaminant intrusion, flooding of properties, transport disruption, etc.) only a subset of those mentioned above has been incorporated into the overall impact model. The following sections will provide details about selected PIs used to capture the impacts caused by low pressure, interruption and discolouration. These impacts are seen as the most important as well as the most practical ones.

Low Pressure Problems

Low pressure problems cause a wide range of direct and indirect adverse effects affecting both the water utility and its customers. In the UK, OFWAT requires low pressure incidents (i.e. drops of pressure below 15m of head at water main) to be reported (i.e. as part of the DG2 PI) by every water utility. Although, short term failures such as those caused by pipe bursts can be excluded from the DG2 register (i.e. list of properties receiving substandard pressure) and thus this PI does not immediately affect the water utilities in the short term operational perspective considered here. Low pressure, although not being as severe as a complete interruption to water supply, causes inconvenience to customers and affects pressure sensitive water consumption. This in turn reduces the revenue of a water utility in case of metered customers (in the UK, approximately 67% of properties are not metered, depending on a particular water utility). Furthermore, inadequate pressure problems occurring in the case of fire might even lead to loss of lives and properties (Filion et al., 2007).

The proposed approach uses the number of affected customers (see Equation 1), the undelivered demand due to low pressure (see Equation 2) and the average low pressure impact duration (see Equation 3) as surrogate measures reflecting the social aspects of low pressure impacts. Furthermore, each of the above indicators should be evaluated for a given type of customer (i.e. residential, commercial, industrial and critical) in order to reflect their importance.

$$LP_{type} = \sum_{i=1}^{N_N} Cust_{i,type} \times \begin{cases} 0 & if \quad P_i(t) \geq \mathrm{P}_{req} \quad for \quad \forall t \in <1,T> \\ 1 & otherwise \end{cases} \tag{1}$$

$$UWLP_{type}[m^3] = \frac{3600}{1000} \times \sum_{t=1}^{T} \sum_{i=1}^{N_N} \begin{cases} \dfrac{\left(D_{i,req}(t) - D_i(t)\right) \times Cust_{i,type}}{Cust_{i,count}} & if \; 0 < P_i(t) < \mathrm{P}_{req} \\ 0 & otherwise \end{cases} \tag{2}$$

$$AVGLPD_{type}[h] = \frac{1}{Cust_{total,type}} \sum_{t=1}^{T} \sum_{i=1}^{N_N} \begin{Bmatrix} Cust_{i,type} & if \; 0 < P_i(t) < \mathrm{P}_{req} \\ 0 & otherwise \end{Bmatrix} \tag{3}$$

where:

- N_N is the number of demand nodes in the system
- t is the simulation time (with assumed time step of 1 hour)
- T is the impact horizon in number of time steps (hours)
- $P_i(t)$ is the pressure at demand node i and time t (m of head)
- P_{req} is the minimum required pressure in m of head to deliver the full requested demand at node i (in this case 15m)
- $D_{i,req}(t)$ is the requested demand at node i and time t in *l/s*
- $D_i(t)$ is the delivered demand at node i and time t in *l/s*
- $Cust_{i,type}$ is the number of customers of particular type supplied from node i
- $Cust_{i,count}$ is the number of customers supplied from demand node i
- $Cust_{total,type}$ is the total number of customers of a particular type affected by the failure at least during one time step over given impact horizon T

In order to represent economic losses of a UK water utility caused by low pressure it is vital to distinguish between metered and unmetered consumption since the water consumption of a large percentage of customers is not metered. Hence it is proposed to use following performance indicator to measure the lost revenue due to undelivered water because of low pressure.

$$UWLR[m^3] = \frac{3600}{1000} \times \sum_{t=1}^{T} \sum_{i=1}^{N_N} \begin{cases} \dfrac{\left(D_{i,req}(t) - D_i(t)\right) \times Cust_{i,M}}{Cust_{i,M} + Cust_{i,UM}} & if \; 0 < P_i(t) < \mathrm{P}_{req} \\ 0 & otherwise \end{cases} \tag{4}$$

where:

- $Cust_{i,M}$ the number of metered customers supplied from node i
- $Cust_{i,UM}$ the number of unmetered customers supplied from node i

Water Supply Interruption

Interruption to water supply is defined here as a drop of pressure at water main to 0 m of head or below this threshold. It is acknowledged that this is a simplified assumption and that in reality an interruption occurs even at less significant pressure drops (e.g. due to the elevation of individual properties and head losses through internal plumbing). Interruption is the most severe failure with the highest impact on customers and as shown by Sadiq et al. (2006) it can also lead to intrusion of contaminants into the WDS and cause health related problems.

The performance indicators used to evaluate the interruption of water supply are similar to those described in previous section by Equations (1), (2), (3) and (4). However, the duration of an interruption is calculated as the number of hours from the beginning of the failure until the supply is fully restored, which is different from the low pressure impact where the duration is calculated as a sum of the number of hours when inadequate pressure is received by the customers. In order to provide a measure which is well understood by the operators in the UK, the interruption duration is categorised in a similar way as suggested by OFWAT (2008). The following classes are introduced: 0-3h, 4-6h, 7-12h, 13-24h and more than 24h. However, even in this case the interruption duration is calculated per customer type (e.g., 4 residential properties affected for 4-6h and 1 industrial customer affected for 0-3h).

Discolouration

Apart from taking into account the effects of failures related to reduced level of service in terms of low pressure or inadequate flow, it is also important to consider water quality related issues. Discolouration caused by disturbance of normal flow regime usually plays a key role for water quality considerations (at least in the UK). A discolouration model based on risk trees developed by a panel of experts (Dewis and Randall-Smith, 2005) has been applied to estimate the increase in discolouration potential of all pipes in the WDS after a failure has occurred. As pointed out by Vreeburg and Boxall (2007) using a discolouration model based on shear stress would be more appropriate, however, no such model was available to the authors. The discolouration impact is expressed as the number and length of pipes experiencing increased discolouration potential due to a failure and also as the total discolouration score increase defined as follows:

$$TotalDiscInc = \sum_{j=1}^{N_P} \begin{cases} Disc_{j,failure} - Disc_{j,norm} & if\ Disc_{j,failure} > Disc_{j,norm} \\ 0 & otherwise \end{cases} \quad (5)$$

where:

- N_P is the number of pipes in the system
- $Disc_{i,norm}$ is discolouration index of a pipe i under normal conditions
- $Disc_{i,failure}$ is discolouration index of pipe i under failure conditions

Nowadays WDS are typically divided into district metered areas (DMA) where inflows and outflows into/from such areas are monitored in order to minimize leakage. Modelling particular types of failures at DMA level might be sufficient in most cases as failures usually have a localised impact. However, it is vital to use an all-pipe model of the whole

WDS in order to model major failures such as pump outages, large pipe bursts and isolations of segments of pipes. Such failures are likely to have impacts on other parts of the WDS that might not be immediately obvious due to WDS in urban areas being looped. Furthermore, when discolouration is considered, the disturbances caused by a failure might spread far upstream and downstream from the actual location of a failure and stretch well beyond the boundaries of a single DMA.

CASE STUDY

The above proposed impact model has been applied to a large WDS (see Figure 1) comprising of about 9,000 pipes and supplying over 25,000 properties (69% of the properties are not metered).

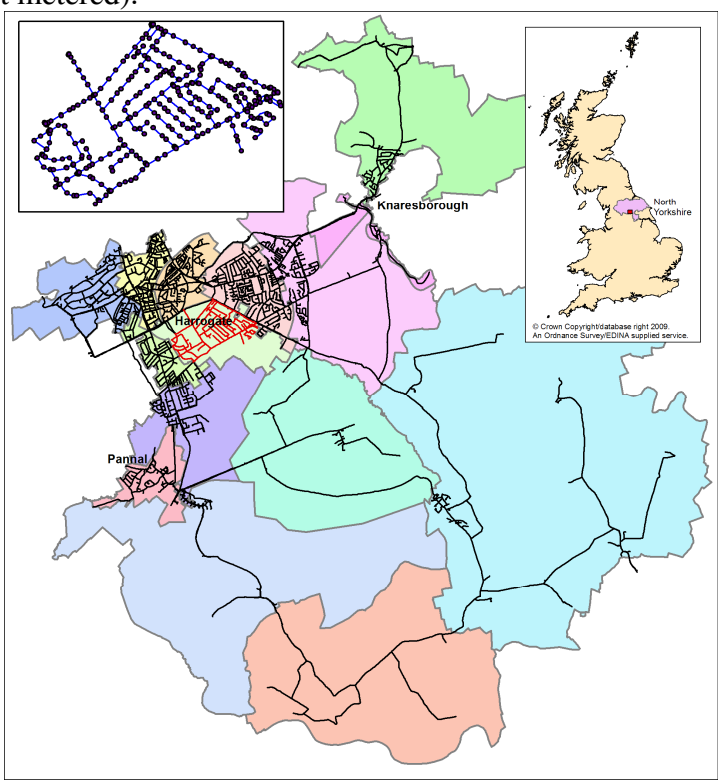

Figure 1. Case Study Area

The model covers an area of 16 DMAs of various types, stemming from fully tree-like networks located mostly in rural areas to highly looped networks in urban areas. A pipe burst of a constant outflow of 10 l/s starting from midnight and lasting for 24 hours has been simulated in the highlighted DMA in Figure 1. The affected DMA provides water to almost 1,600 properties and is located in an urban area. An extended period simulation model has been run using a modified version of EPANET in order to obtain the pressures at demand nodes and the reduced demands delivered due to insufficient pressure.

RESULTS AND DISCUSSION

Although, the magnitude of the burst flow is high (i.e. 10 l/s), which makes it a major event, no interruption to water supply has occurred during the impact horizon of 24 hours

since the pressures have never dropped to 0m of head or below that level. In real life a part of the system would be isolated in order to carry out the repair of the burst, this however has not been considered. Therefore, the performance indicators related to interruptions are not going to be reported here. Figure 2 reports the impact model results for different lengths of the impact horizon and shows the amount of cumulative undelivered demand caused by low pressure. The total undelivered metered demand is also shown as it relates to the loss in revenue for the utility.

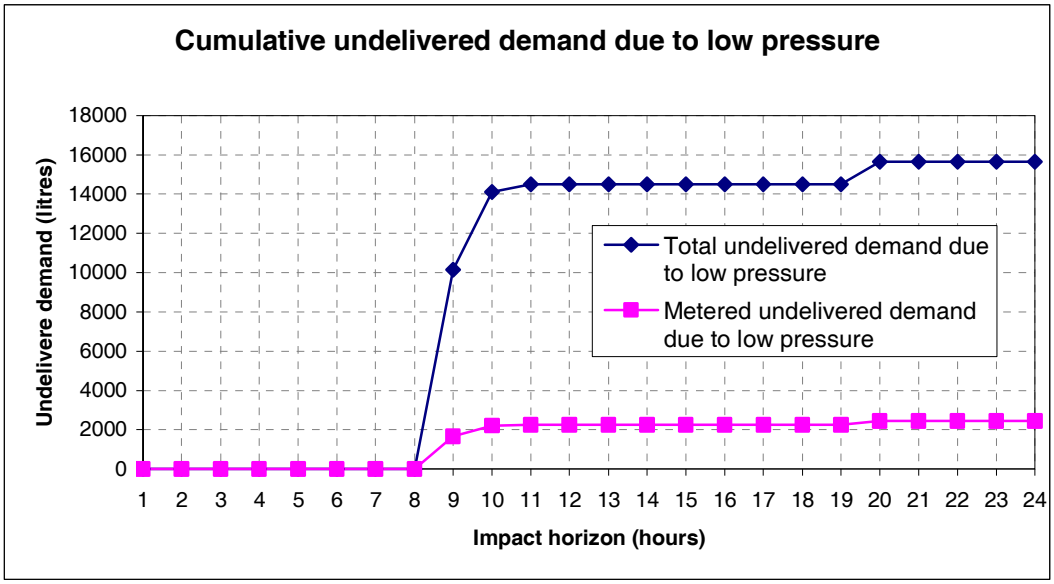

Figure 2. Cumulative undelivered demand in the analysed system due to low pressures

Due to the size of the considered WDS and the localized impact in this case, the fraction of the undelivered demand does not exceed 0.1% of the overall demand for the whole system. The major increases in the undelivered demand occur at peak times (i.e. 8:00AM, 9:00AM, 10:00AM, 7:00PM and 8:00PM) and outside of these critical hours the system remains unaffected (apart from potential discolouration problems). As can be further noticed, the amount of undelivered metered demand is relatively low and does not represent a significant economic loss to the water utility when compared to the amount of water lost due to the burst (i.e. 864,000 litres). In this case the environmental impact can be related indirectly to the amount of water which has escaped from the system by considering the carbon emissions produced during the extraction, treatment and delivery of the leaked water.

Figure 3 is a snapshot, showing the impact at the peak time (i.e. 8:00AM) rather than the cumulative results. The spatial distribution of the affected properties as well as the pipes which are likely to experience an increase in discolouration potential due to the failure are visualised using GIS. It can be seen that the areas of increased discolouration risk can be geographically distant from the location of the failure. In total there were 337 pipes having the length of 12.5km whose discolouration potential increased.

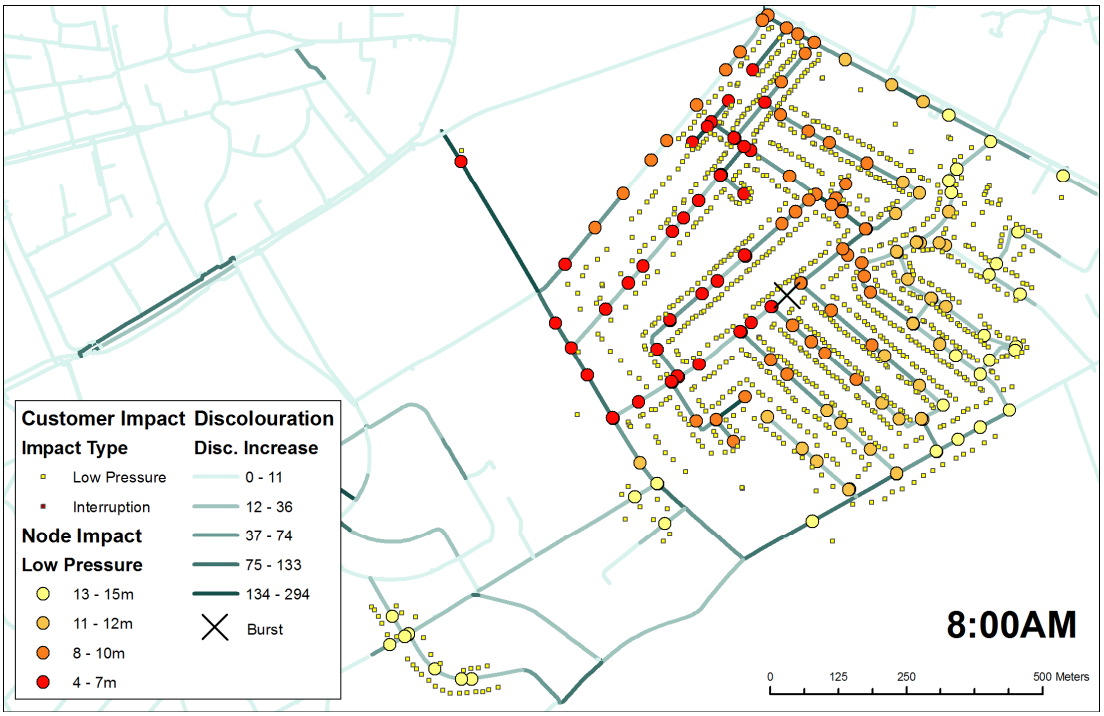

Figure 3. The estimated impact of a pipe burst at peak demand time

CONCLUSIONS

The impact model presented in this paper aims to provide WDS operators with a better insight into the adverse effects of failures and their development in time. That will help them make more informed decisions and prioritise the actions of repair teams. It is argued that in order to meet the high levels of standard of delivery of potable water, the indicators currently used to assess the impact are inadequate and need to be extended. A set of new performance indicators that specifically distinguishes between types of affected customers and incorporates both the duration and magnitude of a failure has been formulated. A pressure-driven hydraulic model based on modified version of EPANET has been coupled with a GIS, in order to consider the sensitivity of the customers. The hydraulic model is also integrated with a model that relates disturbances in normal flow regime to discolouration potential.

The increasing importance of impact evaluation can also be seen in recent attempts to move from traditional and well established WDS reliability studies towards risk-based approaches (e.g. Kapelan et al., 2006; Beuken et al., 2008). These studies take into account not only the likelihood of occurrence of adverse events but also consider their impact. The impact model presented here, forms only one component of a risk-based methodology (Bicik et al., 2008) for the operation of WDS under failure conditions, which is being developed as part of an ongoing EPSRC funded Neptune project (Savic et al., 2008).

This paper has described in detail only a few out of almost 50 performance indicators that form the output of the implemented overall impact model. Although, the number of reported PIs is relatively high, it is believed that the WDS operators will choose the most

representative set of PIs to use themselves according to their experience. As part of future work it is envisaged to focus on finding suitable methods to visualise such a broad range of performance measures using GIS and ways to speed up the computational time required to apply the impact model on large scale WDS.

ACKNOWLEDGEMENTS

The work on the NEPTUNE project was supported by the U.K. Science and Engineering Research Council, grant EP/E003192/1, and Industrial Collaborators. The authors also thank Lewis A. Rossman for providing the pressure-driven modification of EPANET. The kind assistance of Mr Ridwan Patel from Yorkshire Water Services and Dr Mark S. Morley is greatly appreciated.

REFERENCES

Ang, W. K., and Jowitt, P. W. (2006). "Solution for Water Distribution Systems under Pressure-Deficient Conditions." *Journal of Water Resources Planning and Management*, 132(3), 175-182.

Beuken, R. H. S., van den Boomen, M., Blaauwgeers, H. G. P., and van Daal, H. A. (2008). "Feasibility Study on Quantitative Risk Analysis of Drinking Water Networks." *10th Annual Water Distribution Systems Analysis Conference WDSA2008*, Kruger National Park, South Africa, 665-675.

Bhave, P. R. (1981). "Node Flow Analysis Distribution Systems." *Transportation engineering journal of ASCE*, 107(4), 457-467.

Bicik, J., Makropoulos, C., Joksimovic, D., Kapelan, Z., Morley, M. S., and Savić, D. A. (2008). "Conceptual Risk-Based Decision Support Methodology for Improved Near Real-Time Response to WDS Failures." *Proceedings of the 10th Annual Water Distribution Systems Analysis Conference (WDSA2008)*, Kruger National Park, South Africa, 510-519.

Dewis, N., and Randall-Smith, M. (2005). "Discolouration Risk Modelling." *Computers and Control in the Water Industry (CCWI 2005)*, Exeter, UK.

Filion, Y. R., Adams, B. J., and Karney, B. W. (2007). "Stochastic Design of Water Distribution Systems with Expected Annual Damages." *Journal of Water Resources Planning and Management*, 133(3), 244-252.

Giustolisi, O., Kapelan, Z., and Savic, D. (2008). "Extended Period Simulation Analysis Considering Valve Shutdowns." *Journal of Water Resources Planning and Management*, 134(6), 527-537.

Gupta, R., and Bhave, P. R. (1994). "Reliability Analysis of Water-Distribution Systems." *Journal of Environmental Engineering*, 120(2), 447-461.

Kapelan, Z., Savic, D. A., Walters, G. A., and Babayan, A. V. (2006). "Risk- and robustness-based solutions to a multi-objective water distribution system rehabilitation problem under uncertainty." *Water Science & Technology*, 53(1), 61-75.

Mansoor, M. A. M., Gorantiwar, S. D., and Vairavamoorthy, K. (2005). "Quantifying the performance of water distribution system as a result of failure." *Computers and Control in the Water Industry (CCWI 2005)*, Exeter, UK.

Michaud, D., and Apostolakis, G. E. (2006). "Methodology for Ranking the Elements of Water-Supply Networks." *Journal of Infrastructure Systems*, 12(4), 230-242.

OFWAT. (2008). "June return 2008 reporting requirements." <http://www.ofwat.gov.uk/regulating/junereturn/prs_web_jrreportingreq> (accessed 16 January 2009).

Ostfeld, A., Kogan, D., and Shamir, U. (2002). "Reliability simulation of water distribution systems - single and multiquality." *Urban Water*, 4(1), 53-61.

Rahman, S., Vanier, D. J., and Newton, L. (2005). "Social Cost Considerations for Municipal Infrastructure Management." *Report no. B-5123.8*, Institute for Research in Construction, National Research Council Canada, Ottawa.

Rossman, L. A. (2000). "EPANET 2 Users Manual." U.S. Environmental Protection Agency, Cincinnati, Ohio.

Sadiq, R., Kleiner, Y., and Rajani, B. (2006). "Estimating risk of contaminant intrusion in water distribution networks using Dempster-Shafer theory of evidence." *Civil Engineering and Environmental Systems*, 23(3), 129-141.

Savic, D. A., Boxall, J. B., Ulanicki, B., Kapelan, Z., Makropoulos, C., Fenner, R., et al. (2008). "Project Neptune: Improved Operation of Water Distribution Networks." *Proceedings of the 10th Annual Water Distribution Systems Analysis Conference (WDSA2008)*, Kruger National Park, South Africa.

Skipworth, P. J., Engelhardt, M. O., Cashman, A., Savic, D. A., Saul, A. J., and Walters, G. A. (2002). *Whole life costing for water distribution network management*, Thomas Telford Publishing, London.

Vreeburg, I. J. H. G., and Boxall, D. J. B. (2007). "Discolouration in potable water distribution systems: A review." *Water Research*, 41(3), 519-529.

New Concepts for Meter Placement in Water Distribution Systems for Demand Estimation

Doo Sun Kang[1] and Kevin Lansey[2]

[1]Research Associate, Department of Civil Engineering and Engineering Mechanics, The University of Arizona, Tucson, AZ 85721; email: doosun74@email.arizona.edu.

[2]Professor, Department of Civil Engineering and Engineering Mechanics, The University of Arizona, Tucson, AZ 85721; Ph (520)-621-2512; Fax (520)-621-2550; email: lansey@email.arizona.edu.

ABSTRACT

Kang and Lansey (2008a) have shown that water distribution system (WDS) nodal demands can be estimated in real-time using pipe velocity measurements from a supervisory control and data acquisition (SCADA) system. The field measurements are key elements for the real-time state estimation. However, the limited number of metering locations has been a significant obstacle for the real-time studies and identifying locations to best gain information is critical. Previous studies for the data sampling mainly focused on minimizing either parameter or prediction uncertainties. However, reducing uncertainty does not guarantee a good fit for the model predictions in terms of the mean estimate. Therefore, robust objective criteria, that guarantee precise and accurate state estimates, must be applied. Here, an optimal meter placement (OMP) problem is formulated as a multi-objective optimization model. Three distinctive objectives are posed: (1) minimization of nodal demand estimation uncertainty; (2) minimization of nodal pressure prediction uncertainty; and (3) minimization of absolute error between demand estimates and their expected values. Objectives (1) and (2) represent model precision while objective (3) describes model accuracy. The OMP problem is solved using a multi-objective genetic algorithm (MOGA) based on Pareto-optimal solutions. The trade-off between model precision and accuracy is clearly observed from a simple network study and it is strongly recommended to use both criteria as objectives.

INTRODUCTION

Generally, state estimates (SE) improve with more field measurements. However, due to budget limitations, only a few selected key locations are monitored. Given the type and number of measurements, the topological distribution of meters in networks strongly influences the SE quality. If portions of a system are insufficiently measured, the state variables in those regions can not be accurately estimated and will contain a high degree of uncertainty.

Optimal sampling design (SD) for WDS model calibration (parameter estimation, i.e., roughness coefficient) is an important issue and has been completed by a number of researchers. Meier and Barkdoll (2000) used genetic algorithm to find an optimal combination of calibration test locations to maximize a total length of pipes having non-negligible flow velocities (≥ 0.3 m/s). Lansey et al. (2001) proposed a sensitive-based heuristic method for design of data collection using model prediction uncertainty. They used first-order second moment (FOSM) analysis for model prediction uncertainty quantification. Kapelan et al. (2003, 2005) formulated the SD problem as a two objective optimization problem. The objectives were to minimize the relevant uncertainties and to minimize a total SD cost (i.e., number of measurements). The optimal SD problem was solved using genetic algorithms. They used FOSM analysis to estimate parameter and prediction uncertainties. The aforementioned SD problems are usually solved considering multiple demands under steady-state hydraulic conditions to take into account various demand loads.

Yu and Powell (1994) presented optimal meter placement (OMP) algorithm for system-wide pressure estimation. The optimization is based on a systematic extension of a given measurement system, starting from purely pseudo-measurements (nodal demand guesses) and at every stage one metered measurement (nodal pressure head) is added based on maximum covariance of state variables.

The aforementioned SD/OMP studies only considered model precision by minimizing the uncertainties (either parameter or model prediction) as their objective function. However, reducing uncertainty does not guarantee a good fit for the model predictions. In this study, we address a new criterion, accuracy, as one of multiple objective functions. Here, "precision" refers to the uncertainty of state estimates and "accuracy" denotes the unbiased tracking of the target value. Therefore, a meter placement design presented in this study comprises finding the set of meter locations that optimally improve the accuracy and the precision of state estimates. The state condition of concern is the nodal demand.

METHODOLOGY

The OMP problem requires demand estimation and uncertainty analysis. The methods applied are taken from Kang and Lansey (2008b) and described in steps 1-3. The OMP location is determined using a genetic algorithm (step 4).

1. Demand aggregation and field data generation. To reduce the number of unknowns and subsequently the number of measurements for demand estimation, nodal demands are grouped (i.e., aggregated) based on the relative locations and user characteristics, such as industrial, commercial, and residential. Once group total demands are estimated, they are allocated to individual nodes proportionally to the consumption ratio of each node as estimated from population densities or customer

billing records. Field measurement data sets (here, pipe flow rates) are synthetically generated using simulation model by adding Gaussian random errors for actual values.

2. Uncertainty quantification. The uncertainties caused by measurement errors are transferred through the demand estimation process and result in inaccurate demand estimates and subsequently propagated to the predicted output variables. Here, the first-order second moment (FOSM) approximate method is applied in a two step process:
First, the variances of nodal demands caused by measurement errors are estimated by

$$Cov(\mathbf{x}) = E[(\mathbf{x} - \hat{\mathbf{x}})(\mathbf{x} - \hat{\mathbf{x}})^T] \cong (\mathbf{J}^T \mathbf{R}_\mathbf{z}^{-1} \mathbf{J})^{-1}$$

where E is expectation operator, $\hat{\mathbf{x}}$ and $\mathbf{x}$ is the actual and estimated demand, respectively, and $\mathbf{R_z}$ is the covariance matrix of the measurement (pipe flow rates) error. $\mathbf{J}$ is the Jacobian (or sensitivity) matrix of pipe flow rates with respect to the nodal demands evaluated at the base demands. Note the diagonal elements of the covariance matrix, $Cov(\mathbf{x})$, are the variances of the individual nodal demand estimates. Second, the covariance matrix of nodal pressure predictions are estimated using $Cov(\mathbf{x})$ from first step and

$$Cov(\mathbf{y}) = \left[\left(\frac{\partial \mathbf{y}}{\partial \mathbf{x}} \right) Cov(\mathbf{x}) \left(\frac{\partial \mathbf{y}}{\partial \mathbf{x}} \right)^T \right]$$

where $\mathbf{y}$ denotes nodal pressure and $\partial\mathbf{y}/\partial\mathbf{x}$ represents the sensitivities of the nodal pressures with respect to the nodal demands. The diagonal terms of the covariance matrix, $Cov(\mathbf{y})$, are the variances of individual nodal pressure predictions. This FOSM has been successfully applied for uncertainty analysis of hydraulic variables by Xu and Goulter (1998), Lansey et al. (2001), and Kang et al. (2007, 2008).

3. Demand estimation. For demand estimation, a recursive state estimator based on the weighted least squares (WLS) method is applied (Kang and Lansey, 2008a and b). The WLS method has been widely used for parameter estimation (Datta and Sridharan 1994; Reddy et al. 1996) and state estimation (Powell et al. 1988) in WDS.

Consider the non-linear measurement model:

$$\mathbf{z} = \mathbf{h}(\mathbf{x}) + \mathbf{e}$$

where $\mathbf{z}$ is the measurement (pipe flow) vector, $\mathbf{x}$ is the true state vector of nodal demands and $\mathbf{h}(.)$ is a non-linear vector function relating measurements to states. $\mathbf{e}$ is the measurement error vector. The elements of $\mathbf{e}$ are assumed to have zero mean and the corresponding measurement covariance matrix is denoted by $\mathbf{R_z}$. Here, $\mathbf{h}(.)$ are linear/nonlinear equations describing the conservation of mass at each node and the conservation of energy across a pipe. These equations are solved using the hydraulic simulation model as a sequence of steady state conditions.

The demand estimation problem is formulated as a minimization of the squares of the errors or:

$$E(\mathbf{x}) = \frac{1}{2} (\mathbf{z} - \mathbf{h}(\mathbf{x}))^{\mathrm{T}} \mathbf{R}_\mathbf{z}^{-1} (\mathbf{z} - \mathbf{h}(\mathbf{x}))$$

A Taylor series expansion provides an approximation of the non-linear vector function **h(x)**:

$$\mathbf{h}(\mathbf{x}+\Delta\mathbf{x}) \approx \mathbf{h}(\mathbf{x}) + \mathbf{J}(\mathbf{x})\Delta\mathbf{x}$$

The minimization problem is rewritten as:

$$E(\mathbf{x}+\Delta\mathbf{x}) = (\Delta\mathbf{z} - \mathbf{J}(\mathbf{x})\Delta\mathbf{x})^{\mathrm{T}}\, \mathbf{R}_{\mathbf{z}}^{-1}\, (\Delta\mathbf{z} - \mathbf{J}(\mathbf{x})\Delta\mathbf{x})$$

where $\Delta\mathbf{z} = \mathbf{z} - \mathbf{h}(\mathbf{x})$.

The first-order optimality condition for this problem is:

$$\frac{\partial E(\mathbf{x}+\Delta\mathbf{x})}{\partial \Delta\mathbf{x}} = -\mathbf{J}^T(\mathbf{x})\,\mathbf{R}_{\mathbf{z}}^{-1}\,(\Delta\mathbf{z} - \mathbf{J}(\mathbf{x})\Delta\mathbf{x}) = 0$$

Hence, the linear least-squares solution can be expressed as:

$$\Delta\mathbf{x} = (\mathbf{J}^T(\mathbf{x})\,\mathbf{R}_{\mathbf{z}}^{-1}\,\mathbf{J}(\mathbf{x}))^{-1}\mathbf{J}^T(\mathbf{x})\,\mathbf{R}_{\mathbf{z}}^{-1}\,\Delta\mathbf{z}$$

Using the previous time step (*t*-1) solution as the initial estimate for current time *t*, the recursive equation for the multi-scan demand estimation is rewritten as:

$$\mathbf{x}(t_i) = \mathbf{x}(t_{i-1}) + (\mathbf{J}^T(\overline{\mathbf{x}})\,\mathbf{R}_{\mathbf{z}}^{-1}(t_i)\,\mathbf{J}(\overline{\mathbf{x}}))^{-1}\,\mathbf{J}^T(\overline{\mathbf{x}})\,\mathbf{R}_{\mathbf{z}}^{-1}(t_i)\,(\mathbf{z}(t_i) - \mathbf{h}(\mathbf{x}(t_{i-1})))$$

Note that the Jacobian matrix **J** is calculated only once using the base demands, $\overline{\mathbf{x}}$, prior to the multi-scan estimation to reduce the computational time. For a complete description of the demand estimation approach, see Kang and Lansey (2008a and b).

4. Multi-objective genetic algorithm. Genetic algorithms (GAs) are stochastic search techniques based on the evolutionary mechanisms inspired by biological evolution processes such as selection, crossover, and mutation (Goldberg 1989). The GA starts from a population of randomly generated individuals and evolves toward better solutions through many generations. Many design problems involve multiple objective optimizations and, if more than one objective is considered in an optimization problem, there may not exist only one best solution with respect to all objectives. Instead, there exists a set of solutions called Pareto-optimal solutions. All solutions on the Pareto-front are equally optimal but by moving from one Pareto solution to another the improvement in one function value causes deterioration in at least one other function value. Therefore, engineer's experienced judgment is still required to provide a practical solution depending on the application.

Three objectives are formulated: (1) minimize demand estimate uncertainty (Eq. 1a); (2) minimize pressure prediction uncertainty (Eq. 1b); and (3) minimize the RMSE between estimated demands and expected true values (Eq. 1c).

$$F_1 = \sum_{i=1}^{nnode} \sum_{t=1}^{ntime} sqrt(diag(Cov(x_{i,t}))) \tag{1a}$$

$$F_2 = \sum_{i=1}^{nnode} \sum_{t=1}^{ntime} sqrt(diag(Cov(y_{i,t}))) \tag{1b}$$

$$F_3 = \sum_{i=1}^{nnode} sqrt\left\{ \sum_{t=1}^{ntime} (x_{i,t} - \hat{x}_{i,t})^2 / ntime \right\} \tag{1c}$$

where *nnode* and *ntime* are the number of nodes and the simulation time, respectively, and *diag*(.) denotes diagonal elements of covariance matrix. For better comparison, The three objective functions (Eq. 1) are scaled by their corresponding values when

all locations are measured, $F_{i,full}$. The scaled dimensionless objective functions are:

$$Minimize \ \ f_1 = \frac{F_1}{F_{1,full}}$$

$$Minimize \ \ f_2 = \frac{F_2}{F_{2,full}}$$

$$Minimize \ \ f_3 = \frac{F_3}{F_{3,full}}$$

Note that the scaled objective functions are limited below at a value of 1.

RESULTS

The study network and network data are shown in Figure 1. To reduce the unknowns, nodes with similar consumer types are grouped i.e., industrial for node 3 itself, commercial for nodes 2, 4, and 6, and residential area for nodes 7, 8, and 9. Only those seven nodes have demands. Pipe flows are assumed to be measured on an hourly time step. The task here is to find the two best locations among the twelve pipes where the pipe flow rates will be monitored (assuming the flow from the source, i.e., pipe 13 is always measured). Flow transducers are assumed to have 10% measurement error, that is introduced by adding the Gaussian noise, $N(0,\sigma)$, where $\sigma = 0.1\mu/3.27$ to actual flows.

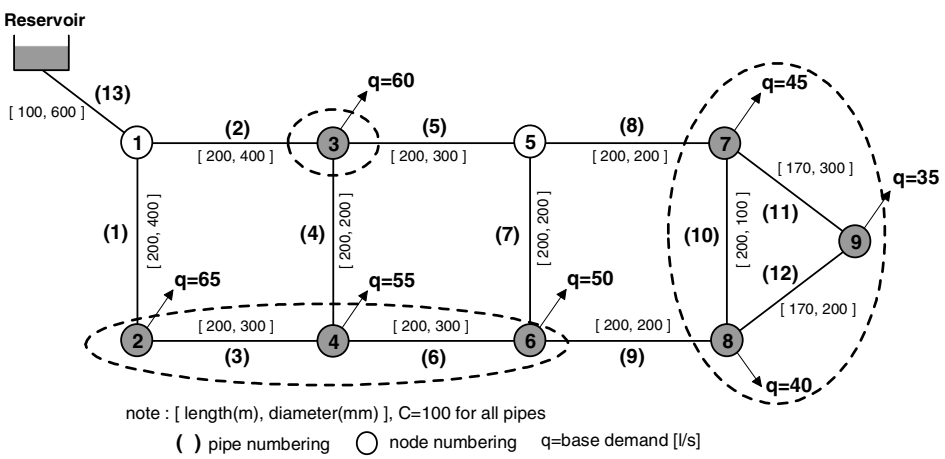

Figure 1. Study network schematic

Full enumerations are performed first by using the total 66 possible combinations (12 combinatorial 2, ${}_{12}C_2$). The problem is then solved using the MOGA. The solutions from the MOGA are compared to the solutions found by a full enumeration (Figure 2). As seen the Pareto solutions obtained from the full enumeration and the MOGA are identical. For the MOGA simulation, we defined 50 populations and 100 generations, i.e., 5,000 function evaluations. The stochastic search methods like GA repeat the same genes and relevant function evaluations. To prevent the costly repetitive

function evaluations, solutions (i.e., genes and relevant function values) obtained from previous generations are stored in the cache and used if the same genes are detected in the current generation. By doing so, GA could save computation time by 1/2 of the full enumeration although it has more function evaluations.

The trade-off between model precision and accuracy is clearly shown in Figures 2a and b. The Pareto-front between f_1 and f_2 (Figure 2c) appear to be correlated suggesting potential redundancy between the uncertainty objective functions.

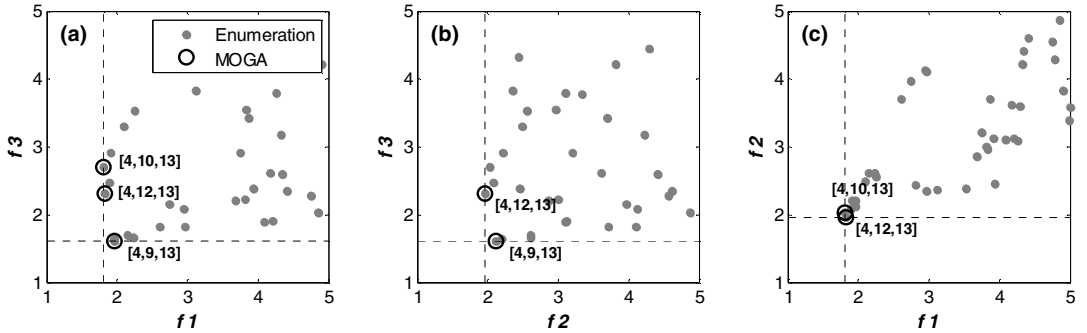

Figure 2. Pareto-front solutions from full enumeration and MOGA for three objective function pairs (OMP sets are in brackets)

To verify the suitability of the applied objective criteria for the OMP problem, the demand estimations are performed using the Pareto-front solutions. Three solution sets (set 1 – pipes 4, 10, 13 / set 2 – pipes 4, 12, 13 / set 3 – pipes 4, 9, 13) are selected. Note that measurement sets 1, 2, and 3 provide minimum values for function f_1, f_2, and f_3, respectively. Figures 3a, b, and c show the demand estimates and associated 95% confidence intervals for node 4 using measurement sets 1, 2, and 3, respectively. Figures 3a and b show precise but inaccurate state estimates. The demand estimates are poor and actual (true) values are frequently out of the estimated confidence bounds. On the other hand, Figure 3c shows relatively wider confidence intervals but more accurate estimates compared to Figures 3a and b. If only uncertainty measures are used as objective functions, sets 1 or 2 would be selected as solutions while set 3 is rejected. Therefore, for robust solutions, both model precision and accuracy should be considered as dual objectives in OMP problems.

Another important result observed from this study is that the OMP problem should be solved considering unsteady hydraulic conditions to take into account the temporal changes of nodal demands. In general, sampling design problems for parameter estimation are solved using multiple demand loads under steady state conditions. For example, demands at peak hour (8 am), average hour (2 pm), and minimum hour (3 am) are used to consider multiple system loading conditions. However, as seen in Figure 3, steady estimations at several points may not provide sufficient information for identifying accurate solutions. Instead, more robust solutions can be obtained by comparing the unsteady simulation results during a certain time period. Here, 24 hour

duration extended period simulation (EPS) has been performed based on an hourly time step.

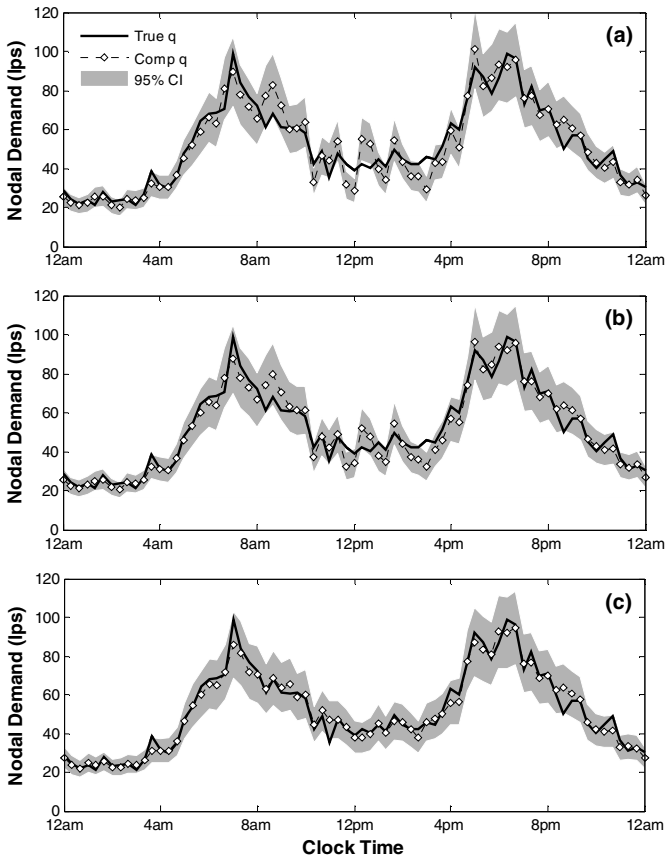

Figure 3. Demand estimates and 95% confidence intervals for node 4 using three Pareto-optimal sets: (a) Set 1 – pipes 4, 10, 13, (b) Set 2 – pipes 4, 12, 13, and (c) Set 3 – pipes 4, 9, 13

DISCUSSION

Optimal meter placement (OMP) for state estimation (SE) is formulated and solved in a multi-objective optimization model. Three objective functions, representing demand estimation uncertainty, pressure prediction uncertainty, and demand estimation accuracy, are defined. The optimization problems are solved using a multi-objective genetic algorithm (MOGA) based on Pareto-optimal solutions. The results from the example problem clearly demonstrate the trade-off between model accuracy and precision. It is seen that a precise state-estimation does not necessarily guarantee an accurate estimation and vice versa. Therefore, both measures should be included in an SE OMP problem as objectives. However, the Pareto-fronts between two uncertainty functions appear to be correlated each other indicating potential redundancy. Further study can be conducted for larger network to investigate the effect of different numbers of meters and solution layout.

REFERENCES

Datta, R. S. N., and Sridharan, K. (1994). "Parameter estimation in water-distribution systems by least squares." *J. Water Resour. Plng. and Mgmt.*, ASCE, 120(4), 405-422.

Goldberg, D. E. (1989). *Genetic algorithms in search, optimization and machine learning*. Addison-Wesley, New York.

Kang, D. S., Pasha, M. F. K., and Lansey, K. (2007). "Approximate methods for analyzing water quality prediction uncertainty in water distribution systems." *World Environmental and Water Resources Congress 2007*, ASCE, Tampa, FL.

Kang, D. S., Pasha, M. F. K., and Lansey, K. (2008). "Approximate methods for uncertainty analysis of water distribution systems." *Urban Water Journal*, in press.

Kang, D. S., and Lansey, K. (2008a). "Real-time demand estimation and confidence limit analysis for water distribution systems." *10th International Water Distribution System Analysis conference,* Kruger, SA.

Kang, D. S., and Lansey, K. (2008b). "Real-time state estimation and confidence limit analysis for water distribution systems." *J. Hydr. Engrg.*, ASCE, under review.

Kapelan, Z., Savic, D. A., and Walters, G. A. (2003). "Multiobjective sampling design for water distribution model calibration." *J. Water Resour. Plng. and Mgmt.*, ASCE, 129(6), 466-479.

Kapelan, Z., Savic, D. A., and Walters, G. A. (2005). "Optimal sampling design methodologies for water distribution model calibration." *J. Hydr. Engrg.*, ASCE, 131(3), 190-200.

Lansey, K. E., El-Shorbagy, W., Ahmed, I., Araujo, J., and Hann, C. T. (2001). "Calibration assessment and data collection for water distribution networks." *J. Hydr. Engrg.*, ASCE, 127(4), 270-279.

Meier, R. W., and Barkdoll, B. D. (2000). "Sampling design for network model calibration using genetic algorithms." *J. Water Resour. Plng. and Mgmt.*, ASCE, 126(4), 245-250.

Powell, R. S., Irving, M. R., and Sterling, M. J. H. (1988). "A comparison of three real-time state estimation methods for on-line monitoring of water distribution systems." *Computer Applications in Water Supply*, vol. 1, 333-348.

Reddy, P. V. N., Sridharan, K., and Rao, P. V. (1996). "WLS method for parameter estimation in water distribution networks." *J. Water Resour. Plng. and Mgmt.*, ASCE, 122(3), 157-164.

Xu, C., and Goulter, I. C. (1998). "Probabilistic model for water distribution reliability." *J. Water Resour. Plng. and Mgmt.*, ASCE, 124(4), 218-228.

Yu, G., and Powell, R. S. (1994). "Optimal design of meter placement in water distribution systems." *Int. J. Syst. Sci*., 25(12), 2155-2166.

On-line hydraulic state prediction for water distribution systems

Ami Preis[1], Andrew Whittle [2] and Avi Ostfeld [3]

[1] Postdoctoral Associate, Center for Environmental Sensing and Modeling, MIT-SMART Center, Singapore; *amipreis@smart.mit.edu*
[2] Professor, Department of Civil and Environmental Engineering, MIT, Cambridge, MA, USA; *ajwhittl@MIT.EDU*
[3] Senior Lecturer, Faculty of Civil and Environmental Engineering, Technion – I.I.T, Haifa, Israel; *ostfeld@tx.technion.ac.il*

Abstract

This paper describes and demonstrates a method for on-line hydraulic state prediction in urban water networks. The proposed method uses a Predictor-Corrector (PC) approach in which a statistical data-driven algorithm is applied to estimate future water demands, while near real-time field measurements are used to correct (i.e., calibrate) these predicted values on-line. The calibration problem is solved using a modified Least Squares (LS) fit method. The objective function is the minimization of the least-squares of the differences between predicted and measured hydraulic parameters (i.e., pressure and flow rates at several system locations), with the decision variables being the consumers' water demands. The a-priori estimation (i.e., prediction) of the values of the decision variables, which improves through experience, facilitates a better convergence of the calibration model and provides adequate information on the system's hydraulic state for real time optimization. The proposed methodology is demonstrated on a prototypical municipal water distribution system.

1. Introduction

The integration of near real-time hydraulic data with computer simulations for on-line operation and control of large-scale urban water distribution systems can be used in a variety of applications ranging from real-time optimization of pump and valve settings for efficient power management; to the detection and quantification of leaks. Such a system can also be used for the implementation of water security systems and for the prediction of system performance during emergency events (e.g., pollution events, main pipe rupture, or significant fire).

Over the last 10 years, computer simulation models of water networks have been widely used by water systems operators (Walski et al. 2003). In conventional practice, model calibration is carried out off-line (USEPA 2005) using a short-term (e.g., one week) sample of hydraulic data (e.g., based on a limited set of flow rate and pressure measurements within the network). Thereafter, uncertain system parameters (e.g., water demands and pipe roughness) are adjusted until an acceptable match is achieved between the model outputs and physical observations. Ormsbee (1989) and Lansey and Basnet (1991) were among the first to develop formal optimization methods for determining the uncertain system elements. Datta and Sridharan (1994), and Reddy et al. (1996) used the regression approach in which parameter uncertainties were estimated as part of the calibration process. Greco and Del Giudice (1999) used a "sensitivity matrix" to minimize the least squares differences between observed and predicted values, and Lingireddy and Ormsbee (1998) developed a calibration method using Artificial Neural Networks (ANN). More recently, Kapelan et al. (2007) used the shuffled complex evolution metropolis (SCEM-UA) global optimization algorithm to solve a least-squares-type calibration problem where both calibration parameter values and associated uncertainties were considered in a single optimization model run.

The current research uses a Genetic Algorithm approach following methods developed by Savic and Walters (1995); Wu and Simpson (2001); Kapelan et al. (2002); Wu et al. (2002); Walski et al. (2006); and Clark and Wu (2006).

Overall, the main limitation of all off-line calibration procedures is that they approximate the unknown parameters using a short-term sample of hydraulic data. The calibration results may represent the system hydraulics during the short period of the sampling procedure but they are not expected to accurately represent the system conditions for the full range of operational conditions that can occur. In the case of water demands this issue is even more critical, since water demands have dynamic/stochastic pattern variations which fluctuate with time-changing economic and demographic characteristics and may even show trends with local climatic conditions *(*Maidment and Miaou 1986; Kenward and Howard 1999; Zhou et al. 2000*).* In principle, much more realistic predictions can be achieved by updating the hydraulic state-

estimation using continuous on-line hydraulic measurements, provided by a sensor network installed on the distribution system.

There have been several recent studies that have assimilated on-line measurements into hydraulic state estimation models. Davidson and Bouchart (2006) propose proportional and target demand methods. These are two techniques for adjusting estimated demands in hydraulic models of water distribution networks to produce solutions that are consistent with available Supervisory Control and Data Acquisition (SCADA) data. The two techniques assume that pipe resistances and SCADA data are accurate and that the combination of SCADA data and demand estimates produce over-determined problems. Nodal demands are regarded as stochastic variables which fluctuate about an estimated mean value. The method of weighted least squares is used to obtain solutions that satisfy all of the constraints imposed by SCADA data with adjusted nodal demands that most closely resemble the estimates. The methods are intended for use in real-time modeling but are limited to quasi-steady state flow.

Shang et al. (2006) presented a predictor-corrector method, implemented in an extended Kalman filter to estimate water demands within distribution systems in real-time. A time-series ARIMA model is used to predict the water demands based on the estimated demands at previous steps. The predictions are corrected using measured nodal water heads or pipe flow rates. As noted by the authors, the proposed methodology is in a preliminary stage and aimed mainly to study the impact of spatial correlation between demand forecast errors on demand estimations. The methodology is demonstrated on EPANET example 3, having 59 demand nodes, through three simulation studies with 20 pressure, 20 flow rate, and 40 flow rate sensors. The main conclusion was that the model performances depend on sampling design, measurement uncertainty, demand forecast error and the spatial correlations among the demand forecast errors. Although only preliminary results were presented, the study provided a modeling framework and mathematical tools for further implementations on more complex case studies.

In this study, a Predictor-Corrector (PC) approach which integrates a limited number of continuous hydraulic observations with a computer simulation model is implemented to continually predict the hydraulic state of a real urban water supply comprised of 10550 demand

nodes. The *M5 Model-Trees algorithm* (Quinlan 1992) is used to forecast future water demands for a rolling planning horizon of 24 h ahead, and *Genetic Algorithms* (Holland 1975) are used to correct (i.e., calibrate) these predicted values in real-time. Thereafter, at each subsequent time step, the corrected outputs of previous iterations are used as inputs for the prediction model. This a-priori estimation of the calibration parameters values, which improves through experience, facilitates a better and quicker convergence of the calibration procedure towards the optimal solution of the problem and provides adequate information on the system's hydraulic state for real time operation and control.

2. Methodology

Model definitions and assumptions

1. Calibration Parameters: The calibration parameters used in this study are the variations in water demands (i.e., defined as demand multiplication factors; see next paragraph for a full description of this parameter). The demand multiplication factors (DMFs) are calibrated at each time step of the overall process. Other uncertain variables are less dynamic and their values are assumed to be constant for a certain period of time. It is assumed that valve and/or pump settings are known inputs, while pipe roughness coefficients are calibrated off-line using conventional procedures (with complete supplementary information on pipe diameter, material type, and age).

2. Demand Multiplication Factors (DMFs): The baseline demand (D_{base}) of each consumption node is a deterministic value that usually equals to the average daily demand (i.e., average daily demand is calculated from monthly or quarterly meter readings and billing records). The patterns in demand on a finer time scale are described by Demand Multiplication Factors (DMFs). For each short-term time step in the demand pattern, the relevant DMFs are multiplied with the baseline demands of the consumption nodes to obtain the actual water consumption (i.e., $D_t = D_{base} \times DMF_t$; where D_t is the actual nodal demand at time step t and DMF_t is the demand multiplication factor at the same time step). It is assumed that the min-max DMFs boundaries are 0 and 3, respectively; previous publications (Walski et al. 2003; Jonkergouw et al. 2008) have shown that these min-max boundaries provide acceptable estimates for hourly basis demand multiplication factors.

3. Calibration parameters grouping: There are thousands of unknown parameters in a typical urban water system and only a relatively small number of direct measurements available. This creates an ill-posed, underdetermined problem which leads to non-unique solutions. This can be overcome by grouping the unknown parameters. Grouping is based on the assumption that water customers in a given area of the system will have the same characteristics and will not need large adjustments to achieve calibration (Wu et al. 2002; Walski et al. 2006). The main advantage of 'grouping' is that the size of the problem is reduced - making it possible to find unique solutions to the optimization problem. In this study, the consumption nodes were grouped based on spatial analysis of the system and each group of consumption nodes is assigned its own set of demand multiplication factors.

4. Time step: the method developed in this study is general and can be adjusted to a wide range of time-step intervals so that even frequent continuous sensor measurements can be used in the model. The current analysis uses a fixed one hour time step in order to match the frequency of available hydraulic data.

5. Time cycle: The common approach (Shang et al. 2006, Alvisi et al. 2007, and Ghiassi et al. 2008) for the time-series forecasting of water demands relies on direct identification of patterns existing in the archived system data. It has been observed that water demand patterns usually follow a 24-h cycle. This cycle is called the Diurnal Demand Pattern (DDP) and is used by many urban water utilities to plan the system operation one day ahead (i.e., to schedule pump operation and plan tank storage). Weekend demand patterns often differ from weekday patterns and usually follow a 168-h (1 week) cycle. In this study, daily and weekly demand cycles were used, so that the DMFs at each time-step are predicted based on previously calibrated DMFs from past hours 24, 25, 168, and 169.

Predictor-Corrector Model

The predictor-corrector loop process starts at t=169 hr, after performing an off-line calibration procedure for the first 168 h (1 week) of the collected data; the aim of this off-line calculation is to generate initial values for the input data-set of the prediction model; no a-priori information on the first 168 h DMFs values is available except of the min-max boundaries which are 0 and 3,

respectively. At t=169 h the prediction-correction process (Fig. 1) is initiated. The following paragraphs describe the model steps:

1. DMF prediction: DMFs values of each group of demand nodes are predicted using the *M5 Model Trees algorithm*, with the inputs being the calibrated DMFs from past hours t-24, t-25, t-168, and t-169

2. EPANET simulation: the system hydraulics are simulated using the steady-state mode of EPANET, with the predicted DMFs as inputs; the hydraulic simulation outputs are nodal pressures and pipe flow rates

3. On-line hydraulic data integration: pressure and flow measurements (from a set of in-line sensors) are inserted to the model at the current time step

4. DMF correction/calibration: a calibration problem is formulated and solved using *Genetic Algorithms*. The objective function is the minimization of the differences between predicted and measured hydraulic parameters (i.e., pressure and flow rates at the measured locations), with the decision variables being the consumers' water demands (i.e., the Demand Multiplication Factors - DMFs). A modified Least Squares fit method (the Huber function) which takes into account noisy measurements is implemented to solve the optimization problem

5. DMF delay: the calibrated DMFs are being delayed for 24, 25, 168, and 169 h before being used as inputs in the prediction model

- Steps 1 to 5 are repeated at each subsequent time step

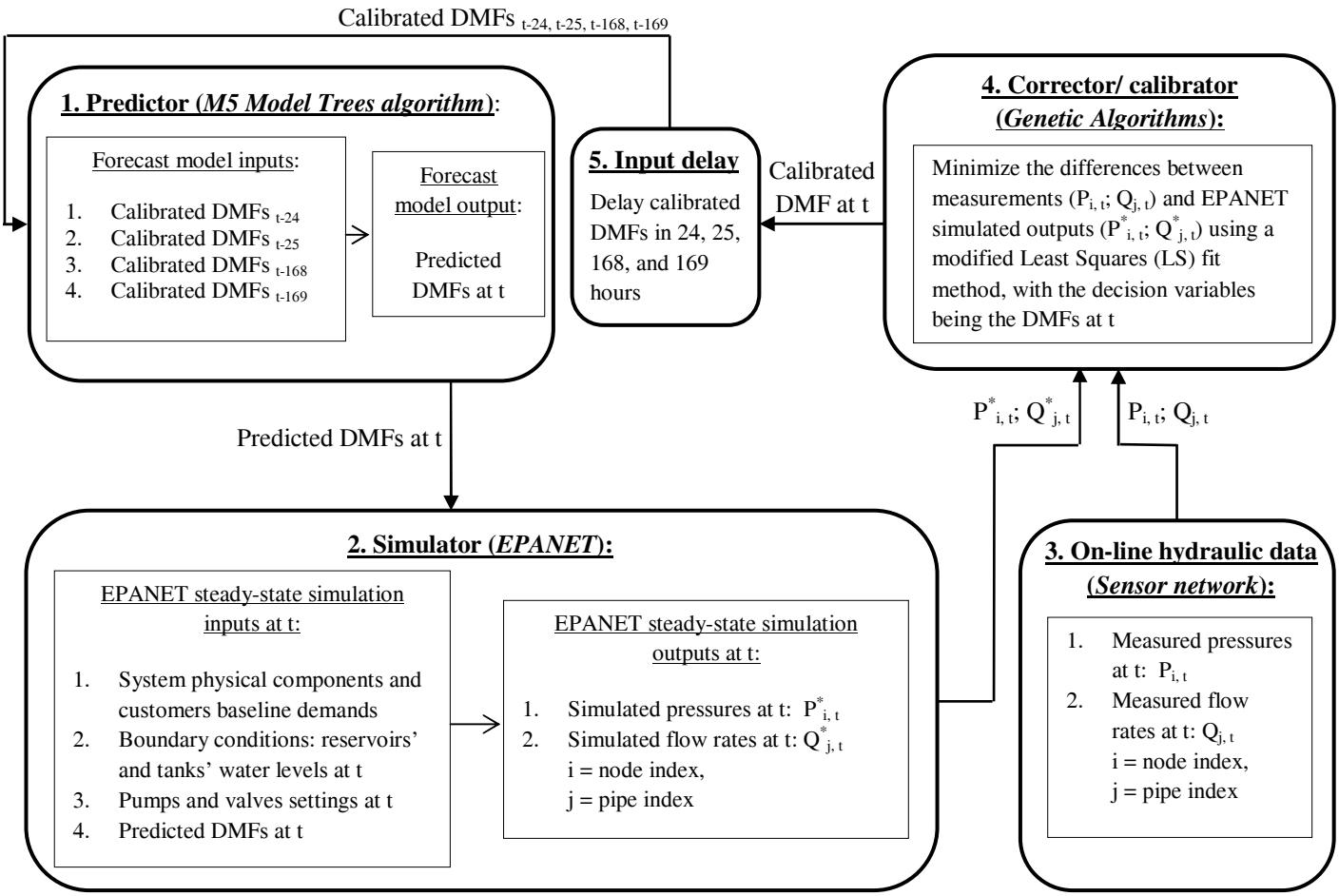

Fig. 1: predictor- corrector loop for Demand Multiplication Factors (DMFs) prediction at the tth time step

The basic building blocks of the predictor-corrector model (e.g., *M5 Model Trees algorithm* and *Genetic Algorithms*) are described in the following paragraphs.

M5 Model Trees algorithm (Quinlan 1992)

The M5 model trees algorithm (Appendix A gives a more comprehensive description of the methodology) builds rule-based predictive models using a top-down induction approach. The tree is fitted to a training data set by recursively partitioning the data into homogeneous subsets based on its attributes. Thereafter, the tree is constructed with all training cases being predicted by the tree leaves (i.e., each leaf is a linear regression model that can explain the remaining variability of each homogeneous subset). In order to simplify the tree structure, and thus to improve its ability to classify new instances, the tree is then pruned from the bottom-up by quantifying the contribution of each attribute to the overall predicted value and removing those

attributes that add little to the model. At the last stage, a smoothing process is performed to compensate for the sharp discontinuities that will inevitably occur between adjacent linear models at the leaves of the pruned tree.

As observed in previous studies (Solomatine and Xue 2004, Bhattacharya et al. 2007, and Ould-Ahmed-Vall et al. 2007), Model Trees have several advantages compared to other data-driven techniques such as Artificial Neural Networks (ANN), Support Vector Machines (SVM), and Regression Trees: Their accuracy is similar to that of both ANN and SVM and much better than that of Regression Trees; they are interpretable to users (in contrast to 'black-box' ANN and SVM models) and hence can provide insights to prevent sources of inefficiencies; and they are much faster in training compared to all other methods.

Genetic Algorithms (GA) (Holland, 1975)

Genetic Algorithms are heuristic combinatorial search techniques that imitate the mechanics of natural selection and natural genetics of Darwin's principles of evolution. The basic idea is to simulate the natural evolution mechanisms of chromosomes (represented by string structures), involving: selection, crossover, and mutation. This is accomplished by creating a random search technique that combines survival of the fittest among string structures with a randomized information exchange. A typical form of a genetic algorithm involves three main stages: 1) Initial population generation: the genetic algorithm generates a bundle of strings (termed population, or generation), with each string (chromosome) being a set of values of the decision variables/optimization parameters. 2) Computation of string fitness: the genetic algorithm evaluates each string's fitness (i.e., the value of the objective function that corresponds to each string). 3) Construction of a new generation: the genetic algorithm establishes the next generation by performing selection, crossover, and mutation. The process of selection involves choosing strings (chromosomes) from the current population for reproduction according to their fitness values. Crossover involves the partial exchange of information between pairs of strings; and mutation is the random change in one of the string locations. The genetic algorithm parameters are the population size, the mating and mutation rates, and the number of generations.

Calibration Problem Objective Function

The objective of the calibration process is to match the computed and measured sensor node data (pressure and/or flow rates), taking into consideration possible noise in the measurements. In this application, calibration is achieved by minimizing a modified least-squares of differences function known as the Huber function (Huber 1973). The Huber function implementation to the hydraulic state estimation problem is described as follows:

1. The differences (i.e., residuals) between modeled and observed pressures and flow rates at each time step, at sensor node *i* - are defined as $R_{i,t}^{P}$ and $R_{i,t}^{Q}$ respectively
2. The Huber function of each residual R is defined as

$$f\left(R_{i,t}^{P\ or\ Q}\right) = \begin{cases} \frac{1}{2}\left(R_{i,t}^{P\ or\ Q}\right)^2, & \left|R_{i,t}^{P\ or\ Q}\right| \le h \\ h\left|R_{i,t}^{P\ or\ Q}\right| - \frac{1}{2}h^2, & \left|R_{i,t}^{P\ or\ Q}\right| > h \end{cases} \quad (1)$$

   where h is a predefined value that represent the tolerance to noise in measurements; for small residuals ($|R| \le h$) that represent low to zero values of noise in sensor measurements, the Huber function minimizes the usual least squares function (i.e., l_2 norm approximation), for large R ($|R| > h$) that represent high values of noise in sensor measurements, it minimizes a linear penalty function which is relatively insensitive to noise (i.e., l_1 norm approximation)
3. The overall calibration problem objective function to be minimized at each hydraulic time-step *t* is defined as

$$\sum_{i=1}^{N_P} f\left(R_{i,t}^{P}\right) + \sum_{i=1}^{N_Q} f\left(R_{i,t}^{Q}\right) \quad (2)$$

   where *i* is the sensor nodes index, N_p is the total number of pressure sensors, and N_Q is the total number of flow rate sensors

- In this application the value of *h* in each sensor node at each time-step is equal to the average of all previous time-steps sensor node residuals multiplied by a factor of 2.

3. Results

The predictor-corrector approach developed in this study was tested against the real input data of Network 2 (Fig. 2) of the "Battle of the Water Sensor Networks (BWSN): A Design Challenge for Engineers and Algorithms" (Ostfeld et al. 2008). The network corresponds to an anonymous but real water distribution system comprising 12,523 nodes, two constant head

sources, two tanks, 14,822 pipes, four pumps, five valves. The system was subject to highly variable demand patterns over a period of 934 hours (~39 days). Hydraulic simulations for this system are considered valid for this entire duration. The original EPANET input file was downloaded from the University of Exeter Centre for Water Systems (ECWS) web-site (http://www.exeter.ac.uk/cws/bwsn).

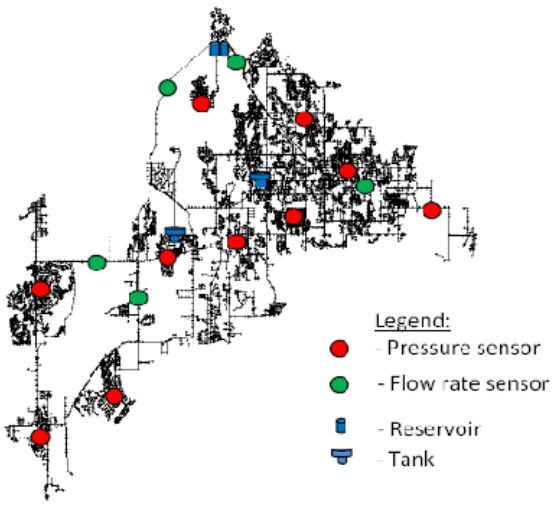

Fig. 2: Network 2 with the sensor nodes locations

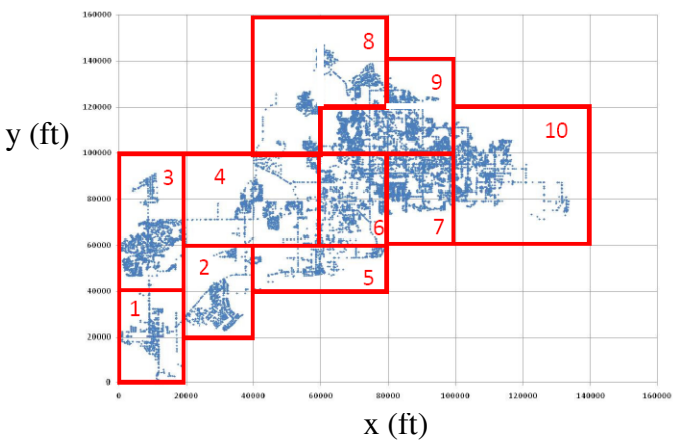

Fig. 3: demand nodes groups on a plane grid of the system

The current application assumes that continuous in-line data are available from 10 pressure and 5 flow rate sensors (Fig. 2). The nodal flow and pressure records from these locations were generated by the EPANET model using real input data for the system. The reservoirs and tank water levels were considered as known inputs. The analysis considers 10 demand zones (i.e., 10 groups of demand nodes; see Fig.3) based on a spatial analysis of the system. It is expected that the consumption nodes in each zone will follow the same demand pattern and each nodal base demand at each zone will be multiplied with the same DMF. Therefore, the number of decision variables to be calibrated/corrected at each time-step is equal to 10.

The total running time on a DELL PC (2.66 GHz, 3.0 GB of RAM) of the GA calibration process (i.e., with a GA population of 48 ‘chromosomes’ and 30 GA generations) is about 5 minutes and the total running time of the data driven prediction process is less than 10 seconds.

Base Run: Demand Multiplication Factors (DMFs) prediction accuracy

Following previous data-driven models implementations (e.g., Solomatine and Xue 2004 and Bhattacharya et al. 2007), about 33% of the data (from t = 680 to 934 hrs, corresponding to a total of 254 hrs) was used for cross validating the model predictions. The predictive ability of the model can be evaluated with several prediction metrics. In this application, the following commonly used metrics were applied to evaluate the fit between predicted (p) and actual (a) values:

1. Correlation Coefficient (CC): measures the degree of correlation between predicted and actual values; it ranges from -1 to 1, with 1 corresponding to an ideal correlation:

$$CC = \frac{Cov(p,a)}{\sigma_p \sigma_a} \quad (3)$$

where $Cov(p,a)$ is the covariance between p and a; and σ_p, σ_a are their standard deviations

2. Root Mean Squared Error (RMSE): RMSE is a frequently-used measure of the differences between values predicted by a model or an estimator and the values actually observed; it ranges from 0 to infinity, with 0 corresponding to ideal fit:

$$RMSE = \sqrt{\frac{\sum_{i=1}^{N}(p_i - a_i)^2}{N}} \quad (4)$$

where p_i and a_i are the predicted and actual values of case i; and N is the number of cases

3. Mean Absolute Error (MAE): MAE is similar to RMSE, except it uses absolute error values instead of the squared errors; it ranges from 0 to infinity, with 0 corresponding to ideal fit:

$$MAE = \frac{\sum_{i=1}^{N}|p_i - a_i|}{N} \quad (5)$$

where p_i and a_i are the predicted and actual values of case i; and N is the number of cases

4. Root Relative Squared Error (RRSE): RRSE value is relative to what it would have been if a naive predictor had been used. More specifically, this simple predictor is just the average of the actual values; it ranges from 0 to infinity, with 0 corresponding to ideal fit:

$$RRSE = \sqrt{\frac{\sum_{i=1}^{N}(p_i - a_i)^2}{\sum_{i=1}^{N}(a_i - a_{av})^2}} \quad (6)$$

where p_i and a_i are the predicted and actual values of case i; a_{av} is the mean of the observed data; and N is the number of cases

The accuracy of the 10 zones DMF predictions is summarized in Table 1:

Zone index	CC	RMSE	MAE	RRSE
1	0.87	0.05	0.06	0.16
2	0.89	0.06	0.06	0.18
3	0.92	0.04	0.05	0.18
4	0.85	0.06	0.06	0.18
5	0.85	0.06	0.06	0.18
6	0.86	0.06	0.07	0.17
7	0.91	0.07	0.06	0.16
8	0.92	0.05	0.06	0.16
9	0.87	0.04	0.05	0.15
10	0.92	0.04	0.05	0.15

Table 1: Predictive metrics for DMFs in 10 demand zones from base run

The results indicate that the predictor – corrector model has relatively good predictive accuracy for all 10 demand zones according to all four metrics. All of the DMFs were predicted with a correlation coefficient exceeding 0.85 with mean absolute error below 10%. Figures 4 to 6 show the improvement achieved in the predictor-corrector model predictions through experience, as demonstrated on one of the system demand nodes (e.g., Junction 7631). In this example, the correlation coefficient (CC) is used as the characteristic measure of predictive accuracy. The data set of results from t = 169 – 934 hrs was divided into 3 segments (Δt_1 =169 - 424 hrs; Δt_2 =425 - 679 hrs; and Δt_3 = 680 to t=934 hrs). Figure 4 shows a correlation coefficient, CC = 0.66 for time period Δt_1. This low value is explained by insufficient input data for the Model Trees predictor in forecasting future DMFs. For the second (Fig. 5) and third (Fig. 6) time periods, with the increase in training data, there is an improvement in the predictor-corrector performances that is refelected in higher correlation coefficients, CC = 0.85 and 0.92, for periods Δt_2 and Δt_3, respectively.

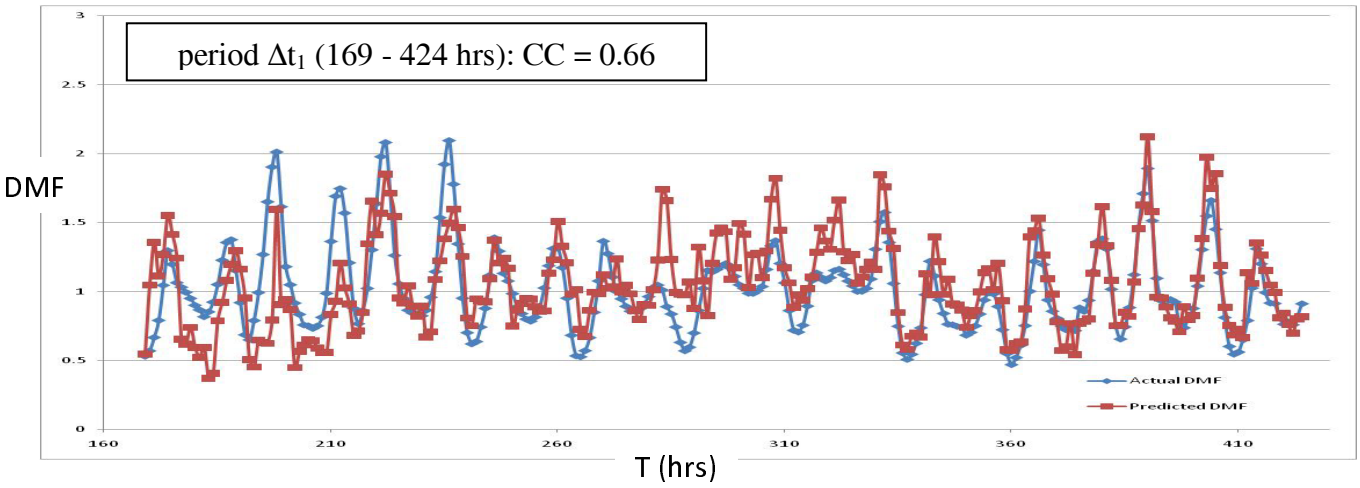

Fig. 4: Comparison between predicted and actual DMFs for time period 1;

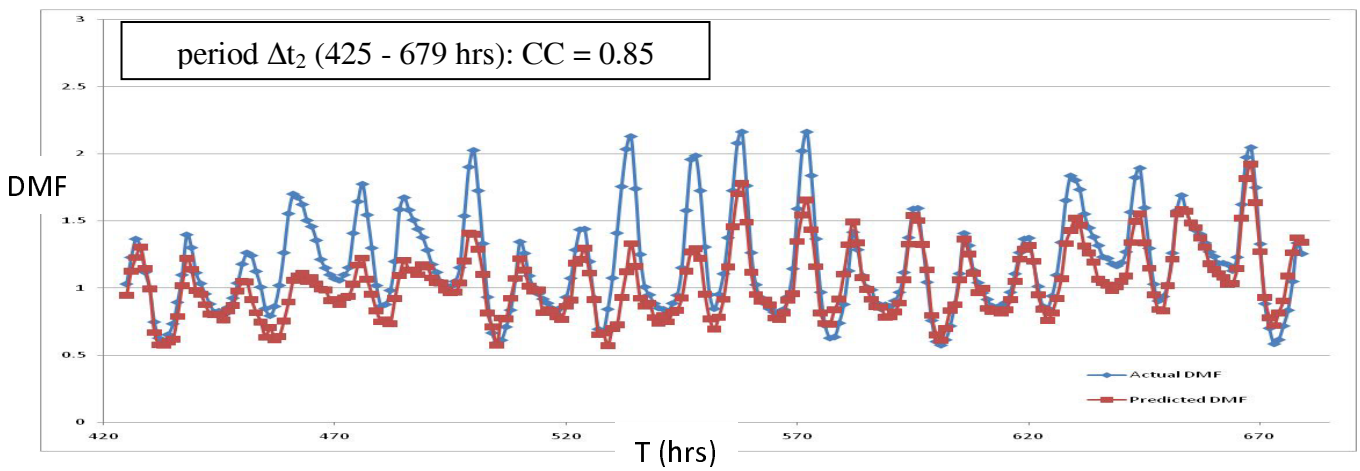

Fig. 5: Comparison between predicted and actual DMFs for time period 2;

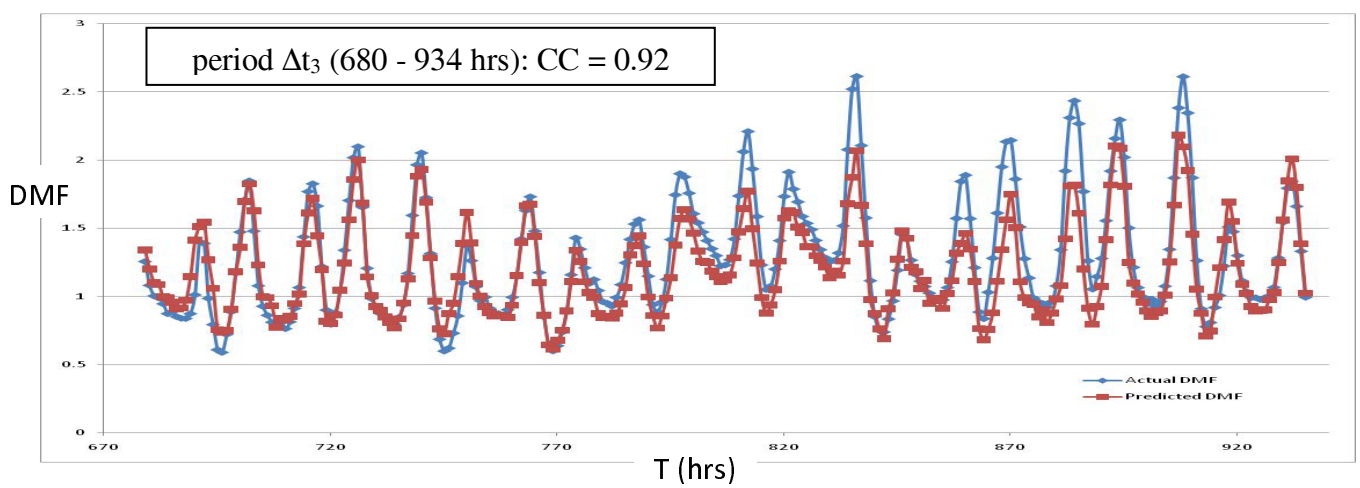

Fig. 6: Comparison between predicted and actual DMFs for time period 3;

Comparison between on-line and off-line calibration model performance

Since the main hypothesis of this study is that on-line hydraulic-state prediction models are more accurate than off-line calibration models in representing the hydraulic state of the water system, the predictive accuracy of the proposed predictor-corrector analysis must be compared with reference results from off-line calibration. The off-line reference result are based on a calibration using the same pressure and flow records for a one-week period ($\Delta t_0 = 0 - 168$ hrs). The off-line calibration process was much more intensive then the on-line model (200 GA iterations instead of 30, with a GA population of 120 decision variables' strings instead of 48) and resulted in a relatively high fit for the DMF's during the calibration time period.

The predicted Demand Multiplication Factors (DMFs) for time period 3 (680 - 934 hrs) were used together with EPANET analyses to calculate unknown hydraulic outputs (e.g., flow rates; flow directions; and nodal pressures). Thereafter, these parameters, which represent the hydraulic state of the water system - were used to evaluate and compare the predictions accuracy of the on-line and off-line models.

1. Flow rate prediction

The statistical evaluation of the predicted flow rates includes 5 ranges of predictive accuracy (i.e., within 5, 10, 15, 20, and 25 % of the actual flow rates for two groups of pipes: 1) pipes with diameters less than 24'' which correspond to more than 80% of the network length and 2) medium and large pipes with diameter greater than 24" The statistics are computed for all the pipes in the system (e.g., 15000 pipes) throughout time period 3 (i.e., over a period of 254 hrs); such that the total number of flow rates considered is 3.76×10^6 (14822x254). The results for pipe groups 1 and 2 are shown in Figures 7 and 8, respectively. The proposed predictor-corrector model outperforms the off-line calibration process and provides significantly better estimates of flow rates for both sets of pipes. The predictions are generally much more accurate for the medium and large pipes (group 2, Figure 8) than for the small diameter pipes (group 1, Figure 7). For the medium and large diameter pipes, the predictor-corrector model is within 5% of the actual flow rates for 68% of the samples and within 25% for 95% of the sample population (Fig. 8). For the smaller pipes the 5% and 25% accuracy rates drop to 48% and 86% of the

population. In contrast, the off-line calibration is only within 5% of the actual flow for 22% of the small pipes and 43% of the medium to large pipe sample population.

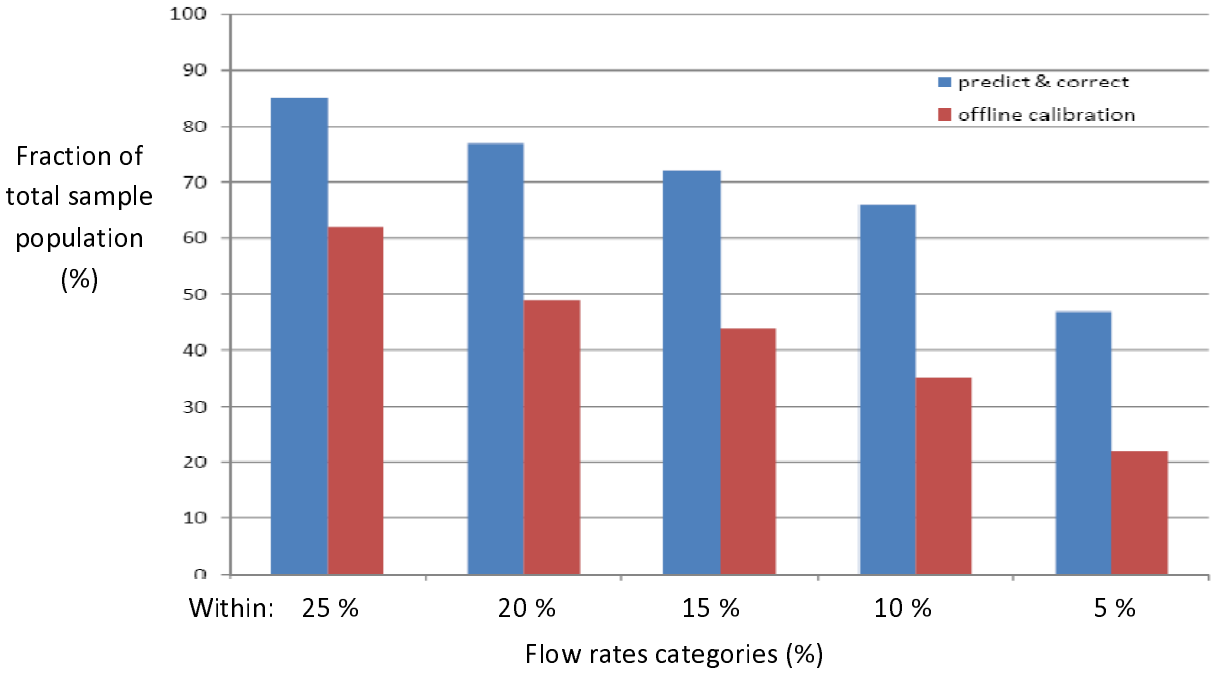

Fig. 7: Comparison of estimated and measured flow rates using the predictor-corrector and off-line calibration methods small pipes (with diameter less than 24")

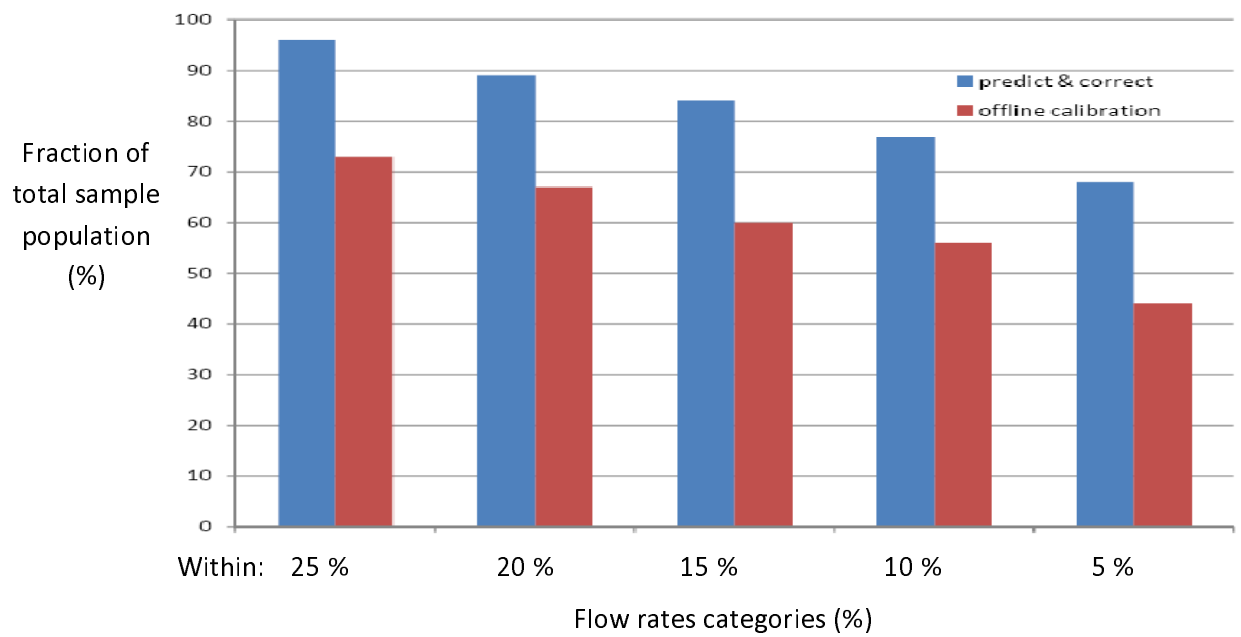

Fig. 8: Comparison of estimated and measured flow rates using the predictor-corrector and off-line calibration methods for medium and large pipes (diameter greater than 24")

The proposed predictor-corrector model correctly estimated the flow direction for 100 % of the sample population of 114822 pipes from t = 680 to 934 hrs while the off-line calibration was accurate for 97% of the actual flow directions in the system. The main conclusion from the above is that flow directions are less sensitive to variations in the DMFs (at least for this reference pipe network) as both the on-line and off-line models were able to provide very accurate estimations of this parameter.

2. Pressure prediction

The statistical evaluation of nodal pressures considers 7 ranges of predictive accuracy (i.e., ± 2, 4, 6, 8, 10, 12 and 14 psi of the actual pressures). The statistics are computed for all the nodes in the system (e.g., 12523 nodes) through time period 3 (t = 680 - 934 hrs); corresponding to a total sample population of 3.81×10^6. It can again be observed that the proposed predictor-corrector model provides significantly better estimations for the pressures than the off-line calibration process. In this case, 87% of the samples are estimated within 4psi using the predictor-corrector scheme compared to 42% using the off-line calibration.

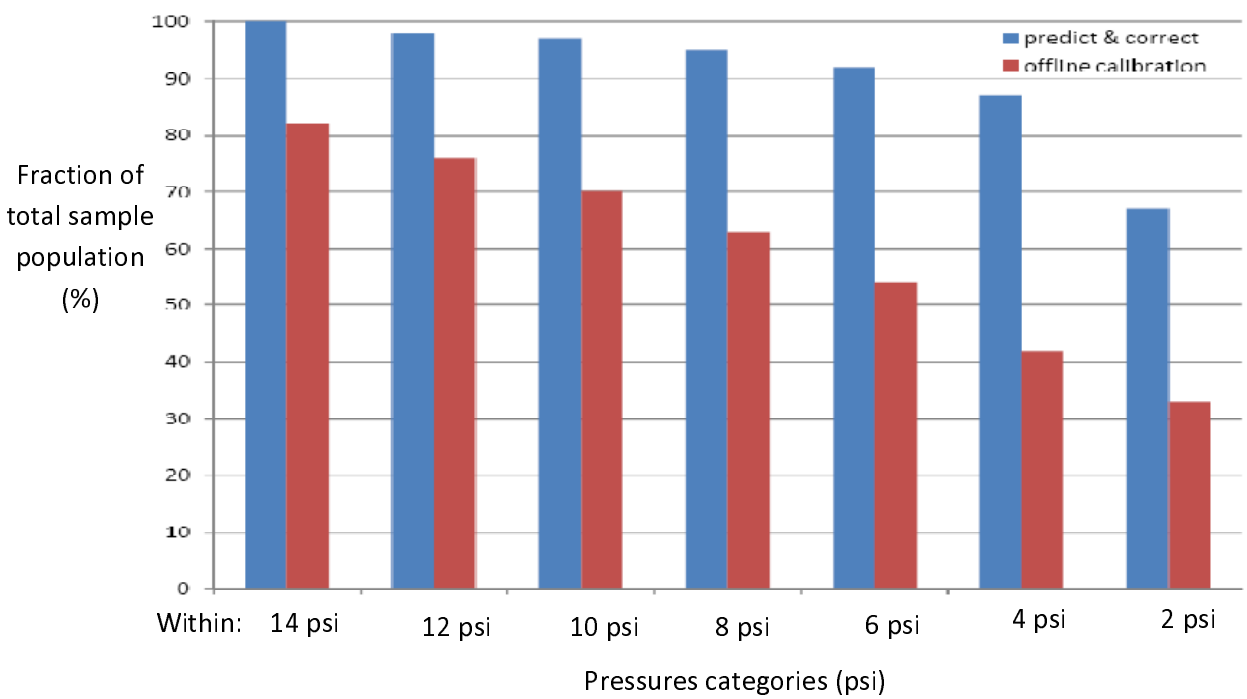

Figure 9: Comparison of predictive accuracy for nodal pressures using the proposed predictor-corrector scheme and an off-line calibration process

Effect of Demand Zone selection

The Authors have carried out a sensitivity analysis to evaluate how the partition of the system into demand zones can affect performance of the predictor-corrector model. Figure 10 shows a revised partition of the network into 20 demand zones. In order to keep the problem slightly over-determined, the number of the sensor locations was increased to 25. In order to comply with the increase in the number of decision variables in the calibration problem, the genetic algorithm parameters were altered to 60 iterations with a population of 96 decision variable strings (vs. 30 and 48, respectively, used in the base run).

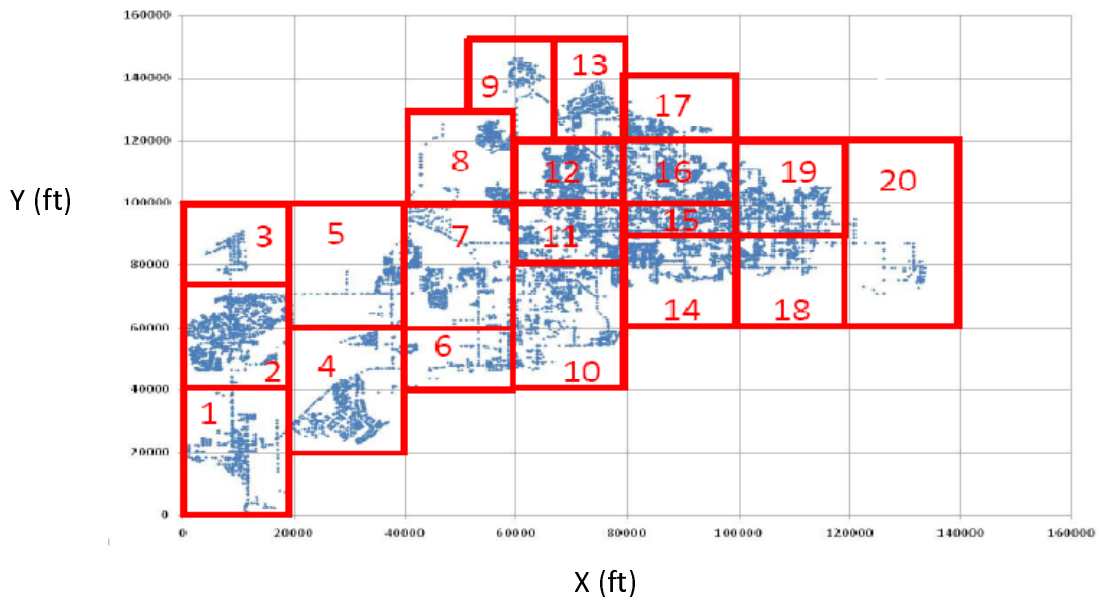

Fig. 10: Sensitivity analysis using 20 demand zones for the reference pipe network

The correlation coefficients for the DMF's in the 20 zones DMF are summarized in Table 2:

Zone index	CC	Zone index	CC
1	0.88	11	0.85
2	0.86	12	0.88
3	0.83	13	0.87
4	0.89	14	0.78
5	0.84	15	0.89
6	0.88	16	0.92
7	0.88	17	0.91
8	0.86	18	0.86
9	0.93	19	0.86
10	0.92	20	0.87

Table 2: Correlation coefficients of DMFs for the 20 zone model of the network

The average correlation coefficient for the entire system (CC = 0.87) is slightly lower than that obtained in the base run (average CC = 0.89) but requires much higher computational effort (e.g., about double the total running time of the base run) making it not worthwhile to change the demand zones selection used in the base run. Although, the revised partition of the network into 20 demand zones need not necessarily improves the predictive accuracy of the model (at least using CC values) this process of testing different system partitions is important as it may improve the model performances. As a conclusion of this sensitivity analysis, grouping demand nodes into demand zones requires high level of judgment based on good knowledge of the system structure. Therefore, if Geographical Information System (GIS) data of the municipality is available, then it is advisable to incorporate it in the demand zone selection procedure and to test the model performances with several system partitions.

4. Summary

This paper has presented and demonstrated a Predictor-Corrector (PC) model for on-line, hydraulic state prediction of urban water networks. The method uses a statistical data-driven algorithm (M5 Model Trees algorithm) to estimate future water demands, while near real-time field measurements are used to correct (i.e., calibrate) these predicted values on-line. The calibration problem is solved using Genetic Algorithms with a modified Least Squares (LS) fit method (Huber function) to account for noisy measurements. The a-priori estimation (i.e., prediction) of the decision variables values, which improves through experience facilitates a better convergence of the calibration model towards the optimal solution of the problem; and provides adequate information on the system's hydraulic state for real time optimization. Future research efforts will focus on the implementation of the developed methodology on large scale urban water system using physical data from an in-situ sensor network. Additional efforts will focus on the ability to detect anomalies such as leakage and burst events in real time. The integration of water networks aggregation methods to reduce the computational time required for the calibration process will also be explored.

References

Alvisi, S., Franchini, M., Marinelli, A., (2007),"A short-term, pattern-based model for water-demand forecasting" Journal of Hydroinformatics, Vol. 9, No. 1

Bhattacharya, B., Price, R.K., and Solomatine, D.P., (2007), "A machine learning approach to modeling sediment transport", ASCE J. of Hydraulic Engineering,133(4), 440-450.

Clark , C., Wu, Z, Y. (2006), "Integrated Hydraulic Model and Genetic Algorithm Optimization for Informed Analysis of A Real Water System", 8th Annual Water Distribution Systems Analysis Symposium, Cincinnati, Ohio, USA, CD-Rom.

Davidson, J. W., Bouchart, F. J.-C., (2006), "Adjusting Nodal Demands in SCADA Constrained Real-Time Water Distribution Network Models", Journal of Hydraulic Engineering, Vol. 132, No. 1

Datta, R.S.N., and Sridharan, K. (1994), "Parameter Estimation in Water-Distribution Systems by Least Squares", Journal of Water Resources Planning and Management, ASCE, 120(4), 405-422.

EPANET. (USEPA 2002) Available on line at: www.epa.gov/ORD/NRMRL/wswrd/epanet.html

Ghiassi, M., Zimbra, D. K., and Saidane, H., (2008), "Urban Water Demand Forecasting with a Dynamic Artificial Neural Network Model", Journal of Water Resources Planning and Management, Vol. 134, No. 2

Greco, M., and Del Guidice, G. (1999), "New Approach to Water Distribution Network Calibration", Journal of Hydraulic Engineering, ASCE, 125(8), 849-854.

Holland J. H. (1975). "Adaptation in natural and artificial systems." The University of Michigan Press, Ann Arbor.

Huber, P. J., (1973), "Robust regression: Asymptotics, conjectures, and Monte Carlo" Ann. Statist., 1, 799-821.

Jonkergouw, P. M. R., Khu, S.-T., Kapelan, Z. S., and Savić, D. A., (2008), "Water Quality Model Calibration under Unknown Demands" Journal of Water Resources Planning and Management, Vol. 134, No. 4

Kapelan, Z. S., Savic, D. A., and Walters, G. A. (2002) ''Hybrid GA for calibration of water distribution system hydraulic models.'' Proc., 1st Annual Environmental & Water Resources Systems Analysis (EWRSA) Symp., CD-Rom.

Kapelan, Z. S., Savic, D. A., and Walters, G., A., (2007), "Calibration of Water Distribution Hydraulic Models Using a Bayesian-Type Procedure" Journal of Hydraulic Engineering, Vol. 133, No. 8,pp. 927-936

Kenward, T. C., and Howard, C. D. (1999). "Forecasting for urban water demand management." *Proc., 26th Annual Water Resources Planning and Management Conf.*, ASCE, Reston, Va.

Lansey, K. E., and Basnet, C. (1991). "Parameter estimation for water distribution networks." Journal of Water Resources Planning and Management, ASCE, 117(1), 126– 144.

Lingireddy, S. and Ormsbee, L. (1998) "Neural Networks in Optimal Calibration of Water DistributionSystems," Artificial Neural Networks for Civil Engineers: Advanced Features and Applications, ASCE.

Maidment, D. R., and Miaou, S. P. (1986). "Daily water use in ninecities." *J. Water Resour. Plann. Manage.*, 110 (1), 90–106.

Ormsbee, L. E. (1989). "Implicit network calibration." Journal of Water Resources Planning and Management, ASCE., 115(2), 243–257.

Ostfeld A. et al. (+ 34 co-authors) (2008). "The battle of the water sensor networks: a design challenge for engineers and algorithms." Journal of Water Resources Planning and Management Division, ASCE, Vol. 134, No. 6, pp. 556- 568.

Ould-Ahmed-Vall, E., Woodlee, J., Yount, C., Doshi, K., (2007) "On the Comparison of Regression Algorithms for Computer Architecture Performance Analysis of Software Applications", First Workshop on Statistical and Machine learning approaches applied to Architectures and compilation**,** Ghent, Belgium

Quinlan J. R. (1992). "Learning with continuous classes." Proceedings 5th Australian Joint Conference on Artificial Intelligence. World Scientific, Singapore, 343-348

Reddy, P.V.N., Sridharan, K., and Rao, P.V. (1996), "WLS Method for Parameter Estimation in Water Distribution Networks", Journal of Water Resources Planning and management, ASCE, 122(3), 157-164.

Savic, D.A., and Walters, G.A. (1995), "Genetic Algorithm Techniques for Calibrating Network Models", Report No. 95/12, Centre for Systems and Control Engineering, University of Exeter, p. 41.

Shang, F., Uber, J., van Bloemen Waanders, B., Boccelli, D. , Janke, R.(2006) "Real Time Water Demand Estimation in Water Distribution System", 8th Annual Water Distribution Systems Analysis Symposium, Cincinnati, Ohio, USA, CD-Rom.

Solomatine, D.P. and Xue, Y., (2004) "M5 model trees compared to neural networks: application to flood forecasting in the upper reach of the Huai River in China" ASCE Journal of Hydrologic Engineering, 9(6)

USEPA (2005), Water Distribution System Analysis: Field Studies, Modeling and Management. A Reference Guide for Utilities. USEPA Cincinnati, Ohio, USA

Walski, T. M. (1983). "Technique for calibrating network models." Journal of Water Resources Planning and Management, ASCE, 109(4), 360–372.

Walski, T.M., Chase, D.V., Savic, D.,A., Grayman, W., Beckwith, S. and Koelle, E., (2003) "Advanced Water Distribution Modeling and Management," Haestad Methods, Inc. Waterbury, CT.

Walski, T.M., Defrank, N., Voglino, T., Wood, R., Whitman, E. (2006), "Determining the Accuracy of Automated Calibration of Pipe Network Models", 8th Annual Water Distribution Systems Analysis Symposium, Cincinnati, Ohio, USA, CD-Rom.

Wu, Z. Y. and Simpson A. R. (2001) "Competent Genetic Algorithm Optimization of Water Distribution Systems." J. of Computing in Civil Engineering, ASCE, Vol 15, No. 2, pp 89-101.

Wu, Z, Y., Walski, T.M., Mankowski, R., Herrin, G., Gurrieri,, R. and Tryby, M. (2002), "Calibrating Water Distribution Models via Genetic Algorithms," Proceedings AWWA Information Management Technology Conference, Kansas City, Mo.

Zhou, S. L., McMahon, T. A., and Lewis, W. J. (2000). "Forecasting daily urban water demand: A case study of Melbourne." *J. Hydrol.*, 236, 153–164.

Appendix A: *Model Trees* Construction using the *M5* Algorithm (Quinlan 1992)

Suppose we have a set of *T* training cases. Each case is specified by its value of a fixed set of attributes and has an associated target value. The aim is to construct a model that relates the target values of the training cases to their values described by the input attributes. The performance of the model will generally be measured by the accuracy with which it predicts the target values of unseen cases (cross-validation data set). Fig. A1 illustrates a set *T* which is described by two input attributes (x_1, x_2) and one target attribute (y):

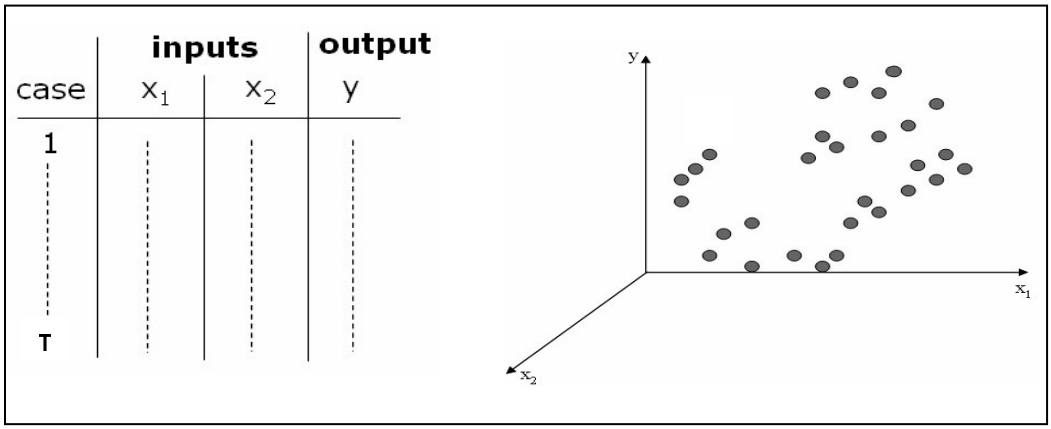

Fig. A1: Set T - described by 2 input attributes (x_1, x_2) and 1 target attribute (y)

In this tree based model, the set *T* is either associated with a leaf, or some test is chosen that splits *T* into subsets corresponding to the test outcomes. The same process is applied recursively to the subsets. This persistent division often produces over-elaborate structures that must be pruned back (i.e., this process is described by the following steps).

Step 1: Building the Initial Tree

The standard deviation of the target values of cases in *T* is computed. Unless *T* contains very few cases (e.g., three examples or less) or their values vary only slightly (e.g., 5% of the standard deviation of the class values of the original set of examples), *T* is split on the outcome of a test. Every potential test is evaluated by determining the subset of cases associated with each outcome; let T_i denote the subset of cases that have the *i-th* outcome of the potential test. If we treat the standard deviation $sd(T_i)$ of the target values of cases in T_i as a measure of error, the expected reduction in error (*SDR*) as a result of this test can be written as:

$$SDR = sd(T) - \frac{1}{|T|}\sum_i |T_i| \, sd(T_i) \qquad \text{(A1)}$$

After examining all possible tests, the model tree chooses one that maximizes this expected error reduction (*SDR*). At this step an initial model tree has been grown and a multivariate linear model is constructed for the cases at each node of the model tree using standard regression techniques. Fig. A2 illustrates this process on the data set *T* introduced in Fig. A1.

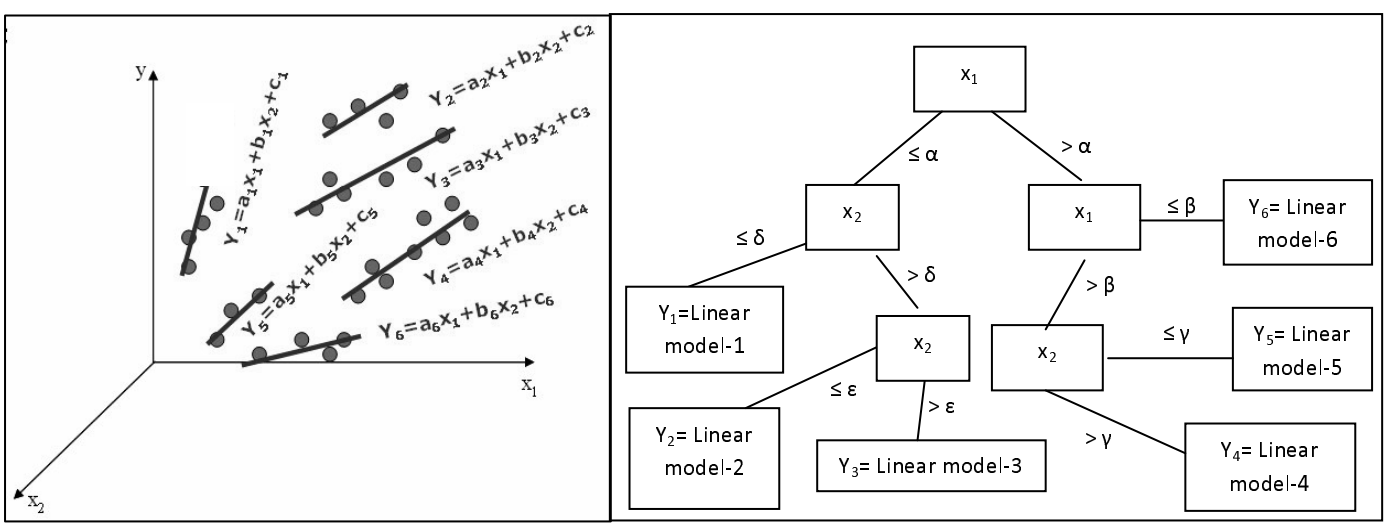

Fig. A2: model tree construction based on the data set - *T*

After that, the tree is transferred into a simple set of *If-Then* rules that simplify the tree structure and make the tree internal structure interpretable to users. Fig. A3 illustrates this process on the data set *T* introduced in Fig. A1.

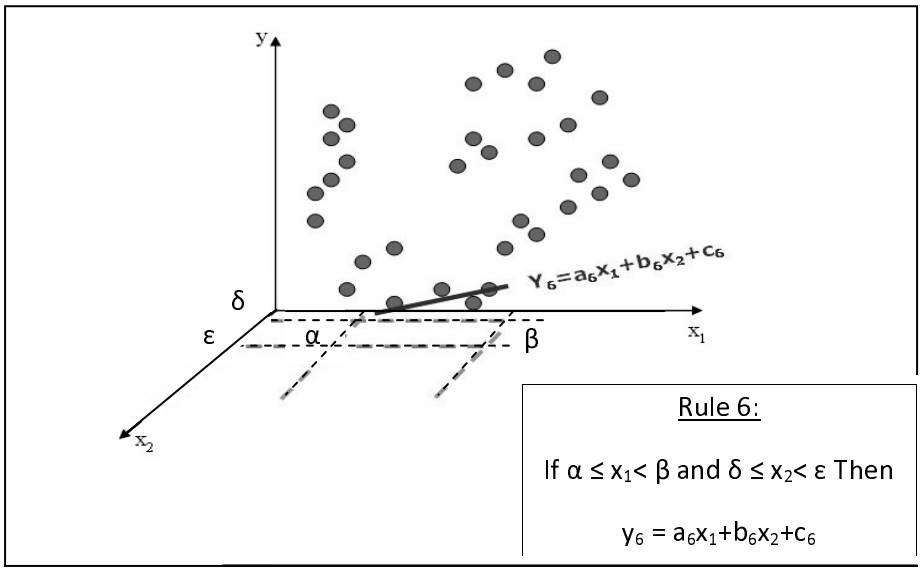

Fig. A3: model tree transformation into an *If-Then* set of rules demonstrated on sub-set Y_6

Step 2: Pruning the Tree

At the second step, the over-elaborated model tree structure is simplified, and pruned bottom-up - and thus its ability to classify new data sets (i.e. cross validation data) is improved. The simplification of the model tree is performed mainly by removing variables that contribute little to the model; in some cases the algorithm removes all variables, leaving only a constant.

Step 3: Smoothing

The smoothing process is performed to compensate for the sharp discontinuities that will inevitably occur between adjacent linear models at the leaves of the pruned tree, particularly for some models constructed from a smaller number of training examples. In smoothing, the adjacent linear equations are updated in such a way that the predicted outputs for the neighboring linear input equations are becoming close in value.

SAMPLING OF RESIDENTIAL WATER USE FOR LEAK CONTROL VIA WATER BUDGETS

C.Arena[1], A. Criminisi[2], A. Fortunato[1] and M.R. Mazzola[1]

[1]Dipartimento di Ingegneria Idraulica ed Applicazioni Ambientali, Viale delle Scienze, Edificio 8, 90128 Palermo, Italy; email arena@idra.unipa.it, antonino.fortunato@libero.it, mazzola@idra.unipa.it
[2]AMAP SpA, Via Volturno 20, 90100, Palermo, Italy; email: crimanto@yahoo.it

ABSTRACT

The paper provides insights into the sampling techniques that may be employed to assess domestic water use for developing water budgets at district scale aimed at losses evaluation. The basic idea is to use only few meters to provide inference on the total use of a district metered area by standard statistical sampling procedures. Random and stratified sampling are compared with reference to the sampling fraction necessary to obtain estimates of the daily use totals (or means) with given precision and confidence level. An application with real data from a small, homogeneous group of connections in Palermo (Italy) shows how stratified sampling allows a considerable reduction of the sampling fraction. A sensitivity analysis on model parameters (group variance, precision, confidence levels) shows how stratified sampling is always a better option than random sampling and that results are mainly driven by precision, with a considerable increase of the required sample size when the desired precision shifts from 5% to 1%.

INTRODUCTION

Developing water budgets is a basic step to assess the level of water losses in district-metered water distribution networks and is hence preliminary to the selection of asset management options such as leak detection and removal, pipe rehabilitation or substitution. It requires knowledge of water use of individual customers. Albeit conceptually straightforward, the water budget methodology has its major drawback in the metering of water use, as the metering system can be (inhomogeneously) old (or even absent in some instances) or it can prove difficult to organise extensive and detailed surveys of consumption data, whose format and information attached are in most cases designed for accounting purposes, rather than for technical ones. In addition, the amount of time required to implement such procedures may be incompatible with the requirements of the asset planning (and subsequent decision-making) process and with a real-time strategy of monitoring losses. This is particularly true whenever heterogeneous types of domestic uses co-exist within the same administrative unit, as is the case for the Italian "Ambiti", groups of neighbouring municipalities where water service is operated by a single company and

therefore sharing the same water tariff and the same investment plan. For such reasons, water budgets are often given up in the diagnosis of water losses in a water distribution network in favour of bottom-up approaches such as continuos night flow measurement (Farley and Tow, 2003).

It can be hence of some interest to explore the option to provide only few districts, or customers, with a perfectly working and updated metering system and to extend the results obtained to similar districts or users. In this paper the focus will be on this latter option, i.e. working with microdata of residential water use to assess water use of the whole district. Evaluation of the feasibility of working at larger scale (i.e. determining the number of districts to meter in order to infer total water use of a larger number of districts) is left to future work.

Curiously enough, the idea has received little attention both from the research community and from water utilities: after the pioneer work by Hanke and Mehrez (1979) on microdata of peak hour water use, although the importance of sampling domestic water use has been recognised and illustrated (Mays, 2004), little research and field work has been produced on the subject: Arreguin Cortes and Ochon-Alejo (1997) apply stratified sampling procedures directly to losses measurements, while Speight et al. (2004) suggest stratified sampling methodology as a suitable procedure for water quality assessment in water distribution systems and propose stratification criteria that are then evaluated via a synthetic data set. To some degree, such reduced set of experiences is in contrast with the considerable development of studies and tools for modelling time series of domestic consumption (e.g. Buchberger and Wu, 1995, Magini et al., 2008). Both aspects, however, should be seen as complementary, as the possibility of extending the results of time series modelling of single or multiple users to an entire district-metered area is also related to the selection of an appropriate sample size.

The paper is organized as follows. After a brief review on the theoretical background of sampling, a case study is introduced and a sensitivity analysis on the variables involved in the methodology is carried out, in order to highlight the ones with the largest impact on the necessary sample size.

SOME RESULTS FROM SAMPLING THEORY

Statistical sampling allows to obtain information on a given characteristic η of a population Ω of size N (η may be the water use of N domestic users) through a subset of Ω, i.e. n sampling units, with $n<N$. Sampled values of the characteristic will be denoted with y, in order to distinguish them from population values η. Information is conveyed through a synthetic value $f(\eta)$, such as the mean of the characteristic or its total, whose estimator will be denoted with h(y). The problem is to assess the number of sampling units to be drawn such that the estimated synthetic value h(y) may be assumed with a certain degree of confidence α to approximate the "true" value with a given precision ε. In statistical terms this implies that $f(\eta)$ has a probability of $1-\alpha$ to fall within interval $[h(y) - \varepsilon, h(y) + \varepsilon]$.

Sampling techniques vary according to how sampling is performed, i.e. to how the n units are selected out of the population. Simple random sampling, for instance, refers to a method of selection of the n sampling units such that the distinct samples

have an equal chance of being drawn. In stratified sampling, the population is first divided into M nonoverlapping subpopulations Ω_k (called groups or *strata*) of size N_k with $1 \leq k \leq M$ and samples of size n_k are then drawn from each stratum. If each stratum is sampled randomly, then the sampling procedure is described as stratified random sampling. Some standard definition and results from sampling theory are reported in the following (Cocchi, 2006).
Let $m(\eta)$ be the population mean and $v^2(\eta)$ the population variance:

$$v^2(\eta) = v(\eta,\eta) = \frac{1}{N}\sum_{\lambda=1}^{N}(\eta_\lambda - m(\eta))^2 \tag{1}$$

An unbiased estimator of (1) is:

$$s^2(\eta) = s(\eta,\eta) = \frac{N}{N-1}v^2(\eta) \tag{2}$$

In stratified sampling, a group mean and a group variance can be defined:

$$m(\eta_k) = \frac{1}{N_k}\sum_{\lambda=1}^{N_k}\eta_{k\lambda} \tag{3}$$

$$v^2(\eta_k) = \frac{1}{N_k}\sum_{\lambda=1}^{N_k}(\eta_{k\lambda} - m(\eta_k))^2 \tag{4}$$

An unbiased estimator of (4) is the following:

$$s^2(\eta_k) = \frac{N_k}{N_k-1}v^2(\eta_k) \tag{5}$$

that is, the variance of the *k*-th subpopulation.
In addition, a within-stratum variance can be introduced...

$$v_e^2(\eta) = \frac{1}{N}\sum_{k=1}^{M}N_k v^2(\eta_k) \tag{6}$$

...and a variance between the strata:

$$v_t^2(\eta) = \frac{1}{N}\sum_{k=1}^{M}N_k\left[m(\eta_k) - m(\eta)\right]^2 \tag{7}$$

$v^2{}_e(\eta)$ is hence the weighted average of the group variances, group size being the weight, and $v^2{}_t(\eta)$ is a measure of the distance of the mean of each group from the mean of population Ω.
It can be shown that the following additive decomposition holds:

$$v^2(\eta) = v_e^2(\eta) + v_t^2(\eta) \tag{8}$$

that is, total population variance is the sum of a within-stratum variance and the between strata variance. The strategy of stratified sampling consists of maximizing the distance among different groups (the variance between strata) thus minimizing within-stratum variance. As sample size is driven by within-stratum variance,

reducing it through appropriate stratification will determine significant reductions of the overall sample size.
Incidentally, from (8) an expression for sample variance follows:

$$s^2 = \frac{1}{(N-1)}\left\{\sum_k N_k\left[m_k - m\right]^2 + \sum_k (N_k - 1)s^2{}_k\right\} \tag{9}$$

The above proposition on the possibility of reducing sample size through the selection of an appropriate stratification criterion can be understood by considering that, whatever the type of sampling procedure, the estimation error ε of a given population characteristic is proportional to the variance $V[h(y)]$ of its estimator:

$$\varepsilon = v_{\frac{\alpha}{2}}\sqrt{V\left[h(y)\right]} \tag{10}$$

where $v_{\alpha/2}$ is a given percentile of the (assumed gaussian) distribution W of standardized $h(y)$.

In random sampling, the number n_{random} of sampling units necessary to obtain an estimation of the population mean with precision ε at a confidence level α is given by:

$$n_{random} = \left(\frac{(\varepsilon/z_{\alpha/2})^2}{s^2(\eta)} + \frac{1}{N}\right)^{-1} \tag{11}$$

where $s^2(\eta)$ is the population variance that can be substituted by its unbiased sample estimator $s^2(y)$.
In stratified sampling, n_{strat} is given by:

$$n_{strat} = \left(\frac{N(\varepsilon/z_{\alpha/2})^2}{\sum N_k s^2(\eta_k)} + \frac{1}{N}\right)^{-1} \tag{12}$$

In n_{strat}, within-stratum variances appear instead of total variance (as in simple random sampling), hence n_{strat} will in general be less than n_{random}.

If sampling fractions f_k in each stratum are the same, i.e. if $f_k = n_k/N_k = n/N = f$ then stratified sampling is called proportional. Optimal stratified sampling consists instead of subdiving n_{strat} among the different strata in such a way that the n_k's minimize estimators' variance. The problem to solve is a constrained minimization. In the case of the mean, it may be stated as follows:

$$\text{Min } V\left[m_s(y)\right] \qquad \text{Subject to:} \qquad \sum_{k=1}^{M} n_k = n \tag{13}$$

The Lagrangian for such problem is:

$$\psi(n_1, n_2, ..., n_M; \theta) = V\left[m_s(y)\right] + \theta\left(\sum_{k=1}^{M} n_k - n\right) \tag{14}$$

in which $V[m_s(y)]$ is given by:

$$V\left[m_s(y)\right] = \frac{1}{N^2}\sum_{k=1}^{M} N_k(N_k - n_k)\frac{s^2(\eta_k)}{n_k} \tag{15}$$

By setting to zero the partial derivatives of ψ with respect to n_1, n_2 ... n_M and q one obtains:

$$n_k = n\frac{s(\eta_k)N_k}{\sum_{k^*=1}^{M} N_{k^*}s(\eta_{k^*})} \tag{16}$$

As expected, the sample size within each stratum is proportional to the subpopulation variance $s(\eta_k)$.

Remarks on the application of sampling procedures to domestic water use

Any sampling procedure assumes population variance to be known, implying that a suitable number of preliminary data should be already available in order to obtain estimates of population variance. In the case of stratified random sampling, such preliminary information should be larger than for random sampling, as the available data will be split into different groups. In addition, stratified sampling requires that appropriate stratification criteria be adopted. Such stratification criteria should be applied to the set of preliminary data to estimate group variances. In the case of domestic water use, reasonable stratification criteria may be household typology (e.g. with or without garden), number of users per connection and probably also income. Unfortunately, in most cases none of such pieces of information is available in the water utilities' databases on customers, which simply contain the contract holder's data, without any specification on household size, number of household occupants etc. This requires that some assumptions on the stratification variables be made, based on statistical information that in many instances is fortunately readily available (e.g. in Italy through ISTAT, the National Institute of Statistics), but may not have the desired spatial resolution (e.g. the distribution of household size may not be available for small municipalities, and data from larger cities should be used). This may induce errors in the sampling procedure, reducing the expected precision of results. In the authors' view, while the impact of the sample size available for sampling plan calibration may be evaluated via standard statistical tools, the assessment of the uncertainty related to the selection of the stratification variables and to the thereto related assumptions should be assessed via a simulation study.

However, one of the advantages of stratified sampling applied to the assessment of water consumption is that in many cases homogeneous districts (subnetworks) may be identified from the standpoint, for instance, of income, thus reducing the need for further stratification.

A CASE STUDY

The above ideas have been applied to a small group of homogeneous users (around 50 connections) located in a council house district in the Noce neighbourhood in

Palermo, Italy. Households share all the same typology (two-storey residential units, each with four flats, no garden, all flats have a surface of around 90 m^2) and inhabitants can be assumed to belong to the same socio-economic level. Albeit homogeneous, daily water use per connection in the district features a considerable variability (average daily water use per connection: 351 l, standard deviation of daily water use per connection: 225 l) to be ascribed to the different number of users in each connection. Thus, this seems to be the classical situation where a possible stratification has already taken place (for instance on income and household typology) and attention can be restricted only to the variability in water use related to the number of persons served by each conection. For large cities, data from 2001 national census include a classification of families according to their size (1 person, 2 person ... ≥5 persons) at neighbourhood scale. We could then assess the percentage of families in Noce neighbourhood belonging to each class. We ranged the available water use data (50 values) in descending order and attributed the water use data to the different family size classes according to the surveyed census percentages. Data belonging to a given stratum were used to estimate group variances. This can be done by assuming that *k*-th subpopulation variance is equal to the variance of the available sample. Admittedly, the uncertainty related to variance estimates can be large owing to the small number of available data in each stratum.

For illustrative purposes, these estimates have been applied to a hypothetical water distribution district, serving the entire population of the Noce neighbourhood (around 10,500 connections), with the same household characteristics as above, i.e. two-storey council houses with no garden and with flat surface of around 90 m^2. Table 1 reports the data for such hypothetical situation.

Table 1. Data for a hypothetical, homogeneous water distribution district – stratum mean and variances have been estimated using real microdata from a council house district in Palermo, Italy.

Number of users per connection	Connection number per stratum, N_j	Stratum water use standard deviation, $s(\eta_k)$ [l/conn.day]	Stratum water use variance, $s^2(\eta_k)$ [l^2/conn.^{2}day^2]	Stratum water use mean, m_k [l/conn.day]	Stratum water use variation coeff., CV_k
1	2,194	35.7	1,275.1	80.2	0.44
2	2,680	39.6	1,566.0	213.0	0.19
3	2,216	59.3	3,517.1	382.0	0.15
4	2,378	40.6	1,650.7	505.3	0.08
≥ 5	1,155	86.7	7,516.5	806.0	0.11
Population	N 10,623	$s(\eta)$ 224.9	$s^2(\eta)$ 50,571.3	$m(\eta)$ 351	CV 0.6412

With such data and assumptions on stratification, assuming one wishes to assess the average daily use per connection with a precision of ± 25 l/day (around 7% of the estimated daily consumption) and a confidence level of 95%, one obtains n_{strat} = 16

(around 0,15 % of connections) and n_{rand} = 303 (circa 2.85% of connections). Whereas this last figure is in good agreement with the application results reported in Mays (2004) (pages 1.5 - 1.6), it is clear how stratified sampling allows a considerable reduction of sample size. Optimal repartition of sampling units among strata, performed according to (16), yields the sample sizes reported in Table 2.

As stated above, however, it is difficult to draw definite conclusions on the effectiveness of the procedure only based on such few calibration data. For this reason, a sensitivity analysis was performed to assess, even roughly, the range of variability of the required sample size for different values of precision, confidence level and model parameters (group variances).

Sensitivity analysis was performed considering all the possible combinations of three different precisions (±1%, ±5% and ±10%), three different confidence levels (90%, 95% and 99%) and five different values of each group coefficient of variation (a "base case" value equal to the CV_k's of Table 1 and four departures from this value equal to 0.50, 0.75, 1.25 and 1.50 of CV_k). Estimated mean water use was not subject to sensitivity analysis as it does not affect sample size. Likewise, subpopulation size N_k was left unchanged. This resulted in 3,215 different combinations (scenarios) of precision, confidence levels and group variances. For each scenario, n_{random} and n_{strat} were computed through the following steps: 1) multiplication of a given combination of CV_k for the corresponding group means m_k provides an estimation of sample group variances s_k by (5); 2) eq. (9) can then be used to assess the overall "scenario" sample variance s^2. Leaving mean values unchanged, but varying s_k, s^2 will also vary. Thus, eq. (11) may be used to estimate n_{random}.

Table 2. Optimal sample sizes for the sampling problem from Table 1.

Stratum, k	Number of users per connection	Sample size, n_k
1	1	3
2	2	3
3	3	4
4	4	3
5	≥5	3
Total sample size		16

Results

Table 3 reports results of the analysis in terms of minimum and maximum sample units for each different precision and confidence level scenario, with both stratified and random sampling. Minimum and maximum sample sizes (n_{min} and n_{max}) are attained for group variances set all at their minimum and maximum value respectively. Overall, sample fractions show a considerable variability, ranging in the case of stratified sampling from 0.02% (precision = ±10%, confidence level 90%, all group variances at their minimum value) to 23% (precision = ±1%, confidence level 99%,all group variances set at their maximum value), and from 1.00% and 73.2% in

the case of random sampling. The advantage of using stratified sampling is clear considering ratio n_{strat}/n_{random} which ranges from 1.5% (±5% precision, 99% confidence level, all group variances at their minimum value) to, at most, 31.1% (precision = ±1%, confidence level 99%, all group variances set at their maximum value).

It is worthwhile observing how the range of variability of the sample coefficient of variation is quite little (min = 0.63, max = 0.68, base case 0.64), as a consequence of the little value of the ratio $v^2_e/v^2_t = 0.04$, meaning that the adopted stratification criterion is able to capture a considerable part of water use variability, leaving the rest to within-stratum variance. Hence, even considerable departures in the scenaios from the base-case within stratum variances do not produce considerable changes in the resulting sample variance. Nonetheless, table 3 shows that sample size seems to be quite sensitive to sample variance in the case of stratified sampling, and much less in the case of random sampling, as should be expected. An increase of around 5% in population standard deviation (equal to the corresponding shift in the coefficient of variation from 0.6288 to 0.6613 documented in Table 3) produces comparable increases in sample size in the case of random sampling, with ratios $(n_{max} - n_{min})/n_{min}$ not exceeding 16%. In the case of stratified sampling, instead, such ratios increase to around 700%. This indicates to what extent within-stratum variability affects sample size. The procedure is however even more sensitive to precision, and quite less to confidence levels.

Table 3. Sensitivity analysis results.

ε [%]	α [%]		CV	n_{strat}	n/N [%]	n_{rand}	n_{rand}/N [%]	n_{strat}/n_{rand} [%]
1%	90%	min	0.6288	140	1.32%	5,331	50.18%	2.60%
		max	0.6613	1,140	10.73%	5,598	52.70%	20.40%
	95%	min	0.6288	198	1.86%	6,252	58.85%	3.20%
		max	0.6613	1,548	14.57%	6,508	61.26%	23.80%
	99%	min	0.6288	337	3.17%	7,562	71.19%	4.50%
		max	0.6613	2,418	22.76%	7,776	73.20%	31.10%
5%	90%	min	0.6288	6	0.06%	412	3.88%	1.50%
		max	0.6613	51	0.48%	454	4.27%	11.20%
	95%	min	0.6288	9	0.08%	575	5.41%	1.60%
		max	0.6613	72	0.68%	632	5.95%	11.40%
	99%	min	0.6288	14	0.13%	955	8.99%	1.50%
		max	0.6613	124	1.17%	1,047	9.86%	11.80%
10%	90%	min	0.6288	2	0.02%	106	1.00%	1.90%
		max	0.6613	13	0.12%	118	1.11%	11.00%
	95%	min	0.6288	3	0.03%	150	1.41%	2.00%
		max	0.6613	19	0.18%	166	1.56%	11.40%
	99%	min	0.6288	4	0.04%	257	2.42%	1.60%
		max	0.6613	32	0.30%	283	2.66%	11.30%

For instance, a shift in precision from 5% to 1% at, say, a 95% confidence level produces an increase of the required sample size from 72 to 1,548 (i.e. samples twenty times bigger) in the case of stratified random sampling and a corresponding increase of around nine times (from 632 to 6,508) in the case of random sampling. Similar increases are also found in the case of minimum values of within stratum variances (samples 21 and 9 times bigger for stratified and random sampling respectively). Confidence level has a softer, albeit always relevant, impact on sample size. With a precision of ±1% and all group variances set at their highest value, for results to be accepted at a confidence level of 99% in the case of stratified sampling, a sample size twice as big as in the case of a confidence level of 90% is required (from 1,140 to 2,418 sampling units). In the case of random sampling sample size should be around 38% larger (from 5,598 to 7,776).

CONCLUSION

The paper has discussed the basic issues in designing a sampling plan for domestic water use, mainly aimed at conducting water balances at the scale of district meter area. After reviewing the main results of sampling theory for two popular types of methodologies, stratified and random sampling, a case study is introduced based on microdata (recorded water uses) from a small, homogeneous council house district in Palermo, Italy, in order to illustrate the methodology and to perform a sensitivity analysis on the relevant variables, namely precision and confidence levels of estimates, as well as group variances.

Results show that, overall, stratified sampling always allows great savings in data collection, compared to random sampling, with sampling fractions varying from less than 0.1% to 23% depending on group variances, precision and confidence level. With the random sampling methodology, sampling fractions vary between 1% and 73%. In stratified sampling, the variable with the strongest impact on sample size is precision, with requested sample sizes eighty times bigger for precision of ± 1% than for precision ± 10%. Sample size is also sensitive to group variances, with requested sample sizes around seven times bigger for twice bigger group variances. The paper also highlights the need for preliminary microdata of water use in order to estimate group variances and for simple stratification criteria, requiring readily available "exogenous" information on people served per connection, household size and typology etc. The impact of the reduced availability of such preliminary and exogenous information on the precision of water use estimates will be assessed via a simulation study.

REFERENCES

Arreguìn-Cortes, F.I., and Ochoa-Alejo, L.H. (1997) "Evaluation of water losses in distribution networks." *J. Water Resources Planning and Management*, ASCE, 123(5), 284-291.

Buchberger, S.G., and Wu,L. (1995). "Model for instantaneous residential water demands." *J. Hydraulic Engineering*, ASCE, 121(3), 232-246.

Cocchi, D. (2006). *Teoria dei Campioni – Corso base*. http://www2.stat.unibo.it/cocchi/dispensa/masteribrido.pdf

Farley, M., and Trow, S. (2003). *Losses in water distribution networks – A Practitioner's Guide to Assessment, Monitoring and Control*, IWA Publishing, UK.

Hanke, S., and Mehrez, A. (1979). "An optimal sampling procedure for the collection of residential water use data." *Water Resources Research* 15(6), 1343 - 1348.

Magini, R., Pallavicini, I., and Guercio, R. (2008). "Spatial and temporal scaling properties of water demand." *J. Water Resources Planning and Management*, ASCE, 134(3), 276-284.

Mays, L.W. (2004). *Urban water supply management tools*, Mc Graw-Hill, New York.

Speight, V.L., Kalsbeek, W.D., and DiGiano, F.A. (2004). "Randomized stratified sampling methodology for water quality in distribution systems." *J. Water Resources Planning and Management*, ASCE, 130(4), 330-338.

Smart Pipe – Nanosensors for monitoring water quantity and quality in public water systems

Yu-Feng Lin[1], Chang Liu[2] and Jordan Whisler[2]

[1]Illinois State Water Survey/Institute of Natural Resource Sustainability, University of Illinois at Urbana-Champaign, 2204 Griffith Dr., Champaign, IL 61820; PH (217) 333-0235; email: yflin@illinois.edu

[2]Department of Mechanical Engineering, Northwestern University, Room L288, Tech Institute, 2145 Sheridan Rd, Evanston IL 60201; PH (847) 467-0701; email: changliu@northwestern.edu

Abstract

A 2005 study by the American Society of Civil Engineers showed that six billion gallons of clean, treated drinking water disappears every day, mostly due to old, leaky pipes and mains. The amount is enough to serve the population of California. The approximate dollar cost, given varied water rates in different U.S. regions, is $12.5 million - $92 million. Moreover, leaking systems have wasted not only dollars but also priceless natural and energy resources for future generations.

A current research project funded by the US Environmental Protection Agency – Midwest Technology Assistance Center is designed to improve water supply infrastructure via a highly-advanced, cost-efficient monitoring system. A research group led by the Illinois State Water Survey, in collaboration with the Department of Mechanical Engineering at Northwestern University, has been developing a “Smart Pipe” prototype: a multi-sensor array to monitor water flow and quality using state-of-the-art nanotechnology. Each sensor unit in the array will include sensors for pressure, flow velocity and temperature on a 2.5mm by 2.5 mm silicon skin. The Smart Pipe will be equipped with a wireless processor and antenna to transfer monitoring data via commercial wireless communication systems.

With several Smart Pipes installed in critical sections of a public water system, real-time monitoring will be able to automatically detect flow rate, pipe pressure, stagnant points, slow-flow sections, pipe leakage, backflow, and water quality without altering flow conditions in the pipe. Moreover, applying this technology at an affordable cost will help small and/or rural public water systems in rule implementation, capacity development, and water systems operations. Further study is intended to improve this prototype via real-life application that includes the study of the frequency of required maintenance, fouling investigation, measurement calibration, real-time data communication software, manufacturing cost efficiency, long term stability, and assessing the precision and accuracy under differing environmental conditions.

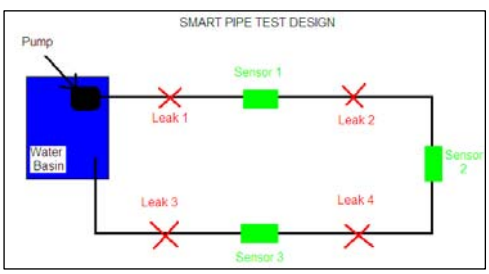

Figure 1

Extended Abstract

This extended abstract is to present the process and results of the development of Smart Pipe. A video of a live demonstration for proving the concept was performed in the Summer of 2008. The video is available at: http://www.youtube.com/watch?v=8xSlLCScIqw. The prototype development of the sensor chip to be packaged in the Smart-Pipe system was completed in the Fall of 2008.



Figure 2

THE PROOF OF CONCEPT

Hardware Design: The system for proving the concept involved the use of an existing commercial sensor instead of the prototype nanosensor since it was in the development stage at the time. The pipe system was constructed using 2-inch PVC pipes with three sensor sets. The dimensions of the test system

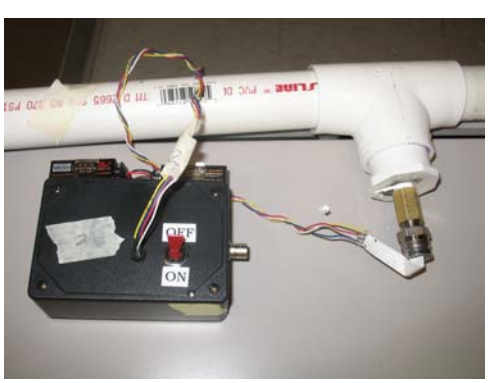

Figure 3

were approximately 4X2 meters as shown in Figure 1. The four controllable leaks were valves that could be opened or closed to simulate a leak, and the sensors were spaced equidistant from each another (Figure 2). Each sensor set used Honeywell pressure sensors (part number 19C100PG5K) that threaded into the pipe using a tee. Each sensor was wired to an amplifier (Figure 3) and was tested successfully using a voltmeter and an oscilloscope to measure the pressure. The nanosensors were packaged or tested at that proof-of-concept stage, but they can be quickly implemented in an existing water system by feeding the wires through a hole drilled into a rubber pipe connector (Figure 4).

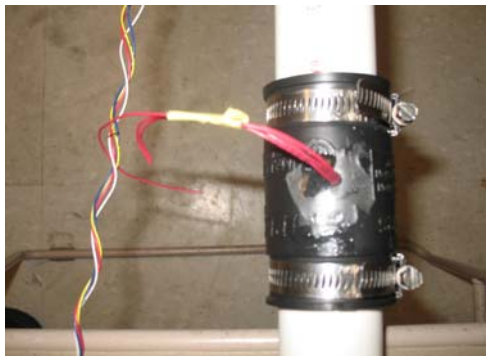

Figure 4

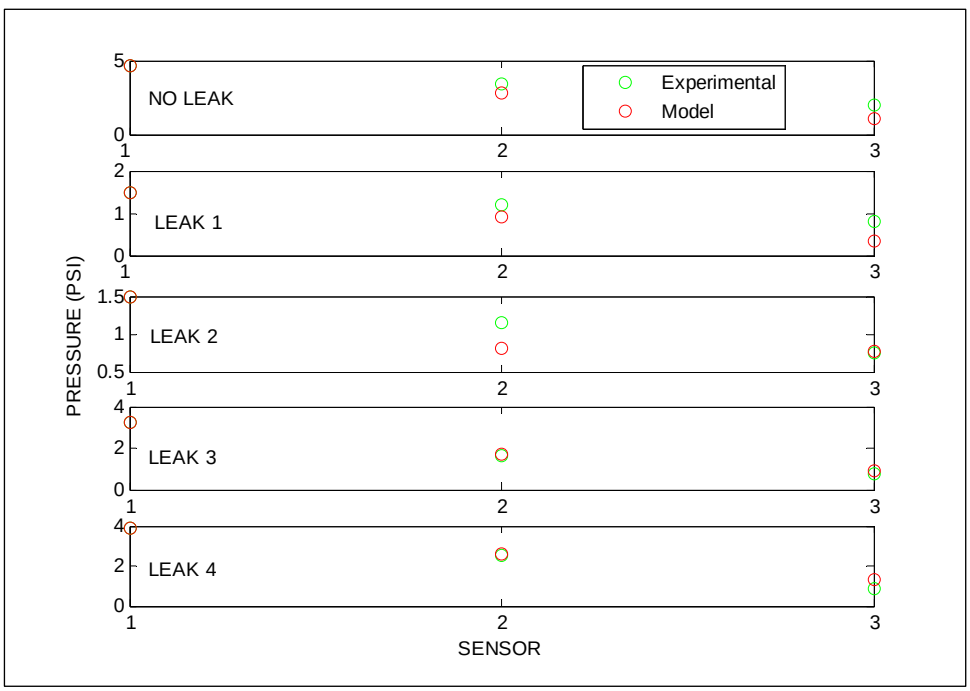

Figure 5. The comparison of experimental results and model results using various leaking scenarios.

Numerical Simulation: A mathematical model was developed using MATLAB to compare the data recorded by sensor set 1 to predict the pressures of the other sensors for each of the possible leak scenarios (Figure 5). The model also showed variance

from the actual collected data, but some variance is to be expected due to the makeshift nature of the pipe system. Also, the experimental data Figure 6 show that the pressure sensors are capable of detecting a unique and distinct set of pressures for the various leak scenarios.

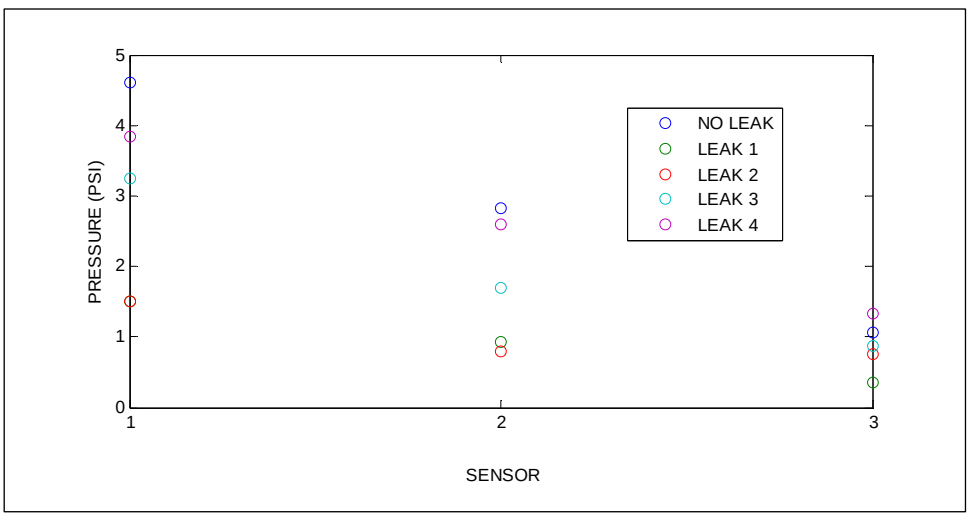

Figure 6. The comparison of experimental results from 5 leaking scenarios.

Real Time Data Acquisition and Detection: There were two versions of a Graphic User Interface (GUI), developed for data acquisition using LabView software. As shown in Figure 7, both versions of Command Center were tested successfully for acquiring test data from a hard-wired system, can continuously monitor the sensor outputs, and can notify the user when and where a leak occurs.

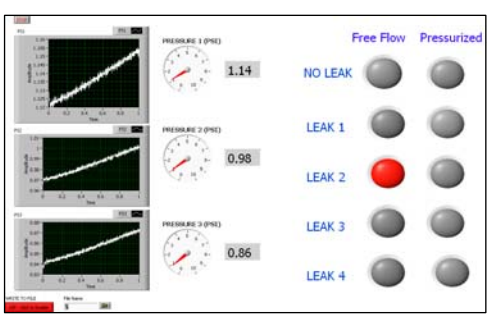

(a)

Figure 7 Command Center

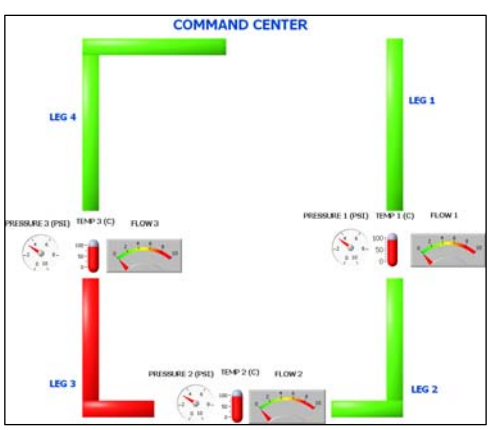

(b)

The software of the wireless system Crossbow is compatible with the Command Center generated by using LabView. Figure 8 shows data taken from the same pressure sensor using both the LabView data acquisition card and the Crossbow wireless data acquisition transceivers. Currently, the signal-processing software is written in LabView code and the signals are acquired through cables connecting the sensors to the computer. The agreement of the two sets of data above shows that the Crossbow devices are capable of supplying the same data but without the need for the sensors to be connected to the computer.

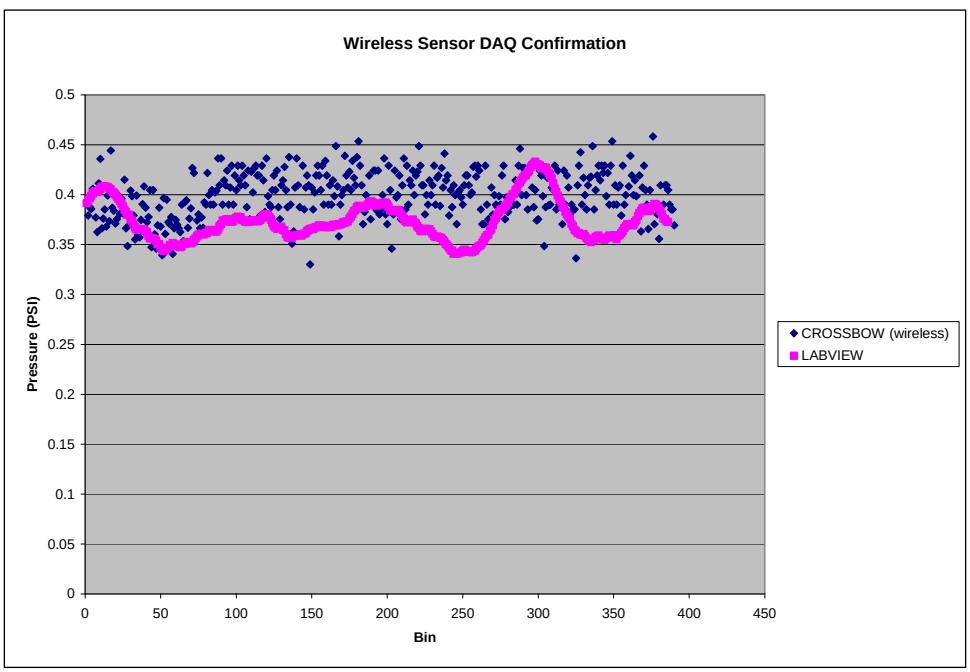

Figure 8. The comparison of data acquisition by wired device (LabView) and wireless device (Crossbow).

NEW GENERATION OF NANOSENSOR CHIP

The new generation of the nanosensor set, G4, has been recently completed. This nanosensor set includes one pressure sensor, one temperature sensor, and two flow sensors (X direction and Y direction) as shown in Figure 9. The flow sensors are the most challenging aspect of the development and testing because of their complex design. Figures 10 and 11 show the test data taken from the flow sensor placed in Smart Pipe sensor number 1 of our experimental setup (Figure 1).

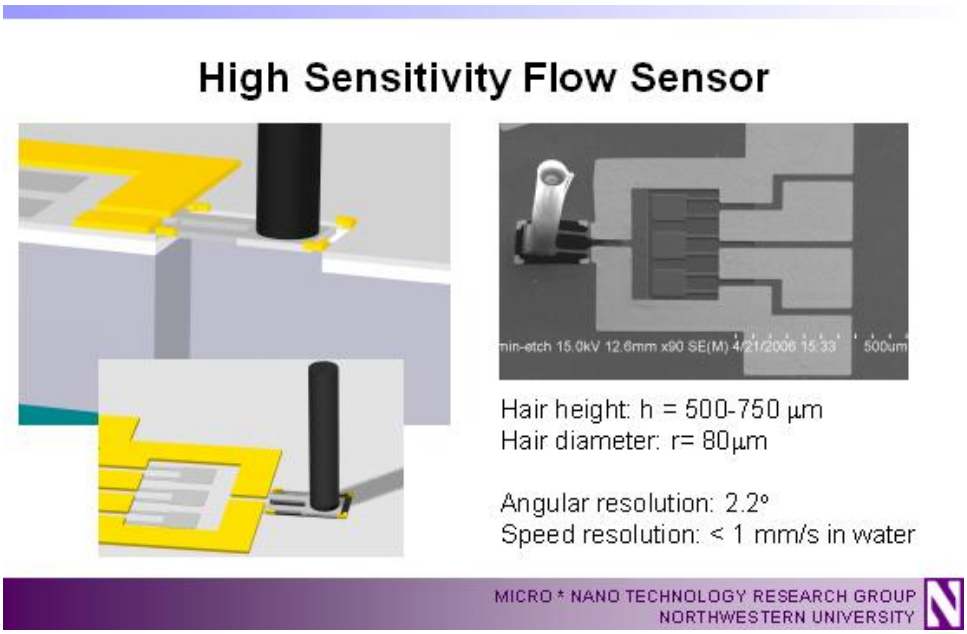

(a) The design diagram and dimensions of the flow sensor

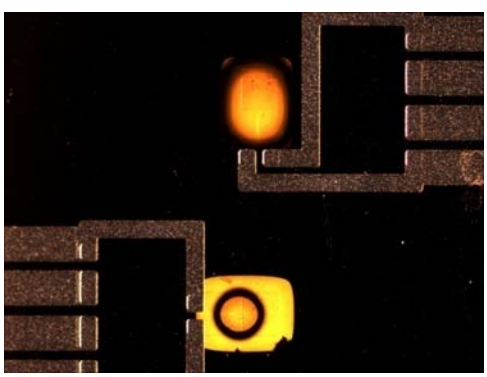

(b) Photos of the actual temperature sensor (above) and the flow sensor (below) taken by microscope

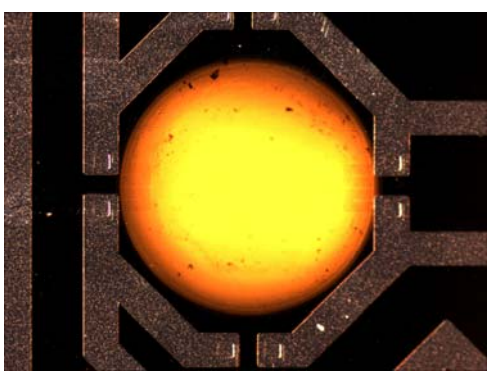

(c) Photo of the actual pressure sensor taken by microscope

Figure 9. The new generation of nanosensor set - G4.

In Figure 10, the first 13 seconds of data represents free flow throughout the entire pipe system. The flow sensor outputs a relatively constant voltage representing the steady state system. At 13 seconds, the valve at the end of the pipe system is shut off, blocking the flow and allowing pressure to build up in the pipes. Although the pressure sensors are unable to detect the motion of the water, the flow sensor data clearly detect that the water has stopped flowing past the sensor after 13 seconds (zero flow is calibrated to -3 Volts.)

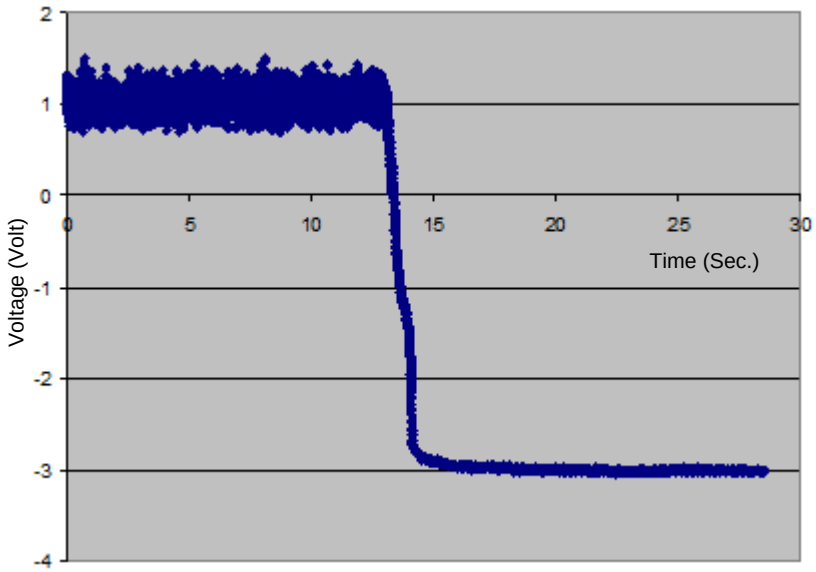

Figure 10. Flow detection by the nanosensor.

In order to test leak detection, we retained the pressurized state shown at the end of Figure 10 and opened the leak at valve 2 at approximately 40 seconds (Figure 11). A spike in the flow past sensor 1 was immediately detected until the valve was shut off again after several seconds before it fell back down to zero flow. Since the end valve remained closed throughout the process, even with the valve at leak 2 opened, no flow was allowed to pass through sensors 2 or 3. Thus, the successful

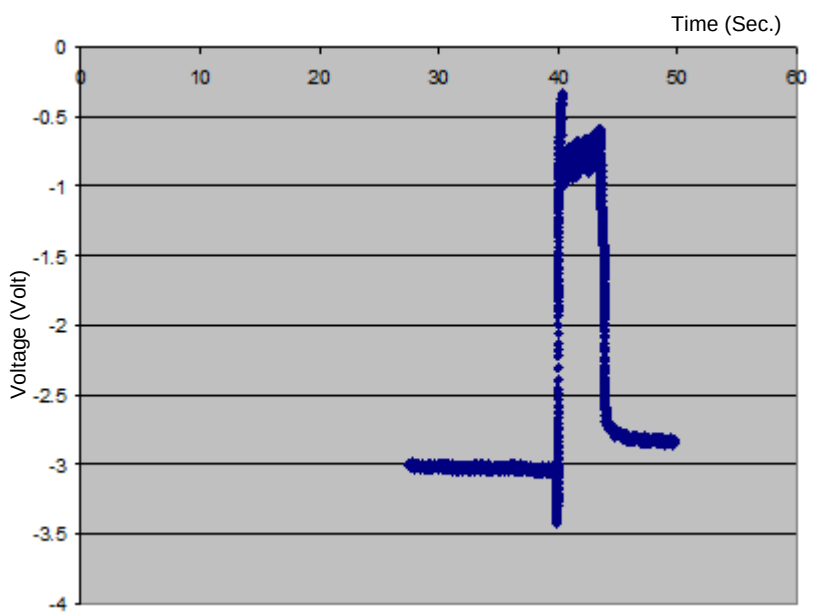

Figure 11. Leak detection by the nanosensors.

detection of flow past sensor 1 determines the existence of a leak between sensors 1 and 2.

SUMMARY

We have presented the proof of concept and the efficiency of nanosensors for the Smart Pipe system, which is still under development. The results from the proof of concept have demonstrated the efficiently of detecting pipe leakage using flow and pressure sensors as well as the feasibility of using a wireless infrastructure. The development of the prototype sensor chip for the Smart-Pipe system was completed in the Fall of 2008. The test results for multiple sensors have shown the feasibility and durability of the nanosensor set. The nanosensor set has greater potential in addition to pipe leakage detection. For example, a temperature sensor has been developed for future tests in water quality detection. The integration between this new generation of nanosensor sets with Smart Pipe is in progress and is dependent on future research funds.

Reference

American Society of Civil Engineers (2005) Report Card for America's Infrastructure. Press Conference Remarks by William P. Henry, President, ASCE, March 9, 2005. http://www.asce.org/reportcard/2005/page.cfm?id=147

An Approach for Integrated Optimization of Wastewater, Recycled and Potable Water Networks

Graeme Dandy[1], Alana Duncker[2], JoelWilson[3] and Xavier Pedeux[4]

[1] MASCE, Professor, School of Civil, Environmental and Mining Engineering, University of Adelaide, Adelaide 5005, Australia, Ph: +618 83035472, email: gdandy@civeng.adelaide.edu.au

[2] Operations Manager, Optimatics Pty Ltd, 11/202 Glen Osmond Rd, Fullarton, SA 5063, Australia, Ph: +618 83797353, email: alana.duncker@optimatics.com

[3] Senior Engineer, Optimatics Pty Ltd, 2/2 Shell Street, Kingscliff, NSW 2487, Australia, Ph: +612 66745723, email: joel.wilson@optimatics.com

[4] Planning Engineer, Yarra Valley Water, Private Mail Bag 1, Mitcham, Vic 3132, Australia, Ph: +613 9872 1152, email: Xavier.Pedeux@yvw.com.au

Abstract

This paper outlines an approach to the integrated optimization of wastewater, recycled and potable water systems in an urban area. The approach will be demonstrated through consideration of a case study of the Hume corridor in Melbourne, Australia. A total of 44,000 new residential lots are planned in this area. These houses will have their garden and toilet connected to a Class A recycled water system. The recycled network will also incorporate some industrial demands.

As the recycled water system will receive its inputs from wastewater treatment plants, the three networks had to be considered in an integrated fashion. The case study considered the development of two optimisation models, one for the wastewater system and the other for the potable and recycled water systems. The interface between the two models occurred at the wastewater and recycled water treatment plants. Values were set for the capacities of these plants for each model and they were adjusted to ensure compatibility between the two models.

The recycled network was designed to the same level of service as the potable water network, e.g. 25 m minimum allowable pressure head at all demand nodes. As potable water top-up of the recycled system is to be considered, it was found that the potable water network needed to carry flows greater than potable peak hour demands.

The results obtained clearly indicated the value of using evolutionary algorithms in an integrated fashion to optimize potable and third pipe systems. Application of this approach to other areas is likely to make third pipe systems more attractive and to lead to significant savings in the use of limited water supplies.

Introduction

Diminishing water supplies and a desire for improved sustainability have highlighted the need for greater reuse of water in urban areas. The efficient use of recycled wastewater requires treatment to a suitable standard and a separate "third pipe" distribution system supplying the recycled water to urban, industrial and/or agricultural users. The distribution network for recycled water is often simpler than the distribution network for potable water as it usually has a smaller number of consumers and does not require the same level of redundancy as the potable network. However, the existence of alternative sources for recycled water and the possibility of topping up this source with potable water mean that the optimization of the recycled network is not a trivial exercise. In fact, there is a strong case for optimizing the potable and recycled networks together, given that the two networks are inter-connected and the demands on the two networks are inter-related. In many cases this integrated optimization should be extended to include the wastewater collection and treatment systems as well.

Considerable research has been carried out into the optimization of water distribution systems (Schaake and Lai, 1969; Alperovits and Shamir, 1977, Quindry Brill and Liebman, 1981; Gessler, 1982). The application of evolutionary algorithms (EAs) to this problem (Simpson et al, 1994, Dandy et al, 1996; Savic and Walters, 1997) has lead to the development of a practical tool that has been applied in master planning and design studies for a large number of cities in the USA, UK, Australia and elsewhere. EAs have the significant advantage that, being guided search procedures, they can be coupled with a detailed simulation model of the system that can include any non-linearities, discontinuities and/or logical variables. In fact, they do not require any simplifications to be made to the hydraulics of the system in the optimization process.

Similarly, the optimization of wastewater system design has received considerable attention in the research literature (Argaman et al, 1973, Mays et al, 1976; Galan and Grossmann, 1998; Swammee, 2001). More recently, evolutionary algorithms (EAs) have been applied to the problem of optimizing wastewater systems (Heaney et al, 1999; Diogo et al et al, 2000). Once again EAs provide a practical tool that can be applied to the optimum design of large scale wastewater networks for similar reasons to the optimization of water supply systems (Savic and Walters, 2001).

A number of water authorities are now developing third pipe systems that distribute recycled wastewater to industrial and domestic consumers. As these are pressured distribution systems, they can be designed and optimized in the same way as potable water distribution systems.

The next level of optimization is to optimize all three networks simultaneously. To the authors' knowledge this has not previously been attempted for a real system. The ideal approach would be to develop a single optimization model that includes all three networks. However, this approach is unlikely to be feasible at the current time because of the long computer run times that would be required. This paper presents an alternative approach that involves linking two separate optimizations models; one for the wastewater system and one for the recycled and potable water systems.

The paper outlines some of the issues involved in developing an integrated optimization model and how they can be addressed. This is described in the context of a case study of the Hume/Epping Corridor in the North of Melbourne, Australia. The water utility is Yarra Valley Water and they funded the study.

Issues in Integrated Optimization of Wastewater, Recycled and Potable Water Systems

It is widely recognised that an integrated approach to urban water management is required, particularly in areas with limited fresh water supplies. A number of urban water utilities are utilising recycled wastewater or stormwater for industrial water use, watering of public or private gardens, toilet flushing, top up of hotwater services or even potable supply. Such developments generally require a "third pipe" network to distribute the recycled water.

The design of the three networks (wastewater, potable water and recycled water) are clearly linked in the following ways:

(1) Recycled water is provided from wastewater treatment plants. The choice of where to locate new or upgraded wastewater treatment plants has significant impact on the location of the source(s) of recycled water and hence on the design of the recycled distribution system.
(2) The seasonal pattern of supply from treated wastewater is unlikely to match the pattern of demand on the recycled network, so significant storages may need to be provided at wastewater or recycled water treatment plants.
(3) It may be cost effective to design the potable supply network so that it can augment the recycled supply when required. This places additional demands on the potable water supply network.

These considerations will be demonstrated in the case study.

Case Study: The Hume/Epping Corridor, Melbourne, Australia

The Hume and Epping North corridors are developing areas serviced by Yarra Valley Water in the North of Melbourne. A total of 44,000 new residential lots are planned in this area

The wastewater collection system needs to be upgraded in response to the expected development of the area. New and upgraded infrastructure needs to be sized, as well as investigating the best strategy to treat, transfer or dispose of the wastewater. The layout of the wastewater system is shown in Figure 1.

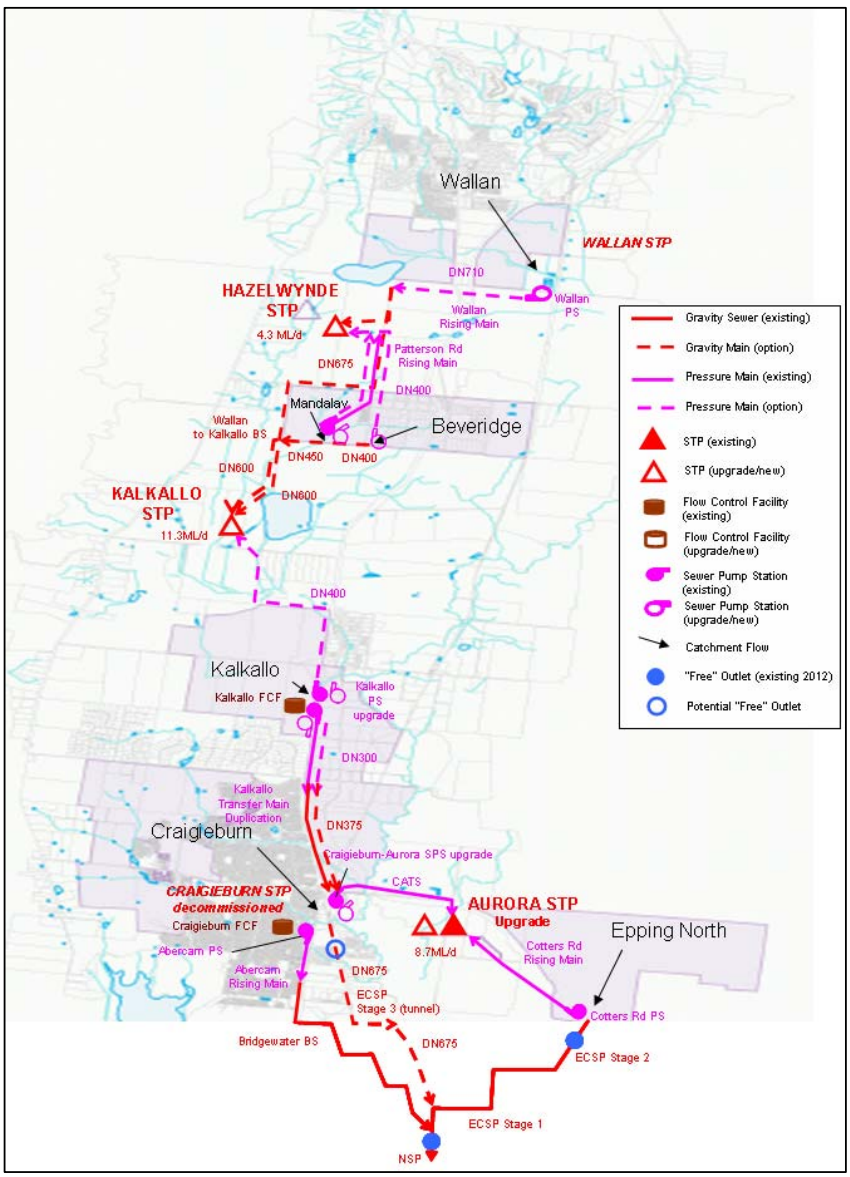

Figure 1: Layout of the Wastewater System

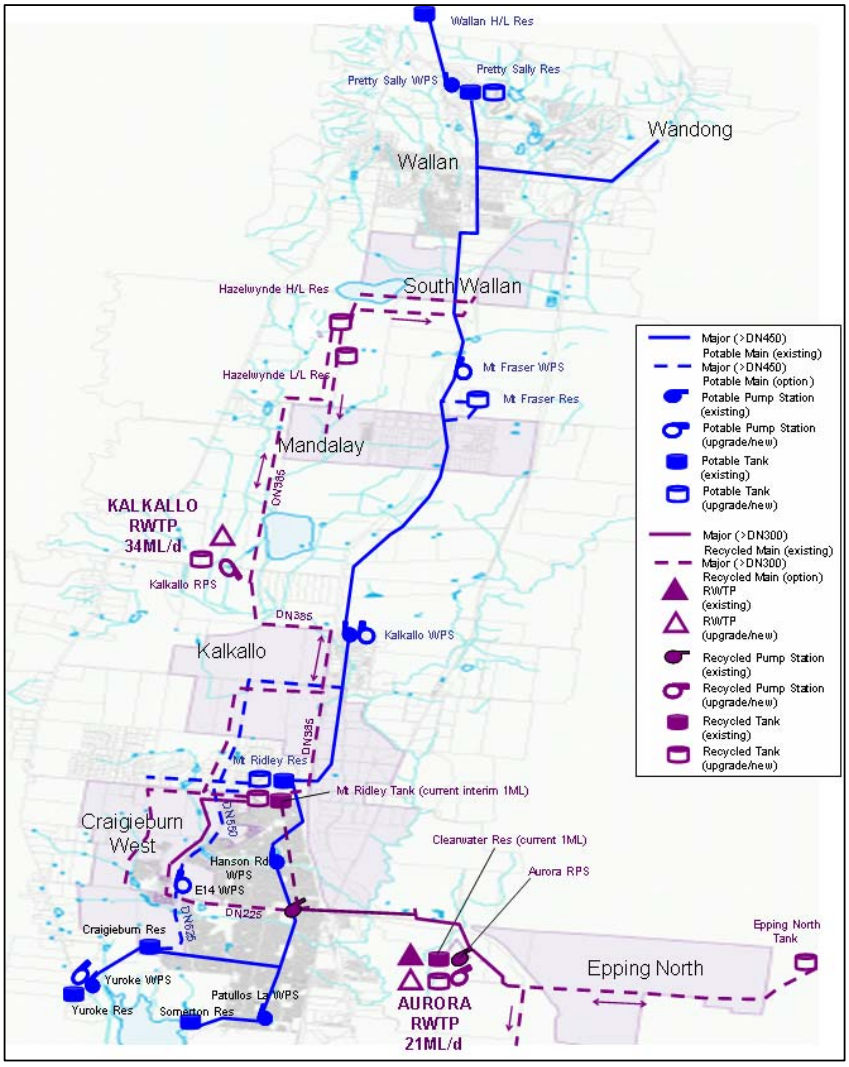

Figure 2: Layout of the Recycled and Potable Water Networks

The layout of the recycled and potable water networks is shown in Figure 2. As the recycled system will receive its inflows from the wastewater system, the wastewater strategy will directly influence the availability and locations of supply to the recycled system. Therefore the wastewater, recycled and potable systems were all investigated together in an integrated study to determine the best overall design and operating strategy.

Optimization of the Wastewater System

The optimization of the Northern Suburbs Sewerage Strategy was completed using Optimizer GA optimization software. The optimization was first completed in 2006 for the wastewater system. However, that initial study did not account for costs associated with the potable and recycled water systems.

The planning options for the wastewater system are characterised by conveyance options and treatment plant options. Ultimately, flow generated in the Northern Suburbs Sewerage Catchment can either be transferred south to the Melbourne Water system or treated locally and disposed or utilised as a recycled water source. The interconnectivity between the

wastewater system and the recycled water system is based on the location and capacity of local treatment plants.

The wastewater optimization study completed in 2006 did not account for the benefit to the potable water system of using local treatment plants. As such, the results from the wastewater only optimization study indicated that local treatment plants were not cost effective and all flow should be transferred south to the Melbourne Water System. The recommendations from the 2006 study suggested that further investigations be carried out to establish the benefit of local treatment plants to the potable water network and that the wastewater optimization be reviewed in light of the findings.

The integrated optimization study completed in early 2009 evaluated the wastewater system improvement and operational costs in conjunction with the recycled and potable systems. The methodology adopted for this study involved conducting individual GA optimization runs for the wastewater system and the potable/recycled water system for selected increments in local wastewater treatment plant capacities. The wastewater system optimization was then completed for each treatment plant capacity scenario and the optimized solution cost wastewater system was then combined with the optimized solution cost for the potable/recycled water system in the same scenario, thus producing a cost-effectiveness curve from which an overall optimal solution for the integrated system could be determined.

The planning alternatives for the Northern Suburbs Sewerage Strategy include upgrade of existing trunk sewers, new diversion sewers, upgrade of existing pumping stations, new pumping stations, new storage facilities and new treatment plants. All feasible combinations of sewer routing and system components are included as multiple pathways in the sewer network model and subsequently evaluated by GA optimization to select an optimal network configuration. Table 1 summarises the performance criteria used in the optimization.

Table 1. Summary of Wastewater Optimization Criteria

Facility Planning Design and Performance Criteria Category	Performance Criteria
Design Storm Event	1 in 5-year, 36-hour design storm
Maximum Surcharge in Gravity Sewers	No flooding or overflows allowed in design storm event
Minimum Velocity in Rising Mains	0.75 meters per second (m/s)
Maximum Velocity in Rising Mains	3.0 m/s for existing rising mains
Treatment Plant Capacity	Existing capacities for some treatment plants, range of treatment capacities for new and upgraded treatment plans depending on the scenario

Optimization of the Recycled and Potable Water Systems

Optimization of the potable and recycled water networks considered a number of different demand options (possible future developments) and also different strategies for the recycled water network (different levels of potable top-up to offset the size of recycled water infrastructure). The optimization was carried out for a 24-hour dry summer day demand (DSD) for ultimate build out (year 2030). The recycled network was designed to the same

levels of service as the potable water network, e,g. 25 m minimum allowable pressure head at all demand nodes

The preferred ultimate solution was subsequently staged in 5 year increments. Table 2 summarises the potable water and recycled water DSD demand for each staging period.

Table 2. Potable Water and Recycled Water Dry Summer Day Demands

Year	Potable Water DSD Demand (ML/d)	Recycled DSD Demand (ML/d)	Total DSD Demand (ML/d)
2010	39.1	6.3	45.4
2015	55.3	19.7	75.0
2020	70.6	33.0	103.6
2025	86.7	45.4	132.1
2030	95.5	54.0	149.5

The different source options for the recycled water network were also considered as separate scenarios so that a matching wastewater solution could be developed for each scenario. This allowed a range of total solutions (wastewater, potable and recycled water) to be developed and compared. The key source scenarios are shown in Figure 3.

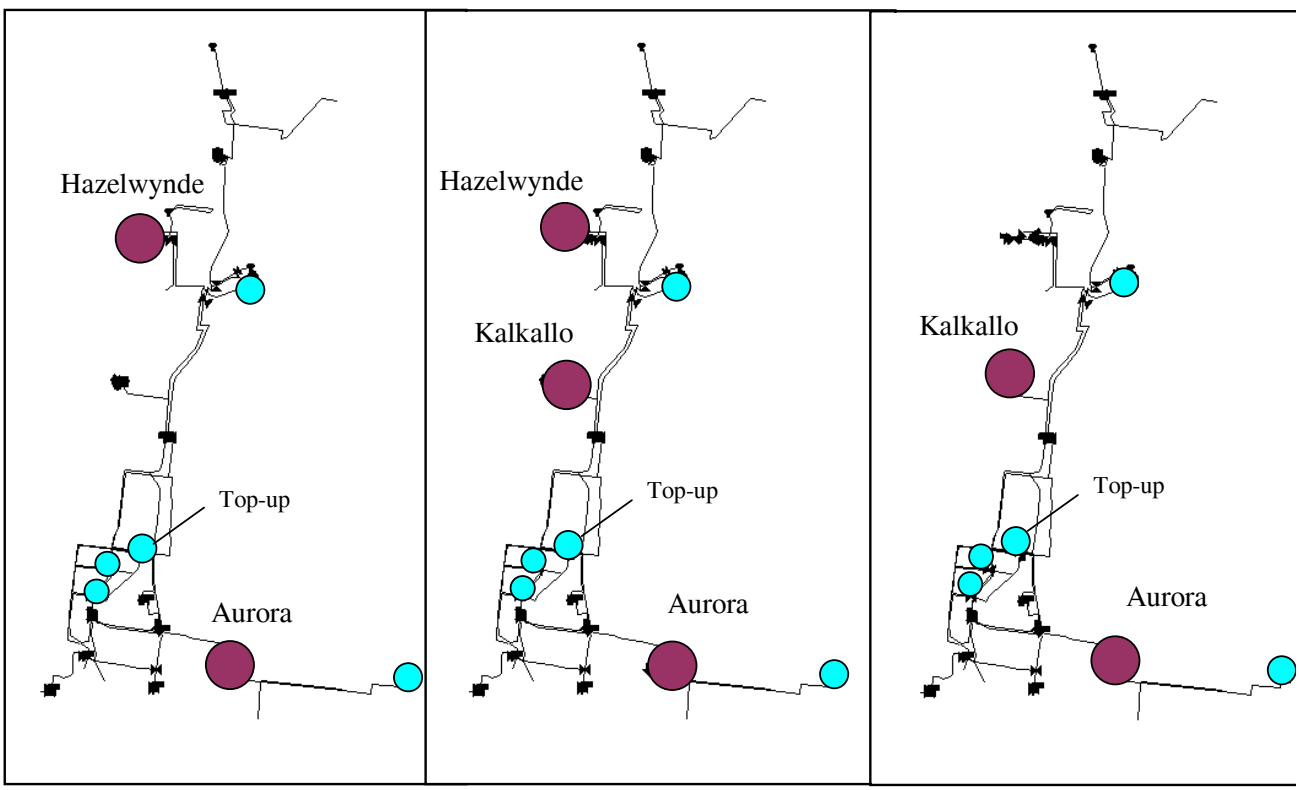

Figure 3: Recycled Water Source Scenarios

The optimization of the potable and recycled water networks involved new and duplicate pipeline options, new and expanded pump station options, new storage options, valve setting options, pump control options and potable top-up options. Flow rates from sources were also

considered as options, but the inclusion of a particular source (or not) was fixed by the scenario being considered.

The potable water top-up options included top-up at number of reservoir sites or emergency cross connections in the system (through pressure reducing valves). The top-up timing and flow rates were determined in the optimization through trigger level controls (either tank levels or downstream pressures) and valve settings (either flow control valves or pressure reducing valves).

Linking the Optimization of the Wastewater, Recycled and Potable Water Systems

Linking the wastewater solution with the potable/recycled water solutions involved pairing solutions from compatible source scenarios, as well as considering the interface between the wastewater treatment plant (WWTP) and the recycled water treatment plant (RWTP). Figure 4 shows a flow chart of the process between the wastewater collection system and the recycled water distribution system.

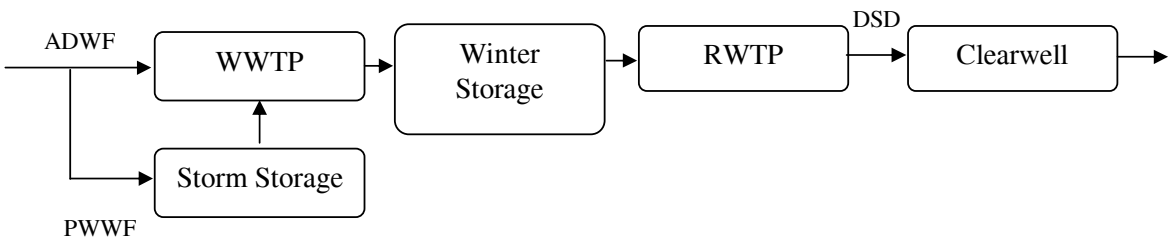

Figure 4: Linking the Wastewater and Recycled Water System

The recycled water treatment plant (RWTP) is sized to meet the dry summer day demands of the area it is supplying. In this optimization, the area supplied by each treatment plant could vary depending on the volume of water supplied from potable water top-up or other treatment plants in the solution. The recycled water clearwell was sized to ensure that any variation in demand over the 24-hour period could be served (this storage was required to refill over the 24-hour period). In this optimization the recycled water diurnal demand varied from 0.12 times to 2.8 times the average hourly flow on a dry summer day.

The wastewater treatment plant is typically sized to meet Average Dry Weather Flow (ADWF). During a storm event the treatment plant can treat up to 4 times ADWF, but any additional flow must be stored in a storm storage tank until it can be treated. The storm storage is sized to hold the peak wet weather flow (PWWF). As part of the optimization process this trade-off between storm storage size and WWTP size was considered.

The interface between the WWTP and the RWTP is the winter storage. This is a large storage designed to store the Class B water produced by the WWTP over the winter when recycled water demands are low, but wastewater continues to be treated. During summer when recycled water demands are high, the winter storage is required to supply the RWTP. If there is a mismatch between the recycled water demands and the wastewater inflow at a particular treatment plant site this can result in a very large winter storage to store excess flows (and then accumulated flows), or a large winter storage required for peak demands, but not enough inflow to fill it.

As part of the optimization, the source scenarios were setup to provide a good match between the wastewater and potable/recycled water solutions. However with some flexibility in each

solution as to how much was used or treated at each source, some solution refinements or re-optimization with fixed flow rates were required for some sources. This ensured that the total solution cost was minimized and the winter storage was sized adequately and used most effectively.

In optimizing the wastewater and potable/recycled water separately a number of different scenarios were required to adequately investigate all source options and determine the best overall solution. This approach also allowed the cost of each different source scenario to be determined and each optimization run was able to focus on a smaller problem and obtain a better solution in a shorter time.

Results

Table 3 summarises the estimated costs of the three key solutions developed. Note that A$1 = US$0.66 (approximately). A range of other solutions considering different rates of top-up and additional demands were also developed. Table 4 summarises the estimated costs of the three key scenarios with the addition of a potential new development area (an additional 100 ML/d demand on the potable/recycled water network and additional flows for the wastewater network).

Table 3. Total Solution Costs – Base Case Solutions (A$millions)

	Waste Water Total Cost	Melbourne Water	Class B Storage	Recycled Solution	Potable Solution	TOTAL
Scenario 1	$88.11	$33.70	$14.90	$176.50	$42.40	$355.60
Scenario 2	$98.59	$31.88	$8.25	$179.97	$43.23	$361.92
Scenario 3	$112.90	$33.15	$14.40	$203.80	$42.40	$406.66

Table 4. Total Solution Costs – Alternative Solutions (A$millions)

	Waste Water Total Cost	Melbourne Water	Class B Storage	Recycled Solution	Potable Solution	TOTAL
ALT 1	$194.78	$30.50	$27.88	$369.16	$75.89	$698.21
ALT 2	$155.00	$31.82	$24.30	$344.35	$75.61	$631.09
ALT 3	$168.39	$36.73	$31.64	$355.07	$75.68	$667.52

Although the Scenario 1 solution was the lowest cost total solution for the current planning assumptions, this scenario (Aurora RWTP + Hazelwynde RWTP) is the most expensive setup when the potential new 100 ML/d development is considered. The potential development outside the current planning boundary adds significant cost to the solution and Scenario 2 (Aurora + Hazelwynde + Kalkallo) becomes the most cost effective scenario.

The preferred solution selected by Yarra Valley Water for staging was the Scenario 2 Base Case solution. This solution was not the lowest cost base case solution, but selecting this solution will give the system flexibility (and save costs) if the potential 100 ML/d development goes ahead in the future.

By developing a range of solutions considering different source options and also different demand scenarios, the sensitivity of the design and the costs can be evaluated. The impact of different assumptions and boundary conditions to the wastewater solution, potable water and recycled water solution can also be measured and evaluated. This optimization analysis has

provided Yarra Valley Water with information that can be taken into account when developing the final service strategy for the corridor. It is expected that a highly cost-effective plan will result.

Summary and Conclusions

With increasing scarcity of water, recycled water systems are becoming more common. It is important to design the wastewater, potable and recycled water systems for an urban area in an integrated fashion. These combined systems can be very complicated as they have a large number of pipe, pump, storage and treatment options. Formal optimization procedures offer considerable potential to identify cost-effective designs for these combined systems.

This paper demonstrates the application of evolutionary algorithms to the optimization of an integrated wastewater, potable and recycled water system in the Hume/Epping Corridor in the North of Melbourne. The study was carried out for Yarra Valley Water (YVW).

Although it is desirable to be able to optimize all three systems simultaneously, in this case study the wastewater system was optimized using one model and the recycled and potable water systems were optimized using a separate model. The interface between the two models occurred at the wastewater and recycled water treatment plants (RWTP). Values were set for the capacities of these plants for each model and they were adjusted to ensure compatibility between the two models. Three different combinations of locations of the RWTPs were considered. Flexibility in terms of possible future demands were also considered in the scenarios modelled by allowing for the demands of a potential new development.

The results obtained provided useful information to YVW on the preferred scheme for development of all three collection and distribution networks. The study demonstrated the feasibility of an integrated approach to this planning problem.

References

Alperovits, E. and Shamir, U. (1977) Design of optimal water distribution systems, *Water Resources Research*, 13 (6), 885 - 900

Argaman, Y, Shamir, U and Spivak, E (1973) Design of optimal sewerage systems, *ASCE Jour of Environmental Eng Div*, Vol 99, No. EE5, 703 - 716

Dandy, G.C., Simpson, A.R. and Murphy, L.J. (1996) An improved genetic algorithm for pipe network optimization, *Water Resources Research*, 32 (2), 449-458

Diogo, A.F., Walters, G.A., de Sousa, E.R, and Graveto, *V.M. (2000)* Three dimensional optimization of urban drainage system, *Computer-Aided Civil and Infrastructure Engineering,* 15, 409 - 426

Galan, B. and Grossmann, I.E. (1998) Optimal design of distributed wastewater treatment networks, *Ind. Eng. Chem. Res*., 37, 4036 - 4048

Heaney, J.P., Wright, L.T., Sample, D., Field, R. and Fan, C-Y (1999) Innovative methods for the optimization of gravity storm sewer design, *Proceedings, 8th International Conference on Urban Stormwater and Drainage,* Sydney, Australia, August, 1896 - 1903

Mays, L.W., Weinzel, H.G. Jr, and Liebman, J.C. (1976) Model for layout and design of sewer systems, ASCE *Jour of Water Resources Planning and Management,* Vol. 102, No. WR2, 385 – 405

Quindry, G., Brill, E.D. and Liebman, J.C. (1981) Optimization of looped water distribution systems, ASCE *Jour of Environmental Engineering Division*, 107 (EE4), 665-679

Savic, D.A. and Walters G.A. (2001) Evolutionary computing in water distribution and wastewater systems, *Proceedings of the World Water and Environmental Resources Congress,* Orlando, Florida, May. Proceedings on CD.

Savic, D.A. and Walters G.A. (1997), Genetic Algorithms for the Least-Cost Design of Water Distribution Networks, ASCE *Jour of Water Resources Planning and Management*, Vol. 123, No. 2, pp. 67-77.

Schaake, J., and Lai, D. (1969). Linear Programming and Dynamic Programming Applications to Water Distribution Network Design. *Report 116*, Department of Civil Engineering, Massachusetts Institute of Technology, Cambridge, Massachusetts.

Simpson, A.R., Dandy, G.C. and Murphy, L.J. (1994) Genetic algorithms compared to other techniques for pipe optimization. ASCE *Jour of Water Resources Planning and Management,* 120 (4), 423-443.

Swammee, P. K. (2001) Design of sewer line, ASCE *Jour of Environmental Eng* , 127 (9), 776 - 781

Application of Optimization Technology to Water Distribution System Master Planning

C.K. Rogers[1], M. Randall-Smith[2], E. Keedwell[3], R. Diduch[4]

[1]Delcan Corporation, 1223 Michael Street, Suite 100, Ottawa, ON K1J 7T2; PH (613) 738-4160; Fax (613) 739-7105; email: c.rogers@delcan.com
[2]Mouchel, Strategic Consulting, Priory Court, Poulton, Cirencester, UK, GL7 5JB
[3]School of Engineering, Computing and Mathematics, University of Exeter, Harrison Building, North Park Road, Exeter, UK, EX4 4QF
[4]City of Ottawa, 110 Laurier Avenue West, Ottawa, ON K1P 1J1

ABSTRACT

This paper presents the application of optimization techniques to the development of a phased expansion plan for the City of Ottawa's water distribution system. The approach involved an iterative process where capacity-driven solutions generated by an optimization model were evaluated for reliability of supply during failure conditions and water quality characteristics in order to update constraints for subsequent re-optimization. An infrastructure solution and phasing plan is presented. It was found that the approach is sound, but the number and variety of alternatives must be limited to achieve reliable results from the optimization model.

INTRODUCTION

When the City of Ottawa, Canada, embarked on a master planning exercise for its water distribution system, staff wanted to take a more systematic and comprehensive approach to evaluating the very large number of potential system expansion alternatives, compared with the traditional methods of the past. This paper describes the development of the expansion strategy for the system using optimization technology that considers growth over a 25 year planning period. The infrastructure solution was optimized by minimizing life cycle costs over this period, considering a range of performance objectives including pressure limits, reliability of supply, and water quality. The development of the solution considered operation of the system under a wide range of conditions.

EVOLUTIONARY ALGORITHMS

Evolutionary algorithms are optimisation techniques based on the principles of evolution and the concept of 'survival of the fittest'. By using the principles of selection, reproduction and mutation, solutions to problems can be evolved rather than explicitly designed. Although the process of evolution itself is slow, the process of simulated evolution is an efficient method of searching spaces that cannot be fully searched by other means. For instance, in the well-known New York Tunnels water

distribution system (Alperovits and Shamir, 1977), with 20 pipes and 16 possible pipe diameters, there would be approximately 1.2×10^{24} unique solutions. Even with very fast computers, it would take hundreds of years to fully evaluate all of these solutions. Therefore a more efficient approach is required.

Evolutionary algorithms have previously been applied to a number of 'trial problem' water distribution systems (Savic & Walters, 1997) and also some industrial networks (Keedwell & Khu, 2003; Savic, Walters & Randall-Smith, 1998; Savic, Walters & Randall-Smith, 2000). In each case, the Genetic Algorithm (GA) has been found to significantly outperform competing techniques, but the examples cited tend to operate on relatively simplistic views of water distribution systems. For instance, Savic & Walters (1997) and Keedwell & Khu (2003) view the network from a pipe-sizing viewpoint only. In the study described in this paper, the objective was to optimise many aspects of the network including pipe sizing and routes, pump settings, pressure zone boundaries, storage and treatment capacity variables.

The GA term was originally coined by John Holland in 1975 (Holland, 1975). The algorithm works by generating a random population of solutions. These solutions are made up of the variable settings for the network (e.g. pipe diameters, pump settings, tank diameters, etc.) and are evaluated against performance criteria by a 'fitness' or 'objective' function. The algorithm takes the variables, applies them to the problem and the fitness function returns a measure of how well that particular solution solves the problem. Once the population has been created, each of the solutions is evaluated and some are selected for progression into the next generation, biased towards those that are best at solving the problem. These solutions are then changed by processes known as 'crossover' and 'mutation' to create new solutions which are then evaluated by the objective function and returned to the population. This process is repeated until it appears that the genetic algorithm has converged on a 'near optimal' solution.

The main tasks needed to apply a GA to a problem are to define a system representation and an objective function. To accomplish this, we must first look at the network which we are proposing to optimise.

EXISTING WATER DISTRIBUTION SYSTEM

Ottawa is a City of about 800,000. An abundant fresh water supply is available from the Ottawa River, which marks the northern boundary of the City. Two water purification plants (WPPs) are located along the river and feed the City's distribution system (Figure 1). The Britannia plant has a rated capacity of 350 million litres per day (MLD) and the Lemieux Island plant is currently rated at 290 MLD. A 110 MLD expansion of the Lemieux plant is currently underway. There are 7 open pressure zones and 4 relatively small closed zones. A Greenbelt separates the core urban area from three distinct urban communities to the east, west, and south. The majority of future urban growth will be taking place in these outlying communities.

There are single 1220mm diameter transmission feeds serving the East and West Urban Communities (EUC and WUC). The South Urban Community (SUC) is

bisected by the Rideau River. A 1220mm main feeds the west portion of the SUC, whereas a 762mm main feeds the relatively small urban area on the east side of the river. There is no link between these two portions of the SUC, which operate at slightly different pressures. With the exception of these single feeds through the Greenbelt, the distribution system is very well looped, providing a high level of redundancy for meeting normal and emergency water needs. However, even in the unlikely event of a critical transmission failure, reservoir storage in the external urban expansion areas will allow supply to be maintained at a restricted rate while emergency repairs are carried out. Major storage reservoirs are located in the core area (108ML) and EUC (82ML). Smaller reservoirs are also located in the WUC (34ML) and SUC (18ML). Some elevated storage is also available in these urban communities.

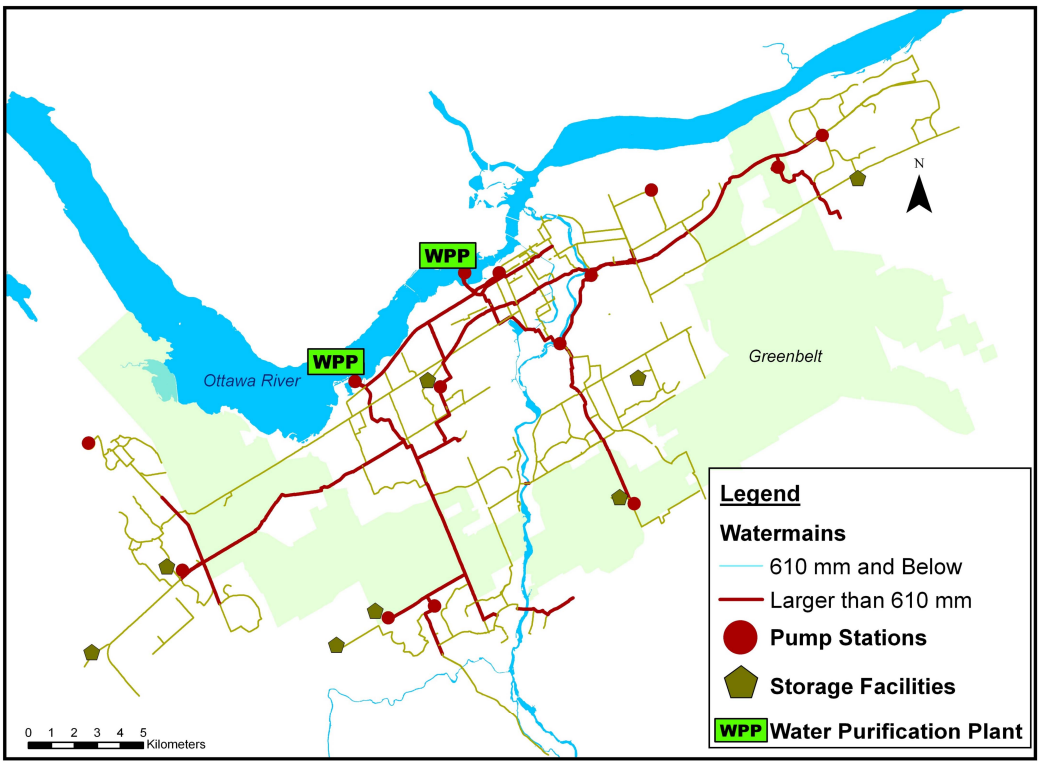

Figure 1. City of Ottawa Water Distribution System

DEMAND PROJECTIONS

At the time of the study, Ottawa's population was expected to increase by roughly 35%, from about 760,000 in 2004 to 1,070,000 by 2021, according to official projections. Although significant intensification is anticipated within the core urban area, the majority of growth will take place in the expansion areas outside the Greenbelt. The 25 year planning horizon selected for the study extends a full 10 years beyond the City's 2021 official planning horizon. The above projections were linearly extrapolated, resulting in an estimated 2031 population of 1,240,000. The current system-wide maximum day demand is in the order of 590 MLD whereas the 2031 maximum day demand would be 1060 MLD based on extrapolation of the

official projections. Basic demand is consistent throughout the year in Ottawa, with peak demands associated with outdoor use in the summer period. There is a downward trend in unit consumption rates, and for conservative results, these rates were assumed to be held constant into the future.

OPTIMIZATION APPROACH

The general approach to solving the optimization problem involved the application of GA technology to an iterative hydraulic system design process that considered a wide range of infrastructure alternatives and a comprehensive set of design criteria. An Optimization Model was developed and used to generate capacity-driven solutions. These solutions were evaluated and further optimization constraints identified to ensure that subsequent solutions would meet reliability and water quality (as indicated by water age) criteria. A number of iterations were required to arrive at a final optimal solution for the year 2031.

The Optimization Model was also used to develop 2011 and 2021 solutions based on an alternatives set corresponding to the 2031 solution. These solutions also involved an iterative design process considering shorter-term reliability objectives. Considerable judgment was involved in the phasing of reliability elements that were not required for interim capacity needs. Consideration was given to risk and affordability issues as part of the phasing plan development. Watermain diameters and elevated storage facilities were fixed based on the 2031 solution, but phasing of pumping station and reservoir expansion was considered as part of the optimization.

OPTIMIZATION MODEL DEVELOPMENT

The Optimization Model was developed based on the Mouchel GA*net* approach, developed jointly with the University of Exeter. The model comprises a GA application (GA*net*), a GIS, and the well-known EPANET hydraulic solver. The GA*net* software is responsible for the creation and evaluation of solutions that are simulated in EPANET. The relationships between the GA*net* software, input files, and EPANET software are illustrated in Figure 2. The GA*net* input file includes all the information needed to control the selection of alternatives including global GA parameters, infrastructure variables, and an objective function that is used to assess the overall 'fitness' of the solutions generated. The infrastructure alternatives are represented as 'dummy' elements in the EPANET model.

GA*net* conforms to the idea of object oriented design. Every element in the network which has some impact on the execution of the GA, is modelled as a separate object. The object types include pipes, tanks, pumps, and water purification plants (WPPs). Each of these object types belongs to one or more 'super-classes' which group the objects together according to the function that they perform in the GA. These groups are: Decision Variable Objects; Cost Objects; Constraint Objects; and Monitor Objects. Each object has capabilities that enable it to perform the function required of it. For instance:

- A decision variable object has the ability to take a value from the GA and make a change to the object in the EPANET Dynamic Link Library (DLL).

- A cost object has functions to calculate the cost associated with making a particular decision. Note that there are instances where objects can incur costs without being a decision variable. For example, where a WPP incurs cost based on the flow through it which is influenced by other decisions that the GA might make.
- A constraint object is able to calculate the violation of a constraint. For example, a network junction where a water demand is specified will be evaluated for minimum pressure against the design criteria.
- A monitor object monitors certain specific values over time. Every constraint object is also a monitor object, but the reverse is not true. For instance the WPPs needs to monitor their flow, but there is not necessarily a constraint on that flow.

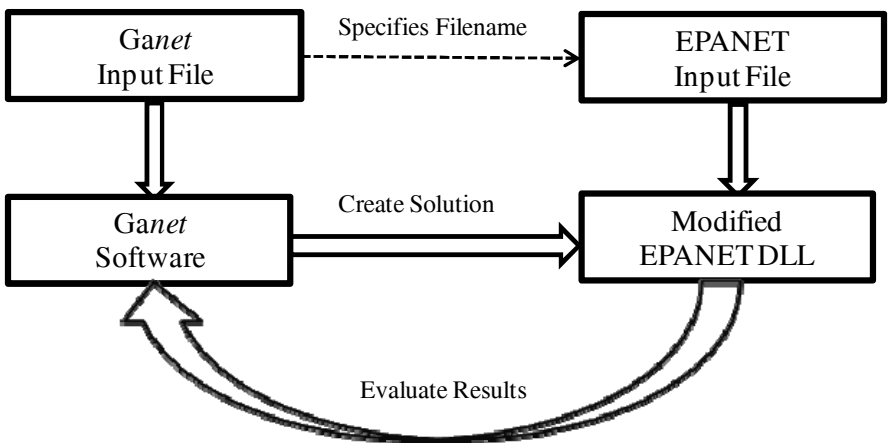

Figure 2: GA*net* / EPANET Relationships

As previously mentioned, each object can belong to one or more of these super-classes. For instance, a pipe is a decision variable (diameter), a cost object (based on the diameter), a constraint object (based on the velocity through the pipe) and a monitor object (to record the velocity). By organising the classes in this way, the software has the capability to model objects with complex behaviour.

There are some engineering alternatives that need to be considered as a single variable. For those alternatives, more than one modification must be made to the network as a result of one decision made by the GA. In this application we have coined the term Custom Decision Variable (CDV) which relates to the fact that any changes can be made to the network and the GA is only aware of the variable as another integer. For example, to adjust a pressure zone boundary, a specific set of pipe closures and openings may be required. These CDVs allow greater flexibility to the range of modifications that may be made to the network, without losing focus on feasible combinations of network modifications.

OBJECTIVE FUNCTION

The objective function is critical to the success of the optimization because it contains the only information that the GA has about the problem at hand. The objective function is used to evaluate the overall fitness of each solution. Those

solutions with a high fitness score have a greater chance of selection for further evolution. There are two primary components of the objective function: the infrastructure cost calculation, and the hydraulic penalty calculation. In essence, the objective function represents the trade-offs between cost and competing performance objectives. The GA can only accommodate the trade-offs by weighting each component of the objective function. In practice, this involves converting measures of non-compliance with performance objectives to costs that are added to the net present value (NPV) of a solution. The GA attempts to minimise the overall 'cost' of the network which is a combination of actual dollar costs and penalty costs.

The NPV cost calculations include capital costs, energy costs, and operations and maintenance costs. Modifications to the GA software were required to include online cost calculations within the software rather than provided as pre-calculated costs via an input file. This was needed to allow for calculations that depended on the hydraulics of the simulation such as flow through the WPPs. The cost models for pipes must also consider river, rail, and highway crossings. Each pipe object can have up to three cost models to account for these crossings.

In addition to the dollar cost, the GA must evaluate whether it is meeting the design criteria. While a number of engineering criteria apply to the problem as described in the following section, many are evaluated as part of post-optimization analyses carried out following each iteration of the design process. The fundamental hydraulic criterion that is evaluated as an integral part of the GA optimization is minimum pressure at each demand node in the system model. In addition to this criterion, the GA also evaluates the solution with respect to minimum and maximum storage facility levels and watermain velocities.

These constraints represent the performance criteria that the GA attempts to meet while minimising the cost of the infrastructure modifications required to deliver them. These constraints are conveyed to the algorithm through the use of penalty functions. These functions compute the violation of the constraint, multiply this value by some penalty factor and add it to the overall 'cost' of the solution. A key part of the model development process involved tuning of the penalty cost factors, so that an appropriate balance between costs and penalties could be achieved as part of the optimization. For example, for each demand node in the Optimization Model, the GA calculates the shortfall (in metres) of the simulated pressure in relation to the target pressure at each time step and multiplies this figure by $1,000,000. This means that some non-compliance with pressure targets can only be accommodated if there are major cost savings associated with the solution compared to other candidate solution. The selected factor was determined by evaluating the results of a number of test runs of the GA to ensure that non-compliance in the solutions was limited and reasonable.

ENGINEERING DESIGN CRITERIA

The optimization was subject to design criteria and constraints established in consultation with the City's Technical Advisory Committee (TAC) for the study. The majority of the criteria are based on well established industry standards. Preliminary reliability criteria were taken from previous City studies. Specific key decisions that

influenced the range of infrastructure alternatives that were ultimately considered included the following:

- Dual transmission is to be provided to the three urban growth areas outside the Greenbelt to provide a high level of supply reliability;
- Elevated storage can be available to provide balancing storage only, with emergency and fire supply provided by redundant watermains;
- Elevated storage must be provided when a minimum pressure of 105 kPa (15 psi) cannot be maintained as a result of the hydraulic grade line (HGL) in the upstream zone should the pump station fail, and when the pressure zone population is greater than 10,000;
- Water age throughout the future distribution system should remain below the desirable limit of 5 days where possible, but should not exceed current values at any existing location where this limit is exceeded.

INFRASTRUCTURE ALTERNATIVES

A broad range of future infrastructure alternatives that could form part of an overall 2031 solution was identified. These alternatives included watermains, new pump stations, pump station expansions, elevated storage facilities, reservoir expansions, control valves, and expansions at the City's two existing WPPs. Over 200 variables were initially considered, each with differing numbers of options, creating a vast combinatorial problem. A number of system reconfiguration options were also considered. In particular, the study terms of reference required that the most appropriate pressure zone configuration for the SUC be determined. Ultimately, 4 different zone configurations were considered for this part of the system.

The potential capacity requirements for future infrastructure alternatives were estimated using supply-storage curves that were developed for the study. These curves are based on mass-balance calculations using diurnal demand curves for specific pressure zones and service areas. The capacity ranges for the alternatives were developed based on two extreme conditions. The first assumes no increase in distribution system storage capacity, and the second assumes no increase in existing transmission capacity, except where required for reliability purposes. From these ranges, a number of discrete sizing alternatives were developed for each future infrastructure component.

SOLUTION DEVELOPMENT

The evaluation of preliminary, capacity driven solutions resulted in updated optimization constraints. These constraints typically involved forcing the selection and/or increasing the minimum sizing of specific infrastructure elements. It was consistently found that the optimal solutions yielded improvements in water age over existing conditions when appropriate operational rules were applied under the most critical conditions. Thus changes in the Optimization Model constraints were driven by reliability needs.

The evaluation of optimization results was carried out using H20Map Water, a GIS-enabled hydraulic simulation package based on ESRI Shapefile technology. The

use of this tool allowed for efficient evaluation of solutions to support debugging of the Optimization Model, penalty factor adjustment, and compliance with design criteria. A long list of operating scenarios were developed and tested as part of the evaluation, most of which involved critical infrastructure failures. Appropriate emergency operational measures were identified for these failures as needed.

The GA is an excellent tool for generating near optimal solutions quickly, but it is slow at arriving at a final optimal solution. In order to minimize manual refinement as part of the post-processing work, a heuristic solver was developed and applied to the solution generated by the GA. The solver identified opportunities to reduce the sizing of watermains selected by the GA.

PRELIMINARY RESULTS

Preliminary optimization trials yielded sub-optimal results. After conducting tasks to troubleshoot the problem set-up, debug the programming, and tune the penalty factors, it was concluded that the number and variety of alternatives needed to be reduced. As per Goldberg (1989), approaches using GA technology are most successful when there is a relatively high degree of independence between the alternatives. In particular, variable storage, pumping and zone boundary characteristics significantly decreases the rate of solution convergence, and the associated options needed to be simplified. There were some logical trends in the preliminary results, and these were used in conjunction with traditional forms of analysis as a basis for reducing the list of alternatives.

The zone configuration alternatives were eliminated from the optimization model. Five separate optimization problems were prepared based on different fixed configurations to relieve the GA of the need to select complex decision combinations. In addition, further analysis of the original list of alternatives was carried out to eliminate those which were judged less likely to form part of the best solution. System detail was also reduced in some areas. The results from these separate optimization runs were considered reliable and contributed to the selection of a preferred future system configuration. Differences in NPV costs between the solutions were small, and the selection was ultimately driven by operational ease and flexibility. The selected pressure zone configuration involves major changes to existing zone boundaries in the SUC. The solution provides the best opportunity for off-peak pressure control, limits peak demand operational requirements, and avoids the need for a major pressure reducing valve station that would have resulted in the creation of numerous dead-end watermains.

DEVELOPMENT OF FINAL 2031 SOLUTION

With a preferred system configuration established, additional system detail was re-introduced, and further iterations of the optimization process carried out to generate a final solution for the 2031 infrastructure requirements (Figure 3). The total capital cost of infrastructure requirements for the solution is estimated at $402M, including $205M for plant expansions, $110 M for new watermains, $45M for pump station projects, $24M for reservoir expansions, and $17M for elevated tanks. The total capital cost estimate for infrastructure needed to meet 2011 demands is $79M,

including a $29M WPP expansion. Infrastructure needed to facilitate zone boundary changes in the SUC are not required until after 2011. The total capital cost estimate for infrastructure to be implemented between 2011 and 2021 is $152M.

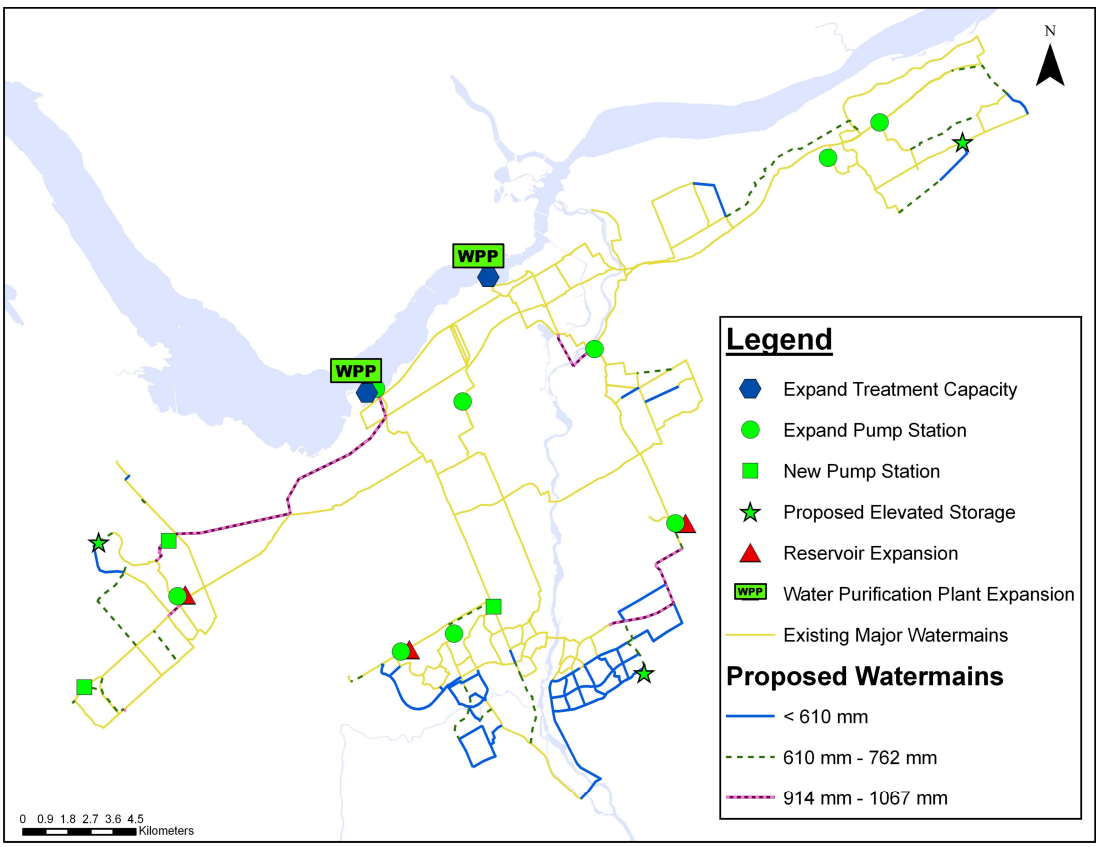

Figure 3: 2031 Infrastructure Solution

MAJOR CONCLUSIONS AND RECOMMENDATIONS

GA technology provides an effective tool that can be used as part of a multi-stage process of developing a water infrastructure Master Plan. However, high level system expansion concepts should be considered based on more traditional methods, with optimization used to assist in the evaluation of these concepts so that a preferred concept can be identified. Optimization can then play a more important role in establishing the details of the preferred concept.

The solution represents a guide to system expansion in the future, but planning efforts will be required periodically over time to update the expansion plan based on the most up-to-date information. Furthermore, the final sizing of infrastructure and specific watermain configurations in growth areas must be confirmed based on more detailed area-specific studies that consider updated growth projections, detailed planning information, and additional operational detail.

Reliable optimization results can best be achieved when a limited range of facility alternatives (i.e. Pump Stations and Storage Facilities) are considered.

Various zone configuration alternatives should not be considered within the context of a single optimization run. Alternatives involving control valves should be considered with caution as they can lead to hydraulic instabilities, leading to unreliable GA results.

High penalty factors are needed to ensure that GA solutions adequately satisfy design criteria. Fine-tuning of these factors is needed to avoid major infrastructure that provides limited benefit beyond ensuring that all criteria are strictly met at all locations. In some cases it was found that post-optimization modelling involving a more detailed representation of the existing watermain network yielded results that exceeded the design criteria in locations that had fallen slightly short of the criteria based on the raw GA results.

ACKNOWLEDGMENTS

This study was funded by the City of Ottawa. We would like to acknowledge the invaluable input provided by various planning, engineering, and operations staff at the City, including Louis Julien, Patrick Leblanc, Fern Marcuccio, Mark Surtees, and Dixon Weir. We would also like to acknowledge the input provided by various researchers at the University of Exeter including Zoran Kapelan and Godfrey Walters.

REFERENCES

Alperovits, E. and Shamir, U. (1977) "Design of optimal water distribution systems". *Water Resour. Res*. 13(6), 885-900

Goldberg, D. E. (1989). *Genetic Algorithms in Search, Optimization and Machine Learning*, Addison-Wesley, Reading, Massachusetts.

Holland, J.H. (1975) *Adaptation in Natural and Artificial Systems*. The University of Michigan Press.

Keedwell E., Khu S.T. (2003) "More choices in water distribution system optimisation." *Advances in Water Supply Management (Proc. of Computers & Control in the Water Industry 2003)* 16-17 Sept. London. 257-265

Keedwell E. and Khu S. T. (2005) "A Hybrid Genetic Algorithm for the Design of Water Distribution Networks." *Engineering Applications of Artificial Intelligence* Vol 18/4, 461-472.

Savic, D. A., and Walters, G. A. (1997). Genetic algorithms for least-cost design of water distribution networks. *J. Water Resour. Plann. Mgmt., ASCE*, 123(2), 67-77.

Savic, D.A. and M. Randall-Smith (1998), "Application of Hydraulic Network Models to Optimisation Problems Using Genetic Algorithms", *IQPC International Conference on Modelling the Distribution System*, London, UK, 15-16 July.

Savic, D.A., G.A. Walters, M. Randall-Smith and R.M. Atkinson (2000), "Large water distribution systems design through genetic algorithm optimisation", *ASCE 2000 Joint Conference on Water Resour. Eng. and Water Resour. Plann. and Mgmt.,* Jul. 30-Aug. 2, Minn., USA, ed. Hotchkiss, R.H. and M. Glade, p. 10.

Industrial Distribution System Simulation for Optimal Water Resource Assignment Using Probabilistic Tabu Search

S.H.H. Nourzad[1] and M.H. Afshar[2]

[1]Master of Science, Department of Civil Engineering, MEWE Consultant Company, P.O. Box 16565-157, Tehran, Iran; PH (+9891) 2294-0829; FAX (+9821) 8821-2355; email: shhn80@gmail.com
[2]Associate Professor, Department of Civil Engineering, University of Science and Technology, P.O. Box 16846, Tehran, Iran; PH (+9821) 7391-3159; FAX (+9821) 7724-0398; email: mhafshar@iust.ac.ir

ABSTRACT

Water of almost any quality has value so all operators need to learn how to use less, recycle more and to keep it as clean as possible. In many cases, the mineral industry, as a significant water user and wastewater producer, has the capacity to substitute poorer quality water for mining and mineral processing. Complex optimization problems and their challenges have been considered by the researchers around the world over several past years. Tabu search (TS) is a powerful searching algorithm based on principles of intelligent search. We propose in this work a probabilistic improvement to the selection procedure of TS. In this article, two methods are presented: Rank Based Probabilistic Tabu Search (RBPTS) and Fitness Based Probabilistic Tabu Search (FBPTS). Finally, we try to find optimal water resource assignment for an industrial copper complex distribution system. Anyhow, this is an applicable case study in industry.

INTRODUCTION

Complex optimization problems and their challenges have been considered by researchers all over the world over several past years. One way to overcome such difficulties is to use heuristic algorithms based on human's intuition or inspiration from nature that seek for near optimum solutions at reasonable computational time, but cannot guarantee that a problem will be solved and obtain the exact solution. The advantage of heuristic approaches compared with exact algorithms is that the heuristics especially when solving large-scaled problems, find high quality solutions much faster than exact algorithms.

Every year, many improved heuristic algorithms are presented. In this article, the focus is on the modern intelligent optimization technique, the well-known tabu search (TS) method. The concept of tabu search was introduced by Hansen and Jaumard and Glover. Since that time, TS has been proved to be among the most powerful tools for solving various combinatorial optimization problems (for example, graph partitioning (Rolland, 1996), scheduling (Thomas, 1998), and vehicle routing problem (Wassan, 2002)). Still, the design of even more effective TS modifications for specific problems is the research topic for many scientists. In this article, our aim is to apply a probabilistic extension in the selection procedure of TS then try to solve

an industrial water resource management problem with this method.

This article is organized as follows: First, the basic definitions of Standard TS and its components are briefly described. Then the extension of TS is outlined and industrial water management is discussed, then a hypothetical water supplying problem for a mineral plant –and its components– are introduced and solved by the proposed TS. Finally, the paper is completed with conclusions.

STANDARD TABU SEARCH

Tabu search (TS) is a powerful searching algorithm based on principles of intelligent search. The very early origins of the tabu search method go to the well-known technique - the descent local search (DLS) (also known as hill climbing) (Papadimitriou, 1982). DLS starts from an initial (maybe, randomly generated) solution. Further, the search process is continued by performing the perturbations of solutions, i.e. making moves from solutions to solutions. A move is applied to the current solution in order to get a new solution from the neighborhood of the current one. The moves are controlled, if the objective function becomes better, the current solution is replaced by the neighboring one, otherwise, the search is continued with the current solution. The whole process is continued until the current solution is a local optimum, that is, no better solution exists in the neighborhood of it.

TS is an extended descend local search. TS enables to escape from local optima and explore a much larger part of the solution space compared to DLS. The key idea of TS is allowing climbing moves when no improving neighboring solution exists, i.e. a move is allowed even if the new solution from the current solution neighborhood is worse than the current one. Obviously, return to local optimum solutions, which have been previously visited, is to be forbidden in order to avoid cycling. TS is based on the methodology of prohibition; some moves become "tabu" from time to time.

The TS algorithm starts from an initial solution in the feasible space. The process is then continued in an iterative way, moving from a solution to a neighboring one. At each step of this procedure, a subset of the current solution neighboring solutions is considered and the move that improves the objective function value more is chosen. Naturally, the new solution must not necessarily be better than the current solution; if there are no improving moves, the algorithm chooses the one that increases the objective function less. In order to eliminate an immediate return to the solution just visited, the reverse move must be forbidden. This is done by storing the corresponding solution (move) (or its "attribute") in the memory (called a tabu list). The tabu list keeps information of last moves which have been done during the search process. This way of proceeding hinders the algorithm from going back to a solution reached within the last steps. However, the straightforward prohibition may sometimes lessen the efficiency of the algorithm. Moreover, it might be worth returning after a while to a solution visited previously to search in another promising direction. Consequently, an aspiration criterion is introduced to permit the tabu status to be dropped under certain circumstances. The search process is stopped as soon as a termination criterion is satisfied.

Therefore TS main components are: Initial solution, Neighborhood and movement, Tabu list, Aspiration criteria and Stopping criteria (Li, 2006).

Theoretically, different *initial solutions* could lead to different local optimum solutions in a highly nonlinear problem. The beauty of TS is that initial solution can be randomly selected but TS optimization process reduces the deviation of optimums.

The basic idea of TS optimization is to *move* from one solution to the best solution, which is not restricted by tabu list, among its *neighborhood*. If the newly found optimum solution is better than any other previously explored optimum solutions recorded in the tabu list, the list will be updated with this solution. Although any new solution may be worse than the current best result, TS keeps moving toward the best neighbor solution until the given stop criterion is met. This is to avoid being trapped in a local optimum. It is noted that different definitions of a solution neighborhood may significantly affect search efficiency as a large neighborhood requires more searching time and less movements, and vice versa.

Better solutions of recent iterations are recorded in the *Tabu list*, serving as a strategic restraint for not moving back to formerly found solutions. The tabu list should not be too short because there it might be trapped in a cycle. However if the list is too long, the search process may become inefficient. Glover (1990) suggested the magic number 7 to be the first guess.

The role of *aspiration criteria* in TS is to provide an exception to the tabu list. When only a part of the decision variable information is recorded in the tabu list, a truly better solution among those in the current solution neighborhood might be ignored. This misjudgment can be resolved by considering an aspiration criteria or recording all decision variable information in the tabu list.

Termination criteria serve as a restriction for not proceeding further searching when the optimum solution has been reached. It can be given as: (1) a defined optimum solution (2) a maximum number of iterations or (3) the number of iterations done with no improvement.

IMPROVED TABU SEARCH METHODS

As described above, in Standard TS, randomization is done at the first step of solving the problem to select the initial solution. In order to escape from local optima, TS allows uphill climbing moves when no improving neighbor solution exists. Considering this idea, two extensions of TS are proposed in the following:

In standard TS, objective function values of all neighbor solutions are calculated and sorted according to the ascending value of the objective function if a minimization problem is at hand. If the best solution of the neighborhood space represented by the first of the sorted list doesn't exist in the tabu list, TS moves to this solution, otherwise the next solution of the sorted list is considered until a solution is found which is not in the tabu list. The aspiration criterion is used if all the neighbor solutions exist in the tabu list. A situation might arise when the best of neighbor solutions isn't better than the current solution representing local optima. Any move in this situation would be a downhill move without any guarantee to get out of the local optima. A remedy to this problem is proposed here by means of a random selection of neighbor solutions. Randomization in TS can help the method not to be trapped in the local optima. In this article two selection mechanism, namely *rank-based* and *fitness-based*, conventionally used in evolutionary algorithms such as GA, are exploited when the above mentioned situation is faced.

Rank Based Probabilistic Tabu Search (RBPTS)

In this case, selection probability is defined as below:

$$Pr_i = \frac{\frac{1}{k_i}}{\sum_j \frac{1}{k_j}}$$

k_i : Rank of the ith solution among the neighborhood space

Pr_i : Probability of selecting the ith solution as the solution to move to.

This selection mechanism would give more chance to the lower ranked, i.e.; better, solutions to be selected as the next point to move to.

Fitness Based Probabilistic Tabu Search (FBPTS)

In this case, selection probability is defined as below:

$$Pr_i = \frac{\frac{1}{(Objective)_i}}{\sum_j \frac{1}{(Objective)_j}}$$

$(Objective)_i$: Objective function of the ith solution

Pr_i : Probability of selecting the ith solution as the solution to move to.

This selection mechanism would also give more chance to the solutions with lower objectives, i.e.; better solutions, to be selected as the next point to move to.

INDUSTRIAL WATER SUPPLY

Water costs money so operators need to learn how to use less, recycle more and to keep it as clean as possible for reuse and ultimate disposal. The mineral industry has an urgent need to demonstrate wise reliable water management and disposal because of public concern about water resources. This extensive concern has put more and more pressure on all significant water users to manage water more sustainable as a key asset with business value. Water plays a significant role in the economic development of regions and communities, and maintenance of the ecology. Water of almost any quality has value. In many cases, the mineral industry has the capacity to substitute poorer quality water for mining and mineral processing - for example, saline and waste water - in place of fresh water. The cost of water supply includes all direct costs of water use in site, such as exploration and extraction of groundwater costs, feasibility study costs, pump costs, license costs, cost of water supply, water treatment costs and cost of maintaining water infrastructure and monitoring equipment.

Water quantity and quality requirements vary significantly across the industry and will be affected by the locality, the mining and processing methods, and the commodity being mined.

A site water management plan should identify operational water supply,

recycling, and disposal needs using water balances, manage treatment of waste water and identify legislative and other regulatory requirements relating to water management. In order to adequately understand the water resource, baseline data relating to water resources, current and predicted water demand and the surrounding environment particularly water dependent ecosystems should be incorporated into the development of site water balances and water management plans.

Measuring and monitoring water -undertaken for the operation life - should include water inputs into the system (i.e. rainfall, supply water, groundwater extraction, surface water pumping, and recycled water), outputs from the system including regulated and unregulated discharges (i.e. rainfall run-off, seepage, evaporation) and water storage (including reconciliation of input and outputs to ensure integrity of storages). (Blum, 2003)

Decision Variables

An industrial water supply system can be modeled with a network consisting of a number of nodes, connecting lines, reservoirs of variable water level and pumping stations. There could be two kinds of connections between network nodes. Some connections transfer water (or slurry containing water) by gravity but some other may contain pumping stations to pump water under pressure. For each node one continuity equation can be written and for each connection line (line discharge) one variable can be considered. Also, for each reservoir node there is an additional variable (flow from spillway). The difference between the equations and variables is the number of decision variables that the optimizer should evaluate.

Objective Function

Objective function in this kind of problem is minimizing the total cost of plant operation. The main expenditure of the plant operation is pumping costs so the objective function is assumed to be minimizing plant pumping costs. First the energy consumption of the plant pumping system should be calculated, and then by multiplying by cost per unit of energy, total cost of operation can be calculated as bellow:

$$ObjectiveFunction: Minimize \sum_{N_{PS}} \left(Energy_i \times CPUE \right)$$

$$Energy_i = Power_i \times T$$

$$Power_i = \frac{\gamma . Q_i . Head_i}{\eta}$$

$Energy_i$: Consumed energy in ith pump station (J)
$CPUE$: Cost per unit of energy (Rials/J)
T : Duration (s)
N_{PS} : Number of pump stations
$Power_i$: Consumed power in ith pump station (W)
Q_i : Discharge of the ith pump station (m3/s)
$Head_i$: Head (m)
η : Pump Efficiency

Constraints

Typically Constraints of this problem are of two types; one type is water demand for each node that should be supplied; the second type is related to pumps and pump stations. For the second type, constraint is derived from ability of pump stations to supply the needed head for pumping the water between nodes.

$$\left(\sum_{n=1}^{N_{PS}} Head_n\right)_j \geq \left(Head_s + Head_f\right)_j$$

$$\left(\sum Q_{in}\right)_i \geq Demand_i$$

$Head_n$: Produced Head by n^{th} Pump Station

$\left(Head_s + Head_f\right)$: Needed Head for Flow in j^{th} Connection

$\left(\sum Q_{in}\right)_i$: Total Discharge to i^{th} Node

$Demand_i$: Water Demand in i^{th} Node that should be supplied

WATER CYCLE COMPONENTS OF A COPPER COMPLEX

Water in industry is used for cooling, transfer, washing, as a solvent and a substance produced in the final product compound. The most important properties of water in industry (the amount of off take, usage and returning water) are strongly related to their production & supply facilities and water systems. Essentially, water in industry is used in two ways; open and closed cycles. In open loop systems, water after off taking and been used (pure or impure), is returned to the river. In a closed looped system, the used water, after necessary productions, is returned to the loop again. In this system, water isn't discharged into the river and by using it repeatedly it remains in the cycle. The amount of off take from the source in industrial water systems is for amending fatalities of industrial producing process and sometimes for replacing water in the water cycle (Aleyasin, 2005).

Water is a vital component in copper production process from mineral rock. After the mineral rock is milled, it is solved in water and some chemical solutions are added so that the copper stands on top of the solution as foam. This foam is collected with large spoons and enters the purring process. The remaining solution in the cauldron, which is called tailing, contains more than 60% water and about 40% unsolved solid matters.

The considered mine is located in a dry region and water resources available are very few. One of these resources is the seasonal river which has little water; this is while one part of this water is allocated for agricultural use. One other water resource for this plant is underground sources.

According to the mentioned conditions, using an open cycle isn't possible. That means that the main resource of this plant should be the return water and the shortcoming should be ensured from surface water and ultimately underground water in case of necessity. For forming a closed cycle, different components are needed; for example pipe lines, pump stations, tailing dams, diversion dam, water reservoirs and treatment plants (Figure 1).

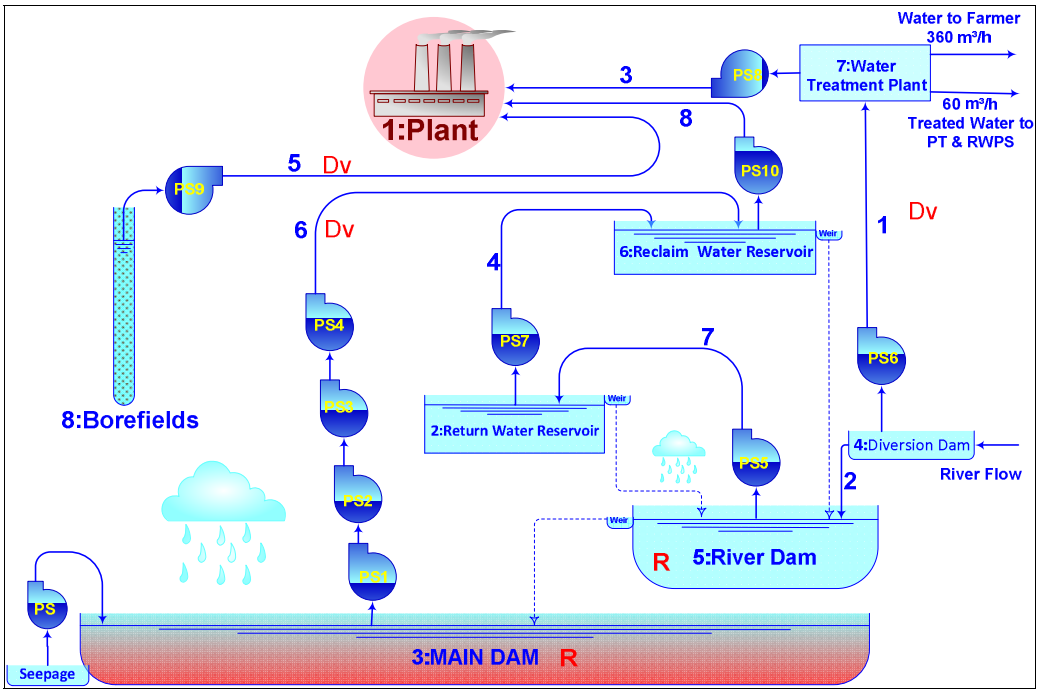

Figure 1: The Copper Complex Water Cycle

According to water components of the complex water cycle (Figure 1), water can be supplied for the complex in three ways: seasonal river, wells and finally returned water from the tailing dam.

MODELING RESULTS

For solving each problem, the needed model inputs are introduced to the model in the format of given files. Inputs are classified in two main groups: one group is inputs related to physical properties which are different for each problem according to their situations. This group is mainly inputs to the simulation model. The other kind of inputs is optimization model constants that are independent from the physical properties. Therefore these constants can be determined for a simple problem and be used for other problems. So the first step for performing a model is parameter tuning. After parameter tuning the model is ready for solving various scenarios of complex operation and decision making.

In this problem, as mentioned above, tailings exported from the plant go directly to the tailing dam pond, sediments settle and decant water is stored behind the dam. This water is pumped to the reclaim water reservoir in several stages.

This problem is solved with all the 3 mechanisms (FBPTS, RBPTS and Deterministic) and as an example the results of one mechanism are presented below (Figure 2, Figure 3 and Table 1).

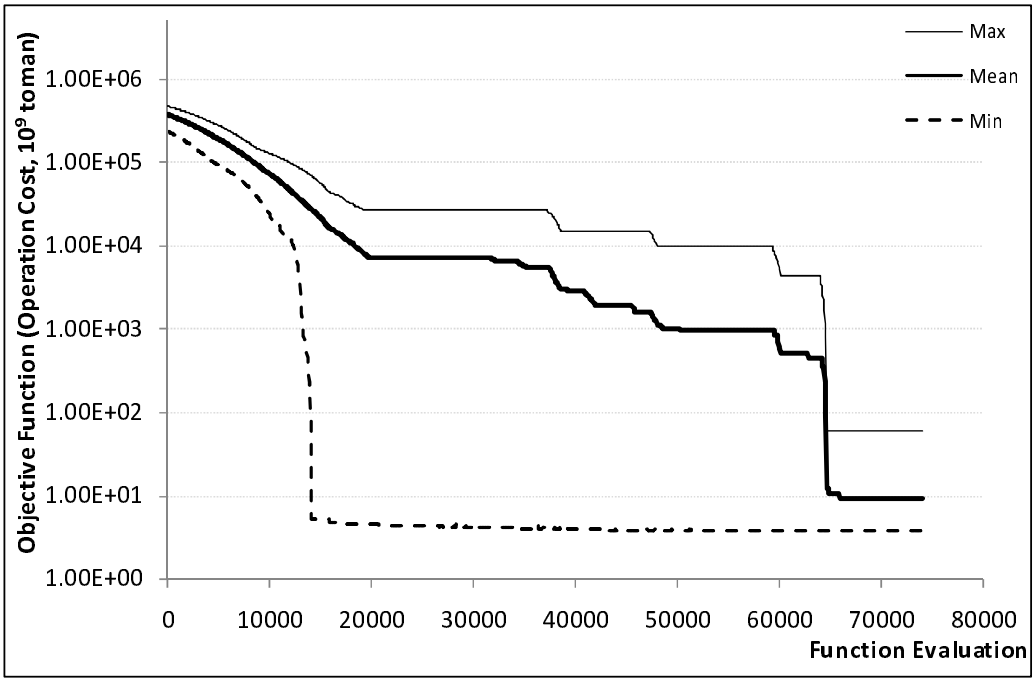

Figure 2: Objective Function Values– RBPTS

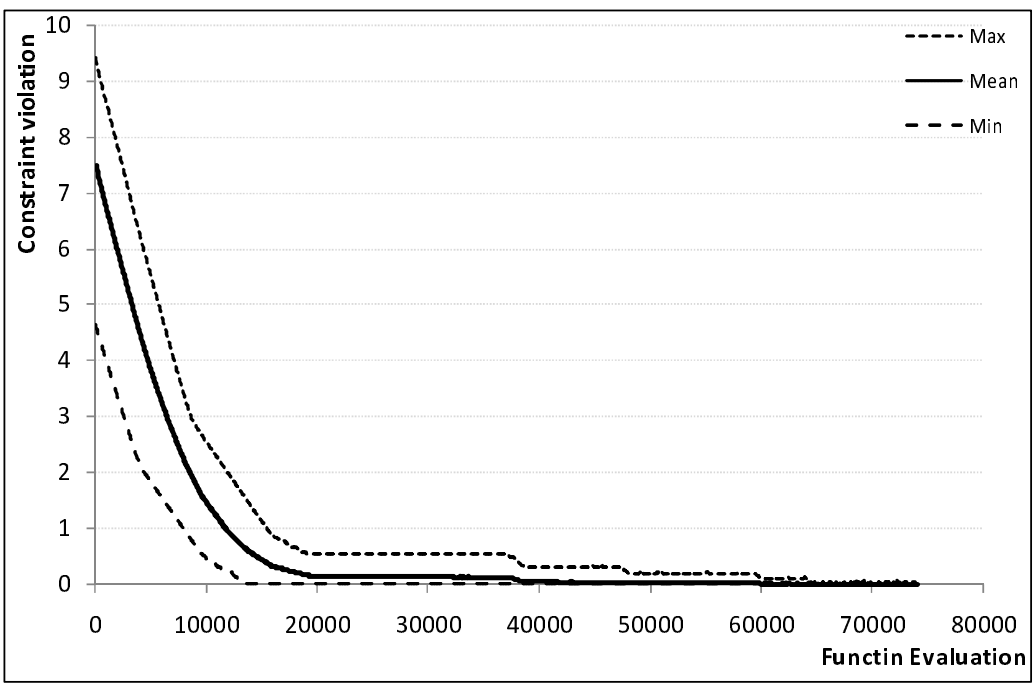

Figure 3: Constraint violation– RBPTS

Table 1: Variable Value (Operation Rule)– RBPTS

	variable		1	2	3	4	5	6	7	8	9	10	11	12
Decision Variable	water from diversion dam to treatment plant	m^3/hr	1,382	652	676	648	673	1,352	1,325	1,800	1,800	1,800	1,800	0
	water from tailings dam to water tank	m^3/hr	0	0	955	781	1,160	655	561	0	0	0	0	0
	water from wells to water tank	m^3/hr	3,500	3,500	3,500	3,500	3,500	3,500	3,494	2,251	2,589	2,948	3,430	0
State Variable	Release from diversion dam to water dam	m^3/hr	113	9	31	7	35	10	39	66	1,378	1,378	1,378	1,378
	water from treatment plant to plant	m^3/hr	858	962	232	256	228	253	932	905	1,380	1,380	1,380	1,380
	water from from return water tank to reclaim water tank	m^3/hr	687	1,338	1,368	1,489	391	687	13	1,140	1,369	1,331	1,372	1,490
	water from water dam to return water tank	m^3/hr	687	1,338	1,368	1,489	391	687	13	1,140	1,369	1,331	1,372	1,490
	water from reclaim water tank to plant	m^3/hr	4,187	4,838	4,868	4,989	3,891	4,187	3,513	4,634	3,620	3,920	4,320	4,920
	tailings dam storage	$milionm^3$	5.00	6.37	8.02	9.18	11.12	12.13	13.64	14.79	16.67	18.65	20.60	22.58
	water dam storage	$milionm^3$	5.00	4.59	3.63	2.67	1.60	1.34	0.85	0.88	0.11	0.13	0.18	0.20

RESULT ANNOTATIONS

According to objective function values, the probabilistic method will improve the objective function value considerably compared with deterministic mechanism. Furthermore, the ranking based mechanism will improve the value better than the fitness based one (**Error! Not a valid bookmark self-reference.**)

Table 2: Annual Costs

Problem / (10^9 toman)		Annual Pumping Cost	Groundwater Cost	Total Operation Cost
Case-Study Solution	Deterministic	2.68	1.48	**4.16**
	FBPTS	2.73	1.07	**3.81**
	RBPTS	2.74	1.07	**3.81**

CONSEQUENCE

In this paper components of a copper complex water distribution system have been introduced and the water flow in this cycle has been simulated and been optimized by Tabu Search method- one of the most powerful meta heuristic methods. Also, two probabilistic extensions have been made to the TS optimization process by authors. Results indicate that these extensions have been remarkably successful in getting closer to optimum solution. Finally, it can be mentioned as an essential consequence for industrial plants that using optimum-closed water cycles is economically and environmentally vital.

REFERENCES

Aleyasin A. (2005) *Water Crisis*, Consultant Engineer Community Publisher, Tehran.

Blum C. et al. (2003). "Metaheuristics in Combinational Optimization: Overview and Conceptual Comparison" *ACM Computing Surveys*, 35(3).

Cunha M. et al. (2004). "Tabu Search Algorithms for Water Network Optimization" *European Journal of Operational Research*,157 ,746–758.

Hansen P., Jaumard B. (1987). "Algorithms for the Maximum Satisfiability Problem" *RUTCOR Research Report*, Rutgers University, USA, 43–87.

Li M.H., Tung C.P., Sui C.H., and Yang F.H. (2006). "Estimating Seasonal Basin Rainfall Using Tabu Search" *TAO*, 17(1), 295-316.

Papadimitriou C.H., Steiglitz K. (1982). "Combinatorial Optimization: Algorithms and Complexity", Prentice- Hall, Englwood Cliffs.

Rolland E., Pirkul H., Glover F. (1996). "Tabu Search for Graph Partitioning" *Annals of Operations Research*, 63, 209-232.

Taillard E. (1991), "Robust Taboo Search for the QAP" *Parallel Computing*, 17, 443-445.

Thomas P., Salhi S. (1998). "A Tabu Search Heuristic for the Resource Constrained Project Scheduling Problem" *Journal of Heuristics*, 4, 123-139.

Wassan N.A., Osman I.H. (2002). "Tabu Search Variants for the Mix Fleet Vehicle Routing Problem" *Journal of the Operational Research Society*, 53, 768–782.

Optimal Pump Scheduling by Linear Programming

M.F.K Pasha[1] and K. Lansey[2]

[1]Water Resources Engineer, Tetra Tech Inc., Tucson, AZ 85711; email: fayzul.pasha@tetratech.com.
[2]Professor and Head, Department of Civil Engineering and Engineering Mechanics, The University of Arizona, Tucson, AZ 85721; Ph (520)-621-2512; Fax (520)-621-2550; email: lansey@email.arizona.edu.

ABSTRACT

Energy is one of the largest water utility expenses. This cost is greatly associated with the pump operation. An optimum pump schedule can reduce the cost significantly while maintaining hydraulics in an acceptable range. In this paper, the pump station relationships are linearized using relationships among energy required, pumping flow, demand factors and tank storage or tank water levels. A linear programming (LP) optimization problem is formulated and solved for a single tank system for the optimal pump schedule to minimize energy cost. This LP model can be solved very quickly for a "near optimal" solution. Available online data can be then incorporated to update the schedule each hour in real-time. This paper describes preliminary methodologies that can be used to optimize the pump schedule and reservoir control. Future work will extend the approach to multiple tanks and pump station systems, better pump curve representations, and spatially variable demands.

INTRODUCTION

Water supply and distribution systems consume a significant amount of energy to transport water through the WDS. This consumed energy used in a form of electrical energy is one of the highest expenses for the water utility industries. Increasing energy prices make the energy expense important to water utilities.

In recent years a significant amount of research has been focused on optimizing pump operation schedules. The full range of linear, nonlinear, and heuristic optimization methods, dynamic programming and brute force search have been applied to solve the problem (Ostfeld and Tubaltzev 2008, Thorstensen 2007, Prasad et. al. 2006, Nace et. al. 2001, Savic et. al. 1997, Brion and Mays 1991). Bunn (2006) and Bunn and Hillebrand (2006) have suggested an LP method but have not presented details of the method. Most of the other method either greatly simplify the complex water distribution system or require significant time to solve the problem which limits their real-time capabilities.

Energy consumption in a water distribution system can be reduced in a number of ways; by lowering pump volumes, by reducing tank or reservoir heads against which pumps are operating for, by operating pumps during off peak hours to decrease the unit energy price, by operating pumps near the best efficiency point. All of these options are possible using online data to optimize pump schedule. We postulate that the most significant portion of these benefits is from proper use of tanks and maintaining pump efficiencies is less important.

The aim of this study is to develop an optimum pump operation model which can be solved quickly enough that online data can be incorporated in the model and solve the problem in real-time. The objective of this problem is to minimize the pump operation energy cost. The approach applies an approximation to the energy use as a function of pump station discharge.

PROBLEM FORMULATION

To date, most of the optimization approaches suggest that 10% to 20% energy cost savings are available compared to trial and error techniques or experience. On the other hand even fairly large linear programming (LP) problems can be solved in seconds on most desktop computers. With online data in hand a linear model can be updated very easily and problem can be solved quickly enough to take real-time decisions. Therefore, LP has been used to solve numerous problems from scheduling to financial market.

A water distribution system is a complex system of pump-tank-node relationship. Since LP requires the objective and constraints functions to be linear, the complex network relationships must be simplified to make the relationship linear so that LP can be adopted. The resulting model may not ensure that the global optimum solution of the pump scheduling problem. However, if a comparable solution (i.e., one within a few percent) can be quickly determined then the benefits of rapid solution may be balanced with inaccuracies introduced by linearization.

The model is formulated to minimize pumping energy such that hydraulic constraints are met. Mathematically the problem can be stated as:

$$\text{Minimize } \sum_{T=1}^{24} C_T E_T(Q_{p,T}, H_T) \tag{1}$$

subject to:

$$H_{min} \le H_T(H_{T-1}, Q_P) \le H_{max} \tag{2}$$

$$Q_{Pmax} \ge Q_P \ge 0 \tag{3}$$

where C_T is a conversion factor to convert energy consumed during period T, i.e., E_T to dollars. E_T is the power function of pump station ($Q_{,Tp}$) and (H_T) is the initial water

level in the tank at time *T*. The tank water level, H_T, is a function of the previous hour water level H_{T-1} and Q_{pT-1} and is constrained to between the minimum (H_{min}) and maximum (H_{max}) allowable tank water levels. The pump station flow is also constrained (Eq. 3) by maximum and minimum limits so that the range of the model does not go beyond the limit of the linear approximation of the system. The model is formulated hourly basis for 24 hours. As seen, this initial model is applicable to a single tank system. Future work will consider multiple tanks. $\boldsymbol{Q_p}$ and $\boldsymbol{H}$ are the sets of LP decision variables with $\boldsymbol{Q_p}$ can be considered as the control variable with $\boldsymbol{H}$ as the state variable.

Eq. 2 is a function of previous hour tank water level and pump station based on conservation of mass or:

$$H_T = H_{T-1} + \frac{(Q_{P_T} - Q_{D_T})\Delta T}{A_T} \tag{4}$$

where Q_{P_T} and Q_{D_T} are the pump station flow and system demand, respectively, at time *T*. A_T is the tank's cross sectional area and ΔT is the length of time step. Since the tank's cross sectional area and time interval are constant in the equation and the demand and previous hour tank's water level are known at the beginning of the time step, H_T can be determined given Q_{pT}

Similarly, the consumed energy is approximated as a linear function of the pump station flow and initial tank level as:

$$E_T = m_T Q_{P_T} + I_T(H_T) \tag{5}$$

where m_T is the slope of the energy curve which is function of pump station flow, Q_{P_T} and I_T is the interceptor of the energy equation which is function of tank water level. The next section describes how this function can be developed.

METHODOLOGY

Pump scheduling by linear programming consists of five steps. The first step is to collect the WDS physical data. Using this data, the energy functions are then developed by extensive simulation. Both of the previous steps are completed off-line prior to the real-time application. In real-time, the third step is to forecast demands. Finally, linear programming model is formed with those demands and the derived functions to determine the optimal pump station discharges for each period. Finally, those discharge values are converted to actual pump operations.

Zhong and Lansey (1991) proposed using a pump station head as a decision variable in an NLP problem with the pump station discharge being an implicit variable computed in the network hydraulic model. They developed a nonlinear

regression relationship between pump station head, discharge and energy consumption. The curve was based on data generated from simulating alternative pump combinations.

The approach here for developing an energy function is different in that it combines the energy consumption to the pump discharge for specific tank level and system demands. For this initial step in formulating this problem, a single linear equation is used. However, this relationship is not necessarily always linear. The shape of the curve suggests that a piecewise linear relationship between these two parameters may be more appropriate than a single linear relationship and will be pursued in the next steps of this research.

EXAMPLE NETWORK

The network that is analyzed in this study consists of 37 pipes, 19 nodes, one tank (node 21) and one source (node 20) with four pumps (Figure 1). The tank elevation and diameter are 215 ft and 40 ft, respectively. The hydraulic time step and pattern time step are each 1 hour. The tank level was permitted to fluctuate between 222 ft to 250 ft. Hourly demand factors ranged from 0.5 to 1.7. Four pumps are installed in the pump station at the reservoir source.

Given the physical and demand data, the energy and flow relationships can be developed. To do so, the network is simulated for each demand factor for each pump combination for a range of water levels. With four available pumps, 15 pump combinations are possible (the no pumping option is not considered). Figures 2a -2c show the plots of energy required and pump station flow for different demand factors. For each demand factor the plots for different tank water levels are similarly concave upward. Only combinations that satisfy pressure requirements are included in the plots. If multiple pump combinations supply the same discharge with different energy demands, the higher cost combination is dropped. The resulting points are the operating points for the pumps at the given demand level and tank level. For a single tank system, the network hydraulics are completely embedded in the energy consumption relationship.

Recall that the pump station flow is the LP decision variable. Since the pump station flow, Qp, and system demand, Q_D, are then known, the flow into the tank and the resulting change in water level can be computed by Eq. 4.

To demonstrate the methodology, the energy consumption versus pump discharge are fit with a single regression line for each tank water level and constant demand factor combination (Figure 3). The largest flow rate point is not included in the regression. The regression line equations are also shown. As seen, the slopes for all combinations are virtually equal so the average slope value is used. The lines do shift vertically. Changes in y-intercepts are related to the tank level that is not known a priori. Tank level, however, is a linear function of the discharge by Eq. 4 and the

energy consumption can be computed using Eq. 5. Figure 4 shows a linear regression to fit for $I_T(H_T)$. This relationship retains the linearity of the problem.

With these energy relationships, the LP can be solved for the optimal pump station discharges. The optimal solution is listed in Table 1.

Table 1: Optimal pump station discharges for application system

Time (hr)	Pump station discharge (gpm)	Time (hr)	Pump station discharge (gpm)	Time (hr)	Pump station discharge (gpm)
0:00	3201	8:00	8852	16:00	8493
1:00	6409	9:00	7	17:00	8141
2:00	10775	10:00	3300	18:00	7718
3:00	1386	11:00	3833	19:00	7679
4:00	5760	12:00	7728	20:00	7646
5:00	10135	13:00	7684	21:00	7041
6:00	94	14:00	11978	22:00	7038
7:00	4489	15:00	3986	23:00	7028
Total required energy to pump 24 hours flow = 21556 kWh					

The next step then is to convert the optimal pump station flow to a discrete set of pumps. An optimal pump discharge that falls on a pump combination point will operate at that discharge and consume the corresponding energy. If the discharge does not fall exactly on a pump combination point, some error will result in the approximate cost and tank water level when a nearby pump combination is chosen. Our supposition is that tank level control is the dominant available energy savings. Thus, small differences in pump operation decisions will not significantly alter the optimal solution cost. In addition, uncertainty in predicting future demands will change the solution over time. Since this approach can update a solution at each time step, the adjustments to demand predictions will mitigate some of the cost differences.

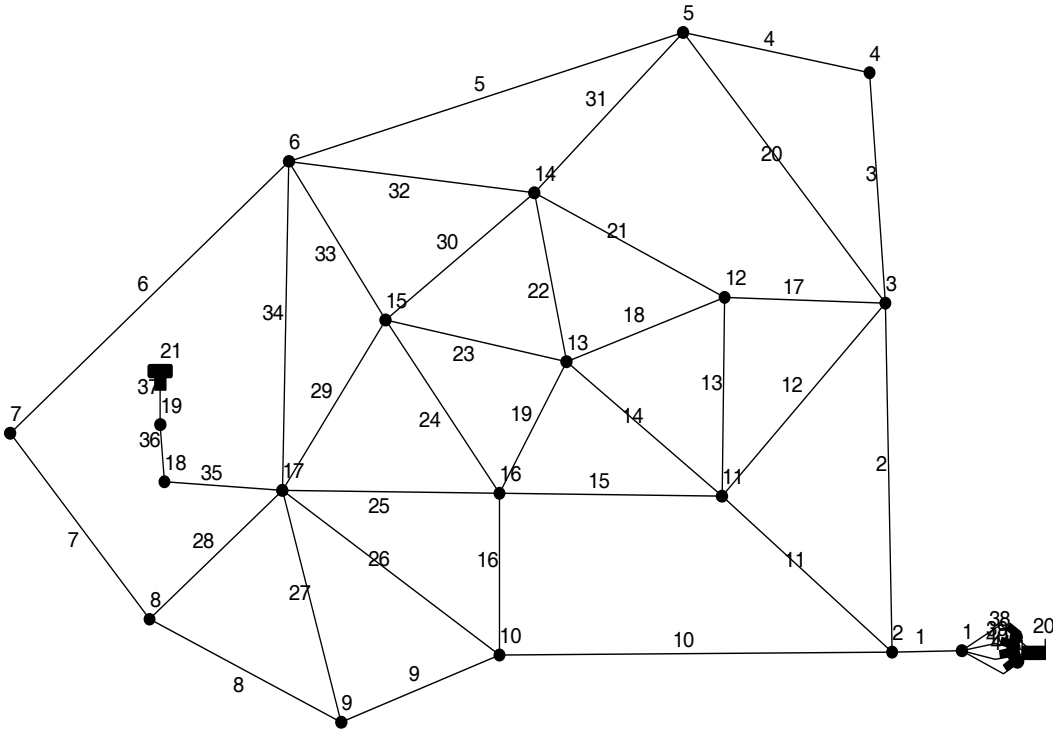

Figure 1. Example network.

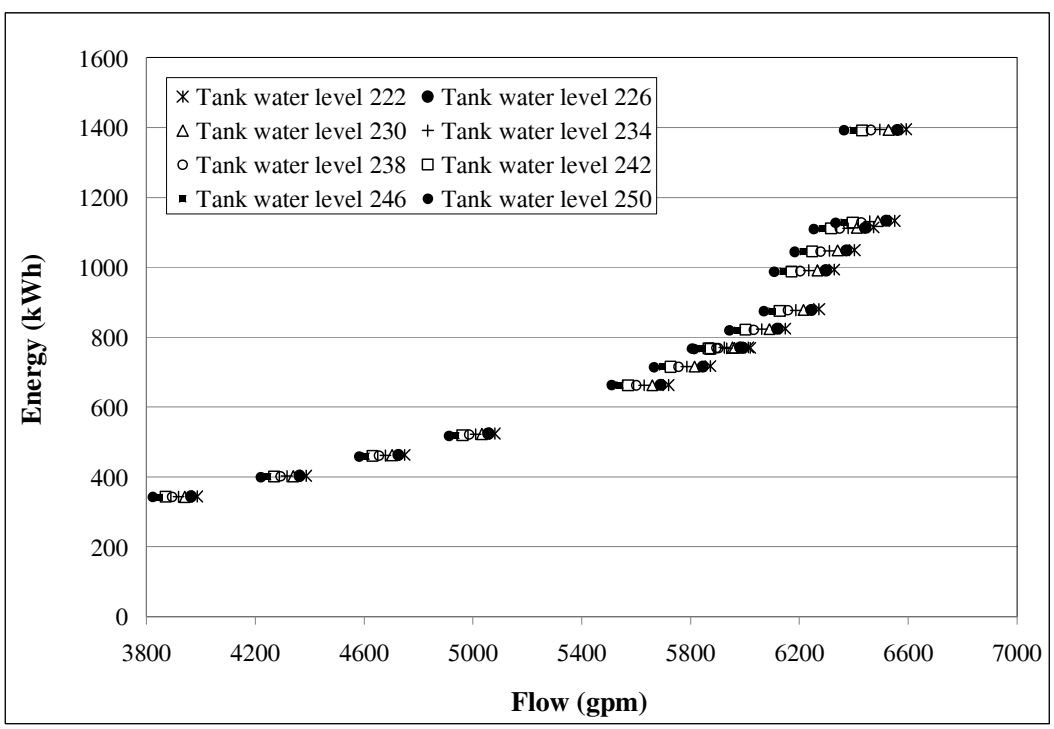

Figure 2a. Plot of energy consumed vs. pump station flow for different tank water levels for demand factor 0.5.

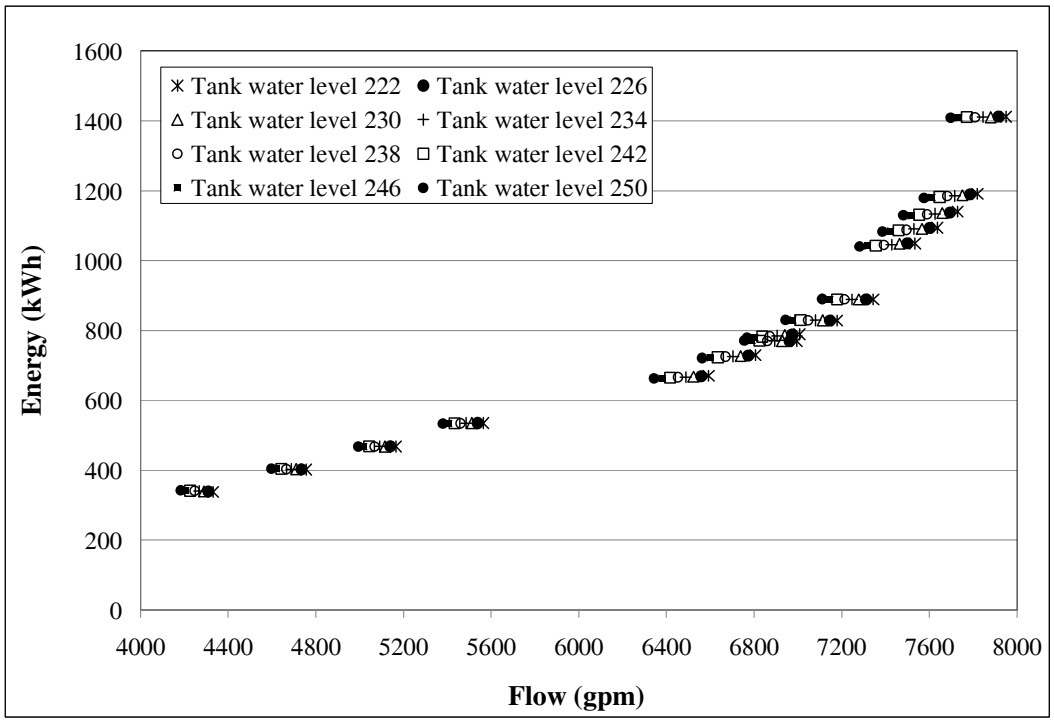

Figure 2b. Plot of energy consumed vs. pump station flow for different tank water levels for demand factor 1.0.

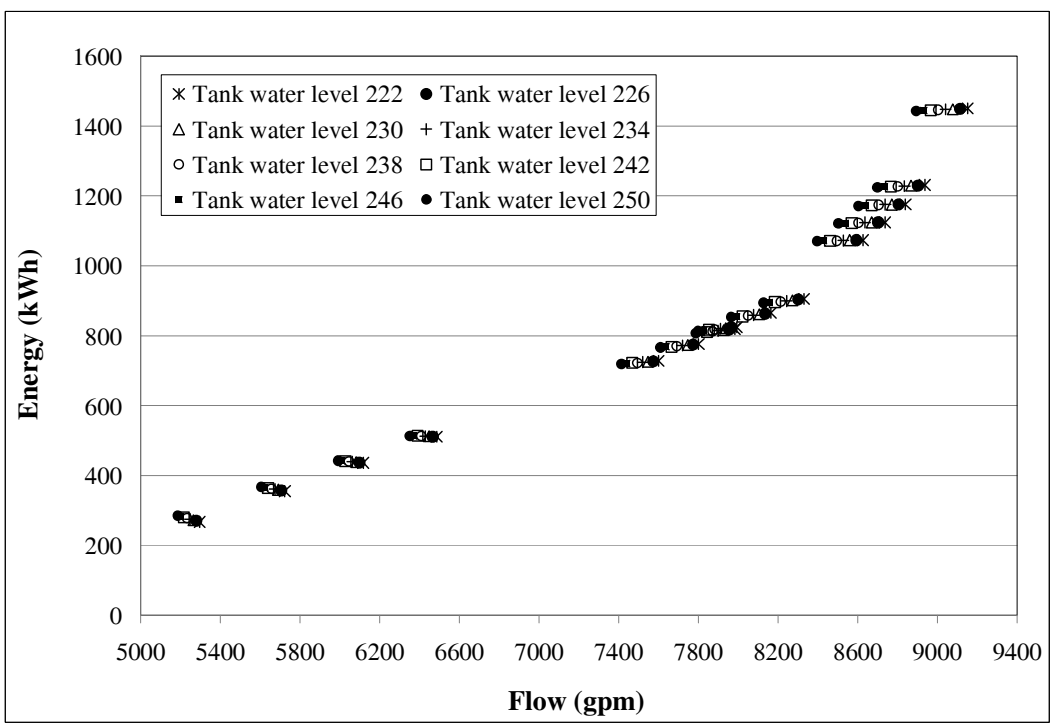

Figure 2c. Plot of energy consumed vs. pump station flow for different tank water levels for demand factor 1.7.

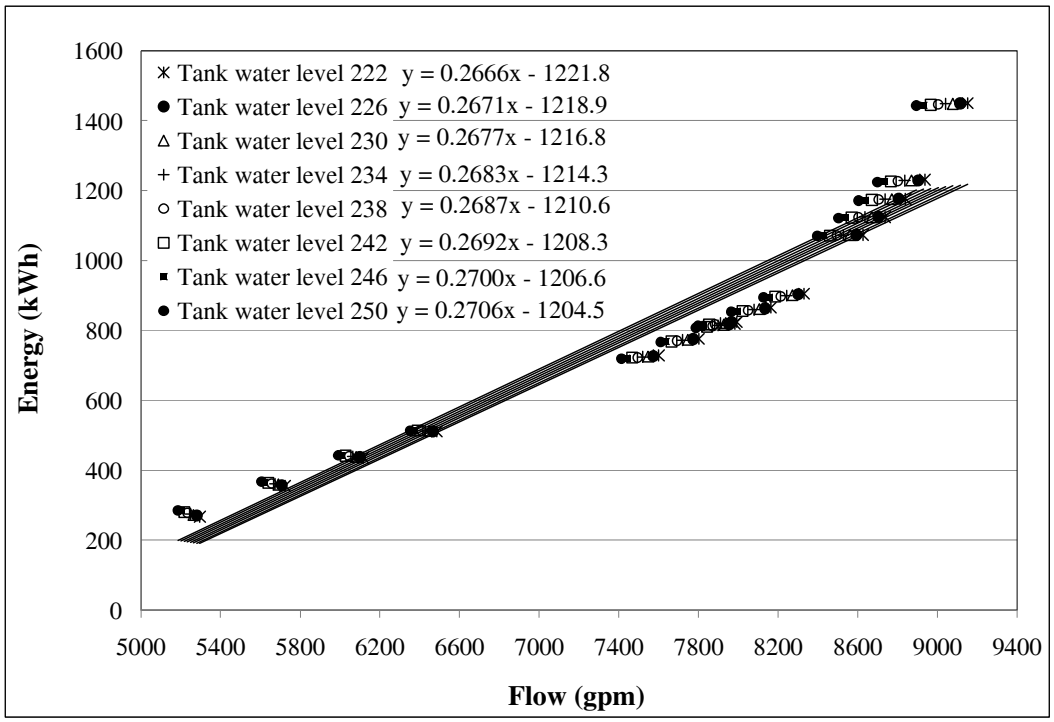

Figure 3. Typical regression relationships between energy required and pump station flow for different tank water levels.

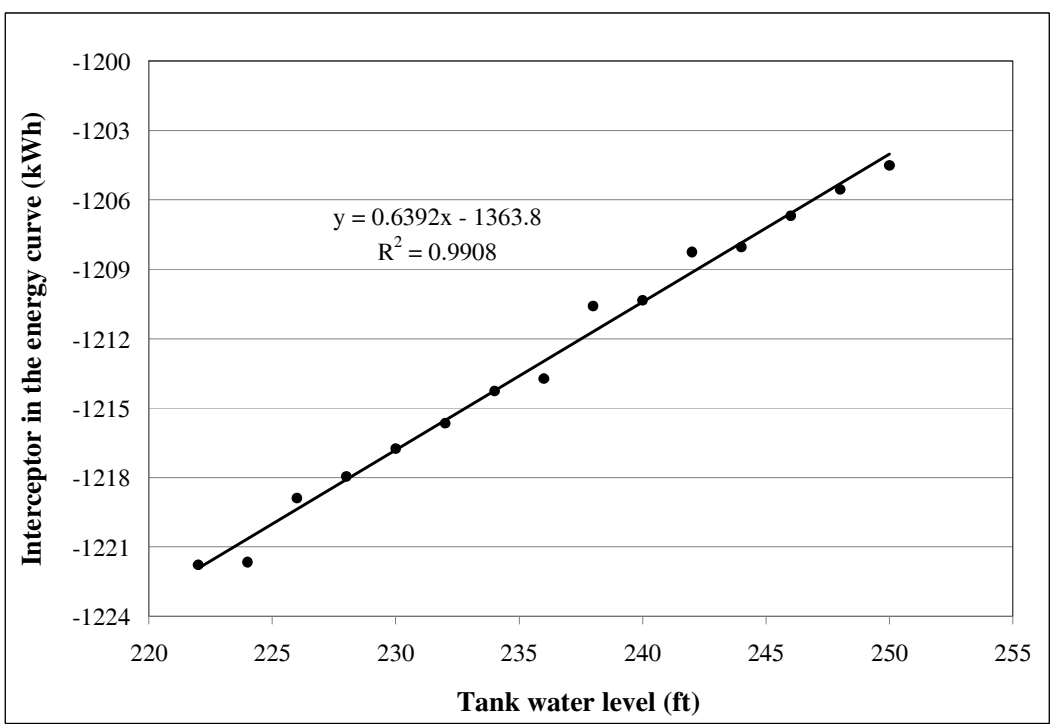

Figure 4. Typical regression relationships between energy curve interceptor and tank water level.

DISCUSSION AND CONCLUSIONS

The advantages of real-time optimal pump schedule have been long discussed. However, most approaches attempt to solve the problem exactly at the expense of high computation time. In this paper, a linear program model is posed that simplifies the complex water distribution system in a reasonable way. The linear programming model is solved quickly so that new data can be incorporated into the model in real-time. Thus, a real-time pump scheduling tool can be created.

Several difficulties arise due to the approximation. The first is converting the LP continuous solution to a discrete solution and the inaccuracies of the linear approximation. As described above, if a discharge at a given time step does not match a pump combination some inaccuracies will occur. Again, however, the majority of cost savings are expected to occur by storage management. A comparison to an exact method should be made to quantify the differences. A possible extension to this methodology is to pass the LP solution to a stochastic search or integer programming with a limited set of pump combinations.

A second problem is the linear regression does not fall through all pump combinations. An obvious improvement is to use a piecewise linear model over the single linear regression. The concave slopes of the energy consumption-discharge function are amenable to a minimization problem.

Next, this approach is only applied to a single tank. Extensions to multiple tank zones may be approximated by the proportion of flows sent to each tank. Finally, pump switch constraints can not be directly included. The two stage approach of passing the solution to a second discrete optimization method that could include these constraints is possible but may result in a local optimum. On the other hand, variable energy costs can be included with no additional difficulty.

Acknowledgement. Authors sincerely thank Surface Water Group of Tetra Tech. Inc. for their supports to present the paper in EWRI, ASCE 2009 conference.

REFERENCES

Brion, L. M. and Mays, L. W. (1991). "Methodology for Optimal Operation of Pumping Stations in Water Distribution Systems." *Journal of Hydraulic Engineering,* ASCE, 117 (11), 1551-1569.

Bunn, S. (2006). " Pump Scheduling Optimization in Four US Cities: Case Studies." *Water Distribution Systems Analysis Symposium, Proceedings of the 2006 EWRI, ASCE Conference*.

Bunn, S. and Hillebrand, C. (2006). "Energy Management in a Deregulated Market." *Proceedings of the AWWA Annual Conference and Exposition in San Antonio, TX. USA*.

Nace, D., Demotier, S., Carlier, J., Daguinos, T., and Kora, R. (2001). "Using Linear Programming Methods for Optimizing the Real-Time Pump Scheduling." *Bridging the Gap: Meeting the World's Water and Environmental Resources Challenges*, *Proceedings of the 2001 EWRI, ASCE Conference*.

Ostfeld, A. and Tubaltzev, A. (2008). "Ant Colony Optimization for Least-Cost Design and Operation of Pumping Water Distribution Systems." *Journal of Water Resources Planning and Management*, ASCE, 134(2), 107-118.

Prasad, T. D., López-Ibáñez, M., and Paechter, B. (2006). "Ant-Colony Optimization for Optimal Pump Scheduling." *Water Distribution Systems Analysis Symposium, Proceedings of the 2006 EWRI, ASCE Conference*.

Savic, D, Walters, G., and Schwab, M. (1997). "Multiobjective genetic algorithms for pump scheduling in water supply." *AISB Workshop on evolutionary computation – selected papers,* pages 227-236, Springer-Verlag, LNCS 1305.

Thorstensen, S. (2007). "Energy Savings Analysis Generated by a Real Time Energy Management System for Water Distribution." *Proceedings of the AWWA Pensylvania/Chesapeake Section Conference, Hershey PA., USA*.

Zhong, Q., and K. Lansey, (1991). "A Comparison of Two Large Scale NLP Strategies for Determining Optimal Pump Station Controls," in ASCE Proceeding of the Water Resources Planning and Management Division Conference on *Urban Water Resources*, 954-958.

An Integrated Approach for Distribution System Hydraulic Criticality and Emergency Response

Laura Jacobsen, P.E., Manager, Planning Division
Sri Kamojjala, P.E., Senior Civil Engineer
Brian Bowler, P.E., Senior Civil Engineer
Las Vegas Valley Water District

Abstract

Determining the hydraulic criticality of distribution system components is key to asset management and emergency response. Evaluation of the hydraulic criticality of large distribution system facilities involves compiling a significant amount of information such as spatial data, customer information and hydraulic model results. An integrated approach which leverages information compiled during the hydraulic demand distribution process for evaluating hydraulic criticality will be outlined. Benefits of the integrated approach for a) asset management, b) shutdown analysis and c) emergency response will be presented.

Introduction

Potential consequences of failure of an individual element of a water distribution system include loss of service to critical customers, entry of contaminants into the distribution system and reduced or no fire protection due to inadequate pressures and inability to maintain sufficient supply resulting out of loss of hydraulic integrity from the failure. Determining hydraulic criticality of a water distribution facility is therefore essential for asset management, emergency response, planning shutdowns and water quality evaluation.

There are almost 1 million miles of distribution piping (excluding service lines) in the United States, the majority of which will be reaching the end of their life spans in the next 30 years (Ray, 2007 and WSTB, 2005). The United States Environmental Protection Agency's (EPA, 2005a) most recent Drinking Water Needs Infrastructure Survey, conducted in 2003 and released in 2005, projects that the US will need to invest $276.8 billion over the next 20 years to repair/replace deteriorating water distribution infrastructure. The size of the drinking water infrastructure funding gap has been estimated by EPA at $45 billion to $267 billion, depending on the revenue growth scenario and spending levels (EPA, 2002a and Marlow, 2009). With limitations on available budgets, prioritizing criticality of assets is essential for optimal repair, rehabilitation and replacement of water distribution facilities.

Traditionally, decisions to rehabilitate or replace water pipes have been based on general indicators such as failure history, age, material, size and type of pipe. Reliance on these indicators alone may lead to sub-optimal decisions. To be optimal, information about the actual condition of pipe and its criticality is needed.

For high risk mains the effects of even a single main break are serious, so prevention becomes much more desirable (EPA, 2005b). The ability to prioritize and schedule repairs and replacements based on pipe condition and hydraulic criticality can be especially valuable for systems that have a substantial amount of high-consequence pipes that are approaching the ends of their service lives, but also have insufficient funds to address all the deteriorated pipes at one time. In this situation, the order in which pipes are repaired, rehabilitated, or replaced is very important, because the adverse effects of failures can be minimized by first addressing the pipes that have the highest failure consequences.

The useful life of pipe, which comprises most of the assets in water systems, varies considerably based on a number of factors. Deterioration rates of pipe will vary considerably as a function of climatic conditions, pipe material, soil properties, and corrosiveness of the water (EPA, 2002a). The best way to determine the remaining useful life of a facility is to conduct a condition assessment. The lack of condition assessment for water facilities can cause repair and replacement to be scheduled either too early or too late. Either error can cause adverse effects (EPA, 2005b). It is cost-prohibitive to conduct condition assessment for every facility in the system. In addition to factors such as material, age and soil characteristics, hydraulic criticality can be used for cost-effective prioritization for water facilities conditional assessment.

Water distribution systems are occasionally subject to emergencies or planned shutdown activities during which the system can no longer provide the minimum level of service to customers. Examples of emergency response situations include facility/equipment failures and power failures (WSTB, 2005). Planned shutdown activities include stopping the treatment plant, shutting down a well, reservoir shutdown for inspection, cleaning or repairs, installation of new pipe connections, pipe rehabilitation or break repairs, and valve repairs. These emergency situations and planned shutdowns can result in a reduction in system capacity and pressure, loss of supply to critical customers and reduced or lack of fire protection. Knowing the hydraulic criticality of a water distribution facility will facilitate a better operational response to emergencies and planned shutdowns, and minimize impact to customers.

Integrated Approach

In simple terms, determination of the hydraulic criticality of a distribution system facility involves:

a) Compilation of spatial and attribute data of system facilities
b) Prediction of system behavior during the failure such as loss of system pressure and capacity

c) Combining predicted system behavior with customer and spatial information to estimate consequences of facility failure

The tasks outlined above for determining hydraulic criticality of large distribution system facilities involve compiling a significant amount of information such as spatial data, customer information and hydraulic model results. The spatial data includes location and spatial relationship (topology) of distribution system facilities such as pipes, valves, pumping stations and storage reservoirs. Customer information includes service criticality, connection point and consumption. Hydraulic model results include system pressures, velocities and supply capacities. In addition, relationships need to be established between system facilities, customers and model results. Because the process and the associated large data requirements are resource intensive, an integrated approach is required to optimize resources and benefits. The following sections describe an integrated approach for evaluating the hydraulic criticality of system facilities.

Prediction of System Behavior during a Facility Failure

As stated above, the first step in evaluating hydraulic criticality is compiling system facilities information. Spatial data (GIS) systems typically keep a good inventory of the system data. GIS software has long supported the concept of topologically connected Geometric Networks with directional flows, sources/sinks, etc. Attempts have been made to predict system behavior during a facility failure using the topology in Geometric Networks. Although these methods, in the absence of a hydraulic model, may indicate portions of the network and customers without supply, they fail to predict the true system behavior for the connected portion of the network. For example, a system might still be connected during a facility failure but the residual pressures might be so low that supply is lost to customers in the connected portion of the network and a potential exists for intrusion of contaminants into the network. Therefore, prediction of system behaviors using geometric networks could result in misleading estimations of failure consequences. Hydraulic models provide a more accurate prediction of system behavior and failure consequences.

Model Construction

Historical emphasis when creating spatial data has been field-accurate mapping to support map generation and spatial analysis. Hydraulic modeling algorithms require a more stringent set of conditions on the data (Jacobsen et al, 2007). The challenge lies in representing system facilities in the hydraulic model and in keeping pace with spatial data updates.

Skeleton Models

Historically, computing power and software limitations necessitated that only the most significant features of the distribution system are represented. This limitation inhibited modeling efforts that attempted to include all the pipes in a large distribution system such as the Las Vegas Valley Water District's (District's) (Jacobsen et al, 2007). In order to work within these hardware and software constraints, the concept of skeletonization was applied. Typically, a model would be

constructed by taking only the most significant portion of the distribution system (for example, all pipes of 12-inch diameter and larger) and by aggregating pipes that have the same diameter, age, material and roughness. The District has been using skeletonized models since 1987. However, it is difficult to accurately represent system looping in skeletonized models. Without proper representation of looping, it is difficult to evaluate system redundancy and response to a facility failure. In addition, because of the conceptual nature of skeletonized models, it is arduous to directly relate system behavior with failure consequences.

All-pipes Model Development

In recent years, advances in hardware and software technologies have provided the ability to include all the pipes in the distribution system. An all-pipes hydraulic model with 170,000 pipes was developed at the District utilizing a one-to-one relationship between model features and GIS features. Figure 1 shows a comparison of a section of the skeletonized model on the left with the same section using all pipes in that area to the right. A one-to-one relationship between model data and spatial data allows seamless spatial analysis capabilities with model output and spatial layers. Figure 2 shows an All-Pipes Model that has a one-to-one relationship with spatial (GIS) data.

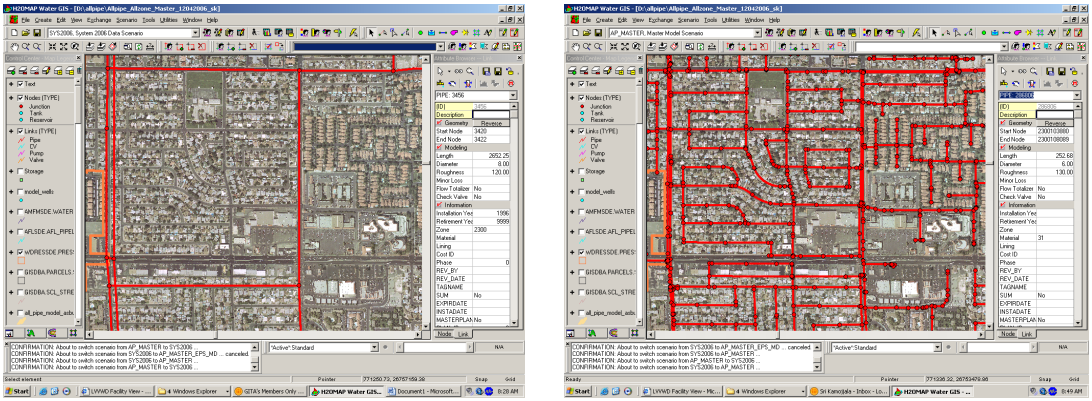

Figure 1. Skeletonized and All-pipes Models

The benefits of utilizing an all-pipes model with a one-to-one relationship with GIS for hydraulic criticality are many:

- More accurate hydraulic modeling, specifically in evaluating system redundancy and looping
- More direct integration with other systems/applications such as customer and spatial information systems
- Streamlined model maintenance
- Better spatial accuracy and quality of data
- More complete water quality analysis

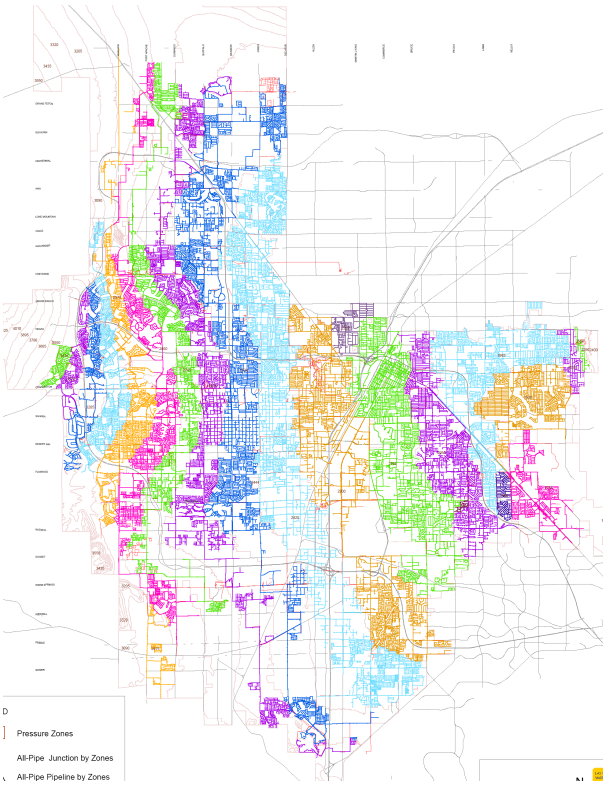

Figure 2. All-pipes Model

Predicting Consequences of a Failure

Once the system behavior is predicted, the behavior of the system needs to be related to customers and spatial data to determine the failure consequences. Simplified methods such as the ratio of demand met with failure to the original system demand have been used to determine the impact to customers (Valkovic, 2004). However, these methods do not provide the information on who is impacted and the criticality of service. To determine the impacted customers, it is essential to tie customers directly to the facilities serving the customers. This can be achieved by identifying all the services connecting to a distribution pipe. The following section describes how relating a pipe to customers served can be accomplished during the hydraulic model demand allocation process.

Demand Allocation and Relating Customers to Pipe Served

There are several methods of demand allocation. All these methods require handling and analyzing a large amount of spatial data, such as landuse and billing (actual consumption) information. Historically, demand has been assigned using semi-automated processes based on the skeletonized model. But with the all-pipes model, manual processing is not feasible; therefore, automated tools are required. Automated methods reported in literature for demand allocation include Meter

Summation, Closest Node and Closest Pipe methods (Jacobsen and Kamojjala, 2005). However, the Connected Pipe method as depicted in figure 3 provides an ideal alternative for hydraulic criticality evaluation.

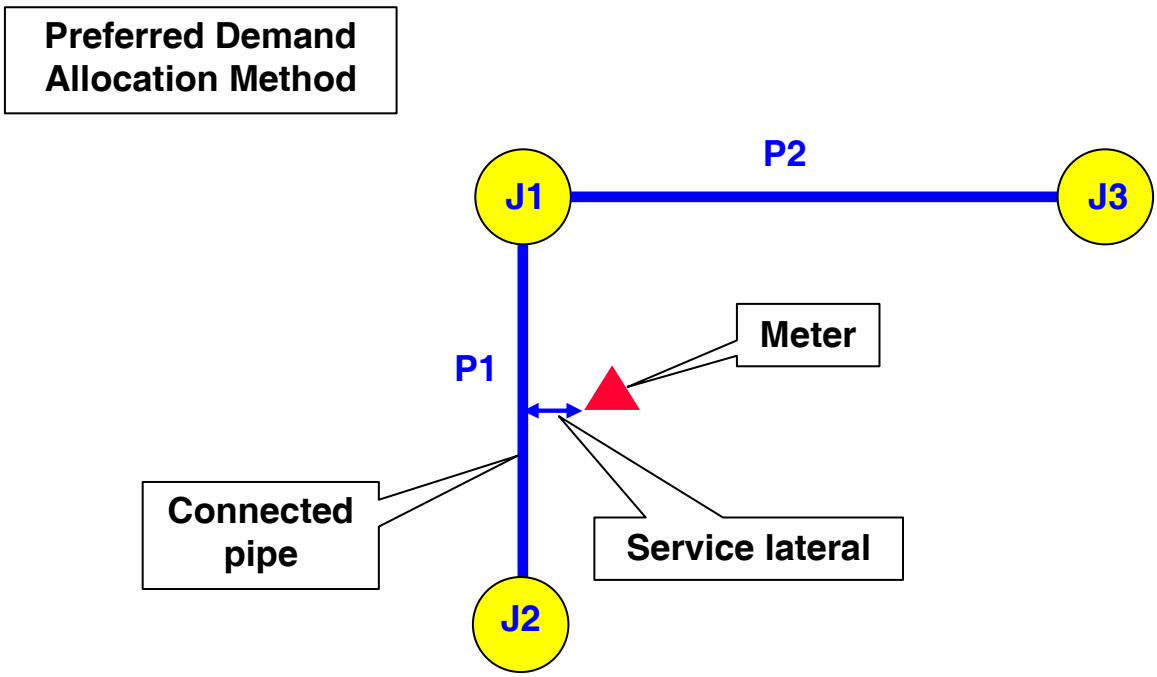

Figure 3. Preferred Method for Demand Allocation

The advantages of this method are:

- It relates pipes to accounts/parcels which in turn makes it easy to relate predicted system behavior during a facility failure to consequences such as impacted customers and is very useful in responding to emergencies or planning a shutdown
- It leverages integration of GIS and CIS
- It provides better spatial distribution for the system model

Determination of Hydraulic Criticality of a Water Main

Evaluating the hydraulic criticality of distribution system water mains involves systematically performing hydraulic analysis for each pipe by closing the pipe and the segments required to isolate the pipe from the hydraulic model. The following example illustrates determination of the hydraulic criticality of a water main. During a water main break (failure), it is critical to quickly identify the distribution system valves that must be closed in order to minimize water loss, potential flooding, or possible contamination. Repairs must be performed quickly so that service can be resumed. Using GIS and modeling tools, valves are rapidly identified for isolation.

After removing the isolated segments from the network, a hydraulic analysis is performed to predict system behavior. System behavior is combined with spatial data and customer information to evaluate the impact on existing services. Figure 4 shows a comparison of pressures before and after a shutdown. Response to emergencies, such as main breaks, can be provided quickly and accurately using integrated tools (Jacobsen and Kamojjala, 2005). A list of affected customers is generated for appropriate notification (Figure 5).

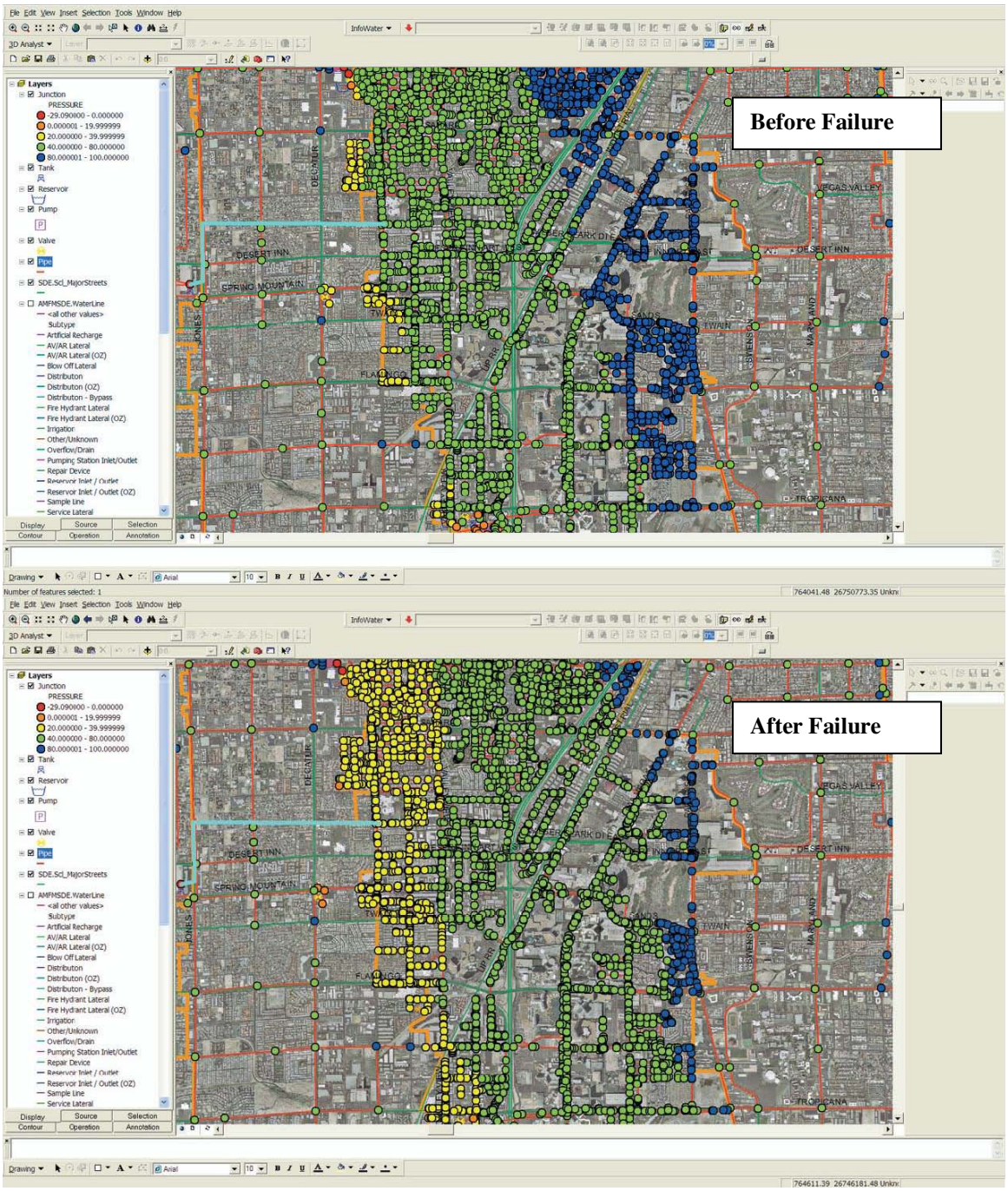

Figure 4. Comparison of Junction Pressures – Before and After Failure

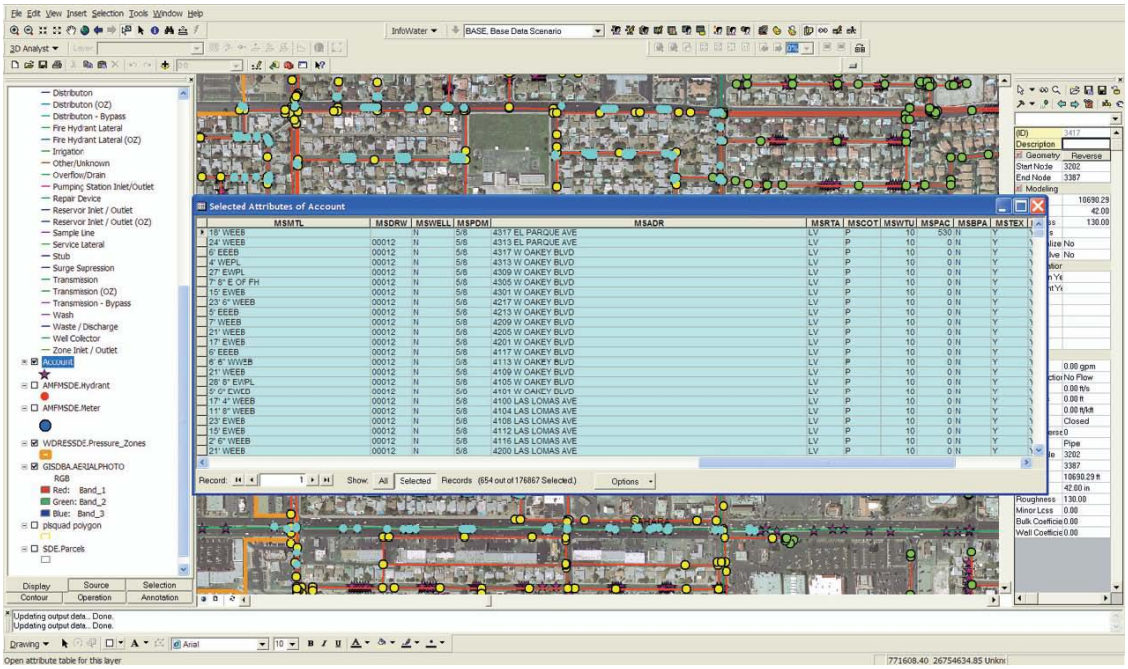

Figure 5. Impacted Customer List

Reducing the Criticality of a Facility

Once a critical facility is identified, it may be possible to mitigate the criticality by installing additional valves, adding pipes to loop the system, providing another feed to the pressure zone or providing a redundant service to a critical customer. Mitigating criticality is very useful in situations where factors such as location, traffic, depth of cover, right-of-way limitations, utility congestion, or unstable soil conditions impose limitations on planned rehabilitation or replacement efforts. By properly evaluating and mitigating criticality of a facility, the impact of an emergency failure may be greatly reduced.

Conclusions

With limitations on available budgets, prioritizing criticality of assets is essential for optimal repair, rehabilitation and replacement of water distribution facilities. Hydraulic criticality of distribution system facilities can be used for prioritizing assets not only for repair and replacements but also for condition assessment. Added benefits of hydraulic criticality evaluation are efficient emergency response and shutdown planning. Recent developments in hydraulic modeling and automated tools help in simplifying the process of evaluating hydraulic criticality. An integrated approach to hydraulic criticality evaluation will optimize resources and benefits.

References

Jacobsen, L., Coffey, R., and Kamojjala, S., 2007. Leveraging GIS to support all-pipes utility modeling. In: GITA Annual Conference, March, San Antonio.

Jacobsen L., and S. Kamojjala, 2005. Full System Models and GIS Integration. AWWA Annual Conference and Exposition, June, San Francisco.

Marlow D. R. and Burn, S., 2009. Effective Use of Condition Assessment within Asset Management. Journal of American Water Works Association, January.

Ray R., 2007. Analyzing Critical Elements in US Water Systems Using Hydraulic Modeling Coupled with GIS, ASCE Conf. Proc. 243, 490 (2007), DOI:10.1061/40927(243)490.

EPA(United States Environmental Protection Agency), 2002a. The Clean Water and Drinking Water Infrastructure Gap Analysis. EPA 816-F-02-017. EPA Office of Water.

EPA(United States Environmental Protection Agency), 2002b. Decision-Support Tools for Predicting the Performance of Water Distribution and Wastewater Collection Systems. EPA/600/R-02/029.

EPA(United States Environmental Protection Agency), 2005a. Drinking Water Infrastructure Needs Survey and Assessment: Third Report to Congress. EPA Office of Water.

EPA(United States Environmental Protection Agency), 2005b. White Paper on Improvement of Structural Integrity Monitoring for Drinking Water Mains. EPA/600/R-05/038. EPA Office of Research and Development.

Valkovic P, 2004. RelNET Help File. Brno University of Technology, Czech Republic.

WSTB (Water Science and Technology Board), 2005. Drinking Water Distribution Systems: Assessing and Reducing Risks. National Academy of Sciences.

Decision making under information constraints

Jianhua Xu[1]; Jeanne M. VanBriesen[2], Member ASCE; Mitchell J. Small[3], Member ASCE; Paul S. Fischbeck[4]

[1]Dept. of Engineering and Public Policy, Carnegie Mellon Univ., 5000 Forbes Ave., Pittsburgh, PA 15213. E-mail: xujianhua.cmu@gmail.com
[2]Dept. of Civil and Environmental Engineering, Carnegie Mellon Univ., 5000 Forbes Ave., Pittsburgh, PA 15213. E-mail: jeanne@cmu.edu
[3] Dept. of Civil and Environmental Engineering, and Engineering and Public Policy, Carnegie Mellon Univ., 5000 Forbes Ave., Pittsburgh, PA 15213. E-mail: ms35@andrew.cmu.edu
[4]Dept. of Social and Decision Sciences, and Engineering and Public Policy, Carnegie Mellon Univ., 5000 Forbes Ave., Pittsburgh, PA 15213. E-mail: pf12@andrew.cmu.edu

ABSTRACT

The purposes of placing sensors in water distribution systems vary from complying with water quality regulations, monitoring accidental contamination events, and detecting intentional contamination events. The information available to water utilities varies: some only have information on the topological structure of their systems; some have calibrated hydraulics models for their systems; and some even have water quality models for their systems. Different sensor location models have been proposed for the different purposes, targeting the objectives of maximizing the coverage, minimizing the contaminant travel time prior to detection, minimizing the contaminated water consumed prior to detection, and/or minimizing the population at risk prior to detection. These different sensor location models require different computational efforts and the availability of information on water distribution systems to different extents. The current sensor location models proposed mainly include graph-theory-based model (network analysis), deterministic optimization models, stochastic optimization models and robust optimization models. In this paper, we develop a protocol to help water utilities to select sensor location models based on the specific purposes of sensor placement, the information available to the water utilities, and the computational requirements of the models.

INTRODUCTION

A typical water distribution system consists of water supply sources, pipes, tanks, pumps and valves. The flow of water in a distribution system is driven by the consumption from consumers and the external pressure from the pumps. Chemical and biological agents in the system travel with water and some even react with other agents in water and the wall of the pipes. It is not feasible to conduct experiments to get information on how water flows and contaminants travel in a water distribution system without interrupting the normal consumption behavior of the consumers. Researchers and practitioners often turn to modeling the structure of water distribution systems, water flow behavior (hydraulics) and contaminants' behavior (water quality) in water distribution systems. Building hydraulic models and water quality models for a water distribution system requires significant calibration efforts. Some water utilities have only the information on the topological structure of their systems, some water utilities have hydraulic models for their systems, and some even have water quality models for their systems.

It is relatively easy to build a mathematical model for the topological structure of a water distribution system. By expressing sources, tanks, and junctions as *nodes*, and pipes, valves and pumps as *edges*, one can use a binary matrix ($N \times N$) to characterize the network structure of a water distribution system, with N being the number of the nodes in the network. In the matrix cell, if there is an edge between node i and node j, then the cell value c_{ij} is equal to 1, and if there is no edge between node i and node j, then the cell value c_{ij} is equal to 0. If a water utility has a calibrated dynamic hydraulic model (based on mass balance and energy conservation) for their system, one can obtain water flow behavior in the system with one run of the simulation and the computational effort is affordable to all the water utilities. If a water utility has a calibrated water quality model for their system, one can simulate contaminant travel behavior in the water distribution system. Without prior knowledge, a contamination event has to be assumed to be possible at any time, any location, and for any duration, which requires the simulation of a large number of contamination scenarios. The computational requirements for a medium-sized to large water distributions systems could be daunting. Krause et al. (2006) shows that it takes 8 days to simulate contamination events that could occur at 5 min intervals over a 24 h period from any of the 12,527 nodes in a modest-sized distribution network by using 30 parallel processors.

Substantial research has been conducted to design sensor location schemes in a water distribution system either for the purpose of enhancing water security (related to intentional and accidental contamination event) or for the purpose of complying with water quality regulations (Lee and Deininger 1992; Kessler et al. 1998; Ostfeld

and Salomons 2004; Berry et al. 2005, 2006; Grayman et al. 2006; Gueli 2006; Krause et al. 2006; Propato 2006; Shastri and Diwekar 2006; Ostfeld et al. 2008; Xu et al. 2008). Research on this topic has evolved from single objective like maximizing the areas covered (Lee and Deininger, 1992), minimizing the contaminated water consumed prior to detection (Kessler et al. 1998; Ostfeld and Salomons, 2004), minimizing the contaminant travel time prior to detection, and minimizing the population at risk prior to detection (Berry et al., 2005) to multi-objectives (Krause et al. 2006). The optimization models developed for placing sensors in water distribution systems so far mainly include graph-theory-based model (network analysis) (Xu et al. 2008), deterministic optimization models (Kessler et al. 1998; Kumar et al. 1999; Krause et al. 2006), stochastic optimization models (Berry et al. 2006), and robust optimization models (Carr et al. 2006; Xu et al. 2009). Figure 1 shows the major models available for placing sensors in water distribution systems and the basic information required from water utilities.

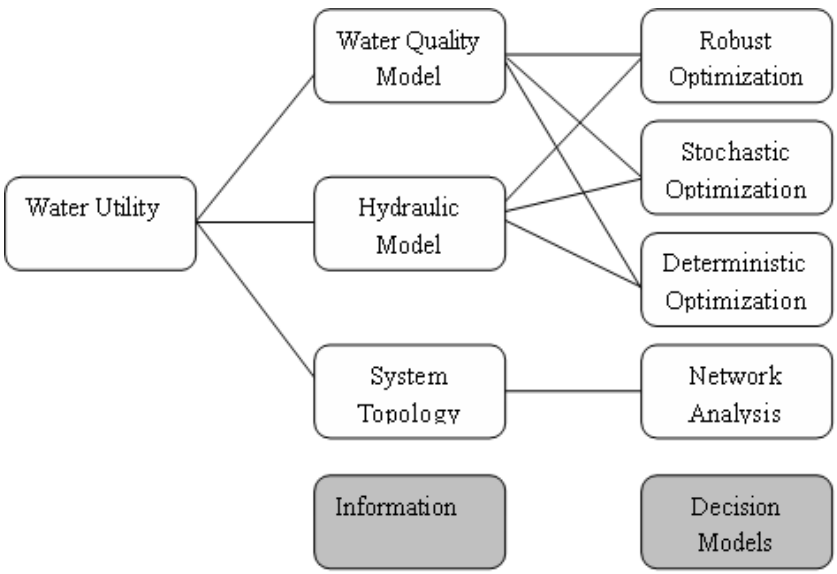

Figure 1. The relationship between the models and the basic information needed for using each type of models

In this paper, we propose a protocol to inform water utilities to make decisions on what models to choose given the information they have about their distribution systems (e.g., topology of the system, hydraulic model of the system, water quality model of the system), their specific purposes (e.g., to detect accidental contamination event, to detect intentional contamination event, or monitor water quality due to internal deterioration), and their computational capacity, based on our previous research (Krause et al. 2006; Xu et al. 2008, 2009). In the following, we describe the details of the models.

MODEL DESCRIPTION

Making difficult decisions with analytical approaches largely depends on what information is available. Two sets of information are needed for making decisions on where to place sensors in water distribution systems: information on the water distribution system, and information on the "contamination events". Some water utilities only have information on the topological structure of their systems, while others have information on how water flows and how chemicals travel in their system. "Contamination events" are also difficult to characterize. For internal deterioration, water quality (e.g., chlorine residual, bacteria etc.) decreases with time and distance from the source, and for external contamination events, there are uncertainties as to where, when and for how long the contamination event might occur (as depicted in Figure 2). Considering these information constraints, four types of models are summarized to locate sensors in water supply networks to detect water quality anomalies: graph-theory based model (network analysis), deterministic optimization models, stochastic optimization models and robust optimization models.

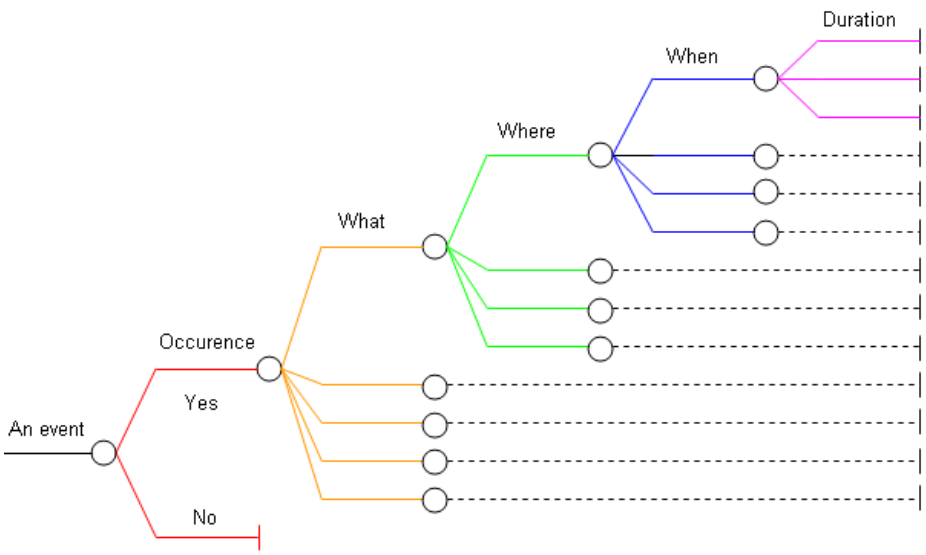

Figure 2. Illustration of the uncertainty of external contamination at a water distribution system with a scenario tree

Graph-theory based network analysis. A water distribution system can be expressed as a network, where *nodes* represent sources, tanks, and junctions, while *edges* represent pipes, valves, and pumps. Xu et al. (2008) express a water distribution system as a network, and adopt the network measures betweenness centrality and receivability to help identify structurally important nodes for sensor placement.

Betweenness centrality defines the centrality of a node in terms of the degree to which the node falls on the shortest path between other pairs of nodes. If a node has a high betweenness centrality, then it lies on the path of many pairs of nodes. In a water distribution network, a node with high betweenness centrality would be between many potential upstream contamination events and downstream receptor populations. Nodes with high betweenness centrality are potential locations for sensors (Xu et al. 2008). For a simple small water distribution network, nodes with high betweenness centrality can be found by visual inspection. For example, in the illustrative 6-node water distribution system (Figure 3), node 4 has a high betweenness centrality. As the size of a water distribution system increases, mathematical equation as proposed in Freeman (1977) are used to determine the betweeness centrality of each node and to identify the nodes with high betweeness centrality.

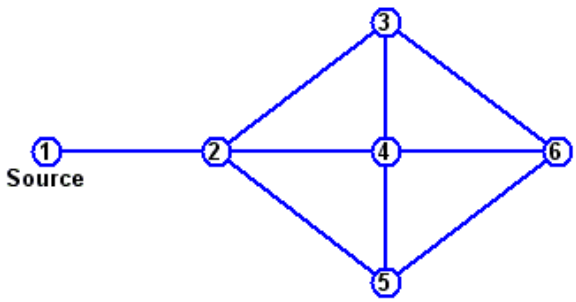

Figure 3. An Illustrative hypothetical water distribution network

Xu et al. (2008) show that nodes with high betweenness centrality in a water distribution system tend to cluster together. If sensors are placed solely based on the value of betweenness centrality, these sensors would be redundant. To avoid this, the water distribution network can be divided into sub-networks and then nodes with high betweenness centrality in each sub-network are selected as sensor location nodes. The merit of this method is that the only information needed is the topological structure of a water distribution system and the computational effort for detecting sub-networks and calculating betweenness centrality for each node is affordable to most water utilities.

Receivability of a node describes the number and set of nodes in a network that have paths to the studied node. Its counterpart, reachabiltiy, has been used extensively in previous research to derive water flow information. The water flow information is then used as input to optimization models used to place monitoring stations or sensors (Kessler et al. 1998, Berry et al. 2005, and Watson et al. 2004). Here, we use receivability to serve as a basis for placing sensors instead of serving as input to an optimization model. A set of nodes that collectively provides the highest

receivability is a potential sensor network. To derive receivability for each node requires a water distribution system be expressed as a directed graph with the direction being water flow direction. Thus, a hydraulic model for the water distribution system is needed to use receivability to identify sensor locations. In identifying the set of sensors which collectively provides the highest receivability (implying a maximum coverage), a greedy heuristic algorithm is used. The computational effort for deriving water flow information with hydraulic models and for identifying the set of sensors locations with greedy heuristic algorithm is likely affordable to all water utilities.

Deterministic optimization model. Various deterministic optimization models have been proposed for placing sensors in water distribution systems. The inputs required for a deterministic model are either a representative instance of water flow and contaminant behavior or the expected value of many instances of water flow and contaminant behavior. Example models include maximum covering model (Lee and Deininger 1992), set covering model (Kessler et al. 1998; Kumar et al. 1999), and a mixed-integer model (Krause et al. 2006) etc..

The inputs (information) required for the different deterministic models vary. Lee and Deininger (1992) applied a maximal covering model to place monitoring stations in water distribution systems; they require water hydraulics of the distribution system. Kessler et al. (1998) applied a set covering model to identify the least number of monitoring stations needed to make sure that the maximum volume of contaminated water consumed does not exceed a certain amount; the information required for this model is the hydraulics of the distribution system. Kumar et al. (1999) modified the model proposed by Kessler et al. (1998) and tried to apply a set covering model to identify the least number of monitoring stations needed to make sure that any contamination events could be detected within a certain time period after the contamination event occurs. Again, the basic information needed for this model is the hydraulics of the water distribution system. Krause et al. (2006) applied a mixed-integer model to place sensors for the objectives of (1) minimizing the contaminant travel time prior to detection, (2) minimizing the population at risk prior to detection, (3) minimizing the contaminated water consumed prior to detection, (4) maximizing the detection likelihood, and/or (5) optimizing the combination of the objectives in (1)-(4). Krause et al. (2006) used simulation of millions of random contamination events, predicting the expected values of water flow and contaminant travel information, and used the expected values as the inputs to the model.

The deterministic models for placing sensors in water distribution systems are mostly facility location models. Most facility location models for a general network are *NP* hard (Drezner and Hamacher 2002). Krause et al. (2006) use greedy

heuristics algorithm to solve their optimization models and found that greedy heuristics algorithm can always find an optimal or near optimal solution in the context of placing sensor distribution systems. In Krause et al. (2006), solving the optimization model with the greedy heuristics algorithm is likely affordable to all water utilities, while the computational efforts required for the initial simulation of random contamination events are daunting.

Stochastic optimization model and robust optimization model. Stochastic optimization models and robust optimization models both address the uncertainties inherent in the problem of placing sensors in water distribution systems. Stochastic optimization models optimize the expected value of an objective (e.g. minimizing the expected volume of contaminated water consumed prior to detection) (Berry et al. 2006). Robust optimization models (Xu et al. 2009) minimize the consequences of the worst cases.

Berry et al. (2006) formulated a *p*-median problem to minimize the expected impact across a set of predefined scenarios. The "distance" x_{ai} is the total impact associated with a contamination scenario (scenario a) until a sensor placed at node i raises an alarm. The authors assume a risk-neutral position in placing sensors and do not give special consideration to extreme scenarios. When the contamination events are intentional events, and the attackers are intelligent attackers, trying to maximize the damage, it is prudent to take this into account in designing sensor placement schemes. One special case is that the attackers have perfect information on the water distribution system. Xu et al. (2009) proposed a set of robust optimization model to minimize the maximum volume of contaminated water consumed, and to maximize the minimum possible number of nodes that are not covered by the sensors. Both stochastic optimization models and robust optimization models require a thorough understanding of how water flows and contaminant travels. Solving the robust optimization models to optimality is much more difficult than solving its deterministic counterpart. Xu et al. (2009) adopt a heuristics algorithm proposed by Serra and Marianov (1998) to solve the robust optimization model.

CONCLUSIONS

When a water utility only has the information on the topological structure of their system and/or their computational capacity is limited, a graph-theory based network analysis method, describing a water distribution system as a network, can be used to identify structurally important nodes. When a water utility has the information on the hydraulics of a water distribution system, water flow behavior can be simulated, deterministic, stochastic and robust optimization models can be applied to identify optimal sensor locations. The computational effort for simulated water

flow behavior with hydraulic model is affordable to almost all the water utilities while the computational effort required for solving optimization models can be high. When a water utility has a water quality model for their system, contaminant behavior can be simulated, and deterministic, stochastic and robust optimization models can be applied to identify optimal sensor locations. The computational load for simulated random contamination event is significant.

ACKNOWLEDGEMENT

This work was funded by the National Science Foundation Sensors Program through the Division of Biological and Environmental Engineering under grant BES-0329549.

REFERENCES

Berry, J. W., Fleischer, L., Hart, W. E., Phillips, C. A., and Watson, J. (2005). "Sensor placement in municipal water networks." *J. Water Resour. Plann. Manage.*, 131(3), 237–243.

Berry, J. W., Hart, W. E., Phillips, C. A., Uber, J. G., and Watson, J. (2006). "Sensor placement in municipal water networks with temporal integer programming models." *J. Water Resour. Plann. Manage.*, 132(4), 218–224.

Carr, R. D., Greenberg, H. J., Hart, W. E., Konjevod, G., Lauer, E., Lin, H., Morrison, T., Phillips, C. A. (2006). "Robust Optimization of Contaminant Sensor Placement for Community Water Systems." *Mathematical Programming*, 107, 337-356.

Drezner, Z., and Hamacher, H. (2002). *Facility location: Applications and theory*, Springer, Berlin.

Freeman, L. C. (1977). "A set of measures of centrality based on betweenness." Sociometry, 40(1), 35–41.

Grayman, W. M., Ostfeld, A., and Salomons, E. (2006). "Locating monitors in water distribution systems: Red team-blue team exercise." *J. Water Resour. Plann. Manage.*, 132(4), 300–304.

Gueli, R. (2006). "Predator-prey model for discrete sensor placement." Proc., Conf. on Water Distribution Systems Analysis, *the 8th Annual Int. Water Distribution Systems Analysis Symp.*

Kessler, A., Ostfeld, A., Sinai, G. (1998). "Detecting accidental contaminations in municipal water networks." *J. Water Resour. Plann. Manage.*, 124(4), 192–198.

Krause, A., et al. (2006)."Optimizing sensor placements in water distribution systems using submodular function maximization." Proc.,Conf. on Water Distribution

Systems Analysis, *the 8th Annual Int. Water Distribution Systems Analysis Symp*.

Lee, B. H., and Deininger, R. A. (1992). "Optimal locations of monitoring stations in water distribution system." *J. Environ. Eng.*, 118(1), 4–16.

Ostfeld, A., and Salomons, E. (2004). "Optimal layout of early warning detection stations for water distribution systems security." *J. Water Resour. Plann. Manage.*, 130(5), 377–385.

Ostfeld, A. et al. (2008). "The Battle of the Water Sensor Networks (BWSN): A design challenge for engineers and algorithms." *J. Water Resour. Plann. Manage.,* 134 (6), 556-568

Propato, M. (2006)."Contamination warning in water networks: General mixed-integer linear models for sensor location design." *J. Water Resour. Plann. Manage.*, 132(4), 225–233.

Serra, D. and Marianov, V. (1998) "The p-median problem in a changing network: the case of Barcelona" *Location Science* 6, 383-394

Shastri, Y., and Diwekar, U. (2006). "Sensor placement in water networks: A stochastic programming approach." *J. Water Resour. Plann. Manage.*, 132(3), 192–203.

Watson, J., Greenberg, H. J., and Hart, W. E. _2004_. "A multipleobjective analysis of sensor placement optimization in water networks." *Proc., 2004 World Water and Environmental Resources Congress: Critical Transitions in Water and Environmental Resources Management*, 4609–4618.

Xu, J., Fischbeck, P., Small, M., VanBriesen, J. and Casman, E. (2008). "Identifying sets of key nodes in dynamic water distribution networks." *J. Water Resour. Plann. Manage.*, 134(4), 378-385.

Xu, J., Johnson, M., Fischbeck, P., Small, M. and VanBriesen, J. (2009). "Robust placement of sensors in dynamic water distribution systems." *European Journal of Operational Research*, (Under review)

Optimal Distribution of Pressure Measurement Points in Water Distribution Networks

Hui Zhang[1] and Tinglin Huang[2]

[1]Ph.D, School of Environmental and Municipal Engineering, Xi'an University of Architecture & Technology, Xi'an 710055, China; email: aoyun9@126.com
[2]Professor, School of Environmental and Municipal Engineering, Xi'an University of Architecture & Technology, Xi'an 710055, China; email: huangtinglin@xauat.edu.cn

ABSTRACT

The pressure similarity method is proposed to get the optimal distribution of pressure measurement points for water distribution networks. This kind of optimal distribution is mainly composed of two steps. Firstly, the pressure similarity coefficients of any two nodes should be calculated to obtain the similarity coefficient matrix. Then all the nodes can be grouped through clustering analysis on the matrix and the pressure measurement points can be chosen out. The application on a practical network shows that the pressure similarity method can reflect the regional characteristics of network pressure and the result is reasonable. This method is very useful for network further study such as state simulation, optimal scheduling and accident early-warning.

INTRODUCTION

Nodal pressure is an important operation parameter of water distribution networks. Proper location of pressure measurement points can accurately reflect the network state which is the basis of optimal scheduling and accident early-warning.
Presently, the optimal distribution of pressure measurement points is based on the influence coefficient method. That is choosing the pressure measurement points according to the nodal pressure changes caused by nodal demands variation (Reddy *et al*. 1996; Huang and Cong 2001; Haestad *et al*. 2003; Davidson and Bouchart 2006). Therefore, this method can be used in monitoring the water use and its influence. But in city water supply it is sometimes necessary for pressure measurement points to reflect the pressure of certain district (Cheryl and James 1998). The influence coefficient method can not meet the requirement. So in this paper another optimal location method based on pressure similarity is proposed to show the regional characteristics of pressure distribution.

PRESSURE SIMILARITY METHOD

Pressure similarity coefficient. Pressure similarity coefficient is proposed to reflect the regional characteristics of pressure distribution. The definition is:

$$\chi_{ij} = 1 - \frac{|H_i - H_j|}{|H_{\max} - H_{\min}|} \quad (i, j = 1,2,\cdots,n) \tag{1}$$

where H_i and H_j are pressure values of node i and j; $H_{\max}$ and $H_{\min}$ are maximum value and minimum value of nodal pressures; n is total number of nodes.
By calculating the pressures under every operation condition, χ_{ij} can be determined by arithmetic mean or weighted average according to Eq.(1) (Shastri and Diwekar 2006). All the coefficients can be written as a matrix $\boldsymbol{X}_{n\times n}$.

Clustering analysis and choosing pressure measurement points. Nodes are grouped through fuzzy clustering, which means classifying the similar objects based on certain clustering principles and fuzzy judging criteria (Wang and Wang 1989). Here the objects are network nodes and the clustering principle is grouping the nodes by comparing χ_{ij} between any two nodes. The procedure can be divided into the following steps:

(1) *Matrix standardization*. Standardization is changing the original data of matrix $\boldsymbol{X}$ to be limited in [0,1] according to the requirements of fuzzy matrix (Xie and Liu 2005). Usually two kinds of transformation are needed. Firstly, the standard deviation transformation should be carried out on matrix $\boldsymbol{X}$:

$$\chi_{ik}^{'} = \frac{\chi_{ik} - \overline{\chi_k}}{S_k} \quad (i, k = 1,2,\cdots,n) \tag{2}$$

where $\overline{\chi_k}$ is average value of column k, $\overline{\chi_k} = \frac{1}{n}\sum_{i=1}^{n}\chi_{ik}$; and S_k is standard deviation of column k, $S_k = \sqrt{\frac{1}{n}\sum_{i=1}^{n}(\chi_{ik} - \overline{\chi_k})^2}$. Thus, the matrix $\boldsymbol{X}^{'}$ composed of $\chi_{ik}^{'}$ can be obtained.
Then the data of column k in matrix $\boldsymbol{X}^{'}$ should be changed as follows:

$$\chi_{ik}^{''} = \frac{\chi_{ik}^{'} - \chi_{k_{\min}}^{'}}{\chi_{k_{\max}}^{'} - \chi_{k_{\min}}^{'}} \quad (i, k = 1,2,\cdots,n) \tag{3}$$

where $\chi_{k_{\min}}^{'}$ and $\chi_{k_{\max}}^{'}$ are minimum value and maximum value in column k. Finally the standardized matrix $\boldsymbol{X}^{''}$ composed of $\chi_{ik}^{''}$ is obtained and $0 \le \chi_{ik}^{''} \le 1$.

(2) *Establishing fuzzy similarity matrix* $\boldsymbol{R}$. Based on the standardized matrix $\boldsymbol{X}^{''}$ the similarity coefficient of any two nodes r_{ij} can be calculated. And the fuzzy similarity matrix $\boldsymbol{R}$ composed of r_{ij} can be obtained as well. The element of $\boldsymbol{R}$ is calculated through Euclidean distance:

$$r_{ij} = 1 - \sqrt{\frac{1}{n}\sum_{k=1}^{n}(\chi_{ik}^{''} - \chi_{jk}^{''})^2} \quad (i, j = 1,2,\cdots,n) \tag{4}$$

(3) *Clustering*. All nodes are grouped by net-making method and several results are achieved with different λ values, which are determined by the values of $\boldsymbol{R}$ elements. Among the grouping results, the optimal one under the optimal λ value can be selected out based on F-statistics:

$$F = \frac{\sum_{j=1}^{r} n_j \| \bar{x}^{(j)} - \bar{x} \|^2 \Big/ (r-1)}{\sum_{j=1}^{r} \sum_{i=1}^{n_j} \| x_i^{(j)} - \bar{x}^{(j)} \|^2 \Big/ (n-r)} \tag{5}$$

where $\bar{x}$ is sample central vector; r, n_j, $x_i^{(j)}$, $\bar{x}^{(j)}$ are classification numbers, sample numbers of class k, sample values and clustering center under certain λ value.

(4) *Choosing pressure measurement points*. In the grouping result under optimal λ value, the nodes, which have the minimum Euclidean distance with other nodes, should be chosen as the pressure measurement points.

COMPUTER PROGRAM DESIGN

According to the procedure of pressure similarity method, a computer program is designed for automatic distribution of pressure measurement points. The flow chart of the program algorithm is shown in Figure 1.

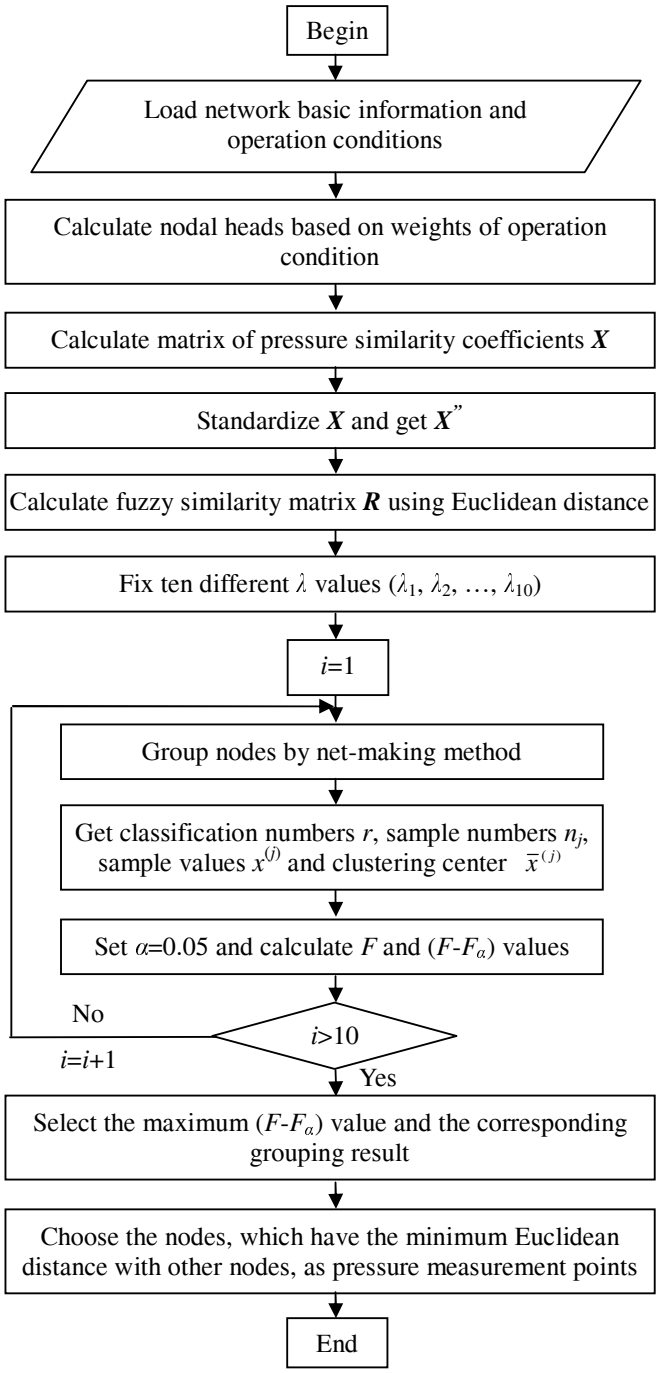

Figure 1. Flow chart of computer program on pressure similarity method.

APPLICATION

Taking an urban water distribution network as an example, the pressure measurement points were analyzed and distributed by the computer program of pressure similarity method. The network was composed of 29 nodes, 44 pipes and 16 loops. The water source was at node 29 and the maximum water supply volume was

173.61L/s. The network structure was shown in Figure 2.

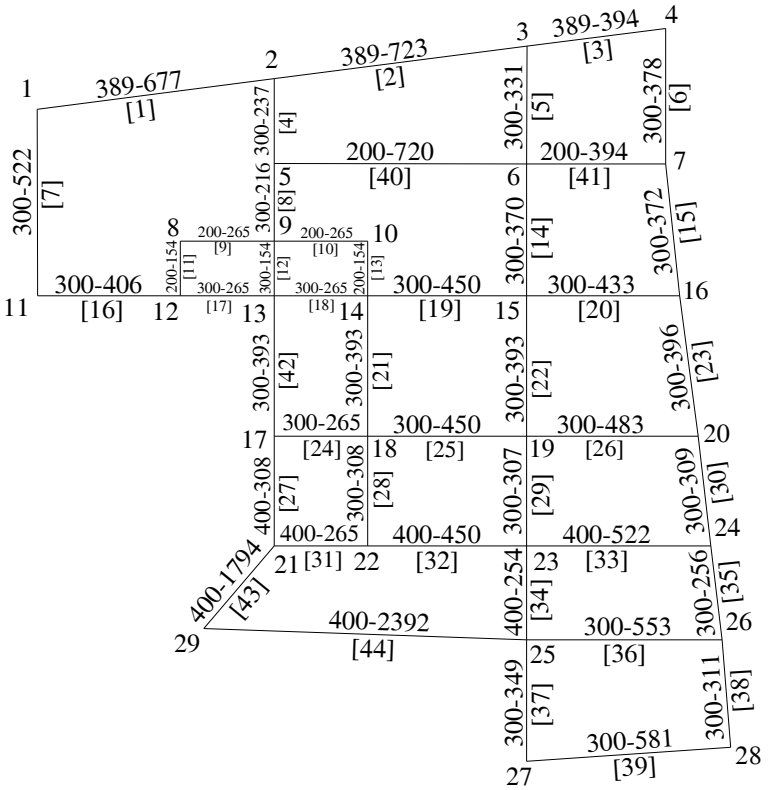

Figure 2. Schematic of example network.

According to the operation conditions and the corresponding weights, the nodal heads were calculated. And the results were shown in Table 1.

Table 1. Nodal heads of the example network.

Node No.	Nodal heads, m	Node No.	Nodal heads, m	Node No.	Nodal heads, m
1	560.58	11	560.69	21	561.26
2	560.59	12	560.64	22	561.17
3	560.60	13	560.70	23	561.15
4	560.60	14	560.73	24	561.10
5	560.61	15	560.73	25	561.15
6	560.62	16	560.72	26	561.13
7	560.63	17	561.06	27	561.17
8	560.64	18	560.98	28	561.13
9	560.66	19	560.94	29	564.84
10	560.69	20	560.92		

According to weighted nodal heads and Eq.(1) to (5), F-statistics under different λ values were work out. Eight F-statistics were higher than $F_{0.05}$ and when λ was 0.990, the discrepancy between F-statistics and $F_{0.05}$ got to the maximum. Therefore, the optimal value of λ is 0.990 and the corresponding result of six groups was the optimal one. F-statistics under different λ values were shown in Table 2.

Table 2. *F*-statistics under different λ values.

λ values	Classification numbers r	F-statistics	$F_{0.05}(r\text{-}1,n\text{-}r)$	$F\text{-}F_{0.05}$
1.000	29	0	249.8	—
0.999	25	10921.4	5.8	10915.6
0.998	19	12596.0	2.8	12593.2
0.996	16	4384.2	2.5	4381.7
0.995	13	3998.7	2.4	3996.3
0.994	9	3976.8	2.5	3974.3
0.990	6	14724.3	2.6	14721.7
0.980	3	1255.0	3.4	1251.6
0.950	2	308.3	4.2	304.1
0.100	1	0	—	—

Based on the optimal grouping result, the pressure measurement points can be chosen out by calculating Euclidean distance of every node in each group. They are node 6, 27, 17, 18, 20 and 28. It was clear that the pressure measurement points were well-distributed and representative. Most of the points were near water source, network ending and dividing line of water supply.

CONCLUSION

The pressure similarity method is proposed for optimal distribution of water distribution networks. And based on the method a computer program is developed. Through the application on an urban water supply network, it is proved that the pressure similarity method is reasonable and most of the points were near water source, network ending and dividing line of water supply. Therefore, the method is useful in district monitoring of water distribution networks.

ACKNOWLEDGEMENTS

The study fulfilled a main part of TRAPOYT (the Teaching and Research Award Program for Outstanding Young Teachers in Higher Education Institutions of MOE, P.R.C.), and also a part of the Project No. GG06200 of Xi'an Key Technologies R & D Program. The authors would like to express their gratitude to the agencies involved and participants of the study.

REFERENCES

Cheryl, A. B. and James, G. U. (1998). "Sampling Design Methods for Water Distribution Model Calibration." *Journal of Water Resources Planning & Management*, 124(6), 335-344.

Davidson J. W. and Bouchart. F. J-C. (2006). "Adjusting nodal demands in SCADA constrained real-time water distribution network models." *Journal of Hydraulic Engineering*, 132(1), 102-110.

Draper, N. R., and Smith, H. (1998). *Applied regression analysis*, Wiley, New York.

Haestad, M., Thomas, M. W., Donald V. C. et al. (2003) *Advanced Water Distribution Modelling and Management*. Haestad Press, USA.

Huang T-L. and Cong H-B. (2001). "Fuzzy Clustering Method for Optimal Distribution of Pressure Measurement Points of Water Distribution Networks." *China Water & Wastewater*, 17(11), 50-52.

Reddy, P. V. N., Sridharan, K. and Rao, P. V. (1996). "WLS method for parameter estimation in water distribution networks." *Journal of Water Resources Planning & Management*, 122(3), 157-164.
Shastri, Y. and Diwekar U. (2006). "Sensor Placement in Water Networks: A Stochastic Programming Approach." *Journal of Water Resources Planning & Management*, 132(3), 192-203.
Wang X-J. and Wang Z-Y. (1989). "Choice of Pressure Measurement Points of Water Distribution Networks". *China Water & Wastewater*, 5(3), 5-12.
Xie J-J. and Liu C-P. (2005) *Fuzzy mathematics and its application*, Huazhong University of Science and Technology Press, Wuhan, China.

Scalable Parallel Computing Framework for Pump Scheduling Optimization

Zheng Yi Wu
Applied Research Group, Bentley Systems, Incorporated, 27 Siemon Co. Dr, Suite200W, Watertown, CT 06795, USA, Email: Zheng.Wu@bentley.com

Qi Zhu
Computer Science & Engineering Department, University of Connecticut, Storrs, CT 06269, USA, Email: qi.zhu@engr.uconn.edu

Abstract

As multi-core personal computers (PC) have become popular and widely available for various computation tasks, developing parallel computing methods are imperative for taking the full capacity of the multi-core machines. This paper reports on the analysis and comparison of different paradigms for portable parallel computation on single multi-core PC and a cluster of PCs. It summarizes the strength and weakness of various parallel and distributed computation models. A scalable and portable parallel optimization framework has been developed and applied to water distribution pump scheduling to improve energy efficiency. It is implemented as a generic optimization method for hydraulic engineers to optimize the pump operation policy in order to maximize energy cost efficiency. An example study is presented to demonstrate the application of the parallel and distributed optimization model. The results show a linear speedup has been achieved for the parallel optimization of pump scheduling.

Keywords: optimization, water distribution systems, parallel computing, pump scheduling and genetic algorithm

INTRODUCTION

Parallel computing has been a research topic for decades. It is employed to achieve the speedup in computation efficiency for solving engineering and scientific problems that requires for intensive computation. Parallel computing is conventionally applied to those computing-intensive cases so that the problems can be effectively solved. In the meantime, sequential computing programs have been benefited from the efficiency enhancement of personal computer (PC) since 1980's. The faster a PC is built, the faster the sequential computing programs could run. Such a 'free lunch' is over when the CPU speed is reaching the limit at which energy consumption is the primary concern so that computer industry has to shift from single-core paradigm to multi-core PCs configuration. It is highly unlikely a faster CPU will be made for PC but multi-core machines are becoming the mainstream of PC industry. Therefore, parallel computing is

not only an approach for solving computation-intensive tasks but also essential for making use of the computing power offered by multi-core PCs that are readily accessible by engineers.

In water distribution system analysis, hydraulic and water quality simulation methods are developed and implemented for sequential computation. Some parallel computing research has been carried out for solving large network simulation and the optimization problems that usually request for iterative execution of the simulation model. Alonso et al. (2000) developed high performance computation (HPC) methods for hydraulic analysis, water quality simulation and leakage minimization. HPC hydraulic simulation was developed by replacing the minimum degree graph search algorithm with the multilevel nested dissection algorithm, which resulted in two triangular linear equation systems solved by using multi-frontal or parallel Choleski factorization. Parallel water quality solution was obtained by partitioning a network into many small portions, each of which was solved by using the previously developed water quality analysis method. Leakage minimization is formulated to optimize the PRV settings at each time step over an extended period of time (e.g. 24 hours) while the leakage optimization is to minimize the emitter flows at nodes. The optimization problem is approximated with a series of quadratic problems that are solved by employing a sequential quadratic programming (SQP) method. The parallel leakage minimization is achieved with the assumption that the leakage is not affected by any control facilities (tanks and pumps) but totally controlled by PRV settings, thus the time-dependent PRV setting optimization is subdivided into an independent optimization problem at each time step and solved on the allocated machine. Balla and Lingireddy (2000) developed distributed genetic algorithm (GA) model for model calibration. The distributed GA optimization is implemented by using Microsoft Window's native peer-to-peer networking/communicating protocol. A cluster of PCs were used to share the computation load in the way that one PC was dedicated as manager process/machine to perform GA search, distribute the solutions to and collect fitness evaluation values from the worker processes/machines, on which hydraulic simulation and fitness calculation were performed, and fitness values were returned to the manager process. Kumar et al. (2006) presented a parallel computing approach for optimal design of water distribution systems. The distributed computing method was based on Java socket interface methods for communication across a network of PCs. In the meantime, great advancement has been made in third party development tools for developing high performance computing method. This paper reports the review on a variety of parallel computing models based on message passing interface (MPI), one of the most popular parallel computing paradigms. Due to its requirement for evaluating hundreds of possible solutions by using extended period simulation (EPS), pump scheduling is chosen as an example for applying the parallel computing paradigm. The ultimate goal is to develop a scalable, portable and robust framework for high performance optimization of water distribution operations.

Parallelism Paradigms

There are two types of computation parallelism at instruction level, data parallelism and task parallelism. Both data and task parallelisms can be achieved by different programming languages, libraries and application programming interfaces (APIs). Message passing interface (MPI) and Open Multi-Processor (OpenMP) are among the most commonly-used libraries for task parallelism and data parallelism.

Task Parallelism

Task parallelism is a parallel computing program that a computing problem is divided into many computing tasks and that different calculations can be performed on different computing processes (CPUs or nodes). Each of the computing tasks can be performed with either the same or different sets of data. Task parallelism usually scales with the number of computing nodes. There are various methods for achieving task parallelism computing, a message passing communication is usually employed for a scalable and portable implementation.

Message Passing Interface is a specification of the application programming interface (API) that allows many computers to communicate with one another. It is used for parallelizing computing task over a cluster of machines or on supercomputers, where each of the CPU is representing a computing node or process. It is a language-independent communications protocol supporting both point-to-point and collective communication. MPI is designed for developing high performance computing applications with scalability and portability. It is one of the popular models used in high-performance computing.

MPI consists of more than 115 functions (Gropp, Lusk and Skjellum 1999). Various MPI implementations are as follows.

1. DeinoMPI is an implementation of MPI-2 for Microsoft Windows. This is the release version 1.1.0 with downloads for both Win32 and Win64 machines.

2. PureMPI.NET is a completely managed implementation of the message passing interface. The object-oriented API is simple, and easy to use for parallel programming. It has been developed based on the latest .NET technologies, including Windows Communication Foundation (WCF). This allows you to declaratively specify the binding and endpoint configuration for your environment, and performance needs. When using the SDK, a programmer will definitely see the MPI'ness of the interfaces come through, and will enjoy taking full advantage of .NET features - including generics, delegates, asynchronous results, exception handling, and extensibility points.

3. MPI.NET is a high-performance, easy-to-use implementation of the Message Passing Interface (MPI) for Microsoft's .NET environment. MPI is the *de facto* standard for writing parallel programs running on a distributed memory system, such as a compute cluster, and is widely implemented. Most MPI implementations provide support for writing MPI programs in C, C++, and FORTRAN. MPI.NET provides support for all of the .NET languages (especially C#), and includes significant extensions (such as automatic serialization of objects) that make it far easier to build parallel programs that run on clusters.

4. MPICH2 is a high-performance and widely portable implementation of the Message Passing Interface (MPI) standard (both MPI-1 and MPI-2). The goals of MPICH2 is to provide an MPI implementation that efficiently supports different computation and communication platforms including commodity clusters, high-speed networks and proprietary high-end computing systems.

5. MSMPI is the Microsoft's implementation of MPICH2 for Windows Compute Cluster Server and High Performance Computing Server.

Data Parallelism

Data parallelism is inherent in program loops, which focuses on distributing the data across different computing nodes to be processed in parallel. Parallelizing loops often leads to similar operation sequences or functions being performed on elements of a large data structure. Many scientific and engineering applications exhibit data parallelism. The most commonly adopted programming language for data parallelism is Open Multi-Processors (OpenMP).

The OpenMP is a set of APIs that support multi-platform shared memory multiprocessing programming in C/C++ and FORTRAN on UNIX and Microsoft Windows platforms. It consists of a set of compiler directives, library routines, and environment variables that influence run-time behavior. Jointly defined by a group of major computer hardware and software vendors, OpenMP is a portable, scalable model that gives programmers a simple and flexible interface for developing parallel applications for platforms ranging from the desktop to the supercomputer. An application built with the hybrid model of parallel programming can run on a computer cluster using both OpenMP and Message Passing Interface (MPI). A brief comparison of MPI and OpenMP is given in Table 1.

Table 1 Comparison of MPI and OpenMP

Criteria	OpenMP	MPI
Platform	Symmetric Multiprocessing(SMP)	Both SMP and Clusters
Parallelism	Fine grain parallelism	Coarse grain parallelism
Performance	Better on SMP	Better on Cluster

With OpenMP computation loops are often parallelized by using compiler directives, so the code runs in serial until it reaches the parallelized loop where concurrent computation is taking place. Conversely, with MPI the entire code is launched on each computing node and computing task is designated to the node by using MPI communication methods and APIs that are rich and flexible enough to implement various parallel computing models to distribute the computing tasks. To ensure the maximum speedup, both task and data parallelism can be mixed in a hybrid model.

Hybrid Parallelism

A hybrid parallelism is to implement both task and data parallel computation in the same application to obtain the maximum speedup. A number of hybrid computation models (Rabenseifner 2003) have been compared and summarized as follows.

1. Pure MPI: Task and data parallelisms are achieved by just using MPI library. The communications within one task process and across multiple task processes are implemented as a flat massively parallel processing (MPP) system.

2. MPI and OpenMP: Task parallelism is implemented by calling MPI communication methods across several computing nodes. Within each parallel task process, OpenMP is used for data parallelism.

3. Pure OpenMP: Based on virtual distributed shared memory systems (DSM), the application is parallelized only with shared memory directives of OpenMP.

The hybrid parallelism models offer advantages for the clusters of SMP computing nodes, but have some serious disadvantages based on mismatch problems between the hybrid programming scheme and the hybrid architecture, including:

1. With pure MPI, minimizing the inter-node communication requires that the application-domain's neighborhood-topology matches with the hardware technology. Otherwise, more data is shipped over the inner-node network instead of using the shared memory based communication within nodes. On the other hand, Pure MPI also introduces intra-node communication on the SMP nodes that can be omitted with hybrid programming.

2. With MPI and OpenMP programming, the intra-node communication overhead, introduced by pure MPI method, can be substitute by direct access to the application data structure in the shared memory. However, this programming style is not able to achieve full inter-node bandwidth on all platforms for any subset of inter-communicating threads. For instance, with manager only style, all non-communicating threads are idling. CPU time is also wasted, if all CPUs are already able to saturate the inter-node bandwidth. With hybrid manager only programming, additional overhead is induced by all OpenMP synchronization, but also by additional cache flushing between the generation of data in parallel regions and the consumption in subsequent message passing routines and calculations in subsequent parallel sections.

3. Overlapping of communication and computation is a chance for an optimal usage of the hardware, but it causes serious programming effort in the application itself, in OpenMP parallelization and load balancing.
4. Although pure OpenMP is simple and runs efficiently in shared-memory multiprocessor platforms, its scalability is limited by memory architecture.

Different programming schemes on clusters of SMPs show different performance benefits or penalties on the hardware platform. In order to obtain the best performance results, we have to choose the schemes bases on both the hardware and computer algorithm. In the project of pump scheduling optimization, we choose the latest release of MPICH2 as our parallel computation interface. It is also readily compatible with MSMPI supported by Microsoft Window Server 2008 and its High Performance Computing Server.

Pump Scheduling

A pump scheduling method (Wu 2002 & 2004) is developed for hydraulic engineers to optimize the pump operation for a water distribution system. It employs a powerful genetic algorithm (GA), a generic search paradigm based on the principles of natural evolution and biological reproduction, to search for optimal pump operation schedule. The solutions are obtained by minimizing the operating cost over a control horizon while meeting the systematic operation criteria of junction pressures, pipe flow velocity and the constraints of system storages given demand loading conditions. The GA used in pump scheduling is fast messy genetic algorithm (fmGA), one of most competent genetic algorithms, to the optimization of pump operation while meeting a set of system operating criteria. Due to its intensive computation required for evaluating many possible solutions, the sequential implementation of fmGA-based pump scheduling is extended to the parallel version of GA-based optimization to improve computation efficiency.

In sequential computing model, one process is used for pump scheduling optimization. The solutions are generated to represent the possible operation strategies for the target pumps to be optimized. All the solutions are evaluated sequentially by calling EPS and objective function. The sequential computing paradigm heavily relies on the computation capability of the single process/CPU. However, the solutions can be evaluated in parallel so that the computing efficiency is expected to be dramatically improved.

Parallel Computation Model

A manager/worker model, as shown in Figure 1, is proposed for pump scheduling optimization. After GA initialization, manager process sends chromosomes to worker processes where EPS and fitness calculation is performed for solution evaluation. Then manager process collects the fitness value of chromosomes from worker processes. The manager process is also responsible for GA operations (selection and reproduction) to search for the optimal chromosome based on the searching criteria. A task parallelism model is implemented over a cluster of computers so that we can greatly enhance our computation capability while making the best use of computer resources. MPICH2 is employed as the communication API among computers. The communication and computation scope for manager/worker task parallelism is as follows:

1. Manager process sends chromosomes to worker processes for evaluation.
2. Worker process performs solution evaluation.
3. Worker processes sends the fitness value back to manager process.
4. Manager process searches for the optimal chromosome based on fitness value.

Pseudo code snippet is below.

```
Manager Process:
        Initialize chromosomes;
        Send chromosomes to workers for evaluation;
        Collect fitness values of chromosomes from workers;
        Find the optimal chromosomes;
Worker Process:
        Receive chromosomes from manager process;
        Evaluate chromosome using objective function;
        Send the fitness value back to manager process;
```

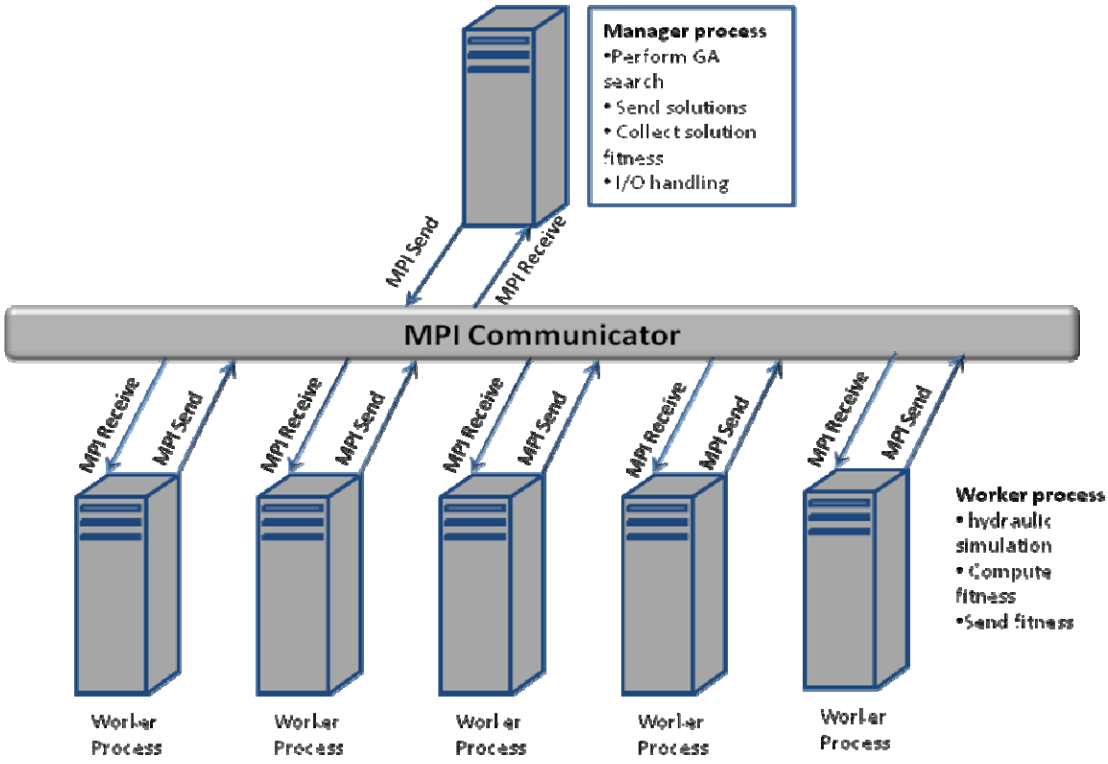

Figure 1: Manager-worker Parallel Computation Model

Example Study

A case study has been conducted by using the example previously studied in sequential computing model (Wu 2004). The sample system was previously studied by using mathematical programming and simulated annealing (Mays et al. 2000). It provides a good comparison basis for testing the pump optimization method.

The example system is illustrated in Figure 3. It consists of 115 pipes, 2 pumps and 3 tanks and 91 junctions and 2 reservoirs. The system is supplied by two water sources including River and Lake through two pumps PMP-10 and PMP-335. The aim is to search for the optimal pump operating status (ON or OFF) or relative speed factor (between zero and the maximum speed limit) for each time interval over a control time horizon such that the energy cost for these pumps is minimized over 24 hours while satisfying system requirements.

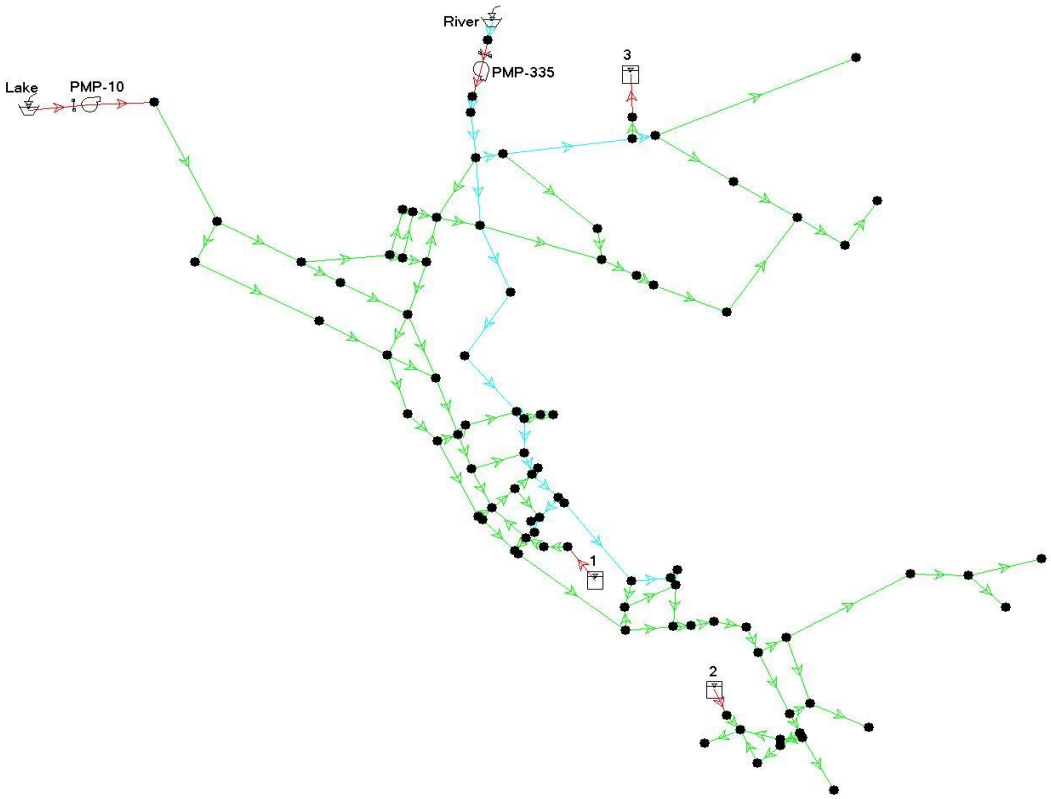

Figure 2: Layout of Case Study Water Distribution System

Test Result

Test runs are performed on a dual core machine with different processes. The parallel computing model has successfully found the same optimal schedule policy as the sequential model, as illustrated in Table 2.

Table 2: Comparison of Search Result

Criteria	Sequential Model	Parallel Model
Trials	30,005	30,005
Fitness	247.95	247.95
Violation	0.0000	0.0000

As shown in Figure 3. the test result shows that 3 processes is achieving the best speedup for running the manager-worker parallel pump scheduling on a single dual-core PC, which is able to save more than 50% of execution time than sequential model. However, if we increase the number of processes from 3 to 4, then the performance deteriorate due

to the resource contention. When the number of worker processes is greater than the number of CPUs available, worker processes are competing for the limited resources and the computing speed is slow. In general, the $(N + 1)$ processes seem to gain the maximum speedup on an N-core CPU for manager-worker parallel computing.

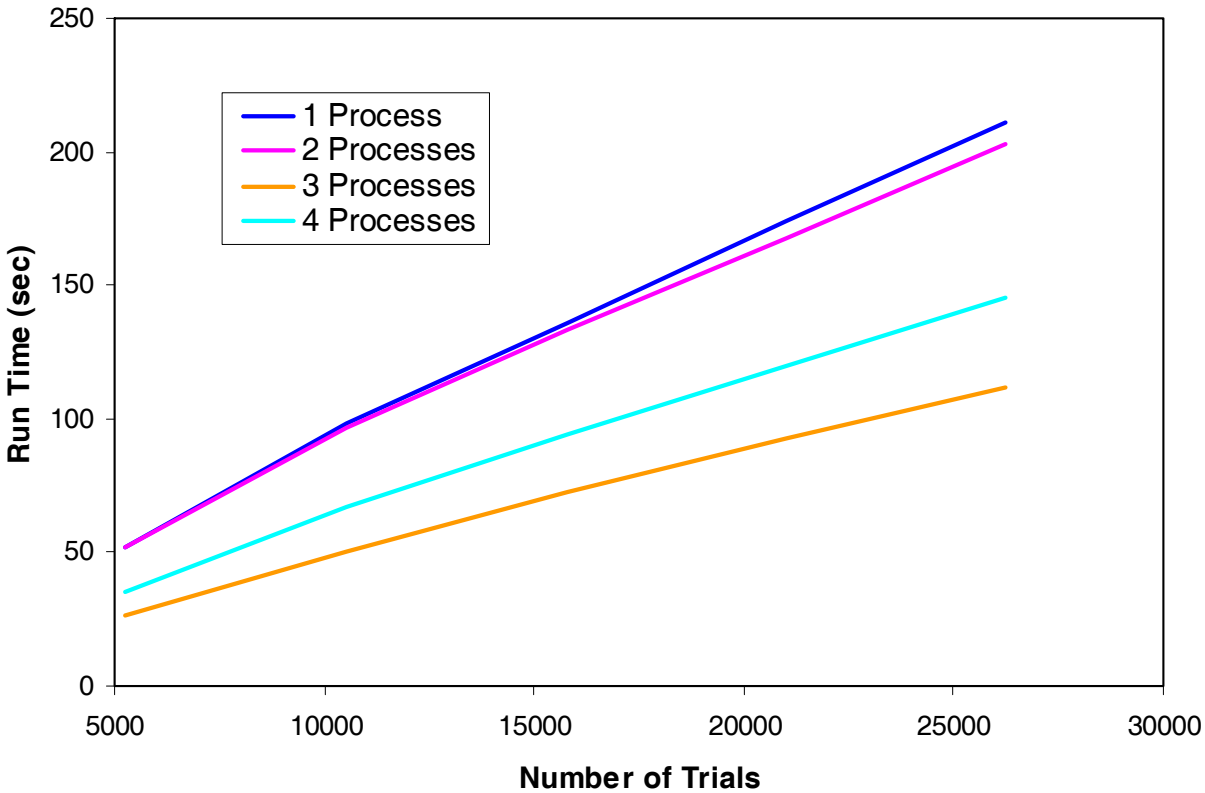

Figure 3 Computation Performance of Parallel Pump Scheduling Optimization

Conclusions

Parallel computation research is not only a promising research topic but also an essential requirement for fully making use of computing capacity offered by multi-core PCs. Computation parallelism shall received more attentions than ever since the computer industry is changing its single core paradigm to multi-core configuration. With mainstream support of computing industry, such as Microsoft concurrency computing libraries, Windows Server 2008 as well as Microsoft High Performance Computing Serve, the paradigm shift is under way from sequential to parallel computing. This research demonstrates the parallel computing speedup in solving for the computation-intensive pump scheduling optimization problem. Parallel computing can be employed for solving many other problems in water distribution analysis with significant speedup. The enhanced computing efficiency enables engineers to make use of the latest many-core PCs and enable them to explore more solution alternatives for enhanced project productivity and solution quality.

Reference

Alonso J. M., Alvarruiz F., Guerrero D., Hernández V., Ruiz P. A., Vidal A. M., Martínez F., Vercher J., and Ulanicki B. (2000) "Parallel Computing in Water Network Analysis and Leakage Minimization." ASCE, *J. Water Resour. Plng. and Mgmt*, Vol.126, No.4, pp. 251-260.

Balla, M.C. and Lingireddy, S. (2000) "Distributed Genetic Algorithm Model on network of Personal Computers." ASCE, *J. Computing in Civil Engineering*. Vol.14, No.3, pp. 199-205.

DeinoMPI, << http://mpi.deino.net>>.

Gropp,W.; Lusk, E. & Skjellum, A. (1999) *Using MPI: Portable Parallel Programming with the Message-Passing Interface*. MIT Press.

MPI, <<http://www.wikipedia.org/wiki/Message_Passing_Interface>>

MSMPI, <<http://msdn.microsoft.com/en-us/library>>

Kumar S. V.; Doby T. A.; Baugh J. W. Jr.; Brill E. D., and Ranjithan S. R. (2006) "Optimal Design of Redundant Water Distribution Networks Using a Cluster of Workstation." ASCE *J. Water Resour. Plng. and Mgmt.* Vol.132, No.5, pp. 374-384.

OpenMP,<< http://en.wikipedia.org/wiki/OpenMP>>

PureMPI,<< http://www.purempi.net/>>

Rabenseifner R. (2003) "Hybrid Parallel Programming: Performance Problems and Chances." *In proceeding of the 45th CUG Conference 2003*, Columbus, Ohio, USA.

Wu, Z. Y. (2002) "Methodology for Optimizing Constant and variable Speed Pump Operation." Haestad Methods Inc., 37 Brookside Ave, Waterbury, CT 06708, USA.

Wu, Z. Y. (2004) "A Benchmark Study on Maximizing Energy Cost Saving for Pump Operation", the 4th International Conference on Watershed Management and Urban Water Supply, Dec. 13-15, 2004, Shenzhen, China.

A Multi-objective Evolutionary Computation Approach to Hazards Mitigation Design for Water Distribution Systems

Lufthansa Kanta[1], Kelly Brumbelow[2], and Emily Zechman[3]

[1] Ph.D. Candidate, Zachry Department of Civil Engineering, Texas A&M University, WERC-205R, 3136 TAMU, College Station, TX 77843-3136, Email: lufthansa_kanta@neo.tamu.edu
[2] Assistant Professor, Zachry Department of Civil Engineering, Texas A&M University, WERC-205L, 3136 TAMU, College Station, TX 77843-3136, Email: kbrumbelow@civil.tamu.edu
[3] Assistant Professor, Zachry Department of Civil Engineering, Texas A&M University, WERC-205M, 3136 TAMU, College Station, TX 77843-3136, Email: ezechman@civil.tamu.edu

Abstract:

One of the critical public safety roles for water distribution systems (WDS) is suppression of urban fire events. Previous studies have investigated WDS rehabilitation for mitigation of potential fire events with a major focus on improving fire flows by pipe enlargement. However, pipe enlargement can cause water quality problems and place public health at risk during normal operational periods. Thus a novel approach is required to effectively address the conflicting goals of the WDS: reliable delivery of water during normal as well as emergency conditions, meeting water quality standards, and finding cost-effective design and rehabilitation options.

In this study an evolutionary computation-based multi-objective optimization-simulation framework is developed to design effective mitigation strategies for urban fire events for water distribution systems with three objectives: (1) minimizing fire damages, (2) minimizing water quality deficiencies, and (3) minimizing the cost of mitigation. An elitist non-dominated sorting genetic algorithm (NSGA-II) is modified by incorporating an evolution strategy (ES) to address difficulties for heuristic algorithms posed by WDS problems. Implementation of this methodology generates Pareto-optimal solution surfaces that express the trade-off relationship between fire damage, water quality, and least cost objectives. Thus, the method provides decision makers with the flexibility to choose a mitigation plan for urban fire events best suited for their circumstances. Each Pareto-optimal solution comprises a set of pipes to be enlarged to achieve increased fire flow and the corresponding diameters of these pipes. The algorithm is illustrated with several test functions. The Micropolis virtual city is then used to demonstrate the application of the proposed methodology to a complex WDS.

Introduction

The goal of a water distribution system (WDS) is to deliver water to the consumers in sufficient quantity and quality, even in case of emergencies such as power outage and urban fire events. Previous studies have investigated WDS rehabilitation for mitigation of potential fire events with a major focus on improving fire flows by pipe enlargement. However, any changes in water demand or water use pattern caused by pipe rehabilitation or new development often cause slower flow through the network which, in turn, results in greater decay of disinfectant, hence cause increase in pathogenic bacteria and influence water quality. This type of water quality problem can be reduced by installing chlorine booster units in the system other than at the water treatment plant.

Kanta and Brumbelow (2008) studied vulnerability and risk of water distribution systems (WDS) posed by urban fire events under both accidental failure and intentional failure scenarios. During the study, several mitigation packages were designed based on hardening sets of pipes to improve the system's resiliency to provide fire fighting flows. Bristow et al. (2007) studied different mitigation strategies to improve water distribution systems' ability to meet fire fighting demand and water main enlargements were generally the most effective strategies but involved relatively high

costs. Main enlargements increased the system's capacity to meet fire fighting demand but also increased water age under normal demand condition. Brumbelow and Bristow (2008) investigated tradeoffs between WDS emergency supply and water quality needs and proposed 17 mitigation packages to improve the system's capacity to provide fire fighting flows without compromising the daily water quality needs. All the previous studies utilized simulation based methodologies which were iterative and hence call for a systematic approach to improve WDS resiliency during fire events without compromising other system goals: meeting water quality standards mandated by regulation and finding cost-effective design and rehabilitation options.

The goal of this project is to develop a methodology to design effective mitigation strategies for urban fire events for water distribution systems with three objectives: (1) minimizing fire damages, (2) minimizing water quality deficiencies, and (3) minimizing the cost of mitigation. This goal can be achieved by identifying pipes for replacement and their corresponding diameters and the location of addition booster units. When more than one objective is considered in an optimization problem, no single solution may produce the best result with respect to all objectives. In such a case a set of solutions known as the Pareto optimal solutions or non-dominated solutions (Hans 1988) exist, none of which is worse than any other with respect to all objectives. The Pareto optimal solutions provide the decision makers more information and flexibility in selection of a solution. In the present study, a novel multi-objective evolutionary algorithm named Non-Dominated Sorting Evolutionary Strategy (NSES) will be used. The following sections describe the development of the methodology, implementation, and results in detail.

Problem Statement

The proposed model has three objectives: (1) minimizing the aggregated fire damage (f_1), (2) minimizing the maximum water quality deficiency (f_2), and (3) minimizing normalized mitigation cost (f_3). The multi-objective optimization problem, therefore, can be mathematically formulated as follows:

$$\text{Minimize } f_1 = \sum_{i=1}^{n} \alpha_i \frac{Q_{i_{\text{Re quired}}} - Q_{i_{\text{Available}}}}{Q_{i_{\text{Re quired}}}} \tag{1}$$

$$\text{Minimize } f_2 = \max_j \frac{C_{j_{\text{Re quired}}} - C_{j_{\text{Available}}}}{C_{j_{\text{Re quired}}}}; \; j=1, 2, \ldots, m \tag{2}$$

$$\text{Minimize } f_3 = \frac{\sum_{k=1}^{np} C_k^P + \sum_{l=1}^{nb} C_l^B}{\sum_{k=1}^{N} C_k^P} \tag{3}$$

Subject to:

$$D_k \in \{d\}; \; k = 1, 2, \ldots, np \tag{4}$$

$$np \le \phi \tag{5}$$

$$nb \le \theta \tag{6}$$

Where, $Q_{i_{\text{Re quired}}}$ = required fire flow (gpm) for hydrant i; $Q_{i_{\text{Available}}}$ = available flow (gpm) at minimum allowable residual pressure at hydrant i (typically set at 20 psi by local code); α_i = weighting coefficient for hydrant i; n= total number of fire hydrants considered for fire flow evaluation; $C_{j_{\text{Re quired}}}$ = minimum required residual chlorine concentration (mg/l) at monitoring node j;

$C_{j_{Available}}$ = available residual chlorine concentration (mg/l) at monitoring node *j*; *m*= total number of monitoring nodes; C_k^P = cost of pipe *k*; C_l^B = cost of booster station *l*; D_k =diameter (inch) of pipe *k*; *d*= commercially available discrete pipe sizes (inch); *N* = total number of pipes in the network; *np*= number of pipe decision variables; ϕ = user defined maximum number of pipes to be replaced; *nb*= number of booster station decision variables; and θ = user defined maximum number of boosters to be installed.

Non-dominated Sorting Evolution Strategy (NSES)

An evolutionary computation (EC)-based approach is used to solve the multi-objective problem. Evolutionary algorithms are population based heuristic search algorithms based on the process of natural selection. Initially developed by Holland, Genetic Algorithm (GA) is the most common EC-based approach among engineering applications. Many genetic algorithm based applications in water distribution system can be found in the literature such as Prasad and Park (2004) and Prasad et al. (2004), among others. Evolutionary Strategy (ES) is another EC-based approach first introduced by Rechenberg and Schwefel which uses a population of individuals to search for the best solution (Eiben and Smith 2007). Each individual (or solution) in the population consists of a set of 'genes' that represent the decision variables. The performance of each individual is evaluated by a fitness function. While GA uses both crossover and mutation, ES is solely based on a probabilistic mutation operator. To mutate a value of a real-valued decision variable, the sample is taken from a normal distribution with mean as the current value of the variable and standard deviation as an algorithmic parameter. The performance of the ES-based search is very sensitive to the value of the standard deviation; thus determination of this parameter requires extensive tuning (Zechman and Ranjithan 2009). ES also allows an alternative approach, called *adaptive mutation*, in which the standard deviations are also included in the chromosome representation (Eiben and Smith 2007).

Several EC-based methodologies are available for addressing multi-objective problems such as, NPGA (Horn et al. 1994), NSGA (Srinivas and Deb 1995), SPEA (Zitzler and Thiele 1999), PAES (Knowles and Corne 1999), and NSGA-II (Deb et al. 2002), among others. The goals of a population-based multi-objective optimization problem are to find: (i) solutions that are close to the Pareto front, and (ii) solutions that are well distributed and spread out along the Pareto front. To solve this multi-objective optimization problem, a fast elitist non-dominated sorting genetic algorithm (NSGA-II) is modified by incorporating an ES to address difficulties for heuristic algorithms posed by WDS problems. Proposed by Deb et al. (2002), NSGA-II is a population based multi-objective genetic algorithm which produces Pareto-optimal solutions in the objective spaces. It has been found in the literature that NSGA-II can converge toward the true Pareto-front uniformly and can distribute non-dominated solutions along the front evenly (Prasad et al. 2004). Traditionally as in GA, NSGA-II utilizes both crossover and mutation operators to facilitate both exploration and exploitation during the heuristic search and generates better solutions in subsequent generations. In WDS problems the significance of the crossover would be exploring an alternate flow path within the distribution network, which could be implemented by introducing a path search algorithm. However, this approach would significantly increase the computation time. Therefore, NSGA-II algorithm is here modified as non-dominated sorting evolutionary strategy (NSES) by implementing evolutionary strategy (ES) based search technique with the elitist non-dominated sorting algorithm. The structure and implementation of NSES operators to the WDS problem are described in the following sections.

Representation: In any population based search, the decision variables are encoded as an array, which, when decoded, represents a solution. The efficiency of an ES-based search depends upon the representation of a solution (Zechman and Ranjithan 2009). For example, if an individual is

represented by a large array of decision variables, it may increase the time of convergence of the algorithm. Typically, ES uses real-valued vectors for representing an individual.

To represent the multi-objective problem, it is assumed that a maximum number of pipes to be replaced for mitigation/rehabilitation is known. In this paper it is assumed that additional chlorine boosters will not be added, but the general problem formulated above includes this possibility. Therefore, the only sets of decision variables are the pipes to be replaced and their corresponding diameters. Rehabilitation locations are represented by an array of integer values, each of which specifies the pipe ID; and the pipe diameters are represented by a separate array of integer values.

An adaptive search is applied during implementation of this methodology. For an adaptive search, each decision variable is represented by a set of two genes. One gene represents the value of the variable, x_j, and another gene represents the standard deviation, σ_{xj}, which is used to mutate the gene representing the variable value. Assuming the number of pipe rehabilitation decisions is *n*, the chromosome representation of the problem is shown in Figure 1.

I_1	I_2	……	I_n	σ_{I_1}	σ_{I_2}	……	σ_{I_n}

Representation: Pipe ID (rehabilitation location)

d_1	d_2	……	d_n	σ_{d_1}	σ_{d_2}	……	σ_{d_n}

Representation: Pipe diameter

Figure 1. Chromosome representation

Mutation: In ES, there is a strong emphasis on the mutation operator for creating offspring. Mutation is migration from the current set of solutions to better solutions using small incremental steps. In ES, the adaptive mutation for each variable value x_j is performed in two steps: first, the standard deviation, σ_{xj}, is mutated using a separate normal distribution to generate $\sigma_{xj}^{'}$; then using the mutated standard deviation, $\sigma_{xj}^{'}$, the variable value x_j is mutated as $x_j^{'}$. The mutation mechanism is specified as follows (Eiben and Smith 2007):

$$\sigma_{xj}^{'} = \sigma_{xj} \cdot e^{\tau^{'} \cdot N(0,1) + \tau \cdot N_j(0,1)} \tag{7}$$

$$x_j^{'} = x_j + \sigma_{xj}^{'} \cdot N_j(0,1) \tag{8}$$

Here, τ and τ′ are parameters such that $\tau^{'} \propto \frac{1}{\sqrt{2n}}$ and $\tau \propto \sqrt{2\sqrt{n}}$; *n* is the problem size (number of decision variables); $N(0,1)$ denotes a draw from the standard normal distribution; and $N_j(0,1)$ denotes a separate draw from the standard normal distribution for each variable *j*. The proportionality constants for both τ and τ′ are external parameters to be set by the users.

To mutate the location of pipe rehabilitation, a special mutation operator is adopted from Zechman and Ranjithan (2009). The current pipe is mutated by random assignment of another topologically close potential pipe using an adjacency list. The adjacency list of each pipe of a water distribution system represents a connectivity map of one pipe to other pipes in the network. In such a

case, the standard deviation value, σ_{I_k}, associated with a pipe ID, I_k, indicates the maximum number of links between that pipe and the pipe to be selected.

Selection: In ES-based algorithm, two different types of selection operators are used: *Parent selection* and *survivor selection* (Eiben and Smith 2007). In the first generation, an initial population of size μ is generated. In each generation, *parent selection* operator is applied based on a uniform distribution to randomly select λ individuals from the pool of μ individuals, where $\lambda > \mu$. Each of these λ individuals is then mutated to create λ offspring.

After creating λ offspring, their fitness values are calculated. The *survivor selection* operator is applied to select best μ individuals deterministically, either from the set of offspring individuals only (denoted as (λ,μ) selection) or from the combined set of parent and offspring individuals (denoted as $(\lambda+\mu)$ selection). In this paper, the investigation is based on a $(\lambda+\mu)$ selection.

Non-dominated Sorting: The non-dominated sorting approach was adopted from Deb et al. (2002). First, elitism is introduced by combining both parent individuals (μ) and offspring (λ). Then each solution is compared with every other solution in the combined population and the individuals are sorted into several fronts such as F_1, F_2, F_3, etc. The first front F_1 contains the best non-dominated solutions in the combined population. Solutions in this front have a non-dominated rank = 1. The second front F_2 contains the solutions that are dominated by the solutions in the first front F_1 but dominate all other solutions in the combined population. Solutions in this front have a non-dominated rank = 2. Similarly, the front F_3 contains the solutions that are dominated by the solutions in the fronts F_1 and F_2 but dominate all other solutions in the combined population. Solutions in this front have a non-dominated rank = 3; and so on.

Crowding Distance Estimation: To maintain the diversity in the population a density estimation technique is adopted from NSGA-II (Deb et al. 2002). This operator measures the density of a particular solution in terms of the average distance of two other solutions on either side of this solution along each of the *m* objectives. Solution with larger crowding distance indicates better diversity in the population.

Algorithmic Steps: The algorithmic steps of NSES procedure are:

1. Generate an initial population of μ individuals.
2. Apply a parent selection operator to select λ individuals.
3. Apply an adaptive mutation operator to create λ offspring.
4. Combine μ individuals with λ offspring to form a pool of $(\lambda+\mu)$ individuals.
5. Evaluate fitness of the combined population with respect to all three objectives using equations (1), (2), and (3).
6. Apply non-dominated sorting operator to sort the solutions into non-dominated fronts.
7. Apply $(\lambda+\mu)$ selection to select best μ individuals deterministically starting from front F_1. If $\mu < |F_i|$ then apply crowding distance operator to select the most diverse solutions.
8. Terminate the procedure if convergence is achieved, otherwise, go to step 2.

Performance Measure of NSES Algorithm

To validate the proposed approach, the NSES algorithm is applied on five test functions, which have been adopted in Deb et al. (2002) and a performance metric Δ is evaluated for each of the test functions. The metric Δ represents a measure of deviation of the solutions of the best non-dominated front in the final population (Deb et al. 2002). In multi-objective problems diversity among the Pareto-optimal solutions is very important. Thus the algorithm with a smaller deviation metric Δ shows better performance. The metric Δ is computed as follows (Deb et al. 2002):

$$\Delta = \sum_{i=1}^{|F_1|} \frac{\left| d_i - \overline{d} \right|}{|F_1|} \tag{9}$$

Where, F_1 = best non-dominated front in the final population; $|F_1|$ = number of solutions in front F_1; d_i = Euclidean distance in the objective space between two consecutive solutions in F_1; and $\overline{d}$ =average of these distances d_i. Table 1 shows the mean deviation $\overline{\Delta}$ and its variance from 10 iterations for each of the test functions using NSES. The performance of NSES algorithm is compared with that of NSGA-II and PAES (Knowles and Corne 1999) listed in Deb et al. (2002) and presented in Table 1. To perform an equal comparison, the total number of function evaluations in NSES is kept the same as that of both NSGA-II and PAES. The smallest values of $\overline{\Delta}$ for all test functions using NSES indicate that the proposed algorithm performs better than the other two.

Table 1. Comparison of mean and variance of performance metric Δ evaluated using NSES, NSGA-II, and PAES

Algorithm	MOP2		MOP3		MOP4		EC4		EC6	
	Mean	*Variance*	*Mean*	*Variance*	*Mean*	*Variance*	*Mean*	*Variance*	*Mean*	*Variance*
NSES	0.1127	0.00038	0.1380	0.00014	0.2635	0.00041	0.2746	0.02791	0.2390	0.00564
NSGA-II	0.3610	0.00068	0.4450	0.00043	0.3870	0.00164	0.3830	0.00099	0.3650	0.01613
PAES	1.6090	0.00671	1.3410	0.00495	1.0870	0.00687	1.5630	0.05723	1.1950	0.05151

Application of Model

A virtual city water distribution system data, Micropolis (Brumbelow et al. 2007), is used to demonstrate the NSES procedure to solve the multi-objective problem. The current version of Micropolis has one pumping station (consisting of 3 pumps), one treatment facility, one storage facility (water tank), 1088 pipes, 1210 non-hydrant nodes, 196 valves, and 52 fire hydrants. Currently, a disinfectant dose of 4 mg/l is added at the treatment plant and there is no additional chlorine booster station in the system. Among 1088 pipes, there are 577 water mains each of which is considered as a potential pipe rehabilitation location. The diameter of rehabilitated pipes could be selected from the set of {6, 8, 10, 12, 14, 16, 18, 20, 24} inch diameter commercially available class 50 ductile iron pipes. The fire fighting capacity of the water system could be evaluated at all 52 fire hydrants; which would make the analyses computationally expensive. Therefore, to represent the system-wide fire fighting performance without contributing to computational burden, three fire hydrants are considered which cover the central business district, industrial area adjacent to the central business district, and heavily populated multi-family residential area on the north-eastern part of the city.

To evaluate the aggregate fire damage (Eq. (1)), the weighting coefficients, α, are determined as replacement building cost of assets within a search radius of 1000 ft of each hydrant over the total cost of assets within the search radius of all three fire hydrants. A required fire flow of 1000 gpm is considered at all three fire hydrants. Apart from the fire hydrants and the demand nodes, there are a total of 751 nodes representing valve nodes and junctions. From the set of 751 nodes, ten are selected as representative water quality monitoring nodes. The Surface Water Treatment Rule (SWTR) requires the water distribution systems to maintain a “detectable” disinfectant residual level of 0.2 mg/l (for chlorine) throughout the system. Therefore, the required minimum residual chlorine

concentration of 0.2 mg/l is used at all ten monitoring nodes to evaluate water quality deficiency (Eq. (2)). A normalized cost is evaluated as cost of pipe replacement over the cost of rebuilding the network (Eq. (3)). The network is shown in Figure 2.

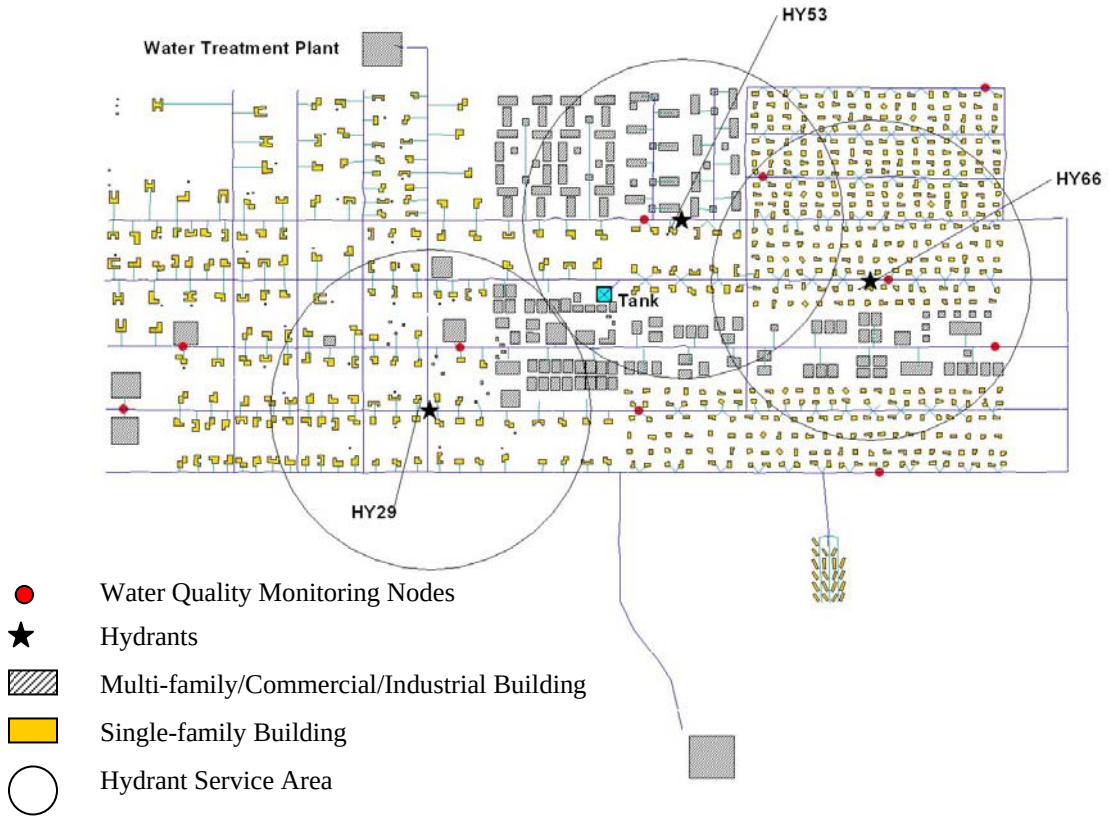

Figure 2. Building map of Micropolis with water distribution system shown in thin lines

The solution approach defined in the previous section is implemented in a computer code in Visual Basic 6.0 that utilizes iterative solution of the water distribution system's hydraulics and water quality under the objectives and constraints defined by equations (1) through (6). The NSES model is coupled with EPANet Programmer's Toolkit (Rossman 1999) to simulate the hydraulics and water quality in the network. To evaluate the aggregated fire damage a single period simulation is performed, and to evaluate the water quality deficiency the hydraulics and water quality in the network are simulated separately without a fire flow over a 168-hour time period to allow the system to reach a dynamic equilibrium condition with respect to disinfectant concentrations. It is assumed that only ten pipes needed to be replaced to increase the system-wide firefighting capability. The NSES procedure was run for 100 generations. The parameters used during implementation of NSES-based search are: μ=15, λ = 100, and *stopping criterion* = number of generations.

Results and Discussion

To test the robustness of the proposed methodology, ten independent trials were performed. The X-Y-Z scatter plots of the Pareto fronts from all of the ten trial solutions are compared in 'fire flow-water quality-cost' objective space where each point represents a solution indicating the aggregated fire flow, minimum residual chlorine, and the corresponding mitigation cost to implement

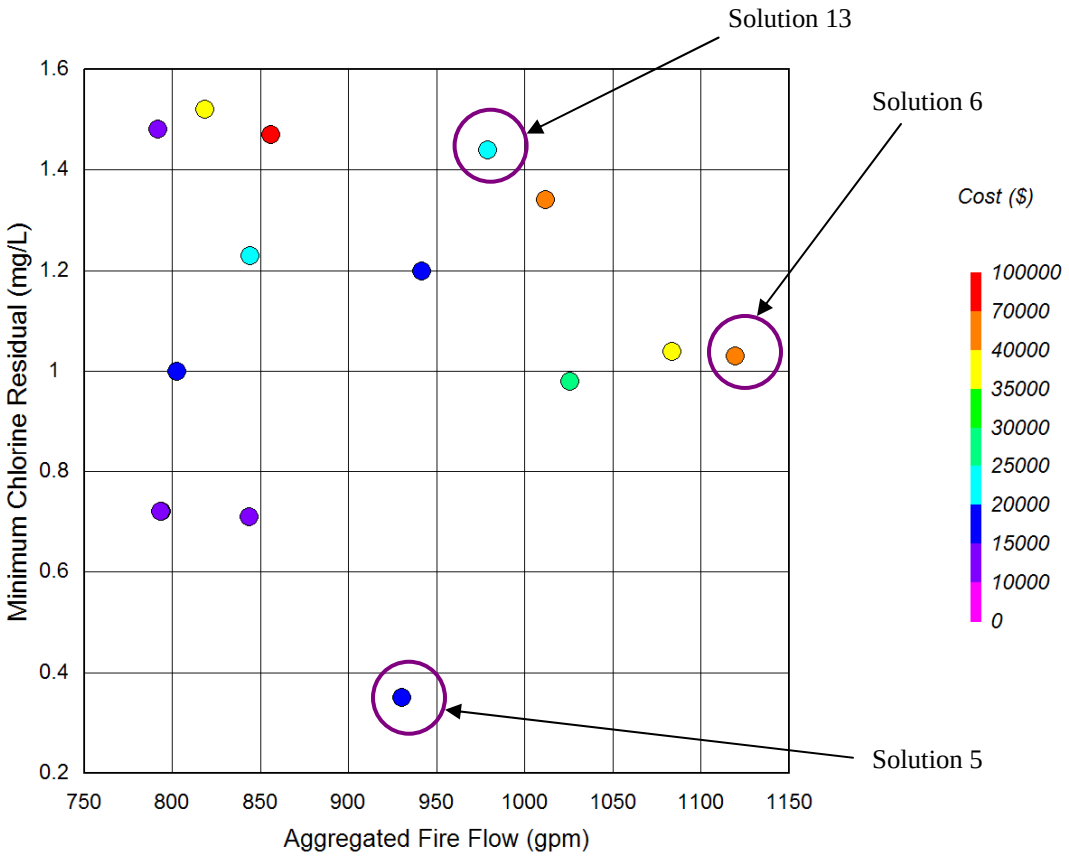

Figure 3. X-Y-Z Scatter plot of Pareto-optimal solutions after 100 generations

that solution. Since the model minimizes the aggregated fire damage, the maximum chlorine deficiency, and the normalized cost of mitigation, consequently, the model returns maximized aggregated fire flow, maximized minimum residual chlorine, and minimum cost solutions. Although the true Pareto front of this problem is not known a priori, the scatter plots of the Pareto fronts represent that the search is consistent for all of the ten trials. To get a better understanding of the Pareto front for the WDS problem, final solutions from a single trial are shown in a scatter plot in Figure 3 and the achieved objectives from the Pareto-optimal solutions are listed in Table 2.

In existing condition, the available fire flows at hydrants HY29, HY53, and HY66 are 469 gpm, 873 gpm, and 869 gpm, respectively. Thus, all 15 solutions yield significant gain at hydrant HY29 and moderate gains at both hydrant HY53 and hydrant HY66 with a few exceptions. The minimum residual chlorine levels in both the existing condition and in the final solutions are above the regulated minimum value of 0.2 mg/l. From the above table, it is evident that the NSES algorithm generates non-dominated solutions in the objective space; which means no one solution is better than the other with respect to all three objectives. To explain the trade-off relations between the objectives in detail, three non-dominated solutions, solution-5, solution-6, and solution-13, are selected. It can be concluded from Table 2 that solution-5 is better than the other two in terms of the third objective: cost, but inferior to the others in terms of both aggregated fire flow and minimum residual chlorine. Solution-6 produces more than required fire flow volume of 1000 gpm and hence superior to the other two in terms of the first objective but inferior to the others in terms of cost. Similarly, solution-13 is superior to the others in terms of the second objective: residual chlorine, but inferior to solution-6 in terms of aggregated fire flow, and inferior to solution-5 in terms of cost. This

comparison clearly indicates that a tradeoff relation exists between the conflicting goals of WDS: fire flow, water quality, and cost.

Table 2. Comparison of solutions in multi-objective space

Solution ID	Hydrant Fireflow *HY29* *gpm*	*HY53* *gpm*	*HY66* *gpm*	Aggregated Fireflow *gpm*	Minimum Residual Chlorine *mg/l*	Cost *$*
Existing	469	873	869	791	0.71	0
1	484	870	866	792	1.48	13,429
2	480	874	869	794	0.72	6,912
3	479	907	895	818	1.52	36,604
4	739	888	878	856	1.47	93,332
5	1138	882	872	930	0.35	16,770
6	1807	942	957	1119	1.03	61,545
7	730	874	869	844	0.71	12,387
8	1422	924	931	1025	0.98	27,972
9	479	874	869	794	0.72	14,421
10	866	1051	1041	1012	1.34	63,504
11	1654	937	949	1084	1.04	37,852
12	1198	880	871	941	1.20	18,674
13	1249	915	902	979	1.44	23,033
14	503	937	911	844	1.23	20,890
15	487	884	875	802	1.00	15,403

Conclusion

This methodology clearly generates Pareto-optimal solution surfaces that express the trade-off relationship between fire damage, water quality, and least cost objectives; thus provides decision makers with the flexibility to choose a mitigation plan for urban fire events best suited for their circumstances. However, the solutions indicate that there were limited or no solutions in 'high fire flow-low water quality-high cost' region. This is due to the fact that the system wide fire flow capacity is evaluated as aggregated fire flow considering three hydrants: HY29, HY53, and HY66 with weighting coefficients of 0.2, 0.55, and 0.25, respectively. Thus, any little improvement at hydrants HY 53 and HY66 contributes to greater aggregated fire flows resulting from small changes in the diameter. Further investigation is required by incorporating more hydrants in evaluating aggregated fire flow and larger number of monitoring nodes needed to be included to evaluate system-wide minimum residual chlorine level.

References

Bristow, E.C., Brumbelow, K., and Kanta, L. (2007). "Vulnerability assessment and mitigation methods for interdependent water distribution and urban fire response systems." *Proceedings World Environmental and Water Resources Congress 2007*, Tampa, FL.

Brumbelow, K., Torres, J., Guikema, S., Bristow, E., and Kanta, L. (2007). "Virtual cities for water distribution and infrastructure system research." *Proc. World Environmental and Water Resources Congress 2007,* ASCE, Reston, VA.

Brumbelow, K. and Bristow, E.C. (2008). "Tradeoffs in water distribution system design for normal versus emergency flows: quantity, quality, and cost/benefits." *World Environmental and Water Resources Congress 2008*, Hawaii.

Deb, K., Agrawal, S., Pratap, A., and Meyarivan, T. (2002). "A fast elitist non-dominated sorting genetic algorithm for multi-objective optimization: NSGA-II." *IEEE Transactions on Evolutionary Computation*, 6(2), 182-197, Piscataway, NJ.

Eiben, A. E. and Smith, J. E. (2007). *Introduction to Evolutionary Computing*, Springer, New York.

Hans, A. E. (1988). "Multicriteria optimization for highly accurate systems." *Multicriteria Optimization in Engineering and Sciences*, W. Stadler (Ed.), Mathematical concepts and methods in science and engineering, 19, 309-352, Plenum Press, New York.

Horn, J., Nafploitis, N., and Goldberg, D. E. (1994). "A niched Pareto genetic algorithm for multiobjective optimization." *IEEE Conference on Evolutionary Computation*, IEEE Service Center, Piscataway, NJ.

Kanta, L. and Brumbelow, K. (2008). "Vulnerability, risk, and mitigation assessment of water supply systems for insufficient fire flows." *World Environmental and Water Resources Congress 2008*, Hawaii.

Knowles, J. and Corne, D. (1999). "The Pareto archived evolutionary strategy: A new baseline algorithm for multi-objective optimization," *Preceedings of the 1999 Congress on Evolutionary Computation*, IEEE Service Center, Piscataway, NJ, 98-105.

Prasad, T.D. and Park, N. (2004). "Multiobjective genetic algorithms for design of water distribution networks." *Journal of Water Resources Planning and Management*, ASCE, 130(1), 73-82.

Prasad, T., Walters, G., and Savic, D. (2004). "Booster disinfection of water supply networks: multiobjective approach." *Journal of Water Resources Planning and Management*, ASCE, 130(5), 367-376.

Rossman, L. A. (1999). "The EPANET programmer's toolkit for analysis of water distribution systems." *29th Annual Water Resources Planning and Management Conference*, Erin M. Wilson, Editor, June, 1999, Tempe, AZ.

Srinivas, N. and Deb, K. (1995). "Multi-objective function optimization using non-dominated sorting genetic algorithms." *Evolutionary Computation*, 2(3), 221-248.

Zechman, E. M. and Ranjithan, R. (2009). "Evolutionary computation-based methods for characterizing contaminant sources in a water distribution system." *Journal of Water Resources Planning and Management*, ASCE (in Press).

Zitzler, E. and L. Thiele. (1999). "Multiobjective evolutionary algorithms: A comparative case study and the strength Pareto approach," IEEE Trans. Evol. Comput., vol. 3, no. 4, pp. 257–271.

Multi-objective Sensor Placements with Improved Water Quality Models in a Network with Multiple Junctions

R.G. Austin[1], C. Y. Choi[1], A. Preis[2], A. Ostfeld[3], and K. Lansey[4]

[1]Department of Agricultural and Biosystems Engineering
The University of Arizona, Tucson, Arizona 85721, U.S.A.
[2]Center for Environmental Sensing and Modeling,
MIT-SMART Center, Singapore
[3]Department of Civil Engineering and Environmental Engineering
Technion, Israel Institute of Technology, Haifa 32000, Israel
[4]Department of Civil and Engineering Mechanics
The University of Arizona, Tucson, Arizona 85721, U.S.A.

Concerns about the security of water distribution systems have lead to increased interest in sensor placement in water distribution systems. Due to the cost of both placing and maintaining these sensors, the number of sensors used must be limited. These constraints make the sensor deployment locations crucial in a water monitoring system. Many studies, based on differing algorithms and objective functions, have sought to determine ways to optimize sensor location. These studies have largely relied on current water quality models that assume perfect mixing at pipe junctions. However, it has been shown that using a water quality model that accounts for imperfect mixing (AZRED) at pipe intersections produces outcomes that differ from those produced by studies that assume perfect mixing and, consequently produces a different scheme for optimal sensor placement. The current work uses a multiobjective approach that relies on the non-dominated, sorted algorithm II. The study seeks, first, to contrast the use of the AZRED water-quality model to the use of water quality models that assume perfect mixing, and, second, to propose a more comprehensive approach to sensor placement. By using a simpler objective of optimizing for complete sensor coverage, the study will expand on pervious work that made this comparison. An example network is analyzed using both AZRED and EPANET, and the results are compared.

1. INTRODUCTION

Sensor Placement in Water Distribution Systems

The Safe Water Drinking Act, issued by the United States Environmental Protection Agency in 1990, requires water utilities to monitor water distribution systems (WDS) for water quality. Since the passing of this act, there has been increased interest in sampling and, in turn, determining the best sampling locations. Lee and Deninger (1992) first approached the problem using optimization tools to determine the best locations; their analysis was based on fractions of water contributed to monitoring locations of a water distribution network. Since that time, there have been many advances in methodologies for monitoring water quality

The terrorist events of September 11th generated a greater demand for increasing the security of water distribution systems, and many subsequent studies, recognizing the possibility of intentional contamination, have focused on sensor placement.

A primary goal in designing a sensor placement scheme should be to give the water distribution operator the best possible tool for making informed decisions about which locations to monitor. Ideal would be a sensor network that provides (1) rapid and (2) accurate detection of an event that takes place anywhere in the system. Obtaining such perfection is, however, simply impossible, given the current technology and budget constraints. Because continuous, ubiquitous monitoring is expensive, the number of sensors deployed must be kept to the minimum needed to achieve threshold levels of accuracy and timeliness as determined by the designer who wishes to make good use of limited resources and must simultaneously weigh the importance of several goals.

Multiobjective Optimization

In contrast to single objective schemes, a multiobjective optimization scheme accounts for several different objective functions simultaneously. Formally, this can be written $F(x) = [f_1(x), f_2(x),..., f_M(x)]^T$ where F(x) is the multiobjective function that is composed of $f_1(x), f_2(x),..., f_M(x)$ which are a set of objective functions, and $x = (x_1, x_2,..., x_n)^T$ is the decision variable vector. The goal of this type of optimization is to find the set of all of the best solutions, subject to any constraints imposed by the problem. The best solutions are solutions such that no other solutions may be found that improve any of the objective functions without making another objective function value worse. This set of solutions is called the Pareto optimal solution set.

AZRED Water Quality Model and Optimization

Most WDS water quality modeling software relies on the assumption of perfect mixing at all junctions within the system. Van Bloemen Waanders et al. (2005) showed, through computational fluid dynamics (CFD), of a cross fitting that this assumption would cause significant errors. They determined that two incoming adjacent flows bifurcate rather than mix. Romero-Gomez et al. (2008a), in describing this mixing phenomenon over a large range of the Reynolds number using CFD and Austin et al. (2008), established an experimental database to model mixing behavior in the turbulent flow regime. Both computational and experimental results demonstrated that nodal mixing could be dramatically different from those produced by a perfect mixing model. Choi et al. (2008b) showed that mixing was mostly dependent on relative inflows and outflows rather than on Reynolds number, and that some modeling simplifications could be made in order to obtain a reasonable estimate of mixing over both the laminar and transitional flow regimes as well. Along with cross fittings, wye and tee junctions have been investigated and shown to exhibit imperfect mixing behavior. These include situations in which more than one tee or wye type fitting have been placed in close proximity. Choi et al. (2008b) developed a database for these other fitting configurations.

The AZRED water quality model is a modified version of EPANET, one that implements an imperfect mixing model for cross, double tee, and tee and wye fittings. The program was created by a group of researchers at the University of Arizona (Choi et al., 2008a; AZRED, 2009) and based on data sets collected through experimental trials.

The program uses EPANET's standard hydraulic water quality solvers but alters the water quality code by calculating concentrations downstream from junctions based on imperfect mixing, when appropriate, and using an interpolation of data. Romero-Gomez et al. (2008b) demonstrated that AZRED could be used as the water quality model in the single objective optimization scheme to maximize system coverage (i.e., likelihood of detection). A minimum hazard level was used in this study to construct a pollution matrix with a binary variable to signal whether or not a contamination above the minimum hazard level had been detected. It was shown that, depending on the minimum hazard level, the water quality model (perfect mixing vs. AZRED) had a significant influence on the number of sensors required for complete coverage and that, due to the increased accuracy of the water quality model, sensor designs based on AZRED should be more reliable than those based on perfect mixing. Here, we pose a multi-objective optimization problem to extend the comparison of perfect and imperfect mixing assumptions.

2. METHODS

Optimization Functions

The optimization problem is formulated using the three objective functions proposed by Preis and Ostfeld (2008): sensor detection likelihood, sensor detection redundancy, and sensor expected detection time.

Detection Likelihood

Detection likelihood is the probability that a random event in the pollution matrix will be detected at one of the sensor locations. This metric is intended to indicate the degree to which the sensor locations cover the network. A network with high detection likelihood has a good chance of detecting a random event, while an arrangement of sensors with low detection likelihood has a low detection probability. More formally, the sensor detection likelihood is given as:

$$f_1 = \frac{1}{S}\sum_{r=1}^{S} d_r \tag{1}$$

where f_1 is the sensor detection likelihood, d_r=1 if there is detection at least one of the sensor locations or d_r=0 otherwise, and S is the total number of pollution events. The detection likelihood indicates the proportion of events in the randomly generated set that would be detected. As such, it is desirable to maximize its value.

Detection Redundancy

Detection redundancy is defined as the probability that if an event occurs, a redundant detection will also occur. Thus, sensor detection redundancy is intended to increase the reliability of the sensor network by reducing the number of false detections that can occur at a single sensor. Mathematically, the term is defined as:

$$f_2 = \frac{1}{\sum_{r=1}^{S} d_r}\sum_{r=1}^{S} R_r \tag{2}$$

where f_2 is the sensor detection redundancy, and R_r=1 if the redundancy condition is met and R_r=0 otherwise. In our specific examples, three sensors are used as the number that must be triggered in order to have a redundant condition. Sensor detection redundancy is to be maximized.

Detection Time

Expected detection time is a metric defining the time that passes from the moment when an event occurs until it is detected. This metric thus specifies the expected time that a given sensor configuration should need in order to initially detect a contamination. The metric is calculated as:

$$f_3 = E(t_d) \tag{3}$$

where f_3 is the sensor detection time, t_d is the time from contamination until the first sensor detection, and $E(t_d)$ is the expected value of t_d. To mitigate harm caused by a contamination event, detection time is minimized in order to minimize the amount of time that passes before action can be taken. The sensor detection time is to be minimized in order to minimize the time that passes before action can be take to mitigate harm caused by a contamination event.

Pollution Matrix Generation

The purpose of the pollution matrix is to organize the results of a set of simulated pollution events into a form that can be easily evaluated by our objective functions (Ostfeld and Salomons, 2004). In this study, a pair of pollution matrices was created for each of the networks. One matrix was derived from a water quality analysis using EPANET, while the second other matrix was developed using AZRED as the simulation model. Aside from the difference of the water quality solver, each matrix was created using the same procedure that was automated through a C++ program using the EPANET toolbox. The program ran both hydraulic and water quality simulations for each pollution event. In the pollution matrix, each line contains the record of a contamination event with a corresponding injection node, mass rate, time, and duration. The pollution information follows the injection information and indicates the concentration of each contamination initially detected for each node being considered. The time of first detection, and the duration of the contamination at that node is also included. Separate pollution matrices were constructed for each minimum detection limit (MDL) that was set to represent which represented the pattern of detection based on the corresponding level where detection would occur.

NSGA-II Optimization Algorithm

The nondominated, sorted genetic algorithm developed by Deb et al. (2000) and implemented by Preis and Ostfeld (2008) was used as the optimization solver by modifying the function evaluation routine to incorporate AZRED as well as EPPANET. Briefly, the NSGA-II algorithm is a multiobjective genetic algorithm that generates a random set of strings to represent the initial population of sensor locations. Each string's fitness is then evaluated for all objective functions. The strings are then sorted and nondominated strings are identified. One string dominates another when:

1. Have a fitness value as good as the other string for all fitness functions
2. Have a fitness value better than the other string for at least one objective function.

Nondominated strings are then sorted according to the average distance between the fitness vectors of the other strings, and solutions that favor greater distances (diversity in the solution) are selected. The algorithm then produces a new generation of strings based on selection, mutation, and a crossover based on the best set of available solutions from the previous generation. This process of evaluation, sorting, and new population generation is repeated until a stopping criteria is reached. In this study, the solutions were all run for 1,000 generations.

Network Descriptions

This exemplary network is part of the EPANET freeware package and consists of 120 links, 90 nodes, 3 elevated tanks, and 2 pumps that connect to 2 reservoirs (a lake and a river). Eight nodes from the network are configured as 4-way junctions (circled in Figure 1) and were thus modified in order to comply with the requirement of AZRED for such junctions. The modifications led to a combination of all the types shown by Choi et al. (2008b): two crosses, two double-tee, one YU-type, and three YN-type junctions. The location and characteristics of the new junctions are listed in Table 1.

EPANET example Network3 is used as the application network in this study. The network was slightly altered so that it would better suite the study. These alterations follow those implemented by Romero-Gomez et al. (2009). Incomplete mixing occurs at nodes (a) having two incoming and two outgoing pipes or (b) that are a special connection. In original Nework3, only cross junctions (type (a)) are available. Therefore, changes were made in the network to introduce special junction types, which were modeled in AZRED (cross, double tee, etc.) and that both the entering and exiting pipes in these nodes where all the same size. The changes introduced 8 special junctions that would produce imperfect mixing: two crosses, two double-tees, one YU-type, and three YN-type junctions (for junction types, see Choi et al., 2009). To ensure that only pipes of the same size entered and exited the special junctions, extra nodes were added around each junction along with a short length of added pipe. These nodes were not used as injection or detection locations.

3. RESULTS

The pollution matrices were created by including events for every possible combination of events from a list of injection mass rates, injection durations and start times. All of the possible event locations were used for each of these combinations. The pollution matrices for Network 3 was done with 2 mass rates of 50000, and 100000 mg/min, durations of 2 and 4 hrs, with 4 start times distributed evenly throughout the day. Sets of pollution matrices were created for each MDL (0, 0.1, 0.01, 0.001, and 0.0001 mg/L).

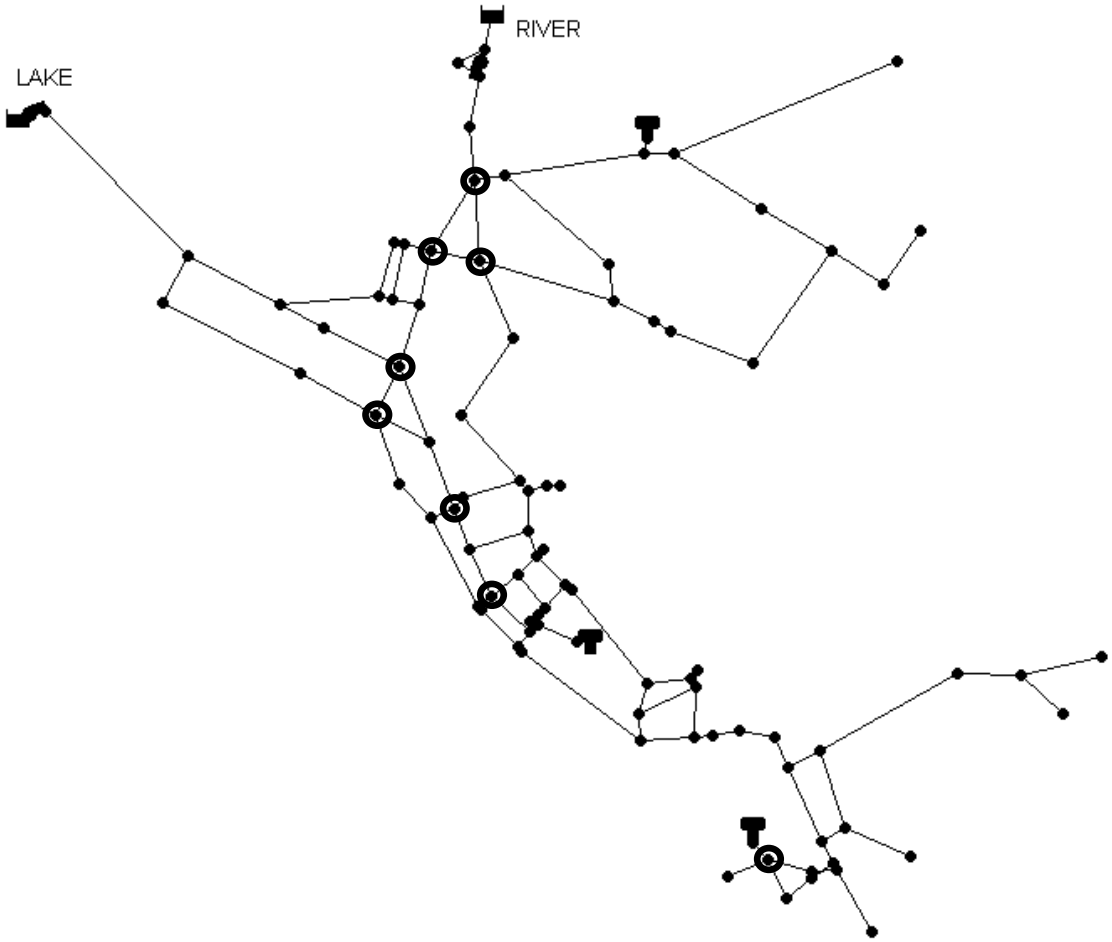

Figure 1. Network 3 from EPANET examples. Network was modified at the circled nodes that correspond to 4-way junctions.

Table 1. Modifications on Network 3 example from the EPANET package (for modified junction types, see Choi et al., 2009).

Node ID	Type	Junction diameter (D)	Dimensionless distance (L/D)
121	YN	24	2.0
120	N	10	1.0
119	X	20	-
115	YN	10	3.0
193	N	12	2.5
189	X	12	-
255	YU	10	1.0
111	YN	12	2.0

Incomplete mixing causes concentration changes downstream of a junction where mixing is incomplete. If additional junctions have incomplete mixing downstream, the difference between the plumes for perfect and imperfect mixing may amplify. The concentration differences are apparent when applying alternative a minimum detection levels (MDL). These differences can be seen between the Pareto fronts for the two mixing conditions. The Pareto fronts for detection likelihood and detection redundancy are shown in Fig. 2 for 4 MDLs.

As the MDL is increased, contamination events are missed at more locations resulting in a shift on the Pareto front. Comparing the results from EPANET and AZRED we see that at most MDLs there is a slight difference between the two methods that diminishes as the MDL is decreased. Little difference can be seen at the 0.0001 mg/L level and with perfect sensors (an MDL of zero) the results for EPANET and AZRED were very similar and are not shown. At low MDLs, any contaminant is detected and a small concentration discharging from an imperfectly mixed node is equivalent to a uniformly mixed higher concentration and will be detected at the assumed precise meters. The differences between the two methods are especially prominent with points that are at the upper range of the detection likelihood parameter. In this portion of the Pareto front differences between EPANET and AZRED are forcing significant changes in concentrations downstream of the special junctions. These changes are not very large but could lead to a better decision for sensor location when using AZRED.

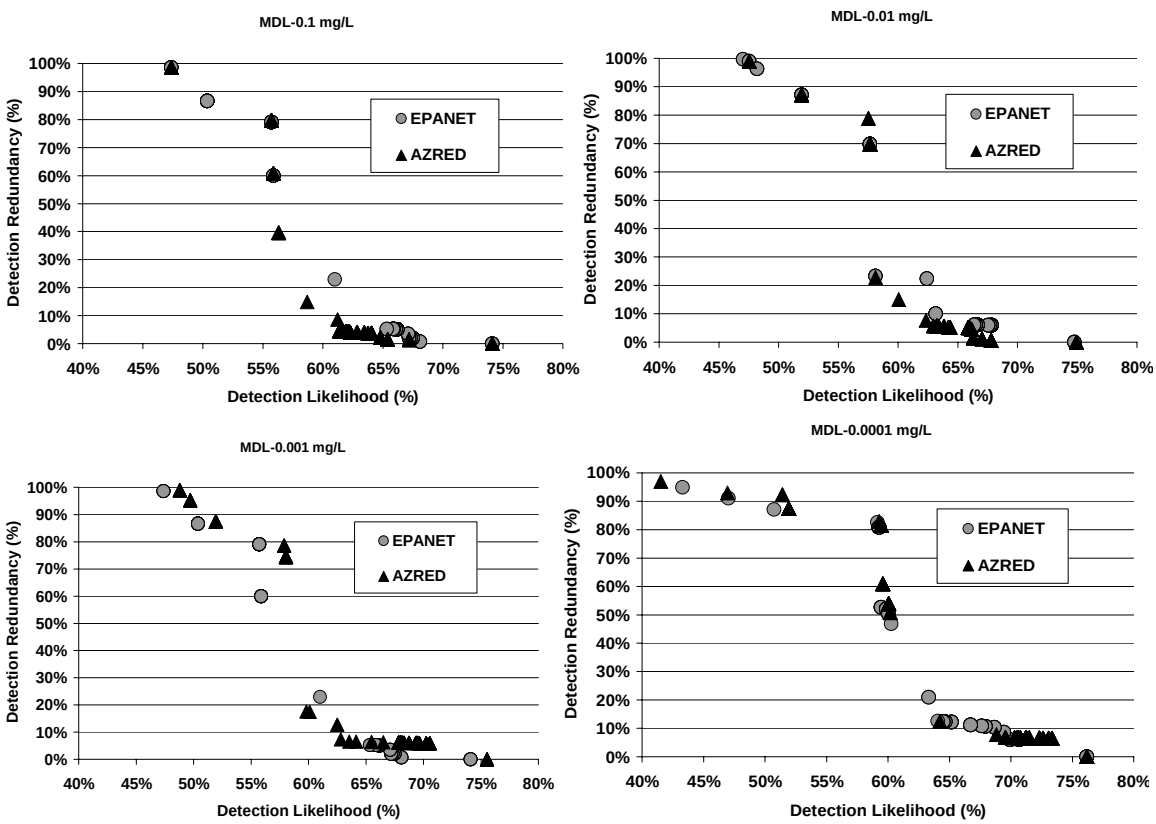

Fig. 2. Pareto fronts for Network3, showing the relationship between detection likelihood and detection redundancy for differing MDLs. Note the detection limit and water quality model's effects on the Pareto fronts.

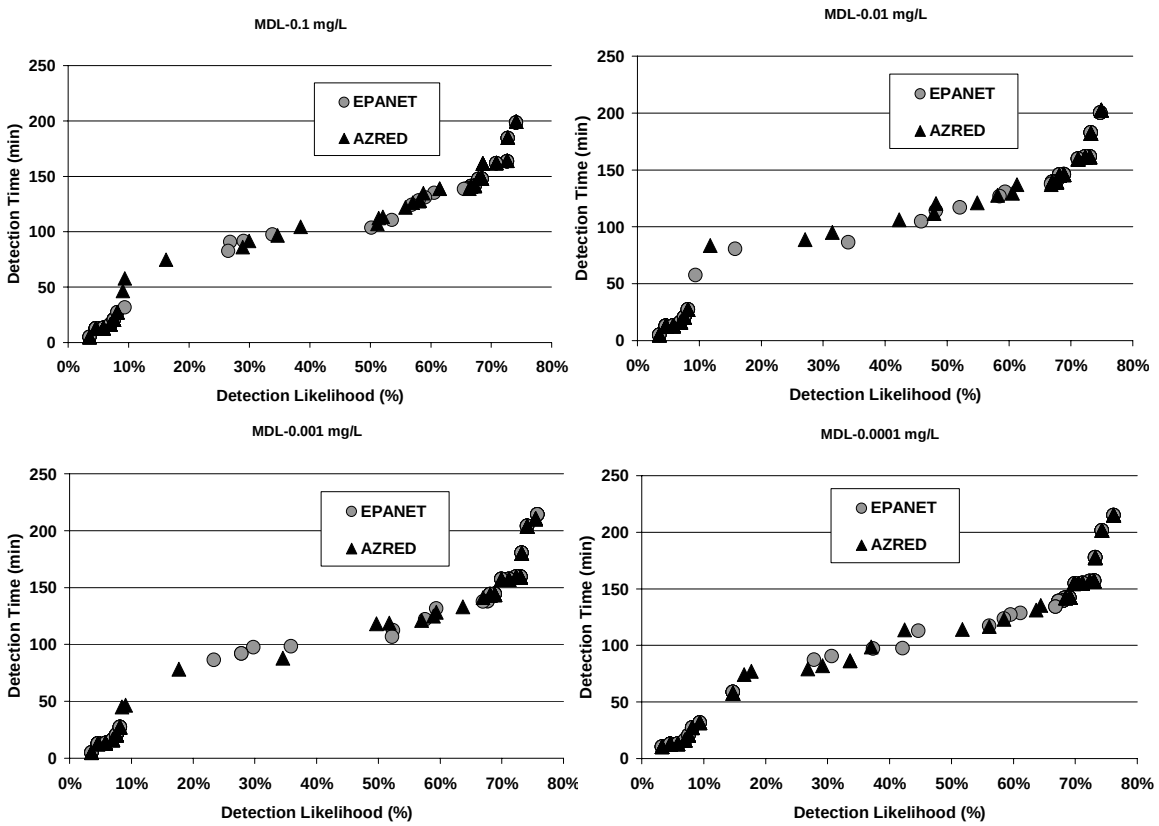

Fig. 3. The Pareto fronts for Network 3 showing the relationship between detection likelihood and detection time for alternative MDL. Note the detection limit and water quality model's effects on the Pareto fronts.

The Pareto fronts comparing the detection likelihood and detection time objectives are shown in Fig. 3 with alternative MDLs. First, the objectives are in conflict smaller detection time and larger detection likelihoods are desirable. Next, the differences between the two mixing models are not as significant as they were for the previous objectives. Given the size and layout of this network, detection time is not sensitive to small changes, while the plume spread is somewhat more variable. A more highly looped or larger network with more nodes that cause incomplete mixing may produce more significant differences compared to those of this system and should be examined.

4. CONCLUSION

Optimal locations for sensor placement in a simple network and under both perfect and imperfect mixing conditions were determined using the multiobjective approach of Preis and Ostfeld (2008). For this network, differences between the two results were not significant. When perfect sensors were assumed (or in any case where concentration is not important but simply the presence of a contaminant), the two mixing models provided very similar results. Differences in the sensor placement designs and the objectives increased with higher (more realistic) MDLs. Although the differences were small in this case, more study should be completed to determine if sensor placement designs would be altered under imperfect mixing conditions in larger and more highly looped networks.

5. REFERENCES

Austin, R. G., van Bloemen Waanders, B., McKenna, S., and Choi, C. Y. (2008). "Mixing at cross junctions in water distribution systems. II: Experimental study." *J. Water Resour. Plann. Manage.*, 134(3), 295-302.

AZRED, Available online at http://cals.arizona.edu/~cchoi/AZRED

Choi, C.Y., Song, I., and Romero-Gomez, P. (2008a). "Solute Transport in a Pressurized Pipe Network with Multiple Cross Junctions." *Journal of Hydraulic Engineering*, submitted.

Choi, C.Y., Shen, J. Y., Austin, R. G. (2008b). "Development of a comprehensive solute mixing model (AZRED) for double-tee, cross, and wye junctions." *Proc. 10th Annual Water Distribution System Analysis Symp.*, Kruger Park, South Africa.

Deb K., Pratap A., Agarwal S., and Meyarivan T. (2002). "A fast and elitist multiobjective genetic algorithm: NSGA-II." *IEEE Transactions on Evolutionary Computation*, Vol. 6, No. 2, pp. 182-197.

Lee, B.H. and Deininger R.A. (1992). "Optimal locations of monitoring stations in water distribution system." *Journal of Environmental Engineering*, 118(1), 4-16.

Ostfeld, A., and Salomons, E. (2004). "Optimal layout of early warning detection stations for water distribution systems security." *J. Water Resour. Plann. Manage.*, 130(5), 377-385.

Preis, A., and Ostfeld, A. (2008). "Multiobjective contaminant sensor network design for water distribution systems." *Engineering Optimization*, in press.

Romero-Gomez, P., Ho, C.K., and Choi, C.Y. (2008a). "Mixing at cross junctions in water distribution systems. I: Numerical study." *J. Water Resour. Plann. Manage.*, 134(3), 285-294.

Romero-Gomez, P., Choi, C.Y., Lansey, K., Preis, A., and Ostfeld, A. (2008b). "Sensor Network Design with Improved Water Quality Models at Cross Junctions." *Proc. 10th Annual Water Distribution System Analysis Symp.*, Kruger Park, South Africa.

van Bloemen Waanders, B., Hammond, G., Shadid, J., Collis, S., and Murray, R. (2005). "A comparison of Navier-Stokes and network models to predict chemical transport in municipal water distribution systems." *Proc., World Water and Environmental Resources Congress*, Anchorage, Alaska.

ACKNOWLEDGMENTS

This study was supported by the Center for Advancing Microbial Risk Assessment (CAMRA) funded by the U. S. Environmental Protection Agency Science to Achieve Results and the U. S. Department of Homeland Security University Programs grant number R3236201.

Robust Sensor Placement for Detecting Adversarial Contaminations in Water Distribution Systems

Andreas Krause* Carlos Guestrin†

Abstract

Drinking water distribution systems (WDS) are complex and dynamic systems. The intentional introduction of a contaminant could theoretically be detected by a network of sensors placed at nodes in the system. Optimizing the placement of these hypothetical sensors for metropolitan area size WDS is an important research challenge. Recently, the Battle of the Water Sensor Networks led to the development of several promising techniques for deploying sensors in large, complex networks. However, this challenge focused on designing sensor networks that detect random, accidental contaminations well. In order to guard WDSs against malicious attacks, sensor network detection performance has to be optimized with respect to the worst possible contamination. We recently developed a new algorithm, SATURATE, that can efficiently solve large robust sensor placement problems. The obtained solutions are provably close to optimal. Our algorithm can handle imprecise sensors that can fail. Our method can also be used to obtain placements that simultaneously perform well both for malicious (i.e., worst-case) contaminations, as well as accidental (i.e., average-case) contaminations. We report results from applying our method to a large hypothetical distribution system with more than 12,000 nodes.

1 INTRODUCTION

Drinking water distribution systems (WDS) are complex and dynamic systems. The intentional introduction of a contaminant disrupts the system and could theoretically be detected by a network of sensors placed at nodes (pipe junctures or households) in the system. Optimizing the placement of these hypothetical sensors for metropolitan area size WDS is an important research challenge. Because the system has many nodes and multiple states, the number of possible contamination events is significant, and the

*Computer Science, Division of Engineering and Applied Science, California Institute of Technology, Pasadena, CA, USA; Email: krausea@caltech.edu

†Computer Science Dept. and Machine Learning Dept., School of Computer Science, Carnegie Mellon University, Pittsburgh, PA, USA; Email: guestrin@cs.cmu.edu

likely number of costly sensors available for deployment is low, the optimal placement of these sensors to minimize the effect of the introduced contaminant on the population is a critical issue.

Recently, the Battle of the Water Sensor Networks [Ostfeld et al., 2008] led to the development of several promising techniques for deploying sensors in large, complex networks with more than 12,000 junctions. However, this challenge focused on designing sensor networks that detect random, accidental contaminations well. In order to guard WDSs against malicious attacks, sensor network detection performance has to be optimized with respect to the worst possible contamination. Existing exact techniques for optimal robust sensor placement are difficult to scale to WDS of metropolitan area size, and so heuristic search procedures, which do not have any guarantees about the quality of the obtained solutions are used. Thus, the resulting sensor placements can potentially perform arbitrarily badly when compared to the optimal solution.

We recently developed a new algorithm, SATURATE, that can efficiently solve large robust sensor placement problems [Krause et al., 2008b]. The obtained solutions are provably close to optimal. Our algorithm can handle imprecise sensors that can fail. Our method can also be used to obtain placements that simultaneously perform well both for malicious (i.e., worst-case) contaminations, as well as accidental (i.e., average-case) contaminations.

We apply our method to a large hypothetical distribution system with more than 12,000 nodes. Optimization was based on multiple criteria including (1) minimizing the time to detection and (2) minimizing population effected prior to detection.

Our results show significant improvement over existing techniques, such as state-of-the-art Simulated Annealing algorithms. Furthermore, they indicate that sensor placements that detect average contaminations well can exhibit very poor detection performance on worst-case contaminations. Using our algorithm, we obtain placements that perform nearly as well in the average case, but significantly better in the worst-case. Further, our optimization algorithm has applications for robust placement of sensors in other complex, dynamic systems, as well as robust experimental design.

2 PROBLEM STATEMENT

Following our approach described by Krause et al. [2008b,a] we model the WDS as a graph $\mathcal{G} = (\mathcal{V}, \mathcal{E})$, where the nodes $\mathcal{V}$ represent the junctions and the edges $\mathcal{E}$ represent the pipes connecting the junctions. In order to model contamination spreading dynamically over this network, we consider a set of *intrusion scenarios* $\mathcal{I}$; each scenario $i \in \mathcal{I}$ models the spreading of contamination starting from a given node $s \in \mathcal{V}$ in the network. By placing sensors at a set of junctions $\mathcal{A} \subseteq \mathcal{V}$, we can detect such a contamination, and thereby minimize the adverse effects on the network.

More specifically, for each possible contamination scenario $i \in \mathcal{I}$ and for each node $v \in \mathcal{V}$ we define the detection time $T_i(v)$ as the time when the contamination affects node v (and $T_i(v) = \infty$ if node v is never affected). We furthermore define a penalty function $\pi_i(t)$ which models the penalty incurred for detecting contamination i at time

t. We require $\pi_i(t)$ to be monotonically non-decreasing in t (i.e., we never prefer late over early detection), and bounded above by $\pi_i(\infty) \in \mathbb{R}$. We extend π_i to observation sets $\mathcal{A}$ as $\pi_i(\mathcal{A}) = \pi_i\left(\min_{s\in\mathcal{A}} T_i(s)\right)$. Equivalently, we can define the *penalty reduction* $F_i(\mathcal{A}) = \pi_i(\infty) - \pi_i(\mathcal{A})$. Krause et al. [2008a] show how realistic objective functions employed in the Battle of the Water Sensor Networks [Ostfeld et al., 2008], such as the reduction in time to detection (Z_1), population affected (Z_2), contaminated water consumed (Z_3) and improvement in detection likelihood (Z_4) can be modeled by appropriate choice of the penalty function π_i.

In the BWSN challenge, a probability distribution over the contamination events is specified, assigning each contamination event $i \in \mathcal{I}$ a probability $p(i)$. The goal is then to place a set of k sensors maximizing the *expected penalty reduction*,

$$\max_{|\mathcal{A}|\leq k} \frac{1}{|\mathcal{I}|} \sum_{i\in\mathcal{I}} p(i) F_i(\mathcal{A}). \tag{2.1}$$

Assuming a probability distribution over contamination events can be appropriate if the goal is to place sensors that effectively detect accidental, random contaminations. However, in order to protect a WDS against an adversary that contaminates the network knowing the sensor locations, it is more appropriate to optimize considering the *worst possible* contamination event. Krause et al. [2008a] show that this can be achieved by optimizing

$$\max_{|\mathcal{A}|\leq k} \min_{i\in\mathcal{I}} F_i(\mathcal{A}). \tag{2.2}$$

3 OPTIMIZATION APPROACH

One can show that the optimization problems (2.1) and (2.2) are computationally complex (NP-hard), such that we cannot expect to find the optimal solution in reasonable time. In this section, we will discuss algorithms, originally proposed by Krause et al. [2008a] and Krause et al. [2008b] that efficiently find provably near-optimal solutions to these problems.

3.1 Placing sensors to detect accidental contaminations

A natural approach to finding approximate solutions is the *greedy algorithm*: This algorithm starts with the empty placement, $\mathcal{A} = \emptyset$, and proceeds iteratively. At the j-th round, it will select the sensor

$$s = \operatorname*{argmax}_{s\in\mathcal{I}} F_{ac}(\mathcal{A} \cup \{s\}),$$

i.e., the sensor which will decrease the expected penalty the most, and adds it to the current set $\mathcal{A} \leftarrow \mathcal{A} \cup \{s\}$. Hereby,

$$F_{ac}(\mathcal{A}) = \frac{1}{|\mathcal{I}|} \sum_{i\in\mathcal{I}} p(i) F_i(\mathcal{A})$$

is the *expected* penalty reduction achieved when placing sensors at locations $\mathcal{A}$. The algorithm stops after k nodes have been selected. Krause et al. [2008a] show that this algorithm performs *near-optimally*: The greedy algorithm will always pick a set $\mathcal{A}$ such that $F_{ac}(\mathcal{A}) \geq (1 - 1/e)F_{ac}(\mathcal{A}^*)$, where $\mathcal{A}^*$ is the optimal placement of k sensors.

The key insight to the analysis of Krause et al. [2008a] is that the penalty reduction satisfies *submodularity*, a diminishing returns property formalizing the intuition that adding another sensor helps more if we have placed few sensors so far, and less if we already have placed many sensors. A fundamental result by Nemhauser et al. [1978] then proves the near-optimal performance of the greedy algorithm.

3.2 Placing sensors to detect adversarial contamination

While the average case objective F_{ac} is submodular, and hence the greedy algorithm provides near-optimal sensor placements, the same does not hold for the *worst case* penalty reduction

$$F_{wc}(\mathcal{A}) = \min_{i \in \mathcal{I}} F_i(\mathcal{A}).$$

In fact, Krause et al. [2008b] show both experimentally and theoretically that the greedy algorithm performs arbitrarily poorly in this setting. Krause et al. [2008b] develop an efficient algorithm, SATURATE, that provides near-optimal solutions for this problem. While we cannot give a detailed description and analysis of the algorithm here due to space limitations, we will present a high level overview. Suppose we would like to find a set of k nodes to place sensors, maximizing the worst-case performance. The SATURATE algorithm proceeds in the following steps. It maintains a search interval $[c_{min}, c_{max}]$ which is reduced in every iteration. Initially, $c_{min} = 0$, and $c_{max} = \min_{i \in \mathcal{I}} F_i(\mathcal{V})$.

1. SATURATE sets $c = (c_{min} + c_{max})/2$. If $c_{max} - c_{min} < \varepsilon$, the algorithm stops and returns the best candidate solution found so far.

2. It applies the greedy algorithm to the *average truncated* objective $\widehat{F}_c(\mathcal{A}) = \frac{1}{|\mathcal{I}|} \sum_{i \in \mathcal{I}} \min\{c, F_i(\mathcal{A})\}$. This algorithm will return a set $\mathcal{A}_c$, such that $|\mathcal{A}_c| \geq k$.

3. If $\widehat{F}_c(\mathcal{A}_c) = c$, then SATURATE considers $\mathcal{A}_c$ a candidate solution, and repeats step 1 with $c_{min} = c$. If $\widehat{F}_c(\mathcal{A}_c) < c$, then it repeats step 1 with $c_{max} = c$.

Hereby, ε is a tolerance parameter that can be chosen arbitrarily small. Krause et al. [2008b] prove that after the algorithm converges, the solution returned is near-optimal, in a strong complexity-theoretic sense, i.e., under widely accepted complexity theoretic assumptions, there cannot exist an efficient algorithm that provides better guarantees about the solution quality in general.

3.3 Trading off average-case and worst-case performance

In some applications, optimizing the worst-case performance $F_{wc}(\mathcal{A}) = \min_i F_i(\mathcal{A})$ might be a too pessimistic approach. On the other hand, ignoring the worst-case and

only optimizing the average-case (the expected performance under a distribution over the objectives) $F_{ac}(\mathcal{A}) = \frac{1}{m}\sum_i F_i(\mathcal{A})$ might make too strong assumptions, and hence be too optimistic. In general, we might be interested in solutions, which perform well both in the average and worst case.

Krause et al. [2008b] describe a multicriterion optimization problem, where we intend to optimize the *vector* $[F_{ac}(\mathcal{A}), F_{wc}(\mathcal{A})]$. In this setting, we can only hope for *Pareto-optimal* solutions [Boyd and Vandenberghe, 2004]. A set $\mathcal{A}^*$, $|\mathcal{A}^*| \leq k$ is called *Pareto-optimal*, if it is not *dominated*, i.e., there does not exist another set $\mathcal{B}$, $|\mathcal{B}| \leq k$ with $F_{ac}(\mathcal{B}) > F_{ac}(\mathcal{A}^*)$ and $F_{wc}(\mathcal{B}) \geq F_{wc}(\mathcal{A}^*)$ (or $F_{ac}(\mathcal{B}) \geq F_{ac}(\mathcal{A}^*)$ and $F_{wc}(\mathcal{B}) > F_{wc}(\mathcal{A}^*)$).

One possible approach to find such Pareto-optimal solutions is constrained optimization: for a specified value of c_{ac}, we desire a solution to

$$\mathcal{A}^* = \operatorname*{argmax}_{|\mathcal{A}|\leq k} F_{wc}(\mathcal{A}) \text{ such that } F_{ac}(\mathcal{A}) \geq c_{ac}. \tag{3.1}$$

By specifying different values of c_{ac} in (3.1), we would obtain different Pareto-optimal solutions. Krause et al. [2008b] show how SATURATE can be modified to near-optimally solve Problem (3.1). In Section 4 we show how this modified algorithm can be used to find sensor placements in WDS that perform near-optimally *both* in the average-case and in the worst-case.

4 EXPERIMENTAL RESULTS

Experimental setup. In August 2006, the Battle of Water Sensor Networks (BWSN) [Ostfeld et al., 2008] was organized as an international challenge to find the best sensor placements for a realistic metropolitan water distribution network, consisting of 12,527 nodes. In this challenge, a set of intrusion scenarios is specified, and each scenario is simulated using EPANET 2.0 [Rossman, 1999] is used to simulate the spread of the contaminant for a 48 hour period. An intrusion is considered detected when one selected node shows positive contaminant concentration [1]. BWSN considered a variety of impact measures, including the time to detection (called Z_1), and the size of the affected population calculated using a realistic disease model (Z_2). The goal of BWSN was to minimize the *expectation* of the impact measures Z_1 and Z_2 given a *uniform distribution* over intrusion scenarios. In our experiments, which are described in more detail by Krause et al. [2008b], we consider scenarios that affect at least 10% of the network, resulting in a total of 3424 scenarios.

Comparison of SATURATE with other algorithms. Figures 1(a) and 1(b) compare the greedy algorithm, SATURATE and a highly fine-tuned simulated annealing (SA) algorithm for the problem of minimizing the worst-case detection time (Z_1) and worst-case affected population (Z_2). The figures show the achieved worst-case penalty reductions achieved by placing an increasing number of sensors using the three algorithms.

[1] As discussed by Krause et al. [2008a], "noisy detection" can be taken into account as well.

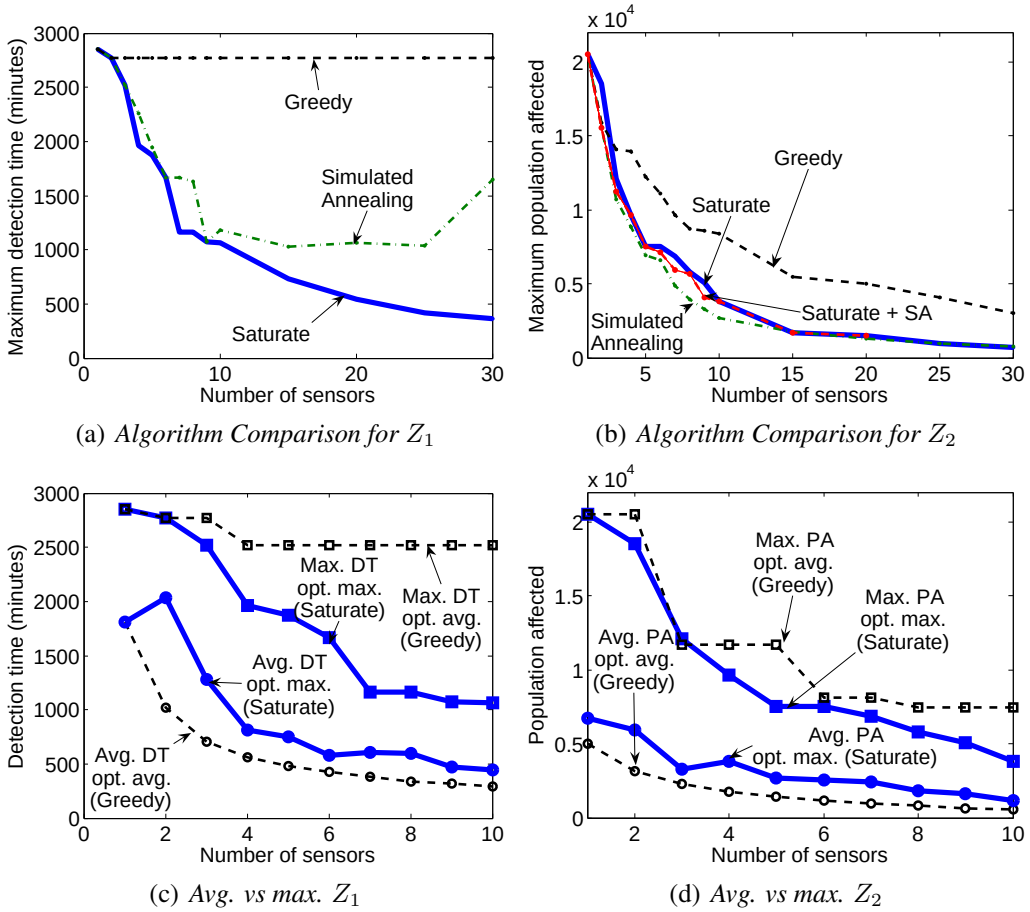

(a) *Algorithm Comparison for* Z_1 (b) *Algorithm Comparison for* Z_2

(c) *Avg. vs max.* Z_1 (d) *Avg. vs max.* Z_2

Figure 1: (a,b) compare SATURATE, greedy and Simulated Annealing (SA), when optimizing worst-case detection time (Z_1, (a)) and affected population (Z_2, (b)). SATURATE performs comparably to SA for Z_2 and strictly outperforms SA for Z_1. (c,d) compare optimizing for the worst-case vs. average-case objectives. Optimizing for the worst-case leads to good average case performs, but not vice versa.

Interestingly, the behavior is very different for the two objectives. For the affected population (Z_2), the greedy algorithm provides acceptable performance, and SA sometimes even outperforms SATURATE. For the detection time (Z_1), however, the greedy algorithm did not improve the objective at all, and SA performs poorly. The reason is that for Z_2, the maximum achievable penalty reduction, $F_i(\mathcal{V})$, vary drastically, since some scenarios have much higher impact than others. Hence, there is a strong "gradient", as the worst-case objective changes quickly when the high impact scenarios are covered. This gradient allows greedy and SA to work well. On other hand, for Z_1, the maximum achievable penalty reductions, $F_i(\mathcal{V})$, are constant, since all scenarios have the same simulation duration. Unless *all* scenarios are detected, the worst-case detection time stays constant at the simulation length. Hence, many node exchange proposals (i.e., steps in the local search) considered by SA, as well as the addition of a new sensor location by greedy, do not change the worst-case objective, and the algorithms have no useful performance metric.

Figures 1(c) and 1(d) compare the placements of SATURATE (when optimizing the

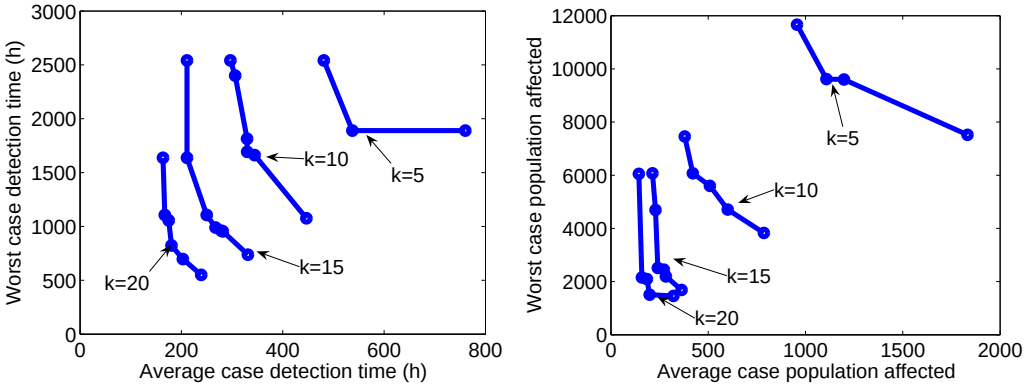

(a) *Pareto curve for* Z_1 (b) *Pareto curve for* Z_2

Figure 2: Experiments on trading off worst-case and average-case penalties minimizing detection time (a) and affected population (b).

worst-case penalty), and greedy (when optimizing the average-case penalty, which is submodular). Optimizing the worst-case performance leads to reasonable performance in the average case performance, but not necessarily vice versa (especially when considering the detection time).

Trading off worst-case and average-case performance. We also performed experiments trading off the worst-case and average-case penalty reductions, using the approach discussed in Section 3.3. We first ran the greedy algorithm to optimize the average-case performance, and then ran SATURATE to optimize the worst-case performance. We considered the average-case performances c_{ac}^{greedy} and $c_{ac}^{Saturate}$ obtained by both algorithms, and uniformly discretized the interval bounded by these average-case performances. For each performance level c_{ac} in the discretization, we use the modified SATURATE algorithm as described in Section 3.3, maximizing the worst-case performance, subject to a constraint on the average-case performance. Each possible value of the constraint on c_{ac} can lead to a different solution, trading off average- and worst-case performances. Figure 2(a) presents the tradeoff curve obtained in this fashion for the detection time (Z_1) metric, for different numbers k of placed sensors. We generally observe that there is more variability in the worst-case performance than in the average-case performance. We can also see that when placing 5 sensors, there is a prominent knee in the tradeoff curve, effectively achieving the minimum worst-case penalty but drastically reducing the average-case penalty incurred when compared to only optimizing for the worst-case performance. The other tradeoff curves do not exhibit quite such prominent knees, but nevertheless allow flexibility in trading off worst- and average-case performances. Figure 2(b) presents the same experiment for the population affected (Z_2) metric. Here, we notice prominent knees when placing $k = 15$ and 20 sensors. We can generally conclude that trading off average- and worst-case performances allows to effectively achieve a compromise between too pessimistic (only optimizing for the worst case) and optimistic (only optimizing for the average case) objectives.

5 RELATED WORK

Carr et al. [2006] consider the problem of robust sensor placements in water distribution networks. They formulate Mixed Integer Programs for selecting sensor placements robust against uncertainty in adversarial strategies and in water demands. Due to computational complexity of Mixed Integer Programming, in their experiments, they used only small networks of at most 470 nodes. SATURATE can potentially be applied to handle uncertainty in demands as well, which is an interesting direction for future work. Watson et al. [2006] consider different notions of robustness in the context of water distribution networks, intended to remove some of the pessimistic assumptions of purely robust sensor placements. They develop integer programs, as well as heuristics, and apply them to networks of similar size as the one considered in this paper. Their local search heuristic performs a sequence of local moves similar to those performed by the simulated annealing algorithm considered in Section 4, and does not provide any theoretical guarantees.

Closely related to the problem of robust sensor placement for contamination detection is the k-*center* problem. In this problem, one is given a graph $\mathcal{G} = (\mathcal{V}, \mathcal{E})$ along with a distance function defined over pairs of nodes in $\mathcal{V}$. The goal is to select a subset $\mathcal{A} \subseteq \mathcal{V}$ of size at most k, such that the maximum distance between any unselected node $s \in \mathcal{V} \setminus \mathcal{A}$ and its nearest center $s' \in \mathcal{A}$ is minimized. For this problem, Minieka [1970] discuss a technique reducing the solution of this problem to a sequence of set cover problems combined in a binary search, similar in spirit to SATURATE. However, they do not discuss any implications regarding approximation guarantees, and do not consider the case of arbitrary submodular functions. Mladenovic et al. [2003] presents a Tabu search heuristic for k-center, also without theoretical guarantees. Gonzalez [1985] and Hochbaum and Shmoys [1985] present a 2 approximation for the k-center problem in the case of symmetric distance functions satisfying the triangle inequality. Panigrahy and Vishwanathan [1998] present a $\log^*(n)$ approximation in the case of distance functions satisfying the asymmetric triangle inequality, which is shown to be best possible by Chuzhoy et al. [2005].

Anthony et al. [2008] consider robust and stochastic notions of facility location problems (such as k-center and k-median, where, instead of the maximum distance the average distance is optimized). In contrast to the robust problems in this paper that require to select k elements to *maximize* the minimum value achieved by these k elements over the m scenarios, the problems described by Anthony et al. [2008] require to select k "centers" in a metric space to *minimize* the maximum cost incurred over the m scenarios—where the cost is some function of the distances between non-selected vertices to the selected centers. For several such robust cost-minimization problems in cases where distances satisfy the symmetric triangle inequality, they present an algorithm that opens k "centers" and achieves an approximation ratio of $\mathcal{O}(\log n + \log m)$ (where n is the number of nodes in the graph, and m is the number of scenarios).

6 CONCLUSIONS

In this paper, we presented our recent results [Krause et al., 2008a,b] addressing the problem of optimizing the placement of sensors for detecting contamination in metropolitan area size WDS. We considered both the problem of placing sensors that detect random, accidental contaminations well (as modeled in the Battle of the Water Sensor Networks challenge), and the problem of guarding WDSs against malicious attacks, where sensor network detection performance has to be optimized with respect to the worst possible contamination. We described an algorithm, SATURATE [Krause et al., 2008b], that can efficiently solve large robust sensor placement problems. The obtained solutions are provably close to optimal. Our algorithm can handle imprecise sensors that can fail. Our method can also be used to obtain placements that simultaneously perform well both for malicious (i.e., worst-case) contaminations, as well as accidental (i.e., average-case) contaminations. We reported results from applying our method to a large hypothetical distribution system with more than 12,000 nodes. Our results show significant improvement over existing techniques, such as state-of-the-art Simulated Annealing algorithms.

References

B. M. Anthony, V. Goyal, A. Gupta, and V. Nagarajan. A plant location guide for the unsure. In *Submitted to SODA*, 2008.

S. Boyd and L. Vandenberghe. *Convex Optimization*. Cambridge UP, Mar. 2004.

R. D. Carr, H. J. Greenberg, W. E. Hart, G. Konjevod, E. Lauer, H. Lin, T. Morrison, and C. A. Phillips. Robust optimization of contaminant sensor placement for community water systems. *Mathematical Programming Series B*, 107:337–356, 2006.

J. Chuzhoy, S. Guha, E. Halperin, S. Khanna, G. Kortsarz, R. Krauthgamer, and J. Naor. Asymmetric k-center is $\log^* n$-hard to approximate. *Journal of the ACM*, 52(4):538–551, 2005.

T. F. Gonzalez. Clustering to minimize the maximum intercluster distance. *Theoret. Comput. Sci.*, 38(2-3):293–306, 1985. ISSN 0304-3975.

D. Hochbaum and D. Shmoys. A best possible heuristic for the k-center problem. *Mathematics of Operations Research*, 10(2):180–184, 1985.

A. Krause, J. Leskovec, C. Guestrin, J. VanBriesen, and C. Faloutsos. Efficient sensor placement optimization for securing large water distribution networks. *Journal of Water Resources Planning and Management*, 136(6), 2008a.

A. Krause, B. McMahan, C. Guestrin, and A. Gupta. Robust submodular observation selection. *Journal of Machine Learning Research*, 9:2761–2801, December 2008b.

E. Minieka. The m-center problem. *SIAM Rev*, 12(1):138–139, 1970.

N. Mladenovic, M. Labbé, and P. Hansen. Solving the p-center problem with tabu search and variable neighborhood search. *Networks*, 42(1):48–64, 2003.

G. Nemhauser, L. Wolsey, and M. Fisher. An analysis of the approximations for maximizing submodular set functions. *Mathematical Programming*, 14:265–294, 1978.

A. Ostfeld, J. G. Uber, E. Salomons, J. W. Berry, W. E. Hart, C. A. Phillips, J.-P. Watson, G. Dorini, P. Jonkergouw, Z. Kapelan, F. di Pierro, S.-T. Khu, D. Savic, D. Eliades, M. Polycarpou, S. R. Ghimire, B. D. Barkdoll, R. Gueli, J. J. Huang, E. A. McBean, W. James, A. Krause, J. Leskovec, S. Isovitsch, Jianhua, C. Guestrin, J. VanBriesen, M. Small, P. Fischbeck, A. Preis, M. Propato, O. Piller, G. B. Trachtman, Z. Y. Wu, and T. Walski. The battle of the water sensor networks (BWSN): A design challenge for engineers and algorithms. *To appear in the Journal of Water Resources Planning and Management*, 2008.

R. Panigrahy and S. Vishwanathan. An $\mathcal{O}(\log^* n)$ approximation algorithm for the asymmetric p-center problem. *Journal of Algorithms*, 27(2):259–268, 1998.

L. A. Rossman. The epanet programmer's toolkit for analysis of water distribution systems. In *Annual Water Resources Planning and Management Conference*, 1999.

J. Watson, W. E. Hart, and R. Murray. Formulation and optimization of robust sensor placement problems for contaminant warning systems. In *Water Distribution System Symposium*, 2006.

SENSOR NETWORK DESIGN AND PERFORMANCE IN WATER SYSTEMS DOMINATED BY MULTI-STORY BUILDINGS

Robert Janke[1], Terra Baranowski Haxton[1], Walter Grayman[2], Rakesh Bahadur[3], Regan Murray[1], William Samuels[3], and Tom Taxon[4]

[1]National Homeland Security Research Center
United States Environmental Protection Agency
26. W. Martin Luther King Drive (MS 163), Cincinnati, OH 45268

[2]Walter Grayman Consulting, 321 Ritchie Avenue, Cincinnati Ohio 45215-2038.

[3]Science Applications International Corporation, 1710 SAIC Dr. McLean, VA 22102

[4]Argonne National Laboratory, 9700 South Cass Avenue, Argonne, IL 60439-4832

ABSTRACT

Understanding the potential health impacts that can occur from contamination events in drinking water distribution systems has been the subject of much research in recent years. Both the characterization of these impacts on distribution systems and the design of contamination warning system (CWS) sensor networks rely on models that vary widely in detail and representation of the actual system. A complete representation of the distribution system for even a medium-sized city can be enormously complex. Macro skeletonization is used to describe the aggregation of the network's nodes and pipes. Micro skeletonization is used to describe the aggregation of all post-service connection piping and system detail to the model node.

Models typically do not include information (pipe detail) beyond the service connection. In water systems dominated by multi-story buildings, such as commercial and residential high-rise buildings, considerable infrastructure (pipes, pumps, and tanks) are absent from the model. Previous work has evaluated the effects that varying levels of macro skeletonization have on the performance of sensor network monitoring designs. However, research investigating the impact to sensor network design performance due to the lack of post service connection piping and system detail is lacking.

This paper reports on the modeling of CWS sensor network designs for two real water systems. The first system is small and simple and the model has been artificially modified to include multi-story buildings. The second water system is actually dominated by multi-story buildings but its base model does not contain any micro-level detail. Geographical information system (GIS) tools and site-specific information are used to construct and arrange reasonable representations of the high rise buildings into the model. For each water system, EPANET simulations are performed along with public health impacts assessments and sensor network design optimizations. Evaluations are made between the skeletonized models (base models without post-service connection detail) and the multi-story building-enhanced models to assess the performance of sensor networks to reduce public health impacts.

1. INTRODUCTION

The intentional or unintentional contamination of a water distribution system can cause significant problems, including public health and economic impacts. Understanding the potential impacts which can occur from contamination events in drinking water distribution systems has been the subject of much research in recent years. For example, Nilsson et al. (2005) and Khanal et al. (2006) examined exposures of small water distribution system networks to contamination events. Murray et al. (2006) developed a model for the spatial and temporal distribution of health impacts in a distribution system. Davis and Janke developed a probabilistic model for the timing of tap water ingestion and illustrated the importance of the exposure model in estimating impacts when a water distribution system is contaminated (Davis and Janke, 2008a and Davis and Janke, 2008b).

Recent research has also focused on the development and application of optimization algorithms to determine where best to place sensor monitoring stations as a principal component of contamination warning systems (CWS) (Berry et al. 2006, Skadsen et al. 2008, Murray et al. 2008). CWS monitor water quality in order to detect intentional or unintentional contamination events.

Grayman and Buchberger (2006) developed an exposure model to estimate human exposures from water contamination events at the building fixture level based on the contaminated water traveling from the service connection and through a residential building. This work provided a conceptual approach for using EPANET to calculate public health exposures to contaminants in the tap water delivered at the fixture level. Later work by Grayman et al. (2008) discusses the potential vulnerability of large venue buildings in New York City by constructing example high-rise buildings to study building occupant exposure patterns. From this work, it was demonstrated how models of high-rise buildings can be constructed to study contamination events that originate from the distribution system supplying the building or from within the building. The study found that contaminant transport in residential buildings was sensitive to detailed fixture level water usage patterns defined by the occupants of the residence. The study also found that for high-rise buildings, contaminant transport into the building from the distribution system was primarily sensitive to the operational conditions of the building's water system, i.e., the timing of pump operation that fill internal tanks within the building.

The accurate prediction of potential impacts from water contamination events and the design of a CWS rely on calibrated hydraulic and water quality models. Distribution system models vary widely in detail and representation of the actual system (Walski et al. 2003). Complete model representations of the distribution system, especially for a large or even medium-sized city, can be enormously complex and difficult to run with available software tools. "S*keletonization"* is known as the process used to select the most significant attributes of the hydraulic network that can collectively still represent the overall behavior of the system (Walski et al. 2003). The level of detail in distribution system models can be described by the number of junctions in the model to the number of customer service connections representing the population served. Ratios of nodes to

service connections in the range of 1 to 5 characterize the most detailed distribution system models. If macro-skeletonization is used to describe the aggregation of the network's nodes and pipes, micro-skeletonization could be used to describe the aggregation of post-service connection piping and system detail to the model node.

Models typically do not include information, i.e., pipe detail, beyond the service connection. For water systems dominated by multi-story buildings, e.g., commercial and residential high-rise buildings, considerable infrastructure (pipes, pumps, and tanks) are absent from the model. Previous work has evaluated the effects that varying levels of macro-skeletonization have on the performance of sensor network monitoring designs; however, research is limited on the impact to sensor network design performance due to the lack of post-service connection piping and system detail (Janke et al. 2007).

This paper investigates the role that complex post-service connection plumbing plays on the estimation of public health impacts from contamination events and the effect that such complexity has on the performance of sensor networks supporting a CWS. The outcomes or performance of the sensor network designs are expressed in terms of potential public health impacts given appropriate intervention on the basis of implementation of a CWS.

The methodology used is provided in Section 2. This includes a description of the network models and the artificial enhancements implemented to include post-service connection detail, a brief overview of the exposure and health impacts assessment approach used, and the modeling and simulation approach used to estimate public health impacts and to design sensor monitoring networks. In terms of notation, impacts refer to the number of people sickened. Sensor design refers to the optimal locations to place sensors to provide useful information to minimize public health exposures.

2. METHODOLOGY

2.1 Model Development

Two real network models were used in the study, Network A and Network B. Their corresponding enhanced, multi-story representations are called Network A-MS and Network B-MS, respectively. Each base model represents a portion of an actual water distribution system. Table 1 provides a description of Network A, A-MS, and B-MS water system models. Data on the base Network B is not provided in order to not reveal the water system.

Table 1. Description of Networks A, A-MS, and B-MS water system models.

Network	Junctions	Reservoirs/Wells	Tanks	Pipes	Pumps	Valves
A	407	1	2	448	3	9
A-MS	959	1	186	1,000	187	9
B-MS	7,692	13	1,107	9,565	1,108	152

Networks A and A-MS represent a relatively small distribution system serving approximately 6,400 people. Figures 1 and 2 show Network A and Network A-MS, respectively. A commercial high-rise and a residential high-rise building were added to most demand nodes in Network A to create its analog network, A-MS. There were approximately 10 non-zero demand nodes which were not enhanced with the multi-story buildings due to network instability. The commercial and residential buildings differed in their demand patterns and the allocation of demand from the central, original model node. Demand from the original, non-zero demand node was randomly allocated to its associated commercial and residential counterparts. The demand patterns for the hypothetical commercial and residential buildings are shown in Figure 3. These demand patterns were developed based on the expert knowledge of the authors. The building representations were constructed in a Microsoft® EXCEL spreadsheet (manually) and then incorporated into EPANET as an input file. Each building representation consisted of three nodes, a pump, and a tank. Included in Figure 2 is an example schematic representation of the commercial and residential high-rise buildings added to the model. Although not easily visible in Figure 2, note that this representative example has been applied to nearly all the demand nodes in the model.

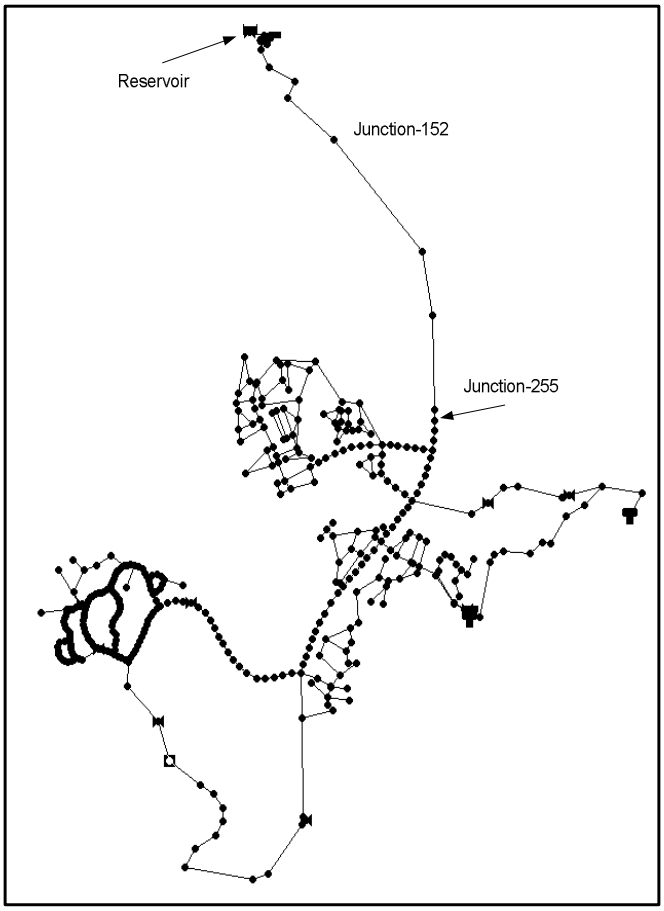

Figure 1. Network A model.

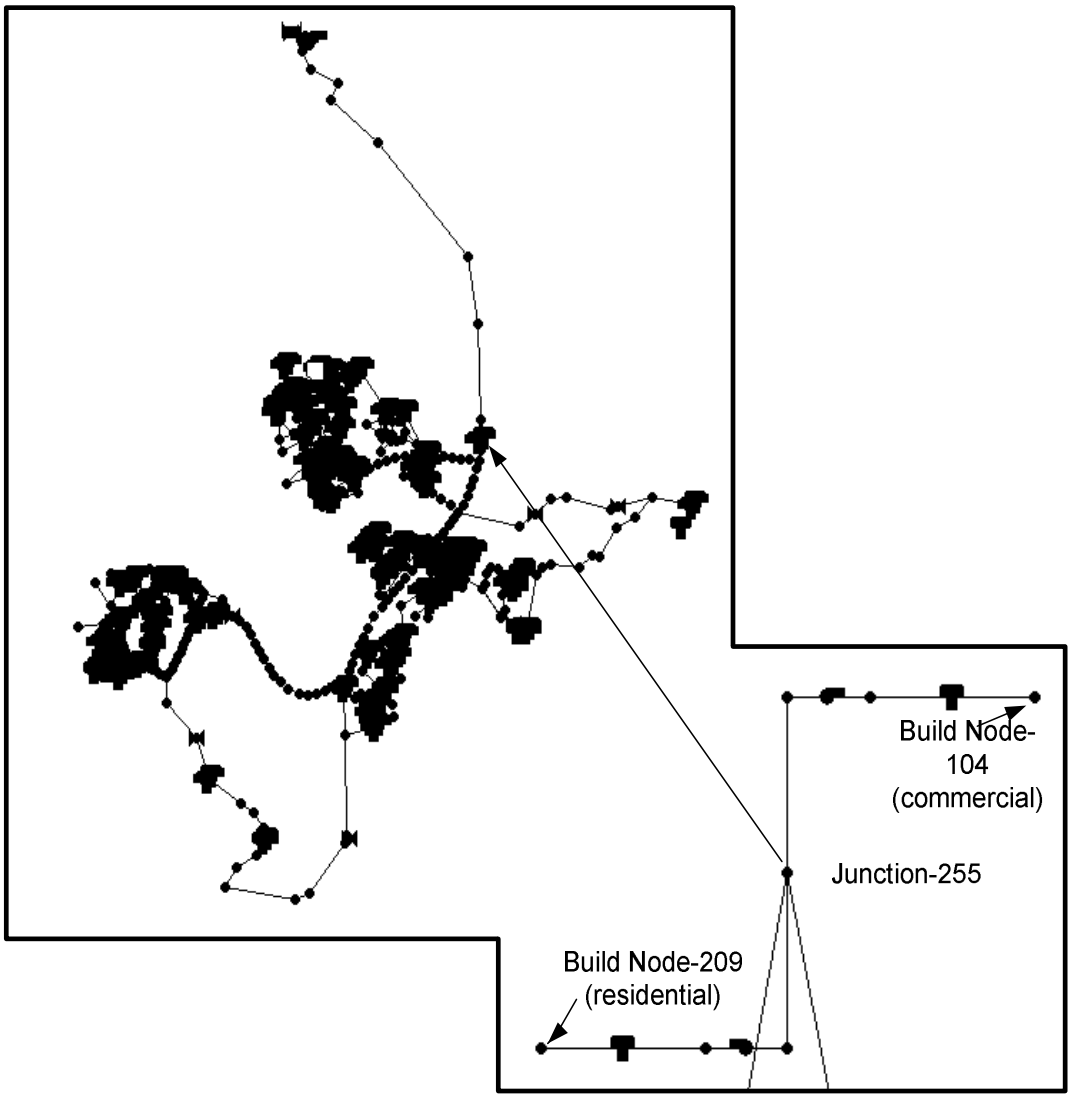

Figure 2. Network A-MS model and representative example of commercial and residential buildings added to nearly all demand nodes in the model.

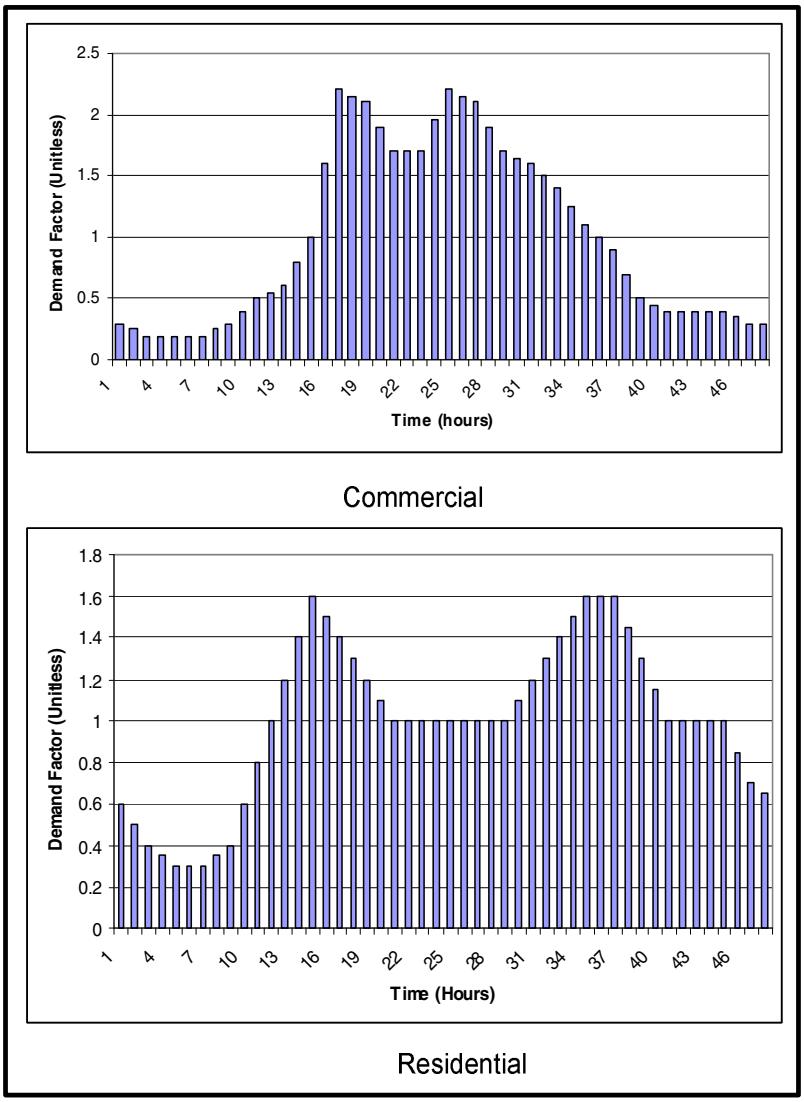

Figure 3: Commercial and residential demand patterns for Network A-MS. Patterns are hypothetical and repeat every 48 hours.

Based on modeling calculations using EPANET, Network A has an average water age of 61 hours and a median age of 59 hours, while Network A-MS has an average water age of 99 hours and median age of 96 hours.

The construction of the high-rise buildings in the Network B-MS model was performed by examining actual water demand data from the utility to determine the number of multi-story buildings to be added to each demand node in the model. Additionally, site-specific geographical information system (GIS) data were used to estimate the number and type of buildings (number of floors) which are served by the distribution system. The Network B model has an average water age of 4 hours and median age of 3 hours; while B-MS has an average water age of 5.3 hours and a median age of 4.5 hours.

Placement of the multi-story buildings in the model was performed manually. In representing the high-rise buildings in the modified model, two types of buildings were added: high-rise and super high-rise buildings. A high-rise building was defined to have an average water use of 20 gallons per minute (gpm); while a super high-rise building was defined to use 60 gpm. Although somewhat arbitrary, these allocations were used to generally reflect the total number of buildings served by the water system, as represented by the base model. When a base model node's demand was less than 20 gpm, no buildings were added to the node. Base nodes were redefined as low-rise buildings. The representations of the two types of high-rise buildings (commercial and residential) added to the model were consistent with Network A-MS. The type of GIS data available and used to determine the number and type (super high-rise, high-rise, low-rise) of buildings added or designated at each demand node in the model consisted, for example, of information on lot size (sq. ft.), building number and area (sq. ft.), and water use billing data. Table 2 illustrates the construction of the super high-rise, high-rise, and low-rise buildings added to each demand node in the B-MS model. Note, for example, Junction-A in Table 2, for this node no super high-rise buildings and only one high-rise building was added to the model. Although approximately 70 gpm remained as the residual demand at the base node, no additional super high-rise or high-rise buildings were added to this node because the total number of buildings added to the model was correlated with the total number and type of buildings present in the actual system.

Table 2. Illustration of how super high-rise, high-rise, and low-rise buildings were allocated using base demand in the Network B-MS model.

Allocation of Demand to Construct Buildings				
Network Nodes & Base Demand		60 gpm	20 gpm	Remaining Residual Demand
Node ID	Base Demand (gpm)	# of Super High-Rise Buildings	# of High-Rise Buildings	Base Node: Low-rise Building (gpm)
Junction-A	110.82	0	2	70.82
Junction-B	163.99	1	1	83.99
Junction-C	6.55	0	0	6.55

2.2 Population Model

Demand-based population models were developed for each network. For Network A, the population was estimated based on a per capita water usage rate of 200 gallons per day, which equated to a network population of approximately 6,400 people. For Network B, the population served represented approximately 600,000 people. The distribution of the 600,000 people across the non-zero demand nodes was performed using a per capita demand rate of 253 gallons per day. The total population of each building-enhanced model was checked to ensure consistency with the base model.

2.3 Contamination Scenario

The following was simulated for each model: (1) the independent injection of a hypothetical contaminant at each of the non-zero demand nodes in the network, (2) transport of the contaminant in the network following injection, and (3) exposure, dose, and dose response to those individuals who ingest the contaminated tap water from the network. A contamination scenario of one hour in duration was evaluated in each model. For example, for the Network A model, 106 independent simulations were run, one for each non-zero demand node. Each of these 106 simulations corresponded to one contamination event resulting from an injection at the particular node of interest. For Network A-MS, the same 106 simulations were run. The same procedure was followed for Networks B and B-MS. For Networks A and A-MS, the contaminant release started at 12:00 AM. For Networks B and B-MS, the contaminant release started at 5:00 AM.

TEVA-SPOT (version 2.1.2) was used to simulate the contamination scenarios in each water distribution system model (EPA, 2009). TEVA-SPOT is a software tool developed to identify and analyze the consequences of intentional contamination introduced into drinking water distribution systems and use the quantitative information gained (termed impacts data) to determine where best to place a limited number of sensors to support a CWS. TEVA-SPOT (version 2.1.2) uses EPANET (Rossman, 2000) (version 2.00.10) as its primary simulation engine.

For each one hour contaminant release scenario, the injection mass was sufficiently large that significant contaminant concentrations and, therefore, exposures were obtained in each network. The same contaminant mass quantity was used for all networks. The contaminant behaves as a conservative constituent following injection.

Public health impacts were determined for ingestion of tap water only. Receptor (a person who ingests contaminated tap water) doses were determined in TEVA-SPOT using the fixed five timing of exposure model, which has been previously described (Davis and Janke, 2008a). The fixed five timing exposure model uses five times for ingestion of water based on results from time-use studies of when ingestion occurs. This timing model is based on the assumption that ingestion occurs in equal amounts at five fixed times, corresponding to three meals and midpoints between meals. Ingestion volume is based on the assumption that all individuals ingest 1 L of tap water per day (EPA, 2000). The resulting dose that a receptor receives of the contaminant is expressed as contaminant mass per unit of body mass (e.g., in units of mg/kg). All exposed individuals are assumed to have the same body mass, i.e., 70 kg, to determine impacts. Probit dose response parameters, e.g., lethal dose to 50% of population and beta slope factor, were input into TEVA-SPOT consistent with the behavior of the assumed contaminant. Public health impacts refer to the number of people sickened. Mean impact results were determined along with the principal percentile scenarios (10th, 25th, 50th, 75th, 90th, and 100th) from the complete ensemble of scenario results.

2.4 Sensor Network Designs

Sensor network designs were developed in TEVA-SPOT (version 2.1.2) using the heuristic algorithm and optimized for mean population exposed (pe-mean) objective. Optimization of average public health impacts means that each contamination release scenario was assumed to be of equal weight and therefore sensor placement was optimized over the average impact of all such releases, i.e., all non-zero demand nodes associated with the base, original model.

Sensor network design set sizes of 2, 5, and 10 sensor locations were selected for Networks A and A-MS. For Networks B and B-MS, additional sensor network design set sizes of 15, 20, 30, 40, and 50 were determined and compared.

Sensors were assumed to behave as perfect sensors and, therefore, able to detect the contaminant at any concentration above zero. TEVA-SPOT offers the capability to specify a contaminant detection limit, i.e., contaminant concentration below which the sensor will not signal the contamination event as well as the ability to specify the probability of sensor failure, but neither of these features was used in these preliminary analyses.

In terms of estimating public health impacts after sensor detection, it was assumed that public health response was instantaneous and, therefore, a zero hour response delay time was used in TEVA-SPOT. Response delay time is defined as the period in time from the initial, uncertain detection of the contaminant, by water quality sensors, to the confirmation of detection and the elimination of further exposures.

Sensor network designs were developed for the base (original) model. Sensor network designs of the same specifications were also created for each enhanced model. The comparison between the original model's sensor network design and the design from its analog was performed in TEVA-SPOT by fixing the optimized, original model's sensor locations into the building-extended model and running TEVA-SPOT. Comparisons of the public health impact results were then made using the percent difference of the original model's design with that of the building-enhanced design. Additionally, each sensor network design (original and building-enhanced) was evaluated for their ability to reduce the impacts from the base case of no sensors. Again, the building-enhanced models were used to assess sensor network design performance.

3. RESULTS

3.1 Impacts – No Sensor Monitoring

Table 3 provides selected percentile and mean public health impact results for each network given no sensor monitoring stations. These are the number of people sickened. For Network A and A-MS, it is the number of people sickened out of a possible 6,400 people. For Networks B and B-MS, it is the number of people sickened out of a possible 600,000. Impacts were rounded to the nearest whole number. The distribution of impacts across all of the scenarios evaluated for Networks A and A-MS do not differ except for the 90th and 100th percentile releases, which increase for the 90th percentile

scenario and decrease for the worst case scenario under the building-enhanced model. Comparing Networks B and B-MS, the results for the building-enhanced model decrease for the higher percentile cases of 75th to 100th and increase for the lower percentile scenarios, with the mean being slightly less under the building-enhanced model.

Table 3. Public health impact results for the no sensors case for Networks A, B, A-MS and B-MS.

Statistic (based on demand node ensemble of base network)	Network A (# of people sickened)	Network A-MS (# of people sickened)	Network B (# of people sickened)	Network B-MS (# of people sickened)
10th	0	0	0	300
25th	10	20	900	1,300
50th	100	100	2,300	2,500
75th	600	600	4,200	4,000
90th	1,200	1,700	6,700	6,000
100th	3,500	2,500	17,000	13,000
Mean	500	500	3,000	2,900

The generally decreased health impacts for the building-enhanced models are consistent with the results reported in the conceptual work by Grayman and Buchberger (2006). This earlier work showed that post service connection plumbing caused a significant delay in time and decrease in concentration for the contaminant to reach the customer when a contaminant was released into the distribution system (Grayman and Buchberger, 2006). Comparing the worst case scenario results for Networks A and A-MS supports these findings with respect to the decreased concentration of contaminant. For Network A, the worst case scenario selected was junction-152; while for Network A-MS, the worst case scenario selected was junction-255. Comparing these two scenarios under just the A-MS model reveals that junction-152 now affected fewer people than under the original model, i.e., 2,000 exposures, with 90% of these impacts spread across 67 receptor nodes; while, junction-255 became the worst case release location with impacts of 2,500, 90% of these impacts were spread across 70 receptor nodes.

3.2 Sensor Network Designs & Performance

Table 4 provides the sensor network design performance results for Networks A and A-MS. Sensor network designs developed for Network A were evaluated in Network A-MS to compare results with the building-enhanced sensor network designs of Network A-MS. Results for percent difference (fourth column) are for Network A designs compared to A-MS designs. For example, for the 5 sensor building-enhanced design of Network A-MS, 10 people are sickened as opposed to 30 people for the Network A design. The percent difference is with respect to the building-enhanced design, hence (30-10)/10 equals 2, expressed as a percentage is 200%. Similarly, the results for percent reduction (fifth column) are with respect to the no sensors case for A-MS. Impact numbers were rounded to the nearest whole number as were the percent difference and percent reduction values. For the 2, 5, and 10 sensor network design sizes evaluated for Networks A and A-MS, the

building-enhanced designs performed between 25 and 200 percent better than their respective designs developed from the original model. The building-enhanced designs reduced public health impacts as compared to the no sensors case an additional 10 percent as compared to the original, Network A model's designs.

For Network A-MS, the optimal design of 2 sensors had an average event detection time of 4.6 hours. Similarly, the median and 95th percentile event detection times were 3.5 and 10.9 hours, respectively, for the optimal A-MS design of 2 sensors. The Network A's 2 sensor design had a average detection time of 5.28 hours, 50th percentile detection time of 4.3 hours, and a 95th percentile detection time of 12.8 hours. The 2 sensor design developed for the original Network A model and then evaluated in the A-MS model did not perform as well. The total number of events detected in the A-MS model was 75 for both designs. The total number of events evaluated in Network A-MS was 106.

Similar results were determined for Networks B and B-MS. For the larger range of sensor set sizes evaluated for Networks B and B-MS, the building-enhanced designs performed between 2 to 27 percent better than their respective designs developed using the original model. Generally, the percent improvements increased with increasing numbers of sensors. The building-enhanced designs reduced public health impacts for the no sensors case from about 2 to 9 percent as compared to the original, Network B model's designs.

For Network B-MS, the optimal design of 5 sensors had an average event detection time of 9.3 hours, median time of 8 hours, and a 95th percentile event detection time of 17 hours. The Network B optimal design of 5 sensors when evaluated in the Network B-MS model had an average event detection time of 10 hours, median time of 8 hours, and 95th percentile time of 26 hours. The optimal design for B-MS detected 1,430 events whereas the original model's design detected 1,240 events. The total number of events evaluated in Network B-MS was approximately 2,200.

For both networks, the building-enhanced sensor network designs differed in location from their original model analogs, with little overlap, although spatially the designs looked very similar. It is important to note that none of the added, building-specific nodes were selected by the sensor placement algorithm for either the A-MS or B-MS models.

Table 4. Comparison of sensor network design performance for Networks A and A-MS. All sensor designs were evaluated in Network A-MS. Mean impact estimates (# of people sickened), percent differences, and percent reductions are rounded to nearest whole number.

Sensor Network Design	Number of Sensors	Mean Impacts (# of people sickened)	Percent Difference from Network A-MS Optimal Design	Percent Reduction from No Sensors Case for A-MS
Network A-MS, No Sensors	0	500		
Network A-MS – Optimal Design	2	40		90
Network A – Optimal Design	2	50	25	90
Network A-MS – Optimal Design	5	10		100
Network A – Optimal Design	5	30	200	90
Network A-MS – Optimal Design	10	4		100
Network A – Optimal Design	10	10	150	100

4. DISCUSSION

The results presented indicate that the lack of post-service connection plumbing in distribution system models can have a significant effect on sensor network design performance. In comparisons of the smaller Networks A and A-MS, the improved sensor network performance obtained from the building-enhanced model designs ranged from 25 to 200 percent over the analogous designs developed with the original model. For the larger Network B, the building-enhanced B-MS sensor network designs improved sensor network performance by 10 to 30 percent over the analogous designs developed with the original model. Analysis of the event detection times further supported these findings for improved performance of the sensor network designs developed with the building-enhanced models. Sensor network designs developed with the building-enhanced models were able to detect contamination events faster than the corresponding designs developed for the base model. These results are preliminary and are based on perfect sensors and an instantaneous response to reduce public health impacts. These results are also only based on contaminant release duration of 1 hour.

The results reported here support earlier findings that by adding post service connection pipe and infrastructure detail to network models results in a significant delay in time and decrease in a contaminant's concentration to occur from the model node to the customer. The delay in time for the contaminant to reach the customer is due to the longer travel path. The decrease in concentration of the contaminant is due to greater mixing and dilution occurring.

5. NEXT STEPS

Research is underway examining the role that response time and contaminant detection limit has on the results presented above. Ongoing research is also examining the role that contaminant release duration has on such results. It is not clear whether the differences reported here represent significant differences, when site-specific and logistical constraints for sensor placement are taken into consideration.

Additionally, it is not clear if the population exposed objective evaluated is the most suitable to assess the sensitivity to post service connection plumbing details. For instance, would the objective to minimize extent of contamination (linear feet of pipe contaminated) be equally, more, or less sensitive? Similarly, would the objective for minimizing the time of event detection provide similar results? Additional research is needed to study and hopefully answer these questions in order to develop guidance on the application of sensor placement optimization tools, like TEVA-SPOT, to water distribution systems dominated by multi-story buildings.

DISCLAIMER

This project has been subjected to the U.S. Environmental Protection Agency's review and has been approved for publication. The scientific views expressed are solely those of the authors and do not necessarily reflect those of the US EPA. EPA does not endorse the purchase or sale of any commercial products or services, so no endorsements should be inferred.

REFERENCES

Berry, J., Fleischer, L., Hart, W. E., Phillips, C. A., and Watson, J.-P. (2006). "Sensor placement in municipal water networks." *J. WaterResour. Plan. Manage.*, 131(3), 237–243.

Davis, M. J., and Janke, R. (2008a). "Development of a Probabilistic Timing Model for the Ingestion of Tap Water." submitted to *J. Water Resourc. Planning Manag*.

Davis, M. J., and Janke, R. (2008b). "Importance of exposure model in estimating impacts when a water distribution system is contaminated." *J. Water Resourc. Planning Manag*., 134(5), p. 449-456.

EPA (U.S. Environmental Protection Agency) (2000). "Estimated Per Capita Water Ingestion in the United States." EPA-822-00-008, Office of Water, Washington, D.C.

EPA. (2009). "Threat Ensemble Vulnerability Assessment Research Program." <http://www.epa.gov/nhsrc/water/teva.html> (January, 2009).

Grayman, W. M., and Buchberger, S. G. (2006). "Fixture-level human exposure calculation model." paper presented at the 8th Annual Water Distribution Systems Analysis Symposium, Cincinnati, Ohio, August, 2006.

Grayman, W. M., Buchberger, S. G., Samuels, W. (2008). "Hydraulic models of buildings for use in contamination studies." paper presented at the 10th Annual Water Distribution Systems Analysis Symposium, Kruger National Park, South Africa, August, 2008.

Janke, R. Murray, R. Uber, J., Bahadur, R., Taxon, T., Samuels, W., Davis, M. (2007) "Using TEVA to Assess Impact of Model Skeletonization on Contaminant Consequence Assessment and Sensor Placement Design." paper presented at the 9th Annual Water Distribution Systems Analysis Symposium, Tampa, Florida, 2007,

Khanal, N., Buchberger, S. G., and McKenna, S. A. (2006). "Distribution system contamination events: exposure, influence, and sensitivity." *J. Water Resour. Plann. Manage.*, 132(4), p. 283-292.

Murray, R., Uber, J., and Janke, R. (2006). "Model for estimating acute health impacts from consumption of contaminated drinking water." *J. Water Resour. Plann. Manage.*, 132(4), 293-299.

Murray, R., Janke, R., Hart, W.E., Berry, J.W., Taxon, T., and Uber, J. (2008). "A decision framework for sensor network design of contamination warning systems." *J. American Water Works Assoc.*, 100(11): 97-109.

Nilsson, K. A., Buchberger, S. G., and Clark, R. M. (2005). "Simulating exposures to deliberate intrusions into water distribution systems." *J. Water Resour. Plann. Manage.*, 131(3), 228-236.

Rossman, L. A. (2000). "EPANET 2 Users Manual." EPA/600/R-00/057, U.S. Environmental Protection Agency, National Risk Management Research Laboratory, Office of Research and Development, Cincinnati, Ohio.

Skadsen, J., Janke, R., Grayman, W., Samuels, W., TenBroek, M., Steglitz, B., and Bahl, S. (2008). "Distribution system on-line monitoring for detecting contamination and water quality changes." *J. American Water Works Assoc.*, 100(7): 81-94.

Walski, T. M, D.V. Chase, D.A. Savic, W.M. Grayman, S. Beckwith, and E. Koelle. *Advanced Water Distribution Modeling and Management.* Haestad Press, Waterbury, CT. pp 112-125. 2003.

COMPARATIVE EVALUATION OF TWO ALGORITHMS FOR LOCATING CONTAMINANT INGRESS POINTS

Hailiang Shen, Edward McBean, Mirnader Ghazali
School of Engineering
University of Guelph
Guelph, Ontario, Canada

ABSTRACT

A procedure involving Data Mining based on Flow Direction and shortest flow time (DMFD) is described, which consists of two components: (i) possible ingress nodes (PINs) identification and (ii) probability quantification. PINs identification is completed based on the flow information, i.e. the flow direction and time in each pipe. Through shortest time which is calculated by Dijksta algorithm, from one node to a specific sensor, ingress time in the node is obtained. A distance metric is described to quantify the probability of one node as PIN. A multi-stage response is described to decrease the elapsed time before a contaminant ingress event is identified and responded to, which is essential to minimize the risk from consumption of the hazard. The roles of two algorithms, namely a Data Mining method based on Injection and Detection information (DMID) and DMFD, are examined. A case study is employed in a network with 285 nodes and 5 sensors. The five sensors all alarm to the injection event. With DMID, the number of PINs is decreased from 44 in the 1st stage to 18, 11, 11 and 11 subsequently; For DMFD, the number is reduced from 44 in the 1st stage to 21, 21, 21 and 21 in the following stages; DMID identifies the true intrusion node 44 with the highest probability in the five stages, while DMFD identifies it with the highest probability in the 3rd and 4th stage; the run time of both DMFD and DMID is less than 2 min, which suggests the two are effective in guiding emergency response.

INTRODUCTION

In recent years, issues related to the quality of water within distribution networks are drawing increased attention from utilities since in most situations the water is beyond the last barrier which can assist in providing safe water to consumers. However, while it is of interest to be concerned with the quality of the water throughout the entire distribution system, it is infeasible to monitor the quality at more than a few nodes within the distribution network.

Given the preceding, and although significant efforts to protect against contaminant intrusion into the water distribution system are being extended, excursion events do occur. In response, of interest is the degree to which in-system monitoring systems with a limited number of sensors in combination with algorithms for contaminant trace back can identify the location of the source of the incursion or, possible injection nodes (PINs). Efforts to minimize the elapsed time to detection are appropriate to reduce health risk to water consumers and accomplished using a "multi-stage response".

LITERATURE REVIEW

A number of algorithms have been proposed for identifying locations of contaminant ingress into water distribution systems. For example, Shang et al. (2002) proposed

particle backtrack algorithms (PBA) to trace back the water parcel to source nodes to construct water quality parameter relationships between outputs and input, assuming a precise hydraulic condition is available. de Santic et al. (2006) extended PBA to locate all PINs and times by assuming contaminant injections occur at network junctions and over discrete time intervals. This approach may identify a large number of PINs. For an emergency response, it is only feasible to respond to a few PINs and hence this algorithm has limited utility since there are no probability assignments.

Preis et al. (2008) formulated the contaminant ingress identification problem as one of optimization and solved it using a Genetic Algorithm (GA). The decision variables (DV) are injection node(s), injection time(s), injection duration(s) and mass rate(s); the single objective is the minimization of the difference between modeled (it is a function of the DV and network parameters) and measured water quality within the sensor alarm period; since an injection event can happen in any node within the network, at any time, with any duration and mass rate, no constraint applies on the optimization problem. The algorithm may incur long running times and issues of convergence.

In DMID (data mining based on injection and detection information), a database containing injection and detection information is constructed to employ the procedure (Huang et al., 2008). The overall time consumed in DMID is related to the initial database construction which may require several days for large networks; however, since the database is constructed prior to a contaminant intrusion event (i.e. as part of a preceding analysis), the database construction time is not a significant issue although this may become a problem when the calibration of an hydraulic model occurs frequently. The ability of DMID in multi-stage response is described by Shen et al. (2008) in detail.

DATA MINING FLOW DIRECTION ALGORITHM

DMFD (data mining based on flow direction and shortest flow time), is based on flow time and direction in each pipe. The flow information is obtained by performing a hydraulic simulation with EPANET software. Two assumptions for the algorithm development are required:

i) If contaminant ingress occurs at one specific node, the contaminant will reach the sensor through the shortest time (through the shortest path). It is assumed that even in the situation of a contaminant which decays and/or is removed via water consumption, the contaminant concentration is sufficiently large that the monitoring system will detect its presence; and,

ii) Contaminant flow velocity is the same as that of water.

In the first stage within the multi-stage response procedure, the DMFD is executed to identify potential locations of ingress (albeit, with only a single sensor response, the range of possible ingress location may be quite large, but this approach avoids the need to wait until the second sensor (and the third, or more sensors) is impacted). Thus, the mean time for identifying the first response may assist in minimizing exposures of water consumers to the contaminant; in the second stage, with an alarm from both the first and second sensors, the PINs are decreased in number. This multi-stage approach, involving successive narrowing of possible source nodes, may be effective in minimizing the

timeframe for response action to the contaminant ingress. The implementation of the multi-stage response is completed with the DMFD, and is compared with DMID in term of PINs identification and probability quantification.

FLOW-DIRECTION MATRIX

A constant hydraulic condition is assumed. The first step in the procedure involves the development of the Flow-Direction Matrix. The data assembly includes: pipe index, pipe start and end node index, the flow direction in each pipe (a value of 1 indicates water flows from a specific node to a specific end node, '0' indicates the hydraulic head is the same in both the start and end node, and thus no flow occurs between the two nodes), velocity within pipe, pipe length, and flow time within the pipe. The assembly of information is stored in tabular format as per illustrated in Table 1, which serves as the base for algorithm development.

Table 1 Flow Information Within Each Hydraulic Time Step

Pipe index	Start node index	End node index	Direction	Velocity	Length	Time

Dijkstra's algorithm (Dijkstra, 1959) is a graphical search algorithm that solves the single-source shortest path problem for a graph with non-negative edge path costs, outputting a shortest path (SP) tree. This algorithm can be used to find the SP between two given vertices, or the shortest paths from source to each vertex in the graph. It searches SP from the source to the target by following the direction of edge flow. A water distribution network is a node-link system, which can be represented by a vertex–edge in a graph, and thus can be searched by graph theory. In contaminant ingress source identification for a water distribution network, of concern is the identification of the upstream node, given the downstream node, a modification of the Dijkstra algorithm is possible. The reverse direction of the flow is 'searched' instead of following the flow direction.

In the contaminant ingress source identification problem, of interest is the procedure to search the shortest flow time is formulated as follows:

Initialize the sensor S alarm time as 0 second, set $N_{DOWN,\ 0,\ N} = S$ (DOWN refers to downstream, 0 is the 0th search forward, N is the node ID), i = 0, set $N_{DOWN,\ i} = N_{DOWN,\ 0,\ N}$.

(i) Find the upstream nodes of $N_{DOWN,\ i}$ based on Table 1 contents, and denote these relationships as $[N_{UP,\ i}]\ N_{DOWN,\ i\ ,j}$ (where UP refers to the upstream, i is the ith search forward, j is the node ID within $N_{DOWN,\ i}$); union of $[N_{UP,\ i}]$ of each downstream nodes need to be put in the Next Search Nodes List (NSNL),

(ii) Update $[N_{UP,\ i,\ k}]$ (k is one node ID within $N_{UP,\ i}$) intrusion time, $N_{UP,\ i,\ k}(t) = N_{DOWN,\ i,\ j}(t)$ + flow time of pipe k-j; for node ID, k may be the upstream node of several downstream nodes, thus, take $N_{UP,\ i,\ k}\ (t) = MIN(N_{UP,\ i,\ k}(t))$,

(iii) Take $[N_{inter}] = [N_{UP,\ i}] \cap [N_{UP,\ i-1}]$, if $[N_{inter}] \neq \phi$ (null), $N_{UP,\ i,\ k}\ (t) = MIN(N_{inter}(t))$; set $N_{DOWN,\ i} = N_{UP,\ i}$,

(iv) The possible contaminant ingress nodes and their intrusion times are PINs= $\bigcup_{0}^{i} N_{UP,i}$ (t); i=i+1,

(v) Repeat step (ii)-(v) until the $N_{UP,\,i} = \phi$, i.e. all nodes reach source node (s).

The outputs of each search forward are:

i) NSNL,

ii) PINs up to the current search step.

To demonstrate the performance of the DMFD algorithm, consider the sample network composed of 5 nodes and 2 loops, where D and A are the source and sink nodes respectively.

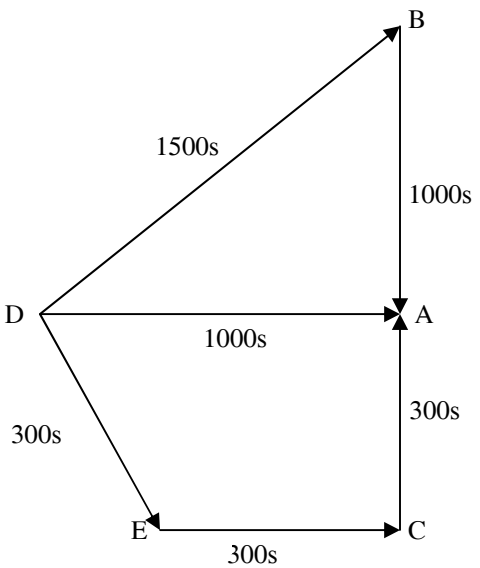

Figure 1 Example Network

Legend: 1000s equals the flow time of water in pipe B-A, (B-A is one pipe, and the water flows from node B to A) A, B, C, D and E are the node IDs.

Example

First search: The first search moves backward or upstream from A to find the PINs related to B, C and D. The relationship is denoted as [B, C, D] A, where A is the downstream node and [B, C, D] are the upstream nodes. The NSNL are B, C, and D.

If the contaminant ingress event happens in node B, the intrusion time should create an alarm at node A minus the flow-time in pipe B-A. Thus, the intrusion time at node B should be 1000s before the node A alarm time, which is denoted as B(1000s), (where B is the possible intrusion node and the label 1000s is the possible intrusion time), likewise for C (300s) and D (1000s).

The outputs of the first search are:

i) NSNL: [B, C, D],
ii) PINs up to this step: B(1000s), C(300s), D(1000s).

Second search: Find upstream nodes, and denote the relationships as [D]B , [E]C , [ϕ]D (D is the upstream node of B, E is the upstream nodes of C, and D has no upstream nodes.)
For node D, since there is no upstream node(s) contributing water to it, NSNL contains only D and E. The upstream node information is updated.
D = B(1000s) + $t_{B\text{-}D}$ = 1000s+1500s = 2500s, and
E = C(300s) + $t_{E\text{-}C}$ = 300s + 300s = 600s.
Compare with the output in the first search to get the outputs of the second search.
D = MIN (D(this step), D(previous step)) = MIN(2500s, 1000s), if contaminant ingress event happens in node D, the contaminant will flow via the shortest flow time 1000s and arrive at A.
There is no node E in the first search, thus E = 600s.
The outputs of the second search are:
i) NSNL: [D, E],
ii) PINs up to this step: B(1000s), C(300s), D(1000s), E(600s).

Third search: Find upstream nodes, and denote the relationships as [ϕ]D, [D]E, (where node D has no upstream node, and node D is the upstream node of E; D is the only node in the NSNL)
Update upstream nodes ingress time: D = E(600s) + $t_{D\text{-}E}$ = 600s + 300s = 900s.
D = MIN (D (this step), D (previous step)) = MIN(900s, 1000s) = 900s.
The outputs of the third search are:
i) NSNL: [D],
ii) PINs up to this step: B(1000s), C(300s), D(900s), E(600s).

Fourth search: Find upstream nodes, and denote the relationships as [ϕ]D, where D has no upstream node, so terminate the search.
The outputs of the fourth search are:
i) NSNL: ϕ,
ii) PINs up to this step: B(1000s), C(300s), D(900s), E(600s).

PINs INDENTIFICATION AND PROBABILITY QUANTIFICATION

Assume only a single intrusion event happens. In the first stage, the first sensor alarm, $PINs^1$ are identified with the procedure described. No probability can be assigned to $PINs^1$, or all $PINs^1$ have the same probability. In the subsequent stages, more sensors alarm, and $PINs^i$ are identified with the following conditions.
i) $PINs^i$ make the ith sensor alarm,
ii) $PINs^i$ are within $PINs^{i-1}$.

Assume node N is the true intrusion node. In the first stage, sensor S1 alarms at time t1; in the following stage i, sensor Si alarms at time ti. From the procedure described above, sensor alarm time is initialized as zero, and the shortest times from N to S1 and Si are

calculated as ST1 and STi respectively. The intrusion time in N is ST1 and STi within the two stages. Without uncertainty from nodal demand and measurement, ST1 – STi is precisely the same as t1 – ti. Thus, the distance between abs(ST1 – STi) and abs(t1 – ti) can be used as one metric to quantify the probability of N as one PIN: the shorter the distance, the higher the probability.

CASE STUDY

The network after Huang et al. (2006) is presented in Figure 1 for the purpose of comparing DMFD and DMID in terms of the ability in PINs identification and probability quantification. The five sensor locations are optimized as per Huang et al. (2006).

In DMID, the following assumptions are made: i) the contaminant is conservative or the decaying coefficients in pipe are zero, ii) only single ingress location exists. Other parameters in database construction are: simulation duration, 72 hours; injection time interval, 1 hour; injection mass rate, 10^{10} to avoid being diluted or consumed to null.

The simulation single ingress event happens in node 44. Its detection information (i.e. the first detection time in each sensor) is listed in Table 2. The PINs in each stage are presented in Figure 2. For DMID, in the five stages, the number of PINs is subsequently narrowed from 44 to 18, 11, 11 and 11. For DMFD, the number of PINs is decreased from 44 in the first stage to 21 in the following four stages.

The procedure for the probability quantification in DMID is described by Shen, et al.(2008), and used herein. The probability is quantified by a Euclidean distance metric in response versus time 2-D coordinate, the shorter the distance, the higher the probability. The probability quantification is presented in Figure 3 through 7. In Figure 3, DMID identifies node 44 with the highest probability; DMFD cannot assign probabilities to each PIN. As presented in Figure 4, DMID identifies node 44 with the highest probability; DMFD identifies node 10 with the highest probability because its corresponding distance is the nearest to zero, and node 44 is identified as one PIN although it is not with the highest probability. In Figure 5 and Figure 6, for both DMID and DMFD, node 44 is identified with the highest probability as the location of ingress. In Figure 7, DMID identifies node 44 with the highest probability, and in the subplot, it shows the magnitude of the probabilities of PINs[5] are quite similar.

RESULTS AND CONCLUSION

This paper describes a multi-stage response procedure and its implementation with DMFD. Within each stage, Dijkstra's algorithm is applied to label the shortest time from each PIN to specific sensor as the ingress time of the PIN. One metric based on distance is used to quantify probability of PIN. In DMID, the database construction process may take hours to days, which limits its application in real time. While DMFD eliminates the database construction process and thus provides possibility for real time application when precise hydraulic condition is available.

As demonstrated in the case study, in the first stage, the two methods can identify the same PINs in the first stage, which suggests the effectiveness of DMFD in PINs identification. In the subsequent stages, DMFD identifies more nodes as PINs, which indicates it is inclined to provide conservative estimates of PINs while more sensors are providing information. In the following stages, DMID can identify the true intrusion node 44 with the highest probability, while DMFD can identify node 44 in the 3rd and 4th stage with the highest probability. The program run time of the two methods is within 2 minutes, and thus is sufficient to guide emergence response.

FUTURE WORK

In DMID, the number of PINs is sensitive to the assignment of value 'm' applied in the query sentences. It is set to 30 min for this research.
DMFD does not have the ability to deal with extended period simulation in the network. This functionality will be incorporated in the future.

REFERENCE

Babovic, V., Drecourt, JP, Keijzer, M., and Hansen, P. (2002). "A Data Mining Approach to Modelling of Water Supply Assets", Urban Water, 4, 401-414.

de Santics, A.; Shang, F. and Uber, J. (2006) "Determining Possible Contaminant Sources through Flow Path Analysis" WDSA Symposium 2006, Cincinnati Ohio USA, Aug27-29.

EPANET 2.0. Toolkits (2000). Available online at: www.epa.gov/ORD/NRMRL/wswrd/epanet.html (accessed Oct 1, 2008).

Huang, J., McBean, E., and Shen, H., 2008. "Data mining as a tool to identify contaminant sources in water distribution system", Proceedings of the 10th annual Water Distribution Systems Analysis conference, Kruger, South Africa, August, pp. 1091-1101.

Huang, J., McBean, E. and James, W. (2006) "Multi-objective optimization for monitoring sensor placement in water distribution systems" WDSA Symposium 2006, Cincinnati Ohio USA, Aug 27-29.

Preis, A., and Ostfeld, A., 2008. "Genetic algorithm for contaminant source characterization using imperfect sensors". Civil Engineering and Environmental Systems, 25(1) : 29 – 39.

Shen. H., McBean, E., and Ghazali, M. (2008). "Multi-stage Response to Contaminant Ingress Into Water Distribution System and Probability Quantification". Canadian Journal of Civil Engineering, under review.

Shang, F., Uber, J. G., and Polycarpou, M. M. (2002) "Particle back tracking algorithm for water distribution system analysis" ASCE Journal of Environment Engineering, 128(5). 441-450.

Thomas H. Cormen, Charles E. Leiserson, Ronald L. Rivest, and Clifford Stein. Introduction to Algorithms, Second Edition. MIT Press and McGraw-Hill, 2001. ISBN 0-262-03293-7. Section 24.3: Dijkstra's algorithm, pp.595–601.

Table 2 First detection information

Alarm sensor	Sensor ID	First detection time (s)
1st alarm sensor	142	148500
2nd alarm sensor	171	150600
3rd alarm sensor	87	156000
4th alarm sensor	212	164400
5th alarm sensor	153	178800

Figure 1 Network of Goderich

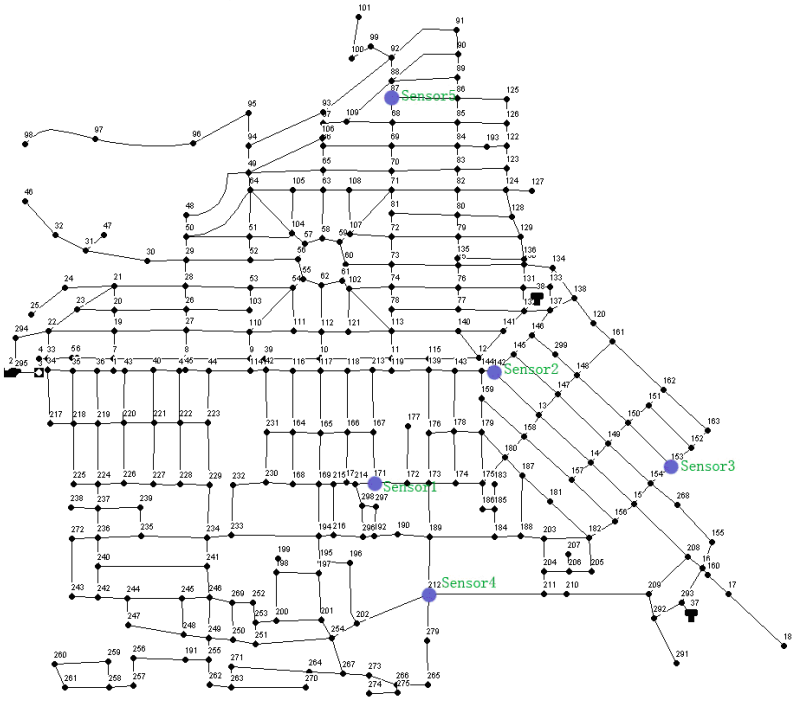

Figure 2 PINs in each stage from DMFD and DMID

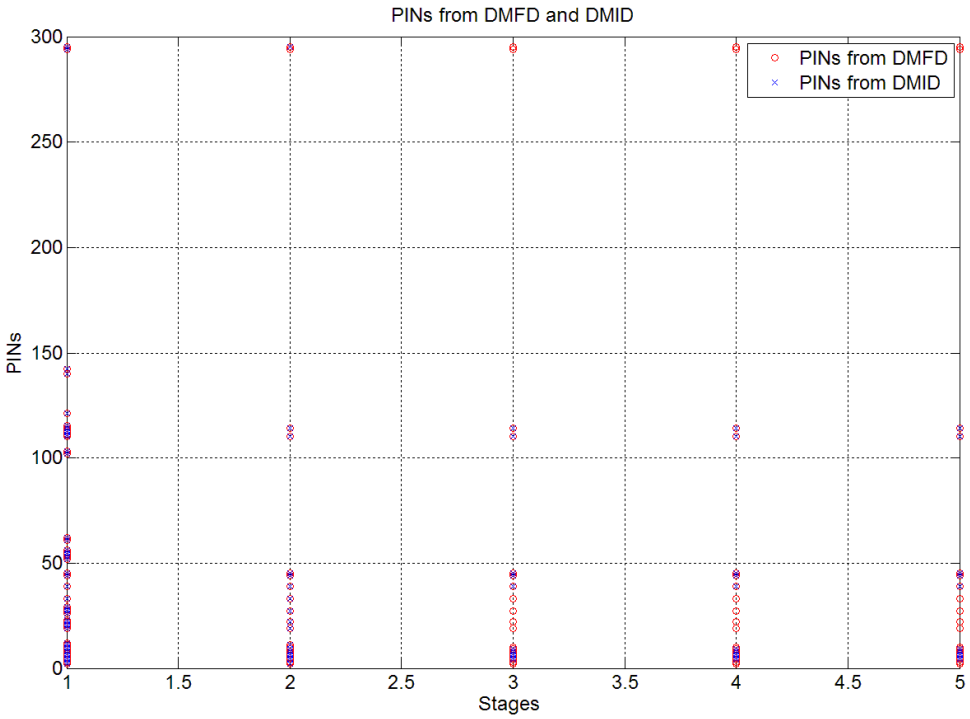

Figure 3 Probability after the 1st sensor alarm

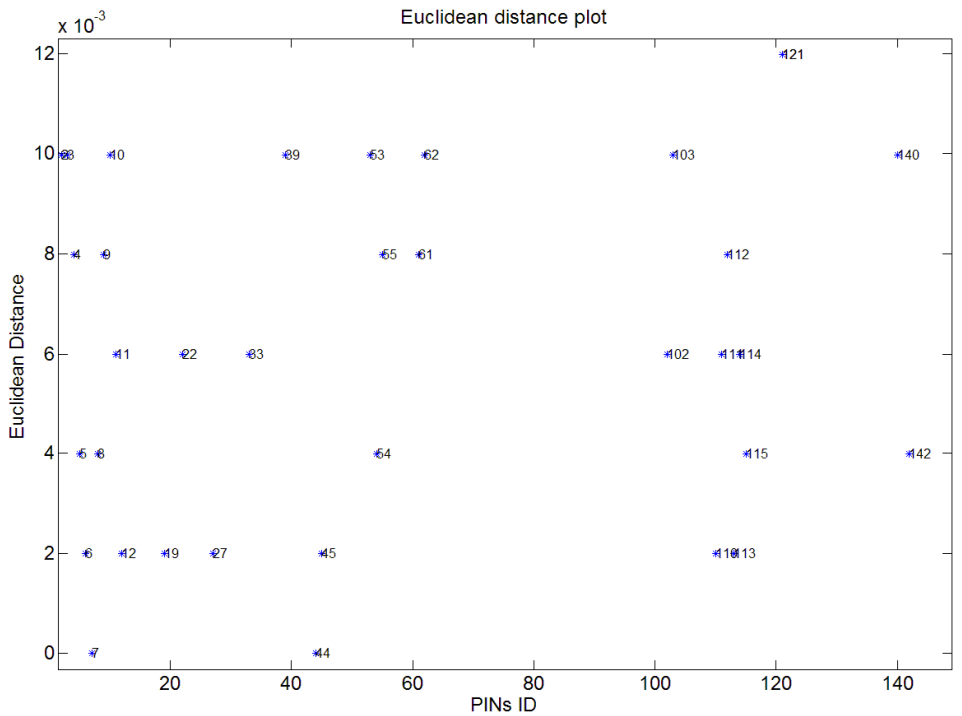

Figure 4 Probability after the 1st, 2nd sensor alarm

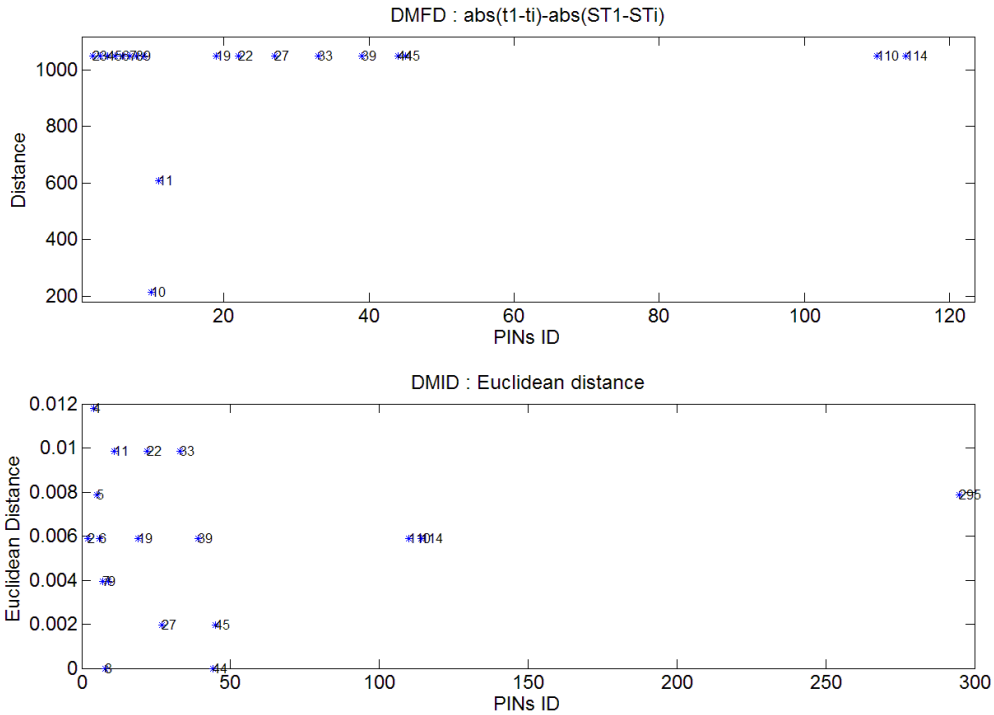

Figure 5 Probability after the 1st, 2nd, 3rd sensor alarm

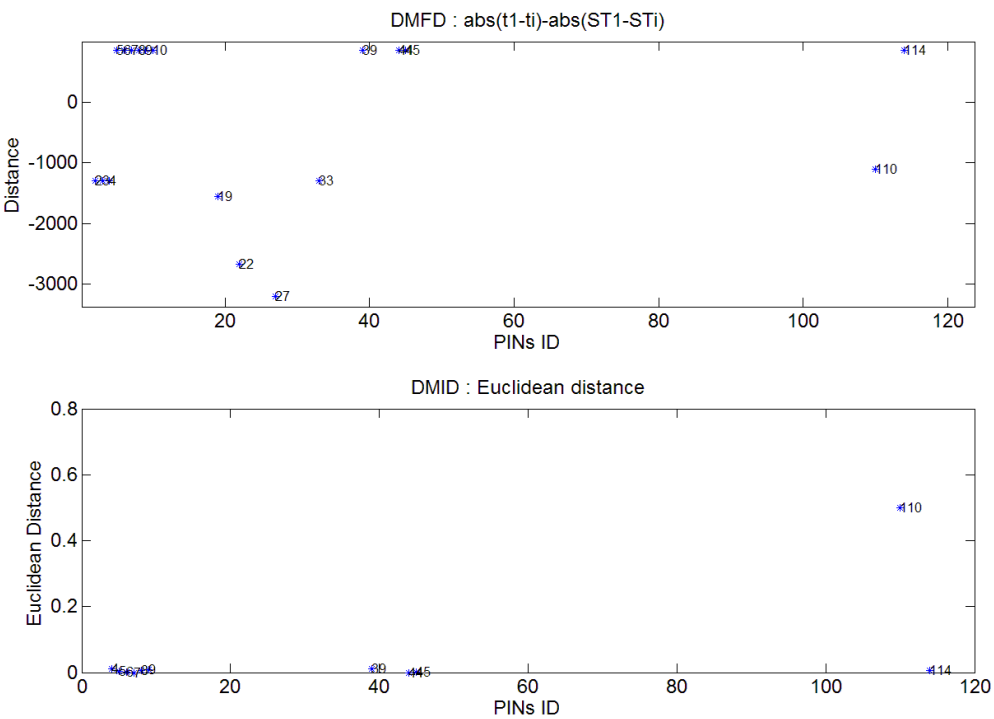

Figure 6 Probability after the 1st, 2nd, 3rd, 4th sensor alarm

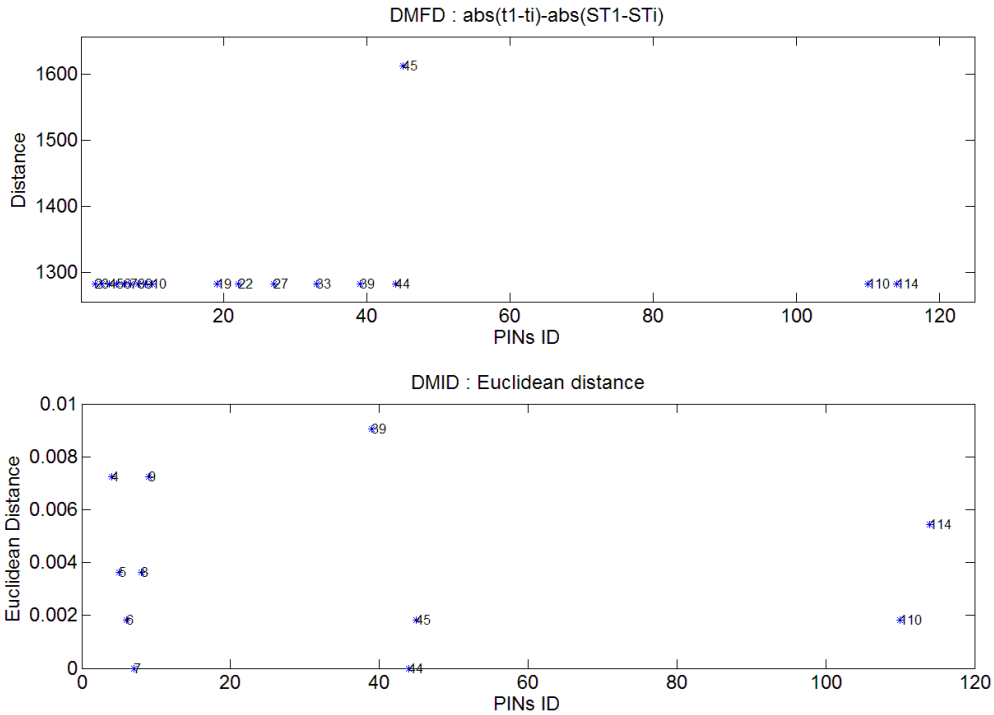

Figure 7 Probability after all sensors alarm

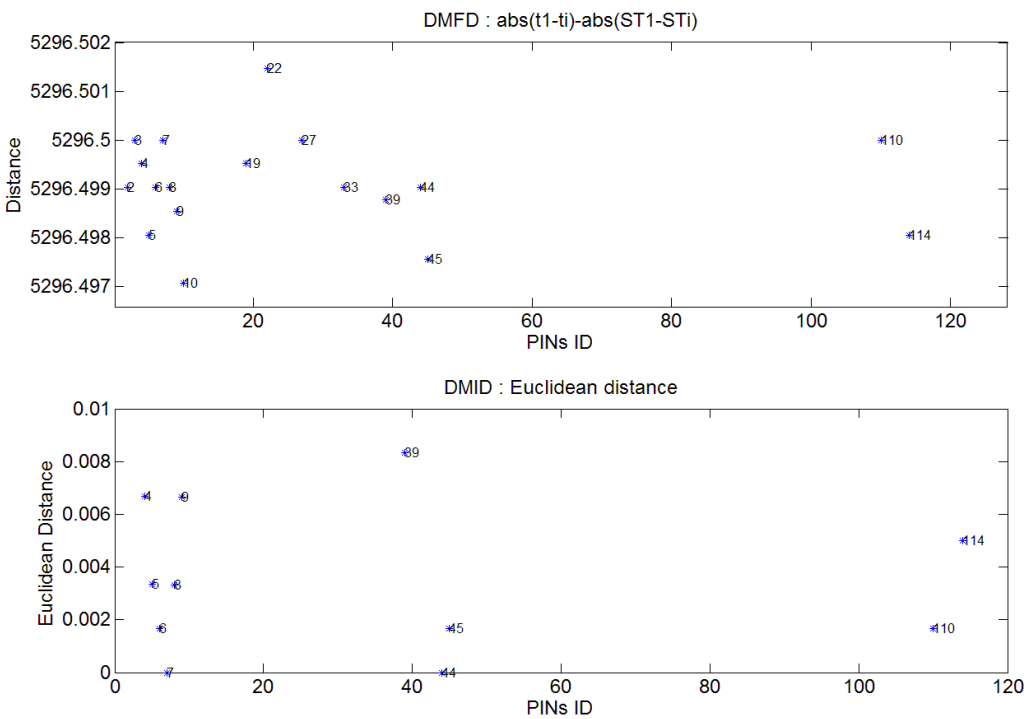

Comparison of Pressures Simulated using Transient Analysis with Field Data from a Full-scale Distribution System

G. Ebacher[1]*, M.-C. Besner[1], J. Lavoie[2], B.S. Jung[3], B.W. Karney[4], and M. Prévost[1]

[1] École Polytechnique de Montréal, NSERC Industrial Chair on Drinking Water, Civil Geological and Mining Engineering, C.P. 6079, Succ. centre-ville, Montréal, QC, H3C 3A7, Canada
* Corresponding author: tel. 514-340 4711 ext. 2975, gabrielle.ebacher@polymtl.ca
[2] Ville de Laval, Usine de traitement Chomedey, 3810, boul. Lévesque, Chomedey, Laval, Québec, H7V 3Z4, Canada
[3] MWH Soft, 618 Michillinda Avenue, Suite 200, Arcadia, CA, 91007, USA
[4] University of Toronto, Department of Civil Engineering, 35 St.George St., Toronto, ON, M5S 1A4, Canada

ABSTRACT

Negative pressures were measured in a full-scale distribution system following low pressure events at a water treatment plant. Transient analysis was used to model three downsurge events and compare the simulated pressure profiles with field measurement data. The objective of this work is to assess the source of uncertainty and variability associated with the estimation of intrusion volumes calculated by a transient analysis model. This assessment was conducted by comparing actual field pressure measurements and model outputs under various model settings (e.g., cavitation head, wave speed). For the three downsurge events, the modeled pressure profiles matched reasonably well with the measured pressures, as long as the pressures remained positive at a site. When the pressures reached negative values, the amplitude of the modeled pressures was larger than that of the recorded pressures. The difference between measured and modeled pressure is strongly related to a greater energy dissipation in the real distribution system, which is affected by the uncertain presence of air in pipes, the level of network skeletonization, and the allocation of demand. The estimation of intrusion volumes and risk for public health is directly affected by the pressure results obtained using transient analysis. Comparison to field data is therefore important to evaluate the accuracy of such a process.

INTRODUCTION

There is a growing interest in the occurrence of negative pressures in drinking water distribution systems and their potentially negative impact on tap water quality. The importance of sustaining positive pressures throughout the distribution system in order to minimize intrusion was pointed out by LeChevallier et al. (2003a). In 2002, the U.S. Environmental Protection Agency (USEPA) listed intrusion as a potentially significant public health concern (LeChevallier et al. 2002). Aggravating factors are the aging of distribution infrastructures, the presence of contaminated water and soil around water mains (Besner et al. 2008; Karim et al. 2003), and the confirmed

incidence of negative pressure events in full-scale water systems (Besner et al. 2007a; 2007b; Fleming et al. 2006; Friedman et al. 2004). However, it is still difficult to determine if intrusion represents a critical risk to water quality. Transient analysis represents an interesting tool, but one must first verify that the transient hydraulic results adequately simulate the field observations. Comparison of computed pressures with corresponding recorded data is the initial step in such a process. Yet, few studies comparing transient field data with transient output from a numerical model are available, though there are several exceptions (McInnis and Karney, 1995; Kirmeyer et al., 2001; LeChevallier et al., 2003; Gullick et al., 2005; Friedman et al., 2004; Fleming et al., 2006). Among these authors, only Friedman et al. (2004) and Fleming and colleagues (2006) compared measured negative pressures with simulated pressures. The largest modelled network included 1700 nodes.

OBJECTIVES

The main objective of this research is to assess the public health risk associated with intrusion events in a distribution system. In order to do so, the source of uncertainty and variability associated with the estimation of intrusion volumes calculated by a transient analysis model must first be assessed. This paper describes the initial phase of this assessment, with the modeling of three downsurge events and the comparison of the simulated pressure profiles with field measurement data.

METHODOLOGY

The distribution system considered serves a population of about 380,000 with an average annual water demand of approximately 210,000 m^3/d (52.8 MGD). It is supplied by three water treatment plants (WTP) using surface water as their raw water source. Each WTP supplies to different network areas that are not delineated by isolation valves, making the three distribution systems hydraulically interconnected. Apart from the clearwells at the WTPs, no storage tanks or pump stations are needed on the water network because of the low profile topography. The distribution system has a total length of 1590 km (988 mi). The distribution system area studied is nominally supplied by a single WTP, as shown in Figure 1.

Ongoing pressure monitoring of the study area and the supplying water treatment plant was carried out for 17 months (June 2006 to November 2007), using high-speed pressure transient data loggers. Modeled events occurred during the summer of 2006.

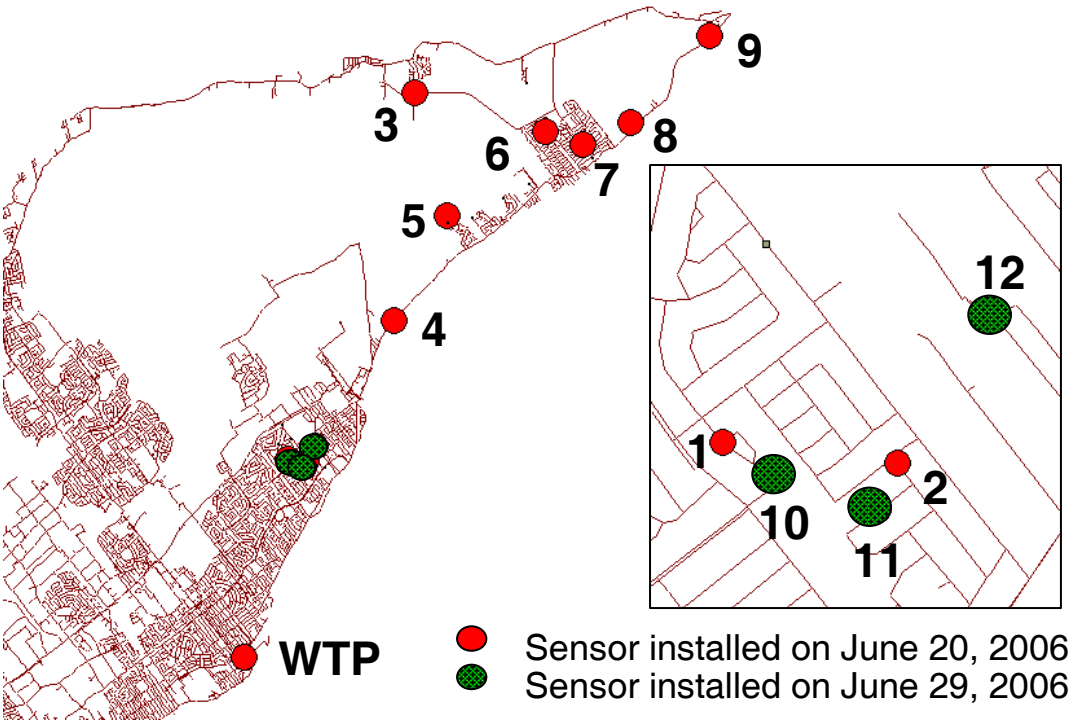

Figure 1. Location of high-speed pressure transient data loggers in the distribution system (number indicates sensor ID).

Pressure monitoring was conducted using two types of high-speed pressure transient data loggers. The RDL 1071L/3 model (Radcom Technologies, Woburn, MA) was installed directly on a transmission main at the outlet of the water treatment plant. This sensor can measure up to 20 pressure values per second within a range of -103 kPa to 1551 kPa (-15 psi to 225 psi). The other type of logger used (HPR31 model, Telog Instruments, Victor, NY) could read up to 4 pressure values per second over its -103 kPa to 1379 kPa (-15 psi to 200 psi) range; it was installed on fire hydrants in the distribution system.

Three specific downsurge events, originating from the water treatment plant and resulting in negative pressures in the distribution system, were modeled. These events were recorded in 2006 on June 27th, August 2nd, and August 22nd. They were caused by a power failure during which the electrical signal was disrupted for a brief moment, requiring the manual restarting of the pumps by the plant operator. Figure 2 illustrates a typical downsurge recorded at the water treatment plant.

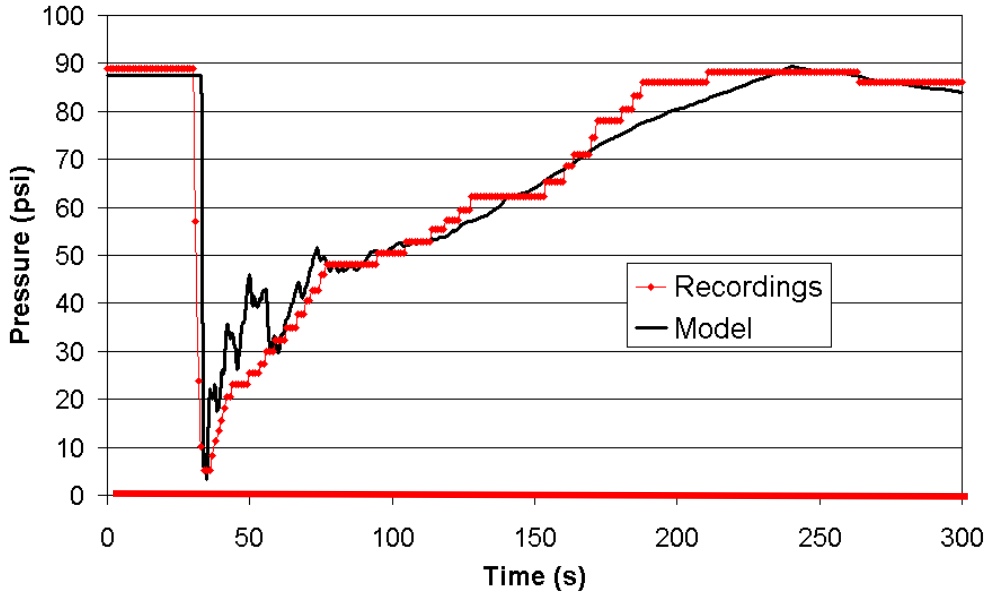

Figure 2. Downsurge recorded at the water treatment plant on August 22nd 2006, together with the modeled pressure profile.

Surge modeling, conducted with the InfoSurge software (MWH Soft, Arcadia, CA), was required to simulate these transient pressure events since they typically lasted less than 5 minutes.

The transient model was built from the extended period simulation (EPS) hydraulic model used by the water utility. Because the original model contains 29,213 nodes and 32,266 links, preliminary steps for the transient model construction included the skeletonization of the EPS model, aiming at reducing the number of links to below 20,000, the maximum limit of the employed software. This was achieved by eliminating the interior nodes of all series pipes with the same attributes (diameter, etc). The model size was decreased to 14,002 nodes and 17,055 pipes, whilst the total length of piping and the total demand remained unchanged.

Typical wave speeds based on pipe material were assigned to mains (Boulos et al., 2006): 1060 m/s (3480 ft/s) for cast iron, 1200 m/s (3940 ft/s) for ductile iron, 600 m/s (1970 ft/s) for concrete, 300 m/s (985 ft/s) for PVC, and 1200 m/s (3940 ft/s) for steel. Minor adjustments in wavespeed for pipe class and bedding conditions were not considered as part of this study.

For each low pressure event, the model's boundary conditions were defined using the pressure and flow out of the 3 WTPs supplying the distribution system. For the WTP supplying the studied area, up to nine high-pressure pumps are available to deliver water into the distribution system. However, because there is no record of which pumps were operating at a specific time in the past, one equivalent pump providing the flow and pressure conditions at the time of the low pressure event was modeled.

The downsurge was created by simulating a sudden pump shutdown using a pump speed change curve.

RESULTS AND DISCUSSION

Before considering the intrusion volumes, the transient model has to be calibrated. It was observed that a calibrated EPS model does not necessarily result in a calibrated transient model. It was also noted that negative recordings may provide useful information to properly calibrate a transient model. Indeed, the pressure profile modeled with a typical wave speed corresponds reasonably well with the measured profiles for locations where the pressure remains above zero for the entire duration of the simulation (Figure 3). However, the correspondence between recordings and pressures computed with typical wave speeds is considerably less accurate for the nodes where the pressure drops below zero (Figure 4).

It should be noted that the cavitation head in the model was set to a very low value (-1000 m) (-1422 psi) instead of the realistic value of -10.1 m (-14.4 psi) (at 20°C). This modeling approach was motivated by the fact that simulation results showed water column separation taking place at some nodes, yet measured data showed that the cavitation head was never reached at the monitoring locations.

As shown in figure 4, the modeled negative pressures were usually lower than the recorded pressures. Hence, the energy dissipation in the real network is greater that the modeled dissipation. This can be explained by attenuation mechanisms happening in the field that are not taken into account in the model. The most likely cause of attenuation in the real system is the presence of accumulated air, which is very difficult to evaluate and cannot be modeled directly with the transient analysis software. A modeling artifice is suggested in order to obtain better-fitting pressure profiles, and, in the end, more realistic intrusion volumes. The proposed solution is to reduce the typical wave speed by 70% in cast iron pipes. This wave speed reduction mimics other attenuation mechanisms. The wave speed was decreased only in cast iron pipes after testing several other alternatives, and because cast iron is the most common material in the studied network. Even if this modeling scheme is introducing a false delay in the arrival of the low pressure wave, it remains an attractive solution because of its simplicity and because of the better pressure fit, and thus can be assumed to be more likely to yield realistic volume estimates and number of nodes affected by negative pressures.

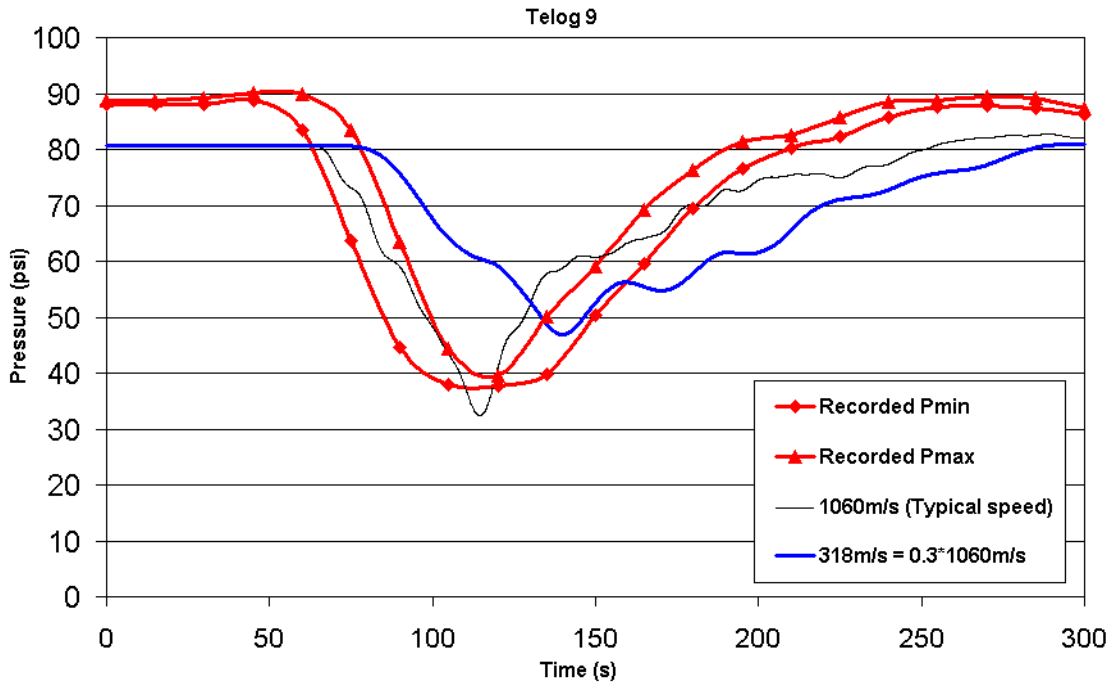

Figure 3. Recorded and modeled pressure profiles at Telog 9.

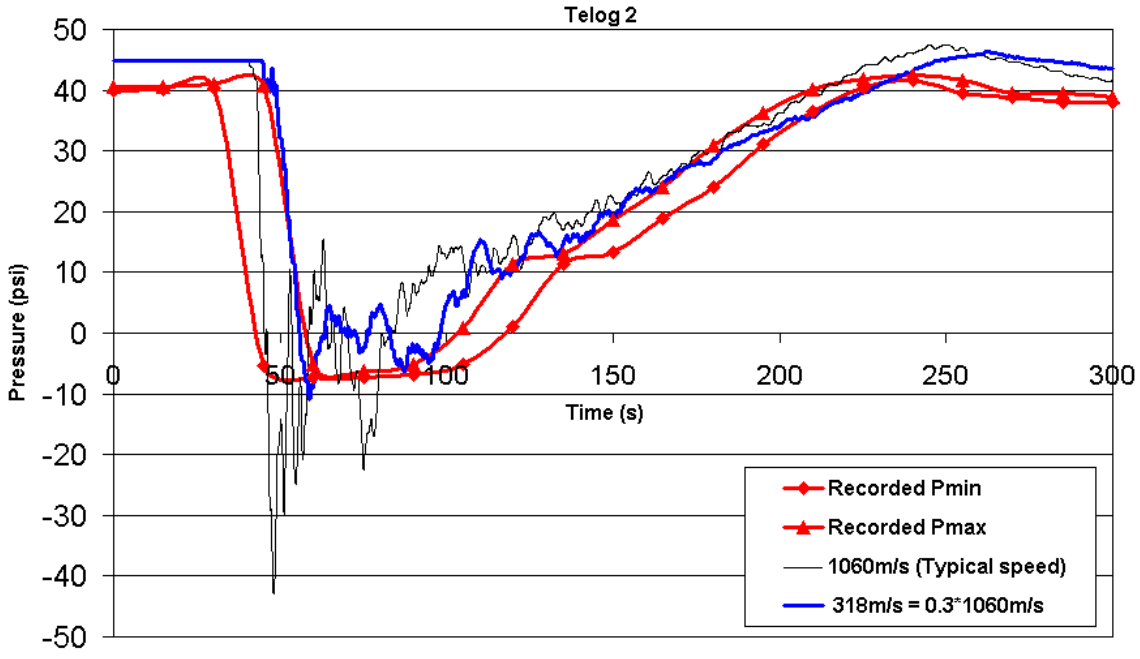

Figure 4. Recorded and modeled pressure profiles at Telog 2.

Intrusion volumes were evaluated for two pathways: pipe leaks and submerged air-vacuum valves located in flooded vaults. The results were based on simulations considering the pressure profiles obtained with 30% of the typical wave speed in cast iron pipes, as these were found to be more in agreement with field pressure results.

For the low pressure event recorded on August 22nd 2006, when the model is run with this wave speed, the total intrusion volume through pipe leaks is 45 L in the entire distribution system (Exit head = 1.4 m, Percentage of leakage = 20%). This volume is six times smaller than the volume computed when the typical wave speeds are used, and represents only $5x10^{-5}$ % of the system's total demand. The intruded volume of 1733 L through submerged air-vacuum valve (45 flooded vaults, Orifice diameter = 50 mm) drops to 102 L when the reduced wave speed in cast iron pipes is used. The wave speed, and its direct impact on the number of nodes experiencing negative pressure, therefore has a significant effect on the intrusion volumes.

CONCLUSION

The objective of this paper is to create a reliable transient model of a large distribution system. The simulated pressure profiles were compared to transient field data. For the three downsurges generated by a power failure at the water treatment plant, the computed pressures matched quite well the measured pressures for the monitoring locations where the pressure remained positive. However, the amplitude of the modeled pressures was larger than that of the recorded pressures whenever the pressure fell below zero. The difference between measured and modeled pressure is strongly related to a greater energy dissipation in the real distribution system, which is possibly accounted for by the uncertain presence of air in pipes, the level of network skeletonization, the allocation of demand and unknown pipe properties (e.g., pipe diameter, friction factor, thickness and material). It should be noted that many uncertain and unknown parameters in transient analysis make the calibration of the model with field data difficult, making the transient system underdetermined. The subsequent work of estimating intrusion volumes and risk for public health is directly affected by the pressure results obtained using transient analysis. Field data are therefore important to evaluate the accuracy of such a process.

ACKNOWLEDGMENTS

This research is funded by the Canadian Water Network (CWN), the Natural Sciences and Engineering Research Council (NSERC) of Canada, and the NSERC Industrial Chair on Drinking Water at École Polytechnique de Montréal. Their support, the one from the participating utility and the following individuals, Jean-François Therrien, Yves Fontaine and Mireille Blais, are gratefully acknowledged.

REFERENCES

Besner, M. C., Ebacher, G., Lavoie, J., and Prévost, M. (2007a). "Low and negative pressures in distribution systems: do they actually result in intrusion?", 9th Annual Water Distribution System Analysis Symposium, ASCE-EWRI World Environmental and Water Resources Congress, Tampa, Florida, USA.

Besner, M. C., Morissette, C., Lavoie, J., and Prévost, M. (2007b). "Pressure transients and water quality changes associated with various O&M activities." American Water Works Association-Distribution Research Symposium, Reno, Nevada, USA.

Besner, M. C., Lavoie, J., Morissette, C., Payment, P., and Prévost, M. (2008). "Effect of water main repairs on water quality." *Journal AWWA*, 100(7), 95-109.

Boulos, P. F., Lansey, K. E., and Karney, B. W. (2006). "Comprehensive water distribution systems analysis handbook for engineers and planners (Second Edition)." MWH Soft, Pasadena, California, USA.

Fleming, K. K., Dugandzic, J. P., LeChevallier, M. W., and Gullick, R. W. (2006). "Susceptibility of distribution systems to negative pressure transients." American Water Works Association Research Foundation, Denver, Colorado, USA.

Friedman, M., Radder, L., Harrison, S., Howie, D., Britton, M., Boyd, G., Wang, H., Gullick, R., LeChevallier, M., Wood, D., and Funk, J. (2004). "Verification and control of pressure transients and intrusion in distribution systems." American Water Works Association Research Foundation, Denver, Colorado, USA.

Gullick, R. W., LeChevallier, M. W., Case, J., Wood, D. J., Funk, J. E., and Friedman, M. J. (2005). "Application of pressure monitoring and modelling to detect and minimize low pressure events in distribution systems." *J. Water Supply Res. Technol. Aqua*, 54(2), 65-81.

Karim, M. R., Abbaszadegan, M., and LeChevallier, M. (2003). "Potential for pathogen intrusion during pressure transients." *Journal AWWA*, 95(5), 134-146.

Kirmeyer, G., Friedman, M., Martel, K., Howie, D., LeChevallier, M., Abbaszadegan, M., Karim, M., Funk, J., and Harbour, J. (2001). "Pathogen intrusion into the distribution system." American Water Works Association Research Foundation, Denver, Colorado, USA.

LeChevallier, M. W., Gullick, R. W., and Karim, M. (2002). "The potential for health risks from intrusion of contaminants into the distribution system from pressure transients." United States Environmental Protection Agency and American Water Works Service Company Inc., Voorhees, New Jersey, USA.

LeChevallier, M. W., Gullick, R. W., Karim, M. R., Friedman, M., and Funk, J. E. (2003a). "Potential for health risks from intrusion of contaminants into the distribution system from pressure transients." *Journal of Water and Health*, 1(1), 3-14.

LeChevallier, M. W., Karim, M., Aboytes, R., Gullick, R., Weihe, J., Earnhardt, B., Mohr, J., Starcevich, J., Case, J., Rosen, J. S., Sobrinho, J., Clancy, J. L., McCuin, R. M., Funk, J. E., and Wood, D. J. (2004). "Profiling water quality

parameters: from source water to the household tap." American Water Works Association Research Foundation, Denver, Colorado, USA.

McInnis, D., and Karney, B. W. (1995). "Transients in distribution networks: field tests and demand models." *Journal of Hydraulic Engineering*, 121(3), 218-231.

Effects of Redesign of Water Systems for Security and Water Quality Factors

Walter M. Grayman[1], Regan Murray[2], and Dragan A. Savic[3]

[1]W.M. Grayman Consulting Engineer, 321 Ritchie Ave., Cincinnati, OH, 45215, PH: (513) 761-1722, email: grayman@fuse.net
[2]US EPA, National Homeland Security Research Center, NG-16, 26 W Martin Luther King Dr, Cincinnati, OH 45268; email: Murray.Regan@epa.gov
[3] University of Exeter, Centre for Water Systems, Harrison Building, North Park Road, Exeter EX4 4QF, UK; email: d.savic@ex.ac.uk

Abstract

Water distribution systems are typically designed based on hydraulic and cost considerations. In the United States, most urban water systems are looped systems with large pressure zones that serve customers in regions of different elevation. In the United Kingdom, water distribution systems are frequently further subdivided into zones of several thousand connections called district metering areas (DMAs) in order to track and control water leakage. In two case studies, starting with existing large looped water system designs, the current systems are redesigned to: (1) approximate a typical DMA design; and (2) provide additional control and isolation capability in order to improve the water security of the system. The systems are then compared in terms of four metrics: (1) fire flow; (2) water age; (3) water security; and (4) reliability. Though the results of the analysis may not necessarily be generalized beyond the case study examples, the methodology provides a mechanism for evaluating alternative water system designs, and provides insight into the effects of water security criteria on system design.

Keywords
Distribution systems, hydraulic modeling, water security, water quality

BACKGROUND

Water supply utilities are facing significant challenges within their distribution systems of both rehabilitating and replacing aging infrastructure, and developing new infrastructure in response to shifting population and development patterns. In most cases, aging infrastructure is replaced with new piping material that approximately mimics the location and characteristics of the original design (i.e., replace an existing cast iron pipe with a PVC pipe of the same size and routing). New infrastructure is generally designed to meet traditional standards associated with water consumption on a typical maximum demand day with a fire flow demand superimposed. Design objectives typically include minimizing cost and providing redundancy and reliability.

In the past decade, concerns about water security and water quality deterioration in distribution systems have been raised. However, there has been only limited work to determine how these concerns may be addressed in the design of new water systems or rehabilitation of existing systems.

In the United States, water distribution systems are typically designed as either looped systems or branching systems or a combination of both. In the United Kingdom, district meter areas (DMA) are frequently superimposed on a looping or branched system and used as an important element of distribution system design. Each approach to design has implications in terms of cost, reliability, system control, and other factors. The characteristics of each of these system designs are described below.

- Looped systems: In a looped system, larger transmission lines and interconnected local delivery pipes are used to deliver water to customers. There is extensive looping in both the transmission system and in the local lines so that there are generally multiple paths that water can follow from the treatment plant to customers.
- Branched systems: A branched system corresponds to a tree with larger pipes feeding smaller branches. In the extreme case, there are no loops and any disruption of a pipe causes outages to all downstream customers. Branched systems are most commonly found in rural water systems.
- District Meter Areas (DMA): A DMA consists of an isolated water distribution system zone for which there can be both control and calculation of flow amounts. It is an important concept in leakage management because the volume of flow into and out of the zone can be measured and abnormal usage can signal the presence of a leak problem. Zones generally contain between 1000 and 5000 connections and all inflow and outflow from each zone is metered.

An alternative design aimed specifically at improving security was suggested in a DHS sponsored study that is currently under review (Baker, 2007). This design incorporates elements of the three basic design concepts described above. The essence of this alternative is provided in the following statement:

> "The strategy is to configure the system using distribution blocks limiting their size to a maximum number based on the "acceptable" size of the contamination dispersion plume within the system. The maximum number of people served by one block could, for example, be limited to 5,000 people. It is important to note that block size and potential exposure are related. The larger the block size, the greater the potential exposure. Depending on the system, there may be a higher cost to implement smaller block sizes. Assuming the contaminant is fed into the distribution system through a house service or hydrant, the strategy is to limit the area of the distribution system where the contaminant could flow. Water would enter the "block" from the transmission system. No water would be allowed to leave the distribution block, i.e., all water entering the block would be consumed within the block."

Many of the concepts inherent in the DHS report are embodied in a distribution system that is divided into DMAs (Farley, 1985; Twort et al, 2000). Areas of similarity

include use of distribution blocks and controlled flow between transmission lines and the distribution blocks.

METHODOLOGY

In order to evaluate the effectiveness of different designs, a case study approach has been employed. Each case study starts with a hydraulic model of an existing water system design. The existing design is then modified to create alternative designs and the response and effectiveness of the original design and the redesigned water distribution systems are tested and compared. The redesigns are based largely on the concepts described in the DHS report (Baker, 2007) and the design of DMA-based systems. In order to evaluate the performance of alternative designs, four separate metrics are applied: (1) ability to provide fire flow requirements; (2) water age (as a surrogate for water quality); (3) water security as measured by health impacts resulting from a contamination event and by the length of pipes contaminated; and (4) a reliability index.

CASE STUDY 1

The initial case study focuses on one of the water systems used as part of the Battle of the Water Sensor Networks (BWSN) competition conducted at the Water Distribution System Analysis Symposium in 2006. This network serves approximately 150,000 people and is composed of 12,523 nodes and 14,822 pipes. An extended period simulation (EPS) EPANET model of the system is available representing average day conditions. The modeled system contains two reservoirs, two tanks, four pumps and five valves. The network is an approximate representation of a real world system. However, the geographic representation and names of the network have been adjusted and distorted in order to protect the identity of the system.

This system is typical of a looped urban distribution system. However, there is little topography in the service area, and as a result, is designed as a single pressure zone.

The present system was manually redesigned using the EPANET model as an aid in order to fit the DMA concept that is popular in the U.K. The system was divided into 43 DMAs by closing selected pipes (representing the closure of valves) and, in a few cases, adding or modifying other pipes. Target size for DMAs was in the range of 500 to 5000 connections each. This encompasses the DMA size of 2000 to 5000 connections suggested by Farley (1985) and the DMA size of 500 to 3000 connections suggested by Twort et al (2000). Preferably there should only be a single feed main for each DMA although this is not always possible. Farley (1985) suggests that feed lines should not exceed 300 mm (12 inches) in order to avoid costly meters. However, this too is not always feasible and may not be as significant an issue given improvements in metering since 1985. In some cases, many small lines serving only a few customers may be connected directly to a transmission line making their inclusion in DMAs difficult. In these cases, such lines may be excluded from the district metering system.

Since information on the number of connections at each node was not available, an average relationship between connections and water demand (known at each node) was developed. The total number of connections in the system is 77,916 and the average water usage is 16,408 gallons per minute. This corresponds to an average water use of 0.211 gpm/connection (or 304 gallons/day/connection). The distribution system network and resulting DMA zones are shown in Figure 1 and the characteristics of the DMAs summarized in Table 1.

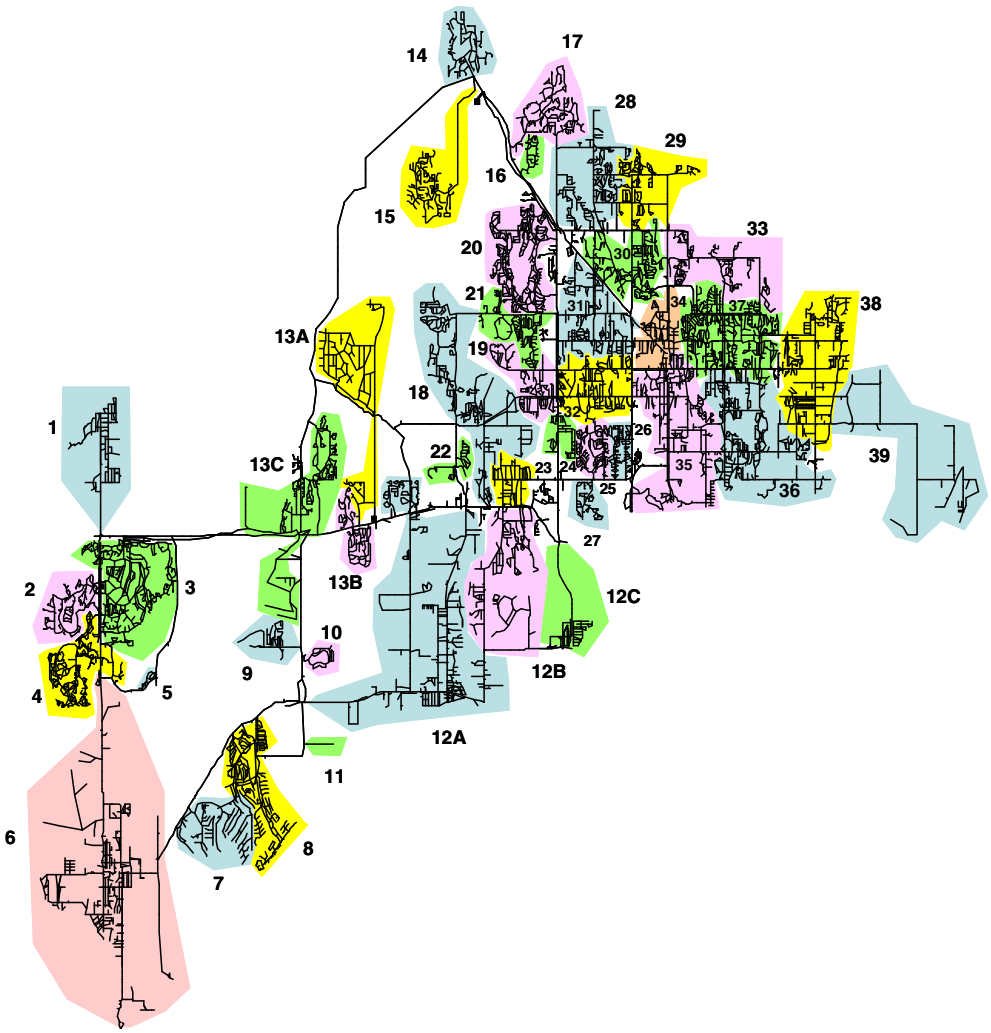

Figure 1. Case Study #1 Distribution System showing DMA Boundaries

The actual process of converting the model to represent a DMA-based water system was a manual, iterative process in which DMA boundaries were defined, feed lines identified, pipes (isolation valves) closed and, in a few cases, pipes modified or added. The modified EPANET model was repeatedly evaluated in the process to ensure the integrity and the hydraulic reliability of the redesigned system. Generally, the process of defining DMAs was more difficult in the central, denser looped part of the network than in the edges of the network. In the outlying parts of the system, frequently a DMA could be defined by simply "installing" a meter. At the other extreme, in the

central part of the system that was highly looped, multiple (sometimes exceeding over a dozen) pipes required closure in addition to multiple feeds and some existing pipe modifications.

In the process of creating the 43 DMAs, a total of 53 feed lines (meters) were defined, 163 pipes were closed, and only 11 pipes were added or modified. In all cases, the modified pipes involved the addition of only short stretches of pipes. In all cases except for one, there is no outflow from a DMA into either the transmission system or into another DMA. Of the 52 meters feeding DMAs, thirty meters are on 12" diameter lines while ten meters are on 8" and 10" diameter lines and ten are on 16" and 18" lines. The average number of connections per DMA is 1996 and, of the 43 DMAs, all but four fell within the target size of 500 to 5000 connections (three were smaller than 500 connections and one is slightly larger than 5000 connections). Less than ten percent of the total pipe length was excluded from DMAs.

The performance of the alternative designs is evaluated in terms of the four general metrics: (1) fire flow; (2) water age; (3) water security; and (4) reliability.

Fire flow Metric

One test of the efficacy of the DMA-modified system is its ability to provide sufficient fire flow. In creating DMAs, some pipes feeding an area are closed and this could have the impact of restricting the amount of flow entering a DMA or reaching remote portions of the DMA. The most critical situation that could be impacted by this would be low pressures resulting from large water demands associated with fire flow. In order to test this situation, the model was tested under a maximum demand day situation with a fire flow demand superimposed. The conditions used in this test approximated typical design standards used in the U.S.

The average day demand conditions represented by the model were converted to maximum day demands by applying a 1.4 global multiplier to all demands. Then, a 2-hour fire flow was superimposed from 12 PM to 2 PM. Initially, a value of 1400 gpm was used as the fire flow demand. Based on industry standards, a typical residential fire flow requirement is 750 to 1000 gpm while commercial fire flow requirements (without sprinklers) typically start at 1500 gpm. For each DMA, an interior node on a 6" or 8" pipe was selected as the location of the fire flow. There is no guarantee that this node would be the most critical node but short of performing an exhaustive test of all nodes, this provides a reasonable test of the ability of the system to adequately respond to a fire condition. The fire flow situation was tested by sequentially and separately applying a fire flow demand to each of the selected nodes. Initially, a 1400 gpm fire flow was applied and pressures at all nodes were checked to ensure that they were greater than 20 psi. If pressures were below 20 psi, then the fire flow demand was iteratively lowered until acceptable pressure levels were reached.

The analysis showed that for 75% of the DMAs, acceptable pressures (i.e., > 20 psi) resulted with the 1400 gpm fire flow. It should be noted that many of these DMAs could support fire flows much greater than 1400 gpm but the actual maximum fire

flow rate was not determined. For the remaining 25% of the DMAs, allowable fire flow values ranged from 400 gpm to 1200 gpm. The same procedure was used to test the same nodes in the looped model. The looped model frequently performed better (i.e., allowed for greater fire flow values), yet the difference between the two models was quite small.

Water Age Metric

Water age is frequently used as a surrogate to represent potential water quality deterioration in a distribution system. In this case study, a 192-hour hydraulic and water age simulation was run in the model for the original looped system and for the DMA-based system. The average water age during the final 24-hour period was then used to compare the results from the model. For each model, both the average water age and the demand-weighted average water age were calculated. The results are presented in Table 1.

Table 1. Comparison of Calculated Water Age for Alternative Designs

	Looped System	DMA System
Average water age (hours)	30.71	31.51
Demand weighted water age (hours)	20.88	20.77

As illustrated, there is no systematic difference in the calculated average water age between the alternative designs. Though there can be significant variations in water age by node, when viewed as a whole, no systematic difference was found.

Water Security Metric

Two water security metrics are used to compare designs. The first metric is the number of persons potentially exposed to a contamination incident. A method to estimate the potential health impacts resulting from contamination incidents in drinking water distribution systems developed by Murray et al, 2006, and implemented in the TEVA-SPOT software (USEPA, 2008), is used for this analysis. The second metric is the number of pipe feet contaminated during a contamination incident.

For this analysis, the contamination incident is assumed to occur when a 55-gallon drum of a biological agent with a concentration of 1E11 organisms/Liter is introduced at midnight for a period of 24 hours into a specific node in the network. The dose response curve is described by a probit function with a slope of 0.52 and an LD50 of 1.94E6. Each person drinks 2 Liters/day of water from the network, timed proportionally to the demand pattern at each node. Contamination incidents are simulated at all network nodes with positive demand (10,551 for this network, labeled Injection Node Set 1) and then the average impacts are calculated over this set of scenarios. A smaller set of all nodes with positive demand *and* within a DMA is also considered (9,924 nodes, labeled Injection Node Set 2) and results for both cases are presented below. The total impacts after 96 hours are shown in Table 2. This analysis assumes that no security measures are in place to prevent or reduce the impacts of

these incidents, nor are any measures taken to provide treatment to exposed persons. Thus, the results are overestimates of the likely public health impacts.

Table 2. Comparison of Water Security Metric for Alternative Designs

Metric	Injection set	Looped System	DMA System
Average # of people exposed	Injection node set 1	1,630	650
	Injection node set 2	1,420	440
Average feet of pipe contaminated	Injection node set 1	230,700	44,600
	Injection node set 2	209,700	23,200

The results show that the DMA System reduces the estimated number of persons exposed by more than 60% as compared to the original looped system, and the number of pipe feet contaminated by more than 80%.

Reliability Metric

An important concept in the design of a water distribution system is reliability in case of some unexpected hydraulic or mechanical failure. Todini (2000, 2008) proposed a resilience index as a measure of the degree of redundancy in a network. Resilience is defined as the intrinsic capacity of a network to overcome sudden failures, and it is measured as the ratio between the surplus of power delivered to users and the maximum power that can be dissipated in the network when meeting exactly the design criteria. A value of 30 psi was used as the design (minimum) pressure criteria. The availability of power allows water to find alternative pathways through the distribution system. Therefore, the resilience index provides an overall relative measure of redundancy with a higher resilience index value corresponding to higher redundancy. The resilience index was calculated over a 51-hour period for both the looped system and DMA system and an average, maximum and minimum value calculated for each system as shown in Table 3.

Table 3. Comparison of Resilience Index for Alternative Designs

	Looped System	DMA System
Average index	0.836	0.802
Maximum index	0.930	0.910
Minimum index	0.644	0.570

In all cases, the resilience index is slightly higher for the looped system than the DMA system (4% higher on average). However, the small differences for the indices between the looped and DMA systems, suggests that in this case, little is given up in reliability when moving from a looped system to a DMA system.

CASE STUDY 2

The second case study focuses on a portion of a municipal water system fed from a single water treatment plant and serving approximately 100,000 people. The distribution system encompasses approximately 400 miles of pipes. The network

model is composed of approximately 3,300 junctions and 3,800 pipes. Average water use for this area is 30 MGD.

An EPS EPANET model of the system was available representing average day conditions. The modeled system contains 34 tanks, 61 pumps and two valves. The service area topography has a range of approximately 900 feet and is divided into multiple pressure zones based on topography and connectivity. The network is an approximate representation of a real world system though the geographic representation and names of the network were adjusted and distorted in order to protect the identity of the system.

A manual procedure similar to the method used in Case Study 1 was employed to divide the service area into DMAs. Based on an estimate of 40,000 connections, an average relationship between connections and water demand (known at each node) was developed. This corresponds to an average water use of 0.53 gpm/connection (or 762 gallons/day/connection). The resulting DMA zones are shown in Figure 2.

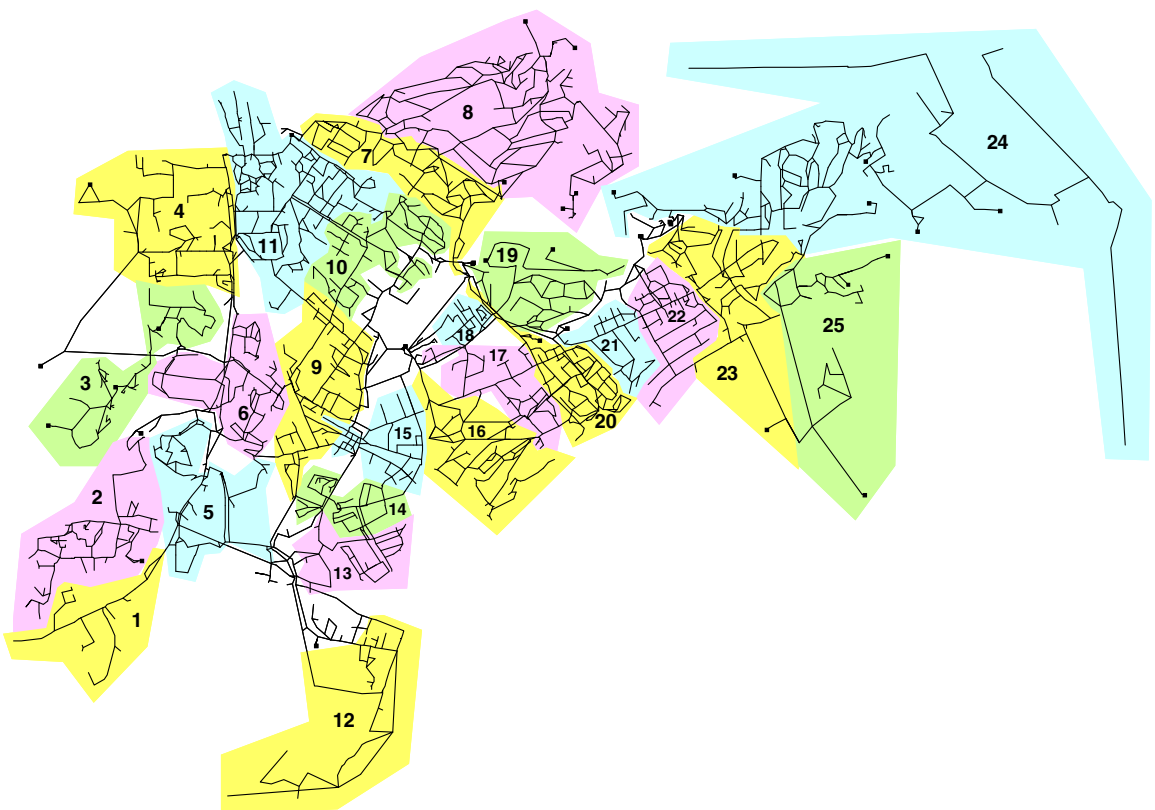

Figure 2. Case Study #2 Distribution System showing DMA Boundaries

The average number of connections per DMA is 1,517 and all DMAs were within the target size of 500 to 5,000 connections with the exception of one DMA that had 469 connections. It is estimated that less than two percent of the pipe length containing service connections was excluded from DMAs. In most cases, these pipes were fed directly from large transmission lines and it was impractical to include them in DMAs.

In most cases, the backbone transmission system was not included within DMAs but rather, delivered water to the DMAs. All but two of the DMAs that were created were fed by a single meter. The remaining two DMAs were fed by two meters. In the DMA creation process, a total of 102 pipes were closed, and only 2 pipes were modified. In all cases except for two sets of DMAs, there is no outflow from a DMA into either the transmission system or into another DMA. In most cases the meters were on pipes with diameters that exceeded the suggested 12" maximum size. This was necessitated by the current pipe configurations.

Fire flow Metric

A similar fire flow analysis similar to that used for Case Study #1 was applied to Case Study #2. The analysis showed that for 19 of the 25 DMAs, acceptable pressures (i.e., > 20 psi) resulted with the 1,400 gpm fire flow. It should be noted that many of these DMAs could support fire flows much greater than 1400 gpm but the actual maximum fire flow rate was not determined. For the remaining six DMAs, allowable fire flow values ranged from 800 gpm to 1,100 gpm. The same procedure was used to test the same nodes in the looped model. In the looped model all but two of the nodes supported a fire flow of at least 1,400 gpm and the difference between the two models was quite small.

Water Age Metric

Water age was used as a surrogate to represent potential water quality deterioration in a distribution system. In Case Study #2, a 960-hour hydraulic and water age simulation was run in the model for the original looped system and for the DMA-based system. The average water age for the last 24-hour period was then used to compare the results from the model. For each model, both the average water age and the demand-weighted average water age were calculated. The results are presented in Table 4. As illustrated, there does not appear to be an appreciable systematic difference in the calculated average water age between the alternative designs.

Table 4. Comparison of Calculated Water Age for Alternative Designs

	Looped System	DMA System
Average water age (hours)	69.14	73.33
Demand weighted water age (hours)	60.39	56.49

Water Security Metric

The simulation methodology and specific contamination incidents described for the first case study are utilized again here. Injection Node Set 1 includes all 1,621 nodes with positive demand, while Injection Node Set 2 includes 1,513 of these nodes that are within the DMA. The results presented in Table 5 show that the DMA System reduces the estimated number of persons exposed by more than 70%, and the number of pipe feet contaminated by more than 85%.

Table 5. Comparison of Water Security Metrics for Alternative Designs

Metric	Injection set	Looped System	DMA System
Average # of people exposed	Injection node set 1	6,500	1,870
	Injection node set 2	5,850	1,180
Average feet of pipe contaminated	Injection node set 1	415,000	55,700
	Injection node set 2	390,520	30,800

Reliability Metric

The resilience index was used as a measure of the reliability (redundancy) of the distribution system with higher values of the index corresponding to greater reliability. The resilience index was calculated over a 48-hour period for both the looped system and DMA system and an average, maximum and minimum value calculated for each system as shown in Table 6.

Table 6. Comparison of Resilience Index for Alternative Designs

	Looped System	DMA System
Average index	0.267	0.276
Maximum index	0.547	0.651
Minimum index	0.075	0.076

In all cases, the resilience index is slightly higher for the DMA system than the looped system (3% higher on average). This suggests that there was no loss in reliability when moving from a looped system to a DMA system and in fact, a slightly greater degree of reliability resulted.

CONCLUSIONS

Two case studies were conducted using computer modeling of distribution systems in the United States to evaluate distribution system design in terms of several metrics. In each case, the current looped water distribution system was redesigned to incorporate aspects of district metering areas (DMAs) and other concepts that may reduce the impacts of security breaches. Following are several conclusions reached concerning these results. Though the results of the analysis may not necessarily be generalized beyond the case study examples, the methodology provides a mechanism for evaluating alternative water system designs, and provides insight into the effects of water security criteria on system design.

1. The process of converting from a looped to a DMA-based distribution system required many pipe closures and additions of check valves. However, on paper, the design changes were relatively minor to implement.
2. Conversion from a looped to a DMA-based distribution system resulted in only slight decreases in the availability of fire flow.
3. The reliability of DMA-based systems as compared to looped systems (as measured by a resilience index) was approximately the same.
4. There was no systematic change in water age when moving from a looped system to a DMA-based system.
5. When the distribution systems were changed from looped systems to DMA-based systems, there was a very significant improvement in water security

related metrics. The two metrics used to represent water security were the number of persons potentially exposed to a contamination incident and the number of pipe feet contaminated during a contamination incident. The DMA-based systems resulted in improved water security as measured by reductions of both metrics by 60 to 85%.

The results of this analysis suggest that significant improvements in water security could be achieved through redesign of both existing and new distribution systems without significantly impacting other design criteria. Further investigation of this concept is certainly warranted.

ACKNOWLEDGMENTS

The authors would like to acknowledge the assistance of the following people: Dr Raziyeh Farmani of the University of Exeter for her assistance in calculating the resilience indices; Don Ballantyne of MMI Engineering for his thoughtful comments and original insights on the design of water systems to improve security; and Robert Janke and Terra Haxton of the United States Environmental Protection Agency's (EPA) National Homeland Security Research Center for their insightful comments and suggestions. The EPA's Office of Research and Development collaborated in and partially funded this work. This research has been subjected to the Agency's review and approved for publication. The views and opinions expressed herein do not necessarily state or reflect those of the Agency.

REFERENCES

Baker (2007). Municipal Water Distribution System Security Study: Recommendations for Science and Technology Investments". Draft report (dated December 2007) prepared for U.S. Department of Homeland Security by a team headed by Michael Baker Jr.

Farley, M.R. (1985). "District Metering. Part 1-System Design and Installation". WRc, Swindon, UK.

Murray, R., Uber, J. and Janke, R. (2006). Model for Estimating Acute Health Impacts from Consumption of Contaminated Drinking Water. *J. Wat. Res. Planning and Manag*. 132(4): 293-299.

Todini, E. (2008). "Design, expansion and rehabilitation of water distribution networks aimed at reducing water losses. Where are we?", Proceedings of the 10th Annual Water Distribution Systems Analysis Conference WDSA2008, Van Zyl, J.E., Ilemobade, A.A., Jacobs, H.E. (eds.), August 17-20, 2008, Kruger National Park, South Africa.

Todini, E. (2000) "Looped water distribution networks design using a resilience index based heuristic approach". Urban Water, Elsevier Pubs., 2(2), 115-122.

Twort, A.C., Ratnayayaka, D.D., and Brandt, M.J. (2000). Water Supply. 5th Edition. Butterworth-Heinemann, Oxford, UK.

U. S. Environmental Protection Agency (2008). User's Manual TEVA-SPOT Toolkit, Version 2.0. EPA 600/R-08/041.

Propagation of chlorine demand signals induced by microbial contaminants in a drinking water distribution system

D.E. Helbling[1], PE, Ph.D and J.M. VanBriesen[2], Ph.D., AM ASCE

[1]Postdoctoral Researcher, Department of Environmental Chemistry, Swiss Federal Institute of Aquatic Science and Technology (Eawag), Ueberlandstrasse 133, 8600-Duebendorf, Switzerland
Email: damian.helbling@eawag.ch

[2]Professor, Department of Civil and Environmental Engineering, Carnegie Mellon University, 5000 Forbes Avenue, Pittsburgh, Pennsylvania 15213.
Email: jeanne@cmu.edu

ABSTRACT

Chlorine residual concentration is used as a protection from accidental and intentional intrusion of microbial contaminants in distribution systems. Monitoring chlorine residual with real-time sensors may enable detection of such intrusions. However, this necessitates prediction of chlorine levels and how they change under normal conditions and in the event of a microbial intrusion event. Existing multi-specie models require knowledge of specific reaction kinetics between chlorine and complex cellular matrices that are unlikely to be known *a priori*. Rather, we propose utilization of a parallel first order rate expression describing microbially-induced chlorine decay over a wide range of conditions. The model can be parameterized using a limited number of batch experiments. The model formulation is then integrated into EPANET-MSX using the programmer's toolkit. We present simulations of a series of microbial events in a small distribution system using the model. Our results indicate that change in residual induced by microbial intrusion events can be simulated in distribution system models. Chlorine residual signals can thus be predicted. Event detection is limited by lack of control of chlorine concentration at the time and location of the contaminant event, the unique species-specific chlorine reaction kinetics, and the changing demand patterns in the system.

INTRODUCTION

While modern drinking water treatment technologies have dramatically improved the biological quality of finished drinking water, emerging deficiencies in the distribution system are resulting in increasing numbers of infectious waterborne

disease outbreaks within the United States (Liang et al., 2006). The rate of incidence of outbreaks is projected to increase due to the aging of drinking water infrastructure beyond its intended design life resulting in more cracked, broken, or otherwise structurally compromised pipes (Geldreich et al., 1992). Also, the increased development of a non-potable water infrastructure for irrigation or industrial uses has resulted in more incidents of inadvertent cross connections which may contribute to biologically compromised water (Lahti and Hiisvirta, 1995). Further, there is on-going concern over threats of intentional biological contamination within distribution systems that could result in catastrophic morbidity and mortality (American Water Works Association, 2002; National Research Council, 2002).

Current regulations require water utilities to monitor the biological quality of distribution system water, which is often accomplished via grab samples and species or group specific assays such as heterotrophic plate counts. These methods result in temporally and spatially sparse data sets that do not provide adequate warning of a biological contamination event. Also, species specific detection is considered an impractical approach for early warning of contamination events given the large number of potential pathogenic biological contaminants that exist. A more practical approach that may enhance the probability of pathogen detection is an intelligent infrastructure equipped with sensors that monitor traditional drinking water parameters that are sensitive to biological contamination. In previous work, we have shown that free chlorine residuals at concentrations typically found within the distribution system are very sensitive to an array of bacterial species, including species that are resistant to chlorine as a disinfectant (Helbling and VanBriesen, 2007). Further, commercially available chlorine sensors have been shown to rapidly respond to injected contaminants within a distribution system (Helbling and VanBriesen, 2008; Hall et al., 2007) and batch determined reaction kinetics have been used to predict *in situ* chlorine response to injected bacterial species, which was validated by sensor response (Helbling and VanBriesen, 2008).

Much research has been published on placement algorithms for drinking water sensors used for contaminant detection, but these studies typically assume the availability of "perfect" sensors that can detect all potential contaminants with very low detection limits (Krause et al., 2008; Ostfeld and Salomons, 2004; Ostfeld et al., 2008; Xu et al., 2008; Berry et al., 2006; Berry et al., 2005). Of course, "perfect" sensors are not likely to ever be available, so in this work we consider the placement of *chlorine sensors* within a distribution system in relation to how *in situ* chlorine concentrations respond to biological contamination downstream from an event. Before we can consider placement algorithms optimized for non-specific detection of contamination events with chlorine sensors, we must first consider how one can model chlorine response to biological contaminants within a distribution system. Under normal operating conditions, free chorine concentrations can be modeled with water quality simulators such as EPANET (Rossman, 2000), which considers chlorine reactions within the bulk water and with pipe walls. An enhanced version of EPANET including an extension for multi-species reactions (EPANET-MSX, Shang et al., 2007) allows for the inclusion of additional reactive species. These reactions

are input within EPANET-MSX as a series of ordinary differential equations that represent all of the reactions between all of the reactants within the system.

With EPANET-MSX and the integral programmer's toolkit, sophisticated user defined scenarios can be simulated. The primary objective of this work was to develop a model within EPANET-MSX capable of simulating the dynamic response of free chlorine within a community distribution system to injected loads of specific bacterial contaminants. By modeling these interactions and the resulting propagation of chlorine response we can assess the potential of chlorine sensors to be used as sentinels of biological contamination within distribution systems. The following describes the development of the model and preliminary results of the simulations.

MODEL

Because EPANET-MSX allows for simple incorporation of rate expressions, the initial attempts at building the model were to define the reactant system as a set of ordinary differential equations. The most logical system of equations to describe chlorine response to biological contaminants is the set of equations:

$$\frac{dC}{dt} = -k_b C - k_w C - \sum_1^n k_n X_n C$$

$$\frac{dX_n}{dt} = \sum_1^n k_n \theta_n X_n C$$

where, k_b is the bulk water chlorine decay rate (determined in batch reactors); k_w is the pipe wall chlorine decay rate (determined from (Hallam et al., 2002)); C is the chlorine concentration; X_n is the total concentration of oxidizable cellular material of each biological reactant n (proteins, lipids, nucleic acids, etc.); k_n is the chlorine decay rate induced by biological reactant n; and θ_n is the stoichiometric coefficient relating how each biological reactant n reacts with chlorine. The parameters k_n and θ_n must be estimated first from experimental data. The parameter Q is used to define the fraction of each biological reactant in the system (for n=2, X_1=Q*X and X_2=(1-Q)*X). We utilized 4th order Runge Kutta to solve this set of ordinary differential equations and to estimate the parameter values based on data derived from over 100 batch experiments conducted over a range of initial free chlorine concentrations and with *Escherichia coli, Staphylococcus epidermidis*, or *Mycobacterium aurum* suspended in a chlorine demand free phosphate buffer (pH=7.2).

The most rigorous approach would be to consider *each* macromolecular reactant as a separate species by assuming $n \rightarrow \infty$. However, this approach is impractical it is not possible to analyze the specific biochemical reactions occurring in such a system with such detail. Further, it is also likely that initial oxidation of a rapidly reacting species would result in a product that also contains viable oxidation sites that react slowly; in other words X_1 can react and form X_2. Although a likely mechanism, it is again impractical to try to estimate the occurrence of these pathways without much deeper biochemical analyses. Therefore, in order to simplify the

conceptual model and for ease of calculation, we first analyze the set of equations considering only X_1 (a concentration of rapidly reacting cellular material) and X_2 (a concentration of slowly reacting cellular material) i.e. n=2.

The first complication in employing this model arose with the need to define input values for X_1 and X_2. How does one quantify an aggregation of cellular material that can be subsequently divided into rapidly and slowly reacting fractions? In reality, chlorine is likely reacting with specific oxidation sites on the various macromolecular components of the matrix. Any given macromolecular component may react differently and contain any number of potential oxidation sites. The decision was made to quantify the amount of total organic carbon (TOC) associated with each microbial suspension via UV-persulfate oxidation (2005) and use that concentration as a surrogate for all oxidizable cellular material. Using the input values of initial chlorine and the measured total organic carbon concentrations, 4th order Runge Kutta was used to estimate the parameters Q, k_1, k_2, θ_1, and θ_2 and the time dependent values of X_1, X_2, and C were obtained for each of the experimental data sets derived from the 100+ batch experiments. The estimated parameter values were obtained by minimizing the sum of the squares of the residuals between the observed and predicted chlorine concentrations (Microsoft Excel 2003, Solver).

The results showed that the estimated parameter values were inconsistent, with Q and k_1 varying over three orders of magnitude and k_2 varying over 6 orders of magnitude with no correlation to initial chlorine or cell concentrations. This suggests that this simplified conceptual model is not adequately representing the mechanisms and reactions occurring in this system. Further, while time dependent values of X_1 and X_2 are provided by the solution, there is no way to check whether these values are realistic as there is no way to quantify the change in concentration of cellular material over time within the experimental setup. A rudimentary sensitivity analysis on the input value X also showed that the estimated parameters are all very sensitive to relatively small changes in X, which is not ideal given the uncertainty inherent within the use of X as an input parameter.

Due to these complications, an alternative way to model the system's reactions was investigated by assuming an excess of cellular material reactant (a logical assumption for a contamination event) and employing pseudo nth order decay models. The models considered included: a pseudo first order model; a pseudo nth order model; a limited pseudo first order model; a limited pseudo nth order model; and a parallel pseudo first order model (**Equation 1**). This approach is consistent with the literature in this field for estimating chlorine decay associated with complex natural organic matter (which also contain several reactive components) within the distribution system (Haas and Karra, 1984; Powell et al., 2000b). Each of these models was used to fit the experimental batch data and values for the correlation coefficient (r^2), the residual mean square error (RMSE), the Akaike information criterion (AIC), and Bayesian information criterion (BIC) were determined. The results of the analysis showed that for nearly all batch studies, the parallel pseudo first order model had the highest r^2, and the lowest RMSE, AIC, and BIC. Further, the

parameter values for the parallel pseudo first order expression were deterministic for each microbial species and the estimated values of Q, k_1, and k_2 were strongly correlated with initial chlorine and cell concentrations (Helbling and VanBriesen, 2009). For these reasons, we continued toward a working model by using the parallel pseudo first order expression. The next challenge was how to incorporate this expression and its dynamic parameters into EPANET-MSX.

The analytical solution of the parallel pseudo first order expression is:

$$C_t = (1-Q) * C_0 * \exp(-k_1 t) + Q * C_0 * \exp(-k_2 t) \quad (1)$$

where, Q is the fraction of the chlorine that reacts with the slowly reacting cellular material (or just the stoichiometricly adjusted fraction of slowly reacting cellular material); k_1 is the rate in which chlorine reacts with rapidly reacting cellular material; and k_2 is the rate in which chlorine reacts with slowly reacting cellular material. Additional parallel terms could be added to account for cellular material that reacts at different rates (n>2), but analysis of the AIC and BIC of data fits after adding additional parallel terms did not improve the ability of the model to fit the data (data not shown). Thus we concluded that, for models of a parallel first order form, a two term model is most suitable for this application. However, EPANET-MSX requires input in the form of rate expressions. The following describes how the parallel pseudo first order expression was incorporated into EPANET-MSX.

The total chlorine concentration within the reacting system is the sum of the chlorine reacting with the rapidly and slowly reacting cellular material. With Q defined as the fraction of slowly reacting cellular material in the system, this is expressed mathematically as shown in Equations 2 - 4.

$$C_t = C_{fast} + C_{slow} \quad (2)$$

$$C_{fast} = (1-Q) * C \quad (3)$$

$$C_{slow} = Q * C \quad (4)$$

The rate coefficients k_1 and k_2 define the rate in which chlorine reacts with the rapidly and slowly reacting cellular material, therefore the rates of change of each of the chlorine fractions are given by Equations 5 and 6.

$$\frac{dC_{fast}}{dt} = -k_1 * C_{fast} \quad (5)$$

$$\frac{dC_{slow}}{dt} = -k_2 * C_{slow} \quad (6)$$

Analytical solutions of Equations 5 and 6 are given as Equations 7 and 8.

$$C_{t,fast} = C_{0,fast} * \exp(-k_1 t) \quad (7)$$

$$C_{t,slow} = C_{0,slow} * \exp(-k_2 t) \quad (8)$$

Substitution of the analytical solutions in Equations 7 and 8 into Equation 2 yields,

$$C_t = C_{0,fast} * \exp(-k_1 t) + C_{0,slow} * \exp(-k_2 t) \quad (9)$$

and substitution of Equations 3 and 4 into Equation 9 yields the final analytical solution for the parallel pseudo first order model (Equation 1), as frequently cited in the literature. Therefore, it is in this form, as two separate pseudo first order rate expressions (Equations 5 and 6), that the parallel first order expression is implemented within EPANET-MSX. This is consistent with the concepts of mass balance and reaction kinetics within EPANET-MSX.

The model was used to simulate the response and propagation of chlorine demand signals throughout a community distribution system. Use of the model is initiated by the following work flow: define network structure, system demand, dosed chlorine concentration, booster locations and doses, k_b, and k_w; initiate a hydraulic and water quality analysis within EPANET; define the time and location of the contamination event; the model determines the chlorine concentration at the time and location of the contamination event; the model determines the dynamic values for the parallel pseudo first order model, which are dependent only on contaminant type and initial chlorine concentration; the model calculates multi-species reactions and concentrations; repeat for each time step over the duration of the pulse contaminant input. The mechanics of the model were written in C++ and incorporated into EPANET-MSX using the programmer's toolkit. More details are available in Helbling and VanBriesen (2009).

RESULTS

Contamination simulations were carried out in the small network shown in **Figures 1** and **2**. This network was used in the Battle of the Water Sensor Networks (Ostfeld et al., 2008) and is available online at (ECWS). System architecture and demands have been previously defined for this network (Ostfeld et al., 2008) and k_b and k_w values were taken as typical values reported in the literature (Hallam et al. 2002; Powell et al., 2000a). A typical EPANET hydraulic and water quality analysis was then performed for an 8-day duration with the first 4-days of data discarded as an equilibration period.

For the first set of contamination simulations, the objective was to determine how chlorine demand signals propagate within a community distribution system. To establish a best-case scenario for signal propagation, Node J-30 (**Figure 1**) was selected as it is the Node with the highest degrees of centrality and reachability (Xu et al., 2008). Because a single Node was selected, we then decided to test how demand patterns may effect chlorine demand signal generation and propagation by selecting 8 contamination times spaced 3-hours apart over a 24-hour period. Therefore, we simulated the injection of *E. coli* and *M. aurum* at Node J-30 at 8:00AM,

11:00AM,…,5:00AM for a 40-minute duration embedded within Days 5 and 6 of an 8-day hydraulic and water quality simulation. Chlorine concentrations at each Node and at each 30-minute water quality time step was compared over Days 5 and 6 between the base case water quality simulation (no contaminant injected) and each of the contaminant injection scenarios. Detectable chlorine demand signals were defined as those generating a change in "typical" background concentration of >25% and are shown in a spatial analysis in **Figure 1**. It is clear from **Figure 1** that, while chlorine demand signal propagation is dependent on temporal demand patterns, significant changes in chlorine residual are evident at locations downstream and distant to Node J-30. Also of note are the differences attributable to the differences in reaction rates of each species tested; *E. coli* reacts quite rapidly while *M. aurum* reacts more slowly. For more details on the injection scenarios and results, see Helbling and VanBriesen (2009).

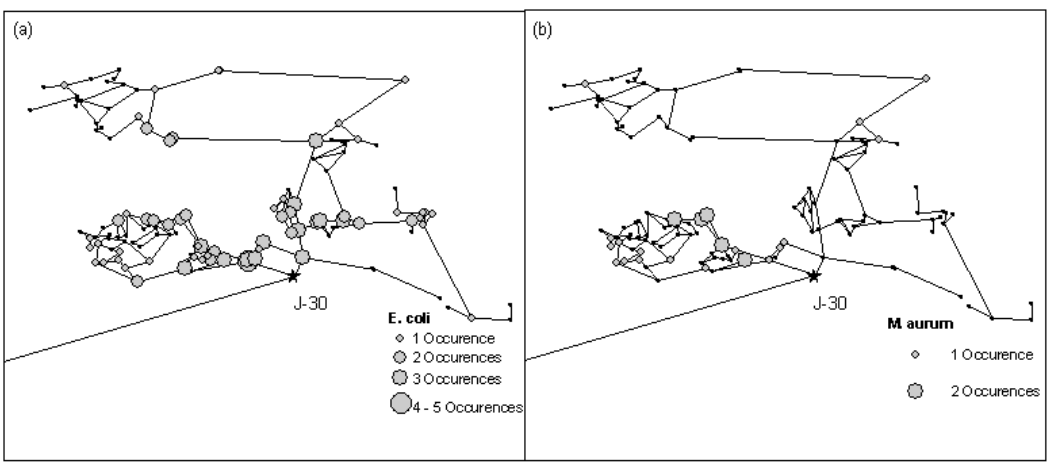

Figure 1: Spatial analysis of the number of occurrences of a >25% change in chlorine concentration for each of the: (a), eight *E. coli*; and (b), eight *M. aurum* injection simulations

Another spatial analysis considers each of the 16 simulations (8 *E. coli* plus 8 *M .aurum)* and determines the 10 nodes that see the greatest change in chlorine concentration during each contamination simulation. These 10 nodes would provide the greatest likelihood of detection in the case of a contamination event acting at Node J-30 while highlighting nodes that are less sensitive to species induced reaction rates. **Figure 2** shows that the majority of these nodes depend on system demand patterns that favor transport to the west of Node J-30. But interestingly, a significant number of nodes downstream and several nodes removed from Node J-30 are also consistently in the top ten nodes that see the greatest change in chlorine concentration. This result emphasizes that, when selecting locations for sensors as sentinel systems, nodes more downstream from centrally located nodes (like J-30) are ideal candidates for placing sensors as they are reachable by a larger number of nodes.

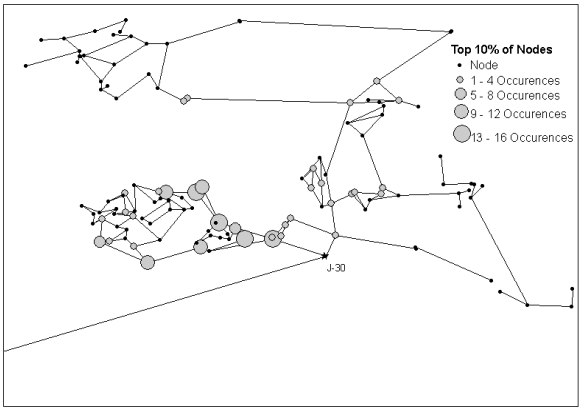

Figure 2: Spatial view of the top 10 most effected nodes over each of the 8 simulated contamination events for each contaminant

Another consideration for placement of chlorine sensors as sentinel systems is whether or not higher "typical" chlorine concentrations at the point of detection (the sensor location) can enhance detection; as it has been previously that higher chlorine residuals may result in greater changes in chlorine concentration during contamination events (Helbling and VanBriesen, 2007). To check this, we located all of the nodes that see a change in "typical" background concentrations of >25% during any of the 16 contaminant simulations and defined them as "sensitive nodes". We then need to determine if the chlorine concentrations are indeed higher at these sensitive nodes at the time of contamination. In **Figure 3**, we plot the distribution of chlorine concentrations at all nodes *and* at only the "sensitive nodes" at the time of maximum detection in the base case. The distribution shows that the median value of chlorine concentration in the system at the time of maximum detection during all simulated contamination events is approximately 0.40 mg/L. The median chlorine concentration at nodes that see a change in "typical" background concentrations of >25% is 0.58 mg/L. These distributions reinforce the hypothesis that higher chlorine residuals may result in greater changes in chlorine concentration during contamination events.

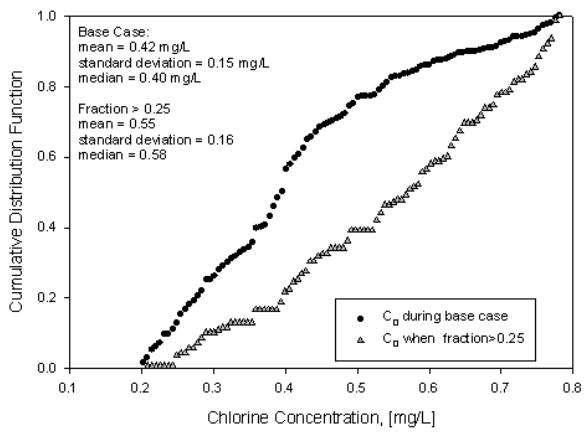

Figure 3: Distribution of chlorine concentrations at all nodes (black circles) and at sensitive nodes (gray triangles).

CONCLUSIONS

- A parallel pseudo first order decay model best fits experimentally determined chlorine demand generated by dense microbial suspensions for each species studied and for any cell or chlorine concentration
- Propagation of chlorine demand signals are dependent on distribution system architecture, demand patterns, and contamination location.
- Propagation of chlorine demand signals are dependent on species reaction kinetics and different species can result in maximum demand at different nodes
- Propagation of chlorine demand signals are dependent on chlorine residual concentrations both at the contaminated node and at the node of detection; greater residual concentrations result in enhanced detection capabilities.

REFERENCES

American Water Works Association (2002). *Water System Security: A Field Guide* AWWA, Denver, CO.

Berry, J., Hart, W.E., Phillips, C.A., Uber, J.G., and Watson, J.P. (2006). "Sensor Placement in Municipal Water Networks With Temporal Integer Programming Models." *Journal of Water Resources Planning and Management-Asce*, 132(4), 218-224.

Berry, J. W., Fleischer, L., Hart, W. E., Phillips, C. A., and Watson, J. P. (2005). "Sensor Placement in Municipal Water Networks." *Journal of Water Resources Planning and Management-Asce*, 131(3), 237-243.

Geldreich, E. E., Fox, K. R., Goodrich, J. A., Rice, E. W., Clark, R. M., and Swerdlow, D. L. (1992). "Searching for a Water-Supply Connection in the Cabool, Missouri Disease Outbreak of Escherichia-Coli O157-H7." *Water Research*, 26(8), 1127-1137.

Haas, C. and Karra, S. (1984). "Kinetics of Wastewater Chlorine Demand and Exertion." *Journal of the Water Pollution Control Federation*, 56, 170-173.

Hall, J., Zaffiro, A. D., Marx, R. B., Kefauver, P. C., Krishnan, E. R., and Herrmann, J. G. (2007). "On-Line Water Quality Parameters as Indicators of Distribution System Contamination." *Journal American Water Works Association*, 99(1), 66-77.

Hallam, N. B., West, J. R., Forster, C. F., Powell, J. C., and Spencer, I. (2002). "The Decay of Chlorine Associated With the Pipe Wall in Water Distribution Systems." *Water Research*, 36(14), 3479-3488.

Helbling DE and VanBriesen, J. (2007). "Free chlorine demand and cell survival of microbial suspensions." *Water Research*, 41(19) 4424-4434.

Helbling, DE and VanBriesen, J. (2008). "Continuous Monitoring of Residual Chlorine Concentrations in Response to Controlled Microbial Intrusions in a Laboratory-scale Distribution System." *Water Research*, 42(12), 3162-3172.

Helbling, DE and VanBriesen, J. (2009). "Modeling residual chlorine response to a microbial contamination event in drinking water distribution systems." Submitted to *Journal of Environmental Engineering*.

Krause, A., Leskovec, J., Guestrin, C., Vanbriesen, J., and Faloutsos, C. "Efficient Sensor Placement Optimization for Securing Large Water Distribution Networks." Submitted to *Journal of Environmental Engineering-Asce.*

Lahti, K. and Hiisvirta, L. (1995). "Causes of Waterborne Outbreaks in Community Water-Systems in Finland - 1980-1992." *Water Science and Technology*, 31(5-6), 33-36.

Liang, J., Dziuban, E., Craun, G., Hill, V., Moore, M., Gelting, R., Calderon, R., Beach, M., and Roy, S. (2006). "Surveillance for Waterborne-Disease and Outbreaks Associated with Drinking Water and Water not Intended for Drinking --- United States, 2003--2004." *Morbidity and Mortality Weekly Report*, 55(SS-12), 31-58.

National Research Council (2002). *Making the Nation Safer: The Role of Science and Technology in Countering Terrorism*. The National Academies Press, Washington, DC.

Ostfeld, A. and Salomons, E. (2004). "Optimal Layout of Early Warning Detection Stations for Water Distribution Systems Security." *Journal of Water Resources Planning and Management-Asce*, 130(5), 377-385.

Ostfeld, A., Uber, J., Salomons, E., Berry, J., Hart, W., Phillips, C., Watson, J., Dorini, G., Jonkergouw, P., Kapelan, Z., Pierro, F., Khu, S., Savic, D., Eliades, D., Polycarpou, M., Ghimire, S., Barkdoll, B., Gueli, R., Huang, J., McBean, E., James, W., Krause, A., Leskovec, J., Isovitsch, S., Xu, J., Guestrin, C., VanBriesen, J., Small, M., Fischbeck, P., Preis, A., Propato, M., Piller, O., Trachtman, G., Wu, Z., and Walski, T. (2008). "The Battle of the Water Sensor Networks (BWSN):A Design Challenge for Engineers and Algorithms." Submitted t o *Journal of Environmental Engineering-Asce.*.

Powell, J. C., Hallam, N. B., West, J. R., Forster, C. F., and Simms, J. (2000a). "Factors Which Control Bulk Chlorine Decay Rates." *Water Research*, 34(1), 117-126.

Powell, J. C., West, J. R., Hallam, N. B., Forster, C. F., and Simms, J. (2000b). "Performance of Various Kinetic Models for Chlorine Decay." *Journal of Water Resources Planning and Management-Asce*, 126(1), 13-20.

Rossman, L. (2000). *EPANET 2 Users Manual*. Risk Reduction Engineering Laboratory, US Environmental Protection Agency, Cincinnati, OH.

Shang, F., Uber, J., and Rossman, L. (2007). *EPANET Multi Species Extension Users Manual*. National Risk Management Research Laboratory, US Environmental Protection Agency, Cincinnati, OH.

Xu, J., Fischbeck, P., Small, M., VanBriesen, J., and , C. E. (2008). "Identifying sets of key nodes for placing sensors in dynamic water distribution systems." *Journal of Water Resources Planning and Management*.

A Markov Chain Monte Carlo Implementation of Bayesian Contaminant Source Characterization in Water Distribution Systems Under Stochastic Demands

Kenneth W. Harrison[a,b], Hui Wang[c]

[a]Earth System Science Interdisciplinary Center, College Park, MD 20740-3823

[b]Hydrological Sciences Branch, NASA Goddard Space Flight Center, Greenbelt, MD, 20771

[c]North Carolina State University, Campus Box 7908, Raleigh, NC 27695-7908

Abstract: Bayesian analysis is applied to the problem of probabilistic source characterization in water distribution systems. An implementation of the Markov Chain Monte Carlo (MCMC) method is tailored to water distribution systems. The likelihood function, a key component of Bayes' rule, is approximated using a Monte Carlo-based stochastic water demand model. Limitations of the approach are also discussed.

keywords: uncertainty, inverse modeling, source identification, infrastructure security

1. Introduction

Research on water distribution analysis is understandably expanding as there is an increased focus on the security of water and other critical infrastructure. An important goal of water security is the development of an early warning system for water distribution systems. This paper focuses on the problem of source characterization immediately following detection of contaminant by a sensor network in a water distribution system.

Generally, contaminant source identification has been treated as an inverse problem without any stochastic modeling and a "best" prediction of the source (e.g., Waanders et al. 2003; Shang et al., 2005; Laird, 2005a; Preis et al., 2006; Guan et al., 2006). Some have adopted a probabilistic approach (e.g., Propato, 2007; Pousakis et al., 2003; Shang et al., 2008), but with the stochastic modeling limited to sensor measurement error. Dawsey and Barbara (2006) use Bayesian belief networks to identify the contamination node but they do not characterize its magnitude nor duration. This paper focuses on the development of a Bayesian approach to address several problem features, including multiple sources of stochastic behavior (e.g., in nodal water demand), uncertainty in multiple source characterization parameters (e.g., magnitude, start time, and location), and prior knowledge relating to possible source characterization scenarios.

In this paper, the serious computational challenges in applying Bayesian analysis to the problem of source characterization are addressed. For computational efficiency, the method of Markov chain Monte Carlo (MCMC) is applied. The contribution of the paper is an

MCMC implementation of Bayesian analysis tailored to water distribution systems.

In the write-up of the MCMC implementation, a simplified contamination case is considered, where the source location, start time, and magnitude are unknown. The anticipated ultimate use of MCMC is to allow for more uncertainty in the description of the source, e.g., allowance for multiple sources and multiple contaminant injection time profiles. The simplified case is targeted because it permits the development of a benchmark solution against which the MCMC implementation can be compared. The numerical scheme to identify the benchmark solution, a compute-intensive grid-based integration of Bayes' Rule, cannot be scaled up further while retaining accuracy.

This emphasis of this paper is on the MCMC method development. The method has been tested for a specific example network (EPANET2 example 3) but with simplifying assumptions with respect to the dynamics; the mean demand is assumed time invariant. A parallel implementation is being developed to relax this assumption and to incorporate hydraulic measurements and will be reported on in future work.

The organization of the paper is as follows. In section 2, the MCMC implementation is developed. In section 3, the limitations of the MCMC implementation are discussed.

2. Methods

In the modeling context, Bayesian analysis provides a basis for updating the probability of alternative model fits θ. In the water distribution source characterization problem, θ may refer to a vector of unobservable model parameters, including for example the contaminant source location, start time, and injection time profile. The initial uncertainty in the source characterization is described with the assignment of the prior probability, p(θ). The prior probability may incorporate expert knowledge regarding, for example, aging parts of the water distribution network that are vulnerable to a contamination incident. The problem of Bayesian analysis is to incorporate data, *y*, so that p(θ) can be revised to posterior probability, p(θ|*y*). In the source characterization problem, the data would originate from the sensors in the sensor network. In Bayesian analysis, this updating of p(θ) to p(θ|*y*) is governed by Bayes' theorem, a rule of probability:

$$p(\theta|y) = \frac{p(y|\theta)p(\theta)}{\int_{\theta} p(y|\theta)p(\theta)d\theta} \qquad (1)$$

The numerator of Bayes' rule consists of the product of the likelihood probability, p(*y*|θ), and the prior probability p(θ); the denominator is the integral of this product over all θ and can be thought to be a normalization constant to ensure that the posterior probabilities sum to unity.

Given a small number of components of θ, a grid-based integration scheme for evaluating the

denominator in Bayes' Rule may be possible and accurate. However, given a large number of components of θ numerical evaluation is often difficult and inaccurate; in such cases, MCMC is required (Gilks et al, 1996, p. 3).

MCMC involves drawing samples θ_j from a target distribution, which for Bayesian analysis is the posterior distribution $p(\theta|y)$, by running a specially constructed Markov chain. Provided the chain was run for a sufficient number of iterations, a random sample from the points in the chain would represent a random sample from the target distribution (Gilks et al, 1996). The Metropolis-Hastings algorithm, of which all MCMC implementations are special cases (Gilks et al, 1996), is given in Figure 1. The attractiveness of MCMC for Bayesian analysis is that in the computation of the ratio R, the problematic integral in Bayes' Rule (which is the same for all θ_j) cancels out.

For j = 1 to J

Sample θ_j^* from $j(\theta_j^*|\theta_{j-1})$

R= TargetDensity(θ_j^*)/TargetDensity(θ_{j-1})

$$A=\frac{j\left(\theta_{j-1}\middle|\theta_j^*\right)}{j\left(\theta_j^*\middle|\theta_{j-1}\right)}.$$

AcceptProb = min(R·A, 1)

If Rand() <= AcceptProb Then

Set $\theta_j = \theta_j^*$

Else

Set $\theta_j = \theta_{j-1}$

End If

Next J

where:

J is the sample size

θ_0 is the starting point (arbitrarily selected)

θ_j is the jth iteration of the Markov chain

θ_j^* is the candidate point for inclusion as the jth iteration of the Markov chain; it is a random draw from the proposal distribution $j(\theta_j^*|\theta_{j-1})$

TargetDensity() is the probability density function from which samples are desired; for Bayesian analysis, the target density is the posterior density as given by Equation 1.

AcceptProb is the acceptance probability for the candidate point θ_j^*

Rand() is a random draw from a uniform distribution with a low=0 and high=1

Figure 1. Algorithm for sampling a target probability distribution with the Metropolis-Hastings algorithm.

The key aspect of the Metropolis-Hastings algorithm is the proposal, or "jumping", probability distribution from which a candidate point for inclusion in the chain, θ_j^*, is proposed based on the previous point θ_{j-1}. The key is to select a proposal distribution to ensure "good mixing" (not getting stuck exploring an area of locally high probability density to the exclusion of other modes of high density). However, other aspects (not shown in Figure 1) are also typically included in the implementation of MCMC: allowance for a "burn-in time" so that results are not skewed by the initial point that often is in a region of very low probability density, the adjustment of the proposal distribution based on the analysis of early results, and use of stopping criterion based on convergence tests. The challenge of this study was to develop an overall algorithm specific to the source characterization problem.

2.1. Application to the water distribution source characterization problem

In the description of the methodology that follows, several important assumptions are made. Among the assumptions, there is a single but unknown node X that is the source of contamination. The contaminant injection rate is a step function, beginning at an unknown time T and continuing indefinitely with a fixed but unknown magnitude M. Thus, overall $\theta=\{X,M,T\}$. Finally, there is one categorical sensor that yields at a time step t an indication of the concentration, C_t:

$$S_t = \begin{cases} U = \text{Undetected} & C_t < C^* \\ L = \text{Low} & C^* \le C_t < C^{**} \\ H = \text{High} & C_t \ge C^{**} \end{cases} \qquad (2)$$

C^* is the detection limit whereas C^{**} marks the cutoff between "Low" and "High". Over time, sensor data $y(t) = [S_0, S_1, \ldots S_{t-1}, S_t]$ is accumulated. Further, it is assumed that the sensor is perfect, i.e., there is no sensor measurement error; this is not a limitation of the approach (see Likelihood Model section below for explanation). The components of θ are a mixture of continuous and discrete variables—start time T and magnitude M are continuous while the contamination node X is discrete. In addition, the observations $y(t)$ are discrete. Hence, the appropriate version of Bayes' Rule should reflect that there is probability of an observation and not probability density:

$$p(\theta|y(t)) = \frac{P(y(t)|\theta)p(\theta)}{\int_\theta P(y(t)|\theta)p(\theta)d\theta} \qquad (3)$$

where P() refers to probability. (Also note that y has been replaced with y(t) to reflect that the data available is a function of time.)

Likelihood Model: P(*y(t)*|θ)

There are several sources of stochastic behavior in a water distribution system: stochastic water demands, sensor measurement error, and hydraulic and contaminant transport modeling errors. Here we focus exclusively on water demands. Sensor error is excluded from the analysis simply to focus on sources of random behavior such as water demand that must be propagated through the water distribution model to obtain a probabilistic prediction of water quality at the location of the sensor; in contrast, sensor error is simpler to incorporate as it can be added to the model prediction with introduction of an error term (e.g., see Shang, 2008).

We selected among the simplest of stochastic water demand models while recognizing that the Bayesian approach does not preclude use of an improved stochastic model. A simple stochastic model is considered: the variation about the deterministically estimated demand for node i, $\overline{D}_i(t)$, is described by a normal distribution:

$$Demand_i(t) = \text{Normal}(\overline{D}_i, \text{COV} \cdot \overline{D}_i) \qquad (4)$$

where the arguments for the Normal distribution are mean and standard deviation, respectively; COV is the coefficient of variation.

The likelihood, P(*y(t)*|θ), can be approximated with application of standard Monte Carlo simulation to the water distribution model EPANET 2.0. EPANET 2.0 is a program that performs extended period simulation of hydraulic and water quality behavior within pressurized pipe networks. N realizations of the water demands across all nodes and time steps can be generated, and for each realization, EPANET can be run to obtain N realizations of *y(t)*. The probability of each signal outcome at the sensor node is equated with the observed frequency within the set of N realizations.

MCMC proposal distribution

The selection of the proposal distribution, $j\left(\theta_j^* \middle| \theta_{j-1}\right)$ is the most important and problem-specific part of the Metropolis-Hasting algorithm. It was necessary to tailor a proposal distribution to the water distribution source contamination problem. The general recommendation of Gelman et al. (1995) was adopted: the proposal distribution was adjusted based on an initial preliminary investigation. We consider three phases: the jumping distributions are referred to as Phase I, Phase II and Phase III jumping distributions, and resulting chains as Phase I, II, and III Markov chains.

Below, one implementation of a general approach is proposed. The approach assumes bounded prior distributions for magnitude and time. As described below, the approach can be adapted to accommodate unbounded prior distributions (e.g., lognormal distribution for magnitude). Here, we use convenient distributions, the uniform and triangular, to emphasize the key aspects of the approach. Figure 2 provides a graphical indication of the approach.

Phase I proposal distribution

The Phase I proposal distribution specifies how the candidate for inclusion as the jth sample in the chain, $\theta_j^* = \{X_j^*, M_j^*, T_j^*\}$ is selected based on the previous sample in the chain, $\theta_{j-1} = \{X_{j-1}, M_{j-1}, T_{j-1}\}$. The Phase I proposal distribution $j^1(\theta_j^* | \theta_{j-1})$, is specified with assignment of independent jumping distributions for the three components of θ:

$$j^1(\theta_j^* | \theta_{j-1}) = j_X^1(X_j^* | X_{j-1}) j_M^1(M_j^* | M_{j-1}) j_T^1(T_j^* | T_{j-1}) \quad (5)$$

With the reasoning that nodes with substantial probability are likely to be located near to one another, the candidate node X_j^* is selected from the set of nodes adjacent to the most recent node X_{j-1}. However, to allow for the possibility that there is more than one pocket of posterior density, we allow for some small probability *p* of randomly jumping to a non-adjacent node in the network:

$$j_X^1(X_j^* | X_{j-1}) = \begin{cases} j \in Adj_{X_{j-1}} & \frac{1}{K_{X_{j-1}}} \\ j \notin Adj_{X_{j-1}} & p \end{cases} \quad (6)$$

In testing, it was observed that often for adjacent nodes there was a large difference in the range of posterior magnitude and start time. As a consequence, for these two components of θ we resorted to an independent MCMC implementation: the candidate magnitude and start times, M_j^* and T_j^*, were drawn from distributions that were independent of M_{j-1} and T_{j-1}, respectively.

Uniform probability distribution functions were used as the proposal distributions for magnitude and start time. Uniform(x,a,b) refers to the probability density of x given lower and upper bounds, a and b; DiscreteUniform(x,a,b) is the discrete version yielding the probability of x. The proposal distributions from which magnitude and start time were selected are:

$$j_M^1(M_j^* | M_{j-1}) = Uniform(M_j^*, a_M, b_M) \quad (7)$$

$$j_T^1(T_j^* | T_{j-1}|) = DiscreteUniform(T_j^*, a_T, b_T) \quad (8)$$

The parameters a_M and b_M, and a_T and b_T, are the lower and upper bounds of the prior distributions assigned to magnitude and start time, respectively.

With the jumping distribution as specified in Eq. 7-9, factor A in Figure 1 can then be computed. The value of A in Phase I, A_1, is:

$$A^1 = \begin{Bmatrix} j \in Adj_{X_{j-1}} & \frac{K_{X_{j-1}}}{K_{X_j^*}} \frac{Uniform\left(M_{j-1}, a_M, b_M\right)}{Uniform\left(M_j^*, a_M, b_M\right)} \frac{DiscreteUniform\left(T_{j-1}, a_T, b_T\right)}{DiscreteUniform\left(T_j^*, a_T, b_T\right)} \\ j \notin Adj_{X_{j-1}} & \frac{p}{p} \frac{Uniform\left(M_{j-1}, a_M, b_M\right)}{Uniform\left(M_j^*, a_M, b_M\right)} \frac{DiscreteUniform\left(T_{j-1}, a_T, b_T\right)}{DiscreteUniform\left(T_j^*, a_T, b_T\right)} \end{Bmatrix} \quad (9)$$

The terms involving magnitude and time cancel out due to the use of uniform distributions, i.e., $Uniform\left(M_{j-1}, a_M, b_M\right) = Uniform\left(M_j^*, a_M, b_M\right)$ and $DiscreteUniform\left(T_{j-1}, a_T, b_T\right) = DiscreteUniform\left(T_j^*, a_T, b_T\right)$. As a result, the expression simplifies to:

$$A^1 = \begin{Bmatrix} j \in Adj_{X_{j-1}} & \frac{K_{X_{j-1}}}{K_{X_j^*}} \\ j \notin Adj_{X_{j-1}} & 1 \end{Bmatrix} \quad (10)$$

Phase II proposal distribution

It is hoped that the Phase I results give some indication of the posterior distribution. This information on the posterior distribution can then be incorporated into the Phase II proposal distribution.

Rather than selecting from the set of adjacent nodes, the candidate node X_j^* is in Phase II based on the frequency with which it was selected in Phase I, $freq_i^1$:

$$j_X^2\left(X_j^* \middle| X_{j-1}\right) = freq_i^1 \quad (11)$$

The proposal distribution for magnitude is revised with knowledge of the Phase I estimate of the posterior mean. This revision is illustrated in Figure 2. The uniform proposal distribution in Phase I is replaced by a triangular distribution. The function Triang(*x,a,b,m*) yields the density of *x* given lower and upper bounds *a* and *b*, and mode *m*. The lower and upper bounds remain unchanged from the Phase I distribution; the mode is set equal to the Phase I-estimated posterior mean, M_μ^1:

$$j_M^2\left(M_j^* \middle| M_{j-1}\right) = Triang\left(M_j^*, a_M, b_M, M_\mu^1\right) \quad (12)$$

Use of this triangular distribution concentrates the sampling of candidate magnitude values around those observed in Phase I but, in acknowledging the approximation error in Phase I, still allows for values from the full range of values in the prior distribution. The revision of the proposal distribution for start time is similar but uses a discrete version of the triangular distribution:

$$j_T^2\left(T_j^* \middle| T_{j-1}\right) = DiscreteTriang\left(T_j^*, a_T, b_T, T_\mu^1\right) \qquad (13)$$

Figure 2 Illustration of the revision of the proposal distribution for magnitude. The revision of the start time proposal distribution differs only in that discrete versions of the distributions are used.

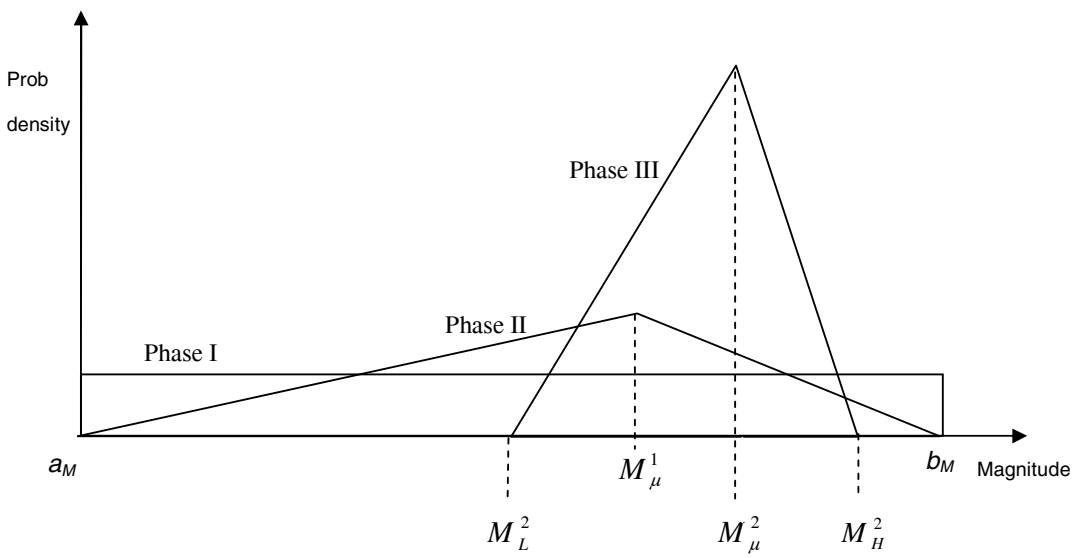

This Phase II jumping distribution is now fully an "independent" MCMC implementation as $j^2\left(\theta_j^* \middle| \theta_{j-1}\right) = j^2\left(\theta_j^*\right)$. The factor *A* in Phase II, is:

$$A^2 = \frac{freq_{X_{j-1}}^1}{freq_{X_j^*}^1} \frac{Triang\left(M_{j-1}, a_M, b_M, M_\mu^1\right)}{Triang\left(M_j^*, a_M, b_M, M_\mu^1\right)} \frac{DiscreteTriang\left(T_{j-1}, a_T, b_T, T_\mu^1\right)}{DiscreteTriang\left(T_j^*, a_T, b_T, T_\mu^1\right)} \qquad (14)$$

Phase III proposal distribution

The proposal distribution for X in Phase III is left unchanged from Phase II, with the exception that frequencies from Phase II, $freq_i^2$, are used:

$$j_X^3\left(X_j^* \middle| X_{j-1}\right) = freq_i^2 \qquad (15)$$

The proposal distributions for the θ components M and T are again based on triangular

distributions with the modes set equal to the best estimate of the posterior means, M_{μ}^{2} and T_{μ}^{2}. However, as was depicted in Figure 2, in this final phase more narrow triangular distributions are used, with the bounds set equal to the minimum and maximum values as observed in Phase II, M_{L}^{2} and M_{H}^{2} for magnitude and T_{L}^{2} and T_{H}^{2} for start time:

$$j_{M}^{3}\left(M_{j}^{*}\middle|M_{j-1}\right)=Triang\left(M_{j}^{*},M_{L}^{2},M_{H}^{2},M_{\mu}^{2}\right) \tag{16}$$

$$j_{T}^{3}\left(T_{j}^{*}\middle|T_{j-1}\right)=DiscreteTriang\left(T_{j}^{*},T_{L}^{2},T_{H}^{2},T_{\mu}^{2}\right) \tag{17}$$

The factor *A* in Phase III is computed as:

$$A^{3}=\frac{freq_{X_{j-1}}^{1}}{freq_{X_{j}^{*}}^{1}}\frac{Triang\left(M_{j-1},M_{L}^{2},M_{H}^{2},M_{\mu}^{2}\right)}{Triang\left(M_{j}^{*},M_{L}^{2},M_{H}^{2},M_{\mu}^{2}\right)}\frac{DiscreteTriang\left(T_{j-1},T_{L}^{2},T_{H}^{2},T_{\mu}^{2}\right)}{DiscreteTriang\left(T_{j}^{*},T_{L}^{2},T_{H}^{2},T_{\mu}^{2}\right)} \tag{18}$$

3. Limitations

A simple categorical sensor with three outcomes (U, L, and H) was considered in the development of the method. With little modification, a sensor with a continuous reading could be incorporated. To accommodate a continuous sensor, from the Monte Carlo-based stochastic model results the probability *density* of measurements would need to be estimated using density estimation methods. To approximate density, kernel density estimation methods can be utilized (Silverman, 1986).

The specific MCMC implementation presented considered three components of θ: the source node (X), the associated magnitude (M) and the start time (T). This set is likely too limiting. As there is a cutoff C* for detection, it may be that two sources are needed to trigger the sensor. The allowance for two sources would add one more component of θ. Moreover, the contaminant injection time profile used, a step function from zero to a fixed magnitude, is too limiting. Other time profiles, including pulses, or ramped up injections into the system could be imagined in addition to profile type; each of these profiles would require additional components of θ such as the duration of the pulse or slope of the ramp-up. The allowance for multiple sources and alternative injection time profiles would quickly increase the number of components of θ.

The main limitation to an MCMC approach will remain computation time. If adding parameters to θ, a parallel or distributed implementation of MCMC likely would be required. Fortunately, the MCMC procedure is amenable to parallel and distributed computing (Altekar et al., 2004). A parallel or distributed computing scheme is needed if additional sensors

(water quality and hydraulic sensors) are to be incorporated; with multiple sensors, larger Monte Carlo sample sizes are needed to estimate the frequencies (or density) for the set of measurements that are observed, as the number of sensor measurement combinations that can occur greatly increases.

Acknowledgements

This work is supported by National Science Foundation(NSF) under Award No. 0540177.

Any opinions, findings and conclusion expressed in this materials are those of the authors and do not necessarily reflect the views of the NSF.

References

Ami Preis and Avi Ostfeld. "Contamination Source Identification in Water Systems: A Hybrid Model Trees-Linear Programming Scheme" Journal of Water Resources Planning and Management, 132(4),263-273,2006

Altekar, G. Dawarkadas, S. Huelsenbeck J.P., A and R.Ronquist. Parallel metropolis coupled Markov chain Monte Carlo for Bayesian phylogenetic inference. Bioinformatics, vol.20, pp 407-415. 2004

Gelman, Andrew, John B. Carlin, Hal S. Stern, and Donald B. Rubin. Bayesian Data Analysis. Chapman & Hall, 1995.

Gilks, Walter R., Sylvia Richardson, and David J. Spiegelhalter. Introducing Markov chain Monte Carlo. In Markov Chain Monte Carlo in Practice, Edited by W.R. Gilks, S. Richardson, and D.J. Spiegelhalter, Chapman & Hall, 1996.

Guan Jiabao, Aral, Mustafa M., Maslia, Morris L., Grayman, Walter M.,(2006) “Identification of contaminant source in water distribution system using simulation-optimization method: Case study”, Journal of Water Res. Planning and Management, 132(4),2006

Larid, Carl D., Biegler, Lorenz T., van Boleman Waanders, Bart G., (2005a), “A Mixed-integer approach for obtaining unique solutions in source inversion of drinking water networks”,World Water Congress 2005, 173(47)

M.Propato., M.E.Tryby, O.Piller,(2007) “Linear Algebra Analysis for Contaminant Source Identification in Water Distribution Systems”, Proceeding of ASCE World and Environmental Congress, Tampa, Florida, 2007

Poulakis, Z., D. Valougeorgis, and C. Papadimitriou. Leakage detection in water pipe networks using a Bayesian probabilistic framework. Probabilistic Engineering Mechanics, vol. 18, pp. 315–327. 2003.

Shang, F., Uber, J. G., van Bloemen Waanders, B. G., Boccelli, D. L., and Janke, R. (2006). “Real Time Water Demand Estimation in Water Distribution Systems.” 2006 Water

Distribution Systems Analysis Symposium, Cincinnati, OH.

Silverman, B.W. Density Estimation for Statistics and Data Analysis. Chapman & Hall/CRC. London. New York. 1986.

Van Bolemen Waanders,B G,Bartlett,R.A.,Bigler, L.T.,and Laird, C.D.(2003) “Nonlinear Programming Strategies for Source Detection of Municipal Water Networks.” Proceeding of the ASCE World and Environmental Congress, Philadelphia, PA Jun 23-26.

Conditioned Backward Probability Modeling to Identify Contamination Sources in a Water Distribution System

R. M. Neupauer[1] and M.K. Records[2]

[1]Department of Civil, Environmental, and Architectural Engineering, University of Colorado, UCB 428, Boulder, CO 80309 USA; PH (303) 492-6274; FAX (303) 492-7317; email: neupauer@colorado.edu
[2]Department of Civil, Environmental, and Architectural Engineering, University of Colorado, UCB 428, Boulder, CO 80309 USA; PH (303) 492-6382; FAX (303) 492-7317; email: michael.records@colorado.edu

ABSTRACT

If a chemical or biological agent is released into a water distribution system, sensors that are installed in the pipe network may detect the contamination as it travels through the system. To minimize the adverse impact of the contaminant release, the source must be characterized to determine the extent of the contamination and to remediate the contaminated area. We develop an adjoint-based backward modeling approach that uses the collected sensor data to identify the location and timing of the release. In the adjoint model, the sensor location is treated as a source of probability, and the probability is transported upgradient and backward in time to obtain probability density functions (PDFs) that describe the random time in the past that the observed contamination was at a particular upgradient position. These PDFs can be used to identify the source location and release time. Conditioning these PDFs on the measured concentrations improves their accuracy and decreases their uncertainty. We demonstrate the effectiveness of this method by using it to characterize a contaminant source in a hypothetical water distribution system.

INTRODUCTION

A water distribution system is made up of pipes and storage tanks that carry water from sources to users. Due to their spatial extent and their many potential injection points, water distribution systems are vulnerable to outside threats such direct injections of chemical or biological agents into the distribution system (Ostfeld, 2006). If a contamination event occurs, the source must be characterized with respect to the contaminant type, injection time and duration, mass loading rate, and location of injection. If sensors are installed to detect contamination in the distribution system, the data recorded at these sensors can be used to provide information about

the source characteristics.

Several inverse methods have been used to characterize contaminant sources in water distribution systems. To determine possible source nodes, release times, and mass loadings, Laird et al. (2005) used a nonlinear optimization method based on multiple sensors. Using an origin tracking algorithm they were able to identify possible source scenarios but were not necessarily able to quantify the number of sources. By applying mixed integer optimization to the array of feasible solutions, Laird et al. (2006) estimated the number of sources. Guan et al. (2006) characterized contaminant sources in the water distribution system of Dover Township, New Jersey using a simulation and optimization approach that was adapted from a method developed by Guan and Aral (1999) and Aral et al. (2001) for use in groundwater contamination. Preis and Ostfeld (2006) used a model tree approach coupled with linear programming. In this method, a water quality simulator such as EPANET is run multiple times with different source scenarios, and the results are formed into a model tree. Classification rules are generated by the model tree, which are then used with sensor data in a linear programming method to characterize contamination sources. Preis and Ostfeld (2007) used a genetic algorithm coupled with EPANET to identify the location, release time, duration, and source mass of a contaminant source in a water distribution system. DiCristo and Leopardi (2008) use a two-step method to identify the source node in a water distribution system. In the first step, the candidate nodes are selected using pathway analysis (Lee and Deininger, 1992); then a linear optimization problem is solved to identify the source node from among the candidate nodes.

These approaches assumed that sensors continuously record concentrations of released chemicals; however cost-effective sensors of this type are not currently available (ASCE, 2004). Rather, sensors are available that measure water quality indicators such as turbidity and pH, and these can be used to detect the presence or absence of contamination. Dawsey et al. (2006) and Preis and Ostfeld (2008) developed methods for determining a source zone using information from this type of sensor. These methods can be used to reduce the number of possible source nodes.

In this paper, we present a conditioned backward probabilistic modeling approach to identify possible sources of contamination in a water distribution system. In backward modeling the sensor location is treated as a source of probability, and the probabilities are propagated upgradient and backward in time. The governing equation for the backward model is the adjoint of the forward transport equation. Adjoint-based backward modeling has been used to identify contamination in groundwater systems (Neupauer and Wilson, 1999, 2001, 2002), in optimal control of point source effluent releases to rivers (Piasecki and Katopodes, 1997) and estuaries (Piasecki and Sanders, 2002), in estimation of historical contaminant distributions (Michalak and Kitanidis, 2004), and other applications. In our method, the adjoint state is related to a probability density function (PDF) of the time in the past that contamination that was observed at a sensor could have been at an upstream node. These PDFs can be used to identify the source location or release time. In the next

section, we present the governing equations of water quality simulations in water distribution systems. Following that, we present the adjoint approach for obtaining the backward travel time PDF. Finally, we introduce a conditioning step in which the backward travel time PDF is conditioned on the measured concentrations at the sensor.

SIMULATION OF WATER QUALITY

Many water distribution models such as EPANET (Rossman, 2000) simulate water quality in pipes using an advection-reaction equation given by

$$\frac{\partial C_i}{\partial t} + \frac{Q_i}{A_i}\frac{\partial C_i}{\partial x_i} = kC_i \tag{1}$$

where C_i, Q_i, and A_i are the concentration, flow rate, and area of Pipe i, t is time, k is a first-order reaction rate, x_i is travel distance in Pipe i, with $x_i = 0$ at the upstream end of the pipe, $x_i = L_i$ at the downstream end of the pipe, and Q_i is defined as positive in the direction of x_i . For each Pipe i, let the upstream and downstream nodes be denoted as u_i and d_i, respectively. Assuming complete mixing at the nodes, the boundary condition for (1) is

$$C_i(x_i = 0, t) = C^*_{u_i}(t), \tag{2}$$

where

$$C^*_j = \frac{\sum_{i \in d_i = j} Q_i C_i\big|_{x_i = L_i} + U_j}{D_j + \sum_{i \in u_i = j} Q_i}. \tag{3}$$

where C_j^* is concentration of water leaving Node j, and D_j and U_j are the demand and source loading, respectively, at Node j. The initial concentration in Pipe i is $C_i(x_i,0) = 0$.

If the source loading U_j is known, (1) - (3) can be solved to obtain concentrations at all nodes as a function of time. These nodal concentrations can be related to a forward travel time probability density function (PDF) that describes the random time T at which a contaminant particle that was released at Node l will be present at Node j. Based on results presented in the groundwater literature (e.g., Jury, 1982; Dagan, 1989, Dagan and Nguyen, 1989), the forward travel time PDF, $f_l(t,j,l)$, is defined as the ratio of max flux of the contaminant at Node j to the total mass of contaminant contributed by the source at Node l, given by

$$f_T(t;j,l) = \frac{C_j^*(t)\sum_{i\in d_i=j} Q_i(t)}{M_l} = \frac{dC_j^*(t)}{dM_l}\sum_{i\in d_i=j} Q_i(t) \quad , \tag{4}$$

where M_l is the mass of contaminant entering Node l, and $dC_j(t)/dM_l$ is the marginal sensitivity of concentration at Node j to a source mass at Node l. The cumulative distribution function (CDF) of travel time, which describes the probability that a particle will travel from Node l from Node j prior to time $t = T$, is obtained by integrating the PDF in (4) from time $t = 0$ to $t = T$.

BACKWARD TRAVEL TIME PROBABILITY DENSITY FUNCTION

If contamination is observed at sensors in a water distribution system, but the source of contamination is not known, (1) - (3) can be used to determine the source characteristics (source location, release time, source mass, etc.); however, the approach is inefficient. The equations would have to be solved for all possible combinations of source location, release time, and source mass, and the simulated nodal concentrations would be compared to the sensor readings, with the final source characteristics identified as the combination that produces the smallest misfit between the simulated concentrations and sensor readings. This process can be automated using various inverse methods, such as those described above.

Alternatively, a backward travel time PDF can be obtained that tracks the movement of the contamination from the sensor where it was measured upgradient to all possible source locations. The governing equation of the backward model is the adjoint of the governing equation of the forward model (1), given by (Neupauer, 2009)

$$\frac{\partial \psi_i}{\partial \tau} - \frac{Q_i}{A_i}\frac{\partial \psi_i}{\partial x_i} = k\psi_i \quad , \tag{5}$$

where ψ_i is the adjoint state of C_i and is identical to the marginal sensitivity of C_i to a source release of mass M_l at Node l, such that $\psi_i = dC_i/dM_l$ (Neupauer, 2009), and τ is backward time which is defined as time prior to observation at the sensor. The main differences between the forward and backward equations are the reversal of the time variable in the backward equation and the change in sign on the advection term. With these changes, the backward equation allows for upgradient movement of the adjoint state in backward time. The initial condition on (5) is $\psi_i(x_i, \tau = 0) = 0$.

The boundary condition on ψ_i is the adjoint state of the nodal concentration C^* at the downstream end of the pipe ($x_i = L_i$), given by (Neupauer, 2009)

$$\psi_i(x_i = L_i, \tau) = \psi_{d_i}^*(\tau) \quad , \tag{6}$$

where

$$\psi_l^* = \frac{\sum_{i \in u_i = l} Q_i \psi_i - h_l}{\sum_{i \in d_i = l} Q_i} \quad , \tag{7}$$

where h_l is a performance functional that depends on the observation of contamination at the sensor, and $\psi_l^* = dC_j^*/dM_l$ is the adjoint of C_j^*. The performance functional in (7) is defined as (Neupauer et al., 2009)

$$h_l(\tau) = \begin{cases} T_d^{-1} & l = j \text{ and } \tau_s < \tau < \tau_s + T_d \\ 0 & \text{otherwise} \end{cases} \quad , \tag{8}$$

where T_d is the duration of the observation at a sensor at Node j, and τ_s is the time in backward time at which contamination was most recently observed at Node j. The adjoint state is related to the travel time PDF through (Neupauer et al., 2009)

$$f_T(\tau; l, j) = \psi_l^*(\tau) \sum_{i \in u_i = l} Q_i(\tau) \quad . \tag{9}$$

From (9), the cumulative distribution function CDF of backward travel time is

$$F_T(\tau; l, j) = \int_0^\tau \psi_l^*(\tau') \sum_{i \in u_i = l} Q_i(\tau') d\tau' \quad .$$

The CDF represents the probability that a contaminant particle that was observed at a sensor at Node j was at Node l prior to backward time τ.

To calculate the backward travel time PDF, the adjoint equations (5) - (7) are solved once for each sensor observation to obtain $\psi_l^*(\tau)$ for all upstream Nodes l. These adjoint states used in (9) to obtain the backward travel time PDF that represents the possible times in the past that the observed contaminant particle was at any upgradient Node j. If contamination is observed at multiple sensors, the backward travel time PDFs for the individual sensors can be combined into a joint backward travel time PDF that represents the backward time τ at which the contaminant particles observed at all sensors could have been at any upgradient Node j. The joint backward travel time PDF is given by

$$f_T(\tau; l, j_1, j_2, \ldots j_{N_s}) = \alpha \prod_{n=1}^{N_s} f_T(\tau; l, j_n) \quad , \tag{10}$$

where $f_T(t;l,j_1,j_2,\ldots j_{Ns})$ is the joint backward travel time PDF, $f_T(\tau;l,j_n)$ is the backward travel time PDF for sensor j_n, N_s is the number of sensor measurements, and α is a constant that ensures that the total probability is unity.

CONDITIONED BACKWARD TRAVEL TIME PROBABILITY DENSITY FUNCTION

The individual and joint backward travel time PDFs described above account for the presence of contamination at sensors, but not for the measured concentrations. If concentrations measurements are available, the travel time PDFs can be conditioned on the measured concentrations. Neupauer and Lin (2006) developed a method for conditioning the backward travel time PDF on the measured concentrations for an instantaneous point release of groundwater contamination at a known location but of unknown mass m. We adapt this method here for a uniform release of contamination at a single node in a water distribution system.

We assume that the measured nodal concentration, $\hat{c}_j^*$, at a sensor at Node j contains normally-distribution random measurement error; and therefore it is a random variable described by a PDF, $f_{\hat{C}^*}(\hat{c}_j^* | M,T;T_d)$, given by

$$f_{\hat{C}^*}(\hat{c}_j^* \mid M,T;T_d) = \frac{1}{\sqrt{2\pi\sigma^2}} \exp\left\{ -\frac{\left(\hat{c}_j^* - c_j^*(M,T;T_d)\right)^2}{2\sigma^2} \right\}, \qquad (11)$$

where σ^2 is the variance of the measurement error and $c^*_j(M,T,T_d)$ is the true concentration at Node j due to a source release of mass M at time T for a duration of T_d. We assume in this work that the contamination is released uniformly at Node l for a known duration of T_d. Other source scenarios are possible; however, for simplicity, we limit our presentation here to this uniform source. The PDF of measured concentration is conditioned on the random source mass M, random release time T, and duration of release of contamination T_d from a source at Node l.

Following the approach of Neupauer and Lin (2006), we first develop a joint PDF, $f_{M,T|\hat{\mathbf{C}}^*}(M,T|\hat{\mathbf{c}}^*,l;T_d)$, of the unknown source mass M and the release time T for a source at Node l conditioned on measured concentrations, where $\hat{\mathbf{C}}^* = [\hat{C}^*_1, \hat{C}^*_2, \ldots, \hat{C}^*_{Ns}]$ is an N_s-length vector of random concentrations, and $\hat{\mathbf{c}}^* = [\hat{c}^*_1, \hat{c}^*_2, \ldots, \hat{c}^*_{Ns}]$ is an N_s-length vector of specific values of concentrations. Using Bayes' theorem, we defined this joint PDF as

$$f_{M,T|\hat{\mathbf{C}}^*}(m,\tau \mid \hat{\mathbf{c}}^*,l;T_d) = \frac{f_{\hat{\mathbf{C}}^*|M,T}\left(\hat{\mathbf{c}}^* \mid m,\tau;T_d\right) f_M(m) f_T\left(\tau;l,j_1 \cdots j_{N_s}\right)}{\iint f_{\hat{\mathbf{C}}^*|M,T}\left(\hat{\mathbf{c}}^* \mid m',\tau';T_d\right) f_M(m') f_T\left(\tau';l,j_1 \cdots j_{N_s}\right) dm' d\tau'}, \qquad (12)$$

where $f_{\hat{\mathbf{C}}^*}(\hat{\mathbf{c}}^* | M,T;T_d)$ is the joint PDF of the vector of measured concentrations, $f(m)$ is a PDF of source mass (which, in the absence of any other information, is assumed to be a uniform distribution), and $f_T(\tau,l,j_1 \ldots j_{Ns})$ is the unconditioned joint backward travel time PDF from (10). Assuming that the measurement error in the sensor measurements are uncorrelated, $f_{\hat{\mathbf{C}}^*}(\hat{\mathbf{c}}^* | M,T;T_d)$ can be expressed as the product of $f_{\hat{C}^*}(\hat{c}_j^* | M,T;T_d)$ for $j = 1, 2, \ldots N_s$. Integrating (12) over the domain of possible source masses results in the backward travel time PDF conditioned on measured concentrations, given by

$$f_{T|\hat{\mathbf{C}}^*}(\tau \mid \hat{\mathbf{c}}^*, l; T_d) = \beta \int \prod_{n=1}^{N_s} \left[f_{\hat{C}_n^* | M,T}\left(\hat{c}_n^* \mid m, \tau; T_d\right) f_T(\tau; l, j_n) \right] dm \quad , \tag{13}$$

where β is defined such that the total probability is unity. In (13), the first PDF on the right hand side comes from (11) and the second PDF comes from (9), and the product is evaluated for all sensor measurements.

REFERENCES

Aral, M.M., Guan, J., and Maslia, M.L. (2001). "Identification of contaminant source locations and release history in aquifers." *J. Hydrologic Eng*., 6(3), 225-2344.

ASCE. (2004). "Interim voluntary guidelines for designing an online contaminant monitoring system." American Society of Civil Engineers, Reston, Virginia.

Dagan G. (1989). *Flow and Transport in Porous Formation*, New York: Springer-Verlag.

Dagan G. and Nguyen, V. (1989). "A comparison of travel time and concentration approaches to modeling transport by groundwater." *J. Contam. Hyrdol*., 4, 79-91.

Dawsey, W.J., Minsker, B.S., and VanBlaricum, V.L. (2006). "Bayesian belief networks to integrate monitoring evidence of water distribution system contamination." *J. Water Resour. Plann. Manage*., 132(4), 234-241.

DiCristo, C. and Leopardi, A. (2008). "Pollution source identification of accidental contamination in water distribution networks." *J. Water Resour. Plann. Manage*., 124(2), 197-202.

Guan, J. and Aral, M.M. (1999). "Optimal remediation with well locations and pumping rates selected as continuous decision variables." *J. Hydrol*., 221, 20-42.

Guan, J., Aral, M.M., Maslia, M.L., and Grayman, W.M. (2006). "Identification of contaminant sources in water distribution systems using simulation-optimization method: Case study." *J. Water Resour. Plann. Manage*., 132(4), 252-262.

Jury, W.A. (1982). "Simulation of solute transport using a transfer function model." *Water Resour. Res*., 18, 363-368.

Laird, C.D., Biegler, L.T., van Bloemen Waanders, B.G., and Barlett, R.A. (2005). "Contamination source determination for water networks." *J. Water Resour. Plann. Manage.*, 131(2), 125-134.

Laird, C.D., Biegler, L.T., and van Bloemen Waanders, B.G. (2006). "Mixed-integer approach for obtaining unique solutions in source inversion of water networks." *J. Water Resour. Plann. Manage*., 132(4), 242-251.

Lee, B.H. and Deininger, R.A. (1992). "Optimal locations of monitoring stations in water distribution systems." *J. Environ. Eng*., 118(1), 4-16.

Michalak, A.M. and Kitanidis, P.K. (2004). "Estimation of historical groundwater contaminant distribution using the adjoint state method applied to geostatistical inverse modeling." *Water Resour. Res.,* 40, W08302.

Neupauer, R.M., (2009). "Adjoint sensitivities of concentrations in water distribution systems." *Journal of Engineering Mechanics*, in preparation.

Neupauer, R.M., Records, M.K., and Ashwood, W. (2009). "Adjoint model to identify contaminant sources in water distribution systems." *J. Water Resour. Plann. Manage*., in preparation.

Neupauer, R.M. and Lin, R. (2006). "Identifying sources of a conservative groundwater contaminant using backward probabilities conditioned on measured concentrations." *Water Resour. Res*., 42, W03424, doi:10.1029/ 2005WR004115.

Neupauer, R.M. and Wilson, J.L. (1999). "Adjoint method for obtaining backward-in-time location and travel time probabilities of a conservative groundwater contaminant." *Water Resour. Res*., 35(11), 3389-3398.

Neupauer, R.M. and Wilson, J.L. (2001). "Adjoint-derived location and travel time probabilities for a multi-dimensional groundwater system." *Water Resour. Res*., 37(6), 1657-1668.

Neupauer, R.M. and Wilson, J.L. (2002). "Backward probabilistic model of groundwater contamination in non-uniform and transient flow." *Adv. Water Resour*., 25(7) 733-746.

Ostfeld, A. (2006). "Enhancing water-distribution system security through modeling." *J. Water Resour. Plan. Manage*., 132(4), 209-210.

Piasecki, M. and Katopodes, N.D. (1997). "Control of contaminant releases in rivers, 1, Adjoint sensitivity analysis." *J. Hydraul. Engg*., 123, 486-492.

Piasecki, M. and Sanders, B.F. (2002). "Optimization of multiple freshwater diversions in well-mixed estuaries." *J. Water Resour. Plann. Manage*., 138, 74-84.

Preis, A. and Ostfeld, A. (2006). "Contamination source identification in water systems: A hybrid model trees-linear programming scheme." *J. Water Resour. Manage*., 132(4), 263-273.

Preis, A. and Ostfeld, A. (2007). "A contamination source identification model for water distribution system security." *Engineering Optimization*. 29(8), 941-951.

Preis A., and Ostfeld, A. (2008). "Genetic algorithm for contaminant source characterization using imperfect sensors." *Civil Engineering and Environmental Systems*, 25(1), 29-39.

Rossman, L.A. (2000). *EPANET 2 :User's Manual*. U.S. Environmental Protection Agency, EPA/600/R-00/057, Cincinnati, Ohio.

Real-Time Implementation of Contamination Source Identification Method for Water Distribution Systems

Annamaria E. De Sanctis, Sam Hachett, James G. Uber, Dominic L. Boccelli, and Feng Shang

Department of Civil and Environmental Engineering, University of Cincinnati, Cincinnati, OH 45221, P.O. Box 210071. Emails: desanca@email.uc.edu, jim.uber@uc.edu, samhatchett@gmail.com, dominic.boccelli@uc.edu, shangf@email.uc.edu.

ABSTRACT

A contamination source identification methodology should be continuously run in real time to provide timely information about contamination event status. The method should be robust with respect to uncertainty and variability in factors affecting the network hydraulic model. This work assesses the impact of hydraulic modeling errors on the performance of a source identification algorithm. Preliminary results evaluate the effect of demand estimation errors on the performance of the identification algorithm. Results suggest the source identification method can be robust to the types of errors investigated. It is stressed, however, that broader conclusions can not be drawn, because the tests consider only one network test case, and the true statistical characteristics of stochastic demands are unknown. Furthermore, the particular example chosen assumes optimistic scenarios for demand estimation. The results provide a methodology and motivation for continuing to investigate the true performance characteristics of real-time contamination source identification algorithms.

Keywords: contamination source identification, real-time calibration model.

INTRODUCTION

A considerable effort has been directed toward developing algorithms for contamination source identification in water distribution systems. Research is underway to extend these algorithms for reliable application in a real-time procedure. To evaluate these methods in a realistic manner, however, various uncertainties must be considered which affect distribution system hydraulics, including model inaccuracies, measurement errors, and calibration errors.

Several methodologies address contamination source identification for water distribution systems assuming system hydraulics are known without error. Unfortunately only limited hydraulic data are available for assessing the state of the system. Further, monitoring stations envisioned for surveillance may fail to detect the real presence/absence of a contamination. Yet the work on source identification has almost exclusively assumed that event detection is also without error.

Disregarding the possibility of false positive and false negative contamination events, and ignoring the uncertainty in hydraulics, could lead to incorrect identification of contamination locations and times. Consequently, this could degrade the effectiveness of remedial actions, and result in greater public health impacts. The contamination source identification approach proposed by De Sanctis et al. (2006) assumes an accurate hydraulic model and perfect water quality sensor information. In De Sanctis et al. (2008), their method is extended to combine imperfect event detection information with the results of a backtracking analysis (EPANET-BTX), to determine the probability of each node-time pair being a contamination source. Here, we retain the original contamination source identification algorithm (De Sanctis et al. (2006)), along with the assumption of perfect event detection, but assume a hydraulic model with real-time water demanded patterns estimated using flow and pressure measurements and an extended Kalman filter predictor-corrector method (Shang et al. (2006)). This method estimates the water demand patterns and the associated uncertainty. By relying on the estimated hydraulic model with water demand uncertainty, it is possible to estimate how reliably the contamination sources can be identified in water distribution systems.

A simulation study using a network with a hydraulic and water quality sensor system is presented to show the time varying candidate contamination sources. The effect of the estimated demand patterns on the source identification is investigated, assuming true stochastic demands described by a time series model with temporal demand correlation. Since the demand estimation performance depends on many factors different cases are examined. One of these cases is the use of several sampling designs for the hydraulic measurements. Furthermore, the performance is evaluated for different magnitudes of the demand pattern variability. This is accomplished by varying the white noise error associated with a time series model.

A comparison is made between the source identification results using estimates of demand patterns, versus perfect hydraulics. The robustness of the source identification is also evaluated with respect to varying the water quality sampling. All the comparisons show the importance for incorporating information regarding demand uncertainty on contaminant source identification.

METHODOLOGY

The *Contamination Status Algorithm* (*CSA*), De Sanctis et al. (2006), is a method to identify all the possible contamination sources in space and time. It updates the contamination possibility status of all nodes and time intervals using the network flow paths that deliver water to water quality monitoring stations. These monitoring stations are assumed to detect the presence/absence of contamination in a water distribution system. The network flow paths for each station are determined using the *particle backtracking algorithm* (Shang et al. (2002)), as implemented in *EPANET-BTX*, a pre-release version of the EPANET backtracking extension that uses the EPANET hydraulic network model. The status assigned to each node-time pair by the CSA is one of the following: *candidate* – possible contamination source, *safe* – not a possible contamination source, and *unknown* – insufficient information to classify the source as candidate or safe.

Here the possible contamination sources are identified using a real time hydraulic model for which the water demands are continuously estimated from hydraulic measurements stored in a SCADA Database. Water quality status from an event detection algorithm is assumed to be perfect (a *probabilistic CSA* has been described to incorporate false positive or false negative rates into the standard CSA algorithm) (De Sanctis et al. (2008)). In order to evaluate the CSA approach for real time source identification we need to verify the robustness of the algorithm with respect to uncertainty and variability in the input data. The deviations between source identification results using accurate hydraulic information, versus those using estimated hydraulic characteristics, is one valid approach to measure the robustness of the identification algorithm under realistic conditions. In this work the time-varying water usage rates at network nodes represent the main uncertain hydraulic model input. Other model parameters are assumed to be accurately identified, including system operation conditions, pipe roughness, and internal diameters. The water demands are estimated using EPANET-RTX, a pre-release version of the EPANET Real-Time eXtension (Shang and Uber (2008)) which implements the predictor-corrector estimation method described by Shang et al. (2006).

The computational procedure implemented here is divided into three main steps:

1. Generation of a synthetic true model
2. Generation of an ensemble of estimated models
3. Comparison of CSA results using different input models

First, the true model is synthetically generated; the true model is intended to represent a realistic set of conditions, incorporating stochastic demand variability. Hydraulic measurements and water quality measurements are simulated using the true model. Simulated flow and head values are used with EPANET-RTX to estimate the real-time water usage rates, while simulated water quality information is converted to a binary alarm/normal state and processed by the CSA.

Second, an ensemble of hydraulic model scenarios is generated based on different sets of estimated real-time demands. Each set of real-time demands is estimated using different simulated measurements for the calibration algorithm. The estimation performance of the calibration system depends strongly on the sampling design (Bush and Uber (1998); Kapelan et al. (2003)). In particular, the performance varies based on the number of measurements, and their locations, accuracy, and frequency. For this reason, random sets of flow and pressure measurement locations are used to study the effects of demand estimation accuracy.

Third, each estimated hydraulic model scenario is used with the CSA to identify possible contamination sources. Then, these results are quantitatively analyzed to evaluate the contamination source identification approach subject to real-time demand estimation errors. Comparisons over time between results from the estimated model and those from the true model are evaluated using various accuracy metrics.

DATA ANALYSIS

In this section four different metrics are presented. Some of them are used to evaluate the influence of hydraulic modeling errors on CSA performance and one is used to evaluate error on the patterns.

1. $Metric\ R_c$, R_s: is the percentage of Candidate (R_c) or Safe (R_s) node-time pairs at any analysis time. R_c represents the number of node-time pairs identified as candidates divided by the total number of node-time pairs in an historical analysis time frame. Similarly, R_s is the percentage of safe node-time pairs, or those excluded as possible contamination sources.

2. $Metric\ \eta$: is the number of times CSA correctly identifies the contamination source, divided by the number of times the CSA misidentifies the source, over a simulation duration (T). At any analysis time, the CSA is considered correct if either of two conditions hold: 1) the true source *is* within the historical analysis time frame, and the group of identified candidate node-time pairs contains the true source, or 2) the true source *is not* within the historical analysis time frame, and the number of candidate node-time pairs is zero. In any other case the CSA methodology is considered to be incorrect.

3. $Metric\ \epsilon$: is the pattern estimation error (Shang et al. (2008)):

$$\epsilon = \frac{1}{T} \times \frac{1}{n_p} \sum_{k=1}^{T} \sum_{j=1}^{n_p} |\frac{\bar{y}_k^j - y_k^j}{y_k^j}| \tag{1}$$

   where $\bar{y}_k^j$ is the estimated pattern value at time step k for pattern j, y_k^j is the true pattern value for time step k and pattern j, and n_p is the number of patterns. Since the estimation performance depends on sampling design, this metric is a way to select sets of measurements that lead to estimated models with varying levels of demand pattern error. For the results presented below, we select two estimated models corresponding to the minimum and maximum pattern estimation error, from among all models estimated.

4. $Metric\ norm$: is the 2-norm (Euclidean distance) between the R_c vector over all time steps using the true model, and that using an estimated model.

APPLICATIONS

Example design

The real-time CSA applications have been carried out to analyze the ability to identify under uncertain condition the correct source injections using a midsize network. The distribution system used for the simulations is the well-known "Net3" network (Figure 1). The network includes 2 reservoirs, 3 storage tanks, 92 junctions, 117 pipes, and

2 pumping stations. Network data, and pumps characteristics are described in Vasconcelos et al. (1996).

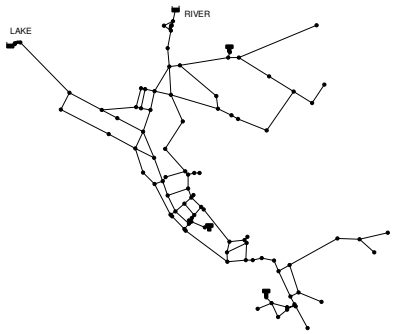

Figure 1: Example network for simulation analysis.

The true model hydraulic scenario includes water four demand patterns that follow the same time series model, with a 1 hour time step. Each pattern uses independent white noise realizations, so the four patterns are independently generated. The assumed true pattern is described as an ARIMA $(0,0,1)(0,1,1)_{24}$ process:

$$y_k = y_{k-24} + (1 - 0.15B)(1 - 0.85B^{24})\epsilon_k \tag{2}$$

where y_k is the pattern value at time step k, ϵ is the white noise distributed with $N(0, 0.06^2)$, and B is the backward shift operator (Box and Jenkins (1976)). The true model water quality scenario includes a single non-reactive contaminant source modeled using a mass booster with a strength of 20000 mg/min and duration of one hour (from time 2:00 h to 3:00 h AM during the third simulation day). For these preliminary results only one source location is analyzed and the true contamination source is node 157 on the north side of the network (Figure 1). The total simulation duration is 10 days. Three water quality monitoring stations are placed at node IDs 35, 203, and 111. Event status (positive/negative) is generated at these locations at the beginning of every hour, and assumed to be perfect. These events are synthetically generated from the water quality simulation using the true hydraulic model, where positive events are generated whenever the simulated concentration was non-zero.

The estimated model includes the same four demand patterns as in the true model, but estimated using the simulated measurements using EPANET-RTX. To calibrate the model four flow measurements and four head measurements were randomly selected from the true model. The hydraulic measurements are assumed to be affected by measurement errors, which are distributed as $N(0, 0.2^2)$ for the flows and $N(0, 1.0^2)$ for the heads. Each estimated pattern is assigned to the same group of nodes as in the true model (perfect pattern assignment). An ensemble of 5000 estimated models was generated using randomized hydraulic measurement locations, and the estimation accuracy ϵ was computed for each estimated model.

Preliminary results

For the true hydraulic model, the CSA gives the results shown in Figure 2. The top plot shows the percentage of candidate sources ($R_c(t)$) versus the simulation time t for a 24 hour historical analysis time frame. The first candidate nodes are identified 9 hours after the true injection time and the percentage of candidate sources is 1.7%. The maximum percentage of candidate sources (14%) is recorded at hour 92:00. The bottom plot in Figure 2 shows the time-varying percentage of safe nodes. As expected, the curve mirrors the plot of candidate node percentage, consistent with higher number of positive status events from the water quality sensors. Further analysis shows CSA results when the hydraulic model is not accurate. The water quality event status information is also obtained from the true hydraulic/water quality model. A time-varying percentage of candidate sources $\overline{R}_c(t)$ versus analysis time t is computed for two estimated models corresponding to the best pattern estimation error ($\epsilon = 0.0164$) and worst pattern estimation error ($\epsilon = 0.795$). Figure 2 shows the comparison of the time-varying percentage of candidate and safe sources for the three models (true, best, and worst estimated models). In these plots it is difficult to discern the differences between the CSA performance for these three models, as those differences are small for this test case.

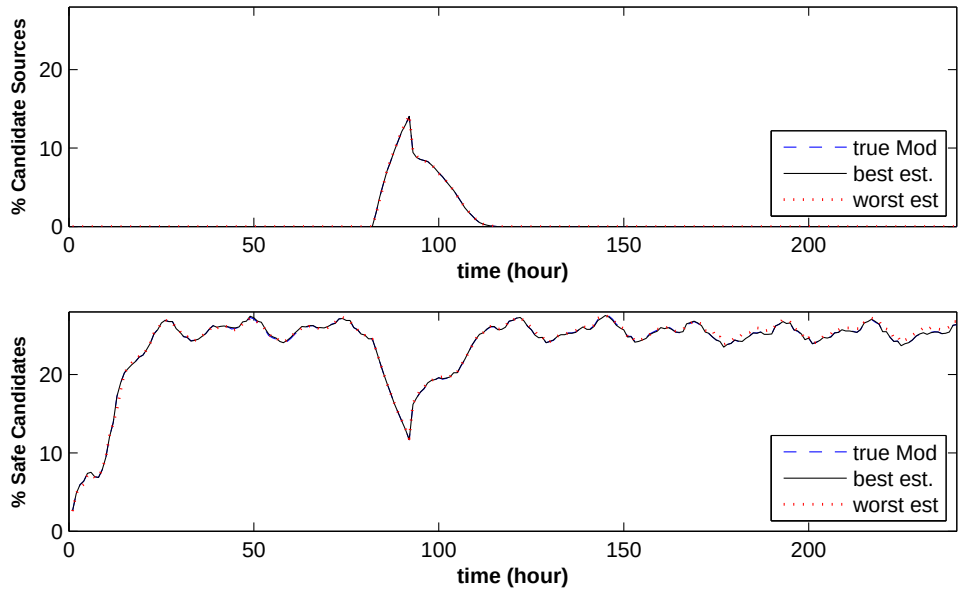

Figure 2: (Top) Percentage of candidate sources for the true model in a 24 hour historical analysis time frame versus analysis time. Comparison with estimated models for best and worst pattern estimation error. (Bottom) Percentage of safe candidates for the true model in a 24 hour historical analysis time frame versus analysis time. Comparison with estimated models for best and worst pattern estimation error.

Figure 3 shows the difference at each analysis time between $R_c(t)$ computed for the true and the two estimated hydraulic models (best estimated patterns, on left, and worst estimates, on right). The first and second row of Figure 3 are the series for the

candidate node-time pairs, and the safe node-time pairs, respectively.

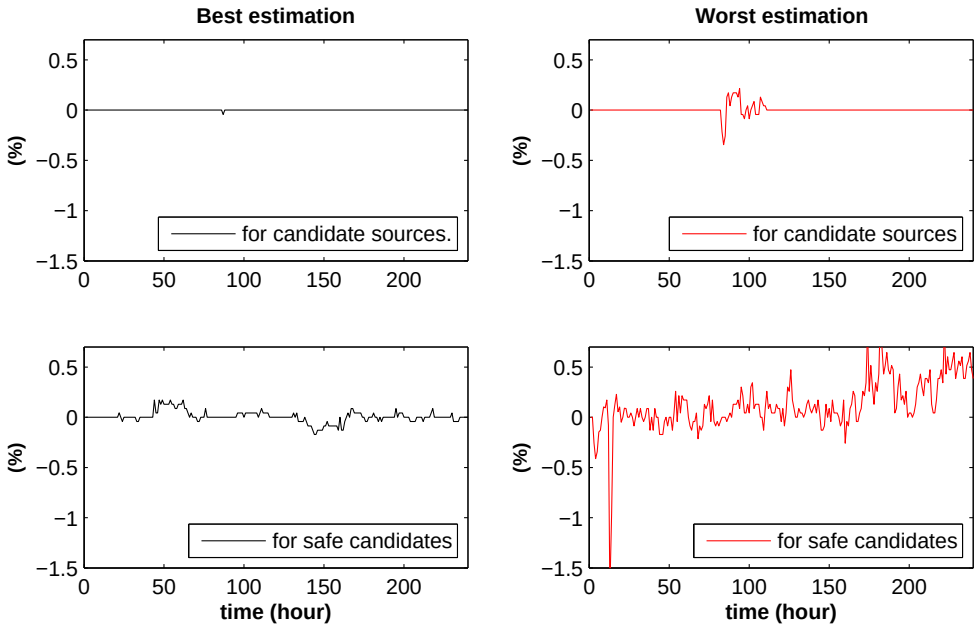

Figure 3: Difference over time between candidate sources for the true model and for the best real-time water demand estimates (left), or fr the worst estimates (right). (Second row) Differences over time for the safe candidates.

To investigate further the sensitivity of the methodology to demand errors, the white noise error standard deviation assumed when estimating the hydraulic models was varied. The standard deviations for the white noise were assumed to equal 0.01, 0.02, 0.04, 0.06, 0.1, 0.2, and 0.4 when estimating the hydraulic models using synthetic data, while the white noise for the true demand model remained 0.06. Figure 4 shows the pattern estimation error for the best and worst estimated models as a function of the assumed white noise standard deviation. For each standard deviation EPANET-RTX was used to estimate an ensemble of demands corresponding to random hydraulic measurement locations; from these a best and worst estimated model were selected. As could be expected, the errors of the worst estimated hydraulic model show a minimum at approximately the true white noise standard deviation of 0.06. Figure 5 shows the 2-norm (Euclidean distance) between the R_c vector over all time steps obtained using the true model, and that using either the best or worst estimated model, as a function of the assumed white noise standard deviation. This difference between true hydraulic model CSA performance, and that using the best and worst hydraulic models, are shown for the candidate node-time pairs, and the safe node-time pairs. As expected, there is a significant degradation of CSA performance between the best and worst estimated hydraulic models, and the results obtained using the true standard deviation (0.06) are near the best performing CSA results.

The accuracy metric η is presented in Table 1 for a varying number of water quality sensors. These represent how well the CSA algorithm performs using the true model.

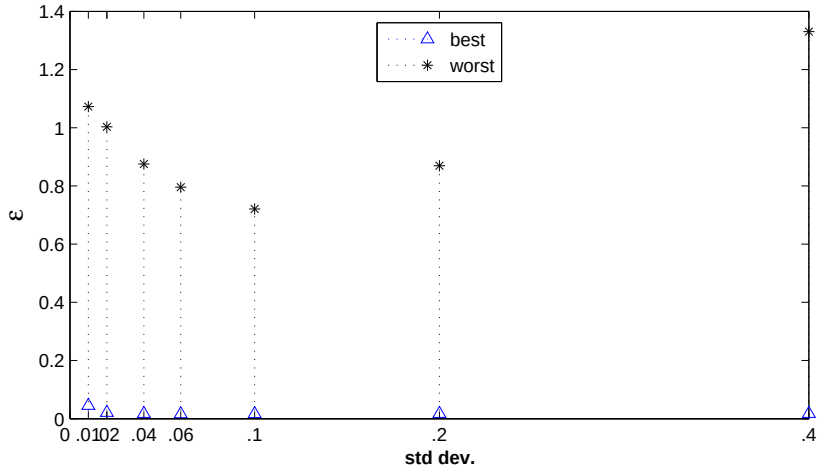

Figure 4: Pattern estimation error for the best and worst estimated models versus the standard deviation used to generate the white noise error for estimated model.

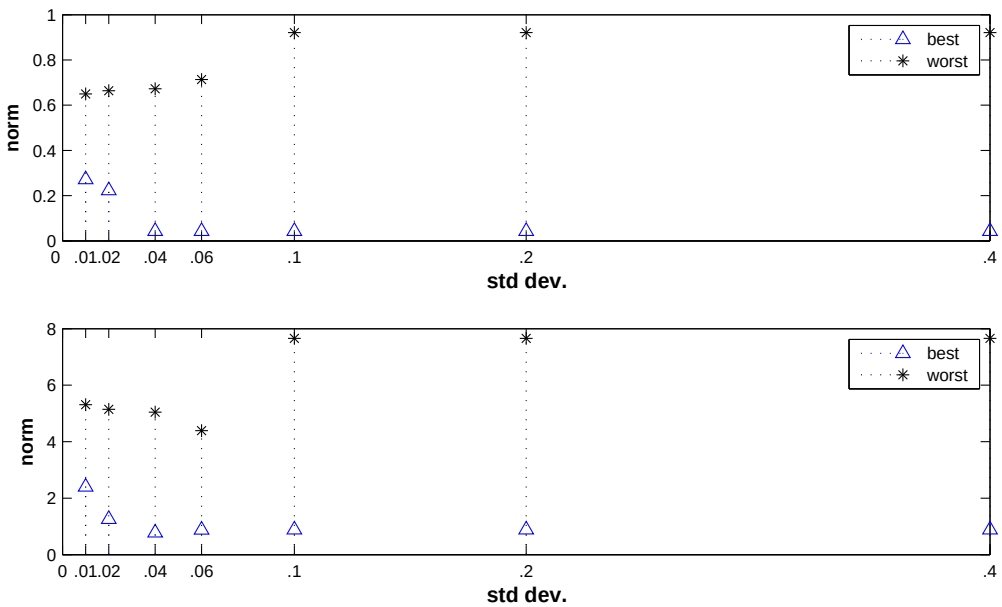

Figure 5: The 2-norm (Euclidean distance) between the percentage of candidatesidentified by CSA using the best or worst estimated models, and the true model (top). The same statistics for the percentage of safe node-time pairs (bottom).

Table 1: Metric η for the true model versus number of sensors

N. sensors	3	6	8	10	12	14	16
Metric η	7.89	6.50	6.50	6.74	6.74	2.81	2.81

Many factors affect the real-time identification of contamination sources, and this work extends the original investigation of the CSA algorithm to include uncertainty and variability in time varying water demands. The analyses here are a first attempt, and further investigations are needed. It is necessary to more accurately and completely model both the true stochastic demands, and the likely errors that are practically unavoidable when trying to estimate them. Further, in a real-time system the true model is not available to the water utilities, instead only a set of different measures from monitoring stations already installed across the system are available. Usually these hydraulic measurements and the system operations are stored in a SCADA Database. For this reason an evaluation of the best and worst pattern estimation can be handle by substituting in eq. 1 the measurements from the database and the synthetic measurements from the estimated models instead of the pattern values. To evaluate the performance of CSA a first set of metrics has been suggested. Metric R_c represents the specificity of the algorithm because gives an indication of how unique is the solution. Smaller is its value and more specific is the algorithm in identifying the true source. The $norm$ of the difference between R_c and $\overline{R}_c(t)$ for true and estimated models seems a valid metric to quantify the effect of patterns estimation on the identified candidate sources. Metric η is a general measure of how correctly the algorithm performs. It can be applied to evaluate CSA results when hydraulic model is accurate or not. For example in case of bad estimated water demands there might be the risk that CSA does not identify the true source among the candidates. η can be also used for the probabilistic CSA approach to compare the effect of perfect or imperfect measurement readings. Despite of these good preliminary results, further analysis is necessary to confirm the efficacy of these metrics.

CONCLUSIONS

A real-time contamination source identification algorithm has been illustrated. The approach uses a hydraulic model with real time estimation of water demands, and could be implemented to reduce the risk of contamination for drinking water. The preliminary results suggest that the contamination source identification process might be robust to errors in the estimated hydraulic model. The number of identified candidates was limited even when using a relatively poor real-time estimation of the demand patterns. Still, it is necessary to more accurately and completely model both the true stochastic demands, and the likely errors that are practically unavoidable when trying to estimate them. Other uncertainties should also be addressed in future work, including false positive and false negative readings from event detection algorithms. By incorporating both realistic water demand uncertainty and imperfect water quality event detection, it is hoped that the true reliability of the contamination source identification process could be identified.

References

Box, G. P. and G. M. Jenkins (1976). *Time Series Analysis: forecasting and control*. Holden-Day.

Bush, C. and J. Uber (1998). Sampling design methods for water distribution model calibration. *Journal of Water Resources Planning and Management, ASCE 124*(6).

De Sanctis, A., D. Boccelli, F. Shang, and J. Uber (2008). Probabilistic approach to characterize contamination sources with imperfect sensors. In *Proceedings of World Environmental & Water Resources Congress*, Honolulu, HI. ASCE-EWRI.

De Sanctis, A., F. Shang, and J. Uber (2006). Determining possible contaminant sources through flow path analysis. In *Proceedings of the 8th Water Distribution System Analysis Symposium*, Cincinnati, OH.

Kapelan, Savic, and Walters (2003). Multiobjective sampling design for water distribution model calibration. *Journal of Water Resources Planning and Management, ASCE 129*(6), 446–479.

Shang, F. and J. Uber (2008). *EPANET-Real Time Extension User's Manual (Draft)*. Cincinnati, Ohio: University of Cincinnati.

Shang, F., J. Uber, R. Murray, and R. Janke (2008). Model-based real-time detection of contamination events. In *Proceedings of the 10th Annual Water Distribution Systems Analysis Conference*, Kruger National Park, South Africa. WDSA.

Shang, F., J. Uber, and M. Polycarpou (2002). Particle backtracking algorithm for water distribution system analysis. *J. Environmental Engineering, ASCE 128*(5), 441–450.

Shang, F., J. Uber, B. van Bloemen Waanders, D. Boccelli, and R. Janke (2006). Real time water demand estimation in water distribution system. In *Proceedings, Water Distribution Systems Analysis Symposium*, Cincinnati, OH, pp. 15 pp.

Vasconcelos, J., P. Boulos, W. Grayman, L. Kiene, O. Wable, P. Biswas, A. Bhari, L. Rossman, R. Clark, and J. Goodrich (1996). Characterization and modeling of chlorine decay in distribution systems. In *AWWA Research Foundation Published by American Water Works Association*, Denver, CO, pp. 258–271.

THREAT PERCEPTIONS AND RISK MANAGEMENT IN URBAN WATER SUPPLY SCHEMES

Mitthan Lal Kansal
Professor,
Department of Water Resources Development & Management, Indian Institute of Technology, Roorkee 247 667, India. E-mail : mlkgkfwt@iitr.ernet.in
&
Aditya Tyagi
Water resources engineer & senior technologist
CH2M HILL, 12301 Research Blvd., Bldg. 4, Suite 250 Austin, TX 78759
E-mail : atyagi@ch2m.com

ABSTRACT

The objective of an urban water supply scheme (UWSS) is to provide safe and adequate drinking water to the public on sustainable basis. Most of these WSSs are vulnerable to natural hazards like earthquake, cyclone, landslides, and excessive rainfall etc., and the willful physical, chemical, biological, and cyber attacks. While the risk due to natural catastrophes remains high, the risk due to man-made disasters has also been increasing during the last few decades. Almost every nation is facing the problem of terrorism, as it is impossible to satisfy all sections of society within a state, a country, or a group of countries at global level. In order to express their dis-satisfaction and anguish, the disillusioned individuals or group of individuals indulge in the terrorist activities targeting the infrastructures so as to create panic among larger section. The events like September 11, 2001, attack on Indian Parliament, religious places, and recent attack of November 26, 2008 in Mumbai (India), and consistent threats of use of chemical & biological weapons in various parts of the world has compelled the researchers and managers to plan the operation and management of water supply schemes from a different perspective as it is one of the most important infrastructure for the sustenance of society. Precautions are required against the physical, chemical, biological, and cyber attacks on water supply systems.

Present study aims at highlighting these security threats and emphasizes on the need for safety review of the water supply schemes in developing countries like India as these are the life-line of a nation. Some of the threats are inherent as almost all the urban water supply schemes in India and other developing countries are of intermittent type. As a result,

pressure in pipelines is low during some part of the day and people are storing water in individual storage tanks, which deteriorates the water quality. Further, there is not much awareness about the emergency do's and don'ts. The actions desired are at all stages of disaster management life cycle that includes response, recovery, mitigation, prevention, and preparedness.

INTRODUCTION

Since the dawn of civilization, mankind has shown a preference to settle near water bodies due to assured supply of water for drinking and water for food, as water and food are the basic necessities for the survival of living beings. With the fast increasing population, and increased human activities, the available water resources are under stress and needs better management. Water resource systems are developed and managed to serve multiple objectives like drinking water, power, irrigation for food, and industrial uses on sustainable basis and are termed as life-line of a nation. These systems may comprise of large storage by creating barrier on rivers in the form of dams and cogent distribution systems. So, any threat to these systems creates panic among people and puts the government under pressure. Recognizing this, water has been used as a strategic objective in armed conflicts throughout the history. For example, in 1948, during the first Arab-Israeli war, Abrab forces cut off the West Jerusalem water supply. In 1982, Israel cut off the water supply of Beirut during the siege. In Kosovo (1999), water supplies/ wells were contaminated by Serbs, who disposed of the bodies of Kosovar Albanians in local wells, etc. Besides the man-made deliberate attempts to endanger the water supply systems, there can be failures of the water resources structures/ water supply system components due to design failure and excessive stresses. Further, there can be natural calamities like that of earthquake, floods, Tsunami, etc. which may affect the supply of water to the public at large.

The objective of this study is to highlight the threat perceptions to water supply systems, vulnerability assessment, and its management so as to reduce the impact of these threats on the survival of mankind.

THREAT PERCEPTIONS TO WATER SUPPLY SYSTEMS

Water utilities construct, operate, and maintain water supply systems. The basic function of these water utilities is to obtain water from a source, treat the water to an acceptable quality,

and deliver the desired quantity of water to the appropriate place at the appropriate time. After utilization, the waste so generated is carried through the sewerage system. The domestic sewage, industrial sewage, and the storm sewage (commonly called as storm drainage or drainage) are collected separately or combined, treated, and finally disposed off. A typical water cycle in an urban area can be divided into following sub systems (Fig.1):

1- Source, treatment and clear water storage

2- Pumping, distribution storage and distribution system

3- Sewage collection system

4- Sewage treatment plant and disposal

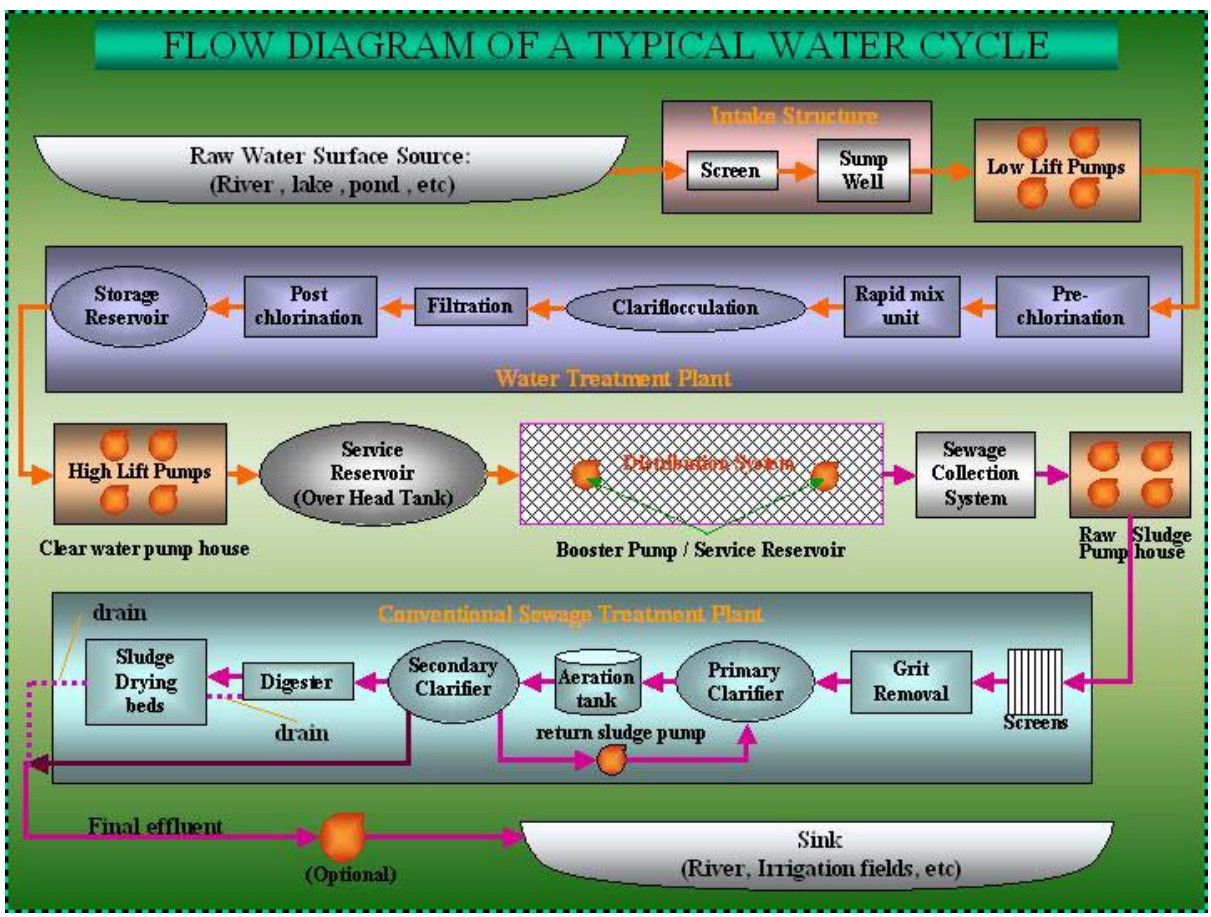

Fig. 1 Line diagram of a typical urban water cycle

The objective of such a WSS is to supply desired quantity of water with desired quality at consumer's tap level and then collect the waste so generated, treat it then dispose off in the

water body. Since the water travels from raw water source to consumer's tap via various components like water treatment plant and distribution system, etc. it is subject to failure due to many reasons. Reasons of failure of one or more components can be classified under two major categories. These are :

i) Natural

ii) Man-made, which may further be classified as unintentional and intentional.

Another way of categorizing the failure of WSS is

i) Physical failure of component(s)

ii) Chemical failure

iii) Biological failure

iv) Cyber failure

The natural causes of water supply system failure are floods, cyclones, earthquakes, windstorms, avalanches, etc. While natural disasters occur on all continents, the number of people affected is greater in the developing world, primarily because the systems are not that much resilient as those in developed countries. The first and foremost effect of natural disasters is on power, roads, and buildings. As a result, the basic infrastructure gets damaged and it takes longer time to restore the basic components to working condition as well as to restore the power which is essential for pumping and other units of the water supply scheme.

The man-made disasters can be because of inadverant decisions taken by the decision makers about the development and the environment, and secondly because of the willful attacks of the terrorist. Terror, which may be defined as a state of intense fear, is often the result of violence committed by one or more group to intimidate individuals, segments of society, or governments to meet the group's demands. Thus, in order to create panic in the society, or among the enemy, people may choose to attack the water supply schemes. These attacks may be in the form of physical, chemical, biological, or cyber. Physical attacks may result in complete disruption of the functioning of one or more components of the water supply scheme. This may include the damage to raw water pumping station, water treatment plants, and over-head service reservoirs, etc. The chemical attacks may include the poisoning of raw water or the potable water in the distribution system itself. Biological attacks may again be

in the form of deteriorating raw or finished water quality biologically. More recent form of attacks is the cyber attacks so that the information system is disrupted which will affect the functioning of the overall management of the water supply scheme.

VULNERABILITY ASSESSMENT

In order to assess the risk and threat perception to water supply schemes, following questions should be addressed (Haimes (1998)):

1. What can go wrong?
2. What is the likelihood that it will go wrong?
3. What are the consequences?
4. What options are available?
5. What are the associated tradeoffs in terms of cost, risks, and benefits?
6. What are the impacts of decisions on future options?

These questions lead to precisely the scope of risk management. The common elements of vulnerability assessments for a typical water supply system includes :

- The elements of the water supply system, including its mission & objectives;
- Identification of adverse consequences and the critical elements that are subject to malevolent acts.
- Assessment of the likelihood of such a malevolent act
- Evaluation of existing countermeasures;
- Analysis of current risk & development of an emergency plan for risk reduction.

In order to develop an infrastructure risk model (IRM), one should carry out the Fault Tree Analysis (FTA) of the system (Kansal, 2005). FTA is a deductive method which is normally used in quantitative way, although it requires initially a qualitative study of the system. FTA of the system will include the identification of its components, hierarchical structure, functions, states, and vulnerability. In order to identify risk to a system, it is desired to know about the system itself. Thus, decomposition of the system into various components and its hierarchical structure is an important input. The vulnerability to risk are function of access and exposure. For example, if a component is easily accessible, it is more vulnerable to risk

as compared to limited access component. Similarly, if a component is more exposed, it is more vulnerable, whereas, the under ground structures are less vulnerable to external attacks. A low vulnerability score for a component is an advantage. Mathematically, if 'α_i' and 'β_i' are the accessibility and exposure of a component on subjective scale (0-1), then the component vulnerability can be expressed as :

$$V_i = \alpha_i * \beta_i$$

If the various components are in series, the overall vulnerability can be estimated as the product of the individual vulnerabilities, whereas, if the components are in parallel, then vulnerability can be taken as the summation of components vulnerabilities.

EMERGENCY RESPONSE PLANNING RISK MANAGEMENT

In the context of prevailing political situation at international level and cross-border terrorism, there is an urgent need to study the vulnerability of such basic amenities. Hardening of water distribution system, which refers to rendering the system less vulnerable to various types of threats, can be grouped into four categories (Haimes et al., 1998) :

- Security
- Redundancy
- Robustness
- Resilience

Many studies have been undertaken in USA (Mays, 2004) for checking the security aspects of various public utilities. For example, the US department of justice conducted a security survey of federal facilities vulnerability (1995)) in response to the bombing of Murrah Federal Building in Oklahoma City in April 1995. The study recommended that where feasible, every federal facility should be brought upto minimum standards specified by the study for its security level. Floyd (1995) has given broad guidelines for developing a security assessment under contract with USEPA and the municipal water systems of Phoenix, Detroit, Atlanta and others. Black and Veatch (1992) have studied the various aspects of security of a major US city. The study has considered the approach of danger to three classes of

community resources such as the human population, business and industry and physical environment.

Redundancy refers to the ability of a certain component of a system to assume the functions of failed components without affecting the performance of the system. For a WDS, redundancy may take the form of properly designed extra pipes in-built in the system, multiple means of system control, duplication in managerial emergency response and the standardization of design of system components. Redundancy can also be achieved through interconnection of WDSs (Castillo et al, 1997). A redundant capability in response to emergency situations assumes a greater chance of containing damage to the system resulting from terrorist act. In other words, redundancy is a corrective measure in case of terrorist attack.

Robustness refers to the degree of insensitivity of a system design to errors in the estimates of certain design parameters that affect the design choice. Hardening a system involves modifying a system's design in effect, choosing a new optimal design. Developing new designs that are robust at a probability level equal to or higher than the original design enhances the hardness of the system rendering it less sensitive to terrorist threats.

Resilience is the ability of a system to be operated close to its optimal design after an adverse event a suitable response to damaging action has been made, such that the economic losses due to aging events may be contained within a certain limit.

Water supply authorities should take urgent note of the requirement of such studies. Approaches are needed for the quantitative analysis of the potential consequences of specific attack scenarios, quantitative risk analysis can be system specific incorporating the case studies like, identification of conventional ways in which a WDS can be disrupted, identification of critical sections of the system that are vulnerable to such attacks which may disrupt the supply for days, for weeks and for months, etc. Accordingly, high priority action plans must be clearly stated and formulated. The cost-benefit analysis of hardening the WDS against the possible attacks should also be studied. The water utilities should have an emergency operations/ response plan in co-ordination with local administration. It should be able to take care of various types of incidents like structural damage (man-made or natural),

contamination event, and events like intrusion through supervisory control & data acquisition (SCADA).

DEVELOPMENT OF NEXT GENERATION ANTI-CONTAMINATION CAPABILITIES FOR WATER SUPPLIES

Water supply systems are spatially diverse and therefore have inherent potential to be vulnerable to a variety of threats like physical, chemical and biological. Water supply systems are designed to deliver adequate water under desired pressure. The disruption could be from raw water source to consumer's tap level. Each of the water supply system element presents a unique challenge to the water utility in safeguarding the water supply. For example, destruction of storage structure, pumping house, treatment facilities, finished water tanks and reservoirs, explosive release of chlorine gas, biological contamination, etc. can cause panic among the people. Since each of these elements is unique it requires a special type of remedial measure.

Contamination if generally viewed as most serious potential terrorist threat to water supply systems. Chemical or biological agents could spread throughout a distribution system and result in sickness or death among the consumers. Some of the contamination might not be noticed unless the emergency rooms report an increase in patients with a particular set of symptoms. There have been report of accidental contamination which resulted in many fatalities in various parts of the world.

Water quality modeling in helps in tracking the water quality changes during the journey from raw water source to the consumer. The water quality simulations to track the propagation of water borne substances in the distribution network are based on the hydraulic characteristics of flow such as flow paths taken by water, the travel and residence time, mixing of water from different sources and corresponding dilution effects. Consumer perception and industry regulation are now focusing on the need for utilities to study water quality variations within the water distribution system and their causes and effects. Recent developments in computer software now provide a capability to build representative models, which can simulate the propagation and concentration of water quality parameters under

steady and dynamic flow condition. The software like EPANET are commonly used for such purposes.

Water quality monitoring is an effort to obtain information on the physical, chemical, biological and radiological characteristics of water via statistical sampling. It is an important aspect of overall water quality management. Quality monitoring in a drinking water supply scheme is undertaken at all the three levels, viz, the source, the treatment plant and the distribution system. A major managerial and technical barrier exists because of lack of proper guidelines for identifying suitable monitoring stations in a WDS. In absence of guidelines, most water utilities go for monitoring at accessible locations. Though it is an important factor, but logically the monitoring station should be those locations that are in low demand zones and are more vulnerable from water quality point of view. However, in most situations, it is not possible to rank the vulnerability of various locations. Thus, a systematic and scientific approach is needed for selecting the monitoring stations which represent the entire network.

The decay in water quality may occur because of (i) internal factors within the distribution system such as long residence time which provides more time for reaction of water borne substances within the bulk and with wall materials; and/ or (ii) external contaminants intruding into the system.

Water quality monitoring in distribution systems of most Indian Metropolitan cities has been carried out in an ad-hoc manner. There is no scientific justification for choosing the location, sampling frequency and the number of sampling stations required to be installed. The monitoring practices can be based on two basic principles (Kumar et al. (1997,1999):

i) Determining the gradual deterioration in quality of finished water within the WDS due to decay of residual disinfectant level, and

ii) Detecting the sudden deterioration of water quality in WDS due to external contamination at one or more nodes.

Strictly speaking, to ensure good water quality at all demand nodes, one should monitor water quality at all the demand nodes, which is practically impossible for a large WDS. To ascertain that internal decay of quality within the WDS is covered with an optimal set of

monitoring stations, one can find out ways and means. Similarly, one can identify the ways & means for identifying the contamination & spread of contamination due to accidental contamination. Some chemical & biological sensors can be developed for identification of contamination so that users can take preventive steps so as to reduce the impact of contamination.

CONCLUSIONS

Drinking water is one commodity in which most of the countries are looking forward to improvements at a massive scale. In this paper threat perceptions to water supply schemes that directly affect quantity and quality of water received by the consumers, and which require attention on an emergency basis, have been discussed. It is felt that the research institutes have potential to develop models in these areas but most of the problems remain unresolved due to absence of coordination between research and field engineers. Thus, there is need industry-institute collaborations in this field of implementing technological up gradations to solve many a pressing problems plaguing the linking water supply systems so that the entire humanity gets better services as far as drinking water is concerned.

REFERENCES

Black and Veatch (1992). "Security system study, city of [a major U.S. metropolitan city]". Rep Index NO. W-904243, S-910802. Kansas city, Mo., May.

Castillo E.T., Rubin S.J., Keefe S.K., and Raucher R.S. (1997). "Restructuring small systems" J.AWWA, Jan. 1997, 65-74.

Floyd, W.R. (1995). "Security Surveys: Guidelines" American Society of Industrial Security, Arlington, Virginia, U.S.A.

Haimes Y.Y., Matalas N.C., Lambert J.H., Jackson B.A. and James.F.R. (1998). "Reducing vulnerability of water supply systems to attack". J. Infrastructure Systems, ASCE, Vol. 4 (4), 164-177.

Haimes Y.Y., (1998). "Risk Modeling, Assessment, and Management". Wiley-Interscience, John Wiley & Sons, New York.

Kansal, M.L., Das, Devadutta, & Mandal, Jeebachh, (2005). "Performance Assessment of a Hydropower Station using Fault Tree Analysis", International Journal of Water & Energy, Vol. 62, No. 3, pp 44-55.

Kumar A., Kansal, M. L. and Arora G. "Identification of monitoring stations in water distribution system", Jour. Env. Engg., ASCE, 123(8), 746-752, (1997).

Kumar A., Kansal M.L. and Arora G., "Tracking accidental contamination in municipal water networks", Proc. of Civil and Environmental Engineering Conference New Frontiers & Challenges, I-67 to I-76, Bangkok, Thailand, 8-12 Nov., (1999).

Mays, Larry W, "Water Supply Systems Security" (Ed.), McGraw Hill handbooks, New York, 2004.

Getting More From Your Investment. Using Water Security Monitoring Technology for Everyday Operations

Dan Kroll[1]

[1]Hach Homeland Security Technologies, Hach World Headquarters, 5600 Lindbergh Drive, Loveland, Colorado, 80539 Phone 970-443-2436. email: DKROLL@hach.com

ABSTRACT

Since 9/11 numerous communities have installed multi-parameter monitoring stations in the distribution system as early warning systems for potential water security threats. These systems have recorded large streams of data relevant to water quality in the distribution systems. In this study data streams from a number of communities are analyzed for pertinent information as to the health and operation of the distribution system. Changes in water quality are correlated with known causes attributable to day-to-day operational changes and also anomalous events (pipe bursts, accidental back flows, cross connections, chemical over feeds, treatment plant problems, nitrification events, etc.). Information concerning what action was taken to ameliorate the problem will also be linked to the data for the identified events. We will need to consider databases such as this before we determine the best course of action to ensure our water supplies meet acceptable levels of safety from source to tap.

INTRODUCTION

The distribution system represents the last analytical frontier in the water quality industry. The monitoring of source water and treatment plant processes has progressed to a level at which we can be confident that we are providing good quality water from the plant to the distribution system. Once the water reaches our aging distribution systems, however; our knowledge as to its continued integrity is limited by the quality and amount of available data. Most monitoring in the distribution system is relegated to the occasional snapshot provided by grab sampling for a few limited parameters or the infrequent regulatory testing required by mandates such as the Total Coliform Rule in the US. The development of water security monitoring in the years since 9/11 has the potential to change this paradigm. Since 9/11 numerous communities have installed multi-parameter monitoring stations in various locations through out the distribution network as early warning systems to detect potential water security threats. These continuous on-line systems have recorded large streams of data (at some sites for a number of years) relevant to water quality in the distribution systems in which they have been deployed.

For the past several years, scientists at Hach Homeland Security Technologies (HST) have been actively engaged in the development and testing of an early warning system for detecting water quality problems including those related to an intentional terrorist attack. This paper gives a brief summary of how the developed system operates and presents results form some of the recent field-deployment efforts that have been undertaken.

In this study, data streams from a number of communities (both small and large) are analyzed for pertinent information as to the health and operation of the distribution system. Changes in water quality are correlated with known causes attributable to day-to-day operational changes and also anomalous events. Case study information concerning what, if any, action was taken to ameliorate the problem will also be reported for the identified events.

This sort of information is critical in understanding and improving the operation of our distribution systems and can also be valuable as we consider regulations that affect that operation. Any future efforts to regulate the distribution system will need to consider databases and monitoring techniques such as the one described here before we can determine the best course of action to ensure our public water supplies meet acceptable levels of quality and safety from source to tap.

THE HACH METHOD AND APPROACH.

Monitoring in the distribution system is a difficult proposition. The shear number and diversity of potential threat agents that could be utilized in an attack against the system makes monitoring for them on an individual basis an effort that is doomed to failure. To counter and detect the unprecedented number and types of compounds that may be encountered, what is needed is a broad-spectrum analyzer that can respond to any likely threat and even unknown or unanticipated events.

Rather than attempting to develop individual sensors to detect contaminants, the Hach HST approach was to utilize a sensor suite of commonly available off-the-shelf water quality monitors such as pH, electrolytic conductivity, turbidity, chlorine residual and total organic carbon (TOC) linked together in an intelligent network. The logic behind this approach is that these are tried and true technologies that have been extensively deployed in the water supply industry for a number of years and have proven to be stable in such situations. One of the difficulties encountered when designing such a device is that the normal fluctuations in these parameters found within the water can be quite pronounced.

The problem then becomes, can we differentiate between the changes that are seen as a result of the introduction of a contaminant or anomalous condition and those that are a result of normal everyday system perturbation? The secret to success, in a situation such as this, is to have a robust and workable baseline estimator. Extracting the deviation signals in the presence of noise is absolutely necessary for good sensitivity. Several methods of baseline estimation were investigated. Finally, a proprietary, patented, non-classical method was derived and found to be effective.

In the system as it is designed, signals from 5 separate orthogonal measurements of water quality (pH, Conductivity, Turbidity, Chlorine Residual, TOC) are processed from a 5-paramater measure into a single scalar trigger signal in an event monitor computer system that contains the algorithms. The signal then goes through a crucial proprietary baseline estimator. A deviation of the signal from the established baseline is then derived. Then a gain matrix is applied that weights the various parameters based on experimental data for a wide variety of possible threat agents. The magnitude of the deviation signal is then compared to a preset threshold level. If the signal exceeds the threshold, the trigger is activated.

The deviation vector that is derived from the trigger algorithm is then used for further classification of the cause of the trigger. The direction of the deviation vector relates to the agents characteristics. Seeing that this is the case, laboratory agent data can be used to build a threat agent library of deviation vectors. A deviation vector from the monitor can be compared to agent vectors in the threat agent library to see if there is a match within a tolerance. This system can be used to classify what caused the trigger event. This system can also be very useful in developing a heuristic system for classifying normal operational events that may be significant enough in magnitude to activate the trigger. When such an event occurs the profile for the vector causing it is stored in a plant library that is named and categorized by the system operator. When the event trigger is set off the library search begins.

The agent library is given priority and is searched first. If no match is found, the plant library is searched and, the event is identified if it matches one of the vectors in the plant library. If no match is found, the event is classified as an unknown and can be named if an investigation determines its cause. This is very significant because no profile for a given event need be present in the libraries for the system to trigger. This gives the system the unique ability to trigger on unknown threats and events. Also, the existence of the plant library with its heuristic ability to learn plant events results in a substantial and rapid decrease in unknown alarms over time and offers a tool for system optimization. The developed system has been subjected to strenuous testing in both laboratory and field scenarios. This has resulted in this approach being the only water quality monitoring system listed by the US Department of Homeland Security as a designated and certified antiterrorist device under the US SAFETY Act.

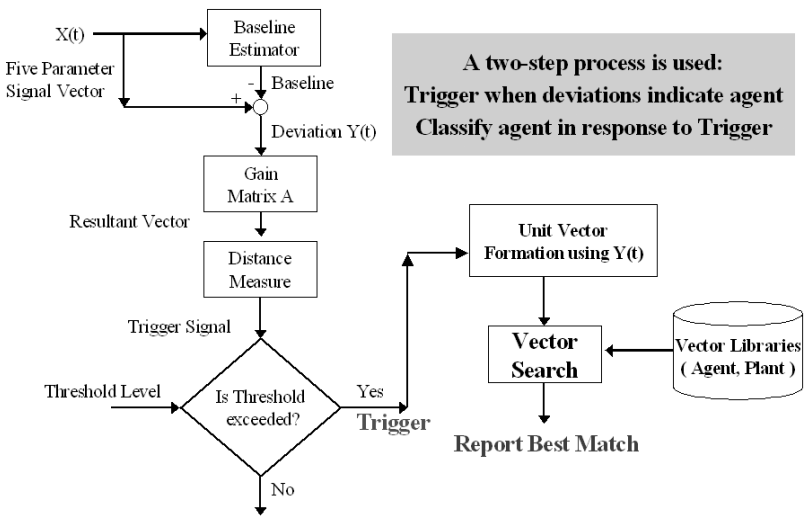

Figure 1. The use of intelligent algorithms with standard bulk parameter monitoring equipment allows for a robust system that is capable of triggering on and classifying a wide diversity of threat agents including unknown events.

FIELD TESTING OF THE DEVELOPED SYSTEM:

Prior to the onset of this project, there was a definite lack of data concerning conditions in the distribution system. Very few utilities carried out data collection in

the distribution system other than periodic grab samples. Those that did have some on-line continuous data were usually limited to only one or two parameters. Since the initiation of this program over, 500,000 hours of real time data has been collected across a wide variety of different distribution systems exhibiting different water matrix profiles revealing many interesting attributes of the distribution systems. These systems represent a variety of water quality conditions and operational situations. The site locations need to remain anonymous due to security considerations and non-disclosure agreements, but they represent a wide diversity of system sizes and geographic locations throughout the United States. The deployments are at both civilian and military sites. At the time of the preparation of this article, all deployments are within the United States. Hach HST has only recently received International Traffic in Arms Regulation (ITAR) clearance from the US Department of State to deploy the systems on an international basis. The following are a few examples of incidents that have been recorded during these real world deployments. These incidents help to demonstrate the systems ability to learn and to become a useful tool not just for security but also for every day operational improvements.

Caustic Overfeed Event

In this deployment scenario, the plant uses caustic feed to control water pH. The system experienced a trigger that when investigated was identified as an operational problem that resulted in the feed of excess caustic. The result was that the overfeed affected the pH and the conductivity of the water, causing the alarm. See figure 2.

The reason behind this was that the vendor from which the casuistic was being purchased had delivered the wrong concentration of the solution. No one had checked to see if the concentration was correct before feeding in the material. New procedures were put in place to verify incoming raw materials. The Event Monitor learned this Plant Event and can identify a recurrence of the event in the future if there is another failure in the system and it is repeated.

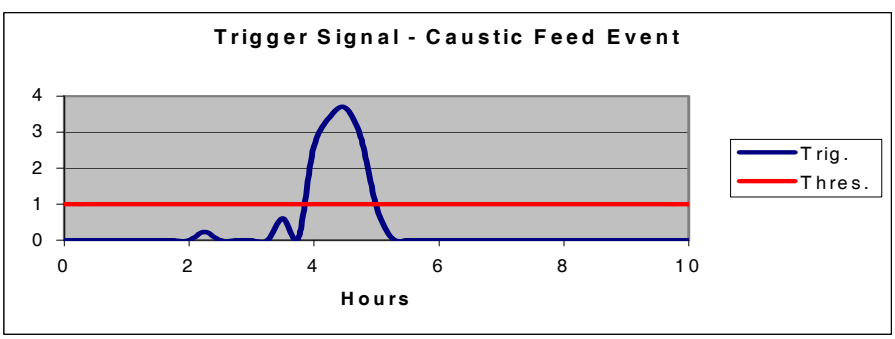

Figure 2. Caustic Event.

Effect of Variable Demand

In this deployment, daily events influencing turbidity, chlorine, pH and conductivity are not completely understood but are suspected to be caused by water

demand fluctuations in the area. This may indicate a need for more routine flushing of the areas pipes and the instillation of a chlorine booster station.

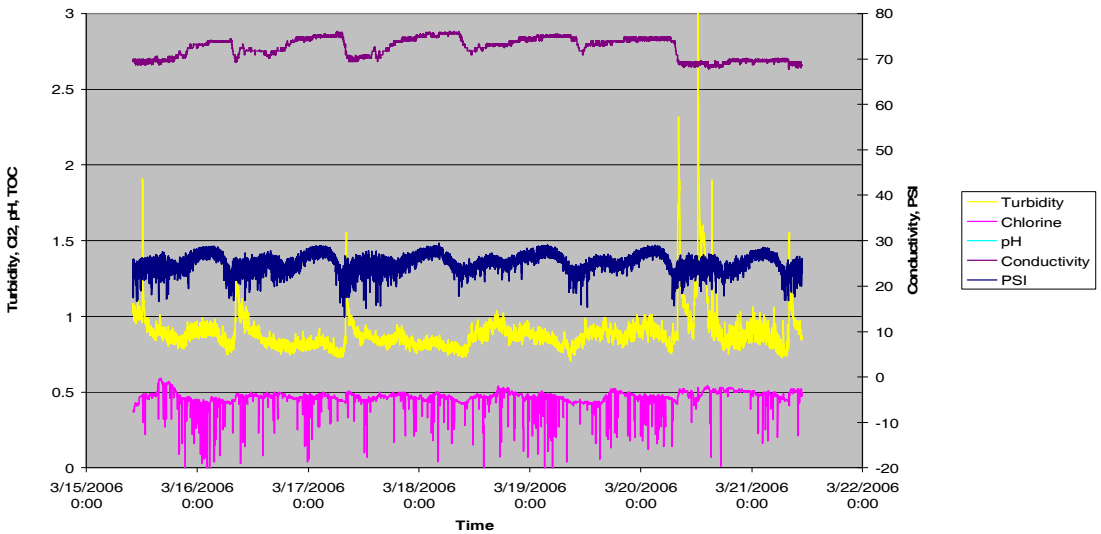

Figure 3. Variable Demand

Ammonia Overfeed Events

On March 26th, 2007; maintenance was performed at the plant supplying water to the distribution system being monitored. After the maintenance was completed, the plant was restarted and the system that feeds ammonia to create monochloramine as a residual disinfectant overfed the chemical. The person in charge of the on-line monitors immediately noticed the increase in pH and notified plant operations. Operations reported a problem with ammonia feed pumps. The problem was temporarily fixed, but a slug of ammonia was sent into the distribution system. Several customers called, complaining about an ammonia smell and taste coming from the tap. The exact amount of ammonia released was unknown, but was believed to be less than 10 ppm. The facility continued operations but temporarily switched to free chlorine as a disinfectant until July 2nd. See figure 4.

On October 3rd, the same treatment plant experienced a brief ammonia overfeed. In this case, a pump was turned on and not switched off at the proper interval. There was a drop in chlorine and a decrease in pH. See figure 5.

Between August 22 and August 23, 2007, three similar events occurred. Increases in turbidity pH and possibly TOC with drops in chlorine caused triggers. These changes resemble the large ammonia event that occurred in March. The operator believes that these could be ammonia feed events, but could not confirm it or find the fault.

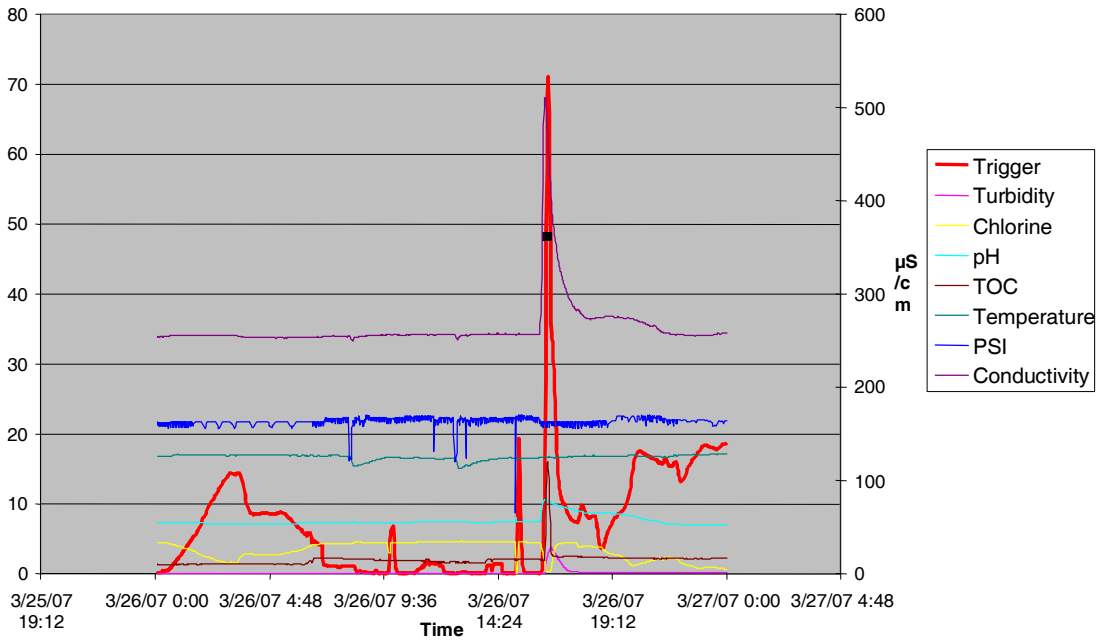

Figure 4. March ammonia overfeed event.

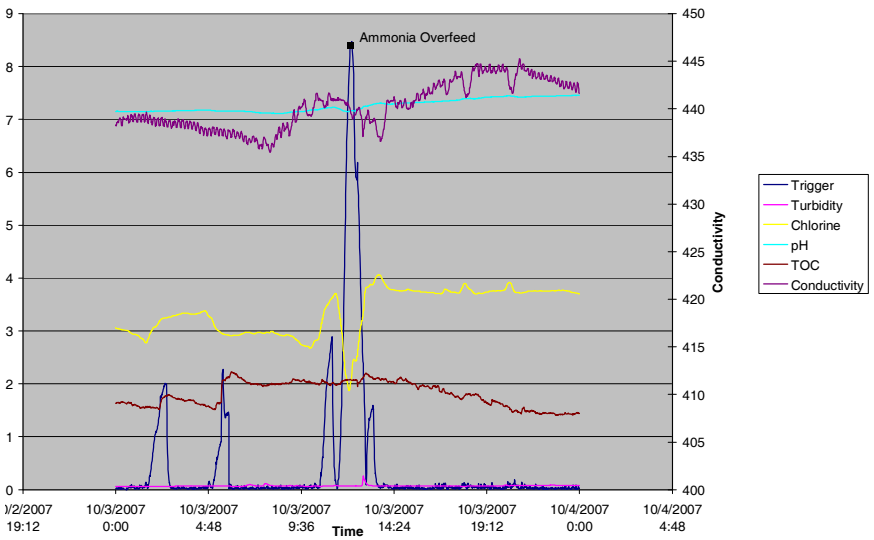

Figure 5. Second Oct 3rd Ammonia Incident

Possible Chlorine Feed Event

An April 3rd, 2007 there was a turbidity and pH increase and a decrease in chlorine and conductivity. The operator suspects that there was a problem with the chlorine feed at the plant. However this cannot be confirmed. The plant was using free chlorine at the time which rules out the possibility of an ammonia feed problem.

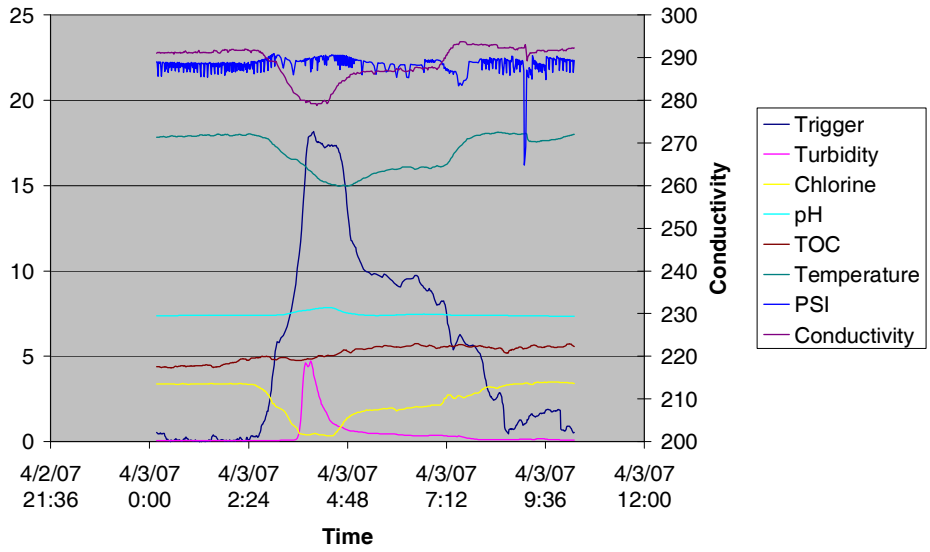

Figure 5. Potential Chlorine Feed Event.

Air Bubble Event.

In one Northern Midwestern city's distribution system, every Friday, the deployed sensors would behave extremely erratically resulting in multiple alarm signals being generated. Investigation led to the discovery of extreme amounts of entrained air bubbles being present in the system's water on Friday afternoons and evenings.

Further investigation into the root cause of the air bubbles being present revealed that school buildings in the area that were to be vacant over the weekend had a policy of using air to blow out their water lines to prevent freezing so that the heat could be turned off over the weekend and holidays. A faulty check valve at one of the schools allowed the air to bleed into the distribution system. The valve was replaced, thus closing a possible backflow route into the system. After this maintenance was performed, the erratic readings ceased.

Distribution Flushing Case Study

In this case, the water utility customers were experiencing poor water quality in certain areas of the distribution system. The systems operations team could not pinpoint the problem. A series of distribution system monitoring devices were installed at various locations throughout the distribution network. The devices were able to help in locating a number of transient dead ends and low flow areas based on the monitoring results. Using this data the team revised the normal flushing schedule for these areas. The results were improved water quality and fewer customer complaints.

Grab Sample Versus On-line Case Study

In this situation, the local water utility had in place an extensive system of water monitoring through grab samples. All indications were that the water quality was good. After installation of several water monitoring panels in the distribution system they found that the turbidity spiked to levels as high as 20 NTU during the

night and early morning hours when typically no grab samples would have been collected. They also found extremely high variability in chlorine levels during these time periods.

A series of changes to their treatment plant operations and distribution system procedures allowed the system to regain control of the water quality in the distribution system. They were able to lower the turbidity spikes to around 1.5 NTU at night and maintain more consistency in chlorine residual levels resulting in better water quality and consistency for the end consumers.

Main Break Events.

In this situation the system had only just been installed a few days previously. Hach HST personnel were informed that the instruments were behaving abnormally and were giving strange readings. An investigation of the sensors found no problems. A short time later a major main ruptured in a catastrophic mode. The system was able to detect the perturbation in water quality parameters that were precursors to the main break and trigger upon them. Unfortunately, the system was newly installed and the event was not recognized until it was too late.

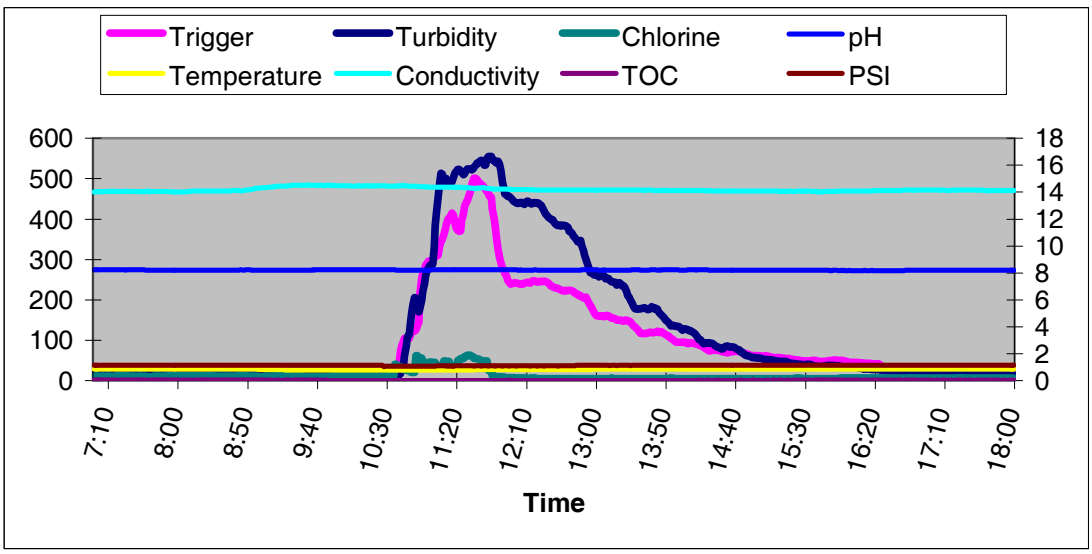

Figure 6. Erratic readings soon after installation.

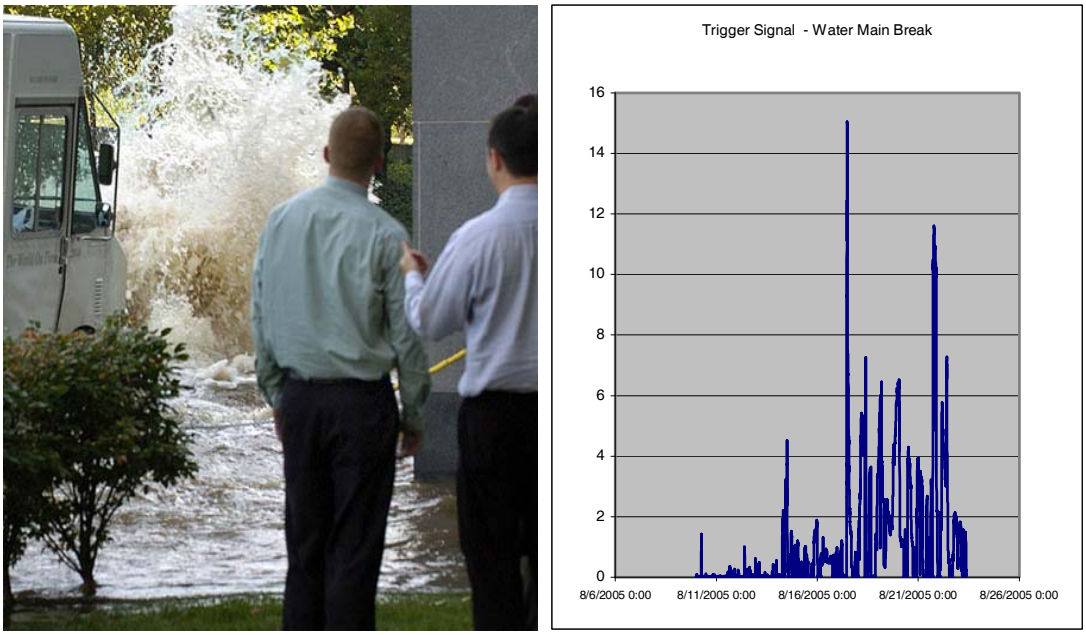

Figure 7. Photo of main break event along with graph of trigger signal.

Another incident occurred on June 29th, 2006 the pipe was an 8-inch line and was located 1.8 miles down stream from the monitoring sensors. There was an increase in turbidity and chlorine. The turbidity appears to have increased the day prior to the break.

A third break occurred on July 30th, 2006. The line was a 36" water main located 1 mile from the monitor. Conductivity, turbidity, and chlorine spiked. There appears to be two water flow interruptions to the WDMP the night before but it's unclear if they are related to the break on the 30th.

This break occurred at night on September 20th, 2006. The exact time of the break is currently unknown, although there appears to be a flow interruption to the monitoring panel the previous morning. The line involved was a 12" water main, which is 0.4 miles from the panel.

CONCLUSION

Extensive laboratory and pipe loop testing that is detailed in a separate papers[1,2,] indicate that these types of monitoring systems appear to be a good choice for detecting water quality excursions that could be linked to water security events. There are a number of advantages to using such systems. The chief advantage is that these instruments are not new. They are based on common everyday parameters with which the average industry worker is quite familiar, thus, adding a degree of comfort in operations not afforded by other new technology. As existing technologies, these instruments have been proven to be robust and dependable in prior field deployments. They represent measurements that would be of interest and use to water utility personnel above and beyond their role as water security devices. The deployment incidents detailed in this paper confirm this and also demonstrate the applicability of utilizing these everyday parameters by linking them with advanced algorithms. The field deployment studies not only demonstrate robustness in the field and the ability to recognize a wide variety of events, but these studies also demonstrate such

system's ability to learn. It is foreseeable that these devices will become much more than a system that is capable of detecting terrorist events. They could easily become a critical tool for improving everyday operations.

For example, through many years of experience, the best old hands at treatment plant operations have developed "a sense" for knowing something in the treatment system is amiss. It can be a smell, color, clarity (or lack there of), sound or just tingling in the nape of the neck. One gains this sense only by extensive experience in a particular facility. These senses do not exist in distribution systems because there has typically been little measurement done upon which to gain these "senses" and, therefore; "Bulk Parameter Monitoring in the Distribution System with Interpretive Algorithms" has the potential to become the artificial "sense" able to quickly "learn" the quirks of the distribution system and have those quirks labeled by those with extensive experience so that less experienced employees have the benefit of that knowledge without having to wait 5, 10 or more years. A good phrase to describe this knowledge base would be "institutional intuition."[3]

With the aging of the work force and rapid employee turnover "institutional intuition" has the chance of quickly dying out. Above and beyond their obvious security benefits, algorithms could be a way to circumvent this loss of knowledge and to build a knowledge base where none has previously existed. This in turn could allow improvements is system operation that may result in cost savings and definitely will result in a higher quality product being delivered to the consumer.

REFERENCES

1) Kroll, Dan and King, Karl "Safeguarding the Distribution System: On-Line Monitoring for Security and Enhancing Operational Performance" Journal of the New England Water Works Association. June 2006.
2) Kroll, Dan "Operational and Laboratory Verification Testing of a Heuristic On-Line Water Monitoring System for Security" International Journal of High Speed Electronics and Systems. Vol. 17, No. 4 (December 2007)
3) Kroll, Dan. 2006. "Securing Our Water Supply: Protecting a Vulnerable Resource. PennWell Publishers. Tulsa, OK.

Modeling a Hydraulic Response to a Contamination Event

Terranna Baranowski Haxton[1] and Thomas M. Walski[2]

[1]U.S. Environmental Protection Agency – NHSRC, Mail Stop: NG-16, 26 W. Martin Luther King Dr., Cincinnati, OH 45268; email: haxton.terra@epa.gov
[2]Haestad Methods Solution Center, Bentley Systems, Incorporated, 27 Siemon Co Dr, Suite 200W Watertown, CT 06795; email: tom.walski@bentley.com

Abstract

In responding to contamination incidents that may occur in a water distribution network, a variety of actions (e.g., public notification and operational changes) can be pursued. A relatively common and effective operational response option utilized by water utilities to address water quality concerns is flushing. The effectiveness of flushing alternatives can be evaluated by modeling the water distribution system dynamics.

Two approaches to modeling hydrant flushing as a hydraulic response are examined in this paper: a fixed flushing rate and flow emitters. In addition, the effects of knowing the source location and the expected contamination spread are explored.

The paper generally demonstrates that the effectiveness of flushing depends on the accuracy with which the initial contaminant plume location is known. In modeling flushing as a response, use of flow emitters instead of fixed flow to model hydrant discharge should provide a more realistic description of system response to flushing.

Introduction

Many utilities across the country are evaluating and considering on-line monitoring systems to address increasing concerns about water quality and the possibility of intentional contamination events. Several research groups have developed methodologies for identifying preferred monitoring locations to provide for a contamination warning system (CWS) or a water quality surveillance program for a utility. Should the CWS detect the presence of a contaminant in a water distribution network, a variety of response actions must be examined in order to implement the most beneficial consequence management strategy, including public notifications and operational changes (e.g., valve closures and flushing). A relatively common and effective operational response option utilized by water utilities to address water quality concerns is flushing. Assuming that flushing is a feasible response, the effectiveness of flushing alternatives can be evaluated by modeling the water distribution system dynamics.

Previous research efforts (Baranowski and LeBoeuf 2008) have used hydraulic/water quality modeling and optimization tools to aid the selection of hydrant locations to flush and valves to close. The optimization objective was to minimize the impact of a

contamination incident in a water distribution system. Flushing was modeled by increasing demand at nodes representing hydrants; however, opening hydrants can occasionally result in negative pressures in the network. Since demand is actually limited by pressure in the real-world, water utility operators cannot simply assign a fixed flow rate to each hydrant. To increase the validity of a hydraulic response, the pressure dependent flushing rate should be modeled as emitter flow.

Therefore, the selected hydrant locations will be modeled as emitters to calculate the feasible flushing rate, since an emitter relates the discharge from the node to the pressure immediately upstream of the node. To evaluate the effect of utilizing emitters, the impacts of contamination incidents in an example network are examined for both fixed flow nodes and emitter nodes for selected hydrant locations.

Methodology

The objective of this research is to identify hydraulic responses that reduce the impact of a contamination event on a water distribution network following successful detection and source identification. The authors, based on knowledge of the system dynamics, selected the locations to flush. Two flushing strategies were utilized; flushing in the center of the expected plume location and flushing near the leading edge of the plume. Since in an actual contamination event the location of a contamination source triggering a sensor and the extent of the contaminant plume will most likely not be known accurately in real time, three assumptions of the plume location were utilized: accurate, over-estimation, and under-estimation.

Following identification of the hydrant locations, flushing was simulated by two different approaches. The first approach increased the demand for these locations to reflect the fixed flushing flow rate. The other approach employed the usage of emitters at the locations to simulate flushing. The emitter equation is given below,

$$Q = K * P^{\alpha}$$

where Q is the flow in gallons per minute (gpm), K is the emitter coefficient in units of gpm/psi$^{0.5}$, P is the pressure in pounds per square inch (psi), and α is the emitter exponent. The emitter coefficient was selected on a system wide basis, while the emitter exponent was set at the default value of 0.5 which is appropriate for orifices.

The metric utilized to determine the effectiveness of the flushing was percent reduction in the extent of contamination. The extent of contamination in the network was calculated for all pipes and times until the end of the simulation. The extent of contamination calculation is,

$$ExtentContamination = \sum_{\substack{i=1..N \\ j=t_{beg}..t_{end}}} contLength_{i,j}$$

where i is the pipe number, N is the total number of pipes, *contLength* is the length of contaminated pipe, and j is time from the beginning of the simulation, t_{beg}, until the end of the simulation, t_{end}. Other metrics of contamination effect could be utilized.

Example

The example network utilized was network two from the Battle of the Water Sensor Networks (BWSN) (Ostfeld et al. 2008), which consists of 12,523 nodes, two reservoirs, two tanks, four pumps, five valves, and 14,822 pipes (Figure 1). For purposes of simulation, a conservative contaminant with a set-point concentration of 100.0 mg/L was injected at the start of the simulation for two hours. Sensors were located at Junctions 3357, 4684, 10874, 11184, and 11304 as determined by Berry et al. in the BWSN (Ostfeld et al. 2008). These sensor locations were chosen based on several criteria and were similar to other designs, such as those by Wu and Walski. The initial simulation ran until detection by one of the sensors, where detection was considered as a concentration greater than 0.01 mg/L.

Starting two hours after detection of the contaminant, flushing was initiated for six hours in order to reduce the total extent of contamination. Two hours represents an optimistic time period in which to confirm that some kind of contamination is occurring, estimate the spread of the plume, determine the best hydrants to flush, mobilize the necessary crews and have them travel to the sites. The overall simulation time was 96 hours, which captured the majority of the contamination spread.

For the purpose of this paper, four flushing locations were chosen for each approach utilized. This number seemed reasonable based on information obtained from a partnering, middle-sized water utility, which stated that to avoid depressurization in their system, the maximum number of hydrants that can be flushed simultaneously is ten. Therefore, four locations were assumed to be feasible for most utilities.

Results

The injection node examined for this research effort was Junction-1742, which is shown in Figure 1 as the red circle. This scenario was detected by the sensor located at Junction-4684, represented as the blue circle in Figure 1, with a concentration of 0.17 mg/L at hour 21 in the simulation. The actual contamination spread at hour 23 (hour at which flushing is begun) is depicted in Figure 2, which is utilized for the accurate estimation of the contamination spread. Figure 3 shows the contaminant plume at hour 23 of another injection scenario detected by the same sensor, which is utilized as the over-estimation of the contamination spread. The under-estimation of the contamination spread at hour 23 is displayed in Figure 4, which is another injection scenario detected by Junction-4684. In Figures 2-4, the selected hydrant locations are represented by diamonds, where the yellow diamonds are the locations selected based on the leading edge of the plume and the orange are locations selected based on the center of the plume.

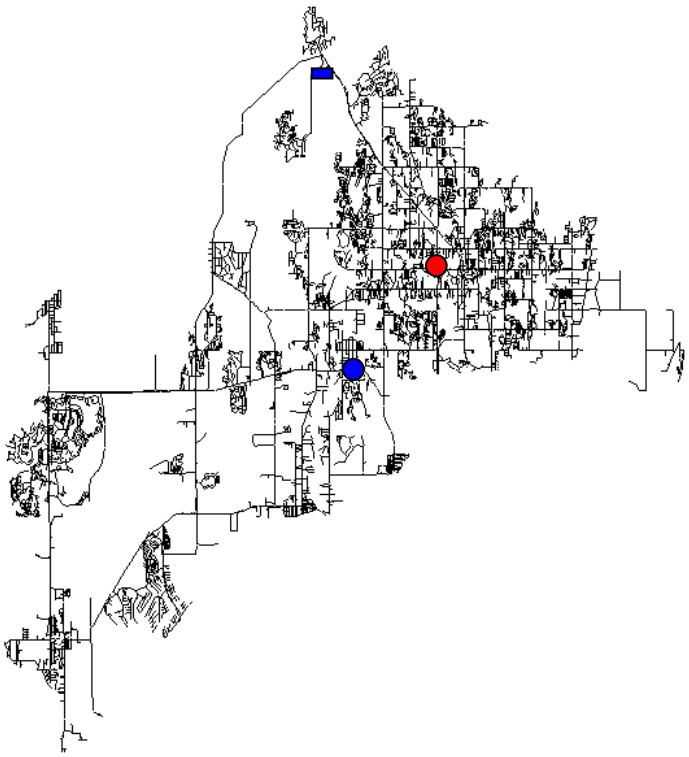

Figure 1. Schematic of example network, BWSN Network 2, where the red circle is the source location, the blue circle is the sensor location, and the blue rectangle is the reservoir.

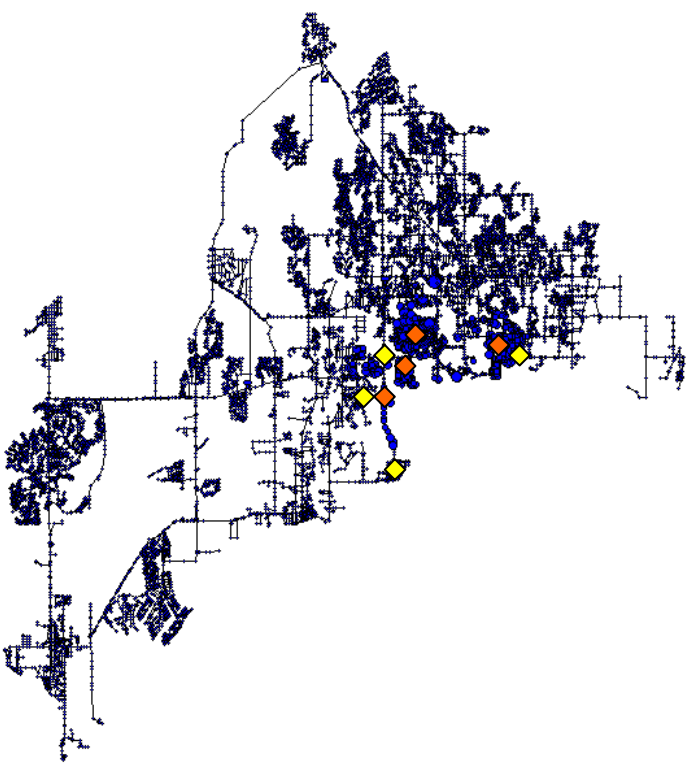

Figure 2. Schematic of accurate contamination spread at the beginning of response, where the diamonds are the hydrant locations: yellow = ahead and orange = center.

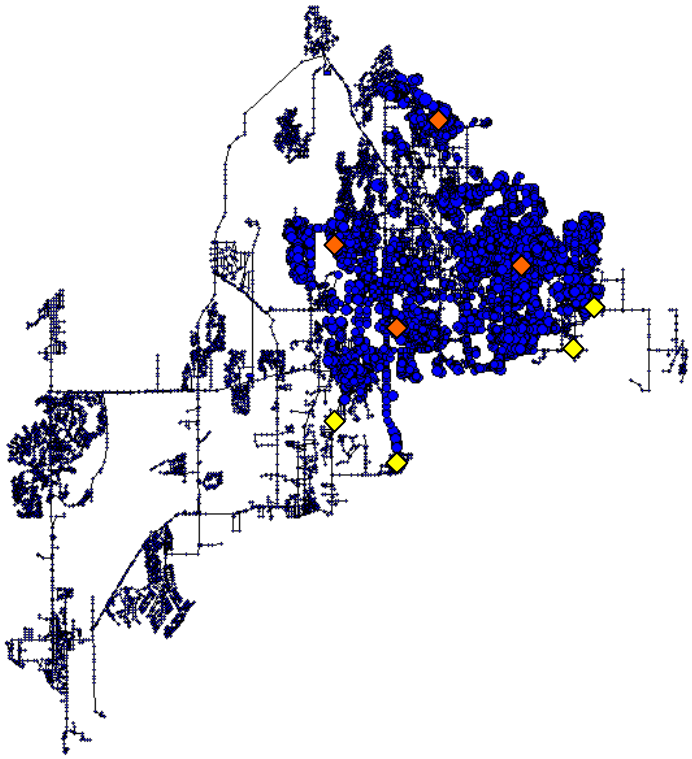

Figure 3. Schematic of over-estimation of contamination spread at beginning of response, where the diamonds are the hydrant locations: yellow = ahead and orange = center.

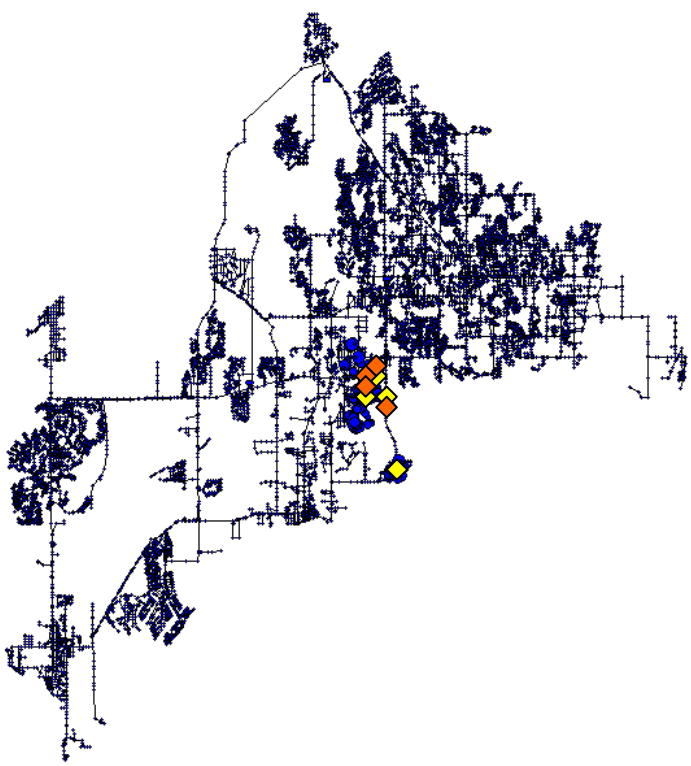

Figure 4. Schematic of under-estimation of contamination spread at the beginning of response, where the diamonds are the hydrant locations: yellow = ahead and orange = center.

The flushing locations for each of the flushing strategies and plume estimation are listed in Table 1. The flushing locations were selected by expert opinion using Figures 2 – 4 (i.e, accurate estimation, under-estimation, and over-estimation of the plume) with consideration of the flushing approach (i.e., locations ahead of the plume and in the center of the plume). The majority of flushing locations were selected on larger service pipes that supply smaller pipes within neighborhoods. The four different emitter coefficients examined in this research effort were 150, 180, 380, and 510 gpm/psi$^{0.5}$. These emitter coefficients were selected based on the lower and upper values for a 2.5 in. outlet and a 4.5 in. outlet (Walski et al. 2003). Utilizing these emitter coefficients and the average system pressure (approximately 77 psi), the corresponding flow was calculated. Based on this calculation, the fixed flushing rates explored were 1300, 1600, 3300, and 4500 gpm.

Table 1. Junction names of hydrant locations for all approaches.

Accurate Estimation of Plume		Under Estimation of Plume		Over Estimation of Plume	
Flushing Ahead	Flushing Center	Flushing Ahead	Flushing Center	Flushing Ahead	Flushing Center
10674	68	5097	1331	545	1172
9976	321	3771	4689	1515	6303
7626	4638	4651	5123	9550	5040
8238	5123	9976	8249	12352	10548

Table 2 shows the percent reduction in extent of contamination for the fixed flushing rate approach, while Table 3 displays the results for the emitter approach. Results from this research effort demonstrate the different modeling techniques that can be applied to simulate a flushing response to a contamination event. By applying the different flushing approaches, similar percent reduction in the extent of contamination objective were obtained. The greatest reduction was achieved by the flushing locations chosen in the center of the plume based on an accurate assumption of the contamination spread. Because the event was not detected until late in the simulation, flushing at four locations only reduced the extent of contamination by 40% or less.

Table 2. The percent reduction in total extent of contamination for the fixed flushing approach.

Fixed Flushing						
Demand (gpm)	Flushing Ahead of Plume			Flushing Center of Plume		
	Accurate	Under	Over	Accurate	Under	Over
1300	27.0%	26.0%	16.9%	34.0%	22.3%	12.1%
1600	26.4%	22.6%	18.6%	37.2%	19.9%	14.0%
3300	30.8%	19.9%	20.4%	40.1%	21.2%	14.9%
4500	31.7%	21.2%	26.4%	42.3%	23.2%	10.3%

Table 3. The percent reduction in total extent of contamination for the emitters approach.

Emitters						
Emitter Coefficient	Flushing Ahead of Plume			Flushing Center of Plume		
	Accurate	Under	Over	Accurate	Under	Over
150	26.0%	25.8%	20.0%	34.3%	22.6%	3.2%
180	25.8%	24.9%	21.8%	36.2%	23.0%	4.9%
380	26.9%	18.1%	20.2%	38.3%	19.0%	4.2%
510	28.9%	19.1%	20.3%	40.2%	20.6%	2.2%

For the majority of analyses, the utilization of fixed flow overestimated the achievable percent reduction by approximately three percent. In a few of the analyses, the percent reduction in the total extent of contamination did not increase with an increase in the flow or emitter coefficient. The reason this might occur is because pipes which were previously uncontaminated may become contaminated due to the flow reversals that are necessary to supply the requested demand. Thus, increasing the demand at some locations increases the number of pipes contaminated.

The benefits of employing emitters are displayed in Tables 4 and 5, which show that the number of nodes with pressures less than 20 psi is more accurately predicted when employing emitters to simulate flushing because it captures the self-limiting nature of hydrant flows. As flow increases, pressure drops to limit flow and using fixed flow fails to capture this effect. In addition, the approach utilizing emitters eliminated any nodes with negative pressures. Table 4 also shows that obtaining flows of 3300 and 4500 gpm at four hydrants is not physically possible in this system and that using those fixed flow rates gives an unrealistic picture of the volume of water that can be flushed.

Thus, to predict a more realistic estimate of the reduction in the extent of contamination, emitters should be utilized to simulate a flushing response. Future work will explore optimization of flushing locations as emitters as well as optimization when the source location is unknown.

Table 4. Number of nodes with pressures less than 20 psi for the fixed flushing approach. The number of nodes with negative pressures are listed in parentheses.

Fixed Flushing Rate	Accurate Ahead	Accurate Center	Under Ahead	Under Center	Over Ahead	Over Center
1300	0	0	0	0	3 (0)	58 (57)
1600	0	0	6 (0)	0	45 (0)	58 (58)
3300	206 (96)	132 (12)	303 (246)	308 (236)	607 (334)	207 (99)
4500	650 (276)	770 (268)	1095 (406)	1123 (389)	1374 (616)	530 (161)

Table 5. Number of nodes with pressures less than 20 psi for the emitters approach. The number of nodes with negative pressures are listed in parentheses.

Emitter Coefficient	Accurate Ahead	Accurate Center	Under Ahead	Under Center	Over Ahead	Over Center
K = 150	0	0	0	0	0	1 (0)
K = 180	0	0	0	0	0	3 (0)
K = 380	0	0	90 (0)	2 (0)	47 (0)	4 (0)
K = 510	88 (0)	7 (0)	107 (0)	15 (0)	161 (0)	4 (0)

Conclusions

This study has implications both in terms of how to decontaminate a system and how to model that decontamination. First, it shows that the effectiveness of decontamination depends heavily on the accuracy of the estimate of the plume location. Overestimating the extent of the plume and flushing accordingly not only is relatively ineffective but can actually spread the plume. If the exact location of the contaminant plume is uncertain it is best to base flushing on a conservative estimate of current spread so as not to expand the plume into clean areas.

Second, based on the results from this example, flushing the system from as close to the center of the plume as possible, can achieve the best containment of the plume. In addition, trying to flush ahead of the plume may be ineffective.

Third, modeling flushing by placing fixed demands on the model can be misleading in that it does not account for the fact that those demands reduce the pressure in the system and may be unachievable or result in negative pressure. Modeling flushing using emitters provides a more accurate estimate of flushing performance.

Disclaimer

This project has been subjected to the U.S. Environmental Protection Agency's review and has been approved for publication. The scientific views expressed are solely those of the authors and do not necessarily reflect those of the US EPA. Mention of trade names or commercial products does not constitute endorsement or recommendation for use.

References

Baranowski, T. M. and E. J. LeBoeuf. (2008). "Consequence Management Utilizing Optimization." *J. Water Resour. Plan. Manage.,* 134(4), 389-394.

Ostfeld, A., J. G. Uber, E. Salomons, J. W. Berry, W. E. Hart, C. A. Phillips, J.-P. Watson, G. Dorini, P. Jonkergouw, Z. Kapelan, F. di Pierro, S.-T. Khu, D. Savic, D. Eliades, M. Polycarpou, S. R. Ghimire, B. D. Barkdoll, R. Gueli, J. J. Huang, E. A. McBean, W. James, A. Krause, J. Leskovec, S. Isovitsch, J. Xu, C. Guestrin, J. VanBriesen, M. Small, P. Fischbeck, A. Preis, M. Propato,

O. Piller, G. B. Trachtman, Z. Y. Wu, and T. Walski. (2008). “The Battle of the Water Sensor Networks (BWSN): A Design Challenge for Engineers and Algorithms.” *J. Water Resour. Plan. Manage.,* 134(6), 556-568.

Walski, T. M., D. V. Chase, D. A. Savic, W. Grayman, S. Beckwith, E. Koelle. (2003). "Operations: Water Distribution System Flushing." *Advanced Water Distribution Modeling and Management*. Haestad Press, Waterbury, CT. 449-456.

Novel, Rapid Molecular-Based Technique for Detecting Contamination in Drinking Water Distribution Systems

Stacia L. Thompson, Ph.D.[1] and Jeanne M. VanBriesen, Ph.D., M.ASCE[2]

[1] 119 Porter Hall, Department of Civil and Environmental Engineering, Carnegie Mellon University, Pittsburgh, PA 15213; PH (412)268-7889; FAX (412)268-7813 email: slthomps@andrew.cmu.edu

[2] 119 Porter Hall, Department of Civil and Environmental Engineering, Carnegie Mellon University, Pittsburgh, PA 15213; PH (412)268-4603; FAX 412-268-7813; email: jeanne@cmu.edu

ABSTRACT

Drinking water distribution systems are vulnerable to biological contamination via many potential intrusion locations; thus, a comprehensive water quality indicator is critical. While previous research has focused on specific pathogen detection using molecular methods, this study seeks to confirm that bacterial indicator classes, specifically, *Alpha-*, *Beta-*, and *Gammaproteobacteria*, can be used as a more comprehensive indicator. The system population exhibits temporal variability in response to changes, such as temperature and disinfectant concentration, but this seasonal bacterial diversity study confirms that these indicator classes are a consistent presence in drinking water. Bacterial class-specific primers were designed to target *Alpha-*, *Beta-*, and *Gammaproteobacteria*, and utilized in Quantitative Polymerase Chain Reaction (QPCR) assays to detect surrogate contaminants. Preliminary results indicate that this QPCR-based approach is a faster, more comprehensive indicator than the culture-based regulatory technique.

INTRODUCTION

Drinking water distribution systems are vulnerable to biological contamination via many potential intrusion locations; thus, a comprehensive water quality indicator is critical for detection of contamination and protection of these systems. Current water quality regulations require testing for total coliform and fecal coliform or *E. coli* concentrations as indicators of possible contamination (USEPA 2001). These culture-based protocols may lead to significant underestimation of microbial diversity and concentration in drinking water (Keinanen et al. 2003, Kalmbach et al. 1997, Von Wintzingerode et al. 1997) and molecular methods may provide public water utilities with more comprehensive water quality information, specifically regarding diversity (Martiny et al. 2005, Schmeisser et al. 2003, Lee et al. 2005).

Proteobacteria constitute the largest fraction within the microbial community identified using 16S rRNA gene clone library analysis for water samples collected

from model and actual distribution systems located in different countries (Williams et al. 2004, Tokajian et al. 2005, Schmeisser et al. 2003, Kalmbach et al. 1997). In these different distribution system studies, the prevalent bacterial classes were *Alpha-*, *Beta-*, and *Gammaproteobacteria* suggesting that these classes may be stable inhabitants of drinking water networks. Although there is a consistent presence of *Proteobacteria* in these systems, some variability has been observed in response to changes in system conditions. For example, *Alphaproteobacteria* is commonly the numerically dominant group in treated bulk water samples because it can survive in the low nutrient, chlorinated environment, while *Betaproteobacteria* are observed more frequently in water with low disinfectant residuals, due to decreased chlorine resistance (Williams et al. 2004, Kalmbach et al. 1997). Seasonal differences in total organic carbon (TOC) or assimilable organic carbon (AOC) may also affect bacterial diversity as nutrient reduction decreases the bacterial re-growth potential (Williams et al. 2005, Eichler et al. 2006, Norton et al. 2000).

It is technically and economically infeasible to develop pathogen-specific sensors for all potential biological contaminants, so a faster and more comprehensive indicator is an alternative approach. If the bacterial populations in distribution systems exhibit stability, with respect to the dominant classes present, then these bacterial classes can be used as indicators and changes in the concentrations of dominant groups, such as *Alphaproteobacteria*, *Betaproteobacteria*, and *Gammaproteobacteria* can be used to signal a contamination event. In order to determine if these bacterial classes are stable enough to be used as indicators, a seasonal study was initiated to evaluate bacterial diversity under different system conditions during the year. After the stability of the bacterial population was determined, this comprehensive indicator, based on dominant bacterial classes, was applied in a more rapid molecular assay (e.g., real-time PCR) appropriate for contaminant detection in drinking water.

METHOD

Total DNA Extraction. Water samples were collected from a continuous flow location in the Pittsburgh Water and Sewer Authority drinking water distribution system. Samples were collected in two 5-liter autoclaved carboys containing sodium thiosulfate (0.03% final concentration) to quench the chlorine reaction and stored at 4ºC until filtration, which occurred within 3 hours of sampling. Samples were filtered through a 0.2 μm filter, the filter was aseptically removed from the apparatus, and placed in a culture plate for storage at -20ºC. The filter was cut into strips using a sterile razor blade, and these strips were placed in two tubes to be used in a modified DNA extraction procedure with the Wizard Genomic DNA kit (Promega, Madison, WI).

PCR. The bacterial community was characterized by 16S rRNA gene clone library analysis, in which a well-conserved sequence, the 16S rRNA gene, is amplified, sequenced, and used to identify the organisms with DNA present in the sample. PCR was used to amplify a section of the 16S rRNA gene present in the extracted DNA sample. *Eubacteria* was targeted with universal primers BAC27F (5'-

AGAGTTTGATCCTGGCTCAG) and BAC805R (5'-GACTACCAGGGTATCTAATCC). PCR reaction mixtures contained template extracted DNA, 1X PCR buffer, 200 µM each deoxynucleoside triphosphate, 2.0 mM $MgCl_2$, 100 nM each forward and reverse primer, and 0.05 U of *Taq* DNA polymerase (Invitrogen, Carlsbad, CA) per ml. The reaction vials were placed in a thermal cycler (Bio-Rad, Hercules, CA) for 3 minutes at 95ºC for initial denaturation, followed by 35 cycles of 94ºC for one minute, 55ºC for 45 seconds, and 72ºC for one minute, followed by a final extension step of 15 minutes.

Clone Library Development. The PCR products were then concentrated (due to the low DNA content) and purified using the QIAquick PCR Purification Kit (Qiagen, Valencia, CA). The purified PCR products were cloned using the TOPO TA Cloning Kit (Invitrogen, Carlsbad, CA) following the manufacturer's instructions and using a modified approach for analyzing transformants by colony PCR with transformed *E. coli* cell culture as template and plasmid-specific primers, M13F (5'-GTAAAACGACGGCCAG) and M13R (5'-CAGGAAACAGCTATGAC), to isolate the PCR products from the vector and 1.0% agarose gel electrophoresis to screen for the correct size DNA fragment. The 16S rRNA gene PCR products were sequenced on an ABI Prism 3730*xl* DNA sequencer at SeqWright DNA Technology Services (Houston, TX).

QPCR Assay. Prior to QPCR, additions of pure culture surrogate bacteria were added to a 10-liter drinking water sample to obtain a concentration of approximately 1.0E+4 CFU/ml. These spiked samples were then filtered and DNA extracted using the methods noted previously. The control sample was collected at the same time and location as the spiked sample, but received no additions prior to filtration and DNA extraction. For each contaminant scenario (control and spiked water samples), extracted DNA was analyzed to determine the quantity of total bacteria using universal primers, and *Alphaproteobacteria*, *Betaproteobacteria*, and *Gammaproteobacteria* using bacterial class-specific primers from literature or designed using Primrose software and Ribosomal Database Project (RDP). All primers were validated for group specificity and optimized prior to use.

Each 25 µl QPCR reaction contained 1X Power SYBR Green PCR Master Mix, 300 nM each forward and reverse primer, and 2 µl of DNA templates, except for the *Alphaproteobacteria* reactions, which contained 600 nM each forward and reverse primer. The real-time thermal cycle was 50ºC for 2 minutes, 95ºC for 10 minutes, followed by 40 cycles of 95ºC for 15 seconds and 60ºC for 1 minute, and a final hold of 7 minutes at 60ºC. All primer sets were run with an annealing/extension step at 60ºC, except for *Alphaproteobacteria* with a hybridization temperature of 55ºC. QPCR assays were run on a 7500 Real-Time PCR System (Applied Biosystems, Foster City, CA) and the DNA concentration of the four target groups: *Alphaproteobacteria*, *Betaproteobacteria*, *Gammaproteobacteria*, and total bacteria, was determined by comparing cycle thresholds of unknown samples against thresholds for plasmid DNA standards with known concentrations ranging from 1.0E+1 to 1.0E+9 copies/µl.

RESULTS AND DISCUSSION

Similar to other bacterial diversity studies in metropolitan drinking water distribution systems, the majority of the 369 seasonal clone sequences were most closely related to 16S rRNA gene sequences found in the *Alphaproteobacteria*, *Betaproteobacteria*, and *Gammaproteobacteria* classes (Martiny et al. 2005, Keinanen-Toivola et al. 2006, Williams et al. 2004). In addition, there were also some sequences identified as belonging to the *Actinobacteria* and *Clostridia* classes. The bacterial diversity of this distribution system is comparable to other systems where *Alpha-*, *Beta-*, and *Gammaproteobacteria* dominate the population, as shown in Figure 1. In all seasonal samples, there is a consistent presence of *Alphaproteobacteria* and *Betaproteobacteria*, which suggests that these bacterial classes may be stable indicators of population diversity, and by extension, system status.

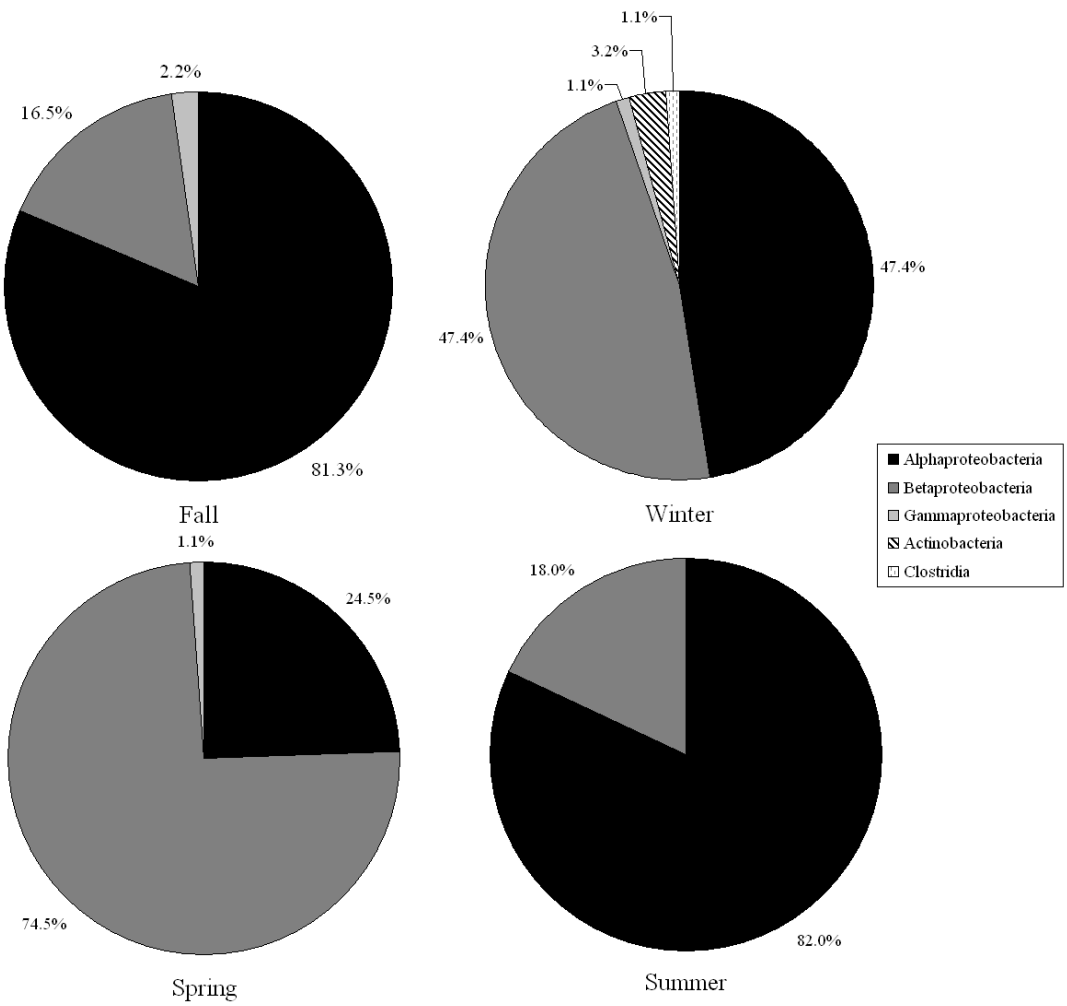

Figure 1. Bacterial class distributions for bacterial populations in drinking water samples collected during four different seasons of the year. Samples were collected starting in November 2006 and finishing in July 2007.

Based on the results of the seasonal bacterial diversity study, which suggests that *Alpha-*, *Beta-*, and *Gammaproteobacteria* are a stable presence within the distribution system and may be used as indicators of biological contamination, some preliminary batch experiments were initiated to test this hypothesis. Assuming that the percentages of *Alpha-*, *Beta-*, and *Gammaproteobacteria* will significantly change from their baseline levels when system disruption occurs, monitoring these bacterial classes is an effective method for detecting contamination in drinking water. Rapid sensing is critical for public health response, so QPCR is used to quantify total bacteria using universal primers and *Alpha-*, *Beta-*, and *Gammaproteobacteria* using class-specific primers. Preliminary results from batch experiments using five different surrogate organisms were favorable. The QPCR-based method detected all contaminants. Statistical analysis of the results is necessary to determine significance and additional experiments need to be run, but preliminary results indicate that this method is a faster and more comprehensive method than current culture-based techniques.

CONCLUSION

This seasonal study of bacterial diversity in a drinking water distribution system corroborates that *Alpha-*, *Beta-*, and *Gammaproteobacteria* are the dominant classes found in these systems. Although there was observed variability in the seasonal bacterial populations due to changes in system conditions, such as temperature and TOC, the bacterial diversity was stable with respect to the presence of the dominant classes. Thus, these indicator classes may be useful indicators of contamination. Although additional experiments and statistical testing should be conducted, preliminary results suggest that a QPCR-based method that targets dominant bacterial classes could be used in drinking water applications as a faster, more comprehensive indicator than current techniques.

REFERENCES

Eichler, S., Christen, R., Holtje, C., Westphal, P., Botel, J., Brettar, I., Mehling, A., and Hofle, M. G. (2006). "Composition and Dynamics of Bacterial Communities of a Drinking Water Supply System as Assessed by RNA- and DNA-Based 16S rRNA Gene Fingerprinting." *Applied and Environmental Microbiology*, ASM, 72(3), 1858-72.

Kalmbach, S., Manz, W., and Szewzyk, U. (1997). "Isolation of New Bacterial Species From Drinking Water Biofilms and Proof of In Situ Dominance With Highly Specific 16S rRNA Probes." *Applied and Environmental Microbiology*, ASM, 63(11), 4164-70.

Keinanen, M. M., Martikainen, P. J., Korhonen, L. K., and Suutari, M. H. (2003). "Microbial Community Structure in Biofilms and Water of a Drinking Water Distribution System Determined by Lipid Biomarkers." *Water Science and Technology*, IWA, 47(5), 143-47.

Lee, D. G., Lee, J. H., and Kim, S. J. (2005). "Diversity and Dynamics of Bacterial Species in a Biofilm at the End of the Seoul Water Distribution System." *World Journal of Microbiology & Biotechnology,* Springer Netherlands, 21(2),155-62.

Martiny, A. C., Albrechtsen, H. J., Arvin, E., and Molin, S. (2005). "Identification of Bacteria in Biofilm and Bulk Water Samples From a Nonchlorinated Model Drinking Water Distribution System: Detection of a Large Nitrite-Oxidizing Population Associated With *Nitrospira* Spp." *Applied and Environmental Microbiology*, ASM, 71(12), 8611-17.

Norton, C. D., and LeChevallier, M. W. (2000). "A Pilot Study of Bacteriological Population Changes Through Potable Water Treatment and Distribution." *Applied and Environmental Microbiology*, ASM, 66(1), 268-76.

Schmeisser, C., Stockigt, C., Raasch, C., Wingender, J., Timmis, K. N., Wenderoth, D. F., Flemming, H. C., Liesegang, H., Schmitz, R. A., Jaeger, K. E., and Streit, W. R. (2003). "Metagenome Survey of Biofilms in Drinking-Water Networks." *Applied and Environmental Microbiology*, ASM, 69(12), 7298-309.

Tokajian, S. T., Hashwa, F. A., Hancock, I. C., and Zalloua, P. A. (2005). "Phylogenetic Assessment of Heterotrophic Bacteria from a Water Distribution System Using 16S rDNA Sequencing." *Canadian Journal of Microbiology*, NRC Canada, 51(4), 325-35.

United States Environmental Protection Agency (USEPA). (2001). Total Coliform Rule: A Quick Reference Guide." *Microbials and Disinfection Byproducts*, http://www.epa.gov/safewater>(April 12, 2007).

United States Environmental Protection Agency (USEPA). (2002). *Method 1604: Total Coliforms and Escherichia coli in Water by Membrane Filtration Using a Simultaneous Detection Technique (MI Medium)*, Washington, DC.

Von Wintzingerode, F., Gobel, U. B., and Stackebrandt, E. (1997). "Determination of Microbial Diversity in Environmental Samples: Pitfalls of PCR-Based rRNA Analysis." *FEMS Microbiology Reviews,* FEMS, 21(3), 213-29.

Williams, M. M., Santo Domingo, J. W., Meckes, M. C., Kelty, C. A., and Rochon, H. S. (2004). "Phylogenetic Diversity of Drinking Water Bacteria in a Distribution System Simulator." *Journal of Applied Microbiology*, Wiley-Blackwell, 96(5), 954-64.

Williams, M. M., Santo Domingo, J. W., and Meckes, M. C. (2005). "Population Diversity in Model Potable Water Biofilms Receiving Chlorine or Chloramine Residual." *Biofouling,* Taylor & Francis, 21(5-6), 279-88.

Trajectory Clustering Approach for Reducing Water Quality Event False Alarms

Eric Vugrin[1], Sean A. McKenna[1], David Hart[1]

[1]Sandia National Laboratories, Energy, Resources and Systems Analysis Center, PO Box 5800 MS 1138, Albuquerque, NM 87185-1138, {edvugri,samcken,dbhart}@sandia.gov

ABSTRACT

Event Detection Systems (EDS) performance is hindered by false alarms that cause unnecessary resource expenditure by the utility and undermine confidence in the EDS operation. Changes in water quality due to operational changes in the utility hydraulics can cause a significant number of false alarms. These changes may occur daily and each instance produces similar changes in the multivariate water quality pattern. Recognizing that patterns of water quality change must be identified, we adapt trajectory clustering as a means of classifying these multivariate patterns. We develop a general approach for dealing with changes in utility operations that impact water quality. This approach uses historical data water quality data from the utility to identify recurring patterns and retains those patterns in a library that can be accessed during online operation. We have implemented this pattern matching capability within CANARY and describe several example applications that demonstrate a decrease in false alarms.

INTRODUCTION

Event detection software (EDS) tools are an integral part of contaminant warning systems being developed and deployed at water utilities. EDS constitute an integral part of contaminant warning systems (Hasan et al., 2004) and can also provide utilities with enhanced monitoring and management of daily operations. Here we focus on the CANARY EDS developed at Sandia National Laboratories (Hart et al., 2007).

A key component of the effectiveness of these EDS tools in actual operating distribution networks is their ability to reduce false positive (false alarm) detections. EDS parameters can be tuned to be more or less sensitive to changes in water quality with increasing sensitivity resulting in fewer missed detections (false negatives), but also increased false alarms. The tradeoff between false negatives and false alarms can be defined through a receiver operating characteristic curve built on historical data with simulated events and an acceptable EDS sensitivity can be defined from the receiver operating characteristic curve (McKenna et al., 2008).

Deployment of EDS tools in distribution networks has shown that changes in water quality at a monitoring location that are caused by changes in the hydraulic operations of the utility are often responsible for false positive alarms. As an example, examination of deployment of the EDS CANARY at the Greater Cincinnati Water Works (GCWW) over six month period has shown a number of instances where

CANARY produces false alarms due to opening or closing of valves, draining of tanks and changes in the status of pumps within the distribution system (Allgeier et al., 2008; Allgeier and Umberg, 2008; Umberg and Allgeier, 2008).

Development of approaches whereby EDS tools can reliably recognize changes in water quality that are due to changes in hydraulic operations are needed. One path towards this development is to incorporate indicators of the hydraulic changes directly as inputs to the EDS. The main difficulty with this approach is that the changes in hydraulic operations often occur at locations that are not near the water quality monitoring station. While these changes can be used as direct input to the EDS, the time lag between the change in operations, e.g., opening a valve to drain a tank, and the change in water quality at a particular monitoring station depends on demands occurring within the system. This dependence on current demands makes the exact timing and the strength of the resulting water quality change difficult to characterize, especially if other operational changes occur within the same time frame. Extensive knowledge and experience of the utility operations can be applied to more directly relate the operational and water quality changes, but this information is utility specific and not easily generalized across utilities. We propose a new approach that adapts trajectory clustering in order to identify patterns of water quality change.

TRAJECTORY CLUSTERING

A number of multivariate clustering algorithms have previously been applied to water quality data with the goal of classifying the water quality into clusters that indicate anomalous or background water quality (e.g., Klise and McKenna, 2006a,b. These previous efforts have been focused on clustering the actual data values to fit within a finite number of water quality classes. However, for event detection, it is not the current state of the water quality that is of interest, it is the time period during which the water quality changes from one classification (e.g., background) to another (e.g., event) that is of the most importance. If only a relatively small number of clusters are employed, the periods of change from one cluster to another will not fit well with any cluster and these data may be improperly classified. This issue led Klise and McKenna (2006a) to consider every previous data point within a moving window of specified length as a separate cluster for comparison to the current water quality. These difficulties with multivariate clustering of water quality data along with the realization that it is the periods of water quality change that are most critical have led us to focus on classification of the period of change in water quality into background or “other” categories.

Time series data streams have received renewed interest in the data mining literature. One promising technique for identifying patterns in time series data is trajectory clustering (see Gaffney, 2004). In this technique time series of data (i.e., trajectories) are clustered rather than discrete data points. Focused applications have been in the area of classifying historical storm tracks (Camargo et al., 2007; Gaffney et al., 2007). Storm track data are the prototypical data sets for trajectory clustering in that they provide a series of latitude and longitude pairs that define the center of the storm at

discrete time intervals (e.g., every 6 hours). Here we increase the dimensionality of the trajectory clustering framework to examine the water quality within n-dimensional parameter space at a series of discrete time steps. For example, we consider trajectories of the water quality within Cl, pH, turbidity and specific conductivity space (n = 4) at a series of discrete time steps as defined by the output of the water utility SCADA systems.

The approach that we propose herein for reducing false alarms in EDS's adapts trajectory clustering methods. This approach consists of two key steps: 1) create a cluster library of events from historical data and 2) compare water quality signals against entries within the library. The following sections detail those processes.

Library Creation

Several months of historical data are used to develop a library of recurring patterns within the multivariate water quality data streams. This library is created using the following process:

- Run the event detection tool. Here we use CANARY (Hart et al., 2007), with a relatively sensitive set of parameters such that large number of water quality events will be identified.
- Record the water quality signal data for a specified time period prior to the initial indication of each event. The number of time steps in the specified period are denoted by N_t.
- For each of the signals, fit a low-order regression model to the N_t recorded data. This is a single variable regression with data from each signal fit independently of the others. Time is the independent variable in each case. In the examples shown in this paper, 3rd order regression models of the form:

  $$y = \beta_1 x3 + \beta_2 x2 + \beta_3 x + \beta_4$$

  are employed resulting in four parameters that define the shape of the water quality signal trajectory over the previous N_t time steps.
- Store the regression coefficients for each event in a library and classify them into different patterns using multivariate clustering. The algorithm simultaneously clusters the regression coefficients for all signals such that the trajectory of the water quality change, rather than the actual data values corresponding to the changes are clustered.
- Calculate cluster statistics for the comparison step.

Here, the fuzzy c-means (FCM) algorithm (Dunn, 1973; Bezdek, 1981) is used to cluster the regression coefficients. It is an iterative, "soft" clustering algorithm that permits events (or in this case, sets of regression coefficients) to belong to multiple clusters. For each event, the FCM algorithm calculates the degree to which each event belongs to each cluster.

The basis of the FCM algorithm is the minimization of the following objective function:

$$J = \sum_{i=1}^{N_E} \sum_{j=1}^{N_C} u_{ij}^m \left\| x_i - c_j \right\|^2, \; 1 \le m < \infty,$$

where

- N_E denotes the number of events being clustered;
- N_C denotes the number of clusters;
- x_i denotes the events that are being clustered;
- c_j denotes the cluster center for the jth cluster;
- u_{ij} is the degree of membership for the x_i to cluster j. Note $0 \le u_{ij} \le 1$, and $\sum_{j=1}^{N_C} u_{ij} = 1$;
- $\| \; \|$ is a norm for measuring the distance of events from cluster centers; and
- m is a "fuzziness" parameter that can be adjusted to affect cluster membership

The FCM requires an "initial guess" for the degree of cluster memberships. To improve the efficiency of the FCM algorithm, we used hierarchical clustering (Johnson, 1967) to assign initial cluster memberships. If hierarchical clustering assigns the ith event to the jth cluster, u_{ij} is assigned an initial value of δ; otherwise, it is assigned a value of $(1-\delta)/(N_C - 1)$. The parameter δ is set to 0.8 in CANARY's implementation of the FCM algorithm.

Additionally, the FCM algorithm requires that the analyst determine the number of clusters *a priori*. CANARY selects the integer between 2 and 10 (inclusive) that maximizes the PBM index (Pakhira et al., 2003). The PBM index is used since Pakhira et al. (2003) assert that the positive integer that maximizes the PBM-index is optimal in the sense that it minimizes the number of clusters while increasing compactness and separation between clusters. The bounds of 2 and 10 clusters were selected since most examples that have been analyzed optimize the PBM index with 3 to 6 clusters.

To perform comparison of water quality events with the library, it is necessary calculate cluster statistics. Under the assumption that the clusters are normally distributed, means (μ_j) and covariance matrices (COV_j) for the jth clusters are calculated as follows:

$$\mu_j = \frac{\sum_{i=1}^{N_E} \left(u_{ij}\right) x_i}{\sum_{i=1}^{N_E} u_{ij}}, \qquad COV_j = \frac{\sum_{i=1}^{N_E} \left(u_{ij}\right)\left(x_i - \mu_j\right)\left(x_i - \mu_j\right)^T}{\sum_{i=1}^{N_E} u_{ij}}.$$

On-line Pattern Comparison

Creation and clustering of a water quality change template library from historical data can be performed in CANARY's off-line mode. When CANARY has a real-time link to a SCADA water quality monitoring system, it can monitor incoming data and assess how similar water quality changes are to patterns already contained in the template library. Sufficiently similar ones are typically caused by changes in operations and are not likely cause for concern. Changes that are significantly different from the template library may merit further investigation. This section describes the process that CANARY uses to compare the real-time signals with the template library.

In its on-line mode, CANARY is connected to a SCADA system that transmits water quality signals to the software. When an event is identified, polynomial regression fits are performed on the incoming data for the same signals that are considered in the template library. This regression uses all of the same parameters that were used to create the template library. The following calculations are then performed for each cluster:

$$xval_j = \left(x_{RT} - \mu_j\right)^T COV_j^{-1} \left(x_{RT} - \mu_j\right), \qquad p_j = 1 - \left[\chi^2_{DOF}\right]^{-1}\left(xval_j\right)$$

where x_{RT} denotes the regression coefficients for the new event and $\left[\chi^2_{DOF}\right]^{-1}$ denotes the inverse cumulative distribution function for the chi-squared distribution with degrees of freedom equal to the total number of regression coefficients per event. Under the assumption that the clusters are multivariate normal distributions, the value p_j denotes the percentile of the jth cluster's distribution to which x_{RT} corresponds. If no p_j values are less than a user defined tolerance level, a new cluster is added to the template library. The cluster is assigned a mean equal to the regression coefficients associated with the new event and a user-specified covariance matrix. If any p_j is less than the tolerance level, no new clusters are added to the template library. Rather, the regression coefficients corresponding to the new event are added to the library, and the FCM algorithm is re-run on the entire supplemented library. Means and covariance matrices are then calculated for each cluster as described in the preceding section.

EXAMPLE CALCULATIONS

An example pattern recognition calculation is shown here to demonstrate this approach. Nine weeks of data are available from the BDWW monitoring station within the PUB network in Singapore. The monitoring station is directly downstream of a water treatment plant and the flow in the pipe past the monitoring station (denoted as "TOPT") varies significantly as shown in the top graphs of Figure 1. Three water quality signals are used: total residual chlorine (TRC), pH and specific conductivity (CDTY) as shown the other graphs in Figure 1. Figure 1 shows nine weeks of data in the left images and an expanded view of 10 days of data in the right images. The data are collected with a 5 minute sampling interval. Figure 1 shows that the flow rate through the pipe has some effect on the water quality values, but the relationship is not straightforward and changes over time.

The linear filtering algorithm within CANARY is used to estimate each future water quality value from the preceding 288 (1 day) values. The differences between the estimated and observed data, the residuals, are shown in Figure 2. The nine week and ten day time periods as shown in Figure 1 are also shown in the left and right images of Figure 2. The residuals demonstrate a more recognizable daily pattern than do the water quality data.

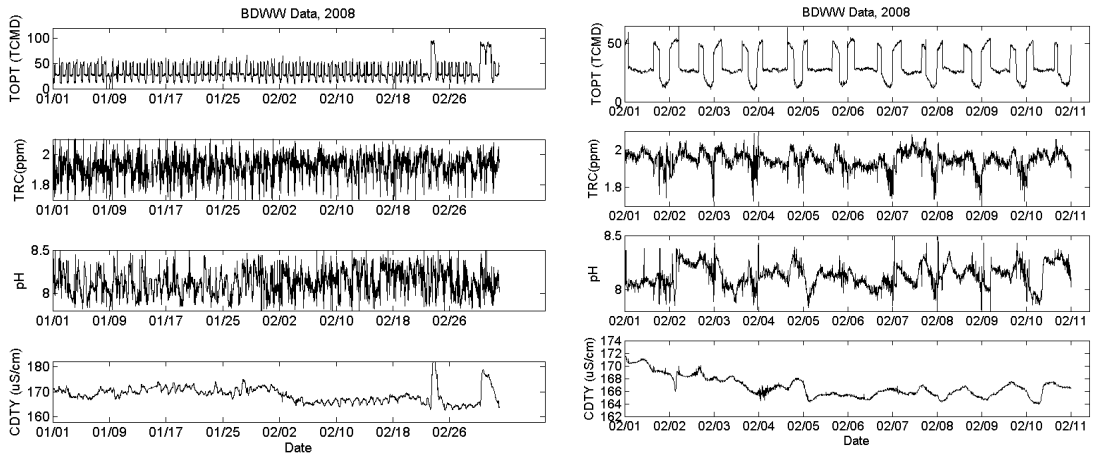

Figure 1. Example data set used for development of the pattern library. The full 9 weeks of training data are shown on the left and an expanded view of 10 days of the data are shown on the right. The total flow in thousand m^3/day (TCMD) is shown in the top graph and the bottom three plots show the water quality signals.

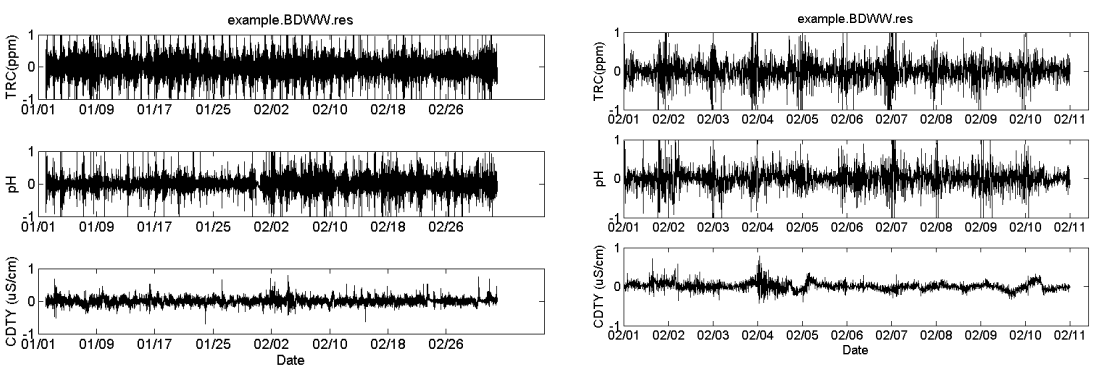

Figure 2. Residuals between estimated and observed water quality data for the example data set. The same time periods as shown in Figure 1 are shown here. The Y-axes have units of standard deviation.

To construct the water quality pattern library, a threshold of 0.8 standard deviations is applied to the residual data seen in Figure 2 and the binomial event discriminator (BED) algorithm within CANARY (McKenna, et al., 2007) is used to calculate the probability of an event (anomalous water quality) at every time step. For times where

this probability exceeds a probability threshold of 0.95, an event is triggered and the previous 90 time steps are retained and a 3rd order regression model is fit to each water quality signal in this 90 time step period. The resulting regression coefficients are then used as input to the FCM clustering algorithm.

A larger data set of roughly 35,000 time steps (approximately 120 days), extending from January 1st to April 30th, 2008 was used to calculate the patterns in the pattern library. The event detection results in a total of 100 unique water quality patterns. These patterns are grouped into 4 clusters by the clustering algorithm. Figure 3 shows the regression models fit to the water quality patterns for the clusters in which they have the highest degree of membership as well as the mean regression pattern for each water quality signal within each cluster. Twenty-three events have the highest degree of membership in Cluster 1, and there are 39, 28, and 10 events assigned to Clusters 2, 3 and 4, respectively.

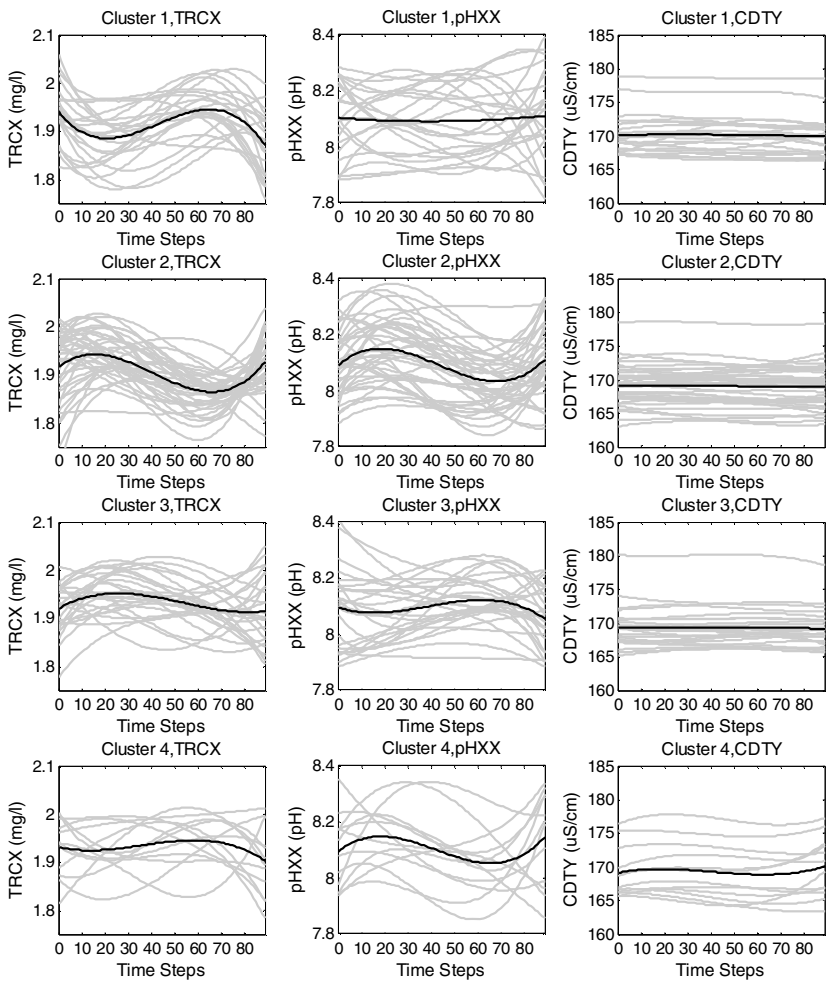

Figure 3. Cluster membership for the water quality patterns in the test data set. The black lines show the mean regression model and the gray lines show the regression models for all members of the cluster.

For each cluster, the distributions of the regression coefficients are shown using box and whisker plots in Figure 4. The clusters are primarily differentiated according to the TRCX and pHXX trajectories closest to the recognition of the event (90 time steps). CDTY does not appear to be as significant a factor in differentiating the clusters. The CDTY coefficients are relatively constant for the first 3 clusters with only Cluster 4 showing significant differences from the other clusters in the CDTY signal.

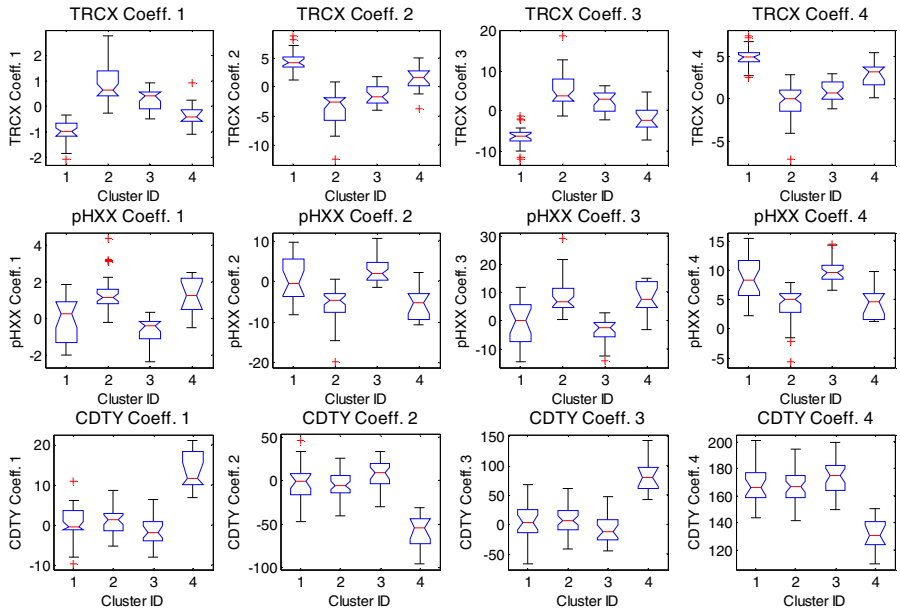

Figure 4. Box and whisker plots showing the distribution of the four regression coefficients for each cluster

Development of the clusters provides a library of recurring water quality patterns that are recognized as background variation in water quality and should not indicate water a water quality event. In order to test the capability of the trajectory clustering approach to recognize previously seen patterns and reduce false positive event detections, CANARY was then run in a manner to simulate its online mode. A testing data set consisting of approximately 30,000 time steps (approximately 100 days), extending from May 1st to August 15th, 2008, was used as input to CANARY. CANARY used the same probability threshold (0.95) to identify 102 water quality events. However, when these events were compared with the pattern library and a tolerance level (see On-Line Pattern Comparison Section) of 0.5 was used, all but 14 fell were rejected as false alarms – an 86% reduction in false alarms. For a tolerance level of 0.75, all but 11 were rejected (89% false alarm reduction). Thus, the library comparison significantly reduced the number of false alarms from CANARY.

CONCLUSIONS

Water quality within distribution networks can display considerable variation and a common source of this variation is due to changes of operational parameters. These operational changes often result in common patterns of water quality change within

multivariate space. While utility-specific rules can be developed to relate operational changes to water quality changes, a general approach that can be applied to any location and any utility is needed. Here we propose and demonstrate trajectory clustering as a general means for classification and subsequent online recognition of recurring water quality patterns. The goal of this approach is to reduce false positive alarms from EDS tools and this approach is successfully demonstrated using the CANARY software.

A training data set was used here to develop a pattern library through offline calculation. Fuzzy multivariate clustering classified distinct patterns of water quality change as summarized with low-order regression models. Event detection and classification of roughly 120 days of data resulted in detection of 100 water quality events which were then classified into four water quality patterns. Subsequent testing using the next 100 days of data resulted in detection of 102 water quality events. Through comparison of these events with the pattern library developed through training, the majority of these events, greater than 80% of them, are recognized as belonging to one of the four existing clusters. Association of these events with water quality patterns in the pattern library eliminates them from being considered as false positive alarms. Further development of this approach will include sensitivity of the results to changes in the event detection parameters and updating of the pattern library as new events are recognized.

ACKNOWLEDGEMENTS

This work was completed as part of the PUB-Sandia project on water security. Sandia is a multiprogram laboratory operated by Sandia Corporation, a Lockheed Martin Company, for the United States Department of Energy's National Nuclear Security Administration under contract DE-AC04-94AL85000.

REFERENCES

Allgeier, S.C and K. Umberg. (2008). "Systematic Evaluation of Contaminant Detection through Water Quality Monitoring" *Proceedings of AWWA Water Security Congress, April 6-8, Cincinnati, Ohio*, 15 pp.

Allgeier, S.C., Y. Lee, K. Umberg, and M. Tyree. (2008). "Operational Experience with Water Quality Event Detection During the Cincinnati Water Security Initiative Pilot." *Proceedings of AWWA Water Quality Technology Conference, November 16-20, Cincinnati, Ohio*, 17 pp.

Bezdek, J.C. (1981), *Pattern Recognition with Fuzzy Objective Function Algorithms*, Plenum Press, New York.

Camargo, S.L., A.W Robertson, S.J. Gaffney, P. Smyth and M. Ghil. (2007) "Cluster Analysis of Typhoon Tracks. Part I: General Properties." *Journal of Climate*, 20, pp. 3635-3653.

Gaffney, S.J. (2004) "Probabilistic Curve-Aligned Clustering and Prediction

with Regression Mixture Models", PhD Dissertation, Department of Information and Computer Science, University of California, Irvine, 281 pp.

Gaffney, S.J., A.W Robertson, P. Smyth, Camargo, S.J.and M. Ghil. (2007). "Probabilistic clustering of extratropical cyclones using regression mixture models." *Climate Dynamics*, 29, pp. 423-440.

Hart, D.B., S.A. McKenna, K.A. Klise, V. Cruz and M. Wilson. (2007) "CANARY: A Water Quality Event Detection Algorithm Development Tool." *Proceedings of ASCE World Environmental and Water Resources Congress, Tampa, FL, May 15-19th*.

Hasan, J., S. States, and R. Deininger. (2004) Safeguarding the security of public water supplies using early warning systems: A brief review*, Journal of Contemporary Water Research and Education*, 129, 27-33.

Johnson, S.C. (1967). "Hierarchical Clustering Schemes" *Psychometrika*, 2:241-254.

Klise, K.A. and S.A. McKenna. (2006a) "Water quality change detection: multivariate algorithms." *Proceedings of SPIE (International Society for Optical Engineering), Defense and Security Symposium 2006, April 18-20, Orlando. Florida*, 9pp

Klise, K.A. and S.A. McKenna. (2006b). "Multivariate Applications for Detecting Anomalous Water Quality." *Proceedings of the 8th Annual Water Distribution System Analysis Symposium, Cincinnati, OH, August 27-30, 2006*.

McKenna, S.A., D.B. Hart, K.A. Klise, V.A. Cruz and M.P. Wilson. (2007) Event Detection from Water Quality Time Series, Proceedings of: ASCE World Environmental and Water Resources Congress, Tampa, FL, May 15-19th

McKenna, S.A., M. Wilson and K.A. Klise. (2008). "Detecting Changes in Water Quality Data." *American Water Works Association Journal*, Vol. 100, No. 1, pp. 74-85.

Pakhira, M. K., S. Bandyopadhyay, and U. Maulik. (2003). "Validity Index for Crisp and Fuzzy Clusters." *Pattern Recognition* 37, 487-501.

Umberg, K. and S. Allgeier. (2008). "Evaluation of Water Quality Event Detection Systems Deployed at the First Water Security Initiative Pilot Utility" *Proceedings of: AWWA Water Security Congress, April 6-8, Cincinnati, Ohio*, 12 pp.

Comparing Single- and Multi-Species Water Quality Modeling Approaches for Assessing Contamination Exposure in Drinking Water Distribution Systems

Stephen Klosterman[1], Sam Hatchett[1], Regan Murray[2], James Uber[1] and Dominic Boccelli[1]

[1]Department of Civil and Environmental Engineering, University of Cincinnati, Cincinnati OH 45220; email: steve.klosterman@gmail.com
[2]Research Scientist, U.S. Environmental Protection Agency, Cincinnati OH 45268

Abstract

New software such as EPANET-MSX enables water quality models that account for multiple reactive species in the distribution system. This allows for a more complete analysis of network water quality, including processes such as adsorption and biological inactivation by a disinfectant. For each of these reaction processes, three models are presented: single-specie conservative, single-specie reactions modeled by wall demand or bulk decay, and multi-species. The implications of model selection on the resulting exposure to contaminants that undergo these reaction processes are investigated for a hypothetical intentional contamination event and a simple single pipe system.

1 Introduction

As concern for public safety and security grows, so has awareness of the vulnerability of drinking water to contamination. Most people in urban and suburban settings get drinking water from their tap via a water distribution system (WDS). Researchers are investigating a range of possible quality changes that can occur within the WDS (Schock, 2005; USEPA, 2001, 2002a,b,c). Computer models are being used to study dynamics within the WDS and to make predictions.

The capabilities of these computer models have grown along with the awareness of WDS water quality issues. Until recently, most water quality software such as EPANET had the ability to account for only a single dissolved specie (Clark and Grayman, 1998). This single specie is advected with the bulk flow, and can undergo decay or growth in the bulk water as well as wall demand from the pipe wall. Since maintaining the minimum disinfectant residual is an area of concern

among WDS operators, the single specie is often used for modeling a disinfectant like chlorine.

Single-specie modeling has several practical limitations. What about the substances that are reacting with a disinfectant? Their concentrations do not remain the same after reaction. However a single-specie approach prevents modeling both these substances and the disinfectant. Lack of ability to account for these substances may be a concern if they are potentially harmful to consumers or if it results in a less accurate model. Previous studies have shown that accounting for these substances may alter the amount and location of disinfectant injection necessary to maintain safe levels in a WDS (Boccelli et al., 2003; Propato and Uber, 2004). What about wall demand reactions? Does a specie disappear after it reacts with the wall? Conservation of mass says this does not happen, and investigators have shown that the pipe wall could act as a reservoir for harmful contaminants which could be released at some later time (Schock, 2005; Lytle et al., 2004; Copeland et al., 2007).

Multi-species modeling presents the opportunity to more realistically predict water quality as it is delivered to the consumer. Few studies on this type of modeling in WDSs have been published (Boccelli et al., 2003; Propato and Uber, 2004; Shang et al., 2008). The new water quality modeling software EPANET-MSX (Shang and Uber, 2007) enables the study of a wide variety of WDS dynamics with multiple species.

This study investigates multi-species reaction models, and how they compare with their single-specie counterparts in the context of public health assessment. In order to make this comparison, two hypothetical intentional contamination scenarios are presented using three models: single-specie conservative, single-specie bulk decay/wall demand, and multi-species. One scenario involves an injection of arsenate, a contaminant with a well-documented affinity for solids like pipe wall materials (Lytle et al., 2004; Copeland et al., 2007). The reaction models for arsenate may involve adsorption to the pipe wall. The other scenario involves an injection of the bacteria E. coli along with a nutrient broth in which the bacteria can grow and which exerts additional demand for the disinfectant. The reaction models for the bacteria may involve the reactions between the contaminant, disinfectant, and nutrient broth.

In this paper results from simulations run on a single pipe will be presented. The results will help explain reaction dynamics in more complicated networks currently being investigated by the authors.

2 Reaction Models

2.1 Multi-Species Adsorption Model for Arsenate

If arsenate were introduced into a WDS, adsorption would be one of the most significant physico-chemical processes affecting its fate and transport. Since arsenate is the oxidized form of arsenic, there is no reaction with oxidizing disinfectants

such as chlorine or chloramine that are typically present in a WDS (Ghurye and Clifford, 2001). However iron particles that may be corrosion products of iron pipes, or carried over from source waters, present a highly adsorptive surface for arsenate. Adsorbed arsenate can also be released from these particles and once again become dissolved in the bulk flow (Lytle et al., 2004; Copeland et al., 2007).

Adsorption is the physico-chemical process by which a substance, called the adsorbate, attaches to a surface, called the adsorbent. The process is reversible, and the substance may also desorb from the surface. A three-species model consisting of bulk arsenate as the adsorbate, iron particles at the pipe surface as the adsorbent, and an adsorbed arsenate specie can be used to model arsenate adsorption in a WDS. Several modeling approaches have been used for this process, also known as sorption. Empirical models such as Langmuir and Freundlich are available (James M. Montgomery, Consulting Engineers, Inc., 1985), while Surface Complexation Models (SCMs) describe the actual chemical reaction taking place between the adsorbate and adsorbent species (Schnoor and McAvoy, 2010; Dzombak and Morel, 1990). An SCM approach is used here. Although a constant pH is assumed for this work, a key strength of the SCM is its ability to handle variable pH, which has been shown to affect contaminant adsorption and desorption in WDSs (Copeland et al., 2007). The following is a simplified general chemical reaction model for sorption. While the focus here is on bulk arsenate, As, as the adsorbate, the model applies to other dissolved species in a WDS:

$$\mathrm{X} + \mathrm{As} \underset{k_{-1}}{\overset{k_1}{\rightleftharpoons}} \mathrm{XAs} \tag{1}$$

where X is an available surface site of the adsorbent, XAs is an arsenic-occupied surface site, k_1 is the rate of the adsorption reaction, and k_{-1} is the rate of the desorption reaction. If no adsorption has taken place at the beginning of the simulation, the initial value of [X] represents the maximum adsorptive capacity of a WDS in terms of available surface sites located at the pipe wall. This model can be implemented as a system of differential equations which describes the time-varying rates of change of the three species (Grossl et al., 1997):

$$\frac{d[\mathrm{As}]}{dt} = A_v(-k_1[\mathrm{X}][\mathrm{As}] + k_{-1}[\mathrm{XAs}]) \tag{2}$$

$$\frac{d[\mathrm{X}]}{dt} = -k_1[\mathrm{X}][\mathrm{As}] + k_{-1}[\mathrm{XAs}] \tag{3}$$

$$\frac{d[\mathrm{XAs}]}{dt} = k_1[\mathrm{X}][\mathrm{As}] - k_{-1}[\mathrm{XAs}] \tag{4}$$

where A_v is the ratio of pipe wall surface area per unit pipe volume in units of $\frac{\mathrm{m}^2}{\mathrm{L}}$. A_v is necessary to reconcile the units of measurement for the surface species [X] and [XAs], which will be expressed as moles per area of pipe surface, and the bulk specie [As], which will be expressed as moles per pipe volume.

To use this model for a contamination of a WDS by arsenate, the rate constants k_1 and k_{-1} must be known, as well as initial values for all the species. This requires

knowledge of the specific substance that arsenate is sorbing to at the pipe wall. While the actual make-up of the pipe wall is highly variable and uncertain, an iron oxide known as ferrihydrite is a typical component of the corrosion layer of iron pipes that is in contact with water (Sarin et al., 2004). Iron oxides such as ferrihydrite may also be present at the pipe wall for other pipe materials, the iron source being dissolved iron that has made it through the water treatment process (Lytle et al., 2004). Ferrihydrite, also known as hydrous ferric oxide or amorphous iron oxide, will be used here to model the pipe wall surface. While this simplifying assumption facilitates the experiments for this work, it is impossible to know exactly what specific reactions are happening in any given WDS without examination of the materials of that system under operating conditions. The results gained from the experiments here indicate what may be happening if these simplifying assumptions are valid.

The forward and backward rates for this reaction have been experimentally determined (Grossl et al., 1997) to be $k_1 = 7.18 \times 10^9 \frac{\mathrm{L}}{\mathrm{mol} \cdot \mathrm{hr}}$ and $k_{-1} = 2.88 \times 10^4 \frac{1}{\mathrm{hr}}$ in the pH range 6.5 - 7.5. It should be noted that these rates pertain to arsenate adsorption on a different iron oxide known as goethite. However ferrihydrite and goethite have similar capacities for arsenate on a surface-area-normalized basis and similar equilibrium constants for the sorption reaction with arsenate (Dixit and Hering, 2003).

In order to determine the initial value of [X], a physical model of the pipe wall needed to be developed. Ferrihydrite particles are often assumed to be spherical (Fuller et al., 1993), so the initial concentration of surface sites [X] was estimated by assuming the pipe wall surface was made up of hemispheres of ferrihydrite organized in a square array. The mean diameter of a ferrihydrite aggregate has been reported as 30 μm (Scheinost et al., 2001), which was used as the diameter of the hemispheres. Using an areal site density of $2.6 \frac{\mathrm{sites}}{\mathrm{nm}^2}$ (Dixit and Hering, 2003) on the surface of the hemispheres, an initial concentration of $6.78 \times 10^{-6} \frac{\mathrm{mol}}{\mathrm{m}^2}$ of surface sites on the pipe surface was calculated. This approach may underestimate the availability of sorption sites because it ignores diffusion-limited sites (Pierce and Moore, 1982; Fuller et al., 1993; Raven et al., 1998). The initial concentration of adsorbed arsenate [XAs] was assumed to be zero, and the initial concentration of bulk arsenate [As] will depend on the particular contaminant source characteristics.

It should be noted that the concentration of a dissolved substance may be different in the boundary layer adjacent to the pipe wall. This accounts for the fact that dissolved species undergo a diffusive mass transfer process to get through the laminar sub-layer of turbulent pipe flow to the pipe wall surface. While it is possible to model this additional concentration as another specie, preliminary analyses indicated that this makes little difference in the resulting bulk concentrations. For simplicity, it is assumed the concentration next to the wall is the same as the concentration in the bulk flow for all models.

2.2 Single-Specie Wall Demand Model for Arsenate

A single-specie wall demand model for bulk arsenate would necessarily fix the wall capacity [X] as a constant. Therefore it is incorporated with the rate constant for the forward reaction from the previous model to make a wall reaction rate constant $k_w = k_1 \cdot [\mathrm{X}] = 4.87 \times 10^4 \frac{\mathrm{L}}{\mathrm{hr} \cdot \mathrm{m}^2}$. In this model, the single bulk arsenate specie undergoes wall demand according to

$$\frac{d[\mathrm{As}]}{dt} = -A_v k_w [\mathrm{As}] \tag{5}$$

2.3 Single-Specie Conservative Transport Model

For both arsenate and E. coli, the conservative transport model represents an assumption that the contaminant is advected with the flow and does not undergo any sort of reaction.

2.4 Multi-Species Model for E. Coli Inactivation

This model addresses concerns of WDS contamination by biological agents. The conceptual model consists of three species: free chlorine, E. coli bacteria, and a nutrient broth. Assuming second order kinetics allows a simple way to model this three-component system as a set of differential equations:

$$\frac{d\mathrm{E}}{dt} = -k_{e1}\mathrm{CE} + k_{e2}\mathrm{BE} \tag{6}$$

$$\frac{d\mathrm{C}}{dt} = -k_{c1}\mathrm{CE} - k_{c2}\mathrm{CB} - k_{c3}\mathrm{C} \tag{7}$$

$$\frac{d\mathrm{B}}{dt} = -k_{b1}\mathrm{BC} + k_{b2}\mathrm{BE} \tag{8}$$

where E is the measure of coliform bacteria in $\frac{\mathrm{cfu}}{\mathrm{L}}$, C is chlorine concentration in $\frac{\mathrm{mg}}{\mathrm{L}}$, and B is the Tryptic Soy Broth (TSB) concentration in $\frac{\mathrm{mL\ TSB}}{\mathrm{L}}$. TSB is a common nutrient growth medium.

Simplifying assumptions reduce the number of parameters that must be estimated. At the time scale of interest, bacterial growth and resulting consumption of TSB is assumed to be negligible ($k_{e2} = k_{b2} = 0$). Chlorine demand exerted by bacterial inactivation and natural organic matter is assumed to be negligible in comparison to that due to TSB ($k_{c1} = k_{c3} = 0$). This leaves the following equations:

$$\frac{d\mathrm{E}}{dt} = -k_e\mathrm{CE} \tag{9}$$

$$\frac{d\mathrm{C}}{dt} = -k_c\mathrm{CB} \tag{10}$$

$$\frac{d\mathrm{B}}{dt} = -k_b \mathrm{BC} \tag{11}$$

Published chlorine survivability data (Rice et al., 1999) for E. coli 0157:H7 were used to estimate k_e by a least squares method. The value of k_e used here is $0.07766 \frac{\mathrm{L}}{\mathrm{mg} \cdot \mathrm{s}}$. Estimation of k_c and k_b is complicated since there is no direct way to measure the time-varying concentration of a broth media, as represented by B. Therefore chlorine measurements are used to estimate these parameters. The chlorine and broth reaction rate equations can be solved simultaneously in a parameterized form (Boccelli et al., 2003):

$$\mathrm{C}(t) = \frac{\mathrm{C}_0 - \alpha}{1 - (\alpha/\mathrm{C}_0)\exp[-(\mathrm{C}_0/\alpha - 1)\beta t]} \tag{12}$$

where $\alpha = \frac{a}{b}\mathrm{B}_0$ and $\beta = k_c \mathrm{B}_0$ (note also that from stoichiometry, $k_b = \frac{b}{a}k_c$).

The parameters α and β depend on three terms: the stoichiometric ratio $\frac{a}{b}$, k_c, and B_0. For the purposes of estimating k_c and $\frac{a}{b}$ (and thus k_b), the value of B_0 is specified as the nutrient broth's volumetric dilution ratio upon initial mixing, and is expressed in units of $\frac{\mathrm{mL\ TSB}}{\mathrm{L}}$. After initial addition, B can be understood as the concentration of a reactive substance with potential to reduce chlorine.

To estimate the parameters for the chlorine-broth interaction, time-varying chlorine concentration data for bench-scale batch mixtures of TSB in a chlorinated buffer were fit by a least-squares method. The parameter values estimated were: $k_b = 0.00937 \frac{\mathrm{L}}{\mathrm{mg} \cdot \mathrm{s}}$ and $k_c = 0.063958 \frac{\mathrm{L}}{\mathrm{mL\ TSB} \cdot \mathrm{s}}$.

2.5 Single-Specie Bulk Decay Model for E. Coli

For a bulk-decay model, pseudo first order inactivation kinetics are assumed:

$$\frac{d\mathrm{E}}{dt} = -k_{e'} \mathrm{E} \tag{13}$$

where $k_{e'}$ is the pseudo first order inactivation rate constant estimated using chlorine inactivation data (Rice et al., 1999), assuming a constant $1.1 \frac{\mathrm{mg}}{\mathrm{L}}$ background chlorine concentration. The value of $k_{e'}$ was determined to be $0.0854 \frac{1}{s}$ using a least squares method.

3 Software

To model multiple reactive species, the water quality modeling software EPANET-MSX is used (Shang and Uber, 2007). EPANET-MSX is the Multi-Species eXtension to the WDS modeling software EPANET, and both are freely available on the web (Shang and Uber, 2007). EPANET models the hydraulics of a system and has the capability to model one specie which can undergo bulk decay or growth and wall demand.

EPANET-MSX emerged to address the need to model reactive systems that can be more accurately described using a multi-species approach, such as those presented here. Using this new software, any number of reactive species in the categories of bulk species that are advected with flow and wall species that are attached to the stationary pipe wall can be accounted for. To accomplish this, EPANET-MSX requires that the number of reaction rate equations or equilibrium equations supplied by the user be equal to the number of species being modeled. For example, Equations (2)-(4) can be used to implement the multi-species adsorption model for arsenate. EPANET-MSX will be used here to run both single-specie simulations such as would be possible with stand-alone EPANET as well as the multi-species simulations they will be compared to.

4 Experimental Design for Arsenate Models

A network consisting of a single pipe was created as an EPANET input file for the hydraulic simulation. The pipe has a diameter of $D = 20$ cm. The flow in the pipe is a constant $Q = 1.6\frac{\mathrm{L}}{\mathrm{sec}}$. The pipe has several zero-demand nodes along its length that are modeled in order to obtain plots of species concentration versus distance. The injection scenarios are based on the assumption of a constant backflow of $0.0082\frac{\mathrm{L}}{\mathrm{sec}}$ with a duration of 1 hour at the start of the simulation. The limiting solubility of arsenic acid at 12.5 °C is $\frac{302\ \mathrm{g}}{100\ \mathrm{mL}}$ (Weast, 1987), which leads to a source mass rate at the beginning of the pipe, $M = 10\frac{\mathrm{mol}}{\mathrm{min}}$ arsenate.

5 Results for Arsenate Models

The concentration profiles of bulk arsenate versus time are shown in Fig. 1(a) for the multi-species adsorption model at several distances and the conservative model. The single specie wall demand model resulted in rapid and complete wall demand of arsenate, at odds with the other models. Complete wall demand occurred within 30 meters of pipe length for this model, so it is not shown here. In a single-specie wall demand model, the adsorbed specie is not modeled and so can never desorb and rejoin with the bulk flow. Also, the rate of wall demand is unrealistically high because it is proportional to the wall capacity. While in reality a pipe surface would lose capacity as it adsorbs more contaminant, the wall capacity in the wall demand model is constant and thus never decreases.

For the conservative and multi-species models, all concentration profiles have similar leading edges and reach the concentration expected from this scenario. The mass injection and flow rate combine to give an expected bulk concentration of $\frac{M}{Q} \approx 10^{-1}\frac{\mathrm{mol}}{\mathrm{L}}$. The multi-species model can be observed to add a tail to the trailing edge of the pulse input which grows as the pulse moves down the pipe.

The concentration profiles of the multi-species adsorption model versus distance are shown in Fig. 1(b). The wall species were converted to bulk concentrations by multiplying by A_v, for direct comparison to the bulk specie. Con-

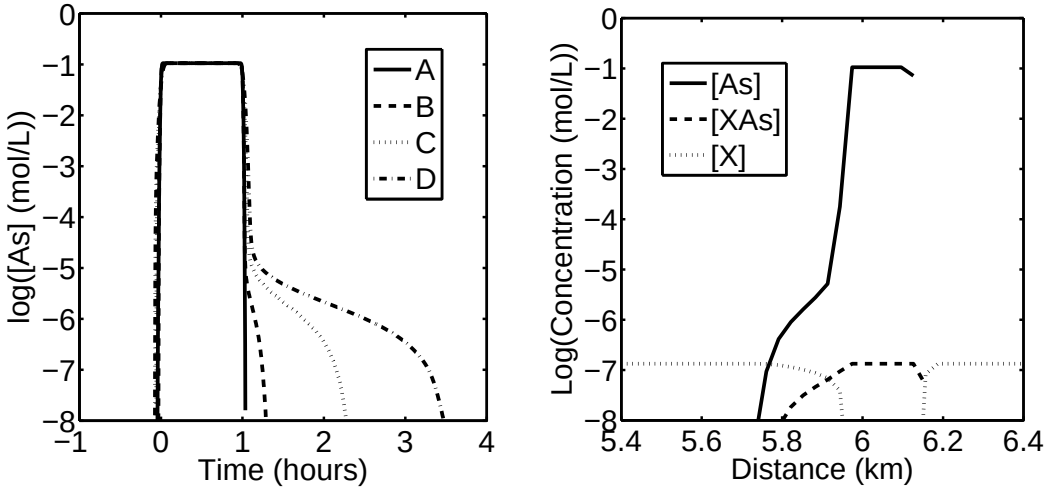

(a) Log concentration of bulk arsenate versus time since pulse arrival at distances = 1.1, 6.1, and 12.2 km from injection site. T_0 represents the arrival time of the pulse at a particular distance. A is the conservative model at T_0 = 6.8 hours. B, C, and D are the bulk [As] specie from the multi-species model at T_0 = 6.8, 34.6, and 69.5 hours respectively.

(b) Log concentration versus distance from injection site at time = 35 hours after start of one-hour injection. [As] = bulk arsenate, [XAs] = adsorbed arsenate, [X] = available surface sites.

Figure 1: Arsenate Models

centrations of wall species expressed in this way can be thought of as the bulk concentration that would result if the wall species at that location were to completely, instantaneously desorb.

Fig. 1(b) shows that the adsorbed arsenate, [XAs], reaches its maximum possible surface loading while the slug of bulk arsenate, [As], is passing by. The maximum surface loading is indicated by the level of unoccupied surface sites [X] prior to contact with the bulk specie. It can also be seen that the bulk concentration in the tail added by the multi-species model can exceed the maximum possible surface loading by more than one order of magnitude at this time in the simulation.

On Fig. 1(a) it can be observed that the pulse input has undergone some numerical dispersion and so the edges of the conservative model graph are not perfectly vertical. The Lagrangian transport scheme used by EPANET as well as EPANET-MSX does not cause dispersive error in pipes, however the pipe used here had several zero-demand nodes along its length.

Nodes have a dispersive effect in this numerical scheme. Accumulation of several discrete parcels of water in the downstream node of a pipe can occur during a water quality timestep. This causes numerical dispersion when the parcels are released as a single parcel with the volume-averaged concentration of the input parcels. Decreasing the timestep will alleviate this numerical dispersion, as illustrated on Fig. 2. Each plot on Fig. 2 is the conservative model and

theoretically would appear as a rectangular pulse. Numerical dispersion causes distortion as the timestep is increased. A timestep of 10 seconds was used for the simulations presented here.

6 Implications for Arsenate Exposure Assessment

In a hypothetical intentional contamination event in a WDS, a public health concern would be the length of time the contaminant remains at a potentially dangerous level in a WDS. For acute arsenate exposure, this level can be determined using the Minimum Risk Level (MRL), which represents the smallest dose of the contaminant considered to be of concern to humans. The MRL for acute arsenate exposure is $0.3\frac{\text{mg}}{\text{person}\cdot\text{day}}$ for a 60 kg person (Center for Disease Control, 2008).

A common ingestion assumption for daily water consumption is $2\frac{\text{L}}{\text{person}\cdot\text{day}}$ (USEPA, 1997). If a consumer were to ingest their 2 L of water all at once, we would want to know if they received a dose equal to or exceeding the MRL for arsenate. A concentration of $\frac{0.3\text{mg}}{2\text{L}} = 10^{-5.7}\frac{\text{mol}}{\text{L}}$ of arsenate. For analysis of exposure to this level a simplified scenario is assumed where there is an uninterrupted path from contaminant source to consumer along the single pipe. In an actual WDS, the problem would be complicated by mixing of other waters, variable flow in pipes, and variable demand. The authors plan to consider these factors in network simulations.

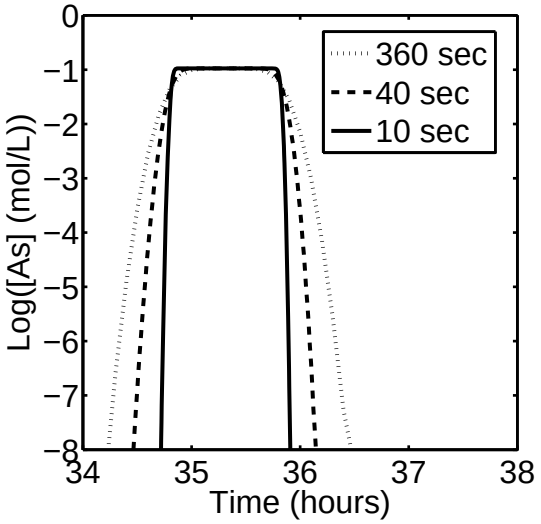

Figure 2: Log concentration of bulk arsenate versus time since beginning of one-hour injection at distance = 6.1 km from injection site. Only the conservative model is shown here to illustrate numerical dispersion. The water quality timestep was varied as indicated in the legend.

In terms of which models are appropriate under these simplified conditions, the wall demand model as formulated here is very different from the other two. Although no physical experiments were conducted, it does not seem appropriate to conclude that an arsenate injection would completely disappear and that consumers at the downstream distances studied here would never receive arsenate in their water. The differences between the conservative and multi-species models are more subtle and are best examined using semi-log plots as on Figs. 1 and 2.

The simulation indicated that the duration of exposure to levels at or above $10^{-5.7}\frac{\text{mol}}{\text{L}}$ of arsenate was 26 minutes longer for the multi-species model than for the conservative model at the location 6.1 km from the injection site pictured in Figure 1. This represents a 38% increase in exposure time. At a distance of

12.2 km downstream of the injection site, exposure time was increased by 75%. Therefore duration of the possible window of time for acute arsenate exposure for a consumer located at these distances downstream of the injection site is significantly affected by use of the conservative model instead of the multi-species model as formulated here.

In addition, there may be more adsorption sites available than are accounted for here, due to the porous nature of the material at the pipe wall (Sarin et al., 2004). Most research of arsenate adsorption onto ferrihydrite indicates the presence of diffusion-limited sites which provide additional capacity for adsorption (Pierce and Moore, 1982; Fuller et al., 1993; Raven et al., 1998). These additional sites may result in increased exposure.

7 Experimental Design for E. Coli Models

For the E. coli simulations, the same pipe diameter D and bulk flow Q are used, as well as a one-hour pulse injection of E. coli at the beginning of the simulation. The pipe has a constant initial chlorine concentration of $1.1\frac{\text{mg}}{\text{L}}$ that will interact with the TSB and E. coli. For this experiment the contaminant injection flow rate Q_i will be varied while the bulk flow Q remains constant. The effect of the changing ratio $\frac{Q_i}{Q}$ on the log inactivation of E. coli at a location 1.2 km downstream of the injection site will be examined for the various models. This distance corresponds to 7.5 hours of contact time. The contaminant injection will consist of TSB and E. coli where the ratio of E. coli to TSB is $1.2 \times 10^6 \frac{\text{cfu}}{\text{ml TSB}}$ (Rice, 2009). Initial concentrations for E. coli and TSB are calculated by dividing their mass or volumetric injection flow rates by the flow in the pipe.

8 Results for E. Coli Models

Since the conservative model has no reactions, the log inactivation of E. coli, $\ln(\frac{[\text{E}]}{[\text{E}]_0})$, will be zero as the pulse propagates down the pipe with concentration $[\text{E}] = [\text{E}]_0$. In contrast, the bulk decay model resulted in near-complete inactivation of E. coli by the time the pulse reached a distance 1.2 km from the injection site. Since a constant chlorine residual is assumed in this model, the rate of bacterial inactivation is artificially high. This phenomenon is similar to that observed in the wall demand model for arsenate and is one drawback of single-specie modeling.

In the multi-species model, the advected pulse had a uniform concentration of TSB, E. coli, and chlorine at a distance 1.2 km from the injection site. The log inactivation or log reduction values for these species using the natural logarithm are plotted on Fig. 3 against the ratio $\frac{Q_i}{Q}$. For reference, $\frac{Q_i}{Q} = 5 \times 10^{-4}$ corresponds to a contaminant injection flow rate of $Q_i \approx 6 \times 10^{-4} \frac{\text{L}}{\text{sec}}$ in this scenario.

9 Implications for E. Coli Exposure Assessment

For purposes of illustration, a 3-log bacterial inactivation criterion is used to compare the different modeling techniques. The nonreactive model has a log inactivation of zero. This model could be thought of as the most conservative when assessing public health impacts for this contaminant, since it does not simulate the disinfecting properties of a chlorine residual. The bulk decay model, similar to the wall demand model for arsenate, seems the least conservative of the three models due to the unrealistically high rate of contaminant loss.

The achievement of 3-log inactivation in the multi-species model is shown to depend on the rate of contaminant injection in Fig. 3. This model predicts that for a contaminant injection greater than $Q_i \approx 6 \times 10^{-4} \frac{\mathrm{L}}{\mathrm{sec}}$, the inactivation criterion is no longer achieved. Preliminary results indicated that with an injection flow $Q_i = 0.3 \frac{\mathrm{L}}{\mathrm{sec}}$, inactivation of E. coli was negligible.

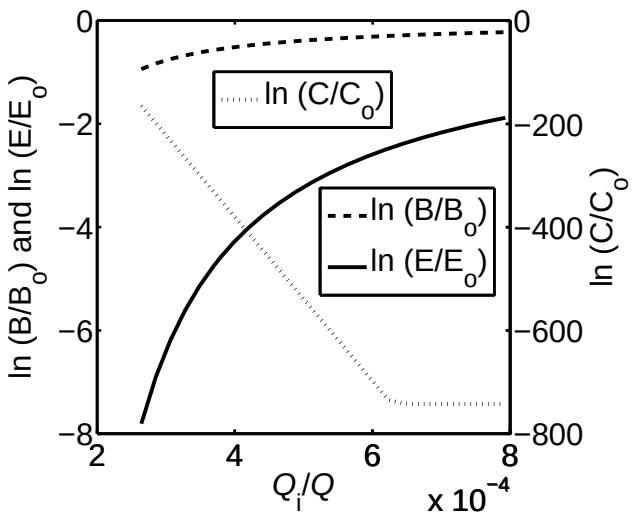

Figure 3: Log inactivation or log reduction of the species simulated by the multi-species model versus the ratio of contaminant injection flow rate to chlorinated flow rate in the pipe. The location is 1.2 km from the injection site, which the pulse input reached 7.5 hours after the beginning of the injection.

However in an actual WDS, other waters would mix with the contaminated water providing additional chlorinated flow which would further dilute the injected material, and likely alter inactivation. Furthermore, chlorinated flow patterns are highly variable and dynamic, making this example an extreme simplification of a contamination scenario. These factors will be assessed in future work.

10 Conclusion

Reaction models for arsenate and E. coli in WDSs were presented to quantify exposure in single pipe scenarios and compare the various modeling approaches. While these results are not directly applicable to more realistic networks with variable flow, demand, and mixing of different waters, they provide some insight as to what difference the models presented here may make in actual distribution system modeling and why. For both contaminants, the reactive models of bulk decay and wall demand as formulated here would likely result in unrealistically

low contaminant concentrations being delivered to consumers.

Compared to the conservative model for arsenate, the multi-species model for arsenate predicts a significantly longer duration of exposure for the particular conditions assumed here. However actual network conditions add factors with unknown impacts on results. Also, multi-species models that account for adsorption to diffusion-limited sites in the pipe wall may indicate even longer exposure times. Development of these models is needed to improve simulation of hypothetical contamination events, as well as pipe-wall accumulation of contaminants that occur at levels that are considered safe in the bulk flow. Even relatively low bulk concentrations of contaminants such as arsenic may cause accumulation at high concentrations in pipe wall materials, providing a possibility of release at higher, possibly dangerous bulk concentrations during changes in pH or other water quality or hydraulic events in a WDS (Lytle et al., 2004; Copeland et al., 2007). The SCM approach can be extended to model changes in pH for these scenarios.

For E. coli bacteria, the multi-species model predicts that inactivation depends on the ratio of contaminant injection rate to chlorinated pipe flow. For significantly large injection flows of a mixture of E. coli bacteria and TSB, 3-log inactivation may not be achieved. A conservative model provides a more cautious assessment of exposure to consumers since no inactivation would take place, however this also means it may over-predict exposure.

Additional work is needed to more accurately determine the parameters of WDS reactions. Several simplifying assumptions were made here to describe and quantify the material at the pipe wall, and the interactions between disinfectant, pathogen and broth. Experimental work that mimics WDS operating conditions could characterize pipe wall materials for more accurate parameter estimates. However WDSs vary widely in their physico-chemical properties due to differences in source water quality and water treatment practices (Sarin et al., 2004). Many WDSs probably also have these types of variation within the individual system. It should also be recognized that no single simulation will be able to characterize as uncertain an environment as a WDS. Further modeling work that employs statistical methods to account for uncertainty in WDS parameters will provide insight into the range of likely behaviors of a system.

11 Acknowledgement/Disclaimer

The U.S. Environmental Protection Agency through the Office of Research and Development funded, managed, and participated in the research described here under a contract with the University of Cincinnati. The views expressed in this paper are those of the authors and do not necessarily reflect the views or policies of the USEPA. Mention of trade names or commercial products does not constitute endorsement or recommendation for use. Work at the University of Cincinnati was sponsored by the USEPA under the Pegasus Contract, Contract Number EP-C-05-056, Work Assignment WA 3-06.

References

Boccelli, D. L., M. E. Tryby, J. G. Uber, and R. S. Summers (2003, June). A reactive species model for chlorine decay and thm formation under rechlorination conditions. *Water Research 37*(11), 2654–2666.

Center for Disease Control (2008, December). `http://www.atsdr.cdc.gov/mrls/`.

Clark, R. M. and W. M. Grayman (1998). *Modeling Water Quality in Drinking Water Distribution Systems*. Denver, CO: American Water Works Association.

Copeland, R., D. Lytle, and D. Dionysious (2007, April). Desorption of arsenic from drinking water distribution system solids. *Environmental Monitoring and Assessment 127*(1-3), 523–535.

Dixit, S. and J. G. Hering (2003). Comparison of arsenic(v) and arsenic(iii) sorption onto iron oxide minerals: Implications for arsenic mobility. *Environmental Science & Technology 37*(18), 4182–4189.

Dzombak, D. A. and F. M. M. Morel (1990). *Surface Complexation Modeling: Hydrous Ferric Oxide*. Wiley-Interscience.

Fuller, C., J. Davis, and G. Waychunas (1993, May). Surface chemistry of ferrihydrite: Part 2. kinetics of arsenate adsorption and coprecipitation. *Geochimica et Cosmochimica Acta 57*(10), 2271–2282.

Ghurye, G. and D. Clifford (2001, March). Laboratory study on the oxidation of arsenic iii to arsenic v. `http://www.epa.gov/nrmrl/pubs/600r01021/600r01021pre.pdf`.

Grossl, P. R., M. Eick, D. L. Sparks, S. Goldberg, and C. C. Ainsworth (1997, February). Arsenate and chromate retention mechanisms on goethite. 2. kinetic evaluation using a pressure-jump relaxation technique. *Environmental Science & Technology 31*(2), 321–326.

James M. Montgomery, Consulting Engineers, Inc. (1985). *Water Treatment Principles and Design*. Wiley-Interscience.

Lytle, D. A., T. J. Sorg, and C. Frietch (2004, October). Accumulation of arsenic in drinking water distribution systems. *Environmental Science & Technology 38*(20), 5365–5372.

Pierce, M. and C. Moore (1982). Adsorption of arsenite and arsenate on amorphous iron hydroxide. *Water Research 16*(7), 1247–1253.

Propato, M. and J. G. Uber (2004, July). Vulnerability of water distribution systems to pathogen intrusion: How effective is a disinfectant residual? *Environmental Science & Technology 38*(13), 3713–3722.

Raven, K. P., A. Jain, and R. H. Loeppert (1998, February). Arsenite and arsenate adsorption on ferrihydrite: Kinetics, equilibrium, and adsorption envelopes. *Environmental Science & Technology 32*(3), 344–349.

Rice, E. (2009, January). Personal Communication with Eugene Rice, USEPA.

Rice, E., R. Clark, and C. Johnson (1999, May-June). Chlorine inactivation of escherichia coli 0157:H7. *Emerging Infectious Diseases 5*(3), 461–463.

Sarin, P., V. L. Snoeyink, D. A. Lytle, and W. M. Kriven (2004). Iron corrosion scales: Model for scale growth, iron release, and colored water formation. *J. Envir. Engrg. 130*, 364–373.

Scheinost, A. C., S. Abend, K. I. Pandya, and D. L. Sparks (2001, March). Kinetic controls on Cu and Pb sorption by ferrihydrite. *Environmental Science & Technology 35*(6), 1090–1096.

Schnoor, J. L. and D. C. McAvoy (2010). *Environmental Modeling: Fate and Transport of Pollutants in Water, Air, and Soil*. Wiley-Interscience.

Schock, M. (2005). Distribution systems as reservoirs and reactors for inorganic contaminants. In M. J. Macphee (Ed.), *Distribution System Water Quality Challenges in the 21st Century : a strategic guide*. American Water Works Association.

Shang, F. and J. G. Uber (2007, October). Epanet multi-species extension users manual. `http://www.epa.gov/nhsrc/water/teva.html#_epanet`.

Shang, F., J. G. Uber, and L. A. Rossman (2008, February). Modeling reaction and transport of multiple species in water distribution systems. *Environmental Science & Technology 42*(3), 808–814.

USEPA (1997, August). Exposure factors handbook. `http://www.epa.gov/ncea/efh/pdfs/efh-front-gloss.pdf`.

USEPA (2001, September). Potential contamination due to cross-connections and backflow and the associated health risks. `http://www.epa.gov/ogwdw/disinfection/tcr/pdfs/issuepaper_tcr_crossconnection-backflow.pdf`.

USEPA (2002a, June). Health risks from microbial growth and biofilms in drinking water distribution systems. `http://www.epa.gov/OGWDW/disinfection/tcr/pdfs/whitepaper_tcr_biofilms.pdf`.

USEPA (2002b, August). Permeation and leaching. `http://www.epa.gov/SAFEWATER/disinfection/tcr/pdfs/whitepaper_tcr_permation-leaching.pdf`.

USEPA (2002c). The potential for health risks from intrusion of contaminants into the distribution system from pressure transients. `http://www.epa.gov/ogwdw000/disinfection/tcr/pdfs/whitepaper_tcr_intrusion.pdf`.

Weast, R. C. (Ed.) (1987). *CRC Handbook of Chemistry and Physics*. Boca Raton, Florida: CRC Press, Inc.

Real-Time Valve Operation for Water Quality Improvement in Water Distribution Systems

Doo Sun Kang[1] and Kevin Lansey[2]

[1]Research Associate, Department of Civil Engineering and Engineering Mechanics, The University of Arizona, Tucson, AZ 85721; email: doosun74@email.arizona.edu.

[2]Professor, Department of Civil Engineering and Engineering Mechanics, The University of Arizona, Tucson, AZ 85721; Ph (520)-621-2512; Fax (520)-621-2550; email: lansey@email.arizona.edu.

ABSTRACT

In order to maintain water quality in water distribution systems, disinfection is performed by chemical addition. Chlorine, the most commonly used disinfectant, decays over time by reaction with organic materials in the water and produces potential harmful disinfection by-products (DBPs). Therefore, it is important to maintain the free chlorine residuals throughout the system within specified limits. Here, optimal valve operation has been combined with booster disinfection for water quality improvement. Valves are operated to alter the flow distribution in the network, prevent isolation of disinfectant and direct disinfectant laden-water to locations where it is required. A real-time optimal valve operation and booster disinfection problem is formulated as a single objective optimization approach. The objective is to minimize chlorine injection while maintaining chlorine concentrations and pressures at consumer nodes. The problem is solved using a single objective genetic algorithm. This paper presents the problem formulation methodology and its uniqueness.

INTRODUCTION

It is necessary to maintain the free chlorine residuals throughout the distribution system between minimum and maximum values. A minimum value (in the range of 0.2 mg/L) needs to be maintained to control the bacteria re-growth, and a maximum limit (at most 4.0 mg/L) is intended to avoid taste and odor complaints and the formation of potentially harmful disinfection by-products (DBPs). Therefore, it is desirable to maintain a uniform low range of chlorine residuals throughout the system.

To improve system-wide water quality, booster disinfection may be coupled with treatment plant disinfection. Multiple water quality sources for disinfection are better than single water plant disinfection to maintain uniform chlorine concentration throughout the system. Water quality can also be improved by shortening travel times within a system. On-line valves can be operated to alter the flow distribution in the

network and direct disinfectant laden-water to locations where it is required. While valve operation helps to spread the disinfectant over the system, part of the system may experience pressure drops due to increased energy loss through the valves.

This study presents algorithms for optimal valve operation coupled with booster disinfection in real-time to improve water quality. This problem is formulated as a single objective optimization approach. The objective is to minimize the injected chlorine mass while maintaining chlorine concentrations and pressure heads at consumer nodes for all times. The problem is solved using a single objective genetic algorithm (GA). To reflect the temporal and spatial variations of system demands, real-time operation schedules are developed based on real-time demand forecasting.

Some studies for booster location design and optimal operating of disinfection boosters have been completed. To reduce the computation demand of dynamic water quality simulations, some works adopted the principle of linear superposition by assuming the first order chlorine reaction and cyclical hydraulic behavior (Boccelli et al. 1998; Tryby et al. 2002; Prasad et al. 2004). Boccelli et al. (1998) showed that location of booster stations and system hydraulics are significant factors in determining the optimal injection schedule. They also reported that the best schedule was found when a booster station was located at a storage tank. Tryby et al. (2002) found that the dosage reduction potential of the designs is related to the injection control (constant dosage or flow proportional dosage) and scheduling (single interval operation and multiple interval operation) decisions, as well as the number and location of booster stations. Prasad et al. (2004) used a multi-objective genetic algorithm (MOGA) to minimize the total disinfectant dose and maximize the volumetric demand within specified chlorine limits.

There were efforts trying to reduce the computational burden of calculating response coefficients for linear superposition method (Propato and Uber 2004a and b; Lansey et al. 2007). Propato and Uber (2004a) formulated a linear least-squares (LLS) model minimizing the deviations of chlorine at the consumer nodes from a desired target value to determine optimal disinfection schedule. They showed that LLS formulation depends only on the number of boosters and their injection rates and is independent of system size, thus computationally efficient compared to earlier approaches utilizing the linear superposition method. Propato and Uber (2004b) extended their previous work to accommodate booster locations as decision variables using a mixed integer quadratic programming (MIQP) formulation. Lansey et al. (2007) used principle of linear superposition but their approach avoids long-term water quality simulations by adding constraints requiring the concentrations at the beginning and end of the design period to be the same. They introduced the initial concentrations as decision variables in the formulation.

Munavalli and Kumar (2003) used a dynamic simulation model to solve the non-first-order reaction kinetics. They used a binary genetic algorithm (GA) to determine the chlorine injection rates that reduce chlorine residuals closest to target minimum. Some studies optimizing pump operations for water quality improvements have been

reported. Sakarya and Mays (2000) optimized the pump operations to improve water quality. The decision variables are discrete-time pump operation schedules and the optimization problem is formulated and solved by interfacing the EPANET (USEPA, 2000) with a nonlinear optimization code, GRG2. Ostfeld and Salomons (2004) developed a methodology optimizing pump operations and booster disinfection. The problem was formulated for a typical demand cycle of 24 hrs given initial tank level and chlorine concentration at all nodes. They showed a trade-off between energy cost and the total chlorine dose injected.

A major assumption of the abovementioned studies is that the chlorine dosage at water quality sources and network hydraulics are periodic (cyclic) over a simulation period, that is mainly appropriate for system planning and design purposes. None of those studies considered temporal/spatial variations of system demands and non-periodic hydraulic behaviors. Study for real-time operation of system facilities considering system demand variations was never completed. Also, studies for optimal operating of valves for water quality purposes are lacking. This study formulates a methodology for optimizing operation schedule for existing control valves and booster chlorination stations in real-time based on a real-time system demand forecasting. The objective is to maintain the required minimum chlorine residual at the consumer nodes subject to constraints of minimum pressure requirement and tank water level.

MODEL FORMULATION

The optimization model is formulated and solved using a genetic algorithm (GA) linked with a water distribution simulation model, EPANET, under extended period simulation (EPS). Details of the methodology are discussed in the following sections.

Demand forecasting. The water demands are variable in space and time. For example, demands on rainy day would be less than the average uses. The pattern of demands during the weekend differs from the work day consuming pattern. Also, the spatial variations of water demands due to fire and pipe break should be reflected for water quality predictions. Here, the demand forecasting is synthetically generated for each node during the simulation period by adding random deviations to base demand patterns.

Pressure estimation. As valve operations cause pressure reductions in portions of the system, a minimum pressure requirement for each node must be maintained. Pressures are computed using EPANET and verified at the critical time in each extended period simulation (EPS) time step. Figure 1 illustrates the pressure estimation scheme used assuming an instantaneous change in demands. In normal EPANET calculations, the pressure head at time $\mathbf{t}$ is estimated based on the tank water level and demand estimates marked as open circle at time $\mathbf{t}$. However, if the demand is higher in the previous EPANET time step (closed circle) the pressure at time $\mathbf{t} - \mathbf{\Delta t}$ will be lower than at time $\mathbf{t}$. Thus, during periods when demands are

declining, the EPANET EPS result tends to overestimate the system pressure. In this study, steady state computation of pressure head using the both sets of demands is completed for each time step and the minimum values are chosen to represent the nodal pressures at that time step.

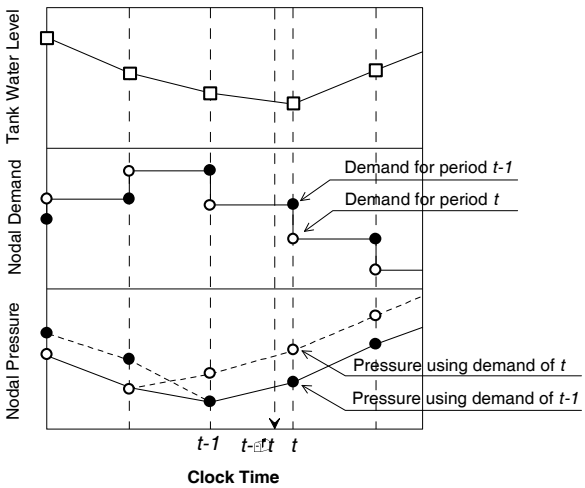

Figure 1. System pressure prediction scheme

Solution schematic. The proposed optimization framework is shown in Figure 2. A single objective genetic algorithm (GA) is linked to the EPANET toolkit that performs hydraulic and water quality simulations. Decision variables are generated through the GA operations and passed to EPANET that simulates the desired conditions and returns the pressure and water quality results to the GA. Based on the simulation results, GA generates new variables and the aforementioned steps are repeated until the predefined maximum number of generations is reached or the objective function converges within a desired tolerance.

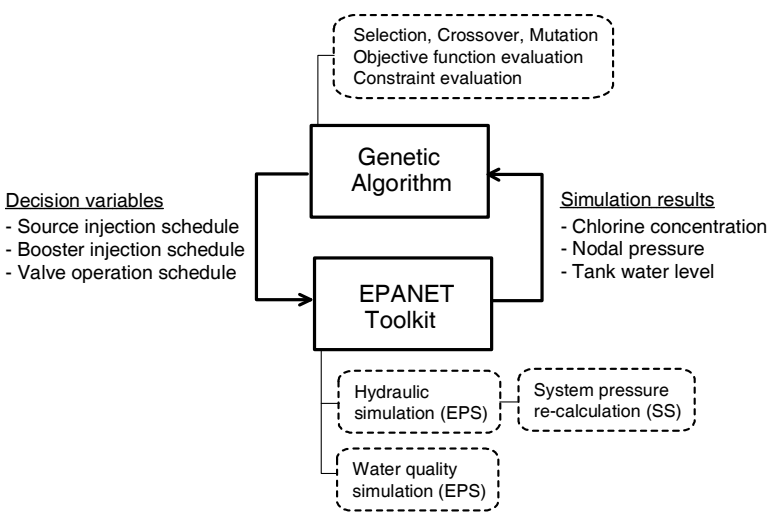

Figure 2. Optimization framework

Objective function. Since excess chlorine is undesirable, the problem objective is to maintain the chlorine concentration at consumer nodes as low as possible but above the minimum limit. The objective function is formulated as:

$$Minimize \quad F = \sum_{i=1}^{N} \sum_{t=1}^{T} q_{i,t} \times \left| C_{i,t} - \underline{C} \right|, \quad i = 1, \ldots, N \text{ and } t = 1, \ldots, T$$

where N and T are the number of nodes and the simulation time, respectively. $q_{i,t}$ and $C_{i,t}$ are the nodal demand and chlorine concentration at node i and time t. $\underline{C}$ is the specified minimum chlorine concentration (mg/L).

Constraints. The bounds for the residual chlorine concentrations are defined:

$$\underline{C} \le C_{i,t} \le \overline{C}$$

where $\underline{C}$ and $\overline{C}$ are the minimum and maximum allowable nodal chlorine concentrations, respectively.

Similarly, nodal pressure head constraints are also included:

$$\underline{P} \le P_{i,t} \le \overline{P}$$

where $\underline{P}$ and $\overline{P}$ are the lower and upper limits, respectively, and $P_{i,t}$ is the pressure head at node i and time t.

Finally, the constraint for the tank water storage is posed as the tank water level at the end of the decision period should be maintained within desired tolerance:

$$y_j^{end} - y_j^{\min} \le H, \quad j = 1, \ldots, K$$

where K is the number of tank. $y_j^{\min}$ is the minimum water surface elevation for emergency storage of tank j and y_j^{end} is the tank water level at the end of the decision period for tank j. H is the user selected tolerance in meters. Note that y_j^{end} cannot be lower than $y_j^{\min}$.

Decision variables. The model decision variables are the source and booster chlorine injection rates and valve settings for each time period. The decision time step is 1 hour. Valve settings are the percentage of valve closure that is converted to the head loss coefficients for the simulation model. The valve closure-head loss coefficient relationship is normally available from a valve manufacturer.

Simulation time window. Since the real-time operation schedules are optimized based on the forecasted demand, the simulation time window should be the same for both. Figure 3 illustrates the simulation time window used for demand forecasting and optimization runs. Here, it is assumed that the demand forecasting is conducted every 6 hours. Note that the demand forecasting time step and decision variable time step are same as 1 hour. For example, simulation (i.e., demand forecasting and model optimization) for Run 1 starts at midnight (12 am) and the next runs are sequentially

conducted with 6 hrs of time interval. Note that each run ends at the same time point, i.e., 8 pm when the lowest tank water level is detected. For each run, only the first 6 hour solutions will be implemented since a new set of decisions will be determined with improved demand forecasts after 6 hours.

A warm up period is needed to accurately depict concentrations at all locations in the system. If this is not applied and nodal concentrations are supplied to the model, EPANET will assume a linearly changing concentration between nodes. Instead, we provide the initial nodal concentrations (including tanks) for a period prior to the decision time frame and simulate that period for each EPANET run using the historical demand and decision data. This provides more accurate pipe concentrations. The warm-up period duration is selected based on system size and travel time.

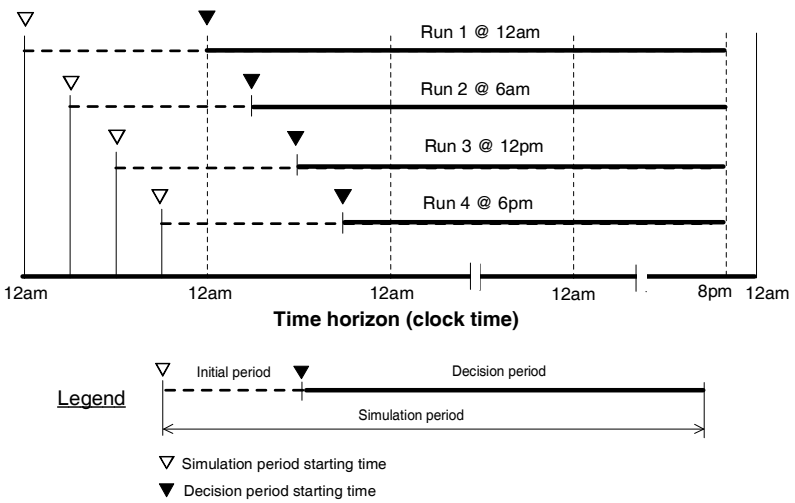

Figure 3. Simulation time window

DISCUSSION

It has been shown that booster disinfection at intermediate locations helps to reduce the total amount of chlorine dose while keeping uniform distribution of chlorine residuals for system wide (Boccelli et al. 1998; Tryby et al. 2002). A potential benefit from the valve operation is to reduce the contact time of disinfectant with the water and prevent slow moving water within the system. Therefore, by combining the valve operation with the multi-sources disinfection, more improvements in water quality are expected resulting in lower chlorine demands. The unique contributions of this study are summarized as follows.

(1) combining valve operation with booster injection to improve water quality
(2) real-time operation considering the variations of water demands and system hydraulics, that are not considered in the early studies where cyclical hydraulic behaviors are assumed for the planning and design purposes.
(3) physically meaningful approach for system pressure prediction by performing the instantaneous steady state pressure computation during changes of demand and comparing with conventional EPS simulation.

REFERENCES

Boccelli, D. L., Tryby, M. E., Uber, J. G., Rossman, L. A., Zeirolf, M. L., and Polycarpou, M. M. (1998). "Optimal scheduling of booster disinfection in water distribution systems." *J. Water Resour. Plng. and Mgmt.*, ASCE, 124(2), 99-111.

Lansey, K., Pasha, F., Pool, S., Elshorbagy, W., and Uber, J. (2007). "Locating satellite booster disinfection stations." *J. Water Resour. Plng. and Mgmt.*, ASCE, 133(4), 372-376.

Munavalli, G. R., and Mohan Kumar, M. S. (2003). "Optimal scheduling of multiple chlorine sources in water distribution systems." *J. Water Resour. Plng. and Mgmt.*, ASCE, 129(6), 493-504.

Ostfeld, A., and Salomons E. (2006). "Conjunctive optimal scheduling of pumping and booster chlorine injections in water distribution systems." *Engineering Optimization*, 38(3), 337-352.

Prasad, T. D., Walters, G. A., and Savic, D. A. (2004). "Booster disinfection of water supply networks: multiobjective approach." *J. Water Resour. Plng. and Mgmt.*, ASCE, 130(5), 367-376.

Propato, M., and Uber, J. G. (2004a). "Linear least-squares formulation for operation of booster disinfection systems." *J. Water Resour. Plng. and Mgmt.*, ASCE, 130(1), 53-62.

Propato, M., and Uber, J. G. (2004b). "Booster system design using mixed-integer quadratic programming." *J. Water Resour. Plng. and Mgmt.*, ASCE, 130(4), 348-352.

Sakarya, A. B., and Mays, L.W. (2000). "Optimal operation of water distribution pumps considering water qualtiy." *J. Water Resour. Plng. and Mgmt.*, ASCE, 126(4), 210-220.

Tryby, M. E., Boccelli, D. L., Uber, J. G., and Rossman, L. A. (2002). "Facility location model for booster disinfection of water supply networks." *J. Water Resour. Plng. and Mgmt.*, ASCE, 128(5), 322-333.

Simulation of Particle Transport in Drinking Water Distribution Systems

Klaus Ripl, Wolfgang Uhl

Technische Universität Dresden, Institute of Urban Water Management,
Chair of Water Supply Engineering Group, 01062 Dresden, Germany;
PH +49 351 463 32337; FAX +49 351 463 37204;
email: klaus.ripl@tu-dresden.de, wasserversorgung@tu-dresden.de

ABSTRACT

Particulate matter in drinking water is one important reason for consumer complains due to discoloured water at customer's taps and further secondary effects. To describe transport of this matter, partices were characterised, important occuring mechanisms described respectively abstracted and, based on known basics for dynamic water quality modelling, a software module developed, which will be linked with a pipe modelling software. Thus, water quality in water supply systems may be predicted and pipe fouling can be described. This shall enhance distribution system operation and planning.

SYMBOLS

c_P	particle volume concentration (1)
D_{brown}	diffusion coefficient ($m^2 * s^{-1}$)
D_{shear}	shear diffusion coefficient ($m^2 * s^{-1}$)
f_{conc}	correction factor for particle volume concentration influence on particle motion (1)
f_{shape}	particle shape factor for the Stokes equation (1)
f_{wall}	correction factor for wall influence on particle motion (1)
g	gravity = 9.81 $m * s^{-2}$
k_{vm}	proportionality constant as a function of the dimensionless distance of the particle to the pipe wall (1)
R_P	particle radius (m)
R_{pipe}	pipe radius (m)
v_{lat}	lateral migration velocity ($m * s^{-1}$)
η_F	dynamic viscosity of fluid ($kg * m^{-1} * s^{-1}$)
ρ_F	water density ($kg * m^{-3}$)
ρ_P	wet density of a particle ($kg * m^{-3}$)

INTRODUCTION

Decreasing water demand in numerous European countries causes varying hydraulic conditions in established drinking water distribution systems. Increased retention times may have an influence on chemical parameters (e.g. chlorine and oxygen depletion), physical parameters (temperature increase) as well as biological parameters (microbial activity) during distribution.

Particulate matter in drinking water is one important reason for consumer complaints due to discoloured water at customer's taps. Particles enter distribution systems at water treatment plant's outlet, may be formed by corrosion of pipe material, microbial activity or after-effects of drinking water treatment, e.g. used coagulation chemicals or adjustment of pH-value.

Investigation subject of a corporate research project was the motion behaviour of particles in drinking water distribution systems for:

- The investigation of established supply networks for impairments with deposits and particle related water quality before consumer complaints occur and
- The accentuation of water quality optimisation as additional parameter for network optimisation strategies beside common optimisation of running and capital costs.

Conclusions of the performed research work were used to write a program, which enables network operators to subsequently minimise particle based water quality impairments.

PARTICULATE MATTER IN DISTRIBUTION SYSTEMS

The main reasons for particle motion in typical pipe flow beside weight/buoyancy are hydraulic forces and weight. In principle, two states can be described for a particle in a pipe:

- Moved by pipe flow, including sedimentation, attachment on surfaces and re-suspension or
- Attached on surfaces or as immobile deposit on pipe bottom.

Particles enter drinking water distribution systems at outlet of water treatment plants or are formed due to corrosion in unlined steel pipe sections. Further sources are amongst others biofilms, chemical precipitation and impurities due to construction works.

In a first step, particulate matter in distribution systems was analysed, focusing on iron oxide particles from a corroding steel pipe. Using Stokes equation, sedimentation experiments in quiescent water yielded a mean wet density of 1430 kg/m³, including influence of particle form. With light microscopy, the sphericity ψ of primary particles could be calculated to 0.859 and the according shape factor f_{shape} for the Stokes equation to 0.945. This denotes that the settling velocity of these iron oxide particles is reduced by roughly five percent due to shape. As the particle density $\rho_{P,pykno}$ calculated with pyknometer was roughly 3300 kg/m³, the settling of these particles was predominantly influenced by particle structure respectively (mean) particle porosity, which could be identified to 77 percent. As the observed particles form stable aggregates in mixed fluids, this value describes the mean aggregate porosity including particle porosity. The real mean wet density ρ_P

of the particles respectively aggregates, including wetted pores but not form influence, is 1539 kg/m³ (at 20 °C water temperature). This is close to the values of Grainger (2002), who got a mean density for mixed samples of suspended particles in distribution systems of 1620 kg/m³. His measuring values for different sampling locations varied from 1180 – 2040 kg/m³.

NETWORK TOPOLOGY AND HYDRAULICS

Water quality modelling in distribution systems is based on network structure and hydraulic conditions. As software for modelling of network structure as well as hydraulics of drinking water distribution systems is provided by several software producers, quality models use the possibilities given by such software packages. Distribution systems are simplified for modelling procedure as links (pipe sections) and nodes.

The quality modelling software described here is bundled with STANET in a first step. STANET, developed by Fischer-Uhrig Engineering in Berlin, is a common commercial software package for modelling of several supply networks (gas, drinking water, power, …). After simulation, results can be saved in structured text files (CSV), which contain network topology, e.g. pipe length, diameter, roughness and so on, as well as hydraulics, e.g. mean flow velocity in the individual pipes, system pressure and water temperature.

Information in text files are imported previous to quality modelling and are prepared respectively stored in PC memory while software is running. For daily consumption patterns, currently used hydraulic data is replaced by new data, when leaving the current hydraulic time step and launching a new one. More details are explained in a later chapter.

TRANSPORT OF MATTER IN DISTRIBUTION SYSTEMS

Particles in pipe flow are exposed to hydraulic induced forces, which results in a motion analogue to fluid motion. In larger time scales of several seconds or even minutes, occurring inertia of particles may be neglected and a simplification is acceptable: inertia due to longitudinal fluctuation resulting from turbulences and varying flow rates are negligible. Therefore, particles move with fluid’s flow velocity in longitudinal direction.

Rossman (1996) describes four methods for the linking of quality models with hydraulic models. The Eulerian discrete volume method (DVM) is one of several methods described. DVM discretise the water body in each individual pipe section (“link”) between two nodes in packages of same size (see figure 1).

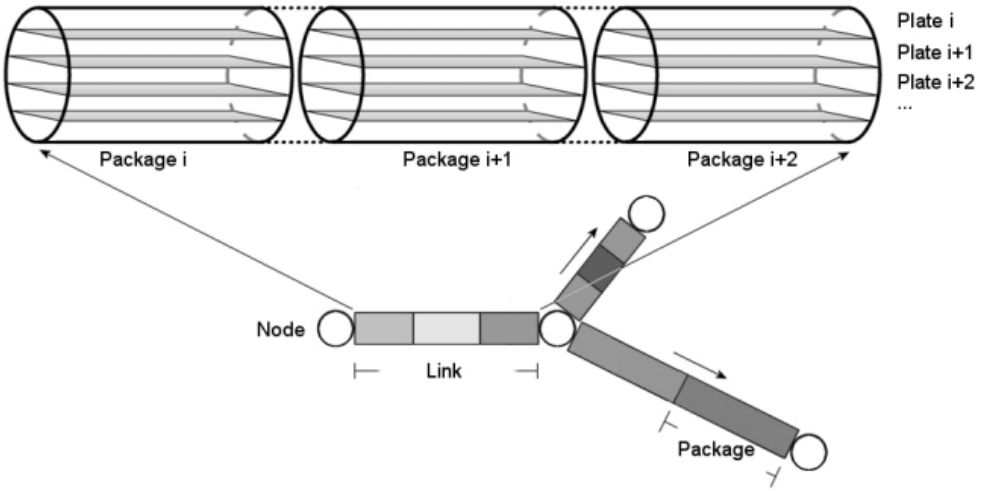

Figure 1. Spatial discretisation of the water body in a distribution system.

Each package is fully mixed, has constant hydraulic conditions (flow velocity) and own water quality parameters (e.g. solid load). Longitudinal, vertical, two-dimensional cuts of all pipes are observed to consider variations of flow velocity in the pipe cross section and therewith varying particle motion velocities.

To reproduce dispersion caused by the typical velocity profile of water in circular tubes, the longitudinal aligned water packages are also vertically segmented in plates with own local flow velocities. All vertically aligned plates of a water package have the same (package) length. This results in dispersion problems, as the length of the water package and the contained plates is adjusted based on the maximum flow velocity in the package and the quality time step length. That means, artificial (numerical) dispersion occurs in plates closer to the bottom respectively top of the pipe, when the content of a plate is assigned to the next package respectively plate downstream.

Beside mobile particulate matter also immobile deposits are modelled and are localised in the pipe by water package boundaries. These deposits do not influence the pipe hydraulics and have no direct influence on particle transport in pipe flow due to reduction of inner pipe diameter in the quality modelling software. However, radial motion of particles in pipe flow is influenced by forces, which are based or influenced on solid concentrations, what is considered in the software.

PARTICLE RELATED PROCESSES IN WATER SUPPLY SYSTEMS

When talking about particle related water quality in drinking water distribution systems, occurring overall measurable effects are the formation of particles as well as changes in particle concentration in bulk water and particle mass in deposits. A breakdown to individual reactions shows figure 2.

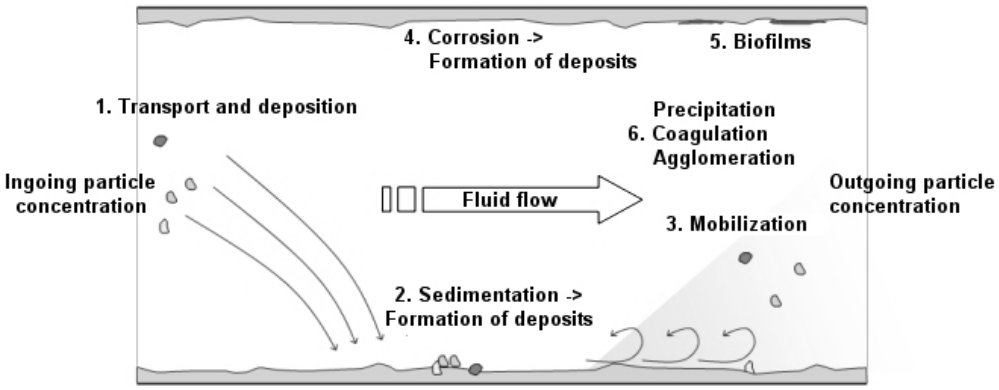

Figure 2. Processes, which affect particle related water quality and fouling of pipes in water supply systems.

A particle in bulk water is carried by fluid flow (1) and may be deposited by sedimentation and attachment on pipe walls. Particulate, soft, water-rich deposits may also result from corrosion (4) of unlined steel and cast iron pipes as well as microbial activity in biofilms (5). Beside mentioned sources, a chemical unstable water can release particles (6), e.g. by precipitation and coagulation of dissolved matter (chemicals used in drinking water treatment). Immobile, deposited particles (2) are exposed to fluid flow and may be re-suspended (3). This hydraulic stress may be described as wall shear stress.

Biofilms and effects of chemical unstable water are not described in the present particle model for drinking water distribution systems.

EXPERIMENTAL INVESTIGATION ON PARTICLE DEPOSITION IN PIPE FLOW

Two identical pipe loops, each with a length of 195 metres and 83 mm inner diameter, were installed for transport and mobilisation experiments. One pipe cycle consists of unlined steel pipes, which allows the formation of particulate corrosion products in a corrosion film under constant flow velocities and their mobilisation due to defined changed hydraulic conditions after a given developmental period for the corrosion film.

The second, identical, system is a PE pipe loop, where the settling and transport behaviour of suspended plastic particles (PVC, Vinnolit E 2078, density 1,400 kg/m³, rounded, solid) and the above described iron oxide particles (wet density 1,539 kg/m³, unshaped, porous) are observed. The pipe water circulates in the pipe loops. Turbidity, particle size distribution and pressure are continuously measured at inlet and outlet of the pipe loops. Furthermore, flow rate and temperature are continuously logged over the duration of the experiments. Differences between ingoing and outgoing particle concentrations result from sedimentation and may be quantified for different particle sizes and flow conditions. Results for the experiments with PVC powder and iron oxide particles are shown in figure 3.

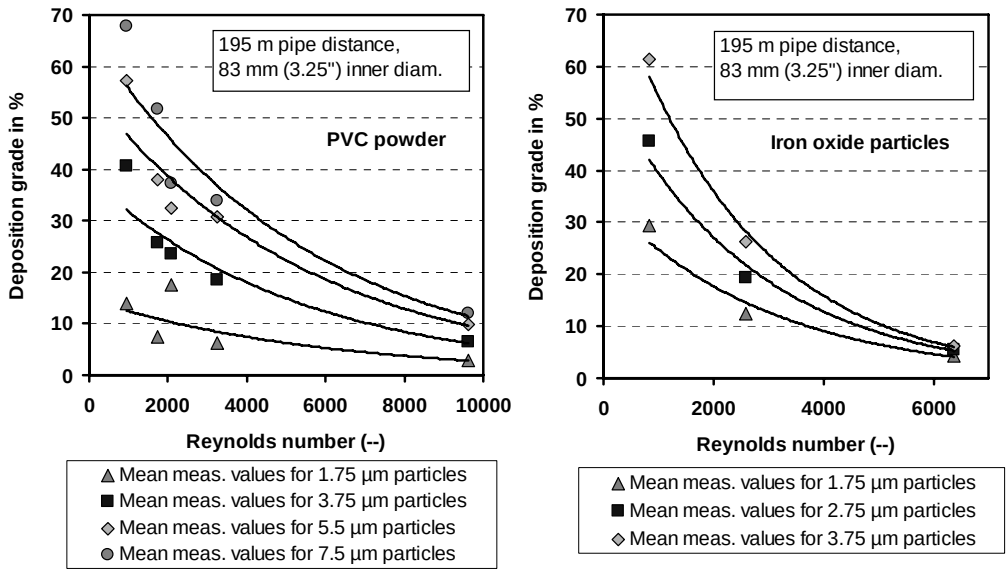

Figure 3. Deposition grade of particles from a PVC powder (LHS) and iron oxide particles (RHS) when transported through a pipe distance of 195 m (83 mm inner diameter).

The diagram on the left-hand side shows, as expected, that with decreasing flow velocity respectively Reynolds number the deposition grade of particulate matter increases, while at higher Reynolds numbers and turbulent flow only less suspended particles settle. This is also noticeable in the diagram on the right-hand side of figure 3. When comparing both diagrams (consider the different x-axes!), it can additionally be reasoned that the iron oxide particles settle „better“, but this observation fits with the particle properties of both particle systems: Even with porosity, the iron oxide particles are more heavy and additionally have surface properties which may possibly advance interaction mechanisms (adhesion) with pipe surfaces. This question is under further investigation.

EXPERIMENTAL INVESTIGATION ON PARTICLE MOBILISATION IN PIPE FLOW

Sediment is stressed by given pipe flow. That is often described as wall shear stress. Slaats et al. (2003) list several values for sediments in water supply systems available from literature, but it is not clearly stated, which type of particulate matter was available and furthermore, situation of sediment resp. pipe (particulate matter, incrustations, …) can’t be defined.

Therefore, mobilisation was experimentally investigated in the steel pipe loop of the pilot plant as described above. After a defined time period for the growth of the corrosion layer, which is situated over the whole pipe perimeter, mean flow velocity was increased by a defined value. Thus, turbidity in the pipe increases and with known relationship between turbidity and solid load, the amount of mobilised

sediment can be determined. After such an experiment, the pipe was flushed and the experiment started again. The result of two series of measurements, each with a constant mean flow velocity v0 for the formation of corrosion layers (=particulate deposit), is shown in the left diagram in figure 4.

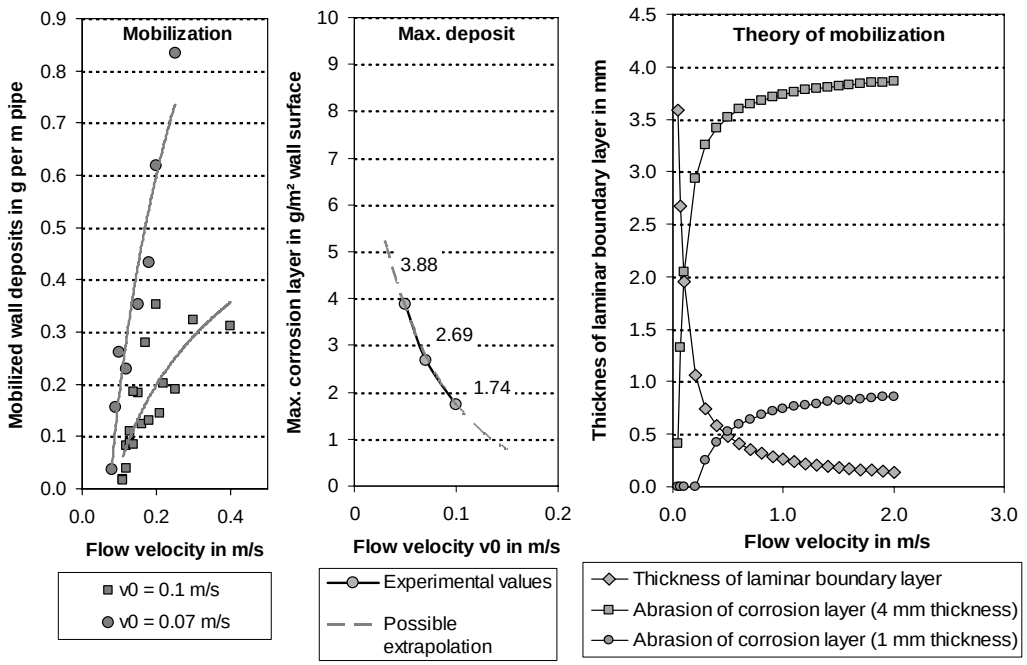

Figure 4. From left to right: Mobilisation of particulate iron oxide wall attachments dependent on mean flow velocity; maximum deposit in a pipe at given constant mean flow velocity; relationship between thickness of laminar boundary layer and mean flow velocity (all diagrams for 83 mm (3.25") inner pipe diameter).

As can be seen, higher flow velocities (the new adjusted velocity higher than v0) result in more mobilised sediments. With long-term experiments, where large amounts of particulate corrosion products could be formed, the maximum amount of attached particulate matter could be determined as can be seen in the middle diagram in figure 4. With increasing flow velocity, the maximum amount of immobile deposits at 80 mm (3.25") inner pipe diameter shows of course a tendency to zero, while at decreasing flow rates the amount of deposits reaches a maximum.

As explained before, the acting wall shear stress is a common value to interpret mobilisation of sediment. However, for particulate deposits in drinking water distribution systems it is important to look at the thickness of the laminar boundary layer, which covers pipe surfaces and attachments. The thickness of this layer δ_{lam} depends on Reynolds number Re and inner pipe diameter D_{pipe} (Bollrich, 2000):

$$\delta_{lam} = 34.2 \cdot D_{pipe} \cdot (0.5 \cdot Re)^{-7/8} \quad (1)$$

The relationship between thickness of the laminar boundary layer and thickness of sediments is illustrated in the right diagram in figure 4. Compared with a thick corrosion layer (here 4 mm), a thin corrosion layer (here 1 mm) is mobilised at higher velocities. If adopted that mobilisation is only possible at turbulent flow conditions with adequate (wall) shear stress on sediments, thickness of the laminar boundary layer decreases with increasing flow velocity and parts of the covered corrosion film may extend into the turbulent core zone of the pipe flow. There, shear stress may abrade this particulate matter. With higher flow, a rapid increase of mobilisation can be noticed at beginning of the mobilisation process, but this development is limited by the maximum available amount of sediment (see the right diagram in figure (4)).

If turbulent flow conditions periodically occur, the typical thickness respectively volume of the laminar boundary layer also describes the amount of maximum settleable matter. As incrustations in unlined pipes may clearly influence the velocity field, the approach described here may be only a first estimation for such pipes.

MODELLING OF PARTICLE MOTION IN PIPE FLOW

The plastic pipe loop of the pilot plant is hydraulically modelled as vertical 2D longitudinal section along the pipe axis in the CFD software package Comsol in full length under single-phase fluid conditions. CFD is the generic term for numerical methods to solve the Navier-Stokes equations. The physical conditions (fluid viscosity, flow velocity) are the same as in the experiments. Also in later descriptions, the x-axis is equal to the pipe bottom and the y-axis is normal to the pipe axis and in the direction of the top of the pipe.

Suspended particles subjected to pipe flow are influenced by various hydraulic induced forces. Lerch (2008) mathematically describes these and additional occurring forces for particles in capillaries of ultrafiltration membranes in detail. These acting forces are described by force balances and are based on the (hydraulic) simulation results of the Navier-Stokes equations. As conditions in pipes are different from capillaries, a simplification of the force model is used to describe particle transport in pipe flow. Table 1 lists the forces, which are required for description of particle motion in y-direction and gives some additional information. The particle motion in x-direction is equal to local flow velocity of the water

Table 1. Forces considered in the model for motion of suspended particles in y-direction transported in pipe flow (adopted from Lerch, 2008).

Force	Equation	#
Sedimentation force	$F_{sed} = f_{shape} \cdot (\rho_P - \rho_F) \cdot \frac{4}{3} \cdot \pi \cdot R_P^3 \cdot g$	(2)
Brownian diffusion	$F_{brown} = -D_{brown} \cdot \frac{dc_P}{dR_{pipe}} \cdot 6 \cdot \pi \cdot \eta_F \cdot R_P$	(3)
Shear induced diffusion	$F_{shear} = -D_{shear} \cdot \frac{dc_P}{dR_{pipe}} \cdot 6 \cdot \pi \cdot \eta_F \cdot R_P \cdot f_{conc}$	(4)
Lateral migration	$F_{lat} = 6 \cdot \pi \cdot \eta_F \cdot R_P \cdot v_{lat} \cdot f_{wall} \cdot f_{conc}$	(5)
Drag force	$F_{drag} = 6 \cdot \pi \cdot \eta_F \cdot v_P \cdot R_P \cdot f_{wall} \cdot f_{conc}$	(6)

According to eq. (2) to (6), the simplified force balance in y-direction for particles in fluid flow is

$$F_{sed} + F_{brown} + F_{shear} + F_{lat} + F_{drag} = 0. \quad (7)$$

Eq. (7) can be solved for the particle velocity v_P in y-direction, which is included in the drag force (see eq. (6)):

$$v_P = k_{correction} \cdot \frac{(F_{sed} + F_{lat} + F_{brown} + F_{shear})}{6 \cdot \pi \cdot \eta_F \cdot R_P \cdot f_{wall} \cdot f_{conc}}. \quad (8)$$

The detailed model with more aspects especially for membrane particularities and the mathematics behind the used equations are described by Lerch (2008).

The modelling results for particle deposition in pipe flow were compared with experimental results (see the according upper chapter “deposition experiments”.) Differences are described as correction factor $k_{correction}$ and used to correct eq. (8) for the particle velocity. With this equation, an individual settling velocity is calculated for particle size classes in all vertically aligned plates in all water packages.

With this force balance (eq. 7/8) it is not possible to model wall attachments, especially on the top of the pipe. However, as the calibration of the model is done with experimental values, also deposition due to attachment on pipe walls is indirectly considered in the modelling results.

INITIAL DESCRIPTION OF THE PARTICLE SOURCE “CORROSION”

An also considered reaction beside deposition and mobilisation is the release of particulate matter due to corrosion. Corroding steel and cast iron pipes may be an

important source for particulate matter in drinking water distribution systems. As there were no sufficient corrosion models available during development of the transport model, which may predict intensity and location of corrosion, a first, simple approach was implemented.

With systematic pipe flushing in present water supply systems, particulate sediments were investigated to determine a mean value for the release of iron (Fe^0) from corrosion in this particulate matter. This work was done by TZW Dresden (yet unpublished results). A small net was flushed with clean water front and after a defined time period, flushing was performed again to investigate the development of the deposits since last flushing and then calculate an "iron formation rate". The mean value 0.0025 g Fe^0/m pipe *day for three supply systems is used to calculate the amount of particulate matter, which is formed due to corrosion. This value can be used, to calculate a mean value for the iron oxide formation rate, when assuming that iron species like Fe_20_3 or FeO(OH) are formed.

All formed particles are attached on the pipe wall over the whole pipe perimeter after formation. It is assumed that no particles are released to bulk water during the formation process. The particle volume concentration of the corrosion layer in the steel pipe loop of the pilot plant was calculated from mobilisation experiments with 0.0415 %. In a first step, this value may also be used for the actual mixed sediment in present distribution systems. This low value indicates the large share of water in the deposits but includes also the irregular distribution and thickness of a natural corrosion layer. Mobilisation is based on this value, which is used to calculate the sediment volume respectively thickness. Thickness of deposits and laminar boundary layer are compared to determine the mobilised amount of particulate matter.

STRUCTURE OF THE SOFTWARE MODULE

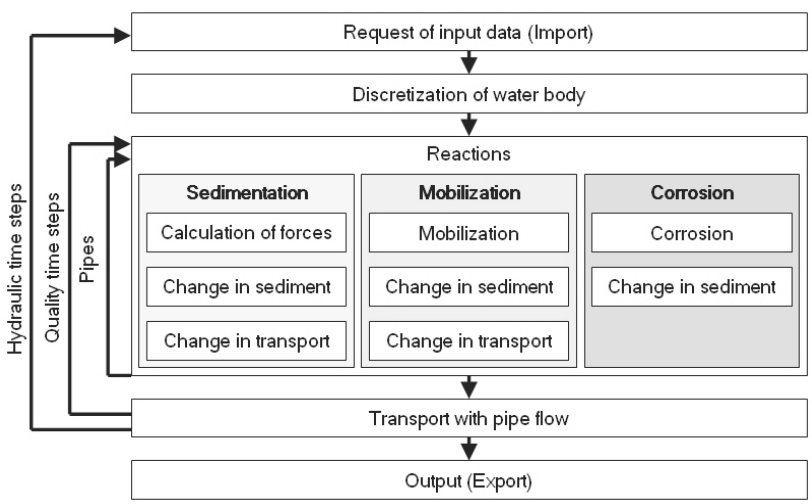

Figure 5. Structure of the software module.

The software module is written in Matlab 7.7 and optimised for Matlab's multiprocessing features. The module structure is shown in figure (5), the GUI in figure (6).

After receiving of input data (net topology and hydraulics) at the beginning of each hydraulic time step, the water body in all pipes is discretised. The hydraulic time step loop only occurs in case of used daily consumption patterns and then is described as a discretisation step of these patterns. As numerical dispersion will occur at each rearrangement of the water packages, it is currently not decided, if, with respect to the sediment, a change in discretisation for each hydraulic time step makes sense.

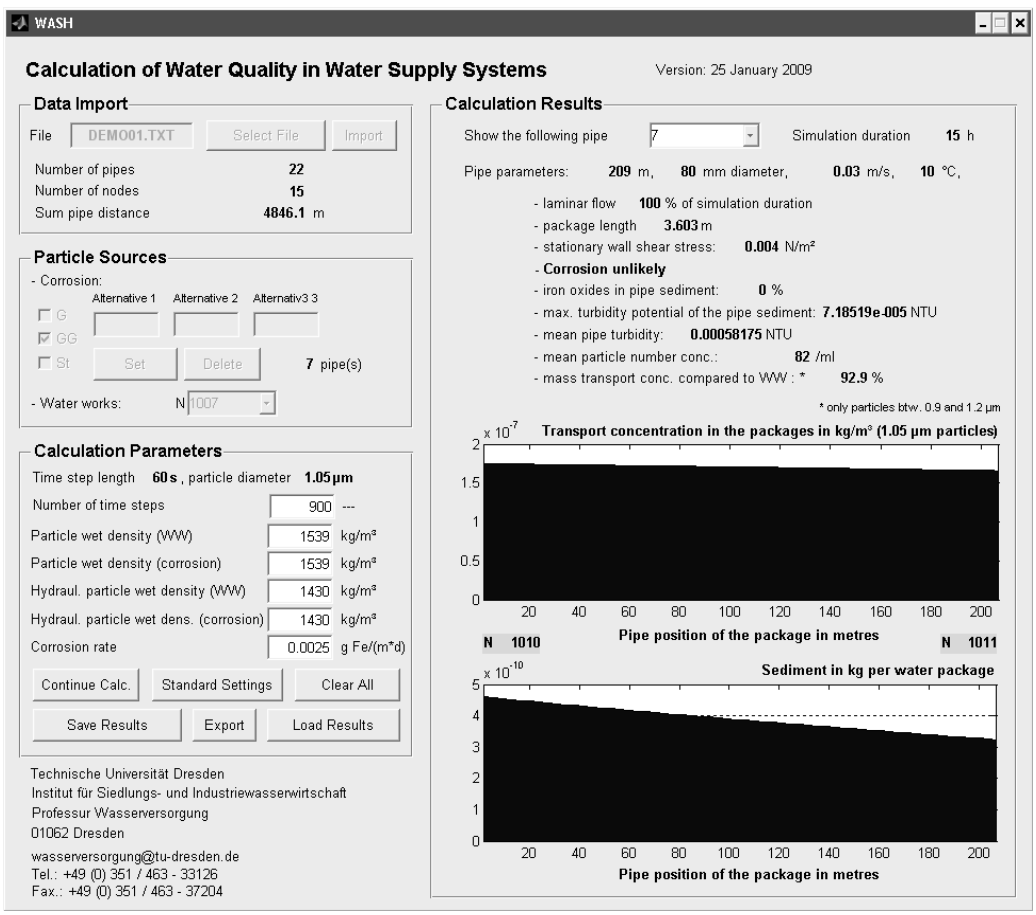

Figure 6. GUI of the software for quality modelling in drinking water distribution systems.

After all reactions and the resulted changes in transport mass concentration and sediment mass, transport with pipe flow is calculated according to Rossman (1996) and EPANET MSX (2008) manual: Initially, transport in the pipes and from the pipes into the nodes is performed. Then, mixing in the nodes is done for all plates and the node content is transported to the downstream pipes. This calculation step,

described in figure 5 as “quality time step” is also implemented as loop and encloses the pipe loop. This inner loop calculates for all pipes in the system the reactions in each quality time step.

The calculation results are stored in the original export file, which is imported to STANET to graphically show the results in whose GUI.

In the current state of the software, the user is guided through the GUI by three steps: import of data from STANET, definition of particle sources and setting up of the simulation parameters as well as handling of simulation results.

EXAMPLE FOR THE TRANSPORT PREDICTION

STANET contains a demo network (demo01), which is used for some first simulations and tests with the developed software. It consists of 22 links (furthermore named as pipes) and 15 nodes (figure (7)).

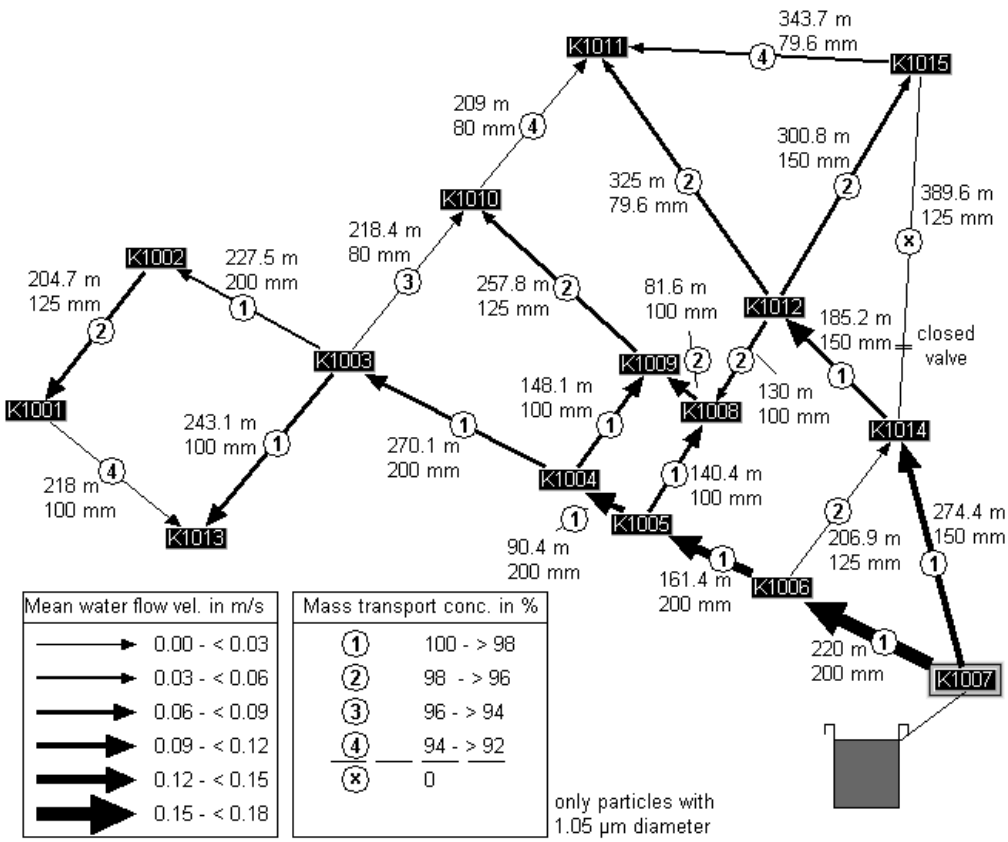

Figure 7. Comparison between particle mass concentration at storage tank outlet (node 1007) and in the pipes as percentage; the storage tank has 100 % (“demo01” from STANET).

This simple network is supplied by a storage tank at node 1007 (K1007). All other nodes are consumers. In this case, only constant consumption was used, as the support for daily consumption pattern in the software is currently in development.

The thickness of the pipe arrows show the mean flow velocities and the symbols on the arrows the mean (steady state) particle concentrations in the pipes compared with the quality in the storage tank. Only transport of particles with 1.05 µm (projection equivalent) diameter is calculated here. The transport simulation results are subsequently manually added to the figure, as file import into STANET isn't finished yet.

A decrease in particle concentration indicates a decrease in turbidity and therewith a better particle related water quality. Hence, it may be reasoned for this simple example that particles settle during water distribution and form deposits. These deposits have a so called "turbidity potential", which may be activated at given hydraulic conditions (Boxall, 2005). When calculating the Reynolds number for the pipes, which indicates turbulent flow conditions, it may also be seen that flow velocity isn't in every case the best choice to predict deposition of particles. For example, the pipe between the nodes 1003 and 1002 has a relatively low flow velocity of 0.05 m/s, but the large inner pipe diameter causes sufficient turbulent flow conditions with Reynolds number 7634, which prevent particles from sedimentation compared with laminar flow conditions (e.g., the pipe between the nodes 1010 and 1011 has RE = 1221 at v_F = 0.02 m/s).

SUMMARY, CONCLUSIONS AND OUTLOOK

A software module is developed for modelling of particle related water quality in drinking water distribution systems. Processes like sedimentation and mobilisation are described as well as required basics for the description of the particle sources "water works" and "corrosion" for a comprehensive approach. As all reactions are based on hydraulics and network topology, the software module was bundled with the pipe modelling software STANET.

Further works will focus on implementation of new, more detailed modelling approaches for the particle related processes corrosion, microbial activity and adsorption. In the mean time, the present model is tested with several hydraulically calibrated distribution systems. The investigation of these systems was done by TZW Dresden.

RFERENCES

Bollrich, G. (2000). "Technische Hydromechanik Band 1." eng.: "Hydromechanics 1.", 5th edition, Verlag Bauwesen, Berlin.

Boxall, J. B., Saul, A. J. (2005). "Modeling Discoloration in Potable Water Distribution Systems." J. Envir. Engrg., 131 (5), 716-725.

EPANET MSX (2008). "User's Manual." US EPA.

Grainger, C., Wu J., Nguyen, B., Ryan, G., Jayaratne, A., Mathes, P. (2002). "Particles in Water Distribution System." CRC 4.3.6 Project Team (Australien).

Lerch, A. (2008). "Coating layer formation by flocs in inside-out driven capillary ultrafiltration membranes." Dissertation at the University Duisburg-Essen.

Rossman, L. A. (1996). "Numerical Methods for ModelingWater Quality in Distribution Systems: A Comparison." J. Water Res. Pl., ASCE, March/April 1996, 137-146.

Slaats, P. G. G., Rosenthal, L. P. M., Siegers, W. G., van der Boomen, M., Beuken, R. H. S., Vreeburg J. H. G. (2003). "Processes Involved in the Generation of Discolored Water." AwwaRF Research Report #90966F.

STANET (2008). www.stafu.de.

TZW Dresden. http://www.tzw.de/en/abteilungen/aussenstelle_dresden/new_concept_for_optimized_flus-82/ (27th January 2009 seen)

WDS Water Quality Parameter Estimation and Uncertainty

M.F.K Pasha[1] and K. Lansey[2]

[1]Water Resources Engineer, Tetra Tech Inc., Tucson, AZ 85711; email: fayzul.pasha@tetratech.com
[2]Professor and Head, Department of Civil Engineering and Engineering Mechanics, The University of Arizona, Tucson, AZ 85721; Ph (520)-621-2512; Fax (520)-621-2550; email: lansey@engr.arizona.edu.

ABSTRACT

During model development and calibration, errors in field measurements propagate to uncertainties in parameter uncertainty. Water distribution water quality models are typically calibrated using tracer test data. Here, we evaluate the uncertainty resulting from the test assuming demands are known exactly and only the wall coefficients are to be estimated.

A meta-heuristic search engine, Shuffled Frog Leaping Algorithm (SFLA) is linked with hydraulic and water quality simulation software EPANET to estimate the pipe wall decay coefficients. A first-order approximation is applied then to estimate the parameter uncertainty. This methodology is applied on a mid sized example network. Results show that with tracer injection parameter can be accurately estimated. It is also found that parameter estimation can be more accurate if the magnitude of the wall decay coefficients is higher.

INTRODUCTION

Chlorine, an oxidizing agent that decays with time, is the most popular water treatment disinfectant in municipal water distribution system. A minimum level of chlorine residual is always desired to be maintained in the distribution system to preserve both chemical and microbial quality of treated water (Vasconcelos et al. 1997, Munavalli and Mohan Kumar 2003). Chlorine reacts with different materials inside the pipe while it travels with water through the distribution system.

Reactants are present in the bulk water and on the surface of the pipe. After a certain age of the systems organic carbon or bio materials deposited on the surface of pipes or tank walls producing a biofilm. Thus, the wall component of reaction may play an important role in chlorine reaction kinetics.

Pasha and Lansey (2005) conducted a thorough study on water quality parameters uncertainty. All the hydraulic and water quality parameters such as pipe diameter and demand, spatial and temporal variation of nodal demand and decay parameters are considered in their uncertainty analysis to observe their impact on

nodal chlorine concentration. The study concluded that chlorine decay and residuals are significantly affected by the decay parameters (bulk and wall). Wall decay parameters are particularly important when the turbulence in the flow is higher.
Although bulk decay coefficient can be determined in a laboratory jar test, there is no direct method to determine the wall decay parameters. A field test is required to estimate wall decay parameters. Several studies have been conducted to estimate the wall decay parameters. A popular way of estimating wall decay parameters is automated calibration in which a water quality simulation model is connected with a search algorithm to estimate their value by minimizing the deviation between measured and simulated chlorine concentrations. However, proper calibration is not an easy task because of various reasons; such as (a) data collection is expensive and requires great effort; (b) most calibration procedures are deterministically based (Lansey et. al. 2001). Measurement error and poor calibration procedure cause uncertainties in the estimated parameters.

The objective of this paper is to estimate parameters and their uncertainty for various field measurement conditions to determine the accuracy that can be expected and the value of alternative measurement and tracer test campaigns.

BACKGROUND

Hydraulic model calibration in water distribution systems analysis was the main focus in the past. A range of optimization methods have been applied (Ormsbee 1989, Lansey and Basnet 1991, Todini 1999, Wu et al. 2000) to solve the hydraulic calibration problem.

Little work, however, has been conducted on water quality model calibration. Clark et al. (1995) estimated wall decay parameter by trial and error approach to simulate chlorine residual. Vasconcelos et al. (1997) calibrated a water quality model by sequentially adjusting the wall decay parameter to give the best fit between simulated and filed measurement. Islam et al. (1997) developed an inverse approach to determine the source concentrations required to meet the specified concentrations at selected nodes. However, no attempts were made in their study to estimate the wall decay parameters.

Munavalli and Mohan Kumar (2003) developed an inverse approach model to estimate reaction parameters in steady state distribution systems and later extended the model to dynamic conditions (Munavalli and Kumar 2005). They applied a weighted least squares method to estimate at most three wall decay parameters for a constant source chlorine injection. Boccelli et al (2004) conducted a network-wide dual-tracer field-scale study and model calibration. They used observed data for manual calibration of the system. No systemic approach was taken to estimate the distribution system parameters. Wall or bulk decay coefficients were not estimated in their studied. Very recently, Pasha and Lansey (2008) estimated best fit wall decay parameters by linking a hydraulic and water quality simulation model with a search engine known as Shuffled Frog Leaping Algorithm (SFLA). Up to six wall decay parameters have been considered with different field conditions. However, parameters uncertainties were not assessed.

METHODOLOGY

The methodology applied here involves two steps. The first is to estimate the parameters and the second step is to evaluate the uncertainties in the estimated parameters.

Parameter estimation. Field data collection is the first step. Due to lack of real world data a simulation model was run to generate data. To create field type condition a random error was added with the exact data. Following calculations can be made to generate the measurement error assuming that the error is normally distributed.

$$CV = \frac{\sigma}{\bar{x}} \tag{1}$$

where σ is the standard deviation and $\bar{x}$ is the mean of the concentrations at specific time and location. Therefore,

$$\sigma = CV * \bar{x} \tag{2}$$

According to normal distribution the measured concentrations can be written as

$$x = \bar{x} + \sigma * Z$$
$$x = \bar{x}(1 + CV * Z) \tag{3}$$

where, Z is the standard normal deviate.

The next step is to estimate the model parameters. The water quality calibration model objective in this paper is to determine the wall decay parameters ($\boldsymbol{k_w}$) so that the difference between the field measured concentration and the simulated values are minimized. Mathematically, the problem can be stated as:

Minimize $f(\boldsymbol{k_w})$ (4)

subject to:

$$\boldsymbol{G_H(H, q) = 0} \tag{5}$$

$$\boldsymbol{G_Q(H, q) = 0} \tag{6}$$

$$\boldsymbol{k_{wlower} \le k_w \le k_{wupper}} \tag{7}$$

where Eq.4 is the objective function that sums the square differences between computed and measured concentrations at selected locations and times. $\boldsymbol{H}$ and $\boldsymbol{q}$ are the vectors of pressure and flow demands for all nodes and demand pattern. $\boldsymbol{G_H}$ and $\boldsymbol{G_Q}$ are the conservation of energy and mass respectively. $\boldsymbol{k_w}$ is decision variable with upper ($\boldsymbol{k_{wupper)}}$ and lower ($\boldsymbol{k_{wlower}}$) bounds.

Equation 4 can be written as:

$$f(\boldsymbol{k_w}) = J = \sum_{l}^{L} \left(CC_l - MC_l\right)^2 \tag{8}$$

where CC_l and MC_l are the computed and measured concentrations at location l for all times considered and L is the total measurement locations. J is optimal objective value.

EPANET version 2.0 (Rossman (2002) is used as the hydraulic and water quality simulation model. Shuffled Frog Leaping Algorithm (SFLA), a meta-heuristic search algorithm (Eusuff and Lansey 2003 and Eusuff et al. 2005) has been linked with EPANET. An initial population (in this case frogs) is randomly generated first.

EPANET then simulates the water quality conditions and the objective function (Eq. 8) is then computed for each frog. New points (frogs) are then generated following the optimization procedure. This iterative process continues until a stopping criterion is reached.

Parameter Uncertainty Evaluation. The next step is to quantify the magnitude of the uncertainty involved with the estimated parameters since the measurement errors are involved. Yeh and Yoon (1981), Mallick and Lansey (1994), Bush and Uber (1998), and Lansey et al. (2001) applied first-order approximation to estimate uncertainties in the hydraulic parameters. This study applies same technique to evaluate the covariance matrix of the estimated parameters in this case the wall decay parameters (Cov($\boldsymbol{k_w}$)) using the concentration sensitivity matrix relative to the parameter ($\frac{\partial C}{\partial k_w}$) and the variance in measured concentrations ($\sigma_C^{\,2}$).

$$\text{Cov}(\boldsymbol{k_w}) = \left[\left(\frac{\partial C}{\partial k_w} \right) \left(\frac{\partial C}{\partial k_w} \right)^T \right]^{-1} \sigma_C^{\,2} \tag{9}$$

The diagonal elements of the Cov($\boldsymbol{k_w}$) are the variances of the individual wall decay parameters and the off diagonal terms are the covariances between the decay parameters. The $\sigma_C^{\,2}$ can be approximated by (Bard 1974)

$$\sigma_C^{\,2} = \frac{J}{M - L} \tag{10}$$

where J = optimal calibration objective (eq. 8); M = total number of field measurements; and L = number of calibrated parameters. The matrix of the sensitivities of the concentrations relative to the wall decay parameters can be estimated analytically or by a numerical approximation (Lansey et al. 2001). The numerical approximation method is used to calculate the sensitivity matrix.

$$\left[\frac{\partial C}{\partial k_w} \right] = \left[\frac{C_\Delta - C}{(k_w + \Delta k_w) - k_w} \right] \tag{11}$$

where C_Δ = concentrations computed by simulation using the perturbed wall decay parameter values; C = simulated concentrations with the best estimate of the wall decay parameters, k_w; and Δk_w = perturbation introduced to k_w. For this study a perturbation of 0.0001 is used.

EXAMPLE NETWORK

The network analyzed in this study is network NET2A from the EPANET with minor modifications (Figure 1). The network consists of 32 pipes, 28 nodes, one source (node 29), one tank (node 30) and three identical pumps at the source. The 24 hour average demand pattern listed in Table 1 was repeated for a 48 hour simulation period.

The source concentration was 3 mg/l. Disinfectants were injected as a pulse injection for the first 2 hours (3 mg/l) simultaneously with the continuous injection of

3 mg/l. The initial concentrations were determined by running the model for a month and then the taking the last hour's concentrations.

Alternative field conditions were examined including different measurement errors, tracer injection times, data collection times, and true wall decay parameter values. In all experiments the number of wall decay parameters (k_w) used is three and hourly data are collected at six locations. k_w is always constrained by upper value of 0.0 day^{-1} and lower value of -1.0 day^{-1}.

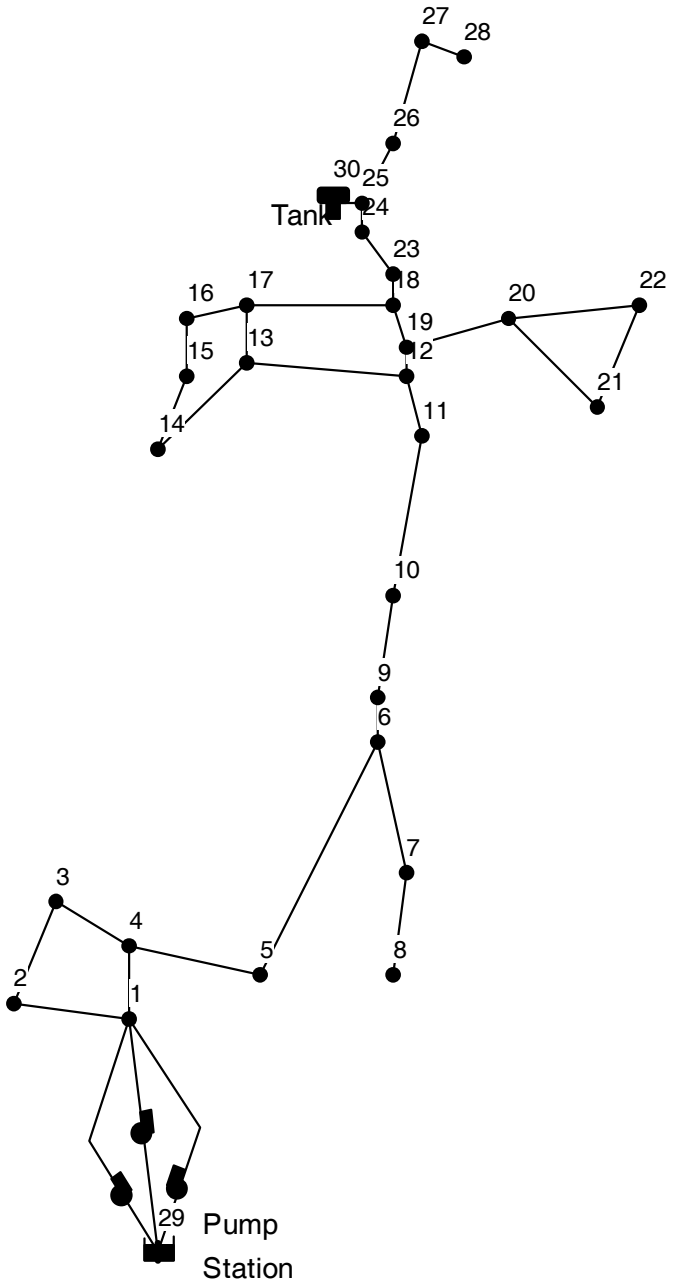

Figure 1. Example Net2A

SFLA parameters values that are used to search the best wall decay coefficients for this network are the number of memeplexes (m) = 50, the number of frogs in a memeplex (n) = 70, the number of frogs in a sub-memeplex (q) =5, the number of evolution or infection steps in a memeplex between two successive shuffling (N) =10, and the maximum step size allowed during an evolutionary step (S_{max}) = 100%. Different experiments are described below with their results.

Tracer injection timing. Four estimation uncertainty analyses are completed by varying the tracer injections timing. The time used are slected to determine the benefit of flow conditions: 12:00 am, 6:00 am, 12:00 pm, and 6:00 pm. A disinfection spike concentration of 3 mg/l is injected for two hours over the continuous injection of 3 mg/l. The measurement errors are introduced using a coefficient of variation of 0.0324.

Results are tabulated in Tables 2 and 3 and show that the impact of the different injection time is not pronounced. However, a closer inspection can find that for the injection at 6 am, the optimal objective value is the highest (Table 2) and that for the injection at 6 pm is the lowest.

Measurement errors can influence the parameter estimation process. As a result, uncertainty may be observed in the parameters. The parameters uncertainties (standard deviations) are calculated for each injection and are tabulated in Table 3. It is found that the parameter standard deviations are highest for the tracer injection at 6am and lowest for a 6 pm injection though the difference is not very significant.

Measurement error magnitude. The purpose of this experiment is to confirm whether the findings in the previous experiment are true for different levels of measurement errors. The previous experiment is repeated here for a coefficient of variation of 0.1 to generate the measurement errors.

It is found that parameters are estimated with highest accuracy at 12 am and lowest accuracy at 6 pm (Table 4). Parameter uncertainties are measured for each injection. Parameter uncertainties show that higher uncertainties (standard deviation of the parameters values) occurred when the parameter estimation accuracy is lower or the lower uncertainties occur when the parameter estimation accuracy is higher (Table 5). In general, uncertainty in the latter case (measurement error coefficient of variation 0.1) is 3 to 3 .5 times higher than the former case (measurement error coefficient of variation 0.0324).

Value of tracer injections and the impacts of the magnitude of wall decay coefficients. Several additional runs were complete to examine the benefits of a tracer injection and to observe the impact of different magnitudes of wall decay coefficients and data collection time. The tracer tests may provide more sensitivity in parameter estimates. This added sensitivity can justify the time of conducing the tracer test. The impact of the wall decay coefficient magnitude should be understood since larger values result in larger decay and higher disinfectant demands. The ability to accurately predict decay under these conditions is especially important.

Results from this experiment are compared with the results performed in the previous experiment (experiment 2). Therefore, previous experiment for the tracer

injection at 12 am is referred as base condition (Tables 6 and 7). To examine the benefit of the tracer, the injection rate is held constant and the process repeated. The result is compared with the base condition in which tracer is injected at 12 am. Parameter estimates are poorer when no chlorine spike is injected (Table 6). However, the relative parameter uncertainty is similar. Thus, the spike condition does benefit the model calibration.

To observe the impact of different magnitudes of wall decay coefficients, the true values k_w's are tripled. The parameter estimation/uncertainty process is repeated and results are compared with the base condition. The first k_w is very poorly estimates (Table 6) but its uncertainty was nearly equal to the previous cases. The other parameters were closer to the true values but the uncertainties increased. One would anticipate that the accuracy might increase because the decay is more significant, thus the parameter would be more sensitive. However, if the measured concentrations are in the slowly changing portion of the decay curve, this may not be the case. The low parameter uncertainty suggests that this may be the case here. This tradeoff between model precision and accuracy should be investigated further, perhaps in a multi-objective formulation.

Table 1. Temporal demand factors at different times in a day

Time	Average demand factors	Time	Average demand factors
12 am	0.50	12 pm	1.16
1 am	0.48	1 pm	1.17
2 am	0.45	2 pm	1.21
3 am	0.40	3 pm	1.23
4 am	0.46	4 pm	1.36
5 am	0.64	5 pm	1.57
6 am	0.85	6 pm	1.75
7 am	1.20	7 pm	1.5
8 am	1.37	8 pm	1.15
9 am	1.27	9 pm	0.85
10 am	1.16	10 pm	0.66
11 am	1.15	11 pm	0.58

Table 2: Estimation of wall decay coefficient for Net2 network for the measurement error CV of 0.0324: pulse injected at different times

True values (day^{-1})	Pulse injection time	Optimal parameter values (day^{-1})	Optimal objective value
-0.5,-0.4,-0.3	12am	-0.507, -0.403, -0.286	1.1233
	6am	-0.482, -0.409, -0.298	1.1246
	12pm	-0.498, -0.399, -0.292	1.18
	6pm	-0.504, -0.398, -0.310	1.0926

Table 3: Parameters uncertainty estimation for Net2 network: pulse injected at different times

Pulse injection time	Standard deviation (day^{-1})		
	k_{w1}	k_{w2}	k_{w3}
12am	0.0109	0.0117	0.0097
6am	0.0108	0.0123	0.0104
12pm	0.0111	0.0114	0.0102
6pm	0.0107	0.0112	0.0101

Table 4: Estimation of wall decay coefficient for Net2 network for the measurement error CV of 0.1: pulse injected at different times

True values (day^{-1})	Pulse injection time	Optimal parameter values (day^{-1})	Optimal objective value
-0.5,-0.4,-0.3	12am	-0.523, -0.386, -0.326	9.8263
	6am	-0.552, -0.365, -0.294	10.194
	12pm	-0.489, -0.437, -0.301	12.748
	6pm	-0.533, -0.382, -0.295	15.272

Table 5: Parameters uncertainty estimation for Net2 network for the measurement error CV of 0.1: pulse injected at different times

Pulse injection time	Standard deviation (day^{-1})		
	k_{w1}	k_{w2}	k_{w3}
12am	0.0325	0.0335	0.0321
6am	0.0341	0.0339	0.0314
12pm	0.0366	0.0407	0.0343
6pm	0.0409	0.0407	0.0364

Table 6: Estimation of wall decay coefficient for Net2 network: different field conditions

Different field conditions	Optimal parameter values (day^{-1})	Optimal objective value
Base condition	-0.523, -0.386, -0.326	9.8263
Without tracer injection	-0.451, -0.472, -0.265	11.168
$\boldsymbol{k_w}$ values are 3 times of base $\boldsymbol{k_w}$	-0.841, -1.314, -1.356	7.3918

*True values for the first two rows were -0.5, -0.4 and -0.3. The true parameter values for the last row were -1.5, -1.2, -0.9.

Table 7: Parameters uncertainty estimation for Net2 network: different field conditions

Different field conditions	Standard deviation (day^{-1})		
	k_{w1}	k_{w2}	k_{w3}
Base condition	0.0325	0.0335	0.0321
Without tracer injection	0.0354	0.0451	0.0307
$\boldsymbol{k_w}$ values are 3 times of base $\boldsymbol{k_w}$	0.0406	0.1064	0.0881

CONCLUSIONS

The impacts of a tracer test on parameter estimations and uncertainty are analyzed in this paper. Analyses include varying tracer test conditions including tracer injection timing, magnitudes of measurement errors and a sensitivity of the tracer test has also been performed. Results show that without tracer injection, parameter can be estimated with less accuracy which can result higher prediction uncertainty.

Acknowledgement. Authors sincerely thank Surface Water Group of Tetra Tech. Inc. for their supports to present the paper in EWRI, ASCE 2009 conference.

REFERENCES

Bard, Y. (1974). Nonlinear parameter estimation, Academic, San Diego.

Boccelli, D. L., Shang, F., Uber, J. G., Orcevic, A., Moll, D., Hooper, S., Maslia, M., Sautner, J., Blount, B., and Cardinali , F. (2004). "Tracer tests for network model calibration." *Critical transitions in water and environmental resources management, Proceedings of the 2004 Conference,* ASCE.

Bush, C. and Uber, J. G. (1998). " Sampling design methods for water distribution model calibration." *Journal of Water Resources Planning and Management*, ASCE, 124(6), 334-344.

Clark, R. M., Rossman, L. A., and Wymer, L. J. (1995). ''Modeling distribution system water quality: regulatory implications.'' *Journal of Water Resources Planning and Management*, ASCE, 121(6), 423–428.

Eusuff, M., Lansey, K., and Pasha, M. F .K. (2005). "Shuffled Frog Leaping Algorithm (SFLA): A Memetic Meta-heuristic for Discrete Optimization." *Journal of Engineering Optimization* (in press).

Eusuff, M. and Lansey, K. (2003). "Optimization of Water Distribution Network Design using the Shuffled Frog Leaping Algorithm". *Journal of Water Resources Planning and Management*, ASCE, 129(3), 210-225.

Lansey, K. E., and Basnet, C. (1991). "Parameter Estimation for Water Distribution Networks." *Journal of Water Resources Planning and Management*, ASCE, 117(1), 126-144.

Lansey, K. E., El-Shorbagy, W., Ahmed, I., Araujo, J., and Haan, C. T. (2001). "Calibration assessment and data collection for water distribution networks." *Journal of Hydraulic Engineering*, ASCE, 127(4), 270-279.

Mallick, K. N., and Lansey, K. E. (1994). ‘‘Determining optimal parameter dimensions for water distribution network models.’’ *Proc., Water Resour. Plng. and Mgmt. Conf.,* ASCE, New York.

Munavalli, G. R., and Mohan Kumar, M. S. (2005). “Water quality parameter estimation in a distribution system under dynamic state.” *Journal of Water Research*, 39(2), 4287-4298.

Munavalli, G. R., and Mohan Kumar, M. S. (2003). “Water quality parameter estimation in a steady state distribution system.” *Journal of Water Resources Planning and Management*, ASCE, 129(2), 124-134.

Pasha, M. F. K, and Lansey, K. E. (2008). “Water quality parameter estimation for water distribution systems.” *Journal of Civil Engineering and Environmental Systems*, first published on 14 August 2008..

Pasha, M. F. K, and Lansey, K. E. (2005). “Analysis of uncertainty on water distribution hydraulics and water quality.” Proceedings of the ASCE World Water and Environmental Resources Congress, May 15-19, 2005, Anchorage, Alaska, USA.

Ormsbee, L. E. (1989). "Implicit Pipe Network Calibration." *Journal of Water Resources Planning and Management*, ASCE, 115(2), 243-257.

Rossman, L. A. (2002). *Epanet User’s Manual, Environmental Protection Agency*, EPA, Cincinnati.

Todini, E. (1999). "Using a Kalman Filter Approach for Looped Water Distribution Network Calibration." *Water Industry Systems: Modelling and Optimisation Applications*. Research Studies Press Ltd., Exeter, United Kingdom, 1.

Vasconcelos, J.J., Rossman, L.A., Grayman, W.M., Boulos, P.F., Clark, R.M., 1997. “Kinetics of chlorine decay.” *Journal AWWA*, 89 (7), 55–65.

Wu, Z. Y., Boulos, P. F., Orr, C. H., and Ro, J. J. (2000). "An Efficient Genetic Algorithms Approach to an Intelligent Decision Support System for Water Distribution Networks." *Proceedings of the Hydroinformatics Conference*, Iowa.

Yeh, W. W.-G., and Yoon, Y. (1981). ‘‘Aquifer parameter identification with optimal parameter dimension.’’ Water Resour. Res., 17(3), 664–672.

A Hybrid Heuristic Search Approach for Contaminant Source Characterization

Li Liu, E. Downey Brill, G. (Kumar) Mahinthakumar, S. Ranji Ranjithan

Department of Civil, Construction, and Environmental Engineering,
North Carolina State University, Raleigh, North Carolina 27695;
email: {lliu2, brill, kumar, ranji}@ncsu.edu

ABSTRACT

The rapid discovery of the contaminant source and its mass loading characteristics in a water distribution system (WDS) is vital for generating an efficient control strategy during a contamination event. Previous work on the Adaptive Dynamic OPtimization Technique (ADOPT), which was developed as an Evolution Strategy (ES) based procedure, presents an approach to estimate the source characteristics adaptively, given dynamically updated observation data. Although this simulation-optimization approach is promising, it is computationally expensive, which poses challenges in the context of real-time solutions. This paper reports the findings of an investigation that builds upon the prior work by introducing a hybrid heuristic search method for the real-time characterization of a contaminant source. This new method integrates the ES-based ADOPT with a logistic regression (LR) analysis and a local improvement method to expedite the convergence and possibly solve the problem quickly. As a prescreening technique, a LR analysis step is performed prior to ADOPT; this step reduces the search space by eliminating unnecessary source nodes as potential source locations. Then, a local search (LS) approach is embedded into some of the algorithmic steps in ADOPT to serve as a postscreening step that potentially speeds up the convergence in localized regions in the solution space. Numerical experiments for the proposed hybrid approach are performed on an example water distribution network, and the results are compared with those of the standard implementation of ADOPT.

INTRODUCTION

Water distribution systems (WDSs) are highly susceptible to various threat attempts, including physical attack, cyber-disruption, and biochemical contamination (Clark and Deininger, 2000). Intentional biochemical contamination has become a major concern recently due to its inherent complexities and the potential hazard to human health. To enhance the response capability in the case of a contamination event, one protective step that should be taken is the installation of monitoring stations within the WDS to measure abnormal water quality resulting from the pollutants. While real-time measurements are collected at these stations, the contaminant source must be determined swiftly to facilitate appropriate decisions in response to the threat. Contaminant sources are typically characterized by the

injection location, starting time, duration, and mass injection rates that correspond to different time intervals.

Contaminant source characterization can be deemed as an inverse problem, the solutions of which are typically ill-posed (e.g., non-existence, instability, or non-uniqueness). Non-existence occurs when no solution exists, given available observations. Instability is caused by the sensitivity of inverse solutions to the observations. Non-uniqueness can be caused by insufficient data when different solutions yield similar explanations for the observations. These ill-posed solutions create challenges, especially in the context of system uncertainties and the need for rapid identification.

One way to address these issues is to formulate the problem as an optimization problem by making use of currently available observation data to inversely seek the best source characteristics. This approach may yield a good explanation for the obtained water quality samples. Most efforts that have been made to solve such a problem use optimization methods to discover the true source information by minimizing the deviation between the observed output from the sensors and the calculated concentration values. Such efforts include direct methods (e.g., Van Bloemen Wannders et al., 2003; Laird et al., 2005) and heuristic-based simulation-optimization approaches (Guan, 2006) that constitute the focus of this research due to their flexibility and robustness. In Liu et al. (2006), the ES-based ADOPT is employed to search for a set of contaminant source characteristics that may result in similar sensor observations. Although ADOPT has shown promise for its dynamically adaptive capability, the simulation-optimization approach suffers because it requires numerous computationally expensive simulations to adaptively recover the contaminant characteristics. The significant computational costs would unavoidably impact not only the identification time but also the resultant solution quality. Thus, to minimize the number of simulations and maintain acceptable accuracy, ADOPT has been enhanced by incorporating techniques that can expedite the solution.

In this paper, an algorithmic framework is introduced for solving a WDS contaminant source characterization problem by integrating ES-based ADOPT with one prescreening and one postscreening technique. The objective of a prescreening technique is to narrow the solution space. While the search is gradually converging to local regions, a postscreening technique is embedded into ADOPT to promote its local convergence capability.

PROBLEM STATEMENT

Given increasingly available observations, a contaminant source characterization can be constructed as a dynamic optimization problem. The objective function is calculated by minimizing the difference between the estimated concentration values and the currently available data, which are time-dependent. The primary goal is to quickly estimate the source characteristics that best explain the observed data at hand. The following mathematical formulation is defined to determine the source location, starting time, and corresponding mass loading history

at any time after the first detection of contamination. Although this definition assumes that the contamination is introduced at only one node in the network, the same model can be extended to consider multiple contamination source locations.

Find $\{L,\ M_{t_c}\ ,\ T_0\}$

$$\text{Minimize } F = \sqrt{\frac{\sum_{t=t_0}^{t_c}\sum_{i=1}^{N_s}(C_{it}^{obs} - C_{it}(L, M_{t_c}, T_0))^2}{N_s * t_c}} \tag{1}$$

where

F = prediction error;
L = contaminant source location;
T_0 = starting time of the contamination event;
t_0 = time of the first detection of the contamination at the sensors;
t_c = current time step;
$M_{t_c} = \{m_{T_0}, m_{T_0+1}, \cdots, m_{t_c}\}$, represented as a vector of mass injected at the source from time T_0 to t_c;
C_{it}^{obs} = the observed concentration at sensor i at time step t;
$C_{it}(L, M_{t_c}, T_0)$ = model (i.e., EPANET)-estimated concentration value at sensor i at time step t;
i = sensor location;
t = time step of observation; and
N_s = total number of sensors.

SOLUTION APPROACH

ES-based ADOPT. Two major challenges that must be faced when addressing a contaminant source characterization problem are: 1) continuously tracking the optimal solutions in dynamic environments, and 2) capturing the potential non-unique solutions that could provide similar explanations to the observations over time. To tackle these challenges, ES-based ADOPT was developed to search for potential solutions that are as different as possible from each other by exploring the decision space through multiple subpopulations. To set a benchmark for the best possible solution, one of the subpopulations searches independently for the solution that best fits the observations. The remaining subpopulations use that benchmark to find other possible solutions that fit the observations equally or nearly as well as the best solution. This procedure is executed for each observation time step. When new information becomes available, the solutions from the previous time step can be adapted to the new environment, if it is assumed that the observation data resulting from one contamination event. Therefore, the number of remaining subpopulations can be adapted according to the dynamic environments. The algorithm terminates when no more available information or only one subpopulation remains. The key steps of this approach are outlined as follows (Liu et al., 2006):

Step 1. Create an initial set of random solutions, equally divided among N subpopulations.

Step 2. Increment time step as t ← t + 1. Set generation index as g = 0. Update monitoring data with additional measurements and construct the prediction error function.

Step 2.1. Increment generation index as g ← g + 1. In the first subpopulation (p = 1), evaluate the fitness based on the prediction error. In other subpopulations (p = 2, 3,…N), evaluate the fitness based on the prediction error and its distance from all other subpopulations.

Step 2.2. In each subpopulation, apply selection and mutation operators, and create a new set of solutions.

Step 2.3. If stopping criterion (i.e., g < max no. of generations) is not met, then go to Step 2.1; otherwise, go to Step 3.

Step 3. Eliminate subpopulations that represent duplicate solutions. If only one subpopulation remains or the current set of solutions is acceptable, then stop.

Step 4. If no more observations are available, then stop; otherwise, return to Step 2.

The efficiency of ES-based ADOPT in characterizing a contaminant source can be improved by eliminating unnecessary nodes as potential source locations. In Liu et al. (2008), a predictive model based on logistic regression (LR) analysis was examined to determine the likelihood that any given node is a source. The resulting location-specific probability values could then be used to reduce the solution space for the optimization search, thus yielding a faster convergence. In addition, as a global optimizer, the ES typically becomes less efficient when the search concentrates on a local region. To further enhance the algorithm's efficiency, a local search (LS) operation is incorporated into ADOPT, which allows the advantage of local fine-tuning.

Logistic Regression Model (LRM). The numerous potential contamination scenarios and system uncertainties collectively contribute to the complexity of source characterization in a contamination event. To offer a fast probabilistic estimation of potential source locations, a linear LRM-based approach was presented in Liu et al. (2008) to model the likelihood of a node as a source, given the sensor observations. The LRM, constructed as follows, describes the relationship between the probability that node i is a source and the observations at time t after the contamination is detected at one or more sensors.

$$\log\left(\frac{p(A_i \mid C_{1t},\cdots,C_{Nt})}{1-p(A_i \mid C_{1t},\cdots,C_{Nt})}\right) = b_{0t} + b_{1t}C_{1t} + \ldots + b_{jt}C_{jt} + \ldots b_{Nt}C_{Nt}\,, \tag{2}$$

where $p(A_i \mid C_{1t},\cdots,C_{Nt})$ denotes the likelihood of the contaminant introduced at node i, given the observations at time t; A_i represents the contaminant entering through node i; (b_{0t}, …, b_{Nt}) are the regression coefficients obtained by the maximum likelihood procedure; and (C_{1t}, …, C_{Nt}) denotes the sensor observations at time t.

While knowledge of an existing WDS and its sensor placements allows simulations of contamination events, the LRMs that correspond to each node at each time interval can be pre-identified through a large number of hypothetical contamination events. Once a contamination is detected, the models can rapidly

return the probability estimation. Thus, the strength of a LRM is that it offers a simple and direct way to make a fast prediction of a small set of nodes that are likely candidates to be a source. In this study, the resulting solutions from the LRMs are used to reduce the search space in ADOPT by eliminating unnecessary nodes, which typically have zero probability as calculated by the LRMs.

Heuristic Search Methods. Heuristic search algorithms have received increasing attention due to their potential in tackling complex optimization problems. In addition to the effectiveness of such algorithms, the objective function evaluation is the only information required to direct the search during the iterative process. This advantage allows wider applications to a variety of complicated problems by coupling search algorithms to simulation models. Evolutionary algorithms (EAs) (Holland, 1975), as one class of heuristic methods, present a global search (GS) mechanism and are of great benefit for solving large nonlinear optimization problems. Making use of a population-based scheme and particular operators (e.g., crossover, mutation), EAs can discover global optima independently of initial guesswork as well as offer easy parallel implementation (Xu et al., 2001). However, as the population gradually moves towards optimal solutions, the efficiency of EAs typically decreases due to the stochastic property of the search process. In the early stages, and because the large search space inherent to early stages contains potentially better solutions, the EAs are more likely to discover improved solutions. As the search approaches the vicinity of local optima, the chance of finding better solutions decreases, and the search yields a slow local convergence (Xu et al., 2001; Gen & Chen, 1997). In contrast, LS approaches, such as the Hooke-Jeeves pattern search and the Nelder-Mead Simplex (NMS) method, focus mainly on locating locally better solutions by using a deterministic strategy, even though these methods are somewhat sensitive to the initial starting points.

Recently, some researchers have investigated hybrid heuristic approaches (i.e., the hybridization of a LS and a GS procedure) that are more likely to be efficient because they take advantage of both capabilities. The methods reported previously can be classified into three categories. The first one employs a GS procedure followed by a LS process (Partheepan, 2003; Espinoza et al., 2005; Mahinthakumar & Sayeed, 2005; and Yeh et al., 2007), where the GS discovers globally promising regions, the subsequent LS continually moves the resulting good solutions towards the optimum. An enhanced solution thus can be acquired through increased computational efforts associated with the LS procedure. The LS does not benefit the GS in this case, however. The second category alternately applies GS and LS procedures (e.g., Espinoza et al., 2005; Hart, 1994; and Land, 1998) whereby the two search procedures support each other. Although this category has the potential to achieve a high solution quality and computational efficiency, the parallel implementation of such an approach is inefficient. The third category of methods embeds a local optimizer into a GS as a genetic operator. One such approach, introduced by Xu et al. (2001), couples a micro genetic algorithm (GA) with the LS to generate two new solutions in place of the two worst solutions using the pattern move operator. Another approach, proposed by Partheepan (2003) links the GA with the NMS method by performing the reflection step as a new operator during the GA evolution process.

Overall, the embedment of the LS into the GS does not yield additional fitness evaluations. This factor is valuable, particularly in the context of complex real-world optimization problems that require time-consuming simulation runs.

Most discussions associated with the hybrid heuristic search methods focus on ways to maximally improve the solution quality with low computational costs. This problem introduces several questions, such as which LS procedure to use, the frequency of the LS, the time that the LS is performed, the way of selecting individuals to conduct the LS, etc. Different LS procedures may bring about quite different solutions. If too many LS procedures are incorporated into a GS, local convergence may result. In addition, it is worth noting that selecting inappropriate solutions or conducting a LS at an improper time can bias the direction of the GS (Hart, 1994; Land, 1998). This paper investigates a hybrid model by embedding a local optimizer into the ES-based ADOPT for characterizing a WDS contaminant source.

Algorithm Framework. Figure 1 shows the framework of the hybrid LRM-ADOPT-LS, starting with the LR analysis. At time step t, when the initial detection occurs, the LRMs input the concentration data collected by the sensors and output the probability of each node as a possible source. This process screens the candidate set, which is composed of nodes with non-zero probability values, for potential source locations. Specifically, the candidate set is employed in the subsequent initialization and mutation operations.

The combination of the ES-based ADOPT with a LS procedure is then applied to determine the source characteristics (i.e., contamination location, start time, duration and mass loading profile). In this phase, the ES-based ADOPT focuses on exploring promising regions, while the LS exploits local characteristics to expedite the convergence in localized regions. In addition to achieving a faster convergence without the expense of additional fitness evaluations, this hybrid search is expected to avoid premature convergence by embedding the pattern move simultaneously within multiple subpopulations. The incorporation of a LS operator into ES-based ADOPT is described in two steps as follows:

Step 1. Assess the need for the LS operator in each subpopulation. Subsequent to the selection operation, assess the necessity of the local optimizer. This process relies on the extent of the convergence of individuals. LS operations that are too numerous or performed too early may lead to premature convergence. Therefore, the LS operator is applied in a subpopulation when the following two conditions are met: 1) The proportion of individuals located at the same node exceeds a specified threshold (denoted as α); 2) The best individual locates at a different node from those in other subpopulations or is better than those in other subpopulations if they are at the same location.

Step 2. Perform the heuristic pattern move. In a subpopulation, the heuristic pattern move is carried out when the current convergence of individuals suggests its necessity. Based on the approach introduced by Xu et al. (2001), the pattern move operates around the current optimum to search for improved solutions.

Step 2.1. Sort individuals according to the prediction error function.
Step 2.2. Record the indices of the best, second best, worst, second worst, and third worst individuals for the same location.
Step 2.3. Generate three new individuals through the linear combination of the best and second best individuals. If I_b represents the optimum, and I_{sb} corresponds to the second best individual with a slightly worse objective value, the new individual $I_{new} = I_b + \beta(I_b - I_{sb})$ is constructed. β is the pattern move step size. (0.2, 0.5, and 1.0 are used in this study.)
Step 2.4. Replace the three worst individuals with the newly generated individuals.

Finally, this hybridization process is repeated over time. At each time step, this procedure leads to a set of possible solutions that is able to match the sensor observations within a specified range of prediction error. With increasingly available measurements, the set of alternatives reduces in number, and eventually reaches a single solution when sufficient sensor information is available. The identified single solution or a set of alternatives is expected to contain the true source. The algorithm terminates when one subpopulation or no additional measurements remain.

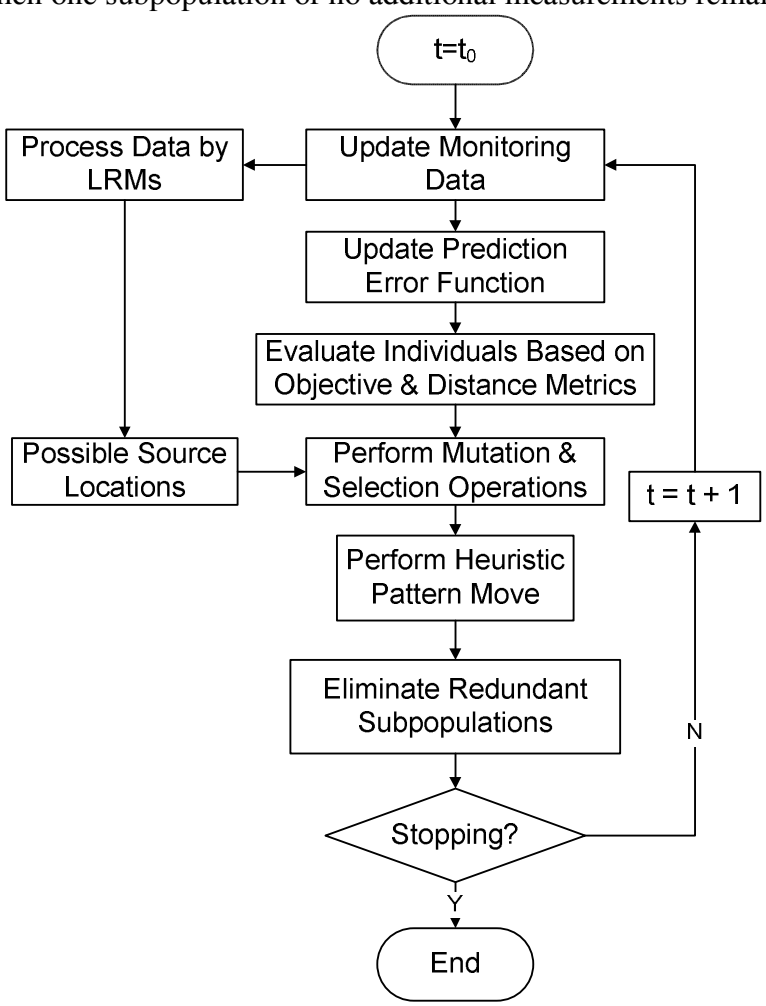

Figure 1. LRM-ADOPT-LS optimization framework.

APPLICATIONS

To test the improvements provided by the LRM and LS, several contamination scenarios in two different WDS networks work studied. In this paper, the results of only two illustrative scenarios are presented. Scenario 1 assumes the intentional intrusion of the contaminant into a small water network. This network is one of the problem scenarios in the EPANET software (Rossman, 2000) and is comprised of 2 sources, 3 tanks, 97 nodes, and 117 pipes. The configuration of this network is depicted in Figure 2(a). Four ideal sensors are randomly placed within the network. A conservative contaminant enters the system through node #267 (denoted as a triangle in Figure 2(a)) at 10:00 a.m., and the event lasts one hour at the time-varying injection rates of 50, 60, 90, 80, 70, 40 g/min, each of which corresponds to a 10-minute interval. The first detection occurred at 12:20 p.m. by sensor S3. No non-zero concentration data were obtained at the other sensors during the observation period. This scenario is used as the baseline in the following discussions.

Scenario 2 represents a contamination event in a large network. This network contains 1574 junctions, 1415 pipes, 8 pumps, 2 reservoirs, and 1 tank. This network was developed for the micropolis virtual city with 5,000 residents, further details of which can be found in Brumbelow et al. (2007). The locations of five ideal sensors are chosen at random within the entire network (see Figure 2(b)). The contaminant entered the network through node VN1468 at the rates of 80, 70, 60 g/min for a duration of 0.5 hour. The contamination was initially detected at sensor S2 after 6.5 hours had elapsed since the first release of contamination. In addition to sensor S2, non-zero concentration data were observed at sensors S2 and S3 during the monitoring period.

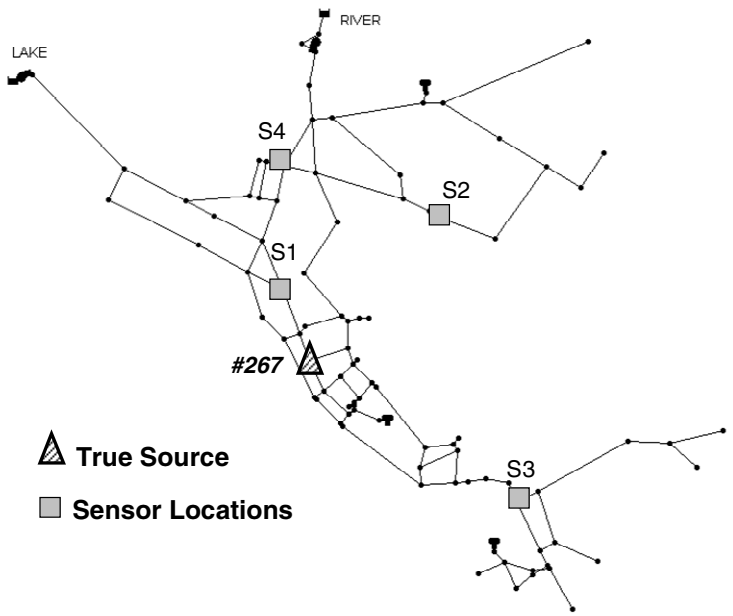

(a)

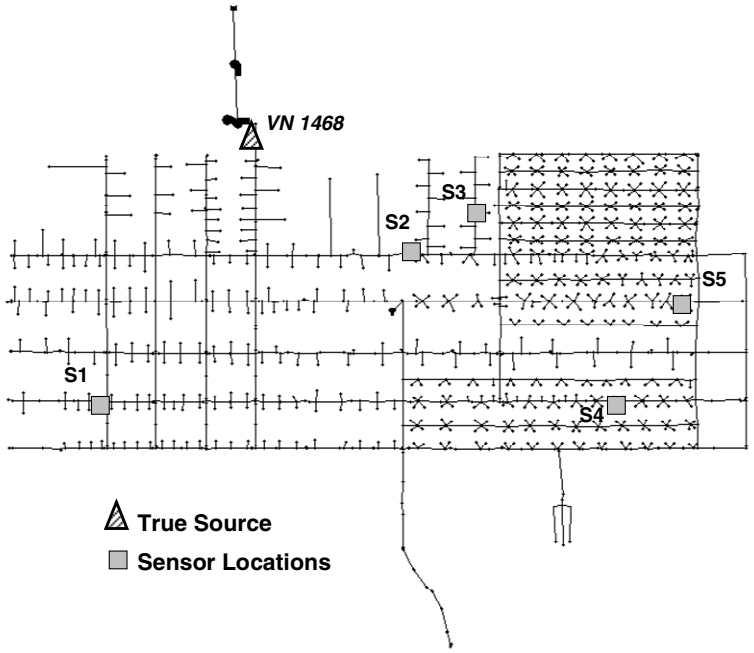

(b)

Figure 2. Layout of the example networks. The triangle represents the injection node, and the square designates the sensor location: (a) Scenario 1; (b) Scenario 2.

SUMMARY

To help better understand the enhancements associated with the LRMs and the LS, a set of experiments were carried out with different enhancements added to ADOPT on the basis of the two scenarios described. The algorithm performance was evaluated in terms of the solution quality as well as the computational costs. In addition to yielding a better understanding of these enhancements, the case studies investigated the performance sensitivity to the coupling strategies along with the mutation sizes. Different strategies of LS selection were investigated to determine the optimal approach to enable the function of the LS. Also, the analysis by looking at the effect of mutation sizes was performed on the solutions when ADOPT is coupled with the LRM and LS. Results from these investigations indicate that the proposed method is able to identify consistently a set of nodes that includes the true source location, and reach this solution state in a computationally more efficient manner compared to the use of just ADOPT.

REFERENCE

Brumbelow, K., J. Torres, S. Guikema, E. Bristow, and L. Kanta. (2007). "Virtual Cities for Water Distribution and Infrastructure System Research." In *Proceedings of World Environmental and Water Resources Congress*, Tampa, Florida, May 15-19.

Clark, R. M. and R. A. Deininger. (2000). "Protecting the Nation's Critical Infrastructure: The Vulnerability of U.S. Water Supply Systems." *Journal of Contingencies and Crisis Management*, 8 (2).

Espinoza, F. P., B. S. Minsker, D. E. Goldberg. (2005). "Adaptive Hybrid Genetic Algorithm for Groundwater Remediation Design." *Journal of Water Resources Planning and Management*, 131 (1): 14-24.

Guan, J., M. M. Aral, M. L. Maslia, and W. M. Grayman. (2006). "Identification of Contaminant Sources in Water Distribution Systems Using Simulation–Optimization Method: Case Study." *Journal of Water Resources Planning and Management*, 132 (4): 252-262.

Hart, W. E. (1994). "Adaptive Global Optimization with Local Search." Ph.D. Thesis, University of California, San Diego.

Holland, J. H. (1975). Adaptation in Natural and Artificial Systems. Ann Arbor, MI: University of Michigan Press.

Laird, C. L., L. T. Biegler, B. G. Van Bloemen Waanders, and R. A. Bartlett. (2005). "Contamination Source Determination for Water Networks." *Journal of Water Resources Planning and Management*, 131 (2): 125-134.

Land, M. W. S. (1998). "Evolutionary Algorithms with Local Search for Combinatorial Optimization." Ph.D. Thesis, University of California, San Diego.

Liu, L., E. D. Brill, G. Mahinthakumar, and S. Ranjithan (2008). "Contaminant source characterization using logistic regression and local search methods." In *Proceedings of the ASCE/EWRI World Water & Environmental Resources Congress*, Honolulu, Hawaii.

Liu, L., E. M. Zechman, E. D. Brill, G. Mahinthakumar, S. Ranjithan, and J. Uber. (2006). "Adaptive Contamination Source Identification in Water Distribution Systems Using an Evolutionary Algorithm-based Dynamic Optimization Procedure." In *Proceedings of Water Distribution Systems Analysis Symposium*, Cincinnatti, OH.

Mahinthakumar, G. K. and M. Sayeed. (2005). "Hybrid Genetic Algorithm – Local Search Methods for Solving Groundwater Source Identification Inverse Problems." *Journal of Water Resources Planning and Management*, 131 (1): 45-57.

Partheepan, R. (2003). "Hybrid Genetic Algorithms." M. Sc. Thesis, North Carolina State University, Raleigh, NC.

Rossman, L. A. (2000) EPANET User's Manual. Risk Reduction Engineering Laboratory, U.S. Environmental Protection Agency, Cincinnati, OH.

Van Bloemen Waanders, B. G., R. A. Bartlett, L. T. Bigler, and C. D. Laird. (2003). "Nonlinear Programming Strategies for Source Detection of Municipal Water Networks." In *Proceedings of the ASCE World Water and Environmental Congress*, Philadelphia, PA, June 23-26.

Xu, Y. G., Li, G. R., Wu, Z. P. (2001). "A Novel Hybrid Genetic Algorithm using Local Optimizer based on Heuristic Pattern Move." *Applied Artificial Intelligence*, 15: 601-631.

Yeh, H. D., T. H. Chang, Y. C. Lin. (2007). "Groundwater Contaminant Source Identification by a Hybrid Heuristic Approach." *Water Resources Research*, 43, W09420.

Analysis of Model Sensitivity and Uncertainty for Chlorine Transport and Decay in a Water Distribution System

W. J. Dawsey[1], B. S. Minsker[2], and A. Ostfeld[3]

[1]Illinois State Water Survey, Institute of Natural Resources Sustainability, University of Illinois; 2204 Griffith Drive, Champaign, IL 61820-7495; Phone: 217-244-8856; dawsey@illinois.edu.
[2]Department of Civil and Environmental Engineering & National Center for Supercomputing Applications, University of Illinois; 3230d Newmark Lab, MC-250 205 N. Mathews Ave., Urbana, IL 61801; Phone: 217-265-5293; minsker@illinois.edu.
[3]Faculty of Civil and Environmental Engineering, Technion–Israel Institute of Technology, Haifa 32000, Israel; Phone: +972-4-8292782; ostfeld@tx.technion.ac.il.

ABSTRACT

There are a number of sources of uncertainty in drinking water distribution system modeling. Uncertain parameters include pipe diameters, consumer demands, hydraulic energy loss coefficients, reaction coefficients and others. Understanding the relative importance of these sources of uncertainty can improve the allocation of resources for model refinement and calibration, as well as, aid knowledge inference from monitoring data. This paper presents an analysis of uncertainty and model sensitivity for chlorine transport and decay in a water distribution system. A clustering and global variance-based sensitivity methodology is proposed to account for spatial inconsistencies found in the results of previous studies of this problem. Results are presented from small and large scale case studies.

This methodology is then used to explore the occurrence of intrusion events in a water distribution system, and the potential to detect such events through online monitoring of chlorine residual concentrations. Noise present in the chlorine monitoring signal has the potential to overwhelm the detection of an upstream intrusion and its associated chlorine demand. Results are presented from simulated intrusion events of varying magnitude and duration.

INTRODUCTION

There are a number of sources of uncertainty in drinking water distribution system modeling. These include, pipe diameters, consumer demands, hydraulic energy loss coefficients, solute reaction coefficients, and others. These parameters can be grouped into two categories. Aleatory uncertainty is inherent to stochastic processes such as rainfall in Hydrology or in this case, consumer demands on a drinking water system. Epistemic uncertainty occurs when processes are unknown or poorly represented by mathematical models. An example of epistemic uncertainty is the variability that occurs in bulk first-order decay coefficients for free within a water distribution system. In this case, a single species first-order decay model does not accurately represent interactions with other species and pipe walls. Thus, the

analysis of uncertainty in any system is highly dependent on the model form and sophistication. Understanding of model uncertainty can be useful in allocating resources to model calibration and exploring novel approaches to modeling.

The objective of this paper is to better understand the sources of uncertainty in water distribution system modeling so that better modeling and monitoring methodologies can be developed. One potential monitoring approach is to use chlorine residual as an indicator of intrusion events. Through the introduction of chlorine demanding species, intrusion events can change the residual chlorine profile in a pipe network. If such a change were detected by a monitoring system, then appropriate response actions could be taken by water system operators to protect public health and restore network integrity. However, variability in network hydraulics and chlorine decay could obscure the detection of such a chlorine demand event. Previous studies have not fully characterized the relative importance of the various sources of uncertainty in this modeling problem.

A methodology is proposed for evaluating the relative effects of uncertain inputs on residual chlorine concentration at a monitoring node. Nodes are divided into upstream and downstream observational pairs that are then clustered into experimental units by mean travel time and node location. These experimental units define spatially and hydraulically similar regions of the network. Latin hypercube sampling and simulation of network hydraulics and chlorine transport using EPANET are proposed for both the undisturbed model condition and a chlorine demand event condition. Simulations are performed for a set of randomly sampled node pairs within each experimental unit. Independent uncertain inputs include nodal demand, pipe diameter, roughness, bulk chlorine reaction coefficient, and wall reaction coefficient. The first step of the sensitivity analysis is to screen input parameters using the Morris method (Saltelli, 2004) to eliminate those that negligibly influence output uncertainty and identify potential interaction effects. The second step is to apply a variance-based sensitivity analysis to determine the sensitivity indices for each input parameter. First-order indices and total sensitivity indices are calculated for each parameter. Higher order indices representing interactions between multiple parameters are calculated as suggested by the results of the Morris screening test. Indices are determined for each experimental unit and aggregated to characterize the total system sensitivity. The chlorine demand event simulations will explore a range of different magnitude chlorine reductions and the effect on downstream monitoring nodes relative to other uncertainties.

BACKGROUND

Uncertainty in water distribution system modeling has for the most part been a secondary topic of study in the research literature. There are several studies that utilize one or two uncertain inputs in developing models of hydraulic reliability (Wagner et al. 1988a and 1988b), optimal design (Lansey et al, 1989), solute fate and transport (Khamal, 2006), optimal monitoring (Jankovic et al., 2007), and to evaluate sensitivity methodologies (Kang et al. 2007). These studies contain some information about the output response to uncertainty in the selected input(s). However, there are very few studies that attempt to quantify the relative importance of multiple uncertain

inputs, and only one Pasha and Lansey (2005) attempt to do so for the case of fate and transport.

Table 1 presents a matrix of model characteristics and the relevant research literature. It is evident from this table that most of the studies have investigated uncertainty in hydraulic input parameters including nodal demand and pipe roughness coefficient. Simulation techniques such as Monte Carlo sampling and analytical approaches such as first order second moment (FOSM) are equally represented in the literature. There are a limited number of papers that have investigated uncertainty in water distribution systems water quality.

Wagner et al (1988a) and Wagner et al. (1988b) present a simulation and an analytical methodology, respectively, for modeling distribution system reliability subject to randomized mechanical failures of network components. Lansey et al. (1989) proposed a chance constrained model to minimize design cost taking into account uncertainties in pipe roughness, demand, and mechanical failure. Xu and Goulter (1999) also proposed a model to optimize design cost and reliability using the same uncertain inputs. Both of these papers utilized first order analytical methods for approximating model output response to input uncertainties. Neither paper makes assertions about the relative importance of input uncertainties.

Bao and Mays (1990) utilized Monte Carlo simulations to determine the effects of uncertainty in demand, pipe roughness, and pressure heads on reliability. Nodal reliability was defined as the probability that flow at a node will meet demand flows at a minimum pressure. The authors found that the choice of probability distribution for input parameters had a significant effect on nodal reliability, and that demand exerted a greater influence on outputs than did pipe roughness (Bao and Mays, 1990). Kapelan (2005) compared a sampling method with a deterministic integral approximation of the uncertain model response for the least-cost design problem. Demand was the only uncertain input for this study. Babayan (2005) proposed a cross entropy approach for multiobjective optimization of distribution system design with uncertain demand and roughness parameters. Babayan (2006) compared an integration based method with Latin hypercube sampling for solving the stochastic optimization design problem for water distribution systems. Again, demand and roughness were uncertain input parameters.

Kang et al. (2007) compared Monte Carlo and Latin hypercube sampling methods with a first order second moment analytical approach for estimating chlorine response to uncertain demand inputs. Sampling methods were found to be more accurate for unsteady flow conditions and the nonlinearities that occur due to flow reversals. First order methods were unable to approximate such nonlinear behavior. Demand was the only uncertain input parameter for this paper. Branisavljevic and Ivetic (2006) proposed a fuzzy approach for uncertainty analysis in a water distribution system. This method does not require the specification of an exact input probability distribution, but rather uncertainty is represented by fuzzy set mapping of input parameters. Outputs were found to be sensitive to the interval over which the fuzzy input set was specified. Pipe roughness was the only uncertain input parameter, and pressure head was the output.

Jankovic et al. (2007) describe a stochastic model for estimating network flows and heads from uncertain demand inputs in order to identify locations for

leakage monitoring. Monte Carlo simulations were used with EPANET to determine output response. Kapelan et al. (2007) proposed a novel analytical method for mapping uncertain input parameters to a set of output calibration data. The probability distributions for a set of input parameters were approximated using Bayesian recursive algorithm. The only uncertain inputs considered by Kapelan et al. (2007) were roughness coefficients.

Two papers in the water distribution system research literature have considered uncertainty analysis for water quality parameters. Khamal et al. (2006) modeled the injection and transport of a conservative solute and introduced an exposure index to quantify the downstream effects for consumers. A generalized sensitivity analysis was performed to determine system response to uncertainty in base demand, storage capacity, injection mass and injection duration. Base demand and injection mass were identified as the input parameters with the greatest influence on exposure index. Latin hypercube sampling coupled to EPANET simulation were used to evaluate system response. Lansey et al. (2005) modeled decay and transport in a water distribution system subject to uncertain demands, bulk decay coefficient, wall decay coefficient, pipe roughness, and pipe diameter. Monte Carlo sampling and EPANET simulation were used to determine the output pressure and chlorine concentration at each node. Results shown at three monitoring nodes suggest that wall decay coefficient, bulk decay coefficient, demand and pipe roughness all exhibit a large influence on output values, with each input taking precedence at different monitoring locations.

The following system of equations is utilized by the EPANET model for hydraulics and water quality in water distribution systems. Additional details may be found in Rossman (2002). Continuity and conservation of energy in a pipe network require that,

$$\sum_j Q_{ij} = D_i \tag{1}$$

and,

$$H_i - H_j = h_{ij} \tag{2}$$

where,
Q_{ij} = pipe flow between nodes *i* and *j*,
D_i = demand at node *i*,
H_i and H_j = total head at nodes *i* and *j* respectively, and
h_{ij} = head loss in the pipe between nodes *i* and *j*.

The head loss may be estimated using the Hazen-Williams equation (US customary units),

$$h_{ij} = K\left(\frac{Q_{ij}}{C}\right)^{1.852} \frac{L_{ij}}{D_{ij}^{4.87}} \tag{3}$$

where,
K = constant,
C = Hazen-Williams roughness coefficient,
L_{ij} = length of pipe between i and j, and
D_{ij} = diameter of pipe between i and j.

Table 1. Matrix of water distribution system uncertainty analysis research literature

		Wagner et al., 1988a	Wagner et al., 1988b	Lansey et al., 1989	Bao and Mays, 1990	Xu and Goulter, 1999	Kapelan et al., 2003	Barkdoll and Didigam, 2004	Babayan et al., 2004	Babayan et al., 2005	Pasha and Lansey, 2005	Babayan et al., 2006	Branisavljevic and Ivetic, 2006	Khamal et al.,2006	Kang et al.,2007	Kapelan et al., 2007	Jankovic et al., 2007
Solute	Chlorine							X			X				X		
	Conservative													X			
	None	X	X	X	X	X	X		X								
	Other																
Uncertain Input Hydraulic Parameters	Nodal demand			X	X	X	X	X	X	X	X	X		X	X		X
	Roughness			X	X	X		X		X	X	X	X			X	
	Pipe diameter							X			X						
	Solute loading condition													X			
	Storage capacity													X			
	Mechanical failure	X	X	X		X											
Uncertain Input WQ Parameters	Wall react. coef.										X						
	Bulk react. coef.							X			X						
	Wall Mass transfer coef.																
	Loading condition																
Input Spatial independence	Full	X	X		X	X	X				X				X		
	Some													X			
	None																
Methodology	Simulation	X			X		X	X	X	X	X	X		X	X	X	X
	Analytical			X		X	X	X	X	X		X			X		
	Other		X							X			X				
Output	Solute Concentration							X			X			X	X		
	Pressure	X	X		X	X		X	X	X	X	X	X		X	X	X
	Reliability	X	X	X	X	X											
	Cost					X	X			X		X					

Solute fate and transport in the distribution system model can be represented by the following set of relationships for a first order decay model with bulk and wall reaction components (Rossman, 1994).

$$\frac{\partial C_i}{\partial t} = -u_i \frac{\partial C_i}{\partial x} + r(C_i) \tag{4}$$

where,
C = concentration
u = average flow velocity
x = longitudinal direction of pipe
t = time

i = pipe index
$r\ (C_i)$ = reaction rate ($M \cdot L^{-3} \cdot T^{-1}$) as a function of concentration, sum of wall and bulk reactions

$$r_{wall} = -\frac{k_w k_f C_i}{R_h\left(k_w + k_f\right)} \tag{5}$$

where,
k_w = wall decay constant ($L \cdot T^{-1}$)
k_f = fluid mass transfer coefficient ($L \cdot T^{-1}$)
R_h = hydraulic radius, pipe volume/area, or 2/radius

$$r_{bulk} = -\ k_b C_i \tag{6}$$

where,
k_b = bulk decay constant ($L \cdot T^{-1}$)

METHODOLOGY

The approach presented here proposes to accomplish two objectives: 1. extend the results from Lansey et al. (2005) to better understand model sensitivity for the fate and transport problem , and 2. model the occurrence of a chlorine demand event and system response within the context of other sources of uncertainty, a problem that has not been addressed previously in the research literature.

Sensitivity analysis (SA) and uncertainty analysis (UA) are terms that are often confused in the research literature. UA is a forward process to quantify the effect of uncertain inputs on output uncertainty, while SA works backward to ascribe uncertainty in the output to the different sources of uncertainties among the inputs. SA attempts to identify the hierarchy of influence that inputs exert on output variability.

There are a large number of sensitivity analysis methodologies (Saltelli, 2000) that have been applied to varying degrees in the Environmental Engineering domain. Variance-based approaches have been shown to be robust for non-monotonic and non-linear problems such as distribution system modeling (Saltelli, 2000). Storage tanks can create pipe flow reversals in nearby regions of a system, thereby causing abrupt nonlinear changes in the chemical profile of water at affected nodes. Variance-based sensitivity analysis is global in that it characterizes model sensitivity over the entire input parameter space.

Lansey et al. (2005) reported that the relative influence of uncertain input parameters varied with choice of monitoring node, and a different parameter was identified as the most important for the three cases shown. This result suggests that an additional spatially heterogeneous parameter may exist that would allow this source of variance to be separated and explained. In addition, Lansey et al. (2005) performed single fixed and single uncertain parameter simulations for each input, and made inferences about input parameter influence based on the standard deviation of chlorine concentration at monitoring nodes. Using the standard deviation is similar to

variance-based methods, however, first or higher order sensitivity indices that are normalized by the output variance were not calculated.

For this study, input probability distributions are consistent with those from Lansey (2005). Pipe diameter will be sampled from a uniform distribution with an interval range of 0.5 - inches, and all other input parameters will be normally distributed with a coefficient of variation equal to 0.1 (Lansey, 2005). The initial case study will be example network 2 from Rossman (2002). This network has been used extensively in the water distribution system research literature for developing novel methodologies.

Spatial Clustering and Sampling

In order to efficiently characterize the spatial variability of the system, a randomized sample of chlorine injection node and downstream monitoring node pairs is proposed. In the language of experimental design, each node pair is considered to be an observational unit. These node pairs are then clustered using the following characteristics:

t_t , mean travel time between the pair of nodes,
(x_1, y_1), coordinate location of node 1,
(x_2, y_2), coordinate location of node 2, and
r_{ud}, upstream-downstream relationship between nodes.

Upstream-downstream relationship refers to the set of three possible flow states that may occur between nodes: 1. no relationship – flow does not pass between nodes, 2. one node is always downstream throughout the simulation period, and 3. upstream and downstream node switch caused by a reversal of flow between the nodes. A schematic is shown in Figure 1 to demonstrate this idea.

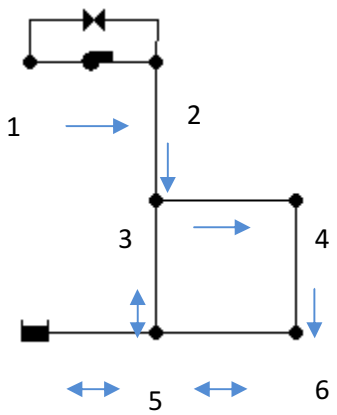

Figure 1. Example network schematic

The matrix shown in Table 2 demonstrates the full set of relationships between nodes in Figure 1. The reason for grouping observational pairs using this criteria is that pairs containing intermediate pathways with flow reversal may exhibit non-monotonic relationships between input and output parameters. Clusters of these six parameters define regions of the node pair space that are hydraulically and

spatially similar. These regions define experimental units that are randomly sampled in order to efficiently characterize the effects of spatial heterogeneity on the results.

Table 2. Matrix of monitoring node pair relationships

	1	2	3	4	5	6
1	n	c	s	c	s	s
2	n	n	s	c	s	s
3	n	n	n	c	s	s
4	n	n	n	n	s	s
5	n	n	s	s	n	s
6	n	n	s	s	s	n

where,
n = no relationship,
c = consistent downstream node
s = switching upstream and downstream node

Morris Screening Method

Screening methods are used to reduce model complexity prior to running exhaustive simulations over uncertain parameters. The Morris method is a means of initially evaluating the influence of inputs to determine if they exert negligible influence, exhibit linearity, or combine to form interaction effects (Saltelli, 2004). The elementary effect for the *i*th input is defined to be:

$$d_i(x) = \frac{\left[y(x_1,...,x_{i-1},x_i+\Delta,x_{i+1},...,x_k)-y(x)\right]}{\Delta} \quad (7)$$

where

y = output
$x = (x_1, x_2,\ldots,x_k)$ set of values selected from set {0, 1/(p-1), 2/(p-1), …, 1},
Δ = a constant value equal to a multiple of 1/(p-1), and
p = the number of input space divisions

The set x is randomly sampled and evaluated until the distribution of elementary effects for input i is found (F_i). The mean and standard deviation of F_i are used to evaluate the relative importance of an input value. The absolute value of d_i may be used in the generation of this distribution for non-monotonic models such as water distribution systems. The mean of F_i is a measure of the input's importance, and the standard deviation indicates non-linearity and interaction effects. These measures are used to refine the model prior to more exhaustive variance-based methods.

Variance-based Sensitivity Analysis

Variance-based sensitivity analysis presumes that variance is a suitable measure of uncertainty in an output. The total variance of the output is attributed to different sources within the set of uncertain input parameters, similar to Analysis of

Variance (ANOVA) techniques in the experimental design literature. The reduction in output variance that occurs if a single input parameter is fixed to its 'true' value is a measure of that parameter's first-order influence. The variance of an output given a single fixed input is,

$$V(Y|P_x = p^t{}_x) \tag{8}$$

where P_x is an uncertain input parameter, Y is the output, $p^t{}_x$ is the true fixed value of the input, V is the variance taken over all input parameters $\neg x$. The true value $p^t{}_x$ is unknown, however, it can be approximated by taking the expected value over P_x:

$$E(V(Y|P_x) \tag{9}$$

The law of total variance states that:

$$V_t = E(V(Y|P_x) + V(E(Y|P_x) \tag{10}$$

where V_t is the total variance of Y over all uncertain parameters. Thus the reduction in the total variance caused by fixing a single input is given by

$$V(E(Y|P_x) = V_t - E(V(Y|P_x) \tag{11}$$

The first order sensitivity index is found by normalizing over the total variance:

$$S_x = \frac{V\left(E\left(Y \mid P_x\right)\right)}{V_y} \tag{12}$$

For water distribution systems, S_x can be determined through Latin Hypercube simulations over all uncertain parameters save the single fixed input. Higher order sensitivity indices represent the interaction effects of multiple parameters. For orthogonal inputs, second order effects are:

$$S_{x1,x2} = \frac{V\left(E\left(Y \mid P_{x1}, P_{x2}\right)\right) - V\left(E\left(Y \mid P_{x1}\right)\right) - V\left(E\left(Y \mid P_{x2}\right)\right)}{V_y} \tag{13}$$

Higher orders are similarly calculated. The total effect ($S_{T,x}$) can be calculated which represents the total contribution of P_x for all orders. A relatively complete picture of a parameter's influence is given by S_x and $S_{T,x}$ and neglecting intermediate orders of interaction (Saltelli, 2004).

Chlorine Demand Simulation

The results of the sensitivity analysis will be used to refine the model and reduce the number of uncertain inputs. The refined model will then be used to estimate the effect of a chlorine demand event on downstream monitoring nodes. Again, monitoring node pairs clustered into similar hydraulic and locational experimental units will be used to characterize the spatial heterogeneity of the model. Random sampling within these units replaces an exhaustive simulation over all nodes.

A chlorine reduction will be simulated at each sampled upstream node. The distribution of chlorine concentration at the downstream node for the chlorine demand scenario will be compared to that of a non-demand scenario at each time step. The statistical difference between these distributions will be estimated. Different magnitudes of chlorine reduction and demand event duration will be simulated in order to determine the severity of event that may be detected. As with

the sensitivity analysis, results will be determined for each experimental unit and aggregated over the full system.

CONCLUSIONS AND NEXT STEPS

This paper presents a methodology to determine a water distribution system model response to uncertain inputs for the chlorine fate and transport problem. It also proposes to model the occurrence of chlorine demand events within the context of other sources of uncertainty. Results from this study will help better understand the potential for chlorine monitoring as an indicator of upstream intrusion events. Results from the methodology presented here also may explain the inconsistent influence that uncertain inputs exhibited on chlorine response shown by Lansey et al. (2005). A clustering and sampling approach for characterizing spatial heterogeneity in water distributions is proposed. The next steps for this study will be to implement conservative solute tracer simulations over the set of uncertain inputs to identify the monitoring pair classifications shown in Table 2 and the mean travel time between pairs. These will be used to cluster pairs into the appropriate experimental blocks.

REFERENCES

Babeyan, A.V., Kapelan, Z.S., Savic, D.A., and Walters, G.A.(2004). "Comparison of two approaches for the least cost design of water distribution systems under uncertain demands." *Proceedings of the ASCE World Water and Environmental Resources Congress, June 27-July 1, 2004,* Salt Lake City, Utah, USA.

Babayan, A.V. ,D. A. Savic, and G. A. Walters (2005). "Multiobjective Optimization for the Last-Cost Design of Water Distribution System Under Correlated Uncertain Parameters". *Proceedings of the ASCE World Water and Environmental Resources Congress 2005, Anchorage, Alaska, USA.*

Babayan, A.V. ,Z.S. Kapelan, D.A. Savic, and G.A. Walters (2006). " Comparison of two methods for the stochastic least cost design of water distribution systems". *Engineering Optimization,* 38(3), 281-297.

Barkdoll, B. D., and Didigam, H. (2004). "Effect of user demand on water quality and hydraulics of distribution systems." *Proceedings of the ASCE World Water and Environmental Resources Congress, June 27-July 1, 2004,* Salt Lake City, Utah, USA.

Bao, Y., and Mays,L.W. (1990)."Model for water distribution system reliability." *Journal of Hydraulic Engineering,* ASCE, 116(9),1119-1137.

Branisavljevic, N.,and M. Ivetic (2006). "Fuzzy approach in the uncertainty analysis of the water distribution network of Becej". *Civil Engineering and Environmental Systems,* 23(3),221-236.

Janković-Nišić,B., N. J. D. Graham, Č. Maksimović, and D. Butler, " Cost-effective leakage reduction through district metering". *Proceedings of the Institution of Civil Engineers: Water Management*, 160(3), 181 – 187.

Khanal, N., Steven G. Buchberger, S. G., and McKenna, S. A., (2006). "Distribution System Contamination Events: Exposure, Influence, and Sensitivity." *Journal of Water Resources Planning and Management*, ASCE, 132(4), 283-292.

Kang,D.S., M.F.K Pasha, and K. Lansey (2007). "Approximate methods for analyzing water quality prediction uncertainty in water distribution systems". *Proceedings of the ASCE World Environmental and Water Resources Congress 2007, Tampa, Florida, USA.*

Lansey, K.E.,Duan, N., Mays,L.W., and Tung, Y.K. (1989)."Water distribution system design under uncertainties." *Journal of Water Resources Planning and Management*, ASCE, 115(5),630-645.

Pasha, M. F. K, and Lansey, K. E. (2005). "Analysis of uncertainty on water distribution hydraulics and water quality." *Proceedings of the ASCE World Water and Environmental Resources Congress, May 15-19, 2005,* Anchorage, Alaska, USA.

Rossman, L. A. (2002). Epanet User's Manual, Environmental Protection Agency, EPA, Cincinnati.

Rossman, L. A., Clark, R. M., and Grayman, W. M. (1994). "Modeling chlorine residuals in drinking-water distribution systems." *Journal of Environmental Engineering*, ASCE, 120(4), 803-820.

Saltelli, A., Tarantola, S., Campolongo, F., and Ratto, M. 2004. *Sensitivity analysis in practice: A guide to assessing scientific models*, Wiley, Chichester, England.

Saltelli, A., Chan, K.,Scot, E., 2000. *Sensitivity analysis,*Wiley, Chichester, England.

Wagner, J.M., Shamir, U., and Marks, D.H. (1988a). "Water distribution reliability: analytical methods." *Journal of Water Resources Planning and Management*, ASCE, 114(3),253-275.

Wagner, J.M., Shamir, U., and Marks, D.H. (1988a). "Water distribution reliability: simulation methods." *Journal of Water Resources Planning and Management*, ASCE, 114(3),276-294.

Xu, C., and Goulter,I. (1999). "Reliability-based optimal design of water distribution networks."*Journal of Water Resources Planning and Management*, ASCE, 125(6), 352-362.

ZS Kapelan, DA Savic, GA Walters (2007). " Calibration of Water Distribution Hydraulic Models Using a Bayesian-Type Procedure". *Journal of Hydraulic Engineering*, ASCE, 133(8), 927-936.

Characterizing reactive contaminant sources in a water distribution system

Jitendra Kumar, E. Downey Brill, G. Mahinthakumar, Ranji Ranjithan,
Department of Civil, Construction and Environmental Engineering
North Carolina State University, Raleigh, NC, USA
{ jkumar, brill, gmkumar, ranji } @ncsu.edu

Abstract

Accurate knowledge of the characteristics of the contamination source during a contamination event is necessary for development of any mitigation and control strategy. Contaminant injected in a system is most likely to be reactive with chlorine; however, it is impractical for water quality monitoring systems to be able to monitor for the presence of all possible contaminants. In any distribution system, chlorine levels and other water quality parameters (pH, conductance, etc.) are routinely monitored to maintain the prescribed disinfection capacity. Any reactive contaminant would affect the chlorine levels resulting in deviations in the expected chlorine levels from those expected under normal operating conditions. Anomalies in the chlorine concentration from that of the expected value can be used as a surrogate to characterize the contaminant source in the system. In the absence of knowing the reactive characteristics of the contaminants, the location of injection, and injection pattern, source identification becomes a difficult problem to solve. Source identification can be posed as an inverse problem. In earlier work authors investigated the effect of the order of reaction kinetics of the contaminant with chlorine and its impact on source identification problem assuming the reaction kinetics to be known. That work is extended to investigate a methodology to address the source identification problem based on chlorine measurements, and the effects of different uncertain contamination conditions. Findings from a range of scenarios will be presented and discussed.

Introduction

Water distribution systems are vital for the supply of safe drinking water to the public. They are prone to accidental or intentional contamination which can endanger the public health. A robust drinking water monitoring program should be able to provide early indication of contamination and minimize the public heath consequences (USEPA, 2005). Also, an early warning system should be able to reliably identify chemical, biological, or radioactive contamination events in source water or distribution systems in time to allow an effective local response to reduce or avoid the potential adverse impacts (ILSI, 1999).

Water distribution system contamination source identification problem has traditionally been approached as an inverse problem. Waanders et al. (2003) used a standard successive quadratic programming approach. An origin-tracking algorithm based on a Lagrangian non-linear programming approach was proposed Laird et al. (2005). Laird et al. (2006) proposed a mixed integer programming-based method for the identification of unique injection scenarios. Zechman et al. (2006) studied the issues related to non-uniqueness in source identification problem, which arises due to the limited availability of the observed water quality data from the sensors in the network. Most of the studies for source identification reported in the literature assume the pollutants to be conservative and a dedicated probe is available to sense that specific contaminant.

In the event of a reactive chemical or biological contamination event, surrogate water quality measurements could be used to source identification. In an earlier work authors (Kumar et al., 2008) used chlorine measurements to characterize the contaminant source location, and examined the effect of the kinetics of contaminant-chlorine reaction on the solution to the source identification problem was investigated. That approach is extended here to investigate the methodology to address the source identification problem using chlorine measurements obtained under uncertain contamination conditions.

Reactive Contaminants

Chlorine is a very commonly used disinfectant in most municipal water distribution systems. Doses of free chlorine are injected in the source water and at other injection nodes to maintain a minimum level of chlorine concentration required as per guidelines to maintain the disinfection capability of water distribution system. Chlorine concentration is routinely monitored in any water distribution system. When a contaminant that is reactive with the chlorine enters the water distribution system, the chlorine concentration in the system would respond according to the contaminant concentration present. Anomaly in the chlorine concentration in the system can be statistically analyzed to issue contamination event alarm (McKenna et al., 2007) and can be used to identify the source characteristics (Kumar et al., 2008). However, the kinetics of reaction between contaminant and chlorine in the water remains unknown during an event. Flow and hydraulic conditions in a water distribution network are highly dynamic, introducing further uncertainties about the interaction of the contaminant with chlorine. Kumar et al. (2008) studied the effect of the order of reaction between arsenic and chlorine on the chlorine concentration level in the system. First and second order reaction kinetics were studied. However, the order of the reaction remains unknown during an event as the type and reactive properties of the contaminant are unknown. This study extends the previous work (Kumar et al., 2008) to develop a methodology for identification of source characteristics for reactive contaminants using chlorine measurements under uncertain conditions.

For the purpose of this study, contamination of water with arsenic (As) is considered. Chlorine is assumed to be present in the form of monochloramine residuals. Arsenic may react with monochloramine leading to the decay of monocloramine as follows.

$$As^{+3} + NH_2Cl \rightarrow AsCl_3 + 3NH_2^+ \tag{1}$$

The reaction system can be solved using the following differential equations:

$$\frac{dAs^{+3}}{dt} = -K_a (As^{+3})^x (NH_2Cl)^y \tag{2}$$

$$\frac{dNH_2Cl}{dt} = -K_b (As^{+3})^x (NH_2Cl)^y - K_c (NH_2Cl)^z \tag{3}$$

where K_a is the decay rate of arsenic (As^{+3}), K_b is the decay rate of monochloramine when arsenic reacts with chlorine in water, K_c is the self decay rate of chlorine, and x, y, and z are the order of reaction of arsenic, monochloramine and self decay of monochloramine in the assumed reaction system. Self decay of monochloramine was assumed to be of first order in the current analysis while the reaction between arsenic and monochloramine was considered to be under first and second order conditions.

Formulation of source identification problem

Anomaly in the chlorine concentration levels in the system can be utilized for the characterization of contamination source. Optimization problem can formulated so as to find solution source with characteristics to match the observed chlorine measurements as accurately as possible. Several different scenarios of optimization problem would be studied using the anomalies in chlorine concentration as observation data. The mathematical problem is defined as:

$$\text{Minimize Error} = \sum_{t=0}^{Ts} \sum_{k=1}^{N_s} \left\{ C_{k,o}(t) - C_{k,p}(t) \right\}^2 \tag{4}$$

The objective function represents the sum squared deviation in the predicted chlorine concentration over chlorine observations at all the sensors over the monitoring period. $C_{k,o}(t)$ is the observed chlorine concentration at sensor k at time t, $C_{k,p}(t)$ is the predicted chlorine concentration at sensor k at time t, T_s is the total time for which the network is being simulated, and N_s is the total number of chlorine measurement locations in the distribution system. The objective is to identify the source characteristics (represented by the junction node where the source is introduced, the reaction order of the contaminant, the start time of the contamination, and the contaminant mass loading profile) that minimizes the prediction error by closely matching the time series of anomalous drop in chlorine concentration in the network.

Methodology

Source identification in water distribution system can be posed as inverse problem and solved using a simulation-optimization method. Evolutionary algorithms (EAs) (Holland, 1975) are a class of heuristic methods that provide a global search mechanism to identify efficiently near-optimal solutions for large optimization problems. Dandy et al., (1996) and Savic and Walters (1997) used genetic algorithms for the optimal design of water distribution systems. Vitkosvsky et al., (2000), and Lingireddy and Ormsbee (2002) solved using EAs the inverse problem associated with calibration of water distribution networks. In the present study, an EA-based procedure is employed for the source identification problem.

Evolution strategies (ES) (Schwefel, 1995) is an EA-based search method that is being explored as a solution approach for the source determination problem. ES works with a population of solutions. The first generation starts with a random population of μ individuals. A set of λ new solutions are created in each generation using a random mutation process. From the combined array of parent and offspring solutions (denoted as (μ + λ)-selection) or from the set of offspring alone ((μ, λ)-selection), the set of λ individuals are selected for the next generation. Zechman et al., (2006) used an ES-based search approach to solve the source identification problem in water distribution systems. The inverse problem was defined in terms of continuous concentration observations assuming the availability of perfect sensors for the specific contaminant. In the present study an ES based methodology will be used for addressing the source identification problem using chlorine observations.

Illustrative case studies

The proposed study is demonstrated through illustrative case studies involving two test networks. First is an example network (Network 1, Figure 1) that is included with the standard EPANET distribution. This network consists of 97 nodes including two sources, three tanks and 117 pipes, and the water distribution system is simulated using EPANET. The second network used in the study is the virtual city of Micropolis (Figure 2) that was developed by Brumbello et al., (2007). It consists of 1236 nodes, 575 mains, 486 service and hydrant connections, 197 valves, 28 hydrants, 8 pumps, 2 reservoirs, and 1 tank. Multiple-species extension toolkit (MSX) for EPANET provides the capability to model the chemical interaction among multiple reactive species.

Synthetic scenarios of contamination events in the example networks have been considered to study the performance of the proposed method. The Network 1 and Micropolis network are simulated for 24 hours and 72 hours, respectively. Hydraulics in network was simulated every hour while the water quality transport was simulated every 5 minutes. A sample network of sensors/monitoring stations was chosen in each network to uniformly cover the entire network. Water quality observations were recorded every 10 minutes at all the monitoring stations.

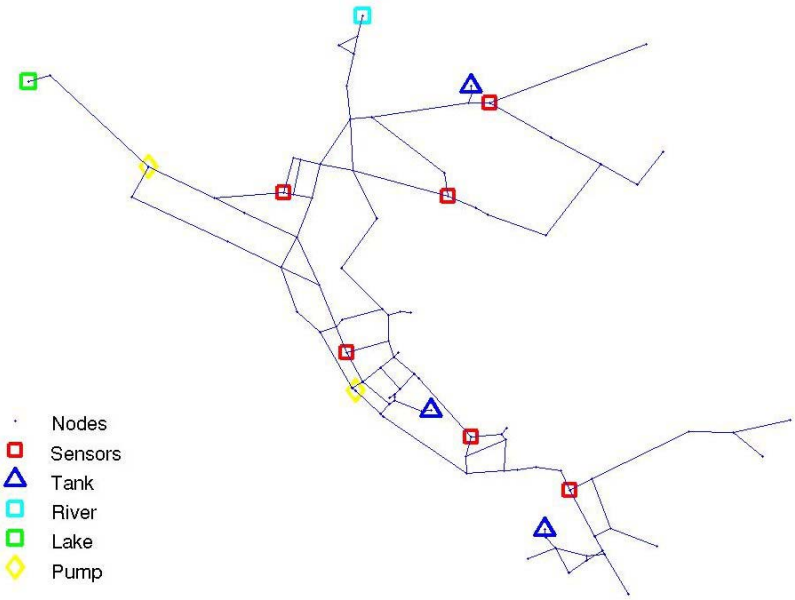

Figure 1. Test Network 1

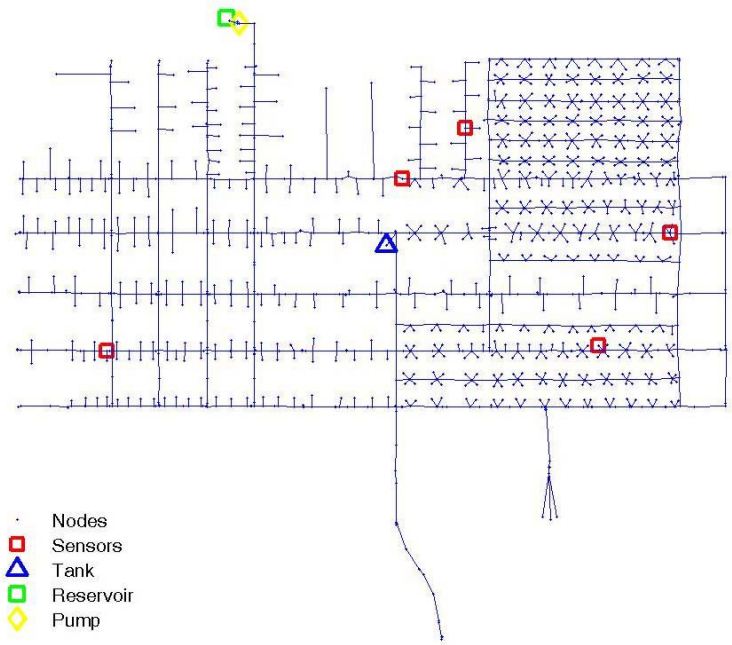

Figure 2. Micropolis network

Arsenic was assumed to undergo a first order or a second order reaction with monochloramine. A part of the source characterization problems is to identify the reaction order, which was assumed to be unknown. Problem was analyzed for two different nodes as contaminant injection location in Network 1. First and second order contamination scenarios were considered in the study, while source identification problem was solved under the conditions of unknown order of reaction. The study was conducted for two different sensor placements scenarios. The methodology was applied to Micropolis network for first and second order contamination scenario. Table 1 summarizes the scenarios studied in this work.

Table 1: Summary of scenarios investigated

Scenario	Network	No. of sensors	True injection source		Order of reaction for solution
			Location	Order of reaction	
1	Network 1	6	12	1st order	1st order / 2nd order
2	Network 1	6	12	2nd order	1st order / 2nd order
3	Network 1	3	12	1st order	1st order / 2nd order
4	Network 1	3	12	2nd order	1st order / 2nd order
5	Network 1	6	54	1st order	1st order / 2nd order
6	Network 1	6	54	2nd order	1st order / 2nd order
7	Network 1	3	54	1st order	1st order / 2nd order
8	Network 1	3	54	2nd order	1st order / 2nd order
9	Micropolis	5	653	1st order	1st order / 2nd order
10	Micropolis	5	653	2nd order	1st order / 2nd order

Summary
This study describes the development and investigation of a simulation-optimization methodology for the identification of source characteristics for contamination events involving reactive contaminants. In this study, the unknown source characteristics are described by the source location, the start time of contamination, the order of the reaction of the contaminant, and the contaminant loading profile. The residual chlorine signature in the system in response to the reactive contaminant is expected to capture the contaminant characteristics. The source characteristics are recreated based on the residual chlorine measurements in the network where the injected contaminant is assumed to undergo reactions with the disinfectant chlorine in the system. The effectiveness of this source characterization procedure under conditions of variability and uncertainty are also investigated. Further, the effect of limited information and data and observation errors on the ability of the method to uniquely identify the source location is investigated by extending the procedure to address non-uniqueness in the solutions. These investigations are conducted for an array of scenarios involving two different water distribution network examples. The preliminary results indicate that the proposed approach is effective in identifying a small set of potential nodes that includes the true contamination source.

References

Brumbelow, K.; Torres, J.; Guikema, S.; Bristow, E. & Kanta, L. (2007). "Virtual Cities for Water Distribution and Infrastructure System Research" World Environmental and Water Resources Congress, 2007, Tampa, FL

Dandy, G. C., Simpson, A. R., and Murphy, L. J. (1996). "An Improved Genetic Algorithm for Pipe Network Optimization" Water Resources Research, 32(2), pp. 449-458.

Holland, J. H. (1975). Adaptation in Natural and Artificial Systems: An Introductory Analysis with Applications to Biology, Control, and Artificial Intelligence. MIT Press, Cambridge, MA

ILSI (1999), "Early warning monitoring to detect hazardous events in water supplies", International Life Sciences Institute-Risk Science Institute.

Kumar, J., Zechman, E.M., Brill, E.D., Mahinthakumar, G., Ranjithan, S., Uber, J., (2007) "Evaluation

of Non-Uniqueness in Contaminant Source Characterization Based on Sensors with Event Detection Methods", World Environmental and Water Resources Congress 2007, Tampa, FL

Kumar, J., Brill, E.D., Mahinthakumar, G., Ranjithan, S., Uber, J., (2008) "Source identification for contamination events involving reacting contaminants", World Environmental and Water Resources Congress 2008, Honolulu, Hawaii

Laird, Carl D., Biegler, Lorenz T., van Boleman Waanders, Bart G., Barlett, Roscoe A., (2005), "Contamination source determination for water networks", Journal of Water Res. Planning and Management, Vol. 131(2)

Laird, Carl D., Biegler, Lorenz T., van Boleman Waanders, Bart G., (2006), "A Mixed-integer approach for obtaining unique solutions in source inversion of drinking water networks", World Water Congress 2005, 173(47)

Lingireddy, S. and Ormsbee, L. (2002). "Hydraulic Network Calibration Using Genetic Optimization." Civil Engineering and Environmental Systems, 19(1)

McKenna, Sean.A., Hart, David., Klise, Katherine., Cruz, Victoria., Wilson, Mark., (2007), "Event detection from water quality time series", World Water and Environmental Congress 2007, Tampa, FL

USEPA (2005), "Technologies and techniques for early warning systems to monitor and evaluate drinking water quality: A state-of-art review."

Savic, D. A. and Walters, G. A. (1997). "Genetic Algorithms for Least-Cost Design of Water Distribution Networks" Journal of Water Resources Planning and Management, 123(2), pp. 67-77.

Schwefel, H.-P. (1995) Evolution and Optimum Seeking, Wiley & Sons, New York

van Bloemen Waanders, B. G., Bartlett, R. A., Bigler, L. T., and Laird, C. D. (2003) "Nonlinear Programming Strategies for Source Detection of Municipal Water Networks." World Water and Environmental Congress 2003, Philadelphia, PA, June 23-26

Vitkosvsky, J. P., Simpson, A. R., and Lambert, M. F. (2000). "Leak Detection and Calibration using Transients and Genetic Algorithms" Journal of Water Resources Planning and Management, 126(4), pp. 262-265.

Zechman, Emily M., Brill, E. Downey., Mahinthakumar, G., Ranjithan, S., Uber, James., (2006), "Addressing non-uniqueness in a water distribution contamination source identification problem", Proceedings of 8th Annual Water Distr. Sys. Anal. Symposium, Cincinnati, OH, August 27-30, 2006.

Low Pressure Propagation at Service Lines

Juneseok Lee[1], Vinod K. Lohani[2], Andrea M. Dietrich[3], and G.V. Loganathan (Late)[4]

[1]Assistant Professor, Department of Civil and Environmental Engineering, San Jose State University, San Jose, CA 95112; email: Juneseok.Lee@sjsu.edu
[2]Associate Professor, Department of Engineering Education, Virginia Tech, Blacksburg, VA 24061; email: vlohani@vt.edu
[3]Professor, Department of Civil and Environmental Engineering, Virginia Tech, Blacksburg, VA 24061; email: andread@vt.edu
[4]Professor in Memoriam, Department of Civil and Environmental Engineering, Virginia Tech, Blacksburg, VA 24061

ABSTRACT

There is copious evidence indicating intrusion of contaminants into the drinking water pipes through the leaking sections due to low pressure events associated with water hammer phenomenon. In this study, an experimental plumbing rig was designed and implemented that replicates the range of pressures encountered in actual service lines and the plumbing systems. This research addresses how a pressure transient triggered within a house and from municipal systems can impact the service lines with a possible suction effect. This experiment also enabled visualization of the various pressure transient phenomena including gaseous cavitation. It is demonstrated that hydraulic transients triggered from water mains result in low pressures events in service lines which can allow possible intrusion of microbial and chemical contaminants at service lines. Structural integrity of service line and hydraulic integrity at water mains should be maintained to minimize any public health risks.

INTRODUCTION

The growth in bottled water consumption, point of use water treatment (including various kinds of filters, distillation, ion exchange, and reverse osmosis) indicates citizens' concern regarding the quality of distributed water at the tap. Cost advantages of public water supply, higher maintenance problems related to the point of use devices and relative marginal improvement in water quality result in the municipal drinking water remaining as the top-ranked water supplier for maintaining established drinking water standards. It is widely believed that because a drinking water distribution system is pressurized, the water can only come out of the system. However, there is evidence that pump trips, opening and closing of fire hydrants, valve closures or malfunctioning, pipe break, and sudden change in demand and resonance can induce significant transients leading to low pressure events within a drinking water system. During such events a greater external pressure can lead to contamination intrusion through available openings. Tests of surrounding soil and pipe specimens from repair locations show the presence of pathogens. In 2000 alone 6,988 water systems affecting about 10.5 million people violated microbial drinking water standards in the US.

Le Chevallier et al. (2003) define intrusion as the specialized backflow situation in which nonpotable/contaminated water from the environment outside of the distribution piping flows into the pipe through leaking sections. Kirmeyer et al. (2001) and Friedman et al. (2004) provided comprehensive reviews and detailed discussions on the pathogen intrusion problems into the municipal drinking water systems. Any breakthrough is considered high risk and probability of occurrence is also considered high. They also point out physical mechanisms grouped as *transitory contamination* due to low pressure propagation in the system drawing in contaminants from the exterior surroundings with a higher pressure; *cross connection* between potable water system and a source that can potentially introduce contaminants into the potable water; *pipe break, repair and installation* that expose the distribution system to the externalities as routes of entries. Storage facilities both covered and uncovered, purposeful contamination, growth and resuspension serve as additional sources for pathogen intrusion.

Friedman et al. (2004) focused on transitory low pressure propagation in the municipal system that typically uses 4 inch to 10 inch pipes. They documented intrusions of contaminants and low pressures of the order of negative 10 psi (gage). They also emphasize that the intruded contaminant is not re-extruded out of the pipe but a portion of it is carried downstream. Distribution mains downstream of pumps, high elevation areas, low static pressure zones, areas far away from overhead tanks, and segments of pipes upstream and downstream of active valves in high flow areas are the most susceptible for low or negative pressures. Locations with frequent leaks and breaks, high water table regions, flooded air vacuum valve vaults, and high risk cross connections have the highest potential for intrusion. Gullick et al. (2004) observed most surge events as the result of pump operations and outages. Novak (2005) provided experimental evidence for a 90 degree bent pipe with a pressure range of less than 10 psi and with a velocity of about 6 ft/sec contamination can be sucked into downstream of the 90 deg bent region of the pipe.

Since the terrorist events of September 11, 2001, water security at water infrastructure has received more attention than before. NRC (2006) categorized drinking water distribution system's integrity into the following components: i) *physical integrity* indicating the physical barrier between pipe externalities and inside the piping, ii) *hydraulic integrity* controlling right pressure, flow, water age, and capacity for providing fire flow, and iii) *water quality integrity* keeping high standard of water quality without any degradation. If any of the components fails to keep the good level of integrity, this will result in serious public health risk. This indicates that drinking water infrastructure bears significant operational and managerial responsibilities towards public health.

Service lines

America's water distribution infrastructure system is old and deteriorating. A water system with its myriad of appurtenances (including pumps, valves, and tanks) is susceptible to hydraulic transients resulting in high and low pressure waves alternatively passing through the network. While the major municipal system is readily recognized as a vast infrastructure system of nearly 1,409,800 km of piping within the United States, the plumbing systems including service lines (minor systems) which are at least 5 to 10 times larger is generally not well addressed.

Leakage rates (water loss while transporting water from treatment plant to minor systems) in drinking water systems reaches 32 percent in some utilities which indicates high potential of

contamination intrusion (Kirmeyer et al., 2001). It is emphasized that 6 billion gallons of treated water is disappearing during distribution (AWWARF, 2007). According to NRC (2006), the majority of water leaks occur at service lines, service fittings, and connections. It is emphasized that the lower total chlorine residuals, lack of dilution, and short detention time before potential consumption might increase the potential health threat to individual consumers if intrusions were to occur at service lines. Also, service line's failure records are not readily available (as they belong to private property) so future prediction of failure is difficult.

To the author's knowledge, no study has been conducted to examine hydraulic impacts at service lines as a result of transients triggered from water mains (major) and plumbing (minor) systems. Also, while it is known water hammer is common inside a home, what pressures exist (when water hammer hits) within the plumbing system is not clearly understood. As plumbing systems and service lines are passive recipients from the water mains; if there is a contamination intrusion event at the service line, it is bound to enter into our tap water which poses health risk issues. The objectives of this research are to design, construct, and implement an experimental plumbing system that replicates the range of pressures encountered in actual minor water distribution systems. The experimental plumbing system is used to i) assess low pressure behavior at the service lines to predict the potential for contamination intrusion from the surrounding soil or water and ii) evaluate the cavitation phenomenon through clear plastic pipe for steady and transient state.

EXPERIMENTAL PLUMBING RIGS

Typical single-story residential house connections to a municipal water main are shown in Figure 1. The average pressure in the main system is 70~ 80 psi and it dictates the pressure at each house level. Cold water plumbing systems are usually branched-type systems that are typically comprised of 'one source, one or more intermediate nodes, and one or more plumbing fixtures' (Bhave, 1991).

In our experiment, we are simulating real plumbing systems by directly connecting to water mains. Three scenarios, referred to as Transient I, II, and III (see Figure 1) that can trigger a transient in a service line are considered. Transient I: In this case, transients are triggered due to actions initiated from inside of the house (e.g., by shutting off the valve, shower heads, or automatic on/off of solenoid valve from laundry room). Transient II and III: In these cases, transient causing actions are initiated from the municipal water systems (e.g., pump trips, opening and closing of fire hydrants, valve closures, pipe break, sudden change in demand and resonance, and malfunctioning of valves). Depending on the flow direction in the system, there are two transients (i.e. transients II and III) which influence the pressure variation at the service line (see Figure 1).

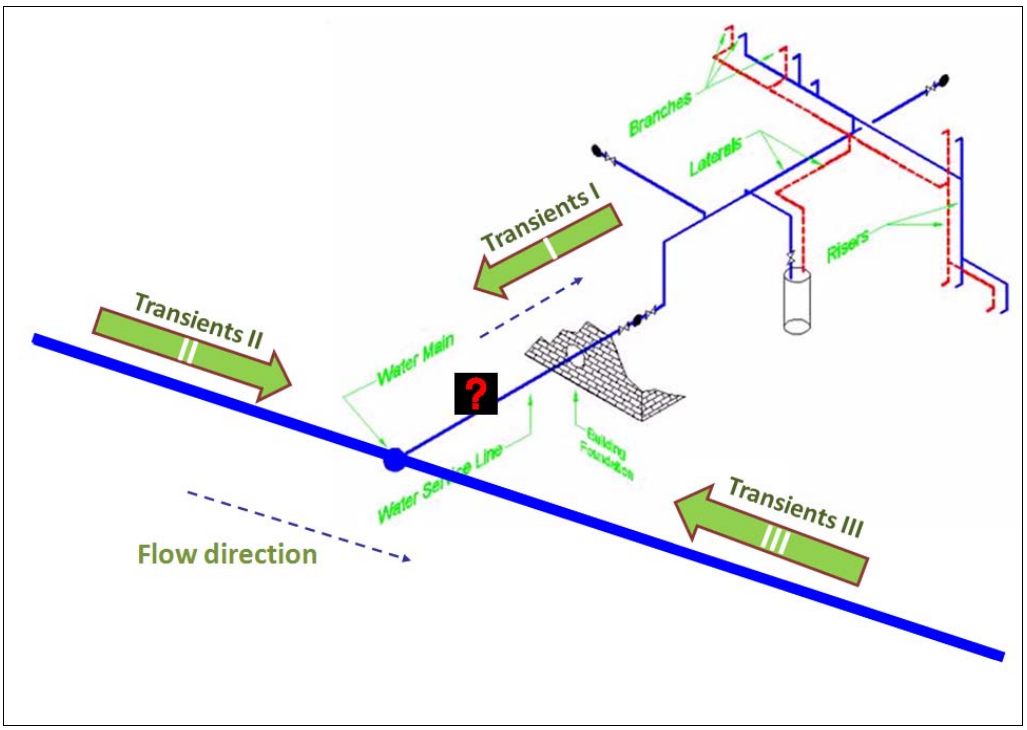

Figure 1 Scenarios of transients that can occur in drinking water distribution systems (modified from Ladd, 2005 with permission)

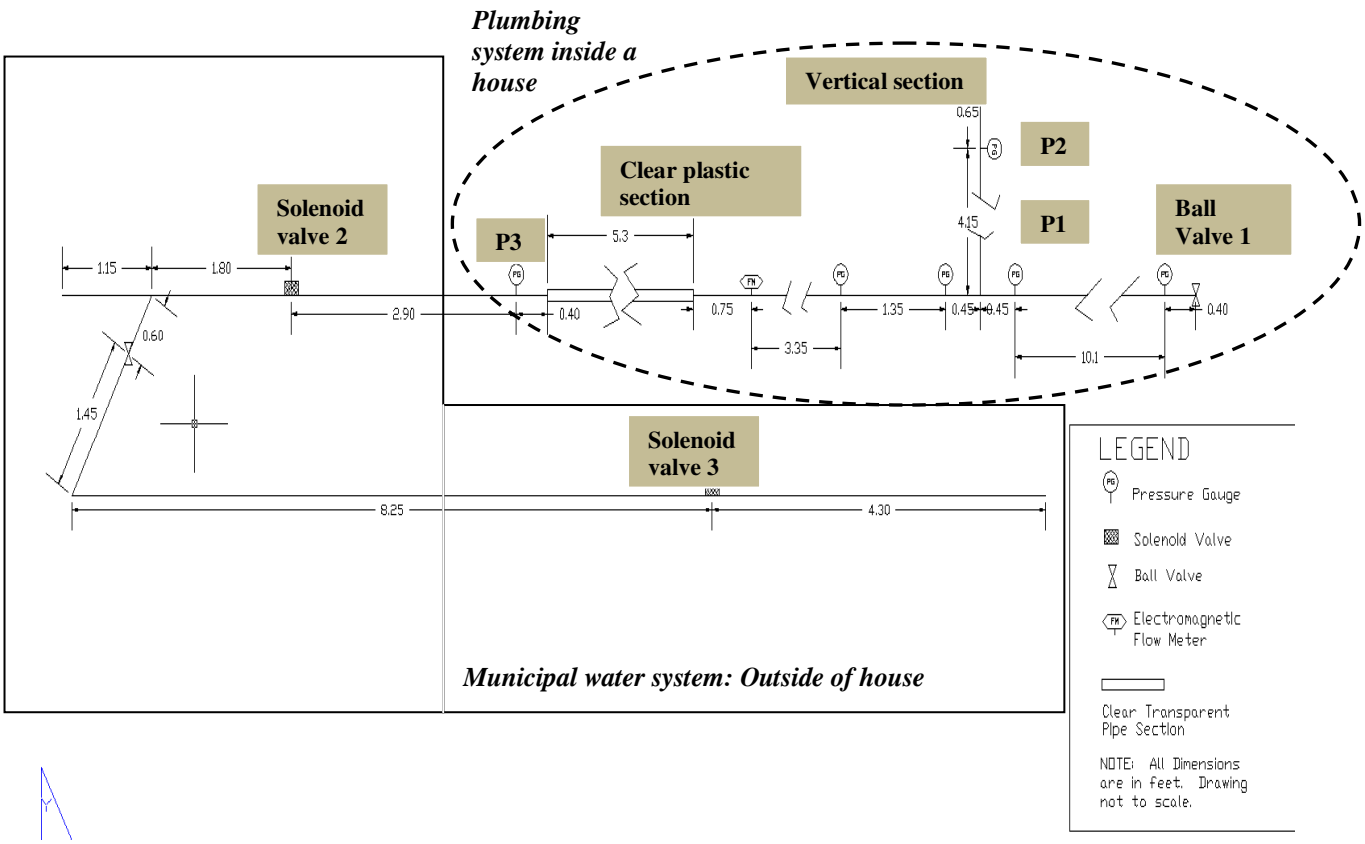

Figure 2 Schematic of the experimental plumbing system

An experimental plumbing rig is built in the hydraulics lab of CEE department at Virginia Tech to simulate these proposed three scenarios. Detailed configuration of the rig is guided by current plumbing code and advice from the plumbers. Main line has 0.75" diameter and we used soldering instead of threaded appurtenances to mimic real home plumbing more closely. Dotted oval shape indicates the plumbing system inside house and solid line is for municipal water system outside of a house (see Figure 2). High sensitive sensors such as pressure transducers and insertion type magnetic flowmeter were adopted to observe the spatial and temporal variation of the flow patterns. Three pressure transducers (P1, P2, and P3) and one flowmeter were installed at locations of interest (see Figure 2). The signals from the sensors were collected by LabVIEW based DAQ (Data Acquisition System) systems using sample and hold technique every 0.01 second so the data from multiple signals are acquired simultaneously. To visualize the phenomenon and study the specific nature of gaseous cavitation inside the piping system, a 5.3' section of clear plastic pipe was installed. We employed a high definition Video camera to capture the cavitation phenomenon for steady state and when water hammer hits.

This experiment involves pressure varying continuously over time over a range of -14.7 to over 250 psig (temperature range is 50 to 90 F [room temperature]). Water hammer occurs if a valve is suddenly closed (ball valve or solenoid valve) in a pipe system, and there is a sudden change in the velocity and pressure. As water hammer passes through the pipe, pressure measurements of the order of hundred readings per second capturing the maximum and minimum are required to visualize the pressure variation. The pressure continuously fluctuates until the transients die out. It was necessary to measure the pressures as they fluctuate continuously with time. To meet these requirements, we chose dynamic application sensors which means sudden change of properties. Water hammer shocks, acceleration, and vibration are examples of dynamic signals. For dynamic applications, piezoelectric pressure sensors are known to be ideal as they are able to measure very high frequencies compared to strain gauge technology due to their stiffness. Stiffness also leads to fast response time. Piezo sensors offer a response time of less than 1 micro-second so there is no trouble making several hundred readings per second as long as sampling rate on the DAQ is high enough (Our DAQ system is able to collect maximum of 1M readings per second).

However, piezoelectric sensors ignore the static pressure component. As such referencing the output to atmosphere or absolute is not possible. The sensor will show the pressure changes in relation to static pressure in the rig. In our application, the baseline pressure is the water line's steady state pressure. So, for the piezoelectric pressure sensor, instead of calling it gage pressure, it is really called a relative pressure measurement; relative to the water line's steady state pressure. For example, water line pressure is 30 psi; the 30 psig static water line pressure will read zero on a piezoelectric pressure sensor. A regular static sensor would read 30 psig. Then, when the water hammer hits, there will be a spike to 250 psi 'relative to 30 psig' and then a reflected pressure wave possibly down to -14.7 psi 'relative to 30 psig.' This -14.7 psi is relative to the static line pressure of 30 psig.

EXPERIMENTAL RESULTS

The experiment plumbing rig was connected to the water main in hydraulics lab to simulate a real household water supply situation (see Figure 2). The average static pressure was 80 ± 5 psig when all the valves were closed. It is opined that this fluctuation comes from water usage in nearby faucets or weak transients from the municipal systems. When the faucets were fully opened (flow rate is (37±5) liter/minute), however, the residual pressure was reduced to 40-45 psig within the experimental system. The level of residual pressure could be controlled by maneuvering the valve at the water main. Initially, the system is set in a steady state of 40 psig (residual pressure). Then the solenoid/ball valves were suddenly closed/ opened following three scenarios. The solenoid valve closing/opening time was known to be less than 0.3 seconds according to the manufacturer. The ball valve closing/opening time is believed to be less than 0.1 seconds after many times of operator's training.

Pressure Variation at Location P3: Representing Service Lines

The relative pressure variations at location P3 (which represents service lines) are explained in this section. Scenario I refers to the open/close at valve1; scenario II refers to open/close at valve 2; and scenario III is open/close at valve 3. When the valve 1 is suddenly closed, the pressure goes up to 70 psi (gage) from the steady state. So, within fraction of a second, service line is going through (40+70=110) psig of pressure. This may result in repetitive fatigue impact on service lines due to constant on/off from inside the house. But when opened, it is causing -30 psig so 80 psig (static pressure) – 30 (instantaneous pressure change) = 50 psig; which is not creating low enough pressure to cause suction.

Transient II scenario results are shown in Figure 3. After sudden closure, the pressure goes below 0 psig (around -10 psig) for a fraction of a second. It is seen that transient II is causing negative pressures (40 (steady state) – 50 (pressure variation) = -10 psig inside the system). When suddenly opened, the pressure goes up to 70 psig. Transient III scenario also showed pressure changes but the magnitudes are not so noticeable compared to scenarios I and II.

Gaseous Cavitation

When the pressure drops to -10 psig (above vaporous pressure values), gaseous bubbles forming inside the clear plastic pipe section was observed; then the bubble disappeared within less than 1 second when pressure goes above gas saturation pressure (see Figure 4). The bubble formation time was very quick (less than 1 second) and this is contrary to traditional theory of gaseous cavitation formation timing (2-3 seconds, Novak (2005)). Pre-existing gas nuclei that was existing on particles in the bulk solution seemed to grow to be the observed bubbles. Using HD video, consecutive phenomenon was captured every 0.033 second (30 frames per second). It is observed that created bubble shape and numbers are near random but gas evolution and dissolution timing seem to be almost consistent (less than 1 second) as long as we control the water hammer triggering mechanism (valve closing time). As the clear plastic's diameter is ¾", rough size of the gaseous cavitation bubbles can be estimated. Observed gaseous cavitation due to water hammer may have implications of noise problems within plumbing systems which bears further research.

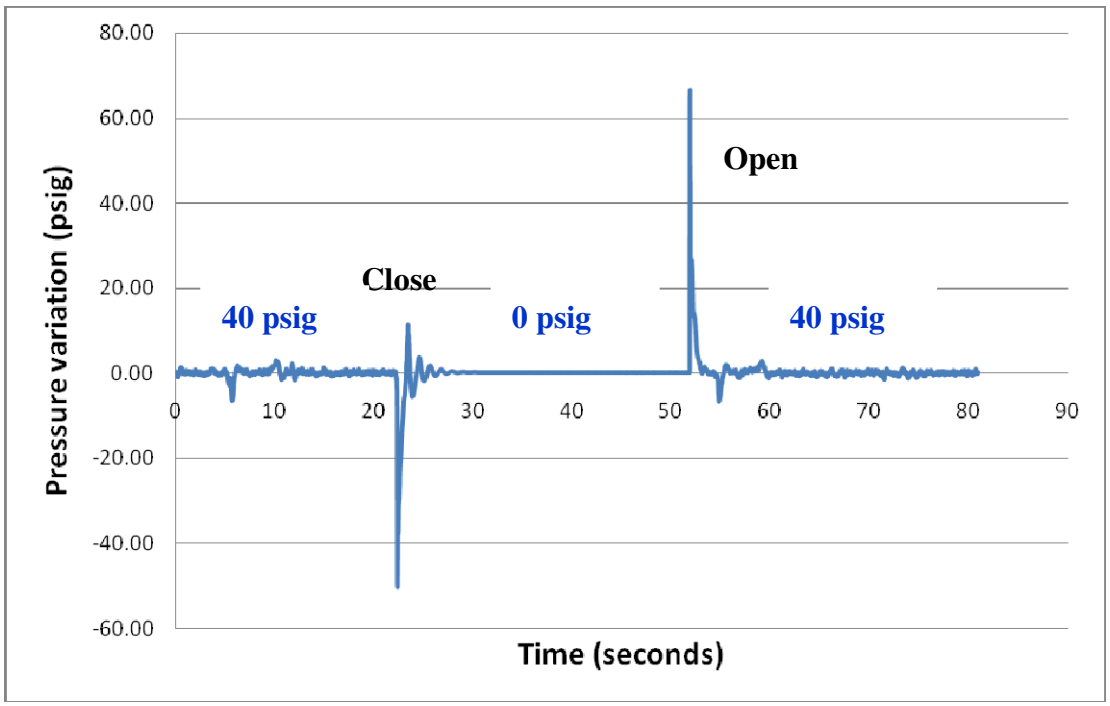

Figure 3 Pressure variation, scenario II, 40 psig residual pressure

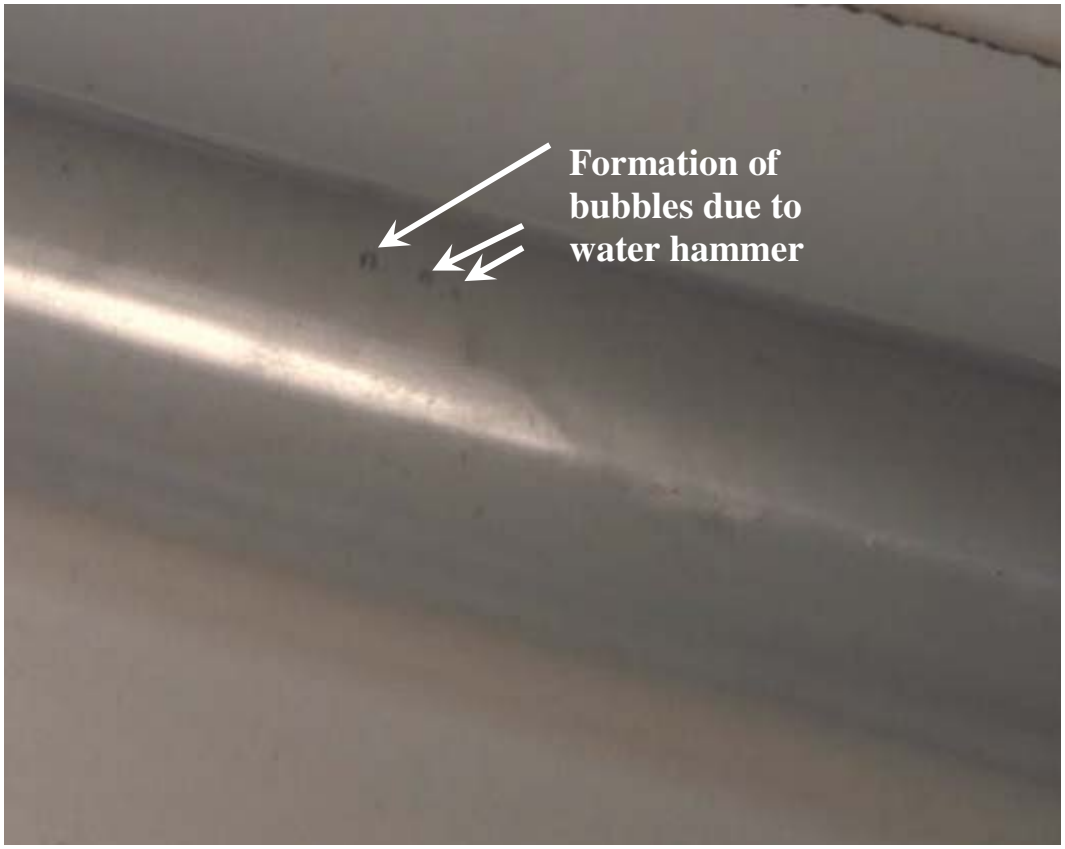

Figure 4 Water hammer induced gaseous cavitation (the pipe diameter is ¾")

CONCLUSIONS

Pressure variations at the service line corresponding to typical street level pressures encountered in a real water supply system are examined in this research. This study was specifically developed for a typical one story house (1800-2200 square foot; water hammer impacts from inside house applies *only to cold water line*) plumbing system which includes 150- 250 feet of pipes. Major findings of this research are following.

1. As a result of a street level transient, low pressure wave (up to -10 psig for fraction of a second) can propagate to the experimental service line. This pressure drop would be sufficient to induce potential contamination intrusion at service line.

2. Gaseous cavitation was observed due to water hammer induced low pressure (as a result of street level transient); also found that bubble formation timing due to gaseous cavitation can be less than 1 second. This phenomenon may have practical implications of implosion or gaseous impingement that is known to erode protective scales on the wall.

To minimize any public health effects, structural integrity of service lines and hydraulic integrity at water mains should be maintained in good condition. Also, this line of research results should be disseminated to the public so they are well aware of these important issues.

ACKNOWLEDGEMENTS

The authors gratefully acknowledge the support provided by the National Science Foundation under the grant DMI-0329474 and DLR-0431779. The authors greatly appreciate Late Mr. Juan Ortiz, and Late Mr. Waleed Shaalan for their founding work. The authors extend their sincere thanks to Drs. Marc Edwards, Paolo Scardina, and Steven Cox for their insightful advice on the experiment. Thanks also go to Mr. Seth Williamson for his physical help on the experiment.

REFERENCES

AWWARF (Awwa Research Foundation) . (2007). *Installation, Condition assessment, and reliability of service lines.* AWWA, Denver, CO.

Bhave, P.R. (1991). *Analysis of Flow in Water Distribution Networks*. Technomic Publishing, Co., Lancaster, PA

Friedman, M., L. Radder, S. Harrison, D. Howie, M. Britton, G. Boyd, H. Wang, R. Gullick, M. LeChevallier, D. Wood, and J. Funk, (2004). *Verification and control of pressure transients and intrusion in distribution systems*. Report 91001F. AWWA Research Foundation, Denver.

Gullick, Richard, M. LeChevallier, R. Svindland, and M. Friedman (2004). Occurrence of transient low and negative pressures in distribution systems. *Journal of the American Water Works Association, 96(11)* p 52-66.

Kirmeyer, Gregory, M. Friedman, K. Martel, D. Howie, M. LeChevallier, M. Abbaszadegan, M. Karim, J. Funk, and J. Harbour (2001). *Pathogen Intrusion into the distribution system*; American Water Works Association Research Foundation: Denver, CO.

Ladd. J. (2005) *An evaluation and pressure driven modeling of potable water plumbing system.* MS Thesis. Virginia Tech.

Novak, J. A. (2005) *Cavitation and Bubble formation in water distribution system*, MS Thesis, Virginia Tech.

NRC (2006). National Research Council. *Drinking Water Distribution Systems, assessing and reducing risks.* The national academic press. Washington D.C.

DRINKING WATER INFRASTRUCTURE ASSESSMENT: THE NATIONAL RESEARCH COUNCIL OF CANADA PERSPECTIVE

Yehuda Kleiner, Balvant Rajani and Rehan Sadiq, National Research Council of Canada

Abstract

The essence of infrastructure asset management and decision-making on its renewal/ rehabilitation is a trade-off between system performance and cost. System performance criteria for water networks include quality, quantity and reliability, i.e., the water should be safe, with acceptable aesthetics, taste and odour; regular and peak demand (including fire flows) should be met with acceptable pressure and with minimal interruptions. Costs comprise capital investment in system design, installation and renewal, operation and maintenance (energy, materials, labour, monitoring, inspection, testing, repair), and indirect and social costs incurred due to failure (property damage, disruption, illness, etc.).

Several challenges need to be overcome in the development of an integrated decision framework for water distribution network. Mechanisms affecting system performance criteria are not all well understood. It is difficult to define and measure performance (which inherently comprises several non-commensurate and often conflicting criteria), let alone decide what level of performance is acceptable. It is also difficult to calculate the costs involved to achieve a specific level of performance. Substantial spatial and temporal variability is inherent in even a moderate-size network, and the collection of data on the performance and condition of these buried assets is often difficult and costly.

At the National Research Council of Canada we have identified the need to address these issues in a holistic way, and in the last 15 years have been involved in a continual effort, both independently and in collaboration with others, to put the pieces of the puzzle together. Although the state of knowledge has advanced significantly since we started, a lot still needs to be achieved. This paper describes our past and current research activities, views and vision for future activities in the field.

Overview

A trade-off between system performance and cost is the essence of decision making on the renewal of infrastructure systems. The general objectives of a water distribution network can be stated as the supply of water that is safe, with acceptable aesthetics, taste and odour; and regular and peak demand (including fire flows) should be met with acceptable pressure and with minimal interruptions. These general objectives are easy enough to understand but their quantification poses a significant challenge because it cannot be done directly but rather through indicators. There are literally hundreds of different performance/condition indicators that have been proposed in the literature by prominent institutions such as the USEPA (2002), the British Office of Water (OFWAT, 1998), the World Bank (Yepes and Dianders, 1996), the International Water Services Association (IWSA) (Alegre, 1999), and many others. This multitude of performance indicators is testament to the complexity involved. Mechanisms affecting the performance criteria are not well understood. It is difficult to define and measure performance, let alone decide what level of performance is acceptable. Furthermore, the costs involved comprise capital investment in system design, installation and renewal, operation and maintenance (energy, materials, labour, monitoring,

inspection, repair) and indirect and social costs resulting from failure (property damage, disruption, illness, etc.). It is difficult to calculate the costs involved to achieve a specific level of performance; and the collection of data on the performance and condition of these buried assets is difficult and costly. All these challenges and difficulties are exacerbated by substantial spatial and temporal variabilities inherent in even a moderate-size system.

The failure of a system is broadly defined as the inability to meet one or more of its performance criteria. The risk of failure can be defined as the expected magnitude of the consequences of failure, i.e.

Risk of failure = E(failure consequence) = f(probability of failure, costs of failure) (1)

Figure 1 illustrates a general, high-level view of the framework within which a water distribution network is managed. In the following sections we shall provide details about NRC's efforts to address the various pieces in this holistic puzzle.

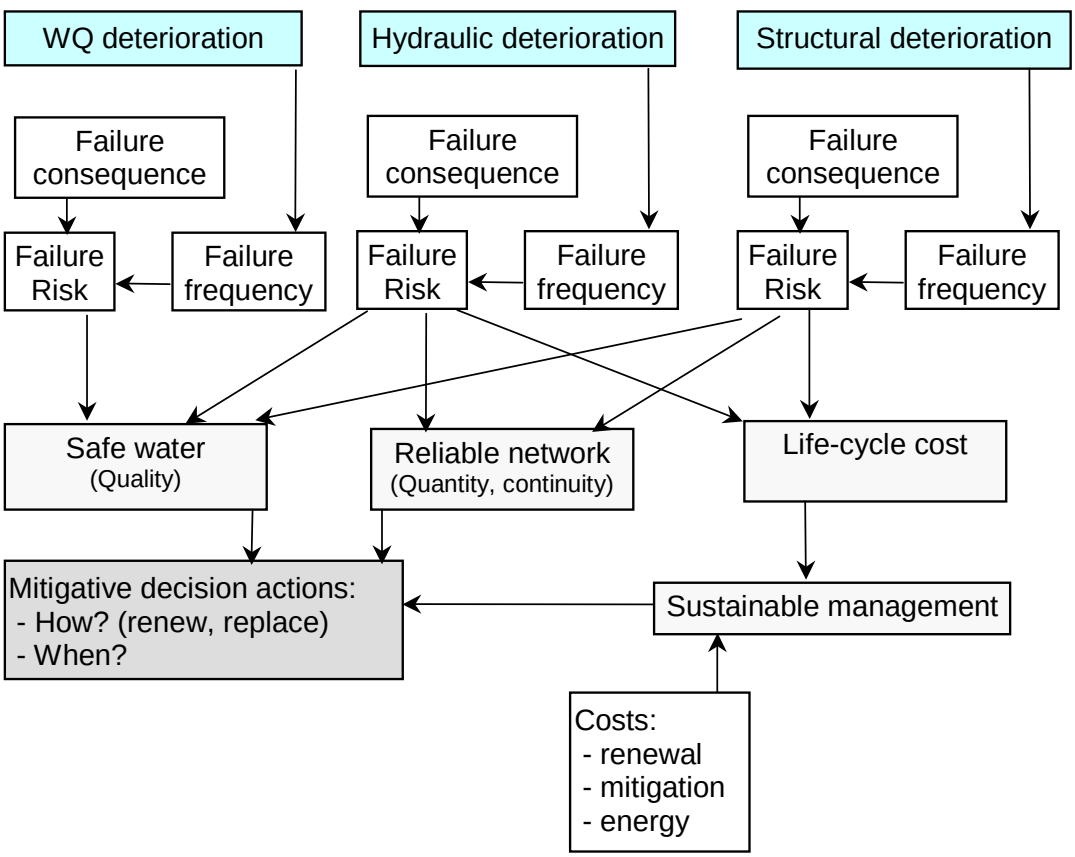

Figure 1. Holistic view of water distribution asset management

Structural deterioration of water mains and failure risk

As water mains age they deteriorate. This deterioration may be classified into two categories: (i) structural deterioration, which diminishes the pipes structural resiliency and

their ability to withstand the various types of stresses; and (ii) deterioration of pipe inner surfaces, resulting in diminished hydraulic capacity, degradation of water quality and even diminishing structural resiliency in cases of severe internal corrosion.

The probability of a water main failure due to structural deterioration can be estimated using physical (mechanistic) models (Rajani and Kleiner, 2001b) and/or statistical (empirical) models (Kleiner and Rajani, 2001a). Statistical models develop empirical relationships between the pipe, its exposure to the external and operational environments and its observed failure frequency while physical models endeavour to mimic realistic field conditions as well as external and operational environments. Empirical models typically over-simplify a complex reality in order to (hopefully) achieve "80% of the answer with 20% of the effort". In contrast, physical models are more general but require a substantial amount of data to represent specific conditions and environments. These data are either unavailable or very costly to obtain for even a modest portion of a distribution network.

The costs of a water main failure event may be classified into three categories: (a) direct, (b) indirect, and (c) social costs. While direct costs are relatively easy to quantify in monetary terms, indirect costs may require much more effort, and social costs are often the most difficult to describe and assess. The magnitude of failure consequence is, strictly speaking, a random value because no two failures have the same consequences. Failures in small distribution mains are usually repaired with little effort and typically collateral damage is relatively small. Failures of large transmission mains are relatively rare, and because only few water utilities attempt to assess total failure damage there are currently insufficient data to assign probability distributions to failure costs.

Figure 2 illustrates qualitatively how these differences between small distribution mains and large transmission mains translate into different forms of management. As a pipe ages and deteriorates (without renewal), its probability of failure (or failure frequency) increases and the risk increases as well. Note that the risk is expressed as the present value (PV) of expected cost. At the same time, the discounted (or PV of) the renewal cost declines as pipe renewal is deferred. The total expected life-cycle cost typically forms a convex shape, whose minimum point depicts the optimal time of renewal (t^*). The top part of Figure 2 illustrates a typical case of small distribution mains, where the optimal time of renewal corresponds to a relatively higher failure frequency. In contrast, due to higher failure cost, the bottom part of Figure 2 illustrates that for large distribution mains the optimal strategy is to avoid failure altogether, i.e., *failure prevention*, rather than tolerate some acceptable frequency, i.e., *failure management*.

Note that Figure 2 illustrates idealized cases, where the minimum point on the convex curve is quite clear. There are cases where this curve is not as well behaved. When the ageing rate (i.e., the rate at which failure frequency increases) is similar in magnitude to the discounting factor, the convexity of this curve can become quite flat, and the point of minimum cost becomes less crisp. When the cost of failure is relatively low compared to the cost of renewal and the discounting factor relatively high, the curve can take the shape

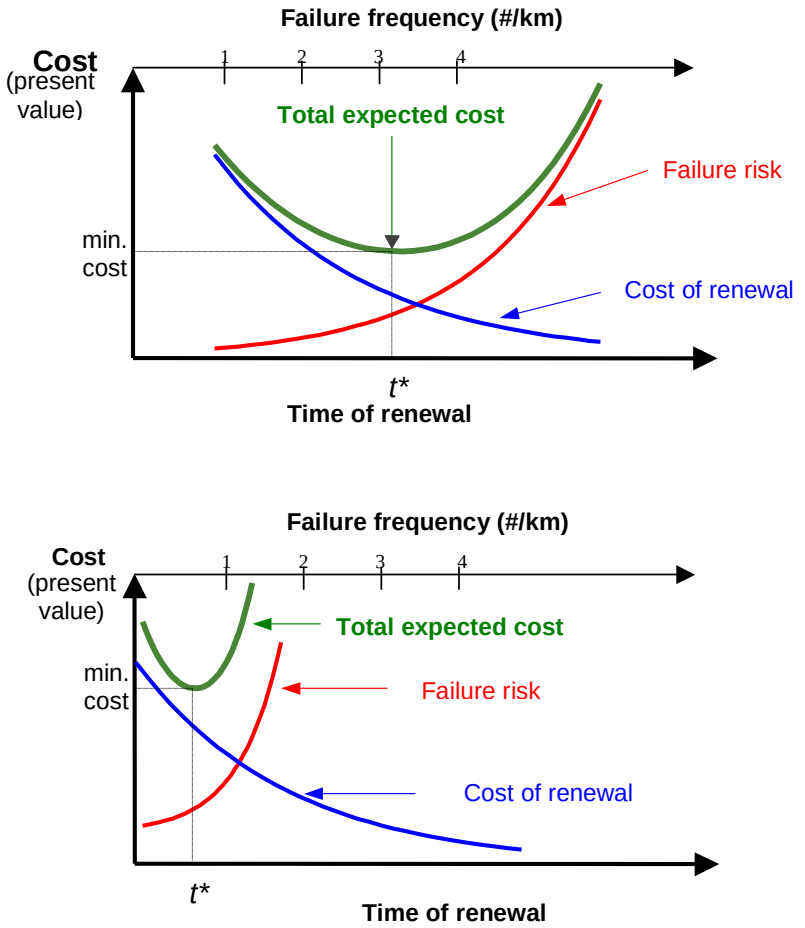

Figure 2. Optimal renewal frequency for distribution mains (top) vs. transmission mains (bottom). Time scale not necessarily same in both graphs.

of the "hammock-chair" as described by Herz (1999), with no definite minimum, indicating that renewal could perhaps be postponed indefinitely.

Asset management of small-diameter distribution mains

At the NRC, we have focused on several aspects of asset management of small-diameter distribution mains, namely investigation of the mechanics of pipe failure, development of statistical/empirical methods to model historical breakage frequency and forecast it in the future, development of leak-detection technologies and investigation of other nondestructive testing (NDT) technologies for the efficient assessment of the condition of pipes.

Numerous approaches have been proposed to decipher historical failure patterns. Kleiner and Rajani (2001b) provided a comprehensive review of the major ones, and more have been published since. Through the investigations of different aspects of the mechanical processes leading to pipe failure (e.g., Rajani and Tesfamariam, 2004; Tesfamariam *et al.*

2006.) we have developed an understanding of what factors need to be considered in asset management models for small distribution mains, which are based on empirical observations. Consequently, we have developed D-WARP (Distribution – Water Main Renewal Planner) and later I-WARP (Individual – Water Main Renewal Planner). Both D-WARP and I-WARP allow the consideration of time-dependent factors, such as climate effects, cathodic protection practices, etc. to be considered in the analysis of failure patterns. While D-WARP deals with high-level planning of groups (or cohorts) of water mains, I-WARP uses a nonhomogeneous Poisson process to model and forecast breakage frequency of individual water mains.

Climatic covariates that are used by both D-WARP and I-WARP are freezing index and rainfall deficit. Freezing index *(FI)* is a surrogate measure for the severity of winter, and rain deficit (*RD)* is a surrogate measure for soil moisture. *RD* can be considered in two separate forms. Cumulative *RD*, which is a measure of the average soil moisture over a given time period, corresponds to the effects described by Rajani *et al*. (1996). Snapshot *RD*, which is a measure of the soil moisture during winter, when the soil is mostly frozen, corresponds to the effects described by Rajani and Zhan (1996).

Cathodic protection can be defined as "… the reduction or elimination of corrosion by making the metal a cathode by means of an impressed direct current or attachment to a sacrificial anode (usually magnesium, aluminium or zinc)" (NACE, 1984). In practice, water utilities can implement two cathodic protection strategies, namely, hotspot and retrofit CP. Hotspot CP (HSCP) is the practice of opportunistically installing a protective (sacrificial) anode at the location of a pipe repair. These anodes are typically installed without any monitoring and stay in the ground until total depletion, usually without replacement. Retrofit CP refers to the practice of systematically protecting existing pipes with galvanic cathodic protection. If the existing water main is electrically discontinuous (e.g., bell and spigot with elastomeric gaskets and no bridging) then an anode is attached to each pipe segment (typically 6 m or 20' length). If the water main is electrically continuous then usually a bank of anodes in a single anode bed can protect several contiguous pipe segments. Figure 3 illustrates, using D-WARP, how an HSCP program that was implemented in 1990 by an East Ontario (Canada) municipality affected the breakage rate in one of its pipe cohorts.

In addition to the aforementioned climate and cathodic protection covariates, I-WARP allows the consideration of user-defined time series that may have impacted historical breakage rates. For example, pumping station failures have been observed to impact failure rates (due to high transient pressures) in a municipality in Western Canada. The inclusion of an appropriate (qualitative) time series helped to 'explain' the resulting outlier breakage rates. Other time series that may impact breakage (or repair) rates are leak detection campaigns, changes in pressure regimes, etc.

D-WARP is available for free download at the NRC-IRC website (NRC-IRC, 2007). A detailed user manual as well as select publications provide detailed information about the model and its application. A complete technical report, as well as a prototype computer application of I-WARP will be available later in 2009 from WRF (Water Research

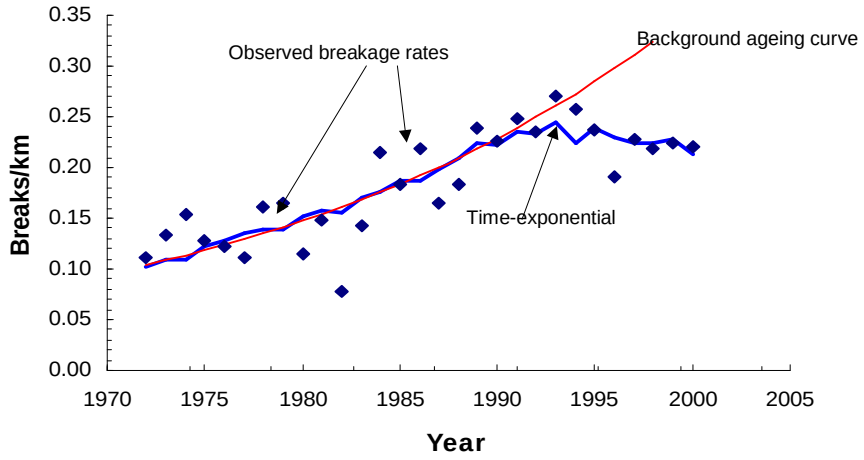

Figure 3 Effect of hotspot CP program on a cohort of cast iron mains.

Foundation – formerly known as the American Water Works Association Research Foundation – AwwaRF), which co-funded the research.

In the area of leak detection we have developed LeakFinderRT, which is a PC based system for locating leaks in all types of water pipes using the leak noise correlation method. It incorporates several new developments, most importantly an "enhanced" correlation function. LeakFinderRT is fully realized in software for PC running under Microsoft Windows. Leak noise is recorded using the PC's soundcard and then correlated via the Fast Fourier Transform (FFT). LeakfinderRT is now a fully commercialised technology, which provides affordable leak detection solutions for small and medium sized municipalities. Based on knowledge generated from leak detection work, a new acoustics-based method is currently in development to discern the average remaining wall thickness of buried pipes. This method has the potential to serve as a screening tool to prioritise some types of water mains for inspection.

In the area of NDT, we are in the early stages of developing a robotic underwater vehicle capable of carrying and manipulating multiple NDT sensors for inspection and early detection of defects in large pipes while in service.

Asset management of large-diameter transmission mains

As discussed earlier, large transmission mains typically have low failure rates but when they fail the consequences can be quite severe. This low rate of failure, coupled with the limitations of currently available inspection tools and high cost of inspection, have contributed to the current situation where most municipalities lack the necessary data to estimate directly or indirectly the deterioration rates of these assets and subsequently to make rational decisions regarding their renewal.

The condition assessment of a large transmission main comprises two steps. The first step involves the inspection of the main using direct observation (visual, video) and/or NDT techniques (radar, sonar, ultrasound, sound emissions, eddy currents, etc.), which reveal distress indicators. The second step involves the interpretation of these distress indicators to determine the condition of the main. This interpretation process is dependent upon the

inspection technique. Interpretation of the visual inspection results, although based on strict guidelines, can often be influenced by subjective judgment. The interpretation of NDT results on the other hand, is often complex (at times proprietary) and can be imprecise.

Managing the failure risk of large transmission mains requires a deterioration model to enable the forecast of the asset condition as well as its possibility of failure in the future. Significant research effort has been carried out in the last two decades to model infrastructure deterioration. The Markov deterioration process (MDP) is one approach that has gained prominence as exemplified by Madanat *et al*. (1997), Kleiner (2001) and others. Examples of other types of statistical models include Lu and Madanat (1994), Ramia and Ali (1997), Flourentzou *et al*. (1999), Ariaratnam *et al*. (2001) and others.

In recent years, increased research effort has been dedicated to the application of soft computing methods to assess infrastructure deterioration. Soft computing methods include techniques such as artificial neural network (ANN), genetic algorithms (GA), belief networks (BN), fuzzy sets and fuzzy techniques. Fuzzy techniques seem to be particularly suited to model the deterioration of buried infrastructure assets where data are scarce and cause-effect knowledge is imprecise. Consequently, we have developed the T-WARP (Transmission – Water Main Renewal Planner) to assess risk of transmission pipelines combining the advantages of both the Markov deterioration process and fuzzy logic.

A fuzzy set describes the relationship between an uncertain quantity x and a membership function which ranges between 0 and 1. A fuzzy set is an extension of the traditional set theory (in which x is either a member of set A or not) in that an x can be a member of set A with a certain degree of membership. Fuzzy techniques help address deficiencies inherent in binary logic and are useful in propagating uncertainties through models.

Membership functions are often represented by triangular fuzzy numbers (TFN), which permit the use of linguistic variables. To illustrate the concept, suppose that the age of a pipe is defined by five fuzzy subsets (or numbers), each representing an age grade; A_1 = "*new*", A_2 = "*young*", A_3 "*medium*", A_4 = "*old*" and A_5 = "*very old*", as illustrated in Figure 4. The fuzzy subset A_3 "*medium*" for example, has a membership function such that for age x below 20 years or above 60 years the membership to "*medium*" is zero, and for age between 20 and 60 years the membership follows straight lines that form a triangle. Fuzzy set A comprises the collection of the five subsets (or numbers) A_i. Further, a crisp (exact) pipe age can be mapped onto the fuzzy set A so that it has memberships of 0.52 and 0.4 to age grades *medium* and *old*, respectively (Figure 4).

In our so-called fuzzy –Markov deterioration approach we use the concept of fuzzy rules that define relationships between variables by means of fuzzy *if-then* propositions. For example: "If 'pipe' *is old* and 'pipe condition' is *good* then 'deterioration' *is slow*", where *old* and *good* and *slow* are linguistic constants represented by fuzzy sets (as in the age example above). An inference can be made, using the Mamdani (1977) algorithm, about how fast deterioration is if the pipe is only partially *old* (say 50% *old* and 50% *medium*) and its condition is only partially *good*. This method has the capacity to capture qualitative and highly uncertain knowledge. To describe the condition of the pipe we used a seven-grade fuzzy set: *excellent, good, adequate, fair, poor, bad,* and *failing.* The fuzzy Markov deterioration process is illustrated in Figure 5.

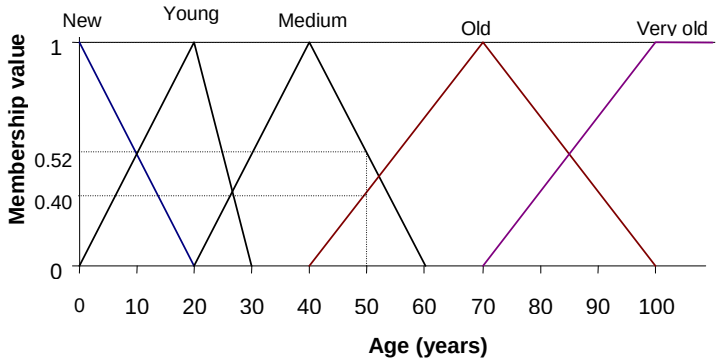

Figure 4. Example of fuzzy sub-sets (numbers).

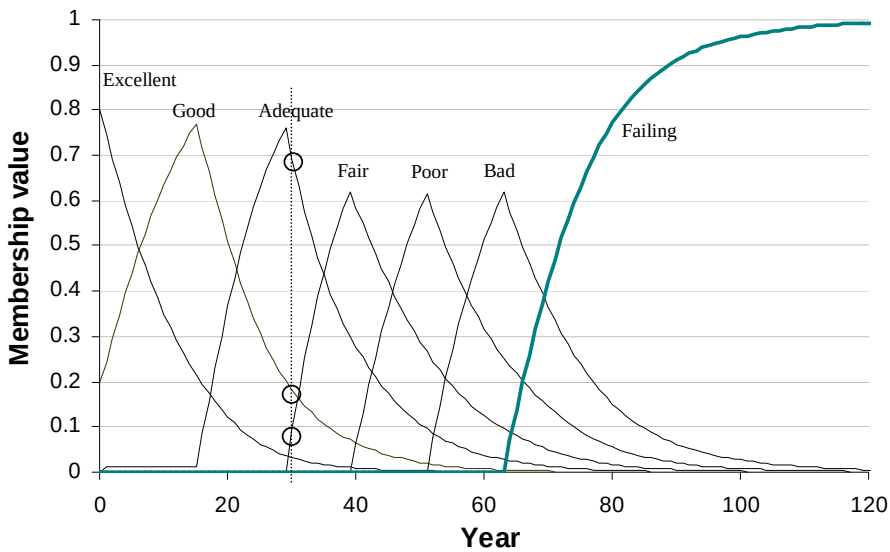

Figure 5. Fuzzy Markov deterioration curves.

As the pipe deteriorates, memberships "flow" from a given condition state to a worse one. The transition process is governed by a set of fuzzy rules (rather than transition probabilities as in the traditional Markov process), which is constructed based on expert opinion. Once deterioration curves are determined they are used to estimate the time in the future when the pipe is expected to approach the *failing* state. The deterioration model can be re-calibrated with each additional inspection and condition assessment. Any pipe inspection, whether visual, NDE or other reveals evidence about the existence and extent of distress indicators on the pipe. These distress indicators have to be interpreted and translated into the fuzzy condition states space described earlier. A condition assessment framework for translating the distress indicators into fuzzy condition states is described in detail by Rajani *et al*. (2006). Kleiner *et al*. (2006a) provide details on fuzzy Markov deterioration. Kleiner *et al*. (2006b), provide details on how to combine fuzzy deterioration

with fuzzy consequences into a life-cycle fuzzy risk of failure. A prototype software application of T-WARP is available from WRF, which co-funded the research.

Water quality deterioration in distribution pipes

Numerous factors affect water quality in the distribution network and interactions amongst them are complex and often not well understood. Water quality failures in distribution networks are scarce, which make it difficult to establish statistically significant generalizations. In such data-sparse circumstances, expert knowledge and judgment can serve as a supplement or even as alternative source(s) of information. Q-WARP (water Quality – Water Main Renewal Planner) is a proof-of-concept model to predict water quality changes in distribution pipe networks, developed at the NRC with co-funding from WRF (Sadiq *et al.*, 2009).

Several mechanisms can compromise water quality within a distribution network. These include (Kleiner, 1998): (1) Intrusion of contaminants into the distribution network through system components whose integrity is compromised or through misuse or cross-connection or intentional introduction of harmful substances in the water distribution network. (2) Formation of corrosion byproducts and leaching of chemicals from the internal pipe surface. (3) Regrowth of microorganisms in the distribution network. (4) Formation of disinfection byproducts (DBPs) and loss of residual disinfectants; and (5) Permeation of organic compounds from the soil through plastic components into the distribution network.

Q-WARP uses a soft computing technique called 'fuzzy cognitive maps' (FCM) to model causal relationship between the numerous factors influencing water quality in the distribution network. FCM is a cyclical graph comprising nodes and arcs (edges), as illustrated in Figure 6. Influencing factors are represented by nodes C_i and causal relationships are represented by directed arches. $w_{ij} \in [-1, 1]$ represents the nature and strength of the relationship between 'causal factor' i and 'effect factor' j and the sign

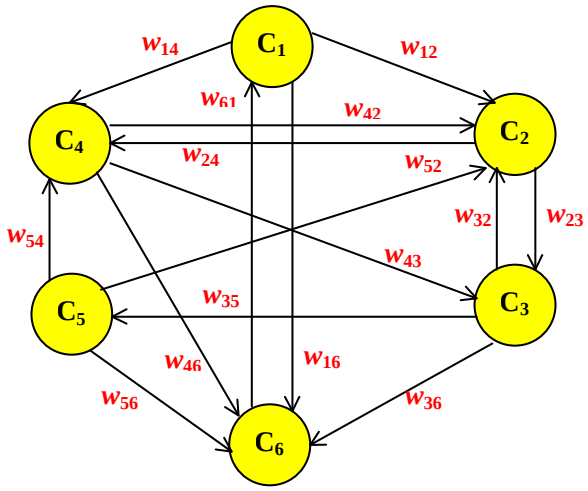

Figure 6. An example of a fuzzy cognitive map (FCM)

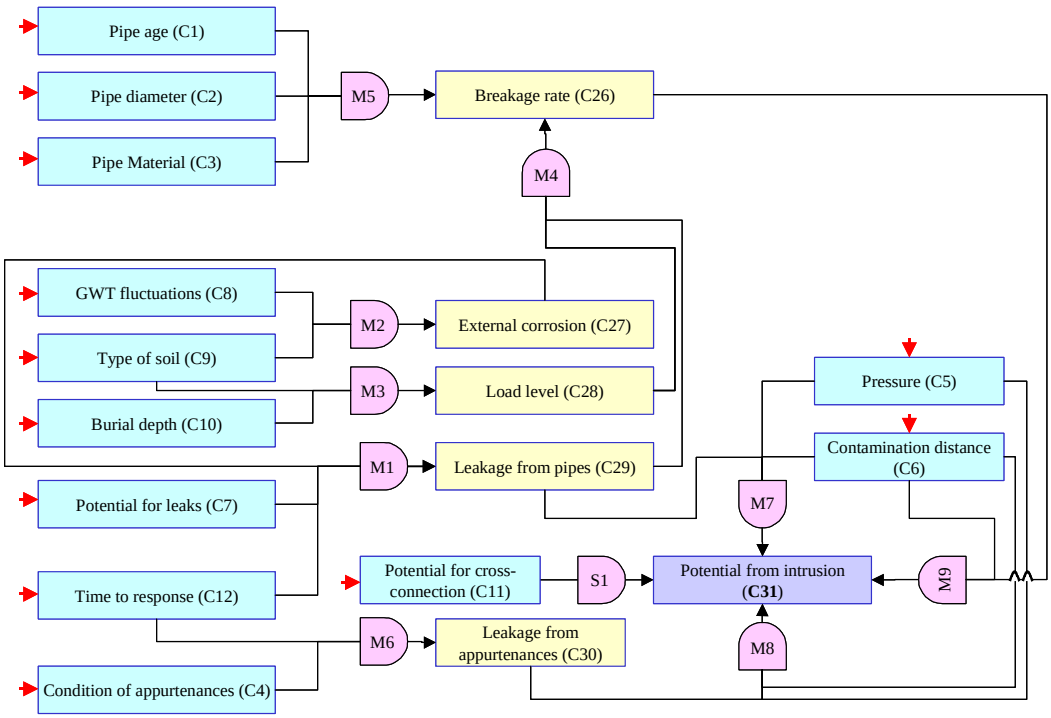

Figure 7. Modular FCM for predicting 'potential for contaminant intrusion'

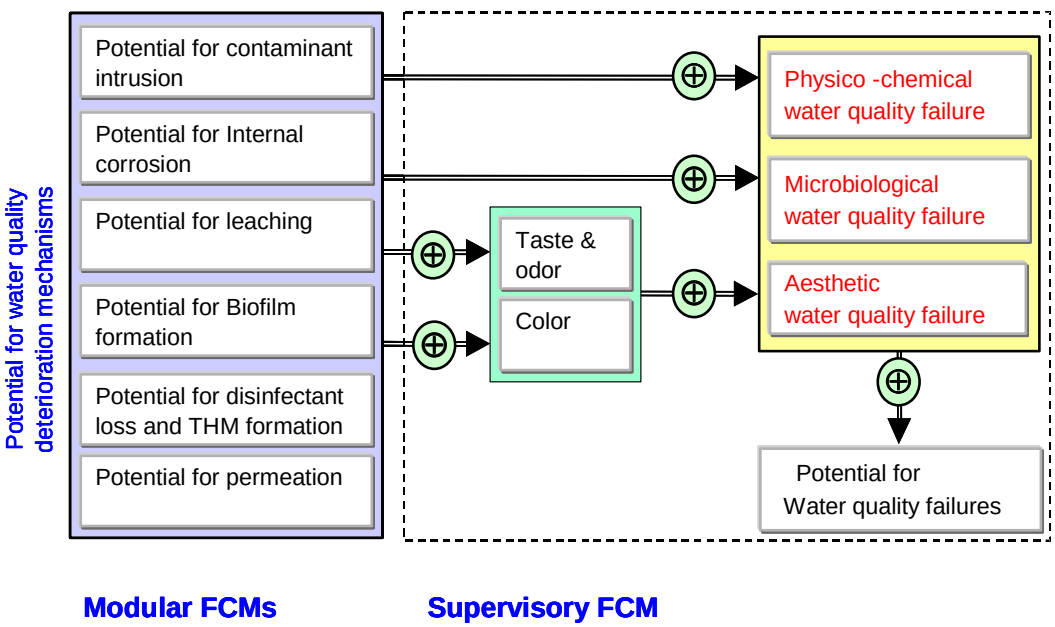

Figure 8. Two-tier (modular and supervisory FCM) framework

represents the type of causation. A positive causality is implied when $w_{ij} > 0$, where an increase in the value of *i* causes an increase in the value of *j* and vice versa. A negative causality is implied when $w_{ij} < 0$, where an increase in the value of *i* causes a decrease in the value of *j* and vice versa; and $w_{ij} = 0$ implies no causal relationship between *i* and *j*. Q-WARP is in fact a rule-base FCM, where causal relationships are defined by rules (e.g., 'if C_1 is high then C_2 is medium) similar to the rules described in the previous section.

Figure 7 illustrates the FCM representing processes leading to contaminant intrusion. The M_i gates represent rule sets that govern relationships between the various factors. Experience shows that if FCM are very large and 'democratic' (every node can be connected to every other node) they become insensitive to perturbations in inputs. Consequently, Q-WARP is designed as a two-tier framework, as is illustrated in Figure 8. Each of the six modular FCMs in tier 1 (representing six different WQ failure mechanisms) is in fact a FCM similar to the one illustrated in Figure 7 for contaminant intrusion. The outputs of the six modular FCMs flows into the supervisory FCM, whose output in turn yield the over potential for water quality failure. A full report on Q-WARP as well as a prototype software application is available from the WRF (Sadiq *et al.*, 2009).

Final remarks

In general, the industry seems to be progressing in the right direction despite many challenges and inherent complexities in the management and operations of water supply and distribution systems. Much progress has been made in the understanding of deterioration processes and failure modes. At the same time, as practices change and new materials are used, the knowledge gap, while decreasing from one end is increasing from the other. However, despite all these advances, too many water utilities still are not aware of the benefits of collecting and organising data that can be used in the various deterioration and decision support models.

As NDT techniques evolve, including the development of various sensors and robots, it appears that failure anticipation and prevention is likely to become technologically feasible as well as affordable. Currently, it seems that only mains prone to high-cost failure (namely transmission mains) can justify the use of these techniques, but this situation is likely to change over time. In the meantime, while the bulk of water distribution networks are comprised of small mains with relatively low failure consequences, NDT techniques can, in some circumstances, be used as complementary means to the empirical models, which rely on historical break records.

REFERENCES

Alegre, H., 1999. "Performance Indicators for Water Supply Systems – Current Trends and On-going Projects", pp. 148-178, *Drought Management Planning in Water Supply Systems*, Ed. by Carbera, E., and Garcia-Serra, J., Kluwer Publishers, Netherlands.

Ariaratnam, S.T., El-Assaly, A. and Yang, Y. 2001. "Assessment of infrastructure needs using logistic models". *Journal of Infrastructure Systems, ASCE,* 7(4): 160-165.

Flourentzou, F., E. Brandt, and C. Wetzel. 1999. "MEDIC – a method for predicting residual service life and refurbishment investment budget". *Proceedings of the 8th*

conference Durability of Building Materials and Components, Edited by M.A. Lacasse and D.J. Vanier, NRC, pp. 1280-1288, Vancouver.

Herz, R. 1999. "Bath-tubs and hammock-chairs in service life modelling". *Proceedings of the 13th European Junior Scientist Workshop*, pp. 11-18.

Kleiner, Y. 1998. "Risk factors in water distribution systems". *British Columbia Water and Waste Association 26th Annual Conference*, Whistler, BC, Canada.

Kleiner, Y. 2001. "Scheduling inspection and renewal of large infrastructure assets", *Journal of Infrastructure Systems*. ASCE, 7(4): 136-143.

Kleiner, Y. and Rajani, B.B. 2001a. "Comprehensive review of structural deterioration of water mains: statistical models". *Urban Water*, 3(3): 131-150.

Kleiner, Y.; Rajani, B.B.; Sadiq, R. 2006a. "Modelling the deterioration of buried infrastructure as a fuzzy Markov process," *Journal of Water Supply Research and Technology: Aqua*, 55, (2), pp. 67-80.

Kleiner, Y.; Rajani, B.B.; Sadiq, R. 2006b. "Failure risk management of buried infrastructure using fuzzy-based techniques". *Journal of Water Supply Research and Technology: Aqua*, 55, (2), pp. 81-94.

Lu, Y. and Madanat, S.M. 1994. "Bayesian updating of infrastructure deterioration models". *Transportation Research Record* 1442: 110-114.

Madanat, S.M., Karlaftis, M.G., and McCarthy, P.S. 1997. "Probabilistic infrastructure deterioration models with panel data". *Journal of Infrastructure Systems, ASCE*, 3(1): 4-9.

Mamdani, E.H. 1977. "Application of fuzzy logic to approximate reasoning using linguistic systems", *Fuzzy Sets and Systems*. 26: 1182-1191.

NACE. 1984. "Corrosion Basics – An Introduction". *National Association of Corrosion Engineers*, Edited by A. deS. Brasunas.

NRC-IRC, 2007. http://irc.nrc-cnrc.gc.ca/ui/software/dwarp/index_e.html

Office of Water (OFWAT) 1998. "Comparing Company Performance". *OFWAT Information Note No. 5*, London, England.

Rajani, B.B.; Kleiner, Y.; Sadiq, R. 2006. "Translation of pipe inspection results into condition rating using fuzzy synthetic valuation technique," *Journal of Water Supply Research and Technology: Aqua*, 55, (1), pp. 11-24.

Rajani, B. and Zhan, C. 1996. "On the estimation of frost load." *Canadian Geotechnical J.*, 33(4): 629-641.

Rajani, B.B. and Kleiner, Y. 2001b. "Comprehensive review of structural deterioration of water mains: physical models". *Urban Water*, 3(3): 151-164.

Rajani, B.B. and Tesfamariam, S. 2004. "Uncoupled axial, flexural, and circumferential pipe-soil interaction analyses of partially supported jointed water mains", Canadian Geotechnical Journal, 41(6): 997-1010.

Ramia, A.P. and Ali, N. 1997. "Bayesian methodologies for evaluating rutting in Nova Scotia's special B asphalt concrete overlays". *Canadian Journal of Civil Engineering*, 24(4): 1-11.

Sadiq, R., Kleiner, Y. and Rajani, B. 2009. "Proof-of-concept model to predict water quality changes in distribution pipe networks (Q-WARP)". Water Research Foundation, Denver, CO (forthcoming)

Tesfamariam, S., Rajani, B.B. and Sadiq, R. 2006. "Possibilistic approach for consideration of uncertainties to estimate structural capacity of ageing cast iron water mains", Canadian Journal of Civil Engineering, 33(8): 1050-1064.

US EPA, 2002. "Decision-Support Tools for Predicting the Performance of Water Distribution and Wastewater Collection Systems". EPA/600/R-02/029, US Environmental Protection Agency, Washington DC.

Yeppes, G., and Dianderas, A. 1996. "Water and Wastewater Utilities Indicators". *Water and Sanitation Division, World Bank.*

National Mains Failure Database Project

Neil S. Grigg[1]

[1]Department of Civil and Environmental Engineering, Colorado State University, Fort Collins, Colorado 80523-1372; PH (970) 491-3369; FAX (970) 491-7727; email: neilg@engr.colostate.edu

ABSTRACT

Water main breaks are a serious problem to utilities, and involve high cost as well as social disruption. Mitigating risk of breaks requires utilities to assess data on past failures and predict which mains are most likely to fail. The UK Water Industry Research has developed a National Mains Failure Database and the US Water Research Foundation has arranged for US utilities to participate. The database is being modified for use by US utilities and a pilot effort is scheduled for 2009. After experience with the database is gained, the Water Research Foundation will work with utility participants to modify and facilitate use of the database.

INTRODUCTION

Breaks in transmission and distribution mains are a serious problem for water utilities because buried pipes are their most costly capital assets and the condition of mains is a major risk factor. Main breaks are an indicator of infrastructure condition, and utilities in the US suffer about 250,000 to 300,000 of them every year. The cost to the nation for these main breaks cannot be quantified exactly, but is on the order of several billion dollars per year. For example, Gaewski and Blaha (2007) analyzed 30 breaks of mains 20-inches and larger and found that the cost of each failure was about $500,000, based on the geometric mean of the data. While many breaks are much smaller and less expensive, the total cost to the nation is high.

Mitigating risk of water main breaks requires utilities to assess which mains are most likely to fail. When utilities prepare business cases for pipe replacement in their capital budgets, they must estimate this risk so they can compute rates of return of remediation projects. While surveys show that utilities are aware that they should undertake pipe renewal programs, it is difficult to decide which pipes to renew because utilities cannot predict probability of failure for individual pipes, although they may be able to estimate the expected number of system-wide failures to expect. Utilities are aware of the need to manage main break data, and guidance is available to establish databases (Wood and Lence, 2007).

To confront this issue, the Water Research Foundation (formerly the AWWA Research Foundation or AwwaRF) has sponsored several projects about main breaks. These include projects on research needs, condition assessment, unique attributes of different pipe types, and modeling of break rates. These projects have provided

valuable information, but many individual utilities are unable to use the information because they lack organized data of their pipe inventories and break rates.

Utility plans to mitigate main break risk must be based on asset data, condition assessment, planning and prioritization, and action plans. While many utilities have basic databases of their water mains, no national register of these exists. Also, no national study of water main breaks across utilities has been conducted.

The UK experiences some 70,000 main failures per year, or roughly one-fourth those in the U.S. In the UK, main break rates are assessed at the national level through water utility regulatory reports. Through the UK Water Industry Research (UKWIR) organization, utilities in the UK have organized a National Mains Failure Database (NMFD) to help them study main breaks and prepare reports. UKWIR is a collaborative water industry research organization based in London which facilitates research projects of common interest to member water companies.

The US Water Research Foundation has decided to sponsor an effort to join the UK effort and organize a US national database. Australia has made the same decision through the Water Services Association of Australia (WSAA). This paper explains the structure and organization of the NMFD and the schedule by which it will be developed. Uses of the database will be explained, with an emphasis on the differences between US and UK conditions and reporting requirements.

OVERVIEW OF THE NMFD

The history of the NMFD has been summarized by MacKellar (2005), one of the developers of the software. The work includes a database of water main failures in the UK, along with a protocol for data collection of mains and failure information.

UKWIR works with twenty-three principal water companies in the UK (England, Wales, Scotland, Northern Ireland), and are regulated by the Office of Water Services (OFWAT). The NMFD managed by UKWIR contains data on known main failures from the water companies presented in the same format and classified by variables that include pipe materials, diameters, dates, land use and failure modes. The database also includes data on pipe stock, and can be viewed as a national asset register of water mains. Sewer failures are also included in the UK NMFD, but are not addressed in this paper.

The goal of UKWIR's NMFD for water mains is to provide "robust, validated data on which deterioration modelling and asset investment strategies can be based." The database includes records of water mains by material, age, diameter and length, along with other attributes such as geographical location. The length of mains covered is about 350,000 km and some 470,000 failures, mostly from 1994 to 2002, are included (UKWIR, 2006).

The planning for the NMFD was explained in (UKWIR, 2003). It includes the principles of the protocol for data management and explains how widespread

reporting differences made comparisons difficult. The protocol proposes best practices to overcome the differences and provide a practical way to manage data.

The UK water companies upload their asset and failure data to the NMFD software, which manages the data and provides tools to generate reports. Anonymity of the data providers is preserved in that companies can get reports of their own data and national reports of all data, which preserve the anonymity of the individual companies. Reports that are currently available include failure rate, number of failures and pipe length involved, failure rate area report, and statistical reports.

UK utilities work with the NMFD through its website, which enables them to upload their pipe and failure data using a "Compilation Tool."[1] This tool enables companies to organize their data in comma-separated-value (.CSV) files, which facilitate the upload. The NMFD software takes over from there to organize and catalog the data.

Examples of pipe data attributes that are included in the UK version are: identification number, diameter, material type, location, lining, ground surface type, installation year, and whether the main has pumped or gravity flow. Failure data items include type of failure, whether third-party damage was involved, location, and other related information.

The Water Research Foundation is working with UKWIR to add and/or change data items to correspond to US conditions and practices, which vary widely among utilities. The challenges to face include how to include geographic information, how to import soils data, and how to coordinate the many different practices for collecting and managing pipe data among US utilities.

US UTILITY PARTICIPATION

The Water Research Foundation is working with a group of utilities for an initial trial of the database. The initial effort to establish the US part of the NMFD is taking place during 2008 and 2009, and is planned to involve around 10 utilities. Plans are to begin data upload in the first half of 2009 and then to assess needed changes. Following completion of this phase, plans will be made to extend and improve the database and its applications.

A US utility participant in the NMFD will upload its water main and break data to the database in the same way as UK water companies do. Utility commitments are limited to uploading and management of their own data. By loading their data into the national database, utilities gain organization and analysis insights for their asset data.

Data will be kept anonymous so that no one other than the utility can see its individual characteristics, while displaying the overall statistics of all utilities to all

[1]The website address is: http://sewersandwatermains.ukwir.org/site/mains/home.

participants. This combined anonymity of individual utilities and transparency of all statistics taken together gives utilities a chance to compare their data with others so they can sharpen their investment planning.

A utility participant will prepare its data for uploading in CSV files in the same way that UK water companies will. The Water Research Foundation will work with the utility's key contact and provide advice for data organization, cleaning, and uploading. Technical support will be provided through UKWIR's existing service desk.

The initial planning by the Water Research Foundation resulted in a few changes to the data formats specified by UKWIR. One important difference is the geographical referencing of pipe and failure locations, which still must be worked out for US utilities. In the UK, a national grid provides a single coordinate system for the nation and is a basis to geo-reference pipe data. The US has a state plan coordinate system, but it does not provide a unified national grid system. Utilities with effective GIS systems are able to use latitude and longitude data for location, but they are not always able to locate pipes and failures using this information. A wide range of practices is in effect, and it is anticipated that initial work with the NMFD may offer a path to more standard approaches.

Looking ahead to the possibility of using the US NMFD as a tool to improve understanding of the causes of main failures, the Water Research Foundation has added attributes to the database that relate to historical US pipe failures. These include several data items that have been identified in reports such as (Kirmeyer et. al., 1994), which reported that the most common causes of main breaks were materials and deterioration, weak joints, earth movement, freezing, internal corrosion, corrosive soils, construction or utility digging, stray DC current, seasonal changes in water temperature, and heavy traffic load.

After the US version of the database is populated, utilities will be able to use models and other predictive methods to assess risk of failure based on their own data or on national experience. A number of mathematical models have been published, and these are summarized in (Grigg, 2005).

MANAGEMENT QUESTIONS FOR US UTILITIES

The general concept of the NMFD is that US utilities will upload water main break data to the US national database, managed by UKWIR. Data will be kept anonymous so that no one other than the utility can see its individual characteristics, but US utilities can obtain the overall statistics of breaks for all US utilities without knowing the sources of the data. This combined anonymity of individual utilities and transparency of all statistics taken together gives utilities a chance to compare their data with others so they can sharpen their investment planning.

A US utility participant will prepare its data for uploading by organizing it in a format supplied by the Water Research Foundation, which will work with the utility's key contact and provide technical advice for data organization, cleaning, and uploading.

Utilities will not have to pay for access to the national database as their commitments are limited to uploading and management of their own data. By loading their data into the national database, utilities gain organization and insights for their asset data. US utility participants who are Water Research Foundation subscribers will be able to generate reports from their data uploaded into the UKWIR database.

Agreements and licenses are needed between the Water Research Foundation and UKWIR and with participating utilities. Currently, UKWIR and each participating company in the UK sign a license agreement to use the software. Details on how these would work in the US are still to be developed. Provisions that will be important to US utilities will include: ownership of data, assurance of anonymity, rights of use, agreement by the water research foundation to finance the database, and access by researchers, among others.

CONCLUSIONS

Main breaks are an important problem for utilities, and are poised to worsen as infrastructure ages. While utilities know of the problem, they are often stymied in their attempts to invest in renewal because they do not know the probable rates of failure of individual pipes. Knowing these rates will always involve some uncertainty, but empirical data through an organized NMFD will improve knowledge of actual conditions in a utility's asset base and offer utilities a good way to organize and manage their pipe failure data.

As UKWIR has already invested in development of the software and website for the NMFD, US water utilities have a good opportunity to take advantage of this emerging tool to manage their pipe failure data. The Water Research Foundation has made arrangements to work with a limited number of US utilities to upload their data and participate in the NMFD. Once a trial period has been completed, additional US utilities may participate and further details on how the database will be managed can be prepared.

A number of management questions must also be answered, including ownership, assurance of anonymity, how to facilitate upgrades to the software, and how to train users and coordinate utility participation in the future. These questions will be faced in cooperation with UKWIR and the Australian utility organizations.

The NMFD offers an excellent opportunity for US utilities to work together to share knowledge about water main failures and their causes. The new knowledge developed will help them to upgrade engineering, construction, and maintenance procedures to reduce the incidence and consequences of water main failures in the US.

REFERENCES

Gaewski, Peter E. and Blaha, Frank J. (2007). *Analysis of Total Cost of Large Diameter Pipe Failures*. AWWA Distribution System Research Symposium. Reno, Nevada, March 2.

Grigg, Neil S. (2005). *Main Break Prediction, Prevention, and Control*. AwwaRF report. Denver.

Kirmeyer, G.J., W. Richards, and C.D. Smith. (1994). *An Assessment of Water Distribution Systems and Associated Research Needs.* Denver, CO: Denver, Colo.:AwwaRF and AWWA.

MacKellar, Steve. (2006). UKWIR National Mains Failure Database. International Conference of Plastics Pipes XIII. Washington, DC, October.

UKWIR. (2003). Nationally *Agreed Failure Data and Analysis Methodology for Water Mains* (two volumes). Report 03/RG/05/7. London.

UKWIR. (2006). *Capital Maintenance Planning: Failure Data and Analysis Methodology for Water Mains*. Report 06/RG/05/16. London.

Wood, Andrew and Lence, Barbara. (2007). "Constructing Water Main Break Databases for Asset Management." *Journal American Water Works Association*, 99(1) 52-65.

Needs and Trends of the Nation's Water Infrastructure - The Utility Perspective

By

Steven Buchberger[1], Robert Clark[2], Walter Grayman[3], Zhiwei Li[1], Matthew McCutcheon[1] and Jeff Yang[4]

[1]Department of Civil and Environmental Engineering, University of Cincinnati, Cincinnati, OH 45221-0071; PH (513) 556-3681, (513) 675-5988; FAX (513) 446-2599; email: steven.buchberger@uc.edu , zhiwei.li@uc.edu, mccutcmd@email.uc.edu

[2]Environmental Engineering and Public Health Consultant, 9627 Lansford Drive, Cincinnati, OH 45242; PH (513) 891-1641; FAX (513) 891-2753; email: rmclark@fuse.net

[3]W.M. Grayman Consulting Engineer, 321 Ritchie Ave., Cincinnati, OH, 45215, PH: (513) 761-1722, email: grayman@fuse.net

[4]US Environmental Protection Agency, ORD/NRMRL/WSWRD, 26 W. Martin Luther King Drive, Cincinnati, OH 45268; PH (513) 569-7655; FAX (513) 569-7185; email: Yang.Jeff@epa.gov

Abstract

*Widespread changes in the climate, demographics, population and economics are expected to impact the quantity, quality and timing of water resources across the globe in the 21st century. Some of these impacts may affect the performance and sustainability of the Nation's urban water resources infrastructure. In anticipation of these imminent global changes and their impact on the Nation's water infrastructure, the U.S. Environmental Protection Agency is implementing the **W**ater **R**esources **A**daptation **P**rogram for Infrastructure (**WRAP-Infrastructure**). **WRAP** seeks to identify and evaluate innovative approaches to improve the planning, design, operation and maintenance of the Nation's water resources infrastructure in the 21st century. A key question to be addressed by the **WRAP** program is, "How can the functionality of the Nation's aging water infrastructure be maintained and sustained to protect human health and preserve the environment for future generations in the face of profound global changes?" To help answer this question, a national data collection effort was conducted with water utilities to identify key factors affecting the current and future performance and sustainability of the water resources infrastructure across the US. Over 60 public and private water and wastewater utilities responded to a detailed web-based questionnaire. Data from this national reconnaissance are reported here.*

Key Words: **water resources, aging infrastructure, climate change.**

BACKGROUND

ASCE President, D. Wayne Klotz, refers to the global infrastructure as the "cathedral of modern civilization" (Klotz 2008). The portion of the national infrastructure responsible for supplying drinking water and disposing of wastewater is ranked among the top five engineering achievements of the 20th century (National Academy of Engineering 2008). These engineering accomplishments have led to an unprecedented standard of living in developed countries around the globe.

Can this standard be sustained? The national inventory of pipes, pumps, plants, and tanks has a high premium. Maintenance of the U.S. water infrastructure has been largely neglected for the past 50 years (Levin *et al* 2002). This lack of attention is reflected in recent ASCE Report Cards on America's Infrastructure which assign "D-" grades to the water and the wastewater areas (ASCE 2005, ASCE 2009).

Clearly, the United States faces an unprecedented challenge in the 21st century: Can the Nation's aging water infrastructure be repaired and restored in a manner that promotes economic and environmental sustainability while protecting human health and preserving the environment for future generations? This daunting assignment is exacerbated by the convergence of national and global trends involving changing climate, evolving institutions, growing population, regulatory issues, and uncertain economics.

In anticipation of these imminent global changes and their impact on the Nation's water infrastructure, the U.S. Environmental Protection Agency has implemented the **W**ater **R**esources **A**daptation **P**rogram for Infrastructure (**WRAP-Infrastructure**). **WRAP** seeks to identify and evaluate innovative approaches to improve the planning, design, operation and maintenance of the Nation's water resources infrastructure in the 21st century (Buchberger *et al* 2008).

A key question considered under the **WRAP** initiative is: How does the Nation's water industry view these impending challenges? To help answer this question, a 40+ question web-based survey was distributed on-line via several national water organizations (AMWA, NACWA, NAWC) to a select subset of the nation's drinking water and wastewater utilities during the summer of 2008. The main objective of the questionnaire was to identify, through the eyes of the Nation's water industry, the most important factors likely to affect the performance and sustainability of the public and private water resources infrastructure across the United States over the next 50 years.

This paper provides a brief overview of some of the key findings from this national survey of the water infrastructure.

METHOD

The research team partnered with three national drinking water and wastewater industry organizations to collect information on utility perceptions of key issues that they will be facing in the future. In each case, the research team worked closely with the organizations to develop a vehicle to collect information from member utilities. Data collection was performed using the Survey Monkey (www.surveymonkey.com) website. The participating water organizations are:

- **AMWA** - The Association of Metropolitan Water Agencies (AMWA) is an organization of the largest publicly owned drinking water systems in the United States. AMWA's membership serves more than 130 million Americans with drinking water from Alaska to Puerto Rico. http://www.amwa.net/

- **NACWA** – The National Association of Clean Water Agencies (NACWA) represents the interests of the country's wastewater treatment agencies, true environmental practitioners that serve the majority of the sewered population in the United States, and collectively treat and reclaim more than 18 billion gallons of wastewater each day. http://www.nacwa.org/

- **NAWC** - The National Association of Water Companies (NAWC) represents all aspects of the private water service industry. The range of members' business includes ownership of regulated drinking water and wastewater utilities and the many forms of public-private partnerships and management contract arrangements. NAWC's membership ranges in size from large companies owning and/or operating many hundreds of utilities in multiple states to individual utilities with only a few hundred customers. http://www.nawc.org/index.html

The on-line survey contained 42 questions and was designed to be completed at one sitting within an hour. The main topics covered in the questionnaire are summarized in Table 1.

Table 1. Main sections of the on-line questionnaire.

Section Number	Number of Questions	Survey Topic
1	0	Motivation
2	9	Utility Profile
3	18	Infrastructure and Operation
4	5	Agents of Change
5	8	Master Plan
6	2	Contact Information (optional)
Total	42	

RESULTS

A total of 55 water utilities responded representing nearly 43 million customers with infrastructure assets that included 91 water treatment plants, over 520 storage tanks, nearly 1200 pumping stations and over 73,000 miles of pipeline. A profile of participating utilities is given in Table 2; the geographic distribution is shown in Figure 1.

Table 2. Participant profile of utilities completing the on-line questionnaire.

Feature	Drinking Water	Wastewater	Total
Number of Utilities	31	24	55
Customers (million)	16.83	25.83	42.7
Summer Flow (mgd)	3,450	2,686	6,136
Water Use (gpcd)	135	160	295
20-yr Projected Growth	24%	17%	~1% per yr
Miles of Pipeline	47,135	26,117	73,252
Pumping Stations	426	735	1,161
Storage Tanks	526	0	526
Treatment Plants	43	48	91

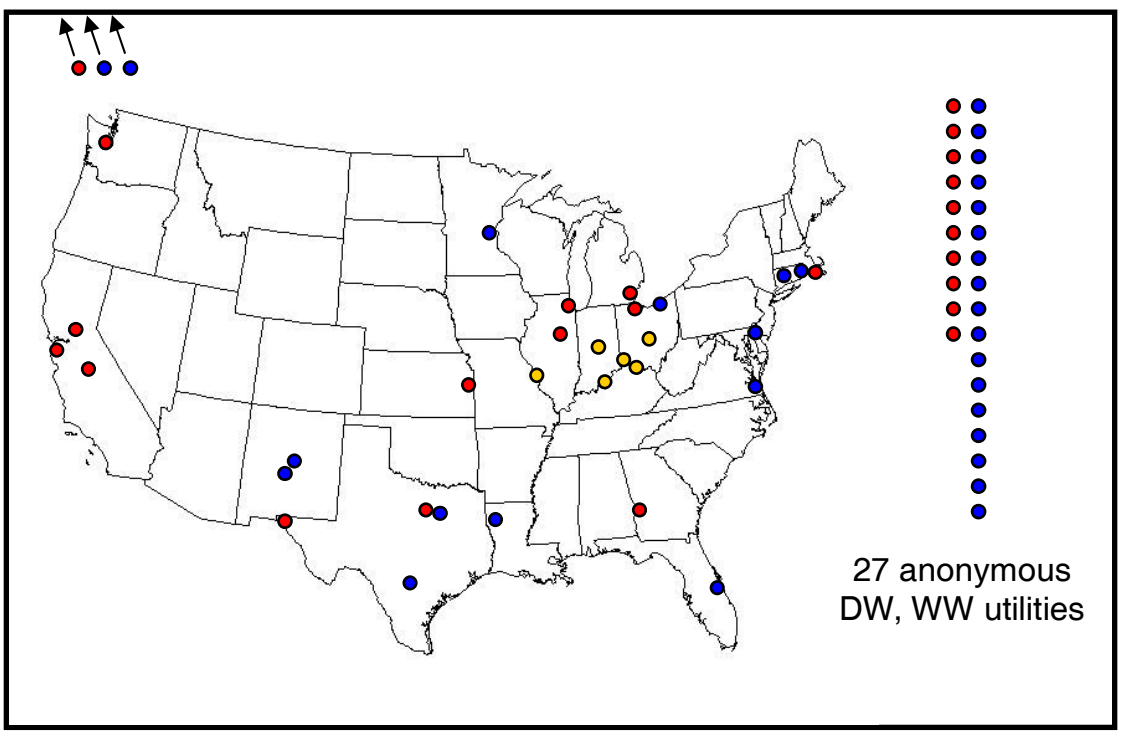

Figure 1. Participants in National Water Infrastructure Survey (red, yellow = wastewater; blue = drinking water)

Projected Growth, Master Plan, Asset Management

Four out of five utility respondents expected demand for water service to increase over the next 20 years with an average annual growth rate of about one percent (see Figure 2). This is consistent with population projections for the United States which forecast the number of U.S. residents to grow from 280 million to 420 million during the period 2000 to 2050 (Hobbs and Stoops 2002). About one in five water utilities expected to maintain the status quo, while one utility in each sector (i.e., drinking water and wastewater, representing less than five percent of the total respondents) anticipated a net decrease in utility size and service over the next 20 years.

Most water agencies had developed a formal master plan (see Figure 3). The master plan response closely mirrors the picture of anticipated growth (e.g., compare to Figure 2). It seems that water utilities who expect growth have a formal mechanism in place to help plan for it. Planning horizons ranged from 5 to 40 years with a median of about 20 years. Surprisingly, however, a significant percentage of water utilities (nearly 40%) have not implemented a formal asset management program (see Figure 4). A recent survey by the U.S. Conference of Mayors found that cities employing asset management practices are "gaining the information and knowledge they seek to determine the level of user rates that can lead to system sustainability" (Anderson 2007). Encouraging widespread adoption of asset management practices holds promise as a relatively simple but practical tool for helping the water industry better cope with anticipated challenges that will confront future utility operation.

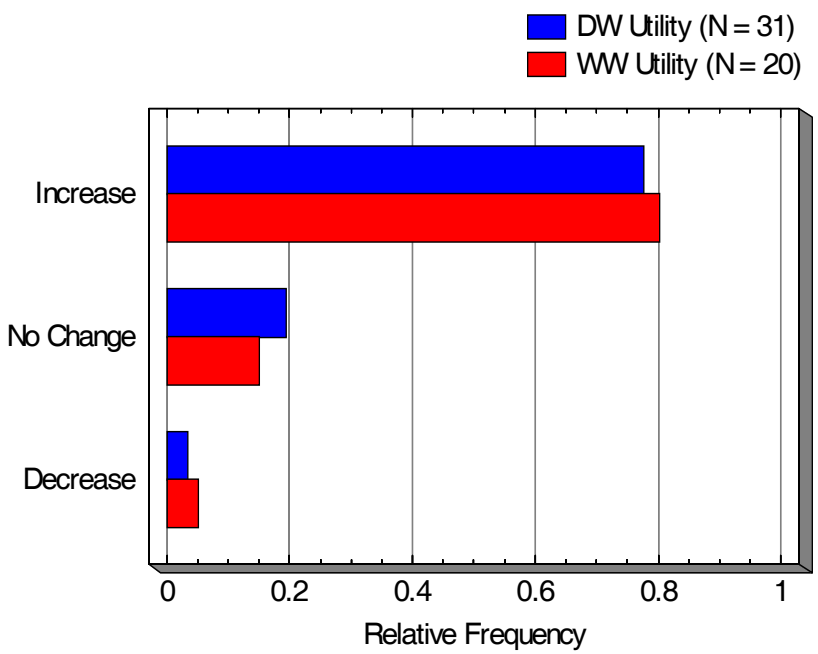

Figure 2. Projected water utility growth over the next 20 years.

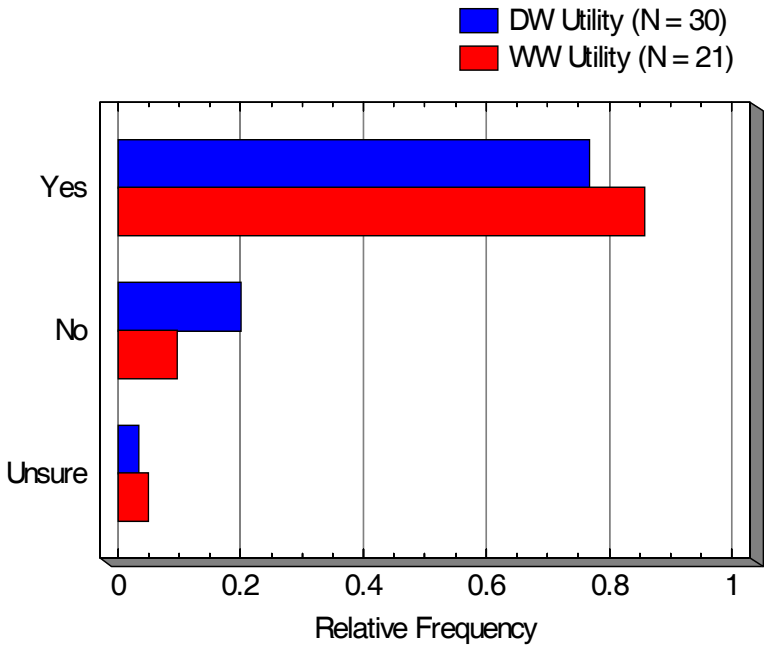

Figure 3. Water utilities with a master plan in place for future growth.

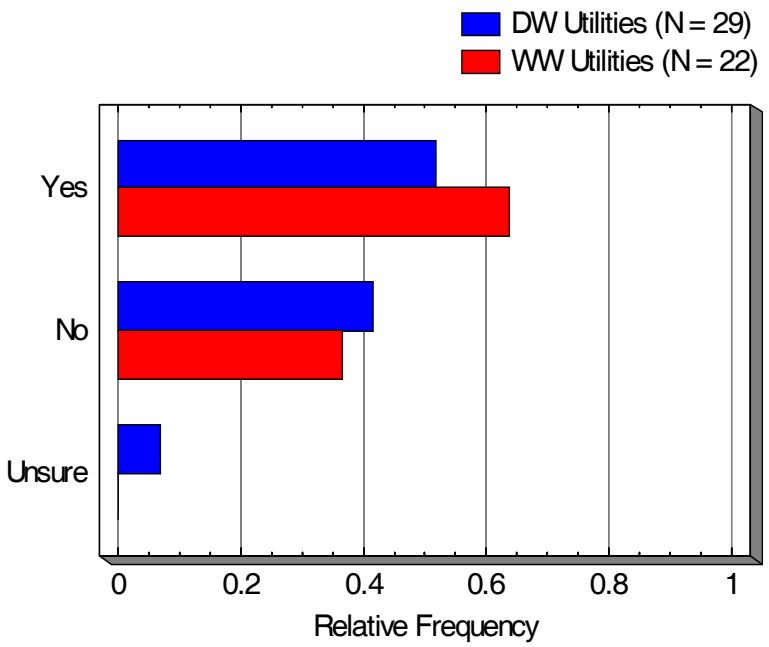

Figure 4. Water utilities with an asset management program.

Water Infrastructure Components

Of the four primary water-related infrastructure categories (pipes, pumps, tanks, plants), the pipeline systems used to distribute drinking water and collect wastewater were judged by the water utilities to be in the worst condition (see Figure 5). The generally poor self-assessment of existing urban water piping systems is consistent with the overall low grade assigned to the drinking water and wastewater sectors in recent ASCE report cards on the Nation's infrastructure (ASCE 2005, ASCE 2009). While the piping network is the portion of the national water infrastructure that is least in the public eye, it often represents the single largest collective capital investment for most water utilities. In comparison to the pipe network, pumping stations, storage tanks and treatment plants tended to fare slightly better in the self-assessment of infrastructure performance and condition.

Critical Future Issues

From a list of ten potential issues, the top three challenges perceived by the water industry to have the greatest impact on the operation and performance of the Nation's water utilities over the next 50 years were identified as: [i] aging infrastructure, [ii] government regulations and [iii] funding shortfalls (see Figure 6). These issues are consistent with the drinking water and wastewater sectors and reinforce key points of the recent infrastructure gap analysis (US EPA 2002). While climate change was recognized as an impending issue, it was viewed as a more distant concern in comparison to the immediate operational needs of the water utility.

SUMMARY

The Nation's water infrastructure ranks among the top engineering achievements of modern society. Public health benefits of this national infrastructure are enormous. Waterborne infectious diseases have been virtually eliminated from the United States. However, this triumph of the 20th century may be in jeopardy. Several major global changes, each with potentially serious consequences for the water industry, loom on the horizon. In the eyes of the engineers and executives from 55 utilities, the three most critical issues facing the water industry at the dawn of the 21st century are: [i] infrastructure decay [ii] federal regulations and [iii] funding sources. Other key concerns include: population growth, institutional evolution and climate change. On an individual basis, any of these issues poses a stiff challenge to the industry-wide mission of producing safe water to protect public health. Taken collectively, the combined impact of these critical factors could catalyze synergistic stresses that exceed the worst-case operating conditions envisioned during design and construction of the original water infrastructure. Fortunately, the national water industry is proactive (Means *et al* 2005; Daigger 2007; Freas *et al* 2008). The industry-wide practice of developing and updating a master plan provides a ready opportunity for incorporating flexible mitigation and adaptation strategies to help water utilities cope with anticipated impacts from aging infrastructure, global climate changes and other impending challenges. The key is recognizing which battle to fight.

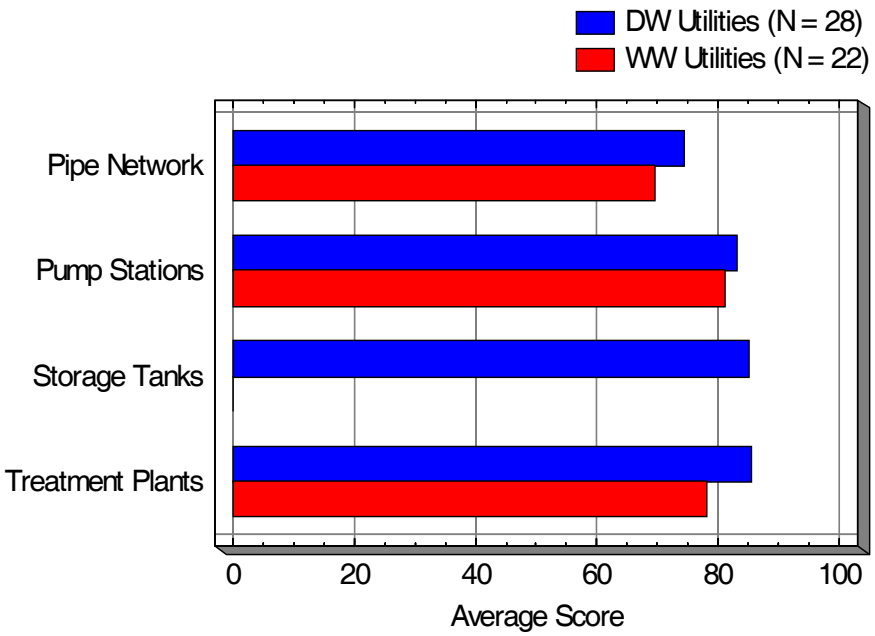

Figure 5. Self assessment of infrastructure performance and condition.

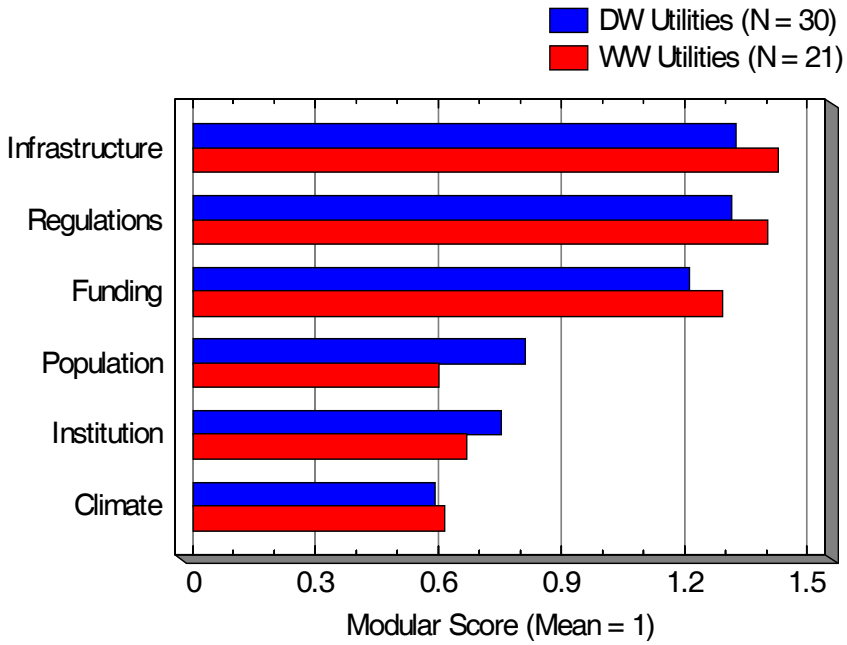

Figure 6. Critical issues facing the nation's water utilities.

ACKNOWLEDGMENTS

This study is part of Water Resources Adaptation Program-Infrastructure supported by USEPA under project/contract EP-C-05-056. This report has not been subject to review by USEPA. Any opinions expressed in this paper are those of the authors and do not necessarily reflect the views of the Agency; therefore, no official endorsement should be inferred. Any mention of trade names or commercial products does not constitute endorsement or recommendation for use. The timely cooperation of AMWA, NACWA and NAWC in assisting with data collection from the dozens public and private water utilities is greatly appreciated.

REFERENCES

ASCE (2005) Report Card on America's Infrastructure: http://www.asce.org/reportcard/2005/

ASCE (2009) Report Card on America's Infrastructure: http://www.asce.org/reportcard/2009/

Anderson (2007) National City Water Survey - The Status of Asset Management Programs in Public Water and Sewer Infrastructure in America's Major Cities, Mayor's Water Council, The U.S. Conference of Mayors, Washington, DC, 28 pp.

Buchberger, S.G., Clark, R.M. Grayman, W.M., Li, Z., Tong, S., Yang, Y.J. (2008). Impacts of global change on municipal water distribution systems. *Proceedings of 2008 International Symposium on WDSA*, Kruger Park, South Africa.

Daigger, G.T. (2007). Wastewater management in the 21st century. J. Environmental Engineering , ASCE. 133(7): 671-680.

Freas, K., B. Bailey, A. Munevar, S. Butler (2008) Incorporating climate change in water planning, *Journal American Water Works Association*, 100(6):92-99.

Hobbs, F. and N. Stoops, (2002) U.S. Census Bureau, Census 2000 Special Reports, Series CENSR-4.

Klotz, D.W. (2008) Infrastructure is cathedral of modern civilization, *ASCE News,* 33(12):1.

Levin, R.B., P.R. Epstein, T.E. Ford, W. Harrington, E. Olson and E.G. Reichard (2002) US drinking water challenges in the 21st century, *Environmental Health Perspectives*, 110(1):43-52.

Means III, E.G., L. Ospina, and R.Patrick (2005) Ten primary trends and their implications for water utilities, *Journal American Water Works Association*, 97(7), 64-77.

National Academy of Engineering (2008). http://www.nae.edu/nae/grainger.nsf

US EPA (2002) The Clean Water and Drinking Water Infrastructure Gap Analysis, *EPA-816-R-02-020.* 50 pages.

Combined Energy and Pressure Management in Water Distribution Systems

P. Skworcow[1], H. AbdelMeguid[1], B. Ulanicki[1], P. Bounds[1] and R. Patel[2]

[1]Process Control - Water Software Systems, De Montfort University, The Gateway, Leicester, LE1 9BH, UK, phone: +44 116 257 7070, emails: {pskworcow, habdelmeguid, bul, plmb}@dmu.ac.uk
[2]Yorkshire Water Services, Western House, Halifax Road, Bradford, BD6 2SZ, UK, email: ridwan.patel@yorkshirewater.co.uk

ABSTRACT

In this paper a method is proposed for combined energy and pressure management via integration and coordination of pump scheduling with pressure control aspects. The proposed solution involves: formulation of an optimisation problem with the cost function being the total cost of water treatment and pumps energy usage, utilisation of an hydraulic model of the network with pressure dependent leakage, and inclusion of a PRV model with the PRV set-points included as a set of decision variables. Such problem formulation led to the optimizer attempting to reduce both energy usage and leakage. The developed algorithm has been integrated into a modelling, simulation and optimisation environment called FINESSE. The case study selected is a major water supply network, being part of Yorkshire Water Services, with a total average demand of 400 l/s.

1. INTRODUCTION

Water distribution systems, despite operational improvements introduced over the last 10-15 years, still lose a considerable amount of potable water from their networks due to leakage, whilst using a significant amount of energy for water treatment and pumping. Due to increasing energy prices, research aimed at the reduction of energy usage via the optimisation of pumps' operation (pump scheduling) has received significant interest in recent years, see e.g. (Bounds et al 2006; Ulanicki et al 2007; Ormsbee et al 2007). Minimisation of leakage, hence reduced losses of clean water and energy used for pumping and treatment, can be achieved by introducing pressure control algorithms (Ulanicki et al 2005). Whilst pump scheduling and pressure control are traditionally considered separately, if the pressure reducing valve (PRV) inlet pressure is higher than required, in many networks it could be reduced by adjusting pumping schedules in the upstream part of the network. Since many modern pumps are equipped with variable speed drives, manipulating their speed can be employed to control the pressure, thus reduce leakage and energy use.

In this paper a method is proposed for combined energy and pressure management via integration and coordination of pump scheduling with pressure control aspects. The developed algorithm has been integrated into a modelling,

simulation and optimisation environment called FINESSE, which utilises GAMS modelling language and CONOPT non-linear programming solver. The research forms a part of the Neptune project (Neptune 2006) and aims to minimize the leakage and the energy usage whilst supplying good service to customers. In Section 2 general description of the proposed method is provided. Section 3 considers formulation of an optimal network scheduling problem. Section 4 briefly describes implementation and in Section 5 case study is presented.

2. GENERAL METHODOLOGY DESCRIPTION

The proposed method for combined energy and pressure management, based on formulating and solving an optimisation problem, is an extension of the pump scheduling algorithms described in (Ulanicki et al 1999; Bounds et al 2006). The main differences between these methods and the one proposed in this paper are in the network model and in the decision variables set.

The proposed method involves utilisation of an hydraulic model of the network with pressure dependent leakage and inclusion of a PRV model with the PRV set-points included as a set of decision variables. The cost function remains as in (Ulanicki et al 1999; Bounds et al 2006), i.e. represents the total cost of water treatment and pumping. Figure 1 illustrates that, with such approach, an excessive pumping contributes to a high total cost in two ways. Firstly, it leads to high energy usage. Secondly, it induces high pressure, hence increased leakage, which means that more water needs to be pumped and taken from sources. Therefore the optimizer, by minimising the total cost, attempts to reduce both energy usage and leakage.

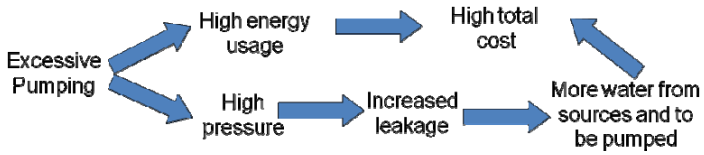

Figure 1. Illustrating how excessive pumping contributes to high total cost when network model with pressure dependent leakage is used.

In the optimisation problem considered some of the decision variables are continuous (e.g. water production, pump speed, and valve position) and some are integer (e.g. number of pumps switched on). Problems containing both continuous and integer variables are called mixed-integer problems and are hard to solve numerically. Continuous relaxation of integer variables (e.g. allowing 2.5 pumps on) enables network scheduling to be treated initially as a continuous optimisation problem solved by a non-linear programming algorithm. Subsequently, the continuous solution can be transformed into an integer solution by manual post-processing, or by further optimisation, see (Bounds et al 2006). For example, the result "2.5 pumps on" can be realised by a combination of 2 and 3 pumps switched over the time step. In this paper only continuous optimisation problem is considered, with the continuous solution of case studies (described in Section 5) being discretised by manual post-processing.

3. OPTIMAL NETWORK SCHEDULING PROBLEM

Network scheduling calculates least-cost operational schedules for pumps, valves and treatment works for a given period of time, typically 24 hours. The decision variables are the operational schedules for control components, such as pumps, valves (including PRVs) and water works outputs. The problem has the following three elements:

1. objective function,
2. hydraulic model of the network,
3. constraints.

The scheduling problem is succinctly expressed as: minimise (pumping cost + treatment cost), subject to the network equations and operational constraints. The three elements of the problem are discussed in the following subsections. The problem is expressed in discrete-time, as in (Ulanicki et al 1999; Bounds et al 2006).

3.1. Objective function. The objective function to be minimised is the total energy cost for water treatment and pumping. Pumping cost depends on the efficiency of the pumps used and the electricity power tariff over the pumping duration. The tariff is usually a function of time with cheaper and more expensive periods. Note that other costs (such as pump switching cost) could be included in the objective function. However, the switching cost is rarely considered due to insufficient data available to formulate it within the objective function (Ormsbee and Lansey 1994). For given time step Δt, the objective function considered over a given time horizon $[k_0, k_f]$ is given by the following equation:

$$\phi = \left(\sum_{j \in J_p} \sum_{k=k_0}^{k_f} \gamma_p^j(k)\, f_j(q^j(k), c^j(k)) + \sum_{j \in J_s} \sum_{k=k_0}^{k_f} \gamma_s^j(k) \times q_s^j(k) \right) \Delta t \qquad (1)$$

where J_p is the set of indices for pump stations and J_s is the set of indices for treatment works. The $c^j(k)$ vector represents the number of pumps on, denoted $u^j(k)$, and pump speed (for variable speed pumps) denoted $s^j(k)$. The function $\gamma_p^j(k)$ represents the electrical tariff. The treatment cost for each treatment works is proportional to the flow output with the unit price of $\gamma_s^j(k)$. The term $f_j(q^j(k), c^j(k))$ represents the electrical power consumed by pump station *j*. The mechanical power of water is obtained by multiplying the flow $q^j(k)$ and the head increase Δh^j across the pump station. The head increase Δh^j can be expressed in terms of flow in the pump hydraulic equation, so that the cost term depends only on the pump station flow $q^j(k)$ and the control variable $c^j(k)$. From mechanical power of water, the electrical power consumed by the pump can be calculated using the pump efficiency or using pump power characteristics (Ulanicki et al 2008).

3.2. Model of water distribution system. Each network component has a hydraulic equation. The fundamental requirement in an optimal scheduling problem is that all calculated variables satisfy the hydraulic model equations. The network equations are non-linear and play the role of equality constraints in the optimisation problem.

The network equations used in this paper to describe reservoir dynamics, components hydraulics and mass balance at reservoirs are those described in (Ulanicki et al 2007). Since leakage is assumed to be at connection nodes, the equation to describe mass balance at connection nodes is modified to include the leakage term:

$$\mathbf{\Lambda}_c \mathbf{q}(k) + \mathbf{d}_c(k) + \mathbf{l}_c(k) = \mathbf{0} \tag{2}$$

where $\mathbf{\Lambda}_c$ is node branch incidence matrix, $\mathbf{q}$ is vector of branch flows, $\mathbf{d}_c$ denotes vector of demands and $\mathbf{l}_c$ denotes vector of leakages calculated as:

$$\mathbf{l}_c = \mathbf{p}^{\alpha} \kappa \tag{3}$$

with $\mathbf{p}$ denoting vector of node pressures, $\alpha \in \langle 0.5,\ 1.5 \rangle$ denoting leakage exponent and κ denoting vector of leakage coefficients, see (Ulanicki et al 2000). Note that $\mathbf{p}^{\alpha}$ denotes each element of vector $\mathbf{p}$ raised to the power of α.

3.3. Constraints. In addition to equality constraints described by the hydraulic model equations, operational constraints are applied to keep the system-state within its feasible range. Practical requirements are translated from the linguistic statements into mathematical inequalities. The typical requirements of network scheduling are concerned with reservoir levels in order to prevent emptying or overflowing, and to maintain adequate storage for emergency purposes:

$$h_f^{\min} \le h_f(k) \le h_f^{\max} \quad for \quad k \in [k_0, k_f]$$

Similar constraints must be applied to the heads at critical connection nodes in order to maintain required pressures throughout the water network. Another constraint is on the final level of reservoirs, such that the final level is not smaller than the initial level. The control variables such as the number of pumps switched on, pump speeds or valve positions, are also constrained by lower and upper constraints determined by the features of the control components.

4. IMPLEMENTATION

Developed energy and pressure management scheduler was integrated into a modelling environment, called FINESSE. The scheduler, as with all tools in FINESSE, is general purpose in that it takes any data model of a network, simulates the network to initialise its decision variables for the network scheduler, and if the model is feasible it calculates the optimal schedules. Using model of a network FINESSE automatically generates optimal network scheduling problem written in a

mathematical modelling language called GAMS (Brooke et al. 1998), which calls up a non-linear programming solver called CONOPT (Drud 1985) to calculate a continuous optimisation solution. CONOPT is a non-linear programming solver, which uses a generalised reduced gradient algorithm (Drud 1985). An optimal solution is fed back from CONOPT into FINESSE for analysis and/or further processing. For further details on using GAMS and CONOPT for optimal network scheduling see (Ulanicki et al 1999).

5. CASE STUDY

5.1. Network description. The case study selected is a major water supply network, being part of Yorkshire Water Services (YWS). The network is fed by two major sources and has two major exports. The network consists of 2074 nodes, 2212 pipes, 4 reservoirs, 12 pumps and 56 valves (including one PRV) with a total average demand of 400 l/s. However, only 8 out of 12 pumps were actually used for scheduling, since other 4 pumps are in standby mode and should not be used unless in an emergency situation such as failure of other pumps. It was also found that only 8 out of 56 valves could be scheduled, while others are to remain fully closed. Schematic of the case study network is illustrated in Figure 2. Description of current operation of the network follows.

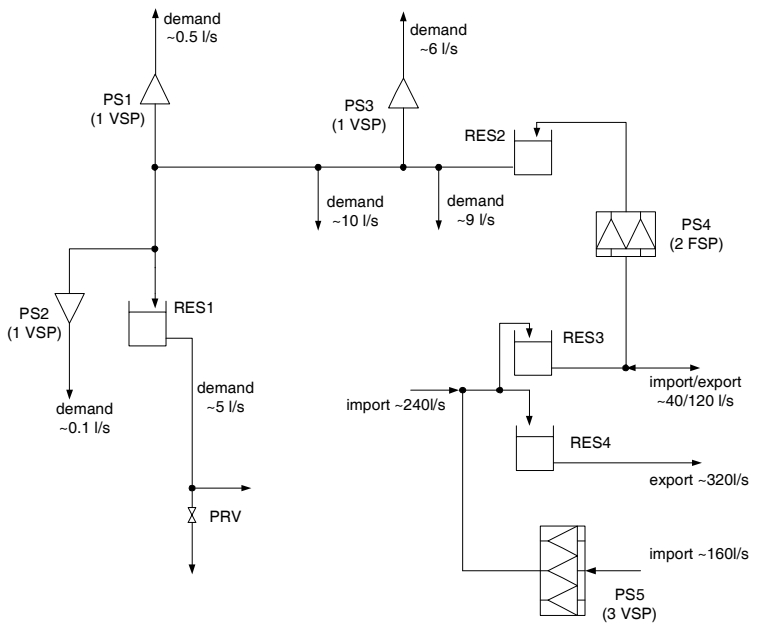

Figure 2. Illustrating schematic of the case study network. Abbreviations denote: PS – pumping station, FSP – fixed speed pump, VSP – variable speed pump, RES – reservoir. Demands and average import/exports are also depicted.

PS1, PS2 and PS3 consist of small pumps that operate to maintain given outlet pressure. Their speed, therefore, changes together with demand. PS4 is

controlled by water level in reservoir RES2 (on/off control with 20 cm water level margin); typically only one pump is used. Due to tight margin (20 cm) the pump in PS4 is switched on/off frequently, every 7 to 30 minutes. PS5 consists of three large pumps with variable speed drives. They operate to number of preset flow bands; typically only one or two pumps are on. Opening of the top-feed valve for RES1 is controlled by water level in RES1. The top-feed valves for RES2-5 are fully open.

Information about the electrical tariffs in the considered water network was not available at the time this work was carried out. For this reason the tariffs were assumed to represent a typical scheme of cheap at night and expensive during day. Assumed tariffs were: 0.1 £/kWh between 22.00 – 07.00 and 0.2 £/kWh between 07.00 – 22.00.

5.2. Modelling and simplification. A model of the network was provided in Aquis format. Structure of nodes and pipes was automatically converted into EPANET format and subsequently imported into FINESSE. Other network element, i.e. reservoirs, pumps and valves, were added manually to the FINESSE model. Pumps, valves and reservoirs parameters were described in FINESSE using data from Aquis model and additional information provided by YWS.

Once the FINESSE model was completed, it was simplified using FINESSE model reduction module (Ulanicki et al 1996) to reduce the size of the optimisation problem. In the simplified model all control elements remained unchanged, but the number of pipes and nodes was reduced to 45 and 43, respectively. Both full and simplified FINESSE models were simulated and compared, with respect to pump flow and reservoir trajectories, against the reference Aquis model. It was found that in Aquis model, which allows variable simulation step, the pump in PS4 was switching at intervals as small as 7 minutes. To represent such irregular switching and model similar operation of the PS4 pump in FINESSE, where minimal time step is 15 minutes, it was assumed that e.g. 0.5 pump is on during a single time step. Both FINESSE models showed satisfactory agreement, see reservoir trajectories illustrated in Figure 3. Since RES3 and RES4 are directly connected, it is considered sufficient to compare average levels for these two reservoirs. Note that for the purpose of comparison of FINESSE models with Aquis model local control rules, such as control of RES1 top-feed valve, were kept. Subsequently, these local rules were removed to enable scheduling of all control elements.

Only limited information about leakage in the considered network was available at the time this work was carried out. For this reason the network optimiser was run for several scenarios, assuming different leakages levels. According to YWS there is a considerable leakage on the connection between PS5 and reservoirs RES3 and RES4, due to significant distance and elevation difference which require high pressure at PS5 outlet. Therefore, in the scenarios described in next subsections the leakage was assumed to be on this connection.

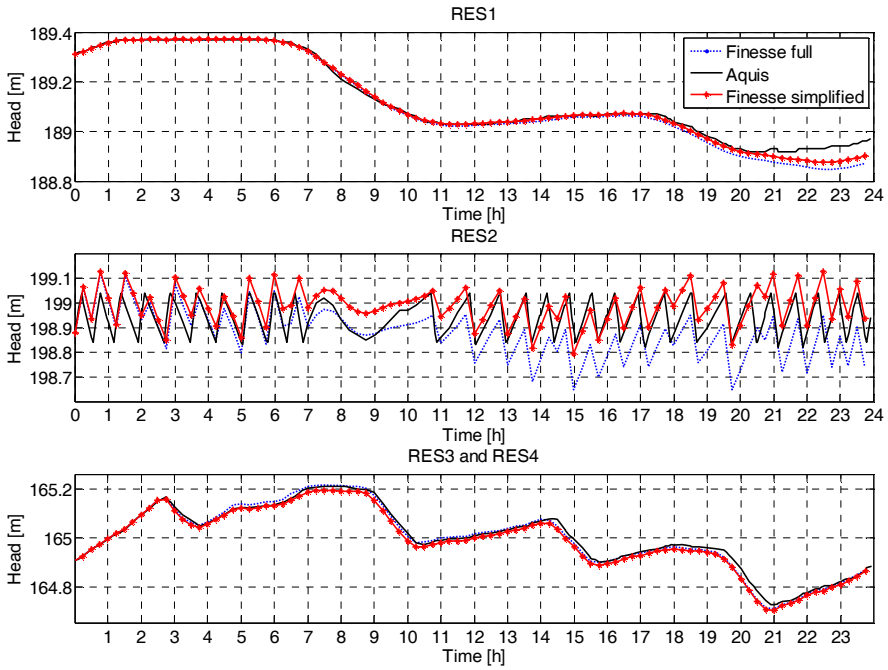

Figure 3. Illustrating reservoir level trajectories for full FINESSE model, simplified FINESSE model and reference Aquis model.

5.3. Network scheduling: no leakage. First, a case with no pressure-dependent leakage was considered, i.e. κ in Equation (3) was zero for all nodes. Time step Δt=1 hour was chosen. The optimisation ran for 2 minutes on a Pentium 4 3GHz PC. Obtained continuous solution was transformed into an integer solution by manual post-processing. Pump schedules for PS4 and PS5 are illustrated in Figure 4 and Figure 5, respectively. Daily cost of electrical energy was as follows: £799 for current network operation, £491 for optimised continuous solution and £494 for integer solution.

5.4. Network scheduling: with leakage term. Three scenarios were considered for different leakage levels. Parameter κ in Equation (3) was chosen such that the leakage at a node close to the outlet of PS5 was approximately 10%, 20% or 30% of the flow for scenarios 1, 2 and 3, respectively. Leakage was assumed to be zero at other nodes. Only continuous solution was considered for simplicity. Obtained pump schedules for PS5 for different scenarios are illustrated in Figure 6. Daily cost of electrical energy was £534, £547 and £562 for scenarios 1, 2 and 3, respectively.

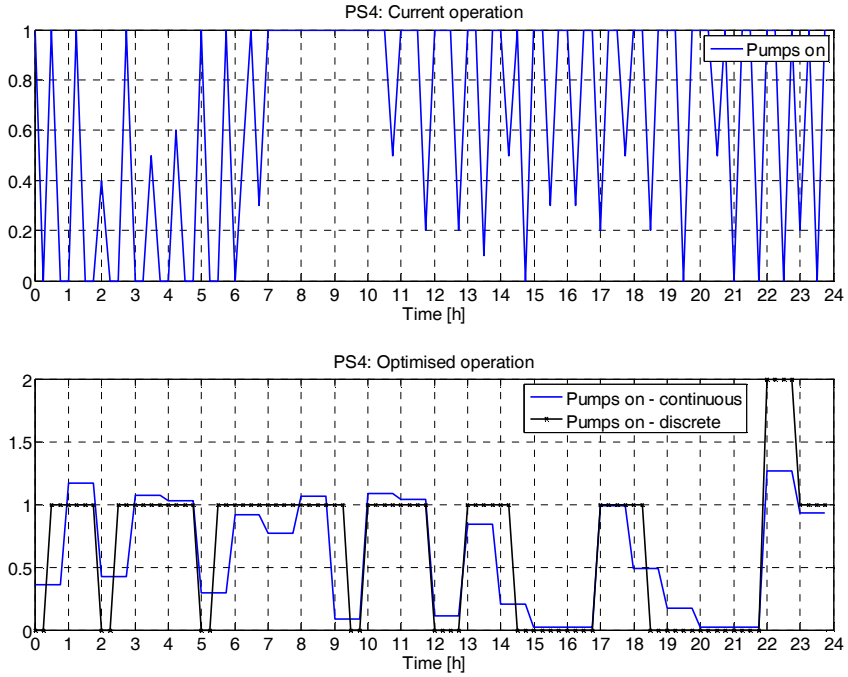

Figure 4. Comparison of current and optimised network operation for PS4.

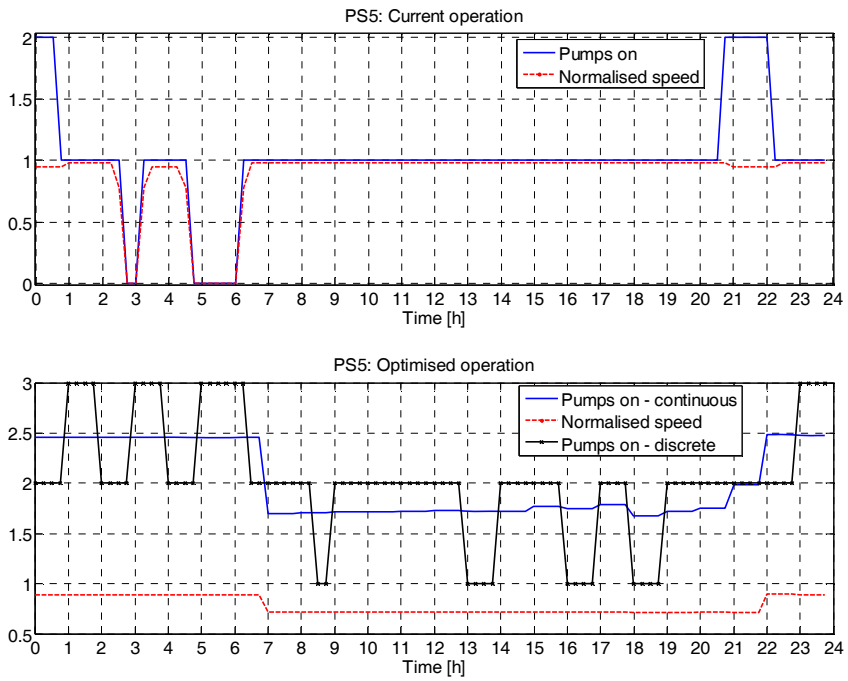

Figure 5. Comparison of current and optimised network operation for PS5.

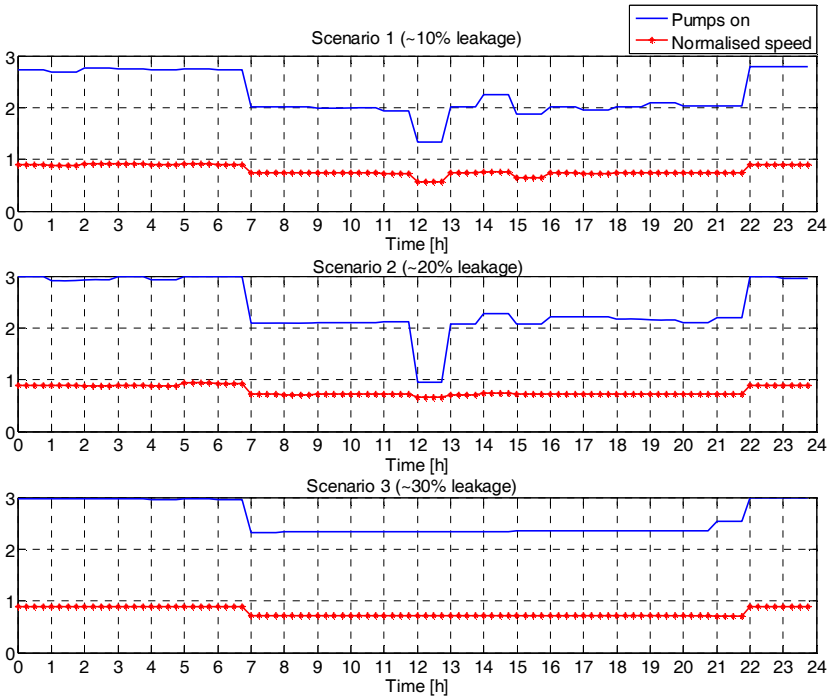

Figure 6. Comparison of PS5 pump schedules for three different leakage levels.

5.5. Discussion. It can be observed in Figure 4 that due to operational constraints not much savings can be achieved for PS4, since current and optimal schedules are similar, i.e. both exhibit switching 0-1 pumps on throughout the 24h period. However, recall from Section 5.1 that PS4 switches frequently due to tight margin (20 cm) for reservoir level controlling the pump operation. Optimal schedules resulted in less frequent switching which is beneficial for pump durability.

In Figure 5 it can be observed that optimal schedules for PS5 cause an intensive pumping during the cheap tariff period to fill RES3 and RES4, which subsequently supply water during the expensive tariff period. The operational speed of PS5 pumps is lower, compared to current operation, during the expensive tariff period, which also contributes to reduced cost. The total cost was reduced by 38%. It should, however, be noticed that these results were obtained for an assumed electrical tariff, which could significantly differ from the actual tariff, and did not take into account standing charge and other costs.

It was found that increased leakage coefficient, not surprisingly, led to increased cost, since harder pumping is required due to increased pump flow. Nevertheless, the pump schedules are similar to the 'no leakage' case, with intensive pumping during the cheap tariff period; compare Figures 5 and 6. It was observed that, despite indirect penalisation of high pressure in the cost function (see Figure 1), increased leakage coefficient did not result in lower PS5 outlet pressure. Analysis of CONOPT logs revealed that this was a result of hydraulic equation constraints: PS5 outlet pressure cannot be decreased, due to significant distance and elevation difference between PS5 and RES3.

6. CONCLUSIONS

In this paper a method was proposed for combined energy and pressure management via integration and coordination of pump scheduling with pressure control aspects. The proposed solution is an extension of the pump scheduling method based on formulation and solving of an optimisation problem. Proposed method utilises an hydraulic model of the network with pressure dependent leakage and takes into account PRV model with the PRV set-points included as a set of decision variables. Such formulation leads to the optimiser attempting to reduce both energy usage and leakage. The developed algorithm has been integrated into a modelling, simulation and optimisation environment called FINESSE, which utilises GAMS modelling language and CONOPT non-linear programming solver.

The method was applied to optimise the operation of a major water supply network, being part of Yorkshire Water Services. A network model provided in Aquis format was converted to Epanet format, imported to Finesse, simplified and validated against original Aquis model. Optimised network schedules resulted in the total cost of electrical energy reduced by 38%, albeit for an assumed electrical tariff, which could significantly differ from the actual tariff. The developed algorithm is currently further investigated using other case studies.

REFERENCES

Bounds P., Kahler J., Ulanicki B. (2006), "Efficient energy management of a large-scale water supply system", *Civil Engineering and Environmental Systems*, Vol 23(3), pp. 209 – 220

Brooke A., Kendrick D., Meeraus, A. and Raman, R. (1998) GAMS: A user's guide, *GAMS Development Corporation*, Washington, USA

Drud A.S. (1985), CONOPT: A GRG Code for large sparse dynamic non-linear optimisation problems, *Mathematical Programming*, 31, pp.153-191

Neptune project website **www.neptune.ac.uk** (2009)

Ormsbee L. and Lansey K. (2007), "Optimal control in water-supply pumping system", *Journal of Water Resources Planning and Management*, Vol. 120(2), pp. 237-252

Ulanicki B., Kahler J., See H. (2007), "Dynamic optimization approach for solving an optimal scheduling problem in water distribution systems", *Journal of Water Resources Planning and Management*, Vol. 133(1), pp. 23-32

Ulanicki B., Bounds P., Rance J., and Reynolds L. (2000), "Open and closed loop pressure control for leakage reduction", *Urban Water*, Vol. 2(2), pp. 105-114

Ulanicki B., Kahler J., and B. Coulbeck B. (2008), Modeling the Efficiency and Power Characteristics of a Pump Group, *Journal of Water Resources Planning and Management,* Vol. 134(1), pp. 88-93

Ulanicki B., Zehnpfund A. and Martinez F. (1996), Simplification of water network models. In:Hydroinformatics 1996, *Proceedings of the 2nd International Conference on Hydroinformatics*, Muller, A. (Eds), vol 2,pp.493-500, Switzerland, 1996

DESIGN OF DUAL WATER SUPPLY SYSTEMS

R. Chee[1], D. S. Kang[2], K. Lansey[3], and C. Y. Choi[4]

[1]Graduate Research Assistant, Department of Civil Engineering and Engineering Mechanics, The University of Arizona, Tucson, AZ 85721; email: ronsonc@email.arizona.edu

[2]Research Associate, Department of Civil Engineering and Engineering Mechanics, The University of Arizona, Tucson, AZ 85721; email: doosun74@email.arizona.edu

[3]Professor, Department of Civil Engineering and Engineering Mechanics, The University of Arizona, Tucson, AZ 85721; email: lansey@email.arizona.edu

[4]Professor, Department of Agricultural and Biosystems Engineering, The University of Arizona, Tucson, AZ 85721; email: cchoi@arizona.edu

Introduction

Water scarcity is causing major concerns throughout the world, especially in arid regions where cities are growing rapidly and are depleting groundwater reserves faster than they can be recharged. The southwestern U.S., Arizona and Nevada in particular, are experiencing the large growth rates with limited water resources and no new sources available. In effort to reduce the amount of water being consumed by people, new engineering technologies are being explored. Water reuse is becoming recognized as the last untapped water resource. However, little research has been conducted on effectively distributing that water to user. In particular, distribution of reclaimed water through a parallel pipe networks system to homes or dual water supply system has not been considered.

Existing distribution systems deliver water via a single system. Meeting flow and pressure requirements for fire conditions are driving factors in designing water distribution systems. Minimum regulatory pipe diameters of six to eight inches are common in most systems and can lead to reduced water quality. The goal of a parallel system is to maximize the usage of reclaimed water. By distributing non-potable water through a separate line to meet non-sanitary uses (i.e., outdoor, fireflow, and toilet flushing), the need for potable water can be greatly reduced. Separating these demands from the potable system can reduce the potable system pipe sizes, improve water quality and reduce the overall cost of the water distribution system.

Some cities in the southwestern U.S. have already implemented this new system in some residential areas through a non-potable "purple pipe" system. However, the efficiency of these new systems has not been thoroughly examined. This paper will

focuses on the design of dual systems by using an optimization algorithm linked to EPANET (USEPA, 2000) via the EPANET toolkit to determine the optimal least-cost design of dual piping systems.

Previous Studies

Optimization of water distribution systems have been under research for some time. A number of optimization algorithms have been applied to water distribution systems with minimizing cost as the objective function and pipe size diameters as the decision variable. Eusuff and Lansey (2003) applied a Shuffled Frog Leaping Algorithm (SFLA) to optimize water distribution systems by minimizing cost. Other works have been done by trying to minimize cost using Genetic Algorithms - Hadji and Murphy (1990), Murphy and Simpson (1992), Walters and Cembrowiez (1993), and Simson et. al. (1994). This paper applies this technique to the least cost optimization of dual supply systems.

Methodology

Implementation of dual supply systems requires designing and optimizing two separate systems for the same network layout in order to analyze the effectiveness of the dual supply system. The objective is to minimize overall piping costs while still meeting the demands and minimum head requirements in the system.

A significant issue from engineering, public perception and regulatory perspectives is the demands that will be supplied in each pipe system. Here, we consider water demands to be composed of four different uses; outdoor, toilet, fire, and drinking/potable. The effectiveness of the dual supply system will be analyzed by determining the least-cost design of four different system configurations:

- Design 1 – (Single System) Outdoor, toilet, fire and drinking use are all distributed via a fully potable system (representative of almost all existing water distribution systems).
- Design 2 – (Dual System) Outdoor use will be distributed via a non-potable system. Toilet, fire, and drinking are delivered in the potable system.
- Design 3 – (Dual System) Outdoor and toilet use will be delivered via a non-potable system. Fire and drinking use is delivered via a potable system.
- Design 4 – (Dual System) Outdoor, toilet and fire use will be delivered via a non-potable system. Drinking use will be delivered via a potable system.

The derivation and proportion of the total demand for each uses is described in detail in the Network Development section. The least cost design, as determined by the optimization program for each of the configurations mentioned above will be compared to the fully potable system. A cost comparison based on pipe sizes will determine cost/benefit of the dual supply systems in terms of pipe construction cost.

Problem Formulation

In this paper, the design of dual water supply systems is formulated as a least-cost optimization problem. The goal is to minimize the pipe cost of the two systems that are composed of commercially available pipes. The layout of the water distribution network, as well as the nodal demands and minimum head requirements in the system are known. The following conditions must be satisfied:

- Conservation of mass: The inflows and outflows must be balanced at each node in the system.
- Conservation of energy: The head loss around a closed loop must equal zero.
- The head loss in each pipe is determined by Hazen-Williams pipe loss equation.
- The minimum pressure in the network must be given as well as the demand(s) in the system,
- Acceptable pipe sizes: Pipe diameters are selected from commercially available pipe sizes (with the exception of small sizes 1 in – 4 in).

The problem formulation subject to these conditions can be represented mathematically by:

$$\min f(D_1,....,D_{npipe}) = \sum_{k \in npipe} C_k(D_k, L_k) \tag{1}$$

Subject to

$$\sum Q_{in} - \sum Q_{in} = Q_e \tag{2}$$

$$\sum_{k \in Loopl} \Delta H_k = 0, \forall l \in nloop \tag{3}$$

$$\Delta H_k = H_{u/snode,k} - H_{d/snode,k} = \omega \frac{L_k}{C W_k^{\beta} D_k^{\gamma}} Q_k \left|Q_k\right|^{\beta-1}, \ \forall k \in npipe \tag{4}$$

$$H_{iN} \geq H_{\min iN}, \forall iN \in nnodes \tag{5}$$

$$D_k \in \{D\}, \forall k \in npipe \tag{6}$$

where (D_1….D_{npipe}) is the discrete pipe diameters selected from commercially available pipe sizes. $C_k(D_kL_k)$ is the cost of pipe with diameter D_k and length L_k. Q_{in} is the flow rate in and Q_{out} is the flow rate out of each node. ΔH_k is the headloss in pipe k and $nloop$ is the number of loops in the system. The headloss equation used is the Hazen-Williams equation with CW as the roughness coefficient which will be 130 for all pipes in the system. $nloop$ and $npipe$ is the number of loops and pipes in the system respectively. H_{iN} is the head in each node must satisfy the minimum head pressure requirement in the system H_{min}. For all designs the minimum head required throughout the system will be 40 psi.

This problem is solved by linking a genetic algorithm (GA) with EPANET as shown in the Figure 1. The GA generates solutions of pipe diameters that are passed to EPANET. The total cost is then calculated. If the pressure requirements (40 psi min.) are not met a penalty term will be added to the objective making the alternative not preferable. The optimization scheme will run until the least-cost of each design is determined or meets the stopping criteria as specified in the GA parameters.

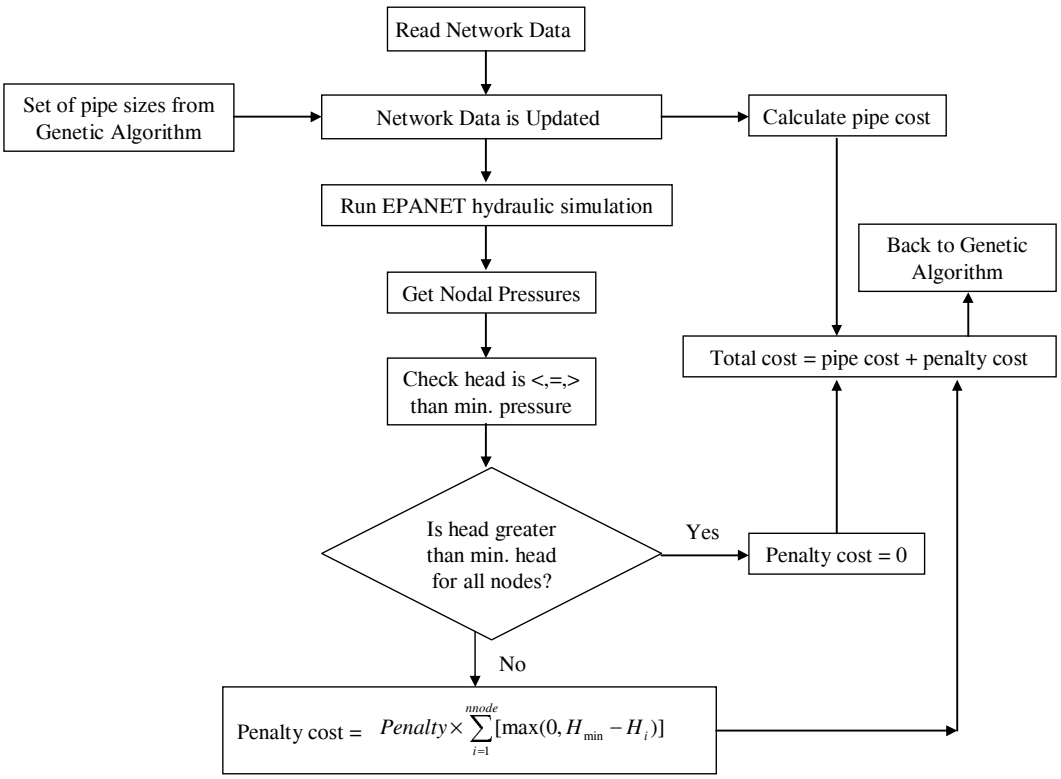

Figure 1 - Flow chart for optimization of a distribution network using GA linked with EPANET

Table 1. Cost function

Diameter (in)	Cost ($/m)
1	2.30
2	2.94
3	3.76
4	4.82
6	7.89
8	12.94
10	21.20
12	34.75
14	56.95
16	93.33
18	152.95

Network Development

A fictitious network was developed that will be designed and analyzed for the dual supply systems. The network was created from a typical residential neighborhood layout in Tucson, Arizona The area chosen for consideration is approximately one square mile and is relatively flat (all nodes assigned zero elevation). (Figure 2).

The source head was modeled as a reservoir with a constant head of 138 feet. This is equivalent to connecting to an existing water main with a pressure of 60 psi. For purposes of this paper the source head was kept constant for each of the designs under consideration. The minimum pressure requirement for each node was 40 psi. Pipe cost for each pipe size is listed in Table 1.

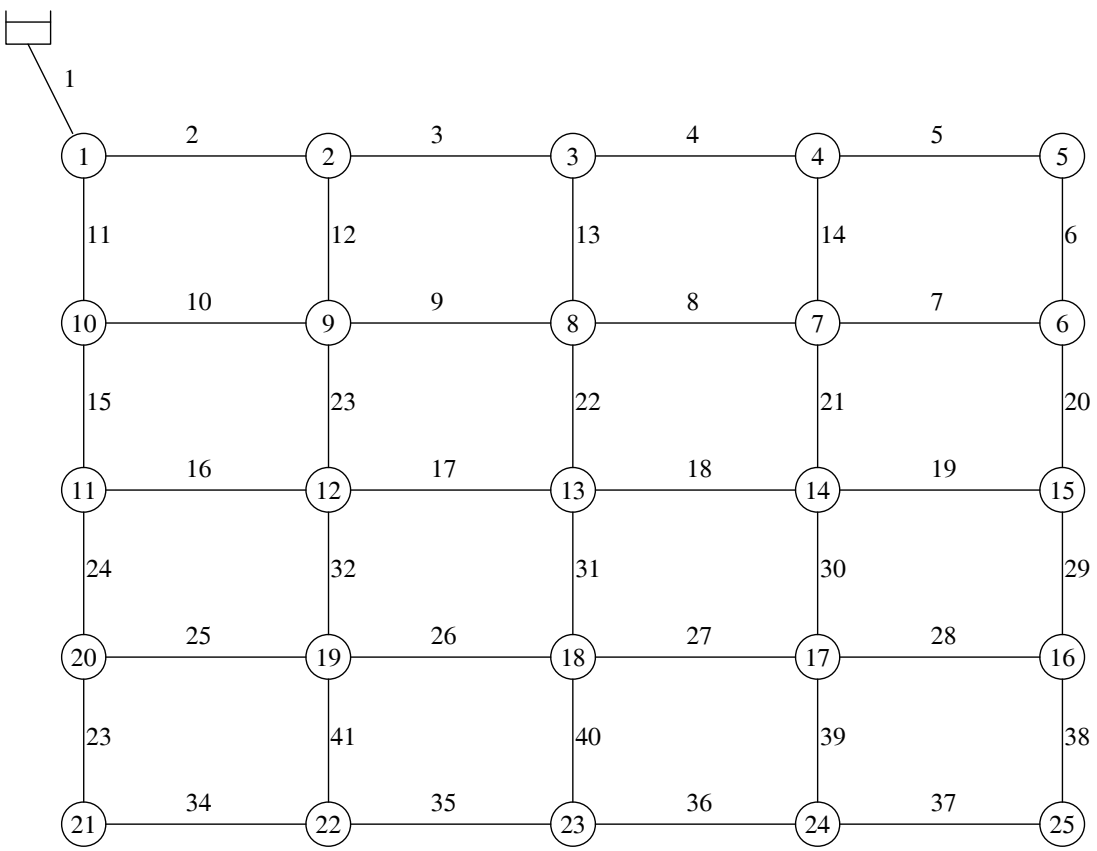

Figure 2 - Network Layout

Nodal Demand Development

Nodes were placed to represent approximately 9 square residential blocks with pipes representing street water mains. Twenty homes per block with 2.5 persons per home consuming 150 gallons/day/per person was used to get a base demand. A peak factor of 2 resulted in a demand of 94 gpm for each node and a simulated fire flow of 2000 gpm at node 25 (furthest from the source) was used for design considerations.

Demand Breakdown

The design demand was divided into outdoor use, toilet use and drinking use with proportions of 47 gpm, 13 gpm, and 34 gpm respectively, for each node. The fire flow will be applied only to node 25. Each of the four designs under consideration requires different combinations of each "type of use" as described above.

Results

Multiple runs were performed for each design to assure that the global minimum is identified. Table 2 shows the best solutions for each of the designs. Some generalization can be made about the design of dual supply systems. As expected, the systems with lower demands require smaller pipes and have lower costs. The fire flow controlled the overall water supply system cost. The system that provided the fire flow required significantly larger pipes and higher cost. Design 1 was the least expensive followed by Design 4, Design 3 and Design 2.

In general, if only pipe costs are considered and the source head is fixed, dual supply systems are more expensive than conventional system on the order of 6% to 14%. However, in this example, only material and construction cost associated with the design are considered. Many other cost factors come into play in distribution systems. Out of the three dual systems considered, the cheapest cost was Design 4, in which only drinking water was delivered via the potable system. This design was 6% more expensive than conventional designs. In theory, this design would be the ideal system if implementation of dual systems was desirable. This system configuration makes the most use of reclaimed water which is the ultimate goal of dual supply systems.

Discussion

In this paper a GA was used to determine optimal designs of dual water supply systems considering construction costs only. With this limitation, dual systems are somewhat more expensive than a single potable system. This results from the economies of scale of pipe diameter and flow relationships. However, considering dual systems functioning as a whole may prove to be more economical in the long run if pumping, source heads and energy costs are taken into account. Benefits of reducing potable demands, and other factors such as system reliability and water quality may also change this conclusion.

A number of factors affect dual water supply system design. Some of those factors are listed in Table 3. For example, here, the source energy was fixed at a constant pressure for the potable and non-potable systems. Additional runs suggest that the network design is sensitive to the source head. Further studies will add the source head as a decision variable to represent pump energy and pump station costs. Further head requirements for alternative systems may not require the same source head and pressure provided. For example, 40 psi may not be necessary for a non-potable system in which outdoor use and toilet flushing are the only uses. Reliability of the

dual systems that must be considered as the two networks may serve as backup systems for each other. Lastly, the type of waters that are socially acceptable to deliver to households must be evaluated. Thus, this study of dual system design must be considered an initial assessment and significantly more effort is necessary to address the value and cost benefits of these networks.

Table 3 – Factors affecting dual water supply system design

Regulatory	*System characteristics*	*Social*
Minimum pipe size	Topography	Water quality by use
Pressure requirements	Demand distribution by use	Reliability
Water quality requirements	Population density	Acceptance of alternative
Reliability	Service area size	waters for different uses
	Demand magnitude	Demands for waste water
	(ex, indoor, outdoor, etc)	Demands conservative
	Water source location/energy	practices
	available	· grey water use
		· rainwater harvesting
		· consumptive use
		reduction
		· indoor use conservation

References

Eusuff, M. M., and Lansey, K. E. (2003). "Optimization of water distribution nework design using the shuffled frog leaping algorithm." *J. Water Resour. Plng. And Mgmt*., ASCE, 129(3), 210-224.

Hadji, G., and Murphy, L. J. (1990). "Genetic algorithms for pipe network optimization." *4th Year Studuent Civil Engineering Research Rep.,* Univ. of Adelaide, Australia.

Murphy, L. J., Simpson, A. R., and Dandy, G. C. (1993). "Pipe network optimization using an improved genetic algorithm." *Research Rep. No. R109,* Dept. of Civil and Environmental Engineering, Univ. of Adelaide, Adelaide, Australia.

Simpson, A. R., Dandy, G. C., and Murphy, L. J. (1994). "Genetic algorithms compared to other techniques for pipe optimization." *J. Water Resour. Plag. And Mgmt.,* ASCE, 120(4), 423-443.

U. S. Environ. Protection Agency (2000). Epanet User's Manual, Cincinnati, OH, 200 pp.

Walters, G. A., and Cembrowicz, R. G. (1993). "Optimal design of water distribution networks." *Water supply system, state-of-the-art and future trends,* E. Cabrera and F. Martinez, eds., Computational Mechanics Inc., Southampton, England, 91-117.

Table 2 - Results for dual supply system

Pipe ID	Length (m)	Pipe Diameters (in)						
		Design 1	Design 2		Design 3		Design 4	
		P	P	NP	P	NP	P	NP
1	225.9	16	14	8	14	10	8	14
2	522.9	10	10	8	10	8	8	12
3	489.6	8	10	6	8	6	6	10
4	482.5	8	8	10	8	6	6	8
5	451.7	8	8	8	10	4	2	8
6	296.8	8	8	4	8	1	4	8
7	449.2	6	6	4	6	3	3	8
8	473.0	10	8	2	8	3	1	8
9	499.2	14	8	2	10	2	6	8
10	525.3	12	10	10	10	12	6	12
11	284.9	14	12	10	12	8	10	14
12	283.2	10	8	4	10	10	2	10
13	288.5	10	12	4	10	8	3	10
14	286.6	12	12	2	10	2	6	10
15	295.1	10	10	6	10	12	4	10
16	513.4	10	8	2	8	1	4	8
17	513.4	8	8	6	8	10	1	6
18	477.7	10	10	1	10	8	1	8
19	444.5	10	10	3	8	6	6	8
20	290.0	10	6	4	8	3	8	10
21	295.2	10	12	4	8	6	6	6
22	290.0	12	10	8	8	4	10	8
23	296.9	12	10	10	10	10	4	10
24	281.5	12	10	3	10	4	8	10
25	513.4	4	8	1	8	2	1	8
26	515.7	10	6	6	8	4	3	12
27	473.0	8	10	8	10	6	6	10
28	446.8	12	10	6	8	3	4	10
29	286.6	10	12	3	10	8	2	8
30	278.1	10	10	3	8	8	4	10
31	281.5	12	8	4	8	4	4	6
32	281.5	14	6	10	10	3	4	12
33	337.6	8	10	4	8	4	4	6
34	508.6	6	8	4	8	4	3	8
35	518.1	8	10	1	8	6	3	8
36	463.4	10	10	1	10	3	3	8
37	456.3	12	10	6	10	3	1	10
38	330.7	10	12	3	10	4	4	10
39	334.1	8	8	8	10	4	4	10
40	330.7	10	8	3	8	8	2	8
41	339.2	8	8	3	8	1	1	8
Individual System Cost ($)		375,242	301,753	123,797	276,751	143,028	95,315	301,828
Total Cost ($)		375,242	425,550		419,779		397,143	

P = Potable System
NP = Non-Potable System

Modeling Domestic Water Demand On A Suburb Level

M.L. Griffioen, J.E. van Zyl and A.S. le Roux

Department of Civil Engineering Science, University of Johannesburg, PO Box 524, Auckland Park, 2006, South Africa; PH (+2711 559-2540); email: mlgriffioen@uj.ac.za

ABSTRACT

In this study it was assumed that a suburb provides a good basis for grouping water demands, and that it is adequate to design for the average suburb AAD (annual average demand). A database on measured domestic water demands was used to determine the average AAD for a large number of suburbs in South Africa, and this data was further linked to sensus and climate data. The combined data set was then subjected to various regression analyses, and a method was developed to compare these models. This method may assist with determining suitable design guidelines for suburb AAD in future.

INTRODUCTION

Domestic water demand is influenced by a large number of factors, including socio-economic (household size, income, stand size, social status, number of household appliances, social patterns, public and school holidays, tourism and water price), climatic (temperature, rainfall, humidity, time since last rainfall and the number of preceding hot days) and structural (number of users, water metering, plumbing fitting properties, pressure and network capacity) (Van Zyl et al 2008). As a result it is impossible to predict water demand with certainty and any prediction model will invariably include significant errors.

The design water demand of a new area is normally determined by first estimating the annual average demand (AAD) and then multiplying this demand by peak factors to determine the design hydraulic load on the distribution network. The AAD may be estimated from measured demands of similar areas, or from design guidelines.

The South African design guideline for AAD provides an upper and lower bound based on stand size. The design engineer estimates the AAD for a particular area between these bounds by taking factors such as climate, income and local conditions into account.

In the last decade, a South African consulting engineering company (GLS) developed a software product called Swift that extracts water meter readings from a municipal treasury system and makes it available for engineering analysis. The product has been

implemented in a large number of municipalities throughout South Africa, and this data was used as the basis for an analysis of domestic water demands.

The data showed that individual water demands have large variations, even when important parameters such as climate, stand size and income are the same. However, if situated in the same geographical area, these extremes will balance each other out, and the designer only needs to consider the average demand for the area.

In this study it was assumed that a suburb provides a good basis for grouping water demands, and that it is adequate to design for the average suburb AAD. The demand database was used to determine the average AAD for a large number of suburbs in South Africa, and this data was further linked to socio-economic and climatic data for each suburb. The combined data set was then subjected to various regression analyses, and a method was developed for using these regression models to propose a new design guideline for AAD in South Africa.

DATA

The data used in this study was obtained from municipal meter readings entered into treasury databases for billing purposes and then extracted using a software package called Swift (GLS, 2007). The data was subjected to a number of verification and cleaning processes to ensure that errors are eliminated in an objective manner.

In the first data verification and cleaning stage, errors in the database were identified and corrected (where possible) or the records removed. Various types of errors were addressed, including missing meter readings, inconsistent reading dates, reading errors, meters that were replaced and duplicate records. After the first phase, the database consisted of 1 353 794 records of monthly water demand for at least a year, as well as other information for each record, such as the stand size and municipal stand valuation.

In the next phase, only residential stands were extracted and then grouped by suburb. The number of suburbs identified was 1 442. To eliminate outlyers in the data, the highest and lowest 2 % of water demands, stand sizes and stand values were removed in each suburb. In addition, filters were applied and records with AAD, stand sizes or stand values outside a reasonable range were removed. The ranges for these parameters were set as follows:

- AAD: between 0.05 and 10 kl/day.
- Stand size: between 50 and 5 000 m.
- Municipal stand valuation: between ZAR 1 000 and 3 500 000.

Climatic and sensus data were obtained from various sources and linked to the demand data. In the final step, all suburbs with no sensus data, or that contained less than 100 records were also removed from the data set.

The final data set consisted of 654 014 residential users in 739 suburbs. For each suburb, the following data was available:

- Location (municipality and suburb)
- Average AAD
- Average stand size
- Average stand value
- Type of water supply (piped water, borehole, spring, etc.)
- Type of sanitation (sewer line, septic tank, chemical toilet, etc.)
- Type of building (house, flat, traditional dwelling, etc.)
- Type of area (urban, smallholding, farm, etc.)
- Income
- Racial distribution
- No of rooms per house
- Mean annual precipitation
- Average maximum daily temperature
- Average minimum daily temperature
- Mean annual evaporation

The current South African design guideline for AAD provides upper and lower guideline values based on stand size. The suburb data was plotted on these guidelines as shown in Figure 1.

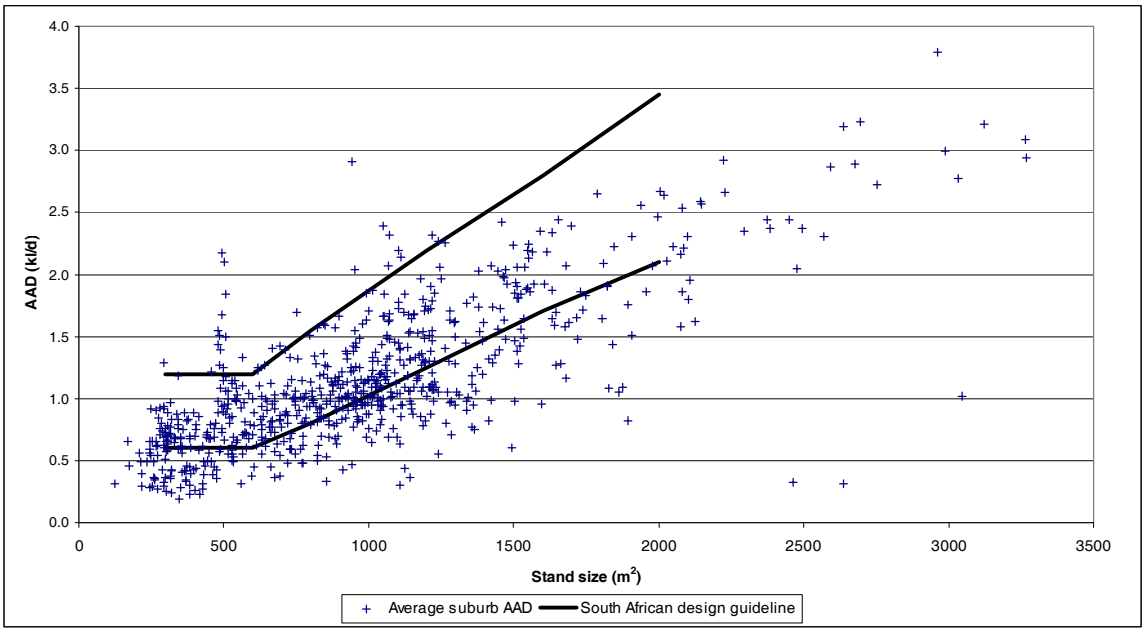

Figure 1 Average suburb AAD compared to the South African design guideline

It is clear that, while the guidelines replicate the general trend, a large fraction of the AAD values fall outside the proposed design envelope, especially on the lower side.

REGRESSION ANALYSES

The data set was then analysed through a number of regression analyses. In the first analysis, a step-wise multiple regression analysis was conducted, which identified the following significant parameters to predict Ln(AAD):

- Ln(fraction of cluster housing)
- Ln(average stand size)
- Mean annual evaporation
- Fraction of houses with piped water
- Fraction of stand-alone houses
- Stand value
- Fraction of African population
- Average number of rooms per house
- Average minimum daily temperature
- Mean annual precipitation
- Fraction of houses with flush toilets

The Adjusted R^2 value for the model was 0.73, which represents a reasonably good prediction for something as variable as water demand.

The step-wise multiple regression identified stand size as the most important predicter of AAD, followed by stand value. To explore these variables further, single regression models were developed for AAD as a function of stand size and value. The logs of the various parameters were also investigated in these models. The results of the single variable regression analyses are summarized in Table 1.

Table 1 Results of single variable regression analyses

Dependent Variable	Independent variable	Adjusted R^2
AADD	Stand size	0.58
AADD	Ln(Stand size)	0.50
Ln(AAD)	Stand size	0.48
Ln(AAD)	Ln(Stand size)	0.51
Ln(AAD)	Stand value	0.50

The model for AADD as a function of stand size produced the best results of all the single regression models with an adjusted R^2 value of 0.58. This model is shown in Figure 2.

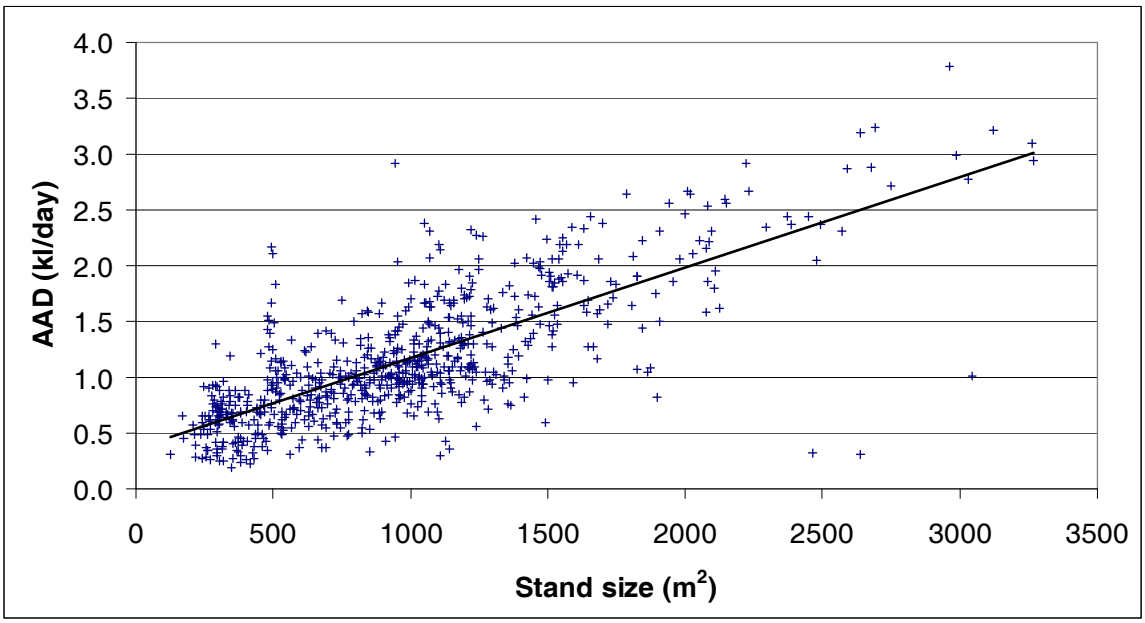

Figure 2 Single regression model for suburb AAD as a function of stand size

COMPARING THE MODELS

The regression analyses showed that the multiple regression model is able to predict suburb AAD significantly better than any of the single regression models. However, this improved accuracy requires data for 11 parameters to be estimated. Single regression equations have the advantage of being much simpler to apply, while still providing reasonable accuracy.

Even the multiple regression model is not perfect, and will underestimate the AAD in roughly half the cases. It is thus necessary to adjust this model to provide a more conservative estimate that will avoid underestimates of AAD, while at the same time not providing excessive over-estimates.

To evaluate and compare the regression models, a trade-off curve was developed by plotting the fraction of data points where the AAD is under-estimated against the average over-estimation error. Each of the regression models was then varied by adjusting its intercept, and the results plotted as shown in Figure 3. The current upper envelope of the South African design guidelines is also shown on the graph.

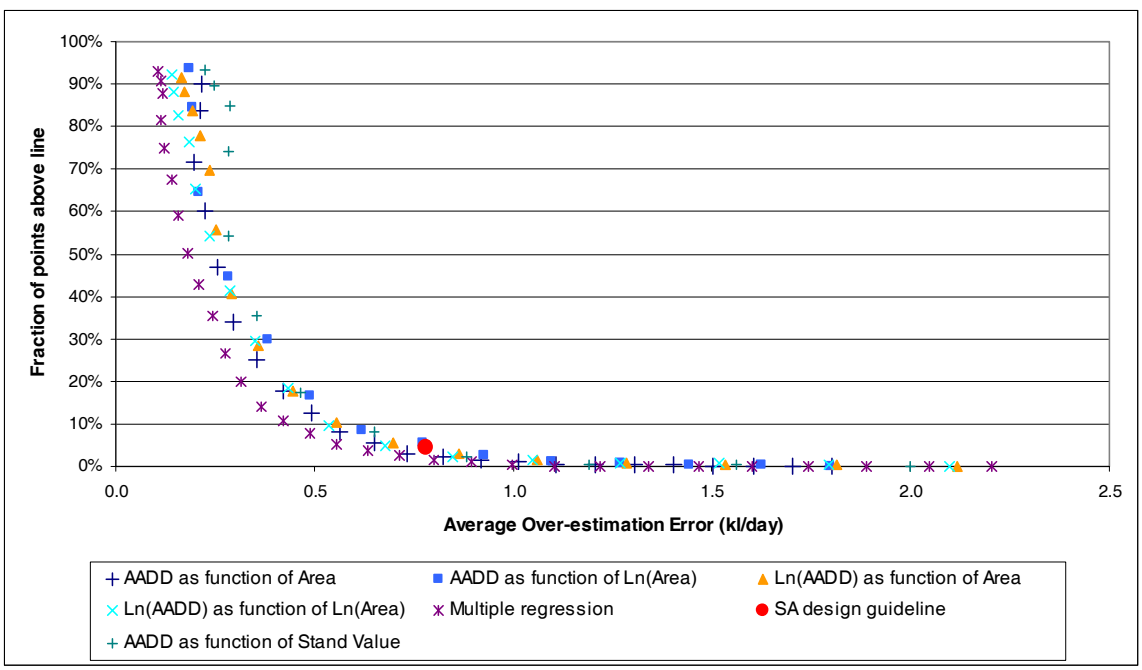

Figure 3 Comparison of different models

Figure 3 shows a that the multiple regression model provides the best prediction for the AAD for any level of safety.

The graph shown in Figure 3 is proposed as a basis for establishing an upper design curve for suburb AAD. It allowes different models to be compared, and allowes the user to pick the optimal curve for a given factor of safety. It is also possible to use the inverse of this method to determine a lower curve for a design envelope.

CONCLUSIONS

This study analysed residential water demand based on the assumption that a suburb provides a suitable grouping to base the design AAD on. A database of AAD values in South Africa was analysed and combined with climate and sensus data. Single and multiple regression models were developed for the data. The multiple regression model was able to predict water demand the best, but is much more complicated and cumbersome than the single regression models, where stand size proved to be the best predictor of AAD.

The different regression models were adjusted to provide better margins of safety for design purposes, and a way to compare the different models was proposed. This may provide a good basis for determining a suitable design envelope for AAD prediction in future.

REFERENCES

GLS (2007) Swift. http://www.gls.co.za/Gls/pages/swift/overview.html. Accessed 27 September 2007.

Van Zyl, J.E., Piller, O., Legat, Y. (2008). “Sizing municipal storage tanks based on reliability criteria”, Journal of Water Resources Planning and Management, 134 (6) 548-555.

Preliminary Spatial-Temporal Statistical Analysis of Hourly Water Demand at Household Level

Ernesto Arandia-Perez[1], James G. Uber[1], Feng Shang[1], Dominic L. Boccelli[1], Robert Janke[2], David Hartman[3], Yeongho Lee[3]

[1]Department of Civil and Environmental Engineering, University of Cincinnati, Cincinnati, OH USA 45221-0071; emails: arandiao@email.uc.edu, jim.uber@uc.edu, fshang@uc.edu, bocceldl@ucmail.uc.edu.
[2]U.S. Environmental Protection Agency, 26 Martin Luther King Drive Cincinnati, OH USA 45268; email: Janke.Robert@epamail.epa.gov.
[3]Greater Cincinnati Water Works, 5651 Kellogg Avenue, Cincinnati, OH USA 45228; emails: David.Hartman@gcww.cincinnati-oh.gov, yeongho.lee@gcww.cincinnati-oh.gov.

Abstract

A methodology for modeling time series of hourly urban water use is presented based on separating the data into three components: trend, seasonality, and autocorrelation. Each component is represented by a model whose parameters are estimated. The series is transformed by removing each of the three components and the last transformation produces only a random error series. In the process of identifying the most suitable model for the autocorrelation component of the series, a large number of alternative autoregressive moving average (ARMA) models are assessed in terms of statistics that measure accuracy, parsimony, and randomness of the residuals. Hourly spatially aggregated water use in Cincinnati, Ohio, during the month of October, 2008 is modeled as an example. The model explains approximately 50% of the variance of this series, divided as trend (8.28%), seasonality (11.51%), and autocorrelation (29.94%). The methodology will be applied in a future study of a large data set of individual service connection hourly demand series, spatially aggregated under different schemes.

Introduction

Network hydraulic models are indispensable in sizing and operating water distribution systems (WDSs), and they may also become essential tools in assessing water quality dynamics at different levels of skeletonization. Increasingly, network water quality models are being used to assess water quality impacts due to intentional or accidental contamination sources, and USEPA regulations even allow the use of such models for assisting in selecting sampling locations, in lieu of more intensive field sampling. Nonetheless, uncertainty in key model parameters is looming as a significant factor

that may limit the promises assigned to network water quality models, especially as the models are applied at finer spatial and temporal resolutions. For many of these current or project applications, it is important to question the accuracy of network hydraulic modeling that is rooted in deterministic assumptions, where evidence and logic suggests a stochastic approach is required.

A sensitivity analysis of a WDS clearly shows that water demands are the parameters that most influence the hydraulic response of a water distribution network. This has been motivating efforts to characterize water demands at finer spatial and temporal resolutions, to support the need for accurate stochastic simulation models. Urban water demand models, which were historically used to quantify systemwide aggregate demand, and determine appropriate price structures, need to evolve toward finer temporal and spatial aggregation scales.

The spatial-temporal variability of urban water demands is assumed to be significant, and it seems natural to rely on the theory of stochastic processes and random fields as the mathematical framework for the development of a demand model that bridges a variety of spatial-temporal resolution scales, from highly aggregated daily demand models applied to entire service areas, to sub-hourly demands assigned to small groups of service connections. It may also be useful to adopt a flexible structure for the model, which at some degree of aggregation can be purely statistical, and at some other can attempt to represent the physical underlying processes. The ultimate goal will thus be to develop a model that adequately represents the statistical properties of water demands at different levels of spatial and temporal aggregation, by giving a reasonably close fit to selected features of data, while allowing a minimum number of parameters to be estimated from commonly available field data

The construction of such a modeling framework requires a stepwise progression. This paper discusses the first preliminary stage, which involves the collection of a large data set of hourly water usage by individual service accounts (ISAs) and an exploratory analysis of such data under different schemes of spatial aggregation. Time series of hourly ISA demands show a predominant random component and several periods of inactivity throughout the day, suggesting an underlying point process as the generating mechanism (Cox and Isham, 1980). As such individual demands are aggregated in space, their temporal variation describes characteristics that may be modeled using time series techniques (Salas and Yevjevich, 1972; Maidment and Parzen, 1984; Maidment and Miaou, 1985), taking benefit from the rich available literature, in particular that relates to Auto Regressive Moving Average (ARMA) models (Box and Jenkins, 1976).

This paper discusses the process of data acquisition and Preprocessing employed to establish a significant demand data set for future model building and testing. Furthermore, it investigates the suitability of different ARMA model structures to spatially-aggregated demand data at hourly resolution. The objectives are to develop a methodology for time series analysis of the aggregated data and to analyze the order of models that can be fitted to residual stationary time series of hourly water usage rates. From a complete analysis using the entire data set (in process, and to be completed at a later date), we expect to better understand the statistical features of urban water usage as a function of various ways to classify them, and the modeling framework that would be required to bridge the various useful scales of demand analysis.

Data Acquisition and Management

For the purpose of this study, water demands are being continuously monitored at approximately 2500 accounts using 4 massive data collectors, with the data being transferred to a centralized database for data processing. The monitored areas were selected through a geographic and demographic study of Hamilton County, Ohio, to include a mixture of single and multi family residences, commercial and industrial establishments.

The system for data collection has three main components. First, at the ISA level, a water meter continuously measures the water inflow, encodes the current cumulated volume, and transmits its value to a radio Meter Interface Unit (MIU) once per hour. The second component is the data collector which is a stand alone unit able to receive the radio signals from the MIUs enclosed in its area of coverage. Also, the unit has the capability of compiling the records into daily binary files that are downloaded through public communication networks. Finally, data is merged into the third component, a centralized database, that can be queried for data retrieval.

The measuring and recording instruments allow a volumetric resolution of 5 gallons (18.93 Liters) and a temporal resolution of 1 hour. The implications are that if less than 5 gal is used, no increment will be recorded. However, the meter does accumulate demand continuously, so the long-term total demand is accurate within a 5-gal increment. On the contrary, for high water usage rates, the limiting resolution will be the temporal, obscuring the actual time at which 5-gal increments occurred between one hour and the next.

For a particular ISA or MIU, the raw data retrieved from the database contains records showing a cumulated water volume and the two times of the day, first and last, at which such volume was registered. For a given period of time, there will be a set of records that needs to be preprocessed to obtain a time series of hourly water usage rates. The preprocessing task includes several operations such as eliminating anomalous records, correcting time sequences, and re-sampling to determine the hourly rates at equal hourly intervals from the cumulated series at uneven time intervals. Figure 1 illustrates the two main steps in preprocessing the raw data for a sample MIU and during the first week of October 2008.

The cumulated series of Figure 1(a) is sampled at uneven intervals as it is generated from the raw data. The time series of Figure 1(b) is created through interpolation using the raw data of the cumulated series, in order to produce water usage time intervals equally spaced by one hour.

Methodology

The study of urban water use based on total system demand has been extensively addressed (Salas and Yevjevich, 1972; Yamauchi and Huang, 1977; Maidment and Parzen, 1984; Maidment and Miaou, 1985; Zhou et al., 2002). As a result, it is well known that spatially aggregated water use can be expressed as the sum of a long-memory or deterministic component and a short-memory or stochastic component. Maidment and

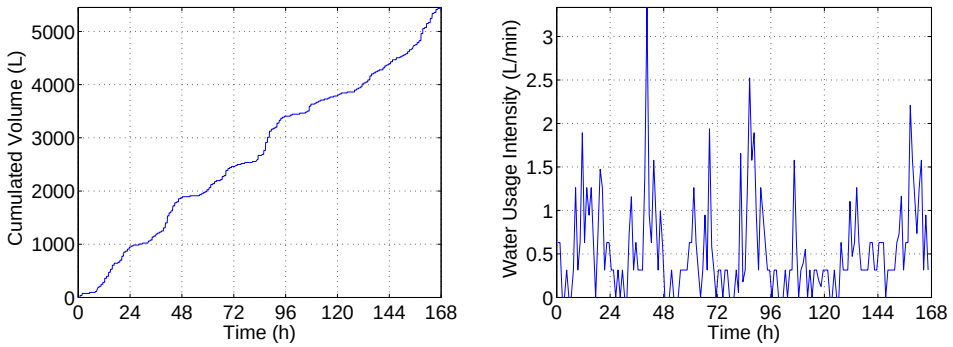

(a) Cumulated volumes (b) Hourly intensities

Figure 1: Sample plots of cumulated volumes and hourly water use rates.

Parzen (1984) define a long-memory time series as one with trends, or periodicities, or very slowly decaying correlations, or very low frequency cycles, or spectral densities with very large dynamic range. The authors also define a short-memory time series as being stationary with an invertible infinite autoregressive scheme representation.

A time series of aggregated water demand is the sequence $X_t = \{X_1, X_2, \ldots\}$ where X represents an aggregated water usage rate and the subscript represents hourly time intervals. The series of observations $x_t = \{x_1, x_2, \ldots, x_n\}$ is regarded as a measured sample realization of the time series X_t or, for simplicity, the data set. The long-memory component of X_t consists of a trend T_t and a seasonal component S_t. On the other hand, the short-memory constituent of X_t can be represented by a residual series Y_t. Thus, the time series X_t is given by

$$X_t = T_t + S_t + Y_t \tag{1}$$

A methodology to find the estimates $\hat{T}_t$, $\hat{S}_t$ and $\hat{Y}_t$, given the availability of the hourly water usage data x_t, is presented in this paper as detailed by the algorithm of Figure 2. The tasks involved and the methods used in every step are explained below.

Trend

The trend in water use time series is caused by several factors, such as household income, water price, number of water connections, and population. Long time series of monthly water demand are likely to show a growing trend that can be modeled by regressing mean annual water use against trend-causing variables (Maidment and Parzen, 1984). Such approach cannot be applied in this study due to the small temporal scale used. Therefore, the trend is considered as the fluctuation of the mean in the data series, produced mainly by sudden changes in population; it is thus estimated by applying the moving average filter (Brockwell and Davis, 2002):

$$\hat{T}_t = \frac{1}{2a+1} \sum_{i=-a}^{a} x_{t+i} \tag{2}$$

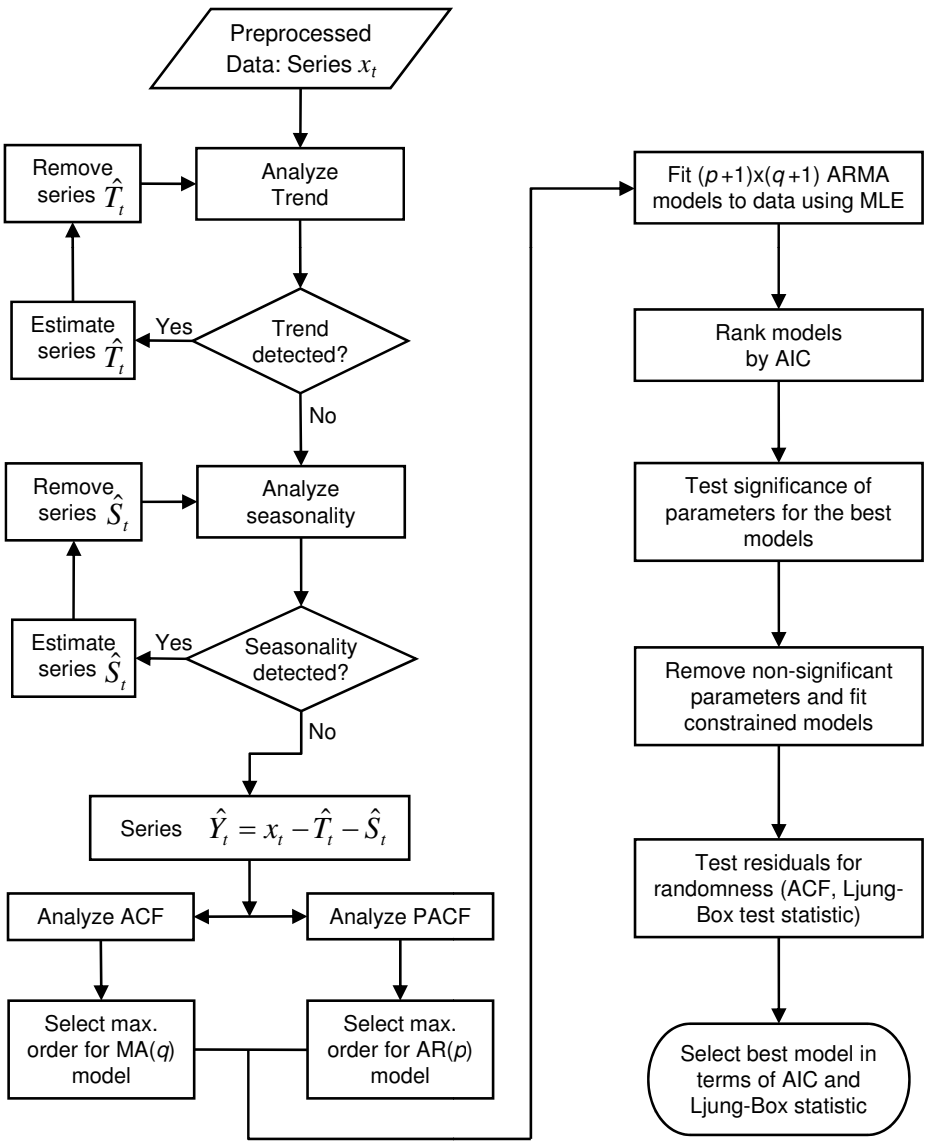

Figure 2: Algorithm for modeling hourly water demand time series.

where $\hat{T}_t$ is the estimated trend at time $t = 1, \ldots, n$, a is a nonnegative integer, and n is the sample size. Therefore, the trend in a time series at a given period τ is represented by its average over the period $t = \tau - a$ to $t = \tau + a$. The larger a the more data values are averaged and the smoother the trend.

Seasonality

Four methods are available for eliminating a seasonal cycle in a detrended water use series: form d-th differences of data (Box and Jenkins, 1976), where d is the estimated period; form an autoregressive model of the detrended series whose coefficients reflect seasonality; regress the series against a seasonal variable such as maximum air temperature; subtract the arithmetic or Fourier-fitted seasonal means. The last method is generally more effective in removing the seasonal cycle in water use and, specifically, the subtraction of Fourier-fitted means produces results that are more physically interpretable and offers an objective basis for determining the significance of seasonal cycles (Maidment and Parzen, 1984). The estimated seasonal series $\hat{S}_t$ expressed as a Fourier series is

$$\hat{S}_t = \alpha_0 + \sum_{m=1}^{M} \left[\alpha_m \cos \frac{2\pi m}{d_m} t + \beta_m \sin \frac{2\pi m}{d_m} t \right] \tag{3}$$

where M is the number of significant harmonics in the series, α_0, α_m and β_m are unknown parameters, and d_m is the period of the mth harmonic. The periods d_m are estimated by inverting the frequency values of the significant peaks in the periodogram (Brockwell and Davis, 2002)

$$I_n(w_k) = \frac{1}{n} \left| \sum_{t=1}^{n} (x_t - \hat{T}_t) e^{-itw_k} \right|^2 \tag{4}$$

where $w_k = 2\pi k/n$, $k = -[(n-1)/2], \ldots, [n/2]$ ($[y]$ denotes the largest integer less than or equal to y), $i = \sqrt{-1}$.

Stationary Model

The detrended and deseasonalized data series is assumed to be a stationary series $\hat{Y}_t$ that can be modeled as an ARMA(p, q) process of the form

$$\phi(B) Y_t = \theta(B) Z_t \tag{5}$$

where $\phi(B)$ and $\theta(B)$ are, respectively, the autoregressive and moving average polynomials of the model, given by

$$\begin{aligned} \phi(B) &= 1 - \phi_1 B - \ldots - \phi_p B^p, \\ \theta(B) &= 1 + \theta_1 B + \ldots + \theta_q B^q, \end{aligned}$$

p and q are, respectively, the autoregressive and moving average orders of the model, B is the backward shift operator ($B^jY_t = Y_{t-j}, B^jZ_t = Z_{t-j}$), $\phi_1, \ldots, \phi_p$ are the autoregressive parameters, $\theta_1, \ldots, \theta_q$ are the moving average parameters, and $\{Z_t\}$ is the white noise, i.e., a normally distributed random variable with mean of 0 and standard deviation σ^2.

The ARMA modeling stage starts by analyzing the Autocorrelation function (ACF) and Partial Autocorrelation Function (PACF) of the transformed data. Given the set of observations $\{x_1, \ldots, x_n\}$ of a time series, the sample autocovariance function is

$$\hat{\gamma}(h) = \frac{1}{n}\sum_{t=1}^{n-|h|}(x_{t+|h|} - \bar{x})(x_t - \bar{x}), \quad -n < h < n \tag{6}$$

where $\bar{x}$ is the sample mean of $x_1, \ldots, x_n$ and h is the time lag. The sample ACF is

$$\hat{\rho}(h) = \frac{\hat{\gamma}(h)}{\hat{\gamma}(0)}, \quad -n < h < n \tag{7}$$

The sample PACF of the same set of observations $\{x_1, \ldots, x_n\}$ with $x_i \neq x_j$, for some i and j, is given by

$$\begin{aligned} \hat{\alpha}(0) &= 1 \\ \hat{\alpha}(h) &= \hat{\phi}_{hh}, \quad h \geq 1, \end{aligned}$$

where $\hat{\phi}_{hh}$ is the last component of the vector of estimated autoregressive parameters

$$\hat{\boldsymbol{\phi}}_h = \hat{\boldsymbol{\Gamma}}_h^{-1}\hat{\boldsymbol{\gamma}}_h \tag{8}$$

where $\hat{\boldsymbol{\Gamma}}_h$ is the sample covariance matrix given by

$$\hat{\boldsymbol{\Gamma}}_h = \begin{bmatrix} \hat{\gamma}(0) & \hat{\gamma}(1) & \ldots & \hat{\gamma}(h-1) \\ \hat{\gamma}(1) & \hat{\gamma}(0) & \ldots & \hat{\gamma}(h-2) \\ \vdots & \vdots & & \vdots \\ \hat{\gamma}(h-1) & \hat{\gamma}(h-2) & \ldots & \hat{\gamma}(0) \end{bmatrix} \tag{9}$$

and $\hat{\boldsymbol{\gamma}}_h = [\hat{\gamma}(1), \hat{\gamma}(2), \ldots, \hat{\gamma}(h)]'$.

Information provided by the ACF and PACF will be used to select the maximum orders p_m and q_m for the autoregressive and moving average components of the ARMA models. The total number of alternative models to be estimated is given by the product $(p_m+1)\times(q_m+1)$. This provides a starting point from which a selection of appropriate values for orders p and q can be attempted.

It is not advantageous from a forecasting point of view to choose p and q arbitrarily large, because the mean squared error of the predictive demand model will depend not only on the white noise variance of the fitted model, but also on errors arising from estimation of the parameters of the model (Brockwell and Davis, 2002). It is therefore necessary to use a criterion based on penalty factors that discourage the fitting of models with too many parameters.

The criterion used here is the Akaike Information Criterion (AIC) (Akaike, 1973), defined as

$$\text{AIC}(\boldsymbol{\beta}) = -2\ln L_X(\boldsymbol{\beta}, S_X(\boldsymbol{\beta})/n) + 2(p+q+1) \tag{10}$$

where $\boldsymbol{\beta} = (\phi_1, \ldots, \phi_p, \theta_1, \ldots, \theta_q)'$, $L_X(\cdot)$ is the Gaussian Likelihood, and $S_X(\cdot)$ is a function of the mean squared errors of the forecasts.

A subset of the total number of preliminary ARMA models will be thus selected using the AIC as the ranking criterion. From that, the significance of the parameters of the selected models is tested, and the nonsignificant parameters are removed. Then, the remaining parameters are "fine tuned" using constrained Maximum Likelihood Estimation.

Finally, the goodness of fit of the remaining models are assessed through the analysis of residuals, which are the rescaled one-step prediction errors,

$$\hat{W}_t = \frac{Y_t - \hat{Y}_t}{\sqrt{r_{t-1}}} \tag{11}$$

where $\hat{Y}_t$ is the best linear mean-square predictor of Y_t based on the observations up to time $t-1$, $r_{t-1} = E(Y_t - \hat{Y}_t)^2/\sigma^2$ and σ^2 is the white noise variance of the fitted model.

The randomness of the residuals $\hat{W}_t$ is tested using the residual ACF $\hat{\rho}_w$ (defined in Equation 7) and the Ljung-Box portmanteau test. By the former, if the sequence of estimated residuals $\hat{w}_1, \ldots, \hat{w}_n$ is a realization of an independent and identically distributed (iid) sequence, about 95% of the residual autocorrelations should fall between the bounds $\pm 1.96/\sqrt{n}$. By the latter, a single statistic is considered:

$$Q_{LB} = n(n+2)\sum_{j=1}^{h} \frac{\hat{\rho}_w^2(j)}{n-j} \tag{12}$$

If $\hat{w}_1, \ldots, \hat{w}_n$ is a finite variance iid sequence, then Q_{LB} is approximately distributed as the sum of squares of the independent N(0,1) random variables $\sqrt{n}\hat{\rho}_w(j), j = 1, \ldots, h$, i.e., as chi-squared with h degrees of freedom. A large value of Q_{LB} suggests that the residual autocorrelations are too large for the residuals to be a sample from an iid sequence. Therefore, the iid hypothesis is rejected at level α if $Q_{LB} > \chi^2_{1-\alpha}(h)$, where $\chi^2_{1-\alpha}(h)$ is the $1-\alpha$ quantile of the chi-squared distribution with h degrees of freedom.

Results and Discussion

This section presents the analysis of a sample data set by means of the methodology illustrated in Figure 2. The data comprises one month of hourly water usage rates from randomly selected ISAs located in one of the areas being monitored in Hamilton County, Ohio.

Sample Analysis

Figure 3 presents the data sample, which was obtained by aggregating hourly usage rates, in L/min, from 10 randomly selected ISAs monitored during the month of October 2008. As shown in Figure 4(a), the series does not exhibit a noticeable trend having

an approximately constant mean of 0.6679 L/min. The variance and the standard deviation of the series are, respectively, 0.1649 $(\text{L/min})^2$, and 0.4061 (L/min).

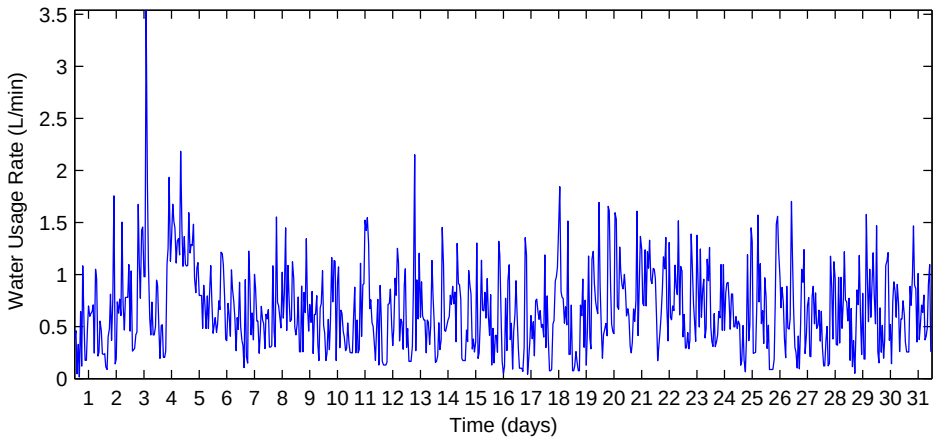

Figure 3: Data

The selection of a in Equation 2 is based on obtaining a smooth series that shows the mean variation of the original series in time. Sudden changes in the level of the trend indicate events that affect the first-order stationarity of the series, such as a considerable increase or decrease in the number of water consumers in the sampled ISAs. A value $a = 36$ was adopted to estimate the moving average trend shown in Figure 4(a). It accounts for 8.28% of the total variance in the data.

To estimate the seasonal cycle in the detrended water use series, first, the periodicity in the series is determined through spectral analysis. Equation 4 is used to estimate the periodogram at frequencies w_k. The inversion of the frequencies of the periodogram allows the determination of periods of the dominant cycles in the series, as illustrated by Figure 5. It should be noted that long term seasonal variation is not being captured by the spectral analysis, given that only one month of data was used.

Three periods are dominant in Figure 5: $d_1 = 24$, $d_2 = 12$ and $d_3 = 8$, therefore three harmonics are considered in Equation 3. The values of parameters in the Fourier series are determined through least squares estimation, and the resulting seasonal model is

$$\begin{aligned} S_t &= 0.00048 - 0.06291\cos\frac{\pi}{12}t - 0.0665\sin\frac{\pi}{12}t \\ &\quad +0.07321\cos\frac{\pi}{6}t - 0.1117\sin\frac{\pi}{6}t \\ &\quad +0.1006\cos\frac{\pi}{4}t + 0.03963\sin\frac{\pi}{4}t \end{aligned} \tag{13}$$

Figure 4(b) illustrates the seasonal model as given by Equation (13). It can be noted that a full cycle of three harmonics in the series is completed after 24 h. The detrended, deseasonalized time series $\hat{Y}_t$ is produced by subtracting $\hat{S}_t$ from the detrended series.

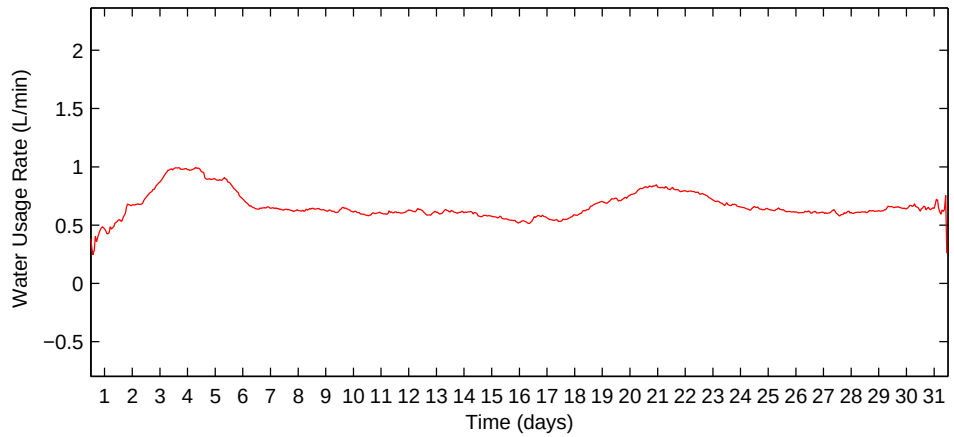

(a) Trend component.

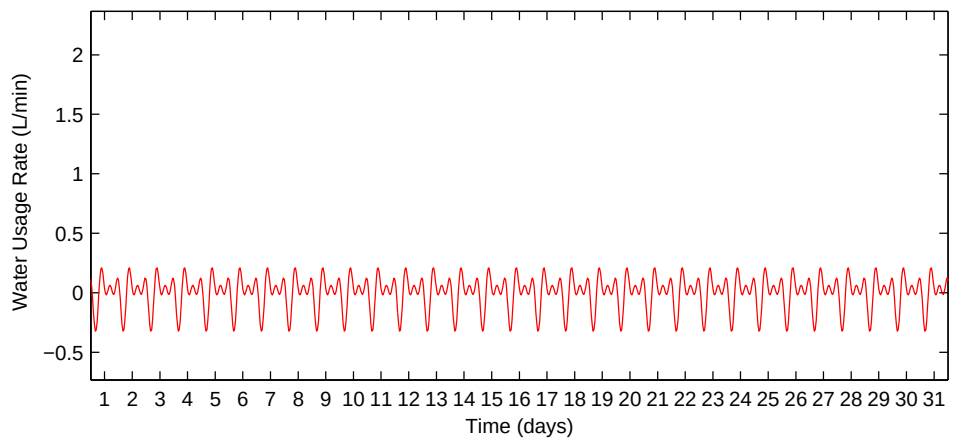

(b) Seasonal series.

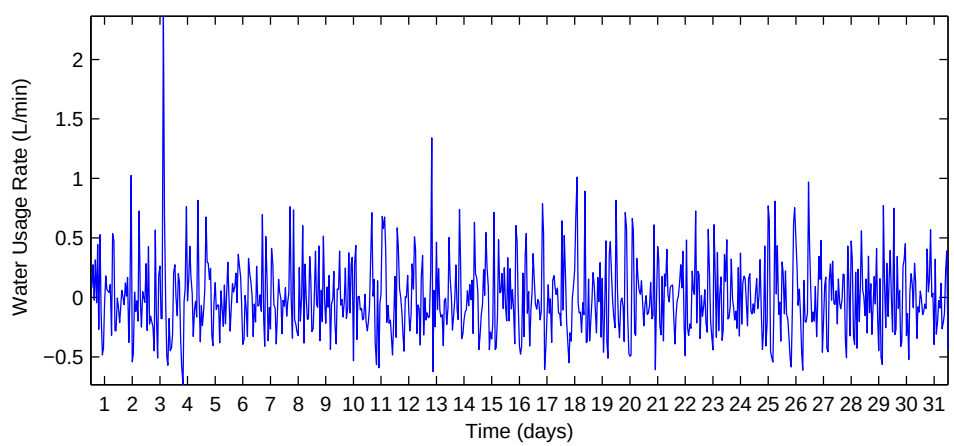

(c) Residual or short-memory series.

Figure 4: Different components of the data series.

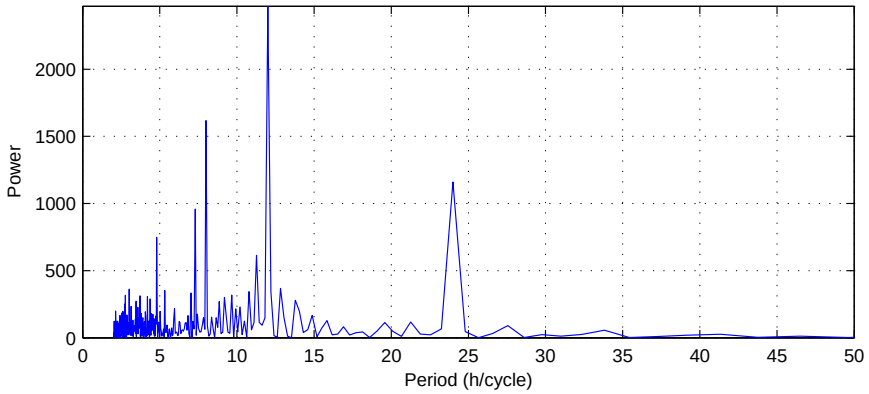

Figure 5: Plot of power of the series vs. period.

As shown in Figure 4(c), this short-memory series oscillates arbitrarily about a zero origin with no apparent trend or seasonal variation. The estimated seasonal component accounts for 11.51% of the original variance.

After transforming the data as described above, the fit of ARMA models to the residual series $\hat{Y}_t$ is attempted. The process starts by calculating and then observing the sample ACF and PACF of Figure 6, where the largest lags with PACF and ACF outside of the 95% confidence interval bounds are, respectively, 22 and 17. Therefore, those are the maximum orders of the autoregressive and moving average components, respectively, of the preliminary time series models to be compared. Thus, the procedure consists in fitting $23 \times 18 = 414$ models, and then selecting only those with the smallest AIC. Fitting is performed by a maximum likelihood estimation method that minimizes the model prediction errors when computing the parameter estimates. Several models were selected, ranked by AIC, and the 5 with the best AIC value were kept for the final selection stage, based on analysis of residuals. The AIC values computed for the 414 models had an average of -2.278, ranging between -2.403 and -1.171. Table 1 summarizes the information about the 5 preliminary models that were selected. The column named *significant lags* indicates the indexes of the model parameters that were found to be significant at 5% level. Values of AIC and estimated error variance presented in the table were computed for the models with all parameters, i.e., before setting the non-significant parameter values to zero.

The models in Table 1 were refined through constrained fitting and their estimated errors were analyzed by statistically testing the hypothesis that the residuals are independent and identically distributed. The tools used in this task are the ACF of the residuals and the Ljung-Box test statistic (Equation 12). This is the final stage in the algorithm of Figure 2 and is intended to lead to the selection of a single best ARMA model to fit the residual series $\hat{Y}_t$. Table 2 presents a comparison of the models in terms of the aforementioned statistics.

It can be noted in Table 2 that the models with largest number of parameters did not pass the test of randomness, having p-values smaller than 0.05. The remaining

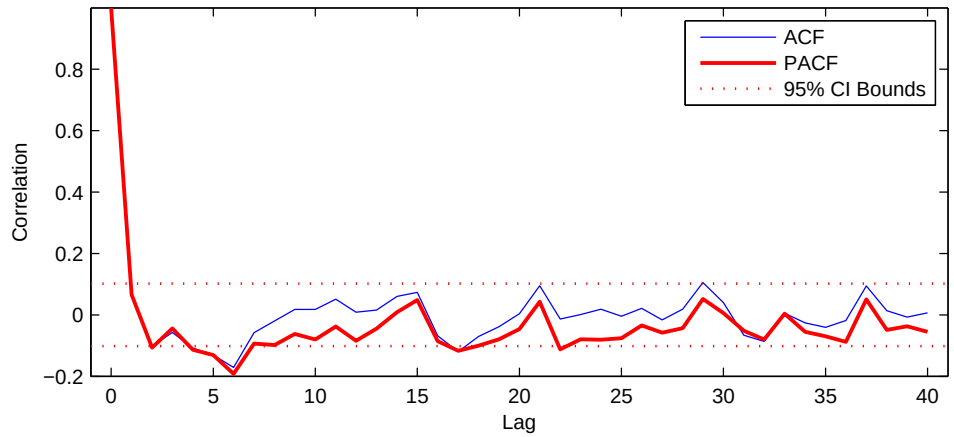

Figure 6: Sample ACF and PACF of the residual or short-memory series.

Table 1: Preliminary ARMA models

Model	Significant Lags		AIC	Error
	AR	MA		Variance
ARMA(22,15)	2, 5, 7, 9, 11, 13, 15, 16	6, 7, 8, 9, 10, 15	-2.403	0.0731
ARMA(12,7)	1, 2, 4, 5, 6, 12	1, 2, 3, 4, 5, 6	-2.385	0.0778
ARMA(8,12)	1, 2, 4, 5, 6, 7, 8	1, 2, 6, 7, 8, 9	-2.380	0.0787
ARMA(0,6)		2, 3, 4, 6	-2.380	0.0837
ARMA(11,11)	1, 4, 5, 7, 10, 11	1, 3, 4, 5, 7, 10	-2.370	0.0785

Table 2: Comparison of refined models

Model	AIC	Error	Analysis of Residuals		
		Variance	Uncorr.	Q_{LB}	p-value
ARMA(22,15)	-2.171	0.0898	90.32%	52.58	0.00009
ARMA(12,7)	-2.288	0.0821	93.55%	20.71	0.4144
ARMA(8,12)	-2.306	0.0806	93.55%	20.29	0.4399
ARMA(0,6)	-2.330	0.0829	93.55%	23.60	0.2603
ARMA(11,11)	-2.299	0.0875	91.13%	32.55	0.0377

models did not pass the criteria of uncorrelated residuals, having less than 95% of ACF values within the confidence interval bounds. This evidences the iterative nature of the selection process and poses a problem that may be solved by going one step backwards, i.e., restituting parameters in the models. The final selection is guided by the AIC, hence the model with smaller AIC, which is an ARMA(0,6), recovers its original parameters and is tested again for residual randomness. The final model passes all the criteria, having AIC, error variance, percentage of uncorrelated residuals, Q_{LB}, and p-value, equal to, respectively, -2.352, 0.0837, 95.16%, 17.61, 0.6129. The structure of the model, including parameter uncertainties is as follows

$$\begin{aligned} Y_t &= 1 - 0.06733(\pm 0.0519)Z_{t-1} - 0.2311(\pm 0.05173)Z_{t-2} \\ &\quad -0.1493(\pm 0.05228)Z_{t-3} - 0.1808(\pm 0.05234)Z_{t-4} \\ &\quad -0.1258(\pm 0.05194)Z_{t-5} - 0.1651(\pm 0.05232)Z_{t-6} \end{aligned} \tag{14}$$

where $Z \sim$ N(0,0.0837). As a result of the methodology used, an ARMA model, which accomplishes imposed statistical conditions was identified. As explained above, the trend and the seasonality account for, respectively, 8.28% and 11.51% of the variance in the original data set. On the other hand, the stochastic model accounts for 29.94% and the residuals represent the remaining 50.27% of the total variance. Such large value is not surprising in an aggregation of 10 hourly water usage series, given the large sources of uncertainty in demand behavior.

Conclusions

A modeling approach for hourly aggregated urban water demand data is presented which identifies the structure of a time series by passing it through a series of filters. Each filter estimates the parameters of an equation describing one property of the time series so that it can be transformed by removing that property. The final result of the transformations is a random error series. The properties identified are trend (related simply to the moving average of the time series), seasonality, and autocorrelation. In the future, the procedure is to be applied to a large ensemble of aggregated data from individual service accounts that are being monitored in Hamilton County, OH.

The concept of partitioning a time series into trend, seasonal, and short-memory components is classical. However, the determination of seasonal periods in the deterministic component of the data series as well as the selection of suitable ARMA models for the stochastic component of the series makes use of tools in a novel manner. The tool used in determining the periods in the series is the periodogram at inverted frequencies. For the stochastic component, the tools are statistics that assess accuracy and parsimony (AIC), as well as randomness in the residuals (ACF and Ljung-Box test statistic).

A sample dataset is analyzed using the methodology proposed and the different stages involved are explained along with the partial and final results. The main advantage of the methodology is that it allows one to explore the suitability of a large number of alternative stochastic models in a systematic fashion, and to select one or

more that best represent the residual (detrended and deseasonalized) series. A limitation of the methodology presented is that the filters which remove trend and seasonality ensure first-order stationarity, but not second-order stationarity. These two conditions are required to validate the assumption that the residual time series is generated by an ARMA process. Additional transformations can be introduced to address this limitation, but they require a comprehensible way to test when they need to be applied.

The advantage mentioned above is to be exploited in the future analysis of a large number of spatially aggregated water demand data sets. Thus, the methodology is to be applied in exploring the suitability of ARMA models to residual time series obtained from different schemes of aggregation. The authors expect to obtain relationships of model orders and levels of aggregation, by grouping ISAs either randomly or by geographic and demographic category. In the analysis of the complete data set, the main goal will therefore be to use the methodology to explore how the spatial aggregation schemes affect the variance in the water demand time series and thus understand how ISAs can be aggregated to reduce such variance.

Acknowledgements and Disclaimer

The U.S. Environmental Protection Agency through the Office of Research and Development funded, managed, and participated in the research described here under a contract with the University of Cincinnati. The views expressed in this paper are those of the authors and do not necessarily reflect the views or policies of the USEPA. Mention of trade names or commercial products does not constitute endorsement or recommendation for use. Work at the University of Cincinnati was sponsored by the USEPA under the Pegasus Contract, Contract Number EP-C-05-056, Work Assignment WA 3-06.

References

Akaike, H. (1973). Information theory and an extension of the maximum likelihood principle. In Petrov, B. N. and Csaki, F., editors, *2nd International Symposium on Information Theory*, pages 267–281, Budapest. Akademiai Kiado.

Box, G. P. and Jenkins, G. M. (1976). *Time Series Analysis: Forecasting and Control*. Holden-Day, 1st edition.

Brockwell, P. J. and Davis, R. A. (2002). *Introduction to time series and forecasting*. Springer, New York, 2nd edition.

Buchberger, S. G. and Wells, G. J. (1996). Intensity, duration, and frequency of residential water demands. *J. Water Resour. Plng. and Mgmt.*, 122(1):11–19.

Cox, D. R. and Isham, V. (1980). *Point Processes*. Chapman and Hall, New York, 1st edition.

Maidment, D. R. and Miaou, S. P. (1985). Transfer function model of daily urban water use. *Water Resources Research*, 21(4):425–432.

Maidment, D. R. and Parzen, E. (1984). Cascade model of monthly municipal water use. *Water Resources Research*, 20(1):15–23.

Salas, J. D. and Yevjevich, V. (1972). Stochastic structure of water use time series. *Hydrology Papers Series 52*.

Yamauchi, H. and Huang, W. (1977). Alternative models for estimating the time series components of water consumption data. *Water Resources Bulletin*, 13(3):599–610.

Zhou, S. L., McMahon, T. A., Walton, A., and Lewis, J. (2002). Forecasting operatinal demand for an urban water supply zone. *Journal of Hydrology*, 259:189–202.

10,000 rain gardens, one green region

Tom Jacobs, Mid-America Regional Council, 600 Broadway, Suite 200, Kansas City, Missouri 64105; PH: (816) 701-8352; FAX: (816) 421-7758; Tjacobs@marc.org

Abstract
The adoption of a broadly stated sustainability framework as the basis for the Overflow Control Plan (OCP) in Kansas City, Missouri is both extraordinary, and reflective of the community's commitment to become America's Green Region. The plan positions the city's wet weather program as a tool to catalyze more integrated water resource management at the neighborhood and watershed scales, and as a strategic initiative that supports sustainable development efforts at the metropolitan scale.

Introduction

The adoption of a broadly stated sustainability framework as the basis for the Overflow Control Plan (OCP) in Kansas City, Missouri is both extraordinary, and reflective of the community's commitment to become America's Green Region. The plan positions the city's wet weather program as a tool to catalyze more integrated water resource management at the neighborhood and watershed scales, and as a strategic initiative that supports sustainable development efforts at the metropolitan scale.

In this plan, water resource management becomes embedded within a larger context of community (re-) development, such that public infrastructure investments support and reinforce achievement of broad community goals and visions. Many of these goals are articulated in related efforts associated with climate protection, growth and development, land use, transportation, housing, parks and greenways, energy, air quality, urban forestry and agriculture.

Metropolitan and Community vision

Seven leading governmental, civic and not-for-profit organizations jointly and formally adopted a goal for the greater Kansas City area to become America's Green Region. A broad community vision seeks to "*create and support a sustainable region that increases the vitality of our society, economy, and environment for current residents and future generations.*"

Similarly, the OCP is rooted in this strong vision, and in the following three guiding principles:

- *Water is a precious resource*. Recognition that water is an asset, not a liability, requires a transition from the conventional practice of collect, convey and discharge to one that manages water resources in ways that maximize community, environmental and economic benefits.
- *Integrated, systems thinking*. Understanding water resource management from a watershed perspective requires integrated, systems thinking. This means approaching problem-solving in a holistic manner, integrating not only multiple disciplines into the decision-making process, but also considering the

interconnectivity of built and natural systems, including energy and material efficiency, and by-product synergies.
- *Adaptive management*. Adaptive management integrates, design, implementation, management and monitoring to systematically test assumptions, learn from results and adapt future plans throughout implementation.

An Adaptive Management Approach

An adaptive management approach frames the Overflow Control Plan. This approach enables the city to minimize risk and uncertainty associated with the performance, acceptability and cost of the various plan components. The plan is founded upon a holistic, watershed perspective to controlling sewer overflows, which will result in more complete, cost-effective solutions that involve watershed stakeholders from various jurisdictions throughout the planning and management process.

As part of the adaptive approach, the OCP focuses on first repairing the existing system, reducing inflow and infiltration and measuring the potential of green infrastructure. Completing these activities early in the program allows for monitoring, modeling and measurement, focused evaluation of program results, and the flexibility to adapt the plan before constructing more expensive structural controls.

An adaptive management program requires rigorous evaluation metrics across the spectrum of social, economic, environmental and regulatory concerns. System-level metrics will address not only the number and volume of combined sewer overflows, but also co-benefits related to air quality, public health, community redevelopment, heat island abatement, education, and energy. Related program-level performance indicators, aligned with long term goals, will help guide shorter term program design and pilot project implementation efforts.

Similarly, appropriate organizational feedback mechanisms will be critical to review program effectiveness, and guide future activity. An organization that is open and receptive to change is necessary to learn from and adapt to changing circumstances.

Integrated planning and design

A sustainable vision for each neighborhood is rooted in an understanding that all aspects of community living will be served better in the future when infrastructure and community assets are integrated to optimize the efficiencies inherent in associated economies of scale and multiple-use programs.

Hawken, Lovins and Lovins characterized elements of sustainable systems in their work, *Natural Capitalism*:

- One is likely to make a system less efficient simply by not properly linking and synchronizing components or tactics
- Optimizing components or tactics in isolation can pessimize the effectiveness or efficiencies of others.

- If components or tactics are not designed to work with one another, they will tend to work against one another.

Broad thinking about sustainability and integrated planning and design suggests consideration of broader principles to guide the implementation of the OCP. These include aspirations to:

- integrate rainwater as a resource, where it falls, in the community.
- secure outdoor venues in which children can play and develop empathy for other living things; in which they can discover that almost all things in nature cannot ever be wholly understood, enhancing awe, wonder and humility.
- secure opportunities for all children to participate in an educational system that preserves their in-born love of learning.
- re-establish mechanisms for authentic, mature, wise elders to be available to children and young people, and to participate meaningfully in community life.
- reconnect with the love and appreciation for beauty in our built environments through a return to local craftsmanship and a renewed appreciation for quality and locally resourced materials. That which is well made is beautiful, that which is beautiful is loved and endures.
- Add beauty and vitality to the community. Sustainable design must be functional *and* beautiful.

The mechanics of an integrated approach

Implementation of a more integrated planning process in Kansas City will be tested through initial pilot projects. Planning processes will likely involve many different elements, from community education and engagement to design charettes or other community-based mechanisms. All relevant public and private stakeholders would be involved. Planning activities would be structured to:

- build neighborhood and community support and partnerships
- create the basis for integrative planning
- identify innovative sustainable design strategies, and
- demonstrate the effectiveness of a participatory planning process.

The institutionalization of green design will require heightened levels of interdepartmental collaboration. Standard engineering drawings and materials will be reviewed and adapted so that water is properly managed for every infrastructure project. Performance standards for water management will be applied to all projects with the goal of updating the city to meet modern water management standards. Even accounting and procurement standards and procedures may need to be adapted to properly account for life cycle benefits and multiple non-project purpose benefits such as social, community development and educational benefits.

From a process standpoint, integration among programs, departments, jurisdictions, and regulatory agencies is imperative. Two significant areas with substantial unrealized opportunity are the integration of stormwater and wastewater programs

in ways that also consider needs for water supply, and the integration of water resource planning with broader city capital investment programs. Opportunities for distributed management and treatment systems for wastewater as well as stormwater will be evaluated. In each area, strong opportunities appear to exist to achieve increased efficiency, impact and financial leverage.

At the regional scale, an integrated Blue River Watershed Management Plan will represent a bi-state, comprehensive effort to improve water quality in the 270 square mile watershed. It is exactly the kind of overarching approach that will be required to significantly reduce structural controls within the plan.

Green infrastructure pilots and partnerships

The plan includes substantial resources to develop large scale, green infrastructure pilots and partnerships in the combined sewer basins. Pilot projects will focus on incorporating and evaluating green infrastructure as part of the proposed basin specific solutions. Green infrastructure partnerships will concentrate on creating private sector participation in both the pilots and final basin solutions.

Pilots will facilitate establishment of standard design, cost, construction and maintenance criteria, as well as create the opportunity to measure the social, economic and environmental impacts of green infrastructure on the neighborhood and community.

The City's first pilot project will occur in the Marlborough neighborhood. The plan includes replacement of two previously proposed underground storage tanks with widespread green infrastructure throughout this 744 acre section of the Middle Blue River Basin. This project will include, in total, approximately 330 catch basin retrofits and nearly 25 acres of rain gardens, bioswales, green roofs and pervious pavement, representing an unprecedented commitment to green infrastructure.

Additional pilot projects will be identified for each primary land use/watershed condition. These projects will provide opportunities to model the full array of innovative, sustainability-oriented program elements that, if successful, may then be applied elsewhere over the long term. These elements would include:

i) development of strong community and public/private partnerships to support plan implementation;
ii) testing and evaluation of alternative incentive programs;
iii) social marketing and community education to support incorporation of water management (e.g. rain garden installation, downspout disconnects and incentives for private participation) on private properties;
iv) design, construction and evaluation of sustainable design strategies;
v) integrated, interdepartmental planning;
vi) creation of green collar jobs and training programs;
vii) development of effective sub-watershed scale models to assess the cumulative impacts of individual design strategies; and

viii) development of specific program and project level performance metrics related to performance goals to serve as a benchmark for future program evaluation.

Early pilot projects create extraordinary opportunities for the community to build new partnerships in support of the regulatory plan and the community vision. Every dollar spent by the city will strive to leverage additional resources. During the course of the proposed 25 year plan, one might expect private investment in re-development to outpace public infrastructure investment by orders of magnitude. Multiple opportunities exist to leverage private investment through creative partnerships with neighborhood, community, civic and development interests. A mix of regulatory approaches (e.g. green development standards), incentives (e.g. discounted utility rates), compliance assistance (e.g. technical assistance) and other mechanisms can facilitate the creation of durable partnerships. Further, contracts might be structured to maximize the creation of local green collar jobs to support planning, education, design, construction and maintenance responsibilities.

Green collar jobs and workforce development

The City's $2.4 billion investment in Kansas City's sewer infrastructure presents significant economic opportunities for local businesses and residents. The plan will support job creation and work force development organizations in the development and implementation of training programs, including a green collar jobs program.

Development of green collar jobs, embedded within community workforce development, job training and green economic development strategies, are strongly recommended as an implementation vehicle for green solutions in the Long Term Control Plan. This approach would simultaneously create jobs within economically distressed communities, build community support for neighborhood scale solutions, address ongoing concerns about green infrastructure maintenance, and catalyze ancillary aesthetic and community development benefits.

Public education and civic engagement

Opportunities for shared learning, whether within city hall or with community partners, will be integral to the overall program. Education may be formal or informal, professional or public, in person or virtual, primary or university level, classroom or field-based. This program will engage diverse constituencies through a range of formats. Greatest emphasis, however, will be placed on creation of experiential, outdoor learning opportunities for children at the primary and secondary levels. Such learning may take place in varied settings, such as green jobs program, summer, church or scout programs. Appropriate investment in the community's children will guarantee the long term program success. Emphasis also will be placed on building the local economy through opportunities such as urban agriculture, urban arts and craftsmanship, and distributed wastewater and stormwater systems management.

Civic engagement, public participation and community education will be married in general outreach efforts. The City will engage neighborhood associations, businesses, civic groups, non-profit entities, universities and citizens in a public dialogue designed to throughout the life of the plan. Extraordinary opportunities exist to expand Kansas City's award winning 10,000 Rain Gardens campaign as part of roust social marketing efforts designed to downspout disconnects and green infrastructure development on private land.

Conclusion

The Kansas City, Missouri effort is buoyed by high aspirations, broad community and political support, and growing scientific consensus about the effectiveness of green infrastructure in meeting prescribed regulatory goals. Substantial work has been undertaken to link community visions with program goals; to integrate community and regional planning efforts; and, to build institutional capacity to achieve an ambitious set of goals. Within that context, the city's adaptive approach is structured to begin implementation of a complex plan in ways that are both programmatic and strategic.

A Level Spreader - Vegetated Buffer System for Urban Stormwater Management

Ryan J. Winston, E.I.[1] and William F. Hunt, P.E., Ph.D.[2]

[1] Department of Biological and Agricultural Engineering, North Carolina State University, Box 7625, Raleigh, NC 27695, rjwinsto@ncsu.edu.
[2] Department of Biological and Agricultural Engineering, North Carolina State University, Box 7625, Raleigh, NC 27695, wfhunt@ncsu.edu.

Abstract. Vegetated filter strips (VFS) have been used to remove pollutants from contributing agricultural watersheds for decades. In order to improve effectiveness of vegetated buffers, level spreaders have been employed to distribute flow evenly across the length of the upstream end of the buffer. In North Carolina, level spreader- VFS systems are now gaining acceptance as a stormwater BMP for urbanized watersheds, as it promotes infiltration and reduces impervious surfaces, two tenets of Low Impact Development. A field study of four level spreader – vegetated filter strip systems was conducted at two urban watersheds in Louisburg and Apex, NC. At each site, stormwater was routed proportionately over two 13 ft long level spreaders, one draining to a 25 ft wide grassed buffer, the other to a 50 ft wide, half grassed, half forested buffer. Flow rates and flow volumes were measured at the inlet and outlets of the system. Composite, flow-weighted water quality samples were collected at the inlet and outlet of the system and analyzed for TKN, NO_3+NO_2, TN, NH_3, TP, Orthophosphate, and TSS. The buffers promoted infiltration, which resulted in a substantial decrease in flow volume and peak flow rate between the inlet and outlet of the system. To date, 46 storm events have been monitored for hydrology in Louisburg, NC. Flow volume was reduced by an average of 83% and 80% for the 25 ft and 50 ft wide buffers, respectively. These buffers also reduced peak flow rate by an average of 86% and 83%, respectively. These results show that a level spreader – vegetated filter strip system can effectively reduce the hydrologic impacts of impervious surfaces. Water quality monitoring has been ongoing since March, 2008, with 19 and 20 storms monitored for Apex and Louisburg, respectively. Reductions in event mean concentrations for all buffer treatments occurred for TKN, TN, and TSS, while the other pollutants studied had mixed results. Because of the large reduction in volume due to infiltration, these BMPs provide a large reduction in mass of pollutants. The median percent mass removal for the Louisburg buffers was greater than 74% for all but one water quality constituent studied. A level spreader is relatively (1) easy to install, (2) inexpensive, and (3) requires little maintenance. Carefully selected and designed level spreader – vegetated buffer systems can be an effective method of controlling stormwater flow and its associated pollutants in small urban watersheds.

Keywords. level spreader, buffer, filter strip, stormwater, LID, urban, bmps, best management practices

Introduction

Urbanization of agricultural and forested landscapes across the U.S. is occurring rapidly, often leading to environmental degradation. Construction leads to a large decrease in permeability. In turn, this causes a decrease in the ability of stormwater to infiltrate or evapotranspire, resulting in increased runoff volumes and peak flow rates. Flow enters water bodies and can cause impairment in water quality in urban streams, lakes, and estuaries. In order to ameliorate these issues, engineers and land use planners have designed and implemented Low Impact Development (LID) practices. Common LID practices include bioretention areas, cisterns (water harvesting), permeable pavement, vegetated swales, decentralized stormwater management, clustered site layouts, disconnected downspouts and reduction of impervious areas. LID practices employ a number of mechanisms to improve water quality and reduce runoff before it enters water bodies. The main purpose of these practices is to reduce runoff volumes to pre-development benchmarks. Ancillary goals of these practices include: removal of pollutants common to urban stormwater, including nitrogen, phosphorous, oil and grease, sediment, bacteria, heavy metals, and thermal pollution and improvements in urban hydrology, including mitigation of peak flows and time to peak.

An LID practice/stormwater BMP that is being used in the state of North Carolina is the level spreader - vegetated buffer system (LS-VBS). The term "level spreader" was first described by Smolen et al. (1988) as "a non-erosive outlet for concentrated runoff constructed to disperse flow uniformly across a slope." A level spreader is designed to receive upslope pipe flow, and create downslope diffuse flow through a vegetated buffer (Hathaway and Hunt, 2008). Design requirements for level spreaders have been produced in several states (IDEQ, 1998; MDEP, 2003; NC DENR, 2007), but past research on their effectiveness is inconclusive and inadequate.

Level spreaders were initially used to disperse runoff from drainage ditches through forested filter zones (FFZ). Runoff from these fields contains high concentrations of nitrogen and phosphorous derived from fertilizers. In an early study of a LS-FFZ system in Granville County, North Carolina (Franklin et al., 1992), stormwater was routed from a planted agricultural field through an unspecified length of wooden level spreader. Stormwater was recollected downslope of the forested filter zone in a wooden flume, with water quality and flow rate measured at the inlet and outlet of the LS-FFZ system. Twenty nine storm events were monitored between October 1989 and July 1990. It was determined that a level spreader-forested filter zone system was effective in reducing concentrations of NH_3-N (75%), TP (32%) and TSS (47%) between the inlet of the level spreader and the outlet of the forested filter zone. Another benefit was that a 36% reduction in flow volume was observed between the inlet and outlet of the LS-FFZ. So, on a mass basis, reduction in pollutants would have been much greater than reported above.

Two quantitative studies on urban water quality and the use of level spreaders can be readily obtained from the literature. The first was completed at a shopping center in Virginia. It involved studying a level spreader-grassed buffer system and its effects

on water quality (Yu et al., 1993). The level spreader in this study was 170 m long and was sized to convey 1.02 m^3/s over the spreader lip. Eight storm events during March-June of 1987 were sampled at three locations: the outlet of the watershed, at the level spreader, and at the outlet of the buffer. The removal efficiency of the level spreader-grassed buffer system was calculated using percent mass removal, with the following efficiencies: TSS, 54-84%; NO_3+NO_2, (27)-20%; TP, 25-40%; Pb, (16)-50%; and Zn, 47-55%, with terms in parentheses representing addition of pollutant. The authors concluded that the low removal efficiencies for NO_3+NO_2-N may be attributable to erosion downslope of the level spreader, and that dense grass cover was not established during the study. The authors also suggested that sedimentation and filtration were the primary methods for solids and metals removal in a vegetated filter strip, while adsorption, precipitation, and plant uptake were likely the means of nutrient removal. This study has three major conclusions: first, the LS-VBS was effective in removal of particulate pollutants such as TSS, but was not as effective at removal of soluble pollutants such as nitrate-nitrite N; second, removal efficiency for all pollutants increased as vegetated buffer width increases; finally, the LS-VBS was at least as cost effective at removal of common stormwater pollutants as a wet pond (Yu et al., 1993).

Another study of a level spreader-vegetated buffer system was conducted in Johnston County, North Carolina, near the intersection of NC 42 and I-40 (Line and Hunt, 2009). Stormwater runoff was collected primarily from the highway (0.35 ha watershed) and conveyed through a vegetated channel to a level spreader 7.3 m in length. Buffer width was 17 m. Reductions in flow volume of 49% were observed, which led to high rates of nutrient, metals, and solids removal. Mass removal efficiencies for the level spreader-grassed buffer system were as follows: 70% total suspended solids, 11% NO_3+NO_2, 36% ammonia nitrogen, 17% total Kjeldahl nitrogen, and an 11% increase in total phosphorous.

The three articles above offer a summary of level spreader-vegetated buffer system performance. For ease of comparison, the following two tables summarize experimental design and results for the three studies. The first table is a summary of level spreader and vegetated buffer characteristics, along with other experimental design parameters of importance to the water quality and hydrology results from each study (Table 1).

Table 1: Summary of LS Research
(Adapted from authors listed in table)

Author	Year Published	Level Spreader Material	Vegetated Buffer Type	Method of Removal Efficiency Calculation	Slope of Buffer (%)	# of Events	Land Use
Franklin et al.	1992	Wooden Trough	Forested (mixed pine-hardwood)	Concentration	4	29	Agricultural
Yu et al.	1993	Concrete	Kentucky 31 Grass	Concentration	6	8	Urban
Line and	In press	Concrete	Bermudagrass	Concentration and	5.2	14	Urban

Hunt				Summation of Loads			

An important note from Table 1 is that urban level spreader studies have been completed on grassed buffers only. Past research has not been documented on level spreader-wooded buffers in an urban setting. Table 2 summarizes the results for pollutant removal. For comparison, the buffer width and the percent of runoff volume reduction are included for each system:

Table 2: Summary of Nitrogen Removal from LS Research
(Adapted from authors listed in table)

Author	Year Published	Buffer Width (m)	% Volume Reduction	% Removal NO_3+NO_2	% Removal NH_4	% Removal TKN
Franklin et al. [a]	1992	30.5	36	NM [c]	75	29
Yu et al. [a]	1993	21	NM [c]	-27	NM	NM
Yu et al. [a]	1993	45	NM	20	NM	NM
Line and Hunt [a]	2006	17	49	11	36	17
Line and Hunt [b]	2006	17	49	49	75	66

Author	% Removal Total Phosphorous	% Removal Orthophosphate	% Removal Lead	% Removal Zinc	% Removal Suspended Solids
Franklin et al. [a]	32	17	NM	NM	47
Yu et al. [a]	25	NM	-16	47	54
Yu et al. [a]	40	NM	50	55	84
Line and Hunt [a]	-11	NM	70	74	70
Line and Hunt [b]	48	NM	81	82	83

[a] These % removal values calculated as concentration reductions between inlet and outlet of the LS/VBS
[b] These % removal values calculated as load reduction between inlet and outlet of the LS/VBS
[c] Indicates that parameter was not measured for this study

Site Descriptions

Two level spreader research sites are currently being monitored in the Piedmont region of North Carolina, where soils are characterized by moderate clay contents. The sites are located in Apex and Louisburg, NC in two of the largest and most urbanized river basins in the state. Each site watershed is approximately 0.40 ha (1 ac) in drainage area, with 89% and 70% imperviousness, respectively, at the Apex and Louisburg sites. Prior to BMP construction, both watersheds drained to curb cuts. Stormwater was then allowed to flow into grassy areas, and eventually to ephemeral streams. Sites were surveyed extensively, and designs were created for two level spreaders at each site. Each level spreader is 3.96 m (13 ft) in length, and was constructed level across its length, in order to aid in dispersal of flow across the length of the buffer. Construction of the BMPs was completed in January 2008, and monitoring of the sites has been ongoing since March 2008.

At each site, incoming flow from the watershed is conveyed from the curb cuts into a forebay to settle out solids and remove trash and debris from the system. Two inlet pipes are used to convey flow proportionally from the forebay to two swales, constructed 9 inches deep. During a storm event, the stage of the water increases until the forebay and swales fill, at which point water flows over the level spreaders, and into one of the vegetated buffers. The buffers differ in width and vegetation type; the first is a 7.6 m wide grassed buffer, and the second is a 15.2 m wide buffer, which is one-half grassed and one-half wooded. This setup is repeated at both experimental sites. Figure 1 shows the level spreaders and associated monitoring equipment in Apex, North Carolina.

After the water passes through the buffer, the remaining surface flow is recollected in a trough downslope of the level spreader. Flow then passes from the trough to a weir box, and then discharges through a drainage pipe offsite. This setup can be seen in Figure 1, and is repeated four times, once for each of the level spreaders.



Figure 1. Level Spreader, Recollection Trough, and Weir Box.

Soil conditions contribute to the functioning of this LID practice, since it is almost solely dependent on infiltration as the volume reduction mechanism. The soils at both the Apex and Louisburg sites are classified as sandy loam. However, there is a tight clayey confining layer at a depth of 60 cm in Apex, which creates a saturated lens during wet periods.

Materials and Methods

Monitoring was conducted at both sites to effectively measure the impacts of a level spreader - vegetated buffer system on water quantity and quality. Hydrology monitoring occurred at four points at each site, using a total of eight ISCO 730 bubbler flow meters. At the inlet, stage measurements were taken in each of the 15 cm (6") diameter inlet pipes on a two minute interval, using ISCO 730 bubbler flow meters. Calculation of flow rates for the inlet was completed using Manning's equation for flow in round pipes, as given below in equation 1. A Manning's n value of 0.01 was used, as is typical for PVC pipes (Fangmeier et al., 2006).

$$Q=A*R^{2/3}*S^{1/2}/n \qquad [1]$$

Outlet hydrology was monitored downslope of the vegetated buffer. Following the initial abstraction, infiltration, and evapotranspiration in the buffer, the remaining flow was intercepted in a triangular cross section wooden trough. Flow was conveyed to one end of the trough, where it entered a weir box. A 30° V-notch weir was used in each weir box, in combination with an ISCO 730 bubbler flow module. The flow module recorded stage measurements at a two minute interval. Flow rates at the outlet were calculated using the standard stage discharge relationship for a 30° V-notch weir, given below in equation 2:

$$Q=0.676*H^{2.5} \quad [2]$$

Following the calculation of flow rates, inlet and outlet flow volumes were calculated by integration of the hydrograph.

Water quality samples were taken from three locations at each site, in order to quantify concentration reductions for each buffer width. During this study, samples were analyzed for the following parameters: Total Kjeldahl Nitrogen (TKN), nitrate-nitrite nitrogen (NO_3+NO_2), total nitrogen (TN), ammonia nitrogen (NH_3N), total phosphorous (TP), orthophosphate (ortho-P), and total suspended solids (TSS). A total of six ISCO 6712 water quality samplers were used to take composite, flow proportional water quality samples during storm events. The inlet sample intake at each site was located in the center of the forebay. The two outlet sample intakes at each site were located in the weir boxes, upstream of each 30° V-notch weir. The inlet water quality samples were used as a baseline for all comparisons, as they represented untreated stormwater runoff.

Hydrology Results

Monitoring has been ongoing at both the Louisburg and Apex, NC sites since March 2008. In Louisburg, forty-six storm events large enough to create inflow have been monitored. Due to minor equipment failures, all of those storm events were not captured for the two buffer lengths. Thirty-one storm events with precipitation depth <1.25 cm, seven events between 1.25 cm and 2.5 cm, and eight events >2.5 cm have been monitored. Median rainfall depth was 0.74 cm, with lower and upper extremes of 0.1 cm and 6.55 cm, respectively. Initial hydrologic results for this site are very promising (Figure 2). For both the 7.6 m buffer and the 15.2 m buffer, percent volume reduction and percent peak flow reduction appear to be correlated to the size of the rainfall event. As precipitation depth increases, the effectiveness of the level spreader - vegetated buffer system decreases. For storm events less than 1.25 cm, this system infiltrates most of the flow volume produced, resulting in >85% volume and peak flow reduction. However, general trends indicate that as rainfall depth increases, volume reduction and peak flow reduction decrease. Therefore, a level spreader - vegetated buffer system may prove more beneficial during events with smaller precipitation depths, similar to the conclusion of Li et al. (2009) for bioretention areas.

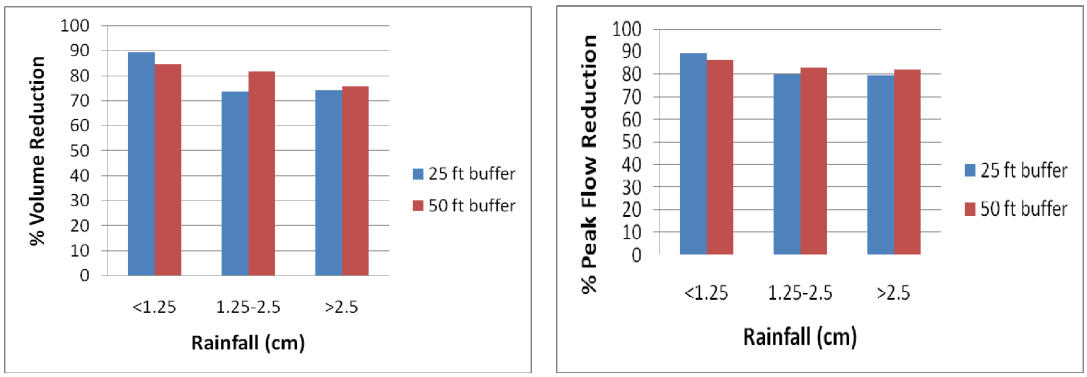

Figure 2. Preliminary Hydrology for Louisburg, NC Site.

At the Apex site, forty-three storm events large enough to create inflow have been monitored. However, accurate hydrology measurements at the site have been difficult to obtain. The slope from the inlet to the outlet of the system is very small (<4%), and this led to a small slope on the inlet pipes (where inlet hydrology is measured). During high intensity portions of the hydrograph, backwater is conveyed from the level spreaders up the inlet pipes, and stormwater is ponded above the bubbler. Because of this, the bubbler gives false readings, since Manning's equation assumes free flow in a pipe. Therefore, inlet hydrology results for the Apex site are not valid. An attempt at creating a rating curve of flow rate versus depth will be made by using area-velocity meters.

Water Quality Results

Monitoring for the water quality portion of this study has been ongoing since March 2008. For a water quality event to occur, a minimum of 0.5 cm of rainfall must occur. Therefore, many of the storm events analyzed above in the hydrology section were not large enough to be considered a "water quality event." In Apex, a total of 19 water quality events have been monitored, while 20 storms have been captured in Louisburg. Median concentration reductions between the inlet and outlet of each buffer can be seen in Figure 3:

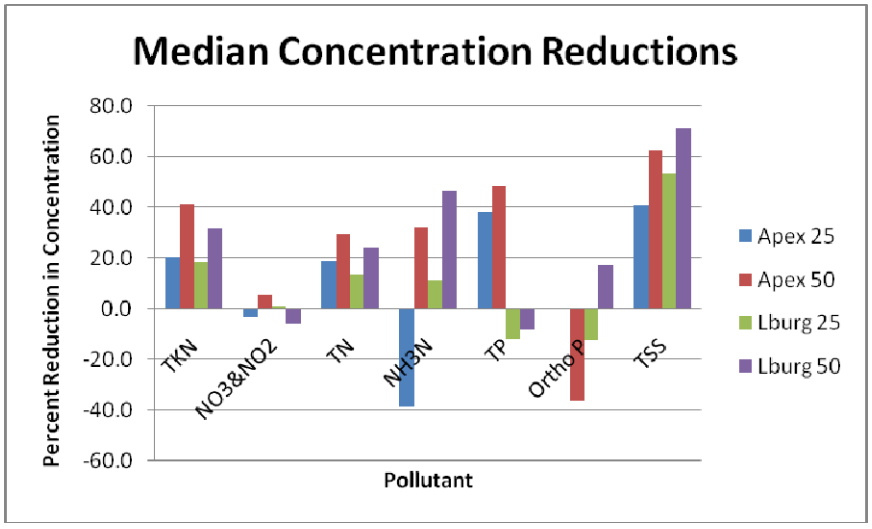

Figure 3. Percent Removal Results.

The terms "25" and "50" refer to the width of the buffer, that is, the 7.6 m (25 ft) buffer the 15.2 m (50 ft) buffer. TKN concentration reductions between 20-40% were seen in each of the buffers studied. However, these systems may be exporting organic nitrogen, since TKN removal rates are generally lower than those for NH_3-N. Nitrate-nitrite nitrogen is a highly soluble nutrient that does not adsorb to sediment due to its negative charge. Since the primary treatment in vegetated buffers is sedimentation, the lack of NO_3-NO_2 nitrogen removal in Figure 3 is logical. Total phosphorus results are mixed. This is disconcerting since TP is most often sediment sorbed, and TSS removal is observed in all four buffers. However, the median inlet TP concentration in Louisburg is 0.13 mg/L, well below the median TP concentration of 1.46 mg/L reported by Frink (1991) for urban runoff. The ortho-P results in Apex may be disregarded, as the inlet ortho-P concentrations are below laboratory detection limits. Removal of ortho-P in Louisburg is mixed, with an increasing width apparently producing greater removal. For TSS, all four buffers perform very well, removing 40-70% of TSS on a concentration basis. In both cases, the 15.2 m (50 ft) buffers removed 20% more sediment than the 7.6 m (25 ft) buffers. Similar results were reported in Robinson et al. (1996), where a 3 m buffer removed 70% of sediment and a 9.1 m buffer removed 85% of sediment.

As shown above, this LID practice is capable of removing sediment-sorbed pollutants on a concentration basis. As shown in Figure 4, this practice can have a large impact on water quality when mass removal of pollutants is considered. This is done by taking into account both the concentration of pollutant and flow volume removed from the system.

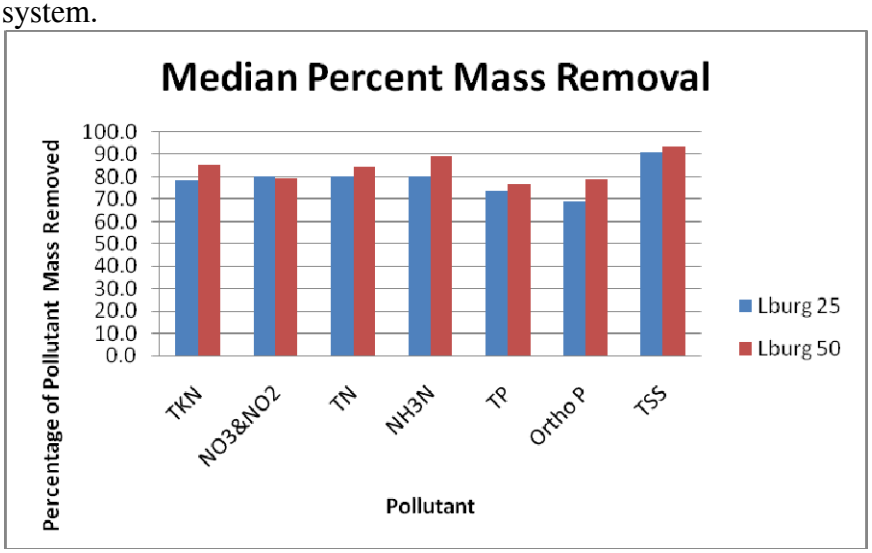

Figure 4. Median Percent Removal Results.

For all pollutants at the Louisburg site, reductions in mass of 68-90% were observed. This is due primarily to the large volume reductions in both buffers of >70%. In every case except $NO_{2\text{-}3}$-N, the wider buffer reduces the mass of pollutant to a greater extent. Overall, the results summarized above are very promising, and show that this system can be used to effectively remove pollutants on a mass basis before they enter downstream rivers, lakes, or estuaries.

Conclusion

Results indicate that level spreader - vegetated buffer systems may perform well in urbanized areas, allowing for greater infiltration, evapotranspiration, and groundwater recharge. Hydrology results show that this BMP performs better during storms with smaller rainfall depths. Water quality results also show promise for reduction in concentration of TKN, TN, TP, and TSS. Load basis calculation of water quality shows between 68-90% reduction in mass across the system.

Preliminary results show that a level spreader - vegetated buffer system can provide substantial peak flow reduction. During small storm events, peak flows were reduced by an order of magnitude. This shows another benefit of this LID practice beyond the traditional volume reductions.

Preliminary results show that a level spreader - vegetated buffer system is a viable LID practice for the management of urban stormwater runoff. In certain situations, level spreaders may be a cost effective method to reduce flow volumes, peak flow rates, and improve water quality in urbanized watersheds. The added green space required for the filter strip is an additional benefit of this practice. Maintenance and construction of these systems is very simple. Level spreader – vegetated filter strips are poised to become one of the most popular stormwater treatment devices in North Carolina.

Acknowledgements

This research was funded by the North Carolina Department of Environment and Natural Resources, Division of Water Quality. The authors would like to thank Dr. François Birgand, Jon Hathaway, Shawn Kennedy, Bill Lord, Dr. Deanna Osmond, Mitch Woodward, and Jason Wright for their assistance throughout the project.

References

Fangmeier, D.D., W.J. Elliot, S.R. Workman, R.L. Huffman, G. O. Schwab. (2006). "Manning Roughness Coefficient n." *Soil and Water Conservation Engineering*. Clifton Park, NY, 479-480.

Franklin, E. C., J. D. Gregory, and M. D. Smolen. (1992). *Enhancement of the Effectiveness of Forested Filter Zones by Dispersion of Agricultural Runoff.* Water Resources Research Institute of the University of North Carolina, UNC-WRRI-92-270, Raleigh, NC.

Frink, C.R. (1991). Estimating Nutrient Exports to Estuaries. *Journal of Environmental Quality*. 20(4): 717.

Hathaway, J. M. and W. F. Hunt. (2008). Field Evaluation of Level Spreaders in the Piedmont of North Carolina. *ASCE Journal of Irrigation and Drainage Engineering*, 134(4): 538.

Idaho Department of Environmental Quality (IDEQ). (1998). Catalog of Stormwater Best Management Practices for Idaho Cities and Counties.

Li, H., L. Sharkey, W.F. Hunt, and A.P. Davis. (2009). Mitigation of Impervious Surface Hydrology using Bioretention in North Carolina and Maryland. *ASCE Journal of Hydrologic Engineering*, 14(4): TBD.

Line, D.E. and W.F. Hunt. (2009). Performance of a Bioretention Area and a Level Spreader-Grass Filter Strip at Two Highway Sites in North Carolina. *ASCE Journal of Irrigation and Drainage Engineering*, in press.

Maine Department of Environmental Protection (MDEP), Bureau of Land and Water Quality. (2003). Erosion and Sediment Control BMPs Manual.

North Carolina Department of Environment and Natural Resources (NC DENR), Division of Water Quality. (2007). Stormwater Best Management Practices Manual.

Robinson, C.A., M. Ghaffarzadeh, and R.M. Cruse. (1996). Vegetative Filter Strip Effects on Sediment Concentration in Cropland Runoff. *Soil and Water Conservation*. 50(3): 227.

Smolen, M.D., D.W. Miller, L.C. Wyatt, J. Lichthardt, A.L. Lanier, and R.G. Jessup. (1988). Erosion and Sedimentation Control Planning and Design Manual. N.C. Sedimentation Control Comm., N.C. Dept. Env. Health and Nat. Resources, Raleigh, NC.

Yu, S. L., M. A. Kasnick and M. R. Byrne. (1993). A Level Spreader/Vegetated Buffer Strip System for Urban Stormwater Management. In *Integrated Stormwater Management,* ed. R. Field, O'Shea, M. L., and Chin, K. K., Boca Raton, FL: Lewis Publishers.

A NEW METHODOLOGY TO EVALUATE POLLUTANT REMOVAL OF GROSS SOLIDS SEPARATION DEVICES

D. P. Smith[1]

[1]Applied Environmental Technology, 10809 Cedar Cove Drive, Tampa, FL 33592; PH (813) 864-5735; email: dpsmith_aet@verizon.net

ABSTRACT

Gross Solids are a set of stormwater components that includes large organic and inorganic materials, litter and trash, and relatively large suspended sediments. A common characteristic of *Gross Solids* is that they are not fully accounted for in BMP monitoring protocols that employ only automatic sampling devices for collection of water column samples. A methodology is presented that provides a quantitative framework for incorporating *Gross Solids* into estimates of the pollutant removal effectiveness of *Gross Solids Separation Devices*. Illustration of the methodology using monitoring data for a full scale Nutrient Separating Baffle Box demonstrates the significance of including *Gross Solids* in estimates of pollutant removal effectiveness. The resulting performance analysis would not be possible using traditional monitoring approaches.

BACKGROUND

Structural Best Management Practices are widely applied for stormwater treatment, but assessing their actual performance is a continuing challenge. Of particular concern is a set of materials that includes large organic and inorganic materials, litter and trash, and coarser stormwater solids. The term *Gross Solids* has been adopted to encompass these materials, which share a common characteristic of not being fully accounted for in typical BMP monitoring protocols that employ automatic sampling devices. A Technical Committee of the EWRI Urban Water Resources Research Council has developed monitoring guidance to assess the ability of treatment devices to remove *Gross Solids* pollutants in stormwater (EWRI, 2007). To rationally incorporate *Gross Solids* pollutants into stormwater and BMP monitoring, practical sampling and analyses protocols must be developed and applied.

METHODS

The Florida Department of Environmental Protection sponsored a monitoring study of a full scale "Nutrient Separating Baffle Box" (aka NSBB) located in Rockledge, Florida. The NSBB is a structural BMP made of concrete or fiberglass

that contains a series of settling chambers separated by baffles (Fig. 1). NSBB are generally deployed as an in-line device in the stormwater

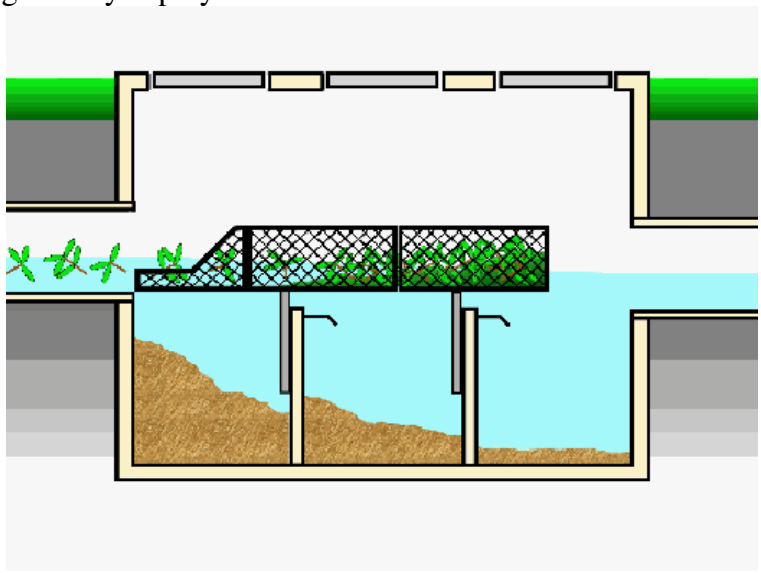

Fig. 1 Nutrient Separating Baffle Box schematic.

conveyance system. Baffle boxes remove stormwater solids that occur as sediment particles suspended in the water column and as larger solids that move by ablation along the bottom of stormwater pipes. The ability to remove suspended sediment solids is related to the settling velocity of solids and stormwater flowrate applied to the baffle box.

The NSBB-type baffle box contains a screen basket located above the bottom chamber baffles with ½ to ¾ in. openings that collect larger floating and suspended materials, including leaves, pine needles, and natural and human derived trash and debris (Fig. 2). Material captured in the NSBB screen is held above the surface of the water column in interevent periods, thus reducing the potential for leaching into the water column and enhancing the opportunity to dry. Material that is captured and retained by the screens can form a mat on the screen surface, which can then remove smaller stormwater particles that would otherwise pass through the screen openings.



Fig. 2 Nutrient Separating Baffle Box screen.

The Rockledge NSBB had a 49 ft^2 plan area (9.8 ft. x 5ft) with 3.5 ft. tall baffles. The NSBB treated stormwater runoff from a 10.6 acre area of predominantly single family residential land use before it discharged into the Indian River Lagoon. The Florida Department of Environmental Protection monitoring protocols for best management practices (BMPs) that require the collection of flow-composited influent and effluent samples for seven to ten storm events (Sutron et al. 2006). The accumulation of sediment in bottom chambers and gross solids in screen baskets occur during storm events, but monitoring of these *Gross Solids* components on a storm event basis would be problematic if not totally impractical. The Rockledge NSBB monitoring program was designed to facilitate a combination of water column and *Gross Solids* pollutant removals by maintaining a temporal linkage between the stormwater event measurements and the discreet Gross Solids cleanouts. Just prior to the start of the test period, the Lincoln baffle box was totally cleaned by removal of all materials deposited in the bottom chambers and all of the contents in the screen basket. The test period was started (t_{zero}) by activating the continuous flowrate acquisition and flowrate-based autosampler collection programs. A Doppler flowmeter provided instantaneous flowrate measurements which were recorded at 5 min. intervals throughout the project duration and used to initiate composite influent and effluent sampling. The methodology required that records be maintained for all removals of *Gross Solids* during the time period corresponding to that of the water column storm event measurements. Cleanout of bottom chambers and screen basket at the end of the operating period (t_{final}) would provide the cumulative removal for mass or volume of *Gross Solids* components.

REMOVAL EFFECTIVENESS

Monitoring of the Rockledge NSBB was initiated on 11/12/2006. All materials accumulated in the bottom chambers and screen basket were removed at the start of monitoring. This paper reports results for the period from start to 11/6/2007 when all accumulated materials were again removed from bottom chamber and screen basket. Continuous flowrate monitoring was conducted throughout the 359 time period, during which a total volume of 1.52 million gallons passed through the baffle box.

Water quality was monitored during seven individual storm events by autosampler collection of flow composited samples from influent and effluent pipes. The average TSS EMC reduction efficiency was moderate (range of -40 to 68%). Average EMC reductions were negative for nitrogen, phosphorus and fecal coliform, indicating net export during monitored storm events (Table 1).

For each bottom chamber the volume of accumulated material was quantified using the chamber cross sectional area and multiple depth measurements. A single sediment sample was assembled for physical and chemical testing characterization by combining sediment subsamples from each chamber in volume-weighted portions. Sediment data are shown in Table 2.

Table 1 Water column EMCs

Constituent	Average $EMC_{influent}$	Average $EMC_{effluent}$	Average % Reduction
Total Suspended Solids, mg/L	50.0	40.1	17.8
Total Nitrogen, mg/L	2.19	2.10	-11.5
Total Phosphorus, mg/L	0.58	0.58	-6.7
Fecal coliform, cfu/100 ml	39,320	89,800	-285

Table 2 Properties of material removed from bottom chambers

Sediment Property	Value
Dry mass removed, lbs.	1280
Bulk density (dry), g/cc	0.69
Water content, %	49.1
Organic matter, %	12.6
Total N, mg/kg	2,310
Total P, mg/kg	247

Material removed from the basket screen was collected, placed in plastic bags, and weighed in an as-received condition. The total mass of material removed from the basket screens was 2724 lbs. over the 359 day period. Screen basket

material collected in the last cleanout was subject to further analysis after weighing. The material was partially air dried and representative subsamples were assembled into a composite screen basket sample. The composite sample was size separated by sieving through a 1 mm nylon screen. Physical measurements and chemical analyses were conducted on each of the two size fractions (Table 3).

Table 3 Properties of material removed from basket screen

Property	Total	> 1 mm	< 1 mm
Wet mass removed, lbs.	**531**		
% Water	**51.6**		
Dry mass, lbs	257.3	106.2	151.0
% Organic Matter	47.88	73.30	30.00
Total N, mg/kg	593	482	670
Total P, mg/kg	834	755	890
Total N, mg/kg OM	1,584	658	2,235
Total P, mg/kg OM	2,167	1,030	2,967

Mass removals were calculated for water column storm events, chamber sediment, and basket screen material. Water column mass removal was estimated by summing mass removal for the monitored storm events and scaling up to the total volume that passed through the baffle box during the study period. The mass removal from each storm was calculated using the flow weighted pollutant concentrations (Event Mean Concentrations) in inlet and outlet and cumulative volume treated:

$$\text{Water Column Removal} = \sum_{i=1,n} \text{Volume}_i \, (\text{EMC}_{\text{inf}_i} - \text{EMC}_{\text{eff}_i})$$

Mass removals of stormwater pollutants in *Gross Solids* were calculated as the product of the accumulated bulk volume of the *Gross Solids* component times its

dry bulk density (i.e. mass *Gross Solids* removed over the study period), times the pollutant concentration (mass pollutant per dry weight solids):

$$\text{Sediment Removal} = \text{Volume}_{sediment} * p_{bulk,\ sediment} * C_{sediment}$$

$$\text{Screen Removal} = \text{Volume}_{screen} * p_{bulk,\ screen} * C_{screen}$$

Mass removal of solids, nitrogen and phosphorus are shown in Table 4. Solids removal in both chamber sediment and basket screen were much higher than in water column, and solids removal in the water column was only 3% of that in *Gross Solids* components. *Gross Solids* nutrient removals were greater than water column removals, which were negative for both nitrogen and phosphorus. Similar calculations are shown in Table 5 for four heavy metals. *Gross Solids* removals exceed those of water column for three of the four metals. The mass removal results using the calculation methodology illustrate that an overall assessment of pollutant removal effectiveness must include the contribution of *Gross Solids* accumulations within the NSBB. Traditional monitoring approaches that include only autosampler-based water column data would not include the *Gross Solids* contributions.

Table 4 Mass removals of solids and nutrients in water column and *Gross Solids* (lbs.)

Constituent	Chamber Sediment	Screen Material		Total Chamber + Screen	Water Column
		> 1 mm	< 1 mm		
Solids	1,280	841	1,196	3,317	98
Total Nitrogen	2.96	0.41	0.80	4.16	-0.77
Total Phosphorus	0.32	0.64	1.06	2.02	-0.08

Table 5 Mass removals of metals in water column and *Gross Solids* (gram)

Constituent	Chamber Sediment	Screen Material		Total Chamber + Screen	Water Column
		> 1 mm	< 1 mm		
Cadmium	0.02	0.25	0.26	0.53	2.04
Chromium	2.67	172	9.8	184	-0.47
Copper	4.75	16.0	19.6	40.3	-2.89
Zinc	34.0	81.4	100	215	58.2

CONCLUSIONS

A methodology was developed to quantify the removal of *Gross Solids* pollutants in stormwater and applied to a full scale Nutrient Separating Baffle Box. It was found that pollutant removal in *Gross Solids* components captured in the NSBB greatly exceeded water column removals calculated with autosampler-based EMCs. The results suggest that pollutant removal estimates for NSBB based solely on water column EMCs are scientifically inadequate. If anything, water column removal efficiencies should be relegated to a lesser status that *Gross Solids* accumulations in bottom chambers and screen basket. The results appear to reflect the inadequacy of water column autosamplers to capture influent pollutants that did in fact accumulate within the Rockledge NSBB. The evaluative framework and results of this study are applicable pollutant removal evaluations of other *Gross Solids Separation Devices*, which share with NSBB a limited water retention time and a primary function of *Gross Solids* removal. Attention should be directed to developing improved protocols for sampling, processing and analysis of *Gross Solids* that can lead to accepted quantitative estimates of pollutant load reduction.

ACKNOWLEDGEMENT

The author is grateful to the Florida Department of Environmental Protection for sponsoring this work.

REFERENCES

Environmental Water Resources Institute (2007) ASCE Guideline for Monitoring Gross Pollutants, B. Rushton, G. England, and D. Smith, Editors, Urban Water Resources Research Council, Gross Solids Technical Committee, available at: http://www.stormwater.ucf.edu/conferences/9thstormwaterCD/documents/ASCEguidelines.pdf

Sutron Corp. et al. (2006) Baffle Box Testing Program Final Quality Assurance Project Plan submitted to Florida Department of Environmental Protection, Tallahassee, Florida.

A simplified model of Combined Sewer Overflows to estimate event driven enteric pathogen concentrations in drinking water sources

Rishab Mahajan[1], James Uber[1], Joseph Eisenberg[2]

[1]Department of Civil Environmental Engineering, University of Cincinnati, Cincinnati,OH-45220; email:mahajarb@email.uc.edu, jim.uber@uc.edu.
[2] Department of Epidemiology, University of Michigan, Ann Arbor, MI-48109, email: jnse@umich.edu.

ABSTRACT

Raw sewage discharges from Combined Sewer Overflows(CSO's) during rainfall can severely impact drinking water quality. Drinking water risk assessment studies in the past have not adequately captured the event driven temporal fluctuations in source water quality. This is despite the knowledge that fecal contamination of source waters is impacted by rainfall and long-term accumulated risks are affected by event driven concentration peaks. This paper presents a simple methodology to estimate the enteric pathogen loadings into the receiving water as a result of combined sewer overflows. The proposed methodology is more suitable for risk assessment studies to formulate policies for public health protection.

1 INTRODUCTION

Enteric viruses are widely reported to be a major cause of non bacterial gastroenteritis resulting in acute diarrhea. About 23 million cases of infection are reported every year in the US alone (Mead et al. (1999)). Enteric viruses, which are shed in faeces of infected individual are of concern in drinking water because of their resistance to environmental stress and disinfection. High concentrations of enteric viruses have been reported in raw and treated sewage (Lodder and de Roda Husman (2005); Lodder et al. (1999)). Some studies also indicated a relationship between a contaminated water source and disease outbreaks (Anderson et al. (2001); Brown et al. (2001)). Rainfall resulting in overflows in combined sewer networks increase the enteric pathogen loading into the receiving water used as drinking water sources. A portion of the public health risk from exposure to drinking water enteric pathogens is thus likely to be event-driven, episodic, and difficult to measure or assess.

Quantitative Microbial Risk Assessment (QMRA) has emerged as a tool to assess the impact of microbial contamination of drinking water on public health. Drinking water QMRA studies in the past (Masago et al. (2006); Westrell et al. (2003)) have not adequately captured the event driven temporal fluctuations in source water quality, despite the knowledge that fecal contamination of source waters is impacted by rainfall and long-term accumulated risks are affected by event driven concentration peaks (Westrell et al. (2006)). This work presents a methodology to estimate the enteric pathogen loadings to source water, incorporating events that are assumed to drive exposure variability.

2 PATHOGEN SOURCE MODELING

Combined sewers are designed to carry both sanitary sewage as well as runoff occurring in a watershed area. During the periods of low flow these deliver the sanitary sewage to the waste water treatment plants. In periods of rainfall, due to limited capacity of conveyance structures and treatment plants, some of the flow is directly discharged into the receiving water through combined sewer overflows(CSO's). These wet weather overflow discharges containing untreated sewage result in pathogen loading into receiving waters. Rodriguez (2007) reported that the concentration of enteric viruses was increased by almost 10 times during overflow events as compared to dry weather.

To model enteric pathogen loading into source water it is assumed that pathogen loading is entirely due to upstream contamination from treated and untreated sewage. Figure 1 illustrates the pathway for source water contamination by enteric viruses. To estimate the time series of pathogen concentrations in source waters a rainfall/runoff driven model is proposed. A simulation of sewer overflow discharges driven by historical precipitation data or synthetic design rain storms, superimposed on pathogen concentration in raw sewage, generates a time series of pathogen concentrations in source water. Detailed sewer network models can be used to predict overflow discharges in combined sewers resulting from rainfall events, using standard hydrodynamic calculations and software such as the EPA Storm Water Management Model (SWMM). Such an approach is, however, data and computationally intensive, particularly for long-term continuous simulation. This renders such an approach practically difficult for QMRA, and precluding useful computational statistics techniques such as Markov Chain Monte Carlo (MCMC) sampling, which can fuse exposure models with data. A simple, phenomenological, "grey-box" modeling approach is proposed here instead to translate precipitation into overflow volumes.

2.1 Combined Sewer Overflow (CSO) model

The simple grey box model to predict combined sewer overflows consists of a hydrological module and a sewer module (Figure 2), described below.

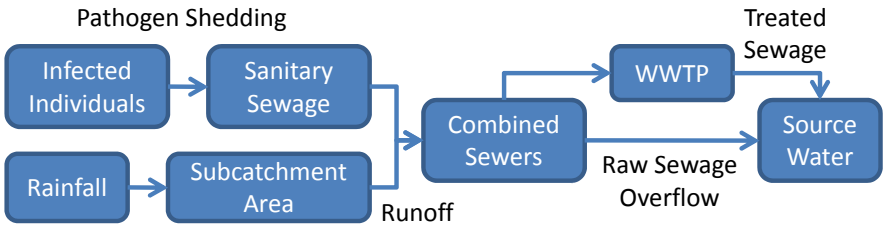

Figure 1: Source water contamination pathway.

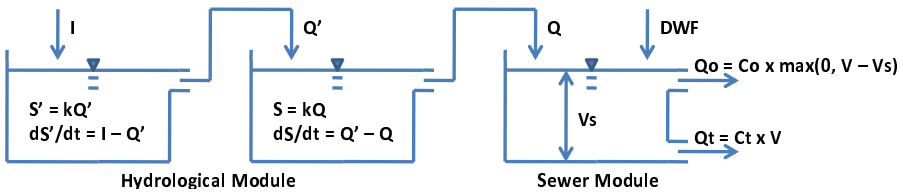

Figure 2: Simplified Grey-Box Model to estimate combined sewer overflows

2.1.1 Hydrological Module

The purpose of the hydrological module is to convert the rainfall falling over an urbanized catchment area into runoff that enters the combined sewer network through roof drain connections and catch basins.

Some amount of initial rainfall will be lost before the runoff occurs. This is accounted for by depression storage or loss potential parameter, L for subcatchment area i. Depression storage for impervious surfaces ranges between 0.05 - 0.1 inches (Rossman (2008)). The loss potential is assumed to recover during the dry period between rainfall events, with complete recovery after an elasped time, R^i with no rainfall. The amount of runoff generated depends on the subcatchment properties. Combining the continuity equations for two reservoirs in series, the subcatchment is conceptualized as a double linear reservoir by the following equation (Ruan and Wiggers (1998)).

$$k^2 \frac{dQ^2}{dt^2} + k\frac{dQ}{dt} + Q = I \times A_z \tag{1}$$

where, Q is runoff generated from the subcatchment area, I is effective rainfall intensity calculated from rain intensity after taking L and R into account, A_z is the impervious area of the subcatchment (assuming that only the impervious area contributes to runoff), and k is the lag coefficient or the concentration time of the subcatchment. The value of k depends upon the subcatchment properties and the storm characteristics. It represents the time lag between the peak rainfall intensity and the peak runoff discharge.
The above second degree ODE can be solved by using a two state space model (The Mathworks Inc. (2007)).

2.1.2 Sewer Module

Simplified sewer reservoir models have been used in the past to predict overflow discharges in large sewer networks. Ruan and Wiggers (1998) developed a model called Sewsim for predicting overflow discharges. Vaes and Berlamont (1999) used a physically based procedure to calibrate parameters for a multi linear sewer reservoir model. Runoff generated from the hydrological module plus the dry weather sanitary sewage flow is used as input into the sewer module. The sewer network is idealized as a reservoir (Figure 2) with an orifice regulating outflow to the treatment plant, Q_t. When the volume in the reservoir exceeds a threshold V_s, an overflow (Q_o) occurs with magnitude given by a weir relationship. Flow continuity for the sewer reservoir yields

$$\frac{dV}{dt} = Q - C_t \times V - C_o \times \max(0, V - V_s) \tag{2}$$

where V is volume in the reservoir, Q is the inflow into the sewer network, and C_t and C_o are lumped discharge coefficients for the fictitious orifice and weir, whose discharges have been simplified as linear functions of hydraulic head or volume.

The above sewer module is a gross simplification of the complex hydrodynamic processes occurring in a sewer network, but it is hoped that such a model can adequately represent the statistics of CSO events, while providing a flexible and more transparent approach for generating synthetic pathogen time series needed for QMRA methodology. The model was applied to a variety of test cases utilizing typical design rainfall storms as well as continuous rainfall input.

2.1.3 Model Calibration

The three parameters of the sewer module (C_t, C_o, V_s) are calibrated using the overflow discharge time series from a hydrodynamic SWMM simulation of a sewer network driven by a precipitation series. A direct search optimization procedure (Hooke and Jeeves (1961)), is used to obtain a least square estimate of the parameters. The objective function used in the calibration procedure is given by the following equation:

$$Z(C_t, C_o, V_s) = \alpha \times \sum_{i \in I_0} Q_i^2 + (1 - \alpha) \times \sum_{i \in I_1} (Q_i - Q_i^S)^2 \tag{3}$$

where, Q_i and Q_i^S are the discharges predicted at the time step i by the model and SWMM respectively, I_0 and I_1 are sets of time step indexes defined as $Q_i^S = 0 \; \forall \; i \in I_0$ and $Q_i^S \neq 0 \; \forall \; i \in I_1$, and α is a weighting coefficient : $0 < \alpha \leq 1$.

The optimization procedure has been tested using a grid optimization procedure to ensure that the least square estimates of the parameters are indeed the true estimates. The estimates of two parameters (keeping the third parameter constant) found using the Hookes-Jeeves algorithm have been found to be in agreement with those obtained from the grid optimization procedure.

2.2 Enteric Pathogen Concentration

The CSO model will be combined with simple statistical models of enteric pathogen concentrations in raw domestic sewage, and attenuation in a surface water environment to estimate the CSO enteric pathogen loadings to receiving waters and the enteric pathogen concentration at a drinking water intake. For estimating the raw sewage concentrations, environmental data on enteric pathogen occurrence in raw sewage from published sources will be used. The pathogen concentration will be adjusted for expected seasonal variability. Preliminary work in this regard has been done by Jeff Soller (Soller (2008)) as part of USEPA Star Grant Project under which the current work is being carried out. CSO enteric pathogen concentrations will be diluted from the dry weather flow concentrations using a simple dilution factor based on CSO overflow discharges.

$$C_s = \frac{Q_d \times C_d}{Q} \tag{4}$$

where, Q_d and C_d are the dry weather flow and pathogen concentration respectively, C_s is the diluted pathogen concentration in sewage after mixing with runoff.

For dilution calculations the overflow discharge Q_o will be assumed negligible in comparison to the discharge in the receiving water body, Q_R. The pathogen concentration in surface water due to overflow at the point of discharge (outfall) i, C_R can be calculated on the basis of mass continuity.

$$C_R = \frac{Q_o \times C_s}{Q_R + Q_o} = (\frac{Q_o}{Q_R}) \times (\frac{Q_d}{Q}) \times C_d \tag{5}$$

Assuming that the pathogen decay in the surface water environment follows first order kinetics, the pathogen concentration at the point of drinking water intake, C_I, can be estimated based on travel time from the overflow outfall i to intake.

$$C_I = C_R \times e^{-k \times t_i} \tag{6}$$

where, k is the decay rate constant, t_i is the travel time from the overflow outfall i to intake.

3 PRELIMINARY RESULTS FOR THE CSO MODEL

The above described modeling methodology has been applied to three preliminary test cases.

3.1 Test Case 1

The first test case consisted of a simple sewer network with one contributing subcatchment and one combined sewer overflow (Figure 3(a)). Initial condition of zero volume in the sewer network was assumed for simulation. For calibration a typical 24 hr design rainfall was used as input into the system. The value of alpha in the objective function was taken to be 0.5 (Equation (3)). Least square estimates of $0.0945\ s^{-1}$, $0.0567\ s^{-1}$,

$13.3812\ m^3$ were obtained for C_t, C_o and V_s respectively, with the optimal value of Z being 101.4154. Figure 4(a) shows the fit obtained as a result of calibration. The estimated set of optimal parameters were then used for the same system with another 24 hr design rainfall as input for validation. Figure 4(b) shows the overflow discharge time series predicted by the model in comparison to SWMM using the estimated set of optimal parameters.

3.2 Test Case 2

In the second test case, a sewer network with one contributing subcatchment area and two overflows (Figure 3(b)) was used. For modeling this system, the discharges from the two overflows were added together to calculate the total system overflow. The objective function was modified so that Q_i and Q_i^s corresponded to the total system overflow discharge. Using the same procedure as in Test Case 1 an optimal estimate of parameters was found to be $0.0395\ s^{-1}$, $0.0272\ s^{-1}$ and $108.6\ m^3$ for the fictitious reservoir system with corresponding optimal value of Z being $2.18E04$. Figure 5(a) shows the fit obtained for the total system overflow. The estimated set of model parameters was then validated using another 24 hr design rainfall as input (Figure 5(b)).

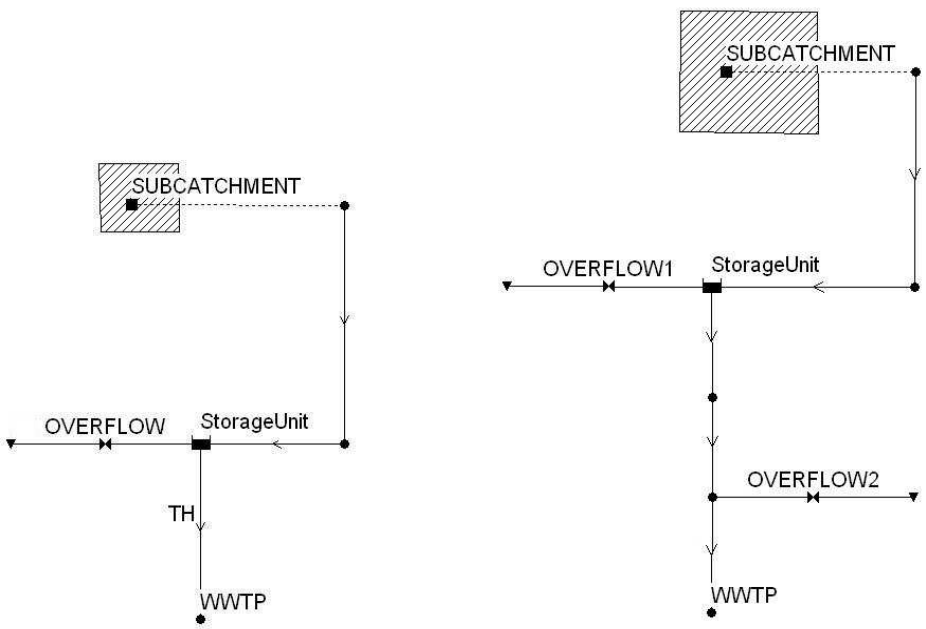

(a) Test Case 1 Network (b) Test Case 2 Network

Figure 3: Simple Test Case Sewer Networks

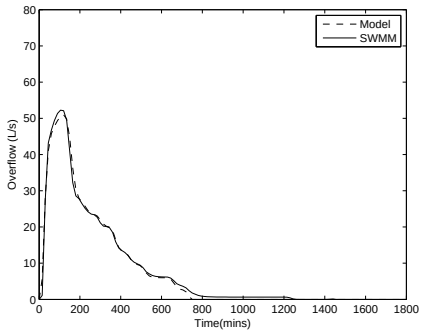

(a) Test Case 1 Calibration: Overflow discharge (L/sec) fit for Rainfall Input1

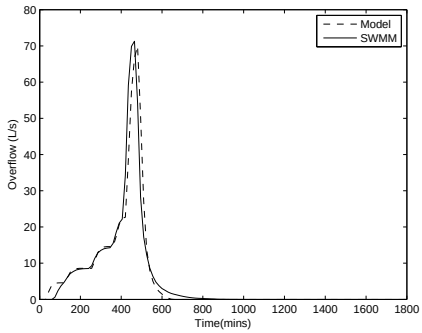

(b) Test Case 1 Validation: Overflow discharge (L/sec) for Rainfall Input2

Figure 4: Test Case 1

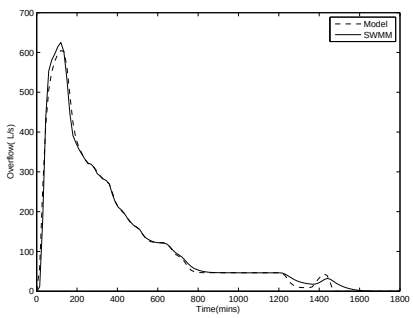

(a) Test Case 2 Calibration: Overflow discharge(L/sec) fit for Rainfall Input1

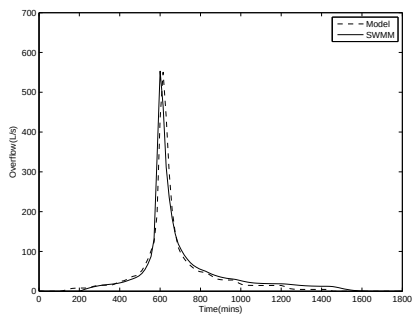

(b) Test Case 1 Validation: Overflow discharge (L/sec) for Rainfall Input2

Figure 5: Test Case 2

3.3 Test Case 3

The CSO model has been found to give promising results with simple sewer networks. A typical urbanized area however has several subcatchment areas and significantly more complex sewer network. The Metropolitan Sewer District (MSD) of Hamilton County is divided into three subdivisions. A portion of Little Miami subdivision was used as a test case. This portion of the Little Miami Subdivision consists of 1625 subcatchments and has four CSO's for discharge (Figure 6).

For the purpose of modeling, the overflows were assumed to be independent. Upstream contributing subcatchments to each overflow were assigned on the basis of network topology. A one year rainfall record for Lebanon, Ohio for year 2001 obtained from National Ocean and Atmospheric Agency (NOAA) database was used as rainfall input for calibration. The objective function used in calibration was obtained by adding the objective function given by equation (3) for each individual CSO location. For each

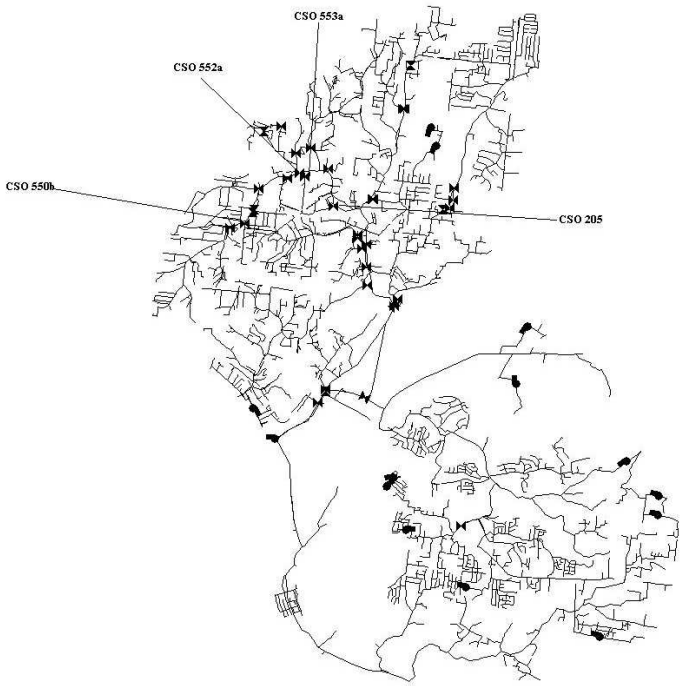

Figure 6: Little Miami Sewer Network

C_t (s^{-1})	C_o (s^{-1})	V_s (m^3)
0.017823	0.3353	54.1
0.00018	0.1991	500
0.001607	0.2417	387.6
0.003613	0.2006	207.2

Table 1: Optimal parameter estimate for Test Case 3

location an optimal set of parameters was thus obtained (Table 1) with $\alpha = 0.5$.

The time series of overflow discharges for total system sewer overflow predicted by model and SWMM are presented in Figure 7. Figure 8 compares the logarithm of non zero overflow discharge predicted by the simplified model to that computed by SWMM at a particular time step. As is clear from the graphs, the model in general tends to underestimate overflow discharge as compared to SWMM simulation. One of the probable reasons for this might be that the error metric compares the discharges at every time step of the continuous simulations, whereas it is likely more important to represent the total CSO loading for individual storm events. The value of optimization parameter, α, used might be another reason for the underestimation.

4 CONCLUSION

In order to assess the public health risk due to combined sewer overflows, a fundamentally different approach is required to incorporate event driven exposure variability. This paper presents a simple approach to model the complex urban sewer system to estimate the overflow discharge into receiving water. The time series of overflow discharges/volumes thus generated, superimposed on the pathogen concentration in the raw sewage, could be used to generate a time series of pathogen loading into source waters. This time series could be then used to drive the QMRA exposure models to assess the public health risk from enteric pathogens in drinking water. The flexibility and simplicity of the model may permit the usage of useful statistical techniques such as Markov Chain Monte Carlo sampling to fuse exposure models with data. The model has been found to give promising results with simple test cases. Further work is required for simulating complex realistic scenarios by calibrating with overflow data from public sewer utilities.

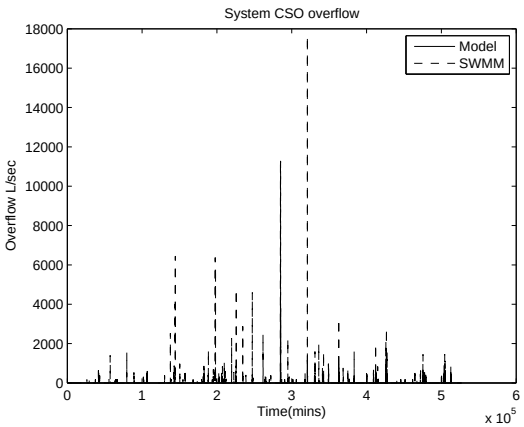

Figure 7: System Overflow discharge

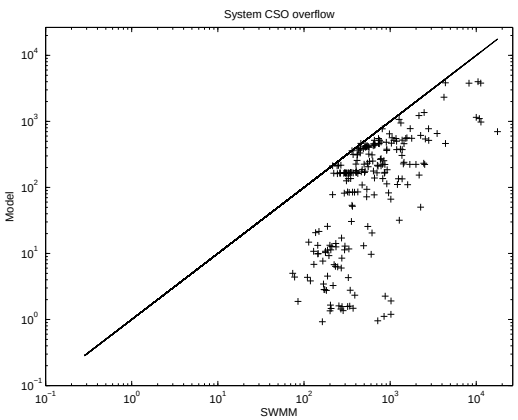

Figure 8: Model Vs SWMM

References

Anderson, A., A. Heryford, J. Sarisky, C. Higgins, S. Monroe, R. Beard, C. Newport, J. Cashdollar, G. Fout, D. Robbins, S. Seys, K. Musgrave, C. Medus, and J.Vinje (2001). A water borne outbreak of norwalk-like virus among snowmobilers-wyoming. *J. Infct. Dis. 187*(2), 303–306.

Brown, C., J. Cann, G.Simons, R. Frankhauser, W. Thomas, U. Parashar, and M. Lewis (2001). Oubreak of norwalk virus in a carribean island resort:application of molecular diagnostics to ascertain the vehicle of infection. *Epidemiol. Infec. 126*(3), 425–432.

Hooke, R. and T. A. Jeeves (1961). Direct search solution of numerical and statistical problems. *Journal of ACM 8*, 212–229.

Lodder, W. and A. de Roda Husman (2005). Presence of norovirus and other enteric viruses in sewage and surface waters in the netherlands. *Journal of Appl. Environ. Microbiology 71*(3), 1453–1461.

Lodder, W. J., J. Vinje, R. van De Heide, A. M. de Roda Husman, E. J. Leenen, and M. P. Koopmans (1999, Dec). Molecular detection of norwalk-like caliciviruses in sewage. *Applied and Environmental Microbiology 65*(12), 5624–5627.

Masago, Y., H. Katayama, T. Watanabe, E. Haramoto, T. Omuru, T. Hirata, and S. Oghaki (2006). Quantative risk assessment of noroviruses in drinking water based on qualitative data in japan. *Environ. Sci. Tech. 40*, 7428–7433.

Mead, P. S., L. Slutsker, P. M. Griffin, and R. V. Tauxe (1999, Nov). Food-related illness and death in the united states. *Emerging infectious diseases 5*(6), 841–842.

Rodriguez, R. (2007). *Occurence of eneteric viruses on Combined Sewer Overflows*. Ph. D. thesis.

Rossman, L. A. (2008). *EPA SWMM Users Manual*. Cincinnati, OH: Water Supply and Water Resources Division, U. S. Environmental Protection Agency.

Ruan, M. and J. B. Wiggers (1998, Dec). A conceptual CSO emission model: Sewsim. *Water Sci. Tech. 37*(1), 259–267.

Soller, J. (2008). Recommendations and basis for a statistical model of norovirus in raw wastewater. Unpublished Manuscript.

The Mathworks Inc. (2007). *Matlab Documentation* (R2007b ed.). The Mathworks Inc.

Vaes, G. and J. Berlamont (1999). Emission prediction by a multi linear resorvor model. *Water Sci. Tech. 39*(2), 9–16.

Westrell, T., O. Bergstedt, T. A. Stenstrom, and N. J. Ashbolt (2003, Jun). A theoretical approach to assess microbial risks due to failures in drinking water systems. *International journal of environmental health research 13*(2), 181–197.

Westrell, T., P. Teunis, H. van den Berg, W. Lodder, H. Ketelaars, T. A. Stenstrom, and A. M. de Roda Husman (2006, Aug). Short- and long-term variations of norovirus concentrations in the meuse river during a 2-year study period. *Water research 40*(14), 2613–2620.

Source Control: The Solution to Stormwater Pollution

Michael A. Ports, PE, PH, D. WRE[1]

Introduction

Another name for source control is pollution prevention. In almost every case, it is easier and cheaper to prevent pollution from occurring in the first place than it is to collect and treat it after the fact. Municipal stormwater managers throughout the United States are coming to grips with the fact that municipal stormwater management requires significant effort and resources and raises numerous legal and financial issues and concerns. More emphasis on source control has the potential to improve system reliability, reduce costs, improve equity, reduce liabilities, as well as improve water quality.

When Phase II of the municipal separate storm sewer system permit program under the National Pollutant Discharge Elimination System began, most stormwater managers relied primarily on end of pipe treatment to meet their goals. Under the Clean Water Act, the United States learned that end of pipe treatments are effective in reducing pollutant loads discharging from municipal and industrial wastewater plants. For example, from 1968 through 1996, municipal wastewater treatment plants reduced BOD entering receiving waters by 45 percent in spite of a significant increase in population served (USEPA 2000). Thus it was no surprise that most municipalities formulated and began their stormwater programs based upon the assumption that, if end of pipe treatment worked so well with municipal sewage, then end of pipe treatment should work with urban stormwater.

Experience, unfortunately, has demonstrated that this is not the case. The flow and composition of municipal waste generally is well known and predictable. Thus, it is relatively easy to design and operate cost effective treatment systems. However, the flow and composition of urban stormwater is highly variable, both spatially and temporally. Municipal wastewater treatment plants are sophisticated, energy intensive operations equipped with elaborate control systems. On the other hand, end of pipe urban stormwater treatments are relatively simple structures with primitive, if any, operational control. At a modern municipal wastewater treatment plant, BOD removal usually reaches 95 percent or more and nutrient removal rates may exceed 85 percent. Removal rates for BOD at a typical structural stormwater BMP may vary by storm from as little as 16 to as much as 93 percent (Strecker, Quigly, and Urbonas 2000). Removal rates vary nearly as much from BMP to BMP regardless of type, size, location, and climate.

---

[1] Principal Water Resources Engineer, Bergmann Associates, 8653 Baypine Road, Suite 100, Jacksonville, Florida 32556. mports@bergmannpc.com

Another problem with structural BMPs is the ultimate fate of the pollutants removed. Stormwater pollutants include a wide variety of substances that build up on both pervious and impervious surfaces and later are transported by the next rainfall. These contaminants include heavy metals, petroleum hydrocarbons, pesticides, fertilizer, and a host of organic chemicals. Some pollutants naturally degrade and convert to harmless byproducts. Other pollutants are taken up by plants or microorganisms. But, many pollutants accumulate in the BMP and must be removed over time by dredging or other means. Some of these pollutants may accumulate to levels requiring classification as hazardous waste (Cox and Livingston, 1997).

In addition, construction costs for most structural stormwater BMPs are higher than for most source controls. Estimated total capital costs, not including land, for typical applications are summarized in Table 1. Total project costs may range from $27,000 to $37,000 per catchment acre. Depending upon the specific project, typical annual maintenance costs range from 5 to 10 percent of the total project cost.

Table 1
Capital Costs of Typical Applications of Structural BMPs

BMP TYPE	TYPICAL COST ($/BMP)	APPLICATION
Retention Basin	$130,000	50-acre residential site with 35 percent impervious cover
Wetland	$162,000	50-acre residential site with 35 percent impervious cover
Infiltration Trench	$58,000	5-acre commercial site with 65 percent impervious cover
Infiltration Basin	$19,000	5-acre commercial site with 65 percent impervious cover
Sand Filter	$45,000 to $91,000	5-acre commercial site with 65 percent impervious cover
Bioretention	$78,000	5-acre commercial site with 65 percent impervious cover
Grass Swale	$4,500	5-acre residential site with 35 percent impervious cover
Filter Strip	$0 to $11,000	5-acre residential site with 35 percent

		impervious cover

(EPA, 1999)

Based upon average removal rates for typical applications with different percentages of impervious cover, urban stormwater treatment costs may range from

- $2,000 to $3,000 per ton of total suspended sediment,
- $1,400 to $2,200 per pound of phosphorus,
- $1,000 to $3,000 per pound of nitrogen, and
- $1,200 to $3,000 per pound of metals.

Structural BMPs are a necessary and important element of any stormwater management program. However, relying solely upon end of pipe treatments is not necessarily the best approach. End of pipe treatments are not always effective. They are expensive. They accumulate pollutants and require diligent maintenance. The proper application of nonstructural, source control BMPs should be an integral part of comprehensive stormwater management programs.

Source Controls

The primary purpose of source control is to prevent pollutants from getting into the stormwater in the first place. By their very nature, source controls have certain advantages that all too often are not appreciated. For some pollutants, source control is more effective than end of pipe treatment. For example, the removal of soluble phosphorus is not effective in BMPs that rely on sedimentation. Because chloride is a soluble pollutant, no structural BMP is effective in removing or trapping chloride from road deicing operations. Hence, only source controls have the potential to reduce the discharge of such containments.

Source controls have the potential to reduce stormwater treatment unit costs. Composting grass cuttings, reducing fertilizer application rates, minimizing pesticide applications, and picking up pet waste can cost little or nothing, yet at the same time can be effective in reducing the discharge of stormwater containments.

Everyone pays for the costs of stormwater pollution through the loss of the use of the public resource. No one can go swimming when the beaches are closed due to stormwater pollution. No one can go angling when the fish are dead or driven away due to stormwater pollution. No one can enjoy the aesthetics of a beautiful water body when it is polluted by stormwater. The public pays the costs of dredging our receiving waters to remove sediments transported from urban construction sites. Source control transfers the cost of pollution control from the public to the polluter. The “polluter pays” philosophy is equitable. It is fair, for example, for the costs of on-site construction

erosion and sediment controls to be borne by the developer. It is not fair for the public to shoulder the burden of subsequent restoration and cleanup downstream. At least for some pollutants, the overall effectiveness and reliability of the stormwater management program may be improved when source controls are combined with end of pipe treatments.

Watershed Approach

When end of pipe treatments alone are implemented, it follows that the stormwater management program tends to be focused on the downstream end of the pipe. Often, stormwater engineers implicitly think that the drainage system consists only of the various constructed elements of the conveyance system, such as the gutters, inlets, pipes, etc. Impervious roadway and parking lot surfaces themselves do not contribute measurably to the overall pollutant loads, although various pollutants mostly from vehicular sources collect on the impervious surfaces. By far most pollutants entering the drainage conveyance system originate from such upstream sources as vehicular traffic, lawns, urban landscapes, tree canopies, and atmospheric deposition. Most impervious surfaces should be considered as part of the conveyance system rather than the source of pollution.

Comprehensive stormwater management should consider the watershed as a whole. Most often, pollutants are brought into the watershed from outside. For example, pet food is purchased at a store, brought home, and fed to the pet. Then the pet excretes the waste onto the lawn or other landscaped surface. When it rains, pollution from that pet waste runs off and enters the conveyance system downstream. For another example, polyphosphates added to municipal water systems for corrosion control may enter urban landscapes through irrigation. Significant pollutants enter the watershed through the streetscape. Copper, zinc, and other heavy metals come from wearing break pads and tires. Road salts and abrasives come from deicing and traction control operations. When considering stormwater pollution, the first question in mind should be "What is the source of the pollution?" The source may be the most effective and least costly place for control.

Characteristics of Stormwater Pollution

Typical pollutant concentrations in stormwater runoff are compared to wastewater and combined sewer overflows in Table 2. There is no apt description of "typical" combined sewer overflow or urban stormwater runoff for that matter. Both are a function of local conditions, including land use, geology, geomorphology, and the many vagaries of weather. Each situation should be evaluated individually, particularly with respect to the receiving water body in question.

Total suspended solids concentrations in typical urban stormwater runoff may be many times higher than found in untreated municipal wastewater or even combined sewer overflow. In addition, total nitrogen and total phosphorus concentrations in urban runoff may be higher than in the effluent from a secondary wastewater treatment plant. Urban

stormwater concentrations of metals also may be problematic. And finally, there is little difference between the fecal coli form concentration in urban stormwater runoff, untreated municipal wastewater, and combined sewer overflow. Other pathogen indicator organism counts, such as total coli form and *e. coli* and *enterococci*, are similar. Research is ongoing to determine the magnitude and characteristics of cryptosporidium and giardia in urban stormwater runoff.

Table 2

Comparison of Stormwater Pollutants to Wastewater

CONTAMINANT SOURCE	UNTREATED MUNICIPAL WASTEWATER	TREATED WASTEWATER (SECONDARY)	URBAN STORMWATER RUNOFF	COMBINED SEWER OVERFLOW
BOD_5 (mg/L)	100-400	<5-30	1-700	25-100
TSS (mg/L)	100-350	<5-30	2-11,300	150-400
Total N (mg/L)	20-85	15-25	0.4-5.0	3-24
Total P (mg/L)	4-15	<1-5	0.5-2.0	1-10
Lead (mg/L)	0.1	0.15	0-1.9	0.37
Zinc (mg/L)	0.28	0.08	0.02	0.17
Copper (mg/L)	0.22	0.03	0.05	0.03
Fecal Coli Form (ct/100ml)	10^7-10^9	<200	10^3-10^7	10^5-10^7

(APWA, 1969 and EPA, 2001)

Urban Forestry Management

Leaves, twigs, nuts, and other tree detritus may be a significant source of nutrients to streets and parking lots. Leaves contain significant amounts of soluble nutrients that can be washed downstream into the storm drainage system. Phosphorus, for example, can be leached out of a dead tree leaf and carried into the storm drainage system without the leaf ever having to move. Phosphorus loadings from streets that are lined with closely-spaced, mature trees with large canopies may be larger than loadings from lawns. An obvious source reduction practice is to sweep the streets more frequently during the autumn leaf dropping period. The potential phosphorus content of leaves and seeds may

range from 1.6 to 11 mg/g (Waller and Hart, 1986). The annual leaf production from trees typically found in urban landscaped environments ranges from approximately 14 to 26 kg per tree.

Pet Waste Management

Pet waste can be a source of fecal bacteria, nutrients, and oxygen-demanding compounds in urban stormwater runoff. Pet fecal matter especially is annoying and polluting in urban residential neighborhoods that are highly impervious. Some European city centers with significant residential populations often suffer from excessive pet waste. In contrast, downtown areas of most large U.S. cities often exclude residential inhabitation, which goes a long way toward solving the pet waste problem but makes the cities look deserted after regular business hours. To control pet waste accumulation, owners should pick up any material deposited by their pets and dispose of it in a clean and safe manner. Pet waste should be placed in the garbage, flushed down the toilet, or buried. To prevent the potential spread of disease, pet waste should not be incorporated into compost piles that will be used on vegetable gardens. Many communities have adopted laws or regulations that require owners to pick up the waste that their pets deposit. The typical pet dog is responsible for as much as 2.6 pounds of phosphate per year (RISE, 2004).

Lawn Management

Stormwater runoff from lawns generally is highly polluted, especially with nutrients, suspended solids, pesticides, and pathogens. Significant concentrations of pollutants are only part of the problem. In too many cases, lawns are compacted during or after construction, increasing the runoff coefficient and thereby the fraction of precipitation that becomes runoff. As the infiltration rate declines, the fraction of the applied fertilizer that enters the runoff increases. It is well documented in the hydrologic literature that the volume of runoff from lawns is an order of magnitude greater than runoff from natural prairie or forest lands. Elevated nutrient loadings coupled with elevated runoff volumes often make lawn runoff the primary source of nutrient pollution in watersheds with significant residential land use. Moreover, nutrients from applied fertilizers, grass clippings, leave mulching, and animal waste all contribute to lawn runoff pollution.

Improved lawn management certainly would reduce the export of pollutants to the runoff. First and foremost, during the initial construction of the lawn, care should be taken not to compact the lawn area. In fact, the soil should be loosened and improved so as to enhance its infiltration ability. Next, care should be taken to apply only low nutrient fertilizers with appropriate irrigation and avoid application on saturated soils prior to rain events. Pretesting soils to determine the optimum application rates should prevent excessive applications and decrease nutrient loads over time.

The comparative phosphorus contributions from different sources within a hypothetical, yet typical small residential catchment is shown in Figure 1. A tree-lined boulevard, one half mile long and 100 feet wide with adjoining residential lots 50 feet by 100 feet in size is assumed. Additional assumptions include:

- Boulevard is lined on both sides by mature trees at 75-foot intervals.
- Half of the households own dogs.
- No dog waste is scooped.
- Half of residential lots drain to boulevard.
- Average runoff coefficient is 0.5 for residential lots.
- Average annual rainfall is 48 inches.

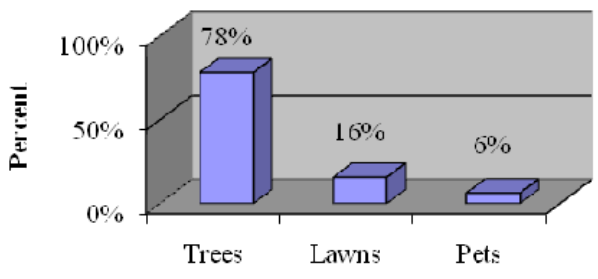

Figure 1
Comparitive P Source Contribution

In such a simplified hypothetical example, the total annual phosphorus contribution from the boulevard trees may exceed 3,000 pounds. But, assuming that half of the leaves fall on the lawns and some of the remainder get blown away, an annual phosphorus contribution of 1,000 pounds is a more reasonable estimate. From the residential lawns, as much as 200 pounds of phosphorus may be contributed annually. The neighborhood dogs may contribute another 80 pounds. Thus, in this hypothetical example, a total of 1,280 pounds of phosphorus is contributed annually to the stormwater runoff. A program to reduce the phosphorus loading should direct most, if not all, of its initial efforts at removing leaves from the public rights-of-way. More frequent street sweeping coupled with mulching and removing leaves from landscaped or grassed areas conceivably could reduce the phosphorus contribution to significantly lower levels, perhaps as low as 200 pounds per year.

Will Citizens Participate?

Many municipal stormwater managers assert that homeowners and other members of the general public will not participate in improved lawn management. Others, especially engineers, assert that they cannot guarantee public acceptance and adoption in the future. They collectively conclude that source reduction is futile and, thus, not worth pursuing.

Actual experience, however, with other environmental programs that include changing environmental behaviors suggests otherwise. For the same reasons, curbside recycling once was regarded as unrealistic. In the early 1970s, only 7 percent of municipal waste was recycled. By 1999, more than 32 percent was recycled nationwide (EPA, 2002).

From 1982 through 2003, soil erosion on U.S. cropland decreased by 43 percent (NRCS, 2007). This significant decline may be attributed to a combination of ongoing education and outreach efforts, incentive payments for adopting conservation practices, encouraging conservation tillage, and removing highly erodible lands from crop production. Farmers also are using fertilizers and pesticides more efficiently and more effectively due to both overall market forces, ongoing public education programs, and peer pressure. Residential water conservation also can be successful. Tampa Bay Water reports that residential water use has declined by more than 40 percent since 1989.

Thus, the historical evidence is clear that private citizens will change their environmental behaviors. The question is, "How should programs be formulated and implemented to result in those changed behaviors?" Anecdotal evidence indicates that successful programs which change environmental behaviors incorporate a mix of education, incentives, penalties, and social marketing. For example, the Tampa Bay Water conservation program includes extensive public education programs, incentives to adopt specific practices, increasing rates for increased consumption, and penalties for certain water uses during drought.

Programs to improve residential lawn management should be formulated differently for different audiences. A program targeted at commercial lawn service companies may be more specific and may be based upon more strict regulatory requirements. A program for avid gardeners and lawn growing homeowners probably should be quite different than a program for the more casual homeowner or renter. Differing program elements may be warranted in different neighborhoods based upon socio-economic indicators, neighborhood organizational context, prevalence and type of pets, population density, and type of housing.

Conclusion

Structural end of pipe treatments alone cannot reduce stormwater pollution sufficiently to meet appropriate water quality goals. Properly designed and implemented source controls should yield major reductions in pollutant loadings. While improved construction and landscaping is most cost-effective when implemented during initial development, significant improvements still are possible with smart retrofits. Significant additional research is needed to improve source control effectiveness and economics. Much may be learned from previous efforts to change environmental behaviors that could be applied to stormwater public outreach programs. More research in lawn ecology and residential lawn behaviors could lead to moving beyond generic, one-size-fits-all recommendations to carefully targeted messages accompanied by appropriate incentives and effective restrictions. Practical research is needed to understand how adaptive management algorithms could be applied to source controls such as road deicing.

Properly designed and implemented source controls offer more potential for reducing pollutant loadings more effectively, more cheaply, and more fairly than end of pipe treatments.

References

American Public Works Association, 1969. Water Pollution Aspects of Urban Runoff. Water Pollution Control Research Series, Federal Water Quality Administration, Report No. WP-20-15, Kansas City, Missouri.

Cox, J. H. and E. H. Livingston, 1997. Stormwater Sediments: Hazardous Waste or Dirty Dirt? Proceedings of the Fifth Biennial Stormwater Research Conference, Southwest Florida Water Management District, Tampa, Florida.

Natural Resources Conservation Service, 2007. 2003 Annual National Resources Inventory – Soil Erosion. U.S. Department of Agriculture, Washington, DC.

RISE, 2004. Phosphorus, Urban Runoff and Aquatic Weeds. Responsible Industry for a Sound Environment, Washington, DC.

Strecker, E., M. Quigly, and B. Urbonas, 2000. Determining Urban Stormwater BMP Effectiveness. Proceedings of the National Conference on Tools for Urban Water Resource Management and Protection, US Environmental Protection Agency, Chicago, Illinois.

Tampa Bay Water, 2008. Compilation of Members' Five Year Conservation Plans, Annual Update. Tampa, Florida.

U. S. Environmental Protection Agency, 1999. Preliminary Data Summary of Urban Stormwater Best Management Practices, EPA-821-R-99-012. Washington, DC.

U. S. Environmental Protection Agency, 2000. Progress in Water Quality: An Evaluation of the National Investment in Municipal Wastewater Treatment, Executive Summary. Washington, DC.

U. S. Environmental Protection Agency, 2001. Report to Congress: Implementation and Enforcement of the CSO Control Policy. EPA-833-R-01-003. Washington, DC.

U. S. Environmental Protection Agency, 2002. Recycling is Working. EPA-5303-F-02-005. Washington, DC.

Waller, D. and W. C. Hart, 1986. Solids, Nutrients, and Chlorides in Urban Runoff. Proceedings, Urban Runoff Pollution, H. C. Torno, et al. (Eds.) Springer-Verlag, Berlin.

A Student-Led Effort to Assess the Effect of Urban Runoff on Potter Lake.

England Porter[1], John Kenny[2], Edward Peltier[2] and C. Bryan Young[2]

1. Environmental Studies Program, University of Kansas, 252 Snow Hall, 1460 Jayhawk Blvd., Lawrence, KS 66045
2. Department of Civil, Architectural and Environmental Engineering, University of Kansas, 2150 Learned Hall, 1530 West 15th Street, Lawrence, KS 66045. Ph: (785)-864-2941; Fax: (785)-864-5379; email: epeltier@ku.edu

ABSTRACT

Potter Lake is a small water body on the University of Kansas campus. Eutrophication and sedimentation are both significant water quality issues for this system. As stormwater runoff provides as significant portion of the total inflow to this system, student-led efforts to develop a restoration and management plan for Potter Lake, have focused on assessing the quantity and quality of this runoff. A water balance model for the Potter Lake watershed was developed using climatological data and watershed characteristics. Runoff samples from four locations were collected for water quality analysis using passive collection bottles suspended in existing storm sewers. Water quality analysis indicates that runoff from Jayhawk Boulevard contributes a disproportionate amount of the total loading of suspended solids and phosphorus, particularly during heavy storms when soils are mobilized from open areas along this street. Improving the water quality in Potter Lake may require treatment of this stormwater prior to discharge into the lake.

INTRODUCTION

Potter Lake is a one and a half acre manmade water body located on the campus of the University of Kansas. Originally created in 1910 to provide a water source for fire protection, the lake became a popular campus feature. At various points in its history, it has been used for swimming, boating and other recreational activities. At present, it serves as a centerpiece for one of the largest remaining open spaces on the main campus, used by students as a place to study and relax. Potter Lake and the adjoining open space are listed as a signature campus feature, is designated for preservation in the current University Landscape Master Plan (Jeffrey L. Bruce and Company 2002), and is apart of a historical Marvin Grove district slated for the National Register of Historic Places. Preserving the aesthetic character of Potter Lake for the future requires addressing two related water quality issues: eutrophication and sedimentation.

Eutrophication is the primary ongoing cause of water quality impairment in Potter Lake. In 1999, the Kansas Department of Health and Environment placed the lake on its list of 120 polluted water bodies in the state due to the effects of repeated algal blooms and vegetation growth. In 2000, a TMDL was issued for nutrients and pH. This TMDL was based on results of a water quality survey conducted in September 1994 that showed the lake as hypereutrophic, with a Carlson trophic state index greater than 70 (Kansas Department of Health and Environment 2000). The report cited total phosphorus as the limiting nutrient for plant growth. Data taken during the survey listed the total phosphorus concentration at 30 ppb, although the report also states that this value was unusually low when compared to the simultaneously measured chlorophyll-a values of approximately 100 ppb. In order to improve lake water quality to acceptable levels, a load allocation of 2.6 lb phosphorus per year was recommended, an 88% reduction from the estimated total loading at that time. The TMDL also noted high pH levels in the lake, ranging from 8.82-9.01, during the September 1994 sampling. More recent sampling, in June of 2007, showed decreased levels of chlorophyll-a (< 10 ppb) and slightly lower phosphorus concentrations (20 ppb); however, excessive plant growth and decay remain a significant issue.

Sedimentation due to transport of suspended solids in stormwater runoff has also been a consistent issue with regard to water quality in Potter Lake. In addition to transporting phosphorus, sediments entrained in stormwater runoff contribute to reducing lake volume and depth. In turn, this increases the potential for growth of rooted aquatic plants, accelerating both eutrophication and further sedimentation. The lake was completely drained, dredged and then refilled in 1958 in a previous attempt to combat the effects of sedimentation. A bathymetric survey conducted in the summer of 2008 shows that most of the lake has once again been substantially filled in from the ~16 foot depth re-established at that time. The maximum lake depth is currently between 12 and 13 feet, while approximately two-thirds of the lake has a depth less than 6 feet. In the southwest quarter of the lake, the depth ranges from <1 to 4 ft. It is in this area that excessive vegetation growth of both rooted and floating plants is most severe.

A student-led group formed during the spring of 2008 has been developing plans for the restoration and long-term preservation of Potter Lake for the continued use and enjoyment of the Lawrence and KU community. The overall objectives of this group are to implement a plan for necessary remediation and restoration efforts (including dredging) that will address current water quality and aesthetics issues at Potter Lake and to develop a long-term strategy to minimize the re-establishment of eutrophic conditions in the lake. The primary focus of this long-term strategy is to evaluate the impact of stormwater runoff and contaminant transport on Potter Lake and to provide management alternatives that would mitigate the effects of this runoff of water quality. In addition to sheet runoff from the surrounding open space, Potter Lake receives channelized stormwater runoff from adjacent locations. The major contributors to this stormwater runoff are two roads (Jayhawk Boulevard and Memorial Drive) south and west of the Potter Lake drainage basin and a parking lot located on the northwest side. Storm sewers at all three of these locations feed runoff into concrete pipes that deposit directly into Potter Lake (from the parking lot and

Memorial Drive) or to an above ground outlet located approximately 15 ft from the lake (Jayhawk Boulevard storm sewers). While this runoff is a significant source of nutrients and sediments, it is also an important part of the water budget for Potter Lake, as the only other significant water source is direct precipitation.

In the current work, we present results of studies conducted during the fall of 2008 to evaluate the impact of stormwater runoff from each of these sources on the hydrology and water quality of Potter Lake. The purpose of this work was to assess the relative contributions of runoff from these locations to lake volume and to contaminant loading and to determine whether some or all of this runoff should be treated or diverted from the Potter Lake watershed in order to improve long-term surface water quality. In order to achieve these objectives, a hydrological model of Potter Lake was developed using available data. This model estimates the relative contributions of different runoff sources to the overall water budget. Model results were combined with runoff water quality data to determine the impact of runoff from each location on total loading of nutrients and suspended solids.

METHODS

Stormwater samples were collected between July and December, 2008 and analyzed for a range of water quality parameters, including total suspended solids, dissolved nitrate and phosphate, and total and dissolved reactive phosphorus. Samples were collected using one liter polycarbonate bottles equipped with a screen to reject large solid materials and a collection funnel with floating ball valve (I-CHEM) to seal the bottle after sample collection was complete. These bottles were suspended from storm grates at four locations: 1.) a storm sewer on the north side of Jayhawk Boulevard, 2.) a storm sewer in the southeast corner of a parking lot on the northwest side of the lake, 3.) one of two storm sewers on the north side of Memorial Drive, 4.) a storm grate collecting sheet runoff from the grassy hill located immediately south of Potter Lake. Sampling locations 1-3 drain primarily from paved surfaces, although locations 1 and 3 also drain from grassy open areas surrounding the roads. The grassy hill at location 4 forms a basin around two sides of Potter Lake. This open space is vegetated with a mixture of fescue grasses and drains directly to the lake. The current landscaping plan calls for minimal to no phosphorus application in this area.

Stormwater samples were transported back to the laboratory for analysis within 24 hours after each storm event. All analyses were conducted using standard procedures (American Public Health Association et al. 2005), with dissolved samples filtered through a 0.45 μm nylon filter prior to analysis . Total suspended solids tests were conducted on the same day as sample collection according to the 2540D procedure. Dissolved nitrate and phosphate concentrations were measured using an ion chromatograph (Dionex Corp.) with a hydroxide eluent. Total and total dissolved phosphorus were determined using the ascorbic acid procedure.

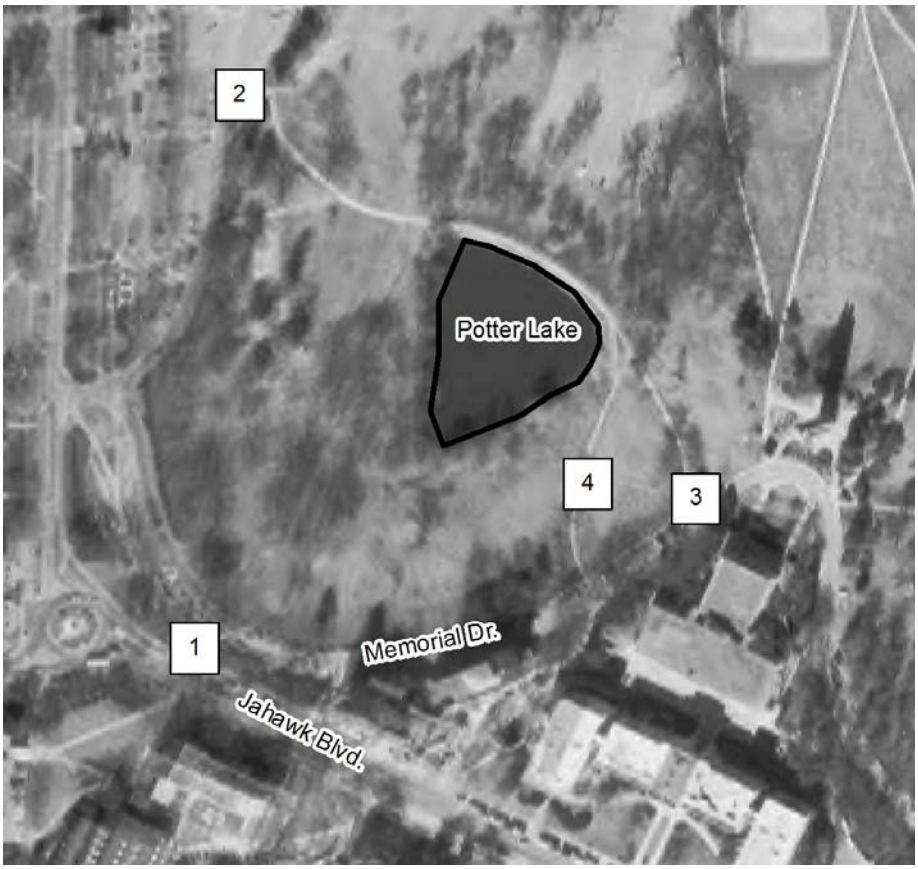

Figure 1. Map of Potter Lake Showing Stormwater Sampling Locations

A hydrological model was developed for the Potter Lake watershed that included two primary components: a water balance simulation for the volume of storage in the lake and simulations of stormwater runoff volumes from discrete regions of the watershed. This model is designed to aid in understanding the hydrologic behavior of the watershed and lake, not to simulate the response to any particular runoff event. Runoff into Potter Lake was simulated for the period March 1964-July 2008 using the NRCS Runoff Curve Number method. The model was driven by daily rainfall data for the NWS weather station in Topeka, Kansas. This gage represents a high quality record with very few missing rainfall values. Translation of the record from Topeka to Lawrence means that the model results are representative of the climate for NE Kansas, but do not simulate the actual daily conditions.

Runoff volumes were computed separately for four areas within the watershed based on the stormwater sampling locations and surrounding land use. The land use for each area was manually classified using aerial photography and field observations. The NRCS hydrologic soil type was determined using the NRCS soil survey for Douglas County, Kansas. The relative runoff contribution was computed for each land use area, making it possible to extrapolate water quality concentrations to annual mass loadings.

RESULTS

Stormwater samples were collected from 8 storm events occurring between July 3 and December 7, 2008. The majority of sampling events (6 of the 8) occurred between August 23 and November 15. The Jayhawk Boulevard site had the highest number of collected samples during this time period, with runoff collected during every storm event. At the Memorial Drive location, however, samples were only collected during higher rainfall events (> 0.4 inches). This is likely due to the smaller drainage area and flatter curbs at this site, which result in lower runoff collection. The sampling location in the open area surrounding Potter Lake had the fewest number of samples (3), a result both of the fact that less runoff is generated from this site and the difficulty of correctly placing the sampler to intercept sheet flow.

Table 1 provides average concentrations of measured pollutants for each of the four sampling locations. As expected, total suspended solids concentrations were substantially higher in the road and parking lot samples than in the sheet flow samples collected immediately around Potter Lake. The highest single TSS concentrations recorded were 594 and 843 mg/L at the Jayhawk Boulevard and Memorial Drive locations, respectively, during the same rainfall event in November, 2008. Since the sampling bottles capture the first liter of runoff, these values are most representative of first flush data for most of the storm events sampled.

Table 1. Water Quality Results from Stormwater Sampling

	Jayhawk Boulevard	Parking Lot	Memorial Drive	Hill
Samples	8	7	4	3
TSS (mg/L)	337	202	438	67
Total P (mg/L)	1.52	1.17	0.766	2.76
NO_3 (mg N/L)	0.37	0.63	0.30	0.64
PO_4 (mg P /L)	0.50	0.14	0.11	1.12

Phosphorus levels from all four sites are higher than values typically found in urban runoff (United States Environmental Protection Agency 1983), with the highest concentrations observed in the sheet runoff adjacent to the lake. The most likely source of this phosphorus is fertilizer application. The sheet runoff collected at location 4 recorded the highest concentrations of dissolved nitrate and phosphate along with very high total phosphorus concentrations, suggesting that fertilizer application may still be occurring in the open space surrounding Potter Lake. Dissolved phosphorus concentrations are much lower for two of the three locations which collect runoff from paved surfaces. The exception is the Jayhawk Boulevard sampling location, which has notably higher concentrations of both dissolved and total P. Total phosphorus and total suspended solids concentrations are strongly correlated at this location (Figure 2). This suggests that the highest loadings of both contaminants occur due to the release of soil from open spaces along the street, including several sets of flowerbeds located within the drainage area. The highest total phosphorus concentrations for this site were recorded after rainstorms totaling

more than 1 inch, allowing for greater washout of soil from the areas surrounding this road.

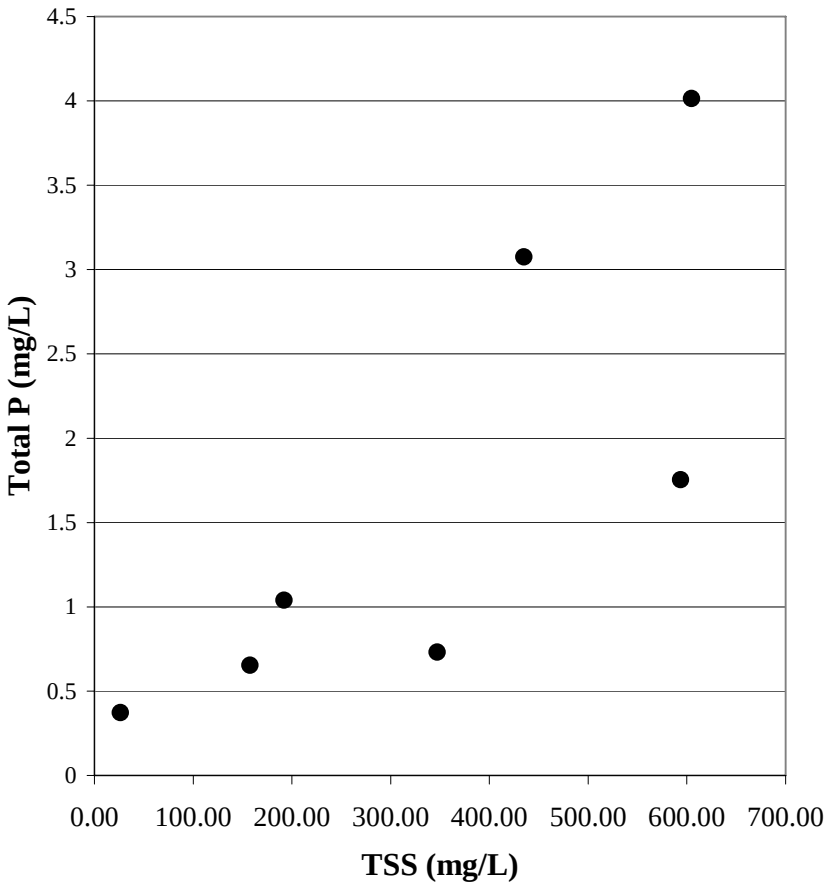

Figure 2. Relationship between TSS and Total P at Jayhawk Boulevard sampling location.

Contaminant Loadings to Potter Lake. The concentrations of total suspended solids and phosphorus found in the stormwater runoff are significantly higher than those found in the lake itself. This indicates that, under current conditions, stormwater runoff entering the lake will continue to impact lake water quality, particularly with respect to eutrophication and sedimentation. In order to better quantify the impact of this runoff and to assess the relative contributions of the different portions of the watershed to water quality degradation, contaminant loadings were calculated for a simulated rainfall event on a mass basis using the average contaminant concentrations reported above.

The relative runoff contributions for the four land use groups in the Potter Lake hydrological model are presented in Table 2. The total annual runoff volume to the lake is approximately 220 ac-ft, or a runoff depth of 9.6 in/yr. Overall, Jayhawk Boulevard (including surrounding areas that drain to the street) is the largest contributor of stormwater runoff to the lake, contributing approximately 37% of the total annual runoff from the watershed. The contributions from Memorial Drive and

from the hill surrounding the lake are approximately equal contributors, while the parking lot on the northwest side has the smallest annual contribution.

The remaining columns in Table 2 show the calculated runoff and contaminant loading to Potter Lake from each drainage region for a simulated 1.0 inch storm event. Estimated runoff volumes were multiplied by the average TSS and total phosphorus concentrations at each sampling location to determine the mass loading of pollutants to the lake as a result of this hypothetical storm event. The total loadings reported here are likely to be high-end estimates, as the concentrations of most contaminants in paved surface runoff will typically decrease in the latter portion of a storm event (Sansalone and Cristina 2004). The concentrations reported in our samples, by contrast, are weighted towards the earlier part of the storm. The calculations do indicate, however, that two of the four regions, Jayhawk Boulevard and the grassy open space, contribute the majority of the total phosphorus received by the lake. The drainage area around Jayhawk Boulevard has a particularly significant water quality impact, as it contributes the highest loading of both suspended solids and total phosphorus.

Table 2. Simulated Runoff and Contaminant Loadings for a 1.0 inch Storm Event

Area	Annual Contribution	Simulated Runoff (ac-ft)	TSS Loading (kg)	Phosphorus Loading (kg)
Jayhawk Blvd	37%	0.240	100	0.424
Hill	24%	0.125	10.4	0.402
JRP	14%	0.101	25.1	0.135
Memorial Drive	25%	0.171	92.4	0.150

CONCLUSION

The results presented here show that stormwater runoff from the watershed surrounding Potter Lake continues to transport a substantial amount of suspended solids and nutrients into the lake. In order to address current water quality and aesthetic problems in the lake resulting from eutrophication, and to preserve the improvements gained by future remediation or restoration actions, this contaminant loading must be significantly reduced. Since stormwater is a significant portion of the total influent to Potter Lake, diversion of these flows to other locations is probably inadvisable. Thus, source reduction and stormwater treatment become the best solutions. The sheet runoff from the gray hill surrounding the lake presents the most difficult challenge from a treatment standpoint. While it may be possible to further adjust fertilizer application strategies in this area to reduce the amount of transportable phosphorus, it would be difficult to intercept and treat this water. The runoff from Jayhawk Boulevard, however, could be more easily treated as it enters or exits the storm sewer that coveys it to the lake. Given the apparent association between suspended solids and total phosphorus in the runoff from this location, the installation of particle collection filter bags at storm sewer inlets could provide substantial reductions to contaminant loading to the lake from this source.

REFERENCES

American Public Health Association, American Water Works Association and Water Environment Foundation (2005). *Standard Methods for the Examination of Water and Wastewater*. Washington, DC, American Public Health Association.

Jeffrey L. Bruce and Company (2002). The University of Kansas Landscape Master Plan Volume 1: Design. Lawrence, KS, University of Kansas.

Kansas Department of Health and Environment (2000). Kansas-Lower Republican Basin Total Maximum Daily Load: Potter's Lake. Topeka, KS, Bureau of Water, KDHE.

Sansalone, J. J. and C. M. Cristina (2004). "First Flush Concepts for Suspended and Dissolved Solids in Small impervious Watersheds." *Journal of Environmental Engineering-ASCE* **130**(11): 1301-1314.

United States Environmental Protection Agency (1983). Results of the Nationwide Urban Runoff Program. Washington, DC, Water Planning Division, USEPA. **1**.

A Tool for the Performance Assessment of Hydrodynamic Separators

Omid Mohseni[1], Janna M. Kieffer[1], and Jennifer A. Koehler[1]
[1] Barr Engineering Company, 4700 West 77th St., Suite 200, Minneapolis, MN 55435

Abstract

Hydrodynamic separators are stormwater treatment devices with small footprints used for removing suspended sediments from stormwater runoff in urban areas. These devices have been tested by different laboratories under a set of specific conditions, e.g. a limited number of flow rates, under a specific water temperature (fluid viscosity), a specific particle size distribution and particle specific gravity. However, the question ahead of the primary users of these devices, i.e. cities, counties and other local government agencies and large retailers is: "How well do these devices remove suspended sediment from our stormwater runoff?"

To address this question a tool has been developed to simulate continuous loading from small drainage basins in urban areas and to simulate the response of these devices in removing the suspended load from stormwater runoff. The tool is comprised of a hydrologic model and a generic device response model. The hydrologic model utilizes the SCS curve number method and the SCS unit hydrograph to simulate runoff. The input data into the hydrologic model are the drainage basin characteristics and 10 years of 15-minute precipitation data. The generic device response model utilizes the removal efficiency performance functions developed from the laboratory testing conducted on hydrodynamic separators. The input data for the device response model are 10 years of daily air temperature data, the particle size distribution, specific gravity, and influent concentration of suspended sediments in stormwater runoff.

The tool has been applied to four small urban drainage basins in Minnetonka, MN using four hydrodynamic separators as stormwater treatment devices. The results of continuous simulation were compared to the performance assessment of the devices under 1-year and 2-year frequency storm events to determine if an event-based simulation is adequate to assess the performance of these devices.

Introduction

Hydrodynamic separators are underground proprietary devices which have been used as stormwater treatment devices for almost two decades. They are primarily used for removing floatables and coarser and heavier suspended sediments from stormwater runoff. They can function as stand-alone treatment devices or as a pre-treatment to other devices such as filters, ponds and infiltration basins to reduce maintenance costs.

Many hydrodynamic separators have been tested by manufacturers and laboratories and many have been monitored by researchers from universities and research institutes (e.g. Fassman, 2006; Roseen et al., 2005; ETV 2005a and 2005b). Subsequently, a number of protocols, e.g. TARP and TAPE, have been developed by different state agencies in the US to make the testing procedure more methodical with well defined parameters and suitable for the projected conditions of those states. Therefore, in most laboratory studies and monitoring programs, the removal efficiencies of these devices have been assessed for a certain flow condition, particle size distribution or a specific drainage basin in a certain climate condition (assuming the monitoring program was conducted for several years), i.e. the results of these studies cannot shed any light on how a tested device may remove the stormwater pollutants for a different location with different storm patterns and suspended loads. Therefore the question ahead of the primary users of these devices, i.e. cities, counties, department of transportations and other local government agencies and large retailers is: "How well do these tested devices remove suspended sediment from our stormwater runoff?"

Recently, Carlson et al. (2006) and then Wilson et al. (2009) introduced a performance function which describes removal efficiency of hydrodynamic separators as a function of a Peclet number. The Peclet number in this application is the ratio of settling of the suspended sediments to the turbulence induced in the sump of hydrodynamic separator and is defined as

$$Pe = \frac{V_s \; h \; d}{Q} \tag{1}$$

In equation 1, *P*e is the Peclet number, V_s is the settling velocity of particles, which is a function of the particles specific gravity and viscosity of water (a temperature dependent parameter), h and d are the height and diameter of the sump, respectively, and Q is the flow rate through the device. Wilson et al. (2009), Mohseni and Fyten (2008) and Fyten and Mohseni (2009) used the Peclet number defined in equation 1 to describe removal efficiency of seven hydrodynamic separators using the results of their field and laboratory tests. The Peclet number-based performance function is a useful tool for predicting the performance of a hydrodynamic separator over a range of storm events, sediment size and sediment density observed in stormwater. In this study, the functions introduced for these devices have been combined with a simple continuous runoff model and thus a computer program has been developed to predict the performance of these devices under a variety of conditions applicable to any location and climate condition.

General Description of the Tool

As stated above, a tool has been developed to predict the amount of suspended sediments removed from stormwater runoff by a given hydrodynamic separator over a period of time. The tool is comprised of a simple continuous runoff model and the performance function of the device. In the following sections, the components of this computer model are described.

Runoff Model

It is well known that the removal efficiency of hydrodynamic separators decreases as the flow rate through these devices increases. However, most storm events are low intensity storms, i.e. storms with high magnitude and intensity are less frequent. In addition, every storm event results in a runoff hydrograph with (a) a period of low flow conditions in its rising limb, i.e. the conditions which are favorable for these devices to remove a considerable amount of sediments from stormwater runoff, (b) a period with relatively higher flow conditions, when the devices are not that effective in treating stormwater, and (c) finally the storm receding period when again the devices are capable of effective treatment of stormwater. In order to accurately assess the performance of these devices, it is necessary to incorporate the entire storm runoff hydrograph as well as the concentration of suspended load throughout the runoff event. Unfortunately, there is not enough information regarding the concentration of suspended sediments in stormwater runoff. There are, however, several particle size distributions (PSDs) recommended by few organizations to estimate the total suspended loads in runoff events (e.g. NURP, and the NJDEP PSD) and so far there is no usable information available on the variability of the suspended sediment concentration throughout a storm event. Therefore, in this study only the variability of flow rate in every event and throughout the year have been incorporated to predict the performance of hydrodynamic separators.

In order to simulate runoff from small urban drainage areas, the SCS curve number method is used to estimate the excess rainfall. Using the SCS curve number method is not the best choice to simulate runoff continuously throughout the year, because the moisture content of the top soil cannot be well incorporated into calculation of runoff. However, since the SCS curve number method is a conventional method often used by city engineers to estimate runoff, it was decided to utilize the method with some minor modification.

Total excess rainfall at each time step is therefore the weighted average of rainfall over the impervious area and the excess rainfall calculated for the pervious area using the SCS curve number method. By default, the initial abstraction is set equal to 20% of the maximum potential retention, however, the amount of initial abstraction can be selected by the user. If there is no rainfall event for 12 hours, the initial abstraction recovers completely.

The SCS synthetic unit hydrograph is used to develop the runoff hydrograph. Each time step of the unit hydrograph is 15 minutes long. Since hydrodynamic separators are used for very small urban drainage basins, i.e. only a few acres, no routing through sewers or curb side is incorporated into the model.

Treatment Model

Wilson et al. (2009) proposed a three-parameter function to describe removal efficiency of hydrodynamic separators as a function of the Peclet number. The function is given in equation 2.

$$\eta = \left(\frac{1}{R^b} + \frac{1}{(aPe)^b} \right)^{-\frac{1}{b}} \quad (2)$$

In equation 2, η is removal efficiency, and a, b and R are the fitted parameters obtained from the non-linear regression analysis of the data obtained from laboratory and field tests.

Particle size distribution and specific gravity are input by the user, and at each time step the model calculates settling velocity of all particles using the equation proposed by Cheng (1997).

$$V_s = \frac{\nu}{D} \left(\sqrt{25 + 1.2 \left(D \left(\frac{g(SG-1)}{\nu^2} \right)^{1/3} \right)^2} - 5 \right)^{1.5} \quad (3)$$

In equation 3, ν is the kinematic viscosity of water, D is the particle size, and SG is the specific gravity of the particle. To estimate ν, it is necessary to know the temperature of water in the sump and runoff. Since the detention time of hydrodynamic separators is very small, runoff temperature is adequate to estimate ν. The runoff temperature is a function of rain temperature and the surface temperature of the ground before the rainfall event. Herb et al. (2008) showed that the rain temperature, dew point temperature and air temperature are very similar during rain storms. During hot summer months, the impacts of paved surfaces on runoff temperature can be very significant at the beginning of the storm events, but soon the surface temperature reaches the rainfall temperature. Since the time step of the model is set at 15 minutes, it was decided to use average daily air temperature to estimate the kinematic viscosity of water for each day. For very hot summer days, this method results in larger value of ν, thus smaller settling velocity and removal efficiency, i.e. using air temperature overall underestimates the performance of hydrodynamic separators.

At each time step, the model estimates the Peclet number of each particle size from equation 1 using the discharge obtained from the runoff hydrograph and the settling velocity of the particle and the total amount of each sediment size removed from equation 2. By utilizing the particle size distribution and the influent concentration, the model calculates the total amount of suspended sediments removed at each time step. In addition, the model updates the available height of the sump in equation 1 by subtracting the average height of the deposit from the height of the device. When the average depth of deposit reaches the maximum storage capacity of the device before cleaning, which is recommended by manufacturers, the model assumes that the device is cleaned and set the height in equation 1 equal to the original height of the device.

Model Input

The runoff model input data are the drainage basin area, the percent imperviousness of the drainage basin, the drainage basin average curve number, the hydraulic length

and average slope of the drainage basin and a time series of rainfall. Rainfall is input at 15-minute time intervals. The 15-minute rainfall data can be obtained from the NCDC web site for more than 3000 rain gages across the country. Since the model does not simulate snowmelt, for regions where air temperature drops below freezing point for an extended period, e.g. Minnesota, Wisconsin and North Dakota, the rainfall time series is for non-snowfall seasons. The weather data can be input for a number of years.

The input data for the treatment module of the model are: influent concentration, particle size distribution and the specific gravity of each particle size in the distribution, daily air temperature time series, the height and diameter of the hydrodynamic separator and the maximum storage capacity of the device before cleaning.

Model Application

The tool was used to estimate the performance of four devices if installed at the outlet of four urban drainage basins in Minnetonka, MN. The four devices selected were a Vortechs 2000, a Stormceptor 4800, a V2B1 Model 4 and an ecoStorm Model 3. The above hydrodynamic separators had already been tested and evaluated by Wilson et al. (2009) and Mohseni and Fyten (2008), therefore, their performance function parameters (a, b and R in equation 2) were available.

The characteristics of the four drainage basins are summarized in Table 1. The particle size distribution and specific gravity of the suspended sediments in stormwater runoff was provided by the City of Minnetonka and is given in Table 2.

Table 1. Characteristics of the urban drainage basins used in this study

Watersheds	Area (hectares)	% imperviousness	Average CN	Hydraulic Length (m)	Average slope
1	2.31	25	51.75	186	0.01
2	4.05	20	65	255	0.0075
3	4.25	77	72	272	0.005
4	2.02	80	61	143	0.0025

Table 2. Particle size distribution recommended by the City of Minnetonka, MN

Particle size (μm)	Percent finer	Specific gravity of the range
2000	100	2.65
400	80	2.65
130	60	2.2
60	40	1.8
20	20	1.3

The model was run for a 10-year period from 1998-2007. For every year of the simulation period, the model was used to estimate runoff at 15-minute time steps from the beginning of April to the end of November. The mean annual removal efficiencies of the four devices for the watersheds in Table 1 are summarized in Table 3. A sample of estimated runoff hydrograph and the sediment load from watershed no. 4, and the amount of sediments removed by Stormceptor SC4800 from that watershed is displayed in Figure 1. It is evident that Stormceptor SC4800 can remove more than 90% of the sediment load, as described in Table 2, from low intensity storm events and at the beginning of each storm event. However, when the flow rate is as large as 40 cfs, removal efficiency drops to 60% and as runoff exceeds 120 cfs, the removal efficiency drops below 50%. It is noteworthy that SC4800 is one of the larger models of Stormceptor and its sump has a 3 m (10 ft) diameter.

Assuming a maximum capacity of 0.6 m (2 ft) for SC4800, before cleaning is required, this device did not require cleaning more than once every two years for the given watershed characteristics. The Stormceptor tested for scour and washout at St. Anthony Falls Laboratory showed no scour (the effluent concentration was measured to be less than 4 mg/l) of the US Silica Sand F110 with a median particle size of about 120 microns. Therefore, it is very likely that the model estimate of removal efficiency for Stormceptor 4800 is a fair estimate, assuming that the particle size distribution given in Table 2 represents the average particle size distribution of the sediments in stormwater runoff in Minnetonka, MN. It is important to note that this tool does not include any function to estimate scouring at this point, because no such function has yet been developed for any hydrodynamic separators. Therefore, the estimates given for mean annual sediment removal efficiency of the other three devices are likely to be higher than what they should be.

To determine whether it is necessary to run a continuous runoff model or only a single storm event to estimate the performance of these four devices, the average annual removal efficiency of devices were compared with their removal efficiencies for 1-year and 2-year 24-hour storm events. The comparison with the 2-year, 24-hour storm events is summarized in Table 3. The removal efficiencies estimated from 2-year 24-hour storm events are within 3% of the 10-year average removal efficiencies. Therefore, it seems that an event based approach can provide a good estimate of the performance of these devices over long periods. However, the scour and washout of deposited sediments should be assessed using a continuous runoff model which is not yet part of this tool.

It is important to note the results summarized in Table 3 do not provide enough information regarding the advantage of one device over another one, because the four devices presented have different sizes. In order to make a fair comparison, the price of each device, and the cost of installation as well as maintenance should be included in the comparison.

Table 3. Estimated removal efficiencies of four hydrodynamic separators based on 10-year average and 2-year 24 storm events in Minneapolis, MN.

Device		ecoStorm31		V2B1-4		Stormceptor4800		Vortechs2000	
Watershed		10-yr Avg	2-yr, 24-hr Event	10-yr Avg	2-yr, 24-hr Event	10-yr Avg	2-yr, 24-hr Event	10-yr Avg	2-yr, 24-hr Event
1	2.31 acres, 25% impervious	56.9	57.4	58.1	57.8	61.7	61.5	52.0	51.8
2	4.05 acres, 20% impervious	53.8	52.4	55.0	52.0	59.3	56.8	48.7	45.4
3	4.25 acres, 77% impervious	44.2	42.5	42.2	40.3	47.0	45.8	35.3	33.1
4	2.02 acres, 80% impervious	49.8	49.0	49.1	47.9	52.6	51.9	42.7	41.2

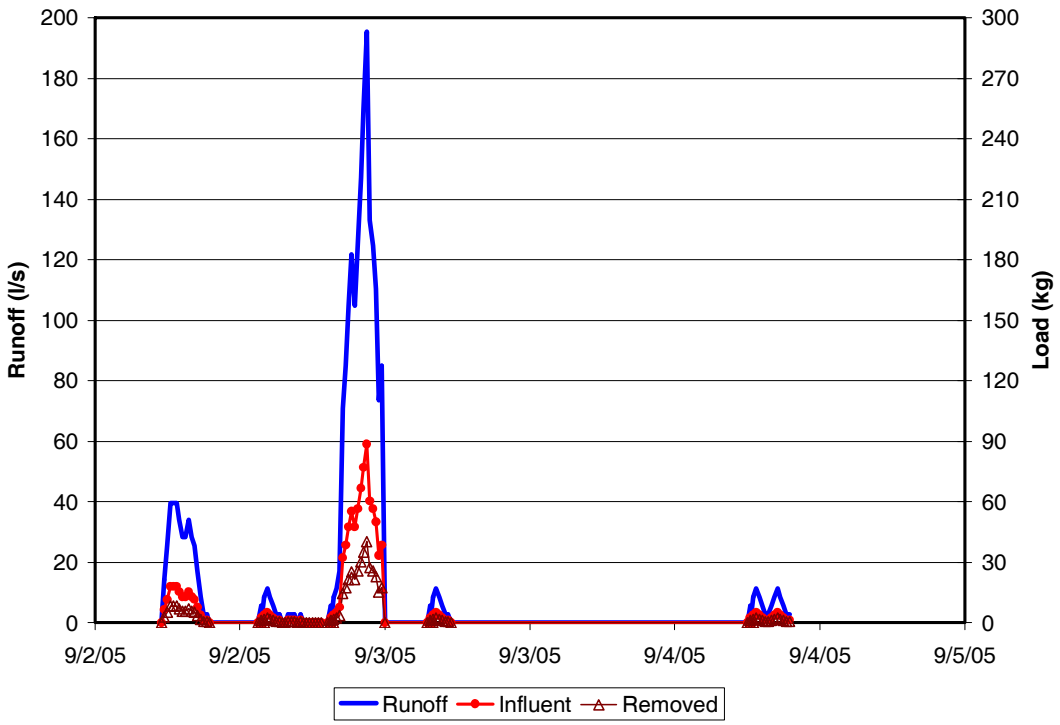

Figure 1. The estimated runoff hydrograph and the load from watershed no. 4, and the amount of sediments removed by a Stormceptor SC4800.

Summary

A tool has been developed to assess the performance of hydrodynamic separators in removing suspended sediments from stormwater runoff. The tool, which is a computer program, includes a continuous runoff model to simulate time variant discharge and a Peclet number-based treatment function to simulate removal efficiency of these devices in treating the suspended load. The continuous runoff model utilizes the SCS curve number method and the SCS synthetic unit hydrograph. The tool was used to estimate the 10-year average performance of four devices in four small drainage basins in Minnesota. The results of continuous simulation were compared to the performance assessment of the devices under 1-year and 2-year

frequency storm events. The removal efficiencies estimated from the 2-year, 24-hour storm events are within 3% of the 10-year average removal efficiencies.

Currently, the model does not include a scour function because no scour function has been developed for hydrodynamic separators. By incorporating scour functions in the model, the maintenance frequency of the devices can be determined with more confidence.

References

Herb, W. R., Janke, B., Mohseni, O., Stefan, H. (2008). "Thermal Pollution of Streams by Runoff from Paved Surfaces". *Hydrological Processes*, 22(7): 987-999.

Carlson, L., Mohseni, O., H. Stefan, and M. Lueker. (2006). *Performance Evaluation of the BaySaver Stormwater Separation System*. St Anthony Falls Laboratory Project Report No. 472, University of Minnesota, Minneapolis, Minnesota.

Cheng, N.S. (1997). "A simplified settling velocity formula for sediment particle." *Journal of Hydraulic Engineering*, 123(2), 149-152.

Environmental Technology Verification (ETV). (2005a). *ETV Report: BaySaver Separation System, model 10k.* NSF International, Ann Arbor, MI.

Environmental Technology Verification (ETV). (2005b). *ETV Report: Vortechs System, model 1000.* NSF International, Ann Arbor, MI.

Fassman, E.A. (2006). "Improving effectiveness and evaluation techniques of stormwater best management practices". *Journal of Environmental Science and Health Part.* 41, 1247-1256.

Fyten, A., and Mohseni, O. (January 2009). "Environment21 V2B1 Model 4 Performance Function." *St. Anthony Falls Laboratory Project Report No. 527*, Minneapolis, Minnesota.

Mohseni, O. and Fyten, A. (June 2008). "Performance Assessment of Modified ecoStorm Hydrodynamic Separator." *St. Anthony Falls Laboratory Project Report No. 495B*, Minneapolis, Minnesota.

Roseen, R.M., T.P. Ballestero, J.J. Houle, and P. Avelleneda. (2005). "Normalized technology verification of structural BMPs, Low Impact Development (LID) designs, and manufactured BMPs". *Proceedings of the Watershed Management Symposium*, ASCE, Reston, VA, 135-146.

Wilson, M., Mohseni, O., Gulliver, J., Hozalski, R., and Stefan, H. (2009). "Assessment of Hydrodynamic Separators for Stormwater Treatment". Submitted to the ASCE *Journal of Hydraulic Engineering*, in press.

Accurate Sampling of Suspended Solids

Gregory P. DeGroot[1], John S. Gulliver[2] and Omid Mohseni[3]

Abstract

Automatic samplers have difficulty with sampling accuracy of inorganic particles larger than silt. The samples are generally at higher concentrations than the true mean concentration in the flow, because of the settling velocity of the particles and the sampling near the bottom of the flow. The vertical mixing is insufficient to overcome the settling of coarse silts and sands. A sampling methodology has been developed to accurately sample suspended solids in stormwater. This methodology is evaluated for its effectiveness, as well as its ability to be transferred to engineering and environmental practice. Emphasis is being placed on developing a methodology which is cost-effective, allowing a method of particle sampling which fits specific users and their projects.

Introduction

Water body impairment due to suspended solids pollution is a common water quality management issue. It is most common for a water body to be primarily or secondarily impaired due to suspended solids pollution (MPCA 2008). In addition, suspended solids are associated with additional pollutants including heavy metals, phosphorus, polycyclic aromatic hydrocarbons (PAHs), and pathogenic bacteria. Thus, removing suspended solids is one of the major water quality improvement objectives of stormwater treatment.

In response to the degraded water quality found in receiving waters due to urban stormwater runoff, the Clean Water Act requires the regulation of municipal separate storm sewer systems (MS4s) and the implementation of a two-phase Storm Water Pollution Prevention Program (SWPPP) (USEPA, 2007). The SWPPP requires discharge detection and elimination, construction and post construction runoff control, and pollution prevention measures. Key to pollution prevention efforts in urban areas are the installation and maintenance of stormwater best management practices (BMPs). Improving the design of best management practices (BMPs) requires more accurate information regarding stormwater particles. For BMPs which treat particles through settling, the particle settling velocity distribution is especially important. For BMPs which remove particles via filtration/infiltration, knowledge of particle size and composition is important. As always, better knowledge of what is coming down the pipe enables better distribution of resources to meet water quality goals.

Monitoring is one means of obtaining particle data. Portable automatic field samplers are common tools for monitoring watersheds – both for establishing baseline conditions and assessing the performance of management practices. Automatic samplers have been used frequently in studies with the goal of characterizing stormwater particles.

St. Anthony Falls Laboratory, Department of Civil Engineering, University of Minnesota, 2 Third Ave SE, Minneapolis, MN 55414;
[1]PH (612) 624-4363; FAX (612) 624-4398; email: degro048@umn.edu
[2]PH (612) 624-4080; FAX (612) 624-7750; email: gulli003@umn.edu
[3]PH (612) 624-4427; FAX (612) 624-4398; email: omohseni@umn.edu

Particle Data: Size Distributions and Treatment by Settling

Particle size distribution data vary widely. Figure 1 compares two examples of stormwater particle data. Data produced by the Nationwide Urban Runoff Program (NURP) is compared with recent data gathered by Kim and Sansalone (2008) for highway runoff. One can see that the median particle size differs by nearly 1.5 orders of magnitude.

Note that when graphically comparing particle size distributions it is important to take note of the minimum and maximum particle sizes considered in the study and rescale all data to fit the narrowest study range. In Figure 1 below, Kim and Sansalone (2008) data has been rescaled to the NURP maximum particle size of 2mm.

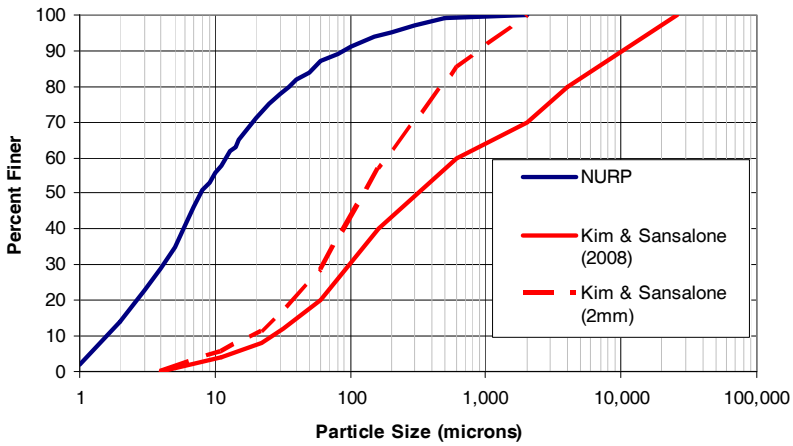

Figure 1. Comparison of Particle Size Distributions.

Particle Distribution in the Flow Column

The main difficulty in sampling suspended solids arises from the behavior of these particles in turbulent flow. Sediment particles are not uniformly distributed with depth in the water column. Suspended solids are composed of an organic portion and an inorganic portion, where the latter is considered to be suspended sediments. The difficulty with sampling suspended sediments has been known for some time. The analysis of Rouse (1937), for example, can be used to develop a suspended sediment concentration relative to the cross-sectional mean concentration based upon particle fall velocity in quiescent fluid, turbulence, and depth.

$$\frac{C}{C_{Ave}} = d\,\frac{(d/y-1)^{\frac{v_s}{\kappa u_*}}}{\int_{y_0}^{d}(d/y-1)^{\frac{v_s}{\kappa u_*}}\,dy} \qquad (1)$$

where C is suspended sediment concentration at depth y, measured from the bed, y_0 is a small distance above the channel bed, C_{Ave} is the cross-sectional mean suspended sediment concentration, v_s is settling velocity, u_* is channel shear velocity, d is channel depth and κ is von Karman's constant. Eq. (1) requires a numerical integration. Shear velocity can be determined from the relation, $u_* = (ghS)^{1/2}$, where S is water surface slope. The particle fall

velocity, in turn, depends upon particle size, density and viscosity of the water. Small particles (< 0.1 mm) have a settling velocity that is described by Stokes law (1851), given in Eq. (2).

$$v_s = \frac{gRd^2}{18\nu} \tag{2}$$

Where g is the acceleration of gravity, R is submerged specific gravity (1.65 for quartz), d is sediment equivalent diameter and v is kinematic viscosity of water. To incorporate larger particles, the empirical equation of Ferguson and Church (2004), with $C_1 = 18$ and $C_2 = 1$ will accurately describe settling velocity for larger sand particles and becomes Stokes Law for smaller particles:

$$v_s = \frac{gRd^2}{C_1\nu + \sqrt{0.75C_2 gRd^3}} \tag{3}$$

Equation (1) was integrated for typical storm sewer conditions of 0.25 m depth of flow and a water surface slope of 0.02. The results, shown in Fig. 2, indicate a substantial vertical variation for suspended sediments greater than 50 μm.

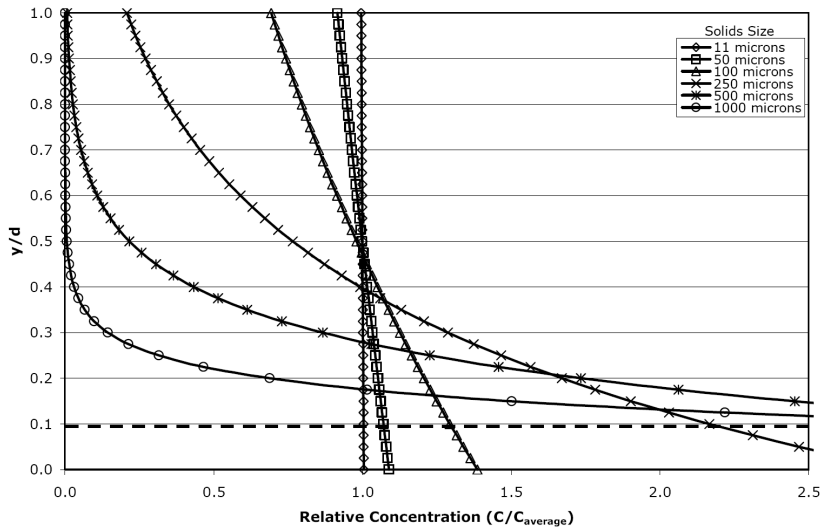

Figure 2. Distribution of suspended sediment concentration with distance from the bed for a depth of 0.25 m and water surface slope of 0.02. The horizontal dashed line indicates the region of sampling, where concentration can be much greater than the cross-sectional mean.

Evaluating Current Sampling Methods

Existing sampling methods were evaluated to establish sampling accuracy. The performance of an automatic sampler was evaluated in a controlled laboratory environment to determine its sampling accuracy for inorganic particles ranging from silt, with a median particle diameter of 20 μm, to medium sand up to 355 μm (Gettel, et al 2009). A laboratory setup was constructed to replicate sampling conditions in a storm sewer conduit. Sediment was fed into a 0.45 m diameter steel pipe at an upstream feed point. Samples were taken with an automatic sampler 10.6 meters downstream of the feed point. Baseline

samples were taken to establish background concentrations and samples were analyzed using the Suspended Sediment Concentration (SSC) method.

Samples were taken with different sediment size ranges and with multiple sampling intake configurations. Intake configurations included a tube oriented parallel to the flow – facing upstream and facing downstream. A manufacturer-recommended sampling manifold was also tested in configurations which included being fixed to the pipe, as well as being allowed to move freely within the flow.

Typical results are shown in Figs. 3 and 4. Results with the intake tube of the sampler indicate that although fine silts and clays (less than 44 μm) were sampled to within 127 percent of the fed concentration, coarse silts and sands were not sampled accurately. Coarse silts sampled at 153 percent of the fed concentration and some sands sampled as high as 6580 percent of the fed concentration. When the intake manifold was used, all silts and clays were sampled within 127 percent of the fed concentration, but fine sands between 180 and 250 μm were sampled at 303 percent of the fed concentration.

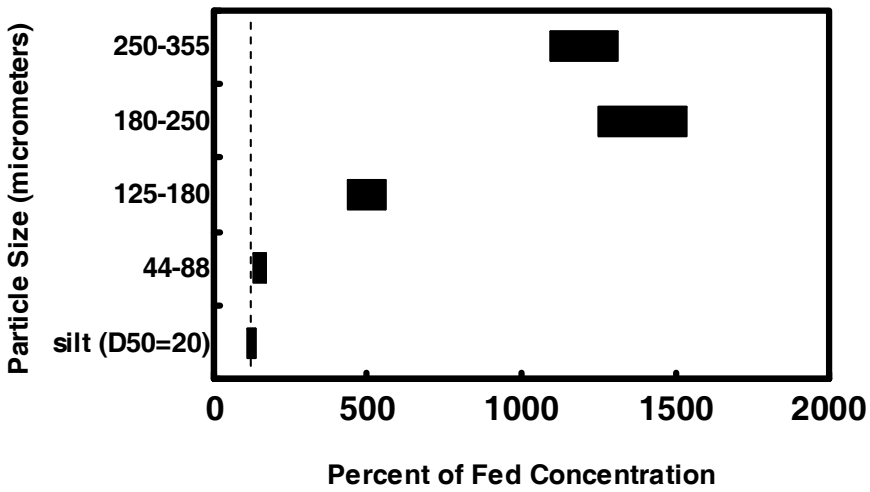

Figure 3. Percent of fed concentration versus particle size for sampling tube facing downstream. Each bar represents a ninety-five percent confidence interval of the mean.

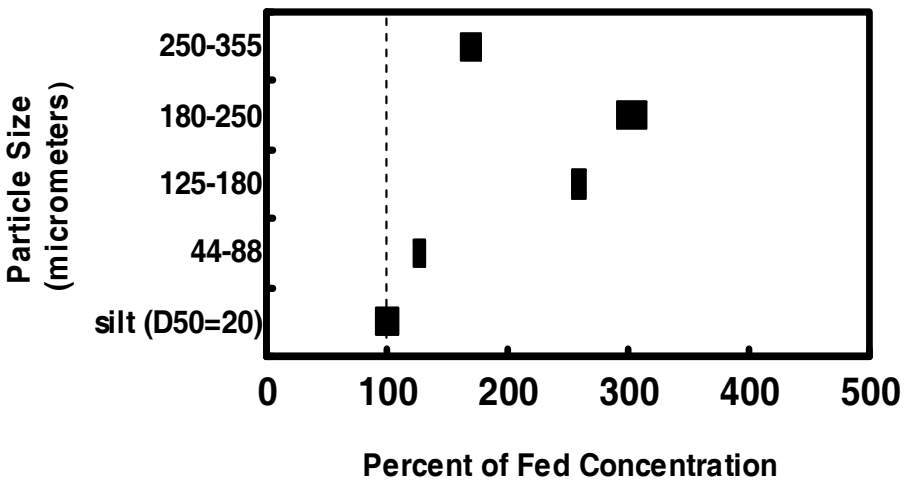

Figure 1. Percent of fed concentration versus particle size for sampling manifold in the fixed configuration. Each bar represents a ninety-five percent confidence interval of the mean.

It is seen that the current sampling technology overestimates most suspended sediment sizes with the sampling tube alone (Fig. 3) and overestimates sand concentration with the sampling manifold (Fig. 4).

Improving Current Sampling Methods

Improvements to sampling mechanisms address two major areas of concern: (1) obtaining an equal volume of sample from multiple regions in the flow column, and (2) ensuring that the lowest section of the flow column is sufficiently mixed. Equal-volume sampling across the flow column ensures the sample is representative of the mean concentration.

Current design iterations of the improved sampling mechanism utilize a passive mixing structure upstream of the intake manifold to ensure the lowest portion of the flow column is well-mixed. The intake manifold itself is hinged from the bottom of the pipe, and a fin is used to provide lift. The intake manifold thus adjusts itself to the depth of flow in the pipe. Equal-volume sampling is attained through variation in the size of the intake ports to account for pressure differences and head loss across the manifold. Figure 5 shows a sketch of the improved sampling mechanism.

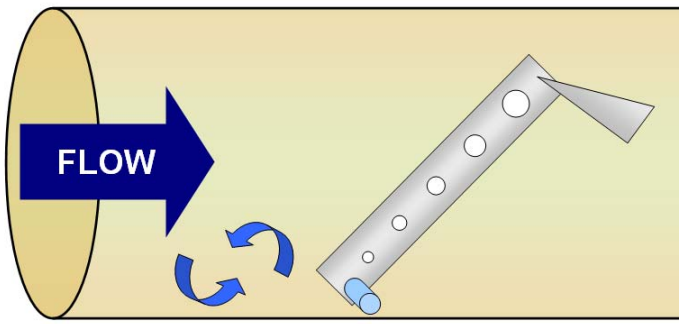

Figure 5. Conceptual Sketch of Improved Sampling Mechanism

Laboratory testing has yielded results as accurate as 119 percent of the fed concentration for fine sand (180 to 250 µm) with a standard sampler. A modified sampler with higher flow rates yielded results as accurate as 103 percent for medium sand (250 to 355 µm).

While this mechanism shows promise for smaller storm sewer pipes, an alternate mechanism is likely necessary for accurate sampling in pipes in excess of 24-inches in diameter.

Conclusions

Previous particle size distribution studies indicate a wide variation in particle size ranges. Taken in concert with the principles of particle settling, an even greater variability becomes apparent with respect to particle settling velocity. Accurate data for particle size and composition is necessary to improve BMP design. Sampling (accurately) with automatic samplers is one means to obtain such data.

Automatic sampling inaccuracy is primarily attributable to the distribution of particles in the flow column. Sampling with a single intake opening does not capture a sample which is representative of the mean concentration. Sampling with multiple intake openings also does not capture a representative sample unless equal-volumes are taken across the flow column and the lowest section of the flow column is well-mixed.

Improved sampling mechanisms have been developed which allow for the sampling of equal-volumes at multiple points in the flow column. These mechanisms are being evaluated for performance over a range of flow conditions, as well as for durability, and resistance to fouling. Future work will also consider methods to accurately sample suspended solids in pipes with very large flow depths.

References

Ferguson, R.I. and M. Church (2004). A Simple Universal Equation for Grain Settling Velocity, Journal of Sedimentary Research, 76(6): 933-937.

Kim, K.Y. and J.J. Sansalone (2008). Event-based size distributions of particulate matter transported during urban rainfall-runoff events, Water Research, 42(10-11): 2756-2768.

Minnesota Pollution Control Agency (MPCA). Minnesota's Impaired Waters and TMDLs. http://www.pca.state.mn.us/water/tmdl/tmdl-303dlist.html

Rouse, H. (1937). Modern conceptions of the mechanics of turbulence, Transactions of the American Society of Civil Engineers, 102(paper 1965), 463-543.

Stokes, G.G. (1851). On the effect of inertial friction of fluids on the motion of pendulums, *Transactions of the Cambridge Philosophical Society*, 9(part II),8.

U.S. EPA. (1983). Results of the Nationwide Urban Runoff Program, Volume 1—Final Report. Office of Water. Washington, D.C.

USEPA (U.S. Environmental Protection Agency). 2007. Phases of the NPDES Stormwater Program. Accessed September 2007. http://cfpub.epa.gov/npdes/stormwater/swphases.cfm.

An Evaluation of Stormwater Wetlands in Series

J.M. Hathaway[1] and W.F. Hunt[2]

[1] Graduate Research Assistant, [2] Assistant Professor and Extension Specialist, Department of Biological and Agricultural Engineering, North Carolina State University, Campus Box 7625, Raleigh, NC 27695; email: jon_hathaway@ncsu.edu

Abstract

Retrofit BMPs are an important tool for achieving water quality goals in urban watersheds, providing treatment to areas not originally developed with stormwater management practices. One such BMP was installed and monitored in Mooresville, N.C. The system includes three wetlands built "in-series" to treat runoff from a highly impervious 30 acre watershed. The configuration of the wetlands allowed monitoring of water quality parameters at the outlet of each of the three stormwater wetlands. The results of this study indicate that water quality improvement for a number of pollutants experiences diminishing returns as it passes through the three wetland cells. For total suspended solids (TSS), approximately 95% of the total concentration reduction took place in the first wetland cell despite it only comprising 60% of the total surface area of the system. Analysis of the effluent concentrations of the first wetland cell indicates that undersized wetlands (roughly 1.5% of the contributing watershed in this case) may still contribute to water quality improvements in urban watersheds. Thus, retrofit BMPs may be desirable even in circumstances when they cannot be sized appropriately for the contributing watershed.

Introduction

Retrofit stormwater Best Management Practices (BMPs) are installed in urbanized areas throughout the United States. These BMPs are designed to treat watersheds which were developed prior to the implementation of stomwater runoff control regulations. Retrofit BMPs are an important tool in watershed management; however, many questions remain regarding their feasibility and performance.

Design guidance for stormwater BMPs in newly developed areas of North Carolina requires the capture and treatment of the water quality volume, that is, the runoff volume associated with either the 2.54 or 3.81-cm (1 or 1.5-inch) storm depending on the physiographic region (NCDENR 2007). This is similar to water quality design criteria in several states, including Maryland (MDE 2000), New York (NYSDEC 2003), Virginia (VDCR 1999). However, in retrofit applications the surface area needed to capture the water quality volume is commonly not available. Thus, innovative designs may be required to maximize available land in urban areas and to optimally treat urban stormwater runoff. The effectiveness of retrofit designs, namely undersized BMPs, is not

well documented. Thus, cost-benefit analyses on urban retrofits are limited by a lack of knowledge as to how undersized BMPs perform.

As efforts continue to reach TMDLs in degraded surface waters, various innovative stormwater treatment designs have been promoted. In North Carolina's nutrient sensitive watersheds, where stormwater nutrient load reductions are required, designers are allowed to place BMPs in series. Each BMP is afforded a state regulated removal rate based on its type (NCDENR 2007). The standard removal rate is applied regardless of a BMP's position in the series (first, second, etc). For example, constructed stormwater wetlands are allotted 85% total suspended solids removal, 40% total nitrogen removal, and 35% total phosphorus removal. Although limited field study has been conducted on the performance of similar kind BMPs in series, most experts agree that this practice is not likely effective for BMPs which rely on similar pollutant removal mechanisms (USEPA 2002, ASCE – WEF 1998, NCDENR 2007). Therefore, NCDENR (2007) only allows two BMPs which rely on similar removal mechanisms to be placed in series. However, both BMPs placed in series are each given full pollutant removal credit, thereby assuming a BMP's location along the series will not significantly impact its performance.

Stormwater BMP efficiency has been shown to vary based on numerous factors including hydraulic loading rate, detention time, characteristics of the storms monitored, and the quality of the stormwater entering the wetland, resulting in a wide performance range when evaluations are based on percent removal calculations (Carleton et al. 2001, Clary et al. 2002, Strecker et al. 2001, Urbonas 1995). Strecker et al. (2001) examined multiple methods of determining stormwater BMP efficiency, concluding that analysis of effluent pollutant concentrations, along with a statistical analysis of influent and effluent pollutant concentrations, was a good measure of BMP performance. Such analysis infers that BMPs receiving relatively clean runoff may not perform as well from a percent removal perspective as BMPs receiving dirty runoff, thus biasing results. This was observed in wetlands studied by Lenhart and Hunt (in review) and Line et al. (2008), where low influent pollutant concentrations led to poor performance based on percent removal calculations despite low effluent concentrations. Various comparisons can be made in an attempt to determine how well a BMP functions, including comparison to effluent concentrations from similar BMPs.

The purpose of this study was to examine a series of stormwater wetlands and (1) evaluate the performance of undersized practices typical of retrofits and (2) document any marginal improvements in pollutant removal provided by wetlands in series.

Site Description

The Dye Branch Stormwater Wetlands were located in the Piedmont of North Carolina in the Town of Mooresville and were constructed between the Fall of 2005 and the Spring of 2006. Complications with one of the outlet structures left the system only in partial operation until December 2006. The wetlands serviced a watershed with an estimated area of 12.5 ha (31 acres), 60% of which was impervious. This does not include the local watershed draining directly to the BMP, which was estimated to be approximately 1.3 ha

(3.3 acres) excluding the BMPs themselves. This adjoining watershed was primarily forested or grassed, and likely only produced a small percentage of the total runoff that the wetlands received during most storm events. The composite curve number for the watershed was estimated to be 87.5. Soils in the watershed were primarily Cecil fine sandy loam.

Stormwater runoff from the watershed drained into a large concrete diversion structure where a 15.2-cm (6-inch) orifice routes stormwater flows up to 133.1 l/s (4.7 cfs) to the wetland (Figure 1). Using a rational method analysis on the watershed, this corresponded to an estimated rainfall intensity of approximately 0.5 cm/hr (0.2 in/hr) (Kuichling 1889, Lloyd-Davies 1906, Mulvaney 1851). During storms which produced flows higher than this value, a concrete bypass weir was overtopped and excess runoff proceeded down an unnamed tributary and in to Dye Branch; the additional hydraulic head on the diversion orifice during overtopping events resulted in increased flow to the wetlands. Debris accumulation in the diversion structure resulted in a minor reduction of pollutants, particularly sediment, entering the wetlands.



Figure 1: Orifice Plate in Diversion Structure Used to Route Flow to Wetlands

Due to topographical and space limitations, the BMP was designed as a treatment train of three wetland cells (Figure 2). The cells had a combined area of approximately 0.33 ha (0.81 acres). The estimated runoff volume during the 2.54-cm (1-inch) storm was estimated by the discrete curve number method (NRCS 2004) to be approximately 1416 m^3 (50,000 cf). Based on the final BMP design, only 575 m^3 (20,300 cf) was expected to be retained by the wetlands. The cells were hydraulically separate, which allowed individualized flow monitoring.

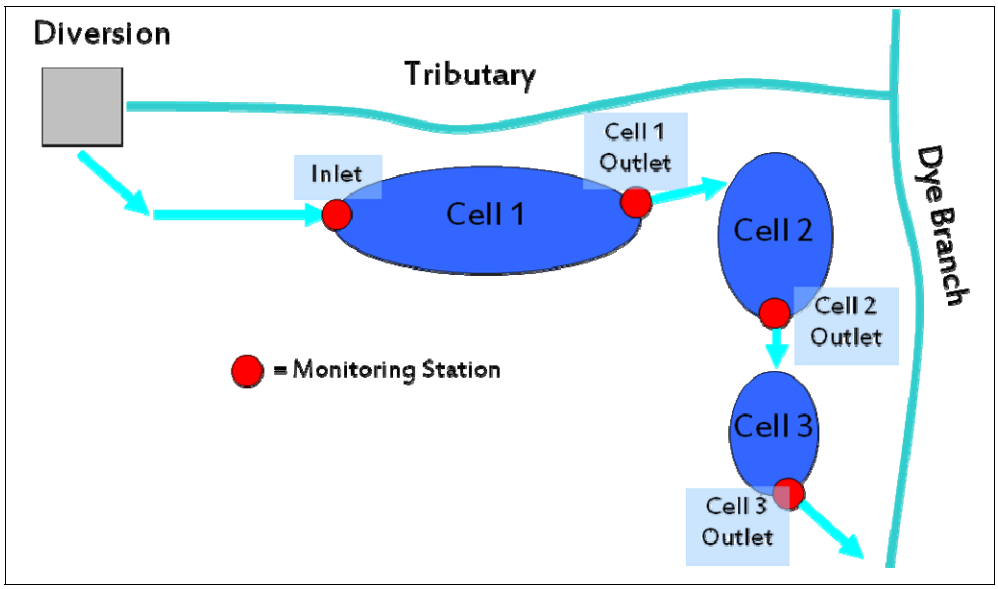

Figure 2: Schematic of Dye Branch Wetlands

Wetland cell 1 was the largest of the three cells (0.19 ha (0.48 acres)). The design included a large forebay (0.02 ha (0.05 acres)). A flashboard riser was used as the outlet of the cell, with two 5.08-cm (2-inch) orifices controlling the normal pool and a 1.16 m (3.8 ft) weir bypassing excess inflow volumes to cell 2. Approximately 23.5 cm (9.25 inches) of freeboard were present between the normal pool and the bypass weir, allowing a design storage volume of 382 m^3 (13,500 cf). However, due to the subsoils of the wetland infiltrating more water than expected, the actual pool of the wetland was frequently lower than the design normal pool, providing more volume storage than anticipated.

Wetland cell 2 was approximately 0.07 ha (0.18 acres), with a forebay which covered 0.01 ha (0.02 acres) of the surface area of the wetland. A flashboard riser was used as the outlet of the cell, with two 5.08-cm (2-inch) orifices controlling the normal pool and a 1.16 m (3.8 ft) weir bypassing excess runoff volumes. Approximately 30.5 cm (1 foot) of freeboard was present between the normal pool and bypass weir, allowing a design storage volume of 193 m^3 (6800 cf). Inter-event infiltration resulted in additional storage in this wetland as well.

Wetland cell 3 was approximately 0.06 ha (0.15 acres), with a 0.004-ha (0.01-acre) forebay. A flashboard riser was used as the outlet of the cell. No detention was present in the cell, as flow was controlled by a 1.16 m (3.8 ft) weir with no drawdown orifice. The normal pool was consistently below the control weir, resulting in some storage occurring during events. A set of three sediment baffles were installed during the construction of the system to be removed after the site had stabilized. Although the site was sufficiently stabilized, these baffles were in place at the start of the monitoring study, and were left in place as to not disturb the cells during the study.

Monitoring Description

Flow monitoring

Flow was measured at the inlet of cell 1 and the outlet of all three wetland cells (Figure 2). After passing through the diversion structure, stormwater runoff was routed into a large concrete structure outfitted with a 120 degree v-notch weir. An ISCO 730 bubbler module was used to measure the hydraulic head on the weir. Standard equations were used to calculate flow using these measurements. Stage-discharge relationships were generated for the orifice / weir combinations at the flashboard riser outlets of wetland cells. ISCO 730 bubbler modules were used to calculate the stage at each riser during storm events, these measurements were used to calculate flow. Due to some questionable flow data, volume and load calculations were not made. However, water quality analyses aided by these data were deemed valid as hydrographs from each location were consistent with the operation of the system.

Water Quality Monitoring

Water quality samples were taken at each flow monitoring point, where monitored hydrographs were adequate to trigger flow weighted samples. A sample was only considered for analysis if at least 5 aliquots were taken during a given event. Samples were collected using ISCO Avalanche™ refrigerated, automatic samplers and were normally collected within 24 hours of a rain event at the inlet and at the outlet of the wetland cells which had substantially drained. For wetland cells which had not substantially drained after 24 hours, a return visit was made to retrieve the samples. During some events, it was necessary to collect the samples prior to the event completely passing through the system due to sample hold times. Samples were preserved as necessary and shipped to an NCDWQ laboratory where they were analyzed for turbidity, total suspended solids (TSS), total Kjeldahl nitrogen (TKN), total ammoniacal nitrogen (TAN), nitrate – nitrite (NO_2-NO_3), and total phosphorus (TP). Total nitrogen (TN) was calculated by adding the concentrations of TKN and NO_2-NO_3. Organic nitrogen (ON) was calculated by subtracting TAN from TKN.

Statistical Analysis

Overall, 27 storm events were monitored at the site; however, sampler power failures and inadequate volumes for analyzing all constituents were sometimes experienced. Further, to provide balanced analysis of the system, only storms where samples were collected from all monitoring points were used for data analysis. Between 10 and 15 paired samples with at least 5 aliquots were collected for each pollutant across the seasons (Table 1).

Prior to in-depth statistical analysis, the data were checked for normality using the Kolmogorov-Smirnov test (REFERENCE). The results of this analysis were verified using box plots and histograms of the data. The data were found to have various distributions. Most data were normally distributed; however, some required log transformation and some could not be matched to any distribution. To maintain consistency in the analyses, and due to the small number of paired samples taken for each pollutant, a non-parametric Wilcoxon signed-rank test (WSR) was chosen to determine the statistical significance of the comparisons being made. Using this non-parametric

analysis allowed evaluation without concerns over the distribution of the data. Efficiency ratios were used as a metric for the amount of pollutant removal provided by each wetland cell. Since flow paced samples were collected, each pollutant measurement from a given sample event was considered to be an event mean concentration (EMC). The following equation was used to determine the efficiency ratio:

$$ER = 1 - (\frac{Average\_Outlet\_EMC}{Average\_Inlet\_EMC})$$

Table 1: Number of Sample Pairs for Each Parameter

Parameter	Number of Paired Samples
Turbidity	12
TSS	10
TKN	14
TAN	15
NO_2-NO_3	15
TP	15
TN	14
ON	14

Results and Discussion

Performance of Undersized Wetland

As retrofit BMPs are commonly constrained by space in urban environments, data evaluating the performance of undersized BMPs such as wetlands are desirable for use in watershed management. Wetland cell 1 was sized to capture approximately 27% of the volume that would leave the treatment watershed during a 2.54-cm (1-inch) water quality rain event. The actual volume captured was somewhat larger because of frequent periods where the water level in the wetland dropped below the normal pool. This is common in some constructed wetlands (Lenhart and Hunt (in review), Line et al. 2008) and likely improves hydraulic performance beyond the design.

Table 2 shows the influent and effluent EMCs for the water quality parameters at wetland cell 1. To provide some comparison for water quality performance analysis, these values are compared to stormwater wetland median effluent concentrations from the ISBD (GCWWE 2008). Although influent concentrations were similar to those exiting stormwater wetlands in the ISBD (GCWWE 2008), effluent values were lower than influent values for each parameter, resulting in significant reductions ($p<0.05$) and ERs of at least 0.39 for each. Further, mean influent concentrations of TKN, NO_2-NO_3, TN, and TP were similar to those determined for eight parking lots in North Carolina by Passeport and Hunt (2009). Although relatively low influent concentrations can result in artificially low efficiency ratios, the undersized wetland cell 1 still performed well. Effluent concentrations at cell 1 were less than those in the ISBD (GCWWE 2008) for each pollutant, indicating good performance relative to other stormwater wetlands. These data indicate that undersized wetlands may provide water quality improvements when space is limited in retrofit designs and may be beneficial in watershed management plans in urban watersheds.

Table 2: Wetland Cell 1 Efficiency Comparisons

Pollutant	Median Effluent EMCs of Wetland Basins in the ISBD – mg/L (reference)	Median Inlet Concentration (mg/L)	Median Cell 1 Outlet Concentration (mg/L)	Efficiency Ratio
TSS	19	80.5	13.5	0.83
TKN	1.09	1.25	0.765	0.39
NO_2-NO_3	0.2	0.4	0.14	0.65
TN	1.21	1.68	0.865	0.49
TP	0.58	0.26	0.11	0.58

Performance of Wetlands in Series

The sampling scheme at the Dye Branch Stormwater Wetlands allowed an analysis of wetlands in series by comparing EMCs and efficiency ratios for the three wetland cells. Table 3 shows the EMCs of pollutants at each monitoring point. Pollutant concentrations decreased at each sequential monitoring point for most pollutants, although slight increases were noted between the wetland cell 2 outlet and the wetland cell 3 outlet for ON and TKN. The EMCs from each cell were lower than concentrations presented in the ISBD (GCWWE 2008). It should be noted that EMCs for ON at the outlet of each wetland cell were very similar at 0.68, 0.63, and 0.64 mg/L for wetland cells 1, 2, and 3, respectively.

Table 3: Pollutant EMCs for Each Monitoring Point at DBW

Pollutant	Inlet	Cell 1 Outlet	Cell 2 Outlet	Cell 3 Outlet
TSS	77	12	11	9
TP	0.31	0.12	0.12	0.10
TN	1.74	0.84	0.74	0.72
ON	1.00	0.68	0.63	0.64
TAN	0.28	0.04	0.03	0.03
TKN	1.30	0.73	0.66	0.67
NO_2-NO_3	0.44	0.14	0.08	0.07
Turbidity	39	15	14	10

Differences in wetland cell performance can be further explored with the efficiency ratios shown in Table 4. These data reemphasize data in Table 3, as efficiency ratios are positive for most pollutants in each wetland cell; however, from wetland cell 2 to wetland cell 3, there are minor increases in ON and TKN. Pollutant efficiency ratios generally experience diminishing returns as stormwater passes through each wetland cell, although efficiency ratios for TSS, TP, and turbidity increased in wetland cell 3. This is potentially due to the sediment baffles still in place in wetland cell 3, which could impact the concentrations of these particle associated pollutants. It should be noted that none of these increases in wetland cell 3 were statistically significant ($p<0.05$). Further, only wetland cell 1 provided statistically significant reductions ($p<0.05$) for all pollutants.

Only nitrogen species were significantly reduced between the outlet of cell 1 and the outlet of cell 2.

Table 4: Efficiency Ratios for Each Wetland Cell

Pollutant	Inlet to Cell 1 Outlet	Cell 1 Outlet to Cell 2 Outlet	Cell 2 Outlet to Cell 3 Outlet
TSS	***0.84***[1]	0.11	0.18
TP	***0.62***	0.03	0.11
TN	***0.52***	***0.12***	0.03
ON	***0.32***	***0.07***	-0.02
TAN	***0.85***	0.26	0.13
TKN	***0.44***	***0.09***	-0.01
NO_2-NO_3	***0.67***	***0.47***	0.12
Turbidity	***0.62***	0.09	0.24

[1]: Significant Differences are italicized and bolded

A number of processes in wetlands affect nitrogen species, resulting in a complex cycle. Microbial transformations change ON to TAN, TAN to NO_2-NO_3, and NO_2-NO_3 to nitrogen-based gasses, including N_2. Simultaneously, various nitrogen species are taken up by plants and microorganisms, becoming organic biomass. Uptake is not considered a permanent removal mechanism, as plant and microbe die-off can lead to a reintroduction of nutrients into the water column (Kadlec and Knight 1996). These processes were likely exhibited in Table 4 above, as wetland processes in each cell continued to remove TAN and NO_2-NO_3 as evidenced by positive ERs for each wetland cell for these nitrogen species. However, reduced or negative ERs were noted for ON and TKN (which includes ON) as stormwater passed through the system. Similar observations were made by Lenhart and Hunt (in review) in a study of a stormwater wetland in the coastal plain of North Carolina.

Conclusions

A system of three wetland cells in series was monitored in this study. Data from the first wetland cell showed that both sediment and nutrients were significantly removed ($p < 0.05$) by a wetland sized only to hold 27% of the 2.54-cm (1-inch) design storm volume. This study indicates that undersized wetlands are able to improve water quality in urban watersheds, which is important when assessing the benefit of installing retrofit stormwater BMPs where space is limited.

The marginal benefit of stormwater BMPs in series was also evaluated in this study. At least 80% of the total concentration change for a given pollutant occurred within the first wetland cell. Further, only the first wetland cell significantly ($p<0.05$) reduced all pollutants tested in the study. Diminishing returns were generally observed in the system, but the ERs associated with nitrogen species continually declined through the wetland cells. TSS, TP, and turbidity showed a minimal, non-significant ($p<0.05$) increase in removal efficiency in wetland cell 3. Based on this study and supporting assertions by others (USEPA 2002, ASCE – WEF 1998, NCDENR 2007), placing BMPs of a similar type in series is not a beneficial management strategy when using effluent concentrations or efficiency ratios as a metric. Percent removal is not constant from BMP to BMP in a

series. While calculations of percent removal may be simple to understand, they should not be exclusively used to evaluate stormwater BMP performance. This is especially the case for systems which have low influent pollutant concentrations, such as the subsequent stormwater wetlands in series

Acknowledgements
The authors would like to acknowledge the North Carolina Ecosystem Enhancement Program for logistical assistance and funding of this study, the North Carolina Division of Water Quality for their monitoring assistance and sample collection, the Town of Mooresville for their logistical assistance and willingness to provide public land for the project, and Jonathan Smith of McKim and Creed for his contributions to the project design, construction, and monitoring set-up.

References

American Society of Civil Engineers (ASCE) and Water Environment Federation (WEF), (1998). "Urban Runoff Quality Management" ASCE, Manuals and Report of Engineering Practice No. 87, Reston, VA. WEF, Manual of Practice No. 23, Alexandria, VA.

Carleton, J.N., T.J. Grizzard, A.N. Godrej, and H.E. Post. (2001). "Factors affecting the performance of stormwater treatment wetlands." *Water Research*. 35(6): 1552-1562.

Geosyntec Consultants and Wright Water Engineers, Inc (GCWWE). (2008). "Analysis of treatment system performance: international stormwater Best Management Practices (BMP) database [1999 – 2008]."

Kadlec, R.H. and R.L. Knight. (1996). *Treatment Wetlands*, CRC Press LLC, Boca Raton, Florida.

Kuichling, E. (1889) "The relation between the rainfall and the discharge of sewers in populous districts." *ASCE Transactions*. 20:1-56.

Lenhart, H.A., and W.F. Hunt. "Evaluating Four Stormwater Performance Metrics with a North Carolina Coastal Plain Stormwater Wetland." *Journal of Environmental Engineering.* (in review)

Line, D.E., G.D. Jennings, M.B. Shaffer, J. Calabria, W.F. Hunt. (2008). "Evaluating the effectiveness of two stormwater wetlands in North Carolina." *Transactions of the ASABE*. 51(2): 521-528.

Lloyd-Davies, D.E. 1906. "The elimination of storm water from sewerage systems." *Inst. Civ. Eng. Proc.* 164:41-67.

Maryland Department of the Environment (MDE). (2000). Maryland stormwater design manual, Vols. I & II, Md.

Mulvaney, J.T. (1851) "On the use of self-registering rain and flood gauges," *Inst. Civ. Eng. (Ireland) Trans.* 4(2):1-8.

New York State Department of Environmental Conservation (NYSDEC). (2003). *New York State stormwater management design manual*. Center for Watershed Protection, Ellicott, City, Md.

Passeport, E. and W.F. Hunt (2009) "Asphalt Parking Lot Runoff Nutrient Characterization for Eight Sites in North Carolina, USA." *Journal of Hydrologic Engineering*, 14(4): TBD.

Natural Resources Conservation Service (NRCS). (2004). *Estimation of direct runoff from storm rainfall*. National Engineering Handbook, Part 620 Chapter 10, USDA, Washington, DC.

Strecker, E.W., M.M. Quigler, B.R. Urbonas, J.E. Jones, and J.K. Clary. 2001. Determining Urban Stormwater BMP Effectiveness. *Journal of Water Resources Planning and Management*. 127:144-149.

United States Environmental Protection Agency (USEPA). (2002). "Considerations in the design of treatment Best Management Practices (BMPs) to improve water quality."

Urbonas, B.R. (1995). "Recommended Parameters to report with BMP monitoring data." *Journal of Water Resources Planning and Management*. 121(1): 23-34.

Virginia Department of Conservation and Recreation (VDCR). (1999). *Virginia stormwater management handbook*, Va.

An Innovative Approach for Modeling Large Urban Hydrologic Systems

J.P. Cantone[1] and A.R. Schmidt[2]

[1]Graduate Research Assistant, Hydrosystems Laboratory, Department of Civil and Environmental Engineering, University of Illinois at Urbana-Champaign, 205 N. Matthews Ave., Urbana, IL 61801, USA; PH (217) 766 5556; FAX (217) 333 0687; email: cantone2@illinois.edu

[2]Research Assistant Professor, Hydrosystems Laboratory, Department of Civil and Environmental Engineering, University of Illinois at Urbana-Champaign, 205 N. Matthews Ave., Urbana, IL 61801, USA; PH (217) 333 4934; FAX (217) 333 0687; email: aschmidt@illinois.edu

ABSTRACT

The dynamics of the urban landscape are ever changing. As the population grows, urban sprawl gathers momentum and the path for a drop of rainfall changes complexion. The physical processes involved from when rain falls until when it reaches a treatment plant or waterway are highly non-linear. In larger urban catchments, these non-linearities have largely been ignored and linearized through development of lumped or semi-distributed models. This linearization is often used to overcome the sheer size and complexity of the urban catchments. The answer to the question of how much network complexity should be included in a model has been pre-empted by the application of conduit skeletonization and subcatchment aggregation. These simplification techniques are not without their dangers and may introduce bias into the predicted hydrographs. This paper provides a review of modeling approaches that are typically undertaken in modeling large urban catchments, highlighting their advantages and disadvantages. The majority of the approaches involve the application of hydrologic models that require calibration and significant knowledge of hydrologic inputs. In many cases the assessment of existing urban hydrologic systems is hindered by the absence of input data and/or calibration data. With this in mind, an innovative approach to modeling large urban hydrologic systems is presented. This approach builds on the fundamentals of the geomorphologic instantaneous unit hydrograph (GIUH) that was developed by Rodriguez-Iturbe and Valdes in 1979, which has been successfully applied to natural watersheds over the past three decades. Application of GIUH has evolved such that it can be applied to ungauged natural watersheds with knowledge of as little as the watershed area and layout of the stream network. The approach proposed in this research, in a similar manner, uses the morphology of the sewer system to route flow through the network. Excess rainfall is determined using the Green and Ampt method based on the physical characteristics of the underlying soils. The kinematic wave approach is used, in conjunction with stochastically generated parameters describing relevant subcatchment and sewer characteristics to establish probability distribution functions (PDF) for overland (both pervious and impervious) and sewer travel times. The PDF's of the travel time and excess rainfall are convoluted to generate an outflow hydrograph. This approach maintains the non-linearity of the physical processes in highly urbanized catchments and allows model development in the

absence of detailed input and calibration data. Through application of this approach an improved understanding of the physical process can be achieved.

INTRODUCTION

The dynamics of the urban landscape are ever changing. Development has seen swamp lands turn into pastures, pastures into corn fields, and corn fields into concrete. As the population grows, urban sprawl gathers momentum and what was once pervious may inevitably become impervious. So as the ground beneath our feet changes complexion so does the path for a drop of rainfall. In order to be able to trace this path it is imperative that the physical processes associated with its travel be better understood. The primary objective of this research is to improve the understanding and representation of the physical processes in highly urbanized catchments.

Urbanized catchments have changed complexion significantly over the past 20 years and will continue to do so into the future. At the simplest level urban consolidation and urban sprawl have seen the imperviousness of urban catchments increase. More complex landscapes are being developed to cater to low impact development and include stormwater best management practices. Sewer systems built in the 20th century often have insufficient capacity to carry post-development flows and are constantly being retrofitted or replaced. Combined sewer systems are seldom built in preference to separated stormwater and sanitary sewer systems. Existing CSO systems that cannot be easily replaced are being intercepted by complex deeper tunnel systems in order to prevent overflows polluting adjacent rivers and waterways in large storm events. All of these changes are unique in their own way but each impacts the behavior of water as it travels through the urban landscape. The question is how one represents the intricate physical processes that are associated with modern urban landscapes?

In order to be able to represent the physical processes one must first understand their high degree of non-linearity. As rain falls, runs off a roof, down a gutter, through a rain garden, onto the street, along a gutter, into an inlet connected to a storm sewer, through that sewer and eventually to a treatment plant or water way, one does not render such a process to be linear. However, traditional approaches to representing such behavior have done exactly that ignoring this obvious non-linearity in the physical processes. In this research the approach that is presented maintains this non-linearity, ensuring a sound fundamental representation of the physical processes.

Since the advent of computer technology the representation of urban catchments has fallen on computer models. Representation has evolved from simple back-of-the-envelope rational-method calculations to more sophisticated DOS based models like ILLUDAS to complex Windows based models capable of solving the full St. Venant equations like InfoSWMM. There are now a plethora of hydrologic simulation packages (including SWMM, HEC-HMS, MOUSE, InfoWorks, etc) that are capable of modeling urban stormwater and combined sewer overflow systems and these are commonly used in practice. Although these models are capable of modeling these systems, there are two key factors that hinder their use in modeling large urban systems. The first problem is that each of the models mentioned require calibration,

and for the most part calibration data are not available. Secondly, the large amount of input data required for these models are often unavailable and are uncertain when they are available. The input data required for the commercially available hydrologic models mentioned above includes:

- Subcatchment data: area, percent imperviousness, slope, length, roughness, soil characteristics, depression storage etc.
- Inlet data: type, size, rating curve etc.
- Pipe data: size, length, roughness, upstream and downstream invert, etc.
- Junction data: surface elevation, invert etc.

For many large urban catchments in densely populated areas, sanitary and storm sewer infrastructure was installed over 50 years ago when documentation was not what it is today. As such this critical input information simple does not exist. In some cases, the only available information is the layout of the sewers themselves. Typically, engineers make simplifying assumptions so that the commercially available simulation packages may be used to model the network. Cantone and Schmidt (2008) explored a number of the commonly employed simplification techniques, including subcatchment aggregation and conduit skeletonization. Tests on a simple CSO network showed that such simplification techniques introduce error in the calculated outflow hydrograph and hence caution must be used in applying them.

Given that the existing models are unable to overcome the problems at hand; this research provides the opportunity to develop a hydrologic model that can be applied in ungauged urbanized watersheds where limited input data are available.

LITERATURE REVIEW

The challenges involved in deriving such a method were met head on by Rodriguez-Iturbe and Valdes (1979) and Gupta et al (1980) when they developed the geomorphologic instantaneous unit hydrograph (GIUH) for natural watersheds. Subsequent development of the GIUH approach has allowed this model to be applied to not only ungauged watersheds, but also to watersheds lacking detailed geomorphologic information (Yen and Lee 1997). In the GIUH approach, rainfall excess is assumed to follow different paths on overland areas and in channels of different stream orders; these different paths can be described probabilistically, according to the drainage pattern to reach the watershed outlet (Yen and Lee 1997).

GIUH applied to watersheds has been the subject of much research since its inception, however little of this research has focused on its application to urban watersheds. Many papers propose different representations for the travel time of the rainfall excess, ranging from exponential (Rodriguez-Iturbe and Valdes 1979), uniform (Gupta et al 1980) and gamma (Jin 1992) distributions to those involving kinematic-wave theories (Lee and Yen 1997). Of particular relevance to this research is a paper published by Yen and Lee (1997) that showed that knowing as little as the watershed area and stream order of each reach a representative unit hydrograph for a

watershed could be obtained using other data acquired from large-region averaged values.

The application of the GIUH concept to urban concepts has not been studied exhaustively. Rodriguez et al (2003, 2005) have published a body of work that utilizes GIUH in the urban setting. Rodriguez et al 2003 showed that the plethora of information contained in Urban DataBanks (UDB) could be used in combination with the GIUH concept to derive Urban Unit Hydrographs (URBS-UHs) for three urban catchments in France with surface areas ranging from 18 to 180 ha. In their formulation Rodriguez et al (2003) make a number of key assumptions:

- Water flows over impervious surfaces and in sewer networks dominate the rapid response of urban catchments. In this way only impervious areas are modeled, pervious areas are ignored.
- UDB's contain enough geometric information to allow the path for the propagation of runoff to be modeled and identified.
- The flow velocity field is a spatial variable depending on the considered flow conditions and available UDB information.
- Flow can be considered a monotonic response to a rain impulse.
- Downstream segments can reasonably be considered to accept the outflow of upstream segments.
- The entire area is assumed to be covered by cadastral parcels and street surfaces. Flow is parameterized over each parcel.
- Street flooding and sewage system overflow is not allowed.
- Street gutter flow is supposed to reach a priori the sewer system at each street network intersection.
- Hydraulic behavior of inlets has been ignored.
- Street gutters are modeled as small-sized pipes (250 mm diameter).
- Hydraulic dispersion along the flow path is ignored.

The approach presented by Rodriguez et al (2003) is highly dependent on the quality and quantity of the information in the UDB. As previously mentioned this type of information is simply not available in many urban catchments. Secondly, Rodriguez et al (2003) ignore runoff from pervious areas. Runoff from pervious areas particularly for wet antecedent moisture conditions can be significant in shaping the surface runoff hydrograph.

In their 2005 paper Rodriguez et al compare the method they developed in 2003 with two other methods usually applied in natural catchments (H2U and FDTF). The three unit hydrograph determination methods make use of varying degrees of the description of drainage network morphology and their combined application requires rainfall and runoff data collected from hydrological recording devices.

Lhomme et al (2004) applied a GIS-based geomorphological routing model to the urban catchment El Batan in the city of Quito, Ecuador. Despite being described as an urban catchment the area of the catchment is some 52 km^2 and a significant portion of the network is made up of natural streams. The formulation presented by the authors

of this paper is reliant on a detailed GIS database of input information and the model is calibrated using hydrologic rainfall and runoff data.

Few researchers have formulated models utilizing morphologic approaches for developing unit hydrographs in urban areas. The model developed by Rodriguez et al (2003) is heavily reliant on detailed catchment description provided through UDB's and utilizes a number of simplifying of assumptions that distinguish it from the approach proposed herein. Similarly, the later work by Rodriguez et al (2005) and Lhomme et al (2004) present approaches that incorporate GIUH but are dependent on rainfall and runoff data and/or detailed catchment description. The approach presented in this paper is not dependant on detailed catchment parameters nor does it require the catchment to be gauged. In addition the approach presented is adaptable and potentially will be able to incorporate important hydrologic processes associated with inlets, lot scale BMP's and runoff over pervious surfaces that are not accounted for in the aforementioned approaches presented in the literature.

METHODOLOGY

The model proposed in this research simplifies the complex hydrologic processes of an urban catchment by initially considering overland surface runoff and conduit flow only. For any given rainfall hyetograph, depression storage in both the pervious and impervious areas is accounted for. For pervious areas, infiltration losses are derived using the Green-Ampt method (as described below). The overland flow for all subcatchments is sub-divided into a pervious and impervious portion with water flowing from pervious to impervious areas by default. By subtracting the depression storage and infiltration losses from the precipitation, the excess rainfall falling on the overland plane is derived for both the pervious and impervious areas. Excess rainfall along with subcatchment parameters are used to determine the overland flow travel time for a given subcatchment using the kinematic wave approach (Yen and Lee 1997).

Green-Ampt Method

Green and Ampt (1911) proposed a physically based approximation to Richard's equation that has an exact analytical solution in order to derive infiltration losses. This approach is well documented in the literature (Chow et al 1988) and so the details are not presented here. Using the infiltration rate calculated using the Green and Ampt equations, and having already subtracted depression storage, the excess rainfall for both the impervious and pervious areas may be determined using:

$$q_{L,perv}(t) = i(t) - f(t) \quad (1)$$

$$q_{L,imp}(t) = i(t) \quad (2)$$

One of the shortcomings of the Green-Ampt model is readily accessible accurate estimates of the Green-Ampt parameters such as the porosity, effective porosity, wetting front soil suction head and hydraulic conductivity. Rawls et al (1983) analyzed approximately 5000 soil horizons throughout the United States and determined average and standard deviation values of the Green-Ampt parameters for

different soil classes (sand, loamy sand, silt loam, etc.). The model presented in this paper only utilizes the expected value of the Green-Ampt parameters, however in the future the model will be adapted to account for the variability in these parameters. The variance in the Green-Ampt parameters will be utilized in a first order second moment (FOSM) analysis to determine the variance in the excess rainfall, which will in turn be used to determine a variance in the overland and conduit travel times. This will allow a more sophisticated probability-density-function, utilizing the mean and variance, to be used in Equation (28).

Travel Time Estimation

Overland Flow

Using the kinematic-wave approach it is possible to simulate the surface-runoff process using the shape, length, slope and surface condition of a subcatchment (Lee an Yen 1997). Implicit to this approach is the assumption that backwater effects are not important and that there is slope on the plane of flow.

Consider an *i*th order basin in the watershed as consisting of two rectangular overland planes as shown in Figure 1. One plane classified as pervious and the other as impervious. Assume that both planes contribute a lateral discharge into a conduit of constant cross-section and slope.

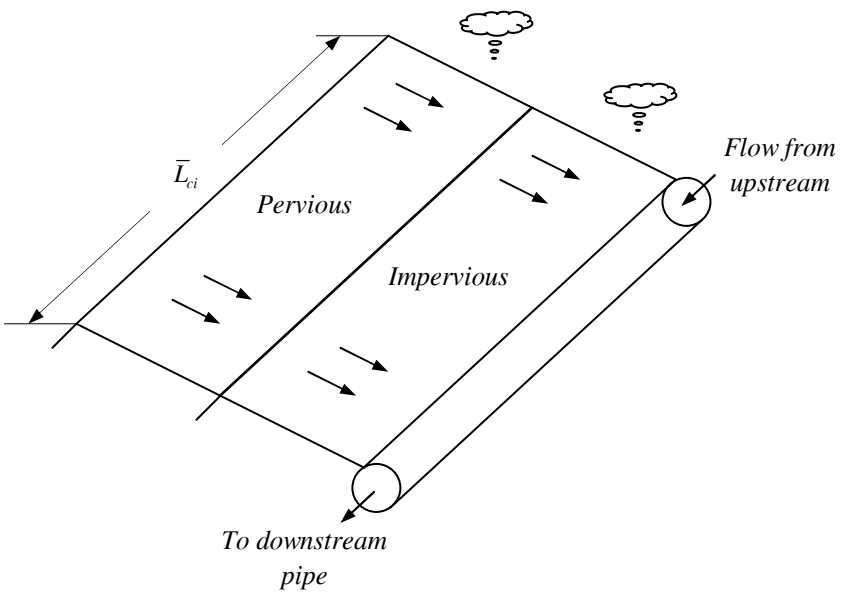

Figure 1 Schematic of surface runoff model

According to Lee and Yen (1997) the mean length of the *i*th order v-shape overflow plane can be estimated by:

$$\bar{L}_{oi} = \frac{AP_{OAi}}{2N_i \bar{L}_{ci}} \tag{3}$$

where P_{OAi} is the probability that a drop of rainfall excess will fall on an *i*th order overland flow region, A is the total area of the catchment, N_i is the number of conduits in the *i*th order, and $\overline{L}_{ci}$ is the average length of the *i*th order conduit.

This formula can be applied to both the pervious and impervious planes shown in Figure 1 using the following equations:

$$\overline{L}_{oi,perv} = \frac{AP_{OAi}}{2N_i\overline{L}_{ci}} \times (1 - \overline{imp}_i) \tag{4}$$

$$\overline{L}_{oi,imp} = \frac{AP_{OAi}}{2N_i\overline{L}_{ci}} \times \overline{imp}_i \tag{5}$$

where $\overline{imp}_i$ is the average fraction of impervious area in the *i*th order catchment.

Lee and Yen (1997) showed that the continuity equation and simplified momentum equation for the kinematic wave overland flow plane may be written:

$$\frac{\partial h_{oi}}{\partial t} + \frac{\partial q_{oi}}{\partial x} = q_L \tag{6}$$

$$q_{oi} = \alpha_{oi} h_{oi}^{\ m} \tag{7}$$

where t is time, x is the flow direction, q_{oi} is the ith order overland flow discharge per unit width, m is a constant, α_{oi} is a parameter reflecting the hydraulic characteristics of the overland flow, h_{oi} is the overland flow depth in ith order plane, and q_L is the lateral flow rate joining the main conduit. For a rectangular plane the constant m can be recognized as 5/3 and the coefficient α_o may be derived from Manning's equation:

$$\alpha_{oi} = \frac{\overline{S}_{oi}^{\ 1/2}}{n_o} \tag{8}$$

where $\overline{S}_{oi}$ is the mean ith order overland slope and n_o is the Manning's roughness coefficient for the overland plane.

Flow over the plane will increase until equilibrium is reached and the longest time for a raindrop to travel through the ith overland plane, T_{xoi}, is the time to reach equilibrium (Wooding 1965):

$$T_{xoi} = \left(\frac{n_o \overline{L}_{oi}}{\overline{S}_{oi}^{\ 1/2} q_L^{\ m-1}} \right)^{1/m} \tag{9}$$

Equation (9) applies for a single overland plane. In this model, flow from the pervious area flows over the impervious area before reaching the conduit. Consequently the longest time for a rain drop to travel is a function of where the rain drop falls. For rain that fall on the impervious portion of the overland flow plane directly, the travel time

is given by Eq.(9) with n_o, $L_{oi\,i}, S_{oi}$ and q_L equal to $n_{o,imp}$, $L_{oi,imp\,i}, S_{oi,imp}$ and $q_{L,imp}$, respectively.

For a rain drop that falls on a pervious area there is a travel time associated with flow over the pervious plane itself as well as the impervious plane. For flow over the pervious plane, travel time is given by Eq. (9) with n_o, $L_{oi\,i}, S_{oi}$ and q_L equal to $n_{o,perv}$, $L_{oi,perv\,i}, S_{oi,perv}$ and $q_{L,perv}$, respectively.

The time for flow from the pervious area over the impervious area is given by:

$$T_{xoi,pervimp}(t) = \left(\frac{n_{o,imp}\overline{L}_{oi,imp}}{\overline{S}_{oi}^{\,1/2}\left(\frac{1-imp_i}{imp_i}q_{L,perv}(t)\right)^{m-1}} \right)^{1/m} \tag{10}$$

Conduit Flow

The total discharge entering an *i*th order pipe from the average *i*th-order overland area includes flow from both the pervious and impervious overland flow planes and is given by:

$$q_{LTi}(t) = q_{L,perv}(t)\overline{L}_{oi,perv} + q_{L,imp}(t)\overline{L}_{oi,imp} \tag{11}$$

Therefore the continuity and simplified momentum equation for the conduit flow are:

$$\frac{\partial A_i}{\partial t} + \frac{\partial Q_{ci}(t)}{\partial x} = q_{LTi}(t) \tag{12}$$

$$Q_{ci}(t) = \alpha_{ci} h_{ci}^{\,m}(t) \tag{13}$$

where Q_{ci} is the ith order conduit discharge, m is a constant, α_{ci} is a parameter reflecting the hydraulic characteristics of the conduit flow, and h_{ci} is the flow depth in the ith order conduit,. For a circular conduit, Wong and Zhou (2003) found that the constant m can be taken as 5/4 and the coefficient α_c may be derived from Manning's equation:

$$\alpha_{ci} = 0.744\frac{\overline{D}_i^{\,1/6}\overline{S}_{ci}^{\,1/2}}{n_c} \tag{14}$$

where $\overline{D}_i$ is the mean ith order conduit diameter, $\overline{S}_{oi}$ is the mean ith order conduit slope and n_c is the manning's roughness coefficient for the conduit.

For a first order channel flow is only conveyed from the overland flow planes and as such the flow depth in the channel, h_{cs1}, is given by:

$$h_{cs1}(t) = \left(\frac{q_{LT1}(t)\overline{L}_{c1}}{\alpha_{c1}} \right)^{1/m} \tag{15}$$

Unlike the open channel flow in natural channels, there is good possibility that the closed conduits encountered in urban conduits will become pressurized. If a conduit becomes pressurized, i.e. $h_{csi} > \bar{D}_i$, then the travel time in a first order conduit is given by:

$$T_{xci}(t) = \frac{\pi \bar{D}_i 2}{4 q_{LTi}(t)} \tag{16}$$

If the conduit does not become pressurized then the travel time in the first-order conduit is given by Wooding (1965):

$$T_{xc1}(t) = \frac{B_1(t) h_{cs1}(t)}{q_{LT1}(t)} \tag{17}$$

For circular conduits, $B_i(t)$ is given by:

$$B_i(t) = \frac{\bar{D}_i}{2} \frac{\left(1 - \cos 2 \arccos\left(1 - \frac{2h_{ci}(t)}{\bar{D}_i}\right)\right)}{\sqrt{1 - \left(1 - \frac{2h_{ci}(t)}{\bar{D}_i}\right)^2}} \tag{18}$$

For higher order channels, the discharge from upstream conduits must be considered. Yen and Lee (1997) found that the water depth at the entrance of an ith (i>1) order conduit is given by:

$$h_{coi}(t) = \left(\frac{q_L^*(t)\left(N_i \bar{A}_i - A P_{OAi}\right)}{\alpha_{c1} N_i} \right)^{1/m} \tag{19}$$

In an urban catchment with overland flow comprising both pervious and impervious flow plains, q_L^* in Eq. (19) is given by:

$$q_L^*(t) = q_{L,perv}(t)\, imp_i + q_{L,imp}(t)\left(1 - imp_i\right) \tag{20}$$

If the flow in the conduit becomes pressurized, i.e. $h_{coi} > \bar{D}_i$, then the travel time in the conduit for an ith order conduit, $T_{xci}(t)$, is given by Eq. (16), where $q_{LTi}(t)$ is given by:

$$q_{LTi}(t) = \frac{\alpha_{ci} {h_{coi}}^m(t)}{\bar{L}_{ci}} \tag{21}$$

If the conduit does not become pressurized then the travel time in the conduit for an ith order conduit, $T_{xci}(t)$, is given by Yen and Lee (1997):

$$T_{xci}(t) = \frac{B_i(t)}{q_{LTi}(t)} \left[\left({h_{coi}}^m(t) + \frac{q_{LTi}(t) \bar{L}_{ci}}{\alpha_{ci}} \right)^{1/m} - h_{coi}(t) \right] \tag{22}$$

Structure of Geomorphic Instantaneous Unit Hydrograph

In an urban watershed rainfall excess occurs randomly over the watershed following a path through an overland flow region to subsequent conduits and eventually to an outlet. As such, an integration of the rainfall excess along all the possible paths in the watershed will yield the outflow hydrograph. The GIUH concept, as originally defined by Rodriguez-Iturbe and Valdes (1979) is reliant on the watershed being ordered according to the Strahler ordering procedure:

1. Channels that originate at a source are defined to be first order channels.
2. When two channels of order *i* join, a channel of order *i+1* is created.
3. When two channels of different order join, the channel segment immediately downstream has the higher of the orders of the two combining channels.

An example of a 3rd order Strahler urban network of conduits is provided in Figure 2. Based on such an ordering scheme a watershed of order Ω can be divided into different states. Overland flow regions are denoted by x_{oi} and conduits by x_{ci}, where $i = 1, 2, ..., \Omega$. Each raindrop (of excess rainfall) falling within the catchment will first fall on an overland region. The order of the region is defined by the order of the conduit receiving the runoff from the overland region. Within this overland region, the rain may fall on either a pervious or impervious overland flow region. If the raindrop falls on an impervious region it is assumed to then pass directly into a conduit, whereas if the raindrop falls on a pervious region it is assumed to travel onto an impervious overland region of the same order before entering the conduit. This unique representation allows for a probabilistic representation of the network geometry by its channel order rather than simulating the overland surfaces and channels individually according to their actual geometry, which is what is done in deterministic modeling.

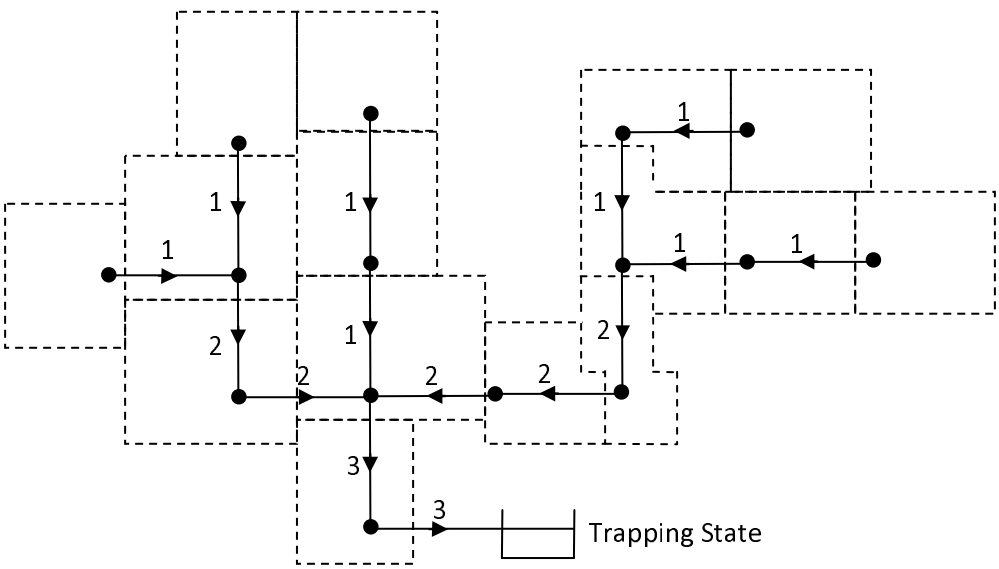

Figure 2 Third order network with Strahler ordering system.

According to the original formation of the GIUH by Rodriguez-Iturbe and Valdes (1979), the travel of a drop is governed by the following rules; (i) when the drop is still in the overland phase, the state is the order of the stream to which the land drains directly; (ii) the only possible transitions out of a state are to a state of a higher order. Under such a formulation the possibility of a rain drop traveling from a pervious region to impervious region is ignored, as is the possibility of a raindrop flowing from one first order channel into another first order channel. Unlike natural catchments the likelihood of a raindrop flowing from a first order conduit into another first order conduit of a different geometry is relatively high and as such must be accounted for. Thus if w denotes a specified path $x_{oi,perv} \rightarrow x_{oi,pervimp} \rightarrow x_i \rightarrow x_j \rightarrow ... \rightarrow x_\Omega$, the probability for a raindrop adopting this path can be expressed as:

$$P(w) = P_{OAi} \cdot P_{x_{oi,perv}x_{oi,imp}} \cdot P_{x_{oi}x_{ci}} \cdot P_{x_{ci}x_{cj}} \cdots P_{x_{ci}x_{c\Omega}} \tag{23}$$

where $i = 1, 2, ..., \Omega$ and $i \le j \le \Omega$, P_{OAi} is probability that a drop of excess rainfall will fall on an ith-order overland region (initial state probability), $P_{x_{oi,perv}x_{oi,imp}}$ is the transitional probability of a raindrop traveling from a pervious region to an impervious region which is equal to the perviousness of the *i*th order overland region, $P_{x_{oi}x_{ci}}$ is the transition probability of a raindrop moving from an ith order overland region to an ith order channel and is equal to unity, and $P_{x_{ci}x_{cj}}$ is the transition probability of a raindrop moving from an *i*th-order conduit to a *j*th-order conduit.

In the literature (Lee and Yen 1997, Kirshen and Bras 1982, etc.) formulations exist for determining intital state probability and transition probability based on the number of channels in each order, N_i, and the average area contributing to an ith-order channel, $\overline{A}_i$. As part of this investigation it was determined that such formulations could not be so readily applied in urban catchments. As such these terms were derived from their physical meanings using an algorithm developed in ArcGIS:

$$P_{OAi} = \frac{\left(\text{total area draining directly into conduits of order i}\right)}{\left(\text{total basin area}\right)} \tag{24}$$

$$P_{x_{ci}x_{cj}} = \frac{\left(\text{number of conduits of order i draining into conduits of order j}\right)}{\left(\text{total number of conduits of order i}\right)} \tag{25}$$

To the best of the authors' knowledge, no study has attempted to apply the GIUH to catchments where the possibility of pipes transitioning from an *i*th-order pipe into another *i*th order pipe is significant. When transitions from an *i*th-order pipe into another *i*th order pipe are not accounted for the number of possible paths for a given order is discrete. For example, in a 5th order catchment there would be 16 (32 if you account for the transition from pervious to impervious overland flow) different possible flow paths that a raindrop could take. However, if you account for the possibility of a raindrop transitioning within a given order, the number of possible flow paths increases dramatically. A Monte-Carlo simulation was performed on a 5th order urban catchment in Chicago (as described in the Results section below) and it was found that the number of possible flow paths exceeded 50,000. This number is

highly dependant on the layout of the network itself. In that particular catchment it was possible for a raindrop to flow through 10 successive 1st order pipes, 13 successive 2nd order pipes, 20 successive 3rd order pipes, 43 successive 4th order pipes, and 10 successive 5th order pipes. To account for each of the 50,000 or more possible flow paths within the model would be intractable. As such the distribution of possible successive flow paths within an order *i* was used to generate a scaling factor for the travel time within the *i*th-order conduit. The scaling factor was taken to be the expected value from the distribution of the number of ith order pipes downstream of an ith order conduit. For example, in the catchment used in the example application of this method there are 472 first order pipes, of which 166 flow directly into conduits of higher order, 119 flow through two first order pipes before transitioning into a higher order conduit, 71 flow through three first order pipes before transitioning into a higher order conduit, etc. It was found that the expected value for the number of first order pipes through which a raindrop would travel before transitioning to a higher order conduit was 2.62. Accordingly then the travel time calculated from Equation (16) or (17) for a first-order conduit would be multiplied by 2.62, effectively lengthening the first order pipe to account for the possibility of a raindrop flowing through multiple first order pipes successively.

In Equations (9), (10), (16), (17),) and (22) above, the travel times for the different states in any path w were defined. Thus the total travel time of a raindrop moving through path w to the watershed outlet, $T_w(t)$, is given by:

$$T_w(t) = T_{x_{oi,perv}} + T_{x_{oi,pervimp}} + a_i T_{x_{ci}} + a_j T_{x_{cj}} + ... + a_\Omega T_{x_{c\Omega}} \quad (26)$$

where $a_i, a_j, ...a_\Omega$ represent the scaling factors accounting for transitions with a given order.

Unlike in deterministic modeling, where it is necessary to find the component travel times for every path in the watershed, the GIUH formulation estimates the travel time collectively and probabilistically for each state by assuming the travel times of different states in the watershed are statistically independent and $f_{x_k}(t)$ is the travel time probability-density-function in state x_k, with a mean value T_{x_k} (Yen and Lee 1997). Using these assumptions Equations (23) and (26) can be combined, for an instantaneous unit input, to yield the instantaneous unit hydrograph (IUH) of the watershed (Rodriguez-Iturbe and Valdes 1979):

$$u(t) = \sum_{w \in W} \left[f_{x_{oi,perv}}(t) * f_{x_{oi,pervimp}}(t) * f_{x_{ci}}(t) * f_{x_{cj}}(t) * ... * f_{x_{c\Omega}}(t) \right] \cdot P(w) \quad (27)$$

where $*$ denotes a convolution integral, and $w \in W$, W being the path space $W = \left\langle x_{oi,perv}, x_{oi,pervimp}, x_i, x_j, ..., x_\Omega \right\rangle$, $(i = 1, 2, ..., \Omega)$.

Many different forms of the travel time probability density function have been explored over the years by researchers. The two most commonly adopted distributions are the exponential and uniform distributions. In this model the travel time for both overland flow and conduit flow was assumed to follow an exponential

distribution with a mean travel time T_{x_k}. In this way the watershed is conceptualized as linear reservoirs in series and/or parallel (Gupta et al. 1980) and is written:

$$f_{x_k}(t) = \frac{1}{T_{x_k}} \exp\left(\frac{-t}{T_{x_k}}\right);\ \forall t \tag{28}$$

EXAMPLE APPLICATION OF MODEL

To demonstrate the application of the model to produce the runoff hydrograph of a given event for an urban catchment and to verify the model by comparison with observed data, a selected rainstorm for the CDS-51 catchment in the Village of Dolton, a southern suburb of Chicago, is presented as an example. This catchment captures storm and sanitary flows for the 341 ha service area contributing to drop shaft CDS51, which feeds the Calumet Tunnel and Reservoir Plan (TARP) system. This catchment was divided into 773 subcatchments collecting inflow from in excess of 800 inlets and feeding a pipe network of 775 pipes ranging in size from 150 mm (6") to 2150 mm (84"). Characteristics (diameter, pipe length, upstream and downstream invert) of the combined sewer network in CDS51 were obtained from the Village of Dolton sewer atlas developed in 1977. Subcatchments were delineated using contours developed from Cook County's LiDAR data, aerial photography and engineering judgment. Imperviousness, infiltration parameters and slope were all obtained from the high resolution synthetic urban watershed developed by Crosa (2008). Manning's roughness for the pervious and impervious overland flow regions were taken to be 0.015 and 0.20 respectively, while a value of 0.014 was used for the conduits. The Green-Ampt infiltration parameters were taken to be homogeneous for the catchment and were derived by taking the weighted average of the parameters throughout the catchment.

CDS-51 is a 5th order catchment and has the geomorphic parameters detailed in Table 1. For this catchment the majority of the required subcatchment and conduit data were available and as such the geomorphic parameters were obtained using all the available data. However, it is not necessary to use all of these data if they are not available. The parameters required for the model could be generated using a subset of the data or perhaps even parameters derived from nearby watersheds were such data available. This is one of the key advantages of this method and these hypotheses will be tested as research continues.

Table 1 Geomorphic data for CDS-51 catchment

Channel Order	N_i	A_i (ha)	L_{oi} (m)	S_{oi}	P_{OAi}	L_{ci} (m)	S_{ci}	D_i (mm)	a_i
1	472	1.04	34	0.0112	0.57	61	0.0061	326	2.62
2	176	4.75	42	0.0115	0.26	60	0.0039	438	5.12
3	60	14.98	27	0.0129	0.07	73	0.0020	704	5.68
4	51	95.90	41	0.0099	0.08	64	0.0014	1179	19.25
5	10	316.10	42	0.0107	0.02	85	0.0056	2073	5.50

The rainstorm used was generated by combining data from four nearby Illinois State Water Survey (ISWS) raingages and NEXRAD data from three nearby radars. The data were combined using a technique developed by Cello et al (2008). The rain storm occurred on the 25th April 2007 and resulting hourly rainfall hyetograph is presented in Figure 3. For brevity, tests of other rainstorms are not reported here.

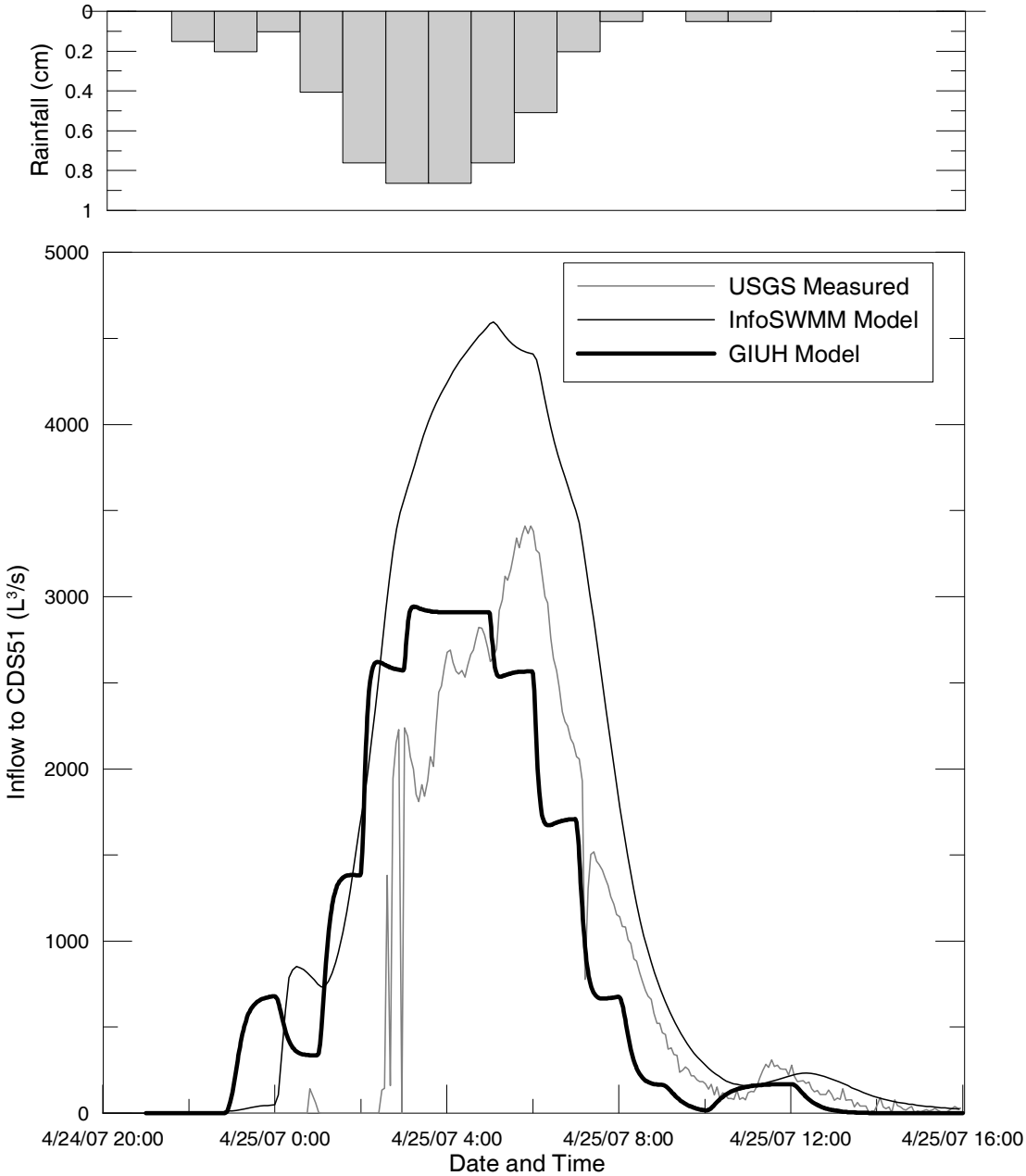

Figure 3 Hydrologic response of CDS-51 to 25th April 2007 storm

Using the input data described above the model was run for the 25th April 2007 storm and the resulting runoff hydrograph is presented in Figure 3. The hydrograph is compared to observed data collected by the USGS at the inflow pipe to drop shaft CDS-51 in the Calumet TARP system. In addition the hydrograph is compared to an

all-pipe InfoSWMM model that was analyzed by Cantone and Schmidt (1008). This model utilizes all of the input parameters available for each of the 773 subcatchments and 775 pipes in the watershed.

Figure 3 highlights that GIUH model is capable of reproducing the observed hydrologic response of CDS-51. The GIUH model predicts a similar volume of runoff, a peak runoff within 10% of the observed peak and shape that mirrors the observed.

CONCLUSIONS

A model, based on conduit ordering and the kinematic wave approximation for estimation of rainwater travel time, has been presented and shown capable of predicting hydrologic response in large urban catchments. This model calculates pervious excess rainfall using the physically based Green-Ampt method and computes travel time in both pervious and impervious overland flow regions, allowing flow to move from pervious to impervious regions prior to reaching a conduit. The model makes use of the known layout of the sewer network and utilizes geomorphic parameters to calculate rainwater travel time through circular conduits under free-surface and pressurized flow conditions. The estimation of travel time through conduits on any given path, allows for the possibility of successive travel in conduits of identical order. The methodology presented does not require runoff and rainfall data for calibration and has the potential to operate without a complete set of conduit and subcatchment input parameters. This work builds on GIUH concept developed by Rodriguez-Iturbe and Valdes (1979) representing the hydrologic response by convoluting a series of probability density functions of travel time.

The model proposed in this paper has large scope for improvement. First, the variability in Green-Ampt infiltration parameters as well as in geomorphic parameters must be explored. This variability can be used to explore different probability density functions for travel time and will account for the uncertainty in the hydrologic inputs. Second, this method must be tested to determine its applicability to catchments where input data are even more limited. This may include the use of only a sub-sample of data or, at the extreme, use of geomorphic parameters from an adjacent or similar urban watershed. Third, the present model only allows for overland flow from pervious to impervious regions but in the future could be adapted to allow flow from impervious to pervious areas. This flexibility would be particularly useful in simulating stormwater BMP's such as rain gardens. Finally, it is necessary to explore the impact of inlet structures on the hydrologic response of the catchment.

ACKNOWLEDGEMENTS

This research would not have been possible without ongoing funding and support from the Metropolitan Water Reclamation District of Greater Chicago as part of the University's work on Chicago's Tunnel and Reservoir Plan.

REFERENCES

Cantone, J.C. and Schmidt, A.R. (2008). "Potential Dangers of Simplifying Combined Sewer Hydrologic/Hydraulic Models.", *Journal of Hydrologic Engineering*, ASCE, Accepted 8th September 2008.

Cello, P.A., Catano, Y.A. and Snook, B.M. (2008). *NEXRAD derived rainfall data calibration for a monitored area in Cook County*, Unpublished draft report, Department of Civil and Environmental Engineering, University of Illinois at Urbana-Champaign.

Chow, V.T., Maidment, D.R., Mays, L.W. (1988). *Applied Hydrology*, McGraw-Hill Book Co., Singapore.

Crosa, C.S. (2008). *High Resolution Synthetic Urban Watershed Data for Hydrologic Model Evaluation*, Masters Thesis, Department of Civil and Environmental Engineering, University of Illinois at Urbana-Champaign.

Green, W.H. and Ampt, G.A. (1911). "Studies on soil physics, Part I, the flow of aire and water through soils", *Journal of Agricultural Science*, 4(1), 1-24.

Gupta, V.K., Waymire, e., and Wang, C.T. (1980). "A representation of an instantaneous unit hydrograph from geomorphology." *Water Resources Research*, 16(5), 855-862.

Jin, C-X. (1992) " A deterministic gamma-type geomorphologic instantaneous unit hydrograph based on path types." *Water Resources Research*, 28(2), 479-486.

Kirshen, D.M. and Bras, R.L. (1983). "The linear channel and its effect on the geomorphologic IUH.", Journal of Hydrology, 65, 175-208.

Lee, K.T. and Yen, B.C. (1997) "Geomorphology and kinematic-wave-based hydrograph derivation." *Journal of Hydraulic Engineering*, 123(1), 73-80.

Lhomme, J., Bouvier, C., and Perrin, J-L. (2004) "Applying a GIS-based geomorphological routing model in urban catchments." *Journal of Hydrology*, 299, 203-216.

Rawls, W.J., Brakensiek, D.L., and Miller, N. (1983). "Green-Ampt infiltration parameters from soils data.", *Journal of Hydraulic Division*, ASCE, 109(1), 62-70.

Rodriguez-Iturbe, I. and Valdes, J.B. (1979). "The geomorphologic structure of hydrologic response." *Water Resources Research*, 15(6), 1409-1420.

Rodriguez, F., Andrieu, H., and Creutin, J.D. (2003) "Surface runoff in urban catchments: morphological identification of unit hydrographs from urban databanks." *Journal of Hydrology*, 283, 146-168.

Rodriguez, F., Cudennec, C. and Andrieu, H. (2005) "Application of morphological approaches to determine unit hydrographs of urban catchments." *Hydrological Processes*, 19, 1021-1035.

Wong, T.S.W. and Zhou, M.C. (2003). "Kinematic wave parameters and time of travel in circular channel revisited." *Advances in Water Resources*, 26, 417-425
Wooding, R.A. (1965). "A hydraulic model for the catchment-stream problem." *Journal of Hydrology*, 3, 254-267.

Yen, B.C. and Lee, K.T. (1997) "Unit hydrograph derivation for ungauged watersheds by stream-order laws." *Journal of Hydrologic Engineering*, 2(1), 1-9.

Analysis of Bioretention Media Specifications and Relationships to Overall Performance

Sean W. O'Neill[1] and Allen P. Davis[1]

[1]Department of Civil and Environmental Engineering, University of Maryland, College Park, MD 20742; PH (301) 405-1958; FAX (301) 405-2585; email: apdavis@umd.edu

Abstract

Bioretention performance specifications differ greatly among jurisdictions. Selected specifications from Prince George's County, MD; MDE; Fairfax County, VA; VDCR; and DNREC are compared for hydrologic management effectiveness, pollutant removal efficiency, construction and maintenance costs, and constructability. Optimal construction and performance requirements are summarized, with the necessity of variable criteria for differing pollutants acknowledged. Specification recommendations are tailored accordingly. Shallow cells with a surface mulch layer are recommended for removal of metals and particulate pollutants. Deeper cells having thick vegetative cover instead of top dressing are recommended for nutrient removal. Additionally, aluminum water treatment residual as a media amendment for phosphorus removal is recommended. This combined with an anoxic saturated zone for nitrogen removal may prove ideal for combined nitrogen and phosphorus removal.

Introduction

Non-point source pollution continues today to be a challenge that needs addressing by engineers, scientists, and regulators. As development continues and the size of urban conurbations continues to increase, so do the associated impervious areas such as roads, parking lots, and roofs. Urban stormwater runoff and the concomitant flux of pollutants to surface water bodies is an especially pressing issue that requires attention. One technology, which also happens to be an EPA Best Management Practice (BMP), that is implemented as a means to reduce runoff pollution discharges is bioretention. Also known as biofiltration or rain gardens, these facilities are effectively shallow depressions filled with sandy media into which runoff is directed. This interception of runoff prevents direct stormwater migration to surface waterways, increases groundwater infiltration, and improves water quality.

Construction and performance specifications for bioretention cells vary markedly depending on the municipal body from which the standard originates. In this project the performance designs from five municipalities were evaluated: Maryland Department of the Environment (MDE); Prince George's County, Maryland Department of Environmental Resources (PGDER); Delaware Department of Natural Resources and Environmental Control (DNREC); Virginia Department of Conservation and Recreation (VDCR); and Fairfax County, Virginia Department of

Public Works and Environmental Services (DPWES). Parameters within the varying standards are compared to show their inconsistencies, as well as highlight optimal criteria leading to performance success as it relates to water quantity management, water quality improvement, reduced construction and maintenance costs, and constructability.

Literature Review

Bioretention has been shown to be a vibrant and viable technology with regard to its use as a means of mitigating stormwater pollution. The technology has been proven both in the field and the laboratory to efficiently mitigate peak flows, minimize surface discharge volumes, and effectively remove stormwater contaminants including heavy metals and nutrients, especially particulate bound.

Maintaining or returning a site's hydrology to a predevelopment state is one of the technology's major advantages. A high media hydraulic conductivity is integral to meeting this goal (Hsieh and Davis, 2005). Even in the harsh environment of the field, bioretention has shown marked improvement of site hydrology (Davis, 2008).

Excellent removal of particulate pollutants has also been shown, including total suspended solids (TSS); metals such as Pb, Cu, Zn, and Cd; and particulate phosphorus (P). In fact, work has shown that effective removal of particulates takes place in approximately the top 20 cm (8 in) of the bioretention media (Li and Davis, 2008a; 2008b). TSS is stopped via filtration mechanisms of the soil and mulch, as are particulate metals. In dissolved form, they will bind to organic matter (OM) such as the mulch top dressing and organics within the bioretention media (Davis et al., 2001).

The majority of P in stormwater is found in particulate form (MWCOG, 1983; Bratieres et al., 2008), which is removed by filtration just as other particulates. However, dissolved P (and nitrogen) is often leached from bioretention cells because of degradation of OM (Davis et al., 2006; Hsieh et al., 2007a; 2007b; Bratieres et al., 2008). Effective removal of nutrients has been observed through proper vegetative coverage (Bratieres et al., 2008; Read et al., 2008), as well as the establishment of an anoxic zone in the media for nitrogen (N) removal via denitrification (Kim et al., 2003; Hunt et al., 2006).

Specifications

Specifications for the design and construction of bioretention systems are inconsistent around the country. The focus of this study is on the Mid-Atlantic States of Maryland, Delaware, and Virginia. It should be noted that with regard to the hydrologic standards reviewed here, the criteria are performance criteria and not design criteria.

An originator for bioretention specifications, Prince George's County, Maryland developed the initial framework on which others built. A summary of relevant county performance guidelines may be found in Table 1. Minimum infiltration rate is 5.1 cm/hr (2 in/hr). Cell media depth is recommended as 76 cm (2.5 ft.); but may be reduced to 46 cm (1.5 ft.) if only shallow rooted plants are used, or increased up to 1.2 m (4 ft.) if trees and/or shrubs are planted. The surface mulch layer may be no more than 7.6 cm (3 in.) deep. The topsoil in the bioretention soil

mixture (BSM); although rated as a loam, sandy loam, or loamy sand (L/SL/LS) per USDA textural classification; must contain 5% or less of clay. The leaf compost component of the BSM is aged leaf mulch.

The Maryland Department of the Environment (MDE) specifies a facility infiltration rate of 1.3 cm/hr (0.52 in/hr) Facilities which cannot meet this requirement are mandated to have an underdrain; once having an underdrain installed, facilities become exempt of the minimum infiltration rate requirement. The BSM for MDE may be rated as a L/SL/LS per USDA; or SM, ML, or SC by the Unified Soil Classification System (USCS). BSM depth must be maintained between 76 and 122 cm (2.5 - 4 ft), with a surface mulch layer of 5.1 – 7.6 cm (3 - 4 in.) thickness. In addition to BSM textural requirements, the ambient soil in which the bioretention cell is situated must contain less than 20% clay and less than 40% silt and clay, which can severely limit siting. A summary of MDE bioretention specifications is found in Table 1.

Table 2 elucidates select bioretention specifications for Virginia facilities. They are required to have an infiltration rate between 1.3 and 21 cm/hr (0.52 - 8.3 in/hr). Media depth must be at least 76 cm (2.5 ft), and the completed facility should have a surface mulch layer of 5.1 to 7.6 cm (2 - 3 in) depth. Alternatively, 70-80% herbaceous plant ground cover may be used instead of a surface mulch layer.

Fairfax County, Virginia, maintains the VDCR infiltration rates, but has augmented drain time requirements as seen in Table 2. Interestingly, underdrains are required on all facilities except those situated on lots containing only single family homes that are not part of a subdivision. The BSM must have a depth of at least 76 cm (2.5 ft), although this is increased to 1.22 m (4 ft) when large trees and/or shrubs are planted. The BSM composition calls for organic compost, which has strict specifications, including: having 50-60% organic matter, a moisture content of 40-50%, and stability as measured by CO_2 evolution of 0-4 mg CO_2-C per g organic matter per day.

The DNREC has promulgated design standards for the state of Delaware, as seen in Table 3. They stipulate a minimum infiltration rate of at least 2.6 cm/hr (1.0 in/hr). Media depth needs to be between 91 and 122 cm (3 - 4 ft). The mulch surface layer is optional in DNREC specifications, but if applied is designated to be between 5.1 and 7.6 cm (3 - 4 in) in depth.

Criteria for Success & Universal BSM

The ultimate goal of any bioretention construction and performance specification is to stipulate limiting requirements needing to be met, which will provide for proper and optimal performance of the structure while minimizing all associated costs. With this in mind, the primary recommendation herein is to accommodate variable construction requirements for the removal of target pollutants. While ideally all contaminants will be removed with a single design, to achieve maximum efficiency this is not practical.

Optimal drain times and infiltration rates for water quantity management and quality improvement are best determined on a situational basis based on local conditions and pollutants of concern. Current standards, however, set limits for facilities which are reasonable, ascertainable, and ultimately lead to rapid water throughput. This allows for runoff control and increased groundwater infiltration, as

well as preventing standing water which may attract disease vectors such as mosquitoes.

Many jurisdictions allow for bioretention cells to be constructed with underdrains which connect directly to municipal stormwater sewers. These devices can reduce the infiltration benefits of bioretention, and add to construction costs. However, underdrains also allow for increased flow rates and drawdown times, and are oftentimes required, such as the MDE requirement when the minimum infiltration rate of 1.3 cm/hr (0.52 in/hr) cannot be attained. Prince George's and Fairfax Counties also require underdrains on facilities situated in certain land use areas: the former on residential plots and sites with infiltration rates less than 2.5 cm/hr (1.0 in/hr); the latter on all sites except single family homes not part of a neighborhood development. This is meant to safeguard against possible flooding which may cause property damage, and has nothing to do with improving facility performance.

The majority of regulations require a media depth of approximately 76 cm (2.5 ft). However, some of the specifications allow for alterations to this range depending on the plantings in the facility. Prince George's County allows the depth to be reduced to 46 cm (1.5 ft) in the event of shallow plants. And both Prince George's and Fairfax Counties increase their minimum to 1.2 m (4 ft) when trees or shrubs are planted. Regulators may want to extrapolate this concept to allow installation of more shallow facilities in areas where dissolved contaminants are not of concern. Evidence suggests that the removal of particulate contaminants including TSS and metals occurs in only the top 10 to 20 cm (8 – 16 in) of media (Li and Davis 2008). Ultimately, a depth of 46 to 91 cm (1.5 - 3 ft) will provide for toxics/metals removal while minimizing construction cost.

Resent research shows that greater infiltration and evapotranspiration for bioretention facilities occurs with increasing maximum depth of cells, especially over 0.9 m (3 feet; Li et al., 2009). Considering this, bioretention facility designers must compromise between the reduced cost of shallow facilities and the improved infiltration and hydraulic performance of deeper ones.

Additionally, a mulch layer on the surface may be ideal to further sorb metals and prevent media clogging by particulates. Minimal OM is necessary in the BSM, as the top dressing and filtration action of the media should be sufficient for metals removal. To provide for plant growth, OM content of 1.5-4% in the final mixture should be sufficient while minimizing nutrient leaching. Additionally, some metals (i.e., Cu) may strongly bind to OM which may become dissolved, leading to leaching from the facility (Li and Davis, 2008). This provides for additional reasoning to reduce unnecessary OM addition to the BSM.

The surface mulch layer provides moisture retention in the BSM, necessary to support plant growth in such sandy media during prolonged dry periods. However, it is detrimental to nutrient removal. Therefore, for nutrient removal cells the top dressing may be replaced with vigorous herbaceous plant growth, such as that specified in the Virginia state specifications. This will not only remove a source of nutrient leaching, but sufficiently thick plant growth will provide adequate shade to retain media moisture, much the same as the top dressing. Additionally, the plants will act as a sink for N and P, contributing to the efficiency of the cell.

Concerning media depth with regard to nutrient removal, sufficient vegetative plant coverage will lead to increased nutrient uptake through plant roots. In fact, while plant coverage is vitally important to effective bioretention N and P removal, it is also strongly affected by variations in plant species (Read et al., 2008; Bratieres et al., 2008). Also, nutrient reduction in bioretention is thought to be best modeled by a first order kinetic decay model, where with increasing travel time or distance through the cell the concentration moves towards a background concentration (Bratieres et al., 2008). Hence, increased media depth will result in concurrent increased nutrient removal. Therefore, the predominant design recommendations in such instances should be vigorous vegetative coverage and sufficient media depth counterbalanced by construction cost.

Consideration should also be given to the installation of upturned underdrains for subrhizomal N treatment anoxic zones (Kim et al., 2003; Dietz and Clausen, 2006; Hunt et al., 2006). This will add to the cost of the facility, but is a viable means of N removal. It should be noted that when utilizing the technology in bioretention facilities, OM as a carbon source for microbes will be needed in the BSM. Ideally, this will be a material which has a high carbon to nutrient ratio (C:N:P). In this way, microbes will utilize the carbon from the OM amendment and the nutrients from the inflowing stormwater, and the nutrient removal capacity of the cell will not be sacrificed. To date, only limited inclusion of this option into specifications has occurred.

In the case of particulate or nutrient removal, the issue of ideal BSM must be addressed. As increased infiltration relative to native soil is of primary concern in most cases, a large proportion of sand is necessary to impart a large hydraulic conductivity and act as a filtering media. Topsoil is necessary to provide nutrients and other qualities for plant growth. Clay and silt content should be kept low, as they limit the ability of water to infiltrate freely. OM, while beneficial for both plant growth and metal sorption, can lead to nutrient leaching.

Ultimately, a final BSM will ideally contain approximately 50-60% construction sand and 40-50% L/SL/LS topsoil on a per volume basis. Clay content of the BSM must be minimized to maintain proper cell hydrology, ideally less than 5-8%. As mentioned above, no additional OM will be necessary in either of the targeted pollutant cases (metals and particulates vis-à-vis nutrients) with the exception of N removal by means of an upturned underdrain. One may note that the mixture ratio of sand and soil is designated on a per volume basis. While many jurisdictions specify mixture on a per weight basis, this is impractical in the field and leads to increased costs. Mixing of the final BSM on a per volume basis allows this activity to occur on site by contractors, providing for increased constructability and therefore reduced cost through fewer labor hours.

Lastly is the consideration of BSM soil amendments for pollutant removal. This has been touched on slightly in consideration of OM as a component of the BSM, and deemed unnecessary for metal removal but essential for N removal via the biological nitrification/denitrification pathway. Consideration has been given as well to P fixation with soil amendments. Coal combustion fly ash has been used in bioretention to immobilize P and has shown excellent removal (Zhang et al., 2008). However, such fly ash is highly alkaline and is not expected to perform optimally

over the long term. It is believed that, given the acidic nature of soils and stormwater on the east coast of the United States, aluminum-based drinking water treatment residual (Al-WTR) is a more viable option. The active component, aluminum (hydr)oxide, is expected to work ideally in the pH range encountered in eastern bioretention facilities, and will remain insoluble and bind P even under reducing conditions found in anoxic environments. Al-WTR utilized as an amendment in conjunction with an anoxic denitrification zone is hypothesized to be an ideal combination for effective and versatile nutrient removal in bioretention facilities.

References

Bratieres, K., Fletcher, T. D., Deletic, A., Zinger, Y. (2008). "Nutrient and sediment removal by stormwater biofilters: A large-scale design optimisation study." *Water Res.,* 42(14), 3930-3940.

Davis, A. P. (2008). "Field performance of bioretention: Hydrology impacts." *J. Hydrol. Eng.*, ASCE, 13(2), 90-95.

Davis, A. P., Shokouhian, M., Sharma, H., Minami, C. (2001). "Laboratory study of biological retention for urban stormwater management." *Water Environ. Res.*, 73(5), 5-14.

Davis, A. P., Shokouhian, M., Sharma, H., Minami, C. (2006). "Water quality improvement through bioretention media: Nitrogen and phosphorus removal." *Water Environ. Res.*, 78(3), 284-293.

Dietz, M. E., Clausen, J. C. (2006). "Saturation to improve pollutant retention in a rain garden." *Environ. Sci. Technol.,* 40(4), 1335-1340.

Hsieh, C. H., Davis, A. P. (2005). "Evaluation and optimization of bioretention media for treatment of urban storm water runoff." *J. Environ. Eng.,* ASCE, 131(11), 1521-1531.

Hsieh, C. H., Davis, A. P., Needelman, B. A. (2007a). "Bioretention column studies of phosphorus removal from urban stormwater runoff." *Water Environ. Res.,* 79(2), 177-184.

Hsieh, C. H., Davis, A. P., Needelman, B. A. (2007b). "Nitrogen removal from urban stormwater runoff through layered bioretention columns." *Water Environ. Res.,* 79(12), 2404-2411.

Hunt, W. F., Jarrett, A. R., Smith, J. T., Sharkey, L. J. (2006). "Evaluating bioretention hydrology and nutrient removal at three field sites in North Carolina." *J. Irrig. Drain. Eng*., ASCE, 132(6), 600-608.

Kim, H., Seagren, E.A., Davis, A.P. (2003). "Engineered bioretention for removal of nitrate from stormwater runoff." *Water Environ. Res.*, 75, 355-367.

Li, H., Davis, A. P. (2008a). "Heavy metal capture and accumulation in bioretention media." *Environ. Sci. Technol.*, 42(14), 5247-5253.

Li, H., Davis, A. P. (2008b). "Urban particle capture in bioretention media. I: Laboratory and field studies." *J. Environ. Eng.*, ASCE, 134(6), 409-418.

Li, H., Davis, A. P., Sharkey, L., Hunt, W. (2009). "Mitigation of impervious surface hydrology using bioretention in North Carolina and Maryland." *In press*.

Metropolitan Washington Council of Governments (MWCOG). (1983). *Pollutant removal capability of urban best management practices in the Washington Metropolitan Area: Final report*, Washington, DC.

Read, J., Wevill, T., Fletcher, T. D., Deletic, A. (2008). "Variation among plant species in pollutant removal from stormwater in biofiltration systems." *Water Res.,* 42, 893-902.

Zhang, W., Brown, G. O., Storm, D. E., Zhang, H. (2008). "Fly-ash-amended sand as filter media in bioretention cells to improve phosphorus removal." *Water Environ. Res.*, 80(6), 507-516.

Table 1. Summary of selected bioretention specifications for Prince George's County and Maryland.

	Prince George's Co., MD DER	Maryland MDE
Drain time, max	48 hr No surface water ponding 3-4 hrs after storm event	48 hr
Infiltration rate, min	5.1 cm/hr	1.3 cm/hr [2] None [3]
Media depth, min/max	76 cm / None specified Min. depth 46 cm when using only shallow rooted plants Min. depth 1.2 m when planting trees/shrubs	76 cm / 1.2 m
Mandatory underdrain?	Yes, on residential sites and sites with infiltration rates < 2.5 cm/hr	Yes, when infiltration rate ≤ 1.3 cm/hr
Top dressing	Max. 7.6 cm mulch Aged ≥ 12 months	5.1 - 7.6 cm mulch Triple-shredded hardwood mulch aged 6 - 12 months
BSM composition	50 - 60% † Sand 20 - 30% † Leaf compost 20 - 30% † Topsoil [4] ↳ ≤ 5 % Clay	35 - 60% † Sand 30 - 55% † Silt 10 - 25% † Clay
Organic Matter	1.5 - 3.0%	1.5 - 4.0% ‡

Table 2. Summary of selected bioretention specifications for Virginia and Fairfax County.

	Virginia DCR	Fairfax Co., VA DPWES
Drain time, max	48 hr	48 hr WQ_V[1] must drain within 24 hrs; Entire facility must drain 48 hrs after WQ_V capture
Infiltration rate, min	1.3 cm/hr max: 21 cm/hr	1.3 cm/hr
Media depth, min/max	76 cm / None specified	76 cm / None specified Min. depth 1.2 m when planting trees/shrubs
Mandatory underdrain?	No	Yes, except on individual single-family detached residential lots that are not part of a bonded subdivision
Top dressing	5.1 - 7.6 cm mulch Well aged shredded hardwood or hardwood chips Alternatively, 70 - 80% herbaceous ground cover	5.1 - 7.6 cm mulch Double shredded hardwood aged 6 - 12 months
BSM composition	50% Sand 30% Leaf compost 20% Topsoil [4] ↳ ≤ 5 % Clay	60 - 75% Sand 5 - 15% Organic compost 10 - 35% Topsoil [4] ↳ ≤ 8 % Clay
Organic Matter	> 1.5%	≥ 1.5% ‡

Table 3. Summary of selected bioretention specifications for Delaware.

	Delaware DNREC
Drain time, max	48 hr Recommended min.: 24 hr No surface water ponding 24 hrs after the end of the 24 hr 5.1 cm (2.0") design storm
Infiltration rate, min	2.6 cm/hr
Media depth, min/max	91 cm / 1.2 m
Mandatory underdrain?	No
Top dressing	Optional; 5.1 - 7.6 cm mulch Triple-shredded aged hardwood
BSM composition	33% † Sand 33% † Sphagnum peat moss 33% † Triple-shredded hardwood mulch
Organic Matter	None specified
	† Per volume basis ‡ Per weight basis 1 Water quality volume: Volume of the facility needed per unit surface area to adequately treat incomir water; specifically defined in county specifications 2 Facilities without underdrains 3 Facilities with underdrains 4 Loam, Sandy loam, or Loamy sand per USDA soil textural classification

Analyzing the Impacts of a Retrofit Detention Basin Flow Control Strategy on Biodiversity in an Urban Stream System.

Natalie A. Postel, P.E., Member ASCE[1], Christine A. Pomeroy, Ph.D., P.E., Member ASCE[2], Tom A. Jacobs, P.E., Member ASCE[3], and Elangovan Karuppasamy, P.E.[4]

[1] CDM, 9200 Ward Parkway, Suite 500, Kansas City, Missouri 64114; PH (816) 444-8270; e-mail: Postelna@cdm.com

[2] Department of Civil and Environmental Engineering, University of Utah, 122 S. Central Campus Drive Room 104, Salt Lake City, UT 84112; PH (801) 585-7300; e-mail: Christine.Pomeroy@utah.edu

[3] City of Lenexa, Kansas, 12350 West 87th Street Parkway, Lenexa, Kansas 66215; PH (913) 477-7680; e-mail: TomAJacobs@ci.lenexa.ks.us

[4] CDM, 9200 Ward Parkway, Suite 500, Kansas City, Missouri 64114; PH (816) 444-8270; e-mail: Karuppasamye@cdm.com

Abstract

Protecting biological diversity of a stream system while supporting development and growth is critical to sustainability. To this end, the City of Lenexa, Kansas has embarked on the Eastern Lenexa Detention Study. The study focuses on 1017 acres (1.6 sq. mi.) of Little Mill Creek watershed in Lenexa, Kansas, a Kansas City suburb. Little Mill Creek drains to Mill Creek, which is listed as an impaired water body under section 303(d) of the Clean Water Act. Water quality impairment parameters include chloride, fecal coliform bacteria, and biology.

This study examined whether modifying 16 existing detention basins to capture and detain smaller storm events would significantly increase biological diversity and reduce erosion potential within Little Mill Creek. The study used biological data and discharge measurements collected at 11 sites within and near Little Mill Creek to develop linkages among hydrologic and biologic metrics.

Computer modeling showed that retrofit of the study area basins, which control only 30% of the watershed, did not change the hydrology in the stream reach sufficiently to expect an increase in biological diversity. Although not quantified by this study, pollutant removal from retrofit implementation is expected to have a positive impact on biological diversity. Controlling a larger percentage of the watershed is expected to show more significant increases in biologic diversity.

Introduction

Protecting biological diversity of a stream, while supporting development and growth, is critical to sustainability. To this end, the City of Lenexa, Kansas has embarked on the Eastern Lenexa Detention Study. The study focuses on 1017 acres (1.6 sq. mi.) of Little Mill Creek Watershed in Lenexa, Kansas, a Kansas City suburb. The Little Mill Creek Watershed is nearly 90 percent developed. Eleven percent of the study area has commercial/institutional land use; 56 percent is in residential use;

the remainder has mixed land use. Little Mill Creek drains to Mill Creek; the Kansas Department of Health and Environment lists Mill Creek as an impaired water body on the Clean Water Act 303(d) list. Chloride, fecal coliform bacteria, and biology have been identified as water quality impairment parameters in the Mill Creek watershed.

The study examined whether modifying 16 existing detention basins controlling 30 percent of the drainage area to capture and detain smaller storm events would increase biological integrity and reduce erosion potential along Little Mill Creek. To make this determination, a continuous simulation model of the watershed was created using the Environmental Protection Agency's (EPA) Stormwater Management Model (SWMM 5). The model was calibrated using rainfall and continuous stream stage information within the watershed. After calibration, the detention basin retrofit projects were incorporated into the model to simulate the impacts on in-stream flows. The resulting changes in in-stream flows were used to infer changes in stream biodiversity.

Methods

Using 2007 Water Environment Research Foundation (WERF) Protocols for Studying Wet Weather Impacts and Urbanization Patterns (Pomeroy *et al.*, 2008) as a guide, macro-invertebrate and discharge data were used to develop linkages among hydrologic and biologic metrics specific to Little Mill Creek watershed. Macro-invertebrate samples were collected at five locations within Johnson County, Kansas, and three locations within Little Mill Creek watershed (Figure 1). Samples were compared to hydrologic metrics derived from measured discharge values for United States Geological Survey (USGS) gage locations outside Little Mill Creek Watershed. Simulated discharge values from the Little Mill Creek SWMM model were used to develop hydrologic metrics for Little Mill Creek and compare them to the biologic metrics at the same location. The SWMM model was then used to simulate the retrofit of 16 detention basins within the study area to include a 40-hour drawdown of the water quality volume (WQv). The results of the proposed SWMM analysis were used to estimate the impact of the retrofits on in-stream biology.

Watershed Characteristics and Hydrologic Modeling

The study area is located in Lenexa, Kansas. It is a sub-basin within Little Mill Creek watershed. Average annual precipitation is 38.5 inches. The following scenarios were examined in this study:

- **Existing without Detention**: In this scenario all sub-basins in the pilot study area are developed with existing land use. Existing detention basins were not modeled in this scenario.

- **Existing with Detention**: Existing detention basins with existing land use are included in this scenario.

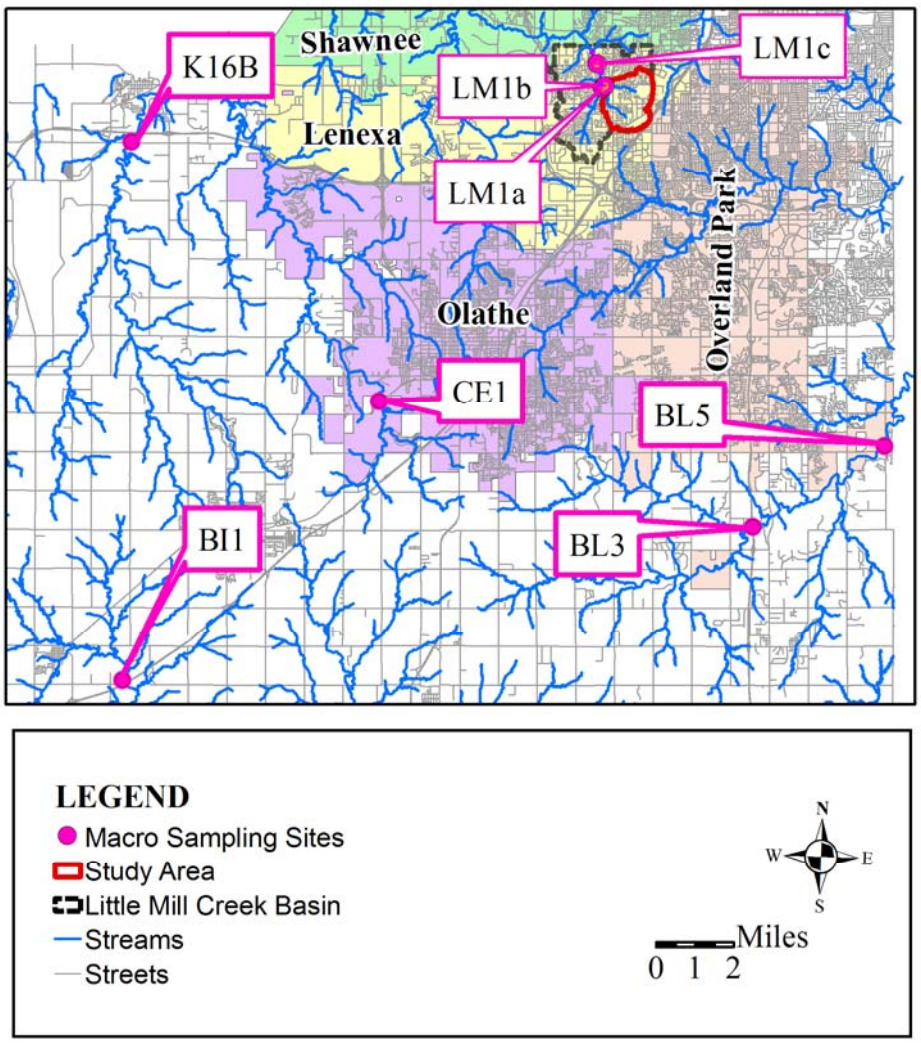

Figure 1 - ELDS Sampling Locations

- **Proposed**: In this scenario retrofits of 16 existing detention basins within the study area are simulated. The retrofit projects incorporate the control of the WQv released over 40-hours. All retrofits were designed to maintain flood control performance for the one percent annual chance event that is achieved in the previous detention scenario.

In Lenexa, Kansas, the WQv is computed as the product of the 90 percent rainfall depth and a runoff factor based on percent imperviousness. The WQv was calculated using the method described in the Manual for Best Management Practices for Stormwater Quality (MARC/APWA 2008) using the following equation:

$$WQv = P*Rv$$

Where WQv = water quality volume (computed as inches across the watershed, the volume is then determined by multiplying the result of this equation by the watershed

area); P = depth of rainfall event for the Kansas City area (1.37 inches) and the Rv (volumetric runoff coefficient) is defined using

$Rv = 0.05 + 0.009*I$

Where I is percent imperviousness.

Computation of Hydrologic Metrics

Studies have shown that the $T_{0.5}$ hydrologic metric is a strong predictor of biotic richness (Booth et al., 2004; Pomeroy et al., 2008). The $T_{0.5}$ metric is the percent of time that the flow is greater than the peak flow of the 0.5-year storm, and is an indicator of stream flashiness. A higher $T_{0.5}$ value indicates that a stream is less flashy than a stream with a lower $T_{0.5}$ value because the length of time the discharge is above the peak flow of the 0.5-year storm is longer. The 0.5-year storm is defined from a partial duration series of flows. By plotting the $T_{0.5}$ and the biologic metric at particular location, a relationship can be drawn between in-stream hydrology and biologic richness.

$T_{0.5}$ was calculated for the locations where macroinvertebrate sampling was performed (Table 3). Measured flow data were used where available. For locations without measured flow data, results from a calibrated continuous simulation hydrologic model were used to estimate the $T_{0.5}$.

The period of flow record from October 2003 to September 2005 was used to calculate $T_{0.5}$ for sites BI1, CE1, BL5, BL3 and K16b. The continuous SWMM model was run for the same period using the existing with-detention scenario and the resulting flows were analyzed to generate $T_{0.5}$ at LM1c, LM1a, LM1b.

Computation of Biologic Metrics

Macro-invertebrate samples were collected during spring and summer 2007 by USGS at eight locations within and near the study area (Figure 1). Data analysis included computations of the Kansas Biotic Index (KBI; Huggins and Moffett, 1988). KBI is a pollution tolerance index used to categorize the macroinvertebrate assemblage's tolerance to organic pollution. Using taxa-specific tolerance values, this index evaluates the tolerance of the macroinvertebrate assemblage to the effects of nutrient and oxygen demanding pollutants. A higher index indicates a community more tolerant of organic pollution exerting oxygen demands in the stream setting.

Tolerance values for the KBI analysis were primarily derived from Table D-1 of *Procedures for Sampling Macroinvertebrates as part of the City of Lenexa Stream Monitoring Plan* (Watershed Institute, Inc.). For a few taxa (*Prostoma*, *Crangonyx*, and *Hyallela*) tolerance values were developed using average regional values from Appendix B of the EPA document, *Rapid Bioassessment Protocols for Use in Streams and Wadeable Rivers: Periphyton, Benthic Macroinvertebrates, and Fish*, Second Edition (2003). Within the family Chironomidae, it was assumed that all taxa would be classified as "non-red," except the genus *Chironomus*.

KBI classifies macroinvertebrate assemblages using the rating scale provided in Table 2.

The formula used to calculate KBI is:

$$\mathbf{KBI = \Sigma(x_i * t_i)/n}$$

x_i = number of individuals within the taxon
t_i = tolerance value of the taxon
n = total number of organisms in the sample

The KBI analyses yielded consistent results. The three Little Mill Creek sampling sites have ratings of "Moderate Impact" (KBI scores of 2.8 – 2.9) from nutrient and oxygen demanding pollutants (Table 3).

Table 2. KBI rating scale

KBI RATING SCALE[1]	
KBI Score	**Rating[2]**
≤ 1.50	No Impact
1.51 – 2.50	Slight Impact
2.51 – 3.50	Moderate Impact
≥ 3.51	High Impact

[1] Adapted from Table 10, Huggins and Moffett (1988)
[2] Impact from nutrient and oxygen demanding pollutants

Table 3 KBI for Macro Sampling Sites

Site ID	Site Name	KBI
BI1	Big Bull C Nr Edgerton, KS	2.2
CE1	Cedar C at Hwy 56 at Olathe, KS	2.3
MI4	Mill C at 87th St Nr Lenexa, KS	3.0
BL5	Blue R at Kenneth Rd, Overland Park, KS	2.0
BL3	Blue R Nr Stanley, KS	2.1
K16b	Kill C at 95th St Nr Desoto, KS	2.4
LM1c	Little Mill C at 79th Street	3.0
LM1a	Little Mill C at 84th Street	3.0
LM1b	Little Mill Trib at 83rd Street	2.9

Results

Linear regression can be used to correlate $T_{0.5}$ and KBI. Figure 2 shows the linear regression of the KBI and $T_{0.5}$ hydrologic metrics. The data show good correlation between $T_{0.5}$ and KBI with an r-squared of 0.78. The regression line in Figure 2 can be used to estimate the response to biologic diversity with changes in stream hydrology. The $T_{0.5}$ at location LM1b Little Mill Tributary at 83rd Street for the proposed conditions scenario was plotted in Figure 2 to indicate the biologic response to changes in hydrology. The proposed conditions $T_{0.5}$ did not change significantly from the existing with detention scenario $T_{0.5}$.

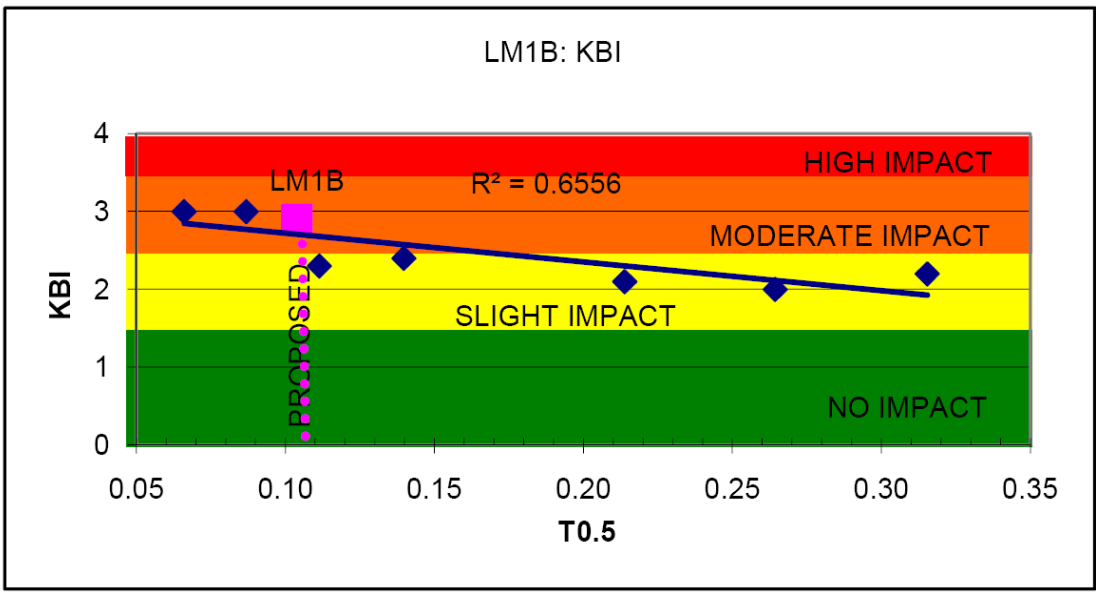

Figure 2 $T_{0.5}$ versus KBI

Conclusions

Regression equations were used to estimate the impact of in-stream biological diversity with changing flow regimes. An increase in $T_{0.5}$ is related to an increase in biological diversity. Many other factors besides hydrology can affect biologic diversity in a stream system, including pollutants and stream bed substrate. Therefore, even if a desired $T_{0.5}$ is reached, biologic diversity may still not be present due to these other factors.

The proposed $T_{0.5}$ showed little change from the existing value, indicating the proposed retrofit projects are not expected to make a large impact on the stream biology from a hydrologic perspective. However, capturing the water quality volume and releasing it between 24 and 48 hours has been reported to remove total suspended solid loads by as much as 80 percent (Debo and Reese, 2003). Therefore, the proposed retrofits should reduce pollutant loads to the stream, improving stream ecology and the aquatic environment.

One possible reason for the small response to hydrology is that only 30% of the area tributary to the reach analyzed is controlled by retrofits. If a larger percentage of the tributary area were controlled to the same degree, a larger positive impact to the $T_{0.5}$ would be expected. The extent of watershed control needed to produce the desired results is not known.

References

Booth, D.B., Karr, J.R., Schauman, S., Konrad, C.P., Morley, S.A., Larson, M.G., and Burger, S.J (2004). Reviving Urban Streams: Land Use, Hydrology, Biology, and Human Behavior. *Journal of the American Water Resources Association* 40(5):1351-1364.

Debo, T.N., and A.J. Reese (2003). *Municipal Stormwater Management, Second Edition*, Lewis Publishers.

Environmental Protection Agency. (2003). *Rapid Bioassessment Protocols for Use in Streams and Wadeable Rivers: Periphyton, Benthic Macroinvertebrates, and Fish, Second Edition.*

Huggins, D.G. & M.F. Moffett (1988). "Proposed biotic and habitat indices for use in Kansas streams." Kansas Biological Survey. Lawrence, Kansas. Report no. 35.

Mid-America Regional Council and American Public Works Association Kansas City Metropolitan Chapter (2008). *Manual of Best Management Practices For Stormwater Quality*.

Pomeroy, C.A., Roesner, L.A., Coleman, J.C., and E. Rankin (2008). *Protocols for Studying Wet Weather Impacts and Urbanization Patterns*, Water Environment Research Foundation, Alexandria, VA.

Watershed Institute, Inc. *Procedures for Sampling Macroinvertebrates as Part of the City of Lenexa Stream Monitoring Plan.*

Are Rational C Values Too Low?

By C. B. Young[1], B. M. McEnroe[2], and A. C. Rome[3]

[1]Dept. of Civil, Environmental, and Architectural Engineering, University of Kansas, 1530 W. 15th St. Rm. 2150, Lawrence, KS 66045; PH (785) 864-2999; FAX (785) 864-5631; e-mail: cbyoung@ku.edu
[2]Dept. of Civil, Environmental, and Architectural Engineering, University of Kansas, 1530 W. 15th St. Rm. 2150, Lawrence, KS 66045; PH (785) 864-2925, FAX (785) 864-5631; e-mail: mcenroe@ku.edu
[3]Wilson & Company, Inc., 8735 Rosehill Road, Suite 200, Lenexa, KS 66215

ABSTRACT

This paper presents empirically derived estimates of the Rational C runoff coefficient for rural watersheds in Kansas. The C values vary with location (there is an east-west trend) and recurrence interval. The C values derived for western Kansas are in line with values commonly assumed for rural watersheds. However, the C values computed for eastern Kansas are much higher than the values found in many hydrology textbooks and design guidelines. The median Rational C values for the watersheds in eastern Kansas are 0.32, 0.63, and 0.97 for the 2-, 10-, and 100-year recurrence intervals.

INTRODUCTION

Over 150 years since its original description, the Rational equation is still widely used by engineers to size drainage structures. Although its use is typically restricted to small watersheds, the Rational method has been used to design billions of dollars worth of drainage infrastructure including storm sewer systems, culverts, and small bridges. The fact that the Rational method has endured as a design methodology caused Yen (1992) to question whether the method persists because it is fundamentally sound, or because the field of hydrology has simply not progressed.

A companion paper in these proceedings (Young et al. 2009) compares the accuracy of the Rational method with regional flood frequency equations. Regional flood frequency equations are often favored over the Rational method for larger, ungaged watersheds. Young et al. (2009) demonstrate that the Rational equation outperforms USGS-style regional flood frequency equations for watersheds up to 30 mi^2 – as long as appropriate values of the Rational C are selected.

The real question, then, is what Rational C values are appropriate? An informal review of hydrology textbooks and design guidelines reveals that most published Rational C values can be traced back to a 1969 sanitary and stormwater sewer design manual produced jointly by ASCE and the Water Pollution Control Federation

(WPCF 1969). Interestingly, the WPCF (1969) manual does not provide justification for the Rational C values selected.

There have been a few research studies that have estimated Rational C values for watersheds. Schaake et al. (1967) used data for twenty small watersheds in the Baltimore, Maryland area to estimate Rational C values. These watersheds were all small (less than 150 acres) and urban in nature. French et al. (1974) carried out a large study of Rational C values in New South Wales, Australia. Rational C values were estimated for 37 watersheds, ranging in size up to 250 km^2. Hotchkiss and Provaznik (1995) estimated Rational C values for 24 rural watersheds in south-central Nebraska. The results for these three studies are discussed along with the findings of this study.

The objective of this study was to establish appropriate Rational C values for rural watersheds in Kansas with drainage areas up to 30 mi^2. A dataset consisting of 72 gaged, rural watersheds was used to compute Rational C values for various recurrence intervals.

Data and Methodology

The Rational equation is commonly written as

$$Q_T = C \cdot i \cdot A \tag{1}$$

where Q_T is the peak discharge for recurrence interval T, C is the Rational runoff coefficient, i is the rainfall intensity, and A is the watershed area. The rainfall intensity is selected for the recurrence interval of interest and for a duration equal to the watershed time of concentration, t_c. The time of concentration is defined as the length of time it would take for water to travel from the most remote point in the watershed to the watershed outlet.

Once Q_T, i, and A are known for a particular watershed, the Rational C value for a particular recurrence interval can be backed out of Eq. 1 using the following relation:

$$C = \frac{Q_T}{i \cdot A} \tag{2}$$

The objective of this study was to determine Rational C values appropriate for rural watersheds in Kansas. As such, a dataset of Q_T, i, and A values was established for 72 gaged, rural watersheds. Figure 1 shows the location of the watersheds used for this study, along with contours of mean annual precipitation (MAP). The watersheds selected for this study all have drainage areas less than 30 mi^2 and streamgage records longer than 20 years.

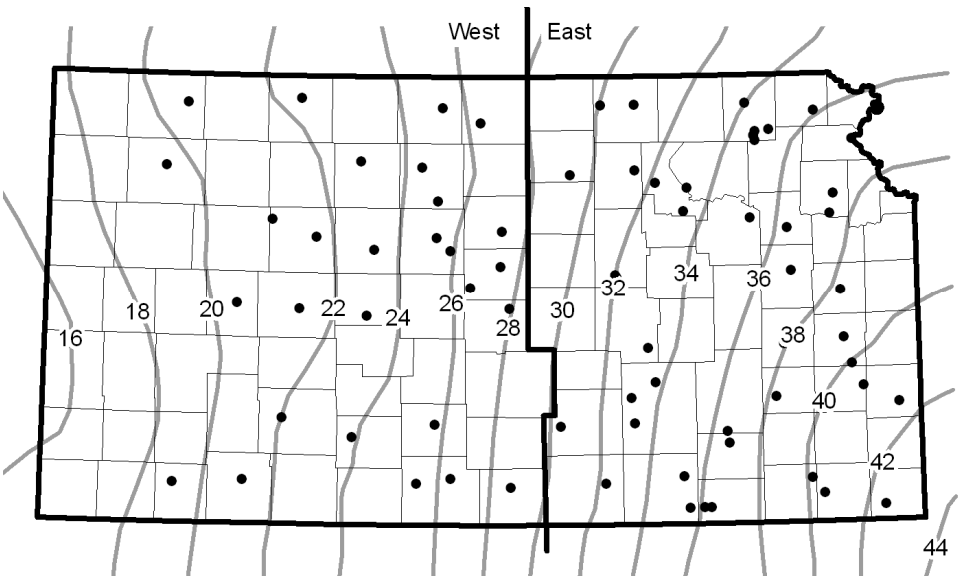

Figure 1. Watershed Locations and Mean Annual Precipitation (in)

Flood frequency analysis was performed according to Bulletin 17B methods for each of the 72 gage records to estimate the flood quantiles (Q_T) for each watershed (Flynn et al. 2006). The drainage areas for each location were determined from digital versions of the USGS 7.5-minute topographic maps. The time of concentration for each watershed was estimated using the following equation for rural streams in Kansas:

$$t_C = 0.0368\left(\frac{L}{\sqrt{S}}\right)^{0.66} \tag{3}$$

where L is the length of the main channel from the outlet to the draingage divide (in ft), and S is the slope of the main channel (in ft/ft) measured between points that are 10% and 85% of the way upstream from the outlet, and t_c is in minutes. This equation for t_c was developed using observed rainfall and streamflow data for nineteen small rural watersheds in Kansas (McEnroe and Zhao 1999). The channel lengths and slopes were measured for each watershed from USGS topographic maps.

Point rainfall intensities for each of the watersheds were selected from the KDOT rainfall tables, which were compiled using data from the National Weather Service (NWS) *Technical Memorandum HYDRO-35* (Frederick et al. 1977) for durations less than or equal to one hour, and from the U.S. Weather Bureau's *Technical Paper No. 40* (Hershfield 1961) for durations in excess of one hour. The point rainfall intensities were extracted for recurrence intervals of 2, 5, 10, 25, 50, and 100 years. These rainfall values were converted to area-rainfall intensities using the point-to-area conversion employed in the U. S. Army Corps of Engineers hydrologic modeling software (Hydrologic Engineering Center 1998).

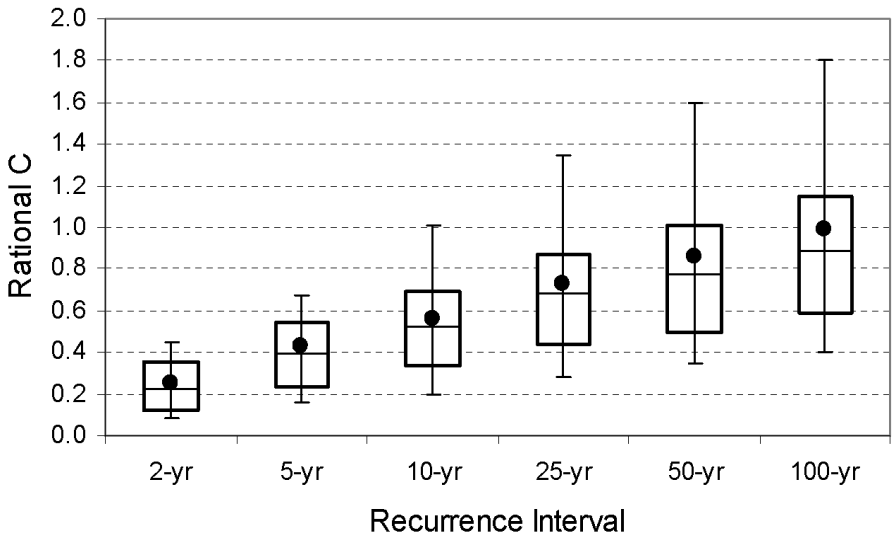

Figure 2. Distribution of Rational C Values for the 72 Watersheds.

RESULTS

Equation 2 was used to compute Rational C values for each watershed for recurrence intervals of 2, 5, 10, 25, 50, and 100 years. Figure 2 presents box-and-whisker plots of the Rational C values plotted versus recurrence interval. The boxes in Figure 2 mark the 25th, 50th, and 75th percentiles, the whiskers mark the 10th and 90th percentiles, and the dots mark the average Rational C value for the 72 watersheds. Table 1 presents summary statistics for the Rational C values.

Table 1. Summary Statistics for Rational C Values for All 72 Stations

Recurrence Interval (years)	Mean	Median	Standard Deviation
2	0.25	0.23	0.15
5	0.43	0.39	0.24
10	0.56	0.53	0.31
25	0.73	0.68	0.42
50	0.86	0.77	0.52
100	0.99	0.89	0.62

It is clear that there is tremendous variability in the Rational C values estimated in this study. Some of this variability is due to uncertainty in the estimate of C for each watershed and recurrence interval, and some of the variability likely results from differences in watershed characteristics.

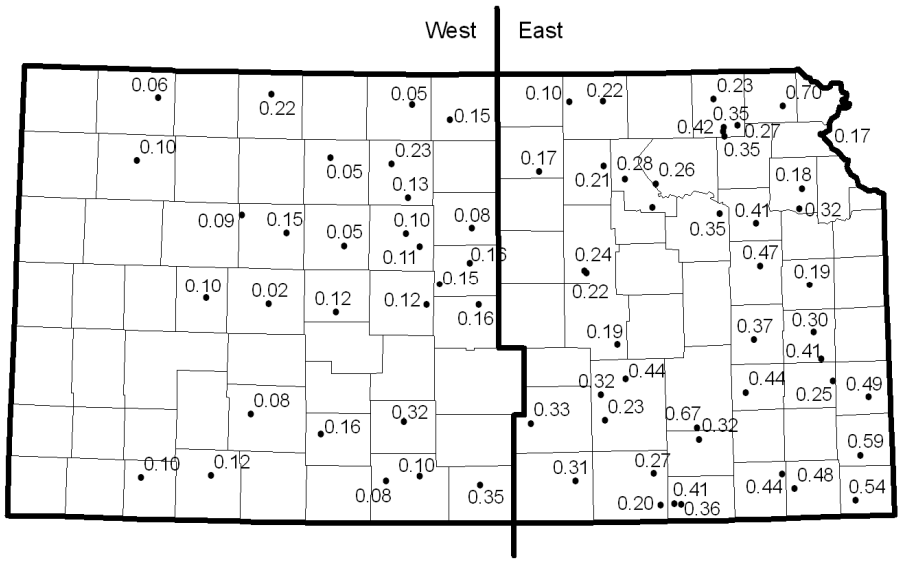

Figure 3. Rational C Values for 2-Year Recurrence Interval

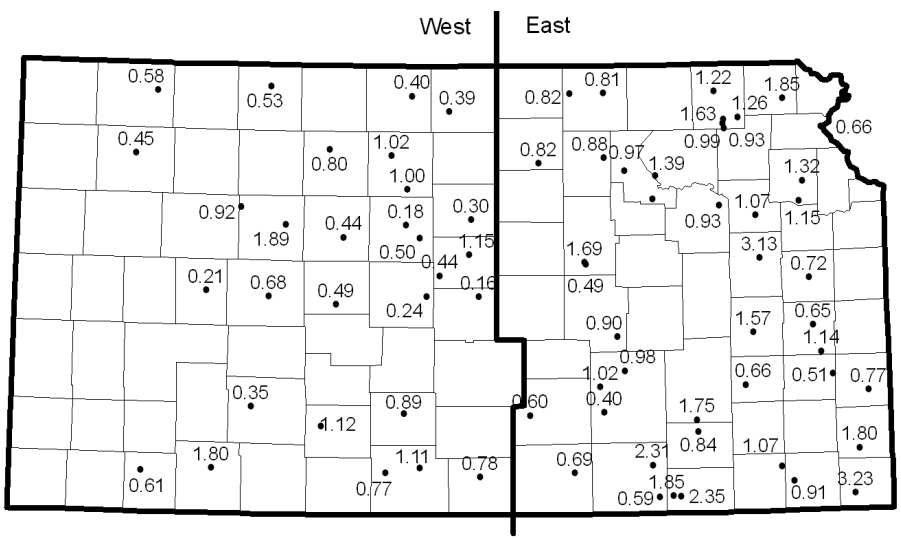

Figure 4. Rational C Values for 100-Year Recurrence Interval

Figures 3 and 4 map out the 2- and 100-year Rational C values. These two figures show a noticeable east-west trend in the Rational C values. In general, Rational C values are higher in eastern Kansas and lower in the western regions of the state. This is likely caused by two main factors. Figure 1 shows the pattern of mean annual precipitation for the state. Rainfall ranges from less than 16 in/yr at the western edge of the state up to nearly 44 in/yr in the southeastern corner. Soil permeability also varies across the state. The eastern half of the state has a mix of NRCS hydrologic soil types B, C, and D. The western half of the state is predominantly hydrologic soil

type B. As such, the eastern portion of the state experiences more rainfall, with lower soil infiltration rates, while western Kansas has higher soil permeability and less rainfall.

Figure 5 shows the median Rational C values for the entire 72-watershed dataset, along with the median values for eastern and western Kansas. As noted in previous studies, the Rational C values increase with recurrence interval.

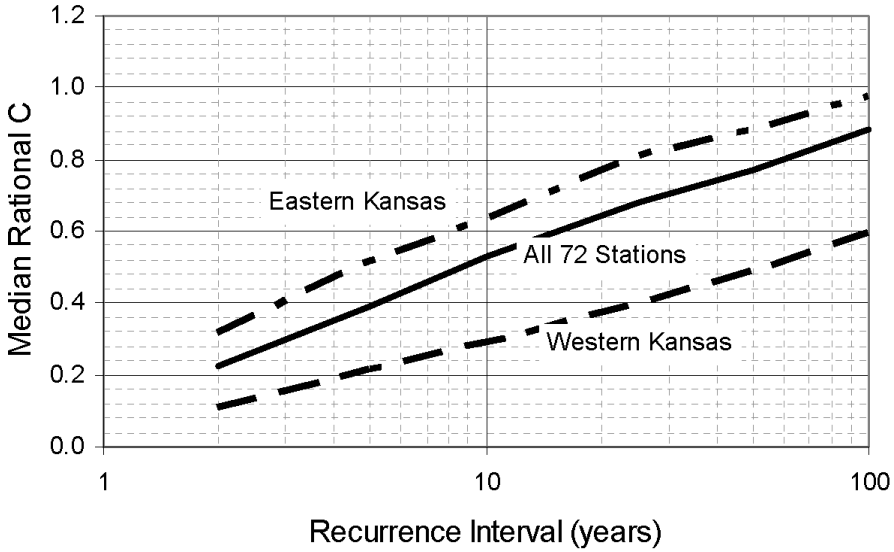

Figure 5. Median Rational C Values vs. Recurrence Interval

DISCUSSION AND CONCLUSIONS

Many modern hydrology textbooks and design guidelines present the Rational C values originally published in WPCF (1969). For unimproved (rural) watersheds, WPCF (1969) recommends a C value of 0.1 for the 2-year recurrence interval and a C value of 0.3 for the 10-year recurrence interval. Based on the results of this study, the C values published in WPCF (1969) appear to be appropriate for western Kansas, but are much too small for use in eastern Kansas. In fact, the Rational C values for eastern Kansas are more than double those recommended in WPCF (1969).

The Rational C values established in this research exhibit greater dependence on the recurrence interval than typically assumed. The ratio of the 100-year to the 10-year C value is 1.68 for all 72 stations, 2.07 for western Kansas, and 1.54 for eastern Kansas. In contrast, Gupta (2001) recommends a ratio of 1.25 for these two recurrence interval.

The findings of this research raise the question of whether the Rational C values currently used for design are too low. This study found the median C value for the 100-year discharge in eastern Kansas to be 0.97. Very few design engineers would

use a Rational C value near 1.0 for a rural watershed – no matter what the recurrence interval.

Other studies have also found Rational C values higher than typically assumed. French (1974) mapped out Rational C values for rural watersheds in New South Wales, Australia. Their findings, reproduced in the *Handbook of Hydrology* (Pilgrim 1993), show Rational C values of over 1.0 for the 10-year recurrence interval on the eastern edge of the study area. C values for the more arid inland areas trend down to 0.1 for the 10-year storm. Hotchkiss and Provaznik (1995) computed Rational C values for 24 rural watersheds in south-central Nebraska. Their C values for the 10-year recurrence interval ranged from about 0.2 to 0.8, with mean C values approximately 20% higher than the WPCF (1969) value.

The Rational C values presented in this paper are based on the analysis of a large number of rural watersheds in Kansas. The results should not be applied to urban watersheds, or to watersheds outside of the study area. However, the findings indicate that conventional wisdom regarding Rational C values may be wrong, and may lead to undersized hydraulic structure. It is critical that engineers examine the basis for Rational C values used in design. Further research should be carried out to establish appropriate values for other areas in the United States. Particular attention should be paid to urban watersheds, where the Rational method is most commonly applied.

ACKNOWLEDGEMENTS

This work was funded by the Kansas Department of Transportation under K-TRAN grant KU-06-4. James Richardson, P.E., of KDOT served as project monitor. This gratefully acknowledged.

REFERENCES

Flynn, K. M., Kirby, W. H., and Hummel, P. R. (2006). *User's Manual for Program PeakFQ, Annual Flood-Frequency Analysis using Bulleting 17B Guidelines,* U. S. Geological Survey.

Frederick, R. H., Myers, V. A., and Auciello, E. P. (1977). *Five- to 60-Minute Precipitation Frequency for the Eastern and Central United States,* NOAA Technical Memorandum NWS HYDRO-35, National Weather Service, U.S. Dept. of Commerce, Washington, D.C.

French, R., Pilgrim, D. H., and Laurenson, E. M. (1974). "Experimental Examination of the Rational Method for Small Rural Catchments." *Civil Engineering Transactions*, The Institution of Engineers, Australia, CE16(2), 95-102.

Gupta, R. S. (2001). *Hydrology and Hydraulic Systems*, 2nd Ed., Prentice-Hall Inc., Engelwood Cliffs, N.J.

Hershfield, D. M. (1961). *Rainfall Frequency Atlas of the United States for Durations from 30 Minutes to 24 Hours and Return Periods from 1 to 100 Years*, Technical Paper No. 40, Weather Bureau, U.S. Dept. of Commerce, Washington, D.C.

Hotchkiss, R. H., and Provaznik, M. K. (1995). "Observations on the Rational Method C Value." *Watershed Management: Planning for the 21st Century*, T. J. Ward, ed., ASCE, New York, 21-26.

Hydrologic Engineering Center (1998). *HEC-1 Flood Hydrograph Package User's Manual*, Report CPD-1A, U. S. Army Corps of Engineers.

McEnroe, B. M., and Zhao, H. (1999). *Lag Times and Peak Coefficients for Rural Watersheds in Kansas*, Kansas Department of Transportation Report No. K-TRAN: KU-98-1.

Pilgrim, D. H., and Cordery, I. (1993). "Flood Runoff." *Handbook of Hydrology*, D. R. Maidment, ed., McGraw-Hill, New York, 9.1-9.42.

Schaake, J. C., Geyer, J. C., and Knapp, J. W. (1967). "Experimental Examination of the Rational Method." *Journal of the Hydraulics Division*, 93(6), 353-370.

Yen, B. C. (1992). "Preface." *Catchment Runoff and Rational Formula*, B. C. Yen, ed., Water Resources Publications, Littleton, Colorado, iii-iv.

Water Pollution Control Federation (1969). *Design and Construction of Sanitary and Storm Sewers*, prepared by a Joint Committee of ASCE and WPCF.

Young, C. B., McEnroe, B. M., and Rome, A. C. (2009). "Regional Regression Analysis and the Rational Method." *Proceedings: World Environmental & Water Resources Congress 2009*, May 17-21, Kansas City, Missouri.

Assessing Hydrodynamic Separators under High Water Flow Conditions

David Saddoris – Graduate Research Assistant, Department of Civil Engineering, University of Minnesota
2 Third Avenue SE
Minneapolis, MN 55414
Phone 612-396-3472
Fax 612-624-4398
saddo002@umn.edu

Omid Mohseni – Adjunct Associate Professor, Department of Civil Engineering, University of Minnesota
2 Third Avenue SE
Minneapolis, MN 55414
Phone 952-832-2665
Fax 612-624-4398
omohseni@umn.edu

John Gulliver – Professor, Department of Civil Engineering, University of Minnesota
122 Civil Engineering Building
500 Pillsbury Drive SE
Minneapolis, MN 55455
Phone 612-625-4080
Fax 612-626-7750
gulli003@umn.edu

Abstract
Underground hydrodynamic separators are widely used in urban areas for removal of suspended solids and floatables from stormwater due to limited land availability for the installation of above ground stormwater best management practices (BMPs). Hydrodynamic separators are sized for applications based on design runoff from the drainage basins that they serve. However, during less frequent storm events, device maximum treatment rates are exceeded and previously captured sediments can be scoured and washed out of these devices. A methodology has been developed to assess sediment retention in hydrodynamic separators under water flow rates exceeding their maximum design treatment rates. This new testing protocol has been used in controlled field and laboratory tests on full-scale commercial devices under high water flow conditions to determine sediment retention performance. Application of this work is primarily to establish the frequency of required cleaning for installed devices.

Background

Hydrodynamic separators are used as best management practices (BMPs) in urban areas for removing contaminants from stormwater. These underground devices are attractive in areas where land is at a premium because of their small footprint. Hydrodynamic separators are flow-through devices used as pre-treatment in a multi-BMP treatment train or as stand-alone BMPs. Water either enters these devices tangentially, thus creating a swirl, or plunges into the main sump. Hydrodynamic separators may be single or multiple sump devices. They have no moving parts and rely on flowing water as their source of energy, so they require no power. Hydrodynamic separators principally function as enhanced settling devices and commonly include a mechanism for capture of floatable solids and liquids. This paper addresses non-floatable solid capture and retention in hydrodynamic separators.

There are two important criteria to consider when determining the overall performance of hydrodynamic separators: 1) their efficiency in removing contaminants under treatment flow conditions and 2) their ability to retain accumulated solids under high flow conditions. Hydrodynamic separators are sized based on the runoff from the drainage basins they serve. As most rainfall events result in flow rates less than the maximum treatment rates for the installed devices, removal efficiency under treatment rates is an important parameter for assessing the performance of these devices. However, during less frequent storm events, maximum design treatment rates are exceeded, and previously captured solids can be subject to scouring, resuspension and washout from these devices.

Historically, monitoring programs have been used to assess the performance of hydrodynamic separators. Monitoring offers the advantage of assessing the performance of BMPs under a wide range of actual hydraulic and pollutant loading conditions for a given drainage basin (Wilson *et al.,* 2009). However, monitoring is limited by the accuracy of sample collection strategies as well as the magnitude and frequency of storm events. In addition, due to the many uncontrolled variables in actual runoff events, it is difficult to use the results of a monitoring study to estimate a device's performance under different flow and sediment particle size conditions than were tested. As a result, new protocols for testing the performance and sediment retention of hydrodynamic separators utilizing controlled field and laboratory testing have been developed.

Performance Testing

Controlled field testing was performed on four commercial devices (Wilson *et al.*, 2009) and laboratory testing was performed on three devices (Carlson et al., 2006; Mohseni and Fyten, 2008; Fyten and Mohseni, 2009) using a range of flow rates and sediment sizes to determine suspended sediment removal efficiencies and develop non-dimensional performance functions. Test procedures, analysis and results from performance testing can be found in the references.

Sediment Retention Testing

The net removal of contaminants by hydrodynamic separators is a function of their performance at capturing pollutants under design storm events and their ability to retain previously captured sediments during high flow events. In hydrodynamic separators two processes cause the wash out of deposited sediments: 1) scouring and resuspension of deposited sediments and 2) turbulence in the sump which overcomes the resettling of resuspended sediments, dispersing them upward to the outlet of the device.

A new methodology has been developed to assess sediment resuspension and washout in hydrodynamic separators under flow rates exceeding their design maximum design treatment rates. The test methodology follows as Procedure 1.

Procedure 1: Sediment Retention Testing Procedure

Procedure:

1) Drain and clean the device
2) Pre-load the device with sediments of known particle sizes
3) Measure the amount of sediments in the device
4) Flow water for a set time duration at rates above device maximum design treatment rates
5) Measure the amount of sediments remaining in the device
6) Determine the sediments washed out via mass balance

Procedure 1 has been applied in the testing of three full scale commercial devices: 1) an Environment21 V2B1 Model 4 in the field and in the laboratory by the authors, 2) a Stormceptor STC 1200 in the laboratory by the authors and 3) an ecoStorm Model 3 in the laboratory (Mohseni and Fyten, 2008).

Environment21 V2B1 – Field Testing

An in-service Environment 21 V2B1 Model 4 was tested in the field in 2007 using Procedure 1. Before and after water flow, a trowel was used to flatten and level the surface of the deposit and a 2 foot level was used to check if the deposit was truly level. After leveling, two methods were used to determine the amount of the sediment in the V2B1 device: 1) A ruler measuring the depth of the sediment to the floor of the device and 2) A laser range finder measuring the distance between the top of the sediment and the ceiling of the device.

Method 1: A standard metal ruler stick was used to measure the depth of the sediment at 18 locations in the device. The same 18 locations were used for each sediment level measurement, and the 18 readings were averaged to obtain average sediment depths.

Method 2: A Hilti Model PD 30 laser range finder was used to measure the distance from the top of the sediment to the ceiling of the device. This laser range finder device has a published accuracy of $\pm 1/16^{th}$ inch over its entire measurement range of 660 feet. A custom bracket was fabricated, and the laser range finder was securely

fastened in the bracket. The bracket incorporates a bubble level. Figure 1 shows the laser range finder with the attached bracket and level.



Figure 1: Laser range finder with bracket and level

The laser range finder was used to measure the distances between the top of the sediment and the ceiling of the device at 28 marked locations. To take a reading, the laser range finder bracket was placed on top of the sediment and positioned until the bracket was level and the laser beam was on target on the mark on the ceiling for the respective reading. Prior to the first test, readings were taken when the device was empty to determine the distances between the floor of the device and the ceiling of the device at each of the 28 points. The depth of sediment at each point was determined by subtracting the distance between the top of the sediment and the ceiling from the distance between the floor and the ceiling of the device. The 28 sediment depths were averaged to obtain the average sediment depth.

The two sediment measurement methods had an average variation in sediment reading of 0.23 cm, a maximum variation of 1.0 cm and a standard deviation of 0.40 cm.

Six tests were conducted in the summer (“Initial Tests”), followed by six duplicate tests in the fall (“Repeat Tests”). These first twelve tests utilized US Silica F110

gradation and two final tests were conducted using AGSCO 70-100 gradation. US Silica F110 and AGSCO 70-100 are commercial silica sand gradations with specific gravities of 2.5. US Silica F110 has a d_{50} of 120 µm, a d_{15} of 80µm and a d_{85} of 170µm. AGSCO 70-100 has a d_{50} of 200 µm, a d_{15} of 120 µm and a d_{85} of 280 µm. Sediment was added to the device prior to each test so that the starting sediment level was approximately six inches. The tests were conducted with water supplied from a fire hydrant, which had water temperatures ranging from 14 to 18 degrees Celsius. The test durations ranged from 30 to 120 minutes. The results of the fourteen retention tests are shown in Figure 2.

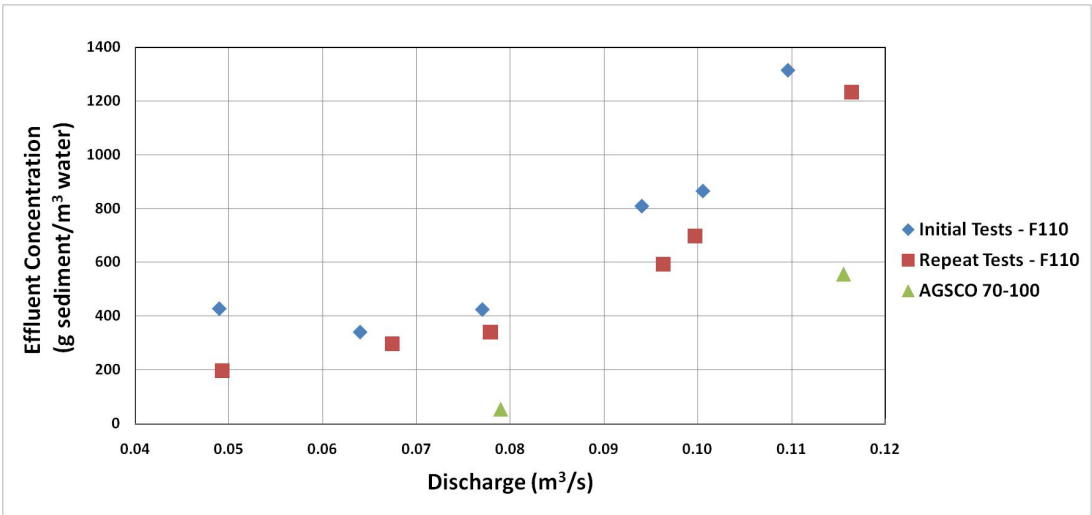

Figure 2: Sediment retention field testing – Environment 21 V2B1 Model 4 (Saddoris et al., 2009)

As anticipated, the larger AGSCO 70:100 sand was better retained than the US Silica F110. Larger particles are less likely to scour, and the larger particles that have been resuspended are more likely to resettle due to their higher settling velocities.

The F110 repeat tests, which were conducted later in the year with lower temperature water, demonstrated higher sediment retention. As water temperature drops its viscosity increases. The effect of water temperature and viscosity on sediment retention in hydrodynamic separators is not yet fully understood.

Environment21 V2B1 – Laboratory Testing

An Environment 21 V2B1 Model 4 was tested in the laboratory in 2008 following Procedure 1. The experimental setup utilized a fiberglass manhole and the Environment21 V2B1 piping placement and baffle wall proprietary design. The device tested in the laboratory in 2008 had a smaller outlet pipe from the first chamber to the second chamber than the device tested in the field in 2007. In addition, a different sediment measurement technique was used for laboratory testing than was used for field testing.

For laboratory testing the entire full-scale device was placed on a frame, which was placed on Tovey Engineering Model FR10 load cells. These load cells have a published non-repeatability of 0.01% of their rated capacity. Numerous tests were conducted on the setup to confirm that load cell measurement drift and non-repeatability were minimized.

The amount of sediment washed out during a test was determined by measuring the weight change of the entire device from the start of the test to the end of the test. Prior to a test, the system was disconnected from the piping and weighted using the load cells, and the water level was recorded. The piping was then connected and a test was conducted at the specified flow rate for the specified duration. At the conclusion of the test the suspended sediment was allowed to settle, and then water was drained from the device to approximately the pre-test water level. The piping was disconnected, and the final weight and water level were recorded. At the end of every test an adjustment was made to the weight to compensate for the difference in water height, and the amount of sediment washed out was calculated based on the weight change of the device and the densities of the sediment and water.

Twelve tests were conducted utilizing US Silica F110 gradation, and five tests were conducted using AGSCO 70-100 gradation. The pre-test sediment level for each test was approximately five inches. The tests were conducted with water supplied from the Mississippi River, which had temperatures ranging from 0 to 2 degrees Celsius. The test durations ranged from 45 to 180 minutes. The results of the retention testing for the V2B21 in the laboratory are included as Figure 3.

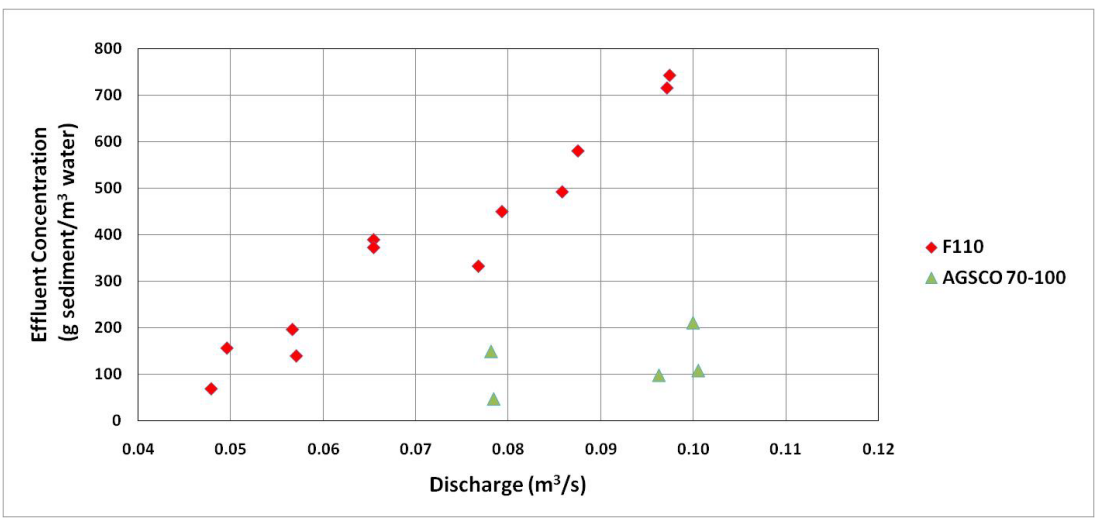

Figure 3: Sediment retention laboratory testing – Environment 21 V2B1 Model 4

As witnessed during field testing of the Environment21 V2B1 in 2007, the larger AGSCO 70-100 sediment was better retained in the device.

Stormceptor STC 1200 – Laboratory Testing

A Stormceptor STC 1200 was tested in the laboratory in 2008 following Procedure 1. The experimental setup utilized a fiberglass manhole and an insert of standard design provided by Stormceptor. Load cells were used for sediment measurement following the same protocol as used for the Environment21 V2B1 laboratory testing (see above). The tests were conducted with water supplied from the Mississippi River, which had temperatures ranging from 0 to 1 degree Celsius. The test durations ranged from 60 to 120 minutes.

Prior to the first test, approximately six inches of US Silica F110 gradation was charged to the sump of the Stormceptor device. Sediment retention tests were conducted at discharges of 0.014 m^3/s (0.5 ft^3/s), 0.085 m^3/s (3 ft^3/s) and 0.14 m^3/s (5 ft^3/s). Measurable sediment removal did not occur during any of these tests, as evidenced by:

1) The weight change of the system was not significant
2) There was no visual appearance of sediment in the discharge water during the tests
3) Sediment did not settle in the outlet channel or on top of the Stormceptor insert after the water flow was stopped
4) As observed through the outside of the fiberglass manhole, the sediment level at the perimeter of the device did not change

Following the F110 tests, approximately 2-1/2" of SCS250 sediment was added to the sump and allowed to settle overnight on top of the F110 sediment. SCS250 is a commercial silica sand gradation with a specific gravity of 2.6. SCS250 has a d_{50} of 28 µm, a d_{15} of 3 µm and a d_{85} of 80 µm. Sediment retention tests were conducted at discharges of 0.014 m^3/s (0.5 ft^3/s), 0.14 m^3/s (5 ft^3/s) and 0.25 m^3/s (9 ft^3/s). After a small initial washout of suspended small solids during the first test, measurable sediment removal did not occur during the SCS250 sediment retention tests.

Sediment retention testing of a Stormceptor STC 1200 at St. Anthony Falls Laboratory indicated there was no measurable scouring and washout of sediments under high water flow conditions.

Scale Model Testing

A 1:10 scale model of a ten foot diameter separator with a swirling flow and two concentric cylinders was built at St. Anthony Falls Laboratory to advance the understanding of the principal processes which govern sediment scouring, resuspension and washout. Velocity measurements were taken in the model under a variety of flow conditions using a 3-dimensional Acoustic Doppler Velocimeter (ADV). Figure 4 shows the model with the ADV setup.

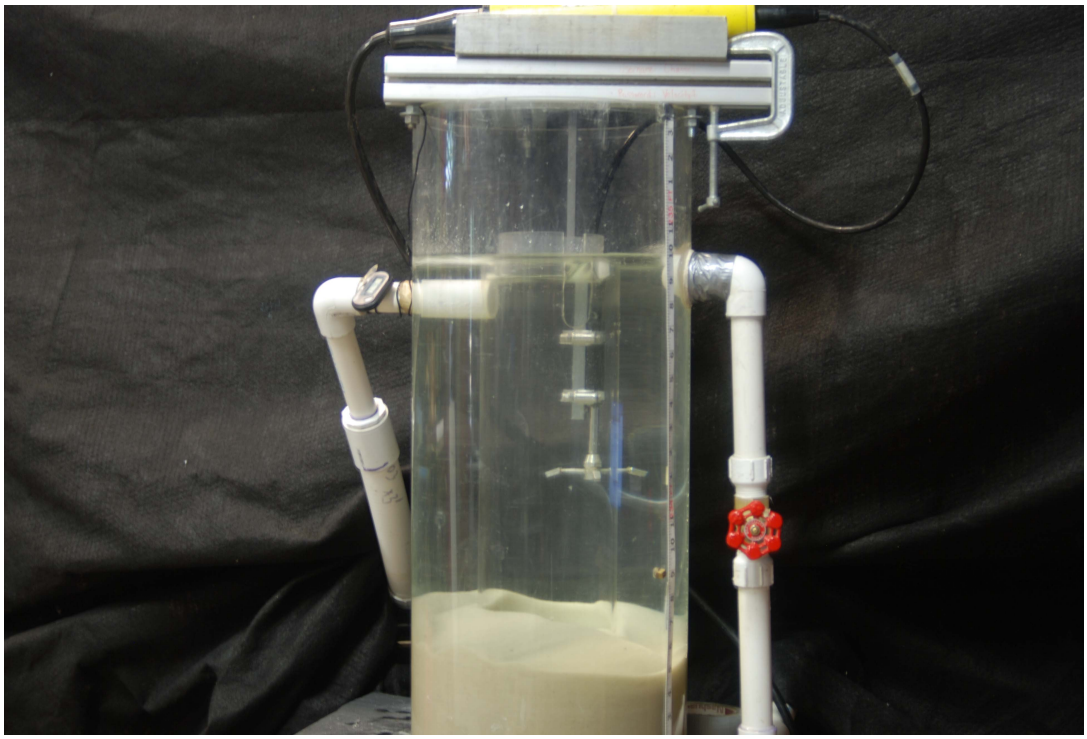

Figure 4: Model hydrodynamic separator with ADV setup (Saddoris et al., 2009)

Vertical velocity profiles were measured at one quarter of the circle downstream of the inlet pipe (1/4 Position in Figures 5 and 6) and at three quarters of the circle downstream of the inlet pipe (3/4 Position in Figures 5 and 6). The velocity readings were taken at a position halfway between the outer cylinder and the inner cylinder of the device. The x-direction was tangential to the radius in the horizontal plane. A variety of discharges were tested, and the results at 0.27 liters per second and 0.92 liters per second discharge are included as Figures 5 and 6, respectively. In Figures 5 and 6, the horizontal axis is the x-direction velocity divided by the average of the x-direction velocity for the position. The vertical axis is the reading height above the sediment bed divided by the height of the water column for the given discharge.

The velocity measurements taken in the model and shown in Figures 5 and 6 indicate:

1) There can be high flow velocities near the bed (3/4 position in Figures 5-7) and therefore substantial energy available for scouring
2) The velocity profiles can be dramatically different at different positions in the device
3) Velocities may be lower near the device outlet, potentially reducing the number of scoured particles that are washed out
4) Flow patterns in swirl flow devices can be complex

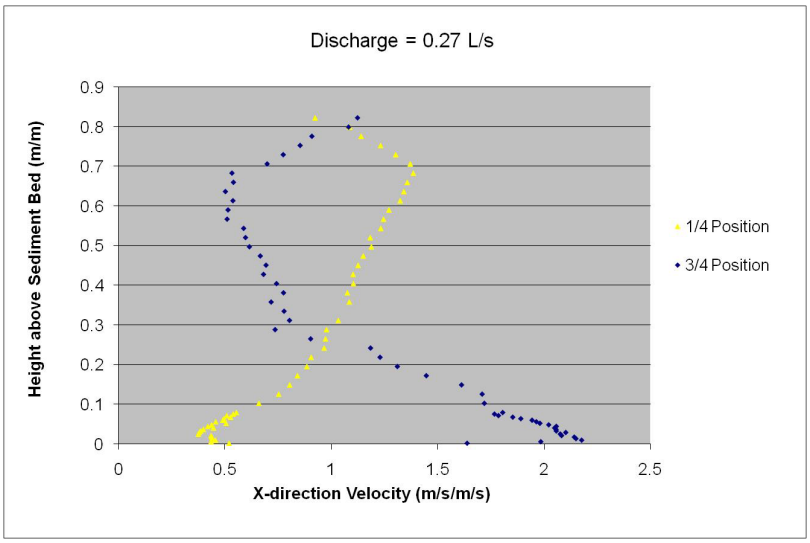

Figure 5: Scale model ADV testing at 0.27 L/s discharge

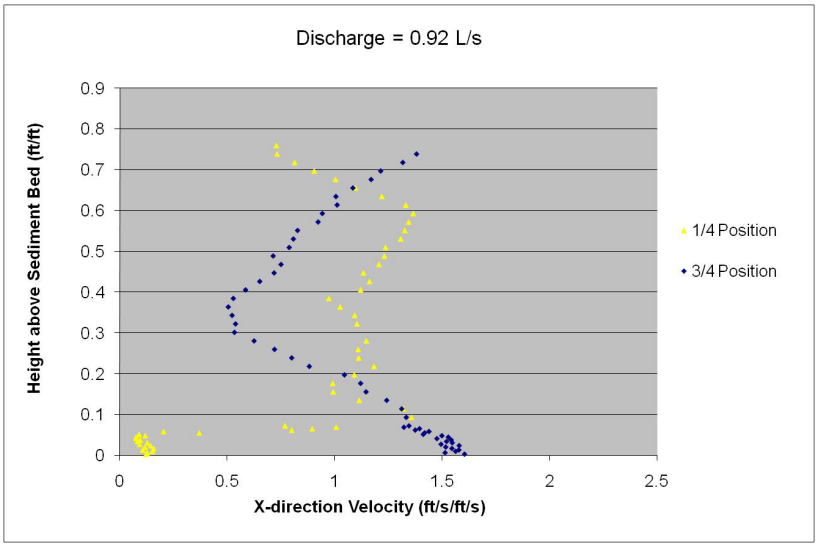

Figure 6: Scale model ADV testing at 0.92 L/s discharge

Further testing and data analysis is required to understand and predict flow patterns in swirl flow devices, which will lend to understanding of scouring, resuspension and washout of deposited sediments.

Maintenance

Future maintenance demands are an important consideration when evaluating hydrodynamic separators as a stormwater treatment option, since full life-cycle costs can be dramatically impacted by maintenance needs.

The primary maintenance activity required with hydrodynamic separators is cleaning of deposited sediments. These devices have design sediment capacities, and sediments must be occasionally removed to minimize resuspension and washout of accumulated sediments. Cleanout is typically accomplished utilizing a vacuum truck,

which is a reasonably costly procedure, so accurate prediction of required cleanout frequency would provide vital information on total life-cycle costs for hydrodynamic separators. However, many variables affect the accumulation of sediments, including watershed hydrology, suspended solids particle size distributions and densities in stormwater runoff, device performance efficiencies and device sediment retention capabilities. Therefore, accurate prediction of net sediment accumulations in a specific device in a specific drainage basin is challenging.

Typically, manufacturers recommend frequent inspections of sediment accumulations for the first one to two years of service so that sediment accumulation rates and cleanout schedules can be predicted. This procedure is time consuming and subject to inaccuracies, as rainfall conditions can vary significantly from year to year, and the results cannot be applied to different devices in different watersheds. If crucial variables affecting net sediment accumulation were well understood, models could be developed to predict cleanout frequencies and better estimate total suspended solids removals for regulatory compliance.

Summary

Solids removal performance, sediment retention and maintenance demands are all important considerations when selecting and sizing hydrodynamic separators for use as an urban stormwater best management practice (BMP).

Field and laboratory sediment retention testing has been completed on an Environment21 V2B1. Sediment compaction and shielding can influence sediment retention under actual operating conditions, so the idealized results obtained cannot be directly adopted as sediment retention rates for in-service devices. However, these results can be applied to help understand the impact of varying conditions on sediment retention, providing information for device design and maintenance. Further work is required to develop non-dimensional retention functions for the Environment21 V2B1 device, so the results so can be applied to a wider range of flow rates, suspended solids sizes and densities and water temperatures.

Laboratory testing has also been completed on a Stormceptor STC 1200. Measurable scouring and washout of sediments under high water flow conditions was not observed for this device.

In one test of a scale model swirl flow hydrodynamic separator the velocity profiles were complex, but could provide important indicators for understanding scouring and sediment washout. Sediment retention in hydrodynamic separators is specific to each design, so additional work is required to test devices and develop retention functions.

With adequate knowledge of drainage area runoff characteristics, suspended solids properties in runoff, device removal efficiencies and sediment retention capabilities, hydrodynamic separators could be accurately selected and maintenance schedules could be optimized to achieve sediment removal targets while minimizing costs.

References

Carlson, L., Mohseni, O., Stefan, H. and Lueker, M. (February 2006). "Performance Evaluation of the BaySaver Stormwater Separation System." *St. Anthony Falls Laboratory Project No. 472*, Minneapolis, Minnesota.

Fyten, A., and Mohseni, O. (January 2009). "Environment21 V2B1 Model 4 Performance Function." *St. Anthony Falls Laboratory Project Report No. 527*, Minneapolis, Minnesota.

Mohseni, O. and Fyten, A. (June 2008). "Performance Assessment of Modified ecoStorm Hydrodynamic Separator." *St. Anthony Falls Laboratory Project Report No. 495B*, Minneapolis, Minnesota.

Saddoris, D., Gulliver, T., Bell, B., Mohseni, O. and Gulliver, J. "Evaluation of Hydrodynamic Separators as an Urban Stormwater BMP." *Proceedings of An International Prospective on Environmental and Water Resources Conference*; 2009 Jan 5-7; Bangkok, Thailand. Environmental and Water Resources Institute (EWRI) of the American Society of Civil Engineers (ASCE); 2009.

Wilson, M., Mohseni, O., Gulliver, J., Hozalski, R., and Stefan, H. 2009. Assessment of Hydrodynamic Separators for Stormwater Treatment. Submitted to the ASCE *Journal of Hydraulic Engineering*, in press.

Assessment of Standard Sumps for Stormwater Treatment

Adam Howard – Graduate Research Assistant, Department of Civil Engineering, University of Minnesota
2 Third Avenue SE
Minneapolis, MN 55414
Phone 712-898-0838
Fax 612-624-4398
howar298@umn.edu

Omid Mohseni – Adjunct Associate Professor, Department of Civil Engineering, University of Minnesota
2 Third Avenue SE
Minneapolis, MN 55414
Phone 952-832-2665
Fax 612-624-4398
omohseni@umn.edu

John Gulliver – Professor, Department of Civil Engineering, University of Minnesota
122 Civil Engineering Building
500 Pillsbury Drive SE
Minneapolis, MN 55455
Phone 612-625-4080
Fax 612-626-7750
gulli003@umn.edu

Heinz Stefan – Professor, Department of Civil Engineering, University of Minnesota
387 St. Anthony Falls Laboratory
2 Third Avenue SE
Minneapolis, MN 55414
Phone 612-625-2810
Fax 612-624-4398
stefa001@umn.edu

Abstract

Although proprietary devices for the treatment of stormwater are used in many urban areas as best management practices (BMPs), their cost has prompted the Minnesota Department of Transportation (DOT) to consider the use of standard sumps to meet stormwater quality goals. However, no data on the effectiveness of sediment removal and proper operation of the sumps exist. Such data is necessary for standard sumps to be considered as a stormwater pretreatment device in Storm Water Pollution Prevention Program regulations.

To determine whether standard sumps remove suspended sediment from stormwater runoff, a sump was tested in a laboratory setting. The removal efficiencies under low flow conditions as well as the flushing effluent concentrations under high flow conditions were determined. In the low flow removal efficiency tests, sediments of specific size and concentration were fed into the influent pipe. At the conclusion of the test, the sediments removed by the sump were collected, dried and weighed. In the high flow condition tests, a predetermined sediment mix was placed inside the sump and the quantity of sediments remaining after the sump had been flushed by high flows for a period of time, was determined.

Sump removal efficiency functions have been developed, and an uncertainty analysis has been conducted as part of the data interpretation.

Background

The standard sump (manhole) has been a key component in stormwater infrastructure. In addition to providing a location for pipe junctions and storm sewer maintenance access, the sump's detention time provides for removal of some particulate and trash. In recent decades, proprietary devices for the treatment of stormwater have become increasingly popular to aid communities in meeting stormwater quality regulations. These regulations are a response to the 1987 amendments to the Clean Water Act (Smith 2001). While these proprietary devices have proven effective as a pre-treatment device that removes inorganic particles larger than silt, their expense has led the Minnesota DOT to seek other avenues to reach their stormwater pretreatment goals.

From 2005 to 2007, a team from St. Anthony Falls Laboratory at the University of Minnesota provided an in-depth laboratory and field performance analyses of several proprietary devices. The focus of these studies was to assess the removal of various sediment sizes from the influent. It was decided to follow the same testing procedure in the evaluation of standard sumps. The results would then be easily compared to that of the proprietary devices and the cost effectiveness of the standard sump can then be determined. In addition to the evaluation of the sump as a sediment capturing device, scour tests have been conducted to determine what flows will cause removal of the previously captured sediment. Guidelines for proper cleaning schedules can be produced with the latter data.

Theory

It is common practice to use monitoring for the evaluation of performance of stormwater best management practices (BMPs). Unfortunately, the use of samplers for monitoring influent and effluent has proven unreliable for the collection of some sediment particle sizes (Wilson et al., 2007). Therefore, in this study a mass balance approach was adopted to assess the performance of standard sumps.

The analysis of sediment removal efficiency will use the Peclet number (Wilson et al. 2009) because it provides a common non-dimensional ground to compare various devices. In this case the Peclet number is directly proportional to the particle settling velocity, device diameter, and depth. It is also inversely proportional to the device flow rate, thus

$$Pe = \frac{Vs * h * d}{Q} \tag{1}$$

When the Peclet number is plotted versus a particle size's measured removal efficiency, a performance function for a specific stormwater treatment device can be developed (Wilson et al., 2009). This performance function is described by the relationship shown in equation 2.

$$\eta = \left[\frac{1}{R^b} + \frac{1}{(a\ Pe)^b} \right]^{-\frac{1}{b}} \tag{2}$$

In equation 2, R, a, and b are fitted parameters, Pe is the Peclet number and η is the corresponding particle's measured removal efficiency. The measurement of η requires the addition of known masses of several particle sizes to the influent in the experiment, and subsequent drying, sieving and weighing of the captured sediment, as described in the next section.

A similar relationship has not yet been developed for the high flow scour tests, so they will be reported as a percent of the initial mass in the sump that is removed by the corresponding high flow.

Experiment Setup

A full scale fiberglass sump was constructed for testing by a local fiberglass manufacturer and placed on a test stand in the St. Anthony Falls Laboratory (SAFL) of the University of Minnesota in Minneapolis, Minnesota. The sump was then connected to the SAFL plumbing system and flow was measured using a pre-calibrated circular weir downstream of the model. The sump was 4 feet in diameter and 4 feet deep (the height of the inlet pipe from the sump bed), and had 15" inlet and outlet pipes at 0 and 180 degrees respectively. There was a one percent drop between the inlet and outlet pipes. Sediment was piped as a slurry from a sediment feeder into the inlet pipe approximately one foot upstream of the sump. The transverse velocity of the slurry allows for proper penetration into the flow within a short development length. The short development length eliminates loss of sediment in the inlet pipe. A manometer is connected to the device for the recording of water surface elevations in the inlet pipe, the sump, and the outlet pipe. Figure 1 is a picture of the fiberglass sump on the test stand.



Figure 1. Sump and Test Stand

Testing Procedure

Flow rates

The flow rates used in testing were determined by first calculating the 80% pipefull discharge using Manning's equation and assuming that this flow would be the design for a 10-year runoff event. Given this flow, the rational equation could be used to develop a representative urban watershed. The maximum flow rate for treatment assessment (MFRT) was then defined as the 1-year storm and calculated.

Performance Testing

Performance testing involves feeding of a known quantity and concentration of sediment with a known particle size to the inflow. A sediment mix was created from three median sediment sizes, 545 μm, 335.5 μm, and 107 μm. This mix was sieved so that particle overlap is not an issue and all three sizes are added to the flow in equal parts with a concentration of 200mg/L for all tests. Twelve tests were conducted with flow rates of 100%, 75%, 50%, and 25% of MTR in triplicate. These flow rates were 2.4 cfs, 1.8 cfs, 1.2 cfs, and 0.6 cfs. Three additional tests were conducted at 0.8 cfs and twice at 0.9 cfs with the 545 μm particle size only. Thus, with the three particle sizes, 39 different Peclet numbers and removal efficiencies could be calculated and fit to the model. Each test involved the addition of 10-15kg of the three part mix of sediment to flow. The amount of sediment added depended on the flow, i.e. low flows had smaller amounts of sediment input. The test duration was varied so the influent concentration remained the same

with lower flowrates having longer durations. Following each test the sediment was collected from the sump, dried, sieved, and weighed.

Scour Testing

Scour testing involved the placement of a predetermined amount of sediment into the sump before flows above the MFRT were applied, and the amount of sediment lost from the sump was recorded. This test involved the use of straight US Silica Sand F-110 which has a median particle diameter of 110 μm. The flow rates used were 100%, 75%, and 50% of the value for the 10 year storm as described above. These flow rates were 5.5 cfs, 4.2 cfs, and 2.8 cfs. All tests had a duration of one hour. After the initial placement of the known mass of sediment before the test, and after the termination of the test, sediment depth measurements were taken to determine the amount of sediment removed from the sump. The average effluent concentration could then be determined. In addition, tests were conducted to determine a mean bulk density of 107 lb/ft^3 for the US Silica Sand F-110.

Model Uncertainty

While the performance function has proven to fit the data nicely, no model or measurement is completely accurate (Kline, 1985). In order to evaluate the model fit it is necessary to evaluate the uncertainty of the model. Quantifying the uncertainty of this model involves the distribution of the residuals. As can be seen in Figure 2, the model residuals are not normally distributed. To deal with this issue, it was decided to use bootstrap resampling method to create pointwise confidence intervals to quantify the error in the fit of the model. Carpenter et al. (2000) provides an overview of the bootstrap method and its application.

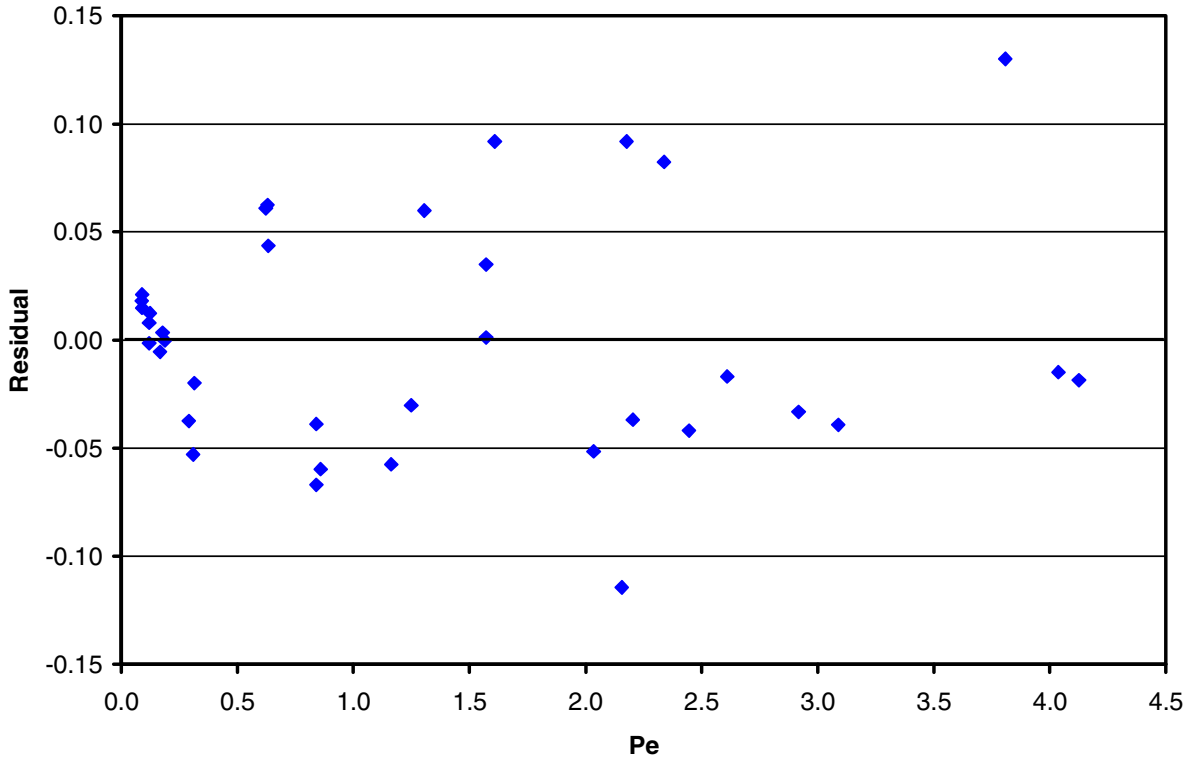

Figure 2. MN/DOT Sump Performance Curve Residuals

Results

Performance Results

Figure 3 shows the results of the performance test as well as the model fit to the data. The results from the performance tests of the standard 4 ft diameter sump indicate that the sump is effective in removing sediment from stormwater. As would be expected, the sump is more effective at higher Peclet numbers, which indicates either low flow rate or larger particle size. The three parameter model also fits the data well with a Nash-Sutcliff Coefficient of 0.97. With this model, it will be possible for designers to predict the removal efficiencies based on particle size, particle density, water temperature and flow. In addition, one can compare the results to various proprietary devices. Figure 4 shows results of a field test on a Stormceptor (Wilson et al., 2009), and of the standard sump. The performance of the two is close up to a Peclet number of two, where they begin to differ. The sump chosen can be expected to remove approximately 75% of the sediment, while the Stormceptor may remove up to 97% of particles. Even though the two performance functions seem to be very similar, it is important to note that dimensionless function was obtained from a Stormceptor with very large dimensions and thus to obtain the Stormceptor removal efficiency for a certain particle size and density, the standard sump flow rate should be significantly smaller than the Stormceptor. If the removal efficiency of standard sumps with different dimensions follow the function showed in Figure 4 for standard sumps, then up to a

Peclet number of about 2, using a standard sump for stormwater treatment is more cost effective than a Stormceptor.

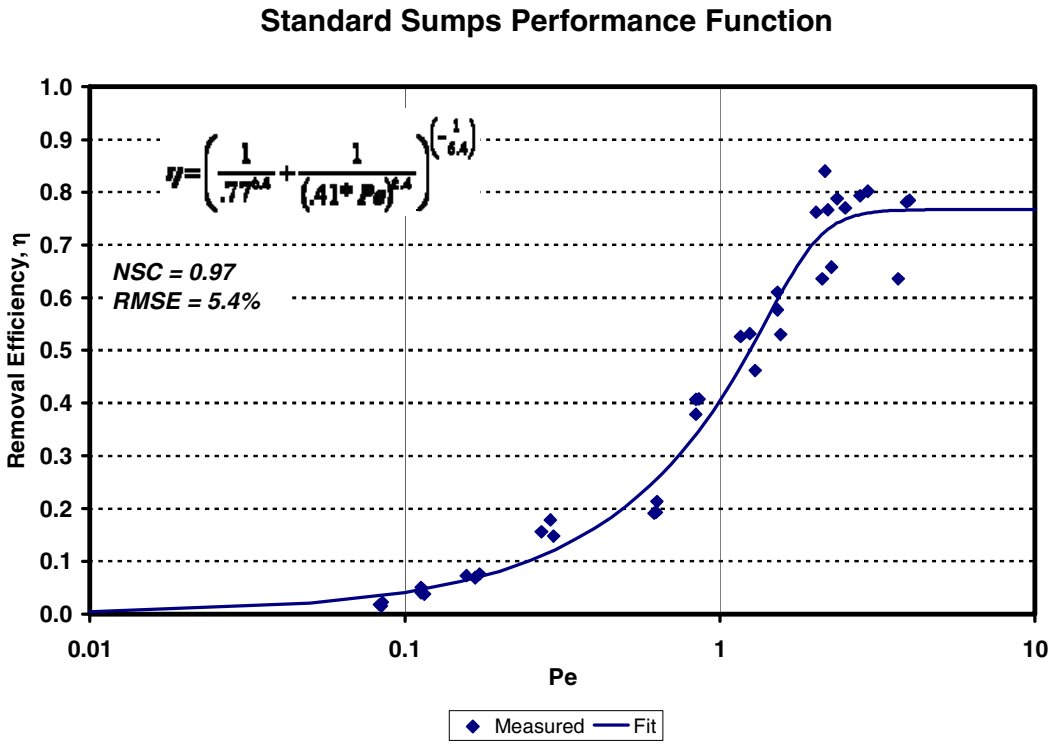

Figure 3. MN/DOT Sump Performance Function

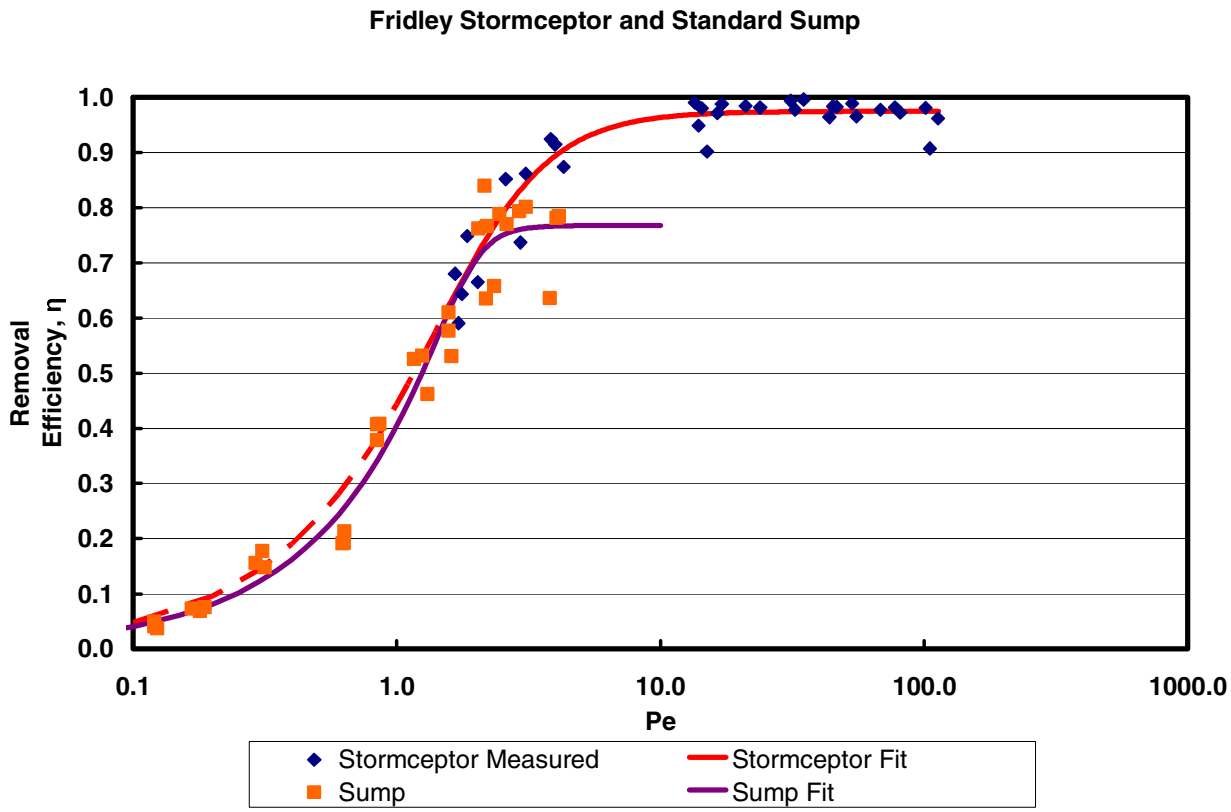

Figure 4. A 10-ft Stormceptor and a 4-ft Standard Sump

Scour Results

The results from the scour tests indicate a discrepancy between measurements and what is expected (Table 2). It would be expected that the higher the flow rate, the more scour would occur. The tests show little scour at the lowest flow rate, then a large increase for the intermediate flow, and finally decreased scour for the highest flow rate. A repeat test of the intermediate flow rate was conducted and showed a lower percent removal, however it was still high when compared to the values for the highest flow rates. On the whole, however, the amount of sediment removed remained low with values not exceeding 30% removal.

Table 2. Scour Test Results

Flow rate (cfs)	Depth Removed (m)	Mass Removed (kg)	Effluent Concentration. (mg/L)	Removed amount (%)
2.69	0.0000	6.21	0.38	1.97
2.88	0.0087	14.93	0.85	4.88
4.17	0.0502	86.04	3.37	27.38
4.17	0.0464	79.47	3.12	24.61
5.7	0.0288	49.28	1.41	14.08
5.41	0.0297	50.88	1.54	13.93
3.92	0.0213	36.53	1.52	12.85

Model Uncertainty Results

The results of the uncertainty analysis provide insight into the quality of the model fit. The uncertainty analysis gives the uncertainty of the model fitting, not the uncertainty in the data. In other words, for a 95% confidence interval 95 out 100 fitted lines will lie within these bounds. Figure 5 shows the fitted model with its 95% confidence bounds.

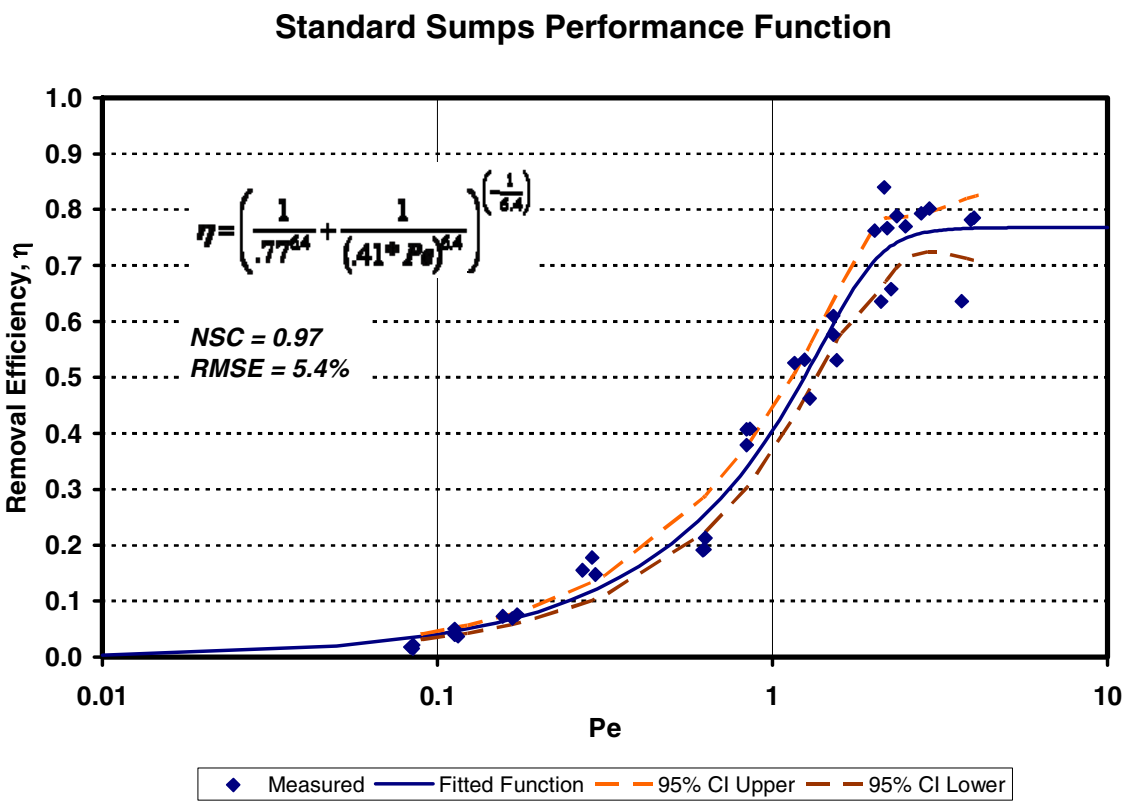

Figure 5. MN/DOT Sump Performance Function With Confidence Intervals

Future Research

The testing of the 4ft diameter sump is the first in a series of tests sponsored by the Minnesota DOT. Future research includes tests on a 4-ft diameter shallow sump and a 6-ft diameter deep and shallow sump. In addition, 90 degree outlets have been constructed on the test sumps to model flows through sumps with different outlet configurations. Acoustic Doppler Velocimeter tests will also be completed to provide information on the flow characteristics.

Conclusion

The performance of a standard sump for stormwater BMP has been assessed in this project. While the sump cannot attain the high removal efficiencies for typical flow rates and sediment particles seen by the proprietary devices, it could prove effective under some conditions. Communities which would expect higher removal efficiencies may find that a standard sump can reach their stormwater pretreatment goals. In these cases the sump would be a good option because of its simplicity and low costs. In addition, scour remains low at flow rates slightly higher than the MFRT. This ensures that captured particles will remain in the sump as long as the municipality follows a regular cleaning schedule.

Acknowledgements

We would like to thank the Minnesota Department of Transportation for providing funding for this project. In addition, thanks is due to Julia Molony of the University of Minnesota Statistical Clinic for her help with the uncertainty analysis. Also Andrew Sander, Teigan Gulliver, Benjamin Plante, and Andrew Fyten at the St. Anthony Falls Laboratory provided great help and support through the setup and testing process.

References

Carpenter, James, and John Bithell. "Bootstrap Confidence Intervals: when, which, what? A practical Guide for Medical Statisticians." Statistics in Medicine 19 (2000): 1141-164.

Kline, S. J. "The Purposes of Uncertainty Analysis." Journal of Fluids Engineering 107 (1985): 153-60.

Smith, Edward. "Pollutant Concentrations of Stormwater and Captured Sediment in Flood Control Sumps Draining an Urban Watershed." Water Resources 35 (2001): 3117-126.

Wilson, Matthew A., John S. Gulliver, Omid Mohseni, and Ray M. Hozalski. Performance Assessment of Underground Stormwater Devices. SAFL Proj. Rep. 494. St. Anthony Falls Laboratory, Univ. of Minnesota, Minneapolis, 2007. 1-94.

Wilson, M., Mohseni, O., Gulliver, J., Hozalski, R., and Stefan, H. 2009. Assessment of Hydrodynamic Separators for Stormwater Treatment. Submitted to the ASCE Journal of Hydraulic Engineering, in press.

Bayesian Load Duration Curves for Bacterial Total Maximum Daily Loads: Urban Case Study

Mary Schoen[1], Mitchell Small[2], and Jeanne VanBriesen[2]

[1]National Exposure Research Laboratory, U.S. Environmental Protection Agency, 26 W. Martin Luther King Drive, Cincinnati, OH 45268; PH (513) 569-7647; email schoen.mary@epa.gov

[2]Department of Civil and Environmental Engineering, Carnegie Mellon University, Pittsburgh, PA 15213-3890

Abstract

A Bayesian load duration curve approach is developed to estimate indicator bacterial load reductions for a small, urban watershed with stormwater and animal inputs. The Bayesian load duration curve approach uses the truncated bivariate normal probability distribution to predict flow, in-stream bacterial concentration, and the resulting load for a specified number of flow conditions. Using non-informative priors, the Bayesian approach propagates the uncertainty resulting from the natural variability in observed concentrations through to the predicted in-stream indicator bacterial concentration and load. Using the best estimate 90th percentile in-stream loads, the Bayesian method predicts indicator bacterial load reductions ranging between 68% for low flows and 99.9% for high flows. The predicted distributions of in-stream bacterial concentration are then compared pre- and post-implementation of stormwater filtration. The pre-implementation distribution of in-stream indicator bacterial concentration demonstrates that the stream exceeds the standard of 235 cfu/100ml *E. coli* 76.1% of the time during the recreational season with a 95% credible interval CI(74.6, 78.0). The post-implementation distribution of indicator bacterial concentration predicts that the concentration of indicator bacteria exceeds the limit set by the water quality standard 72.4% CI(70.6, 74.3). Alternatively, the Bayesian model is then used to predict in-stream concentration post-implementation of an aggressive ultra-violet disinfection process.

Introduction

The formulation of water quality management plans in the United States is driven by the US Environmental Protection Agency (US EPA) rules and guidance for the determination of Total Maximum Daily Loads (TMDLs) (NRC 2001). As required by section 303(d) of the Clean Water Act (1987), each state must identify the waters within its borders that are not in attainment of water quality standards, not protecting a balanced wildlife population, or not supporting their designated use. There are over 60,000 listed impairments for waterbodies on the US EPA 2004 303(d) list of impaired waters. For these impaired waters, the TMDL program general guidance requires a base level of analysis (EPA 2005): (1) the identification of pollutants causing impairment; (2) the wasteload allocations from point sources, the load

allocations from nonpoint sources, and natural background conditions necessary to implement the applicable water quality standard; and (3) a margin of safety (MOS) and a consideration of seasonal variations. Beyond the base level of analysis, the program remains flexible in terms of the methodology used to accomplish 2 and 3. The benefit of this flexibility is the variety of methodologies possible for addressing the overwhelming number of impaired waterbodies.

The objective of the work is to demonstrate and apply the use of a new Bayesian water quality model for TMDL application when the impairment source is presumed to be pathogen contamination (as measured by indicator organisms). Further, we will demonstrate this model's predictive power given alternative control strategies for stormwater. The new model is designed to increase TMDL progress by relaxing the data requirements inherent to existing models while adding the capability to model control strategies. In addition, the new model incorporates uncertainty analysis by treating the model parameters and predictions probabilistically. The new TMDL method is based on the traditional load duration curve approach, but with added capability to predict control strategy performance under uncertainty.

The new Bayesian load duration curve approach is presented and then applied to an urban case study with non-point source bacterial contamination to calculate the required load reductions and evaluate alternative control strategies. The following section provides background on the Bayesian process; the recommended methods for TMDL bacterial analysis, including the traditional load duration curve approach; and each model's ability to formulate control strategies.

Background

Alternative TMDL Bacterial Models

The TMDL program is flexible in the methodology allowed for load allocations and reductions. EPA technical documents (EPA 2001; EPA 2007) as well as research (Donigian and Huber 1991; Wilkinson, Jenkins et al. 1995; Borah and Bera 2003; Borah and Bera 2004; Horn, Rueda et al. 2004; Benham, Baffaut et al. 2006) summarize the strengths and weaknesses of the recommended and popular methodologies for bacterial TMDLs. These reviews categorize the models into many different types including dilution models, continuous dynamic models, and empirical models. Dilution models, primarily used for point source allocation, specify the maximum load for the critical low-flow period (EPA 2001). To model both non-point and point sources, continuous or empirical models are employed.

Continuous models include QUAL2E, WASP, and HSPF, which provide time-series estimates of concentration based on point and non-point source loading. Of the three, only HSPF also allows certain Best Management Practices (BMPs) to be modeled using a constant percent load reduction. QUAL2E was developed to examine waste load allocations under steady flow conditions with limited non-point source representation (Shanahan, Henze et al. 1998). WASP and HSPF are dynamic models with the ability to model both point and non-point source loading; WASP requires

non-point source loading inputs while HSPF allows a "buildup and washoff" sub-routine (Donigian and Huber 1991; EPA 2001). These tools simulate the variation in in-stream concentration over long periods of time at multiple locations to allow identification of critical conditions and locations. These tools also allow simulation of changes to source loading to identify viable load reduction alternatives. Although useful for exploring alternative loading scenarios, the dynamic models require numerous types of data for model formation and comprehensive datasets for calibration (Donigian and Huber 1991; EPA 2001; Borah and Bera 2003). In addition, the large number of model parameters prevents a thorough uncertainty analysis. An alternative to the data-intensive continuous, dynamic models for specifying both point and non-point source allocation is the load duration curve approach.

In guidance provided by the US EPA Office of Water, the load duration curve (LDC) TMDL approach is recommended over difficult to construct and run dynamic models when the primary driver of contamination is flow (EPA 2007). A load duration curve is an empirical method that plots the percent of time that an observable quantity of interest is exceeded. In other words, a duration curve is the complement of the cumulative distribution function F(y) for a quantity of interest y:

$$DC(y) = 1 - F(y) = P(Y \geq y)$$

Duration curves have been used in water resources planning to communicate the variability of water quality and quantity characteristics and to evaluate the impact of management options on those characteristics (Vogel and Fennessey 1995). In TMDL applications, the quantity of interest is the in-stream allowable contaminant load, W. A load duration curve DC(W) can be constructed to estimate a TMDL for a waterbody from the flow duration curve DC(Q) given an in-stream water quality target concentration, S:

$$DC(W) = DC(Q) * S$$

where the $DC(Q)$ is created from a long-term record of average hourly or daily flow measures (Searcy 1963). The load duration curve specifies the allowable in-stream load over the range of possible flow conditions and can be used as the base for the TMDL allocation process. The TMDL for each flow condition is the minimum allowable in-stream load for that flow condition as specified by the $DC(W)$. Load reductions can be specified by comparing the $DC(W)$ to the 90th percentile observed in-stream load under each flow condition (2007).

Although the traditional LDC approach is sufficient for meeting the minimal TMDL requirements, using the approach, it is difficult to map loads to specific sources. Bonta and Cleland (2003) suggest that source tracking techniques be paired with the LDC approach to identify differences in source between flow conditions. In addition, the traditional LDC approach can not facilitate the prediction of water quality or BMP effect on water quality. To facilitate prediction, Bonta and Cleland (2003) present a

load duration curve method that predicts water quality for flow conditions with no observed samples using ordinary least squares regression (OLS). The Bayesian approach outlined in the present work is similar to the regression approach in that it extends the observations in a monitoring record to predict in-stream load for any given flow, but the process proposed here assumes a statistical model for both flow and concentration that allows prediction of future in-stream concentration given a control strategy.

Bayesian Basics

Bayesian data analysis is the process of making inferences from data using probability models for observed quantities as well as unobservable quantities of interest (Gelman, Carlin et al. 2004). For example, given an observable quantity of interest *y*, Bayesian data analysis can estimate an unobservable quantity θ, such as population parameters for *y,* if the two quantities can be expressed as a joint distribution function,

$$p(\theta, y) = p(\theta)p(y \mid \theta)$$

where p(θ) is the prior distribution of the unobservable quantity, which is designed to represent the uncertainty about θ, and p($y|\theta$) is the sampling distribution of the observed quantity. All inferences about θ are based on Bayes rule which estimates a posterior distribution for the unobservable quantity p($\theta|y$) from the joint distribution function by conditioning on the known value of observable quantity *y,*

$$p(\theta \mid y) = \frac{p(\theta)p(y \mid \theta)}{\int p(\theta)p(y \mid \theta)d\theta}$$

In addition to making inferences about θ by formulating the posterior distribution p($\theta|$y), Bayes rule can be used to make inferences about future observations of the observable quantity $\tilde{y}$ through the posterior predictive distribution p*($\tilde{y}|y$),

$$p*(\tilde{y} \mid y) = \int p(\tilde{y} \mid \theta)p(\theta \mid y)d\theta$$

The posterior predictive distribution is expressed as an average of the conditional predictions over the posterior distribution of θ. In this way, Bayesian analysis propagates the uncertainty from model parameters through to the final prediction. The qualities of Bayesian data analysis, including the probabilistic representation of quantities of interest and propagation of uncertainty, makes it a powerful tool for water quality planning (Hobbs 1997).

Bayesian Model

The Bayesian model predicts the distribution of in-stream indicator bacterial concentration over the recreational season using a bivariate likelihood model relating the natural log of indicator bacterial concentrations *y* to the natural log of flow *x* for

different flow conditions *c*. By dividing the flow into conditions, each with equal probability *P*, the joint distribution for each condition $f_{T,c}(x, y)$ is a singly truncated bivariate normal distribution, expressed here as the product of the marginal distribution of *x* and the conditional distribution of *y*,

$$f_{T,c}(x,y) = \frac{1}{\sigma_x P\sqrt{2\pi}} \exp\left\{-\frac{1}{2}\left[\frac{x-\mu_x}{\sigma_x}\right]^2\right\} \times \frac{1}{\sigma_{y|x,c}\sqrt{2\pi}} \exp\left\{-\frac{1}{2}\left[\frac{y-\mu_{y|x,c}}{\sigma_{y|x,c}}\right]^2\right\}$$

where

$$u_{y|x,c} = \alpha_c + \beta_c(x - \bar{x}_c)$$

$$\beta_c = \frac{\rho_c \sigma_{y,c}}{\sigma_x}$$

$$\sigma^2_{y|x,c} = \sigma^2_{y,c}(1 - \rho^2_c)$$

$$\alpha_c = \mu_{y,c} - \beta_c(\mu_x - \bar{x}_c)$$

and for a given sample of *n* specimens in the truncated section, $\bar{x} = \sum_1^n \frac{x_i}{n}$. In this form, the conditional distribution of *y* is normally distributed with a standard deviation $\sigma_{y|x,c}$ and mean $u_{y|x,c}$. The conditional expected value $u_{y|x,c}$ is equivalent to an OLS regression between *x* and *y* in each flow condition.

The Bayesian model creates posterior estimates of the parameters of *y* for the truncated bivariate normal distribution $\theta_{y,c} = (\mu_{y,c}, \sigma_{y,c}, \rho_c, \mu_{y|x,ci}, \sigma_{y|x,c})$ for each flow condition (i.e. low, normal, and high) using Markov chain Monte Carlo (MCMC) samples implemented through the WinBUGs program (Spiegelhalter, Thomas et al. 1999). Non-informative priors are used to reduce the influence of the model structure on the predicted results. Three chains of 40,000 iterations with over dispersed starting points were used for posterior inference. The burn-in period was 20,000 iterations and was identified when the Rubin Diagnostic $\hat{R}$ (Gelman and Rubin 1992) converged to 1.

To calculate the load reduction for a particular flow value x_i, the posterior MCMC samples of parameter estimates are used to generate samples of the posterior predictive 90th percentile in-stream load for flow x_i. To do this, one sample of concentration is generated from each MCMC sample of mean and standard deviation of conditional concentration $(\mu_{y|x,ci}, \sigma_{y|x,c})$ for the select flow x_i. These samples make up the posterior predictive distribution of concentration at flow x_i. The posterior predictive concentration samples are then used to generate a series of loads for flow x_i from which the 90th percentile load is estimated. This process is repeated 1000 times for each flow x_i to create a 95% credible interval of 90th percentile load. The percent

reduction is found by taking the difference between the selected confidence of the 90th percentile in-stream load and the allowable in-stream load specified by the load duration curve *DC(W)*.

To evaluate model performance, posterior predictive checks were generated for the parameters $\theta_{y,c} = (\mu_{y,c}, \sigma_{y,c})$ using the MCMC samples and sample data. The posterior predictive distributions of $\theta_{y,c} = (\mu_{y,c}, \sigma_{y,c})$ are compared to the maximum likelihood parameter estimates using the data:

$$\hat{\mu}_{y,c} = \bar{y}_c + \bar{r}_c \left(\frac{\bar{s}_{y,c}}{\bar{s}_{x,c}}\right)(\bar{x}_c - u_{x,c})$$

$$\hat{\sigma}_{y,c} = \bar{s}_{y,c} \sqrt{\frac{1 - (1 - \frac{\bar{s}_{x,c}^2}{\sigma_{x,c}^2})(1 - \bar{r}_c^{\,2})}{(1 - (1 - \frac{\bar{s}_{x,c}^2}{\sigma_{x,c}^2}))}}$$

where r_c is the sample correlation coefficient and bars over the parameters indicate that only observed data from within the condition are used in estimation (Cohen 1955).

Site

Panther Hollow Stream is located within a 115 acre watershed encompassing Pittsburgh's central park, Schenley Park, and the surrounding urban neighborhood. The stream feeds a small lake created for recreational purposes in the early 1900s. Panther Hollow Stream contributes large loads of indicator bacteria from stormwater runoff, wildlife, and pets that presently prevent recreational activity. The Bayesian LCD analysis is used to predict bacterial concentrations at the outlet of the stream during the recreational season to determine the load reductions necessary to meet the recreational grab sample standard of 235 cfu/100ml *E. coli* as well as evaluate alternative control strategies.

Flow and *E. coli* concentration were monitored in Panther Hollow Stream over the recreational season of May-August in 2006 and 2007. Weekly samples were collected at the outlet of Panther Hollow Stream in order to assess compliance with the federal recreational water quality standard. Water samples were collected using sterilized and sealed 500 ml Nalgene bottles. Samples were transported on ice and refrigerated (4°C) until processing, which occurred within six hours of collection. All laboratory tests were run in duplicate and a blank was run for 10% of the samples. EPA Method 1603 (modified mTEC) and EPA approved ColiQuant Membrane Filtration methods were used to determine the concentration of *E. coli* (cfu/100ml) in the samples. Flow (cfs) at the time of sampling was estimated using a FP101-FP201

Global Flow Probe to measure stream velocity at mid-stream and the estimated stream cross-sectional area.

The scatterplot in Figure 1 shows the range of observed in-stream $\log_{10}$ concentration and flow for Panther Hollow Stream. The figure shows that as flow increases, the observed in-stream concentration increases above the maximum grab sample standard of 235 cfu/100ml *E. coli*, shown as a dashed line. Figure 1 also shows the equal probability flow conditions, roughly matching the observed weather conditions of dry weather and raining. As evidence in support of the structural assumption of normality, Figure 2 shows histograms of $\log_{10}$ concentration for each of the three flow conditions along with normal Q-Q plots, where alignment with the straight diagonal line indicates a normal probability distribution.

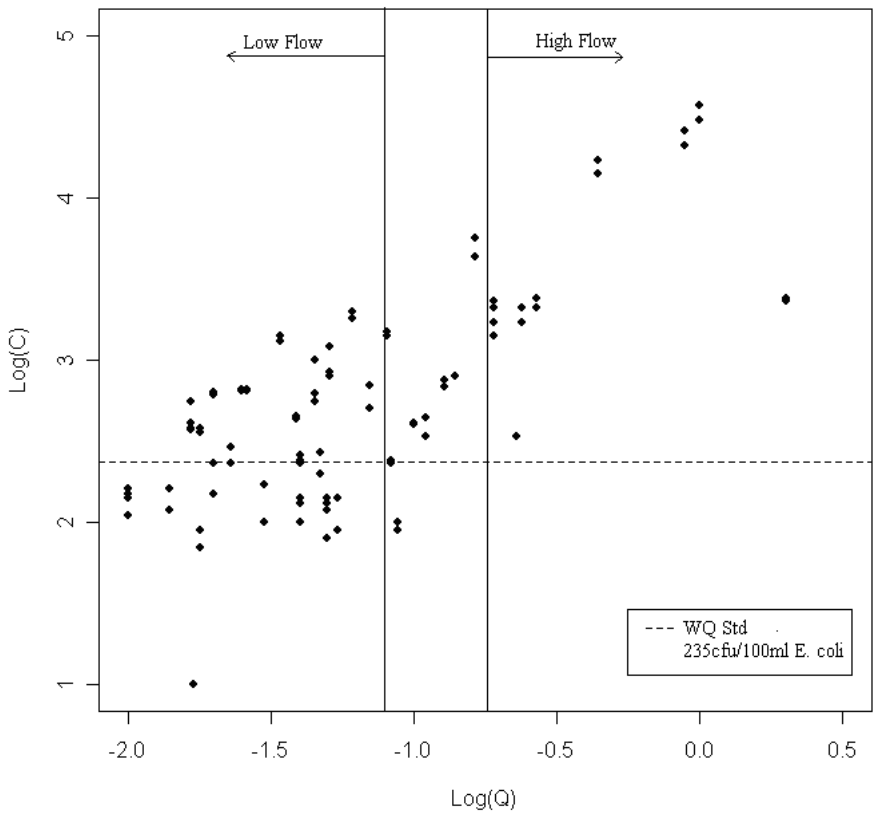

Figure 1. Scatterplot of E. *coli* Concentration and Flow for the 2006 and 2007 Recreational Seasons. The vertical lines show the divisions between low, normal, and high flow conditions.

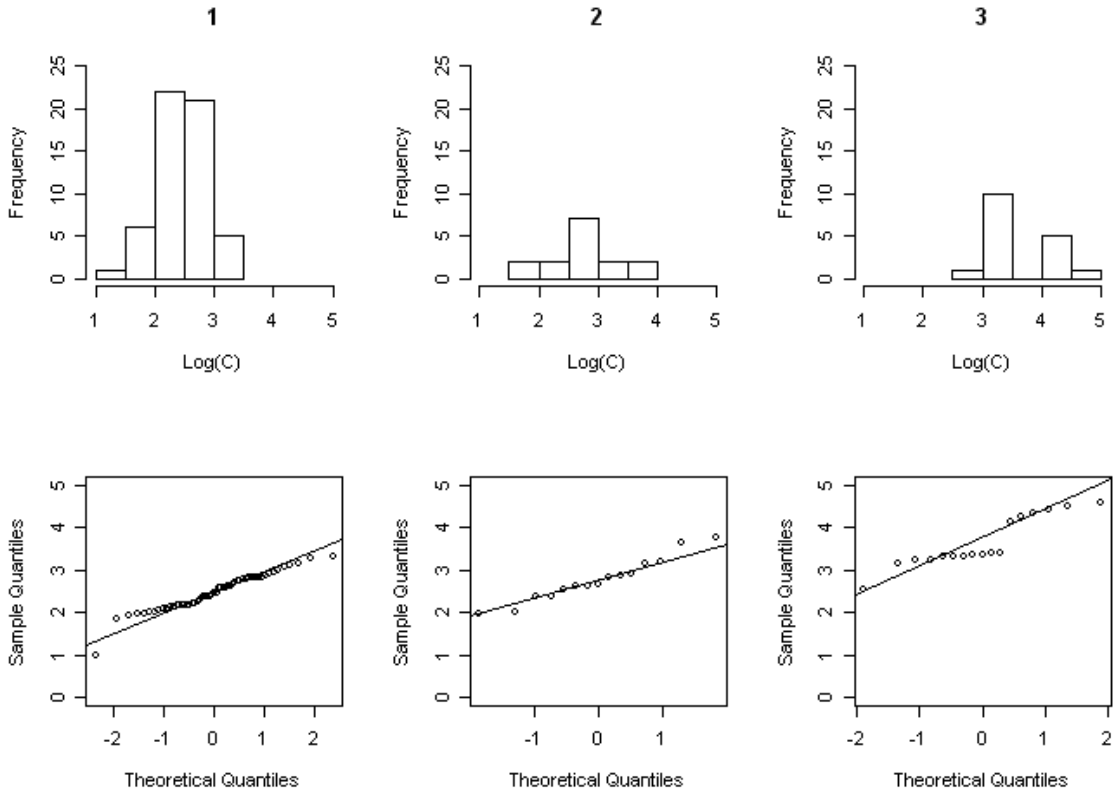

Figure 2. Histograms and normal Q-Q Plots of Recreational Season E. *coli* Concentration for Each Flow Condition. Histograms for the low, normal, and high flow conditions (i.e. 1,2,3) show the sample distribution of $\log_{10}$ *E. coli* concentration. The normal Q-Q plots show fit to the normal model represented by the diagonal line.

Flow Model

The LDC methodology requires a long-term, continuous flow record. Since no streamflow gauge is located in the watershed to provide this type of data, a dynamic watershed model was built in Hydrological Simulation Program-Fortran (HSPF) to simulate hourly flows for Panther Hollow Stream over the recreational seasons 2001-2007. The series of average hourly flows were used to estimate the empirical period-of-record *DC(Q)* as well as parameterize the truncated bivariate normal model.

HSPF models unidirectional flow through completely mixed streams segments using a storage-routing method (Bicknell, Imhoff et al. 2001). Input into the model includes information about the stream segments, watershed, and meteorological conditions. The watershed characteristics are used to estimate overland and subsurface wet weather flows. The Panther Hollow Stream watershed is approximately 115 acres (10% impermeable and 90% permeable) with slopes ranging between 0.1 and 0.6. The calibrated hourly precipitation for years 2001-2007 is

provided at a 1km x 1km resolution for the city of Pittsburgh using NEXRAD radar and a 30 rain gage network by Three Rivers Wet Weather (2007).

The main parameters in the flow calibration process include nominal soil moisture storage and infiltration capacity. The infiltration capacity was initially set within the range common of SCS Hydrologic Soil Group C with moderate to high runoff potential. Soil moisture storage was initially set at 25% of the annual average rainfall. These key parameters were then adjusted in the calibration process to achieve good model performance using the 2006 sample season data. Model performance was evaluated by two measures. The reliability index *RI* (Leggett and Williams 1981) quantifies the average factor by which simulated hourly flows differ from the observations. The modeling efficiency (MEF) measures how well the model predicts the observed values relative to the average of the observations. A MEF value near one indicates a close match between observations and model predictions (Stow, Roessler et al. 2003). A value of zero indicates that the model predicts no better than the average of the observations, and a value less than zero indicates that the average predicts better than the model. The MEF at the stream outlet is 0.76, indicating a close match between observations and model predictions. The RI at the stream outlet is 2.0, indicating that a model predicts the observations within a multiplicative factor of two, on average.

Control Strategies

Two alternative control strategies are compared for achieving the recreational water quality standard: a stormwater sand-filtration best management practice and an ultraviolet (UV) disinfection process. The two alternatives represent the two extremes of commonly implemented stormwater control strategies; the BMPs are generally less expensive but have uncertain performance, while the UV disinfection process has well documented performance at a great expense (Perdek, Arnone et al. 2003). The posterior predictive distributions of concentration in each flow condition are used to compare the percent of time that the waterbody is in compliance with the recreational standard pre- and post- control strategy implementation.

The first control strategy, the stormwater BMP is a sand-filtration sock or box that fits into the stormwater culverts and filters only the collected stormwater. The BMP performance was estimated by Hipp *et. al.* using benchscale testing with bacterial suspensions ranging between 10,000-80,000 cfu/100ml at a flow rate of 0.1 cfs (2006). The BMP performance is incorporated into the model using three alternative approaches; all three approaches assume that all stormwater is treated without bypass. The first is a constant load reduction approach, similar to what is assumed in HSPF. The constant load reduction is set at 46.0% as reported from the benchscale removal efficiency by Hipp *et. al.* (2006). This constant load reduction is applied to the posterior predictive distribution of load for the high flow condition.

The aggregated data on stormwater Best Management Practices (BMP) performance in the National Pollutant Removal Performance Database (Winer 2000) and the

International Stormwater BMP Database (Wright Water Engineers 2007) indicate that there is significant variability in the performance of BMPs. Therefore, the second two techniques incorporate uncertainty in load reduction performance. A lognormal distribution with parameters estimated using the method of moments, a sample mean of 46.0%, and sample standard deviation based on the benchscale performance at 36.0% is used to represent variability in the BMP performance. In addition, a uniform distribution is compared with lower and upper limits set at 9.0% and 92.0% to match the mean performance and standard deviation. Each method is applied to the posterior predictive distribution of load for the high flow condition through Monte Carlo sampling of percent reduction.

The BMP performance is compared to a more aggressive control strategy, an ultraviolet (UV) disinfection process using low-pressure mercury lamps with a wavelength of 25.7 nm. The performance of the UV disinfection process is measured as a rate of inactivation. The natural log of the rate of inactivation is assumed to follow the first-order reaction (Droste 1997):

$$\log(\frac{N}{N_0}) = -KD$$

where
N and N_0 are the concentration of bacteria at time t and initially (cfu/100ml)
K is an inactivation coefficient (cm^2/J)
D is radiation dose (mW/cm^2)

The radiation dose D is a function of the initial intensity of radiation and the time to which the organism is exposed to radiation:

$$D = (I_0 e^{-kd})t$$

where
I_0 is the initial intensity of radiation (mW/cm^2)
k is the absorbance coefficient (base e) (cm^{-1})
d is the depth of water (cm)
t is the exposure time (s)

The radiation dose is affected by flow in two ways. The time of exposure and intensity of radiation decreases as flow increases, decreasing the radiation dose. Here, the depth is assumed to increase proportional to the flow rate while time decreases proportional to the flow rate. In this way, the performance of the UV process changes based on the flow conditions.

To model UV performance, the absorbance coefficient k is set at 0.125 cm^{-1} to represent natural waters and the model is parameterized to achieve a 0.01 rate of inactivation for the 90th percentile stormwater flow rate of 0.25 cfs. The linear relationship between log inactivation and radiation dose is then used to solve for the

rate of inactivation given an observed flow and concentration from the posterior predictive distribution. This process is repeated for the 80th percentile flow of 0.15 cfs. In contrast to the stormwater BMP, the UV disinfection process treats the in-stream bacterial loads under all flow conditions.

Results

The Bayesian LDC results include the posterior predicted distribution of in-stream *E. coli* concentration during the recreational season for the outlet of Panther Hollow Stream, the estimated load reductions necessary to meet the recreational water quality standard, and the predicted distribution of bacterial concentration post-implementation of the various control strategies. All results are based on the posterior distributions of the truncated bivariate normal parameter estimates.

Table 1 shows the mean posterior parameter estimates $\theta_{y,c} = (\mu_{y,c}, \sigma_{y,c}, \rho_c, \sigma_{y|x,c})$ along with 95% credible intervals (CI). The mean posterior parameter estimates of bacterial concentration, standard deviation, and conditional standard deviation for the high flow condition are larger than those of the low flow condition. This suggests that during periods of high flows, the concentration of indicator bacteria is higher and more variable than during periods of lower flow; however, there is overlap in the 95% CI among parameter estimates for the different conditions. Looking at the correlation coefficients, the high and low flow conditions have strong positive relationships between flow and concentration. The differences in parameter estimates among the flow categories are displayed in Figure 3. The posterior predictive checks in Figure 3 show the posterior predictive distributions, observed maximum likelihood parameter estimates, and Bayesian p-values for the mean and standard deviation of concentration for each flow condition, $\mu_{y,c}$ and $\sigma_{y,c}$. The Bayesian p-value range between 0.21 and 0.62 indicates that the observed data are plausible under the posterior predictive distributions.

Table 1. MCMC Parameter Estimates. Parameter estimates for concentration are shown in $\log_{10}$ units for low, normal and high flow conditions (1,2,3). Mean estimates are shown in the first row and the 95% CIs are shown in parenthesis.

	Condition		
Parameter	**1**	**2**	**3**
$\mu_{y,c}$	2.792	2.655	3.172
	(2.391,3.003)	(2.413, 2.879)	(2.669, 3.670)
$\sigma_{y,c}$	0.500	0.673	0.700
	(0.364, 0.708)	(0.370, 1.384)	(0.482, 1.013)
ρ_c	0.490	0.240	0.564
	(-0.050, 0.813)	(-0.846, 0.931)	(0.033, 0.839)
$\sigma_{y\|x,c}$	0.409	0.476	0.544
	(0.337, 0.502)	(0.336, 0.702)	(0.383, 0.769)

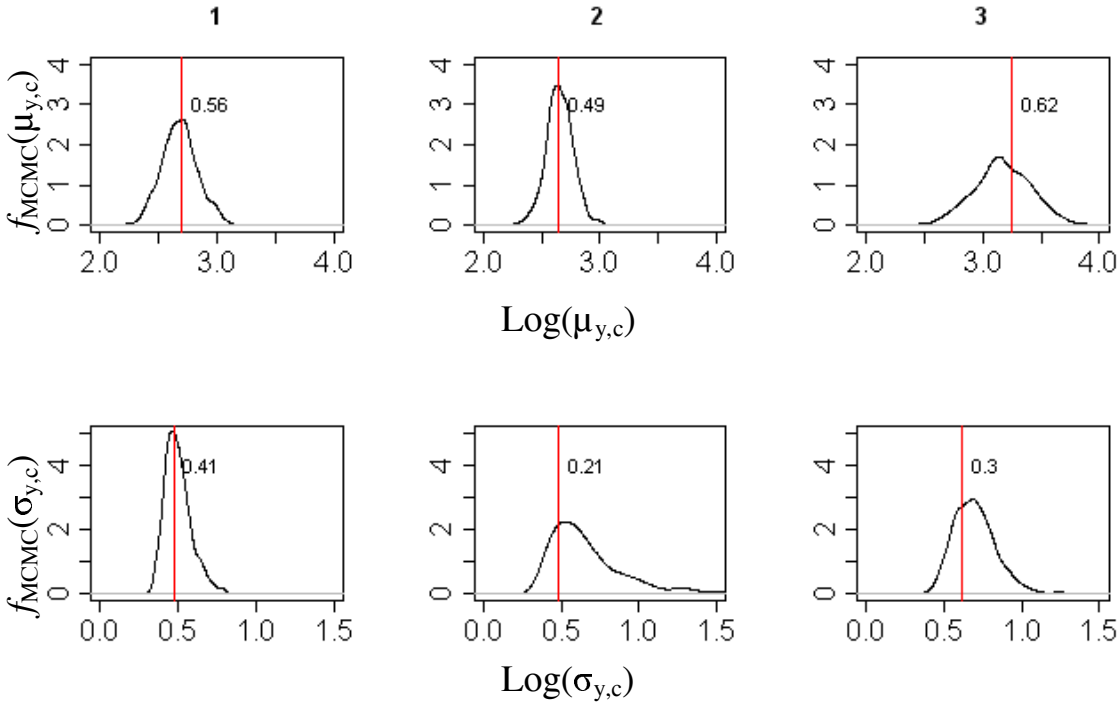

Figure 3. Posterior Predictive Check. The posterior predictive distributions, observed maximum likelihood estimates, and Bayesian p-values for $\mu_{y,c}$ and $\sigma_{y,c}$ are shown for $\log_{10}$ transformed variables with the flow conditions increasing in magnitude from left to right.

The resulting posterior predictive cumulative distribution function (CDF) of recreational season concentration at the stream outlet is shown in Figure 4. In Figure 4, the CDF for bacterial concentration is represented as a bold line with the allowable in-stream *E. coli* concentration set by the standard (235 cfu/100ml) shown as a vertical line. The posterior predictive CDF predicts that the in-stream indicator bacterial concentration exceeds the limit 73.4% of the time during the recreational season with a 95% credible interval CI(71.9%, 74.8%). Figure 4 also shows the CDFs for each flow condition, with exceedance probabilities 57.4% CI(54.2%, 60.1%), 73.5% CI(70.7%, 76.0%), and 97.8% CI(96.9%, 98.6%). Since each flow condition has a unique posterior predictive CDF, the load reductions required to meet the water quality standard vary for each flow condition.

The estimated load reductions necessary to meet the recreational water quality standard for Panther Hollow Stream are shown in Figure 5. Figure 5 displays the components of the traditional LDC approach necessary for a TMDL analysis: the flow CDF (the complement to the *DC(Q)*), represented as a dashed line; the CDF of the allowable in-stream bacteria load for the recreational season (the complement of *DC(W)*), represented a solid line; and estimates of the 90th percentile in-stream bacterial load, represented as closed circles. The x-axis of Figure 5 measures flow

$\log_{10}(Q)$ (cfs) and in-stream bacteria load $\log_{10}(W)$ (cfu/s), and the y-axis measures density values. Unlike the traditional approach, the Bayesian LDC displays the expected posterior predictive estimate of the 90th percentile in-stream load E[90th[log[W]|log[Q]]] for six representative flows. The black bars show the 95% CI for the predicted 90th percentile loads. All of the Bayesian model predictions of expected 90th percentile load are to the right of the allowable in-stream load, indicating that load reductions are necessary. The Bayesian percent load reductions (*PRB*) for each flow are presented using the mean of the posterior predictive 90th percentile loads.

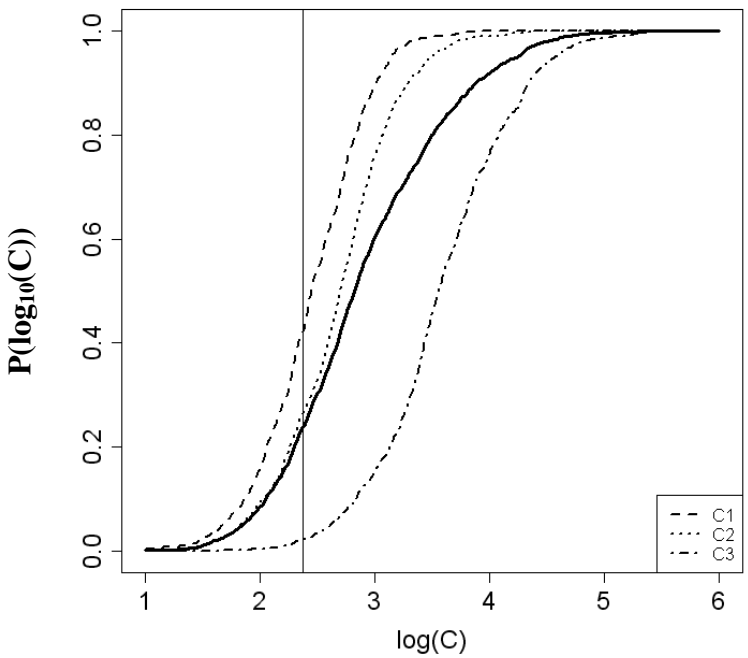

Figure 4. Posterior Predictive Recreational Season Cumulative Distribution of Concentration. The CDF for $\log_{10}(C)$ (boldface) is compared to the recreational standard of 235 cfu/100ml *E. coli*. The posterior predictive CDFs for each flow condition are also shown (C1, C2, and C3).

Looking at the *PRB* estimates, the lower flows with $P(\log_{10}(Q))\leq 0.1$ have the lowest percent reductions with a best estimate of 68%, respectively. As flow increases, the load reduction also increases so that at high flows ($0.9<P(\log_{10}(Q))\leq 1.0$) a 99.9% reduction in load is required to meet the water quality standard. These results are consistent with the bacterial load reductions estimated for other urban streams under high flow conditions; for example, the bacterial load reductions during periods of high flow estimated in the US EPA technical guidance are 99% for Muddy Creek, VA; 93% for Pee Dee River, SC; and 92% for Waldo Creek, MI (EPA 2001, 2007).

The posterior predictive cumulative distribution of recreational season concentration for Panther Hollow watershed incorporating the control strategy reduction in load is

displayed in Figures 6 and 7. Figure 6 presents the predicted concentration distributions for the BMP control strategy and Figure 7 presents the results for the UV disinfection process. Both figures display the CDF for the no-control strategy for comparison. Figure 6 also displays the CDFs for the high flow condition to illustrate the effect of BMP performance uncertainty on predicted exceedances. The low and normal flow conditions' CDFs are not displayed and remain the same as the no-control strategy for the stormwater BMP control strategy and are reduced to zero cfu/100ml for the UV disinfection process.

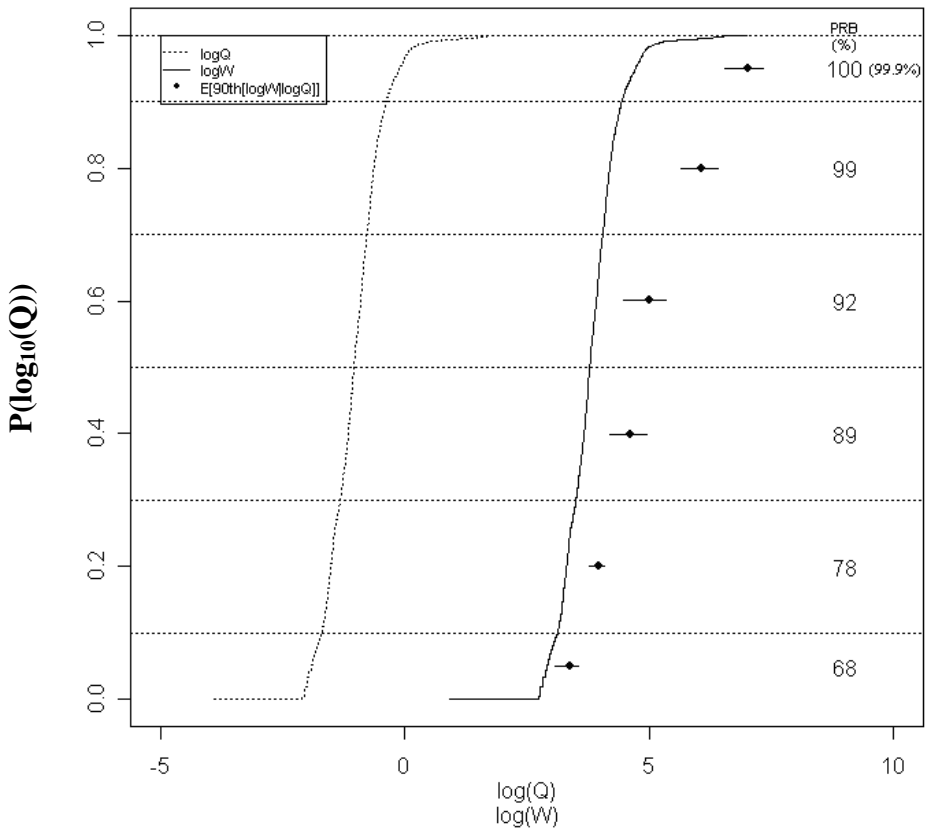

Figure 5. Cumulative Distribution Function of Allowable Load for the Recreational Season with 90th Percentile In-Stream Load Predictions. The figure displays the CDF for flow along with the CDF of the allowable in-stream bacteria load for the recreational season. The x-axis measures flow, $\log_{10}(Q)$ (cfs), and in-stream bacteria load, $\log_{10}(W)$ (cfu/s), and the y-axis measures density values. The Bayesian model predictions of expected 90th percentile load, E[90th[log[W]|log[Q]]], for six representative flows are shown as dots. The black bars show the 95% CI for the Bayesian predicted loads. The Bayesian percent load reductions *PRB* for each percentile are presented using the best estimate 90th percentile loads at each flow.

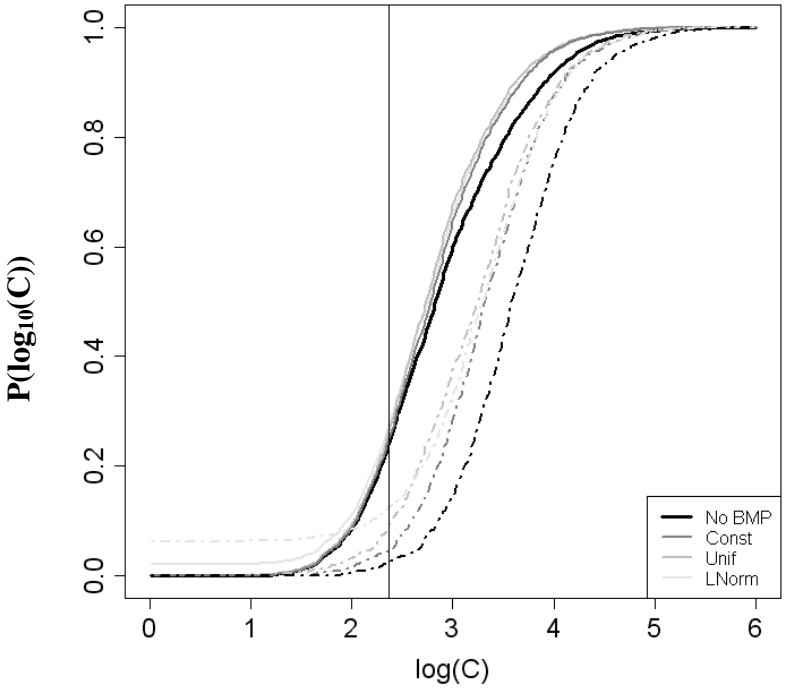

Figure 6. Posterior Predictive Cumulative Distribution of Recreation Season Concentration with BMP Percent Reduction. The overall CDF for $\log_{10}(C)$ with and without BMP load reduction is compared to the standard of 235 cfu/100ml *E. coli*. The high flow condition CDF is shown as dashed type for comparison.

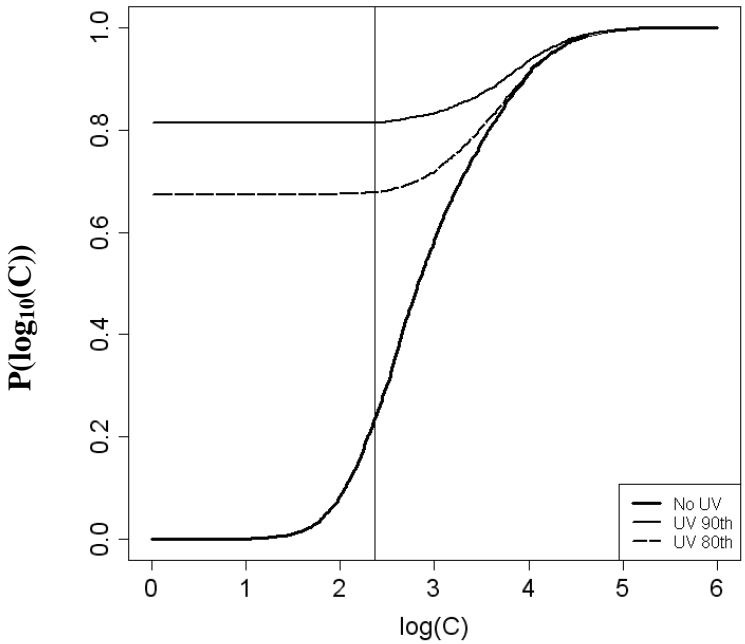

Figure 7. Posterior Predictive Cumulative Distribution of Recreation Season Concentration with UV Disinfection. The overall CDF for $\log_{10}(C)$ with and without UV disinfection is compared to the standard of 235 cfu/100ml *E. coli*.

In the high flow condition, the constant 46.0% load reduction *Const* and the uniform representation of load reduction *Uniform* predict percent exceedances not significantly different from the no-control strategy simulation *None* for the high flow condition, 94.4% CI(92.7, 95.9) and 93.7% CI(92.1, 95.2). Table 2 lists the percent exceedances for each control strategy along with the 95% CI. The percent of time that the outlet of Panther Hollow Stream is above the maximum water quality limit is listed for the stormwater BMP control strategy and the ultraviolet disinfection process designed for the 80th and 90th percentile flows. The percent exceedances for alternative methods of representing the performance measure of the stormwater BMP are compared. The alternative methods include no-control strategy implementation, a constant 46% load reduction, a uniform distribution for load reduction, and a lognormal distribution for load reduction.

Table 2. Percent Exceedances for Each Flow Condition Under Alternative Control Strategies.

C	*None*	*Const*	*Uniform*	*LNormal*	*UV 80th*	*UV 90th*
1	57.4 (54.2,60.1)				0 (0,0)	0 (0,0)
2	73.5 (70.7,76.0)				0 (0,0)	0 (0,0)
3	97.8 (96.9,98.6)	94.4 (92.9,95.6)	90.3 (88.6,92.2)	87.1 (84.7,89.3)	95.0 (93.6,96.4)	54.3 (51.5,56.7)
Overall	76.1 (74.6,77.3)	75.1 (73.5,76.4)	73.8 (72.0,75.8)	72.7 (71.1,74.9)	31.1 (31.2,32.2)	18.1 (17.1,18.9)

*95%CI in parenthesis

Similar to the high flow condition, the *Const* and *Uniform* overall percent exceedances are not significantly different from the no-control strategy. The predictions using the lognormal representation of the BMP performance *LNormal* for the overall and high flow conditions are significantly lower than that of the no-control strategy. The lognormal representation of percent load reduction with mean 46.0% and standard deviation 32.0% predicts that the high flow condition exceeds the standard 86.5% CI(84.7, 88.7) of the time during the recreational season with an overall exceedance of 72.4% CI(70.6, 74.3). Overall, the stormwater BMP shows minimal improvement in indicator bacterial concentration from the no-control strategy.

The water quality after the UV disinfection process, displayed in Figure 7, shows dramatic reductions in in-stream *E. coli* concentration. In Figure 7, the CDF of concentration with no intervention is compared to the CDFs given a UV process designed to eliminate 99% of the organisms at the 90th and 80th percentile flows. As expected, the percent exceedance of the water quality standard drops to 18.1% CI(17.1, 18.9) and 31.1% CI(31.2, 32.2) using the aggressive UV disinfection process. Still, the variability in UV disinfection performance due to changes in dilution and exposure time results in in-stream bacterial concentrations in exceedance of the recreational water quality standard during extreme flow events.

Discussion

The motivation for this work is the need for a TMDL model that will increase TMDL development and implementation progress. The Bayesian model is able to utilize sparse, diffuse data to increase TMDL progress while explicitly communicating uncertainty in load reduction results. The new TMDL model also enables the prediction of water quality given a specific control strategy performance and its associated performance uncertainty. In the Panther Hollow TMDL demonstration, the Bayesian water quality model is used to predict water quality pre- and post-implementation of alternative control strategies. The post-implementation predictions using a sand-filter BMP and aggressive disinfection process demonstrate that it is not possible to bring the waterbody into compliance without aggressive, potentially expensive controls. However, as pointed out by the TMDL program reviews, an evaluation of the control strategy is not part of the minimal TMDL requirements (EPA 2002). Without this evaluation, the implementation of BMPs is likely to have minimal effect on the overall water quality of urban streams with high levels of bacterial contamination.

The structure of the model presented here allows for evaluation of alternative control strategies and the propagation of uncertainty in control strategy performance through to the predicted distribution of post-implementation indicator bacterial concentration. The US EPA has identified the lack of knowledge about BMP performance as a crucial research gap (EPA 2002). Here, the predicted distribution of bacterial concentration for a sand-filter stormwater BMP using a constant percent load removal assumption has a percent exceedance statistically different than that of a variable load removal. Although the predicted water quality may be sensitive to the uncertainty in BMP performance, the representation of control strategy performance uncertainty in existing models is limited and is difficult to incorporate given the lack of field performance data.

The presented Bayesian Load Duration Curve model is a potentially powerful approach for creating management plans for watersheds with limited data. Still, progress in TMDL implementation will continue to be limited until evaluation of the control strategy is mandatory as part of the minimal TMDL requirements, and additional research provides more detailed performance measures for Best Management Practices.

Acknowledgments
Funding for this work was provided by the Center for Water Quality in Urban Environmental Systems (WaterQuest) at Carnegie Mellon University and by Three Rivers Wet Weather, Inc. and by the Pittsburgh Parks Conservancy (PPC).

Benham, B. L., C. Baffaut, et al. (2006). Modeling bacteria fate and transport in watersheds to support TMDLs. ASABE Annual International Meeting Portland, Oregon.

Bicknell, B. R., J. C. Imhoff, et al. (2001). Hydrological Simulation Program - Fortran (HSPF). Reston, VA, EPA National Exposure Research Laboratory, Athens, GA, in cooperation with U.S. Geological Survey, Water Resources Division.

Bonta, J. V. and B. Cleland (2003). "Incorporating natural variability, uncertainty, and risk into water quality evaluations using duration curves." Journal of the American Water Resources Association **39**(6): 1481-1496.

Borah, D. K. and M. Bera (2003). "Watershed-scale hydrologic and nonpoint-source pollution models: Review of mathematical bases." Transactions of the ASCE **46**(6): 1553-1566.

Borah, D. K. and M. Bera (2004). "Watershed-scale hydrologic and nonpoint-source pollution models: Review of applications." Transactions of the ASAE **47**(3): 789-803.

Cohen, A. C. (1955). "Restriction and selection in samples from bivariate normal distributions." Journal of the American Statistical Association **50**(271): 884-893.

Donigian, A. S. and W. C. Huber (1991). Modeling of nonpoint source water quality in urban and non-urban areas. U. S. E. P. Agency.

Droste, R. L. (1997). Theory and Practice of Water and Wastewater Treatment. New York, John Wiley & Sons, Inc.

EPA (2007). An approach for using load duration curves in the development of TMDLs.

EPA, U. S. (2001). Protocol for developing pathogen TMDLs. Office of Water.

EPA, U. S. (2002). The Twenty Needs Report: How Research Can Improve the TMDL Program. Office of Water.

Gelman, A., J. B. Carlin, et al. (2004). Bayesian Data Analysis. New York, Chapman and Hall/CRC.

Gelman, A. and D. B. Rubin (1992). "Inference from iterative simulation using multiple sequences." Statistical Science **7**(4): 457-472.

Hipp, J. A., O. Ogunseitan, et al. (2006). "Optimization of stormwater filtration at the urban/watershed interface." Environmental Science & Technology **40**(15): 4794-4801.

Hobbs, B. F. (1997). "Bayesian methods for analyzing climate change and water resource uncertainties." Journal of Environmental Management **49**(1): 53-72.

Horn, A. L., F. J. Rueda, et al. (2004). "Implementing river water quality modeling issues in mesoscale watershed models for water policy demands - an overview on current concepts, deficits, and future tasks." Physics and Chemistry of the Earth **29**(11-12): 725-737.

Leggett, R. W. and L. R. Williams (1981). "A Reliability Index for Models." Ecological Modeling **13**(4): 303-312.

Perdek, J. M., R. D. Arnone, et al. (2003). "Managing Urban Watershed Pathogen Contamination." Cincinnati, OH, National Risk Management Research Laboratory, US EPA.

Searcy, J. K. (1963). "Flow Duration Curves." Department of the Interior, U.S. Government Printing Office.

Shanahan, P., M. Henze, et al. (1998). "River water quality modeling: II. Problems of the art." Water Science and Technology **38**(11): 245-252.

Spiegelhalter, D. J., A. Thomas, et al. (1999). WinBUGS Version 1.2 User Manual, MRC Biostatistics Unit.

Stow, C. A., C. Roessler, et al. (2003). "Comparison of estuarine water quality models for total maximum daily load development in Neuse River Estuary." Journal of Water Resources Planning and Management-Asce **129**(4): 307-314.

Three Rivers Wet Weather (2007). Calibrated Rainfall Data.

Vogel, R. M. and N. M. Fennessey (1995). "Flow Duration Curves 2: A Review of Applications in Water-Resources Planning." Water Resources Bulletin **31**(6): 1029-1039.

Wilkinson, J., A. Jenkins, et al. (1995). "Modeling feacal coliform concentrations in streams." Oxfordshire, U.K., Institute of Hydrology.

Winer, R. (2000). National Pollutant Removal Database for Stormwater Treatment Practices. Ellicott City, MD, Center for Watershed Protection.

Wright Water Engineers, WERF, the American Society of Civil Engineers (ASCE)/Environmental and Water Resources Institute (EWRI), the American Public Works Association (APWA), the Federal Highway Administration (FHWA), and the U.S. EPA (2007). International Stormwater BMP Database.

Bioretention/Bioinfiltration Performance in the Mid-Atlantic

R. A. Brown,[1] W. F. Hunt,[2] A. P. Davis,[3] R. G. Traver[4], and J. M. Olszewski[5]

[1]Graduate Research Assistant, Department of Biological and Agricultural Engineering, North Carolina State University, Campus Box 7625, Raleigh, NC 27695-7625; e-mail: rabrown4@ncsu.edu
[2] Assistant Professor & Extension Specialist, Department of Biological and Agricultural Engineering, North Carolina State University, Campus Box 7625, Raleigh, NC 27695-7625; PH(919)515-6751; e-mail: bill_hunt@ncsu.edu
[3] Professor, Department of Civil and Environmental Engineering, University of Maryland, College Park, MD 20742; PH(301)405-1958; e-mail: apdavis@umd.edu
[4] Professor, Department of Civil and Environmental Engineering, Villanova University, 800 Lancaster Avenue, Villanova, PA 19085; e-mail: robert.traver@villanova.edu
[5] Undergraduate Student, Department of Civil and Environmental Engineering, University of Maryland, College Park, MD 20742; e-mail: jolszew2@umd.edu

Abstract

Researchers in Maryland, North Carolina, and Pennsylvania have been conducting parallel bioretention/bioinfiltration research since fall 2007. Various designs have been tested including those that rely on underdrains, have internal water storage (IWS) layers, or are underdrain-free. The cells provide a range of watershed practice size ratios and employ a variety of land covers. Researchers are pooling water quantity and quality data to help create new design standards. Initial results from the shared data will be presented, with specific attention to bioretention design parameters that control flow modification and water quality improvement.

Two bioretention cells of varying vegetative cover are being monitored in Rocky Mount, NC. This site is located in the upper coastal plain with sandy in-situ soils. These cells were designed with a 0.9 m media depth and a 0.6 m deep internal water storage (IWS) layer. Another bioretention cell is being monitored in Silver Spring, MD. It was constructed with a 0.9 m media depth and a 0.3 m pooling depth. Finally, there are two bioinfiltration cells being monitored in Villanova, PA. The first is the "Traffic Island" bioinfiltration cell, which has been monitored since 2003. The bowl is only designed for 1.2 cm over the impervious surface, yet overflow rarely occurs for events less than 5.1 cm. The site had groundwater wells installed in 2007 and is the subject of an ongoing study on the groundwater effects. The second site has only been monitored for approximately six months.

Cumulatively, the four bioretention cells extensively examined have dramatically reduced outflow volumes, completely assimilating all events less than 1.2 cm – and in some designs much greater events. By aggregating the data, runoff reduction by bioretention can be profound.

Keywords: Bioretention; bioinfiltration; low impact development; hydrology; pollutant removal; and nutrients.

Introduction

Stormwater managers are faced with controlling increased flooding, altered hydrology, and high pollutant loads associated with impermeable and reduced permeability surfaces (USEPA, 1983). Streets and parking lots generate a large proportion of urban runoff, and these areas derive most of their pollutant loads from automobiles (Barrett et al., 1998). Atmospheric deposition also contributes a substantial amount of certain pollutant loads (Wu et al., 1998). As part of the National Water Quality Inventory, 32% of estuaries and 47% of lakes/reservoirs that were assessed were identified as impaired. Nutrients were the main cause of impairment, and urban stormwater runoff was the number three source (U.S.EPA, 2007). Regionally, two of the most productive estuaries in the U.S. are the Pamlico and Albemarle Sounds in North Carolina (NCDWQ, 2003) and the Chesapeake Bay in the Middle Atlantic States (Chesapeake Bay Program, 2008).

To reduce the negative effects caused by urbanization and to meet the new stormwater rules, strategies such as stormwater Best Management Practices (BMPs) or Low Impact Development (LID) technologies are used. The goal of LID is to develop a site that preserves or meets target hydrologic conditions (Davis, 2008). Bioretention is a very common LID practice, as it serves three major functions: (1) hydrologic, (2) water quality, and (3) aesthetic.

Bioretention combines a natural and engineered system to manage stormwater from developed areas. One design goal is treating the "first flush" runoff (Davis et al., 2009). Bioretention removes pollutants from runoff through adsorption, biological decomposition, filtration, and sedimentation. Metals are removed in the mulch layer through its high capacity for binding metals (Davis et al., 2001). Evapotranspiration (ET) and exfiltration play major roles in volume reduction in a bioretention cell, which are important for pollutant load reduction (Heasom et al., 2006; Hunt et al., 2006; and Li et al., 2009).

Previous bioretention research shows good removal rates and low effluent concentrations for total nitrogen (TN), total Kejhdhal nitrogen (TKN), heavy metals, oil/grease, and total suspended solids (TSS) in both field (Dietz and Clausen, 2006; Davis et al., 2006; Hunt et al., 2006; and Hunt et al., 2008) and laboratory studies (Davis et al., 2001; Hsieh and Davis, 2005; and Davis et al., 2006).

Kim et al. (2003) proposed including an overdrain to create a continuously submerged anoxic zone to promote denitrification. The results from pilot-scale bioretention studies were 70 to 80% mass removal rates of nitrate plus nitrite ($NO_{2,3}$-N). Despite these positive laboratory results, later field studies by Hunt et al. (2006) and Dietz and Clausen (2006) were inconclusive about adding a saturated layer (Figure 1) to create anaerobic conditions required to convert nitrate into nitrogen gas. A field study by Davis (2007) had limited data, but it showed high removal rates of nitrate. Passeport et al. (2009) also had promising field results. Two grassed bioretention cells with different in-situ soils were studied. The study showed significant reduction in nitrate for one of two cells examined. Passeport et al. (2009) believed this was due to the longer saturation period maintained in the one cell surrounded by tight clay, but recommended that the role of in-situ soils be further explored in future studies.

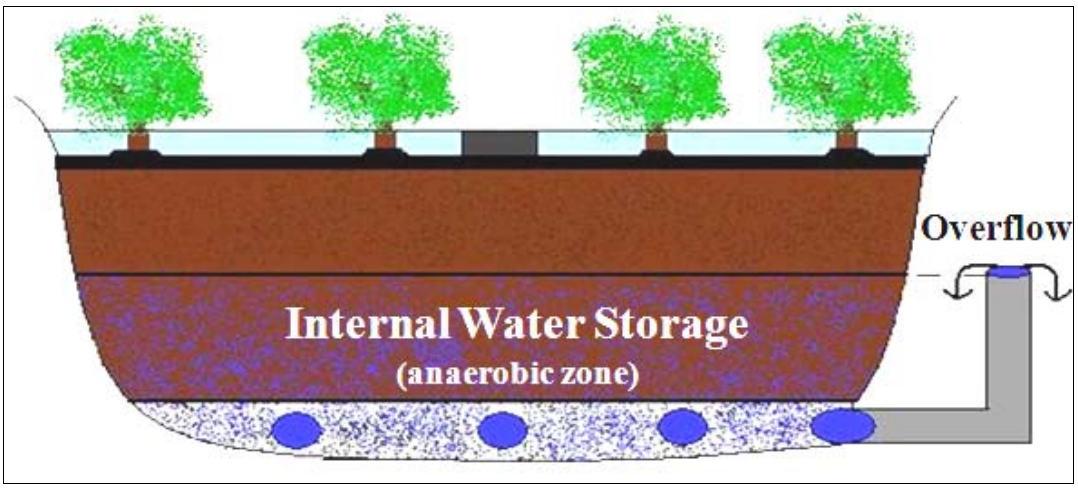

Figure 1. Schematic of bioretention cell with internal water storage (IWS) zone.

Site Descriptions

Rocky Mount, North Carolina

Two bioretention cells are situated in the parking lot for the Imperial Centre in downtown Rocky Mount. They were constructed in the winter of 2005/2006. Current monitoring began in September 2007. There are two bioretention cells at this site (Figure 2). One was planted with shrubs, perennials, and trees (mulch/shrub cell) and the other with centipede turf (grassed cell). Both cells were designed with a 0.6 m (2 ft) deep IWS zone. The IWS zone was created by attaching a 90 degree PVC elbow to the underdrain. The fill media is 0.9 m (3 ft) deep for both cells. In January 2009, the IWS layer was reduced to 0.3 m (1 ft) deep to characterize performance with a shallower IWS zone. Data presented herein are only for the 0.6 m IWS condition.

The range of the P-Index (Hardy et al., 2007) in both cells was low (6-15). Particle size analyses on the fill media were measured using the hydrometer method and determined the fill media was 98% sand and 2% fines (silt & clay). The sand content in the fill media at this site is greater than the sand content (85-88%) recommended in the North Carolina bioretention design guidelines (NCDWQ, 2007). A summary of the site characteristics are found in Table 1.

Table 1. Rocky Mount bioretention watershed and cell characteristic summary.

Actual Characteristics	**Grassed Cell**	**Mulch/Shrub Cell**
Bioretention Cell Area	146 m^2 (1575 ft^2)	142 m^2 (1530 ft^2)
Watershed Area	2200 m^2 (0.54 ac)	2450 m^2 (0.61 ac)
Watershed % Impervious	76%	72%
Fill Media Depth	0.9 m (3 ft)	
IWS Depth (2007-2008)	0.6 m (2 ft)[1]	
IWS Depth (2009-current)	0.3 m (1 ft)	
P-Index of Fill Media	6-15 (Low)	

[1]Only data from this design configuration are presented



Figure 2. Bioretention cell images: mulch/shrub (left) and grassed (right).

Silver Spring, Maryland

Located at the base of the Dennis Avenue Health Center parking lot, the Silver Spring cell was constructed in 2005. Current monitoring began in May 2008. Shrubs and trees were planted in a top layer of mulch. Below the mulch is a permeable soil layer, followed by a sand layer, and finally a gravel layer. The design for the media required a minimum of 10% clay, 30-55% silt, and 35-60% sand. In the gravel layer, 15.2 cm (6 in) perforated PVC pipes were installed to conventionally drain the cell to the existing stormwater network. A summary of the site characteristics is given in Table 2. Images of the bioretention cell and an aerial view of the entire site appear in Figure 3. In the aerial view, the cell is outlined in red.



Figure 3. Silver Spring bioretention cell (left) with aerial view of the site (right).

Table 2. Silver Spring bioretention cell characteristic summary.

Characteristic	**Values**
Bioretention Cell Area	102 m^2 (1096 ft^2)
Watershed Area	4500 m^2 (1.11 ac)
Watershed % Impervious	85%
Fill Media Depth	0.9 m (3 ft)

Villanova Pennsylvania

The bio-infiltration BMP is located in a grassy traffic island in the parking lot of Villanova's West Campus. The West Campus parking lot serves a dormitory complex and a recreation area. The traffic island was retrofitted into the shape of a shallow bowl, allowing the inflow of water to accumulate within. Constructed in 2001, the site has been monitored for water flow since 2003 and for quality in 2004. Bio-infiltration is accomplished by using a combination of porous soils and vegetation. The media consists of a 4-foot layer of sand mixed with the existing soil located at the traffic island. The species of vegetation planted at the site can survive in both dry and wet conditions over long periods of time. The area also has a grass buffer zone extending from the curb to the fill media. Outflow is through a bypass weir utilizing the original culvert system or by infiltration. The traffic island has no underdrains. A summary of the site characteristics is given in Table 3. Images of the cell along with a close up during a storm event are shown in Figure 4.

Table 3. Villanova bioinfiltration characteristic summary.

Characteristic	**Values**
Cell Area (Bottom)	149 m^2 (1600 ft^2)
Post Rainfall Bowl Recession Rate	0.5 to 2.5 cm/hr (0.2 ~ 1 in/hr)
Watershed Area	5261 m^2 (1.3 ac)
Watershed % Impervious	50%
Bowl Storage (Watershed cm)	1.5 cm (0.59 in)
Fill Media Depth	1.22 m (4 ft)



Figure 4. Villanova bioinfiltration cell (left) and close up during storm event (right).

Methods

Rocky Mount, North Carolina

The monitoring equipment used at both sites include: ISCO 6712 Automated Portable Samplers to monitor hydrology and collect flow-weighted composite samples, ISCO 730 Bubbler Flow Modules in combination with 30° weirboxes to measure outflow at both sites, and ISCO 674 Rain Gauges to measure rainfall. The Soil Conservation Service - Curve Number (SCS-CN) discrete method was used to estimate runoff volumes at Rocky Mount. Runoff enters the cells as diffuse flow from all angles, so a collection trough was installed to collect a representative sample of

runoff. Rainfall (0.51 mm in 15 min) triggers the sampler to enable, and once enough liquid has ponded in the trough, the sampler pulls a sample. Flow-weighted composite samples were analyzed for nutrients and TSS. The nutrient species being analyzed include: Ortho-P, TP, NH_3, $NO_{2,3}$-N, TKN, and TN.

Silver Spring, Maryland

A concrete channel conveys runoff from the parking lot through a 23-cm Parshall flume into the cell. A bubbler meter connected to an ISCO 6712FR Refrigerated Sampler monitoring station records the water level every two minutes. A rain gage placed on top of this inflow station also monitors rain depth. After the runoff infiltrates through the cell, it enters the underdrain and passes through a 15-cm ThelMar plug-in weir connected to a second ISCO 6712FR Refrigerated Sampler, which records the outflow water level at two-minute increments. Based on the dimensions of the flume and weir, set equations were employed to determine the corresponding inflows and outflows. The inflow and outflow volumes are also estimated by using the trapezoidal rule with the inflow and outflow values.

Water samples have not yet been analyzed for water quality values. However, TSS, phosphorous, and other tests will be run in the near future to examine water quality improvement in water exiting the cell compared to the runoff entering it.

Villanova University

A level detector is used to measure the rate of infiltration from the surface bowl, and outflow, which is solely overflow at this site, is measured using a weir in the culvert leaving the site. Soil moisture meters and lysimeters have been placed under and within the cell. Water samples for quality analysis are taken from the water bowl above the fill material. As considerable removal in the stone beds leading to this BMP has been observed, "first flush" flow samplers have been installed to better represent the inflows to the site. These devices are installed to capture water samples where the runoff enters the site through curb cuts. Vadose zone water quality (outflow) is measured using lysimeters located at the bottom of fill material (multiple depths and locations). Surface water outflow (only large storms) grab samples are taken from the bowl. A well was added to the site in 2006 to learn more about the site interaction with the groundwater. In 2007 several more were drilled, and pressure transducers with conductivity meters were added to allow for study of the groundwater hydrology from both the hydrology and environmental perspective.

Results and Discussion

Rocky Mount, North Carolina

Data were collected at Rocky Mount under the 0.6 m deep IWS zone configuration from September 15, 2007, through January 7, 2009. Sixty-eight runoff producing events were monitored for hydrology. The mean and median event sizes were 17.9 and 13.7 mm, respectively. Four events generated outflow from each cell. The magnitude of the events that produced outflow in the grassed cell were 83.3, 65.3, 53.1, and 49.3 mm (3.28, 2.57, 2.09, and 1.94 in). Of these four events, only the 65.3 mm event also produced outflow in the mulch/shrub cell because the other events were of much longer duration and lower intensity. It appeared that the

mulch/shrub cell had higher exfiltration because outflow was not generated by these events. The mulch/shrub cell's runoff was generated by three smaller depth events (38.3, 25.4, and 22.8 mm; 1.51, 1.00, and 0.90 in). Two of these had durations under one hour, so these events were characterized by short duration and high intensity.

Outflow volume vs. runoff volume relationships for the grassed cell and mulch/shrub cell are displayed in Figures 5 and 6, respectively. From field visits during the larger storms, it was observed that runoff entered the emergency overflow for the mulch/shrub cell twice, but it did more frequently for the grassed cell due to a less permeable layer in the surface from a clay layer underlying the centipede turf. Based on survey data, a 19.1 mm (0.75 in) event would generate enough influent volume to produce overflow, assuming no "in storm" infiltration occurred. All of the events that did not produce overflow or outflow had pollutant load removals from the stormwater network of 100%. This site had excellent pollutant removal ability because of its sandy in-situ soils coupled with the internal water storage zone.

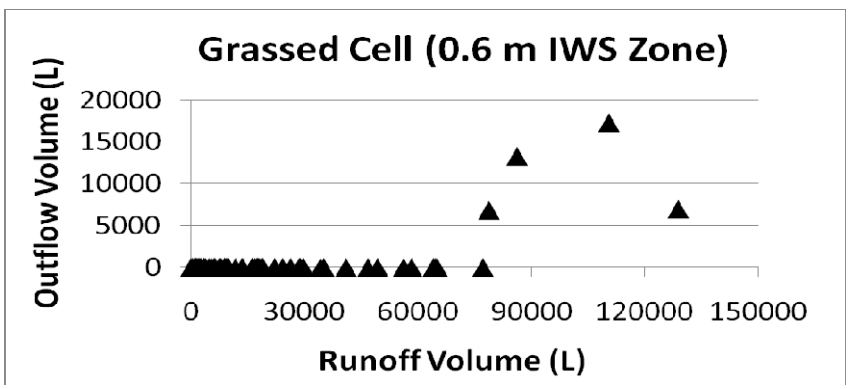

Figure 5. Outflow volume vs. runoff volume for grassed cell in Rocky Mount.

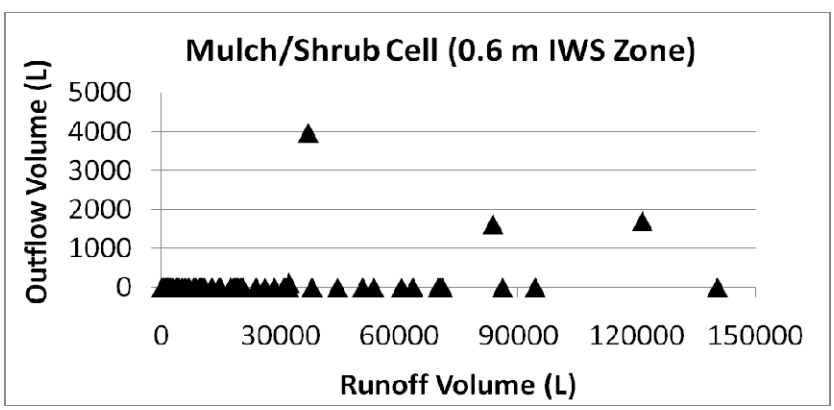

Figure 6. Outflow volume vs. runoff volume for mulch/shrub cell in Rocky Mount.

In January 2008, once it was realized that outflow would not be a regular occurrence due to the presence of the IWS zone, grab samples were taken from the underdrains within 24 to 48 hours after an event. Seventeen events with influent and effluent samples from the grassed cell have been analyzed for all water quality constituents, except for TSS, which has had 14 events analyzed. The grassed cell had a TN, TP, and TSS reductions of 81%, 67%, and 93%, respectively. The water quality results are displayed in Table 4.

Table 4. Preliminary water quality concentration results at Rocky Mount grassed bioretention cell.

	TKN	**$NO_{2,3}$-N**	**TN**	**NH_3-N**	**TP**	**Ortho P**	**TSS**
	(mg/L)	(mg/L)	(mg/L)	(mg/L)	(mg/L)	(mg/L)	(mg/L)
Inflow	1.41	0.36	1.77	0.44	0.18	0.016	122
Grass Cell	0.20	0.15	0.35	0.04	0.06	0.008	8.5
Removal %	**86%**	**59%**	**81%**	**91%**	**67%**	**48%**	**93%**
N	17	17	17	17	17	17	14

Forty-two ambient water quality samples were taken from 1997 to 2002 at the Tar River by NC-97 in Rocky Mount, which is less than 1.2 km (0.75 mi) from the Rocky Mount bioretention site (NCDWQ, 2003). The results indicate the parking lot runoff is a lot dirtier than the water in the Tar River, exceeding the 90th percentile sample for all constituents. The runoff treated by the grassed cell was cleaner than or comparable to ambient conditions in the Tar River. TKN, $NO_{2,3}$-N, and TN were all below the 25th percentile, and NH_3-N and TP were nearly the 50th percentile. The results from TN were especially profound, with inflow exceeding the 90th percentile and outflow similar to the 10th percentile.

Silver Spring, Maryland

Inflow and outflow data have been recorded from 76 events. All storms have shown a reduction in both volume and flow rate from inflow to outflow, and 41 of the events had no outflow. Figure 7 shows the relationship between inflow volume and outflow volume, which has a reduction of volume of 36%. Events with higher inflow produced more outflow. The volumetric capacity of the cell, which is the minimum inflow volume that produces outflow, is estimated to be approximately 16,700 liters or the equivalent of 0.37-cm of rain over the drainage area.

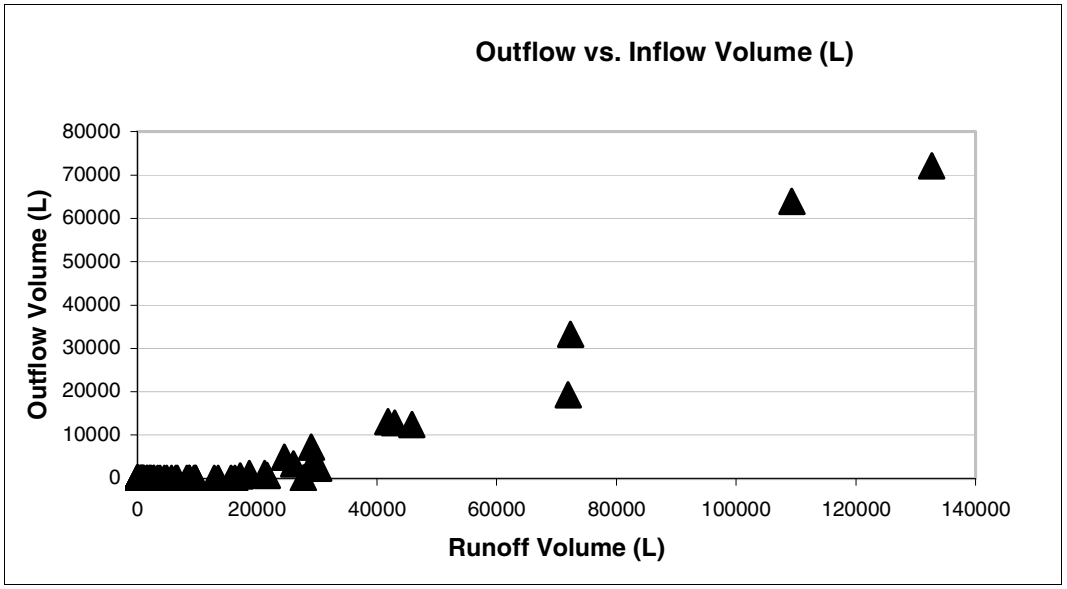

Figure 7. Outflow volume vs. inflow volume at Silver Spring bioretention cell.

Villanova, Pennsylvania

Inflow and outflow data have been recorded from a multitude of events since 2003. Routinely 70 – 85% of the yearly rainfall is captured and infiltrated. Repeating the lessons from Maryland and North Carolina, Volume is reduced for all storms, and a considerable number of events have no outflow (Figure 8).

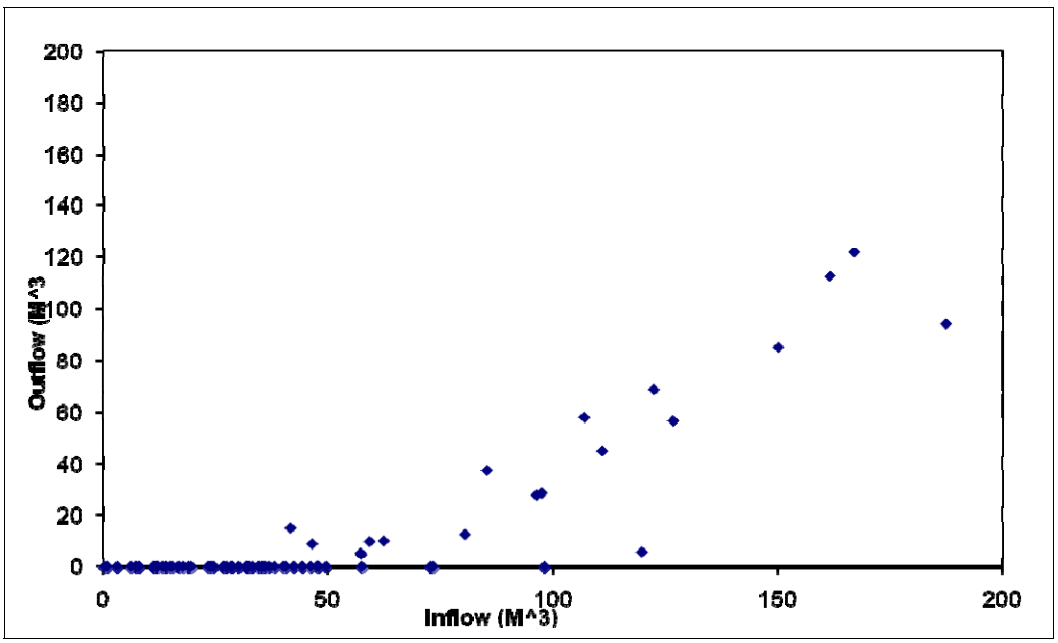

Figure 8. Outflow volume vs. inflow volume at Villanova, PA.

Conclusions and Design Recommendations

- Cumulatively, all four bioretention cells presented have dramatically reduced outflow volumes, often eliminating outflow altogether. All cells completely assimilated events less than 1.2 cm, with some design configurations assimilating even larger events.
- One specific design configuration that was very successful incorporated an internal water storage (IWS) zone at a site with sandy in-situ soils. In Rocky Mount, only four events out of 68 generated outflow in both the grassed and mulch/shrub cell under this design.
- Large flow reduction can have a great effect on pollutant load reduction.
- In a new way to quantify bioretention performance, Rocky Mount bioretention cell data were compared to ambient conditions in the nearby Tar River. The data from this site showed the parking lot runoff was much dirtier than ambient conditions (exceeded the 90th percentile of ambient conditions), while the water treated by the Rocky Mount grassed bioretention cell was cleaner than or comparable to median ambient conditions.

Acknowledgements

This research was funded by The Cooperative Institute for Coastal and Estuarine Environmental Technology (CICEET). The authors would also like to thank Shawn Kennedy, Bill Lord, and Ryan Smith for their assistance and support.

References

Barrett, M. E., Irish, L. B., Malina, J. F., and Charbeneau, R. J. (1998). "Characterization of highway runoff in Austin, Texas, area." *Journal of Environmental Engineering*, 124(2), 131.

Davis, A. P., Hunt, W. F., Traver, R. G., and Clar, M. E. (2009). "Bioretention technology: an overview of current practice and future needs." *ASCE Journal of Environmental Engineering* (in press).

Davis, A. P. (2008). "Field performance of bioretention: hydrology impacts." *Journal of Hydrologic Engineering*, 13(2), 90-95.

Davis, A. P. (2007). "Field performance of bioretention: water quality." *Environmental Engineering Science,* 24(8), 1048-1064.

Davis, A. P., Shokouhian, M., Sharma, H., and Minami, C. (2006). "Water quality improvement through bioretention media: nitrogen and phosphorus removal." *Water Environment Research*, 78(3), 284-293.

Davis, A. P., Shokouhian, M., Sharma, H., and Minami, C. (2001). "Laboratory study of biological retention for urban stormwater management." *Water Environment Research*, 73(1), 5-14.

Dietz, M. E., and Clausen, J. C. (2006). "Saturation to improve pollutant retention in a rain garden." *Environmental Science and Technology*, 40(4), 1335-1340.

Hardy, D. H., Tucker, M. R., and Stokes, C. E. (2007). "Crop fertilization based on North Carolina soil tests." *Circular No. 1,* North Carolina Department of Agriculture and Consumer Services, Agronomic Division, Raleigh, N.C.

Heasom, W., Traver, R. G., and Welker, A. (2006). "Hydrologic modeling of a bioinfiltration best management practice." *Journal of the American Water Resources Association*, 42(5), 1329-1347.

Hsieh, C., and Davis, A. P. (2005). "Evaluation and optimization of bioretention media for treatment of urban storm water runoff." *Journal of Environmental Engineering*, 131(11), 1521-1531.

Hunt, W. F., Jarrett, A. R., Smith, J. T., and Sharkey, L. J. (2006). "Evaluating bioretention hydrology and nutrient removal at three field sites in North Carolina." *Journal of Irrigation and Drainage Engineering*, 132(6), 600-608.

Hunt, W. F., Smith, J. T., Jadlocki, S. J., Hathaway, J. M., and Eubanks, P. R. (2008). "Pollutant removal and peak flow mitigation by a bioretention cell in urban Charlotte, NC." *Journal of Environmental Engineering*, 134(5), 403-408.

Kim, H., Seagren, E. A., and Davis, A. P. (2003). "Engineered bioretention for removal of nitrate from stormwater runoff." *Water Environment Research*, 75(4), 355-367.

Li, H., Sharkey, L. J., Hunt, W. F., and Davis, A. P. (2009). "Mitigation of impervious surface hydrology using bioretention in North Carolina and Maryland." *ASCE Journal of Hydrologic Engineering* (in press).

NCDWQ. (2003). Basinwide assessment report: Tar River basin: April 2003. Raleigh, NC: North Carolina Division of Water Quality.

NCDWQ. (2007). Chapter 12: Bioretention. In *Stormwater Best Management Practices Manual*, 12-1–12-31. Raleigh, NC: North Carolina Division of Water Quality.

Passeport E., Hunt, W. F., Line D. E., Smith R. A., and Brown, R. A. (2009). Field Study of the Ability of Two Grassed Bioretention Cells to Reduce Stormwater Runoff Pollution. *ASCE Journal of Irrigation and Drainage Engineering.* (in press).

USEPA. (1983). Results of the nationwide urban runoff program: Volume I – Final Report, WH-554. Washington, DC: U.S. Environmental Protection Agency.

Wu, J. S., C. J. Allan, W. L. Saunders, and J. B. Evett. (1998). "Characterization and pollutant loading estimation for highway runoff." *Journal of Environmental Engineering*, 124(7), 584-591.

Breaking Down the Barriers to Low Impact Development in Colorado

By Andrew Earles, Ph.D.[1], P.E., D.WRE, Derek Rapp, P.E., CPESC[2], Jane Clary, CPESC[3] and Janice Lopitz[4]

The Keep it Clean Partnership (KICP) is a group of municipalities including Boulder, Erie, Longmont, Louisville and Superior and Boulder County in the Boulder and St. Vrain watersheds that are permittees under the Phase II Stormwater National Pollutant Discharge Elimination System (NPDES) Program. Recognizing that infiltration-based best management practices (BMPs) are often not planned and implemented in situations where they potentially could be successfully used, KICP initiated a study to identify barriers to implementation of Low Impact Development (LID) practices in their watersheds. Barriers identified are broad and include physical, institutional, technical, social and economic factors, some perceived and some real, which act as impediments to more widespread implementation of LID.

The KICP study has included development of a questionnaire that has been circulated to municipal staff, engineers, developers and other parties involved in the development review and approval process. As a part of the study, KICP has developed a checklist for use by developers and by municipal staff reviewing plans to identify potential opportunities for LID and to be sure that the relevant factors that can lead to success or failure of a LID approach are considered in the development review process. Checklists were applied to several proposed development projects to refine the checklists and to identify additional barriers to LID based on "real world" projects. This paper presents the results of the KICP study. Major components of the study discussed in this paper included the following:

1. Identification of potential barriers to design and implementation of LID practices. This was accomplished through a series of several meetings in which participants identified barriers they had encountered and through interviews with planners, engineers and developers.

[1] Vice President of Water Resources, Wright Water Engineers, Inc., 2490 West 26th Avenue Suite 100A, Denver, Colorado 80211. Ph: (303) 480-1700, email: aearles@wrightwater.com.

[2] Project Engineer, Wright Water Engineers, Inc., 2490 West 26th Avenue Suite 100A, Denver, Colorado 80211. Ph: (303) 480-1700, email: drapp@wrightwater.com.

[3] Project Coordinator, Wright Water Engineers, Inc., 2490 West 26th Avenue Suite 100A, Denver, Colorado 80211. Ph: (303) 480-1700, email: clary@wrightwater.com.

[4] KICP Coordinator, Boulder County Public Health , 3450 Broadway, Boulder, CO 80304. Ph: 303-441-1439, email: jlopitz@bouldercounty.org.

2. Development of questionnaire based on barriers identified by the group. The questionnaire was distributed to municipal staff involved in KICP as well as to engineers and developers working in the KICP watersheds. The Homebuilders Association (HBA) of Metropolitan Denver also distributed the questionnaire to members of its water quality committee.

3. Identification of conceptual level strategies to address barriers identified as a part of the study.

The following sections provide an overview of LID and discuss the primary components of the project.

What is LID?

The Low Impact Development Center provides the following definition for LID:

> *Low Impact Development (LID) is an innovative stormwater management approach with a basic principle that is modeled after nature: manage rainfall at the source using uniformly distributed decentralized micro-scale controls. LID's goal is to mimic a site's predevelopment hydrology by using design techniques that infiltrate, filter, store, evaporate, and detain runoff close to its source. Techniques are based on the premise that stormwater management should not be seen as stormwater disposal. Instead of conveying and managing/treating stormwater in large, costly end-of-pipe facilities located at the bottom of drainage areas, LID addresses stormwater through small, cost-effective landscape features located at the lot level. These landscape features, known as Integrated Management Practices (IMPs), are the building blocks of LID. Almost all components of the urban environment have the potential to serve as an IMP. This includes not only open space, but also rooftops, streetscapes, parking lots, sidewalks, and medians. LID is a versatile approach that can be applied equally well to new development, urban retrofits, and redevelopment/ revitalization projects. (http://www.lid-stormwater.net).*

LID is currently included in the water quality guidance published by the Denver Urban Drainage and Flood Control District (UDFCD), a reference used by many municipalities in the area. The LID concept of runoff volume reduction is the first step in the "Four Step Process" for design of best management practices in Volume 3 of the UDFCD Urban Storm Drainage Criteria Manual. LID practices currently included in Volume 3 are planning, minimization of directly connected impervious area, infiltration practices, porous landscape detention, grassed swales and buffers and pervious pavement practices. UDFCD is currently in the process of updating Volume 3 of the USDCM to place more emphasis on volume reduction/LID practices.

Identification of Potential Barriers to LID

Through meetings with KICP, discussions with nationally recognized experts who are members of the American Society of Civil Engineers (ASCE) Environmental and Water Resources Institute (EWRI) Urban Water Resources Research Council (UWRRC), discussions with local municipal reviewers, engineers and developers, the following were identified as potential barriers to implementation of LID in the Front Range of Colorado:

- Fear of liability (engineers, owners, reviewers approving design)
- Reluctance to try something new/lack of demonstration projects
- Lack of education and training
- Lack of common nomenclature (rain garden versus porous landscape detention)
- Limited design examples/good technical documentation
- Costs—design, construction, operation and maintenance, life cycle
- Safety concerns
- Public perception
- LID not integrated early in planning process
- Guidance versus requirements
- Compatibility with existing developments
- Water rights
- Potential for mixed messages from government (different departments)
- No clear economic incentive for using LID
- Difficulty in measuring benefits of LID
- Semi-arid area hydrology
- Maintenance and durability
- Long term ownership/maintenance
- Standing water “nuisance” problems
- Fear of lengthening review process
- Conflicts with municipal code requirements
- American Disabilities Act considerations
- Poorly drained soils and/or high groundwater table
- Expansive soils and construction defect lawsuits
- Other alternatives are “easier”

- LID does not altogether eliminate need for other types of BMPs and drainage infrastructure
- HOA or covenant restrictions (i.e. requirement for irrigated blue grass versus xeriscaped bioretention area)
- Different guidance/criteria from different groups (Center for Watershed Protection [CWP] versus UDFCD versus others)
- Examples of LID failures
- Conflicts with landscaping requirements (i.e. sensitivity of some types of plants to periodic inundation)
- Confusing ordinances
- Iterative versus linear process in coordination with landscapers, planners and others
- Criteria for individual LID BMPs versus overall LID design philosophy
- Requires specialized construction techniques

Many of these barriers were identified as a part of an initial set of workshops with input from KICP and participants from the development community, and others emerged as a part of the development review case studies. For example, in the review of the Redstone Ranch development in Erie a suggested opportunity for improving implementation of LID was limiting sidewalks to one side of the street in selected areas to reduce the overall site imperviousness. Participants in the design review indicated that this would not likely be feasible because a goal of municipal officials and an expectation of the public was to have an easily accessible integrated trail system for pedestrians and cyclists, while minimizing street crossings to get from one trail to another to avoid conflicts with motorized traffic.

Questionnaire

To assess the relative importance of each of these barriers, the project team created a questionnaire to gage participants' experience level with LID and to examine the relative importance of each of these barriers. The questionnaire also requested that participants note their role in the development process (municipal, engineer, developer, etc.) and to rank the significance of barriers on a scale of 1 to 5, with 1 corresponding to a minor barrier and 5 corresponding to a significant barrier. Overall, there were 33 responses to the one page questionnaire, predominantly municipal respondents, but with good representation (more than 25%) from the development community as well. Table 1 shows the overall results of the questionnaire.

Questionnaire results in Table 1 are sorted from those identified as most significant barriers to least significant barriers. In addition, the table shows the number of "1" and "5" responses for each barrier to illustrate which barriers received the most extreme ratings.

Table 1. Summary of Questionnaire Results

KICP LID BARRIERS SURVEY			
Participant Information			
Name (optional):			
Organization (optional):			
Email (optional to receive survey results):			
Municipal Respondents:			
Private Sector (Consultants, Developers):			
Not Specified:			
General questions--Please answer yes or no. If filling out electronically please indicate selection with larger font.			**Responses**
Are you familiar with the term Low Impact Development (LID)?	Y	N	31 Y, 2 N
As a reviewer, designer or constructor have you ever considered LID as an alternative or complement to traditional stormwater management practice such as storm sewers and detention ponds?	Y	N	23 Y, 9 N
Have you been involved in a project where LID measures were implemented?	Y	N	16 Y, 17 N
Have you been involved in a project where LID measures were proposed or planned but not ultimately implemented?	Y	N	13 Y, 20 N

Table 1. Summary of Questionnaire Results (Continued)

KICP LID BARRIERS SURVEY								
Which of the following do you see as barriers to implementation of LID? Please rate on scale of 1 to 5. 1 = not at all, 5 = Very much.	**Not at All**				**Very Much**	**Avg.**	**No. of 1 Responses**	**No. of 5 Responses**
Perceived design, construction, maintenance costs	1	2	3	4	5	4.2	0	15
"Mixed messages" from different governmental departments (planning versus engineering versus open space versus street maintenance)	1	2	3	4	5	4.2	1	15
Maintenance and durability concerns	1	2	3	4	5	4.1	0	14
No clear economic incentive for using LID	1	2	3	4	5	4.0	0	11
LID not integrated early enough in planning process	1	2	3	4	5	4.0	0	12
Other types of BMPs and drainage infrastructure may still be required even with LID	1	2	3	4	5	3.9	0	5
LID "recommended" in guidance rather than "required"	1	2	3	4	5	3.9	0	11
Lack of successful demonstration projects in area	1	2	3	4	5	3.9	1	7
Concerns with swelling soils	1	2	3	4	5	3.9	0	10
Specialized construction techniques may be required	1	2	3	4	5	3.9	0	9
Other water quality alternatives are "easier" to design, construct and maintain	1	2	3	4	5	3.8	1	11
Long term ownership (private versus publicly owned and maintained)	1	2	3	4	5	3.8	1	13
Difficulty in measuring benefits of LID	1	2	3	4	5	3.8	1	10
Reluctance to try something new	1	2	3	4	5	3.8	1	6
Limited technical design guidance	1	2	3	4	5	3.8	1	10
Poorly drained soils/low infiltration capacity	1	2	3	4	5	3.8	1	11
Conflicts with municipal code requirements (i.e. curb and gutter required)	1	2	3	4	5	3.7	0	7
Different or conflicting LID guidance or criteria from different groups (UDFCD versus Center for Watershed Protection versus others)	1	2	3	4	5	3.7	1	10
Semi-arid climate (i.e. difficulty in supporting green rain gardens)	1	2	3	4	5	3.6	2	7
Iterative coordination process with planners, designers, landscapers and others is required	1	2	3	4	5	3.6	1	6
Confusing or unclear ordinances related to LID and/or disconnected impervious area	1	2	3	4	5	3.6	0	8
Education and training do not provide skills to design and implement LID	1	2	3	4	5	3.4	2	10
Potentially longer review process	1	2	3	4	5	3.4	0	6
Fear of liability (engineers, owners, reviewers)	1	2	3	4	5	3.4	1	4
Standing water nuisance problems	1	2	3	4	5	3.1	3	6
Public perception (temporary ponding on lots, standing water, mosquitoes and other factors)	1	2	3	4	5	3.1	3	3
High groundwater table	1	2	3	4	5	3.1	2	2
Water rights considerations	1	2	3	4	5	3.0	3	4
Confusing nomenclature--lack of consistent names for practices (rain gardens versus porous landscape detention versus bioretention)	1	2	3	4	5	3.0	3	3
Compatibility with existing developments that do not use LID practices	1	2	3	4	5	2.9	4	3
Examples of LID failures	1	2	3	4	5	2.9	3	3
Conflicts with landscaping requirements	1	2	3	4	5	2.9	2	3
Safety considerations	1	2	3	4	5	2.6	3	3
Americans with Disabilities Act considerations	1	2	3	4	5	2.4	5	0

Conceptual Strategies for Addressing Barriers

Although the scope of work for the KICP Barriers Identification project was limited to identification of barriers, development of the checklist and conducting design reviews using the checklist, the project team developed conceptual approaches for beginning to address barriers. Conceptual strategies are listed in Table 2.

Table 2. Conceptual Strategies for Addressing LID Barriers

Identified Barriers	Conceptual Strategies
Perceived design, construction, maintenance costs	Examples of successful LID pilot studies in the Rocky Mountain Region including economic analysis and long-term performance monitoring and documentation of maintenance.
"Mixed messages" from different governmental departments (planning versus engineering versus open space versus street maintenance)	Development of improved regional guidance (Volume 3), model ordinances and criteria, better coordination between engineering, planning, parks and recreation, etc.
Maintenance and durability concerns	Long-term performance monitoring and documentation of maintenance activities for existing LID installations.
No clear economic incentive for using LID	Develop incentives for LID implementation (reduced storage requirements for water quality event and potentially larger events) to provide credit. Consider expedited variances to shorten review process for proven methods. Documentation of savings on LID projects in region.
LID not integrated early enough in planning process	Checklist at pre-application meeting to identify opportunities for LID.
Other types of BMPs and drainage infrastructure may still be required even with LID	Examine potential reduced sizing of other "traditional" BMPs when LID measures are adopted.
LID "recommended" in guidance rather than "required"	Evaluate ordinances and requirements in other communities where LID has been more widely adopted.
Lack of successful demonstration projects in area	Consider municipal demonstration projects to "showcase" LID.
Concerns with swelling soils	Better coordination with geotechnical engineers and consideration of soil treatment and amendments.
Specialized construction techniques may be required	Examine construction techniques used for successful LID projects and construction techniques that have contributed to LID failures. Consider contractor education programs and/or certification.
Other water quality alternatives are "easier" to design, construct and maintain	Emphasize importance of "Step 1--Volume Reduction" from UDFCD Manual. Provide updated design details, specifications.
Long term ownership (private versus publicly owned and maintained)	Evaluate need for easements, deed restrictions, public authority to maintain/repair LID BMPs on private property and back-charge owners. Public education for property owners.
Difficulty in measuring benefits of LID	Increased monitoring of LID hydrologic and water quality benefits on individual BMP and site scales (local data). Develop tools for quantifying effects of LID on sizing of other drainage facilities.
Reluctance to try something new	Municipal examples to lead the way. Publicity of successful implementation of LID.
Limited technical design guidance	Updated criteria and focus on planning and volume reduction. Development of detailed specifications templates. More involvement of engineers for construction observation/clarifications during construction.
Poorly drained soils/low infiltration capacity	Better coordination with geotechnical engineers and consideration of soil treatment and amendments. Understand there are some circumstances where LID is not feasible.

Table 2. Conceptual Strategies for Addressing LID Barriers (Continued)

Identified Barriers	Conceptual Strategies
Conflicts with municipal code requirements (i.e. curb and gutter required)	Consider expedited variance requirements where LID features are desired and conflict with standard code requirements.
Different or conflicting LID guidance or criteria from different groups (UDFCD versus Center for Watershed Protection versus others)	Develop LID criteria specific to semi-arid region and incorporate into regional guidance (UDFCD Manual).
Semi-arid climate (i.e. difficulty in supporting green rain gardens)	Use drought tolerant species. Do not expect "green" rain gardens. More emphasis on xeriscaping coupled with infiltration.
Iterative coordination process with planners, designers, landscapers and others is required	Early coordination between developers, engineer and municipal staff from multiple departments to define LID approach for project and identify specific barriers.
Confusing or unclear ordinances related to LID and/or disconnected impervious area	Improved model ordinances and criteria.
Education and training do not provide skills to design and implement LID	Expanded training courses through municipalities and professional organizations. Consider webinars, field tours, symposia.
Potentially longer review process	Integrate LID concepts as early as feasible in planning process. Improved familiarity of municipal reviewers with LID concepts and methods.
Fear of liability (engineers, owners, reviewers)	More local examples of successful LID implementation, Consider in municipal projects to set example for private development community.
Standing water nuisance problems	Include underdrains in designs. Clearly define maintenance requirements. Avoid grading plans that specify very mild (unconstructable slopes).
Public perception (temporary ponding on lots, standing water, mosquitoes and other factors)	Public education on benefits of LID. Better LID design can reduce nuisance water.
High groundwater table	Require submittal of geotechnical information including groundwater levels early in review process. Recognize that LID may not be feasible in all situations.
Water rights considerations	Avoid storage/harvesting of runoff for beneficial use. Directing downspouts from roof to pervious areas is not a problem for water rights (incidental use), but collecting runoff from downspouts, storing it (i.e. rain barrels, then beneficially applying the collected water is not legal.
Confusing nomenclature--lack of consistent names for practices (rain gardens versus porous landscape detention versus bioretention)	Develop glossary of LID terminology as a part of regional guidance.
Compatibility with existing developments that do not use LID practices	Involvement of Landscape Architects and Planners to better define "community identity and character."
Examples of LID failures	Forensic investigation of LID failures. Identify specific factors leading to unsuccessful applications and learn from mistakes.
Conflicts with landscaping requirements and ordinance requirements	Better coordination with Landscape Architects.
Safety considerations	Generally not considered a major barrier, but evaluate safety, especially in areas where the general public will be in close physical proximity to LID BMPs (e.g. Drop off into infiltration swale between sidewalk and street in areas where street parking is likely).
Americans with Disabilities Act considerations	Provide alternate surfaces for disabled access if there is potential for pervious surface to impede mobility.

Conclusion

The results of this project demonstrate that there are many significant barriers to implementation of LID in the Front Range of Colorado, some very real and some largely perceived. Identification of these barriers is an important first step in encouraging wider use of LID practices in this region, because once barriers are identified, strategies can be developed to overcome the barriers. Strategies may include improved communication between municipal departments (engineering, planning, parks and recreation, etc.), updated design guidance and details for developers and engineers, increased public education efforts and other outreach programs. Communities' will also need to determine how LID supports their development and water quality goals - as any new standards will need to be approved by policy boards (councils, advisory boards, etc.)

Fortunately in Colorado, there are a number of organizations ranging from watershed groups to Colorado AWARE (Addressing Water and Natural Resources Education) to municipal permittees such as KICP and governmental organizations such as UDFCD and the Colorado Department of Public Health and Environment that are keenly interested in encouraging the use of LID. Additional efforts by these groups, potentially in collaboration with one another, has great potential to overcome many of the barriers identified in this study.

Challenges in Attaining Recreational Stream Standards for Bacteria: Setting Realistic Expectations for Management Policies and BMPs

Jane Clary[1], Jonathan Jones, P.E., D.WRE[1] and Ben Urbonas, P.E., D.WRE[2]

[1]Wright Water Engineers, Inc.; 2490 W. 26th Ave., Suite 100A; Denver, CO 80211; (303) 480-1700; clary@wrightwater.com, jonjones@wrightwater.com.
[2]Urban Watersheds, LLC; 845 S. Cove Way; Denver, CO 80209; bru@uwllc.org.

ABSTRACT

Attainment of U.S. Environmental Protection Agency (EPA) recreational water quality criteria and state water quality standards for bacteria presents significant challenges to water resource managers in communities throughout the U.S. From a regulatory perspective, many communities are faced with Total Maximum Daily Loads (TMDLs) for bacteria, typically for either *E. coli* or fecal coliform. For local governments responsible for National Pollutant Discharge Elimination System (NPDES) Municipal Separate Stormwater (MS4) permits, this issue can be particularly challenging and many questions arise with regard to whether stormwater best management practices (BMPs) can reduce bacteria in stormwater runoff. Many valid questions exist regarding how attainable current stream standards are and what measures are truly meaningful in reducing bacteria in streams and in development of meaningful TMDLs.

This paper provides a synopsis of Best Management Practice (BMP) performance data provided for bacteria in the International Stormwater BMP Database and discusses implications of these findings for stormwater managers. Findings from analysis of these data are used to provide some recommendations regarding the types of efforts that are expected to provide meaningful results in terms of water quality management policy and bacteria reduction in stormwater and receiving waters. Implications for development of TMDLs with the potential to provide real improvement of water quality is also discussed.

INTRODUCTION

Attainment of U.S. Environmental Protection Agency (EPA) recreational water quality criteria and state water quality standards for bacteria presents significant challenges to water resource managers in communities throughout the U.S. As one example, in some watersheds, largely uncontrollable natural sources of bacteria can cause or contribute to the exceedance of bacteria standards. When natural sources are comingled with controllable anthropogenic sources, it can be extremely difficult to establish realistic and meaningful strategies for attaining bacteria standards. As a result, draconian measures are sometimes implemented (e.g., prohibiting human use of recreational trails along waterways) or considered.

From a regulatory perspective, many communities are faced with Total Maximum Daily Loads (TMDLs) for bacteria, typically for either *E. coli* or fecal coliform. For local governments responsible for National Pollutant Discharge Elimination System (NPDES) Municipal Separate Stormwater (MS4) permits, this issue can be particularly challenging and many questions arise with regard to whether stormwater best management practices (BMPs) can reduce bacteria in stormwater runoff. Many valid questions exist regarding how attainable current stream standards are and what measures are truly meaningful in reducing bacteria in streams and in development of meaningful TMDLs. The International Stormwater BMP Database provides data that can

begin to help communities answer some of these questions. A summary of bacteria data in the BMP Database follows, along with findings and recommendations based on these data.

STORMWATER BMP MONITORING RESULTS FOR BACTERIA IN INTERNATIONAL STORMWATER BMP DATABASE

The International Stormwater BMP Database contains nearly 500 paired fecal coliform monitoring events at 61 sites (Table 1) and over 100 paired *E. coli* monitoring events at 12 sites (Table 2). The majority of the *E. coli* data sets are in Portland, Oregon and are from sites with Low Impact Development BMPs such as bioswales and green roofs. The fecal coliform data set is more geographically diverse with studies in California, Florida, Virginia, Ontario, New York, Texas, Georgia, North Carolina and Oregon. A few caveats related to this data set include:

- Although a few event mean concentration (EMC) data sets for bacteria exist in the Database, the majority of samples are grab samples, typically because a six hour maximum holding time is specified for bacterial analysis, making it inconvenient and difficult to collect samples for a representative hydrograph using automated samplers and to deliver the samples to the laboratory within this timeframe. Thus, the limitations of grab samples, which are well documented in the technical literature, apply. Additionally, some monitored storm events in the database are based on a single pair of grab samples of the influent and effluent, whereas others are based on arithmetic averages of several grab samples, and some are flow-weighted averages.
- The number of events sampled for studies presented in Tables 1 and 2 varies. For the E. coli data set, an average of 10 storms per BMP was monitored. For fecal coliform, an average of eight storms per BMP was monitored; however, six of the studies (10 percent of the studies) had fewer than three sampling events, resulting in their exclusion from subsequent analysis.
- Prior to 2008, the water quality data entered into the Database were based on "Legacy STORET" nomenclature, which many people found confusing. (The new Water Quality Exchange (WQX) format developed by the U.S. Environmental Protection Agency (USEPA) is more intuitive and has been adopted in 2007 updates to the Database). The authors have assumed that the reported data with various STORET codes fall into these three categories: fecal coliform, *E. coli* and fecal strep.
- A complicating issue when evaluating *E. coli* data from multiple sources is that unlike most conventional chemical and physical parameters, bacteria has an upper quantitation limit that can vary by orders of magnitude between studies, or sometimes even within studies. The upper quantitation limit is influenced by the dilution of the sample during analysis. As a result, statistical analysis of lumped data sets can be problematic and it may be necessary to examine the performance of each BMP individually.

Table 1. Summary of Fecal Coliform Data for 485 Monitoring Events in the International Stormwater BMP Database 2009[1]

BMP	City	State	# of Events	Geometric Mean Inflow (#/100 mL)	Geometric Mean Outflow (#/100 mL)
Bioswales					
Altadena (strip)	Altadena	CA	3	386	459
Carlsbad Biofiltration Strip[2]	Carlsbad	CA	2	84,853	47
I-605/SR-91 Strip[2]	Cerritos	CA	2	490	1,122
US 183 at MoPac Grass Filter Strip	Austin	TX	10	59,606	37,321
Cerritos MS[2]	Cerritos	CA	2	20,199	2,915
I-605/SR-91 Swale[2]	Cerritos	CA	1	5,000	900
I-5/I-605 Swale[2]	Downey	CA	2	65	105
I-605 / Del Amo	Lakewood	CA	4	9,460	9,168
SR-78 / Melrose Dr	Vista	CA	3	1,366	239
Key Colony Swale	Key Colony Beach	FL	6	355	380
BES Bioswales - East Swale	Portland	OR	6	1,116	3,176
BES Bioswales - West Swale	Portland	OR	6	1,116	2,852
Russell Pond Bioswale	Portland	OR	4	677	795
WPCL Bioswale East	Portland	OR	10	2,924	4,724
WPCL Bioswale West	Portland	OR	10	2,924	4,134
Alta Vista PUD w/ swales	Austin	TX	19	36,193	25,428
Monticello High School Bioretention Area	Charlottesville	VA	3	5	1
Dayton Biofilter - Grass Swale	Seattle	WA	5	2,628	7,336
Detention Basins					
I-605 / SR-91 EDB	Cerritos	CA	7	654	813
I-5/Manchester (east)	Encinitas	CA	4	978	6,708
I-15/SR-78 EDB	Escondido	CA	9	438	766
I-5 / SR-56	San Diego	CA	9	NA	1,103
The Reserve at DeBary	DeBary	FL	48	682	45
Key Colony Detention Pond	Key Colony Beach	FL	10	95	68
Mountain Park	Lilburn	GA	9	168	1,839
BMP 13, West Lake Drive	Valhalla	NY	13	14,184	5,454
Lexington Hills - Detention Pond	Portland	OR	7	529	289
I-5 / I-605 EDB	Downey	CA	5	2,237	325
Green Roof					
Hamilton Ecoroof East Roof 2001	Portland	OR	4	NA	34
Hamilton Ecoroof East Roof 2002	Portland	OR	3	NA	11
Hamilton Ecoroof West Roof 2001	Portland	OR	4	NA	13
Hamilton Ecoroof West Roof 2002	Portland	OR	3	NA	28

Table 1. Summary of Fecal Coliform Data for 485 Monitoring Events in the International Stormwater BMP Database 2009[1]

BMP	City	State	# of Events	Geometric Mean Inflow (#/100 mL)	Geometric Mean Outflow (#/100 mL)
Media Filter					
BMP 57, Nannyhagen Road	Mt. Pleasant	NY	6	NA	765
Kearny Mesa MS	San Diego	CA	7	200	170
Clear Lake Packed Bed Filter	Orlando	FL	11	2,653	1,012
Lake Olive VVRS	Orlando	FL	5	4,710	859
Hal Marshall Bioretention Cell	Charlotte	NC	14	1,278	172
Lakewood P&R	Downey	CA	6	122	175
Via Verde P&R	San Dimas	CA	6	393	232
La Costa P&R	Carlsbad	CA	7	538	33
Escondido MS	Escondido	CA	8	377	182
Foothill MS (Sand Filter)	Monrovia	CA	4	8,284	1,531
I-5/SR-78 P&R	Vista	CA	7	510	1,254
Eastern Regional MS SF	Whittier	CA	6	627	200
Parkrose Sand Filter	Portland	OR	4	1,602	83
Manufactured Device					
I-210 / Filmore Street	Lake View Terrace	CA	18	1,972	2,676
I-210 / Orcas Ave	Lake View Terrace	CA	13	2,681	4,187
Retention Pond					
I-5 / La Costa (east)	Encinitas	CA	6	4,619	42
DUST Marsh Debris Basin	Fremont	CA	9	1,929	515
Indialantic Project H Pond[2]	Indialantic	FL	2	387	77
Largo Regional STF	Largo	FL	24	58	5
FL Blvd Detention Pond	Merrit Island	FL	5	8,746	530
Jungle Lake (1993)	St. Petersburg	FL	4	2,320	241
Jungle Lake (1995+)	St. Petersburg	FL	7	2,247	411
Shawnee Ridge Retention Pond	Suwanee	GA	5	946	35
BMP 12, Malcolm Brook	Valhalla	NY	16	4,231	2,475
Heritage Estates Stormwater Manag. Pond	Richmond Hill	ON	22	1,446	133
Wetland					
BES Water Garden	Portland	OR	5	7,087	108
DUST Marsh System A	Fremont	CA	8	455	223
DUST Marsh System B	Fremont	CA	8	566	291
DUST Marsh System C	Fremont	CA	9	280	405

[1]Two porous pavement studies and one vegetated buffer strip were excluded from the analysis due to data limitations.

[2]BMPs with less than three studies have been excluded from subsequent analysis due to small sample size, but have been retained in this table for general information. The geometric mean is not a meaningful statistic for these studies.

NA = not available.

Table 2. Summary of *E. coli* Data for 114 Monitoring Events in the International Stormwater BMP Database 2009

BMP Name	City	State	# of Events	Geometric Mean Inflow (#/100 mL)	Geometric Mean Outflow (#/100 mL)
Bioswale					
Bureau of Environmental Services (BES) Bioswale Native[1] East	Portland	OR	6	1,079	3,035
BES Bioswale Non-Native West	Portland	OR	6	1,079	2,529
Russell Pond Bioswale	Portland	OR	7	780	575
WPCL Bioswale East	Portland	OR	10	2,121	3,789
WPCL Bioswale West	Portland	OR	10	2,121	3,286
Bioretention					
Hal Marshall Bioretention Cell	Charlotte	NC	13	275	17
BES Water Garden	Portland	OR	6	5,024	184
Green Roof					
Hamilton Ecoroof East Roof 2001 & 2002	Portland	OR	8	NA	27
Hamilton Ecoroof West Roof 2001 & 2002	Portland	OR	8	NA	25
Ponds and Sand Filters					
Heritage Estates Stormwater Manag. Pond	Richmond Hill	ON	25	1,271	109
Lexington Hills - Detention Pond	Portland	OR	10	399	272
Parkrose Sand Filter	Portland	OR	5	2,099	79

[1] Refers to vegetation types planted in bioswales.

In addition to review of the tabulated data, graphical presentation of the data is useful in identifying potential trends. The International Stormwater BMP Database analysis protocols (Geosyntec and WWE 2007) used for conventional water chemistry analysis focus on the effluent concentrations achieved by various BMPs (e.g., is the BMP helping to protect receiving water quality?) and whether there is a statistically significant reduction between influent and effluent concentrations (e.g., is the reduction in reported means real?). Several other factors such as changes in runoff volumes are also considered. In keeping with this approach, Figure 1 provides notched box and whisker plots of the fecal coliform data according to BMP type for several categories of BMPs. The geometric mean is used as a benchmark in these plots because attainment of stream standards is based on the geometric mean of the bacteria data. The USEPA promulgated instream standard for primary contact recreation is currently 126/100 mL for *E. coli* and was 200/100 mL for fecal coliform prior to USEPA's adoption of *E. coli* as a pathogen indicator. Figure 1 indicates that swales (GS) and detention basins (DB) do not appear to effectively reduce bacteria in effluent concentrations and may possibly increase bacteria concentrations. Although the effluent values are still above primary contact recreation standards, media filters and retention ponds show potential promise in reducing bacteria counts, based on statistically significant differences between the influent and effluent medians (i.e., the 95th percentile confidence limits for the medians of the influent and effluent data sets do not overlap). Data sets for wetlands and manufactured devices are not of adequate size to draw meaningful conclusions.

Figure 1. Notched Box and Whisker Plots Summarizing Paired Fecal Coliform BMP Monitoring Results (Source: International Stormwater BMP Database 2007)

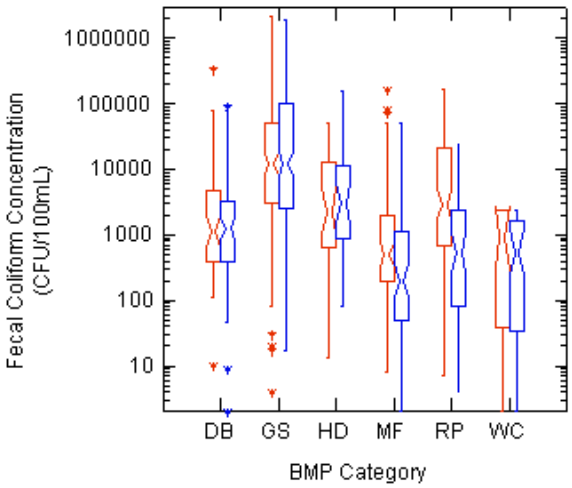

Key:

Inflow (Red)
Outflow (Blue)

DB= Detention Basin
GS= Grass Swales
HD=Manufactured Devices
MF= Media Filters
RP= Retention Ponds
WC=Wetland Channels

It is also worthwhile to evaluate the performance of individual BMPs. Bar charts presenting the geometric mean concentrations for the influent and effluent for each study were prepared. Figure 2 provides the geometric mean influent and effluent concentrations for *E. coli* studies in the database. A series of similar plots for fecal coliform were also prepared according to BMP type (Clary et al. 2008) based on the data summarized in Table 1, but are not reproduced in this paper due to space limitations.

Figure 2. Comparison of Geometric Mean E. coli Data for Stormwater BMPs in International Stormwater BMP Database

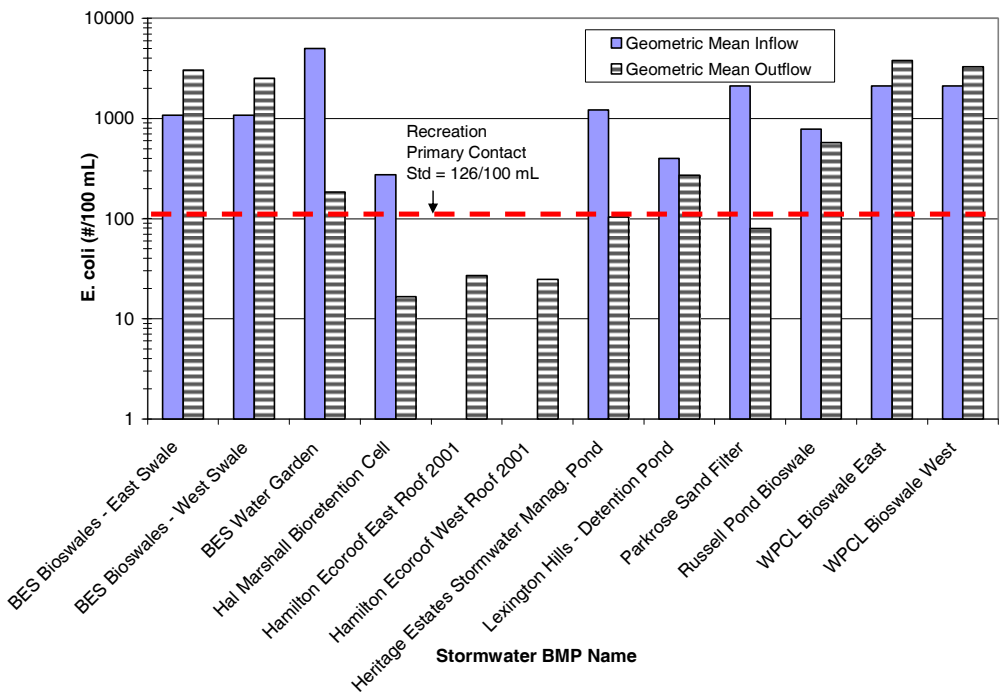

FINDINGS AND IMPLICATIONS FOR STORMWATER MANAGERS

Findings and implications for stormwater managers based on a review of the bacteria data in the International Stormwater BMP Database include:

- Bacteria concentrations in untreated runoff were consistently high for the majority of the BMP study sites, with the influent concentrations varying substantially. The variation may be due to both site-specific conditions as well as the upper quantitation limit for the study.
- The ability of structural BMPs to reduce bacteria varies widely within BMP categories. No single BMP type appears to be able to consistently reduce bacteria in surface effluent to levels below instream primary contact recreation standards. As a result, stormwater managers, permit writers and TMDL participants should not assume that structural BMPs can meet numeric effluent limits for bacteria for all storms and under all conditions. This is consistent with 2006 findings from a Storm Water Panel Recommendations to the California State Water Resources Control Board regarding the feasibility of numeric effluent limits for stormwater in general (CSWRCB 2006).
- Computer modeling of bacteria in stormwater should incorporate significant variability in both untreated runoff (influent) and BMP effluent and should be undertaken with caution. Feedback from some environmental engineers and consultants who apply common models to pathogen and fecal indicator transport suggests that the models provide highly uncertain predictions for pathogen and indicator concentrations and fluxes (USEPA 2007, based on input from Ali Boehm, Stanford University). Additionally, modeling assumptions related to microbe association with particles are typically not well developed (Characklis and Camper 2009). Models should be kept simple, with results not reported in unrealistically precise terms. TMDLs should acknowledge this variability and incorporate terms of compliance based on real-world monitoring data.
- BMP categories that appear to have potential for bacteria reduction in effluent include retention ponds and media filters and bioretention practices, with these considerations:
    - Retention ponds may be well suited for development with significant land area and adequate water rights (typically a challenge in semi-arid and arid states such as Colorado) or abundant rainfall. In ultra-urban areas, infill development, and arid/semi-arid climates, retention ponds are often impractical. Another potential disadvantage with retention ponds if bacteria removal is an objective is that they can attract waterfowl and wildlife, which can increase bacterial levels. Research related to unit treatment processes that are potentially effective for retention ponds is needed. For example, Characklis and Camper (2009) are conducting ongoing research related to microbe association with particles. This is important because the degree to which microbes in the water column associate with settleable particles has important implications for microbial removal via sedimentation-based BMPs.
    - Media filters and bioretention cells show promise in removing bacteria at the site-level. These findings are consistent with recent research by Hathaway and Hunt (2008) in North Carolina. For new developments based on Low Impact Development techniques, the use of bioretention cells or rain gardens is becoming more common in some part of United States. The key unit treatment process (filtration) associated with media filters is well proven in the drinking water arena, so it is not surprising that these BMPs would reduce bacteria, provided that the facilities are properly maintained. For existing developments, some targeted retrofitting in bacteria "hot

spot" areas could be possible, but costs of watershed-wide retrofits with many media filters will likely be cost prohibitive. One of the important aspects of long-term functioning of distributed controls such as bioretention cells is ensuring that these facilities are maintained and continue to function as designed in perpetuity. In many cases, local governments are already stretched to ensure maintenance of regional stormwater facilities, so although these practices may hold promise, "ensuring" their continued function may be administratively challenging.

- Swale and extended detention (dry) pond BMPs appear to have low effectiveness in reducing bacteria and in some cases have the potential for exporting bacteria. The authors hypothesize that potential causes could include that fact that these types of BMPs tend to attract geese, wildlife and domestic pets, which may contribute to bacteria loading. Regardless, these BMPs can still be effective at reducing pollutant concentrations such as total suspended solids (TSS), total metals, and other constituents, as demonstrated in the 2007 analysis of the International Stormwater BMP Database (Geosyntec and Wright Water Engineers 2007), and are valuable components of stormwater management programs. Some infiltration may also occur in these facilities, as well.
- Several BMP categories have data sets too small to warrant interpretation; these include the wetland, porous pavement and manufactured device categories. However, one could anticipate how some of these BMPs may perform by evaluating BMPs with similar unit processes. For example, properly designed porous pavements, such as those with a sand layer above the sub-surface underdrains, could potentially perform similarly to media filters.
- In addition to the ability of a BMP to reduce concentrations of bacteria, it is also important to consider whether the BMP reduces the volume of stormwater runoff and the frequency of discharges. BMPs such as bioretention, vegetated biofilters, and, in some cases, dry-extended detention basins have shown the ability to reduce runoff volumes via infiltration and/or evapotranspiration losses. These factors should also be considered in BMP selection.

As part of the data analysis, the authors also compared the conclusions based on International Stormwater BMP Database to previous findings reported by others such as Pitt (2004) and Schueler and Holland (2000). A few representative excerpts from previous findings include:

- *A natural outcome of discussions after examining microorganism levels in urban waters focuses on their potential control. Unfortunately, there does not appear to be an easy (inexpensive) solution to reduce the often-times very high indicator bacteria levels found in stormwater…The most basic control program would incorporate the required inappropriate discharge detection and elimination program…included in the NPDES stormwater permit program, and dog feces controls. These can be highly effective and of low to moderate (or higher) cost… Dog feces control programs are a basic public health and aesthetic benefit and should also be implemented (including enforcement)…the remaining indicator bacteria, although possibly still quite high in comparison to the current criteria, would indicate minimal risks, as they should mostly originate from urban wildlife…In order to reduce the bacteria levels to criteria levels, much more costly control programs will be needed. These should only be implemented after a local risk-assessment is conducted and actual human health impairments are identified* (Pitt 2004).
- *Concentrations of bacteria in urban stormwater are notoriously variable on a site-specific basis, even for similar land use types and even at the same sampling location. Due to the*

wide variability of bacterial data, it is difficult to make accurate estimates of expected pollutant loading and pollutant removal that are transferable from site-to-site with any degree of confidence. Even with the significant variability, all of the databases and literature sources agree that bacteria concentrations in untreated urban stormwater are very high (estimates range from 15,000/100 mL to over 50,000/100 mL for fecal coliform) and difficult to reduce to instream standards (Schueler and Holland 2000).

CONCLUSIONS AND RECOMMENDATIONS FOR ADDITIONAL RESEARCH

The International Stormwater BMP Database provides a relatively large and growing bacterial data set that is useful in evaluating the effectiveness of various structural BMPs with regard to bacteria removal. Media filters and retention ponds were most effective based on the current data set; however, effluent concentrations for these BMPs remained above primary contact recreation standards in many cases. Although several BMP types such as extended detention basins and grass swales did not appear to be effective at reducing bacteria concentrations, these BMPs can be effective at removing other pollutants such as TSS and total metals and may help to reduce runoff volumes and frequencies (thereby reducing bacteria loading). The bacteria-related findings reinforce earlier research by investigators such as Pitt (2004) and Schueler and Holland (2000). Recommendations for additional research include:

- Analysis of site specific conditions at BMP studies may help to identify factors such as exposure to sunlight, meteorological conditions, natural (non-human) contributions of bacteria associated with the BMP, and other factors that help to explain why some BMPs perform better than others. A more refined level of statistical analysis may also be valuable (e.g., hypothesis testing to determine statistically significant differences between influent and effluent concentrations, along with other techniques).
- Continued submittal of bacteria monitoring data for BMPs to the International Stormwater BMP Database is needed to continue to refine these findings and enable more statistically robust conclusions. Even though the overall number of paired storm events is fairly large, the number of studies per BMP category remains relatively small, as does the number of storm events monitored for some BMP studies. It is essential that evaluation of BMP performance related to bacteria include geometric mean effluent concentrations due to the fact that even when large percentage removals are present (and the BMP appears to be "doing something"), the effluent concentrations still typically exceed primary contact stream standards. This is critical for realistic expectations in BMP-based stormwater permits.
- Continued national data-based dialogue and research regarding bacteria levels in stormwater runoff relative to instream recreational water quality criteria is needed, in keeping with USEPA's expert workshop and critical path science plan for revising recreational water quality criteria (USEPA 2007) that acknowledges that many unanswered questions exist regarding recreational standards for bacteria. Near-term "critical path" research identified as part of the USEPA (2007) workshop includes addressing issues such as the significance of natural versus human-induced sources of bacteria, determination of acceptable risk levels, and other factors. This is critically important research to ensure that time and effort expended by regulators and MS4 permit holders is meaningful in terms of protection of human health. As an example, recent microbial risk assessment conducted for the Chicago Waterways Project (Petropolou et al. 2008) showed relatively low risk to human health due to secondary contact recreation in waters, despite elevated bacteria concentrations. Ideally, EPA would also support bacteria-related monitoring for BMPs so that a national baseline

expectation regarding the ability of structural BMPs to effectively treat bacteria could be developed.

- From a practical standpoint, state and federal regulators should carefully consider whether appropriate recreational use classifications are assigned to streams. Assigning primary contact recreation standards to streams that are not truly used for primary contact recreation can result in unnecessary 303(d) listing of streams and costly TMDL efforts that may result in BMP-based requirement to treat bacteria in MS4 permits. These situations do not provide meaningful increases in protection of human health and can be costly, diverting resources away from other real water quality issues. Aside from source control BMPs such as pet waste ordinances and illicit discharge detection and removal, MS4 permit holders may find themselves with unachievable permit requirements. This situation can also result in dilemmas for state regulators who may ultimately find themselves unable to issue a permit that contributes to an exceedance of a water quality standard. Some states (e.g., Kansas and Texas) have recently worked to develop more detailed recreational use standards that focus on streams where true primary contact recreation is occurring.
- Development of cost-benefit data for stormwater BMPs relative to bacteria reduction for municipal stormwater managers is important. Most local governments need this type of information for decision-making when determining how to best allocate limited resources.

REFERENCES

California State Water Resources Control Board (CSWRCB). 2006. Storm Water Panel Recommendations to the California State Water Resources Control Board: The Feasibility of Numeric Effluent Limits Applicable to Discharges of Storm Water Associated with Municipal, Industrial and Construction Activities. June 19.

Characklis, G. and A. Camper. 2009. Microbial Partitioning to Settleable Particles in Stormwater. Seminar hosted by Urban Wet-Weather Flow Research Program, National Risk Management Research Lab, USEPA, January 26.

Clary, J., J. Jones, B. Urbonas, M. Quigley, E. Strecker and T. Wagner. 2008. "Can Stormwater BMPs Remove Bacteria? New Findings from the International Stormwater BMP Database." *Stormwater*. May, 2008. Vol. 9, No. 3.

Petropolou, C., Tolson, J., DeFlaun, M., Lanyon, R., Granato, T., Rijal, G., Gerba, C., Lue-Hing C., and Patterson Environmental Consultants. 2008. Disinfection vs. Non-disinfection Microbial Risk Assessment for Recreational Use of Chicago Area Waterways. WEFTEC, October 21.

Hathaway, J. and W. Hunt. 2008. Removal of Pathogens in Stormwater, North Carolina State University Extension Urban Waterways Fact Sheet.

International Stormwater BMP Database website: www.bmpdatabase.org.

Pitt, R. 2004. *Control of Microorganisms in Urban Waters*. (http://unix.eng.ua.edu/~rpitt/Class/ExperimentalDesignFieldSampling/MainEDFS.html).

Schueler, T and H. Holland. 2000. "Microbes in Urban Watersheds: Implications for Watershed Managers" in *The Practice of Watershed Protection*. The Center for Watershed Protection: Ellicott City, MD.

U.S. Environmental Protection Agency (USEPA). 2007. *Report of the Experts Scientific Workshop on Critical Research Needs for the Development of New or Revised Recreational Water Criteria*, March 26-30, 2007. EPA 823-R-07-006. (http://www.epa.gov/waterscience/criteria/recreation/).

Characterizing Water Inputs to Catchments in the Santa Monica Mountains with δ18O and δD

W. Hu[1], B. Hibbs[1] and R. Bugarin[1]

[1]Department of Geological Sciences, California State University, Los Angeles, 5151 State University Drive, Physical Sciences Building Room 256, Los Angeles, CA 90032; PH (323) 343-2414; FAX (323) 343-2435; email: whu@calstatela.edu

ABSTRACT

Water inputs to Santa Monica Mountains National Recreation Area (SMMNRA) watersheds include local precipitation, runoff of imported water and treated wastewater derived from imported water. Imported water from northern California is isotopically distinct from southern California precipitation. This contrast allows source flow differentiation.

To determine the relative contributions of water sources to creeks and streams in the SMMNRA, stable water isotopes [δ18O, δD] are used.

Sampling of rainwater, stream water, tap water and treated wastewater was done from January through December 2008. Analysis includes a focused study of McCoy Creek.

Results show tap water and treated wastewater to be fairly reliable end members and local precipitation to be unreliable as an end member. The isotopic signatures of McCoy Creek samples appear to be affected either by evaporation or changes in imported waters' isotopic signatures.

SMMNRA STUDY AREA

Land Use and Hydrology. The [SMMNRA] covers a gross area of 153,250 acres with various land use designations: urban, residential, commercial, agricultural, parks & recreation and natural preservation (National Park Service 2007.) Local precipitation, runoff of imported water and treated wastewater derived from imported water are all potential water inputs to SMMNRA watersheds.

In many creeks, groundwater baseflow accounts for much of the dry season stream flow (Hibbs and Andrus 2007.) Shallow groundwater in SMMNRA watersheds may be sourced from recharge by local precipitation or from recharge by imported water applied to irrigated landscapes.

Other studies on Las Virgenes Creek, a major tributary to Malibu Creek, indicate that Las Virgenes Creek is fed mainly by groundwater baseflow. Baseflow feeding into Las Virgenes Creek is derived primarily from local precipitation, not from recharge of imported water. These results were obtained during the dry season (Hibbs and Andrus 2007.)

This is a key observation because Las Virgenes Creek flows through the City of Calabasas before entering state park lands. Urban runoff (from residential and

municipal application of imported water) was only a small percentage of the flows in Las Virgenes Creek (Hibbs and Andrus 2007.)

Climate and Topography. The study area has a Mediterranean climate. The rainy season is from November to April. The dry season is from May to October. Precipitation is not constant during the rainy season but limited to rain events or occasional snow. Average yearly rainfall is roughly 15 inches along the coast, 22 to 27 inches along inland ridges (Dale, Brown and Thomas 2009.)

The Santa Monica Mountains form a 72 km long, west-trending coastal range that drains south from the Simi Hills (Dibblee 1987.) Elevations are mostly between 1000 feet and 2000 feet. Sandstone Peak, close to the western end, is 3111 feet high. Water flow has cut deeply into the mountains; gorges cut by the Topanga and Malibu Creeks are hundreds of feet deep (Dale, Brown and Thomas 2009.)

MCCOY CREEK

McCoy Creek is located in the City of Calabasas. Most of the creek is south of the Ventura Freeway between Las Virgenes Road and Old Topanga Canyon Road. The creek's watershed begins in the New Millennium development at the very western end of Parkway Calabasas (City of Calabasas Public Works Department 2006.) Its general direction of flow is toward the northeast. From head to mouth, much of McCoy Creek is adjacent to land developed for residential or recreational purposes. Consequently, McCoy Creek is ideal for observing imported water's effects on local water chemistry.

East of the New Millennium development, McCoy Creek emerges from an underground cement culvert below Parkway Calabasas. McCoy Creek then flows through a natural channel in an area with native vegetation before entering the Calabasas Golf Course and Country Club. The golf course flanks both sides of the creek for 0.6 mile (City of Calabasas Public Works Department 2006.)

After McCoy Creek exits the golf course, a tributary flows into McCoy Creek from the south by crossing underneath Parkway Calabasas. The confluence is concrete-lined (City of Calabasas Public Works Department 2006.)

McCoy Creek then flows beneath Parkway Calabasas via two box culverts before emptying onto property owned by Countrywide Financial. There, the property is maintained as a park (City of Calabasas Public Works Department 2006.)

McCoy Creek leaves Countrywide Financial's property by flowing under a road named Park Capri and into the park next to Lake Calabasas. In the park's western area, high-density residential land borders the creek to the north. The natural southern bank has oak woodland vegetation, which gives way to turf grass by the lake. A concrete overflow structure drains the lake into McCoy Creek "south of the Calabasas Tennis and Swim Center" (City of Calabasas Public Works Department 2006.)

By Calabasas' northern boundary, McCoy Creek flows under Calabasas Road in Old Town Calabasas. The creek then crosses under the Ventura Freeway before joining Dry Canyon "Creek to form Calabasas Creek" (City of Calabasas Public Works Department 2006.)

Five sites for observing McCoy Creek were selected: two upstream near the New Millennium housing development [Gate Upper and Gate Middle,] one site just after McCoy Creek enters the Calabasas Country Club and Golf Course [Golf Course Site 1,] one site just before McCoy Creek exits the golf course [Golf Course Site 5] and one site at the Calabasas Tennis and Swim Center [23400 Park Sorrento] (see Figure 1). Sampling took place about every 6 weeks beginning in July 2008.

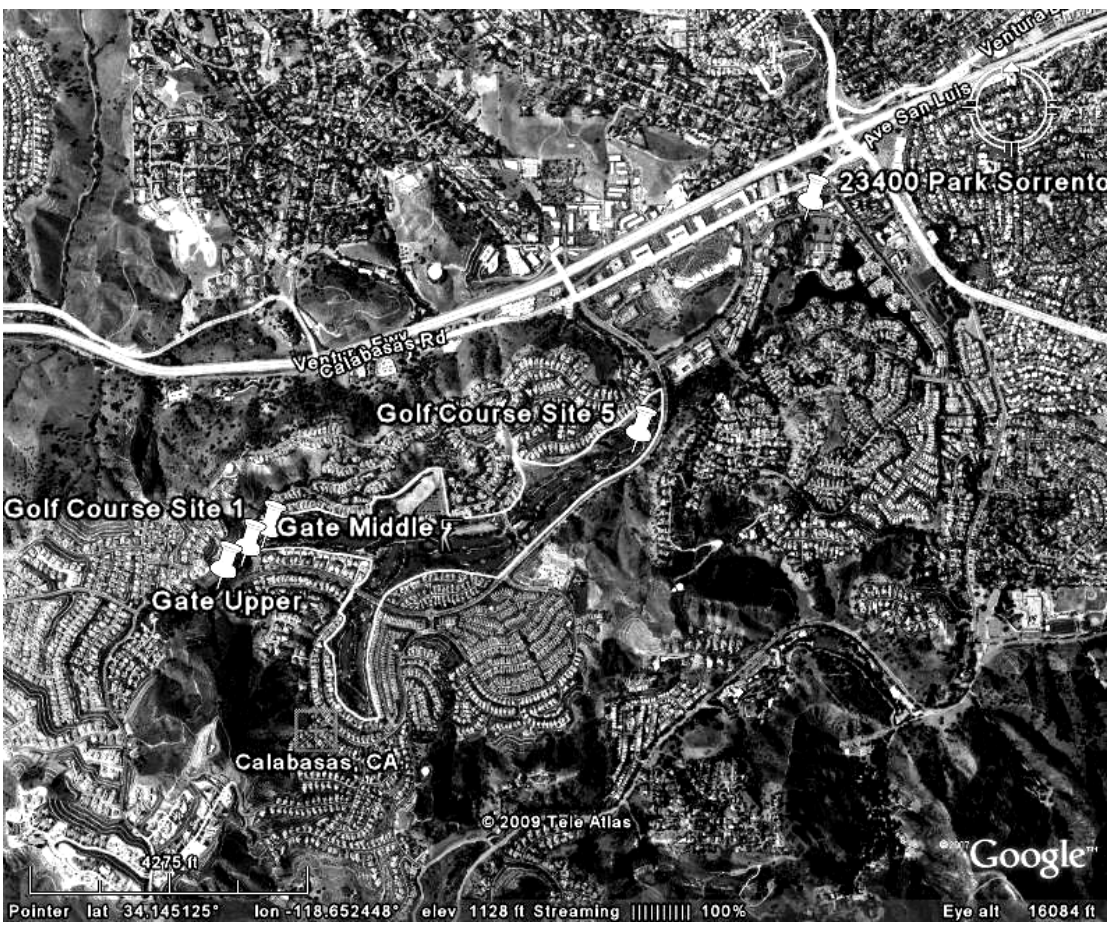

Figure 1. McCoy Creek sampling sites indicated by virtual tacks (Google Earth 2007.)

METHODS: STABLE WATER ISOTOPES

Unpreserved samples were collected in LDPE bottles. In each instance, containers were filled to the rim to minimize headspace. Minimizing headspace is necessary to prevent isotopic fractionation caused by evaporation, which could produce inaccurate results.

Stable isotopes of water, δ18O and δD, were measured in per mille [‰]. Mass spectrometry analysis for δ18O and δD was at the Environmental Isotope Laboratory at the University of Arizona's Geosciences Department. Analytical precision was 0.08‰ or better for δ18O and 0.9‰ or better for δD based on repeated internal standards. Standardization was based on Vienna Standard Mean Ocean

Water [VSMOW] & Standard Light Antarctic Precipitation [SLAP] (Christopher J. Eastoe, Lab Director, personal correspondence, January 12, 2009.)

Measurements of δ18O and δD were taken with a Finnigan Delta S gas-source isotope ratio mass spectrometer. To test hydrogen isotopes, samples were reacted with Cr metal at 750 degrees Celsius "using a Finnigan H/Device coupled to the mass spectrometer" (Christopher J. Eastoe, Lab Director, personal correspondence, January 12, 2009.) To test oxygen isotopes, samples were equilibrated with carbon dioxide gas at about 15 degrees Celsius "in an automated equilibration device coupled to the mass spectrometer" (Christopher J. Eastoe, Lab Director, personal correspondence, January 12, 2009.)

RESULTS & DISCUSSION

SMMNRA Study Area. Stable water isotopic signatures of all samples gathered January 2008 through December 2008 are plotted in relation to the Global Meteoric Water Line (see Figure 2).

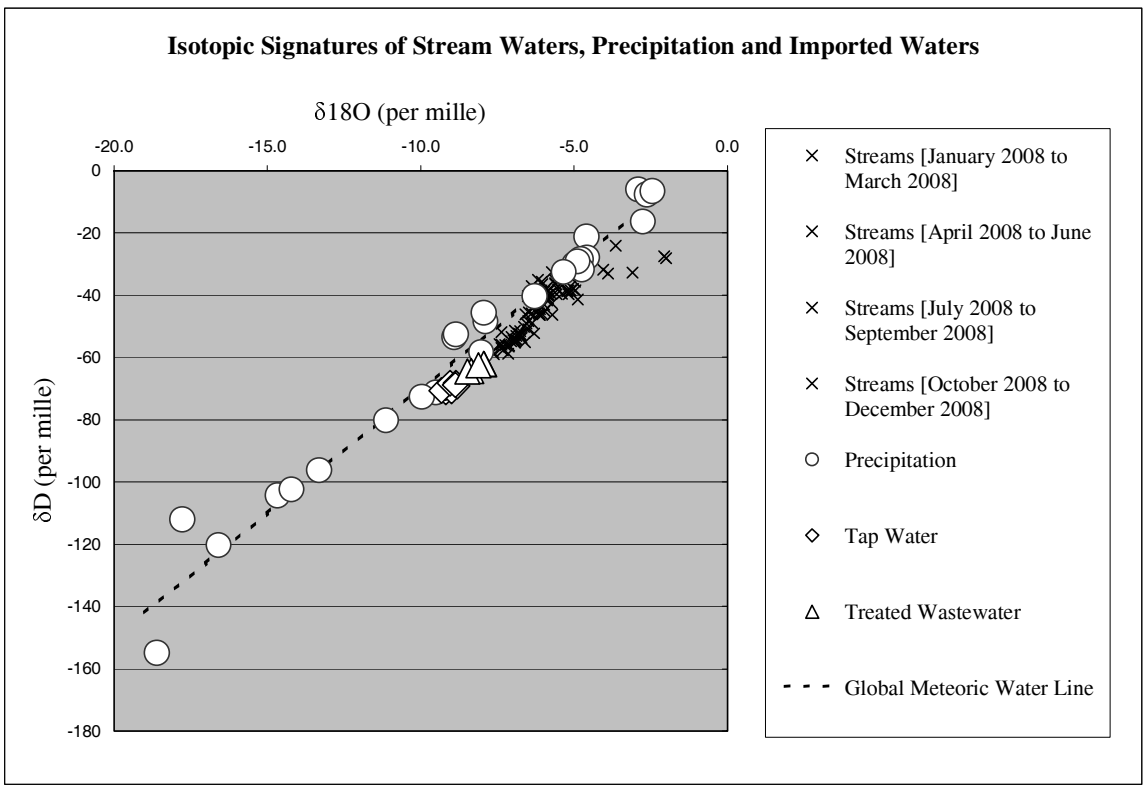

Figure 2. Isotopic signatures of stream waters, precipitation and imported waters relative to the Global Meteoric Water Line.

The isotopic signatures of tap water and treated wastewater remain fairly regular, which indicates that tap water and treated wastewater are reliable end members. Treated wastewater is isotopically heavier than tap water due to 1) evaporation of treated wastewater during reservoir storage and 2) infiltration of isotopically heavier groundwaters into pipes transporting untreated sewage.

Precipitation samples' isotopic signatures vary widely. There are a number of possible causes for this variation: orographic effects as a storm moves inland and higher in elevation, weather patterns such as whether a storm comes from the north or the south, how long a storm event had been occurring at the time of sampling, etc. Due to rainwater's wide-ranging isotopic signatures, precipitation is not reliable as an end member for analysis.

Stream waters also vary greatly in their isotopic signatures. None are isotopically lighter than tap water and treated wastewater, however. Also, stream samples appear to plot between imported water and most precipitation samples in terms of isotopic enrichment or lightness. Therefore, it seems likely that most stream waters are composed of different proportions of imported waters and local precipitation.

McCoy Creek. Stable water isotopic signatures of McCoy Creek sites and end members are plotted in relation to the Global Meteoric Water Line (see Figure 3). From upstream to downstream, the McCoy Creek sampling sites were Gate Upper, Gate Middle, Golf Course Site 1, Golf Course Site 5 and 23400 Park Sorrento. Because no rainwater was collected in the immediate vicinity of McCoy Creek, isotopic signatures from the nearest precipitation samples are shown. These samples' locations are the Las Virgenes Municipal Water District [LVMWD] in the southwest and Gates Canyon Park in the northwest.

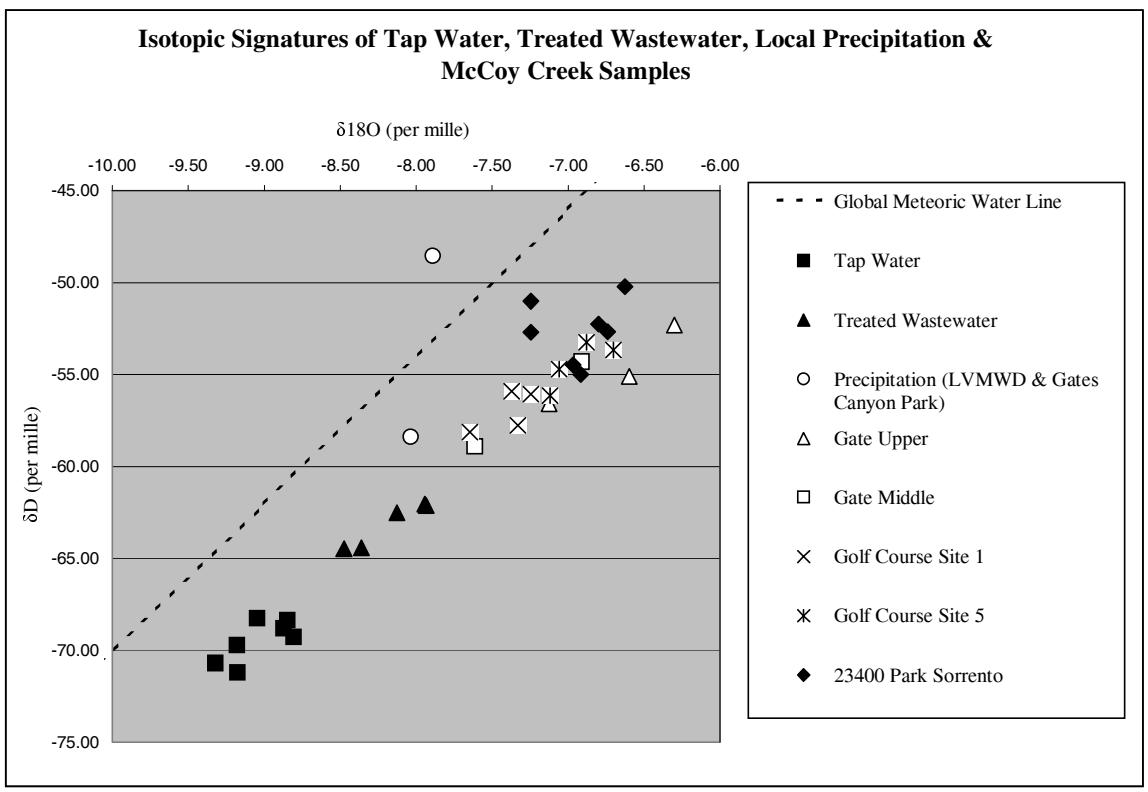

Figure 3. Isotopic signatures of imported waters, precipitation and McCoy Creek samples relative to the Global Meteoric Water Line.

Isotopic signatures at Gate Middle are usually lighter than at Gate Upper. Golf Course Site 1 samples plot between Gate Middle samples. Isotopic signatures at Golf Course Site 5 are heavier than at Golf Course Site 1 and heavier at 23400 Park Sorrento than at Golf Course Site 5.

There appears to be a significant contribution of isotopically lighter imported water to McCoy Creek as it flows from the New Millennium development into the golf course. Although the golf course and 23400 Park Sorrento water their lawns with treated wastewater that is isotopically lighter than stream water, McCoy Creek's water leaves the Calabasas Country Club and Golf Course more isotopically enriched than when it arrived. Also, McCoy Creek is more isotopically enriched at 23400 Park Sorrento than at the Calabasas Country Club and Golf Course.

An explanation for McCoy Creek's heavier isotopic signature at sites with potential inputs of isotopically light imported water could be that conservative watering practices result in most treated wastewater being taken up by plants. With input of treated wastewater to McCoy Creek thus minimized, the isotopic signature of the stream water could become enriched by evaporation or rainfall.

Isotopic signatures of imported waters and McCoy Creek waters monitored over time suggest that the creek waters' isotopic signatures might vary due to local evaporation or due to influence by fluctuations in imported waters' isotopic signatures (see Figures 4 and 5).

The isotopic signatures of both tap water and treated wastewater were relatively light from mid-spring to midsummer. They then became heavier from mid-summer through late September. After late September, the isotopic signatures of tap water and treated wastewater began to become isotopically lighter.

Fluctuations of isotopic signatures of McCoy Creek water at 23400 Park Sorrento closely follow fluctuations of imported waters' isotopic signatures. δD at the other sites appears to mimic fluctuation of δD in imported waters, but with a delay that affects all these sites. $\delta 18O$ results at these sites have a similar-looking delay in fluctuation relative to imported waters' $\delta 18O$ results, but the delay in fluctuations of $\delta 18O$ does not occur consistently.

CONCLUSION

Because the stable water isotope signatures of tap water and treated wastewater remain fairly stable, they are useful end members for analyzing relative contributions to stream flow in the SMMNRA. Precipitation, however, varies greatly in isotopic signature for multiple possible reasons, so rainwater is not reliable as an end member.

Fluctuations of isotopic signatures in tap water and treated wastewater appear to be reflected in the isotopic signatures of McCoy Creek samples. Inputs of treated wastewater to McCoy Creek may be limited by plant uptake.

Possible explanations for stream waters' different isotopic compositions in relation to imported waters include evaporation as well as the quantity of input by imported waters to stream flow.

Results from samples collected in January 2009 and February 2009 may reveal clearer patterns regarding imported waters' effects on stream waters by extending the time over which isotopic signatures are observed.

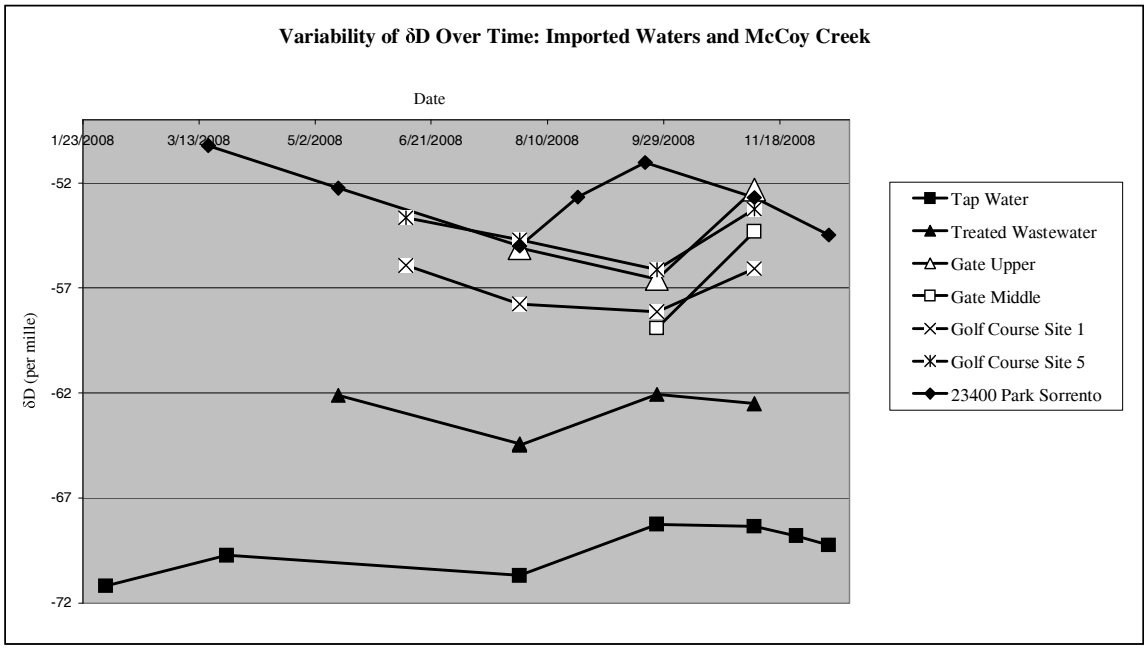

Figure 4. Variations in δD over time.

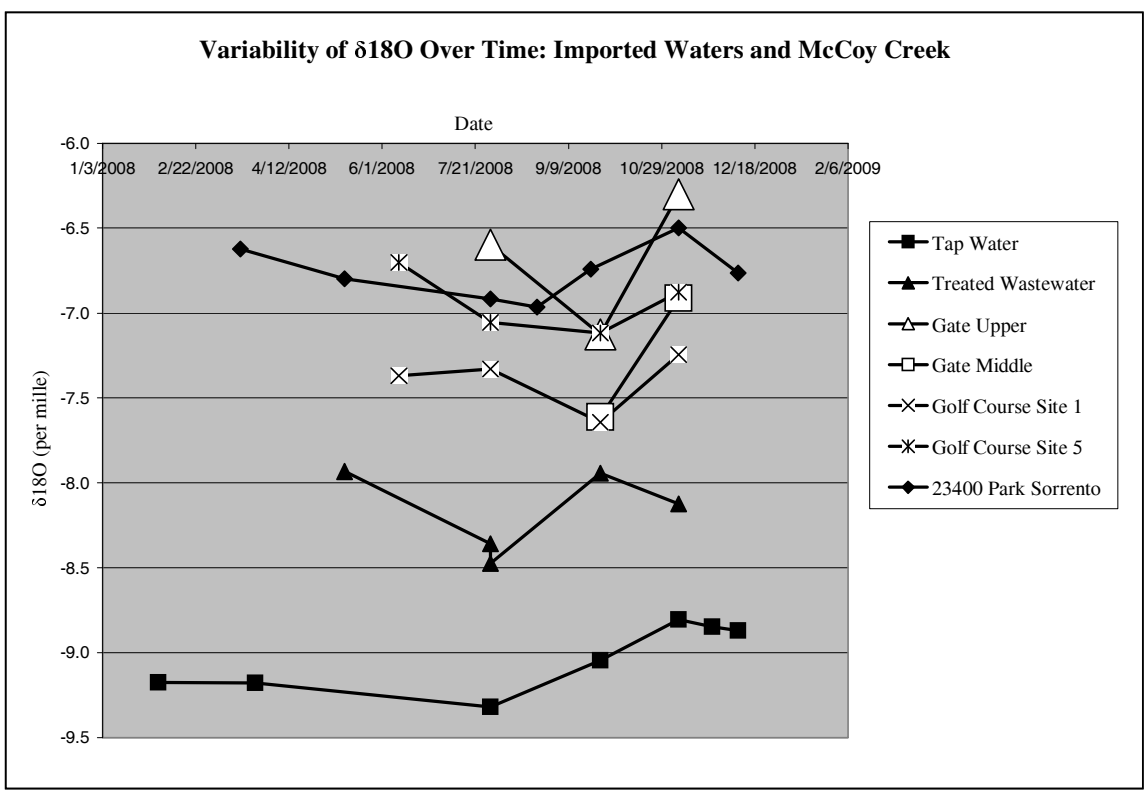

Figure 5. Variations in δ18O over time.

REFERENCES

City of Calabasas Public Works Department (2006). "Creeks Master Plan." <http://www.cityofcalabasas.com/pdf/creek-masterplan/creeks-master-plan.pdf> (January 15, 2009).

Dale, N., Brown, D., and Thomas, T. (2009). "About the Santa Monica Mountains." California Native Plant Society. <http://www.lasmmcnps.org/santamonicamtns.html> (January 8, 2009).

Dibblee, T. W. Jr. (1987). "Geology of Santa Monica Mountains and Simi Hills, California: ABSTRACT." *AAPG Bulletin*. vol. 71. (2005). <http://search.datapages.com/data/doi/10.1306/94887118-1704-11D7-8645000102C1865D> (January 11, 2009).

Google Earth version 4.2.0205. (Build date 2007). (Computer software.) Server <kh.google.com> Google Inc. Mountain View, California. (January 23, 2009).

Hibbs, B., and Andrus, R. (2007). "New Models on Sources of Selenium in Las Virgenes Creek." <www.cityofcalabasas.com/environmental/PDF/selenium-sources-2007.pdf> (January 21, 2009).

National Park Service. (2007). "Santa Monica Mountains National Recreation Area Park Statistics." <http://www.nps.gov/samo/parkmgmt/statistics.htm> (August 15, 2008).

Clark County Regional Flood Control District Arc Hydro (CCRFCD Arc Hydro): Toward on-going Stormwater Master Planning

Stephen Bourne, PE[1]; Kevin Eubanks, PE, CFM[2];
Harshal Desai, PE, CFM[3]; Brian Rowley, PE, CFM[3]

[1]PBS&J, 1800 Parkway Place, Suite 1200, Marietta, GA 30067; PH (404) 895-0753; FAX (770) 426-5316; e-mail: sfbourne@pbsj.com
[2]PBS&J, CCRFCD, 600 S. Grand Central Parkway, Suite 300, Las Vegas, NV 89106; PH (702) 685-0000; FAX (702) 685-0001; e-mail: keubanks@regionalflood.org
[3]PBS&J, 2270 Corporate Circle, Suite 100, Henderson, NV 89074; PH (702) 263-7275; FAX (702) 263-7200; e-mail: hdesai@pbsj.com; bjrowley@pbsj.com

ABSTRACT

The Las Vegas Valley represents an extreme hydrologic condition in that its high density population must manage discrete but very heavy rainfall events in an erstwhile arid climate. The runoff from these events is routed by way of an elaborate existing and proposed flood control facility system which is composed of washes, channels, storm drains and detention basins. First developed in 1986, the CCRFCD Master Plan has been an excellent planning document for major flood control facilities within the Las Vegas Valley. Currently, the CCRFCD uses a periodic (every 5 years) stormwater infrastructure master plan update process, which requires hydrologic modeling to understand system response to major storm events. Over time, the Master Plan Update (MPU) has evolved into a technical tool for guiding local governmental agencies and private consultants in the development of both public and private property.

This paper will describe the design and on-going development of an Arc Hydro based GIS database for the Las Vegas Valley. This database will provide the geographic and technological foundation for regional hydrologic modeling, efficient permitting, and emergency response modeling. Benefits of moving to this standard include 1) an in-built geometric network that can be used for delineation of drainage area and stream tracing, 2) the integration of existing CCRFCD GIS and hydrologic modeling data into a single database, and 3) making accessible the broad variety of tools that already exist for the Arc Hydro platform.

The development of the database focuses on the workflow of converting existing stormwater GIS coverages into the Arc Hydro database schema. Existing HEC-1 stormwater models are also used in the workflow to 1) describe the catchment-to-catchment connectivity as prescribed by the current master plan models, and 2) to populate the database with information necessary for hydrologic modeling in the future. An ESRI ArcMAP extension called CCRFCD Arc Hydro Tools has been built to facilitate the database development process. To enhance user friendliness and power, this toolset introduces some novel concepts, such as in-built workflow accounting, intelligent map interaction, and environmentally driven network

construction. The design process for this extension, plus some examples of its use, will be described.

INTRODUCTION

The Las Vegas Valley represents an extreme hydrologic condition in that its high density population must manage discrete but very heavy rainfall events in an erstwhile rain-less climate. The runoff from these events is planned to be routed by way of an elaborate, and evolving, flood control facility system which is composed of washes, channels, storm drains and detention basins. The Clark County Regional Flood Control District (CCRFCD), in which the Las Vegas Valley lies, is responsible for planning out regional scale development of this system. First developed in 1986, the CCRFCD Master Plan has been an excellent planning document for major flood control facilities within the Las Vegas Valley. Currently, the CCRFCD uses a periodic (every 5 years) stormwater infrastructure master plan update process, which requires hydrologic modeling to understand system response to major storm events. Over time, the Master Plan Update (MPU) has evolved into a technical tool for guiding local governmental agencies, private developers and engineering consultants in the development of both public and private property.

The next step in the evolution of the MPU process will be to move to an on-going update process, where the stormwater drainage system will be modeled in a GIS-based framework. Through a maintenance tool, used each time a new development is constructed, the system model will be continually updated as new construction occurs within the Las Vegas Valley. To get started on this evolutionary step, CCRFCD plans on converting their existing stock of model data – which includes Arc Info coverages of facilities and HEC-1 model input files – into a fully functional Arc Hydro database.

This paper will describe the planning and development of the CCRFCD Arc Hydro solution. Topics covered will include a discussion of the value of on-going stormwater master planning, a description of the CCRFCD Arc Hydro technological solution including the powerful set of tools developed to help automate the process of converting CCRFCD's existing stock of ArcInfo coverages using HEC-1 hydrologic modeling files into the new Arc Hydro geodatabase, and extensions to the Arc Hydro database design necessary for modeling the stormwater system in Las Vegas Valley.

THE NEED FOR ON-GOING STORMWATER MASTER PLANNING

Like many communities around the country, CCRFCD conducts a periodic master planning process to set the direction of stormwater system enhancement. Every five years, a new MPU plan is produced that specifies the set of stormwater facilities that will be built/maintained over the next five years and quantifies how the entire system will perform with the new set of facilities in place. This quantification is accomplished through a comprehensive hydrologic modeling processing, which traditionally has used the Hydraulic Engineering Center (HEC), HEC-1 model.

At each five year MPU, the most up-to-date model input data available is used. This data includes 1) geo-spatial information about the stormwater facilities, their connectivity and hydraulic properties, 2) updated landuse data that reflects ultimate future development, and 3) updated characterizations of regional storms that occur in the region. This data is collected and formatted to form model input at each master plan update – the data collection effort typically represents the largest task in the MPU development process because it requires collecting data from hundreds of new developments via public entities, and others.

The result of the MPU process is an accurate and reliable characterization of the Las Vegas Valley ultimate condition stormwater system. With extremely high rates of new development – motivated by a high rate of regional population growth – it is becoming clear that an opportunity for improvement of the master planning effort is to continually update the hydrologic models as information about new development becomes available.

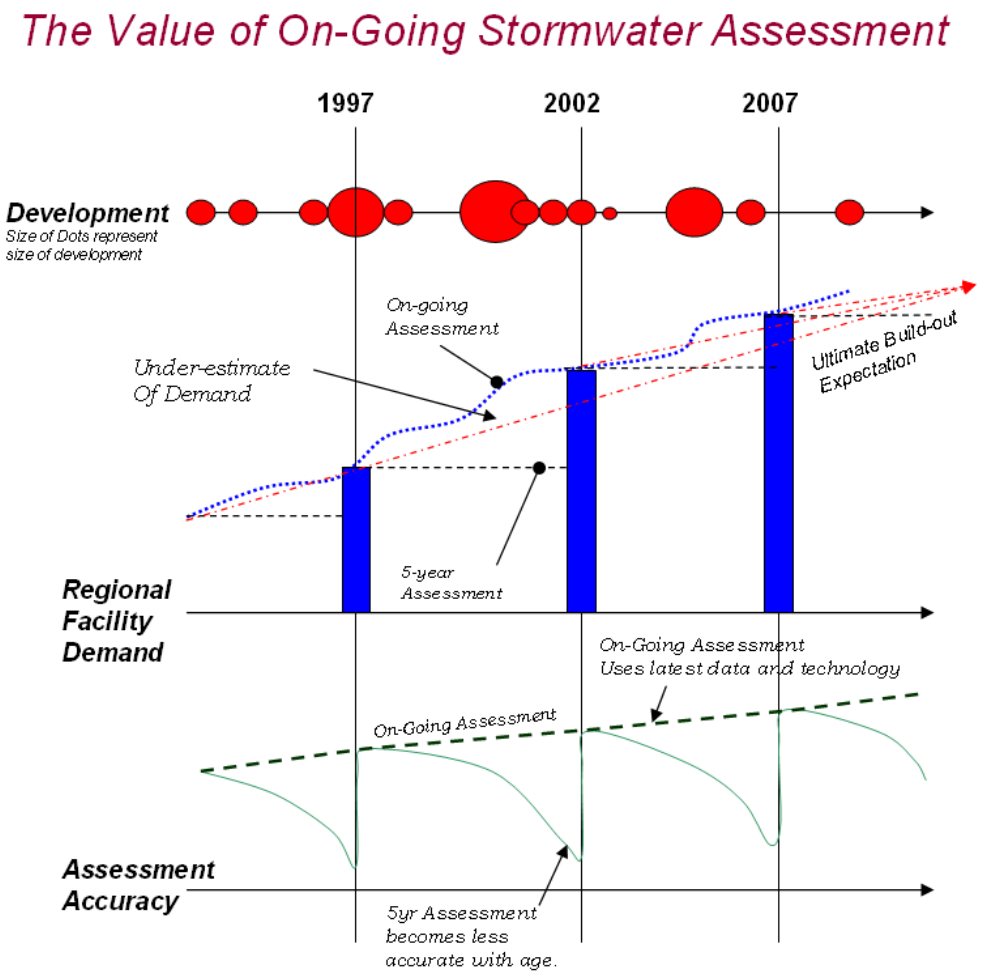

Figure 1. Schematic illustrating the value of an on-going stormwater assessment process.

Figure 1 shows a schematic of the value of such an on-going stormwater assessment process. The top panel in the figure represents new development. The red dots each represent a new development, with the size of the dot representing the size of the development. The middle panel shows the effect of new development on facility demand. As each new development is built, demand on the stormwater facilities increases. A periodic update will capture an accurate estimate of demand at the time of the preparation of the master plan model. The periodic plan will also estimate growth in demand based on perhaps linear interpolation to an ultimate build-out situation that occurs several decades in the future. As time passes, the estimate of growth of demand will become less accurate as unanticipated high growth occurs. The lower panel in the figure shows the accuracy of the estimates of facility demand. In general, accuracy will increase over time due to improved hydrologic modeling methods, but the accuracy will decrease over time in a five year cycle as the time since the last master plan update increases.

Figure 1 provides a good illustration of the value of continuous update of the master plan. If a continuous update occurs, new developments will be captured in the models as they occur. As a result, the accuracy of the modeling effort will remain high, as illustrated by the dashed line in the lower panel of the figure.

THE CCRFCD ARC HYDRO SOFTWARE SOLUTION

The need for on-going stormwater assessment establishes a need for an information solution capable of assimilating new data about land use, hydrologic parameters, and regional stormwater facilities in a relatively automated way. Moreover, the information solution should be able to generate input for hydrologic modeling and organize the output of the models into a useful product for interpretation and reporting. Ideally, the solution will be able to facilitate the entire modeling process in a seamless, single user interface, process.

These needs point to an information solution that is centered on a digital depiction of the real physical stormwater system. This digital depiction should also contain data about terrain and geology – which may be required for understanding the topography and to determine the initial abstraction – and data on the man-made and interpreted environment – which may include roads, rail lines, utility information, landuse data, census information, political boundaries, and parcel definitions. We refer to this digital depiction of reality as the digital watershed (Hampson et.al. 2008).

Figure 2 illustrates the CCRFCD Arc Hydro information solution. The digital watershed database will be composed of an extended Arc Hydro that represents 1) the hydrologic system, 2) the geologic system including soils and land cover, and 3) the man-made environment including land use and political boundaries, etc. The Arc Hydro database design is the natural choice for the CCRFCD solution as it has been developed over many years by a national community of experts in hydrology (Maidment, 2002). Arc Hydro works on the Environmental Systems Research

Institute (ESRI) ArcGIS platform, which is the platform used at CCRFCD and around the country. There is a large body of examples of application of the Arc Hydro system, an ESRI-supported suite of tools for working with Arc Hydro geodatabases, and a national community of Arc Hydro users. The Arc Hydro design has pre-existing feature classes for each part of the stormwater system. Several modifications of the design are necessary to facilitate the modeling of man-made water conveyances – as opposed to natural river systems for which the Arc Hydro design was originally conceived. Specific modifications will be covered in a later section.

A suite of applications will work with the digital watershed database to facilitate 1) exploration of data and model inventory, 2) maintenance of the system through check in/out of new models reflecting new development, 3) hydrologic modeling with newly received input data, 4) automated production of master planning analysis products, and 5) compliance with federal and state regulatory processes. The applications will be built as extensions to the ESRI ArcMap application, which is already in use at CCRFCD as the primary GIS application.

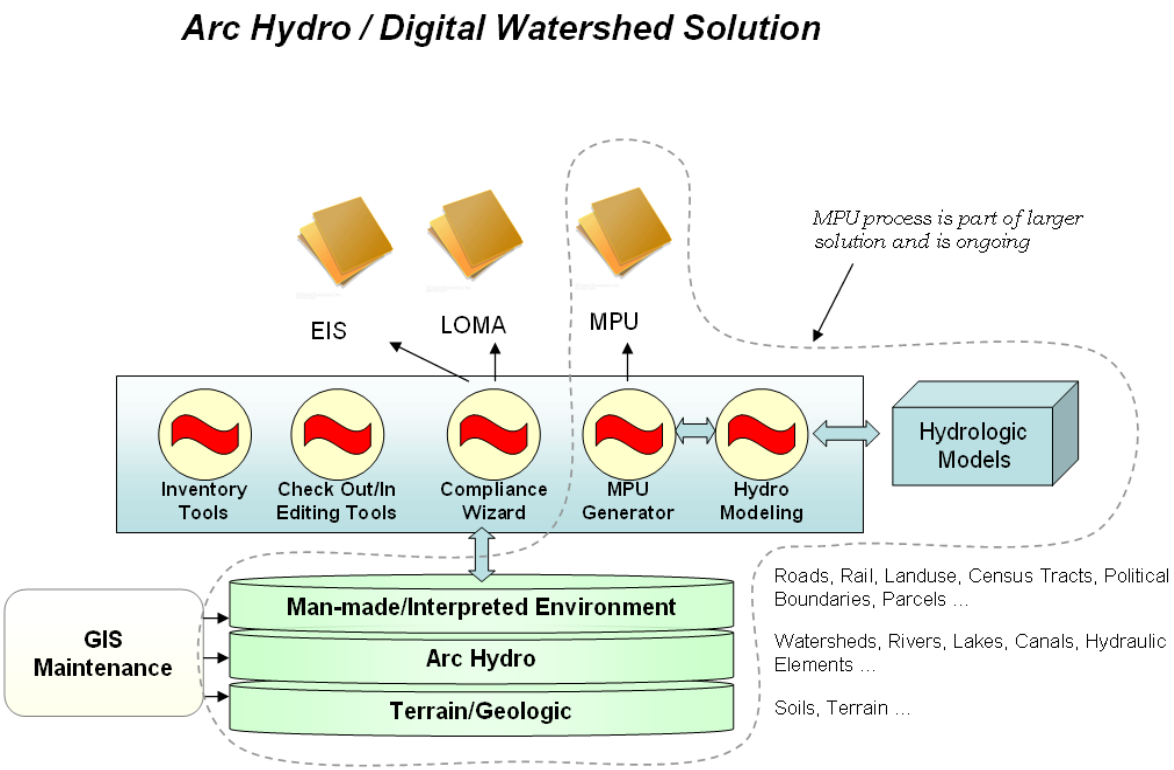

Figure 2. Conceptual Architecture of the CCRFCD Arc Hydro Solution.

MODIFICATIONS TO THE ARC HYDRO DESIGN TO ACCOUNT FOR DESERT ENVIRONMENT STORMWATER INFRASTRUCTURE

The Arc Hydro geodatabase has been created using 1) a set of basic GIS shape files depicting the stormwater channels and detention basins, and the catchments draining

to them, and 2) a set of HEC-1 model input files used to understand the connectivity from the catchments to the stormwater infrastructure and the connectivity of infrastructure itself. A tool was developed to automatically import this data and infer from it a proposed Arc Hydro database.

Modifications to Arc Hydro Connectivity Feature Classes

We found it necessary to modify the basic Arc Hydro design during this process to accommodate the stormwater infrastructure system, which essentially replaces the dendritic natural stream system that is the heart of the Arc Hydro design. Specifically, for the HydroEdge feature class, we added sever subtypes of hydroedge including:

- ***Regional Facilities****: These included the stormwater channels and other mand-made conveyances and natural washes that convey water.*
- ***Schematic Links:*** *A Family of schematic link types was created to establish full connectivity of the system while maintaining the exact shape and dimension of the regional facility features – as the length and size of the regional facilities is used in applications like maintenance cost estimation. The schematic link types include:*
    - ***Catchment Links****: Catchments were linked to the conveyance system via a set of phantom hydroedges called catchment links. These linked the centroid of the catchment directly to the point in the stormwater infrastructure where the catchment is considered to drain.*
    - ***Detention Basin Flow Line****: Stormwater channels drain to detention basins in several locations in the system. Schematic links were created to establish connectivity through the detention basins. Schematic links were used, as opposed to extending the facility hydroedges through the detention basin, so as to preserve the exact shape of the facilities and the associated attributes like length, which are used in stormwater system maintenance cost estimation.*
    - ***Diversions****: In HEC-1 modeling, a diversion can be created that diverts flow from one location to another.*
    - ***Floodway Centerline****: Natural washes exist in Las Vegas, which are wide and full during flooding. Connectivity through these washes was established through using Floodway Centerlines.*
    - ***Route****: A route in the hydrologic model (HEC-1) is used when the hydrograph needs to be routed from one location to another. These routes impact the shape and timing of the hydrograph due flow attenuation and translation. The routes used in the model either represent the regional conveyance system or other local flood conveyances.*

For the HydroJunction feature class, we also added several sub types to accommodate HEC-1 type hydrologic modeling. They included:

- ***CPoint****: These junctions are known as combination points. They represent the hydrojunctions where flows from two or more separate sources join.*
- ***Catchment:*** *These junctions represent the centroid of catchments*
- ***Detention Basin:*** *These junctions represent the centorid of detention basins*
- ***MultiNode:*** *These junctions represent locations where the modeler may want to partition the incoming flows to a hydrojunction simply for modeling purposes. For example, two channels may drain to a single hydrojunction. The local catchment may drain to the only one of the channels. Given this situation, the modeler will want to add the flow from the catchment plus the flow in the channel from upstream catchments to get the total flow in the channel. For the other channel, the flow will be defined as only that flow from the upstream catchment. In this case, the modeler will need to specify one channel flows to one hydrojunction with one HydroID and the other channel flows to another hydrojunction with another HydroID, despite the fact that the channels are actually flowing to a single physical location. To avoid duplication of hydrojunctions in the same location, the multinode has the ability to have up to 5 separate HydroIDs. The multimode, of course, introduces some extra complexity to the Arc Hydro design, as it conflicts with the rule that geographic features should have only one HydroID, but its elegance and respect for the physical nature of the system was deemed worth it. Upstream and downstream path queries were created in the CCRFCD Arc Hydro tools to enable searching through the multi-nodes as a result.*

Finally, the waterbody feature class was used to model the detention basins within the system and the catchment feature class was used to model catchments. With the exception of adding CCRFCD indexing and naming fields, few structural changes were made to these tables. They included:

Extensions to the Arc Hydro Geodatabase Schema for Non-Hydrologic Components

As the CCRFCD Arc Hydro geodatabase will be used eventually for hydrologic modeling, the database was extended to included data for soils, land use, and a working layer for calculating curve numbers.

A TOOL FOR MAINTAINING THE ARC HYDRO DATABASE

Currently under development is a maintenance tool for the CCRFCD Arc Hydro database. This tool will allow developers and engineers to extract portions of the enterprise SDE geodatabase as personal geodatabases. The developers will then be able to modify the facilities, and modeling parameters of that portion of the database according to planned development, or simply to improve the accuracy of GIS-data and modeling data. Then, the developer will be able to submit the personal geodatabase back to CCRFCD, where it will first be quality controlled to ensure acceptability, and then checked back into the CCRFCD enterprise geodatabase, thereby updating the enterprise geodatabase with the most recent data.

Through continuous use of the maintenance tool, the enterprise geodatabase, on which master planning updates are founded, will be continually maintained. The need for data collection at the next MPU, will be diminished drastically. The maintenance extends only to the geodatabase for the current MPU period (2008 – 2013). In 2013, when the MPU is conducted again, a valley-wide modeling effort will be required. Eventually, both the new GIS-data and the model will be run on each new submission of data, so that both the geodatabase update and the model update happen continuously, and there is no need for a periodic update.

CONCLUSIONS

The Clark County Regional Flood Control District (CCRFCD) has made a substantial move toward facilitating on-going stormwater master planning. An Arc Hydro database has been created that contains the entire stormwater infrastructure system and understands connectivity from the catchment to the stormwater conveyance system, through the detention basins, and eventually to the Las Vegas Wash and Lake Mead. Moreover, the features and attributes within the Arc Hydro database will contain sufficient data to re-create the hydrologic models that make up the master plan update model set. Currently a maintenance tool is being created to keep the Arc Hydro database up-to-date over time. As CCRFCD moves into the future, on-going modeling updates will soon be achievable, and the value of on-going master planning will be realized.

ACKNOWLEDGEMENTS

The authors would like to thank Clark County Regional Flood Control District for its support during the development of this project. We would also like to thank Gale Fraser, Stan Clawson, and Michael Moore of CCRFCD, and Matt Baird and Jack Hampson of PBS&J for their support and advice.

REFERENCES

Arc Hydro GIS for Water Resources, David R. Maidment, June 2002

Codorus Creek Restoration – A Case Study for the Chesapeake Bay

Matthew P. Hoch, Ph.D.[1], Christina Y.S. Siu[2*], Shirley E. Clark, Ph.D., P.E., D.WRE, M. ASCE[3], Katherine H. Baker, Ph.D.[4]

[1]Chair and Associate Professor of Biology, Department of Biology, Lamar University, 4400 MLK Blvd., P.O. Box 10037, Beaumont, TX 77710; PH (409) 880-8256; FAX (409) 880-1827; email: matt.hoch@lamar.edu.
[2]Research Scientist, Penn State Harrisburg, School of Science, Engineering, and Technology, 777 West Harrisburg Pike, TL 123; Middletown, PA 17057; PH (717) 948-6304; FAX (717) 948-6580; email: cys106@psu.edu
[3]Assistant Professor of Environmental Engineering, Penn State Harrisburg, Environmental Engineering Program, 777 West Harrisburg Pike, TL 105; Middletown, PA 17057; PH (717) 948-6127; FAX (717) 948-6580; email: seclark@psu.edu
[4]Associate Professor of Environmental Microbiology, Penn State Harrisburg, School of Science, Engineering, and Technology, 777 West Harrisburg Pike, TL 105; Middletown, PA 17057; PH (717) 948-6308; FAX (717) 948-6580; email: khb4@psu.edu

*Corresponding author

ABSTRACT

Healthy streams have the physical characteristics and chemical water quality to support healthy and diverse populations of organisms. The Codorus Creek, a tributary to the Susquehanna River, which eventually drains to the Chesapeake Bay, is being restored in several locations. Penn State University (York and Harrisburg campuses) is evaluating the effectiveness of the state-funded restoration activities. We examine the current pollutant loadings of two branches of this stream in conjunction with land use practices, particularly agriculture and wastewater treatment plants. Fish, macroinvertebrates, and periphyton are routinely sampled. Streamwater sampling for water chemistry analyses occurs during both baseflow and storm event conditions. Restored sites are being compared to both impaired and control sites to determine whether restoration has any significant reduction in a pollutant's load. Preliminary results indicate that the southern branch has greater impairment than the eastern branch. The southern branch impaired site showed greater annual mean loads of total nitrogen and total phosphorus, a macroinvertebrate community dominated by pollution tolerant organisms, and a greater number of fish with parasitic diseases. All sources contributing to the total nitrogen load to Codorus Creek have not been identified. Although restoration activities may decrease pollutant loads, such as as suspended solids, restoration is not believed to be effective in decreasing nitrogen loads. Nitrogen is found more readily in the aqueous phase (streamwater) rather than adsorbed to sediment particles. Therefore, more effective ways to remove nitrogen in water is to decrease or eliminate the source or to treat the streamwater directly. Further monitoring and comparison of restored sites to control and impaired sites are

needed. In addition, future work on the toxicity of the legacy sediments has been proposed.

INTRODUCTION

The Chesapeake Bay has pollutant concentrations that affect the fisheries, tourist, and recreational industries. The main pollutants of concern are nutrients and suspended sediment. Large increases in nutrients cause eutrophication. Suspended sediment affects aquatic organisms such as shellfish populations by smothering the shellfish and degrading or eliminating its habitat. Because many of Pennsylvania's streams eventually enter the Chesapeake Bay, it is prudent to control the pollutant sources upstream if the Bay is to recover. Agriculture, a dominant land use in Pennsylvania, is the leading source of both suspended sediment and nutrient contributions to streams and rivers. However, erosion from streambanks is a source for suspended sediment as well.

Historically, the dominant land use in the South-central Pennsylvania area was agriculture. Up until the early industrial revolution (mid-1800s) this agriculture depended on a large number of mills, most of which were powered by the hydro-mechanical forces of small streams. During colonial times, there were in excess of three hundred mills and their associated mill dams in some counties (Natural Streams Project 2008, Lloyd 2007). These dams collected sediment over the years, including any contaminants present. When most of these mills were eventually abandoned, their respective dams breached or eroded away. The collected sediments, or legacy sediments, began eroding and washing downstream. Walter and Merritts (2008) recognized legacy sediments as a source of suspended sediments and nutrients in South-central PA. These sediments are still problematic as erosion continues into the present.

The Codorus Creek empties into the Susquehanna River, which then flows into the Chesapeake Bay. Historically, forty-five mills were located along the three branches of this stream, (Natural Streams Project 2008). Suspended solids and nutrients from the remaining legacy sediments and the erosion of surrounding farmland contribute to the stream's pollutant loads. Restoration of the Codorus Creek is a high priority and several restoration projects are being planned or recently have been initiated on both the Eastern and Southern branches of the creek. This study, under a Pennsylvania Department of Environmental Protection's Growing Greener Grant (#SC30462), examines the loadings of pollutants in Codorus Creek along with biological metrics to determine the health of the stream at reference, restoration, and impaired sites.

Restoration activities were slated for specific portions of the stream. To date, restoration has been completed at several study sites on both the eastern and southern branches. The intent of the study was to determine what effect restoration has in improving stream health. The working hypothesis of this research proposes that natural stream channel restoration will initiate a cascade of shifts in the physical,

chemical, and biological characteristics of the stream, ultimately leading to greater ecosystem health.

SITE DESCRIPTION

Located in South-central Pennsylvania, Codorus Creek flows through York County. The mainstem of Codorus Creek originates in West Manheim Township, Maryland and empties into the Susquehanna River (near Saginaw, Pennsylvania) (Pennsylvania Department of Natural Resources [PA DCNR] 2002). Three branches of this creek (east, south, west) join the mainstem before it empties into the Susquehanna River. Considered a trout stream and warm water fishery, the stream flows in the northeast direction, including two manmade lakes that serve as reservoirs. The drainage area is 720km^2 (278mi^2) (PA DCNR 2002). Primary land use is cropland, followed by woodland. Urban areas (*e.g.*, the city of York) comprise of a lesser percentage of land use in the Codorus watershed (Smith 2003). Nonetheless, these urban areas impact Codorus Creek.

The initial phase of the project focused on pre-restoration characterization of the East and South Branches of the creek. A reference site (upstream of the proposed restoration), impaired, and proposed restoration sites (both downstream of the reference site) were monitored for both branches of the creek. A total of nine sites were sampled on the two branches, five on the eastern branch and four on the southern branch.

METHODOLOGY

Physical/Chemical Parameters

Baseflow and storm event samples are taken throughout the study period for nutrient (total phosphorus and total nitrogen) and suspended sediment analysis. Precipitation data was obtained from the WeatherBug® network. Average values for stations in each watershed were used in modeling storm-event volume and loads for suspended solids, total nitrogen (TN) and total phosphorus (TP). Suspended solids (SS) was determined by gravimetric analysis of particles collected on Whatman GF/F filters (American Public Health Association [APHA], American Water Works Association [AWWA], and Water Environment Federation [WEF] 1996). Total nitrogen and total phosphorus were determined using the alkaline persulfate thermal digestion and subsequent analysis of phosphate and nitrate ions (Valderrama 1981). One multiparameter sonde (YSI model 6600M) was placed on each branch at an impaired site. The sondes continually measured sonde depth, turbidity, specific conductivity, dissolved oxygen, pH, and water temperature.

Biological Parameters

Habitat assessments for each study site were made using the U.S. EPA Rapid Bioassessment Protocol III for wadable streams (Barbour *et al.* 1999). Periphyton samples were collected at approximately bimonthly intervals. The exact timing of the periphyton sampling depended on stream discharge; periphyton samples were only collected after at least ten days without a scouring precipitation event. Samples were collected and analyzed for chlorophyll *a* (chl*a*), dry mass, and ash-free dry mass (AFDM) (Steinman, Lamberti, and Leavitt 2006). Macroinvertebrates were collected twice a year (spring and autumn) using a proportionate habitat approach (Barbour *et al.* 1999). Biological metrics for macroinvertebrates was determined by using macroinvertebrate abundance data which, in turn, allowed for the calculation of the index of biotic integrity for macroinvertebrates (IBI_M) (PADEP 2007; Stribling *et al.* 1998). Fish were surveyed once a year (summer) using an electrofishing approach recommended by Barbour *et al.* (1999). Data from the electrofishing was used to determine an index of biological integrity for fish (IBI_F) (Roth *et al.* 2000).

RESULTS AND DISCUSSION

Physical/Chemical parameters

Suspended sediment: Both branches showed greater concentrations at the impaired sites during baseflow conditions. Storm events created conditions where more sediment was available for transport than at baseflow conditions. SS at the Reference sites on both the Eastern and Southern Branch were significantly lower ($p < 0.05$) than at the impaired sites throughout the year. There were no significant differences when the reference sites on both branches or the impaired sites on the branches were compared to each other (Hoch 2007).

Nutrients: Total nitrogen concentrations were similar for both branches at baseflow conditions. Seasonality was not a factor and concentrations were not significantly different for either total phosphorus or total nitrogen between reference and impaired sites on the eastern branch. Total phosphorus concentrations at the southern impaired site were greater than those found at the reference site. During stormflows, total phosphorus concentrations were higher on the eastern branch than the southern branch. Total nitrogen concentrations appeared to be dependent on storm intensity and stream branch. Greater releases of total nitrogen occurred in storms of 1 – 4cm on the southern branch. On the eastern branch, storms of the same size or greater released more total nitrogen than the smaller storms (Hoch 2007).

SS concentration was a poor predictor of TN concentrations in both watersheds supporting the possibility that erosion of legacy sediments are not the dominant source of TN to downstream areas. In contrast, the TN, TP concentration was positively related to SS concentrations, indicating that the bulk of the input of the

phosphorus to the stream was particle-bound and associated with erosion (Hoch 2007).

Biological Parameters

Periphyton – chlorophyll α: Chlorophyll *a* was used to assess the biomass of primary producers in the stream. In both reaches, pool samples tended to contain lower chlorophyll α than riffle samples. In addition to differences between habitats, seasonal differences were found with greater concentrations in winter and the lowest in summer months. The highest chlorophyll *a* concentration was found at the impaired site in the South Branch. This site is downstream of the discharge of the New Freedom Wastewater Treatment Plant. Not surprisingly, the concentration of TP at this site was significantly higher at this site than at any of the other sites (Hoch 2007).

Periphyton – ash free dry weight: Greatest dry weight concentrations were found in pools. However, mineral content was greater than organic content. This higher mineral content was due to the silt found in the stream. Little differences were observed between sites on each branch and between the branches themselves (Hoch 2007).

Macroinvertebrates: Macroinvertebrate data indicated no consistent differences overall between the control and impaired sites in the overall density of macroinvertebrates, although the seasonal variability makes it difficult to detect differences when yearly averages are compared. Macroinvertebrate diversity was always greater at the Southern branch reference site than at the impaired site on this branch. On the East Branch, diversity at the reference site was only greater than the impaired site for 4 of the 7 total samples obtained. In addition, the average IBI_M scores for each watershed were significantly higher ($p < 0.05$) at reference reaches compared to impaired reaches. There were no differences in the IBI_M scores between the reference sites on the two watersheds while the scores for the East branch impaired site was generally higher than that for the South Branch.

Fish: Twenty-two species of fish were observed in the surveys. Interestingly, a greater number of species were found at the impaired sites rather than the reference sites. Black nose dace was the dominant species at reference sites and the long nose dace was dominant at the impaired sites. Biomass was dominated by two other species. All sites, except the southern branch reference site, were dominated by the white sucker. The southern branch reference site was dominated by brown trout. Although the eastern branch demonstrated more diversity, there was no significant difference between the two branches. Some captured fish showed disease anomalies: black spot parasite or parasitic flatworms. Using the index of biological integrity for Maryland streams (Roth *et al.* 2000), all sites were in the poor range except for the reference site on the southern branch. This site was considered fair (Hoch 2007).

Overall, the southern branch is more impaired than the eastern branch. Data are still being collected and analyzed. Three sites are proposed to be restored in summer 2009 (R.L. Irwin, personal communication 2009).

REFERENCES

Barbour, M.T., Gerritsen, J., Snyder, B.D., Stribling, J.B. (1999). *Rapid Bioassessment Protocols for use in streams and wadeable rivers: Periphyton, benthicmacroinvertebrates and fish*, Second edition. EPA 841-B-99-002. U.S. Environmental Protection Agency, Office of Water, Washington, D.C.

Codorus Creek Watershed Association. (2009). Accessed online at http://www.codoruscreek.net.

APHA (American Public Health Association), American Water Works Association (AWWA) and Water Environment Federation (WEF) (1996). in *Standard Methods for the Examination of Water and Wastewater*, 19th edn., Eds. L. S.Clesceri, A. D. Eaton, A. E. Greenberg, and M.A.H. Franson, APHA, AWWA and WEF, New York, NY.

Hoch, M.P. (2007). *Codorus Creek Restoration Efficacy Program: Pre-restoration Assessment Final Data Report (#SC30462)*. Southcentral Regional Office, The Pennsylvania Department of Environmental Protection, Harrisburg, PA.

Irwin, R.L. (2009). Personal communication. Aquatic Resource Restoration Company, Seven Valleys, PA.

Lloyd, J. (2007). "Many, many mills in York County, Pennsylvania". December 13, 2007. York Daily record/Sunday News and York Newspaper Company: York, PA. Accessed online at http://www.yorkblog.com/universal/2007/12/many_many_mills.html.

Pennsylvania Department of Conservation and Natural Resources (PA DCNR). (2002). "Upper Codorus Creek Watershed (August 19, 2002)". Accessed online at http://www.dcnr.state.pa.us/brc/rivers/riversconservation/registry/upper_codorus.aspx .

Pennsylvania Department of Environmental Protection (PA DEP). (2007). *Index of biological integrity for wadeable freestone streams in Pennsylvania*. Pennsylvania Department of Environmental Protection, Harrisburg, PA.

Natural Streams Project. (2008). Franklin and Marshall College, Lancaster, PA. Accessed online at http://edisk.fandm.edu/michael.rahnis/index.html.

Roth, N.E., Southerland, M., Chaillou, J.C., Kazyak, P.F., and Stranko, S.A. (2000). "Refinement and validation of a fish index of biotic integrity for Maryland streams". Report # CBWP-MANTA-EA-00. Chesapeake Bay and Watershed Programs, Maryland Department of Natural Resources, Annapolis, MD.

Smith, R.V. (2003). *Soil survey of York County, Pennsylvania*. United States Department of Agriculture and Natural Resources Conservation Service: Washington, DC. Accessed online at http://soils.usda.gov/survey/printed_surveys/state.asp?state=Pennsylvania&abbr=PA.

Steinman, A.D., Lamberti, G.A., and Leavitt, P.R. (2006). "Biomass and pigments of benthic algae". *In*: Hauer, R.F. and G.A. Lamberti (eds.), *Methods in stream ecology*. Academic Press, San Diego, CA. 357-380.

Stribling, J.B., Jessup, B.K., White, J.S., Boward, D., and Hurd, M. (1998). "Development of a benthic index of biotic integrity for Maryland streams". Report # CBWP-MANTA- EA-98-3. Chesapeake Bay and Watershed Programs, Maryland Department of Natural Resources, Annapolis, MD.

Valderrama, J.G. (1981). "The simultaneous analysis of total nitrogen and total phosphorus in natural waters". *Mar. Chem.*, 10, 109-122.

Walter, R.C. and Merritts, D.J.. (2008). "Natural streams and the legacy of water-powered mills". *Science,* 319, 299-304.

Combining GIS, BMP Performance, and Strategic Planning to Support Water Quality Implementation Planning

Ken Susilo[1], PE, D.WRE, CPSWQ, Marc Leisenring[2], PE, and Eric Strecker[3], PE

[1]Geosyntec Consultants, 2566 Overland Ave., Suite 670, Los Angeles, CA 90064; PH (310) 839-6040; FAX (503) 839-6041; email: ksusilo@geosyntec.com
[2]Geosyntec Consultants, 55 SW Yamhill St., Suite 200, Portland, OR 97204; PH (503) 222-9518; FAX (503) 242-1416; email: mleisenring@geosyntec.com
[3]Geosyntec Consultants, 55 SW Yamhill St., Suite 200, Portland, OR 97204; PH (503) 222-9518; FAX (503) 242-1416; email: estrecker@geosyntec.com

ABSTRACT

Numerous efforts to improve storm water quality on a watershed-wide basis have lacked a reproducible, transparent, methodical approach to optimize the selection and implementation of structural Best Management Practices (BMPs) to meet receiving water quality goals. For urban stormwater retrofit projects, structural BMPs are primarily selected in an opportunistic, site-specific fashion, focusing on one or a few pollutants, stakeholder inputs, or local funding availability. As geographic information systems (GIS) technologies improve, computing power increases, and pollutant loading and treatment efficiency datasets become more robust there is an opportunity to improve watershed-based implementation planning efforts.

The authors have developed methods to prioritize water quality improvement needs and identify structural BMP opportunities on a watershed scale to maximize the return on investment for improved water quality. Opportunity evaluation considers property ownership and the potential for retrofitting to achieve multiple benefits, such as water quality, aesthetics, recreation, and habitat. It is recognized that different types of land parcels typically have different types of opportunities and constraints. BMP opportunities can be regional or distributed in nature depending on the land use, size, and location of the public parcel, among other things. By utilizing GIS-based parcel and land use information in the context of water quality need, potential opportunities, and constraints, as well as BMP unit processes and performance data, watershed-wide benefits of BMP implementation can be assessed.

An analysis tool has been developed in the ArcGIS™ environment that automates many of these spatial prioritization and identification processes, while allowing for stakeholders and decisions-makers to provide meaningful input that supports BMP implementation decisions. Once candidate BMPs have been identified for a high priority area, the tool can estimate the potential pollutant load reductions and planning level costs associated with site-specific implementation. Example studies are provided to illustrate the concepts and GIS methods employed.

INTRODUCTION AND PURPOSE

Agencies in Southern California, like many others throughout the United States, are facing a number of challenges and opportunities with respect to stormwater quality. The challenges lie in the implementation of TMDLs and planning for future MS4 Permits while considering limited space, aging infrastructure, and numerous other constraints. Opportunities lie in funding opportunities such as successful local ballot propositions, Integrated Regional Water Management Planning efforts, and coordinated redevelopment and urban retrofit projects.

With the advent of geographic information systems (GIS), watershed-wide stormwater BMP implementation planning and prioritization efforts have the potential to significantly improve. However, the general approach with many efforts is to identify opportunities based on limited spatial analyses and stakeholder inputs without considering *a priori* the spatial distribution of relative water quality improvement need. The prioritization of potential opportunities, if conducted, often lacks a reproducible, updateable and methodical approach that considers both the relative need for water quality improvement and the constraints of BMP implementation.

Once opportunities have been prioritized, the selection of candidate BMPs must consider site-specific constraints and the potential for improving water quality. Quantifying water quality improvements can be particularly challenging given uncertainties in rainfall, hydrologic response, water quality loading, and BMP effectiveness. By combining long-term hydrologic simulations with stochastic water quality modeling methods, the storm-to-storm variability of loads and load reductions can be quantified for selected site-specific scenarios. This quantification of uncertainty provides a more realistic estimate of the confidence in model predictions and the range of potential improvement to water quality. Site-specific scenario model results can then be extrapolated to inform watershed-wide water quality improvement planning.

The purpose of this paper is to present some of the approaches and considerations for identifying opportunities and assessing potential benefits of watershed-wide BMP planning and implementation efforts. The Structural BMP Prioritization and Assessment Tool (SBPAT; Geosyntec 2008) is then introduced and used to demonstrate these methods and illustrate how site-specific modeling can be used to assess various watershed-wide BMP implementation scenarios.

WATERSHED WIDE PRIORITIZATION APPROACHES

The identification and prioritization of stormwater BMP retrofit projects should consider water quality improvement needs and BMP implementation opportunities. Water quality improvement need may be quantified by estimating runoff volumes, pollutant loads, and stressors by analyzing land use, imperviousness, receiving water impairments, and local monitoring data. BMP implementation opportunities may be identified by considering parcel attributes such as size, ownership, land use, and distance to storm drains. Depending on the specific goals of the watershed

prioritization additional spatial data sets may also be included. As examples, two different watershed-wide prioritization approaches are described below.

Los Angeles County Structural BMP Prioritization Methodology (Methodology). The BMP Prioritization Methodology (Geosyntec 2006) provides a four step procedure for prioritizing catchments by water quality need and BMP implementation potential and then ranking BMP types based on relative cost, effectiveness, implementability, and other benefits. The four steps of the Methodology are shown in Figure 1.

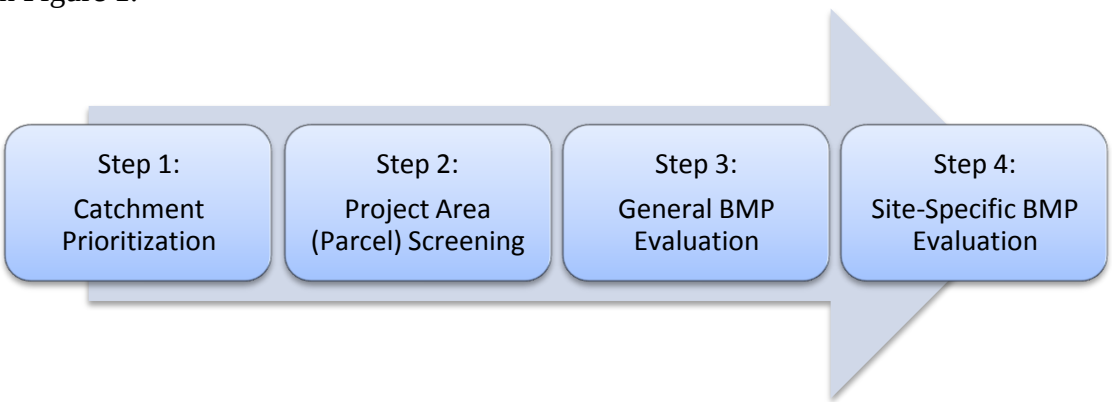

Figure 1. Overall Methodology flowchart.

During Catchment Prioritization (Step 1), the relative need for retrofitting a catchment within a watershed is quantified by developing a Catchment Prioritization Index (CPI) and a Nodal CPI. The CPI is calculated by estimating normalized pollutant loads or concentrations for every catchment and weighting each pollutant according to downstream receiving water impairments and TMDLs. Downstream receiving water impairments are determined using a defined catchment network where every catchment has a unique identifier and a unique downstream catchment identifier. The Nodal CPI is calculated as the area-weighted average of the CPI values from all upstream tributary catchments. The CPI provides a relative measure of the need to address pollutants of concern generated directly from the catchment. A Nodal CPI provides a measure of the need to address pollutants of concern generated upstream from the catchment. Both the CPI and Nodal CPI serve as the basis for prioritization of catchments for BMP implementation.

Project Area Screening (Step 2) identifies parcels in or downstream of high-priority catchments that provide the greatest opportunities for structural BMP implementation. Two different types of structural BMPs are explicitly considered:

- Regional/subregional BMPs: centralized stormwater facilities, typically placed near the outlet of a catchment or subwatershed (a group of catchments) ,designed to treat stormwater from larger drainage areas (order of magnitude:100-200 acres).

- Distributed/onsite BMPs: stormwater devices and landscaping practices dispersed throughout a catchment and typically serving smaller drainage areas (order of

magnitude: <10 acres), such as a large single parcel, rooftop, or section of roadway.

If a catchment is identified as having a high water quality improvement need but regional and distributed structural BMP opportunities are limited, then non-structural or institutional BMPs must be considered.

Potential BMP opportunities are determined by calculating distributed and regional BMP scores for every catchment. The BMP scores are determined by first calculating parcel scores according to their size, ownership, land use, and distance from major storm drains. An area-weighted parcel score is then calculated for every catchment. An overlay analysis compares the distributed BMP scores to the CPI values and the regional BMP scores to the nodal CPI values. Catchments with high BMP scores and high CPI values are considered high priority catchments for retrofit BMP implementation. Figure 2 provides examples of regional and distributed BMP priority and opportunity maps generated for the Ballona Creek watershed in Los Angeles, California. These maps represent the final products of Steps 1 and 2 of the Methodology.

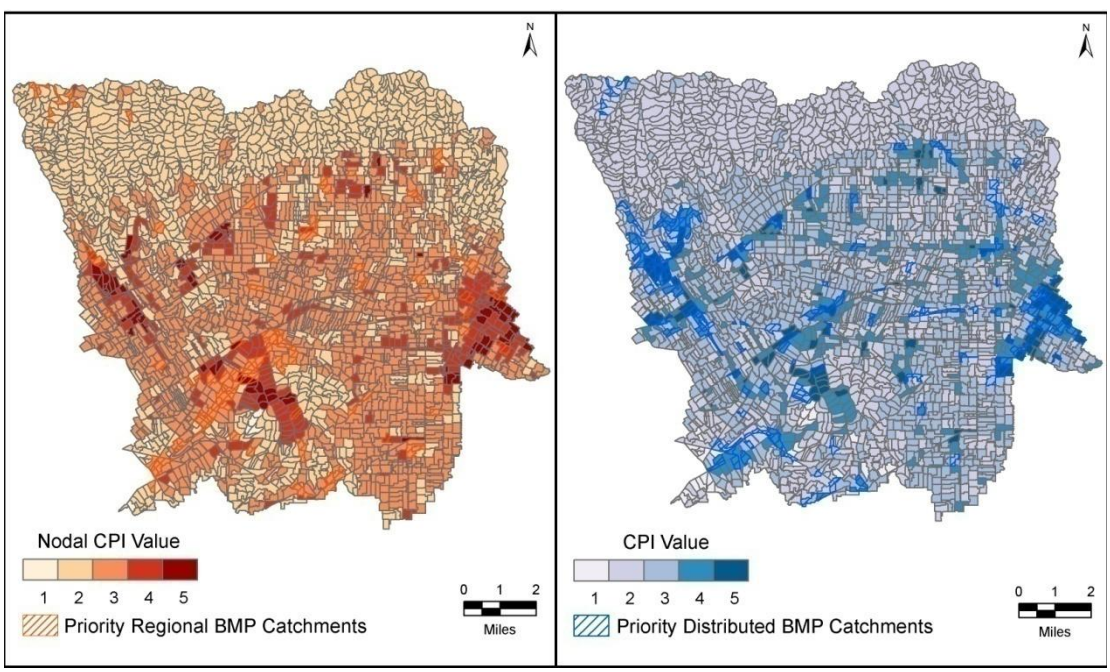

Figure 2. Example Regional (left) and Distributed (right) BMP Priority and Opportunity Maps.

Once regional and distributed BMP priority catchments are identified, during Steps 3 and 4 of the Methodology BMP comparison matrices are produced using user-defined weights of the relative importance of various BMP implementation factors, such as cost, effectiveness, site-specific constraints, and other benefits. These matrices can then be used to identify which BMPs should be further evaluated for specific priority catchments.

The Green Solutions Project. Similar to the BMP Prioritization Methodology, the Green Solutions Project (Geosyntec and GreenInfo, 2008) involved watershed-wide assessment of water quality improvement need and potential BMP implementation opportunities. However this project focused was on multi-use, multi-benefit "green" BMPs that can be implemented on publicly owned parcels. The overall purpose of the Green Solutions Project was to quantify the number of acres needed and the amount of existing public lands suitable for stormwater quality retrofit projects to effectively treat runoff while also providing new park, recreation, natural habitat or other green open space lands.

Water quality treatment needs and BMP implementation opportunities were identified for each major watershed in the County (Figure 3) by applying various assumptions regarding treatment areas, BMP design, parcel and land use suitability, treatable areas, and water quality priorities.

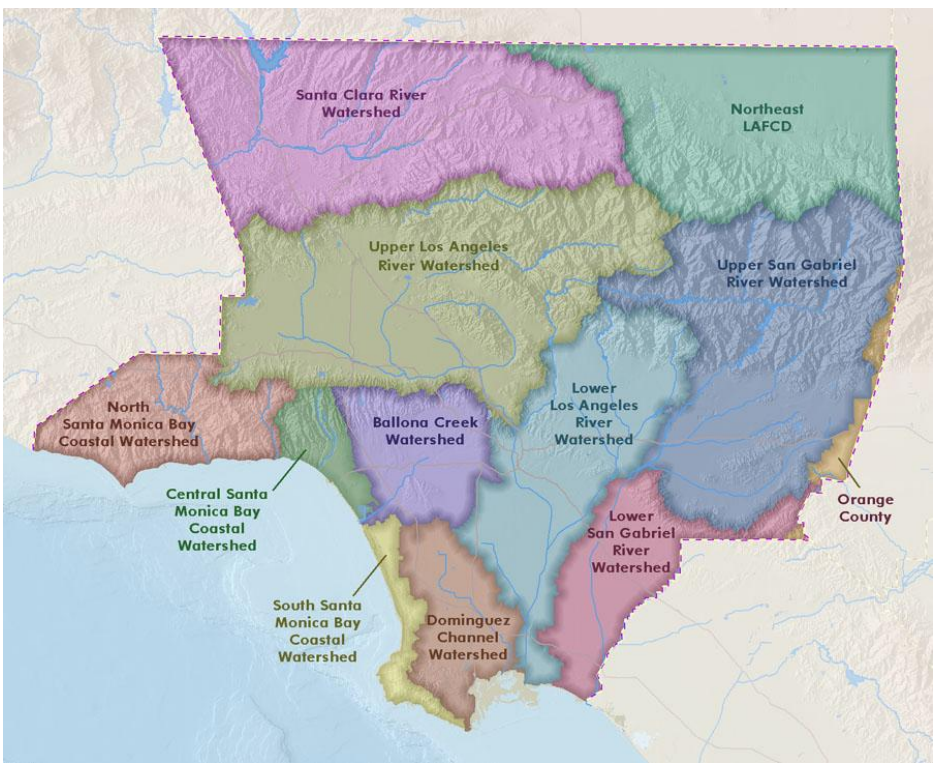

Figure 3. Los Angeles County Watersheds (Geosyntec and GreenInfo 2008).

Effective drainage areas, or area contributing to direct runoff, were estimated for each subwatershed based on Los Angeles County's runoff coefficient equation:

$$A_E = (0.9 \times A_T \times Imp) + [0.1 \times A_T \times (1 - Imp)]$$

Where: A_E = Effective Drainage Area (acres)
A_T = Total Drainage Area (acres)
Imp = Proportion Impervious (0 to 1)

By applying typical BMP design assumptions and analyzing runoff capture efficiencies from long-term hydrologic simulations of historical Los Angeles area rainfall, treatment area ratios (TARs), or the ratio of BMP footprint to the effective tributary area (Figure 4), were estimated to range between 5-10%. This range was then used to estimate a range of potential land needed to capture 80% of the average annual runoff volume from the effective drainage areas.

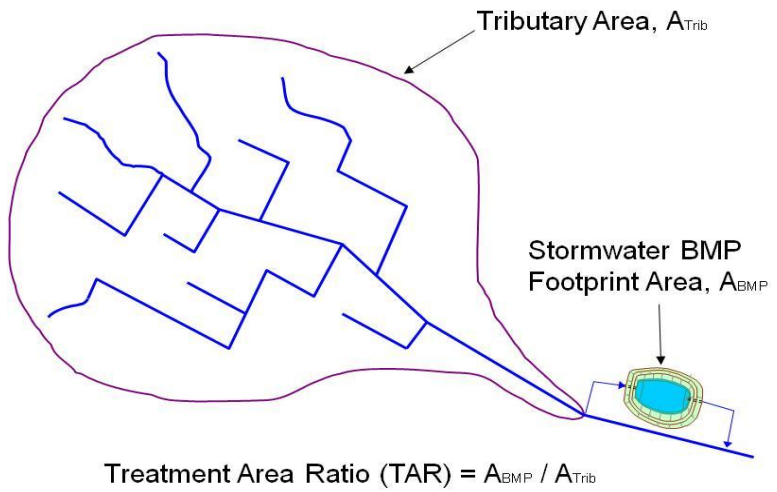

Figure 4. Conceptual Illustration of the Treatment Area Ratio (TAR) (Geosyntec and GreenInfo, 2008).

Suitable acres of publicly owned land for BMP implementation were then estimated by evaluating aerial photographs of a subset of parcels for each major land use category. Ranges of suitable acres were then assigned to all public parcels by land use. Public parcels greater than 100 acres were evaluated and assigned suitable acreages individually. A range of total suitable acres for each subwatershed was then computed by summing the values assigned to all public parcels.

Finally, comparisons of needed BMP footprint areas to suitable acres were then used to identify subwatersheds with adequate or deficient public land to meet stormwater treatment goals. Figure 5 summarizes the estimated BMP acres suitable as a percentage of the needed acres for all watersheds in Los Angeles County. The wide range illustrates the high level of uncertainty associated with this planning level analysis, but clearly indicates which watersheds have few or many opportunities for water quality improvement through the retrofit of public lands. Figure 6 shows the average percent suitable acreages by subwatershed for each L.A. County watershed. The catchment prioritization index (CPI) from the BMP Prioritization Methodology has also been overlain to illustrate which watersheds have the most pressing needs.

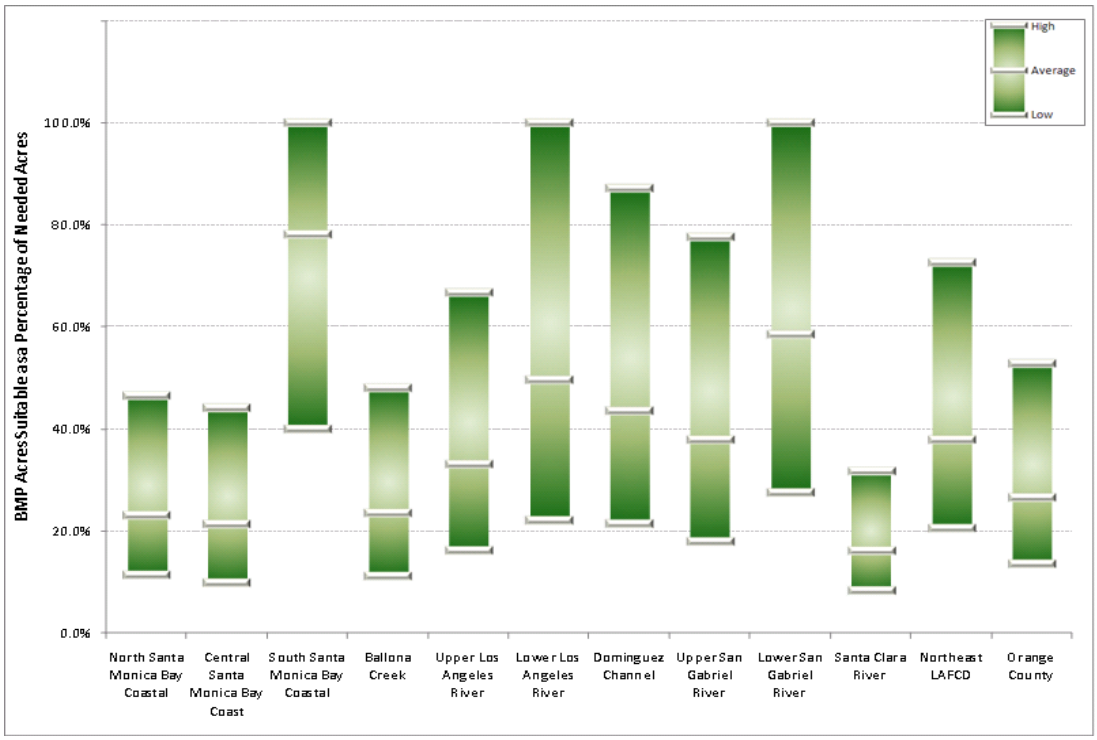

Figure 5. Percent of BMP Area Needs Potential Met by Suitable Public Lands (Geosyntec and GreenInfo, 2008).

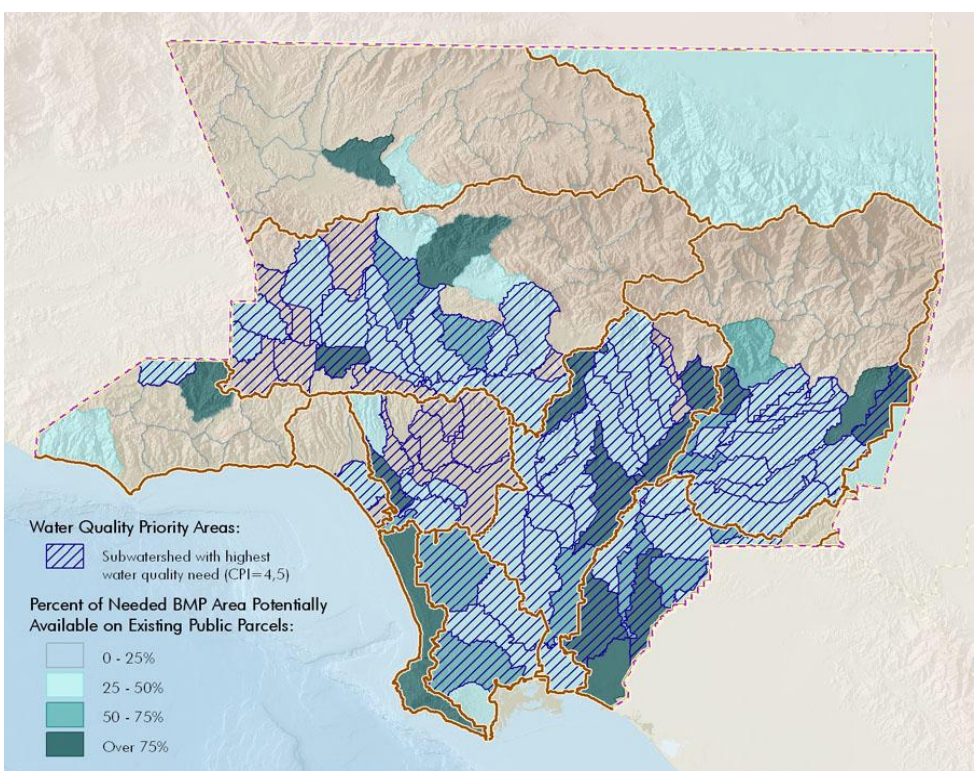

Figure 6. Average BMP Area Needs Potentially Met versus Water Quality Improvement Priority (Geosyntec and GreenInfo, 2008).

STRUCTURAL BMP PRIORITIZATION AND ANALYSIS TOOL (SBPAT)

The Structural BMP Prioritization and Analysis Tool (SBPAT) is a GIS-based decision support tool that has been developed as an ArcGIS™ extension (Geosyntec, 2008). SBPAT includes two primary elements: a Prioritization component and a Modeling component. The Prioritization component implements the Los Angeles County Structural BMP Prioritization Methodology, as described above. The Modeling component is intended to help evaluate the costs and benefits of implementing specific BMP types within prioritized catchments by modeling the hydrology and quality of runoff before and after BMP implementation. It utilizes a modified U.S. EPA Storm Water Management Model (SWMM) and a Monte Carlo water quality model to estimate average annual runoff volumes and loads and average storm EMCs before and after BMP implementation. The predicted uncertainty of these estimates and planning-level capital and O&M costs are also provided to assist in risk-based decision making regarding BMP implementation.

Primary inputs for SBPAT include spatial and non-spatial data sets. A pre-populated geodatabase includes many of the necessary inputs including catchments, slopes, soils characteristics, land uses, imperviousness, long-term rainfall records, land use EMCs, and BMP effluent concentrations. Land use EMCs were estimated using Los Angeles County data (LACDWP, 2001 & 2002) and BMP effluent concentrations were estimated using data from the International BMP Database (WWE and Geosyntec, 2008). The primary user inputs are catchment prioritization parameters and site-specific information such as extent of BMP implementation and BMP design parameters. Figure 7 illustrates the primary inputs and components of SBPAT.

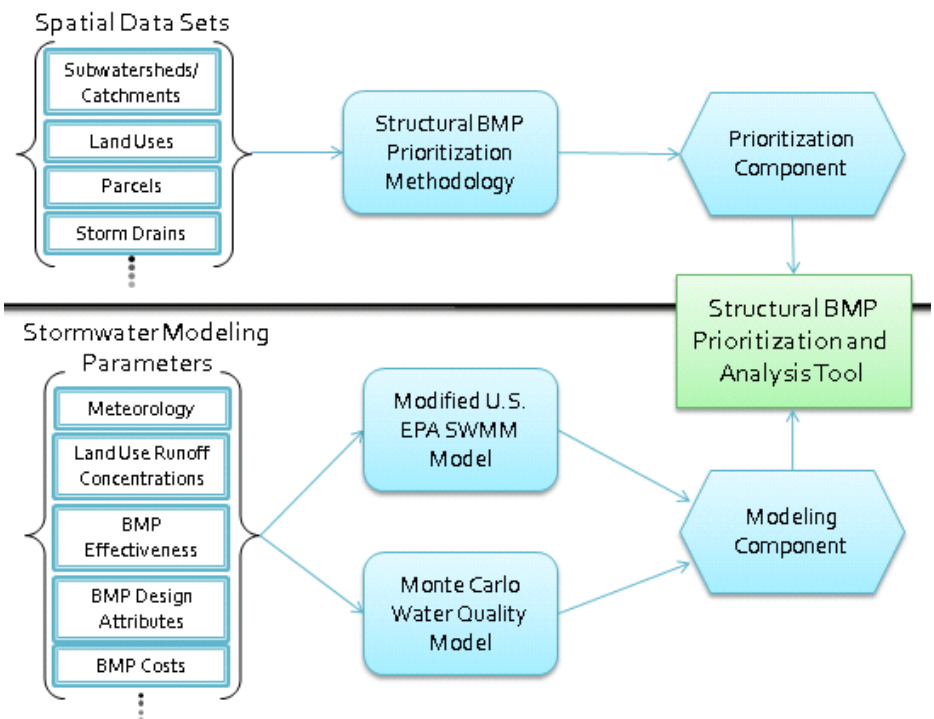

Figure 7. Primary Inputs and Components of SBPAT.

SBPAT DEMONSTRATION OF BMP MODELING ANALYSIS

The catchments of the Ballona Creek watershed were prioritized using the Prioritization Component of SBPAT. A 238-acre, 85% impervious study area was selected by choosing a high priority group of catchments as shown in Figure 8.

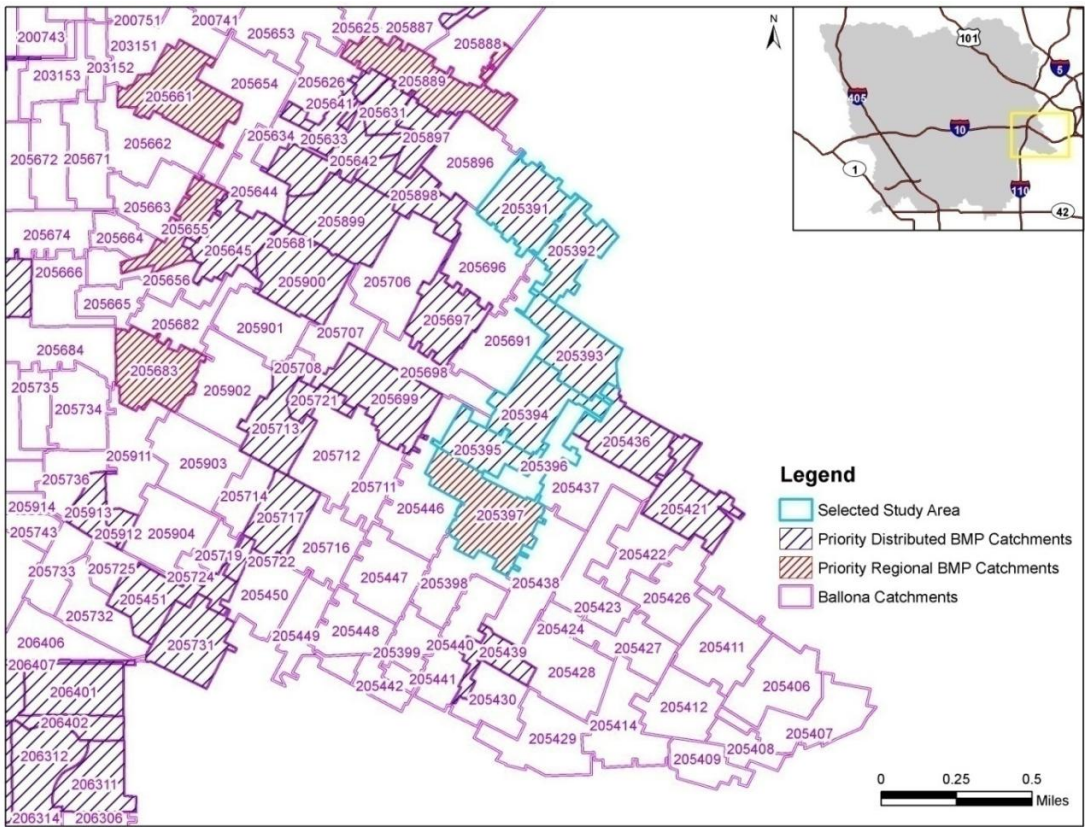

Figure 8. Selected Study Area and Priority Catchments.

BMP Implementation Scenarios. Due to a Metals TMDL (LARWQCB, 2007), BMP types were selected for this example that would likely reduce loads or concentrations of metals based on fundamental unit treatment processes (Strecker et al., 2005). Within SBPAT, the user identifies distributed BMPs by land use (in terms of percent implementation). Regional BMPs are assumed to be placed at the downstream end of the study area and will treat runoff from the entire area. The BMP design capacities determine the quantity of runoff that is treated over the simulation period.

Four different BMP modeling scenarios were simulated as follows:

- Scenario 1: Distributed BMPs only with the land use-based percent implementation strategy described below.
- Scenario 2: A regional extended detention basin sized to fit within a 0.75-acre playfield of a City-owned park; estimated design volume of 4.5 ac-ft.
- Scenario 3: A regional hydrodynamic separator sized to treat 0.2 in/hr design intensity for the entire study area; estimated design flow rate 39 cfs.

- Scenario 4: A regional subsurface flow wetland sized to fit beneath the 0.75-acre playfield in the City-owned park (design flow rate of 1.4 cfs), including an equalization basin designed to capture a 0.2-inch storm from the entire study area.

For Scenario 1, aerial photographs were examined to estimate available areas for distributed BMP implementation within each land use type. Distributed BMP assignments (Table 1) were based on estimated available areas and the following target treatment levels:

- Since metals are priority pollutants, industrial, commercial, and transportation land uses should be highest priority; target level of distributed BMP implementation was set to 80%.
- Multifamily and educational land uses are generally lower priority; target level of distributed BMP implementation was set to 50%.

Table 1. Distributed BMP Assignments by Land Use.

Land Use	*Cisterns*	*Bioretention*	*Perm. Pvmt*	Media Filters
Commercial	0%	0%	30%	50%
Education	20%	30%	0%	0%
Industrial	0%	0%	20%	60%
MF Residential	30%	20%	0%	0%
Transportation	0%	0%	5%	75%
Vacant	0%	0%	0%	0%

Default sizing parameters for each BMP type were not changed; distributed BMPs would be sized to capture and treat the Los Angeles County Standard Urban Storm Water Mitigation Plan (SUSMP) design storm criteria (LACDPW, 2002).

The three regional BMP scenarios (Scenarios 2-4) were an extended detention (ED) basin, hydrodynamic separator (HD separator), or a subsurface flow (SSF wetland). The ED basin and SSF wetland were limited to available space within the City-owned park, but it the hydrodynamic separator was sized to meet a BMP design criteria of 0.2 in/hr (the device can be placed underground and in-line with a major storm drain).

Summary of Results. Table 2 summarizes the total influent volume and the percent captured (reduced or treated) and untreated for each individual BMP. Scenarios 1 and 3 capture the largest total volume of runoff as these BMPs were sized using the SUSMP size criteria and default design assumptions. The ED Basin (Scenario 2) and SSF wetland (Scenario 4) were sized according to the estimated available space for implementation and therefore resulted in much smaller percent captures.

Table 2. Average Annual Percent Reduction, Treated, and Untreated Volumes.

BMPs	*Influent Vol (ac-ft)*	*% Reduced*	*% Treated*	*% Untreated*
Cisterns	10	46%	0%	54%
Bioretention Areas	8.7	52%	0%	48%
Permeable Pvmt	40	88%	0%	12%
Media Filters	106	0%	87%	13%
Total Dist. BMPs (Scenario 1)	164	20%	42%	38%
ED Basin (Scenario 2)	220	0%	30%	70%
HD Separator (Scenario 3)	220	0%	86%	14%
SSF Wetland (Scenario 4)	220	1%	16%	83%

Figure 9 graphically compares the average annual metal load and average storm EMC reductions between the scenarios. As indicated in the figure, Scenarios 1 and 3 produce the highest load reductions for total copper (TCu), total lead (TPb), and total zinc (TZn). However, despite the small percent volume capture for the SSF wetland (18%), it outperforms the HD separator for dissolved metals load reductions and outperforms both the distributed BMPs and the HD separator for dissolved metals concentrations reductions. The SSF wetland also does nearly as well for total metal concentration reduction. The high load reductions for all constituents for the distributed BMP scenario can be largely attributed to the 20% volume reduction.

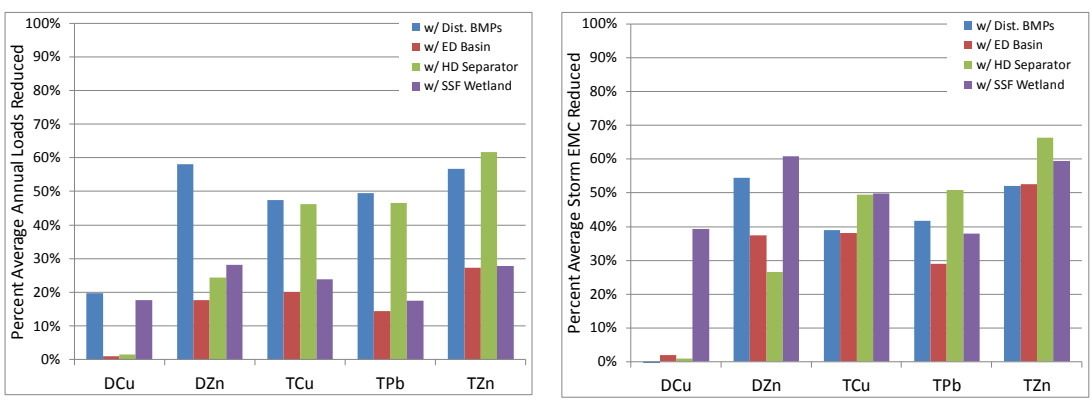

Figure 9. Scenario Comparison of Percent Average Annual Volume and Load Reductions.

In addition to evaluating relative changes in volumes, loads, and concentrations with the implementation of BMPs, a comparison to in-stream numeric water quality objectives was evaluated. The Ballona Creek Metals TMDL (LARWQCB, 2007) lists the wet-weather water quality objectives shown Table 3.

Table 3. Wet-weather Numeric Targets for Ballona Creek.

	Dissolved(µg/L)	*Total Recoverable (µg/L)*
Copper	11	18
Lead	49	59
Zinc	94	119

Table 4 summarizes the storm event exceedance probabilities with and without BMPs for several constituents. As shown in the table, the exceedance probabilities for all total metals are expected to be reduced significantly by the distributed and regional BMP implementation scenarios. Only the SSF wetland is predicted to reduce the exceedance probabilities of dissolved copper or fecal coliform. The distributed BMP scenario and the SSF wetland scenario are predicted to reduce exceedance probabilities of dissolved zinc, but the other two regional BMP scenarios are not predicted to have an effect. Dissolved copper exceedances are expected to increase slightly for the distributed BMP scenario due to volume losses from land uses with lower average dissolved copper EMCs.

Table 4. Storm Event Exceedance Probabilities Before and After BMP Implementation.

Pollutant	*DCu (ug/L)*	*DZn (ug/L)*	*TCu (ug/L)*	*TPb (ug/L)*	*TZn (ug/L)*
Threshold	11	94	14	59	119
Pre-BMP	62%	90%	91%	3%	96%
Dist. BMPs (Scenario 1)	65%	55%	66%	0%	66%
ED Basin (Scenario 2)	62%	90%	64%	1%	58%
HD Separator (Scenario 3)	62%	90%	51%	0%	39%
SSF Wetland (Scenario 4)	24%	38%	46%	1%	46%

SBPAT provides planning level estimates of capital and annual maintenance for each modeled BMP type. Capital costs do not account for engineering, design, or permitting, but a default of 25% is added to all capital and maintenance costs to account for contingencies. Figure 10 compares life-cycle costs for the four modeled scenarios assuming all BMP types have the same life span (30-years) and annual discount rate of 2%. The much higher costs for distributed BMP is due high capital costs for permeable pavements and high annual maintenance costs for media filters.

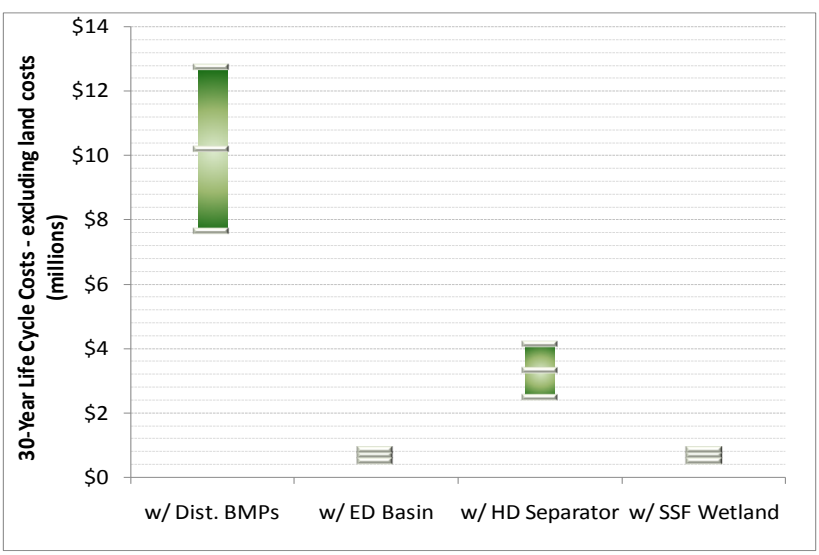

Figure 10. Life-Cycle Cost Comparisons between the Modeled Scenarios.

After several example study areas of various sizes and land use distributions are simulated, it may be possible to extrapolate the results from this site-specific simulation to the larger watershed. Care must be taken not to over-generalize BMP implementation feasibility, especially for regional BMPs where site-specific constraints can be more limiting than for distributed BMPs. Due to the generally small number of regional BMP retrofit opportunities in urbanized watersheds, it may be feasible to evaluate all of these individually. The extrapolation of distributed BMP results is more appropriate since these BMP types are not as dependent on the routing of concentrated flows and it may be possible to generalize BMP implementation based on land use and parcel ownership.

SUMMARY AND CONCLUSIONS

Various methods are available for identifying and prioritizing water quality improvement projects within a watershed. A GIS provides a framework for assimilating many spatial datasets at the watershed scale so that multiple objectives and constraints can be simultaneously considered. The Structural BMP Prioritization Methodology is a transparent, reproducible method for prioritizing BMP retrofit projects at a catchment scale that accounts for both water quality improvement need and BMP implementation opportunities. The Green Solutions Project provides an alternative method that identifies potential opportunities at a subwatershed scale for implementing multi-use, multi-benefit BMPs on public lands and identifies where there is a lack of suitable public lands to address water quality concerns. SBPAT is an ArcGIS™ extension that automates the Prioritization Methodology and allows users to model BMP implementation scenarios within priority catchments. Planning level costs and benefits of the scenarios can then be compared against water quality objectives. Site-specific assessments can be extrapolated across an entire watershed to assist with the development of strategic water quality implementation plans.

REFERENCES

Geosyntec Consultants (2006). *Los Angeles County-wide Structural BMP Prioritization Methodology - A Guidance Manual for Strategic Water Quality Project Planning.* Prepared for Heal the Bay, the County of Los Angeles, and the City of Los Angeles.

Geosyntec Consultants (2008). *A User's Guide for the Structural BMP Prioritization and Analysis Tool (SBPAT v1.0).* Prepared for Heal the Bay, the County of Los Angeles, and the City of Los Angeles.

Geosyntec Consultants and GreenInfo Network (2008). *Green Solution Project – Identification and Evaluation of Urban Runoff Quality Retrofit Projects in Los Angeles County.* Prepared for Community Conservancy International.

Los Angeles County Department of Public Works (LACDPW). (2000). *Los Angeles County 1994-2000 Integrated Receiving Water Impacts Report*. http://dpw.lacounty.gov/wmd/npdes/IntTC.cfm (Jan. 26, 2009).

Los Angeles County Department of Public Works (LACDPW). (2001). *Los Angeles County 2000-2001 Stormwater Monitoring Report.* http://dpw.lacounty.gov/wmd/NPDES/2000-01TC.cfm (Jan. 26, 2009).

Los Angeles County Department of Public Works (LACDPW). (2002). *Development Planning for Storm Water Management. A Manual for the Standard Urban Storm Water Mitigation Plan (SUSMP).* http://www.ladpw.org/wmd/NPDES/SUSMP_MANUAL.pdf (Jan. 23, 2009).

Los Angeles Regional Water Quality Control Board (LARWQCB). (2007). *Ballona Creek Metals TMDL, Regional Board Resolution No. 2007-015, Attachment A (Final Basin Plan Amendment.* http://63.199.216.6/larwqcb_new/bpa/docs/2007-015_RB_BPA.pdf (Jan. 23, 2009).

Strecker, E.; Huber, W.; Heaney, J.; Bodine, D.; Sansalone, J.; Quigley, M.; Leisenring, M.; Pankani, D.; and Thayumanavan, A. (2005). *Critical Assessment of Stormwater Treatment and Control Selection Issues*. Final report to the Water Environment Research Foundation. WERF 02-SW-1.

Wright Water Engineers (WWE) and Geosyntec Consultants (2008). *International Stormwater Best Management Practices (BMP) Database Project*. http://www.bmpdatabase.org/. Sponsored by the Water Environment Research Foundation (WERF), ASCE Environmental and Water Resources Institute (EWRI), USEPA, Federal Highway Administration (FHWA) and the American Public Works Association (APWA)

Considerations, Opportunities, and Strategies for Infiltration Stormwater BMPs

Ken Susilo[1], PE, D.WRE, CPSWQ; Neven Matasovic[2], Ph.D., PE, GE;
Ronald S. Johnson[3], PE, GE

[1]Geosyntec Consultants, 2566 Overland Ave., Suite 670, Los Angeles, CA 90064; PH (310) 839-6040; FAX (310) 839-6041; email: ksusilo@geosyntec.com
[2]Geosyntec Consultants, 2100 Main Street, Suite 150, Huntington Beach, CA 92648 PH (714) 465-1244; FAX (858)674-6586; email: nmatasovic@geosyntec.com
[3]Geosyntec Consultants, 10875 Rancho Bernardo Rd, Suite 200, San Diego, CA 92127, PH (858) 674-6559; FAX (714)969-0820 email: rjohnson@geosyntec.com

ABSTRACT

Infiltration as a Best Management Practice (BMP) is strongly encouraged by many who are focused on water quality, water resources, and regulatory compliance. It is often considered the ideal solution that solves multiple problems. Many practicing engineers, designers, and project approvers however, are concerned about the widespread implementation of infiltration measures, and have initiated restrictive conditions that significantly limit their use. This paper discusses benefits and considerations that should be made when proposing infiltration BMPs, offers potential methods to meet what can be limiting site conditions, and discusses recent applied research/design efforts that been initiated in southern California.

Infiltration has numerous potential benefits, particularly in urbanized watersheds. Infiltration BMPs when implemented properly can lead to a) restoration of natural hydrologic cycles; b) mitigation of the degradation of creeks; c) management of water resources; and d) comprehensive watershed-wide water quality improvement.

There are, however, numerous design considerations that should be evaluated when proposing infiltration BMPs. These include a) soil type/infiltration capacity; b) groundwater;, c) pre-existing contamination; d) design and hydraulic issues; e) long-term issues such as groundwater mounding and ground settlement; f) introduction of geological hazards such as landsliding, soil liquefaction and their impacts; and i) other issues such as mold and waterproofing that may result from the presence of wet soil. While many of these considerations can be fatal flaws, in some cases innovative engineering approaches can be implemented to increase the viability of infiltration, particularly where choice of satisfactory alternatives is limited. This paper explores some of these methods and impacts related to implementation of these methods. In addition, some recently initiated projects that are expected to contribute to the body of knowledge regarding infiltration concerns and opportunities, and are worthy of further examination and tracking are outlined.

INTRODUCTION

Infiltration (through infiltration basins, infiltration trenches, bioretention, and/or drywells) as a Best Management Practice (BMP) is strongly encouraged by many who are focused on water quality and water resources. It is often considered an ideal solution to stormwater quality mitigation that solves multiple problems. Many practicing engineers, designers, and project approvers however, are concerned about the widespread implementation of infiltration measures, and have initiated restrictive conditions that significantly limit their use. This paper discusses benefits and considerations that should be made when proposing infiltration BMPs, offers potential methods to meet what can be limiting site conditions, and discusses recent applied research/design efforts that been initiated in southern California.

Infiltration has numerous potential benefits, particularly in urbanized watersheds. Infiltration BMPs when implemented properly can lead to restoration of natural hydrologic cycles, through the introduction of subsurface and groundwater flows to shallow aquifers would have been effectively sealed off by urbanization. Infiltration contributes to the restoration of natural hydrological cycles and can assist or mitigate the degradation of creeks (hydromodification effect), by reducing the increased volumes, durations, frequencies, and erosive power of post-urban stormwater. Infiltration, in areas where groundwater is a resource, can help encourage integrated water resources practices, and in doing so can support comprehensive watershed-wide water quality improvement. Large scale infiltration practices may assist with infrastructure requirements, potentially reducing required capacities and frequency of use of drainage systems.

The authors have observed that some documented criteria relating to infiltration can be qualitative or oversimplified, and as such, may not provide specific details or may not necessarily providing a consistent factor of safety. The following is a list of some more quantitative design limitations found in various sources (EPA 2004, CASQA 2003, MassDEP 2008, Stormwater Center and others):

- May not be appropriate where spills may occur.
- The maximum contributing area to an individual infiltration practice should generally be less than 5 acres.
- Infiltration basins require a minimum soil infiltration rate of (range varies 0.15 to 0.5) inches/hour, not appropriate at sites with Hydrologic Soil Types C and D.
- If infiltration rates exceed 2.4 inches/hour, then the runoff should be fully treated prior to infiltration to protect groundwater quality.
- Not suitable on fill sites or steep slopes.
- Risk of groundwater contamination in very coarse soils.
- Upstream drainage area must be completely stabilized before construction.
- Provide significant separation distance (2-feet to 10-feet, depending on standard cited) from the bottom of infiltration basin.
- Provide pretreatment.

The authors recommend caution implementing generic criteria/limitations, and present some evaluation considerations that should be examined on a site specific basis. This paper presents a general discussion only, and provides suggestions on analyses that might be appropriate with the confirmation of the project's geotechnical engineers and geologists.

ENGINEERING MITIGATION / DESIGN CONSIDERATIONS

Infiltration BMPs are simple in principle; however, there are a number of key elements that need to be considered in the feasibility and design stages to achieve the desired performance. These elements include the soil and geology, groundwater, pollutant accumulation, and a wide variety of geotechnical considerations that could affect neighboring structures, slopes, and groundwater conditions.

SOIL AND GEOLOGIC CONDITIONS

The critical success factor for infiltration BMPs is the capacity of the soil to convey the storm water. The basic principles governing flow in a porous media was formulated by Henri Darcy. Darcy's law describes a steady-state flow in the form of $Q = kiA$, where k = the hydraulic conductivity, i = gradient (dh/dl) and A = area of flow. As illustrated in Darcy's equation, the capacity for soil to convey water is a function of three basic components hydraulic conductivity, head, and the area available for infiltration. Ideal soil conditions are primarily granular materials consisting of sand, gravel, or a combination. Coarse-grained soil has a greater hydraulic conductivity than fine grained materials (silt and clay) and therefore can convey water more readily. Most storm water infiltration facilities that have failed are the result of poor or marginal soil conditions that are inconsistent with infiltration demand. Soil having a hydraulic conductivity greater than approximately 1×10^{-3} cm/s is generally considered to be excellent for infiltration. Hydraulic conductivity between 1×10^{-3} and 5×10^{-4} cm/s are good, and below 5×10^{-4} cm/s are marginal.

Marginal soils have a much higher propensity to clog from sediment accumulation and biofouling. Regardless of the soil conditions, reductions in flow capacity due to clogging is addressed by lowering the design hydraulic conductivity by a half or full-order of magnitude. Infiltration characteristics can be maintained over the long-term by adequate pre-treatment, such as fore bays or basins, to remove trash, sand, and silt sized particles that could restrict the flow of water into the soil.

A thorough geotechnical field exploration program should be performed to evaluate the soil and geologic conditions. The investigation should include soil borings to permit direct observation and sampling of the soil. Cone Penetration Test (CPT) soundings will provide detailed stratification and an indirect indication of density, hydraulic conductivity, and material type, but should not be used without conventional soil sampling. Groundwater observation or vadose zone monitoring probes installed in the borings provides a means to perform the in-situ testing of hydraulic conductivity and observation of groundwater elevations. The groundwater surface elevation should be monitored over a wet season to understand the seasonal fluctuations. The grain-size distribution and density are the two soil parameters that

indicate whether the planned site is appropriate for infiltration. Of greatest importance is the presence of fine-grained materials such as silt and clay, as small fraction of these materials can result in a substantial reduction in permeability. For example, the addition of just two percent of minus #100 standard US sieve material can reduce the hydraulic conductivity of the sand by one or two orders of magnitude (Cedergren, 1989).

In addition to identifying the subsurface stratigraphy, the investigation must include an evaluation of the permeability in the vadose zone. One of the greatest shortcomings of vadoze zone permeability testing is the attempt to measure saturated hydraulic conductivity of unsaturated materials. Saturated conductivities are generally lower than their unsaturated counterparts. Generally, an evaluation of the in-situ hydraulic conductivity for free-draining soil requires ground saturation. As such, a large volume, constant-head test such as USBR Test Method 7300-89, is likely to yield results that are more representative of conditions that the infiltration facility will experience during operation (USBR, 1990). The standard of practice is to measure the hydraulic conductivity using in-situ methods rather than laboratory testing. Urbonas and Sathre (1993) suggest that at least three measurements of in-situ hydraulic conductivity be made both within and down gradient of the infiltration area. The hydraulic conductivity selected for design is sometimes selected as the lowest recorded measurement, or as the values that are most representative of the proposed infiltration zone characteristics. Hydraulic conductivity may also be tested in geotechnical laboratory, but this testing should not substitute for the high-volume in-situ measurements.

DESIGN CONSIDERATIONS

Marginal sites

If a site is underlain at depth by fine grained soil, then infiltration should not be considered. Typically sedimentary materials are horizontally stratified as materials have been sorted naturally according to the depositional energy. This sorting often results in near horizontal beds of sand, silt, or clay, of variable lateral extent. So, it is possible to have a site that has clays near the ground surface, but sand or granular materials at a greater depth. In these cases, if a hydraulic connection is made between the two strata, then it is possible to direct the storm water to a zone that is more conducive for infiltration. Engineering controls such as large-diameter gravel-filled borings can be placed in the bottom of the basin to provide the hydraulic link to the deeper highly permeable soil.

Aside from the soil conditions, there are urbanized settings that may be inappropriate for infiltration. Heavy industrial sites may have constituents that would be problematic if introduced into the soil and groundwater. It is absolutely imperative that the designer understand the groundwater basin plans and the constituents in the industrial storm water effluent, so that the infiltrated storm water is consistent with the basin plan.

Groundwater

As previously mentioned, many infiltration BMPs have failed by attempting to force infiltration in sites having marginal hydraulic conductivity. The presence of shallow groundwater has also caused basins to fail through a reduction in transmissitivity due to groundwater mounding. Mounding occurs when the volume of water entering the basin is too great to be timely conveyed away from the basin through the soil. In general, the infiltration capacity increases as the separation from groundwater increases. There are numerous literature guidance documents that provide hydraulic, soil, and performance criteria. For example, the recommended minimum separation from groundwater ranges from 2 to 10 feet, (EPA, 2004). In some cases these minimum amounts may be insufficient to infiltrate the desired flow volume, particularly if the soil has marginal infiltration characteristics. The recent Water Augmentation Study in the Los Angeles Basin (LASGRWC) (Los Angeles and San Gabriel Rivers Watershed Council, 2005), indicated that the separation guidelines are not only based on the physical ability for water to move through the soil, but also to allow time for sufficient biological activity before reaching groundwater.

Unfortunately, the greatest infiltration capacity is needed during the wet season, when groundwater is often at its highest levels. For this reason, it is important to understand the sequence of storm events that the infiltration BMP will be required to accommodate. Steady-state seepage analyses may be appropriate for small-footprint, low volume infiltration BMPs. Larger, high-volume BMPs will likely require transient modeling to understand the complex behavior of unsaturated / saturated, time dependent scenarios. Using these models, the designer can model the anticipated storm water impulse flow and its gradual infiltration into the soil. These models also allow for a long-term evaluation of ground water mounding and can identify the seasonal decay in the ground water mound at the infiltration point and at selected distances away from the infiltration point. Understanding the lateral development of a groundwater mound is helpful in the geotechnical analyses of potential collateral impacts (e.g., settlement, expansion, and/or soil liquefaction). An example of a transient analysis for a large infiltration facility is presented in Figure 1. This example depicts the seasonal rise and fall of the groundwater mound at various distances from the center of the infiltration facility over a 10-year time-frame and the corresponding storm water inflows.

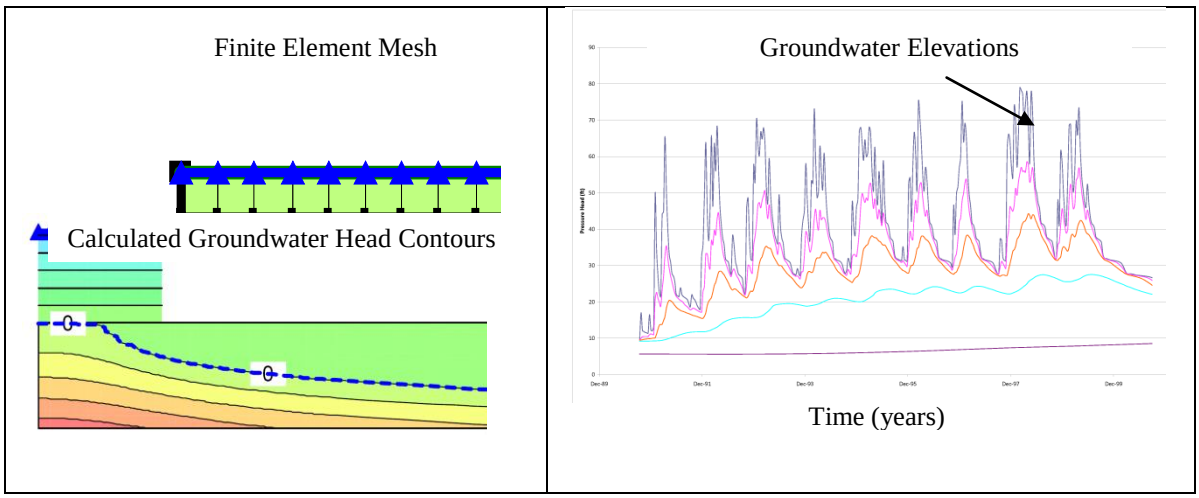

FIGURE 1. A) FINITE ELEMENT MESH AND CALCULATED PRESSURE HEAD CONTOURS DURING INFILTRATION; B) PLOT ILLUSTRATING GROUNDWATER MOUND DEVELOPMENT OVER A 10 YEAR PERIOD.

Modeling the development of groundwater mounding also provides an indication of where the infiltration water will migrate and to what extent the vadose zone will become saturated. These changes not only have geotechnical implications, but also may affect existing pollutant plumes in groundwater or mobilize constituents in the vadose zone. During the basin feasibility stage, it is important to identify known release areas near the infiltration facility.

VOLUME OF WATER/MODELED RAINFALL

The volume of water to be infiltrated is governed by the design storm event and the tributary area. This event may be regulatory driven or may be derived from a hydrological / statistical evaluation of historical precipitation to arrive at a "capture" ratio. The 90th percentile year is commonly utilized for the basis of design. In the example presented above, hydrological records were available for many decades, and the decade of the 1990s represented the 90th percentile decade in this example. An appropriate capture ratio is dependent upon a large number of factors such as watershed area, constituents of concern and their variation in concentrations throughout the wet season, receiving waters, groundwater basin plans, or on regulatory mandated reductions in constituent concentrations.

Where infiltration BMPs are proposed as subregional facilities, the tributary area can be 10 to over 100 times the infiltration area. This results in a significant concentration of flow, well above natural infiltrative conditions.

POLLUTANT ACCUMULATION

One consideration for infiltration as a stormwater BMP is the quality of the influent. While pre-treatment is a design requirement, it often is focused on the removal of gross solids and sediment to prevent clogging. Table 1, below presents an analysis of potential pollutant accumulation loading rates calculated for a hypothetical site in

Southern California. Key constituents in this hypothetical example are analyzed per land use (e.g., copper for transportation land use), and accumulation rates are compared to various disposal thresholds. Figure 2 illustrates that, based on the typical event mean concentrations and land uses, regular maintenance can help avoid significant pollutant accumulation, but that even with some deferred maintenance, under normal circumstances high concentration levels may accumulate for a number of years before becoming problematic.

Example Mass Balance: Metal Accumulation in Bioretention BMPs

Input	Copper	Lead	Zinc	Cadmium
Land Use with Highest Concentration	Transportation	High Density Single Family Residential	Light Industrial	Transportation / Commercial
Rate of Accumulation in Media, R_{accum}, mg/kg/yr	**4.2**	**0.59**	**40**	**0.054**
Human Health Thresholds[5], mg/kg	3,000	150	23,000	1.7 (Res) 7.5 (Com/Ind)
Time to Human Health Thresholds, years	**709**	**256**	**579**	**31 (Res)** **139 (Com/Ind)**
TTLC, mg/kg	2,500	1,000	5,000	100
Time to TTLC, mg/kg	**590**	**1706**	**126**	**1842**

FIGURE 2. EXAMPLE (SOUTHERN CALIFORNIA) OF POLLUTANT ACCUMULATION VS. VARIOUS THRESHOLDS

GEOTECHNICAL CONSTRAINTS OF INFILTRATION

General

The introduction of surface water into the ground through infiltration can result in a variety of issues related to characteristics of certain deposits, such as settlement through collapsible soil, expansive soil movement, slope instability, and increased soil liquefaction potential. However, in most deposits, these issues are, constrained to relative proximity of the infiltration facility and hence readily identifiable and mitigated.

In order to mitigate infiltration impacts, a geotechnical investigation should be performed prior to (preferably conceptual) design of the infiltration facility. Potential geotechnical issues due to infiltration should be considered along with other relevant issues affecting the design and, if necessary, design should be enhanced and/or modified.

Relevant, infiltration-induced geotechnical issues and related evaluation requirements are discussed in the balance of this section. Mitigation measures are just hinted as numerous possibilities exist, yet their implementation is dictated by the size and importance of the project, severity of impact, and many other parameters that are beyond the scope of this paper.

Slope Stability

Stability of native and man-made slopes near the infiltration facility can be affected even by a temporary rise in groundwater elevations and/or by change in groundwater flow direction. Therefore, geotechnical investigation coupled with a groundwater mounding analysis should be performed to assess changed conditions within and around the infiltration facility. If significant change in groundwater elevations is evaluated and/or downslope groundwater flow is anticipated, formal slope stability evaluation is required. This evaluation may trigger supplemental geotechnical investigation to better define slope stratification, saturation, and material properties. Mitigation measures, if any, will depend on the continuation and duration of the elevated groundwater levels, assessed potential for concurrence of infiltration and seasonal increases in groundwater regime, and slope face inclination, keying and drainage, to name a few.

Soil Liquefaction and its Impacts

Soil liquefaction is a phenomenon in which loose to medium dense, saturated granular materials partially or entirely lose its strength when subjected to ground shaking. Soil liquefaction may also occur in fine-grained materials such as some low-plasticity silts and clays and can affect deposits in excess of 100 ft. Partial or complete loss of soil strength due to liquefaction can have a range of consequences on buildings and their foundations, but also on slopes and even on nearly-level ground. Severe consequences of soil liquefaction, commonly referred as the soil liquefaction impacts, include liquefaction-induced total and differential settlements, cracking of ground surface, lateral spreading of mild to nearly-horizontal slopes, soil liquefaction-induced downdrag on pile foundations, and impact of liquefied soils on shape of acceleration response spectra used for structural design.

Storm water infiltration may cause increase of ground water elevation and hence, indirectly, in increased soil liquefaction potential in not only infiltration-saturated layers, but also in layers below. Therefore, a groundwater mounding analysis should be conducted along with assessment of the duration of mounding. The assessment of duration is especially important as it is not likely that the maximum (design) earthquake coincides with the highest mounding that may exist only briefly during rainy season. If long-term impacts of stormwater infiltration are found likely, mitigation of increased soil liquefaction potential and impacts should be considered.

Expansive Soils

Expansive soil is generally defined as soil or rock material that has a potential for shrinking or swelling under changing moisture conditions. These soils, commonly present in coastal areas, typically contain clay minerals that expand in volume when water is introduced and shrink when the water is removed or the material is dried. When expansive soil is present near the ground surface, even a temporary change in moisture conditions from either direct infiltration or indirectly from rise in groundwater elevation cause these soils to swell. Conversely, as soils dry or the

groundwater surface falls after infiltration, these soils will shrink in response to the loss of moisture in its structure.

The effects of expansive soil movement (swelling and shrinking) is typically greatest near ground surface and affects near surface structures such as shallow foundations, roadways, rail lines, and concrete pavements. Basements or below-grade parking structures can also be effected as additional loads are applied to the basement walls from potentially large swelling pressure generated by soil expansion. The geotechnical investigation should identify if these materials are present near the proposed infiltration facility, and if so, geotechnical engineers should evaluate soil expansion potential on a site-specific basis and assess if the surface water infiltration will, through shrinkage and swelling cycles, induced damage to nearby and/or planned structures.

Collapsible Soils

Typically, collapsible soils are most commonly observed in sediments that are loosely deposited, separated by coatings or particles of clay or carbonate. When saturated, these soils may collapse and thus induce damage to foundations, structures and slopes.

Infiltration of stormwater may result in a temporary flooding of collapsible soils. Similarly, even temporary rise in groundwater elevations could change the soil structure by dissolving or deteriorating the intergranular contacts between particles of certain soils, resulting in a sudden collapse referred to as "hydrocollapse." This hydrocollapse phenomenon generally occurs during the first saturation episode of natural deposits, i.e., repeated cycles of saturation are not likely to result in additional collapse. The magnitude of hydrocollapse is proportional to the thickness of the soil column where infiltration is occurring.

It is important to evaluate the hydrocollapse potential of soils during the geotechnical investigation. However, in many cases, this is difficult, if possible task. Luckily, at most instances, the magnitude of hydrocollapse is small and hence not likely to cause significant damage at the ground surface. When hydrocollapse is suspected, but not demonstrated, network of surface settlement monuments is typically installed around the infiltration site, adjacent roadways, and in the neighboring developments. These monuments are typically monitored prior to completion of infiltration facility, after the first infiltration event, and periodically thereafter. If settlement-sensitive structures are present at or in the vicinity of the site, mitigation measures may be required.

SUMMARY

Both the benefits and considerations of infiltration BMPs have been presented. Infiltration has numerous potential benefits, particularly in urbanized watersheds. The locations of these urban BMPs often require numerous design considerations that need to be evaluated when proposing infiltration BMPs. These considerations may identify fatal flaws or may require the necessity for innovative engineering solutions,

particularly where choice of satisfactory alternatives is limited. Current advancements on projects in southern California have identified the need for more careful examination of the design approach and considerations of the BMP impacts on existing structures

ACKNOWLEDGEMENTS

The authors acknowledge Lisa Austin, Aaron Poresky, Chris Conkle and Simon Gudina of Geosyntec Consultants for their contributions to this paper.

REFERENCES

California Stormwater Quality Association (CASQA) 2003. Stormwater Best Management Practice Handbook: New Development and Redevelopment (www.cabmphandbooks.com). January.

Cedergren, H.R., 1989. *Seepage, Drainage, and Flow Nets*, John Wiley & Sons, New York, NY.

EPA, 2004. "The Use of Best Management Practices (BMPs) in Urban Watersheds." United States Environmental Protection Agency, Cincinnati, OH.

Los Angeles and San Gabriel Rivers Watershed Council, 2005. "Los Angeles Basin Water Augmentation Study, Phase II Final Report," Los Angeles, CA.

Massachusetts Department of Environmental Protection (MassDEP) 2008. Massachusetts Stormwater Handbook. February

Stormwater Center. Stormwater Management Fact Sheet: Infiltration Basin. http://www.stormwatercenter.net/Assorted%20Fact%20Sheets/Tool6_Stormwater_Practices/Infiltration%20Practice/Infiltration%20Basin.htm

U.S. Bureau of Reclamation, 1990. *Earth Manual, Part 2*, U.S. Department of the Interior, U.S. Government Printing Office, Denver, Colorado.

Urbonas, B. and Sathre, P., 1993. "Stormwater, Best Management Practices and Detention for Water Quality, Drainage, and CSL Management," Prentice-Hall, Inc., Englewood Cliffs, NJ.

Construction and Performance of Bioretention Cells

G.O. Brown[1], R.A. Chavez[2], D.E. Storm[3], and M.D. Smolen[4]

[1] Biosystems and Agricultural Engineering, Oklahoma State University, 219 Ag Hall, Stillwater, OK 74078; PH (405)744-8425; email: gbrown@okstate.edu
[2] Biosystems and Agricultural Engineering, Oklahoma State University, 214 Ag Hall, Stillwater, OK 74078; PH (405)744-5427; email: rebecca.chavez@okstate.edu
[3] Biosystems and Agricultural Engineering, Oklahoma State University, 121 Ag Hall, Stillwater, OK 74078; PH (405)744-8422; email: dan.storm@okstate.edu
[4] Biosystems and Agricultural Engineering, Oklahoma State University, 218 Ag Hall, Stillwater, OK 74078; PH (405)744-8414; email: michael.smolen@okstate.edu

ABSTRACT

Bioretention cell are gaining popularity as a stormwater best management practice (BMP). This can be largely attributed to the fact that they present a broad range of potential benefits such as decreased runoff, thermal attenuation, aesthetics and improved water quality through various physical, chemical and biological processes. Ten prototype cells were constructed in Oklahoma as part of an ongoing demonstration project. The cells ranged in size from 19 m^3 to 435 m^3, and the filter media incorporated fly ash to enhance phosphorus and heavy metal retention. Eight of the cells were installed in Grove, Oklahoma by a contractor, while the other two were constructed in Stillwater by the authors. This paper discusses engineering considerations, general design procedures, cell specifications, construction costs and issues that arose during construction.

INTRODUCTION

Non-point source pollution from urban runoff is a major concern in many watersheds. Nutrients, heavy metals, and organic chemicals and pathogens contained in non-point source pollution, while at low concentrations, negatively impact water quality due to the large volumes and widespread nature of flow. Bioretention cells (BRC) are gaining popularity as a stormwater BMP and are in essence "functional landscaping." They are landscaped areas that treat storm water runoff and present a broad range of potential benefits including decreased runoff; improved water quality through various physical, chemical, and biological processes; thermal attenuation; and aesthetics for a limited drainage area (Hunt and White, 2001).

Ten BRC have been constructed in Oklahoma, in a variety of land use settings, as part of an ongoing study to demonstrate the effectiveness of this technology. Eight are located in Grove, and two are located in Stillwater. Of the ten cells, two are residential properties, six are public or municipal properties, and two are commercial properties.

This paper provides an overview of the engineering considerations, general design procedures, site parameters, construction specifications, construction costs, lessons learned during construction, and initial water quality analysis.

CELL DESIGN

In general, the designs for this project are consistent with the BRC guidelines set by Prince George's County (2002), Hunt, et al (2001 and 2005), and the LID Center (2003). Figure 1 depicts a typical section of the BRC design for this project. Variations from the references cited include a 1:1 side slope for improved safety during construction, sand plugs for adequate infiltration through the top soil layer, the addition of a blend of sand and fly ash as a filter medium, and vegetation criteria suitable for eastern Oklahoma. Construction for this project was formally bid through the Oklahoma Department of Central Services, requiring a complete Plans, Specifications, and Estimate (PS&E) package.

It was arbitrarily decided that the cell would catch the first ½ inch of runoff from any storm event in the designated ponding area. There is an expectation that the majority of the pollutants will be present in that first flush. However, there is little supporting data for that assumption. Given the drainage area from the site survey, the volume of the first flush, V_R (ft^3) is,

$$V_R = \frac{0.5}{12} A_D$$

The filter layer consisted of a blend of sand and 5 percent fly ash by weight. As with the ponding area, the water storage volume of the filter was arbitrarily set to equal ½ inch of runoff from the drainage area. The volume of this layer, V_F (ft^3), is based on a porosity, φ, of 0.30.

One cell was constructed with a biozone. The biozone was designated as an anaerobic layer within the BRC to encourage denitrification. An inverted siphon was used to create the anaerobic condition by increasing the amount of head necessary for water to leave the system, thereby maintaining a constant saturated zone. This layer consisted of sand with a specification to contain no more than 5 percent fines. The volume of the biozone was again arbitrarily set to accommodate ½ inch of runoff

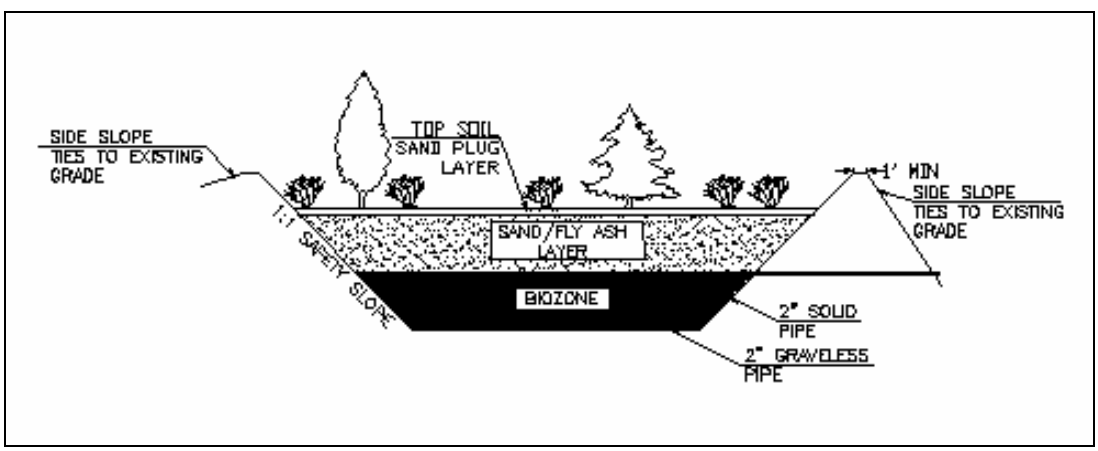

Figure 1. Bioretention cell typical section

from the drainage area. Volume and depth of this layer were calculated based on a porosity of 0.39, which is a typical value for a clean, uniform sand (Holtz and Kovacs, 1981).

Inlet channel dimensions were calculated using a combination of the rational method for surface flow and Manning's equation. An overflow bypass was designed as a broad-crested weir on the back end of the cell.

The topsoil available in Grove, Oklahoma is a silty loam, with a hydraulic conductivity much less than 1 in/hr. The Stillwater site had a deep clay loam. Even blending equal parts sand and topsoil did not provide adequate hydraulic conductivity to ensure infiltration into the filter layer. Sand plugs were introduced as a solution for increased infiltration into the cell, and were designed for ease of construction. Sand plugs were randomly placed, such that no two plugs touch each other, as shown in Figure 2 below.

Since BRC are usually in landscaped areas, plantings should be aesthetically pleasing. With that requirement in mind, the horticultural planting list was developed using the following criteria: plants had to be wet and dry tolerant, not N fixers, noninvasive species, low-maintenance requirements, offer color variety, plants had to be easily attainable and replaceable, and include trees, shrubs, flowering perennials, ornamental grasses, and rock accents. A conscious effort was made to include native species in the cell vegetation. To maintain landscaping aesthetics and to help retain moisture for the vegetation, a 2 inch hardwood mulch layer was applied over the top soil / sand plug layer after planting the vegetation. Hardwood was used to minimize mulch floating out of the cell.

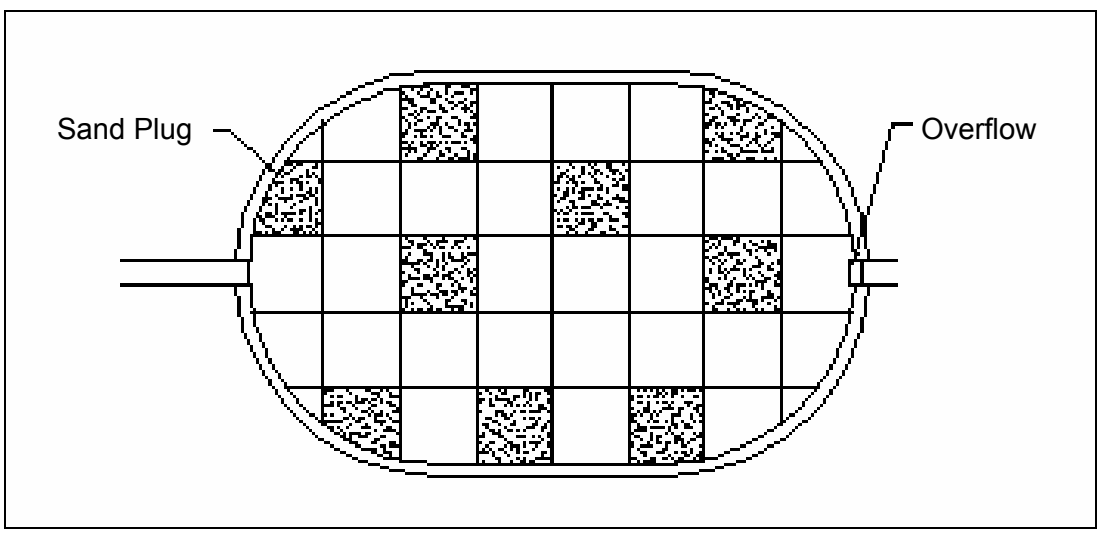

Figure 2. Example of sand plug layout.

FILTER MEDIA SELECTION

Phosphorus removal in BRC has been highly variable in previous research (Hsieh and Davis, 2003; Hunt, 2003). As phosphorus is a contaminant of concern in the Grand Lake watershed, it was necessary to find a means to improve phosphorus removal in BRC. Zhang. (2006) conducted a series of experiments to find a cost effective filter medium with both a high phosphorus sorption capacity and an

adequate hydraulic conductivity to improve the removal of phosphorus in BRC, and concluded Class C fly ash was suitable.

Sorption isotherms and desorption experiments were conducted to characterize phosphorus sorption and desorption of Dougherty sand and various mixtures with fly ash. The fly ash exhibited a high phosphorus sorption predominantly due to calcium phosphate precipitation. With the addition of 5% fly ash, the distribution coefficient, K_d, of Dougherty sand was elevated from 2.08 mL/g to 398 mL/g (5.77 to 1100 in^3/lb), and phosphorus removal increased from 9.4% to 94.2%. Desorption results indicated that Dougherty sand released a large amount of phosphorus, averaging 42% of the initially sorbed phosphorus. However, Dougherty sand with 5% fly ash released negligible amounts of phosphorus, even when the initial phosphorus concentrations were increased. The end result of the study was that, in a hypothetical scenario, the sand/fly ash infiltration layer provides satisfactory phosphorus removal over a long period and enhances phosphorus retention significantly.

The infiltration capacity of filter media is an important parameter for BRC. It is not recommended to leave water in the ponding area of BRC for longer than four days because it restricts the use of water-intolerant plants and encourages the breeding of mosquitoes and other insects (USEPA, 1999). PGDER (2002) recommends that the infiltration rate should be greater than 2.54 cm/hr (1 in/hr) in a BRC intended for runoff infiltration. The infiltration rate may be directly calculated with the hydraulic conductivity by Darcy's law and the hydraulic gradient. In the limiting case of a saturated medium with no ponding, the hydraulic gradient is equal to one, and the infiltration rate is equal to the hydraulic conductivity. Hunt (2003) suggested that the desired range of hydraulic conductivity in BRC is 1.26 cm/hr to 5.04 cm/hr (0.5 to 2.0 in/hr). However, the hydraulic conductivity requirement depends on the BRC design.

A falling head permeameter (McWhorter and Sunada, 1977) was used to determine the saturated hydraulic conductivity (K_s) of Dougherty sand (Thermic Arenic Haplustalf), and the mixtures of the sand with various levels of fly ash. The hydraulic conductivity (K_s) of Dougherty sand was 34 cm/hr (13 in/hr). Fly ash had an extremely low hydraulic conductivity, which could not be measured by the procedure used. The hydraulic conductivity of Dougherty sand and its mixtures with various levels of fly ash are presented in Figure 3. The hydraulic conductivity dropped exponentially with increasing fly ash content. To keep the hydraulic conductivity of amended soils higher than 2.54 cm/hr (1 in/hr), the incorporation rate of fly ash should be less than 6% calculated from the exponential relationship (Figure 3).

Due to the pozzolanic nature of fly ash and hydration reactions, the hydraulic conductivity of the sand/fly ash mixtures may decrease with an extended saturation period. To assess the effect of saturation period on the hydraulic conductivity of the sand/fly ash mixtures, Dougherty sand, D+2.5%F, and D+5%F were kept in saturation in the testing columns for 28 days and the hydraulic conductivity measured periodically. Dougherty sand was examined for comparison in this case.

The change of hydraulic conductivity over the extended saturation period for Dougherty sand, D+2.5%F, and D+5%F is shown in Figure 4. The trends were

different for Dougherty sand and the sand/fly ash mixtures. Hydraulic conductivity of Dougherty sand dropped slightly first, and then recovered to the previous level. This behavior was probably due to movement of the fines through the column. However, the hydraulic conductivity of D+2.5%F and D+5%F decreased rapidly during the first 24 hours, and then stabilized after 14 days. Because of the pozzolanic

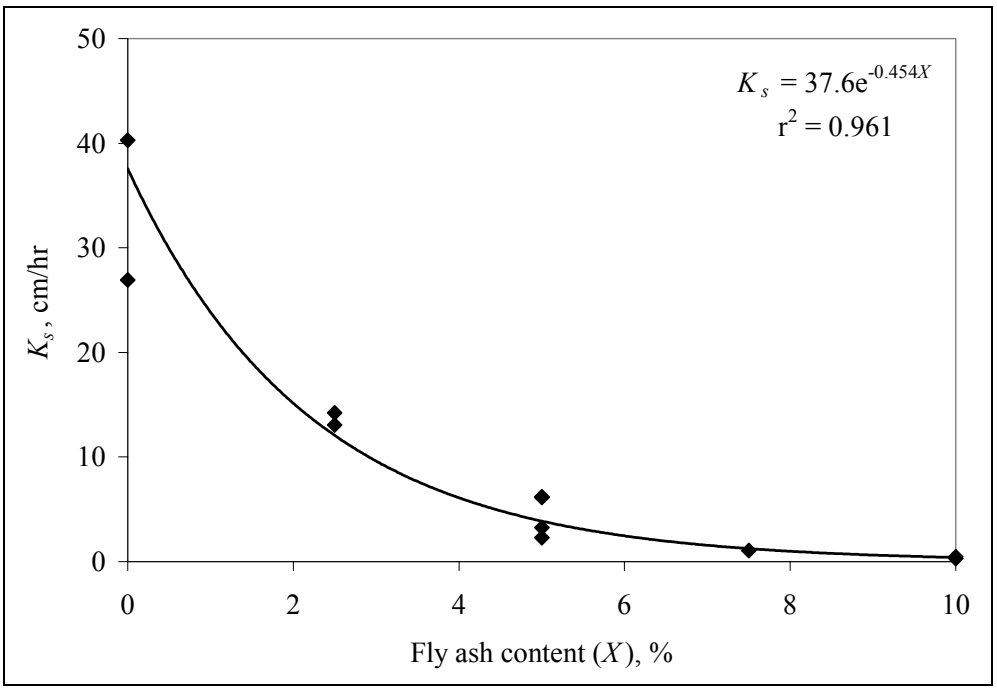

Figure 3. Effect of the fly ash addition on hydraulic conductivity of Dougherty sand.

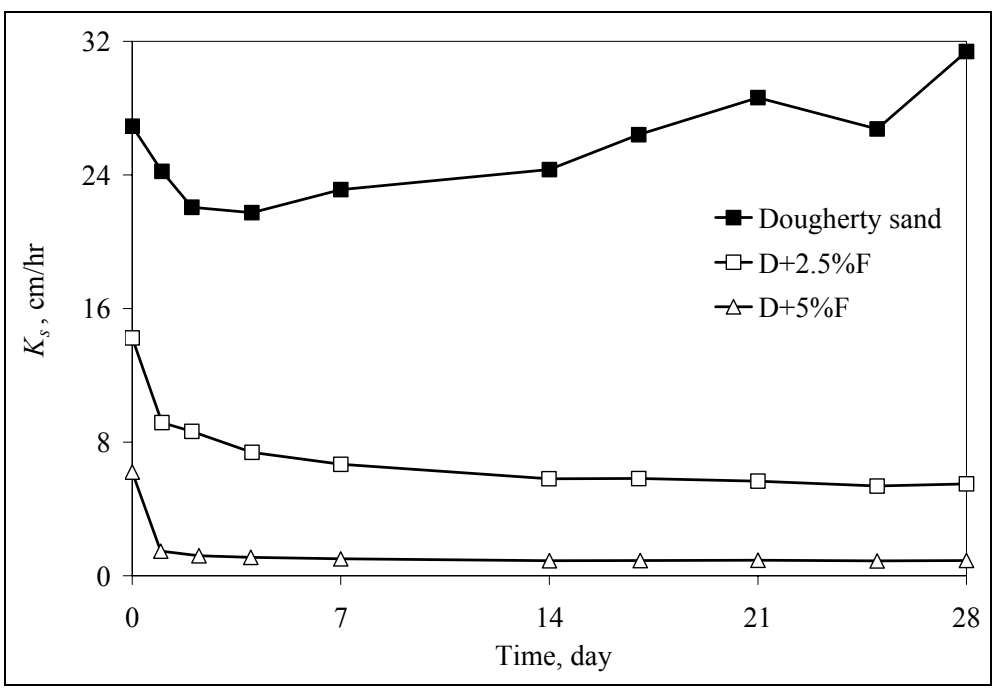

Figure 4. Effect of extended saturation period on saturated hydraulic conductivity of Dougherty sand, D+2.5%F, and D+5%F.

reactions that occurred in the water-saturated sand/fly ash mixtures, the permeability of D+2.5%F and D+5%F was decreased. The stabilization of hydraulic conductivity after 14 days indicated the end of the pozzolanic reactions. At the end of the 28-day experiments, the hydraulic conductivity of D+2.5%F and D+5%F was 5.50 cm/hr and 0.91 cm/hr (2.2 and 0.36 in/hr). This characteristic of the sand/fly ash mixtures implies that their 4-day or 7-day hydraulic conductivity should be evaluated to ensure the adequate infiltration. With the final hydraulic conductivity of 0.91 cm/hr (0.36 in/hr), D+5%F still possesses an adequate hydraulic conductivity to drain 30 cm (1 ft) ponding water within 33 hours.

Installation of the filter medium consisted of 6 inch lifts to keep the mixture as consistent as possible and to prevent preferential flow through this layer of the BRC. The sand specified in the design was a clean sand with less than 5% fines. Fly ash utilized was Class C, obtained from the Chouteau power plant for the Grove sites and from the Sooner power plant for the Stillwater site.

Combining the sand and the fly ash in the field was accomplished in two ways. The first method involved mixing with heavy equipment before placement in the cell. A load of sand was deposited near the cell site and the appropriate amount of fly ash was then mixed into the sand by repeatedly filling the bucket of a front end loader and pouring it back over the pile containing the sand and fly ash, until an even blend was achieved. The second method entailed using a roto-tiller to mix media in lifts inside the cell. A 6 inch lift of sand was placed into the cell. The appropriate amount of fly ash was then evenly distributed on top and tilled into the sand.

CONSTRUCTION COSTS

Sites were chosen based on grade, location, drainage area, visibility, and access. Of the sites chosen, two are commercial properties, two are residential, and six are public. Land use includes both paved and grass. There is one site where the paved surface and the grass surface are approximately equal and one where the runoff is intercepted primarily from a roof surface. Drainage areas vary from 0.11 acre to 1.90 acres, with all but one being less than one acre.

The first eight sites listed in Table 1 were constructed by a contractor selected through a formal state bidding process. All eight sites are located in Grove, Oklahoma. Cost was bid on a volume basis and includes mulch but not vegetation. Cell cost ranged from $7,368 at the Clark residence, which is the second smallest cell with a volume of 27 m^3 (35 yd^3), to $29,172 at the Grand Lake Association, which had a volume of 435 m^3 (569 yd^3). The cell at Lendonwood Gardens was the smallest, but cost more to construct because of site conditions requiring tree removal and traffic control.

The two BRC (Cell A and Cell B) constructed at the Oklahoma State University Botanical Gardens in Stillwater, Oklahoma are also listed in Table 1. These cells were constructed primarily “in house.” Excavation was professionally contracted, though not through a bidding process as were the cells listed in Table 1. Final costs for both Cell A and Cell B were $4,753 and $11,479, respectively.

Table 1. Bioretention cell area, volume and cost as constructed by a contractor in Grove, Oklahoma and by Oklahoma State University in Stillwater, Oklahoma

Location	Drainage Area (Acres)	Land Use	Area (m^2)	Volume (m^3)	Final Cost
Elm Creek Plaza 36°34'47" N, 94°46'08"W	0.62	Paved	63	128	$12,496
Lendonwood Gardens 36°34'59" N, 94°47'13"W	0.54	Turf	23	19	$8,847
Grove High School 36°37'19" N, 94°44'50"W	0.65	Paved	149	161	$17,071
Grand Lake Association 36°36'39" N, 94°48'14"W	1.90	Paved/Turf	172	435	$29,173
Cherokee Queen Riverboats 36°38'05" N, 94°48'54"W	0.45	Paved	116	108	$13,796
Early Childhood Development Center 36°35'12" N, 94°46'57"W	0.11	Paved (Roof only)	48	70	$10,715
Spicer Residence 36°38'59" N, 94°46'08"W	0.39	Turf	101	93	$13,271
Clark Residence 36°35'18" N, 94°49'36"W	0.18	Turf	30	27	$7368
Cell A 36°07'00" N, 97°06'01"W	0.32	Paved	28	66	$4,753
Cell B 36°07'01" N, 97°06'01"W	0.90	Paved	160	208	$11,479

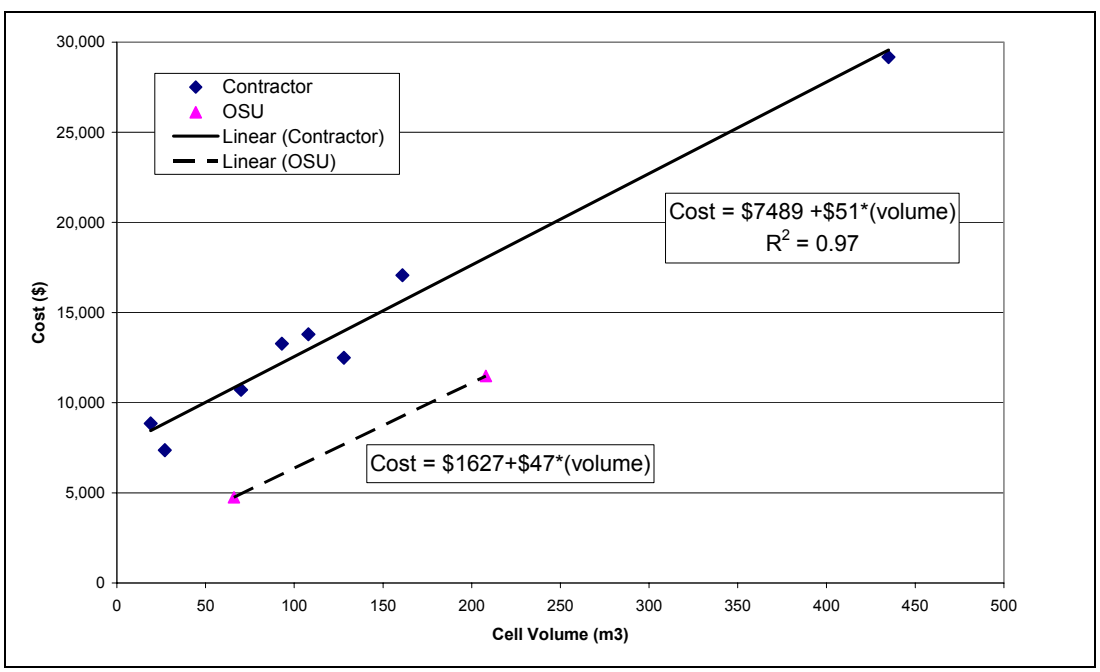

Figure 5. Comparison of Bioretention Cell costs; contractor versus OSU constructed cells

A linear regression equation was fit to cell cost as a function of volume for both contractor and in-house constructed cells in Figure 5. There is a difference of approximately $6,000 between contractor and in-house construction costs for cells of comparable sizes. However, the price difference may decrease as BRC technology becomes more common in the region and contractors learn more about what cell construction entails. Competition may also contribute to a decrease in the cost of contractor constructed projects.

MONITORING

Monitoring of the cells in Stillwater began in July 2008. Cell B is divided into two hydraulically separate regions. One region contains the sand/ fly ash media blend for the filter layer, and the second contains only sand in the filter layer. This was done in an effort to observe the effectiveness of the fly ash in a quantifiable manner.

Nitrate and phosphorus contents were measured in the effluent of the cell, as exhibited in Table 2. Effluent pH values were lower for the sand only side of Cell B than for the fly ash side. Alkalinity was lower in the effluent samples taken from the fly ash side of Cell B, than for the sand only side of Cell B. NO_3-N was lower in the effluent collected from the sand only side of Cell B. However, Ortho-P content measured in the effluent from the fly ash side of Cell B were lower than that measured in the effluent from the sand only side of the same cell.

Metal contents were also measured in the effluents as listed in Table 2. Marked differences are visible in the Fe contents when comparing both sides of Cell B. The effluent from the fly ash side of Cell B had lower Fe contents, ranging from 0.06 ppm to 0.19 ppm, than the sand only side which had contents ranging from 0.10 ppm to 5.81 ppm.

Table 2. Effluent pH, nutrients, alkalinity, and metal content by cell.

Cell	Sample #	pH	NO3_N (ppm)	Alkalinity (ppm)	Ortho - P	Fe (ppm)	Cu (ppm)	Pb (ppm)
Cell B-South - No Fly Ash	2	7.9	4.53	226	0.16	0.10	<.02	<.02
	5	8.1	3.61	223	0.1	0.13	<.02	<.02
	7	8.1	3.88	263	0.18	0.35	0.03	<.02
	10	7.6	6.78	342	0.13	0.44	<.02	<.02
	12	7.3	6.6	365	0.14	0.11	<.02	<.02
	15	7.3	0.71	206	0.06	5.77	<.02	<.02
	18	7.5	0.51	219	0.07	5.60	<.02	<.02
	21	6.8	0.93	190	0.08	5.81	<.02	<.02
Cell B-North - Fly Ash	1	10.4	3.59	158	0.07	0.06	0.03	<.02
	4	9.7	2.85	92	0.07	0.13	0.02	0.05
	8	10	3.13	111	0.07	0.19	0.02	<.02
	14	9.3	8.73	106	0.05	0.14	0.02	<.02
	17	9.3	8.73	106	0.06	0.08	0.02	<.02
	20	10	8.68	148	0.06	0.13	0.02	<.02

LESSONS LEARNED

Overall, the design process translated well to the construction of the BRC for this project. However, lessons were learned in the field.

Mixing fly ash in the field presented a challenge and was approached using the two previously described methods. The challenge arose in ensuring an adequately mixed medium on such a large scale, and neither method was considered adequate Samples were taken during placement and the variability is being quantified now and will be reported at a later date.

Fly ash storage is an issue that needs to be addressed. During the construction phase of this project, Oklahoma experienced significant rain. Fly ash exhibits pozzolanic characteristics when exposed to even small amounts of moisture. Clots of fly ash are formed and it is difficult to sift through the large quantities of fly ash to effectively remove them. This poses many issues of concern such as effective sorption capacity, preferential flow within a non-uniform medium, and achieving an even blend of sand and fly ash. The contractor stored the fly ash underground in a pit and covered it with a tarp. A similar method was used for short term storage at the Stillwater site. Under typical climate conditions this would be appropriate. However, a better solution would be to store the fly ash in weather proof/resistant vessel such as a trailer.

Another point of interest is to observe the differences in capabilities and costs when comparing construction by a contractor versus construction in-house. On average, the contractor was able to complete a cell within four days, with three people, a backhoe and a bobcat. The cells constructed by OSU averaged six days, using five people, two tractors, a dingo, and a roto-tiller. Most of the additional time required for the in-house construction was during the backfilling process. The contractor was able to use heavy equipment with a greater capacity for moving soil than the process employed by the in-house team, which relied more on man-power and smaller, more readily available equipment. It costs approximately $6,000 more to have a contractor build a cell. However, it takes half the time and considerably less man power and equipment. Differences in cost and labor are attributed to the issues surrounding man versus machine and in-house versus contractor labor.

There were two cell failures. The first was at Elm Creek Plaza, where the cell receives runoff from a parking lot and sits on a stream bank. Berm failure occurred due to fugitive water from a neighboring property during a 50 year storm, providing roughly twice the design flow. The flow destroyed the overflow weir that was poorly placed on the streambank. The cell was repaired and reinforced, and the overflow was moved to a different location to alleviate the possibility of a repeated failure. The property owner also had the channel between the two properties cleaned out and deepened. One positive outcome is that immediate benefits with regard to erosion have been observed at this site. During construction it was necessary to rebuild the bank as it had eroded substantially in the time between the design and construction phases, and the cell would not have fit as designed.

The second failure was at the Spicer residence. The cell is located near the lakefront, above the GRDA takeline and the U.S. Army Corps of Engineer's regulation line. Excessive rains after a long period of drought have caused the lake to rise to unusually high elevations. The shore effects at the high lake elevations

caused erosion of the cell berm. Repairs commenced once the water receded. The berm was repaired and reinforced. High water levels around the lake area also delayed construction and submerged the Cherokee Queen cell, but caused no significant damage.

CONCLUSION

The constructed cells appear to be operating as intended. Planned future monitoring will define actual performance. Bioretention cells designs are evolving and reflecting the need to attenuate specific contaminants based on land use. This is an important development that will make bioretention more effective and more attractive as a BMP. Costs associated with this technology will be better understood with time and experience, and may also decrease as designs and construction processes become more efficient. Overall, bioretention cells will be most effective in mass quantities, and could have a significant impact on water quality in Oklahoma.

REFERENCES

Holtz, R. D. and W. D. Kovacs. 1981. *An Introduction to Geotechnical Engineering*, 104-105. Englewood Cliffs, NJ: Prentice Hall.

Hsieh, C.; Davis, A.P. 2003. Evaluation of bioretention for treatment of urban storm water runoff. *Proceedings of 2003 ASCE World Water & Environmental Resources Congress*, Philadelphia, PA.

Hunt, Bill. Bioretention / Rain Garden Hydraulic & Hydrologic Design Worksheet. NCSU, Raleigh, NC. Available at: http://legacy.ncsu.edu/classes-a/bae/cont_ed/bioretention/lecture/rain_garden.pdf. Accessed on 12 October 2005.

Hunt, W. F and N. White. 2001. Designing Rain Gardens (Bio-Retention Areas). Urban Waterways. AG-588-3. Raleigh, NC: North Carolina Cooperative Extension Service.

Hunt, W.F. (2003) Pollutant removal evaluation and hydraulic characterization for bioretention stormwater treatment devices. PhD dissertation. Department of Agricultural and Biological Engineering, the Pennsylvania State University, PA.

Low Impact Development (LID) Center. 2003. Urban Design Tools. Beltsville, MD:Low impact Development Center, Inc. Available at: www.lid-stormwater.net. Accessed 5 October 2005.

McWhorter, D.B.and D.K. Sunada, 1977. Ground water hydrology and hydraulics. Water Resources Pub., Fort Collins, CO.

Prince George's County Department of Environmental Resources (PGDER). 2002. Bioretention manual. Program & Planning Division, Department of Environmental Resources, Prince George's County, MD.

U.S. Environmental Protection Agency (USEPA). 1999. Storm water technology fact sheet: Bioretention. *EPA 832-F-99-012*, USEPA, Washington, DC.

Zhang, W. 2006. Improvement of Phosphorus and Heavy Metal Retention in Stormwater Treatment. MS thesis. Stillwater, Oklahoma: Oklahoma State University. Department of Biosystems and Agricultural Engineering.

Cost Estimating Tools for Low-Impact Development Best Management Practices

C. Dasch Houdeshel[1] and Christine A. Pomeroy, Ph.D., P.E. M.ASCE[1], Lisa Hair[2] and Robert Goo[2]

[1] Department of Civil and Environmental Engineering, University of Utah, 122 S. Central Campus Drive Room 104, Salt Lake City, UT 84112; PH (801) 585-7300; e-mail: daschh@gmail.com and Christine.Pomeroy@utah.edu
[2] Office of Water, Environmental Protection Agency. USEPA Office of Water, 1301 Constitution Ave, N.W. Washington, D.C. 20004. PH, Lisa Hair: (202) 566-1043 E-mail: Hair.Lisa@epamail.epa.gov, and Goo.Robert@epamail.epa.gov

ABSTRACT

The stormwater community has a critical need for evaluating the life-cycle costs of Low-Impact Development (LID) Best Management Practices (BMPs) as part of encouraging communities to incorporate LID. Great effort has gone towards demonstrating that LID BMP techniques can mediate negative stormwater effects including increased discharge volume from impervious surfaces and pollution loading as water travels through urban settings. However, LID BMPs must be proven to be cost effective as well as technically functional.

The current suite of cost tools available through the Water Environment Research Federation (WERF) is being expanded to include vegetative roofs, rainwater catchment systems, and bioretention facilities. These tools provide a detailed framework to facilitate cost estimation for capital costs, operation and maintenance costs, and life-cycle net present value. The tools can serve as a format for cost reporting for past, current and future projects, and also provide users with planning-level cost estimates.

The cost tool includes both a parametric cost estimation to demonstrate approximate cost per drainage area, and a line-itemized engineer's cost estimation tool. The line-item engineer's estimate allows the user to customize their project, while exposing the user to an extensive list of potential costs and opportunities to maximize stormwater management value. The use of this cost tool will enable consistent reporting of cost data on LID BMPs, so that users will be able determine the cost of each component of the project, both in materials and in planning and design. The standard format will also improve the ease of preparing cost estimates, since the necessary line items are broken out for consideration. Creating an understanding of the life-cycle cost benefits of LID will lead to more use of LID and green infrastructure in development and redevelopment.

INTRODUCTION:

A set of whole life cost (WLC) models designed to assist in planning-level cost estimation of various stormwater Best management Practices (BMPs) has been

expanded to include single-site, decentralized low impact development (LID) stormwater management practices. Included in this new set of tools are WLC estimating models for green roofs, residential rain gardens, parking-lot scale curb contained bioretention, in-curb planter vaults, and cisterns collecting runoff from commercial buildings. In addition to providing a general cost estimate based on drainage area, the tool synthesizes basic design concepts and parameters from multiple BMP and LID references in order to clearly describe the type of facility for which cost estimates are generated.

Each spreadsheet estimates capital costs as well as operation and maintenance costs to provide the user a WLC estimate for a selected LID facility. Default capital costs as well as operational and maintenance costs are provided, however, the model allows the user to enter known site-specific costs through all aspects of the model in order to produce a more accurate cost estimate for any specific project. For each facility type, two cost estimation methods are presented: a parametric estimate based on assumed default values; or an engineer's estimate with an extensive list of project-specific line items for which the user can enter known costs. The model combines either capital cost method with whole life operation and maintenance costs to estimate the WLC of the facility.

Currently, cost information on LID BMP infrastructure development is limited, and expanding this information is a critical part of the campaign to encourage LID development around the country. Managers around the country are hesitant to adopt LID practices because the cost factor is not well known. In addition to predicting costs, the model is designed to be used as a cost-reporting tool. The provided format can be used to enter costs of a completed project so that LID cost information can be shared and the model may be improved in the future.

BACKGROUND:

In 2005, the Water Environment Research Foundation (WERF), in collaboration with the United Kingdom Water Industry Research (UKWIR) and with funding support from the Environmental Protection Agency (EPA), released a cost estimation spreadsheet tool as part of a report titled, "Performance and Whole Life Cost of Best Management Practices and Sustainable Urban Drainage Systems" (Lampe, et al 2005). These spreadsheets include tools for costing traditional stormwater BMPs: retention ponds, planted swales, and extended detention basins. Permeable pavement, a source control BMP, is also included in the tool set. Capital costs for these BMPs are based on parametric equations derived from costs reported by agencies that had completed projects fitting the descriptions of each model. Capital, maintenance, and operating costs are separated into line items to provide the user details of each cost component for individual BMP installations.

The EPA has determined that providing better cost information to land owners and agencies should encourage expansion of LID and BMP approaches to stormwater management. As part of an effort to encourage agencies to adopt LID and BMP

approaches to stormwater management, the EPA has decided to expand the WERF cost estimation tool.

WLC MODELS:

The first spreadsheet in the WLC models requires a user to specify a series of design guidelines and system characteristics, such as drainage area, project size, and/or the primary objectives of the project. Each model requires the user to answer a different series of questions relative to that specific model. For example, the design options in the Cisterns model are shown in Figure 1.

Design & Maintenance Options

STORAGE REQUIREMENTS	Unit	Model Default	User	Chosen Option
Drainage Area, DA (often roof area)	sq ft	5,000		5,000
Max Design Rainfall Event	in	2		2
Precipitation Volume Generated per Event	gallons	6,233		6,233
Total Storage Needed	gallons	6,300		6,300

SYSTEM CHARACTERISTICS	Unit	Model Default	User	Chosen Option
Type of Tank Desired (*P=Plastic, M=Metal, F=Fiberglass, C=Concrete. See sizing suggestions below*)	-	C		C
Primary Use (*I = Indoor, Non-potable O = Outdoor Irrigation*)	-	O		O
Height of Building (Used to calculate 'Indoor' Use costs)	story	3		3
Number of Fixtures per Floor (toilets, used to calculate 'Indoor' Use costs)	ea	10		10

DESIGN & MAINTENANCE OPTIONS	Unit	Model Default	User	Chosen Option
Choose Level of Maintenance, Irrigation (*"H"=high; "M"=medium; "L"=low*)	-	M		M

Figure 1: Design and Maintenance Options from the Cisterns WLC model.

Each design option and system characteristic controls a major cost component used to calculate the simple cost estimate on the "Capital Costs" page. As in the example above, the user enters "Drainage Area" and the desired "Max Design Rainfall Event" to calculate storage size needed for the facility. This storage volume is then used to estimate the appropriate tank size and tank cost. In the "System Characteristics" box, the "Type of Tank Desired" tells the model which cost curve to use in estimating the cost of the tank, and the "Primary Use" option tells the model which equation to use to most appropriately size the distribution pump.

The user may also select a level of maintenance they estimate to be appropriate for their project in the "Maintenance Options" window on the first spreadsheet. Each level of maintenance assumes a different maintenance cost structure, explained on the "Maintenance Cost" page of each model.

Figure 2 shows the "Capital Cost Option A", or simple cost estimation, from the Cisterns model. This page estimates costs based on the information entered in the "Design Options" page, displays default costs, and allows the user to adjust the cost

of each item as appropriate. Totals entered in the "User" column are read in the "Chosen Options" column, allowing the user to adjust some cost values and rely on the model defaults for others. Advanced users may use this function to compare two separate sets of design options or system characteristics. In Figure 2, the user has specified that a one horsepower motor is needed instead of a 0.5 horsepower motor, and the costs in the "Chosen Option" column have re-calculated a separate user-chosen cost estimate. This "Chosen Option" cost is the cost used to calculate the WLC through the rest of the model.

Cistern

CAPITAL COSTS

Site Name:
Site Location:

Implementation Date:

Choose Capital Costing Option

A	Total Facility Cost	$ 17,920

"A" - Simple Cost based on Drainage Area
"B" - User-Entered Engineer's Estimate

C	User entered 'Concrete' for Tank Material in Design Options
O	User entered 'Outdoor' as Primary Use Option in Design Options

Method A: Simple Cost Based on Tank Volume*

Cost Based on Drainage Area	Cost per Acre of DA Treated		Chosen Option
	Model Default	User	
Tank Size	6,300		6,300
Tank Costs per Gallon	$ 1.66		$ 1.66
Estimated Tank Cost	$ 10,458		$ 10,458
Installation Cost	$ 6,275		$ 6,275
Pump Size Needed (horsepower)	0.5	1.0	1.0
Pump Cost	$ 599		$ 1,188
Culinary Re-Supply	$ -		$ -
Tank Installation Base Cost	$ 17,332		$ 17,920
System Design Cost	$ 1,387		$ 1,434
Total Facility Cost	**$ 17,332**		**$ 17,920**

Figure 2. Capital Cost Option A from Cisterns WLC tool.

On the "Capital Costs" page, "Cost Option B" is an engineer's estimate outline for each project type. "Cost Option B" is designed to serve three functions: 1) provide a user the opportunity to incorporate their own project-specific costs into the WLC model; 2) to provide an extensive list of anticipated cost items to the user to assist with planning; and 3) to serve as a form for record keeping and cost reporting so that agencies may share LID BMP cost information in a useful and efficient way. If "Cost Option B" is selected as the capital costing option, the engineer's estimate is used to estimate the WLC for the project.

Maintenance costs are calculated on the third worksheet in the model. Similar to the "Capital Cost" page, the model makes literature-based assumptions where available (or Best Professional Judgment if literature values are not available), and the user may adjust these assumptions to their needs. Maintenance costs are calculated by estimating hours per service event, hourly cost of labor, hourly cost of equipment, and cost of any materials used. Maintenance costs are divided into two types in the model: routine and corrective or infrequent. The user may control the schedule of these activities, which affects the WLC calculations. In the models representing smaller-scale projects, the costs of equipment and materials (such as a weed trimmer

or garbage bags for litter removal) is included in the hourly labor cost. Two tables are shown on this page, as shown in Figure 3. The top table is used to estimate labor costs per service event. The lower table is the reference table that shows the costs that the upper table uses to calculate cost, based on the user-chosen level of maintenance. The user may change maintenance costs in two locations, either in the look-up table or in the "user" columns in the upper cost-calculating table.

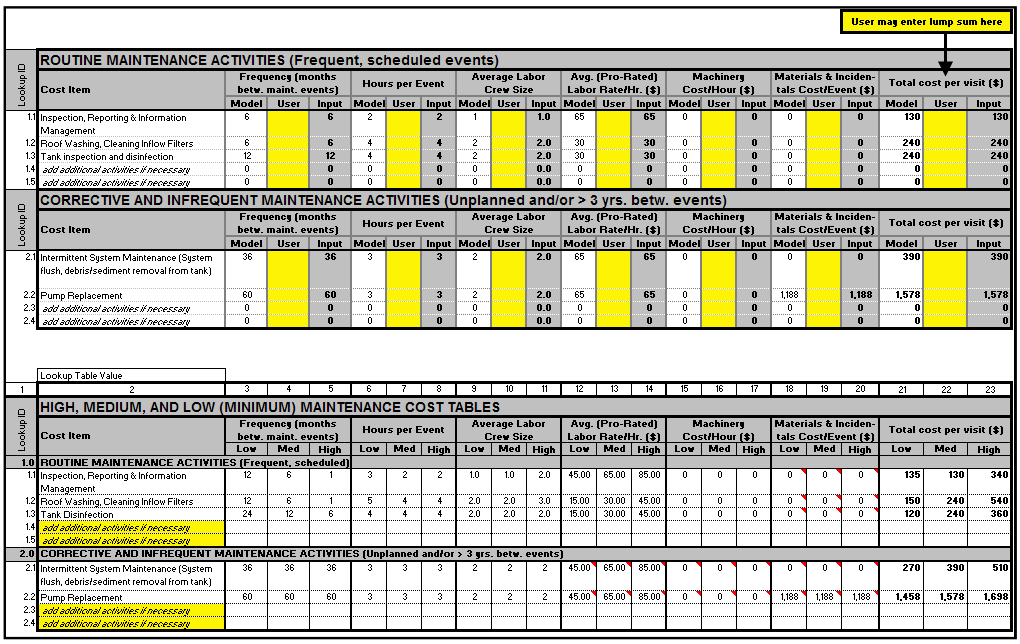

Figure 3. Maintenance Cost Worksheet from Cisterns WLC Model

After capital and maintenance costs have been estimated, each WLC model compiles all costs into an estimate on the "Cost Summary" page (Figure 4). This page summarizes annual costs for routine maintenance, corrective or infrequent maintenance, and capital costs. From this summary, the model builds a 50-year lifetime cost estimate for the facility (shown in the "Whole Life Costs" page) including a discount rate that the user may adjust on the "Design and Maintenance Options" page, and is then graphed to show the user a year-by-year facility cost for planning. Three graphs are presented: Present Value of Costs over 50 years (Figure 5), a Cumulative Discounted Costs over 50 years, and a Discounted Costs per Time.

Cost variability of LID BMP infrastructure across the United States is significant, as is climate variability which drives LID objectives. Because of this, the WLC models are designed to produce a default planning level cost estimate and allow the user to enter more specific cost values for every component tracked by the model. The existing WLC tools were designed to provide cost estimations for stormwater agencies in the United States and the United Kingdom. This expanded suite of WLC tools is targeted more towards single-lot scale LID stormwater controls because of the scale of projects addressed. This likely will increase variability in actual costs because the agencies available to construct the LID facilities are greatly increased. In

some instances, this includes opportunities for land owners to provide their own labor and sources for materials with the potential to drastically decrease whole life cost. Although many of the practices addressed by the tool are more applicable to smaller land areas, municipalities and regional management agencies can use these tools to examine future policy change options to shift a large-project, regional management paradigm of conveyance to a decentralized paradigm of many smaller projects that address catching the rain where it lands.

CAPITAL COSTS	Included in WLC Calculation			Total Cost
	Model	User	Chosen Option	
Tank Costs	$ 10,458		$ 10,458	$ 10,458
Total Associated Capital Costs (Install, pump, ect)	$ 7,463		$ 7,463	$ 7,463
Capital Costs				$17,921

REGULAR MAINTENANCE ACTIVITIES	Months Between Events	Cost per Event	Total Cost per Year	Included in WLC Calculation		
				Model	User	Chosen option
Inspection, Reporting & Information Management	6	$ 130	$ 780	$ 780		$ 780
Roof Washing, Cleaning Inflow Filters	6	$ 240	$ 1,440	$ 1,440		$ 1,440
Tank Disinfection	12	$ 240	$ 2,880	$ 2,880		$ 2,880
add additional activities if necessary	0	$ -	$ -	$ -		$ -
add additional activities if necessary	0	$ -	$ -	$ -		$ -
Totals, Regular Maintenance Activities				$5,100		$5,100

CORRECTIVE AND INFREQUENT MAINTENANCE ACTIVITIES (Unplanned and/or >3yrs. betw. events)	Years Between Events	Cost per Event	Total Cost per Year	Included in WLC Calculation		
				Model	User	Chosen option
Intermittent System Maintenance (System flush, debris/sediment removal from tank)	3	$ 390	$ 130	$ 130		$ 130
Pump Replacement	5	$ 1,578	$ 316	$ 316		$ 316
add additional activities if necessary	0	$0	$0	$0		0
add additional activities if necessary	0	$0	$0	$0		0
Totals, Corrective & Infrequent Maintenance Activities				$446		$446

Figure 4. Cost Summary Spreadsheet for the Cisterns WLC model

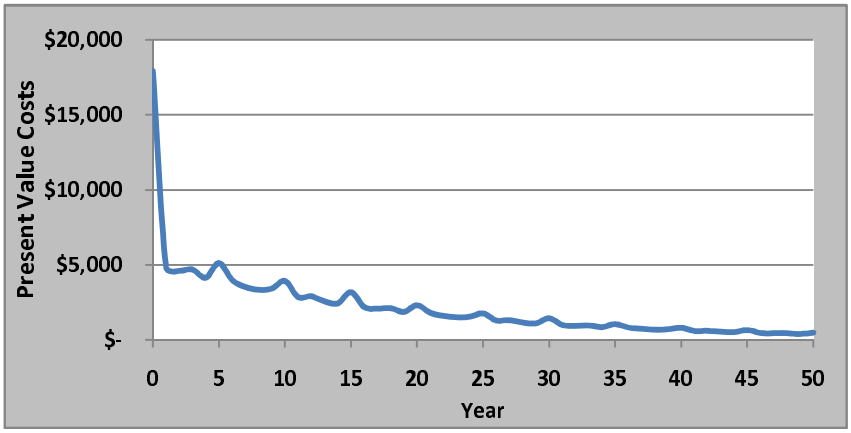

Figure 5. Whole Life Cost Presented as a Present Value of Costs Graph for the Cisterns WLC tool.

Capital and maintenance default costs used in the tool are generated from literature available in the public domain. In some instances, sufficient data were not available, or reported cost information was not sufficiently transparent to ensure appropriate cost comparisons. In such cases, design guidelines for each respective facility were summarized from multiple sources and, based on these design guidelines, cost estimates were constructed from component cost in the RS Means 100 and from national providers. In the parametric estimate, efforts have been made to present the

model as transparently as possible in order to both display how costs are generated and to allow the user to adjust many of the cost components in each model to improve the accuracy of the cost estimate generated for the user's specific scenario. For each facility type, different methods to establish default costs are used based on the availability of information in the public domain. These methods are discussed specifically for each WLC model below.

Green Roofs

Green Roofs evaluated by this model are "extensive" roofs, which are defined as having shallow soils and low plant cover, with limited roof access. "Extensive" roofs were evaluated because they minimize the need for structural reinforcements that may be required for "intensive", or deeper soil roofs, which would further complicate cost estimation. Many green roof arrangements evaluated by this model will weigh around 35 lb/ft^2; the most basic configuration may weigh as little as 20 lb/ft^2 and the more elaborate configuration can weigh over 50 lb/ft^2 (Roofscapes, 2008). The model can automatically generate two cost estimates based on roof area, building height, and roof function: one cost based on a pre-manufactured modular style installation ("Option A" on "Capital Costs") and a custom installation consisting of a root boundary layer, vegetative cover, and if elected, engineered soils ("Option B" on "Capital Costs"). A template is also provided for a user-entered engineer's estimate.

All costs are assumed to be in addition to the cost of a traditional roof covering. Green roof designs are not intended to be used as a substitute for a traditional roof covering. Instead, green roofs are designed to be installed on top of a conventional roof. One suggested benefit of green roofs is the increased lifespan of a conventional roof membrane due to the shading and insulating effects of the green roof installation. Conventional roofs have a typical life span of approximately 25 years; installation of a green roof on top of the conventional roof has been reported to prolong the life of the conventional roof two-fold (Toronto and Region Conservation, 2005).

A literature review suggests that the driving factor in the cost of green roof installations is the selection of landscaping options. In the development of the green roof cost tool, roof size and final cost were obtained for 48 buildings from the City of Portland (2005), the Chesapeake Bay Foundation (2008), and the Toronto and Region Conservation (2005). However, developing a parametric cost equation from the available literature was not feasible due to a combination of inconstancies in cost reporting and variations in design. This WLC model assumes the most basic type of installation, and allows the user to create a more elaborate installation including botanical upgrades, walkways, and irrigation. In order to account for the high variability in design options, the user may include or omit many green roof components and/or over-ride all default costs on the "Capital Costs" and "Maintenance Costs" pages. This model is designed to estimate costs for extensive roofs, however, it can be used to estimate costs for intensive roofs by increasing the soil depth and increasing the vegetative costs. This will substantially increase the weight of the roof, which may require structural reinforcements as noted previously.

Residential Rain Gardens

Design guidelines and general cost information for residential rain gardens are readily available in the public forum. Many community water quality-focused organizations and municipalities encourage the installation of rain gardens on residential properties because of the efficiency of rain gardens in reducing runoff volume, the relatively low expense of installation and maintenance, and limited regulations of landscaping practices on residential lots (Edgewood College, 2003; Kassulke, 2003; Belan and Otto, 2004; City of Lincoln, 2008; EPA, 2008; James City County, 2008; Maryland Department of the Environment, 2000). Unlike other larger scale stormwater management approaches, single home owners have access to the equipment and technology required to install a rain garden in their yards. Because this access is so broad, designs and costs of installments are also broad.

Based on the literature surveyed, two sets of cost information are reported for this tool. The first cost set includes estimates for land owners installing and managing residential rain gardens with labor provided at no cost, i.e. their own labor or volunteer labor. This cost set includes only costs of materials from local nurseries and hardware stores averaging $4.40 (normalized to 2008 US$) per square foot of garden installed. The second cost set includes rain gardens installed and managed by professional landscapers and averages $16.00 per square foot of garden installed (Edgewood College, 2003; Kassulke, 2003; City of Lincoln, 2008; EPA, 2008; James City County, 2008).

Labor, plants, and mulch costs drive the capital cost of most residential rain garden installations. EPA (2008) discusses the advantages of a developer installing multiple rain gardens during the initial development stage of large sub-divisions; this tool includes a cost-adjustment for this installation approach. However, this WLC model is best suited to provide planning-level WLC estimates for small-parcel land owners and managers interested in installing small rain gardens and comparing different cost options.

Curb-contained Bioretention

Many bioretention concepts take advantage of different ecological processes; however, they are often similar in construction approaches, design, and function. This WLC model is designed to incorporate bioretention concepts that can be contained by curbing and are designed to mitigate stormwater runoff from the surrounding pavement. Specifically, the model is designed to produce a planning-level cost estimate for a series of smaller basins that are back-filled with highly porous media and planted with vegetation that encourages infiltration and/or evapotranspiration and reduces stormwater peak runoff from expansively paved areas. These depressions are typically surrounded by curbing to maximize storage during large events, and to prevent drive-over in vehicle areas, and often include an overflow outlet or underdrain to conventional stormwater systems. The RS Means cost estimate

provided does include cost of demolition in the case of a retrofit. In the “Design and Maintenance Options”, the user may select “New” construction or “Retrofit” construction. If “Retrofit” is selected, a cost adjustment of 16% of the estimated base facility cost is added to the total cost estimate (Clar et al, 2004). Costs for this type of installation throughout the literature reviewed may be higher than current practice, as this is a relatively new technology. It is expected that as familiarity with the design concepts increases, cost should decrease.

The need for underdrains is dependent on soil type and overflow drain options, and underdrains represent a major percentage of the total project cost. Because of this, the WLC model includes the option for the installation of underdrains as part of the bioretention cells. If the user does not feel that this model fits their design criteria, the user should refer to the first suite of WLC models designed for large-scale LID installations such as extended detention basins, retention ponds, or swales.

In-curb Planter Vaults

Runoff reduction for small events with small drainage areas may be accomplished with in-curb planter vaults, defined as sub-grade storage vaults built into curbs to allow road or parking lot drainage to enter the vault's planter. In addition to reducing runoff volume, the planter facilitates passive precipitation storage to provide for urban vegetation in traffic islands or sidewalks. The vaults are filled with engineered structural soils to facilitate root growth, maximize porosity/water storage capacity, and support the load of the sidewalks and streets above them. These vaults can be capped by a normal sidewalk or street, and include a planted opening (often planted with a shrub or small tree).

The user can choose between two installation options in this model. The first installation option is a pre-cast vault, supplied by a manufacturer. In a review of available literature, for sources that reported costs for pre-cast vaults (EPA, 2005; Fairfax County, 2005; Unified Facilities Criteria, 2005; Calkins, 2008) the vaults were supplied by the same manufacturer. Differences in cost were functions of local construction and transportation costs; these values were averaged to create a per-pre-fabricated box installed cost estimate. Pre-fabricated vaults are substantially less expensive than vaults that are formed and poured in-situ and often include installation and service contracts to minimize inconvenience to the developer/manager.

The second installation option is vaults that are formed and poured in-situ. In-situ installations allow greater flexibility in all aspects of the design implemented, including water quality volume and landscaping components. In-situ installations include increased design, engineering and construction management costs in addition to a longer construction phase. Only the City of Portland (2005) reported costs for this type of installation. Instead of reporting this cost directly in the model, the Portland-style installation costs are averaged with an RS Means-based cost estimate of a similar project. This reduces the cost reported in the WLC model compared to Portland’s reported costs, which should be representative of future projects. Portland

noted that their installations, which were pilot in nature, included a number of unexpected costs that could be reduced in the future as the practices become more routinely implemented.

Cisterns for Commercial Buildings

In this model cisterns are defined as water catchment systems that channel rainwater from impervious surfaces into a storage tank for later use. This model is designed to estimate the cost of cistern systems for commercial buildings. Components included in this cost estimation model are the water tank, tank installation, and a re-distribution pump. The costs in the model were derived from a combination of literature review (CFM, 2008; Hicks, 2008; Miller, 2008; Nicklas, 2008; Ohio State Extension, 2008), component cost analysis, and an RS Means-based estimate of standard pump, tank, and installation costs.

The model allows the choice of two re-use options to more accurately estimate component costs. These options are “Outdoor Use”, assumed to be an automated spray irrigation system, or “Indoor Use”, assumed to use the collected water for toilet flushing. Indoor use is assumed to require a larger distribution pump in order to lift water to the upper stories of a building. The parametric cost estimate model does not include any costs of irrigation systems or double-plumbing that may be necessary depending on local regulations. Also, the model assumes that any gutters or internal conveyance systems from the roof to a storm drain are required components of a conventionally drained building. Although conventional storm water conveyance systems and cistern conveyance systems will differ in design (for example the downspouts will need to be directed into the cistern instead of a gutter or storm drain and more screening may be required), the model assumes that the cost difference is negligible. This model assumes minimal screening as the only method of treatment for stored water and intends for water supplied by the cistern not to be used as a potable source. Depending on the project location, different levels of treatment may be required by the local health department before the water can be used inside a building.

Summary and Conclusions

The expanded set of WLC models for LID BMP infrastructure provides planning-level estimates, describes system design approaches, and provides a standardized cost reporting form for agencies and developers to record and share development cost information. Many projects described in these models will vary greatly in design and cost based on the specific project goal and location. Flexibility has been built into the model to allow a user to compensate for design aspects specific to their project based on climate, regulatory environment, or other factors, as well as general regional cost differences in materials and labor.

The scale of any given project will also likely affect the final cost of the project. Every effort has been made to scale costs appropriately according to the size of the

project (related to, for example, drainage area, garden area or roof area); however, many of the cost models are based on limited cost data, and a limited number of varying project sizes. Economies of scale may not be entirely captured in these cost models. The scale of the project may also affect sourcing of materials and labor. Single-lot owners and managers may have many sourcing options for materials and labor for costs ranging from volunteer labor to more expensive labor, depending on quality or skill level required for the project. On larger -scale projects, a manager working for a municipality may be limited in their sourcing options for labor and materials.

To minimize the effects of the above-mentioned issues, each cost model was designed independently. Cost estimating approaches varied greatly from one model to another because the required infrastructure varied. For example, many sources are available on the internet to assist a home owner in designing, installing, and estimating the cost of a residential rain garden. Based on this information, the derivation of a per-garden size cost formula was direct. However, the cost reporting for green roofs was too unspecific to ensure that appropriate comparisons were made between sources and even within the same source. Most information sources reviewed (Toronto and Region Conservation, 2005, Peck and Kuhn, 2008) suggest that as roof area increases, the cost per square foot of an installation decreases. However, when comparing reported costs, the larger roof areas tended to be much more elaborate in design, and therefore, more expensive per square foot. Deriving a per-roof area cost proved unreliable. To overcome this, the two approaches described in the green roofs section above were created (one based on a modular green roof supplier's estimate and one based on component cost analysis) instead of one literature-based cost equation. In all instances, if the area-based estimate is insufficient for a particular project, a form is included in the cost tool to allow the user to create an engineer's estimate for a green roof project.

Regional LID BMP design considerations vary greatly, and therefore, so does infrastructure cost. The WLC models described here allows a user to modify cost information sufficiently to compensate for these variations and provide adequate planning-level cost estimations. In addition to providing cost estimates, the design concepts presented in each model provide factors to consider during the planning stages of an LID project. The model's function as a cost reporting tool will help agencies record and share cost information. These three model components will help to fill the lack of LID BMP cost information available to managers, thus encouraging the expansion of the use of LID BMP practices.

References

Belan, G. and B. Otto. 2004. Catching the Rain, A Great Lakes Resource Guide for Natural Stormwater Management. Retrieved September 2008, from American Rivers Web Site: http://www.americanrivers.org/site/DocServer/CatchingTheRain.pdf

Calkins, R. 2008. City of Ventura Administrative Report, Subject: Policy Direction for Incorporating Green Street Elements into Street Maintenance Projects and Authorization to Continue with a Demonstration project on South Catalina St.

Canada Freshwater Management (CFM). 2008. Retrofit . Accessed October 2008, from Canada Fresh Water Management. web site: http://www.ec.gc.ca/Water/en/manage/effic/e_retro.htm.

Chesapeake Bay Foundation. 2008. *Green Roof Demonstration Project Final Report.*

City of Lincoln, Nebraska. 2008. Alternative Stormwater Best Management Practices: 3.13 Rain Gardens. Retrieved October 2008, from Lancaster, NE, web site: http://lancaster.ne.gov/city/pworks/watrshed/educate/bmpguide/pdf/3.13.pdf.

City of Portland, OR. 2005. SW 12th Avenue Green Street Project. Retrieved August 2008, from: http://www.portlandonline.com/shared/cfm/image.cfm?id=167503.

Clar, L.M., Barfield, B.J., O'Connor, T.P. 2004. Stormwater Best Mangement Practice Design Guide. Volume 2: Vegetative Biofilters (Document No. EPA/600/R-04/121A). National Risk Management Research Laboratory Office ofCincinnati, OH. Research and Development. U.S. Environmental Protection Agency, Cincinnati, OH.

Edgewood College. 2003. Ten Steps to Building a Rain Garden. Retrieved October 2008, from Edgewood College web site: http://natsci.edgewood.edu/wingra/management/raingardens /rain_build.htm. Madison , WI.

Environmental Protection Agency. 2005. Quality Assurance for Nonpoint Source Best Management Practices: Tree vault Filters. Retrieved October 2008, from: http://www.lowimpactdevelopment.org/qapp/treevaultfilter_cost.htm.

Environmental Protection Agency. 2008. Urban Design Tools: Bioretention. Retrieved October 2008, from LID Center web page: http://www.lid-stormwater.net/bio_costs.htm.

Fairfax County, VA. 2005. LID BMP Fact Sheet, Tree vault Filters. Retrieved October 2008, from: http://www.lowimpactdevelopment.org/ffxcty/1-6_treevault_draft.pdf . Feb 2005.

Hicks, B. 2008. A Cost-Benefit Analysis of Rainwater Harvesting at Commercial Facilities in Arlington County, Virginia. Retrieved October 2008, from Duke Space web page: http://dukespace.lib.duke.edu/dspace/bitstream/10161/512/1/MP_wdh11_a_200805.pdf.

James City County. 2008. Rain Garden Guide. Retrieved October 2008, from: http://www.protectedwithpride.org/images/pdfs/Rain%20Garden%20Guide_web.pdf.

Kassulke, N. 2003. A Run on Rain Gardens. Wisconsin Natural Resource Magazine. Retrieved October 2008, from WNRM magazine: http://www.wnrmag.com/supps/2003/feb03/run.htm.

Lampe, L., Andrews, H.O., Hollon, M., Jefferies, C., Kellagher, R., Matin, P. 2005. *Performance and Whole-Life Costs of BMPS and SUDS*. Project # 01CTS21TA. Water Environment Research Foundation, Alexandria, VA.

Maryland Department of the Environment (MDE), 2000. 2000 Maryland Stormwater Design Manual, Appendix B-3 prepared by the Center for Watershed Protection

and the Maryland Department of the Environment, Water Management Administration, Baltimore, MD.
Miller, M. 2008. Personal communication Oct. 2008 with Mark Miller, Owner of Mark Miller Toyota concerning the cistern installation at his dealership. Salt Lake City, UT.
Nicklas, M. 2008. Rainwater, the Untapped Resource. Retrieved October 2008, from High Performance Buildings Online Magazine: http://www.hpbmagazine.org/images/stories/articles/Rainwater.pdf.
Ohio State Extension. 2008. On-Site Sprinkler Irrigation of Treated Wastewater in Ohio. Bulletin number 912. retrieved Oct. 2008, from Ohio University web site: http://ohioline.osu.edu/b912/step_5.html.
Peck, S. and M. Kuhn. 2008. Design Guidelines for Green Roofs. City of Chicago. Retrieved Oct. 2008 from City of Chicago Web Site: http://egov.cityofchicago.org/webportal/COCWebPortal/COC_ATTACH/design_guidelines_for_green_roofs.pdf.
Roofscapes. 2008. Web Site retrieved in Sept. 2008, from: http://www.roofmeadow.com/Inc.
Toronto and Region Conservation. 2008. An Economic Analysis of Green Roofs: Evaluating the costs and savings to building owners in Toronto and surrounding regions. Retrieved Sept. 2008 from Sustainable Technologies web site: http://www.sustainabletechnologies.ca/Portals/_Rainbow/Documents/GR_Econ.pdf.
Unified Facilities Criteria (UFC). 2004. Low Impact Development. UFC Publication No 3-210-10. Retrieved September 2008, from: http://www.wbdg.org/ccb/DOD/UFC/ufc_3_210_10.pdf.

Data Reporting Guidelines for Certification of Manufactured Stormwater BMPs: Part II

CE Database: Stormwater management, best management practice, performance characteristics, water quality, certification

Authors: Robert M. Roseen M.ASCE[1], Ernie Carrasco[2], Yuan Cheng[3], Bill Hunt[4], Charlene Johnston[5], Jim Mailloux[6], Walt Stein[7], Tim Williams[8]

Abstract

Data Reporting guidelines presented here were developed as part of the ASCE/EWRI Task Committee on Guidelines for Certification of Manufactured Stormwater BMPs. This work is the collaboration of the Stormwater Infrastructure Committee of EWRI's Water, Wastewater, and Stormwater Council (WWSC) and the Wet Weather Flow Technology Committee of the Urban Water Resources Research Council (UWRRC). These guidelines were developed by review of the major manufactured treatment device certification protocol requirements drawing primarily from the Technology Assessment Protocol-Ecology (TAPE) and the Technology Assessment Reciprocity Partnership (TARP). These reporting guidelines have been broadened to support the International Stormwater Best Management Practices (BMP) Database. With the increasing need for the field testing of proprietary devices comes the importance of consistent data reporting guidelines to be used when reporting to regulatory agencies or designers. The need for standardized reporting is underscored by the tremendous impact the range of testing factors can have upon testing results. These factors include the testing environment, experimental design, testing methodologies, statistical analysis, and data presentation. The need for consistency is underscored by the complex influence these factors have upon performance results. A clear and consistent data reporting approach can ensure that these biases are minimized, well understood, and that representative field testing can be effectively evaluated by the regulatory agency. A consistent reporting format is also needed to aid vendors to efficiently navigate the complicated application process for device certification. Finally, an independent third-party is needed to either conduct or review the testing to ensure testing impartiality. The committee membership includes stakeholders from the regulatory, academic, manufacturing, and design communities.

[1]Corresponding Author, Subcommittee Chair , The University of New Hampshire Stormwater Center, Department of Civil Engineering, 35 Colovos Road, Durham, NH 03824; PH 603-862-4024; FAX 603-862-3957; e-mail: robert.roseen@unh.edu; web: www.unh.edu/erg/cstev/
[2] Rinker Materials, ECarrasco@rinker.com
[3]Century Engineering, ycheng@centuryeng.com
[4]North Carolina State University, wfhunt@ncsu.edu
[5]AMEC Earth & Environmental, 3800 Ezell Road, Nashville, TN 37219, PH 978-761-0663, Charlene.Johnston@amec.com, www.amec.com
[6]Alden Labs, jmailloux@aldenlab.com
[7]Contech, steinw@contech-cpi.com
[8]Foley Products Company, TWilliams@foleyproducts.com

Introduction

The need for a strict coherent approach to the testing of manufactured treatment devices (MTD) for stormwater management is ever increasing. MTD abound in the marketplace; however, there is limited information about system performance by third-party verification, and third-party verification protocol is not consistent This makes it difficult for consumers and stormwater managers to make informed decisions. A few states are making progress on this front, but there is no recognized consensus in the approach. To address this issue, both prescriptive testing protocols for laboratory and field conditions are required. The data acquired through those processes requires detailed reporting. The certification process itself can arguably be as difficult as the device testing process. Because of a lack of reporting guidance for the dominant testing protocol, vendors are left to discover the reporting requirements. This can lead to an inefficient, incomplete, and multi-stepped review process that can take years to negotiate effectively.

The ASCE/EWRI Task Committee on Guidelines for Certification of Manufactured Stormwater BMPs was convened in 2007 and is comprised of a range of stakeholders from academics, industry, and regulatory communities. By the end of 2009, the subcommittee on Data Reporting is responsible for preparation of the reporting guidelines for the presentation of testing results, so the data can be readily interpreted by the regulatory community.

The result of effective data reporting is a System Performance Evaluation Report that presents sufficient information to determine if an MTD meets the requisite performance standards within a reasonable level of statistical confidence. The System Performance Evaluation Report includes both summary data and sufficient experimental data to provide a detailed review of system performance. A critical review of leading testing protocols was performed and used as the basis for these guidelines. The first and only approved certification report for a MTD was also included. These reporting guidelines may need to be further adapted based on the synthesis of the subcommittee's products on both Field Testing and Data Analyses.

Background

Prescriptive testing protocols are needed because the range of influences upon testing and performance data is wide and not always well understood. Influences include watershed characteristics, storm event characteristics, maintenance requirements, system sizing, and testing methodologies. A testing protocol that does not dictate methods introduces biases that are challenging to account for.. In addition for performance characteristics to be compared across a range of different MTDs similar analytical methods and monitoring strategies must be used. The function of existing protocols is often to provide both a uniform testing environment and an accelerated review process that aids in the acceptance of stormwater technologies. Arguably, the current protocols have mixed success as measured by the existence of very few approved technologies despite programs existence for over 7 years.

If the testing protocol adequately addresses these issues, the testing results must be presented in order that a committee of scientists is not necessary to synthesize and interpret the results. This last point is significant, because the staff of the many regulatory agencies that reviewing the test results can not be expected to decipher the range of factors influencing system performance. As such, reporting results require sufficient information ranging from detailed appendices of experimental data to summary data indicating whether the systems met requisite performance standards within a reasonable level of statistical confidence.

A consistent reporting format does not currently exist; this leads to an , which has lead to a non-transparent and inefficient application and review process. Consistent and thorough data reporting requirements will aid regulatory review and vendor application alike.

The technology protocols and reports reviewed as part of this effort included:

- TARP Tier II Guidance Document: Protocol for Stormwater Best Management Practice Demonstrations. (NJCAT, 2003).
- New Jersey Tier II Stormwater Test Requirements - Amendments to Tarp Tier II Protocol. (NJCAT, 2006).
- TARP (Technology Acceptance Reciprocity Partnership) Tier I Guidance Document. TARP. (2001).
- NJCAT Technology Verification: Stormwater Management Stormfilter (CONTECH Stormwater Solutions, Inc. 2007).
- ETV Verification Protocol Stormwater Source Area Treatment Technologies. US EPA Environmental Technology Verification Program, Washington DC. (USEPA, 2002).
- Technology Assessment Protocol- Ecology's (TAPE) by the State of Washington, Department of Ecology. (WADOE, 2002).
- Improved Protocol for Classification and Analysis of Stormwater-Borne Solids. Water Environment Research Foundation, Alexandria, Virginia. (WERF, 2007)
- Urban Stormwater BMP Performance Monitoring. (USEPA and ASCE 2002)
- International Stormwater BMP Database. (ASCE et al, 1996))

International Stormwater BMP Database

The reporting framework was broadened to include data reporting criteria that will also meet the requirements for inclusion in the International Stormwater BMP database (BMPDB). The purpose of the BMPDB is to provide scientifically sound information for improved the design selection, and performance of stormwater management strategies. Continued population of the database and assessment of its data will lead to a better understanding of factors influencing BMP performance and help to promote improvements in BMP design, selection, and implementation. Statistical performance reporting requirements consistent with those used in the BMPDB are proposed as part of the MTD reporting framework. The database is only as valuable as the information that is included in it. The breadth and depth of the testing that will be done for MTD certification are ideal for inclusion in the BMPDB.

Work Plan

The subcommittee work plan for year one was to develop a consensus on a Reporting Framework. This was accomplished by the review of existing protocols, literature, and technology evaluation reports. Next, the framework was to be developed in the form of an annotated outline and sample mock-up. By year two, final input from the subcommittee will be completed. The next stage is for the draft Reporting Framework to be circulated amongst the full committee. The Final Data Reporting Guidelines will be completed in 2009. At which point, the full committee guidelines will be presented at the EWRI Annual Meeting.

DRAFT Reporting Framework

The reporting framework includes information ranging from the testing location, MTD specific information, test methods and procedures, and testing and sampling conditions. The test methods section will be determined largely from the subcommittee on Field Testing Methodology. The performance results and discussion are presented from two perspectives: 1) complete testing summary statistics and 2) on an individual event basis. Overall system performance is needed to determine the basic MTD performance. The summary statistics reflect largely the BMPDB (ASCE, 1996). The individual storm reports (ISR) on system performance enables understanding of the system variability with respect to storm event characteristics. This section has been adapted largely from existing reporting protocols for TAPE (2008).

The framework is listed below.

1. Summary: Executive Summary with rated performance rating, Study Summary, Data Collection Summary
2. Definitions
3. Site Conditions: longitude, latitude, land cover type, land use activities, site conditions, site elevations and slopes, location of sampling equipment, location of on-site stormwater collection system, and a description of any upstream BMPs
4. Technology Description:
   a) The specific device used (model number, size)
   b) Functionality of treatment mechanisms including pretreatment and bypass requirements
   c) Physical description: engineering plans, site installation requirements
   d) Cost of system and installation
   e) Sizing methodology: flows, volumes, etc.
   f) Maintenance procedures
5. Test Methods and Procedures
   a) Particle size for influent, effluent, and residuals, mass based, concentration based
   b) Water quality parameters monitored
   c) Data Quality Objectives (DQO), QA methods, and measurement accuracy for the observations
   d) Measuring instruments, sampling frequency, and sampling program information
   e) Sampling Locations and Peak Concentration Timing
6. Testing and Sampling Event Characteristics:
   a) Storm date, depth, antecedent dry period, intensity, duration, season, type of runoff (precipitation, snowmelt, groundwater, etc.)
   b) Number of influent and effluent aliquots; storm volume, % storm treated influent, effluent, peak flow rate, calculation of peak reduction and lag coefficients, number of storms exceeding design criteria.
   c) Comparisons with Data Quality Objectives
7. MTD Performance Results and Discussion:
   a) Event mean concentrations for influent and effluent with summary statistics (N, mean, median, coefficient of variation, standard deviation, one –tailed sign t-test)
   b) Detection limits and confidence intervals
   c) Performance metrics: removal efficiency, efficiency ratio

d) Statistical Evaluation: time series plot, box and whisker with confidence intervals, effluent probability method, linear regression . Statistical analyses should be consistent with the International BMP Database (bmpdatabase.org).
e) Solids characterization: influent, effluent, residuals particle size analysis
f) Accumulated mass reductions
g) Individual Storm Reports with event characteristics (6a and 6b), combination event hydrograph and hyetograph with sample times; system performance characteristics (7a-c), monitoring details
h) Quality Assurance, rejection criteria and rejection summary.
i) Maintenance findings: discussion on recommended maintenance schedules

8. Conclusions, Performance Claims, and Limitations
9. Appendices: Raw data and credentials
10. Third Party Review. The testing and reporting, if not performed by an independent professional third party, must be reviewed. The independent review should include a review summary and observation of at least one monitoring event.
11. Appendices

Conclusions

Guidelines produced by the Data Reporting subcommittee will be completed in 2009. The Committee's intentions are to facilitate a rapid review, so emerging technologies can be brought to market with the confidence of both third-party verification and regulatory approval. To accomplish this, a thorough and effective System Performance Evaluation Report reviewed by an independent third party is needed. The challenge is to balance the complex science of technology verification with the need for thorough review and a clear presentation of results. The collaboration of stakeholders from the regulatory, academic, manufacturing, and design communities will ensure an appropriate balance is achieved.

1. ASCE, U.S. Environmental Protection Agency, Water Environment Research Foundation, Federal Highway Administration, American Public Works Association, Wright Water Engineers, Geosyntec Consultants (1996). "International BMP Database." http://www.bmpdatabase.org/
2. CONTECH Stormwater Solutions, Inc. (2007). "NJCAT Technology Verification: Stormwater Management Stormfilter." http://www.resourcesaver.com/file/toolmanager/CustomO56C145F75793.pdf
3. NJCAT. (2003). "TARP Tier II Guidance Document: Protocol for Stormwater Best Management Practice Demonstrations." N. J. Department of Environmental Protection (NJDEP).
4. NJCAT, NJDEP. (2006). "New Jersey Tier II Stormwater Test Requirements - Amendments To Tarp Tier II Protocol."
5. TARP. (2001). "TARP (Technology Acceptance Reciprocity Partnership) Tier I Guidance Document."
6. USEPA. (2002). "ETV Verification Protocol Stormwater Source Area Treatment Technologies." N. International and U. E. N. R. M. R. Laboratory, eds., US EPA Environmental Technology Verification Program, Washington DC.

7. USEPA, ASCE. (2002). "Urban Stormwater BMP Performance Monitoring." *EPA-821-B-02-001*, Washington DC.
8. WADOE. (2002, 2008). "Technology Assessment Protocol- Ecology's (TAPE) by the State of Washington, Department of Ecology."
9. WERF. (2007). "Improved Protocol for Classification and Analysis of Stormwater-Borne Solids." L. A. Roesner and A. Pruden, eds., Water Environment Research Foundation, Alexandria, Virginia.

Design of Integrated Bioinfiltration-Detention Urban Retrofits with Continuous Simulation Methods

William C. Lucas, S.M. ASCE

Griffith University, Nathan Campus, Brisbane Australia Bill.Lucas@Student.Grifith.edu.au, wlucas@integratedland.com

ABSTRACT

This paper presents the elements involved in the design of a bioretention planter/trench infiltration-detention system as an urban retrofit project. The system was designed to intercept all of the runoff from a synthetic 5.08mm 24-hr rainfall event. Diverted flows were conveyed into bioretention planter for treatment. The bioretention systems were fingerprinted into areas comprising 0.8% of the contributory drainage areas, with an associated stone trench comprising another 3.4%. The system was modeled using SWMM 5.0.014 continuous simulation (CS) software. Under existing conditions, over 80% of annual runoff exceeded the 3.50 L-s^{-1}-ha^{-1} (0.05 cfs-ac^{-1}) threshold for initiation of combined sewer overflows (CSOs). Nearly all runoff was intercepted by the planter/trench infiltration system, and even with a soil infiltration rate of only 2.54 mm-h^{-1}, nearly 46% was infiltrated, and less than 8% was discharged at rates that could initiate CSOs. The number of CSO events was reduced from 74 to 4, a reduction of 95%. The volume of flows exceeding the threshold decreased by over 91%.

KEYWORDS: Bioretention; Infiltration; Routing; Modeling; Continuous Simulation; SWMM

INTRODUCTION

Because it determines runoff capture performance for a given area, infiltration is one of the most important processes in bioretention systems. However, infiltration is an element that remains poorly understood, let alone effectively addressed in their design. As such, computational approaches that realistically address infiltration are urgently needed. The Green-Ampt formulation can be quite precise if its parameters are properly determined. It has the ability to account for head, and the resulting changes in infiltration rates according to Darcy's Law. These aspects of the Green-Ampt formulation make it very attractive for modeling.

Many biological processes also affect infiltration properties. The beneficial effects of native plants on infiltration rates persist even in depositional situations where sediments accumulate (Rachman et al, 2004). Plant movement in the wind tugs at the soil surface, breaking clogging mats, and cracking through deposits. Ponded rainfall can then more easily penetrate clogged surface layers, increasing infiltration rates. Root turnover promotes the formation of macropores. These processes associated with vegetation are remarkably effective in restoring and/or enhancing infiltration rates. Field infiltration rates in native grass hedges are much higher than found in adjacent croplands (Rachman et al, 2004; Blanco-Canqui et al, 2004a,

2004b; Seobi et al, 2005). In bioretention columns, Culbertson and Hutchinson (2004) have documented that switchgrass (Panicum virgatum.) increased infiltration rates in bare soils from 0.5 cm-h-1 to 128 cm-h-1, an increase well over two orders of magnitude. The presence of vegetation can result in infiltration rates several orders of magnitude higher than predicted by underlying soil properties (Ralston, 2004). Therefore, the presence of vegetation can play as much of a role in determining the infiltration and percolation response as the underlying soil texture composition. It is only recently that the literature has begun to address how media properties such as texture and organic matter interact with soil structure and vegetation to affect the matrix infiltration and percolation response (*e.g.*, Sharma et al, 2006).

In addition to the complexity of infiltration responses, there are several different compartments through which runoff flows in bioretention systems. There is a surface pool compartment that infiltrates into the media compartment, but also has the capability of bypassing surface flow in excess of storage. Flows initially pass slowly from the media into a stone layer as unsaturated flow, which increases in rate until saturated. Flows from the stone layer infiltrate into the surrounding soil which typically controls system capture because media flow rates are typically much faster than that of the surrounding soils. As such, the hydraulic gradient is initially rapid, but eventually decays to the rates determined by the surrounding soil. Where soils have very low infiltration rates, an underdrain can be installed to permit more flow to be captured and treated by the media. A key aspect of this arrangement is the fact that flows under saturated conditions are driven by hydraulic gradients, so backwater created by any of these nodes will control system response.

Given the complexity of this system, there is still uncertainty about how to properly model infiltration processes in bioretention systems. A method that mimics the Green-Ampt initial infiltration response needs to be combined with standard level pool routing that takes into account hydraulic gradients. This paper presents the elements involved in the hydraulic routing of bioretention systems as part of an urban retrofit project in Columbus Square, Philadelphia, Pennsylvania.

METHODS

System Design

Two bioretention planters linked by a stone trench were designed to provide storage of at least 25.4 mm (1") of runoff from the surrounding impervious areas. These systems are intended to not only intercept runoff from frequent events, but also to infiltrate as much of it as possible. The balance that doesn't infiltrate is released through a small orifice to reduce flows below the 3.50 $L\text{-}s^{-1}\text{-}ha^{-1}$ CSO threshold. Each planter comprises a 5.08cm long by 91cm wide (16.67' by 3.0') cast in place concrete cell. The planter media is placed at a depth of 81cm (32"), with the top being 41cm (16") below the lip of the planter. This results in the media being 10cm (4") below street elevation. Runoff from the street is intercepted by a 91cm wide curb cut, with a sump 91cm deep. It is covered with a metal cover to permit access to remove coarse debris. Collected runoff then flows through a 91cm wide slot that is 10cm high, placed 5cm above the media to prevent backwash of mulch from the planter. The planters are placed upon a stone bed of AASHTO no. 57 stone with a compacted void percentage of at least 40%. Figure 1 displays the planter section.

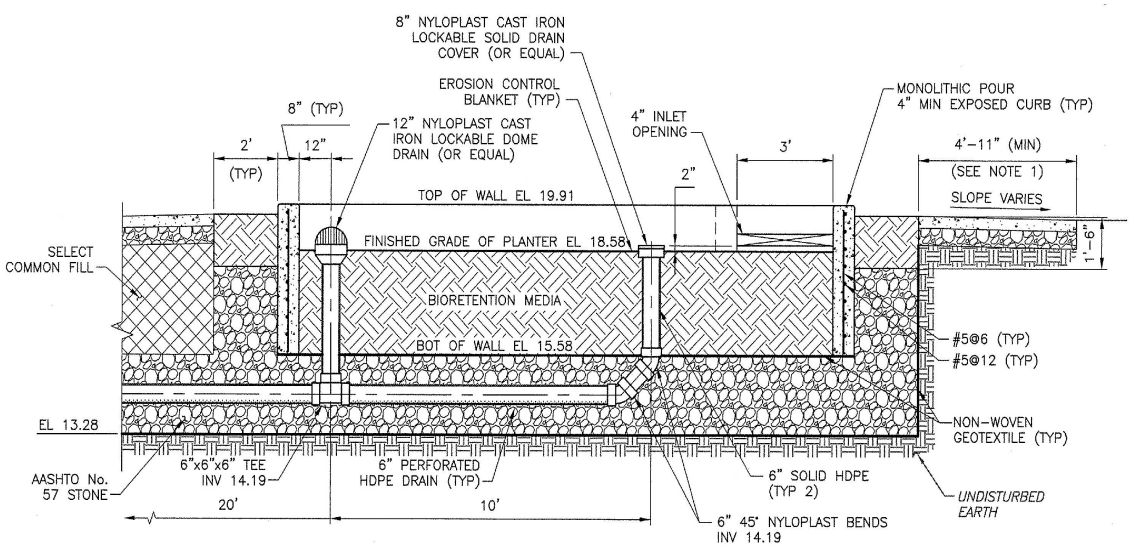

Figure 1: Section View of Typical Planter System (Courtesy of CDM and PWD)

Runoff collected in the planters initially passes through the planting media, and once ponding depths exceed 5cm, also pass through an 46cm circular inlet and then into an 20cm (8") distribution manifold into the underlying stone. Given this internal bypass arrangement, these systems are capable of intercepting runoff very effectively in even large events, while treating the smaller events as flow through the media for better treatment performance. Between the planters, there is a 23.9m long by 1.5m wide (78.5' by 5') infiltration trench 152cm deep, with its bottom set this distance below street elevation. This trench is also filled with no. 57 stone. Runoff accumulated in the stone system is collected by a perforated underdrain which discharges into a control structure comprising a 13mm (0.52'') circular orifice at the underdrain invert, and a 61cm (24") wide overflow compound v-notch weir 122cm (48") higher. Although infiltration tests at the locations of the planters indicated negligible infiltration, the extent of the area exposed by the trench is likely to encounter areas of some infiltration. As a result, the nominal infiltration rate of the soil surrounding the trench was projected at 2.54 mm-h^{-1} (0.10 in-h^{-1}) per hour.

Routing Setup

To represent the system, it is necessary to disaggregate the various components so they can be modeled discretely. As shown in the routing diagram in Figure 2, this is accomplished through modeling the contributing subareas individually. Each bioretention/surround system is then subdivided into three nodes: an Inlet node, a Planter Pond node, and a Media node. The Planter Trench node is filled by flows through the media and bypass flows from the surface pond of each planter. The inlet orifices are modeled explicitly to ensure that they do not constrain flows. Overflows down the street represent bypass flow to surface inlet node that is not intercepted by the planters.

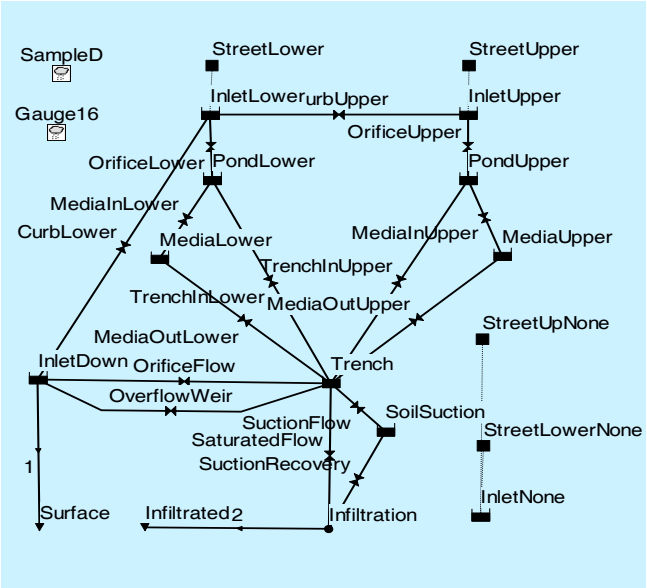

Figure 2: SWMM 5.0.14 Model Routing Diagram

To route flows into the media, an alternative approach is needed to reproduce such vertical flow dynamics. One approach is to model the flows into the media and as if it was routed through an orifice. This obviously does not replicate the complexity of unsaturated flow dynamics into and through a complex media/soil system of several layers. Furthermore, orifices increase flow at the half power of head, while Darcy's Law through media of a uniform length bears a linear relationship to head. Therefore orifice responses will be only an approximation at best. However, because the ponding depths that increase flows into media are so shallow, allocating an orifice several inches below the surface is an effective method to mimic inflows into the media. Flows are initially higher than stabilized rates until head in the media rises, thus mimicking Green-Ampt response, while the orifice will then respond to the hydraulic gradient when the media is saturated.

For flow through the media, SWMM5 now offers a flow routing option that permits flows through elevation-dependent rating curves that reflect the difference in head between nodes. With this option, the rating curve flow declines once there is less effective head. This often occurs when outflow is controlled by infiltration into the surrounding soils. In this manner, the outflows can respond according to the limiting condition. To do this, the hydraulic grade line must be carried upward from the surrounding soils through the media into the pond, and even back out the inlet in extreme events. As a result, there can be minimal flow into or through the media once the surrounding stone is filled up and outflows are restricted by its discharge response. This method can provide quite a reasonable representation of flows into and through the media when it is saturated.

Because the planter area of the systems is only 0.8% of the effective source area, even relatively small events will exceed the infiltration rates into the media, resulting in surface ponding. Once the surface ponding exceeds the bypass inlet grate set 5cm higher, the resulting flows are also routed through the bypass inlet into the stone surround and trench system as primary flows. Accumulated runoff into the combined surround and trench stone system is collected by a perforated underdrain which discharges into a control structure comprising an orifice and the compound v-notch overflow weir. Because infiltration rates are so low, this system is designed to release accumulated runoff at low rates into the InletDown node.

Flows passing through the trench node infiltrate into the surrounding soil at a K_{sat} projected to be 2.54 mm-h^{-1}. Outflows from this node can be allocated by rating curves computed according to the corresponding wetted area and K_{sat}. However, in

addition to saturated flows, it is necessary to mimic the response of capillary suction response of the surrounding soil. This is accomplished by creating a dummy SoilSuction node created 444cm (13.55') below the bottom of the trench. This dummy node area is sized according to the projected capillary suction volume divided by this depth. Flows enter the node through an orifice at the bottom sized to represent the initial rate, which is based on the ratio of capillary suction to K_{sat}, divided by a peak factor.

Given this configuration, flow rates into this node are initially rapid due to the high head across the orifice, and then decline as the SoilSuction node fills up (saturates) and the effective head differential declines. To replicate recovery, flows leave this soil node at the initial K_{sat} applied to the bottom of the trench, divided by a recovery factor. This is applied as a constant rating curve. In this manner, there will be minimal suction flow for events that occur when the SoilSuction node is full (wet), while events that occur when it has drained will have more of a suction response. The recovery rate is subtracted from the K_{sat} applied to the surrounding soils as a function of wetted area. In essence, this SoilSuction node operates as a sponge with the capacity representing the suction head volume, designed in a manner that accelerates the same infiltrated volume that would be encountered with a constant K_{sat}. While these artifices vastly oversimplify the actual processes involved, the system response throughout an event is quite similar that expected from a more physically process-based model, while requiring considerably fewer computational resources.

SWMM used a CS time series rainfall file to project annual responses. This distribution is the 2005 "synthetic year" distribution developed by Camp Dresser and McKee (CDM) based on 26 years of rainfall records. This design year was selected as being hydrologically representative of annual rainfall distributions, subject to including a range of larger events to address flooding design. An uncontrolled system without the SMPs (InletNone) was established for comparison purposes. The model was then used to compare flow distributions of the uncontrolled system to the Planter-Trench LID system in terms of reducing overall runoff, and in particular, reducing combined sewer overflows (CSOs). A threshold of 3.50 L-s^{-1}-ha-1 (0.50 cfs-ac-1) was set as the runoff rate at which CSOs are likely to occur. This disaggregated routing results in unexpected behavior during events as the various compartments fill and empty at different rates.

RESULTS AND DISCUSSION

Figure 3 displays the response for two events in January 2005. The upper row displays the response for the upper and lower media, the middle row displays the relative elevations of the Media, Trench and SoilSuction nodes, while the bottom row shows both the surface and exfiltration outflows from the Trench. In this case, the first event is 12 mm precipitation over 8 hours, while the second is a 43.4 mm event that occurs over 14 hours. This latter event is the fourth largest event in the 2005 rainfall time series.

In the first event, initial orifice controlled inflow rates into the media are as high as inflow rates into the pond until the media approaches saturation, after which and inflows are then controlled by the system based on Darcy's Law. There is relatively rapid drainage from both the upper and lower media. Because soils are

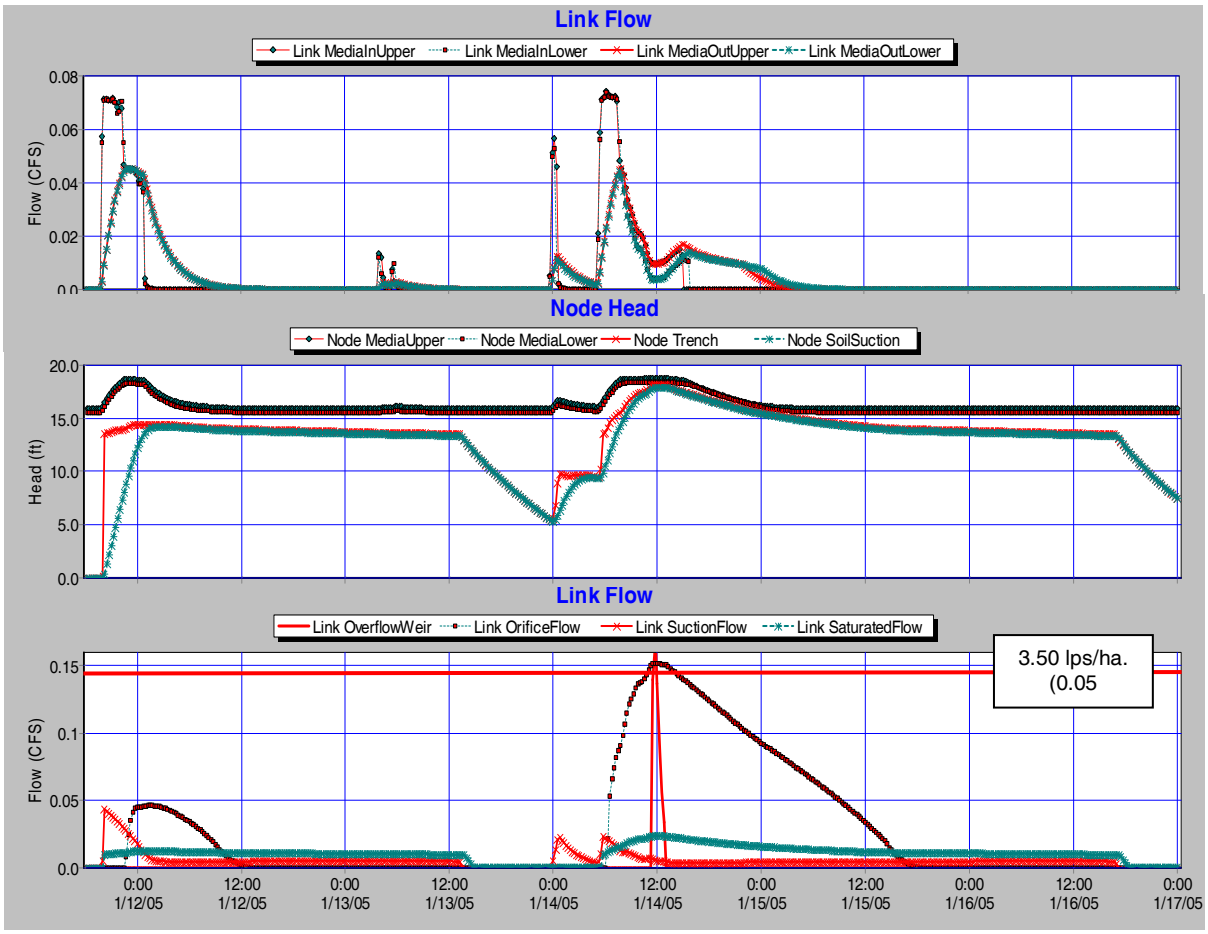

Figure 3: Flow Rates and Node Depths, Jan 12 and January 14, 2005 Events. Top Row displays Flow into and out from Media, Middle Row displays Media Trench and Suction Node Elevations, while Bottom Row displays Trench Outflow into Surrounding Soil via Suction and Saturated Flows, as well as Flows through Orifice and Overflow Weir.

initially dry, the elevation of the trench in the middle row is initially much higher than SoilSuction, resulting in a corresponding peak in the SuctionFlow response shown in the bottom row. Note how OrificeFlow discharge is delayed well after media outflows, and is well under the 3.50 L-s^{-1}-ha-1 threshold for CSOs.

The response of the latter event is similar to the first in terms of media inflows. However, during peak runoff, there is a characteristic double peak in the media response, in which the dip is matched by a corresponding peak in the overflow weir flow. The dip between the peaks occurs as the trench elevation approaches that of the media. There were two precipitation pulses in this event, in which the SoilSuction node had not fully recovered from the first event. This resulted in two SuctionFlow responses, of which neither was as pronounced as the first event. There was a slight CSO exceedance as shown in the OverflowWeir discharge.

The preceding events were examined in detail to present the dynamic interactions between the various nodes so as to get a better of the overall system response. The entire 2005 design year was then run to evaluate the cumulative annual performance of the system. The full dynamic wave option was used, with a time step

of 6 seconds to avoid instabilities. The annual flow routing continuity error was 0.06%. To examine sensitivity of the system to underlying infiltration rates, runs were also made with the nominal rate of 2.54 mm-h^{-1} doubled to 5.08 mm-h^{-1}, and halved to 1.27 mm-h^{-1}.

Figure 4 displays the resulting distribution of CSO exceedances, and their magnitude. Table 1 presents the resulting runoff and infiltration volumes, as well as the number of CSO exceedances and their total volume. The total runoff from the uncontrolled system was 1175 cu.m., representing an effective depth of 1.13 m. This comprised 113 different runoff events, of which 73 exceeded the CSO threshold. With the SMP systems at the lowest infiltration rate 1.27 mm-h^{-1}, the runoff volume was reduced by 40.8% to 680 cu.m. While this is a substantial reduction in annual runoff, the number of CSO exceedances declined to only 4 events, a decrease of 95%. Likewise, the volume of exceedances was reduced from 947 to 103 cu.m, a reduction of 89%. This emphasizes just how effective the SMP system can be due even when constrained by very low infiltration rates into the surrounding soil. This is due to the effective interception and retardance of flows.

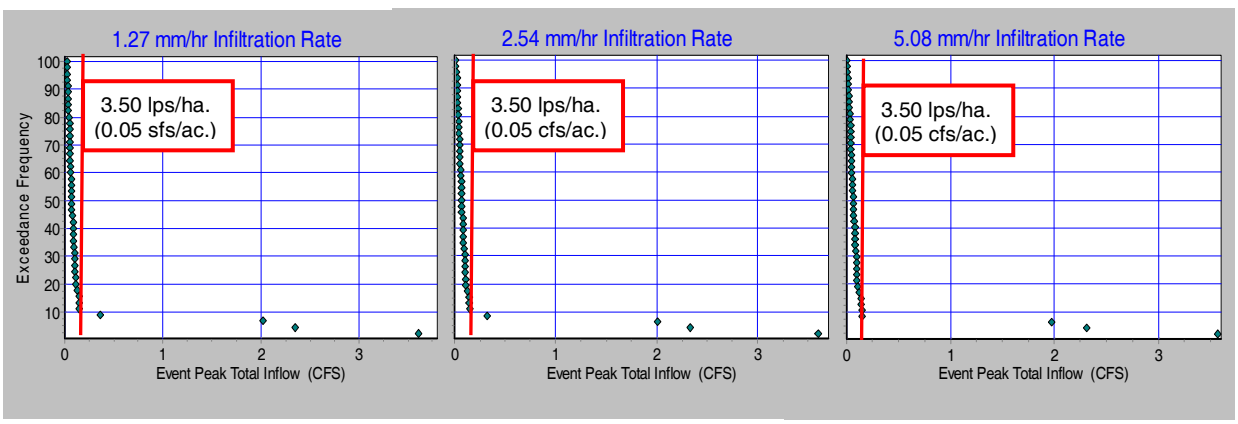

(a) (b) (c)

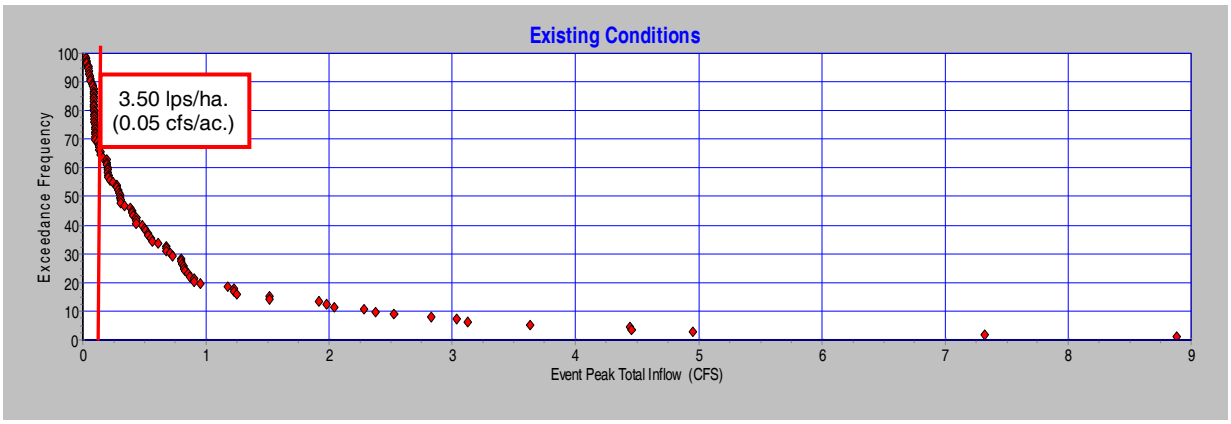

d)

Figure 4: Peak Flow Exceedance Frequencies: (a) Planter-Trench LID, Infiltration Rate at 1.27 mm-h^{-1} (0.05 in.-h^{-1}); (b) Planter-Trench LID, Infiltration Rate at 2.54 mm-h^{-1} (0.10 in.-h^{-1}); (c) Planter-Trench LID, Infiltration Rate at 5.08 mm-h^{-1} (0.20 in.-h^{-1}); (d) No LID Inlet Flows.

Table 1: SWMM Routing Results, 2005 Design Year, Uncontrolled Runoff Compared to Planter Trench LID System, Infiltration Rates at 1.27-, 2.54- and 5.08-mm-h^{-1}

Scenario	Uncontrolled Runoff	LID Planter Trench Controlled Inlet		
		1.27 mm-h^{-1}	2.54 mm-h^{-1}	5.08 mm-h^{-1}
Runoff Volume (cu.m.)	1175	680	637	535
Infiltrated Volume (cu.m.)	0.0	479	538	640
Infiltrated Depth (m.)	0.00	0.46	0.52	0.62
Percentage Infiltrated	0.0%	40.8%	45.8%	54.5%
Treated Volume (cu.m.)	0.00	512	513	514
Percentage Treated	0.0%	43.6%	43.6%	43.8%
Number of CSO Exceedances	74	4	4	3
CSO Exceedance Volume (cu.m.)	947	103	91	81
CSO Percentage Exceedance	80.6%	8.8%	7.7%	6.9%

When the infiltration rate was set at 2.54 mm-h^{-1}, the percentage infiltrated increased to 45.8%, with 538 cu.m. infiltrated. The number of exceedances was the same. The volume of exceedances was reduced to 91 cu.m., a reduction of 90%. With the infiltration rate increased to 5.08 mm-h-1, 54.5% of the inflow volume was infiltrated, representing 640 cu.m. The number of exceedances further declined to 3, a reduction of 96%, and the volume of exceedances was reduced to 81 cu.m., a reduction of 92%. Note that these latter results were obtained at infiltration rates that are still quite low. Table 3 also presents the extent of flows that are treated by the media. In all three scenarios, the percent treated is nearly 44%, a remarkable proportion for a SMP with a surface area of only 0.8% percent of the source area. While the remaining runoff volume may not be treated by the media, it represents less polluted flows that occur after the first flush, which flows are both filtered by passing through the planter vegetation and then through the stone.

Figure 5 graphically displays how the resulting annual flows are distributed. This graph uses the typical percent exceedance display as shown on the upper abscissa. However, flows are not only altered in terms of their distribution, they are also reduced in terms of total volume and duration. Therefore, comparisons of normalized cumulative frequencies can be misleading in terms of seeing what the actual effect may be. To better display the comparison of the LID scenario to the uncontrolled scenario, the data is plotted on the bottom abscissa in terms of 15 minute flow intervals. While this method shows very similar trends in flow distributions, their origins are different. In the exceedance distribution, flows are apportioned across the entire range of percentages, because they are normalized in terms of total flow. On the other hand, because the cumulative flows are not normalized against themselves, they represent the true comparison between treatments with different flow volumes and durations.

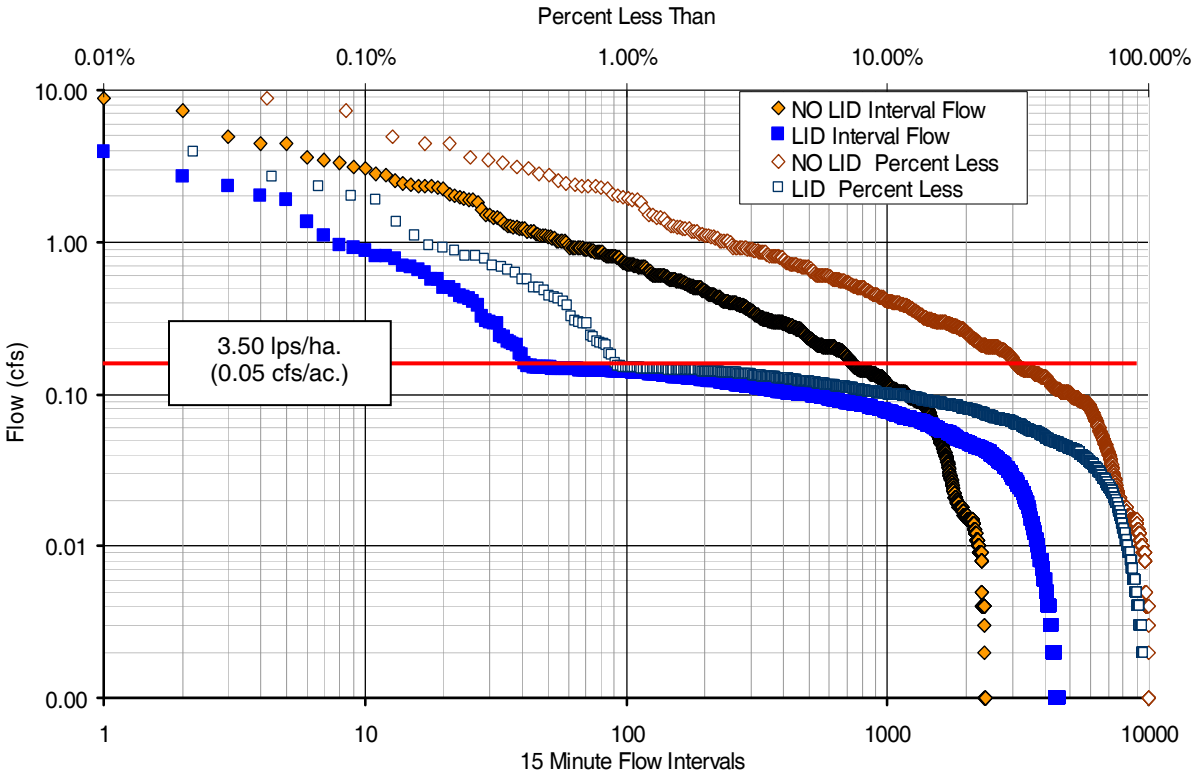

Figure 5: Flow Exceedance Frequency and Cumulative Flow Distribution: Uncontrolled Runoff Compared to Planter-Trench LID System, 2.54 mm-h^{-1} (0.10 in.-h^{-1}) Infiltration Rate.

Without SMP controls, flows exceed the CSO threshold over 20% of the time. With the SMP system at the nominal infiltration rate, the percent of time that flows exceed the CSO threshold then declines to 1% of total runoff duration. However, because total flow volumes and durations are different between these scenarios, it is difficult to determine what this difference in percentage really means.

In contrast, the interval flow plots show a more comprehensive picture. In the No LID scenario, there are 800 flow intervals over the CSO threshold, with the remaining 1600 or so intervals less than the threshold. In contrast, there are only 40 intervals over the threshold in the LID scenario, while there are some 3400 flow intervals are below the threshold. So even though there are many more flow intervals in the LID scenario, their flow rates are relatively low. In essence, these low flows are meant to make up for the low infiltration rates. This type of observation is not so readily apparent from the percentage graphs. Furthermore, it can be seen that the few flows that are over the threshold in the LID scenario are much lower than the corresponding uncontrolled flows. This is partly because the low flow outflow from the orifice releases so much more runoff at rates below the threshold. This restores storage volume so that even large peaks can be reduced.

CONCLUSIONS

Flows in bioretention systems should be represented vertically in addition to the horizontal routing approaches typically used in conventional stormwater design. By judicious selection of orifice parameters and properties allocated to the dummy

node for surrounding soils, it is possible to realistically model the dynamics of the system using the power of a CS model. With this discrete routing approach, the benefits of urban retrofits can thus be better documented. Given the computational efficiency of this method of analysis, it can be applied to many discrete subcatchments to address specific outfall discharge criteria in a comprehensive manner, and under many scenarios.

Based on this comprehensive approach at the street scale, the combined planter-trench system is capable of transforming the runoff response from urban source areas into a runoff response more typically found in pervious areas. Where infiltration rates are favorable, the resulting runoff response could approach that of a forested condition. This is accomplished with only 0.8% of the contributory source area used for the surface facility, in association with an underground trench system comprising an additional 3.4% of the source area. These possibilities make integrated bioretention-infiltration systems a viable approach to contribute materially to Philadelphia's Long Term Control Plan to reduce Combined Sewer Overflows.

ACKNOWLEDGEMENTS

This work was done under a contract with Camp, Dresser and McKee on behalf of the Philadelphia Water Department, Office of Watersheds. The author wishes to thank to these organizations for the opportunity to undertake this analysis.

REFERENCES

Blanco-Canqui, H., C. J. Gantzer, S. H. Anderson, E. E. Alberts, and A. L. Thompson. 2004a. "Grass Barrier and Vegetative Filter Strip Effectiveness in Reducing Runoff, Sediment, Nitrogen, and Phosphorus Loss" *Soil Sci. Soc. Am. J*. 68:1670–1678.

Blanco-Canqui, H., C. J. Gantzer, S. H. Anderson, and E. E. Alberts. 2004b. "Grass Barriers for Reduced Concentrated Flow Induced Soil and Nutrient Loss" *Soil Sci. Soc. Am. J*. 68:1963–1972

Rachman A., S. H. Anderson, C. J. Gantzer, and A. L. Thompson. 2004. "Influence of Stiff-Stemmed Grass Hedge Systems on Infiltration" *Soil Sci. Soc. Am. J.* 68:2000–2006

Ralston, M.R. 2004. Fox Hollow Infiltration Facility. In: Rustia B, (ed.), Putting the LID on Stormwater Management. Proc. First Nat. Low Impact Development Conference. College Park, MD, Sep.21-23, 2004.

Seobi, T., S. H. Anderson, R. P. Udawatta, and C. J. Gantzer. 2005. "Influence of Grass and Agroforestry Buffer Strips on Soil Hydraulic Properties for an Albaqualf" *Soil Sci. Soc. Am. J.* 69:893–901

Sharma, S K. B P. Mohanty, and J Zhu. 2006. Including Topography and Vegetation Attributes for Developing Pedotransfer Functions *Soil Sci. Soc. Am. J.* 70:1430–1440

Design Optimization of Hydrodynamic Separators

James H. Lenhart, PE, D.WRE, Joanna B. Ogintz, PE and Scott A. de Ridder

CONTECH CONSTRUCTION PRODUCTS INC., 11835 NE Glenn Widing Drive, Portland, OR, 97220; PH (800) 548-4667; FAX (503) 240-9553; email: lenhartj@CONTECH-cpi.com

ABSTRACT

Typically, the sizing of hydrodynamic separators (HDS) for stormwater treatment is based on two factors. The first factor is the ability to remove a designated fraction of a particle size distribution, usually with a d_{50} of 100 μm or greater. The second factor designates the magnitude of flow that needs to be treated from a given site.

The techniques for determining the magnitude of flow vary, but two basic methods dominate. The first is a fairly simplistic method that requires the HDS to be sized to remove a target percentage of a specified particle size at a defined flow rate. The flow rate can be determined using a specified rainfall intensity and storm return period with a hydrologic model output, such as the Santa Barbara Urban Hydrograph. The second method, sometimes called the average annual load method, is based on calculations which use the storm depth (or intensity) frequency distributions converted to flows through a unit, which are then used to predict the removal performance. The removal performance prediction is based on laboratory studies of specific gradations of silica sediment, which have been tested to create a performance graph. These graphs often show plots of removal performance to the point where zero removal is achieved. These flows at zero removal are sometimes termed the "peak treatment flow".

This paper provides a perspective on this methodology and an approach to how sizing methods can be changed to optimize the total load reduction of a system by throttling the flow to a rate that is less the "peak treatment flow".

As a simple example, if a system's performance graph demonstrates that the HDS is 0% efficient at 5 cubic feet per second (CFS), then when that "peak treatment flow" reaches the system, no removal will occur. However, if the system is operated at a lower operating rate by bypassing a portion of the "peak treatment flow", this would result in some degree of treatment for a portion of the flow, and would therefore be more efficient overall. Say, in the example above, the system is designed to bypass at 4 CFS to get a 20% removal for the 4 CFS portion of the flow and a zero percent removal for the 1 CFS bypass flow. The total efficiency would be 16% (20%

removal for 80% of the flow) as compared to a total efficiency of 0%, resulting from no bypass at all.

The question becomes: Given the characteristic curve of an HDS system, at what point is it best to bypass the system to optimize removal on a total flow basis? This paper presents a method to accomplish this task.

BACKGROUND

Hydrodynamic separators (HDS) are compact water treatment devices that are effective for the treatment of coarse and gross solids. (WERF, 2008) Since they rely principally on the physics of settling governed by Stokes Law, the devices become less efficient with increasing surface loading or volumetric flow rates. However, based on system geometry and the management of the hydraulic grade line, some systems are more efficient at a given flow rate for a set particle size gradation of coarse solids. Hence, performance curves, plotted as flow rate vs. removal efficiency, are used to design these systems. The curves are typically generated in a laboratory setting using known gradations of silica sand at concentrations typically found in stormwater runoff (NJDEP, 2006). These curves typically show the removal efficiency range from 100% to 0% removal. The flows at zero removal are sometimes termed the "peak treatment flow".

To meet jurisdictional design requirements for coarse solids removal, two basic methods dominate. The first is a fairly simplistic method that requires the HDS to be sized to remove a target percentage of a specified particle size at a defined flow rate. For example, the design flow rate is determined using a specified rainfall intensity and storm return period with a hydrologic model output, such as the Santa Barbara Urban Hydrograph. Then the system must be sized to remove 80% of a specified particle at that design flow rate.

The second method, sometimes called the average annual load method (CONTECH, 2006), is based on the notion that a jurisdiction needs to remove 80% of the designated solids on an average annual load basis. Since flow, relative removal efficiency, and mass load, through the unit are dependent on rainfall, calculations which use the storm depth (or intensity) frequency distributions converted to flows are used to "model" the overall annual removal performance. However, this approach should be considered more of a method than a model since critical factors such as particle size and load are assumed constant, when in reality they vary with storm depth, and intensity. This method and others utilize the entire efficiency curve such that bypass around the unit does not occur until the peak treatment flow (0% efficiency) is reached.

TOTAL FLOW OPTIMIZATION

This approach raises the question: Would the overall annual removal increase by bypassing the flow sooner? At first, this may seem counter-intuitive but if one

considers the peak treatment flow rate it becomes clearer. Given a total inflow into the system that results in 0% removal, it would be better to bypass a portion of that flow and achieve some removal efficiency of that portion such that there would be some removal at the total flow.

The question then becomes: Given the characteristic curve of an HDS system, at what point is it best to bypass the system to optimize removal on a total flow basis?

METHOD TO OPTIMIZE HDS OPERATION

Figure 1 below shows a general schematic of an HDS configured with a bypass. Typically the bypass is configured to operate when the total inflow (Q_{TOTAL}) exceeds the 0% efficiency flow rate of the HDS and scouring and resuspension of solids would occur.

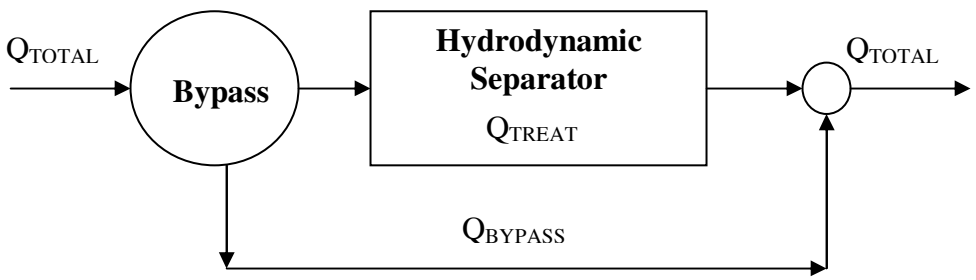

Figure 1: A schematic of an HDS with a high flow bypass.

Given Figure 1, the following relationships can be established:

$$\text{Eqn 1:} \quad Q_{TOTAL} = Q_{TREAT} + Q_{BYPASS}$$

$$\text{Eqn 2:} \quad E_{BYPASS} = 0$$

Let's assume that the removal efficiency (E) for any of the bypass flow is 0% and the HDS has some characteristic removal efficiency curve resulting from laboratory testing. For the demonstration purposes of this paper a hypothetical HDS curve is created. The hypothetical functional relationship between the flow and efficiency is:

Eqn 3:

$$E_{TREAT} = -0.0065\ Q_{TREAT}^2 - 0.3338\ Q_{TREAT} + 100$$

Graph 1 is a plot of the efficiency curve given by equation 3.

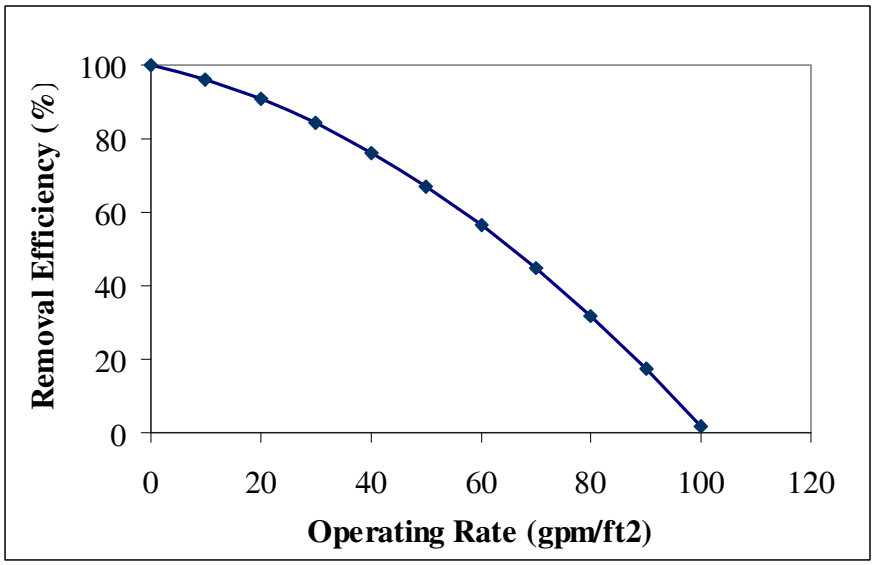

Graph 1: An efficiency plot for a hypothetical hydrodynamic separator.

The total system treatment efficiency can then be calculated using Equation 4:

$$\text{Eqn 4:} \quad E_{TOTAL} = [(E_{TREAT} \times Q_{TREAT}) + (E_{BYPASS} \times Q_{BYPASS})]/[Q_{TOTAL}]$$

Since $E_{BYPASS} = 0$, then

$$\text{Eqn 5:} \quad E_{TOTAL} = [(E_{TREAT} \times Q_{TREAT})/[Q_{TOTAL}]$$

Equation 5 can be used to solve for the most optimal system operating rate. Equation 3 can be substituted into equation 5 and differentiated with respect to Q. The first differential can then be set to zero and solved for a value of Q with corresponds to the maximum E_{TOTAL}. However a numerical solution is very easy to calculate with a spreadsheet. Given the equations above, a spreadsheet was created to calculate the E_{TOTAL} for the entire operating range of the separator. The spreadsheet calculations are shown in Table 1. In this example, the peak treatment rate is 2.8 CFS and therefore the total flow (Q_{TOTAL}) is set to 2.8 CFS. Column 1 is the flow through the HDS and the removal efficiency (column 2) is calculated using Equation 3 (E_{TREAT}), Q_{BYPASS} (column 3) is calculated from Equation 1 and the total efficiency (column 4) is calculated from Equation 5. The percent peak operating rate (column 5) is simply the ratio of the Q_{TREAT} to Q_{TOTAL}. Graph 2 below is a plot of the results.

Table 1: Numerical Total Efficiency Model of Hypothetical Hydrodynamic Separator.

Q_{TREAT} (cfs)	Removal Efficiency (%)	Q_{BYPASS} (cfs)	Total Efficiency (%)	% of Peak Operating Rate
0.00	100.0	2.80	0.000	0%
0.10	98.7	2.70	3.490	4%
0.20	97.3	2.60	6.877	7%
0.30	95.7	2.50	10.144	11%
0.40	93.9	2.40	13.272	14%
0.50	92.0	2.30	16.243	18%
0.60	89.9	2.20	19.041	21%
0.70	87.6	2.10	21.646	25%
0.80	85.1	2.00	24.042	29%
0.90	82.5	1.90	26.211	32%
1.00	79.8	1.80	28.134	36%
1.10	76.8	1.70	29.794	39%
1.20	73.7	1.60	31.174	43%
1.30	70.5	1.50	32.254	46%
1.40	67.0	1.40	33.019	50%
1.50	63.4	1.30	33.449	54%
1.60	59.7	1.20	33.528	57%
1.70	55.7	1.10	33.237	61%
1.80	51.6	1.00	32.558	64%
1.90	47.4	0.90	31.474	68%
2.00	43.0	0.80	29.967	71%
2.10	38.4	0.70	28.019	75%
2.20	33.6	0.60	25.612	79%
2.30	28.7	0.50	22.730	82%
2.40	23.6	0.40	19.352	86%
2.50	18.3	0.30	15.463	89%
2.60	12.9	0.20	11.045	93%
2.70	7.3	0.10	6.078	96%
2.80	1.5	0.00	0.547	100%

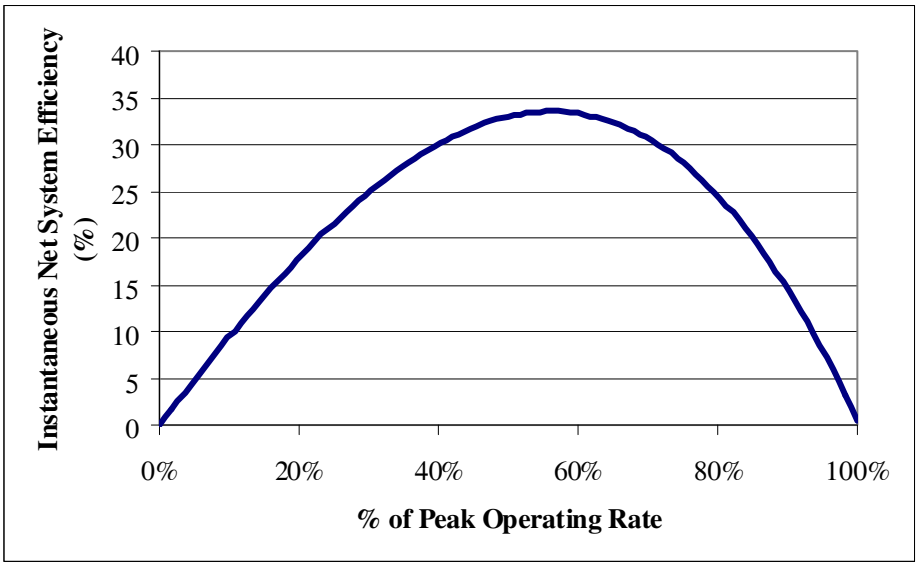

Graph 2: Determination of the optimum operating rate.

Observing this graph, it is clear there is an optimal operating rate, which for this characteristic curve is about the 55% operating rate. This rate corresponds to a treatment efficiency of about 62% (Graph 1). In other words, if a flow rate of say 5,000 gpm (11 CFS) was to be treated, the unit would be sized such that the maximum flow rate would occur at 11 CFS and flows in excess of 6 CFS should be bypassed. Graph 3 represents an overall performance curve for the hypothetical separator for the flow range from 0 to the maximum operating rate (2.8 CFS), considering the case of no bypass as well as bypassing at 60% of the maximum operating rate.

DISCUSS AND CONCLUSIONS

From this analysis it can be concluded that operating hydrodynamic separators to the point of zero efficiency is not the most efficient use of their operational characteristics when looking at the entire flow regime. One thing that may appear surprising about this example is that the instantaneous net system efficiency was 34% and one may say that this is the absolute best the average annual load reduction the unit could achieve. What this model does not address is that frequency distribution of the incident runoff, which is heavily weighted toward small storms and which may result in higher efficiencies. In addition this model is really applicable to a total flow at or less than the peak operating rate. Flows less than those bypassed will be removed at the efficiency of the separator.

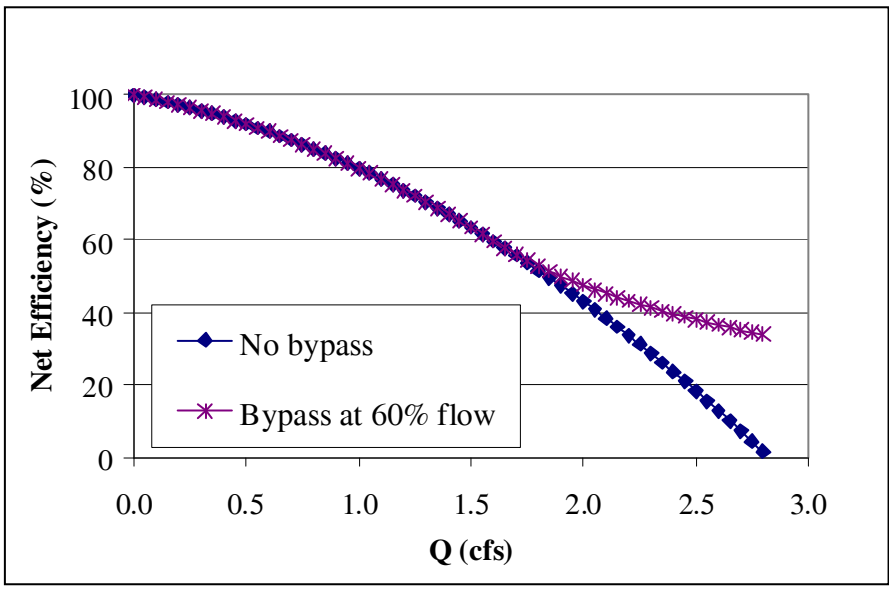

Graph 3: Combined efficiency curve showing two bypass conditions (bypass at 60% of peak treatment rate and no bypass)

REFERENCES

CONTECH Stormwater Solutions Inc. (CONTECH) (2006). Vortechs® Technical Bulletin 3 – Sizing for Net Annual Sediment Removal. Portland, Oregon: Author.

New Jersey Department of Environmental Protection (NJDEP). (2006). New Jersey Tier II Stormwater Test Requirements – Amendments to TARP Tier II Protocol. Trenton, New Jersey: Author. Available online: http://www.state.nj.us/dep/dsr/bscit/NJStormwater_TierII,pdf

Water Environment Research Foundation (WERF). (2008). Improved Protocol for Classification and Analysis of Stormwater-Borne Solids. Alexandria, VA: Author.

DEVELOPING A WATER BUDGET FOR A CONSTRUCTED STORMWATER WETLAND

KRISTEN MOGAVERO[1], GERRAD JONES[1], AND BRIDGET WADZUK[1]

[1]Department of Civil and Environmental Engineering, Villanova University, 800 Lancaster Avenue, Villanova, Pennsylvania, 19085;PH (610) 519-5365, FAX (610) 519-6754; email: gerrad.jones@villanova.edu, kristen.mogavero@villanova.edu, bridget.wadzuk@villanova.edu, M.ASCE

ABSTRACT

A thorough understanding of the hydrology of a constructed stormwater wetland (CSW) is essential to develop a water budget; that is a comprehensive view of all inputs and outputs in the system. Two of the principal functions of a CSW are to 1) reduce peak flows and 2) improve water quality. The latter is achieved through biological, chemical, and physical processes that are ultimately governed by the hydraulics and hydrology of the system. As these built systems populate the watershed management landscape, it is necessary to account for all flows that pass through the CSW to ensure that it is providing a benefit and does not have any deleterious effects on the watershed. One of the most significant and least understood aspects of a CSW is the groundwater-surface water exchange. This exchange is difficult to quantify, but is deserving of consideration because of the potential impact this exchange has on groundwater and surface water quantity and quality in a CSW system. Therefore, the goals of this study are to 1) use hydraulic and hydrologic computer models to create a water budget of the CSW, with a focus on quantifying groundwater-surface water fluxes, and 2) discuss the implications of how hydraulic and hydrologic processes affect the water quality within a CSW.

1 INTRODUCTION

A growing amount of research is dedicated to identifying the conditions necessary for the successful construction of treatment wetlands. Items commonly cited for a successful design are hydrologic analysis, water source and quality, site selection criteria, plant material selection, soil and geologic conditions, buffer zone placement, and maintenance procedures (Kusler and Kentula 1996). Hydrology has commonly been cited as one of the primary factors in controlling wetland functions (Hammer 1989, Owen 1995). Wetland hydrology has a bearing on the soils and nutrients in the wetland, and therefore has an influence on the character of the ecosystem. The flows and storage volume dictate the retention time of the wetland, and thus, the opportunity for interactions between waterborne substances and the wetland ecosystem. Therefore, the design of a treatment wetland attention must emphasize the system hydrology since treatment efficiency is dependent upon the extent of water-biota interactions and the proximity of waterborne substances to sites of biological and physical activity. (Kadlec & Knight, 1996)

The hydrologic characteristics of constructed stormwater wetlands (CSW) are usually described through development and analysis of a water budget. The water budget is a way to describe the processes through which water is introduced, temporarily stored, and

removed from the CSW. Water is introduced to a CSW through direct precipitation, overland flow, overbank flow, and groundwater discharge. Temporary storage includes channel, overbank, basin, and groundwater storage. Water is lost from the CSW through evaporation, plant transpiration, channel, overland flow, and groundwater recharge (WRP, 1993).

Water budgets are essential for understanding the fluxes of constituents between the hydrologic, biochemical, and ecological systems of a CSW. They also provide information regarding the relationship of the CSW to the surrounding terrain (Dexler et al., 1999). However, there has been very few water budgets compiled for CSW, or wetland systems in general. The development of water budgets for wetlands is hindered by the need for long term monitoring, the difficulty in estimating certain hydrologic components (e.g. the groundwater – surface water exchange), and the laborious nature of data collection (Dexler et al., 1999). The purpose of this research is to develop a water balance for the Villanova CSW that can aid future research in understanding the fate of pollutants within the system, the mechanisms that result in high pollutant removal efficiencies, and the possibility that the CSW is functioning as a volume-reducing BMP. In the present study, an integrated hydraulic and hydrologic model of the CSW is developed using the Danish Hydraulic Institute's (DHI) MIKE 11 and MIKE SHE modeling software. The MIKE SHE software has a water balance tool that will be used to develop a water budget for the Villanova CSW.

2 SITE DESCRIPTION

The Villanova CSW is a mature wetland system that is located on Villanova University's campus in Villanova, Pennsylvania (Figure 1). The CSW was originally a detention basin that was retrofitted in 1999. It was noticed that the soils in some areas of the detention basin were perpetually saturated and thus it seemed an eligible site for a CSW; however, a formal evaluation of the water budget was never conducted. Water is primarily introduced to the system from two pipes that drain part of Villanova University's campus. The total drainage area is approximately 23 hectares, and of this area, 57%, 31%, and 12% of the surfaces are impervious, semipervious, and pervious respectively.

Since 2003, the Villanova CSW has been monitored for quantity and quality performance (Rea 2004; Woodruff 2005; Flynn 2008). During 2007, approximately 20% more water entered the system than exited for the entire year (Unpublished data). Due to infrequent calibration, however, the quality of historical quantity data must be interpreted with caution. According to past research, during base flow conditions average removal efficiencies of total phosphorous and total nitrogen were 60% and 80%, respectively (Rea 2004).

3 MIKE SHE AND MIKE 11 MODELING SYSTEMS

To model the Villanova CSW, the Danish Hydraulic Institute's (DHI) MIKE SHE and MIKE 11 modeling systems were used. MIKE SHE is capable of modeling all processes of the land phase of the hydrologic cycle; these include: precipitation, evapotranspiration, overland flow, channel flow, unsaturated subsurface flow, and saturated groundwater flow. Furthermore, MIKE SHE is capable of simulating interactions between the

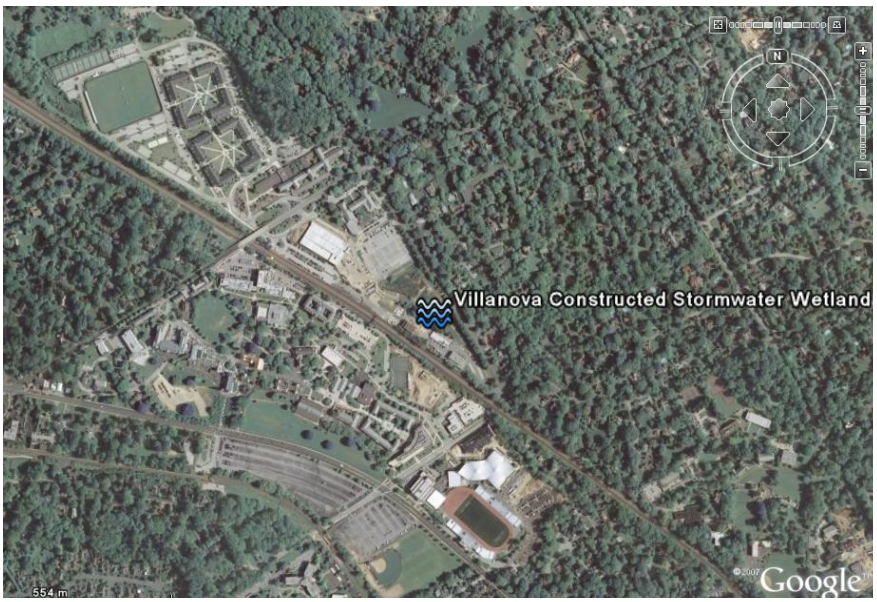

Figure 1. Aerial photograph of Villanova University and the Villanova University Constructed Stormwater Wetland

groundwater and surface water. Geotechnical investigations of the area surrounding the Villanova CSW indicate that the groundwater table may be at or above the bottom of the CSW.

MIKE 11 is a one-dimensional modeling system for rivers and channels. MIKE 11 generates a one-dimensional (1D) simulation of river flows and water levels using the fully dynamic Saint-Venant Equations. It is also able to simulate a wide range of hydraulic control structures, such as weirs, gates, and culverts. The model is based upon user-defined network geometry, cross-sections, resistance, and boundary conditions. MIKE 11 is ideal for modeling the CSW as flow is approximately 1D with some backwater conditions that can be mathematically described by the Saint-Venant Equations.

MIKE 11 and MIKE SHE can be integrated to model overland flow to and from the MIKE 11 river network and to model surface and sub-surface flow processes between the two. The ability to dynamically integrate the channel and overland flow is crucial to the modeling of the CSW since it is essentially a main channel with a wide, heavily vegetated floodplain. The interactions between the river channel and overland flow are modeled using the "overbank spilling option," which treats the river bank as a weir. When the overland flow water level or the river water level is above the left or right bank elevation, then water will spill across the bank based on the standard weir formula:

$$Q = \Delta x \cdot C \cdot (H_{us} - H_w)^k \cdot \left[1 - \left(\frac{H_{ds} - H_w}{H_{us} - H_w} \right)^k \right]^{0.385}$$

where Q is the flow across the weir, Δx is the cell width, C is the weir coefficient, H_{us} and H_{ds} refer to the height of water on the upstream side and downstream side of the weir respectively, H_w is the height of the weir, and k is a head exponent. If the water levels are such that water is flowing to the river, then the overland flow to the river is added to

MIKE 11 as lateral inflow. If the water level in the river is higher than the level of ponded water, then the river water will spill onto the MIKE SHE cell and become part of the overland flow.

4 MODEL DEVELOPMENT

4.1 Field data

The Villanova CSW is a highly monitored research site. As such, a greater than normal amount of input data is available for model compilation. For example, precipitation, inflow, and outflow are measured continuously at five minute intervals. The field data used in compiling the MIKE 11 and MIKE SHE models is discussed in this section.

The flow from the contributing drainage area is conveyed through a storm sewer system and is accounted for as an upstream boundary condition in the MIKE 11 simulation. The flows entering the CSW from the inlet pipes are monitored using Sigma 950 area/velocity bubbler probes. Measurements are taken every five minutes and the equipment is calibrated monthly.

Precipitation is measured at the CSW using a "tipping bucket" rain gauge (American Sigma Model 2149) that is connected to the Sigma 950 located at the inlet. Readings are taken continuously in five minute intervals. This measured rainfall data was input to the model as a uniform distribution over the entire catchment. Based upon the small area of the catchment it is assumed that any variation within the catchment would be negligible.

Kadlec & Knight (1996) recommend that wetland evapotranspiration can be estimated as 80 percent of the evaporation from a Class A evaporation pan. The website for the Pennsylvania State Climatologist posts average daily Class A evaporation pan data for south east Pennsylvania and it is assumed that this data is representative of the CSW. To verify this assumption two plastic containers, approximately 0.7m x 0.45m x 0.25m in size, were filled with water and placed at the CSW. During August, September, and October 2008 daily evaporative losses were recorded on a random basis. The observed losses correlated well with those reported by the Pennsylvania State Climatologist. The Pennsylvania State Climatologist evaporation pan values were multiplied by 0.8 and input into the model as reference evapotranspiration rates.

In 2006, David Blackmore and Associates, Inc. completed a geotechnical investigation of the area adjacent to the CSW. Their investigation consisted of 40 borings and a laboratory soil analysis. The report indicates three layers in the soil profile. Based upon the elevation of the CSW and the elevations of the soil strata described in the report, it was assumed that the soil in the CSW is similar to the soil layer that the geotechnical report refers to as "Stratum III." Stratum III is described as "an orange brown, brown, tan, and gray decomposed/weathered gneiss. The upper portion of this stratum is considered medium dense to dense. The lower portion of this stratum is considered dense to very dense". The soils in Stratum III were classified by Blackmore (2006) as SM soils. The assumption that the CSW soils were similar was visually verified by soil samples taken within the CSW in fall 2008 and near the CSW when wells were drilled in January 2009.

Soil samples collected from the CSW were analyzed in the laboratory to determine the saturated hydraulic conductivity. A flexible wall falling head permeameter test indicated a saturated hydraulic conductivity of 3.55×10^{-6} m/day (0.0014 in/day) and a constant head permeater test indicated a value of 0.23 m/day (9.20 in/day). For compacted SM

soils, published values for saturated hydraulic conductivity range from 0.048 – 0.28 m/day (1.90-10.90 in/day) (Johnsen and Jensen 2001). The saturated hydraulic conductivity in the vertical direction was set to 0.051 m/day (2.0 in/day) because it falls within the range of values and is a conservative estimate. The DHI user manual (2007) states that the horizontal hydraulic conductivity is typically five to ten times greater than the vertical hydraulic conductivity. Therefore, the horizontal hydraulic conductivity was set to 0.382 m/day (15 in/day), 7.5 times the vertical hydraulic conductivity.

In order to model flow between the groundwater and surface water in the CSW the groundwater table must be defined in the model. Since the elevation of the groundwater table is not known explicitly, the water table in the CSW was approximated using a linear regression model between four points at which the water table was known: three boring wells and Mill Creek, the downstream receiving water body. The water table between the three wells and Mill Creek formed a near perfect linear relationship ($y = -0.0184x + 419.44$ ft, $y = -0.0184x + 127.87$m, $R^2 = 0.9999$, Figure 2). Based upon this linear regression, a groundwater table was defined and entered in the MIKE SHE model.

The bedrock constitutes the lower boundary of the model. Blackmore (2006) reports that gneiss bedrock was encountered in four of the test borings. The maximum elevation at which bedrock was encountered was 417.92 feet. However, one of the boring was extended to 50 feet without encountering bedrock. For this model, the bedrock elevation was estimated to exist at an elevation of 375 ft.

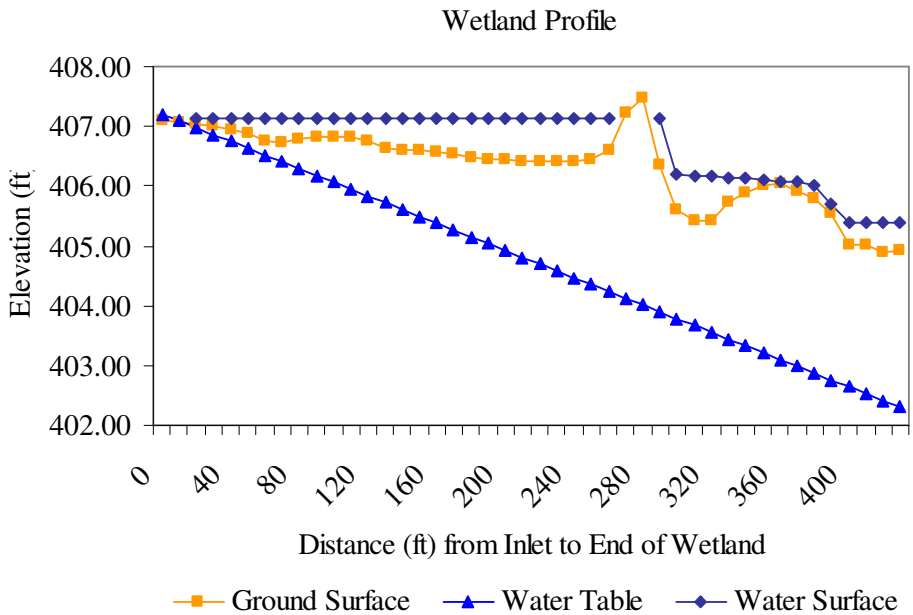

Figure 2. Estimated Surface Water, Ground Surface, and Groundwater Profiles

4.2 MIKE SHE

The first step in developing a MIKE SHE model is setting the simulation specifications. This includes the simulation period, time step controls, and computational control parameters. All the phases of the hydrologic cycle were selected, including overland flow, rivers and lakes (channel flow), unsaturated flow, evapotranspiration, and saturated flow. The simulation period for this model is May 1, 2007 to May 31, 2007. The time

steps are set to the recommended default values as per the MIKE SHE User Manual (2007).

The second step in developing a MIKE SHE model is defining the model domain and grid. The domain is defined as the perimeter of the CSW. A topographic survey of the CSW from the summer of 2007 was used to delineate this area. This topography was also used to define the ground surface in MIKE SHE and the cross-sections in the MIKE 11 simulation. The grid size was set to one meter by one meter on a 200 meter by 250 meter grid.

The overland flow in MIKE SHE is simulated using an explicit numerical solution of the diffusive wave approximation. The input data required for the calculation of overland flow are the Manning's number, detention storage, and the initial water depth on the ground surface. A Manning's number of 0.08 was used based upon recommended values for a floodplain with medium to dense brush (Chow, 1959). The detention storage is used to limit the amount of water that can flow over the ground surface and is equivalent to the trapping of surface water in small ponds or depressions within a grid cell. The detention storage was set to 0.25 millimeters. The surface area of the CSW having an initial water depth (standing water) was delineated using aerial photographs of the CSW and ArcMap 9.2.

The soil information gathered from the geotechnical report and laboratory analyses was used to define the soil properties in the unsaturated and saturated zones. The vertical flow in the unsaturated zone is calculated using a simple two-layer water balance, which is suggested in the DHI User Manual (2007) when there is a shallow water table, such as in the CSW. The main purpose of this method is to calculate evapotranspiration and the amount of water that recharges the saturated zone. The model assumes that if sufficient water is available in the root zone, the water will be available for evapotranspiration. The output is an estimate of the actual evapotranspiration and the groundwater recharge.

In the saturated zone, spatial and temporal variation of the hydraulic head are described mathematically by the three-dimensional Darcy equation and solved numerically by an iterative implicit finite difference technique. The saturated zone component interacts with the other components of the MIKE SHE model by using the boundary flows from other components implicitly or explicitly as sources and sinks.

4.3 MIKE 11

As previously mentioned, MIKE 11 is a one-dimensional hydrodynamic software package based on the complete dynamic wave formulation of the Saint Venant equations for open-channel flow. It was used to simulate flow and water level through Villanova's CSW and is integrated with MIKE SHE as part of SHE's Rivers and Lakes module. Cross-sections were created approximately every 20 meters along the main channel. The cross-section geometry is based upon the topographic survey from 2007. The upstream boundary condition is the inflow from the inlet pipes. As previously described, this inflow is continuously monitored using Sigma 950 area/velocity bubbler probes. The model was run several times with varying Manning's numbers to see which value generated an outflow hydrograph most similar to the actual, measured outflow hydrograph.

4.4 WATER BALANCE

After developing and running an integrated MIKE11/MIKESHE model, the output is used by the water balance editor to generate a water balance for the simulation. As described in the MIKE SHE User Manual (2007), the water balance editor is "a post processing tool which provides a clear, unambiguous summary of flow and storage changes for the individual model components as well as for the entire model." It also provides an "analysis of errors occurring in the model due to input data or numerical instabilities." The compilation of a water balance for the CSW is the primary goal of this study.

5 RESULTS

Before attempting to integrate the MIKE SHE and MIKE 11 models, each model was run separately to verify the simulations. Outflow hydrographs created by the MIKE 11 hydraulic model of Villanova's CSW are only moderately correlated with actual measured hydrographs ($r = +0.70$). Figure 3 depicts the actual measured outflow hydrograph as well as outflow hydrographs generated by MIKE 11 based upon Manning's numbers of 0.04 and 0.12. Although the modeled inflow exactly mirrors the actual inflow of the CSW, the hydraulic models consistently overestimate the volume of water exiting the system. MIKE 11 consistently overestimates the volume of outflow by 32%, indicating that nearly a third of the total volume is unaccounted for. There is also a distinct spike at the beginning of the actual hydrograph that has not been replicated by MIKE 11.

As a free-standing model, MIKE SHE has been run successfully. Without being linked to MIKE 11, direct precipitation on the wetland is the only input to the system. The majority of flows introduced to the system come from the inlet pipes. These flows are introduced to the wetland system via MIKE 11, and cannot be simulated in MIKE SHE until it is integrated with MIKE 11. The current conditions simulated in MIKE SHE are considered unrepresentative of the CSW and as such the results from MIKE SHE are extraneous. However, the model was pre-processed and a water movement simulation was run without errors or warnings, indicating that it will be capable of simulating the system when integration occurs.

Both models are properly functioning independently, however, MIKE 11 and MIKE SHE have not been successfully integrated yet. The main technical problem with integrating the two models is the geo-referencing. The world is properly represented as a three dimensional object; however, maps can only represent two of those dimensions. Frequently, designs are created in abstract space without any geographic reference point. The 2007 topographic survey of the CSW was created in abstract space. The input files for MIKE 11 were generated from this survey, while the input files used for MIKE SHE were generated from spatially referenced data. A spatial reference point can be applied to non-referenced data, such as the CSW survey. By providing the CSW survey with a spatial reference the input files for both MIKE 11 and MIKE SHE can be created in the same geo-spatial data frame. After correcting the spatial referencing it will be possible to integrated the models and generate a preliminary water budget of this CSW.

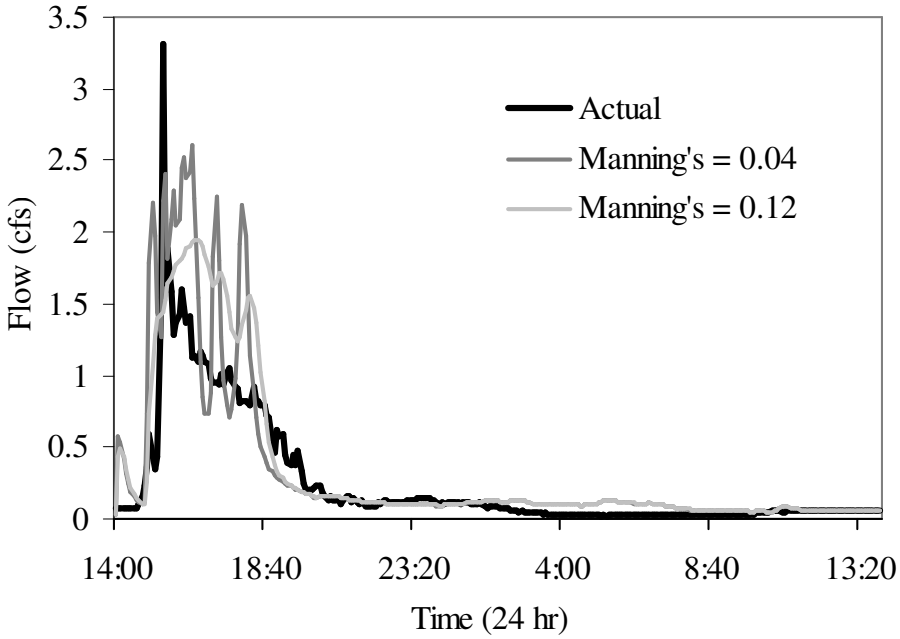

Fig 3. Actual Outflow Hydrograph and MIKE11 Model Outflow Hydrographs for a Manning's numbers of 0.04 and 0.12

6 Discussion & Future Work

The MIKE11 model has consistently overestimated the volume of water leaving the wetland when compared with the measured outflow volume. This overestimation has occurred in several trials with varying values of Manning's number. A possible reason for this overestimation is that there are real losses that are not accounted for in the MIKE 11 model alone, such as infiltration, evaporation and transpiration. It is anticipated that this discrepancy in outflow volume will be resolved by incorporating the MIKE11 model with the MIKE SHE model since the SHE model can account for system losses such as infiltration, evaporation, and transpiration.

Furthermore, the MIKE11 model has been unable to replicate the spike observed at the beginning of the actual hydrograph. This initial spike in outflow is most likely due to direct overland flow and precipitation on the CSW. MIKE SHE is capable of simulating precipitation and overland flow, and when integrated with MIKE 11 will account for this spike.

When completed, the integrated model of the CSW is expected to be a useful tool for discerning the movement of water and waterborne constituents through the system. However, the output generated by the model must be interpreted with caution. The input data used to compile this model is based predominantly on approximations and assumptions. If actual conditions in the CSW vary from the conditions specified in the model than the output may be misleading. For example, it is commonly recognized that a great deal of spatial variation may exist when considering hydraulic conductivity and other soil properties. Thus, continued calibration, verification and collection of monitored data will continue to build an exhaustive dataset of varied CSW conditions. In addition, current research is focused on investigating the effects of temperature on water viscosity and thus on the infiltrative capacity of soils (Emerson, 2008). It is

recommended that future models be designed to investigate the impact of such variations as opposed to using a single value to represent the entirety of the system, as was done in this study.

This model also utilizes water table elevations that were estimated based upon a geotechnical investigation completed over 18 months prior to the simulation period of the model. The water table elevation is susceptible to fluctuations based upon antecedent dry or wet weather. Therefore, the available groundwater data may not be representative of the groundwater elevations occurring for the specified time duration of the model. Wells were installed around the CSW in January 2009 and will be equipped with monitoring data to continuously record the water table elevation.

There is also uncertainty surrounding the estimated evapotranspiration rates. Although the regional evaporation pan data was reduced by 20% to estimate evapotranspiration, as per Kadlec and Knight (1996), this technique is merely a general rule of thumb. Furthermore, the location of the reference evaporation pan was approximately 75 miles from the CSW. Variations in solar radiation, temperature, wind speed, and humidity between the two locations could cause error in the estimated evapotranspiration values. A parallel study at Villanova is examining evaporation; this data can be used in the future for localized rates.

Although there may be inherent error in the model, uncertainty in assumptions can be reduced by continuing to build the library of data for the CSW. The model serves as a valuable tool for understanding the hydrology of the CSW and provides the research team with a preliminary water balance. The development of a water balance clarifies the significance of each component of the budget on the CSW's functions. Additionally, the budget is the first step towards understanding the fate of nutrients and other contaminants in the CSW system on a unit process scale.

WORKS CITED

Blackmore, D. (2006) "Report of Geotechnical Investigation", Technical Report, David Blackmore and Associates, Inc., Project 3492G1R1, Pottstown, Pennsylvania

Chow, V.T. (1959) "Open Channel Hydraulics", McGraw Hill, New York City, New York

Danish Hydraulic Institute. (2007) *MIKE SHE User Manual, Vol. 1 and 2.*, Horsholm, Denmark, 1-632.

Dexler, J.Z., B.L. Bedford, A.T. DeGactano, and D.I. Siegel (1999) "Quantification of the Water Budget and Nutrient Loading in a Small Peatland*", Journal of American Water Resources Association*, 35:753-769

Emerson, C. (2008) "Evaluation of Infiltration Practices as a Means to Control Stormwater Runoff", Dissertation, Villanova University, Villanova, Pennsylvania

Flynn, K. (2008), "Pollutant Removal Efficiency of a Mature Constructed Stormwater Wetland Over the Course of a Year," Thesis, Villanova University, Villanova, Pennsylvania

Hammer, D.L. (1989) "Constructed Wetlands for Wastewater Treatment", Lewis Publishers, Chelsea, MI

Johnson, H.E., and Jensen, D.M. (2001). "Transmittal of Test Results for: Old Burial Ground Cap, Geotechnical Testing Services"*, WSRC Site Wide – Task Release*

No. 61, Law Engineering Project No. 50161-7-0108 (Phase 61). Law Engineering and Environmental Services, Inc., Atlanta, Georgia

Kadlec, R.H. and R.L. Knight. (1996) "Treatment Wetlands", CRC Press, Boca Raton, Florida, 81-116

Kusler, J.A. and H.E. Kentula (1996) "Wetland Restoration and Creation- the Status of the Science", Island Press, Washington, D.C.

Owen, C. (1995) "Water Budget and Flow Patterns in a Urban Wetland", *Journal of Hydrology* 169, 171-187

Rea, M. (2004). "Pollutant Removal Efficiency of a Stormwater Wetland BMP during Baseflow and Storm Events." Thesis, Villanova University, Villanova, Pennsylvania, 1-126

Woodruff, G.L. (2005). "Pollutant Removal Efficiency and Seasonal Variation of a Storm Water Wetland BMP." Thesis, Villanova University, Villanova, Pennsylvania, 1-104

Wetlands Reserve Program (1993), "Wetland Surface Water Processes", Technical Note HY-EV-2.1, Army Engineer Waterways Experiment Station, Vicksburg, Mississippi

Effects of Media Depth on Bioretention Performance in the Upper Coastal Plain of North Carolina and Bioretention Construction Impacts Study

R. A. Brown,[1] and W. F. Hunt[2]

[1]Graduate Research Assistant, Department of Biological and Agricultural Engineering, North Carolina State University, Campus Box 7625, Raleigh, NC 27695-7625; e-mail: rabrown4@ncsu.edu

[2] Assistant Professor & Extension Specialist, Department of Biological and Agricultural Engineering, North Carolina State University, Campus Box 7625, Raleigh, NC 27695-7625; PH(919)515-6751; e-mail: bill_hunt@ncsu.edu

Abstract

Bioretention is a principal low impact development (LID) practice. This paper examines two critical questions associated with bioretention design and construction. First, fill media is perhaps the major cost in constructing bioretention cells, so shallower media depths would be preferred, were they to work as well as deeper media systems. Two sets of bioretention cells of varying media depths in the upper coastal plain of North Carolina have been monitored since April 2008. They treat an impervious asphalt parking lot watershed in Nashville, NC. The bioretention cells were constructed with media depths of 0.6 and 0.9 m. Performance is being measured with respect to hydrology and water quality. Data show the deeper media depths meet the LID hydrology goal of volume reduction more frequently (35% compared to 9% of 45 events monitored).

The second question examines how bioretention cells are excavated. Two excavation techniques, the conventional "scoop" method which purposefully smears the underlying soil surface and the "rake" method which uses the teeth of an excavator's bucket to scarify the underlying soil surface, were tested. Field tests were conducted on three soil types (sand, loamy sand, and clay) and under a variety of antecedent soil moisture conditions. Saturated hydraulic conductivity, surface infiltration, and soil compaction were measured for each excavated condition. In all cases, the rake method of excavation yielded more permeable, less compacted soils than the scoop method. The difference of infiltration and hydraulic conductivity between the two excavation techniques was statistically significant ($p<0.05$) when tests were conducted in wet soil conditions. Also, the infiltration rate at the clay site was significantly lower ($p<0.05$), and the hydraulic conductivity at the sandy site was significantly lower ($p<0.05$), when the scoop methodology was used. Based on results of this experiment and because there is essentially no extra cost associated with the rake method of excavating bioretention cells, the rake method of excavation is recommended over the conventional scoop method. The use of the rake method is expected to increase long term exfiltration from bioretention cells.

Keywords: bioretention; low impact development; media depth; exfiltration; construction impacts; stormwater runoff.

Introduction:

As part of the National Water Quality Inventory, 32% of assessed estuaries and 47% of assessed lakes/reservoirs were identified as impaired. The main cause for impairment was nutrients. Urban stormwater runoff was among the top three sources

for the impairment in these water bodies (USEPA, 2007). Historically, flooding had been the primary concern related to urban runoff because of reduced pervious land surfaces to infiltrate water. Newer concerns of water quality issues have arisen because of excess amounts of nitrogen, phosphorus, and heavy metals found in urban stormwater (USEPA, 1983).

In order to minimize the negative effects caused by urbanization and to meet the new stormwater rules, strategies, such as Low Impact Development (LID), that employ infiltration are increasingly adapted. The goal of LID is to plan and construct a site so that the hydrology and water quality mimic that of the initial undeveloped site (Davis, 2008). Bioretention is a very common LID practice, which meets several design goals: (1) hydrologic, (2) water quality, and (3) aesthetic.

Bioretention combines a natural and engineered system to manage stormwater from developed areas. They are designed to at least treat the water quality volume of runoff. Bioretention removes runoff pollutants through adsorption, biological decomposition, filtration, and sedimentation. Evapotranspiration (ET) and exfiltration play major roles in volume reduction in a bioretention cell, which are important for pollutant load reduction (Hunt et al., 2006 and Li et al., 2009).

Previous field (Dietz and Clausen, 2006; Davis et al., 2006; Hunt et al., 2006; and Hunt et al., 2008) and laboratory studies (Davis et al., 2001; Hsieh and Davis, 2005; and Davis et al., 2006) have shown that bioretention has good removal rates of and low effluent concentrations for total nitrogen (TN), total Kejhdhal nitrogen (TKN), heavy metals, oil/grease, and total suspended solids (TSS). However, removal of nitrate has been poor in conventionally drained systems.

In NC, media depth requirement is based on vegetation. The minimum media depth is 0.6 m for cells vegetated with grass or shallow rooted plants and 0.9 m for cells vegetated with shrubs or trees (NCDWQ, 2007). In comparing six bioretention cells in NC and MD, Li et al. (2009) showed that deeper media depths appeared to promote more infiltration and ET and that the deeper media depths more closely mimicked pre-development hydrology. They concluded that media depth may be a controlling design parameter to meet target hydrologic performance goals.

With all of the research published on bioretention, limited data exist on how construction activity impacts their performance. One study by Tyner et al. (2009) studied innovative construction techniques to improve exfiltration from permeable pavement, in regions with clay in-soil. They treated the subgrade with boreholes, a subsoil ripper, and trenches. Disturbing the compacted bottom layer created a significant increase in exfiltration compared to the undisturbed control plot (Tyner et al., 2009). If construction processes are optimized to promote higher exfiltration rates from the bottom layer of bioretention cells, outflow volume will decrease, which will consequently decrease pollutant loads released to the storm drain network.

Compaction has an important influence on soil hydraulic properties, including soil water retention, soil water diffusivity, and hydraulic conductivity. All of which govern infiltration rates (Horton et al., 1994). Natural infiltration is negatively affected by removal of surface soils and exposure of subsurface soils. Earth moving equipment can compact the soil, which decreases subsoil permeability (Gregory et al., 2006). Also, rainfall on exposed subsoil has also been shown to cause surface sealing, which will decrease infiltration rates (Gimenez et al. 1992).

Gregory et al. (2006) examined the effects of compaction on infiltration at urban construction sites in North Central Florida. Infiltration was measured in non-compacted and compacted soils from three land types. Overall, construction activity reduced infiltration rates 70 to 99% at all sites. Pitt et al. (2008) showed results similar to Gregory et al. (2006): typical compaction considerably reduced infiltration rates. Tests on both clay and sandy soils showed that infiltration rates were significantly reduced in compacted soils, and clay soils were less able to withstand low levels of compaction compared to sandy soils.

One way bioretention cells function to remove pollutants is by reducing the ratio of outflow to influent runoff (Hunt et al., 2006; and Li et al., 2009). Promoting more exfiltration from the bottom layer of the bioretention cell will improve pollutant removal capabilities of bioretention. This can be accomplished through varying construction techniques and conditions to minimize compaction and promote exfiltration. Understanding hydraulic properties of the in-situ soil are important to estimate bioretention performance and its ability to enhance groundwater recharge (Shuster et al., 2007).

Media Depth

In answering the first of the two critical questions associated with bioretention design and construction, the effects of bioretention performance were examined based on fill media depth. Fill media is perhaps the major cost in constructing bioretention cells, so shallower media depths would be preferred if they to work as well as deeper media systems.

Site Description

The field site is located in the parking lot of a Wal-Mart Supercenter in Nashville, NC. The store was constructed from June 2007 to February 2008, and monitoring began on April 12, 2008. There are seven bioretention cells that treat runoff from the front half of the Wal-Mart parking lot. Three are connected to one outlet drain, and the other four are connected to another outlet drain. The set of three cells have a media depth of 0.9 m, and the set of four cells have a media depth of 0.6 m. Due to backwater constraints, the last cell in each set was not monitored. All the cells are designed to capture and treat the 2.5 cm storm. The bioretention cells were covered by mulch, shrubs, perennials, and trees, and these cells were designed with conventional drainage. The asphalt parking lot, which drains to the bioretention cells, experiences heavy use.

After several months of data collection, it was realized that the bioretention cells were undersized. The actual ponding depth and surface storage area of the bioretention cells were much less than the design specifications. The actual surface storage volume is only 38% and 45% of the designed surface storage volume for the 0.6 m and 0.9 m media depth cells, respectively. Monitoring of this configuration will continue through March 2009. All data presented herein were collected from these "undersized" cells. In April 2009, the surface storage volume will be increased to be closer to the design volume. Monitoring will continue for 12 more months to compare the difference in performance of undersized cells to those designed to treat the water quality event. A summary of the site characteristics are given in Table 1.

Table 1. Summary of characteristics for monitored bioretention cells in Nashville.

Design Characteristics	**0.6 m Media Depth**	**0.9 m Media Depth**
Number of Cells Monitored	3	2
Drainage Area	6580 m^2 (1.62 ac)	4310 m^2 (1.06 ac)
Impervious Area	79%	94%
Design Cell Storage Volume	97 m^3 (3430 ft^3)	69 m^3 (2440 ft^3)
Actual Cell Storage Volume	37 m^3 (1300 ft^3)	31 m^3 (1110 ft^3)
Actual Storage Capacity Compared to Design	**38%**	**45%**
P-Index (Fill Media)	11-18 (Low)	
Fill Media Composition	86-89% Sand & 11-14% Fines	

Methods

The monitoring equipment used include: ISCO 6712 Automated Portable Samplers to monitor hydrology and collect flow-weighted composite samples, ISCO 730 Bubbler Flow Modules in combination with weirs to measure outflow, and ISCO 674 Rain Gauge to measure rainfall. In Nashville, runoff enters each bioretention cell at two curb cuts. A rectangular weir with end contractions was installed at one of the curb cuts to collect a representative sample of the entire parking lot. Initial abstraction values of 2.0 mm (0.08 in) for the impervious asphalt parking lot (CN = 98) and 13.5 mm (0.53 in) for impervious surfaces (CN = 79) were subtracted from rainfall to calculate runoff volumes.

Flow-weighted composite samples were analyzed for nutrients and TSS. The nutrient species being analyzed include: Ortho-P, TP, NH_3, $NO_{2,3}$-N, TKN, and TN. Samples are collected and taken to the NCSU Center for Applied Aquatic Ecology laboratory within 24 hours (EPA-certified laboratory).

Results and Discussion

In Nashville, forty-five runoff producing events were monitored for hydrology, since monitoring began on April 12, 2008. Of these events, the mean and median rainfalls were 19.4 mm and 13.3 mm, respectively. Hydrology performance was analyzed by examining the 24 hour volume reduction – a LID hydrology goal first proposed in Davis (2008). With this performance measure, it was found that the bioretention cells with 0.9 m deep media met the LID hydrology goals more frequently (35%) compared to the 0.6 m deep cells (9%). Davis (2008) proposed that if the inflow volume is reduced by two-thirds, the site will meet the LID hydrology goal of 24 hour volume reduction. The 24 hour time period was selected because outflow from bioretention occurs for long periods of time at very low rates. Two-thirds reduction was chosen because the rational method C coefficient of a highly pervious surface is about 0.9, and it is about 0.3 for an undeveloped area (Davis, 2008). This is represented by the dashed line in Figure 1. In comparing these results to the six sites of varying media depths presented in Li et al. (2009), the 0.6 m media depth cells performed worse than all six sites. It even performed worse than the lined cell with 0.5-0.6 m media depth in Louisburg, NC, and this was the only site that the 0.9 m media depth cells performed better than.

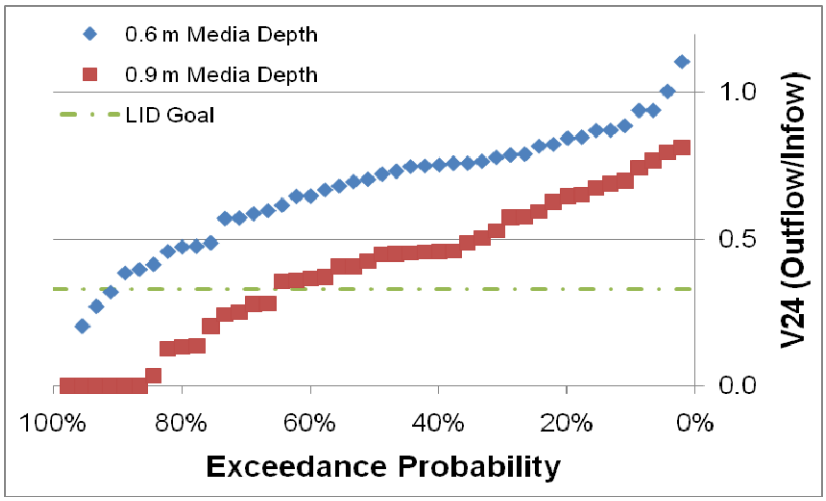

Figure 1. Exceedance of 24 hour volume reduction in Nashville bioretention cells.

Combined underdrain and overflow are being monitored in the outflow. Runoff not measured in the outflow has been lost through exfiltration and ET. Since the cells have the similar surface areas and vegetation, it is assumed that the difference in ET between the two cells is small. In the 0.9 m media depth cells, 38% of runoff is lost through ET and exfiltration compared to 23% for the 0.6 m media depth. This supports Li et al. (2009), in that deeper cells promote more exfiltration. In comparing the overflow, the 0.9 m media depth has 37% of the influent water leaving as overflow, where the 0.6 m media depth has 41% as overflow. The reason for the 0.6 m media depth having slightly more overflow is that it has a smaller surface storage volume compared to the 0.9 m media depth. The remaining flow is released by the underdrains, as seen in the water balance in Figure 2.

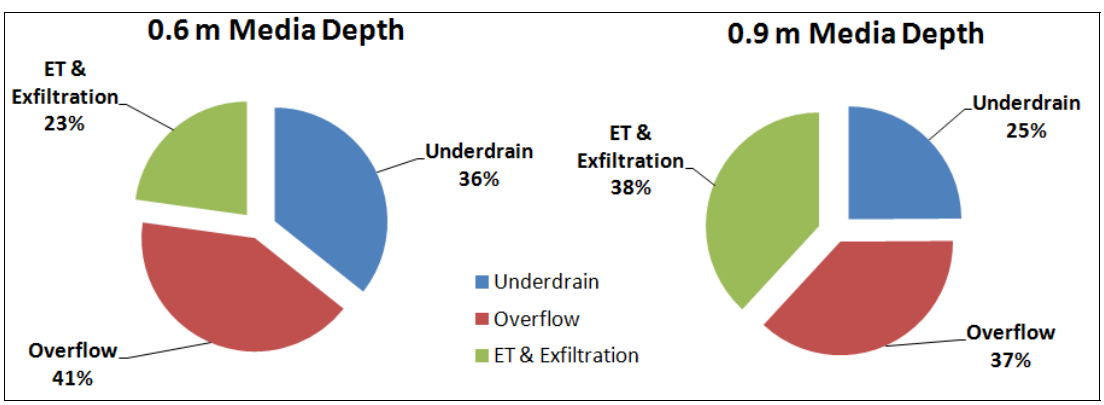

Figure 2. Fate of runoff in Nashville bioretention cells.

Out of the 45 monitored events, ten have been greater than the design storm (2.5 cm), so there should have been at most ten events producing overflow. However, due to the reduced surface storage, 29 and 26 events produced overflow in the 0.6 m and 0.9 m deep cells, respectively. For properly constructed cells, better performance would be expected. However, the data still show that the deeper media cells are performing better with respect to meeting the hydrologic goal of volume reduction than the shallower media cells.

Construction Impacts Study

The second critical question associated with bioretention design was to find ways to improve exfiltration through the bottom of bioretention cells during construction. Excavation technique, soil moisture condition, and soil type were all examined to find ways to improve exfiltration to the in-situ soil.

Construction Description:

Bioretention cells were constructed in an area of clay soil, representative of the Piedmont region of NC (NCSU Lake Wheeler Field Research Facility in Raleigh), and in an area of sandy soil, representative of the upper coastal plain of NC (Nash County Agricultural Center in Nashville). In order to be consistent with typical bioretention construction, a fill media depth of 0.6-0.9 m was used.

The excavation techniques used were a "rake" versus a "scoop" approach. Examples of the two methods can be seen in Figure 3. The "rake" approach used the teeth of the backhoe bucket to scarify and till the surface, where the "scoop" technique had more smearing and compaction associated with it. The "scoop" technique is consistent with sewer and utility line placement, where the surface is smoothed and compacted to minimize shifting and settling. Due to the maximum compaction levels occurring between 20 to 30 cm during construction, emphasis was placed on using consistency in technique for excavating the final 30 cm of soil (Gregory et al., 2006).



Figure 3. Demonstration of excavation – rake method (left) vs. scoop method (right).

Another method was excavating in different soil moisture conditions – wet soil versus dry soil. In order to test the difference of these conditions, excavation in dry soil took place after several consecutive dry, warm days. To test for excavation in wet soil, the cell was manually irrigated overnight to saturate the soil. One cell was randomly selected as the "wet" cell and the other was designated as the "dry" cell, and each of these was randomly divided into two roughly equal sized sections to test the different excavation techniques.

Monitoring Methods:

After excavation was complete, field testing took place. The order of testing was as follows: (1) soil samples were weighed on site to test for gravimetric soil moisture content at the time of construction, (2) double ring infiltrometers and soil cores were placed at test sites to avoid foot traffic, (3) soil was tested for compaction, and (4) infiltration tests were run and soil cores were taken. For each combination of

excavation technique, soil type, and antecedent moisture condition, there were two soil samples collected for measuring gravimetric soil moisture content; six soil cores to test for hydraulic conductivity, bulk density, and porosity; three infiltration tests; and fifteen soil compaction measurements. A summary of the methods and devices used to determine the soil properties are in Table 2.

Table 2. Summary of devices and methods to determine soil properties.

Soil Property	Testing Device	Method	Notes
Permeability	Amoozemeter	Amoozegar, 2006	Pre-excavation
Gravimetric soil moisture content	Scale	ASTM D 2216 (ASTM, 2005)	Field
Infiltration	Double ring infiltrometer	Bean et al., 2007	Field, 30 and 61 cm diameter rings
Soil compaction	Spectrum Field Scout SC-900 hand cone penetrometer		Field, five tests per infil. test (Gregory et al., 2006)
Sat. hydraulic conductivity	Constant head test	Klute, 1986	Laboratory, 7.6 cm diameter cores
Dry bulk density	Weigh oven-dry core		Laboratory, bulk density = mass solids / total volume
Particle size analysis	Hydrometer method	Gee and Bauder, 1986	Laboratory

The pooled dataset of infiltration and saturated hydraulic conductivity were not normally distributed. A Box-Cox transformation was applied to the infiltration and saturated hydraulic conductivity data, with shift parameters of 0.22 and 0.44, respectively (Box and Cox, 1964). Box-Cox transformation was used because it provided the most consistent variances, and Levene's test (homogeneity of variance test) showed it was the best method of transformation. Once the transformed dataset was normally distributed, ANOVA was run using SAS version 9.1.3

Results:

Nashville (Sandy Soil Site):

Bioretention cell construction at the Nash County Agricultural Center took place from August 2-3, 2008. The antecedent weather conditions for the two weeks prior to construction were hot and dry. Despite being separated by 1.5 m, the soil texture differed between the two test plots. The soil texture, as classified by the USDA, was loamy-sand for the "dry" test plot and sand for the "wet" test plot.

For both soil conditions tested, infiltration and saturated hydraulic conductivity decreased when the scoop method was used. This was due to increased soil compaction associated with more scoop method bucket contact, which consequently increased the bulk density. As the compaction and bulk density increased, water movement through the soil slows down (Horton et al., 1994).

Plotting the residuals of hydraulic conductivity versus the residuals of bulk density and taking into account the effects of excavation technique and soil moisture

condition, there was a statistically significant negative association of hydraulic conductivity to bulk density (p-value = 0.017). As bulk density increases, hydraulic conductivity is reduced, which was seen for soil samples from the "scoop" method.

Raleigh (Clay Soil Site):

Bioretention cell construction at Lake Wheeler Field Labs, in Raleigh, took place from October 10-12, 2008. The antecedent weather conditions for nine days prior to construction were warm and dry. Similar to the results from the Nashville site, infiltration and saturated hydraulic conductivity were lower when the scoop method was used. This was due to increased soil compaction associated with more bucket contact from the scoop method. Based on particle size analysis and the USDA classification, the soil texture for the "dry" cell was sandy-loam for the rake method and clay for the scoop method, and the soil texture of the "wet" cell was clay.

Combined Results:

The datasets were pooled to test the impacts that excavation technique, antecedent moisture condition, soil type, and interactions among the three had on infiltration and saturated hydraulic conductivity. P-values for the combinations based on soil condition are presented in Table 3. Analyzing the data based on soil condition showed there was a significant impact of excavation technique on infiltration and saturated hydraulic conductivity for the wet condition (p-values = 0.036 and 0.005, respectively), but no significant impact existed for the dry condition.

Table 3. Effects of soil condition on infiltration and hydraulic conductivity (p-values)

Factor (Soil Condition – dry vs. wet)	Excavation Technique	Excavation Technique & Soil Type
Infiltration (dry)	0.153	0.932
K_{Sat} (dry)	0.508	0.573
Infiltration (wet)	**0.036**	0.499
K_{Sat} (wet)	**0.005**	0.623

P-values for the combinations based on soil type are presented in Table 4. There was a significant impact of excavation technique on hydraulic conductivity in sandy soil (p-value = 0.024) and infiltration rate in clay soil (p-value = 0.047), but no significant impact existed for infiltration rate in sandy soil or hydraulic conductivity in clay soil. There was no effect on soil condition in the clay site, but there was a significant impact on infiltration and saturated hydraulic conductivity at the sandy site. This was due to the "dry" cell having loamy-sand in-situ soil, compared to sand.

Table 4. Effects of soil type on infiltration and hydraulic conductivity (p-values).

Factor (Soil Type – clay vs. sand)	Excavation Technique	Soil Condition (dry vs. wet)	Excavation Tech. & Soil Condition
Infiltration (clay)	**0.047**	0.511	0.629
K_{Sat} (clay)	0.173	0.952	0.202
Infiltration (sand)	0.148	**<0.0001**	0.845
K_{Sat} (sand)	**0.024**	**0.030**	0.222

Conclusions

The Nashville bioretention cell data are similar to those found in the literature. Deeper media depths meet the LID hydrology goal of volume reduction more frequently than the shallower media depths (35% compared to 9% of 45 monitored events). This is because the cells with deeper media depths are exfiltrating more water. For properly constructed cells, better performance would be expected. Despite the relatively poor performance, the results still show that deeper media cells perform much better with respect to meeting the hydrologic goal of volume reduction.

Using the teeth on the bucket to rake the final 30 cm of soil, instead of scooping the soil improved the soil properties that govern infiltration. The rake method scarified the bottom layer in the bioretention cell. This increased the soil's ability to exfiltrate water from bioretention cells to the underlying soils. Using the scoop method reduced the potential for exfiltration because it compacted the soils to a greater extent, as evidenced by higher bulk densities and compaction measurements.

In particular, when excavating in wet conditions, the hydraulic conductivity and infiltration rate associated with the rake method were significantly more than that of the scoop method (p-values = 0.005 and 0.036, respectively). The hydraulic conductivity associated with the rake method of excavation were significantly more at the sandy soil sites (p-value = 0.024), and the infiltration rate associated with the rake method of excavation were significantly more at the clay soil sites (p-value = 0.047). Based on the results of this study and because there is no extra cost associated with the rake method, it is recommended to use the rake excavation technique in preference to the "conventional" scoop method for future bioretention or other infiltration BMP projects to decrease outflow volume and pollutant loads.

Acknowledgements:

The authors would like to acknowledge the Cooperative Institute for Coastal and Estuarine Environmental Technology (CICEET) and NC Department of Environment and Natural Resources (NCDENR) for funding this project. Thanks to NCSU faculty, Dr. Aziz Amoozegar, Dr. Greg Jennings, and Dr. Jason Osborne. The authors sincerely appreciate Joe Wright for his help in excavating the bioretention cells exactly how they needed to be. Thanks to everyone involved with this project at the Lake Wheeler Research Facility and Nash County Ag. Center for their cooperation, in particular Mike Wilder, Bill Lord, Joni Tanner, and Ken Snyder. Also thanks to NCSU-BAE staff and students for their assistance.

References

Amoozegar, A. (2006). Amoozemeter. In *Encyclopedia of Soil Science*, 86-92. London: Taylor and Francis.

American Society for Testing and Materials (ASTM). (2005). "Standard test methods for laboratory determination of water (moisture) content of soil and rock by mass." *ASTM D 2216-05*, West Conshohocken, PA.

Bean, E.Z., Hunt, W. F., and Bidelspach, D. A. (2007). "Field survey of permeable pavement surface infiltration rates." *Journal of Irrigation and Drainage Engineering*, 133(3), 249-255.

Box, G. E., and Cox, D. R. (1964). "An analysis of transformations." *Journal of the Royal Statistical Society,* 26(B), 211–246.

Davis, A. P. (2008). "Field performance of bioretention: hydrology impacts." *Journal of Hydrologic Engineering*, 13(2), 90-95.

Davis, A. P., Shokouhian, M., Sharma, H., and Minami, C. (2006). "Water quality improvement through bioretention media: nitrogen and phosphorus removal." *Water Environment Research*, 78(3), 284-293.

Davis, A. P., Shokouhian, M., Sharma, H., and Minami, C. (2001). "Laboratory study of biological retention for urban stormwater management." *Water Environment Research*, 73(1), 5-14.

Dietz, M. E., and Clausen, J. C. (2006). "Saturation to improve pollutant retention in a rain garden." *Environmental Science and Technology*, 40(4), 1335-1340.

Gee, G. W., and Bauder, J. W. (1986). "Particle-size analysis." *Methods of soil analysis: Part 1 - Physical and mineralogical methods*, A. Klute, ed., Soil Science Society of America, Madison, WI, 383-411.

Gimenez, D. C., Dirksen, R., Miedema, L. A., Eppink, A. J., and Schoonderbeck, D. (1992). "Surface sealing and hydraulic conductances under varying-intensity rains." *Soil Science Society of America Journal*, 56(1), 234-242.

Gregory, J. H., Dukes, M. D., Jones, P. H., and Miller, G. L. (2006). "Effect of urban soil compaction on infiltration rate." *Journal of Soil and Water Conservation, 61*(3), 117-124.

Horton, R., Ankeny, M. D., and Allmaras, R. R. (1994). "Effects of compaction on soil hydraulic properties." *Soil compaction in crop production*, B. D. Soane and C. van Ouwerkerk, eds., Elsevier Science B. V., London, 141-165.

Hsieh, C., and Davis, A. P. (2005). "Evaluation and optimization of bioretention media for treatment of urban storm water runoff." *Journal of Environmental Engineering*, 131(11), 1521-1531.

Hunt, W. F., Jarrett, A. R., Smith, J. T., and Sharkey, L. J. (2006). "Evaluating bioretention hydrology and nutrient removal at three field sites in North Carolina." *Journal of Irrigation and Drainage Engineering*, 132(6), 600-608.

Hunt, W. F., Smith, J. T., Jadlocki, S. J., Hathaway, J. M., and Eubanks, P. R. (2008). "Pollutant removal and peak flow mitigation by a bioretention cell in urban Charlotte, NC." *Journal of Environmental Engineering*, 134(5), 403-408.

Klute, A. (1986). "Water retention: laboratory methods." *Methods of Soil Analysis: Part 1 - Physical and Mineralogical Methods*, A. Klute, ed., Soil Science Society of America, Madison, WI, 635–662.

Li, H., Sharkey, L. J., Hunt, W. F., and Davis, A. P. (2009). "Mitigation of impervious surface hydrology using bioretention in North Carolina and Maryland." *ASCE Journal of Hydrologic Engineering* (in press).

NCDWQ. (2007). Chapter 12: Bioretention. In *Stormwater Best Management Practices Manual*, 12-1–12-31. Raleigh, NC: North Carolina Department of Environment and Natural Resources – Division of Water Quality.

Pitt, R., Chen, S., Clark, S., Swenson, J., and Ong, C. (2008). "Compaction's impacts on urban storm-water infiltration." *Journal of Irrigation and Drainage Engineering*, 134(5), 652-658.

Shuster, W. D., Gehring, R., and Gerken, J. (2007). "Prospects for enhanced groundwater recharge via infiltration of urban storm water runoff: a case study." *Journal of Soil and Water Conservation, 62*(3), 129-137.

Tyner, J. S., Wright, W. C., and Dobbs, P. A. (2009) "Increasing exfiltration from pervious concrete and temperature monitoring." *Journal of Environmental Management* (in press).

United States Environmental Protection Agency (U.S.EPA). (2007). "National water quality inventory: report to Congress, 2002 reporting cycle." *EPA 841-R-07-001*, U.S.EPA, Washington, D.C.

United States Environmental Protection Agency (U.S.EPA). (1983). Results of the nationwide urban runoff program: Volume I – Final Report, WH-554. Washington, DC: U.S.EPA.

Engineered Waste Materials as Amendments to Prevent Erosion and to Stabilize Contaminated Sites

S. P. Kakuturu[1], M. Xiao[2], and L. N. Reddi[3]

[1]Corresponding author, Department of Civil, Environmental, and Construction Engineering, University of Central Florida, Orlando, FL 32816, USA, Ph. 1-407-823-1361, e-mail: skakutur@mail.ucf.edu

[2]Department of Civil and Geomatics Engineering and Construction, M/S EE94, California State University, Fresno, California 93740, USA, Ph. 1-559-278-7588, e-mail: mxiao@csufresno.edu

[3]Department of Civil, Environmental, and Construction Engineering, University of Central Florida, Orlando, FL 32816, USA, Ph. 1-407-823-1374, e-mail: lreddi@mail.ucf.edu

ABSTRACT

Erosion is an important consideration in remediation strategies of slopes at contaminated sites such as mine tailings. Pelletized waste materials offer the dual advantages of waste utilization and soil erosion prevention at such sites. These materials could be designed to reduce stormwater runoff by optimizing their infiltration capacities, to trap the eroded soil particles and pollutants before they get to the nearby lakes and streams, and store sufficient moisture for supporting vegetation. In this paper, we present the results of our study that focused on flow, erosion, and filtration through an erosion control blanket built with three different particle size ranges of pelletized waste materials. The finest gradation is used on the upper portion of the slope, and the medium and coarse gradations are used in the lower portions to act as graded filters for the upper portion. The density, gradation, and erodibility properties of the waste materials are used for calculating the flow, internal erosion, filtration, and moisture retention in the erosion control blanket. The model is intended to aid in the engineering design of erosion-resistant blankets on slopes. It optimizes the physicochemical and hydraulic characteristics of the pelletized waste materials to fulfill diverse functions of an erosion blanket, viz., erosion resistance, runoff inhibition, moisture retention to support vegetation, and controlled infiltration.

INTRODUCTION

Soil erosion is a world-wide problem that is causing early deterioration of public infrastructure, and pollution of surface and ground waters. As compared to vegetated landscapes, exposed soil slopes of earth structures and waste disposal sites experience

higher levels of erosion due to rainfall. Engineering suitable methods to prevent erosion for protecting environment is now a statutory requirement in many countries. In the United States of America (USA), the Clean Water Act (CWA) and the National Pollutant Discharge Elimination System (NPDES) are being enforced to prevent pollution of surface and ground waters from point and non-point sources of pollution.

In the United States, the annual soil loss due to erosion is estimated at 4 billion tons. Soil erosion results in loss of fertility, leaching of nutrients and pesticides, increased sedimentation of drainage systems and water bodies, and increased cost of drinking water treatment. In USA, the estimated annual economic loss considering these costs is put at 44 billion dollars (Brady and Weil, 2004). As per NPDES Phase II, that is in force from 2003 in USA, any activity disturbing soil on areas measuring 1 acre or over must have an approved storm water pollution prevention plan (SWPPP).

Faucette et al (2005, 2007), and Osorio and Ona (2006) studied the suitability of compost for preventing soil erosion and compared the stormwater quality with other options for erosion control. Gyasi-Agyei (2004, 2005) described the use of compost for preventing erosion and establishment of grass on slopes.

In this paper, we have presented the results of our recent studies on the performance of erosion control blankets composed of pelletized waste materials. Several waste materials, including compost, can be pelletized to result in particle aggregates of desired properties and gradations. Successful erosion control blankets can be designed based on the properties and gradations of pelletized waste considering their resistance to erosion, self-filtration potential, and capacity to retain moisture and nutrients for promoting growth of vegetation.

WASTE MATERIALS IN EROSION CONTROL

Utilization of waste materials in erosion control reduces the need for disposing them in landfills, which are becoming increasingly expensive due to cost of urban lands. The treated wastes for erosion control should have low self-erodibility characteristics, long-term chemical stability, and capacity to retain moisture and nutrients for supporting vegetation. Pelletization of compost and similar materials increases their particle sizes, and improves their resistance to degradation and self-erosion.

In USA, the Environmental Protection Agency (EPA), the Composting Council Research and Education Foundation (CCREF), the U.S. Composting Council (USCC), and the federal and state Departments of Transportation (DOTs) have started to advocate and regulate the use of compost for preventing soil erosion. Similar efforts are underway to utilize pelletized inorganic industrial wastes in pollution prevention applications. However, the use of pelletized waste as erosion control blankets is hindered due to lack of understanding of their mechanism, design methods, and performance histories.

In this study, we are developing a mathematical model that considers the flow through different sections of an erosion control blanket, erodibility of waste pellets, and migration and filtration of eroded particles. Fig. 1 shows the schematic of a three-section erosion control blanket. The gradation of pellets is finer in the top section, medium in the middle section, and coarser in the bottom section. This variation is chosen to allow the water to flow freely inside the blanket without emerging on the slope. It is also meant for filtering and retaining any soil particles and contaminants that are getting eroded in the upper sections.

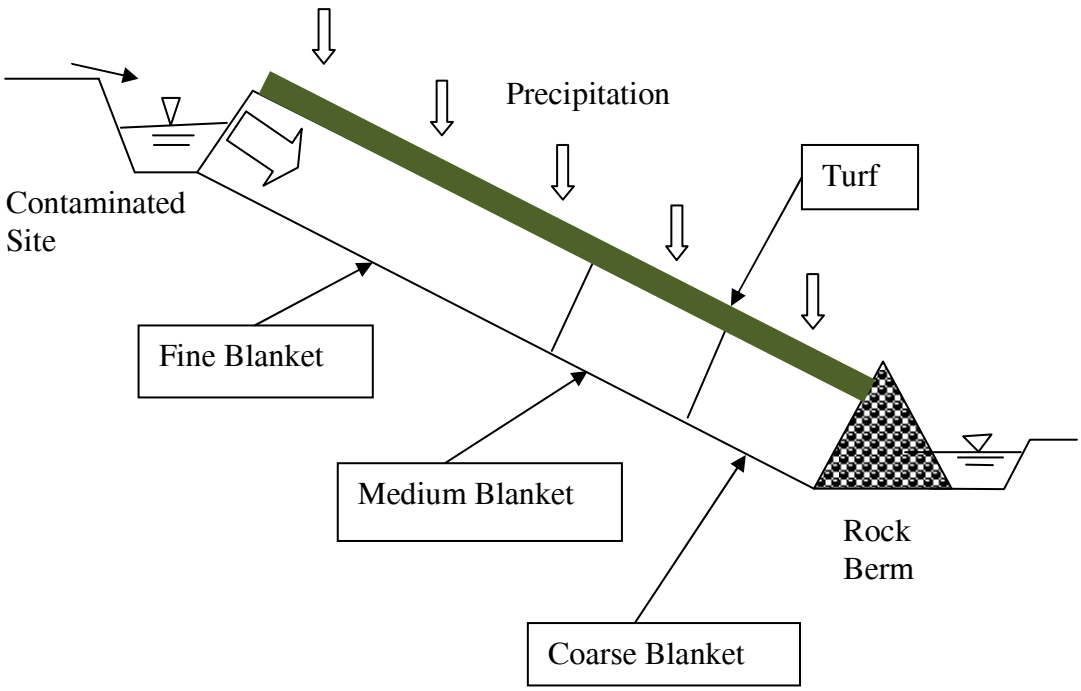

Fig. 1. Schematic of a three-section erosion control blanket of pelletized waste

As shown in Fig.1, the top ditch collects all the discharge from the contaminated site and facilitates flow of that influent through the erosion control blanket. The turf prevents erosion of blanket due to rainfall, but allows some infiltration. The thickness of the erosion control blanket shall be sufficient to safely conduct the inflow entering at the top and rainfall infiltration, without seepage emerging on the top of the blanket. Also, the blanket shall have suitable particle gradation for retaining moisture to support vegetation during dry seasons. The gradation of medium blanket and coarse blankets shall satisfy the filtration criteria with respect to their upper section so that the seepage would not result in soil loss or pollution.

INTERNAL & SURFACE EROSION AND MOISTURE RETENTION

The success of an erosion control blanket depends on the design choices of particle gradations and section thicknesses. Such a design exercise shall consider possible surface erosion (before and after establishment of vegetation), the internal erosion

and filtration processes, and moisture retention. The hydraulic conductivities of any particulate material can be estimated for initial and life-cycle stages by considering void ratio, particle characteristics, and particle gradation. These parameters change during the life cycle due to erosion, and escape/entrapment of particles due seepage.

Surface Erosion

The Revised Universal Soil Loss Equation (RUSLE), Renard et al (1997), is a widely used method for estimating annual soil losses due to surface erosion. It is given as:

$$\mathbf{A = RKLSCP} \qquad \mathbf{(1)}$$

where A is the long-term annual average soil loss, R is the rainfall-runoff erosivity factor, K is the soil erodibility factor, L is the slope length factor, C is the crop and cover management factor, and P is the support practice factor. Kinnell (2007) reported that RUSLE over estimates small event soil losses and under estimates large event soil losses. Alternative advanced models of rainfall induced surface erosion were described by Tayfur (2001), Lie et al (2005), Liu et al (2005), Raff and Ramirez (2005), Visser et al (2005), and Walter et al (2007).

Internal Erosion

The internal erosion of the finer blanket can be estimated by idealizing its pore space as a bundle of capillary tubes and calculating the shear stresses causing erosion. The model reported by Kakuturu and Reddi (2006) can re-written in this context as:

$$\mathbf{m_{er} = E\{\tau(t) - \tau_{cr}\}p\Delta t} \qquad \mathbf{(2)}$$

where m_{er} = the mass eroded in time interval Δt,

E = erodibility rate expressed as mass eroded per shear stress difference, area

$\tau(t)$ = the shear stress on the walls of that idealized pore tube at any given time

τ_{cr} = the critical shear stress of the material, and

p = the surface area of that idealized pore tube

The shear stress, $\tau(t)$, can be estimated using the discharge as:

$$\mathbf{\tau(t) = 4\eta Q(t)/(\Pi\, r_{cc}^3)} \qquad \mathbf{(3)}$$

where η = dynamic viscosity of the seeping water,

Q(t) = the flow rate at any time t, and

r_{cc} = the radius of the idealized pore tube.

The internal erosion and subsequent partial re-deposition of eroded particles gradually reduces the hydraulic conductivities of medium and coarse sections during the life-cycle. Therefore, the design objective is to ensure that their hydraulic conductivities remain more that the desired values even at the end of life cycle. Reddi et al (2000) reported a model for estimating permeability reduction due to the entrapment of eroded particles in pore spaces.

Moisture Retention

The variation of gradation along the different parts of such a blanket configuration results in differences in the moisture retention capacity. This impacts the growth of vegetation and surface erodibility. Moreover, internal erosion of finer blanket may, over several years, reduce the moisture retention capacity of finer blanket. On the other hand, entrapment of eroded particles may increase the moisture in lower parts.

EXPERIMENTAL INVESTIGATIONS

For verifying the potential of pelletized compost blankets to resist erosion, a series of laboratory experiments were conducted at the Kansas State University, Manhattan, KS (USA). As shown in Fig. 2, a laboratory model of compost erosion control blanket was tested by simulating the precipitation using a rainfall simulator.



Fig 2. Erosion testing of a 3-section compost blanket using a rainfall simulator

Pelletized compost (patent pending) manufactured by Earth Solutions, LLC, was used in our study. Two configurations were tested: (1) Mixed compost, with same gradation throughout, which was a mixture of three particle size ranges viz., fine, medium, and coarse; (2) Filtered compost, a 3-section blanket with fine, medium, and coarse size ranges arranged in separate sections from top to bottom, respectively. The compost sections were filled up in the test box (914 mm x 305 mm x 178 mm). The test box was placed at a slope of 1:3 (V:H), a typical value of slopes where erosion control is critical.

Six repeated rainfalls at an average intensity of 63.5 mm/hour were created for 1-hour duration each time. Six tests on each configuration were first conducted without vegetation. Four tests were repeated after establishing vegetation by embedding grass seeds between the base soil and compost blanket. In all the tests, the eroded material

was collected and weighed for obtaining erodibility rate. The results of the tests on un-vegetated and vegetated blankets are presented in Fig. 3 and Fig. 4, respectively.

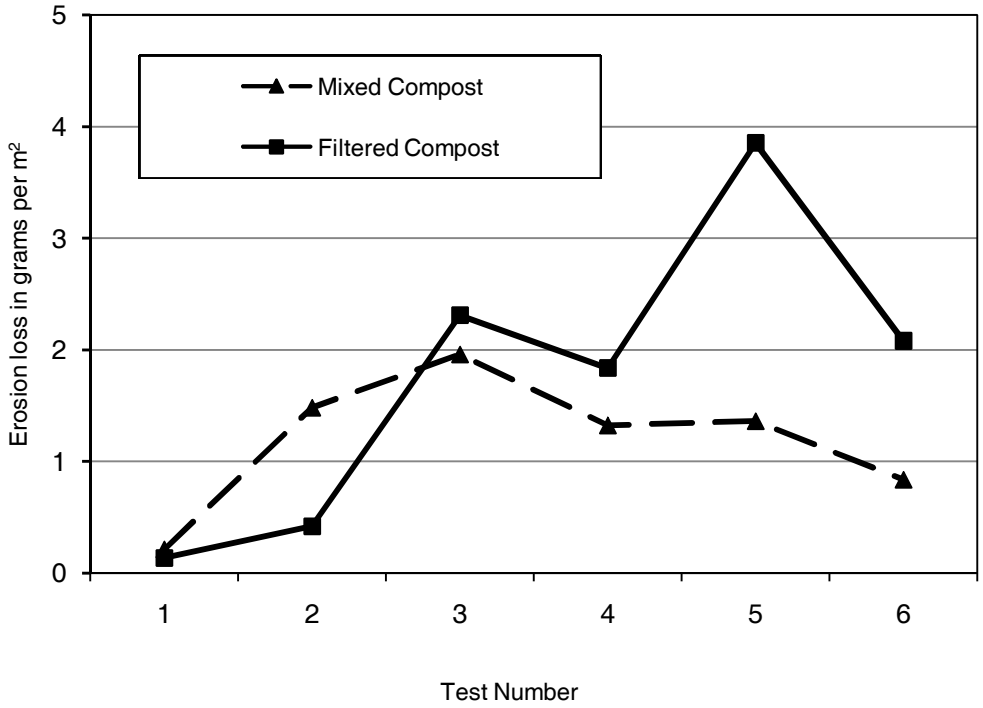

Fig. 3. Comparison of surface erosion losses of compost blankets (without vegetation)

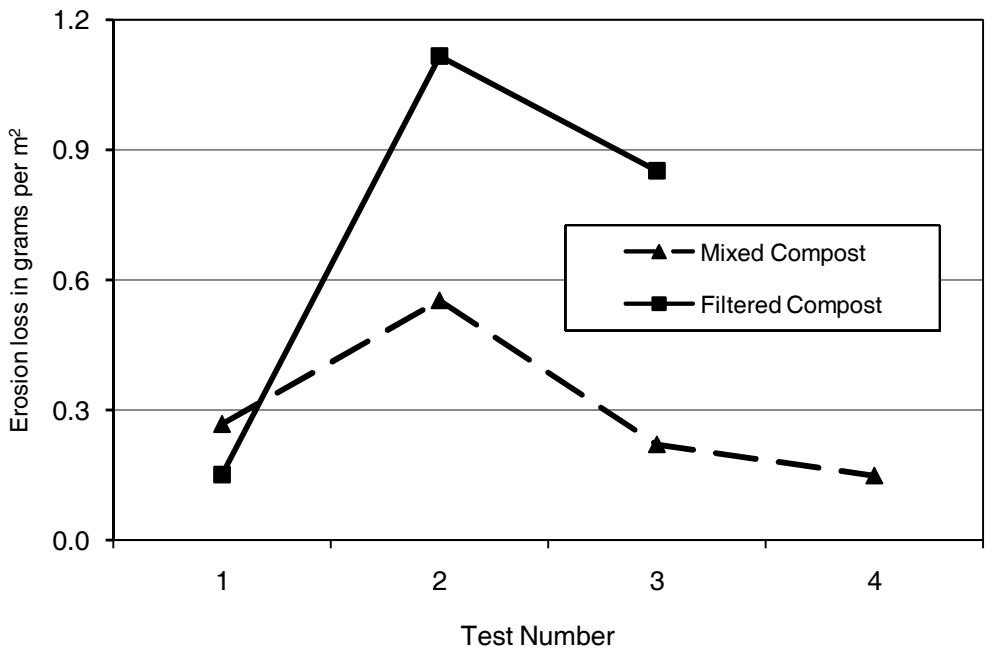

Fig. 4. Comparison of surface erosion losses of compost blankets (without vegetation)

DISCUSSION AND CONCLUSIONS

It is seen from the experimental results that the mixed compost resulted in lower values of surface erosion losses compared with filtered compost. These results suggest that mixed compost, that is very well graded, has more resistance to surface erosion than filtered compost whose sections are not well graded. The surface erosion losses were smaller with vegetation than without vegetation. These results suggest that vegetation substantially reduces surface erosion of compost blankets.

Until now, the experimental part of our study was focused on surface erosion caused by precipitation on the slope. However, it is also needed to study the base flow (as shown in Fig.1) for considering erosion and filtration within the blanket. A comprehensive approach considering all the surface and internal phenomena could result in better mechanistic understanding of erosion control blankets.

Acknowledgments

The authors wish to thank Kansas Livestock Association and Agri Beef Co. who have supported some of the research reported in this paper. We are also thankful to David Suhling, Research Technologist in the Department of Civil Engineering at Kansas State University, for his important role in the design and construction of the experimental apparatus. The authors greatly appreciate the contributions of Joshua Howard, Alice Devine, and Rick R. Stott to this research.

References

Brady N.C., and Weil R.R. (2004). The Nature and Properties of Soils, 13th edition. Upper Saddle River, NJ: Prentice Hall.

Faucette L.B., Governo J., Jordan C.F., Lockaby B.G., Carino H.F., and Governo R. (2007), "Erosion control and storm water quality from straw with PAM, mulch, and compost blankets of varying particle sizes", Journal of Soil and Water Conservation, 62(6), 404-413.

Faucette, L.B., Jordan C.F., Risse L.M., Cabrera M., Coleman D.C., and West L.T. (2005), "Evaluation of storm water from compost and conventional erosion control practices in construction activities", Journal of Soil and Water Conservation, 60(6):288-297.

Gyasi-Agyei Y. (2004), "Optimum use of erosion control blankets and waste ballast rock mulch to aid grass establishment on steep slopes", Journal of Hydrologic Engineering, 9(2), 150–159.

Gyasi-Agyei Y. (2005), Errata for "Optimum use of erosion control blankets and waste ballast rock mulch to aid grass establishment on steep slopes", Journal of Hydrologic Engineering, 10(2), 171-172.

Kakuturu S., and Reddi L. N. (2006), "Mechanistic Model for Self-Healing of Core Cracks in Earth Dams", Journal of Geotechnical and Geoenvironmental Engineering, 132 (7), 890–901.

Kinnell P. I. A. (2007), "Runoff dependent erosivity and slope length factors suitable for modeling annual erosion using the Universal Soil Loss Equation", Hydrological Processes, 21 (20), 2681–2689.

Lei T., Pan Y., Liu H., Zhan W., Yuan J. (2006), "A run off on ponding method and models for the transient infiltration capability process of sloped soil surface under rainfall and erosion impacts", Journal of Hydrology, 319, 216–226.

Liu Q. Q., Xiang H., and Singh V. P., (2006), "A simulation model for unified inter-rill erosion and rill erosion on hill slopes", Hydrological Processes, 20, 469–486.

Osorio, F. and O˜na, J. (2006), "Using compost from urban solid waste to prevent erosion in road embankments", Journal of Environmental Science and Health, Part A, 41, 2311–2327.

Raff D. A., and Ramirez J. A. (2005), "A physical, mechanistic and fully coupled hill slope hydrology model", International Journal for Numerical Methods in Fluids, 49, 1193–1212.

Reddi L. N., Xiao M., Hajra M. G., and Lee I. M., (2000), "Permeability reduction of soil filters due to physical clogging", Journal of Geotechnical and Geoenvironmental Engineering, 126 (3), 236–246.

Renard K. G., Foster G. R., Weesies G. A., McCool D. K., Yoder D. C. (1997), "Predicting soil erosion by water: a guide to conservation planning with the Revised Universal Soil Loss Equation (RUSLE)", U.S. Department of Agriculture Agricultural Handbook, Vol. 703, USDA, Washington, DC.

Visser S. M., Sterk G., and Karssenberg D. (2005), "Modeling water erosion in the Sahel: application of a physically based soil erosion model in a gentle sloping environment", Earth Surface Processes and Landforms, 30, 1547–1566.

Walker J. D., Walter M. T., Parlange J. Y., Rose C. W., Meerveld H.J. T., Gao B., Cohen A. M. (2007), "Reduced raindrop-impact driven soil erosion by infiltration", Journal of Hydrology, Vol. 342, 331-335.

*****

Enhancing Rain Garden Design to Promote Nitrate Removal

Emilie K. Stander[1], Michael Borst[2], Thomas P. O'Connor[3], and Amy A. Rowe[4]

[1]U.S. Environmental Protection Agency, National Risk Management Research Laboratory, Urban Watershed Management Branch, 2890 Woodbridge Ave, MS-104, Edison, NJ 08837; PH (732) 906-6898; FAX (732) 321-6640; email: stander.emilie@epa.gov
[2]U.S. Environmental Protection Agency, National Risk Management Research Laboratory, Urban Watershed Management Branch, 2890 Woodbridge Ave, MS-104, Edison, NJ 08837; PH (732) 321-6631; FAX (732) 321-6640; email: borst.mike@epa.gov
[3]U.S. Environmental Protection Agency, National Risk Management Research Laboratory, Urban Watershed Management Branch, 2890 Woodbridge Ave, MS-104, Edison, NJ 08837; PH (732) 321-6723; FAX (732) 321-6640; email: oconnor.thomas@epa.gov
[4]U.S. Environmental Protection Agency, National Risk Management Research Laboratory, Urban Watershed Management Branch, 2890 Woodbridge Ave, MS-104, Edison, NJ 08837; PH (732) 906-6823; FAX (732) 321-6640; email: rowe.amy@epa.gov

ABSTRACT

Rain gardens effectively remove some stressors from stormwater, but in most cases they show much smaller removal rates of nitrate, likely due to the media's high sand and low organic matter content that inhibit nitrate removal by denitrification. EPA's pilot-scale research explores the use of shredded, unprinted newspaper as a carbon source to fuel denitrification. A bench-scale experiment was conducted to test the drainage capability of media containing shredded newspaper layers. Stormwater was introduced at low and high rates to bins containing zero, one, and two layers of newspaper at varying depths. While there were differences in effluent flow rates between control and newspaper treatments, surface ponding occurred in all three treatments, suggesting that some other factor besides the newspaper had an effect on drainage properties. Grain size and clay mineralogy analyses indicated that migration of finer particles into the deeper soils could have inhibited drainage.

Key words: rain gardens, bioretention, low-impact development, urban stormwater, nitrate, denitrification, soil media, carbon amendment, newspaper

INTRODUCTION

Excess nitrogen (N) is among the most widespread and pervasive pollutants in surface waters throughout the United States (USGS, 1999). The U.S. Geological Survey's National Water Quality Assessment program findings show that elevated

nitrate (NO_3^-) in streams and groundwater is as common in urban areas as in agricultural areas (USGS 1999). In urban watersheds, stormwater runoff from impervious surfaces carries an associated N load to storm drains that empty into receiving waters (Klein, 1979; Lee et al., 2004). Some practitioners are championing low-impact development practices, such as rain gardens, as a more sustainable approach than conventional stormwater management approaches for mitigating the hydrologic flows and environmental stressor loads associated with urban stormwater (Walsh et al., 2005; Dietz, 2007). Rain gardens have been shown to be particularly effective in removing total suspended solids, heavy metals, phosphorus, and some N species (Davis et al., 2001; Davis et al., 2003; Dietz and Clausen, 2005; Davis et al., 2006; Dietz and Clausen, 2006; Hunt et al., 2006; Davis, 2007; and Hsieh et al., 2007).

Practitioners currently specify rain garden media with high sand content and low organic matter content to promote infiltration and sorption of heavy metals and phosphorus (Dietz, 2007). However, this design inhibits denitrification, the biological transformation of NO_3^- to nitrogen gas (N_2) that is released to the atmosphere. Denitrification requires anaerobic conditions and organic carbon as an energy source to drive the reaction. The few NO_3^- removal studies in laboratory, pilot-scale, and field-scale rain gardens have mostly shown low rates of NO_3^- removal (Davis et al., 2001; Kim et al., 2003; Dietz and Clausen, 2005; Hsieh and Davis, 2005; Davis, 2007) and in some cases, NO_3^- production (Davis et al., 2001; Barrett, 2003; Davis et al., 2006). However, Dietz and Clausen (2006) did find reasonable rates of nitrate removal in another study.

Through the manipulation of soil media, vegetation, and rain garden size, pilot-scale rain garden mesocosms at the Urban Watershed Research Facility (UWRF) in Edison, New Jersey, will be designed to facilitate denitrification and NO_3^- removal by providing organic matter hotspots, soil media saturation at depth, plant uptake, and larger media volume and depth. The pilot-scale test adds shredded, unprinted newspaper, a recalcitrant organic carbon source, to the rain garden media. Newspaper's high lignin and cellulose content and ability to retain moisture may allow it to act as a hotspot for denitrification in rain garden systems over the long term (McClain et al., 2003). In a column study Kim et al. (2003) demonstrated that adding shredded newspaper to rain garden media increased NO_3^- removal rates more than other carbon sources tested, including wood chips, wheat straw, leaf mulch compost, sawdust, and alfalfa.

In Kim et al.'s (2003) column study the shredded newspaper was mixed homogeneously with the sandy media. While feasible in small-scale applications, this becomes more difficult for full-scale rain gardens because it requires mixing large volumes of media and shredded newspaper. In the UWRF pilot-scale rain gardens the shredded newspaper will be added into the media in layers rather than mixed homogeneously; however, there are concerns that this layered approach may make the newspaper act like a boundary layer. Consequently, a bench-scale test of the system is necessary to ensure that the shredded newspaper layers do not impede stormwater infiltration and drainage and thus result in saturated or ponded conditions for an unacceptable period.

The primary objectives of this study are to 1) test the ability of bench-scale

rain gardens to drain stormwater through sandy media containing layers of shredded newspaper, and 2) isolate the components of the bench-scale system which may impede drainage. Drainage capability will be tested using sandy media only, sandy media plus one-newspaper layer, and sandy media plus two-newspaper layer treatments. This paper presents the results of the completed bench-scale study; the pilot-scale study will be initiated in the spring of 2009.

METHODS

Experimental Apparatus

The bench-scale test system consisted of three 90-cm long x 60-cm wide x 60-cm deep plastic bins raised 90 cm above the floor on cinder blocks in a greenhouse. The bins were elevated to enable gravity drainage to cylindrical containers (55.9 cm diameter, 85.1 cm deep). All three bins contained a horizontal, 3.75-cm slotted PVC pipe 2 cm from the bottom that routed water through the wall of the bin and to the collection container. The slotted pipes were wrapped in nonwoven, permeable, polypropylene geotextile fabric (US Fabrics Inc., Cincinnati, OH, model 115NW) to prevent clogging and media loss.

The first bin, which served as a control treatment, was filled with a sand-clay soil mix used for baseball infields in New Jersey (NJ Gravel and Sand, Wall, NJ). State infield mixes are commonly used in rain garden applications. Media characteristics are presented in Table 1.

Table 1. Characteristics of Bench-Scale Study Media

Soil Characteristic	Value
% Passing Sieve # 270	10-20%
% Sand	81%
% Silt	9%
% Clay	10%
Compacted Bulk Density	1.80-1.86 g cm^{-3}
Organic Matter Content	1.56%

Note: Sieve data and compacted bulk density were specified by the manufacturer. Organic matter content was measured at EPA's laboratory facility. All other parameters were measured at the Rutgers University Soil Testing Laboratory.

A freeboard of 5 cm was maintained above the media during installation; this was true in all three bins. The media was added as gently as possible to reduce compaction, and it settled about 2 cm before, and an additional 2 cm following, stormwater introductions. The second bin, which served as the one-newspaper layer treatment, was filled with media and included one 2.5-cm layer of shredded, unprinted newspaper (American Veterans Group, Riva, MD) 11 cm from the top of the bin. Newspaper was also added gently by hand to reduce compaction during initial installation. The third bin, which served as the two-newspaper layer treatment, was filled with media and contained two 2.5-cm layers of shredded newspaper 48 and 11 cm from the top of the bin. Newspaper was shredded using a conventional office cross-cut shredder which produces confetti-type shred with dimensions of 3.125 cm x

0.125 cm.

Stormwater Additions

Urban stormwater runoff from a 9.75-acre area of an adjacent community college parking lot and high-density residential development was collected from an outfall at the UWRF and stored on site in an 11-m^3 holding tank in the greenhouse. Mixed stormwater was introduced to the bins at a set rate using a spray bar secured slightly above the media surface.

During the low-flow test, 40 L of stormwater were introduced to each bin during a two-hour interval, a rate equivalent to 333 mL min^{-1}. Bins were run one at a time, once per day, for two work weeks (i.e., 10 runs in each bin) during June 2008. The order in which the bins were run was changed daily. During the subsequent high-flow test, 100 L of stormwater were introduced to each bin during a two-hour interval, again, once per day, for two weeks during July 2008. This rate of introduction is equivalent to 833 mL min^{-1}. Both the high- and low-flow rates are relatively low (both are two orders of magnitude lower than one gallon min^{-1} ft^{-2}).

The cylindrical drainage containers were placed under the drain in each of the three bins to collect all effluent. Each drainage container was instrumented with a water level logger (Global Water model WL16) to measure effluent depth at six-minute intervals. The rate of change of the measured effluent depth was used as a surrogate for effluent flow rate.

Media Analysis

Following the hydraulic experiments, tests were performed on the media to quantify grain size and soil characteristics. One soil core was taken in the center of each bin to the bottom of the bin using a ¾ inch-diameter Oakfield corer. Cores were separated into 3-cm profile segments and stored at 4°C until analysis. The number of profile segments varied from four to six among bins due to varying amounts of media settling and compaction during coring. Samples were prepared and analyzed for particle size distribution on a Coulter counter model LS 230 (Beckman Coulter, Inc., Fullerton, CA). A sample of the original, uncompacted media used to fill the bins was sent to the Rutgers University Soil Testing Laboratory for texture analysis. Approximately 10 g of the original air-dried media were sent to EPA's AWBERC Laboratory for clay mineralogy analysis.

Data Analyses

One-way analysis of variance (ANOVA) tests were used to compare effluent flow rates and volumes among treatments. On each day from Tuesday through Friday, all three bins experienced approximately the same amount of drying time since the previous stormwater introduction; therefore, these runs were treated as statistical replicates. Tests were performed using Statistica 7 (StatSoft, Inc., Tulsa, OK). Fisher's LSD, Bonferroni, Scheffe, and Tukey's HSD post hoc tests were used to compare treatment means; reported results are from Tukey's HSD tests.

Particle size distribution of the soil depth profiles is presented in the results as the 10th, 25th, 50th, 75th and 90th percentiles (D_{10} through D_{90}). Mean particle size in each depth profile was analyzed separately for each percentile using one-way

ANOVA. Overall mean and median particle sizes were also analyzed for each depth profile using ANOVA. Coefficient of uniformity (C_u) was calculated as D_{60}/D_{10}, and particle size range was calculated as D_{90}/D_{10}. ANOVA was used to analyze differences in C_u and range by soil depth. The three bins were treated as statistical replicates for all particle size tests because the same media was used in all three treatments.

RESULTS

Effluent Flow Rates

The control treatment had larger effluent flow rates than both newspaper treatments during the low-flow test (Figure 1).

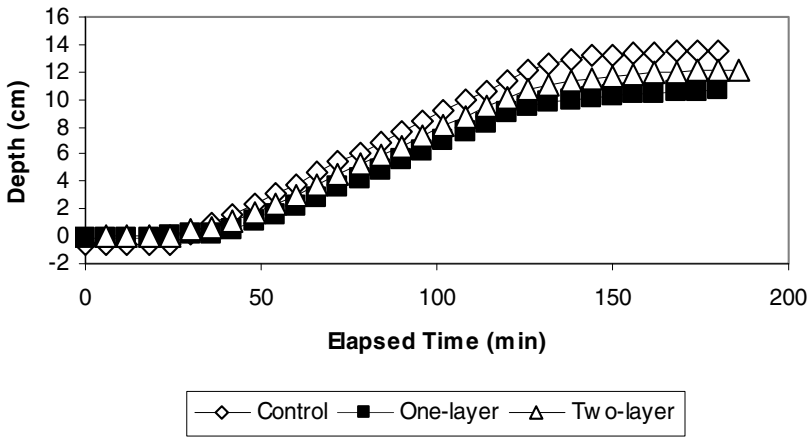

Figure 1. Effluent depths from one representative day (6/23/08) of the low-flow test.

This difference was statistically significant for the Tuesday through Friday runs when composited over both Week One and Week Two (Table 2a).

Table 2. Results of ANOVA Tests Comparing Differences in Effluent Flow Rates

a

Test	Overall Model[a]	Control vs. One-Layer[b]	Control vs. Two-Layer[b]	One-Layer vs. Two-Layer[b]
Full Test	$F_{2,16} = 9.03$ $p < 0.01$	$p < 0.05$	$p < 0.01$	ns
Week One	ns			
Week Two	$F_{2,5} = 11.8$ $p < 0.05$	$p < 0.05$	$p < 0.05$	ns

b

Test	Overall Model[a]	Control vs. One-Layer[b]	Control vs. Two-Layer[b]	One-Layer vs. Two-Layer[b]
Full Test	ns			
Week One	$F_{2,9} = 6.84$ $p < 0.05$	$p < 0.05$	ns	ns
Week Two	$F_{2,9} = 21.6$ $p < 0.001$	ns	$p < 0.05$	$p < 0.001$

[a] Results from one-way ANOVA tests. Post hoc tests were performed when ANOVAs were significant.

[b] Results from Tukey's HSD post hoc tests.

Note: Tuesday through Friday results from the low-flow test are presented in part a; Tuesday through Friday high-flow test results are in part b. Nonsignificant results are indicated by the abbreviation "ns".

The two newspaper treatments were not significantly different from each other. There were no significant differences in flow rates during Week One Tuesday through Friday runs, but the control treatment had significantly higher flow rates than both newspaper treatments during Week Two Tuesday through Friday runs (Table 2a).

A much different pattern emerged during the high-flow test. Surface ponding occurred in all three treatments, and drainage times increased. Overall, the two-layer treatment had much smaller effluent flow rates than the other two treatments (Figure 2).

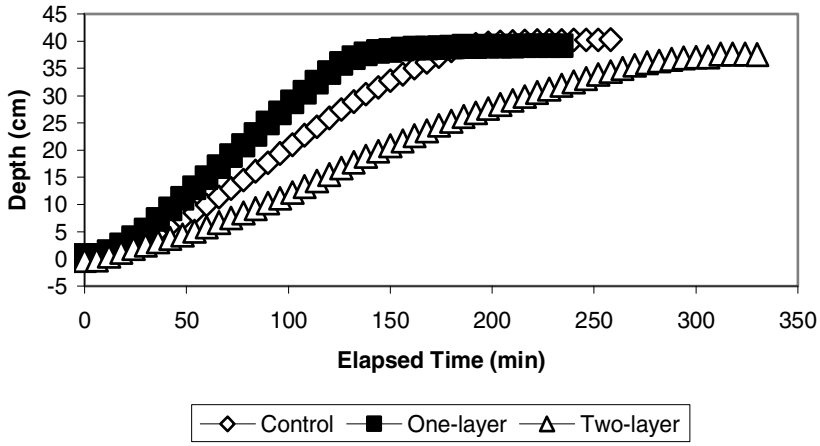

Figure 2. Effluent depths from one representative day (7/23/08) of the high-flow test.

The Tuesday through Friday runs demonstrated no significant differences in flow rates during the high-flow test taken as a whole (Table 2b). During Week One Tuesday through Friday runs, flow rates were significantly larger in the control treatment than the one-layer treatment (Table 2b). However, during Tuesday through Friday runs of Week Two, the two-layer treatment had significantly smaller flow rates than both the control and one-layer treatments (Table 2b).

Media Grain Size Analysis

The media was found to contain a high percentage of silt and clay and had a low organic matter content (Table 1). No significant differences were found in particle size distributions among 3-cm depth profile increments in any of the parameters tested. However, there were some nonsignificant trends in the data. Overall, there was a trend toward smaller particle sizes with depth in overall mean particle size and mean particle size in the 90th, 75th and 10th percentiles (Figures 3a-c).

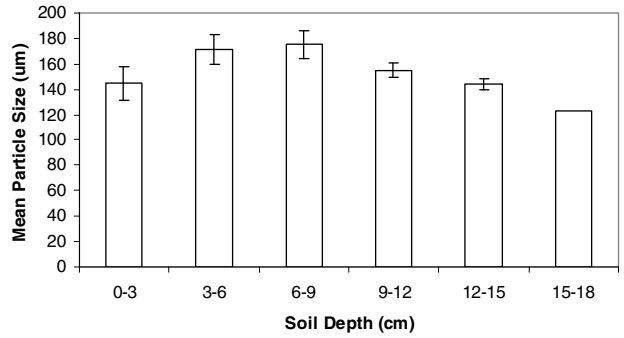

a

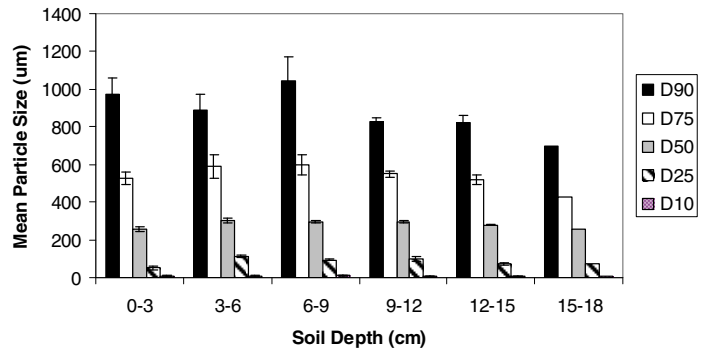

b

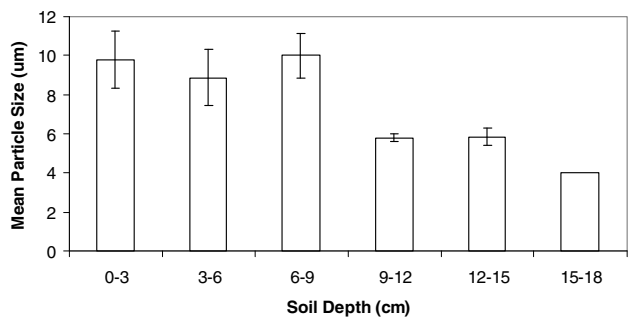

c

Figure 3. Mean particle size overall (a), by percentile (b), and for D_{10} (c). Error bars represent standard errors at each soil depth increment.

The trend was particularly apparent in comparing the first three depth increments (0-3, 3-6, and 6-9 cm) with the last three depth increments (9-12, 12-15, and 15-18 cm), so the analyses were rerun compositing the first three and last three depth increments. Mean particle sizes were significantly larger in the upper 9 cm of media compared to the bottom 9 cm when the first three and last three soil depths were composited for analysis. The primary clay minerals contained in the media were illite, kaolinite, goethite, gibbsite, and a vermiculite/chlorite-like mineral.

There was also a trend of increasing coefficient of uniformity and particle size range with depth in the media profile (Figures 4a-b), again, with the most visible difference between the first three and last three depth profiles. Both coefficient of uniformity and particle size range were significantly lower in the upper 9 cm of the

media compared to the bottom 9 cm when the first three and last three soil depths were composited for analysis.

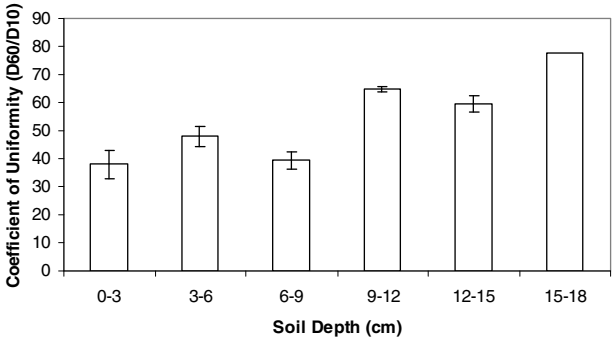

a

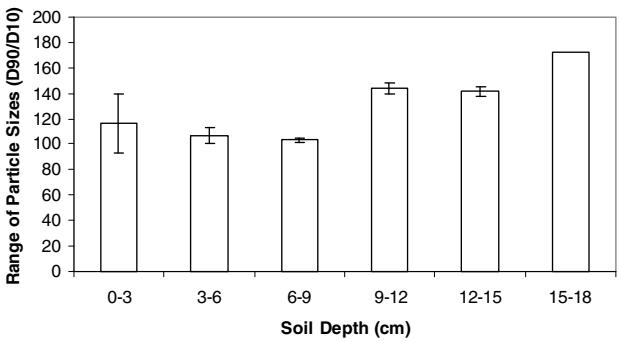

b

Figure 4. Coefficient of uniformity (a) and range of particle sizes (b) by soil depth. Error bars represent standard errors at each soil depth increment.

DISCUSSION

There were some differences between the control treatment and the two newspaper treatments, but because all three treatments demonstrated extensive surface ponding and slower drainage times during the high-flow treatment, the shredded newspaper is likely not the only factor impeding drainage. Other likely factors include the nonwoven geotextile wrapped around the drainage pipe and the relatively large percentage of clay particles in the media. The results from the media grain size analysis suggest the clay may be playing a role in reduced drainage capability. In particular, smaller mean particle sizes, both overall and at D_{10}, in the lower 9 cm of the media compared to the upper 9 cm, suggest that the smaller clay particles may be migrating to the lower half of the media profile (Figure 3) and forming a clay layer that impedes drainage. The larger coefficient of uniformity and range in the lower 9 cm compared to the upper 9 cm of the media (Figure 4) suggest that the particle size distribution is less uniform and spans a wider range of particle sizes at depth. This pattern points to the presence of more small clay particles in the lower half of the media profile, which could inhibit drainage. The clay contained in the media consists of minerals which are not typically prone to swelling; however, illite is known to absorb water and become gel-like if saturated. This could have a negative effect on drainage.

The shredded newspaper does affect effluent flow rates. There are some indications that the newspaper may be impeding drainage compared to media that does not contain the newspaper (Figures 1 and 2). The difference in flow rates is not large enough to conclude that shredded newspaper layers are an impractical soil amendment in rain garden applications.

CONCLUSIONS

Results of this bench-scale study indicate that layers of shredded, unprinted newspaper in rain garden media reduce stormwater effluent flow rates. However, the reduction in flow rates is not large enough to preclude the use of shredded newspaper layers in rain garden applications. Findings also suggest that great care should be taken in choosing engineered media. A media with too much clay or too great a range in particle sizes could result in downward migration of small particles. This could negatively impact drainage rates.

ACKNOWLEDGEMENTS

This research at the Urban Watershed Management Branch, Edison, NJ, is supported by the Office of Research and Development, U.S. EPA. We would like to thank Clarence Smith, John Lapinski, Christa Casciolini, and Mike Cerrato at PARS Environmental for sample collection under EPA contract EP-C-04-064. We also thank Kirk Scheckel at EPA's Land Remediation and Pollution Control Division for conducting the clay mineralogy analysis.

Notice

The U.S. Environmental Protection Agency, through its Office of Research and Development, funded and managed, or partially funded and collaborated in, the research described herein. It has been subjected to the Agency's peer and administrative review and has been approved for external publication. Any opinions expressed in this paper are those of the author (s) and do not necessarily reflect the views of the Agency, therefore, no official endorsement should be inferred. Any mention of trade names or commercial products does not constitute endorsement or recommendation for use.

REFERENCES

Barrett, M. E. (2003). "Performance, cost, and maintenance requirements of Austin sand filters." *J. Wat. Res. Plan. Man.,* 129(3), 234-242.

Davis, A. P., Shokouhian, M., Sharma, H., and Minami, C. (2001). "Laboratory study of biological retention for urban storm water management." *Wat. Env. Res.,* 73(1), 5-14.

Davis, A. P., Shokouhian, M., Sharma, H., Minami, C., and Winogradoff, D. (2003). "Water quality improvement through bioretention: lead, copper, and zinc removal." *Wat. Env. Res.,* 75(1), 73-82.

Davis, A. P., Shokouhian, M., Sharma, H., and Minami, C. (2006). "Water quality improvement through bioretention media: nitrogen and phosphorus removal." *Wat. Env. Res.,* 78(3), 284-293.

Davis, A. P. (2007). "Field performance of bioretention: water quality." *Env. Engin. Sci.,* 24(8), 1048-1064.

Dietz, M. E. (2007). "Low impact development practices: a review of current research and recommendations for future directions." *Wat., Air and Soil Poll.,* 186, 351-363.

Dietz, M. E. and Clausen, J. C. (2005). "A field evaluation of rain garden flow and pollutant treatments." *Wat., Air, and Soil Poll.,* 167, 123-138.

Dietz, M. E. and Clausen, J. C. (2006). "Saturation to prove pollutant retention in a rain garden." *Env. Sci. Tech.,* 40(4), 1335-1340.

Hsieh, C. H. and Davis, A. P. (2005). "Evaluation and optimization of bioretention media for treatment of urban storm water runoff." *J. Envir. Engin.,* 131(11), 1521-1531.

Hsieh, C. H., Davis, A. P., and Needelman, B. A. (2007). "Bioretention column studies of phosphorus removal from urban stormwater runoff." *Wat. Env. Res.,* 79(2), 177-184.

Hunt, W. F., Jarrett, A. R., Smith, J. T., and Sharkey, L. J. (2006). "Evaluating bioretention hydrology and nutrient removal at three field sites in North Carolina." *J. Irr. Drain. Engin.,* 132(6), 600-608.

Kim, H., Seagren, E. A., and Davis, A. P. (2003). "Engineered bioretention for removal of nitrate from stormwater runoff." *Wat. Envir. Res.,* 75(4), 355-367.

Klein, R.D. (1979). "Urbanization and stream quality impairment." Wat. Res. Bull., 15(4), 948-963.

Lee, H., Lau, S.-L., Kayhanian, M., and Stenstrom, M. K. (2004). "Seasonal first flush phenomenon of urban stormwater discharges." *Wat. Res.,* 38(19), 4153-4163.

McClain, M. E., Boyer, E. W., Dent, C. L., Gergel, S. E., Grimm, N. B., Groffman, P. M., Hart, S. C., Harvey, J. W., Johnston, C. A., Mayorga, E., McDowell, W. H., and Pinay, G.. (2003). "Biogeochemical hot spots and hot moments at the interface of terrestrial and aquatic ecosystems." *Ecosys.,* 6, 301-312.

U.S. Geological Survey. (1999). The Quality of Our Nation's Waters – Nutrients and Pesticides. *U.S. Geological Survey* Circular 1225, 82 p.

Walsh, C. J., Fletcher, T. D., and Ladson, A. R. (2005). "Stream restoration in urban catchments through redesigning stormwater systems: looking to the catchment to save the stream." *J. N. Amer. Benth. Assoc.,* 24(3), 690-705.

EPA Aging Water Infrastructure Research Program: State of the Technology for the Condition Assessment and Rehabilitation of Wastewater Collection Systems

Daniel J. Murray, Jr., P.E., M.ASCE[1]

[1]U.S. Environmental Protection Agency, Office of Research and Development, National Risk Management Research Laboratory, 26 W. Martin Luther King Drive (689), Cincinnati, Ohio, 45268, PH (513) 569-7522, e-mail: murray.dan@epa.gov

ABSTRACT

In 2007, the U.S. Environmental Protection Agency's Office of Research and Development (ORD) initiated a new research program to address our nation's aging water infrastructure. Under this new program, ORD established the goal to conduct research and demonstrations, and develop technical guidance to transfer innovative technologies and approaches for:

- More cost-effective operation, maintenance, repair and replacement of aging and failing drinking water and wastewater systems and
- Development and application of advanced designs and management approaches for drinking water and wastewater systems.

In addition, in its research plan for this new program, ORD structured the program following an advanced asset management framework. Under this framework, the program would focus primarily on buried water infrastructure and investigate new and innovative technologies and approaches for condition assessment, rehabilitation and infusion of advanced concepts. This paper presents the issues and state of the technology for the condition assessment and rehabilitation of wastewater collection systems, as defined to support this new research program.

CONDITION ASSESSMENT OF WASTEWATER COLLECTION SYSTEMS

Since the passage of the Water Pollution Control Act Amendments, better known as the Clean Water Act (CWA), in 1972, the major focus of sewer system condition assessment and rehabilitation has been the reduction of infiltration and inflow (I&I). Requirements for sewer system assessments were codified in the Rules and Regulations for Sewer Evaluation and Rehabilitation (40CFR35.927) and stated that U.S. EPA construction grants could not be approved unless there was documentation that sewer systems contributing to municipal wastewater treatment plants were not exhibiting "excessive infiltration and inflow." (EPA, 1991)

The focus of sewer system condition assessment and rehabilitation on the reduction of I&I, almost exclusively targeted excessive hydraulic loading in collection systems and at treatment facilities to lower capital and operation and maintenance costs, and to prolong the lifetime-capacity of the treatment facility. (EPA, 1991) While I&I still plague our current wastewater collection systems and is linked to our current challenges relating to sanitary sewer overflows (SSOs) and wastewater blending, comprehensive asset management is broadening the focus of sewer system condition assessment. In addition to condition assessment that seeks to determine

excessive hydraulic loading and I&I, currently practiced comprehensive asset management assesses the likelihood that a capital infrastructure asset will deteriorate and potentially fail, and the consequences of that deterioration and failure in terms of costs and effect on the system's ability to deliver desired services and meet performance measures. (GAO, 2004)

As the focus of condition assessment continues to broaden to include targets beyond the reduction of excessive hydraulic loading due to I&I, sewer system inspection technologies and investigation approaches must evolve. More innovative technologies will take advantage of observation and detection technologies, such as sonar, laser, ultrasonic, and infrared, not traditionally applied to sewer system investigation. In addition, the deployment of these non-traditional technologies will be supported by emerging digital, modular, and robotics technologies to greatly expand the "reach" of sewer system inspection techniques.

Corrosion of wastewater collection infrastructure, especially concrete sewers, is a significant cause of deterioration and premature failure. When exposed to the internal atmosphere of gravity sewers which is characterized by high humidity and the presence of hydrogen sulfide, sulfuric acid corrosion negatively affects concrete surfaces, mortar, and metal reinforcement material. Given this universal challenge for wastewater utilities, this research program will look into innovative inspection technologies and condition assessment methods that address corrosion-related wastewater infrastructure issues.

Deteriorating collection systems can result in excessive infiltration of rising groundwater during high water table seasons and wet weather events, and the export of recharge water from watersheds. When this is combined with increased impervious surfaces and water withdrawals resulting from urban growth, the effect of these man-made influences on the natural water balance can result in reduced flows in streams affecting aquatic ecosystems and decreased water availability. The application innovative assessment techniques to determine relationships between aging infrastructure and altered water balances, leading to measures to reduce or mitigate resulting adverse consequences is needed.

Force mains are a relatively small, but important, segment of the wastewater collection system infrastructure needing assessment. Force mains convey pumped sewage. There are about 30,000 miles of force mains in the nation. Based on a sewer pipe inventory of approximately 600,000 miles, force mains comprise about 5% of the total, by length. Because of hydrogen sulfide generation in wastewater collection systems, force mains are more prone than drinking water pipes to corrosion at the crown of the pipe. The average length of force mains is around 3600 ft. About 60% of the total length of force mains is constructed of ferrous materials, with ductile iron being the dominant material. A significant percentage of ductile iron installed has an internal lining that is most commonly cement mortar. For diameters of 36 inches and greater, pre-stressed concrete cylinder pipe (PCCP) and concrete cylinder pipe (CCP) are the dominant types. For diameters up to 20 inches, asbestos cement has a small but not insignificant percentage. For diameters less than 12 inches, polyvinyl chloride (PVC) and polyethylene (PE) account for about a third of the length installed. Because most force mains are in constant service and cannot be accessed internally for inspection without expensive by-passing arrangements, condition assessment is often difficult. Innovative, external condition assessment technologies are needed to facilitate inspection of force mains while they are in operation.

Related to wastewater collection system inspection and condition assessment is the evaluation of sewer system security vulnerabilities. In today's climate, vulnerability assessment of the collection system should be an integral part of an overall system condition assessment program. A recent GAO report found that few utilities have or are planning to install monitoring or security devices to detect and prevent system intrusions. (GAO, 2006) Recent work, funded by EPA, has been conducted by ASCE and WEF on monitoring systems and physical security enhancements, including security measures for wastewater collection systems. This program will coordinate with EPA's Water Security Division and National Homeland Security Research Laboratory to assist wastewater utilities in developing and implementing comprehensive inspection and condition assessment programs.

STATE OF THE TECHNOLOGY

The ability to visually examine the internal condition of a gravity sewer using internal cameras, usually closed circuit television (CCTV), has been the most important development in the area of inspection and condition assessment, leading to the current operation, maintenance and rehabilitation techniques employed by wastewater utilities. Incremental improvements continue to be made to CCTV technology and as electronic components become more affordable, this technology can be applied by most contractors and plumbers. Basic CCTV systems which can inspect small-diameter sewer and drain pipes can be purchased for less than $1500. Also, a standard investigation of a sewer line can cost a utility no more than $1 per foot. (WERF, 2004) In addition, the National Association of Sewer Service Companies (NASSCO) provides a wide range of training programs to standardize the application of condition assessment techniques. NASSCO's programs address the assessment of sewer pipe, manholes and service laterals.

Most utilities have established fairly simple rating systems which use the results from CCTV investigations to make an overall assessment of each section of sewer being inspected. This rating can then be combined with other data and information, such as results from hydraulic evaluations, sewer location, known soil conditions, and operational records, to determine maintenance and system rehabilitation priorities. However, CCTV assessments are qualitative and rely heavily on the skill of the investigation personnel to make judgments on the condition of the sewer. Also, this technology does not provide quantitative data to determine variations in sewer dimensions, subtle deformations, or debris level. Also, CCTV does not permit assessment of pipe condition below the water line within a sewer. While many sewers can be inspected during dry weather conditions to limit this issue, most trunk sewers maintain a fairly high flow and diverting these flows for inspection purposes is difficult. (WERF, 2004)

The application of CCTV in combination with newer technologies is currently being used in sewer inspections. Sonar technology, which uses high-frequency sound waves, can identify defects, especially large cracks, in the wall of sewer pipes and because it is almost exclusively designed to work underwater, it can overcome one of the shortcomings of CCTV. Laser technology can be used to identify variations in sewer pipes above the water line. Comparison of laser images of the interior dimensions of a sewer over time can be an effective method to determine temporal deterioration. (WERF, 2004)

One potential research issue emerges from this analysis of the state of technology for condition assessment. Given the ubiquitous application of CCTV for sewer inspections and condition assessment, a state of the art evaluation and technology transfer product on optimized application of CCTV results for condition assessment could be generated in the early phases of this research program. Wastewater utilities that are well known for their innovative application of CCTV could be identified and a best practices assessment and tool produced. In addition, this effort could include optimizing the use of existing and historical data and information, in combination with CCTV information to establish baseline assessments.

REHABILITATION OF WASTEWATER COLLECTION SYSTMES

The objective of system rehabilitation is to ensure the overall viability of the collection system to maintain operational and structural integrity and to prevent or reduce infiltration, inflow and exfiltration and their negative environmental impacts. There are several primary concerns related to deteriorating sewers. On a daily basis, significant pipe defects can cause blockages that lead to dry weather sewer overflows and backups into buildings. Water that flows into sewer pipes through defects (holes, cracks, failed pipe joints) can weaken the critical soil-pipe structure. Fine soil particles carried into the sewer can eventually reduce soil support to a point causing pipe deformation and/or subsidence. Exfiltration of water from the sewer into the surrounding soil can also weaken support provided by the soil. Soil movement due to traffic movement can exceed design assumptions and result in soil-support related problems. Deposition of material and sewer blockages can result in septic conditions due to flat grades, high ambient temperatures and poor ventilation. These conditions are ideal for the development of sulfuric acid and resulting crown corrosion which reduces the structural integrity of concrete material and the reinforcing steel, commonly used sewer materials. High rates of infiltration and inflow can lead to sewer overflows, basement backups, significant system capacity issues and excessive peak flows at pumping stations and at treatment plants. Although an infrequent occurrence, exfiltration of sewage into the surrounding soil can lead to groundwater and soil contamination. In some instances, water pressure drops in water distribution pipes adjacent to exfiltrating sewers can result in contamination of the potable water supply. In many cases, these problems are the result of faulty sewer designs. In addition, inadequate inspection, quality assurance and poor construction workmanship during sewer installation can result in long-term problems due to poor workmanship. (Tafuri and Selvakumar, 2002)

Generally, rehabilitation includes a broad spectrum of approaches, from repair to replacement that attempt to return the system to near-original condition and performance. Rehabilitated systems can be improved to provide hydraulic conditions and structural integrity better than the original sewer. Repair techniques are used when the existing sewer is structurally sound, provides acceptable flow capacity and can serve as the support or host of the repair method. When the existing sewer is severely deteriorated, collapsed, or increased flow capacity is needed, it is usually replaced. Current rehabilitation methods generally address unsound structural conditions. A wide range of causes can be responsible for sewer line deterioration and failure. These include:

- inadequate or improper bedding material,
- chemical attack,

- traffic loadings,
- soil movements,
- root intrusion,
- compromised joint integrity,
- subsequent construction damage,
- groundwater fluctuations,
- poor design and installation, and
- inadequate maintenance. (WERF, 2000)

Effective system rehabilitation programs require a complete understanding of the condition and performance of the collection system, including factors that affect system integrity and operations. Pipe age is a factor; however, pipe deterioration is very complex and it is usually a combination of several factors that causes failures and influences rehabilitation decisions, leading to a very complex decision-making process. Pipe materials, bedding and backfill materials, surrounding soil conditions, loads and stresses on the pipe, groundwater levels, sewage and soil acidity, sewage dissolved oxygen levels, and electrical and magnetic fields are factors that negatively impact long-term integrity and operational performance of the collection system. The results from a sound system inspection and condition assessment program provide critical input to decision support tools that evaluate the condition of the system based on structural, hydraulic, service delivery, water quality and economic factors.

Building connections to street sewers, referred to as house or service laterals, can contribute as much as 70 to 80% of the infiltration to a sewer. Fluctuating ground water, variable soil characteristics and conditions, traffic, erosion, washouts, etc., cause enormous stresses on house/service lateral pipes and joints. Connectors and fittings in many cases do not retain their watertight integrity while adjusting to these factors. Some connections react to soil acid and may totally disintegrate in a few years. These conditions often result in major points of infiltration at the connection of the house/service lateral to the street lateral or main. With current technology, rehabilitating building connections has become technically feasible but, because of the shear number of connections and cost for service renewals, is a significant additional cost. Economics and conditions of service renewals may make this difficult to address systematically. The problem is both critical and sensitive because of legal jurisdiction, private ownership and costs associated with disturbance to the occupant and destruction of valuable landscaping. Because of this, municipalities are often reluctant to address infiltration and inflow problems from these sources. (Tafuri and Selvakumar, 2002)

STATE OF THE TECHNOLOGY

Collection system rehabilitation includes a wide range of repair and replacement options that can be used to return the system to acceptable levels of performance. Pipeline rehabilitation procedures are usually preceded by some form of cleaning to remove foreign materials before other phases of rehabilitation. The removal of roots, sediments, and debris is also a critically important practice for maintaining operational performance levels including ensuring proper flow conditions, reducing infiltration and exfiltration and preventing structural damage to the pipeline. Common repair methods of chemical and cement grouting address problems associated with groundwater movement, washouts, soil settlements, collapses, and soil voids. Grouting is

marginally effective in reducing or eliminating infiltration but will not significantly improve the structural condition and has a limited life-cycle. It does, however, help stabilize the surrounding soil mass. Other system repair approaches include sliplining, spiral-wound pipe, segmented liner pipes, cured-in-place pipe (CIPP), fold and form pipe, close-fit-pipe, coatings, mechanical sealing devices, and spot repair. Many rehabilitation methods marginally reduce pipe cross-sectional area and can reduce hydraulic performance, but generally improve the system hydraulics.

Trenchless technologies have moved to the forefront of sewer system rehabilitation. Many are proprietary systems and the details of installation procedures and materials are trade secrets, limiting the ability to compare and evaluate competing approaches. For some techniques, codes and standards have been developed; however, because of the rapidly evolving technology in rehabilitation, standards and codes often lag behind. Trenchless technologies are applied in both repair and replacement situations. Pipe replacement technologies include pipe bursting, pipe splitting, pipe reaming and pipe eating. These trenchless replacement techniques install a new sewer in the location of the old pipe without total surface digging and accompanying traffic and business disruptions.

It is significant to mention that past studies have found that rehabilitation of sewers at the street alone does not completely solve the infiltration problem. Successive rainfalls can elevate the groundwater table to levels where entry occurs through service laterals. When performed, rehabilitation of service laterals is generally done by point repair or replacement; cured-in-place lining, sliplining and pipe bursting are sometimes used. These approaches do not overcome the private ownership problem or the problems associated with the location and configuration of the line (sharp bends/transitions) or the line condition (massive roots).

System rehabilitation includes repairing or replacing appurtenances (manholes, pump stations, wet wells, and siphons) which is an important component of a comprehensive program. About 30 to 50 percent of system infiltration and inflow is due to defects in or near appurtenances, in particular, manholes. For example, manhole covers submerged in one inch of water can allow as much as 75 gallons per minute to enter the system depending on the number and size of holes in the cover. Rehabilitation of manholes, pump stations, and wet wells includes spray-on coatings, spot repairs, structural liners, and replacement. Rehabilitation of siphons includes some of the options available for pipelines such as grouting and lining. Many siphons have been rehabilitated using either CIPP or high density polyethylene (HDPE) liners. (Tafuri and Selvakumar, 2002)

Selection of rehabilitation methods and materials suitable for various parts of the wastewater collection system remains an issue, especially due to ever emerging new materials and methods of construction. Uncertainty in the selection of appropriate repair and replacement techniques is partly related to the lack of understanding of the capabilities of each methodology to solve the problem in the long term. Reliable rehabilitation product performance under actual field conditions, especially over longer periods of performance, is lacking. Data on the effectiveness and longevity of rehabilitation technologies and materials and life-cycle cost information will be useful in determining whether rehabilitation or replacement is more cost effective.

The introduction of sewer pipes made from plastic materials has replaced in the market the more traditional sewer pipes constructed from concrete, clay and ductile iron. Plastic pipe has and continues to be an area of innovation for sewer pipes. The most commonly used materials for wastewater applications are polyvinyl chloride (PVC), polyethylene (PE) and glass reinforced plastic (GRP). Plastic pipe innovations include structured wall pipe and composite pipe that use different pipe materials to address both structural and corrosion issues. The application of plastic pipe in wastewater is becoming standard practice, resulting in the need for determining long-term performance and related testing. In addition, raw materials and formulations can vary widely, resulting in different quality pipe for the same plastic.

REFERENCES

Tafuri, Anthony, N. and Ariamalar Selvakumar, Wastewater Collection System Infrastructure Research Needs in the USA, Urban Water, Vol. 4, Issue 1, 2002.

U.S. Environmental Protection Agency, Handbook – Sewer System Infrastructure Analysis and Rehabilitation, EPA/625/6-91/030, October 1991.

U.S. Government Accountability Office, Water Infrastructure – Comprehensive Asset Management Has Potential to Help Utilities Better Identify Needs and Plan Future Investments, GAO-04-461, March 2004.

U.S Government Accountability Office, Securing Wastewater Facilities – Utilities Have Made Important Upgrades but Further Improvements to Key System Components May Be Limited by Costs and Other Constraints, GAO-06-390, March 2006.

Water Environment Research Foundation, New Pipes for Old: A Study of Recent Advances in Sewer Pipe Materials and Technology, 97-CTS-3, 2000.

Water Environment Research Foundation, An Examination of Innovative Methods Used in the Inspection of Wastewater Systems, 01-CTS-7, 2004.

Evaluation and Optimization of Distributed Stormwater Controls in Spreadsheet

Joong Gwang Lee[1], Ph.D, M.ASCE and Scott D. Struck[2], Ph.D., M. ASCE

[1]Tetra Tech, Inc., 350 Indiana St., Suite 500, Golden, CO 80401; PH: (720) 881-5871; FAX: (303) 217-5705; email: joong.lee@tetratech.com
[2]Tetra Tech, Inc., 350 Indiana St., Suite 500, Golden, CO 80401; PH: (720) 881-5837; FAX: (303) 217-5705; email: scott.struck@tetratech.com

ABSTRACT

Maximizing on-site stormwater management is one of the key concepts of distributed stormwater controls, such as those used as a part of Low Impact Development (LID) and sustainable sites approaches. These approaches are usually expressed as (1) maximize on-site depression storage and infiltration, (2) minimize runoff discharge by minimizing directly connected impervious area (DCIA), (3) maximize flow paths and time of concentration, and (4) maximize the potential for evaporation and/or evapotranspiration (ET). A few process models are available to evaluate these types of distributed stormwater control alternatives directly. The purpose of this paper is to describe how to evaluate and optimize distributed urban stormwater control options in a spreadsheet environment. One methodology to evaluate stormwater control alternatives is to compare total runoff volume from long-term continuous simulation. Using a lumped simulation model, it can be difficult to adequately represent the physical characteristics of distributed onsite LID options. Another alternative evaluation and optimization method based on lot-level detailed functional spatial information and explicit rainfall-runoff estimation is presented in this paper.

INTRODUCTION

Excess runoff drainage and flood control have been the main targets of stormwater management in the past. This approach generally relied upon designing for larger storm events and larger watersheds. Usually, 5- to 10-year return periods were used for designing drainage systems and 25- to 100-year periods were used for designing flood control facilities. However, the most frequent and highly contaminated urban runoff is typically contributed by storm events with a two-year or less return period (Guo and Urbonas 1996; Pitt 1999). Guo and Urbonas (1996) show nearly 95 percent of runoff producing events may be smaller than a two-year storm as demonstrated by the runoff event distribution for Denver, Colorado. Shueler (1992) described 6-month or shorter frequency storms likely contribute approximately 90% of the annual pollutant load. A number of technical approaches have been applied to reduce the negative impacts of these smaller storms. Those efforts are usually a suite of best management practices (BMPs) termed LID or Sustainable Urban Drainage Systems (SUDS) (British terminology).

Most of the LID/SUDS style approaches are developed with a highly distributed spatial pattern. Maximizing onsite stormwater management is a key concept of distributed stormwater controls. One of the most effective runoff quality controls is reducing the quantity of runoff, i.e. peak and volume (ASCE-WEF 1992). One of the more effective ways to solve urban runoff problems is to control them as close to the source as possible (Dunne and Leopold 1978; ASCE-WEF 1992) by maximizing onsite infiltration and minimizing runoff discharge as summarized below.

- Maximize onsite depression storage and infiltration
- Minimize runoff discharge by minimizing directly connected impervious area
- Maximize flow paths and time of concentration
- Maximize the potential for evaporation and/or evapotranspiration (ET)

A few process models are available to evaluate these types of distributed stormwater control alternatives directly. This paper will describe a methodology to evaluate and optimize distributed urban stormwater control options in a spreadsheet environment.

EVALUATION OF DISTRIBUTED ONSITE STORMWATER CONTROLS

Process dynamic models can be applied to evaluate the performance of distributed stormwater controls. However, the models usually need a number of modeling parameters and relatively high level of technical experience. It is difficult to conduct a wide range of onsite BMP scenario analyses and apply design optimization when using stand-alone models. Some organizations have arranged relatively simple evaluation tools for the purpose of evaluating onsite LID/SUDS and other BMP options. For example, the Emeryville spreadsheet BMP model (Emeryville, CA) uses a runoff coefficient (i.e., Rational Method) for analyzing lot-level to neighborhood-scale BMP sizing. The Green Calculator (Center for Neighborhood Technologies, http://greenvalues.cnt.org/calculator) estimates the benefit of onsite LID BMP options on a neighborhood-scale by applying the curve numbers (i.e., TR-55) and the Modified Rational Method. The Northern Kentucky Spreadsheet Tool uses a TR-55 based approach for sizing BMPs with lot or site-level spatial scales. However, little background information is available to customize the models for other locations.

The Rational Method was originally developed to estimate a peak discharge from a site by a selected frequency design storm. This approach is frequently used for drainage system design. In applying this method, all of hydrologic conditions (e.g., surface condition, soil types, slope, depression storage, infiltration loss, etc.) at a drainage area are expressed in a single implicit modeling parameter, i.e., the runoff coefficient. Most available reference data for runoff coefficients are usually arranged by surface conditions and soil types. It may be difficult to model smaller areas with varied land use characterizations and soils when applying stormwater controls by manipulating a single lumped runoff coefficient. The NRCS Curve Number (CN) method was initially developed to estimate total runoff volume by applying a design storm (USDA-SCS 1986). The original model was introduced to aid in the design of flood controls based on agricultural and rural watershed conditions. The CN method

estimates runoff volume by using a single modeling parameter, i.e., the CN. This CN implicitly represents all of land surface and soil conditions at the drainage area as well.

Runoff occurs when rainfall satisfies surface storage and infiltration capacity during a certain period. Instead of using a single implicit parameter, it would be better to apply surface storage and infiltration rate directly in estimating runoff volume. Surface storage and infiltration capacity can explicitly represent a wide range of surface and soil conditions, including distributed onsite LID/SUDS and BMP options. Estimating runoff from rainfall can be expressed as follow:

$$Runoff = Rainfall - Storage - Infiltration$$

Storage in the above equation can include depression storage (DS) or initial abstraction for the runoff from a given contributing area. *Storage* also includes the stormwater control practice design storage volume, as well. Infiltration typically occurs only in pervious areas. *Infiltration* can be modeled by using a fixed infiltration rate, the time-dependent Horton's infiltration equation, or the physically based Green-Ampt equation. In this paper, a long-term continuous rainfall-runoff model was arranged by applying DS, design stormwater storage of a control practice, and a fixed infiltration rate. Each runoff estimation model for subareas and runoff control practices are presented in the next section.

MODEL ARRANGEMENT

A spreadsheet model was developed to evaluate the performance of distributed onsite LID options based on a conceptual residential lot. The lot consists of a rooftop, driveway, and yard. Four onsite BMP options were considered in the model: bioretention; paver blocks on driveway; grass swale in yard, which can drain and infiltrate rooftop runoff; and a green roof. Lot layout and potential BMPs are schematically presented in Figure 1. Table 1 shows sizes of each surface component with its DS and infiltration rate.

Table 1. Status of a Residential Lot.

Surface	Rooftop	Driveway	Yard	Sum
Area (m^2)	200	40	760	1000
DS (mm)	2.5	2.5	5.1	
Infiltration (mm/hr)	0	0	5.1	

It is assumed that 10% of rooftop runoff drains to the driveway and the remaining 90% runoff drains to the surrounding yard. The yard area that receives rooftop runoff was modeled as a grass swale in this analysis. This grass swale area was assumed to be 10% of the yard, which represents the existing condition.

In this analysis, the ultimate goal of onsite management controls was to manage the same runoff volume of pre-development condition runoff with post development

management controls by applying 10 years of data using continuous simulation. The pre-development condition was assumed to have grass or shrub covered pervious area, which has a higher DS (7.6 mm or 0.3 inches) and infiltration rate (6.35 mm/hr or 0.25 inch/hr) than the existing yard.

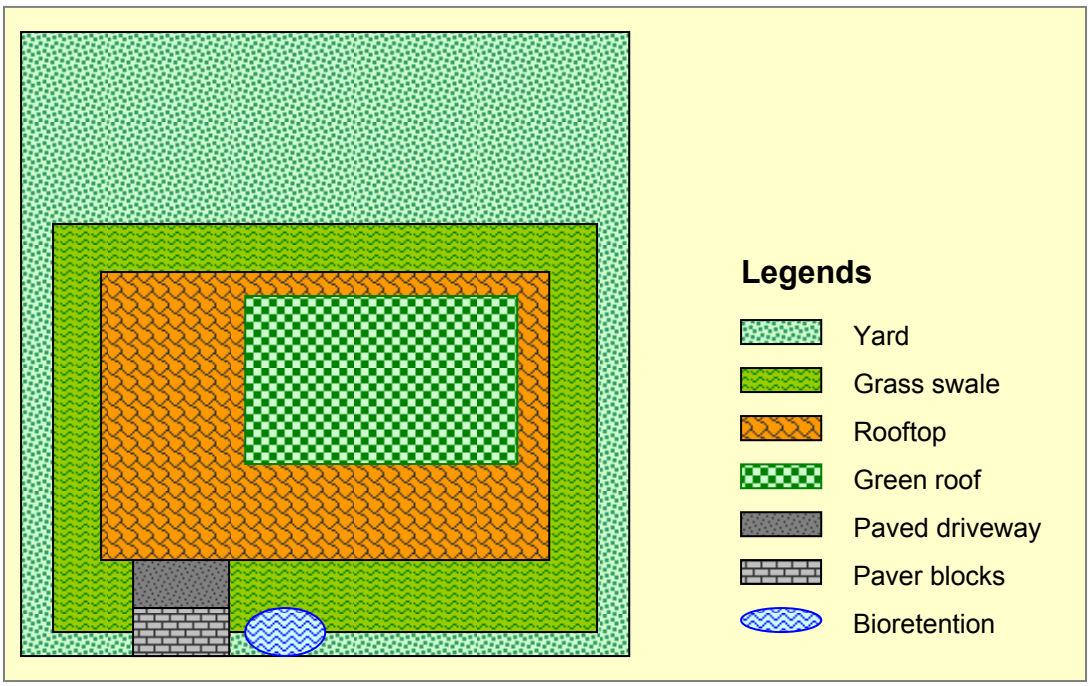

Figure 1. Schematic Lot Layout with Potential Onsite Control Practices.

Stormwater flow paths with onsite runoff management options are presented in Figure 2. If a certain BMP system is not included (i.e., no selection of the BMP), stormwater flow is simply bypassed to the next component.

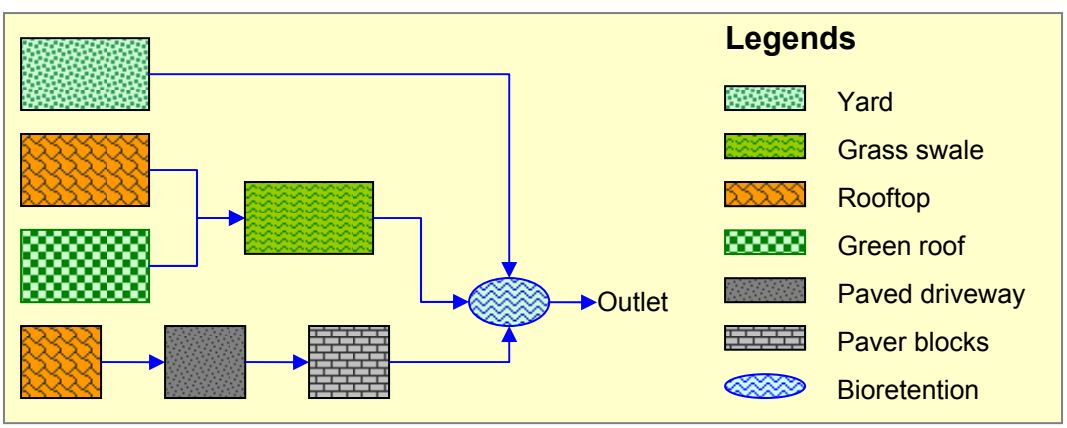

Figure 2. Stormwater Flow Paths with Potential Onsite Control Options.

During wet periods, runoff from each subarea and control practice was estimated as follows:

- Runoff from rooftop = *Rainfall – DS*

- Runoff from yard = *Rainfall – DS – Infiltration*
- Runoff from paved driveway = (*Rainfall* + *Runon* from rooftop) – *DS*
- Runoff from green roof = *Rainfall – Design Storage*
- Runoff from paver blocks = (*Rainfall* + *Runon* from paved driveway) – *Design Storage – Infiltration*
- Outflow from grass swale = (*Rainfall* + *Runon* from rooftop and green roof) – *DS – Infiltration*
- Outflow from bioretention = (*Rainfall* + *Runon* from yard, grass swale, and paver blocks) – *Design Storage – Infiltration*

While DS and design storage of a control practice would be filled by stormwater during wet periods, both can recover (dry out) during dry periods. Recovery could occur through evaporation and infiltration for paver blocks; ET for green roofs; and ET and infiltration for bioretention systems. Existing monthly average pan evaporation data from Chapel Hill, NC (Robinson 2005), which is close to Raleigh, NC. were used in this analysis. Using the pan evaporation data, monthly average ET was estimated by the following equation (Brouwer and Heibloem 1986):

$$ET = K_{pan} \cdot Evaporation$$

where, K_{pan} = pan coefficient; and *Evaporation* = pan evaporation from a free water surface.

The pan coefficient (K_{pan}) was assumed to be 0.75 in this analysis. Infiltration was estimated by applying soil infiltration rates and durations. To avoid any negative numbers or unrealistic values beyond the management practice design characteristics, MIN and MAX functions were used in the spreadsheet model.

MODEL APPLICATION

A case study was conducted by applying 10 years of long-term hourly precipitation records from Raleigh, NC to the model. Annual average precipitation is 1,116.2 mm (43.94 inches) during the period from January 1997 to December 2006. In order to conduct least-cost design optimization of distributed onsite control practice options, required cost functions for individual systems were arranged by applying site specific cost data from the same area (Hathaway and Hunt 2007) as shown below:

- Cost for bioretention ($) = 49.649 $(Area)^{0.9037}$
- Cost for green roof ($) = 135.71 $(Area)^{0.9596}$
- Cost for permeable pavement ($) = 103.44 (Area)
- Cost for swale ($) = 8.18 (Area)

where, (Area) = surface area of each BMP (m^2)

In this case study, design characteristics and surface areas of individual LID management controls were assumed as follows:

- Bioretention
  - Surface area: up to 3% of the lot
  - Design storage: 152.4 mm or 6 inches (e.g., 18 inches of media with 33% void space)
  - Infiltration: 5.1 mm/hr or 0.2 inch/hr (It is assumed to be the same as yard.)
- Green roof
  - Surface area: up to 50% of rooftop
  - Design storage: 26.7 mm or 1.05 inches (e.g., 3.5 inches of media with 30% void space)
  - No infiltration was assumed at green roof.
- Paver blocks
  - Surface area: up to 90% of driveway
  - Design storage: 61.0 mm or 2.4 inches (e.g., 12 inches of media with 20% void space)
  - Infiltration: 3.8 mm/hr or 0.15 inch/hr (It is assumed to be a little lower than yard, which has 0.2 inch/hr because of possible compaction during paver block installation.)
- Grass swale
  - Surface area: up to 40% of yard (Actually, it varies from 10 to 40% because 10% of the yard was already assumed as grass swale based on the existing condition as described earlier.)
  - DS: 6.35 mm or 0.25 inches (It is assumed a little higher than other grass area, which has 0.2 inches of DS.)
  - Infiltration: 5.1 mm/hr or 0.2 inch/hr (It is assumed to be the same as yard.)

Based on the goal of managing long-term runoff volume from developed areas to match pre-development runoff, the performance of onsite control practices was estimated as:

$$Performance = \frac{(Runoff_{current} - Runoff_{BMPs})}{(Runoff_{current} - Runoff_{pre-dev})}$$

where, $Runoff_{current}$ = runoff from the currently existing condition;
$Runoff_{BMPs}$ = runoff from the lot with management practices; and
$Runoff_{pre-dev}$ = runoff from pre-development condition.

If the performance reaches 100%, the onsite runoff control practices exactly mimic the pre-development conditions based on long-term runoff volume control.

Given the cost functions and the design constraints of individual onsite control options, then optimal solutions for specific stormwater volume control performances can be found by solving the following optimization problem:

Minimize *Total cost*
Subject to *Volume control performance ≥ Specific performance level*
Satisfy the design constraints of individual control options

In this case study, a number of least cost optimizations for sizing onsite control options were conducted with 5% increments of the stormwater volume control performance. Optimal sizing of required onsite runoff control practices for achieving a wide range of the volume control performance are presented in Figure 3. Because of the cost functions, bioretention was picked first and green roof was picked last as target performance increased.

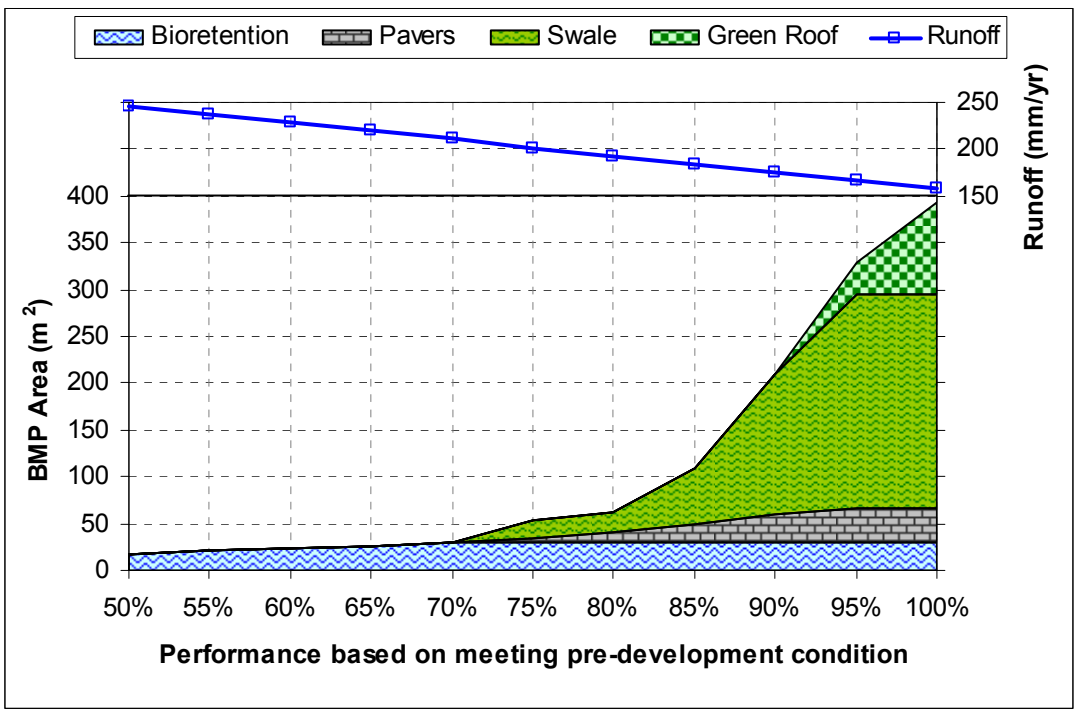

Figure 3. Optimal Sizes of Onsite Control Practices based on Performance Optimization.

Removed stormwater volumes by onsite control practices are presented in Figure 4. The figure indicates that bioretention and paver blocks controlled a greater portion of runoff volume even though their sizes, based on percent of surface area, were smaller than the other control options. These two control practices could facilitate both onsite storage and infiltration while the other two practices could provide only one of the two processes for reducing volume (i.e., grass swale could provide little storage of stormwater (beyond the small DS) and green roof could not infiltrate stormwater). Once runoff was captured through storage of onsite control practices during wet periods, the captured stormwater could be removed within the site by infiltration and ET (or evaporation for paver blocks). The removal functions can extend to the dry periods following the rainfall event until the captured stormwater has been removed from the control systems. While the grass swale was implemented in a larger area,

especially for higher performance ranges, the effective stormwater control volume was smaller than other practices because infiltration in the grass swale could occur only during wet periods. If the grass swale is designed with some storage capacity (e.g., by applying check dams), this control practice may perform more like a bioretention system. Storage volumes managed through bioretention systems and grass swales were decreased when implementing upstream control options based on controlling the runoff before reaching theses management controls.. Similarly, the runoff volumes necessary at downstream control options were decreased as the sizes of upstream control options increased.

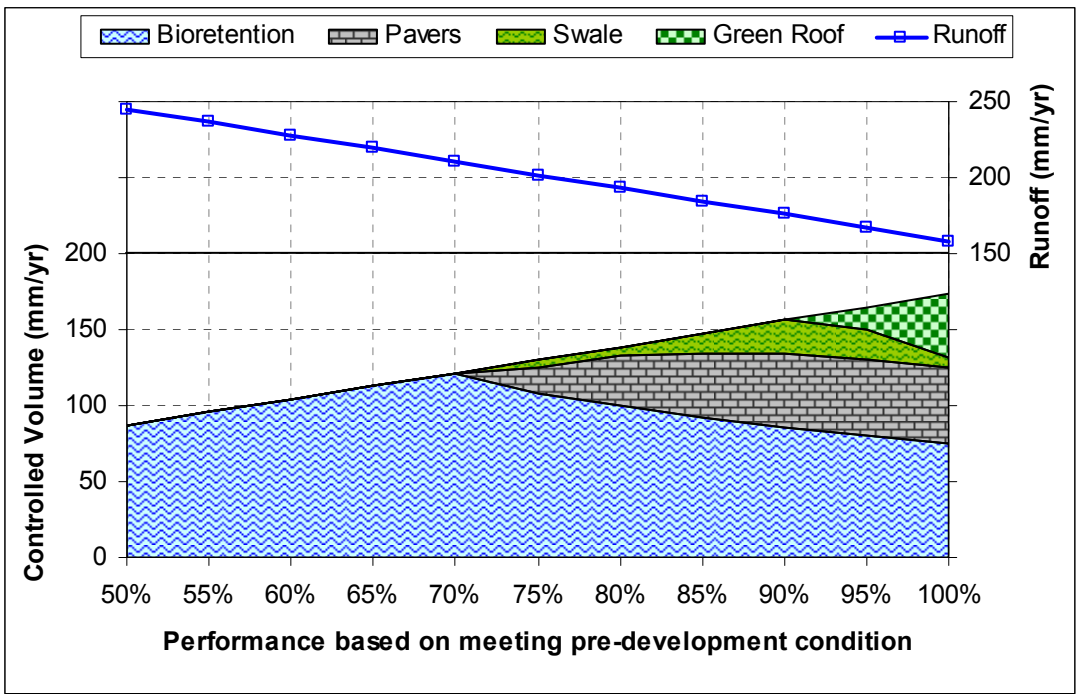

Figure 4. Volume Controlled by Onsite Control Practices based on Performance Optimization.

The total and marginal costs of the runoff control practice options are shown in Figure 5. As shown in the figures, to achieve higher performance in order to meet the goal of matching pre-development condition requires larger sizes of onsite BMPs and, similarly, requires a higher cost. This trend is most notable as the marginal costs of controlling unit runoff by onsite control practices increases to achieve greater than 90% performance. Instead of achieving 100% performance within the site, utilizing centralized regional control practices (e.g., a detention basin) could be a more cost-effective approach for the higher performance ranges. In this case, highly contaminated frequent smaller storms can still be controlled by distributed onsite practices.

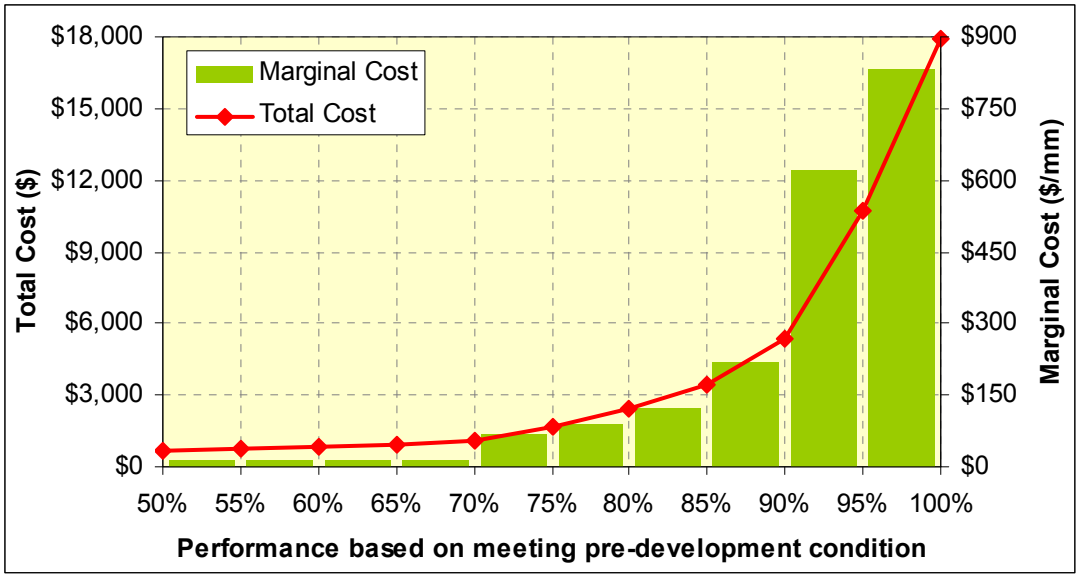

Figure 5. Costs of Collective Onsite Control Practices based on Performance Optimization.

SUMMARY AND CONCLUSIONS

This paper introduced an evaluation and optimization method for lot-level onsite LID control practice options using explicit modeling parameters. Four onsite management practice options for a residential lot were considered meeting pre- and post-development long-term runoff volumes. The four management practices modeled were bioretention, green roof, paver blocks, and grass swale. The application of this methodology may be applied to larger areas with additional runoff management options. Water quality simulation can be incorporated into the developed model if additional modeling parameters are available (e.g., buildup/washoff, inflow concentration, background concentration, pollutant removal rate, etc.). Applying site-specific data is critically important in finding the optimal management practice configuration because results could be varies substantially based on local site conditions. Because of this sensitivity analysis should also be considered when doing this kind of optimization.

REFERENCES

ASCE-WEF. (1992). *Design and Construction of Urban Stormwater Management Systems.* American Society of Civil Engineers. Water Environment Federation. ASCE No.77. WEF FD-20. ASCE, New York, NY

Brouwer, C. and Heibloem, M. (1986). *Irrigation Water Management: Irrigation Water Needs.* Training Manual No. 3. Food and Agriculture Organization (FAO) of the United Nations. Rome, Italy.

Dunne, T. and Leopold, L.B. (1978). *Water in Environmental Planning*. W.H. Freeman and Company, New York, NY.

Guo, J. and Urbonas, B. (1996). Maximized detention volume determine by runoff capture probabilistic models 1. runoff volumes. *Water Resources Research*. 34(12): 3421-3431.

Hathaway, J., and Hunt, W.F. 2007. Stormwater BMP Costs. North Carolina Department of Environment and Natural Resources. http://www.bae.ncsu.edu/stormwater/PublicationFiles/DSWC.BMPcosts.2007.pdf

Pitt, R. (1999). Small storm hydrology and why it is important for the design of stormwater control ponds. *New Applications in Modeling Urban Water Systems*. Ed. James, W. Computational Hydraulics, Inc., Chelsea, MI.

Robinson, P.J. (2005). *North Carolina Weather & Climate*. UNC Press, ISBN 0807856258, 9780807856253

Schueler, T.R. (1992). *Design of Stormwater Wetland Systems: Guidelines for Creating Diverse and Effective Stormwater Wetland Systems in the Mid-Atlantic Region*, Metropolitan Washington Council of Governments.

USDA-SCS. (1986). *Urban Hydrology for Small Watersheds. Technical Release No. 55*. Second Edition. U.S. Department of Agriculture, Soil Conservation Service. Washington, D.C.

Evaluation of Atriplx Shrubs Growth in Semi Arid Area

Mehemed A. Razzaghi

Associate Professor at Civil Engineering Department, Faculty of Engineering,
Al-Gabel Al-Gharbi University
P.O.Box 13688, Al-Fateh University, Tripoli, Libya.
PH: (218)913119629; FAX: (218)412634210; email: m_razzaghi@yahoo.co.uk

The effect of rainwater harvesting systems on the growth of Atriplx shrubs in semi arid land in western part of Libya was evaluated using two of rainwater harvesting systems (Contour lines and Negarim). Plant height, crown length, crown circumference and maturity were evaluated as measures to the effectiveness of these rainwater harvesting systems. Three micro-catchments area (10.2, 12.5, and 15.5 m^2) for each system were used. The catchment area was calculated on the basis of the average annual rainfall, surface runoff coefficient, plant water requirement, and root zone area. The ratio of the cultivated area to the catchment area was found to be 1:15. The growth of Atriplx shrubs was evaluated for two consecutive years. Both contour lines and negarim rainwater harvesting systems gave better results compared with the growth of the control shrubs (shrubs that were planted outside the W.H. systems). The overall efficiency of the systems varied from system to system and from catchment area size to other size. The contour line system and the larger ratio of the catchment area to the cultivated area were found to be strongly related to the growth of the shrubs.

Keywords: rainfall; rainwater harvesting systems; Atriplex; Negarim basin; contour ridges

INTRODUCTION

Rainfall is the major source of livelihood to the farming communities in Libya. The average annual rainfall drops from 350 mm near Mediterranean coast in the north to less than 100 mm in the central zone, where semi-desert/ desert climate dominates. Further in the south, full desert conditions prevails. Only a narrow northern band receives reasonable rain. Most of the area of the country is either rainless or receives negligible rain that does not help much in biomass production.

The rain-fed agriculture that contributes to production of grains and oils, mainly concentrates in the western mountains, green mountains in the east and valleys or wadies of deep soils and areas of runoff concentration. Traditionally, dams, cisterns and semi-circular (*lunar*) bunds are used as a way for rainwater harvesting. The existed water-harvesting infrastructure deteriorated due to lack of maintenance and being at low-priority, and it continued to be abandoned till recent past when the water resources became very limited and deteriorated in quantity and quality. Recently the government lunched a program to improve the existing rainwater harvesting systems with the adoption of latest technology and development in this field. As a result of that, the Agricultural Research Center (ARC) in Libya in cooperation with the International Center for Agricultural Research of Dry Areas (ICARDA) had conducted a field experiment in order to demonstrate the usefulness of water harvesting systems that suits to the country environment. The experiment aims at real-time testing and evaluating two potential micro-catchment rainwater harvesting systems in order to improve bio-mass production in a certain agro-climatic and geo-physical environment, which largely prevails in the northern areas of Libya.

EXPERIMENT SITE

The experiment site was chosen at the Gharian Pasture Project which is located at region of Qdama. Qdama is about 40 km south of Gharian city (13° 6' longitude and 31° 55' latitude). Figure 1 shows the project location. The site represents a large area with similar characteristics and it is in easy approach to manage. Moreover, it is located in a region designated as grazing area, which is in match with the project objectives. Australian Atriplex was tested for its succession by using contour ridges and Negarim basin rainwater harvesting systems. The main characteristics of the area around and the experiment site are as follows:

Climate

The experiment site is characterized by its semi-desert climate. Longtime data of nearby stations shows an average annual rainfall of 144 mm, and average annual of maximum and minimum temperatures being 23.3^{O}C and 13.3^{O}C respectively. Temperature may go above 40°C in summer and drop below zero in winter. Monthly climatic data shows that rainfall is likely to exceed evaporation during December, January and February and thus moisture storage should take place. Rainfall in March might just balance the evaporation. This balance might shift in April, when evaporation is likely to higher than the rainfall; however, residual moisture might cover a part of the moisture deficit. May, June, July and August being no rainfall, should be high moisture deficit months, when the plants should suffer from very low

evaporation and thus little or no growth. Rainfall in September, October and November might partly cover the moisture deficit till the time when rainfall is higher than the evaporation. So, the rainfall is one of the most important climatic parameters for the survival and succession of biomass in an area, which does not have other source of fresh water resources.

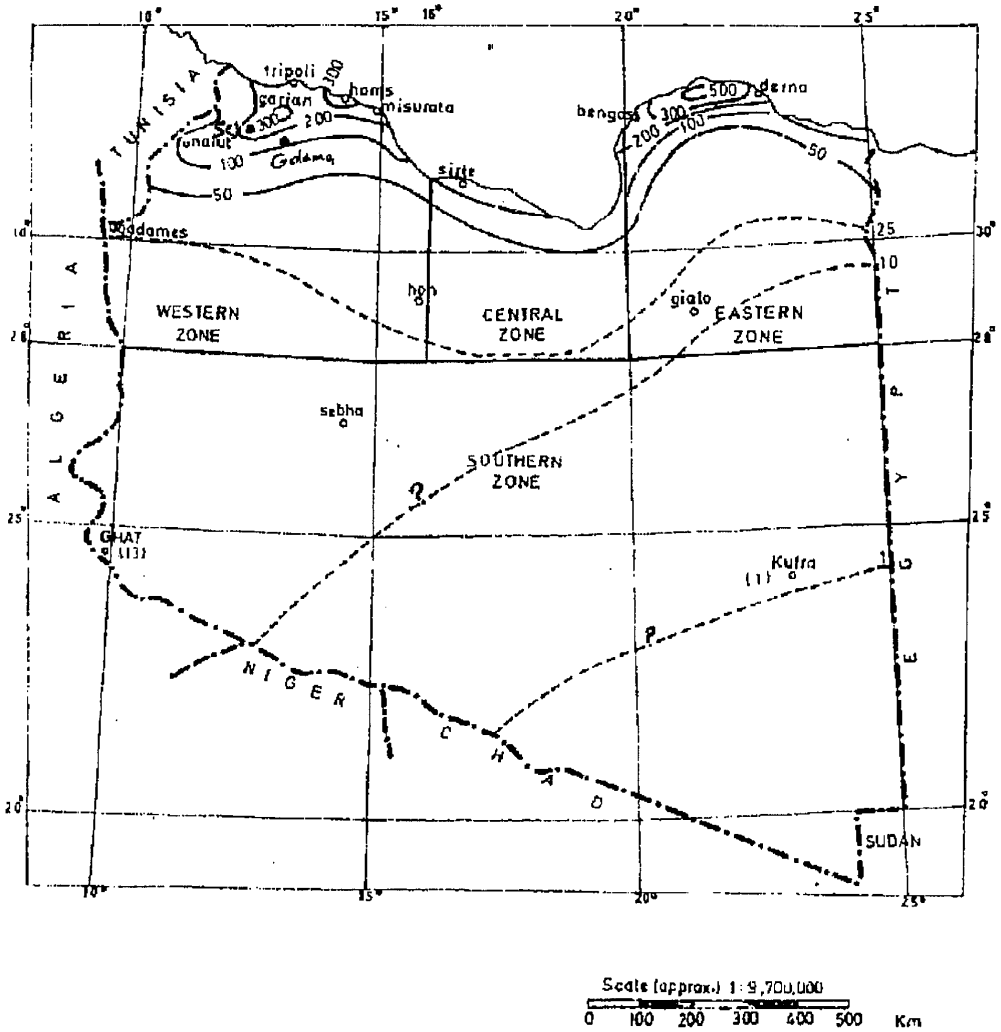

Figure 1: Isohyftal Map also shows the project location

Topography, Soil and Land Cover

The topography is rolling and undulating with slope variation between 2 and 20%. Dominant ground slope at experiment site is about 5%. A soil profile at the site indicates that the soil consists of 30 cm thick silt over a deep fragile layer limestone. It was noticed that plant roots have penetrated deeply into this layer. The soil can be classified as *Calcic Xerofluvents*. The family of *Artemisia Herb Alba* and *Hamada Scoparium* generally dominate in the area of the experiment. *Stipa Tenacissima* also sparsely exists.

EXPERIMENTAL DESIGN

The experiment aims at verifying the difference of biomass production with and without using water-harvesting systems and to quantifying this difference among control and two treatment cases. A recording rain gage was available near the experiment site and is the main source of site-specific rainfall data. Two potential rainwater harvesting systems, contour ridges and Nigarim basin, were evaluated. Three replicas of each were tested in order to minimize the experimental error.

The ratio of catchment to cultivated area (C/CA) was calculated on the basis of average annual rainfall, effective root zone and crop-water requirement with the use of values of runoff coefficient (50%). A C/CA value of 15:1 works out for the experiment site. Therefore, three sets with C/CA of 15:1, 12:1 and 18.75:1 were developed. The design parameters for contour ridges and Negarim basin are given in Table 1.

Table 1*:* Design parameters of contour ridges and Negarim micro-catchment water harvesting basins

C/CA	Contour ridges			Negarim basin		
	Mark	Total area (m^2)	Distance between ridges (m)	Mark	Basin total area (m^2)	Basin dimensions (m*m)
12:1	C1	10.2	6.8	N1	10.2	3.2*3.2
15:1	C2	12.5	8.4	N2	12.5	3.6*3.6
18.75:1	C3	15.5	10.4	N3	15.5	3.95*3.95

Field layout of experiment is shown in Figure 2. *Atriplex* was cultivated in each micro-catchment.

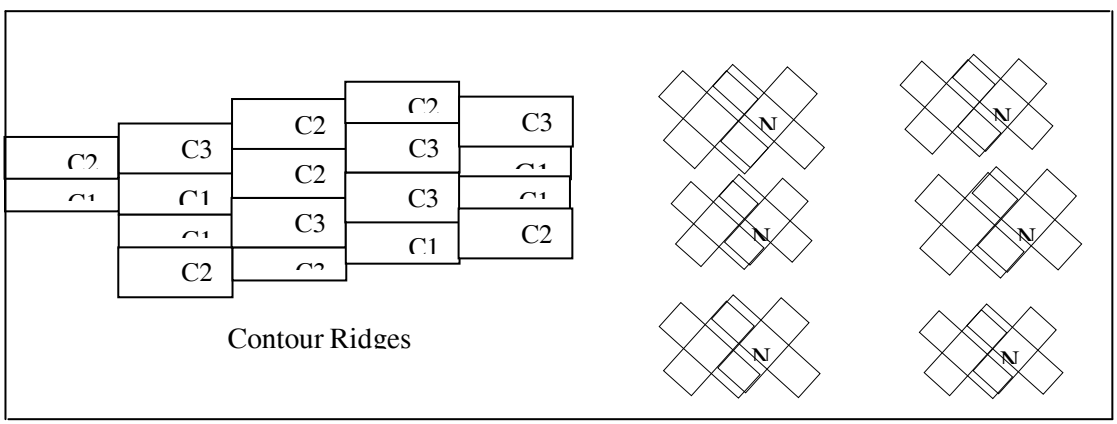

Figure 2: Field Layout of the Experiment

DATA COLLECTION ANALYSIS

The rainfall events for a period from 1998 – 2001 were recorded at rain gauge. Rainfall data of these events was collected from the rain gauge record.

Monthly and mean-monthly rainfall in mm at Qdama for period 1997-2001

Year	Sep	Oct	Nov	Dec	Jan	Feb	Mar	Apr	May	June	July	Aug	Annual
1997-98	74.5	38.0	0.0	26.5	49.0	13.0	54.2	0.0	0.0	0.0	0.0	0.0	255.2
1998-99	0.0	0.0	17.5	17.0	26.0	61.1	24.1	0.0	0.0	0.0	0.0	13.5	159.2
1999-2000	8.7	0.0	19.8	54.0	16.2	75.9	0.0	0.0	6.2	0.0	0.0	0.0	180.8
2000-01	0.0	94.0	0.0	0.0	16.3	80.8	0.0	6.2	0.0	0.0	0.0	0.0	197.3
Mean-monthly rain	***20.8***	***33.0***	***9.3***	***24.4***	***26.9***	***57.7***	***19.6***	***1.6***	***1.6***	***0.0***	***0.0***	***3.4***	

Atriplex growth was recorded at each micro-catchment, by the end of year 2000/2001, which includes plant height, crown diameter and plant maturity. A summary of collected data is given in Table 2 below.

Table 2: Summary of collected data on plant succession

Treatment	Cultivated area	Catchment area	Total area	Avg plant height	Avg crown length	Avg diameter	Biomass	Maturity
	m^2	m^2	m^2	cm	cm	cm	cm^3	%
Control				53.0	26.0	49.0	49004	16
C 1	0.785	9.4	10.19	59.0	57.0	90.0	362435	66
C 2	0.785	11.7	12.49	53.0	53.0	71.0	209731	51
C 3	0.785	14.7	15.49	62.0	58.0	110.0	550913	79
N 1	0.785	9.4	10.19	56.0	25.5	75.0	112598	44
N 2	0.785	11.7	12.49	55.5	39.0	71.0	154330	50
N 3	0.785	14.7	15.49	58.0	42.0	83.5	229875	62
C for Contour ridges and N stands for negarim basin								

RESULTS AND DISCUSSION

Rainfall

Rainfall data at Qdama from years 1997-2001 is presented in Figure 3(a), which shows an average annual rainfall of 199 mm. A comparison between long-time average (144 mm) and the average during study period reveals that as a whole the study period yielded high average and can be regarded as relatively wet period. Examining the data infers that 2–3 events of rainfall equal to or greater than 30 mm occur in every season. This means that a significant chunk of the annual rain falls in these 2–3 events and is thus available for shorter duration if not properly stored

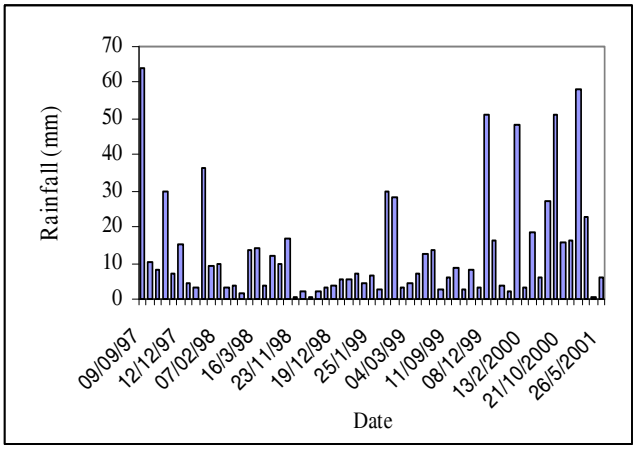

Figure 3(a): Event rainfall at Qdama, from 1997-2001 (Near water harvesting site)

Knowledge of month-wide distribution of rainfall is important to know the amount of water available for the biomass in rain-fed areas. Figure 3(b) shows mean-monthly and monthly rainfall at Qdama for the study period. Monthly rainfall also shows a high variability. Based on four-year data, it also shows zero rainfall in one of the four years (December is rainless for 25% of time), two out of four years (September, October, November and March are rainless for 50% of time), three of the four (April and May are rainless for 80% of time). January and February receives rainfall for 100% of time. The variability along mean is also high. It could negatively affect the biomass, if rainless conditions for the above-mentioned months continue for a couple of consecutive years.

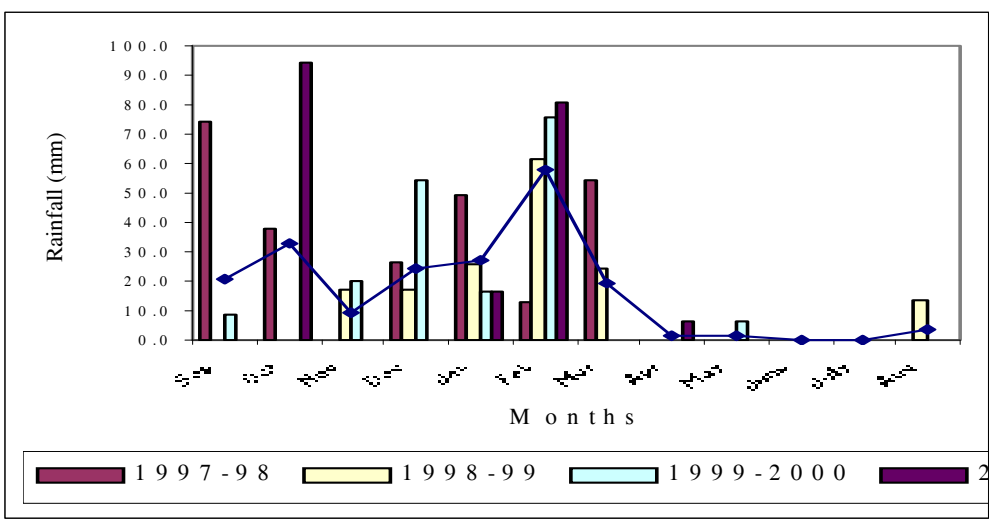

Figure 3(b): Monthly and mean-monthly rainfall at Qdama for the study period (1997 – 2001)

Atriplex succession in relation to treatments

Figure 4(a) is based on summary results, which shows the variation in plant height, crown sizes and plant maturity in relation to control, and three treatments of each contour ridges and Negarim basins. The results show a good survival rate for both the treatments and control case. These also indicate that for plant succession, both treatments performed better than control case, when the performance of contour ridges with a catchment area of 14.7 m^2 was the best among all treatments.

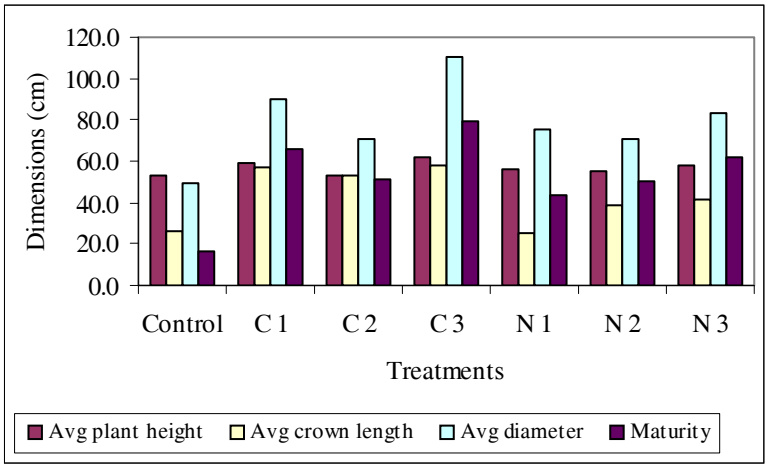

Figure 4(a): Plant height, crown sizes and maturity in relation to treatments

Figure 4(b) shows the variation of biomass in relation to size of catchment area for Negarim basins and contour ridges. It indicates that biomass growth was higher in case of contour ridges as compared with Negarim basin for all three catchment sizes, however, the catchment area of 14.7 m^2 performed better than the catchment areas of 11.7 and 9.4 m^2 for both the treatments. The performance of contour ridges with the catchment area of 14.7 m^2 was best among all alternatives. The volume of biomass for treatments as compared with control case is higher by 2.3 to 11 times, which shows the usefulness of water harvesting techniques. Figure 5 shows views of the shrubs growth.

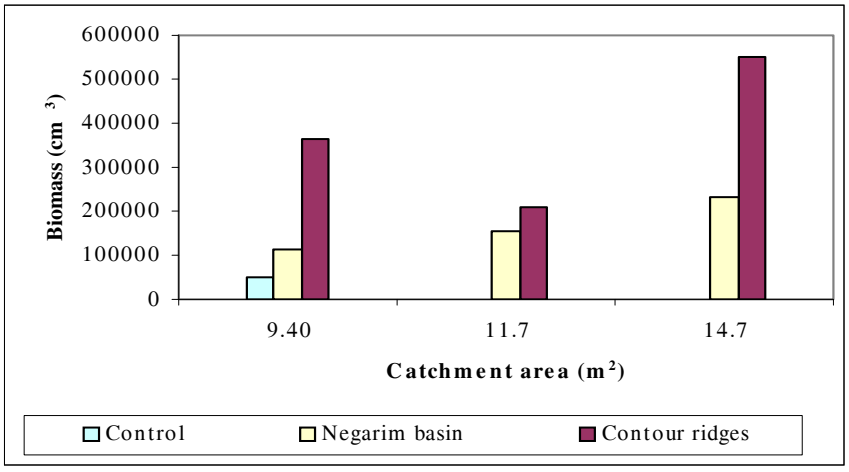

Figure 4(b): Biomass variation in relation to catchment area and treatments



Figure 5: General view of Atriplex growth inside the W.H. techniques

CONCLUSION:

As a result of this experiment, Contour ridges technique gave better results than the Negarim but we can not generalize this conclusion from a first evaluation unless the experiment is repeated.

The Experiment has proved that the Atriplx can be planted in downhill areas where was believed that in semi arid areas, only the bottom of the valley can be cultivated. The techniques used in the experiment are very simple and they can be constructed manually or by simple machines. The Contour ridges technique can be used for more than purpose, for example the area between the ridges can be cultivated by another grazing species.

REFERENCES:

[1] Bazz, M.; Tayaa, M. and Hassan, Iav ; "Operation and management of water Harvesting Techniques" Proceedings of the FAO Expert Consultation, Cairo, Egypt, 21 –25 November 1993. Doc. No. TD.17.

[2] FAO, 1994.Water harvesting for improved agricultural production, water report 3. Proceeding of the FAO Expert Consultation, Cairo, Egypt, November 1993. Rome, Italy: FAO.

[3] Frasier, G.W. 1994. Water harvesting/runoff farming systems for agricultural production. In: Water harvesting for improved agricultural production. Proceedings of the FAO Expert Consultation, Cairo, Egypt, Nov 1993. Rome. Italy: FAO.

[4] Frasier, G.W. and L.E. Myers. 1993 Handbook of water harvesting. Agricultural Handbook No. 600. USA: United States Department of Agriculture, Agriculture Research Service.

[5] Gintzburger, G. and Huxley, P.A. ; "Surface Water Micro-Catchment and Range Plant Establishment – A Preliminary Investigation" FAO/ARC Accn.234/79, March 1979

[6] Oweis, T., Hachum, A., Kijne, J. Water Harvesting and Supplemental Irrigation for Improved Water use Efficiency in Dry Areas, International Water Management Institute, 1999.

[7] Oweis, T. , and A.T. Taimeh. 1996 Evaluation of a small basin water harvesting system in the arid region of Jordan. Water Resources Management 10:21-34.

[8] Oweis, T., and D. Prinze. 1994. Identifacation of potential water harvesting areas and methods for the arid regions of West Asia and North Africa: A proposal for a regional research project. In: Water harvesting for improved agricultural production. Proceeding of the FAO Experts Consultation. Cairo, Egypt, Nov. 1993. Rome. Italy: FAO.

[9] Siegert. K. 1994. Introduction to water harvesting some basic principles for planning. Design and monitoring. In: water harvesting for improved agricultural production. Proceeding of the FAO Expert Consultation, Cairo, Egypt, Nov. 1993, Rome, Italy: FAO.

Evolutionary Optimization of Combined Sewer Overflow Control

Andrea Zimmer[1], David Hill[2], Barbara Minsker[1], Avi Ostfeld[4], Arthur Schmidt[1]

[1]Civil and Environmental Engineering, University of Illinois at Urbana-Champaign, [2]National Center for Supercomputing Applications, University of Illinois at Urbana-Champaign, [4]Civil and Environmental Engineering, Technion - Israel Institute of Technology

ABSTRACT

Model predictive control (MPC) is coupled with a real-coded Genetic Algorithm to predict a decision sequence that minimizes combined sewer overflow (CSO) volume for a 3-hour rainfall event over a hypothetical sewer system. Rainfall is transformed to overland runoff through the cell model which depicts each sewershed (draining to an overflow dropshaft) by two linear reservoirs in series, and water entering the interceptor is routed downstream to establish water levels at the dropshaft connections. A pumping rate at the most downstream end of the interceptor plus one sluice gate position for each dropshaft connection will be altered to produce the best control strategy. Resulting management scenarios disperse overflows differently throughout the sewer, but may yield similar overflow volumes. This paper describes the simulation approach taken and displays the overflow distribution for favorable control sequences.

INTRODUCTION

Combined sewers, such as those found in the Chicago region, are susceptible to overflows during severe rainfall events when runoff from urban sewersheds enters interceptor conduits through sluice gate connections. This runoff combines with sanitary sewage and may overwhelm the interceptor capacity. In an effort to minimize overflows that occur when flows exceed the sewer capacity, a genetic algorithm has been applied to a generalized hydrologic-hydraulic model to generate optimal management scenarios for a hypothetical sewer network.

Recent advances in the real-time control of sewer overflows include work by Darsono and Labadie (2007) to minimize overflow volumes and maximize flow to a wastewater treatment plant. A volume-based overflow control strategy is determined to be preferable to a pollution- or emission- based control. Pleau et al. (2005) use a multi-objective non-linear programming algorithm to minimize overflows (among other goals) in the Quebec sewer system by computing water levels for a control horizon discretized into 5-minute intervals. Generalized reduced gradient search has been applied to reduce combined sewer overflows by Cembrano et al. (2004); water levels are predicted for a 30-minute horizon at 5-minute control intervals. Rauch and Harremoes (1999) apply model predictive control in conjunction with a genetic algorithm to maximize the mean dissolved oxygen concentration below an urban wastewater system.

Application of model-based predictive control for real-time decision support has also been applied to the problem of aircraft arrival scheduling; Hu and Chen (2005) minimize the airborne delay of aircraft approaching a runway. Lee et al. (2005) utilize rolling horizon control and a binary coded genetic algorithm to minimize vehicle delays in real-time traffic signal control. Naeem et al. (2005) apply a genetic algorithm and model predictive control to the operation of an autonomous underwater vehicle. Further investigation of genetic algorithms used for predictive control has indicated that population initializing and sizing should be altered slightly for the specific predictive application (Onnen et al., 1997). A real-coded GA is appropriate for the CSO application addressed in this paper because it eliminates the need for the control variables to be converted to binary coding and enables the problem to be optimized without restructuring the physical formulation.

METHODS

The MPC formulation involves minimizing the predicted volume of overflow, V, calculated at sequential 15-minute time increments Δt, to be evaluated out to time horizon $t + (\Delta t \times N)$ based on system information available at time t.

$$\text{minimize} \sum_{k=1}^{N} \{V(t + (k \times \Delta t))|t\} \tag{1}$$

The variable t indicates the current time, and N is the number of time intervals in the prediction horizon. The value of N is set to 8 to designate a 2-hour prediction horizon divided into 15-minute intervals. The volume depends on the values of the current and future control signals which consist of one pumping rate and three sluice gate positions and are designated by the vector Y in Eqn. 2.

$$\sum_{k=0}^{N-1} \{Y(t + (k \times \Delta t))|t\} \tag{2}$$

The summation indicates the inclusion of all control signals within the prediction window. At time $t+1$, the control signal $Y(t)$ is implemented in the hydrologic-hydraulic model, and the computation is repeated with the prediction horizon (k) moving forward one interval. The interval t is advanced with k at Δt until no additional overflows are predicted within the window $t + (\Delta t \times N)$.

Within the MPC algorithm for the hydrologic-hydraulic system, the cell model introduced by Diskin et al. (1984), and further utilized by Karnieli et al. (1994) and Ostfeld and Pries (2003) is utilized to route excess rainfall water overland to each connecting structure. The model convolutes rainfall in accordance with a unit hydrograph U that has been created for the two linear reservoirs in series (Dooge, 1973) that represent each sewershed.

$$U(t) = \frac{e^{-t/K_1} - e^{-t/K_2}}{K_1 - K_2} \tag{3}$$

The variables K_1 and K_2 are the storage coefficients of each reservoir (in units of 1 over time); in this case $K_2 = 0.1K_1$ and K_1 is proportional to the sewershed area (A_c)

and an overall mean reservoir coefficient (A_{KC}) that can be used for calibration during implementation in an actual sewershed. The mean sewershed area is given as A_m.

$$K_1 = A_{KC}\left[\frac{A_c}{A_m}\right]^{0.5} \tag{4}$$

The hydrograph unit U is the inverse of time. The resulting hydrograph flows (Q_n) are generated for each sewershed through convolution of the linear system, where M is the number of input rainfall pulses (P_m) and n is the current time step.

$$Q_n = \sum_{m=1}^{n\leq M} P_m U_{n-m+1} \tag{5}$$

The precipitation P is a volume. Flows from each sewershed into the interceptor are calculated by equations derived by Swamee (1992) for flow under a sluice gate. Flow can occur either from the connecting structure to the tunnel or from the tunnel to the connecting structure. If the sluice gate is not submerged, the flow can be calculated by Eqn. 6

$$Q = 0.864ab\sqrt{gh_0}\left(\frac{h_0 - a}{h_0 + 15a}\right)^{0.072} \tag{6}$$

where a represents the height of the sluice-gate opening, b is the width of the gate opening, h_0 is the upstream water depth (the higher of the tunnel and the connecting structure water surface elevation), and g is gravitational acceleration. The same variables hold for the case of submerged flow in Eqn. 7

$$Q = 0.864ab\sqrt{gh_0}\left(\frac{h_0 - a}{h_0 + 15a}\right)^{0.072}(h_0 - h_2)^{0.7}\left[0.32\left[0.81h_2\left(\frac{h_2}{a}\right)^{0.72} - h_0\right]^{0.7} + (h_0 - h_2)^{0.7}\right]^{-1} \tag{7}$$

where h_2 is the tailwater depth (the lower of the connecting structure water surface elevation or the tunnel water elevation at that point.) Water is permitted to flow only when h_0 is larger than h_2. Revised sluice gate calculations may be implemented in the final model.

Currently, hydraulic routing computations are simplified by assuming a level pool solution (LMNO Engineering, 2008) for interceptor water level. This results in Eqn. 8, where the volume (V) is calculated from the sluice gate equations and the time step, and the distance along the tunnel wall to which the water rises, S, is translated to a water surface elevation. The slope of the interceptor Φ is 0.0015, and r is the pipe radius.

$$V = \pi r^2\left(S + \frac{r}{\tan\emptyset}\right) \tag{8}$$

Once water elevations are established throughout the system, the elevations in the interceptor at the connecting structures can be compared with the water surface

elevations within the connecting structures. The sluice gate equations (6 and 7) can then be applied to determine the direction and the magnitude of flow.

The MPC algorithm implemented for this study is similar to the algorithms used by Onnen et al. (1997) and Naeem et al. (2005) and is illustrated in Figure 1. Chromosome genes represent percentages of sluice gate closures or the percent of maximum pumping rate and are coded between 0 and 1 and rounded to one decimal place. After initialization and mutation, the gene values are set to 0 or 1 if they are negative or greater than 1, respectively. Each gene can take one of 11 possible values.

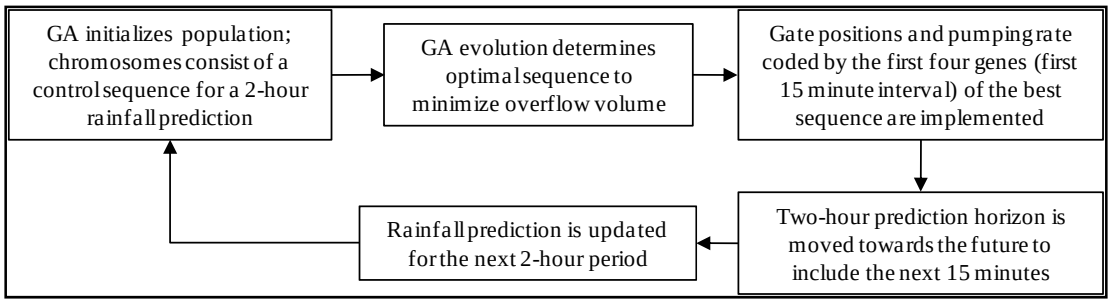

Figure 1: MPC Schematic

The genetic algorithm initializes a population of chromosomes composed of genes, and iteratively applies the operators of selection, crossover, and mutation to produce chromosomes of higher fitness. Real-coded genes increase the algorithm search space, and as a result, mutation rates and/or population sizes should be increased to ensure adequate search (Tate and Smith, 1993). Wright (1991) also supports higher mutation rates. Herrera et al. (1998) summarize numerous methods for real coded GA crossover and mutation; they resolve that non-uniform mutation (NUM) appears to yield fine tuning and the best results in later stages of the GA. Chen (2003) and Chang and Chen (1998) resolve that in terms of crossover, blended crossover (BLX-0.5) exhibits the best performance.

The GA used in this study uses binary tournament selection with replacement where the individual with maximum fitness (minimum overflow volume) is chosen. BLX-0.5 crossover is implemented as described by Herrera et al. (1998) and Eshelman et al. (1993). This method requires the definition of two limits and one integer.

$$c_{min} = \min(c_i^1, c_i^2), c_{max} = \max(c_i^1, c_i^2), I = c_{max} - c_{min} \quad (9)$$

Where the c values represent the gene values from the parent individuals at the ith location. The value of each of two new genes, h_i, is computed to be a random number on the closed interval given in Eqn. 10.

$$[c_{min} - I \cdot \alpha, c_{max} + I \cdot \alpha] \quad (10)$$

To enable local search, the GA used in this study also employs non-uniform mutation based on a mutation size that decreases as the number of generations increase (Herrera et al. 1998; Michalewicz 1992). For this operator applied in generation t, where g_{max} is the maximum number of generations, the value of the mutated gene c_i' is given in Eqn. 11.

$$c_i^{'} = \begin{cases} c_i + \Delta(t, b_i - c_i) \; if \; \tau = 0 \\ c_i - \Delta(t, c_i - a_i) \; if \; \tau = 1 \end{cases} \tag{11}$$

where τ is a random number that can be either 1 or 0 with 50% probability, b is the closed domain to which the mutated gene is constrained, and Δ is the function in Eqn. 12.

$$\Delta(t, y) = y\left(1 - r^{\left(1 - \frac{t}{gmax}\right)^b}\right) \tag{12}$$

where r is a random number from the closed interval 0 to 1 and b is a parameter taken to be 5 in accordance with the value applied by Herrera et al. (1995). For all steps, the maximum number of generations is set to 100; this number must be specified when using non-uniform mutation.

Three approaches are compared for population initialization at each new time interval. The first involves randomly initializing every chromosome (by generating 32 new genes with values between 0 and 1). The other methods constitute identifying the best chromosome from the last time window, and shifting the genes 4 places to the left to retain system knowledge gained in the last interval. Four new randomly generated values are placed at the end of the string to simulate decisions for the next 15 minutes of rainfall. The gene shifting procedure is shown in Figure 2.

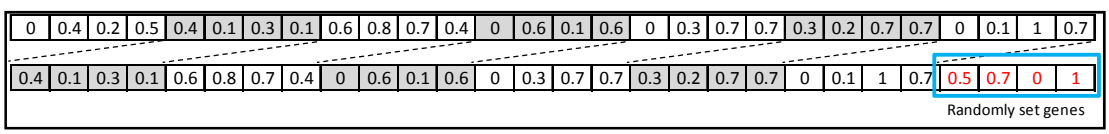

Figure 2: Gene Shifting Method

The second method reinitializes the entire new population with the chromosome of shifted genes (as a result the population only differs by the last four genes of each chromosome). The third strategy entails reinitializing only two members in the next population with these genes. Two chromosomes in the initial GA population for the next time window are replaced with the shifted values, while the remaining chromosomes are randomly initialized.

CASE STUDY

The combined generalized hydraulic model, MPC algorithm, and GA system is demonstrated using a small test case that is roughly based on a portion of the Chicago Tunnel and Reservoir Plan (TARP) system. Case study results are analyzed in order to facilitate development of the decision sequence optimization system as well as provide insight as to regions of the hydrologic-hydraulic system where more accurate modeling is needed.

The coupled hydrologic-hydraulic model used to simulate the rainfall to runoff process is depicted in Figure 3. The system consists of three sewersheds, represented by squares 1 through 3 that are connected through connecting structures (nodes 1 through 3) to conduits 1 through 3 that convey water to a downstream treatment plant and pumping station; arrows designate the flow direction.

The conduit diameters (D), upstream elevations (El_u), downstream elevations (El_d) and lengths (L) are included in Figure 3. Sluice gates that restrict water flow to and from the conduits are located in each connecting structure. The area of watershed 1 is 161 hectares, the area of watershed 2 is 243 hectares, and the area of watershed 3 is 81 hectares. The flow from each of the three sewersheds that enters the conduits is routed downstream to establish water levels throughout the sewer. Water levels at each connecting structure determine whether an overflow will occur. Overflows can occur in the following three ways, volume from each of which is given equal weight within the optimization.

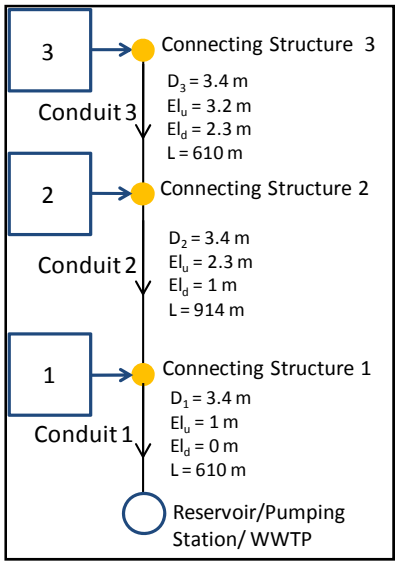

Figure 3: Hypothetical System

1) Local CSO: Water can overflow the connecting structure if the flow in from overland is greater than flow permitted to leave through the sluice gate to the conduit.
2) Pump Station CSO: If the pumping station lifts more water than the treatment plant capacity, water must overflow as opposed to entering the treatment plant.
3) Global CSO: Flows into the reservoir may be greater than the pumping capacity, and water can back up along the interceptor. When the elevation of water in the interceptor is greater than the water level in any of the connecting structures, flow exits the conduit into the connecting structure through the sluice gate, constituting an overflow.

The minimum cumulative volume of sewer overflow events throughout a 3-hour storm (and resulting 5-hour overflow duration) is sought for the watershed-interceptor system. This volume will be achieved through the optimal sequence of management decisions (consisting of a single pumping rate and three sluice gate positions at multiple time steps) derived using model predictive control. Three random number generator seeds, constituting trials 1 through 3, are utilized to provide an overview of possible sequences.

In the results presented, the algorithm is implemented assuming the rainfall is known for the 3-hour storm (displayed in Table 1) and no changes in the prediction occur.

Table 1: Simulated Rainfall

15 minute interval	0	1	2	3	4	5	6	7	8	9	10	11	12	13	14	15	16	17	18
Rainfall (cm/hr)	0	1.3	1.3	1.3	1.3	2.5	2.5	2.5	2.5	1	1	1	1	0	0	0	0	0	0

The 0 cm/hr rainfall input is continued until all overflows have subsided.

Each gene is represented by one integer (that takes a value from 0 to 10) and four genes represent the system at each 15-minute interval. For a 2-hour prediction horizon, the chromosome length is determined in Eqn. 13.

$$4\left(\frac{variables}{interval}\right) \times 2(hours) \times 60\left(\frac{minutes}{hour}\right) \Big/ 15\left(\frac{minutes}{interval}\right) \qquad (13)$$

Eqn. 13 indicates a total of 32 genes per chromosome. The population size will be set to the chromosome length times a constant value of 8 for a value of 256, as suggested by Onnen et al. (1997.) This population size may be reduced when a more physics-based hydrologic-hydraulic model is implemented in order to allow all chromosomes to be evaluated within 15 minutes.

RESULTS AND DISCUSSION

Initially, a crossover probability of 0.5 is used for single point real crossover; nonuniform mutation is used for 100 generations and a mutation probability of 0.01. Figure 4 demonstrates the spatial and temporal overflow distribution when the GA initializes a generation and does not perform further operations for the optimization routine for the 20 interval (5-hour) decision sequence. Only one value of the random seed is used.

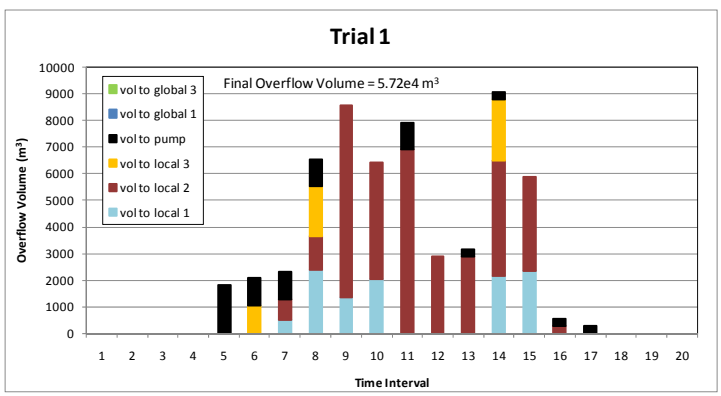

Figure 4: Implemented Sequence for Trial 1

The cumulative overflow volume is 5.72e4 cubic meters. The overflow distribution demonstrates that the largest volume is partitioned as a local overflow out of dropshaft 2 (at the sewershed with the largest drainage area.) CSOs at the pump station also exhibit a large volume, indicating that the pumping rate is increased substantially above the treatment plant capacity.

Initial GA Results

The GA is utilized to transform chromosomes over 100 generations, and three different random seeds (trials) are utilized. Figures 5 through 7 show the implemented sequences for each trial produced by the lowest fitness chromosomes in the final generation at each time increment.

Results show that decisions made at time intervals when very little rainfall has entered and/or remains in the system do not significantly impact the total overflow volume. Many different decision sequences, which differ in the decisions made during early and late time intervals, demonstrate equivalently optimal fitness. For a 2-hour window starting at time step 1, the only overflow that is predicted to occur is at the eighth time step at dropshaft 2. All chromosomes for all seeds predict this local overflow; but the series of gate closures and pumping rates previous to this interval differ.

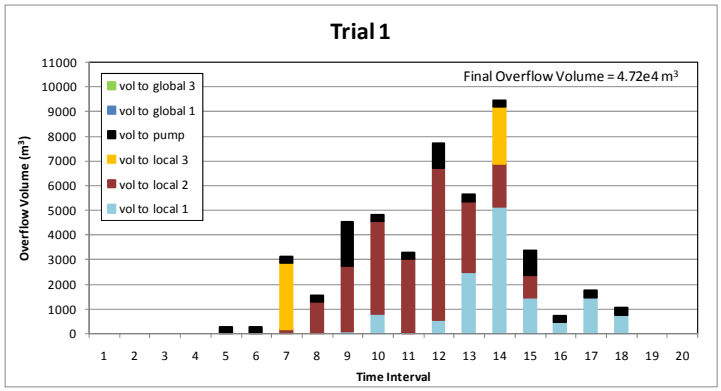

Figure 5: Implemented Sequence for Trial 1

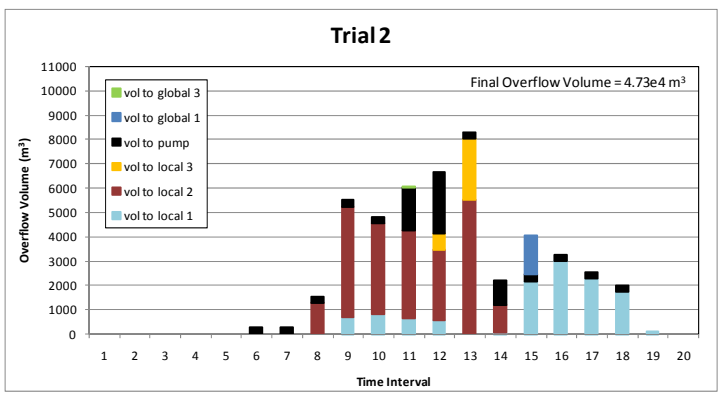

Figure 6: Implemented Sequence for Trial 2

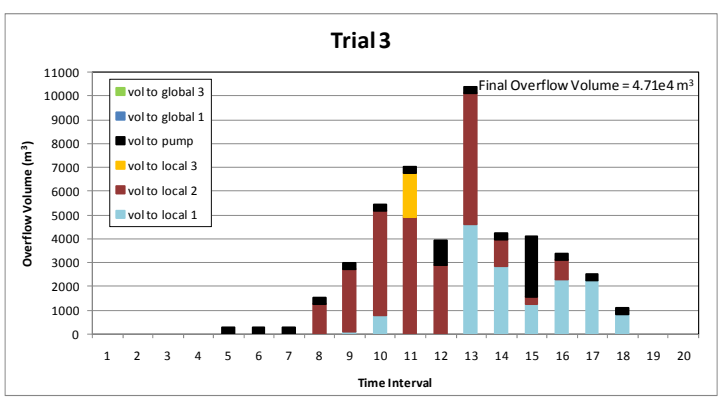

Figure 7: Implemented Sequence for Trial 3

The strategies proposed by the different seeds differ significantly; however local overflows at connecting structure 2 dominate for early time intervals for all seeds and a large number of local overflows at dropshaft 1 occur later in the storm. Local overflows at structure 1 indicate that sluice gate 1 is closed to prohibit global overflows that may be caused at that location because once more water enters the sewer, connecting structure 1 will be the first affected by backups.

The population size used in this algorithm is fixed, and a high mutation rate is necessary to expand the breadth of the search at least for early generations. The mutation rate is increased to 0.05 to aid in the search for good solutions for a large

real-coded alphabet, and elitism is introduced. BLX-0 and BLX-0.5 crossover are introduced, and although they have no effect on their own, introduction of chromosome shifting significantly effects the overflow volumes obtained.

Results for Revised GA Parameters

Introduction of the gene shifting strategy for population initialization significantly reduces the overflow volumes, and leads to a convergence among spatial and temporal overflow partitioning for all three trials. At the same time period for all three trials, the volume is partitioned to the same local or global overflows. The average volume generated over the storm duration decreases from 4.72e4 cubic meters to 4.60e4 cubic meters. The improved performance obtained by gene shifting may be amplified by the deterministic rainfall assumed in this problem. Further work will implement more realistic, changing precipitation forecasts necessary to validate the superiority of the gene shifting strategy.

The distribution of overflows throughout the system is shown in Figures 8 through 10 for population initialization with two chromosomes with shifted genes. The predictions (final chromosomes) for intervals beginning at time steps 1 through 4 and from steps 18 though 21 differ the most due to lack of water in the system.

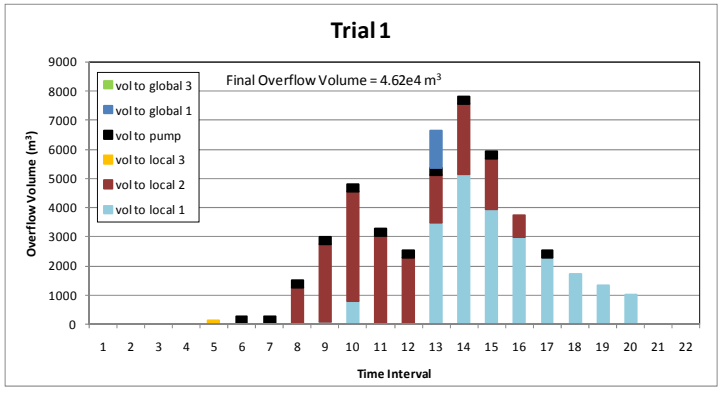

Figure 8: Implemented Sequence for Trial 1

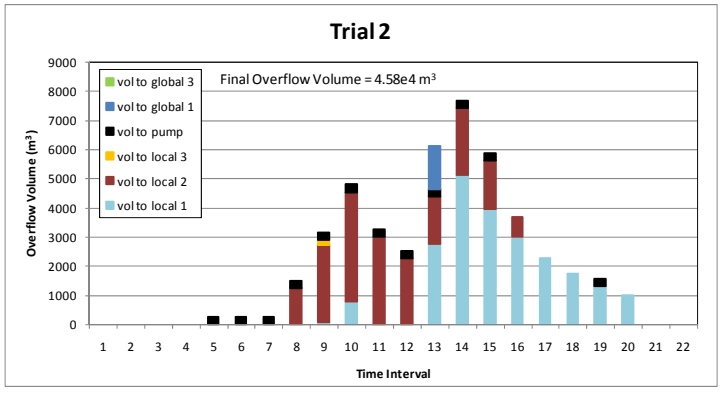

Figure 9: Implemented Sequence for Trial 2

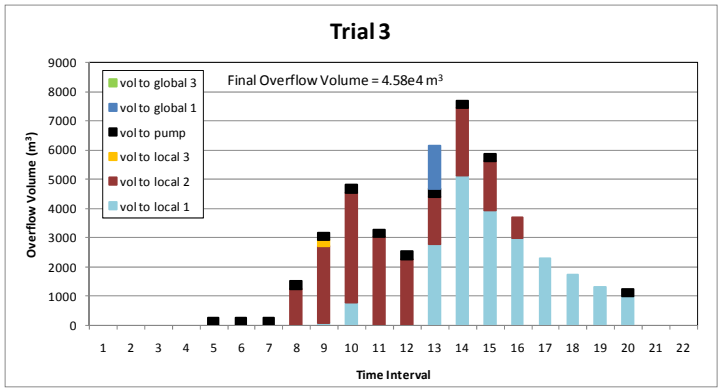

Figure 10: Implemented Sequence for Trial 3

The implemented decision variables demonstrate that that the best management strategy is to keep the pump on at the capacity closest to the treatment plant rate throughout the storm event rather than pumping at higher rates at inconsistent intervals. All trials also indicate that sluice gate 2 should be fully open for the middle intervals of the rainfall, and towards the end of the rainfall, sluice gate 1 should be fully closed and sluice gate 3 should be partially closed while water from sewershed 2 is pumped out of the system. The three strategies extend the number of intervals for which overflows occur from 19 to 20. For all trials, one global overflow occurs at time interval 13, and no overflows occur after interval 20.

CONCLUSIONS AND FUTURE WORK

This study develops a real-time GA-based control system for managing CSOs. The system employs a real coded genetic algorithm to develop management strategies that most effectively reduce overflow volume over a 5-hour window using 15-minute control intervals and a 2-hour planning horizon. At each control interval, the system re-evaluates the optimal 2-hour decision sequence to account for changing precipitation conditions. The system is implemented in a case study roughly based on a portion of the Chicago TARP system.

The decision sequences that produce the lowest CSO volume are obtained when the genes for the best chromosome in the previous time window are shifted for initialization in the next window; this method of initialization propagates knowledge of the best management strategy to the next generation. Additionally, this method of population initialization allows decision sequences derived from different random seeds to converge to similar partitioning of overflow volume for the entire 5-hour optimization period. It may prove beneficial to initialize only two members of the subsequent population with the shifted genes, allowing the remainder of the chromosomes to be randomly generated, thus enlarging the search space. This method may also save computational effort; fewer GA generations may be required to reach a good solution when genes shifted from the previous time interval are utilized.

Future work will include further evaluation of the genetic algorithm. New strategies of population initializing at each time window should incorporate evaluation of the necessity of rerunning the algorithm at every 15 minute interval for low changes in rainfall rate. A threshold change in rainfall rate may exist below which the decision

sequence remains consistent for the initial steps of a new time window. The effects of population size on minimum fitness and the types of chromosomes of minimum fitness should be further examined; high mutation rates should be evaluated as a substitute for increases in population size.

Different weights could be assigned to the location and timing of overflows. This extension would be valuable for possible use within a water quality model in which portions of the receiving waterway downstream of certain sewersheds are more sensitive to overflow contamination than others. The analysis may restructure the spatial and temporal patterns observed for the equivalent weighting presented.

The insight into GA parameters and physical characteristics for this case study will be applied to a more physics-based model, in which interceptor hydraulics will be based on the methodology proposed by Hoy (2005). A hydraulic performance graph (HPG) and a volumetric performance graph (VPG) will be established for each conduit. The HPG ensures conservation of momentum for the reach and is a collection of the backwater profiles of the reach created through the gradually varied flow equation (Chow, 1959).

$$\frac{dh}{dx} = \frac{S_0 - S_f}{1 - F^2} \tag{14}$$

The HPG has been used to analyze open channel stage-discharge relations (Schmidt, 2002) and applied to unsteady flow routing by Gonzalez-Castro (2000). The VPG introduced by Hoy (2005) describes the volume stored in the reach for each flow condition described by the HPG, and ensures conservation of mass for the reach.

$$\frac{\partial A}{\partial t} + \frac{\partial Q}{\partial x} = q_{lateral} \tag{15}$$

The change in flow area with respect to time plus the change in flow rate with respect to distance is equal to any lateral inflows to the reach. All water entering the conduit system is immediately transferred to the downstream reservoir and from there is routed back upstream to establish conduit water level in accordance with work done by Oberg et al. (2001). The HPG and VPG files are created offline for a range of flow rates and downstream boundary conditions for the sub-conduits through tools scripted in *C++* (Oberg, 2008). The graphs will be used for interpolation during the MPC algorithm.

At each time step, the HPG is used to find the upstream water surface elevation for each conduit given the average flowrate and the downstream water surface elevation. The VPG is used to determine the storage in each reach for the current time step, using the same inputs utilized for the HPG. Optimization is performed to find the minimum least squares solution that equates the change in storage with space to the change in storage with time, that is, to minimize the difference: $\Delta S_{time} - \Delta S_{space}$ for each conduit. The solution will provide flow rates for each sub-conduit which can then be utilized to find upstream water surface elevations throughout the system.

The finalized coupled hydrologic-hydraulic model will be used to evaluate the sensitivity of local, global, or pump station overflows to system management. The procedure will eventually be extended to the Metropolitan Water Reclamation

District of Greater Chicago's (MWRDGC) Tunnel and Reservoir Plan (TARP). The system will be utilized with real-time precipitation updates, and calibrated to CSO data provided by the MWRDGC.

REFERENCES

Cembrano, G., Quevedo, J., Salamero, M., Puig, V., Figueras, J., and Marti, I. (2004). Optimal control of urban drainage systems. A case study. *Control Engineering Practice*, 12, 1-9.

Chang, F., and Chen, L. (1998). Real-Coded Genetic Algorithm for Rule-Based Flood Control Reservoir Management. *Water Resources Management*, 12, 185-198.

Chen, L. (2003). Real Coded Genetic Algorithm Optimization of Long Term Reservoir Operation. *J. of the American Water Resources Association*, 39(5), 1157-1165.

Chow, V. T. Open Channel Hydraulics. McGraw-Hill, New York, 1959.

Darsono, S., and Labadie, J.W. (2007). Neural-optimal control algorithm for real-time regulation of in-line storage in combined sewer systems. *Environ. Modelling and Software*, 22, 1349-1361.

Diskin, M.H., G. Wyseure, and J. Feyen. (1984). Application of a Cell Model to the Bellebeek Watershed. *Nordic Hydrology*, 15, 25-38.

Dooge, J. (1973). Linear Theory of Hydrologic Systems. US Dep. Agric. Tech. Bull., 1468, 327.

Eshelman, L.J., and Schaffer, L.D. (1993). Real-Coded Genetic Algorithms and Interval-Schemata. Foundations of Genetic Algorithms 2, L. Darrell Whitley (Ed.), Morgen-Kaufmann Publishers, San Mateo, 187-202.

Goldberg, D.E. (1989). Genetic algorithms in search, optimization, and machine learning. Reading, MA: Addison-Wesley.

Goldberg, D.E. (2002). The Design of Innovation. Norwell, MA: Kluwer Academic Publishers.

Gonzalez-Castro, J.A. (2000). Applicability of the Hydraulic Performance Graph for Unsteady Flow Routing. Ph.D. Thesis, Department of Civil Engineering, University of Illinois at Urbana-Champaign.

Herrera, F., Lozano, M., and Verdegay, J. (1998). Tackling Real-Coded Genetic Algorithms: Operators and Tools for Behavioral Analysis. *Artificial Intelligence Review*, 12(4), 265-319.

Hoy, M. (2005). Unsteady Flow Routing Using Predetermined Solutions to the Equations for Conservation of Mass and Momentum. MS Thesis, University of Illinois at Urbana-Champaign.

Hu, X., and Chen, W. (2005). Receding Horizon Control for Aircraft Arrival Sequencing and Scheduling. *IEEE Trans. on Intelligent Transportation Systems*, 6(2), 189-197.

Karnieli, A.M., M.H. Diskin, and L.J. Lane. (1994). CELMOD5 – a semi-distributed cell model for conversion of rainfall into runoff in semi-arid watersheds. *Journal of Hydrology*, 157, 61-85.

Lee, J., Abdulhai, B., Shalaby, A., and Chung, E. (2005). Real-Time Optimization for Adaptive Traffic Signal Control Using Genetic Algorithms. *Journal of Intelligent Transportation Systems*, 9(3), 111-122.

LMNO Engineering, Research, and Software, Ltd.
http://www.lmnoeng.com/Volume/InclinedCyl.htm.

Michalewicz, Z. (1992). Genetic Algorithms + Data Structures = Evolution Programs. Springer-Verlag, New York.

Naeem, W., Sutton, R., Chudley, J., Dalgleish, F.R., and Tetlow, S. (2005). An online genetic algorithm based model predictive control autopilot design with experimental verification. *International Journal of Control*, 78(14), 1076-1090.

Oberg, N., A.S. Leon, A.R. Schmidt, and M.H. Garcia. Illinois Hydraulic Conveyance Analysis Program (ICAP) Version 1. University of Illinois at Urbana Champaign, June 2008.

Onnen, C., Babuska, R., Kaymak, U., Verbruggen, H.B., and Isermann, R. (1997). Genetic Algorithms for Optimization in Predictive Control. *Control Eng. Practice*, 5(10), 1363-1372.

Ostfeld, A., A. Pries. (2003). *Lake Kinneret watershed contamination transports – a GIS based hydrological model*. Water Science and Technology, 48(10), 63-70.

Pleau, M., Colas, H., Lavallee, P., Pelletier, G., and Bonin, R. (2005). Global optimal real-time control of the Quebec urban drainage system. *Environ. Modelling and Software*, 20, 401-413.

Schmidt, A. (2002). Analysis of stage-discharge relations for open-channel flows and their associated uncertainties. Ph.D. Thesis, Department of Civil Engineering, University of Illinois at Urbana-Champaign.

Swamee, P. (1992). Sluice-Gate Discharge Equations. *Journal of Irrigation and Drainage Engineering.* 118(1), 56-60.

Tate, D.M., and E.A. Smith. (1993). Expected allele coverage and the role of mutation in genetic algorithms. In: Proc. 5th Int. Conf. Genetic Algorithms, S. Forrest, Ed. San Mateo, CA: Morgan Kaufmann, 1993. 31–37.

Wright, A. (1991). Genetic Algorithms for Real Parameter Optimization, in: G.J.E. Rawlins, *Foundations of Genetic Algorithms,* Morgan Kaufmann, San Mateo, CA, 205-218.

Examinations of Pervious Concrete and Porous Asphalt Pavements Performance for Stormwater Management in Northern Climates

Kristopher M. Houle [1], Robert M. Roseen [2], Thomas P. Ballestero[3], Joshua F. Briggs[4], James J. Houle[5]
University of New Hampshire, Durham, NH

[1] Graduate Research Assistant, Water Resources, Department of Civil Engineering, 35 Colovos Road, University of New Hampshire, Durham, NH 03824; PH 603-862-1172; FAX 603-862-3957; e-mail: khoule@unh.edu; web: www.unh.edu/erg/cstev/.

[2] Corresponding Author, Director, The UNH Stormwater Center, Ph.D., Department of Civil Engineering, 35 Colovos Road, University of New Hampshire, Durham, NH 03824; PH 603-862-4024; FAX 603-862-3957; e-mail: robert.roseen@unh.edu; web: www.unh.edu/erg/cstev/.

[3] Associate Professor, Civil Engineering, P.E., Ph.D., P.H., C.G.W.P., P.G., Department of Civil Engineering; Principal Investigator, The UNH Stormwater Center, 35 Colovos Road, University of New Hampshire, Durham, NH 03824; PH 603-862-1405; FAX 603-862-3957; e-mail: tom.ballestero@unh.edu; web: www.unh.edu/erg/cstev/.

[4] Post-graduate Research Assistant, Water Resources, Department of Civil Engineering, 35 Colovos Road, University of New Hampshire, Durham, NH 03824; PH 603-862-1172; FAX 603-862-3957; e-mail: briggs@unh.edu; web: www.unh.edu/erg/cstev/.

[5] Program Manager, The UNH Stormwater Center, Department of Civil Engineering, 35 Colovos Road, University of New Hampshire, Durham, NH 03824; PH 603-767-7091; FAX 603-862-3957; e-mail: james.houle@unh.edu; web: www.unh.edu/erg/cstev/.

ABSTRACT

In northern climates, runoff from standard pavements has varying seasonal effects on the surrounding environment. Year-round runoff carries transportation associated contaminants into surface waters. During the winter and spring, deicing practices for pavements result in high levels of chloride-laden runoff that is both toxic to aquatic biota and degrades drinking water supplies. The use of pervious pavements for parking lots for new and redevelopment projects are one watershed-based strategy that can both mitigate impacts for new development and reverse impacts in areas with redevelopment. This study presents the findings from 2 pervious pavements, a pervious concrete and a porous asphalt parking lot, studied at the University of New Hampshire Stormwater Center. Winter in particular places great demands on pavements however it was observed that due to the well-drained nature of the reservoir base that freeze thaw was limited. Surface infiltration rates, frost penetration, degree of snow and ice cover, and surface friction were measured on a monthly basis to assess winter performance. Frost penetration was observed to reach depths of eighteen inches however, surface infiltration capacities remained in excess of 200-in/hr. Analysis of snow and ice cover and pavement skid resistance demonstrated that up to 75% less salt was needed for porous asphalt to maintain equivalent or better surface conditions as the reference dense mix asphalt lot. The annual median snow and ice surface cover for the porous asphalt lot was not significantly different than the reference lot with salt applications four times greater ($p=0.749$ @95% CI). The annual median weighted skid resistance for the porous asphalt lot was 12% greater than the reference lot with greater salt application ($p=0.061$ @95%CI). Pervious concrete did not demonstrate substantial salt reduction capabilities during storm events; however, 'black-ice' formation did not occur during freeze-thaw conditions indicating possible annual reductions. Pavement color and shading were found to be major factors influencing the amount and duration of snow and ice cover on the pervious concrete lot.

INTRODUCTION

The implementation of the National Pollutant Discharge Elimination System (NPDES) Phase II regulations has helped to fuel the research, development, and implementation of innovative Best Management Practices (BMP) for managing and treating stormwater runoff. Since 2003, the University of New Hampshire Stormwater Center (UNHSC) has set out to evaluate over twenty types of BMPs in a fully-monitored field setting. One class of BMP that is at the forefront of the industry and is being adopted in both the public and private sectors is permeable pavements. One of the major benefits of permeable pavements is their dual function as a transportation surface and self-contained stormwater management device. The research has demonstrated that porous asphalt may allow for a 77% annual salt reduction for winter maintenance over conventional practices on impermeable asphalt (Houle, 2008). To date, the UNH Stormwater Center (UNHSC) has constructed and tested two types of permeable pavement parking lots: porous asphalt and pervious concrete, both of which are located at the UNH campus in Durham, NH. The objective of this study is to compare and contrast a series of winter performance metrics of porous asphalt (PA) and pervious concrete (PC). Topics discussed include frost penetration, hydraulic performance as measured by infiltration capacity, winter performance based on snow and ice cover and surface friction. Historically, there has been some debate among the engineering community on how permeable pavements perform in northern climates; part of this debate stems from the confusion between a true porous asphalt stormwater management system versus open-graded friction course (OGFC), for example, which is typically used in highway application and differs from PA by its impermeable asphalt base (Kandhal and Mallick, 2002). This paper to addresses these misconceptions and identifies the potential benefits of permeable pavements.

BACKGROUND

Permeable pavements differ from standard dense-mix asphalt in that the "fines" (particles smaller than 600 microns) are removed from the aggregate mix, thereby allowing the formation of pores for water to pass (Cahill et al., 2003; Ferguson, 2005). Porous asphalt typically consists of stone aggregate, binder material, and other modifiers and should demonstrate a void space of 18% to 20% (Briggs, 2006). Pervious concrete, on the other hand, consists of hydraulic cement, stone aggregate, water, and a combination of various chemical additives (admixtures) to enhance the performance, strength, and ease of placement. Typical void space of a pervious concrete pavement should be between 15% and 25% (NRMCA, 2007). In the case of the UNHSC designs, the porous asphalt lot was placed in one, four-inch lift while the pervious concrete lot was poured to a six-inch depth. Both of these surfaces were placed over a choker (stone) course underlain by 12-inches or more of a bank run gravel filter course. Design specifications can be found online at the UNHSC (2007).

Many of the sub-base design considerations for porous asphalt and pervious concrete stormwater management systems are similar to those that would be inherent of most infiltration-based BMPs. For instance, both UNHSC designs consist of a bank-run-gravel (BRG) filter course underlain by crushed-stone reservoir layer. The

thicknesses of these layers vary between systems, ranging from 14-inches (PC) to 24-inches (PA) of filter course and 4-inches (PC) to 21-inches (PA) of crushed-stone reservoir. The total sub-base depth of the PA site was greater than the PC design in order to meet seasonal-high-groundwater separation restrictions and due to the presence of a less permeable native sub-grade soil. Historically, the sub-base of many porous asphalt systems consisted of only crushed stone; however, with the addition of the filter course, the water quality performance of the porous asphalt system is substantially improved, resulting in the removal of most stormwater contaminants (hydrocarbons, microorganisms, sediment, metals) (Roseen et al., 2009). The major differences between these systems (PA and PC, in general) are primarily in the wearing course mix designs.

The UNHSC porous asphalt (PA) site is a hydraulically isolated 5,000 ft^2, 17-space parking lot that was installed in 2004. Directly adjacent to this PA lot is an equally-sized dense-mix asphalt (DMA) parking area that is also hydraulically isolated. The DMA lot was constructed concurrently with the PA site to serve as a control for most performance metrics. Both lots are located along the perimeter of a nine-acre, asphalt commuter parking lot. The UNHSC pervious concrete (PC) site was installed in August, 2007. It is approximately 20,000-ft^2 and includes 75 parking stalls. It serves as a parking lot for several nearby dormitories and is used to capacity primarily from September to May. Adjacent to the PC site, is a university-maintained standard asphalt lot that was used as an additional reference location for the study.

The winter climate (January through March) in Durham, NH generally consists of average temperatures near 27.7 ^{o}F, with maximum and minimum temperature of 37.5 ^{o}F and 17.3 ^{o}F, respectively. Total precipitation during this time period is approximately 16.4 inches and snowfall is around 63.1 inches (NHSCO, 2008).

METHODOLOGY

Frost depth penetration within the two types of permeable pavement was measured using a field assembled frost gauge (Ricard et al., 1976) installed in a screened, PVC groundwater monitoring well. Frost depth was determined by measuring the depth of frozen water-methylene blue solution. Frost depth and air temperature were recorded regularly from December 2007 to April 2008.

Surface Infiltration Capacity. Hydraulic performance of the permeable pavements was evaluated by measuring the surface infiltration capacity (IC) on a near-monthly basis beginning soon after installation. A falling head surface inundation (SI) test (Bean, 2005) was used for this process. This involved pouring a known volume of water into a cylinder and measuring the time required for the water to enter the pavement surface. Measurements were taken at three randomly selected locations (A-C) on the PA lot beginning in 2004, and at six locations (A-F) on the PC lot beginning in 2007. A double-ring infiltrometer (DRI) test was used at one location at the PA lot (Point C) because the IC rate was too low to be accurately represented with the SI device (Briggs, 2006) and further explanation can be referenced in Houle (2008).

Salt Application. Salt was applied to the parking lots in a manner designed to mimic municipal anti-icing and de-icing strategies, and consistent with the general practices employed by the University of New Hampshire. Application rates were selected based on percentages of the recommend standard of practice rate of 3.0-lbs per 1000-ft^2 of application area (MPCA, 2006). The rates used in Houle (2008) (100%, 50%, 25%, and 0%) were applied to 20-ft by 20-ft sections of the driving lane through the pervious concrete lot (Figure 1). The remaining driving lane area received a 100% application rate. The salt used was standard rock salt with less than 10% added fines by mass; it was identical to the mix used in the '06-'07 study.

The number of salt application rates for the porous asphalt and dense-mix asphalt lots was altered from the previous winter. The entire PA lot received a rate of 25% of the standard of practice while the DMA lot received a 100% rate (Figure 1). Evaluation areas included isolated parking stalls, as was the case in Houle (2008) and the lots as a whole. This change in methodology was performed in order to quantify any differences that may exist between driving lanes and parking stalls.

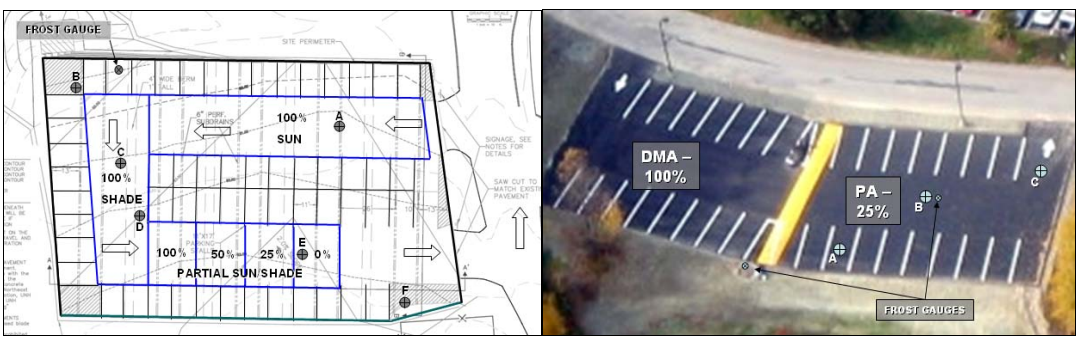

Figure 1: Pervious concrete (PC) (left) and Porous asphalt (PA) and dense mix asphalt (DMA) (right); Salt application rates, frost gauge and IC locations shown

Visual Observations and Documentation. Before, during, and after storm events, photos were taken of each study area and the specific event characteristics were recorded. Pavement conditions, type and amount of snow and ice cover, and weather conditions were of primary interest. Apparent effects from shading or direct sunlight was also recorded. Photo documentation was necessary to substantiate the findings and to display comparative results of the different pavements. Evaluations typically occurred at various times during and up to three days after precipitation events.

Friction Measurements. The skid resistance of all pavement types was measured using a Munro Stanley London British Pendulum Skid Resistance Tester. Each measurement was classified based on the form of surface cover that was present during the reading, including: dry, wet, snow, slush, compacted-snow, and ice covered pavement. The method for using the skid resistance tester followed ASTM Standard E 303–93 (2004). As explained in Houle (2008), the device measures the energy loss of a rubber slider as it is swung against the test surface. A British Pendulum Number, or BPN, is generated and can be directly related to a pavement coefficient of friction (Munro Environmental, 2007). The higher the frictional resistance of the surface, the greater the resulting BPN.

Skid resistance measurements were taken at various locations within each study area, repeated five times, and seasonally averaged in order to characterize the variability in friction between each type of pavement cover. The mean values were then multiplied by their respective surface cover type percentages in order to develop a weighted friction value for each observation. The significance of the weighted friction value was to obtain a number that can easily be related to safety for each of the varying salt application rates.

Statistical Comparison Methods. A 'Student's t' means comparison test was employed for all portions of this study to determine differences in central location (mean) for two independent data sets (Helsel and Hirsh, 2002). Group comparisons with p-values less than 0.05 (with a 95% confidence interval) were deemed statistically different. These analyses include surface infiltration capacity, snow & ice cover, and skid resistance.

RESULTS AND DISCUSSION

Frost Depth Penetration. A time-series from November 2007 to April 2008, displaying frost depth in the porous asphalt and pervious concrete lots, is shown in Figure 2. Frost depth within the systems is plotted against average daily air temperature and frost depth at one reference location in soil adjacent to the PC study areas. Rain events as occurrences are plotted as vertical dashed lines. A clear repeatable phenomena is observed where depth of frost penetration is reduced following a rain event. This occurs on 6 occasions. The same response is not observed in the reference location, likely due to lack of infiltration of meltwater as is observed in the corresponding open-graded materials. The degree of response has not been examined with respect to rain depth or other important factors. Rain events occur throughout the winter and are commonly mixed with snow and ice. It is apparent from the figure that the PC responded quicker to lower air temperatures and maintained a greater frost depth than the PA system until early February when a sudden decrease in depth of frost was observed. It is believed that the rapid decrease in frost depth was due to a 1.66" rain-equivalent snow and rain event on 2/5/08 that thawed the systems, which is consistent with findings by Backstrom (2000) and Houle (2008). This was observed for another large storm on the 2/26 of nearly 1" rain-equivalent. Shortly after this rapid thawing process, the PA lot refroze to a frost depth of about thirteen inches while the frost depth in PC lot stayed nearly constant at eight-inches. A possible explanation for this may be due to water levels and latent heat within the two systems. The PC frost gauge well is located at the low-point of the lot and in an area where the total system depth is about 30-inches. At the time of observation, the water level was consistently about 26-inches below the pavement surface (at the base of four-inch perforated sub-drains). The water level in the PA lot on the other hand, was approximately 37-inches below the pavement surface. Researchers in Sweden discovered that high water content in the sub-soils beneath permeable pavements creates a high level of latent heat within the system, which can help resist freezing of the sub-base materials (Backstrom, 2000). The higher ground water level in the pervious concrete system may have supplied enough latent heat to minimize its frost depth.

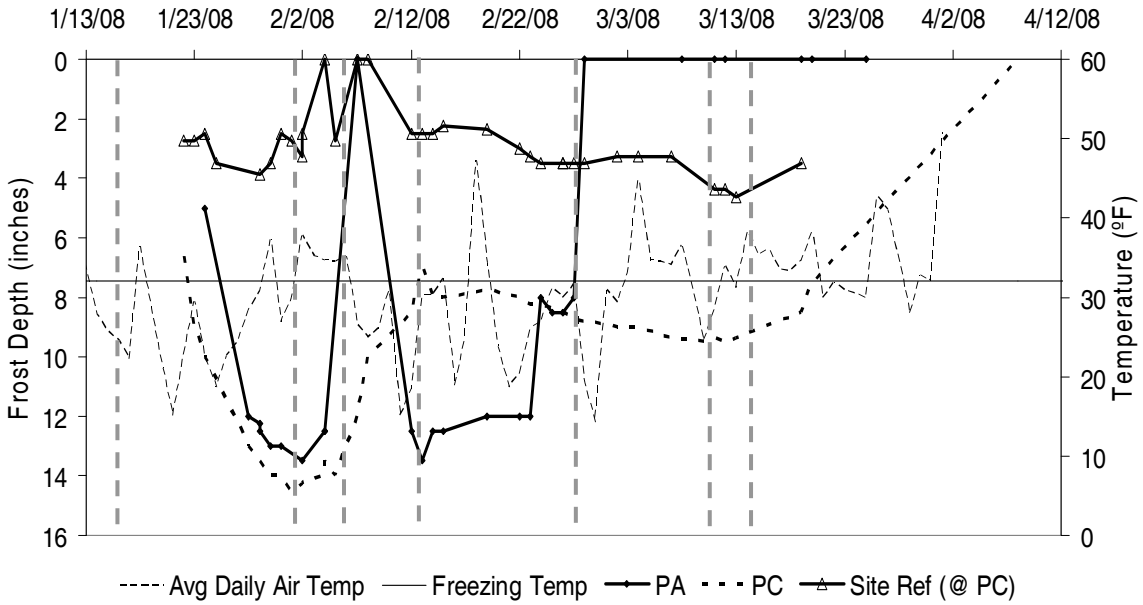

Figure 2: Frost depth penetration comparison between permeable pavements and reference soil sites (11/07 – 4/08); (Rain events shown with vertical, dashed lines)

Another interesting finding from this data is that frost depth in the PA system reached zero, and was sustained, over four weeks earlier than the PC lot. This discovery can be explained by the fact that the black PA surface possesses low albedo and therefore retains more solar energy in the winter than lighter colored surfaces and the more rapid response in frost depth variability in the dark colored pavement. Concrete pavements have been shown to exhibit surface temperatures up to 10-degrees Fahrenheit lower than asphalt pavements when subjected to similar sun exposure conditions (Cambridge Systematics, 2005). Shading of the PC lot may have also contributed to the longer frost depth duration.

In addition, the permeable pavements demonstrated similar freezing depths to the tree filter treatment unit, suggesting that frost penetration can be comparable to other existing stormwater BMPs, even with several inches of open-graded surface material (Houle, 2008). The one major difference between the pavements and the tree filter is the time it took to reach the maximum frost depths. The lag of the tree filter may be attributed to snow-pack insulation that was present much of the winter. It is also worth noting that no damage or heaving due to freeze-thaw was observed at these lots since their respective installations.

Surface Infiltration Capacity. The surface infiltration capacity was measured at both permeable pavement lots. Figure 3 is a time series and box and whisker plot of the IC data for the PA lot. In the time series plots, each point on the figure represents an average IC measurement; the location and testing method used is indicated by the

different markers. The average daily air temperature (A.D.A.T.) is also shown on the figure. In the box and whisker plots, the maximum and minimum observations are represented by the upper and lower whiskers, respectively, and the median values are shown by the gray bar through the 'boxed' segment of the data. The infiltration rates for the PA lot were typically found to be greater than 500 in/hr (Houle, 2008). During the first year of study, IC rates were highest during the winter and spring seasons, even with frost penetration reaching up to six-inches (Briggs, 2006). Since the first year of testing, higher IC rates were typically observed during the summer months; however, winter rates never dropped below 250 in/hr at Locations A and B. Asphalt binder drain-down of approximately 0.5% was identified (Houle, 2008) and thought to contribute to the infiltration rate decline observed during the first summer of study. The low infiltration capacity at Location C was determined to be an anomaly due to over-compaction during placement and clogging from tracked/blown sediments. Further explanation of the IC results can be referenced in Houle (2008) and Briggs (2006).

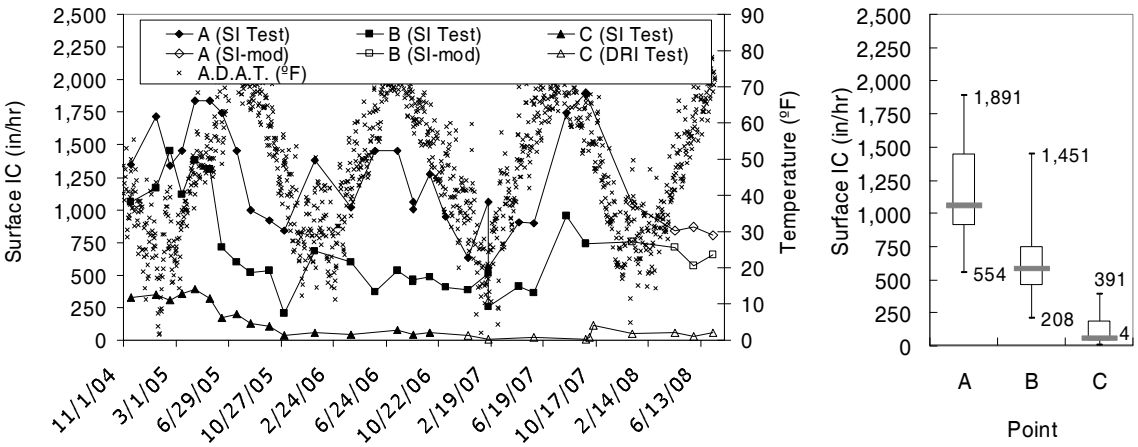

Figure 3: Porous asphalt surface infiltration capacity (Houle, 2008; Briggs, 2006); Time-series of surface IC (left); Box and whisker plots of surface IC (right); [(SI = surface inundation; DRI = double-ring infiltrometer; SI-mod. = modified SI), (Mod. SI appears to report lower infiltration rates, further study needed for correlation), (Pavement cleaning occurred 9/23/07)]

The IC testing at the PC lot was monitored at six locations. Even though considerable variability existed between locations, five of the six sites exhibited median IC rates in excess of 1,600-in/hr, nearly matching the highest values recorded on the PA lot (Figure 4). The only site below this value was near the entrance of the lot, a location where sand and other debris was commonly tracked and deposited from the nearby roadway. Nevertheless, all of the observed rates surpass rainfall intensities that one might experience in New England. [The 50-yr rainfall intensity for a 5-minute time of concentration in Strafford County, NH is approximately 8.0-inches per hour (NHDES, 1992)].

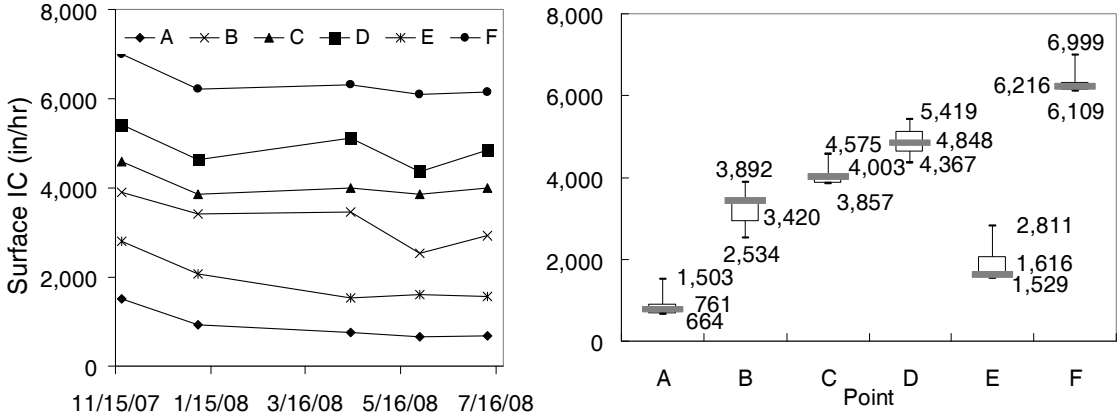

Figure 4: Pervious concrete surface infiltration capacity ('07-'08); Time-series of surface IC (left); Box and whisker plots of surface IC (right)

Winter Storm Event Characteristics. The results for one season of winter precipitation events are presented beginning in December 2007 and ending in March 2008. The types of storms evaluated during this season consisted of light to heavy snowfall, sleet, freezing rain, rain, and various combinations of each, with air temperatures ranging between -5ºF and 62ºF (UNHWS, 2008) (Table 1).

Visual Observations. Provided that plowing occurred shortly after the end of snow events, it was commonly observed that the PA pavement became clear of snow and ice earlier than the dense-mix asphalt lot. This observation is exemplified by the photos in Figure 5. These illustrate the PA and DMA lots at 11:20AM after morning plowing. A thin layer of snow is present on both lots because most plowing operations have difficulty removing all cover due to vehicular compaction and irregularities of the pavement surface as well as the plow blade itself. The figure show the same lots one-hour and forty-minutes later. The PA lot is distinctively clear of snow and ice while the conditions of the DMA lot only exhibit minimal melting. Estimates of surface cover amounts at 1PM were 15% snow for the PA lot and 50% snow for the DMA lot. Air temperatures ranged from 31.3ºF at 11:20AM and 37.6ºF at 1PM. These observations correlate well with assessments made during the 2006-2007 winter on the same parking lots (Houle, 2008).

Figure 6 shows the two pavements after a freezing-rain event (air temperature of 42.3ºF). It is clear from these photos that the ice on PA had melted and drained through the pavement far earlier than the DMA lot based on the amount of standing water and ice on the DMA surface. Standing water on pavements is a problem because it will often refreeze during the night creating unsafe surface conditions that require deicing salt applications. Standing water was never observed on the porous asphalt lot. It should be noted that freezing-rain events often created icy conditions on both the PA and DMA pavements when air temperature remained near or below 32ºF. When temperatures exceeded this point, the porous asphalt typically responded quicker than the DMA, as is the case in the figure.

Table 1: Winter storm event characteristics ('07-'08); (S = Snow; R = Rain; I = Ice) (NCDC, 2008; NHSCO, 2008; UNHWS, 2008)

Date	Precipitation Type	Snow Depth (in.)	Water Equivalent Depth (in.)	Max Temp (ºF)	Min Temp (ºF)
11/20/2007	S	1.5	0.19	35	30
12/3/2007	S	5.5	0.74	33	21
12/10/2007	S	1.5	0.13	34	14
12/12/2007	I	0.04	0.35	44	31
12/14/2007	S	5	0.13	39	17
12/16/2007	S/I	8	0.99	19	10
12/20/2007	S	7	0.39	29	21
12/27/2007	S/R	2	0.21	35	29
12/31/2007	S	13	1.3	36	14
1/14/2008	S	7	0.47	36	12
1/18/2008	S/R	2	0.67	44	18
1/27/2008	S	3	0.31	28	17
2/1/2008	I/R	0.5	1.23	44	33
2/5/2008	S/R	0.75	1.66	37.5	32
2/8/2008	S	4	0.51	29	21
2/10/2008	S	2	0.29	35	16
2/13/2008	S/R	5	2.77	36	21
2/22/2008	S	5	0.36	26.5	13
2/26/2008	S/R	3	0.94	39.5	20
3/1/2008	S	3	0.44	35	21
3/11/2008	S/R	1	0.21	41	17
3/15/2008	S/R	1	0.69	40	33
3/28/2008	S	4	1.02	42	32
Nov. avg.	-	14.4	4.84	49.1	29.3
Dec. avg.	-	14.4	4.46	36.8	18.2
Jan. avg.	-	19	4.11	33.4	13
Feb. avg.	-	16.9	3.48	35.4	14.4
Mar. avg.	-	12.8	4.31	44.4	23.7

The PC lot demonstrated mixed results based on the amount of shading that each section of the lot received. Much of the lot was shaded due to dense fir tree cover around the perimeter; some areas were in shade at all times of the day. The lot was divided up into three main sections in order to characterize this spatial variation. The photos in Figure 7 demonstrate the shading trends that were common through the majority of the winter; all were taken concurrently at 11AM on 2/27/08. The figure depicts the variations of three shaded conditions: the driving lane that was typically in the sun with clear weather conditions; a driving lane that received partial sunlight; the driving lane almost always in the shadow of the surrounding trees.



Figure 5: Changing pavement conditions with time: PA vs. DMA; (12/14/07) PA at 11:20AM (top-left); PA at 1PM (top-right); DMA at 11:20AM (bottom-left); DMA at 1PM (bottom-right)



Figure 6: Instantaneous pavement conditions after freezing-rain: PA vs. DMA; (1PM on 2/2/08) PA (left); DMA (right)



Figure 7: Pervious concrete surface conditions with varying levels of shading; (11AM on 2/27/08) In sun (left); In partial sun (center); In shade (right)

Despite the difficulties created by shading, the PC lot performed extremely well during freezing and thawing weather conditions as measured by the amount of black ice formation. Figure 8 is a comparison the PC lot and the adjacent standard asphalt reference lot that is maintained by the university. The photo shows a driving lane of the PC lot that is completely dry and nearly free of snow while the nearby standard lot in is almost entirely covered with black-ice and water. These photos were taken at 12:50PM on 2/16/08 when the air temperature was approximately 22.5ºF; a low of 14ºF was reached at 7:15AM (UNHWS, 2008). The standard winter maintenance practice for the UNH Grounds & Roads Dept. is that when nightly air temperatures are below freezing, salt is applied to most roads and parking lots to combat the formation of black ice. The DMA reference lot in the photo was treated in this manner. Conversely, no salt was needed on the PC pavement under these weather conditions since standing water was never an issue. In these photos, snow is observed in the parking stalls. The stalls are not plowed because often cars remain there before, during, and after snowfall events.



Figure 8: Pavement conditions after thawing and refreezing of meltwater; (12:50PM on 2/16/08) PC at 12:50PM (left); Stnd. Ref. lot at 12:50PM (right)

Snow/Ice Surface Cover Analysis. The amount and type of snow/ice surface cover (dry, wet, slush, snow, compacted-snow, or ice) that was observed on each study area after storm events was recorded in order to make comparisons between salt applications and pavement type. Data for the entire '07-'08 winter season was grouped and compared statistically and graphically. Figure 9 presents the snow and ice cover for all study areas; the median surface cover percentages are displayed next

to each data set. The salt application rates for each study area are specified as 100%, 50%, 25%, or 0% of the recommended application rate (3.0-lbs per 1000-ft^2; MPCA, 2006).

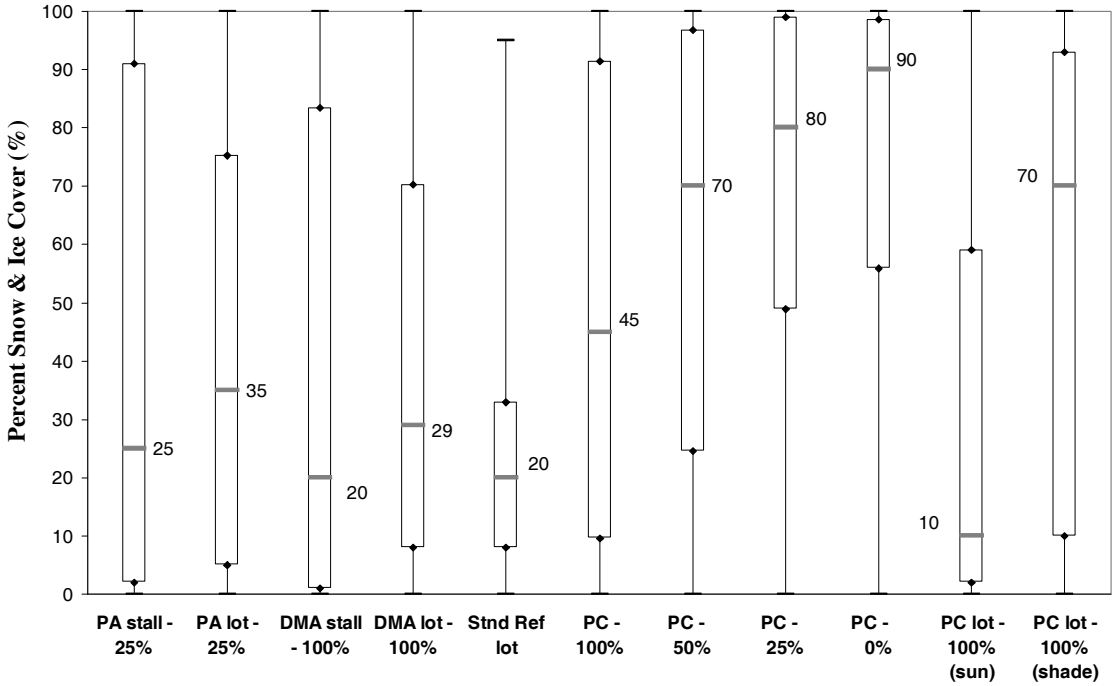

Figure 9: Comparison of snow & ice percent cover for all study areas ('07-'08); (Pavement type and salt application rate as percentage of 3-lbs/sf shown on x-axis)

The median snow/ice surface cover at the "DMA lot" is not significantly different (@95%CI, P=0.749) than at the "PA lot" even though the DMA received a salt application rate four times as great as the PA. A slightly higher application rate on the PA surface may have produced equivalent results between the two pavements.

When comparing the parking "stall" snow and ice cover data to the "lot" data in Figure 9, a difference of about 10% is shown for both the PA and DMA pavements even though each received the same salting rate. This disagreement can be explained by the amount of vehicular snow compaction at each observation area. The driving lanes, which make up a portion of the area included in the "lot" snow/ice surface cover observations, often experienced longer melting times than the parking stalls due to the difference in traffic and amount of snow compaction. Despite this disparity, no statistical difference in snow/ice surface cover was found between the data sets for the "lot" and "stall" areas at either the PA or DMA site (based on a p-value of 0.05).

The snow/ice surface cover measurements for the PC lot were considerably higher than the PA and DMA lots, but as one might expect, snow/ice surface cover increases with decreasing salt use. As mentioned previously, a possible explanation for the dramatic difference can be attributed to shading of the PC lot. The four PC study areas were located in an area that received only partial sunlight. This claim is supported when comparing the data sets for the PC lot that were in the sun and in the shade. A strong statistical difference exists between the sunny and shaded study areas

at the PC lot (p = 0.001) demonstrating that a factor other than salt application was contributing to the amount of snow/ice surface cover.

Frictional Properties of Pavement Surfaces. Frictional measurements were taken on all pavements with the British Pendulum Tester during and after storm events. All types of pavement conditions observed were evaluated, including dry, wet, snow-, slush-, compacted snow-, and ice-covered pavement. The data were grouped by pavement type and analyzed statistically to determine median skid resistance values for each type of surface cover (Figure 10). The median values for each group are displayed on the figure below each data set. Student's t-tests were performed to show how porous asphalt and pervious concrete compare to the conventional pavements in this study (Houle, 2008).

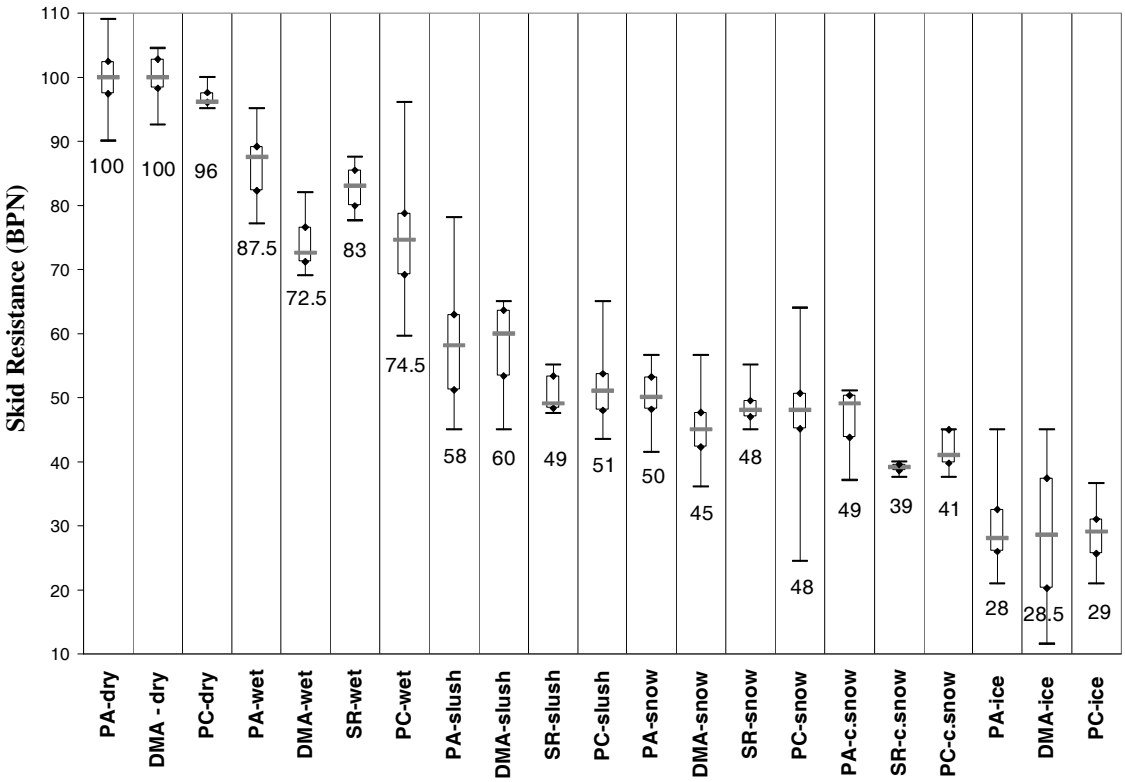

Figure 10: Skid resistance for all pavements and winter surface conditions ('07-'08) [(PA = porous asphalt; DMA = dense-mix asphalt; PC = pervious concrete; SR = standard (asphalt) reference), (Median skid resistance value displayed under each group)]

Of the four pavement types studied, porous asphalt was found to have the highest skid resistance for wet, snow-, and compacted snow-covered pavement, this is likely due to the large aggregate gradation (Figure 11) and the lack of fine particles in the mix. Literature suggests that coarser aggregate gradations will produce rougher pavement surface textures (Asi, 2007; Manuba et al., 2007). The PC demonstrated moderate skid resistance values for dry, wet, and snow-covered pavement. The smooth PC surface finish may have also contributed to the lower skid resistance when compared to the tackiness of asphalt mixes. It is significant to note the similarities in

skid resistance for PA and DMA between this winter and the '06-'07 winter presented in Houle (2008) despite differences in winter charateristics. The median values exhibit only slight differences between seasons, some of this variation may be due in part to the inclusion of additional snow/ice surface cover types (slush and compacted snow) in the '07-'08 winter.

By multiplying the mean skid resistance values by the snow and ice surface cover percentages a weighted skid resistance value was developed (Figure 11). The purpose of a weighted skid resistance was to assign a single number that can describe the pavement safety when compared to standard, dry conditions. The median skid resistance for the "PA lot" was 12% higher than the "DMA lot" even though the salt application rate was a quarter of that which was applied to the DMA surface. Similarly, the standard reference lots, which received regular plowing and salting by the UNH Grounds & Roads Dept., also demonstrated lower frictional resistance than the porous asphalt lot. The weighted skid resistance for the PA "stall" measurements in Figure 11 correlate extremely well with the data from the '06-'07 winter. A median value of 77 BPN was observed for the '07-'08 winter with the 25% salt application rate, whereas for the '06-'07 winter, a BPN of 79 was shown (Houle, 08). The "stall" measurements serve best for making comparisons between winters because the '06-'07 study focused only on areas that were not utilized for parking. A p-value of 0.662 was calculated between winters for the PA lot, suggesting that annual differences in weather conditions did not statistically change the results. The difference between the two seasons for the DMA parking stall study areas was 7 BPNs with a p-value of 0.298, also suggesting no statistical difference between winters (@95% CI).

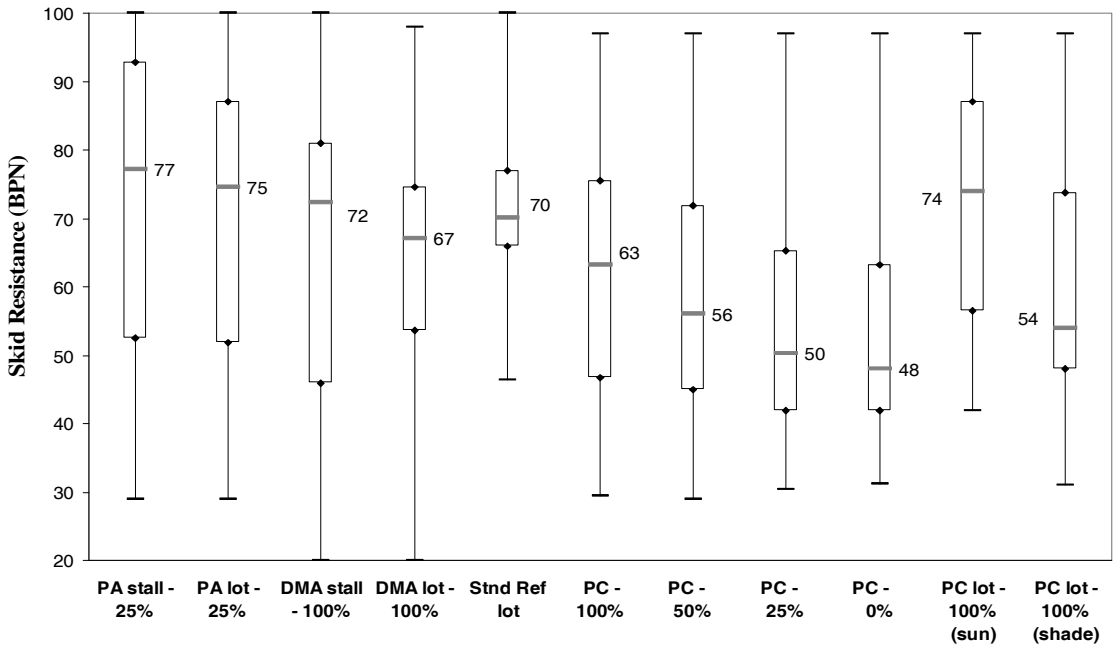

Figure 11: Weighted skid resistance as a function of surface cover ('07-'08) (Pavement type and salt application rate as percentage of 3-lbs/sf shown on x-axis)

The weighted skid resistance values for the pervious concrete parking lot study areas were considerably lower than both the PA and DMA pavements, despite salt application. This is likely due in part to a number of factors. As mentioned previously, the four main study areas did not receive as much sunlight as the other pavements because of a heavily wooded perimeter. Additionally, the pervious concrete lot is a much more trafficked parking lot due to its proximity to three adjacent dormitories; therefore, vehicle compaction of snow cover prior to plowing was often a problem. Operational constraints limited plowing maintenance for this project to one time per storm event. For this reason it was not uncommon for snow in the lanes to be driven on for several hours before plowing. Lastly, the measured skid resistance values for most types of pavement cover on the PC were lower than the other pavements, which will inherently produce lower weighted skid resistance values. Conversely, when looking at the data for the section of the PC lot that did receive sunlight, the skid resistance is similar to the results for the PA data set. This is a significant finding considering that permeable pavements may be most applicable for large, commercial settings where heavy tree cover is uncommon, and should be further investigated.

P-values less than 0.05 indicate that a statistical difference may exist between weighted skid resistance data sets. When comparing the results for PA to DMA using a Student's t-tests, the p-values are only slightly greater than 0.05, suggesting that the data sets may be marginally different and that PA with a 25% salt application may be safer than DMA with the recommended 100% application rate. This finding is consistent with results from Houle (2008). When comparing the PC study area that is primarily in the sun to the study area primarily in the shade a p-value of 0.004 is shown, suggesting a strong difference. Also of importance are certain data sets that are not statistically different. The PC lot study area in the sun compared to the PA lot demonstrate very similar weighted skid resistance results ($p = 0.847$). This is a notable finding because it shows that pervious concrete may exhibit similar surface conditions to porous asphalt if used with full sun exposure. A comparison between results for the DMA lot and for the Standard Reference Lot also exhibits a high p-value. This fact helps to verify that the winter maintenance methods used in this study were similar to the methods used by UNH Grounds & Roads.

CONCLUSIONS

Two years of winter performance evaluations have demonstrated that PA can perform extremely well in northern climates. Frost depth penetration and freeze-thaw temperature cycles have not compromised the integrity of the system structurally, visually, or hydraulically. Research has shown (both through literature and field testing) that PA exhibits greater frictional resistance and can become clear of snow and ice faster than conventional pavements. Substantial reductions in annual salt loads for anti-icing/deicing practices were observed, reaching over 70% during the study. Providing that plowing was regularly performed, salting was needed only for events where freezing rain created icy conditions. No salt was required on days when refreezing of meltwater was a problem on standard asphalt.

The results obtained from studying PC varied from PA but showed strengths in other areas. The surface infiltration rates measured on the PC lot exceeded those

that were observed on the PA. The benefit of this is that the PC will have a greater tolerance for clogging if sand or organic debris is present at the site. Additionally, binder drain-down is not a consideration with PC, as is the case with some PA mixes, making for a possible longer service life. Overall, the skid resistance and salt reduction capabilities for the PC lot were not as great as was shown for the PA. It is suspected that shading was the main contributing factor for this finding. The reasoning for this can be explained when looking at sections of PC pavement where shading was not as prominent and trees did not obstruct direct sunlight. Under these conditions the results drastically improve and the weighted skid resistance is shown to surpass that of the DMA lot. In addition to the shading, it is believed that the white pavement color of the PC contributed to the high levels of snow and ice cover. White pavements are more efficient at reflecting radiation, which can be beneficial in the summer months by lowering surface and air temperatures and consequently reducing the urban 'heat island' effect often associated with black, asphalt-based pavements, but non-ideal during the winter since the absorption of heat into the pavement will help to melt snow and ice (USEPA, 2007). Salt reductions during freeze-thaw events were achievable provided the lot was adequately plowed after storm events, an important consideration for all pavements not just PC.

REFERENCES

Asi, Ibrahim M. 2007. Evaluating skid resistance on different asphalt concrete mixes. *Building and Environment,* 42: 325-329

ASTM (American Society for Testing and Materials). 2004. Standard test method for measuring surface frictional properties using the British Pendulum Tester: E 303-93. *Annual Book of ASTM Standards,* 4 (3).

Backstrom, Magnus. 2000. Ground temperature in porous pavement during freezing and thawing. *Journal of Transportation Engineering,* 126 (5): 375-381.

Backstrom, M. and Bergstrom, A. 2000. Draining function of porous asphalt during snowmelt and temporary freezing. *Canadian Journal of Civil Engineering*, 27: 594-598.

Bean, E. Z. 2005. A field study to evaluate permeable pavement surface infiltration rates, runoff quantity, runoff quality, and exfiltrate quality. *Biological and Agricultural Engineering*. North Carolina State University, Raleigh.

Briggs, Joshua F. 2006. Performance assessment of porous asphalt for stormwater treatment. *M.S. Thesis*. University of New Hampshire, Durham.

Cahill, T., M. Adams, and C. Marm. 2003. Porous asphalt: The right choice for porous pavements. *Hot Mix Asphalt Technology,* September/October: 26-40.

Cambridge Systematics. 2005. Cool pavement report: EPA Cool pavements study – Task 5 (draft report). Prepared for *Heat Island Reduction Initiative, U.S. EPA*. August 18, 2008 (http://www.epa.gov/hiri/resources/pdf/CoolPavementReport_Former%20Guide_complete.pdf).

Ferguson, Bruce K. 2005. Porous Pavements: Integrative Studies in Water Management and Land Development. *CRC Publishing*, Boca Raton, FL.

Helsel, D.R. and R.M. Hirsch. 2002. Statistical methods in water resources. *USGS – TWRI Book 4,* Chapter A3 (online). August 15, 2008

(http://pubs.usgs.gov/twri/twri4a3/).

Houle, Kristopher. 2008. A winter performance assessment of porous asphalt and its function for chloride source control (In preparation). *Winter performance assessment of permeable pavements (Chapter 2), M.S. Thesis.* University of New Hampshire, Durham.

Kandhal, P. and R. Mallick. 2002. Design, construction and maintenance of open-graded asphalt friction courses: Information Series 115. National Asphalt Pavement Association.

Manuba, Chiba, Tako Jun, and Abe Ryuji. 2007. Effectiveness of open-graded pavements as a measure against snowy/icy winter roads. *Civil Engineering Research Institute for Cold Region: Monthly report,* 644: 21-27.

MPCA (Minnesota Pollution Control Agency). 2006. Winter parking lot and sidewalk maintenance manual. *Minnesota Snow and Ice Control Field Handbook for Snowplow Operators.*

Munro Environmental. 2007. Portable skid resistance tester operating instructions. *The Munro Group,* England.

NCDC (National Climatic Data Center). 2008. Record of climatological observations: Durham, NH. National Oceanic and Atmospheric Association (NOAA). June 2, 2008 (http://cdo.ncdc.noaa.gov/dly/DLY?stnid=20018620).

NHDES (New Hampshire Department of Environmental Services). 1992. Stormwater management and erosion and sediment control handbook for urban and developing areas in New Hampshire. *NH Greenbook.*

NHSCO (New Hampshire State Climate Office). 2008. NH data: Durham. *University of New Hampshire: Department of Geography.* June 3, 2008 (http://www.unh.edu/stateclimatologist/).

NRMCA (National Ready Mixed Concrete Association). 2007. (Text reference for) Pervious concrete contractor certification. *NRMCA Publication #2PPCRT.*

Ricard, J.A., W. Tobiasson, and A. Greatorex. 1976. The field assembled frost gauge. U.S. Army Cold Regions Research and Engineering Laboratory (CRREL), Hanover, NH.

Roseen, R.M., T.P. Ballestero, J.J. Houle, P. Avellaneda, R. Wildey, and J.F. Briggs. 2006. Storm water low-impact development, conventional, structural, and manufactured treatment strategies for parking lot runoff: Performance evaluations under varied mass loading conditions. *Transportation Research Record: Journal of the Transportation Research Board,* No. 1984: 135-147.

Roseen, R. M., Ballestero, T. P., Houle, J. J., Avellaneda, P., Briggs, J. F., Fowler, G., and Wildey, R. (2009). "Seasonal Performance Variations for Stormwater Management Systems in Cold Climate Conditions." *Journal of Environmental Engineering-ASCE.*

UNHSC. (2007). "UNHSC Design Specifications for Porous Asphalt Pavement and Infiltration Beds." University of New Hampshire Stormwater Center.

UNHWS (University of New Hampshire Weather Station). 2008. UNH Weather Statistics. *University of New Hampshire*: *Thompson Farm,* Durham, NH. June 3, 2008 (http://www.weather.unh.edu/).

USEPA (United States Environmental Protection Agency). 2007. Heat island effect: basic information. *Heat Island Reduction Initiative.* July 17, 2008 (http://www.epa.gov/hiri/about/index.html).

Field Evaluation of Indicator Bacteria Removal by Stormwater BMPs in North Carolina

J.M. Hathaway[1*], W. F. Hunt[2], J.D. Wright[3] and S.J. Jadlocki[4]

[1] Graduate Research Assistant, [2] Assistant Professor and Extension Specialist, and [3] Extension Associate, Department of Biological and Agricultural Engineering, North Carolina State University, Campus Box 7625, Raleigh, NC 27695; email: jon_hathaway@ncsu.edu
[4]Charlotte-Mecklenburg Storm Water Services, Charlotte, N.C., USA

Abstract: In the United States Environmental Protection Agency's National Water Quality Inventory in 2000, 13% of the river and stream miles that were surveyed were impaired by pathogen indicator bacteria (USEPA 2002). Stormwater runoff is a transport mechanism for indicator bacteria to receiving waters, resulting in an increased risk to public health through consumption of contaminated shellfish or ingestion by swimmers. Urban stormwater is commonly treated by stormwater Best Management Practices (BMPs), each of which provides some combination of natural treatment mechanisms and fosters certain environmental conditions. Although BMPs have been studied in detail for many pollutants, little peer-reviewed literature is available which documents their ability to remove or inactivate indicator bacteria. The North Carolina State University Department of Biological and Agricultural Engineering evaluated 10 stormwater BMPs in Charlotte and Wilmington, NC, to evaluate their efficiency with respect to indicator bacteria removal. The study practices included two bioretention cells, four stormwater wetlands, two wet ponds, and two dry detention areas. Data collected from these studies indicates that positive removal of indicator bacteria is possible in many types of BMPs; however, removal can be highly variable from practice to practice. Further, stormwater BMPs may foster environments where indicator bacteria can persist, becoming sources of indicator bacteria. Finally, even if positive reductions in indicator bacteria are noted, research indicates that achieving effluent concentrations of indicator bacteria consistent with USEPA standards may be difficult with many types of BMPs.

Introduction

In the United States Environmental Protection Agency's (USEPA 2008) National Water Quality Inventory in 2006, approximately 12% of the river and stream miles that were surveyed were impaired by indicator bacteria. Of the stream and river miles designated as impaired, either unable or partially unable to meet their designated use, more were impacted by this pollutant than by any other. Indicator bacteria were also the number one source of impairment in bays and estuaries, the number two source of impairment in oceans and near coastal areas, and the number three source of impairment along coastal shorelines (USEPA 2008). In light of the negative impact that indicator bacteria have on surface waters in the United States (indicating the

possible presence of pathogens), TMDLs have been established for impaired water bodies. Municipalities across the country are exploring options to reduce indicator bacteria inputs from point and non-point sources.

Numerous studies have indicated that development in watersheds leads to increased export of indicator bacteria. In a study of 18 mixed land use watersheds in West Georgia, Schoonover and Lockacy (2006) indicated that watersheds consisting of greater than 24% imperviousness exhibit higher fecal coliform concentrations than watersheds with impervious percentages less than 5% during both base and storm flow. Studies by Line et al. (2008) and Mallin et al. (2000) conclude similarly that urbanization in watersheds leads to increases in indicator bacteria export.

To test for the presence of harmful pathogens in surface waters, indicator species are used. Various indicator species have been used to assess water quality degradation due to pathogens including: total coliform, fecal coliform, *Escherichia coli* (*E. coli)*, and enterococci. In 1986, the EPA's Ambient Water Quality Criteria for Bacteria report (USEPA, 1986) discussed the merits of these various indicator species, and set a criteria whereby *E. coli* and enterococci are suggested as indicators in freshwater environments and enterococci is suggested as an indicator in marine environments. This criteria states that for fresh waters designated for use as full body contact recreational waters, the geometric mean over a 30 day period should not exceed 126 col/100 ml for *E. coli* and should not exceed 33 col/100 ml for enterococci. For marine waters designated for use as full body contact recreational waters, the geometric mean over a 30 day period should not exceed 35 col/100 ml for enterococci. The recommendation for fecal coliform, set in 1976 by the USEPA, is that the log mean over a 30-day period should not exceed 200 CFU/100ml (colony forming units per 100 ml) and no more than 10 percent of the samples should exceed 400 CFU/100ml (USEPA 1976).

Indicator bacteria can be removed from surface waters and stormwater through a number of natural processes, such as ultraviolet light (from sunlight), sedimentation, filtration, and various environmental factors. These environmental factors can include temperature, moisture conditions, and salinity (USEPA, 2001; Schueler, 2000; Arnone, 2007; Davies-Colley et al., 1994). Urban stormwater is commonly treated by way of stormwater Best Management Practices (BMPs), each of which provides some combination of natural treatment mechanisms. These BMPs include wet ponds, dry detention basins, wetlands, bioretention areas, and proprietary devices.
Although BMPs have been studied in detail for many pollutants, little peer-reviewed literature is available which documents their ability to remove or inactivate indicator bacteria. Six sites in Charlotte, NC, and 4 sites in Wilmington, NC, were monitored to determine indicator bacteria removal efficiency.

Site Descriptions

The stormwater BMPs evaluated in this project were monitored as part of the Charlotte – Mecklenburg Stormwater Services (CMSS) Pilot BMP Program and the

Burnt Mill Creek Watershed Restoration program in Wilmington, NC. As part of these studies, grab samples were taken and analyzed for both fecal coliform and *E. coli* from 6 stormwater BMPs in Charlotte, NC, and 4 stormwater BMPs in Wilmington, NC. In Charlotte, data were gathered from two dry detention basins, one wet pond, two stormwater wetlands, and one bioretention area. In Wilmington, data were gathered from one wet pond, two stormwater wetlands, and one bioretention area. Although data collection has been completed in Charlotte, the study in Wilmington was ongoing at the time of this publication. The characteristics of the BMPs from each city are given in Table 1.

Table 1: BMP and Watershed Characteristics

Site (Charlotte)	Watershed Size (ha)	Description	Estimated Curve Number
Dry Detention 1	2.4	Office Park - Buildings and Parking	85
Dry Detention 2	1.5	Office Park - Buildings and Parking	94
Wet Pond	48.6	Residential	75
Wetland 1	21	Residential	80
Wetland 2	6.4	Residential and School	83
Bioretention	0.4	Municipal Parking Lot	98
Site (Wilmington)	**Watershed Size (ha)**	**Description**	**Estimated Curve Number**
Bioretention 2	0.14	Parking Lot	98
Wetland 3	12.7	School Parking Lot and Fields	73
Wetland 4	2	Mulit-Family Residential	80
Wet Pond 2	4.7	Commercial	81

Dry detention basins fill with runoff during storm events and provide temporary detention while slowly draining over a span of approximately 48 hours. The primary pollutant removal mechanism in these systems is sedimentation. Charlotte, dry detention 1 was an extended dry detention basin which received runoff from a 2.4 ha watershed comprised of an office park and its associated parking areas, landscape features and buildings. The dry detention facility was well vegetated with grass and had good sun exposure. There was some evidence of erosion and sedimentation within the facility. Charlotte dry detention 2 was sited in a similarly sized watershed, 1.5 ha, also comprised of an office park. Like dry detention 1, this facility had good sun exposure, was well vegetated with grass, and had evidence of some erosion and sedimentation. Both facilities appeared to be mowed frequently. CMSS staff noted the frequent presence of birds around the basins, with bird droppings noted on the boxes which housed flow and water quality sampling equipment.

Wet ponds work on the principle of plug flow whereby influent runoff enters the pond and theoretically replaces the runoff that has been stored since then last storm event. Sedimentation in the basin is the primary pollutant removal mechanism as the stormwater slows, but some treatment is also provided via other mechanisms such as plant uptake, oxidation-reduction reactions, and adsorption as contact is made

between the soils and plants in the pond and the captured stormwater. The Charlotte wet pond was fed by a small, perennial stream and received stormwater runoff from a 48.6 ha watershed that was primarily residential. This pond was likely not originally created for stormwater management, and was constructed with no detention component. The estimated age of the pond was between 50 and 70 years old. Waterfowl were frequently observed at the pond during site visits. The pond was retrofit in the late 1990's to include a littoral shelf; however, the shelf was not planted and exhibited little vegetation during the study period. Despite the presence of trees around the BMP, there was good exposure on the pond. Wet pond 2 in Wilmington, NC, received runoff from a 4.7 ha commercial property which included a highly impervious 2 ha parking lot.

Wetlands are commonly installed as water quality devices, whereby they are sized to treat small (2.5 cm) storm events. These BMPs promote sedimentation much like wet ponds, but provide more intense contact between the captured stormwater and wetland soils and plants in shallow a system. Charlotte wetland 1 received stormwater from approximately 21 ha of residential area. This wetland exhibited common wetland topography, and consisted predominantly of shallow water depths. During the course of the study, however, there was very little vegetation in the wetland, likely due to poor soil conditions, prolonged periods of high water levels due to slow drainage, and the impact of waterfowl grazing. This lack of vegetation resulted in a larger amount of full sun exposure to water in the wetland than would typically be expected. Waterfowl were commonly observed at this site. Charlotte wetland 2 was constructed with similar topography, but exhibited exceptional plant growth. Charlotte wetland 2 received stormwater from 6.4 ha of residential area and a school. This wetland had two inlets, thus, weighted average influent fecal coliform and *E. coli* concentrations were calculated by weighting the grab samples at each inlet based on the total flow they contributed to the system. Wildlife was observed at Charlotte wetland 2 during the study. Wilmington wetland 3 treated runoff from 12.7 ha of a school, which included parking lots and practice fields. Wilmington wetland 4 is located in a multi-family residential complex. This wetland exhibits high amounts of infiltration in between storm events resulting in a normal pool where water is held mostly inside the deep pools.

Bioretention areas are filtration and infiltration BMPs. Stormwater enters the system and passes through a permeable soil media where pollutants are filtered, functioning similarly to sand filter systems. The BMP may pond water as much as 6 to 12 inches; however, it is drained within 12 to 24 hours. The system is intended to dry out in-between storm events. The Charlotte bioretention site received stormwater from a highly impervious 0.4 ha parking lot. This bioretention cell was studied and described in detail by Hunt et al. (2008). On at least one occasion, a diaper was observed in the parking lot, providing a potential source of bacteria to the BMP. Additionally, trees in the parking lot attract birds, and evidence of bird droppings have been observed by CMSS staff. Sun exposure in the BMP was fair, as it was limited by fairly dense vegetation. Wilmington bioretention area 2 was a sodded bioretention that treated the

runoff from a 0.14 ha parking lot at the headquarters of a coffee shop chain. The Wilmington bioretention area is broken into two paired cells, one with a 30 cm (1-foot) soil depth and one with a 60 cm (2-foot) soil depth. Observations have been made that the 30 cm deep cell receives more stormwater due to parking lot grading. This cell characteristically appears to stay more moist, likely due to the shallow soil depth and greater watershed area. Detailed surveys of the watershed area for the Wilmington bioretention area are planned to determine the exact sub-watersheds for each cell. Sun exposure at the Wilmington bioretention area is high.

With such highly variable uses, design specifications for the BMPs varied. Thus, there are some inherent differences in the function of the BMPs selected for this study with respect to both hydrology and water quality, making normalization problematic. However, these BMPs were selected because they are representative of the types of BMPs common to the City of Charlotte, NC, the City of Wilmington, NC, and elsewhere.

Monitoring Methods

Charlotte

As part of the Pilot BMP Program, grab samples were taken due to the small sample hold times required of bacteriological samples (USEPA, 2002). Grab samples were tested for fecal coliform and *E. coli*. Samples were collected at the various sites in Charlotte between March 2004 and October 2006. The monitoring period and number of samples collected at each site varied (Table 2).

Wilmington

Grab samples were also collected at each Wilmington, NC, site beginning in August of 2007. The samples from Wilmington were analyzed for enterococci and *E. coli*. Enterococci has proven to be a more reliable indicator species in environments with higher salinity (USEPA, 1986). Table 3 shows the number of samples collected at each site.

Table 2: Monitoring Period and Number of Samples Taken at Each Study Location

Site	Start	End	Number of Sample Tested For Fecal Coliform	Number of Samples Tested For *E. coli*
Dry Detention 1	Feb-05	Jul-06	9	9
Dry Detention 2	Jan-05	Dec-05	12	12
Wet Pond	Aug-04	Apr-06	14	10
Wetland 1	Mar-04	Jun-05	9	6
Wetland 2	Sep-04	Dec-05	15	10
Bioretention	Aug-04	Mar-06	19	14

Table 3 Number of samples taken at each Wilmington Study Site

Site (Wilmington)	Number of enterococci	Number of *E. coli* Samples
Bioretention 2	9	9
Wetland 3	9	8

Wetland 4	8	8
Wet Pond 2	8	8

Data Analysis

To adequately describe the bacteria sequestration and removal performance of each BMP, various analyses were performed. This included a calculation of concentration reduction efficiency and an analysis of effluent concentrations. The concentration reduction efficiency (CR) was determined by calculating the geometric mean of the influent and effluent indicator bacteria concentrations and using them in equation 1 below:

Equation 1: CR = 1 – (geometric mean outlet concentration / geometric mean inlet concentration)

Lastly, the geometric mean effluent concentrations of fecal coliform and *E. coli* leaving each site were compared to the maximum 30-day geometric mean for each indicator as established by the USEPA for full body contact (EPA, 1986; EPA 1976). This will aid in evaluating not only the efficiency of indicator bacteria removal for each system, but also the practicality of using stormwater BMPs to improve runoff from urban watersheds to indicator bacteria concentrations equal to or below targeted concentrations.

Results and Discussion

Table 3 presents the results for fecal coliform and Table 4 presents the results for E. coli for the BMPs studied in Charlotte, NC. Table 4 presents the results for *E. coli* and table 5 presents the results for enterococcus for the BMPs studied in Wilmington, NC. It should be noted that not all BMPs exhibit similar performance for both indicator bacteria for which they were tested. This indicates that BMP removal percentages generated for one indicator bacteria may not be applicable to other types of indicator bacteria data.

For the Charlotte BMPs, the wet pond, wetland 1, wetland 2, and bioretention area, exhibited greater than 50% removal of fecal coliform. The high fecal coliform removal determined for wetland 1 and wetland 2, 99% and 70%, is similar to that found by Birch et al. (2004) and Davies and Bavor (2000). For *E. coli*, only wetland 1 and the bioretention area provided high (> 50%) concentration reductions. Overall, wetland 1 and the bioretention proved most proficient at reducing influent concentrations of both kinds of bacteria. Wetland 1 had good sun exposure, likely leading to higher die off rates. Stormwater wetlands and bioretention areas also facilitate sediment removal through sedimentation and, in the case of bioretention, filtration and drying. All of these factors likely have some impact on indicator bacteria removal in stormwater BMPs. The poorest performing BMPs were the two dry detention basins. These systems had good sun exposure but remained moist for a substantial period of time after each rain event (per CMSS staff observation). It is possible that the wet soil provided an environment where the indicator bacteria could

persist for an extended period of time. Bird droppings were also noted by staff, likely leading to additional bacteria inputs to the BMP.

Table 3: Fecal Concentration Efficiency for BMPs in Charlotte, NC.

BMP Type	Fecal Coliform Concentrations (col/100ml)		
	Geometric Mean Influent	Geometric Mean Effluent	Concentration Reduction[1]
Dry Detention 1	1985	2873	-0.45
Dry Detention 2	1327	1590	-0.20
Wet Pond	9033	2703	0.70
Wetland 1	9560	184	0.98
Wetland 2	8724	3874	0.56
Bioretention	2420	258	0.89

1: Negative values indicate an increase in concentration
2: Significant reduction between the influent and the effluent

Table 4: *E. coli* Concentration Efficiency for BMPs in Charlotte, NC.

BMP Type	*E. Coli* Concentrations (MPN/100ml)		
	Geometric Mean Influent	Geometric Mean Effluent	Concentration Reduction
Dry Detention 1	915	1121	-0.22
Dry Detention 2	655	658	0.00
Wet Pond	2122	1153	0.46
Wetland 1	2400	106	0.96
Wetland 2	1295	864	0.33
Bioretention	241	20	0.92

For the Wilmington BMPs, the deep Bioretention cell 2, Wet Pond 2, and Wetland 4 all showed a fair ability to remove both types of indicator bacteria. The best performing of the BMPs was the Wet Pond 2, which removed a high percentage of *E. coli* and enterococcus. Further investigation is planned to determine factors which may lead to the high concentration reduction noted for this site. There is good sun exposure to the Wet Pond, potentially aiding bacteria removal. Studies by Mallin et al. (2002) and Davies and Bavor (2000) showed variable performance by Wet Ponds; however, two of the wet ponds evaluated in Wilmington, NC, by Mallin et al (2002) did show concentration reductions of greater than 50%.

Wetland 4 showed good performance for both indicator bacteria while Wetland 3 only removed enterococcus. However, influent *E. coli* concentrations to Wetland 3 were low, having a geometric mean of 255 MPN / 100 ml. It is possible that some natural background concentration of indicator bacteria is present and low influent concentrations of indicator bacteria result in poor performance when the data is evaluated using percent removal metrics.

Perhaps the most interesting relationship in the Wilmington data is the performance of the deep Bioretention 2 compared to the shallow Bioretention 2. The shallow cell showed poor performance for both *E. coli* and enterococci, and essentially acted as a source of bacteria. Further investigation of this cell has revealed that the shallow cell is potentially more moist due to a larger drainage area and shallow soil. This would provide a more favorable environment for indicator bacteria persistence and is concerning considering the potential for indicator bacteria removal that is seen in Bioretention 1 in Charlotte, NC, and in bioretention soil column studies performed by Rusciano and Obropta (2007).

Table 5: *E. coli* Concentration Efficiency for BMPs in Wilmington, NC.

BMP Type	*E. Coli* Concentrations (MPN/100ml)		
	Geometric Mean Influent	Geometric Mean Effluent	Concentration Reduction
Bioretention 2 (shallow cell)	111	792	-6.11
Bioretention 2 (deep cell)	111	44	0.60
Wetland 3	255	293	-0.15
Wetland 4	1315	720	0.45
Wet Pond 2	1621	83	0.95

Table 6: Enterococci Concentration Efficiency for BMPs in Wilmington, NC.

BMP Type	Enterococci Concentrations (MPN/100ml)		
	Geometric Mean Influent	Geometric Mean Effluent	Concentration Reduction
Bioretention 2 (shallow cell)	248	576	-1.32
Bioretention 2 (deep cell)	248	35	0.86
Wetland 3	1617	827	0.49
Wetland 4	2198	861	0.61
Wet Pond 2	497	52	0.89

Analysis of the geometric mean effluent concentrations from all BMPs reveals that not every BMP was able to reach EPA target concentrations for surface waters. The bioretention areas showed good performance for indicator bacteria. Other than the shallow bioretention cell, target concentrations were approached for fecal coliform, *E. coli*, and enterococcus via the bioretention cell in Charlotte, NC, and the deep bioretention cell in Wilmington, NC. Wetland 1 was also able to reach target concentrations for fecal coliform and *E. coli*, and Wet Pond 2 was able to reach or approach target concentrations for *E. coli* and enterococcus.

Conclusions

The results of this study support the literature that urban watersheds are a non-point source of bacterial pollution in surface waters. Even in watersheds consisting primarily of parking lots, concentrations of indicator bacteria entering BMPs can be higher than government assigned maximum values. Unfortunately, there are limited

data regarding bacteria removal in the stormwater BMPs commonly used to treat runoff from these urban watersheds.

This study suggests that some stormwater BMPs may effectively sequester and remove bacteria. Stormwater BMPs in both Charlotte, NC, and Wilmington, NC, were able to reduce indicator bacteria concentrations by over 50%. Bioretention cells in Charlotte, NC, and Wilmington, NC, performed well; however, the shallow bioretention cell in Wilmington, NC, indicates that some design features may impact the ability of a bioretention area to remove indicator bacteria. The Charlotte Wetland 1, which performed well for both fecal coliform and enterococcus, was atypical due to its lack of vegetated growth. The shallow water depths present in wetland 1 (15 – 45 cm) and minimal vegetative coverage led to more sun exposure than would normally be expected in a stormwater wetland. This high sun exposure may have led to increased indicator bacteria inactivation and removal by way of exposure to ultraviolet light. The substantial indicator bacteria removal in Wilmington Wet Pond 2 must be further explored to determine factors leading to its performance.

If the proper environment exists, it may be possible for stormwater BMPs to be sources of indicator bacteria. This may be due to both animal activity and to indicator bacteria persistence within BMPs. This was potentially the case for the two dry detention basins in Charlotte and the shallow Bioretention 2 studied in Wilmington, NC. This emphasizes the need for further study as to which environmental factors impact indicator bacteria sequestration, inactivation, and persistence in stormwater BMPs.

Acknowledgements
The authors would like to thank Charlotte – Mecklenburg County Stormwater Services for funding the research in Charlotte, NC, and collecting the data discussed herein. In particular, the authors thank Ron Eubanks, John Beller, and Jeff Price for their sample collection and analysis. The authors also would like to thank the Cape Fear River watch for their support with samples collection in Wilmington, NC. In particular, the authors wish to thank Joe Abbate.

References

Arnone, R.D. and J.P. Walling. (2007). “Waterborne Pathogens in Urban Watersheds.” *Journal of Water and Health*. 5(1): 149-162.

Davies, C.M. and H.J. Bavor. (2000). “The fate of stormwater-associated bacteria in constructed wetland and water pollution control pond systems.” *Journal of Applied Microbiology*, 89, 349-360.

Davies-Colley, R.J., R.G. Bell, and A.M. Donnison.(1994). “Sunlight Inactivation of Enterococci and Fecal Coliforms in Sewage Effluent Diluted in Seawater.” *Applied and Environmental Microbiology*. 60(6): 2049-2058.

Hunt, W.F., J.T. Smith, S.J. Jadlocki, J.M. Hathaway, and P.R. Eubanks. (2008). "Pollutant Removal and Peak Flow Mitigation by a Bioretention Cell in Urban Charlotte, NC." *Journal of Environmental Engineering*. 134(5): 403-408.

Line, D.E., J. Wu, J.A. Arnold, G.D. Jennings, and A.R. Rubin. (1997). "Water quality of first flush runoff from twenty industrial sites." *Water Environment Research*, 69(3), 305 – 310.

Mallin, M.A., K.E. Williams, E.C. Esham, and R.P. Lowe. (2000). "Effect of human development on bacteriological water quality in coastal watersheds." *Ecological Applications*, 10(4), 1047-1056.

Mallin, M.A., S.H. Ensign, T.L. Wheeler, and D.B. Mayes. (2002). "Pollutant removal efficacy of three wet detention ponds." *Journal of Environmental Quality*, 31, 654-660.

Rusciano, G.M. and C.C. Obropta. (2007). "Bioretention column ctudy: fecal coliform and total suspended solids reductions." *Transactions of the ASABE*, 50(4), 1261-1269.

Schoonover, J.E. and B.G. Lockacy. (2006). "Land Cover Impacts on Stream Nutrients and Fecal Coliform in the Lower Piedmont of West Georgia." *Journal of Hydrology*. 331:371-382.

Schueler, T. (2000). "Microbes and Urban Watersheds: Ways to Kill 'Em." Technical Note 67. Watershed Protection Techniques. 3(1):566-574.

USEPA. (1976). "Quality criteria for water." EPA-440/9-76-023, Office of Water, Washington, DC.

USEPA. (1986). "Ambient Water Quality Criteria for Bacteria – 1986." EPA 440/5-84-002. Office of Water, Washington, DC.

USEPA. (2001). "Protocol for developing Pathogen TMDLs." EPA-841-R-00-002. Office of Water, Washington, DC.

USEPA and American Society of Civil Engineers. (2002). "Urban Stormwater BMP Performance Monitoring: A Guidance Manual for Meeting the National Stormwater Database Requirements." U.S. EPA. EPA-821-B-02-001. Washington, DC.

USEPA. (2008). "Water quality assessment and total maximum daily loads information (ATTAINS)." < http://www.epa.gov/waters/ir/index.html> (November 29, 2008)

Field Testing Guidelines for Certification of Manufactured Stormwater BMPs: Part II

John Sansalone[1], Jeff Benty, Ernie Carrasco, John Gulliver, Jon Hathaway, Bill Hunt, Masoud Kayhanian, Uday Khambhammettu, Robert M. Roseen, Betty Rushton, Tim Williams

John Sansalone, University of Florida, Environmental Engineering Sciences, 218 Black Hall, Gainesville, FL 32611 (email: jsansal@ufl.edu) for Field Verification Sub-Committee

ABSTRACT

Guidance from information and field testing concepts examined by the ASCE/EWRI Subcommittee on Field Testing is presented. Field-testing of manufactured treatment devices requires critical planning and implementation through all steps of the verification process from watershed/catchment selection, to testing and analytical protocols, to data evaluation and quality assurance and control measures, to data reporting guidelines. Ultimately the goal of field testing is to provide verification of analytical or numerical models for BMPs that have been developed through scaled or full-scale controlled physical model testing. The desired goals and outcomes must be known and designed into the entire verification process. Ultimately, the entire process leads to a defensible model that represents a quantitative yardstick for both deterministic and probabilistic evaluations of a BMP for stakeholders across a range of regional conditions.

This committee is focused on field verification of a BMP for separation of particulate matter (PM) from rainfall-runoff and snowmelt. Towards this goal, the entire gradation of PM requires characterization for a BMP field evaluation, in particular the suspended fraction because of the mobility and acute bio-availability of this finer fraction. On the other hand, the coarse sediment fraction is of particular importance because this coarse fraction fills many BMPs and is most labile. A fundamental, transferable and defensible methodology is considered which includes particle size distributions (PSD) combined with gravimetric index tests for PM: total suspended solids (TSS) and suspended sediment concentration (SSC). TSS by definition is the PM fraction remaining suspended in an Imhoff Cone after one hour, although current methods utilize sub-sampling generate controversy as to the meaning of the measurement. However TSS remains in use because of ubiquitous usage, regulatory significance and as an important index of treatability. In contrast, SSC provides a gravimetric analysis of the entire sample and therefore limited bias, and outstanding reliability and repeatability. Quality assurance and feedback protocol are a necessary part of the testing protocol. We must recognize the range of challenges and collect sufficient representative data within an event and across events so that the role of such uniqueness can be quantified for the specific BMP or BMPs tested.

The committee is developing a multi-tiered approach to field testing predicated on the intended utilization and rigor required for the defensible and transferable examination of BMP behavior; thereby removing BMPs from the category of "black-boxes". Testing protocols with a basis of scientific knowledge are needed because the complexity for field testing of uncontrolled and episodic events is significant. This complexity extends to watershed characteristics, rainfall-runoff event characteristics, operation and maintenance requirements, system sizing tied to hydrologic and PM loadings, testing methodologies including mass balances and the non-stationary behavior of the BMP. A testing protocol must dictate methods to minimize bias, such that system performance can be effectively evaluated within a defensible level of statistical confidence. Additionally, such testing must ensure that valid comparisons between BMPs can be

conducted and that the protocols and results for such BMP testing are provided in a transparent and available format. The dataset provided should be sufficiently populated with an event and between events that defensible models can be developed from the results of the BMP testing and comparisons between BMPs can be made with statistically significant inferences.

As the committee moves forward, major technology protocols and reports will be reviewed. Guidance documentation will also be compared with TARP (Technology Acceptance Reciprocity Partnership) and TAPE (Technology Assessment Protocol- Ecology's) considerations. Field Testing guidance are developed as part of the ASCE/EWRI Committee on Guidelines for Certification of Manufactured Stormwater BMPs.

KEYWORDS

Best Management Practices, Unit Operations, Unit Processes, Stormwater, Rainfall-Runoff, Mass Balances, Watersheds, Hydrology, Particulate Matter, Particle Size Distributions

INTRODUCTION: Transferability of Hydrologic and PM Loadings

Controlled or uncontrolled field-testing of manufactured BMPs (unit operations and processes) still relies to a large extent on measurements of hydrologic loadings and particulate matter (PM). The most common measurements include TSS and SSC, both gravimetric indices as well as turbidity. A focus on PM has a fundamental rationale. While the dissolved fraction must be addressed and is bio-available; pollutants can partition to and from PM in many watershed and BMP conditions. PM measurements are coupled with hydrologic loadings from the watershed and hydraulic measurements in the BMP. In general, while watershed processes can be categorized and modeled, each watershed is different and unique with respect to BMP loadings of hydrologic, chemical, biological and PM quantities. Climates are different across the USA. However, despite such differences small watershed that commonly load manufactured BMPs can exhibit similar loading behaviors for different climates. For example, Figure 1 compares Trenton NJ to Gainesville, FL and Figure 2 summarizes the frequency distribution of events for each locations.

Annual average	Gainesville, FL	Trenton, NJ
Temperature	68.4 °F / 20.2 °C	54.8 °F / 12.7 °C
Humidity	78.2%	65.0%
Mean PDD*	3.1	2.3
# of events / yr	117	159
Precipitation	45.7 in / 1116 mm	41.6 in / 1057 mm

*: Previous dry days

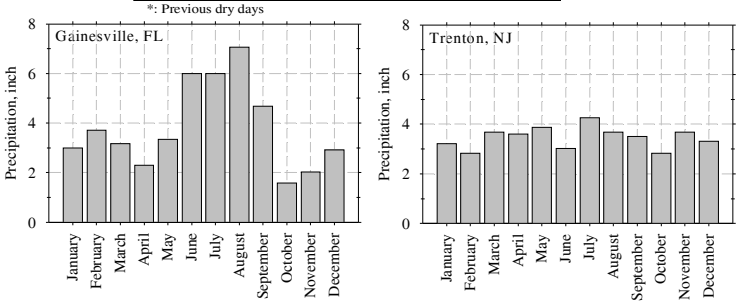

Figure 1. Comparison of the annual average and monthly average climate data for Gainesville, FL and Trenton, NJ.

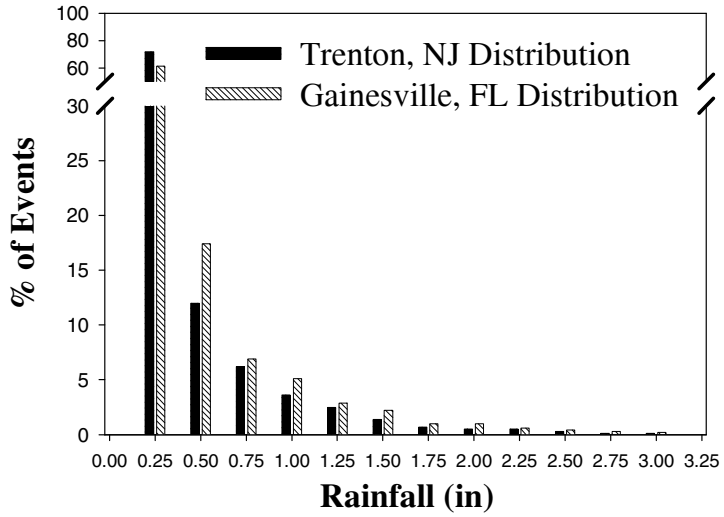

Figure 2. Frequency distribution of rainfall depths based on 30+ years of data from NOAA for both localities.

Despite specific climate differences, the two locations on the eastern seaboard of the USA have many rainfall frequency similarities with similar total annual rainfall depths. We can recognize these differences and similarities and collect sufficient representative data so that the role of such uniqueness can be quantified for the specific BMP or BMPs tested. What is more challenging than minor differences in climate are the very disparate methodologies of PM protocols that range from gravimetric index tests such as the traditional total suspended solids (TSS) method adopted from wastewater treatment evaluations, or the more recent suspended sediment concentration (SSC) method, index tests such as turbidity testing, to more fundamental methods of particle size distributions (PSDs). Each index method provides an indication of BMP performance with respect to PM; however a more fundamental, transferable and defensible methodology includes PSD (and specific gravity) and turbidity testing that are paired with a representative gravimetric index test for PM. In other words, SSC and PSD must be paired to provide a complete gravimetric description of the gradation. Field testing is predicated on the intended utilization and the rigor required for the defensible and transferable application of BMP performance results between localities of reasonably similar hydrologic loadings. Differences can be addressed through collecting a sufficient number of events to provide a distribution of hydrologic loadings that are comparable across regions. In addition to hydrologic loadings, knowledge of PM loadings is important. While both the fine suspended fraction and coarse sediment fraction are each important for BMP field testing, field testing requires the transport of a hetero-disperse PSD so that the BMP can be tested and examined across the gradation. This committee has the benefit of protocols such as TAPE and TARP that can be used as examples. The guidance that each protocol provides, while not universal is instructive when considering PM and the BMP separation of PM and building further guidance. It should be recognized that the entire gradation of PM should be representatively characterized for a BMP, in particular the suspended fraction, because of the mobility and acute bio-availability of this finer fraction. Figure 3 illustrates an example of an event mean PSD for a small watershed in Gainesville, FL. This urban catchment on the University of Florida campus is loaded by biogenic and anthropogenic PM loadings. The event mean PSD illustrated is compared to that of the NJCAT gradation. Again, despite the differences between New Jersey and Gainesville, Florida, the

similarity between PSDs is striking. It should be noted however that there is variability around the event mean; as there would be for any constituent.

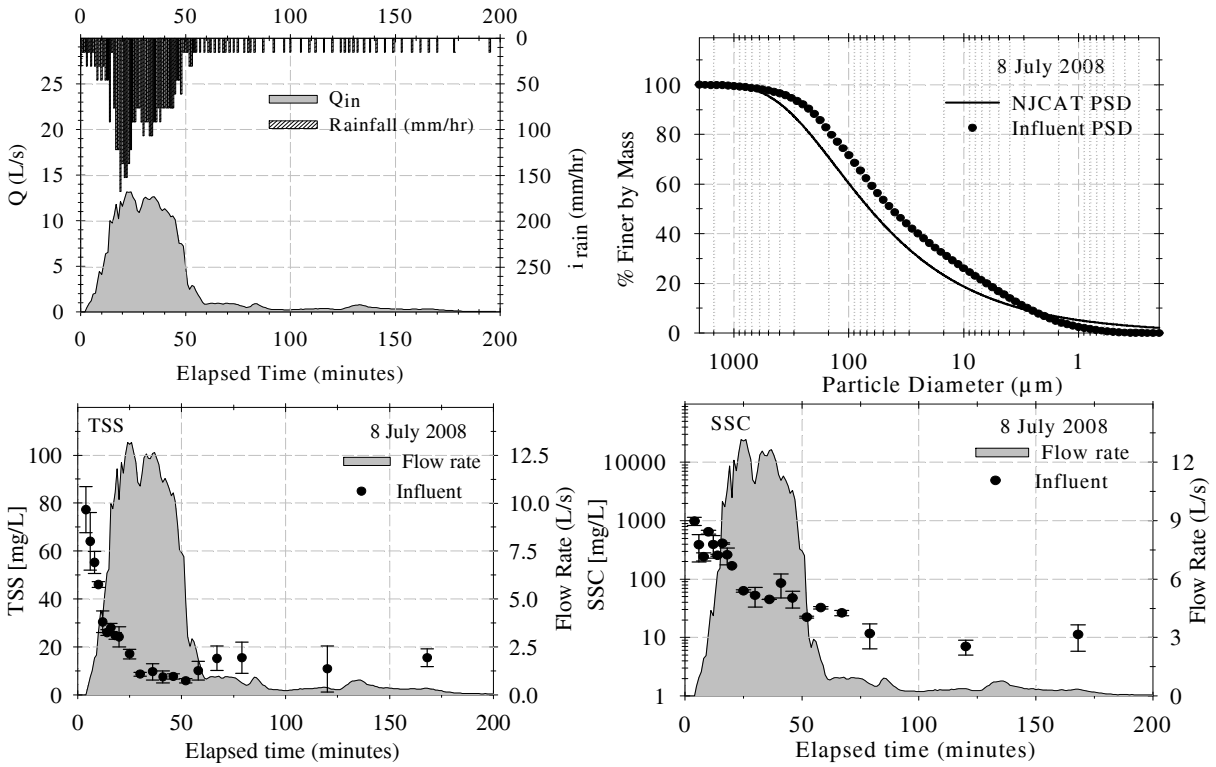

Figure 3. Coupling of hydrologic loads with PM measurements. The PSD illustrated is the event mean PSD.

Figure 3 illustrates a number of important phenomena that the committee is addressing. First, the highly unsteady nature of the hydrologic phenomena provides a far more challenging testing environment for a BMP and for the evaluators. The temporal hydrologic behavior is not known a-priori nor is the arrival of the event. Certainly, representative hydrologic measurements and sampling are challenging with such unsteady behavior. BMP behavior is directly impacted by such unsteady behavior that is not represented by controlled testing. However, such uncontrolled testing is not as readily amenable to model development or parametric analysis. Despite such unsteady behavior the event mean PSD is very similar, albeit slightly finer than an NJCAT gradation. The event-mean PSD and NJCAT are equally hetero-disperse. Such results suggest that a hetero-disperse NJCAT gradation for regulatory testing not only has the attributes of a defensible testing gradation, the NJCAT gradation has a reasonable granulometric resemblance to real gradations, albeit an event mean PSDs. If we step back and examine aggregate gravimetric indices such as TSS (PM < ~ 25 µm) there are a number of important observations. First, there is a clear mass-limited behavior between flow and TSS concentration that is driven by hydrology. The function of a BMP will be driven by this relationship between hydrology and load, with the caveat that such behavior is not known a-priori. When comparing TSS to SSC, it can be observed that TSS for this catchment is a small fraction of SSC. This is a result of the small watershed and source area configuration of the watershed. The high levels of SSC early in

the event are biogenic and larger anthropogenic sediment (> 75 μm) that are transported but not replenished during the event. This SSC material was generated between events and washed off during the rising limb of the runoff hydrograph. Early in the event the BMP (and the field sampling) is challenged by high flows, neutrally-buoyant biogenic material and coarse (> 75 μm) anthropogenic PM. SSC follows a more attenuated mass-limited behavior. Given the hetero-disperse nature of the PSD, representative automated sampling is challenging.

GENERAL DESCRIPTION OF BMP FIELD VERIFICATION AND MODELING

The basis of transport and fate of PM and other pollutants in natural and engineered BMPs, at the most rigorous macroscopic level of description, are the Navier-Stokes (NS) equations. Derivation of the NS equations to examine fate and mitigation strategies starts with the basic laws of conservation of mass, momentum and energy which apply to all natural and engineered BMP systems. The resulting equations would be the Navier-Stokes (NS) system of non-linear partial differential equations (PDEs) for multi-phase hydrodynamics and the fate (separation) of entrained pollutants (for example, particles) and the partitioning to these particles. While such a defensible analysis of field BMP performance is rare it is important to recognize that BMPs are amenable to such rigorous analysis whether the BMP is a simple batch settling tank or a screened hydrodynamic separator. The transport and fate of particles and pollutants (such as phosphorus that partition and distribute to particles) with such a defensible methodology for a BMP requires the following components.

Field Verification Components (with general BMP assessment needs)

1. **Geometric data component**: These are the data which geometrically define the domain of the BMP, essentially the BMP control volume (overall dimensions of the BMP system). For example the BMP system could be a wet vault, a hydrodynamic separator pre-treatment device or a combination of multiple unit operations and processes (UOPs) such as a wet vault followed by a cartridge filter. The geometric data are commonly generated by as-built drawings, as-built surveying data, manufacturer's drawings/specifications and surveying data for inflow and outflow geometries (pipe dia., slope, material, outflow geometry, soil cover, elevations, etc.). In modeling efforts, a Computer Aided Design (CAD) module is used to generate and modify (in the case of design or retrofits) the geometry of the BMP system. The data inputs are:
    a. A three dimensional description of BMP system through detailed CAD drawings or engineered drawing, including all inflow and outflow conveyance geometries. From such data, stage-storage, stage-outflow, inflow-storage functions are developed.
    b. This should be a common and conventional requirement for urban drainage and BMP system design/construction. Those who are carrying out the modeling, the CAD tasks, and those gathering field data and geometric data inputs should have the background and experience for such tasks.
    c. This is not significantly different than conventional as-built data, but with the need for standardization across protocols.

2. **Boundary-initial conditions data component:** These are the data that define the "quantity" and "quality" parameters at the BMP system boundaries. These parameters are classified as:

- **Hydrologic** (rainfall, previous dry hours, wind, air temperature, relative humidity, infiltration, evaporation, watershed storage, watershed characteristics),
- **Hydraulics** (flow rate, velocity, cross-sectional flow area, wetted perimeter, roughness, shear stress, hydrodynamic regime, temperature, degree of saturation, residence time distributions, RTD as developed from tracer studies),
- **Chemistry** (chemical species concentrations, temperature, turbidity, dissolved gas concentrations, partitioning, kinetics, pH-redox couples), and
- **Particulate** (particle size distributions, PSDs, particulate matter measured as suspended sediment concentration - SSC, suspended solids measured as TSS, trash, floatables, constituent distribution on PSDs, specific gravity, surface area, surface charge, solubility, exchange capacity, leaching, sludge and sediment properties including depth, density and cohesive-frictional properties)
- **Porous medium, soil or filter matrix** (porosity, pore size distribution, media or soil size distribution, tortuosity, effective porosity, surface area, exchange capacity, mineralogy, aquifer dynamics, equilibria, kinetics, breakthrough, hydrodynamics, moisture content – hydraulic conductivity relationships and head loss, leaching)
- **Vegetation** (species, hydraulic and friction properties, uptake and release equilibria, growth and uptake kinetics, leaching, specific gravity, flexural properties)
- **Microbiological** (species, size, charge, number, specific gravity, growth kinetics, uptake rates, hydrodynamic selection criteria and washout)

These parameters apply to the inflows, the BMP system and outflows. Even this list of parameters provided herein is not exhaustive and it should be recognized that the scope of this committee is most directly towards PM separation. However, these are coupled phenomena, and as such the role of vegetation (such as in an infrastructure-constrained bio-detention cell), microbiology and chemistry are important for the fate of PM across a BMP. It is readily apparent that such boundary and initial condition data requirements are significant and many are significantly different as compared to conventional data collection practices, as can be seen from the list of parameters in each category. Therefore, at this point in time, three levels of boundary/initial conditions field verification requirements are proposed. These field verification requirements will be defined in three levels:

- "***Level 1***" field verification requirements are for event-based BMP examinations. ***"Level 2***" field verification requirements are more detailed, are appropriate for monitoring and modeling event-based BMP examinations, and require temporal input and output data, as well as event-based system data.
- "***Level 3***" requirements are research or specialized datasets for BMP examinations examining specific pollutants beyond PM, nutrients or metals, for example, microbiological, that is combined with modeling and water chemistry examinations such as charge, volume and mass balances.

Commensurate with the available length of the paper, the following is a draft summary of the field verification requirements for a BMP under a detailed Level 1 requirement.

Number of Events Monitored: (12 calibration, 3 verification events for modeling)

a. A minimum of 12 calibration and 3 verification events are required for a BMP system. Events should occur in a one year period, and event rainfall depth should be at least 0.25 inches. There should be at least 24 previous dry hours. This is similar to

other BMP testing protocols around North America. Event mean flows should be reasonably distributed between 25 and 75 % of the BMP design flow rate.

Hydrologic: (initial storage depth required for CFD)

a. A ***watershed delineation*** so that a rainfall-runoff model can translate rainfall loadings to runoff loadings at the BMP system location for the watershed of interest. This is a hydrologic modeling input and should be a current and conventional requirement for BMP systems in any protocol.
b. A ***frequency distribution of the historical rainfall record*** for the watershed or locality. The maximum time increment between rainfall depth measurements during the event should be no greater than the time of concentration for the watershed. This is a hydrologic modeling input and should be a current and conventional requirement for BMP systems in any protocol.
c. A ***watershed-based and event-based temporal rainfall record*** for storm events captured. Representative rainfall depths should be recorded in increments of 0.01 inches or in time at increments no greater than 5 minutes for the watershed. This is a hydrologic modeling and should be a current and conventional requirement for BMP systems in any protocol.
d. A measurement of ***previous dry hours (pdh), wind speed and direction, air temperature, evaporation indices, and relative humidity*** for the watershed or locality on an event-basis. These data are readily available from a number of sites around most MS4s and do not require a weather station for the watershed where the BMP system is located.
e. A measurement of ***initial runoff storage depth and sludge depth*** should be made in the BMP.

Hydraulic:

a. ***Flow depths and velocities*** at increments no greater than 5 minute intervals for the entire inflow and outflow duration for each inflow and each outflow of the BMP system. These are direct BMP verification inputs and should be a current and conventional on-line measurement requirement for BMP systems.
b. ***Temperature***, for simplicity at increments to match hydraulic flow measurements for the entire inflow and outflow duration for each inflow and each outflow of the BMP system, as well as initial storage and final storage temperatures. These are indirect BMP inputs (to specify aqueous viscosity and density), and should be conventional on-line measurement requirement for BMP systems.
c. A ***temporal RTD*** for a high-flow calibration event and a lower-flow calibration event using a conservative tracer. This is carried with a known mass input of conservative tracer in the influent and temporal automated sampling of effluent with temporal discrete samples (not composited).
d. ***Pressure measurements*** should be made as a function of volume treated for BMP systems that contain a porous media including in-situ soil filters, taken on-line just upstream and downstream of filter. This is a critical need for porous media systems.
e. A ***calibration curve*** should be provided for each hydraulic measurement for each event. This should be required in any quality assurance plan.

Chemistry:

a. ***Constituent species and phases*** are analyzed from duplicated composite samples to provide event mean concentrations (EMCs). Recognizing that automated samplers cannot reproduce a representative PM; but to avoid endless debate over this topic, this methodology will nominally refer to "sampling" but not a method. These duplicate composited samples for an event will be composited by representative samplers for the entire duration of influent and effluent flow. The sampler is setup to house 4, 4 L (minimum composite volume) samples, unless larger volumes (i.e. 6 L composite samples) are possible. This additional volume is important for effluent samples. It is fully recognized that EMCs eliminate any temporal understanding of influent and effluent transport, and automated samplers cannot representatively sample influent and effluent flows (particularly influent particulate matter (PM) larger than approximately 75 μm and neutrally-buoyant material). However, for the sub-75 μm PM and the operationally-dissolved fraction of constituents such index methods will have to suffice until more representative measurements become more viable for common "Level 1" applications. Constituent selection is dependent on the receiving water impairments, BMP system and watershed. Calcium and alkalinity are also important measurements. An event-mean analysis of rainfall should be conducted.
b. All ***constituent analyses are conducted on fractionated (filtered) samples***; creating a dissolved fraction and a particulate fraction, operationally-separated using a 0.45 μm membrane filter. As with automated sampling and EMCs this masks the continuum of partitioning, but is a Standard Method, recognized by most laboratories, and will have to suffice. A digestion process is utilized to examine the constituent concentration associated with the dry PM (as TSS) retained on the membrane filter after the dry filter with dried TSS is weighed and the dry filter weight subtracted. The exact volume filtered to generate the TSS is also recorded along with the dry TSS mass retained on the membrane filter. It is noted that this fractionation occurs after the sample is pre-screened by passing each composite sample separately through a #200 (75 μm) stainless steel or nylon sieve (discussed in the particulate section).
c. A ***sample holding time of less than 24 hours***. No sample shall be held for more than 24 hours before analysis between the time the sample was taken and fractionation between dissolved and particulate-bound fractions, even under refrigerated conditions. While partitioning occurs at much shorter time intervals, within hours, there is currently no practical method to fractionate rapidly without on-site personnel.
d. ***On-line temporal chemistry measurements*** should include pH, redox (hydrogen-based offset provided), temperature, turbidity, total dissolved solids – TDS and conductivity for influent and effluent. The on-line measurement technology has advanced to the point that these are commonly deployed applications for BMP systems.
e. A ***calibration curve*** should be provided for each chemistry measurement for each event. This should be required in any quality assurance plan.

Particulate:

a. A ***measured volume for each duplicated composite sample*** should be determined to the nearest 10 mL. Duplicated 4-L (or larger if possible) and 20-L composite sample should be prepared with the exact volumes recorded. The 4-L duplicated influent and effluent composite samples will be used for obtaining datasets d, e and f. The 20-L influent and effluent composite samples will be used for obtaining datasets b, c and h.

b. ***A pre-screening through a #200 (75 μm) stainless steel or nylon sieve*** of each duplicated 4 L composite sample and 20 L composite sample should be first carried out before fractionation at the 0.45 μm level by passing the entire volume that is free of any holes or grid weighed and gently disaggregated. This dried material will then be dry-sieved through the standard (#50) 300 μm, (#80) 180 μm, (#100) 150 μm and (#140) 106 μm sieves. A mass balance shall be made by summing the mass components on each sieve allowing no greater than a 5% mass balance error from the original dry weight.
c. A ***determination of constituent mass distribution as a function of PSD*** is made through the appropriate extraction or digestion process for each particle size. This is more easily carried out for the influent samples. For the effluent samples, there may only be sufficient PM to carry out a larger than 75 μm analysis and a smaller than 75 μm analysis since a digestion process requires approximately 0.2 to 0.4 g of dry PM. This may require the utilization of larger effluent volumes to pass through the 75 μm pre-screen and the 0.45 μm membrane filter.
d. A ***set of 3, 500 mL TSS sub-aliquots is taken*** from each pre-screened duplicated composite sample that is well-mixed and these aliquots are taken and labeled in a consecutive manner. Before each sub-aliquot is taken, a turbidity measurement at mid-depth is taken. Each aliquot is taken from mid-depth of the composite volume. Each aliquot shall be completely filtered through a 0.45-μm filter, dried and analyzed for TSS and VSS using Standard Methods protocol. The relative percent difference between sub-aliquots must be < 10% on a gravimetric basis for TSS. The filtrate is saved, separated as required, and preserved for dissolved constituent analyses.
e. A ***set of 3 alkalinity sub-aliquots*** are also taken for alkalinity and other constituent measurements of choice for the filtrate.
f. A ***set of 3 PSD sub-aliquots***, approximately 750 mL will be used for PSDs for the sub 75 μm fraction. It is recommended that as part of any database these sub 75 μm fractions be compiled and also combined with the matching fraction larger than 75 μm to create a database that is available for BMPs, land use, cover conditions, hydrologic regions, seasons, etc. These PSD sub-aliquots must be matched with their TSS or SSC sub-aliquot partners in order to convert % volume of particles to an absolute gravimetric value in mg. Note that turbidity measurements are also included to examine the relationship for a site between turbidity and TSS (or SSC).
g. An ***estimation of sludge (sediment) depth*** should be made at the beginning and end of the monitoring. A 2000 dry grams sludge (sediment) sample should taken from the BMP (location determined from modeling or measurement of short-circuiting) for determination of PSD, specific gravity and contamination levels as a function of PSD.
h. ***A determination of specific gravity for the sub 75 μm and larger than 75 μm fractions*** for each 20 L composite sample should be made for 2 calibration events. Analysis will require the entire dry mass for each fraction of influent and effluent.

Porous medium, soil or filter matrix: (datasets a and b are required for CFD)

a. A ***representative set of porosities*** of a porous medium, whether surrounding soil of an infiltrating BMP or as a filter matrix should be measured.
b. A ***representative set of filter or soil media size distributions*** should also be measured.

Vegetation:

a. An ***identification of the vegetation species*** and approximate size should be provided.

Microbiological:

a. An ***identification of the redox conditions and microbial consortium*** and their numbers in the water column or media (or soil) column should be approximated.

CONCLUSIONS

While field verification of manufactured BMPs is more complex and uncertain than controlled, scaled or full-scale BMP testing utilized for numerical (or analytical) model development, parametric evaluations, or controlled performance evaluations; field verification of a BMP is a logical and required step. The Field Verification Sub-Committee of the Guidelines for Certification of Manufactured Stormwater BMPs Task Committee is in the process of developing guidance for field verification protocols for manufactured stormwater BMPs. This paper illustrates the complexity of uncontrolled field loadings with respect to hydrology and PM while outlining one level of requirements involved with defensible and transferable field verification for a BMP. The requirements and level-of-effort increase with the level of field verification required; as illustrated herein. When combined with controlled laboratory testing and scaling for the same BMP; that allow rigorous mechanistic analysis and model development, the combination of such testing/monitoring campaigns with field verification of the same BMP results in a tripartite verification of BMP behavior. While data from controlled studies are more readily amenable for BMP comparisons, although there still seems to be some murkiness regarding simple concepts such as creation of an NJCAT gradation, field verification is much more challenging given the lack of control. Despite such uncontrolled conditions, existing protocols such as TAPE and TARP are a reasonable starting point with reasonable applicability across regions. An example is provided comparing Trenton, New Jersey loadings to Gainesville, Florida. Rainfall frequency distributions, annual depths and event mean PSDs for Gainesville are relatively similar to Trenton. Even if similarities are somewhat more disparate than the example given, tools such as frequency distributions, fundamental data collection (as opposed to indices such as an EMC) such as PSDs and the coupling of hydrology with PSDs allow the transferability of field verification. Such verification should be sufficient in scope, depth and quality that a public database of testing should be available to cut through the murkiness of BMP claims. With the inherent requirement for accuracy and representativeness, the more fundamental and precise is the data collection, the greater the potential for transferability and comparability of BMPs. Even though the Committee focus is limited to PM the Sub-Committee and Task Committee have more work to carry out. This document as well as future documents will not be without controversy but are intended as a significant step forward. The creation of a more uniform defensible and transferable laboratory, scaling and field verification program for BMPs allows a representative “chili-cookoff” for BMPs which benefits all stakeholders and most importantly the environment.

From Grey to Green: Strategies and Concepts for Implementing Green CSO and Wet Weather Solutions

James C. Schlaman[1] and Bryce Lawrence[2] and Scott Schulte[3]

[1] Black & Veatch, 8400 Ward Parkway, Kansas City, MO, 64114; PH (913) 458-3359; email: schlamanjc@bv.com
[2] Patti Banks Associates, 929 Walnut Street, Kansas City, MO, 64106; PH (816) 756-5690; email: blawrence@pbassociates.com
[3] Patti Banks Associates, 929 Walnut Street, Kansas City, MO, 64106; PH (816) 756-5690; email: sschulte@pbassociates.com

ABSTRACT

Sustainable wet weather and Combined Sewer Overflow (CSO) solutions that utilize green infrastructure and solutions are an increasing topic of interest. Identifying suitable locations for green infrastructure, developing appropriate concepts and quantifying their impact can be challenging. In the content of this paper, the authors will provide three strategies that address these challenges and present a comprehensive and holistic approach to incorporate green solution technologies into wet weather and CSO Long Term Control Plans.

KEYWORDS

Sustainable planning, watershed planning, green infrastructure, green solutions, best management practices (BMPs), natural systems, BMP locator, Green Filter, combined sewer overflow (CSO), stormwater management, geographic information system (GIS), source control, water quality, Hydrologic and Hydraulic Modeling.

INTRODUCTION

Black & Veatch (B&V), in collaboration with Patti Banks Associates (PBA), is developing Combined Sewer System (CSS) solutions for communities across the country. Specifically, their efforts in two Midwestern cities; Kansas City, Missouri and Omaha, Nebraska are of interest. Recently the regulatory community has focused on "green infrastructure" to help supplement communities' Combined Sewer Overflow (CSO) Long Term Control Plans (LTCPs). In March of 2007, the Environmental Protection Agency (EPA) released guidance encouraging the use of green infrastructure stating that green solutions "could be both cost effective and an environmentally preferable approach" in helping to solve CSO problems.

The following discussion addresses specific approaches for using green infrastructure for CSO control. The approaches attempt to answer some of the more challenging questions regarding their use which include:

- How should the best sites for incorporating the technologies be located and prioritized?
- What type of green technologies and concepts make the most sense at specific locations?
- How can the benefits of green infrastructure be quantified?

The authors present a methodology for locating green infrastructure at a macro scale, develop green infrastructure concepts for identified locations and present a method for quantifying the benefits of green infrastructure. These three methodologies can be used in conjunction to create a more sustainable and holistic approach for developing CSO and wet weather solutions.

Green infrastructure includes a universe of technologies that offer a wide variety of benefits. Green infrastructure technologies focused on CSO and stormwater runoff control include, but are not limited to: detention and retention practices such as wetlands, dry and wet extended detention and retention basins, infiltration and filtration practices like pervious pavement and bioretention, conveyance practices such as vegetated swales and bioswales and rainwater harvesting practices like cisterns and rain barrels. Dispersed detention and retention practices are particularly interesting because they have the potential to maximize source control while efficiently using available land.

Over the last several years, the use of green infrastructure technologies, or Best Management Practices (BMPs), has increased within the stormwater and CSO communities. Green infrastructure is a break from more traditional wet weather engineering practices, where conveyance was maximized and hydrologic residence time was minimized. The traditional approaches to controlling wet weather runoff focused on removing water as quickly as possible through engineered pipes and conveyance channels. However, the focus on conveying water quickly has led to unanticipated and significant problems in the nation's receiving streams. Urban stream corridors around the country are becoming degraded; pollutant loadings in runoff are left unfiltered and are conveyed directly to receiving streams; impaired waters are negatively impacting wildlife and natural ecosystems; beach closings still occur on the coasts; fecal coliform and E. coli concentrations in receiving streams continue to exceed, sometimes by orders of magnitude and the list of problems goes on.

Green infrastructure departs from the traditional engineered schemes in the developed landscape by attempting to mimic eco-systems and return the landscape to a more natural state. For example, these technologies can provide wet weather runoff control by:

1. Increasing infiltration
2. Increasing evapotranspiration
3. Adding surface detention and retention storage
4. Increasing initial abstraction
5. Lengthening the hydrologic residence time
6. Disconnecting impervious areas from the sewer system

7. Filtering runoff and removing pollutants before they enter receiving water bodies
8. Enhancing chemical, typically through biological processes, and physical break down of contaminants before reaching receiving water bodies.
9. Providing CSO and stormwater runoff source control

In addition to the technical benefits, green infrastructure can typically be incorporated with less impact and disturbance to the surrounding community while offering multipurpose benefits not associated with traditionally engineered wet weather solutions. The multipurpose benefits can include community aesthetic enhancements, added recreational opportunities, greater public acceptance and enhanced economic vitality and property values. Also, unlike many traditional solutions, green infrastructure can provide highly tangible and visible solutions which stakeholders can better appreciate and value.

The CSO and wet weather benefits provided by green infrastructure technologies are the main topic of this paper. CSO problems are often complex and encompass vast sewer systems serving highly developed areas. Traditional CSO solutions (i.e., grey solutions) such as deep tunnels, storage tanks, high rate treatment systems and treatment plant and pump station upgrades will continue to be the main components of any CSO LTCP. However, green solutions specifically targeted at reducing the inflow to combined sewer systems may potentially minimize the cost and magnitude of the grey CSO solutions. Water quality will be improved and a wide range of the benefits previously noted will be provided.

The excitement surrounding green infrastructure and sustainable planning efforts, specifically those focused on CSO control, has created an interest in incorporating these technologies into ongoing wet weather and CSO planning and solution efforts. Several distinct schemes may be used to incorporate green solutions into a CSO LTCP and such schemes are discussed herein. First, the Green Filter (i.e., green infrastructure locator) identifies and prioritizes locations across a community that is suitable for green infrastructure technologies. Second, concepts and rendering of specific green solution approaches for use in developed areas is presented. Finally, a Hydrologic and Hydraulic (H&H) Modeling exercise is presented that attempts to estimate the effectiveness of green infrastructure technologies on reducing the wet weather runoff from a basin.

The goal and objective is to find sustainable approaches and solutions for current and future complex wet weather problems. As the world continues to remind us, nothing we do is truly independent. As we learn the hard lessons of the past, reinventing our thinking to promote sustainable environmental, social and economic solutions for all future generations is now, more than ever, paramount.

METHODOLOGY AND DISCUSSION

As discussed in the introduction, the authors presented a process herein to link the identification and prioritization, design and modeling of green infrastructure. Although each of the three processes are discussed below in independent sections,

the intent of this paper is to show how these concepts can be used together to achieve more sustainable CSO and wet weather control solutions.

1. Green Filter

a. Methodology

In fully developed communities, which are those typically targeted by CSO regulations and in need of better wet weather control, frequently few large open spaces remain that are suitable for land-intensive green solution technologies such as wetlands and detention basins. Therefore, a computerized analysis that can quickly process and locate existing open space of all sizes across wide area is an invaluable tool. For both the Kansas City and Omaha CSO programs, the ESRI ArcGIS ModelBuilder tool was used to develop such a model. The Green Filter model was based on the following data:

1. High resolution Digital Elevation Models (DEMs)
2. One-acre Resolution Landsat Enhanced Thematic Mapper Plus (ETM+) images
3. Parcel Data and Right of Way Boundaries
4. Impervious Coverage
5. National Wetland Inventory (NWI) and Flood Insurance Rate Maps
6. Soil Data
7. Natural Resources Inventory Land Cover Classifications or GAP Analysis Land Cover Analysis
8. High Resolution Surface Drainage Network

Figure 1 provides a graphical representation of the ArcGIS ModelBuilder tool along with the input data used to identify green infrastructure opportunities for the Omaha, Nebraska CSO program. A similar configuration was used for the Kansas City, Missouri CSO program. It should be noted that the ArcGIS Model Builder is flexible and can be adjusted depending upon local conditions and needs. The subsequent text describes the Omaha green infrastructure locator methodology in greater detail as one example of this tools' capabilities.

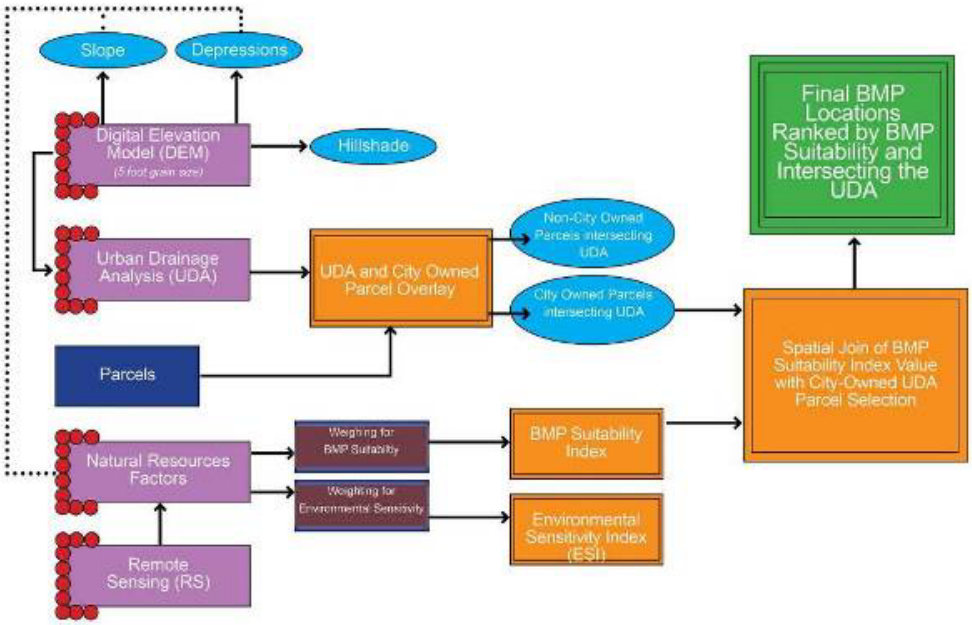

Figure 1. Green Solutions Locator Model Overview

The Green Filter uses a raster-based analysis to classify natural resources and identify green solution opportunities and constraints. The rasterization process converts spatial data into pixels as opposed to polygons or linear features as performed with vector analyses. Raster analyses are more appropriate for the green solutions modeling process because much of the base information (such as the DEM and Landsat data) is already in raster format. In addition, raster data can be more easily compiled and incorporated into statistical models to generate useful outputs.

Initially, a 5-foot grid cell DEM for the entire city of Omaha, derived from 2-foot contours provided by the City, was developed. The DEM was the basis for the subsequent evaluation of urban hydrology and catchments, slope, hillshade, and existing depressional storage areas.

In lieu of local natural resources mapping, the modeling team used 1-acre Landsat satellite imagery to classify and rank land cover types. Multispec image processing software (Purdue Research Foundation, 1994-2008) was used to classify the cover types. ETM+ bands 2 (0.52-0.6m), 5 (1.55-1.75m), and 7 (2.08-2.35) were classified to identify tree canopy land cover, open / under story land cover, and open / agricultural land cover. The results were statistically verified using Multispec.

In Omaha, the modeling team developed two distinct weighting distributions, one which weighted the sensitivity of natural resources from the most sensitive to the least sensitive (the environmental sensitivity index or ESI), and one which weighted the natural resources from the most to the least appropriate for constructing BMPs on them (BMP weighted ESI or Green Filter).

For the Green Filter suitability index weighting, wetlands, high quality vegetation and 100-year floodplains were devalued because it didn't make sense to construct BMPs in areas that are environmentally sensitive and already functioning in a natural way. Areas that were identified in the ESI to be highly sensitive natural resources were not considered to be good locations for the future incorporation of BMPs. Conversely, depressions, alluvial valleys and poor quality vegetated spaces were increased in value for the BMP weighted ESI. This would highlight those areas that could potentially provide the greatest wet weather benefit if they were to be retrofitted with BMPs. The Green Filter weighting factors were determined through discussions with the Omaha CSO Program Management Team (PMT) and City staff. The modeling team further refined the weighting factors based on experience and research (Dunne et al., 1978). A schematic of the GIS Green Filter model inputs and corresponding weighting factors to develop the Green Filter Suitability Index used by the Omaha CSO program are presented by Figure 2. Note that each parcel with the City limits was assigned a green infrastructure "suitability score" based on this screening criterion.

Next, using contour data, an urban drainage analysis (UDA) was developed for the entire City. The UDA reviews hydrology and City parcel data to identify those parcels that currently intercept and/or are adjacent to "significant" overland flow paths (i.e., for Omaha, flow paths that drain greater than approximately 2 acres). The ArcGIS ARChydro extension was used in combination with City topography to create a this detailed flow line network, which was overlaid on the City's parcel mapping to identify properties that intersect or are adjacent to these major surface flow lines. A 15-foot buffer was applied to the flow line to identify adjacent rights-of-way or roadways that could be used to capture runoff along a flow line. Parcels intersecting surface flow lines were identified and extracted for further consideration.

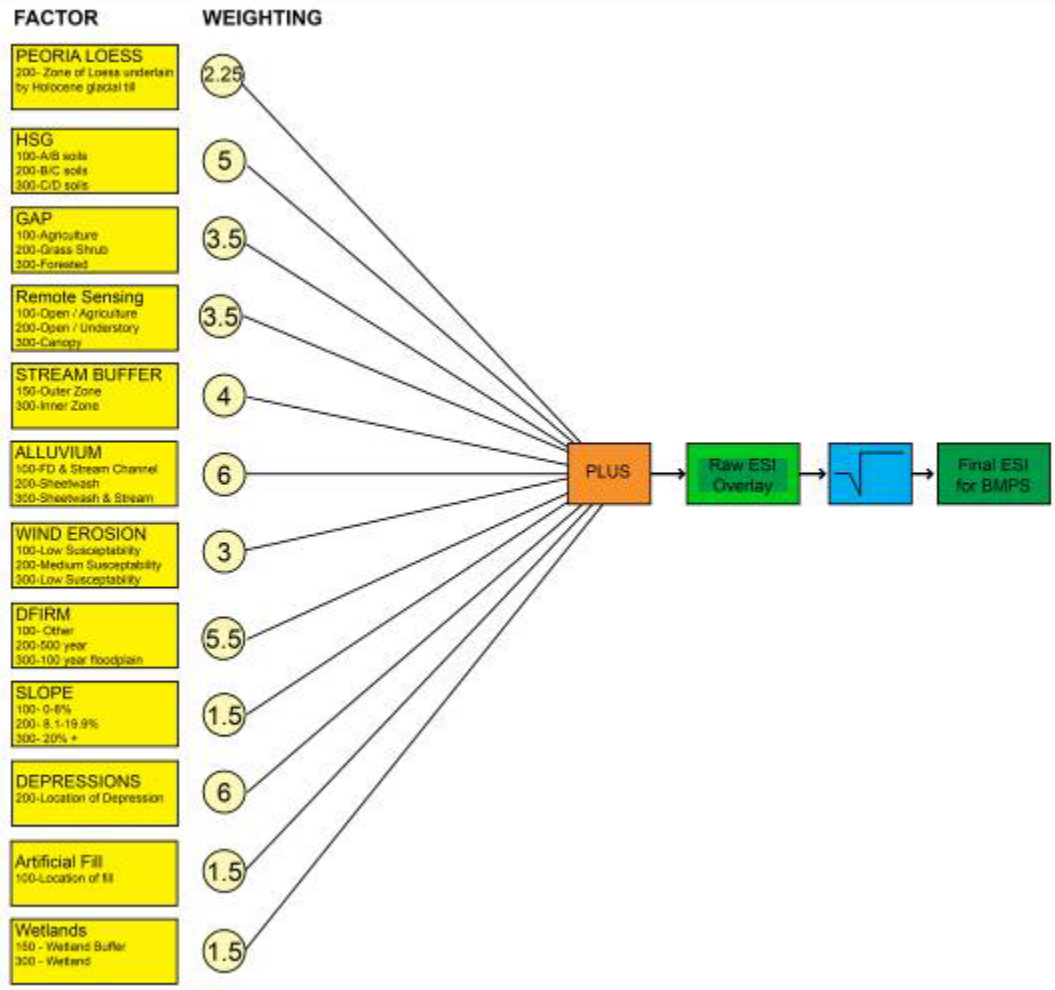

Figure 2. BMP Suitability Index

To complete the Green Filter effort, the value of the BMP suitability index was joined to City-owned and non-City-owned parcels identified by the UDA analysis. This created a prioritized green solution opportunities GIS layer which is located near significant overland flow paths. In other words, the process highlighted areas most suitable for wet weather green infrastructure retrofits. Output and results from the Omaha Green Filter process are presented within the following section.

b. Results of Green Filter

The Green Filter was used to produce maps of possible green CSO BMP opportunities across the 100-square mile area of the City of Omaha. In addition, the identified locations were prioritized and ranked depending upon the suitability of each location to be modified into a highly valuable green solution technology. The suitability of each site is color coded on a spectrum where the color red denotes the least suitable locations and the color blue indicates locations most suitable for green solution technologies. Per the request of the City, the modeling

team developed a tiered result system by varying the inclusivity of ownership records in the parcel codes within the model. This variation allowed the team to screen out parcels based on ownership. The following parcels are displayed in descending order according to those of most interest to The City.

- City owned parcels (i.e., Tier 1)
- Educational and institutionally owned parcels (i.e., Tier 2
- All property parcels (i.e., Tier 3).

The graphic results from the Green Filter GIS model are presented for each tier by Figure 3 Figure 4 and Figure 5, respectively.

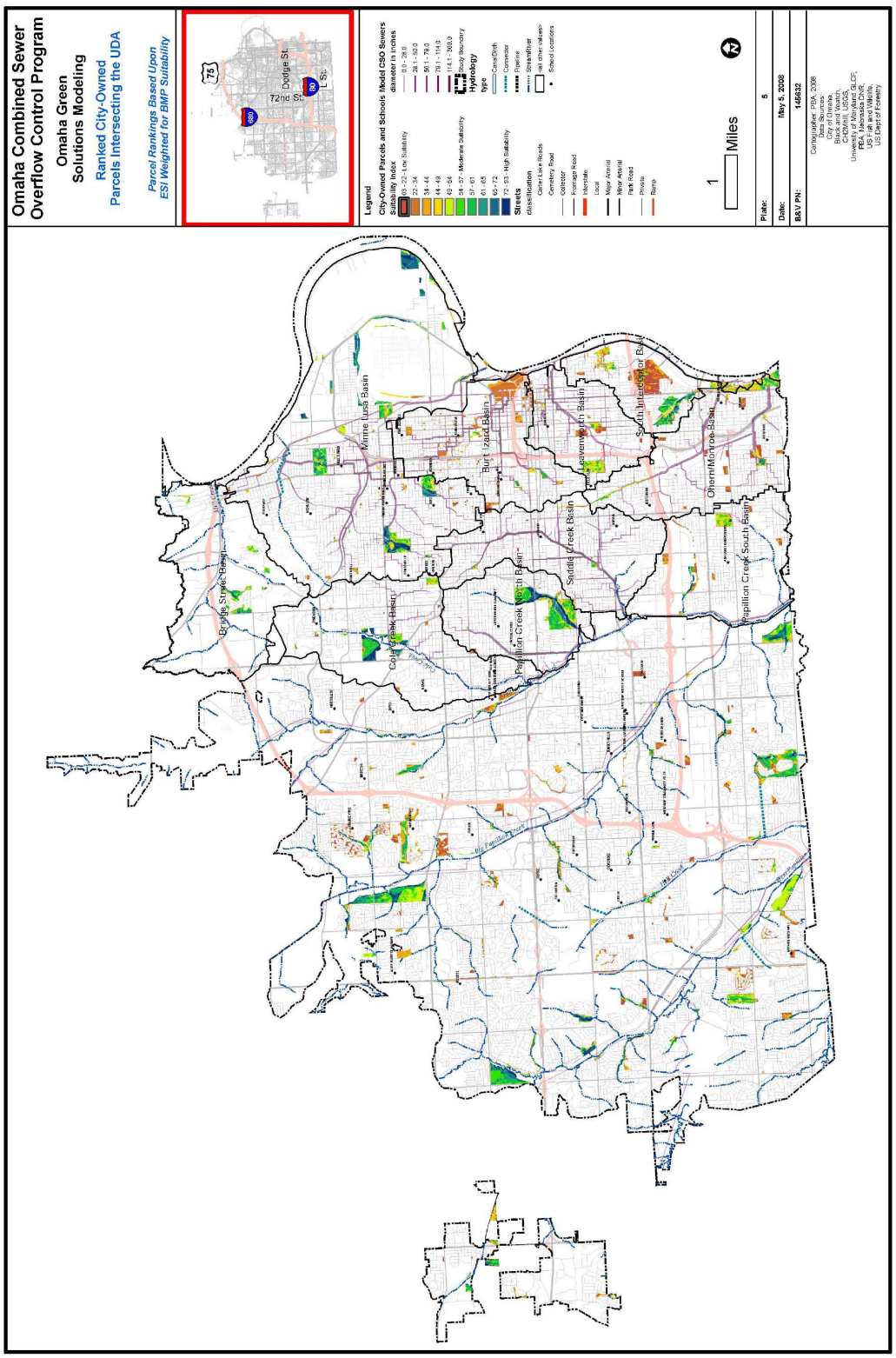

Figure 3. Green Filter Tier 1: City-Owned Green Infrastructure Opportunities

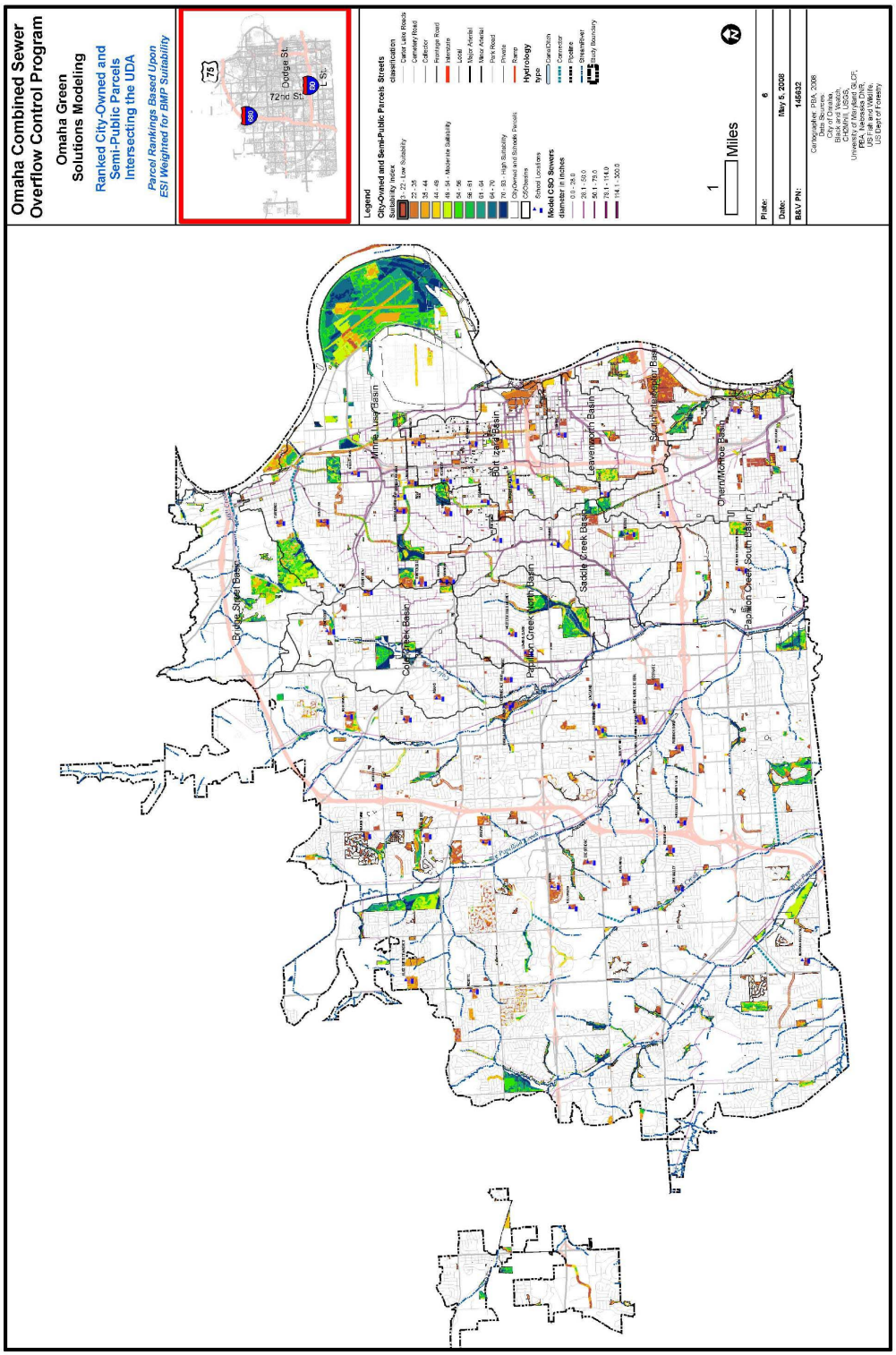

Figure 4. Green Filter Tier 2: City-Owned, Educational, and Institutional Green Infrastructure Opportunities

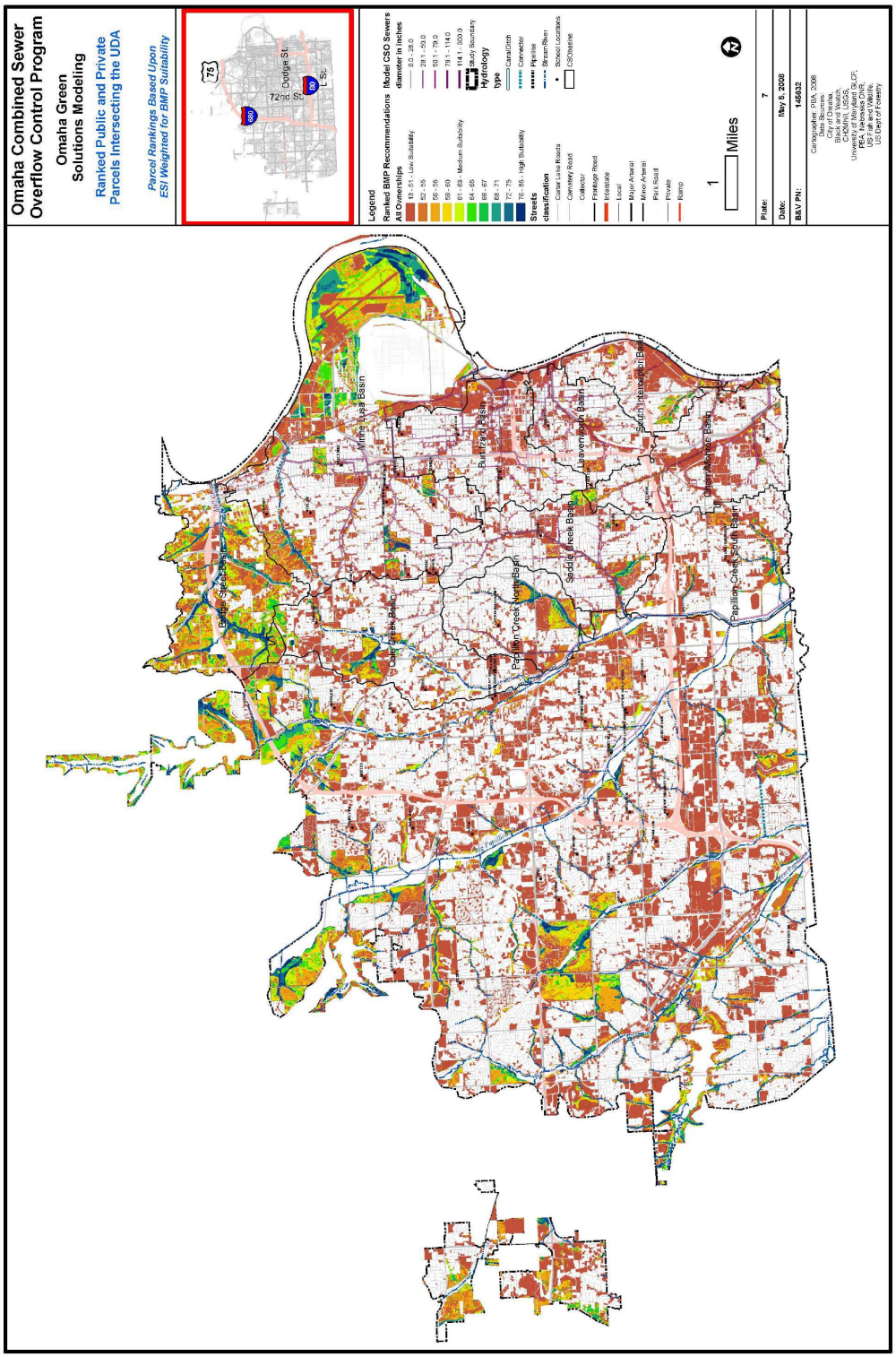

Figure 5. Green Filter Tier 3: All Green Infrastructure Opportunities

In total, the City-Owned Tier 1 analysis identified 1,291 publicly owned sites totaling 6,111 acres that could be considered for public green infrastructure within the Omaha area. The most suitable locations for those technologies are shown in blues and greens by Figure 3. Most of the identified City-Owned opportunities can be categorized as open spaces in the urban core, or remnant alluvial valleys and stream channels in the suburban areas. Many of the opportunities received high Green Filter suitability scores as these opportunities are well suited for receiving, treating and detaining large volumes of wet weather runoff. Basically, these sites, which could create opportunities for larger public amenities (such as new ponds, wetlands, and detention facilities located within existing parks and City owned open spaces) while reducing wet weather runoff and CSO frequency, would provide The City with the most value for their dollar.

When the City, Educational and Institutional Green Filter Tier 2 analysis was considered, 2,852 opportunities were identified within the Omaha City limits. If green solutions were to be considered at these locations, partnerships between the City and educational / institutional groups would need to be established. For Omaha, this tier identified some large natural features such as land owned by the airport authority and large swaths of privately held forested land. Furthermore, the suitability of some private BMP opportunities identified within Tier 2 was more mixed than the City owned Tier 1 opportunities. This occurred because the soils, vegetation and hydrology have been disrupted by development and the ArcGIS model reflected this within its calculated BMP suitability ranking of each site. Other sites within Tier 2 have large open spaces, such as playgrounds, fields, tracks, lawns and gardens which are located adjacent to large buildings. It may be feasible that the large educational and institutional sites could be retrofitted with green solution technologies so that runoff from the site would be captured within the available, directly adjacent, open space.

If all parcels (i.e., Tier 3) that intersect major overland flow paths were considered, a very detailed fluvial pattern would emerge within the City. Within Tier 3, more than 645,000 green solution opportunities were identified in Omaha. Prior to Omaha's development, these parcels were once part of the natural riparian corridor that conveyed overland runoff from the area to the local surface waters. As a result of years of development, the majority of the identified opportunities within Tier 3 were calculated by the GIS Green Filter to have a medium to low BMP suitability ranking. Furthermore, it is neither feasible nor pragmatic for the City to attempt installation of small green solution technologies on each identified parcel. In most cases, scattered and uncoordinated green solutions would be ineffective at solving the wet weather and end-of-pipe problems on a watershed scale. The usefulness of this layer is better targeted for comprehensive planning purposes. For example, the Tier 3 findings could be used as a guide to more systematically incorporate wet weather BMPs into a City's long-range planning and development.

Now that the Green Filter GIS model, which identifies appropriate locations for BMPs, has been detailed, specific concepts and BMP designs for the identified locations will be discussed.

2. Concepts, Layouts and Sizing of Identified BMP Opportunities - Minne Lusa Basin; Omaha, Nebraska

Based upon the Green Filter GIS process, the Program Management Team (PMT) and City requested that the best opportunities identified by the Green Filter be selected and refined. With the top opportunities identified (see Figure 6), detailed locations and sizing of appropriate green infrastructure technologies were developed for each site. Note that the Green Filter identified two general sites within the Omaha Minne Lusa Basin. There were:

1. Larger City-Owned Open Spaces
2. City-Owned Rights-of-Way (i.e., street and boulevard corridors)

For this paper, three of the Green Filter identified locations have been included herein for discussion. To size and cost out each facility, the runoff from the 1" design storm was used. The runoff was calculated using the "Short-Cut Method" (MARC and APWA, 2008) and is presented below. Note that although planning level costs for each site were developed, this information has not been included herein.

Short-Cut Method Equation:

$WQv = P * Rv$

Where:

WQv = Water Quality Volume (inches)
P = Rainfall event in inches (the Water Quality Storm of 1.37 inches or other appropriate amount, with the approval of the city engineer)
Rv = Volumetric runoff coefficient = 0.05 + 0.009(I). I = Percent site imperviousness (%)

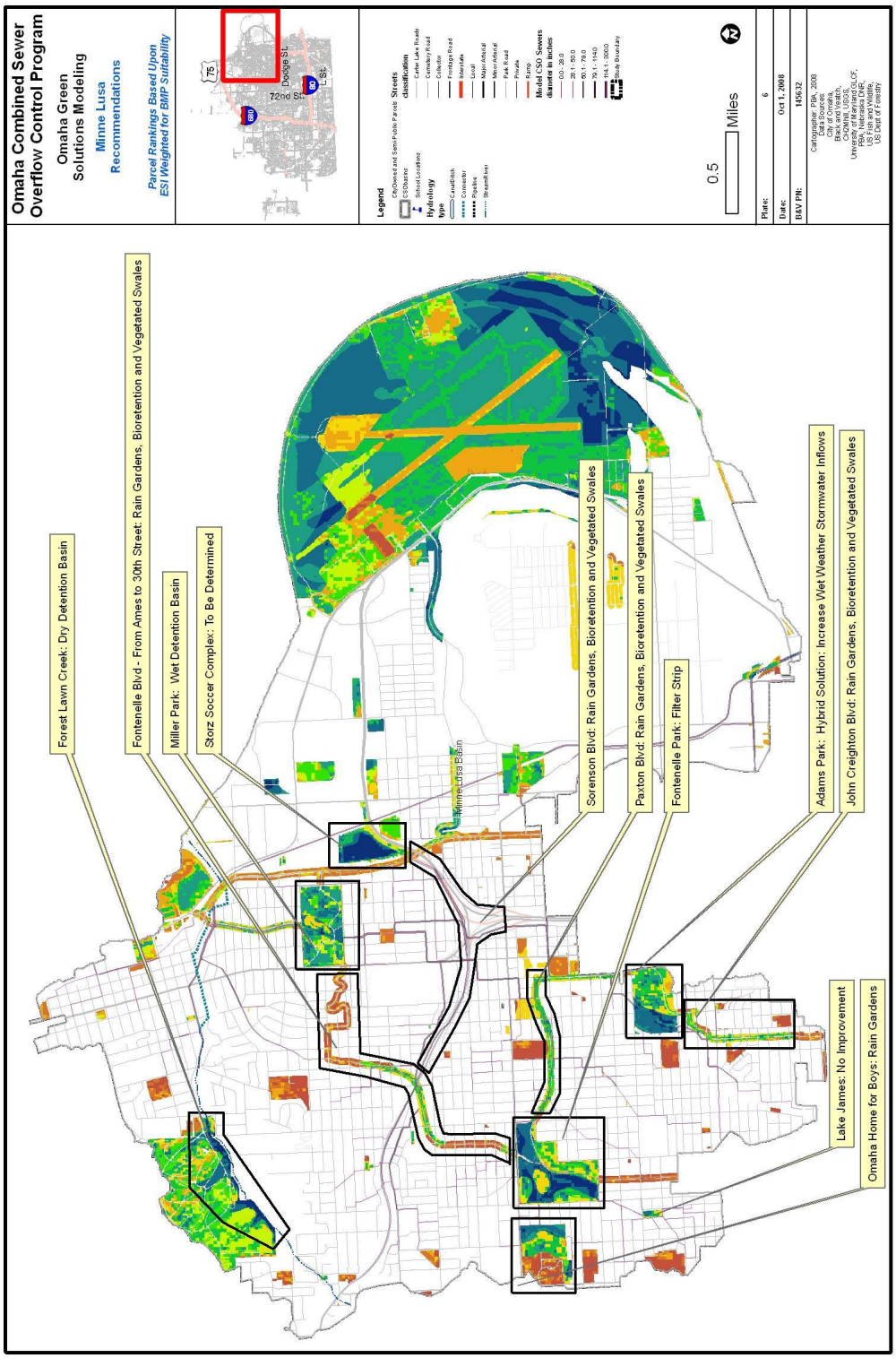

Figure 6. Top Minne Lusa Basin Green Infrastructure Locations and Recommendations

c. Adams Park Wetland and Lagoon Green Solutions Concept

Adams Park, as shown by Figure 7, is a publicly owned site with an existing wetland and lagoon. The Green Filter identified this location as an optimal place to add more BMPs. Upon review, it appears that the existing wetland and lagoon at the Park site could be enhanced by reconfiguring the upstream combined sewer collection system. It was determined that upstream sewer separation could be expanded to supplement stormwater inflow to Adams Park. In addition, downstream sewer separation was proposed which would allow stormwater from Adams Park to remain separated by a dedicated stormwater outfall.

Results from the detailed hydrologic evaluation of Adams Park showed that the proposed modifications could result in the storage of 9.1 acre-ft of wet weather runoff from 1-inch rain event. Furthermore, the modifications would allow Adams Park to receive more stormwater inflow, assist in improving the water quality of additional stormwater, serve to detain more wet weather runoff, and, in combination with downstream sewer separation, would keep stormwater runoff from mixing back into the combined sewer system.

In other words, this specific concept provides an integrated wet weather and CSO solution. The Green Filter identified the site, while the specific concept presented maximizes the sites ability to achieve multiple wet weather treatment solutions.

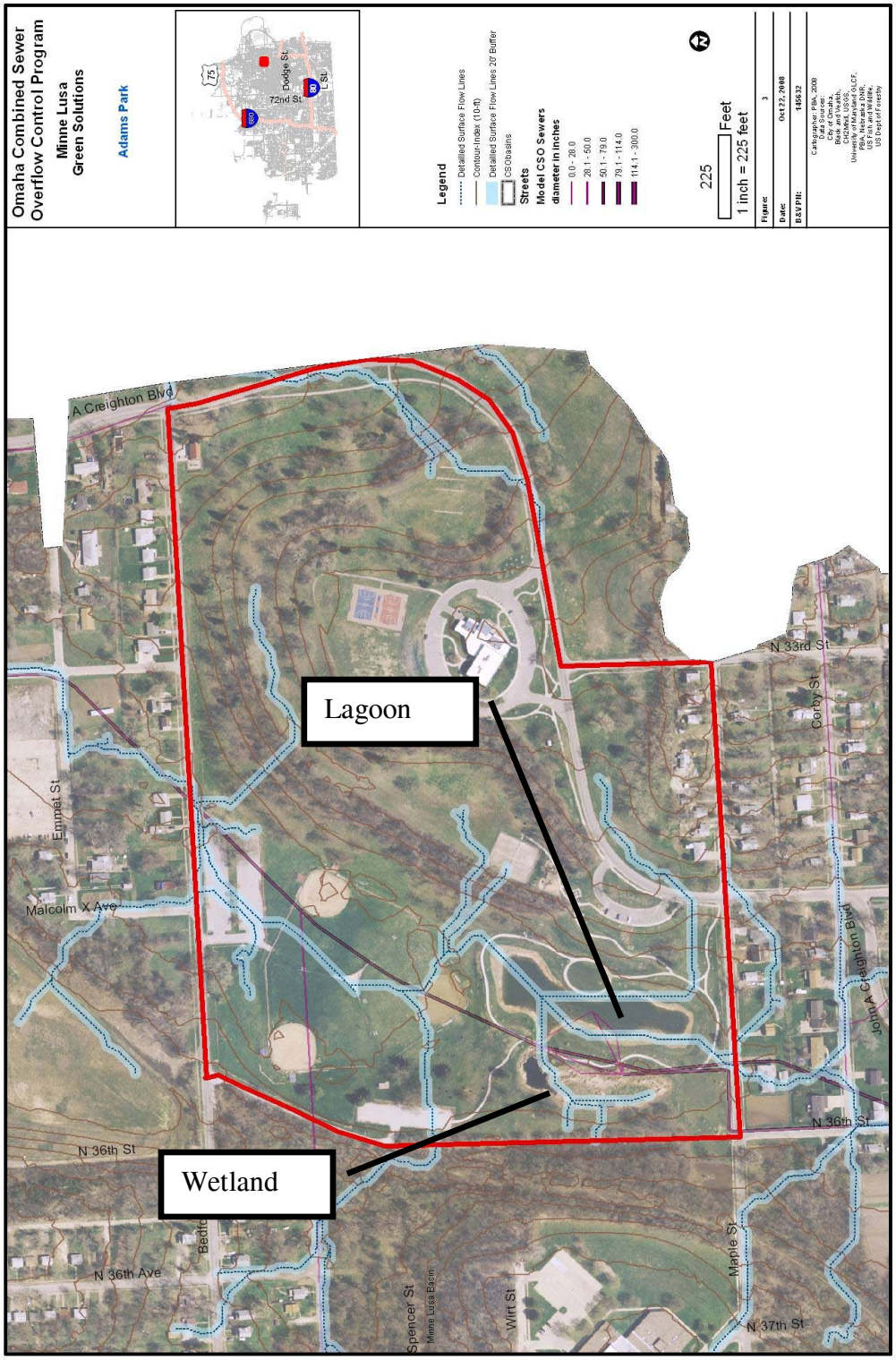

Figure 7. Adams Park Green Solution

d. Omaha Home for Boys Green Solutions Concept

Although the Omaha Home for Boys site is a privately held site, it has a significant amount of open space (approximately 66 acres) and was identified by the Green Filter as a good site for BMPs. Upon review, the site is located on a hill therefore making it a good location for potential green solutions along the extremities of the site (positioned to capture runoff from the site). Two areas on the site were proposed to be transformed into rain gardens, and would collect runoff from the Omaha Home for Boys site. The proposed watershed areas and corresponding rain gardens are presented by Figure 8. Since ample space exists on the site, the footprints of the rain gardens were sized so that runoff would be no greater than 1 foot deep following a 1-inch storm within the proposed rain gardens. The runoff calculation was performed using the Short-Cut Method, as previously discussed, and the drainage areas to the rain gardens were calculated using the GIS model. Results from the detailed hydrologic evaluation of the Omaha Home for Boys showed that the proposed modifications could result in the storage of 0.5 acre-ft of wet weather runoff from a 1-inch rain event.

Note that because the Omaha Home for Boys site is a private entity, the City of Omaha is not currently pursing the green solution option presented herein. Obviously, buy-in from the land owner would be a necessary step before the propose option discussed herein could become a reality. However, this option does show that opportunities exist on privately held sites that could benefit the overall basin.



Figure 8. Omaha Home for Boys Green Solution Concept

3. John Creighton Boulevard Green Solutions

The Green Filter also identified old riparian corridors where public right-of-way open space now exists. For example, the John Creighton Boulevard corridor, as presented by Figure 9, is an example. This Boulevard Corridor could be retrofitted with a number of small rain gardens, bioretention and vegetated swales that would be located in the existing right-of-way. Rain gardens could be built where the exiting topography is flat and the ratio of the watershed area to open space is small. Bioretention could be built where the existing topography is flat and the ratio of the watershed area to open space is high. Vegetated swales could be used on areas that are steeper to convey overland flow into the adjacent rain gardens and bioretention facilities.

A detailed hydrologic evaluation was performed within GIS to identify the specific watershed areas that drain into the Green Filter identified right-of-way open spaces. Using the Short-Cut Method, runoff estimates were calculated to determine the approximate runoff volume to each open space from a 1" rainfall. Results from the detailed hydrologic evaluation of this boulevard corridor determined that a combination of rain gardens, bioretention and vegetated swales located within the wide right-of-way could store the 1.0 acre-ft of runoff from a 1-inch rain event. Furthermore, there are 2 acres of available open space along this boulevard corridor so the average depth in the available right-of-way green solutions following a 1-inch rain would only be 0.5 ft.

Thus, John Creighton Boulevard corridor may be well suited for a green solution retrofit having a number of small rain gardens, bioretention and vegetated swales. Additionally, the boulevard corridor was historically a stream channel, so development of a green infrastructure system is a partial restoration of the historic riparian corridor.

Although parkways have a good potential (i.e., available open space) for being retrofitted with green infrastructure, utility conflicts such as water, sewer, gas, and electrical lines in addition to large trees could be encountered. This would make parkway retrofits potentially complicated and problematic which would increase the project's uncertainty and corresponding project costs. Due to the potential of utility conflicts, the boulevard alternatives are not being carried forward as viable CSO green solution at this time by the City of Omaha. However, the concept will remain open for further discussion and analysis as the CSO program moves forward.

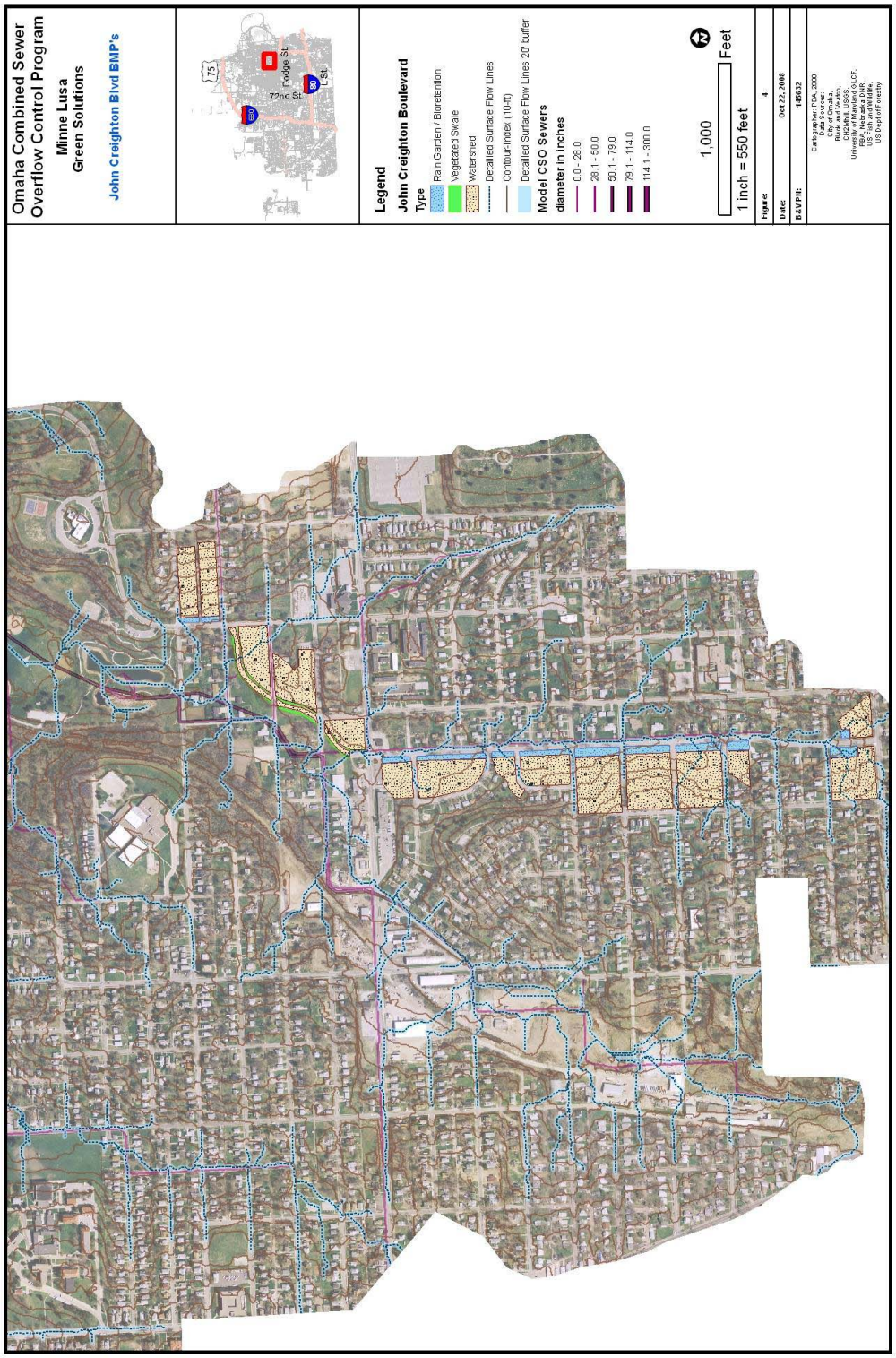

Figure 9. John Creighton Boulevard Right of Way Green Infrastructure Concept

4. Hydrologic and Hydraulic Modeling of Green Infrastructure – An Estimate of Effectiveness

The Green Filter has been discussed previously and presents a method to systematically identify, on a large scale, appropriate sites for BMPs. Furthermore, some specific green technologies have been presented that could work well on specific identified sites within urban areas. However, another important part of the Green Solutions process is to quantify, on a large scale, what impact multiple dispersed green infrastructure has on the overall basin-wide runoff characteristic.

Typically, to achieve CSO reduction and treatment goals established by the regulatory agencies, communities have relied on heavily engineered solutions (i.e., grey solutions). Grey technologies include sewer separation, deep storage tunnels, tank storage, high rate wet weather treatment facilities and pump station and treatment plant upgrades. Since traditional grey technologies are large in scale and focused on addressing in-system combined sewer flows, modeling and estimating the effect of these grey technologies is straight forward using common hydrologic and hydraulic (H&H) pipe and node models.

One of the difficulties of incorporating green infrastructure is determining the overall benefit from numerous distributed green infrastructure technologies on the reduction of the CSO frequency and volume. As presented earlier, green solutions technologies, unlike most grey CSO solutions, are typically smaller in scale. Because communities targeted by CSO regulations are generally fully developed, large open spaces for sizable green solution technologies, such as wetlands and detention basins, may be limited. The lack of available and sizable open space requires that green solution plans include smaller and more distributed practices. Examples of more distributed technologies include, but are not limited to, rain gardens, rain barrels, swales, bioretention cells, bio-swales, and infiltration basins (also referred to as Low Impact Development green solution technologies).

The challenge with quantifying numerous and highly distributed wet weather control green technologies is that the complexity of standard H&H models must be significantly increased to estimate their effectiveness. For example, instead of having one major structure to incorporate into an H&H model (like a large deep storage tunnel or detention basin), there may be dozens or hundreds of proposed distributed green technologies across an area of interest. To physically represent each green solution technology, the H&H model must be of sufficient resolution to capture each BMP and its associated processes. Furthermore, without the use of models to represent the complex nature of the collection system interactions, it is difficult to truly evaluate what impact distributed green infrastructure can have on basin wide runoff characteristics as well as on proposed large scale grey solutions.

To help answer the question regarding how much green infrastructure can reduce the frequency and volume of wet weather runoff and CSOs, a pilot H&H model was developed. The model was set up to estimate the effectiveness of a

distributed network of residential, parcel-scale BMPs for controlling the stormwater runoff from a combined sewer subbasin within Kansas City, Missouri. Using the Green Filter GIS model discussed previously along with some standard green technology designs, a dispersed network of green solutions was modeled. The modeling team assumed suitable open space identified by the Green Filter would be retrofitted with shallow extended dry detention basins. The selected locations for the green infrastructure retrofits within the subbasin are shown in red by Figure 10.

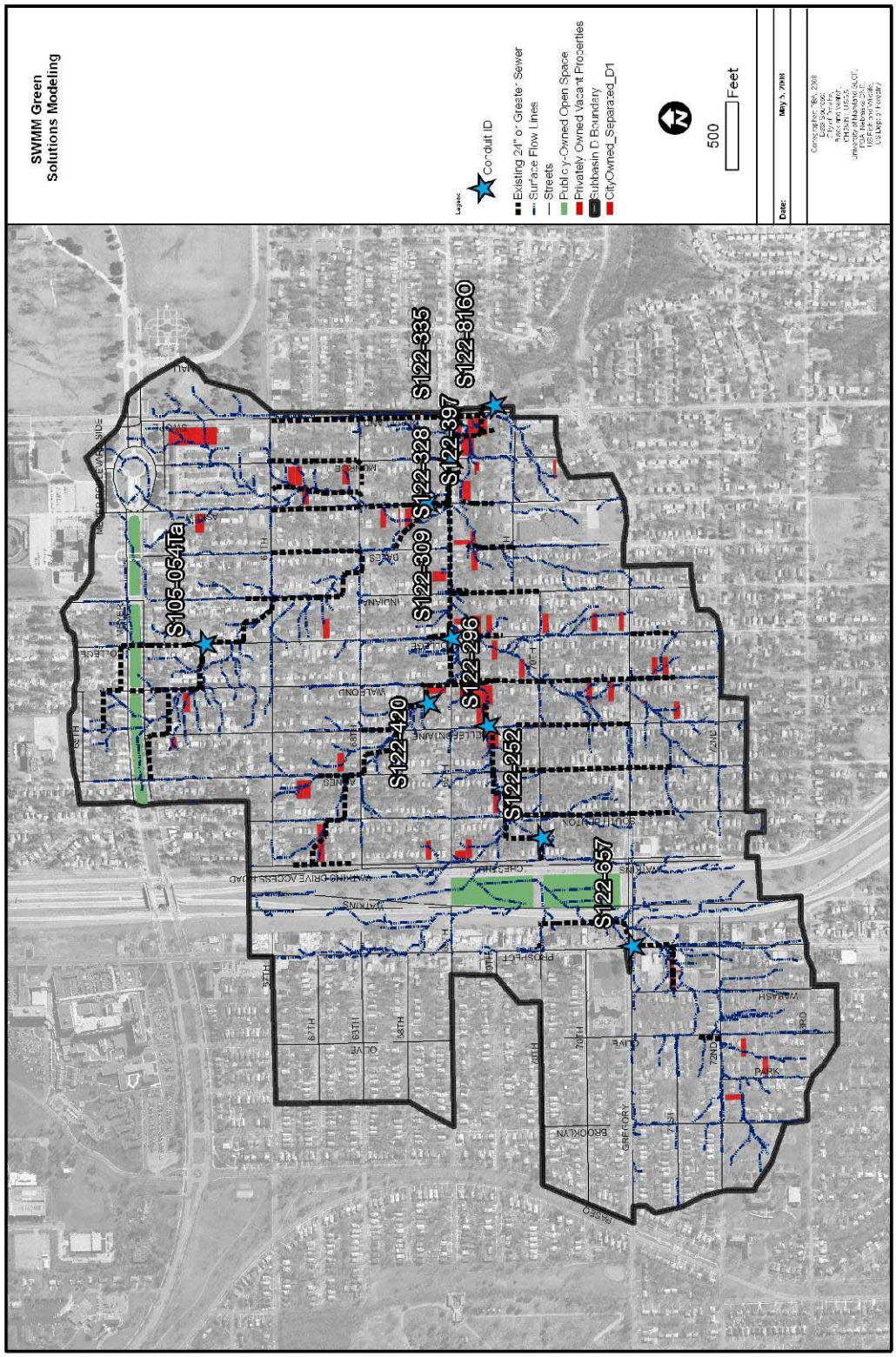

Figure 10. Dispersed Green Solution Modeling

The identified green solution locations were then input into an existing (developed previously for use in characterizing the CSS wet weather response), system-wide, XP-SWMM Version 9.51 (XP Software, Inc.) H&H model to determine their effectiveness at providing CSO control. The green infrastructure retrofits were input by breaking up (i.e., finer resolution) the existing model hydrologic subcatchments to capture and represent each parcel-scale green solution technology independently. Figure 11 illustrates the concept.

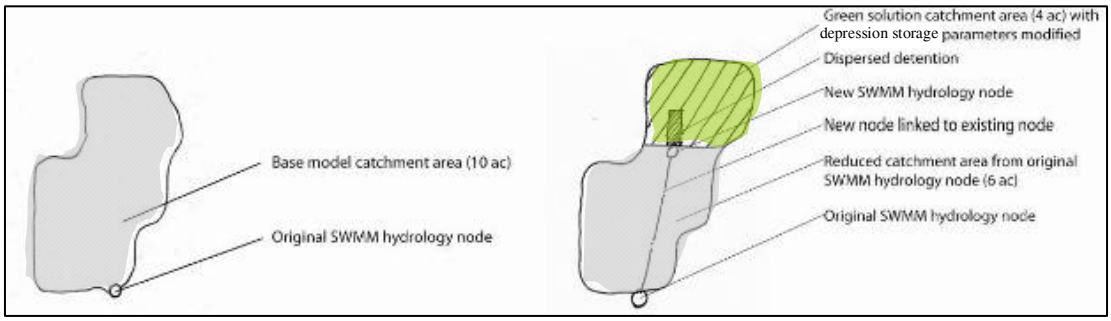

Figure 11. Green Solution Modification of a Traditional H&H Model

The detailed process to add each green solution to the existing XP-SWMM H&H model is summarized below:

1. One new SWMM runoff node was added for each green solution and a new conduit was added to link the new runoff node to the existing model catchment runoff node.
2. The catchment area for each green solution was defined as the Residential Block Area draining to the green solution (i.e., the area above the 6-inch curb and gutter system typically referred to as a "block". Streets were assumed to break up hydrologic connections).
3. For simplicity, roof areas were excluded from the catchment area. It was assumed that runoff from the roofs was directly connected to the sewer system. This was done because an accurate estimate of the number of directly connected roof areas was not available at the time of model development.
4. All green solutions catchments were assumed to be 100-percent pervious.
5. A Manning's C value of 0.03 was input for all green solutions catchment areas to represent mature vegetation (i.e., trees, grass, and shrubs).
6. The catchment infiltration parameters were set to reflect silty clay soils.
7. Each green solution was assumed to be 0.914 meters (3-feet) deep. The dispersed detention area was multiplied by two-thirds to define the useable detention area (i.e., assumes 0.3 meter [1 foot] of freeboard). The total detention storage for each green solution was calculated.
8. The storage volume for each green solution was converted into an area-depth. This value was then input into the H&H model as the updated depression storage for the BMP catchment.

After configuring the XP-SWMM model by incorporating the green solution technologies, a 20-hour, 4.57 cm (1.8 inch) storm was simulated within the model. This storm is equivalent to a rain event in the Kansas City, Missouri region that occurs approximately 4 times per year (Design Year for CSS Analysis Technical Memorandum, 2006), a design frequency that many regulators select as a level of control for CSO LTCPs. If a community can store and treat combined sewer flows from a wet weather event of this frequency without having a CSO event occur, they are presumed to have met receiving water quality standards. Therefore, the H&H model was configured to determine the effect that the green infrastructure had on this specific wet weather event. For reference, a hyetograph for this design storm is presented by Figure 12.

In total, 33 dispersed green infrastructure retrofit opportunities were identified within the investigated subbasin and input to the H&H model. Figure 13 shows the location of the BMP retrofits (in red) along with their corresponding catchment or tributary areas (in blue). A review of this figure shows that a significant area (shown in blue) of the overall watershed could be drained to the proposed 33 dispersed BMPs within this area.

The green infrastructure XP-SWMM model incorporated all 33 identified green solutions opportunities within the 20-hour, 4.57 cm (1.8 inch) rainfall event simulation. The output from the modified H&H model was compared to the baseline H&H model (i.e., without green solutions) already developed for the CSO program. The comparison focused on two main parameters of interest, peak flow and runoff volume reduction from the identified subbasin of interest.

The pilot green solution modeling effort indicated that dispersed green infrastructure covering approximately 4 percent of the total surface area of sub-basin, as shown by Figure 13, could reduce the peak runoff flow rate by approximately 60 percent and total runoff volume by approximately 55 percent. While the results are preliminary and should be refined through further conceptual design and model development, the analysis indicates that these technologies have considerable potential to affect and reduce the runoff loading to the CSS if applied basin-wide. Furthermore, although B&V and PBA are not directly involved, the City of Kansas City is investigating a green solutions concept within the Marlborough neighborhood, similar in concept to the one presented herein, as part of their CSS Long Term Control Plan. Flow monitoring performed for that work will help to better define the effectiveness from green solution strategies such as the one presented herein.

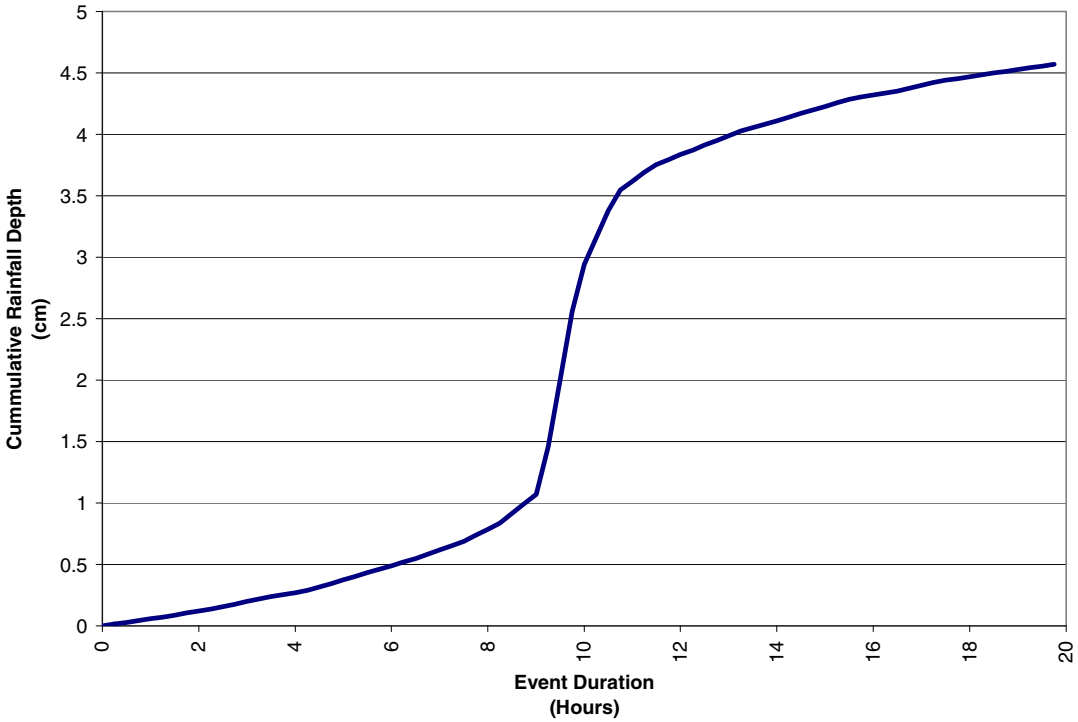

Figure 12. Design Storm Cumulative Hyetograph

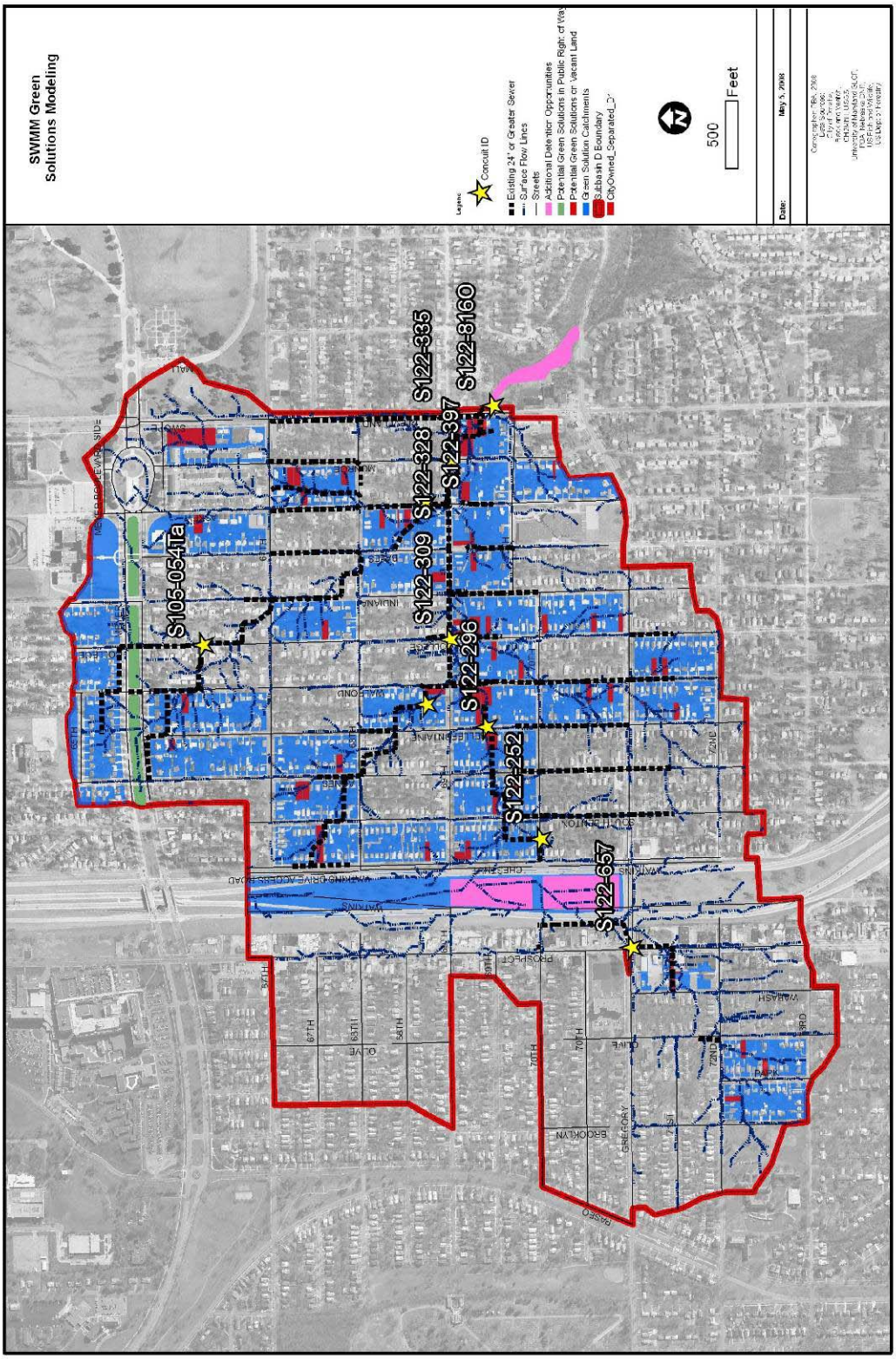

Figure 13. Dispersed Green Solution Hydrologic and Hydraulic Modeling Example

SUMMARY AND CONCLUSION

It is proposed that locations for green infrastructure should be identified and prioritized first to determine where spending time, money and resources would be the most beneficial. It serves little purpose to incorporate green infrastructure simply for the sake of doing it, if the economic, technical and societal impacts are not maximized. The Green Filter provides a flexible, GIS methodology for both identifying and prioritizing these locations, based on a community's specific conditions, to help satisfy its unique needs and objectives.

Second, detailed layouts and concepts for possible green infrastructure ideas should be considered that match the specific locations identified by the Green Filter with appropriate green solution concepts and technologies. Concepts were shown herein that could be effective in both open space applications and linear right-of-way boulevard applications located within developed areas.

Lastly, a preliminary H&H modeling exercise was presented that estimated the effectiveness of green infrastructure on wet weather runoff. The preliminary results showed that green solutions could result in a sizable reduction of wet weather runoff and corresponding CSOs from a specific area. It appears that these technologies could be used as a source control to reduce both the magnitude and cost of wet weather grey infrastructure. Furthermore, with communities (i.e., Kansas City) actively investigating green solutions strategies such as the ones presented herein, more data will soon be available to better refine the H & H modeling procedures. Through refinement and ongoing work, these models will continue to get better at quantifying the benefits of wet weather green infrastructure on CSO and wet weather solution schemes.

There is much work to be done as sustainable planning concepts and green infrastructure are incorporated into traditional wet weather and CSO solutions. However, the initial results are promising. By locating, selecting and quantifying specific green infrastructure for use in a community's long term wet weather and CSO solutions, we are closer to achieving our collective goal of attaining a more sustainable future. The past demanded that we change, the present shows opportunities where we can, and the future is more promising because we are now, more than ever, committed to seizing sustainable opportunities wherever they are found.

ACKNOWLEDGMENTS

Black & Veatch and Patti Banks Associates would like to acknowledge the City of Kansas City, Missouri and the City of Omaha, Nebraska as well as their program management teams. A significant portion of the material presented herein was developed by Black & Veatch and Patti Banks Associates in coordination with the two communities' ongoing CSO programs. The CSO programs consist of multiple engineering and planning firms and Black & Veatch and Patti Banks Associates are a part of those larger team efforts.

In addition, Mark Seip with HDR Engineering in Kansas City, Missouri is acknowledged for providing data and background information so that the green solution H&H modeling discussed herein could be performed.

REFERENCES

Design Year for CSS Analysis Technical Memorandum (2006) City of Kansas City, MO: Kansas City, MO.

Dunne, Thomas; Leopold, Luna G (1978) Water in Environmental Planning. W. H. Freemand and Company: New York, NY.

Forman, Richard T.T. (1995) Land Mosaics, The Ecology of Landscapes and Regions. Cambridge University Press: UK.

Forman, Richard; T.T.; Godron, Michel (1986) Landscape Ecology. John Wiley and Sons: New York, NY.

Mid-America Regional Council (MARC) and American Public Works Associates (APWA). "Manual of Best Management Practices for Stormwater Quality", March 2008. pp. 69.

Purdue Research Foundation (1994-2008) Multispec: A Freeware Multispectral Image Data Analysis System, Version 5.3.01. http://cobweb.ecn.purdue.edu/~biehl/MultiSpec/

Generalized Storage-Reliability-Yield equations for rainwater harvesting systems

Lars S. Hanson[1], Richard M. Vogel[2], Paul Kirshen[3], and Peter Shanahan[4]

1 GKY & Associates, 4229 Lafayette Center Dr., Suite 1850, Chantilly, VA 20151 (ph) 7038707000
Email: lhanson@gky.com
2 Professor. Dept. of Civil and Environmental Engineering, Tufts University, Medford, MA
Email: richard.vogel@tufts.edu
3 Professor. Dept. of Civil and Environmental Engineering, Tufts University, Medford, MA
4 Senior Lecturer. Dept. of Civil and Environmental Engineering, Massachusetts Institute of Technology, Cambridge,MA

Abstract: Although rainwater harvesting (RWH) is gaining popularity as a sustainable water supply source in urban as well as rural areas, estimating required storage remains an important design challenge. This paper develops a robust, yet computationally simple equation for calculating required storage capacity for a RWH system, which is generally applicable in the United States (U.S.). A simulation model with a daily time step and a yield-after-spill algorithm is used to generate empirical Storage – Reliability – Yield (SRY) relationships for RWH systems at 232 U.S., first-order precipitation gaging stations with long daily precipitation records. A regional regression modeling approach is used to combine system parameters (daily yield, collection area, reliability) with climatic variables (e.g. standard deviation of daily rainfall) to predict required storage capacity. Nationwide regression models for fixed reliability cases (80, 90, 95, 98%) demonstrate good fits (R^2> 0.95) between model predictions and simulated storage capacities. The fits improve (R^2>0.97) when the nation is broken down into smaller, more climatically homogeneous regions.

1. Introduction

Recently, rainwater harvesting has drawn increased attention in many regions of the world as a sustainable and economic water source. Rainwater harvesting has maintained its importance as a water source for small-scale agriculture and as a primary water sources in remote locations in rural areas and islands. In the past few decades, rainwater harvesting has also become a popular supplemental (and generally non-potable) water source in urban and suburban areas.

As the variable costs of rainwater collection tend to be quite small, the largest economic consideration is the initial capital cost to construct the system. In most cases, the most important design decision is how much storage capacity to build. While the performance of rainwater harvesting systems depends on only a few system parameters, and the location's rainfall pattern, estimating required storage can be difficult and is often performed through a collection of rules-of-thumb, local experience, rough calculations, and judgment. The performance and sizing of rainwater harvesting systems have been explored in the past with a range of approaches including water balance and mass-curve analysis (Handia et al., 2002; Goel and Kumar, 2005; Panigrahi et al., 2007 among others), probabilistic methods (Ree et al., 1971; Lee et al., 2000; Guo and Baetz, 2007), economic optimization (Pandey et al., 1991; Dominguez et al., 2001; Liaw and Tsai, 2004), and detailed simulation and performance analysis (Hermann and Schmida, 1999; Fewkes, 2000; Villareal and Dixon, 2005; Ghisi et al., 2007).

If RWH is to become a more widely used method of water supply, a simpler, more generalized method of storage design would be invaluable. Examining the behavior of the system, and specifically, the relationship between the storage, demand, collection area, and reliability is crucial to designing the storage.

Although not specifically recognized in most of the RWH literature, this relationship is directly analogous to the common Storage-Reliability-Yield (SRY) relationship used for reservoir analysis (see for example, McMahon and Adeloye, 2005; Vogel and McMahon, 1996; and Vogel and Stedinger,1987). Conceptually, the RWH system is remarkably similar to a reservoir system. Both have a fixed storage capacity, a characteristic volumetric demand, and a volumetric inflow determined by natural hydrologic processes. A reservoir's inflow is determined by the volumetric flow of the stream or streams that feed it. The flow in the stream however, is a function of the precipitation falling in its (finite-area) watershed, which is directly analogous to precipitation falling on a RWH system's fixed collection area. The SRY framework, therefore, is well suited to analyzing the characteristics of a RWH system.

Though they have not recognized the analogy to the reservoir SRY relationship, many RWH modelers have recognized the relationship of the key storage, reliability and yield variables (Schiller and Latham, 1987; Fewkes, 2000; Villareal and Dixon, 2005). None of these authors, however, have sought to generalize the relationships they discovered over larger areas. Looking to the analogy of reservoir behavior, at least two methods of generalizing behavior-based statistical properties of the hydrologic inputs appear in the literature.

The first method is the Gould-Dincer equations which calculate the reservoir storage for a desired reliability using an estimate of the critical drawdown sequence length based on several properties of the streamflow sequence (mean flow, coefficient of variation, Cv) and the reservoir yield. This approach has been extended to a wide range of streamflow distributions (see Gould, 1964; Vogel and McMahon, 1996; McMahon and Adeloye, 2005), but the differences in statistical character of rainfall versus streamflow, and the fact that the method does not take into full consideration the sequential nature of the inflows, make it unsuitable for RWH analysis. Thus, we turn to a second approach.

Regional regression approaches have proven extremely valuable in estimating a range of hydrologic parameters over a geographic area, most notably, streamflow (Jennings et al., 1994; Vogel et al.,1999a). More recently, however, regional regression has proven capable of estimating reservoir storage on a global geographic scale calculated by a sequent peak algorithm or behavioral model by using reservoir yield and various annual streamflow statistics as regression variables (McMahon et al., 2007).

Multivariate regression has been used to investigate RWH system behavior by Lee et al. (2000), who apply it to a RWH irrigation system in China. They use a single-site regression equation to predict the relationship between the system parameters including collection area, reliability, storage, and irrigable area (a measure of yield). Since only a single site is considered, the character of the hydrologic input (rainfall) is built into the model, and they focus instead on relationships between failure probability, collection area, storage, and other system parameters. Guo and

Baetz (2007), spurning the regression approach in favor an approach grounded in stormwater detention theory, demonstrate analytically that differences in RWH system behavior can be explained by statistical properties of the rainfall sequence. The research in this paper differs significantly from all previous research because it is our goal to develop a generalized regression model suitable for determining the relationship among rainwater harvesting system storage, reliability and yield over the entire continental U.S.

2. RWH Simulation and the Storage-Reliability-Yield Relationship

In order to understand the behavior of rainwater harvesting systems over large geographic areas, simulations using daily precipitation as input were performed. A set of 232 first-order precipitation gages from the National Weather Service's Cooperative Station Network with high-quality daily records are selected for simulation. The stations are well distributed across the continental United States and have a median record length of 59 years.

The simulation approach was designed to develop the SRY relationship by generating constant reliability curves at several useful reliabilities for a rainwater harvesting system. The reliabilities chosen for analysis are 0.80, 0.90, 0.95, and 0.98. The Yield-After-Spillage algorithm, widely used in the rainwater harvesting literature (Jenkins et al., 1978; Schiller and Latham, 1987; Fewkes, 1999; among others), is selected for the simulations. The simulations run for a single combination of yield and storage, track daily storage and whether the daily yield is met each day. The number of days with failure is recorded, and used to compute time reliability, q_t, defined in Equation 1.

To allow comparability between stations, all simulations are run for a unit collection area (Ac). Additionally, the yield is normalized to the mean daily rainfall (μ_{dp}) of each station to generate the unitless yield ratio, α (Equation 2), which describes the average fraction of available water used. The simulations were performed at 20 yield ratios per station to define each constant reliability curve, with α ranging from 0 to 1. The storage was then varied for each yield ratio to generate the desired reliability. Storage is normalized to collection area to generate the physical storage ratio, Sr (Equation 3).

$$q_t = 1 - \frac{d_f}{n} \qquad \textbf{Equation 1}$$

$$\alpha = \frac{y}{\mu_{dp} \cdot A_c} \qquad \textbf{Equation 2}$$

$$S_r = K/A_c \qquad [ft^3/ft^2] \qquad \textbf{Equation 3}$$

Where d_f is the number of days when yield is not met, n is the simulation length in days, y is daily volumetric yield, and K is total volumetric storage capacity.

For the purposes of modeling, a few assumptions are necessary. The runoff coefficient is assumed to be one, and no first flush is modeled. The precipitation gages, which melt snow, treat all precipitation as rain. .

The constant reliability curves generated by the modeling can effectively describe the full SRY relationship when plotted. Figure 1 shows a full set of reliability contours generated from the model by using precipitation data from Los Angeles, CA.

This is the typical shape of the SRY relationship, with lower reliability contours lower and less curved than the higher reliability contours because greater storage is required to satisfy higher reliabilities. The position of the individual contours varies considerably by station, however, as Figure 2 illustrates. Figure 2 displays the 90 % reliability contour from a range of cities with widely ranging climate types.

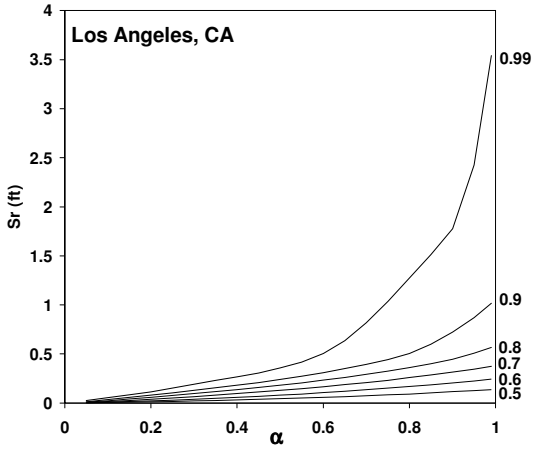

Figure 1. Constant reliability Storage-Yield contours for Los Angeles, CA

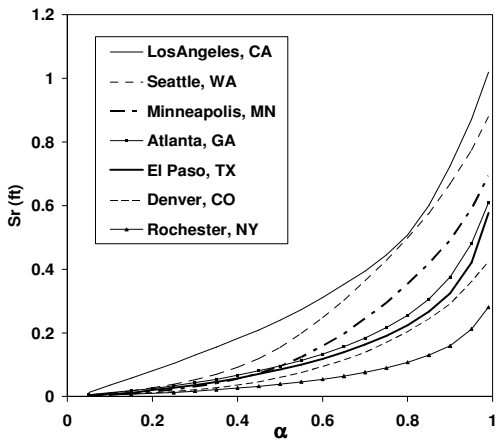

Figure 2. Comparison of modeled 90% reliability curves for 7 cities.

3. Regression Analysis

This study employs multivariate least-squares regression as the method of generalizing the SRY relationship across the entire U.S. The physical storage ratio is the dependent variable in all cases. The independent variables are a combination of system parameters and statistical parameters of the climate record.

The two goals of the regression modeling in this study are (1) to determine which precipitation parameters affect the SRY relationship, and (2) to develop an accurate, generalized predictive model for required system storage.

All the analyses use ordinary least squares (OLS) regression with the dependent variable (response) being the physical storage ratio (S_r). The regression equation is of the general form:

$$Sr = e^{\beta_0} \cdot X_1^{b_1} \cdot X_2^{b_2} \cdot \ldots X_m^{b_m} \cdot Y_1^{c_1} \cdot Y_2^{c_2} \cdot \ldots Y_n^{c_n} \qquad \textbf{Equation 4}$$

where X_i, i= 1…m, describe physical system parameters such as the demand fraction (α). Y_j, j = 1 …n, describe local climate parameters.

The following sections detail the system parameter variables and the climatic variables selected for evaluation in the regression model, followed by the generalized storage regression.

Rainwater Harvesting System Parameters

This study considers as major RWH system parameters reliability, yield, and collection area. Reliability and yield parameters are clearly important to the SRY relationship, and must be in any regression unless held constant. Reliability has been held constant, as four constant reliability storage-yield relationships are evaluated. Collection area clearly has an impact on the amount of rainwater that can be captured, but in this study, both the storage and yield parameters are normalized to collection

area, so it does not require a separate variable. Thus, yield is clearly the most important system parameter. Besides yield ratio (defined in Eqn (2)), some common transformations of α are investigated.

The parameter m, known as the resilience index (or drift), defined as (1-α)/Cv is well known as a useful parameter describing storage reservoir behavior. Reservoirs with m values greater than Cv tend to exhibit within-year behavior (they refill in most years), and those with m < Cv tend to exhibit over-year behavior (Vogel et al., 1999b). For this study, Cv is the coefficient of variation of the *daily* precipitation record. It was found that stations were overwhelmingly *over-day* systems.

With these parameters, it is also possible to apply additional transformations to further linearize them with respect to S_r. One way to investigate such transformations is to attempt single-site regression models relating storage only to system parameters. A single-site regression analysis was performed for all stations to try to find the form of the regression model describing the relationship between S_r and α for a constant reliability curve. The model in Equation 5 is sufficient to explain more than 99% of the variability (adjusted $R^2 = 0.99$) at any site in the study for any of the reliability curves.

$$ln(S_r) = b_0 + b_1 (-ln(\alpha))^d \qquad \textbf{Equation 5}$$

Equation 5 is basically a log-linear model with one key difference. The logarithmically-transformed dependent variable (α in this case) is further transformed by raising it to the "d" power. While the overall model is not log-linear, the transformation caused by the d parameter can still be incorporated in a log-linear model. Replacing $\ln(X_1)$ in (6) with $(-\ln(\alpha))^d$, we find that exponentiating both sides to base e results in Equation 7, a formulation similar to that of Equation 4. (We will refer to $(-\ln(\alpha))^d$ as the a^d transformation.) Note that for the generalized regression, d must be solved from Equation 5 using data from all stations before Equation 6 is used to fit all of the other parameters.

$$Sr = e^{\beta_0} \cdot e^{b_1 \cdot (-\ln(\alpha))^d} \cdot X_2^{b_2} \cdot \ldots X_m^{b_m} \cdot Y_1^{c_1} \cdot Y_2^{c_2} \cdot \ldots Y_n^{c_n} \qquad \textbf{Equation 6}$$

Initial regression trials demonstrated that m did not have nearly as much explanatory power as α or a^d, so only the latter two were tested further.

Climatic Variables

The system parameters alone may well explain a large portion of the variability of regional regression models. After all, at every station, S_r generally increases as α increases. It is clear, however, from Figures 1 and 2 that the SRY relationship can vary considerably by station, and is dependent on more than reliability and yield alone. This study investigates a range of possible input parameters for use in making an improved general regression model for predicting storage. Table 1 identifies the rainfall parameters investigated. The parameters are divided into three classes by their relative ease of calculation and requisite knowledge of statistics by the user. Class 1 is composed of traditional descriptive and order statistics of the complete daily rainfall series for a given location. Additionally, we include the lag-1 daily serial correlation (ρ), which can serve as a rough indicator of the general arrival pattern of

storms, and the transformation, $(1+\rho)/(1-\rho)$ derived using two completely independent approaches by both Phatarfod (1986) and Vogel and McMahon (1996).

Table 1. Daily rainfall parameters used in regression modeling

Class	Variable	Description
Class 1 Full Record	μ	Mean
	σ	Standard deviation
	Cv	Coefficient of variation
	γ	Skewness
	κ	Kurtosis
	p_{zero}	Proportion of days in rainfall record with zero rainfall
	ρ	lag-1 serial correlation (autocorrelation)
	$(1+\rho)/(1-\rho)$	transformation of ρ
Class 2 Wet-day only (zeroes removed)	μ_w	Mean
	σ_w	Standard deviation
	Cv_w	Coefficient Of Variation
	γ_w	Skewness
	κ_w	Kurtosis
	$x_{1/2,W}$	median of wet-day rainfall
Class 3 L-moment and Fitted Distribution Parameters	τ_2, τ_3, τ_4	2nd, 3rd, and 4th L-moment ratios of the full rainfall record
	$\tau_{2W}, \tau_{3W}, \tau_{4W}$	2nd, 3rd, and 4th L-moment ratios of the wet-day rainfall record
	$\alpha_{P3}, \beta_{P3}, -\xi_{P3}$	Shape, scale, and (negative) position parameter of fitted Pearson-III distribution to the full rainfall record
	$h_K, \alpha_K, -\xi_K$	"h" shape, scale, and (negative) position parameter of fitted Kappa distribution to the wet-day rainfall record
	$(1+k_K)/(1-k_K)$	transformation of k_K, the "k" shape parameter of fitted Kappa distribution to the wet-day rainfall record

Class 2 includes similar types of statistics, but instead of the complete rainfall series, the wet-day series is used. The wet-day series excludes all zeros (and trace rainfall) in the record. The statistics available are virtually identical to Class 1, except that ρ becomes meaningless as removing the zeros destroys serial correlation. The median value, however, becomes meaningful, as it now has a value other than zero.

Both Class 1 and 2 precipitation parameters can be easily calculated with nothing more than the built-in functions in almost any basic statistical package, or spreadsheet program. Class 3 variables are different in that they require understanding of L-moments and fitting parameters to a probability distribution. Hanson and Vogel (2008) found that daily rainfall depth could be well approximated by the Pearson-III distribution for the complete series and the Kappa distribution for the wet-day series of rainfall. The parameters were fit to each rainfall sequence using L-moment estimators and the equations in the appendix of Hosking and Wallace (1997).

Fixed Reliability Regression Results

Regression results for the four fixed reliability cases are presented in Table 2. For each reliability case, the best regression for Class 1, Class 1 and 2 only, and all Classes of climate variables are included. Column 1 indicates the regression region, constant reliability, and the classes of variable considered. Column 2 gives the regression constant value and associated T-value in parentheses, while Column 3

gives the yield parameter, including the d value, the coefficient value and the T-value in parentheses. Columns 4-6 present the chosen climatic variables with the most explanatory power, with coefficients and T-values indicated beneath. Columns 7-9 contain the maximum variance inflation factor introduced by any single variable, the standard model error (SE), and the adjusted R^2 value.

Table 2 : Fixed Reliability Regression models for for q = 0.8, 0.9, 0.95 and 0.98.

(1)	(2)	(3)	(4)	(5)	(6)	(7)	(8)	(9)
Region Reliability Case	**Constant β_o (T)**	**a^d b (T)**	**Y_1 c_1 (T)**	**Y_2 c_2 (T)**	**Y_3 c_3 (T)**	**Max VIF**	**SE**	**Adj R^2**
US		a^0.667	σ	ρ	γ	1.3	0.5815	95.3
0.8	3.07251	-2.38083	0.89371	0.91667	0.5655			
1	(50.16)	(-289.47)	(89.28)	(66.6)	(27.26)			
US		a^0.667	σ_W	(1+ρ)/(1-ρ)	p_{zero}	1.1	0.5108	97
0.8	-0.70985	-2.30993	1.00286	2.3591	0.76 686			
1,2	(-39.56)	(-363.93)	(119.75)	(82.94)	(25.44)			
US		a^0.667	β_{P3}	(1+ρ)/(1-ρ)	h_K	1.1	0.4984	97.3
0.8	-2.0501	-2.31008	0.943373	2.52637	0.40697			
1,2,3	(-87.56)	(-380.23)	(117.93)	(98.83)	(14.15)			
US		a^0.645	σ	ρ	p_{zero}	1.4	0.5524	96.5
0.9	5.67481	-2.55626	0.958948	0.92204	1.55977			
1	(104.55)	(-334.43)	(101.26)	(72.23)	(39.46)			
US		a^0.645	σ_W	(1+ρ)/(1-ρ)	Cv	1.1	0.5217	97.1
0.9	-0.71068	-2.55664	0.987521	2.46851	0.39156			
1,2	(-33.1)	(-370.11)	(113.05)	(83.23)	(21.81)			
US		a^0.645	β_{P3}	(1+ρ)/(1-ρ)	h_K	1.1	0.5085	97.4
0.9	-1.37645	-2.55703	0.920987	2.63134	0.49013			
1,2,3	(-56.36)	(-387.35)	(110.38)	(93.75)	(16.33)			
US		a^0.577	σ	ρ	p_{zero}	1.4	0.5391	96.9
0.95	6.23851	-2.93638	0.951784	0.87947	1.46556			
1	(118.83)	(-360.3)	(104.2)	(71.26)	(38.45)			
US		a^0.577	σ_W	(1+ρ)/(1-ρ)	p_{zero}	1.1	0.5180	97.4
0.95	0.69506	-2.93483	0.977263	2.32063	0.60727			
1,2	(36.95)	(-386.62)	(112.37)	(78.55)	(19.28)			
US		a^0.577	β_{P3}	(1+ρ)/(1-ρ)	h_K	1.1	0.5072	97.5
0.95	-0.59861	-2.93473	0.910102	2.4591	0.45917			
1,2,3	(-24.3)	(-401.42)	(108.84)	(86.99)	(15.27)			
US		a^0.483	σ	ρ	p_{zero}	1.4	0.5523	96.9
0.98	6.94232	-3.55193	0.946599	0.79692	1.38041			
1	(125.79)	(-359.85)	(98.77)	(61.64)	(34.63)			
US		a^0.483	σ_W	(1+ρ)/(1-ρ)	p_{zero}	1.1	0.5398	97.2
0.98	1.64098	-3.55169	0.97017	2.4392	0.49578			
1,2	(79.29)	(-374.62)	(103)	(64.99)	(14.64)			
US		a^0.483	β_{P3}	(1+ρ)/(1-ρ)	h_K	1.1	0.5328	97.3
0.98	0.45805	-3.55213	0.908436	2.17216	0.38001			
1,2,3	(16.84)	(-383.33)	(98.92)	(70.12)	(11.55)			

Table 2 indicates that remarkably powerful regression models (adjusted $R^2 > 95$) for predicting required storage capacity can be generated for the entire U.S at fixed reliabilities. Somewhat surprisingly, the adjusted R^2 values actually increase as reliabilities increase. The coefficients of the a^d values are virtually unaffected by the class of climate variables are used. The less-easily-calculated Class 3 parameters lead to only somewhat improved regressions over the Class 1 and 2 variables, though variance inflation is considerably lower.

The climatic parameters selected demonstrate some definite patterns in the models. Of the Class 1 and 2 variables, the standard deviation of the wet-day series (σ_W), and (1+ρ)/(1-ρ) seem to occur most frequently. The β_{P3} parameter seems to be the precipitation parameter with the most explanatory power when all variable classes are included. It should be noted that β_{P3} and σ_W are highly correlated, so including both in a model leads to high variance inflation factors.

The models generally perform quite well, but an analysis of the residuals indicates some significant lacks of fit in certain geographic areas such as the Pacific Coast, South Florida, certain areas near the Great Lakes, and a few other places. Though it would be desirable to have a model that could predict storage at any location in the United States or world, regional regression analyses on smaller, more climatically homogenous regions should result in improved predictive power.

Regional Regression Results

Though the nationwide regressions were surprisingly powerful, considerable improvement may be gained by examining smaller, more homogeneous regions. The intent of this study is not to identify how to select appropriate regions for regional regression analysis for RWH system design. A diverse body of literature exists on how to select appropriate climate regions for regional regression analyses. In further studies, this may be an important element in developing more accurate regional regressions for designing RWH systems. One key requirement for any regional regression is data availability and spatial representativeness.

This study does not include enough stations to break the study area down significantly, so fixed reliability regressions are performed for only the three regions in Figure 3. The divisions roughly follow watershed boundaries and general climate character, but no specific methodology was applied in their selection, as that was not the intent of this study. The East, Midwest, and West Region contain 95, 85, and 52 stations respectively.



Figure 3: Three regions for regional regression analyses

Tables 3 displays the fixed reliability regression results for the East, Midwest, and West Regions, respectively, in much the same format as Table 2. An additional climatic variable is included in some models, and all models include all three classes.

In general, Table 3 displays better regressions than those performed for the entire U.S. R^2 values are higher than nationwide ones for comparable models for the East and Midwest Regions, but only slightly better for the West Region. One possible explanation for this difference is merely that fewer stations are included in the West, and station density is lower.

A more probable explanation is that the range of climates in the West is greater than in the East or Midwest, considering the West includes both arid deserts in the Southwest and temperate rainforests in the Northwest. This may be supported by the prominence of α_K in the West results, which discounts the influence of zeroes. Further division of the West region by climate type may then be recommended.

The East and Midwest Regions display high R^2 values overall. As in the nationwide regressions, either the σ_W or β_{P3} variables appeared prominently. Interestingly, ρ was more significant than $(1+\rho)/(1-\rho)$ for the Midwest, unlike the other regions. One especially peculiar feature of the Midwest regressions is that the value of d in the a^d parameter was greater in the 90% regression than the 80 %. The value of d in a^d generally exhibits a decreasing pattern as reliabilities increase.

Table 3. Fixed reliability regressions for the East, Midwest, and West Regions

Region Reliability	Constant β_o (T)	a^d b (T)	Y_1 c_1 (T)	Y_2 c_2 (T)	Y_3 c_3 (T)	Y_4 c_4 (T)	Max VIF	SE	Adj R^2
East 0.8	-1.96397 (-33.14)	a^0.675 -2.17313 (-408.99)	σ_w 1.04691 (86.14)	(1+ρ)/(1-ρ) 2.18117 (34.45)	- ξ_{P3} -0.12119 (-15.28)		1.3	0.3685	98.9
East 0.9	-1.39324 (-19.71)	a^0.589 -2.69436 (-394.73)	σ_w 1.05685 (77.02)	(1+ρ)/(1-ρ) 2.70974 (38.39)	- ξ_{P3} -0.16096 (-16.87)		1.3	0.3885	98.9
East 0.95	-0.60691 (-7.74)	a^0.516 -3.22189 (-380.77)	σ_w 1.0438 (68.86)	(1+ρ)/(1-ρ) 2.81609 (35.86)	-ξ_{P3} -0.16463 (-15.53)		1.3	0.4098	98.8
East 0.98	0.4067 (3.87)	a^0.468 -3.72534 (-287.28)	σ_w 1.02204 (49.32)	(1+ρ)/(1-ρ) 2.79194 (25.24)	- ξ_{P3} -0.14288 (-10.03)		1.3	0.4836	98.1
Midwest 0.8	-0.59732 (-12.69)	a^0.655 -2.49948 (-308.9)	β_{P3} 0.67958 (56.45)	τ_4 1.23239 (24.04)	ρ -0.16862 (-6.38)		1.5	0.4356	98.4
Midwest 0.9	-0.27956 (-4.68)	a^0.671 -2.6124 (-329.98)	β_{P3} 0.61513 (51.51)	τ_4 1.05546 (16.81)	h_K 0.3351 (6.64)	ρ -0.18098 (-6.55)	1.8	0.4332	98.6
Midwest 0.95	0.34209 (5.85)	a^0.630 -2.83048 (-344.35)	β_{P3} 0.64737 (55.53)	τ_4 0.95194 (15.44)	h_K 0.32824 (6.68)	ρ -0.14024 (-5.23)	1.8	0.4243	98.7
Midwest 0.98	1.20711 (19.38)	a^0.537 -3.33354 (-301.71)	β_{P3} 0.70686 (56.49)	τ_4 0.61031 (10.13)	h_K 0.40059 (7.37)		1.4	0.4618	98.3
West 0.8	-1.2118 (-11.14)	a^0.696 -2.20977 (-169.62)	a_K 1.10021 (50.68)	(1+ρ)/(1-ρ) 2.13427 (27.58)	γ 0.29347 (9.08)		2.8	0.5114	97.5
West 0.9	-0.32869 (-5.1)	a^0.695 -2.28795 (-178.16)	a_K 1.08413 (48.03)	(1+ρ)/(1-ρ) 2.00892 (31.28)	γ_w 0.2943 (7.2)		1.7	0.5064	97.7
West 0.95	-0.23892 (-4.43)	a^0.613 -2.62834 (-179.2)	a_K 0.88535 (49.94)	(1+ρ)/(1-ρ) 2.29544 (44.26)	γ_W 0.39129 (9.28)		1.7	0.5154	97.6
West 0.98	3.513 (19.75)	a^0.505 -3.20343 (-180.99)	a_K 0.67744 (27.74)	(1+ρ)/(1-ρ) 1.07145 (11.9)	σ 0.48433 (14.04)		4.4	0.5172	97.6

On the whole though, these regression results demonstrate that statistical parameters of rainfall can be used very effectively to predict required storage over considerably broad geographic areas.

Conclusion

Calculating the required storage for a rainwater harvesting system often presents a difficult design challenge. This study considered the problem of how to simplify the calculation of storage by incorporating the robustness of information about a RWH system provided by a wide range of simulation experiments. Considering a rainwater harvesting system as a simple storage reservoir, a daily simulation model computed empirical SRY relationships at 232 U.S. locations.

We hypothesized that differences in SRY relationships between stations could be explained by daily rainfall parameters, which would make possible a generalized regression model capable of calculating required storage anywhere in the study area (United States). By including daily rainfall statistics along with system parameters in an ordinary least squares, a log-linear regression framework can lead to a surprisingly powerful generalized storage equation. When considering three sub-regions of the United States, the regression fits improved, presumably due to greater homogeneity in hydroclimatic characteristics.

The regression models presented can be used to get a relatively good estimate of how large to build a storage tank based on desired yield and reliability, collection area, and local rainfall statistics. The regression approach presented could easily be extended and, enables the creation of improved storage equations in the U.S. and other regions of the world.

References

Coombes, P.J. and M.E. Barry (2007). The effect of selection of time steps and average assumptions on the continuous simulation of rainwater harvesting strategies. *Water Sci. Technol.*, **55(4)**, 125 – 133.

Dominguez, M.A., E. Schiller and N. Serpokrylov (2001). Sizing of Rainwater Storage Tanks in Urban Zones. Proceedings of the 10th International Rainwater Catchment Systems Conference. Mannheim, Germany. 10 – 14 September, 2001.

Fewkes, A. (1999). The use of rainwater for WC flushing: The field testing of a collection system, *Building and Environment*, **34 (6)**, 765-772.

Fewkes, A. (2000). Modeling the Performance of Rainwater Collection Systems: Towards a Generalized Approach. *Urban Water*, **1(4)**, 323-333.

Goel, A.K. and R. Kumar (2005). Economic analysis of water harvesting in a mountainous watershed in India. *Agricultural Water Management*, **71**, 257 – 266.

Guo, Y. and B. Baetz (2007). Sizing of rainwater storage units for Green Building applications. *Journal of Hydrologic Engineering*, **12(2)**, 197 – 205.

Handia, L., J.M. Tembo, and C. Mwiindwa (2002). Potential of rainwater harvesting in urban Zambia. Proceedings of the 3rd WaterNet/Warsfa Symposium 'Water Demand Management for Sustainable Development.' Dar Es Salaam, Tanzania. 30 – 31 October, 2002.

Hanson, L., and R.M. Vogel (2008). The Probability Distribution of Daily Rainfall in the United States, ASCE-EWRI, World Water & Environmental Resources Congress 2008, Hawaii, 2008.

Herrmann, T., and U. Schmida (2000) Rainwater utilisation in Germany: Efficiency, dimensioning, hydraulic and environmental aspects. *Urban Water,* **1(4)**, 307-316.

Herrmann, T., and K. Hasse (1997) Ways to get water: Rainwater utilization or long-distance water supply? A holistic assessment. *Water Sci. Technol.,* **36(8-9)**, 313-318.

Jenkins D., F. Pearson, E. Moore, J.K. Sun and R. Valentine (1978). *Feasibility of rainwater collection systems in California*. Contribution No. 173, California Water Resources Center, University of California.

Lee, K. T., C-D. Lee, M-S. Yang, and C-C. Yu (2000). Probabilistic design of storage capacity for rainwater cistern systems. *J. Agric. Eng. Res.*, **77(3)**, 343–348.

Liaw, C.H. and Y.-L. Tsai (2004). Optimum storage volume of rooftop rainwater harvesting systems for domestic use. *Journal of the American Water Resources Association,* **40(4)**, 901 – 912.

McMahon, T. A., and A. J. Adeloye, 2005. *Water Resources Yield.* Water Resources Publications, Littleton, Colorado

McMahon, T.A., Vogel, R.M., Pegram, G.G.S., Peel, M.C. and D. Etkin (2007). Global streamflows – Part 2 Reservoir storage-yield performance, *J. Hydrol.*, Vol. 347, No. 3-4, pp. 260-271..

Pandey, S. (1991). The economics of water harvesting and supplementary irrigation in the semi-arid tropics of India. *Agricultural Systems*, **36**, 207 – 220.

Panigrahi, B., S.N. Panda, and B.C. Mal (2007). Rainwater conservation and recycling by optimal size on-farm reservoir. *Resour. Conserv. Recycl.*, **50**, 459-474.

Phatarfod, R.M. (1986) The effect of serial correlation on reservoir size, *Water Resour. Res.*, **22(6)**, 927-934.

Schiller, E.J. and B.G. Latham (1987). A Comparison of Commonly Used Hydrologic Design Methods for Rainwater Collectors. *Water Resources Development,* **3(3)**, 165-170.

Vogel, R. M., and T.A. McMahon (1996). Approximate Reliability and Resilience Indices of Over-year reservoirs fed by AR(1) gamma flows. *Hydrol. Sci. J.,* **41 (1)**, 75 – 96.

Vogel, R.M., I. Wilson and C. Daly (1999a). Regional Regression Models of Annual Streamflow for the United States, *Journal of Irrigation and Drainage Engineering*, ASCE, **125(3)**, 148-157.

Vogel, R.M., M. Lane, R.S. Ravindiran and P. Kirshen (1999b). Storage Reservoir Behavior in the United States, *Journal of Water Resources Planning and Management*, ASCE, 125(5), Sep/Oct, 1999.

Vogel, R.M. and J.R. Stedinger (1987). Generalized Reservoir Storage-Reliability-Yield Relationships, *J. Hydrol.*, **89**, 303-327.

Villarreal, E.L., and A. Dixon (2005). Analysis of a rainwater collection system for domestic water supply in Ringdansen, Norrköping, Sweden. *Building and Environment.*, **40 (9)**, 1174 – 1184.

How the Heart of America is *Goin' Green* to Solve Water and Sewer Issues

Lynn Hinkle[1] and Michael Ports, PE, PH, D. WRE[2]

To become "America's Green Region," here's how a city in the Heart of America created a strategy for green infrastructure with a unique public engagement effort that created a groundswell of grassroots support for stormwater management.

As budgets tighten and the economy shows stresses from high energy costs, leaders are putting on their thinking caps and becoming creative problem solvers. In one aging American city that straddles a state line, Kansas City, such regional initiatives as 10,000 Rain Gardens, Conversations on the Environment, a regional Sustainability Academy, and the Kansas City Power and Light utility agreement with the Sierra Club to use more alternative energy sources such as wind power, have brought national attention and widespread acclaim. The appeal of *goin' green* as a region means that Kansas City can become a national model for sensible, sustainable growth.

One way to be a national model is to learn from others about solving common urban issues like polluted stormwater runoff and raw sewage overflowing during wet weather due to antiquated combined sewers. Kansas City leaders have traveled to Seattle and Portland to view green solutions that treat water as a resource, capturing and using stormwater to recharge the water table. They have seen green infrastructure such as rain gardens, bio-retention facilities, and stream buffers, which reduce storm water runoff and water pollution, create recreational amenities, and protect natural resources. These green solutions are integrated and include renewable energy, solid waste recycling, mass transit, bike/pedestrian infrastructure and other measures that reduce greenhouse gas emissions and improve environmental quality.

[1] President, ASTRA Communications, 7908 NW Pleasant Ford Road, Kansas City, Missouri 64152.
[2] Principal Water Resources Engineer, Bergmann Associates, 8653 Baypine Road, Suite 100, Jacksonville, Florida 32256.

Aside from the environmental benefits, defining Kansas City as the premier green solutions region is a brilliant stroke that could attract commerce and increased federal funding for innovative approaches.

As the nation's center of sustainability, Kansas City would be uniquely positioned to attract new businesses and relocating existing ones, particularly those that dominate the green industry. The current green industry has no center the way other industries do. The technology industry has San Francisco's Silicon Valley, the American auto industry has Detroit, and Connecticut is home to most of the insurance industry. Could the green industry be "goin' to Kansas City"? That is the goal that a number of visionary leaders have been planning for the past three years.

Everyone wants to do their part to make Kansas City the premier clean, green community. The Mid-America Regional Council (MARC) has announced a plan to create "America's Green Region" including a suite of training symposiums for area professionals. MARC is the regional planning organization for the Greater Kansas City area, including transportation and mass transit. Currently there is no light rail and mass transit is limited to a bus system. The automobile is king in a city that stretches for 250 miles from north to south and east to west. The region lies within two states, Missouri and Kansas, and encompasses eleven counties and ___ municipalities. A new transit plan has been under development and a suggested starter route for light rail will be presented to voters in November 2008.

The private sector is squarely behind the sustainability movement. The Greater Kansas City Chamber of Commerce recently launched a Climate Partners initiative with 181 business members who pledge to assess, measure, and reduce their carbon footprints. Taking a similar tack, twenty mayors in the region have signed a Climate Protection Pledge. Not only do these leaders from both groups see environmental benefits, they also understand that the incorporation of sustainability improves the quality of life for their citizens as well as increase their bottom lines through new efficiencies.

The Kansas City, Missouri is preparing a Long-Term CSO Control Plan for the EPA to describe how the City will reduce six billion gallons of polluted stormwater runoff and sewage that is discharged into local waterways each year. Like many of America's older cities, the aging infrastructure and combined sewer systems in an 85-square block area of the city are in severe need of relief and repair. Traditional approaches are projected to cost more than four billion dollars over 25 years. A citizen group known as the Wet Weather Community Panel, has been meeting for five years and advocates the use of green solutions, resulting in a unanimous City Council Green Solutions Policy Resolution. The administrative regulation that went into effect on February 25 directs all City departments to incorporate green solutions into their policies, projects, and programs.

To ensure efficient adoption across City departments, the administrative regulation directs more than ten City divisions and departments to explore and implement green solutions. The policy also provides for the creation of a Green Team Committee, which will direct the City's green solutions efforts, approve modification of internal business processes necessary to implement green solutions throughout the City, and provide direction on innovative ways to add green solutions to City projects.

"City projects will be approached as opportunities to incorporate green solutions in a creative way to provide multiple benefits for the residents of Kansas City," said Dennis Murphey, chief environmental officer in the Office of Environmental Quality. "Solutions include reducing sewer overflows and basement flooding, improving water quality in area streams, making our city a more bike and pedestrian-friendly community, improving air quality, and reducing greenhouse gas emissions that contribute to climate change."

The City Council has unanimously embraced the two year Climate Protection Plan led by Murphey's office using a collaborative, all-volunteer workforce to investigate the best approaches for Kansas City to reduce its carbon footprint, setting a city government goal and a community goal. The plan covers policy and public outreach, carbon offsets and waste management, transportation, buildings, and infrastructure.

For the homeowner, multiple short-term benefits stem from the use of green solutions. Many are easy and affordable. Property owners in other cities such as Portland, Oregon, and Maplewood, Minnesota, have welcomed the addition of large rain gardens installed by the city in the rights-of-way along streets because they help alleviate street flooding. Additionally, a street lined with rain gardens creates a beautiful neighborhood amenity that increases property values. Green street landscape designs called "bumpouts" have been used as traffic calming features in some communities. An excellent example in Kansas City is found near City Hall on 12th Street. The benefits include improved air quality, and a cooling effect from the urban environment's heat island effect.

In the long run, Kansas City residents also will benefit. Homeowners that support the visionary efforts of their regional leaders and take their cue to apply green solutions at the home level will help keep costs of renovating sewer system infrastructure in line. By disconnecting downspouts that send thousands of gallons of roof runoff directly into sewers, and redirecting that flow into a beautiful rain garden or a practical rain barrel, we begin to be part of the wet weather solution, one home or business at a time.

Workshops and training seminars for the public and for professionals held the key to Kansas City's successful 10,000 Rain Gardens initiative. Organizers held to one rule: KISS….Keep It Simple Stupid! Many gardeners are willing to "dig in" with just a little direction. The active involvement of Master Gardeners and other professionals helped improve a series of half-day training classes on the fundmentals of rain gardens, and reached thousands of citizens. A 45-minute video, "How to Build a Rain Garden," takes the mystery out of rain gardens and demonstrates the required planning, installation, and maintenance.

Workshops for teachers helped them to establish living classrooms. Youth groups and schools are a natural path to creating watershed management curriculum that grows with the students. Training the Trainer programs were created to help master gardeners continue their outreach to the community.

Professional training seminars helped experienced nursery owners, landscapers, planners, engineers, and others in the community's green industry to learn the design and planting of rain gardens, bioswales, and green roofs. Even seasoned professionals can be intimidated or overwhelmed by new ways of landscaping for stormwater management. Workshops geared to professionals included materials on native plants that are appropriate regionally, which invasive plants to avoid, proper preparation of the bed material, and basic hydrology, site issues, standard designs and templates, practical exercises in designing rain gardens, design evaluation, common pitfalls and troubleshooting, how to handle slopes, and a way to network the group for future business opportunities through the website that was designed for 10,000 Rain Gardens, www.RainKC.com.

Rain garden designs that are provided to the public must be customized to the region. Creating the website allows citizens, government officials, and businesses to find good information that is appropriate for the Kansas City rain fall and weather patterns. Kansas City's average storm yields 1.37 inches of rain. The green solutions approach helps the city to absorb more of the rainfall naturally, keeping it from running off into the sewer system and overloading it during a storm. Cities are looking for locations in their built environment to add a layer of green, from flat rooftops in the urban core, to alleyways that can become pervious through the use of different materials, to rain gardens or rain barrels that allow the disconnection of downspouts from the sewer system and a place to catch and use the rain water productively.

Modern marketing and advertising techniques were employed in Kansas City's 10,000 Rain Garden initiative that helped to create awareness and interest in stormwater management. Statistics from citizen opinion polls demonstrated a fifty percent increase in knowledge about sources of pollution in local waterways after just three weeks of the initial television campaign on local news channels. The female mayor, Kay Barnes, was featured in the ads to lend credibility and to demonstrate the commitment of the City's political leadership to green solutions. The use of humor assisted in the engagement of citizens and civic leaders in the campaign.

Other outreach included a Speaker's Bureau of local rain garden and native plant experts, volunteers such as Master Gardeners, who had received the appropriate training, and landscape architects. Requests for speakers came through the website, which was prominently featured in the television ads. Signage and displays at large events assisted in reaching the targeted audiences. An intensive public relations effort extended every paid dollar and allowed for a larger national story to develop, attracting the attention of federal regulators at the Environmental Protection Agency, who became strong advocates for this initiative.

In spring of 2008, after a $2.3 billion plan for the sewer overflows was submitted to city leaders and was found to be lacking in green solutions, the leadership of Kansas City, Missouri, worked with regulators to extend the timeline for a completed plan by six months to allow for a more progressive and integrated approach to be developed. The goal of the City Council was to fund green solutions with as much as twenty percent of the $2.3 billion gray infrastructure plan, thus positioning the city to develop a stronger local economic engine of small, minority-owned and women-owned businesses to design, install and maintain the green roofs, green streets, and rain gardens that would relieve the aging sewer system of a significant amount of stormwater runoff by diverting and infiltrating it naturally.

The local congressional leadership agreed to support the City's efforts by seeking funding for research projects from federal agencies, and made it a top priority to develop a Green Collar Job Corps in the region. As Congressman Emanuel Cleaver noted, green collar jobs are always needed in the community, and cannot be shipped overseas. The development of a green work force will depend upon small businesses and entrepreneurs, and is a critical asset that will stabilize the local economy through good times and bad.

Measuring success includes quantitative measures that indicate how many jobs are created in a new market sector, how many gallons of runoff are diverted from the sewer system, how many rain gardens, green roofs, rain barrels are installed, how many

corporate partners participate, and the number of students educated about their watershed. A change in attitudes and knowledge about stormwater management can be measured as well. A baseline for future public surveys was established in 2005.

Changing behavior by engaging hearts and minds in the Heartland of America creates a template that is applicable to cities anywhere in the world. Water is at the core of the effort, and it is important to remember that citizens care about beauty, clean water, and wildlife, even when they live in the heart of a big city. Empowering citizens and leaders to be innovative, and to take an active role in solving community issues, has paid off for Kansas City in helping it retain its quality of life. By *goin' green*, this region expects to create long term benefits for all citizens that balances the economic, social and environmental needs of all.

Graywater Irrigation as a Means to Meet Water Demands in Arid Regions

Sybil Sharvelle[1], Masoud N Azar[2], Mary Stromberger[3], Larry Roesner[4]

[1] Department of Civil and Environmental Engineering, Colorado State University, Fort Collins, CO 80523; PH (970) 491-6081; FAX (970) 491-7727; email: sybil.sharvelle@colostate.edu
[2] Department of Civil and Environmental Engineering, Colorado State University, Fort Collins, CO 80523; PH (970) 491-8314; email: masazar@engr.colostate.edu
[3] Department of Soil and Crop Sciences, Colorado State University, Fort Collins, CO 80523; PH (970) 491-5283; FAX (970) 491-6873; email: mary.stromberger@colostate.edu
[4] Department of Civil and Environmental Engineering, Colorado State University, Fort Collins, CO 80523; PH (970) 491- 7430; FAX (970) 491-7727; email: roesner@engr.colostate.edu

Abstract

Graywater irrigation systems offer many benefits, however the use of such systems has not become widespread due to concerns about safety issues. While some states have begun to legalize and regulate the practice of graywater reuse for residential landscape, little guidance based on scientific data has been provided for the safe operation of graywater irrigation systems. Limited scientific data is available on the fate of graywater chemical and microbiological constituents and the effect of these constituents on plant health after graywater is applied for irrigation. In this research we have examined the long-term effects of graywater irrigation. We selected three households where graywater has been applied for irrigation for more than five years to include in this study located in California, Colorado, and Texas. Sampling locations were selected to encompass a variety of soil types and climatic conditions. Soil and plant samples have been collected in an area irrigated with graywater as well as a control area with analogous soil and landscaping that has been irrigated with potable water. Soil cores have been taken to a depth of 1 m and we have analyzed the presence of antimicrobials, and indicator organisms at depths of 0 - 13 cm, 13 – 30 cm, and 30 – 100 cm separately. Soil samples also were analyzed for indictor organisms including total coliforms, *E. coli*, *Enterococci*, *Clostridium perfringens*. In addition, infiltration tests were conducted in each sites to evaluate the effect of graywater on infiltration rate of soil.

1. Introduction

As communities throughout the United State and abroad are becoming interested in innovative approaches to water resource sustainability, household graywater reuse for landscape irrigation is gaining popularity. In a typical household, graywater (near 28 gallons per person per day) is nearly 50% of the total wastewater generated. If used for irrigation of a typical residential landscape, it could supply about 30% of the demand, and with increasing emphasis on xeriscape in the semi-arid West, it has the potential to supply 100% of the irrigation demand in some areas. A study conducted by the Soap and Detergent Association (SDA) in 1999 revealed that 7% of U.S. households were reusing graywater (NDP Group, 1999). Another study in the same year (Little, 1999)

found that 13% of the households in Arizona used graywater for irrigation with the most utilized source being from clothes washers (66%). Some states, including California, Arizona, and New Mexico have legalized the practice.

However, there are potential risks associated with graywater reuse for irrigation. The physical, chemical, and microbial characteristics of graywater are highly variable based upon the sources connected to the collection system, household inhabitants, household chemicals used by the residents for personal hygiene and house cleaning, personal care, plus medications and waste products disposed of in sinks (Eriksson et. al., 2002). Application of graywater may result in increased levels of pathogens, negative impacts to soil quality, potential groundwater contamination with chemical constituents present in graywater, or negative impacts to plant health. These risks should be further evaluated and methods of graywater application that minimize these risks should be understood.

A number of studies have inferred fecal contamination of graywater via the presence of indicator organisms (e.g., Novotny, 1990; Rose et al., 1991; Christova-Boal et al., 1996; Casanova et al., 2001; and Ottoson et al., 2003). A primary concern is the possibility of graywater irrigation being a pathway for the spread of human diseases. However, the fate of pathogens after graywater application is not well understood.

Application of graywater for irrigation may impact soil chemistry. Potential effects of graywater on soil chemistry include changes in pH, salinity, and concentrations of chemicals, specifically organics and metals, introduced by the graywater. Very few published studies were found that evaluated these changes in the soil. The Gray Water Pilot Project in the City of Los Angeles, CA (1992) conducted research on eight voluntary residential sites retro-fitted with graywater systems for the purpose of residential sub-surface irrigation. Results showed an increase in sodium levels (Na^+) and in the Sodium Adsorption Ratio (SAR).

While graywater reuse for household irrigation is widespread, potential effects to soil quality, groundwater quality, and plant health have not been adequately assessed. The application of any irrigation water will introduce chemicals to the soil and potentially have short- and long-term effects. This potential depends on application rate, chemical concentrations in the water, biodegradation rate of the chemical, sorption, leaching, and plant uptake. Graywater chemical constituents can potentially migrate to groundwater, surface water, and drinking water sources. In addition, pathogens present in graywater may persist and pose human health risks. Previous researches have not addressed impacts of graywater chemical constituents and pathogens on soil quality, groundwater quality, and plant health. In addition, household graywater has not been adequately characterized. The study presented herein describes scientific experiments to alleviate these information gaps regarding household graywater irrigation.

The objective of this research project is to elucidate information on the fate and occurrence of graywater chemical constituents and pathogens and their long-term potential impacts on soil quality, as a result of its application for residential landscape irrigation with the experiments on households with existing graywater irrigation systems. Soil samples have been collected and analyzed at households where graywater

has been applied for irrigation for at least five years. Results will provide guidance to decision makers, water agencies, regulators, product manufactures and consumers so that safe graywater irrigation systems can be installed and operated for household irrigation.

2. Materials and Methods

2.1. Site Description

Soil samples were collected from three selected households where graywater has been applied for irrigation for more than 5 years in California, Colorado, and Texas. A control area at each household was selected with similar landscape irrigated with fresh water. Soil samples were collected at different depths of 0-15, 15-30, and 30-100 cm. The diameter of soil cores was 0.8 inch and cores were collected within the root zone of irrigated landscape. Site specifics and sampling dates are summarized in Table 1.

Table 1. Sites Specification and Sampling Dates

Location	Graywater Source[a]	Pretreatment	Storage Tank	Years in Use	Months Irrigated	Household Population	Sampling Date
Fort Collins, CO	L, S, W, B	No	Yes	5	May-Oct.	2	11-Aug-08
Escondido, CA	L, S, W	Sand Filtration	Yes	10	10	2	20-Oct-08
Dallas, TX	L	No	No	31	12	2	15-Sep-08

a: L = Laundry, S = Shower, B = Bath, W = Washbasin

2.1.1. California

The existing household in Escondido, California was equipped with a more advanced irrigation system than other households studied here. The system was comprised of a slow sand filter, which was automatically backwashed daily, pump, and submerged drip system. Underground emitters were placed in the root zone of graywater irrigated plants. The installed emitters were very effective in that they prevent clogging resulting from root growth. The system was installed by ReWater. No problems operational have been encountered with this system in its 10 years of operation. Landscape was irrigated on a daily basis. Some problems were encountered with sampling at this household. Depth sampling was not feasible due to a layer of bedrock present at around 4-8" below ground surface (bgs). Because a very extensive area was irrigated with graywater at this site with varying landscape, samples were collected at various locations rather than conducting depth sampling to 3 feet. It was decided that depth sampling would not provide useful information at this site since water was observed to flow down-slope rather than vertically, due to the layer of bedrock. Soil samples were collected from three different areas of the yard irrigated with graywater, one area amended with manure and two areas with native soil. One sample was collected where graywater had migrated to the soil surface.

2.1.2. Colorado

The household with an existing system in Fort Collins, Colorado was equipped with a simple irrigation system consisting of a storage tank, pump, and coarse filter. No problems were encountered with sampling at this household.

2.1.3. Texas

Samples were collected from a household in Dallas, Texas where wastewater from a laundry machine has been drained to landscape for more than 30 years. Turf grass in the graywater irrigated area appeared very healthy. Of particular note was that free range chickens and a dog defecate in the area irrigated with graywater.

2.2. Materials

Triclosan >97% (HPLC) and triclocarban 99% were obtained from Sigma-Aldrich. LC/MS grade methanol, acetonitrile, water and acetone were from Honeywell Burdick and Jackson.

2.3. Analytical Methods

Soil samples were analyzed for total coliforms, *E. coli*, and *Enterococci* using the IDEXX Quanti-Tray® enumeration procedure with Colilert® reagent for total coliforms and *E. coli* and Enterolert™ reagent for *Enterococci*. In addition, *Clostridium perfringens* was measured according to the plate count method specified in the Bacteriological Analytical Manual (FDA BAM). Microbial biomass, microbial respiration, and dehydrogenase enzyme activity were determined in all samples by the method described by Horwath and Paul (1994).

Soil samples were assessed for presence of antimicrobials. Extractions were performed on all soil samples upon arrival in our labs by methods as describe by Dyer et al. (1996) and Halden and Paull (2005). In addition, common antimicrobials in personal care products, triclosan and triclocarban, were also be monitored by LC/MS (Halden and Paull, 2005). An Agilent 1200 (Agilent Technologies) High-throughput HPLC systems coupled with Agilent 6220 Accurate Mass Time of Flight mass spectrometer (Agilent Technologies) was used for determination of triclocarban and triclosan. Chromatographic separation was carried out at a HyperClone ODS C18 column (5 μm, 150×2.00 mm) from Phenomenex. The data were controlled and processed using MassHunter Workstation software. Sample volumes of 5 μL were introduced to the instrument with an auto-sampler. Column temperature was maintained at 35 ^{o}C at both right and left sides. A gradient method with a mixture of water (A) and methanol (B) was used as follows: initial mix of 40% water, 60% methanol, linear increasing to 100% methanol within 5 min and held for 11 min, then linear decreasing to initial 60% methanol within 2 min and finally a postrun at initial condition for 10 min, at flow rate of 0.32 mL/min. Electrospray ionization (with negative ion mode) mass spectrometer was used for the determination of triclosan and triclocarban. Several methods described in the literature were evaluated for the analytical determination of triclosan and triclocarban in extracted soil samples with LC-MS techniques. Chromatographic separation of the analytes was evaluated under various conditions. For the first runs, water and acetonitrile elution containing 0.1% formic acid as an additives were performed with different isocratic and gradient conditions. These conditions did not result in adequate separation. Acetonitrile and water mobile phases with 10 mM acetic acid reported by Halden and Paull (2005) were used through different isocratic and gradient methods. Although acidic mobile phase was recommended for determination

of triclosan and triclocarban, it was found that acid addition caused reduction in sensitivity. A mobile phase with 10 mM ammonium acetate reported by other researchers may improve chromatographic resolution slightly, but it reduces sensitivity as well. Chu and Metcalfe (2007) used methanol and water as mobile phases quantification of triclosan and triclocarban without additives by monitoring of specific transition ions for each analyte. Our work showed that optimum results were achieved when water and methanol were used for the mobile phases. Although chromatographic separation of the analytes is still poor, this method results in more sensitive chromatograms in much less time in compare with other methods.

Widely used surfactants including soap, linear alkyl benzene sulphonates, alcohol ethoxylates, and alcohol ether sulphates will be quantified by liquid chromatography/mass spectrometry LC/MS, (Levine et al., 2005) in the near future.

A single ring infiltrometer test was applied to each household site to estimate the infiltration capacity of graywater irrigated and control soils. The single-ring infiltrating device (approximately 20 centimeters (cm) diameter) was driven 5-6 cm into the ground using a large mallet and sealed by compacting native soils around the outside edges. At the beginning of the test, the device was filled with approximately 15 cm of fresh (i.e. tap) water. Water depth measurements were collected at intervals ranging from 30 seconds to 5 minutes for a minimum of 30 minutes. If the water depth dropped below 2 cm before the test was completed, the device was refilled back to a depth of 15 cm. With a few exceptions, two tests were conducted at each site, one at a location irrigated with fresh water (control site) and another at a location currently (or planned to be) irrigated with graywater (graywater site).

Table 2. Soil Microbial Data for Households with Existing Graywater Systems

State	Treatment	Soil Depth	Total Coliforms	E. coli	Enterococci	Clostridium perfringens	MBC[1]	Respiration rate	Dehydrogenase
			No. cells g^{-1} soil			cfu g^{-1} soil	mg kg^{-1} soil	mg CO_2 kg^{-1} soil d^{-1}	µg INT kg^{-1} soil h^{-1}
CA	Control 1	with manure	69,574	BDL[2]	150		1,048	47.1	2,015
	Control 2	no manure	9,321	BDL	30.8				
	Graywater 1	with manure	82,884	BDL	803		553	27.3	4,967
	Graywater 2	no manure	13,560	BDL	35,583				
	Graywater 3	citrus	15,275	BDL	726				
CO	Control	0-15 cm	1,964	106	299	BDL	622	27.3	358
		15-30 cm	37.1	1.2	11.5	BDL			
		30-100 cm	BDL	BDL	23.0	BDL			
	Graywater	0-15 cm	15.6	11.8	BDL	BDL	539	10.3	489
		15-30 cm	10.8	BDL	BDL	BDL			
		30-100 cm	BDL	BDL	BDL	BDL			
TX	Control	0-15 cm	5,640	136	14,000	375	5,478	71.7	3,584
		15-30 cm	8,500	43.3	850	BDL			
		30-100 cm	23,200	216	546	BDL			
	Graywater	0-15 cm	137,000	543	31,000	BDL	6,210	95.5	3,688
		15-30 cm	17,600	160	1,220	BDL			
		30-100 cm	28,300	1,093	2,230	BDL			

[1]MBC = Microbial Biomass Carbon
[2]BDL = Below the Detection Limit

3. Results and Discussion

3.1. Soil Microbial Data

Pathogen indicator organisms were measured in soil samples to assess their fate after graywater application. Soil microbial data with existing graywater system has been summarized in Table 2. Numbers of total coliforms ranged from very low (11 cells g^{-1} soil in Colorado) to 137,000 cells g^{-1} soil in Texas. Total coliform numbers generally decreased with soil depth, with the exception of Texas soil receiving fresh irrigation water (Figure 1). No clear trend of an effect of graywater irrigation was observed on total coliform numbers in soil samples. Total coliforms were not higher in graywater irrigated soils compared to contol soils. Numbers were similar between control and graywater-treated soils at California, greater in control soil in Colorado, and greater in graywater-irrigated soil in Texas.

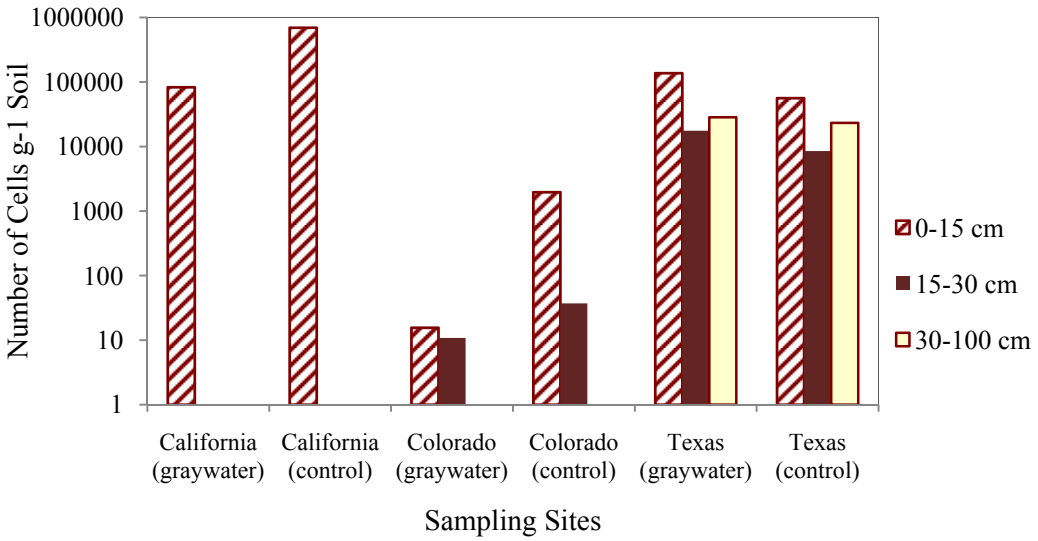

Figure 1. Number of Total coliform in soil samples

Numbers of *E. coli* were generally low or below detection limits in soils from California and Colorado (Figure 2). In Texas, *E. coli* numbers increased with soil depth for the graywater treatment, indicating downward movement of *E. coli* in soil receiving graywater. Numbers of *Enterococci* were highly variable, ranging from below the detection limit to greater than 35,000 cell g^{-1} soil, which occurred in graywater-irrigated soil in California (Figure 3). In Texas, surface soil receiving graywater contained more than twice the number of *enterococci* as surface soil receiving fresh water, potentially attributable to chickens in the area.

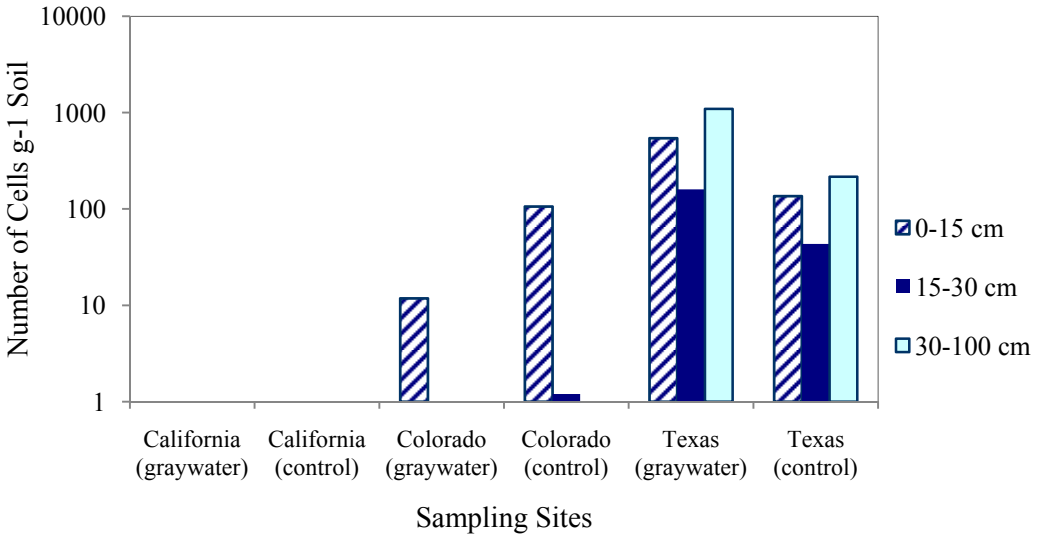

Figure 2. Number of *E Coli* in soil samples

No clear trend was observed regarding graywater effects on soil microbial biomass and respiration (Table 1). Microbial biomass and respiration were lower in graywater-treated soil in California, slightly lower in graywater-treated soil in Colorado, and higher in graywater-treated soil in Texas. Overall, Texas soils contained very large amounts of microbial biomass and had the greatest rates of respiration. Dehydrogenase is an intracellular enzyme involved in aerobic metabolic processes and is an indicator of microbial activity. Overall, rates of this enzyme were low in the Colorado soils, which corresponded to the relatively low microbial biomass at this site. Graywater did not affect dehydrogenase activity in Colorado or Texas. In California, dehydrogenase activity was greater in soil irrigated with graywater, despite the smaller microbial biomass in graywater-treated soil.

1.1. Soil Antimicrobial Analysis

The optimized analytical method previously described was applied to the analysis of extracted soil samples collected from different sites in CA, CO, and TX. Triclosan and triclocarban were not detected in any of the soil samples. The mass of soil extracted was 40 g, so the lower detection limit on the instrument was near 0.04 ng/g soil for both antimicrobials. Triclosan and triclocarban do not appear to be present in graywater irrigated soils at concentrations of concern.

1.1. Soil Infiltration Data

Each site offers unique conditions that exist due varying soil characteristics, particle sizes and varying depths to restrictive layers that may limit the vertical migration (and promote the horizontal migration) of graywater. Results from infiltration tests are summarized in Table 3. Preliminary results from paired infiltration tests comparing control (freshwater irrigated) locations to graywater irrigated locations suggest that long-term application of graywater may enhance infiltration; however, additional tests

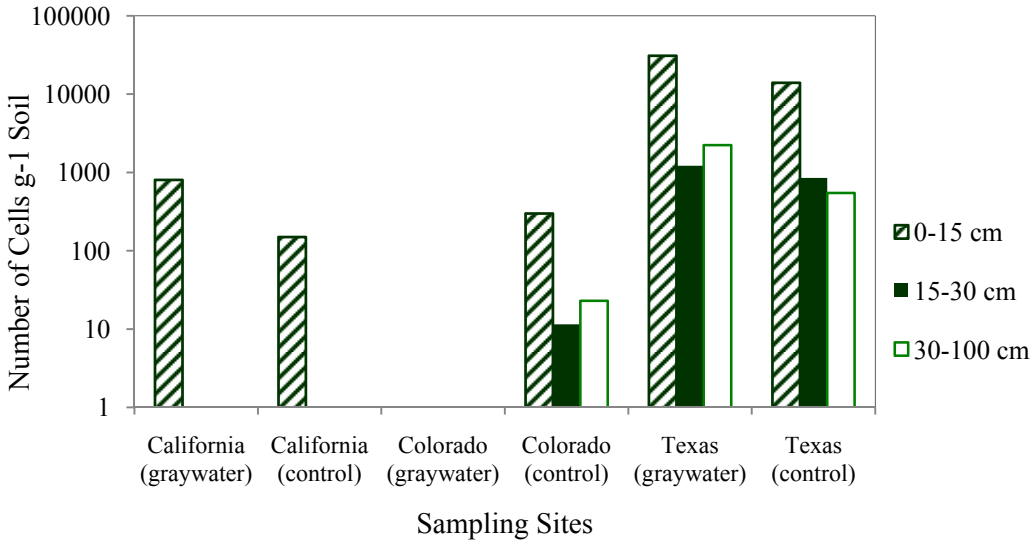

Figure 3. Number of *Enterococci* in soil samples

and analysis should be conducted before reporting definitive conclusions. Of note is that the site where the infiltration test conducted in the control area at the California site was highly sloped whereas the area within the graywater irrigated soil was not as sloped, resulting in substantial horizontal flow of water. Therefore, results from the California infiltration study were not interpreted. Two infiltration tests were conducted at each site; one where graywater is currently used for irrigation and another where freshwater is used for irrigation. This one set of paired tests may not be adequate to conclude with certainty whether or not graywater irrigation has a significant impact on the infiltration rates of soils. In the future, it may be useful to conduct infiltration sites at multiple locations within each site to better understand the influence of graywater on soil infiltration rates. A modified method of the single-ring infiltration test developed by Bouwer (1999) could be conducted during future field visits to better estimate the vertical and horizontal proportions of hydraulic conductivity.

Table 3. Summary of infiltration test results

Site	Dominant Soil Type	30 min Infiltration (in)		Restrictive Layer	Max. Soil sample Depth (in)	GW Impact to Infiltration Rate
Colorado	Loam	Graywater	1.6	20 - 40 (bedrock)	36	yes
		control	2.3			
Texas	Silty Clay	Graywater	40.0	20 - 40 (bedrock)	36	yes
		control	55.0			
California	Gravelly Loam	Graywater	15.3	4 - 20 (bedrock)	< 6	n/a
		control	10.0			

2. Conclusion

Pathogen indicator organisms were measured in soil samples to assess their fate after graywater application. No clear trend of an effect of graywater irrigation was observed. However, it is notable that pathogen indicators were generally not found to be higher in soils irrigated with graywater than control soils irrigated with freshwater. Pathogen indicators were highest in soils where animals defecated in the area and where soils were amended with manure. No clear trend was observed regarding graywater effects on soil microbial biomass and respiration. Triclosan and Triclocarban were both below detection limit in soil samples, which may indicate that graywater irrigation has no effect on the presence of these compounds in soil. Preliminary infiltration test results suggest that long-term application of graywater may enhance infiltration; however, additional tests and analysis should be conducted before reporting definitive conclusion.

3. REFERENCES

Casanova, L.M., V. Little, V., R. J. Frye, and C. P. Gerba 2001. A Survey of the Microbial Quality of Recycled Household Graywater. *Journal of the American Water Resources Association.* 37(5): 1313-1319.

Christova-Boal, D., Eden, R.E., and McFarlane, S. 1996. Investigation into Greywater Reuse for Urban Residential Properties, *Desalination.* 106 (1-3): 391-397.

Chu, Shaogang, and Chris D Metcalfe. 2007. Simultaneus determination of triclosan and triclocarban in municipal biosolids by liquid chromatography tandem mass spectrometry. *Journal of Chromatography* 1164: 212-218.

City of Los Angeles: Office of Water Reclamation. 1992. Nov. *Graywater Pilot Project* – Final Project Report.

Dyer, S. D.;Sanderson, H.;Waitte, S. W.;Van Compernolle, R.;Price, B.;Nielsen, A. M.;Evans, A.;Decarvalho, A. J.;Hooton, D. J.;Sherren, A. J. 2006. Assessment of Alcohol Ethoxylate Surfactants and Fatty Alcohols Mixtures in River Sediments and Prospective Risk Assesment. *Environmental Monitoring and Assessment.* 120:45-63.

Eriksson, E., Auffarth, K., Eilersen, A.M., Henze, M., and Ledin, A. 2003. Household Chemicals and Personal Care Products as Sources for Xenobiotic Organic Compounds in Grey Wastewater, *Water SA.* 29: 135-146.

Halden, R. U.;Paull, D. H. 2005. Co-Occurence of Triclocarban and Triclosan in U.S. Water Resources. *Environmental Science and Technology.* 39:1420-1426.

Horwath, W.R., and E.A. Paul. 1994. Microbial biomass. p 753-773 *In* R.W. Weaver, J.S. Angle, P.S. Bottomley, D. Bezdicek, S. Smith, A. Tabatabai, and A. Wollum (eds.) Methods of Soil Analysis. Part 2. Microbiological and Biochemical Properties. Soil Science Society of America, Madison, WI.

Levine, L. H.;Garland, J. L.;Johnson, J. V. 2005. Simultaneous Quantification of Poly Dispersed Anionic, Amphoteric, and Nonionic Surfactants in Simulated Wastewater Samples Using C18 High-Performance Liquid Chromatography-Quadropole Ion-Trap Mass Spectrometry. *Journal of Chromatography A.* 1062:217-225.

Little, Val L. 1999. Residential Graywater Reuse: The Good, The Bad, The Healthy. Water Conservation Alliance of Southern AZ.

NPD Group, The. 1999. for the Soap and Detergent Association. *Graywater Awareness & Usage Study.*

Novotny, V. 1990. Potential and prospects for reclamation of graywater. Proceedings of Conserv 90.

Ottoson, J. and Stenström, T.A. 2003. Faecal Contamination of Greywater and Associated Microbial Risks. *Water Research.* 37: 645-655.

Rose, Joan B., Cho-Shing Sun, Charles P. Gerba, and Norval A Sinclair. 1991 Jan. Microbial Quality and Persistence of Enteric Pathogens in Graywater from Various Household Sources. *Water Research*. 25(1):37-42.

HCFCD M3 System
Maximizing and Maintaining Local Investments in Floodplain Modeling

Karl McArthur, PE[1], CFM; Stephen Bourne, PE[2];
Yu-Chun Su, PhD, PE, CFM[3]; Jacob Spenn, PE, CFM[4]

[1]PBS&J, 6504 Bridge Point Parkway, Suite 200, Austin, TX 78730; PH (512) 327-6840; FAX (512) 327-2453; e-mail: kemcarthur@pbsj.com
[2]PBS&J, 1800 Parkway Place, Suite 1200, Marietta, GA 30067; PH (404) 895-0753; FAX (770) 426-5316; e-mail: sfbourne@pbsj.com
[3]PBS&J, 1250 Wood Branch Park Drive, Suite 300, Houston, TX 77079; PH (281) 529-4195; FAX (281) 493-1047; e-mail: ycsu@pbsj.com
[4]Harris County Flood Control District, 9900 Northwest Freeway, Houston, TX 77092; PH (713) 684-4000; FAX (713) 684-4140; e-mail: Jacob.spenn@hcfcd.org

ABSTRACT

Harris County, Texas, one of the most heavily populated and fastest growing areas in the nation, has 25% of its 1800 square miles located within the 1% annual chance floodplain. The District, in association with the Federal Emergency Management Agency (FEMA) recently completed a county-wide Flood Insurance Study for Harris County, Texas (Houston, Texas) also known as the Tropical Storm Allison Recovery Project (TSARP), which encompassed the restudy of 22 major watersheds and approximately 1300 miles of channels. The hydrologic and hydraulic (H&H) models produced as part of this study became effective in June 2007 and the citizens, developers and engineers within Harris County are now actively using them. It is HCFCD's desire to protect their significant investment in these models by ensuring their efficient management and update into the future. As a result, the number of requests for the effective Flood Insurance Study models and the resultant frequency of updates to these models have prompted Harris County Flood Control District (HCFCD) to implement an automated system for model management.

The solution currently under development is known as the Model and Map Management System (M3). The M3 will tackle the difficult problem of the on-going management and update of models in the highly active floodplain-related development environment of Harris County. A major part of this problem is that multiple projects tend to impact the same streams and watersheds, which can lead to the development of hydrologic and hydraulic studies based on out-of-date or conflicting H&H models. The effective model at the time a floodplain development permit application was started may have been replaced with a revised model by the time of the permit application submission. The M3 system will provide HCFCD and the development community with a set of tools that will address this contemporaneous permitting issue through the maintenance of up-to-date models, provision of notifications of potentially overlapping studies, provision of efficient model distribution and submittal functionality, and seamless integration into the FEMA LOMC process.

In addition to efficiently managing the use and update of models through the FEMA process, the M3 also will provide the District with powerful tools for their own internal management and planning activities. The M3 system includes management tools, such as a Model Explorer, that will provide comprehensive documentation of and access to all the H&H modeling and supporting documentation developed for studies within their jurisdiction. Having this information at their finger tips will allow the District to thoroughly evaluate the impacts of capital projects, plan more effectively for periodic watershed-scale master planning and study updates, and provide a higher level of service in their planning and management operations.

INTRODUCTION

Harris County is one of the fastest growing communities in the nation with 25% of its 1800 square miles located in the 1% floodplain. The numbers of requests for effective floodplain models and the resultant frequency of updates to those models have prompted HCFCD to implement an automated system to manage the models. With the system in place, the potential flooding risk to Harris County citizens will be reduced, by insuring that engineers are always using the best and most up-to-date information for planning and development.

In response to Tropical Storm Allison, which caused severe flooding in Houston, the Harris County Flood Control District (HCFCD) in association with the Federal Emergency Management Agency (FEMA), did a county-wide update of its floodplain models. Recently completed, the Tropical Storm Allison Recovery Project (TSARP), resulted in the restudy of 22 major watersheds and approximately 1300 miles of channels using HEC-HMS and HEC-RAS. FEMA has recently accepted the models and the citizens, developers and engineers within Harris County are actively using the models.

A model and map management program has been created by the HCFCD to protect the 30 million dollar investment that FEMA and the HCFCD made in TSARP. Through the model management program, HCFCD will update the HEC-HMS and HEC-RAS models and implement policy which will standardize the processes used to keep the models valid, up to date, accurate, and consistent into the future.

The objective of the model management program is to standardize the process through which developer engineers will be able to modify the models. The reasons for these modifications could range from flood control or development projects of varying size to hydraulic changes such as new bridges. With the standardization, new policies have been implemented to help in the review of the models and to protect the integrity of the models. Furthermore, with standardization, the final product received by the HCFCD from the engineer will be consistent and all new or modified hydrologic or hydraulic features will be consistent from one project or study to another. The goal is to provide consistent, up to date models and to ensure coordination between the end users and regulatory entities on all potentially

conflicting studies. Internal polices will be defined and clarified to allow for quick, efficient decisions during the model review process.

A key component of the model management program is the model and map management system, or the M3 system. The M3 system is comprised of (1) a geographic information system (GIS)–based, Arc Hydro compliant, enterprise database of spatial information that describes the watershed and stream network for Harris County and provides linkages to associated hydrologic and hydraulic models, (2) a directory structure and allocated server space for the archival of models and supporting data, (3) a web portal for checkout and submittal of models and tracking of study status, and (4) an accompanying Environmental Systems Research Institute (ESRI®) ArcMap-based extension for internal processing and data management. The extension can best be described as a workbench for the retrieval, distribution, and management of the effective and legacy models for Harris County. This paper discusses the process which the HCFCD has undertaken to ensure efficient management of hydrologic and hydraulic models for the Harris County area and to develop the M3 tools to provide this management and coordinate the use of the models into the future.

THE PROBLEM OF CONTEMPORANEOUS FLOOD STUDIES

The efficient management and maintenance of flood models presents a number of challenges. These challenges include effective coordination of the FEMA update process, rapid development, and the resultant changes in land use and topography, changes in HEC-HMS and HEC-RAS versions, and standardization between studies performed by various contractors. However, the key issue in the day to day management and maintenance of floodplain models is the handling of multiple studies that involve the same stream(s) and model(s).

Growth and development within unincorporated Harris County has been rapid during the past decade. This is clearly reflected in the statistics for approved plan sets since 2001 in the three most active watersheds within Harris County. These statistics, shown in Table 1 are based on HCFCD Watershed Department data.

Table 1. Approved Plan Sets by Watershed from 2001 to 2007.

Watershed	Total	Average/Year
Greens Bayou	1520	253
Cypress Creek	1652	275
Addicks Watershed	895	149

While many of these developments are small and will not be reflected in the effective models, there will be a significant number that result in the need for a FEMA Letter of Map Revision (LOMR). In addition, the HCFCD has completed a number of Capitol Improvement Projects (CIP) since 2001 that must also be reflected in the

models. Invariably there will be situations where multiple development and/or CIP projects result in simultaneous studies on the same modeled stream.

The central issue associated with the maintenance of the effective model set is the need to address and manage this contemporaneous use of the same models for multiple permit requests (studies). The situation will arise when ongoing studies by more than one engineer, developer, municipality or other entity require the use of the same hydrologic and hydraulic models or hydraulic models that have direct impacts on each other (near confluences). This situation is illustrated in Figure 1.

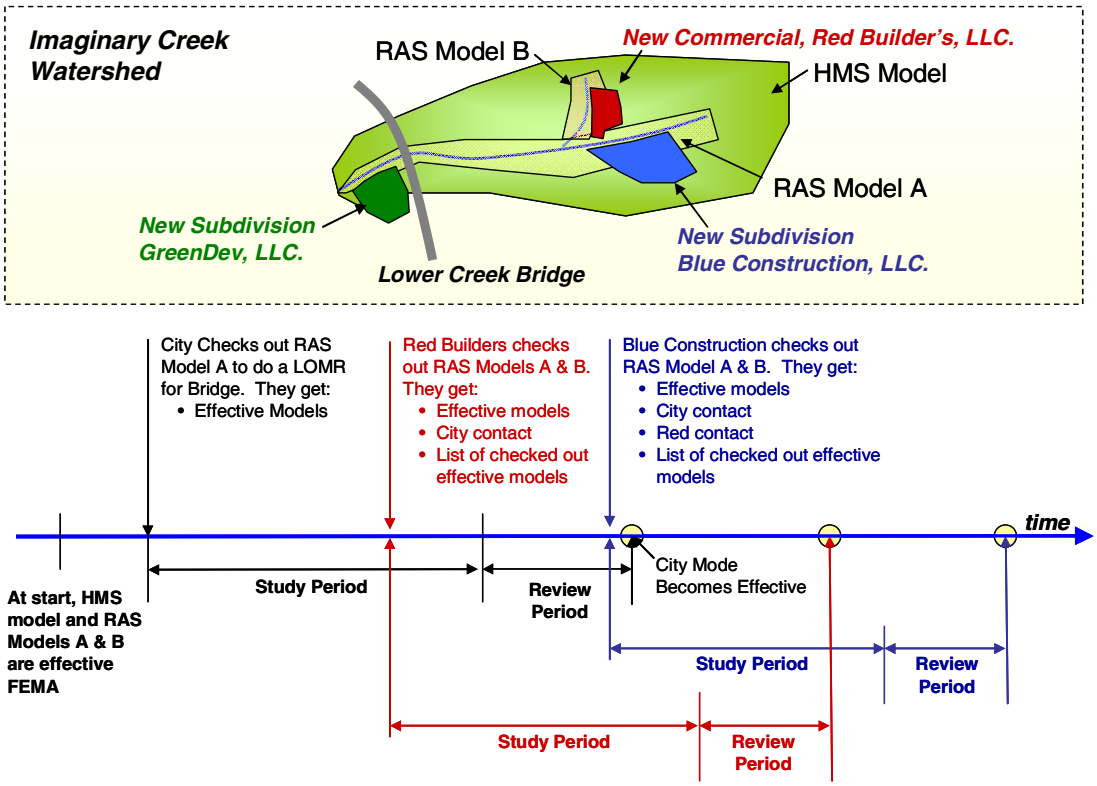

Figure 1. Hypothetical Usage Timeline Illustrating Contemporaneous Permitting Issues Addressed by the M3 System.

The figure shows a hypothetical watershed that is subject to heavy development. Three separate entities study the creek at the same time. First, the city in which the creek lies uses the effective hydraulic model to produce a LOMR for a bridge crossing the river. The process of creating this LOMR may take several months and consists of a stage during which the city is producing the new model, and a phase during which that model is being reviewed. Collectively, the life cycle of the process may take more than one year. While the city produces its new model, Red Builders, LLC starts the process of applying for a permit for a new development. Red Builders request the effective model before the City has had the chance to submit their revised model and so Red Builder's permit is based on the effective model in existence before the city revises it. While both the city and Red Builders are revising the effective model, Blue Construction, LLC, requests the effective model for a hydrologic study

of a new subdivision they plan to build. They request the model after the City has submitted their new version of the effective model, but before that model has been approved and made effective.

This figure illustrates the potential for study time frames to overlap for the same stream. This situation is most critical when one or more of the permits associated with the requests will require the submission of a Letter of Map Revision (LOMR). The submission of a LOMR will result in a change in the effective hydraulic model for the stream. This change in the effective model will need to be reflected in any uncompleted studies on the same stream. The issue is further complicated by the fact that the initial requestor may not ultimately be the first to resubmit their revised model.

Due to the ramifications of the contemporaneous permit request issue, it is critical that the M3 system efficiently manage multiple overlapping requests and provide timely notification to impacted requestors. The management of this issue was a focal point in the ultimate configuration and capabilities of the system.

MODEL MANAGEMENT SOLUTION APPROACH

To properly document, develop, and implement a solution for the issues described above, a four phase plan was developed by HCFCD for the Model Management Program. These four phases include 1) an update of the HCFCD modeling standards, 2) development of a process to update the supporting data for modeling, 3) a systematic approach for the update of watershed studies, and 4) development of a system to facilitate the distribution and update of models and supporting data – the M3 system.

The key components of Phase 1 of the plan were the development of consistent model standards and identification of the processes required for model management and tracking. The standards developed in Phase 1 will ensure that any revisions made to the effective models by users after the June 18th, 2007 effective date for the Harris county-wide study will be efficiently incorporated and disseminated. This phase also included the initiation of preliminary tracking of projects through the model checkout and check in process. This will allow HCFCD staff to efficiently track the potential changes to the models and facilitate the notification of the end users in the occurrence of overlapping or adjacent studies. This preliminary tracking system has subsequently been incorporated into the more comprehensive M3 system.

The objective of Phase 2 of the solution approach was to develop the processes required for management of the support data associated with the effective HEC-HMS and HEC-RAS models and to prepare data that will be used during Phase 3, the Model and Map Update Program (MMUP). First the watersheds must be evaluated and prioritized to determine which watersheds will be updated first. Second, the data supporting the models must be processed and updated. This supporting data includes catalogs of on-site detention ponds, LiDAR data, land use data and model calibration

data. An evaluation matrix was developed for each of the watersheds in Harris County to rank the watersheds relative to the following three issues: 1) rate of development, 2) existing modeling issues and inconsistencies, and 3) CIP projects constructed or planned for the watersheds. Rankings were assigned for each of the three issues and each issue was weighted equally. While all of the watersheds will be updated on a regular basis, the watersheds with the highest rankings will be updated first and potentially more frequently. This effort has occurred in parallel to the development of the M3 system and will ultimately be managed by M3.

The objective of Phase 3, the MMUP, is to systematically update the models and associated data. These updated models will be used to properly document the benefits of proposed HCFCD design projects. The level of effort for MMUP can be split into three tiers with respect to the type and size of the modeling effort. A Tier 1 model update will apply to watersheds that are very active from a development and CIP perspective. Tier 1 updates will consist of land use updates, LiDAR updates, modifications to unit hydrograph parameters (TC&R and DET variable), updated storage routing (SV-SQ relationships), update/fix of modeling inconstancies, updates to reflect CIP projects, and updates to the current version of HEC-HMS and HEC-RAS. Tier 2 will focus on updating or fixing modeling inconsistencies, updates to reflect CIP projects, and updates to the current version of HEC-HMS and HEC-RAS. Tier 3 will be used on watersheds with significantly less development activity, but that need to be updated to the current version of HEC-HMS and HEC-RAS.

Phase 4 focuses on the Model and Map Management (M3) System. The M3 lies at the heart of the HCFCD model management solution and will integrate the MMUP with the ongoing, incremental evolution of models due to projects that generate LOMCs. Version 1.0 of the M3 system has been implemented and is currently being used to manage the model request and study tracking process. Development of additional components and capabilities for the M3 is ongoing. The design and functionality of the system is discussed in the following sections.

MODEL AND MAP MANAGEMENT SYSTEM DESIGN

The design strategy for the M3 system focused on collaborative development of requirements between the HCFCD and the development teams. This collaboration was necessary primarily due to the complex nature of the problem that the M3 system is intended to solve. As discussed previously, the processing and tracking of contemporaneous development permit applications for a stream and associated models is the key issue that must be addressed in order to effectively manage model updates. *The general solution for this problem is careful management of permit applications, the use of algorithms for identifying possible conflicts, the pro-active notification of all involved system users of potential conflicts, and the general encouragement of communication among users through technology*.

Figure 2 illustrates the M3 design. The M3 system is based on an enterprise SDE ArcGIS geodatabase. In addition to the enterprise database there is an archive of

hydraulic and hydrologic models that is maintained in a carefully defined directory structure.

The public face of the M3 system is a web portal, which is maintained outside the HCFCD firewall. As requests for models are received, they are communicated securely to the M3 system via custom web services. Web services also handle communication about the status of requests to the public. For example, if a developer has previously requested models for a river with intent to write a permit application for development, the M3 system will inform the developer if another request comes in with the same intent. Transfer of effective models is done via secure ftp. The M3 web services are currently under development and represent an exciting new way of conducting secure public-to-regulatory agency permitting processes.

The M3 workbench component is an ESRI ArcMap 9.2 extension. This component is the user interface for most of the functionality provided by the Request Processing functional component. The workbench will be installed on several HCFCD machines and will be the primary tool used by HCFCD staff for working with the M3 system. As the tool is an ArcMap extension, it will immediately fit within the GIS solution that HCFCD is currently using.

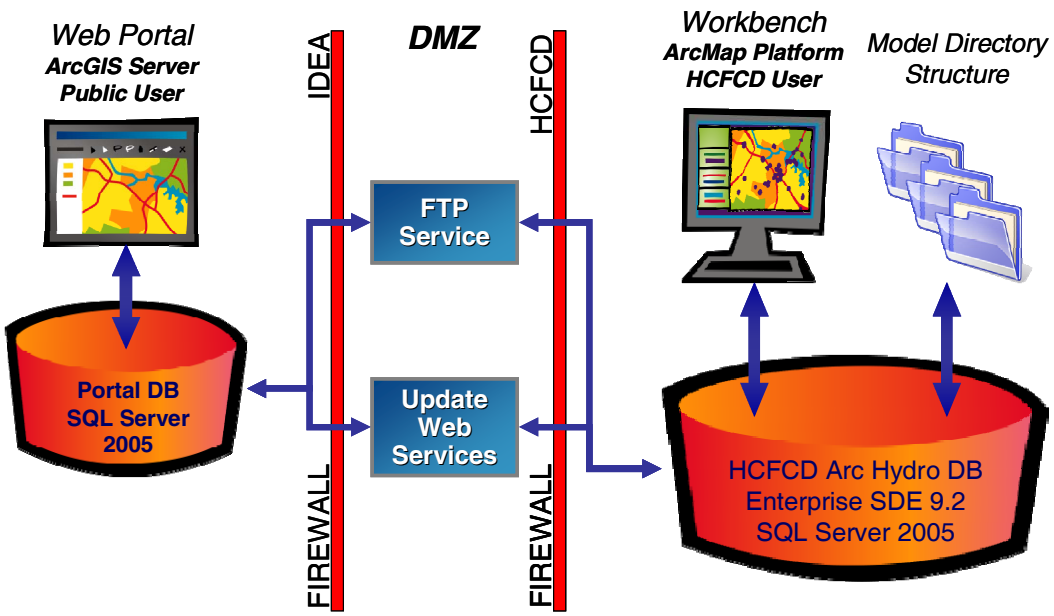

Figure 2. Physical System Components Comprising the Solution Architecture.

The workbench provides essentially two sets of functionality: model exploration and request processing, which are described in detail below:

M3 MODEL EXPLORATION

The M3 workbench includes a section dedicated entirely to model exploration called the model explorer. With the tools provided, the user can select a stream and

immediately see all the available models for that stream or its watershed. The model explorer interface is illustrated in Figure 3. In this example, the cyan colored stream segment indicates the stream that has been selected by the user. The tree on the left displays 1) all the hydraulic models available for the selected stream, 2) all the hydraulic models for the streams within the watershed that includes the selected stream, and 3) the hydrologic models for that watershed.

Once a particular stream has been selected, there are several options available to the user. They have the option to graphically compare profiles or cross sections from the various models. The user can also open a selected model directly in the software in which it was developed. For example, the user can open the hydraulic model directly in HEC-RAS. The M3 system protects effective and legacy models from being directly edited by dynamically controlling the read-only properties of the models and offering the user the option to copy the entire model to another directory for editing and other uses.

Perhaps the most valuable function of the model explorer is its model catalog editing capabilities. Any authorized HCFCD user may add models to the catalog so that other users can access them in the future. Moreover, users are required to add metadata to the models to describe why they were created, who was involved, and other important information related to the development of the model.

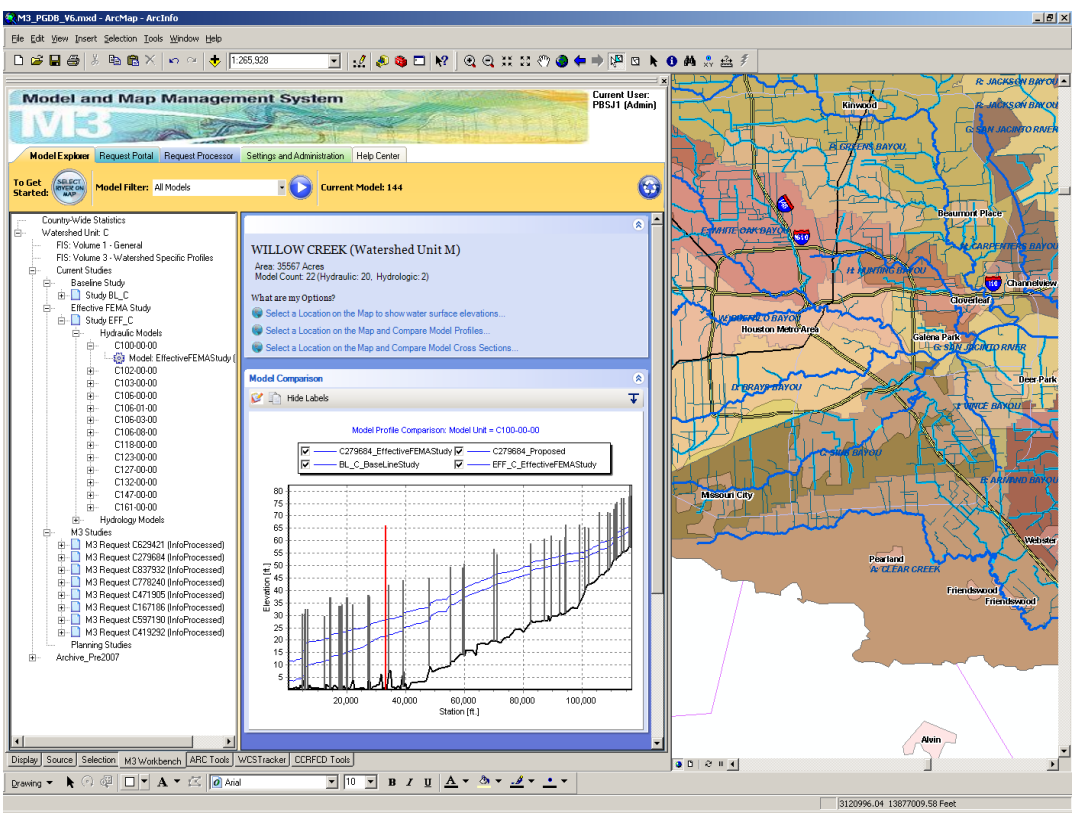

Figure 3. The M3 Model Explorer – Comparison of modeled river profiles from two HEC-RAS models for the same river.

M3 MODEL REQUEST PROCESSING

Version 1.0 of the M3 system, which is currently deployed and in use for the management of HCFCD models, consists of the enterprise geodatabase and workbench components along with partial versions of the internal and external web portals. These tools provide HCFCD staff with the ability to review model requests and quickly bundle the resultant models and supporting data for distribution; track the status of a study generated by a model request; coordinate notification of potentially impacted parties and accept submitted models from end users. Key among this functionality is the component for coordination of notification. This component will automatically generate notifications for studies impacted by the contemporaneous permitting issue. Notifications will be generated for many events. Some examples are a) when a new model request is received that indicates the need for a LOMR, b) when a study that includes a CLOMR or LOMR is submitted to and accepted by HCFCD, and c) when a CLOMR or LOMR has been approved by FEMA. The M3 workbench will allow HCFCD staff the opportunity to review the default notification and either add additional information or send the notification in its default form. The default notification includes a map showing the location of the requestor's study along with the locations of the other study or studies that may impact the models for the requested stream, the study identifiers and basic information about these other studies and HCFCD staff contact information for coordination with the parties involved with the other studies. An example of the workbench interface is shown in Figure 3. The timeline chart in this figure shows the active requests for the selected river. We can see from the chart that there are several contemporaneous requests, each of which may lead to a permit application.

In addition to the coordination and notification features of the M3, version 1.0 of the system provides a number of additional tools that will help HCFCD staff manage, distribute, and maintain the effective set of floodplain models. The workbench allows HCFCD staff to quickly review model requests generated by the external web portal, add or delete models from the default set of models identified by the system and efficiently bundled the models, and associated support data for distribution through the FTP site. The system allows HCFCD staff to track and update the status of studies, modify the submittal and review dates initially generated for studies, and graphically visualize the status of studies. The system also will flag requests that require HCFCD attention for processing or review.

Version 2.0 of the M3 system will provide a number of additional capabilities that will facilitate the review of submitted studies, allow internal users to access and retrieve both the FEMA effective model set and other legacy models that will be incorporated into the directory structure, add additional notification and coordination functionality, facilitate the management of studies and associated models through the full review process including review and acceptance of FEMA CLOMRs and

LOMRs, and add other miscellaneous functionality. Version 2.0 of the system is currently under development and will add this and other functionality over the next year.

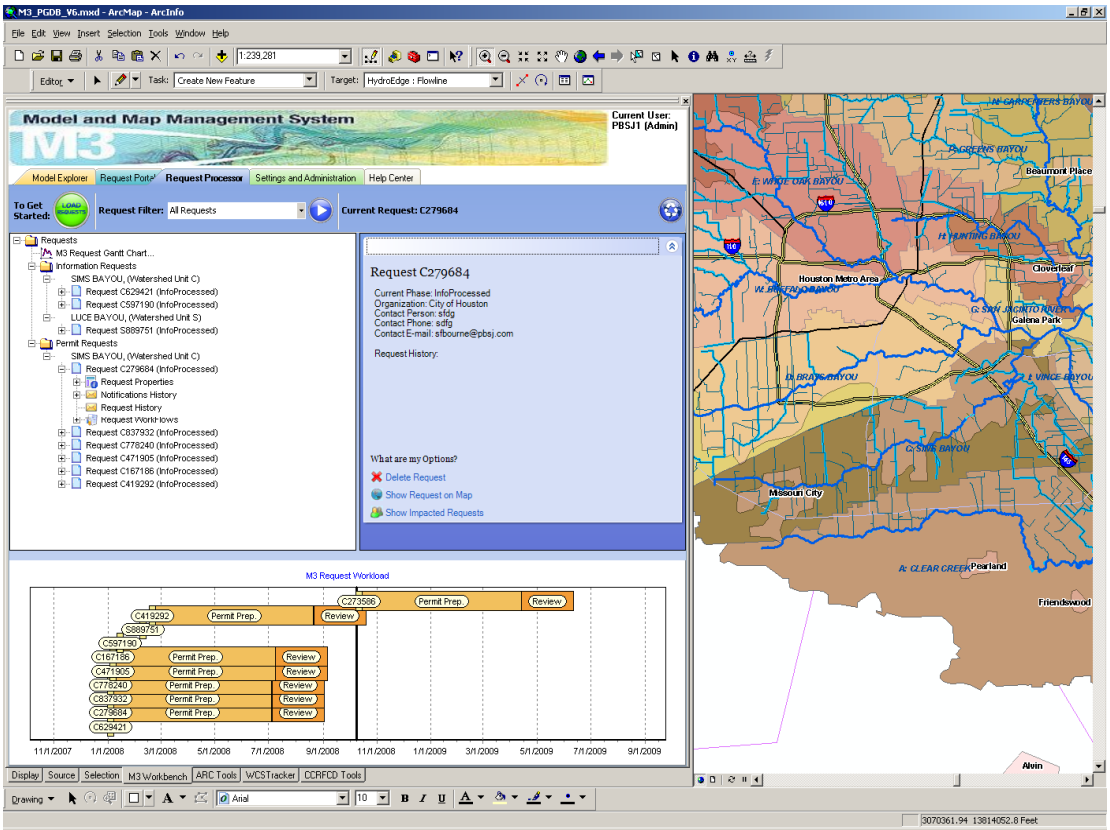

Figure 3. M3 Request Processor Interface

CONCLUSIONS

The ultimate goal of the model management program is to serve the residents of Harris County by ensuring that the models used to address floodplain permitting issues are as up-to-date, consistent, and accurate as possible. It will also serve to protect and enhance the significant investments made in the models developed for Harris County. These models will continue to evolve, as managed by the M3 system, to reflect the current conditions within the various watersheds. This approach suggests an obvious synergy with the FEMA LOMC process. HCFCD has initiated discussion with FEMA to become the "custodian" of the effective models for Harris County. This role could ultimately include the centralization of the LOMC process with the HCFCD as part of their existing Cooperating Technical Partnership Agreement (CTP). Such a partnership with FEMA should help to ensure better communication between the various entities within Harris County and more efficient update and distribution of hydrologic and hydraulic models.

Hydrologic Footprint Residence: A New Metric to Assess Hydrological Alterations Due to Urbanization

M. H. Giacomoni[1] and E. M. Zechman[2]

[1]MsC – Graduate Research Assistant, Environmental and Water Resources Engineering, Zachry Department of Civil Engineering, Texas A&M University, 205-R Wisenbaker Engineering Research Center, 3136 TAMU, College Station, TX 77843-3136; PH (979) 587-0684; FAX (979) 862-1542; ghmarcio@tamu.edu.

[2]Ph.D.- Assistant Professor, Environmental and Water Resources Engineering, Zachry Department of Civil Engineering, Texas A&M University, 205-M Wisenbaker Engineering Research Center, 3136 TAMU, College Station, TX 77843-3136; PH (979) 845-2875; FAX: (979) 862-1542; ezechman@civil.tamu.edu.

ABSTRACT

Urbanization modifies hydrological processes in a watershed as surface alterations, such as the use of impervious cover, increase runoff volumes and modify the temporal patterns of the hydrograph. Higher peak flows and increased flood duration often lead to erosion and degradation of ecosystems. Typically, the peak flow for a design storm is used to assess the impact of land use change on the hydrological cycle. This approach, however, does not capture the extent of hydrologic change and impact on downstream communities. Floodplains have an important function in controlling downstream floods and sustaining sensitive ecosystems. This research proposes a new metric to quantify the effects of development based on the change in floodplain areas. The Hydrologic Footprint Residence (HFR) is proposed to evaluate the modification of floodplain areas and duration of a flood's residence. HFR can be used to analyze hydrological changes, gauge riparian ecosystem health, and develop watershed management plans. The use of HFR is demonstrated for a case study located on the Texas A&M University campus to evaluate the hydrologic impact of watershed development.

Keywords: hydrologic sustainability, floodplain modeling, urbanization, watershed management.

INTRODUCTION

Many regions in the world suffer with the impacts of change in land use and land cover. For example, urbanization converts natural cover, such as forest and grassland to urban areas. Urbanization transforms the landscape through the construction of roads, sidewalks, buildings and parking lots, which directly impact the hydrologic cycle. Increased impervious areas result in higher volumes of runoff, higher and faster peak flows, and more frequent and severe floods. In dry periods, increased imperviousness results in a deficit of groundwater recharge, lowering the base flow (EPA 1993, Bertrand-Krajewski et al. 2000, Tang et al. 2005). These impacts directly affect humans and ecosystems communities, which according with Richter et al. (1996) are directly dependent on the duration, frequency, and magnitude

of high and low flows. Human communities may experience extreme water shortages during dry weather, loss of property due to increased flooding, and loss of water supply due to poor water quality (EPA 2004). Management of increased stormwater runoff volumes is needed that will prevent degradation of the natural hydrologic flow regime and enable a balance among economic prosperity, environmental responsibility, and social fairness.

Development can be planned to maintain pre-development hydrologic flow characteristics through low impact development (LID) or Best Management Practices (BMPs), which are a set of techniques, measures, or structural controls that mitigate the volume of stormwater runoff and improve the quality of stormwater runoff (EPA 2004). BMPs that are designed to reduce alterations in runoff volumes, such as detention ponds, are typically designed based on a peak flow value, where the discharge for a certain frequency does not exceed pre-development conditions. Typical flow-based criteria, however, do not provide a comprehensive measure of the downstream impact of development, as urbanization changes both the inundated area of a floodplain and the duration of a flood. For example, the placement of a detention pond will sustain high flows for long periods of time, potentially causing a dramatic shift in the health of the in-stream ecosystem. A peak flow-based metric does not capture the extent of alteration in the hydrologic flow regime. A metric that better represents the extent of hydrologic change and the impact on downstream communities is needed to facilitate a sense of ownership of the impact of urbanization on downstream communities.

The objective of this work is to present a hydrologic sustainability metric to better quantify the impact of urbanization on downstream water bodies. The Hydrological Footprint Residence (HFR) is designed to capture both temporal and spatial hydrological changes due to urbanization by calculating the inundated areas and the duration of a flood.

HYDROLOGICAL FOOTPRINT RESIDENCE

Consider a flood that passes through a river reach in a hypothetical watershed (Fig. 1). At each time step, the flowrate in the channel is based on the rainfall-runoff relationship that governs the watershed response. The quantity of flow in the channel inundates a corresponding area of land, as specified by the elevation of the water surface and the geometry of the channel and floodplain, and the time series of inundated land is plotted similar to the hydrograph. The extent of flooding in the reach due to the specific rainfall event can be evaluated as the area under the inundated land curve, which represents the amount of land that was inundated and the duration of the time that each unit of land was inundated. The area under the inundated land time series curve is termed the Hydrological Footprint Residence (HFR).

ILLUSTRATIVE CASE STUDY

The HFR is simulated for an illustrative watershed for a set of design rainfall events. The selected case study is the west campus watershed of Texas A&M University (TAMU). The campus straddles two watersheds, with a portion of the campus drainage traveling southeast through Wolf Pen Creek towards the Navasota

River. The west campus area drains southwest through White Creek toward the Brazos River (Fig. 2). Due to increasing development, storm water runoff discharged to White Creek has steadily increased. The creek has undergone a transformation from a small and slow moving creek to a large creek that moves large amounts of storm water during typical rainfall events, and erosion has undermined the creek bank at several critical locations.

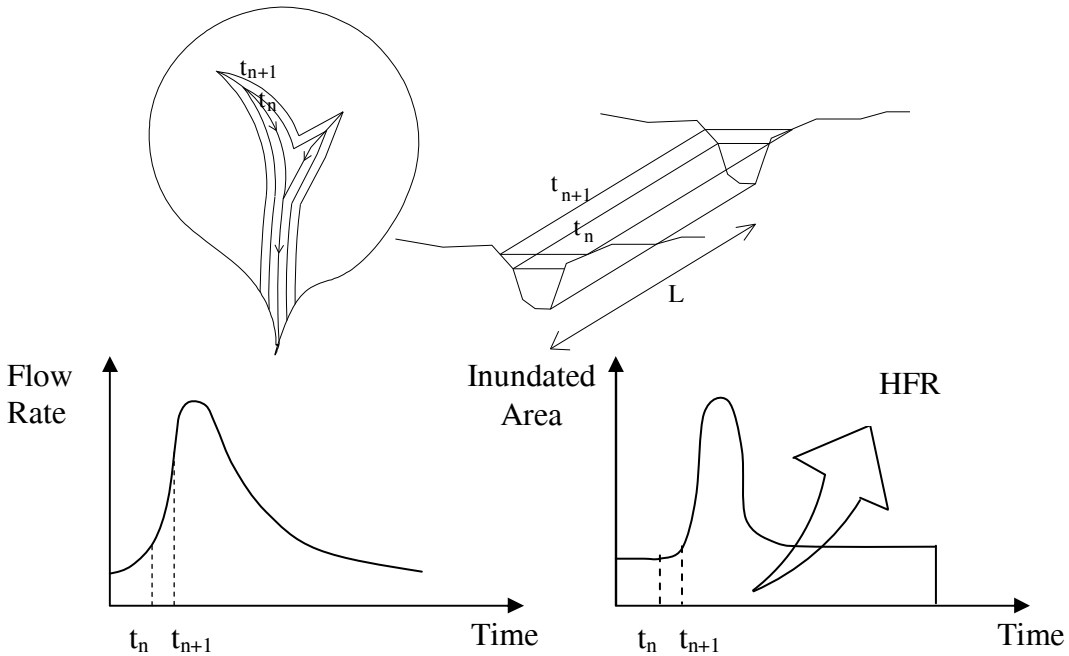

Figure 1. Illustrative calculation of HFR in a hypothetical watershed.

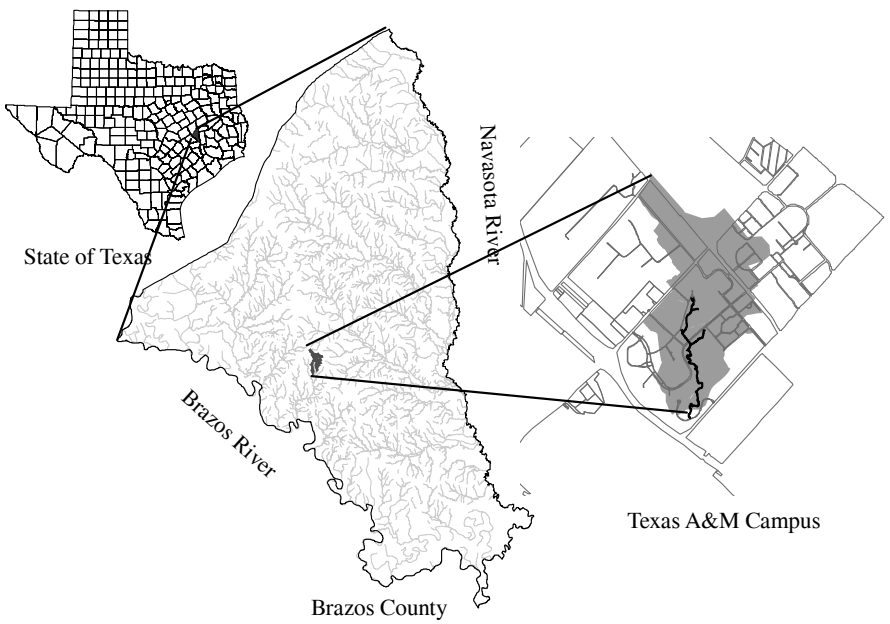

Figure 2. Location of Texas A&M West Campus

A hydrological and hydraulic model of West Campus has been developed to study the increased flows and corresponding erosion issues (AECOM 2008). The hydrological model, implemented within HEC-HMS (Army Corps of Engineering 2006), is used to convert the rainfall into overland runoff, and the hydraulic model Stormwater Management Model (SWMM) (EPA 2008), to route the runoff in the drainage network and open channels.

The main watershed of the West Campus covers 3.18 km² and discharges into Tributary D (Fig. 3). The percent of imperviousness of the watershed is approximately 40.7 %, and for the main cover type of the watershed, landscaped areas, the curve number is 77, according to the Bryan/College Station Unified Stormwater Design Guidelines (Bryan/College Station 2007). The drainage network in the watershed is composed of 442 segments, classified as round, box, elliptical storm sewer and open channel. The length of the open channel section of Tributary D is approximately 2 km.

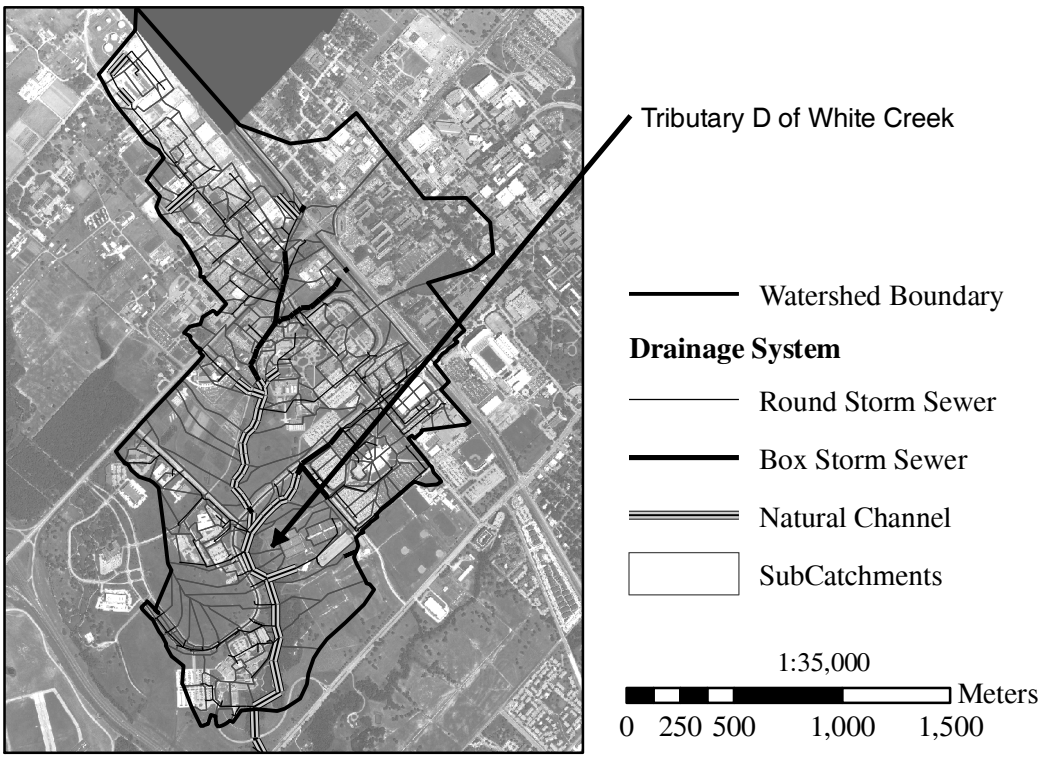

Figure 3. Watershed D located on TAMU West Campus.

PRELIMINARY RESULTS

To simulate the HFR for a rainfall event, the hydrograph and time series of depth of flow were simulated using the HEC-HMS/SWMM modeling framework. The time series of inundated area was calculated for each of the 26 reaches in Tributary D (Fig. 4), based on the geometry of the reach and the depth at each time step. For each reach, the HFR was calculated as the area under the inundated land curve, and the composite HFR for the total watershed is the sum of the incremental HFR values.

HFR was simulated for three 24-hour rainstorm events, corresponding to 2, 10 and 100-year return periods. The accumulated depths of these design storms are 112.3, 189 and 288.3 mm, respectively. Each rainstorm was modeled using the Type III SCS distribution, which simulates the highest intensity rainfall at 50% of the rainfall duration.



Figure 4. Twenty-six reaches of Tributary D.

The simulation results for the three storms are shown in Table 1. The total runoff generated by the simulation was 74.5, 142.2 and 240.4 mm, respectively. The peak flows computed for the last reach of the watershed were 28.3, 61.3 and 93.7 m³/s. The three hydrographs at the outlet of Watershed D are shown in Fig. 5.

Table 1. Simulation results for 2, 10 and 100 years - 24 hours storms.

Storm	Precipitation	Run Off	Peak Flow	HFR
(24 hours)	(mm)	(mm)	(m3/s)	(m² x hours)
2 yr	112.3	74.5	28.3	196141
10 yr	189.0	142.2	61.3	258060
100 yr	288.3	240.4	93.7	330691

The values of HFR calculated using the described approach are 198141, 258060 and 330691 m².hours. Figure **Figure** 6 presents the time series of the inundated area for the entire reach.

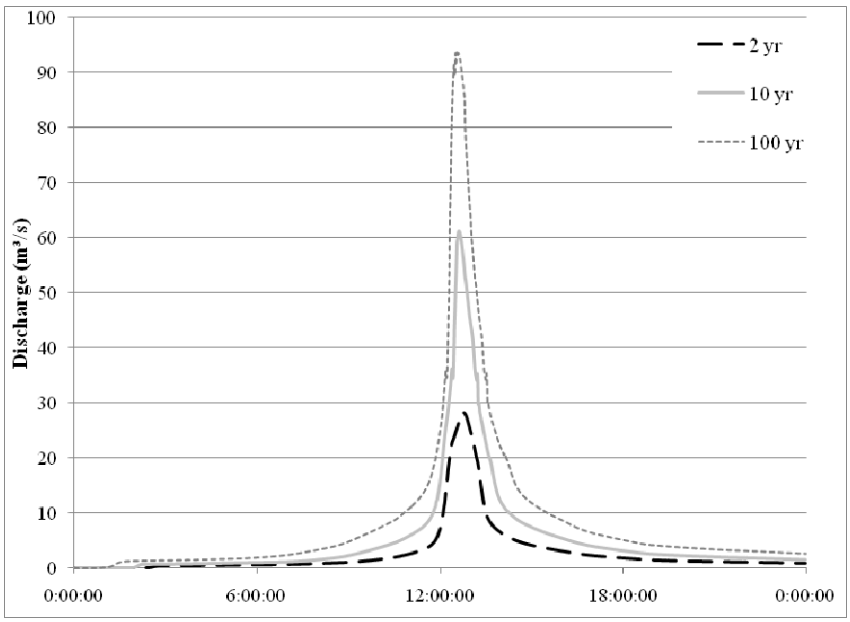

Figure 5. Hydrographs at the outlet of Watershed D for three design storms.

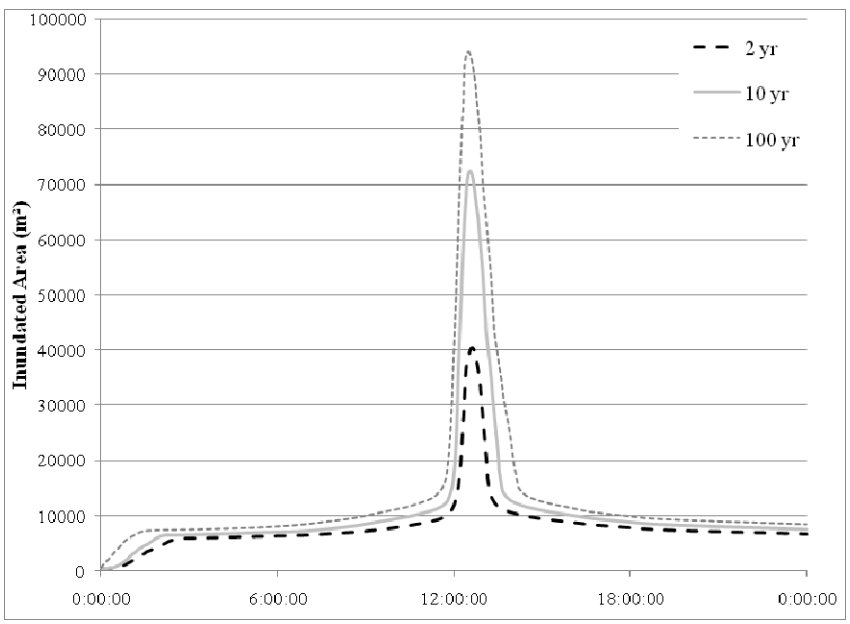

Figure 6. Inundated areas at all reaches in Tributary D for three design storms.

ON-GOING INVESTIGATIONS

The HFR is presented here as a new metric that is designed to assess the hydrological alteration of a receiving water body due to urbanization and development. Calculation of the HFR was demonstrated for a watershed on TAMU West Campus using a hydrological and hydraulic model for three design storms.

Future investigations will assess the use of HFR to compare watershed management and development scenarios. Further development of campus, best management practices and LID strategies will be simulated and evaluated by comparing HFR values to those for pre-development conditions.

ACKNOWLEDGEMENT

Although the research described in this article has been funded wholly or in part by the United States Environmental Protection Agency through Grant #SU833944, it has not been subjected to the Agency's required peer and policy review and therefore does not necessarily reflect the views of the Agency and no official endorsement should be inferred.

The authors express their thanks and appreciation to the Texas A&M Physical Plant, Engineering Design Services (TAMU PP/EDS), College Station, Texas, Gary Struzick of Klotz Associates, and Anthony Holder of Turner, Collie and Braden, both of Houston, Texas for their help and sharing of valuable storm water, rainfall, survey, and data base information. This additional information was gathered in a separate project funded by Texas A&M Utilities, College Station, Texas and managed by TAMU PP/EDS.

REFERENCES

AECOM (2008). West Campus Storm Drainage Modeling. College Station, Texas A&M University: 67.

Bertrand-Krajevski, J.-L., Barraud, S., and Chocat, B. (2000). Need for improved methodologies and measurements for sustainable management of urban water systems, Environmental Impact Assessment Rev., 20, 323-331.

Bryan/College Station (2007). Unified Stormwater Design Guidelines. www.bcsunited.net/2007_Files/Design_Manual/Streets_2007.pdf> (Dec. 20, 2008).

Richter, B. D., J. V. Baumgartner, et al. (1996). "A Method for Assessing Hydrologic Alteration within Ecosystems." Conservation Biology 10(4): 1163-1174.

Tang, Z., B. Engel, K. Lim, B. Pijanowski, J. Harbor (2005). Minimizing the Impact of Urbanization on Long Term Runoff, Journal of the American Water Resources Association, 1347-1359.

Texas A&M (2004) Campus Master Plan. 12/12/07 http://www.tamu.edu/campusplan/final_report.html > (Dec. 12. 08)

U.S. Army Corps of Engineering (2006). Hydrologic Modeling System User's Manual, Version 3.0.

U.S. EPA (1993). Urban Runoff Pollution Prevention and Control Planning, EPA/625/R-93/004.

U.S. EPA (2004). The Use of Best Management Practices (BMPs) in Urban Watersheds, EPA/600/R-04/184.

U.S. EPA (2008). Storm Water Management Model User's Manual, Version 5.0.

Hypothesis-based flow monitoring for green solutions

Deb O'Bannon[1], F.ASCE and Erich Schmitz[2]

[1]Department of Civil and Mechanical Engineering, University of Missouri-Kansas City, 5100 Rockhill Road, Kansas City MO 64110; PH (816)235-1287; FAX (816)235-1260; email: obannond@umkc.edu
[2]TranSystems, 2400 Pershing Road, Kansas City MO 64108; PH (816)329-8656; FAX (816)329-8602; email: egschmitz@transystems.com

ABSTRACT

A demonstration project to show the efficacy of stormwater best-management practices deployed in an urban midwestern neighborhood. The large-scale demonstration depends on reliable flow monitoring to verify stormwater invention by the green solutions and reduction of flows to the combined sewer collection system. The flow monitoring includes both temporal and spatial controls.

BACKGROUND

The City of Kansas City has a combined sewer collection system in the older part of the city, approximately 56 mi^2 (145 km^2). Detailed analysis of appropriate engineering controls to reduce overflows (CSOs) were tailored to each watershed.

The Middle Blue River watershed (shown in Figure 1) was initially recommended to have two large underground detention tanks ($3.5x10^6$ gallons ($13.25x10^3$ m^3) total) from a strict, traditional engineering analysis to reduce overflows to the Blue River.

Figure 1. Middle Blue River watershed location

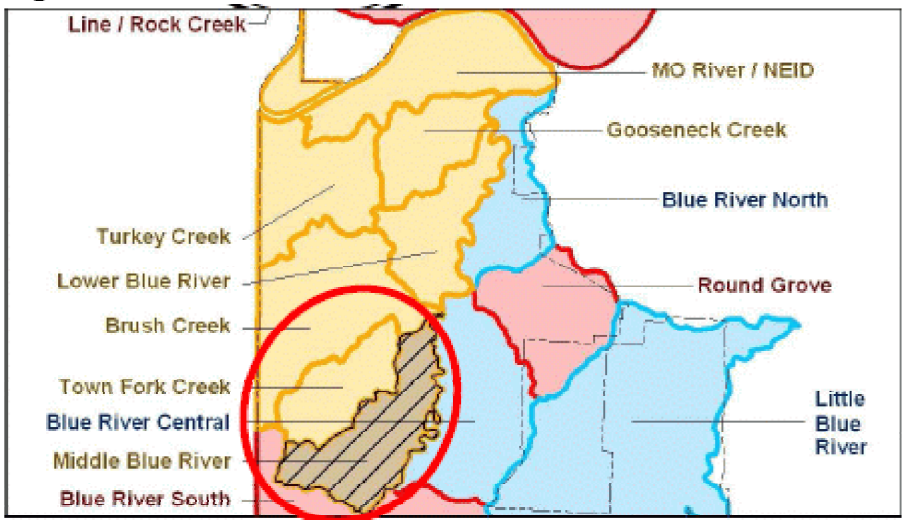

GREEN SOLUTIONS

A groundswell of interest in raingardens and other stormwater best-management practices (BMPs) happened about a year before the CSO correction plan was finalized. A combination of cost-benefit analysis and a desire include green solutions in the plan indicated an excellent candidate watershed for a significant implementation of green solutions was the Middle Blue River watershed.

The choice of the Middle Blue watershed is optimal for urban, midwestern sites for the following reasons:

- clay soils (low permeability)
- older neighborhood -- soils probably compacted
- middle-class neighborhood (no vacant/abandoned properties)
- traditional neighborhood - no raingardens or early-adoptors of progressive technologies
- 90% residential/single-family homes
- high-intensity, low-duration thunderstorm rainfalls
- mild slopes
- no public parks in demonstration area

While the study area may be optimal for demonstrating the efficacy of green solutions in reducing stormwater inflow to the combined sewer system, thereby reducing overflows, this study area presents significant placement challenges for green solution installations. Green solutions will be limited to public right-of-way along the streets.

FLOW MONITORING

A double-control flow monitoring program was evaluated to (a) establish the rainfall-runoff response in this small watershed, and (b) measure any reductions in stormwater runoff after installation of the green solutions. The flow metering was installed at four locations in September 2008, as shown in Figure 2. The temporal control data will run from September 2008 to September 2009, when construction of the green solutions will be largely complete and some interception of the stormwater will begin.

The spatial control will be monitored throughout the project life. The demonstration project area is ~100 acres (40 ha) and the control area is 86 acres (35 ha). One can observe that the control area is contiguous to the demonstration area and will receive virtually identical rainfall events.

RAINFALL MONITORING

Detailed, rainfall intensities and total daily rainfall depths will be recorded within and close to the demonstration and control areas, subject to placement constraints.

CONCLUSIONS

A carefully-designed flow monitoring program will support hypothesis-testing for green solutions performance in a combined sewer area. Control data for the flow monitoring is in both the temporal and spatial domains.

Acknowledgments

U.S. Environmental Protection Agency

Kansas City, Missouri Water Services Department

Figure 2. Middle Blue River demonstration (pink) and control (blue) project area.

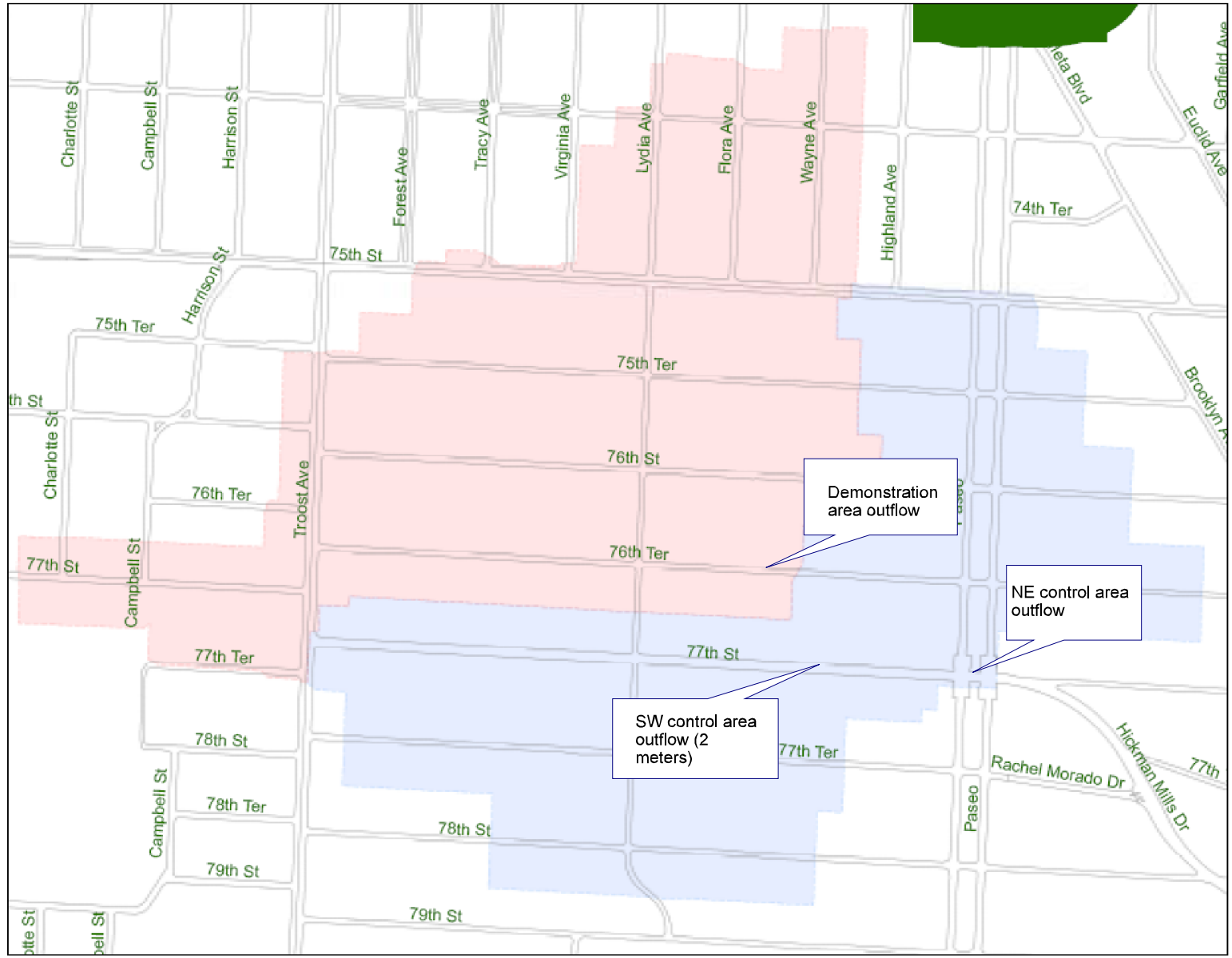

Impact of Wet-Weather Peak Flow Blending on Disinfection Performance

(To be presented at the 6th Urban Watershed Management Symposium, ASCE World Environmental & Water Resources Congress, May 17-21, 2009, Kansas City, Missouri)

Mary K. Stinson[1], Richard Field.[2], R. Boris Rukovets[3]

[1]United States Environmental Protection Agency, National Risk Management Research Laboratory, Water Supply and Water Resources Division, Urban Watershed Management Branch, 2890 Woodbridge Avenue, Edison, NJ 08837; PH (732) 321-6683; email: stinson.mary@epa.gov
[2]United States Environmental Protection Agency, National Risk Management Research Laboratory, Water Supply and Water Resources Division, Urban Watershed Management Branch, 2890 Woodbridge Avenue, Edison, NJ 08837; PH (732) 321-6674; email: field.richard@epa.gov
[3]Interstate Environmental Commission, 311 W 43rd St., Suite 201, New York, NY 10036 PH (212) 582-0380, email: brukovets@iec-nynjct.org

ABSTRACT

A U.S. EPA study evaluated the impact on disinfection during peak flows (wet-weather flow events) when a portion of the flow to the wastewater treatment plant (WWTP) bypasses secondary treatment prior to disinfection. The practice of bypassing secondary treatment during peak flows, referred to as "blending," takes place when the volume of primary treatment flow exceeds the capacity of the secondary treatment. The bypassed flow is only treated by primary clarification before it is recombined with the fully treated secondary effluent prior to disinfection. Blending practice prevents passing of excess flow to secondary treatment, which could result in inactivation and destruction of the vulnerable biological process. The trade-off is that during blending only a portion of the total flow receives full secondary treatment.

The study was conducted at three WWTPs in New York City, ranging from 60 MGD to 275 MGD capacity. A total of four dry-weather and 12 wet-weather events were sampled and analyzed. Three samples from four sampling points of the treatment train in the WWTP were collected per event. The principal analytical parameters were fecal coliform, *Enterococcus*, viruses, and protozoa. Other parameters included total residual chlorine, BOD_5 , and TSS.

The difference between wet-weather blending and dry-weather final effluent results ranged from a half order of magnitude to one order of magnitude higher at two plants for fecal coliform and at one plant for *Enterococcus.* A difference of three orders of magnitude higher, which represents a significant impact, was observed at one plant for fecal coliform and at two plants for *Enterococcus.* During blending, average effluent BOD_5 and TSS concentrations remained above 30 mg/l at two out of three plants. The third plant had average effluents above 30 mg/l for both BOD_5 and TSS; however, the plant was undergoing a partial construction at the time of sampling, which was causing lower treatability. When blending occurred, the sampled WWTPs removed, on average,

between 97% coliphage and enteric viruses, approximately 71% of *Cryptosporidium* and between 40% and 88% of *Giardia.*

A maceration procedure was used for disinfected, final effluent samples prior to analyses for fecal coliform and *Enterococcus.* Maceration exposes the occluded and clumped-together bacteria. For the majority of samples, particle maceration of effluent samples resulted in some (in most cases, less than half an order of magnitude) increase in both fecal coliform and *Enterococcus* values during both wet- and dry-weather. At one out of three plants, in each instance, maceration of effluent samples resulted in one order of magnitude increase in fecal coliform during wet-weather and *Enterococcus* during dry-weather.

KEYWORDS

Disinfection, blending, pathogens, peak-flow, wastewater treatment plant, fecal coliform

INTRODUCTION

This study evaluated the effect of wet-weather blending on the concentration of fecal coliform and *Enterococcus* indicator bacteria, protozoa, viruses, total residual chlorine, 5-day Biological Oxygen Demand (BOD_5), and Total Suspended Solids (TSS) in the treatment plant final effluent (1). The practice of bypassing secondary treatment during peak flows, referred to as "blending," takes place when the flow rate of primary treated effluent exceeds the capacity of secondary treatment. Accordingly, the bypassed flow is only treated by primary clarification before it is recombined with the treated secondary effluent prior to disinfection. Blending practice prevents passing of excess flow to secondary treatment, which could result in inactivation and destruction of the vulnerable biological process. The trade-off is that during blending only a portion of the total flow receives full secondary treatment.

The U.S. Environmental Protection Agency's (EPA's) 1994 CSO Policy (2) encourages delivery of maximum flows to the WWTPs, while ensuring that bypasses would not result in effluent water quality violations. Consistent with that principle, blending of flows at treatment plants serving combined sewer systems is economically viable provided that acceptable treatment is achieved. As a protective measure of public health, the practice of blending is much superior to the release of untreated combined sewer overflows (CSOs) and/or incidents of basement flooding.

This study was designed by the U.S. EPA's Urban Watershed Management Branch in Edison, NJ as an cooperative effort of several EPA groups (National Risk Management Research Laboratory, National Exposure Research Laboratory, Office of Policy, Economics, and Innovation, Office of Wastewater Management and Office of Science and Technology under the Office of Water, EPA's Region 2 Laboratory in Edison), and two non-EPA agencies (Interstate Environmental Commission (IEC) – a tri-state (New York, New Jersey and Connecticut) regulatory water pollution control agency and the New York City Department of Environmental Protection (NYCDEP). Under contract to

the EPA, the IEC was the main performing organization. The IEC selected the WWTPs, prepared the Quality Assurance Project Plan (QAPP), interacted with the NYCDEP, collected and distributed the samples for analyses, and reported on the results.

This study was conducted at three WWTPs in New York City, whose capacities ranged from 60 MGD to 275 MGD. The three plants selected, receive their flow from combined sewer systems. The treatment process at each of the plants, typical of all 14 NYCDEP plants, includes: coarse screening and de-gritting, preliminary treatment, primary treatment, secondary treatment, disinfection, and sludge treatment. It is important to mention that the disinfection process used at NYCDEP plants is hypo-chloride disinfection. Dechlorination is not used at NYCDEP plants.

PROJECT DESIGN

The principal element of the project design was the selection of four sampling points (SPs) along the WWTP's treatment train. (Figure1). The sampling locations were: SP1 at entrance of flow to plant, SP2 after primary treatment, SP 3 after secondary treatment and point of blending, and SP 4 after disinfection. SP4 was the critical sampling location, as it was the final plant effluent for release to the receiving waters, where the apparent impact of blending could be measured. Figure 1 also shows the schematic of the blending practice during peak flow wet-weather which typically happens at NYCDEP plants after the influent flow exceeds one and a half times the permit flow limit for the plant.

Another important part of project design was an ample sampling period that included a total of four dry-weather and 12 wet-weather events. For bacterial sampling, three samples from each sampling of the four sampling points shown in Figure 1 were collected per event. The study had a generous selection of pathogens in addition to conventional pollutants to be evaluated in the disinfected effluent generated from both wet- and dry-weather events. Analyses of protozoa and viruses are not routinely done at the WWTP but were done in this study.

Figure 1. WWTP Wet-Weather Blended And Dry-Weather Non-Blended Sampling Locations

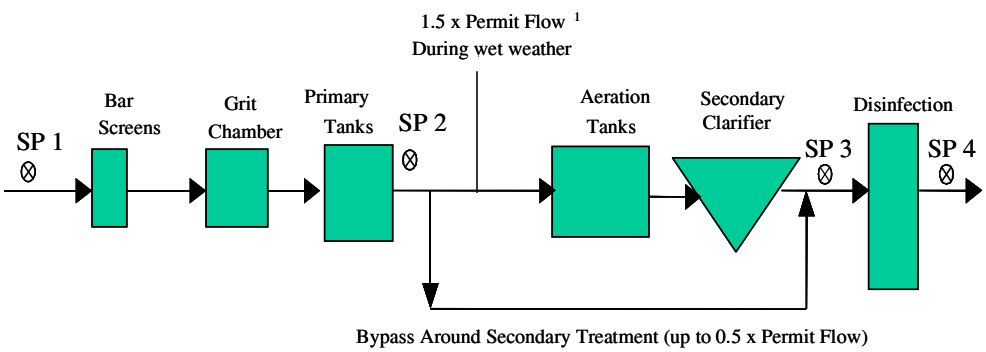

Notes:

(1) Permit Flow = 12 Month Rolling Average Flow

(2) SP1, SP 2, SP3, SP4 – IEC Sampling Location

Bacteria Sampling, Analyses, and Maceration Procedure

During each sampling event, three grab influent samples each were collected at SP1 (prior to any treatment), at SP2 (primary effluent), at SP3 (prior to chlorine contact tank), and SP4 (post chlorination). The samples were analyzed for fecal coliform and *Enterococcus* using the most probable number (MPN) method. There were a total of five sampling events per plant with at least one dry-weather (non-blending) event and four wet-weather (blending) events. During wet-weather events, all samples were collected at peak flows, after plants started bypassing secondary treatment. The dry-weather event was used for comparison purposes.

A maceration procedure was conducted for a limited number of bacteria analyses. Maceration exposes the particle-associated and occluded, and clumped together bacteria and achieves a thorough enumeration. The study consisted of two parts: maceration optimization and maceration of final effluent samples (SP4) to determine if maceration had any impact on results. The maceration optimization procedure was conducted during one wet-weather blending event and one dry-weather non-blending event at one of the WWTPs to determine the optimum speed (revolutions per minute (rpm)) and time (seconds) of the multi-speed (3,500-22,000 rpm) laboratory blender that was used for maceration of effluent samples during the subsequent wet- and dry-weather runs. Upon completion of the maceration optimization - achieved at speed of 22,000 rpm and time of 60 seconds - 36 dry-weather and 36 wet-weather macerated analyses were performed for fecal coliform and for *Enterococcus.* Each of the three final effluent samples involved in the experiment was analyzed as a regular unmacerated sample for comparison purposes. The macerated samples showed higher concentrations of bacteria.

Protozoa, Virus, and Coliphage Sampling and Analyses

At two of the Plants (selection of two Plants instead of three Plants was due to the budgetary constraints), four sampling events - three during wet-weather blending and one during dry weather - were conducted for protozoa (*Giardia* and *Cryptosporidium*), viruses (adenovirus, astrovirus, enterovirus, reovirus, rotavirus, norovirus and Hepatitis A (HAV), and coliphage (male-specific and somatic). Each sampling event at a Plant was comprised of ten grab samples for protozoa analyses and ten grab samples for viral analyses. The protozoan and viral sampling consisted of three grab influent (SP1, prior to any treatment), one grab primary effluent (SP2), three grab pre-chlorinated effluent (SP3, prior to chlorine contact tank) and three grab effluent (SP4, post chlorination) samples collected at 45-minute intervals.

For the protozoan portion of the study, *Giardia* and *Cryptosporidium* were detected and enumerated using EPA Method 1623 (3). Since this method provides for quantification of *Giardia* and *Cryptosporidium*, but does not determine viability or infectivity, ten split samples per plant were sent for infectivity analyses for *Cryptosporidium* using a published method with some modification (4 & 5). Following infectivity determination, molecular confirmation of the genotype was ascertained by PCR analysis for all samples, except for the positive control (6). For the virus portion of the study, ten samples per plant were submitted to quantitative analyses using EPA ICR Methodology (3). In addition, analyses for the detection and quantification of male-specific and somatic

coliphage were performed on all samples using a soft agar overlay procedure. The EPA report from the study provides a complete list of references for all of the above methods. (1).

RESULTS

Bacteria

For both fecal coliform and *Enterococcus* concentrations in the disinfected final effluent during wet-weather blending were higher than the corresponding dry-weather non-blending concentrations. For both fecal coliform and *Enterococcus* at Plant 3 and for fecal coliform at Plant 1, the concentrations of wet-weather blending and dry-weather non-blending effluent were between a half and one order of magnitude higher. Disinfected effluent fecal coliform and *Enterococcus* concentrations were significantly higher (three orders of magnitude) during wet-weather blending versus dry-weather non-blending for both parameters at Plant 2 and for *Enterococcus* at Plant 1 (Table 1). In addition, the order of magnitude reduction between influent and effluent ("kill") was at least two orders of magnitude higher in most (five out of six) cases at all three plants during dry-weather non-blending as compared to wet-weather blending (Table 1).

Table 1. Fecal Coliform and *Enterococcus* Concentrations

Plant	Average Flow (MGD)	Operating Mode	Fecal Coliform –Geometric Mean (MPN/100ml)			*Enterococcus* –Geometric Mean (MPN/100ml)		
			Influent	Effluent	Order of Magnitude Reduction	Influent	Effluent	Order of Magnitude Reduction
Plant 1	239	Wet Blending	4,200,000	4,900	10^3	890,000	17,000	10
	122	Dry	19,000,000	890	10^5	470,000	20	10^4
Plant 2	125	Wet Blending	1,100,000	19,000	10^2	260,000	14,000	10
	31	Dry	5,000,000	16	10^5	220,000	3	10^5
Plant 3	469	Wet Blending	1,600,000	520	10^4	280,000	870	10^3
	238.5	Dry	5,600,000	31	10^5	1,700,000	120	10^4

Graphic representation of fecal coliform and *Enterococcus* concentrations, during dry-weather non-blending and wet-weather blending is shown in Figures 2 and 3 below.

Figure 2. Fecal Coliform Concentrations at All Three Plants

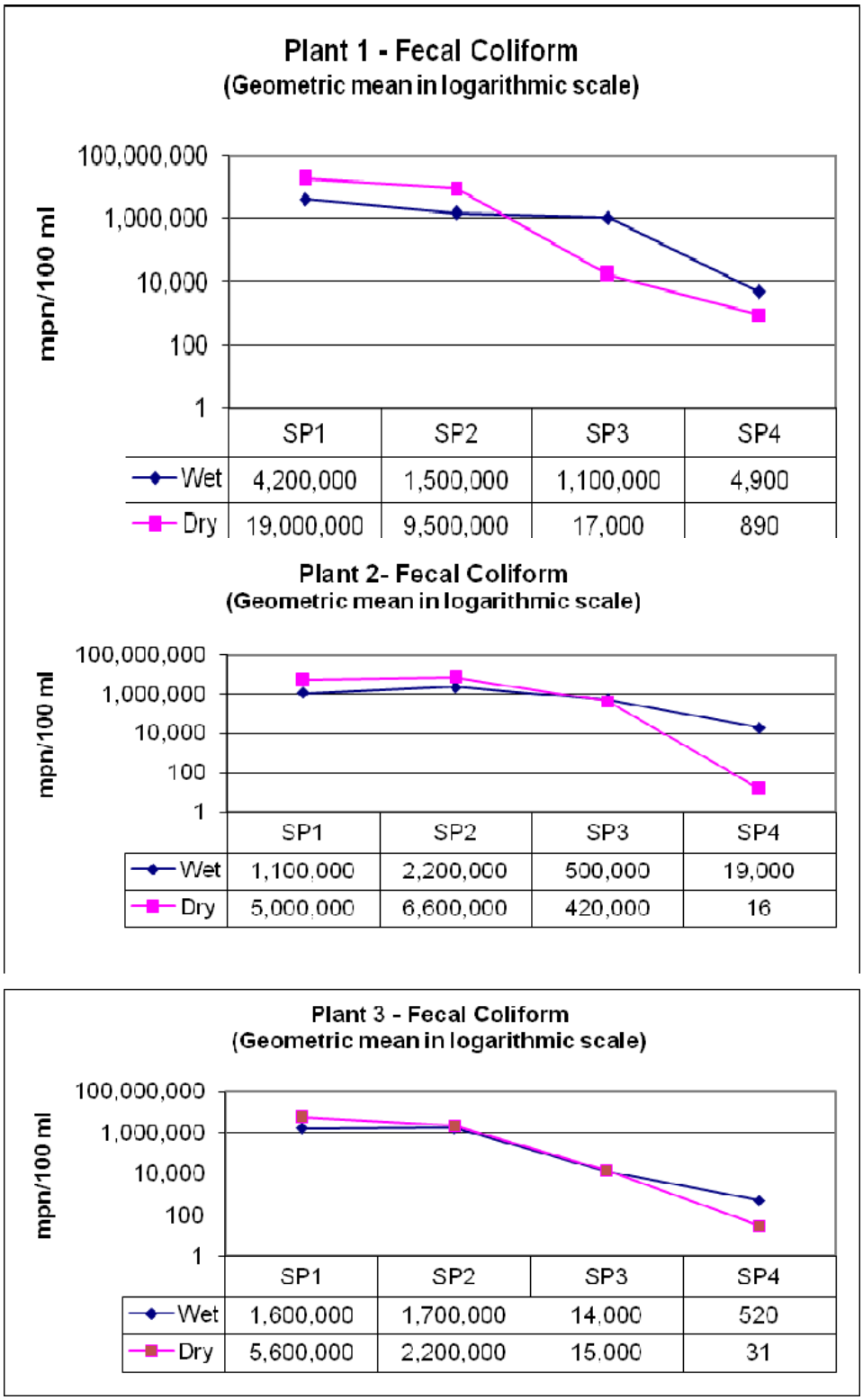

Figure 3. *Enterococcus* Concentrations at All Three Plants

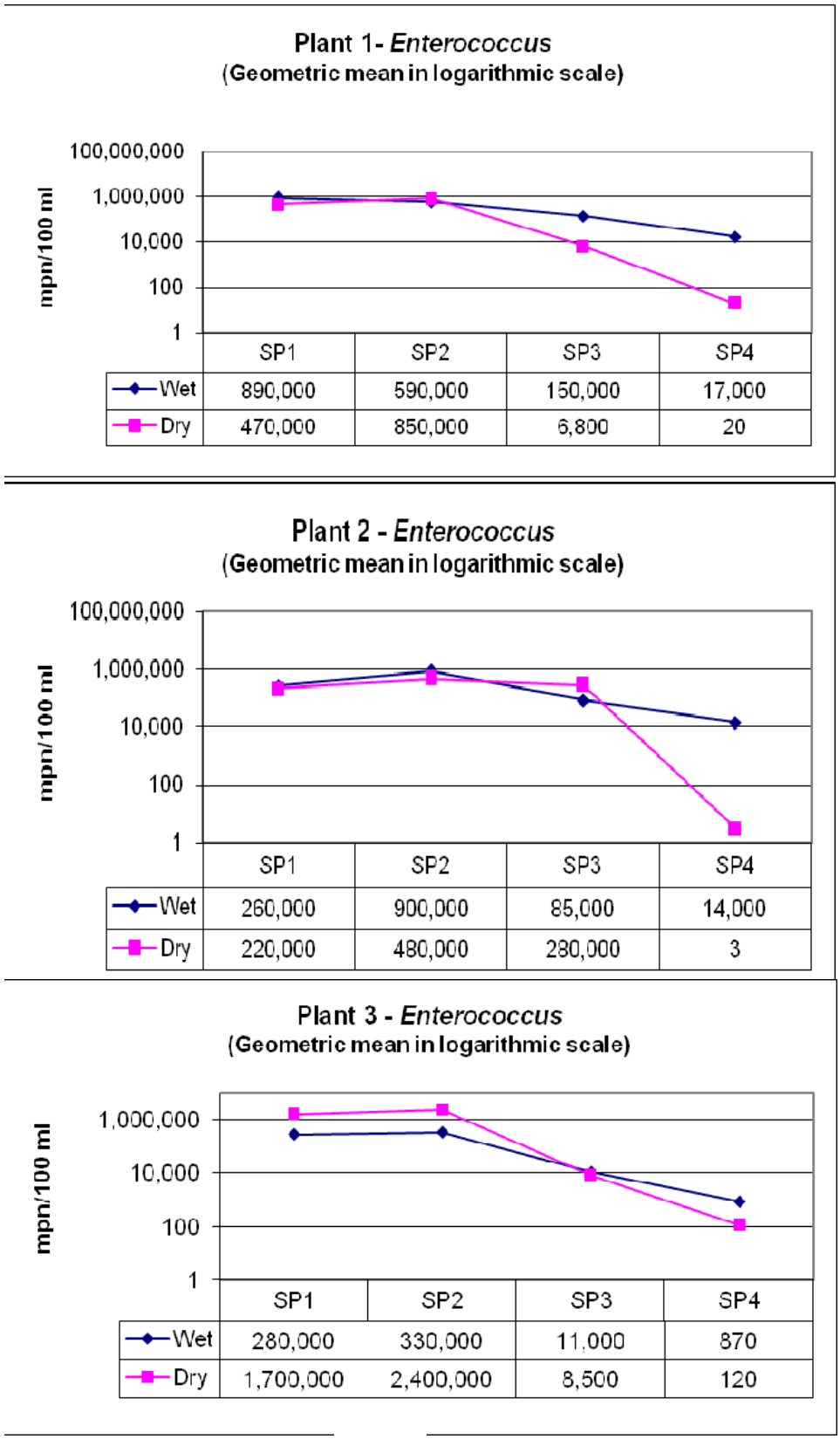

Protozoa

Effluent concentrations of *Cryptosporidium* parvum were higher during wet-weather blending at one plant (Plant 1) when compared to dry weather non-blending. The *Crypotosporidium* parvum effluent concentrations during wet-weather were low, mostly in single or low double digits, with average percent removal of 71% at Plant 1. Average percent removal for Plant 2 could not be estimated, since less than three detectable results were reported (Table 2 and Figure 4).

Infectious *Cryptosporidium* parvum concentrations at both plants were mostly low or non-detectable. Only two out of nineteen infectious *Cryptosporidium* parvum effluent samples showed a detectable value; only one of these two samples showed the presence of *C. Parvum* Genotype II.

Effluent concentrations of *Giardia* were one order of magnitude higher during wet-weather blending versus dry weather non-blending at both Plant 1 and Plant 2. The geometric mean of *Giardia* effluent results during wet weather were at in low triple digits, with 88% removal, at Plant 1 and with 40% removal, at Plant 2. (Table 2 and Figure 5).

Table 2. Range of Final Effluent Concentrations for Protozoa

Plant	Operating Mode	*Giardia* cysts/ L (enumerated values)		*Cryptosporidium* oocysts/ L (enumerated values)		Infectious *Cryptosporidium* *MPN/L*	
		Range	Geometric Mean	Range	Geometric Mean	Range	Geometric Mean
Plant 1	Dry	6 – 21	12	1 – 8	2	<0.2	NA
	Wet Blending	40 – 720	148	<0.2 – 52	8	<0.3 - <9.2	NA
Plant 2	Dry	2 – 4	3	2 – 4	2	<0.2	NA
	Wet Blending	7 – 720	105	<0.2 – 2	NA	<0.5 – <2.4	NA

Note: NA =Less than three detectable results were reported, hence geometric mean could not be calculated

Less than three detectable *Giardia* results were reported for the SP2 location at Plant 1 during dry weather, hence geometric mean could not be calculated. Dry-weather results for SP1 and SP2 locations at Plant 1 were affected by clogged filters and, hence, prevented the full detection of *Giardia* and *Cryptosporidium.* Therefore, dry-weather SP1 and SP2 results for Plant 1 should not be used for deriving conclusions for this study.

Figure 4. *Cryptosporidium* Concentrations

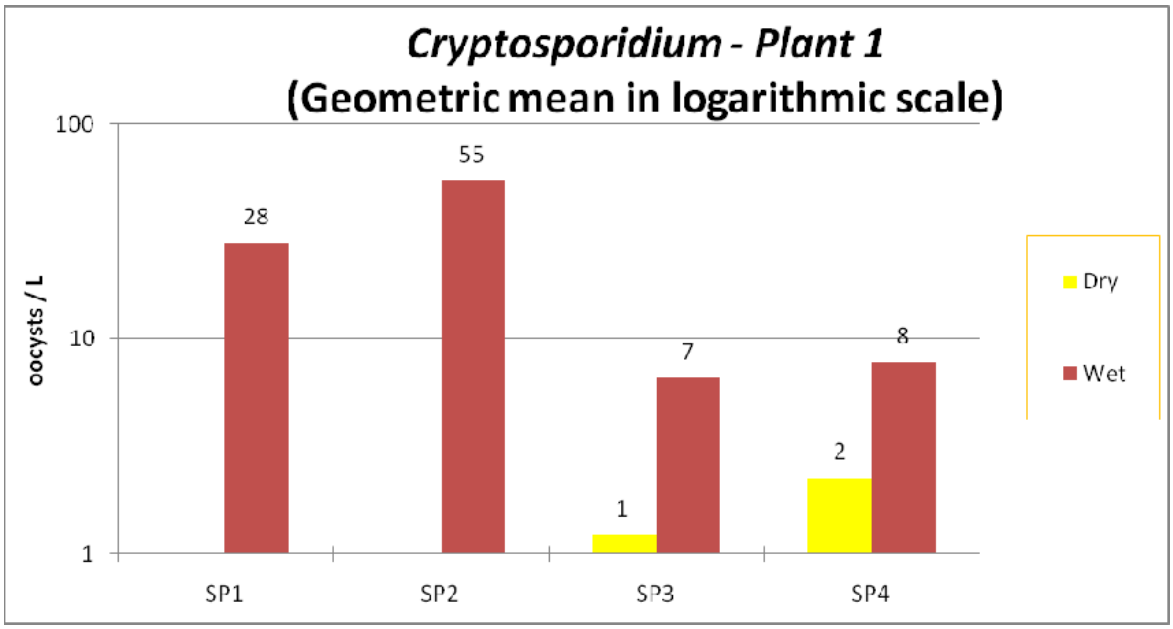

Viruses

With relatively high plant influent results during wet-weather blending, the effluent results for enteric viruses were, on average, in single digit or low double-digit infectious units/L in final effluents, with average percent removal between 98% and 99% for Plant 1 and 99% for Plant 2. (Table 3). Cell lines are human or animal cells that are grown in a laboratory and used for detection of the presence of a particular organism. In this study, four cell lines were used for detection of enteric viruses:

1. BGM – Buffalo Green Monkey cell line
2. MA-104 – derived from Rhesus monkey kidney
3. PLC/ PRF/5 – human hepatoma cell line
4. CaCo-2 – human intestinal cell line

Table 3. Average Percent Removal of Viruses during Wet Weather

Plant	% Removal of BGM	% Removal of MA-104	% Removal of PLC/PRF/5	% Removal of CaCo-2 cells
Plant 1	98%	98%	98%	99%
Plant 2	99%	99%	99%	99%

The cell lines that were used for detection of enteric viruses using ICC-PCR and/or PCR methods are shown in Table 4.

Table 4. Detection by Cell Line

Cell Line	Viruses Targeted for PCR Detection
BGM:	Enterovirus, Reovirus
MA104:	Enterovirus, Rotavirus, Reovirus
PLC/PRF/5	Adenovirus
CaCo-2	Enterovirus, Astrovirus

Table 5. Range of Final Effluent Concentrations for Viruses

Plant	Operating Mode	BGM Infectious Units/L		MA-104 Infectious Units/L		PLC/PRF/5 *Infectious Units/L*		CaCo-2 *Infectious Units/L*	
		Range	Geom. Mean	Range	Geometric Mean	Range	Geom. Mean	Range	Geom. Mean
Plant 1	Dry	1 – 3	2	1 – 5	2	2 – 5	3	<1 – 1	NA
	Wet	3 – 143	14	<2 – 393	21	9 – 32	18	1 – 34	4
Plant 2	Dry	3 – 6	5	5 – 14	8	4 - 5	5	<3 – 8	NA
	Wet	<1– 25	6	<1 – 12	4	<1- 104	11	<1 – 21	5

Coliphages

Coliphages are bacteriophages that infect *Escherichia coli* (*E. coli*). They are frequently viewed as alternate bacterial indicators, representing enteric virus contamination. Analysis of the results for the two plants, at which the coliphage samples were collected, shows that male-specific coliphage was consistently lower during wet-weather blending vs. dry-weather conditions throughout - Plant 1. At both SP3 and SP4 for Plant 2, there were no significant differences between wet-weather blending and dry-weather non-blending conditions.

Graphical representation of viruses results is shown below by each of the four cell lines (Figures 6, 7, 8, and 9).

Figure 5. ***Giardia*** **Concentrations**

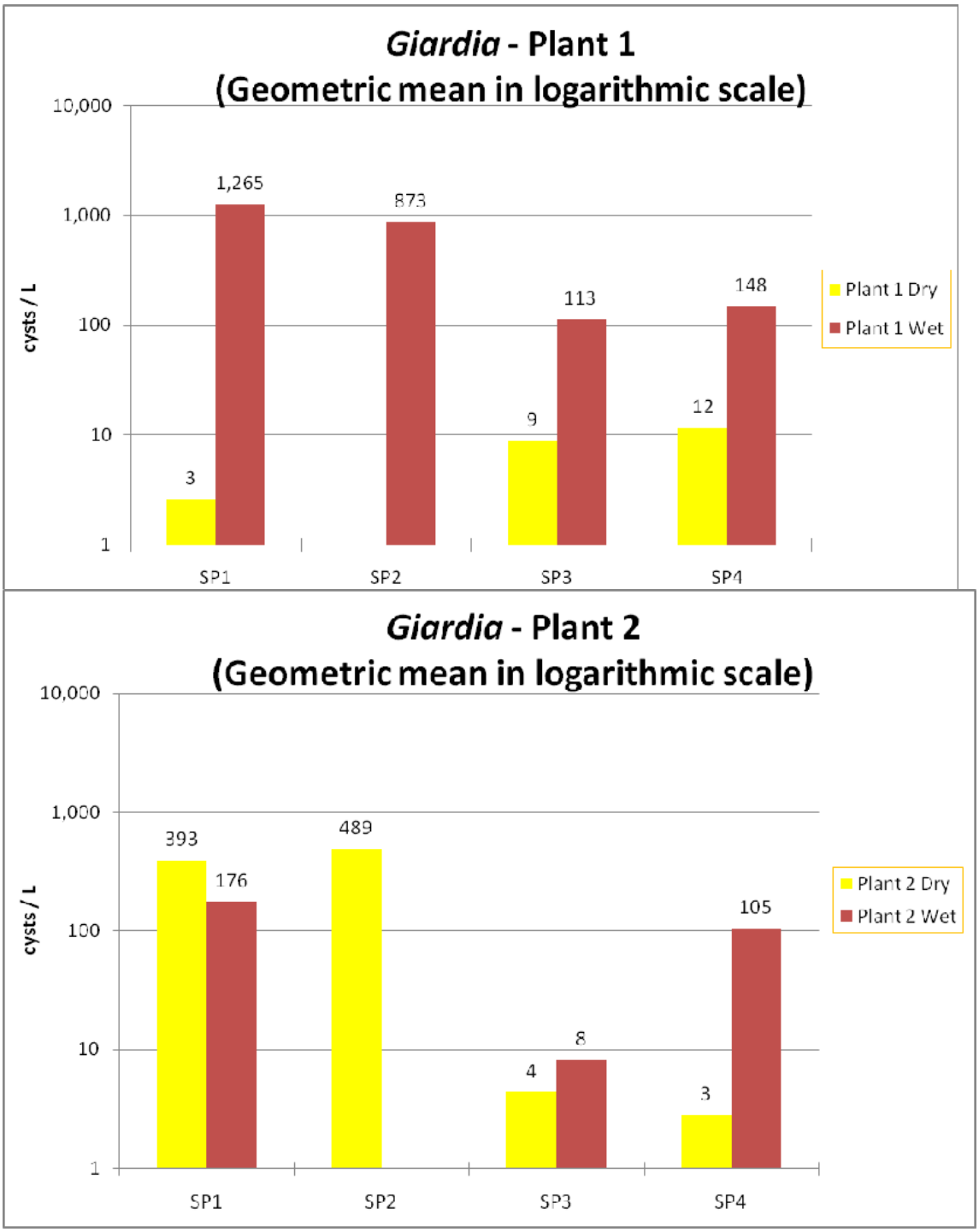

Figure 6. Buffalo Green Monkey Cell Line Viruses Concentrations

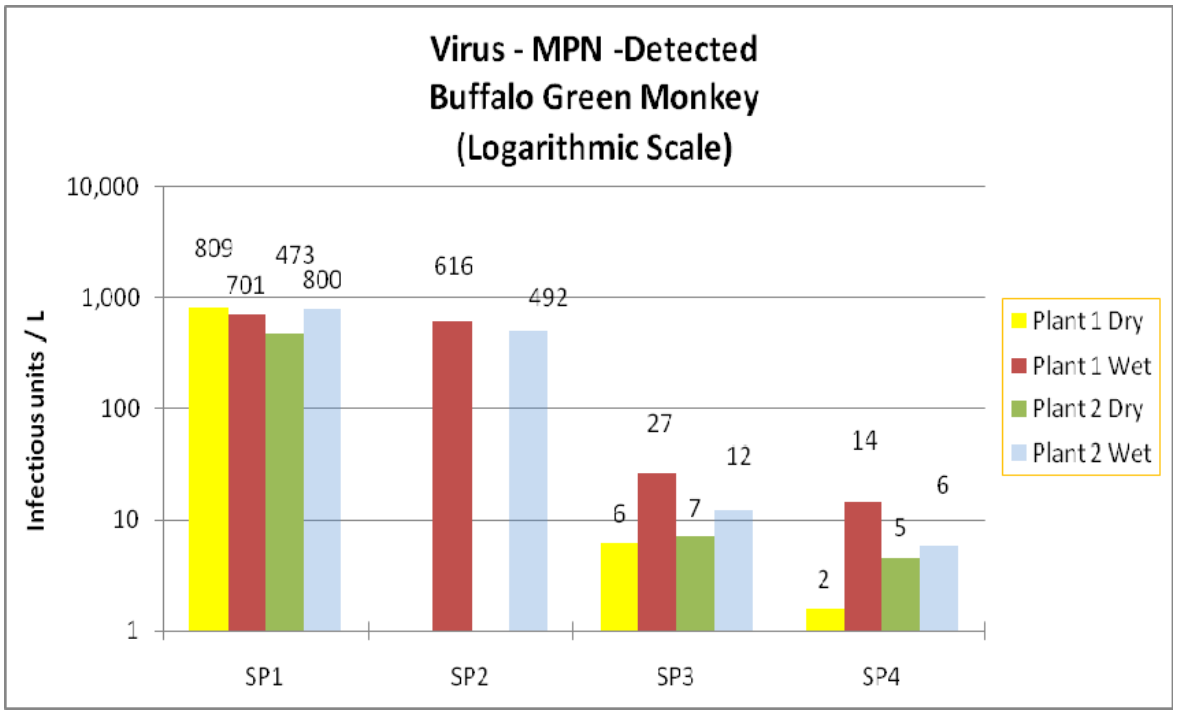

Figure 7. MA-104 Cell Line Viruses Concentrations

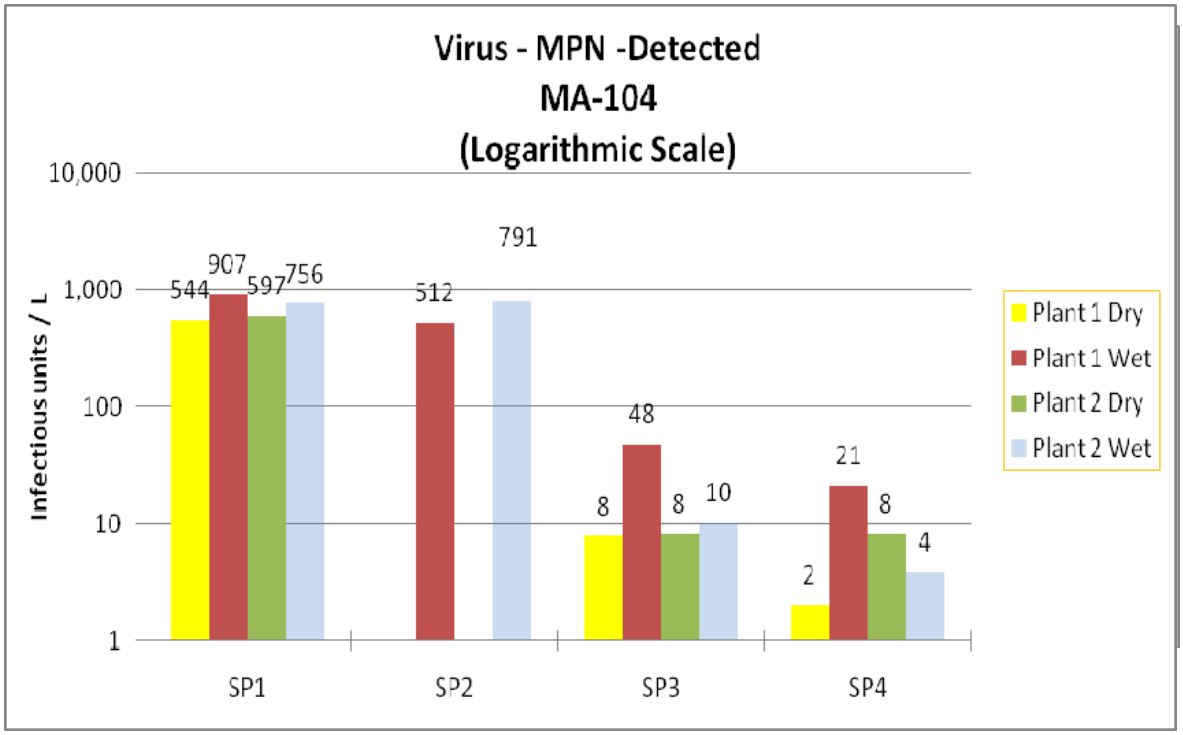

Figure 8. PLC/PRF/5 Cell Line Viruses Concentrations

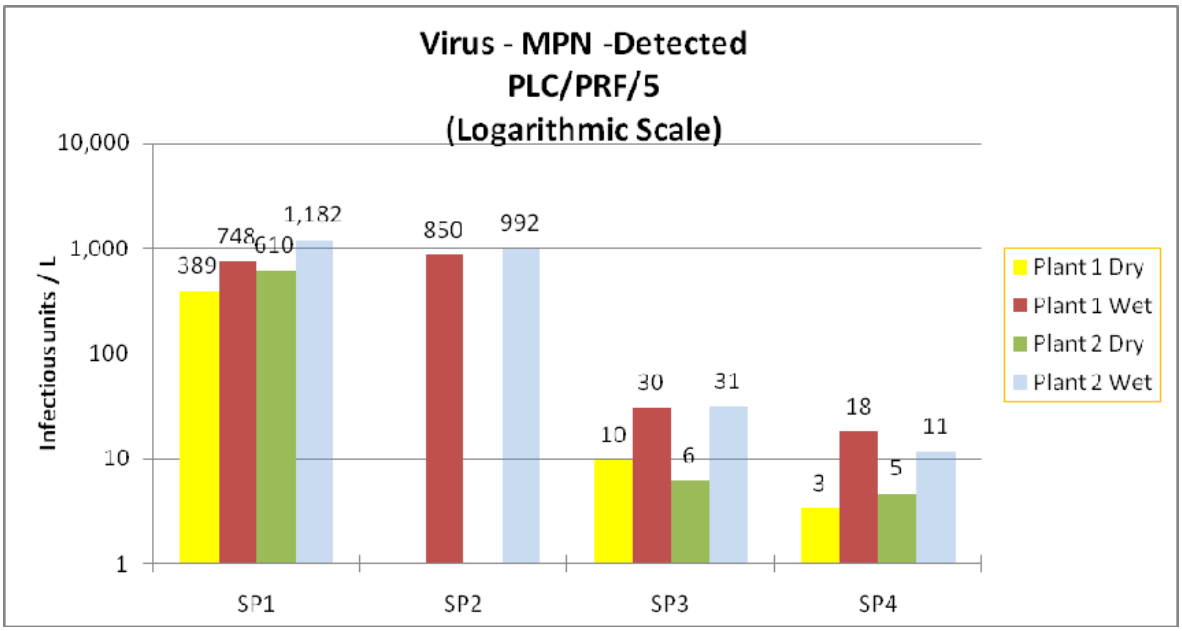

Figure 9. CaCo-2 Cell Line Viruses Concentrations

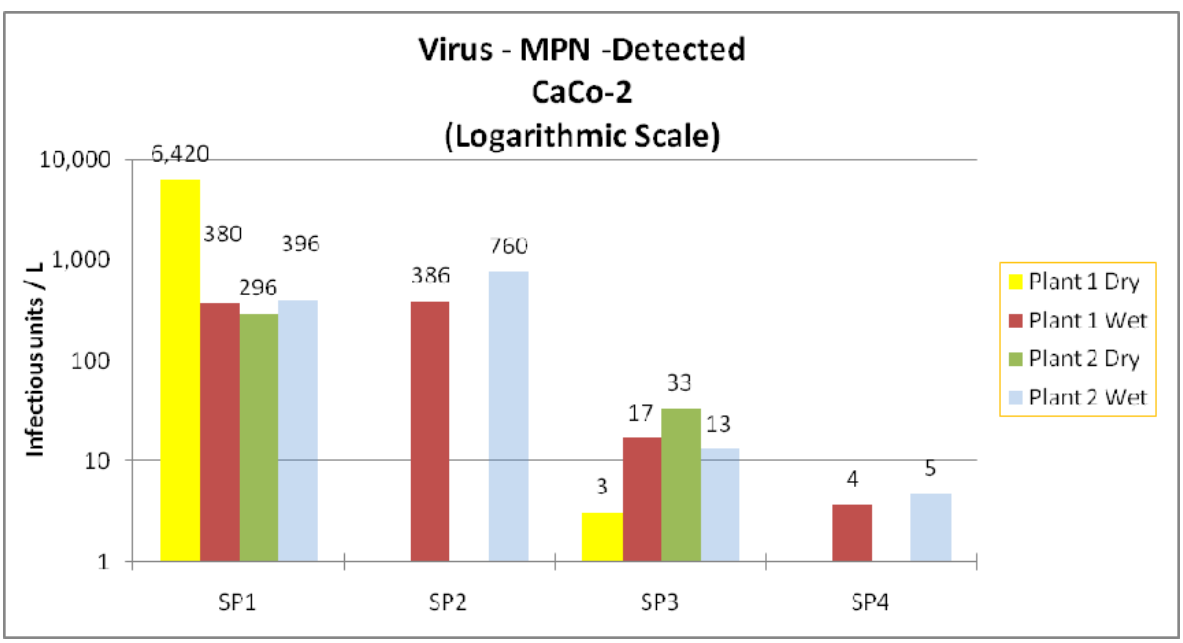

Maceration Results

For the majority of samples, maceration of effluent samples did result in increase in both fecal coliform and *Enterococcus* concentrations for both wet and dry weather. After maceration, significant increase in concentrations of one order of magnitude was observed only during dry weather for *Enterococcus* at Plant 1 and during wet weather for fecal coliform at Plant 2. A smaller increase of half order of magnitude was observed for fecal coliform during dry weather at Plant 1.

Figure 10. Wet-Weather Fecal Coliforms Macerated versus Unmacerated

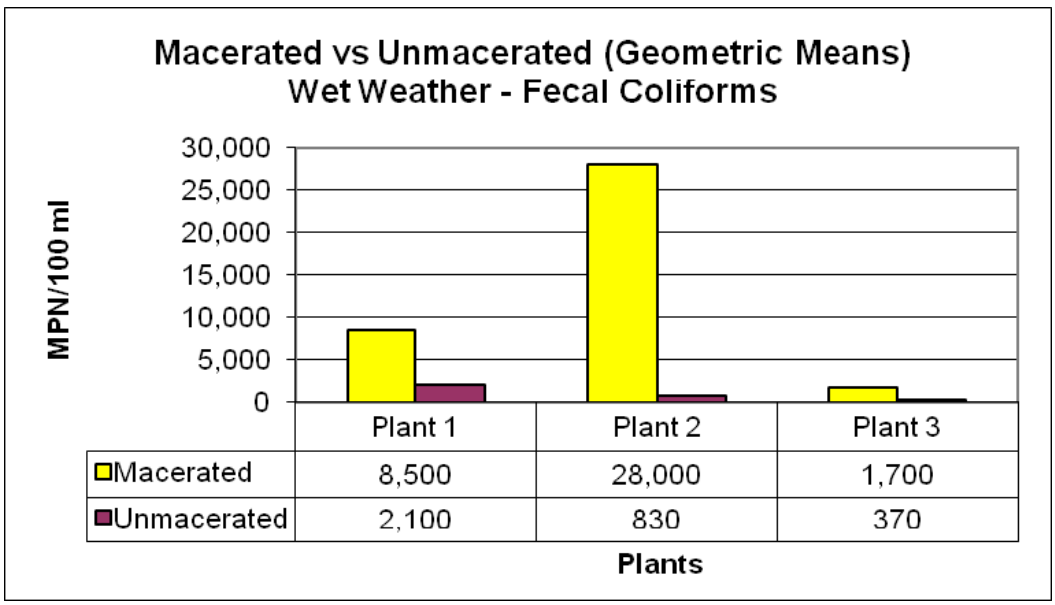

Figure 11. Wet-Weather *Enterococcus* Macerated versus Unmacerated

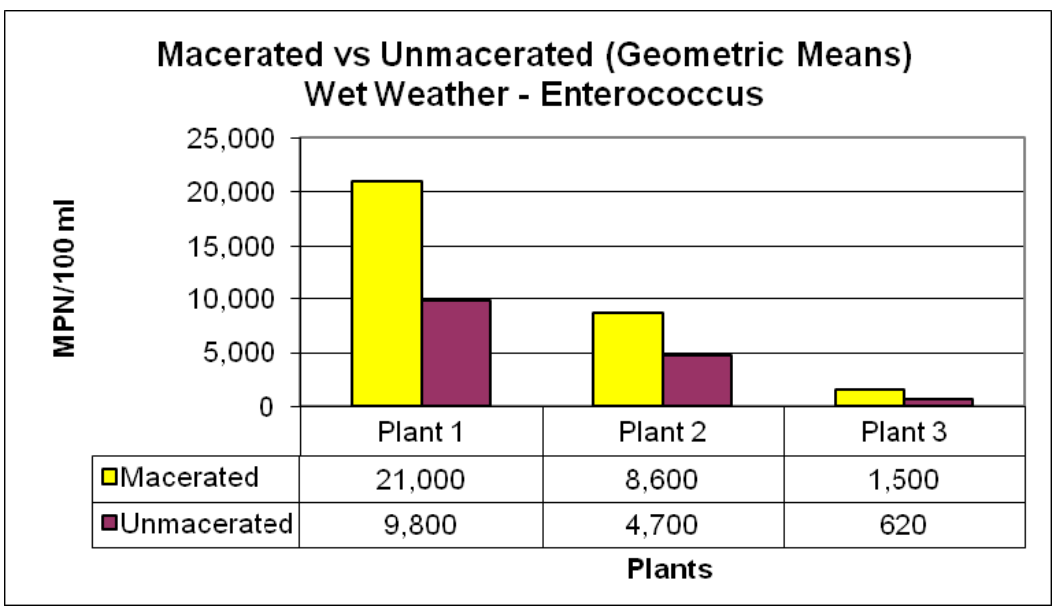

BOD_5 and TSS Results

The study showed that during blending, effluent BOD_5 and TSS concentrations at Plant 1 and Plant 2 were, on average, below 30 mg/l, and effluent BOD_5 and TSS concentrations at Plant 3 were, on average, above 30 mg/l. BOD_5 and TSS percent removal during blending remained, on average, above 80% at Plant 2, above 70% at Plant 1 and showed a more significant decline at Plant 3 where it was 45% for BOD_5 and 17% for TSS. The most probable reason for a poorer performance of Plant 3 was an occurrence of a major upgrade during sampling. See Table 6.

Table 6. BOD_5 and TSS Total Percent Removal

Plant	BOD_5 % - Dry Weather	BOD_5 % - Wet Blending	TSS % - Dry Weather	TSS % - Wet Blending
Plant 1	92%	77%	89%	71%
Plant 2	88%	81%	99%	89%
Plant 3	93%	45%	93%	17%

The average of BOD_5 wet-weather blending effluent concentrations was 24 mg/l at Plant 1 (values ranged from 9.5 to 37 mg/l), and 22 mg/l at Plant 2 (values ranged from 9 to 30 mg/l). The average of TSS wet-weather blending effluent concentrations was 29 mg/l at Plant 1 (values ranged from 22 to 33 mg/l) and 20 mg/l at Plant 2 (values ranged from 13 to 26 mg/l).

Total Residual Chlorine (TRC) Results

There was no significant correlation between TRC versus plant flow. Chlorine residual concentrations were, on average, higher during wet-weather blending versus dry weather at all three Plants. It has been observed that the chlorine contact times were shorter during blending events due to higher flow rates.

CONCLUSIONS

As presented in the previous sections, the data on key pathogens, pathogen indicators, TSS and BOD show a negative impact of the blending practice on the WWTP performance and on the quality of the final effluent. A definite impact of blending is clearly visible when comparing the dry-weather non-blending to wet-weather blending results. This comparison showed that at two plants fecal coliform and *Enterococcus* concentrations in disinfected effluent were on average one to three orders of magnitude higher during wet-weather blending versus dry-weather non-blending. *Cryptosporidium* and *Giardia* effluent concentrations were also higher during wet-weather blending versus dry weather. Effluent concentrations of viruses were between a half and one order of magnitude higher during wet-weather blending versus dry weather at Plant 1 and similar at Plant 2.

However, there are several important reasons why these data should be accepted with caution and why this or similar studies should be continued:

1. This study was an ambitious undertaking, but it was conducted in a single geographic area and with a limited number of data points. These results should be viewed as plant specific. Conclusions should not be drawn on a national scale, and the results from this study should not be used in support of any regulations.
2. During the sampling period, Plant 3 was undergoing a major upgrade, which appeared to have an adverse impact on treatment quality, especially during wet-weather blending. Therefore, all results for Plant 3 should be viewed with caution.
3. The blending practice, although undesirable compared to non-blending, provides considerable protection of public health compared to the release of untreated overflows. It is possible that the design and operational characteristics of the individual treatment plants are significant factors affecting the ability of individual plants to perform satisfactorily during wet-weather blending.
4. Capability of the secondary treatment to reduce viruses concentrations to the double digit levels sheds good light on the WWTP performance in wet-weather.
5. The results of this study need to be supported by additional data collected not only at the WWTPs studied by this project but also by WWTPs with separate sewer systems and WWTPs located in other geographical areas.
6. Other studies of this type, such as the ongoing *blending study* conducted by the Water Environment Research Foundation (WERF) should be followed to exchange ideas, compare results and reinforce findings.
7. Continuation of the study at the same three or at different New York City plants would be a start in the right direction. Such a study would substantially increase the number of data points needed for reaching valid conclusions. This continuation would involve analyzing for fecal coliform, *Enterococcus, Cryptosporidium*, *Giardia*, and viruses in samples collected during one dry weather, three wet-weather non-blending (not done in this study), and three wet-weather blending events. For bacteria, maceration of the final effluent samples would be also done to achieve truer enumeration.

REFERENCES

1. U.S. Environmental Protection Agency (2009), Impact of Wet-Weather Peak Flow Blending on Disinfection and Treatment: A Case Study at Three Wastewater Treatment Plants. (Draft Report). National Risk Management Research Laboratory, Office of Research and Development, Cincinnati, Ohio 45268.
2. U.S. Environmental Protection Agency (1994), Combined Sewer Overflow (CSO) Control Policy. *Federal Register* Vol.59, Issue 75 p. 18688.
3. U.S. EPA Microbiology Home page; http://www.epa.gov/microbes.

4. Slifko, T.R., D.E. Friedman, and J.B. Rose. (1999). A most-probable-number assay for the enumeration of infectious *Cryptosporidium parvum* oocysts. *Applied and Environmental Microbiology* 65(9):3936-3941.
5. Rochelle, P.A., M.M. Marshall, J.R. Mead, A.M. Johnson, D.G. Korich, J.S. Rosen, and R.D. Leom. (2002). Comparison of InVitro Cell Culture and a Mouse Assay for Measuring Infectivity of *Cryptosporidium parvum. Applied and Environmental Microbiology* 68 (8):3809-3817
6. Quintero-Betancourt, W., A. L. Gennaccaro, T. M. Scott, and J. B. Rose. (2003). Assessment of Methods for Detection of Infectious *Cryptosporidium* Oocysts and *Giardia* Cysts in Reclaimed Effluents. *Applied and Environmental Microbiology* 69(9): 5380–5388.

BIBLIOGRAPHY

1. American Public Health Association, American Water Works Association, and Water Environment Federation. 1998 "Standard Methods for the Examination of Water and Wastewater," 20th Edition.
2. Tchobanoglous, G. and F.L. Burton (1991), Wastewater Engineering: Treatment, Disposal, and Reuse, Metcalf & Eddy, Inc., McGraw-Hill, New York, 1991.

DISCLAIMER

The U.S. Environmental Protection Agency (EPA) through its Office of Water, Office of Policy, Economics and Innovation, and Office of Research and Development has financially supported and collaborated in the research described herein. The views expressed in this paper are those of the individual authors and do not necessarily reflect the views and policies of the U.S. Environmental Protection Agency.

ACKNOWLEDGMENTS

Significant contributions to this project were made by the following fellow professionals**:**

- Mohammed Billah, Kevin Weiss, and Stephen Schaub, U.S. EPA-Office of Water
- Sarah Garman, U.S. EPA –Office of Science and Technology
- Jennifer Cashdollar and Daniel Murray, U.S EPA-Office of Research and Development
- Deborah Szaro, Ruth Sykes and Irwin Katz, U.S. EPA- Region 2 Laboratory (Edison, NJ) (*Giardia* and *Cryptosporidium* analyses)
- Troy Scott and George Lukasik, Biological Consulting Services (Viruses, *Giardia*, and *Cryptosporidium* analyses)
- Caitlyn Nichols, Interstate Environmental Commission. (Sampling Plan execution)
- Brian J. Mitchell, Interstate Environmental Commission. (Final Project Report).

IMPROVING HYDROLOGIC SUSTAINABILITY OF TEXAS A&M UNIVERSITY CAMPUS

Prakash Khedun[3], Chandana Damodaram[1], Marcio Giacomoni[1], Andrea Ryan[2], Hillary Holmes[2], Ross Klein[4], William Saour[2], Michelle Hollingsworth[1], Troy Berthold[3], Meg Davis[5], Philip Bullock[2], Neetha Ravikumar[1], Emily Zechman[6,9], Georgianne Moore[7], Bryan Boulanger[6], Radu Stoleru[8]

[1]Graduate Student, Zachry Department of Civil Engineering, Texas A&M University, College Station, TX
[2]Undergraduate Student, Zachry Department of Civil Engineering, Texas A&M University, College Station, TX
[3]Graduate Student, Water Management & Hydrologic Sciences, Texas A&M University, College Station, TX
[4]Graduate Student, Department of Ecosystem Science & Management, Texas A&M University, College Station, TX
[5]Undergraduate Student, Department of Computer Science and Engineering, Texas A&M University, College Station, TX
[6] Assistant Professor, Zachry Department of Civil Engineering, Texas A&M University, College Station, TX
[7] Assistant Professor, Department of Ecosystem Science & Management, Texas A&M University, College Station, TX
[8] Assistant Professor, Department of Computer Science and Engineering, Texas A&M University, College Station, TX
[9] Corresponding Author: 205-M Wisenbaker Engineering Research Center, 3136 TAMU, College Station, TX 77843-3136; PH (979) 845-2875; FAX: (979) 862-1542; ezechman@tamu.edu

ABSTRACT

This research investigates the hydrologic sustainability of urban development and stormwater management for a watershed on the Texas A&M campus. The main Texas A&M campus has become increasingly urbanized, resulting in areas of imperviousness that generate higher rates of runoff. This growth has proceeded unchecked, and significant growth and development are planned for the future. Both increased rates of runoff from previous development and the impact of anticipated development should be addressed through mitigation efforts. This research provides a means to assess watershed health through biological indicators, water quality indicators, riparian ecosystems, the floodplain footprint, and the long term flow regime. A modeling framework is implemented to couple hydrologic and hydraulics models to simulate a set of watershed management plans that employ alternative best management practices. Development plans will be evaluated based on a set of comprehensive metrics that synthesize ecological, hydrologic, and environmental aspects of watershed health. The selection of management plans based on these metrics will enhance the environmental sustainability of further campus development.

INTRODUCTION

Urbanization of watersheds leads to an increase in peak flow and volumes of stormwater runoff and fundamentally alters the characteristics of the flow regime and therefore the health of the in-stream ecosystem. More sustainable development in a

hydrologic context would enable the stream to maintain its natural variability and flow characteristics. Best Management Practices (BMP) are a range of technologies and methods for mitigating increased stormwater runoff and have provided an appropriate approach for controlling the volume of flow and limiting the amount of sediments and pollutants that would otherwise be washed into the stream. For example, detention ponds are typically designed to match pre-development peak flows (EPA 2004). While centralized BMP placement may reduce peak flows and may effectively remove pollutants, the natural hydrology may become dominated by inadequate base flow or flashy hydrology, which negatively affects the ecosystem (Coffman 2000). Alternatively, Low-Impact Development (LID) is a selected set of BMPs that enable the design of management strategies with the goal of either maintaining or replicated the pre-development hydrologic regime. LID principally uses the tactic of controlling stormwater at the source through the use of micro-scale stormwater retention areas, landscapes that act as stormwater facilities, and the protection of riparian buffers and other environmentally sensitive site features (EPA report 2000). LID strategies include permeable pavements, rainwater harvesting systems, green roofs, and vegetated swales.

The purpose of this paper is to explore through a simulation study the placement of LID strategies, including rainwater harvesting systems, permeable pavement, and riparian buffer systems, on a campus watershed for improvement of the hydrologic sustainability. The watershed has experienced development in recent years, through the construction of buildings, roadways, and parking lots. To simulate the pre-development flow regime, data from 1940 is incorporated into a hydrologic modeling framework. The flow regime for the current conditions and different LID placement scenarios are simulated and compared to the predevelopment flow regime to evaluate hydrologic sustainability.

TEXAS A&M UNIVERSITY CAMPS: PAST, PRESENT, AND FUTURE

The main Texas A&M University (TAMU) campus, located in College Station, Texas, covers an area of 5,280 acres (21.37 square kilometers), most of which are not densely developed. Since 1962, the campus witnessed unprecedented growth with a student population increasing from 7,500 to 45,000. The main campus consists of a mix of old and new structures which reflect the evolution of the university footprint over the past 130 years. Construction and development have led to degraded hydrologic conditions, especially during peak flow conditions, which lead to street flooding and in-stream erosion.

The two sections of campus, Main Campus and West Campus (3.03 and 4.39 square kilometers, respectively), are separated by a four-lane road and railway track (Fig. 1). The campus straddles two watersheds, and the Main campus drains southeast toward the Navasota River while West campus drains southwest through White Creek into the Brazos River. While West Campus is less developed than Main Campus, development that has taken place over the last 50 years on West Campus has greatly increased the impervious surface and volume of storm water draining into White Creek, subsequently degrading the structure of the creek and the ecosystem. Tributaries C and D that contribute to White Creek have undergone a transformation from small and slow moving creeks to large creeks that move large amounts of storm

water during a typical 2-5 year rainfall event. The TAMU Physical Plant Utilities commissioned a study to assess the extent of erosion within the watershed and to propose the most effective engineering solutions (JF Thompson, 2005). The study documented the erosion and massive slope failure that has occurred throughout the extent of the creek's channel, and predicted that, if left unmitigated, erosion would likely undermine adjoining structures including buildings, roads, bridges, and ponds. As a result of this study, immediate protection of critical locations was recommended, and riprap and gabions with vegetation were implemented to decrease velocities in stream.

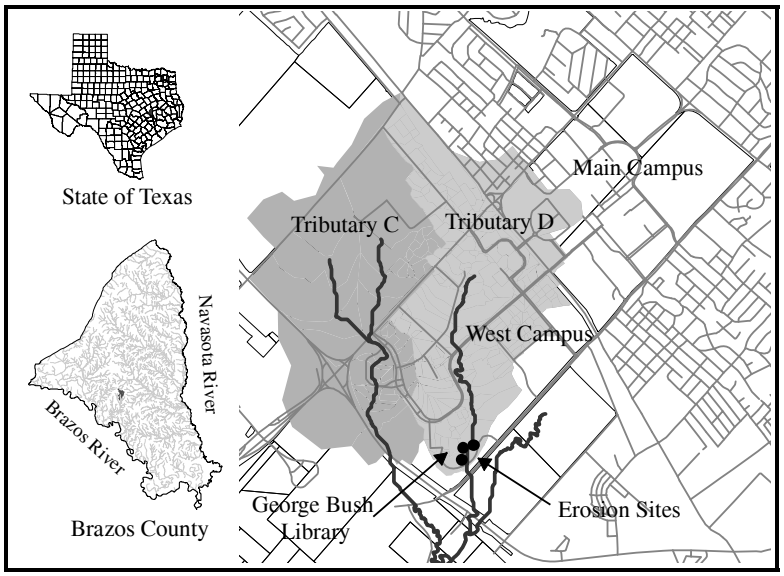

Figure 1. Location of Texas A&M campus; West Campus Watersheds C and D; Tributaries C and D; and the location of erosion problems

To prevent further damage and improve the aesthetics of the campus as a whole, a master plan was commissioned and was released in July 2004 (Barnes Gromatzky Kosarek Architects and Micheal Denis & Associates, 2004). It assesses the present strength and weaknesses of the campus and sets the tone for future construction and landscape development as the university enhances its physical environment. The master plan proposes an extension of the civic structure and landscape that exists on Main Campus into West Campus. As the number of buildings on West Campus is expected to approximately double, the replacement of parking areas with green spaces, buildings, and garages is suggested to mitigate environmental implications of increased impervious areas. Thompson (2005) suggests that a more comprehensive stream restoration plan is required to address erosion and hydrologic problems in the long term and plan for the further development of West Campus as proposed in the master plan.

LOW IMPACT DEVELOPMENT STRATEGIES

Three LID strategies, including a riparian buffer system, permeable pavement, and rainwater harvesting systems, are considered for mitigating the impacts of development in the campus watershed.

Riparian Buffer System. The campus master plan suggests that Tributary D should be developed as a greenway. The area can be restored to its natural state by encouraging the use of native Texas riparian landscape. A 300 feet (approximately 90 meter) wide riparian buffer, divided into three cores (inner, middle and outer) is proposed (Fig. 2). It is expected to act the backbone of the natural enhancement around which other segments will be organized.

The proposed Greenway is a strip of riparian buffers and linear strips of vegetation between the aquatic ecosystem and the upland habitats. Such systems are usually located adjacent of streams, rivers, lakes, reservoirs, and other inland aquatic systems. They are different from riparian corridors, which primarily facilitate the movement of wildlife. Their purpose is to improve water quality (Fisher et al., 2000). Riparian buffer strips can reduce stream sedimentation in several ways. They trap terrestrial sediment in the surface runoff and reduce the velocity of the sediment bearing storm-water, allowing more time for the sediment to settle out. They also stabilize stream banks and prevent excessive channelization, they moderate flows during floods, and they contribute large wood to the stream, assisting stabilization by acting as soil rebar (Wenger, 1999).

The first five meters on the outer side of the strip is the most important as it screens out large particles. Smaller sized particles are more difficult to remove by filtering through grass, and generally require a zone of woody vegetation to intercept them (Garabaghi et al., 2001). Vegetation already existent along the riparian zone will be retained and protected and it must be ensured that drainage does not interfere with the hydrology of the buffer. The buffer tree canopy should be maintained to balance both understory and overstory vegetation. The buffer can also include sedimentation detention structure, such as depressions in the ground, vegetative filter strips, permeable barriers, and infiltration structures such as gravel trenches.

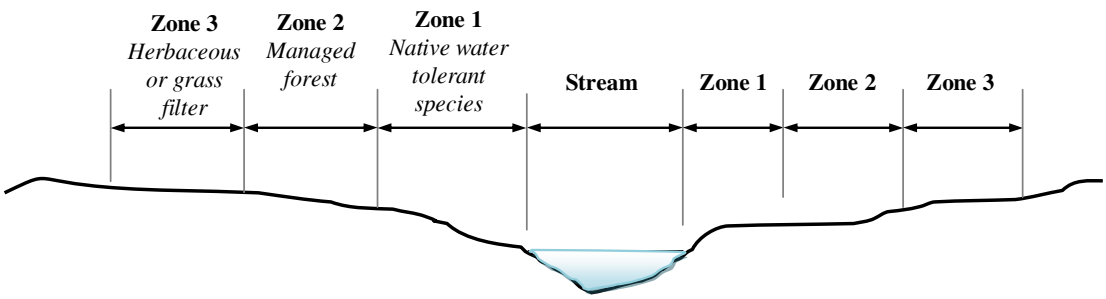

Figure 2. Schematic of riparian buffer system

Permeable Pavement. Permeable pavements systems generally consist of a matrix of concrete blocks or plastic web-type structure with voids that are filled with a material of high permeability (sand, gravel or even soil). The voids hold the precipitation, allows water to infiltrate and be retained within the highly permeable matrix as it slowly infiltrates into the underlying soil (Brattebo and Booth 2003). Permeable pavement may replace traditional pavement or concrete infrastructure for sidewalks, roads, and parking lots. A set of studies have documented the ability of permeable pavement to reduce the volume of stormwater runoff and the amount of

contaminant washed from parking lots into surface water bodies (Braune and Wood 1999).

Rainwater Harvesting Systems. Rainwater harvesting is an ancient practice that has been receiving attention, fueled by water shortages from droughts, pollution and population growth (Nolde 2007). While originally used to collect water in depressions for irrigation, the practice of collecting rainfall from rooftops was later adapted for domestic water supply in rural areas and islands (Kahinda et al. 2007; Michaelides and Young 1983). More recently, environmental concerns have increased the appeal of green building practices, including rainwater harvesting systems, in urban areas. Rainwater harvesting is especially appealing as it combines the benefits of water reuse with runoff reduction and groundwater recharge, and has been proposed as a means to conserve rainwater and reuse it for landscaping (Porter et al. 2007).

MODELED SCENARIOS

A hydrologic and hydraulic model of Watersheds C and D in West Campus for current conditions was developed by AECOM (AECOM 2008). Geographical, hydrologic, and meteorological information were incorporated within HEC-HMS (Army Corps of Engineering 2006) for hydrologic simulation. Watersheds C and D were divided into sub-watersheds, delineated corresponding to storm sewer manholes, culverts, channel junctions, buildings, and streets. Curve numbers for the watershed, specified in the Bryan-College Station Unified Design Guidelines (2007), range between 75 for natural woodlands and natural grasslands and 77 for landscaped area. Streets, building roofs, and parking lots contribute to the percentage imperviousness for each sub-catchment. The Storm Water Management Model (SWMM) (EPA 2008) was used for hydraulic simulation. SWMM is a dynamic rainfall-runoff simulation model for both flow and water quality of a single storm event or a long-term continuous storm event. It extracts the flow hydrograph information from HEC-HMS at subbasins to route hydrographs through sewers, conduits, and open channels (AECOM 2008). As the storm water infrastructure on West Campus consists of box and circular storm sewers and two tributaries of White Creek, the hydraulic model consists of a combination of links and nodes representing the storm water infrastructure.

A set of scenarios were considered and compared to the Existing Conditions, which are represented in the current model. A 2-year 24-hour rain event with a cumulative depth of 4.42 inches (112.3 mm) (TxDOT 2004) was used to evaluate new scenarios, including Predevelopment Scenario, Riparian Buffer System, Permeable Pavement, and Rainwater Harvesting.

Predevelopment Scenario. An aerial photograph from 1940 is available (Texas A&M University Libraries Map & GIS Collection and Services) and was used to build the model of the predevelopment conditions. In 1940, most of the university infrastructure was concentrated on Main Campus, and West Campus was generally undeveloped and covered with natural grassland. A curve number of 75 was adopted for these areas (Bryan-College Station Unified Design Guidelines 2007).

In the current scenario, delineation of sub-watersheds was forced by curb gutters, inlets, conduits, and manholes. As the storm sewer infrastructure had not been implemented in 1940, the existing delineation of the sub-watersheds was restructured to reflect the natural topography of the watersheds for pre-development conditions. After this restructuring, the total number of sub-watersheds modeled in the predevelopment scenario is 52, compared to 327 in the existing conditions. The present channel configuration and cross section of the open channel in Tributaries C and D were adopted from the 2008 conditions.

Riparian Buffer System. The riparian buffer system is modeled using the recommendations of the campus master plan which proposes a riparian buffer along the creek. The buffer is divided into three zones; the outer zone being an herbaceous or grass filter strip, the middle zone consisting of managed forest of fast growing or native species, and the inner zone being native species that are water-loving or water-tolerant. A model of the buffer strip is incorporated within the HEC-HMS-SWMM model. Appropriate sub-catchments were delineated representing the buffer on both sides of the creek. While the standard design manual specifies a curve number of 75 for both natural grassland and natural forest (The Bryan-College Station Unified Design Guidelines 2007), other research suggest a wide range of curve numbers for grass, brush and woods based on hydrologic condition (e.g. McCuen, 1989). To simulate the presence of a buffer strip, a sub-catchment is created for each zone (outer, middle, and inner) with a curve number that reflects the type of vegetation.

Permeable Pavement. Few studies have investigated the mechanistic modeling of pervious pavements. Leming et al. (2007) identified a method for calculating a curve number for pervious pavement, which is implemented for this study. This method approximates the initial abstraction as the volume of water stored by the pervious pavement, based on the depth and porosity of the pavement. The following equations are used to calculate the corresponding curve number for a system of permeable pavement designed to store a 24-hr 2-yr storm, as demonstrated in Leming et al. (2007):

$$I_a = P_{24-hr,2-yr} \text{ (mm)} \quad (1)$$

$$S = \frac{I_a}{0.2} \text{ (mm)} \quad (2)$$

$$CN = \frac{100}{\left(\frac{S}{254}+1\right)} \quad (3)$$

where $P_{24\text{-}hr,2\text{-}yr}$ is the depth of a 24-hr 2-yr storm (mm); I_a is the initial abstraction (mm); S is the maximum potential retention (mm); and CN is the curve number.

For the 24-hr 2-yr storm of 112.3 mm, the curve number is calculated as 31.2. Currently in West Campus, 41% of the watershed is total impervious area and 6.5% of the watershed is uncovered asphalt parking lots. A weighted curve number approach is taken to calculate the new curve number for each sub-watershed, based on the acreage of pavement in that subbasin.

Rainwater Harvesting Systems. The approach taken to simulate the rainwater harvesting is similar to the simulation procedure for the permeable pavement, employing the assumption that the precipitation from a 2-year 24-hour storm event will be collected from the roof of buildings within the watershed. The curve number is calculated as 31.2, based on Eqns. 1-3. Buildings on West Campus provide a total roof area of 227,150 square meters, or 3.2% of the total area.

PRELIMINARY RESULTS

Based on the modeling approaches described above, the characteristics for four scenarios as implemented in Watersheds C and D were calculated and summarized in Table 1.

Table 1. Scenario characteristics

Scenario	Total Pervious Area (%)	Total Impervious Area (%)	Area Represented as LID (%)	Weighted Curve Number
Pre-development	93%	7%	-	76.6
Existing Conditions	73%	27%	-	82.7
Permeable Pavement	73%	20.6%	6.4%	78.4
Rainwater Harvesting System	73%	23.8%	3.2%	80.5

A set of preliminary results have been generated to demonstrate the hydrologic differences between the existing and pre-development conditions. Four catchments in West campus were further examined (Fig. 3). The characteristics of these catchments under pre-development and existing conditions are summarized in Table 2. Values for curve numbers increase by 5-13% (Table 2) for these catchments. The hydrographs at the outlets are generated for existing and pre-development conditions for the 24-hr, 2-yr rainfall event (Fig. 4). The impact of increased imperviousness is seen clearly in both the increased peak flow and decreased time to peak.

Table 2. Physical characteristics of four selected sub-watersheds.

Catchment	Area (km^2)	Pre-development Conditions			Existing Conditions		
		CN (perm. areas)	% Imp.	Weighted CN	CN (perm. areas)	% Imp.	Weighted CN
C North	0.48	75	3%	75.6	77	11%	79.3
C South	0.15	75	0%	75.0	77	20%	81.1
D North	0.84	75	26%	81.0	77	51%	87.8
D South	0.36	75	16%	78.6	77	60%	89.5

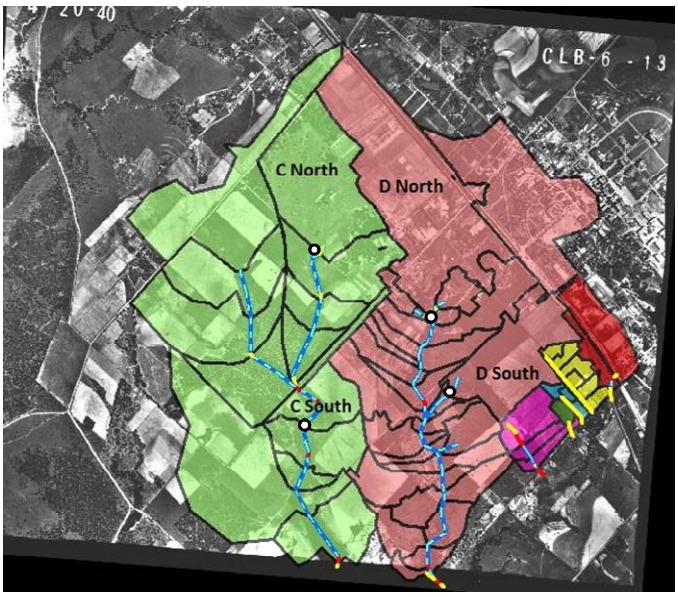

Figure 3. Location of four selected sub-watersheds on West Campus: C North, C South, D North, and D South, overlaying aerial photograph (Texas A&M University Libraries Map & GIS Collection and Services). Open circles show location of sub-watershed outlet.

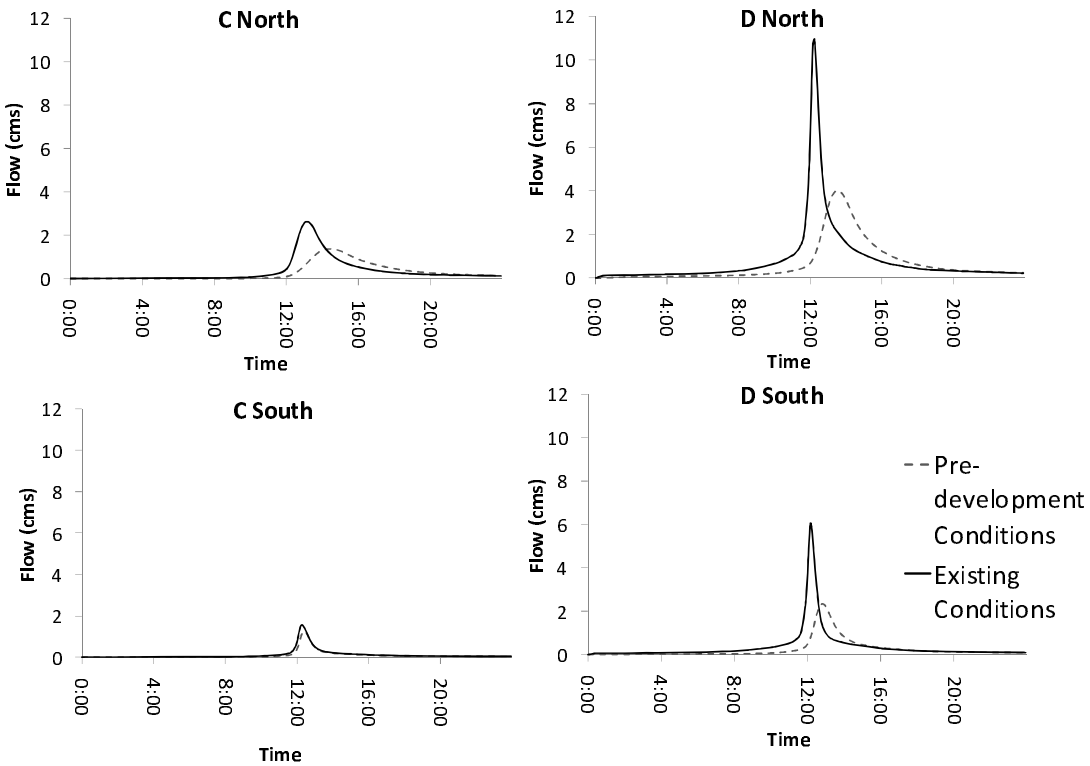

Figure 4. Hydrographs for pre-development and existing conditions at four selected sub-watersheds.

ONGOING WORK

This paper presents preliminary work to explore more hydrologically sustainable options for the current level and planned level of development in a campus watershed, as compared to pre-development conditions. LID strategies under consideration include both structural and ecological changes that may be designed and implemented to restore the creek to its predevelopment flow regime.

A Riparian Buffer System is suggested to improve both hydrological conditions and conditions for ecosystems. This system will be simulated to evaluate its contribution to hydrologic sustainability of the tributary. Two structural LID strategies, permeable pavement and rainwater harvesting systems, are designed to retain a 2-year 24-hour storm event so that there would be no runoff from these areas. Further modeling techniques will be explored to investigate the hydrologic performance of these LID strategies for 10-year and 100-year rainfall events. For larger events, rainfall that is not captured by the porous pavement will runoff as sheet flow. Rainfall that overflows the rainwater harvesting storage system will be discharged through the existing sewer system.

For future work, we will model the hydrologic effects of the development proposed in the master plan and investigate the effects of utilizing the three LID strategies described here.

ACKNOWLEDGEMENTS

Although the research described in this article has been funded wholly or in part by the United States Environmental Protection Agency through Grant #SU833944, it has not been subjected to the Agency's required peer and policy review and therefore does not necessarily reflect the views of the Agency and no official endorsement should be inferred.

The authors express their thanks and appreciation to the Texas A&M Physical Plant, Engineering Design Services (TAMU PP/EDS), College Station, Texas, Gary Struzick of Klotz Associates, and Anthony Holder of Turner, Collie and Braden, both of Houston, Texas for their help and sharing of valuable storm water, rainfall, survey, and data base information. This additional information was gathered in a separate project funded by Texas A&M Utilities, College Station, Texas and managed by TAMU PP/EDS.

REFERENCES

AECOM (2008), West Campus Storm Drainage Modeling - Texas A&M University, College Station, Texas, US.

Barnes Gromatzky Kosarek Architects and Micheal Denis & Associates (2004), Campus Master Plan, Texas A&M University, 229 pp, College Station, Texas, US.

Brattebo, B. O., and D. B. Booth (2003), Long-term stormwater quantity and quality performance of permeable pavement systems *Water Research*, *37*, 4369-4376.

Bryan-College Station (2007), Unified Stormwater Design Guidelines, Texas, US.

Coffman, L. (2000) Low-Impact Development Design Strategies, An Integrated

Design Approach. EPA 841-B-00-003. Prince George's County, Maryland.

Department of Environmental Resources, Programs and Planning Division.

Fischer, R. A., et al. (2000), Improving riparian buffer strips and corridors for water quality and wildlife, paper presented at International Conference on Riparian Ecology and Management in Multi-Land Use Watersheds, American Water Resources Association, Middleburg, VA.

Gharabaghi, B., et al. (2001), Sediment removal efficiency of vegetative filter strips, paper presented at ASAE Meeting, St. Joseph, MI.

JF Thompson Inc. (2005), White Creek Drainage Study, 70 pp, College Station, Texas, US.

Kahinda, J.-m., et al. (2007), Domestic rainwater harvesting to improve water supply in rural South Africa, *Physics and Chemistry of the Earth, Parts A/B/C*, *32*, 1050-1057.

Leming, M. L., et al. (2007), *Hydrologic Design of Pervious Concrete, EB303*, Portland Cement Association, Skokie, Illinois, and National Ready Mixed Concrete Association, Silver Spring, Maryland, USA.

McCuen, R. H. (1998), *Hydrologic Analysis and Design*, Prentice Hall, Upper Saddle River, NJ.

Michaelides, G., and R. Young (1983), Rainwater harvesting for domestic use in rural areas, *Ekistics*, *303*, 473-476.

Nolde, E. (2007), Possibilities of rainwater utilisation in densely populated areas including precipitation runoffs from traffic surfaces, *Desalination*, *215*, 1-11.

Porter, D. O., et al. (2007), *Rainwater Harvesting*, Agrilife Extension, Texas A&M University, College Station, Texas.

Texas A&M University Libraries Map &GIS Collection and Services, Brazos County Aerial Photos from 1940, Available at http://library.tamu.edu/about/collections/map-gis-collections-services/collections/brazos-aerial-1940, accessed October 15, 2008.

Texas Department of Transportation (2004), Hydraulic Design Manual, Texas, US.

U.S. Army Corps of Engineering (2006). Hydrologic Modeling System User's Manual, Version 3.0.

U.S. EPA (2000) Low Impact Development (LID): A Literature Review, EPA/841/B/00/005

U.S. EPA (2004) The Use of Best Management Practices (BMPs) in Urban Watersheds, EPA/600/R-04/184

U.S. EPA (2008). Storm Water Management Model User's Manual, Version 5.0.

Wenger, S. (1999), A review of the scientific literature on riparian buffer width, extent, and vegetation, Institute of Ecology, University of Georgia, Athens, Georgia, US.

AN INVESTIGATION OF INFILTRATION IN A CONSTRUCTED STORMWATER WETLAND AND IMPLICATIONS FOR GROUNDWATER QUALITY

Gerrad Jones[1], Kristen Mogavero[1], and Bridget M. Wadzuk[1]

[1]Department of Civil and Environmental Engineering, Villanova University, 800 Lancaster Avenue, Villanova, Pennsylvania, 19085;PH (610) 519-5365, FAX (610) 519-6754; email: gerrad.jones@villanova.edu, kristen.mogavero@villanova.edu, bridget.wadzuk@villanova.edu, M.ASCE

ABSTRACT

Traditionally, detention basins and constructed stormwater wetlands (CSW) have been used primarily for peak flow reduction and water quality improvement and are assumed to possess negligible infiltrative capabilities. However, the potential for storm water infiltration within these structures and the associated non-point source pollution of groundwater can not be ignored based on untested assumptions. The purpose of this research was to assess the infiltration capacity of a mature CSW on Villanova University's campus, in Villanova, Pennsylvania. Piezometers located within the CSW were monitored to develop a water budget and a chloride mass balance. The vertical gradients in the piezometers alternated between recharge and discharge patterns, with downward recharge gradients for baseflow conditions and upward discharge gradients after rainfall events. Preliminary water budget and chloride mass balance analyses suggest considerable reductions in volume and chloride load over a 6.5 day baseflow period in December, 2008. Although these findings suggest infiltration contributes to the water budget, it is unclear whether other explanations (e.g. perched water table or chloride stratification) could account for these patterns. Infiltration may be the most parsimonious explanation, but further research needs to be conducted to determine whether the negligible infiltration assumption is valid.

1 INTRODUCTION

Increased impervious surfaces around urban areas has adversely affected watersheds directly and indirectly (Arnold and Gibbons 1996). Water intercepted by impervious surfaces is conveyed to gutters, drains, or directly into bodies of water. The resulting flow has higher velocities and greater volumes when compared to similar watersheds with less impervious cover, which affects biota within the watershed and results in scour and erosion (Arnold and Gibbons 1996).

Water that is intercepted by impervious surfaces collects pollutants including sediments, nutrients, metals, petrochemicals (Weiss et al. 2008). Non-point source pollution from stormwater runoff is documented as a leading cause of impairment in freshwater lakes, rivers, and estuaries (U.S. EPA 2005). Although the concentration of these pollutants may be relatively small at their source, the total sum of these pollutants can become toxic as they collect in downstream receiving water bodies.

To mitigate the effects of large volume, high intensity flows generated from urban stormwater runoff, infiltration best management practices (BMPs) have become increasingly popular. Infiltration BMPs reduce runoff volumes by infiltrating stormwater into the soil where it is transported by sub-surface flow and/or recharges groundwater aquifers (PSBMPM 2005). Peak rate reduction BMPs are thought to have minimal volume reducing capabilities. Such BMPs include detention basins and CSWs, which are surface stormwater structures that provide temporary storage of stormwater runoff to prevent downstream flooding. These systems are thought to be relatively impermeable because the soils have been compacted and have low hydraulic conductivities (PSBMPM 2005).

With the rise in popularity of infiltrating stormwater management techniques, concern has arisen regarding potential groundwater contamination. Kwiatkowski et al. (2007) concluded that infiltration BMPs do not adversely affect the groundwater when properly located; however, the placement of BMPs can be dictated by necessity instead of ideality and ponded infiltration should not be ignored when considering the fate of pollutants and the potential for groundwater contamination (Weiss et al. 2008). Because infiltration within CSW's has largely been disregarded, the overall goal of this study was to assess the infiltration capacity of a CSW on Villanova University's campus. This was accomplished by 1) monitoring piezometers to discern vertical groundwater flow gradients, 2) constructing a water budget for Villanova University's CSW, and 3) performing a chloride mass balance on a chloride tracer study. If surface and ground water interactions are negligible, anomalous losses or gains of water and chloride should be minimal. Conversely, if anomalous losses or gains of water and chloride comprise a substantial portion of the total inflow or load, than surface and ground water interactions cannot be ignored.

2 SITE DESCRIPTION

The Villanova CSW is a mature wetland system located on Villanova University's campus in Villanova, Pennsylvania. The CSW was originally a detention basin that was retrofitted in 1999. During base flow conditions, a continuous flow of water enters the system from two pipes that drain Villanova University's campus and serves as the primary inputs of water into the system. The drainage area is approximately 23 hectares, and of this area, 57%, 31%, and 12% of the surfaces are impervious, semipervious, and pervious, respectively.

Since 2003, the Villanova CSW has been monitored for quantity and quality (Rea 2004; Woodruff 2005; Flynn 2008). During 2007, approximately 20% more water entered the system than exited for the entire year. Due to infrequent calibration, however, the quality of historical quantity data must be interpreted with caution. There is 60% and 80% removal efficiency of total phosphorus and total nitrogen, respectively for base flow conditions (Rea 2004); however, no research had been done to determine interactions between surface water and groundwater, which could have implications for the observed water quality improvements. Rea (2004) found that chloride concentrations between the inlet and outlet were similar for base flow conditions, with a 5% maximum removal. This suggests that chlorides within Villanova's CSW are relatively nonreactive and that infiltration may be negligible. A water budget and a chloride mass balance are developed as part of the current

research to further investigate the validity of these findings. A series of four piezometer nests in the CSW are monitored to discern vertical flow gradients and identify whether groundwater recharge or discharge is most probable.

3 METHODS

3.1 Piezometers

In November, 2007 four piezometer nests were installed within the CSW. When two or more piezometers are installed at the same location but at different depths, the vertical differences in head between the piezometers is indicative of vertical flow patterns. Each nest consists of three piezometers installed to depths of 0.9, 1.8, and 2.7m (3, 6, and 9 ft) below the ground surface. The water level in the piezometers was measured two to four times a week from January 2008 to December 2008. A downward gradient is indicative of a groundwater recharge system (i.e infiltration is occurring) while an upward gradient indicates groundwater discharge.

3.2 Water Budget

A water budget is a method for balancing the input and output of a system. Based on the conservation of mass, the water budget for the CSW can be summarized as follows:

$$\frac{dV_{sys}}{dt} = Q_{in} - Q_{out} \pm Q_{accumulation} \quad (1)$$

where $\frac{dV_{sys}}{dt}$ is the change in surface water volume within the system over time, and Q_{in}, Q_{out}, and $Q_{accumulation}$ are the volume rates of water coming into , out of , and accumulating within the system, respectively. Due to conservation of mass, and assuming constant density, the change in volume over time is zero. Equation 1 is reduced and rearranged to:

$$Q_{in} = Q_{out} \pm Q_{accumulation} \quad (2)$$

The flux terms (Q_{in} and Q_{out}) can be summarized as follows:

$$Q_{in} = Q_{inlet} + \frac{P}{\Delta t} \quad (3)$$

and

$$Q_{out} = Q_{outlet} + \frac{(E + T + I)}{\Delta t} \quad (4)$$

where Q_{inlet} and Q_{outlet} are the volume rates of water entering and exiting the system though pipes respectively, P is precipitation, E is evaporation, T is transpiration, I is infiltration, and Δt is the time step. Substituting equations 3 and 4 into 2 yields:

$$Q_{inlet} + \frac{P}{\Delta t} = Q_{outlet} + \frac{(E + T + I)}{\Delta t} + Q_{accumulation} \quad (5)$$

The present study for water budget analysis was conducted from December 4-10 under base flow conditions (steady state) resulting in negligible accumulation.

During this time, the average temperature was 2.5°C, so evaporation and transpiration were assumed to be negligible. Precipitation was zero. Reducing equation 5 and rearranging for infiltration yields:

$$\frac{I}{\Delta t} = Q_{inlet} - Q_{outlet} \quad (6)$$

To measure water inflow and outflow, three American Sigma 950 Flow meters were used at the inlet and outlet pipes at five minute intervals. The inlet and outlet flow rates were inserted into equation 6 to determine the volume of water infiltrated.

Darcy demonstrated that the discharge rate of water flowing through a soil under a hydraulic gradient is related to the hydraulic conductivity:

$$q = K_s iA \quad (7)$$

where q is the discharge rate, K_s is the saturated hydraulic conductivity, i is the hydraulic gradient, and A is the cross sectional area of the sample. If equation 7 is multiplied by time, the resulting equation is:

$$I = K_s iAt \quad (8)$$

which represents the volume of water infiltrated over a given time interval (from equation 6).Rearranging equation 8 to solve for saturated hydraulic conductivity yields:

$$K_s = \frac{I}{iAt} \quad (9)$$

The hydraulic gradient, *i*, is $\frac{dh}{dL}$, the change in head over the length of soil sample assuming saturated conditions. For the CSW, dh represents the depth of ponded water above the water table and dL represents the length of the soil column above the water table. Because the CSW has continuously ponded water, the soil beneath the system was assumed saturated. The water table was approximated using a linear regression model between four points at which the water table was known: three boring wells and Mill Creek, the downstream receiving water body (Blackmore 2006; Figure 1). The surface water elevation of the CSW was subtracted from the extrapolated groundwater table to calculate dh. A 2007 land survey of Villanova's CSW was used to get the ground elevation. The dL was determined by subtracting the ground elevation from the water table elevation. The hydraulic gradient was calculated at 40 points in five foot intervals along the cross section of the CSW shown in Figure 2. These estimates were averaged to estimate the total hydraulic gradient for the CSW. The ponded surface area of the CSW was used as the cross sectional area (A) and was determined using aerial photographs of the CSW and ArcMap 9.2. The time interval encompassed the duration of the study (6.48 days). Using these values it was possible to derive the average saturated hydraulic conductivity value for the CSW soils. The calculated hydraulic conductivity values were compared to values obtained from flexible wall falling head permeameter and a constant head permeameter tests that were conducted in October, 2008. The

calculated values were also compared to published values for similar soils (Johnson and Jensen, 2001).

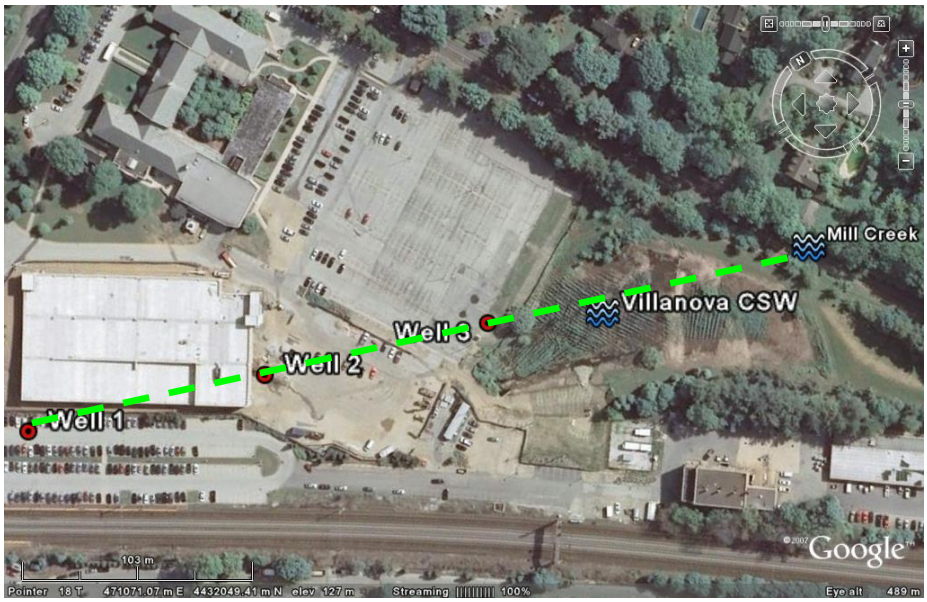

Fig. 1 The water table surrounding the CSW was determined from four locations on upstream and downstream ends (image obtained from Google Earth).

3.3 Chloride Mass Balance

Similar to the water budget, the mass balance is an application of the conservation of mass. The mass balance can be summarized as follows:

$$\frac{dM_{sys}}{dt} = \frac{M_{in} + M_{generated} - M_{out} - M_{reacted} \pm M_{accumulated}}{\Delta t} \qquad (10)$$

where $\frac{dM_{sys}}{dt}$ is the change in chloride mass within the system, M_{in} and M_{out} are the chloride mass entering and exiting the CSW respectively, $M_{generated}$ and $M_{reacted}$ is the mass of chloride generated or removed through chemical reactions, and $M_{accumlation}$ is the chloride mass that accumulates with the system. Chlorides move through natural systems unchanged so $M_{generated}$ and $M_{reacted}$ are negligible; assuming negligible accumulation and conservation of mass, equation 10 reduces to:

$$Mi_n = M_{out} \qquad (11)$$

On December 4 2008, 1080 grams of deicing salt was added to the inlet of the CSW. On December 6, 2008 a snow event introduced an additional unknown mass of chlorides into the wetland system as a result of roadway de-icing. Therefore, the initial chloride loading was unknown and was calculated by multiplying the inflow by the measured chloride concentrations and time. The chloride concentrations were monitored continuously (every five minutes) using conductivity probes (CTD-Divers by Schlumberger) at the inlet and outlet. The equipment was calibrated prior to the start of the study and was tested for accuracy using a solution of known conductivity at the end of the study to insure the divers were taking accurate measurements.

A relationship between the conductivity readings and chloride concentration was established. The maximum conductivity recorded by the probes was 2500 µS/cm. Deicing salt was added to each of three water samples until conductivity readings reached 1500, 2000, and 2500 µS/cm. The chloride concentration of the prepared samples was tested and the corresponding conductivity and chloride values were used to create the calibration curve (Figure 2). The calibration curve was used to obtain chloride concentrations based upon conductivity readings. The chloride concentration was multiplied by time and the flow of water entering and leaving the CSW to obtain a chloride load at the inlet and outlet, respectively. The mass of chloride entering the system was compared to the mass of chloride leaving.

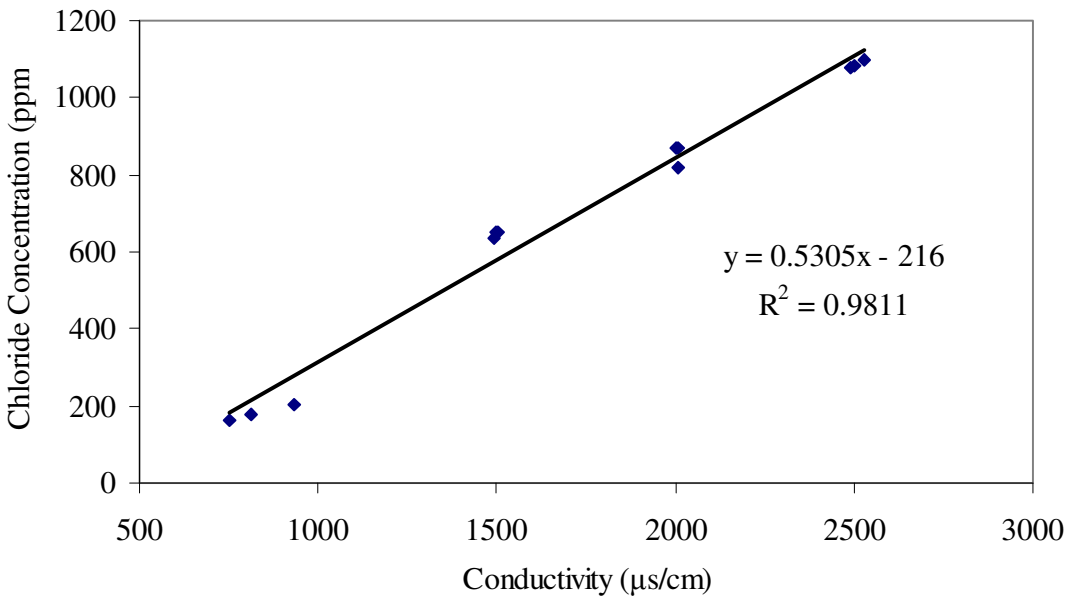

Fig. 2 Conductivity chloride calibration curve.

4 RESULTS

4.1 Piezometers

The piezometer readings indicate the existence of downward vertical flow gradients within the CSW, which occurs predominantly during baseflow conditions. The occurrence of precipitation and the number of days since a storm event seem to be the driving force behind whether an upward or downward flow gradient exists. During baseflow periods (i.e. no precipitation for at least 72 hours), downward flow gradients are predominant. However, storm events induce a reversal to an upward gradient, indicating groundwater discharge to the CSW. Figure 3 shows the water levels in the piezometers at one of the nests from August 1 to September 14, 2008 and the resulting gradient reversal following storm events.

4.2 Water Budget

Based on the water budget analysis, the inflow volume was greater than outflow volume by 57.8% during the 6.48 day experiment (Table 1). This suggests that infiltration was a large contributor to the overall water budget since other sources of water loss have been assumed negligible for the duration of the study.

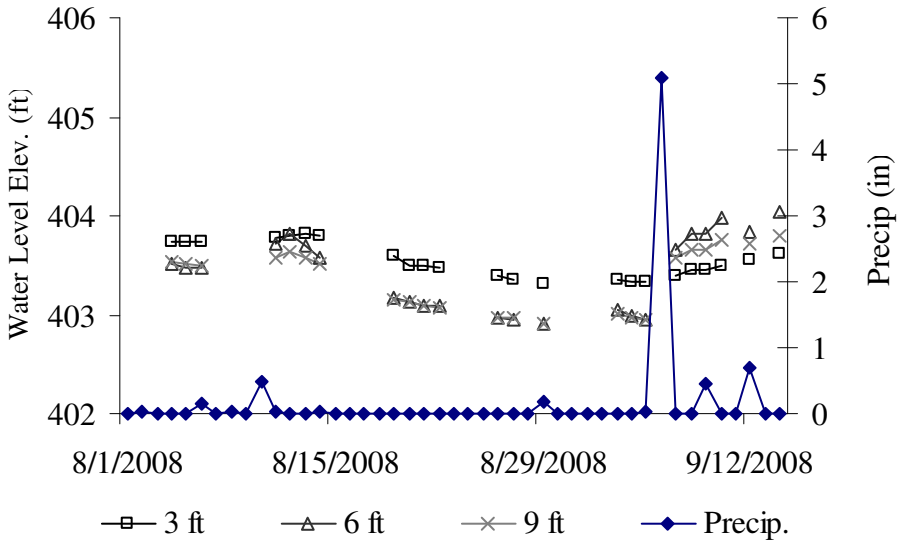

Fig. 3 Piezometer Readings and Precipitation

The water table between the three wells and Mill Creek formed a near perfect linear relationship (y = -0.0184x + 419.44 ft, y = -0.0184x + 127.84m, R^2 = 0.9999, Figure 4). Using the Darcy Equation (equation 9), the average saturated hydraulic conductivity for the entire CSW was calculated to be 2.61 cm/day (1.03 in/day) (Table 1), which is between the two values determined using a flexible wall falling head permeameter and a constant head permeameter, which ranged from 0.0014-9.20 in/day. Furthermore, Blackmore (2006) classified soils immediately adjacent to Villanova's CSW as ML and SM soils. For compacted ML soils, the hydraulic conductivity ranged from 0.92-5.40 in/day, and for compacted SM soils, the hydraulic conductivity ranged from 1.90-10.90 in/day (Johnsen and Jensen, 2001).

Table 1. Values used to calculate the average hydraulic conductivity (Equation 9).

Total Inflow (Qin)	55,372 ft^3, 1567m^3
Total Outflow (Qout)	31,928 ft^3, 904m^3
Total Volume Infiltrated (I)	23,444 ft^3, 663m^3
Ponded Surface Area (A)	42,549 ft^2, 3957m^2
Avg. Hydraulic Gradient (i)	1.44
Total Time (t)	6.48 days
Avg. Hydraulic Conductivity (Ks)	1.03 in/day, 2.61cm/day

4.3 Chloride Mass Balance

Conductivity is a good surrogate measure of chloride concentration (R^2=0.98, Figure 2). The chloride loading leaving the CSW was 500% less than that of the inlet, suggesting a significant removal of chlorides through the CSW (Figure 5). Previous estimates of the retention time under baseflow were about 50 hours (Wadzuk et al. 2006).

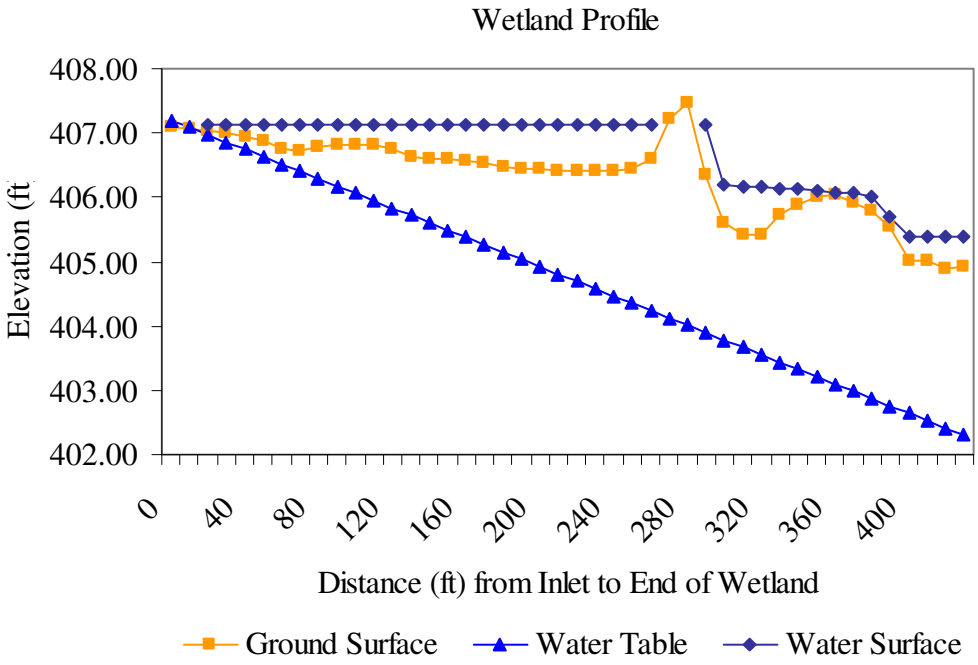

Fig. 4 Cross sectional profile of the wetland was used to calculate the gradient over 40 intervals. Note the groundwater intersects the surface at one location, the inlet.

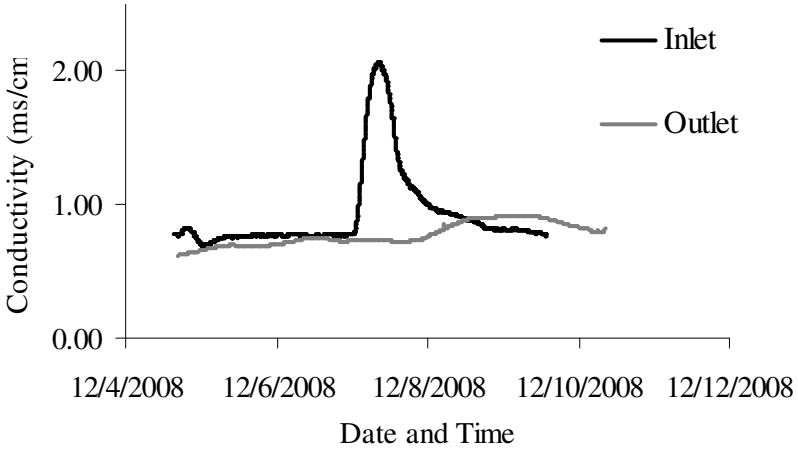

Fig. 5 Inlet and outlet conductivity readings

5 DISCUSSION

The downward flow gradients observed in the piezometers during baseflow conditions suggest that infiltration is occurring. Forty to 49% percent of the total flow moving through the wetland over the year occurs during baseflow conditions (Woodruff, 2005) and any pollutants introduced to the CSW during baseflow, as well as storm flow conditions, could be infiltrated into the groundwater. The downward flow gradients, however, do not conclusively show that infiltration is occurring, but rather that it could be occurring if the soil is permeable enough to allow infiltration to occur. The results of the water budget and chloride mass balance analyses further

suggest considerable infiltration is occurring within Villanova's CSW; however, in order to draw accurate conclusions based on these results, the major assumptions made within the water budget, the chloride mass balance, and the Darcy Equation need to be addressed.

Due to the low average temperature (2.5°C) in conjunction with high average relative humidity (84%), evaporation and transpiration were assumed to be negligible. Additionally, plants lose water through transpiration during metabolic activities and for cooling. The occurrence of low temperatures and the assumption that plants were dormant during the study period provides validation for the assumption of minimal water losses due to transpiration.

During this study the flows were measured using Sigma 950 flow meters. These sensors are prone to take inaccurate readings at low flows. Given that this was a low flow study, some inherent error surrounds the flow readings; however, all the flow meters were the same and were likely to have responded similarly to low flows thereby minimizing the effects of this problem. Furthermore, all instrumentation was calibrated daily to ensure the most accurate flow readings.

Twenty-four hours after chlorides were added to the inlet, conductivity readings were taken in a vertical cross section of the water column. Within this cross section, the conductivity at the surface was 800 μS/cm while that at the bottom (~0.5 m below the surface) was 5000 μS/cm. Like other wetland systems, Villanova's CSW has a deep organic litter layer. It is possible that within this litter layer, chloride stratification occurred within the water column. Because little water flows through this layer, it is possible that chlorides could have accumulated within the CSW. Therefore, the accumulation assumption may have been violated. Rea (2004) noted, however, that inlet and outlet chloride concentrations were similar and suggested that chloride concentrations pass uninhibited through the system. Regardless, any conclusions based on the fate of chlorides should be made with caution.

The ground surface elevation of the CSW averaged 0.45m (1.5 ft) above the estimated groundwater table. The logical question to follow is, "how is the surface water ponding on top of the groundwater?" It is possible that the CSW is atop a perched water table. In this case, the CSW would be on top of a limiting layer resulting in a gradient of zero (dh=0). As a result, infiltration would be negligible. However, a perched water table does not explain the 43% reduction in water moving through the CSW. Furthermore, a perched water table would not explain the reduction in chloride concentration since chlorides would not have been able to penetrate the limiting layer. It is possible that the CSW is actually a mounded system that resulted from the constant inflow of water from Villanova's campus. Villanova's CSW was originally a detention basin that was designed to retain water. Therefore, overland flow and any discharge from the University's campus would collect within the basin. If the infiltration rate over the entire area of the CSW was less than the inflow rate ($I/\Delta t < Q_{inlet}$), then water would pond on the surface of the CSW. This condition would also result in saturated soils, an assumption on which the Darcy Equation is based, which validates the calculation of the hydraulic conductivity. The correlation of the hydraulic conductivity value obtained using the Darcy Equation with published values for similar type soil indicates that the estimated volume of infiltrated water is realistic. Therefore, using the Darcy Equation to account for

anomalous losses within the water budget seems plausible.

6 CONCLUSIONS & RECOMMENDATIONS

Urban stormwater runoff is one of the greatest sources of water quality impairment in rivers and lakes (U.S. EPA 2005). With the rise in popularity of stormwater management techniques that infiltrate polluted runoff, there is concern regarding potential groundwater contamination. Because of the risk of polluting groundwater, the goal of this research was to determine whether infiltration was negligible within peak rate reducing BMPs. In constructing a water budget over a 6.48 day base flow period, anomalous losses accounted for 43% of the total volume of water within the system. Infiltration is the most parsimonious explanation accounting for losses within the system. Similarly, chloride loadings were reduced by 500%; however, due to stratification and a thick litter layer within the CSW, it is unknown whether or not losses in chlorides were due to movement into the groundwater or storage within the wetland system.

Before any definitive conclusions can be drawn about infiltration within this system, multiple base flow water budgets need to be conducted. Furthermore, low flow equipment should be used in order to have the most accurate readings of inflow and outflow data. Finally, more research needs to be conducted to determine the fate of chlorides within the system. Specifically, how does adding chloride to the surface water affect the chloride concentration in the ground water? This could easily be examined using piezometers at varying depths with the soil column below the CSW. Chloride concentrations leaving the CSW could be compared to chloride concentrations at the headwaters of Mill Creek. If chlorides are leaving the CSW and entering the water table, they should appear within the headwaters of Mill Creek.

The findings of this study suggest that infiltration may be a substantial portion of the CSW water budget; however, before any definitive conclusions can be drawn, more research needs to be conducted, specifically addressing the low flow measurement problem and the fate of chlorides within the system. Research regarding infiltration in this CSW will be on-going, and any associated water quality impacts will be investigated.

WORKS CITED

Arnold, C.L., and Gibbons, C.J. (1996). “Impervious Surface Coverage: The Emergence of a Key Environmental Indicator.” *Journal of the American Planning Association*, 62(2), 243-258

Blackmore, D. (2006) “Report of Geotechnical Investigation”. *Technical Report, David Blackmore and Associates, Inc.,* Project 3492G1R1 Pottstown, Pennsylvania

Flynn, K. (2008), "Pollutant Removal Efficiency of a Mature Constructed Stormwater Wetland Over the Course of a Year." Thesis, Villanova University, Villanova, PA

Johnson, H.E., and Jensen, D.M. (2001). “Transmittal of Test Results for: Old Burial Ground Cap, Geotechnical Testing Services.”*, WSRC Site Wide – Task Release No. 61, Law Engineering Project No. 50161-7-0108 (Phase 61). Law Engineering and Environmental Services, Inc.,* Atlanta, Georgia

Kwiatkoski, M., T. Ladd, R. Traver, M. Vanacore, and A. Welker (2007), "Evaluation of an Infiltration Best Management Practice Utilizing Pervious Concrete", *Journal of the American Water Resources Association* 43(5): 1208-1222

"Pennsylvania Stormwater Best Management Practices Manual" (PSBMPM) *Technical Report Draft 2, Cahill Associates*, No. 2003-WWEC-1, 2005, West Chester, Pennsylvania

Rea, M. (2004). "Pollutant Removal Efficiency of a Stormwater Wetland BMP during Baseflow and Storm Events." Thesis, Villanova University, Villanova, Pennsylvania, 1-126

U.S. EPA. (2005). "Stormwater Phase II Final Rule: Small MS4 Stormwater Program Overview" *Technical Report*, Office of Water (4203), EPA 833-F-00-002, Washington D.C.

Wadzuk, B.M., W.C. Heasom, and R.G. Traver (2006), "Modeling and Optimizing the Design of Villanova University's Constructed Stormwater Wetland", *Proceedings of the AWRA 2006 Annual Water Resources Conference*, Baltimore, MD

Weiss, P.T., LeFevre, G., and Gulliver, J.S. (2008) "Contamination of Soil and Groundwater Due to Sormwater Infiltration Practices." *Technical Report, University of Minnesota, St. Anthony Falls Laboratory*, Project Report No.515, Minneapolis, Minnesota, 1-38

Woodruff, G.L. (2005). "Pollutant Removal Efficiency and Seasonal Variation of a Storm Water Wetland BMP." *Unpublished Masters Thesis*, Villanova University, Villanova, Pennsylvania, 1-104

Integration of Low Impact Development Studies into the International Stormwater BMP Database

Jane Clary[1], Marcus Quigley, P.E.[2], Andrew Earles, P.E., Ph.D.[1], Marc Leisenring, P.E.[3], Eric Strecker, P.E.[3], Jonathan Jones, P.E.[1]

[1]Wright Water Engineers, Inc.; 2490 W. 26th Ave., Suite 100A; Denver, CO 80211; (303) 480-1700; clary@wrightwater.com, aearles@wrightwater.com, jonjones@wrightwater.com.
[2]Geosyntec Consultants; 1330 Beacon Street, Suite 317; Brookline, MA 02446; (617)734-4436; mquigley@geosyntec.com.
[3]Geosyntec Consultants; 55 SW Yamhill Street, Suite 200; Portland, OR 97204; (503) 222-9518; mleisenring@geosyntec.com; estrecker@geosyntec.com.

ABSTRACT

Low Impact Development (LID) strategies are being encouraged in many communities as an approach to reduce potential adverse impacts of development on receiving streams. Many questions exist regarding how well various LID strategies perform in different settings, just as similar questions have been raised regarding performance of traditional stormwater best management practices (BMPs). Over a decade ago, Urban Water Resources Research Council (UWRRC) members worked to develop a set of standardized monitoring and reporting protocols for traditional BMPs and establish a master database for the purpose of evaluating BMP performance and the factors affecting performance. This effort culminated in the International Stormwater BMP Database (www.bmpdatabase.org), which contains data for over 350 BMPs and continues to operate as a clearinghouse for stormwater BMP data and performance analyses. During 2008-2009, the Stormwater BMP Database project expanded to better integrate LID into the database. This paper provides a condensed overview and progress report on the LID-focused effort, including the following topics: 1) monitoring guidance for LID at the overall site development level; 2) an overview of recent changes to the stormwater BMP database to better accommodate LID studies, 3) a summary of LID studies currently included in the database; and 4) initial concepts related to evaluating performance of LID studies.

ACKNOWLEDGEMENTS

The International Stormwater BMP Database project is a long-term project that was conceptualized in 1996 by Urban Water Resource Research Council members and funded by the U.S. Environmental Protection Agency. The project has grown and been sustained by support from many individuals and organizations, both financially and through submission of BMP studies. Supporting organizations include the Water Environment Research Foundation, the U.S. Environmental Protection Agency, the Environmental and Water Resources Institute of the American Society of Civil Engineers, the Federal Highway Administration, and the American Public Works Association. During 2008-2009, the primary project focus has been on better integration of LID into the database. This effort has included monitoring, standardized reporting protocols, and analysis approaches that better assess hydrologic performance of BMPs and overall LID sites. In December 2008, an expert panel was convened to provide input and guidance on this effort. Geosyntec Consultants and Wright Water Engineers (WWE) would like

to acknowledge the following experts who were instrumental in developing many of the concepts included in this paper:

Richard Horner, P.E., Ph.D., University of Washington
Bill Hunt, P.E., Ph.D., North Carolina State University
Bob Pitt, P.E., Ph.D., University of Alabama
Robert Roseen, P.E. Ph.D., University of New Hampshire
Robert Traver, P.E., Ph.D., Villanova University
Ben Urbonas, P.E., Urban Watersheds, LLC

INTRODUCTION

Low Impact Development (LID) strategies are being encouraged in many local communities as an approach to reduce potential adverse impacts of development on receiving streams. Many questions exist regarding how well various LID strategies perform in different settings, just as similar questions have been raised regarding performance of traditional stormwater best management practices (BMPs). This paper highlights work completed under the International Stormwater BMP Database Project during 2008-2009 to provide guidance related to LID monitoring, reporting and analysis. *(Note: At the time of submission of this paper, key aspects of these efforts had been released in draft form for review and comment; therefore, the www.bmpdatabase.org website should be referenced for the most current version of recommendations provided in this paper.)*

GENERAL FRAMEWORK FOR LID MONITORING GUIDANCE

While many of the individual LID techniques are comparable to some types of traditional stormwater BMPs, LID is an overall design philosophy based on the implementation of multiple, distributed small-scale controls throughout a development site. Monitoring guidance applicable to traditional BMPs can generally be followed when monitoring individual LID BMPs. However, effectively monitoring overall LID sites can offer a unique challenge and is the focus of a stand-alone chapter in the 2009 update to the *Urban Stormwater BMP Monitoring Manual* (Geosyntec and WWE 2009). In order to provide guidance for LID monitoring studies, it is important to understand the type of LID site being monitoring, included the following general settings:

1) **Individual LID Practice Monitoring**: In this case, an individual LID practice (e.g., a bioretention cell, a biofilter, or permeable pavement parking lot) is isolated to monitor performance. This may also include monitoring a combination of practices in series within a relatively small drainage area such as a biofilter preceding a bioretention cell in a parking lot. These types of monitoring programs can generally follow the guidance for traditional stormwater BMPs, with particular attention to designing studies in a manner that incorporates a robust hydrologic monitoring component and properly addresses the challenges that come with monitoring small watersheds with often poorly structured inflow and outflow monitoring stations. A number of studies exist that demonstrate individual LID practice monitoring approaches such as Hunt et al. (2008), Davis (2008), Emerson and Traver (2008), Barrett et al. (2006), Roseen et al. (2009), and Li et al. (2009).

2) **Overall Site Level LID Monitoring**: In this case, the composite site level performance which includes multiple distributed controls is monitored. Fewer examples exist for these types of studies, with several notable examples including the Somerset Development in Maryland (Cheng et al. 2003), Jordan Cove in Connecticut (Claussen 2007) and Burnsville, MD (Barr 2006). Due to the varying types, number, and spatial distribution of the LID practices, and the lack of specific discharge locations, these types of monitoring study designs can present significant challenges to the researcher. In many cases, the designs of sites must specifically incorporate features to facilitate effective monitoring. Historically, reference or "parallel" watershed study designs have often been used to assess performance at the site level. Alternatively, "before and after" studies can provide insight into how well a LID site is performing relative to pre-development hydrology, which is a fundamental goal for LID projects.
3) **Hybrid LID-Traditional Site Level Monitoring**: In this case, a site to be monitored may include multiple distributed controls and LID principles, but it may also incorporate some traditional larger-scale stormwater management components at the downstream end of the study site, particularly for flood control. For example, a study by Selbig and Bannerman (2008) involves a Cross Plains, WI LID site with multiple distributed controls and a larger-scale infiltration basin located at the downstream end of the drainage. Retrofits of existing subdivisions would often fall into this category. Historic approaches to monitoring these types of sites are similar to those for the overall LID-based site development described above. These types of sites may be more straightforward to monitor relative to the overall LID-based sites because there is often a centralized discharge point to facilitate sample collection.

ENTERING LID STUDIES INTO THE INTERNATIONAL STORMWATER BMP DATABASE

When submitting a LID study to the BMP Database, data must be entered in accordance with BMP Database Reporting Protocols specified in the 2009 Excel spreadsheet package downloaded from www.bmpdatabase.org/DataEntry.htm. Figure 1 provides a simple overview of the general types of data requested, followed by brief descriptions of each major component.

Figure 1. Overview of Data Requirements for Submittal to the BMP Database

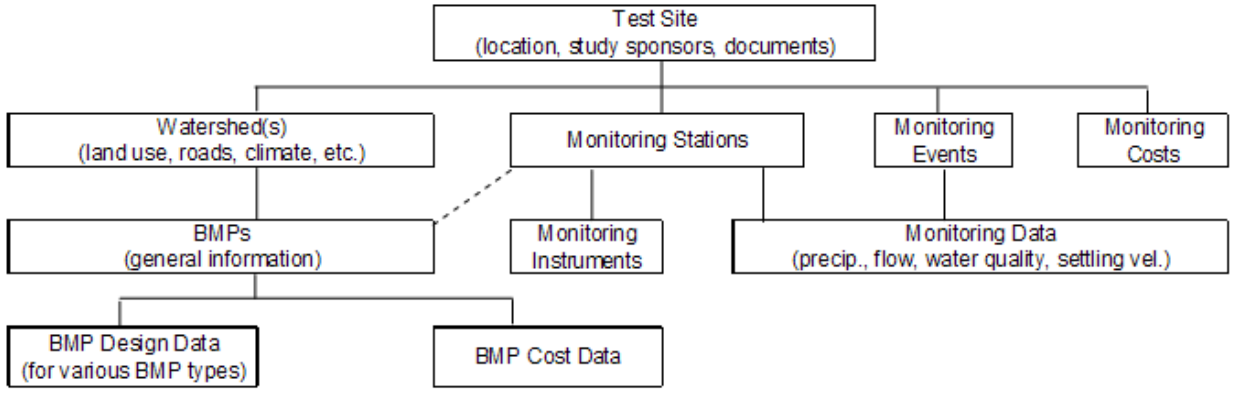

General Test Site Information

The purpose of the general test site data set is to identify the study, its location, climate characteristics, involved parties and cost of monitoring for the study. Additionally, the "study documents" spreadsheet enables the user to attach supporting information such as links to published studies, quality assurance plans, photos, BMP and site layouts, and other information.

Watershed Information

The purpose of the watershed table is to identify the conditions in the area tributary to the BMP. For example, important factors for successful designs of infiltration-type BMPs include watershed parameters such as soil type, imperviousness, and storm drainage system efficiency. More than one watershed may be entered for LID studies that use a reference (i.e., control) watershed to assess performance. For LID studies, there may also be more than one reference watershed in cases where pre-development hydrology and water quality for the site are monitored, along with a comparative watershed developed using traditional development designs. In order to conduct valid comparisons of performance between test watersheds and reference watersheds, it is critical to thoroughly document the watershed conditions for both. For example, a test and reference watershed could have a similar tributary area and number of homes (e.g., "look the same"), but the underlying soil types could be dramatically different, which would be a critical difference between the two watersheds in terms of evaluating performance of the LID design.

General BMP Information

General information and cost data for BMPs are requested for all BMP types, including structural and non-structural BMPs and site-scale LID sites. General information requested includes parameters such as date of installation, various basic design parameters, maintenance and rehabilitation types and frequencies, and cost data. Additionally, BMP-specific design parameters are also requested. An overview of the types of information requested for structural, nonstructural, and LID sites is provided below.

Structural BMPs

Data requested for each structural BMP vary according to the following common groups of BMPs: Detention (Dry) Basins, Retention (Wet) Ponds, Infiltration Basins, Percolation Trenches/Dry Wells, Porous Pavement, Wetland Basins, Wetland Channels/Swales, Biofilters (buffer strips and swales), Media Filters, Bioretention, Stormwater Harvesting (cisterns), Green Roofs, and Manufactured Devices. An "Other" BMP category is also provided to enable flexibility for entry of BMPs that may not fit a pre-defined category. A "Treatment Train" BMP option is also provided. Most of the design parameters requested in the structural BMP tables are required in order to compare the effectiveness of various BMP designs. Table 1 provides a summary of LID practices currently entered into the database. Table 2 provides a summary of design data requirements proposed for bioretention practices, including the "general" BMP information requested for all BMP types.

In order for monitoring data to be interpreted in proper context, it is important to provide thorough documentation of the BMP as constructed in the field, identify whether engineering oversight was provided during construction, and provide a proper description of the BMP's condition during the study. For example, a common problem with bioretention cells and pervious pavements is that the as-built conditions deviate from the design. Without such

information, poor performance of a BMP may be falsely attributed to design characteristics, when the design conditions did not actually exist in the field. Additionally, a well designed and properly installed, but poorly maintained BMP, is unlikely to perform well. It is important to clearly document the maintenance and/or rehabilitation status of the BMP so that researchers using data from the study can appropriately group BMPs with comparable maintenance conditions for performance analysis. The BMP Database accepts properly conducted studies, regardless of whether the BMP performs well, because one of the primary long-term purposes of the BMP Database is to identify factors affecting BMP performance. Improper installation and poor maintenance are key factors that must be properly documented.

Table 1. Overview of Bioretention, Green Roof and Porous Pavement Studies in the BMP Database as of January 2009

LID Techniques Monitored	Source of Studies
Porous Pavement (10)	Southwest Florida Water Management District; Urban Drainage and Flood Control District, Denver CO; City of Austin, TX
Bioretention (10-15)	University of New Hampshire Stormwater Center; North Carolina State University; Villanova Urban Stormwater Partnership; City of Portland, OR, Bureau of Environmental Services
Green Roofs (4)	City of Portland, OR, Bureau of Environmental Services

Non-Structural BMPs

Non-structural BMP data requested are generally narrative/descriptive information on the type and extent of BMP practice being implemented, as well as cost data. Non-structural BMPs are divided into the general categories of education, maintenance, recycling, and source controls. Non-structural practices are often a component of LID sites.

LID Sites

Because LID sites attempt to mimic pre-development site hydrologic conditions by controlling runoff close to its source, BMPs are typically dispersed throughout a development site. Reporting for LID sites includes both individual practices and performance for the overall site. In cases where individual LID practices (e.g., bioretention cells) are monitored, reporting protocols for the individual practices described under "structural BMPs" would be used. When site-scale LID monitoring is conducted, a set of parameters describing the extent to which a broad suite of LID practices is implemented would be entered, as summarized in Table 3. These reporting parameters would be requested in addition to the previously described watershed and monitoring data provided for conventional studies. As discussions related to reporting parameters and performance evaluation approaches for LID sites progress, it is anticipated that additional hydrologic parameters or metrics may also be requested for site-scale LID studies.

Table 2. Example of BMP Design Information Requested for Bioretention Practices
(Draft Released for Review and Comment January 2009; Subject to Revision)

General Information (all BMP types)	Bioretention Design Information
Type of BMP Being Tested (*from Pick-List)*	BMP Name
Basis of Design (e.g., 2-yr, 24 hr storm, water quality volume in watershed inches, etc.)	Type of Bioretention (Pick List: bioretention cell (non-linear), off-line bioretention, in-line bioretention, sloped (weep garden), sloped biodetention vegetative barrier, tree filter box)
Source of Design Guidance for BMP	Ratio of Tributary Area to Bioretention Surface Area (hydraulic loading)
Date Facility Placed in Service	Is Pretreatment Provided? (Y/N)
Number of Inflow Points	Description of Pretreatment, if present
BMP Designed to Bypass or Overflow	Description of Flow Entrance
Upstream Treatment Provided?	Bioretention Surface Area
Describe Upstream Treatment (if any)	Ponding Volume above Bioretention Media Surface
Name of Upstream BMP(s) (comma separated list upstream to downstream)	Average Ponding Depth above Bioretention Media Surface
General Configuration of BMP in Tributary Watershed (i.e., end of pipe, source control, off-line, on-line)	Is "Internal Water Storage Zone" Created? (Y/N)
Was qualified engineering oversight provided at construction? (Y/N)	Subsurface Storage Volume
Was structure installed as designed? (Y/N)	If subsurface storage provided, then height of outlet above bottom of bioretention media
Maintenance and Conditions of BMP	Bioretention Media: Natural or Amended
Maintenance Type and Frequency	Bioretention Media Depth
Last Rehabilitation Date	Bioretention Media Design Specifications
Type of Rehabilitation	Bioretention Media "P" Index (Phosphorus Index)
Description, Types, and Designs of Outlets	Description of Supplemental Bioretention Media Characteristics (clay content, pH, cation exchange capacity, carbon:nitrogen ratio, moisture content, metals contents, inerts content)
Qualitative evaluation of condition	Description of Vegetation Community (canopy layers and their approximate cover [stems/acre], species)
For BMPs without permanent pool, does surface ponding exist beyond design drain time?	Description of Mulch (if present)
If clogging present, estimate % of total surface area of structure affected	Surface Infiltration Rate
Describe BMP/Comments	Design Infiltration Rate (including safety factor for clogging)
	Is an Underdrain Provided? (Y/N)
	Description and Dimensions of Underdrain, if present
	Underdrain Gravel Layer Thickness, if present
	Description and Dimensions of Surface Overflow, if present
	Is a Hydraulic Restriction Layer (Liner) Provided? (Y/N)
	Description of Hydraulic Restriction Layer, if present

Table 3. Site-scale Low Impact Development
(Released for Review and Comment January 2009; Subject to Revision)

Low Impact Development at Site Level Design Information (Source: Horner 2009)	
Parameter	**Explanatory Comment**
BMP Name	Name of the Overall LID Site
Describe Site Design	Provide a brief overall description providing context for how specific design elements fit together.
Describe Monitoring Design	Provide a brief description of monitoring design to ensure proper use of data by others.
Comments/Other Description	Additional information, as desired by data provider.
Describe the Extent to Which the Following LID Practices Were Implemented in Site Design:	**Instructions:** These are narrative fields, but quantitative data should be provided to the extent it is available. If the practice is not implemented, this should be stated instead of leaving the field blank. For discrete practices (e.g., permeable pavement, bioretention), design data should also be provided in their respective BMP tables.
Conservation	Conserving natural areas including existing trees, other vegetation, and soils.
Minimizing Disturbance	Minimizing soil excavation and compaction and vegetation disturbance.
Minimizing Building Coverage	Minimizing impervious rooftops and building footprints.
Minimizing Travelway Coverage	Constructing streets, driveways, sidewalks, and parking lot aisles to the minimum widths necessary, provided that public safety and a walkable environment for pedestrians are not compromised.
Maintaining Natural Drainage Patterns and Designing Drainage Paths to Increase Time of Concentration	Maintaining natural drainage patterns and designing drainage paths to increase time of concentration—Maintaining depressions, natural swales, emphasizing sheet flow instead of concentrated flow; increasing the number and lengths of flow paths; maximizing non-hardened drainage conveyances; and maximizing vegetation in areas that generate and convey runoff.
Source Controls	Minimizing pollutants; isolating pollutants from contact with rainfall or runoff by segregating, covering, containing, and/or enclosing pollutant-generating materials, wastes, and activities; conserving water to reduce non-stormwater discharges.
Permeable Pavements	Constructing low-traffic areas with permeable surfaces such as porous asphalt, open-graded Portland cement concrete, coarse granular materials, concrete or plastic unit pavers, and plastic grid systems (areas that should be considered for permeable surfaces include, but are not limited to, driveways, patio slabs, walkways and sidewalks, trails, alleys, and overflow or otherwise lightly-used parking lots).
Natural Drainage System Elements	Bioretention area (rain garden), vegetated swale, vegetated filter strip.
Stormwater Harvesting	Cisterns, rain barrels.
Green Roof (vegetated)	Vegetated roofs with stormwater-related design components.

Monitored Events, Monitoring Stations and Monitoring Results

The BMP Database requires information to be provided regarding the events monitored, instrumentation at monitoring stations, and monitoring results. For sites also monitoring groundwater levels, soil moisture or particle size distributions, the water quality spreadsheet can be used to enter such data. Data types requested for LID studies include:

- **Precipitation:** Date/time that the event began and ended, total depth and peak one-hour precipitation rate. This is important because performance may be significantly different depending on the type of storm event.
- **Flow (Runoff, Bypass, Base Flow):** Storm runoff directly affects the hydraulics of BMPs. Types of runoff data requested include runoff volumes into, from or bypassing the BMP, and peak flow rates.
- **Water Quality:** Water quality data in combination with flow data for a monitoring event are used to calculate loads of each constituent, which are fundamental for comparing the performance of BMPs at different sites, locations and regions.

EVALUATING PERFORMANCE FOR LID STUDIES

When comparing LID (and/or other distributed controls) sites, performance metrics are needed that move beyond water quality and into evaluation of site hydrology. This can be facilitated by reporting a set of composite site characteristics and hydrologic performance metrics that collectively quantify the extent of LID implemented at a site. Some of these metrics are easier to obtain than others; however, a broad list is provided below for consideration and represents initial brainstorming for performance metrics that could be applied to LID studies. These concepts will continue to be refined during 2009. (*Water quality evaluation would follow approaches similar to traditional BMP studies as described in Geosyntec and WWE [2009] and are not repeated below, but can be obtained from* www.bmpdatabase.org.)

Composite Site Characteristics

An ideal set of composite site characteristics allows for quantification of the extent of LID at a site so that comparisons can be made among LID sites regardless of size, location, and other environmental factors. These characteristics can be estimated for a site, regardless of whether LID techniques have been implemented or whether development has yet occurred. Some composite site characteristics that could be considered include:

- Hydrologically available temporary storage at the site, potentially including these components:
    - Surface storage, including natural, pervious, and impervious depression storage and surface detention that is not surface discharged. This would represent volume that is eventually lost through ET and/or infiltration but would not become a surface discharge.
    - Surface storage, including natural, pervious, and impervious depression storage and surface detention that is eventually surface discharged, but after detention and/or filtration that slows the discharge.
    - Subsurface LID practice temporary storage including all pore space within LID practices (e.g., in bioretention soils, stone infiltration trenches, planter media, green roof media, etc.) that it is not surface discharged. This would also represent volume that is eventually recovered through ET and/or infiltration.

  - Subsurface LID practice temporary storage including all pore space within LID practices (e.g., in bioretention soils, stone infiltration trenches, planter media, green roof media, etc.) that is eventually surface discharged via an underdrain system.
  - Volume in tanks or surface or subsurface detention facilities that is eventually recovered through ET and/or infiltration.
  - Volume in cisterns and rain barrels in excess of average long-term retained volume that is eventually recovered through ET (e.g., irrigation reuse, cooling water makeup reuse, drip hose, etc.) and/or infiltration.
- The tributary areas and characteristics to each of the components above, perhaps expressed as weighted site averages.
- Estimated volume of pore space within the natural duff layer, compost, mulches, etc.
- Maximum (summer), minimum (winter) and annual average potential vegetative canopy interception.
- Area weighted saturated hydraulic conductivity and field capacity of the top foot of native or post construction soils not within LID features.

Hydrologic Performance Metrics

Another method for comparing sites is to treat certain hydrologic performance metrics as indicators of the extent of LID present at a site. Such metrics should represent the combined long-term effects of all LID practices on the surface water flows at a site. In December 2008, an expert panel was convened to provide input on potential approaches to evaluating LID sites, an initial set of potential metrics was proposed for evaluating LID sites (Horner 2009) and include:

- Largest rainfall event (depth and duration) producing no discharge.
- Long-term cumulative discharge volume per unit rainfall (long-term volumetric runoff coefficient).
- Largest rainfall quantity producing no discharge with a "wet" versus "dry" Antecedent Precipitation Index (API). API is defined as APIt = Rt-1 + k*APIt-1, where APIt is the index for day t, APIt-1 is the index for the previous day, Rt-1 is the rainfall depth for the previous day in inches, and k is a coefficient reflecting the relative rate of soil drying (Linsley, Kohler and Paulhus 1982). The value of k can range from approximately 0.85 (sand) to 0.98 (clay). "Wet" is considered to be API > 0.6 and "dry" as API <0.6.
- Average of storm-by-storm volumetric runoff coefficient under wet and dry API.
- Largest rainfall quantity producing no discharge with a varying 7-day antecedent rainfall.
- Peak flow rates for specific average rainfall intensities over the time of concentration. For example, if the time of concentration for a site is 10 minutes, the peak flow rate resulting from an average intensity of 0.1 in/hr, 0.2 in/hr, 0.3 in/hr, etc., over 10 minutes under varied antecedent moisture conditions.
- Hydrograph lag time (time to center of mass of outflow hydrograph volume minus time to center of mass of outflow hydrograph).
- Time of concentration under varied rainfall intensities and APIs determined from analysis of hyetographs and hydrographs.

Additionally, other metrics are also being considered, such as those proposed by Davis (2008) for evaluation of bioretention cells. These metrics include: three metrics for describing the restoration of hydrologic conditions by bioretention facilities: 1) the peak flow rate ratio of effluent to influent (R_{peak}), 2) the peak discharge time span ratio of effluent to influent (R_{delay}),

and 3) the effluent/influent volume ratio (f_V). An example of application of the Davis metrics to six bioretention cells is provided by Li et al. (2009).

CONCLUSIONS

During 2008-2009 substantive revisions to the International Stormwater BMP Database have been completed and others are underway. These include development of monitoring guidance for LID studies, data reporting protocols, and initial development of concepts enabling assessment of performance among LID sites. See the www.bmpdatabase.org website for the most up-to-date monitoring and reporting protocols.

REFERENCES

Barr Engineering Company (2006). *Burnsville Stormwater Retrofit Study*, prepared for City of Burnsville.

Cheng, M.S.; Coffman, L.S.; Zhang, Y.; and Licsko, J.Z. (2003). "Comparison of Hydrological Responses from Low Impact Development with Conventional Development," *Proceedings of World Water & Environmental Resources Congress 2003*, EWRI, American Society of Civil Engineers, June 23-26, 2003, Philadelphia, Pennsylvania.

Claussen, J.C (2007). *Jordan Cove Watershed Project: Final Report.* Prepared for U.S. EPA and Connecticut Department of Environmental Protection.

Davis, A.P. (2008). Field Performance of Bioretention: Hydrology Impacts. *Journal of Hydrologic Engineering* 13:2(90).

Emerson, C.H. and Traver, R.G. (2008). "Multiyear and Seasonal Variation of Infiltration from Storm-Water Best Management Practices." *J. of Irrigation and Drainage Engineering*. 134(5): 598-605.

Geosyntec Consultants, Wright Water Engineers, 2009. *Urban Stormwater BMP Monitoring*. Prepared with support from the U.S. Environmental Protection Agency, Water Environment Research Foundation, and the Urban Water Resources Research Council.

Horner, R. (2009). Personal Communication following Stormwater BMP Database Expert Panel Meeting in Denver, CO. (unpublished written communication).

Hunt, W. F.; Smith, J.T.; Jadlocki, S.J.; Hathaway, J.M.; and Eubanks, P.R. (2008). "Pollutant Removal and Peak Flow Mitigation by a Bioretention Cell in Urban Charlotte, NC." ASCE *Journal of Environmental Engineering*.

International Stormwater BMP Database website: www.bmpdatabase.org.

Li, H., Sharkey, L., Hunt, W., and A. Davis (2009). "Mitigation of Impervious Surface Hydrology Using Bioretention in North Carolina and Maryland," *ASCE Journal of Hydrologic Engineering*. April.

Linsley, R. Kohler, M. and Paulhus, J. (1982). *Hydrology for Engineers*, 3rd ed. Whitby, ON, Canada McGraw-Hill.

Roseen, R. M., Ballestero, T. P., Houle, J. J., Avellaneda, P., Briggs, J. F., Fowler, G., and Wildey, R. (2009). "Seasonal Performance Variations for Stormwater Management Systems in Cold Climate Conditions." ASCE *Journal of Environmental Engineering*.

Selbig, W.R., and Bannerman, R.T. (2008). A Comparison of Runoff Quantity and Quality from Two Small Basins Undergoing Implementation of Conventional- and Low-impact-development (LID) Strategies. Cross Plains, Wisconsin, Water Years 1999–2005. U.S. Geological Survey Scientific Investigations Report 2008–5008, 57 p.

KANSAS CITY – BALANCING GREEN INFRASTRUCTURE WITH TRADITIONAL APPROACHES FOR CSO CONTROL

Scott D. Struck, Ph.D. [1]; Tom Jacobs [2], Ginny Moore, J.D.[2], Robert Pitt, Ph.D., P.E., D.WRE[3]; Michael A. Ports, P.E., D.WRE[4,] Deborah O'Bannon Ph.D., P.E.[5], Erich Schmitz P.E.[5], Richard Field P.E., D.WRE[6]

[1] Tetra Tech, Inc., 350 Indiana Street, Suite 500, Golden, CO 80401; PH (720) 881-5837; e-mail: scott.struck@tetratech.com
[2] Mid-America Regional Council, 600 Broadway, Suite 200, Kansas City, MO 64105 (816) 474-4240; e-mails: tjacobs@marc.org, gmoore@marc.org
[3] University of Alabama, Department of Civil, Construction, and Environmental Engineering, Box 870205, Tuscaloosa, Alabama 35487 Tuscaloosa, AL; PH (205) 348-2684; e-mail: Rpitt@eng.ua.edu
[4] University of Missouri - Kansas City, 352G Flarsheim, 5100 Rockhill Rd, Kansas City, MO 64110; PH () - ; e-mails: ObannonD@umkc.edu,schmitzeg@umkc.edu
[5] Bergmann Associates, 8653 Baypine Rd, Suite 100, Jacksonville, FL 32256; PH (904)363-3203 ; e-mail: mports@BERGMANNPC.com
[6] EPA-ORD Urban Watershed Management Branch,2890 Woodbridge Ave, MS-104 Edison, NJ 08837; PH (732) 321-6674; e-mail: field.richard@epa.gov

Abstract

The City of Kansas City Missouri is perfectly positioned for demonstrating the use and effectiveness of applying green infrastructure for combined sewer overflow (CSO) control. The Kansas City Water Services Department (WSD) provides wastewater collection and treatment for approximately 650,000 people, located within the City and in 27 tributary or "satellite" communities. Approximately 56 square miles within Kansas City, south of the Missouri River, are served by combined sewers. The City's combined sewers overflow to a number of receiving streams, including the Kansas River, the Missouri River, the Blue River and Brush Creek. Kansas City has also suffered from severe flooding issues. Lives have been lost and significant property damage has occurred as a result of flooding, in large part due to substantial increases in stormwater runoff from ever-increasing impervious surfaces.

Kansas City's WSD has conducted extensive modeling and economic studies of its combined sewer system over the last 5 years, in preparation for submittal of its long term control plan to EPA, in January 2009. These studies and recent funding opportunities have provided the impetus for selection of Kansas City as a case study location to demonstrate the efficacy and sustainability of green infrastructure approaches in an urban-core neighborhood served by a combined sewer system. The intent of this project is to compile data and demonstrate the water quality and quantity results from larger scale application of LID or micro-BMP retrofits in a subcatchment.

---

[1] Tetra Tech, Inc., Golden CO
[2] Mid-America Regional Council, Kansas City, MO
[3] University of Alabama, Tuscaloosa, AL
[4] University of Missouri-Kansas City, Kansas City, MO
[5] Bergmann Associates, Jacksonville, FL
[6] EPA-ORD Urban Watershed Management Branch, Edison, NJ

Installed monitoring equipment will measure changes in peak flow, total volume and pollutant mass of storm events and overflows for a two-year period. The project also includes working with community-based partners to plan, design, implement, monitor and evaluate green infrastructure acceptance from a socio-economic context. Economic, hydraulic, and water quality modeling is also being done. Results from pre-implementation monitoring and expected modeling outcomes developed to date will be presented.

Key Words: Urban Stormwater and Wastewater Management, CSO Reduction, Modeling, Economic Analyses, Wet Weather Flow

Introduction

Advanced design concepts such as Low Impact Development (LID) and Green Solutions (or upland runoff control techniques) are currently being encouraged by the U.S.EPA (EPA) as a management practice to contain and control stormwater at the lot or upland residential parcel level. These controls have shown that when implemented and maintained properly, they can increase retention at the runoff source – decreasing the runoff volume entering the drainage system and the demand on a drainage system. Both developed stormwater and combined sewersheds can benefit from the added storage from areas retrofitted with bioretention cells or rain gardens and other management, e.g., inlet retrofits or curb-cuts with tree plantings.

This paper documents an effort by the U.S. EPA to demonstrate the efficacy of implementing integrated, green infrastructure-based solutions to support control of wet-weather flow pollution problems in an urban core neighborhood within a combined sewer system. This pilot project is part of a larger adaptive management approach to incorporate Green Solutions into the Kansas City long term control plan. The project involves local and regional efforts to provide the "basis-for-success" of the implementation of Green Solution infrastructure and stormwater management at the neighborhood, watershed, and regional levels. The project will demonstrate the strategy and methodology, including model support, for identifying where and how Green Solutions will be implemented within Kansas City, Missouri.

The key objectives in this project are to:

- Demonstrate the efficacy and sustainability of green solutions in an urban-core neighborhood having a combined sewer system
- Develop a methodology for implementation of Green Solutions
- Compile data to demonstrate the effects on the receiving system of Green Solutions for an urban watershed
- Measure the changes in both the peak flow, total volume and pollutant mass of a storm event in the receiving system or the reduction of combined wastewater volumes, pollutant loads and overflows
- Develop a model for predicting the quality and quantity benefits of implementing Green Solutions

- Compare economic costs and benefits of integrated green and grey solutions

Background

The City of Kansas City Missouri is perfectly positioned for demonstrating the use and effectiveness of applying green infrastructure for combined sewer overflow (CSO) control. The Kansas City Water Services Department (WSD) provides wastewater collection and treatment for approximately 650,000 people, located within the City and in 27 tributary or "satellite" communities. Approximately 56 square miles within Kansas City, south of the Missouri River, are served by combined sewers. The City's combined sewers overflow to a number of receiving streams, including the Kansas River, the Missouri River, the Blue River and Brush Creek. Kansas City has also suffered from severe flooding issues. Lives have been lost and significant property damage has occurred as a result of flooding, in large part due to substantial increases in stormwater runoff from ever-increasing impervious surfaces.

Kansas City's WSD has conducted extensive modeling and economic studies of its combined sewer system over the last 5 years, in preparation for submittal of its long term control plan to EPA, in January 2009. These studies and recent funding opportunities have provided the impetus for selection of Kansas City as a case study location to demonstrate the efficacy and sustainability of green infrastructure approaches in an urban-core neighborhood served by a combined sewer system.

The study area is a 100 acre subcatchment shown in Figure 1. The selected sewershed contains commercial, medium density, and some high density residential land uses. An adjacent 80 acre subcatchment has been selected as a control

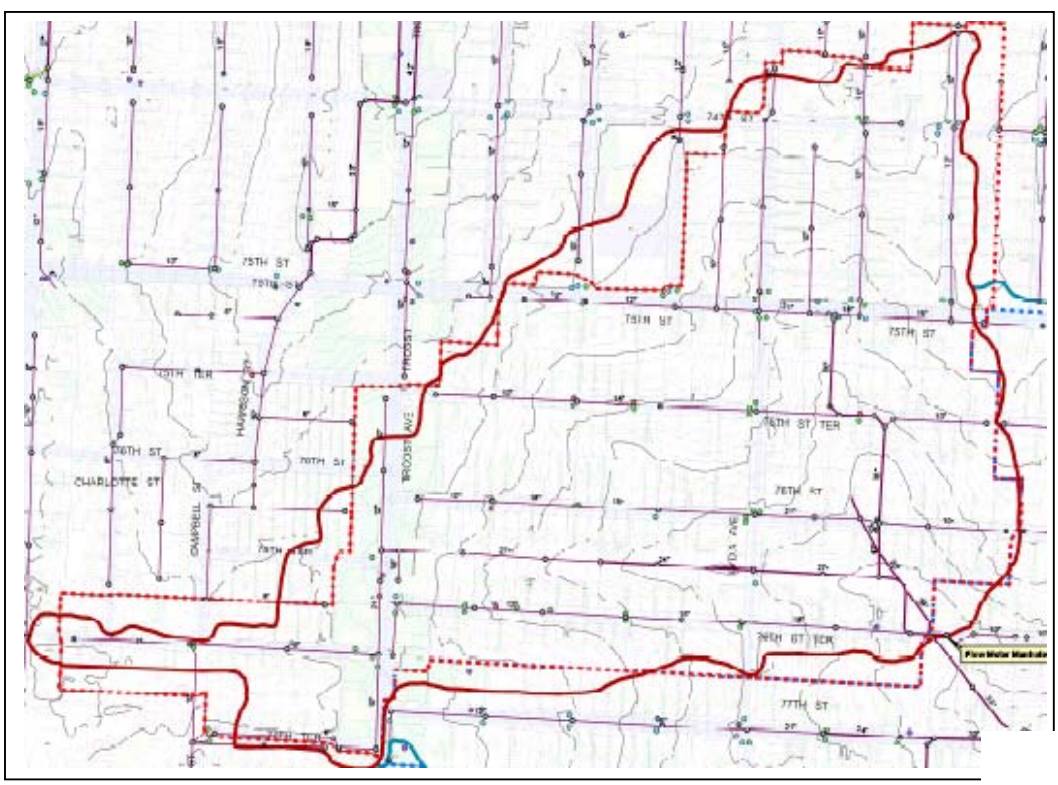

Figure 1. Sewershed of the pilot project. Solid red line indicates the watershed boundaries while the dashed red indicates the sewershed boundaries.

watershed.

Technical Approach for Monitoring and Modeling Interactions

Pre and post-control installation monitoring of the combined sewer flows in the drainage area below the area where the stormwater management controls are being installed are critical components to this project. The stormwater management controls in the demonstration area drain to the municipal combined sewer drainage system in the Middle Blue River watershed. This drainage pattern will allow isolation of the benefits of the upland stormwater controls with minimal flows coming from outside areas. The watershed model (WinSLAMM) and the sewerage model (SWMM) will be calibrated for this area using the pre-construction flow, Land use characterizations and water quality data. Both dry and wet weather flow data will be recorded. The calibrated models will be used early in the project to predict the benefits of the upland controls, and these predictions will be verified as the controls are installed. After the models are calibrated and verified for the demonstration area, they will be used to predict the benefits of wider application of the upland controls across the city. Specifically, the models will predict the decreased runoff volumes and peak runoff rates associated with upland stormwater controls to alleviate problems in the combined sewer system. Water quality benefits associated with stormwater pollutant discharge reductions of wet weather particulates (including particle size distributions), nutrients, bacteria, and heavy metals will be quantified. WinSLAMM will be used to calculate the stormwater contributions to the combined sewerage system during wet weather by providing a time series of flows and water quality conditions, for various types of upland controls, while SWMM, with its detailed hydraulic modeling capabilities, will focus on the interaction of these time series data with the sewage flows and detailed hydraulic conditions in the drainage system. Both models will be used interactively emphasizing their respective strengths.

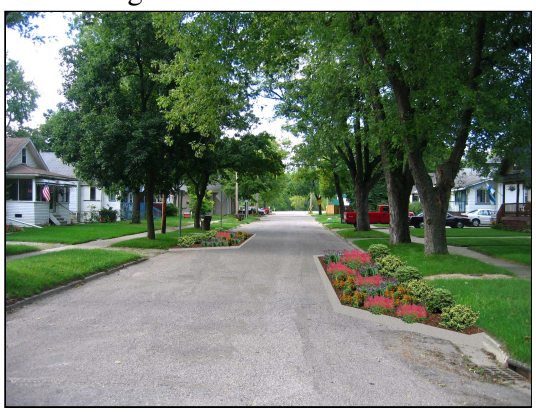

Figure 2. Rendering of Curb Extension Swales.



Figure 3. Rendering of Permeable Pavement Sidewalk and Bioretention.

Detailed monitoring of the upland stormwater controls (rain gardens, biofiltration devices, rain barrels and larger cisterns, inlet inserts) will be used to calibrate and verify the stormwater models reflecting local conditions (soils and rainfall patterns). WinSLAMM contains numerous upland control options, including development conditions (such as downspout disconnections and other impervious

area disconnections, and amended soils), and specific controls that focus on runoff reduction (grass swales, biofilters, rain gardens, beneficial reuse of stormwater, etc.) that can be modeled (Figure 2 and 3). It can be applied to individual control locations, to land use areas having many controls, and to larger areas having multiple land uses. WinSLAMM has been successfully used to produce detailed hydraulic calculations of infiltration

devices considering detailed geometries of the device, underlying soils, amended soils, gravel storage layers, and hydraulic outlets. Variabilities in soil properties affecting infiltration can be large. WinSLAMM therefore includes stochastic elements that consider these variabilities in the resulting calculations. Newer additions to the model that will be used for this project include detailed evapotranspiration calculations that consider specific plants and root characteristics.

Completed Monitoring

This project is compiling data to demonstrate the water quality and quantity results from larger scale application of LID or micro-BMP retrofits in a subcatchment. To date over four months of quantity data has been collected from seven locations in the test watershed. Table 1 indicates the flow meter identification number, pipe size, owner and their purpose for the study.

Table 1 – Flow Monitoring Site Summary

Subsystem	Manhole	Diameter (inch)	Flow Meter Owner	Purpose
UMKC01	S128-498	42	KCMO (OCP)	Pilot Project Flow Basin
UMKC02a	S128-422	30	KCMO (OCP)	Control Flow Basin
UMKC02b	S128-420	24	GBA	Control Flow Basin
UMKC03	S128-426	30	KCMO (OCP)	Control Flow Basin
KCMO01	S128-556	18	GBA	Pilot Project Flow Basin
KCMO02	S128-555	27	GBA	Pilot Project Flow Basin
KCMO03	S128-471	18	GBA	Pilot Project Flow Basin

This data has captured four wet weather flow events as shown in Figure 4. Flow of one of these events for three of the seven monitoring locations is shown in Figure 5.Water quality monitoring equipment will be installed in close proximity to three of the flow monitoring stations and will also record control practice in and out measurements.

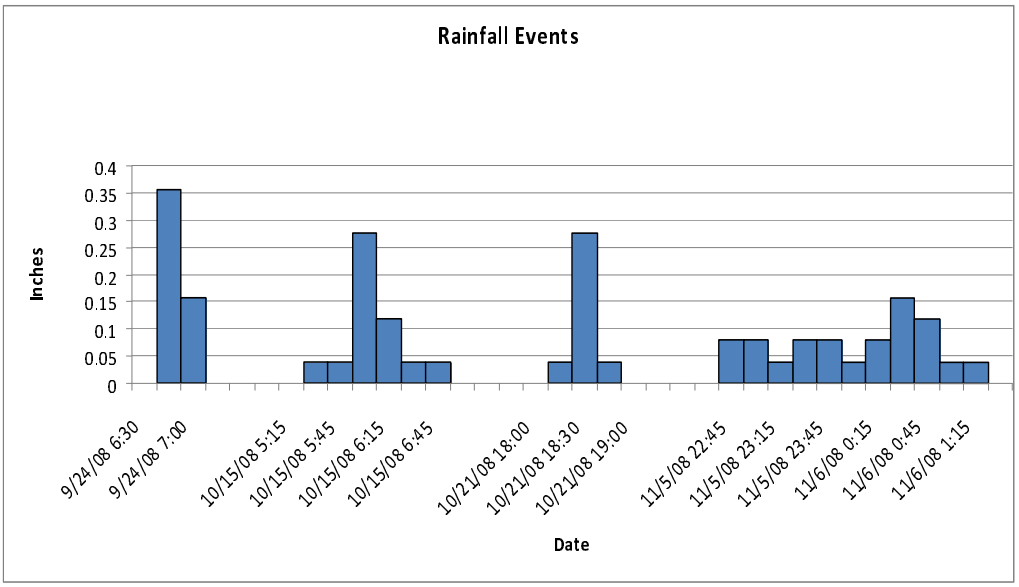

Figure 4. Rainfall data from four events.

Overall, this monitoring scheme will measure changes in peak flow, total volume and pollutant mass of storm events and overflows for a two-year period. Detailed monitoring of selected controls (rain gardens, biofiltration devices, rain barrels and larger cisterns, inlet inserts; green roofs) will be used to calibrate and verify the stormwater models reflecting local conditions (soils and rainfall patterns). Water quality samples will be collected using automatic samplers and data will be downloaded from data acquisition modules following rainfall events. The practices will be inspected for general conditions regularly. Data collected will include the rainfall record and flow data. Laboratories for analyses will include University of Missouri – Kansas City (analytes will include fecal coliform, COD, suspended solids, pH and turbidity), University of Alabama (analysis of solids), and The City's WSD laboratories (analytes include nutrients, metals, pesticides and/or oil & grease). All laboratory analyses and data collection follow an EPA approved quality assurance project plan.

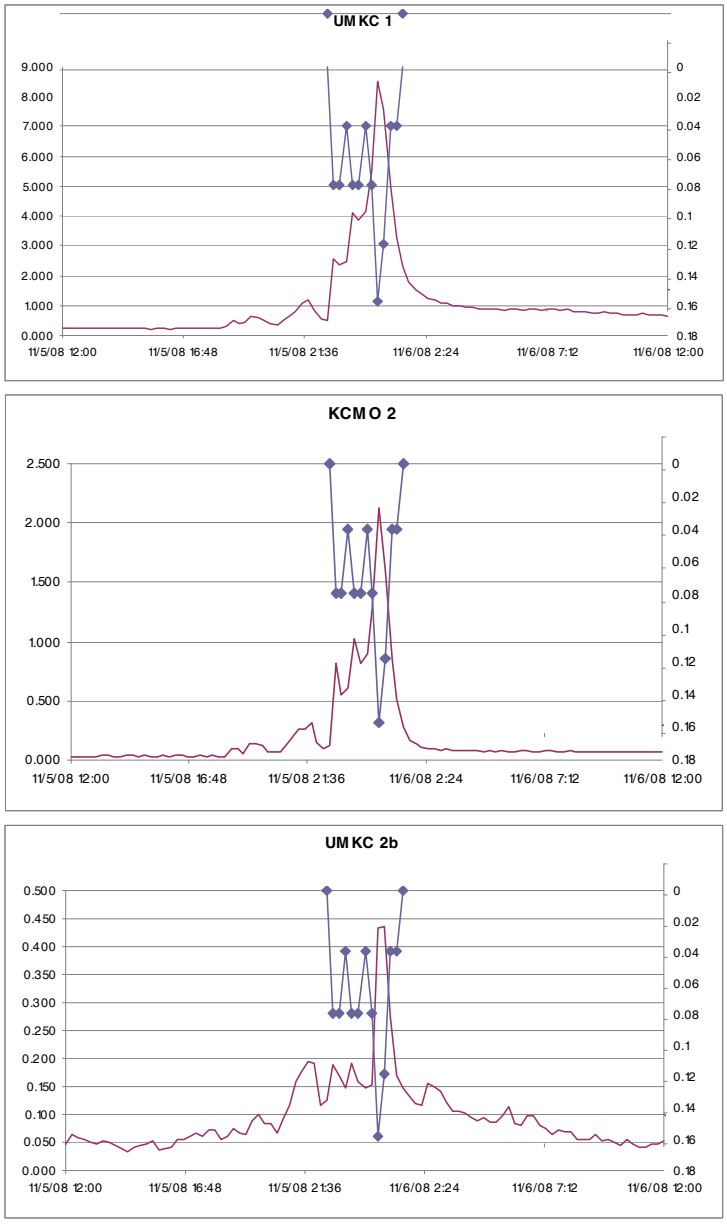

Figure 5. Rainfall data and flow data from three gauges for a November wet weather events.

Selection of the Most Appropriate Combination of Controls

There are many control options that can be used to reduce stormwater discharges to combined sewer systems. Infiltration of excess stormwater will be one method examined during this Kansas City project. Other options will include development modifications associated with disconnection roof rains and other impervious areas from direct connections to the combined sewer, and the beneficial use of the stormwater during dry weather. Combinations of these approaches will

likely be the most effective, depending on specific characteristics of each area being examined.

The selection of the most appropriate combination should use decision analysis methods. Decision analysis is a systematic procedure that enables one to study the trade-offs among multiple and usually conflicting objectives. An alternative procedure is to separately determine the programs necessary to meet each objective and to use the least costly program that satisfies all the identified critical objectives. This is an acceptable procedure some of the time, but it may not result in the most cost-effective program, especially when multiple and conflicting objectives need to be considered. Pitt and Voorhees (2007) presented a description and examples of using decision analysis methods with WinSLAMM for complex stormwater projects and the following summary is from that publication.

There is a great deal of information calculated by WinSLAMM during an analysis for a site and stormwater management alternative. In most cases, just a few of the values are sufficient for quick comparisons. These include the overall percent runoff and particulate solids reductions, the final Rv and runoff volume, and the resulting particulate solids yields and concentrations. Recent enhancements to WinSLAMM also now enable the costs and the expected habitat conditions of the receiving waters to be directly calculated and compared, in addition to flow-duration information. The batch processor option of WinSLAMM is frequently used to automatically examine all the land use and stormwater control options for a relatively large area, such as for city-wide analysis, especially when used in conjunction with GIS data.

The techniques of decision analysis, as described by Kenney and Raiffa (1976), can be used to aid in the selection process. This method uses utility curves and trade-offs between the different attributes. The utility curves should be based on data and not reflect personal attitudes or objectives, while the trade-offs between the attributes reflect different viewpoints. This decision analysis method is a powerful tool that can be used to compare the rankings of alternative stormwater management programs for different groups. In many cases, final rankings may be similar amongst the interested parties, although their specific reasons vary. This tool also completely documents the decision making process, enabling full disclosure.

Current Status of Project

Results from pre-implementation monitoring and expected modeling outcomes developed from monitoring data will be presented to support detailed hydraulic and water quality analyses providing before and predicted post Green Solution implementation information for planning and design at the site, sewershed, and watershed levels.

Refined land use characterizations have recently been completed to assess accuracy of GIS land use layers and to verify existing land use metadata is defined in the same manner as land use codes to be used in the WinSLAMM model for accurate model predictions.

Project Outcomes

It is expected that the methodology used to determine site selection will provide the best technical, political, social, and cost effective location based on modeling and considered needs of the neighborhood, WSD, and for water quality benefits. The modeling approach will provide a scientifically sound basis for the locations, types, and design of the stormwater management practices selected for this project. The initial outcomes from this project including planning and design process determination and modeling approach will be of interest to other engineering and planning professionals.

References

Pitt, R. and J. Voorhees. "Using decision analyses to select an urban runoff control program" Chapter 4 in: *Contemporary Modeling of Urban Water Systems*, ISBN 0-9736716-3-7, Monograph 15. (edited by W. James, E.A. McBean, R.E. Pitt, and S.J. Wright). CHI. Guelph, Ontario. pp 71 – 107. 2007.

Keeney, R.L. and H. Raiffa. 1976. Decision Analysis with Multiple Conflicting Objectives. John Wiley & Sons. New York.

KANSAS CITY, MISSOURI
OVERFLOW CONTROL PLAN SUMMARY

January 2009

Terry Leeds[1], **Scott Struck**[2]
[1]Water Services Department, City of Kansas City, MO, [2]Tetra Tech, Inc

Kansas City's Sanitary Sewer System

Kansas City began building the basic sewer infrastructure that would allow the City to grow and prosper over 150 years ago. Amazingly, some of that infrastructure is still in use today. While focused on controlling overflows, a significant portion of the Overflow Control Plan addresses repairing, improving, and maintaining the City's basic sanitary sewer system so that it can be used by Kansas Citians for years to come.

Kansas City's overall sanitary sewer system is comprised of both combined and separate sewer systems. A combined sewer system is simply a single sewer system that carries both sewage and stormwater. Kansas City has 58 square miles of combined sewers. Typically these systems are in the oldest areas of the City and are not capable of carrying the large amounts of stormwater that now run off of our urban landscape. During moderate to heavy rainfall events, the system will reach capacity, overflow, and discharge a mixture of sewage and stormwater directly to our streams and rivers. Although there is a desire to minimize these overflows, the discharge of combined sewer overflows is not uncommon from combined sewer systems and is allowed under a National Pollutant Discharge Elimination System (NPDES) permit issued to Kansas City's Water Services Department by the Missouri Department of Natural Resources.

The remainder of Kansas City's sanitary sewer system is considered a separate system. A separate sanitary sewer system collects sewage and a relatively small percentage of inflow (stormwater) and infiltration (ground water which gets into the sewers through cracks) and is not designed to overflow unless a storm occurs which exceeds the sanitary sewer design capacity. In Kansas City, however, the separate sanitary sewer system is in great need of repair. Stormwater entering through joints, broken pipes and manholes, and unpermitted direct connections causes the system to overload during rain events much smaller than its design storm. When flows in the sanitary system exceed its capacity, it too overflows a mixture of sewage and stormwater. Unlike combined sewers, however, overflows from the separate sanitary system are not currently authorized in the City's discharge permit.

Developing the Overflow Control Plan

In 2003, Mayor Kay Barnes appointed the Wet Weather Community Panel to help guide the City's efforts in addressing combined sewer overflows and flooding issues. This group has met extensively over the last five years and established goals by which the Overflow Control Plan and Kansas City's stormwater initiatives have developed.

Goals and objectives of the Wet Weather Community Panel are as follows:

- Minimize loss of life and injury and reduce property damage due to flooding
- Improve water quality
- Maximize economic, social and environmental benefits

Almost 300 different alternative solutions were evaluated during the five year development of the Overflow Control Plan. Alternatives were evaluated by cost, feasibility, ability to control overflows, and multi-benefit potential to help control stormwater. In an effort to maximize benefits received from the investment, final alternatives were also evaluated for potential to incorporate green infrastructure as part of the proposed solution.

TRIPLE BOTTOM LINE
People, Planet, and Prosperity: Sustainable design establishes a balance between social, economical and environmental factors – between people, prosperity and the planet. Within the triple bottom line cycle, the benefits propagate naturally into other areas.

SYSTEMS THINKING
Systems thinking is a unique approach to problem-solving that examines systems in a holistic manner. Essentially, the only way to fully comprehend why a problem or issue occurs is to understand the part in relation to the whole.

INTEGRATED DESIGN
Through a process of integrated design, which is both an organized collaboration between disciplines and an interweaving and interconnectivity of man made and natural systems, teams create design solutions that are both environmentally responsible and that achieve the highest level of design excellence. The practices of our civic leaders, ecologists, engineers, architects, landscape architects, and craftsmen requires an understanding of a number of complex and varied issues and the ordering of those issues, based on project needs, desires and abilities. Successful design requires a process that includes all stakeholders in its dialogue and encourages feedback in a process of continuous refinement and improvement.

Adaptability in Future Years

This Overflow Control Plan is premised on an adaptive management approach. Adaptive management integrates design, management, and monitoring to

systematically test assumptions, learn from results, and adapt future plans throughout implementation. Its uniqueness is grounded in the flexibility it can bring to the Overflow Control Plan and the City's ability to meet regulatory requirements and achieve "triple bottom line" results. Integrating adaptive management principles into the Overflow Control Plan will require strong leadership, strategic business planning, an effective performance measurement system, and a "continual improvement" operational framework.

The adaptive management framework will be applied to the Overflow Control Plan on various levels. Adaptive management will be part of the overall programmatic approach, and will also be specifically applied at the basin and project level. Data gathered through project implementation will provide opportunities for feedback loops that subsequently inform decision-making at the basin level and ultimately at the overall program level.

A critical aspect of adaptive management is the ability to measure and evaluate project activities, which requires the identification of performance indicators, or measures of success. As this Overflow Control Plan moves forward, performance indicators that relate to overall program development and implementation will be formulated to measure program success in reducing sewer overflows and maximizing social, economic and environmental opportunities for the Kansas City community. Additionally, specific performance indicators will be devised to evaluate success at both the project and basin level.

As part of the adaptive management approach, the proposed Overflow Control Plan focuses on first repairing the existing system and reducing inflow and infiltration, while also measuring the potential of green infrastructure. Completing these activities early in the program will allow the City to use monitoring, modeling and measurement tools to evaluate program results, and adapt the plan accordingly, before constructing more expensive structural controls.

In addition to conducting a regulatory review of the plan every five years, the Overflow Control Plan incorporates intermediate, internal program reviews occurring at the mid-point of each 5-year cycle that will focus on the direction of the Plan and its benefit to the rate payers and citizens of Kansas City.

Public Policy Changes

The Overflow Control Plan is just one element of a comprehensive approach to position Kansas City as America's Green Region. The broader approach will systematically incorporate low impact development strategies, tools, and practices that focus on maintaining the natural hydrologic cycle. A great example of this strategy is the City's recent adoption of a stream setback ordinance in August of 2008. Other initiatives which will enhance the effectiveness of this plan include:

INTEGRATION WITH OTHER CITY AND REGIONAL EFFORTS
The Overflow Control Plan will complement and be integrated with other city and regional programs related to integrated water resource management, climate protection, land use, community development, parks and trails, air quality, and transportation.

DEVELOPMENT REGULATIONS FOR PUBLIC AND PRIVATE PROPERTY
A review of the full city development code to support broad low impact development strategies will be used to formulate proposed code revisions to be submitted to the City Council for its review and approval.

STORMWATER ENGINEERING CRITERIA, STANDARDS AND SPECIFICATIONS FOR NEW AND REDEVELOPMENT PROJECTS
Existing standards applied to public and private projects alike, will be reviewed to ensure that low impact development benefits are maximized through state-of-the-art stormwater management practices.

URBAN AND COMMUNITY FORESTRY PROGRAM
Expanded urban forestry programs will achieve multiple benefits, such as improved air and water quality, reduced energy use and urban heat islands, and restored habitat and biodiversity.

STANDARD OPERATING PROCEDURES
City operations and maintenance practices will be guided by new procedures to capitalize on the many opportunities to implement more distributed, green infrastructure solutions, and to ensure the long term effectiveness of these practices.

Cost and Affordability

A financial capability assessment for the recommended Overflow Control Plan was prepared using procedures suggested by the EPA. The EPA's approach calls for an evaluation of costs of the proposed improvements against Kansas City's median household income. In general, the EPA considers wastewater costs below two percent of median household income to be an acceptable cost burden to ratepayers.

As suggested by the EPA, costs for implementing the Overflow Control Plan were estimated in current day dollars at $2.4 billion. Based on the cost and a preliminary 25-year implementation schedule, the affordability assessment determined that the Overflow Control Plan would result in a cost to Kansas City residents of approximately 1.7% of median household income. This will impose a heavy financial burden on Kansas City residents.

Overflow Control Plan

The Overflow Control Plan was developed to meet regulatory requirements put forth by the Environmental Protection Agency (EPA) and the Missouri Department of Natural Resources (MDNR) related to minimizing overflows from the combined and sewer separate sewer systems. This plan meets those objectives by providing a planned list of improvements targeted at capturing for treatment, approximately 88% of combined sewer overflows, and controlling sanitary sewer overflows during a 5-year rainfall event. While it would be desirable to completely eliminate all wet weather sewer system overflows, the financial burden that would be placed on the rate payers to achieve those goals would simply be too great.

The Overflow Control Plan addresses issues beyond combined sewer overflows, such as deferred maintenance, repairs, and overflow control in all parts of the sanitary sewer system. Completing these repairs not only extends the life of the system for future generations, but they also help in reducing the size of the problem which Kansas City must overcome.

While this Overflow Control Plan is recognized as one of the "greenest" ever developed, WSD will strive to make it even greener through the adaptive management approach described above. There is a desire to utilize above ground, green infrastructure in a manner which provides substantial ancillary benefits to Kansas Citians beyond sewer overflow control, such as cleaner air, cooler ambient air temperatures, recreational and aesthetic amenities, and economic opportunities. This plan lays the ground work for Kansas City to realize those benefits with a substantial, initial investment in green infrastructure and an adaptive management approach that will allow additional green infrastructure to be utilized as its benefits to the system and the City are measured and confirmed.

PUBLIC EDUCATION AND OUTREACH

Active citizen participation will be critical to the overall success of the Overflow Control Plan. To facilitate this participation, the City will partner with neighborhood associations to develop a public education and outreach program that helps inform citizens of the problem and their role in the solution. Creating successful individual projects is also highly reliant on positive citizen participation. Throughout the life of the plan, public education and outreach will also focus on informing citizens about proposed project designs, schedules and progress towards completion. Funding for public education and outreach has been estimated at $12 million, to be spent over the life of the program.

RAIN GARDENS AND DOWNSPOUT DISCONNECTS

Since 2005, Kansas City's award-winning 10,000 Rain Gardens Campaign has focused on educating homeowners on the positive effects of rain gardens. In the Overflow Control Plan, the campaign's focus will be expanded to include an aggressive rain garden establishment program along with a new downspout disconnection program. Funding for the program is estimated at $5 million. The

initiative, which will incentivize citizens to disconnect their downspouts, will also include assistance and information related to helping homeowners and businesses manage and hold water on their own property.

GREEN COLLAR JOBS AND WORKFORCE DEVELOPMENT

Preparing our community for the work required in the Overflow Control Plan is critical. Every dollar of this $2.4 billion investment that can be kept within Kansas City is a dollar of economic development opportunity for our local businesses and residents. To keep those dollars home, local minority and woman owned business enterprises, design firm, contractors, and the City itself will have to ramp up their capabilities and skill sets. The plan includes $5 million to be utilized in job creation and work force development initiatives related to program specific objectives. The City will work with job training and work force development organizations to develop a green collar jobs program related to green infrastructure and sustainable projects proposed in the program. New jobs will help address many concerns, among them unemployment, community support and long term maintenance obligations for green infrastructure.

MONITORING AND MODELING

One of the first activities in the Overflow Control Plan will be to install additional flow meters and level sensors in both the combined and separate sanitary sewer systems. The results of monitoring will help in the development of enhanced system models, evaluating enhanced performance in the system and potential water quality improvements.

Current system models analyze performance characteristics in pipes 24 inches in diameter and larger. In order to evaluate the potential impact of green infrastructure solutions, these models will need to be extended further up the drainage basins. Technical models will be complemented by a triple bottom line evaluation framework including well specified social, economic, and environmental metrics. Once system models and related evaluation frameworks are developed, adjustments to the design, construction, and operation of remaining components will be analyzed throughout implementation of the Overflow Control Plan. Funding for the enhanced monitoring and modeling activities has been estimated at $24 million over the life of the program.

Blue River Watershed Management Plan

One important premise of this Overflow Control Plan, and indeed the City's more comprehensive approach to managing water resources, is to approach planning and management from a holistic watershed perspective. The benefits of watershed-based planning and management are many. Approaching water resource management from a watershed perspective allows the resource itself to become the focal point of study, leading to a more complete understanding of the various impacts on the water body. A watershed approach is also more cost-effective, because it embraces the

involvement of key stakeholders in the process and allows for coordination and communication in addressing pollution sources and issues. Moreover, a watershed approach is the best method of maximizing social, economic, and environmental benefits, because the approach itself is grounded in a broader focus on all activities within a watershed that might have an impact on human health and the environment.

A large portion of the flow and bacterial loading in the Blue River comes from upstream of Kansas City. For this reason, simply reducing overflows from Kansas City's sewer system may not be enough to meet MDNR's water quality standards in the stretch of the Blue River between 59th and 95th Streets. The water quality standard in this stretch of the Blue River is more stringent than the standards applicable to adjacent upstream and downstream reaches of the Blue River. For these reasons, the Overflow Control Plan includes $2 million as Kansas City's contribution to the preparation of a Blue River Watershed Management Plan. A watershed management plan for the Blue River, developed together with Johnson County and other significant watershed stakeholders, is critical to determining the best methods to address the pollution issues that affect this waterway, and to determining appropriate water quality standards for all reaches of the Blue River.

COMBINED SEWER SYSTEM

About 58 square miles within Kansas City are served by combined sewers. This area is generally bound by the Missouri/Kansas state line on the west, 85th Street on the south, the Blue River on the east, and the Missouri River on the north. The area served by the combined sewer system is subdivided into seven principal basins, Gooseneck Creek, Lower Blue River, Town Fork Creek, Brush Creek, Middle Blue River, Northeast Industrial District, and Turkey Creek/Central Industrial District. North of the river, the Charles B. Wheeler Municipal Airport is also served by combined sewers.

The estimated overflow volume from Kansas City's combined sewer system in a typical year is 6.3 billion gallons. Overflow frequency varies significantly within the individual basins, with the average overflow frequency estimated at more than 18 times in a typical year.

In the combined sewer system, repairs to the existing system are scheduled to occur early in the implementation of the Overflow Control Plan. The early years of the plan will also include aggressive pilot projects focused on developing green infrastructure solutions, which will modify proposed structural solutions scheduled for construction in the later years of the plan. The middle years of the plan will focus on maximizing the capacity within the existing system and analyzing the results of source volume reductions and pilot projects, together with improvements to the City's wastewater treatment plants. The final years of the plan will address necessary improvements to the City's wastewater treatment plants and adjustment and construction of proposed structural storage solutions.

NEIGHBORHOOD SEWER REHABILITATION

The first objective of the Overflow Control Plan is to maximize the effectiveness of the existing system. The Overflow Control Plan includes $122 million in capital maintenance and repairs to neighborhood sewers in the combined sewer system. These repairs will help reduce the amount of stormwater entering the system, will address significant outstanding maintenance items, and will improve system performance and life span. To minimize disruption to the neighborhood and improve efficiencies, the City will coordinate sewer rehabilitation efforts with other planned infrastructure projects.

GREEN INFRASTRUCTURE PILOTS AND PARTNERSHIPS

The Overflow Control Plan includes $28 million of funding dedicated to developing green infrastructure pilot projects and partnerships in the combined sewer basins. While proven individually or as part of small systems, green infrastructure has yet to be utilized in a widespread effort to address combined sewer overflows. By developing large scale pilots, the City will be gathering the information required to effectively implement green infrastructure on a much broader scale while simultaneously constructing a portion of the basin specific solution. Green infrastructure partnerships will focus on creating private sector participation in the pilots and proposed basin solutions.

The first pilot project will be implemented in the Middle Blue River Basin as part of the Marlborough Green Infrastructure Project. In this pilot, green infrastructure is planned to provide distributed storage of stormwater throughout a 100-acre area of the neighborhood. The area is primarily residential, but does include commercial businesses. In addition to gaining valuable information about the effectiveness of green infrastructure in controlling combined sewer overflows, this initial pilot will evaluate alternatives to achieve additional plan objectives, including:

- Effectiveness of green infrastructure as a systematic solution;
- Codes and ordinances in conflict with green infrastructure utilization;
- Socio-economic benefits/change;
- Construction techniques and costs on a wide-scale programmatic level;
- Interdepartmental coordination to minimize neighborhood disruption;
- Development of preliminary green design standards for Kansas City;
- Maintenance approaches and costs;
- Public/Private partnership opportunities; and
- Community interaction and support of green infrastructure practices.

Other pilot projects will be developed in the early years of the plan based on the specific basin solutions proposed. In order to develop green infrastructure strategies that will be applicable across Kansas City, it is important that the development of those pilots consider different land uses such as industrial areas and urban areas.

The 100-acre Marlborough Pilot Project area represents the largest focused installation of green infrastructure for combined sewer overflow control in the United States currently.

MARLBOROUGH GREEN INFRASTRUCTURE PROJECT

As mentioned in the previous section, the Marlborough Pilot Project will help define the utilization of green infrastructure across many areas of the City. However, this 100-acre pilot project is only a portion of the area in Marlborough where the use of green infrastructure looks very promising.

Four basin areas in the combined sewer system were evaluated to determine the opportunity for green infrastructure utilization. Based on this analysis, it was determined that an area in the Middle Blue River Basin, was a prime candidate to implement a green infrastructure approach. This area, located in and around the Marlborough neighborhood, is comprised of approximately 744 acres draining to combined sewer overflow outfalls 059 and 069.

The draft Overflow Control Plan called for two underground storage tanks and associated pumping equipment to store and transfer approximately 3.5 million gallons of anticipated overflow from these outfalls. In the selected Plan, these tanks have been replaced with an equivalent amount of storage in the basin itself through the use of green infrastructure.

While final designs will be modified based on results of the pilot project in the basin, initial estimates indicate that green infrastructure in the 744-acre area could include as much as 330 curb inlet modifications, and 25 acres of rain gardens, bioswales, permeable pavement, and green roofs.

A capital budget of $40 million has been included in the plan for the remainder of green infrastructure construction in this 744-acre area. The proposed sole reliance on utilizing distributed green infrastructure to achieve combined sewer overflow control performance goals in an area of this size is unprecedented in both scale and scope at the national level.

SYSTEM IMPROVEMENTS

Many of the improvements proposed in the Overflow Control Plan relate to improving the performance of the sanitary sewer system itself. The investment in these facilities will help the City in their daily duties of collecting and treating sewage, as well as help reduce overflows and system backups by pushing more flow through the system. Additionally, some areas of the system have extra capacity and can be modified to store flows within the system itself. This approach of maximizing the use of the City's existing investment is fundamental in the proposed Overflow Control Plan.

SEPARATION PROJECTS

In many areas of the combined sewer system, it is less costly to modify the existing system so that it functions as a separate sanitary and storm sewer system. These areas typically have a separate sanitary sewer system already functioning in the general area, which at some point connects to the combined sewer system. Separating the systems involves eliminating those interconnection points and providing new sewer lines that convey sewage only.

While these separation projects may be small in scope, their proximity to neighborhoods makes them disruptive to the everyday life of citizens. The City will focus on minimizing disruption through the use of innovative design, construction and management techniques aimed at shortening construction times, limiting disruption, and coordinating with other planned improvements in the neighborhoods.

STORAGE PROJECTS

Despite all of the significant system repairs and improvements and green infrastructure projects proposed in this Overflow Control Plan, the potential still exists that these improvements may not be sufficient to reduce sewer overflows to the levels intended. In that case, structural storage components will have to be relied upon to meet regulatory requirements. For that reason, this Overflow Control Plan includes contingency plans for the construction of structural storage facilities.

It is important to understand that the adaptive management approach used throughout this plan gives the City the opportunity to gauge the effectiveness of the system repairs and improvements and green infrastructure projects as Overflow Control Plan implementation progresses. If those activities result in meeting the sewer overflow requirements in effect in the later years of this plan, then the need for structural storage facilities will be greatly diminished, if not eliminated. The intent of this Overflow Control Plan is to focus on all reasonable methods of reducing or eliminating the need for structural storage facilities, yet retain the option to construct some or all of those storage facilities if no other reasonable alternatives are available to meet regulatory requirements in effect in the later years of this plan.

The structural storage projects currently proposed as the contingency approach in the Overflow Control Program are comprised of deep tunnels used to store and convey sewer overflows during rain events until such time as the sewer system has capacity to accept those flows. Deep tunnel storage has been proven to be a cost effective method of storage on a per gallon basis. It is also less disruptive than above ground storage solutions. The disadvantage of utilizing a tunnel system is that for the most part, the tunnels serve only one purpose, storing combined sewer overflows.

Throughout implementation of the Overflow Control Plan, the City will actively evaluate emerging technologies and other storage alternatives. Final evaluations will take into account social, economic, and environmental aspects of the proposed solutions as they pertain to meeting regulations and improving the economic vitality and quality of life in Kansas City.

SEPARATE SANITARY SEWER SYSTEM

Kansas City's separate sanitary sewer system is comprised of nine principal basins, covering 250 square miles of the City. The four separate sanitary sewer system

basins north of the Missouri River are the Northern and Northwestern watersheds and the Line Creek/Rock Creek and Birmingham/Shoal Creek basins. The five separate sanitary sewer system basins south of the Missouri River are the Blue River North, Round Grove, Blue River Central, Blue River South, and Little Blue basins.

Under existing conditions, the collection systems and wastewater treatment plants have adequate capacity to convey and treat dry weather flows. During heavy rainfall, however, the amount of water infiltrating into the sewers exceeds the system's capacity.

In addition to the uncontrolled overflows from the separate sanitary sewer system, a constructed sanitary sewer overflow is present at the lower end of the Line Creek system. The plan addresses flows from this structure as an early priority.

Recommended strategies in the separate sanitary sewer system include reducing inflow and infiltration of stormwater by repairing the existing system where cost-effective. A combination of wet weather storage and treatment will also be provided to address inflow and infiltration determined to be too expensive to keep out of the system. Because work in the separate sanitary sewer system relates only to repair of the sanitary sewer system, green infrastructure is not included in the proposed plan.

In the separate sanitary sewer basins, a design storm with duration of 24 hours and a depth that would be equaled or exceeded, on average, once every five years was utilized to develop the Overflow Control Plan. In Kansas City, that design storm would result in a rainfall depth of 4.68 inches.

INFLOW/INFILTRATION REPAIR WORK

Many parts of the separate sanitary sewer system are in need of general repair and have experienced deferred maintenance. In addition to extending the life of the system, these repairs will help reduce the amount of rainwater inflow into the system. Inflow, however, is not the only problem. The age of the system and the construction techniques utilized at the time of construction create many challenges in keeping rainwater from entering the system below ground. To combat these issues, the Overflow Control Program proposes an aggressive infiltration reduction initiative focusing on lining existing pipes within the system to combat infiltration through pipe joints and connection points. While effective, the system itself is so large geographically that inflow and infiltration reduction efforts are only expected to partially reduce the amount of stormwater entering the system.

SYSTEM IMPROVEMENTS

Addressing overflows from the constructed sanitary sewer overflow located within the Line Creek/Rock Creek basin, just upstream from the Line Creek Pumping Station, is a priority to the City. The plan provides $37 million for construction of a 30 million gallon per day high rate treatment facility to be constructed near the Line Creek Pumping Station early in the program. This facility will allow the City to begin treating sewage overflows early in the program and will stay in service until final solutions are implemented.

Ultimately, it is anticipated that wet weather flows from the Line Creek/Rock Creek and Northwestern basins will be transported through a conveyance and storage tunnel to the Birmingham Wastewater Treatment Plant. The Plan also provides $44 million in funding for a high rate treatment facility to be added to the Birmingham plant to address peak wet weather inflows.

STORAGE PROJECTS

Two major structural storage projects are currently proposed in the separate sanitary sewer areas. Similar to the storage projects in the combined sewer area, through an adaptive management approach, the City will retain the flexibility to reduce the size or eliminate these storage projects depending on actual flow reductions achieved in early phase projects.

The North Bank Tunnel is proposed as the primary solution to store sanitary sewer overflows from the entire separate sanitary sewer system north of the Missouri River. In addition to providing 42 million gallons of storage, this tunnel also provides conveyance capacity in an undersized portion of the system.

South of the Missouri River, the plan proposes 68 million gallons of tank storage to hold excess inflow and infiltration from the Blue River South Basin and flows from Johnson County Wastewater. The adaptive management approach of the plan gives the City the flexibility to postpone final decisions on storage capacity until the results of ongoing technical and contractual discussions between Kansas City and Johnson County Wastewater are fully evaluated. The cost for addressing Johnson County Wastewater flows to the 87th Street Pumping Station will be recovered through either increased rates charged to Johnson County Wastewater or other funding agreements. Should Johnson County choose to manage the flows themselves, the proposed storage necessary will be reduced accordingly.

Preliminary Schedule

Financial projections prepared for the Overflow Control Plan suggest that between 25 and 33 years will be needed to complete construction of the projects identified in the Plan and other presently identified wastewater utility capital needs. Each of those projections is predicated upon acceptance of a heavy financial burden by the City and its ratepayers. Wastewater rates are expected to almost quadruple over the next 13 years, eventually leading to a cost to residents in the City's retail service area equivalent to 1.7 percent of the City's median household income. Completing the Overflow Control Plan at the lower end of the 25-33 year range will require the identification of revenues other than presently projected user rate increases sufficient to comply with any new regulatory requirements and other wastewater utility capital improvement needs.

As we continue to work with the agencies to finalize our commitment to protecting our region's streams and rivers, we will continue our efforts to establish a final implementation schedule acceptable to the agencies that maximizes our opportunities

to benefit from the adaptive management approach and recognizes our responsibility to properly operate and maintain the system while responding to future requirements in an ever-changing regulatory environment.

Estimated Cost of Selected Plan in 2008 Dollars

Project Description	Estimated Cost (in Millions, 2008 $)	
	Capital	Annual
Programmatic Elements		
Enhanced Monitoring and Modeling	$24	$1.0
Public Education and Outreach	12	---
Rain Gardens and Downspout Disconnects	5	---
Green Collar Jobs and Workforce Development	5	---
Blue River Watershed Management Plan	2	---
Subtotal, Programmatic Elements	**$48**	**$1.0**
Combined Sewer System		
Green Infrastructure Pilot Projects and Partnerships in CSS	$28	$1.40
Neighborhood Sewer Rehabilitation	122	---
Sewer Separation	104	0.26
Outfall Consolidation Piping	35	0.06
Increased Collection System Capacity	39	0.58
In-Line Storage and Other Improvements in Existing System	22	0.16
Distributed “Green” Storage (Outfalls 059 and 069)	40	2.00
Deep Tunnel Storage and Pumping	576	5.34
High Rate Treatment and Other WWTP Improvements	428	15.63
Subtotal, Combined Sewer System	**$1,393**	**$25.44**
Separate Sanitary Sewer System		
I/I Reduction	$172	---
Increase Collection System and Pumping Capacity	26	$0.03
North Bank Tunnel System	371	1.78
Tank Storage at 87th Street Pumping Station	265	1.13
Interim Line Creek Wet Weather Treatment Plant	37	0.53
Additional Pumping Capacity and Wet Weather Treatment at Birmingham WWTP	72	3.16
Subtotal, Separate Sanitary Sewer System	**$943**	**$6.63**
TOTAL ESTIMATED COST	**$2,384**	**$33.07**

Kansas City's Stream Setback Ordinance: A Case Study on the Benefits of Stream Buffers in Urban Areas

Laurie Brown, Scott Schulte, and Bryce Lawrence[1]

[1]Patti Banks Associates, 929 Walnut, Suite 200, Kansas City, MO 64106; PH (816) 756-5690; FAX (816) 756-1606); email: llbrown@pbassociates.com, sschulte@pbassociates.com, blawrence@pbassociates.com

Abstract

Riparian buffers provide direct public and environmental benefits by stabilizing streams, separating people and structures from flood hazards, protecting public infrastructure from damage, and improving water quality. They also provide indirect benefits such as habitat preservation, recreational opportunities, public amenities and increased property values.

Over the past 5 years the City of Kansas City, Missouri (City) systematically evaluated stream quality throughout the city and quantified the relationship between riparian buffers and stream quality. A comprehensive stream asset inventory demonstrated that the health and stability of the City's streams is influenced by the quantity and quality of riparian buffers. The results are bolstered by other studies from the Kansas City region, and support national research on the importance of stream buffers as a watershed management tool.

For this reason, the City adopted a stream setback ordinance in August 2008 that prohibits floodplain development, while focusing on preserving adjacent riparian buffers through development controls, low-impact development provisions, and incentives. This groundbreaking stream setback ordinance uniquely addresses stormwater management, natural resource protection, and future development by protecting sufficient riparian buffer to maintain the City's streams and environmental quality, while providing development incentives and flexibility to developers affected by the buffer. Flexibility, through the provision of "conservation development" options protects significant riparian resources while at the same time allowing development within the outer zone of the buffer.

Introduction

Management of stormwater runoff is a critical issue for both urban and rural communities. The conversion of once well vegetated land into homes, institutions, commercial or other urban related developments radically changes what happens to stormwater runoff. Where it once was slowed down by nature and allowed to gradually soak into the ground, now it is directed to storm sewers or detention basins that simply send the problem downstream to someone else. As a result, communities throughout the country are looking for innovative ways to deal with wet weather issues and are focusing specifically on stormwater runoff and municipal sewer systems.

In the past, solutions have often been highly engineered, expensive, and unsightly, with little regard for natural resources. Recently communities have begun looking into their future and are seeing green, including money savings and natural resource conservation. The City is currently faced with a $4 billion bill to fix its wet weather problems. Of this total bill, approximately $1.8 billion is for the stormwater program and $2.2 billion is for the combined and sanitary sewer overflow control program. Kansas citians are looking to their City to lead the way in integrating protection of water resources and wildlife habitat into the solutions derived for wet weather problems. The stream setback ordinance is just the initial step the City is taking to solve wet weather problems, save money, and literally green the city for future generations.

Setback ordinance implementation presents some interesting challenges and opportunities to developers, planners, and City staff. This paper discusses the ordinance and describes two project examples that show how the ordinance is being applied to urban sites, illustrating its application and implications for design and development. These projects include a data center and a major industrial/commercial development. In each case, the setback ordinance has required the designers to rethink site design and stormwater management. By addressing stream setbacks early in the development planning process, riparian buffers were integrated into these projects as design elements and site amenities without sacrificing project objectives.

Ordinance

The City began developing a stream setback ordinance in 2005 as part of a comprehensive Development Code update. At the same time, the City was also addressing stormwater issues through its' KC-

One Stormwater Master Plan Program and combined sewer overflows through the Overflow Control Program, which are included under the City's Wet Weather Program.

City staff and consultants working on the ordinance implemented public involvement early in the ordinance development process by meeting frequently with a variety of stakeholders inside and outside of City government, particularly development attorneys and engineers. These particular stakeholders and members of the Development Code Steering Committee requested that the ordinance meet certain criteria, including:

- Clearly defining regulated streams
- Being easy to understand and administer
- Applying uniformly and equally to all streams and projects
- Using common information
- Incorporating the latest scientific research and buffer recommendations

The final adopted stream setback provisions were significantly influenced and improved by this group's comments and suggested improvements.

The final ordinance includes a three-tiered riparian (stream) buffer system to reduce flooding and protect water quality and city infrastructure. Regulations within this ordinance are stricter closer to the stream. Thus, the type and number of allowable uses increases with distance from the stream as dictated by the buffer zones. The outer zone offers the greatest flexibility to developers, guaranteeing them the right to develop. The outer zone is regulated for higher quality development use.

The ordinance (see Figure 1) requires a 25 foot streamside zone where uses are strictly limited to infrastructure and trail crossings. The middle zone incorporates the Federal Emergency Management Agency (FEMA) or city-designated 1 percent (100-year) floodplain or the limits of the 1 percent (100-year) conveyance and jurisdictional wetlands. Uses allowed within the middle zone are infrastructure and trail crossings, utility corridors, and recreational trails. The outer zone extends at least 75 feet from the outer edge of the middle zone and includes slopes greater than 15 percent or mature riparian vegetation areas contiguous with the middle zone. If steep slopes or mature riparian vegetation is present, the outer zone is expanded to encompass these resources. The maximum extent of the outer zone is established at the landowner's election, it can be 75, 150, or as much as 250 feet from the outer edge of the middle zone. At all times the

landowner has the option of developing up to 40 percent of the outer zone provided that a continuous 25 foot strip of outer zone vegetation is maintained to avoid fragmenting the vegetated area. The Open Space and Conservation Development portion of the City's Development Code provides the flexibility to maximize development of the cleared portion of outer zone.

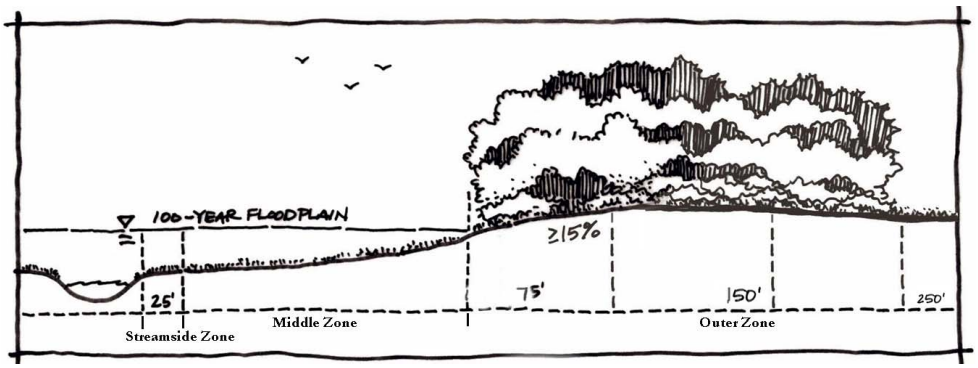

Figure 1. Three-tiered buffer zones in the setback ordinance.

The final Stream Setback Ordinance and Conservation Development Code were adopted by City Council on August 20, 2008. The ordinance and code became effective February 14, 2009.

Implementation

Implementation of the setback ordinance is presenting challenges and opportunities for the City and the development community. The stream setback ordinance guarantees developers the right to develop 40 percent of the outer zone area and the conservation development ordinance provides options to maximize its value. In the following two examples, the designers were required to rethink site design and stormwater management in order to successfully integrate stream buffers into these projects as design elements and site amenities without sacrificing project objectives.

Data Center

A 40-acre greenfield site in northern Kansas City was identified as an ideal location for a large data center. The site, post-agricultural fallow land, is a wide open hilltop with a major roadway on the north and west, a residential subdivision on the south, and pasture on the east. A narrow strip of fencerow vegetation and one wet pond are located on the eastern side of the proposed development site. The developer believed the land had minimal constraints and would easily accommodate the 100,000 square foot facility.

Natural resources on the development site include a first or second order stream tributary that is regulated subject to the City's stream setback ordinance, and two jurisdictional wetlands. One wetland is in the floodplain (middle buffer zone) and the other is outside of the floodplain by approximately 10 feet (see Figure 2).

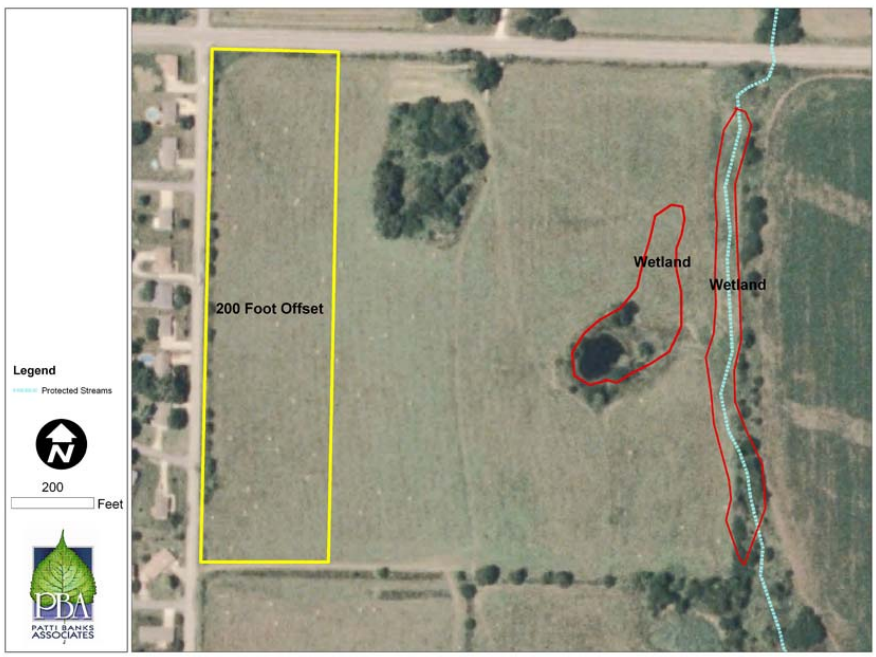

Figure 2: Data Center natural resources and development constraints base map.

The developer was advised that site development must comply with the City's newly adopted stream setback ordinance and that a riparian buffer must be established. Additionally, a 200-foot no-build offset was required on the western side of the property to screen the project from nearby residences.

Runoff from the proposed 100,000 square foot data center roof and parking area would significantly impact the adjacent wetlands and stream. Additionally, the large amount of impervious surfaces would require significant detention and water quality treatment as required by City stormwater engineering regulations.

Full site development, placement of stormwater facilities, and the space needed for the stream buffer presented a challenge to the design team. The designers met the challenge and created an amenity for nearby residents.

Fortunately, the outer zone of the buffer may be varied in width as long as 60 percent of its area is preserved as permanent open

space. This flexibility allowed designers to meet stormwater design requirements, comply with the riparian buffer, protect the wetlands, and meet the developer's goals. The buffer was narrowed on the north end to accommodate a power substation and was widened in the central site to incorporate the two wetlands, reconnecting these to the riparian system and improving the ecological function of the existing site. The stormwater detention facilities were designed and placed within the 200-foot offset on the western side to create a green stormwater solution (see Figure 3) and a visual amenity on the otherwise unusable space. The project is considered a success by everyone involved.

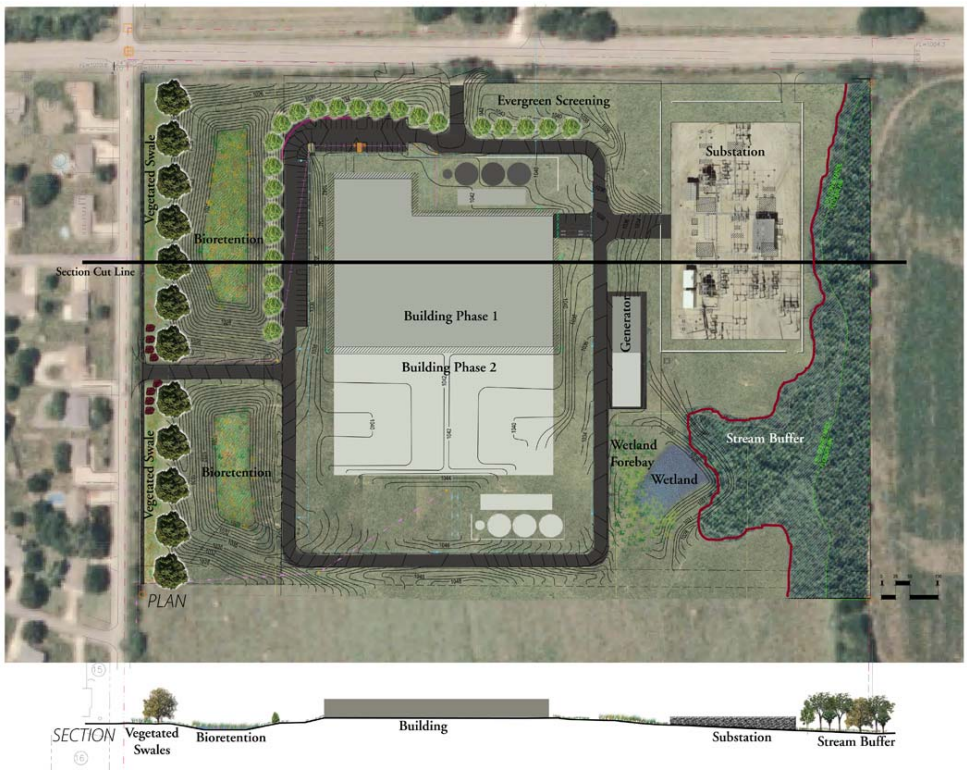

Figure 3: Data Center design protecting the stream buffer and wetlands.

Intermodal BusinessCentre

The Kansas City International Airport (KCI) Intermodal BusinessCentre (IBC) project consists of a 602-acre commercial development that will include distribution centers, air cargo facilities, light manufacturing, office space and commercial businesses. The project is located adjacent to the southeastern corner of Kansas City International Airport on City-owned land (see Figure 4).

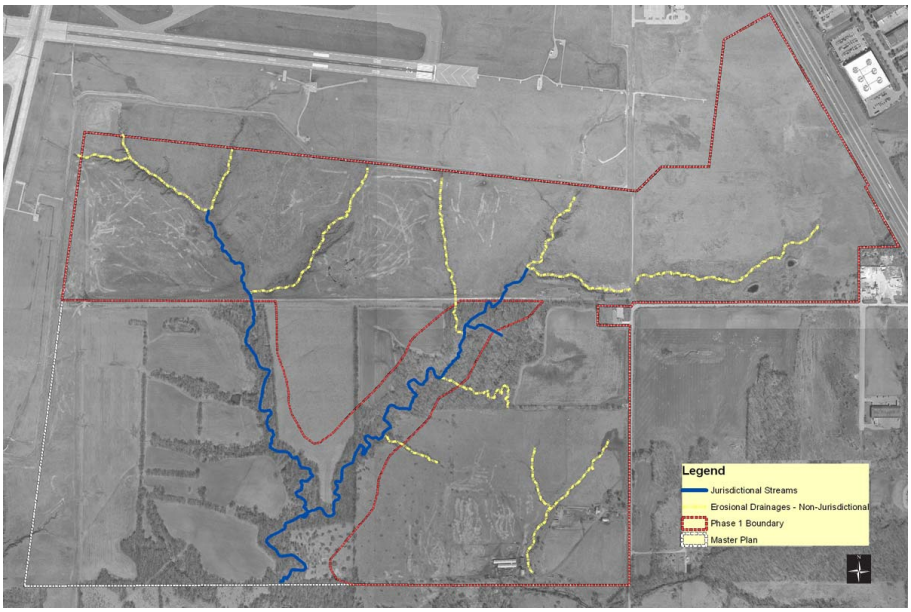

Figure 4. The KCI IBC development site.

The project site lies within the headwaters of the Brush Creek watershed which contains valuable natural resources, including wetlands, prairies, forests, high quality streams, and lakes. While still mostly undeveloped, the Brush Creek Watershed is expected to experience rapid development over the next decade. Thus, it is critical to protect the headwaters of Brush Creek during the development process. Topography throughout the project site is gentle to moderately steeply rolling hills with steeper topography adjacent to the stream channels. The project site's primary resources are located within the riparian corridor associated with Brush Creek.

Past management of natural resources within the project area was dictated by federal regulations. The Federal Aviation Administration (FAA) provides regulations and guidance to airports regarding land management practices aimed at minimizing human/wildlife conflicts at airports and on surrounding lands. The airport is located in a predominantly agricultural area with significant wildlife that poses a potential hazard to aircraft operations.

Project impacts are limited to Brush Creek as there are no jurisdictional wetlands within the development site. Other natural resources have been removed closest to the airport to minimize human/wildlife conflicts.

From the initiation of this development project, the developer proposed a stream buffer zone to avoid impacts to the higher quality stream resources located within the central portion of the project site (independent of the stream setback ordinance). The design team was

able to focus development and management of stormwater outside of the primary Brush Creek channel and the stream buffer area. The developer's buffer averages between 150 and 200 feet from the top of bank on each side of the stream (see Figure 5). Comparison of this buffer to the City's stream setback ordinance showed that this buffer actually exceeds requirements of the stream setback ordinance. Riparian vegetation will be restored in portions of the buffer to improve the quality and function of the stream corridor.

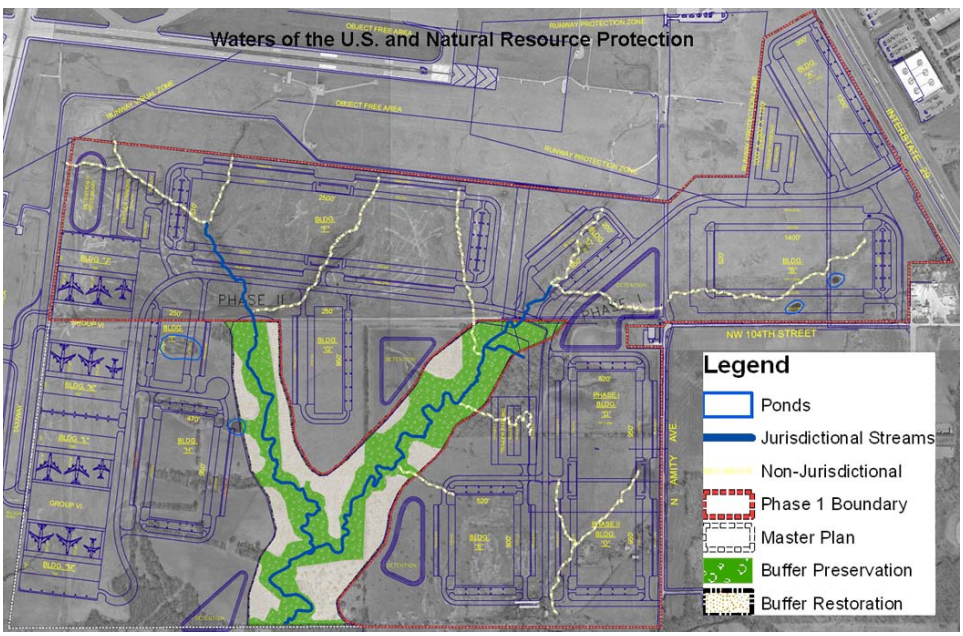

Figure 5. Site Plan with riparian buffer and natural resources to be protected during development.

In addition to the stream setback, all stormwater discharges have been designed to maintain stream stability and provide water quality treatment in accordance with American Public Works Association (APWA) Section 5600 Stormwater Design Criteria (APWA 2006) and the *Manual of Best Management Practices for Stormwater Quality* (BMP Manual; APWA and Mid-America Regional Council (MARC) 2008).

Summary

The stream setback ordinance developed and adopted by the City sets new precedents nationally by protecting mature riparian vegetation and incorporating conservation development. Developers are guaranteed the right to develop while the City is guaranteed the protection of its valuable water resources.

The design teams for both the Data Center and the Intermodal BusinessCentre realized the critical value and necessity of integrating existing resources into their development plans. Valuable natural resources were integrated into the overall site design to create plans that offer amenities to both the site users and adjoining landowners while protecting valuable water resources for the City and meeting the goals of the developers.

The stream setback ordinance is just the first major step the City has taken as it works to solve numerous wet weather problems. The riparian buffers that will be protected by this ordinance will greatly enhance the City's ability to protect water quality while promoting wildlife habitat and creating public amenities such as trails while encouraging development. It should attract new development while avoiding creating costly future infrastructure problems for the City.

References

American Public Works Association. 2006. Section 5600 Stormwater Design Criteria.

Mid-America Regional Council and American Public Works Association. March 2008. *Manual of Best Management Practices for Stormwater Quality,* Second Ed.

KC-One: Comprehensive City-Wide Management Plan Creates Leading Stormwater Management Program

J. W. Henson[1] and R. Gaskin[2]

[1]Black & Veatch, 8400 Ward Parkway, Kansas City, MO 64114; PH (913) 458-3410; FAX (913) 458-3518; email: hensonj@bv.com
[2]City of Kansas City, Missouri, 4800 E. 63rd Street, Kansas City, MO 64130: PH 816-513-0352; FAX (816) 513-0366; email: Richard_Gaskin@kcmo.org

ABSTRACT

Introduction. Major floods have caused millions of dollars of damages, taken lives, and degraded Kansas City's streams. The City's Stormwater Management Program identified needed improvements over the last decade for the 320 square miles within the corporate boundaries. Approximately 1,000 projects were identified with estimated costs of about $1.8 billion to upgrade the drainage system and protect the residents, homes, and businesses in Kansas City.

Goals and Objectives. The City implemented the KC-One project to develop the tools needed to make Kansas City's Stormwater Management Program a leader in the region. The City needed to develop a Capital Improvements Program to equitably prioritize the large number of identified projects. More importantly, it needed to identify more sustainable solutions to flooding problems and land development than the traditional methods used in Kansas City, develop policies and regulations to manage stormwater in a sustainable manner, develop a funding plan, and identify the staff needed to adequately manage the program.

KC-ONE

KC-One is a comprehensive City-wide stormwater management plan for the City of Kansas City, Missouri. The KC-One plan, part of the City's overall Wet Weather Program, clarifies responsibilities within the City, recommends policies and procedures, establishes priorities, provides timelines and schedules, and offers funding recommendations for comprehensive stormwater management. The comprehensive plan includes recommendations in the following areas:

- Policy: incorporates best management practices (BMPs), stream protection, land use planning, development plan approval, floodplain management and permit compliance.
- Administration: defines roles and responsibilities of City departments, staffing needs, operations and maintenance.

- Stormwater Master Plan Review: combines watershed master plans into a coherent and usable access system, creating a centrally organized geographic information system.
- Capital Improvement Program: re-prioritizes improvements in 35 watersheds after applying "Green" multi-purpose solutions while complementing the overflow control program (OCP) and improving Municipal Separate Storm Sewer Systems MS4 permit compliance.
- Public Involvement: lays the foundation for expanded stormwater management and the use of green solutions.
- Funding: identifies approaches and options to address capital, administrative, and operational needs.
- Implementation: formulates a comprehensive plan to achieve results.

TWO PHASES

The work for KC-One was segmented into two phases. The purpose of Phase I was to establish the vision, principles, and priorities for the new stormwater management program in Kansas City, Missouri. These key elements then guided the development of the scope of work, budget, and schedule for the remainder of the project during Phase II. Phase I involved working with numerous stakeholders, including the City's Water Services Department, other City departments, elected officials, regulators and other stakeholders. Thus, the stakeholders helped formulate the scope of work, budget, and schedule for development of the comprehensive city-wide stormwater management program. A series of one-on-one interviews and stakeholder workshops culminated in a consensus on the vision, guiding principles, and priorities for stormwater management.

The results from the majority of the one-on-one interviews yielded certain recurring themes. Those recurring themes may be summarized as follows:

1. Focus on reducing flooding, protecting natural resources and improving water quality.
2. The primary obstacle is funding. Innovative approaches and solutions are needed that combine local, state and federal sources of funding.
3. A big picture view is needed that incorporates "Green" infrastructure into multi-objective and multi-use solutions.
4. Public involvement and education is the key to building support and implementing effective programs.

KC-ONE VISION AND MISSION

Four conclusions may be drawn from the major outcomes of Phase I. The first is that there is wide understanding among the identified stakeholders. Not only do they understand the current situation and its problems, they seem to understand what is needed to solve the problems and improve the situation. Secondly, a majority of the stakeholders have the will to make tough decisions and implement solutions. That will is underpinned by the political support of the local elected officials. The third is a general desire to improve the City's overall quality of life--in all

neighborhoods and communities. The fourth is the realization that no program will be accepted by the community unless it is accountable to the community. Actions or specific solutions will be accepted and funded only if they are effective and economical.

Specific Phase I deliverables included a vision, mission statement, set of guiding principles, stormwater management strategy, and scope of work for Phase II. The KC-One vision is

Stormwater management in KC is a holistic regional watershed planning, operating, and growth strategy.

That vision is supported by the KC-One mission to

- Protect and benefit citizens
- Provide sound and consistent development policy
- Conserve and restore natural resources
- Be regional in scope and implementation

During Phase I, consensus was reached on the following policy issues:

- The stormwater management program should apply throughout the entire City, including the areas with combined sewers, where different regulations apply;
- Water quality should be improved and protected throughout the City;
- Floodplain management criteria should be based upon the 100-year flood;
- Stormwater facility designs should be based upon the regionally developed American Public Works Association (APWA) Section 5600 design standards.
- Stormwater facility design should also be based on the APWA BMP manual, which requires new development to manage both quality and quantity of runoff.

POLICIES

Recommendations have been developed throughout the course of the project from its inception in 2004 through preparation of the final report. Many of these recommendations have been implemented and are already providing benefits. Two of the most important recommendations were to adopt new drainage design standards and to implement a stream buffer ordinance to protect the City's streams. Regulation and management of the City's natural resources are the most effective means to protect the City's streams and to achieve the goals of the Wet Weather Program.

Adoption of the new drainage design standards was accomplished in October 2006. These new standards were developed to protect streams from erosion and sedimentation that often occurs during construction, to reduce water pollution carried into streams and treatment facilities during storm events, and to leave a buffer zone between waterways and development to reduce property damage and protect the stream corridor. New standards include:

- APWA 2100-Clearing and Site Preparation Standards: These standards give builders and developers guidelines and criteria for preparing their site(s) for construction. This includes clearing, demolition, grading, erosion control, tree

protection, dust control, waste disposal, temporary entrances and fencing, vegetative buffers, etc.

- APWA 5100-Sediment and Erosion Control Standards: These design criteria and engineering standards address erosion control issues from project planning stages and construction stages to mitigation methods and engineering solutions for roadways. Many temporary and longer-term solutions are described as well as educational and certification requirements. Erosion controls address prevention, while sedimentation controls mitigate erosion already occurring.
- APWA 5600-Storm Drainage and Facilities Standards: These design standards provide developers and cities with guidelines for stormwater drainage and treatment infrastructure. They include a Channel Stability Assessment Matrix and methods for estimating runoff and flows/capacity of gutters, culverts, etc. These standards also address the benefits and issues of using natural streams as part of stormwater management plans as well as engineered channels and engineered structures in stream channels. These criteria make open channels the highest priority and strive to maintain pre-development runoff conditions for a full range of storms.
- BMP Manual: The Manual of Best Management Practices for Stormwater Quality describes BMPs for stormwater management in the region. It requires new development to manage runoff water quality based on changes in runoff conditions. These practices include many of nature's own stormwater management strategies such as using native species, wetlands, bioretention, and rain gardens to filter pollution out of runoff and slow the water down, which allows it to percolate into the soil. Better stormwater infrastructure are also addressed, including pervious pavements, constructed wetlands, and engineered stream corridors, making water quality management choices flexible. The BMP methods described can help treat 1.4 inches of rainfall daily (instead of overloading treatment facilities) providing treatment for runoff from over 90 percent of the region's storm events.

  The hierarchy of priorities for stormwater quality management that the BMP Manual promotes is as follows:

  1. Preserve and promote natural hydrology: Preserve open space, preserve native vegetation and soils, and restore native vegetation and soils;
  2. Infiltrate the runoff through constructed systems;
  3. Filter the runoff through constructed systems; and
  4. Store and treat the runoff.

While adoption of the APWA and BMP standards cited above is an important first step in protecting the City's streams, a stream buffer ordinance was needed to further regulate the floodplains and protect habitats along the streams. Under the City Planning and Development sponsored project to update the Zoning Ordinance and Subdivision Regulations, a stream buffer ordinance was developed to implement the recommendations of KC-One. The stream buffer ordinance will become effective February 14, 2009.

- Stream Buffer Ordinance: Stream buffers are a component of the Zoning Ordinance and Subdivision Regulation Update designed to keep homes, businesses and other built infrastructure away from stream banks, to prevent property damage from flooding and other water quality issues resulting from development occurring too close to streams. The stream buffer ordinance is considered the most effective BMP, and establishes zones to enhance stormwater management.
    - Streamside zone
        - 25 feet wide, each side of stream
        - Allows utility crossings
    - Middle zone
        - Includes 100-year floodplain and wetlands
        - Allows utility and recreational corridors
    - Outer zone
        - Extends a minimum of 25 feet outside of middle zone
        - Includes steep slopes and adjacent wildlife habitat areas
        - Allows conservation development

While the City has made great progress in proactive stormwater management and natural resource protection, additional policy recommendations will further improve natural resources and prevent flooding. These include stormwater management design standards that require the reduction of runoff from new development and redevelopment, provide incentives for homeowners and business owners to install stormwater best management practices, and proactive management of floodplains to prevent development in areas that are projected to flood as the City develops.

ADMINISTRATION

The Administration Plan includes a discussion of organizational theory, industry trends, and considerations for change with respect to how the Stormwater Utility Division is organized. This section also includes a review of the key processes that either the Stormwater Utility Division executes or should be executing as it looks to increase its level of service and effectiveness. Major recommendations include the following:

- Elevate Stormwater within the Water Services Department (WSD) organizational chart to "peer" status with Water and Wastewater, to be led by an Assistant Director.
- Conduct an annual Stormwater Summit: This approach would gather the managers who lead organizations that either own or contribute to key stormwater processes to a workshop designed to clearly delineate the following stormwater issues:
    - Strategic direction and priorities
    - Identify process owners and accountability plans
    - Promote dialogue among stormwater contributors and mutual ownership of challenges

Attendees would include WSD departments as well as other City and external departments which are relied upon to achieve stormwater goals.

- Update the business plan annually: This recommendation is intended to increase the frequency of strategic planning performed for stormwater functions. The plan would develop annual stormwater goals and should address major objectives related to all stormwater functions. Strategic, quantifiable priorities would be highlighted, and tactics to achieve those priorities would be identified. The plan should be accompanied by a set of financial projections and related operational metrics for a minimum of a 5 year period.
- Add incremental staff and resources over time as available funding and additional responsibilities increase.
    - Priority should be placed on adding identified resources in the areas of Maintenance and Watershed Management, which includes staff to manage capital improvements projects and support "green" initiatives.

CAPITAL IMPROVEMENTS PLAN

The Stormwater Utility Division has developed Watershed Management Plans for the City's 35 drainage basins over the last decade. These Watershed Management Plans have identified approximately 750 projects to upgrade the drainage system to reduce flood hazards and to meet drainage design standards. Each of these projects was prioritized within the watershed that they occurred, but a comprehensive prioritization process including all of the projects was not completed. Therefore, one of the primary Phase II tasks of KC-One was to develop the comprehensive list of projects and reprioritize them. The table below provides a summary of the recommendations.

Watershed	Total Projects	Total Cost	Total Green Cost	Total Transportation Cost
Birmingham Bottoms	6	$13,080,000	$12,340,000	$0
Blue River	113	$426,190,000	$28,200,000	$30,310,000
Brush Creek North	33	$256,410,000	$7,460,000	$1,330,000
Brush Creek South	8	$109,890,000	$0	$0
Buckeye	5	$6,550,000	$2,690,000	$0
Burlington	13	$2,410,000	$1,360,000	$660,000
Dyke's Branch	22	$5,940,000	$50,000	$280,000
East Fork Shoal	8	$960,000	$0	$960,000
First	11	$1,250,000	$0	$510,000
Fishing	16	$7,170,000	$220,000	$4,710,000
Hickman Mills	22	$8,630,000	$0	$5,120,000
Indian	42	$62,880,000	$26,310,000	$6,210,000
Line	98	$63,130,000	$30,140,000	$9,200,000
Little Blue	101	$44,710,000	$14,560,000	$15,320,000
Little Shoal	15	$12,130,000	$9,850,000	$2,210,000
Mill	19	$7,690,000	$2,750,000	$1,310,000
NEID (All)	17	$86,080,000	$18,770,000	$700,000
Randolph	2	$8,830,000	$0	$0
Rock	6	$1,970,000	$1,120,000	$290,000
Rocky Branch	20	$6,460,000	$360,000	$3,770,000
Round Grove	43	$28,550,000	$14,990,000	$13,280,000
Rush/Walnut	30	$10,230,000	$6,250,000	$0
Searcy	7	$39,610,000	$3,320,000	$1,690,000
Second	20	$6,310,000	$2,060,000	$6,310,000
Shoal (Lower)	8	$970,000	$330,000	$0
Todd	7	$3,750,000	$1,430,000	$330,000
Town Fork	16	$72,420,000	$25,000,000	$460,000
Turkey (including CID)	15	$574,840,000	$0	$0
Upper Shoal	49	$15,550,000	$8,030,000	$4,100,000
TOTAL	**772**	**$1,884,600,000**	**$217,590,000**	**$109,050,000**

The final Capital Improvements Plan will be defined by the available funding. Projects have been categorized by well-known historic flooding problems, projects that can be solved by green solutions, transportation projects that have historically been funding through Public Improvements Advisory Committee sales tax revenues, and remaining projects.

Following are the general recommendations for defining the highest priority projects:

- Projects that address historic flooding areas such as Southwest Boulevard, Westport, Freighthouse District and Gardner Avenue;
- The top 100 projects that involve green solutions; and
- The top 100 remaining projects that provide the most benefit for the lowest cost.

FUNDING PLAN

Funding stormwater management programs for the City may be achieved through various methods, some of which are applicable to funding operating costs and others to funding major capital improvement costs. Only a few of these methods have sufficient flexibility and revenue generating ability to be used as a primary source of funding. The City should take into account the implications of the Hancock Amendment when considering new funding sources or adjustments to existing fees and charges.

A stormwater utility user fee is a flexible, reliable source of revenue, and with proper design, is an equitable method of charging for stormwater services. It is therefore recommended that the City adopt a policy to transition to a stormwater user fee as the primary source of funding the City's stormwater management program over the long-term, including both operation and maintenance expenses and capital related costs. State and Federal grant funding should be used to leverage the local revenues. Other funding sources such as in lieu of construction fees, inspection fees, and plan review fees should be utilized as appropriate as supplemental funding. Although the supplemental sources will not generate a significant amount of revenue, they will enhance the overall equity of the stormwater user fee structure.

Based on the estimated cost of anticipated stormwater capital projects, a significant increase in the stormwater utility user fee will be required to fund both operating and capital costs. A transition period of several years should be allowed for this conversion, during which time stormwater utility user fees can be increased at a rate that is deemed acceptable to customers and by the City Council. During this transition period the stormwater utility needs assurance that funding of capital improvements will be made available either through the current sales tax or an alternative mechanism. It is recommended that the City consider seeking approval of additional sales taxes under House Bill RSMo 644.032 (for stormwater control and/or parks), or other statutory provisions to supplement current revenue sources during this transition period.

Revenues from system development charges will provide a new source of income for funding capital improvements related to growth and development, and will enhance the equitability of cost recovery.

PUBLIC INVOLVEMENT

The *10,000 Rain Gardens* program, which was begun in November 2005, led by Kansas City's Water Services Department, and supported by then-Mayor Kay Barnes, was contained within the scope of KC-One to begin community outreach for the purposes of "education, communication, and public involvement." KC-One took *10,000 Rain Gardens* through its first year; its management was then shifted to the Overflow Control Plan (OCP) City-wide program.

10,000 Rain Gardens has called upon the creativity of citizens, corporations, educators and non-profit organizations to join with government in creating pieces of the solution to the City's stormwater challenges. By providing both homeowner-based information and professional-level training and certification, *10,000 Rain Gardens* has succeeded in bringing the enormity of the challenge down to a personal scale. This alone helps citizens relate to the City's challenge and feel empowered by contributing to the stormwater solution on a yard-by-yard basis.

IMPLEMENTATION PLAN

Implementing the recommendations of the KC-One Plan will help the City achieve the goals of its Wet Weather Solution program:

- Minimize loss of life and injury and reduce property damage due to flooding;
- Improve water quality; and
- Maximize economic, social, and environmental benefits, optimize infrastructure investment and enhance natural habitats.

Achieving these goals will take many years and require new sources of revenue, changes in policies, additional staff, and the construction of stormwater management facilities across the City.

Implementation recommendations are categorized as either high priority or medium priority. This distinction is made based on a balance of considerations including the expected degree of impact and the availability or anticipation of funding. Within the high or medium priority designations, recommendations are further stratified to reflect a relative time line for implementation as follows.

- Critical – as soon as possible
- Near-term - within the next three years
- Mid-term – within the next three to five years
- Long-term – more than five years

CONCLUSION

KC-One has provided the foundation for increasing the scope and influence of the City's Stormwater Management Program. Key to success of the Program is providing additional funding to implement the recommendations from KC-One. As stormwater revenues increase, the level of service provided by the Program will increase and the goals of the Wet Weather Program will be achieved.

Laboratory Testing Guidelines for Certification of Manufactured Stormwater BMPs

Bannerman, Roger[1]; Bruijn, Hans de[2]; Karimipour, Shohreh[3]; Kayhanian, Masoud[4]; Mailloux, Jim[5]; McDonald, Jon[6]; Miller, Mark[7]; Mohseni, Omid[8]; Osei, Kwabena[9]; and Perry, Scott[10]

[1] Wisconsin Department of Natural Resources [2] Terre Hill Stormwater Systems, [3] New York State Department of Environmental Conservation, [4] University of California Davis, [5] Alden Laboratory, [6] Kristar Enterprises, Inc., [7] AquaShield, Inc., [8] St. Anthony Falls Laboratory, [9] Hydro International, [10] Imbrium Systems Corporation

Abstract

For the past decade, manufactured stormwater best management practices (BMPs) have been widely used in urban areas to remove suspended solids from stormwater runoff to meet the local and federal government agencies' standards. The ASCE/EWRI Task Committee on Guidelines for Certification of Manufactured Stormwater BMPs formed a subcommittee to develop the laboratory testing guidelines. The focus of this subcommittee has been on developing laboratory testing guidelines to assess the efficiency of the devices used for physical separation of the full spectrum of stormwater-borne non-dissolved solids. In general, these devices include hydrodynamic separators and filters.

After reviewing the protocols developed by organizations, but not limited to, the state of Washington Technology Assessment Protocol-Ecology (TAPE), the state of Wisconsin Method for Predicting the Efficiency of Proprietary Storm Water Sedimentation Devices, the TARP Protocol for Stormwater Best Management Practice Demonstrations, the subcommittee utilized the experience obtained from the laboratory tests conducted on these devices and employed the material in the existing protocols to develop the testing guidelines. These guidelines are designed to conduct robust laboratory testing with stated repeatability. The guidelines encompass three separate series of tests for addressing three different processes: (1) Testing to determine the efficiency of hydrodynamic separators in removing suspended sediments, (2) testing to quantify sediment retention of hydrodynamic separators, and (3) testing to determine the efficiency of filters in removing suspended solids.

Introduction

For the past decade, manufactured stormwater treatment devices, also known as manufactured best management practices (BMPs), have been widely used in urban areas with the goal of removing pollutants from stormwater runoff. The main advantage of these devices is their small foot print where space is limited. These

devices can be divided into two main categories: (1) settling devices, and (2) filters. The settling devices, primarily hydrodynamic separators, remove pollutants by settling the particles, while filters remove pollutants through the attachment of particles to the media filter. Hydrodynamic separators are often designed to remove floatables, e.g. oils from stormwater runoff.

These devices have been monitored in the field and tested by either the manufacturers' laboratories or other independent laboratories under a set of specific conditions. There are few protocols or guidelines for the performance assessment of these devices. Therefore, in 2007, the Stormwater Infrastructure Committee of EWRI's Water, Wastewater, and Stormwater Council (WWSC) in collaboration with the Wet Weather Flow Technology Committee of the Urban Water Resources Research Council (UWRRC) formed a committee to develop guidelines for certification of manufactured BMPs. In May 2007, six subcommittees were formed to develop the guidelines. This paper is a summary of the work done by the members of the Laboratory Testing Subcommittee.

Development of the Laboratory Testing Guidelines

The goal of the subcommittee has been to develop laboratory testing guidelines to assess the efficiency of the devices, i.e. hydrodynamic separators and filters, used for physical separation of particles (the full spectrum of stormwater-borne non-dissolved solids) from stormwater runoff. The guidelines are intended to include scouring of the removed particles under high flow conditions. The guidelines do not include removal of trash, leaves and hydrocarbon products.

The first task of the subcommittee members was to review and assess the existing protocols. Some of the protocols reviewed have not been finalized, however, the subcommittee decided to review all the existing knowledge in the community before attempting to draft new guidelines. Therefore, several protocols were reviewed and their pros and cons were summarized. Among them were (1) Technology Assessment Protocol-Ecology (TAPE 2002) papered by the Washington Department of Ecology as part of their Stormwater Management Manual (SWMM) that includes stormwater treatment facility design criteria, performance goals, and a process evaluating the performance of stormwater treatment facilities, (2) the New Jersey Department of Environmental Protection (NJDEP 2003) for evaluating hydrodynamic separators, (3) the protocol developed by the Wisconsin Department of Commerce and the Wisconsin Department of Natural Resources (WDC & WDNR 2007) for evaluating hydrodynamic separators, (4) the draft standard for Measurement of Suspended Sediment Removal Efficiency of Hydrodynamic Stormwater Separators and Underground Settling Devices prepared by the ASTM, (5) the Laboratory Testing Specifications for Manufactured Water Quality Structure prepared by the Ohio DOT, (6) the Laboratory Testing Protocol for Manufactured Stormwater Treatment Systems prepared by the City of Indianapolis, (7) the Procedure for Lab-based Testing of a Hydrodynamic Separator by the Direct Method prepared by Hydro International, and (8) Procedure for Lab-based Testing of a Hydrodynamic Separator by the Indirect Method prepared by Hydro International.

In addition to summarizing the pros and cons of all these protocols, the main features of the first three protocols were compared and summarized in a single table (Figure 1). The main three protocols specified target removal efficiencies and designed the procedure to meet the targets.

Table 1. Summary of the parameters used in the NJDEP, WDNR and TAPE protocols.

FEATURE	NJCAT/NJDEP	WA DOE	WI DNR
Specified Test Material	5% - 500-1000 µm 5% - 250-500 µm 30% - 100-250 µm 15% - 50-100 µm 25% 8-50 µm 15% 2-8 µm 5% 1-2 µm (d50 ~67 µm)	OK-110 (d50 ~110 µm)	0.90 lb US F-95 1.2 lb OK-110 0.25 lb Sil-Co-Sil 250 4.0 lb Sil-Co-Sil 106 1.0 lb Sil-Co-Sil 52 2.0 lb Min-U-Sil 40 1.0 lb Min-U-Sil 30 1.0 lb Min-U-Sil 15 4.0 Min-U-Sil 10 (d50 ~8 µm)
Target Influent Concentration	100, 200, 300 mg/l	100, 200 mg/l max.	150-250 mg/l
Flow Increments	25%, 50%, 75%, 100% and 125% of unit's rated treatment capacity	50%, 75%, 100% and 150% of unit's rated treatment capacity	5%, 20%, 50% and 100% of unit's rated treatment capacity
# of Tests	3 for each flow rate and concentration (15 total)	2 for each flow rate and concentration (8 total)	1 for each flow rate and concentration for 2 models min. (8 total)
Preloaded Sediment for Resuspension Test	Specified test material at 50% and 100% of unit's rated sump capacity	Specified test material at 100% of unit's rated sump capacity	15% ASTM C33 Conc. Sand 10% NJ 0 Sand 20% NJ 4 Sand 15% Flint #12 Sand 10% Flint #15 Sand 15% F60 Grade Sand 10% 20/40 Oil Frac 5% HI-50
Resuspension Test	2 tests at maximum hydraulic operating rate w/preloaded sediment & clean water	Maximum flow without negative removal efficiency w/preloaded sediment	30 min or $5t_r$ 5 paired grab samples Max. +25 mg/l effluent w/clean water
Min. Performance	70% as SSC/50% as TSS at rated treatment capacity	80% removal as TSS at rated treatment capacity	Flow limited to 83% of allowable based on resuspension test
Sampling Method	Not specified	Not specified (grab samples or compositing inferred)	Total mass fed & collected in separator + 5 grab samples for influent/effluent SSC & TSS + PSD from all
# of Models	One	One	Two minimum (Ratio between surface areas of primary settling chambers of at least 2.5)
PSD Analysis	None specified	Optional laser diffraction	Feed per ASTM C117, C136 and D422 Influent/Effluent residuals per same methods for >63 µm, Coulter counter for <63 µm
Temperature	73-79 °F max.	None specified	50-80 °F

FEATURE	NJCAT/NJDEP	WA DOE	WI DNR
Other Aspects			False floor allowed to simulate 50% sediment load – system run clean Recommended 5 lbs of accumulated sediment in unit
Pros	1. Flow increments cover wide range of operation	1. Single, commercially available feed material in range of expected removal capability 2. Simple, conservative resuspension test	1. Direct sediment collection w/sampling backup 2. Resuspension test using material representative of captured sediment 3. Testing more than one model allows more direct scaling method
Cons	1. Preloaded sediment conflicts with direct collection to determine removal efficiency 2. Complex feed and resuspension test material mixture 3. Sampling methods not clarified	1. Sampling methods not clarified 2. Resuspension test method needs clarification	1. Fine feed material largely not captured at typical flow rates 2. Complex feed and resuspension test material mixtures 3. Mandatory PSD analysis expensive

The subcommittee decided to prepare the guidelines using the existing protocols. However, instead of specifying the flow rates, the particle size distributions, influent concentrations, etc., the committee has organized the guidelines with the goal of developing performance functions for the tested devices. A performance function for a tested device allows the cities, counties, and other local government agencies and end users to evaluate the performance of a tested device under a variety of climatic and environmental conditions without the requirement of further testing of that device. In order to develop the performance function of a device, only the range of tested flow rates, particle size distributions, and influent concentrations would be determined in the guidelines.

Subsequently, the Laboratory Testing Subcommittee formed three task groups to prepare the first drafts for (1) removal efficiency testing of hydrodynamic separators, (2) sediment retention testing of hydrodynamic separators, and (3) removal efficiency testing of filters.

Since hydrodynamic separators are primarily cost effective for removing sand and very coarse silt particles, and sampling these particles could cause large errors in the results, especially in the effluent pipe, the subcommittee agreed to recommend a semi-mass balance method for testing hydrodynamic separators. In a semi-mass balance method, it is required to weigh the amount of sediment to be fed into a hydrodynamic separator prior to each test, and at the end of each test to collect, dry and weigh all the sediments removed by the device. For testing filters, however, sampling of influent and effluent is allowed if the non-organic particles fed into the device during the test are fine silt or smaller.

The Laboratory Testing Certification Guidelines is comprised of four main sections. The first section is on the terminology used in the guidelines. The other three sections are the documents prepared by the task groups on testing the removal efficiency of hydrodynamic separators, sediment retention testing of hydrodynamic separators and filter testing. Each section includes the general features of the laboratory test stand, characteristics of the materials fed into the system or used to preload the system, measurement of the hydraulic characteristics of the device during a test, measurement of the materials removed by each device, and measurement of the materials washed out of a preloaded device. Testing filters includes (a) removal efficiency test, sediment retention test and clogging test which is to measure the changes in head and discharge over time.

Summary

The ASCE/EWRI Task Committee on Guidelines for Certification of Manufactured Stormwater BMPs formed a subcommittee to develop the laboratory testing guidelines. The objective of this subcommittee was to develop guidelines for laboratory testing to assess the efficiency of manufactured devices for physical separation of the full spectrum of stormwater-borne non-dissolved solids.

The laboratory testing guidelines includes a terminology section, and three sections on testing the removal efficiency of hydrodynamic separators, sediment retention testing of hydrodynamic separators and filter testing. The foundation of these laboratory testing guidelines are based on the existing protocols, however, the main difference is in developing performance functions for the tested devices which can be used under a variety of climatic and environmental conditions.

References

New Jersey Department of Environmental Protection (2003). Total Suspended Solids Laboratory Testing Procedures, Division of Science, Research and Technology, NJDEP, Trenton, New Jersey, December 23. http://www.state.nj.us/dep/dsr/bscit/TestProcedure_Dec%2703_.pdf

Washington State Department of Ecology (2002). Guidance for Evaluating Emerging Stormwater Treatment Technologies, Technology Assessment Protocol - Ecology(TAPE), October 2002 (Revised June 2004), Publication Number 02-10-037. http://www.ecy.wa.gov/biblio/0210037.html

Wisconsin Department of Commerce & Wisconsin Department of Natural Resources (2007). Method for Predicting the Efficiency of Proprietary Storm Water Sedimentation Devices (1006), September 15 draft. http://www.socwisconsin.org/pdf/Broad%20Review/Proprietary%20Stormwater%20Devices%20Std.-Draft6.pdf

Land Use and Runoff Uncertainty

Celina Bochis*[1] and Robert E. Pitt[2]

[1]Department of Civil, Construction and Environmental Engineering, The University of Alabama 260 H.M. Comer, Box 870205, Tuscaloosa, AL 35487-0205; FAX (205) 348 – 0783; email: cbochis@bama.ua.edu
[2]Department of Civil, Construction and Environmental Engineering, The University of Alabama 374B H.M. Comer, Box 870205, Tuscaloosa, AL 35487-0205; PH (205) 348-2684; FAX (205) 348 – 0783; email: rpitt@eng.ua.edu

ABSTRACT

Data from about 160 neighborhoods in six Jefferson County, AL drainage areas were intensively investigated to determine the surface covers for each land use type. The data shows that the watersheds are highly impervious, with three of them having more than 50% of the watershed area composed of impervious cover. However, TR-55 (USDA 1986) guidance still shows that the impervious cover for all land uses investigated to be much greater than we observed for our area. It was also concluded that the variabilities of the surface covers within the different land uses for the investigated areas was small, especially for the impervious covers.

The percentage of directly connected impervious cover (DCIA) was determined by direct field observations and this data was also compared to commonly use empirical equations. Equations for determining DCIA developed during prior studies were fitted with our observed DCIA for our data, but they did not result in good relationships, especially when analyzed at the land use level. There was a good comparison between Sutherland's "highly connected basins" equation and the fitted equation for our overall data. However, the residual analysis for the regression model was poor, suggesting that the power equation may not be applicable to our data in our region. Suitable equations were developed for each land use separately, showing that a single equation could not be accurately used to estimate DCIA for all regions and land uses.

KEYWORDS: land use, land cover, imperviousness, impervious cover, runoff

INTRODUCTION

An urban area inventory for watershed development conditions should be part of any comprehensive stormwater management plan, when the goal is to understand the sources of pollution and the magnitude of the expected runoff. The watershed inventory would, therefore, assist in the selection of the most beneficial stormwater control practices. The type of urban development in an area can have a major impact on the local hydrology and water environment. This inventory can therefore be used to support many decision making activities and to increase the success of local stormwater monitoring. Past studies (Schueler 1994; USEPA 1994; Arnold and Gibbons 1996; Booth and Jackson 1997) have demonstrated the importance of knowing the areas of the different land covers in each land use category and the storm drainage characteristics (grass swales, curb and gutters, and the roof drains). Increasing levels of impervious surfaces

associated with urbanization result in higher volumes of runoff with higher peak discharges, shorter travel times, and more severe pollutant loadings. Urban imperviousness is an important indicator for urban watersheds in measuring the impact of land development on drainage systems and aquatic life (Schueler 1994). However, there are many different types of impervious surfaces and their direct connectivity to the drainage system is an important attribute affecting stormwater runoff.

The purpose of this research was to provide more details on impervious surfaces for different land uses in the Southeast, as the literature information on impervious cover is not very accurate when applied to local conditions. There are a lot of assumptions about impervious area characteristics for different types of land uses, but very little data has been available to support these assumptions. As part of this research, the Little Shades Creek watershed (Jefferson County, near Birmingham, AL) and five highly urbanized drainage areas situated in Jefferson County, AL (in and near the city of Birmingham) were surveyed in detail to determine the actual development characteristics and their variability. Jefferson County is the largest county by population and fifth by size (NACO 2001) in the state of Alabama having Birmingham as the county seat. This was historically a heavily industrialized area. Rainfall occurs year around, although is generally driest in the fall. About 55 inches of rainfall occurs in a normal year, but recent years have been marked by a significant drought. With the decreased rainfall, more attention is being placed on regional water resources, including stormwater.

To determine how land development variability affects the quantity and quality of runoff, different land surfaces (roofs, streets, landscaped areas, parking lots, etc.) for different land uses (residential, commercial, industrial, institutional, etc.) were directly measured. Surface cover of 125 neighborhoods located in the Little Shades Creek watershed and 40 neighborhoods located in five of Jefferson County's highly urbanized drainage areas were analyzed to determine the actual development characteristics and their variabilities. The locally verified WinSLAMM model (Pitt and Voorhees 1995 and 2002) was then used to determine the sources of critical pollutants, and to predict their loads and concentrations. Statistical analyses were conducted at several levels to establish the quantitative and qualitative runoff sensitivity associated with variations of site characteristics.

ESTIMATION OF IMPERVIOUS AREA

Imperviousness is an important indicator for analyzing and measuring the impact of urbanization on drainage systems and aquatic life because the impervious cover is a variable that can be quantified for different types of land development and has long been found to be directly related to the amount and rate of runoff from an area (Schueler 1994; Arnold and Gibbons 1996; Booth and Jackson 1997).

Urban imperviousness is site-specific and can be complicated to measure. There are several methods used to measure the actual and "effective" impervious cover, some of which are more accurate than others. These methods include direct measurement from aerial photographs and satellite imagery, estimation of impervious cover based on land use, estimation from road density (length of road per unit area), and estimation of impervious cover from population data. The most common methods of determining directly connected impervious cover are field measurements and empirical equations. Several studies have dealt with imperviousness and its estimation (as reported by Heaney et al. 1977; Boyd et al. 1993 and 1994; Novotny and Olem 1994; Debo and Reese 1995). Table 1 shows some of the studies that have estimated or measured impervious cover for different regions. Booth and Jackson (1997) explained the limitations of

using total impervious area (TIA) in urban hydrology analyses and suggested using directly connected impervious area (DCIA) to describe urban development, but noted that its direct measurement is complicated. Consequently, empirical equations for determining DCIA have been developed as part of several different studies (Alley and Veenhuis 1983; Laenen 1983; Sutherland 2000).

Alley and Veenhuis (1983) developed an empirical equation that shows the relationship between the directly connected impervious area and the total impervious area for a highly urbanized area in Denver, CO:

$$DCIA = 0.15 * TIA^{1.41} \quad (1.1)$$

Sutherland (2000) developed an equation based on USGS work completed in Portland and Salem, OR that describes the relationship between effective impervious area (EIA or DCIA) and total impervious and has its general form as:

$$EIA = A\ (TIA)^{B} \quad (1.2)$$

This equation has the same form as used by Alley and Veenhuis (1983), where *A* and *B* are coefficients that satisfy the following criteria: TIA = 1 then EIA = 0% and TIA = 100 then EIA = 100%. This equation has several alternatives known as the "Sutherland Equations" (Sutherland 2000) developed to apply to various conditions of subbasins which might exist in a watershed.

Values of imperviousness can vary significantly according to the method used to estimate the impervious cover (Lee and Heaney 2003; Ackerman and Stein 2008). These researchers concluded that the main focus should be on DCIA when examining the effects of urbanization on stormwater quantity and quality. Reducing the DCIA by disconnecting the impervious surfaces (sidewalks, rooftops, parking areas, and streets) from the drainage system will not restore hydrologic function to pre-development levels, but will improve the base flows, lessen the frequency of bank erosion, and improve stream functions. From a hydrological point of view, road-related imperviousness usually exerts larger impacts than the rooftop-related imperviousness, because roadways are usually directly connected while roofs can be hydrologically disconnected (Schueler 1994).

FIELD DATA COLLECTION

For this study, a locally calibrated version of WinSLAMM was used to compute the runoff quantity and quality for Little Shades Creek watershed near Birmingham, AL and for five additional Jefferson County drainage basins.

The field data used for modeling was gathered manually as part of a cooperative study conducted by the University of Alabama at Birmingham, the Jefferson County office of the U.S. Natural Resources Conservation Service (NRCS), the U.S. Army Corps of Engineers, and other city and county governments. The field data collection effort for the five additional Jefferson County drainage basins reported in this paper was performed during the author's master thesis research (Bochis 2007). Every impervious surface was checked to estimate its properties and connectivity. Streets were classified according to their drainage system: with curb and gutter (directly connected to the storm drainage system) or with swales (disconnected). Also, the pavement material of every street and parking lot was examined and classified.

Table1. Reported Percent Impervious Cover for Various Land Uses

Land Use	Density (units/ac)	Source									
		Northern Virginia (NVPDC, 1980)	TR-55 NRCS (USDA, 1986)	Puget Sound, WA (Aqua Terra, 1994)	Rouge River, MI (Kluitenberg, 1994)	Olympia, WA (COPWD, 1995)	Holliston, MA (CRWA, 1999)	Connecticut (Prisloe, 2000)	Chesapeake Bay (CWP, 2000)	Birmingham, AL (Bochis, 2007)	Simple Method (Schueler 1987)
Forest	-	1	-	-	2	-	1	-	-	-	-
Agriculture	-	1	-	-	2	-	1	-	2	-	-
Urban Open Land	-	-	-	-	11	-	7-23	-	9	13	-
Water/ Wetlands	-	-	0	-	-	-	-	-	-	-	-
Low Density Residential	<0.5	2-6	-	10	19	-	12	7-10	-	-	10
	0.5	9	12						11	-	
	1	12	20						14	18	
Medium Density Residential	2	18	25	-	19	-	14	14-21	21	22	30
	3	20	30	40		40			-		
	4	25	38						28		
High Density Residential	5-7	35	65	40	38	40	19	28	33	30	40
Multifamily all >7 units/acre	Townhouse	40	65	60	51	48	47	39	41	35	60
	Apartments	50							44	42	-
	High Rise	60-75	-	-	-	-	-	-	-	-	-
Industrial	-	60-80	72	90	76	86	60	53	53	59	75
Commercial	-	90-95	85	90	56	86	45	54	72	73	85
Roadway	-	-	-	-	-	-	-	-	-	58	80

DESCRIPTION OF STUDY AREAS

The Little Shades Creek watershed has an area of about 8 square miles and was about 70% developed at the time of the initial surveys (mid 1990s). It lies under the jurisdiction of several municipal governments as well as the county government, which made land development highly variable and uncoordinated. Many types of land development are represented, even though the residential areas, mostly as single family residential units, are predominant. Sixteen land use categories belonging to major land uses such as residential, commercial, institutional, industrial, and open space were surveyed by investigating about 10 neighborhoods for each land use. The predominant land use in the watershed was residential land, subdivided according to the density type, and age (Table 2).

The stormwater drainage system was predominantly formed of curbs and gutters in good or fair condition with very little use of grass swales. Most of the roofs (pitched in residential and institutional areas and flat in the other areas) were found to be directly connected to the drainage system. The streets and most of the commercial parking lots had asphalt pavement, but industrial parking lots and residential sidewalks/driveways had smooth concrete as their predominate surface cover. As expected, the largest fraction of impervious cover was found in the commercial areas, followed by industrial, freeway and institutional land uses.

Table 2. Imperviousness Percentage based on Land Cover in Birmingham, AL Land Uses (Bochis 2007)

Land Use	Total Impervious Area (%)	Directly Connected Impervious Area (%)	Pervious Area (%)
High Density Residential	30	19	70
Medium Density Residential	22	13	78
Low Density Residential	18	9	83
High Rise Res/Apartments	42	17	58
Multi Family	35	27	65
Commercial	73	72	27
Institutional	46	41	54
Industrial	59	50	41
Open Space	13	9	87
Freeways	58	0	42

RESULTS AND DISSCUSIONS

Impervious Cover Variability

Regardless of the method used to estimate imperviousness, field verification is necessary. Field verification is also the only accurate method that can be used to estimate the directly connected portion of the impervious area (Gregory, et al. 2005). Therefore, in addition to field surveys, aerial photographs and satellite images were used to assist in the measurement of the actual coverage of each type of surface in each neighborhood studied, and were used to supplement the field collection information. Table 2 shows the percentage impervious and pervious coverage for the land uses found in the Birmingham, AL study areas. Table 3 shows the existing land uses with their average DCIA and the corresponding coefficients of variation.

Table 3. Directly Connected Impervious Areas in Birmingham, AL Area (Bochis 2007)

Land Use	Directly Connected Impervious Area (%) Local Conditions	COV	TR-55 Estimates (using interpolation)
High Density Residential	19	0.48	52
Medium Density Residential	13	0.68	39
Low Density Residential	***9****	***1.03****	23
High Rise Res/Apartments	17	0.97	65
Multi Family	27	0.53	-
Commercial	***72***	***0.29***	85
Institutional	41	0.61	-
Industrial	50	0.66	72
Open Space	***9***	***1.21***	-

* Bold values represent the extremes of DCIA (%) and their coefficient of variation

Those drainage basins have most of the impervious surfaces directly connected to the drainage system, except for the low density residential and open space land uses which have the lowest connectivity and the greatest coefficient of variation. The other extreme case is the commercial land use, which has almost all impervious cover connected and little variability.

A power equation was fitted to the data based on the empirical equations for determining DCIA from TIA as suggested in the literature. The plot shown in Figure 1 relates the percent directly connected impervious areas to the total impervious areas for all of the individual homogeneous land use sites investigated (Bochis 2008).

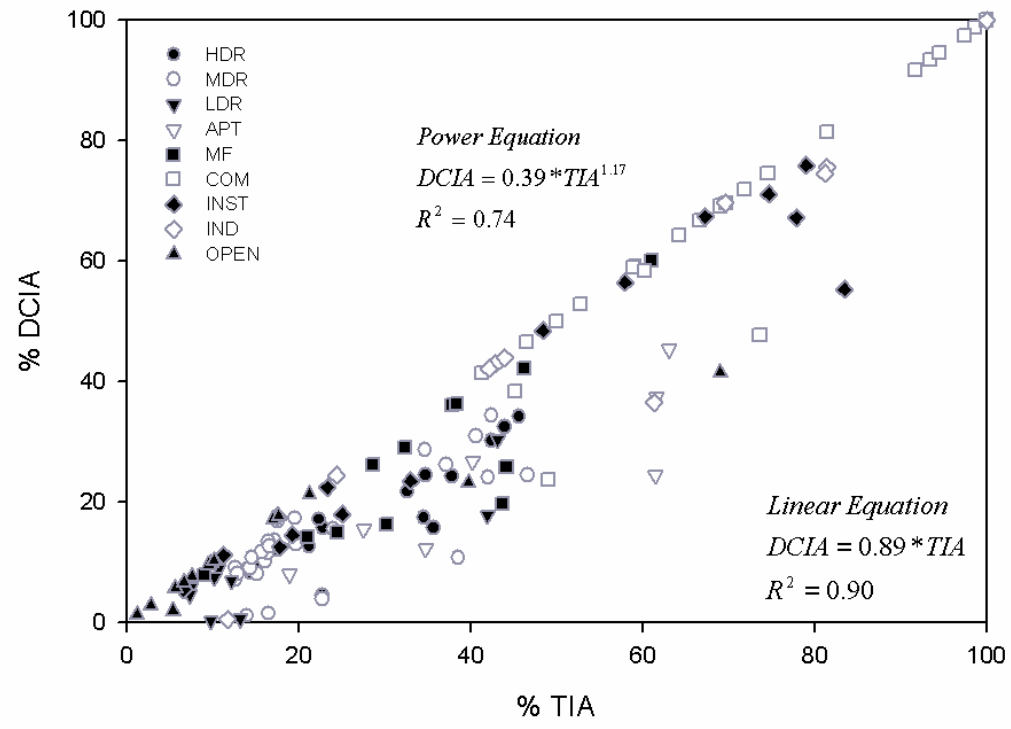

Figure 1. Empirical Estimation of DCIA based on TIA for Birmingham, AL Study Areas (Bochis 2008)

This figure shows that the combined study areas' DCIA might be a power function of TIA, as suggested by Sutherland (highly connected basin, 2000), and Alley and Veenhuis (1983). For these drainage basins, most of the impervious surfaces are directly connected to the drainage system. The fitted equation for the entire study areas is comparable to one of the Sutherland equations used for highly connected areas where the drainage collector is a storm sewer with curb and gutters, and the roofs are connected. The power equation was fitted separately for each individual land use in the study areas. The *A* and *B* equation coefficients, along with their coefficients of determination and residual P-values are presented in Table 4. This data shows that DCIA of each land use is not always a power function of TIA, suggesting that power fitting cannot be successfully applied to Alabama's local condition. We found that the linear equations better fit our data (Table 4).

Table 4. Equation Coefficients for Each Land Use Existent in Birmingham, AL Study Area (Bochis 2008)

	Power Equation				**Linear Equation**		
Land Use	**A coeff.**	**B coeff.**	**R^2 value**	**Residuals p-value**	**A coeff.**	**R^2 value**	**Residuals p-value**
High Density Residential	0.34	1.16	0.64	**0.008***	0.64	0.78	0.061
Medium Density Residential	0.42	1.09	0.36	**<0.005**	0.63	0.65	0.061
Low Density Residential	0.22	1.16	0.27	0.415	0.55	0.78	0.292
High Rise Res/Apartments	0.22	1.22	0.83	0.823	0.56	0.74	0.943
Multi Family	0.74	1.00	0.77	0.714	0.80	0.72	0.527
Commercial	0.49	1.16	0.82	**<0.005**	0.98	0.90	0.048
Institutional	0.75	1.04	0.97	0.106	0.88	0.93	0.153
Industrial	0.04	1.78	0.75	0.068	0.95	0.94	0.382
Open Space	1.05	0.92	0.91	**<0.005**	0.67	0.87	0.373

* Bold values represent statistically significant equations

Other reported literature impervious cover conditions are not very accurate when applied to local conditions. The TR-55 (USDA 1986) (Table 1) method overestimate the impervious cover for all land uses investigated, because TR-55 likely assumes that most of the impervious areas are directly connected to the drainage system. Table 2, Table 3 and Figure 2 show that impervious areas in the six Jefferson County watersheds are almost entirely directly connected, and that there is a large variability among and within the land uses. In the case of residential land uses (high, medium and low density), the predominant land use in the study area, the TR-55 method gave values of impervious cover which are about three times higher than the observed values. This overestimation will lead to significant overestimations in runoff volume.

We used a Pearson correlation matrix to relate the magnitude of the relationships between the field measurements and predicted concentrations for those highly urbanized drainage areas. The matrix illustrated that runoff volume can be mostly predicted by using DCIA, TIA, and parking lot areas. Also, there are high correlations between several pairs of parameters, showing that some pollutants concentrations (COD and phosphorus) are directly related to the particulate solids concentrations.

Expected Biological Conditions as a Function of Impervious Area

Table 5 is a summary of the existing land uses that were monitored as part of this research. The data shows that three watersheds are highly impervious, with more than 50% of watershed being composed of impervious cover. The expected biological conditions of the receiving waters were calculated by WinSLAMM to be "poor" for the base conditions having no stormwater controls (based on the Center for Watershed Protections' Impervious Cover Model). The highly impervious watersheds (ALJC001 and ALJC012), which have mainly industrial and commercial land uses respectively, have higher values of Rv (about 0.6) but lower values of TSS concentrations, compared to the watersheds dominated by residential land uses (ALJC009, ALJC010, and Little Shades Creek). In this area, the main sediment sources are the landscaped areas, and not the parking or storage areas, or streets.

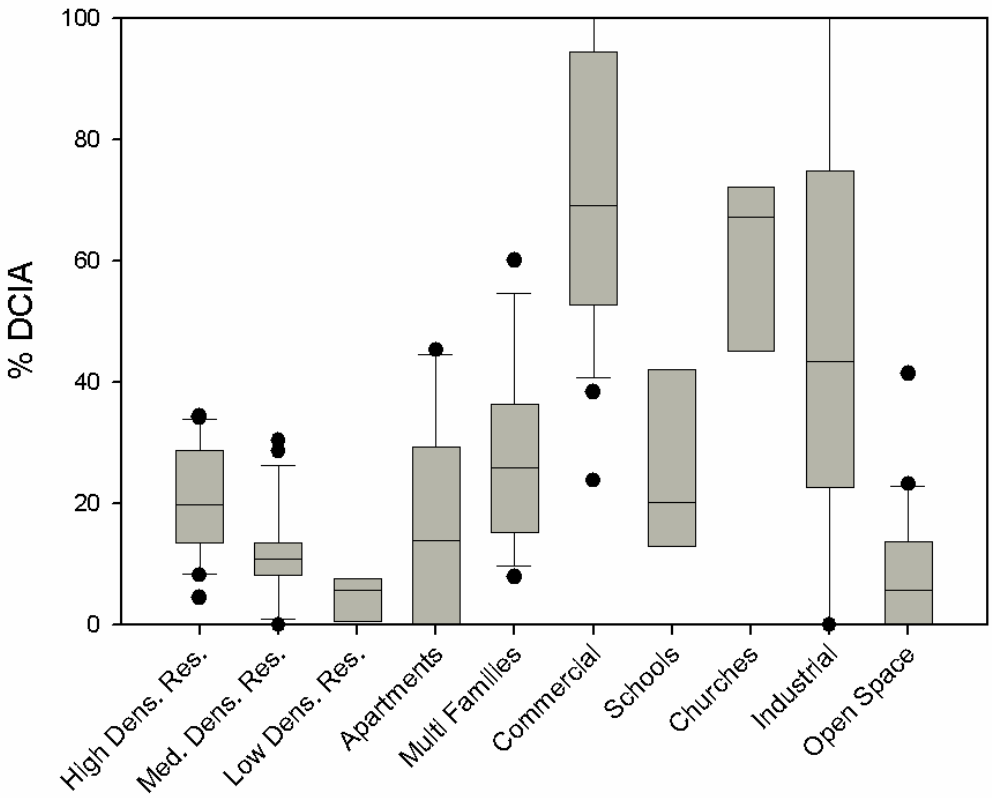

Figure 2. Percent of Directly Connected Impervious Area by Land Use for Little Shades Creek and Jefferson County, AL Watersheds (Bochis 2007)

The residential watersheds are closer to the threshold between fair and poor expected biological conditions (an Rv of about 0.25) than the industrial and commercial watersheds, as expected. WinSLAMM was used to investigate the relationship between watershed and runoff characteristics for each of the individual 160 neighborhoods investigated. An example evaluation of the relationships between the directly connected impervious area percentages (DCIA %) and the calculated volumetric runoff coefficients (Rv) for each land use category (using the average land use characteristics) in the Little Shades Creek watershed, based on 43 years of local rain

data showed that there is a strong relationship between these parameters for both sandy and clayey soil conditions.

Table 5. Runoff Quantity and Source Area Drainage Connections by Land Use for Birmingham, AL Sites (Bochis 2007)

Watershed ID	Major Land Use	Area (ac)	Pervious Areas (%)	Directly Connected Impervious Areas (%)	Disconnected Impervious Areas (%) (draining to pervious areas)	Volumetric Runoff Coefficient (Rv)	Expected Biological Conditions of Receiving Waters
ALJC 001	Industrial	341	25	72	2.8	0.67	Poor
ALJC 002	Industrial	721	40	53	7.3	0.51	Poor
ALJC 009	Residential High Density	102	54	34	12	0.37	Poor
ALJC 010	Residential Medium Density	133	64	28	7.9	0.30	Poor
ALJC 012	Commercial	228	36	61	3.4	0.61	Poor
Little Shades Creek	Residential	5120	67	21	12	0.29	Poor

The fitted exponential equations are (Bochis and Pitt 2005):

$$\text{Sandy soils: } R_v = 0.062e^{0.031*DCIA} \quad (R^2 = 0.83)$$

$$\text{Clayey soils: } R_v = 0.15e^{0.017*DCIA} \quad (R^2 = 0.72)$$

It is interesting to note that the Rv is relatively constant until the 10 to 15% directly connected impervious cover values are reached (at Rv values of about 0.07 for sandy soil areas and 0.16 for clayey soil areas), the point where receiving water degradation typically is observed to start. The 25 to 30% directly connected impervious levels (where significant degradation is observed), is associated with Rv values of about 0.14 for sandy soil areas and 0.25 for clayey soil areas, and is where the curves start to greatly increase in slope.

CONCLUSIONS

The data collected for the Jefferson County watersheds show that this area in Birmingham, AL, has an average impervious cover of about 39%, of which about 25% is directly connected to the drainage system and 14% drains to pervious areas (Tables 2). Table 5 is a summary of the discharge conditions for the study drainage areas and shows that three urban areas are highly impervious, with more than 60% of the watershed areas being composed of impervious covers. It also shows the expected conditions in the local receiving waters due to the measured amounts of impervious cover from these local land uses. The stream quality is damaged to severely damaged, a fact confirmed by in-stream investigations by the Storm Water Management Authority Inc. biologists. As expected, the land use with the least impervious cover is open space (parks, cemeteries, golf course), and the land uses with the largest impervious covers are commercial areas, followed by industrial areas. It was found that the impervious areas in the Little Shades Creek and Jefferson County watersheds are almost entirely directly connected, but

that there is a large variability between the land use categories. It was found that for a typical residential land use located in the Birmingham area, the total amount of impervious area does not vary much. There is an apparent variability in front landscaped vs. back landscaped areas, the reason being the position of the house on the lot, but the total amount of landscaped areas has a low variability for residential land use areas.

Urbanization radically transforms natural watershed conditions and introduces impervious surfaces into the previously natural landscape. Total impervious areas are mostly composed of rooftop and transportation related components that can be either directly connected or disconnected to the drainage system. The impervious areas that are directly connected to the storm drainage system are the greatest contributor of runoff and stormwater pollutant mass discharges under most conditions. The amount of impervious cover has become recognized as a tool for evaluating the health of a watershed and serves as an indicator of urban stream quality. Knowledge about the impervious surfaces, and how they can be managed, is an effective stormwater management tool and can be used to help reduce the impacts of developments within watersheds.

ACKNOWLEDGEMENT

The authors acknowledge Stormwater Management Authority Inc. at Birmingham, AL for their help with the monitoring data and satellite images, and the Jefferson County "Earth Team" of the local USDA office, that in a volunteer effort, collected the Little Shades Creek field information during the mid 1990s. Also, a special thanks to The University of Alabama graduate students who helped in the Jefferson County drainage areas field data collection.

REFERENCES

Ackerman, Drew, and Eric Stein. 2008. Estimating the Variability and Confidence of Land Use and Imperviousness Relationships at a Regional Scale. *Journal of the American Water Resources Association* 44 (4): 996-1008.

Alley, William M., and Jack E. Veenhuis.1983. Effective Impervious Area in Urban Runoff Modeling. *Journal of Hydraulic Engineering*, 109 (2): 313-319.

Arnold, Chester, and James Gibbons. 1996. Impervious Surface Coverage. The Emergency of a Key Environmental Indicator. *Journal of the American Planning Association* 62 (2): 243-258.

Bochis-Micu, Celina and Robert Pitt. 2005. Impervious Surfaces in Urban Watersheds. *Proceedings of the Water Environment Federation*, WEFTEC 2005, Washington D.C. Session 37: 3124-3141(18).

Bochis, Celina. 2007. *Magnitude of Impervious Surfaces in Urban Areas*. Master Thesis. Department of Civil, Construction, and Environmental Engineering. The University of Alabama. Tuscaloosa, AL.

Bochis, Celina and Robert Pitt. 2008. Characteristics of Land Development in Central Alabama. *Proceedings of the Water Environment Federation*, WEFTEC 2008, Chicago, IL. Session 73.

Booth, Derek, and Rhett Jackson. 1997. Urbanization of Aquatic Systems - Degradation Thresholds, Stormwater Detention, and the Limits of Mitigation. *Journal of the American Water Resources Association* 33 (5): 1077–1090.

Boyd M.J., M.C. Buffil, and R.M. Knee. 1993. Pervious and Impervious Runoff in Urban Catchments. *Hydrological Sciences* 38: 463–478.

Boyd M.J., M.C. Buffil**,** and R.M. Knee.1994. Predicting Pervious and Impervious Storm Runoff from Urban Drainage Basins. *Hydrological Sciences* 39: 321-332.

Debo, Thomas, and Andrew Reese. 1995. *Municipal Stormwater Management,* Lewis Publishers, CRC Press, LLC, Boca Raton, FL.

Gregory, Michael, John Aldrich, Amy Holtshouse, and Kyle Dreyfuss-Wells.2005. Evaluation of Imperviousness Impacts in Large, Developing Watersheds. In: *Intelligent Modeling of Urban Water Systems, Monograph 14.* (Edited by W. James, K.N. Irvine, E.A. McBean, and R.E. Pitt). CH I Guelph, ON, Canada: 115-150.

Heaney, J. P., Huber, W. C., and Nix, S.1977. Storm water management model: Level I - Preliminary Screening Procedures. *U.S. Environmental Protection Agency Rep. EPA-600/2-76-275*, Washington, D.C.

Laenen, Antonius. 1983. *Storm Runoff as Related to Urbanization Based on Data Collected in Salem and Portland and Generalized for the Willamette Valley, Oregon.* USGS Water Resources Investigations Report 83-4143: 88

National Association of Counties (NACO).2001. http://www.naco.org/Template.cfm?Section=Find_a_County&Template=/cffiles/counties/county.cfm&id=1073

Novotny, Vladimir, and H. Olem. 1994. *Water Quality: Prevention, Identification, and Management of Diffuse Pollution*. Van Nostrand Reinhold, New York, NY.

Pitt, Robert, and John Voorhees. 1995. Source Loading and Management Model (SLAMM). *Seminar Publication: National Conference on Urban Runoff Management: Enhancing Urban Watershed Management at the Local, County, and State Levels*. March 30 –April 2, 1993. Grant No. EPA/625/R-95/003. U.S. Environmental Protection Agency. Center for Environmental Research Information. Cincinnati, OH: 225-243.

Pitt, Robert, and John Voorhees. 2002. SLAMM, the Source Loading and Management Model. In: *Wet-Weather Flow in the Urban Watershed: Technology and Management* (Edited by R. Field and D. Sullivan). Lewis Publishers, CRC Press, LLC, Boca Raton, FL: 103- 139.

Schueler, Thomas. 1994. The Importance of Imperviousness. *Watershed Protection Techniques*. Center for Watershed Protection 1(3): 100-111.

SCS (U.S. Soil Conservation Service, now Natural Resources Conservation Service).1986. *Urban Hydrology for Small Watersheds*. U.S. Department of Agriculture Technical Release No. 55.

Sutherland, Roger. 2000. Methods for Estimating the Effective Impervious Area of Urban Watersheds. In: *The Practice of Watershed Protection (*Edited by T. R. Schueler and H. K. Holland). Center for Watershed Protection, Ellicott City, MD: 193-195.

Linking Environmental Assessment and Solutions

L Gosselink[1], C. Herrington[1], and R.H. Glick[1]

[1]Watershed Protection and Development Review Department, City of Austin, PO Box 1088, Austin, TX 78767 ph: (512)974-2550 email: leila.gosselink@ci.austin.tx.us, chris.herrington@ci.austin.tx.us; roger.glick@ci.austin.tx.us

Abstract

The City of Austin is proposing a revised water quality problem score calculation for its master-planning process, which is used to direct allocation of resources for capital projects, programs and regulations. This change is proposed to address the challenge that Resource Managers face in identifying ecological assessment methods appropriate to their resource setting and particular information needs. Ecological assessment tools such as the City's Environmental Integrity Index (EII) include such a comprehensive suite of parameters that teasing apart the data to identify solutions and quantify potential benefits is difficult and not well documented. The revised problem score methods are more transparent and targeted to specific solution opportunities.

Background

Protection of our nation's waters has risen in priority as effects of urbanization began to impact what are characterized as the many "beneficial uses" of the surrounding water bodies. The focus has gradually grown to encompass protecting not only our water supply sources, but the stream systems that lead to it, flowing through our parks, neighborhoods, and wildlands. In addition to water quality measures, the health of the benthic community is often measured as a reflection of long-term impacts from flow variation, sedimentation, erosion and loss of riparian vegetation. The degradation of the stream systems reduces support of the aquatic ecosystem, and impacts to the urban environment by limiting contact and noncontact recreation.

The nation continues to look at water chemistry, and more recently biological communities, to assess large streams with standards and to direct efforts to reverse impairments. However, the complex issues of setting impairment levels for other concerns have not yet been addressed in many states and municipalities, examples including nutrient levels that cause algae blooms, toxins in sediments, riparian vegetation and litter. So, while some problems are addressed and prioritized separately by programs such as TMDLs or stream restoration projects, it is more

difficult to prioritize a multitude of different problems from a single funding source such as a drainage fee.

The City of Austin began a comprehensive assessment program under its drainage-funded department (WPDRD, the Watershed Protection and Development Review Department), where flood and erosion projects focus on safety issues and property damage. The Environmental Resource Management Division, meanwhile, generated an Environmental Integrity Index (EII) using six sub indices as a measure of the (1) health of the aquatic life, support of (2) contact and (3) non-contact recreation, (4) the physical integrity, (5) water quality, and (6) sediment quality. The specific field measures under each of these categories were selected after careful review of other current water quality monitoring and assessment protocols. In particular, the US Environmental Protection Agency (USEPA) Rapid Bioassessment Protocols (Plafkin, et al. 1989) and the Texas Natural Resource Conservation Commission, (TNRCC) Use Attainability Assessment and Physical Characteristic Assessment (TNRCC, 1988) were useful references. The EII generates an overall score of watershed health reported on a 0-100 scale (bad to good); the methodology for the EII is provided in "Environmental Index Methodology" (COA 2002).

Prior City of Austin Work

The solutions, Capital Improvement Projects (CIP), programs such as education programs and regulations are provided primarily through the City's drainage fee, in addition, problems and projects may be allocated to other departments such as the Austin Water Utility. A prioritization of all problems is required for planning and funding allocation for these programs. Thus, EII scores are translated to problem scores which are used in the prioritization process.

Previous water quality problem scores were calculated by the formula:

$$\text{Problem Score} = \sum_{i=1}^{n} [(W_{cur}*RV_{cur}*CPS*) + (W_{fut}*RV_{fut}*FPS)]$$

where n = number of receiving waters
W_{cur} = Weight assigned to Current problems
RV_{cur} = Resource Value for Current Conditions
CPS = Current Problem Severity Score (see Table 1 for measured parameters)
W_{fut} = Weight assigned to Future problems
RV_{fut} = Resource Value for Future Conditions
FPS = Future Problem Severity Score

Previous water quality problem score calculation methods for each of these factors have been characterized as overly complex, lacking transparency and strongly influenced by the various weighting factors. Problem severity was based on a "goal gap." Current and future scores were combined, although programmatic and regulatory changes (i.e., new or revised development ordinances) are the preferred

solution for future problems. The previous problem score method, based on the average of all six EII sub-indices and their many factors, tended to dilute scores resulting in an indirect linkage between problems and specific solutions. Predicting and measuring the performance of solutions was also difficult and measureable success of one type of problem was diluted by those problems not addressed.

The method for calculating the water quality problem score has been revised and updated generally following the methods used by the WRE to address unacceptable decreases in EII scores according to the departmental action plan (COA 2003, COA 2005, COA 2007).

The field measurements were evaluated with field staff and problem score components were selected that met the following criteria:

a. Solutions will provide direct or indirect protection or enhancement of beneficial uses such as aquatic life support (ALS) and for receiving waters (RW) such as lakes.
b. There is an identifiable and feasible solution through City funding or actions
c. The problem and benefits can be quantified with specific performance measurements and environmental indicators.

Ten problem components were selected that met the criteria.

1. Toxins in sediments –
    a. Benefits: Reducing toxins (PAHs, metals, pesticides) in sediments improves Aquatic Life Support and Receiving Water conditions.
    b. Solutions include engineered controls, such as water quality ponds to capture sediment-sorbed contaminants in stormwater, and regulations such as the City's ban of coal tar-based sealants.
    c. Performance Measures: Estimates can be made of loads reduced and sediment toxin concentrations will be measured after solution implementation.
2. Bacteria from animals (dogs, livestock, wildlife) –
    a. Benefits: Reducing bacteria protects contact recreation in both the stream segment and the receiving water body. .
    b. Solutions include primarily programmatic solutions such as the "Scoop the Poop" education program.
    c. Performance Measures: Bacteria concentrations will be measured.
3. Sewage (bacteria, nutrients, algae) –
    a. Benefits: Reductions in bacteria, nutrients and algae growth protects contact recreation, noncontact recreation, water quality and aquatic life uses in the streams and receiving water bodies
    b. Solutions will be mainly referred to the Austin Water Utility for CIP projects.
    c. Performance measures: Bacteria and nutrient concentrations as well as algae presence will be measured.

4. Fertilizer Runoff (nutrients, algae)
    a. Benefits: Reduction in nutrients reduces algae and enhances recreational opportunities in the stream segment and the receiving water body. .
    b. Solutions can include both engineered controls and programs such as the City's "Grow Green" education program..
    c. Performance measures: Nutrient concentrations as well as algae presence will be measured.
5. Litter
    a. Benefits: Reduction in litter, trash & debris enhance recreational uses of streams and lakes.
    b. Current solutions including the City's Keep Austin Beautiful Program; the lake cleanup program can also be targeted to the most problematic areas.
    c. Performance measures: The litter assessment (part of EII) as well as the Ladybird Lake Visual Index of Pollution are the current measures for this problem.
6. Construction runoff (TSS)
    a. Benefits: Reduction in sediments washing into stream segments will enhance habitat for Aquatic Life Support.
    b. The principal solution would be to notify the City's Code Enforcement staff of targeted areas or specific site problems to enforce construction BMP requirements..
    c. Performance will measured by a reduction in the TSS in baseflow as well as sediment depth in the streambed.
7. Unstable channels (erosion)
    a. Benefits: Improved bank stability and channel restoration to a more natural condition will benefit the aquatic life by providing better habitat as well as reducing erosive sediment loads
    b. Solutions are comprised of bank and channel restoration projects.
    c. Performance will be measured by an improved habitat score, reductions in suspended sediments in the stream and transported to the receiving waters, and reduced sediment depth on the streambed.
8. Poor riparian vegetation (poor riparian zone width and quality)
    a. Benefits: Improved riparian vegetation and width will provide better habitat and environment for aquatic communities. In addition, improvements may enhance the aesthetics for noncontact recreation activities. as well as the ancillary benefit of capturing washoff pollutants draining through stream buffer areas.
    b. Solutions will take the form of re-vegetation programs which will frequently be combined with erosion control and bank restoration projects.
    c. Performance will be measured by a the direct assessment of vegetative protection and riparian width.

9. Altered hydrology (current flow regime, flashiness & baseflow presence)
    a. Benefits: Enhancing baseflow & reducing flashiness may be perhaps the most beneficial action for improving benthic community health in the Austin area. Recreational opportunities associated with water resources are enhanced too by increased presence of baseflow. Water quality improvements will also be seen with a reduction in stagnant pools.
    b. Solutions for enhancing current baseflow conditions are difficult, but the use of ponds with infiltration capacity and the cumulative effects of programs to encourage and build small scale rain management systems such as rain gardens may show some results.
    c. Performance will be measured by long-term flow monitoring and analysis of the flow parameters used to identify problems as well as the direct measure of aquatic life.
10. Future problems (future flow regime, flashiness & baseflow presence)
    a. Benefits: Preventing degradation of the natural flow regime where it still exists in Austin creeks is, likewise, a critical factor for maintaining aquatic life. Recreational use will likely degrade with reduced baseflow. Additionally, the development and increased impervious cover that degrade flow regimes are also the primary factors for many of the other problems identified for current conditions (fertilizer, bacteria, toxins), thus the future flow assessment will be used as an indicator for all future water quality problems.
    b. Solutions for preventing baseflow degradation will most likely be regulatory protective measures, protection of undeveloped lands and headwater areas through purchase programs or buffer protection, engineering flow control requirements, and cooperative agreements with regulatory agencies in the stream segments outside of the City's jurisdiction.
    c. Performance will be estimated with hydrologic modeling exercises and long-term monitoring of both streamflow and aquatic life..

These proposed problem factors will better reflect actual environmental conditions; the worst problems will have the highest scores, will use the most indicative factors, and will enable more specific evaluation of post-implementation solution effectiveness.

Methods

Using functional methods such maxima of critical parameters, the WQ score calculation allows a simplified illustration of stream segment conditions as well as source specific interpretation to inform the public and provide geographical targeting information to program managers. A major revision includes the substitution of hydrologic parameters for the direct use of benthic community health indices.

There are currently 118 EII reaches monitored by the WRE surface water team (watersheds with relative EII condition shown in Figure 1), selected on the basis of similar hydrology, geomorphology, land use, point sources and predicted future impacts. Note that the narrative scales of the EII and the problem score are reversed such that a larger EII score reflects a more positive condition while a larger problem score reflects a more negative condition. Flow information will be taken from long-term gauging stations. Soil and Water Assessment Tool (SWAT) models, calibrated for gauged watersheds and extended to all monitored reaches by Water Quality Monitoring team (WQM) staff, will be used to predict reach flows. Future flow conditions will be predicted by replacing current land use with predicted future land use provided by planning staff.

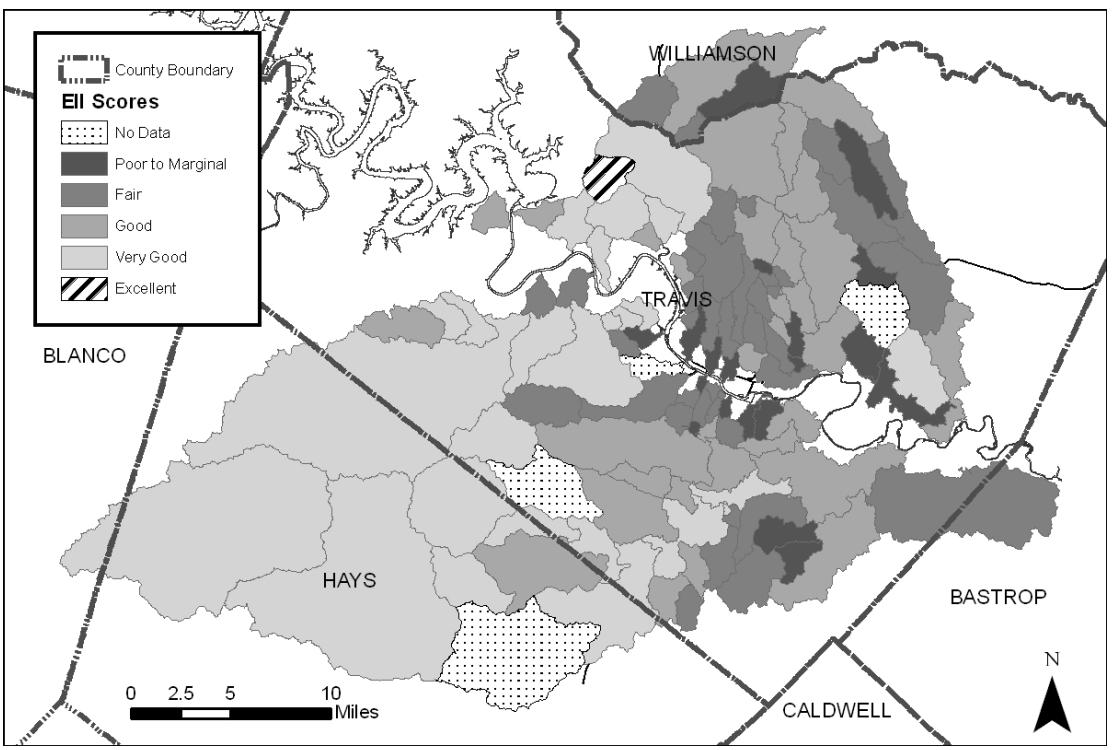

Figure 1. EII reach conditions (2005-2007 sampling events), Austin, TX

The calculation method for each problem score component is detailed below. EII scores are scaled 0-100 (bad to good) and are thus frequently "inverted" (subtracted from 100) to yield a problem score that are scaled 100-0 (bad to good). Problem scores may be less than zero for some problems resulting from the subtraction of two unrelated EII components, and negative problems should be considered as low priority and set to zero in any score combination method.

Toxins in Sediment = 100 – min(PAH, pesticide or metal EII)

Sediment data are collected from the mouth of each EII-monitored watersheds and analyzed for PAHs, pesticides and metals. Sediment EII scores are intended to be

representative of the toxic load for the entire watershed. The worst (lowest) EII component (PAH, pesticide or metal) is used in the calculation.

Litter = 100 – (Litter EII)
Litter EII component scores collected for the aesthetics sub-index are subtracted from 100 to identify reaches with litter problems. EII litter scores are based on a visual assessment litter quantity and type at the representative monitoring site for each reach. Potential solutions include creek cleanups organized through groups like Keep Austin Beautiful and further source investigation through creek walks or aerial photography analysis.

Bacteria from animals = min(nutrient or %algae EII) – (bacteria EII)
The problem of bacteria from animals, e.g. pets or livestock, was constructed to identify reaches with low concentrations of nutrients (ammonia, nitrate and orthophosphorus) and algae (as characterized by the percent algae coverage component of the aesthetics sub-index) but high fecal bacteria indicative of fecal contamination from animal sources and not leaking wastewater infrastructure. Areas with high fecal bacteria concentrations that are influenced by runoff from high-traffic dog parks would exemplify high priority problem reaches. The dual use of the worst (lowest) nutrient or algae EII component allows for reaches that may have low instream nutrient concentrations because of high algal biomass accrual and are thus nutrient enriched systems. Example solutions include education programs like the COA Scoop the Poop campaign to reduce fecal contamination within the reach.

Sewage = 100 – average[bacteria EII and min(nutrient or %algae EII)]
The sewage problem was designed to identify reaches with both high nutrients (ammonia, nitrate or orthophosphorus) and fecal bacteria typical of areas affected by leaking wastewater infrastructure. Again, the worst (lowest) nutrient or algae component EII score is used to more accurately represent the level of nutrient enrichment present. Problem areas could be recommended to the Austin Water Utility for further investigation and remediation of failing wastewater infrastructure.

Fertilizer Runoff = (bacteria EII) – min(nutrient or %algae EII)
Effectively the inverse of the bacteria from animals problem, the fertilizer runoff problem is constructed to identify reaches with low bacteria and high nutrients or algae cover indicative of reaches affected by nutrient enrichment from excessive or improper lawn fertilizer usage. Note that EII scores are 0-100 (bad to good) such that the subtraction of a good bacteria EII component score from a bad nutrient or algae EII component score would yield a large fertilizer runoff problem score. Programs like the COA Grow Green education campaign and CIP projects to capture and treat stormwater runoff are example solutions that could be targeted to problem reaches.

Construction Runoff = (bank stability EII) – average(TSS, sediment deposition EII)
The sediment from construction runoff problem score was designed to identify reaches with stable channels but high instream total suspended solids (TSS from the EII water quality sub-index) and high substrate embeddedness (from the sediment

deposition component of the EII habitat quality sub-index). The worst of left or right bank stability are used in the calculation. Bank stability is included in the calculation to exclude highly depositional reaches where the source of stream sediments is likely bank sediments from erosion of unstable areas. Revised regulations and increased environmental inspections for code compliance are potential solutions which could be targeted to problem reaches.

Poor riparian vegetation = 100 – [(vegetative protection EII/100)*(riparian width EII)]

The inadequate riparian vegetation problem was designed to prioritize reaches with both low quality (i.e., low diversity) and low quantity (i.e., narrow) riparian zones. The calculation is done separately for the right and left banks and then the worst is used to represent the reach. Division of the bank vegetative protection score by 100 effectively converts it to a weighting factor to modify the riparian zone width component. Riparian zone assessments are completed as part of the habitat quality (a.k.a. physical integrity) EII sub-index. An optimal EII reach would have wide and diverse riparian zones on both sides of the creek. Stream bank restoration and re-vegetation are potential solutions for problem areas.

Unstable Channels = 100 – ¾*bank stability EII – ¼*channel alteration EII

The unstable channel problem score was designed to identify unstable creek reaches. The differential weighting of bank stability and channel alteration ranks altered, unstable reaches with the highest problem priority followed by unaltered, unstable reaches. The unstable channel problem will and the construction runoff problem are effectively mutually exclusive. Bank stability and channel alteration are collected during the habitat EII sub-index. The worst (lowest) of the left and right bank stability EII scores are used in the calculation.

Altered Hydrology = f(Annual avg. # of dry periods, Ln of 90th flow percentile)

The current altered hydrology problem was developed from a multiple linear regression of EII aquatic life scores versus a set of metrics describing the flow regime of the reach by the WQM team. The selected flow metrics are:

Annual avg. # of dry periods = Average of the number dry periods for each site
Ln of the 90 percentile = Natural log of the 90th percentile of flow (flow in cfs)

Flow metrics will be calculated from the output of SWAT models for all reaches for a pre-determined length of time preceding the evaluation year. The targeted problem is altered hydrology including both lack of baseflow and flashiness in response to runoff events. Flow is most likely the best predictor of future environmental conditions and can be predicted with SWAT models even in watersheds without continuous flow monitoring with reasonable accuracy. Because of the reliance of aquatic life community function on flow regime, hydrology is likely to be a good predictor of aquatic life integrity.

Future Problem = Future – Current Altered Hydrology Problem

The future problem score is simply the difference between the future altered hydrology problem score, calculated using the SWAT models incorporating predicted future land use, and the current altered hydrology problem score. Highest priority reaches would be reaches with more stable flow regimes now that are threatened in the future to exhibit flow regimes that lack baseflow and are more flashy in response to runoff events. A potential solution to future problem reaches would be targeted regulatory action to limit connected impervious cover and provisions for specific types of stormwater controls.

Results

The simplicity of the separate problem scores allows combining in more than one manner. Figure 2 below shows selected scores for several reaches with individual problem scores stacked. The staff who prioritize for CIP engineering solutions looked at the total of four components that may be remediated by ponds, revegetation and channel work. The highest priority segment was identified as TAN1, not the highest overall total score. The litter score of two segments below, WLR1 and EBO3, indicate that these two segments in the most highly urbanized area of Austin may need programmatic fixes for sewage & litter, but may not show the most benefit for CIP funds spent. Likewise, inspections to prevent construction TSS runoff in GIL4 may be the most cost-effective improvement in that reach rather than a CIP project.

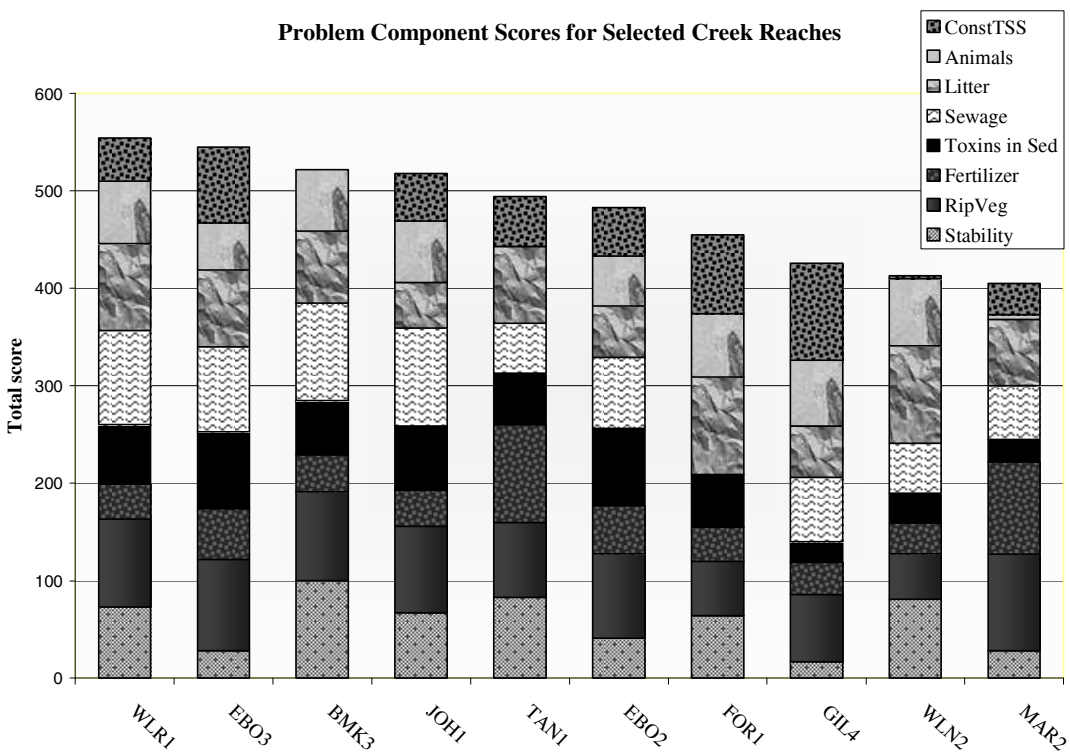

Conclusions

The revised problem score method provides prioritization of specific water quality problems with practical solutions. The calculation of the individual scores is simple and maximizes the specificity of the EII field observations to discriminate between pollution sources. A creek segment such as WLN2 above has an overall EII score of good, yet has some creek stability problems and the highest reach litter score. These individual problems may be used to prioritize solutions for any of the programs or processes affected, and the overall combined score may be used in the mission integration process for the selection of CIP projects.

The easy visualization of the component parts of the proposed score will be implemented to test transparency in public venues, reflecting observed conditions by citizens; to test practicality, whether specific solutions tied to the indicated problems; and predictable, whether estimated benefits will match improvements from solution implementation.

References

City of Austin (COA). 1997. Environmental Integrity Index Water Quality Technical Assessment Methodology. City of Austin Drainage Utility Department, Environmental Resources Management Division. Water quality report series COA-ERM/WRE 1997-03.

City of Austin (COA). 2001. Watershed Protection Master Plan Phase I Watersheds Report, Volume 1. Watershed Protection Report Series COA-WPD-2001-02. City of Austin Watershed Protection Department.

City of Austin (COA). 2002. Environmental Integrity Index Methodology. City of Austin Watershed Protection Department. Water Quality Report Series COA-ERM 1999-01.

City of Austin (COA). 2003. Change in Environmental Integrity Index Values in the Austin, Texas, area (1996-2002). City of Austin Watershed Protection and Development Review Department. SR-03-06.

City of Austin (COA). 2005. Action Plan Items Related to EII Scores—Fiscal Year 2005. City of Austin Watershed Protection and Development Review Department. SR-05-08.

City of Austin (COA). 2007. Action Plan Items Related to EII Scores—Fiscal Year 2005. City of Austin Watershed Protection and Development Review Department. SR-07-03.

Long-term Effectiveness of a Bioretention System Treating Road Runoff in Northeastern Kansas

Edward Peltier[1], Xiaolu Chen[1], Kelly Kindscher[2] and C. Bryan Young[1]

1. Department of Civil, Architectural and Environmental Engineering, University of Kansas, 2150 Learned Hall, 1530 West 15th Street, Lawrence, KS 66045. Ph: (785)-864-2941; Fax: (785)-864-5379; email: epeltier@ku.edu
2. Kansas Biological Survey, University of Kansas 135 Higuchi Hall, 2102 Constant Ave. Lawrence, KS 66045

ABSTRACT

Recent studies have indicated that the use of ecologically-based methods for stormwater treatment, including bioretention systems, may provide increased pollutant removal and protection of downstream receiving waters. However, there is little data addressing the long-term performance of these systems in the field or the effects of contaminant accumulation over time on treatment effectiveness. In this study, we present results from an ongoing three-year study of bioretention performance and contaminant fate at a 0.1 acre bioretention cell located in northeastern Kansas. Samples of influent and treated stormwater from storm events during 2007 and 2008 were analyzed for a range of water quality parameters, including total suspended solids, nutrients and total and dissolved Cu and Zn. Results of this sampling show that the bioretention system successfully removes > 70% of suspended solids and more than half of influent total metals. Removal of dissolved constituents is much lower, with the exception of nitrate, which had removal rates of up to 50% during the study. Improvements to the mulch material and vegetative establishment could potentially increase system performance for these constituents.

INTRODUCTION

Mitigating the impact of non-point source pollution has become increasingly important to maintaining surface water quality in the United States, particularly as point source pollutants have been reduced through effective regulatory control. The 2000 National Water Quality Inventory (United States Environmental Protection Agency 2002) reported that 40% of the nation's water bodies do not meet water

quality standards and identified non-point source pollution (NPS) in general, and urban stormwater runoff in particular, as a leading cause of surface water degradation. Stormwater runoff can contain a wide range of pollutants that can degrade receiving water quality and aquatic ecosystems, including suspended solids, excess nutrients, and toxic organic and inorganic compounds. Runoff from roads and other paved surfaces is particularly likely to contain elevated levels of heavy metals, including Cu, Zn, Pb and Cr, as well as suspended solids and nitrate (Shaver et al. 2007). Treatment strategies that address this broad spectrum of pollutants are required in order to minimize the effects of these contaminants on downstream receiving waters.

Engineered best management practices (BMPs) for stormwater must simultaneously provide for stormwater storage during high flow events and improve the quality of effluent water released from the system through contaminant removal. While a variety of design options exist for these systems, recent studies have indicated that the use of ecologically-based (or low-impact) BMPs provide superior pollutant removal to other treatment approaches (Weiss et al. 2007). The presence of soil, vegetation, and microbes in these systems allows for the removal and transformation of influent contaminants through multiple chemical, physical and biological processes, making them particularly useful for treatment of stormwater runoff containing a mixture of pollutants. The presence of a self-sustaining vegetative ecosystem can also aid in reducing maintenance and operating costs over the treatment lifetime.

For locations with relatively small watersheds and/or limited available space for BMP placement, bioretention cells represent one of the most attractive ecologically based treatment options. A bioretention cell is a compact system (as small as 0.05 acres) consisting of a thin layer of mulch over a filter layer composed of a sandy soil mixture, with a planted vegetative cover. Stormwater is channeled to the top of the treatment cell where it initially ponds and then slowly infiltrates into the soil matrix over a period of 8-24 hours. Sedimentation at the surface and filtration within the soil matrix are the primary removal mechanisms for suspended solids and solid-associated contaminants. Dissolved species are removed primarily through sorption to the filter material, although biological uptake and degradation may also play a role in the removal of nutrients and organic compounds. Previous studies have shown good potential for removal of metals and suspended solids with these systems, but poorer removal rates for nutrient compounds, particularly NO_3-N (Hsieh et al. 2007).

With their small footprint and potential to remove multiple types of contaminants, including toxic metals, bioretention systems may become an effective approach to improving the quality of stormwater runoff from roads and other paved surfaces. However, there is currently little data regarding the long-term performance of these systems in the field or the effects of contaminant accumulation over time on treatment effectiveness and lifespan. Additionally, there are likely to be regional issues involved in implementing these BMPs in the Great Plains region related to

growing season, storm frequency and duration, and soil drainage. (Many of the soils in this region have relatively high clay and low sand contents, leading to slower drainage and longer periods of standing water.) In order to address these issues and develop long-term data on system performance, we are conducting a three-year study of a bioretention cell located in northeastern Kansas. In this study, we present results from this ongoing study related to hydrological performance and contaminant removal at this location.

METHODS

The field site is a 0.1 acre bioretention cell built in 2005 to treat runoff from a 4-lane road prior to discharge into an adjoining lake. The surrounding area is undergoing rapid development, with several residential and commercial development projects currently underway or in the planning stages. Road traffic and associated pollutant loading from roadway runoff are therefore expected to increase over the next several years. Stormwater is collected in curbside sewers and transported to the cell through a single concrete pipe. A mesh bag trap in the storm sewer filters large particulates and debris from the runoff before it enters the bioretention cell. The cell itself consists of a 3 inch layer of wood chip mulch overlying a 2.5 foot layer of sandy loam soil. Treated effluent is collected in a perforated pipe that serves as a cell underdrain and then discharged into the lake through a surface level outfall pipe. An overflow sewer in the center of the cell allows for short-circuiting by a portion of the stormwater runoff during high rainfall events.

Rainfall data for storm events during the sampling period was obtained from the 9 stations of the Johnson County ALERT rain gauge data network (Young and McEnroe 2003) located within 3 miles of the field site. Total precipitation amounts were verified using an on-site rain gage. Runoff depths were calculated using tabulated runoff curve values based on a survey of ground cover in the watershed drained by the bioretention cell. The hydrological properties of the system were monitored in two ways: by observing the drawdown time for standing water after heavy rainfalls using an automated camera set to take pictures of a staff gage every hour, and by collecting data on water depth in the effluent pipe using a pressure sensor attached to a datalogger.

Water samples were collected at three locations within the treatment system. The first location was at the curbside storm sewer, prior to passing through the solids catch basin. Runoff was funneled through a plastic tube placed on the road surface and into a 1 L plastic bottle. The second collection site was at the discharge point of the storm sewer into the bioretention cell. Samples at this location were collected using a programmable auto-sampler (ISCO 6700) with attached flow meter. The third collection site was at an underground drainage pipe containing effluent from the bioretention cell. Treated water from the bioretention cell passes through this drain

prior to draining to the adjacent lake. Composite samples were collected from this location using an automated sampler and flow meter. Additional samples were collected by hand within 24 hours of storm events.

Samples of influent and treated stormwater from each storm event were collected within 48 hours of each storm event and then stored at 4 ºC until analysis. Samples for dissolved ion analyses were filtered through a 0.45 μm nylon filter prior to analysis. Total suspended solids tests were conducted on the same day as sample collection according to the 2540D procedure (American Public Health Association et al. 2005). Concentrations of major inorganic anions, including nitrate and phosphate, were measured using an ion chromatograph (Dionex Corp.) with a hydroxide eluent. Sample digestion for total metals analysis was carried out using concentrated nitric acid at a 10:1 sample:acid ratio. Inductively-coupled plasma mass spectrometry (ICP-MS) was used to screen initial samples collected in the spring of 2007 for dissolved and total metals. Based on these initial results, Cu and Zn were chosen for monitoring in subsequent samples. These samples were analyzed using flame or graphite-furnace atomic absorption spectroscopy, depending on the concentrations encountered.

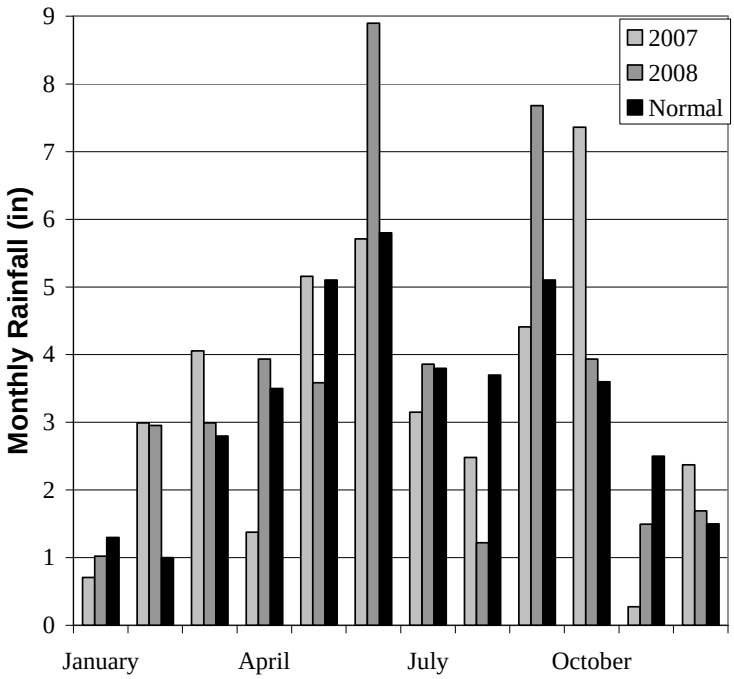

Figure 1. Average Monthly Rainfall during the Study Period.

RESULTS

The bioretention field study began in April, 2007. Figure 1 shows the monthly rainfall totals during the study period compared to normal rainfall amounts for these months based on historical data. Total yearly rainfall was 40.0 and 43.3 inches for 2007 and 2008, respectively, both slightly higher than the typical yearly value of 39.7 inches. The highest monthly rainfall was recorded in June 2008, at 8.9 inches. This unusually wet month resulted in sustained inundation of the bioretention cell for a period of approximately 2 weeks, and the only use of the site's overflow sewer during the sampling period. With the exception of this period, site drainage was within target design parameters, with drawdown occurring within 24-36 hours. The average drawdown rate was determined to be 0.18 inches/hour.

Table 1. Mean Suspended Solids and Metal Concentrations at Bioretention Cell Sampling Locations. All values in μg/L unless otherwise noted

	TSS	Zn		Cu	
	(mg/L)	Total	Dissolved	Total	Dissolved
Storm Sewer	343 ± 129	653 ± 150	44.9 ± 11.0	159 ± 54.4	9.83 ± 3.83
Bioretention Cell Influent	34.6 ± 13.7	303 ± 45.6	49.5 ± 11.9	82.8 ± 30.4	6.45 ± 3.58
Bioretention Cell Effluent	25.7 ± 13.5	194 ± 34.4	52.0 ± 15.8	50.0 ± 14.2	2.81 ± 0.97

Mean values for suspended solids and total and dissolved metal concentrations during the study period are listed in Table 1. Total suspended solids and metal concentrations were substantially higher than those reported in the 1983 USEPA Nationwide Survey (United States Environmental Protection Agency 1983). The effect of the particulate trap located in the storm sewer can be seen in the approximately 90% decrease in average suspended solids concentration from the roadway to the bioretention cell influent. Total metal concentrations also decrease between the two influent sampling locations, but by a much smaller factor than that for suspended solids. This indicates that both Zn and Cu are disproportionately bound to smaller particulates, which will be less likely to be removed in the large mesh filter bags used in the storm sewer.

Comparison of the average TSS values for the three sampling locations suggests that there is little additional removal of suspended solids provided by the bioretention cell itself. However, these average values do not take into account the substantial variations in influent TSS loading between different storm events. In order to account for this variation, removal rates for TSS and metals in the bioretention system were calculated on an event basis by assessing the difference between contaminant concentrations at each sampling location for each storm and then averaging these

removals. Removal rates were calculated based on the difference in concentration between the influent and outlet sampling location for three zones: the system as a whole (storm sewer to cell effluent), the bioretention cell itself (cell influent to cell effluent) and the storm sewer particulate trap (storm sewer to bioretention cell influent). Concentration-based data were used in all cases, with no attempts to account for loss of water volume in the bioretention cell due to evapotranspiration. Storm events where one of the influent concentrations was at or below detection limits were not used included in the datasets for these calculations.

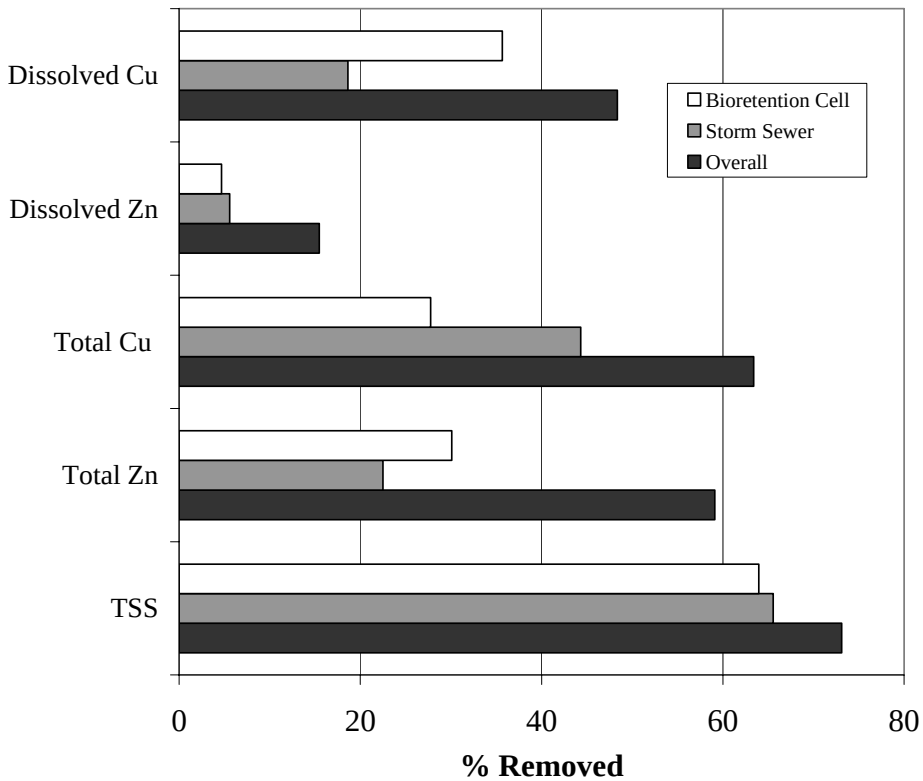

Figure 2. Contaminant Removal in the Components of the Bioretention Treatment System.

The effectiveness of the bioretention system at removing influent contaminants is shown in Figure 2. While the majority (~ 65 %) of suspended solid removal from the roadway runoff occurs in the storm sewer particulate trap, the bioretention cell also effectively removes the same percentage of influent solids. For both zones, as well as for the overall system, the percentage of influent solids removed increases with increasing concentration in the influent stormwater. TSS removal is in excess of 90% for most storm events where the concentration in the roadway runoff is greater than 100 mg/L. Total Zn and Cu removal percentages are lower in both the particulate trap and the bioretention cell itself. For Zn, in particular, this is partially due to very low dissolved metal removal rates of less than 20%. Dissolved Zn makes up almost 25%

of the total Zn in the bioretention cell effluent. The bioretention cell appears to be somewhat more effective at removing both dissolved and total copper, potentially due to the greater affinity of Cu for complexation with organic matter in the soil matrix.

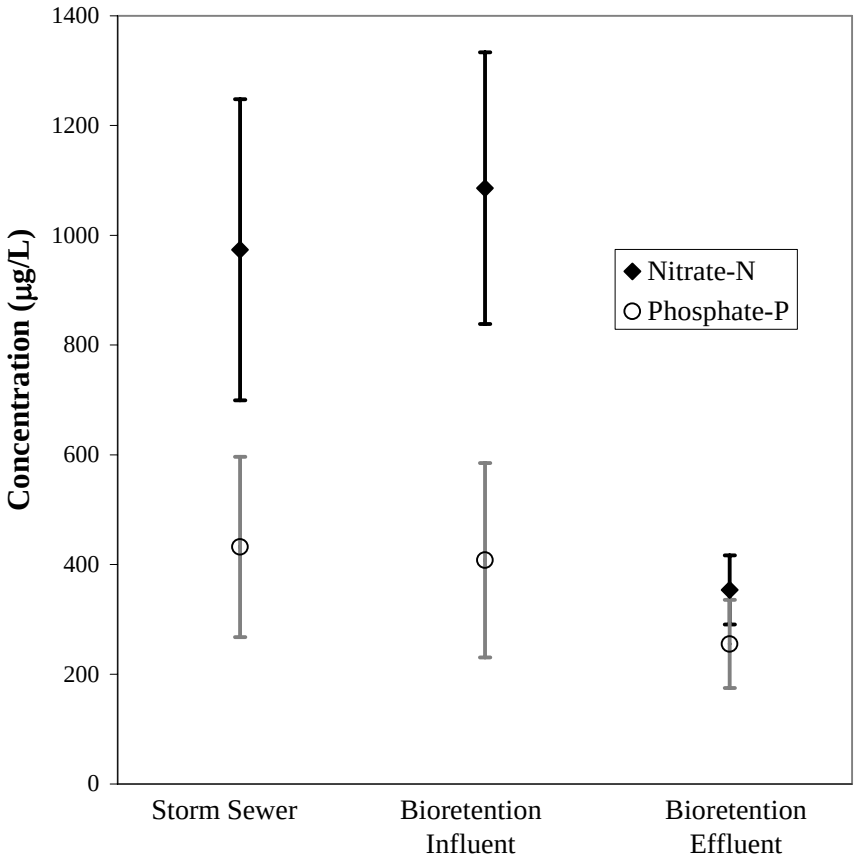

Figure 3. Mean Nitrate and Phosphate Concentrations at each Sampling Location in µg-N/L and µg-P/L.

Nutrient Removal: Mean nitrate and phosphate concentrations at the three sampling locations are shown in Figure 3. While phosphate concentrations are similar throughout the bioretention system, the nitrate concentration increases somewhat between the storm sewer and the bioretention cell influent. This increase is unlikely to be related to changes in total volume, since water is not retained for long in the storm sewer system. Possible sources of nitrate in the drainage area of this system include the vegetated berm surrounding the bioretention cell and the surface of the cell itself. In particular, water buildup on the cell surface during larger storm events may result in water mixing and nitrate release from the soil and vegetation immediately surrounding the storm sewer exit. Nitrate concentrations then drop substantially between the bioretention cell influent and effluent. While average phosphate concentrations are somewhat lower in the cell effluent than in the influent

stormwater, there were also multiple individual events in which an increase in dissolved phosphate was observed across the treatment system, suggesting that dissolved phosphorus retention may be a long-term cell performance issue.

Calculated removal percentages for these two compounds confirm that the bioretention cell removes a substantially higher fraction of influent nitrate (40%) than is typically observed for these systems. Nitrate removal has been improved in model systems by stimulating biological denitrification through the addition of biodegradable material at the cell effluent (Kim et al. 2003). Based on these results, it appears that a similar process is naturally occurring in this system. Biological denitrification may be enhanced in this system by relatively long stormwater detention times (24-36 hours, compared to recommendations of 8-12 hours in most design manuals). There is considerable biofilm growth on the inside of the bioretention cell effluent collection pipe, which may also play a role in the observed denitrification.

CONCLUSIONS

Sampling results presented here show that influent stormwater quality for the bioretention treatment system is typical of paved surface runoff, with elevated concentrations of suspended solids and total Zn and Cu. The use of a particle trap in the storm sewer considerably reduces loading of these contaminants to the bioretention cell itself, particularly with respect to suspended solids. This design choice adds to the maintenance requirements for the system, as the particle trap must be cleaned on a monthly basis, but will also likely prolong the lifespan of the bioretention cell by preventing clogging at the filter surface and reducing the rate of metal accumulation in the bioretention cell soil matrix.

The performance of the bioretention cell with respect to solid phase contaminants is in line with results from published field studies. Removal of suspended solids and particulate-associated metals is in the range of 50-70%, with little seasonal variation. Short circuiting of the treatment process occurred on several occasions due to extremely high rainfall in the first two weeks of June 2008, but the hydrological performance of the system is otherwise within the requirements for maintaining good vegetative cover and removing water from the site. System performance is weakest for dissolved metals and phosphorus, which show consistently low removal percentages. The high rates of nitrate removal observed here suggest that the 24 hr drawdown time observed in most storms is sufficient to allow for establishment of denitrifying bacteria in the bioretention cell. The overall effect on total nitrogen removal, however, is still under investigation. Further work for this study will focus on resolving this issue, and on improving system performance with respect to dissolved metal and phosphorus removal through changes or amendments to the soil mulch layer and/or the type and amount of cell vegetation.

REFERENCES

American Public Health Association, American Water Works Association and Water Environment Foundation (2005). *Standard Methods for the Examination of Water and Wastewater*. Washington, DC, American Public Health Association.

Hsieh, C. H., A. P. Davis and B. A. Needelman (2007). "Nitrogen removal from urban stormwater runoff through layered bioretention columns." *Water Environment Research* **79**(12): 2404-2411.

Kim, H. H., E. A. Seagren and A. P. Davis (2003). "Engineered bioretention for removal of nitrate from stormwater runoff." *Water Environment Research* **75**(4): 355-367.

Shaver, E., R. Horner, J. Skupien, C. May and G. Ridley (2007). *Fundamentals of Urban Runoff Management: Technical and Institutional Issues*. Madison, WI, North American Lake Management Society

United States Environmental Protection Agency (1983). Results of the Nationwide Urban Runoff Program. Washington, DC, Water Planning Division, USEPA. **1**.

United States Environmental Protection Agency (2002). National Water Quality Inventory: 2000 Report. Washington, DC, Office of Water, USEPA.

Weiss, P. T., J. S. Gulliver and A. J. Erickson (2007). "Cost and pollutant removal of storm-water treatment practices." *Journal of Water Resources Planning and Management-ASCE* **133**(3): 218-229.

Young, C. B. and B. M. McEnroe (2003). "Sampling Adjustment Factors for Rainfall Recorded at Fixed Time Intervals." *Journal of Hydrologic Engineering* **8**(5): 294-296.

Looking Upstream and Into the Watershed for the Big Picture of Stream Health

Christina Y.S. Siu[1]*, Shirley E. Clark, Ph.D., P.E., D.WRE, M. ASCE[2], Ruth A. Sitler, and Katherine H. Baker, Ph.D[3]

[1]Research Scientist, Penn State Harrisburg, School of Science, Engineering, and Technology, 777 West Harrisburg Pike, TL 123; Middletown, PA 17057; PH (717) 948-6304; FAX (717) 948-6580; email: cys106@psu.edu

[2]Assistant Professor of Environmental Engineering, Penn State Harrisburg, Environmental Engineering Program, 777 West Harrisburg Pike, TL 105; Middletown, PA 17057; PH (717) 948-6127; FAX (717) 948-6580; email: seclark@psu.edu

[3]Associate Professor of Environmental Microbiology, Penn State Harrisburg, School of Science, Engineering, and Technology, 777 West Harrisburg Pike, TL 105; Middletown, PA 17057; PH (717) 948-6308; FAX (717) 948-6580; email: khb4@psu.edu

*Corresponding author: cys106@psu.edu

ABSTRACT

When examining impaired river reaches, the primary focus is improving streamwater quality in the reach and downstream. The degree of damage to the river channel, the biological functions, and the river chemistry are assessed and restoration plans implemented. Few examine the causes of the degradation from upstream and upland areas and manage those problems before performing restoration work downstream. Without watershed management in the upper river system that addresses the stream's stressors, any restoration downstream becomes useless either relatively immediately or over time. Continued and potentially increased high peak flows from development during storms can wash out many restoration elements. Here, we examine the water management in the upper watershed of an unnamed tributary that passes through the Penn State Harrisburg campus, empties into the Susquehanna River, and eventually into the Chesapeake Bay. We also demonstrate the linkages between the lack of integrated water management and the current status of this tributary. The biota within the stream and surrounding the stream lack both diversity and richness. The streambanks are highly eroded and unstable. Current practices on campus (irrigation, grass cutting, etc.), as well as in the agricultural, residential, and industrial areas upstream, and any future campus development can hinder improving the stream's health. As restoration is being planned and implemented, the fact that this is an educational institution allows us to assess the stream's physical, chemical, and biological health both during dry-weather and wet-weather flows, as well as before and after restoration. We plan to evaluate whether on-land restoration and improved

stormwater management will affect the effectiveness of in-stream and stream buffer activities. We also plan to continue both biologic and chemical health evaluations of the stream as a function of land-use improvements. This project has supported several years of both undergraduate and Masters'-level research.

INTRODUCTION

Stream restoration, in recent years, has become a popular method in addressing water quality problems. Projects range from small undertakings such as creating a buffer zone along the streambank to large scale activities like repositioning the stream channel within the landscape. These projects can follow traditional engineering practices or be more holistic in nature. The primary focus, no matter the technique used, is to improve the present quality of water flowing in the stream.

Although the water quality can be improved at the point of restoration and further downstream, the potential for further degradation exists, particularly when degradative practices located upstream still exist and when future land development does not look off-site in evaluating its effects. With the lack of upstream water management, many type of restoration already in place will become useless. They may be removed due to uncontrolled high peak flows during storm events. Increasing the development in the upper watershed simply adds new pressure to the system, increasing the likelihood of failure of the restoration activities in the stream.

Using Penn State Harrisburg's natural resource, an unnamed tributary to the Susquehanna River, we examine the idea of water management both on campus and in the upper watershed to demonstrate how past and present management activities have affected the current state of an unnamed tributary to the Susquehanna River, which flows through campus. Chemical water quality assessments have been made as well as some biological assessments through the use of the stream as a living classroom for students. The stream has been used in ecology and engineering classes, as well as presenting research opportunities to both undergraduate and graduate students. We discuss what research and activities have been performed and possible outcomes of future activities that directly impact the stream.

SITE DESCRIPTION

The Campus Stream watershed has a rich history. Once farmland, the watershed was home to the United States Army's Camp (George Gordon) Meade in July, 1898. By July 1899, Camp Meade was returned to civilian use as a pickle farm for the H. J. Heinz Company until it was reclaimed for military use by the United States Air Force. The Olmsted Air Force Base was established in 1947 and retained ownership of a majority of the watershed until it was sold to the Pennsylvania State University in 1966 for establishment of the University's Capital College campus (Sitler 2007).

Located in south central Pennsylvania, an unnamed stream found on the campus of Penn State Harrisburg empties into the Susquehanna River and eventually into the Chesapeake Bay. Evidence of multiple engineering activities can be found along the stream (Figure 1a). The drainage area of the daylighted portion of the stream is 1.54 km (Sitler 2007). From where the stream daylights to the main entrance of the campus, the stream length is approximately 1.61 km (~1mi) long. Streambanks are steep, vertical, and easily erodible (Figure 1b). Located in the Piedmont Province, rock types in the study area comprise of sedimentary rock (red sandstone, shale, and conglomerate) and diabase intrusions (Siu 2006).

(a)  (b) 

Figure 1: (a) Past engineering practices at the campus stream downstream site, (b) Steep, vertical, erodible bank of campus stream.

Most of the drainage area surrounding the stream is behaves as an impervious surface. Immediately around the stream lie residential, institutional, commercial, industrial, and agricultural areas. The upper watershed contains more of the same. The impervious area in the watershed is shown in Figure 2. Using traditional definitions of impervious surface containing pavement and roofs, the pink color represents known impervious areas (rooftops, parking, etc.). The cyan color represents residential areas which are partially impervious (roofs, driveways, some sidewalks).

The campus history as the land use moved from agriculture to military to institutional has created unusual site conditions. The campus is in an area known historically for flooding. In addition, past military, agricultural, and other development activities appear to have left much of the ground on the campus itself compacted. While compaction has not been measured directly on campus, an analysis of the soils along the stream bank by Sitler (2007) found that the stream bank soils had bulk densities that were greater than the range listed for soils with limited grass growth and in the range of soils compacted by construction. Therefore, in order to minimize the land flooding and drain stormwater rapidly away from the land surface, a series of underground drainage pipes was installed. The storm drain network on campus, which discharges into the stream at several points along its daylighted and underground lengths, collects water directly roof drains, parking lots, and grassy surfaces.

(a)  (b) 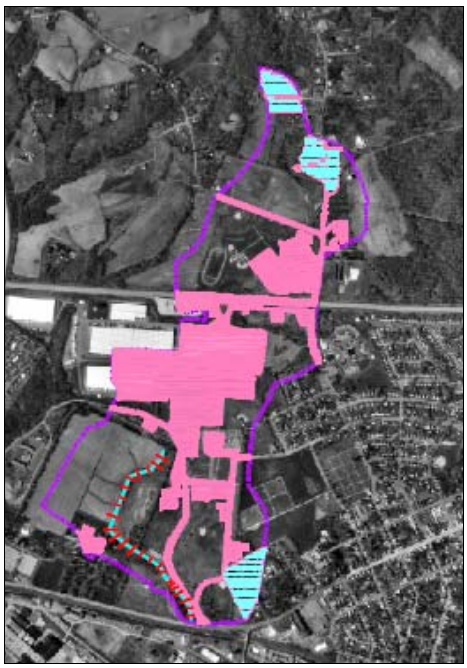

Figure 2: Watershed Boundary and Imperviousness (a) The drainage area of the Campus Stream encompasses a variety of land uses. The lack of stream channel, however, is indicative of the severity of channel impoundment through underground piping. (b) The current watershed is approximately 32% impervious. The pink areas may be considered totally impervious while the cyan color is residential and assumed to be partially pervious.

PAST AND CURRENT STORMWATER MANAGEMENT AFFECTING THE STREAM

Upper watershed: The upper watershed consists of a trucking/warehouse storage facility directly adjacent to the campus on the upstream side. Immediately upstream of the warehouse facility is the Pennsylvania Turnpike and a rest area, followed by (going upstream) a regional high school with outdoor athletic facilities, agricultural land and newer residential developments. The limited stormwater management in the upper watershed appears to consist of detention facilities.

Campus management: Current management at Penn State Harrisburg still reflects the historical stormwater management of previous land uses on that same land. Buildings from the military era are still in use today. These buildings and the more modern ones are directly connected to stormwater pipes, which empty into the stream that runs through campus. At some point in the stream's history, the stream channel was straightened and diverted at several locations. Bank destabilization, which still occurs today, has resulted in high vertical banks and the placement of riprap on portions of the stream (see Figure 1a,b). High peak flows during storms contribute to this bank destabilization. A detention pond, located alongside the stream, was intended to

decrease high peak flows by retaining nearby surface runoff from roads and open areas for release into the stream over a slower time period. The pond has not functioned properly, evidenced by high flows and bank erosion (Figure 3). In 2006, the detention pond was improved through area enlargement and more riprap placed at outfalls. High peak flows are evident still, regardless of these enhancements. The underlying problems in the pond design were not addressed.



Figure 3. Campus stream at bankfull conditions (< 1 year storm event). The detention pond is in the upper left corner and appears to be detaining little water, even during storms that cause bank full conditions in the stream.

Other problems and activities on campus contribute to poor stream health. For instance, water usage for gardening purposes has not been conservative. Watering grass has included directing the sprinkler into the storm drain as shown in Figure 4.



Figure 4: Campus lawn maintenance and water management.

Watering has occurred also on the same day forecast for rain or recently after a rainstorm. On occasion, watering has lasted for several hours. Lawn mowing near the stream impacts the stream's health as well. Grass clippings typically are left on the lawn instead of collected. Clippings also fall into the stream as the areas next to the stream channel are mowed. Figure 5 illustrates this and the fact that a riparian buffer does not exist. Grass is mowed up to the edge of the streambank. Grass clippings in

streams can increase the nutrient and pesticides concentrations as these compounds are released into the water. The lack of overstory cover increases the thermal radiation to this stream, thereby raising water temperatures and allowing stream evaporation in the summer to occur.



Figure 5: Grass clippings in the campus stream.

While the current conditions are not favorable for stream health, there is an interest in the administration in improving the campus' ecological health. Included in that is the desire to beautify the front entrance to the campus, which requires improving the stream. The activities described below have been designed to provide baseline information on the stream's health and prospects for improvement. Additional activities are ongoing in terms of determining effective watershed management. As described earlier, the stream and the land use activities are intertwined. The stream's health will not improve and restoration will not last unless sustainable stormwater management is implemented on campus. This campus provides an excellent opportunity for documenting the effects of retrofitting stormwater management practices – both structural and non-structural. The land is available and the people are interested.

EDUATIONAL ACTIVITIES AND RESEARCH

This stream offers many opportunities to students and for outreach activities. Students of all ages learn ecological, hydrological, engineering, and chemical concepts and their application to a real world situation. Examples of classes using the stream for projects or labs include Ecology, Hydrology, and Open channel hydraulics. Water quality monitoring techniques can be demonstrated also. Several Masters' papers and theses have revolved around different aspects of the stream. Subjects include streambank stability over time, modeling stormwater practices within the watershed, and gathering baseline data with the anticipation of changes to water quality as campus development continues.

Stream ecology: As part of several laboratory activities using the stream as a classroom, ecology students have learned about macroinvertebrate distribution, periphyton, and energy budgets. A project starting in February 2009 will measure stream water chemistry, flow, rainfall, macroinvertebrates and periphyton concurrently to elucidate relationships between them on this small headwater stream.

Siu (2006) noted green filamentous algae (*Cladophora* and possibly *Stigeoclonium*) growing in the streambed at various times of the year throughout the length of the stream. Observations also found a continual growth and decay cycle including algal mats at one study site during the study period. Stream organisms were low in diversity and individuals. Observations of gopher, bullfrog, minnows, and crayfish were made. Flocks of Canadian geese were observed to frequent the stream during migration periods. Samples of algae were taken to determine the presence and diversity of macroinvertebrates. Little diversity and few individuals were present. Most of the macroinvertebrates found were either pollutant tolerant or moderately so. Pollution sensitive species that would indicate good stream quality were mostly absent.

Stream chemistry: Data collection for baseline data of the stream began in 2005. Siu (2006) reports on a six-month water quality study examining baseflow conditions and conditions immediately after storm events. The study encompassed three seasons, late summer, autumn, and winter. General chemistry metrics such as pH, conductivity, turbidity, dissolved oxygen, and temperature were measured. Nutrients (nitrate, orthophosphate, and ammonia), total suspended solids, chemical oxygen demand, detergent, and fluoride were examined as well. Seasonal trends were found for nitrate and orthophosphate concentrations (Figure 6), turbidity, dissolved oxygen, and temperature.

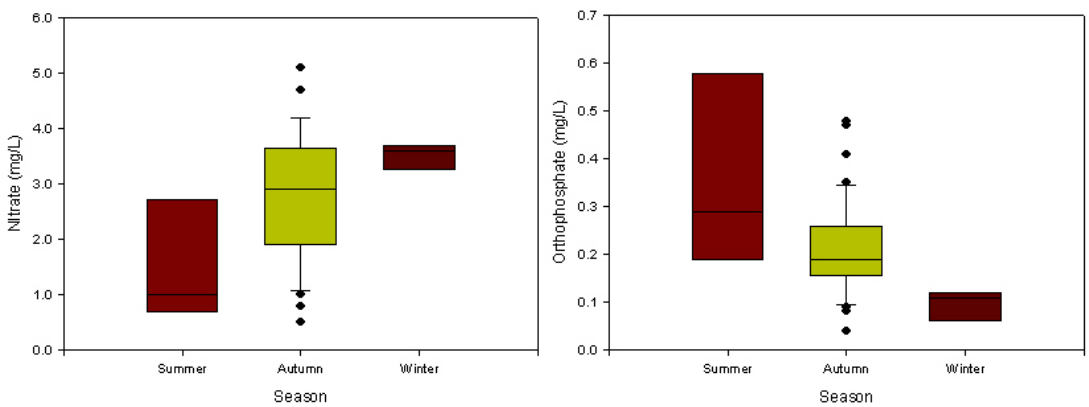

Figure 6: Seasonal nitrate and orthophosphate concentrations.

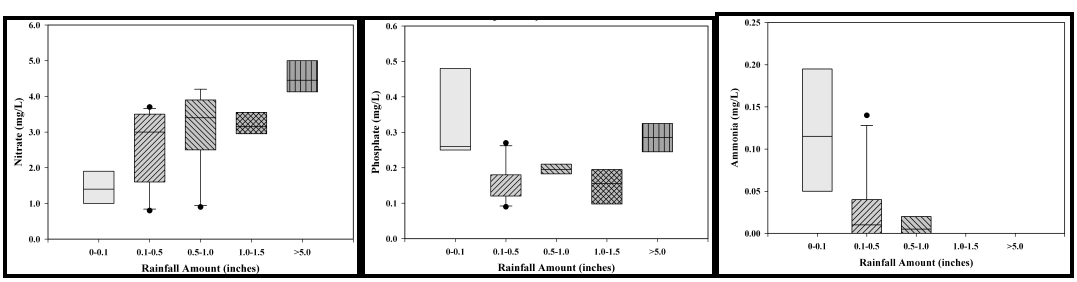

Figure 7: Nitrate, orthophosphate, and ammonia concentrations affected by rainfall intensity.

Nutrients (nitrate, orthophosphate, and ammonia) were affected by rainfall intensity (Figure 7). In both seasonal and rainfall intensity trends, orthophosphate and nitrate showed inverse relationships. Nitrate concentrations increased through the seasons and with an increase in rainfall intensity. Orthophosphate concentrations decreased as the seasons passed. Greater concentrations of orthophosphate occurred with the smallest amount of rain (0-0.1in). Ammonia concentrations were greatest also at this same rainfall intensity.

Work performed by Clark and Treese (2008) and Clark et al. (2009) determined concentrations of copper and other pollutants in campus stormwater that originated from roofing materials. Many building roofs on campus contain copper sheets or copper flashing. During storm events, copper is washed off these surfaces and enters receiving waters. To date, only stormwater runoff has been tested for copper. Campus streamwater has not been tested yet for heavy metals or organics. It would be anticipated that the sediments nearest the discharges from pipes draining the roofs with copper flashing most likely would contain elevated copper concentrations. The travel time in the stream is relatively short; therefore, without analysis, it would be difficult to predict whether equilibrium occurred and the copper had time to move from the water column (stormwater) into the sediment.

Engineering: Stream geomorphology and stormwater runoff volume, flow rate, and duration were modeled by Sitler (2007) to investigate what flows were likely to cause streambank erosion. Visual surveys of the stream during this period showed continued slumping of the streambanks after storms such as the one shown in Figure 3, which was a bankfull storm by flow but was smaller than the traditional bankfull definition of a 1 – 2 year storm. This event had a return interval of < 1 year. The modeling demonstrated the need for models that could work in the small size of the stream. The model showed no streambank slumping during the storms, while the visual observations noted substantial erosion.

Engineering classes such as hydrology and open channel hydraulics have used the stream in classroom projects to further enforce concepts taught in the classroom. These classes are concerned with the quantity of stormwater runoff and elevation of the water surface profile and spread of water in the floodplain during a flooding event. The results show that as the campus develops, the need for improved stormwater management will increase exponentially.

FUTURE PROJECTS

The Penn State Harrisburg campus is continuing to grow with the increase of students. Plans for future buildings and facilities on campus are underway. Students and others have been asked for their input in the decision making of future buildings and facilities. However, campus development must consider how construction can affect the campus stream. All phases of construction may become a risk to the stream's health. Improper installation or unintentional breach of stormwater control systems,

particularly for erosion control, can increase sediment loads and cause greater peak flows into the stream. In-stream habitats can become covered or lost. Stream organisms can become injured and there may be loss of oxygen. Continuation of streamwater monitoring is anticipated with the expansion of analytes for analysis to include heavy metals, organic pollutants, and chlorides.

The immediate area around the stream has the potential to be made into a space that can be enjoyed by the campus community and benefit the stream's inhabitants. Care needs to be taken that these types of improvements will not further impact the stream. For example, increasing or maintaining pervious cover rather than impervious cover will help decrease additional runoff entering the stream. Adding tree cover visually improves stream appearance but also improves soil quality, reduces pollutants and runoff entering the stream, stabilizes the ground, and reduces erosion. Reducing soil compaction or diverting stormwater runoff away from areas that behave as impervious, such as to rain gardens and other amenities, will mitigate the impacts on the stream.

Although improving campus stormwater controls will improve the stream's health, the quantity and quality of water from the upper watershed is crucial as well. This campus and its continued development provide an excellent opportunity for studying the impacts of relatively minor and inexpensive changes, as well as major ones, on stormwater generation, stream water quality and stream stability. Future campus stormwater management activities may include rainwater harvesting for irrigation, conversion of traffic islands to rain gardens, green roofing. The potential of these small, relatively-inexpensive changes on stormwater flow rates and duration currently are being modeled by a graduate student with the results available in May 2009. Future work will include monitoring the effectiveness of newly implemented practices on the stormwater and on the stream.

The education of students and the community about streamwater quality and stormwater through outreach activities will continue. The stream remains an outdoor classroom and living laboratory for present and future students and campus visitors. The size of the campus relative to the watershed, the location of the campus at the downstream end of the watershed, and the willingness of the campus community to engage in improved stormwater management for stream health makes it an ideal location to study the linkages between land use and ecology.

REFERENCES

Clark, S.E., Steele, K.A., Spicher, J., Siu, C.Y.S., Lalor, M.M., Pitt, R., and Kirby, J.T. 2009. Roofing Materials' Contributions to Stormwater Runoff Pollution. *Journal of Irrigation and Drainage Engineering,* 134(5):638-645.

Clark, S.E. and Treese, D.P. *Pollutant Transport Within the Vadose Zone of Natural Soils: Interactions of Pollutants and Soil Horizons*. 2008 International Low Impact Development Conference, November 16-19, 2008, Seattle, WA.

Sitler, R. (2007). *Streambank stability: channel evolution and pollutant transport in an urban stream*. M.Eng. Paper. The Pennsylvania State University, Middletown, PA.

Siu, C.Y.S. (2006). *Characterization of an urban stream for stormwater control – A baseline study on the campus of Penn State Harrisburg*. M.S. Thesis. The Pennsylvania State University, Harrisburg, Middletown, PA.

LID-SWM Practices as a Means of Resilience to Climate Change and Its Effects on Groundwater Recharge

Iulia A. Barbu[1], Thomas P. Ballestero[2] and Robert M. Roseen[3]

[1]UNH Stormwater Center, Environmental Research Group, University of New Hampshire, 214 Gregg Hall, 35 Colovos Road, Durham, NH, 03824; Phone: +1(603) 862-1172; Fax: +1(603) 862-3957; email: iaj4@unh.edu
[2]UNH Stormwater Center, Environmental Research Group, University of New Hampshire, 238 Gregg Hall, 35 Colovos Road, Durham, NH, 03824; Phone: +1(603) 862-1405; Fax: +1(603) 862-3957; email: tom.ballestero@unh.edu
[3]UNH Stormwater Center, Environmental Research Group, University of New Hampshire, 242 Gregg Hall, 35 Colovos Road, Durham, NH, 03824; Phone: +1(603) 862-4024; Fax: +1(603) 862-3957; email: robert.roseen@unh.edu

ABSTRACT

Many surface water bodies have been severely degraded by runoff from the centuries of continuous human development without regard to the impacts of stormwater. Local governments are beginning to responsibly respond to the need for action about increased imperviousness by adopting local Low Impact Development (LID) ordinances. The purpose of this study was to evaluate the hydrologic abilities of LID development to: reduce peak runoff flow rates to the pre-development values; to infiltrate the recharge volumes mandated by current criteria; and to attenuate the impacts of extreme storm events. A numerical simulation was performed on a 4-hectare site for pre-development as well as residential development with Conventional and LID stormwater management design scenarios. Research results from four years of intense monitoring of LID systems at the University of New Hampshire Stormwater Center were integrated into these hydrologic models. Analyses were performed for hydrologic soil types A and C, for storms with recurrence intervals of 0.17-, 2-, 10-, and 100-years, as well as 2-, 10-, and 100-years adjusted for climate change. The results show that the LID site design: generated much lower runoff volumes than the Conventional and Pre-development site conditions; infiltrated more than the recharge volumes required by current regulations; and attenuated the impacts of extreme storms modified for climate change.

KEY WORDS:
Low impact development, stormwater management, climate change, water scarcity, groundwater recharge, design storms, hydrologic impacts.

INTRODUCTION

In the last half century, water resources management has become increasingly problematic. In the summers we face more frequent limited drinking water availability, while in the spring and fall, we struggle with floods and repair flood damages. Sometimes the same repairs have to be repeated in consecutive years due to the same cause: increased runoff peak flow. These peak flows are exacerbated by human development as well as due to storm depths greater than the design events for the infrastructure.

The rate of climate changes directly affects how we design infrastructure and how we can mitigate its impacts on our communities and daily life. Evaluations of the last six decades of precipitation data in the US have found that storms with extreme precipitation have increased in frequency by about three percent per decade, varying regionally (Kunkel et al., 1999) and they are prone to increase by 10-40% by the end of the 21st century in the northern latitudes of North America (Parry et al, 2007). Warmer climate increases the risk of both floods and droughts, since the precipitation variability is also projected to increase. We will see precipitation events with increasing storm depths but with longer dry periods between events and subsequently extended periods of low streamflow (Union of Concerned Scientists 2006).

Stormwater infrastructure is usually designed to safely pass a 10-, 25-, 50-, or 100-year storm, depending on the degree of importance of the site. Storm depth values for each design storm are computed from the statistical evaluation of regional historic precipitation events. Unfortunately, these statistical analyses have not been updated for current precipitation patterns, and are based on decades old rainfall data. This means that infrastructure designed nowadays based on these criteria's are obsolete from their first day of installation. Comparing the precipitation data from the first and second half of the last century in the Chicago area (Angel and Huff, 1997), it was found that the rainfall intensities for the storm durations of interest in urban drainage design have had statistically significant changes. Increases of 28, 36, 43, 50, and 60% for return periods of 2-, 5-, 10-, 25-, and 50-years, respectively, were detected in the second half of the last century (Guo, 2006). According to Stack et al., (in review) who studied the rainfall data for southwest New-Hampshire, what were once 10- and 25-year storms, will become 25- and 100-year storms, respectively, in the mid-21st century.

Additional stress on infrastructure comes from connecting runoff from new developments to the existing stormwater sewer systems designed for past needs. In urbanized areas serviced by combined sewer systems, additional contributing areas can result in more frequent combined sewer overflows (CSO's). This contributes to both degradation of receiving water body quality and increases of peak flow rates and runoff volumes discharging into these surface water bodies.

The stormwater management challenges of the 21st century are to develop strategies that encompass climate change for the increasing impervious surfaces of

urbanization, while maintaining watershed health and fulfilling governmental requirements for stormwater quality. Several local governments responded favorably to the need to take action about increasing runoff volumes by adopting local LID ordinances. In addition, stakeholders have included LID practices in their planning. Although researchers have found that LID practices can address the main problems of current stormwater management, and many State Agencies have developed new manuals for stormwater management that include design guidance, there are still impediments to the full implementation of LID practices. Engineering teams find that there is not enough understanding of how the hydraulic response of LID practices change with system design variables, such as hydraulic conductivity, filter media thickness, distances between under-drains or the lack of them, and infiltration rates of the native soils. For the same reason, reviewing agencies do not yet have clear modeling guidelines for applicants.

Since 2003, the University of New Hampshire Stormwater Center (UNHSC) set out to evaluate stormwater treatment systems in a fully-monitored field setting. The systems are studied in a side-by-side setting (all receiving equivalent water quantity and quality) and can be categorized as: conventional practices (retention pond, detention pond, and swales), LID practices (sand filter, bioretention, gravel wetland, pervious concrete, porous asphalt, tree filter) and manufactured devices (subsurface sand filter, filtration, hydrodynamic separators). UNHSC research results show that the pollutant removal efficiencies and peak flow reduction obtained by LID systems are superior of those obtained by conventional and manufactured systems. (Ballestero et al., 2007).

The overall goals of this study were: to research the abilities of structural LID systems to attenuate the hydrologic impact of storms, compared to conventional stormwater designs; to study the ability of these systems to infiltrate stormwater ; and to assess how management strategies perform for expected climate changes. As an example of infiltration requirements, the New Hampshire Department of Environmental Services (NHDES) requires that for each new development, for the 2-year, 10-year, 25-year and 50-year, 24 hour design storms: “post-development peak flow rate shall not exceed the pre-development peak flow rates”; “post-development total runoff volume shall be equal to 90 to 110 percent of the pre-development total runoff volume” and “the annual average recharge volume for the major hydrologic soil groups found on the site should be maintained” (NHDES, 2007).

These recharge requirements are similar to those of other states in United States. (Table 1). These volumes can vary by state and they are normally meant to match the infiltration volumes of pre-development conditions. Since design precipitation intensities are predicted to increase (Kunkel at al., 1999) in the context of climate change, runoff volumes could increase to the detriment of infiltration. Milly et al, (2005) found that runoff would increase in the higher latitudes of North America by 10-40% by 2050. Although the goal of recharging stormwater is to preserve the water balance of the pre-developed conditions, current requirements regarding recharge

volumes are not meant to compensate for recharge loss in the context of climate change or for groundwater withdrawal for human consumption.

Table 1- Recharge depths required by different states and different soil types.

Hydrologic Soil Group	NHDES	MADEP	Philadelphia/for CSO-sheds
Type A	1cm (0.40in)	1.5cm (0.60in)	2.5cm (1in)
Type B	0.6 cm (0.25in)	0.9cm (0.35in)	2.5cm (1in)
Type C	0.3 cm (0.1in)	0.6cm (0.25in)	2.5cm (1in)
Type D	Not required	0.3cm (0.10in)	2.5cm (1in)

For this research, it was decided to hydrologically model a 4-hectare site for pre-development conditions, developed conditions with conventional stormwater management, and an LID approach. Special interest in this study was given to peak flow rates, recharge volumes, and runoff volumes generated under the same design storms by the different land use scenarios.

For the Jordan Cove project, where the LID hydrologic response was monitored and compared to the hydrologic response from a conventional site design, it was found that the LID site was performing better than the conventional site only for storm events smaller than 25 millimeters or shorter than 4 hours and for low antecedent moisture conditions (AMC). (http://www.jordancove.uconn.edu/index.html).

METHODOLOGY

Numerical simulation of the stormwater management of ten 0.4-hectare residential lots was studied for three scenarios: Pre-development, Conventional design, and LID design. Three hydrologic models were developed using the runoff modeling software HydroCAD 8.50. The three models are meant to represent the change in land use and how this alters the hydrologic responses of the site for the same design precipitation events. For the Pre-development site, the land use was chosen to be four hectares of woods and grass combinations in fair conditions and with a general slope of 5%. For the Conventional design, land use was 5% road, 3.6% driveways, 4.6% rooftops and the rest being 86.8% lawns. The site configuration is presented in Fig.1(a). Stormwater management for this site included a series of five catch basins, connected by underground pipes, which were designed to convey the 24 hour-10 year storm event. Each catch basin collects runoff from the lawns and impervious surfaces of two 0.4-hectare lots. The catch basins were modeled as ponds with the interconnecting pipes modeled as outlets. For the LID site design, the land use was 5% road, 3.6% driveways, 4.6% rooftops, 21.8% lawn and the rest of the 65% was conserved as the pre-development land use of woods and grass. The LID site configuration is presented in Fig.1(b).

Stormwater management for the LID site included nonstructural practices (land conservation and the use of natural features of the original site) and structural

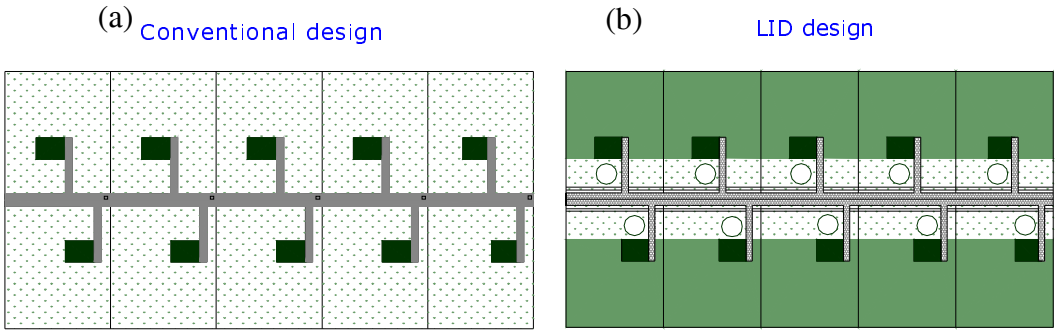

Figure 1. Conventional and LID site design configuration; dark green represent rooftops, grey represent the driveways and the road and light green represents undisturbed cover.

practices (porous pavement for driveways and road, bioretention systems that collect the rooftop runoff, and grassed swales on the sides of the main road which convey the runoff from lawns). Culverts underneath the driveways connect the grassed swales, which were designed to pass the 24 hour-10 year storm event. Bioretention systems were modeled as ponds which also allowed infiltration; they were designed to retain the "first flush" (the first 25 millimeters of rainfall), and had an overflow for larger events, which was directed towards the porous pavement driveways. As the modeling software did not contain special features for LID systems, the porous pavement was modeled as a pond with 30% void space, and for the outlets, a 15-centimeter diameter underdrain with exfiltration. This was considered to be a conservative approach, which gives an approximation of outflow through drains similar to the outflows observed at the UNHSC porous pavement site. In order to simulate the filtering time of runoff through the sand filter layer (the sub-base of the porous pavements), the inflow hydrograph was delayed by a time equal to the annual average lag time observed for monitored storms at the UNHSC porous pavement lot. The sub-base thickness for the driveways is represented by 7.5 centimeters of porous asphalt, 5 centimeters of crushed stone, and 20 centimeters of gravel on top of 10 centimeters of crushed stone. The gravel layer contains a 15-centimeter diameter underdrain, wrapped in 5 centimeters of crushed stone. In a similar way, the sub base for the road is represented by 10 centimeters of porous asphalt, 7.5 centimeters of crushed stone, and 35 centimeters of gravel on top of 20 centimeters of crushed stone. A 15-centimeter diameter underdrain is placed 10 centimeters above the bottom of the system (in the underlying crushed stone). This allows infiltration in between storms. The sub bases of the driveways and road are interconnected, allowing the water to travel from the driveway sub base into the road sub base. The grassed swales were modeled as ponds, which allow infiltration, with the primary spillway represented by the driveway culverts, and the secondary outlet represented by broad-crested rectangular weirs discharging into the porous pavements. This was meant to simulate the porous pavement run-on from swales after their capacity is exceeded.

These three site models were analyzed for hydrologic soil types A and C, with infiltration rates of 6.25 millimeters per hour and 50 millimeters per hour, respectively. The models were run and analyzed for type III, 24 hour storm events with recurrence intervals of 0.17-, 2-, 10-, and 100-years, as well as 2-, 10-, and 100-

years adjusted for climate change. Soil moisture conditions were selected as AMC-II. The total storm depths used in the analyses are summarized in Table 2.

Table 2 – Values of design storm depths for present conditions and those predicted for the climate change scenario

Design storm (yr)	2	10	100
Climate Change Depth Increase (%)	17	28	45
Current depth –cm (in)	7.53 (3.01)	10.86 (4.35)	15.75 (6.3)
Increased depth –cm (in)	**8.8 (3.52)**	**13.93 (5.57)**	**22.85 (9.14)**

RESULTS

Hydrographs from Pre-development, Conventional, and LID sites were analyzed by each design storm depth. The results were compared at the final site outlet structure, which was identical for the LID and Conventional sites, and then divided by ten, in order to find the hydrologic response of each residential lot (0.4 hectares).

Results for Hydrologic Soil Group A

For the hydrologic soil group A, the Pre-development site generated runoff for the 10- and 100-year storms, but not for storms smaller than the 10-year return period. The LID site generated runoff only for the 100-year storm, and the Conventional site generated runoff for all design storms investigated in the analysis. In the context of climate change, the Pre-developed site generated runoff starting with the 2-year storm, and for the LID site, only the 100-year storm generated runoff. Since the LID site generated runoff starting with a storm depth which is somewhere between the 10-year and the 100-year storm, this particular site was also analyzed for intermediate storm depths, and it was found that runoff was generated starting with the 50-year storm. The 50-year storm represents a 24-hour duration rain event with a total depth of 14.5 centimeters of precipitation.

Interestingly, a 45% increase in the 100-year storm (representing the effect of climate change), resulted in an increase of runoff volume of 170% for the Pre-developed site. The same change in the storm depth resulted in a 363% increase of runoff volume from the Conventional site and a 74% increase from the LID site. Analyzing the total depth of storms and their distribution as runoff and infiltration (Fig.2a and Fig.3a), it was found that the LID site retained up to 44% more water on the site than the Conventional site and up to 15% more than the Predevelopment site. Surprisingly, peak flow rate results show that the LID site reduced the peak flow rates to values smaller than those generated by the Pre-development site. Peak flow rates for the LID site were up to 58% less than the Pre-development values; while the Conventional site values were up to 188% more than the Pre-development site (the Conventional design objective was solely to drain the development of stormwater).

Results for Hydrologic Soil Group C

For the hydrologic soil group C, all three development scenarios generated runoff for all storms, the only exception being the LID site which did not generate runoff for storm depths up to 25 millimeters. The results are similar as those for the type A soil, but the changes were not as dramatic, because the initial infiltration capacity of the soil is lower. The 45% increase in the 100-year storm depth (representing climate change) resulted in an increase of runoff volume of 70% for the Pre-developed site. The same change in the storm depth resulted in an 82% increase of runoff volume for the Conventional site and a 36% increase for the LID site. Analyzing the total depth of storms and their distribution as runoff and infiltration (Fig.2b and Fig.3b), it was found that the LID site retained on the site up to 67% more water than the Conventional site and up to 24% more than the Predevelopment site. Results show that peak flow rates for the LID site were up to 73% less than the Pre-development values, while the Conventional site values were up to 76% more than those for the Pre-development site were.

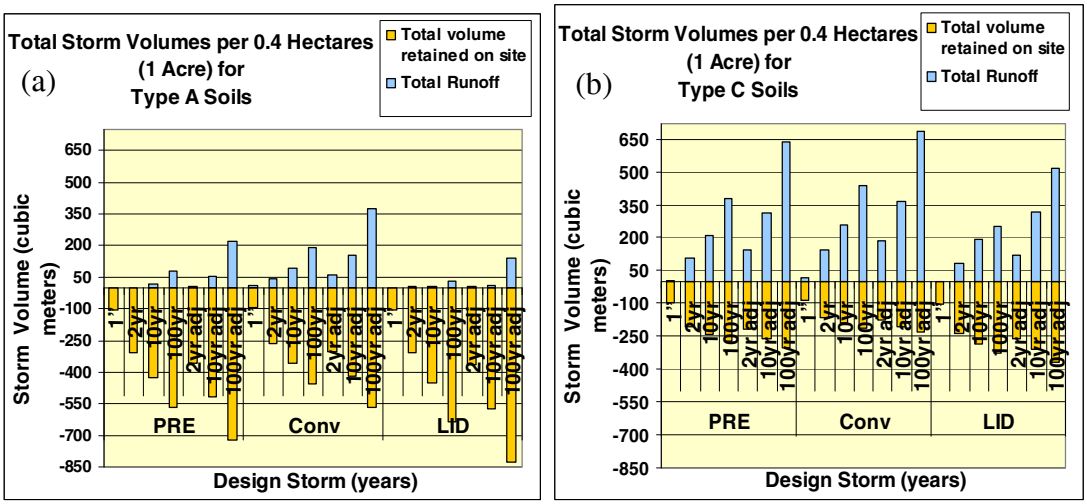

Figure 2. Total storm depth distribution: positive values represent runoff and negative values represent infiltration.

The study of daily precipitation data from 1915 to 2007 for Durham, NH shows that 99% of daily precipitation depths are 75 mm or smaller, with an annual average precipitation of 115 cm. As seen in Fig. 2, each site generates runoff starting with a certain storm depth. For example, the LID site generated runoff starting with the 2-years storm in a type C soil and with the 50-years storm in a type A soil. Assuming that all precipitation events smaller than the ones which generate runoff are retained on the site, Fig.4 show the summation of annual rainfall retained on the site by each land use scenario for hydrologic soil types A and C, for all storms of 75 mm and smaller. The results indicate that in a type A soil, the LID site recharges annually the same amount as the pre-developed site, while in a type C soil, the LID site recharges even more than the Pre-developed site. The Conventional site recharges the least out of the three sites for both types of soil, with an annual recharge decrease of 9.3 cm and 9.6 cm for type A and C soils, respectively, compared to pre-development conditions.

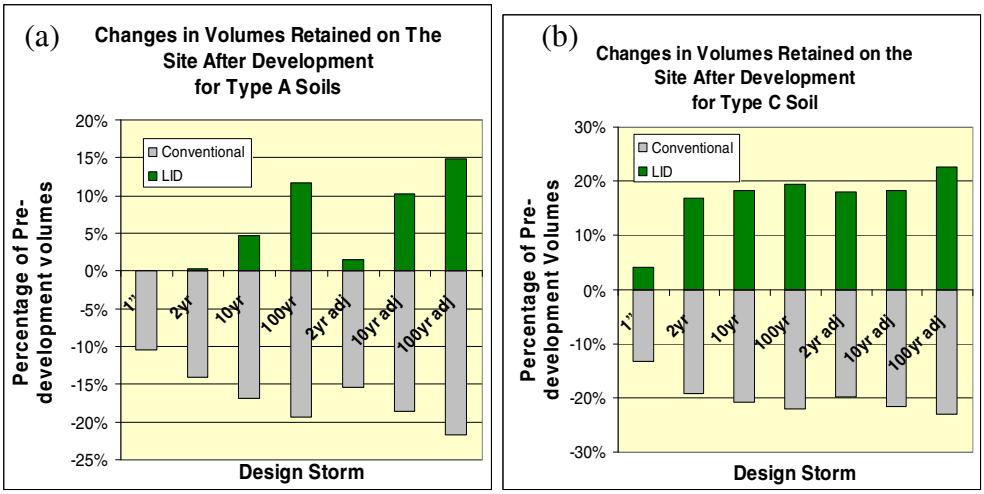

Figure 3. Total infiltrated volumes by Conventional and LID sites compared to the Pre-development site: the zero line represents the Pre-development. Positive values represent an increase of infiltrated volumes, while negative values represent decrease of recharge compared to Pre-development conditions.

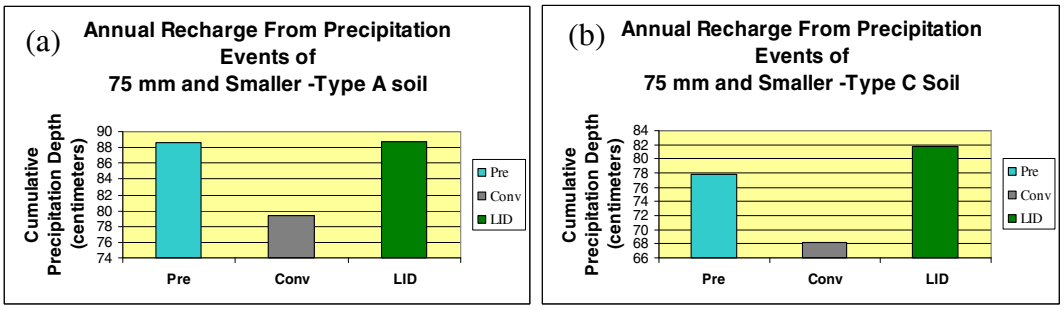

Figure 4. Summation of retained water volume (as depth) on the site for annual precipitation events up to the 2-year storm for type A soil(a) and type C soil(b).

DISCUSSION

The results of this study show that by using structural and nonstructural LID practices in stormwater management, the hydrologic characteristics of developed sites can be improved over that of a conventionally designed site by providing for additional storage in the LID systems, increasing infiltration, reducing runoff peaks, and delaying the runoff peak by routing the water through low hydraulic conductivity layers. The longer residence time of water in the LID systems allows groundwater recharge over a longer period, which in turn results in higher total volumes recharged per storm event. Contrasting this to conventional stormwater management practices which are meant to collect, concentrate, and convey runoff off site, LID principles imply that the runoff should be managed at the source and infiltrated at the source, when possible. These principles were reflected in the models used in this study, and the results showed that the requirements regarding peak flow rates, total runoff volumes, and recharged volumes could be met by using LID practices. The LID site generated runoff starting with the 2-year storm (7.5 cm) in a type C soil and with the

50-year storm (14.5 cm) in a type A soil, which implies that smaller storms are retained on the site. These values are much higher than the 1 to 2.5 cm required for type A soil and 0.3 to 2.5 cm required for type C soil found in Table 1.

LID systems are usually designed to retain, treat, and infiltrate the first 2.5 cm of rainfall: higher storm depths are by-passed. This explains, in part, the results of the Jordan Cove Project and is also a forewarning that LID design could be effective and more efficient if designed with built-in redundancy. In the model presented in this study, the bioretention system was also designed to retain the first 2.5 cm of rainfall, but a secondary spillway was designed to direct the higher bypass flows into the porous pavement driveways. Grassed swales were designed to pass the 10-year storm, but the swale secondary spillway was directed into the porous pavements. Porous pavement systems are usually designed for load capacity and frost depth (in cold climate zones) and then they are analyzed for their storage capacity. In most cases, the sub-base designed for these structural criteria allows for retention of much more than 2.5 cm of rainfall. When the porous asphalt hydraulic capacity is exceeded in a model, the sub-base depth can be increased in order to obtain additional storage. Routing the secondary spillways for swales and bioretention systems through the porous pavement sub-base makes a good use of the extra storage capacity available in the porous pavement system. This represents the site redundancy in this study and explains the peak flow rates and runoff volumes for the LID site being lower than the Pre-development conditions.

The overall results show that the LID site design:

- generated much lower runoff volumes than the Conventional and Pre-development site conditions;
- infiltrated more than the recharge volumes required by current regulations; and
- attenuated the impacts from extreme storms for both hydrologic soil groups A and C, since peak runoff flows rates from the LID site were lower than the peak runoff flow rates from the Conventional and the Pre-development sites.

Given the fact that the hydrologic conditions of the soils were improved by providing extra storage in the LID systems when developing only 13.2 % of the total site, it is believed that LID developments with greater densities could reduce the impacts of large storms even more.

Although this modeling approach is considered conservative and reflects research results from studying the porous pavement site at the UNHSC, assumptions used in this study should not be used for porous pavements with sub base materials different from those of the studied site (http://www.unh.edu/erg/cstev/pubs_specs_info/unhsc_pa_spec_07_07_rev_4_08.pdf). Future research efforts regarding hydrologic performances of LID systems should include the relationship between the outflow hydrograph and its design variables such as: porous media thickness, hydraulic conductivity, system geometry, and/or infiltration rates of native soils. Future research should focus on how runoff will change as a result of changes in precipitation patterns in the context of climate change and accurate estimates of

recharge needs in order to maintain the natural water balance of a site for different hydrologic soil types and for different groundwater withdrawal patterns.

CONCLUSIONS

Current stormwater management regulations are moving towards requiring hydrologic transparency of developments (post-development hydrology should match the pre-development hydrology). The only means of accomplishing this, particularly the infiltration aspects, is through LID designs. With new legislation paying closer attention to the implementation of sustainable development patterns, regulations for development that address recharge should encompass all the factors which impact groundwater and not only the lack of recharge due to land use changes.

In conclusion, it should also be mentioned that by practicing LID stormwater management, we are a step closer to sustainable development. Recharging precipitation is instrumental in maintaining the natural water cycle, and the results of this study showed that LID-SWM practices have the ability to infiltrate amounts of water that may compensate in the water balance of aquifers for both the lack of recharge due to impervious surfaces and withdrawal of groundwater for water supply.

REFERENCES

Angel, J. R., and Huff, F. A. (1997). "Changes in heavy rainfall in Midwestern United States". J. Water Resour. Plan. Manage. 123(4), 246–249.

Ballestero, T. P., Roseen, R., and Houle, J. (2007). "UNH Stormwater Center 2007 Annual Report", Cooperative Institute for Coastal and Estuarine Environmental Technology, Durham, NH.

Guo Y.(2006). "Updating Rainfall IDF Relationships to Maintain Urban Drainage Design Standards", Journal of Hydrologic Engineering © ASCE, Sept/Oct, 506-509.

Kunkel, K. E., Andsager, K., and Easterling, D. R. (1999). "Long-Term Trends in Extreme Precipitation Events Over the Conterminous United States and Canada". J. Clim., 12(8), 2515–2527.

Milly P.C.D., Dunne K.A., Vecchia A.V (2005). "Global Pattern of Trends in Streamflow and Water Availability in a Changing Climate". Nature 438;17 November 2005, 347-350.

NHDES (2007). "Innovative Land Use Planning Techniques: A Handbook for Sustainable Development", New Hampshire.

Parry M., Canziany O., Palutikof J., Linden P., Hanson C. (2007). "Climate Change 2007: Impacts, Adaptations and Vulnerability", published for the Intergovernmental Panel on Climate Change (IPCC).

Stack, L., Simpson, M., Crosslin, T., Spearing, W., Hague, E. (in review). "A Point Process Model of Drainage System Capacity Under Climate Change".

Union of Concerned Scientists (2006). "Climate Change in the U.S. Northeast - A report of the Northeast Climate Impacts Assessment". UCS publications, Cambridge, MA.

Maintenance of Stormwater BMPs

Andrew J. Erickson[1], Joo-Hyon Kang[2], Peter T. Weiss[3], C. Bruce Wilson[4], and John S. Gulliver[5]

[1]St. Anthony Falls Laboratory, Department of Civil Engineering, University of Minnesota, 2 Third Ave SE, Minneapolis, MN 55414; PH (612) 624-4629, FAX (612) 624-4398; email: eric0706@umn.edu
[2]Dept. of Environmental Science and Engineering, Gwangju Institute of Science and Technology, Republic of Korea
[3]Department of Civil Engineering, Valparaiso University, 1900 Chapel Drive, Valparaiso, IN 46383; PH (219) 464-5220; FAX (219) 464-5065; email: peter.weiss@valpo.edu
[4]Minnesota Pollution Control Agency, St. Paul, MN, USA
[5]Department of Civil Engineering, University of Minnesota, 500 Pillsbury Drive SE, Minneapolis, MN 55455, PH (612) 625-4080, FAX (612) 626-7750; email: gulli003@umn.edu

ABSTRACT

Many stormwater management manuals and guidance documents have stated the importance and estimated the necessary frequency of maintenance for stormwater best management practices (stormwater BMPs), but few have been able to document the actual frequency and intensity of maintenance required to maintain a desired level of performance and efficiency. Increased attention to mass balance, numerical goals, total maximum daily loads (TMDLs), and non-degradation requirements has created the need for more emphasis on stormwater BMP operation and maintenance (O&M) in order to meet permitting and reporting requirements. The purpose of this paper is to advance knowledge about routine and non-routine maintenance so as to develop more useful O&M plans. To do so, we reviewed literature throughout the United States for maintenance costs and developed, distributed, and analyzed the results of a detailed municipal public works survey.

The specific goals of the survey were to identify and inventory O&M efforts and associated costs for stormwater BMPs. Survey questionnaires were sent to 106 cities, 28 of which responded. The survey related to the following topics: number of stormwater BMPs in the city, frequency of inspections and maintenance, average staff-hours spent per routine inspection or maintenance, complexity of maintenance, most frequent causes of performance deterioration, and cost of non-routine maintenance activities. The results of the survey revealed that most (89%) cities perform routine maintenance once per year or less. The most common causes of performance deterioration and the greatest expense were sediment buildup and litter/debris for most stormwater BMPs. The nationwide literature review resulted in predictive equations for O&M cost of stormwater BMPs as a function of total construction cost. A general rule of thumb is provided for estimating the relative importance of O&M in life-cycle costs.

INTRODUCTION

Structural stormwater ***BMP operation*** is the optimization of (1) pollutant removal and (2) reduction of runoff volume and rate via the management of stormwater networks or treatment trains. Stormwater ***BMP maintenance*** is the purposeful management of a stormwater BMP so as to maintain a desired level of performance and efficiency and consists of short-term (routine or more frequent), long-term (non-routine or less frequent), and major (rare) actions (Figure 1).

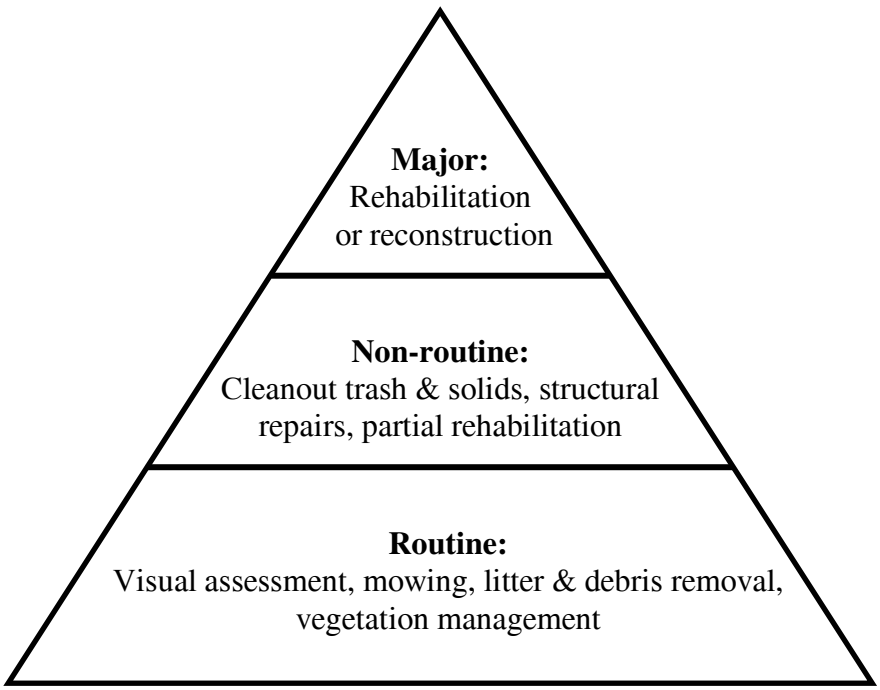

Figure 1: Stormwater BMP Operation & Maintenance Pyramid

Performance longevity of stormwater BMPs from their creation (design and construction) through operative stages (functional or not) is dependent on operation and maintenance actions. Because maintenance involves a significant amount of resources (personnel, equipment, materials, sediment disposal expense, etc.), the more that is learned about stormwater BMP operation, the easier it will be to maintain optimal performance as well as improve cost-effectiveness. The purpose of this article is to advance knowledge about short and long-term maintenance so as to develop more useful operation and maintenance (O&M) plans. To do so, we reviewed nationwide literature on maintenance costs and developed, distributed and analyzed the results of a detailed municipal public works survey.

The specific goals of the survey were to identify and inventory stormwater BMP maintenance activities. Survey questionnaires were sent to 106 cities in Minnesota, 28 of which responded. The survey included questions on the following topics:

- How many, and what type of, stormwater BMPs are in your watershed?
- How often are your stormwater BMPs inspected?
- What is the average staff-hours spent per regular inspection/maintenance?
- How complex is the maintenance of your stormwater BMPs?

- Which factors most frequently cause the performance deterioration of your stormwater BMPs?
- What are the costs for non-routine maintenance activities?

The questions for the survey were chosen to reflect key parameters necessary to reasonably budget and schedule inspection and maintenance. These factors will vary based upon stormwater BMP design, climate conditions, stormwater BMP accessibility, desired level of stormwater BMP performance, personnel and budgetary constraints, and maintenance strategies.

SURVEY RESULTS AND DISCUSSION

Inspection Frequency

As listed in Table 1, the majority (89%) of cities conduct routine maintenance actions once a year or less. Inspection frequency varies significantly due to stormwater BMP accessibility and management strategy (proactive vs. reactive). "We are working on and around the site every business day, and so inspections happen informally every day," said Julie Vigness-Pint, stormwater BMP Cost Share Coordinator at Ramsey-Washington Metro Watershed District, MN. A more common response was voiced by Jim Hafner, the stormwater manager for the City of Blaine, MN who stated "Our city has not had a proactive program for stormwater BMP maintenance. It has generally occurred when problems have popped up." The difference between proactive and reactive maintenance strategies and the execution of maintenance plans has resulted in a wide variation in the type and frequency of inspection and maintenance activities.

Table 1: Frequency of routine inspection and maintenance activities

Stormwater BMP Type	Number of Responses (n)	Less than once	Once per year	Twice per year	More than twice
		Percentage of Responses			
Wet Ponds	27	52%	44%	0%	4%
Dry Ponds	23	52%	48%	0%	0%
Constructed Wetlands	16	38%	56%	6%	0%
Surface Sand or Soil Filter	9	67%	33%	0%	0%
Infiltration Basins or Trenches	17	18%	76%	0%	6%
Rain Gardens	19	21%	42%	16%	21%
Porous Pavements	12	25%	50%	8%	17%
Filter Strips or Swales	12	58%	33%	0%	8%
Underground Sedimentation Devices	16	13%	56%	31%	0%
Underground Filtration Devices	9	44%	56%	0%	0%
Average		**39%**	**50%**	**6%**	**6%**

Staff Hours

Descriptive statistics for staff-hours spent on routine inspection and maintenance are shown in Table 2. For most stormwater BMPs, staff-hours per activity range from 1 to 4 hours, except constructed wetlands and rain gardens which

reportedly require more time for inspection and maintenance (typically between 1 and 16 hours). Rain gardens and constructed wetlands may require more staff-hours for inspection and maintenance because vegetation management can be significant in these practices.

Table 2: Staff-hours spent on routine maintenance actions

Stormwater BMP Type	Number of Responses (n)	Staff-hours				
		Max.	75th %tile	Median	25th %tile	Min.
Wet Ponds	24	120	3.5	2	1	0.5
Dry Ponds	19	5	2	1	0.5	0.5
Constructed Wetlands	14	60	9.5	1.5	1	0
Surface Sand or Soil Filter	7	3	2	1	0.5	0.5
Infiltration Basins or Trenches	17	60	2	1	0.5	0.5
Rain Gardens	13	80	16	1	1	0.5
Porous Pavements	9	6	4	2	1	0.5
Filter Strips or Swales	11	30	1.75	1	0.5	0.5
Underground Sedimentation Devices	14	360	3	1.25	1	0.5
Underground Filtration Devices	7	5	3.5	1	0.75	0.5

Maintenance Complexity

To assess maintenance complexity, a scale from 1 to 4 was used with 1 being minimal complexity (i.e. stormwater professional or consultant is seldom needed) and 4 being most complex (i.e. stormwater professional or consultant is always needed). For most stormwater BMP types, most respondents indicated that maintenance was minimal or simple, as listed in Table 3. Maintenance was viewed as moderate to complex most often for constructed wetlands (47%), porous pavements (46%) and surface sand and soil filters (38%). Porous pavements are fairly new in Minnesota, which may explain the more frequent requirement for evaluation by stormwater professionals.

Factors reducing stormwater BMP performance

Respondents were also asked to choose from a list of possible factors that most frequently caused deterioration in the performance of their stormwater BMPs. Sediment buildup and litter & debris accumulation were reported most frequently for most stormwater BMPs and possible factors, respectively (Table 4). Pipe clogging was reported frequently for wet ponds and dry ponds while invasive vegetation was reported frequently for dry ponds, constructed wetlands, rain gardens, filter strips, and swales.

Table 3: Complexity of maintenance activities

Stormwater BMP Type	Number of Responses (n)	Maintenance Complexity*			
		Min.	Simple	Mod.	Comp.
Wet Ponds	23	57%	30%	4%	9%
Dry Ponds	21	67%	29%	0%	5%
Constructed Wetlands	15	40%	13%	40%	7%
Surface Sand or Soil Filter	8	63%	0%	25%	13%
Infiltration Basins or Trenches	15	33%	40%	13%	13%
Rain Gardens	17	41%	29%	12%	18%
Porous Pavements	13	46%	8%	38%	8%
Filter Strips or Swales	13	62%	31%	0%	8%
Underground Sedimentation Devices	15	40%	33%	7%	20%
Underground Filtration Devices	10	50%	20%	10%	20%

*Maintenance Complexity is defined as:
Minimal - stormwater professional or consultant is seldom needed
Simple - stormwater professional or consultant is occasionally needed
Moderate - stormwater professional or consultant is needed about half the time
Complicated - stormwater professional or consultant is always needed.

Table 4: Percentage of respondents who indicated the factors listed most frequently for causing deterioration of stormwater BMP performance

	Number of Responses	Sediment buildup	Litter & Debris	Pipe Clogging	Invasive vegetation	Bank erosion	Groundwater level	Structural problems	Oil spill	Mechanical problems
Wet Ponds	90	26%	19%	21%	10%	11%	7%	7%	0%	0%
Dry Ponds	49	24%	31%	18%	16%	8%	2%	0%	0%	0%
Constructed Wetlands	37	24%	19%	14%	22%	11%	8%	3%	0%	0%
Surface Sand or Soil Filter	10	50%	30%	10%	0%	0%	0%	0%	10%	0%
Infiltration Basins or Trenches	39	36%	21%	10%	5%	5%	13%	5%	3%	3%
Rain Gardens	27	33%	22%	7%	26%	0%	7%	0%	4%	0%
Porous Pavements	9	67%	11%	11%	0%	0%	0%	0%	11%	0%
Filter Strips or Swales	19	21%	26%	5%	26%	11%	5%	5%	0%	0%
Underground Sedimentation Devices	19	58%	21%	11%	0%	0%	5%	5%	0%	0%
Underground Filtration Devices	8	50%	25%	13%	0%	0%	13%	0%	0%	0%

Maintenance Cost

Maintenance for sediment removal, converted to an annual cost, was the most reported and costly maintenance activity. There was also considerable variation in the maintenance costs, as illustrated in Figure 2 for sediment removal. The highest

median sediment removal costs were for porous pavement ($1700/yr) and underground sedimentation devices ($1000/yr).

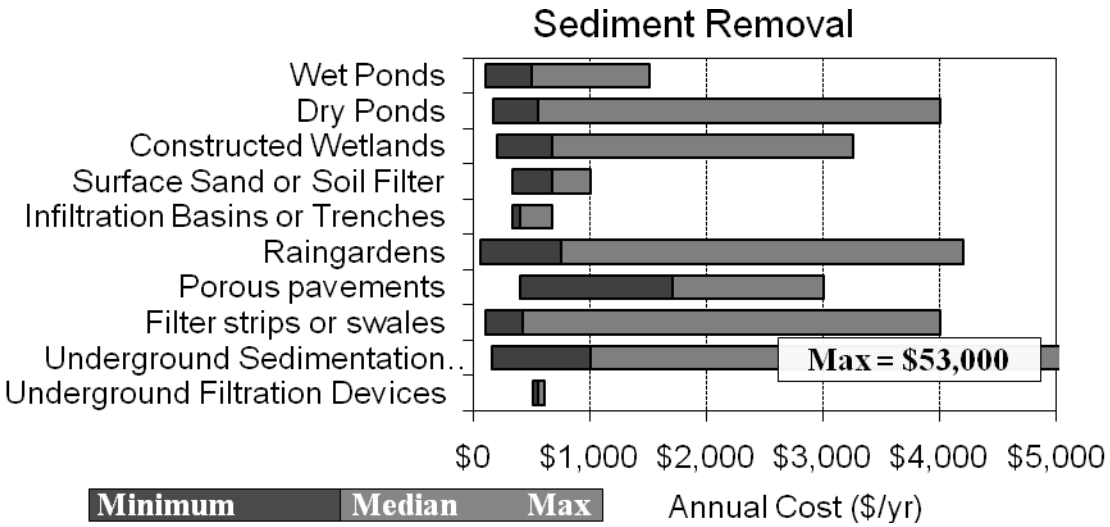

Figure 2: Annual cost of sediment removal for stormwater BMPs

OVERALL OPERATION AND MAINTENANCE COSTS

Publications throughout the United States that contained cost estimates of typical maintenance schedules for common stormwater BMP categories were reviewed. Cost estimates of annual operation and maintenance (O&M) expenses as a function of construction costs were developed for dry ponds, wet ponds, constructed wetlands, rain gardens, sand filters, and grassed/vegetative swales. All costs were adjusted by means of a 'Regional Cost Adjustment Factors' (USEPA, 1999) to reflect 2005 costs in Minnesota.

The U.S. Environmental Protection Agency (USEPA, 1999) published expected annual stormwater BMP O&M costs, as a percentage of total construction cost ranging from less than 1% for dry ponds to a maximum of 20% for infiltration trenches. More recent analyses (Landphair, et al., 2000; Wossink and Hunt, 2003) have expanded this range. Cost estimate data from the literature are shown on log-log scale in Figure 3 (Weiss et al., 2005) with the best-fit line (dashed line) and 67% confidence intervals (solid lines). Using known total construction costs excluding land costs and the equation of the best-fit line, the annual expected maintenance for each type of stormwater BMP can be estimated.

It is apparent from Figure 3 that O&M costs indicate an economy of scale for all stormwater BMPs. Predicted annual O&M cost, as a percentage of construction cost (excluding land cost), decreases with increasing total construction cost. Therefore, more expensive (and presumably larger) stormwater BMPs require a smaller fraction of the original construction cost for annual operation and maintenance. This trend is slight for sand filters and rain gardens (bioretention practices), and greater for wet ponds, dry ponds, constructed wetlands and swales.

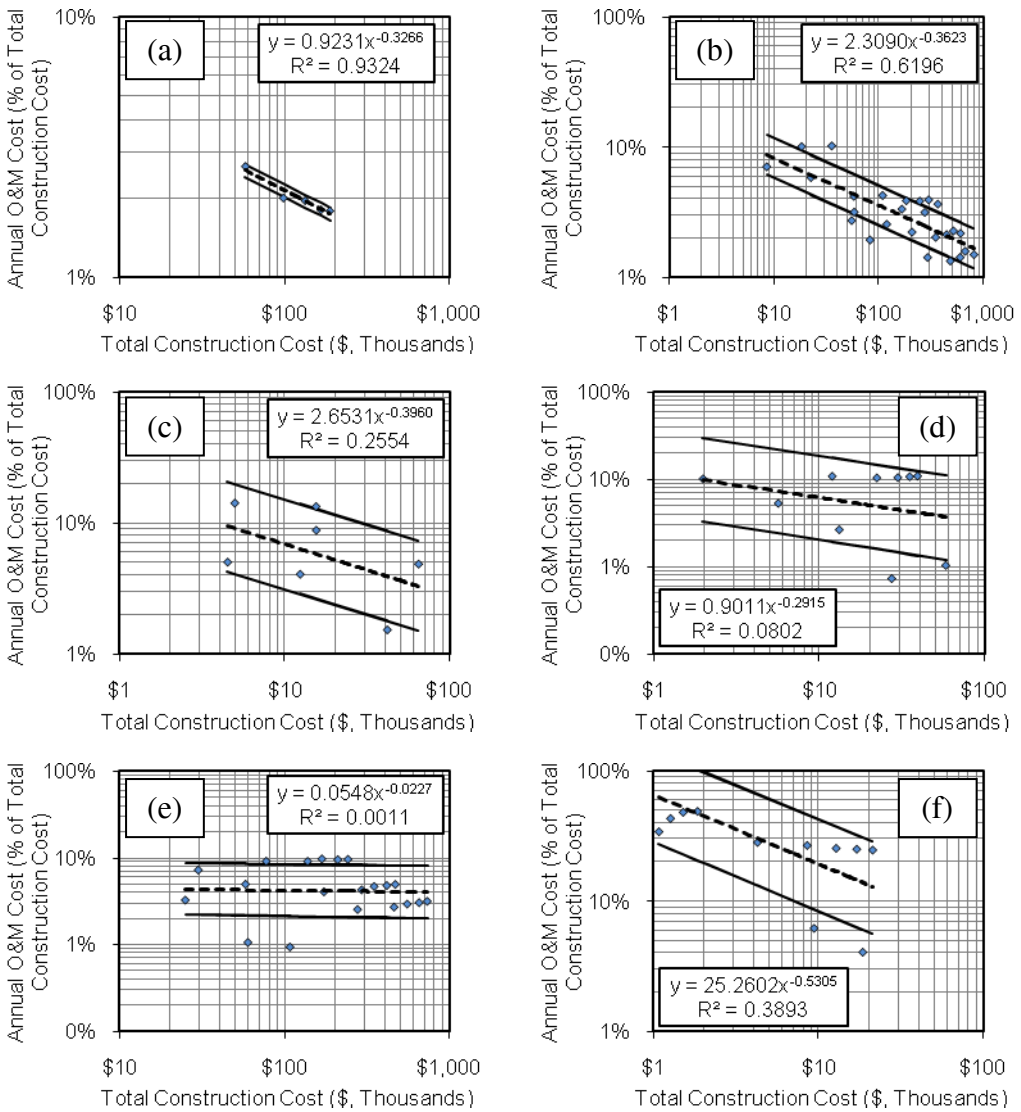

Figure 3: Predicted annual life-cycle O&M costs as a function of total construction costs in 2005 USA dollars (Weiss et al., 2005). (a) dry ponds, (b) wet ponds, (c) constructed wetlands, (d) rain gardens, (e) sand filters and (f) grassed/vegetative swales. Data from SWRPC (1991), Landphair, et al. (2000) and Wossink and Hunt (2003).

Operation and maintenance costs are a substantial portion of life-cycle stormwater BMP costs. As shown in Figure 3, the annual predicted O&M cost is roughly 10% of total construction costs for stormwater BMPs that cost $10,000 (2005 dollars) to construct. Therefore, O&M cost of these stormwater BMPs will roughly equal total construction cost after 10 years (in constant dollars). Similarly for stormwater BMPs that cost $100,000 (2005 dollars) to construct, O&M cost is roughly 5% and will roughly equal total construction cost for these BMPs after 20 years (in constant dollars). This estimation can be used as a general rule of thumb when planning, designing, and budgeting for installation of stormwater BMPs.

CONCLUSIONS

Many communities are struggling to define stormwater BMP operation and maintenance needs without readily available guidelines. As a step towards providing this information, a survey of cities was conducted to quantify the frequency of inspection, level of effort needed for routine maintenance, stormwater BMP deterioration factors, and maintenance complexity. In addition, a nationwide literature review was conducted to estimate operation and maintenance (O&M) costs for stormwater BMPs.

The results of the survey revealed that most (89%) cities perform routine maintenance once per year or less. The most common causes of performance deterioration were sediment buildup and litter/debris for most stormwater BMPs. Sediment removal is the most costly maintenance activity reported for all stormwater BMPs.

The nationwide literature review resulted in predictive equations for O&M cost of stormwater BMPs as a function of total construction cost. Operation and maintenance (O&M) cost is also shown to be a substantial portion of life-cycle cost for all stormwater BMPs and requires serious consideration. As a general rule-of-thumb, O&M cost for stormwater BMPs will roughly equal the construction cost (in constant dollars) after 10 years for a $10,000 installation and 20 years for a $100,000 installation (2005 dollars).

ACKNOWLEDGEMENTS

This study was performed as part of the research project "Assessment and Maintenance Stormwater Best Management Practices" funded by Minnesota Pollution Control Agency. We thank Lisa Thorvig, Roger Karn and Don Jakes for their support of this work. We are also grateful to the 28 cities for responding to our survey and providing information related to their experience with stormwater BMPs.

REFERENCES

Landphair, H.C., McFalls, J.A., and Thompson, D. (2000). *Design methods, selections, and cost-effectiveness of stormwater quality structures*, Texas Transportation Institute, Texas A&M Univ. System, College Station, Tex.

Southeastern Wisconsin Regional Planning Commission (SWRPC). (1991). *Costs of urban nonpoint source water pollution control measures*, SWRPC, Waukesha, Wis.

U.S. Environmental Protection Agency (USEPA). (1999). "Preliminary data summary of urban stormwater best management practices." EPA-821-R-99-012, Washington, D.C.

Weiss, P.T., J. S. Gulliver and A. J. Erickson, (2005). "The Cost and Effectiveness of Stormwater Management Practices," Minnesota Department of Transportation Report 2005-23. http://www.cts.umn.edu/Publications/ResearchReports/reportdetail.html?id=1023

Wossink, A., and Hunt, B. (2003). "The economics of structural stormwater BMPs in North Carolina." *Water Resources Research Institute Rep. No. UNC-WRRI-2003-344*, Univ. of North Carolina, Raleigh, N.C.

Modeling Performances of Detention Basins with Uncertainty Analysis

Daeryong Park[1]and Larry A. Roesner[1], PhD, P.E., Fellow ASCE

[1]Department of Civil Engineering Colorado State University, Fort Collins, Colorado 80523-1372, USA; PH (970) 491-2838; FAX (970) 491-7727;
Email: Daeryong.Park@colostate.edu, and Larry.Roesner@colostate.edu,

Abstract

Best Management Practices (BMPs) correspond to actions and practices used to reduce flow rate and the constituent concentration in urban runoff. The extended detention basin is the most widely used among various types of BMPs. This study addresses the design guidelines for extended detention basins by applying uncertainty analysis to predict the magnitude of the widely varying urban nonpoint source pollution concentration expected in the BMP influent and effluent. With uncertainty analysis considered, urban nonpoint source pollution can be predicted with greater accuracy and better detention basin design criteria can be established for the protection of receiving waters.

The International BMP Database (www.bmpdatabase.org), used for observed data in this study, is the database of monitored water quality data for nationwide BMP sites maintained by the U.S. Environmental Protection Agency (U.S. EPA) and the American Society of Civil Engineers (ASCE), et al.

This study uses and Total Suspended Solid (TSS) as the representative water quality parameter from extended detention basin. Hydrologic and BMP geometric data of watersheds correspond to the location of these detention basins. This study incorporates the k-C* model with uncertainty analysis to represent observed data. The k-C* equation was chosen for the detention basins performance model because this model has been widely used for representing wetland treatment performances, but also can consider the performance effect for the physical dimensions of the BMP. This study will be able to support stormwater management decision makers in building detention basins of appropriate sizes with a better idea of the expected performance and risk.

Introduction

Many attempts have been made to evaluate BMP performance. Historically, the efficiency of BMPs has been represented as percent removal of pollutants. Strecker et al. (2001 and 2004) argued that using percent removal as an indicator of efficiency often gives inaccurate results. They suggested that the efficiency of several BMPs might be better characterized by the effluent Event Mean Concentration (EMC) and that design standards should consider hydrologic losses that take place with some BMP types.

Many mathematical models have been developed to analyze and predict the water treatment. They attempt to represent complex treatment mechanisms through

simple mathematical expressions. One of the most popular mathematical model for wastewater treatment is the k-C* model, which has been widely used to describe pollutants removal in wetlands (Kadlec and Knight, 1996; Kadlec, 2000; Braskerud, 2002; Kadlec, 2003; Rousseau et al, 2004; Lin et al., 2005). International Water Association (IWA) (2006) provides design and condition guidelines of wetland using the k-C* model.

Uncertainty analysis is a tool commonly used in all disciplines of civil engineering. Various approaches have been used in uncertainty analysis including analytic methods, approximation methods and different types of Monte Carlo Simulation (MCS). One of the most well-known approximation methods is the First Order Second Moment (FOSM) method, also referred as the First Order Error Method or the First Order Variance Estimation method. The Latin Hypercube Sampling (LHS) method is a modified stratified sampling of MCS. It can provide accurate estimates of statistical variables of model output at much smaller computational loads than MCS (Melching, 1995).

The objective of this study is to presents a BMP performance model that evaluates TSS removal in detention basins by incorporating uncertainty analysis. The distribution of effluent EMC can be represented depending on the uncertainty of variables, both influent EMC (C_{in}) and areal removal rate constant (k) in the k-C* model. Data uncertainty, such as C_{in}, is evaluated with selected TSS data from BMP database. Model uncertainty is estimated from a regression relation of q and k.

Two uncertainty estimation methods are used to estimate effluent concentration, referred to plot the probability density function (PDF). The LHS has been chosen as the numerical estimation method and FOSM has been selected as the analytical approximation method.

The classical mathematical model of water treatment is the first-order decay model widely used to describe pollutant removal in wetlands, swales etc. (Careleton et al., 2001; Braskerud, 2002; Wong et al., 2006). Storage BMPs performance in stormwater is very similar to water treatment in wetlands. Similar aspects include variables such as geometric storage condition, inflow and outflow rates, and influent/ effluent concentrations. Thus, the models for water treatment have been applied to represent storage BMPs performance.

One of these models is the k-C* model. Many researchers applied this model to constructed wetland performance and proved good reproducibility of real situations (Kadlec, 2000; Rousseau et al, 2004; Stone et al, 2004; Kadlec, 2003). It can apply an "irreducible minimum concentration" to the first decay equation because the observed effluent concentration is converged with a constant value. Assumptions of the model are steady and plug flow conditions, which are valid assumptions used in representing flow hydrodynamics within wetland systems (Kadlec and Knight, 1996). The k-C* model is given by:

$$q\frac{dC}{dy} = k(C - C^*) \tag{1}$$

Considering y, the fraction of distance from inlet to outlet, setting y=1, integration of equation (1) gives

$$C_{out} = C^* + (C_{in} - C^*)e^{-k/q} \quad (2)$$

where:

C_{out} = effluent EMC (mg/L),

C_{in} = influent EMC (mg/L),

C* = background EMC or minimum output EMC (mg/L),

k = areal removal rate constant (m/day), and

q = hydraulic loading rate, defined as the ratio of the inflow discharge divided by the surface area of the system (Q/A) (m/day)

Despite these applications, the model has some drawbacks. It assumes steady-state flow condition and output concentrations are extremely sensitive to the areal removal rate constant, making it difficult to predict effluent concentration.

The k is related to q with the power function as shown in Figure 2. However, the output of the k-C* model is too sensitive to estimated k. Therefore, it is necessary to apply a prediction interval in k and q regression line. A Prediction interval is focused on variance of individual data while a confidence interval is focused on variance of a regression line. This study chooses the prediction interval of k since it is more necessary to know the performance for an individual event rather than the prediction of the average performance for many similar events (Barrett, 2005). The prediction interval in the regression line relating k and q are calculated by Equation (3) (Kutner et al. 2004).

$$t_{0.05} s \sqrt{1 + \frac{1}{n} + \frac{(X - \overline{X})^2}{\sum_{i=1}^{n} (X_i - \overline{X})^2}} \quad (3)$$

where

t = the t distribution for the appropriate degree of freedom (n-2),

n = the number of total data,

s = standard error of the regression,

X = average q at which the confidence interval calculated,

$\overline{X}$ =mean of observed q from monitoring data, and

X_i =individual observed q from monitoring data.

Study Approach

BMP performance data were collected from the International Stormwater BMP Database (www.bmpdatabase.org) maintained by ASCE and US EPA categorized as illustrated in Figure 1. For different BMPs, the database includes geometric information, event runoff volumes, water quality data, and other general information.

Table 1. Selected Best Management Practices in this study

BMP Type	BMP name, Location	Number of Data Set	Volume (m^3)	BMP size Surface area (ha)	Length (m)
Detention Basin	15/78, CA	17	1122.54	0.0977	60.96
	5/605 EDB, CA	2	364.66	0.0598	47.24
	605/91 edb, CA	5	69.57	0.0114	22.86
	Manchester, CA	12	252.79	0.0304	22.86

Based on the results obtained by the Nationwide Urban Runoff Program (NURP) study (US EPA 1983) and Van Buren et al. (1997), Strecker et al. (2001) remarked that stormwater constituents can be well represented by a lognormal distribution. Lognormal distribution was adjusted to C_{in} and C_{out} data to verify this statement. Figure 1 shows this distribution together with the empirical histogram for the site. It is observed that the lognormal distribution represent the data well. Similar results were obtained for the other locations in this study.

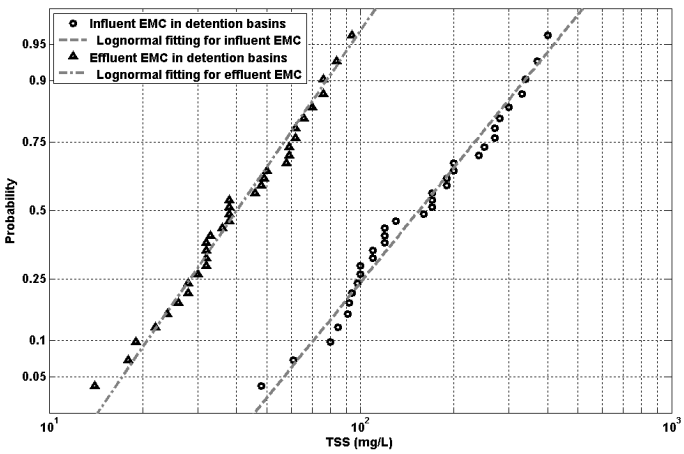

Figure 1. Lognormal probability plots of observed EMCs in detention basins

The k-C* model presented is used for simulating the performance of BMPs. Both parameters of the model, k and C*, depend on pollutant characteristics such as the particle size and settling velocity (Wong et al. 2002). Treatment systems receiving large particles concentrations will have a high removal rate and low C* since there is more sedimentation. Thus, there is a relationship between the parameter, k, and the settling velocities (or particle size) of suspended particles in the watershed. Parameter calibration for the k-C* model should be performed based on local conditions such as particle size distribution. Usually, C* depends on temperature and inflow concentration (Kadlec and Knight 1996). Although the areal removal rate constant, k ,has a theoretical link to settling velocity, field studies have shown that it is not necessarily the case for particles finer than about 40 μm (Wong, THF et al. 2002). Thus, the estimation of k is not straightforward. Scherup et al. (1990) found that the

k-values of the k-C* model are strongly dependant on the Hydraulic Loading Rate (HLR) (q). They proposed the following power relationship with coefficients a and b:

$$k = aq^b \tag{4}$$

This relationship is used in this study to estimate the value of k. However, k-values in the model are very sensitive and they must be estimated with more accuracy in order to obtain accurate effluent EMCs. Therefore, the need of high accuracy in the model causes the need of k for uncertainty analysis. A plot of k versus q based on storm event is shown in Figure 2 with a 95% prediction interval from Equation (4) for TSS in detention basins. Data are categorized by BMP and location. Values of the coefficients a and b in Equation (4) are 1.4841 and 0.9721. The distance between the median line and the prediction interval line means uncertainty in k. Thus, the log-transformed k is 0.437 from Figure 2.

This study suggested one constant value, 10 mg/L, for C*. Table 2 shows the required given information of input variables for uncertainty analysis of uncertainty in both C_{in} and k.

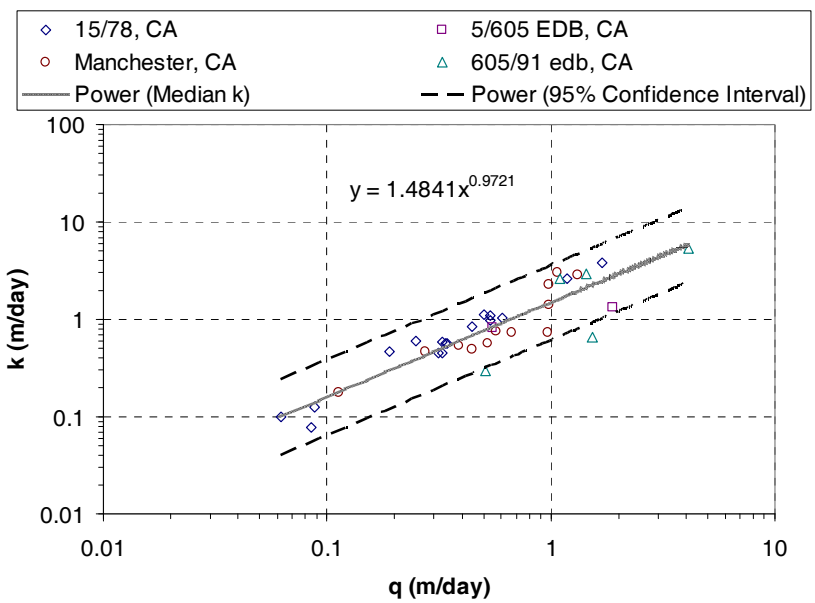

Figure 2. Estimated k vs. q using individual storm events

Table 2. Required parameters information of C_{in} and k for uncertainty analyses

Input Parameters	C_{in}		k	
Log-transformed Statistical Properties	mean	standard deviation	mean	standard deviation
Value	5.038	0.6083	$\text{Log}(1.4841q^{0.9721})$	0.4370

Results

This study assumes that there is no correlation between C_{in} and k for simpler calculations and the LHS method provides similar results with analytical simulations such as the derived distribution method. Thus, the LHS method is used in this section to evaluate the FOSM method. To apply the FOSM method, it is assumed that C_{out} is lognormally distributed. Figure 3 shows the PDF of effluent EMC depending on the q with the LHS and the FOSM methods. Most probability density values of effluent EMCs are placed below 50 mg/L without regards to q values.

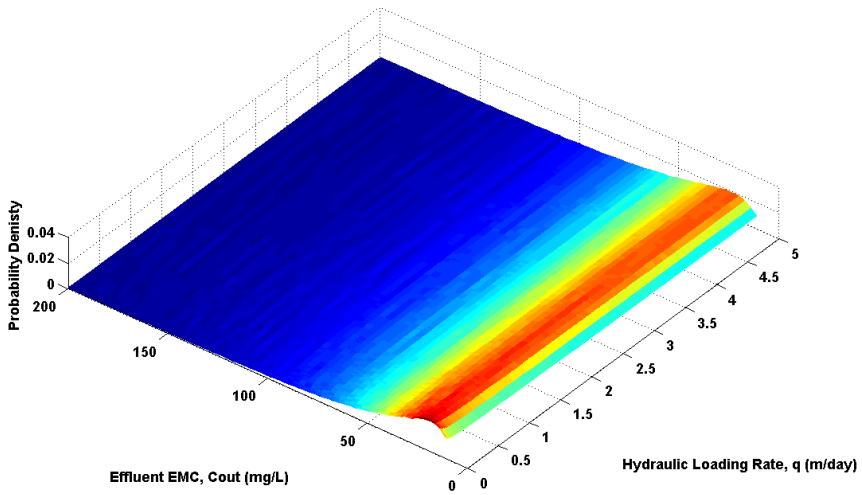

(a)

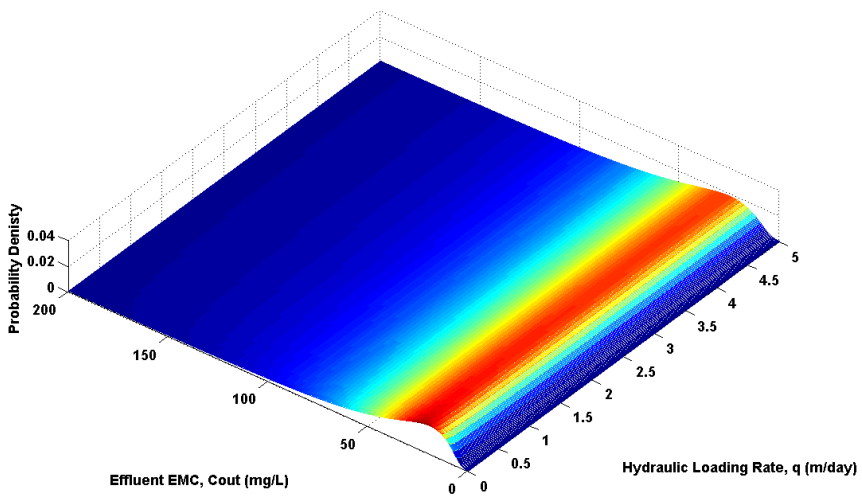

(b)

Figure 3. $f(C_{out})$ **as function of q on considering uncertainty in both** C_{in} **and k ;(a) LHS, (b) FOSM**

Figure 4 shows a comparison of both PDFs for q=0.01 and q=5 m/day. Both distribution are more similar for q=5 m/day, but differences in the peak value and the shape are observed for q=0.01 m/day. The distribution of C_{out} for high q resembles a lognormal distribution. However, that is not the case for C_{out} distribution when low values of q are used.

LHS does not require identifying the type of distribution of output. In other words, it can be represented by any unknown types of distributions. However, FOSM assumes the distribution of output as lognormal distribution. Thus, the shape of the PDFs generated by the LHS and the FOSM method differ.

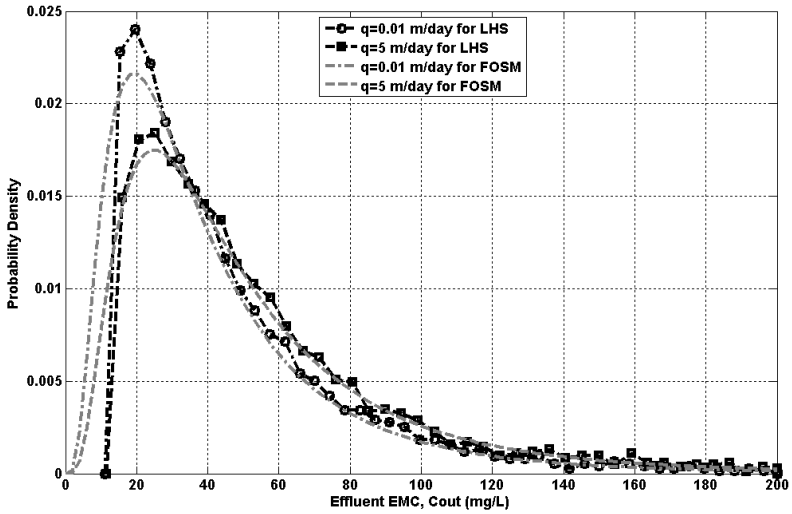

Figure 4. Comparison of $f(C_{out})$ as function of q on considering uncertainty in k between LHS and FOSM

Figure 5 shows PDFs obtained with LHS with confidence intervals of 50% and 95% and the observed data. About 70% of the total data are located within the 50% confidence interval and all observed data are located within the placed 95% confidence interval. Therefore, TSS treatment in detention basins is well explained by an uncertainty analysis that considers variability in both C_{in} and k.

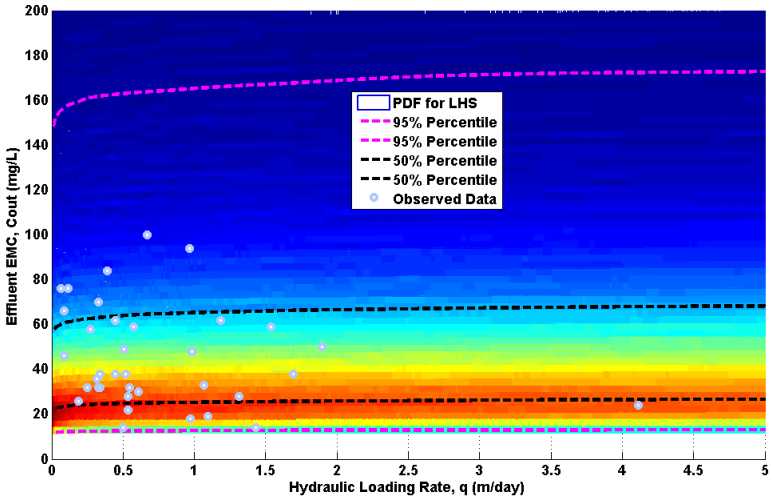

Figure 5. Uncertainty in both C_{in} and q: probability density functions of LHS including confidence intervals and observed data

Figure 6 compares the 50% and 95% confidence intervals obtained using LHS and FOSM when uncertainties in C_{in} and k are considered. They are different because the FOSM analysis assures a lognormal distribution for C_{out} while LHS method does not. This assumption is supported by the observed data, as shown in Figure 4. Thus, the assumption of lognormal distribution for C_{out} seems to be reasonable for estimating the variance of C_{out}.

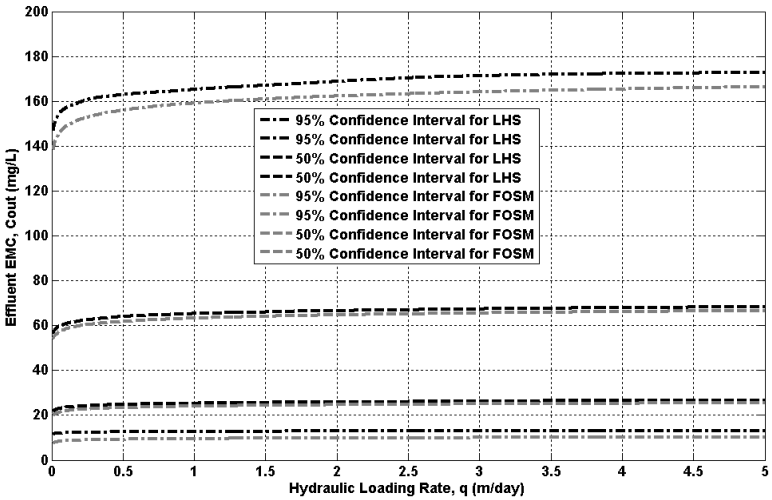

Figure 6. The comparison of confidence intervals between LHS and FOSM on considering uncertainties in C_{in} and k

Conclusion

This study has investigated the application of two uncertainty analysis methods in using the k-C* model to characterize the variability of C_{out} at the outlet of stromwater detention basins. Two methods were studied:

- FOSM is simple analytic method for uncertainty analysis. However, this method requires the distribution of the results to a known continuous distribution. Thus, the applicability of this method is reduced in the case that output distribution is not known.
- LHS is a stratified sampling method on MCS. It generates results through an appropriate sampling of the input variables and provides very accurate results even when distribution of the input variables is unknown and not unique.

Therefore, it is concluded that LHS is more efficient method to characterize the uncertainty of C_{out} when there is more than two variable parameters in the k-C* model.

With respect to the k-C* model and detention basins performance under uncertainty in input variables, the following is concluded:

- Observed variance of C_{in} is very large. This variance significantly affects the computation of effluent EMC using the model. For large values of q, the PDF of C_{out} resembles a lognormal distribution. This similarity is lost for smaller values of q.

Finally, it can be concluded that the k-C* model incorporating uncertainty analysis, represents the detention basin performance very well.

References:

Barrett, M. E. (2005). "Performance comparison of structural stormwater best management practices." Water Environment Research, 77(1), 78-86.

Braskerud, B. C. (2002). "Factors affecting phosphorus retention in small constructed wetlands treating agricultural non-point source pollution." Ecological Engineering, 19(1), 41-61.

Carleton, J. N., Grizzard, T. J., Godrej, A. N., and Post, H. E. (2001). "Factors affecting the performance of stormwater treatment wetlands." Water Research, 35(6), 1552-1562.

International Water Association (IWA) (2006). Constructed wetlands for pollution control : processes, performance, design and operation, IWA Pub., London.

Kadlec, R. H. (2000). "The inadequacy of first-order treatment wetland models." Ecological Engineering, 15(1-2), 105-119.

Kadlec, R. H. (2003). "Effects of pollutant speciation in treatment wetlands design." Ecological Engineering, 20(1), 1-16.

Kadlec, R. H., and Knight, R. L. (1996). Treatment wetlands, Lewis Publishers, Boca Raton.

Lin, Y. F., Jing, S. R., Lee, D. Y., Chang, Y. F., Chen, Y. M., and Shih, K. C. (2005). "Performance of a constructed wetland treating intensive shrimp aquaculture wastewater under high hydraulic loading rate." Environmental Pollution, 134(3), 411-421.

Melching, C. S. (1995). "Reliability estimation." Computer models of watershed hydrology, V. P. Singh, ed., Water Resources Publications, Littleton, Colo., 69–118.

Rousseau, D. P. L., Vanrolleghem, P. A., and De Pauw, N. (2004). "Model-based design of horizontal subsurface flow constructed treatment wetlands: a review." Water Research, 38(6), 1484-1493.

Stone, K. C., Poach, M. E., Hunt, P. G., and Reddy, G. B. (2004). "Marsh-pond-marsh constructed wetland design analysis for swine lagoon wastewater treatment." Ecological Engineering, 23(2), 127-133.

Strecker, E. W., Quigley, M. M., Urbonas, B., and Jones, J. (2004) "Analyses of the expanded EPA/ASCE international BMP database and potential implications for BMP design." Proceedings of the 2004 World Water and Environmental Resources Congress: Critical Transitions in Water and Environmental Resources Management, 363-372.

Strecker, E. W., Quigley, M. M., Urbonas, B. R., Jones, J. E., and Clary, J. K. (2001). "Determining urban storm water BMP effectiveness." Journal of Water Resources Planning and Management-ASCE, 127(3), 144-149.

U.S. EPA (1983). "Results of the Nationwide Urban Runoff Program. Volume 1. Final Report." Water Planning Division, Washington, DC.

Van Buren, M. A., Watt, W. E., and Marsalek, J. (1997). "Application of the log-normal and normal distributions to stormwater quality parameters." Water Research, 31(1), 95-104.

Wong, T. H. F., Fletcher, T.D., Duncan, H.P., Coleman, J.R., and Jenkins, G.A. (2002). "A model for urban stormwater improvement conceptualization." the Ninth International Conference on Urban Drainage, Portland, Oregon.

Wong, T. H. F., Fletcher, T. D., Duncan, H. P., and Jenkins, G. A. (2006). "Modelling urban stormwater treatment - A unified approach." Ecological Engineering, 27(1), 58-70.

MONITORING THE HYDROLOGIC EFFECTS OF AN EXTENSIVE GREEN ROOF

Nathaniel Hanna Holloway, Charles J. Werth and Arthur R. Schmidt[1]

[1]*Graduate Research Assistant, Associate Professor and Research Assistant Professor, respectively; Department of Civil and Environmental Engineering, University of Illinois at Urbana-Champaign, 205 N. Matthews Ave., Urbana, IL 61801, USA*
email: hnnhllwy@illinois.edu, werth@illinois.edu, aschmidt@illinois.edu

Abstract

A well known consequence of urbanization is an increase in impervious area (parking lots, streets, roofs, etc), which carries along with it a number of undesirable side effects; such as an increase in storm water runoff and often a degradation of downstream water quality. Storm water best management practices (BMP's) are currently being implemented in many communities across the United States to address these consequences. BMP's increase the pervious area in an urban environment and thus imitate natural storm water processes (i.e. infiltration, filtration, evaporation, etc). BMP's have been shown to reduce runoff quantity whilst improving runoff quality. One specific BMP, green roofs, are proposed to reduce storm water runoff through storage and improve water quality through filtration. While there are data that support these assertions, they are largely insufficient to describe the processes that produce the runoff and water quality changes. As a result, prediction of the hydrologic effects of green roofs (and other BMP's) over a range of conditions often relies on assumed adjustments to empirical parameters such as percent impervious or runoff curve number. In order to provide process-scale data describing hydrologic effects of green roofs, a monitoring system has been installed on an extensive green roof and an adjacent conventional roof on the new Business Instructional Facility on the University of Illinois Urbana-Champaign campus. The green roof being monitored is approximately 280 square meters with 0.20 meters of soil and a variety of sedums planted. The conventional roof is approximately 45 square meters. The green roof station is monitoring: volumetric water content at 15 locations, soil temperature at 9 locations, air temperature and relative humidity at two heights, rainfall, runoff, incoming and reflected solar radiation, and temperature underneath the roof at 5 locations. The conventional roof station is monitoring: roof surface temperature at two locations, air temperature and relative humidity at two heights, rainfall, horizontal wind velocity, runoff, incoming and reflected solar radiation, and temperature underneath the roof at 2 locations. In addition, automated samplers collect water quality samples from the runoff of both the green and conventional roofs and a passive atmospheric sampler monitors deposition of particles. To date atmospheric condition data and soil moisture and temperature data have been collected for 20 storm events.

Introduction

Urbanization in developed countries is increasing [Mentens et al., 2006]. With this increase in urbanization there are a number of adverse effects associated with stormwater runoff. Urbanization has been found to generally increase the size and frequency of floods due to the increase in stormwater runoff caused by a greater proportion of impervious surfaces [Konrad, 2003]. Furthermore, groundwater recharge is diminished, downstream ecosystems are degraded, and channels become unstable [Stone, 2004; Walsh et al., 2001; Bledsoe and Watson, 2001]. Stormwater BMP's can be incorporated into new development, or retrofit into existing infrastructure, to increase the amount of pervious area in urban environments. This increase in pervious area has been shown to reduce runoff quantity and improve runoff quality.

Green roofs, a structural BMP, manage stormwater in four ways: (1) through the process of infiltration the time to peak runoff is delayed, (2) the time to initial runoff is delayed due to infiltration and storage, (3) total volume of runoff is reduced due to storage of water by the soil and vegetation, and (4) pollutants deposited on the roof from the atmosphere are filtered out (Mentens et al, 2006). Moreover, green roofs may also reduce the urban heat island effect, as well as heating and cooling loads on buildings.

Previous Monitoring

A study conducted by the National Research Council of Canada provided thermal and stormwater runoff data from two different green roofs and a conventional roof. This study showed a greater reduction in heat flux through the green roof in summer than in winter. Furthermore, an annual average reduction in runoff volume of 57% was achieved by the green roof [Liu, 2005]. Another study conducted in Portland, Oregon showed the green roof could absorb approximately 69% of rainfall. The study also showed that water quality was improved through volume (loading) reduction as well as pollutant removal [Hutchinson et al., 2003]. A third study, which examined the effect of media depth and slope on water retention, found increasing the depth and decreasing the roof slope increased water retention and, surprisingly, vegetation had little effect [VanWoert et al., 2005]. Although helpful in illuminating general characteristics of green roofs, previous monitoring lacks in high resolution data that describes the physical processes. The goal of this monitoring is to provide a dataset such that these processes may be evaluated.

Experimental Method

The study area consists of an extensive green roof made up of four sections of vegetated beds and an adjacent conventional roof, see Figure 1. Figure 1 shows the location of:

1. The green and conventional roof weather stations.
2. Roof drain sets.
3. Soil moisture and temperature sensors.
4. The placement of the water quality and passive samplers.

5. The placement of the flow measurement devices (CR1, GR1, GR2, GR3) in the operational drains.
6. Conventional roof temperature probes.

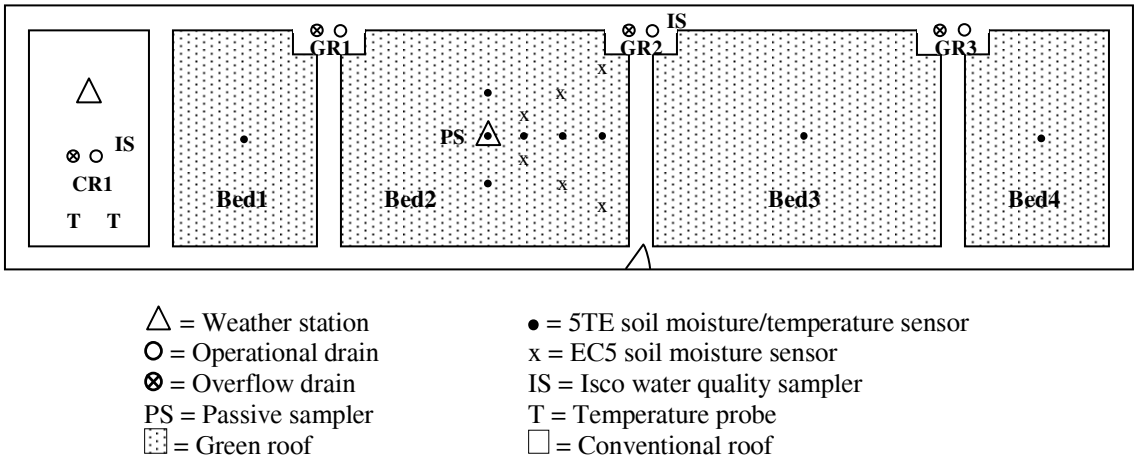

Figure 1. Schematic of green roof and conventional roof monitoring (not to scale)

The conventional roof, which covers approximately 45 square meters, is one story above the green roof and is accessed via a ladder. The total green roof area comprises of four beds with a total area of approximately 280 square meters. Each bed is surrounded by a vegetation free zone. The green roof was planted in July 2008 and therefore vegetation coverage is minimal, full vegetation coverage is attained after two years. Figure 2 shows a cross section of the green roof, vegetation free zone and drainage chamber. The green roof consists of six basic layers:

1. The substrate soil – approximately 20 cm.
2. A geotextile filter membrane, which prevents fine material from escaping the bed.
3. A water storage panel.
4. Moisture retention mat.
5. Insulation.
6. Root stop, protection membrane and roofing membrane.

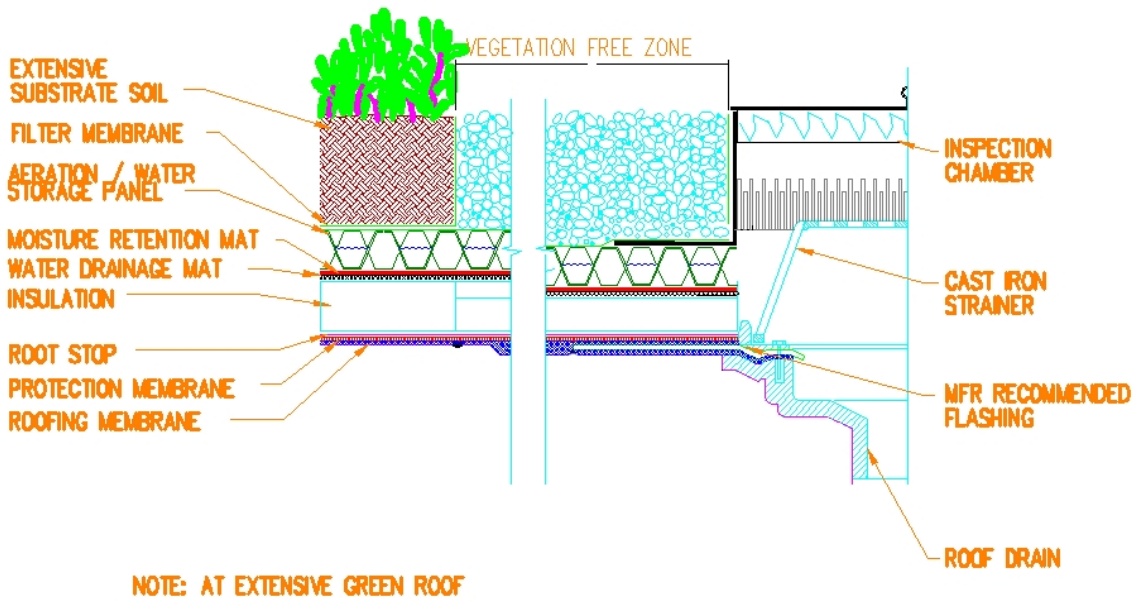

Figure 2. Cross section of green roof (courtesy Gilbane Inc.)



Figure 3. Conventional roof weather station

Weather Stations

Each weather station measures a number of atmospheric conditions and is powered by a solar panel which charges a battery. The weather stations are comprised of: a 10 foot tripod to which the sensors and solar panel are attached, an enclosure box which contains the datalogger and battery, see Figure 3. At each station a datalogger (Campbell Scientific CR1000) controls the sensors and stores the data. The green roof station incorporates a multiplexer due to the number of sensor inputs. All data are stored at one minute time intervals except for the flow measurement output which is stored at half second intervals when triggered. The flow measurement devices will be discussed in further detail later.

At each station relative humidity (RH) and air temperature probes are mounted on two foot crossarms at two heights above the roof, approximately 1.2 m and 2.2 m. The placement of the sensors was chosen to facilitate sensible and latent heat flux calculations. These conditions are measured using Campbell Scientific CS215's with radiation shield, see Figure 4. The temperature measurements have an operating range of -40 to +70°C and the relative humidity operating range is 0 to 100% RH (-20 to +60°C). The RH readings are temperature compensated to better than ±2% over the entire temperature range [CS215, 2008]. Table 1 shows the precision of the probe reading for different operating ranges. The output is percent relative humidity and degrees Celsius.

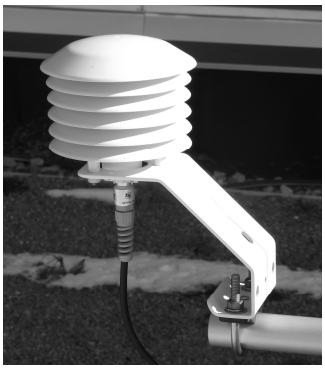

Figure 4. Air temperature and relative humidity sensor with radiation shield

Table 1. Precision of temperature and RH readings

	Accuracy	
Operating Range	Temperature	RH (at 25°C)
-40 to +70°C	±0.9°C	X
25°C	±0.3°C	X
+5 to +40°C	±0.4°C	X
10-90%	X	±2%
0-100%	X	±4%

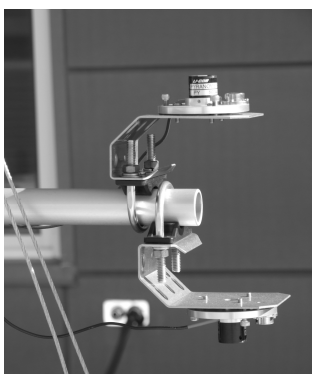

Figure 5. Up-looking and down-looking pyranometers

Both stations also measure incoming and roof reflected solar radiation using an up-looking and down-looking pyranometer (Campbell Scientific LI200X), see Figure 5. The LI200X uses a silicon photovoltaic detector to measure solar radiation (400 to 1100 nm). Like the CS215's the pyranometers are mounted on a 2 foot crossarm. The absolute error in natural daylight is ±5% but typically ±3% [LI200X, 2008]. Data is output in Watts/m^2 for each data interval and totalized in Mega Joules/m^2.

Precipitation is measured at both stations using a tipping bucket rain gage (Texas Electronics TE525WS), see Figure 6 . The gage measures rainfall in 0.254 mm increments. The gages were placed in close proximity to investigate the spatial variability of rainfall. Table 2 shows the precision of the rain gage for different rainfall rates [TE525WS, 2008]. Precipitation depth is totalized over the data interval.



Figure 6. TE525WS rain gage

Table 2. TE525WS rain gage precision

Rainfall Rate	TE525WS
Up to 2.54 cm/hr	±1%
2.54 to 5.08 cm/hr	+0, -2.5%
5.08 to 7.62 cm/hr	+0, -3.5%



Figure 7. Sonic anemometer

An ultrasonic anemometer (Gill Instruments WindSonic 2-D Sonic Anemometer) mounted on a two foot crossarm is used to measure horizontal wind speed and direction at the conventional roof station, see Figure 7. The sensor takes readings at a height of approximately 2.5 m above the roof and is oriented towards true north. Table 3 shows the operating range, precision and output resolution for the wind speed and direction readings [Gill, 2007].

Table 3. Specifications for sonic anemometer

	Wind Direction	Wind Speed
Operating Range	0-360°	0-60 m/s
Precision	±3°	±2% of reading
Output Resolution	1°	0.01 m/s

The roof temperature of the conventional roof will be measured at two locations. These measurements will be taken using Campbell Scientific CS107 temperature probes. Table 4 shows the specifications for these probes.

Two temperature probes will be placed inside the building under the conventional roof, while five probes will measure temperature under the green roof. Two probes will be placed under Bed3; all other beds will have one probe under them. Campbell Scientific

CS109 temperature probes will be used for the under roof applications. These probes are used in conjuction with two Campbell Scientific CR200 dataloggers placed under each roof. Table 4 shows the specifications for these probes [CS107, 2008 and CS109, 2008] . At the time of submittal no under roof probes had been installed.

Table 4. Temperature probe specifications

Sensor	Measurement Range	Thermistor Error	Equation Error
CS107	-35 to +50°C	<±0.2°C (0 to 60°C); ±0.4°C @ -35°C	<±0.01°C
CS109	-50 to +100°C	<±0.2°C (0 to 70°C); ±0.5°C @ -50°C	max error ±0.03°C @ -50°C

Soil Moisture and Temperature Sensors

Volumetric water content (VWC) is measured at 15 locations using two different sensors: Decagon Devices EC-5 and 5TE. The placement of these sensors can be seen in Figure 1. The placement was chosen to track moisture fronts on a process scale as they move through the growing media. All sensors are placed in a vertical position at the same depth, with the dielectric VWC probes extending from 10 to 5 cm deep. The EC-5 measures VWC while the 5TE measures: VWC, electrical conductivity (EC) and soil temperature. Both sensors were calibrated to the specific soil using five samples at different moisture contents. Moisture content was determined by drying the samples in a vacuum oven set at 70°C for 48 hours, for further details on the process see Decagon Application Note [Cobos, 2008]. Table 5 shows the specifications for the soil moisture sensors [ECH_2O, 2008 and 5TE, 2008].

Table 5. Specifications for EC-5 and 5TE sensors

	EC-5		5TE	
Parameter	Precision	Resolution	Precision	Resolution
VWC	0.02m^3/m^3	0.001 m^3/m^3	±0.01-0.02 m^3/m^3	0.0008 m^3/m^3
EC	X	X	±10% (0-7 dS/m)	0.01 dS/m (0-7 dS/m) 0.05 dS/m (7-23 dS/m)
Temperature	X	X	±1°C	0.1°C

Water Quality Sampler and Passive Sampler

Water quality samples will be taken at the conventional roof and green roof using ISCO automated samplers. A passive sampling device will be placed at the green roof station to sample atmospheric deposition of particles and polycyclic aromatic hydrocarbons (PAHs). The water quality samples will be analyzed for: organic compounds, major and trace elements, organic carbon, nitrates, radionuclides and suspended sediment. The atmospheric deposition samples will be analyzed for the same constituents sans suspended sediment. The automated sampler will be triggered by the datalogger based on the output of the flow measurement devices (described below).

Roof Drain Sets

Runoff from both the conventional and green roof areas is drained from the roof by paired sets of roof drains. The conventional roof has one set of drains while the green roof has three. Each set of drains consist of one operational drain and one overflow drain, see Figure 8. Runoff entering the operational drain is routed through the building to a stand pipe in cast iron pipe. The stand pipe is connected directly to the storm sewer. Runoff entering the overflow drain is routed to the outside of the building to notify maintenance personnel in the event the operational drain becomes clogged. The conventional roof overflow drain has a 5 cm tall collar, while the green roof drains have a 12 cm tall aluminum collar. These collars prevent runoff being routed to the overflow drain unless the operational drain is clogged and runoff begins ponding on the roof.

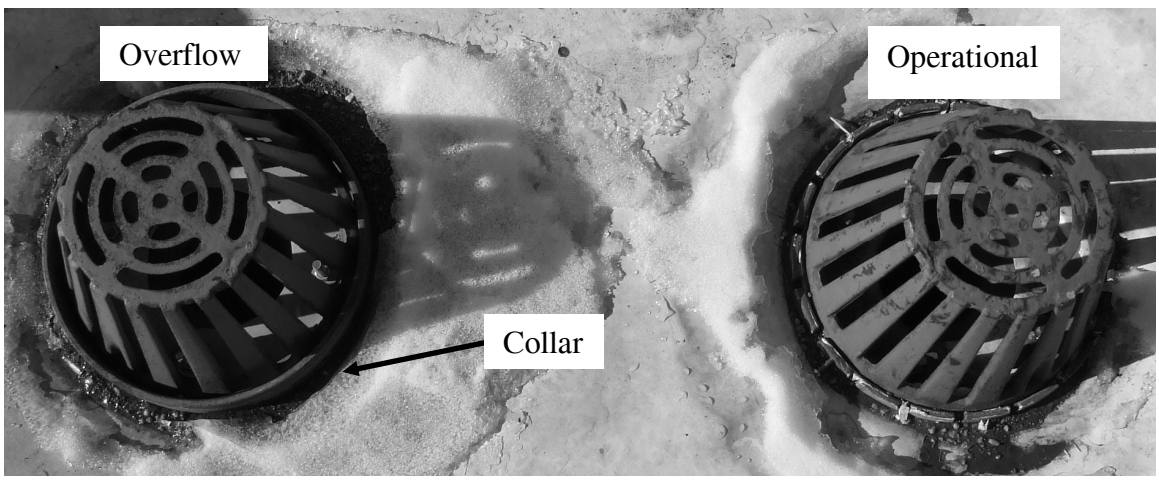

Figure 8. Conventional roof drain set

Flow Measurement Devices and Calibration

The flow measurement devices were designed and fabricated by the authors. Several options were discussed, including: tipping bucket devices located at an external downspouts, electromagnetic flow meters and a Wenzel flume [Wenzel, 1973]. These options were eventually abandoned due to prohibitive cost or access issues. The final design is a multi-stage combination weir and orifice that is retrofit to the existing roof drain. This design includes a 28 cm diameter plate with a vertical 10 cm length of 7.62 cm (3 inch) PVC pipe running through the center of the plate down into the drain pipe (Figure 9 and Figure 10). For low flow conditions a series of six, 0.64 cm orifices in the pipe; two 0.32 cm above the plate and four 0.95 cm above the plate convey the flow to the drain pipe. For larger flows a scalloped sharp crested weir conveys flows in excess of the capacity of the six orifices. The crest of the weir is approximately 2.2-2.5 cm above the plate. A pressure transducer (Keller of America Acculevel) is recessed 3.8 cm below the surface of the plate and outputs depth of water. Table 6 shows the specifications for the pressure transducer [Acculevel, 2008]. The 28 cm diameter plate is designed to sit on top of the operational roof drain flashing with the transducer sending data back to the

datalogger. The plate is caulked in place to insure all flow passes through the meter. Due to non-uniformity in the fabrication each device was calibrated separately. To date the meters have not been installed due to roof conditions and other delays.

Table 6. Acculevel specifications

	Acculevel
Pressure Range	0-90 cm WC*
Precision	0.25%

* WC = water column

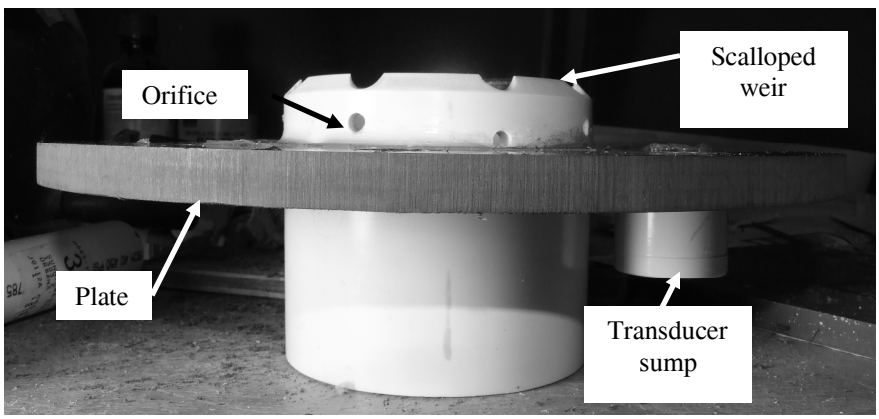

Figure 9. Side view of flow measurement device without pressure transducer

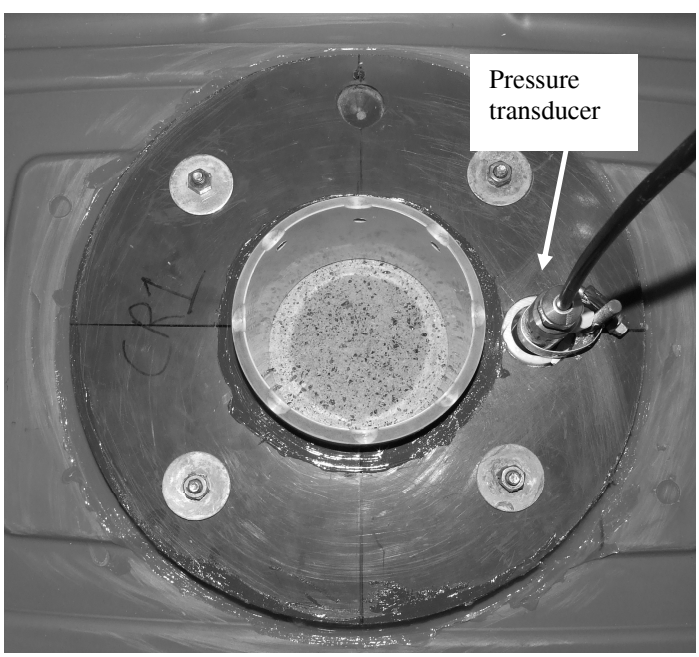

Figure 10. Top view of flow measurement device with pressure transducer

Calibration of the flow measurement devices was performed in the Ven Te Chow Hydrosystems Laboratory using volumetric measurements and a 5.1 cm (2 inch) electromagnetic flow meter (McCrometer UltraMag). Volumetric flow measurements were used for lower flows ranging from 0.3 liters/minute to 30 liters/minute. The

electromagnetic flow meter was used for higher flows (7 l/min to 200 l/min). A sample rating curve can be seen in Figure 11. The transitions between orifice and scalloped weir flow can be seen in the change of the curve slope. Furthermore, at higher flows (>200 l/min) above the scalloped weir a change in slope can be seen where the flow transitions from weir flow to orifice flow due to the weir becoming submerged. The standard deviation across the entire curve is approximately 10 l/min, most of this error originates from the transition at the scalloped weir.

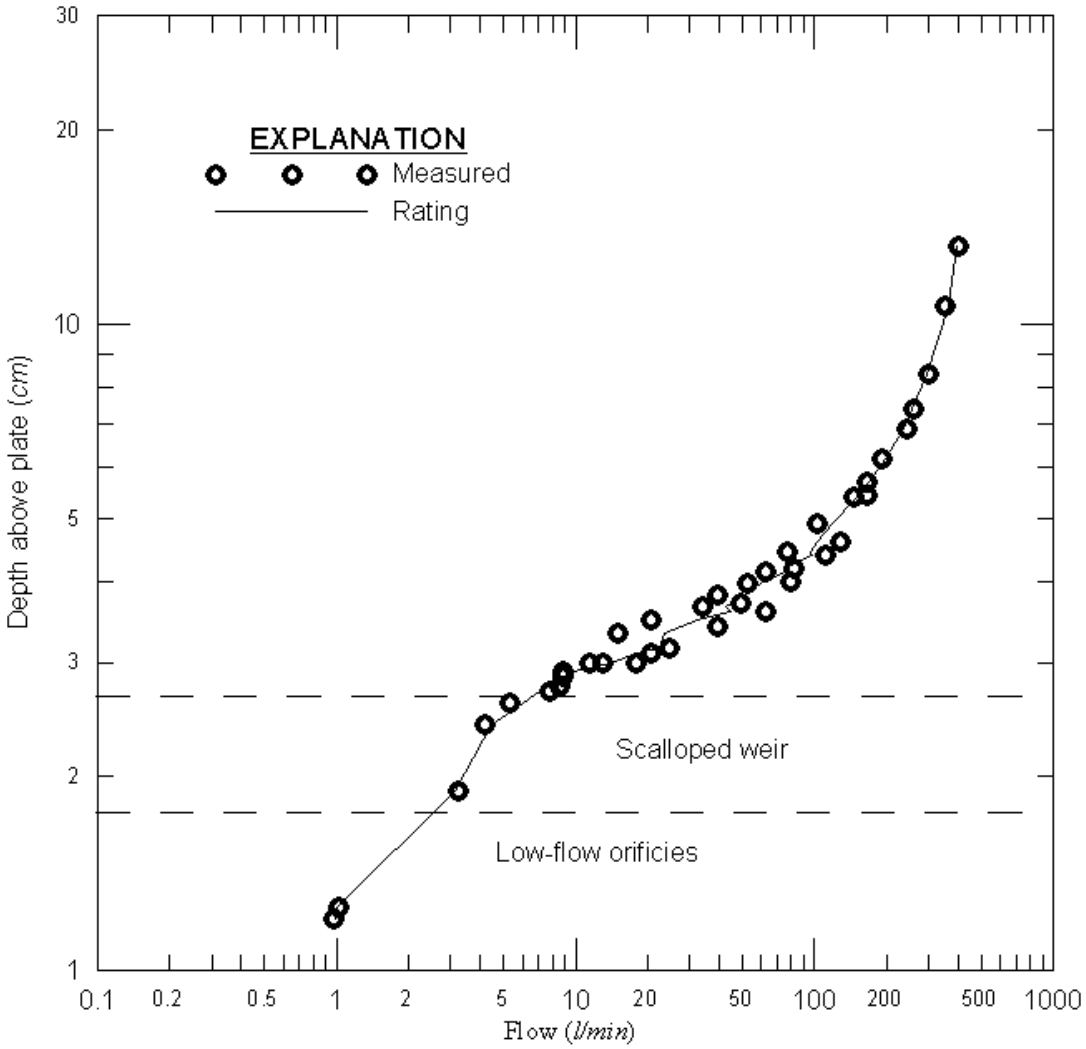

Figure 11. Sample rating curve for flow measurement device

Communications

Four wireless devices (Lantronix WiBox) will be used, one at each datalogger, to enable real-time monitoring and control of all devices. At the time of submittal data was being downloaded manually from the weather stations.

Sample Data and Discussion

To date atmospheric condition data and soil moisture and temperature data have been collected for 20 storm events.

Precipitation Data

Figure 12 shows all the precipitation data for the green roof gage for approximately 20 rainfall events to date. The storms range in duration from almost 8 hours with a total rainfall depth of 10.64 cm to small trace events.

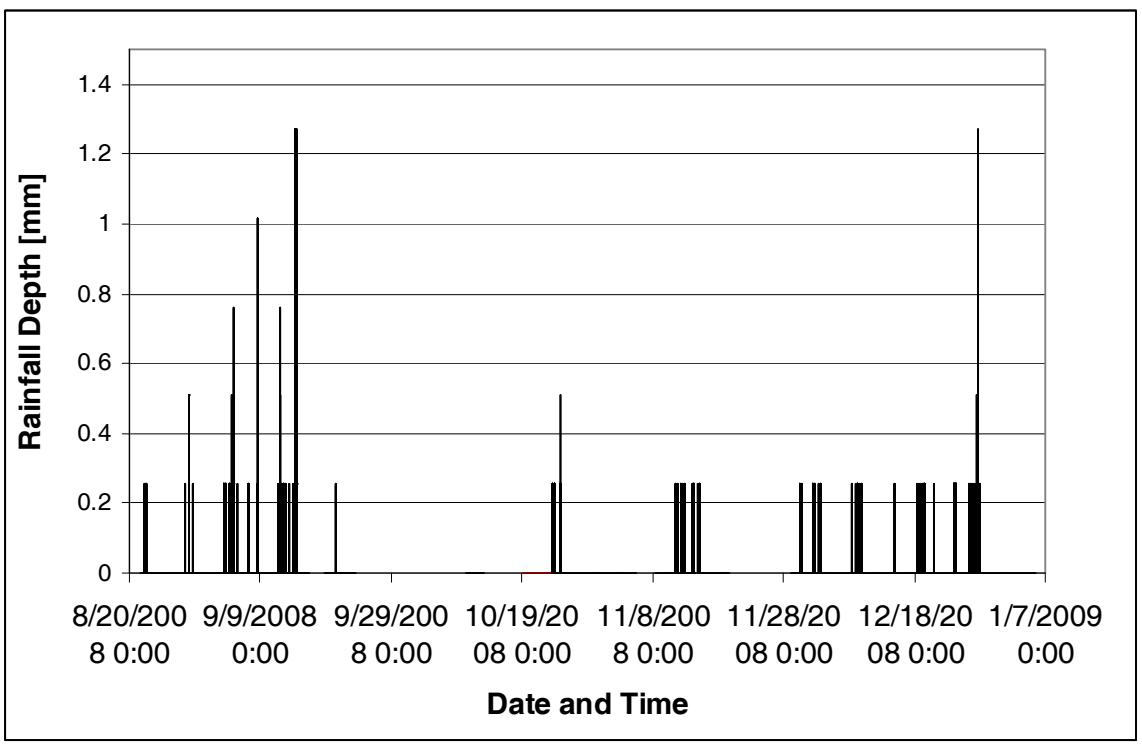

Figure 12. Entire green roof gage rainfall record

Figure 13 shows a comparison of the conventional roof raingage with the green roof raingage for a small rainfall event. Table 7 shows the duration and rainfall depth for the two gages, it can be seen that there is very little difference between the two. This is most likely due to the magnitude of the event. Unfortunately, due to data loss larger storm events were not able to be compared.

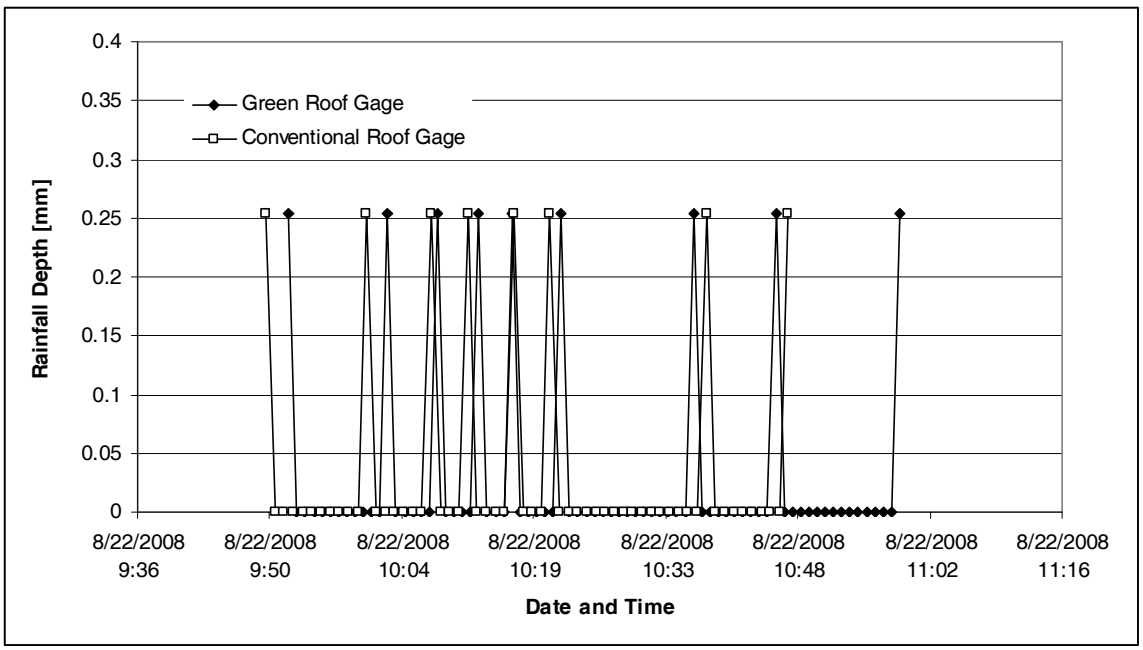

Figure 13. Comparison of gages for small rainfall event

Table 7. Comparison of rainfall events

Gage	Duration [min]	Rainfall Depth [mm]
Green roof	67	2.286
Conventional roof	57	2.032

Air Temperature and Relative Humidity

Figure 14 shows a comparison of lower air temperature at the green and conventional roofs. It can be seen that the temperature above the green roof is less than that above the conventional roof. This may be an indication of the insulating properties of the green roof, but more analysis is required. Figure 15 shows a comparison of RH at the green and conventional roofs. This plot shows the RH at the green roof is higher during the daytime, possibly indicating evapotranspiration.

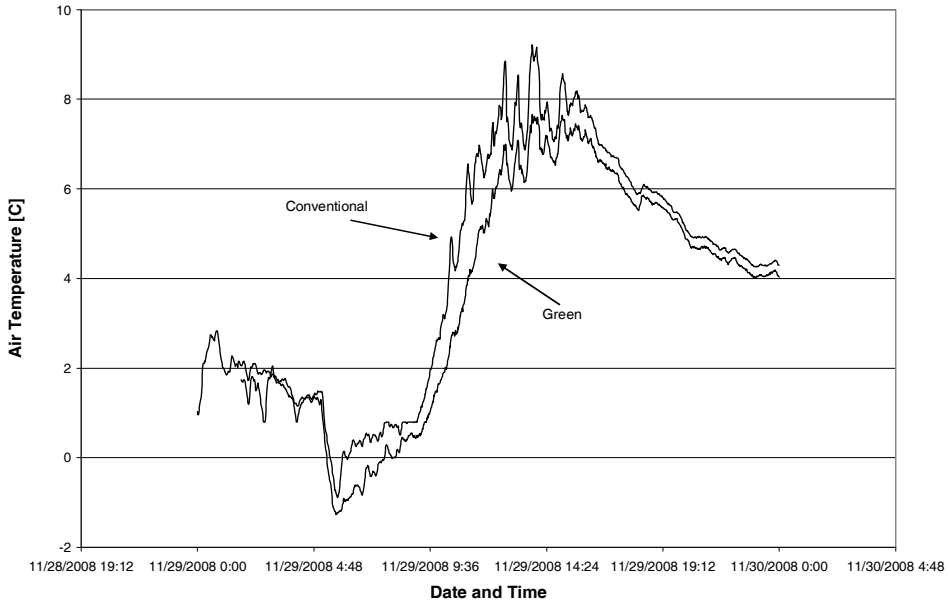

Figure 14. Comparison of lower air temperature at green and conventional roofs

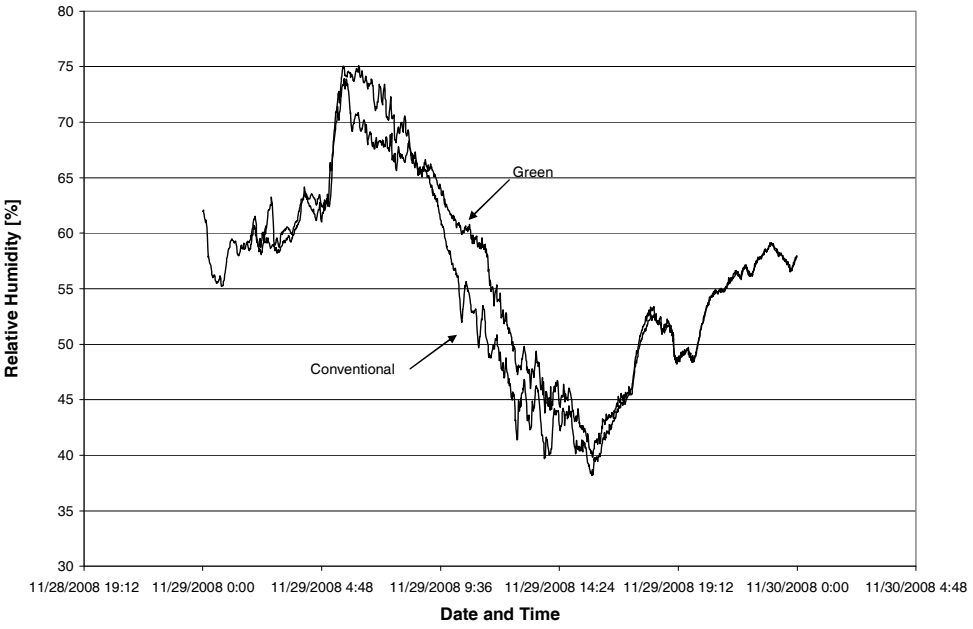

Figure 15. Comparison of lower RH at conventional and green roofs

Solar Radiation

Figure 16 shows a comparison of the up-looking pyranometers at each station. The plot illustrates the difference in shading the two roofs receive. Beyond the shading there is

little difference in the incoming solar radiation. Figure 17 shows a comparison of the down-looking pyranometers. Interestingly, these results show the effect of the smaller albedo of the green roof. The brown growing media reflects far less solar radiation than the white roofing membrane on the conventional roof.

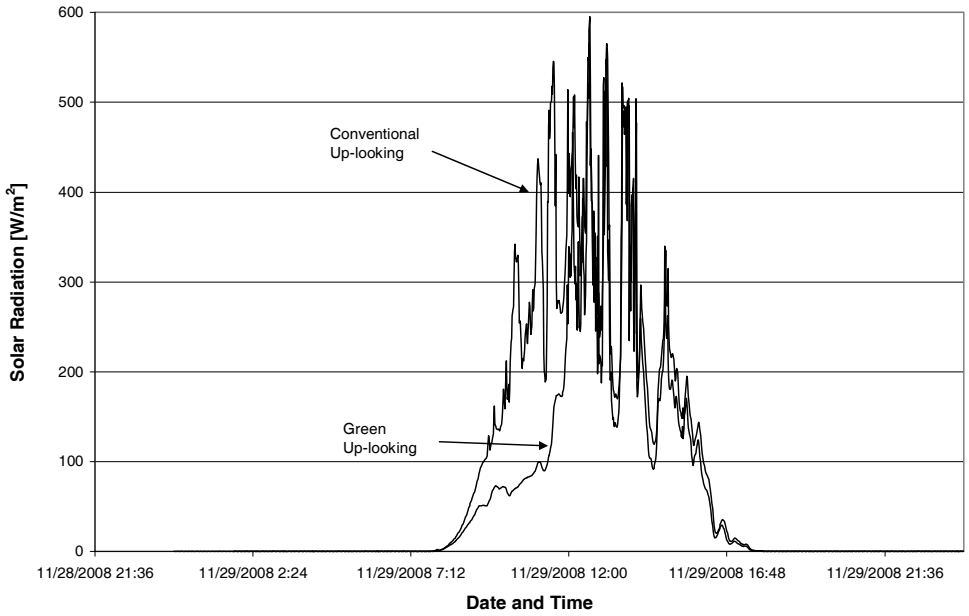

Figure 16. Comparison of up-looking pyranometers

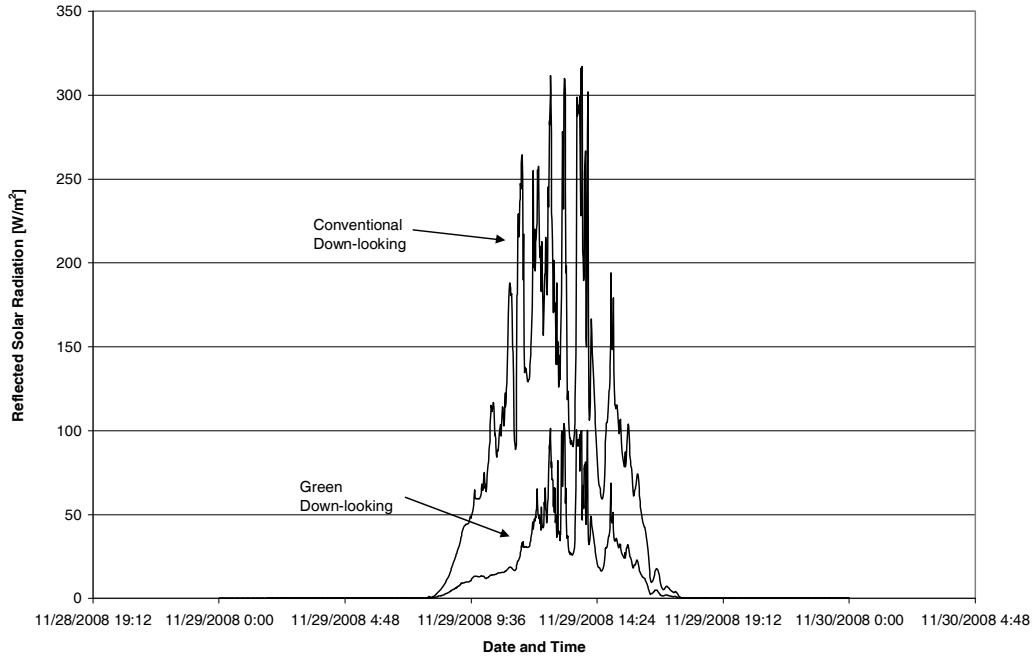

Figure 17. Comparison of down-looking pyranometers

Soil Moisture

Changes in soil moisture due to a 6 hour, 25 mm rainfall event can be seen in Figure 18. The most intriguing results show the response of the bed is relatively fast for higher intensities of rainfall. However, once the rainfall has ceased, detention of the water in the pore spaces can be seen. The green roof effectively detains some of the runoff and releases it slowly.

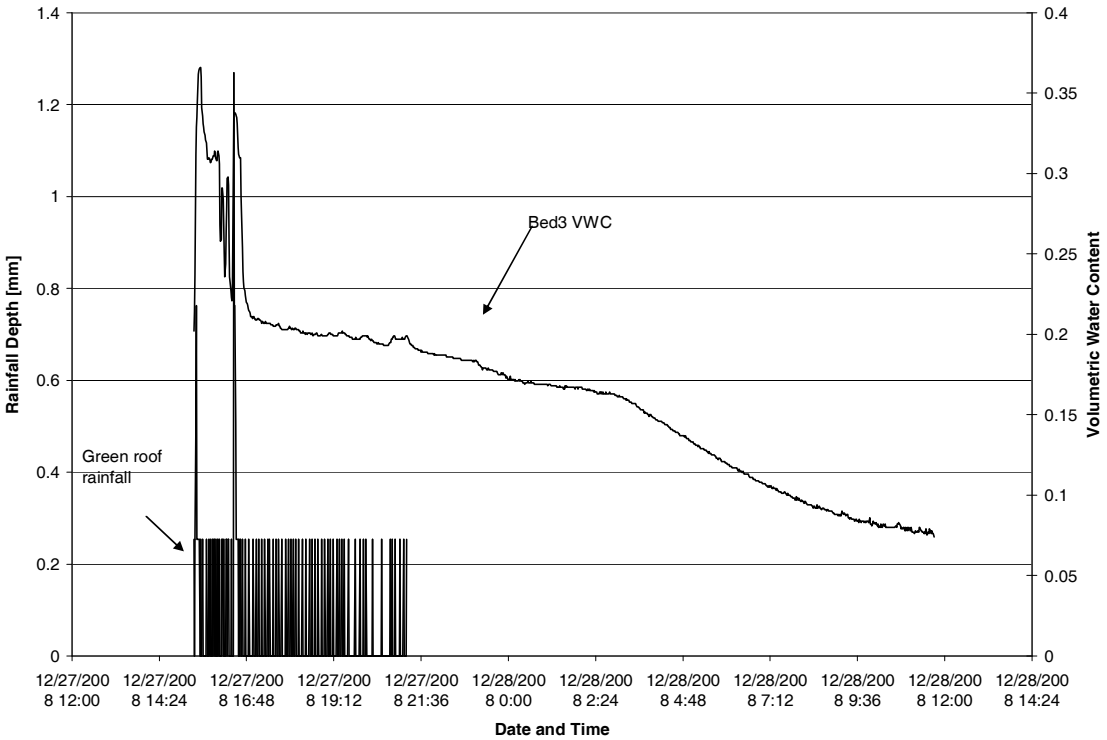

Figure 18. Effect of 6 hour, 25 mm storm on VWC in green roof Bed3

Wind

Wind data from the anemometer were analyzed, finding the prevailing wind direction is South-Southwest at an average speed of 3 m/s. Gusts up to 53 m/s (120 mph) were recorded; gusts strong enough to blow the top off of the raingage causing damage and loss of precipitation data for the conventional roof station.

Conclusions and Future Work

The current dataset contains data for atmospheric conditions and soil moisture and temperature for 20 rainfall events. Indications of differences in insulating properties can be seen, however more rigorous analysis of the data can be complete when the under roof temperature sensors are installed. Furthermore, evaporation and infiltration processes can be seen. However, few strong conclusions can be drawn without the aid of runoff data.

In the near future: the flow meters will be deployed, the passive and water quality samplers will be installed, the under roof temperature probes will be installed and the wireless communications network will be set up. Moreover, once a suitable dataset is obtained for the current configuration of soil moisture sensors, a new configuration of sensors will be implemented. The new configuration will place the sensors horizontally at different depths to collect process scale data to investigate the soil moisture profile. Ultimately, the goal is to provide real-time monitoring and control of the sensors and dataloggers, with real-time data being uploaded to a website.

References

5TE: Water Content, EC and Temperature Sensors Operator's Manual. (2008). Decagon Devices, Inc. Version 1.

Acculevel: High Accuracy Submersible Level Transmitters. Keller America, Inc. Date accessed: 7 July 2008. < http://www.kelleramerica.com/pdf/Acculevel.pdf>.

Bledsoe, B.P. and Watson, C.C. (2001). Effects of urbanization on channel instability. J. of the American Water Resources Association, Vol. 37, No. 2: 255-270.
Cobos, D.R. (2008). Calibrating ECH$_2$O Soil Moisture Sensors Application Note. Decagon Devices, Inc. Date accessed: 7 July 2008. <http://decagon.com/literature/app_notes/CalibratingECH2OSoilMoistureProbes.pdf>.

CS107 Temperature Probe Instruction Manual. (2008). Campbell Scientific, Inc. Date accessed: 12 Aug. 2008. <http://www.campbellsci.com/documents/manuals/107.pdf>.

CS109 Temperature Probe Instruction Manual. (2008). Campbell Scientific, Inc. Date accessed: 12 Aug. 2008. <http://www.campbellsci.com/documents/manuals/109.pdf>.

CS215 Temperature and Relative Humidity Probe Instruction Manual. (2008). Campbell Scientific, Inc. Date accessed: 12 Aug. 2008. <http://www.campbellsci.com/documents/manuals/cs215.pdf>.

ECH$_2$O Soil Moisture Sensor User Manual. (2008). Decagon Devices, Inc. Version 7.
Gill Instruments WindSonic Two Dimensional Sonic Anemometer Instruction Manual. (2007). Campbell Scientific, Inc. Date accessed: 12 Aug. 2008. <http://www.campbellsci.com/documents/manuals/windsonic.pdf>.

Hutchinson, D., Abrams, P., Retzlaff, R., and Liptan, T. (2003). Stormwater Monitoring Two Ecoroofs in Portland, Oregon, USA. City of Portland, Bureau of Environmental Services. Date accessed: 10 Jan. 2009. <http://www.seattle.gov/DPD/cms/groups/pan/@pan/@sustainableblding/documents/web_informational/dpds_009575.pdf>.

Konrad, C.P. (2003). Effects of Urban Development on Floods. United States Geological Survey: Fact Sheet 076-03.

LI200X Pyranometer Instruction Manual. (2008). Campbell Scientific, Inc. Date accessed: 12 Aug. 2008. <http://www.campbellsci.com/documents/manuals/li200x.pdf>.

Liu, K. and Minor, J. (2005). Performance Evaluation of an Extensive Green Roof. National Research Council of Canada: NRCC-48204. Date accessed: 20 Dec. 2008. <http://irc.nrc-cnrc.gc.ca/pubs/fulltext/nrcc48204/nrcc48204.pdf>.

Mentens, J., Raes D., and Hermy M. (2006). Green roofs as a tool for solving the rainwater runoff problem in the urbanized 21st century? Landscape and Urban Planning, 77: 217-226.

Stone Jr., B. (2004). Paving over paradise: how land use regulations promote residential imperviousness. Landscape and Urban Planning, 69:101–113.

TE525 Tipping Bucket Rain Gage Instruction Manual. (2008). Campbell Scientific, Inc. Date accessed: 12 Aug. 2008. <http://www.campbellsci.com/documents/manuals/te525.pdf>.

VanWoert, N.D., Rowe, D.B., Andresen, J.A., Rugh, C.L., Fernandez, R.T., and Xiao, L. (2005). Green Roof Stormwater Retention: Effects of Roof Surface, Slope and Media Depth. J. Environ. Qual. 34: 1036-1044.

Walsh, C.J., Sharpe, A.K., Breen P.F., and Sonneman J.A. (2001). Effects of urbanization on streams of the Melbourne region, Victoria, Australia. I. Benthic macroinvertebrate communities. Freshwater Biology, 46: 535-551.

Wenzel, Jr., H.G. (1973). Development of a Meter for Measurement of Sewer Flow. University of Illinois at Urbana-Champaign Water Resources Center Research Report No. 74.

Multiple Watershed Scales Approach for Placement of Best Management Practices in *SUSTAIN*

Fu-hsiung Lai,[1] Jenny Zhen,[2] John Riverson,[2] Khalid Alvi,[2] and Leslie Shoemaker[2]

ABSTRACT

Since 2003, the U.S. Environmental Protection Agency has been developing a decision support system for placement of best management practices (BMPs) at strategic locations in urban watersheds. This system is called the **S**ystem for **U**rban **S**tormwater **T**reatment and **A**nalysis **IN**tegration (*SUSTAIN*).

One dominant technical requirement for *SUSTAIN* is the ability to place management practices at multiple scales. To manage the complexity of larger watershed scale applications, *SUSTAIN* uses a tiered approach to evaluate both individual and multiple nested watersheds. In addition, for distributed BMPs in residential parcels of a new development or an existing neighborhood, *SUSTAIN* uses an optional *lumped* approach to aggregate BMPs by two generic BMPs, representing infiltration and storage processes. This paper describes the procedures for performing a tiered evaluation of BMPs at various spatial scales and aggregation of distributed BMPs. It illustrates framework features and performances through selected examples that are typical of the conditions and scenarios of watershed stormwater management.

The tiered optimization implemented in *SUSTAIN* provides an efficient and manageable means for large watershed scale decision makings and allows users the flexibility in placing assessment points throughout a watershed where flow and pollutant load reduction goals are to be met.

KEYWORDS

Stormwater management, decision support, watershed scale, best management practices (BMPs), cost optimization, tiered approach, aggregation, distributed BMPs.

INTRODUCTION

In 2003, the U.S. Environmental Protection Agency (EPA) initiated development of a decision support system that is based on sound science and engineering for selection and placement of best management practices (BMPs) and low impact development practices (LIDs) at strategic locations in urban watersheds. The BMP/LID assessment tools would help develop, evaluate, select, and place BMP options on the basis of cost and effectiveness. Called the **S**ystem for **U**rban **S**tormwater **T**reatment and **A**nalysis **IN**tegration (*SUSTAIN*), it provides a means for objective analysis of management alternatives among multiple interacting and competing factors. The desired outcome from the system application is a thorough, practical, and informative assessment of BMP/LID placement options considering the significant water quantity

[1] U.S. Environmental Protection Agency, Office of Research and Development; E-mail: Lai.Dennis@epa.gov; Urban Water Management Branch, Woodbridge Avenue, Edison, NJ 08837
[2] Tetra Tech, Inc., 10306 Eaton Place, Fairfax, VA 22030

and quality factors in urban watersheds and associated restoration or mitigation costs. The tool is designed for experienced watershed and stormwater practitioners to develop, evaluate, and select optimal BMP options for various watershed scales on the basis of cost and effectiveness. The beta version of *SUSTAIN* is to be released in 2009.

SUSTAIN is intended to support local and county government engineers and planners, federal and state regulatory reviewers, private consulting engineers, concerned citizens, stakeholders, and academicians in developing watershed-based stormwater management plans. The users are expected to have a fundamental understanding of watershed and BMP modeling processes.

SUSTAIN is being developed in phases because of its comprehensive scope and budgetary constraints. The Phase 1 work was completed in 2005, and the Phase 2 work is underway and scheduled to be completed in 2009. *SUSTAIN* has seven key components: ArcGIS framework manager, BMP siting tool, watershed module, BMP module, optimization module, post-processor, and BMP cost database. They are integrated under a common ArcGIS platform. In Phase 1, a conceptual framework design was developed, and major components were programmed and preliminarily tested. The systematic development of the framework through a critical review of modeling needs, current and emerging data management technology, and available watershed and BMP models has been previously presented (Lai et al. 2003; Lai et al. 2004; Riverson et al. 2004; Lai et al. 2005; Lai et al. 2006; and Lai et al. 2007). The systematic design process ensures that *SUSTAIN* provides a platform that satisfies the needs of environmental managers with technical sophistication consistent with current and emerging technology. The Phase 1 work adopted the then existing BMP module and parts of the optimization module in the Prince George's County BMP evaluation model (Tetra Tech 2001). The ongoing Phase 2 work expands the capabilities and functionalities of the system. Key enhancements include a preprocessor to facilitate selection of placement sites, more tightly integrated and flexible post-processors, expanded cost-estimating functions, and additional BMP types and improved BMP simulation processes. The optimization module is significantly expanded to incorporate an additional solution technique—the Non-dominated Sorting Genetic Algorithm II (Deb et al. 2002)—and provides a means to perform a multi-tier evaluation of individual or multiple, nested watersheds. The Phase 2 work also includes an aggregated BMP approach to represent regionalized distributed BMP/LID practices.

TIERED OPTIMIZATION APPROACH

A relatively large watershed can usually be subdivided into several smaller subwatersheds or subareas. For each subarea, users select an appropriate suite of feasible BMP options (types, configurations, and costs) at strategic locations. *SUSTAIN* generates time series rainfall-runoff data from BMP drainage areas and routes them through BMPs, in parallel or in series, and predicts quantity and quality at selected locations. For each subarea, *SUSTAIN* produces output for deriving optimal cost-effectiveness curves that relate flow or pollutant load reductions with

their associated costs as shown in Figure 1. Each point on the cost-effectiveness curve represents an optimal combination of BMPs that will collectively remove the targeted amount of pollutant load at the least cost.

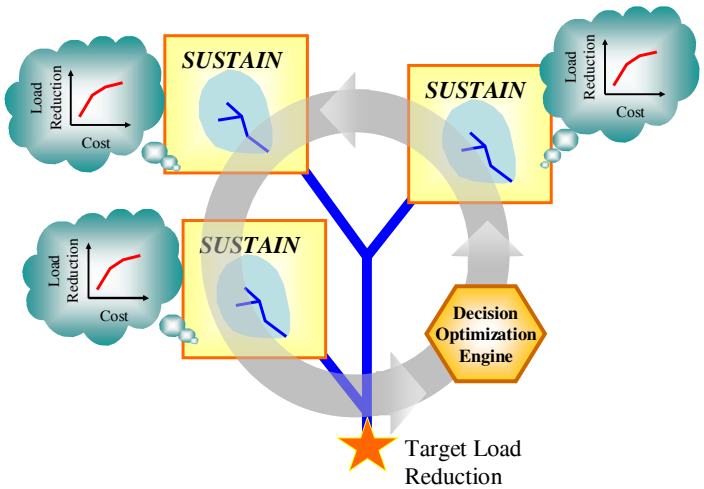

Figure 1. Tiered application of *SUSTAIN* for developing cost-effectiveness curves.

One important requirement in developing *SUSTAIN* is the ability to place management practices at multiple scales. This is because placing BMPs at different spatial levels, i.e., on-site, subregional, and regional, affects the overall cost-effectiveness of the stormwater control system (Zhen et al. 2004). In an urban setting, the on-site scale can be exemplified by building lots or neighborhoods with a drainage area in the range of 10–100 acres. LID technologies are normally applied on this scale. Other BMPs collect runoff at hydrologic junctions further downstream, at a level typically associated with the township scale with a drainage area of approximately 100–5,000 acres. At the larger, regional scale, the benefits of management are often measured by effects on receiving streams, lakes, or other larger waterbodies. The regional scale usually represents a watershed on a county level with a drainage area greater than 5,000 acres. Management plans often need to reflect the cumulative benefit of management practices at multiple scales on downstream water quality in rivers, lakes, or estuaries. Detailed simulation can be performed at the site scale or small watershed scale to evaluate the effects of various combinations of practices and treatment trains on localized water quantity and quality. For evaluation and placement at a larger scale watershed, there could be hundreds or thousands of individual management practices that compose the aggregated treatment. To manage the complexity of larger-scale applications, *SUSTAIN* uses a tiered evaluation approach conceptualized in Figure 1 that allows for evaluation of both individual watersheds and multiple, nested watersheds.

As the first step of the tiered optimization analysis, cost-effectiveness curves for each subwatershed (tier 1) are generated by performing multiple optimization runs for the defined incremental flow/pollutant reduction targets. The second step is to construct

the search domain for a combination of subwatersheds (tier 2). The search domain contains the discrete solutions on the tier-1 cost-effectiveness curves at various assessment points *i* and *j* in the watershed. Figure 2 illustrates the search domain construction process.

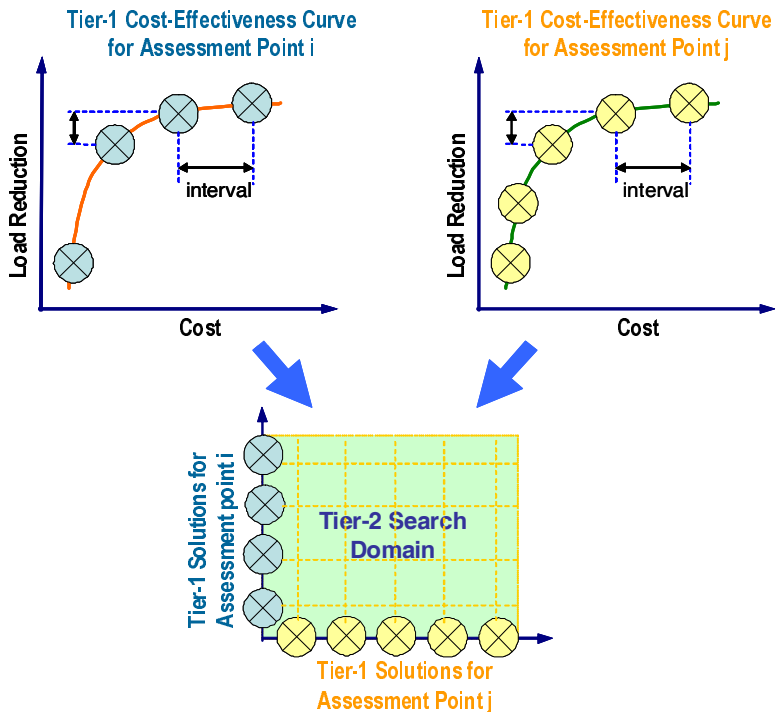

Figure 2. Construction of the tier-2 search domain using tier-1 results.

The third step is to perform the tier-2 optimization on the search domain. The optimization engine is designed to strategically sample within the search domain. The cost-effectiveness of each sample is measured, stored, and analyzed to guide the next search direction. Figure 3 illustrates the simulation process that generates the results used for measuring each iteration run's cost-effectiveness. The simulated time series output for each set of tier-1 solutions (assessed at smaller location point ★) are stored and used every time the solution is sampled. Similarly, the watershed area that is not covered by the tier-1 assessment points can either be represented by a pre-simulated time series or by real-time simulation during the tier-2 search process (assessed at larger location point ★). Because tier 2 typically represents modeling at a larger watershed scale, time of concentration is an important factor that must be incorporated into the solution approach. For every iteration run, the transport module can be used to route the time series data from the tier-1 subwatersheds and the watershed area between the tier-1 and tier-2 assessment points. The tiered approach is flexible and can apply to both large watersheds that contain several subwatersheds and small watersheds that require a BMP/LID plan at a street block or a parcel level.

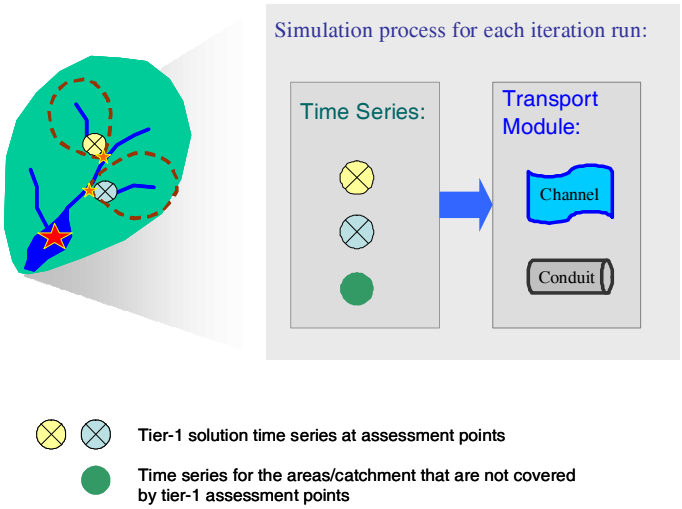

Figure 3. Simulation process for every iteration run.

A hypothetical exercise was carried out to further demonstrate the tiered optimization approach. The objective of this optimization search was to find the lowest cost combinations of BMP options for the desired total phosphorous (TP) load reductions at the specified assessment points. The hypothetical watershed consists of two tier-1 subwatersheds (subwatersheds A and B in Figure 4 below), each with three sets of BMP treatment trains. Each train has an infiltration facility and a detention pond in series. Subwatershed A directly drains to the watershed outlet, while subwatershed B is further upstream and drains to the watershed outlet through a conduit. Figure 4 depicts the entire watershed layout.

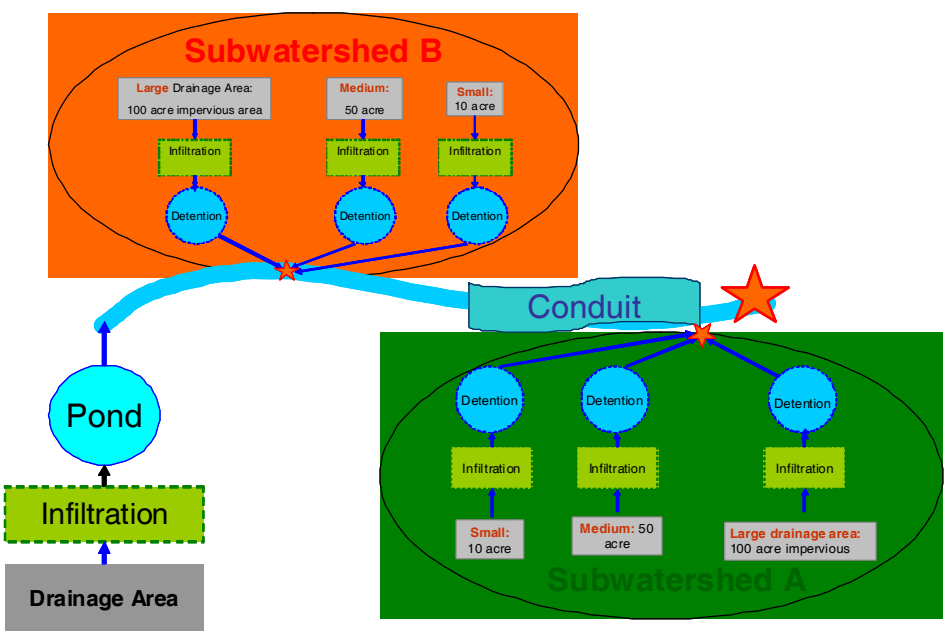

Figure 4. Tiered watershed schematic.

For the tier-1 optimization analysis, the decision variables are the sizes of the infiltration and detention ponds. The outcome of the tier-1 optimization analysis is the identification of optimal solutions along the cost-effectiveness curves shown in red and green diamonds in Figure 5.

Each optimal solution on the tier-1 cost-effectiveness curve contains a combination of decision variables that achieve the desired load reduction at the lowest cost. For the tier-2 optimization, the decision variables included the sizes of the BMPs corresponding to the discrete optimal solutions on the two tier-1 cost-effectiveness curves. The search engine is used to find the tier-2 optimal solutions shown as blue squares in Figure 5. Figure 6 shows the decision variable values (normalized by the maximum value) for each optimal solution along the tier-2 cost-effectiveness curve. For example, at the 18 percent tier-2 TP load reduction target, the tier-1 solutions with 20 percent reduction for both subwatersheds A and B were selected, while the upstream infiltration facility and detention pond were not chosen. As the target tier-2 TP load reduction increases, the tier-2 solutions tend to allocate more TP load reduction to the subwatershed A, which directly drains to the watershed outlet. The upstream pond and infiltration facility were selected only at significantly high load reduction targets, preferring pond over infiltration facilities.

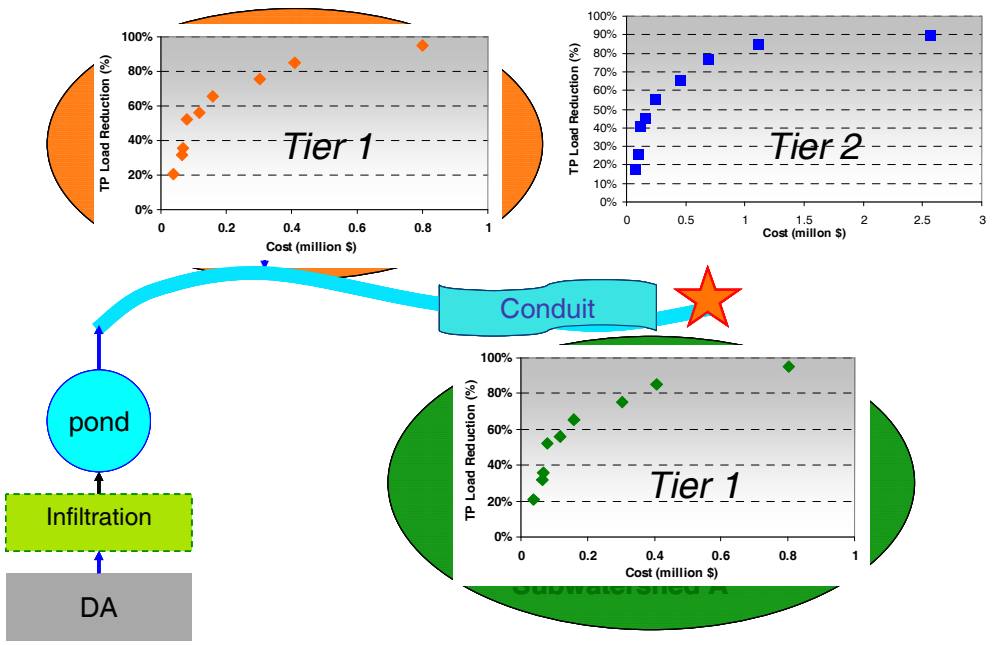

Figure 5. Tier-1 and Tier-2 cost-effectiveness curves.

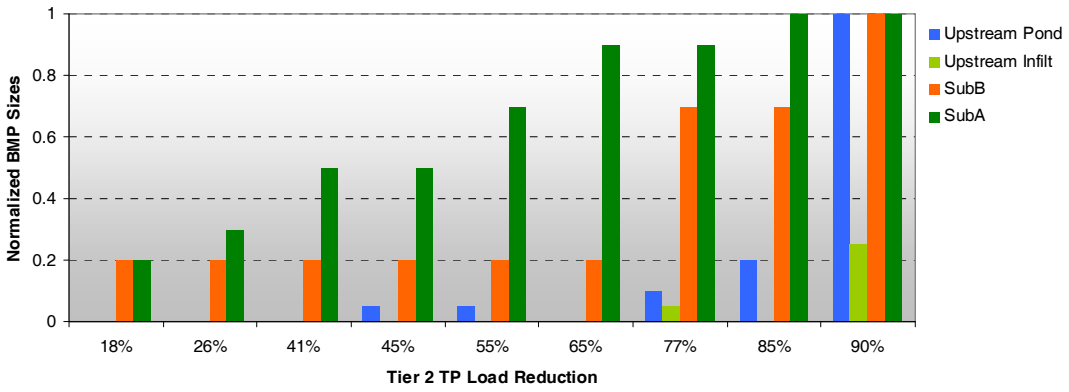

Figure 6. Breakdowns of the tier-2 optimization solutions.

One advantage of the tiered optimization approach is that it significantly improves search efficiency. For this hypothetical case, the total number of solutions for each tier-1 subwatershed is 5^6 (each BMP has 5 possible sizes, and there are 6 potential BMPs in each subwatershed). The possible number of solutions for the tier-2 run is 10^2 x 5^2 (10 tier-1 discrete solutions for both subwatersheds and 5 possible sizes for the two upstream BMPs). The total number of possible combinations using the tiered approach is $5^6 + 5^6 + 10^2 \times 5^2 = 33{,}750$. In comparison, if the optimization is performed in a single run, the total number of combinations of decision options that need to be evaluated would be $5^{14} = 6{,}102{,}515{,}625$ (for the 14 potential BMPs in the entire watershed with five possible sizes for each BMP). This is approximately 180,000 times more searches than that required for the tiered approach. As shown in Figure 3, a tiered optimization can involve transport routing, which can be computationally time consuming. Hence, the reduction of needed search by the tier-approach would also significantly reduce the computational efficiency.

AGGREGATE BMP APPROACH

The BMP module in *SUSTAIN* performs explicit simulation of individual BMP practices for a defined management area. For larger-scale watershed applications, there could be hundreds, even thousands of BMP units scattered throughout the landscape. This poses a challenge in evaluating the collective benefits of distributed BMP units. The required simulations and cost comparisons of these distributed options could significantly burden the modeling effort and require a compromise between the accuracy of the results and computer time required. Hence, an aggregate BMP modeling approach to represent the characteristics of distributed BMPs was developed in *SUSTAIN* aiming at the reduction of computational effort while providing comparable time series data output.

As illustrated in Figure 7, a typical aggregate BMP consists of a series of optional components, including on-site interception, on-site treatment, routing attenuation, and regional storage/treatment. Each component can be used to represent a number of individual BMPs. For example, on-site interception can be represented as a cistern, rain barrel, or green roof, while on-site treatment can be bioretention, porous

pavement, or an infiltration trench. Each individual component can be enabled or disabled on the basis of the desired functionality and can use the BMP template to input the sizes and parameters. Users are asked to input the gross drainage area and the number of units for each aggregate BMP components. For example, as illustrated in Figure 8, one unit bioretention cell with the size of 10 feet long by 10 feet wide is designed to treat runoff from a 0.1-acre drainage area.

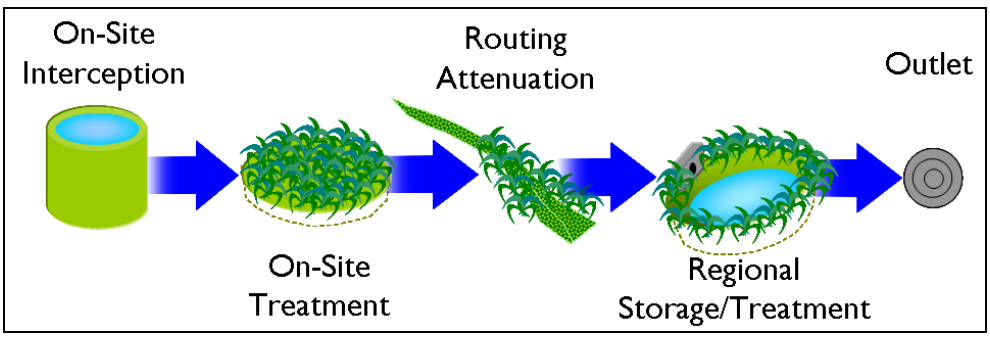

Figure 7. Generic aggregate BMP schematic.

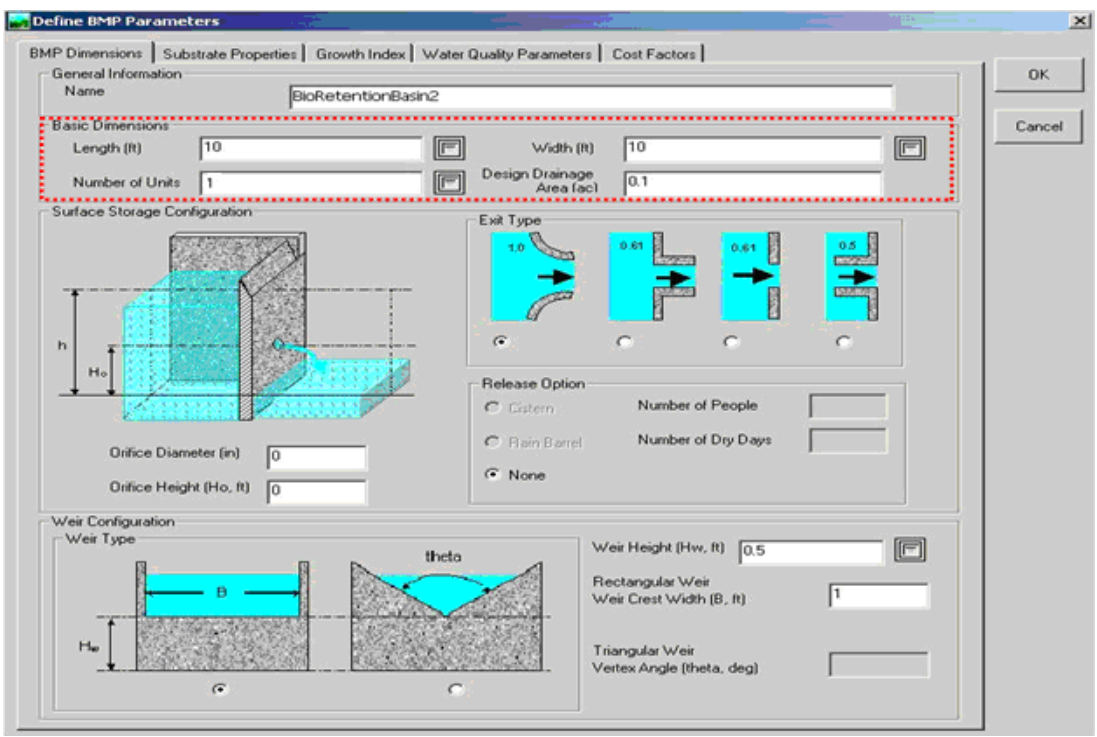

Figure 8. Aggregate BMP sizing interface.

To apply the aggregation procedures, the land use distribution of the drainage area shown in Figure 9 is calculated on the basis of the land use map. Users then assign the percentage of each land use group that could drain to each of the aggregate BMP components (Figure 9). Runoff and pollutant loads from the total drainage area of

each component is lumped and routed through the respective component, preserving the overall routing order shown in Figure 9. The relative scales and sizes of individual BMPs are preserved in the aggregate representation. For the example shown in Figure 8 where one unit bioretention cell with the size of 100 ft^2 is assumed to treat runoff from a 0.1-acre drainage area, one lumped bioretention representing 500 units of bioretention cells with the size of 50,000 square feet would be used to treat runoff from a watershed area of 50 acres.

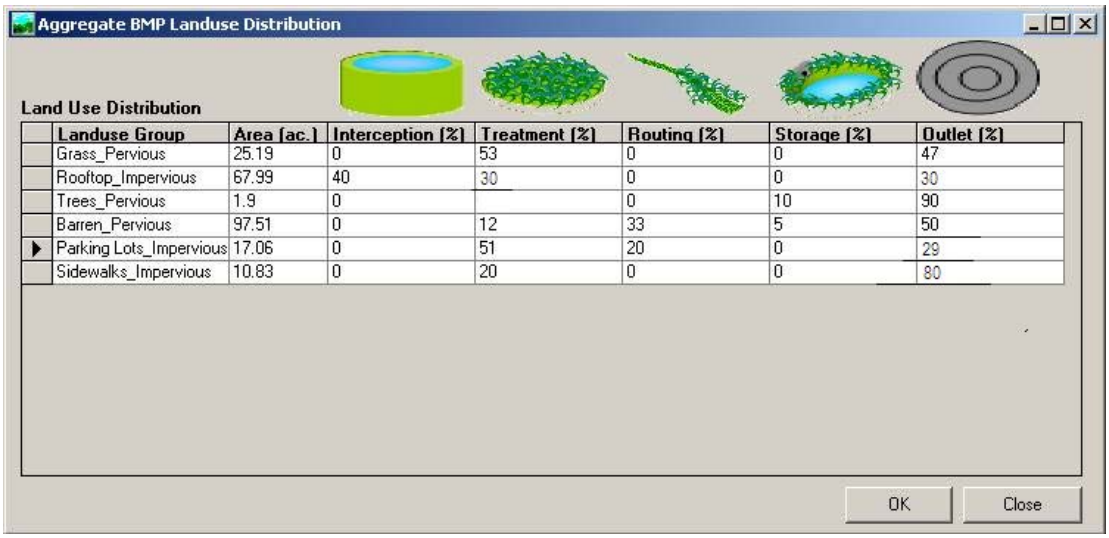

Landuse Group	Area (ac.)	Interception (%)	Treatment (%)	Routing (%)	Storage (%)	Outlet (%)
Grass_Pervious	25.19	0	53	0	0	47
Rooftop_Impervious	67.99	40	30	0	0	30
Trees_Pervious	1.9	0		0	10	90
Barren_Pervious	97.51	0	12	33	5	50
Parking Lots_Impervious	17.06	0	51	20	0	29
Sidewalks_Impervious	10.83	0	20	0	0	80

Figure 9. Example of land use area assignment to aggregate BMP components.

CONCLUSIONS

The tiered optimization procedures implemented in *SUSTAIN* and described in this paper provide an efficient means for developing cost-effective stormwater management solutions in multiple-scale watersheds. The described aggregate BMP modeling approach to represent distributed BMPs at a larger scale has been separately tested, though not described in the paper, and shown to result in a significant reduction of computational effort while providing a comparable time series data output. Both the tiered optimization and aggregate approach are being applied to two watershed case studies and the results will be reported in the near future.

ACKNOWLEDGMENTS

The authors thank Dr. Sabu Paul and Ms. Teresa Rafi of Tetra Tech for their technical contributions to developing *SUSTAIN*.

DISCLAIMER

Any opinions expressed in this paper are those of the author(s) and do not necessarily reflect the official positions and policies of EPA. Any mention of products or trade names does not constitute recommendation for use by EPA.

REFERENCES

Deb, K., A. Pratap, S. Agarwal, and T. Meyarivan. 2002. A fast and elitist multi-objective genetic algorithm: NSGAII. *IEEE Transactions on Evolutionary Computation* 6(2):182–197.

Lai, F.-h.,C. Fan, L, Shoemaker, and R. Field. 2003. Development of a decision-support framework for placement of BMPs in urban watersheds. In *Proceedings of the Water Environment Federation Specialty Conference TMDL 2003*. November 15–19, 2003, Chicago, IL.

Lai, F.-h., L. Shoemaker, and J. Riverson. 2004. Framework for placement of BMP/LID in urban watersheds. In *Proceedings of the LID Conference: Putting the LID on Stormwater Management*, September 21–23, 2004, College Park, MD.

Lai, F.-h., L. Shoemaker, and J. Riverson. 2005. Framework design for BMP placement in urban watersheds. In *Proceedings of the ASCE EWRI World Water and Environmental Congress*. May 15–19, 2005, Anchorage, AK.

Lai, F.-h. J. Zhen, J. Riverson, and L. Shoemaker. 2006. *SUSTAIN*—An evaluation and cost-optimization tool for placement of BMPs. In *Proceedings of the ASCE EWRI World Water and Environmental Congress*. May 21–25, 2006, Omaha, NE.

Lai, F.-h., T. Dai, J. Zhen, K. Alvi, J. Riverson, and L. Shoemaker. 2007. *SUSTAIN*—An EPA BMP process and placement tool for urban watersheds. In *Proceedings of the TMDL Conference*. May 21–25, 2007, Omaha, NE.

Riverson, J., J. Zhen, L. Shoemaker, and F.-h. Lai. 2004. Design of a decision support system for selection and placement of BMPs in urban watersheds. In *Proceedings World Water and Environmental Resources Congress 2004*. June 27–July 1, 2004, Salt Lake City, UT.

Tetra Tech. 2001. Low-Impact Development Management Practices Evaluation Computer Module User's Guide. Prepared for Prince George's County, MD, by Tetra Tech., Fairfax, VA.

Zhen, X., and S.L. Yu. 2004. Optimal location and sizing of stormwater basins at watershed scale. *Journal of Water Resources Planning and Management,* 130(4).

Nexus Projects in Kansas City's Suburban Watersheds

Brian Rast, PE, CFM, PMP[1]

[1]Planning Branch, U.S. Army Corps of Engineers, Kansas City District, 700 Federal Building, 601 East 12th Street, Kansas City, Missouri 64106-2896; PH (816) 389-3337; FAX (816) 389-2025; email: brian.t.rast@usace.army.mil; Member American Society of Civil Engineers (ASCE) and Association of State Floodplain Managers (ASFPM).

ABSTRACT

Two studies in Kansas City will benefit from the U.S. Army Corps of Engineers' emphasis on multipurpose plans and focus on systems. The Upper Turkey Creek and the Brush Creek Basin are both watersheds facing complex circumstances with many stakeholders. The studies are *nexus projects*, or planning efforts, using the watershed perspective to address the array of interrelated water resource issues through solutions that involve Federal, state, and local programs and projects. These nexus projects are defined by several characteristics, especially the strong integration uniting local, state, and Federal initiatives and recommendations for future stormwater management goals in the watersheds, including water quantity and water quality. An important characterization of nexus projects is the establishment of helpful processes in the watersheds, ranging from communication techniques to a decision process for evaluating best management practices and stream corridor restoration measures. The studies are providing forward looking, collaborative planning efforts to assemble multipurpose alternatives to address flood risk management, environmental degradation, and even recreation. The paper shows how nexus projects in an urban setting can lead to watershed management plans that establish useful processes, integrate the cities in achieving the goals of a shared watershed vision, and get the right projects implemented by first building strong partnerships.

INTRODUCTION

No one can live in a vacuum, and similarly, the work in the discipline of planning cannot be done by one. The water resource planners at the U.S. Army Corps of Engineers (Corps) achieve their best planning alternatives for solving water resource problems when these planners include input from the many relevant disciplines affected by a potential construction project. Planning studies include the effort to write a good report that acts as a decision document on the most feasible alternatives. To do this, water resource planners must integrate the ideas from many stakeholders, whether local, state, or Federal agencies, or simply individuals. Only then can the selected plan best represent a balance between human development and environmental sustainability. To do this, planning leaders must fully understand the missions of other agencies that are affected.

In April 2007, floodplain and stormwater managers met to discuss how two Federal agencies coordinate their programs. In their joint recommendations, those floodplain

and stormwater managers sought "to improve flood risk management with the specific focus on the nexus between Corps and FEMA programs" (ASFPM 2007). That simple word, *nexus*, is defined as a means of connection; tie; link; or the core situation. The word can serve to widen our awareness to other programs that planners should be aware of. This paper coins the phrase *nexus projects* to refer to projects that are defined by their need for using a systems approach, requiring interagency cooperation, transcending political boundaries, seeking a multipurpose solution, and/or integrating local, state, and Federal initiatives.

The Corps addresses nexus projects in many mission areas. As an example, look at the great river, the Missouri River, also known as the Big Muddy. The Missouri River Recovery Program seeks to address a nexus with a budget that now rivals the Everglades. The Missouri River has many interests and uses, all of which are considered in the river's recovery program. They include social, economic, historical and cultural uses such as agriculture, commerce, conservation, energy, environmental, natural resources, navigation, recreation, residential, urban uses, and water supply. These uses have resulted in significant impacts to the Missouri River ecosystem. This example involves many states and agencies and is very large nexus project. Nexus projects can be found on smaller scales, such as the situation in two small, tributary watersheds to this river.

The word nexus goes further than acknowledging systems. Nexus projects require an understanding of other agencies' missions, roles, and capabilities. Nexus projects reach beyond the confines of political boundaries, seeking to integrate initiatives. This describes the essence of collaborative planning, as described by the Corps Engineering Circular, *Planning in a Collaborative Environment* (Corps 2005). Projects that apply collaborative planning involve many stakeholders. Since watershed-level projects also require these considerations, they are good case studies for nexus projects.

As further constraints on water resources funding occur at all levels, the need for thought out approaches, or addressing nexus projects, is becoming more important for decision makers dealing with our water resources. Coordinating efforts, leveraging resources, and avoiding duplication are critical. This means the watershed perspective is one system approach that water resources planners must improve at. In 2008, the Corps completed Five Pilot studies on a watershed basis. The large scale watershed studies that the Corps fully funded began in 2006 with the purpose of determining how that type of study assists stakeholders and the Nation. The Five Pilot studies involve multiple states, multiple stakeholders, and one involves Canada. Figure 1 presents the five studies as either states with cross hatching or a large star. The findings of the Five Pilot studies and the two studies appearing in this paper point at the benefits of presenting nexus projects to decision makers for prioritizing funding choices.

Urban areas are another setting where nexus projects can occur. Many Federal agencies are actively addressing urban watersheds. For several years, one of the fastest growing parts of Corps' Civil Works budget has been the restoration of streams in urban environments (Fischenich 2001). This paper presents two studies in Kansas City as examples of nexus projects.

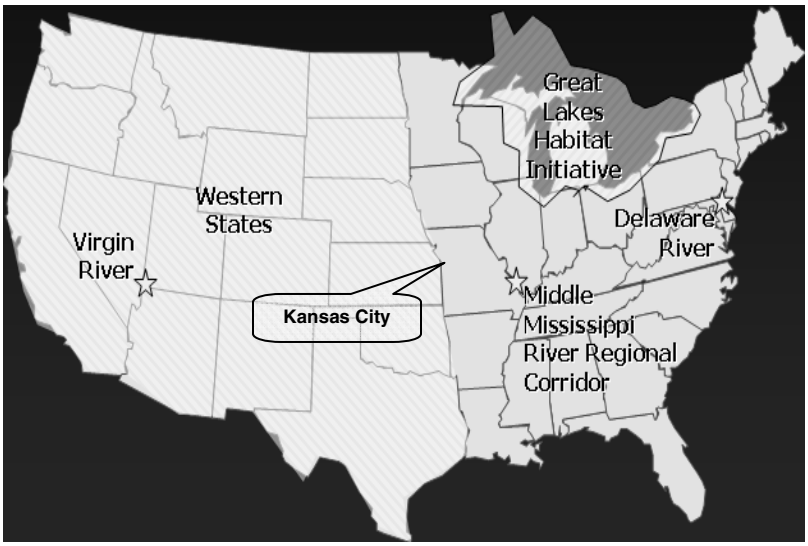

Figure 1. Five Pilot Watershed Studies.

TWO NEXUS PROJECTS

The Brush Creek Basin project and Upper Turkey Creek project are two studies that are nexus projects. Each has a watershed about 30 square miles in area. Their needs are best visualized by a watershed map that both de-emphasizes political boundaries, as shown in Figure 2, and captures the complexity of the situation, later, in Figures 3 and 4. Both creeks flow northeasterly towards Downtown Kansas City, Missouri, which is shown with a star in Figure 2. Nexus projects, like these, do not need to have big watersheds that cover multiple states, as the Five Pilot watershed studies did. Smaller, urban watersheds also face complex circumstances.

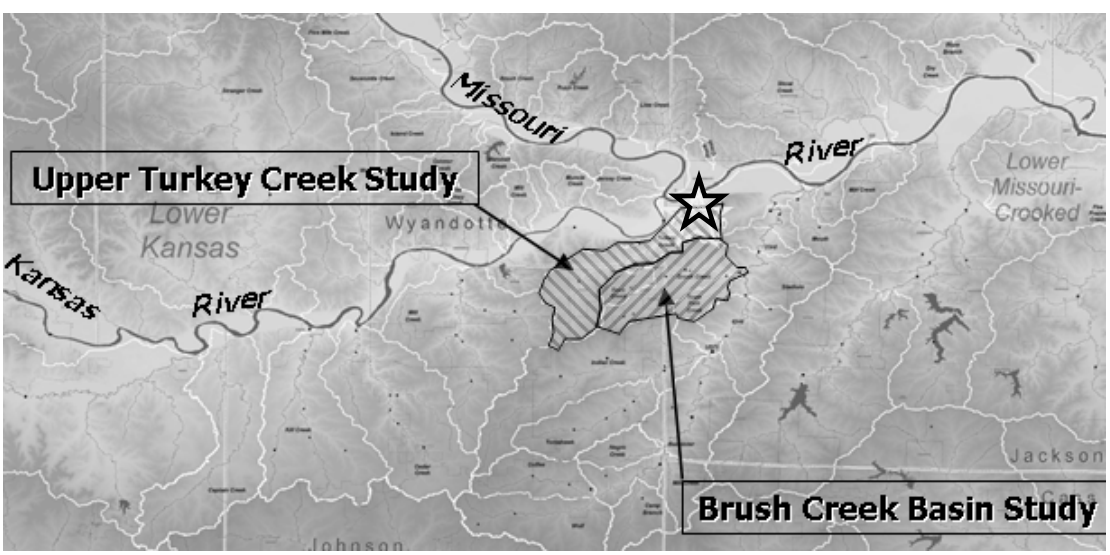

Figure 2. Corps Studies Using Watershed Perspective in Kansas City Metro-Area.

Upper Turkey Creek. This project is an investigation, referred to as a study, that is in the feasibility phase, which is a planning phase. The sponsors who are cost sharing on this project are the City of Merriam, Kansas and the Unified Government of Wyandotte County, Kansas and the City of Kansas City, Kansas. Notable stakeholders include the Downtown Merriam Partnership, the Merriam Drainage District, and the Turkey Creek Coalition. The historical circumstances include a significant flood in 1998 that both cause flood damages and endangered lives as water overtopped Interstate 35. $12 million in flood damages occurred in Merriam's downtown reach, and Interstate 35 overtopped in five spots. Downstream, the Corps is currently constructing the Lower Turkey Creek flood project, consisting of a diversion tunnel, over 20-feet in diameter and a channel widening and bridge project. Those sites are not part of the Upper Turkey Creek (UTC) work. The current feasibility study is authorized to address flooding with structural (i.e. channels, floodwalls) and non-structural (i.e. flood warning systems, relocations, buyouts) recommendations. Under the watershed perspective, the study can also address ecosystem restoration, as found acceptable in an urban situation.

UTC is a nexus project because the study involves several small cities in Johnson County and the Unified Government in Wyandotte County. The planning efforts must integrate local efforts and address a variety of stormwater infrastructure. As an example, the study established one contiguous hydraulic model that can evaluate existing conditions and proposed work within both counties as a system.

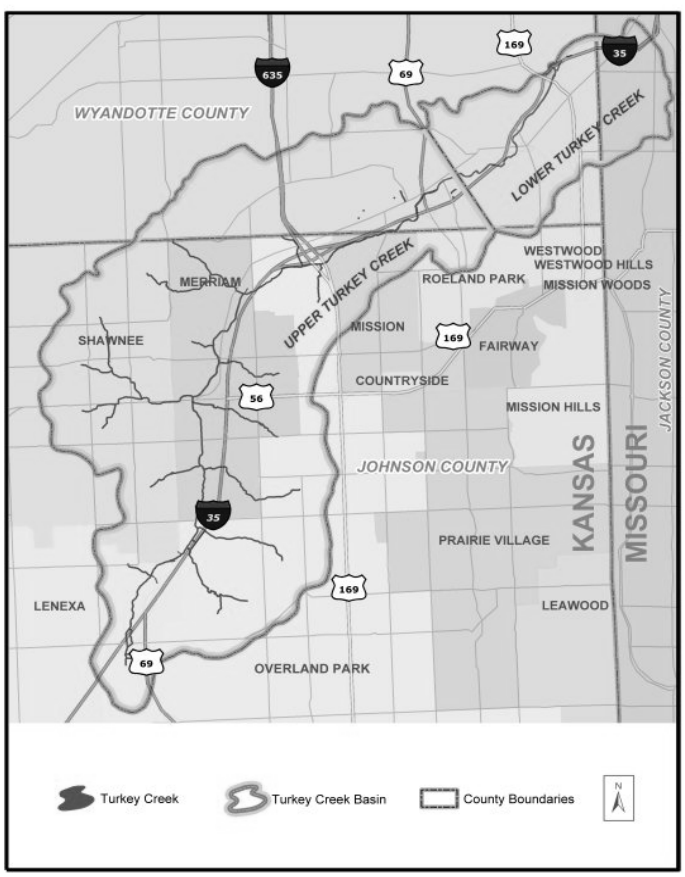

Figure 3. Watershed Map for Turkey Creek.

Another reason this is a nexus project is that the UTC watershed has several agencies and levels of government active here. Activity includes the Corps, the Environmental Protection Agency (EPA), the U. S. Geological Survey (USGS), the Federal Emergency Management Agency (FEMA), and the State of Kansas. EPA has proposed a special area management plan. USGS has been helping Johnson County with studies addressing watershed contaminants, and under the National Flood Insurance Program (NFIP) FEMA is receiving updates to Flood Insurance Rate Maps (FIRMs) for all of Johnson

County. The State has expressed concerns with water quality in a Use Attainability Assessment. All of the technical planners from many disciplines and from the many agencies must work openly, so the need is to provide a framework for interagency cooperation.

Brush Creek Basin. This project is also an investigation in feasibility phase. The sponsors sharing the cost are Johnson County, Kansas and the City of Kansas City, Missouri. Stakeholders include the Brush Creek Community Partners. The history of Brush Creek is well known in this region for the flood of 1977, which unfortunately resulted in the deaths of 25 people. Over $66 million in flood damages resulted, including damages in the Country Club Plaza shopping district. In 1996 the Corps and Kansas City completed construction of a $48 million channelization project.



Figure 4. Watershed Map for Brush Creek.

However, in 1998 the creek flooded again and 8 people died downstream of the project. The feasibility study has a multipurpose authorization, addressing flooding and allied purposes, possibly water quality and recreation. This planning effort recognizes the combined sewer overflows and the non-point source problem identified by the USGS in a recent study of the Blue River watershed, of which Brush Creek is a sub-basin of (Wilkison 2006).

The Brush Creek Basin (BCB) study is a nexus project, because this project involves two states, and this means the need is to overcome this separation and integrate the fractured local efforts. Additional complexities include the need to recognize the

water quality goals that must address not only combined sewer overflows and sanitary sewer overflows, as regulated by the EPA, but especially the non-point sources throughout the watershed. USGS specifically pointed out the degree of impairment of the streams and the effects on water quality, explaining that half of the problem is non-point sources. Best management practices (BMPs) are being implemented by many of the cities, and the Corps has assisted in planning some using the funding program, Planning Assistance to States, within the Rock Creek tributary for the City of Mission, Kansas. Johnson County's strong stormwater management program has aided smaller cities in implementing some BMPs. The watershed's planners understand the need to look beyond their own jurisdictions to implement solutions. All of these are evidence of the presence of a nexus project.

CHARACTERISTICS OF NEXUS PROJECTS

Developing Characteristics. The idea of nexus projects is characterized by water resource initiatives that develop by

- acknowledging the systems approach
    - transcending political boundaries
    - managing stormwater comprehensively
- integrating efforts by local, state, tribal, & Federal agencies
    - avoiding repetitive efforts or combining initiatives
    - leveraging funds & grants
    - requiring interagency cooperation
- considering multipurpose solutions
    - pursuing sustainable projects
    - addressing environmental conditions with creative and compatible alternatives that balance with economic development
- establishing useful processes to aid in achieving long-term goals
    - engaging in collaborative planning
    - applying processes that will find and evaluate alternatives that meet agreed objectives

The planners at local governments, the state level, the tribes, and the Federal agencies must be aware of when there is a significant nexus. A nexus among their mission statements. A nexus for water quality goals. For the Corps planners, this means realizing that urban water quality cannot be trivialized. For planners in EPA, this means realizing flood hazards overlap with local environmental priorities. For all, this may mean re-examining transportation to enhance multipurpose alternatives. Planners must be aware of the nexus surrounding infrastructure to find the most sustainable alternatives. In pursuing this concept of the nexus among cities, states, tribes, or agencies, the many disciplines involved in solving water resource planning

problems should strive to lay down a process to implement best practices in any system.

A closer look will explain why BCB and UTC have prominent nexus project characteristics. The two watersheds are experiencing the same prevalent problems, flooding concerns and environmental degradation associated with urbanization. These nexus projects are developing because planners are acknowledging the main characteristics. The cities are reaching out from their political boundaries. Cities are interested in stormwater management alternatives. Stakeholders are voicing their desire to improve the environment. Collaboration is happening. Tax payers are happier seeing an interest in reducing repetitive efforts, and they realize that funds can be invested better by applying multipurpose measures and by wrapping these studies into comprehensive watershed management plans or floodplain management plans. In fact, the studies call for defining and pursuing specific processes inside watershed management plans that are proving very valuable.

Systems As a Characteristic. The Corps' acknowledgement of nexus projects has grown and is leading to more guidance about using a systems approach. In the mid-1990s, a priority mission for the Corps' budget became restoring the environment. Planning procedures show increasing concern for watersheds and ecosystem restoration between the late 1990s and the current Water Resources Development Act of 2007. Within the Corps, the ecosystem restoration mission now has a recognized Planning Center of Expertise. The Corps understands the need for having the planning discipline address nexus projects. More recently, the Chief of Engineers has emphasized the need for a systems approach, and for these two studies in Kansas City, this means applying a watershed perspective. Systems appeared specifically in first of four themes in the Chief's *Actions for Change* (Corps 2008), which enhances the version that first appeared in August 2006:

Theme 1: Comprehensive Systems Approach. In space, time, and function: Use a flexible and adaptive system in conjunction with all stakeholders/partners to facilitate collaborative planning, design, and construction.

> *Action 1 -- Employ an integrated, comprehensive, systems-based approach.*
>
> *Action 5 -- Employ adaptive planning and engineering systems.*
>
> *Action 6 -- Focus on sustainability.*

This idea of a systems approach, or watershed perspective, is in harmony with this concept of nexus projects. The relevance of nexus projects and systems continues to mature.

When Congress authorizes investigations by the Corps, the degree to which a study examines watershed level work may be described in several degrees. In the first degree, a study, or "investigation," may use a watershed perspective, as explained in *Policy Guidance Letter #61* (Corps 1999). In the second degree, pure watershed planning work produces a watershed study and sometimes a watershed management plan. A draft engineering circular (EC) for these true watershed studies is due to come out in the spring of 2009 (Corps 2007). The EC explains that the Corps may lead the study or may be simply a team member in the effort. The Federal

government shows an incentive for addressing such planning needs with an additional 10% cost share, or 75% total cost share that a true watershed planning effort is eligible for, versus the normal 65% for most studies. These first two degrees of watershed level work can be compared to what occurs frequently at the local level: Stormwater master plans attempt to provide a city or county with a watershed perspective. However these local master plans often are constrained by political boundaries and stop short of reaching out to the watershed borders. In this third degree, what results is a list of capital improvement projects, prioritized by some criteria other than the needs of a watershed. Often the focus is on very localized problems that get just a band aid, even though overall watershed health is at stake.

Watershed planning is an efficient and effective way to address the problems of urban stormwater management, which are sometimes nexus projects. Since the 1990s, much has developed at the Corps for nexus projects that are in the watershed planning arena. More recently, the science for detecting water quality parameters has also been refined. This is important in stormwater management as this allows engineers and scientist to test implementation with better water quality sampling and use adaptive management to improve. Both of these facts are relevant for these watershed projects.

The Multipurpose Characteristic. This is another strong characteristic of nexus projects. An urban stream corridor is a good example for examining multipurpose alternatives. The Corps now recognizes benefits in combining missions, for example, the "marriage" of business lines, unifying corrective measures from ecosystem restoration mission and the flood risk management mission into a suite of alternatives that would address a given water resources problem. Recreation is another, albeit more minor, consideration, and recreation may be used to address transportation in the multipurpose nexus characteristic.

As an example, consider transportation in terms of bike trails. As Gilbert White, one of the fathers of floodplain management, observed: Do not put the parks on the hilltops, put them in the stream corridors. Planners have observed this since the 1960s. If they can serve as parks, the stream corridors can serve as linear parks, including hiking and biking trails. In harmony with this, the Mid-America Regional Council (MARC) established a master plan, called their *MetroGreen* trails system, and Johnson County and associated cities have embraced the idea with their *Streamway Parks*. This concept is even more important when you consider other facts and what might encourage use by bicyclists that might commute. Streamway trails have a less variable, lower grade compared to the roads laid out in a grid that inevitably include a roller-coaster ride on hills and valleys. Not to mention all the intersections requiring starts and stops. As far as efficiency in moving, the lowest demand for force is in the valleys, which is what the railroads have known for more than a century. The point is that the communities could amplify the amenity of a stream corridor, when they include hike and bike trails in combination with flooding and environmental issues, and they can establish a much more biker friendly area than the current situation, where bikers on UTC must brave two lane roads with trucks supporting the industrial road traffic. Who knows how popular enabling such a corridor along UTC would be considering the fact Turkey Creek parallels the main

interstate connecting the county having the highest income in the State of Kansas with both Kansas Citys' downtowns. A final thing worth mentioning is how the stream corridors could double as utility corridors too, as many do already with sanitary sewers, and the trails could double as equipment paths for comprehensive maintenance. Multipurpose projects extend beyond water quantity and water quality, as transportation issues also are relevant when striving for sustainable solutions, considering the need to reduce our carbon footprints and basically just survive the high cost of gasoline.

The Corps is attempting to unite the efforts in these watersheds with these nexus projects in light of multipurpose needs. For the BCB study, the planners are recognizing that the alternatives identified in the planning phase may be either implemented in the short-term with local funding or constructed later with Corps assistance. Issues span the stormwater spectrum, from water quantity to water quality, while touching on transportation and recreation. The issues and players make these nexus projects.

The UTC study is further along in feasibility phase. Planners have taken the hydraulic and hydrologic models used for the FEMA FIRM updates and expanded their use to evaluate a variety of alternatives that reduce flood hazards for several reaches. The current set of alternatives for urban stream corridors, in Merriam's downtown reach and in the vicinity of the Unified Government's Roe Lane Industrial Park, could be levees or floodwalls measures to protect property. Another alternative could be channel widening with minor ecosystem restoration of habitat and possible buyouts or relocations, as compatible with stream corridor restoration mentioned earlier. State flood hazard mitigation funding has been available for that alternative; however, the local residents and/or businesses must be willing to go forward with this. In the short-term, this would be a very big step for those affected by such an extreme alternative. Planners are pointing out the trade-off on UTC: gaining a channelized reach similar to the current Brush Creek Federal project with little environmental value and ignoring possible improvements that might address urban degradation. For UTC structural alternatives, more likely is that a combination of channelization and floodwalls may be most feasible. Although in the long-term, say 50 to 100 years out, planning goals for reclaiming land along the stream corridor throughout the watershed could be identified.

Both studies are looking at the possibility of multipurpose stream corridors. These multipurpose, nexus projects can include recreation in the form of trails. The Corps can include recreation for up to 10% of the total project cost. With the cost of alternatives currently averaging a million dollars, asphalt biking trails would be a small addition that could be covered in the cost sharing agreement. Again, a nexus project addresses complex circumstances and uses collaborative planning to find similar, acceptable multipurpose projects.

In Figure 5, the case for a multipurpose project is made on UTC. The variety of beneficial functions of stream corridors or floodplains, in alignment with the missions of many agencies, could be addressed by ecosystem restoration. The benefits are shown as the arbitrarily chosen symbols of fish, birds, or turtles, representing the respective amount of aquatic habitat restored, as reasonably acceptable for the urban

stakeholders that need these. Multipurpose alternatives have the most maximized benefits, as shown in the final column at the bottom.

Named Alt.s	Measure	Mission Area	Cost	Benefits
Alt. 1	Channelization Only	Flood Risk Management.		
Alt. 2	Levees & Flood Walls Only	Flood Risk Management.		
Alt. 3	Combo: Channelization with Levees & Flood Walls	Flood Risk Management.		
Un-named	Bank Stabilization	Ecosystem Restoration		
Un-named	Restore Streamway (Native Vegetation, Wetlands)	Ecosystem Restoration		
Un-named	**Combo (channel benching), Relocations, & Streamway Restoration**	**Multipurpose** FRM, ER, & Recreation		

Figure 5. Initial Planning Alternatives for Upper Turkey Creek.

The finalize details about both planning projects' multipurpose analysis will appear in their respective decision documents, the feasibility reports, but much public involvement work remains. Producing these products takes time because of the interaction needed among many stakeholders. Funding comes intermittently. Both facts can delay planning projects. The UTC feasibility report will be finalized after significant public involvement occurs in 2009 and will likely see design work on acceptable alternatives in late 2010. BCB is about a year or so behind UTC, however planning work is introducing useful tools for the local cities and counties to use, as described below. Similar to UTC, the BCB planners are seeking feedback via various public involvement techniques to gage acceptability of alternatives.

THE PROCESSES AS A CHARACTERISTIC OF NEXUS PROJECTS

The most prominent characteristic that allows nexus projects to develop are the various processes that contribute to wise planning and development. These processes include communication tools: maps, geographic information systems, on-line maps, websites, collaborative web tools like e-rooms, and especially documents such as watershed management plans or floodplain management plans. Another process is getting a group to reach consensus on the right organizational structure for the area, whether a floodplain or a watershed. A final process that is needed is one that evaluates, and sets the priority for, water resource measures that provide the most benefits per dollar of investment.

Communication Processes. As a first example, the damage to property and the threat of loss of life due to flooding leads to useful communication process found in

the flood insurance rate maps (FIRMs) under FEMA's National Flood Insurance Program. Both BCB and UTC are affected by Johnson County's county-wide revisions to the FIRMs. From year-to-year for the same frequency of storm, rising water surface elevations at any one location on a stream comes with the development of any upstream land to more impervious conditions. Many downstream creeks have serious flooding concerns. ASFPM points out this serious issue with one of their mottos, "Today's floodplain is not tomorrow's floodplain." The revised FIRMs show continuous reaches of homes and business inundated by the base flood's water surface extents, and this helps define the first set of opportunities. If the base flood is the extents of inundation that the public agrees to use as a screening tool for achieving some objectives, then several reaches of streams are already identified for possible Federal interest-multipurpose project sites. However, FIRMs are just one communication process to be aware of.

These nexus projects develop because several communication processes contribute to their momentum. Communication techniques, such as web tools and geographic information systems share information quickly and transparently. However, creating and using a watershed management plan (WMP), or a floodplain management plan, allows them to unite and begin to achieve long-term goals. A WMP is a living document that looks at a vision associated with a specific planning horizon, such as 50 to 100 years. The WMP documents all processes for identifying the best project sites for environmental improvements and for resolving real estate issues. This alone is not enough.

Processes & Organizational Structure. Additional processes must be addressed, especially the need for an organizational structures for managing any WMP. Without identifying an organizational structure, the WMP would be simply one more study that collects dust on a shelf. This group must be funded locally to have any endurance. The organizational structure will manage communication techniques, such as web tools, maps, on-line forums and calendars for communicating meeting dates. The Corps' Five Pilot watershed studies have shown that going through these processes and funding these types of collaborative software tools yield benefits, including active participation and contributions from stakeholders to build consensus, facilitate implementation, and head in the direction of the goals agreed upon. Also, the Five Pilot studies have shown that these nexus projects need Federal investment to establish these processes.

Both the BCB and UTC studies are striving to establish vision, mission, goals & objectives shared among the stakeholders in the watersheds, and this is a process that requires patience. Figure 6 below illustrates the Three-Prong Approach, which is the process that the BCB project is using. The figure shows a conceptual timeline for these three prongs. The Corps, represented in the figure with the hatched boxes, is working through a planning effort and identifying nexus projects that can be either implemented by the locals or other projects that may be cost shared with the Federal government. The Three-Prong Approach is being launched under the coordination of Johnson County, Kansas, the City of Kansas City, Missouri, and the Mid-America Regional Council (MARC), with assistance from the Corps. The success that they have had can be attributed partially to the forum they are using, called the Brush

Creek Coordinating Committee (BCCC). The BCCC has convened many stakeholders and captured a vision. This is a framework of collaboration, which is the heart of the integrated effort. Throughout 2007 and 2008, the BCCC has met monthly to gradually establish the vision and mission statements. Kansas City, Missouri launched the BCCC in the 1980s. The BCCC has a diversity of technical people involved, ranging from biologists, to parks staff, to engineers. MARC has acted to facilitate the meetings and help the BCB study establish needed management measures and processes, although the formation of the BCCC was a needed process in itself.

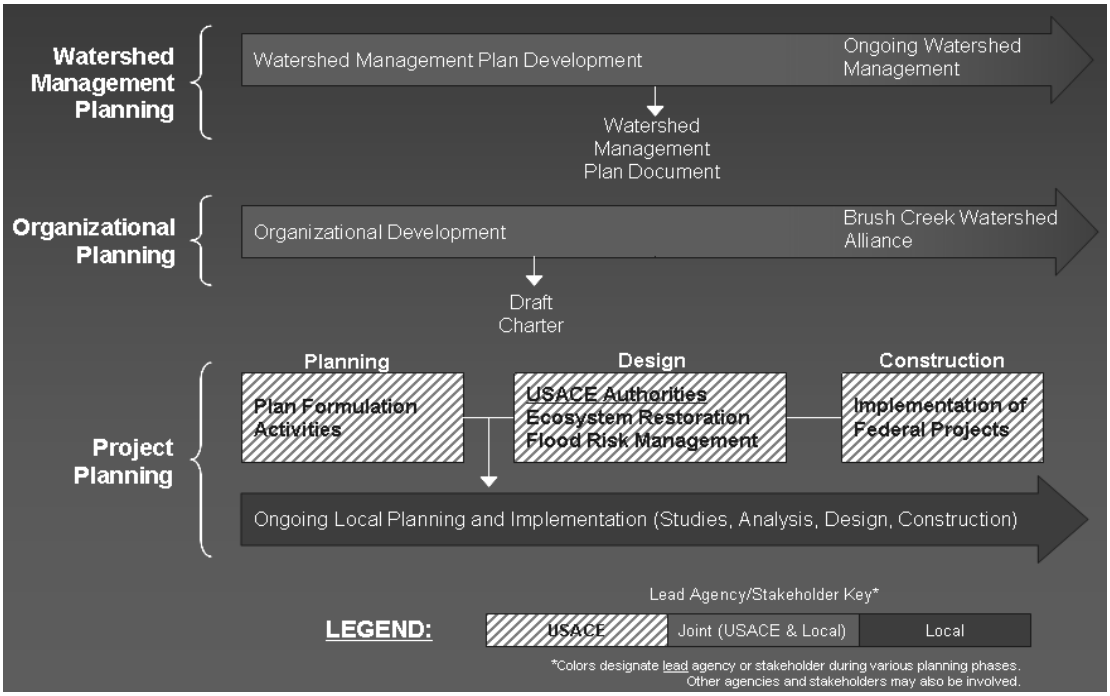

Figure 6. Brush Creek's Process: The Three-Prong Approach.

The persistence of the planners that have given time to the collaborative effort on the BCB planning work has allowed them to create meaningful vision and mission statements and goals:

Vision Statement: *A healthy, sustainable Brush Creek Watershed, where communities work together to protect, restore, and enhance resources in a cost effective manner.*

Mission Statement: *Create a sustainable watershed employing a balanced approach to manage resources and infrastructure while building a healthy community.*

Goals: Manage flood risk; improve water quality; preserve, enhance, and restore riparian and aquatic ecosystems; promote and enhance recreational opportunities; establish and implement organizational framework for watershed management; increase public education, understanding, and participation in watershed stewardship; promote sustainable economic development. Goals have also been sorted to these themes: *Environmental Design & Construction, Advocacy & Education, Integrated Collaborative Management, Economic Development.*

Objectives: The BCCC has identified only qualitative objectives at this time.

The Ultimate Characteristic of Nexus Projects: A Decision Process. A decision process is the most valuable process that defines nexus projects. For BCB and UTC, evaluating the urban environmental nexus can address the Federal interest and unite the constituents in the watersheds. The biggest process that defines these as nexus projects is the one that helps identify the water resource solutions with the most benefits for urban stormwater.

This means addressing not just flooding but also water quality conditions, which currently has the attention of many. In parts of each watershed, combined sewers are being addressed as the cities seek to comply with the Clean Water Act. Kansas City, Missouri is preparing to spend billions of dollars to address combined sewer overflows, or CSOs, with their Wet Weather Program and KC-ONE. USGS studies indicate a large part of the water quality issues are non-point sources, though. A significant effort went into the USGS reports on stream health on the Blue River (Wilkison 2006). The stormwater program under Johnson County, Kansas Public Works has several on-going USGS studies for Johnson County watersheds (Rasmussen 2008). On UTC, EPA proposed special area management plan, or SAMP, which could begin to establish firm guidelines to start to address water quality. On a National scale, EPA released a green infrastructure memo (Grumbles 2007) that acknowledges the structural BMPs, such as Kansas City's *10,000 Rain Gardens* and also including those the Corps planned for Mission, Kansas, as appropriate solutions to water quality challenges. The situational awareness continues: American Public Works Association (APWA) and MARC released a *BMP Manual*. Even the U.S. Department of Agriculture, through the Forest Service, contributes to addressing physical component of water quality: In the *2006 Ten-year Action Plan National Urban & Community Forestry Advisory Council* the goal is to offer grants and to recognize "urban and community trees and forests are vital parts of America's infrastructure and essential to the well-being of our individual human health and welfare." Communities addressing urban forest will see improved urban environments, where benefits include cooler summer air, warmer homes in winter, cleaner air and water, quieter streets, peaceful neighborhoods, healthy and productive local economies. Finally, a situational awareness identifies good changes in regional real estate practices to address water quality. Setback ordinances are being implemented by several cities in developing areas. Similar to APWA's *Stormwater Design Criteria* stream setback details, one by one, cities in the Metro-Area have adopted stream setback ordinances for the developing areas of Overland Park, Lenexa, and Kansas City, Missouri. However, the areas already developed are the real challenge, and land trusts, generally not accepted in the area in the past, may be a useful measure to solve the problems in these nexus projects. Within the Kansas City Metro-Area, the interest in stormwater is clearly a part of needed situational awareness.

The state of watershed protection for both watersheds begs the question where is the most cost effective place to begin? Downstream stakeholders bear the flood waters that runoff of sites upstream. Development has been degrading urban water quality gradually overtime. A helpful step is to establish a decision process for addressing these issues. A good process that does a good job of telling the story, and as a result, can unify the stakeholders, is a characteristic of nexus projects.

The planners at the Corps can offer at least two decision processes. Flood damage analysis is one, and the process uses projected water surface profiles and a thorough economic analysis of flood damages. This is the most well known strength that the Corps offers in the flood risk management mission area. The process that is less well known is the ecosystem restoration mission. This may be the process that can help stakeholders unify and want to stand behind a given set of water resource improvements.

But first, what is urban ecosystem restoration? The idea of restoring the ecologic conditions to pre-settlement time is not realistic. The definition of urban ecosystem restoration is not an easily defined thing. This is a grey area of many different opinions, and none are perfect. The definition also varies with location, and views vary depending on which lenses of the various groups or agencies are used to see it. That definition of how to balance economic development and environment is needed, and time must be spent collecting input.

For the Kansas City Metro-Area, two areas of focus in addressing a decision process that involves urban ecosystem restoration are BMPs and wise floodplain management. First, consider BMPs. Land use practices across the Nation have increasingly acknowledged a practice of keeping rain where it falls over the past 40 years. Low impact development, or LIDs, curb-cuts, and rain gardens are examples of BMPs. Secondly, consider the wise use of floodplain management in light of the condition of the urban stream. These streams are characterized by highly eroded banks with the channel cut-off from the floodplain. A sustainable condition in the stream corridors is needed. A nexus of many cities, states, and agencies exists in the stream corridors. Ecosystem restoration priorities for the Nation typically center on endangered resources, where significance can be addressed, and these are not found in urban areas. However, when sustainability is considered, the question becomes what are we not doing that could reduce adverse anthropogenic effects to the environment? Also relevant, urban ecosystem restoration brings back the intangible socio-economic benefits of having a natural retreat in the proximity of stakeholders in urban areas. Looking at the mission statements of more than one single agency again shows the nexus: EPA's sustainable watersheds and Multi-Objective Management, the FEMA NFIP concept behind Beneficial Functions of floodplains, states like Kansas and Missouri that use EPA's 319 grants, and the Corps' variety of programs, including Regional Sediment Management. A decision process might help integrate all these initiatives.

Without a guiding decision process on both BMPs and stream corridor measures, determination of what achieves a watershed vision can be a vague and wandering search, but consider the stream corridors more closely. Alternatives in the stream corridors have the multipurpose opportunity to address flooding and erosion. Over a 50 or 100 year timeframe, the re-establishment of stream buffers in these developed areas would open the door to more sustainable solutions to the erosion of stream banks. Opportunities have been revealed with the recent FEMA FIRM updates showing continuous reaches of properties subject to flooding from the 1% event. Restoration of a contiguous reach is of more significance than a single property. Within watershed management plans, the cities could gradually, over many years,

reclaim at risk properties in these floodplains and use those lands to address the water quality challenges. A helpful step is to establish a decision process for addressing these stream corridors and BMPs.

To define a decision process, consider the nexus of all the agencies and cities on BCB and UTC (see Figure 7) and reflect on the variety of mission statements each has. The Corps cannot ignore urban water quality. For the Corps, water quality measures fit best under ecosystem restoration. If you are a municipality that shares a watershed with others, how do you make the decision for whether to apply BMPs or whether to apply bank stabilization for eroding creek banks? A process is needed that juxtaposes these and describes what output you would get for some land based BMPs versus the improvements to establish a sustainable stream corridor. Maybe a combination is the best approach?

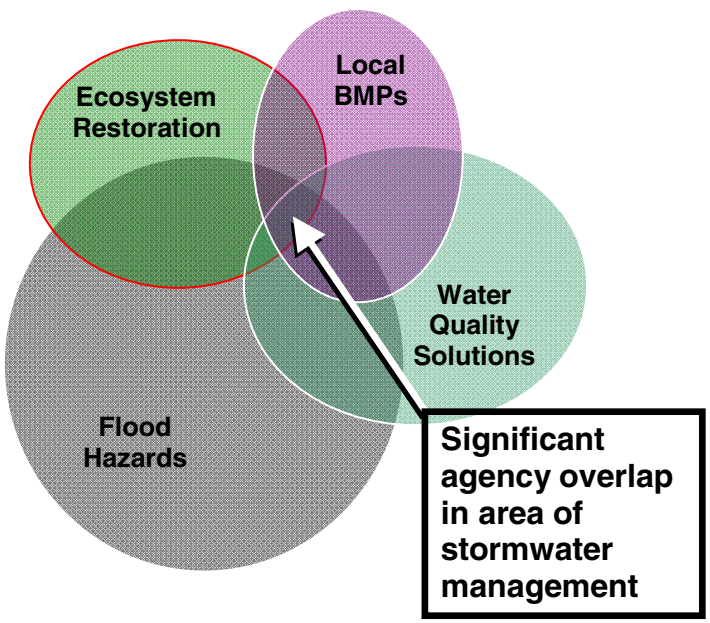

Figure 7. Relevant Water Resource Funding Nexus

The most prevalent water quality contaminant is sediment, because the sediments serve to transport the remaining pantheon of water quality offenders. In urban watersheds, this comes from the changed conditions caused by land development that goes from pervious conditions, such as native planted ground, to impervious conditions, like roofs and pavement. This change increases rainfall runoff. That moves streams out of balance, specifically in how flows and sediment react (Lane 1955). Indeed, the rate of loss of sediment in urban watersheds can be ten times greater than agricultural watersheds. Therefore, any management measures that can address this will help.

The Decision Process. A process for evaluating which alternatives provide the most benefits for the buck exists. The measures must be chosen based on how well they address both water quality and water quantity problems. If the stakeholders know which measures provide the best results, they can make informed decisions about the alternatives that include combinations of these measures. A process that tells the whole story of the watershed is missing from simple capital improvement programs that ignore watershed boundaries. A good process is presented in the principles behind cost effective analysis (Robinson 1995). So to answer the question on how to juxtapose the various BMPs on the UTC project, the Corps offers a process that applies two tools to address environmental degradation in the urban watersheds.

First, from the ecologic or biologic disciplines, a conceptual model is needed that describes the environmental degradation in terms of aquatic habitat. A conceptual model is a tentative description of a system that serves as a basis for intellectual organization and represents the modeler's current understanding of the relevant system processes and characteristics (Fischenich 2008).

This would be a habitat model that could satisfy the Corps' ecosystem restoration mission requirements and characterize water quality conditions. The habitat model chosen is going to make the difference. For the Corps, the habitat model must tie to the aquatic habitat. The model should also be based on watershed variables. Finally, the model should be locally accepted. The UTC planners are proposing the Kansas Department of Wildlife and Parks' habitat model, *Subjective Evaluation of Aquatic Habitat* (KDWP 2004). Combining this with the economic discipline is the step that makes the process begin to take shape.

In 2004 UTC planners began juxtaposing watershed protection measures in an interim report, *Upper Turkey Creek Basin Environmental Restoration Report Feasibility Phase* in August 2004. The report presents a medley of BMPs and stream corridor restoration measures. In 2009, funding will allow the Corps to complete the feasibility report, which will use these initial plan formulation measures and compare them to bank stabilization measures. The planners will show the cost effectiveness of the various alternatives, extending the study beyond the single purpose of flood damage reduction.

The ecosystem restoration measures could be a menu of measures that includes recommendations for treating streambank erosion, or the ecosystem restoration measures may be watershed-wide BMPs that meet the water quality needs under the Clean Water Act. This has been of increasing concern since EPA has begun enforcing rules that apply to municipal separate storm sewer systems (MS4s), and operators of these MS4s must comply with the National Pollutant Discharge Elimination System. Below in Table 1 is a short list of possible measures, or features, which could be formulated into appropriate alternatives and then built to treat the spectrum of stormwater problems, whether attributed to water quantity or water quality.

Second, a cost effectiveness and incremental cost analysis (CE/ICA) is needed for the subject process, and CE/ICA can answer the question of which measures are most effective to achieve an urban watershed's vision. On the UTC feasibility study, the Corps proposes combining the Kansas aquatic habitat model with the CE/ICA done within the IWR-PLAN software. These processes allow the Corps to satisfy the *Principles and Guidelines*: "Efficiency is the extent to which an alternative plan is the most cost effective means of alleviating the specified problems and realizing the specified opportunities, consistent with protecting the Nation's environment." (U.S. Water Resources Council, 1983). At the same time the Corps satisfies the Federal Objective: "The Federal objective of water and related land resources planning is to contribute to national economic development consistent with protecting the Nation's environment, pursuant to National environmental statutes, applicable executive orders, and other Federal planning requirements."

Table 1. Measures for Improving Water Quality.

Streambank Treatments (Corps 1998)	Instream Practices (Corps 1998)	Best Management Practices (BMPs) (APWA 2003)
Bank Shaping and Vegetation	Bank toe stability measures	Filter Strip
Branchpacking and Brushlayering	Bendway Weirs	Native Landscaping (rain gardens)
Coconut Fiber Roll	Boulder and Log Weir	Open Space
Dormant Posts or Dormant Cuttings	Channel Block	
Gabions and Gabion Mattress	Channel Constrictor	Engineered Swales
Hedge - Brush Layering	Cross Channel Log and Revetment	Sand Filters
Joint Planting or Vegetative Riprap	Deflectors	Infiltration Trench
Live Fascines and Wattlings	Grade control structure	Bioretention Filters
Live Siltation	Log Cover (Whole, Half and Slab)	
Live Staking	Longitudinally Peaked Stone Toe Protection (LPSTP)	Extended Detention Wetlands
Log, Rootwad and Boulder Revetment (Native Material Revetment)	Lunker Structure	Wetland Treatment Systems
Overhanging Bank Cove	Newbury Rock Riffle	Pervious Pavement
Riprap	Rock and Wood Spur Dikes	Wet Ponds
Rootwad/Rootball	Tree Drop Deflector and other Midchannel Deflectors	
Stream Debrushing, Brush Bundles and Brush Mats	Vortex Rock Weir with Floating Logs	
Vegetation/Revegetation	"W" Rock Weir	
	Water Control Structure	

This process is the essence of the role that economics has in environmental planning. As with flood damage reduction, CE/ICA seeks to maximize the net benefits, and helps to answer the decision makers' question of whether the level of output is worth the investment. If improved water quality means better habitat, then decision makers should focus on the units of habitat restored in a watershed, not just the levels of contaminants. A good habitat model applied with a watershed perspective could be a valuable tool for decision makers.

The decision makers typically get an analysis summarized in the graph in Figure 8. Each alternative is compiled of compatible measures that establish a coordinate composed of cost and habitat output. Each proposed alternative has a horizontal component, or environmental output, determined by multiplying the area of the project site by the associated habitat index. This index can be either the U.S. Fish & Wildlife's Habitat Suitability Index from the Habitat Evaluation Procedure, or in the case of the two Kansas watersheds, the Kansas habitat model provides a similar habitat index via the R-value. The area is tied to the width of the stream corridor and the length of stream deemed to be affected directly by the proposed measures. The cost of those measures is the vertical component. A certain stream corridor with proposed measures can be grouped as a single alternative, which would be a single point on the graph. BMPs used throughout the watershed would be assessed by looking at the beneficial affect to a reach of stream that lies downstream from the BMP alternative, in terms of affected area. Together, the graph would include both types, where the BMPs are the solid dots in the Figure 8 example. With the graph complete, some alternative points end up on the cost effective frontier and some are best buys. Both streambank treatments and watershed-wide BMPs address water quality challenges. This process would then capture the intended watershed

perspective, and decision makers, whether local or Federal, could begin focusing first on the measures with the most benefits for aquatic habitat.

Good environmental planning ought to look at the whole problem. Urban stream corridors have disconnected habitat due to erosion and channel incisions. BMPs address a host of other contaminants. The Corps' economic process for evaluating ecosystem restoration measures could be very useful in this case.

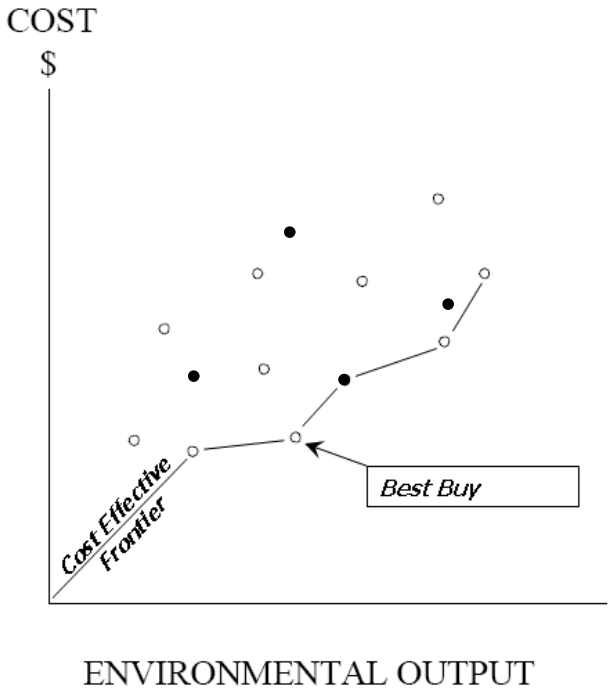

Figure 8: Concept of Cost Effectiveness and Incremental Cost Analysis.

The process described above is needed for nexus projects. As far as the Corps' feasibility study goes, the process defined by the CE/ICA has to be done anyways to evaluate alternatives. When the CE/ICA is done to integrate the efforts in an entire watershed, the reward is a decision tool that provides a means for focusing and coordinating the efforts of local stakeholders. The next process may be an even grander plan that looks at the long-term identification of the easements or property needed for the alternatives. In this regards, the use of geographic information systems could be used to identify needed acquisitions and track the status. As properties become available over 50 or 100 years, they could gradually be acquired.

These two watersheds are recognized as nexus projects, and the stakeholders will benefit from the planning work that will improve the degraded environmental state and reduce flood hazards as well. This is how the Corps can provide planning assistance to show a way to integrate stakeholders and to achieve more sustainable stream corridors throughout the urban watersheds in Kansas City Metro-Area.

CONCLUSION

Water resource planners should recognize the characteristics of nexus projects. They must understand the commitment they require, and they must be patient in taking the time needed for collaboration. They should consider all facets of stormwater management. In doing this, all those involved in the nexus project should see the importance of long-term planning that addresses gradual processes that will achieve the objectives and attain the shared vision. The nexus projects are these watershed studies that are showing how to solve problems for their shared water resources.

The BCB and UTC projects are providing forward looking collaborative planning efforts to the Kansas City Metro-Area. They are establishing and applying a process

for restoring stream corridors is a central theme, and they are defining what urban ecosystem restoration is. Planners are realizing the importance of looking at the 50 to 100-year planning horizon and documenting the goals with a systems approach. A key realization is that urban stream corridors that could be restored are wise floodplain management, and that is also a best management practice. Even without a cost shared project, the Corps will have provided a way forward, allowing locals to work towards their agreed upon vision for sustainable stream corridors. The studies will reduce redundant efforts and leverage funds.

Planning studies are requiring planners to think about the nexus of many things. The decision makers they serve continue to encourage the acknowledgement of the concept of nexus projects. Nexus projects develop because they have characteristics that build strong partnerships during the planning work. The reward from this synergy can benefit many down the road.

REFERENCES

American Public Works Association and Mid-American Regional Council. 2003. *Manual for Best Management Practices for Stormwater Quality*. American Public Works Association, Kansas City Metropolitan Chapter. Sep.

Association of State Floodplain Managers. 2007. *Joint Recommendations on Levee Policy developed by the Association of State Floodplain Managers and the National Association of Flood and Stormwater Management Agencies December 2006*. Flood Risk Policy Summit, 29 April.

Association of State Floodplain Managers. 1996. *Using Multi-Objective Management to Reduce Flood Losses in Your Watershed.* http://www.floods.org/PDF/Using_MOM_in_Watershed.pdf

City of Kansas City, Missouri, Parks Department. 2007. *Brush Creek Parks Master Plan*.

City of Kansas City, MO Water Services Department. 2007. Wet *Weather Solutions Program Home*, website. Kansas City, MO: http://www.kcmo.org/water.nsf/web/defaultww?opendocument

City of Kansas City, Missouri, Wet Weather Solutions Program. 2007. *Green Solutions Position Paper*.

City of Kansas City, Missouri, *Stream Setback Ordinance: Fact Sheet*. Wet Weather Solutions. http://www.kcmo.org/water/KCWetWeatherCityNav/images/pdfs/BasinCoordinatingMeetings/MiddleBlueRiver/MiddleBlueRiverBCC3/setback_HANDOUT_final_011707.pdf

City of Overland Park, Kansas. 2002. *Designation of Stream Corridor*. Unified Development Ordinance, Chapter 18.365.040. http://www.opkansas.org/_Assets/law/opmc/opmc_by_chapter/18-365.pdf

Fischenich, C. (2008). "The Application of Conceptual Models to Ecosystem Restoration." *ERDC/EBA TN-08-1,* U. S. Army Engineer Research and Development Center, Vicksburg, MS.

Fischenich, C. 2001. *Technologies for Urban Stream Restoration and Watershed Management, Ecosystem Management and Restoration, EMRRP Bulletin No. 01-1,* May.

Ecosystem Management and Restoration Research Program. http://www.wes.army.mil/el/emrrp

Grumbles, Benjamin H. 2007. *Memorandum to EPA Regional Administrators, Using Green Infrastructure to Protect Water Quality in Stormwater, CSO, Nonpoint Source and other Water Programs*. 5 Mar.

Robinson, R., Hansen, W., and Orth, K. 1995. *Evaluation of Environmental Investments Procedures Manual Interim: Cost Effectiveness and Incremental Cost Analyses.* Institute for Water Resources, Water Resources Support Center, IWR Report 95-R-1.

Johnson County, Kansas Public Works Department, Stormwater Section. 2005. *Northeast Johnson County Watershed Study*. May.

Johnson County Stormwater Management Program. 2007. Olathe, KS: Johnson County Public Works. http://stormwater.jocogov.org/default.shtml

Kabbes Engineering, Inc & HNTB. August 2004. *Upper Turkey Creek Basin Environmental Restoration Report Feasibility Phase*.

Kansas City Metropolitan Chapter American Public Works Association. 2005. *Division V, Section 5600, Construction and Material Specifications, Storm Drainage Systems & Facilities, Stormwater Standards*.

Kansas Department of Wildlife & Parks Environmental Services Section. 2004. *Subjective Evaluation of Aquatic Habitats*.

Lane, E. W. (1955). "Design of stable channels." *Transactions*, 1234-1279.

Mid-America Regional Council. 2007. *Environmental Programs*. http://www.marc.org/Environment/Water/

Rasmussen, T.J., 2008. *Water quality of streams in Johnson County, Kansas*, 2002-07: U.S. Geological Survey Fact Sheet 2008-3090, 4 p.

Rast, B., 2008. *Brush Creek Basin Flood Damage Reduction & Ecosystem Restoration Kansas City, Missouri and Johnson County, Kansas Feasibility Phase Project Management Plan*. U.S. Army Corps of Engineers Kansas City District. 1 Apr.

Wilkison, D.H., Armstrong, D.J., Norman, R.D., Poulton, B.C., Furlong, E.T., and Zaugg, S.D., 2006. *Water Quality in the Blue River Basin, Kansas City Metropolitan Area, Missouri and Kansas, July 1998 to October 2004*: USGS Scientific Investigation Report 2006-5147, 170.

U.S. Army Corps of Engineers. 2008. *Actions for Change*. Feb.

U.S. Army Corps of Engineers. 2004. *Civil Works Strategic Plan: Fiscal Years 2004-2009*.

U.S. Army Corps of Engineers. 2005. *Engineering Circular, Planning in a Collaborative Environment, EC 1105-2-409*, 31 May.

U.S. Army Corps of Engineers. 2007. *Engineering Circular, Watershed Planning, EC 1105-2-410* (draft), 22 May.

U.S. Army Corps of Engineers. 2000. *Engineering Regulation, Planning Guidance Notebook, ER 1105-2-100*, 22 Apr.

U.S. Army Corps of Engineers. 2007. *Planning Community of Practice, Watershed*, website. http://www.usace.army.mil/cw/cecwcp/psa/watershed.htm

U.S. Army Corps of Engineers. 1999. *Policy Guidance Letter #61- Application of Watershed Perspective to Corps of Engineers Civil Works Programs and Activities*. 27 Jan.

U.S. Army Corps of Engineers Institute for Water Resources. 1998. *Illustrations of Environmental Engineering Features for Planning, IWR Report 98-R-8*. Dec.

U.S. Army Corps of Engineers Kansas City District. 2005. *Brush Creek Basin Flood Damage Reduction & Ecosystem Restoration Kansas City, Missouri and Johnson County, Kansas Reconnaissance Study, Section 905(b) Analysis*. Feb.

U.S. Army Corps of Engineers Kansas City District. 2001. *Upper Turkey Creek Basin Johnson and Wyandotte Counties, Kansas Reconnaissance Study, Section 905(b) Analysis*. Jul.

U.S. Department of Agriculture Natural Resources Conservation Service. 1998. *Stream Visual Assessment Protocol*. National Water and Climate Center, Technical Note 99–1. http://www.nrcs.usda.gov/technical/ECS/aquatic/svapfnl.pdf

U.S. Environmental Protection Agency. 1999. *EPA Rapid Bioassessment Protocol for Habitat Assessment and Physiochemical Parameters of Streams*.

U.S. Environmental Protection Agency. *NPDES*, website. http://cfpub.epa.gov/npdes/allfaqs.cfm?program_id=0#1

U.S. Environmental Protection Agency. 2007. *Wetlands, Oceans, & Watersheds*, website. EPA. http://www.epa.gov/owow/watershed/regulations.html

U.S. Geological Survey. *Watershed Management*, website. 2007. http://water.usgs.gov/wsc/management.html

U.S. Water Resources Council. 1983. Economic and Environmental Principles and Guidelines for Water and Related Land Resources Implementation Studies. March 10.

NON-POINT SOURCE NUTRIENT LOADING IN AN URBAN WATERSHED

Eric Gurr and Fidelia (Ola) Nnadi

University of Central Florida, Civil and Environmental Engineering Department, Orlando Florida; PH: (407) 823-2105; email: egurr@mail.ucf.edu

ABSTRACT

The United States Environmental Protection Agency (EPA) passed the Federal Clean Water Act (CWA) in 1972 which set the framework for the water quality standards for the entire United States. As a result of the CWA many point sources were eliminated, but in the process it became apparent that non-point source loads represented even more of a threat. To further study the physical and chemical characteristics of urban runoff the Nationwide Urban Runoff Program (NURP) was established in 1978. This lead to series of management options, named Best Management Practices (BMPs) which proposed various structural and non-structural methods to reduce nutrient loads.

The present study attempts to generate accurate and effective water quality and quantity data that future stormwater management decisions can be based upon. The main objective of this study is to determine the nutrient loadings into the tributaries of Lake Tohopekaliga, using automatic monitoring sites established throughout the City of Kissimmee, Florida. These monitoring sites were located to monitor subbasins within the watershed such that inflows from outside the city limits can be isolated and external pollutant loads quantified. Additional internal monitoring sites were established to determine the pollutant loads of sections within the city.

The nutrient removal efficiency was performed using both the event mean concentration method and the summation of loads method to check for seasonal variation. Analysis was based on 25 discrete grab samples collected on a bi-monthly basis over a twelve month period. The concentration levels of total nitrogen did not seem to vary significantly from its mean value of 0.90 mg/l throughout the year, while there were some relatively lower values in late spring. The study found that concentration levels of total phosphorus ranged from 0.02 mg/l to 0.48 mg/l, but not in relation to either season or flow volume fluctuations. The wet pond showed no net removals of total nitrogen and was actually found to be releasing total phosphorus to the downstream receiving waters.

Background

Florida is surrounded by water, and its many internal lakes and rivers have long been recognized for their excellent fishing and boating. This notoriety draws land developers to the lake shores to establish residential and commercial infrastructure. The altering of the natural environment during the urbanization of watersheds can cause harmful side effects such as decreased infiltration of rainfall, increased runoff volumes and increased occurrences of flooding. These hydrologic factors lead to streambank erosion which is the main transport mechanism for pollutant export to receiving waterbodies (Schueler, 1987). The influx of these nutrients carried by the runoff from developed watersheds can lead to algae blooms which reduce water quality levels.

The United States Environmental Protection Agency (EPA) passed the Federal Clean Water Act (CWA) in 1972 which set the framework for the water quality standards for the entire United States. As a result of the CWA many point sources were eliminated, but in the process it became apparent that nonpoint source loads represented more than 65 percent of pollutants entering our nation's waterbodies (Rushton and Dye, 1993, Livingston, 1985). Research that began prior to the adoption of the CWA documented that a large source of nonpoint pollution is the runoff from urban and industrial areas (Whipple and Hunter, 1977). The Nationwide Urban Runoff Program (NURP) was established in 1978 to collect basic data on the physical and chemical characteristics of urban runoff across the country (EPA, 1983).

A series of management options, named Best Management Practices (BMPs) were developed to control the pollutants transported in urban runoff (Schueler, 1987). These BMPs can be either maintenance or development practices that do not include the construction of a permanent stormwater management structure like street sweeping or Low Impact Development (LID) which are referred to as "non-structural" or they can be actual ponds, swales or physical processes which are referred to as "structural". The effectiveness of each of these BMPs varies according to the targeted pollutant, pollutant concentration, and site conditions.

Scope and Objectives

The study area encompasses approximately twenty (20) square miles of surface area with a relatively flat topography and poorly drained soils. A mixed land use of residential, commercial and agricultural can be found throughout the City of Kissimmee. Stormwater runoff in the city is conveyed to Lake Tohopekaliga by six (6) distinct tributaries which receive flow from the runoff of their respective watersheds.

The goal of this study is to generate accurate and effective water quality and water quantity data to aid in future stormwater management decisions. Specifically, this study aims to establish automatic monitoring sites throughout the City of Kissimmee, Florida to determine the pollutant loadings into the tributaries of Lake Tohopekaliga. These monitoring sites were located such that inflows from outside the city limits were isolated and external pollutant loads quantified. Also, additional internal monitoring sites were established to determine the pollutant loads of internal sections of the city. These internal monitoring sites were used to determine the variable pollutant removal efficiencies and hydraulic fluctuations of natural, irregular riverine systems.

The objective of this paper was to create a pilot study to verify the results of a nationwide urban runoff program conducted by the Environmental Protection Agency which rated permanent wet pool detention basins as very effective in reducing nutrients from urban runoff (EPA 1983). This objective was met by collecting nutrient data at the inflow and outflow points of an in-line, wet detention lake to provide more information on effectiveness of essential nutrient removal.

Discrete grab samples in tandem with the continuous hydraulic and hydrologic data from monitoring stations were gathered on the man-made lake. The data were analyzed to determine if there are any seasonal variations in pollutant loading or removal efficiencies. For the purpose of this study, only total nitrogen and total phosphorous were examined.

The man-made lake selected for the pilot study has an area of 15 acres and ranges from 3 to 8 feet deep with an average depth of approximately 5 feet. This lake receives an average annual flow of 3.5 cubic feet per second, which results in a residence time of 11 days with no littoral zone. Monitoring stations are located at the influent and effluent sections of the lake which provided data on the hydraulic and hydrologic parameters.

Methodology

The essential chemical compounds that all plants require to grow and flourish are nitrogen and phosphorus. Nitrogen compounds are primary constituents of concern in surface waters due to their limiting role for plant growth. The most important forms of inorganic nitrogen in surface waters are ammonia, nitrite, and nitrate. Organic nitrogen is also an important constituent of surface waters and occurs in both dissolved forms and in particulate organic matter. Nitrogen is the critical element required for protein synthesis and, hence, is critical to life of all plants.

Phosphorus occurs as soluble and insoluble complexes in both organic and inorganic forms in aquatic systems. The principal inorganic form is ortho-phosphate and is the preferred form for plant (macrophyte) growth. Dissolved phosphorus includes both phosphate and dissolved organic phosphorus. Particulate phosphorus includes biological matter such as plankton (microbiota) and phosphorus sorbed on biotic and abiotic suspended particles. Dissolve organic phosphorus and insoluble forms of organic and inorganic phosphorus are generally not biologically available until they are transformed into soluble inorganic forms.

Phosphorus may be permanently or semi-permanently lost from aquatic ecosystems to the sediments and to a lesser extent as phosphine gas to the atmosphere. Because organic phosphorus can be transformed and used by plants, it is generally sufficient to consider the ambient concentrations of total phosphorus in natural water bodies to anticipate ecological effects. Naturally occurring inputs of phosphorus originate from surface inflows, groundwater inflows, leaching from soils, and atmospheric deposition. Anthropogenic inputs are typically from the use of inorganic phosphorus fertilizers for agriculture and landscaping, the use of animal feeds rich in phosphorus, and from discharges of phosphorus in wastewaters and stormwaters.

Wet detention ponds use permanent pool of water to achieve nutrient removal. To maintain a permanent pool it is important to have sufficient surface runoff, fairly impermeable soils, and an adequate base flow to the pond. The effectiveness of these permanent pools at removing nutrients depends on the inflow rate and detention time, which are both functions of the storm intensity, runoff volume, and pond size (Gurr, 2007). These parameters determine the fraction of nutrients captured in the pond for treatment, especially during quiescent periods between events (Woodward-Clyde, 1986)

The influent-effluent approach is the most effective method for estimating the pollutant removal efficiency of a structural BMP. This is because pollutant removal efficiencies are based on calculating the difference between influent and effluent loads (Urbonas, 1994). Since the locations of the sampling points are immediately upstream and downstream of the BMP, it makes it possible to isolate the pollutant loads for the mass balance calculations.

The nutrient load transported at any time interval is determined by mass balance. The United States Environmental Protection Agency proposed two different mass balance methods for computing nutrient removal efficiency in a lake. The first method, called the average event mean concentration efficiency ratio (E_{emc}), uses an average of the event mean concentrations from all of the samples distributed over the sum of the sample volumes. The E_{emc} expressed as percentages is computed as follows:

$$E_{emc} = (1 - E_{emc\ (ave)out} / E_{emc\ (ave)in}) \times 100$$

where $E_{emc\ (ave)in}$ is the averaged inflow E_{emc} and $E_{emc\ (ave)out}$ is averaged outflow E_{emc}. The loads are computed as the product of event mean concentrations and the associated volume. Since the average event mean concentration efficiency method averages all of the event volumes, it gives equal weight to each storm event.

The second method, which is the summation of loads efficiency ratio (E_{sol}), sums the product of each sample volume multiplied by its corresponding event mean concentration. The E_{sol} expressed as percentages is computed as follows:

$$E_{sol} = (1 - SOL_{out} / SOL_{in}) \times 100$$

where SOL_{in} is the summed inflow loads and SOL_{out} is the summed outflow loads. Loads are then computed as the product of event mean concentrations and the associated volume. However, unlike the average event mean concentration method, sample data is required for each events input and output loads.

Although, both of these methods are independent of the number of samples collected and assume that their results represent the storms that normally occur in the region, the summation of loads method however assumes the collected samples represent all significant input and output loads (Martin, 1986). Even though the average event mean concentration method is capable of providing efficiencies of BMPs, the summation of loads method was found to be a better measure of the overall efficiency of a BMP (Martin, 1986). Additional research on BMPs found that where there is a permanent pool, computing pollutant removal effectiveness for individual storms may not be meaningful since the outflow typically has limited relationship to the inflow. For wet detention ponds, it may be more appropriate to use total loads over the monitored period to compute removal efficiencies (Strecker, 1992).

Data Results and Analysis

The physical data to fulfill the goal of the study were gathered by continuous monitoring equipment installed at nineteen permanent sites located within the six tributaries of Lake Tohopekaliga. Two of these monitoring sites were located at the upstream and downstream channels of the pilot study lake (Figure 1). The multi-parameter water quality instrument used to measure temperature, dissolved oxygen, pH, Chlorophyll, conductivity, salinity, turbidity and total dissolved solids was the YSI 6600 EDS Component. While Sontek Argonaut (SW) instrument was installed along the bottom of the channel to measure water level, velocity and temperature. The automatic samplers were not in place during some of the initial water quality sampling so the data used in this study were limited to a twelve-month data period.

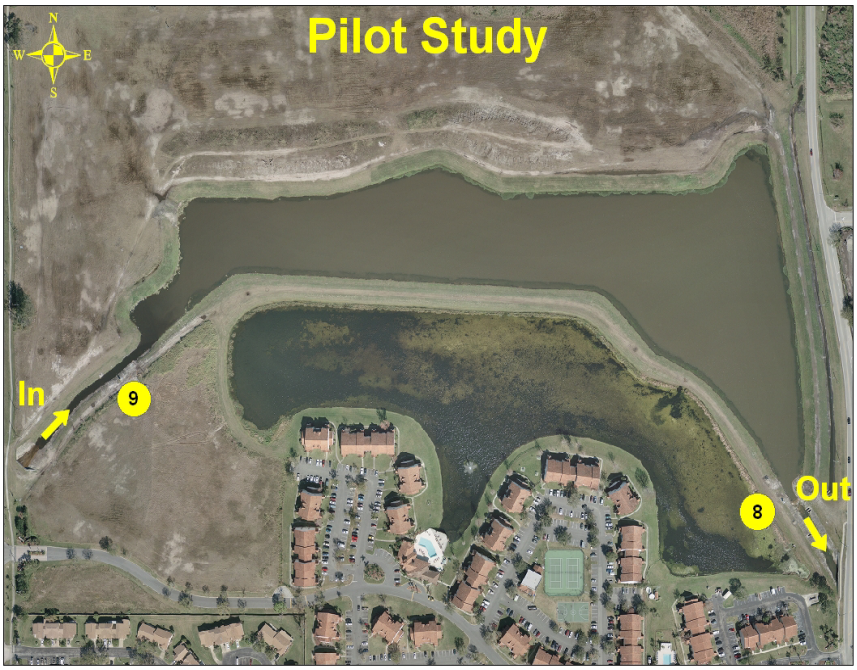

Figure 1: Study site location

Frequency of sample collection and the level of detail for the water quality analysis were within budgetary constraints. Water quality sampling protocols were established to cover field sampling procedures, sample labeling conventions, sample transit and laboratory result verification. All analysis of water quality samples were required to be conducted by laboratories certified in the state of Florida and the continuous field monitoring equipment needed to be maintained on a daily basis by personnel licensed by the equipment manufacturers.

The laboratory results from the collected grab samples in the pilot study lake show little variation of total nitrogen concentration levels from their mean value of 0.90 mg/l whereas the concentration levels of total phosphorus ranged from 0.02 mg/l to 0.48 mg/l during the year-long study period. The levels of total nitrogen and total phosphorus in the lake were within the range for algae bloom generation of 1.5 mg/l and 0.15 mg/l for total nitrogen and total phosphorus, respectively. During the study period, only two minor algae blooms were observed and they only lasted a few days each.

Both E_{emc} and E_{sol} approaches were used to compute the mass balance for nutrient loads. The E_{sol} approach was performed on a bi-monthly and monthly basis whereas the E_{emc} approach was performed for the entire year. Figures 2 and 3 represent the

seasonal nutrient loads flowing into and out from the lake for total nitrogen and total phosphorus, respectively.

CONCLUSIONS AND RECOMMENDATIONS

The laboratory results from the collected grab samples show slight variation of total nitrogen concentrations and moderate variation of total phosphorus concentrations throughout the year. The concentration levels of total phosphorus ranged from 0.02 mg/l to 0.48 mg/l, but not in relation to either season or flow volume variations.

A review of the data shows that the E_{emc} and E_{sol} methods yielded approximately the same results. This is mostly because the study period was short duration of only one year. It is interesting to note that the magnitude of total nitrogen loads coming into the lake were basically identical for either pollutant load analysis method. In contrast, the total phosphorus levels increased at the outlet of the lake, which suggests that the study lake was actually releasing total phosphorus into the downstream receiving waters.

The nutrient loads flowing into and out from the lake were evaluated for wet and dry cycles, but no significant variation of nutrient concentration levels nor removal efficiencies were found with respect to season. The only nutrient that showed any seasonal variation was nitrogen and it only showed slightly lower values towards the later part of spring and early summer.

LIMITATIONS

Resuspended pollutants from the lake floor were not accounted for in the analysis since sediment data was not collected during this study. Atmospheric contributions of pollutants to the lake were expected to be insignificant, but the data was not available to verify this assumption. The initial and final pollutant loads within the lake were not measured, so an assumption was made that it remained unchanged from year to year. Also, any contribution from waterfowl was not accounted for even though there is a rather large roust of birds along the maintenance berm of the lake.

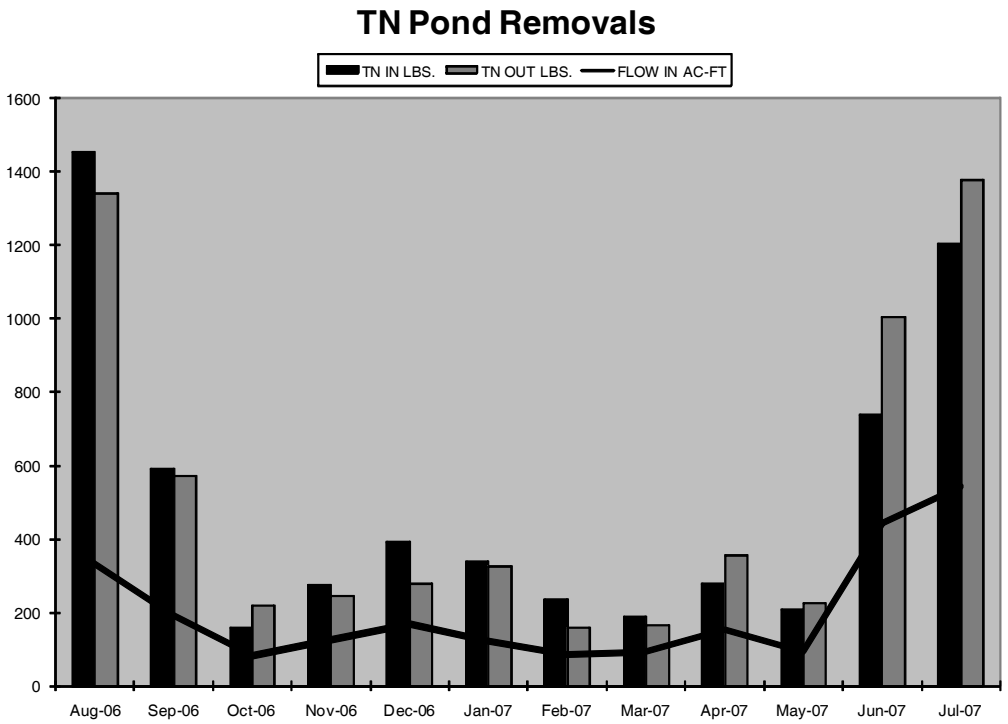

Figure 2: Total Nitrogen Loads

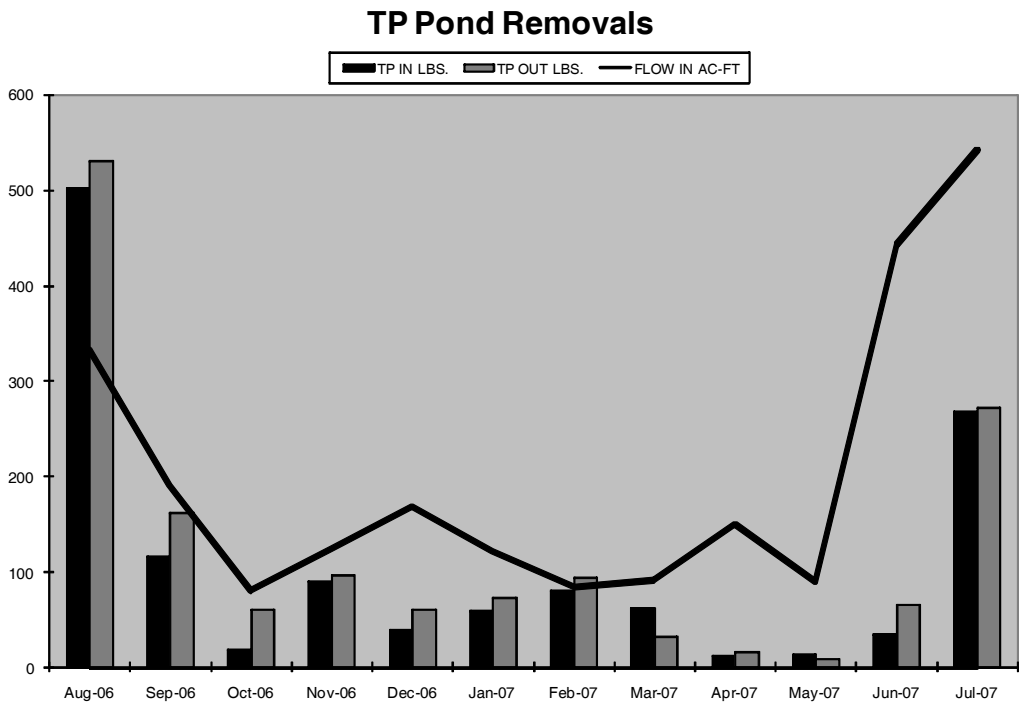

Figure 3: Total Phosphorus Loads

LIST OF REFERENCES

Gurr, Eric, "Pilot Study of Nutrient Loading in a Wet Detention Lake", Univ. of Central Florida, Orlando, FL (2007)

Livingston, E.H., "The Stormwater Rule: Past, Present and Future", in: Wanielista, M.P. and Yousef, Y.A. (Eds.) Stormwater Management: "An Update", Univ. of Central Florida publication #85-1, Orlando, FL (1985).

Martin, E.H., and Smoot, J.L., Constituent-Load Changes in Urban Stormwater Runoff Routed Through a Detention Pond-Wetlands System in Central Florida, USGS Report 85- 4310 (1986).

Rushton, B.T., and Dye, C.W., C., Effectiveness of Permitted Stormwater Systems for Water Quality Control (1993).

Schueler, T.R. Controlling Urban Runoff: A Practical Manual for Planning and Designing Urban BMPs, Metropolitan Washington Council of Governments (1987).

Strecker, E.W., Kersnar, J.M., Driscoll, E.D., and Horner, R.R. The Use of Wetlands for Controlling Stormwater Pollution, prepared for U.S. EPA by Woodward-Clyde Consultants (1992).

Urbonas, B., Carlson, J., and Vang, B., "Joint Pond-Wetland System Performance in Colorado, U.S.A.", Internal Report of the Urban Drainage and Flood Control District, Denver, CO (1994).

Whipple, W. and Hunter, J.V., "Nonpoint Sources and Planning for Water Pollution Control", Journal of the Water Pollution Control Federation, 49:15-23 (1977).

Woodward-Clyde Consultants, Methodology for Analysis of Detention Basins for Control of Urban Runoff Quality, prepared for U.S. Environmental Protection Agency, Office of Water, NTIS #PB93-223576 (1986).

Pervious Pavement System Evaluation

Amy A. Rowe[1], Michael Borst[2], and Thomas P. O'Connor[3], and Emilie K. Stander[4]

[1]Oak Ridge Institute of Science and Education postdoctoral fellow at U.S. Environmental Protection Agency (U.S. EPA), Office of Research and Development, 2890 Woodbridge Ave., Edison, NJ, 08837. rowe.amy@epa.gov Phone: 732-906-6823 Fax: 721-321-6640

[2]U.S. EPA, Office of Research and Development, 2890 Woodbridge Ave., Edison, NJ, 08837. borst.mike@epa.gov Phone: 732-321-6631 Fax: 721-321-6640

[3]U.S. EPA, Office of Research and Development, 2890 Woodbridge Ave., Edison, NJ, 08837. oconnor.thomas@epa.gov Phone: 732-321-6723 Fax: 721-321-6640

[4]U.S. EPA, Office of Research and Development, 2890 Woodbridge Ave., Edison, NJ, 08837. stander.emilie@epa.gov Phone: 732-906-6898 Fax: 732-321-6640

Abstract

Pervious pavement is a low impact development stormwater control. The Urban Watershed Management Branch of the U.S. Environmental Protection Agency in Edison, NJ, is evaluating concrete pavers as a popular implementation. The pollutant removal of a bench-scale permeable interlocking concrete paver system was evaluated using urban stormwater runoff from a 9 ¾-acre drainage area. Stormwater was delivered to the pavement system twice daily to accelerate aging of the system, while monitoring clogging and long-term pollutant removal. The role of microbial communities within the pervious pavement system in pollutant removal is also being examined. It is important to evaluate stormwater quality after filtration through pervious pavement systems to see if the exfiltrate has improved sufficiently for release to surface or ground waters. The bench-scale phase of this study examined materials and system hydraulics to optimize for the full-scale experiment. The project evaluated system performance with the presence of a geotextile between gravel layers using both woven and nonwoven fabrics along with control systems with no geotextile.

Background

Permeable interlocking concrete pavement is a stormwater best management practice (BMP). The pavers themselves are not permeable, but the spaces in between the pavers allow water to infiltrate. The gaps are filled with washed, graded stone that allows infiltration and also provides structural support for the pavers. Recent

literature has shown that the concentration of stressors in exfiltrate is substantially lower than the infiltrate for other pervious pavement systems partly because the gravel layers under the surface provide some filtration (James and Thompson 1997, Rushton 2001, Clausen and Gilbert 2003, Ellis et al. 2004). Studies showed that annual pollutant export in runoff from driveways was 86% less for paver driveways than impervious asphalt driveways (Clausen and Gilbert 2003, Gilbert and Clausen 2006). The system can also potentially reduce the urban heat island effect because the pavers reflect sunlight rather than absorbing it (James and Thompson, 1997).

Objectives

The overall objective of this ongoing project is to assess the long-term pollutant removal performance of a pervious pavement system receiving parking lot runoff. A bench-scale hydraulic study determined the flow rates and materials necessary for the full-scale experiment. A separate bench-scale microbial study will examine the role of microbial colonies in pollutant removal performance of this pervious pavement. Results from these two bench-scale experiments will be used to refine the full-scale investigation.

This paper focuses on the hydraulic bench-scale study. The primary objectives of the hydraulic bench-scale study are to:

(1) Determine the flow rate of stormwater through the system;
(2) Compare the total suspended solids (TSS) of the influent stormwater with that of the effluent; and
(3) Determine the performance effects of the presence/absence of a permeable geotextile in the system and to determine performance differences between a woven and nonwoven geotextile.

Secondary goals of this hydraulic study are to:

(1) Determine the discharge volume of the system;
(2) Determine the breakthrough time of the effluent discharging from of the system; and
(3) Monitor clogging of the system as the study progresses.

Experimental Design

Four small-scale pervious paver systems were constructed in 60cm x 60cm x 90cm HDPE bins. Pavers of a minimum of 7.6cm thickness were placed on a 2.5cm layer of 1-cm diameter crushed stone. The 1-cm crushed stone also fills the gaps between the pavers. These pavers were surrogates for the interlocking pavers and were spaced accordingly. There is a maximum of 1.27cm space between the pavers. Below the 1-cm layer is a 12.7-cm deep layer of 1.6-cm diameter angular crushed stone, and a 3.8-cm diameter slotted PVC pipe is positioned near the bottom of the bin that routes discharge through the bin wall. The bins are placed at a 1% longitudinal slope, the same as that of the full-scale pervious pavement design. Two

systems were installed with a woven permeable geotextile (manufacturer reported apparent opening size = 0.425mm, flow rate = 204 L/min/m^2) between the gravel layers, while the other two systems have no geotextile (Figure 1). The permeable geotextile separates the gravel layers to prevent migration and possibly increases the solids removal from the stormwater infiltrate.

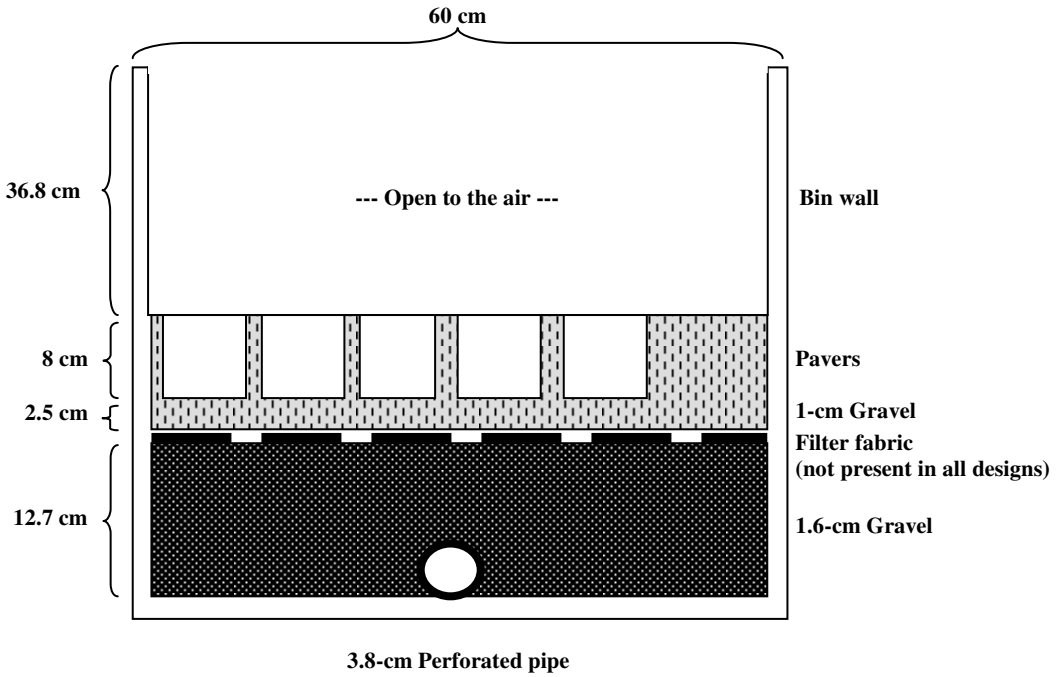

Figure 1. A schematic of the bench-scale pervious pavement system. This schematic is not drawn to scale.

Approximately 17L of collected, homogenized, stormwater were "rained" over each bin every workday, twice daily, for 12 weeks. The stormwater gravity-drained from a 19-L bucket through 5-mm holes drilled in the bottom. The bucket was positioned over the center of each bin to ensure that the water landed on the pavers and did not flow down the sides of the bin (Figure 2). The stormwater drained from the influent bucket in less than 1 hour. The 17L stormwater introduction is the equivalent of a 3cm rain event for the bench-scale paver system (90cm x 60cm). After 12 weeks the study boxes received the equivalent of 380 cm of rain, which is 3 times the mean annual precipitation for New Jersey (124 cm/year) (Robinson 2007). By simulating 3 years of rainfall/runoff (introduced as collected stormwater), the solids loading on the system was accelerated and the effects on the hydraulic and pollutant removal performance on the system were observed.

The discharge from the bins was collected. The depth changes with time in both the influent and effluent bucket were recorded using water level loggers (Global Water, Inc.). Both the influent (stormwater) and the effluent were analyzed for TSS according to Standard Method 2540 D (Clesceri et al, 1999).

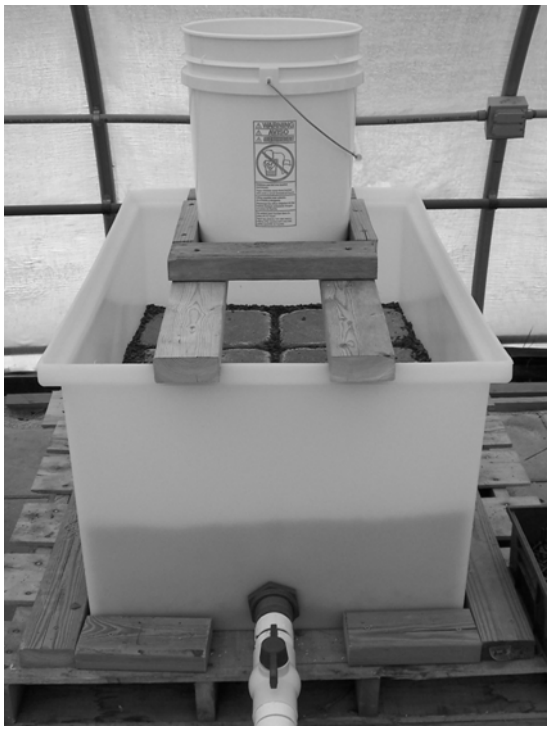

Figure 2. Bench-scale pervious pavement system demonstrating stormwater delivery method.

A second four-bin study was run with two boxes containing a nonwoven geotextile (manufacturer-reported apparent opening size = 0.212mm, flow rate = 6095 L/min/m^2) between the gravel layers, and two bins were used as controls with no geotextile. This allowed a performance comparison between the two geotextile types. The woven geotextile has a grid-like polypropylene weave, the apparent opening size is relatively large, and the flow rate is relatively low, while the nonwoven geotextile is made up of needle punched, polypropylene staple filaments, has a smaller apparent opening size, and has a relatively high flow rate.

The first four-bin study (woven geotextile) was run for 12 weeks and then extended an additional 12 weeks for a total of 24 weeks (Six years of equivalent New Jersey rainfall). The second four-bin study (nonwoven geotextile) was run for 12 weeks concurrently with the second 12 weeks of the first set of bins. Stormwater introductions were made twice daily for the studies.

Preliminary Results and Discussion

The TSS removal for both the woven and nonwoven pervious pavement systems was 89% ($R^2 > 0.96$) (Figure 3).

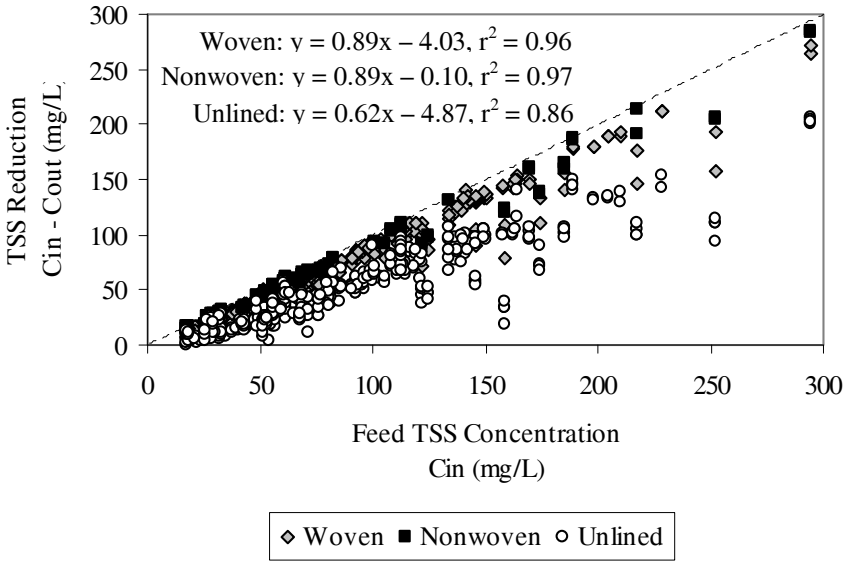

Figure 3. TSS concentration reductions compared to feed concentrations for woven, nonwoven, and unlined systems.

The unlined systems removed 62% of solids, indicating that the gravel and block paver system, with no geotextile, does provide some TSS reduction. The performance of the unlined control systems was more variable than the systems with geotextiles. The presence of a geotextile in pervious block systems increased TSS removal efficiency ($p < 0.01$), but the two geotextile types are not statistically different ($p = 0.06$).

The effluent flow rates from the woven and nonwoven systems were statistically different ($p = 0.04$) and both differ from the unlined systems ($p<0.01$, $p <0.01$ woven and nonwoven, respectively). The unlined bins had the largest effluent flow rates. The nonwoven bins had larger mean flow rates than the bins with the woven fabric, which was expected given the manufacturer's geotextile flow rate differences (constant head test) (Figure 4).

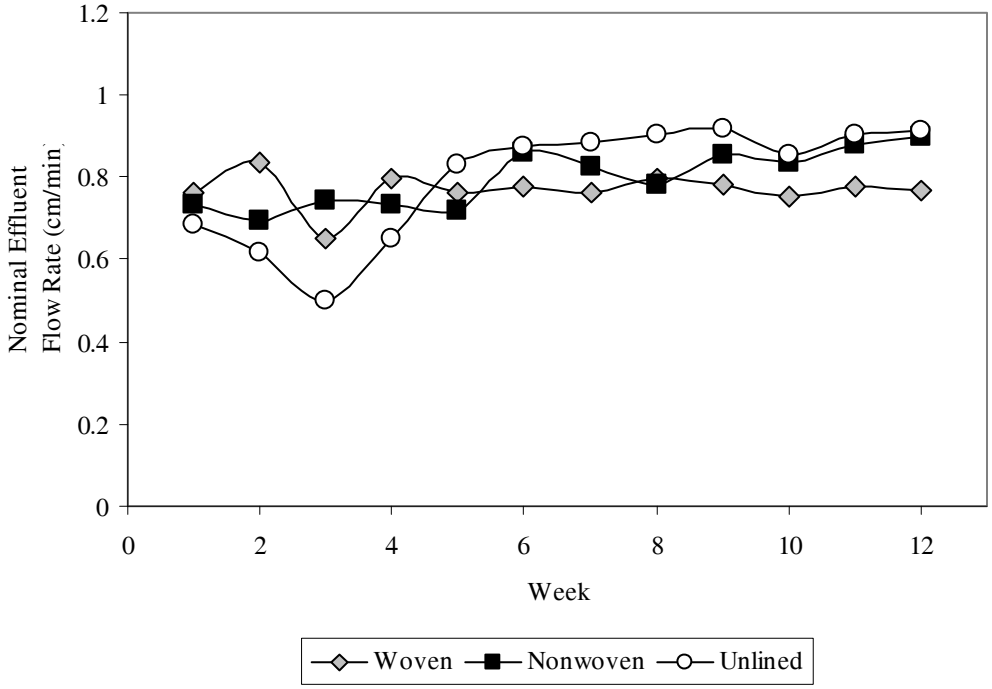

Figure 4. Effluent flow rates for woven, nonwoven, and unlined systems during the first 12 weeks of operation.

The experiment simulated the rainfall/runoff from an equivalent of six years of New Jersey rainfall. The effluent flow rates from the lined and unlined bins at the start of the experiments showed no statistically significant difference from the flow rates at the end of the experiment. This suggests that the systems had no measurable clogging during the experimental period.

Future Work

Once the hydraulic studies are complete, the microbial bench-scale study will begin to examine the role of microbial communities on the performance of the pervious pavement systems. Microbial removal of pollutants can be an effective method for reducing concentrations at contaminated sites (Hutchins et al. 1998, Ellis et al. 2000, Townsend et al. 2003, Shi et al. 2005).Therefore, pollutant removal in pervious pavement systems may be enhanced by expediting the establishment of microbial colonies in the gravel layers. Microbial growth effects will be observed with respect to the following variables: inoculation of microbes on the geotextile, the presence and location of a carbon source in the system, and the detention of stormwater in the system.

The full-scale parking lot construction has started and monitoring study is expected to start in the summer of 2009. The full-scale study, in cooperation with EPA's Region 2, will focus on a 1-acre parking lot with 110 parking spaces that will have three pervious pavement systems: pervious asphalt, pervious concrete, and pervious pavers. The roadways of the parking lot will be conventional asphalt and the parking islands will be pervious. The pervious asphalt parking area will be installed

to the specifications of the National Asphalt Pavement Association, the pervious concrete will be constructed following Standard 522.1 of the American Concrete Institute, and the pervious pavers will be installed to the specifications of the Interlocking Concrete Pavement Institute.

The subsurface of the pervious pavement parking areas of the lot will have both lined and unlined sections. The lined sections will have impermeable liners and underdrains to collect the infiltrate and the unlined sections will drain to the underlying soil. There will be four lined and five unlined sections for each pervious pavement type to allow for comparisons.

The exfiltrate from the lined sections of the pervious parking areas will be collected and monitored for volume, rate, and environmental stressors (e.g., solids, pathogens, nutrients, metals, and semi-volatile organic compounds). Instruments are being installed in the parking lot to record a variety of other parameters such as: sub-grade moisture, sub-grade temperature, water depth, ambient temperature, meteorological conditions, and parking lot usage (car counter). The lot will be maintained (sweeping, vacuuming), but schedules will be varied to determine maintenance recommendations for these types of pervious surfaces. The parking lot will also be observed for signs of aging, surface degradation, clogging of surfaces, and system failure. The parking lot lifetime is projected to be 20 years, but it may last longer if it is well-maintained. This project is being undertaken because there has not been a definitive, long-term, multi-stressor, statistically-valid investigation on multiple pervious pavement systems at the same site.

Conclusions

The hydraulic bench-scale study yielded results that are critical for achieving success in the full-scale parking lot study. Both lined and unlined systems removed TSS, and the lined systems showed 89% relative TSS removal, on average. The systems with the woven and nonwoven geotextiles were not statistically different from each other for TSS removal, but the nonwoven systems had statistically larger flow rates than the woven ones. Both woven and nonwoven systems were different from the unlined for both TSS removals and effluent flow rates. After six years of New Jersey rainfall, no measurable clogging of the systems was seen and solids removal was still robust. The success of the full-scale parking lot is dependent on proper design and these bench-scale studies will help direct those design decisions.

Disclaimer: The U.S. Environmental Protection Agency, through its Office of Research and Development, funded and managed, or partially funded and collaborated in, the research described therein. It has been subjected to the Agency's peer and administrative review and has been approved for external publication. Any opinions expressed in this paper are those of the author(s) and do not necessarily reflect the views of the Agency, therefore, no official endorsement should be inferred. Any mention of trade names or commercial products does not constitute endorsement or recommendation for use.

Acknowledgment

All sample collection and analysis was performed by PARS Environmental. This project was supported in part by an appointment to the Research Participation Program at the National Risk Management Research Laboratory administered by the Oak Ridge Institute for Science and Education through an interagency agreement between the U.S. Department of Energy and EPA**.**

References

Clausen, J. C., Gilbert, J.K. (2003). Annual Report, Jordan Cove Urban Watershed Section 319 National Monitoring Program Project., Department of Natural Resources and Engineering, College of Agriculture and Natural Resources, University of Connecticut.

Clesceri, L. S., Greenberg, A. E., Eaton, A.D. Editors (1999). Standard Methods for the Examination of Water and Wastewater, 20th Ed. Washington, DC: American Public Health Association.

Ellis, D. E., Lutz, E.J., Odom, J.M., Buchanan, Jr., R.J., Bartlett, C.L., Lee, M.D., Harkness, M.R., DeWeerd, K.A. (2000). "Bioaugmentation for accelerated in situ anaerobic bioremediation." Environ. Sci. Technol. **34**(11): 2254-2260.

Ellis, J. B., Scholes, L., Revitt, D.M., Oldham, J. (2004). "Sustainable urban development and drainage." Proceedings of the Institution of Civil Engineers-Municpal Engineer **157**(4): 245-250.

Gilbert, J. K., Clausen, J.C. (2006). "Stormwater runoff quality and quantity from asphalt, paver, and crushed stone driveways in Connecticut." Water Research **40**: 826-832.

Hutchins, S. R., Miller, D.E., Thomas, A. (1998). "Combined laboratory/field study on the use of nitrate for in situ bioremediation of a fuel-contaminated aquifer." Environ. Sci. Technol. **32**(12): 1832-1840.

James, W., Thompson, M.K. (1997). Contaminants from four new pervious and impervious pavements in a parking-lot. Advances in Modeling the Management of Stormwater Impacts. W. James. Guelph, Ontario, Canada, Computational Hydraulics, Inc. **5:** 207-222.

Robinson, D. A. (2007). Historical Monthly Station Data, Office of the NJ State Climatologist.

Rushton, B. T. (2001). "Low-impact parking lot design reduces runoff and pollutant loads." Journal of Water Resources Planning and Management - ASCE **127**(3): 172-179.

Shi, W., Bischoff, M., Turco, R., Konopka, A. (2005). "Microbial catabolic diversity in soils contaminated with hydrocarbons and heavy metals." Environ. Sci. Technol. **39**(7): 1974-1979.

Townsend, G. T., Prince, R.C., Suflita, J.M. (2003). "Anaerobic oxidation of crude oil hydrocarbons by the resident microorganisms of a contaminated anoxic aquifer." Environ. Sci. Technol. **37**(22): 5213-5218.

Planning for Sustainable Growth and Water Resources in the Chesapeake Bay Watershed

Thomas E. Dumm, PE[1]

[1] O'Brien & Gere, 8401 Corporate Drive, Landover, MD 20785; PH (301) 731-1160; FAX (301) 577-4737; email: dummte@obg.com

ABSTRACT

Over the past several decades, a multitude of strategies, policies, and programs have been formulated and implemented in an effort to protect the quality of a most precious resource – the Chesapeake Bay. In 2006, Maryland passed a new law known as House Bill (HB) 1141 which directly addresses the relationship between planned growth and water resources. The Water Resources Element of HB 1141 ensures that future county and municipal comprehensive plans reflect the opportunities and limitations of the local and regional water resources.

Situated on a peninsula in the Chesapeake Bay, Kent County, Maryland is nationally recognized for its rural character and serene beauty. Less than a two hour drive from Philadelphia, Baltimore and Washington DC, growth and development pressures have the potential to impact the sustainability of the water resources of the County. This paper includes a discussion of the following topics related to the update of the County's Water & Sewerage Plan which incorporates the Water Resources Element of HB 1141:

- Overview of the Water Resources Element of HB 1441.
- Tools and data sources (i.e., Source Water Assessments, TMDL's, land use plans, Chesapeake Bay Critical Areas, etc.).
- Water resources limitations (i.e., infrastructure, susceptibility of potable water sources to pollutants, point source nutrient load caps, and TMDLs).
- Methods for managing growth where there is limited resource availability (i.e., building permit limitations, down zoning, etc.).

INTRODUCTION

A multitude of strategies, policies, and programs have been formulated and implemented in an effort to protect the quality of the Chesapeake Bay. In 2006, Maryland passed a new law known as House Bill (HB) 1141 which requires counties and municipal jurisdictions to complete a Municipal Growth Element and Water Resources Element. In 2008, Kent County retained O'Brien & Gere to prepare its Water Resources Element including information that could be used by elected officials and decision-makers as a roadmap for addressing the sustainability of planned growth and water resources.

OVERVIEW

Situated on a peninsula on the eastern side of the Chesapeake Bay, Kent County, Maryland is nationally recognized for its rural character and serene beauty. Less than a two hour drive from Philadelphia, Baltimore and Washington DC, growth and development pressures have the potential to impact the sustainability of the water resources of the County. The Water Resources Element of HB 1141 requires that counties and municipal jurisdictions answer the following questions related to sustainability:

- Is there adequate water supply to meet current and future needs?
- Is there adequate wastewater and septic capacity to meet current and future needs?
- How much development can the watersheds accommodate before the nutrient load thresholds is exceeded?

The answers to these questions are intended to link land use decisions and water resources and ultimately improve the health of the Chesapeake Bay. One key aspect of this linkage is the prediction of pollutant loading which is dependent upon a variety of factors, including point sources of pollutants (i.e., wastewater treatment plants) and non-point sources of pollutants (i.e., stormwater, septic, agriculture, etc.). Water quality regulations have traditionally focused on point source pollutants because they are easier to define, test and control; however in the Upper Eastern Shore Basin which includes Kent County point sources constitute only six percent of the total nutrient loading. To address both point and nonpoint source pollution, Maryland has developed the Tributary Strategy Implementation Plan which consists of a comprehensive list of river-specific cleanup strategies that detail the "on-the-ground" actions needed to reduce the amount of nutrients and sediment flowing into the Chesapeake Bay. The Tributary Strategy Implementation Plan includes a multitude of programs within each of the following strategies:

- Point Source
- Growth Management
- Onsite Sewage Disposal System
- Agricultural
- Urban Sources
- Stormwater
- Air Deposition

The overall goal of the Tributary Strategies is to achieve roughly a 50 percent reduction in nitrogen and phosphorus from the Agricultural Strategy and 50 percent from the remaining strategies. In the Upper Eastern Shore Basin which includes Kent County, approximately 70 percent of the nitrogen and phosphorus pollutant load is from agriculture and 5 percent is from point sources.

NUTIRENT LOADING METHODOLOGY

The Maryland Department of Planning developed a non-point source nutrient loading analysis to determine how growth trends and land use decisions could impact future nutrient loading. The expectations for the loading analysis were three-fold: (1) simple

non-point source analysis for nutrient loading, (2) reasonable assurance that future land use scenarios have been considered, and (3) discussions of future steps for running analyses and tailoring the analyses for Kent County. The loading analysis was in the form of an MS Excel spreadsheet and was intended to be applied on a county-wide basis using the loading rates provided by the State for a multitude of land uses (i.e., development, agriculture, forest, wetlands, etc.). Baseline simulations for loading (lbs/yr) were conducted using nitrogen and phosphorus loading rates (lbs/acre/year) and 2002 and 2030 land use (acres). These baseline results can be compared to alternative land use scenarios to assess the loading impacts associated with changes in land use.

FINDINGS

The methodology for conducting the loading analyses outlined in the Water Resources Element was developed to provide counties and municipal jurisdictions with a means for generating a simple and technically defensible prediction of the non-point source loading. For the Upper Eastern Shore, approximately 70 percent of the nitrogen and phosphorus loading is attributed to agriculture. However, in Kent County, the non-point source loading analyses conducted in this study indicated that because of the large quantity of agricultural land in the County the percentage of nitrogen and phosphorus pollutant loads from agriculture were significantly higher (greater than 95 percent) than the Upper Eastern Shore. Although the loading analyses is simplistic, it illustrates that the improvements in water quality will in large part be driven by the ability to achieve the reductions in nutrient loads associated with the Agriculture Strategy. This challenge is one faced by jurisdictions throughout the Chesapeake Bay Watershed.

CONCLUSIONS

Numerous strategies can be implemented to address point and non-point source loading and the improvement in water quality will be defined, in part, by the overall reduction in pollutant loading achieved by a combination of strategies. At this time, the County will initially focus its efforts on the following areas:

- On-site Sewage Disposal Systems
- Capacity Management Plans for Water and Sewer
- Wellhead Protection and Aquifer Recharge Areas
- Stormwater

Implementation of the Agriculture Strategy will likely be directed by the Natural Resources Conservation Service and is paramount to achieving the pollutant loading reductions outlined in the Tributary Strategy Implementation Plan and improving water quality. The challenges involved in moving forward and implementing the tributary strategies will likely be significant and will require the cooperation of a number of organizations. However, recognizing that the Water Resources Element is in its infancy and needs further refinement, the State of Maryland has taken a bold first step toward linking land use decisions with sustainability of water resources in the Chesapeake Bay Watershed.

Pollutant Transport within the Vadose Zone: Interactions of Soil Horizon Chemistry on Water Quality

Daniel P. Treese*, Shirley E. Clark, Ph.D., P.E., D. WRE, J. Bradley Mikula, Katherine H. Baker, Ph.D.
*Corresponding Author: dpt117@psu.edu

Environmental Pollution Control Program,
The Pennsylvania State University, Harrisburg

ABSTRACT

Hydrologic cycle restoration is the primary objective of stormwater management. Infiltration and biofiltration systems composed of engineered soils have become a preferred tool for obtaining this objective while also providing pollutant removal. It is desirable, though, to limit soil disturbance and incorporate native soils. The use of native soils requires a fundamental understanding of their behavior towards water transport and pollutant treatment. Their structure is not homogeneous but instead contains several layers, or "horizons," each with differing pollutant removal capacity. The ability of the various horizons to treat runoff was investigated over 40 simulated storm events in two soil types, a Wharton silt loam and Leetonia loamy sand. Effluent water results showed leaching of total nitrogen and removal of total phosphorus by all soil horizons of both soil types. Potassium leached from the organic horizons of both soils, the silt loam showed removal by lower horizons while the loamy sand did not. All soil horizons of both soil types lowered the pH of influent stormwater and increased conductivity, turbidity, color, and hardness.

INTRODUCTION

Urban sprawl has created large areas of impervious surfaces, increasing surface stormwater runoff peak rates and volumes which amplify erosion rates and flood occurrences. Along with increased surface runoff, the urban environment creates increased levels of pollutants that are washed into steams at levels that may deleteriously impact recreational usage, and aquatic life and habitat, as well as increasing the cost of drinking water treatment. Infiltration units have become a preferred method for reducing runoff rates, volumes, and pollutant loads. Clark et al. (2006) provides an extensive literature review on water quality passing through the infiltration device and the International BMP Database provides results regarding improvements in surface runoff quality after passing over or through an infiltration basin. To maximize the benefit of infiltration as a stormwater management tool, understanding of the biogeochemical processes that control both the quantity and quality of water passing through a soil (natural or engineered) is required.

Because natural soils have transitional layers, called horizons, of varying biological activity, chemical reactions and physical qualities, it is important to understand the properties and interactions of these individual horizons when evaluating a soil's pollutant removal capacity. Most soils have five basic horizons: O, A, B, C, and R. The O-horizon, or organic horizon, consists of vegetative matter that is still in a recognizable condition. Once this organic matter decays beyond recognition of its origin and begins to mix with mineral particles, an A-horizon, commonly called topsoil, is defined. Below the A-horizon, minerals and metals leached from above accumulate and form a B-horizon. Similarly, the C-horizon is a mineral layer formed from material raised by groundwater from the consolidated bedrock of the R-horizon.

This study tested the ability of two natural, undisturbed soil columns representing both the entire available horizon and the individual soil horizons to treat local stormwater runoff. In addition, soil horizons samples were periodically removed from the study and will soon be tested to measure accumulation of pollutants and release of exchangeable ions over time. In the end, correlations between soil parameters and pollutant migration will be studied and the results incorporated into design guidance for determining the proper application, predicted lifespan, and maintenance requirements of infiltration devices. This research, in particular, focuses on the pollutant removal capacity below the organic horizon of the soil where it is believed that much removal occurs but that has historically been ignored. This information is crucial to providing an accurate picture of the movement of pollutants in the subsurface, regardless of the infiltration method used (Clark and Pitt 2007).

MATERIALS AND METHODS

Ten-centimeter diameter columns of two soil types, a Wharton silt loam and Leetonia loamy sand, were vertically encased in PVC pipe and removed intact from two central Pennsylvania sites. The descriptions of the columns are given in Table 1. The Wharton silt loam contains four test groups of soil horizons: O, A, AB, or OAB. The Leetonia loamy sand columns also contain four test groups of soil horizons: O, A1, A1A2, or OA1A2. Control columns of each soil type, representing pre-infiltration conditions, were also collected for soil analysis.

Table 1. Collected soil column descriptions

Soil Type	Horizon(s)	# of Columns	Depth (cm)
Wharton silt loam	O	5 study	5
	A	5 study	15
	AB	5 study	32
	OAB	5 study,1 control	37
Leetonia loamy sand	O	5 study	10
	A1	5 study	11.5
	A1A2	5 study	20.5
	OA1A2	5 study, 1 control	30.5



The Wharton silt loam columns come from a sloped field with a shallow soil that is less than one meter to bedrock. Currently, the land is maintained as a lawn but there has been agricultural activity in the past and plowing may have occurred; the O-horizon is barely three centimeters deep but was slightly exaggerated in the O-horizon columns to keep the soil intact. The A and B-horizons are moderately rocky.

The Leetonia loamy sand columns come from a wooded section of state gameland about 15 meters from a timber harvest landing and 100 meters from abandoned strip mines. Also present are the remains of the village of Dougherty; the small average size of the trees in the area and the presence of a concrete spring water containment structure suggest that the collection site was once part of the village. The O-horizon is fairly deep and consists almost entirely of forest canopy leaf litter. The A-horizon is very sandy and mostly rock free. Impenetrable compaction was encountered at a depth of about 30 centimeters, before a B-horizon was reached, so the obtained section of A-horizon was divided into two sub-horizons in order to make observations similar to the Wharton columns. Also the creation of two depths of the A horizon will enable comparisons to be made of removal as a function of depth.

Roughly 3800 liters of stormwater runoff was collected from the Penn State Harrisburg campus during Fall 2007 and kept in an indoor storage tank. This stormwater includes runoff from copper or tar rooftops, campus roadways/parking lots, and lawns. Approximately once a week, the stormwater was circulated inside the tank for 30 minutes, 135 liters pumped into a barrel, and 600 ml distributed into each column. The 600 ml volume is equivalent to a 7.5 mm storm event on a site where the infiltration system occupies 10% of the surface area. Each soil type received a total of 40 simulated storm events. Effluent was collected from each column weekly and volumes recorded.

A 500 ml bottle of water was collected from the barrel each week for influent water quality analysis and the effluent samples of the soil columns were analyzed bi-weekly on an alternating schedule. Water quality analysis was performed for the effluent of each column; the columns represent true replicates and the error bars on the graphs represent ± 1 standard deviation.

Water quality tests included pH and conductivity (indirect measure of dissolved salts); total hardness (calcium/magnesium); turbidity, color, total nitrogen, total phosphorus (phosphate), potassium, and sulfur (sulfate). Samples for future heavy metals analysis by graphite furnace were passed through a 0.45µm filter and preserved with a 2% addition of 67-70% nitric acid solution; copper, lead, and zinc are planned for testing early Spring 2009. Samples for future total organic carbon analysis by TOC analyzer were preserved with a 2% addition of 5N sulfuric acid.

At the start of the research and in intervals of 8-storm events, a column of each representative test group of each soil type was sacrificed for future soil testing at the Penn State College of Agricultural Sciences Agricultural Analytical Services Lab. Each sacrificed column is subdivided into ~3 inch segments and will be tested for

water pH, buffer pH, soluble salts, total carbon and total nitrogen through combustion, and phosphorus, potassium, magnesium, calcium, zinc, copper, and sulfur. Sieve analysis for soil texture has been completed and the soil analysis at State College is expected to be complete in early Spring 2009.

The initial plan was to have undisturbed natural soil columns, but the Wharton columns showed preferential flow along the pipe, with stormwater not flowing through the soil. It was decided that these columns would be removed from the PVC, divided into three-inch sections, broken apart, air dried, and then the sections repacked in their initial order. The Leetonia columns performed as intended and were left intact. Results for the Wharton silt loam are post-disturbance and may reflect the interaction of the soil type and the soil disturbance.

RESULTS

Results of water analysis reveal leaching of total nitrogen by all soil horizons of both soil types. While the leached concentrations of the Wharton soil started high (> 100 mg/L) and then sloped towards the influent (< 10 mg/L), the total nitrogen concentrations leached from the Leetonia soil started near the influent and then gradually increased to 20 – 30 mg/L (Figure 1). Two questions are raised by this data. First, did disturbing the Wharton soil expose parts of the soil where nitrogen was readily release? Second, what differences exist between the two soils that lead to the differences in stable effluent concentrations?

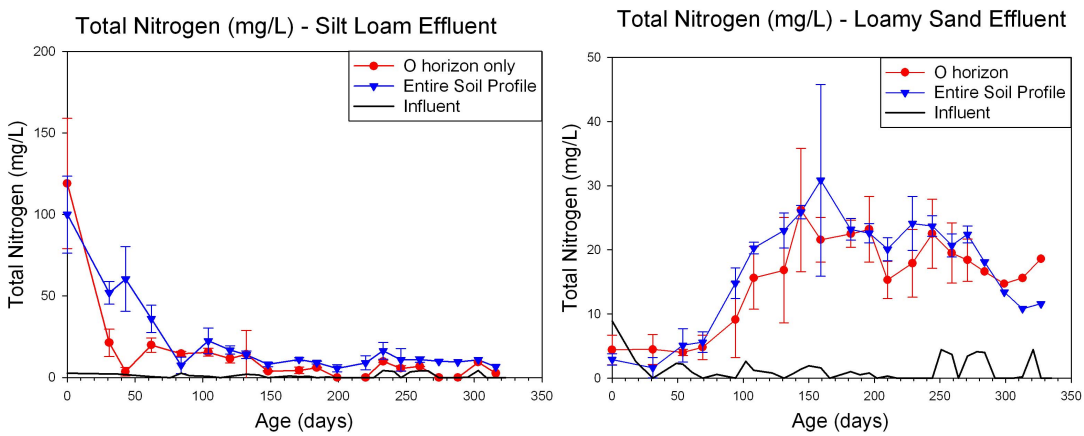

Figure 1. Effluent Total Nitrogen: Wharton silt loam and Leetonia loamy sand

The O-horizon had no impact on the total phosphorus concentration, after the elevated O-effluent concentration during the first two events (Figure 2). This elevated phosphorus concentration that decreased rapidly may be an artifact of the soil disturbance, especially since it correlates well with the elevated nitrogen concentrations from the Wharton soil. The less-organic soil horizons remove the phosphorus from the influent water, and as seen during the two earliest events for the Wharton soil, the lower mineral horizons remove the phosphorus that is released from the organic horizon. This indicates that an increasing mineral concentration and/or a

decreasing organic concentration, where phosphorus content is less likely to be bioavailable and more likely to be bound into soil minerals, can improve phosphorus removal in infiltration systems.

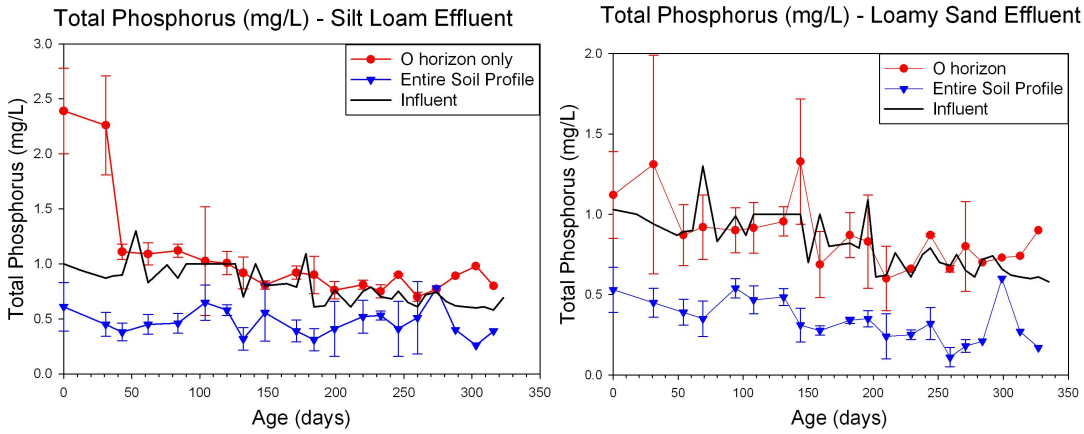

Figure 2. Effluent Total Phosphorus: Wharton silt loam and Leetonia loamy sand

Since potassium carries a +1 valence charge, it is likely to have limited competition in a media where the sorption/ion-exchange locations prefer a polyvalent cation. Interestingly, the potassium was not leached from the Wharton silt loam, although it was leached from the loamy sand (Figure 3).

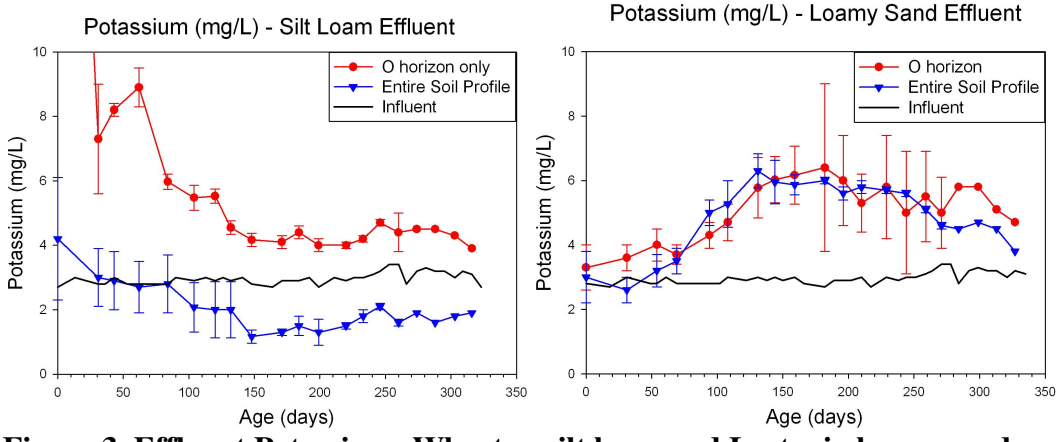

Figure 3. Effluent Potassium: Wharton silt loam and Leetonia loamy sand

Sulfate removal would require the soil to have a substantial anion exchange capacity (AEC). However, our observations indicate that the AEC of these two soils is small (Figure 4).

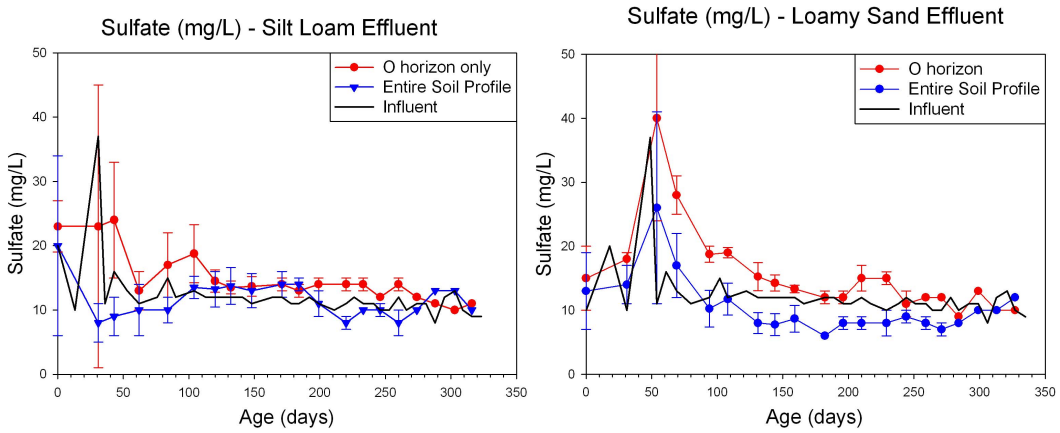

Figure 4. Effluent Sulfate: Wharton silt loam and Leetonia loamy sand

All soil horizons of both soil types lowered the pH of influent stormwater (Figure 5). Effluent pH was slightly lower for the Leetonia loamy sand. The Wharton silt loam has a slight upward trend in the effluent pH for the O and A horizons, indicating a potential loss of acidity. However, the acidity of the AB horizons together and the entire profile increase the acidity of the effluent water. For the Leetonia loamy sand, no change in pH has been observed. Until soil analysis is complete, the question remains as to whether changes in pH will herald changes in soil chemistry that affect removal.

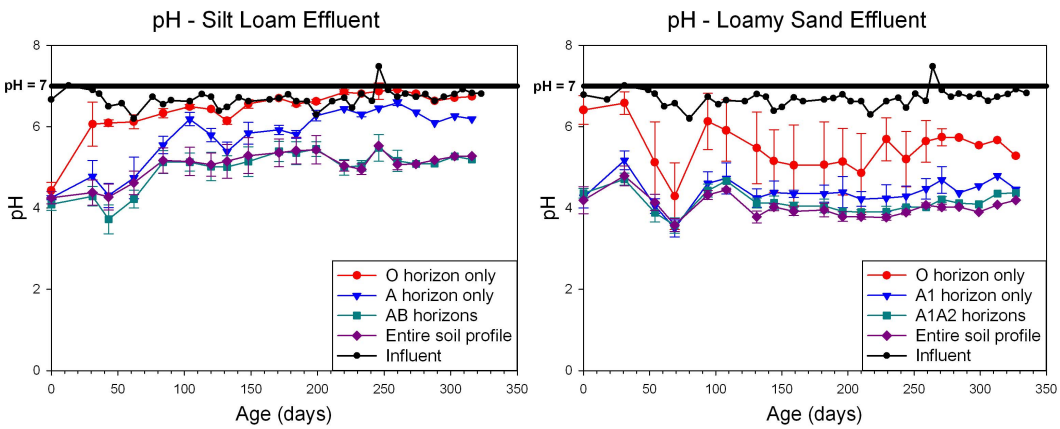

Figure 5. Effluent pH: Wharton silt loam and Leetonia loamy sand

All horizons increased conductivity, hardness, turbidity, and color of the passing stormwater. The hardness results (Figure 6) show a distinct contrast between the soils. The Wharton silt loam, the disturbed soil, had concentration trends similar to those of total nitrogen. The initial concentration of the hardness components was elevated compared to the influent and, after the first few filtering events, the effluent concentrations resemble the influent. This indicates that over time, a slight release of calcium and magnesium from the media is occurring, agreeing with what is known about calcium and magnesium's participation in ion-exchange reactions with other polyvalent cations. In general, if the passing water has a polyvalent cation that will

sorb to the soil stronger than calcium or magnesium, then the calcium or magnesium is released into the flowing water and is replaced by the polyvalent cation (typically heavy metals). This appears to be occurring in the Wharton soil. The early elevated concentrations may be an artifact of having to disturb the soil. Later in the soil's lifespan as a filtering media, it appears that the hardness increases through the soil profile, indicating potential sorption/ion-exchange sites for the polyvalent cations.

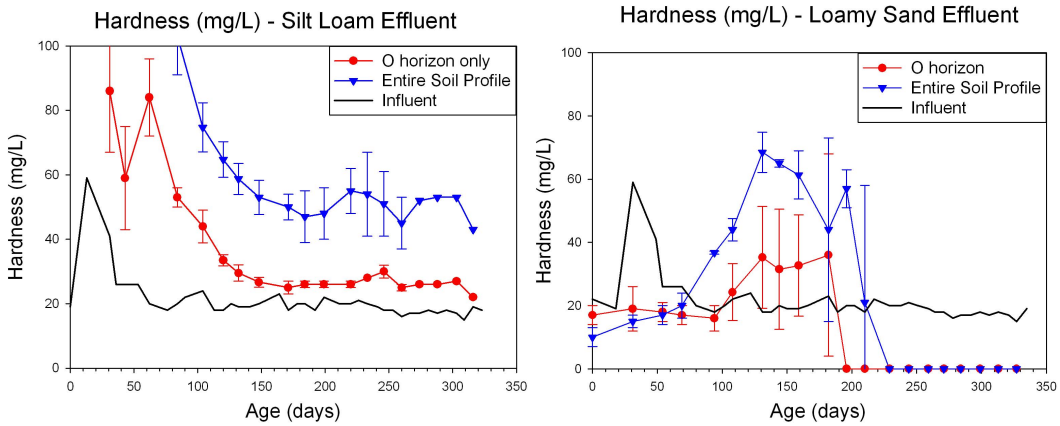

Figure 6. Effluent Hardness: Wharton silt loam and Leetonia loamy sand

The Leetonia loamy sand results are different. First, likely because the soil column was not disturbed during construction, hardness components such as calcium and magnesium were removed from the stormwater, indicating that removal sites existed for the entire group of polyvalent cations. However, after approximately eight weeks (four filtering events), hardness was released from the column. One explanation for the sudden leaching of hardness is that the sorption/ion-exchange sites were full, but that the calcium and/or magnesium were loosely bound. When a polyvalent cation with a stronger affinity for that soil component was near enough to the site to react and replace the calcium or magnesium, then the replacement occurred, washing out calcium and/or magnesium. What is unexpected is the decrease to zero hardness in the effluent near the end of the filter run – first for the organic horizon and then for columns containing the entire soil profile. This indicates that soil chemistry in the column has changed sufficiently to make removal of calcium and magnesium competitively favorable. It is unknown why this occurs.

DISCUSSION

The initial drastic leaching of some tested parameters by the Wharton soil columns, which had to be air-dried and repacked, may resemble what occurs after construction of infiltration units. The release of nitrogen especially is of concern because of the attention that nutrient pollution receives. The nitrogen release of the Wharton soil columns quickly reduced but the nitrogen release of the Leetonia soil columns slowly increased. This increase in nitrogen release by the Leetonia may be a result of decaying organic matter. These results are in contrast with those of Hsieh and Davis (2005), who found that nitrate removal increased with increased organic matter

(Hsieh and Davis, 2005). Additionally, field removal of nitrogen by infiltration units has also been observed (Hunt et al., 2006).

In contrast, a neutral impact on phosphorus content by the O-horizon columns of both soil types was observed and removal of phosphorus was seen by all other soil horizons of both soil types. The influent concentration of phosphorus in this study started around 1.0 mg/L and slowly decreased to 0.70 mg/L. Phosphorus removal has also been seen with influent concentrations of 3 mg/L but may or may not be independent of organic matter (Hsieh and Davis, 2005). In this study, the neutral interaction of the O-horizon and slightly greater removal of phosphorus by soil columns containing a B or A2 horizon suggest that phosphorus removal is independent of organic matter and is dependent on one or more components of the mineral matter. A limit to the phosphorus removal capacity of soils has been observed before in a groundwater recharge study (Schneider et al., 1987) and it is unknown whether removal would continue long term for infiltration applications.

In addition to the created nitrogen pollution, all soil horizons of both soil types lowered the pH of influent stormwater and increased the conductivity, hardness, turbidity, and color of effluent. The O-horizon columns of the Wharton soil had little impact on pH, but an influent pH of 6.7 was been reduced to 5-6 in the effluent of other Wharton columns. The Leetonia soil reduced pH to 4-5 in the effluent of all horizons. An influent conductivity of 40 µS/cm steadily increased in the effluent of all Leetonia columns and reached levels of around 150 µS/cm in the effluent of OA1A2 columns. The conductivity of Wharton column effluent leveled out at 60-90 µS/cm. Hardness slowly decreased in the effluent of the Wharton columns while it increased from the Leetonia columns, perhaps because of Leetonia's sandy composition. Until soil analysis has been completed, the cause of these changes can only be speculated. Despite low turbidity and color present in the influent, 4-7 NTU and 50-100 PtCo respectively, both the Wharton and Leetonia produced greatly increased levels in the effluent of their columns; especially the Wharton, which was air-dried and repacked.

CONCLUSIONS

Infiltration units may or may not be helping the stormwater dilemma but with continued research and changes in design they could definitely be a proper solution. Although only half completed and still in the process of obtaining some key data, this study has already provided interesting data for insight into the functions of individual soil horizons and their impacts on the suitability of infiltration units. The phosphorus removal shown by horizons with little organic matter is of significance and will be further researched. It is believed that the results of planned soil analysis will help answer some unknowns. A closer look at pollutant loadings and the influence of the outflow to inflow volume ratio upon pollutant removal will also be required since a connection has been seen before (Hunt et al., 2006). Finally, analysis of heavy metals is in progress and may help complete the picture.

REFERENCES

Clark, S.E., and Pitt, R. (2007). "Influencing factors and a proposed evaluation methodology for predicting groundwater contamination potential from stormwater infiltration activities." *Water Environment Research*. 79(1), 9-36.

Clark, S.E., Baker, K.H., Mikula, J.B., Burkhardt, C.S., Lalor, M.M. (2006). *Infiltration vs. Surface Water Discharge: Guidance for Stormwater Managers.* Water Environment Research Foundation. Project Number 03-SW-4. 2006. 220 pages.

Hsieh, C. and Davis, A.P. (2005). "Evaluation and optimization of bioretention media for treatment of urban storm water runoff." *Journal of Environmental Engineering*, 131(11), 1521-1531.

Hunt, W.F., Jarrett, A.R., Smith, J.T., Sharkey, L.J. (2006). "Evaluating bioretention hydrology and nutrient removal at three field sites in North Carolina." *Journal of Irrigation and Drainage Engineering*, 132(6), 600-608.

Schneider, B.J., Ku, H.F.H., and Oaksford, E.T. (1987). "Hydrologic effects of artificial-recharge experiments with reclaimed water at East Meadow, Long Island, New York." U.S. Geological Survey, Water Resources Investigations Report 85-4323.

Potential Data Analysis Methodology to Evaluate the Performance of Manufactured BMPs

Masoud Kayhanian[1*], Robert M. Roseen[2], James H. Lenhart[3], Greg Williams[4]

[1*]Department of Civil and Environmental Engineering, University of California, One Shields Avenue, Engineering III, Davis, CA 95616; PH (530) 752-8957; FAX (530) 752-7872; email: mdkayhanian@ucdavis.edu

[2]The University of New Hampshire Stormwater Center, Department of Civil Engineering, 35 Colovos Road, Durham, NH 03824; robert.roseen@unh.edu

[3]CONTECH Stormwater Solutions Inc., 11835 NE Glenn Widing Dr., Portland, OR 97220, LenhartJ@contech-cpi.com

[4]Monteco Research & Development Centre, 2596 Dunwin Dr., Mississauga, ON L5L 1J5 gwilliams@monteco.com

ABSTRACT

Evaluating the performance of manufactured BMPs on a consistent and scientifically sound approach is beneficial for both the service provider and the services recipient. To do this properly, it is important that these devices need to be tested under a standard set of protocols. The testing data must be collected, reported, and validated prior data analysis. The testing, data collection, data reporting and validation will be addressed under a separate ASCE/EWRI subcommittee. The focus of this paper is to address the data analysis and performance evaluation of manufactured BMPs.

To address this issue the existing statistical data analysis methods and performance evaluation that potentially could be used for manufactured BMPs have been examined in this paper. Special attention was devoted to the data distribution and the issue of normality since that will influence the selection of suitable data analysis approach. In general, it has been concluded that the stormwater data is log-normally distributed. The existing BMP performance evaluation has also been evaluated and the effluent probability plot has been recommended to determine the performance evolution of manufactured BMPs.

INTRODUCTION

Background. Since the passage of the United State Clean Water Act in 1972 and consequently through NPDES amendment in 1983, many local, state and industry are obligated to treat the stormwater runoff before discharging them to a receiving water. Initially with Phase I, the regulatory compliance was only applicable to communities with population higher than 100,000. Since as early as 2002, Phase II extended the same regulatory framework to communities with population of 10,000 or higher and to areas along the urban fringe that together have a residential population of at least 50,000 and an overall population density of at least 1,000 people per square mile. For this reason, demand for the use of compact treatment systems has increased and as a result numerous manufacturers responded and developed wide ranges of structured best management practices (BMPs) to remove different pollutants. These treatment systems are defined as manufactured treatment devices (MTDs). Some organizations such as Caltrans, who had the technical capability and financial resources tried to develop their own treatment systems that is more suitable on their right-of-way facilities (http://www.dot.ca.gov/hq/env/stormwater/special/newsetup/index.htm#new_technology). In recent years, however, the use of MTDs are rapidly increasing in order to meet escalating water quality regulatory requirements; particularly in re-development and new development areas where land space is limited and potential use of other BMPs are not practical. As the use of MTDs has been increased, the demand for some type of certification for their effectiveness in pollutant removal and meeting water quality standard has also been increased on national level. Several attempts have been made on

state and regional level (TAPE, TARP, ETV). However, no consistent protocol has been established for national use.

In response to this national demand, a manufactured BMP certification committee was established under the EWRI's stormwater infrastructure committee of water, wastewater, and stormwater council (WWSC) and the wet weather flow technology committee of the urban water resources research council (UWRRC) (Guo et al., 2007). In addition, parallel efforts are being undertaken by ASTM and WERF. To avoid inconsistencies between the organizations, liaisons from the task committee were established for these other groups. To develop the certification guidelines, several subcommittees were established and each subcommittee was responsible for specific task to develop the final certification guidelines document. The subcommittees to tackle specific tasks include: data reporting, data analysis and performance evaluation, lab testing, field monitoring, scaling, and maintenance. Deliverables from each sub-committee will be a technical guidance manual that will be published by EWRI. The work of each sub-committee will be presented at the annual ASCE/EWRI Congress conference meeting and finally will be published as a peer reviewed ASCE journal paper.

This effort has been broadened to be consistent with the reporting requirements for the International Stormwater BMP database (BMPDB) developed by a broad coalition of partners including the Water Environment Research Foundation (WERF), ASCE Environmental and Water Resources Institute (EWRI), USEPA, Federal Highway Administration (FHWA) and the American Public Works Association (APWA). The purpose of the BMPDB is to provide scientifically sound information to improve the design, selection and performance of BMPs. Continued population of the database and assessment of its data will lead to a better understanding of factors influencing BMP performance and help to promote improvements in BMP design, selection and implementation.

Focus of the paper. The objective of this paper is to summarize the data analysis and performance evaluation task and to prepare a conference manuscript to be presented at the ASCE/EWRI Congress conference at Kansas City, 2009. The specific objectives of this manuscript are to present (1) the potential data analysis approaches, and (2) to evaluate potential methodologies for assessing manufactured BMP performances. From this preliminary work, there will be an opportunity to recommend consistent protocol to evaluate the performance of manufactured devices.

POTENTIAL DATA ANALYSIS APPROACHES

Data Quality and Reporting Prior Statistical Analysis. The central goal of a BMP verification program is first to collect scientifically defensible data in fulfillment of the verification objectives. Statistical methods may be used in the design of the lab, pilot, or field testing to determine data quality objectives (DQOs). DQOs are an important and useful step to ensure that the data produced by laboratory or field testing is sufficient, both in terms of quality and quantity, to establish meaningful confidence levels for the BMP performance evaluation.

The use of standardized procedures to collect BMP performance data and reporting them is essential for successful verification program – not just from one BMP to another, but also from project to project, region to region, year to year. If consistent methods are not applied, it may be difficult to perform data comparisons, and the value of the data may be diminished. For instance, flow can vary significantly throughout a runoff event, and rainfall intensity and runoff volume (Kayhanian et al., 2007). Flow-proportioned composite samples are therefore considered to be the most representative sampling regimen for runoff monitoring. The preferred set-up for water quality evaluation in BMPs is to employ automated monitoring equipment to collect an equal sample volume (aliquot) for every increment of a pre-set runoff flow volume. The composite sample ideally needs to cover the full event hydrograph and accounts for variation in flow and/or runoff quality throughout the runoff event. Grab sampling, or even time-proportioned compositing, by contrast, may generally produce data that are not representative of any given runoff event. Grab sampling provides no information on the contaminant mass load, which in many cases is the ultimate goal. Depending on the sample timing and the nature of the events monitored, this can lead to a substantial bias in the reported results. However, grab samples

are typically needed for collecting solid samples (including sediment and litter) where automatic samplers may be impractical.

Regardless of method of sampling collection, the verification protocol should provide a series of steps to be taken both in the field and in the lab to ensure the overall quality of data. The product of hard work related to representative sample collection, analytical testing method, and proper QA/QC will still be a relatively useless pile of data reports if there isn't consistency in and an established protocol for data reporting. The data reporting protocols help ensure that data from all tested BMPs will be reported in consistent format – and that the data records will include sufficient information to permit their full use within a common database. For instance, if half of data for total suspended solids are reported as TSS and the remaining half as "Total Suspended Solids", extracting the data from a database may not include all dataset. Similarly, reporting inconsistent unit for TSS as PPM or mg/L may create similar problem on data extraction and data analysis. In addition, a well-designed database having a user-friendly interface feature can be developed to provide an efficient and uniform data storage and data retrieval as an important and essential component of a successful verification program.

Performing detail statistical analysis and performance evaluation of manufactured BMPs will require additional data collection such as flow, physical characteristics of the manufactured device, monitoring site characteristics, and storm event characteristics. These data can be included as part of the same database. The principal data components potentially to be collected under each category are summarized in Table 1. Fields and content guidelines for each of these categories will be described in detail by the Data Reporting subcommittee.

Table 1. Summary of potential data to be collected as part of the manufactured BMP verification.

Data collection category	Data component collected under each category
WQ Parameter and solids characteristics	*Water Quality:* conventional, nutrients, aggregate organics, metals (total and dissolved) PAHs, etc…… *Solids:* trash, total suspended solids (TSS), total dissolved solids (TDS), suspended solid concentration (SSC), particle size distribution (PSD)
Storm event and hydraulic characteristics	Storm event starting and ending time, rainfall characteristics, inflow and outflow volume, antecedent dry period, etc…….
Device physical characteristics	Device name, principal pollutant removal mechanism, design characteristics, size, etc…….
Monitoring site characteristics	Drainage area, imperviousness, number of lanes for highway, AADT, etc…….

Statistical Analysis. This section of the paper is organized to deal with some of the basic statistical analysis that can be performed to address specific question. General questions and statistical approach that are commonly used to address them are summarized in Table 2.
Detail discussion of each topic presented is beyond the scope of this paper and will be presented in final certification guidelines documentation. An overview of recommended statistical analyses for BMP performance monitoring can be found in the recently updated EPA manual (EPA, 2009). The selection of an appropriate statistical test based on the distribution of data (e.g., normality verification) is further discussed below.

Testing the Normal Distribution of Data. Various methods are available to test the normality of data distribution. The best method to verify normal distribution of stormwater runoff data is the probability plot of the original data and transformed data. Based on the past experience, the majority of the environmental data including stormwater runoff characterization and BMP performance data typically are not normally distributed. Log transformation is commonly the most suitable method to verify the normal distribution of data. A sample distribution of stormwater data for TSS prior to transformation

and after log-transformation is shown in Figure 1. As shown, the data distribution before transformation resembles an exponential function. After log-transformation of the data, the majority of the data plots linearly (at least between 10 percentile and 90 percentile range) and hence assumption of log-normal distribution is appropriate. The assumption of log-normally distributed data is important when performing a comparative statistical analysis (Shumway et al, 2002; Kayhanian et al, 2002).

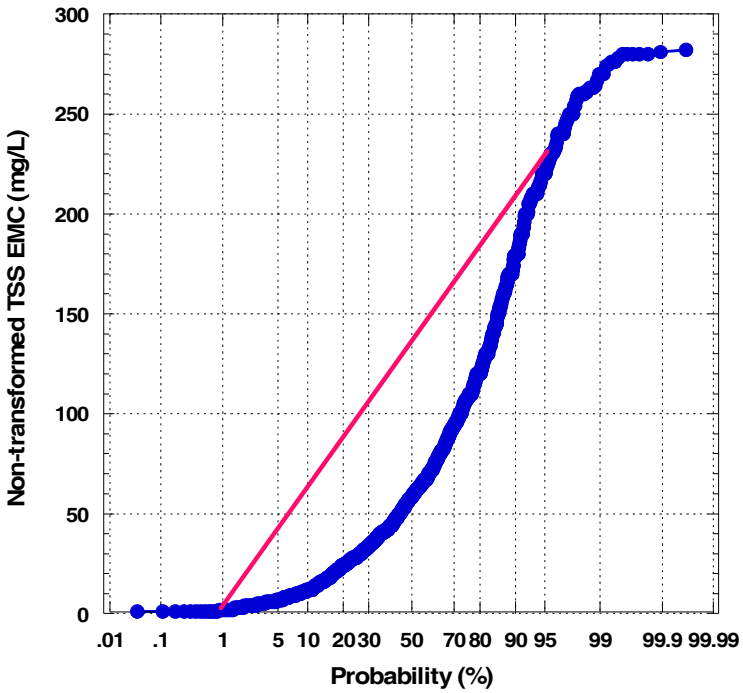

(a) non-transformed TSS data

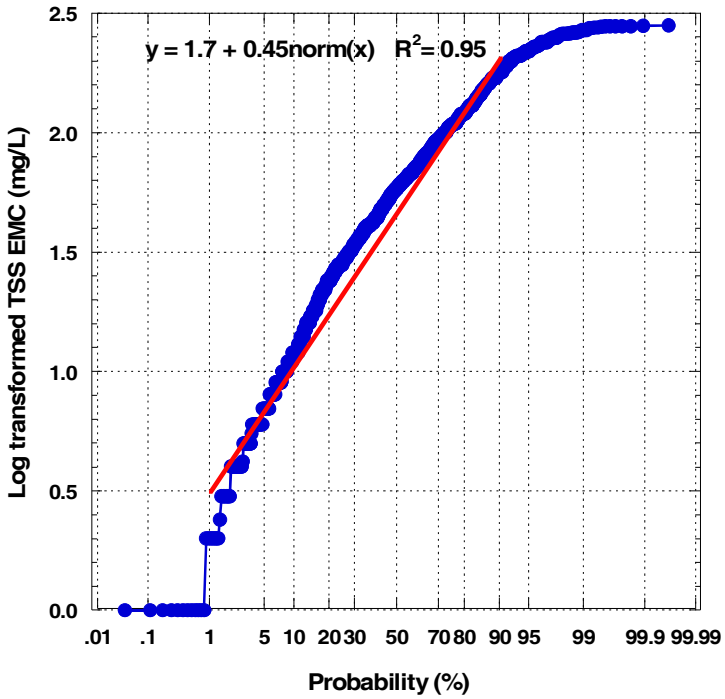

(b) Log-transformed TSS data

Figure 1. Probability distribution of TSS EMC before and after log-transformation.

Table 2. Summary of Statistical Approach Addressing Specific Question in BMP Testing.

Statistical topic	Question to be addressed	Statistical approach
Sample size	How many samples are needed to achieve desired confidence? After a few years of field sampling or number laboratory testing, how would we decide whether we need more samples than initially planed?	USEPA statistical methods for practitioners: EPA QA/G-9S
Selection of an appropriate statistical test	How do we verify whether data are normally distributed? How do we very that the data variability of two or more groups is similar? This question is specifically useful when preparing the BMP probability plots.	Graphical data presentation using histogram, box plot, normal probability plots. Numerical evaluation through Shapiro-Wilk W test
Addressing non-detect in data set	How do we account for non-detect results?	Regression on order statistics (ROS)
Examining outlier in data set	How do we prepare graphical and numerical data summaries to identify potential outliers?	Histogram, box plot, standard and log-transformed probability plots, and scatter plot
Probability of meeting water quality requirements	How do we estimate how often the average BMP effluent concentration would meet a water quality standard or regulatory discharge limit? How do we estimate the BMP percentage removal of a pollutant with a specified confidence level?	This should be available directly from the effluent probability plot of laboratory or field testing data, assuming the field data sample is large enough to be representative.
BMP effectiveness for specific pollutant removal	In an influent-effluent approach or before-after approach, how do we decide whether a given BMP is effective in removing a pollutant?	Hypothesis testing through null hypothesis (H_0) or alternative hypothesis (H_A). Statistical test performed include student's t-test with equal variance and t-test with unequal variance. Both tests assume a particular probability distribution.
Comparing effectiveness of two or more BMPs	How do we compare the effectiveness of two or more pilot BMPs under similar test condition or under a given geographic location?	Paired t-test comparing the mean of effluent concentration for normal or log-normally distributed data. Comparing three or more BMPs use the analysis of variance (ANOVA). Specific analysis include: parametric ANOVA (equal variances), Welch ANOVA (unequal variance).
Developing a linear regression equation	How does BMP effectiveness vary as a function of factors such as storm event characteristics, BMP design variables, operational, maintenance practices?	Multiple linear regression using the following form: $y = \beta_0+\beta_1x_1+\beta_2x_2+\ldots\beta_mx_m+\varepsilon$ where, y=response variable, x=model variable, β = model parameters, and ε random error
Effectiveness of BMPs over time	How can we tell if the effectiveness of a BMP is changing over time within a year or multiple years?	Graphic representation using time-series plot or Mann-Kendall test.

The normality can further be tested using goodness of fit test applying the Shapiro-Wilk W test. For example the data presented in Table 3 can be tested for normality using graphical representations of data using standard probability, histograms, or box and whisker plots. The results of the Shapiro-Wilk W test for the previous data set are shown in Table 3 and illustrates that the original data did not fit the normal distribution but was log- normally distributed. The brief discussion presented here could justify the log-transformation of manufactured BMP data and may be used as a basis to perform other statistical analysis.

Table 3. Summary of Shapiro-Wilk W test to verify the normal distribution of a typical data.

Test #	BMP effluent	Shapiro-Wilk W test result
1	10.9	*Parameter estimate prior transformation:*
2	4.3	*Parameter* *Estimate* *Lower 95%* *Upper 95%*
3	6.9	μ 11.84 8.75 14.94
4	0.7	σ 13.90 12.03 16.47
5	2.9	
6	79.6	*W test result:*
7	9.6	*W = 0.642* *Prob<W = <0.0001*
8	4.0	
9	4.8	*Since the probability is less than 0.05, we can conclude that the assumption of normal distribution is not reasonable.*
10	14.3	
11	14.5	
12	4.4	*Parameter estimate after log- transformation:*
13	12.2	*Parameter* *Estimate* *Lower 95%* *Upper 95%*
14	13.5	μ 1.99 1.77 2.22
15	8.6	σ 1.02 0.88 1.21
16	8.4	
17	11.7	*W test result:*
18	9.7	*W = 0.974* *Prob<W = <0.105*
19	17.8	
20	3.8	*Since the W is much higher that the W of the original data and probability is greater than 0.05, we can not reject the normal distribution of log-transformed data.*
21	4.6	
22	11.6	
23	3.6	
24	1.5	
25	10.3	
26	16.0	

MANUFACTURED BMP PERFORMANCE EVALUATION

Review of the historical approaches. During the past ten years numerous methods have been applied to evaluate the performance of constructed and manufactured BMPs. These methodologies are summarized in Table 4. A few of the performance evaluations shown in Table 4 (e.g., influent and effluent concentration or load basis) are more commonly used while others are less common. The approach for using the performance evaluation in most cases is straight forward. Two other methods specifically the "lines of comparative performance" (Minton, 1999) and "performance expectation function" (Lenhart, 2007) have also been introduced and their application have not universally been adapted. However, among all performance evaluation the probability method may be the most comprehensive way to evaluate manufactured BMPs and it is gradually being recognized as method of choice as it has been recommended by the USEPA/ASCE (2002). The potential application of this technique is further discussed below.

Table 4 Summary of Methodologies used for BMP Performance Evaluation.

Method	BMP Performance Evaluation Method	Approach/Formula	Applicable certification program
1	Pollutant EMC reduction for single test or storm event	$\text{Efficiency} = 100 \times (1 - \frac{\text{Effluent EMC}}{\text{Influent EMC}})$	ETV, TARP, TAPE, EPA
2	Pollutant load reduction for single test or storm event	$\text{Efficiency} = 100 \times (1 - \frac{\text{Effluent load}}{\text{Influent load}})$	ETV, TARP, TAPE, EPA/ASCE
3	Pollutant load reduction for multiple tests of storm events	$\text{Efficiency} = 100 \times (1 - \frac{B}{A})$	ETV, TARP, TAPE, EPA/ASCE
4	Mean pollutant concentration removal efficiency	$\text{Efficiency} = 100 \times (1 - \frac{\text{Average effluent Conc.}}{\text{Average influent Conc.}})$ This technique does not require flow measurement and it might be useful for pollutants with grab sampling where no flow weighted data is available.	EPA/ASCE BPM performance monitoring
5	Regression of loads (ROL)	Compute effluent and influent load same as method 2; perform linear regression based on outflow and inflow load and determine the R^2 and slope of regression line. Under special circumstance, the regression lines may be forced through (0,0) as it may produce a more realistic lead removal.	EPA/ASCE BPM performance monitoring
6	Relative to achievable	$\text{Efficiency} = 100 \times (1 - \frac{\text{Attainable limit Conc.}}{\text{Average influent Conc.}})$	EPA/ASCE BPM performance monitoring
7	Relative to water quality standard	$\text{Efficiency} = 100 \times (\frac{\text{avg. infl. conc.} - \text{avg. effl. conc.}}{\text{avg. infl. conc.} - \text{WQ standard conc.}})$	EPA/ASCE BPM performance monitoring
8	Effluent probability method	This method provides comprehensive BMP performance evaluation by presenting the standard parallel probability plot of both influent and effluent EMCs for all storm events or performance tests.	EPA/ASCE BPM performance monitoring

Effluent load = effluent EMC × effluent volume
Influent load = influent EMC × influent volume

$$B = \left[\sum (\text{effluent EMC}_1 \times \text{flow V}_1) + (\text{effluent EMC}_2 \times \text{flow V}_2) + \ldots\ldots\ldots (\text{effluent EMC}_n \times \text{flow V}_n)\right]$$

$$A = \left[\sum (\text{influent EMC}_1 \times \text{flow V}_1) + (\text{influent EMC}_2 \times \text{flow V}_2) + \ldots\ldots\ldots (\text{influent EMC}_n \times \text{flow V}_n)\right]$$

Effluent Probability Method. Effluent probability method is probably the most comprehensive method that could be used to determine the performance evaluation of manufactured BMPs. Under this approach, a standard probability plot is prepared for both inflow and outflow pollutant EMC or load. Before, preparing the probability plot, however, non-parametric (or if applicable parametric) statistical tests should be conducted to indicate if the difference between influent and effluent are statistically significant. In addition, the log normality should be checked and the probability plot may be prepared based on log transformed data. If the log transformed data deviates significantly from normality, other transformations can be explored to fit the data distribution. Three example of log-normally distributed probability plots are shown in Figures 1 through 3. Figure 1 shows the probability plot for TSS data for a BMP that there is a clear difference between influent and effluent event mean concentration. Figure 2, shows the TSS data for another BMP that there is no distinct difference between influent and effluent EMC. Under this situation, no removal efficiency can be expected. Figure 3 shows the results for TSS data for a condition when a BMP performed fairly well when influent TSS concentration was high but achieved no removal when TSS concentration was low.

One problem associated with the probability method is the lack relationship with direct influent and effluent measurement. For instance, a BMP performance is much higher under correlated data shown in 2 vs. 1 (see top Figure). Ideally, the BMP performance can remain within a narrow range with high probability of meeting effluent requirement regardless of influent concentration or testing condition. For example, the sample probability plots could be used to determine if BMP could meet certain regulatory or standard effluent quality requirement. As an example, under ideal BMP performance (see top Figure 3), the probability plot shows that effluent TSS quality of 30 mg/L can be met at all time. Multiple probability plots can also be produced under a single plot to compare the performances of two or more BMPs.

Another issue that worth to discuss with respect to BMP performance is that the pollutant removal generally decreases as influent concentration decreases. This may not be a practical problem since the point where BMP performance starts to decrease is often close to the point where the influent concentration is low enough that is does not exceed the discharge requirement and hence a high level of treatment is not needed. Similarly, if majority of pollutants are associated with smaller particle size, some manufacturer devices may not be able to sufficiently meet the discharge load requirement at full capacity flow rate. However, it has been shown that this phenomenon is largely dependent on the dominant unit process used in certain MTDs and as such filtration systems do not exhibit much variability in removal (Roseen et al, 2006). Nevertheless, there is value in requiring BMPs to report performance even at low concentrations, recognizing that removal may not as important if discharge limits are being met. At the other extreme, discharge limits may exceeded at very high influent concentrations even though the BMP were capable of removing 80% of influent concentration. Therefore, testing the manufacture BMPs under wide ranges of influent flow and pollutant concentration is essential in order to determine the true performance characteristics.

SUMMARY AND CONCLUSIONS

Generally, the manufactured BMP performance data collected over a range of flow rates is not normally distributed. This can impact the choice of statistics used to describe performance. Log transformation found to be a good choice for normal distribution and hence the statistical data analysis should be performed accordingly. The choice of statistical method usually related to question to be addressed and must be performed on consistent basis throughout the verification program.

Consistent, data collection, data management, data retrieval, and data analysis is an important and essential integrated component of a successful manufactured BMP verification program. This may apply to both laboratory and field testing; although it is more realistic for laboratory generated data so lab data collection should be a requirement. For proper performance evaluation, the manufactured BMP may be tested at 25, 50, 100 and 125 percent of designed flow. BMP testing at or above 100 percent of designed flow rate is especially useful to assess scouring.

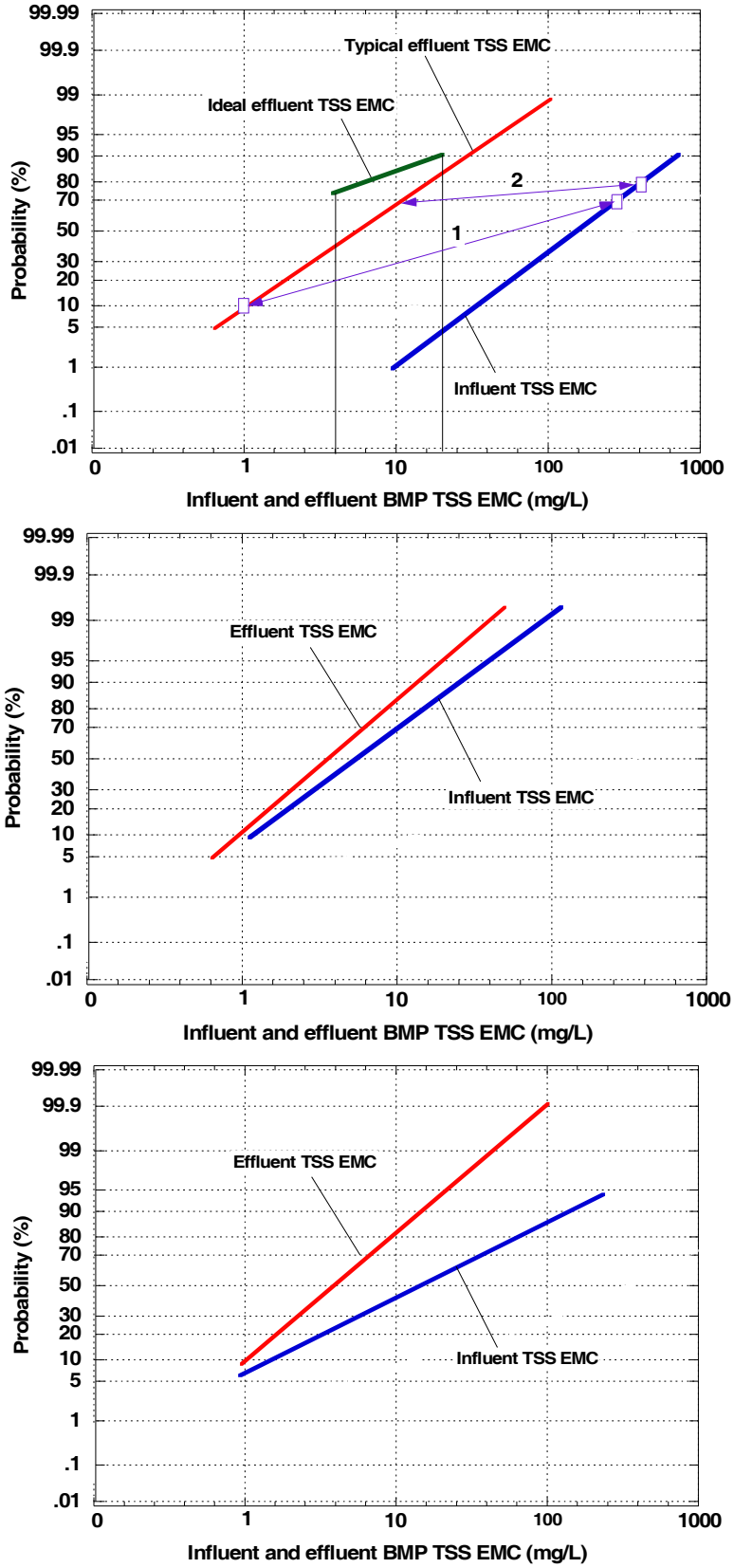

Figure 3. Probability plot for influent and effluent BMP TSS EMC under three different performance conditions.

ACKNOWLEDGEMENTS
The lead author greatly acknowledges the contribution of Robert Roseen, Jim Lenhart, and Greg Williams for their valuable comments and suggestions. This paper will be presented at the EWRI congress conference at Kansas City and the travel expense for the paper presentation will partially be supported by the ASCE/EWRI task force committee.

REFERENCES

American Society of Civil Engineers and U.S. Environmental Protection Agency (2002). *Urban Stormwater BMP Performance Monitoring, A Guidance Manual for meeting the National Stormwater BMP Database Requirements*, April, EPA-821-B-02-001. http://www.bmpdatabase.org/docs/Urban/Stormwater/BMP/Performancemonitoring.pdf

ETV Verification Protocol (2002). *Stormwater Source Area Treatment Technologies*, Draft 4.1, March. http://www.epa.gov/etv/pubs/04_vp_stormwater.pdf

Guo, Q., G. England and E,C. Johnston (2007) Development of Certification Guidelines for Manufactured BMPs. Proceedings of EWRI conference, Hawaii, May 17-21.

Kayhanian, M., A. Singh, and S. Meyer (2002). " Impact of non-detects in water quality data on estimation of constituent mass loading." *Water Science and Technology,* 45(9), 219-225.

Kayhanian, M., A. Singh, C. Suverkropp, S. Borroum (2003). "The Impact of Annual Average Daily Traffic on Highway Runoff Pollutant Concentrations." *Journal of Environmental Engineering*, Vol. 129(11), 975-990.

Kayhanian, M., C. Suverkropp, A. Ruby, and K. Tsay (2007). "Characterization and Prediction of Highway Stormwater Pollutant Event Mean Concentrations." *Environmental Management*, 85(2), 279-295.

Lenhart, James (2007) "BMP Performance Expectation Functions – A Simple Method for Evaluating Stormwater Treatment BMP Performance Data." 9th Biennial Stormwater Research and Watershed Management Conference, Orlando, FL.

New Jersey Department of Environmental Protection (2006). *New Jersey Tier II Stormwater Requirements – Amendments to TARP Tier II Protocol*, Division of Science, Research and Technology, NJDEP, Trenton, New Jersey, January. http://www.state.nj.us/dep/dsr/bscit/NJStormwater_TierII.pdf

Minton, Gary (2005). Stormwater Treatment. Resource Planning Associates, Seattle, Washington, U.S.A.

Roseen, R. M., Ballestero, T. P., Houle, J. J., Avellaneda, P., Wildey, R., and Briggs, J. F. (2006). "Performance evaluations for a range of stormwater LID, conventional structural, and manufactured treatment strategies for parking lot runoff under varied mass loading conditions." *Transportation Research Record: Journal of the Transportation Research Board*(No. 1984), 135–147.

Shumway, R., R. Azari, and M. Kayhanian (2002). Statistical Approaches to Estimating Mean Water Quality Concentrations with Detection Limits. *Environmental Science and Technology*, Vol. 36, No. 15, 3345-3353.

Technology Acceptance Reciprocity Partnership (2003). *Protocol for Stormwater Best Management Practice Demonstrations*, Endorsed by California, Massachusetts, Maryland, New Jersey, Pennsylvania, and Virginia, Final Protocol August 2001, Updated July 2003. http://www.state.nj.us/dep/dsr/bscit/StormwaterProtocol.pdf

USEPA, ASCE, Consultants, G., and District, U. D. a. F. C. (2009). "Urban Stormwater BMP Performance Monitoring." *EPA-821-B-02-001*, Washington DC.

Washington State Department of Ecology (2002). *Guidance for Evaluating Emerging Stormwater Treatment Technologies, Technology Assessment Protocol – Ecology (TAPE)*, October 2002 (Revised June 2004), Publication Number 02-10-037. http://www.ecy.wa.gov/biblio/0210037.html

Proposed scaling relations for manufactured stormwater BMPs

John S. Gulliver, Qizhong Guo, John J. Sansalone, Gregory Williams, and J.S. Wu
for the Scaling Sub-Committee,
Guidelines for Certification of Manufactured Stormwater BMPs Task Committee

Manufactured stormwater best management practices (BMPs) generally apply one or both of two unit operations to remove particles from stormwater runoff: hydrodynamic separation and filtration. Hydrodynamic separation is best used to remove sand particles, while filtration is used to remove organic particles as well as silt and clay. Many manufactured stormwater BMPs also have a chamber designed to remove floatables, or particles that are lighter than water. The numerous designs and multiple sizes of these manufactured stormwater BMPs suggest the need for scaling criteria to size and apply designs in the field. This paper reviews the scaling criteria research that has been completed, the research that may be adopted from other areas, and the needs for developing scaling criteria in manufactured stormwater BMPs.

KEYWORDS

Best Management Practices, Unit Operations, Unit Processes, Stormwater, Particulate Matter, Particle Size Distributions, Dimensionless Numbers, Scaling

Introduction

Most manufactured stormwater BMPs (M-BMPs) function as either hydrodynamic separators or filters. Hydrodynamic separators utilize the difference in density to settle suspended solids into the bottom of the device and to retain floatables, such as hydrocarbons and trash at the surface of the device, while the effluent flows through an intermediate elevation. Filters use a media to retain particles of a given size while the effluent flows through the filter. These devices are generally placed below ground, and therefore are suited for high density locations and retrofits to existing infrastructure. There is a great need for these underground devices, and manufacturers have responded to this need. M-BMP units supplied by each vendor are manufactured with specific capacity/size categories. Scaling criteria help in developing performance specifications for various sizes of M-BMP and in utilizing model-scale tests to develop performance specifications. However, an industry-wide, uniform methodology to scale and size these devices does not currently exist. This paper will review the need for scaling criteria in M-BMPs, and propose scaling criteria for head loss and flow, particle separation, scour and filtration.

Need for Scaling Relations

Because of interaction with a complex flow field, the need for scaling criteria is probably greatest in hydrodynamic separators. The vertical velocity relative to water causes separation while the turbulence of the flow field tends to mix the media that is being separated back into the water. There are three issues that need to be addressed: 1)

settling of heavier-than-water particles out of the flow, 2) rise of lighter-than-water compounds such as oils and trash out of the flow field, and 3) the tendency to entrain both after separation has been accomplished in high flow. Experimental tests are possible on model-scale or full-scale devices, but these tests will need to be scaled to another size of device in order to meet demand. In addition, if an accurate scaling procedure can be developed and verified, it will be possible to perform smaller-scale model studies on each device which can be scaled to full device size with a known accuracy.

A filter media can be tested through column studies. However, the parameters that need to be controlled (e.g., grain size versus column diameter) and scale-up to full scale filters needs to be documented. In addition, many filters are partially self-cleaning, utilizing turbulence in the flow field to remove caked material from the filter. The scaling relations developed in item 3) above may be sufficiently general to apply to this case as well. Tests would still be required on the devices to demonstrate and measure the self-cleaning properties. To apply the results of such tests to a multiple of device sizes would require scaling criteria.

Dimensionless Numbers and Scale Effects

One goal of scaling is to have one dimensionless number that represents the important processes of the device. This is not generally possible at all scales, so criteria are developed on the appropriate model scale. These criteria include a critical Reynolds number value that must be exceeded to assure that turbulent flow occurs:

$$\mathbf{Re} = \frac{Q}{\nu d} \geq \mathbf{Re_C} \tag{1}$$

and a critical Weber number that must be exceeded to assure that surface tension does not alter the flow field:

$$\mathbf{We} = \frac{\rho Q^2}{\sigma d^3} \geq We_C \tag{2}$$

where Q is discharge through the device, ν is kinematic viscosity, ρ is density of the liquid, σ is liquid surface tension, g is the acceleration of gravity, and d is the smaller of the important length scales in the flow field, such as the diameter of the device or depth of water. It is also common practice to enhance the wall roughness in a physically-scaled model to result in a similar relationship of wall shear stress to flow velocity (similar friction factor or drag coefficient) as in the full scale.

Fenner and Tyack (1997) reviewed the scaling criteria for removal efficiency and head loss of hydrodynamic separators and, in addition to geometric similarity, came up with the following dimensionless similarity criteria:

Removal Efficiency: Hazen number = $\mathbf{Ha} = \frac{AV_s}{Q}$ (3)

$$\text{Froude number} = \mathbf{Fr} = \frac{Q}{\sqrt{gd^5}} \quad (4)$$

Pressure loss:

$$\text{Euler number} = \mathbf{Eu} = \frac{\Delta P d^4}{\rho Q^2} \quad (5)$$

$$\text{Friction factor} = \mathbf{f} = \frac{u_*}{V} \quad (6)$$

where A is the plan area of the separator, V_s is the settling velocity of the particles, V is a mean flow velocity, g is the acceleration of gravity ΔP is pressure drop, ρ is the density of the fluid, and $u_* = (\tau_{wall}/\rho)^{1/2}$ is the shear velocity at the walls. The Hazen number is designed for similarity of settling in a quiescent flow field, Froude number similarity is required for fluid flow driven by gravity, Euler number similarity will appropriately scale up pressure loss and friction factor similarity is required for the influence of turbulence in the flow field. Friction factor similarity would also be important for removal efficiency, because of the impact of turbulence on particle settling.

Based upon previous experience with settling of suspended sediments in lakes (Dhamotharan, et al. 1981), the Peclet number (**Pe** = $V_s L /D_t$) and a dimensionless time, are appropriate and sufficient dimensionless scaling parameters to explain sediment deposition rates. In the definition of the Peclet number V_s is particle settling velocity in quiescent water, L is settling depth, and D_t is a vertical eddy diffusion coefficient. Peclet number is defined as the ratio of convection to diffusion: in this case the convective, settling process is opposed by eddy diffusion in the system tending to keep solids in suspension. Similar to the approach taken for lakes and reservoirs, Wilson, et al. (2007, 2008) scaled convection with the settling velocity (V_s), used the settling depth (h) as a vertical length scale L, and a flow velocity times a length scale for the vertical diffusion coefficient (D_t). When the diameter is the shortest dimension of the flow, $D_t \sim Ud$, and by continuity $D_t \sim Qd/A$. In most hydrodynamic separators, flow enters the chamber from above and turbulence is stronger where plunging occurs. Therefore, if A is taken as the horizontal projection of the chamber (the cross-sectional area of mixing) which is proportional to d^2, then $D_t \sim Qd/d^2 = Q/d$. The Peclet number for the stormwater treatment device therefore becomes;

$$\mathbf{Pe} = V_s\, h\, d/Q \quad (7)$$

If the smallest dimension of the device is its height, or settling distance, as is the case for detention ponds, then inflow is relatively horizontal and thus A becomes the cross-section of the pond, hd. Therefore $D_t \sim Qh/dh = Q/d$ and **Pe** = $V_s\, h\, d/Q$. In both cases, one obtains the same equation for the Peclet number. The resulting Peclet number resembles the Hazen number, $V_s\, d^2/Q$, which is the ratio of settling velocity to overflow rate and was not developed to scale eddy diffusion.

Scaling of Removal Efficiency for Hydrodynamic Separators

Fenner and Tyack (1997) investigated the performance of a 1.6 m and 0.3 m diameter hydrodynamic separators with plastic beads of specific gravity equal to 1.04. They found that Froude scaling was most accurate at low removal efficiencies and Hazen

scaling was more successful at higher removal efficiencies. They proposed a hybrid scaling formula which incorporates the impact of each dimensionless number:

$$\frac{Q_{prototype}}{Q_{model}} = \eta_m L_r^{\,2} + (1-\eta_m) L_r^{\,2.5}\left(1+\frac{d_p}{3mm}\right) \tag{8}$$

Where η_m is the fraction of removal in the model, d_p is the mean particle diameter in mm and L_r is the length ratio (prototype/model). To be used in practice, Eq. (8) should be adjusted for the specific gravity of the particles, which typically will differ from those used in Fenner and Tyack's experiments, or arranged to use the settling velocity of the particles. The latter was performed on Fenner and Tyack's data to result in:

$$\frac{Q_{prototype}}{Q_{model}} = \eta_m L_r^{\,2} + (1-\eta_m) L_r^{\,2.5}\left(1+\frac{V_S}{25mm/s}\right) \tag{9}$$

where V_S is settling velocity of the particles in mm/s.

A relationship for settling velocity has been developed by Ferguson and Church (2004)

$$V_s = \frac{gRd_p^{\,2}}{18\nu + \left(0.75CgRd_p^{\,3}\right)^{1/2}} \tag{10}$$

where v is kinematic viscosity of the fluid, d_p is particle diameter, g is the gravitational acceleration, R is the specific gravity in water (1.65 for silica sand) and C is a constant equal to 0.4 for spheres and 1 for typical sand grains. Equation (10) becomes Stokes law at small particle diameters and results in a constant drag coefficient for large particle diameters.

A criticism of Eq. 8 is that it mixes flow scaling with particle settling into one equation. The result is that Eq. (8) and (9) will be applicable only to the particles that Fenner and Tyack tested. This is not necessary, and it is possible to separately scale settling velocity and flow. One proposal for scaling is outlined in the following sections.

Flow and Head Loss in Hydrodynamic Separators

Flow in most hydrodynamic separators is controlled by gravitational forces. The field of physical hydraulic models has been performing this type of scaling for many years. The criteria are as follows:

1. The model should be sufficiently large that surface tension (Weber number effects) does not alter performance and scaling of the model.
2. Reynolds numbers in the model should be sufficiently large such that the flow is not close to laminar. For open channels this is Re = 2,000 and for closed conduits, Re = 8,000 is recommended.
3. The friction factor in the model should be close to the prototype value. This often means adding some roughness to the model. This will make the ratio of turbulence to flow velocity similar in the model and prototype.

4. Froude number scaling is now possible:

$$Fr_p = Fr_m \tag{11}$$

where subscripts *p* and *m* indicate prototype and model scales, respectively. Then,

$$\frac{Q_p}{Q_m} = \left(\frac{L_p}{L_m}\right)^{5/2} \tag{12}$$

Settling and Rise in Hydrodynamic Separators

Scaling for settling with both retention (Hazen number) and turbulent mixing (Peclet number) result in a similar scaling parameter for settling of solids in hydrodynamic separators. Froude number scaling, Eq. (12), should also be followed. The final result is:

$$\frac{Q_p}{Q_m} = \frac{V_{Sp}}{V_{Sm}}\left(\frac{L_p}{L_m}\right)^2 \tag{13}$$

It is possible to satisfy both Eqs. (12) and (13) because of the addition of settling velocity to equation (12). Although model-prototype tests are needed to verify this scaling technique, the fact that both mixing and retention result in the same scaling parameters is encouraging. In addition, rise velocity for floatables should follow the same scaling parameters as settling.

Scour in Hydrodynamic Separators

Collected solids in hydrodynamic separators, if not cleaned, will eventually reach the height where scour of the collected solids will occur. In addition, some hydrodynamic separators are exposed to higher flows, beyond the design flow, and are therefore subject to potential scour of collected solids. Scour is physically modeled by equating (dimensionless) Shields stress, the presumed bottom stress where sediment begins to move off of the bottom, divided by parameters of the sediment. Shields stress is given by:

$$\tau^* = \frac{u_*^2}{gRd_P} \tag{14}$$

where $u_* = \sqrt{f/8}V$ is shear velocity.

Equating Shields stress for model and prototype results in

$$\frac{Q_p}{Q_m} = \sqrt{\frac{f_m d_{pp} R_p}{f_p d_{pm} R_m}}\left(\frac{L_p}{L_m}\right)^2 \tag{15}$$

As with settling, Froude number scaling, Eq (12) should also be followed. The process of scour in a Hydrodynamic separator is a combination of lifting sediment off of the bed and settling of that sediment back to the bed. Thus, scour similarity needs to simultaneously satisfy Eqs. (13) and (15). To get similarity relations (13) and (15) to both be satisfied, relatively large sediment is necessary, such that Eq. (10) becomes

$$V_s = \sqrt{\frac{gRd_p}{0.75C}} \tag{16}$$

This is often difficult to achieve.

Removal Efficiency for Filters

The particle trapping of a filter is a local phenomenon, dependent upon the characteristics of the media and the particle size distribution of the suspended solids. This can be relatively well simulated with a bench-top column test, where the media filtration efficiency is tested with the particle size distribution of interest. The scaling parameters of most interest are the media Reynolds number,

$$\boldsymbol{Re} = \frac{Q}{\varepsilon^{1/3} A^{1/2} \nu} \tag{17}$$

and the suspended solid-media size ratio:

$$L_s = \frac{d_p}{d_{med}} \tag{18}$$

where ε is the porosity of the filter media and d_{med} is the equivalent spherical diameter of the media. Then, scaling of discharge and media would follow the relations:

$$\frac{Q_p}{Q_m} = \left(\frac{\varepsilon_p}{\varepsilon_m}\right)^{1/3} \frac{L_p}{L_m} \frac{\nu_p}{\nu_m} \tag{19}$$

and

$$\frac{d_{med,p}}{d_{med,m}} = \frac{d_{p,p}}{d_{p,m}} \tag{20}$$

The scaling of one particle size distribution to another, and scaling with filter flow rate is of interest because it would reduce the required filtration tests. In addition, filters are often placed in the turbulent flow field of the device, resulting in differential pressure drop across the filter that varies spatially.

In the application of filters, one needs to also consider the fouling that will occur at the filter surface. Fouling will increase the frequency of cleaning and could reduce the filter life. The cleaning of particle cake which has accumulated on the surface of the filter, however, cannot be simulated with column tests because cleaning is often provided by turbulence generated in the chamber of the filter device. This would require a scaling

analysis similar to high flow scour, since both are based upon the resuspension of collected material.

Conclusions

1. Scaling laws have been proposed for head loss, settling, scour and filtration. These laws need to be tested with combined model and prototype studies of manufactured BMPs.
2. The scaling relation of Fenner and Tyack is not recommended, because it combines settling and head loss similarity and is applicable only to the type of spheres used in their experiments.
3. Froude number scaling, with approximately equal friction factors, should be used in all model studies.
4. Settling can be modeled with Peclet number or Hazen number scaling. They are equivalent, and encompass the important processes of settling.
5. Scaling for scour should follow Shields stress and Hazen (Pecltet) number scaling. This will be difficult, but is possible if the sediment is sufficiently large, such as with plastic beads.
6. The scaling of filtration units is dependent upon the size of the particles relative to the size of the media and the pressure distribution in the filtration chamber. Froude scaling with equal friction factors should be sufficient for pressure distribution. In addition, cleaning of a filter unit is similar to scour, such that the scour scaling parameters should also be followed to simulate cleaning of the filter fouling. While bench tests are acceptable to test the filter media, the operation of the filter as a whole deserves a full scale prototype test, because of the complexities of pressure distribution and fouling. Model scaling relations would help in determining the performance of manufactured filtration units.

The ability to scale the performance of manufactured stormwater BMPs through similitude relationships will help size and design these products for municipalities. In addition, it will focus the research and experiments on items that are truly essential to performance. The result will be more focused research, improved quality of tests, and better manufactured stormwater BMPs. Although there is much work to be completed in improving scaling relations for these devices the committee believes that the benefits will outweigh the costs.

References

Dhamotharan, S., J.S. Gulliver and H.G. Stefan. (1981). Unsteady One-Dimensional Settling of Suspended Sediment. *Water Resources Research,* 17(4), 1125-1132.

Fenner, R. A. and Tyack, J. N. (1997). "Scaling laws for hydrodynamic separators." *Journal of Environmental Engineering*, 123(10), 1019-1026.

Ferguson, R.I. and M. Church (2004). A Simple Universal Equation for Grain Settling Velocity, *Journal of Sedimentary Research*, 74(6), 933–937.

Wilson, M, J.S. Gulliver, O. Mohseni, R.M. Hozalski (2007). *Performance assessment of underground stormwater treatment devices*. St Anthony Falls Laboratory Project Report No. 494, University of Minnesota, Minneapolis, Minnesota.

Wilson, M. A., O. Mohseni, J. S. Gulliver, R. M. Hozalski and H.G. Stefan (2008). "Assessment of hydrodynamic separators for stormwater treatment," *Journal of Hydraulic Engineering*, In press.

Wisconsin Department of Commerce & Wisconsin Department of Natural Resources (2007). *Method for Predicting the Efficiency of Proprietary Storm Water Sedimentation Devices* (1006), September 15 draft, http://watertech.rutgers.edu/VerificationProtocols/Wisconsin/.

Rainwater Harvesting for Non-Potable Use in Gardens: A Comparison of Runoff Water Quality from Green vs. Traditional Roofs

Natasha Nicholson[1]*, Shirley E. Clark[1], Ph.D., P.E., D. WRE, Brett V. Long[2], Julia Spicher[3], Kelly A. Steele[1]

[1*]Penn State Harrisburg, 777 W. Harrisburg Pike, Middletown, PA 17057, emails: ntn113@psu.edu, seclark@psu.edu, kel95us@hotmail.com

[2]GTS Technologies, Inc., 441 Friendship Road, Harrisburg, PA 17111, email: blong@gtstech.com

[3]Greeley and Hansen, Inc., 1818 Market Street, Suite 3400, Philadelphia, PA, 19103, email: jspicher@greeley-hansen.com

ABSTRACT

Sustainable stormwater management involves ensuring that site runoff not exceed the pre-development peak flow rate and volume, typically accomplished through the use of water retention, infiltration, and reuse onsite through rainwater harvesting. Certain roofing materials, however, may be a pollutant source, thus, influencing the runoff's potential for harvesting. This project focuses on the first year of roof life for several traditional roofs and an extensive green roof. Substantial and significant releases of zinc and copper originated from an uncoated galvanized roof and from two treated woods, respectively. Roof runoff concentrations during early life indicated potential toxicity concerns for zinc and copper both in the water and from the potential buildup in the soil. Periodic elevated nutrient concentrations also were seen. Additionally, periodic spikes in pollutant concentrations after periods of low water concentrations indicated that elevated pollutant levels simply were not a result of washoff from excess preservative remaining on the surface of the material at installation.

KEYWORDS

Green roof; galvanized roof; shingles; roofing; cedar shakes; treated wood; runoff; source control; metals; early life; nutrients

INTRODUCTION

Impervious surfaces, such as rooftops and pavements, occupy a large part of the urban landscape. They often are directly linked directly to urban receiving waters through the storm drainage system. It is common, for example, in older cites in the northeastern United States to have the roof drains directly connected to the storm sewer or combined sewer system. This direct transport system for impervious-area-

generated pollutants has led to quantifiable degradation in urban receiving waters. Prior research links either total impervious area or directly-connected impervious area (as a percent of total urban land) to stream degradation with threshold values of no alteration/degradation typically found at approximately 10 – 15% impervious surfaces (Klein, 1979; Schueler, 1994; U.S. EPA 2002; Wang and Kanehl, 2003; Wang et al., 2001; Wang et al. 1997; Walsh and Breen 2001). Roofing is a substantial fraction of the urban impervious surface area (Akbari et al., 2003; Bochis et al., 2008).

Laboratory studies of common construction materials have demonstrated the potential for many construction materials to leach pollutants into the environment (Clark, 2000, Clark et al., 2004). Other studies have confirmed the important role played by roofs, paved surfaces, treated woods, and other construction materials to wet weather flow pollutant contributions, with primary emphasis on metals' release from these materials (Clark et al., 2008; Boller, 1997; Good, 1993; Brown and Peake, 2006; Adeniyi and Olabanji, 2005; Athanasiadis et al., 2006; Tobiason et al., 2004; Khan et al., 2006; Bailey et al., 1999; Davis and Burns, 1999; Kingette Mitchell, 2003; Wallinder et al., 2007). Clark et al. (2008) also have investigated nutrient contributions from these roofing materials. Extensive green roofing, where the media depth is shallow and the plants are typically drought and heat tolerant alpine-types, has been examined as a means of reducing the volume of and improving the quality of stormwater runoff (Berghage et al., 2007a,b; Berghage et al., 2008; DeNardo et al., 2003; Emilsson et al., 2007; Kohler and Schmidt, 2003; Moran, 2004; Teemusk and Mander, 2007; Long et al., 2008; Wanielista et al., 2007). In general, green roofs have been shown to remove metals from runoff, with nutrient releases being mixed and potentially dependent on the form and content of nutrients in the growing media.

Although pollutant releases can occur at any point in time, generally, it is thought that there are two periods of concern for pollutant release – early and late life. During the early life (such as within the first few months to one year), excess sealants and potential surface contamination wash off. This release decreases over time with environmental exposure. The second time of concern is the end of life where the material has degraded so greatly that the subsurface/subbase materials are exposed and pollutants released.

Green roof lifespans are currently estimated at 30 – 50 years, based on functioning installations in Europe approximately 30 years in age. For green roofs, the early stage encompasses plant establishment and washout of fines in the media mix. Also, depending on the growth media or substrate used, initial runoff may have excess nutrients leached out before stabilizing. For other materials, this lifespan is typically approximately the same or smaller. For example, asphalt shingle roofs often are guaranteed for approximately 15 – 20 years.

The purpose of this research is to compare the runoff quality from several types of roofing early in their life spans (defined for this research as approximately 4 months): galvanized (uncoated) steel roofing, asphalt shingles, cedar shakes, and green roofing with an expanded shale and peat moss media. The underlying question for this research is whether the green roof improved runoff quality compares to the traditional

roofing materials investigated here. If improved runoff quality is seen, then the follow-up question to be answered is whether the green roof actually "cleaned" the rainfall or whether its presence, in place of a traditional material, prevented the release of pollutants.

METHODS

This paper compares the results from two projects – one focusing on commercially-available roofing materials and one focusing on green roofing – as the materials aged over the first twelve months of operation, defined here as the early life of a roof. This designation is arbitrary. It is the time of initial aging and includes the period where washoff of excess surface coatings or cross-contamination due to storage near fertilizers at the retail location would occur for traditional roofs. For the green roof, this time period incorporates the early plant establishment phase and potential aging of the organic growth substrate. The data reported herein for the traditional roofs was collected from August 2005 through July 2006 (results from the first two years of testing is reported in Clark et al., 2008). Green roof samples were collected June 2007 through May 2008 (full test results since installation can be found in Clark et al., 2008). With the exception of the green roof materials, all roofing materials were purchased from Lowes Home Improvement Stores in Harrisburg, PA. The description of the green roof materials and their sources can be found in Long et al. (2008).

These roofing materials were installed on test frames on the Penn State Harrisburg campus. The roof frames for traditional roofs were designed to mimic residential roofs; both installation practices and materials mirrored those used in the field to the maximum extent practicable. The treated woods, cedar shakes, uncoated galvanized metal, asphalt shingles, and a plexiglass control panel were installed in August 2005.

The extensive green roofs were installed in late May 2007. The roof slope was 1:4, which is near the upper slope range for non-baffled roofs. The green roof consisted of a drainage layer of coarse expanded shale, topped by a geotextile layer, and finally the media mix (42.5% medium-grade expanded shale, 42.5% fine-grade expanded shale, 10% peat moss, and 5% granular activated carbon). The media mix was determined through the laboratory testing reported in Long et al. (2008).

Samples were collected from almost every storm for both roofs within each respective early lifespan except when the forecast was for less than 0.05 inches of rain. Samples were collected and analyzed for pH, nutrients (nitrate, ammonia, total nitrogen, and total phosphorus) and heavy metals (lead, copper, cadmium, arsenic, nickel, iron and zinc) using methods outlined in APHA (2005). The lists of analytical methods were described in Clark et al. (2008) and Long et al. (2008). The HDPE and plexiglass roofs were used to measure atmospheric deposition and their results were background subtracted from the runoff concentrations of the other materials. With the exception of pH, for which background subtraction would not be valid, the results shown in this paper were corrected for atmospheric contributions and reflect only the contributions from the materials themselves.

Statistical analysis was performed for each parameter using a multivariance one-way analysis of variance (MANOVA) on ranks in SigmaStat 3.5 (SPSS, Inc.) with the post-hoc Dunn method for pairwise comparison. The MANOVA on ranks was used because the assumptions of normality and/or equal variance were not met for each parameter. The MANOVA on ranks used a significance level of 0.05.

RESULTS AND DISCUSSION

All pollutant concentrations have been background corrected for atmospheric deposition, allowing for direct material comparisons. pH values presented here are direct measurements without any background corrections. Only total pollutant concentrations are presented. Although more bioavailable, dissolved species of pollutants have not been analyzed for this dataset.

Figure 1 shows the results for pH. The pH of the control was included in this figure to highlight the pH of the rainwater after it was returned to the lab. It ranged between approximately 4 and 6, slightly acidic. Periodic samples of rainwater pH also were collected and analyzed in real-time at the test site. Rainwater pH was occasionally slightly lower than that measured in the lab in the samples, ranging from 3.7 to 6.0. The results showed that the green roof was able to neutralize the acidic rainwater to above 7.0. Neutralization also occurred with both the galvanized and shingle roofs from the traditional roofs.

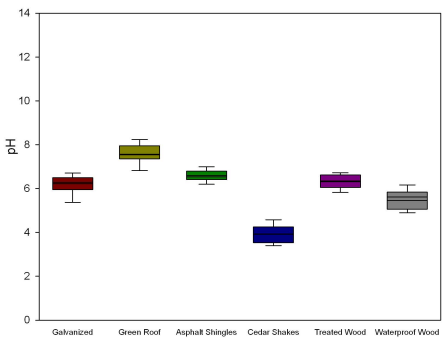

Figure 1. Runoff pH from roofing materials and control (rainfall pH range between 3.9 and 6).

For pH, the three categories statistically different categories were high (pH > 6), middle (pH = 4 – 6), and low (pH < 4). The highest pH group included the green roof, the galvanized metal, and the asphalt shingles. The middle group was comprised of the treated and waterproof woods plus the control. The low pH group contained the cedar shakes. Compared to the control and the rainwater samples, the cedar shakes consistently acidified the samples and were statistically different from the other materials.

Figure 2 highlights the nutrient release for nitrate. The results for ammonia and total nitrogen are similar to those seen for nitrate. All materials had several storm events for which no measurable nitrate was found in the runoff water. The nutrient runoff

concentrations for the galvanized metal and green roofs never exceeded 1 mg/L. The galvanized metal was not a source of total phosphorus (data not shown), in contradiction to other work performed by this research team on galvanized metal, which found measurable concentrations of total phosphorus in the runoff water. Of these materials, the cedar shakes were the greatest source of nitrate, potentially due to the degradation of the surface of the wood and the splitting of the shingles as the materials age. The asphalt shingles were the greatest source of phosphorus. Unlike for nitrate, the green roof was a source of phosphorus. It has been hypothesized that the phosphorus results from the release of nutrients in the peat used to supply organic matter to the green roof. Research by Hunt et al. (2006) on bioinfiltration media, which is currently under investigation for applicability to green roof media, indicated that if a low-phosphorus organic media is used and maintenance on the roof can be managed to add only the phosphorus required for the plants, phosphorus content in the runoff may be reduced to levels that are not an aquatic concern.

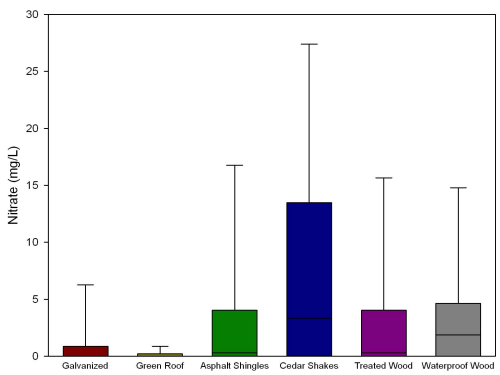

Figure 2. Runoff nitrate concentration from roofing materials (background corrected).

The statistical analysis for both nitrate and phosphorus found that the roofs were not distinguishable from each other, with the exception of the difference in runoff nitrate concentrations between the cedar shakes and green roof. This likely was due to the large variabilities seen in the runoff data and several non-detections of nitrate and phosphate in the runoff from the woods and shingles. The concern was whether surface contamination existed on the roofs at the beginning of testing that washed off during subsequent storms. Sources of this contamination could be excess surface sealants or fertilizer potentially stored nearby at the home improvement store. The runoff concentrations were graphed as a function of material age (Clark et al., 2008 contains the graphs for all roofing materials but the green roof) to examine any potential temporal trends. No trends were noted for the green roof. For the other roofing materials, spikes were seen during the testing period; however, a general trend of decreasing concentrations was noted for total phosphorus (but not for the nitrogen compounds).

The results for the metals are shown in Figures 3 and 4 for copper and zinc, respectively. The results for lead, cadmium, chromium, nickel, and arsenic are not shown because the concentrations were regularly near or below the method detection limit. Iron results are not included because they mirror the results seen for zinc, with elevated concentrations associated with the galvanized metal roof. Several materials had small releases of copper: galvanized metal, green roof, asphalt shingles, and cedar shakes. The median runoff concentrations were < 25 µg/L, which were well below the caution level for terrestrial plant toxicity. This concentration, however, is in the toxic range of certain aquatic plants (US EPA, 2007). Large variabilities were seen in the runoff concentrations for the cedar shakes and asphalt shingles. Figure 4 shows the upper ranges for the runoff copper concentrations and the large range of runoff concentrations for the two treated wood products. Statistically, the roofs could be divided into two groups – high (treated woods) and low (galvanized metal, green roofs, cedar shakes, and asphalt shingles) runoff concentrations.

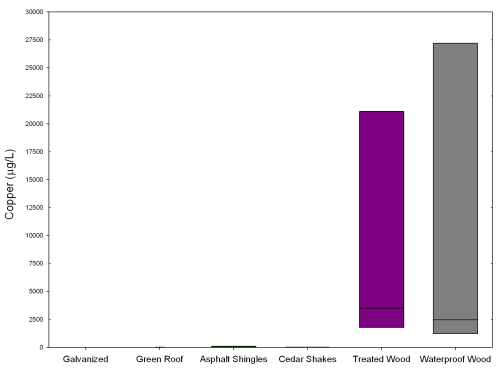

Figure 3. Runoff copper concentrations from roofing materials (high runoff concentration materials, background corrected).

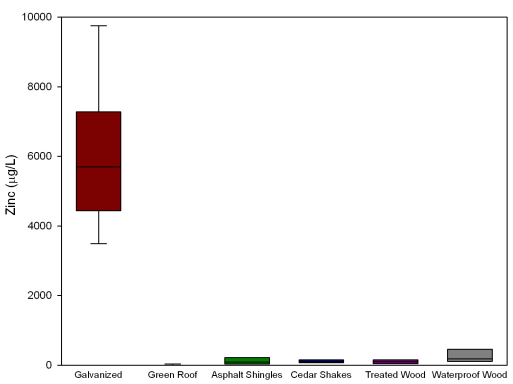

Figure 4. Runoff zinc concentration from roofing materials (background corrected).

For zinc, statistically, the materials were separated into high concentration (galvanized metal) and low concentration (green roof, asphalt shingles, cedar shakes, and the treated woods) materials. The high zinc concentration in the runoff from the uncoated galvanized metal was not surprising since zinc is added in the hot-dip galvanizing process as the sacrificial cation and may have been released as the roof captures the hydronium ion and neutralizes the acid rain. Comparison of the runoff concentrations from the uncoated galvanized metals to the aquatic toxicity criteria established by the U.S. Environmental Protection Agency (120 µg/L) showed that the median runoff concentration was approximately 1,400 times greater than the criteria.

The underlying hypothesis of this research was that there were two periods in the life-span of these materials that were of concern environmentally. The first, and the focus of this investigation, was the early life, when excess surface coatings and surface contamination from storage would wash off into the runoff. In the case of the green roof, this early life coincided with plant establishment and aging of the organic materials in the media mixture, likely characterized by nutrient release. The second would be when substantial visible degradation occurred. It was assumed that this degradation would expose to the atmosphere substrates that were not designed for environmental exposure.

This research does not focus on the fate and transport of these pollutants. However, the discharge location of the roofing runoff may affect whether these compounds are receiving water concerns. The runoff concentrations, particularly of zinc and copper from the galvanized metal and treated woods, respectively, may be problematic for rainwater harvesting for landscape irrigation. Concerns are raised not only because of the water quality itself but also because of the potential for metal buildup in the uppermost soil layer. The uppermost soil layer typically has a relatively high organic content, which often results in strong binding of the metals to the soil. Treese et al. (unpublished data) has shown a substantial buildup of copper in the upper 5 cm of the soil profile after approximately 1 year worth of rainfall. This rapid rate of soil buildup may be an exception since the runoff source was primarily a roof with substantial copper flashing. However, metal accumulations in the root zone must be considered when selecting a roofing material appropriate for rainwater harvesting.

Future research, in addition to developing models of degradation and resultant runoff concentrations as a function of the environmental parameters causing degradation, also should focus on whether a first flush exists, which would require treatment prior to reuse and possibly prior to discharge. It also should focus on the speciation of the pollutants in the runoff. This research analyzes only the total pollutant concentrations and does not analyze for the fraction that was dissolved and likely more bioavailable.

CONCLUSIONS

These results show that during the early life of a roofing system, several of the traditional roofing materials (shingles, cedar, galvanized) release pollutants into the

rainwater. These pollutants may then be transported in the storm drain system to receiving waters. Green roofs have been advocated as a means to control the volume of the runoff, but limited information is available about their water quality contributions. This research tests an extensive green roof along with several traditional roofing materials. Based on these early-life results, it appears that, while the green roof may not clean up relatively clean rainwater further, with the exception of acidic rainfall, it may be a roofing system that contributes few pollutants to the runoff water.

Sustainability initiatives typically focus on rainwater harvesting for landscape irrigation. This research highlights the water quality concerns, and potential need for treatment, in the runoff from several common building materials advocated for harvesting. Further research will be required to determine whether the pollutants seen in this research are bioavailable. Based on this research, exposed treated woods and uncoated galvanized metals appear to be inappropriate for rainwater harvesting, and possibly for direct receiving water discharge as well, during their early life (measured to date as four months in the U.S. Mid-Atlantic region).

ACKNOWLEDGMENTS

The authors would like to express their gratitude to Dr. Robert Pitt, Betsy Graham, and Noboru Tagawa of the University of Alabama for their assistance in digesting and analyzing the metals samples. Additionally, the authors would like to thank the following Penn State Harrisburg undergraduate and graduate students for their assistance in constructing and maintaining the test set-ups: James Elligson, J. Bradley Mikula, Daniel Treese, and Natasha Nicholson. Funding for this research was supplied by the Penn State Harrisburg Graduate Research Council and the School of Science, Engineering, and Technology.

REFERENCES

Adeniyi, I.F.; Olabanji, I.O. (2005) The physico-chemical and bacteriological quality of rainwater collected over different roofing materials in Ile-Ife, southwestern Nigeria. *Chem. Ecol*., 21, 149 - 166.

Akbari, H.; Rose, L.S.; Taha, H. (2003) Analyzing the land cover of an urban environment using high-resolution orthophotos. *Landscape Urban Plan.*, 63, 1 – 14.

APHA (American Public Health Association); American Water Works Association (AWWA); Water Environment Federation (WEF). (2005). *Standard Methods for the Examination of Water and Wastewater, 22nd ed.*; Clesceri, L.S., Greenberg, A.E., Eaton, A.D., Eds.; APHA, AWWA, WEF: New York.

Athanasiadis, K.; Helmreich, B.; Wilderer, P.A. (2006) Infiltration of a copper roof runoff through artificial barriers. *Water Sci. Technol.,* 54, 281 - 289.

Bailey, H.C.; Elphick, J.R.; Potter, A.; Zak, B. (1999) Zinc toxicity in stormwater runoff from sawmills in British Columbia. *Water Res.*, 33, 2721 - 2725.

Berghage, R.; Jarrett, A.; Beattie, D.; Kelley, K.; Husain, S.; Rezai, F.; Long, B.; Negassi, A.; Cameron, R.; Hunt, W. (2007) *Quantifying evaporation and transpirational water losses*

from green roofs and green roof media capacity for neutralizing acid rain. National Decentralized Water Resources. Research project report. www.ndwrcp.org.

Berghage, R.; Beattie, D.; Jarrett, A.; O'Conner, T. (2007b) Greenroof runoff water quality. *Greening Rooftops for Sustainable Communities 2007 – Conf. Proc.* Minneapolis, MN.

Berghage, R.; Wolf, A.; Miller, C. (2008) Testing green roof media for nutrient content. *Sixth Annual International Greening Rooftops for Sustainable Communities Conf. Proc.* April 30 – May 2, 2008, Baltimore, MD.

Bochis, C., R. Pitt, and P. Johnson. "Land development characteristics in Jefferson County, Alabama." In: *Stormwater and Urban Water Systems Modeling*, Monograph 16. (edited by W. James, E.A. McBean, R.E. Pitt and S.J. Wright). CHI. Guelph, Ontario, pp. 249 – 282. 2008.

Brown, J.N.; Peake, B.M. (2006) Sources of heavy metals and polycyclic aromatic hydrocarbons in urban stormwater runoff. *Sci. Total Environ*., 359, 145 - 155.

Clark, S.E.; Steele, K.A.; Spicher, J.; Siu, C.Y.S.; Lalor, M.M.; Pitt, R.; Kirby, J.T. (2008) Roofing materials' contributions to stormwater runoff pollution. *J. Irrigation Drainage Eng*., 134. October 2008 (in production).

Davis, A.; Burns, M. (1999) Evaluation of lead concentration in runoff from painted structures. *Water Res.*, 33, 2949 - 2958.

DeNardo, J.C.; Jarrett, A.R.; Manbeck, H.B.; Beattie, D.J.; Berghage, R.D. (2003) Stormwater detention and retention abilities of green roofs. *World Water and Environmental Resources Congress 2003*, Philadelphia, PA. American Society of Civil Engineers, Reston, Virginia.

Emilsson, T.; Berndtsson, J.C.; Mattson, J.E.; Rolf, K. (2007) Effect of using conventional and controlled release fertiliser on nutrient runoff from various vegetated roof systems. *Ecol. Eng*., 29, 260 - 271.

Good, J.C. (1993) Roof runoff as a diffuse source of metals and aquatic toxicity in stormwater. *Water Sci. Technol*., 28, 317 - 321.

Hunt, W.F., A.R. Jarrett, J.T. Smith, and L.J. Sharkey. 2006. "Evaluating Bioretention Hydrology and Nutrient Removal at Three Field Sites in North Carolina." *ASCE Journal of Irrigation and Drainage Engineering* 132(6): 600-608.

Khan, B.I.; Solo-Gabriele, H.M.; Townsend, T.G.; Cai, Y. (2006) Release of arsenic to the environment from CCA-treated wood. 1. Leaching and speciation during service. *Environ. Sci. Technol*., 40, 988 - 993.

Kingette Mitchell Ltd.,; Diffuse Sources Ltd. (2003) *A study of roof runoff quality in Auckland New Zealand: Implications for stormwater management*. Kingette Mitchell Ltd., Takapuna, Auckland, New Zealand.

Klein, R.D. (1979) Urbanization and stream quality impairment. *Water Resour. Bull*., 15, 948-963.

Kohler, M.; Schmidt, M. (2003) *Study of extensive green roofs in Berlin: Part III Retention of contaminants* (Translated by Saskia Cacanindin), Technical University of Berlin, Berlin, Germany.

Moran, A.C. (2004) *A North Carolina field study to evaluate greenroof runoff quantity, runoff quality, and plant growth*. M.S. Thesis, North Carolina State University, Raleigh, North Carolina.

Scheuler, T. (1994) The importance of imperviousness. *Watershed Protection Techniques*, 1 100 - 111.

Teemusk, A.; Mander, U. (2007) Rainwater runoff quantity and quality performance from a greenroof: The effects of short-term events. *Ecol. Eng.*, 30, 271 - 277.

Tobiason, S. (2004) Stormwater metals removal by media filtration: Field assessment case study. *Watershed 2004 Conf. Proc.* (CD-ROM). Water Environment Federation, Alexandria, Virginia.

U.S. EPA (U.S. Environmental Protection Agency). (2002) *National management measures to control nonpoint source pollution from urban areas - draft*. Office of Wetlands, and Watersheds (Ed.): United States Environmental Protection Agency.

U.S. EPA (U.S. Environmental Protection Agency). (2007). *Aquatic life ambient freshwater quality criteria: Table 4*. Office of Water (Ed.): U. S. Environmental Protection Agency. http://www.epa.gov/waterscience/criteria/copper/2007/table-4-freshwater-plant.pdf.

Wallinder, I.O.; Bahar, B.; Leygraf, C.; Tidblad, J. (2007) Modeling and mapping of copper runoff for Europe. *J. Environ. Monitor.*, 9, 66 - 73.

Walsh, C. J.; Breen, P.F. (2001) A biological approach to assessing the potential success of habitat restoration in urban streams: Verhandlungen der Internationalen Vereinigung für theoretische und angewandte. *Limnologie.*, 27, 3654 - 3658.

Wang, L.; Kanehl, P. (2003) Influences of watershed urbanization and instream habitat on macroinvertebrates in cold water streams. *J. Am. Water Resour. Assoc.*, 39, 1181 - 1196.

Wang, L.; Lyons, J. L.; Kanehl, P.; Gatti, R. (1997) Influences of watershed land use on habitat quality and biotic integrity in Wisconsin streams. *Fisheries.*, 22, 6 - 12.

Wang, L.; Lyons, J.; Kanehl, P. (2001) Responses of stream habitat, macroinvertebrate, and fish to watershed BMPs: Lessons from Wisconsin. *Watershed 2000 Management Conference*, July 2000, Vancouver, British Columbia. Water Environment Federation, CD-ROM.

Wanielista, M.; Hardin, M.; Kelly, M. (2007) *The effectiveness of green roof stormwater treatment systems irrigated with recycled green roof filtrate to achieve pollutant removal with peak and volume reduction in Florida*. FDEP Project Number: WM 864, University of Central Florida and Stormwater Academy. 175 pages.

Redesigning Constructed Stormwater Wetlands: an integrated modeling approach to optimize form and function

G.D. Jones[1], K.A. Mogavero[1], and B.M. Wadzuk[1]

[1]Department of Civil and Environmental Engineering, Villanova University, 800 Lancaster Avenue, Villanova, Pennsylvania, 19085;PH (610) 519-5365, FAX (610) 519-6754; email: gerrad.jones@villanova.edu, kristen.mogavero@villanova.edu, bridget.wadzuk@villanova.edu, M.ASCE

ABSTRACT

Constructed stormwater wetlands (CSWs) have tremendous potential in managing stormwater runoff. These systems are shallow marsh environments that are built to minimize both peak flow rates and contaminant loads to aquatic ecosystems following storm events. In order to meet these goals, CSWs are constructed with few guiding principals. Despite these principles, little research has been conducted to optimize the biological, chemical, and physical processes involved in stormwater mitigation.

A four tiered modeling approach is underway to redesign Villanova's CSW, however, this paper focuses on MIKE 11 a hydraulic model. Four plan view designs were created which included a one pond, two pond, one pond and meander, and continuous meander design. Using the same inflow data, a modeled outflow hydrograph was simulated. Three parameters were obtained from this hydrograph: peak flow rate, time to discharge, and time rate of change of flow.

The best performing design was the continuous meander design which had the lowest peak flow rate, longest stormwater discharge time, and lowest mean change in flow rate. The second best performing design was the one pond design. As a general rule of thumb, increasing the length to width ratio increases the hydraulic performance. Although this may be true, the single pond design had the lowest length to width ratio but was the second best performing model. Based on these results, volume storage was the best predictor of model performance.

INTRODUCTION

Constructed stormwater wetlands (CSWs) are shallow marsh systems planted with emergent vegetation that are designed to treat stormwater runoff (PADEP 2007). Because of their high capacity to reduce pollutant loads, CSWs are becoming increasingly popular for mitigating stormwater runoff (Koob et al. 1999; PADEP 2007). Furthermore, CSWs are capable of reducing peak flow rates associated with stormwater runoff. Despite their benefits, their large size requirements are a limiting factor in their implementation (PADEP 2007). Therefore, in order to maximize their efficiency in the smallest available space, having an understanding of how the features of a CSW affect its performance is critical.

When designing CSWs, stormwater managers have few design criteria to aid in creating the most efficient system for their needs. Walker (1998) found that the residence time of

polluted stormwater was the key factor in treatment efficiency of wetlands. Persson et al (1999) concluded that large length-to-width ratios, wide uniform depths, and wide wetlands with transverse baffles were the key characteristics that made an efficient wetland. These design suggestions were also corroborated by Conn and Fiedler (2006). Although the body of literature on CSWs is growing, Scholz and Lee (2005) concluded that detailed processes within constructed wetlands contributing to the treatment performance is lacking. Furthermore, it appears that good performance designs are obtained through trial and error instead of applying mathematical principles to maximize the performance at a particular location.

Because creating an optimum design for CSWs is critical for meeting stormwater regulations, and because little research exists for understanding the mathematical relationship between CSW features and their affect on performance, the ultimate goals of this research are two-fold. First, an optimum redesign will be created for CSW on Villanova University's campus. This design will incorporate hydrodynamic designs using MIKE 11 in addition to biochemical designs using ECOLAB (Danish Hydraulic Institute, Hørsholm, Denmark). Second, multivariate statistical techniques, such as linear regressions or discriminate function analysis, will be used to understand the relationship between physical CSW parameters and design performance. This paper focuses on the results for creating an optimum hydrodynamic redesign using MIKE 11 for Villanova's CSW.

METHODS

Site Description

Villanova's CSW is a mature wetland system that is located on Villanova University's campus in Villanova, Pennsylvania (Figure 1). It was originally a detention basin that was retrofitted in 1999. During base flow conditions, a steady flow of water enters the system from two pipes that drain Villanova University's campus. These pipes serve as the primary inputs of water into the system. Additionally, a single pipe allows water to leave the system. The drainage area is approximately 56.6 acres, and of this area, 57%, 31%, and 12% of the surfaces are impervious, semipervious, and pervious respectively.

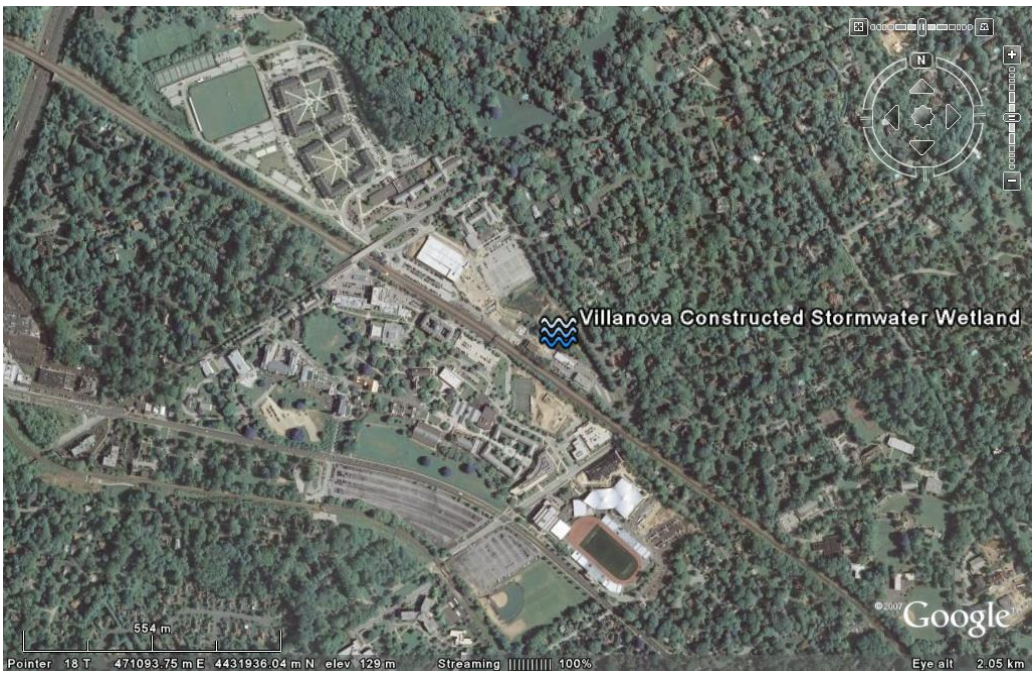

Figure 1. Aerial photograph of Villanova University and the Villanova University Constructed Stormwater Wetland. Image was obtained from Google Earth.

Simulated Designs

The physical design of a CSW – the shape, depth and length – affects the hydraulic and biological and chemical optimum performance. The hydraulic performance was evaluated for four CSW designs, which included one large pond, two equal sized ponds, one pond followed by meanders, and continuous meanders (Figure 2). The total plan view surface area of each of design and the position, elevation, and orientation of the inflow and outflow structures for all designs were identical. These designs were chosen because they represent a broad range of typical hydraulic features.

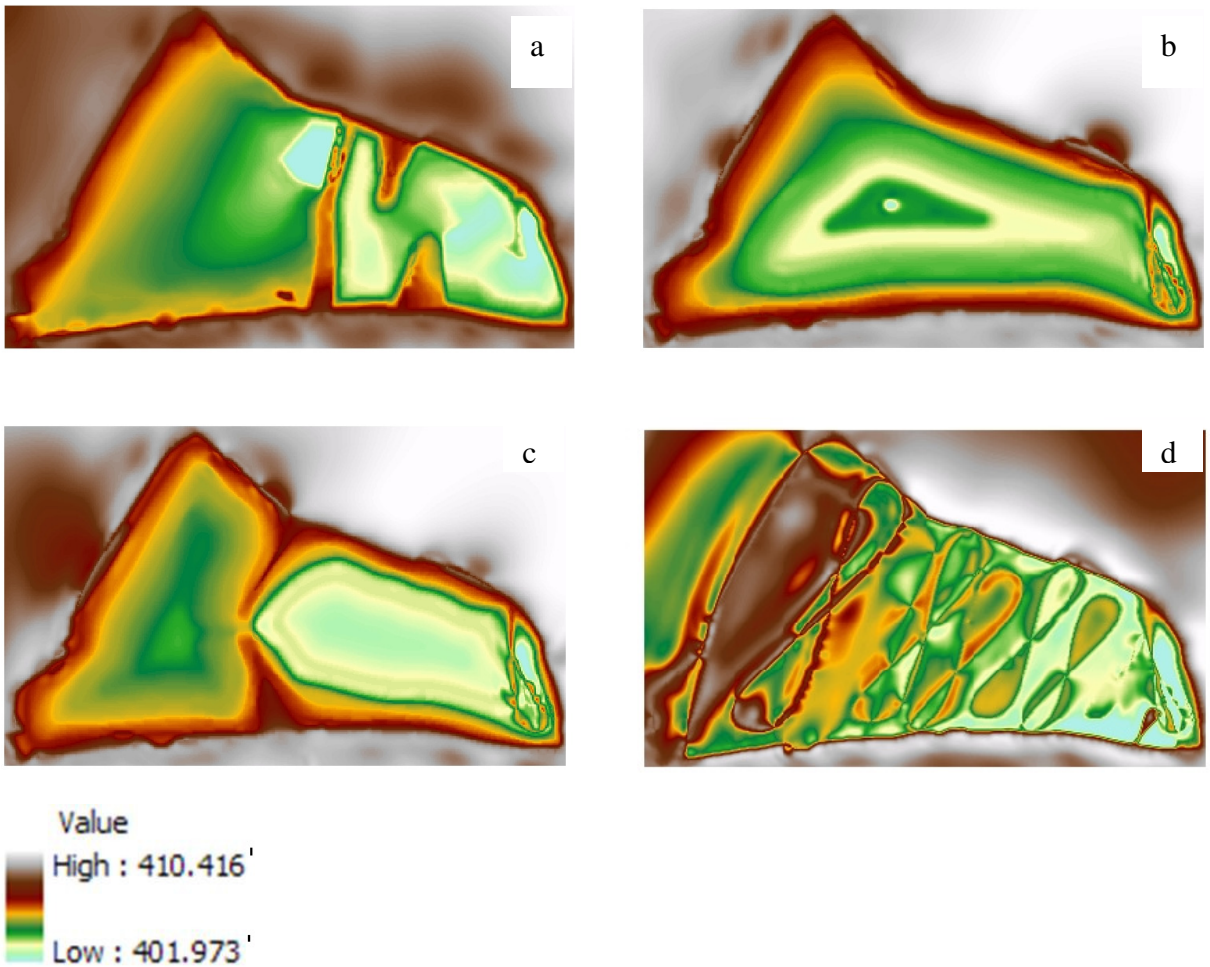

Figure 2. A 3-D digital elevation model (DEM) was created for each of the four designs (a= pond and meander, b= 1 pond, c= 2 ponds, and d= continuous meander).

Design Performance

The performance of each CSW design was evaluated based on 1) the maximum peak flow rate, 2) stormwater discharge time, and 3) flow rate of change. The design(s) with the lowest peak flow rate, longest stormwater discharge time, and lowest flow rate of change was ranked the best design. The performance of each design was compared to the inflow hydrograph which served as a no treatment or control design. By minimizing peak flow rate, maximizing discharge time, and minimizing change in flow rates, the energy carried in the stormwater would be minimized which would minimize scour and erosion within and downstream from the wetland channel.

Peak flow rates were determined by finding the maximum flow of the hydrograph. The stormwater discharge time was evaluated as the time difference between the initial increase in

flow due to stormwater runoff and the time for the system to return to baseflow conditions (~0.3 ft^3/s) at the outlet of the CSW. The flow rate of change was determined by averaging the absolute value of the slope for the entire hydrograph. The absolute value of the flow rate of change was used since positive changes in flow rate (before peak flow) and negative changes in flow rate (after peak flow) would average to zero. Differences among the mean change in flow rate were evaluated using a One-way analysis of variance (ANOVA). Analysis of variance can determine if at least one mean value is statistically different from another. In order to determine which value(s) are statistically different, a post hoc test is used to determine which mean(s) is (are) different. For this analysis, Tukey's HSD post hoc test was used to determine which designs had statistically higher and lower flow rates of change (Lomax 2001). All statistical significance values were evaluated at an alpha (α) level of 0.05.

MIKE 11

Performance metrics for each CSW design were obtained from MIKE 11 simulations, which is a one-dimensional hydrodynamic modeling package based on the complete dynamic wave formulation of the Saint Venant equations for open-channel flow. The Mike 11 model simulated flow and water level through Villanova's CSW. The model operates from four basic data inputs: network, cross section, boundary, and hydrodynamic parameters.

In 2007, a ground surface elevation survey was conducted of Villanova's CSW. This survey served as the base map for the pond and meander design. The survey topographic lines were imported into MIKE 11 GIS, an extension of ArcMap 9.2, and a 3-D digital elevation model (DEM) of the surface of the CSW was created (Figure 2a). The network and cross section files needed in Mike 11 were created from the DEM. The network, or thalweg, was created by following the path of lowest elevation from the inlet to the outlet. Cross sections were taken along the network at approximately 20 meter intervals. Each cross section extended the width of the CSW or to the width of a limiting structure, such as a berm. The roughness coefficient for weedy streams with underbrush range from 0.075-0.15 (Mays 2005); for this simulation, the lower extreme was used. Subsequent models were created in AutoCAD, and network and cross section files were created in a similar manner (Figure 2 b-d).

The upstream and downstream ends of the CSW were modeled as open boundaries. The input data for the model was the inflow (ft^3/s) entering the CSW from the two pipes previously described. The flow exiting the system was calculated by MIKE 11 using a Q-h curve that was previously established for the outlet of the system. The total duration of the simulation was 24 hours, and included 40 minutes of base flow conditions prior to a 0.71 inch rain event that lasted 3.5 hours in May 2007. The time preceding this storm was considered base flow conditions (>36 hours without rain).

Finally, Mike 11 has various hydrodynamic parameters that can be used for setting supplementary data for a simulation. These parameters include flood plain resistance factors, sand bars, wind conditions, wave approximations, etc. Default values for all parameters were used which are sufficient for obtaining satisfactory simulation results in most cases (DHI 2008).

RESULTS

Peak Flow Rate

When comparing the inflow hydrograph to the modeled results, the inflow had the greatest maximum flow rate, followed by the pond and meander, 2 ponds, 1 pond, and continuous meander designs (Table 1.) Overall, the modeled designs reduced the peak flow rate by 46-58%.

Table 1. Performance results for the four designs and the control (Inflow). Flow units were cubic feet per minute (cfs). Mean flow rate of change represent absolute values.

	Peak Flow (cfs)	Time to Discharge (hr)	Mean Change in Flow Rate (Δcfs/min)
Inflow	4.48	4.42	0.62
1 Pond & Meanders	2.40	4.25	0.15
2 Ponds	2.26	4.50	0.10
1 Pond	2.16	4.58	0.10
Continuous Meanders	1.87	5.58	0.03

Time to Discharge

The pond and meander design had the shortest time to discharge, followed by inflow, 2 ponds, 1 pond, and the continuous meander designs (Table 2, Figure 3). With the exception of the pond and meander design, each modeled design increased the time to discharge by 2-26%.

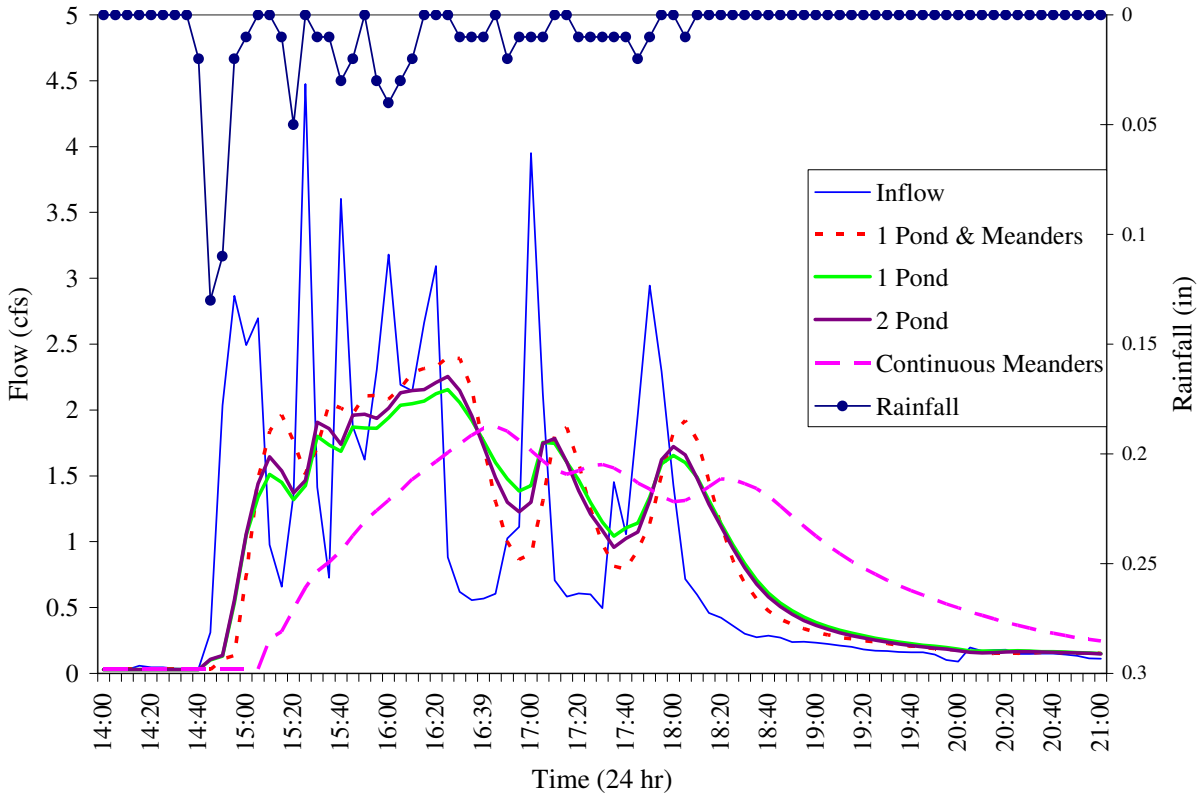

Figure 3. Modeled hydrographs were used to evaluate each model. Only seven hours were plotted to highlight flows during and immediately following the modeled storm event.

Flow Rate of Change

The inflow had the greatest mean change in flow rate, followed by the 1 pond and meanders, 2 ponds, 1 pond, and continuous meanders designs (Figures 3 and 4, Table 1). Overall, the modeled designs decreased the mean change in flow rate by 76-95% from the inflow. Based on the One-way ANOVA, a statistical difference existed among the means of the four designs and the inflow control ($df=4$, $F=24.32$, $P<0.001$). Using Tukey's HSD post hoc test the inflow's mean flow rate of change was statistically greater than all other designs, while the continuous meander's mean flow rate of change was statistically lower than all other designs (Figure 4). The 1 pond and meanders mean flow rate of change was statistically greater than those of the 1 pond and continuous meander designs (Figure 4).

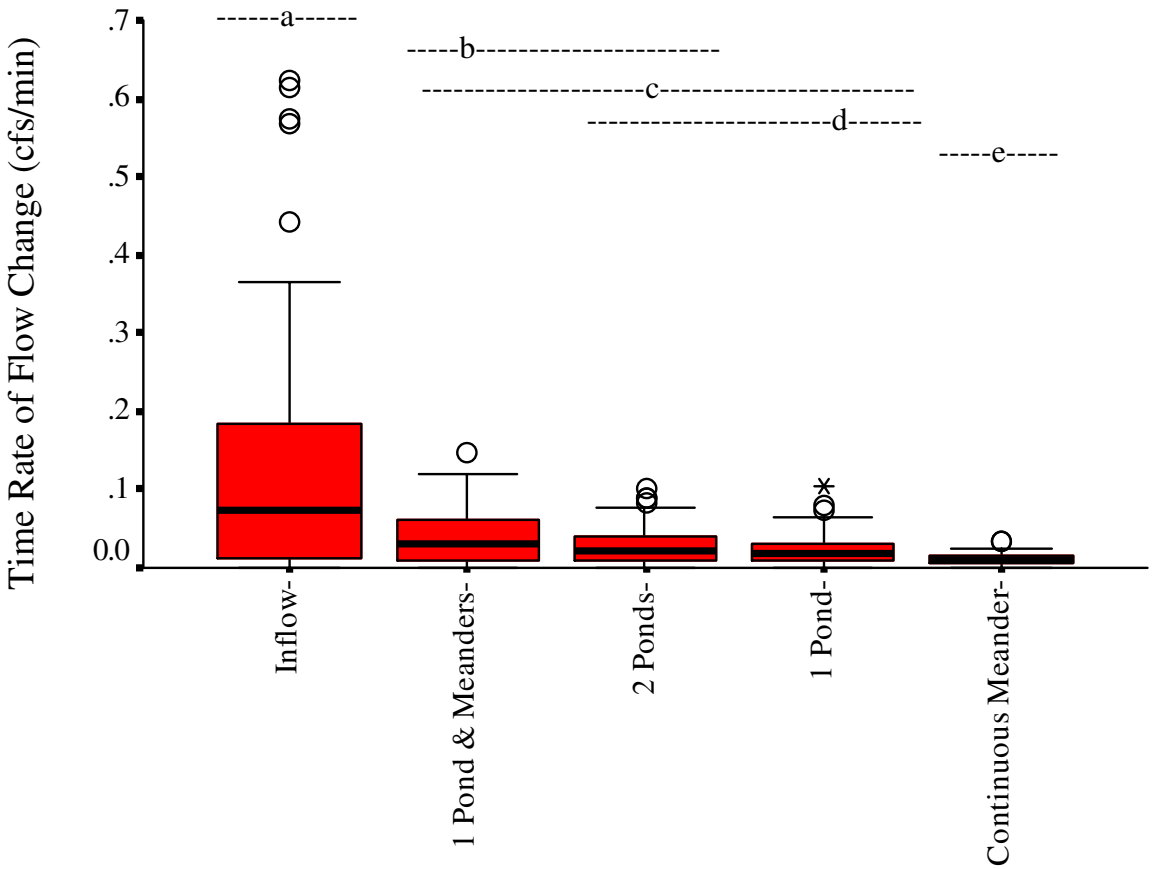

Figure 4. Box and whisker plots of the four wetland designs and control (no treatment). Letters above plots correspond to treatment (a=no treatment, b=2 ponds, c=current design, d=1 pond, and e =continuous meander). Bars above each boxplot represent statistical differences among boxplots. Bars that do not span other boxplots were statistically different ($P<0.05$). No difference in means was detected for bars that span other boxplots.

DISCUSSION

The continuous meander design outperformed all other designs in the three categories. Both pond designs performed similarly while the pond and meander design was consistently the worst design. All models outperformed the inflow model in most categories, which was expected since any treatment is likely better than no treatment (Table 1). Only the pond and meander design had a shorter time to discharge than that of the inflow hydrograph. The pond and meanders design represents the current state of Villanova's CSW and was the only model to contain a sediment forebay. It is possible that the small storage capacity of the sediment forebay caused a temporary backwater as stormwater initially entered the CSW. Early stormwater inputs would have been temporarily retained before water levels increased enough to negate the storage effects. Therefore, the temporary storage in the sediment forebay could have caused an accordion effect shortening the time to discharge. To verify this, future research will compare the current pond and meander system to one where the sediment forebay is removed.

The continuous meander design had the greatest length to width ratio while the single pond design had the shortest. It is surprising then that these two designs were the best hydraulic designs and that the composite designs (two ponds and pond with meanders) performed worse. These results are somewhat contrary to previous literature in which the general conclusion is that increasing the length to width ratio also increases the performance (Walker 1998, Person et al. 1999, Conn and Fiedler 2006).

The difference between the observed results for the continuous meander and single pond designs and the composite designs are likely explained by increased storage capacities within the single pond and continuous meander designs; however, the underlying mechanism is different for both. The mechanism controlling the continuous meander design is the longer length, leading to the longer travel time through the CSW that dampens the hydrograph. The mechanism controlling the single pond model is that there is a large volume to absorb the inflow and damp the outflow hydrograph. For example, consider the volume of two sphere systems. One system is composed of a single sphere with a radius of two while the second contains two spheres each a radius of one. The total volume of the single sphere system is four times greater than the total volume of the composite system. For a unit increase in water depth in either the single of two pond designs, the single pond design would store more volume. Therefore, it is not surprising that the composite systems have less storage volume than the non-composite systems.

In addition to geometry, storage was affected by vegetation (modeled as roughness) within the CSW itself. Although the roughness coefficient was held constant (0.075) for all models, the length to width ratio varied and was greatest for the continuous meander model. Within each design, vegetation acted as a regulating device, causing water to pond locally behind it. With a high length to width ratio, the total volume of water must pass a greater proportion of vegetation thereby causing and increase in localized ponding throughout the system. This increase in localized ponding would result in greater storage volume.

The dynamics of stormwater runoff are complex and are unlikely to be fully described using the analysis within. For example, if high resistance and high length to width ratio was the best practice for decreasing peak flows generated from stormwater management, than the pond and meanders model should have performed better since it has the second greatest length to width ratio. But it is shown by the performance of the single pond design that increasing the storage volume is one way to mitigate stormwater runoff. The conventional wisdom of CSW has been to extend the travel path. The present research shows, however, that while a high length to width ratio will improve hydraulic performance, it is necessary to understand all the mechanisms that are driving volume storage and peak flow rate reduction.

CONCLUSIONS

The continuous meander design had the best performance; however, the metrics do not identify which variables inherent to each design have the greatest contribution to the performance to each design. Furthermore, there is a qualitative element in interpreting and evaluating performance metrics for each design. Are the differences among the models meaningful? For example, will a 0.10 cfs difference in peak flow rate between the two and one pond design impact biochemical processes within the system? The next step of this research will be to derive mathematical relationships between design parameters, such as length to width ratio

or roughness, and the other performance variables. Future research should focus on determining the variables that are most important to mitigate the effects of urban stormwater runoff. This can be done through discriminate function analysis, or other multivariate statistical analyses. Optimizing the physical aspects is only one part of the solution to minimizing the required area of constructed stormwater wetlands. In addition to modeling various physical parameters, optimizing the biological and chemical processes is an area for future research that needs to be investigated, and questions like, "what physical dimensions optimizes biological removal or chemical degradation of nutrients?", should be addressed.

WORKS CITED

Conn, R.M. and Fiedler, F.R. (2006) *Treatment wetlands with designed bottom topography.* Water Environment Research. 78(13):2514-2523

Danish Hydraulic Institute. (2008) MIKE 11 A modelling system for Rivers and Channels User Guide. Hørsholm, Denmark

Koob, T.; Barber, M.E.; Hathhorh, W.E. (1999) *Hydrologic Design Considerations of Constructed Wetlands for Urban Stormwater Runoff.* Journal of the American Water Resources Association. 35(2):323-331

Lomax, R.G. (2007). *Statistical Concepts: A Second Course for Education and the Behavioral Sciences*. Lawrence Erlbaum, Mahwah, N.J.

Mays, L.W. (2005) *Water Resources Engineering*. John Wiley & Sons, Hoboken, NJ.

Pennsylvania Department of Environmental Protection. (2007). *Pennsylvania Stormwater Best Management Practices Manual*. Bureau of Stormwater Management, Division of Waterways, Wetlands and Erosion Control, Harrisburg, Pennsylvania.

Persson, J. S.; Somes, N. L. G.; Wong, T. H. F. (1999) *Hydraulics Efficiency of Constructed Wetlands and Ponds*. Water Science Technology. 40(3):291-300

Scholz, M. and Lee, B. (2005) *Constructed Wetlands: a Review.* International Journal of Environmental Studies. 62(4): 421-447

Walker, D. J. (1998) *Modeling Residence Time in Storm Water Ponds*. Ecological Engineering. 10: 247-262

Research of Hydrologic and Water Quality Performance of 4 Linear Wetlands in Eastern North Carolina

J. D. Wright[1], W. F. Hunt[1]

Abstract. *The North Carolina Department of Transportation is charged by an agreement with the North Carolina Department of Environment and Natural Resources to treat stormwater from NC DOT facilities across North Carolina. One heretofore unaccounted treatment is hundreds of miles of right-of-way swales in eastern North Carolina. It is possible that these serendipitous practices are improving runoff quality along theses highways. If so, an assessment of their performance is needed.*

Four existing right-of-way linear swales along I-40 east of I-95 will be monitored to determine their hydrologic and water quality effectiveness. Two different treatments are being examined: one swale that is unaltered and one that has been allowed to establish wetland conditions. There are two examples of each. Monitoring will also address the impact of the vegetated filter strip between the shoulder and the edge of the swale. Monitoring began in August of 2008. Samples are being collected from 18 events and analyzed for TN, TKN, NH_4-N, NO_{2-3}-N, TP, and TSS.

Keywords. Stormwater, BMPs, road side swales, Wetlands, Permeable Pavement

Introduction

The North Carolina Department of Transportation (NC DOT) is charged by an agreement with the North Carolina Department of Environment and Natural Resources (NC DENR) to treat stormwater runoff from NC DOT facilities across North Carolina. To date, NC DOT has installed scores of retrofits across North Carolina and has researched the hydrologic and water quality function of several. One unaccounted for treatment is hundreds of miles of right-of-way linear wetlands in eastern North Carolina. It is possible that these serendipitous practices are improving runoff quality along these highways. If so, an assessment of their performance is needed.

A research team in Northern Sweden studied several different grassed swales (Backstrom 2003). They found that the swales retained significant amounts of particulate matter during high pollutant loading events. However, when the swales received low pollutant concentrations, some of the swales released pollutants. Disssolved pollutants did not receive any perceptible treatment. The swales studied were regarded as facilities that even out pollutant peak loads, but were not able to consistently reduce pollutant loads. In eastern North Carolina where nitrogen deposition is an important issue, a standard dry swale, such as those studied in Sweden may not provide ample treatment.

[1] Department of Biological and Agricultural Engineering, North Carolina State University, Campus Box 7625, Raleigh, NC 27695

Another study conducted in Florida examined a series of dry grass swales in a low impact parking lot (Rushton, 2002). The swales were associated with permeable pavement applications. The system, which included a pond, permeable pavement, and sand filters was able to reduce pollutants and reduce runoff. The swales that were individually examined often added phosphorus to the pond, where the phosphorus was later removed. Evaluated alone, the dry swales were not a very effective practice. Perhaps this was due to high amounts of phosphorus present in the swale or inadvertent fertilization. It is apparent that the swales studied in Florida and Sweden would not adequately treat nutrients associated with North Carolina. Both of these swales were designed to be dry.

Stormwater wetlands, however, have repeatedly been shown to reduce nitrogen and phosphorus concentrations and loads from small watersheds. Some wetland studies have been conducted in highway interchanges (Farrel and Scheckenberger 2003) and have shown promising pollutant removal. A pair of wetlands was recently studied in North Carolina for approximately two years; each treating relatively small watersheds (Johnson 2007). One wetland in Charlotte was able to reduce the nitrogen concentration by 40% and phosphorus concentrations by 55%. A less sophisticated study in Smithfield showed nitrogen removal rates exceeding 80% and phosphorus removal rates higher than 70% at a high school in Johnston County. These studies indicate that wetlands have a significant potential to reduce nitrogen and phosphorus. To date no research has been conducted of either existing wetland swales or standard swales in the NC DOT linear right-of-way.

The goal of this research is to examine whether linear swales will significantly reduce nutrients and solids from highways and the impact of allowing swales to develop wetland conditions. Four linear swales in the right-of-way of interstate 40 between interstate 95 and mile marker 360 were identified for study.

Methods

Four linear swales were monitored along the right of way of interstate 40. Two swales with wetland vegetation (Figure 1) were each paired with a swale that was not vegetated (Figure 2). The first non wetland vegetated site is along the east bound lane of I-40 around mile marker 332. This site is paired with a wetland vegetated site located along the shoulder of the east bound lane between mile marker 332 and 333.



Figure 1 Wetland Vegetated Swale



Figure 2 Non Vegetated Swale

The next wetland vegetated site is located along the east bound shoulder between mile marker 353 and 354 in Sampson County and is paired with a non wetland vegetated site near mile marker 360 at the boundary between Sampson County and Duplin County (Figure 3). Samples were also collected to quantify the effect of the shoulder between the edge of the pavement and the wetland (referred to as the filter strip). A section of the swale approximately 100 feet long was monitored. Monitoring required a slot drain be installed along the shoulder at the edge of the pavement (Figure 4) and at the edge of the filter strip (Figure 5).

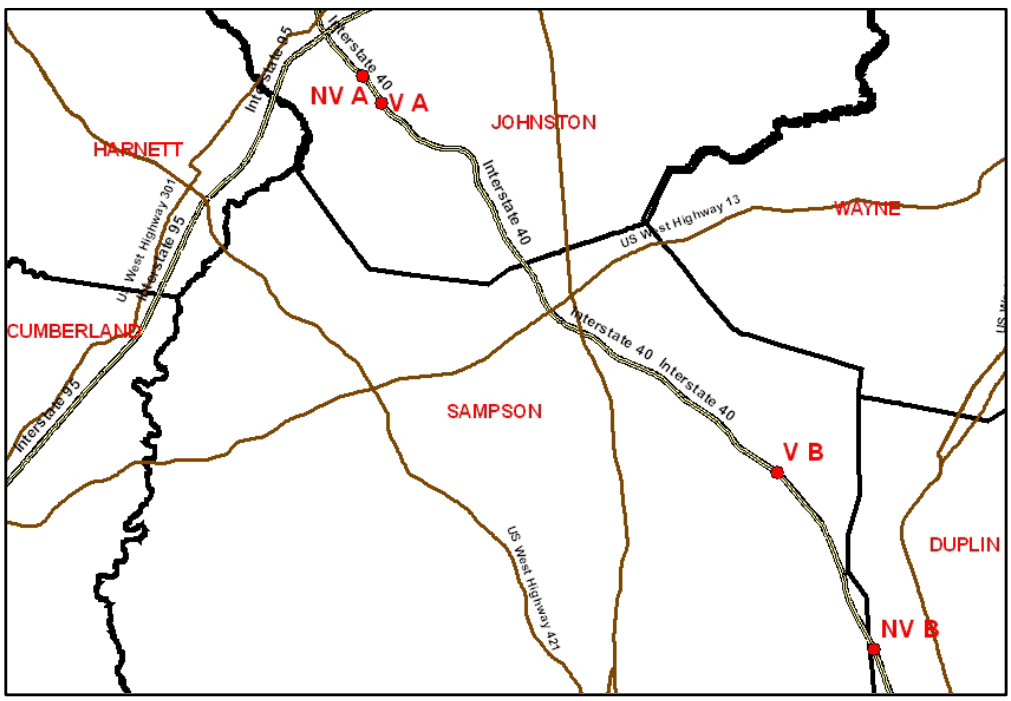

Figure 3 Swale Locations



Figure 4 Pavement Slot Drain



Figure 5 Filter Strip Slot Drain

Figure 6 shows the monitoring set up. An outlet structure with a 30° v-notch weir was installed in the swale to measure the flow rate and to be able to collect water quality samples (Figure 7).

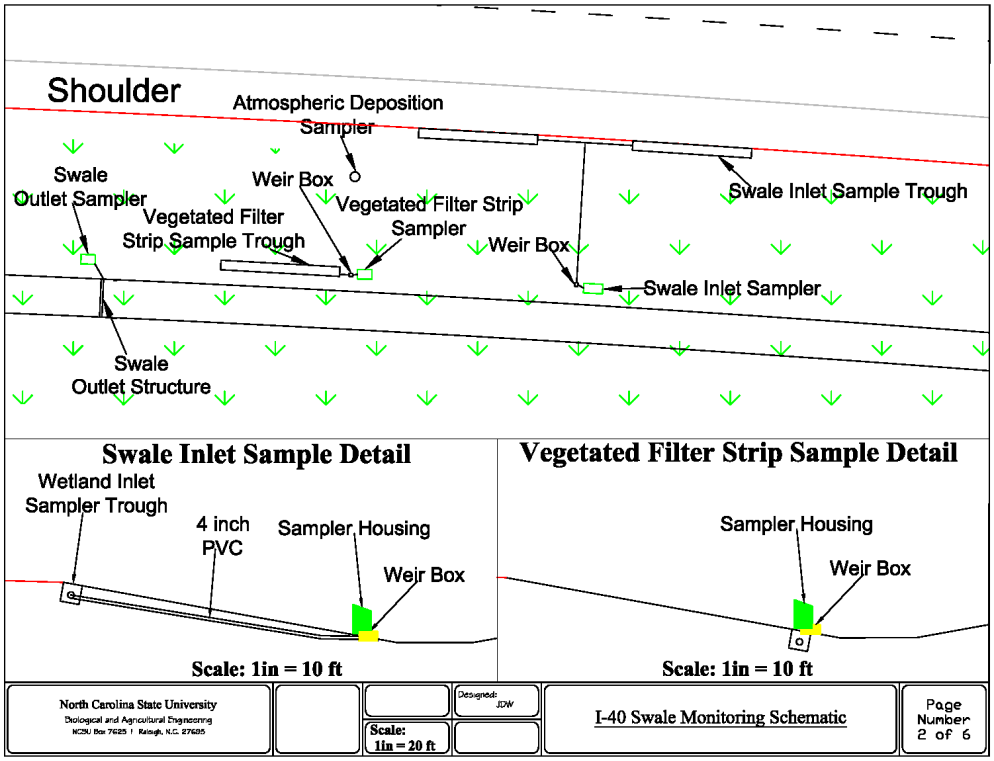

Figure 6 Monitoring Layout



Figure 7 Outlet Structure

Weir boxes with 30° v-notch weirs were used to measure the volume of water that passed through the slot drains at the edge of the pavement and the filter strip (Figure 8). ISCO 730 bubbler modules were used to measure the depth of flow over the weirs and calculate flow rate. The bubblers triggered ISCO 6712 automatic samplers to take flow-weighted composite samples for the storm. The sampler received pulses from the bubbler each time a pre-defined volume of water passed over the weir and then took a sample. Runoff from storm events up to 37.5 mm (1.5 inch) in size was expected to be fully captured by the bioretention cells. Rain fall samples are being collected to determine the impact of atmospheric deposition at each site.



Figure 8 Weir Box

Results and Discussion

Data collection began in September of 2008. Seven storms have been collected to date with data from three of those storms presented in Table 1. After samples from one storm at NV B and three storms at the other sites have been collected, initial analysis indicates some reduction in nitrate and nitrite nitrogen between the inlet and outlet at each swale and a reduction in NH_3 at each swale with the exception of NV B. The filter strip at NV A showed a reduction in nitrate and nitrite nitrogen. There was an increase in TSS at each swale. It is possible that the sites have not had a chance to stabilize after the equipment was installed causing sediment to wash into the swales. Further analysis will be possible after more storms are collected.

Conclusions

NC DOT has hundreds of miles of swales throughout the state of North Carolina. It is important to adequately characterize how much treatment these swales are providing in their current state. Additionally, if a slight modification of linear wetlands that would allow them to develop wetland vegetation improves nutrient and other pollutant removal, NC DOT may be able to provide simple retrofits to improve performance. This research may allow for NC DOT to account for thousands of pounds of nitrogen and phosphorus removal in eastern NC. In addition to pollutant removal the NC DOT may be able to save a substantial amount of money by justifying reduced maintenance practices along the right of way and and in the swales by not mowing or spraying and allowing wetland vegetation to establish.

Acknowledgements

The authors would like to thank the NC DOT for their support financially and logistically. We would like to specifically thank the Sampson County Maintenance crew for their support in installing the monitoring equipment.

Table 1 Water Quality Data from the Linear Stormwater Wetland Study
(all values in mg/L)

Date Sampled	Sample Site	TKN	NO_3&NO_2		NH_3N	TP	TSS	Ortho P
9/6/08	NVA IN	0.27	0.10	0.37	0.17	0.02	5.80	0.01
9/6/08	NVA FS IN	0.35	0.03	0.37	0.07	0.16	6.70	0.13
9/6/08	NVA OUT	0.55	0.01	0.56	0.06	0.06	6.70	0.02
9/6/08	VA IN	0.35	0.13	0.48	0.19	0.03	4.60	0.01
9/6/08	VA OUT	0.39	0.02	0.40	0.07	0.04	2.90	0.02
9/6/08	VB IN	0.26	0.18	0.45	0.11	0.04	4.60	0.01
9/6/08	VB OUT	0.58	0.03	0.61	0.03	0.08	7.20	0.03
9/17/08	NVA IN	0.39	0.33	0.71	0.19	0.02	4.50	NS
9/17/08	NVA FS	1.05	0.09	1.14	0.35	0.21	26.70	NS
9/17/08	NVA OUT	0.90	0.12	1.01	0.12	0.08	17.10	NS
9/17/08	VA IN	1.56	0.71	2.27	0.74	0.09	6.30	NS
9/17/08	VA OUT	0.70	0.09	0.79	0.10	0.07	22.40	NS
9/17/08	VB IN	0.97	0.92	1.89	0.47	0.07	5.50	NS
9/17/08	VB OUT	1.25	0.01	1.26	0.22	0.10	25.80	NS
9/29/08	NVA IN	0.36	0.25	0.61	0.12	0.03	7.10	NS
9/29/08	NVA FS	0.68	0.08	0.75	0.08	0.18	23.80	NS
9/29/08	NVA OUT	0.70	0.05	0.75	0.03	0.07	9.40	NS
9/29/08	VA IN	0.29	0.24	0.53	0.06	0.03	8.00	NS
9/29/08	VA OUT	0.73	0.07	0.80	0.04	0.06	12.30	NS
9/29/08	VB IN	0.43	0.27	0.70	0.19	0.07	7.80	NS
9/29/08	VB OUT	0.71	0.08	0.79	0.03	0.07	15.70	NS
9/29/08	NVB IN	0.35	0.35	0.69	0.06	0.07	8.80	NS
9/29/08	NVB FS	1.03	0.09	1.13	0.07	0.24	26.60	NS
9/29/08	NVB OUT	1.06	0.05	1.11	0.11	0.14	53.00	NS

NVA = Non Vegetated site A
NVA IN (slot drain @ edge)
NVA FS (slot drain @ filter strip)
NVA OUT (outlet weir)

VA = Vegetated site A
VA IN (slot drain @ edge)
VA OUT (outlet weir)

VB = Vegetated site B
VB IN (slot drain @ edge)
VB OUT (outlet weir)

NVB = Non Vegetated site B
NVB IN (slot drain @ edge)
NVB FS (slot drain @ filter strip)
NVB OUT (outlet weir)

References

Backstrom, M. 2003. Grassed swales for stormwater pollution control during rain and snowmelt. *Water Science and Technology*, v 48, n 9, 2003, p 123-132

Ferrel, A.C. and R.B. Schenkenberger. 2003. An assessment of long-term monitoring data for constructed wetlands for urban highway runoff control. *Water Quality Research Journal of Canada*. v 38, n 2, p 283-315

Rushton, B. 2002. Enhanced parking lot design for stormwater treatment. In: Proceedings of the Ninth International Conference on Urban Drainage. Eds. E. Strecker and W. Huber. Portland, Ore. 16p.

Johnson, Jennifer Lee. (2007) Evaluation of Stormwater Wetland and Wet Pond Forebay Design and Stormwater Wetland Pollutant Removal Efficiency. A thesis published by the Graduate School of North Carolina State University, under the direction of Dr. William Hunt, III.

Reservoir Sedimentation Estimation Using Genetic Programming Technique

Vaibhav Garg[1] and V. Jothiprakash[2]

[1]Research Scholar, Department of Civil Engineering, Indian Institute of Technology Bombay, Powai, Mumbai – 400 076, Maharashtra, India; PH (+91) 9869321798; email: vaibhavgarg@iitb.ac.in
[2]Assistant Professor, Department of Civil Engineering, Indian Institute of Technology Bombay, Powai, Mumbai – 400 076, Maharashtra, India; PH (+91) 22 25767315; FAX (+91) 22 25767302; email: vprakash@iitb.ac.in

Abstract

To a certain extent, all reservoirs are subjected to the problem of sediment deposition universally. Depending on the amount of material deposited the shortening of reservoir capacity and useful life result in several unpredictable consequences. To determine the total quantity of deposition, as well as the pattern and distribution of deposits in a reservoir, hydrographic survey is the only direct measurement method. These hydrographic survey methods are being considered as expensive, time consuming and cumbersome. In the present study, an attempt has been made to employ genetic programming (GP) soft computing technique to estimate the volume of sediment retained (S_v) in the Pong Reservoir, India. It was found that GP model captured the trend and magnitude of S_v very well. Moreover, GP model provided input-output relationship in the form of computer programs which may be easily used by end user. Also, GP can be effectively used to capture the non-linear relationship between the input and output with short length of data.

Introduction

Hitherto, humankind has been trying to harness the available surface water resources by creating reservoirs. Reservoirs have well known primary purposes such as water supply, irrigation, flood control, hydropower and navigation. The total storage capacity of reservoirs in the world has been estimated by various sources. One of the estimation is 4000 to 6000 x 10^9 m^3, and another is 5 per cent of the total runoff in the world (38830 x 10^9 m^3), i.e. 2 000 x 10^9 m^3 (Yang, 2003). While according to Siyam et al. (2005), the potential quantity of water that can be controlled through reservoirs in the future varies between 9000 and 14000 km^3 annually. Thus reservoirs are key infrastructures for humankind survival and well being.

Despite the benefits realized, reservoirs are also having some drawbacks. Reservoirs are often threatened by loss of capacity due to sedimentation. Globally, the overall annual loss rate of reservoir storage capacity due to sedimentation is estimated as 1 to 2 per cent of the total storage capacity (Yoon, 1992; Yang, 2003). In India, many

reservoirs have been subjected to reduction in their storage capacities due to sedimentation. Analysis of sedimentation survey details with respect to 43 major, medium and minor reservoirs in the country indicate that the sedimentation rate varies between 0.34 – 27.85 ha m/100 km^2/ year for major reservoirs, 0.15 – 10.65 ha m/ 100 km^2/ year for medium reservoirs and 1.0 – 2.3 ha m/ 100 km^2/ year for minor reservoirs (Shangle, 1991). Thus, the accuracy in prediction of the volume of sediment deposited in a reservoir is very important for planning, design and operation of reservoirs. In the present study, an attempt has been made to simulate the volume of sediment retained (S_v) in the Pong Reservoir at Beas Dam on Beas River, Kangra district, Himachal Pradesh, India using Genetic Pogramming (GP) soft computing technique. It was observed that the GP model captured both the trend and magnitude of S_v with small set of data easily.

Study Area

To study the suitability of the GP model for estimating the S_v of a reservoir in India, Pong Reservoir has been selected as a case study. Pong Reservoir is located on Beas Dam, a multipurpose river valley project commissioned in 1974, on Beas River at village Pong in Kangra district of Himachal Pradesh, India. The Beas catchment along with location of Pong dam is shown in Figure 1. The catchment area of river Beas is fan shaped.

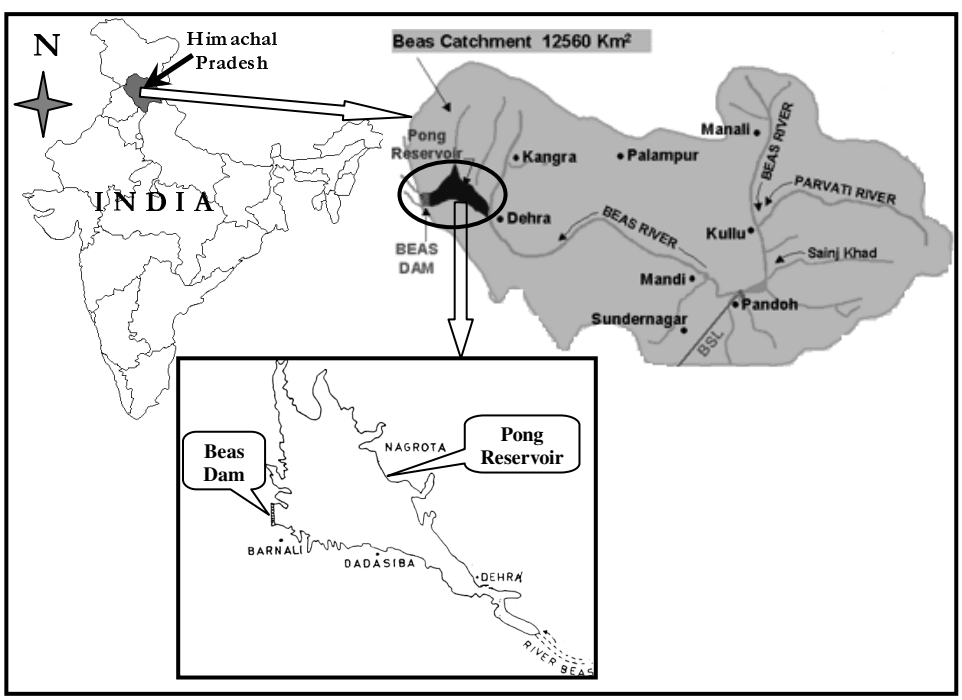

Figure 1. Location of Pong Reservoir on Beas River

It has an enormous water-spread of 260 km^2 at full reservoir level and impounds 8578.99 x 10^6 m^3 of water with spread length of 42 km and maximum width 16 km at normal storage. The live storage of the reservoir is 7291.22 x 10^6 m^3 and the dead storage is 1287.773 x 10^6 m^3. The total catchment area above the dam site is 12,562 km^2 out of which only 777 km^2 is under snow and rest of the area is covered by forests, degraded forests, cultivated land and uncultivated withered rocks (BBMB, 2006). The annual yield of the catchment is about 10,720 x 10^6 m^3. Pandoh dam, constructed about 140 km upstream of Pong Dam, diverts the normal flow of river to River Satluj (Beas-Satluj Link Project) and intercepts an area of 5278 km^2. With the construction of Pandoh Dam the sediment contribution of river has reduced by a large percent, as major sediment load brought in the river upto Pandoh gets deposited in the Pandoh reservoir. Thus, the Pandoh Dam acts as a check dam for Pong Reservoir.

Methodology

The Darwin's natural selection theory of evolution based GP, is a relatively new technique and member of the evolutionary algorithm family (Koza 1992). The generalized form of Genetic Algorithm (GA), GP, operates on parse trees structures composed of function and terminal sets, rather than on bit strings as in a GA. GP is an inductive form of machine learning as it evolves a computer program to perform a underlying process defined by a set of training samples (Whigham and Crapper, 2001). It approximates the solution that best describes the input-output relationship. The algorithm considers an initial population of randomly generated programs, derived from the random combination of input variables, random numbers and functions, which include arithmetic operators (+, -, *, /), mathematical functions (sin, cos, exp, log), logical/comparison functions (OR, AND) etc., appropriately chosen based on some understanding of the underlying process. This population of potential solutions is then subjected to an evolutionary process and the fitness measures of the evolved programs are evaluated. The individual programs that best fit the data are then selected from the initial population, discarding no-so-fit programs. The programs that best fit are selected to exchange part of the information between them to produce better programs through crossover (exchanging the parts of best programs with each other) and mutation (randomly changing programs to create new programs). This evolution process is repeated over successive generations and is driven towards finding best solution describing the process. It has been successfully applied to complex non-linear hydrological problems by various researchers like Savic et al. (1999); Whigam and Crapper (2001); Khu et al. (2001); Liong et al. (2002); Dorado et al. (2002); Harris et al. (2003); Babovic (2005); Drunpob et al. (2005); Jayawardena et al. (2006); Makkeasorn and Chang (2007); Sivapragasam et al. (2007); Parasuraman et al. (2007); Singh et al. (2007); Wang et al. (2007); Aytek and Kisi (2008); Sivapragasam et al. (2008). The detailed description of the GP method can be seen in Koza (1992); Babovic Keijzer (2000); Babovic et al. (2001).

Results and Discussion

The GP soft computing technique, which provides input-output relationship in the form of computer program, has been employed to estimate S_v. In the present study, the Discipulus Pro Version Lite 4.0 has been used for implementing GP. The available capacity (C_t), annual rainfall (R_t) and annual inflow (I_t) data for 33 years (1974-2006) were considered as input parameters. The S_v was considered as output parameter for the same period. For analysis, first 70% (1974-1996) and remaining 30% (1997-2006) of the available data length has been chosen for training and testing respectively. The objective function was to find the minimum mean square error of the estimated S_v. The relevant GP parameters and their chosen values, which provided the best input-output relationship, are shown in Table 1. It has been noticed that the large population size provides high search space for GP solution. The parameter "initial program size" and "maximum program size" indicate the maximum size of the program of the initial population and of the population from subsequent generations, respectively.

Table 1. Values of GP Control Parameters

Parameter	Value
Population Size	500
Mutation Frequency (%)	95
Crossover Frequency (%)	50
Program Size	
Initial	80
Maximum	512
Total runs started	53
Cost function	MSE
Set of functions	+,-, ×, ÷, √, sin, cos, exp, log, x^2

The large initial program size of 500 leads to good initial exploration of the search space and provides better result after 53 numbers of runs for this problem. The evolved GP computer program is presented in Appendix I. The performance of the present GP model has been evaluated by common statistical parameters such as coefficient of correlation (R); root mean square error (RMSE); mean absolute error (MAE); Nash and Sutcliffe (1970) efficiency (E) as presented in Table 2. The R value for training and testing are obtained as 0.991 and 0.896 respectively. This correlation analysis shows an outstanding performance of GP model.

The results of the GP model are presented in form of scatter plot in Figure 2. The results in terms of trends of observed and estimated S_v during the testing period are shown in Figure 3. From these figure, it can be seen that not only the pattern, but also

the magnitude of S_v was well captured by the proposed GP soft computing techniques. These figures confirm the good performance of the ANN model.

Table 2. Performance Statistics of the S_v Estimation Models

Performance Criteria	Value	
	Training	Testing
R	0.991	0.896
RMSE ($10^6 m^3$)	1.441	2.413
MAE ($10^6 m^3$)	1.071	1.786
E	0.991	0.762

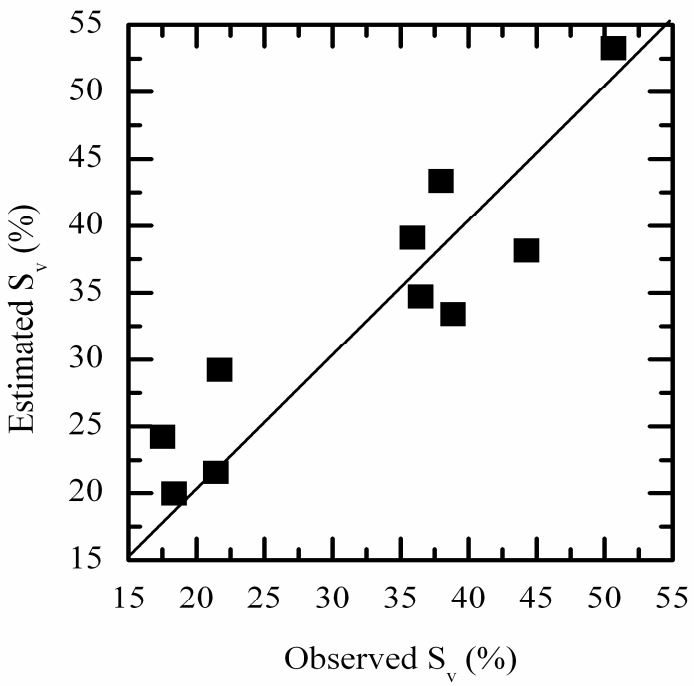

Figure 2. Scattered Plot of Observed vs Estimated S_v using GP

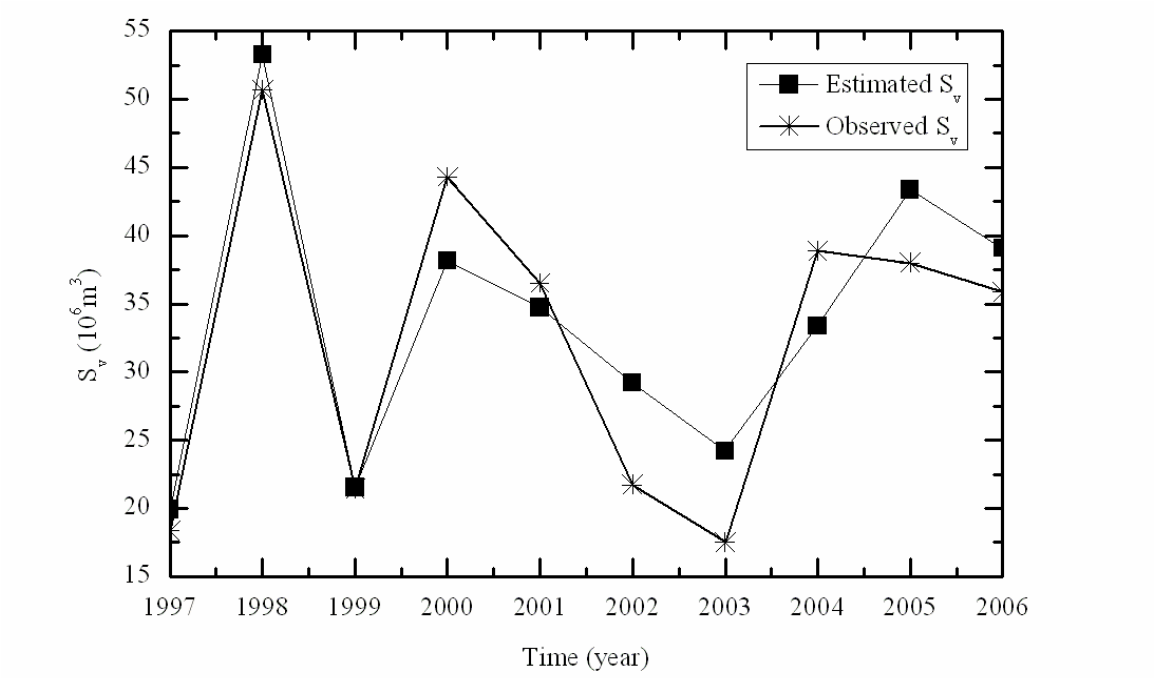

Figure 3. Comparison Plot of Observed and GP Estimated S_v for Pong Reservoir

The impact of each input parameter was analyzed by taking into account the number of times an input appears in a way that contribute to the fitness of the programs containing them (as presented in Table 3). A value of 1.00 in the frequency column indicates that the particular input variable appeared in set of all best programs. The average and maximum effect of removing all instances of a particular input from each best program is also presented. The results are scaled between 0 and 1.0. A value of 1.0 represents the largest impact value possible (Francone, 2001)

Table 3. Relative Impact of Input Parameters (GP)

Input Parameter	Frequency	Average Impact	Maximum Impact
C_t	1.00	0.77	0.96
R_t	0.33	0.23	0.61
I_t	0.67	0.35	0.64

The impact analysis of input parameters shows that C_t is the most important input parameter in estimating S_v of Pong Reservoir.

Conclusions

The volume of sediment retained (S_v) in Pong Reservoir on the river Beas in Kangra district, Himachal Pradesh, in the foothill of Himalayas, India has been estimated using GP soft computing technique. It was observed that GP model captured the trend and magnitude of S_v estimation very well. It was realized that the emerging soft computing techniques such as GP can estimate S_v easily. The outperforming GP model provided input-output relationship in the form of computer programs which may be easily used by end user. It was also found that GP can be effectively applied to capture the relationship between input and output with short length of data. This study shows that the use of soft computing tools can improve the accuracy of estimation significantly as compared to the conventional cumbersome hydrographic survey method.

References

Aytek, A., and Kisi, O. (2008). "A Genetic Programming approach to suspended sediment modeling." *Journal of Hydrology*, 351, 288-298.

Babovic, V. (2005). "Data mining in hydrology." *Hydrological Processes*, 19, 1511-1515.

Babovic, V., and Keijzer, M. (2000). "Genetic Programming as model induction engine." *Journal of Hydroinformatics*, 2(1), 35-60.

Babovic, V., Keijzer, M., Aguilera, D.R., Harrington, J. (2001). "An evolutionary approach to knowledge induction: genetic programming in Hydraulic Engineering." *World Water and Environmental Resources Congress 2001*, ASCE, D. Phelps, and G. Sehlke, eds., Orlando, Florida, USA, 20-24 May.

BBMB (2006). "Pong reservoir sedimentation studies." *Sedimentation Survey Report 2005-2006*, BBMB, Pong Dam Circle, Talwara, India

Dorado, J., Rabunal, J.R., Puertas, J., Santos, A., Rivero, D. (2002). "Prediction and modelling of the flow of a typical urban basin through Genetic Programming." *Proceedings of the EvoWorkshops*, S. Cagnoni, J.Gottlieb, E. Hart, M. Middendorf, and G. R.Raidl, eds., Kinsale, Ireland, April 3-4, 190-201.

Drunpob, A., Chang, N.B., and Beaman, M. (2005). "Stream flowrate prediction using Genetic Programming Model in a semi-arid coastal watershed." *World Water and Environmental Resources Congress 2005,* ASCE, Raymond Walton, Ed., Anchorage, Alaska, USA, May 15–19.

Francone, F.D. (2001). Owner's Manual Discipulus. Fast Genetic Programming Based on AIML Earning Technology.

Harris, E.L., Babovic, V., and Falconer, R.A. (2003). "Velocity prediction in compound channels with vegetated floodplains using genetic programming." *International Journal of River Basin Management*, 1(2), 117-123.

Jayawardena, A.W., Muttil, N., and Lee, J.H.W. (2006). "Comparative analysis of data-driven and GIS-based conceptual rainfall-runoff model." *Journal of Hydrologic Engineering*, 11(1), 1-11.

Khu, S.T., Liong, S.Y., Babovic, V., Madsen, H., and Muttil, N. (2001). "Genetic Programming and its application in real-time runoff forecast." *Journal of the American Water Resources Association*, 37(2), 439-451.

Koza, J.R. (1992). *Genetic Programming: On the programming of computers by means of natural selection*, The MIT Press, Cambridge, Massachusetts, USA.

Liong, S.Y., Gautam, T.R., Khu, S.T., Babovic, V., Keijzer, M., and Muttil, N. (2002). "Genetic Programming: A new paradigm in rainfall-runoff modeling." *Journal of the American Water Resources Association*, 38(3), 705-718.

Makkeasorn, A., and Chang, N-B. (2007). "Short-term stream flow forecasting with the aid of global climate change indices." *Environment Informatics Archives*, 5, 440-454.

Muttil, N., and Liong, S.Y. (2001). "Improving runoff forecasting by input variable selection in genetic programming." *World Water and Environmental Resources Congress 2001*, D. Phelps, and G. Sehlke, eds., Orlando, Florida, USA, 20-24 May.

Nash, J.E., and Sutcliffe, J.V. (1970). "River flow forecasting through conceptual models. 1. A discussion of principles." Journal of Hydrology, 10, 282–290.

Parasuraman, K., Elshorbagy, A., and Carey, S.K. (2007). "Modelling the dynamics of the evapotranspiration process using genetic programming." *Hydrological Sciences Journal*, 52(3), 563-578.

Savic, D.A., Walter, G.A., and Davidson, J.W. (1999). "A genetic programming approach to rainfall-runoff modelling." *Water Resources Management*, 13, 219-231.

Shangale, A.K. (1991). "Reservoir sedimentation status in India." *Jalvigyan Sameeksha, INCOH*, NIH Roorkee, VI (1&2).

Singh, A.K., Deo, M.C., and Sanil Kumar, V. (2007). "Neural Network – Genetic Programming for sediment transport." *Journal of Maritime Engineering,* The Institution of Civil Engineers, London, 160(MA3), 113-119.

Sivapragasam, C., Maheswaran, R., and Venkatesh, V. (2008). "Genetic Programming approach for flood routing in natural channels." *Hydrological Processes*, 22, 623-628.

Sivapragasam, C., Vincent, P., and Vasudevan, G. (2007). "Genetic Programming model for forecast of short and noisy data." *Hydrological Processes*, 21, 266-272.

Siyam, A.M., Mirghani, M., El zein, S., Golla, S., and El-sayed, S.M. (2005). *Assessment of the current state of the Nile basin reservoir sedimentation problems*, NBCN-RE (Nile Basin Capacity Building Network for River Engineering), River Morphology, Research Cluster, Group – I Report.

Wang, T-S., Chen, L., and Wu, M-M. (2007) "Application of genetic programming to stream-flow extension." *Proceedings of the Sixth International Conference on Machine Learning and Cybernetics*, Hong Kong, 19-22 Aug, 974-977.

Whigham, P.A., and Crapper, P.F. (2001). "Modelling rainfall-runoff using genetic programming." *Mathematical and Computer Modelling*, 33, 707-721.

Yang, X. (2003). *Manual on sediment management and measurement*, World Meteorological Organization, Operational Hydrology Report No. 47, WMO-No. 948, Secretariat of the World Meteorological Organization – Geneva, Switzerland.

Yoon, Y.N. (1992). "The state and the perspective of the direct sediment removal methods from reservoirs." *International Journal of Sediment Research*, 7(20), 99–11.

Sediment Monitoring Bias by Autosampler in Comparison with Whole Volume Sampling for Parking Lot Runoff

George D. Fowler [1], Robert M. Roseen [2], Thomas P. Ballestero [3], Qizhong Guo[4], James Houle[5]

[1] Graduate Research Assistant, Water Resources, Department of Civil Engineering, 35 Colovos Road, University of New Hampshire, Durham, NH 03824; e-mail: deforestfowler@unh.edu
[2] Corresponding Author, Director, The UNH Stormwater Center, Ph.D., P.E., Department of Civil Engineering, 35 Colovos Road, University of New Hampshire, Durham, NH 03824; e-mail: robert.roseen@unh.edu
[3] Associate Professor, Civil Engineering, P.E., Ph.D., P.H., C.G.W.P., P.G., Department of Civil Engineering; Principal Investigator, The UNH Stormwater Center, 35 Colovos Road, University of New Hampshire, Durham, NH 03824; e-mail: tom.ballestero@unh.edu
[4] Associate Professor, Ph.D., P.E., Department of Civil and Environmental Engineering, Rutgers University, 623 Bowser Road, Piscataway, NJ 0885; email: qguo@rci.rutgers.edu
[5] Facility Manager, The UNH Stormwater Center, M.A., C.P.S.W.Q., 35 Colovos Road, University of New Hampshire, Durham, NH 03824; e-mail: james.houle@unh.edu

ABSTRACT

A field study was conducted to assess biases of suspended sediment concentration (SSC) analyses (ASTM standard D 3977-97) performed on discrete samples obtained by auto-sampler in comparison with actual sediment concentrations from whole volume sampling. Research results indicate that the biases attributed to monitoring of sediment event mean concentration (EMC) and particle size distribution (PSD) in parking lot runoff by automated samplers (non-isokinetic) can be insignificant. Large volume samples (~15,000 L) of the full pipe cross-section were taken from a stormwater sewer system for eighteen storm events over two years to monitor for EMCs and PSDs. Concurrently, flow weighted grab samples were obtained by automatic samplers throughout the entire large volume sampling period. Thus characteristics of sediments were compared from a "whole storm" sample with that of "sub-samples" obtained by an autosampler using non-isokinetic sampling. SSCs and particle size distributions were compared for the two respective field sampling methods. The two methods showed a strong correlation for median sediment EMCs (R^2=.9801, n=18). Biases to particle size distributions were found to be largely confined to the large particles (>160 um) representing less than 25% of the load by mass. Moreover, sediment particles captured by the whole volume sampling and autosampler were not significantly different (α=0.05) for D_{50}'s=0.067 and 0.047 microns respectively (particle size at which 50% of the sample mass is less).

INTRODUCTION

Stormwater has been identified as the greatest threat to surface water quality (EPA, 2002). Sediment concentration is the pollutant that most regulating bodies have identified as a surrogate pollutant to measure stormwater quality. (EPA, 1993, TARP 2003). Several guidelines have been developed to standardize the protocol for monitoring sediment concentration in stormwater runoff through the use of automatic samplers and their deployment in: storm sewer systems, swales, or other effluent discharge infrastructure (EPA, 1992, TARP 2003, TAPE, 2008). These guidelines also provide insite into the location of the sampling probe in the water column and the method of extracting water samples.

However, the type of automatic sampler used in stormwater monitoring can bias results. A review of the protocol for sampling suspended sediment in surface water, suggest isokinetic samplers are necessary to accurately collect sand size particles and correctly calculate sediment concentrations (USWQ, 1998, Horowitz, 2008). An isokinetic sampler possesses the ability to adapt its sampling intake velocity to the velocity of the incoming discharge. In order to obtain an accurate sample of particles with varying specific gravity

and momentum characteristics, the samples should be withdrawn at the same velocity as the discharge (Othmer, 2002).

The majority of automatic samplers used in stormwater monitoring programs are non-isokinetic samplers. A non-isokinetic sampler does not possess the ability to create a velocity within the sampling tube that mimics the incoming velocity of the stormwater. Another potential bias with sediment monitoring is the location of the sampling probe intake itself. The location of the intake could influence the reporting accuracy of sediment concentration (Horowitz, 2008). If the intake is located on the invert, it might draw in more sediment and overestimate sediment concentration (ISCO, 2001).

This research followed federal and state guidelines to monitor sediment concentration in stormwater runoff and evaluated its utility. This was accomplished by monitoring effluent from a stormwater sewer system with non-isokinetic automatic samplers whose sampling intakes where located at the storm sewer invert. The results from these effluent samples were compared to the data obtained by capturing the entire volume of effluent passing by the samplers, to determine the actual sediment concentration.

Site Description. This research characterized sediment concentration in stormwater runoff at the terminal end of a storm sewer that drained a curbed and guttered 10-acre commuter parking lot built in 1996 (Roseen et al., 2006). The West Edge parking lot is located on the University of New Hampshire campus in Durham, NH and is at nearly 80% capacity eight months of the year. The lot is plowed, sanded, and salted regularly during the winter months. The climate is temperate and the 42 inches of annual precipitation is typically evenly distributed throughout the year.

The time of concentration for the parking lot is 22 minutes with land slopes between 1.4-2.0%. At the terminal end of the drainage system, a distribution box was built, in order to distribute this stormwater to a system of ten 15-inch pipes, configured to each receive equal parts of the runoff (Roseen et al, 2006). The sediment pollutant concentration in the stormwater runoff at this site is typical for this type of land use, Figure 1.

MATERIALS AND METHODS

Equipment Description. A removable seal in the distribution box controlled flow into one of the 15-inch pipes. At the terminal end of this pipe were two ISCO 6700 samplers with intakes set along the pipe invert, 12-cm behind a 15-inch Thel-mar compound weir. The location of the intakes, flow measurement method, and rainfall collection data followed regulatory guidelines (EPA, 1992, EPA, 2002). The suction head for the automatic samplers was 13.0 ft. Downstream of the 15-inch weir, a sedimentation forebay of a sand filter was used as the initial collection area for the stormwater that passed by the sampler intakes. This basin was lined with two tarps: a 2.5 mm, 30-ft by 20-ft polyethylene tarp, which could be removed and cleaned; and larger 2.0 mm thick multipurpose polyethylene liner underneath.

Figure 1: Total Suspended Solids (TSS) Event Mean Concentration (EMC) for varied land uses and at the UNH Stormwater Center (UNHSC) (NSQD 2005). Data in (mg/L).

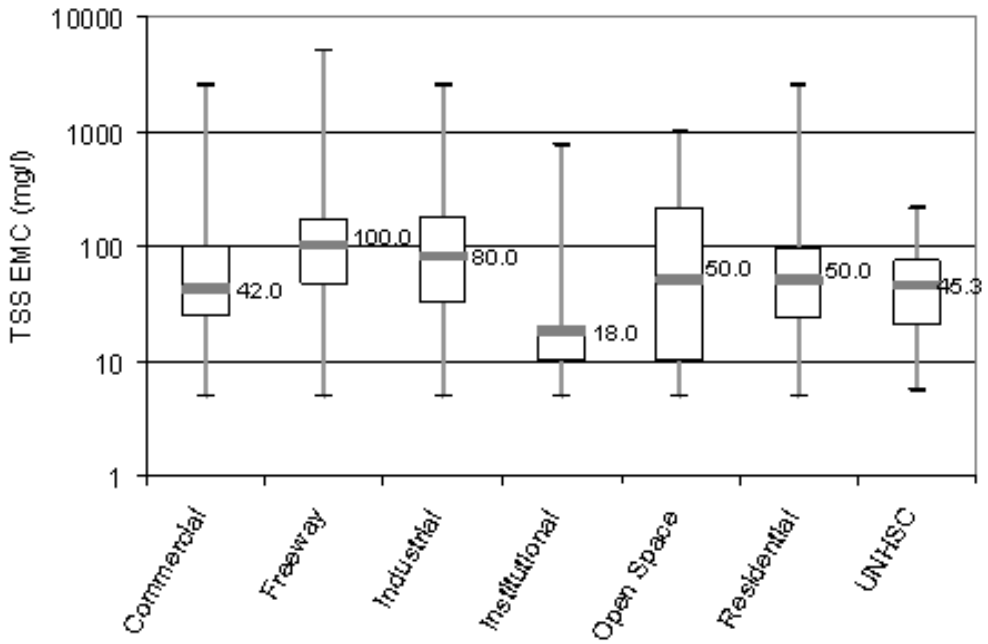

Sample Collection. Generally a storm a month was targeted for capture. As soon as runoff began to flow out of the 15-inch weir, water was allowed to fall onto the tarp and the sampling programs were turned on. One sampling intake collected 1L flow-paced grab samples at short time intervals during the entire time the sedimentation bay filled. This sampling approach followed regulatory sampling guidelines, (EPA, 2002). The second intake took a "Constant Volume - Time Proportional to Flow Volume Increment", single composite sample, also following EPA guidelines. Depth of flow (ft) was measured using an ISCO 730 bubbler and a Global Water WL400 pressure transducer located at the intakes and was subsequently converted into discharge (gpm) using the stage-discharge rating curve provided by Thelmar for their 15-inch weir, an acceptable flow measurement procedure within EPA recommendations.

Once the sedimentation forebay filled, water was diverted away from tarp, the programs were shut off and the seal in the distribution box closed

Analytical Method. Generally, 20-24 1L flow-paced samples were collected by automatic sampler per storm event. Eight to nine of these samples were selected for sediment analysis in order to develop an Event Mean Concentration (EMC).

The EMC calculation used for this study split the mid-point between two consecutive concentration samples which is standard practice (Charbeneau, 1998 and Stenstrome, 2005). These samples were kept at 4ºC temperature and sent to an analytical lab for analysis following EPA recommendations for sample preservation and holding. These samples were analyzed for sediment concentration using the Suspended Sediment Concentration analysis (SSC) following ASTM D397 protocol (ASTM 2000) for each sample. The use of the SSC method was used instead of the traditional Total Suspended Solids (TSS) analytical test because of the influence sand-size particles have on the reporting accuracy of TSS (Gray, 2000).

The single composite sample was kept at 4ºC temperature and sent to a lab for Particle Size Distribution analysis using Tri-laser photo-detection. The usual time lapse between collection and analysis was 24-30 hours.

The water captured in the tarp-lined basin was allowed to settle for 48 hours and followed with a volume-measured decant of the upper half of the water in which grab samples were collected. The remaining water, and any remaining sediments on the liner, were transferred into a 13,000 liter tank. After another 48 hours of settling, another volume-measured decant with grab samples was completed and the remaining 37-55 liters of slurry was recovered. This slurry was wash sieved (sieve sizes 2.5 mm-0.075 mm) and a hydrometer test was completed on sediments less than 0.075mm following ASTM D422D.

Reporting Method. Flow weighted event mean concentrations (EMC) were developed using discrete sample analyses from the automatic samplers. (EPA, 2002, Huber, 1993). Sediment concentrations for the total capture (TC) sample was determined by totaling the mass of the sediments divided by the total volume of runoff.

Table 1: Analytical Experimental Design for Sediment Characterization

Method of Sample Collection	EMC	PSD
Total Capture (TC)	Measured Decant Volume/Weight of Recovered Sediments	Wash Sieve and Hydrometer
Automatic Samplers (AS)	SSC analysis of 1L Discrete Samples	Microtrac Tri-Laser Device

RESULTS

Sampling and Event Characteristics. Eighteen events, over the course of two years were monitored. Figure 2 shows the depth of rainfall over the watershed compared to the effective precipitation captured for the Total Capture (TC) sample. The rain captured occurred during the first flush of rain events. During this first flush, the pollutant concentration is assumed to be highest (Li 2006, Aryal 2006,). High discharge rates reduced sampling time, as seen in Figure 2 and usually occurred during summer thunderstorms.

The intake velocity in the sampling tube of the automatic sampler, with 13.0 ft suction head, is 2.8 ft/s. The range of velocities in the stormwater pipe during these events can be seen in Table 2. Three of 18 storms that occurred exceeded the intake velocity of the sampler. The remaining storms were less than the sampler intake capacity.

Table 2: Pipe Velocities (ft/sec) Observed During Storm Events.

Storm Profile	# of Storms	Median Velocities (ft/s)	Max (ft/s)	Min (ft/s)
I	5	0.01-0.50	0.47	0.09
II	8	0.51-1.00	0.81	0.51
III	3	>1.01	3.52	1.3

Figure 2: Sampling and Event Duration and Depth with Maximum Discharge

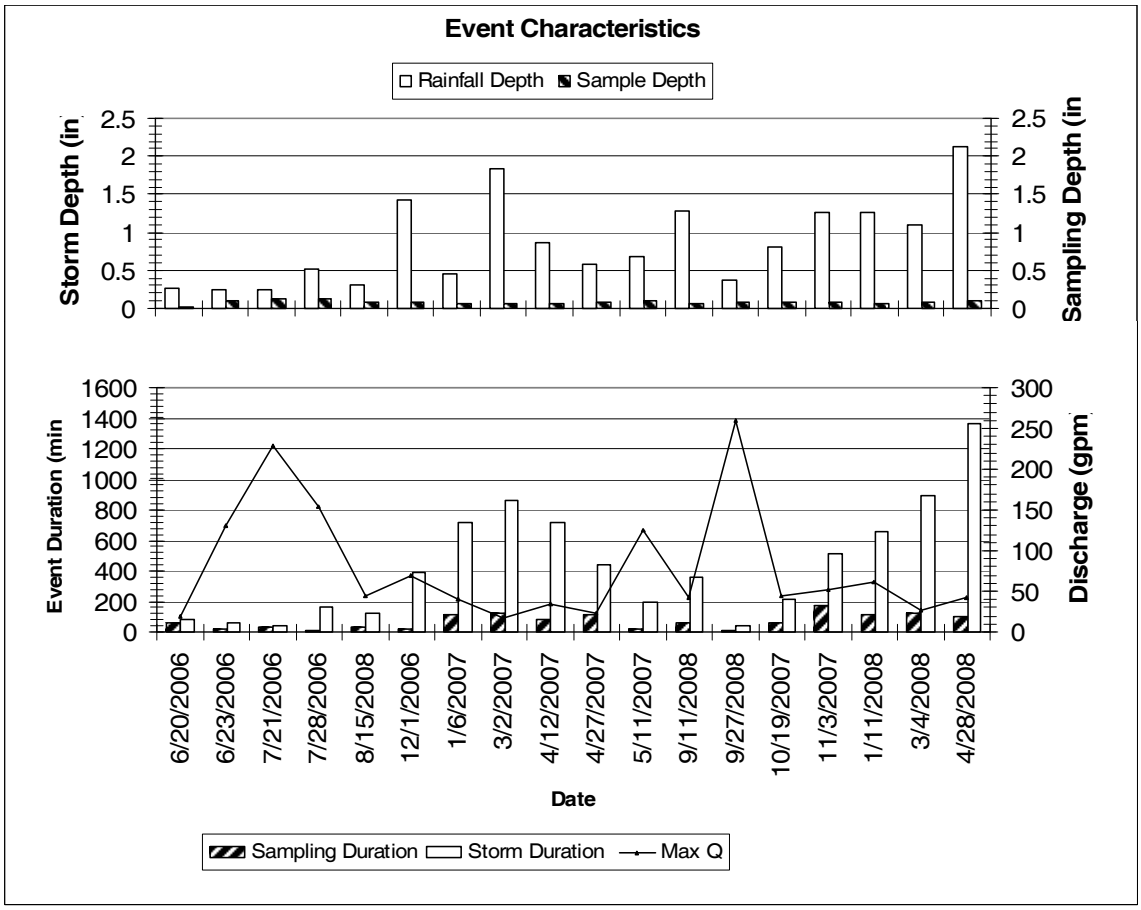

Total Capture and Sampling Methods. The median sediment EMCs from the total capture (TC) and suspended sediment concentration (SSC) b y autosampler (AS) are 69.0 and 70.1 mg/L, respectively, as seen in Figure 3. The median concentration for both methods is higher than what is expected for the this land use type as would be expected for first flush sampling. In Figure 1, the values for sediment EMC were determined using the TSS analytical method which previous research has shown to have inaccuracies (Gray 2000).

Typical median sediment concentration values for light transportation land use (45mg/L) are illustrated in Figure 3 by the reference line. The distribution of the sediment concentration for TC and SSC-AS are similar to each other as illustrated in Figure 3. The box represents the interquantile range (IQR) of the distribution, An extreme outlier "*" exists in the AS PSD and is more than three times the IQR from the end of the box. This outlier occurred during the 9/27/07 event. The greatest outlier from the TC method also occurred during this event but was not outside 3 times the IQR. Figure 4 present the comparison of sediment concentrations by the 2 methods by date and illustrates the range of observations.

Figure 3: Sediment EMC for Total Capture (TC) Versus SSC by Auto-Sampler (AS) (mg/l)

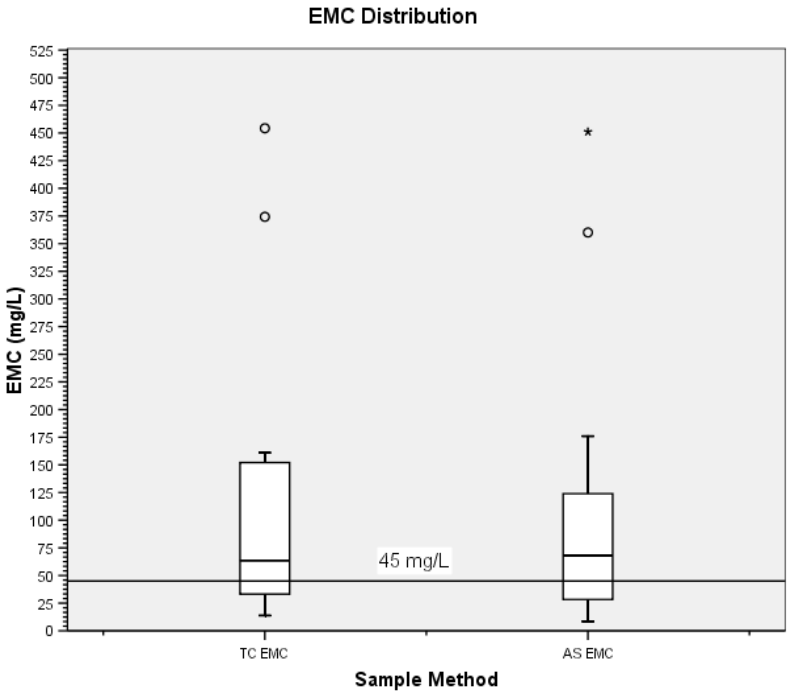

Higher sediment concentrations typically occurred during storms in the summer months, which experience events with large discharge rates.

Figure 4: Sediment Concentration by Date for Total Capture (TC) Versus SSC by Auto-Sampler (AS)

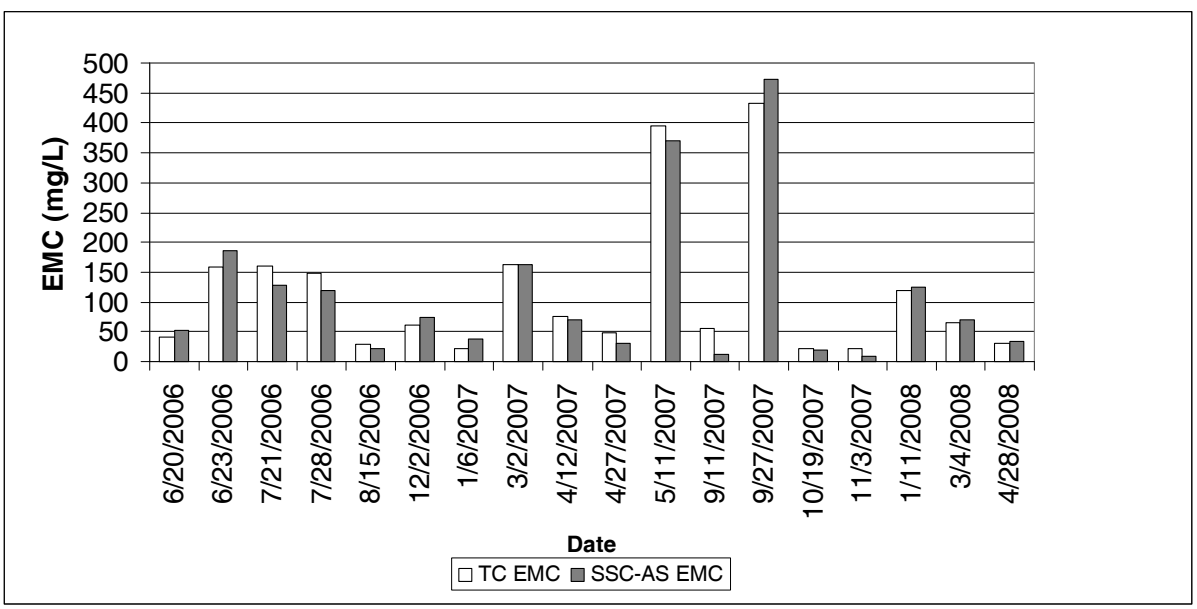

Correlation between Methods and Sediment Concentration Results. The correlation between the sediment EMCs for the two methods, SSC by auto-sampler and the TC is strong (R^2=.974) as observed in Figure 5. The results of sediment concentration for each method

were normally distributed and the two methods were found not to be significantly different at a 95% confidence level (Table 3).

Figure 5: Correlation between Sediment Concentration by Total Capture (TC) Versus SSC by Auto-Sampler

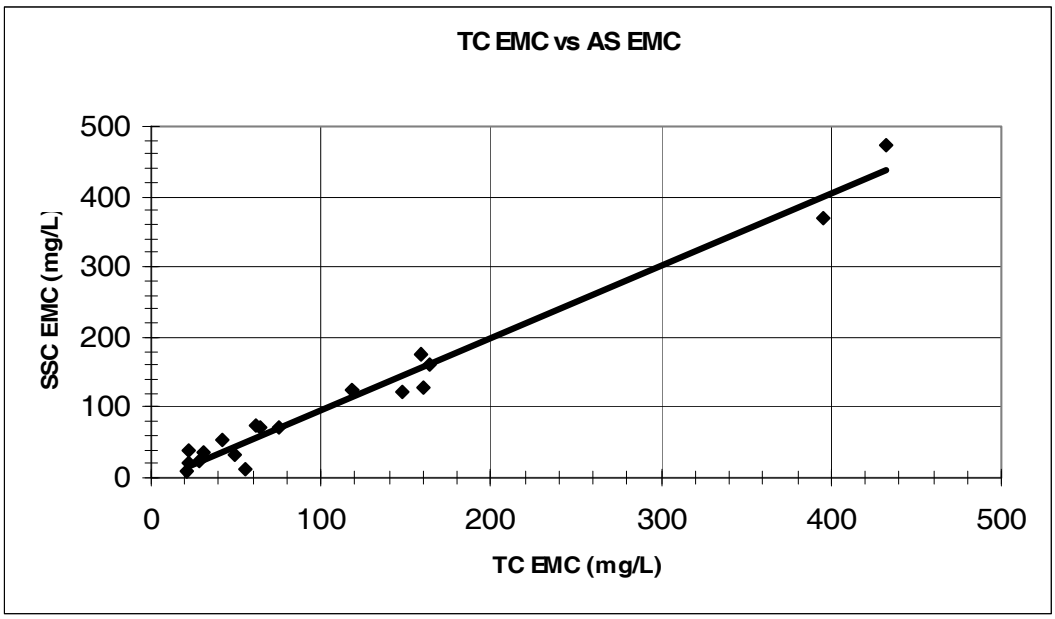

Table 3: T- Test for Significance of Sampling Methods: TC vs SSC

N	Mean (mg/L)	St. Dev.	95% Confidence Interval		Signifigance
			Lower	Upper	
18.00	7.40	18.40	-1.77	16.50	0.11

Suspended Sediment Particle Size Distribution (PSD). The range of particle sizes found in stormwater runoff varies significantly with land use however the presence of sand size sediments or coarser are commonly found in stormwater. (Sansalone, 1999) The median value of all D_{50} values for sediments recovered in the total capture samples and SSC samples taken by auto-sampler is 0.067 mm and 0.046 mm respectively. The distribution of three particle size percentiles is illustrated in Figure 6 (n=11). This size distribution fits well within the range for PSD of sediments from this type of land use (Fumari, 2002, Li, 2005). PSDs were not completed on sediments captured by automatic samplers for every event. A sand size reference line can be seen in this figure and all values above this line are sand size or coarser.

CONCLUSION

This study demonstrated that the use of auto-samplers combined with the suspended sediment concentration (SSC) method was an effective means for determining actual measured sediment loads (TC). This was for a site where the median particle size was in the 46-67 micron range (depending on method), common of stormwater sediments. Much press has been given to the notion that auto-samplers are fundamentally ineffective at sampling

Figure 6: Distribution of PSD Fractions by Method

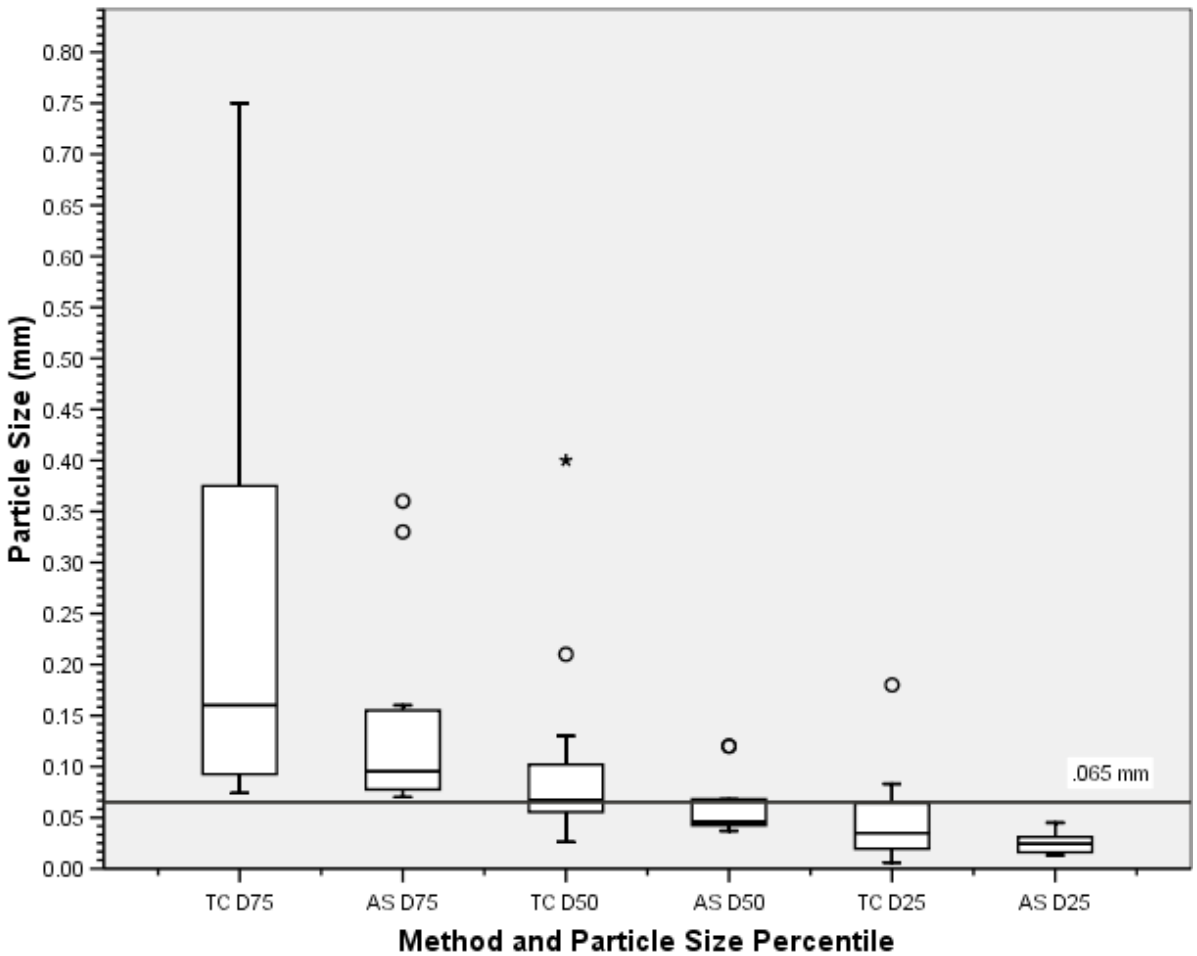

sediment loads. However, most of these studies have focused on the use of total suspended solids (TSS) with auto-samplers.

There are a source of potential errors when measuring sediment concentration, including samplers, sediment concentration methodology (TSS, TS, TVS, SSC, turbidity), sample splitters (cone and churn splitters), to name a few. For the combination of SSC with auto-sampler, there was no significant difference from the actual sediment load. Biases to particle size were observed, especially for the larger particles above 65 micron. The D_{75} particles were substantially underrepresented by the auto-sampler. For the range of 18 storms studied, only 3 storms had pipe velocities that exceeded the sampler intake velocity at 2.8 ft/s, another potential source of error. A sediment concentration monitoring method that employs a non-isokinetic automated sampler can provide an accurate measure of sediment concentration in a common stormwater sewer system.

REFERENCES

American Society for Testing and Materials. (2000). Standard Test Methods for Determining Sediment Concentration in Water Samples. D 3977-97. Pp. 395-400

Aryal, R.K,. et alt. 2006. Characteristics of particle associated PAHs in a first flush of a highway runoff. Water Science & Technology. Vol 53 No 2 pp245-254

Charbeneau, R.J. and Barrett, M.E. (1998). "Evaluation of methods for estimating stormwater pollutant loads." Wat. Evniron. Res. 70(7). 1295-1302.

Furumai, H., Balmer, H., Boller, M. (2002). Dynamic Behavior of Suspended Pollutants and particle Size Distribution in Highway Runoff. Water Science and Technology. Pp. 413-418.

Gray, J., Glysson, D., Turcios, L., Schwarz, G. 2000. Comparability of Suspended-Sediment Concentration and Total Suspended Solids Data. USGS WRIR 00-4191 Han, Y.H. 2006. Correlation analysis among highway stormwater pollutants and characteristics. Water Science & Technology Vol 53 No 2 pp 235-243

Horowitz, A. 2008. Determining annual suspended sediment and sediment associated trace element and nutrient fluxes. Science of the Total Environment.

Huber, W. 1993. Contaminant Transport in Surface Water. Handbook of Hydrology, McGraw-Hill Book Co., Inc., Pp. 14.1-14.50

ISCO. 2001. 6700 FR Refrigerated Sampler Instruction Manuel.

Kayhanian, M. (2006). "Online and Continuous Flow-Through Particle Size Distribution Measurement of Stormwater Runoff." Stormwater, 7(5): 94-103.

Li, Y., Lau, S., Kayhanian, M. (2005). Particle Size Distribution in Highway Runoff. Journal of Environmental Engineering. Pp. 1267-1276.

Li, Y. et alt. 2006 First flush and natural aggregation of particles in highway runoff. Water Science & Technology Vol 54 No 11-12 pp 21-27

Liebens, J. 2001. Heavy metal contamination of sediments in stormwater management systems: the effect of land use, particle size, and age. Environmental Geology 41:341-351.

National Stormwater Quality Database. 2005

Othmer, E. Berger, B. 2002. Future Monitoring Strategies with Lessons Learned on Collecting Representative Samples. Presented at: StormCon 2002

Roseen, R., et alt. 2006. Storm Water Low-Impact Development, Conventional Structural, and Manufactured Treatment Strategies for Parking Lot Runoff. Transportation Research Record: Journal of the Transportation Research Board, No. 1984.

Sansalone, J.J. and Tribouillard, T. 1999. "Variation in characteristics of abraded roadway particles as a function of particle size.". Transportation Research Record, 1690. Transportation Research Board, Washington, D.C.,

Stensome, M., Kayhanian, M. 2005. First Flush Phenomenon. California Department of Transportation Division of Environmental Analysis. CTSW-RT-05-73-02.6

Technology Acceptance Reciprocity Partnership. 2003. The TARP Protocol for Stormwater Best Management Practice Demonstrations

Technology Assessment Protocol-Ecology (TAPE). 2008 Guidance for Evaluating Emerging Stormwater Treatment Technologies. Washington State Department of Ecology

USEPA, 1992 NPDES Stormwater Sampling Guidance Document. EPA 833-92-001

USEPA, 1993 Guidance Specifying Management Measures for Sources of Nonpoint Pollution in Coastal Waters. EPA 840-B-92-002

USEPA, 2002 National Management Measures to Control Nonpoint Source Pollution from Urban areas-draft. EPA 8421-B-02-003, Office of Water, Washington, D.C.

US Office of Water Quality. 1998. Guidance for Collecting Discharge-Weighted Samples in Surface Water Using an Isokinetic Sampler. Office of Water Quality Technical Memorandum 99.01 and 99.02

SELECTING OPTIMAL WATER SUPPLY OPTIONS – A REGIONAL WATER SUPPLY CASE STUDY IN THE UPPER KISSIMMEE BASIN, FL.

Aditya Tyagi[1], Mitchell Griffin[2], Richard Nevulis[3] and Chris Sweazy[4]

[1] CH2M HILL 12301 Research Blvd., Bldg. 4, Suite 250, Austin, TX 78759; PH (512)453-1980; FAX (412)453-4109; email: aditya.tyagi@ch2m.com
[2] CH2M HILL 3011 S.W. Williston Road, Gainesville, FL 32608; PH (352) 335-5877; FAX (352) 271-4906; email: Mitch.Griffin@ch2m.com
[3] South Florida Water Management District, 3301 Gun Club Road (33406), P.O. Box 24680, West Palm Beach, FL 33416-4680; PH (561) 686-8800; email: rnevul@sfwmd.gov
[4] South Florida Water Management District, 1707 Orlando Central Parkway, Suite 200. Orlando, FL 32809 (407) 858 - 6100. Fax: (407) 858-6121, email: csweazy@sfwmd.gov

ABSTRACT

Central Florida's population is growing at a rapid pace and is approaching the limits of its available groundwater supplies. Considering this fact, the South Florida Water Management District (SFWMD), St. Johns River Water Management District (SJRWMD), and Southwest Florida Water Management District (SWFWMD) foresee that additional groundwater withdrawals in Central Florida to meet future water demands beyond 2013 will be restricted. The objective of this initial feasibility study is to evaluate the availability of surface water in the upper Kissimmee River basin as an alternative supply source for Central Florida. As part of the Upper Kissimmee Basin Regional Water Feasibility Study, 28 integrated water supply options were identified and evaluated by developing a reservoir optimization model that minimizes both capital and O&M costs of various water supply components, such as intakes, reservoirs, water treatment plants, pumps, pipelines, and groundwater withdrawals, and so forth, and satisfies necessary physical constraints.

The optimization approach appropriately sized the various water supply system components from both surface and groundwater sources to meet a desired yield target while addressing the primary environmental performance measures identified for the Kissimmee River restoration effort. In addition to minimizing water supply cost, reliability was also maximized using a multi-objective genetic algorithm. A key component of the feasibility study is to provide a planning-level estimate of surface-water availability and reservoir sizing for one or more project locations within the study area. This work was completed in August 2008 using interim operational criteria for the Upper Kissimmee Chain of Lakes. Additional refinements to the estimates of water availability and reservoir sizing are anticipated in the future as the current environmental criteria and operation schedules of the lake structures are modified in 2009.

INTRODUCTION

The three Florida Water Management Districts that border each other in Central Florida (SFWMD, SJRWMD, and SWFWMD) have determined that additional groundwater from current wellfields in Central Florida will be restricted beyond 2013 unless it can be demonstrated that the additional withdrawals do not add to the cumulative affects of current withdrawals. The Districts have indicated to the water utilities that alternative water supplies are needed to meet their future demands (beyond 2013). The Upper Kissimmee River Basin surface water has been identified as a potential source of alternative water supply.

In recent years, several water resource management issues have emerged as competing for the water resources in the Upper Kissimmee Basin (UKB). Four specific items that have come to light include: 1) meeting hydrologic requirements for the Federally-authorized Kissimmee River Restoration Project (Water Resources Development Act, 1992), 2) meeting the hydrologic requirements for the health of the upper basin lakes, 3) finding alternative storage to reduce flows to Lake Okeechobee, as directed in the Northern Everglades and Estuaries Protection Program (Section 373.4595 Florida Statute), and 4) finding water supply alternatives to the Floridian aquifer as a source of water to meet municipal consumptive uses in the upper basin.

CH2M HILL assisted SFWMD by conducting this feasibility study for developing a new surface water supply in the UKB to provide alternative supplies to Central Florida utilities consistent with the Central Florida Coordination Area (CFCA) plans and agreements. The study area for this project is the drainage basin of the Kissimmee River upstream and including the S-65 spillway structure at the discharge of Lake Kissimmee. Key components of the feasibility study was to provide a planning-level estimate of surface-water yield given a pre-defined surface water availability after environmental and programmatic needs of the watershed are met and reservoir sizing for one or more project locations within the study area. Figure 1 presents a map of the study area.

OBJECTIVE

In a previous study CH2M HILL (2008a) developed a reservoir spreadsheet model for the UKB System to evaluate the relationship between reservoir sizing and water yield based upon the surface-water availability information provided by the District. The reservoir spreadsheet model was used to determine the size of reservoirs to meet a given target yield via a water balance analysis. This study illustrated that the surface water for alternative supply may not be available constantly. So in addition to available surface water supplies the optimization model included the use of supplemental groundwater sources that may be needed to improve the reliability and increase the potential quantity with which future water demands can be met from this system.

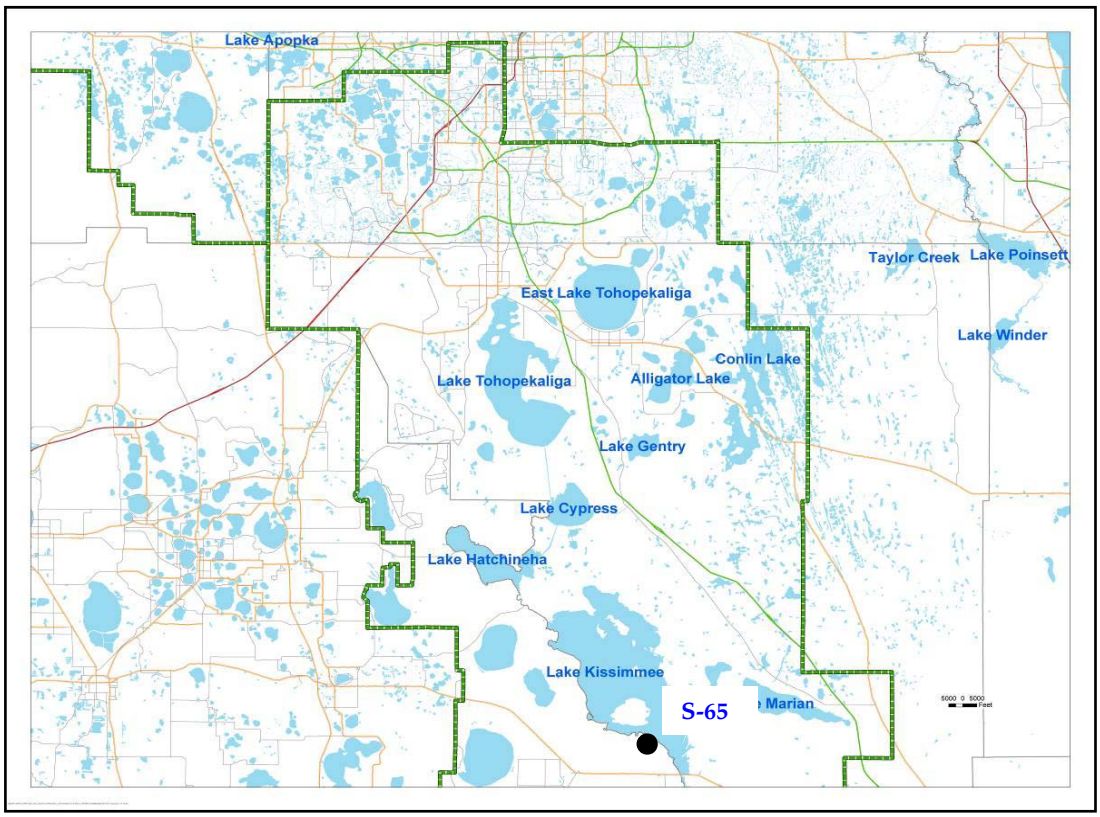

Figure 1. Upper Kissimmee Basin Water Supply Feasibility Study Area.

The objective of follow-up study was to develop an optimization model and apply it to a broader UKB water supply infrastructure system. To identify the best combination of pre-identified candidate project configurations that meet the project objectives, an optimization approach was applied around the reservoir spreadsheet model to incorporate the sizing of pumps and pipelines need for the UKB water supply system. For a given scenario, the optimization model identified an optimal solution that both minimizes costs and satisfies necessary physical constraints.

INTEGRATED WATER PLANNING SCENARIOS

Targeted water supply yields included for this analysis are 10, 20, and 40 million gallons per day, annual average daily flow (mgd, AADF). These target supply quantities are less than the expected cumulative water supply deficit between 2013 and 2025 of the stakeholders which is greater than 80 mgd, AADF (CH2M HILL, 2007). These smaller supply quantities were considered because the preliminary work concluded that only 20 mgd of water was available 50 percent of the time from Lake Kissimmee. Therefore to meet supplies greater than about 10 mgd additional sources other than solely surface water are needed to provide even the modest rates studied here.

A preliminary strategy regarding the locations of water supply system components within the UKB was developed based on the local knowledge of CH2M HILL and SFWMD. Figure 2 provides an overview of the system components including surface water inlets, transmission pipelines, groundwater withdrawal points, storage reservoirs, and points of connections (POCs). Water storage is believed to be an important component required to utilize "water of opportunity" to the fullest degree so storage reservoirs are also central in the water supply scenarios. For purposes of this study, the identification of water-storage options is conceptual in scope. SFWMD identified publicly-owned land areas to be initially considered as potential locations for surface storage impoundments until more detailed available land assessments can be conducted.

Once the potential water supply system layout was developed, a variety of scenarios capable of meeting target water yields of 10, 20, and 40 mgd at four potential connection points to utilities were identified. Twenty-eight scenarios were selected for evaluation because these would include most potential alternatives. The associated water supply sources, treatment alternatives, delivered water quality, transmission routes, and delivery points were specified for each scenario. The development of these scenarios and the formulation of model objectives and constraints were coordinated with the SFWMD. Table 1 provides a list of the 28 water planning scenarios selected for evaluation.

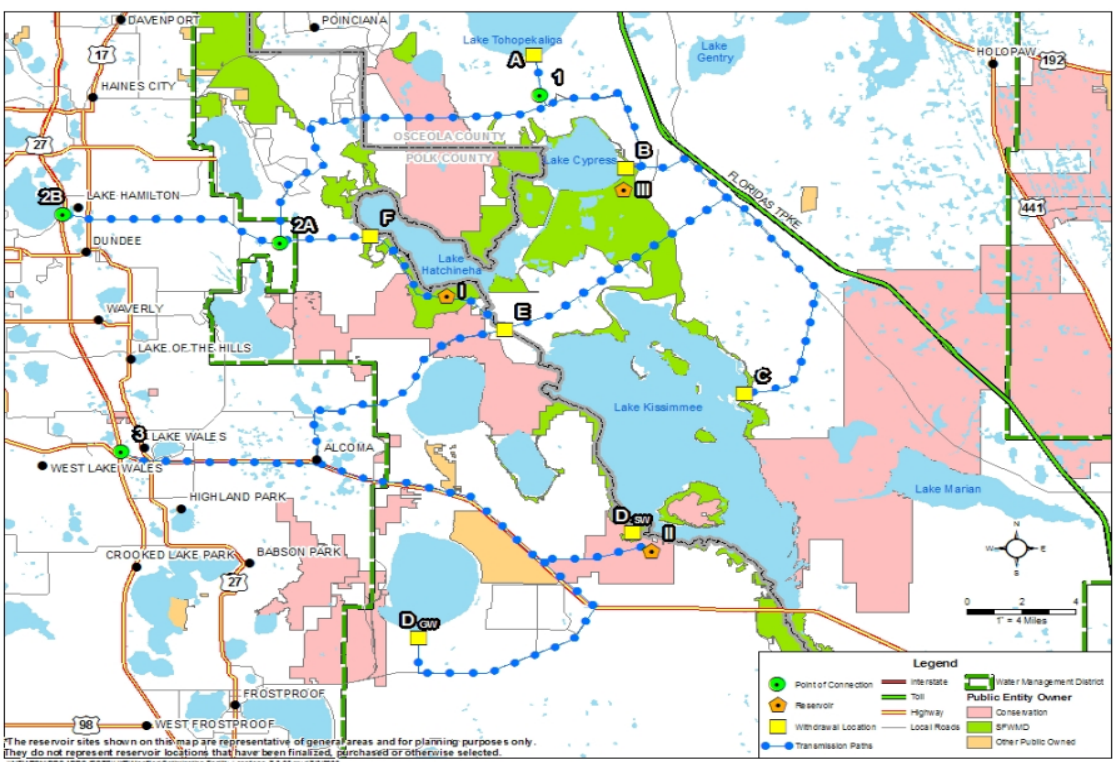

Figure 2. Upper Kissimmee Basin Transmission and Facility Infrastructure used for Optimization Analysis.

Table 1. Integrated Water Supply Planning Scenarios

S.No.	POC Demand (mgd)					Inlet						Reservoir		
	1	2A	2B	3	Sum	A	B	C	D	E	F	I	II	III
1	10				10	x	x	x		x		x		x
2	20				20	x	x	x		x		x		x
3	40				40	x	x	x		x		x		x
4	10				10		x	x						x
5	20				20		x	x						x
6	40				40		x	x						x
7				10	10				x				x	
8				20	20				x				x	
9				40	40				x				x	
10		5	5		10						x	x		
11		10	10		20						x	x		
12		15	5		20						x	x		
13		20	20		40						x	x		
14	10			10	20					x		x		
15	20			10	30					x		x		
16	20			20	40					x		x		
17	10				10					x		x		
18	20				20					x		x		
19	40				40					x		x		
20	10				10	x				x		x		
21	20				20	x				x		x		
22	40				40	x				x		x		
23				10	10					x		x		
24				20	20					x		x		
25				40	40					x		x		
26	10		10		20	x	x	x		x		x		x
27	20		10		30	x	x	x		x		x		x
28	20		20		40	x	x	x		x		x		x

SYSTEM COMPONENTS AND OPTIMIZATION LAYOUT

As shown in Table 1, multiple sources from which one or two points of connection must be supplied are specified for each model scenario. Figure 3 shows a schematic of a typical path from supply source to point of delivery. Supply system components include surface water intakes, reservoirs, pump stations, treatment plants, and transmission booster pump stations and pipes. The size of the system's physical components determines the system's ability to meet yield targets and minimize costs. For a given scenario, the optimization model determines the cost of the withdrawal, treatment, and delivery of surface water and groundwater supplies to a particular POC.

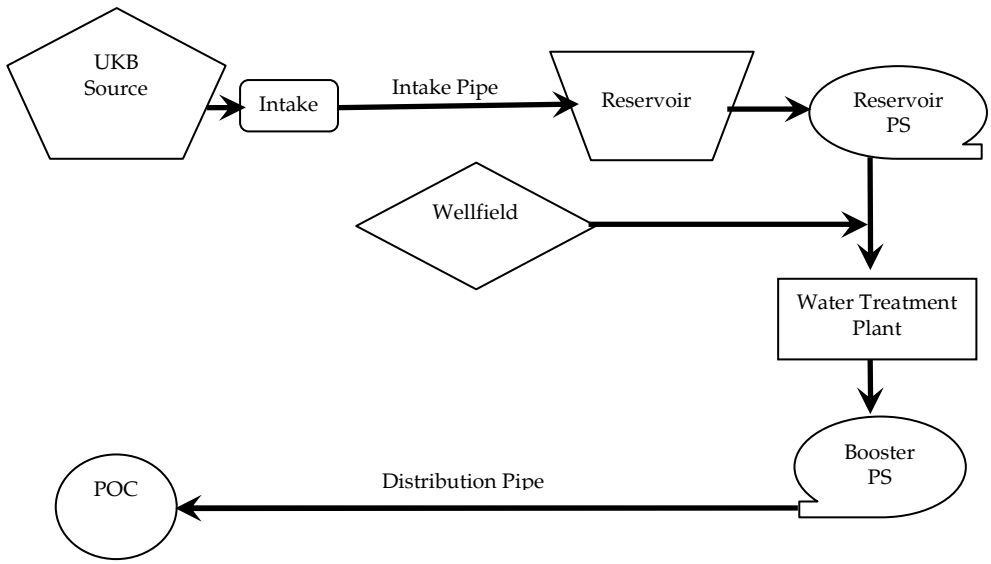

Figure 3. Water Delivery Schematic for the Upper Kissimmee Basin

Optimization Model Approach. The UKB optimization model was developed to size water supply components, such as intakes, reservoirs, water treatment plants, pumps, pipelines, and groundwater withdrawals to meet a given target yield. In addition to minimizing the cost-based objective function, the optimal solution must also meet certain assumptions and physical constraints which are described below. For this study, the model was run on a daily time step over the period of January 1, 1970, through December 31, 2005 using the time series of available water that provided the greatest yield identified in the previous reservoir study. This time series of available water was provided to CH2M HILL by the SFWMD. This data stream represented the then-best estimate of surface water available at S-65 that would meet environmental objectives for the multiple projects in the basin. However, since then the District is moving forward on additional evaluations to better refine the objectives and available surface waters from the UKB (to be completed in approximately 2010).

Objective Function. The optimization model determines the optimal supply system configuration by minimizing the following objective function:

*Total Performance Cost = Capital Cost*PF1+ O&M Cost*PF2 + GW Penalty*PF2*

Where: *Capital Cost* = Capital cost of Intake, Intake Pipe, Reservoir, Booster Pump Station, & Distribution Pipeline*; O&M Cost* = O&M cost of Intake Pumps, Reservoir Pumping, Groundwater Pumping and Distribution Pumping*; PF1 & PF2* = Present worth factors, *PF1* = 1.0 assuming interest rate equals inflation rate*, and PF2*= $(1+NIR)^t$; NIR = Nominal Inertest Rate based on the annual interest rate of 5%, t = no. of days; *Penalty* = A penalty is applied to discourage groundwater use

While the cost of groundwater withdrawals is presented in the final results, this cost was not incorporated in the objective function because surface water is the preferred supply source at all times, regardless of treatment costs. Groundwater supply will be less expensive than surface water so it would always be the preferred low cost solution. However, by adding groundwater use as a penalty cost, this forces the model to minimize groundwater use.

Cost Functions. The optimization model requires cost to be included to evaluate the least-cost solution as part of the objective function. To satisfy this requirement, appropriate capital and O&M cost equations were determined for the physical components of the water supply system. The cost functions used included surface water intakes, transmission pipe, reservoirs, pump stations, wellfields, water treatment plants, and booster pumps.

Except where otherwise noted, these functions were based on reported costs that were originally developed in February 2008 (Black and Veatch, 2008). These cost opinions were based on an Engineer News Record Construction Cost Index equal to 8,005 and are appropriate for planning-level evaluations. The "capital costs" listed below do not include all potential owner project costs (management, engineering, permitting, land and easements, etc.). The purpose of these opinion-of-cost functions is for developing order-of-magnitude scenario comparisons like was done for this evaluation.

Physical Constraints. Certain assumptions have been incorporated into the model to provide boundaries, such as maximum size and peak withdrawal rates from the reservoir and each well. In addition to minimizing the objective function, selection of an optimal solution is subject to the following physical constraints:

- $\sum$ (Supply – Demand) $\geq$ 0 for the study period (1970 – 2005)
- Daily groundwater supply $\leq$ an assigned Maximum Groundwater Capacity
- Maximum Groundwater Capacity $\leq$ Demand per scenario
- Surface Water Storage $\leq$ an assigned Maximum Reservoir Capacity
- Reservoir Capacity $\leq$ 9.38 Billion Gallons each (about 3 mi^2)

- Intake Capacity = Maximum Allowable Lake Withdrawal
- Maximum Allowable Lake Withdrawal ≤ 600 mgd (±1,000 cfs).
- Maximum reservoir depth = 16 ft
- Reservoir initial depth = 8 ft
- Supplies from Inlet A ≤ 24% of S-65 flows
- Supplies from Inlet B ≤ 60% of S-65 flows – Supplies from Inlet A
- Supplies from Inlets C, D, & F ≤ S-65 Flows – Supplies from Inlets A & B

MODEL RESULTS

Figures 4 through 7 provides a summary of the results for the 28 scenarios which includes the amount of surface and groundwater used; capital and O&M costs; and the size of the reservoirs. Figures 4 and 5 show the estimated capital and average annual O&M costs associated with each scenario. Figure 6 depicts the distribution of supplies from surface and groundwater sources, while Figure 7 shows total reservoir storage capacity for each scenario. In each figure, the scenarios are grouped by their specified target yield: 10, 20, 30, or 40 mgd, AADF, respectively.

The capital costs of most of the scenarios varied from $550 to $800 million. The capital cost per mgd delivered was more cost-effective for the larger yields. However, the scenarios with higher yield also used a greater fraction of groundwater (Figure 6), as expected. The overall scenario costs are generally affected by the cost of the pipelines because the reservoir costs did not vary greatly except for the few where the costs are much higher (Scenarios 3, 26, 27, and 28; Figure 7). Therefore, scenarios that reduced the pipeline costs had somewhat smaller capital costs. The O&M costs generally increased with the increase in yield, but not in direct proportion so the larger yield projects again would have lower unit O&M costs.

A maximum reservoir size of approximately 3 square miles was used in the model because increasing the size only provided small increases in yield (CH2M HILL, 2008a). The optimization model picked the largest size reservoir in most cases because of the penalty function applied to the groundwater to discourage its use. In practice there will be real-world limitations on the reservoir size.

These results are consistent with the previous results utilizing the preliminary estimates of "available water." A different data stream for available water will likely provide different results but these estimates provide an idea of the scale of projects required to develop a surface water supply in the UKB**.**

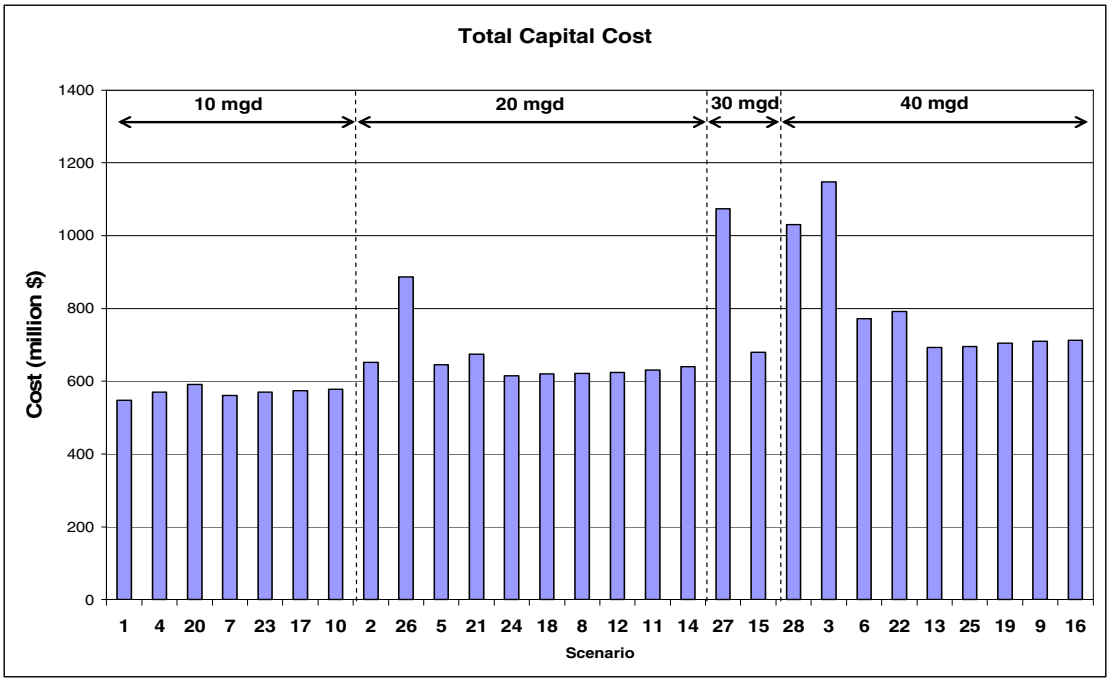

Figure 4. Total Project Capital Cost for 28 Scenarios

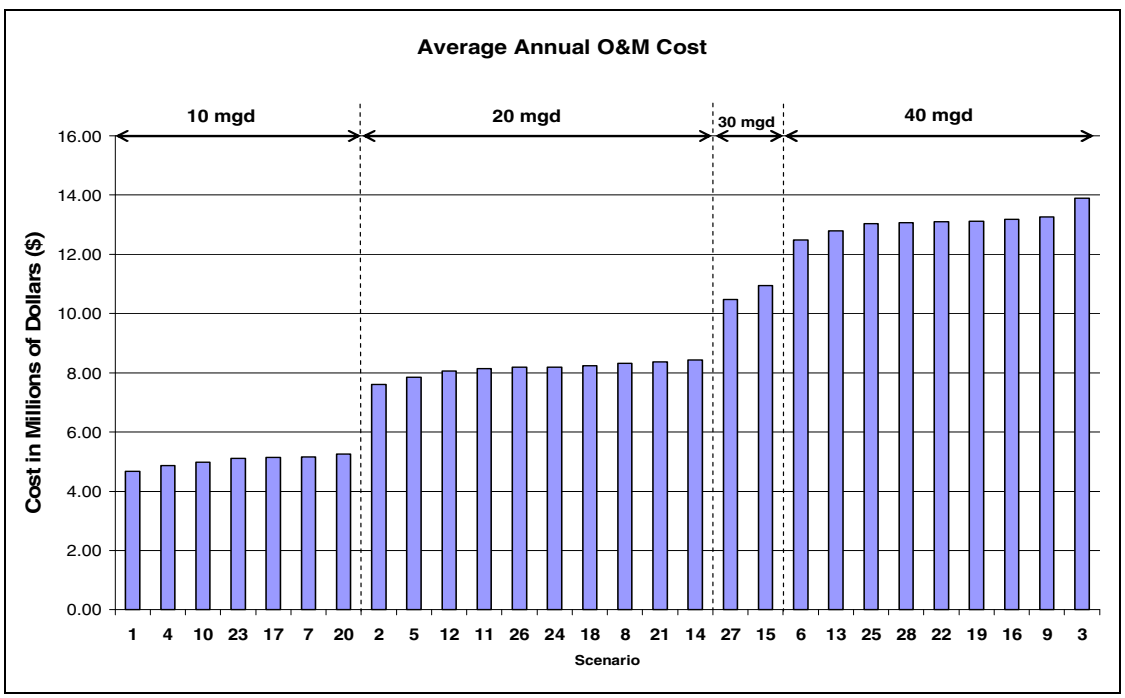

Figure 5. Average Annual O&M Cost for 28 Scenarios

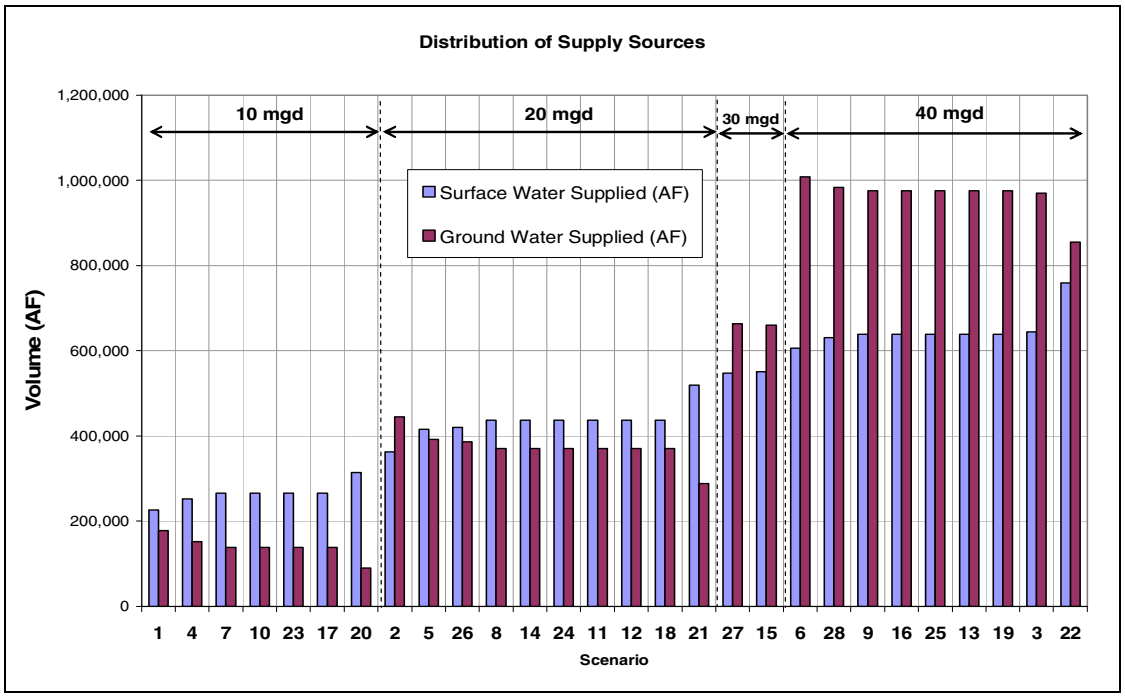

Figure 6. Total Volume Groundwater and Surface Water Supplied During Project Lifetime

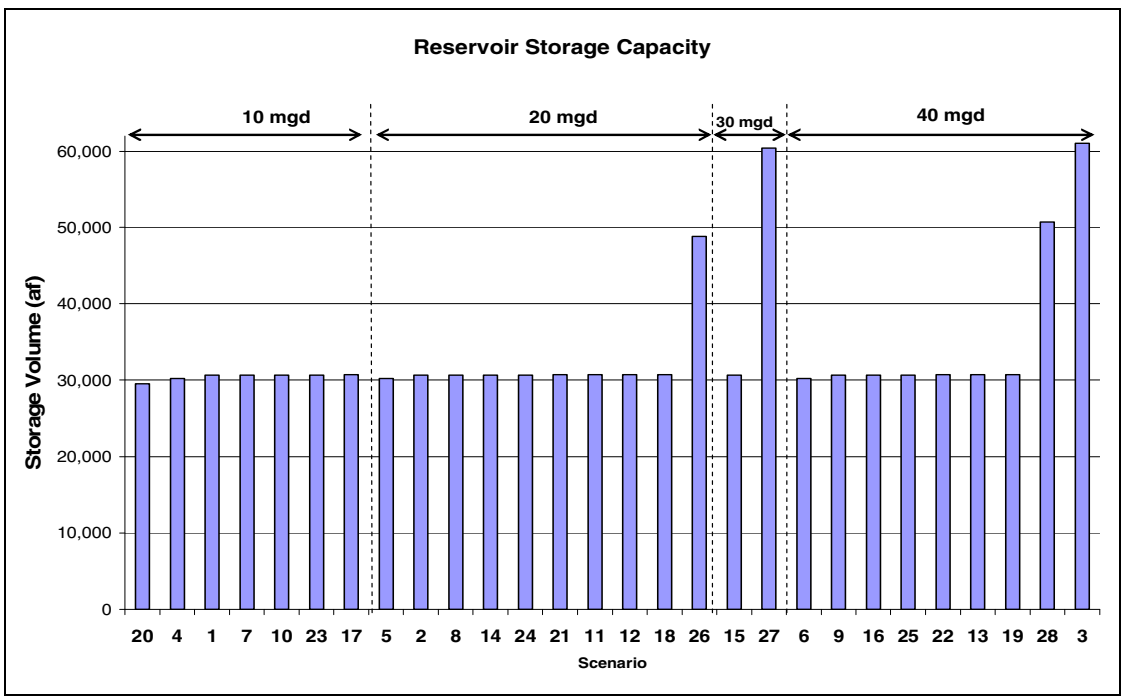

Figure 7. Total Required Reservoir Storage Capacity for 28 Scenarios

CONCLUSIONS

The SFWMD conducted a feasibility study for the purpose of developing a new surface water supply in the UKB to provide a new source of water supply to stakeholder utilities in Central Florida. As part of the Upper Kissimmee Basin Regional Water Feasibility Study, 28 integrated water supply options were identified and evaluated using a reservoir spreadsheet optimization model.

The optimization model was applied separately for each scenario to identify a solution that both minimizes costs and satisfies necessary physical constraints by appropriately sizing supply system components to meet a given target yield. In addition to available surface water supplies, the optimization model considered the use of groundwater supplies that may be needed to improve the reliability with which future water demands can be met, but only after surface water was used first. The overall conclusions of this study are listed below.

- The capital cost per mgd of delivered water was more cost effective for the larger yields. However, the scenarios with higher yield used greater fraction of groundwater, as expected.
- Consistent with previous analysis, the amount of surface water that could be applied to a constant demand will be limited with the given "available water" used in this evaluation.
- Integrated water supply planning is a complicated mix of alternatives that includes engineering, environmental, and policy decisions to be incorporated into the planning effort. The optimization model was very effective in finding integrated water supply systems given a set of physical constraints. Additional issues have been highlighted through this work, like the potential size of storage reservoirs.
- A different flow record of available water may provide significantly different results, thus additional work is being focused on improved estimates of excess water from the UKB. Environmental and programmatic water needs are being established by the SFWMD. In addition, the SFWMD is in the process of a Kissimmee Basin Modeling and Operations Study (KBMOS) that includes a detailed, linked groundwater and surface-water model that is being concurrently developed for the Kissimmee River Restoration Project and adapted for water supply assessments.
- The predicted overall cost of a potential surface water supply infrastructure gives the utilities and districts better information to use in their overall planning efforts.

The results of this optimization study are meant to serve as a precursor to an improved analyses that will jointly review water supply and restoration goals in future water supply evaluations.

REFERENCES

Black and Veatch (2008). *Engineering Assistance in Updating Information on Water Supply and Reuse System Component Costs*, Prepared for St. Johns River Water Management District, District Project No. SK30712.

CH2M HILL (2007). *Regional Water Demands, Upper Kissimmee Basin Regional Water Feasibility Study*. TM2, December 14, 2007.

CH2M HILL (2008a). *Upper Kissimmee Basin Regional Water Feasibility Study: Regional Availability of Surface Water in the Upper Kissimmee Basin*, TM4, May 15, 2008.

CH2M HILL (2008b). *Upper Kissimmee Basin Water Treatment Facility Conceptual Cost Estimate Basis and Assumptions for Comparison Purpose*. TM3, May 15, 2008.

HDR (1999). *Studies level engineering and costing methodology for pipelines pump stations, and other facilities*, HDR Engineering, Inc., Austin, TX.

SIMPLIFIED SOLUTION FOR GROUNDWATER MOUNDING UNDER ROUND STORMWATER INFILTRATION FACILITIES

Kaveh Zomorodi[1]

ABSTRACT

A study was conducted to derive new groundwater mounding equations that are simple in their structures but produce reasonable values for conditions most commonly found in stormwater infiltration facilities. This paper presents the new simplified equations and their theoretical development. The equations apply to Steady–uniform recharge rate to infinite homogenous aquifers with initially horizontal water table and bedrock surfaces. Separate sets of equations were derived for recharge strips (infiltration channels/trenches) and infiltration basins (round or square facilities). The equations for recharge strips were published previously. This paper presents the equations for round or square facilities. The new equation sets require minimum input data in terms of the size and shape of the facility, the properties of the saturated layer and the recharge rate and are convenient for routine engineering calculations. Example applications of the new equation sets for conditions typical in New Jersey are presented.

INTRODUCTION

Excessive groundwater mounding under an infiltration facility could cause various problems including water logging, structural instabilities, wet basements, declined recharge rates, groundwater quality problems by reduction or loss of the unsaturated layer under infiltration facilities, and the possibility of interflow or surface water discharge leading to untimely or undesirable contribution to baseflow. Both the maximum rise of the central mound and the areal extent of the mound are important for the above concerns.

Low Impact Development (LID) quantitative calculation tools have been developed for the State of New Jersey that deal both with surface water and groundwater (Zomorodi, 2003, and Dewberry, 2002). The New Jersey regulations encourage infiltration practices mainly to help maintain groundwater recharge under post-development conditions. In the design of any infiltration facility, the potential for excessive groundwater mounding must be checked. However, the existing methods for evaluation of groundwater mounding are complex and usually difficultto apply.

[1] Ph.D., P.E., CFM, M. ASCE, Dewberry, 8401 Arlington Blvd., Fairfax, VA 22031, 703.849.0336 (P); 703.849.0104 (F); E-Mail: kzomorodi@dewberry.com

This paper presents new simplified equations that can be used for a general approximation of mounding under stormwater infiltration facilities. Separate equations were derived for recharge strips (infiltration channels/trenches) and infiltration basins (round or square facilities). The equations for recharge strips have been published previously (Zomorodi, 2003). The author has since received many requests for the second set of equations applicable to round (and with approximation to square) facilities. This paper presents the derivation and application of the equations for round and square infiltration facilities.

Limitations in Application of the Existing Solutions to Stormwater Infiltration

There are a number of issues and considerations that limit the applicability of current groundwater mounding calculation methods in everyday design of a stormwater infiltration facility. One issue is the fact that these methods require knowledge of the local groundwater system and its various hydrogeological parameters. The water resources engineers who traditionally work on BMP design are not familiar with groundwater issues and data sources. Moreover, local groundwater studies are typically not available and the regional groundwater studies (if they are available) do not accurately apply to micro-scale urban drainage conditions. Some studies indicate a need for even a larger information base that is required in application of most of the existing equations. For example, a recent study by Gua (2001) suggests that the hydraulic conveyance capabilities of not only the saturated layer but also that of the unsaturated layer must be considered in estimating the groundwater mounding.

A number of researchers such as Swamee and Ojha (1997) have tried to simplify existing solutions, but the resulting equations are still too complicated for routine applications in stormwater management design and require an iterative solution methodology.

Besides the relatively accurate estimates of groundwater parameters, most existing solutions require knowledge of the boundary conditions. Boundary conditions must satisfy assumptions of the formulas. These assumptions include factors such as an infinite aquifer extent or known head at a known distance. Bouwer et. al. (1999) and Bouwer (2002) presented simplified mounding equations. However, these equations predict only the central mound rise and not the mounding depth at a given distance from the facility and they require the depth and distance of the controlled saturated zone. The controlled saturated zone is the water table that is held constant by regional recharge/discharge activities. This means that the boundary conditions have to be prescribed and constant. Therefore, these equations may be applicable

to large artificial recharge facilities that are integrated into regional groundwater pumping plans, but they are not usable for small stormwater recharge facilities. In most cases the radius of influence of a stormwater facility on the water table is what we need to estimate and not a given parameter of the problem. The simplified equations we developed (presented later) are based on the general approach of Bouwer (2002) but they overcome the problem of controlled prescribed boundaries by the use of additional equations.

Another major issue is that the traditional groundwater mounding equations are valid for steady state recharge subject to uniform and constant recharge rates and the effect of the unsaturated zone is ignored. The few existing unsteady mounding equations typically entail other application restrictions. For example, Youngs (1977) presented an equation for unsteady groundwater mound but it assumes no water table prior to recharge. An infiltration facility receiving stormwater runoff would cause unsteady intermittent recharge in which the rate of infiltration and recharge is variable and the mound actually dissipates between recharge operations. Typically groundwater mounds below recharge basins are one to six feet after a rain event and the mound usually disappears within five days of a heavy rainfall. Zomorodi (1988, 1991) studied the response of water table to intermittent-variable rate recharge and showed that the mounding under a variable recharge rate could be quite different from mounding under a constant recharge rate even with an equivalent recharge depth for both cases. The proposed solution method in that study, however, was for artificial recharge ponds receiving water in regular cycles that allow a repeating predictable cycle of recharge. This condition is not satisfied with recharge of stormwater that occurs on an irregular time basis. Manglik and Rai (2000) presented an analytical solution for modeling of water table fluctuations in response to a variable recharge and withdrawal rate. However, this equation is too complex for routine use in stormwater management studies. Zomorodi (2002) developed a numerical model on a spreadsheet that can predict mounding due to unsteady infiltration rate and considers the effect of the unsaturated zone. The model predicts the position of the central mound and so, conceivably it can be used in verifying stormwater regulation requirements of a given minimum thickness of unsaturated layer under a recharge facility. However, to provide the shape and extent of the mound the model in Zomorodi (2002) model must be combined with another technique that provides the typical shape of the mound.

A number of complicating factors preclude development of general solution charts for groundwater mounding. For example, according to Vauclin et. al. (1979), because of the shape of the soil suction curve, it is not possible to use a series of nomographs

to predict the time of transfer (time it takes for the infiltrated water to reach the water table) for a given soil, even if the infiltration rate and depth to water table are known.

There have been attempts to develop coupled surface water-groundwater models to address the problem of a retention pond operation and its interaction with underlying aquifer. However, these models are usually integrated into proprietary software packages and their application is very data and labor intensive and is possibly justified only for the final design of large retention ponds.

Development of New Equation for Round Recharge Facilities

If the recharge area is circular or approximately square or has an irregular shape that can be interpolated to an equivalent circle, then the flow out of the facility can be simulated by assuming radial flow. Figure 1 shows the general layout and configuration of the problem. Due to symmetry of the system only the layout on one side of the pond is shown in Figure 1.

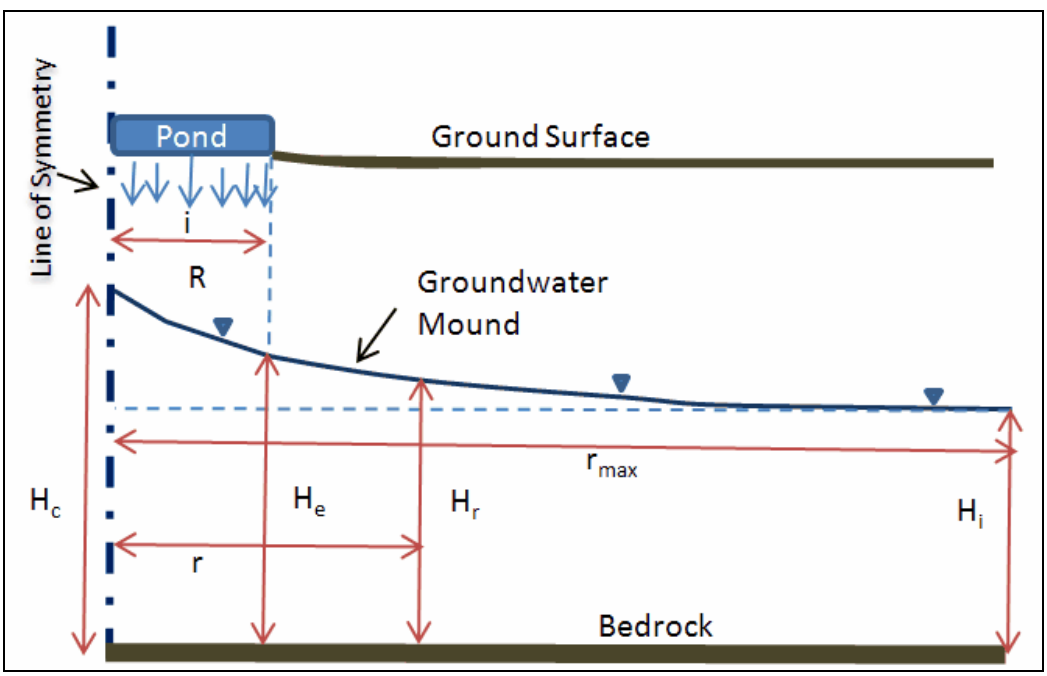

Figure 1. Circular Recharge Area Problem layout and Parameters.

Several assumptions need to be made to allow derivation of the required solution:

- Steady – uniform recharge rate from a circular recharge source (pond),
- Average recharge rate is smaller than the horizontal saturated hydraulic conductivity of the aquifer,

- Infinite aquifer extent with horizontal initial water table and bedrock,
- Horizontal flow in the aquifer,
- Homogenous aquifer,
- No source/sink terms outside of pond boundaries,
- Effective transmissivity is approximated by hydraulic conductivity times pond diameter.

The last assumption above may be justified based on review of several sources in Zomorodi (1988) that led to the conclusion that the active (effective) thickness of the saturated layer in transmitting the recharged water away from the pond is not larger than the pond width. This means that the rate of mound rise does not depend on saturated thickness of the aquifer as long as this thickness exceeds the width of the basin. Under a given design condition, whether these assumptions are valid or not depends on local conditions. The solution methodology developed here does not require an exact knowledge of the initial saturated thickness of the aquifer. As long as a rough estimate of this thickness indicates that it is larger than the pond diameterthe equations apply and an arbitrary value can be used in the equations. The effective transmissivity may be assumed to be equal to hydraulic conductivity multiplied by the basin diameter.

Assuming a constant uniform recharge rate from the circular pond which is equal to the average infiltration rate "i" in the pond, the flow from the pond to aquifer at a distance "r" from the pond center (but still under the pond) can be written as:

$$q = i\pi r^2 \qquad (1)$$

From Darcy's equation the flow away from the pond in the underlying aquifer at a given distance "r" would be:

$$q = 2\pi r K H\left(\frac{-dH}{dr}\right) \qquad (2)$$

Combining Equations 1 and 2 and rearranging the terms allows integrating the equations for limits between the pond center and the pond edge:

$$\int_0^R i\pi r\, dr = \int_{H_c}^{H_e} 2\pi K H\,(-dH) \qquad (3)$$

Based on the assumption of the effective transmissivity being equal to hydraulic conductivity times pond diameter, "H" can be replaced in the above equation with 2R as long as $H_i > 2R$. Making this substitution and simplifying the equation leads to an equation that relates the maximum saturated thickness at the edge of pond (H_e)

to the maximum saturated thickness under the pond center when the stable mound is fully formed (H_c):

$$H_e = H_c - \frac{i\,R}{8\,K} \tag{4}$$

To equate the total flow out of the pond to the total flow moving radially away to a distance "r" from the pond center in the aquifer when equilibrium is reached we can write:

$$i\,\pi\,R^2 = 2\pi\left(\frac{r}{2}\right)K\,H\left(\frac{-dH}{dr}\right) \tag{5}$$

We can write the flow balance for up to the maximum radius of influence of mounding r_{max}:

$$i\,R^2\int_R^{r_{\max}}\frac{dr}{r} = -2\,K\int_{H_e}^{Hi} H\,dH \tag{6}$$

Using the assumption of the effective transmissivity being equal to 2R x K and integrating both sides and rearranging terms we can express the natural logarithm of the mound's maximum radius of influence by:

$$\ln(r_{\max}) = \frac{4\,K(H_e - H_i)}{i\,R} + \ln(R) \tag{7}$$

Replacing H_e by its equivalent from Equation 4 yields:

$$\ln(r_{\max}) = \frac{4\,K((H_c - H_i) - \frac{i\,R}{8\,K})}{i\,R} + \ln(R) \tag{8}$$

H_c and r_{max} are both unknowns of the above equation and a second equation will be needed to solve the problem.

Bouwer (1962) proposed the following equation for the groundwater flow rate moving away from a recharge facility,

$$q(t) = \frac{K\,h'(t)Q'}{1 + h'(t)Q'} \tag{9}$$

Q' is an intermediate flow parameter. Under steady state equilibrium q (t) = i and h' (t) = H_c – H_i, and so the above equation can be used to yield:

$$H_c - H_i = \frac{i}{Q'(K-i)} \tag{10}$$

Bouwer (1962) used an analogue model to generate curves that related Q' to the two factors of the width of the infiltration bed and the original thickness of the aquifer. Zomorodi (1991) fitted an equations to the original Bouwer data or Q' which is valid as long as the width of the infiltration bed is smaller than half the original thickness of aquifer, a condition easily satisfied under most common field conditions. Modifying the equations in Zomorodi (1991) for Q' for the case of radial steady-state flow yield to:

$$Q' = \frac{12.8/(2R)}{10 + \left(\frac{2R}{H_i}\right)^{2.2}} \tag{11}$$

Substituting Q' from Equation 11 into Equation 10 and rearranging the terms yield to the equation for the final central mound rise:

$$H_c - H_i = \frac{0.156\, i R \left(10 + \left(\frac{2R}{H_i}\right)^{2.2}\right)}{(K-i)} \quad for\ i < K\ and\ 2R < H_i \tag{12}$$

Equation 12 gives the stable central mound rise and is valid as long as i < K and 2R< H_i. However, the use of Equation 12 requires a good estimate of the original saturated thickness of the aquifer. Note that in the equations developed for long strip recharge (Zomorodi, 2005) the exact value of the original saturated thickness of the aquifer is not needed as long as it is larger than the width of the recharge strip (infiltration channel). In derivation of Equation 12, it was assumed that the effective thickness of the aquifer is not larger than the diameter of the pond. However, this does not mean that the initial thickness of the aquifer may be simply replaced by the pond diameter. In fact, replacing H_i on the right side of Equation 12 with 2R would yield an inaccurate equation. In order to make the system of equations independent of the original aquifer thickness an analysis was made in which the rise was calculated by Equation 12 for various values of $2R/H_i$ and K and i. It is generally known that beyond a given thickness of the aquifer, the effect of any additional depth of the saturated layer on the mound rise is nominal. The idea here was to define the limiting value (the largest quantity) of $2R/H_i$ as a function of K and i (both of which are known parameter). For different values of K and i the values of $2R/H_i$ were identified where the calculated central mound rise would only change by a

nominal value (0.01 inch or 0.00083 ft) when the value of $2R/H_i$ changed by 10% . The results for the critical value of $2R/H_i$ were recorded for a range of K and i values and are presented here as the data points in Figure 2.

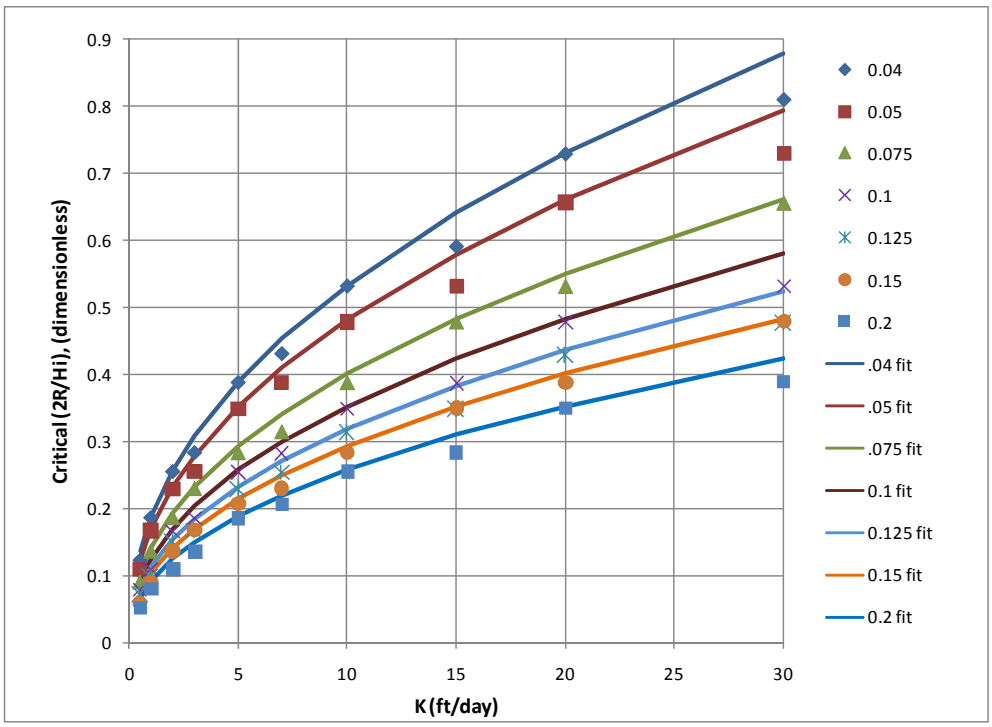

Figure 2. The Critical Values of $2R/H_i$ as a Function of K and i.

The number next to each data symbol in Figure 2 legend is the i value in ft/day. A power curve can well represent the data points for each i value in Figure 2. However, one equation was derived to represent all data points in Figure 2 and at the same time allow simplification of Equation 12:

$$\frac{2R}{H_i} = 0.0434\left(\frac{K}{i}\right)^{(1/2.2)} \qquad (13)$$

The fit curves produced by Equation 13 to the data points in Figure 2 are shown as solid curves in Figure 2. Equation 13 implies that as long as $(2R/H_i)$ is equal to or smaller than the value calculated by Equation 13 a change of $2R/H_i$ by more 10% does not appreciably impact the calculated value of the central mound rise and we don't need to know the exact value of the original thickness of the aquifer. This presents an opportunity to simplify the problem formulation. For example, if K= 15 ft/day and i= 0.069 ft/day, then the pond diameter should be no more than half of the aquifer thickness. Only a rough knowledge of aquifer thickness is required to verify this. In this example if the actual thickness of the aquifer is less than half of

the pond diameter we would expect errors in estimating the central mound rise equal to or larger than 0.00083 ft. For many stormwater management applications (especially Low Impact Development provisions) the value of 2R would be relatively small and this condition would be easily satisfied and so we could use Equation 13 to simplify Equation 12. This leads to the following equation for the central mound rise:

$$H_c - H_i = \frac{0.156\, i\, R\,(10 + 0.001\frac{K}{i})}{K - i} \qquad (14)$$

Note that even for large values of K compared to i, the term (0.001 K/i) is relatively small. Samplecalculations showed that this term can be disregarded without significantly changing the values calculated by Equation 14. This leads to the final form of the equation for the central mound rise under a round infiltration basin:

$$H_c - H_i = 1.56\frac{i\,R}{K - i} \qquad (15)$$

The maximum radius of influence of mounding can be found by calculating the rise from equation 15 and using the resulting value in Equation 8. An equation to directly calculate r_{max} can be found by combining equations 15 and 8, simplifying like terms, and taking exponential of the two sides of the equation which yields:

$$r_{\max} = e^{\left(\frac{5.74\,K + 0.5\,i}{K - i}\right)} \times R \qquad (16)$$

Where r_{max} represents the radial distance from the pond center beyond which mounding is negligible.

Having the value of the central mound rise, the rise of the mound at the pond edge can be found by using the value of the rise in Equation 4. Alternatively a direct equation for the mound height at the pond edge it can be derived by using Equations 15 and 4:

$$(H_e - H_i) = (\frac{1.56\,K}{K - i} - 0.125)\frac{i\,R}{K} \qquad (17)$$

The water table position at any radial distance between the pond center and the pond edge can be simply estimated by linear interpolation.

The water table rise at any point between the edge of the pond and r_{max} can be found by writing Equation 7 for an arbitrary “r” and subtracting the original

thickness of the saturated layer from H_r which is the thickness of the saturated layer including the mound at a radial distance "r" from the pond center:

$$(H_r - H_i) = (\frac{1.56K}{K-i} - 0.25\ln(\frac{r}{R}) - 0.125)\frac{iR}{K} \qquad (18)$$

As "r" approaches r_{max} , the value of the rise calculated by Equation 18 approaches zero and when r= r_{max} the rise drops to zero. This can be verified by replacing r in Equation 18 by its equivalent formula for r_{max} from Equation 16.

Example Calculation for Mounding under an Infiltration Pond

In this example let us consider a hypothetical infiltration pond in New Jersey. The pond is roughly circular in shape with a surface area 25 feet in radius and it overlays a homogeneous aquifer with a horizontal water table and a horizontal bedrock. The aquifer horizontal hydraulic conductivity is 3 ft/day. The exact thickness of the aquifer is not known, however, there are indications that it is at least 100 feet thick, allowing us to assign an arbitrary value of 100 feet to its lower limit estimate. There are no other major sources or sinks either recharging or discharging the aquifer in the vicinity of the pond. Calculations through New Jersey main Recharge Spreadsheet (Zomorodi, 2004) have shown that during a typical year, the total recharge depth from the pondto the aquifer is about 547 inches. The dimensions of the stable mound under and around the pond need to be estimated.

First, we must check the three conditions for equation application as explained under Equations 12 and 13:

1) Check $2R \leq H_i$: 2R = 50 ft which is smaller than the lower estimate of the aquifer thickness (100 ft).

2) Check i < K, the average recharge rate over a year would be 547/ (12 x 365) or about 0.125 ft/day which is smaller than hydraulic conductivity of 3 ft/day.

3) Check $2R/ H_i$: from Equation 13 the critical value of $2R/H_i$ is calculated to be 0.184. Assuming a value of at least 100 ft for the initial aquifer thickness, the value of 2R should be less than or equal to 100 x 0.184 or about 18 ft. But in our example, the value of 2R=50 ft. Therefore, if the aquifer thickness in reality is only about 100 ft, the central mound rise calculated here could be slightly underestimate. The required thickness of the aquifer for no errors would be 50/0.184 or about 270 ft. Note that in this example the value of K=

3 ft/day is relatively small. The larger the value of K the more relaxed the above restrictions would be. If K= 27 ft/day the 100 ft aquifer thickness would be sufficient for our estimates to have no errors.

The solution steps for this problem are as follows:

1. For the pond center use Equation 15:

$$H_c - H_i = 1.56\frac{i\,R}{K-i} = \frac{1.563\times 0.125\times 25}{3-0.125} = 1.70\,ft$$

2. At the pond edge where r=R=25 ft, the rise ($H_e - H_i$) can be calculated by Equation 17:

$$(H_e - H_i) = (\frac{1.56\,K}{K-i} - 0.125)\frac{i\,R}{K} = (\frac{1.56\times 3}{3-0.125} - 0.125)\frac{0.125\times 25}{3} = 1.57\,ft$$

For any radial distance from the pond center to pond edge the rise may be estimated by linear interpolation. For example 10 ft away from the pond center the rise would be about 1.64 ft.

3. For all points between the pond edge and r_{max}, apply Equation 18. For example 75 ft from the pond center (50 ft from the pond edge) the mound would be 1.28 ft as calculated by:

$$(\frac{1.56\,K}{K-i} - 0.25\ln(\frac{r}{R}) - 0.125)\frac{i\,R}{K} = \left(\frac{1.56\times 3}{3-0.125} - 0.25\times\ln(\frac{75}{25}) - 0.125\right)\left(\frac{0.125\times 25}{3}\right)$$

4. The maximum radius of influence is calculated from Equation 16:

$$r_{\max} = e^{\left(\frac{5.74\,K+0.5\,i}{K-i}\right)}\times R = e^{\left(\frac{5.74\times 3+0.5\times 0.125}{3-0.125}\right)}\times 25 = 10{,}200\,ft$$

For all distances beyond r_{max} assume no mounding. In this case r_{max} is rather large distance. Application of a groundwater recharge Software to this example also indicates very large radius of influence. Note that this is the limit of radial distance around the pond where there will be any rise. In practice, a certain amount of rise at a given distance may be acceptable. For example, suppose that the lowest foundation elevation of a proposed residential house is to be set 1 foot above the maximum water table. At least how far away from the pond center should this structure be located to keep the mound level below the foundation level? This

question can be answered by solving Equation 18 for the "r" value that would make $H_r - H_i = 1$ foot. The answer is r = 223 ft which, given the 25-ft radius of the pond suggests a minimum distance of about 200 ft between the structure and the edge of the pond. Figure 3 shows the mounding under the pond and its vicinity as calculated for this example by the new equations (due to symmetry only half of the pond and one side of the aquifer are shown).

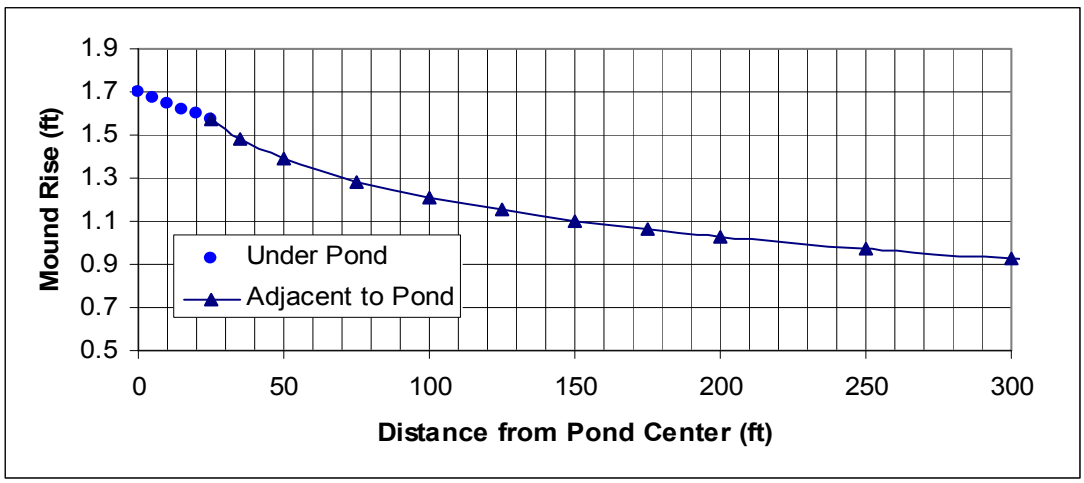

Figure 3. Mounding under the Pond of Example Calculation.

Notice that the results are sensitive to the value of hydraulic conductivity. The value of K used in this example K= 3 ft/day is expected to be exceeded in most field conditions where large scale infiltration BMPs are implemented. For example, if the value of K is increased to 6 ft/day the central mound rise drops to 0.83 ft and 223 ft from the pond center the rise would be only about 0.48 ft.

Comparison of Results with an Existing Solution

In order to check the performance of the equations derived above a couple of example cases were solved by these new equations and by the Sunada Software "Artificial Recharge" which is an artificial recharge mounding program developed by Molden et. al. (1984a and 1984-b). This software package uses the well-known analytical solution by Glover (1960) for rectangular basins. The equations implemented in this package cannot be easily solved by manual calculations. The input values and assumptions of the example calculation as laid out in the previous section were used in this comparison. Sunada Software is a specialized computer program and its use requires parameters additional to the requirements of our simplified equations. To make sure that we are solving an almost equivalent problem using both methods several provisions had to be made. While for the new equations a circular pond with a radius of 25 feet was used, in the Sunada Software

a square pond with an equivalent area of the circular pond was used. The value of transmissivity used in the Sunada Software was calculated by multiplying the K value by 2R. The Sunada Software also needed a value for Specific Yield, a parameter not appearing in our equations. For this parameter the default program value of 0.1 was used. Sunada software is provides the shape and size of the mound for various time period after a constant recharge rate is initiated. Figure 3 compares the values of the central mound calculated by Sunada (labeled Sunada K=3) as a function of recharge period in years to the central mound value calculated by the new equation. Sunada software predicts a central mound value that rises in time and for 100-years of recharge approaches the value calculated by the new equation. The central mound rise continues to slightly increase beyond 100-years but more or less stabilizes in time. The results by the two methods are also compared in Figure 3 for a K value of 6 ft/day. In this case due to larger hydraulic conductivity of the aquifer the rise of the central mound is milder. In this case, the value calculated by the new equation corresponds to the calculated central mound rise by Sunada software calculated for almost 50-years of recharge. In general, Figure 3 shows that the new equation provides a good estimate of the long-term central mound rise when compared to the results of the Sunada Software.

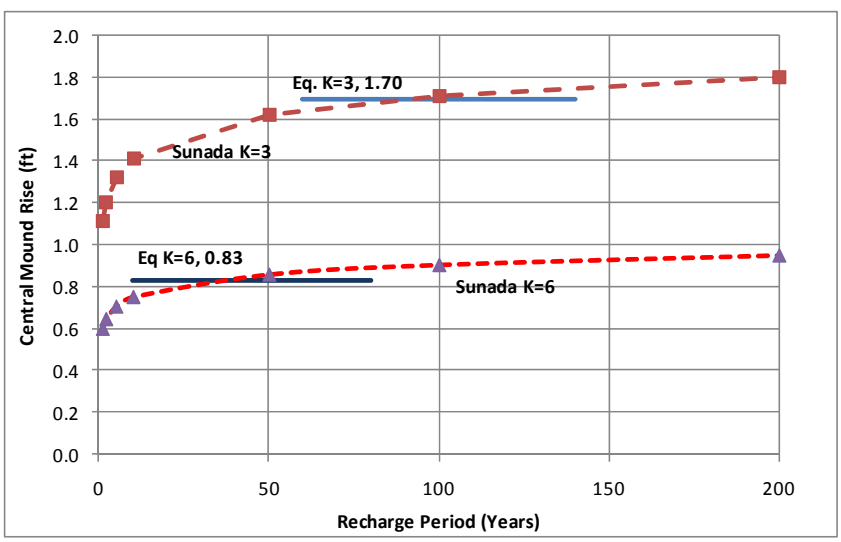

Figure 3. Comparison of the Central Mound Rise Calculated by the New Equation and the Sunada Software.

Figure 4 compares the shape of the mound calculated by the new equations to the values calculated by Sunada Software for a recharge period of 100-years. For K=3, the two sets of results are almost identical. For K=6, the new equations slightly under predict the values calculated by Sunada software but the results follow the

same shape of the curve. The values calculated by the new equations in this case more closely correspond to Sunada values calculated for 50-years of recharge.

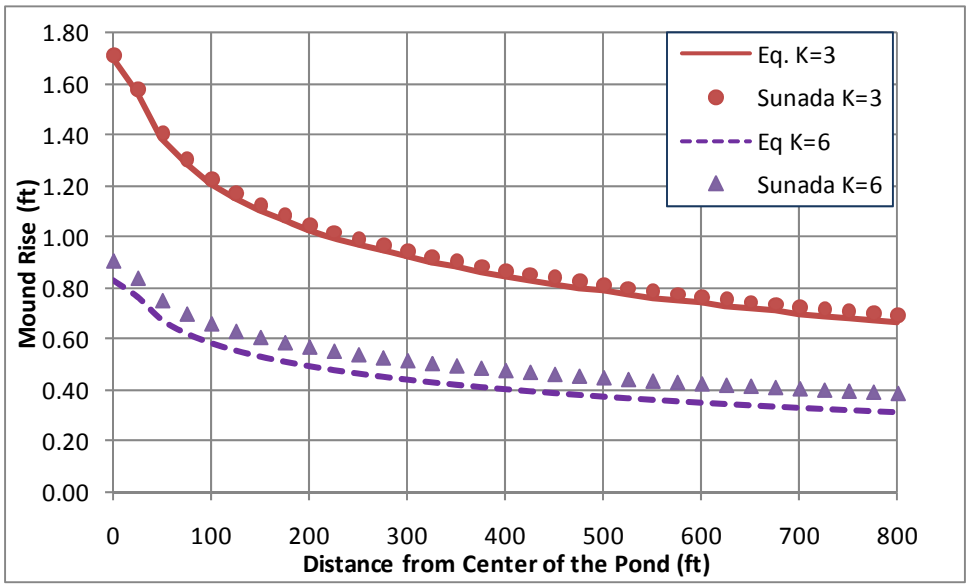

Figure 4. Comparison of the Mound Shape by Sunada Software (for 100-years of recharge) and by the New Equations.

CONCLUSIONS

The new equations developed and presented in this paper provide a simple means of predicting the rise of the groundwater mound under a round or square stormwater infiltration facility or recharge basin. The equations apply to steady–uniform recharge rate to infinite homogenous aquifers with initially horizontal water table and bedrock surfaces. The new equations require minimum input data in terms of the size and shape of the facility, the properties of the saturated layer and the recharge rate and are convenient for routine engineering calculations. Example applications of the new equation sets for conditions typical in New Jersey showed that the new equations are easy to use and provide reasonable results. The results obtained by the new equations were shown to generally agree with the results from a more elaborate analytical solution implemented in a software package.

NOTATION

The problem parameters as used in this paper are as follows:

C= a constant equal to the slope of linear relationship between $2R/H_i$ and K, (day/ft),

h’ (t)= Rise of the mound above the original aquifer thickness at time “t”, (ft),

H_C = Maximum saturated thickness (original aquifer thickness plus mound rise) under the centerline of the facility under the stable mound condition, (ft),

H_e = maximum saturated thickness at the edge of pond under the stable mound condition, (ft),

H_i = Initial thickness of the saturated layer (aquifer), (ft),

H_r= Thickness of saturated layer under the stable mound condition a radial distance "r" from the pond edge, (ft),

i = Average Infiltration from pond (assumed to be also equal to Recharge Rate to aquifer), (ft/day),

K = Horizontal Saturated Hydraulic Conductivity of the saturated layer (ft/day),

q(t)= Downward flux of groundwater at water table at time t, (ft/day),

Q'= a flow parameter that depends on the two factors of the width of the infiltration bed and the original thickness of the aquifer, (ft^{-1}),

r= an arbitrary radial distance from the pond center, (ft),

r_{max}= Maximum radius of influence of the mound beyond which mound rise is zero, (ft),

R= Radius of Pond (for non circular shapes the radius of an equivalent circle may be used for "R"), (ft).

ACKNOWLEDGMENTS

This project has been wholly funded by a 319(h) Grant to the New Jersey Department of Agriculture. The author would like to thank Mr. Charles Kuperus, Secretary of Agriculture, and Mr. Hunter Birckhead, State Erosion Control Engineer, State Soil Conservation Committee, NJDA.

REFERENCES

Bouwer, H. 2002 Artificial Recharge of Groundwater: Hydrogeology and Engineering, Hydrogeology Journal 10:121-124. Published online: 26 January 2002.

Bouwer, H., Back, J.T., and Oliver J.M., 1999, Predicting Infiltration and Groundwater Mounds for Artificial Recharge, ASCE Journal of Hydrological engineering, 4(4):350-357.

Bouwer, H. 1962 “Analyzing Groundwater Mound by Resistance Network”, ASCE Journal of Irrigation and Drainage Engineering, 88(IR3):15-36.

Dewberry, 2002, “Evaluation of Groundwater Mounding Under Stormwater Infiltration Facilities”, Report submitted to New Jersey Department of Environmental Protection, September 2002, 18 pages.

Glover, R. E. (1960) Mathematical derivations as pertain to groundwater recharge. Agric. Res.
Serv., USDA, Fort Collins, Colorado, USA.

Gua, J.C.Y. (2001) “Design of Circular Infiltration Basin under Mounding Effects”, ASCE Journal of Water Resources Planning and Management, Vol. 127, No. 1, January/February 2001, pp. 58-65.

Manglik, A., and Rai, S.N. (2000) “Modeling of Water Table Fluctuations in Response to Time-varying Recharge and Withdrawal”, Kluwer Academic Publishers, Water Resources management 14- pp. 339-347.

Molden, D., Sunada, D.K., and Warner, J., 1984-a, Artificial Recharge, Computer Program, Enhanced and Expanded for IBM PC by Glen U. Sunada, Colorado State University, 1984.

Molden, D., D.K. Sunada and J.W. Warner. 1984-b. Microcomputer Model of Artificial Recharge Using Glover’s Solutions. Ground Water. Vol. 22, No. 1.

Swamee, K.P., and Ojha, C.S.P., 1997, “ Ground-water Mound Equation for Rectangular Recharge Area”, ASCE Journal of Irrigation and Drainage Engineering, May/June 1997, Vol. 123(2):215-217.

Vauclin, M., Khanji, D. and Vachaud, G., (1979) “ Experimental and Numerical Study of a Transient, Two-dimensional Unsteady-Saturated water Table Recharge Problem, Water Resources Research Vol. 15, No. 5, pp. 1089-1101.

Youngs, E.G. (1977) “The Unsteady Groundwater mound Below an Irrigation Ditch or Leaky canal”, Journal of Hydrology, Vol. 34, pp. 307-314.

Zomorodi, K. 2005, “Simplified Solutions for Groundwater Mounding under Stormwater Infiltration Facilities”, Conference Proceedings, 2005 American Water Resources Association Annual Conference, November 7-10, 2005, Seattle, Washington, Session 8, Stormwater management-II, pp 1-4.

Zomorodi, K. 2004, "Curve Number and Groundwater Recharge Credits For LID Facilities in New Jersey", Proceedings of the Conference "Putting the LID on Stormwater Management!", The Inn and Conference Center- Marriott, College Park, Maryland, September 21-23, 2004. Proceedings published electronically on a CD, to reach this paper on the CD first select "Program and BIOS" and then "Read BIOS and papers". PP. 508-514.

Zomorodi, K. 2003, "Quantitative Runoff Volume and Groundwater Recharge Credit Charts for LID Practices", Proceedings, Virginia Water Conference 2003, "Navigating the Regulatory Environment: NPDES, TMDLs, Section 404, and Beyond", Virginia Lakes and Watersheds Association, held in Virginia Beach, VA, March 23-25, 2003, p. 61.

Zomorodi, K., 2002, " A New Infiltration Pond Model for Shallow Water Table Conditions", Proceedings of Virginia Water Conference 2002, Virginia Lakes and Watersheds Association, Virginia Beach, VA, March 11-12, 2002, P. 57.

Zomorodi, K., 1991, "Evaluation of the Response of Water Table to a Variable Recharge Rate". Journal of Hydrological Sciences, 36(1):67-78.

Zomorodi, K., 1988, "Optimization of Design and Operation of Artificial Recharge Facilities", Ph.D. Dissertation, Utah State University, Logan, Utah.

South Lake Park Bioretention Gardens

J. J. Dremsa[1] and T. A. Hartsig[2]

[1]Applied Ecological Services, Inc., Regional Contracting Manager, 701 East 22nd Street, Lawrence, KS 66046; PH (785) 842-3300; FAX (785) 842-3313; email: jason.dremsa@appliedeco.com

[2]Olsson Associates, 7301 West 133rd Street, Suite 200, Overland Park, KS 66213; PH (913) 381-1170; FAX (913) 381-1174; email: thartsig@oaconsulting.com

ABSTRACT

The South Lake Park Bioretention Garden project consists of a survey, layout, design, and plans for parking lot reconstruction and bioretention grading and underdrain system. The layout and grading for both the parking lots and bioretention cells were challenging aspects for the following reasons: matching the existing grade for adjacent constraints, regulating the amount of water that each cell received, and taking special care to evenly distribute how the water flowed into the cells to minimize erosion and possible cell damage. Applied Ecological Services, Inc. (AES) was asked to design alternative BMPs as demonstration projects at two parks in Overland Park, KS. AES was selected because of its expertise in natural systems and ecological restoration. Understanding that failure of poorly designed BMPs has resulted in public doubts, AES anchored their design by conducting infiltration tests of engineered bioretention soils. The attention the team gave to the site layout, construction sequence, and native plant selection has lead to successful results.

INTRODUCTION

A bioretention cell is a shallow basin filled with a soil media and planted with native grasses, trees, and shrubs. Bioretention cells collect stormwater and hold it for a short period of time, allowing water to infiltrate into and be stored in the soil. The pollutants in the water are removed through various plant and soil processes. The bioretention cell design includes a subsurface perforated drainage pipe that allows subsurface drainage to flow to the storm sewer and nearby water bodies.

The project goals for the bioretention cells at South Lake Park included reducing stormwater discharge volume, improving water quality, enhancing natural beauty of park setting, and reducing erosion activity of the feeder streams and overflow channel that cause deposition of silt in the lake

The bioretention cells at South Lake Park function by retaining and treating storm runoff from the nearby roads, parking lots and buildings at the site. The site is located

south of W. 86th street and Valley View drive in Overland Park, KS. The site serves as an educational site and field experience for the community at South Lake Park and for adult education and demonstrations on the design, construction, and function of bioretention cells. The project was designed and constructed by Applied Ecological Services, Inc. an experienced ecological consulting firm that has demonstrated knowledge and skill at creating ecologically valid and functional natural wetland and native habitat areas. The education and demonstration programs will be supported by the Parks and Recreation Department of Overland Park as part of the city park system. The Parks and Recreation Department will provide appropriate public notice of the availability and opportunity of the site through their established public outreach efforts.

The site is designed as a functional natural area with locally valid ecological groupings of native plant species. Native landscape concepts will be used to demonstrate the approach to combining ecological functionality and an attractive park amenity. Design elements are included that allow public access to specific educational aspects such as particularly notable native or historic species, important or essential ecological processes of the site, or specific construction aspects that are important to successful retention and natural treatment.

INFILTRATION CAPACITY AND HYDRAULIC CONDUCTIVITY OF ENGINEERED BIORETENTION CELL SOIL

A simple benchscale study was conducted to determine the most effective soil matrix to facilitate water infiltration and permeation, as well as holding capacity, in bioretention cells and similar alternative best management practices for stormwater. There has been substantial discussion about the "best" soil mix to use in bioretention cells, including the type of material and amounts of different constituents. For this study, it was determined that an engineered soil matrix of sand and compost would be evaluated. Sand was chosen because it will not foul as a result of fine soil particles being translocated in the profile during the initial year of bioretention cell operation. Compost was selected because it increases water-holding capacity of the engineered soil and because of its nutrient holding capacity.

Methods

The benchscale study was completed using packed columns and measuring the rate of falling head of water at the top of the column. Infiltration was measured into unsaturated and saturated media, followed by measurement and calculation of hydraulic conductivity by rate of falling head into saturated media.

Sand and compost were obtained from Missouri Organic Recycling in Kansas City, Missouri, and staged in the AES workshop in separate piles. Sand and compost in mixes of 30% sand/70% compost, 50% sand/50% compost, and 70% sand/30%

compost (volumetric measurements) were homogenized in a plastic tub using a wide mixing spatula for several minutes to assure consistent media texture. After homogenizing the representative sand/compost mix, the soil media was placed into 4-inch (inner diameter) PVC pipe (27 inches long). The soil was placed in approximate 9-inch lifts and packed using a wooden rake handle before the next lift was added. The finished column was 24 inches of packed sand/compost media with approximately 3 inches (7.5 cm) of void space at the top of the column. A series of three columns was used, providing three replicates of each treatment. The PVC column was prepared prior to packing by placing screen material underlain by a paper coffee filter affixed (with rubber bands) to the bottom of the PVC pipe. After each column was packed, it was placed on an elevated holding platform, with metered collection buckets below each column. Water was placed into a graduated measuring cup in 600 ml increments. The volume of water was verified by weighing on a balance to assure 600 grams of water were placed in the cup (assuming 1 g/cubic centimeter (cc) density of water). Each 600 ml increment provided a hydraulic head of 7.0 cm at the top of the column. Infiltration was measured for movement into the dry column, and with each subsequent 600 ml increment of water, with four increments added to each column. The fourth increment of water reflected wet, and assumed saturated, conditions. The rate of falling head was measured as the time it took for water to infiltrate into the soil mix from the moment of placement into the column until the instant that no water remained on the soil mix surface.

The amount of water collected after infiltrating and passing through the column was measured for each column. After equilibration of each column after 6 hours, the amount of water collected was subtracted from the amount of water poured through the column. The packed column volume (approximately 4,970 cc) was multiplied by the calculated bulk density (see below) to obtain an approximate weight of the material in the soil column. Water holding capacity could then be calculated as the amount of water remaining in the column after equilibration (in grams) divided by the weight of the soil media in the column. The soil water holding capacity is measured as grams of water per gram of soil.

After four increments of water were added to each column and measured for infiltration, we assumed saturated conditions existed. Saturation was assumed to be achieved after water was allowed to equilibrate in the column for a period of 18 to 24 hours. To measure hydraulic conductivity in the profile as a reflection of falling head, 600 ml increments were again added to the top of each column and the rate of falling head recorded, with the first measurement being the last measurement of the infiltration tests.

To measure porosity of the soil mixes, each soil mix as packed into a 500-ml vessel (measuring cup). The packed cup was weighed, and the weight of the empty cup was subtracted to obtain the weight of the soil mix. Bulk density of the sand/compost mix was calculated as the weight of the soil media divided by 500 ml (or cc's) to obtain an approximate density measurement of the engineered soil. This value was used for estimating water holding capacity.

Water was slowly added to the packed soil mix, allowing time for displacement of gasses and saturation of the soil pores. Trapped air was removed by repeatedly inserting a narrow rod into the mix to release gasses. After the saturated soil mix was allowed to equilibrate, the soil/water weight was measured. The weight of the water equals the weight of the soil/water mix minus the weight of the soil mix and cup. Because water density is assumed to be 1.0 gm/cc, the volume of pore space was assumed equal to the weight of the water in the soil mix, and measured as cc per cc of soil, or as a percent of the soil volume.

Results

Results of the benchscale study are summarized in Table 1. A discussion of the measurements of each of the parameters examined is provided below.

Table 1: Mean Values for Measured Soil Parameters

	30% Sand 70% Compost	50% Sand 50% Compost	70% Sand 30% Compost
Water Holding Capacity (gm water/gm soil)	0.18	0.14	0.18
Soil Bulk Density (gm/cc soil)	1.15	1.30	1.26
Porosity (percent)	35	35	30
Infiltration Rate (cm/sec)	0.029723	0.019821	0.03663
Hydraulic Conductivity (cm/sec)	0.006459	0.007693	0.009599

Water Holding Capacity and Bulk Density

The calculated water holding capacity of the soil mixes appears to be reasonably consistent between all soil mixes, ranging from 0.14 to 0.18 gm water per gram of soil. The lower water holding capacity in the 50% sand/50% compost mix should not be interpreted as indicative of conditions, and more data is necessary to determine the true water holding capacity of these soil mixes.

Bulk density was measured and estimated to aid in determining the water holding capacity of the soil mixes. As with water holding capacity, the bulk density appears to vary little, with the lowest density being in the mix with 70% compost, as would be expected. Variability in the degree of packed media in the columns and in other vessels probably contributes to the relative uniformity in the data.

Infiltration Rate

Infiltration rate, from the measurements collected, projected a trend as demonstrated in Figure 1 (with upper and lower standard deviations). Figure 1 demonstrates relatively consistent infiltration of water into each of the soil mixes, with slower movement into water into the 50% sand/50% compost mix.

Figure 1: Infiltration Rate into Sand/Compost Soil

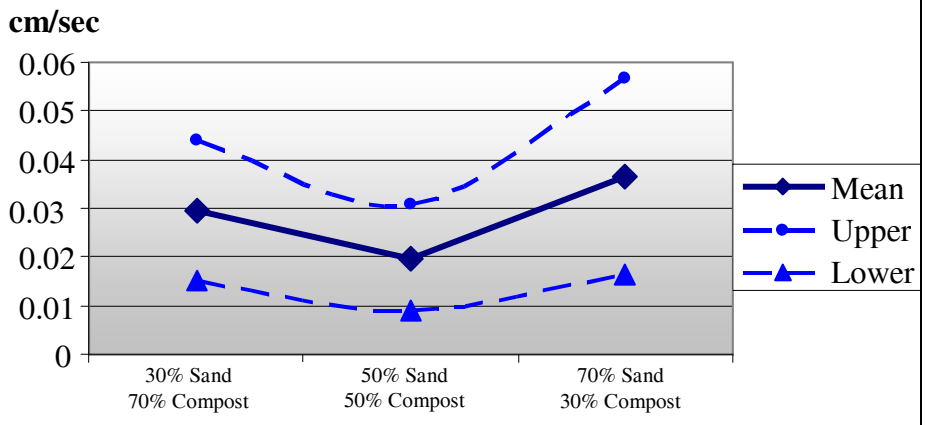

Data represents average of 4 measurements on 3 replicates of each treatment

The decrease in infiltration rate in the 50/50 soil mix appears to be a function of the higher bulk density and lower water holding capacity, indicating greater compaction for this treatment Overall trend, if this would be examined as a linear regression, would indicate relatively uniform infiltration, with a slight upward capacity with increased sand content. On the whole, the expected infiltration rate of water into any of the sand/compost mixes would be expected to be between 0.02 to 0.04 cm per second. The data of first infiltration measurements into the dry soil mixes indicates that infiltration is expected to be between 0.03 to 0.06 cm per second when the soil mix surface area is dry.

Hydraulic Conductivity

Hydraulic conductivity, from the measurements collected, projected a trend as demonstrated in Figure 2 (with upper and lower standard deviations). Figure 2 displays a more notable trend of water movement through the soil, with increasing movement of water through the mix with increasing sand content.

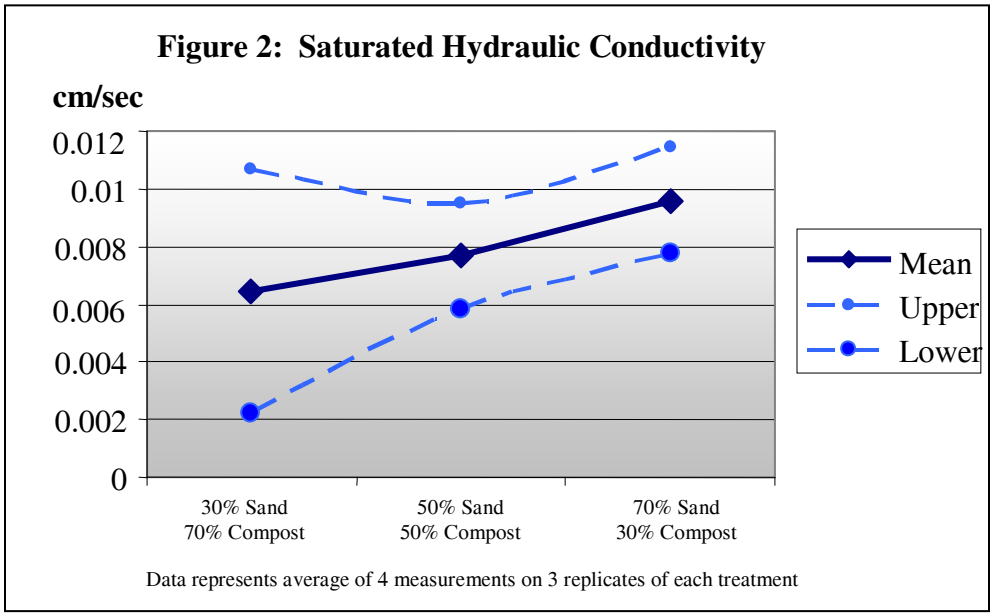

The upper and lower standard deviations of the data indicate more variability in hydraulic conductivity measurements with the increased amounts of compost (treatment 1). This is not unexpected, as increased compost will likely have more varied density depending on the degree of packing into the columns. This may be reflective of what could also occur under field conditions.

Summary

The benchscale measurement of water infiltration into and hydraulic conductivity through engineered soil provides a preliminary indication of expectations of flow dynamics for bioretention cells and similar stormwater best management practices. In general, with a sand and compost mix for the treatment media of bioretention cells, movement of water through the cell can be expected to be at a rate between 0.006 and 0.01 cm per second (6×10^{-3} to 1×10^{-2} cm per second) under saturated conditions, and faster under dryer conditions.

Because of the apparent relative uniformity in the data, with a trend of increasing hydraulic conductivity with increased sand content, it would be appropriate to recommend that a moderate approach be utilized for obtaining the appropriate sand/compost mix for the design of bioretention cells. Therefore, from the data obtained, it is appropriate to designate a soil mix of 50% sand and 50% compost for the bioretention cell. The 50/50 sand/compost mix offers the most positive attributes of both the sand and the compost by providing adequate infiltration of water through the bioretention cell, good water holding capacity, strong nutrient holding capacity in the compost, and a very good root-growing medium. Too much compost in the mix (such as at the 70% level) could result in excessive subsidence as compost decays.

Too little compost (such as at the 30 % level, or less), may not provide adequate water holding and/or nutrient holding capacity, and water treatment through biological actions, as desired for the treatment unit.

DESIGN AND CONSTRUCTION

Site Inventory and Analysis and Infrastructure Design Support

AES staff and associates prepared basemaps including all applicable and available site information for use in constructing the selected BMPs. Available topographic surveys, boundary surveys, and park layout were compiled in AutoCAD format. AES's ecological site design team visited the site to become familiar with the opportunities and constraints of the specific property and to become familiar with its surroundings. An AES soil scientist conducted a preliminary soils assessment and survey to determine the appropriateness of certain native plants and sustainable stormwater elements. Compilations and conclusions were documented for use in site design.

AES received technical support from BHC Rhodes for the design of the parking lot and associated infrastructure in consideration of elements that could affect the bioretention cells.

Initial Planning Meeting and Design Charette

An initial planning and concepts meeting was held to start the project work. The meeting was necessary to finalize contracts, clarify tasks and schedule, obtain any additional data, and begin the project coordination process. The Design Charette was an interactive, collaborative process with the goal of achieving a consensus schematic/conceptual design. Participants included members of the design team, BHC Rhodes, the Owner, and appropriate City personnel.

Preparation of Conceptual Landscape Plans

AES refined schematic drawings of recommended design solutions developed during the charette process and prepared Draft Conceptual Plans for the bioretention cell, including soil treatment, planting areas, stormwater flow, and other elements. The Draft Conceptual Plan consisted of a plan view drawing of the bioretention cell layout and surrounding park areas and features, and was presented to BHC Rhodes for review, input, and approval. A memorandum describing project elements, a Conceptual Plant List, and Conceptual Opinion of Probable Construction Cost was prepared for dissemination with the Draft Conceptual Plan. AES incorporated BHC Rhodes comments into the plan for presentation to the City. AES incorporated revisions requested by the BHC and the City to create an approved Final Design Documents.

Design Documents

AES prepared the design documents defining the improvements shown on the Draft Conceptual Plan in sufficient detail to obtain City approvals and proceed with project implementation. The following documents were provided by AES:

Design Drawings: AES prepared five sets of design drawings for use in permitting and construction that included: summary sheet, design plan, planting plan (Figure 3), erosion control plan, and construction details.

Specifications: AES staff prepared specifications to supplement and clarify the design drawings as necessary for communication to the General Contractor, any subcontractors, and to the City for necessary approvals.

Opinion of Probable Construction Costs: AES staff prepared a final Opinion of Probable Construction Cost for the proposed design.

Design Calculations: AES staff reviewed and incorporated engineering calculations demonstrating stormwater runoff and water quality improvements for City approvals.

PROJECT APPROVALS, PERMITTING, AND MEETINGS

AES prepared necessary ecological, environmental, and stormwater management regulatory submittals and secured project approval from the City of Overland Park and other governing agencies. These included stormwater management permits and approvals, water quality certifications, and erosion and sedimentation control plans, among others. BHC Rhodes kept abreast of requirements and progress. The City had a standard permit guidance and format that was closely followed for this process, and permits were completed with minimal comment from the City.

Participation in public meetings helped to educate locale public offices, residents, neighbors, etc. on the project design, methods, and philosophy. This proved to be very effective in alleviating public discontent and dispelling misconceptions.

CONSTRUCTION OVERSIGHT

AES oversaw construction of the final design. Complexity of the final design determined the Lead Designer's involvement in construction observation. However, construction oversight required that an AES restoration supervisor to visit the site daily during construction to review progress and conduct construction quality assurance. Construction quality assurance was necessary to verify that the design was being built and vegetation established according to design specifications. During each site visit progress was examined, quality of workmanship and materials was evaluated, and a CQA checklist was completed.

CONSTRUCTION AND FUNDING

AES completed these projects as design-build programs. The contracting division of AES provided constructed bioretention garden cells as specified in the design plans and specifications. Funding for the project included a City of Overland Park & Johnson County Stormwater Management Advisory Council (SMAC) Partnership, a research and development grant to evaluate BMP performance for the region, and a cost share for design construction and monitoring – SMAC 75% City 25%.

EDUCATION PROGRAMS AND OUTREACH

The City Parks and Recreation Department will provide the resources for maintaining the site and accommodating tour groups and education classes. Announcements of the availability of the site appeared in school resource materials, city catalogs, activity calendars and other public information materials. Coordination and response to requests for field trips, tours, workshops and other educational experiences was provided as needed. The site will be maintained as an educational area that is safe, has informative signs in place, and displays healthy natural elements.

CONCLUSION

AES successfully designed a series of bioretention gardens as alternative stormwater best management practices (BMPs) for reducing peak stormwater discharge and creating ecologically functional units that sustain native habitat. These biorention cells also allow some of the stormwater to infiltrate and recharge the natural water cycle. A measure of success of the project is that the community of Overland Park, KS appreciates the site for its benefits to the environment. It continues to serve as a local example of a successful bioretention cell.

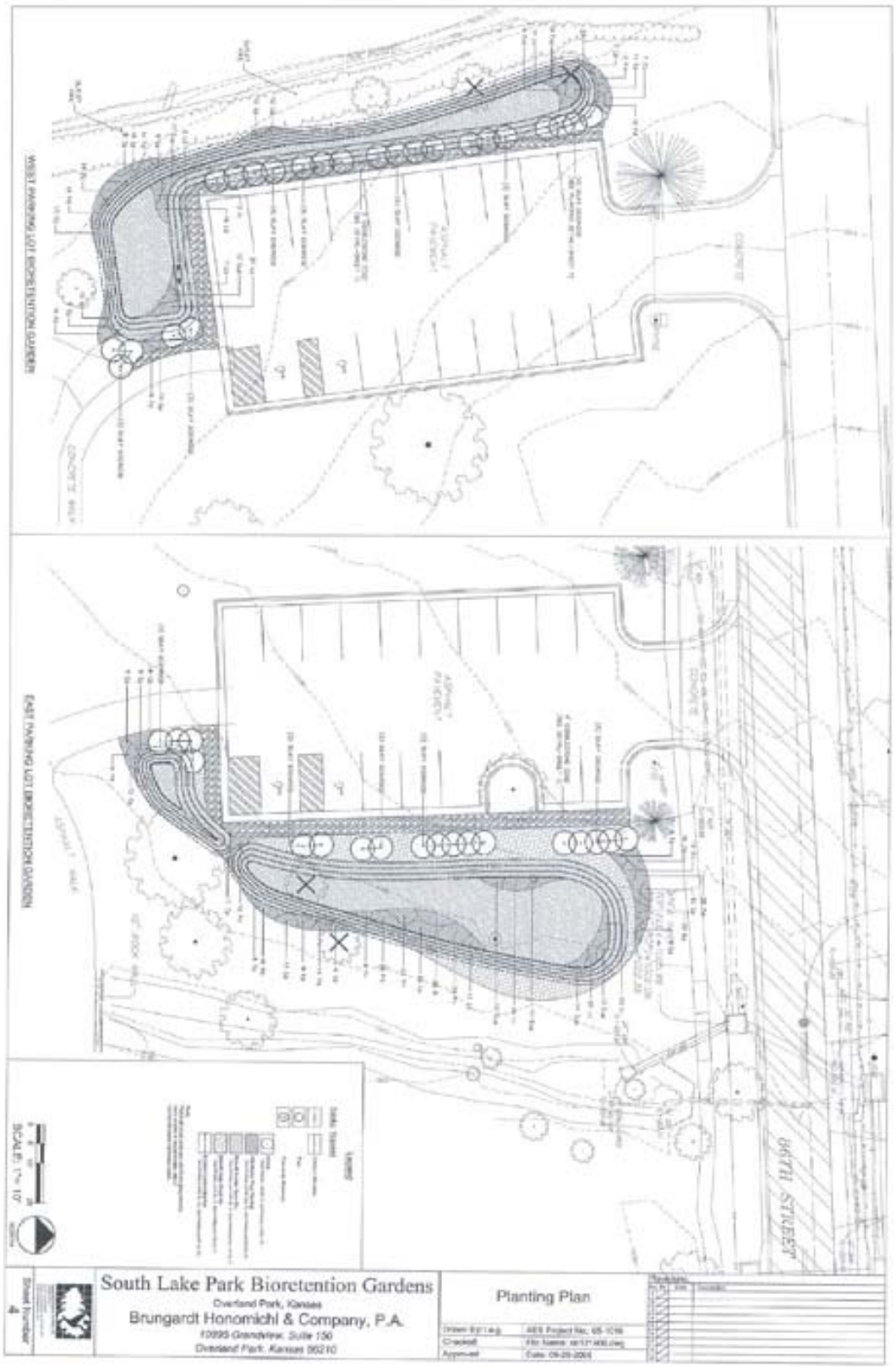
WEST PARKING LOT DIRECTION OF FLOW
EAST PARKING LOT DIRECTION OF FLOW
86TH STREET
SCALE: 1"=10'
South Lake Park Bioretention Gardens
Overland Park, Kansas
Brungardt Honomichl & Company, P.A.
10895 Grandview, Suite 150
Overland Park, Kansas 66210
Planting Plan
Sheet Number
4

Figure 3.

State of the Practice of Wet Weather Flow Analysis

Mitchell Heineman, P.E., M. ASCE, D.WRE

CDM, 50 Hampshire Street, Cambridge MA 02139; HeinemanMC@cdm.com

ABSTRACT

Engineers analyze wet weather flow in collection systems using a variety of computer tools and analytical techniques. Tools and data available for performing these analyses have greatly advanced since software for this purpose was first standardized in the 1970s. The practicing engineer today has access to GIS-based modeling software, high-resolution land cover and elevation datasets, and enormous hydrologic databases. Methods used for typical engineering work have advanced quite modestly by comparison. Furthermore, there is little standardization of how analyses of drain, combined sewer, and sanitary sewer collection systems are carried out, despite considerable commonalities among their wet weather performance.

This paper reviews the state of the practice of collection system modeling, considering software availability and selection, model complexity, calibration criteria, and simulation methods. Urban modeling protocols for drain, combined, and sanitary sewer systems are discussed. Uniform approaches for model calibration are suggested. Finally, the paper identifies research and development needs where the state of the practice is limited by current technology.

INTRODUCTION

Engineers analyze wet weather flow in collection systems using a variety of computer tools and analytical techniques. Tools and data available for performing these analyses have greatly advanced since initial development of software such as USEPA's SWMM and USACE's HEC models in the early 1970s. Today's engineer has access to GIS-based modeling software, high-resolution digital land cover and elevation datasets, and enormous precipitation, streamflow and groundwater databases. However, methods used for typical engineering work have advanced quite modestly by comparison. There is little standardization of how analyses of drain, combined sewer, and sanitary sewer collection systems are carried out, despite considerable commonalities among these systems in wet weather performance.

Analysis of existing collection systems today often uses dynamic models, but construction and application of these models remain rooted in historic methods which were constrained by limited flow data availability and computer resources. Many models are still developed with minimal calibration and validation datasets, only weakly emulate key components of system hydrology, and are applied with design

storms that do not represent local meteorology and bear limited statistical relevance to design standards they are intended to inform. The UK *Wastewater Planning Users Group Code of Practice for the Hydraulic Modelling of Sewers* (2002) defines standards for model calibration and verification that are rooted in an historical approach where it was not practical to simulate more than a few storms. USEPA's *Combined Sewer Overflows: Guidance for Monitoring and Modeling* report (1999) states little more than that, "…calibration and validation are frequently done with two to three storms each."

Whereas urban runoff models originally focused on combined sewer overflows and drain system flooding, sanitary sewer systems are now a principal focus of many studies, and key components of most combined sewer studies. Various methods have been identified to simulate sanitary sewer rainfall-derived infiltration and inflow (RDII), such as described in Bennett *et al.* (1999), and recently discussed by Lai (2008). However, the state of practice generally remains based in event simulation, whereas RDII in many sewer systems depends on longer term processes that are only well-represented via continuous simulation.

This paper reviews the state of the practice of collection system modeling with regards to software availability and selection, model complexity, calibration criteria, and simulation methods.

MODEL SELECTION

Engineers today are faced with many choices in software selection. While good engineering design should not depend on computer software choices, the software used has important implications for the engineering approach ultimately used and the design of facilities.

Two important distinctions affect software selection and, ultimately, facilities design. First, available software is generally segregated into steady state versus dynamic models. Second, for dynamic modeling, some engineers favor design storm analysis while others favor multi-storm and/or long-term analyses. A third, lesser distinction, also divides collection system modeling software and engineers: some software packages are linked to CAD programs and environments, some to GIS software/environments, and some use schematic or non-visual interfaces.

Many state-of-the-art wet weather flow analyses use dynamic collection system modeling software. However, many engineers use steady-state analyses, as this is a common norm and software for these analyses are generally easy to use. Typically, new sewer and stormwater systems designs are based on steady-state models; engineers plan systems that conform to a standard based on peak runoff and/or inflow/infiltration rates. These rates are typically driven by local or state guidelines that dictate use of a peak runoff rate determined using rational method or comparable methodologies.

Dynamic collection system modeling for analysis of combined and sanitary sewer systems in the US commonly uses models based on USEPA SWMM, Wallingford Software's InfoWorks CS, or DHI's MIKE URBAN CS. InfoWorks is a comprehensive package that uses its own proprietary modeling engine and GIS. Its beginnings date to 1980, corresponding with development of the UK Wallingford Procedure. MIKE URBAN CS is a GIS-based modeling framework built around MOUSE. MOUSE was developed by the Danish Hydraulic Institute (now DHI Water & Environment) in 1983. MIKE URBAN also supports SWMM 5 within the same interface.

SWMM was first released in 1971. It was completely reprogrammed by USEPA in 2004. SWMM 5 is available free from EPA, or via commercial packages that incorporate it in various ways. Vendors offering products built around SWMM 5 include Bentley Systems (SewerGEMS and CivilStorm), BOSS International (StormNET), Computational Hydraulics International (PCSWMM.NET), DHI (MIKE URBAN), and MWHSoft (InfoSWMM and H2OMap SWMM). Additionally, XP Software offers xpswmm, which was derived from USEPA SWMM 4 in the 1990s. InfoWorks incorporates algorithms adapted from SWMM 4 among its various hydrologic methods. While all the dynamic models can model single storms or continuous simulations, the ease and speed of performing long-term or multi-storm simulations differs greatly among packages. Similarly, there is a wide range of connectivity and interoperability with CAD and GIS among these programs.

MODEL COMPLEXITY

Until early in this decade, computer models of existing urban sewer systems were typically built by assembling design drawings, record drawings, and sewer maps and then digitizing critical data into text files. This approach, combined with limitations on computing power, necessarily yielded parsimonious models that incorporated the minimum detail needed to reasonably model collection systems. Today, many existing systems models are developed in part from GIS collection system asset databases. This shift, combined with greatly increased computing power, has resulted in many models being built with much higher levels of detail. Whereas a decade ago, a one thousand pipe model was considered large, collection system models with many thousands of pipes are now becoming common.

There is a strong drive to implement models that bear close resemblance to their prototype systems. However, growth in model size has not been matched by corresponding growth in the use of models to perform long-term simulations, or process model sophistication. The design storm approach, coupled with simple surface hydrology, remains favored by most engineers for facilities analysis and design.

The balance between model network realism and parsimony is driven in part by vendors touting their software's ability to store large databases and run faster than competitors' products. There remains a significant gap in the demonstrated accuracy

of models as a function of their level of detail, and there is little movement or understanding of the use of approaches that require more than single storm simulation for facilities analysis.

Model complexity has also grown in recent years, although many models today still omit processes that may be of considerable import in identifying engineering solutions. Many dynamic sewer models traditionally focused on simulating inflow peaks and, to a lesser extent volumes, during and immediately after rainfall. Sanitary flows were often modeled as an averaged constant, and minimal attention was paid to infiltration and baseflows, which have lesser bearing on management of peak inflows. Today's more powerful computers and database management tools facilitate detailed simulation of wastewater flows. Many engineers now model diurnally varied flow, as this is relatively easy to specify, and bears directly on calibration of dry weather flow. However, little attention is devoted to understanding and simulating sewer and drainage baseflows; these flows are beyond the scope of existing calibration standards, and have a less recognized bearing on facilities design for peak flow management. While the major dynamic collection system models can simulate pipe infiltration and stream baseflow as a function of groundwater conditions, few models are built that account for this major contributor to the overall water balance in many collection systems.

CALIBRATION CRITERIA

Standards for collection system model calibration differ widely and generally lag the modeling state-of-the-art. USEPA's 1999 *Combined Sewer Overflows: Guidance for Monitoring and Modeling* report states little more than that, "calibration and validation are frequently done with two to three storms each." The UK Wastewater Planning Users Group (WaPUG) *Code of Practice for the Hydraulic Modelling of Sewers* has clearly defined standards for model calibration and verification, but these standards are rooted in an historical approach whereby it was not practical to simulate more than a few storms. Whereas the WaPUG standards identify acceptable tolerances for calibration to two days of dry weather flow and three wet weather events, it is today practical to calibrate models to much broader datasets. Temporary flow metering programs accompanying model development typically are deployed for three months, while many cities now have long-term sewer metering data that may be available for a year or longer. Long-term urban drain system metering is less widely available than sewer system data, but numerous local studies exist, as do extensive long-term USGS streamflow records.

Some US communities and regulatory agencies today refer to the WaPUG standards when identifying criteria for model calibration. However, these standards are primarily appropriate for traditional CSO (combined sewer overflow) studies, and lack relevance for SSO (sanitary sewer overflow) or stormwater studies. Even for combined systems, the WaPUG guidelines are inadequate for evaluating calibration of models to the large datasets and broadly scoped models that are now being routinely developed.

The WaPUG guidelines identify criteria for model calibration based on:
- two days of dry weather
  - timing of peaks and troughs
  - peak discharge
  - flow volume
- wet weather calibration to three events
  - timing of peaks and troughs
  - peak discharge
  - flow volume
  - surcharge depth
  - unsurcharged depth at key points

Given the many advances in computing technology since the initial version of these criteria was promulgated in 1993, it is appropriate that more rigorous standards be developed today. Some areas for consideration include:
- dry weather flow calibration to two seven-day periods
- dry and wet weather velocity
- comparison of volumes, peak discharge, peak velocity, and peak depth for all storms over an extended flow metering period
- if seasonal baseflows variation is modeled, it should be measured via assessment of discharge distribution frequency
- for combined sewer systems, models should be calibrated to long-term records of overflow frequency
- for all sewer systems, models should be checked against long-term treatment plant flow records
- conformance of calibration to statistical goodness-of-fit criteria
- sensitivity and uncertainty analysis

DESIGN SIMULATIONS

Design storms. Despite the exponential growth of computing power, single design storms remain a primary basis for many facilities studies. Synthetic design hyetographs using standard distributions are commonly used for facilities assessment. Hyetographs developed following the NRCS (formerly SCS) TR-55 methodology (Natural Resources Conservation Service, 1986) are often used in US rainfall-runoff modeling. NRCS hyetographs are 24-hour events that exhibit nearly the same recurrence frequency at all durations. Thus a 10-year NRCS storm ideally nests a 10-year 15-minute rainfall within a 10-year 24-hour depth. Since only four hyetograph shapes identified for the entire United States, NRCS hyetographs only approximate this ideal in many locations.

NRCS-type hyetographs have several limitations that restrict their applicability:
- NRCS hyetographs are not realistic in locations where short-duration convective storms cause short duration extrema whereas long-duration cyclonic storms drive long-duration extrema

- NRCS hyetographs are centrally peaked, whereas extreme rainfall is typically front- or back-loaded in many locations
- An n-year rainfall likely does not yield an n-year runoff response. This is especially true where baseflow is important, such as in sanitary sewer systems where seasonal infiltration can contribute as much excess flow to a system as direct inflow.
- Synthetic hyetographs are more difficult to explain to the public than historic events.
- In some areas and for certain types of facilities, a 24-hour storm may not be sufficiently long to analyze performance
- Single event analysis does not consider effects of consecutive storms
- In tidally-influenced areas and other locations where a time-varying tailwater condition must be considered, the modeler must develop an appropriate tailwater to accompany the design storm that yields the intended recurrence frequency

The use of synthetic hyetographs shapes other than NRCS can mitigate or eliminate some of these restrictions. Use of selected historical storms as design events potentially offers several advantages, but poses its own difficulties. For example, data analysis identified 21 storms in Norfolk, Virginia from 1948 to 2006 that were a 5-year or larger event at three or more durations at select durations from 1 to 96 hours. For a study where 5-year, 10-year, and 25-year storms were needed for design analyses, one possible solution would be to select the 15 June 2001, 23 August 1990 and 27 July 1969 events listed in Table 1 to represent the respective recurrence periods. While the 1990 storm is larger than the 2001 storm at nearly all durations, and the 1969 storm is similarly generally larger than the 1990 storm, none of these events conforms to the characteristic return period across a range of durations.

A further limitation is encountered when applying a single hyetograph over a large area. Proper correspondence of areal total rainfall with return period may require substantial reduction of the rainfall totals, with differing reduction factors applied at different durations, as discussed by Huff and Angel (1992).

Table 1. Norfolk, Virginia rainfall depths for select storms

Date	1-h	2-h	3-h	6-h	12-h	24-h	48-h	96-h
27 July 1969	2.9	3.5	3.8	4.2	4.7	5.6	6.7	7.8
23 August 1990	1.7	2.8	3.5	4.2	4.3	4.3	4.7	5.0
15 June 2001	1.1	2.1	3.0	3.7	4.1	4.4		
25-year depth	2.8	3.6	3.9	4.8	5.7	6.8	7.8	8.4
10-year depth	2.4	3.0	3.2	3.9	4.7	5.5	6.3	6.9
5-year depth	2.0	2.5	2.7	3.2	3.9	4.6	5.3	5.8

Frequency estimates from "Precipitation-Frequency Atlas of the United States" NOAA Atlas 14, Volume 2, Version 3 reported for Virginia 36.872 N 76.209 W (Norfolk)

Other constraints challenge modelers when selecting design storms:

- In many parts of the US, 1960s and 1970s-era rainfall atlases remain the official National Weather Service precipitation frequency publications. These atlases are based on much more limited datasets than are now available
- Rainfall atlases usually assume stationarity of datasets. Collection system planners should ideally incorporate climate change uncertainty into their designs.
- Most rainfall atlases do not report precipitation estimates for recurrence intervals shorter than one year, while some facilities designs, such as for combined sewer overflows, must examine performance in more frequent events

Event versus continuous simulation. Approaches used for assessing collection system performance differ widely. Many sewer and stormwater design studies evaluate steady-state peak discharge only. This approach is common for design of new sewer and stormwater development and for flood studies. Many large-scale urban collection system analyses use single event design storm approaches. Representative, or "typical", year simulations are used for some urban combined sewer systems, while five-year simulations have been used in other studies. True long-term simulations are rarely used. An approach where select large storms are simulated and performance statistics tabulated from model results offers many advantages for extreme event analysis, but is not commonly used.

Steady-state peak discharge computation remains the most common basis for designing new sewer and drain facilities. This approach has the advantage of simplicity, but typically yields more conservative (i.e. larger) facilities design than would be obtained from dynamic simulation. Steady state analyses can be performed using a wide variety of spreadsheet methods and software.

Single-event design storm simulations using a dynamic collection system model can today be performed on very large models with most of the complexity of the prototype system incorporated into the model. This approach remains limited in that it may not yield a design flow commensurate with the intended recurrence frequency. It is further compromised where factors other than rainfall-driven inflows, such as infiltration or tailwater, affect system performance.

Representative year simulations have been used in many communities to assess combined sewer overflows. Some investigators use historic precipitation data directly, while others adjust historic data by adding and removing events to obtain a record closer to a statistical ideal (Tsay *et al.*, 2007). The representative period may be one year or a longer period such as five years. When true historic data are used, this approach can be used realistically in conjunction with other environmental data. Examples of these situations are where a large river influences local system hydraulics but is statistically independent of the local system, or where temperature data is used to simulate snow processes. When complex collection system models are used, representative year simulation is restricted by limits on computing power and speed, computer storage capacity, and post-processing of large datasets. InfoWorks and MOUSE have built-in functionality for speeding long-term simulations and

controlling output size; SWMM has no comparable inherent capabilities, although some vendors have added some functionality in this area.

A one to five year representative period simulation is useful for combined sewer system analysis, where design criteria have return periods of one year or less; it has limited use for analyzing system performance in extreme events. Selection of a representative period from a long precipitation record requires considerable analysis, although the process becomes less critical as longer representative periods are used (Yeboah and Heineman, 2004).

True long-term simulation relies on the availability of long-term precipitation data. Most major US airports today have continuous digital hourly datasets dating to 1948. This enables statistically robust assessment of system performance for events with recurrence frequencies of 5 to 100 years. There are important constraints limiting adoption of long-term simulation:

- There is minimal demand for its use; most communities and regulatory agencies accept and understand the use of design storms for facilities planning
- Long-term simulations using complex models strain computational resources and are time-consuming to analyze
- Many engineers are not familiar with appropriate statistical techniques for assessing system performance based on results from long-term simulation
- Most collection system models omit seasonal and long-term variability; results from short simulations of select storms thus yield the same results as true long-term simulations

Long-term simulations are especially useful for extreme event analysis (e.g. flood or SSO) where the extreme events cannot be identified *a priori*. Thus, in a sanitary sewer system that is equally influenced by both rainfall-driven inflow and groundwater-driven infiltration, which is in turn controlled by long-term precipitation, it may not be possible to identify the most extreme events in a long record other than by simulation. Long-term dynamic collection system simulations may be performed by reducing model complexity. This can be achieved by, for example, simplifying the collection system, simulating rainfall-runoff without conduit hydraulics, or using a simpler model such as STORM (Heineman, 2004).

Many of the benefits of long-term simulation can be achieved by identifying select large rainfall events and developing statistics for those select events. For instance, a facilities design for 10-year performance could be developed from a 50-year precipitation record by simulating 20 pre-screened storms expected to yield the largest responses and identifying the conditions which fall at a 10-year plotting position (approximately the fifth largest event in the 50-year record) or along a fit of the results to a log-normal or other appropriate statistical distribution. InfoWorks and MOUSE have built-in capabilities for performing the batch-type simulations needed for this type of analysis; some of the commercial SWMM packages have similar capabilities.

Use of long-term simulations must be based on quality datasets. Where precipitation is the only external data, good long-term datasets are available for major US cities. However, these datasets must be assessed for stationarity and evaluated against potential climate change impacts. Similar attention must be paid to other external boundary data such as temperature and river and ocean levels.

RECOMMENDATIONS

While it is the engineer's responsibility to select appropriate software and engineering methods, there is little formal guidance available for design of collection system modeling studies. WaPUG's standards are somewhat dated and are primarily oriented towards combined systems. New standards that address all types of urban collection systems and consider the range of available datasets will help align contemporary studies with current technology.

USEPA SWMM is the most commonly used model for US dynamic collection system modeling. While SWMM was originally designed for combined sewer systems, it has long been used for sanitary and stormwater system analysis worldwide. The hydraulic aspects of SWMM have continually evolved throughout its history, and are much stronger in SWMM 5 than in older versions. However, the model's hydrology is constrained by limited scientific inquiry and by a lack of demand for more rigorous approaches. Some areas where the model's hydrology could be improved are listed below.

- The groundwater infiltration module works well for natural streams. It is usable for simulating pipe system infiltration, but does not simulation a complete sub-surface system where groundwater can enter pipes and streams or flow laterally.
- Raster-based drainage models have been developed, but have had limited application to urban collection systems. The catchment and inlet paradigm used in SWMM, InfoWorks, and Mouse works at many scales, but advances in computer technology warrant re-assessment of runoff simulation fundamentals.
- SWMM 5.0.14, released in January 2009, implements a seasonal soils recovery parameter that has not been experimentally tested. SWMM's surface infiltration models were originally designed for single event analysis, and were later modified for continuous simulation. They have not previously been adapted to simulate seasonal variation in infiltration processes.
- SWMM's surface water and groundwater components are not well-coupled. While surface water infiltration influences groundwater conditions, the water table has no impact on surface infiltration.
- SWMM's process models were not designed to simulate the complexity of sanitary sewer RDII processes. These processes are generally simulated by manipulating the process models in ways that make it difficult to translate field data into model parameters. For instance, representing sump pumps in SWMM requires either considerable aggregation and many assumptions or a highly detailed model.
- The principal dynamic collection system models are deterministically driven by rainfall. Adding a stochastic component to runoff hydrology or to dry weather

flow processes may yield more realistic models in some cases. This may be especially valuable in sewer systems with minimal RDII where random wastewater load variation is a significant stressor.

This paper has reviewed current practice in urban collection system modeling, identifying the state-of-the-art, opportunities for standardization, and research needs. The currently strong national interest in civil infrastructure projects creates an opportunity to address the issues associated with the advanced age of many US urban collection systems. Modest investment in research and development of updated guidance protocols for this field will yield great return in the value of the models used for urban facilities planning, improving the science of collection system modeling and yielding strong returns in reliable public works.

REFERENCES

Bennett, D., *et al.* (1999). *Using Flow Prediction Technologies to Control Sanitary Sewer Overflows.* Water Environment Research Foundation Project 97-CTS-8.

Heineman, M.C. (2004). "NetSTORM — A Computer Program for Rainfall-Runoff Simulation and Precipitation Analysis," *World Water and Environmental Resources Congress 2004*, ASCE.

Huff, F. A. and J. R. Angel (1992). *Rainfall Frequency Atlas of the Midwest (Bulletin 71)*. Illinois State Water Survey.

Lai, F. (2008). *Review of Sewer Design Criteria and RDII Prediction Methods.* EPA/600/R-08/010.

Natural Resources Conservation Service (1986). *Urban Hydrology for Small Watersheds*, U.S. Dept. of Agriculture, Conservation Engineering Division, Technical Release 55.

Tsay, S., D. Brocard, W. Lee, and G. Braswell (2007). "Developing a Typical Rainfall Period for Long Term CSO Analysis in San Francisco," *WEF Collection Systems 2007*.

USEPA (1999). *Combined Sewer Overflows Guidance For Monitoring And Modeling. EPA 832-B-99-002*.

Wastewater Planning Users Group (2002). *Code of Practice for the Hydraulic Modelling of Sewers*.

Yeboah, M. and M. Heineman (2004). "Selection of a Representative Long-Term Period for Continuous Model Simulation," *World Water and Environmental Resources Congress 2004*, ASCE.

The application of Environmental Site Design Processes to design a residential subdivision

Steven D. Trinkaus, P.E., CPESC, CPSWQ; Trinkaus Engineering; Southbury, CT

ABSTRACT:

Strategies of Low Impact Development (LID) are best known as alternative treatment systems to reduce the impact of storm water runoff on the environment. A more important aspect of LID is the implementation of Environmental Site Design (ESD). ESD is a design process to evaluate the environmental conditions on a parcel of land prior to the creation of a land development project. This process is most important for residential developments. While ESD can work with any land use regulations, the most environmentally sound developments will occur in those communities, whose land use regulations that permit "cluster" or "open space" designs.

This paper will explore the strategies and steps necessary to create a residential subdivision utilizing ESD.

THE KEY CONCEPTS OF ENVIRONMENTAL SITE DESIGN:

The strategies of ESD are designed to achieve certain benchmarks during the development process for all types of development. The overall benchmarks are as follows:

a) Establish Increased on-site recharge rates and Volumetric Reductions for Runoff,
b) Establish Nutrient-Based Storm water Loading Criteria,
c) Conservation of Forest Area,
d) Protect wetlands, watercourses, including zero-order streams and provide minimum width buffers for these systems,
e) Map and preserve the most permeable soils on the site,
f) Utilize Site Fingerprinting and define maximum limits of site clearing,
g) Utilize well defined and effective construction phasing plans,
h) Utilize decompaction and reaeration of soils following the construction period to restore infiltrative capacity.

For lower density development, the following are additional benchmarks for the application of ESD:

a) Allow the cluster or open space designs that reduce lot sizes in exchange for the conservation of natural areas,
b) Reforest turf areas to maximize area covered by tree canopy,
c) Conserve forests, wetlands and other natural areas with a goal of 65% of the site area being preserved,
d) Utilize restrictions on clearing and grading, implement filter strips and natural vegetation to disconnect impervious areas,
e) Maximize controlled sheet flow to naturally-vegetated area,
f) Limit residential street width to 22',
g) Disconnect rooftop runoff and direct to rain gardens, cisterns or filter strips,

h) Keep total site imperviousness to 10% or less. Design drainage systems to prevent direct connections to streams from the impervious areas,
i) Consider alternative road design standards to facilitate the use of grass swales in lieu of conventional curb/gutter systems.

ZONING REGULATIONS:

In this particular community, the zoning regulations permit Open Space subdivisions by Special Permit under Section 4.3 – OPEN SPACE SUBDIVISIONS. The goals of this regulation are as follows:

a) Permit flexibility in land development by allowing fro a variation in the lot sizes in all residential zones except R-4 without increasing the density permitted with the zone in which the property is located,
b) Provide open space, conservation and recreation areas (both active and passive),
c) To the extent practicable, preserve the natural and scenic qualities of the site and its surrounding neighborhood, including wetlands, watercourses, ridge tops, existing stands of mature vegetation, rock outcrops, scenic and historic sites,
d) Protect water quality, natural drainage systems and areas affording housing in conformance with the policies set forth in the plan of development.

SUBJECT PROPERTY:

The subject property comprises 104.5 acres and is located on the east side of Platt Hill Road, west and significantly above Highland Lake in Winchester, CT.

THE PROCESS OF ENVIRONMENTAL SITE DESIGN:

The following are the steps necessary to obtain the base mapping to create a residential subdivision using ESD:

1) Obtain field delineation of inland wetlands and watercourses on the site by a Certified Soil Scientist. In Connecticut, wetlands are solely determined by the presence of low chorma coloring within the upper 20" of the soil. The soil scientist will also approximate the boundaries and types of upland soil types on the site. These boundaries are typically sketched on a preliminary map of the site.
2) Obtain a boundary survey of the site along with the field location of all delineated inland wetlands and watercourses.
3) Obtain a topographic base map of the property based upon current aerial photographs which will provide existing contours at a 2' interval.
4) Investigate the presence of 100-year flood boundary limits on the site from the available mapping by the Federal Emergency Management Agency (FEMA).
5) Obtain an inspection of the site by an environmental consultant to determine the presence of vernal pools or other high quality wetland/watercourse areas.

Create an initial base map showing the information obtained above. This base map is used to begin the site assessment/analysis process.

A. Soils: Utilize local soil manuals or information from National Resource Conservation Service (Website: www.websoilsurvey.nrcs/usda.gov/app/) to determine the range of infiltration rates for soils on the site. Highlight those soils with the highest infiltration rates on the plan. Test pits may be necessary to verify the location of the infiltrative soils on the site.

Hydrologic Patterns: Determine watershed boundaries on the site tributary to wetland or watercourse systems. Verify in field if necessary.

Vegetation: Determine and highlight different types of forest cover.

Wetland/Watercourse/Floodplains: Determine on the map those wetland areas which are of high quality or possess unusual biological habitat.

Slopes: Determine all slopes on the site in excess of 25% and highlight on plan.

ACTUAL SITE FOR ESD ANALYSIS:

The site contains 104.5 acres and was farmed until the mid 1950s'. Wetlands were delineated by soil scientist. There are three intermittent stream/wetland corridors and a large Red Maple Swamp. Two isolated wetland areas were determined to be small vernal pools by environmental consultant.

The majority of the soils on the site are Paxton and Woodbridge. There are two large areas of Charlton soils as shown. While the soil permeability of the A horizon for all three of the soils range between 1.26 ft/day to 12.6 ft/day. The permeability of the B horizon for the Paxton and Woodbridge soils is significantly less at 0.4 ft/day, while the range for a Charlton is 4.0 ft/day to 12.6 ft/day. Clearly, most of the proposed development should occur on the Paxton and Woodbridge soils, thus saving the Charlton areas for use as infiltration areas or for low intensity residential use.

With the exception of two small meadow meadows, the majority of the site is densely wooded. The brush areas are in succession from meadow to woods and are also found along the intermittent stream corridors on the site. The site does contain a good mixture of Red & Black Oak, Sugar & Red Maple, Silver Beech, Black Cherry and some Northern White Pine. The pines are concentrated in the area of the Charlton Soils in the south central portion of the site.

The 25% slopes were delineated using the two foot topographic mapping. These slopes are primarily located above the eastern wetland system. In general development should not occur on these soils due to concerns of erosion during the construction period and these soils pose difficulties with stabilization after construction due to their fine grained nature.

Figure 1 shows the topography, wetlands/watercourses/vernal pools, watershed divides and soils.

Figure 2 shows 25% slopes, soil types and generalized vegetative cover.

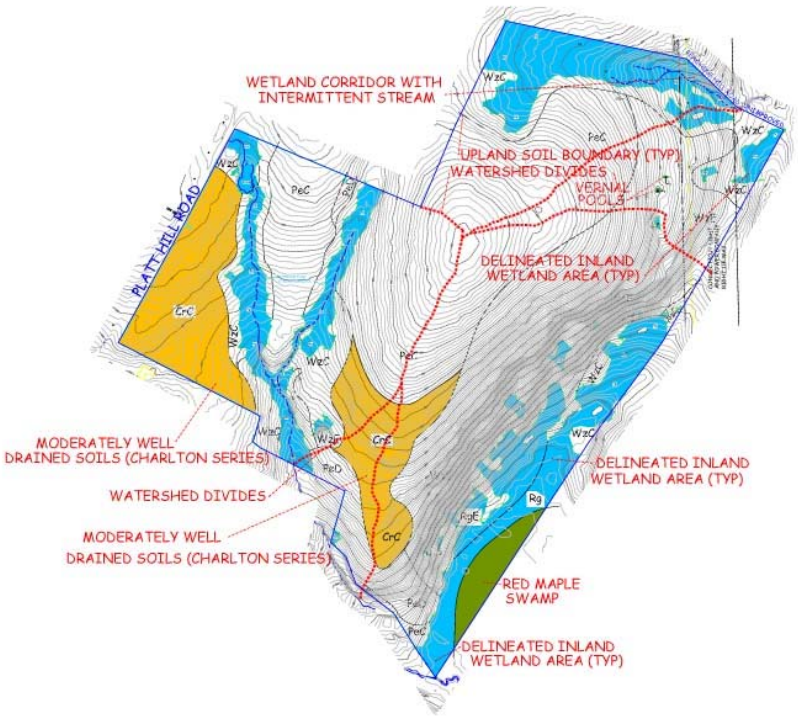

Figure 1 - Wetlands/Soils/Watersheds

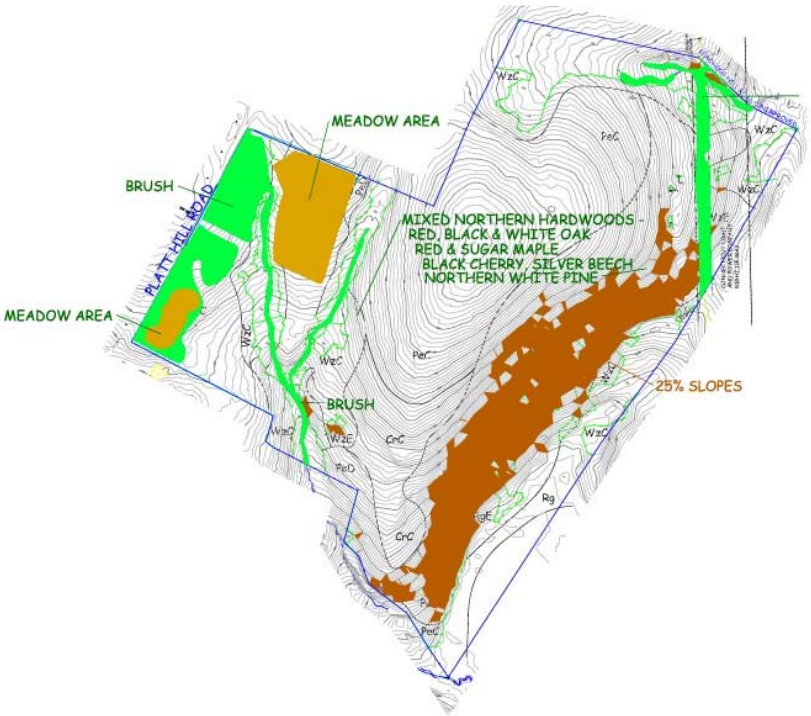

Figure 2 - 25% slopes/Vegetation Types/Soils

DEVELOPABLE AREA:

Of the total 104.5 acres, slightly over 49 acres is available for development. This area is shown in Figure 3 below. The next step is to determine the suitability of the site for the installation of subsurface sewage disposal systems (SSDS) for each proposed lot. The local health district required a 75' separation from a SSDS to a wetland or watercourse, so those areas were excluded from the developable areas. Over 150 deep test pits were excavated on the site. In general, the testing was done on the lower portions of the site to permit gravity flow systems to be utilized on each lot.

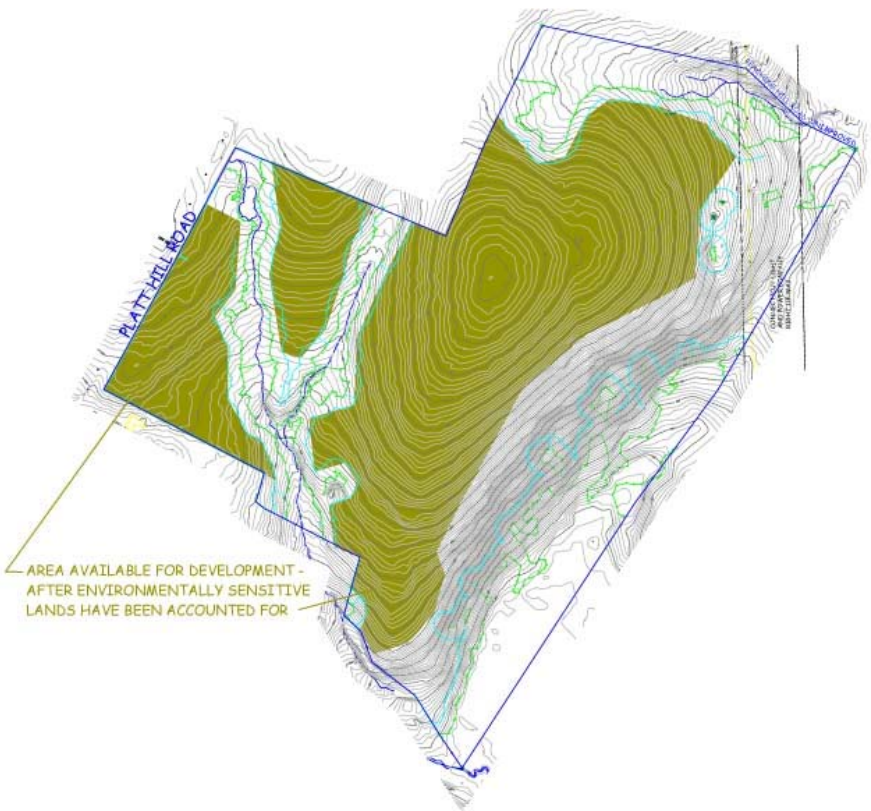

Figure 3 - Area available for development

The next step in this process was to compute the maximum allowable density permitted on the site in accordance with the town's regulations.

Density Calculation: For all residential zones, the total land area must be reduced as follows to determine the Developable Land Area (DLA). You must exclude 50% of all lands with inland wetlands soils, land subject to flooding, water bodies or watercourses, or land with slopes in excess of 25%. Once this calculation is done, Section 4.3 has further requirements to be met. First, 15% of the total land area must be taken out to for future street rights of way. Next, any land subject to utility easements must be taken out. Once these calculations have been done, the DLA shall be divided by the minimum lot requirements for the zone to determine the maximum number of lots permitted on the tract.

The calculation is as follows:

Total Site Area:	104.50 acres
- 15% (roads):	- 15.67 acres
- Utility Easement:	- 5.12 acres
- 50% of wetlands:	- 10.83 acres
- 50% of 25% slopes:	- 6.12 acres
Net Area:	66.76 acres
Current zoning: 1 house/1.9513 acres	
Max. Allowable density:	66.76/1.9513 = 34.2 lots

A layout conforming to current zoning is prepared to determine if ESD strategies can be implemented under this scenario. Figure 4 shows the conventional plan, while it appears feasible, many of the environmentally sensitive areas are not protected and a significant amount of road must be constructed, including reconstruction of 700'+ of an unimproved road to the north. This plan does not conform to the benchmarks of ESD. In order to achieve the ESD benchmarks, a reduction in density is necessary as is the consideration of an Open Space Design.



Figure 4 - Conventional Design

SITE DESIGN AND ACCESS:

Zoning regulations in this community permitted the use of an Open Space subdivision concept, where lots areas could be reduced from 85,000 sq.ft. to 40,000 sq.ft.

Septic soil test results were evaluated to determine the carrying capacity of the land to disperse the anticipated effluent loads. Based upon this analysis, a density of about 25 – 27 lots would be appropriate on the site. A conceptual layout of the road and lots is then prepared for the previously defined Developable Area. The following design elements need to be considered:

a) Road alignment should follow existing contours to the maximum extent possible in order to minimize site disturbance and limiting of grading.
b) Building lot should be sited with an eye toward providing easy access to the proposed residences with minimal changes in grade.
c) Use common driveways where practical to reduce impervious areas.
d) Subsurface sewage disposal systems are generally located below the proposed residences in order to facilitate gravity flow.
e) How will storm water from the impervious area be handled? It is very important that storm water be evaluated early in the design process to achieve ESD goals.

ENVIRONMENTAL SITE DESIGN STRATEGIES THAT CAN BE APPLIED ON THE SITE:

a) Preserve a large portion of the site as permanent Open Space,
b) Cluster Development Utilize Site Fingerprinting to minimize the extent of clearing for each lot,
c) Utilize rain gardens for the roof drains,
d) Utilize filter strips for overland flow prior discharge into natural areas,
e) Encourage the disconnection of impervious areas such as driveways from road,
f) Infiltrate runoff from impervious areas where the soil is suitable,
g) Implement storm water treatment systems to remove common pollutants from runoff,
h) Require soil tilling (min. 12” deep) of the disturbed soils around the house and yard area prior to the installation of topsoil to increase the infiltration ability of the soil.

Due to the regulations of the this community, conventional structural drainage systems had to be utilized for the road conveyance system. To provide enhanced settlement of coarse grained particles, 48” deep catch basin sumps are to be installed on the last catch basin prior to discharge. All other catch basins have 24” sumps. However, there was the opportunity to utilize LID storm water Best Management Practices (BMPs) to treat the runoff after it left the road right of way.

WHAT ESD STRATEGIES WERE APPLIED ON THIS SITE?

1. Cluster twenty four lots proposed on 104.5 acre site,

2. 64.1 acres preserved as Open Space, including ridge top,
3. Road design follows existing contours, minimizing site grading,
4. All roof drains are directed to rain gardens,
5. Runoff from driveways downhill of road discharged as overland flow across vegetated areas,
6. Installation of wildflower meadow strip with 3" micro-berm at edge of lawn area prior to natural area,
7. Four common driveways were used to reduce impervious areas,
8. Storm water treatment systems consisted of Subsurface Flow Gravel Wetlands, Constructed Shallow Marsh Wetlands, Linear Vegetated Level Spreader, Stone Infiltration Trenches, Vegetated Swale with Gravel Filter Berms.



Figure 5- Final Site Design

HYDROLOGIC ISSUES:

The site has two major drainage divides, one goes to the south to Taylor Brook (a perennial stream) and the north goes to Sucker Brook (an intermittent stream). For pre-development conditions, the RCN was 71 for Taylor Brook and 70 for Sucker Brook. Without the disconnection of impervious areas, the RCN values increased to 72.3 for Taylor Brook and 74.9 for Sucker Brook.

The preservation of over 60% of the land in its natural state has a significant positive effect on the Runoff Curve Numbers (RCN) for post-development conditions.

When the roof areas and those driveways downhill of the road system are removed from the total impervious area, the RCN's are reduced. For Taylor Brook the RCN is reduced to 71.2 (virtual match to pre-dev value of 71) and is reduced to 70.1 for Sucker Brook (virtual match to pre-dev value of 70).

Total impervious cover on the site is 4.4%, well below the desired 10% threshold. When the effective impervious area is considered, only 3.2% will be impervious. This minimization of impervious cover is best way to minimize impacts of development on water quality.

All of the storm water treatment systems are designed to contain the required Water Quality Volume (1" of rainfall). This applies to the subsurface flow gravel wetlands, constructed shallow marsh wetland, vegetated level spreader, rain gardens and infiltration trenches.

Because of the necessity of using conventional storm water conveyance system on the road, there will be increase of the Time of Concentration to the treatment systems. However, this initial increase of the Tc will be mitigated by the long residence times within the treatment systems, so that the Tc to the design point on the property line will match or exceed the pre-development Tc.

In addition, the preservation of significant natural areas below the proposed lots will also help to maintain pre-development times of concentration for overland flow from the individual lots.

The rain gardens, infiltration trenches and the preservation of over 60% of the site will allow the pre-development recharge rate to be maintained on the site. The other storm water treatment systems will also remove significant pollutant loads, especially the subsurface flow gravel wetlands and constructed shallow marsh wetlands so water quality goals will easily be achieved.

CONCLUSION:

The application of ESD early in the design phase and the application of LID strategies and treatment systems clearly demonstrate how land can be developed in an environmentally friendly manner. These strategies not only protect sensitive environmental areas, but also create a very livable community for future residents.

AUTHOR CONTACT INFORMATION:
Steven David Trinkaus, P.E., CPSEC, CPSWQ; ASCE Member Grade; Trinkaus Engineering, LLC; 114 Hunters Ridge Road; Southbury, Connecticut 06488; Phone: 203-264-4558; Fax: 203-264-4559; email: strinkaus@earthlink.net; Website: www.trinkausengineering.com

References:

1. "Consensus Proposal - Core Environmental Site Design Principles for the Implementation of the Maryland Stormwater Management Act of 2007"; August 2007
2. "Conservation Design for Stormwater Management – A Design Approach to Reduce Stormwater Impacts from Land Development and Achieve Multiple Objectives Related to Land Use" – A Joint Effort Between the Delaware Department of Natural Resources and Environmental Control and The Environmental Management Center of the Brandywine Conservancy; September 1997.
3. "Low Impact Development – Technical Guidance Manual for Puget Sound"; January 2005 and Revised to May 2005 by the Puget Sound Action Team.
4. "Technical Memorandum: The Runoff Reduction Method"; April 18, 2008 by David Hirschman and Kelly Collins of the Center for Watershed Protection and Tom Schueler of the Chesapeake Stormwater Network.

Effect of Bioretention on Runoff Temperature in Trout Sensitive Regions

Matthew Jones, Ph.D., E.I.[1] and William F. Hunt, Ph.D., P.E.[2]

[1] Department of Biological and Agricultural Engineering, North Carolina State University, Box 7625, Raleigh, NC 27695; email: Matthew_Jones@ncsu.edu
[2] Department of Biological and Agricultural Engineering, North Carolina State University, Box 7625, Raleigh, NC 27695; email: Bill_Hunt@ncsu.edu

Abstract

Although it has been established that thermal pollution from urban stormwater can negatively impact the aquatic ecosystem, there are few mechanisms available to reduce the temperature or urban stormwater runoff. A monitoring study was conducted at 4 bioretention areas in western North Carolina, located along the southeastern extent of United States trout populations, to examine the effect these systems have on runoff temperature and identify any design criteria pertinent to temperature reduction. Median runoff temperatures leaving the pavement surfaces, based on storm events, exceeded the 21°C upper avoidance temperature of trout at all sites during the months of June through September. Of the bioretention areas studied, the two systems that covered an area smaller than 10% of their contributing watershed were able to significantly ($p<0.01$) reduce both maximum and median storm temperatures between the inlet and outlet. At the two bioretention areas that were larger than 10% of their contributing watershed area, maximum effluent temperatures were significantly ($p<0.01$) cooler than influent temperatures; however, there was no significant ($p<0.05$) difference between median influent and effluent temperatures. Despite reductions in temperature, effluent temperatures were not significantly ($p<0.05$) cooler than the upper avoidance temperature for trout at any of the monitoring locations. There was evidence that substantial reductions in runoff volume occurred at all bioretention areas, especially the systems that were larger than 10% of their contributing watershed. Overall, monitoring results indicated that bioretention areas served as effective treatment mechanisms for reducing, but not eliminating, the thermal impacts associated with urban stormwater runoff.

Introduction

As advances in aquatic ecology have coincided with increased urbanization, it has become evident that warm stormwater runoff can negatively impact coldwater stream environments. Due to the thermal properties of asphalt, pavement surfaces can reach temperatures in excess of 60 °C, with much of the heat concentrated near the surface (Asaeda et al., 1996). During a storm event, runoff collects this heat and distributes it throughout the watershed. Although water temperature in streams naturally fluctuates in response to changes in solar radiation and the ambient air temperature, temperature changes are typically limited to a 0.6-0.8°C temperature increase for every 1°C increase in air temperature (Morrill et al., 2005). The discharge of stormwater runoff into coldwater creeks can raise stream temperatures above normal levels, with runoff temperatures elevated even during the night and early morning (Kieser et al., 2004; Lieb and Carline, 2000).

Heated stormwater runoff is a concern because of the negative impact it can have on the aquatic ecosystem. Because many aquatic organisms lack the ability to regulate their body temperature, temperature increases in the aquatic environment can impair major biological functions. Increases in stream temperature can negatively impact the behavior, metabolism, reproduction, growth, and vulnerability to disease of many aquatic organisms. Moreover, because various organisms respond differently to elevated temperatures, thermal pollution can have substantial impacts on community structure. Trout and salmon, which serve as important game fish in many parts of the United States, are among the fish most sensitive to elevated water temperatures. Due to a variety of complex factors, it is difficult to predict the specific effects of elevated temperatures on fish behavior and survival (Hocutt et al., 1980). In spite of these complexities, it has been determined that trout generally avoid water temperatures in excess of 21°C (Coutant, 1977).

Despite evidence that the thermal impacts or urban stormwater runoff have a negative effect on the aquatic ecosystem, there are few mechanisms available to cool stormwater runoff. Stormwater best management practices (BMPs) have been installed throughout the United States in order to reduce the impacts of sediments, nutrients, metals, and other pollutants; however, the effect of these systems on runoff temperature is not well understood. A study of a wet pond found that temperatures increased between the inlet and outlet (Kieser et al., 2004). Because wet ponds are not typically shaded, solar radiation can heat the water within the pond above the temperature of the ambient air. A stormwater wetland has been shown to reduce runoff temperatures when well shaded, with the net heat reduction attributed to evapotranspiration and infiltration (Kieser et al., 2004).

Although bioretention areas have been shown to reduce runoff flows, their effect on runoff temperature has not been thoroughly examined (Hunt et al., 2006). Soil temperature is largely governed by radiation and convective heat transfer near the soil surface. Because thermal conduction through a soil column is relatively slow, deeper layers of soil are able to maintain relatively stable temperatures over long periods of time (Mohseni et al., 2002). During irrigation with warm water, it has been shown that water temperature approaches the temperature of the surrounding soil as it infiltrates, resulting in minimal temperature variations at soil depths greater than 100 cm (Wierenga et al., 1970). At shallow drain depths, heat exchanges between the soil and infiltrating water may have little impact on water temperatures. For example, seasonal mean water temperatures between rooftop runoff and underdrain outflow were not significantly different at a relatively shallow (60 cm) bioretention area in the northeastern United States (Dietz and Clausen, 2005).
In order to examine the effect of bioretention areas on runoff temperature, a monitoring study was conducted at 4 locations in western North Carolina, along the southeastern extent of United States trout populations. Effectively managing thermal pollution is important in this region, since many coldwater stream environments approach the temperature limits of trout under natural conditions.

Methods

The monitoring sites consisted of bioretention areas in Asheville, Lenoir, and two adjacent bioretention areas in Brevard, North Carolina. Monitoring was

conducted during the summer months, generally from May through mid-October. Data were collected at all monitoring sites during 2006 and 2007.

To measure outflow at all bioretention areas, pulley-float stage recorders were used in conjunction with v-notch weirs. Pulley-float stage recorders with v-notch weirs or measured rainfall were used to estimate inflow at all monitoring sites. Due to complications with the flow monitoring equipment, flow data were primarily used to identify periods of flow over the temperature sensors. Rainfall data were collected for each monitoring location using tipping bucket rain gauges with a resolution of 0.25 mm. HOBO™ Water Temp Pro (H20-001) and HOBO™ 4 channel loggers (H08-008-04 & U12-008) with temperature sensors attached (TMCX-HD), which were all manufactured by Onset Computer Corporation, were used to collect temperature measurements. All temperature and flow measurements were logged at a 5 minute interval.

Statistical analysis was conducted using SAS® software, Version 9 (SAS Institute Inc., Cary, NC). The potential thermal impact to trout populations was ascertained by comparing water temperatures to 21° C, the temperature at which trout begin to experience thermal stress, using a signed rank test. Comparisons of influent, effluent, and soil temperatures were conducted using the Wilcoxon Rank Sum test (Wilcoxon, 1945). Storm medians and maximums were used in the analysis of BMP influent and effluent temperatures. Statistical significance was established within a 99% confidence interval ($p<0.01$), unless otherwise noted.

Site Description

The Asheville bioretention area (35°36'46"N, 82°33'54"W) covered 45m² and received runoff from 280 m² of asphalt parking lot. During the summer of 2005, when the bioretention area and contributing parking lot were constructed, a light colored chip seal was applied to the parking surface in an attempt to reduce pavement temperatures. The bioretention area was located approximately 6 m from the parking lot and runoff was routed into the BMP within an asphalt channel. Perforated PVC pipes, 10 cm in diameter, were used to drain the bioretention area and 38 cm smooth walled corrugated plastic tubing (CPT) discharged the bioretention effluent into nearby Reed Creek. The bioretention area did not contain mulch and naturally progressed from no vegetative cover in June of 2005 to an estimated 55% vegetative cover in late August, 2006. Temperature probes were installed at the inlet channel, inside the outlet weir box, and at 5 evenly spaced depths within the soil column from the surface to the underdrain depth of 135 cm.

The Lenoir bioretention area (35°55'20"N, 81°31'24"W) covered a 30 m² area. Runoff originated from a 675 m² asphalt parking lot and two sections of concrete sidewalk, which covered a combined area of 95 m². The bioretention surface was covered by hardwood mulch and vegetation within the BMP shaded 79% of the area, while the bioretention area and adjacent parking surface were shaded by a mature tree canopy. A network of 12 cm perforated CPT underdrains located 95 cm below the ground surface collected infiltrating runoff and discharged the water onto a street curb located approximately 10 m away. Temperature probes were installed in the inlet pipe, outlet weir box, and at 4 evenly spaced depths within the soil column from the

surface to the underdrain depth. Soil temperatures were only monitored at this site during the summer of 2007.

Adjacent bioretention areas were monitored in Brevard, NC (35°14'20"N, 82°43'52"W). Water from these bioretention areas, as well as others in the parking lot, was routed by an underground drainage network to Kings Creek, which was adjacent to the property. Both systems were mulched with pine straw. The Brevard east bioretention area covered a 37 m² area and received runoff from approximately 525 m² of asphalt parking lot (Fig. 4). Water left the bioretention area through a 12 cm perforated CPT underdrain network located approximately 48 cm below the soil surface. An estimated 43% of this bioretention area was shaded by low-lying plants. Temperature probes were located in the inlet weir box and outlet pipe. Soil temperature was measured at a depth of 48 cm during the summer of 2007.

The Brevard west bioretention area covered a 36 m² area and received runoff from approximately 325 m² of asphalt parking lot. Water left the bioretention area through a 12 cm perforated CPT underdrain network located approximately 43 cm below the soil surface. An estimated 43% of this bioretention area was shaded, primarily from 2 maple trees. Periods of inflow and outflow were identified with weir boxes mounted at the inlet and outlet, where temperature probes were also located.

Results and Discussion

Runoff temperatures directly leaving the parking surfaces were significantly ($p<0.05$) warmer than 21°C during the months of June through August at all monitoring sites. Runoff temperatures were typically warmest at the beginning of a storm event and cooled as the storm progressed. The coolest runoff temperatures were observed leaving the parking surface at the Asheville bioretention area, likely due to the presence of a light colored chip seal on the parking surface. Over the course of the monitoring period, runoff temperatures at the Asheville bioretention area were not significantly ($p<0.05$) different from those measured at a nearby parking lot that benefited from an older asphalt surface and shading from a perimeter of mature trees.

At the Asheville bioretention area, there was no significant ($p<0.05$) difference between median effluent temperatures and the 21°C threshold when examining the entire monitoring period; however, median effluent temperatures were significantly ($p<0.05$) cooler than 21°C when the month of August was excluded. There was no significant ($p<0.05$) difference between median influent and effluent temperatures at the Asheville bioretention area, indicating that the bioretention area was not able to consistently reduce runoff temperatures over the course of an entire storm (Figure 1). Although maximum effluent temperatures were not significantly ($p<0.05$) different from the 21°C threshold, maximum effluent temperatures were significantly ($p<0.05$) cooler than the maximum influent. A reduction in maximum water temperatures suggests that the bioretention area was able to reduce the initial runoff temperature spike, but unable to convey the benefits of cooler runoff as a storm progressed.

Median and maximum effluent temperatures at the Lenoir bioretention area were both significantly lower than influent temperatures, which indicated that the bioretention area was able to reduce the thermal impact associated with the

stormwater runoff. Despite the reduction in water temperature resulting from bioretention treatment, median effluent temperatures were not significantly ($p<0.05$) different from 21°C and maximum effluent temperatures were significantly warmer than 21°C. Although thermal impacts were reduced, the effluent from this bioretention area still posed some risk to the thermal environment of trout waters. At the Brevard east bioretention area, median and maximum effluent temperatures were significantly cooler than influent temperatures; however, effluent temperatures were also significantly warmer than 21°C. Similar to the Lenoir bioretention, the Brevard east bioretention was able to reduce, but not eliminate the thermal impact to a coldwater stream environment. At the Brevard west bioretention area, there was no significant ($p<0.05$) difference between median influent and effluent temperatures; however, there was a significant difference between maximum temperatures. Similar to the Asheville bioretention area, these temperature results suggest that the bioretention area was able to reduce the initial spike in runoff temperatures, but could not convey the benefit of cooler runoff temperatures later in a storm. Median and maximum effluent temperatures were both significantly warmer than 21°C, indicating potential thermal impacts to a coldwater stream environment. Seasonal trends in influent and effluent temperatures were not as well defined during 2007, possibly due to the impact of the drought throughout the region.

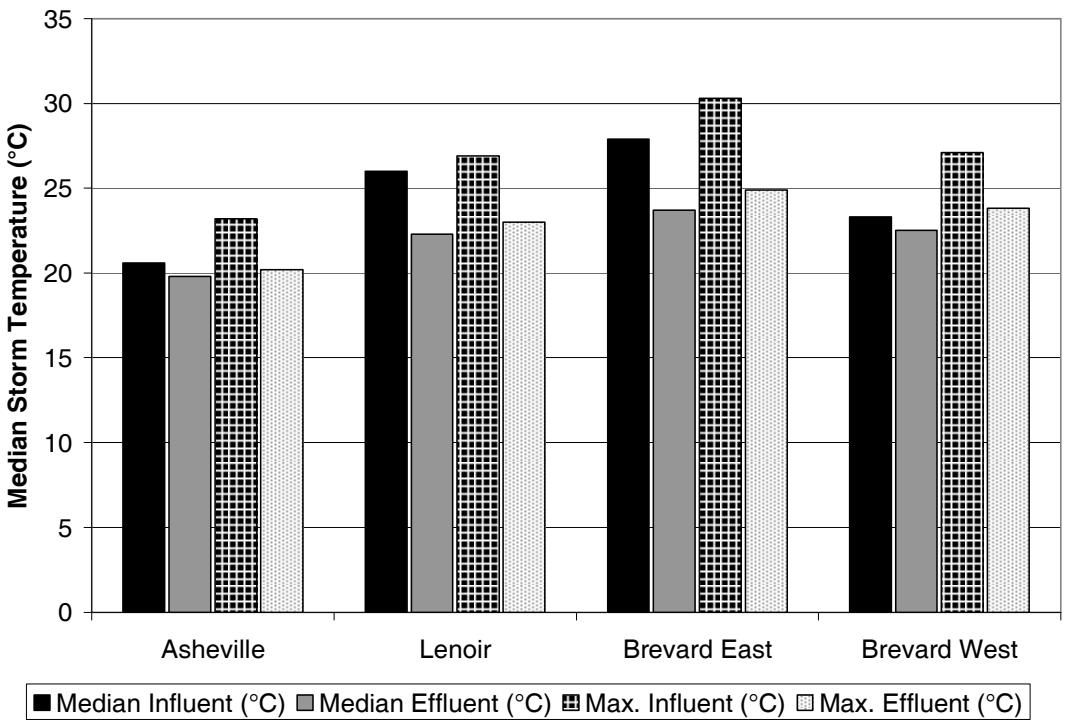

Figure 1. Median storm temperatures observed at each bioretention area for 2006

Despite significantly warmer median influent temperatures at the Brevard east bioretention area, there was no significant ($p<0.05$) temperature difference between median effluent temperatures at the Brevard east and Brevard west bioretention areas. The primary difference between these bioretention areas was the size of the contributing watershed, since they shared immediately adjacent locations, similar soil

properties, drain depth, and bioretention size. The area occupied by the Brevard east bioretention area was equivalent to 7% of the contributing watershed, while the area of the Brevard west bioretention was equal to 11% of the contributing watershed. Based on temperature results alone, there appears to be minimal thermal pollution benefits associated with moderately oversizing a bioretention area. One major benefit of a proportionally larger bioretention area that does not directly relate to effluent temperatures is the ability of a larger system to infiltrate runoff without generating outflow. When water exfiltrates, or leaves the bioretention area through the underlying soil and not the drainage pipes, the thermal impact from that runoff is effectively eliminated. Although the adjacent bioretention areas received the same rainfall, measurable outflow occurred in response to 76% of rainfall events at the Brevard east bioretention area, but only 27% of rainfall events at the Brevard west bioretention area. A similar outflow reduction finding was made by Li et al. (2009).

Analysis of temperature trends at specific soil depths provided insight into optimum underdrain depths. With the exception of nighttime surface temperatures, soil temperatures were coolest at the bottom of the bioretention soil column during the summer months. Soil temperatures at the bottom of the bioretention areas also exhibited the smallest fluctuations in response to storms or diurnal and seasonal temperature changes. However, the stability of soil temperatures at greater depths poses a potential risk of increasing the temperature of infiltrating water during later portions of a storm when cooler runoff prevails. Although there were several exceptions during late night storms, soils at a depth of 90 cm or greater remained cooler than soils at shallower depths for most storms. Beginning in September, soil temperatures were often warmest at the bottom of the bioretention areas, which raises potential concerns of warm effluent from deep bioretention areas during spawning seasons in the fall when temperature preferences are cooler.

Conclusion

Based on monitoring results, it appears that bioretention areas were able to effectively reduce the thermal impacts of urban stormwater runoff. Thermal load reductions can be attributed to initially warm runoff dissipating heat within the cooler soil depths of a bioretention area, and the ability of these systems to reduce runoff volumes. Although these systems effectively reduced thermal pollution from urban stormwater runoff, thermal impacts were not eliminated, since effluent temperatures were often warmer than the 21°C trout temperature threshold. Results of this research show that when runoff temperature is considered in BMP design, it should be possible to reduce thermal loads or minimize temperature increases, while maintaining the water quality and quantity benefits of bioretention.

Acknowledgements

This research was funded by the North Carolina Department of Environment and Natural Resources (NCDENR), Division of Water Quality. The authors would like to thank Jonathan Smith, Dr. Dan Willits, Dr. Garry Grabow, Dr. Aziz Amoozegar, Jon Calabria, Allen Caldwell, Eric Caldwell, Seth Nagy, and Jason Zink, all of whom are currently or formerly of NC State University, for their assistance in selecting research sites and support throughout the project.

References

Asaeda, T., Ca, V. T., and Wake, A. (1996). Heat Storage of Pavement and its Effect on the Lower Atmosphere. *Atmospheric Environment*, 30(3), 413-427.

Coutant, C. C. (1977). Compilation of Temperature Preference Data. *Journal of the Fisheries Research Board of Canada,* 34 740-745.

Dietz, M. E., and Clausen, J. C. (2005). A Field Evaluation of Rain Garden Flow and Pollutant Treatment. *Water, Air, and Soil Pollution,* 167 123-138.

Hunt, W. F., Jarrett, A. R., Smith, J. T., and Sharkey, L. J. (2006). Evaluating Bioretention Hydrology and Nutrient Removal at Three Field Sites in North Carolina. *Journal of Irrigation and Drainage Engineering*, 132(6), 600-608.

Kieser, M. S., Spoelstra, J. A., Feng Feng, A., James, W., and Li, Y. (2004). *Stormwater Thermal Enrichment in Urban Watersheds.*

Li, H, Sharkey, L.J., Hunt, W.F., and Davis, A.P. (2009). Mitigation of Impervious Surface Hydrology Using Bioretention in North Carolina and Maryland. *Journal of Hydrologic Engineering*, 14(4): TBD.

Lieb, D. A., and Carline, R. F. (2000). Effects of Urban Runoff from a Detention Pond on Water Quality, Temperature and Caged *Gammarus minus* (Say) (Amphipoda) in a Headwater Stream. *Hydrobiologia,* 441(1), 107-116.

Mohseni, O., Erickson, T. R., and Stefan, H. G. (2002). Upper Bounds for Stream Temperatures in the Contiguous United States. *Journal of Environmental Engineering,* 128(1), 4-11.

Morrill, J. C., Bales, R. C., and Conklin, M. H. (2005). Estimating Stream Temperature from Air Temperature: Implications for Future Water Quality. *Journal of Environmental Engineering,* 131(1), 139-146.

Wierenga, P. J., Hagan, R. M., and Nielsen, D. R. (1970). Soil Temperature Profiles During Infiltration and Redistribution of Cool and Warm Irrigation Water. *Water Resources Research,* 6(1), 230-238.

Wilcoxon, F. (1945). Individual Comparisons by Ranking Methods. *Biometrics*, 1(6), 80-83.

The Lawrence Technological University Greenroof Performance Evaluation Project

Donald D. Carpenter, Ph.D. AM ASCE[1] and Preethi Kaluvakolanu[2]

[1]Civil Engineering Department, Lawrence Technological University, 21000 W. Ten Mile Road, Southfield, MI 48075 PH 248 204-2549; FAX 248 204-2568; Email: carpenter@ltu.edu

[2]Graduate Student, Civil Engineering, Lawrence Technological University, 21000 W. Ten Mile Road, Southfield, MI 48075, Phone: 248-579-3215; Email: prityraju@gmail.com

Abstract

Lawrence Technological University is a private university located on a 120-acre campus in highly urbanized Southfield, Michigan (Detroit Metropolitan Area). The campus was primarily developed over the last several decades with limited or no stormwater controls as was customary with regulations of the time. However, the opening of a student services center in 2005 provided the opportunity for the campus to commit itself to green design and the use of low impact development (LID) techniques. The 40,000 square-foot A. Alfred Taubman Student Services Center (Center) is a Leadership in Energy and Environmental Design (LEED) Silver Certified green building that features a 10,000 square foot green roof; geothermal heating and cooling; cistern water harvesting; a bioswale, and other energy efficient technologies. As such, the Center provides a living laboratory for Lawrence Tech architecture and engineering students, local municipal officials, community planners, and design engineers to learn about LID techniques and LEED certification.

Of specific interest to stormwater management, the building features a 10,000 square foot Hydrotech Garden Roof™ and gray water cistern that recycles roof water. The presence of the green roof provided an unique opportunity to compare and contrast the hydrologic performance of a full-scale greenroof with other more traditional roofs on campus. This was accomplished by outfitting three separate roof drains (a traditional blacktop asphalt roof, a rock ballasted roof, and the green roof) with water quality and quantity sensors. Objectives of the Greenroof Performance Evaluation Project include the overall volume of precipitation retained and detained by the green roof compared to the other roofs on campus; the peak discharge and run-off coefficient reduction of the greenroof for various storm events, the nutrient loading attenuation capabilities of the greenroof; the reduction in ambient temperature associated with the greenroof; and the educational benefit of establishing a long-term monitoring station capable of determining the temporal performance of the green roof that could be integrated into the curriculum.

Introduction

A green roof, or vegetated roof, is a roofing system that includes a layer of engineered soil planted with vegetation. The two basic varieties are extensive and intensive with extensive roofs being lighter and more commonly used to treat stormwater runoff. The green roof at Lawrence Technological University is an extensive HydroTech Garden Roof™ (Figure 1). Green roofs represent a type of stormwater best management practice (BMP) that focuses on volume reduction and water quality in addition to water quantity and peak discharge attenuation

(Hutchinson et al., 2003; Hunt et al., 2005; Hunt et al., 2004; Moran et al., 2005; Liptan, 2003; Carter and Rasmussen, 2005 and Kolb, 2004). Green roofs have been used as a stormwater BMP for decades in Germany and are gaining in popularity in the United States. However, common acceptance of green roofs as a structural stormwater BMP has been slow in many communities. One reason is the lack of published full-scale performance data on their performance in a variety of climatological settings. Regional differences in hydrology, climate, plant material, and background water quality make the transference of results from one region to another questionable. Finally, there are numerous green roof design configurations and data is needed to evaluate the effectiveness of different designs. All of these factors indicate the necessity of more research studies on green roof performance.

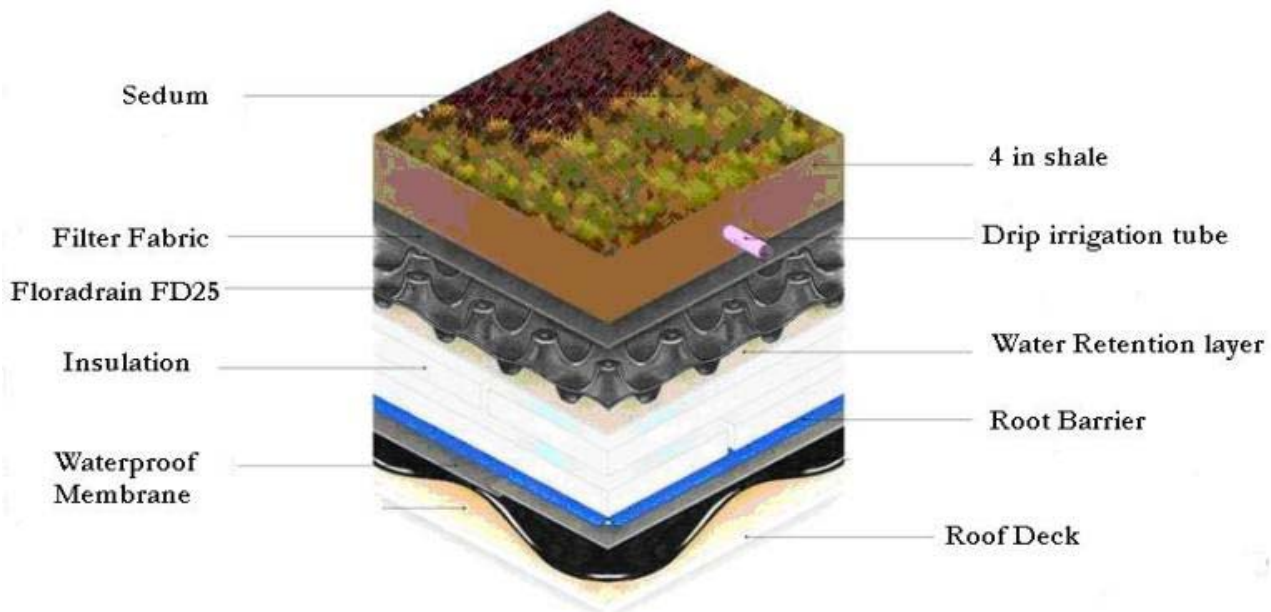

Figure 1: Cross section of HydroTech Garden Roof™ (schematic courtesy of HydroTech).

Project Objectives

The green roof constructed at Lawrence Technological University (LTU) was designed as a stormwater BMP in an urban environment (Figure 2). It was constructed over the A. Alfred Taubman Student Services Center (SSC) and was designed to retain approximately 60 percent of the annual rainfall while the remainder drains into a 10,000 gallon cistern to be used as "gray" water for sanitary purposes. To evaluate the performance of the greenroof, it is compared with runoff data collected from two additional full-scale roofs on Lawrence Tech's campus adjacent to the SSC - a rock ballast roof and a black asphalt roof. The black asphalt roof also acts as the control station from which to compare the green roof too.

The goals of this research and demonstration project are as follows:

1. Determine the overall percent of precipitation retained and detained by the green roof (water quantity).

2. Determine the peak discharge reduction of the green roof (water quantity)
3. Determine the nutrient loading attenuation capabilities of the green roof (water quality).
4. Determine the reduction in ambient temperature associated with the green roof (air quality).
5. Establish a long-term monitoring station capable of determining the temporal performance of the green roof as well as provide data that can be integrated into the curriculum (water quantity and education).



Figure 2: Green roof on the A. Alfred Taubman Student Services Center.

Monitoring Equipment

To monitor discharge from the roof, three Palmer-Bowlus flumes of 4 inch diameter were installed into existing roof drains at the three locations (Figure 3). The flumes were inserted into existing roof drains. When runoff from the roof reached a certain level in the flume, water was siphoned from the flume into the Avalanche Sampler which has a refrigerated compartment with a 14 bottle configuration for discrete collection of water samples. A second tube connected the flume to a 730 Bubbler Flowmeter, which measured the level of the runoff in the flume based on the pressure necessary to release a bubble air. The runoff discharges were calculated based on the water level readings in the flumes using Equation 1.

$$Q = 1.68 \times H^{1.9} \qquad \text{(Equation 1)}$$

where, Q = Flow in ft^3/sec (cfs),
H = Level reading in flume (ft).

The discharge rate from Equation (1) was integrated over the entire time runoff was observed to obtain volumes of the runoff was observed to obtain volumes of the runoffs:

$$V = \int_0^t Q(t)dt \qquad \text{(Equation 2)}$$

where, V = Volume of runoff (cubic feet)
Q = Runoff discharge (cfs),
t = Time (seconds)

The percent retained was then determined using the equation:

$$\%\ \text{Retained} = \frac{\text{Amount retained (inches)}}{\text{Total rainfall (inches)}} \times 100\% \qquad \text{(Equation 3)}$$

where the total rainfall was measured via the rain gauge and the amount retained is the volume from Equation (2).

Water Retention

One of the objectives of the green roof research was to determine the water retention capabilities of the green roof. Precipitation is retained on the greenroof and then stored in the soil media and the drainage layers below until moisture goes back into atmosphere via evapotranspiration. Percent retained on the green roof is calculated as the difference between rainfall depth and runoff depth on green roof as determined by Equation (3). Data was collected for six months from April to September 2008. During that time there were a total of twenty one measurable rainfall events for a total precipitation of 13.40 inches. The green roof retained 9.14 inches of rainfall depth, which represents a 68.24% retention rate. The total percent retained on the LTU green roof is comparable to a green roof study in Portland 69% of 44 inches was retained over a 15 month period (Hutchinson et al., 2003). It is also comparable to a study conducted at Michigan State University where 66% rainfall retention was reported over 24 rainfall events (Rowe et al., 2003).

Table 1. Summary of monthly water retention for LTU greenroof.

Period	Rainfall (inches)	Runoff (inches)	Amount Retained (inches)	Percent Retained %
Apr-08	0.68	0.09	0.59	86.59
May-08	2.12	0.11	2.00	94.40
Jun-08	3.52	0.66	2.85	81.01
Jul-08	2.55	0.60	1.94	76.30
Aug-08	0.29	0.00	0.28	99.44
Sep-08	4.24	2.77	1.47	34.66
Total	13.4	4.25	9.14	68.24

Table 1 provides a summary of monthly water retention values where monthly retention percentages varied from approximately 35% to 100%. A similar range of water retention was recorded for individual storm events. This variation represents the various factors that affect the

rainfall retention including rainfall intensity/duration/frequency, initial soil moisture, and evapotranspiration. For example, the green roof is able to retain more water from smaller rainfall events. When the soil media on the green roof is already saturated from a previous event, it was unable to absorb additional water. In addition, when there was a longer time period between storm events, evapotranspiration played a role and water temporarily stored in the soil media and drainage layer was either evaporated or transpired by the vegetation. For example, May exhibited a total recorded rainfall of 2.12 inches over four events that were at least 4 days apart. Whereas in the month of June, the total rainfall was 4 inches over six events with several events occurring two or three days apart. For June, the green roof retained 81% of the total precipitation compared with 94% for May.

A similar analysis was conducted for the other two roofs and compared against the green roof. The percent retained and total rainfall depth retained for each month is shown in Figure 3. In total, the black asphalt roof retained 1.4 inches for a retention percentage of 10.44% with the rock ballasted "stoneroof" retaining 6.88 inches for a retention percent of 48.58%.

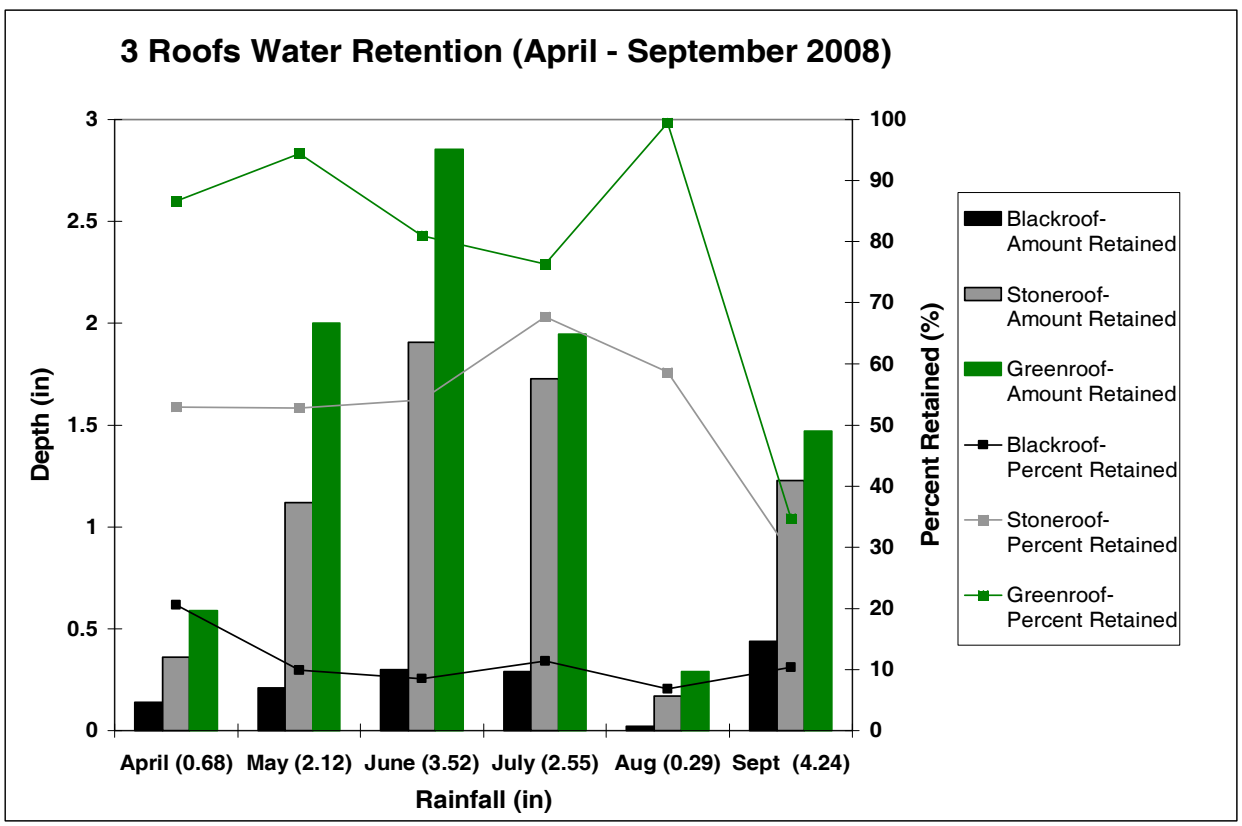

Figure 3. Display of monthly retention for the three roofs.

A rational coefficient (C) is a dimensionless number that is used to determine the peak discharge of an area for a given rainfall intensity. The rational coefficient is often used in hydrologic calculations and is included in many stormwater ordinances which rely on the rational formula for determining peak discharge for small watersheds. The rational coefficient can be calculated based on volume:

$$C = \frac{\text{Volume of roof runoff (cu.ft)}}{\text{Volume of rainfall (cu.ft)}} \qquad \text{(Equation 4)}$$

To demonstrate the impact rainfall intensity has on the runoff coefficient of a green roof, the rainfall events from April to September 2008 have been categorized into three sizes: rainfall intensities that varied between 0.1 inch to 0.5 inch were considered as of small size, intensities with a range of 0.5 inch to 1 inch were categorized as medium events and rainfall amounts greater than 1 inch were termed as large events. Table 2 displays the range of runoff coefficients for the types of rain events. From the table it is clearly seen that the runoff coefficients for the green roof increase with increasing rainfall intensities. The black asphalt roof and the stone roof have similar runoff coefficients values regardless of rainfall intensity.

This effect can clearly be seen in Figure 4 which plots measured runoff from the three roofs versus rainfall for all storms of less than 1 inch total depth. Statistical best-fit trend lines indicated a linear relationship for the black roof and the stone roof (although the stone roof had significant variability) whereas the green roof exhibited a power relationship indicating increased run-off with increasing rainfall.

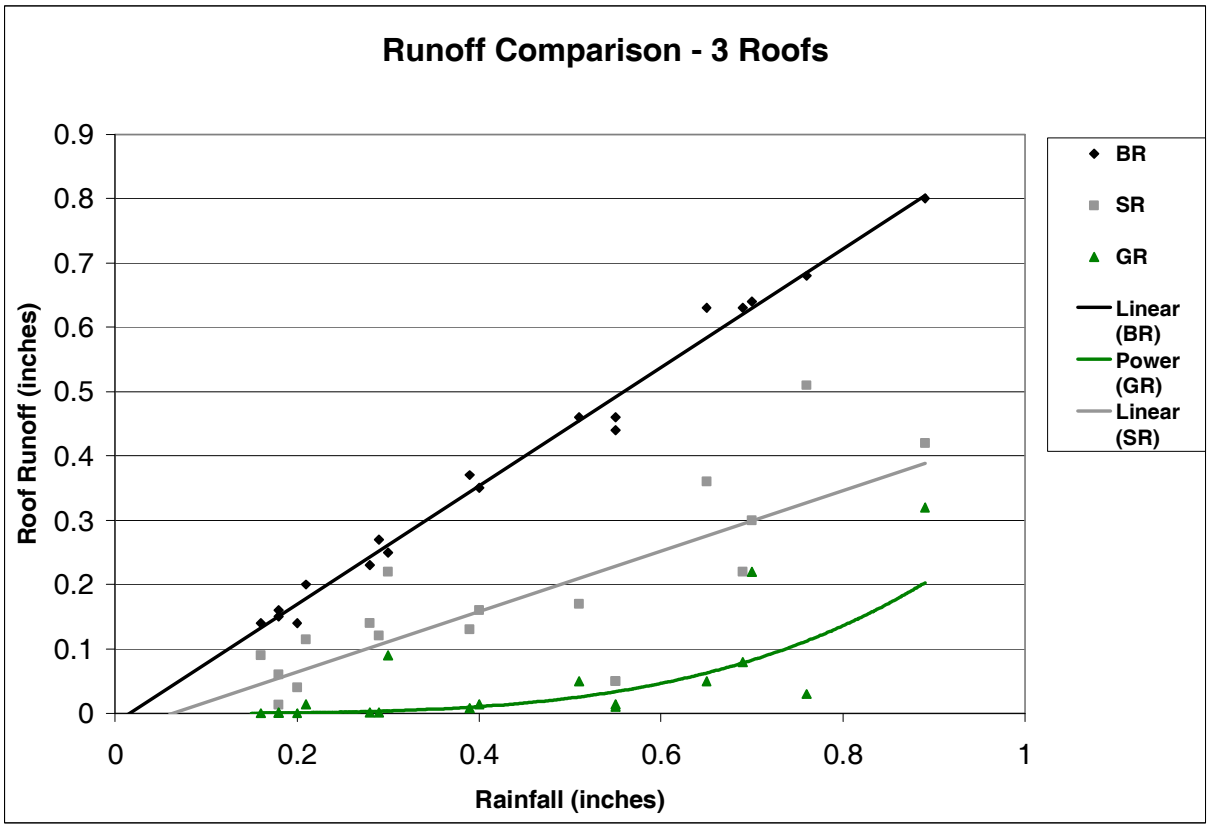

Figure 4: Display of runoff comparisons for the three roofs, less than 1 inch.

Table 2. Rational coefficients for the three roofs based on selected storm sizes.

Size Category	Storm Size	Number of Observations	Green roof	Black roof	Stoneroof
Small	0.1 -0.5 (in)	9	0.037	0.88	0.44
Medium	0.5 – 1 (in)	8	0.13	0.91	0.36
Large	> 1 (in)	3	0.55	0.92	0.62

Peak Discharge Attenuation

Reduction of peak discharge is another major benefit of green roofs and was included in the LTU greenroof research's objectives. The soil media and the drainage layer on the greenroof absorb rainwater and runoff occurs after the soil is saturated and drainage layer is at capacity. This process causes a delay for the runoff to occur and thus a time delay is observed between the time when the rainfall begins and the time when the greenroof exhibits measured runoff. This difference can vary from several minutes to several hours depending upon the initial conditions of the green roof media and the intensity/duration/frequency of the rainfall event. To compare the three roofs, which were different in size, the flows were normalized per 1000 square feet of the corresponding roof areas and represented as hydrographs based on Equation 1.

Figure 5 is an example of one of the 21 hydrographs measured in this investigation. The graph shows time (hours) on the x-axis and discharge (cfs) on the y-axis along with 15-minute rainfall data. For this example, the green roof observed a delay of 2.5 hours from the start of the rainfall event until discharge was measured. During this time the soil media was getting saturated and the drainage layer was filling. In addition, runoff from the greenroof was observed for 1.5 hours after the precipitation ended. Finally, all of the initial peaks measured on the black roof are not captured on the green roof discharge record. The green roof peak discharge occurs around 3.75 hours and is significantly less than the corresponding black asphalt roof peak measured around 2.5 hours into the storm record. Overall, the green roof showed significant reduction of flow rates for the entire study from April to September 2008. Individual reductions in peak discharge varied from 99.9% for the smallest 0.1 inch of rainfall to 54.23% for the largest single measured rainfall event (2.54 inches of rain) with an average percent reduction of 84.06%.

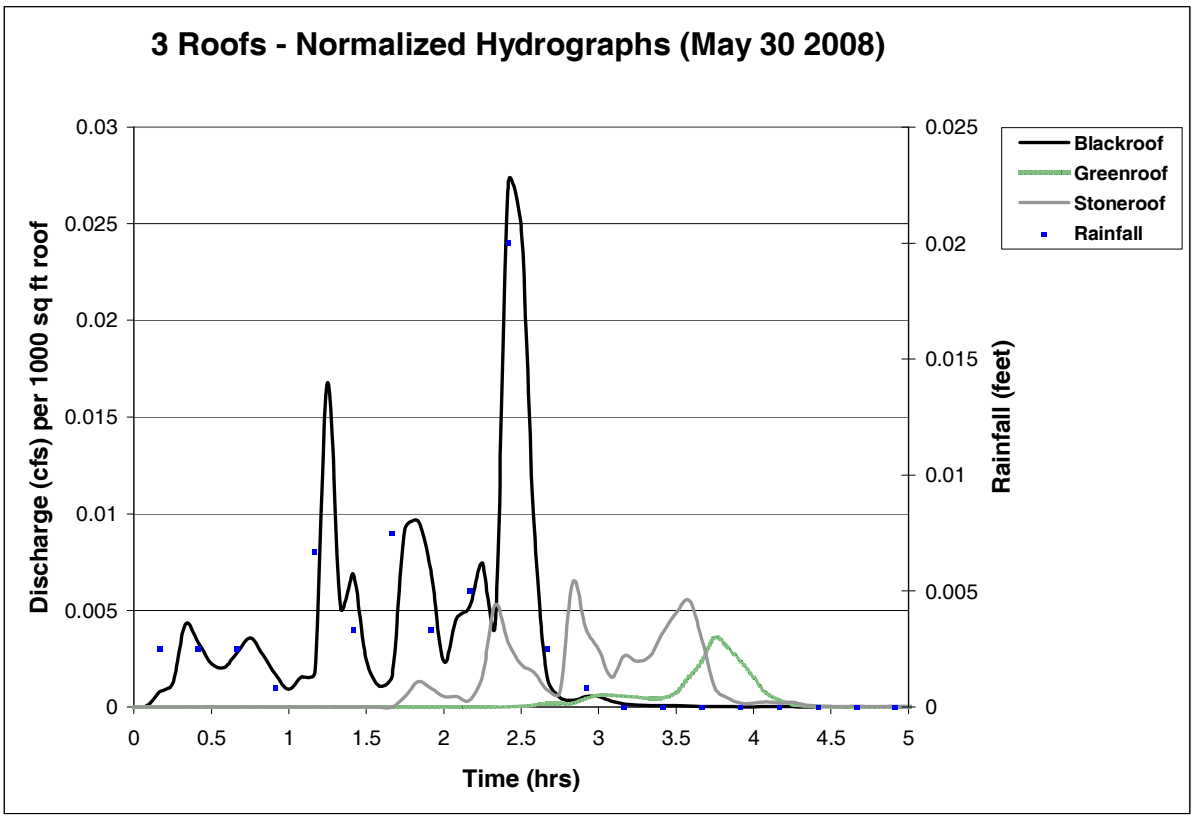

Figure 5. Peak flow hydrograph of three roofs (May 30 2008).

Laboratory Study – Water Quality Data

The water quality tests were conducted on nutrients that included total phosphates (TP) and Nitrates (NO_3^--N), and also total solids (TS). Data is available for a total of five rain events from May 2008 to September 2008. The Avalanche Samplers installed at the three sites have collected water samples required for the water quality tests. Equal amounts of water were then taken from the samplers, composited into a container, and then were utilized for the pollutant testing using procedures found in Water Quality with Computers (Johnson et al., 2008). A summary can be found in Table 3. Overall, there was significant variability between individual rainfall events and the nutrient removal and water quality performance portion of the investigation is inconclusive. However, given the significant reduction in discharge associated with green roofs, the mass loadings are significantly better than the concentrations.

Table 3. Average pollutants derived on the 3 roofs.

Type of Pollutant	Average Rainfall (inches)	Greenroof Concentrations (mg/L)	Blackroof Concentrations (mg/L)	Stoneroof Concentrations (mg/L)
Total Solids	1.19	190	108	152
Total Phosphates	1.19	0.12	0.18	0.10
Nitrates	1.19	0.41	0.37	0.80

Ambient Temperature Reduction

The temperature difference between the urban areas and the surrounding natural areas is called as urban heat island effect and this is found to be significantly reduced by green roofs. Three temperature sensors (Microlite USB from Fourier Systems) were used as the temperature measuring devices on the three roofs. Temperature data was collected starting from the month of December 2007 to June 2008 and daytime average temperatures were calculated. Table 5 shows the values calculated for the three roofs which indicate the green roof was always cooler than the other two roofs. However, the temperature sensors failed on several occasions and the quality of the temperature data collected is questionable. That said, the ambient temperature reduction of green roofs has been well documented in other investigations (Getter and Rowe, 2006; Liu and Baskaran, 2003; Tan & Sia, 2005; Liu, 2004; Oke, 1987; Scholz, 2001 and Laberge et al., 2004).

Table 5. Average daytime temperatures of three roofs for selective months.

	Average Daytime Temperature °C		
Month	Blackroof	Stoneroof	Greenroof
February 2008	2.28	1.30	1.74
March 2008	11.97	9.95	9.10
May 2008	28.02	27.12	21.0

Education

The final goal of the LTU Green Roof Performance Evaluation Project was the ability of the green roof to provide educational benefits to university students, municipal engineers and planners, and the general public. This goal was definitively met. Research data from the green roof has been utilized by two Master students for their thesis (Kaluvakolanu, 2009; Biman, 2009) and has been incorporated into undergraduate and graduate level engineering and architecture courses. The roof has been the subject of many regional presentations and tours in an effort to

inform the populace on the benefits of green roofs. In addition, the University is setting up partnerships with regional public school districts and community colleges to assist them in implementing green roofs on their campuses as well as to utilize the green roof as part of their curriculums. Finally, the LTU green roof served as a case study for the new Michigan Low Impact Development Manual.

Summary

Water quantity data was collected for six months from April to September 2008, with a total of twenty one rain events. A total precipitation of 13.40 inches was observed for which the greenroof retained 9.14 inches, which accounted to 68.24% of retention. The retention observed at the blackroof was 10.44% and stoneroof showed total retention of 48.55%. The variability of rainfall retentions on the greenroof ranged from 33% to 100% for monthly data and this was dependant on the rainfall patterns. The greenroof also showed significant reduction of peak flows with an average of 84.06% for the total rain events. Average Rational Formula runoff coefficients were developed from the runoff flows observed on the greenroof. For storms ranging from 0.1 inch – 0.5 inch, the coefficient was 0.037, for storms in the range of 0.5 inch to 1 inch, coefficient of 0.13 and 0.55 was observed for storms greater than 1 inch; typical rooftop runoff coefficients range from 0.75 to 0.95.

Water quality samples were collected from the three roofs for five selected rain events. Laboratory tests were conducted to determine the concentrations of total phosphates (TP), nitrates (NO_3^--N) and total solids (TS). Greenroof showed higher concentrations of total solids and nitrates compared to the other two roofs, while it showed lower concentrations of total phosphates.

Temperature data was collected on the three roofs from December 2007 to June 2008. The results showed that greenroof was efficient in reducing rooftop temperatures in summer when compared to the black and stoneroofs. The average daytime temperatures of summer were 28.45 °C on greenroof, 32.55 °C on blackroof and 31.6 °C on stoneroof.

References

Biman, P. (2009). "Modelling and Evaluation of an Extensive Green Roof for Stormwater Management" thesis, submitted to University of Windsor, Windsor, ONT, in partial fulfillment of the degree requirements for Master of Science.

Carter, T., and Jackson, T. C. (2006). "Vegetated roofs for stormwater management at multiple spatial scales." *Landscape Urban Planning*, 80(1-2), 84-94.

Carter, T.L., and Rasmussen, T. C. (2005). "Use of greenroofs for ultra-stream restoration in the Georgia Piedmont (USA)." *Proc., 3rd North American Green Roof Conference: Greening rooftops for sustainable communities,* Washington, D.C., 526-539.

Getter, K. L., and Rowe, D. B. (2006). "The role of extensive green roofs in sustainable development.' *HortScience,* 41(5), 1276-1285.

Hunt, B., Moran, A., and G. Jennings. (2004). "A North Carolina field study to evaluate green roof runoff quantity, runoff quality and plant growth." *Proc., 2nd North American Green Roof Conference: Greening rooftops for sustainable communities,* Portland, OR, 446-460.

Hunt, W.F., Moran, A., and Smith, J.T. (2005). "Hydrologic and water quality preformance from greenroofs in Goldsboro and Raleigh." *Proc., 3rd North American Green Roof Conference: Greening rooftops for sustainable communities,* Washington, D.C.

Hutchinson, D., Abrams, P., Retzlaff, R., and Liptan, T. (2003). "Stormwater monitoring two ecoroofs in Portland, Oregon, USA." *Proc., 1st North American Greenroof Conference: Greening Rooftops for Sustainable Communities*, Chicago, IL, 372-389.

Johnson, R., Redding, K., and Holmquist, D. (2008). *Water quality with computers*. Beaverton, OR.

Kaluvakolanu, P. (2009). "Evaluating green roof performance in improving stormwater quantity, quality, and reducing ambient air temperatures," thesis, submitted to Lawrence Technological University, Southfield, MI, in partial fulfillment of degree requirements for Master of Science.

Kolb, W. (2004). "Good reasons for roof planting – Green roofs and rainwater." *International. Conference on Urban Horticulture,* Acta Horticulturae, Waedenswil, Switzerland, 643, 295-300.

LaBerge, K., Mulvaney, P., and MWH. (2005). "City of Chicago greenroof test plot study". Stormwater and Temperature Results." *Proc., 3rd North American Green Roof Conference: Greening rooftops for sustainable communities,* Washington, D.C.

Liu, K., and B. Baskaran. (2003). "Thermal performance of green roofs through field evaluation." *Proc., 1st North American Green Roof Conference: Greening rooftops for sustainable communities,* Chicago, IL, *273*–282.

Liu, K. (2004). "Sustainable building envelope – garden roof system performance." *Proc., Symposium on Building Envelope Technology,* New Orleans, L.A., 1-14.

Liptan, T. (2003). "Planning, zoning and financial incentives for ecoroofs in Portland, Oregon." *Proc., 1st North American Green Roof Conference: Greening rooftops for sustainable communities,* Chicago, IL, 113-120.

Moran, A., Hunt, W.F., and Smith, J.T. (2005). "Greenroof hydrologic and water quality performance from two field sites in North Carolina." *Proc., 2005 Watershed Management Conference* , ASCE, Reston, VA.

Oke, T. R. (1987). *Boundary layer climates.* John Wiley and Sons, New York, New York.

Scholz-Barth, K. (2001). "Green Roofs: Stormwater management from the top down." 63-70, http://www.edcmag.com/CDA/Archives/d568f635d8697010VgnVCM100000f932a8c0 (accessed 1/10/2008).

USEPA. (2003). "Protecting water quality from urban runoff." *EPA 841 – F-03-003*, United States Environmental Protection Agency, Washington, DC.

The Road to LID Plan Approval in Coastal North Carolina

Development of a Spreadsheet Modeling Tool for LID Based Designs

by Hunter Freeman P.E.
Withers & Ravenel, Cary, NC

Introduction

North Carolina has an abundance of natural resources and a climate that has helped make it one of the fastest growing states in the nation. With the growth and the jobs, comes the challenge of protecting the environment and quality of life that makes it such a desirable place to live. This is especially true for the 20 coastal counties, where stormwater policies are being updated to protect shellfish habitats and enhance water quality.

In theory Low Impact Development (LID) practices are one means to achieve high water quality standards, but until recently guidance for implementing this type of program at any level has been scarce. To that end the North Carolina Coastal Federation (NCCF) with National Oceanic and Atmospheric Administration (NOAA) grant funding and contributions from three jurisdictions: the City of Wilmington, New Hanover County, and Brunswick County, spearheaded the development of LID specific stormwater design manuals and a spreadsheet based modeling tool for each local government. The model was developed to assist engineers and developers with the permitting and approval of LID stormwater management plans as well as act as a tool for the reviewing agencies to use in the approval process.

Withers & Ravenel worked with the NCCF and the three local governments to tailor the model to meet specific requirements of each jurisdiction, combining the governmental needs with the calculation requirements of the engineer.

A Background on Stormwater Regulations in NC

While the current emphasis of North Carolina's LID initiative is to reduce the impact of runoff from new impervious surfaces, challenges to North Carolina's water quality are hardly new or limited strictly to urban development.

Virtually none of the North Carolina's coastal plains resemble the natural habitat the early settlers found when they arrived. The practice of draining wetlands to establish fertile cropland was commonplace. The conversion of North Carolina's pristine forest to agricultural use impaired nearly 50% of the estimated 8 million acres of natural coastal wetlands. These impacts deprived coastal habitats of their natural system for pollutant removal – functional wetlands.

Today, land development represents the greatest environmental impact from non-point source pollution in North Carolina, and sedimentation pollution, primarily from construction sites, is the largest non-point source pollutant by volume.

In 1974, North Carolina was one of the first States to enact statewide Erosion and Sedimentation Control regulations. North Carolina moved to protect water supply watersheds and other sensitive waters from non-point source pollution in the late 1980's with water quality regulations primarily targeting total suspended solids (TSS).Nonetheless some of North Carolina's river basins, in addition to the majority of the coastal estuaries, have proved to be more sensitive to pollution than others and needed more protection.

In the early 1990's fish kills in the Neuse River were traced to the proliferation of an organism which flourishes in nutrients from fertilizers, waste water discharges and runoff from impervious surfaces. In 1997, the State passed some of the nations strictest regulations for the Neuse River Basin. These rules were followed by Tar-Pamlico River Basin Rules, Randleman Lake Watershed Rules, and now the Jordan Lake Watershed Rules which are currently in development. The goals remained constant – reduce pollutant loading rates resulting from wastewater treatment processes and new development.

While new impacts to the water quality have been greatly reduced due to these regulations, the quality of coastal waters and habitat continues to degrade, due largely to the explosion of development within North Carolina's Inner Banks – the mainland development adjacent to the estuaries themselves.

The Challenge of Coastal Development

The natural amenities of the southeastern North Carolina coast have attracted new residents on a daily basis. Coastal North Carolina has been one of the fastest growing regions of the nation over the past 30 years. The number of housing units has increased by 127% in that time period, ranking the area as 5th in national growth. More specifically, Brunswick County, located between Wilmington, NC and Myrtle Beach, SC, was recently ranked as the 17th fastest growing county in the nation (source: US Census).

With the influx of development, and the increased impervious cover that accompanies it, stormwater runoff has become a major contributor to the pollution of North Carolina's sensitive coastal waters. The NCCF estimates that over 100,000 acres of shellfish habitat has been contaminated due to pollution from all sources, but principally stormwater runoff.

In July 2008, the North Carolina Senate passed a bill modifying stormwater regulations in the 20 coastal counties. The previous regulations, originally adopted in 1988, have remained unchanged since 1995. The recent efforts to revise the rules were met with significant opposition from developers and local governments alike. The newly revised regulations lower density thresholds for sensitive watersheds, require permitting for small projects previously exempt from regulations, and also

allow for a wider variety of stormwater treatment facilities, and best management practices (BMPs) including Low Impact Development techniques.

The Road to LID

In 2005, the NCCF, using EPA grant funding, formed the Lockwood Folly Roundtable in Brunswick County, NC. Water quality experts from a number of State agencies presented the Roundtable with evidence that demonstrated a long-term deterioration of water quality in the Lockwood Folly River. These presentations showed that between 1980 and the present, widespread areas in the Lockwood Folly failed to meet State water quality standards set for shellfishing. As a result, the percentage of the river's shellfishing areas that are closed increased from 18% in 1980 to the current level of 55%.

The group of eight stakeholders spent 18 months identifying key strategies in an attempt to protect, preserve and possibly restore local shellfish habitats. From the roundtable eight strategies were accepted by the County Commissioners in February 2007. Included among them were plans to "*Incorporate low impact development (LID) technology into county site design and development policies. The strategy will include methods to integrate this tool into the County's existing development management program."* In addition, a second strategy was to coordinate "*State, local, and federal regulatory programs with Brunswick County taking lead enforcement role and fostering inter-local cooperation,"* and to "*Suggest policy changes and financial plan to accomplish."*

Technical Advisory Committees

In 2006, the NCCF received grant funding from the NOAA to develop LID based ordinances for Brunswick and New Hanover counties, and the City of Wilmington.

Beginning in January 2007, the two counties organized Technical Advisory Committees consisting of local government staff, engineers, planners, developers, and local stakeholders. The Coastal Federation also contracted with Larry Coffman, a widely recognized LID expert, and implementer of a successful LID program in Maryland. He offered a wealth of knowledge and assistance in writing the ordinances, resolutions, and design manuals being used by both counties. With one of the largest obstacles being how to engineer and regulate LID in the fast moving pace of land development, Mr. Coffman's experience proved invaluable. The committees immediately began working towards drafting resolutions to encourage Low Impact Development practices; writing LID design manuals for use by engineers and developers; and identifying obstacles to LID implementation.

The three jurisdictions are highly motivated to get the necessary tools in place to encourage LID developments within their boundaries. While having similar overall

objectives, development patterns in the two counties are very different, and thus each of the three tasks mentioned above took on slightly different structures during the development process.

Development Patterns and LID

Brunswick County is largely undeveloped, and while it is a quickly growing area there is still the latitude to implement plans to manage growth, protect open space, and create watershed management strategies for areas such as the Lockwood Folly River. Conversely, New Hanover County is relatively densely developed. With much of the county being incorporated within the city limits of Wilmington, the county as a whole is rapidly becoming an urban area.

Brunswick County is tailoring their resolution and design manual to emphasize strategies to incorporate LID within new development. The county is projecting that development will involve more large scale master plans rather than individual single lot residential or commercial developments. In keeping with those projections, LID practices can be employed over large tracts of land with planners and developers starting from an essentially clean slate.

New Hanover County and the City of Wilmington are more inclined to focus their LID efforts on retrofit opportunities, small scale new developments, and urban infill projects. While there are some large tracts within the county which still remain undeveloped, there is a higher premium on redevelopment and infill projects closer to the center of Wilmington. .

The challenges of implementing LID practices in each county were had considerably more in common than differences stated above might suggest. It became apparent during these discussion that the overall development patterns and future land use goals of the two areas was less critical in identifying challenges to LID implementation. The list of recognized issues could be generally categorized as development, but one primary focus area became the ability, or lack thereof, to obtain necessary stormwater permits.

Identification of the Problem

The ability of any project to gain permit approval is a vital component of all successful designs, stormwater management plans, and developments. While the technical advisory committees were looking for ways to promote and encourage LID designs, one challenge to LID design which was identified by nearly every stakeholder was that the permit process timetable would increase exponentially unless a process was created specifically for LID designs. The root of the issue was simply the number of BMPs being used. Conventional designs used small numbers of large BMPs, while LID designs used large numbers of small BMPs. This meant that

preparation of calculations, reports, and supplemental worksheets in addition to permit reviews, would all take more time simply because there were more structures to review, not to mention more structures to operate and maintain

It is important to note that in these communities, as well as across most of coastal North Carolina, the stormwater permitting process is implemented by the North Carolina Division of Water Quality (DWQ). The water quality regulations are also set by the State, and then often supplemented with local flood control ordinances which are regulated by each individual jurisdiction. So at the very least, two stormwater permits are required for most projects.

On the whole, the regulations themselves posed little or no problem for LID implementation; it was the design and review process that needed to change. Moreover, for the permit process to work efficiently, projects would need to begin preparing for LID permit submittals from day one, long before the permit reviewer would ever see the first submittal. Conceptually, if the stakeholders could agree on revised standards for engineering calculations and reporting, then this could be used as the foundation of the revamped permit process. Withers & Ravenel, with the support of the NCCF, involved the State of North Carolina as a stakeholder in this process, putting them on an equal playing field with the local jurisdictions.

Regulatory Cooperation

In a separate initiative, State officials in North Carolina are spending considerable effort developing LID standards, policies, and a State LID design manual, scheduled for publication in late 2008. Past efforts by the State have opened the door for LID. The most recent version of the State stormwater BMP design manual included references to LID and had some allowances and guidance information for LID projects. In 1995, the DWQ developed their first stormwater BMP design manual in response to Clean Water Act amendments. Recently, the DWQ has made significant revisions to the manual, reflecting improved technologies and updated construction practices. The major focus of the manual is to spell out required design parameters for structural BMPs.

In 2007, Withers & Ravenel participated in a second set of stakeholder meetings with the City of Wilmington, New Hanover and Brunswick counties, the NCCF, and the State DWQ to discuss the methodologies, assumptions, and equations which would be accepted for LID designs.

The goal of this second set of stakeholder meetings was to involve the State permit reviewers in the discussions related to the technical requirements of LID. Once those general principles were in place, the group could move on to discussing possible changes to the LID permit review process. In a limited number of meetings, the group was able to thoroughly examine the technical aspects of LID, as well as a myriad of

areas within the design and approval processes where current policies posed a challenge for LID implementation.

It was apparent in these stakeholder meetings that to facilitate LID designs in the short term, the LID permitting process in North Carolina would need to closely align with the current permit process for conventional designs. Larry Coffman's experience with LID permitting in Maryland was relevant and valuable during these discussions. With LID permitting, Brunswick and New Hanover counties and the City of Wilmington were blazing a new trail for stormwater permitting in the State, and that created numerous decision points that required concurrence from all regulatory stakeholders before any permitting plan could take shape.

The regulatory stakeholder meetings centered on calculation methods for LID submittals. In an effort to promote LID as well as standardize the calculation methods, Withers & Ravenel was contracted by the NCCF to develop a spreadsheet based computational tool for the calculations, which was later dubbed LID-EZ.

Developing LID-EZ

Withers & Ravenel, using experience in writing analytical tools for Wake County's volume based stormwater ordinance, stepped in to help remove the calculation obstacle from LID permitting. LID-EZ is a spreadsheet based program developed to aid in the implementation of Low Impact Development stormwater management strategies on residential and commercial development projects. LID-EZ utilizes basic pre and post development land use and storage device design information input by the user, combined with established engineering methods, to quantify the impact of proposed development on stormwater runoff rates, volumes, and pollutant loads. The calculations and results are presented in an easy-to-read format and can be tailored to include specific site and stormwater data to address compliance with specific local stormwater regulations.

The engineering equations and methodology used in LID-EZ are based on the Soil Conservation Service Curve Number Method (described in Part 630 of the Natural Resources Conservation Service (NRCS) National Engineering Handbook), Technical Release 55 (TR-55) also published by NRCS, and TR-20 for time of concentration calculations. A number of current State policies and recommendations are also used in the software.

Above and beyond the calculations, LID-EZ's value is that it is customized to the individual preferences and policies of the four regulatory agencies involved in this project. The discussion during the regulatory stakeholder meetings was instrumental in delivering a spreadsheet that could actually be completed by the engineer, reviewed by a permit reviewer, and checked for regulatory compliance in less time than it took to perform the same tasks for a conventional design.

The Uses of LID-EZ

LID-EZ has two distinct uses. The first is a quick calculator, which is a single sheet form design to compute preliminary estimates of required storage volumes to meet State regulations. This sheet is completely independent of the remainder of the program. Because the sheet is not intended for use with final permit submittals, there are significantly fewer input requirements, warning messages, and data verification tools. The objective of incorporating this sheet was to provide a tool for engineers and planners who wish to determine the total required storage volumes for development sites at the time of sketch plans or preliminary submittals. Because land planning is such a critical aspect to successful LID design, having the ability to quickly evaluate numerous site plans using only the information typically known at the sketch plan stage (land area, soil types, and basic residential or commercial site data) is helpful in optimizing land use and maximizing the benefit of LID devices.

The second function is the detailed computational tool. This section of LID-EZ requires more detailed user input necessary and the results are intended for permit submittals and review. The user entry data is divided into three main input forms. One each for pre-development conditions (land use, soil types, time of concentration), post development (with the same inputs are pre-development) and the third for BMPs and storage devices. After completing the first two sheets, LID-EZ will report accurate values for required storage volumes, pre and post development curve numbers and time of concentrations, total runoff volumes for numerous storms, and estimated peak flows for each storm event.

The storage input sheet requires four critical inputs: the type of device being used, the impervious area draining to the device, the volume provided, and the downstream BMP (if applicable). Using those three inputs, in combination with the results already reported after filling in the land use data, LID-EZ computes and reports all the remaining data required for permit review. Other than reporting the storage volumes required and provided, the results include summary data on the size of each BMP relative to the upstream drainage area, estimated pollutant removal efficiencies for the entire site, and anticipated post development curve numbers for each storm event after accounting for the storage volume.

The curve number output is critical because of the local flood control requirements. The regulatory stakeholder group realized that it may be difficult to achieve flood control for larger storm events using only LID devices. The curve number reported (calculated using methods established by the Maryland Department of the Environment) reflects post development land use as well as the impact of the numerous LID techniques and devices used in other areas of the watershed. This allows the developers to reduce the size of required flood control devices in proportion to the extent to which they apply LID practices to their site.

Specific Limitations in North Carolina

In using the curve number method, which is included in the current version of the State BMP manual as an allowable method for computing runoff volume from LID projects, calculation methods were being used which had not been widely used in North Carolina for permit approval. Although the core equations have been previously published and generally accepted, restrictions were needed on the limit to which certain variables could be employed.

These areas of the curve number method were discussed during the regulatory stakeholder meetings. In establishing allowable input ranges, we consulted papers from many experts on the curve number method, used our experience from the Wake County stakeholder meetings, and consulted with staff from the Soil Conservation Service. The information we gathered was used throughout the regulatory stakeholder meeting. The stakeholder discussions were, to our knowledge, the first in depth analysis of how to take LID from a conceptual planning tool to a viable permitting option in North Carolina.

Some unique aspects of LID-EZ were included in the program to simplify input parameters. These included restricting pre-development land use to woods, pasture, or impervious area, and restricting post development land use to woods, open space, residential lots, connected impervious area, and disconnected impervious area. A separate input section includes information on the residential lots, such as proposed impervious area and preserved woods on each lot, resulting in computations which generate a composite curve number for residential areas.

Other decisions were made to assist with permit review and reduce the number of potential errors in the submittals. This included limits on sheet flow length, restrictions on the use of impervious area in pre-development conditions, and inclusion of multiple warning and error messages to alert the applicant of potential errors. The programming behind LID-EZ includes numerous checks for consistency between pre-development and post-development land areas, composition of soils, and calculators to assure that adequate storage volumes are provided to meet State standards.

Recent Updates to LID-EZ

The original development of LID-EZ was limited to holistic calculations for entire tracts of land. After consulting with State regulatory officials, we identified the need for more detailed information, resulting in the addition of input fields for the impervious area drainage to individual BMPs and the identification of downstream BMPs. In this case, two simple inputs significantly increase the potential for high quality LID designs.

Conventional stormwater permitting in North Carolina requires detailed information about each structural BMP to ensure that minimum design requirements are met for volume control and pollutant removal. Using the two additional inputs, we were able to add computational checks to ensure that the storage volume provided was proportional to the impervious area draining to the device. Impervious area was also used to compute pollutant loading figures for total suspended solids, nitrogen, phosphorous, fecal coliform and temperature. Combining pollutant removal data previously published by the State with the user input of the downstream BMP, we could reconstruct the treatment train effect of multiple BMPs in series and report the anticipated pollutant removal rates for the entire site.

In addition, we are updating the spreadsheet with tools enabling the user to receive credit for pervious pavement installations in accordance with DWQ guidance, and we are developing a separate program targeted specifically at the analysis of retrofit opportunities.

Withers & Ravenel is currently in the process of preparing a presentation and an intensive day long training session for regulators from the Division of Water Quality. We hope to educate permit reviewers about the equations and methods being used, and establish a permit application process specifically for LID projects in coastal North Carolina.

The current version of the spreadsheet has been distributed on a case by case basis to a limited number of engineers. The revised spreadsheet, with added functionality, will be released for use in late September 2008 in conjunction with publication of LID design manuals for Brunswick and New Hanover counties.

Conclusions

The end result of the stakeholder and task force meetings was multi faceted. On one level, we achieved concurrence between all the local agencies, as well as buy-in from the State regulators on all of the issues known at the time. On an entirely different level, but perhaps even more importantly, we had initiated a long term dialogue between State regulators, local officials, and the development community which continues today and is a key component in establishing a more complete approach to LID design and permitting

Since the conclusion of the stakeholder meetings, it has become easier to achieve consensus on key decision points in development of LID tools, largely due to the fact that each stakeholder in the regulatory meetings was open minded and believed that Low Impact Development would lead to a better living environment, and had a willingness to make LID happen.

While we are still in the process of product development, we look back with satisfaction on the accomplishments of the past 18 months. Significant progress has been made on LID resolutions in each community, which is a key step in promoting

LID for new developments. The design manuals are nearly complete, and the spreadsheet program is already in its second version. We continue to increase the number of tools and resources available to local developers and are looking forward to the day when LID designs become the standard for high quality stormwater management plans in North Carolina.

References:

State of the Coast Report 2008, *The North Carolina Coastal Federation*, 2008

Low Impact Development for the North Carolina Coast, *The North Carolina Coastal Federation*, 2008

Lockwood Folly River Water Quality Strategy, *Lockwood Folly Watershed Roundtable*, 2007.

About the Author

Hunter Freeman is a stormwater managerl in the water resources department in the Cary, North Carolina office of Withers & Ravenel. He has ten years of engineering experience, specializing in hydrology, Low Impact Development design, stormwater management and flood plain management. He has worked on stormwater management plans for projects throughout North Carolina, and has also assisted multiple piedmont and coastal municipalities with Low Impact Development (LID) ordinance implementation and specific LID software needs. He has served on the Wake County Collaborative Stormwater Management Task Force, Brunswick County and New Hanover County LID Technical Advisory Committees, and recently completed his duties on the Wake County Stormwater Ordinance Implementation Team.

The Runoff Reduction Method

Kelly A. Collins*[1], Dave Hirschman[2], Greg Hoffmann[3], and Tom Schueler[4]

[1] *Water Resources Engineer, Center for Watershed Protection, 8390 Main Street, 2nd Floor, Ellicott City, MD 21043*
[2] *Program Director, Center for Watershed Protection, 1107 Calhoun Street, Charlottesville, VA 22901*
[3] *Program Director, Center for Watershed Protection, 8390 Main Street, 2nd Floor, Ellicott City, MD 21043*
[4] *Coordinator, Chesapeake Stormwater Network, 117 Ingleside Avenue, Baltimore, MD 21228*

* *Corresponding Author email: kac@cwp.org*

ABSTRACT

In 2008, the Center for Watershed Protection and the Chesapeake Stormwater Network developed the Runoff Reduction Method. The method was developed as part of a project to research and update best management practice (BMP) performance and, in particular, ascertain the ability of various BMPs to reduce post-development runoff volumes. The method focuses on the capability of conventional and innovative stormwater management practices (e.g., permeable pavement, green roofs, rainwater harvesting, bioretention, downspout disconnection, etc.) to reduce runoff, as well as remove pollutants, and incorporates built-in incentives for environmental site design, such as forest and open space preservation. Because of the high runoff reduction capabilities of various site design and innovative stormwater practices, implementing these innovative practices at a site reduces the overall number and size of structural BMPs required. This approach helps put innovative stormwater management practices on a level playing field with conventional stormwater management practices, such as wet and dry ponds.

Currently, various state programs are in the process of using or adopting the Runoff Reduction Method as part of regulatory and non-regulatory programs. The Virginia Department of Conservation and Recreation (DCR) is integrating the Runoff Reduction Method into proposed stormwater management regulations and an updated stormwater management handbook. The Georgia Department of Natural Resources is modifying the method for a new Coastal Stormwater Management Manual Supplement. The State of Delaware is using the concept of runoff reduction in proposed statewide regulations. With the incorporation of the Runoff Reduction Method into these programs, communities are poised for the wide-spread implementation of low impact development and innovative stormwater management practices on development sites.

Keywords: Runoff reduction, volume, nutrients, site design, BMPs, LID, regulations, Virginia

INTRODUCTION

The Runoff Reduction Method was developed in early 2008 by the Center for Watershed Protection (CWP) and the Chesapeake Stormwater Network (CSN) in order to promote better stormwater site design and as a compliance tool for Virginia's proposed stormwater regulations. The method focuses on the capability of both conventional and innovative stormwater management practices (e.g., permeable pavement, green roofs, rainwater harvesting, bioretention, downspout disconnection, etc.) to reduce runoff and remove pollutants, and incorporates built-in incentives for site design approaches that preserve forest and open space.

Runoff reduction is defined as the average annual reduction in stormwater runoff volume. Various BMPs are capable of reducing the overall volume of runoff based on the post-development condition. Runoff can be reduced via canopy interception, soil infiltration, evaporation, transpiration, rainfall harvesting, engineered infiltration, or extended filtration. Depending on the BMP or series of BMPs, runoff reduction processes can be combined with processes that remove pollutants through settling, filtering, adsorption, biological update, or other mechanisms. The Runoff Reduction Method includes BMPs that achieve runoff reduction (RR), pollutant removal (PR), or both.

The field of stormwater management has recently seen many new terms being adopted to describe related and overlapping approaches and philosophies. Runoff reduction describes a process or function of BMPs. As such, it is an important components of other stormwater terms, such as low impact development (LID), environmental site design (ESD), and green infrastructure. For the purposes of this paper, the term runoff reduction will be used, but the other terms are also applicable. Independent of what it is called, the suite of practices and site design techniques that reduce runoff volumes has the potential to reduce the size and number of structural or conventional best management practices (BMPs) and put innovative practices on a more level playing field with the commonly used wet and dry ponds.

The Runoff Reduction approach also moves beyond managing stormwater solely for peak rate and water quality treatment by attempting to replicate a more natural (or pre-development) hydrologic condition. More specifically, it moves towards a more comprehensive approach that addresses runoff volume, duration, velocity, frequency, groundwater recharge, and protection of stream channels. When used in conjunction with site pollutant limits, the approach can help meet the pollutant reduction goals (i.e. nutrient strategies, TMDLs) of the larger watershed.

THE METHOD

The Runoff Reduction Method relies on a three-step compliance procedure, as described below:

Step 1: Reduce Stormwater Runoff by Design

Step one focuses on implementing better site planning and design techniques during the early phases of site layout. The goal is to minimize impervious cover and mass grading, and maximize retention of forest cover, natural areas and undisturbed soils (especially those most conducive to landscape-scale infiltration). The Runoff Reduction Method assigns runoff coefficients for forest, disturbed soils, and impervious cover to calculate a site-specific target treatment volume.

Step 2: Reduce Volume of Post-Construction Stormwater Runoff. In this step, a designer uses combinations of small-scale, distributed and conventional practices that are effective at reducing runoff from the site. In each case, the designer estimates the area to be treated by each runoff reduction practice to incrementally reduce the required treatment volume for the site. The designer is encouraged to use these practices in series within individual drainage areas (such as rooftop disconnection to a grass swale to a bioretention area) in order to achieve a higher level of runoff reduction.

Step 3: Capture and Treat Remaining Stormwater Runoff.
In this step, the designers apply pollutant reduction values to the runoff reduction practices used in Step 2. If the target pollutant limits are not reached, the designer can select additional, conventional BMPs - such as filtering practices, wet ponds, and stormwater wetlands - to meet the remaining pollutant reduction requirements.

<table>
<tr><th>Step 1: Site Planning and Design Practices</th><th>Step 2: Runoff Reduction (RR) Practices</th><th>Step 3: Pollutant Removal (PR) Practices</th></tr>
<tr><td>Forest Conservation</td><td>Sheetflow to Conservation Area or Filter Strip</td><td>Filtering Practice</td></tr>
<tr><td rowspan="2">Site Reforestation</td><td rowspan="3">Rooftop Disconnection:
▪ Simple
▪ To Soil Amendments
▪ To Rain Garden or Dry Well
▪ To Rain Tank or Cistern</td><td>Constructed Wetland</td></tr>
<tr><td>Wet Swale</td></tr>
<tr><td>Soil Restoration (combined with or separate from rooftop disconnection)</td><td rowspan="2">Wet Pond</td></tr>
<tr><td rowspan="4">Site Design to Minimize Impervious Cover & Soil Disturbance</td><td>Green Roof</td></tr>
<tr><td colspan="2">Grass Channels
Permeable Pavement</td></tr>
<tr><td colspan="2">Bioretention</td></tr>
<tr><td colspan="2">Dry Swale (Water Quality Swale)
Infiltration</td></tr>
<tr><td colspan="2">Extended Detention (ED) Pond</td></tr>
<tr><td colspan="3">Practices in shaded cells achieve both Runoff Reduction (RR) and Pollutant Removal (PR) functions</td></tr>
</table>

Figure 1. Practices Included in the Runoff Reduction Method

In reality, the process is iterative for most sites. When compliance cannot be achieved on the first try, designers can return to prior steps to explore alternative combinations

of site planning, site design, runoff reduction practices, and pollutant removal practices to achieve compliance. A possible Step 4 would involve paying an offset fee (or fee-in-lieu payment) to compensate for any pollutant load that cannot feasibly be met on particular sites. A related, but simpler option would be to allow a developer to conduct an off-site mitigation project in lieu of full on-site compliance. **Figure 1** includes a list of site design and stormwater practices that can be used for each step.

RUNOFF COEFFICIENTS AND TREATMENT VOLUME

The negative impacts of increased impervious cover (IC) on receiving water bodies have been well documented (CWP 2003, Walsh et al. 2004; Shuster et al. 2005; Bilkovic et al. 2006). Due to widespread acceptance of this relationship, IC has frequently been used in watershed and site design efforts as a chief indicator of stormwater impacts. More recent research, however, indicates that other land covers, such as disturbed soils and managed turf, also impact stormwater quality (Law et al, 2008). Numerous studies have documented the impact of grading and construction on the compaction of soils, as measured by increase in bulk density, declines in soil permeability, and increases in the runoff coefficient (OCSCD et al, 2001; Pitt et al, 2002; Schueler and Holland, 2000). These areas of compacted pervious cover (lawn or turf) have a much greater hydrologic response to rainfall than forest or pasture. Further, highly managed turf can contribute to elevated nutrient loads. Typical turf management activities include mowing, active recreational use, and fertilizer and pesticide applications (Robbins and Birkenholtz 2003).

An analysis of Virginia-specific data from the National Stormwater Quality Database (Pitt et al. 2004) found that runoff from monitoring sites with relatively low IC residential land uses contained significantly higher nitrogen concentrations ($\alpha = 0.05$) than sites with higher IC non-residential uses (CWP & VA DCR, 2007). This suggests that residential areas with relatively low IC can have disturbed and intensively managed pervious areas that contribute to elevated nutrient levels.

The failure to account for the altered characteristics of disturbed urban soils and managed turf can result in an underestimation of stormwater runoff and pollutant loads generated from urban pervious areas. Therefore, the computation and compliance system for stormwater runoff should take into account impervious cover as well as other land cover types.

The runoff coefficients provided in **Table 1** were derived from research by Pitt et al (2005), Lichter and Lindsey (1994), Schueler (2001a), Schueler, (2001b), Legg et al (1996), Pitt et al (1999), Schueler (1987) and Cappiella et al (2005). As shown in this table, the effect of grading, site disturbance, and soil compaction greatly increases the runoff coefficient compared to forested areas.

The Runoff Reduction Method uses runoff coefficients to calculate a site-specific target treatment volume (Tv). A site's Tv is calculated by multiplying the "water quality" rainfall depth by the three site cover runoff coefficients (forest, disturbed

soils, and impervious cover) present at the site, as shown in **Figure 2**. The "water quality" rainfall depth is often defined as the rainfall depth associated with 90 percent of runoff-producing storm events on an average annual basis. Use of this depth as a design requirement for stormwater BMPS ensures that 90% of all storm events will be completely treated, as will the first portion of all larger storm events. The 90% storm event approach to defining the treatment volume is widely accepted and is consistent with several state stormwater manuals (MDE, 2000, ARC, 2002, NYDEC, 2001, VTDEC, 2002, OME, 2003, MPCA, 2005).

Table 1. Site Cover Runoff Coefficients (Rv)

Soil Condition	Runoff Coefficient
Forest Cover (R_{vF})	0.02 to 0.05*
Disturbed Soils/Managed Turf (R_{vT})	0.15 to 0.25*
Impervious Cover (R_{vI})	0.95
*Range dependent on original Hydrologic Soil Group (HSG) Forest A: 0.02 B: 0.03 C: 0.04 D: 0.05 Disturbed Soils A: 0.15 B: 0.20 C: 0.22 D: 0.25	

$$T_v = \frac{P \times \left[\left(R_{vI} \times \%I \right) + \left(R_{vT} \times \%T \right) + \left(R_{vF} \times \%F \right) \right] \times SA}{12}$$

Where
T_v = Runoff treatment volume in acre feet
P = Depth of rainfall for "water quality" event
R_{vI} = runoff coefficient for impervious cover[1]
R_{vT} = runoff coefficient for turf cover or disturbed soils[1]
R_{vF} = runoff coefficient for forest cover[1]
% I = percent of site in impervious cover (fraction)
%T = percent of site in turf cover (fraction)
%F = percent of site in forest cover (fraction)
SA = total site area, in acres
[1] R_v values from **Table 1.**

Figure 2: Determining the Stormwater Treatment Volume

The proposed treatment volume has several distinct advantages when it comes to evaluating runoff reduction practices and sizing BMPs. In effect, Tv provides an objective measure to gage the aggregate performance of runoff reduction practices and conventional BMPs together using a common currency (runoff volume). Calculating the Tv explicitly acknowledges the difference between forest and turf cover and disturbed and undisturbed soils, which creates incentives to conserve forests and reduce mass grading. Further, runoff is a direct function of impervious cover and disturbed soils, which provides designers incentives to minimize both at a

development site. Additionally, the Tv captures approximately 90% of the annual runoff volume from the site, and partially captures for larger storms. Managing this volume through the Runoff Reduction Method provides effective treatment of pollutants for a range of storm events, which is important since the first flush effect has been found to be modest for many pollutants (Pitt et al 2005).

DOCUMENTING BMP PERFORMANCE

After implementing environmental site design and site planning techniques to minimize the site treatment volume generated, the next steps of the Runoff Reduction Method involve the selection of BMPs to reduce Tv, and in effect, the pollution load of a site. CWP and CSN made a significant effort through an extensive literature search to identify the capabilities of various BMPs to reduce overall runoff volume (*runoff reduction*) in addition to pollutant concentrations (*pollutant removal*). Historically, BMP performance has been evaluated according to the pollutant removal efficiency of a practice. In some cases, this underreported the full capabilities of BMPs to reduce pollutant loads. Depending on the method used to calculate pollutant removal, reported removal efficiencies of stormwater best management practices (BMPs) can vary widely and are often inconsistent. Further, removal efficiencies do not always address runoff volume reductions in BMPs (Strecker et al, 2004; Jones et al, 2008). More recent BMP performance research has focused on runoff reduction as well as overall pollutant removal. In order to isolate the pollutant removal mechanisms of a BMP apart from runoff reduction, EMC based pollutant removal efficiencies were researched.

For several practices, there were a limited number of studies available that reported runoff reduction or EMC based nutrient removal efficiencies. As a result, some of the values listed in the tables below will be subject to change as more studies and data become available. The values represent the authors' best judgment based on currently-available information. Further documentation on the derivation of these values can be found in Hirschman et al, 2008.

RUNOFF REDUCTION PRACTICES

As described earlier in this paper, various BMPs are capable of reducing the overall volume of runoff based on the post-development condition. Runoff can be reduced via canopy interception, soil infiltration, evaporation, transpiration, rainfall harvesting, engineered infiltration, or extended filtration. Extended filtration includes bioretention or dry swales with underdrains that delay the delivery of stormwater from small sites to the stream system by six hours or more.

Runoff reduction data were limited for most practices. However, many recent studies have started documenting runoff reduction performance. Based on the research findings, runoff reduction rates were assigned to various BMPs, as shown in **Table 2**. A range of values represents the median and 75th percentile runoff reduction rates based on the literature search. Several BMPs reflected moderate to high capabilities

for reducing annual runoff volume. Others – including filtering, wet swales, wet ponds, and stormwater wetlands -- were found to have a negligible affect on runoff volumes, and were not assigned runoff reduction rates. The accuracy of these runoff reduction numbers can depend upon the characteristics and BMP geometry of specific sites, so specific design criteria are associated with each BMP to ensure that the runoff reduction numbers are appropriately applied.

Table 2. Runoff Reduction for various BMPs (based on average annual rainfall in the Virginia Piedmont area)

Practice	Runoff Reduction (%) *
Green Roof	*45 to 60*
Rooftop Disconnection	*25 to 50*
Raintanks and Cisterns	*40*
Permeable Pavement	*45 to 75*
Grass Channel	*10 to 20*
Bioretention	*40 to 80*
Dry Swale	*40 to 60*
Wet Swale	*0*
Infiltration	*50 to 90*
ED Pond	*0 to 15*
Soil Amendments	*50 to 75*
Sheetflow to Open Space	*50 to 75*
Filtering Practice	*0*
Constructed Wetland	*0*
Wet Pond	*0*

*Range of values is for median (Level 1) and 75th percentile (Level 2) designs

POLLUTANT REMOVAL PRACTICES

In order to isolate the pollutant removal mechanisms of a BMP and offer a better approach to assessing BMP pollutant removal performance (as distinct from runoff reduction), EMC based pollutant removal rates for nitrogen and phosphorus were researched. EMC based pollutant removal is accomplished via processes such as settling, filtering, adsorption, and biological uptake. This does not account for changes in the overall volume of runoff entering and leaving the BMP.

Based on the research findings, EMC-based pollutant removal rates were assigned to various BMPs, as shown in **Table 3**. A range of values represents the median and 75th percentile runoff reduction rates based on the literature search. It should be noted that the data used to estimate pollutant removal were derived from practices in good condition; most studies focused on BMPs that were constructed within three years of monitoring. Further, the actual EMC pollutant removal performance can be strongly influenced by the influent quality. As with runoff reduction, since pollutant removal rates are dependent on site characteristics and BMP geometry, these EMC-based pollutant removal numbers are associated with specific design criteria.

Table 3. EMC-based pollutant removal for various BMPs

Practice	Total Phosphorus Pollutant Removal (%)*	Total Nitrogen Pollutant Removal (%)*
Green Roof	*0*	*0*
Disconnection	*0*	*0*
Raintanks and Cisterns	*0*	*0*
Permeable Pavement	*25*	*25*
Grass Channel	*15*	*20*
Bioretention	*25 to 50*	*40 to 60*
Dry Swale	*20 to 40*	*25 to 35*
Wet Swale	*20 to 40*	*25 to 35*
Infiltration	*25*	*15*
ED Pond	*15*	*10*
Soil Amendments	*0*	*0*
Sheetflow to Open Space	*0*	*0*
Filtering Practice	*60 to 65*	*30 to 45*
Constructed Wetland	*50 to 75*	*25 to 55*
Wet Pond	*50 to 75*	*30 to 40*

*Range of values is for median (Level 1) and 75th percentile (Level 2) designs

ACCOUNTABILITY FOR BETTER BMP DESIGN

A range of performance values associated with design are introduced in the Runoff Reduction Method (see **Tables 2 and 3**). A standard, or Level 1 design can be expected to achieve the median value of Runoff Reduction and Pollutant Removal from the research), while an enhanced, orLevel 2 design achieves the 75th percentile values.

Based on the evaluation of BMP performance in the literature, design factors – such as sizing, pretreatment, flow path geometry, vegetative condition, and treatment processes – that enhance nutrient pollutant removal and runoff reduction of BMPs were isolated. These design factors were then applied to Level 1 and Level 2 BMPs. In order to achieve established RR and PR rates, the specific design factors associated with these levels must be met.

The scientific rationale and assumptions used to assign sizing and design features to the standard and enhanced BMP levels involved identifying the "standard" design features that should be included in all designs (i.e., not directly related to differential nutrient removal or runoff reduction rates), a review of individual BMP studies, and the modification of design point tables in the *Stormwater Retrofit Manual, Appendix B* (Schueler et al, 2007) to reflect the more specific goal of reducing runoff and nutrient removal for BMPs.

Importantly, it should be understood that the assigned rates are based on the assumption that BMP designs will meet certain "eligibility criteria." That is, the BMPs will be located and designed based on appropriate site conditions and limitations with regard to soils, slopes, available head, flow path, and other factors.

The specific design factors and eligibility criteria for various BMPs are detailed in the Runoff Reduction Technical Memo (Hirschman et al, 2008).

TRANSFERABILITY OF THE RUNOFF REDUCTION CONCEPT

While the Runoff Reduction Method was originally developed in tandem with the Virginia Department of Conservation and Recreation (DCR) efforts to update the stormwater regulations and handbook, the concept is widely applicable to other state and local stormwater planning procedures. The focus on runoff volume as the common currency for BMP evaluation is gaining wider acceptance across the county (U.S. EPA, 2008). Currently, various state programs are in the process of using or adopting methods similar to the Runoff Reduction Method as part of regulatory and non-regulatory programs. With the incorporation of the Runoff Reduction Method into these programs, communities are poised for the wide-spread implementation of runoff reduction practices on development sites.

- *Virginia* – The Virginia DCR is integrating the Runoff Reduction Method into proposed stormwater management regulations and an updated stormwater management handbook. The method focuses on compliance to meet site-based pollutant load limits, aimed at limiting the total nutrient load leaving a new development site. A site design compliance spreadsheet was developed to ensure runoff reduction and nutrient loading requirements for the site are met.

- *Georgia* - The Georgia Department of Natural Resources is modifying the Runoff Reduction Method for a new Coastal Stormwater Management Manual Supplement. The manual requires that the stormwater runoff volume from the 1.2" rainfall event (85th percentile event) be retained, reused, or reduced to the maximum extent practical, on a new development or redevelopment site. A runoff reduction volume is calculated based on site impervious cover, and volume reduction "credits" are given to green infrastructure and stormwater management practices that reduce overall runoff.

Additional efforts to incorporate the concept of runoff reduction into updated stormwater regulations and design manuals are underway in the States of Delaware, Maryland, and the District of Columbia (Capiella et al., 2007; DeBlander et al., 2008; MSC, 2008). The *Pennsylvania Stormwater Best Management Practices Manual* (PA DEP, 2006) already incorporates standards for volume control achieved by structural and nonstructural BMPs.

CONCLUSION

Clearly, the concept of runoff reduction marks an important philosophical milestone that will help define the next generation of stormwater design. The promise of runoff reduction is that the benefits go beyond water quality improvement. If site and stormwater designs can successfully implement runoff reduction strategies, then they will do a better job at replicating a more natural (or pre-development) hydrologic

condition. This goes beyond peak rate control to address runoff volume, duration, velocity, frequency, groundwater recharge, and protection of stream channels. Important future work will involve integrating the runoff reduction concept with stormwater requirements for channel protection and flood control, so that stormwater criteria can be presented in a unified approach.

REFERENCES:

Atlanta Regional Commission (ARC). (2001). *Georgia Stormwater Design Manual,* Volume 2: Technical Handbook. Atlanta, GA.

Bilkovic, D.M., Roggero, M., Hershner, C. H., and Havens, K. H. (2006). Influence of Land Use on Macrobenthic Communities in Nearshore Estuarine Habitats. *Estuaries and Coasts*, 29(6B), 1185-1195.

Capiella, K., Hirschman, D.H., and Kitchell, A.C. (2007). *Memorandum: Proposed Stormwater Philosophy to Guide Revisions to the Sediment and Stormwater Regulations (Delaware).*

Cappiella, K., Schueler, T., and Wright, T. (2005). *Urban Watershed Forestry Manual.* Part 2: Conserving and Planting Trees at Development Sites. USDA Forest Service, Newtown Square, PA.

Center for Watershed Protection (CWP). (2003). *Impacts of IC on Aquatic Systems*. Center for Watershed Protection, Inc., Ellicott City, MD.

Center for Watershed Protection (CWP) and Virginia Department of Conservation & Recreation (VA DCR). (2007). *Virginia Stormwater Management: Nutrient Design System, Version 1.2.* June 23, 2007.

DeBlander, B., Caraco, D., and Harper, G. (2008). *Memorandum: The District of Columbia Stormwater Management Guidebook Expansion, Issue Paper #1* (in production).

Hirschman, D.H, Collins, KA, and Schueler, T. (2008). Technical memorandum: the Runoff Reduction Method. Center for Watershed Protection and the Chesapeake Stormwater Network.

Jones, J., Clary, J., Strecker, E., and Quigley, M. (2008). 15 Reasons you should think twice before using percent removal to assess BMP performance. *Stormwater Magazine*. Jan/Feb 2008.

Law N.L., Cappiella, K., and Novotney, M.E. (2008). The need to address both impervious and pervious surfaces in urban watershed and stormwater management. *Journal of Hydrologic Engineering* (accepted).

Legg, A. Bannerman, R., and Panuska, J. (1996). Variation in the relation of runoff from residential lawns in Madison, Wisconsin. *USGS Water Resources Investigations Report 96-4194*.

Lichter J. and Lindsey, P. (1994). Soil compaction and site construction: assessment and case studies. *The Landscape Below Ground*. International Society of Arborculture

Maryland Department of the Environment (MDE). (2000). *Maryland Stormwater Design Manual*. Baltimore, MD.

Maryland Stormwater Consortium (MSC). (2008). Core environmental site design principles for the implementation of the Maryland Stormwater Management Act of 2007. Chesapeake Stormwater Network. Baltimore, MD

Minnesota Pollution Control Agency (MPCA). (2005). *Minnesota Stormwater Manual*. Minneapolis, MN

New York State Department of Environmental Conservation (NYDEC). (2001). *New York State Stormwater Management Design Manual*. Prepared by the Center for Watershed Protection. Albany, NY.

Ocean County Soil Conservation District (OCSCD), Schnabel Engineering Associates, Inc. and U.S. Department of Agriculture (USDA) Natural Resources Conservation Service. (2001). *Impact of Soil Disturbance During Construction on Bulk Density and Infiltration in Ocean County, New Jersey*. OCSCD, Forked River, NJ.

Ontario Ministry of the Environment. (OME) (2003). *Final Stormwater Management Planning and Design Manual.* Aquafor Beech Ltd. Toronto, Canada

Pennsylvania Department of Environmental Protection (PA DEP). (2006). *Pennsylvania Stormwater Best Management Practices Manual.*

Pitt, R., Chen, S., Clark, S., and Lantrip, J. (2005). Soil structure effects associated with urbanization and the benefits of soil amendments. World Water and Environmental Resources Congress. Conference Proceedings. American Society of Civil Engineers. Anchorage, AK.

Pitt, R., Maestre, A., and Morquecho, R. (2004). "National Stormwater Quality Database. Version 1.1." <http://rpitt.eng.ua.edu/Research/ms4/Paper/Mainms4paper.html> (Jan. 28, 2008).

Pitt, R., Chen, S., and Clark, S. (2002). "Compacted Urban Soils Effects on Infiltration and Bioretention Stormwater Control Designs."*Proceedings of the Ninth International Conference on Urban Drainage: Global Solutions for Urban Drainage*, American Society of Civil Engineers, Reston, VA.

Pitt, R., Lantrip, J. and Harrison, R. (1999). Infiltration through disturbed urban soils and compost-amended soil effects on runoff quality and quantity. Research Report EPA/600/R-00/016. Office of Research and Development. U.S. EPA. Washington, D.C.

Robbins, P., and Birkenholtz, T. (2003). "Turfgrass revolution: measuring the expansion of the American lawn." *Land Use Policy*, 20, 181-194.

Schueler, T. (1987). Controlling urban runoff: a practical manual for planning and designing urban best management practices. Metropolitan Washington Council of Governments. Washington, DC.

Schueler, T., Hirschman, D., Novotney, M, and Zielinski, J. (2007). Urban Stormwater Retrofit Practices. Center for Watershed Protection, Ellicott City, MD.

Schueler, T.R., and Holland, H.K. (2000). "The Compaction of Urban Soils." *The Practice of Watershed Protection,* Center for Watershed Protection, Ellicott City, MD, 210-214.

Schueler, T. (2001a). The compaction of urban soils. *Watershed Protection Techniques*. 3(2): 661-665.

Schueler, T. (2001b). Can urban soil compaction be reversed? *Watershed Protection Techniques.* 3(2): 666-669.

Shuster, W.D., Bonta, J., Thurston, H., Warnemuende, E., and Smith, D. R. (2005). Impacts of impervious surface on watershed hydrology: A review. *Urban Water Journal,* 2(4), 263-275.

Strecker, E., Quigley, M., Urbonas, B., and Jones, J .(2004). Stormwater management: State-of-the-art in comprehensive approaches to stormwater. *The Water Report.* Issue #6. Envirotech Publishers Inc., Eugene, OR.

U.S. Environmental Protection Agency (USEPA). (2008). Urban BMP Performance Tool (online). http://cfpub.epa.gov/npdes/stormwater/urbanbmp/bmpeffectiveness.cfm.

Walsh, C.J. (2004). Protection of In-Stream Biota from Urban Impacts: Minimize Catchment Imperviousness or Improve Drainage Design? *Marine and Freshwater Research,* 55(3), 317-326.

Vermont Department of Environmental Conservation (VTDEC). (2002). The Vermont Stormwater Management Manual. Vermont Agency of Natural Resources.

Unit Process Modeling of Stormwater Flow and Pollutant Sorption in a Bioretention Cell

Zhuangxiang He and Allen P. Davis
Department of Civil and Environmental Engineering,
University of Maryland, College Park, MD 20742

Abstract

Bioretention is a mulch/soil/plant-based low impact development facility employed to collect, store, infiltrate and treat urban stormwater runoff. This work focuses on modeling to describe the fate of stormwater and the adsorption of pollutants in bioretention facilities. A two dimensional Variable Saturated Flow and Transport Model is developed based on partial differential equation modes in COMSOL Multiphysics, in which both fluid flow and solute transport are under transient analysis. Model results indicate that the outflow volume is less than the inflow due to the storage and the extent of initial unsaturation in the media. The outflow volume from loamy sand media (with larger K_s) is larger than that from sandy loam media. The flow peak is reduced. Concentrations of naphthalene (NP) and pyrene (PY) in runoff vary with depth and most NP and PY (> 90%) is removed within about 3 cm media depth.

1 Introduction

Bioretention, also known as rain gardens, is a low-impact development (LID) best management practice (BMP), providing a mulch/soil/plant-based trapping media to collect, store, infiltrate and treat urban stormwater runoff. A diagram of a bioretention cell is presented in Figure 1. Besides a thin mulch layer on the top of the cell, the primary media consists of a sand/soil/organic matter mixture with high hydraulic conductivity, surrounded by native (possibly less permeable) soils. A vegetative layer provides evapotranspiration, pollutant uptake, and enhanced porosity of the planting soil. A ponding area serves as a storage reservoir, and thereafter extends the time for water to infiltrate into the media.

Bioretention was developed to improve post-development hydrology. Field studies have demonstrated the ability of bioretention to increase the lag time and reduce the peak flow rates as well as the total volume of effluent water (Dietz and Clausen 2005; Hunt *et al*. 2006; Davis 2008). A variety of numerical models, describing variably saturated flow by Richards' equation, have indicated that the primary factors influencing the hydraulic performance of infiltration systems similar to bioretention are initial water content, characteristics of infiltration media and surrounding soils, stormwater loading and duration (Duchene *et al*. 1994; Harada and Ichikawa 1994; Li *et al*. 1999; Sansalone and Teng 2004, 2005). However, limited modeling work is available to show the impacts of these factors on the performance of a bioretention cell.

Recently, bioretention was found to improve the quality of stormwater runoff before discharge to receiving waters. Pollutants in runoff are removed mainly through physical and chemical mechanisms during rainfall events, such as adsorption. After rainfall events, captured pollutants continue to be impacted by chemical or biological processes. Laboratory and field work have been completed indicating that bioretention is a promising management practice for controlling several urban pollutants, including total suspended solids (Hsieh and Davis 2005a, 2005b), nutrients (Davis *et al*. 2006; Hsieh *et al*. 2007), heavy metals (Davis *et al*. 2001, 2003; Li and Davis 2008), and polycyclic aromatic hydrocarbons (PAHs) (Hong *et al*. 2006). However, in order to continue the maturation of BMP research, comprehensive modeling ventures must be undertaken to complement ongoing experimental and monitoring programs. This work focuses on modeling to describe the fate of stormwater flow and the adsorption of two common PAH compounds, i.e., naphthalene (NP) and pyrene (PY), in a bioretention cell.

2 Methodology

2.1 *Geometry*

Figure 2 shows the geometry of a bioretention cell with width of 3.6 m and height of 0.8 m. Water is ponded above the surface layer when the media is saturated. The circle within bioretention media subdomain represents the underdrain with a diameter of 0.3 m. The height of the ponding space is 0.3 m, as bioretention practices are often designed to treat ponding water no higher than 0.25 m. Because the boundary conditions between the soil media and surrounding soils are unclear, a large modeling geometry is generated by extending the surrounding soil subdomain for 4.2 m wide on each side and 1.2 m deep under the bioretention media. The mulch and vegetated layers are not included in this simple representation.

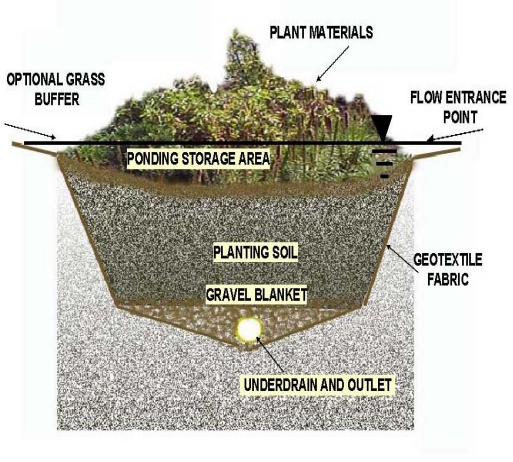

Figure 1. Typical bioretention cell (DER, 2001)

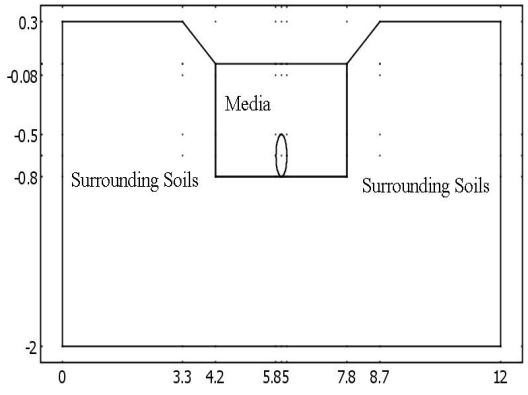

Figure 2. Geometry of a bioretention cell (Unit: meter)

2.2 Governing Equations

A two dimensional Variable Saturated Flow and Transport Model is developed based on partial differential equation modes in COMSOL Multiphysics (formally named FEMLAB). Richards' Equation Application Mode and Solute Transport Application Mode in the Earth Science Module are employed to simulate both subsurface flow and pollutant fates (COMSOL AB, 2005), using a unit operations approach to consider mass balances under unsteady state conditions.

Subsurface flow and solute transport are linked by fluid velocities from Darcy's law.

$$\mathbf{u} = K_s k_r \nabla(H_p + D) \tag{1}$$

Here, **u** is a vector of directional velocities (m/d). In the two dimensional modeling, *u* and *v* represent the x- and y- velocity, respectively. *D* represents vertical elevation (e.g., *x* or *y*).

The Richards' equation application mode uses the Richards' equation interface to describe the nonlinear relationship between retention and permeability properties according to van Genuchten. Richards' equation governs the saturated-unsaturated flow of water in soil.

$$[C + \mathrm{Se}S]\frac{\partial H_p}{\partial t} + \nabla \cdot [-K_s k_r \nabla(H_p + D)] = Q_s \tag{2}$$

Here, *C* represents specific moisture capacity (m^{-1}), Se is the effective saturation of the soil, *S* is a storage coefficient (m^{-1}), and Q_s represents fluid sources and sinks (d^{-1}). $S = \theta_s - \theta_r$, where θ_s and θ_r are water volume fraction at saturation and after drainage, respectively.

Equation 3 is implemented in the Solute Transport application mode, describing advection, dispersion, sorption, volatilization, and decay of solute in soil.

$$\left[\theta + \rho_b \frac{\partial c_p}{\partial c} + a_v \frac{\partial c_G}{\partial c}\right]\frac{\partial c}{\partial t} + \left[(1 - k_G)c\frac{\partial \theta}{\partial t}\right] + \nabla \cdot [-\theta D_{LG} \nabla c + \mathbf{u}c] = R_L + R_P + R_G + S_c \tag{3}$$

On the left side, the first bracketed term shows the change of liquid-, solid-, and air-phase concentrations with time. The second term explains changes in storage because water content in the soil media varies in time. The third term represents the overall solute flux due to dispersion, diffusion, and advection with moving water. The right side represents reactions (liquid phase, solute attached to soil particles, and air phase) and sources. In this work, adsorption is assumed as the main pollutant removal mechanism and the reactions in three phases are not considered.

2.3 Boundary Conditions

The surface boundary of bioretention media is crucial as it is not easy to handle the varying rainfall boundary. Non-steady state flow and pollutant concentration

conditions typical of urban stormwater runoff are input. Specifically, the inflow rate is modeled as a Gaussian distribution and coefficients a, b and c in the Gaussian equation are employed to represent the peak, density and duration of rainfall, respectively. The influent concentration of PAHs is assumed as 120 *u*g/L (Pitt *et al*. 1995). The concentration decreases exponentially and the minimum pollutant concentration in runoff after a decay period is assumed to 10% of the highest concentration.

The boundary of the underdrain is also important. The water from a bioretention cell enters a drainage system though holes on the top of the drainage pipe. The boundary conditions at the top half circle are set to be atmospheric pressure in the fluid flow mode and convection in the solute transport mode. The boundary conditions of the under half circle are described as no flux. All boundary conditions for surrounding soils are set to no flux for both water flow and solute transport.

2.4 Parameters

Simulations are run to evaluate the impacts of inflow rate, input concentrations, and some key parameters of bioretention performance and design, such as the soil types and properties for both cell media and surrounding soils (K_s, θ_s, θ_r, α, n, and ℓ). Some important parameters for bioretention performance and design are listed in Table 1. The impact of the linear partition coefficient (K_p) of NP and PY is also evaluated. This parameter is determined based on solubility and media organic matter content (foc). K_p of PAHs is calculated by the following equations:

$$K_p = f_{oc} K_{oc} \quad (4)$$

$$\text{Log } K_{oc} = 0.4057 \log K_{ow} - 0.4155 \log S + 2.3739 \quad (5) \quad \text{(Gao } \textit{et al}. \text{ 1996)}$$

Here, K_{oc} is the partition coefficient of pollutant in the organic fraction of the soil. K_{ow} is the partition coefficient of organic matter between octanol and water. S is the PAH solubility in water.

Table 1. Important Parameters for Bioretention Performance and Design

Parameters	Definition	Units	Values	Comments
$\mathbf{K_s}$	Saturated hydraulic conductivity	m/d	*	
$\mathbf{\theta_s}$	Saturated volume liquid fraction	-	*	
$\mathbf{\theta_r}$	Residual volume liquid fraction	-	*	
α, n, ℓ	Parameters for Van Genuchten	**α**: m^{-1}.	*	$\ell = 1\text{-}1/\mathbf{n}$
$\mathbf{H_p}$	Pressure head of ponding	M	0 ~ 0.25	
$\mathbf{H_{p0}}$	Initial pressure head in soil	M	**	
$\mathbf{K_p}$	PAH partition coefficient	m^3/kg	***	
$\mathbf{f_{oc}}$	Fraction of organic matter in soil		1 ~3%	
$\mathbf{C_0}$	Initial concentration in soil	Kg/m^3	0	

* Values of K_s, θ_s, θ_r, α, n, and ℓ of media and surrounding soils are listed in Table 2.

** H_{p0} is defined using expressions in which initial pressure head varies with soil depth.

*** K_p of PAHs is calculated using equation (4) and (5).

Table 2. Hydraulic Parameters of Bioretention Media and Surrounding Soils (Li *et al*. 1999)

Soil Type	K_s[m/d]	θ_s	θ_r	α [m^{-1}]	n	ℓ
Media						
Sandy Loam [a0]	1.0627	0.41	0.065	0.075	1.89	0.471
Loamy Sand	3.450	0.41	0.057	0.124	2.28	0.5614
Surrounding Soils						
Sandy Clay Loam [b0]	0.314	0.39	0.1	0.059	1.48	0.324
A: Sand	7.128	0.43	0.045	0.145	2.68	0.627
B: Sandy Loam	1.063	0.41	0.065	0.075	1.89	0.471
C: Clay Loam	0.0624	0.41	0.095	0.019	1.31	0.237

[a0]: standard soil type of bioretention media

[b0]: standard soil type of surrounding soils

3. Results and Discussion

3.1 Hydrology performance

The Bioretention media is a sandy loam with a saturated hydraulic conductivity, K_s, of 1.06 m/d, surrounded by sandy clay loam with a smaller K_s of 0.314 m/d. Flow volumetric flux (m^2/d) is used in the results of this two dimensional model instead of flow rate (m^3/d). Under the assumed Gaussian distribution influent (solid line), the dashed line in Figure 3 shows that the peak of the effluent from the underdrain was delayed and reduced. The total volume of outflow is much less than that of inflow.

Davis (2008) employed three metrics to quantify the hydrological benefits of two field bioretention facilities with lined bottoms in Maryland, including the peak flow rate ratio of effluent to influent $R_{peak} = q_{peak\text{-}out}/ q_{peak\text{-}in}$, the effluent/influent volume ratio $f_{V24} = V_{out\text{-}24}/V_{in}$, and the peak discharge time ratio of effluent to influent $R_{delay} = t_{q\text{-}peak\text{-}out} / t_{q\text{-}peak\text{-}in}$. An $R_{peak} < 1$ indicates peak reduction. An $f_{V24} < 1$ indicates runoff volume reduction and ground water recharge. The target f_{V24} value proposed is $f_{V24} <$ 0.33 with the same rationale for R_{peak}. Peak delay ($R_{delay} > 1$) is expected for 75-88% of rainfall events at field bioretention facilities (Davis 2008). In this simulated event, f_{V24}, R_{peak} and R_{delay} are 0.086, 0.08 and 1.67, respectively, which all indicate good hydrological performance of this bioretention cell.

3.2 Water quality

Figure 4 shows the influent concentration of NP and the concentration at the depth of 0.5 m, at the top of the underdrain. The effluent NP concentration is nearly zero and hence the removal efficiency is nearly 100%, mainly due to the high adsorption of NP by the organic matter in the media. In this model, adsorption is considered as the primary removal mechanism. Figure 5 shows that the NP concentration varies with depth (negative values of depth indicate depths beneath the surface). Most NP (>90%) is removed within about 3 cm depth. Similar results are also obtained for PY, although the PY has a larger K_p than NP. This is probably due to the very high K_p values of both NP and PY, calculated as 0.023 and 1.311 m^3/kg, respectively.

These simulation results of PAH concentrations agree well with the field data collected by DiBlasi *et al* (2009), reporting that the PAH event mean concentration reduction ranged from 31 to 99%, with a mean discharge EMC of 0.22 μg/L at a Maryland bioretention cell. Also, the intercepted PAH compounds penetrated only a few centimeters vertically beneath the surface. Similarly, laboratory, field and modeling studies showed high metals removal within the top soil layers (first 20 cm), significantly decreasing with media depth (Davis *et al*. 2001, 2003; Li and Davis 2008). This suggests that a shallow bioretention cell design may be recommended when PAHs and heavy metals are the pollutants of interest.

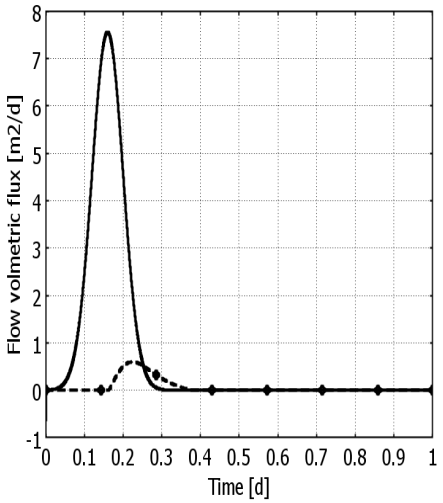

Figure 3. Gaussian Distribution Influent flux (solid line) and effluent flux from underdrain (dash line)

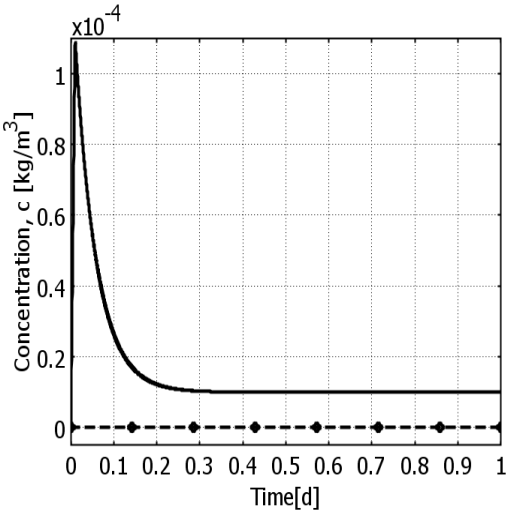

Figure 4. Influent NP concentration (solid line) and effluent NP concentration (dash line)

3.3 Soil types for media and surrounding soils

For the same hydraulic loading, the outflow volume varies for different media types. Figure 6 shows the effluent flow from sandy loam media, and from loamy sand media (with larger K_s), surrounded by the same surrounding soils of sandy clay loam. Media with higher K_s (i.e., loamy sand) generates higher flow peak, larger total volume, and shorter lag time.

Figure 7 shows that, under the same hydraulic loading and with the same sandy loam media, the outflow also changes for different characteristics of surrounding soils. Surrounding soils with higher K_s, such as sand, generate lower discharge peak and less total volume. Two-dimensional modeling of the partial exfiltration reactor (PER) by Sansalone and Teng (2005) supports the results in Figure 7, except that in Figure 7 the time to peak flow does not change much with surrounding soils.

In Figure 8, for sand with K_s of 7.1 m/d, the peak flow rate is 3.5 times that of clay loam with K_s of 0.0624 m/d. With the more permeable surrounding soils (larger K_s),

more water enters into surrounding soil layer, resulting in less effluent discharge from a bioretention cell. Therefore, total outflow volume decreases.

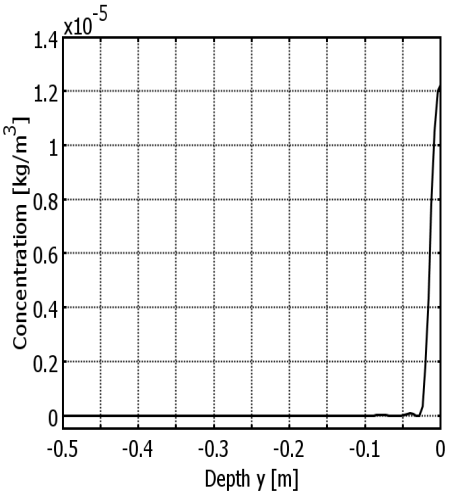

Figure 5. Concentrations of NP vary with depth when t = 0.2 day.

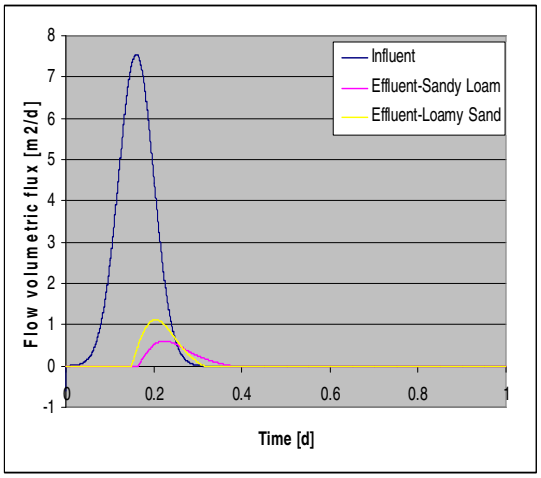

Figure 6. Simulated hydrograph with different media soils.

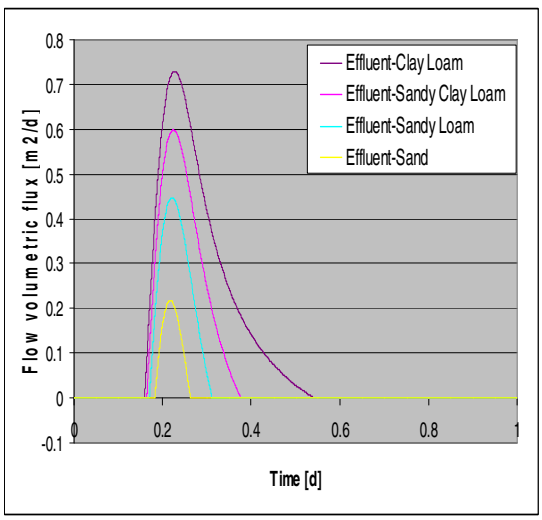

Figure 7. Effluent for different surrounding surrounding soils

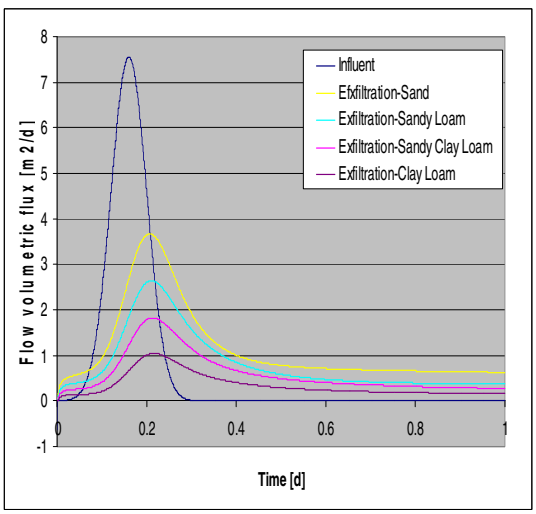

Figure 8. Exfiltration for different soils

Conclusions

In this study, a two dimensional Variable Saturated Flow and Transport Model is developed based on application modes in COMSOL Multiphysics. This model is tested under transient hydraulic and pollutant loading. Model results indicate that the outflow volume is less than the inflow. The flow peak is reduced and delayed. Concentrations of NP and PY in runoff vary with depth and most NP and PY (> 90%) is removed within about 3 cm media depth. This suggests the possibility of a shallow bioretention cell design.

Different soil types with different hydraulic properties in both media and surrounding soils impact the outflow from a bioretention cell. The outflow volume from loamy sand media (with larger K_s) is larger than that from sandy loam media. However, surrounding soils with larger K_s, such as sand, produce less outflow volume than those with smaller K_s. This suggests that careful consideration of the soil types of both media and surrounding soils is important in the design and function of a bioretention cell.

Continuing work evaluates more complicated geometry such as multi-layer soil media including the mulch layer and vegetative layer. Other mechanisms of pollutant removal in bioretention facilities such as biodegradation will be considered in order to evaluate long-term performance.

References

COMSOL AB (2005). "*COMSOL* Multiphysics earth science module user's guide (Version 3.2)."120p.

Davis, A.P. (2008). "Field performance of bioretention: hydrology impacts." *J. Hydrologic Engg.,* ASCE*,* 13(2), 90-95.

Davis, A. P., Shokouhian, M., and Ni, S. (2001). "Loading estimates of lead, copper, cadmium, and zinc in urban runoff from specific sources," *Chemosphere*. 44, 997-1009.

Davis, A. P., Shokouhian, M., Sharma, H., Minami, C., and Winogradoff, D. (2003). "Water quality improvement through bioretention: lead, copper, and zinc Removal." *Water Environ. Res*., 75 (1), 73-75.

Davis, A. P., Shokouhian, M., Sharma, H., Minami, C., and Minami, C. (2006). "Water quality improvement through bioretention media: nitrogen and phosphorus removal." *Water Environ. Res*., 78 (3), 284-293.

DiBlasi, C., Li, H, Davis, A.P., and Ghosh, U. (2009). **"**Removal and fate of polycyclic aromatic hydrocarbon pollutants in an urban stormwater bioretention facility." *Environ. Sci. Technol.*, 43 (2), 494–502.

Department of Environmental Resources (DER) Prince George's Country, Maryland. (2001). "Bioretention manual: Chapter 1 Introduce to bioretention." http://www.co.pg.md.us/government/agencyindex/der/LID/pdf/intro_bioretention.pdf, last accessed, Aug. 2006.

Dietz, M. E. and Clausen, J. C. (2005). "A field evaluation of rain garden flow and pollutant treatment." *Water, Air, Soil Pollut*., 167(1–4), 123–138.

Duchene, M., McBean, E. A., and Thomson, N. R. (1994). ''Modeling of infiltration from trenches for storm water control.'' *J. Water Resour. Plng. and Mgmt.,* ASCE, 120(3), 111–116.

Gao, C., Govind, R., and Tabak H. H. (1996). "Predicting soil sorption coefficients of organic chemicals using a neural network model." *Environ. Toxicol. Chem.*, 15, 1089–1096.

Harada, S., and Ichikawa, A. (1994). "Performance of the drainage infiltration strata: Statistical and numerical analysis.'' *Water Sci. and Technol.,* 29(1-2), 255–265.

Hong, E., Seagren, E.A., and Davis, A.P. (2006). "Sustainable oil and grease removal from stormwater runoff hotspots using bioretention." *Water Environ. Res.,* 78(2), 141.

Hsieh, C.H., and Davis, A.P. (2005a). "Evaluation and optimization of bioretention media for treatment of urban storm water runoff." *J. Environ. Eng*., 131(11), 1521-1531.

Hsieh, C.H., and Davis, A.P. (2005b). "Multiple-event study of bioretention for treatment of urban storm water runoff." *Water Sci. Technol*., 51(3–4), 177-181.

Hsieh, C.H., Davis, A.P. and Needelman, B.A. (2007). "Bioretention column studies of phosphorus removal from urban stormwater runoff." *Water Environ. Res*., 79(2), 177-184.

Hunt, W.F., Jarrett, A.R., Smith, J.T., and Sharkey, L.J. (2006). "Evaluating bioretention hydrology and nutrient removal at three field sites in North Carolina." *J. Irrigat. Drainage Eng.,* 132(6), 600-608.

Li, H., and Davis, A.P. (2008). "Heavy metal capture and accumulation in bioretention media." *Environ. Sci. Technol.*, 42 (14), 5247–5253.

Li, Y., Buchberger, S.G., and Sansalone, J. J. (1999) "Variably saturated flow in storm-water partial exfiltration trench." *J. of Environ. Eng.,* 125(6), 556-565.

Pitt, R.,Field, R., Lalor, M. and Brown, M. (1995). "Urban stormwater toxic pollutants: assessment, sources, and treatability." *Water Environ. Res*., 67, 260-275.

Sansalone, J., and Teng, Z. (2004). "In situ partial exfiltration of rainfall runoff. I: Quality and quantity attenuation*." J. Environ. Eng*., 130 (9), 990–1007.

Sansalone, J. J., and Teng, Z. (2005). "Transient rainfall-runoff loadings to a partial exfiltration system: Implications for urban water quantity and quality." *J. Environ. Eng*., 131(8), 155 –1167.

Use of the Basin Development Factor to Evaluate Urban Watershed Response

Shiva Sunder[1], Theodore G. Cleveland[2], and David B. Thompson[3]

1. ABSTRACT

The Basin Development Factor (*BDF*) is a reasonably straightforward categorical variable that has promise for estimating urban hydrologic response. The objective of this study is exploratory — the goal is to learn whether the *BDF* improves the explanation of the rainfall and runoff responses of watersheds. This particular metric is attractive as an alternative to other metrics in use.

The *BDF* was determined for more than 100 watersheds in Texas and then used to generate estimates of unit hydrograph timing characteristics and peak discharge characteristics. Simulated responses using these values are compared to both observed and prior simulated responses for the same watersheds.

Inclusion of *BDF* as an explanatory variable in the regression analyses in this study to generate hydrologic responses did not materially reduce, or enhance performance in models of selected watersheds. This finding indicates that use of *BDF* cannot make estimates worse, but does not improve estimates either (and thus *BDF* as implemented here could be ignored). The result was discouraging, but the particular effort overlooked that the regression models used could estimate zero discharges, when, in fact, the actual database did not contain zero values.

Despite the discouraging result, the authors believe that the BDF bears further study and suggestions for such studies are offered.

2. INTRODUCTION

Hydrologic response of a watershed is controlled in large part by its topography, storage properties, and loss (or runoff generation) properties. The study reported herein was motivated by an observation that topography is relatively unchanged in urban watersheds as they develop, but hydrologic response certainly changes — no doubt in some proportion to changes in storage, runoff generation, and conveyance efficiency to the outlet.

Liscum and Massey (1980), Liscum et al. (1996), and Liscum (2001) in a series of studies addressed the effect of change by a variety of watershed properties as explanatory variables

[1]Department of Civil and Environmental Engineering, University of Houston, Houston, Texas 77204-4003. email: ssunder@uh.edu

[2]Department of Civil and Environmental Engineering, Texas Tech University, Lubbock, Texas 79404-. email: theodore.cleveland@ttu.edu (corresponding author)

[3]R.O. Anderson Inc., 1603 Esmerelda Blvd., Minden, Nevada 89423. email: dthompson@roanderson.com

in rainfall-runoff regression models of the Houston area. One promising explanatory variable was the Basin Development Factor (*BDF*) (Sauer et al., 1983). The *BDF* is a measure of runoff transport efficiency of the drainage systems in a watershed, and thus indirectly addresses the storage and transport components of a watershed's runoff signal. *BDF* is a categorical variable, whose value is assigned based on the prevalence of certain drainage conditions that result from urbanization of a watershed.

Cleveland et al. (2008) used a particle tracking approach for parametrizing unit hydrographs from topographic information for selected watersheds in Texas. That work demonstrated that topographic information explained a large portion of variability in response, yet the use of a binary categorical variable for developed and undeveloped watersheds was insufficient to capture the spectrum of change as a watershed urbanizes; the *BDF* potentially extends the range of responses by 11 categories.

Southard (1986) examined an alternative urban basin characteristic, called the percentage developed area, to simplify the computation process of evaluating the percentage of impervious area within a basin. At the time, he speculated that the field reconnaissance of a watershed with an area of 20 square miles would take 1 to 6 hours but computation of percentage of developed area would take less than 2 hours for basins with area 22 square miles or less. Field reconnaissance necessary to determine BDF would be impractical if the user is located a considerable distance from the basin, however since that time tools like Google Earth make the prospect of computing a BDF as practical as percentage impervious area.

This study examines the *BDF* on urban hydrologic response. The objective of this research is to determine how the *BDF* explains the rainfall and runoff responses of watersheds and if this metric is a useful alternative to other metrics in use. The BDF is applied to more than 100 watersheds in Texas and the results compared to prior efforts on these watersheds.

3. METHODOLOGY

The database used for this research contains rainfall and runoff values, physical and dimensional parameters of 133 watersheds in Texas. The database combined the contents of Asquith et al. (2004) with recent computations of BDF using Google Earth, as well as recent additions to the original rainfall-runoff database.

The Basin Development factor is computed from analyst interpretation of the presence or absence of the following physical features, of which three (of four) are detectable using aerial imagery. Borrowing from Sauer et al. (1983) the four components and their meanings are:

(1) Channel Improvements: The improvements are noted by taking into consideration the phenomenon of straightening, deepening, clearing and enlarging. If all or any of the above phenomena are present in at least 50% of the main channel and its

tributaries, then, a value of one is given to the third of the watershed taken into consideration; else it takes the value zero.

(2) Channel linings: If more than 50% of the main channel length is lined with an impervious material like concrete, then a value of one is given to the third of the watershed under study, else the value of zero is assigned. Usually, if the drainage channel is lined with an impervious material, it will have a good channel improvement. Hence this aspect is an added factor to portray a highly developed drainage system.

(3) Storm drains or storm sewers: the enclosed drainage structures (usually pipes) that are used on the secondary tributaries, that collect the drainage from the parking lots, streets etc., and drain into open channels in most cases or into channels enclosed as pipe or box culverts are called storm drains. So, when over 50% of the secondary tributaries are found to have storm drains, then a value of one is given else zero value is given.

(4) Curbs and gutters: this factor reflects the actual urbanization of the watershed area. If more than 50% of the area is industrially developed or used in constructing residential or commercial buildings and if streets and freeways are constructed using curbs and gutters, then the value one is assigned. Else the value zero is given. Curbs and gutters take drainage to storm drains.

The authors acknowledge that storm sewers are likely undetectable from Google Earth imagery and thus there is considerable subjectivity in these last two components of the BDF, nevertheless the analysts proceeded using their best judgement to arrive at a defendable value.

The computation of BDF for one watershed is illustrated as an example. Figure 1 is a screen capture of a Google Earth image with a watershed delineated. The boundaries are approximate which is sufficient for this task.

The watershed is divided into three approximately equal parts that are examined for channel improvements, channel linings, storm drains and curbs and gutters. The component scores for the watershed are listed in Table 1. The upper portion of the watershed has no visible channel, thus these two components are scored zero. Storm sewers probably exist and are scored one on this conjecture and the obvious curb and gutter component is scored one in this portion. The middle portion has visible channels, and there is some evidence of improvement (there are linear features when the image is zoomed), but there is no visible evidence of lining. Hence the channel improvement is scored one, as is the curb and gutter, and storm sewer. The lower third has all components and each is scored one, for a total $BDF = 9$.

As an observation (from several dozens of urban watersheds) a $BDF = 9$ is a reasonably developed watershed. Several different analysts will arrive at different values of BDF but

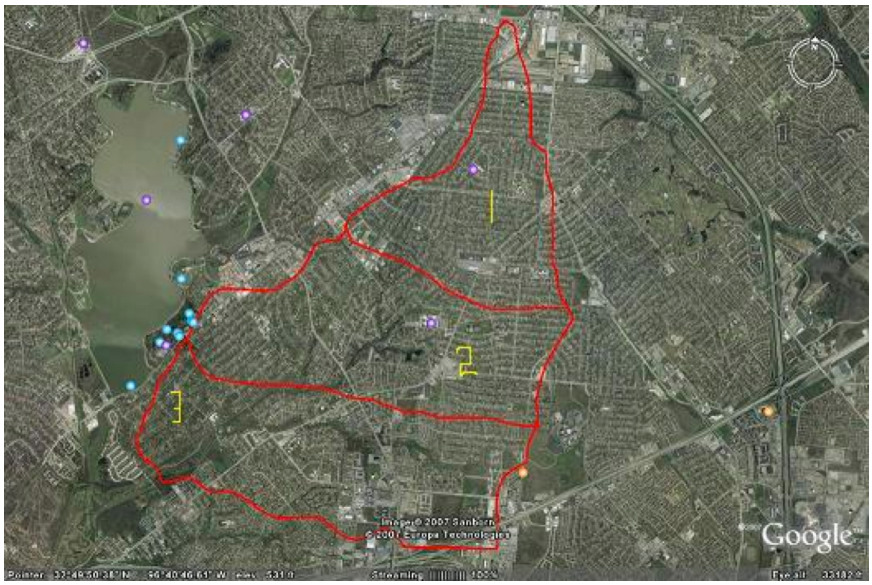

FIGURE 1. Station 0807320 Ashcreek Watershed, Dallas, Texas. Boundaries are approximate.

TABLE 1. Ash Creek BDF component scoring

Area	Imp. Channel	Lined Channel	Storm Drain	Curb and Gutter
(1) Upper $\frac{1}{3}$	0	0	1	1
(2) Middle $\frac{1}{3}$	1	0	1	1
(3) Lower $\frac{1}{3}$	1	1	1	1

generally will be within a score of one, thus the subjectivity is not so large that two analysts will score at opposite ends of the scoring range.

Figure 2 is a plot of the relationship of a characteristic time, T_p, and a characteristic spatial dimension, A/S_o, for each watershed examined. The figure exhibits considerable variability, but when these results are segregated by *BDF* value, the watersheds with greater *BDF* value plotted closer to the lower envelope of the marker cloud (i.e. along the lower line in the figure), while the watersheds with lower *BDF* plotted along the upper envelope. This result is anticipated and important for the potential use of *BDF* as an explanatory variable[4].

The values of T_p were determined from the observation data using methods described in Thompson et al. (2007) and Asquith et al. (2006) and can be considered metrics of the actual watershed response (as opposed to estimates obtained by regressions). The differences in the characteristic time were found to be meaningful enough to consider *BDF* as an explanatory, categorical variable. These values of *BDF* were then used to generate regression equations

[4]The differences are visible when the figure is plotted in color. The authors were unsure of the manuscript would be in color, so the text was written as if only black and white were available.

to estimate values of initial abstraction, I_a, loss rate, C_l, characteristic time to peak, T_p, and a peak rate factor, Q_p. The meanings of these values are analogous to the same terms used in the collective works of Cleveland et al. (2008), Thompson et al. (2007), Asquith and Roussel (2007), and Asquith et al. (2006).

Of particular importance, to reduce the effort required to analyze the database, station median values were used to generate the estimation equations that were used to generate the responses to rainfall input in the cases where *BDF* was considered as an exploratory variable, while the other results presented herein were computed on a storm-by-storm basis.

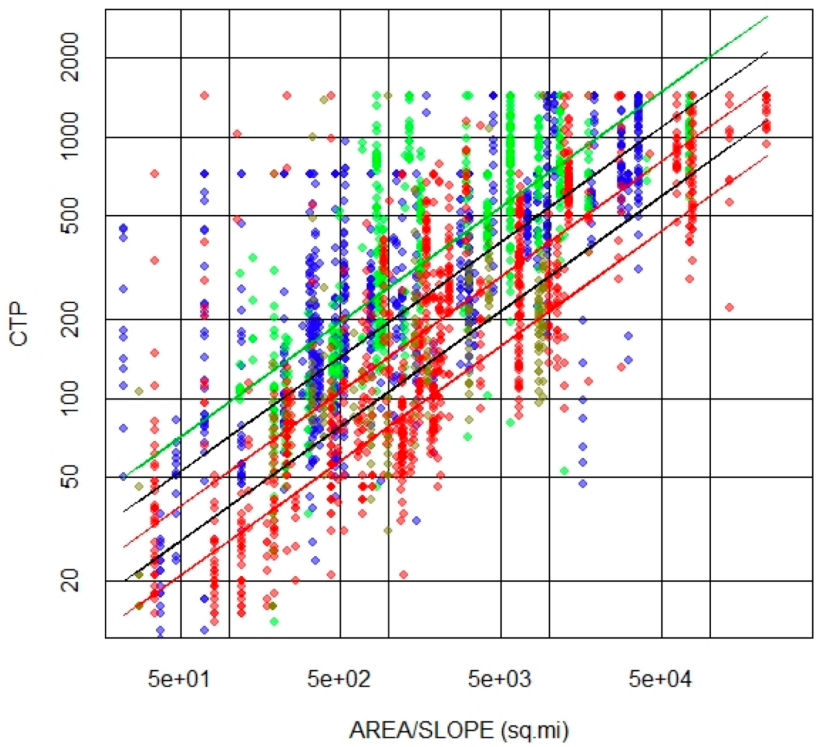

FIGURE 2. Observed characteristic time, T_p, and ratio of watershed area to slope (a characteristic spatial dimension) for all storms all watersheds. Markers indicate individual rainfall-runoff paired events. Marker density is indicative of relative number of markers in a particular location. Color is segregation by *BDF* value.

Once these regression equations were generated, estimated responses from these regressions were compared with those of Asquith and Roussel (2007) where similar analysis was performed on a subset of these watersheds and Cleveland et al. (2008) where only a minimal set of categories related to basin development was examined. The desirable result would be

a measurable reduction in variability explained by the additional categories; an undesirable result would be added variability, and a null result would be acceptable (but not particularly useful).

4. RESULTS

The *BDF* results presented here incorporate the loss model of Asquith and Roussel (2007), and only the characteristic time is different when comparing these two estimation procedures. The *NO_BDF* model uses the results from Cleveland et al. (2006), and represents storm-fitted unit hydrographs. The Digital Terrain Runoff Model (*DTRM*) results are from Cleveland et al. (2008) which incorporated a proportional loss model.

Figure 3 is a plot of the peak discharge values computed using the three different models. Ideally all models would plot along an equal value line. The markers representing the *BDF* model exhibit more variability than anticipated, but are still within reasonable values for most of the storms simulated.

Figure 4 is a plot of the time of peak discharge values computed using the three different models. Ideally all models would plot along an equal value line. Of particular note in this plot is the significant number of zero times in the *BDF* model. These values are attributed to the choice of loss model used in these simulations — and initial abstraction constant loss model that for some storms simulated zero runoff (when, in fact, actual runoff was non-zero). The markers representing the *BDF* model exhibit about the same variability as the prior efforts[5], and could be argued to reduce variability slightly.

The upper panel of Figure 3 is a boxplot of the information depicted in the scatterplots of Figure 3. The boxplots (and associated non-parametric tests) indicate that all the models perform the same when compared to each other or to their associated observations. Likewise the lower panel of figure 4 is a boxplot of the same information depicted in the scatterplots of Figure 4. These boxplots (and associated non-parametric tests) also indicate that all the models perform the same when compared to each other or to their associated observations.

5. DISCUSSION AND INTERPRETATION

Inclusion of *BDF* as an explanatory variable in a regression analysis to generate hydrologic responses did not materially reduce, or enhance performance in models of selected watersheds.

The implementation here was essentially an application of the loss models of Asquith and Roussel (2007) with an adjustment for the value of *BDF*, without re-analysis of the entire database — thus the method admits zero discharge cases when, in fact, such cases were not

[5]the zero values being ignored for this statement

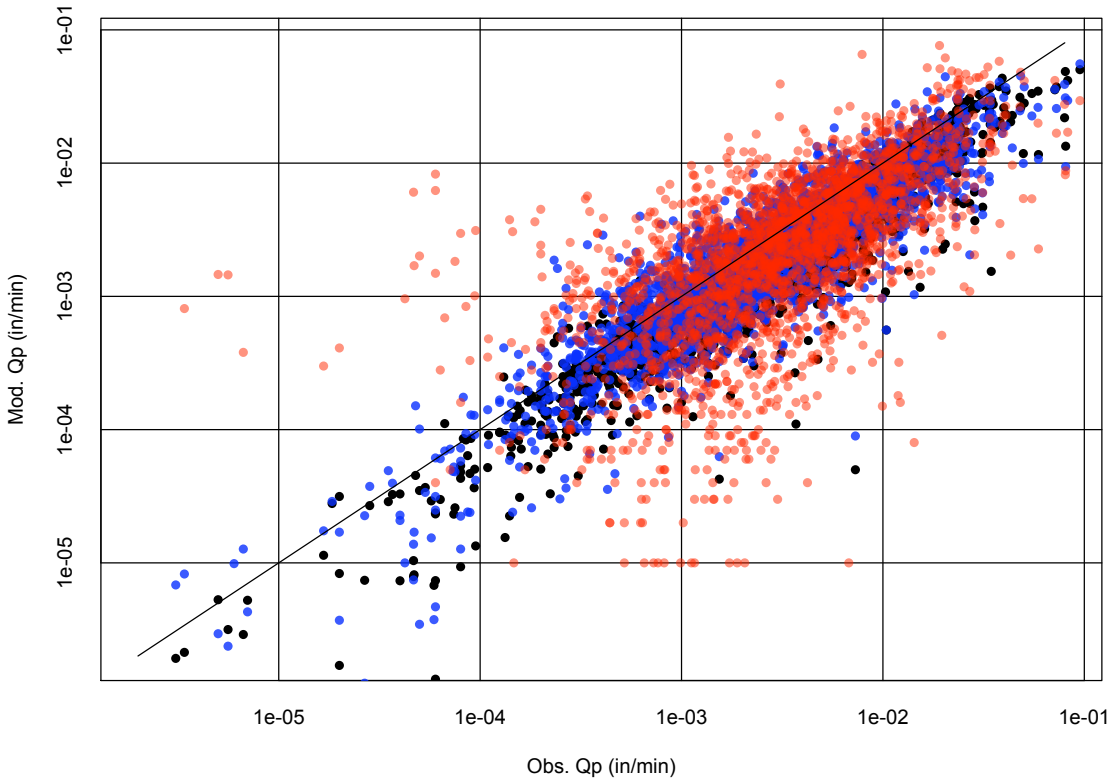

FIGURE 3. Plot of observed and model peak discharge values for individual storms on the study watersheds. Black markers (narrow marker cloud) are storm-optimized (storms fitted to unit hydrographs), blue circles are terrain-based unit hydrographs (Cleveland et al., 2008), and red markers are results estimated using a regression model that incorporates *BDF*.

in the original data, and this substantial difference is an issue needing further clarification. Furthermore, the authors did not re-analyze the entire database, instead choosing to apply regression to the station median values to incorporate the effects of *BDF* on response. This particular conceptual error is why the *BDF* did not perform as well as anticipated[6].

The simulated characteristic times, if the zero-discharge cases are censored, qualitatively reduces the variability in the responses, weakly supporting the original conjecture that *BDF* could confer additional accuracy in such modeling. Once loss (runoff generation) processes are accounted for, the simulated responses are sensitive to values of *BDF*.

[6]Or the BDF is simply not useful as an explanatory variable — yet its value in other venues suggests the conceptual error is a better explanation

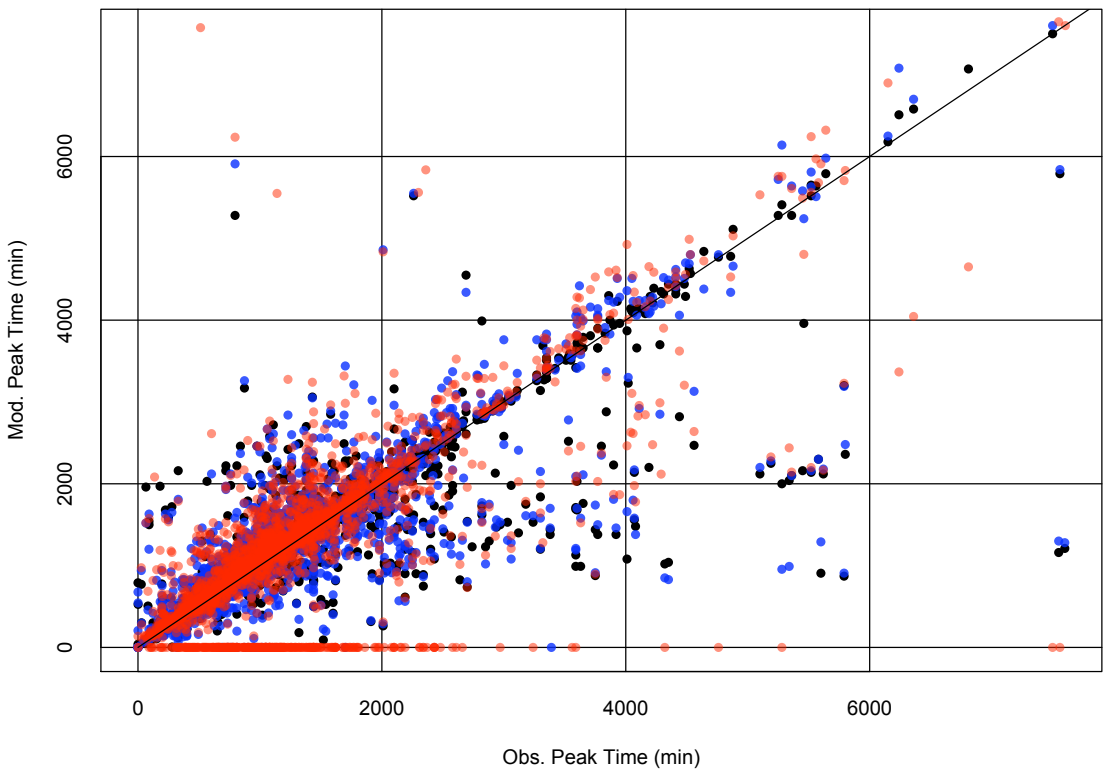

FIGURE 4. Plot of observed and model time of peak discharge values for individual storms on the study watersheds. Black markers (narrow marker cloud) are storm-optimized (storms fitted to unit hydrographs), blue circles are terrain-based unit hydrographs (Cleveland et al., 2008), and red markers are results estimated using a regression model that incorporates *BDF*.

Future efforts would be to re-analyze the entire database with *BDF* as an explicit explanatory variable (instead of a de-coupled analysis done in this work) and combine this effort with the terrain based model to determine if the inclusion of *BDF* improves the simulation value of that model. Additionally, the issue of runoff generation appears to be the crux of these kind of simulations and this issue is not adequately addressed in this work.

6. ACKNOWLEDGEMENTS

The research reported herein was supported in part by the Texas Department of Transportation and the Harris County Flood Control District. Their financial support is greatly appreciated and acknowledged.

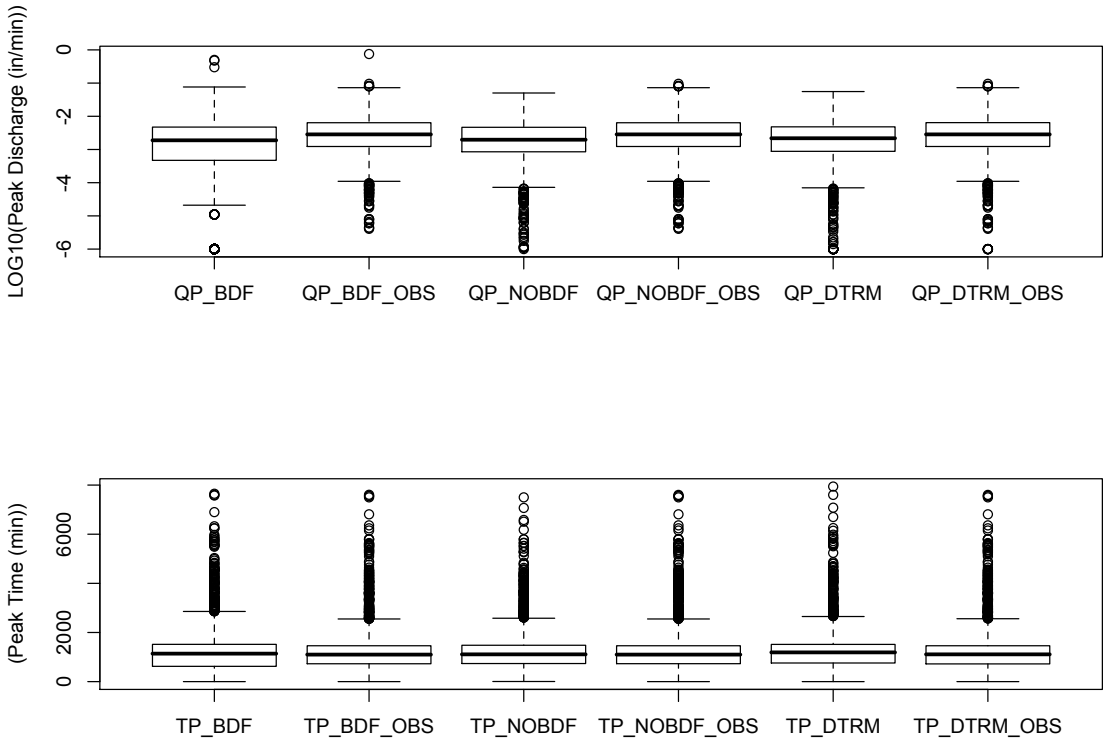

FIGURE 5. Upper Panel: Boxplot of the peak discharge for the three models (BDF, NO_BDF, and DTRM) and their respective observed (paired) values.

Lower Panel: Boxplot of the time of peak discharge for the three models (BDF, NO_BDF, and DTRM) and their respective observed (paired) values.

The authors further wish to acknowledge the guidance of their colleagues who contributed to this effort: G. R. Herrmann (Texas Department of Transportation) , T. Luong (Texas Department of Transportation) , W. H. Asquith (U.S. Geologic Survey) , M. S. Roussel (U.S. Geologic Survey), F. Liscum (PBS&J) , S. Johnson (LJA) , D. Schwertz (Natl. Weather Service) . and D. Barrett (R.G. Miller).

The contents of this report reflect the views of the authors who are responsible for the facts and the accuracy of the data presented herein. The contents do not necessarily reflect the official view or policies of the Harris COunty Flood Control District, the Texas Department of Transportation or the Federal Highway Administration. This report does not constitute a standard, specification, or regulation.

References

Asquith, W. H. and M. C. Roussel (2007). An Initial-Abstraction, Constant-Loss Model for Unit Hydrograph Modeling for Applicable Watersheds in Texas. Scientific Investigations Report SIR 2007-5243, U.S. Geological Survey.

Asquith, W. H., D. B. Thompson, T. Cleveland, and X. Fang (2004). Synthesis of Rainfall and Runoff Data Used for Texas Department of Transportation Projects 0-4193 and 0-4193. Open-File Report OFR 2004-1035, U.S. Geological Survey.

Asquith, W. H., D. B. Thompson, T. G. Cleveland, and X. Fang (2006). Unit hydrograph estimation for applicable Texas watersheds. Research Report TechMRT/TxDOT 0-4193-4, Texas Department of Transportation.

Cleveland, T. G., X. He, W. H. Asquith, and D. B. Thompson (2006). Instantaneous Unit Hydrograph Evaluation for Rainfall-Runoff Modeling of Small Watersheds in North and South Central Texas. *ASCE J. of Irrigation and Drainage Engineering 132*(5), 479–485.

Cleveland, T. G., D. B. Thompson, X. Fang, and X. He (2008). Synthesis of Unit Hydrographs from Digital Elevation Model. *ASCE J. of Irrigation and Drainage Engineering 134*(2), 212–221.

Liscum, F. (2001). Effects of Urban Development on Stormwater Runoff Characteristics for the Houston, Texas, Metropolitan Area. Water-Resources Investigations Report 01-4071, U.S. Geological Survey.

Liscum, F., D. Brown, and M. Kasmarek (1996). Summary of Surface-Water Hydrologic Data for the Houston Metropolitan Area, Texas, water years 1964 – 89. Open-File Report 96-250, U.S. Geological Survey.

Liscum, F. and B. Massey (1980). Technique for Estimating the magnitude and Frequency of Floods in the Houston, Texas, Metropolitan Area. Water-Resources Investigations Report 80-17, U.S. Gelogical Survey.

Sauer, V. B., W. O. Thomas, V. A. Stricker, and K. Wilson (1983). Flood characteristics of urban watersheds in the United States. Water Supply Paper 2207, U.S. Geological Survey.

Southard, R. E. (1986). An Alternative Basin Characteristic for use in Estimating Impervious Area for Urban Missouri Basins. Water-Resources Investigations Report WRIR 86-4362, U.S. Geological Survey.

Thompson, D. B., T. Cleveland, and X. Fang (2007). Loss Rate Functions for Selected Texas Watersheds. Research Report TechMRT/TxDOT 0-4193-5, Texas Department of Transportation.

Water Quality and Hydraulic Properties of the Permeable Friction Course

Michael Barrett[1], Ph.D., P.E., D.WRE, Brandon Klenzendorf[2] M.S., Brad Eck[3] M.S., and Randall Charbeneau[3], Ph.D., P.E., D.WRE

[1]Center for Research in Water Resources, PRC #119 (R8000), University of Texas, Austin, TX 78712; PH (512) 471-0935; FAX (512) 471-0935; email: mbarrett@mail.utexas.edu
[2]Center for Research in Water Resources, PRC #119 (R8000), University of Texas, Austin, TX 78712; PH (512) 471-3131; FAX (512) 471-0935; email: jbklenz@mail.utexas.edu
[3]Center for Research in Water Resources, PRC #119 (R8000), University of Texas, Austin, TX 78712; PH (512) 471-3131; FAX (512) 471-0935; email: brad.eck@mail.utexas.edu
[4]Department of Civil, Architectural, and Environmental Engineering, 1 University Station C1700, University of Texas, Austin, TX 78712; PH (512) 471-0070; FAX (512) 471-0935; email: charbeneau@mail.utexas.edu

ABSTRACT

The objective of this study is to document the water quality benefits and the hydraulic properties of PFC. Stormwater runoff from a four-lane divided highway in Austin, Texas, USA was monitored at the edge of pavement at two sites before and after the installation of a PFC. Observed concentrations of total suspended solids and pollutants associated with particulate material were much lower in the runoff from the PFC than that derived from the conventional asphalt surface. Significant concentration reductions were observed for total suspended solids, total lead, total copper, and total zinc. The reduction in TSS concentration is about 90 percent and the average discharge concentration is less than 10 mg/L. Concentrations of dissolved constituents were not significantly different at either site. These results are generally consistent with findings of research conducted in Europe.

Results of this study indicate that PFC performs as well as many types of structural controls for reducing the pollutants in highway runoff. Consequently, this material that has historically been used primarily for safety benefits should also be considered where reduction in pollutant discharge is desired. This material incorporates runoff treatment within the pavement itself, which facilitates its use in retrofit situations where additional right-of-way may not be available for stormwater treatment.

In addition, to the water quality measurements, cores of the pavement have been collected at a number of sites of different ages and traffic densities to determine porosity and hydraulic conductivity. Laboratory measurements of the hydraulic conductivities of the cores indicate that the testing regime commonly used results in conditions where Darcy's Law is no longer valid.

INTRODUCTION

Porous asphalt overlays are used increasingly by state transportation agencies in the U.S., including those in Georgia, Texas, California, and Utah, to improve drivability in wet weather conditions and to reduce noise from highway traffic. Acknowledged benefits include reduced splash and spray, better visibility, better traction, reduced hydroplaning and less noise (Stotz and Krauth, 1994; Berbee et al., 1999). These pavements also may reduce the runoff volume and peak runoff velocity, as well as increase the lag time between rainfall and runoff, especially for smaller storm events.

The impact of PFC on stormwater runoff quality has been evaluated in only a few scientific studies; however, improved runoff quality has been consistently observed by researchers (Berbee et al., 1999; Pagotto et al., 2000; Stotz and Krauth, 1994) There are several reasons to think that improved water quality may result from the installation of this material. PFC might be expected to reduce the generation of pollutants, retain a portion of generated pollutants within the porous matrix, and impede the transport of pollutants to the edge of the pavement.

It has been reported that the concentrations of selected constituents in highway runoff were affected by the number of vehicles passing the site during a storm event (Irish et al., 1998). These constituents included oil/grease, copper, and lead. Spray generated from tires was assumed to wash pollutants from the engine compartments and bottoms of vehicles. It is reasonable to expect that the amount of material washed off vehicles while driving in the rain will be reduced since PFC reduces splash and spray. This reduction in the amount of material washed from vehicles is expected to decrease the concentrations of these pollutants in the runoff generated from roads paved with PFC. In addition, the porous structure of PFC also may act as a filter of the stormwater. Runoff enters the pores in the overlay surface and is diverted towards the shoulder by the underlying conventional pavement. Pollutants in the runoff can be filtered out as the water flows through the pores, especially suspended solids and other pollutants associated with particles.

In order to properly maintain the benefits of the PFC layer, stormwater runoff must be contained within the pore space. Several researchers have addressed the issue of flow in porous pavements. Jackson and Ragan (1974) were among the first to model flow through an entirely porous pavement. They developed numerical solutions to the Boussinesq equation for a pavement with zero slope in order to determine the effect of underdrain spacing on discharge rates. Ranieri (2002) was the first researcher to model water depths specifically within PFC. He developed a runoff model to determine the required PFC thickness necessary to contain the entire runoff within the pore space based on the roadway geometry, rainfall intensity, and PFC hydraulic

conductivity. The theoretical model was validated with a laboratory experiment that simulated rainfall on PFC and measured the water depth within the pore space. Ranieri (2007) expands on the earlier work and provides some minor corrections to the original model.

Tan et al. (2004) used a three-dimensional finite element model to determine the effects that roadway geometry (slopes and widths), design rainfall, and PFC thickness have on the water depth within the PFC. Finally, Charbeneau and Barrett (2008) provide analytic solutions to the governing equations of flow through PFC for a variety of boundary and rainfall conditions. In addition, Charbeneau and Barrett address the issue of completely saturated PFC flow with the addition of surface runoff, and suggest a method for determining the spacing of underdrains.

In order to model flow within PFC knowledge of the hydraulic conductivity of the pavement is required. There are two main obstacles to direct measurement of hydraulic conductivity: 1) the high permeability may result may result in a non-Darcy flow regime, and 2) in-situ measurement results in two dimensional flow patterns, rather than the one dimensional regime commonly associated with most permeability testing.

OBJECTIVES

The main objective of this study was to compare the water quality of stormwater runoff derived from a PFC overlay with that from a conventional hot mix asphalt pavement. This comparison was made by collecting runoff samples at the same location along a highway in the Austin, Texas area before and after a PFC overlay was applied. The second objective was to determine a method to accurately characterize the hydraulic properties of the PFC.

METHODOLOGY

Stormwater runoff quality was monitored at two sites located on Loop 360 in Austin, Texas, USA during the period from February 2004 through December 2007. Loop 360 is a four-lane state highway in the western part of Austin. The original monitoring site is adjacent to the two southbound lanes of the highway, while the second site is located a short distance away on the northbound lanes. The average daily traffic count is estimated at 48,000 (Campo, 2005).

GKY FirstFlush Samplers were installed to collect the runoff from a site on Loop 360. In October 2004, TxDOT implemented a PFC overlay project at this location. The overlay was applied on top of the existing conventional asphalt according to TxDOT specifications. New instrumentation was installed at the site in November 2006 including an H-flume and an automatic sampler. Consequently, at this site there has now been collection of runoff samples since the initial installation of the PFC more than 4 years ago.

In February 2007, two GKY First Flush samplers were installed about 1.5 km away adjacent to the northbound lanes. When the overlay was initially installed, conventional pavement was retained at stop lights along the highway because of fears that the PFC might be damaged by the acceleration/deceleration of vehicles at the lights. The samplers were placed about 60 m apart, one located adjacent to the PFC portion and one adjacent to the conventional pavement. This allowed comparison of the water quality from the same events for the two pavement types.

At the original site, five samples of runoff were collected from the conventional pavement and 36 samples of runoff were collected after the PFC overlay, while a total of 13 storms have been monitored at the site with paired samplers.

PFC cores were extracted by saw cutting from pavement surfaces. Typical coring will recover the PFC layer along with part of the underlying conventional pavement. The laboratory test specimen thus has a circular shape with an open PFC surface and impermeable base. This research has used PFC core samples with diameters of 15.1 and 21.8 cm taken from three locations around Austin, TX. The small diameter cores were extracted in March 2007, and the large diameter cores were extracted in February 2008. The impermeable conventional pavement base is removed from the PFC layer resulting in core thicknesses of 2.5 to 5 cm. The cores are analyzed in the laboratory to determine hydraulic conductivity using constant head tests and porosity. In addition, a falling head test protocol developed for the field is proposed to determine the in-situ hydraulic conductivity. Determination of in-situ hydraulic conductivity is necessary to easily evaluate the drainage potential of the PFC throughout its life cycle without the extraction of core samples.

RESULTS

The EMCs measured during the sampled storm events at the two monitored sites are shown in Table 1. Concentrations of TSS, total phosphorus, and total lead, copper, and zinc are significantly lower in runoff generated from the PFC surface than in runoff generated from the conventional asphalt surface. A negative sign on the removal efficiency indicated that an increase in concentration was observed; however, these differences were not statistically significant.

The data indicate that the runoff generated from the PFC surface has consistently lower concentrations of particles and particle associated pollutants than that from the traditional asphalt surface. This difference in water quality also was noted upon visual inspection of the runoff samples collected at the edge of pavement. The concentrations of nitrate/nitrite, dissolved copper and zinc, and total and dissolved phosphorus did not exhibit a significant difference between the two road surfaces. These data indicate that the PFC has little to no effect upon the concentrations of dissolved constituents in the stormwater runoff.

Table 1 Constituent EMCs for Conventional Asphalt (HMA) and PFC

	Original Site			Second Site		
Constituent	HMA	PFC	Removal %	HMA	PFC	Removal %
TSS (mg/L)	117	9.0	92	159	17	89
TKN (mg/L)	1.13	1.03	9	1.12	0.93	17
NO3/NO2 (mg/L)	0.43	0.40	9	0.17	0.28	-65
Total P (mg/L)	0.13	0.08	40	0.15	0.06	60
Dissolved P (mg/L)	0.06	0.07	-12	0.04	0.04	0
Total Copper (ug/L)	27	14	49	30	13	57
Dissolved Copper (ug/L)	5.9	10.6	-78	5.9	9.3	-58
Total Lead (ug/L)	12.6	1.5	88	11	1.4	87
Dissolved Lead (ug/L)	<1.0	<1.0	NA	<1.0	<1.0	NA
Total Zinc (ug/L)	167	31	82	132	21	84
Dissolved Zinc (ug/L)	47	23	51	16	11	31
COD (mg/L)	64	62	3	77	62	19

After more than 3 years of monitoring, no significant correlation between discharge concentrations at the edge of pavement and time since installation or cumulative rainfall volume has been observed. As an example, Figure 1 presents the concentrations of total suspended solids for each of the monitored events at the original site. The measurements prior to 8/1/04 were of runoff from the conventional pavement. The measurements made after 10/06 were from flow weighted composite samples and the average concentrations from this sampler were all lower than those collected with the passive sampler, but not by a large amount. To date, no significant relationship has been ascertained between time and concentration. The dramatic difference in TSS concentrations for each of the monitored events at the second site is illustrated in Figure 2.

A critical component in the assessment of the water quality benefits of PFC is whether the relatively low pollutant concentrations observed in this study is a function of removal of pollutants within the pavement, reduced generation of pollutants through reduction in washoff from vehicles, or the lack of accumulation of pollutants on the new road surface. It is unlikely that the latter is the cause of the low observed concentrations since this research has shown that 4-year old PFC pavement still had better runoff quality than a conventional asphalt roadway. As particles and particle associated pollutants accumulate within the pore structure it seems likely that more runoff will travel on the surface of the pavement resulting in concentrations that might not be significantly different from those observed in runoff from conventional asphalt pavements unless maintenance is performed to remove the accumulated material.

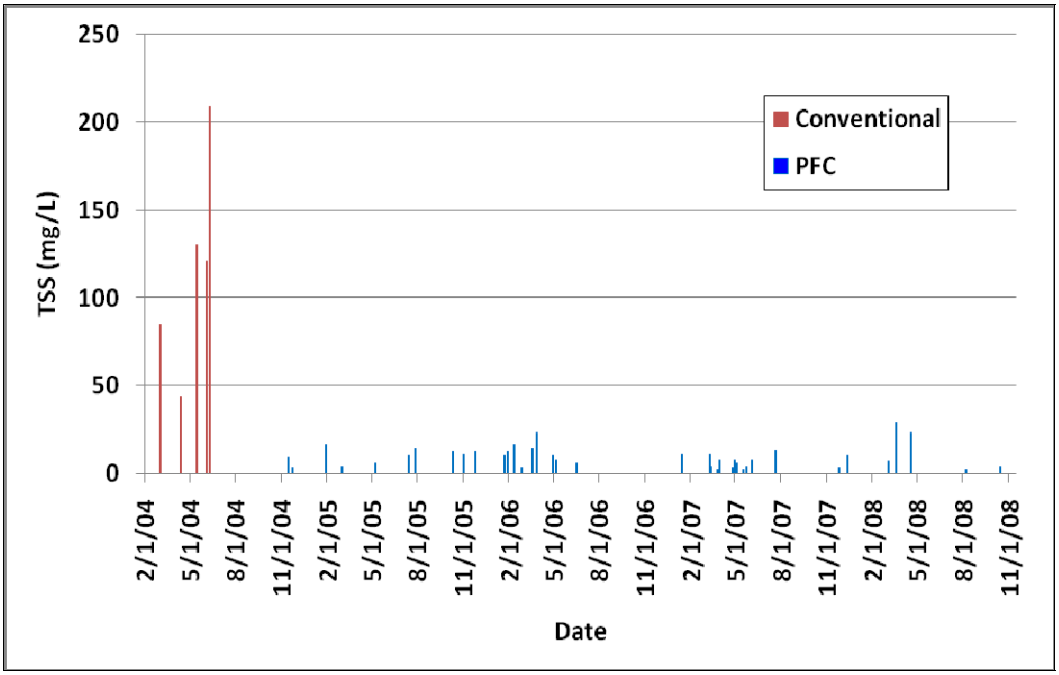

FIGURE 1 TSS concentrations for monitored events original site.

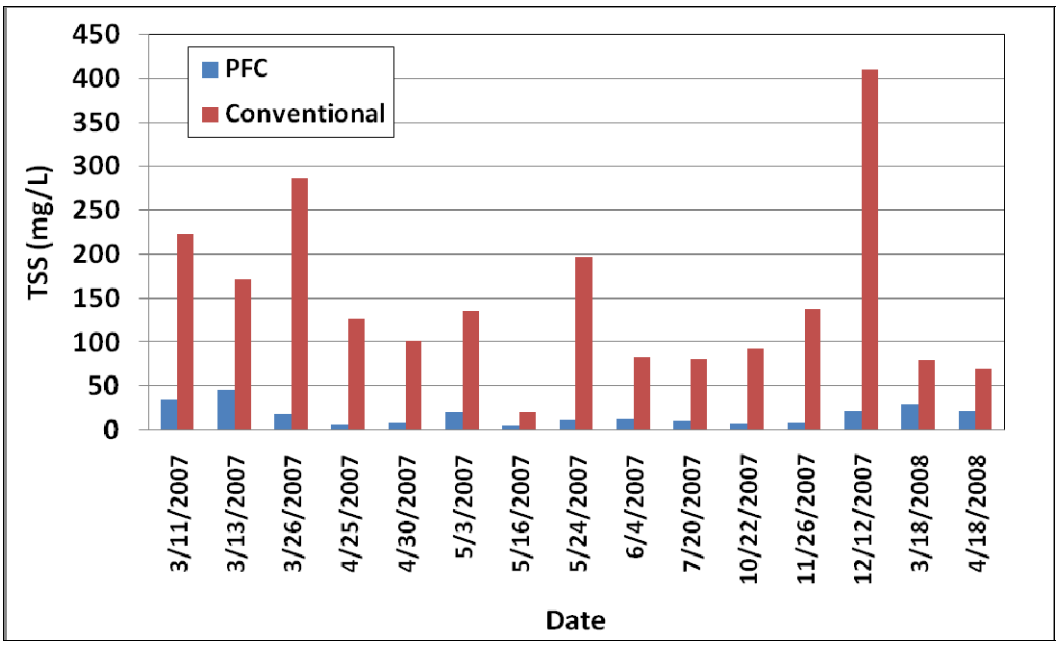

FIGURE 2 TSS concentrations for paired events at new site.

Laboratory analysis of the porosity and hydraulic conductivity of PFC core samples were conducted for both the small diameter and large diameter cores. Analysis of the porosity showed a decrease in effective porosity between the two core samples (taken within a year of each other). This decrease in porosity suggests the trapping of particles within the pore space as a removal method.

Determination of the PFC hydraulic conductivity is conducted by a series of constant head tests. Testing consists of submerging the PFC core in a water tank and placing the core between two pliable rubber membranes which create no flow boundaries on the top and bottom surfaces. A standpipe centered on the top surface of the PFC core serves as the inflow boundary. The outflow boundary is the circumference of the core. Therefore, flow enters the core in the vertical direction, and exits the core radially. A constant flow rate is established in the standpipe using a peristaltic pump. Steady state conditions are established, and the head in the standpipe is measured with an ISCO bubbler with the datum taken as the water elevation in the tank. Multiple flow rates are tested in order to create a curve of the standpipe head as a function of flow rate.

The Forchheimer equation can be modified for the global conditions of the core, since the hydraulic gradient and specific discharge cannot be easily measured for two-dimensional flow.

$$h_s = \alpha Q + \beta Q^2 \tag{1}$$

Equation (2) is the modified Forchheimer equation used for this research. The specific discharge has been changed to the total volumetric discharge, Q. The hydraulic gradient is taken as the head on the standpipe, h_s. These changes from the original Forchheimer equation alter the Forchheimer coefficients to the modified Forchheimer coefficients, α [T/L^2] and β [T^2/L^5]. Experimental data can be fit to Equation (2) for measured values of h_s and Q in order to determine α and β for each core. Figure 3 shows the results for a typical core. The data shown is in good agreement with the constant head equation using the modified Forchheimer equation, and shows a clear nonlinear relationship. In anticipation of the use of a falling head test in the field, a falling head test was conducted in the laboratory. The falling head curve shown in Figure 3 closely matches the constant head curve, particularly for the low flow rates which are more likely to be observed in the field.

In order to determine a representative core hydraulic conductivity, we must examine the equations governing flow in cylindrical coordinates. Carslaw and Jaeger (1959, pg. 215) provide an equation for the flow rate through an "infinite" core using a linear Darcy-type flow. The use of the method of images and the addition of a shape factor can be included to incorporate the finite core dimensions. The modified solution of Carslaw and Jaeger for a finite core is:

$$Q = 4Kh_s R_s F \tag{2}$$

Equation (3) relates the flow rate to the hydraulic conductivity K, the head on the standpipe, the radius of the standpipe R_s, and the shape factor F. If only the linear portion of the modified Forchheimer Equation (2) is considered, a representative

hydraulic conductivity can be obtained as a function of the core and standpipe geometry (F and R_s), as well as the modified linear Forchheimer coefficient given in Equation (4).

$$K = \frac{1}{4\alpha R_s F} \tag{3}$$

The resulting hydraulic conductivity obtained in the lab is on the order of 0.5 to 2.0 cm/s.

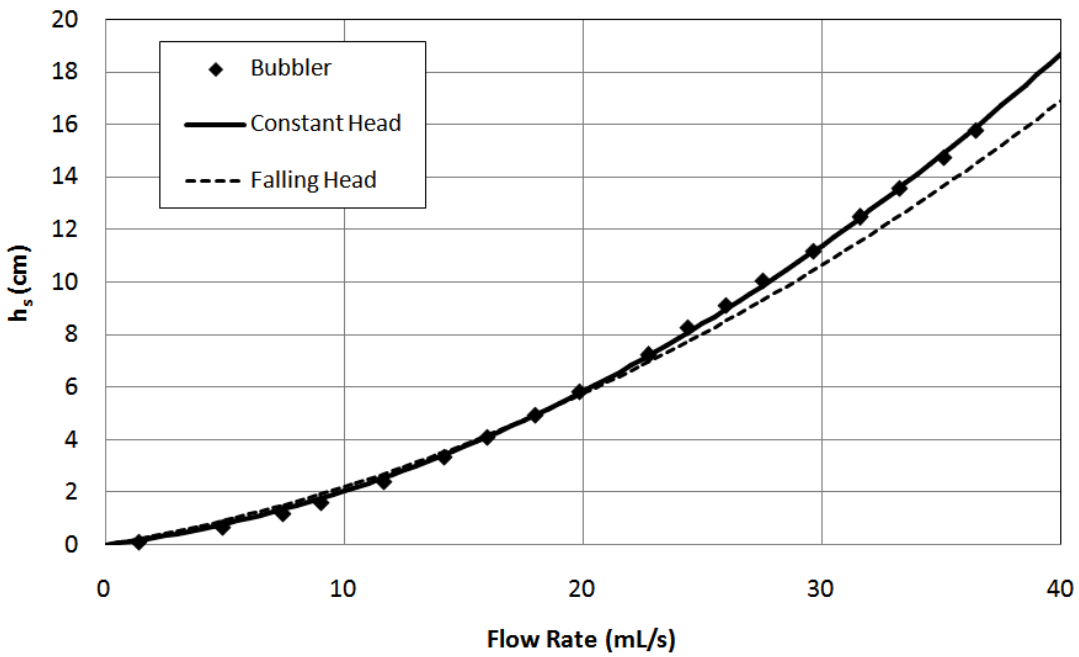

FIGURE 3 Head versus flow rate data and model fit for typical PFC core

Falling head tests are analyzed by solving the modified Forchheimer equation for the flow rate. Laboratory tests have shown that constant head and falling head tests result in approximately the same relationship, particularly at low flow rates, when a set of three time-head measurements are taken. Therefore, falling head tests in the field should provide an adequate alternative method for obtaining the in-situ hydraulic conductivity throughout the life of the PFC overlay. Current in-situ hydraulic conductivity test results are of the same magnitude as those obtained in the lab.

CONCLUSIONS

This research examined the quality of runoff from a conventional asphalt pavement and a permeable friction course. This research was unique in that it provides a direct comparison of the two surface types at the same research sites, and analyzes runoff produced during discreet storm events over a 4-year sampling period.

Concentrations of TSS, total metals and total phosphorus were found to be significantly lower in runoff generated from the PFC surface than in the runoff from the conventional hot mix asphalt surface. Average concentrations of TKN, COD, nitrate-nitrite and the dissolved forms of lead, zinc, and phosphorus show little change between the two surface types. From these results it is evident that the runoff generated from the PFC surface is of better quality than that from the traditional asphalt surface. Many regulatory agencies in the US require an 80 percent reduction in the amount of TSS discharged from new developments. The TSS removal observed during this project easily exceeds this threshold; consequently, this type of overlay may be considered a Best Management Practice (BMP) for highways in lieu of ponds, filters, or other structures commonly constructed to treat stormwater runoff. This improvement may be the result of several factors. Fewer pollutants may be derived from the bottoms of vehicles since splash and spray are reduced. In addition, these pollutants could be retained in the pores of the overlay and thereby prevented from leaving the paved area.

Core samples can be extracted from a layer of PFC and analyzed in the laboratory through a series of constant head tests to determine a representative hydraulic conductivity. The hydraulic conductivity depends on a shape factor which incorporates the geometry of the core assuming linear Darcy-type flow through the core. Laboratory testing has shown that nonlinear flow occurs in PFC for the large head values experienced during the constant head tests. The nonlinear effects can be modeled using a modified Forchheimer equation for the global conditions of the core. With the experimentally determined modified Forchheimer coefficients and the linear shape factor, a representative hydraulic conductivity can be calculated.

Additional research is needed in order to fully incorporate the nonlinear effects of flow through PFC. The approximations used here for determining the linear head distribution through a PFC core and the linear shape factor do not precisely represent the nonlinear flow observed in the lab constant head tests or field falling head test, nor the necessary boundary conditions. However, this provides a good first approximation for characterizing the hydraulic properties of PFC as well as a defined test procedure.

ACKNOWLEDGMENTS

The Texas Department of Transportation provided funding for this project under projects #0-4605 and 0-5220. Special thanks to Gary Lantrip of TxDOT's Austin Division. He has been a consistent proponent for the use of porous pavements and is currently overseeing continued research by TxDOT on its water quality benefits.

REFERENCES

Barrett, Michael, and Shaw, Christopher. (2007). Water Quality Benefits of a Porous Asphalt Overlay, Transportation Research Record, Vol. 2025, pg 127-134.

Berbee, R., Rijs, G., de Brouwer, R., & van Velzen, L. (1999). Characterization and Treatment of Runoff from Highways in the Netherlands Paved with Impervious and Pervious Asphalt. *Water Environment Research*, Vol. 71, No. 2, 183-190.

Capital Area Metropolitan Planning Organization. (2002). TxDOT 5 County Annual Average Daily Traffic Counts [Data file]. Retrieved March 20, 2005 from http://www.campotexas.org/programs_gis.php

Carslaw, H.S. and J.C. Jaeger (1959): *Conduction of Heat in Solids*, Second Ed., Oxford University Press, Amen House, London.

Charbeneau, R.J. and M.E. Barrett (2008): "Drainage Hydraulics of Permeable Friction Courses", *Water Resources Research*, Vol. 44, W04417.

Irish, L. B., Jr., Barrett, M. E., Malina, J. F., Jr., & Charbeneau, R. J. (1998). Use of Regression Models for Analyzing Highway Storm-Water Loads. *Journal of Environmental Engineering*, Vol. 124, No. 10, 987-993.

Jackson, T.J. and R.M. Ragan (1974): "Hydrology of Porous Pavement Parking Lots", *Journal of the Hydraulics Division*, Vol. 100, HY 12, pg. 1739-1752.

Mahler, B. J., Van Metre, P. C., & Wilson, J. T. (2004). *Concentrations of Polycyclic Aromatic Hydrocarbons (PAHs) and Major and Trace Elements in Simulated Rainfall Runoff from Parking Lots, Austin, Texas, 2003*. Open File Report No. 2004-1208. U.S. Department of the Interior & U.S. Geological Survey. Retrieved January 13, 2005 from http://tx.usgs.gov/.

Pagotto, C., M. Legret and Le Cloirec, P. (2000). Comparison of the Hydraulic Behaviour and the Quality of Highway Runoff Water According to the Type of Pavement. *Water Resources*, Vol. 34, No. 18, pp. 4446-4454.

Ranieri, V. (2002): "Runoff Control in Porous Pavements", *Transportation Research Record*, No. 1789, pg. 46-55.

Ranieri, V. (2007): "The Functional Design of Porous Friction Courses", *2007 Annual Meeting of the Transportation Research Board*.

Stotz, G., and Krauth, K. (1994). The Pollution of effluents from pervious pavements of an experimental highway section: First results. *The Science of the Total Environment*, Vol. 146/147, 465-470.

Tan, S.A., T.F. Fwa, and K.C. Chai (2004): "Drainage Considerations for Porous Asphalt Surface Course Design", *Transportation Research Record*, No. 1861, pg. 142-149.

Water Quality Design Storms for Stormwater Hydrodynamic Separators

Victoria J. Fernandez-Martinez[1] and Qizhong Guo[2]

[1]Rutgers University, Department of Civil and Environmental Engineering, 623 Bowser Road, NJ 08854

[2]Corresponding Author, Rutgers University, Department of Civil and Environmental Engineering, 623 Bowser Road, NJ 08854; Phone: 732-445-4444; Fax: 732-445-0577; E-mail: Qguo@rci.rutgers.edu

Abstract

When measure of the device performance is based on laboratory data, NJCAT calculates the average annual removal efficiency using the NJDEP-specified weighting factors. In this study, ten years of precipitation records were used to quantify frequency distributions of runoff volumes/depths as well as runoff peak flow rates. The SWMM model was used to simulate the runoff events produced by the given precipitation events. The model results indicate that the weighting factors, based on frequency distribution of the peak runoff rates normalized by the peak runoff rate generated by the uniform-intensity water quality design storm, are close to the NJDEP-specified weighting factors. The impact of using two different water quality design storms, uniform vs. non-uniform intensity distribution, to size an interim-certified hydrodynamic separator was also evaluated. The SWMM model was used to continuously simulate solids loading to the treatment device. The lab-measured relationship between flow rate and removal efficiency was used to specify the removal rate of solids within the storm event. The model results also indicate that sizing with the uniform-intensity design storm would achieve a removal efficiency close to the one verified. Sizing with the non-uniform intensity design storm, although could be taken as a conservative approach, would achieve the removal efficiency considerably higher than the one verified.

1. Introduction

In the State of New Jersey the Stormwater Management Rules (NJDEP 2004a) require Stormwater Best Management Practices (BMPs), for major new developments, to achieve an annual average of Total Suspended Solids (TSS) removal efficiency equal or greater than 80%, and for major re-developments, 50% TSS removal. Regulations require this efficiency as an annual average. Therefore, the treatment devices do not have to be designed to achieve 80 or 50 percent of TSS reduction for every individual storm event that occurs in a year.

The rules (NJAC 7:8-5.5) also specify a “water quality design storm” which consists of 1.25 inches of rainfall falling non-uniformly over two hours. This design storm substituted the one specified in NJAC 5:21-7.6 and 7:13-2.8(b), defined as 1.25 inches of rainfall falling in two hours with a uniform intensity of 0.625 in/hour. According to the proponents of the non-uniform quality storm, although the previous one provided “sound basis for the design of stormwater

quality treatment facilities that require an estimate of the total runoff volume that will flow to the facility" it did not provide information for the design of those facilities that required an accurate estimate of the runoff peak flow rate that would flow through them. The non-uniform water quality storm provides estimates of total runoff volume as well as peak runoff rate for the same storm event.

Based on the described regulations the New Jersey Best Management Practices Manual (NJDEP 2004b) indicates that the design of flow-through devices, such as the hydrodynamic separators, must be based on the runoff peak flow rate generated by the current non-uniform water quality design storm. Therefore under such specification, project engineers will size the devices to achieve the required solid removal efficiency when the treatment flow rate, in the drainage area, equals the runoff peak flow rate generated by the water quality design storm, with non-uniform intensity distribution.

This study intends to compare the hydrodynamic separator sizing methodology based on the uniformly distributed quality design storm with the sizing methodology based on the non-uniformly distributed design storm.

Two approaches were taken to determine the removal efficiency that a hydrodynamic separator could achieve when sized with different design storms. The first approach consisted of calculating the removal efficiency of the device using weight factors which are based on the frequency distribution of the runoff depths and peak runoff rates generated by precipitation over 10 years. The second approach consisted of continuous simulation of the solids removal performance of a hydrodynamic separator during 10 years of precipitation events.

2. Methodology

2.1. Curve Fitting of Hydrodynamic Separator Performance

Many hydrodynamic separator manufacturers have tested the solid removal performance of their devices at full scale and under laboratory controlled conditions. The results from many of those tests have been submitted to the New Jersey Corporation of Advanced Technology (NJCAT) for verification and performance of many devices has been certified by the New Jersey Department of Environmental Protection (NJDEP).

When this study was started, the NJCAT verification report most recently available corresponded to the FloGard® Dual-Vortex Hydrodynamic Separator (model DVS-48), manufactured by Kristar Enterprises Inc. Therefore, the FloGard® was the device selected for evaluating the impacts of using different water quality design storms to size the hydrodynamic separators.

The removal efficiency of the device was tested following the Total Suspended Solids Laboratory Test Procedure developed by NJDEP (2003). Tests were run at flow rates of 25, 50, 75, 100 and 125 % of the FloGard® DVS-48 treatment flow rate (280 gpm) (NJCAT 2007).

Figure 1 shows the TSS removal efficiencies measured at all the five tested flow rates and at three TSS influent concentrations (100 mg/L, 200 mg/L, and 300 mg/L). TSS was measured as Suspended Sediment Concentration (SSC). It can be observed that the solids removal efficiency

of the device decreases as the operating flow rate increases and the removal efficiency does not vary significantly with the influent concentrations. An exponential regression of the measured removal efficiencies vs. the operating flow rates yields the following mathematical expression for the model DVS-48:

$$RE = 100e^{-0.00299Q}$$

where

RE = removal efficiency (%)

Q = operating flow rate (gpm)

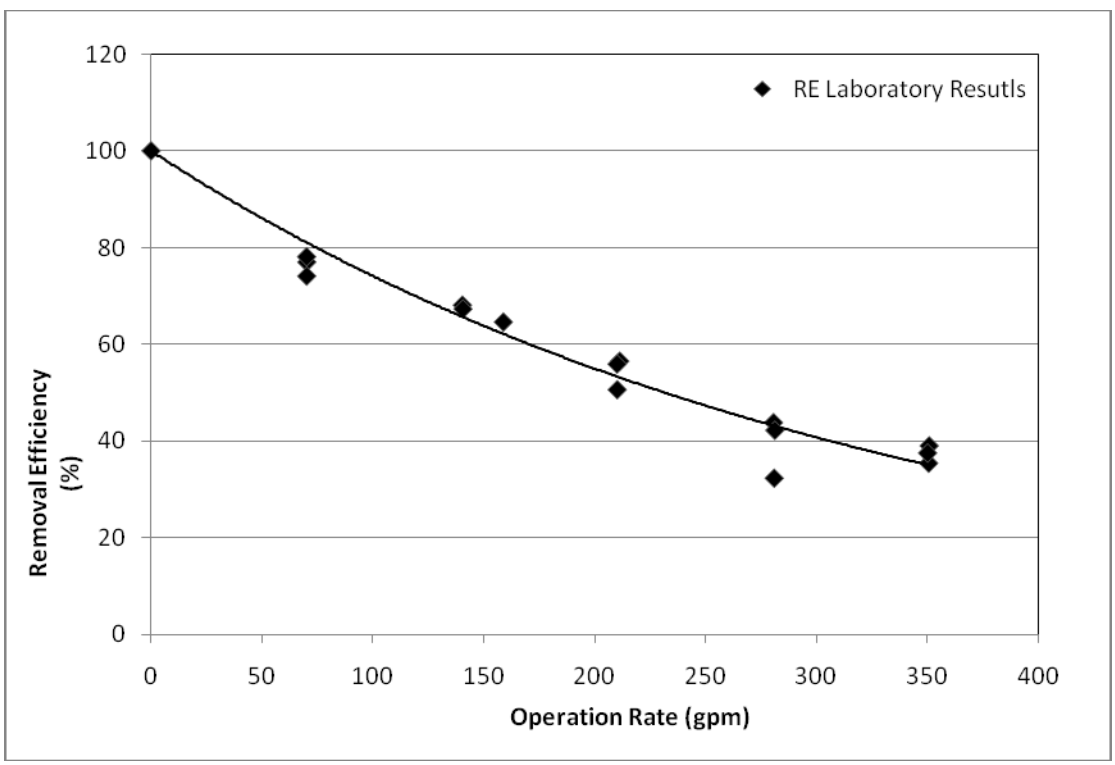

Figure 1. Measured FloGard® SSC Removal Efficiencies vs. Operating Flow Rates

2.2. Collection of Precipitation Data

Hydrodynamic separators on site receive stormwater runoff under non-uniform flow rates that change in small time steps. Such variations affect the removal efficiency of the device since the removal performance of the device depends on its influent flow rate, as discussed above. For that reason precipitation data with small-time-interval readings was needed for the intended simulation. The National Climatic Data Center (NCDC) reports precipitation readings every 15 minutes, for 19 stations in New Jersey. At the time of this study, reliable readings with even smaller time steps were not available from national or regional climatologic services.

Trenton, New Jersey was the meteorological station selected to collect 10 years of precipitation data from the NCDC website since New Jersey Rainfall Intensity-Duration-Frequency Curves were developed from Trenton rainfall data between 1913 and 1975 (NJDEP 2004b). The available data at the mentioned website covered the period between 1977 and 2001.

The daily data of each year was summed in order to calculate the annual precipitations to select 10 years in a row with an annual precipitation close to the long term annual mean precipitation in New Jersey, which is 40.24 inches, according to the Office of the New Jersey State Climatologist. Years 1981 to 1990 were selected, with annual rainfalls of 45.0, 37.1, 46.2, 46.1, 27.4, 37.0, 50.9, 33.5, 49.4, and 42.2 inches, respectively. Average annual precipitation during the studied period was 41.48 inches, close to the long term average.

2.3. Determination of Weighting Factors

Stormwater Runoff Continuous Simulation

EPA Storm Water Management Model (EPASWMM), version 5.0, was used to simulate the peak flow rates generated by the collected precipitation data over a defined subcatchment. The properties of the subcatchment introduced in SWMM intended to represent highly impervious drainage areas, such as parking lots, where hydrodynamic separators are usually installed. The subcatchment was defined as having 80% of impervious area, 20% of pervious area, evaporation of 0.1 in/day, impervious depression storage of 0.1 inches, pervious depression storage of 0.2 inches and slope of 0.1%. The infiltration loss was calculated in SWMM using the Horton Method.

The drainage area of the subcatchment, which would be an input to SWMM, was calculated assuming that the runoff peak flow rate, generated by the former New Jersey water quality design storm (uniform intensity of 0.625 in/hour), was equal to the treatment operating rate of the FloGard® DVS-48, i.e., 280 gpm (0.63 cfs). Applying the Rational Method and assuming a runoff coefficient of 0.8, the subcatchment area obtained was 1.26 acres. From the SWMM modeling results, the uniform design storm generated a peak flow of 0.638 cfs in a drainage area of 1.26 acre. Such peak flow was slightly higher than the FloGard® treatment operating rate. For that reason a smaller drainage area of 1.25 acre was used. This drainage area generated a peak flow rate of 0.63 cfs.

Frequency Distribution of Runoff Volumes/Depths

After providing SWMM with the collected precipitation data and defining the subcatchment area to study, the following steps were performed:

1. The model was run using the collected 10-year precipitation data.
2. A rank ordered report was obtained from SWMM. The report contained the magnitude of the total volume of each runoff event, the starting date and time, the duration, its exceedance frequency and the return period in years.
3. The runoff volume was divided by the area of the subcatchment in order to obtain the stormwater runoff depth.

4. The runoff volumes generated by the uniform and non-uniform design storms were determined by SWMM and the correspondent depths were calculated. Since the obtained depths had almost the same values, an average design storm runoff depth was calculated.
5. The runoff depths generated by the collected precipitation data were expressed as a percentage of the average depth generated by the design storms.
6. The obtained values were ranked from the lowest to the highest in order to obtain the probability (P) of values being equal to or less than the ranked one. The probability was calculated using the Weibull plotting position formula.
7. The runoff depths, expressed as a percentage of the average runoff depth generated by the design storms, were plotted versus their probability of no-exceedance.

Frequency Distribution of Runoff Peak Rates

In order to obtain frequency distribution of the peak runoff flow rates the following steps were performed:

1. The runoff peak flow rate that the water quality design storm of uniform intensity would generate over the defined area was obtained using SWMM.
2. The runoff peak flow rate that the water quality design storm of non-uniform intensity would generate over the defined area was obtained with SWMM.
3. The peak runoff flow rates generated by the collected precipitation data over 10 years were simulated by SWMM.
8. A rank ordered report was obtained. The report contained the magnitude of peak flow rates of each storm event, the starting date and time, the duration, the exceedance frequency and the return period in years.
4. The runoff peak flow rates were expressed as percentages of the peak flow rates obtained from the simulated design storm events. Two sets were obtained.
5. The obtained values were ranked from the lowest to the highest in order to obtain the probability of values being equal to or less than the ranked one. The probability was calculated using the Weibull plotting position formula.
6. The runoff peak flow rates, expressed as percentages of the peak runoff rate generated by the uniformly distributed design storm, were plotted versus their probability of no-exceedance.
7. The runoff peak flow rates, expressed as percentages of the peak runoff rate generated by the non-uniformly distributed design storm, were plotted versus their probability of no-exceedance.

Weighting Factors

Figure 2 shows the frequency distribution of the runoff depth and the peak flow rates, generated by the collected 10-year precipitation data, expressed as percentages of the average runoff depth as well as the peak flow rates generated by the uniform and non-uniform design storms, respectively.

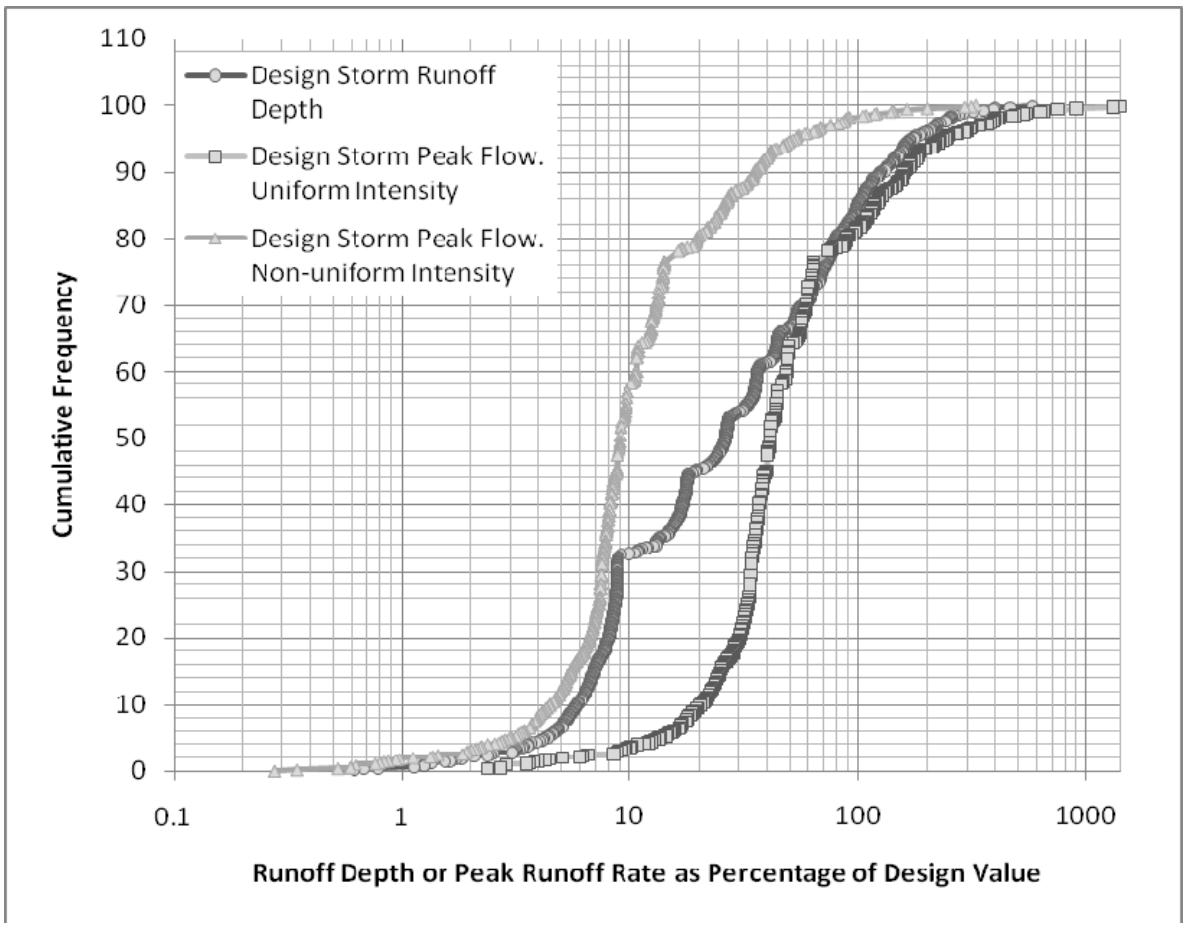

Figure 2. Frequency Distribution of Runoff Depths and Peak Flows

Table 1 shows the cumulative frequency distribution of the runoff depths produced by the collected precipitation data, expressed as percentages of the average runoff depth generated by the water quality design storms (0.930 inches). The same table also shows the frequency distribution of peak runoff flow rates expressed as percentages of the peak flow rates generated by the uniformly and the non-uniformly distributed water quality design storms (0.63 cfs and 2.85 cfs, respectively).

The difference between two adjacent cumulative frequencies is the probability of occurrence for range between two adjacent design values, and it is defined as the weighting factor. Five weighting factors for the ranges of 0-25, 25 -50, 50-75, 75-100 and 100-125 % of the design value were calculated. These ranges of flows were evaluated by the FloGard® manufacturer, as required by the NJDEP lab testing procedure. Table 2 shows the obtained weighting factors. The probability (thus the weighting factor) for the range larger than 125% of the design value was added to the probability (thus the weighting factor) for the range between 100-125%.

Table 1. Cumulative Frequency Distribution of Runoff Depth and Peak Flow Rates Generated by Precipitation over Ten Years (expressed as percentages of the design values)

% of Design Value	Cumulative Frequency (%)		
	Runoff Depth	Peak Flow Rate (uniform design storm)	Peak flow rate (non-uniform design storm)
25	48.00	13.00	84.05
50	66.81	60.00	94.60
75	78.00	78.00	96.87
100	85.75	81.50	98.00
125	90.31	83.50	98.60

Table 2. Weighting Factors of Runoff Depth and Peak Flow Rates Generated by Precipitation over Ten Years (expressed as percentages of the design values)

% of Design Value	Weighting Factors		
	Runoff Depth	Peak Flow Rate (uniform design storm)	Peak flow rate (non-uniform design storm)
25	0.48	0.13	0.84
50	0.19	0.47	0.10
75	0.11	0.18	0.03
100	0.08	0.04	0.01
125	0.14	0.18	0.02

2.4. Calculation of Weighted Removal Efficiency from Weighting Factors

The FloGard® weighted removal efficiency was calculated using each set of the weighting factors. Each weighting factor was multiplied by the removal efficiency measured from the laboratory tests at the corresponding flow rate (25, 50, 75, 100, and 125% of the device treatment rate, respectively). The total weighted removal efficiency is the sum of the five products.

2.5. Continuous Simulation of Removal Efficiency

Stormwater Runoff Simulation

The stormwater runoff from two subcatchments of different sizes was simulated using SWMM. The area of each subcatchment was specified according to two sizing criteria. The first criterion considered the treatment flow rate of the FloGard® DVS48 as equal to the peak flow rate generated by the water quality design storm with a uniform intensity of 0.625 in/hr. The second criterion considered the treatment rate of the FloGard® DVS-48 as equal to the peak flow rate generated by the water quality design storm with a non-uniform intensity distribution.

The areas were calculated using the Rational Method and assuming a runoff coefficient of 0.8. The first sizing criterion yielded a subcatchment area of 1.25 acres and the second sizing criterion yielded a subcatchment area of 0.25 acre. The subcatchments were meant to represent a typical watershed were the hydrodynamic separators are usually installed. The subcatchments were defined as having 80% of impervious area, 20% of pervious area, 0.1 in/day of evaporation, 0.1 inches of depression storage in the impervious zone, 0.2 inches in the pervious zone, and a 0.1 % slope. The infiltration loss was calculated in SWMM using the Horton Method.

Water Quality Simulation

The pollutant buildup was simulated in SWMM assuming a linear accumulation of the dust on the subcatchment surfaces (Huber and Dickinson 1988).

According to New Jersey BMPs Manual (NJDEP 2004b), an annual accumulation of 200 pounds per acre can occur in a commercial area. Dividing this value by 365 days a daily accumulation rate of 0.55 lbs/day was obtained. This value was used in the linear dust accumulation equation.

SWMM simulates the washoff process of the accumulated pollutants through the following expression:

$$C_t = C_w \times r^w \times P$$

where

C_t= pollutant washed off at time t (pounds)

P = quantity of constituent still available on the surface at time t (pounds)

C_w= washoff coefficient

r = runoff rate (cfs)

w = modeling exponent

The parameters C_w and w are inputs to SWMM by the user. The remaining material on the surface at the end of a time step is calculated by SWMM during the simulation.

In this study, three different cases were simulated by varying the values of the parameters C_w and w in order to generate concentration distributions that reflected the first flush effect (FF) during the storm event.

However there is no standard quantitative definition of the first flush effect. Different authors proposed different mass-based indicators. For this reason, three pairs of coefficients were selected to generate pollutant washoff distributions that would reflect the most common definitions of the mass-based first flush effect. Case 1 simulates a FF of 80% total pollutant load transported by the first 20% of the total runoff volume (Sansalone and Chad 2004). Case 2 simulates a first flush effect of 80% of the total pollutant load transported by the first 30% of the total runoff volume (Bertrand-Krajewski, et al. 1998) and case 3 simulates a first flush effect of 80% of the total pollutant load transported by the first 40% of the total runoff volume.

Among all the continuously simulated storm events, three were selected to evaluate distribution of the solids mass (solids concentration multiplied by runoff volume). These events were selected because their peak flow frequency exceedance was close to 50%, according to SWMM statistic report for subcatchment 1 (1.25 acres). That is, they are "average" storm events. Different exponent-coefficient combinations were tried until the desired distributions were achieved.

Table 3 shows the selected coefficients for the simulation and the resulted distribution of the solids mass.

Table 3. Study Cases of Pollutants Washoff

Case	W	C_w	% Volume at 80% mass
1	1.6	50	20
2	1.7	50	30
3	1.9	50	40

A simulation of the removal efficiency of the device was additionally performed for the case when 80% of the mass is transported by 80% of the volume, i.e., the runoff mass is uniformly distributed through the event. The washoff process was modeled using an exponent (w) equal to 2.5 and a washoff coefficient (C_w) of 2.0.

Removal Efficiency Continuous Simulation

As described above, the laboratory test of the FloGard® Dual Vortex showed that its removal efficiency depends on the flow rate. If the flow rate is less than the hydraulic capacity (560 gpm for the tested model DVS-48), the fitted relationship between the removal efficiency and the flow rate is assumed to be applicable. After the hydraulic capacity is exceeded, the removal efficiency is assumed to be zero since the removal efficiency of the treated part of the flow is small and the bypassed part will not receive any treatment. However, the use of positive and

zero removal efficiency may not be appropriate if a significant bottom sediment resuspension occurs under the flow beyond the tested maximum flow rate. The removal efficiency could actually be negative if a severe sediment resuspension occurs during high flows that would pass through an online system.

At the end of the event the total mass of pollutant that entered the device will equal the sum of the calculated influent mass during each time step of the entire storm (= the simulated flow rate multiplied by the simulated concentration and the time interval). The total mass removed from the storm water runoff will equal the sum of the mass removed during each time step of the entire storm (= the influent mass multiplied by the removal efficiency at the specific flow rate at that time step). The removal efficiency of the device for the entire event is obtained by dividing the total mass removed by the total mass that entered the device. See Fernandez (2008) for additional modeling details.

3. Results and Discussion

3.1. Calculated Weighted Removal Efficiency

The weighted removal efficiencies calculated using three different sets of weighting factors are listed in Table 4.

Table 4. FloGard® DVS-48 Weighted Removal Efficiencies based on Frequency Distribution of Runoff Depths and Peak Flow Rates, Expressed as Percentages of Design Values.

% Operating Rate	Av Removal Efficiency	Runoff Depth		Runoff Peak Rate, Uniform Design Storm		Runoff Peak Rate, Non-uniform Design Storm	
		Weighting Factors	Removal Efficiency	Weighting Factors	Removal Efficiency	Weighting Factors	Removal Efficiency
25	74.6	0.48	35.81	0.13	9.70	0.84	62.66
50	67.6	0.19	12.84	0.47	31.77	0.10	6.76
75	55.6	0.11	6.12	0.18	10.00	0.03	1.67
100	43.8	0.08	3.50	0.04	1.75	0.01	0.44
125	38.7	0.14	5.42	0.18	6.97	0.02	0.77
Total weighted removal efficiency		63.69%		60.19%		72.30%	

The results shown in Table 4 suggest that the weighted removal efficiency (63.69%) calculated from the weighting factors based on frequency distribution of runoff depths is close to that (60.19%) calculated from the weighting factors based on frequency distribution of peak runoff flow rates expressed as percentages of the peak runoff rate generated by the uniform intensity design storm. However, the weighted removal efficiency (72.30%) calculated from the weighting factors based on frequency distribution of peak runoff flow rates expressed as percentages of the peak runoff rate generated by the non-uniform intensity design storm is considerably larger than that normalized by the uniform intensity design storm (60.19%). It is approximately 12% larger in terms of absolute difference.

The weighted removal efficiency (60.19%) calculated from the weighting factors based on frequency distribution of peak runoff flow rates expressed as percentages of the peak runoff rate generated by the uniform intensity design storm is strikingly similar to that (60%) calculated using the NJDEP-specified weighting factors (NJCAT 2007).

The performance claim verified by NJCAT reads:

"The FloGard® Dual-Vortex Hydrodynamic Separator, Model DVS-48, at a flow rate of 280 gpm (0.63 ft3/s), has been shown to have a 60% total suspended solids (TSS) removal efficiency, measured as suspended solids concentration (SSC) (as per the NJDEP methodology for calculation of treatment efficiency) using NJDEP specified material with an average d50 particle size of 70 microns, an average influent concentration of 202 mg/L and 100% initial sediment loading in laboratory studies using simulated stormwater."

The weighted removal efficiency of 60% was calculated using the NJDEP-specified weighting factors.

3.2. Continuously Simulated Removal Efficiency

Tables 5 and 6 summarize the results of simulated total influent and effluent mass and the correspondent removal efficiency for two different drainage areas (1.25 acres and 0.25 acres, respectively). See Fernandez (2008) for detailed model results.

The SWMM continuous simulation indicates the FloGard® model DVS-48 can achieve an average annual removal efficiency of approximately 70%, on a drainage area of 1.25 acres sized from the peak runoff flow rate generated by the design storm with uniform intensity.

The simulation shows that the same device can achieve a removal efficiency of approximately 90% over a drainage area of 0.25 acres sized from the peak runoff flow rate generated by the design storm with non-uniform intensity. The use of uniform rainfall distribution is already a conservative criterion with the simulated approximately 70% removal efficiency that is larger than the verified 60%. The use of non-uniform rainfall distribution is even more conservative with the simulated approximately 90% removal efficiency that is much larger than the verified 60%.

Table 5. Simulated Influent Mass, Effluent Mass and Removal Efficiency for the FloGard® DVS-48 in Subcatchment 1 (1.25 acres)

	Subcatchment 1		
Case	Influent Mass (lbs)	Effluent Mass (lbs)	Removal Efficiency (%)
1	2352.78	692.09	70.58
2	2352.45	713.70	69.66
3	2352.45	765.94	67.44
Runoff mass uniformly distributed	2345.91	1042.16	55.58

Table 6. Simulated Influent Mass, Effluent Mass and Removal Efficiency for the FloGard® DVS-48 in Subcatchment 2 (0.25 acres)

	Subcatchment 2		
Case	Influent Mass (lbs)	Effluent Mass (lbs)	Removal Efficiency (%)
1	477.61	47.45	90.06
2	477.61	48.56	89.83
3	477.60	50.73	89.38
Runoff mass uniformly distributed	474.76	121.69	74.36

For the drainage area of 1.25 acres sized with the uniform-intensity design storm and in the case where the runoff mass was assumed to be uniformly distributed within the storm event, the continuous simulation yielded a removal efficiency of 55.58%, which is reasonably close to the removal efficiency (60%) calculated using the NJDEP-specified weighting factors and verified by NJCAT. This result is consistent with the assumption behind application of the weighting factors that the runoff mass is uniformly distributed through the event.

It should be cautioned that the above-described SWMM modeling results may not fully represent the field performance of the device. Size and density of the particles used in the lab testing and the lab-measured flow rate-removal efficiency relationship that was an input to the model may not accurately represent the field conditions.

4. Conclusions

The current NJ stormwater rules define the water quality design storm as 1.25 inches of rainfall non-uniformly distributed over two hours. This is a significant change from the previous definition of uniform rainfall distribution. The current definition leads to a higher peak runoff rate in small watersheds in comparison to the previous definition although the runoff volume remains essentially the same.

The runoff frequency analysis suggests that setting design treatment flow rate equal to the peak flow rate generated by the uniform-intensity water quality design storm is more consistent with the use of existing weight factors in calculating the average annual solids removal efficiency. Use of the non-uniform intensity water quality design storm to size the treatment device is probably too conservative. The SWMM modeling of the solids removal performance also suggests that sizing the treatment device with the uniform intensity water quality design storm is more appropriate than sizing with the non-uniform intensity design storm.

5. Acknowledgements

The first author was sponsored by the Fulbright Program while the research was conducted at Rutgers University. The support is gratefully acknowledged.

6. References

Bertrand-Krajewski, J. L., Ghassam, C. and Agnes, S. (1998). "Distribution of pollutant mass vs. volume in stormwater discharges and the first flush phenomenon". *Water Research,* 32(8), 2341-2356

Fernandez-Martinez, V. J. (2008). *Water Quality Design Storms for Stormwater Hydrodynamic Separators*, MS Thesis, Rutgers University, New Brunswick, NJ, May.

Huber, W and Dickinson, R (1988). *Storm Water Management Model Version 4, User's Manual.* EPA/600/3-88/001a (NTIS PB88-236641/AS), US Environmental Protection Agency, Athens, GA.

New Jersey Corporation of Advanced Technology (NJCAT) (2007). *FloGard® Dual-Vortex Hydrodynamic Separator, Verification Report*, August.

New Jersey Department of Environmental Protection (2003). *Total Suspended Solids Laboratory Testing Procedure*, December.

New Jersey Department of Environmental Protection (2004a). *N.J.A.C. 7:8 Stormwater Management Rules*, February.

New Jersey Department of Environmental Protection (2004b), *New Jersey Stormwater BMP Manual*, April.

Sansalone, J. and Chan, M (2004) "First flush concepts for suspended and dissolved solid in small impervious watersheds." *Journal of Environmental Engineering,* 130 (11), 1301-1314.

Water Sustainability Index: Application of CWSI for Ahwaz County

J. Attari[1] and S.A. Mojahedi[2]

[1]Assistant Professor, Water Engineering Department, Power and Water University of Technology, P.O. Box 16765-1719, Tehran, Iran; email: attari@pwut.ac.ir
[2]Expert, Water Resources Planning Department, Ministry of Energy, Valiasar and Neyayesh crossing, Tehran, Iran; email: ali.mojahedi@gmail.com

ABSTRACT

Sustainability of water resources is vital especially for developing countries such as Iran which are located in the Middle East and North Africa (MENA) region where water is scarce. To balance the high demand of water for economical growth and at the same time preserve the environment for present and future generations, sustainability of water resources should be considered by monitoring and data mining. For this purpose, several quantified indices have been proposed and applied world wide recently. In this paper, the Canadian Water Sustainability Index (CWSI) proposed by PRI, has been trailed for the case of Ahwaz County, a community located in South West of Iran fed by Karun River. Required data for the composite CWSI score which is the average of five major theme-based components (i.e. resource, ecosystem health, infrastructure, human health capacity) was collected according to the PRI evaluation method. In addition to the standardized CWSI, the final index was also calculated considering weight estimation for the five components by pair-wise comparison, using Expert Choice version 2000. Results showed that application of this index as a policy tool, with some modifications in weights, was satisfactory for the educational case study and could be replicated for other communities in Iran.

Keywords: Water Resources Sustainability, Sustainability Index, CWSI

INTRODUCTION

Sustainability of water is vital for preservation of this resource in the world. This is more prominent for developing countries and especially for those located at the Middle East and North Africa (MENA) Region, where water is scarce (World Bank 2007). Iran is one of these countries which suffers from limited renewable water supply while intends to develop its economy which highly demands water resources. To balance these two contradictory factors and at the same time preserve the environment for present and future generations, sustainability of water resources should be considered by monitoring and data mining.

Mays (2007) defines water resources sustainability as : "the ability to use water in sufficient quantity and quality from the local and global scale to meet the needs of humans and environmental ecosystem for the present and future to sustain life, and to protect humans from the damages brought about by natural and human-caused disasters that affect sustaining life." Whichever definition is used, there is a

need for measurement or quantification of water impacts on the environment for present and future generations so that plans for sustainable water resources management can be carried out accordingly.

Sustainability indicators and composite index are increasingly recognized as a useful tool for policy making and public communication in conveying information. They simplify, quantify, analyze and communicate otherwise complex and complicated information. There are currently several initiatives working on the frame works for sustainable development in different fields such as environment (Singh et al. , 2008).

The Canadian Water Sustainability Index (CWSI) has been developed by the Policy Research Initiative (PRI) for evaluating the well-being of Canadian communities with respect to fresh water resources. This index integrates a range of water-related data and information into a series of 15 indicators, classified in five major theme-based components (i.e. resource, ecosystem health, infrastructure, human health capacity). The CWSI which is the arithmetic average of scores of the indicators provides a holistic profile of a community's key water issues, allowing for comparison and analysis (PRI, 2007).

The primary objective of this paper is to assess the water resources sustainability and well being in the Ahwaz County, a community located in South West of Iran fed by Karun River. In the absence of any local index, the Canadian Water Sustainability Index (CWSI) has been trailed for this purpose.

METHODOLOGY

In the absence of any local index, the CWSI has been trialed for the Ahwaz County in Iran. Most of the water and wastewater data for calculation CWSI indicators in this community were collected form the local (AWWC, 2006) and national sources (NWWEC, 2006), while the demographic information were acquired from the latest census carried out (SCI, 2006).

In this study, the standard CWSI score which is the simple average of five major theme-based components was first calculated according to the PRI evaluation method. Furthermore, the index was also calculated considering weight adjustments. For this purpose, importances of five components relative to each other were first estimated on the basis of an internal data analysis and weights were further calculated by pair-wise comparison, using Expert Choice version 2000. In this regard, arithmetic weights were considered for the components. On this basis the final CWSI of the five components were calculated according to the following formula:

$$CWSI = \frac{\sum_{i=1}^{N} w_i \times X_i}{\sum_{i=1}^{N} w_i} \tag{1}$$

where: X_i refers to component i of the index for a particular community

w_i is the weight applied to that component.

Finally the standardized CWSI score was compared with the weighted average.

STUDY AREA

Ahwaz City is the center of Khuzestan province, located in South West of Iran (Figure 1). Ahwaz County (City of Ahwaz and subsidiary cities) has a population of 1,166,287 people (NWWEC, 2006). Karun River, the most important river of Iran, passes through this county which is located about 12 meters above the sea level (Figure 1). This river is the main source of supplying drinking water to the citizens and abstraction from the ground water resources is negligible. Total length of the water supply network is 2349 km which covers 278,000 connections (AWWC, 2006).

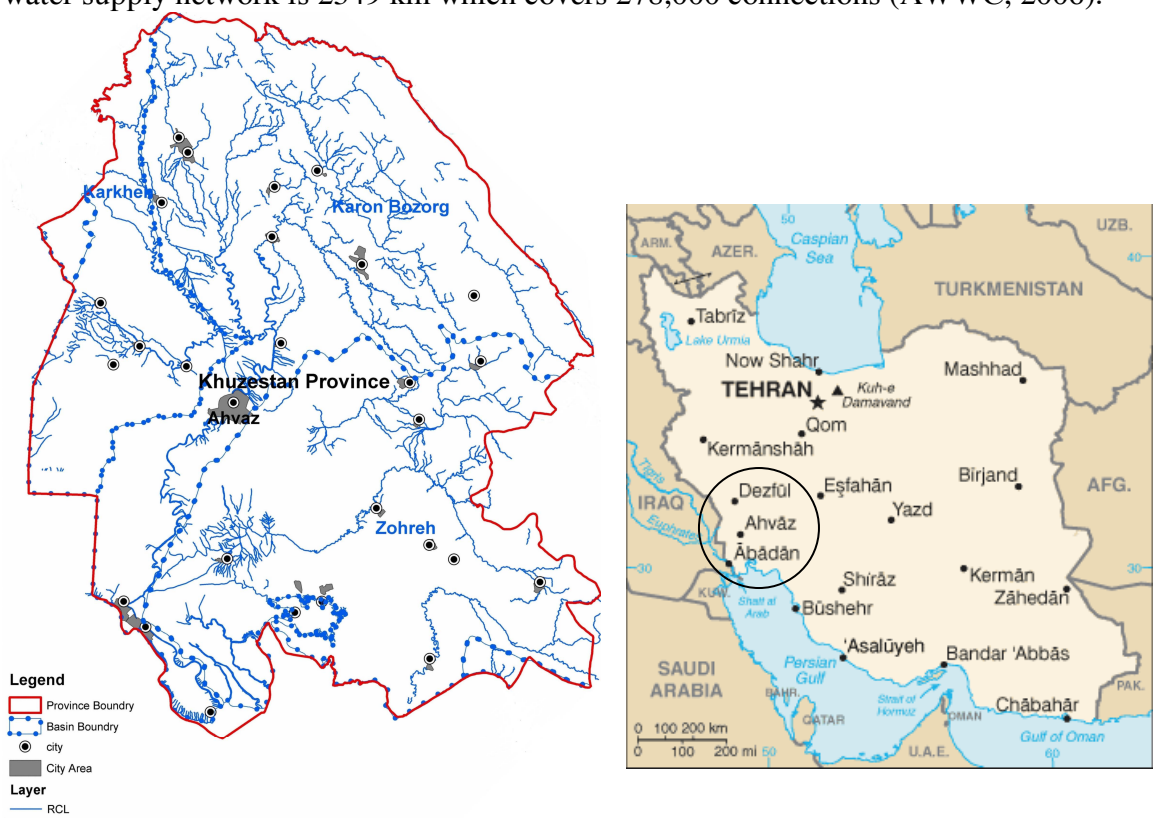

Figure 1. Location of Ahwaz County in Khuzestan Province

The flow rate of Karun river, measured at Ahwaz station, are 90 m^3/s in low water seasons, 2500 m^3/s high water season and about 5000 m^3/s in maximum floods. This River suffers from discharge of pollution loads from industrial, agricultural, agro-industrial and domestic sources. Increasing water withdrawal from and wastewater discharge to the river has endangered the aquatic life of this important ecosystem. Furthermore, the drinking and in-stream water quality standards have been violated in many instances. (Karamouz et al., 2008).

RESULTS

The indicators of CWSI for Ahwaz County were calculated according to the mentioned methodology. Results for estimation of each of the 15 sub-components, grouped in the 5 thematic components, are summarized below.

1. Resource: This component, evaluated at the river basin scale, scores the natural endowment of freshwater and comprises three indicators of Availability, Supply and Demand as follows:

1.a. Availability: This indicator assesses the annual amount of renewable fresh water available which is 21.8 BCM for the population of 1,166,287 persons for Ahwaz county. Considering the Falkenmark water stress indicator as a bench mark, the score for this component would be $R_a=100$.
1.b. Supply: This indicator considers the seasonal variability of the supply only as the ground water resources depletion does not occur in Ahwaz. Using discharge time series of the Karun River at Ahwaz location, run-offs exceeded 5% and 95% of the year are $244 m^3/s$ and $1715 m^3/s$ respectively. By dividing the last tow figures, the score for this component would be $R_s=100$.
1.c. Demand: This indicator assesses the current level demand of water on the basis of water license allocations. In Ahwaz County, the total amount of water consumed for municipal, irrigation and industrial use were 1.3 BCM in 2006. This amount in relation to the total amount of renewable freshwater (21.8 BCM), scores $R_d=94$.

2. Ecosystem Health: This component examines the health of the river basin's aquatic system with three indicators of Stress, Quality and Fish as mentioned below:
2.a. Stress: This indicator is intended to reflect the pressures imposed on ecosystem by pollution as well as excessive water use. In Ahwaz County, 20.5 BCM of water is removed from the ecosystem which leads to score of Es=*85*.
2.b. Water Quality: This indicator assesses the quality of water with respect to protection of aquatic life. For this purpose CWSI relies on the Water Quality index (WQI). This tool was also employed for the case of Ahwaz County (Mojahedi & Attari, 2009) which provided a result of $E_{wq}=85$.
2.c. Fish: This indicator reflects the health of native fish species that are economically and culturally important for the community. These fish population trends are not considered to have much influence in Ahwaz County and therefore collection of limited data for estimation of this indicator was not considered.

3. Infrastructure: This component assesses the state of water and wastewater infrastructure by combination of its ability to meet future demand, its condition and the level of treatment it provides as follows:
3.a. Demand: This indicator assesses the capacity of the water infrastructure to meet future demand due to population growth. The Water distribution network of the Ahwaz county currently covers the entire community but this would not be enough for a population growth of about 1.28% in this area and therefore $I_d=8$.

3.b. Condition: This indicator reflects the condition of water and wastewater infrastructure by considering the system losses. Unfortunately, the un-accounted for water in Ahwaz network is more than the limiting value of 25% and therefore $I_c=0$.
3.c. Treatment: This indicator focuses on the level of wastewater treatment. In Ahwaz County, 85% of populations are connected to the municipal sewers but only 28% receive secondary treatment in which insoluble matter and biological impurities and therefore $I_t=18.6$.

4. Human Health: This component considers three issues of Access, Reliability and Impact of water supply which are directly related on the health and well being of the community.
4.a. Access: This indicator measures the amount of potable water which is available to each person. In the Ahwaz County, about 230L/cap/day is available which is larger than the bench mark value of 150L/cap/day and therefore $H_a=100$.
4.b. Reliability: This indicator reflects reliability of a community's water supply in terms of services disruptions days per person. This figure for the City of Ahwaz is estimated to be 0.35 day per person which rewards a high score of $H_r=100$.
4.c. Impact: This indicator assesses the number of registered water borne incidences per 1000 people. Such an official data was not available for the Ahwaz County at the time to the authors.

5. Capacity: This component measures the capacity of the community to manage their water resources in terms of Financial Capacity, Education and Training as mentioned below:
5.a. Financial: This indicator examines the financial capacity of a community to manage water resources in relation to the communities with the highest surplus and debt in the country. Unfortunately, all of the water and wastewater companies in Iran face deficits now days as they are not functioning on a full cost recovery basis. Therefore, the companies with the maximum (-12.45$) and minimum amount of loss (-2.23$) per capita in the country were selected for the sake of this comparison. In the Ahwaz County, the amount of surplus in relation to the expenditures is -8.61$ per capita which leads to a score of $C_f=38$.
5.b. Education: This indicator considers the level of education in the community to address local water issues. In Iran, 45% (the maximum) and 18% (the minimum) of the population, aged between 20 to 64, have at least high school education. This figure for the Ahwaz County is 34% and therefore $C_E=58$.
5.c. Training: This indicator specifically addresses the level of training that water and wastewater treatment plant operators have received. In the Ahwaz water and wastewater company, roughly about 60% of the operators have had no training, 25% had other trainings and 10% have industrial certified trainings. This leads to a score of $C_o=27.5$.

DISCUSSION

The results of estimation of the indicators as well as an average of their sub-components are summarized in Table 1. The final CWSI index was first evaluated according to standardized method and then by consideration of weights using Equation 1. Comparison of these results did not show a significant effect once weights were adjusted for this county. Therefore, application of the standardized index is more appropriate especially for intra-community comparison purposes.

Table 1. Results of final CWSI for Ahwaz County

No.	Component	Indicator	Code	Score	Component Score w_i	Component Weight X_i	Component $w_i X_i$
1	Resource	*Availability*	R_a	100	98	0.329	0.267
		Supply	R_s	100			
		Demand	R_d	94			
2	Ecosystem Health	*Stress*	E_s	85	675	0.199	0.181
		Quality	E_{wq}	50			
		Fish	E_f	NA			
3	Infrastructure	*Demand*	I_d	8	8.9	0.179	0.171
		Condition	I_c	0			
		Treatment	I_t	18.6			
4	Human Health	*Access*	H_a	100	99.5	0.171	0.221
		Reliability	H_r	99			
		Impact	H_i	NA			
5	Capacity	*Financial*	C_f	38	41.2	0.122	0.160
		Education	C_e	58			
		Training	C_o	27.5			
Final CWSI Score			*Weighted Average=63.0*			*Weighted Average=69.3*	

CONCULSION

In this paper, the Canadian Water Sustainability Index (CWSI) was trialed for the case of Ahwaz County, in the South Western part of Iran. Results showed that:

- In the absence of any local water sustainability index, the first attempt to apply CWSI index for the case study in Iran was found satisfactory, despite economical and ethical differences.
- The final standardized CWSI score, calculated for Ahwaz, were found to be in the range of the figures calculated for the six communities in Canada.
- The final CWSI score for Ahwaz County has most benefited form the large amount of resources component while the poor infrastructure component has dramatically lowered the average score. To improve this, wastewater treatment plants with large investments are currently under construction.

- Modifications of the CWSI index by weight adjustments, using pair-wise, did not show a significant effect. Therefore, application of the standardized index is more appropriate especially for intra-community comparison purposes.
- This educational case study can be replicated for other communities in Iran which further facilitates comparison of the indices.

ACKNOWLEDGMENTS

The authors are grateful to the National Water and Wastewater Engineering Co. as well as Ahwaz Water and Wastewater Engineering Co. for some of the data taken from their web-sites.

REFERENCES

AWWC, (2006). Ahwaz Water and Wastewater Company. http://www.aww.co.ir (1 Jan. 2009).

Karamouz, M., Kerachian, R., Akhbari M. and Hafez B. (2008). "Design of river Water Quality Monitoring Networks: A Case Study.", *Environ Model Assess,* Springer, DOI 10.1007/s10666-008-9172-4.

Mays, L. W. (2007). "Chapter 1: Water Sustainability." *Water resources sustainability,* McGraw-Hill, New York, 2-15.

Mojahdi, S. A., and Attari, J. (2009). "A Comparative Study of Water Quality Indices for Karun River.", *World Environmental and Water Resources Congress*, ASCE*,* Kansas City, Missouri.

NWWEC, (2006). National Water and Wastewater Engineering Company of Iran. http://www.nww.co.ir (1 Jan. 2009).

Policy Research Initiative (PRI). (2007). "The Canadian Water Resources Sustainability Index (CWSI)." *PRI Project Report,* Ottawa, 1-27.

SCI, (2006). Statistical Center of Iran. http://www.sci.org.ir (1 Jan. 2009).

Singh, R. K. et al. (2008). "An overview of sustainability assessment methodologies.", J. of Ecological Indicators, Elsevier, In-Press,1-24.

World Bank, (2007). "Making the most of scarcity: Accountability for better water management results in the Middle East and North Africa.", MENA Development Report. 1-227.

Development of watershed management modeling system: the Los Angeles County Flood Control District's watershed based approach for urban runoff and stormwater quality

Youn Sim, Ph.D., P.E., M. ASCE

Los Angeles County Flood Control District, 900 South Fremont Ave, Alhambra, CA 91803; PH (626) 458-4314; email: ysim@dpw.lacounty.gov

ABSTRACT

Improving the quality of urban runoff and stormwater in the Los Angeles County's coastal watersheds is challenging. Thousands of separately permitted discharges with multiple Total Maximum daily Loads flow into the same receiving water bodies simultaneously. This makes it necessary and economical to address many different pollutant sources concurrently. In order to help overcome such challenges, the Los Angeles County Flood Control District is developing a watershed modeling system (WMMS) that would ultimately identify cost-effective projects through an integrated, watershed based approach. Using WMMS, collective impact of a variety of pollutant sources from point to non-point is evaluated and thereby comprehensive, long-term strategies for overall water quality improvement of the entire watershed will be planned. In addition, the WMMS will be used as an integrated watershed management tool for future planning of projects that achieve multiple benefits besides water quality such as water conservation, flood control, and open space development. This would eventually allow for an effective stormwater resource management.

Background

- **Watersheds in the Los Angeles County, California**

The Los Angeles County's coastal drainages flow from the highlands in the east to the Pacific Ocean in the west. Total size of coastal watersheds is approximately 3,100 square miles. Major surface waters originate from pristine mountains, flow through urbanized foothill and valley areas, high density residential and industrial coastal areas, and terminate at highly utilized recreational beaches and harbors. Drainages in the northern and western part of the County flow through un-developed or developing areas. Alluvial fans in low lying areas such as the San Fernando Valley, San Gabriel Valley, Oxnard Plain, and the Los Angeles Coastal Plain contain layers of sediment that form aquifers. The aquifers are important sources of ground water in the basin. The Los Angeles County's coastal watersheds include the following six watersheds. See Figure 1 for watershed locations:

1. San Gabriel River,
2. Los Angeles River,

3. Dominguez Channel,
4. Ballona Creek/Coastal,
5. Malibu Creek, and
6. Santa Clara River Watersheds.

- **Land Use**

Land use within the County varies considerably from vacant land to industrial. Overall land use in the County is dominated by undeveloped vacant land, which encompasses 64 % of the total land use. Residential areas comprise 19% of the total land use in the region, followed by commercial and public areas which comprise 6%. All other land use categories including agriculture, transportation and utilities, industrial, open space and water make up the remaining 11% of the County.

- **NPDES Permittees**

Typical artificial discharges (distinguished from stormwater discharge) regulated under NPDES program include discharges from: publicly owned treatment works (POTWs), generation stations, refineries, and other minor industrial facilities. Currently approximately 600 permits are issued under this category in the County.

The storm water program consists of three components; municipal, industrial and construction. The goal of the program is to reduce/eliminate the discharge of pollutants in storm water and dry weather flows from urban, construction, and/or industrial environments. Municipal stormwater discharge (MS4) in the County is currently regulated only by two permits while industrial and construction stormwater discharges are regulated by approximately 5,000 permits.

It should be noted, however, that among the total 5,600 permits in the County, TMDLs are enforced in only one permit, Los Angeles County MS4 permit.

- **TMDL Parameters and Source Characterization**

Stormwaters in the County include flows from mountain areas through urbanized areas, high-density residential and industrial coastal areas. The water bodies that carry the runoff have been identified as impaired for various pollutants including bacteria, metals, nutrients, and also carry trash. These water bodies are identified, listed, and updated by the USEPA under Section 303(d) of the Clean Water Act as Impaired Water bodies.

Specific pollutant sources, their transport mechanisms, and processes that influence the magnitude and patterns of pollutant distribution vary significantly depending on the locations. Controlling the impairment of these water bodies by these pollutants has been a challenge to local governments.

- **TMDLs developed**

  To date total 23 TMDLs have been developed for water bodies in the County. They include trash, metals, toxics pollutants, bacteria, nutrients, and chlorides. TMDLs of most pollutants are allocated to POTWs, MS4, California Department of Transportation (freeway owner), and industrial and construction sites. Nutrient and chlorides TMDLs mainly focus on effluents from wastewater treatment plants. Most of TMDLs have both point and non-point source components. Typical non-point sources identified in the TMDLs are aerial deposition, natural sources (forests and birds), and urban runoff. In particular, since the County's watersheds are highly urbanized, a majority of pollutants in stormwater runoff is from non-point sources.

Watershed based approach to current challenges

As indicated above, among the total 5,600 permits in the County, TMDLs are enforced only in one permit, Los Angeles County MS4 permit. TMDLs are allocated to storm drain outlets. However, since there are thousands of drain outlets into receiving waters, TMDL compliance for MS4 is typically determined based on water quality measured at receiving waters instead of quantifying total loads at all storm drain outlets. It should be noted that besides MS4, 5,600 other individually permitted discharges also impact the water quality of the same receiving waters. Therefore, it is almost impossible for MS4 dischargers to demonstrate the effect of their efforts toward TMDL compliance at the receiving waters. At any given time, deterioration of water quality can be attributed to any one of 5,600 separate discharge activities.

In order to overcome such challenges, a watershed based approach was needed to address the water quality of entire watersheds. In the watershed based approach, collective impact of a variety of pollutant sources from point to non-point is evaluated and thereby comprehensive, long-term strategies for overall water quality improvement of the entire watershed can be planned. Projects can be developed to achieve multiple benefits besides water quality such as water conservation, flood control, and open space development. This would eventually allow for an effective stormwater resource management.

- **Project goals**

  To help implement the watershed based approach to urban runoff and stormwater quality, the Los Angeles County Flood Control District has initiated a project to develop a watershed management modeling system (WMMS) that would ultimately be used to identify cost-effective pollution reduction projects. The WMMS simulates hydrologic and pollutant transport process and subsequently identifies cost-effective combinations of local scale (often referred to as LID type BMPs) and watershed scale BMPs. Identified local scale BMPs present a great option for individual cities and the unincorporated County areas to implement to

control pollution at the sources. Watershed scale BMPs treat residual runoff from the entire watershed. The WMMS and its results will be made available to all cities for their use in making decisions on how to best address pollution in runoff within their jurisdictions.

Specific goals include:

a. To develop WMMS for all major watersheds within the County boundary that simulates hydrologic and pollutant generation and transport process. See Figure 2 for illustration of WMMS.

b. To develop water quality improvement plan for the unincorporated County areas (WQIP) as a comprehensive plan for long-term TMDL implementation.

c. To provide technical guidance for LID implementation at new and re-development projects in the unincorporated County areas by quantifying water conservation and pollution reduction benefits.

d. To develop a watershed management tool for future planning of multi-benefit projects involving water quality, flood control, water conservation, and open space development components in the unincorporated County areas.

- **Project components**

1. WMMS based on USEPA's watershed models and BMP selection system based on an optimization algorithm.
2. WQIP for the unincorporated County areas that includes a thorough list of optimally selected, cost-effective BMP projects at local and regional scales and estimated pollution load reduction and associated costs.
3. Continuous update of watershed condition and subsequent BMP adjustment based on data from Countywide monitoring plan

- **Project Benefits**

1. Provides a system for phased BMP implementation with quantified pollutant load reduction to be achieved.
2. Allows for integrated watershed management with multi-benefits in addition to water quality benefit.
3. Allows for an iterative adaptive approach to water quality improvement goals through continuous refinement and improvement of the WQIP. See Figure 3 for illustration of an iterative and adaptive process using WMMS and WQIP.

Latest Progress

- **Watershed model development**

Existing watershed models for the Los Angeles County's coastal watersheds were developed by a multi-agency cooperation among the Los Angeles Regional Water Quality Control Board, U.S. Environmental Protection Agency (EPA), Southern California Coastal Water Research Project (SCCWRP), Tetra Tech, Inc., the Ventura County Watershed Protection District, the U.S. Army Corps of Engineers, and the Los Angeles County Flood Control District. The models employed a regional modeling approach that has been developed to simulate the hydrology and transport of sediment and metals. The approach is based on EPA's Hydrologic Simulation Program–FORTRAN (HSPF) and the Loading Simulation Program C++ (LSPC) (a version of HSPF, recoded into C++).

The models have mostly been used to support Metals TMDLs for Ballona Creek, the Los Angeles River, and the San Gabriel River, Dominguez Channel estuary, and and Los Angeles and Long Beach harbors, and Indicator Bacteria TMDLs for Santa Monica Bay beaches.

To provide a regional modeling approach to meet watershed planning needs, all previously developed models of the County's watersheds are currently being re-configured into a single modeling system based on the latest version of LSPC. This consistency provides a foundation for modifications for tailored applications, including representation of key watershed and pollutant source characteristics, management considerations, environmental conditions, spatial resolution, and other factors determined important for planning purposes.

- **Hydrologic Response Units**

In a watershed model, land unit representation should be sensitive to the features of the landscape that most affect hydrology and pollutant transport. In urban areas, it is important to estimate the division of land use into pervious and impervious components. In rural areas, vegetative cover is more important. Agricultural practices and crops (or crop rotations) should be well represented when present, although this component is less a factor in Los Angeles (where about 1 percent of the total sub watersheds area is agricultural) than in other areas. Depending on the goals of the model, if soil hydrologic groups are not homogenous in a watershed, it may be important to further divide pervious land cover by soil hydrologic group so that infiltration processes are better represented. Slope may also be an important factor, especially if steep slopes are prevalent; high slopes influence runoff and moisture-storage processes. The combination of land use, soil hydrologic group, and slope was used to define the HRUs. The HRU approach simplifies the selection of model parameters and provides a clear physical basis for parameter assignment.

Based on intensive analysis using nationally and locally available database for land use, soil types and slopes, the followings haven been found for HRU development:

a. The developed areas are concentrated in areas that have relatively poorly draining soils (Hydrologic Soil Group D).
b. Nearly half of the vacant land is composed of D soils, but the other half is almost evenly divided between B and C soils.
c. The developed areas are almost exclusively in areas that have slopes of less than 10 percent.
d. The highly sloped areas (> 10 percent slope) are almost exclusively vacant.

Figure 4 shows the spatial distribution of HRUs in the Los Angeles County.

Figure 1: Illustration and facts of Los Angeles County's coastal watersheds

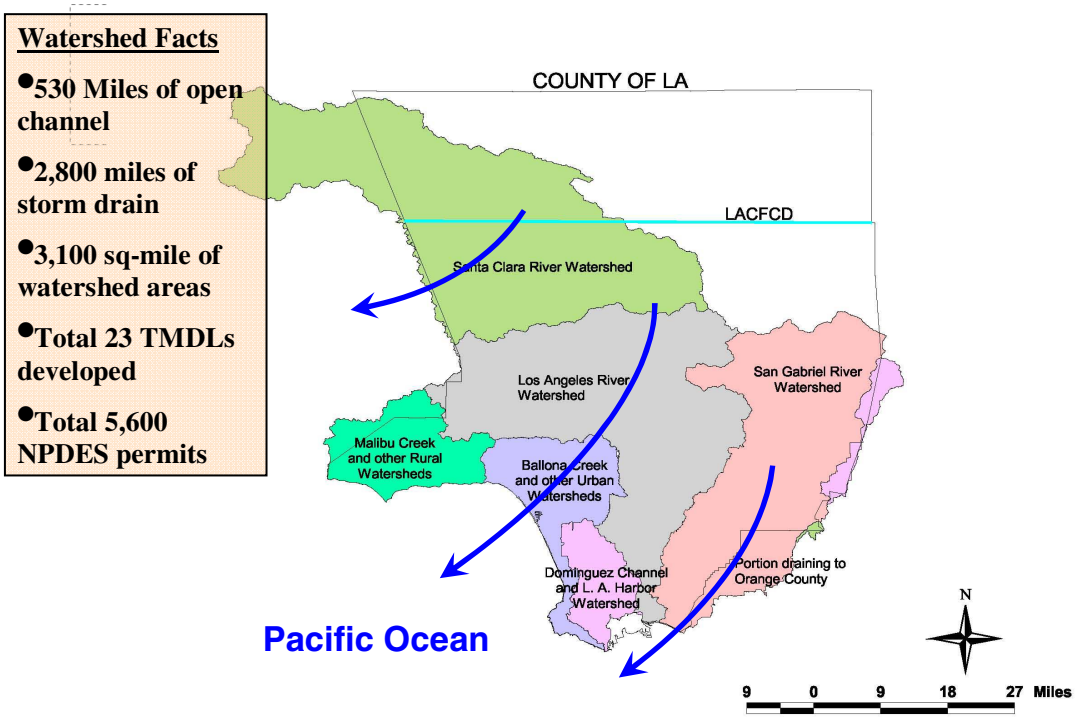

Figure 2: Illustration of Watershed Management Modeling System's main structure

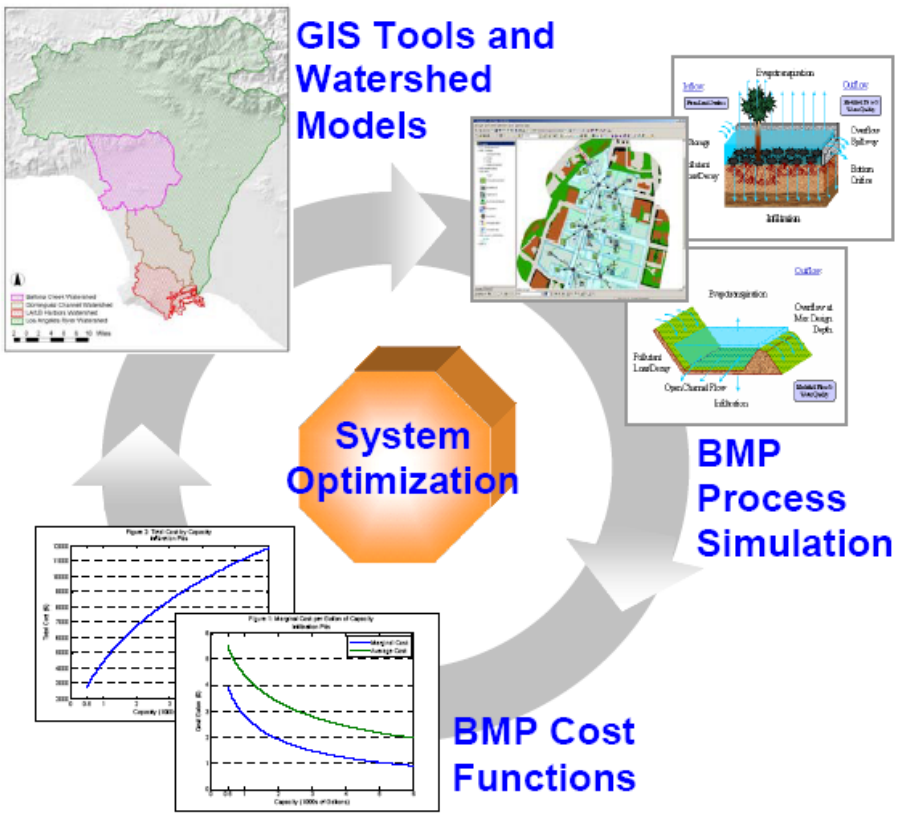

Figure 3: illustration of an iterative and adaptive process using WMMS and WQIP.

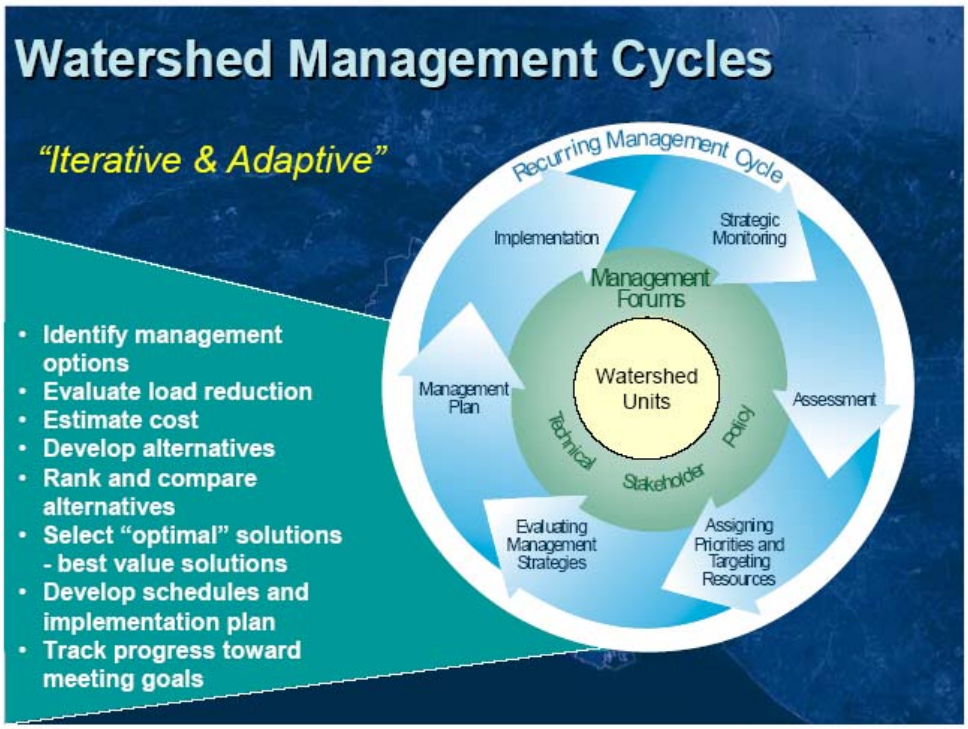

Figure 4: Hydrologic Response Units representation in Los Angeles County coastal watersheds

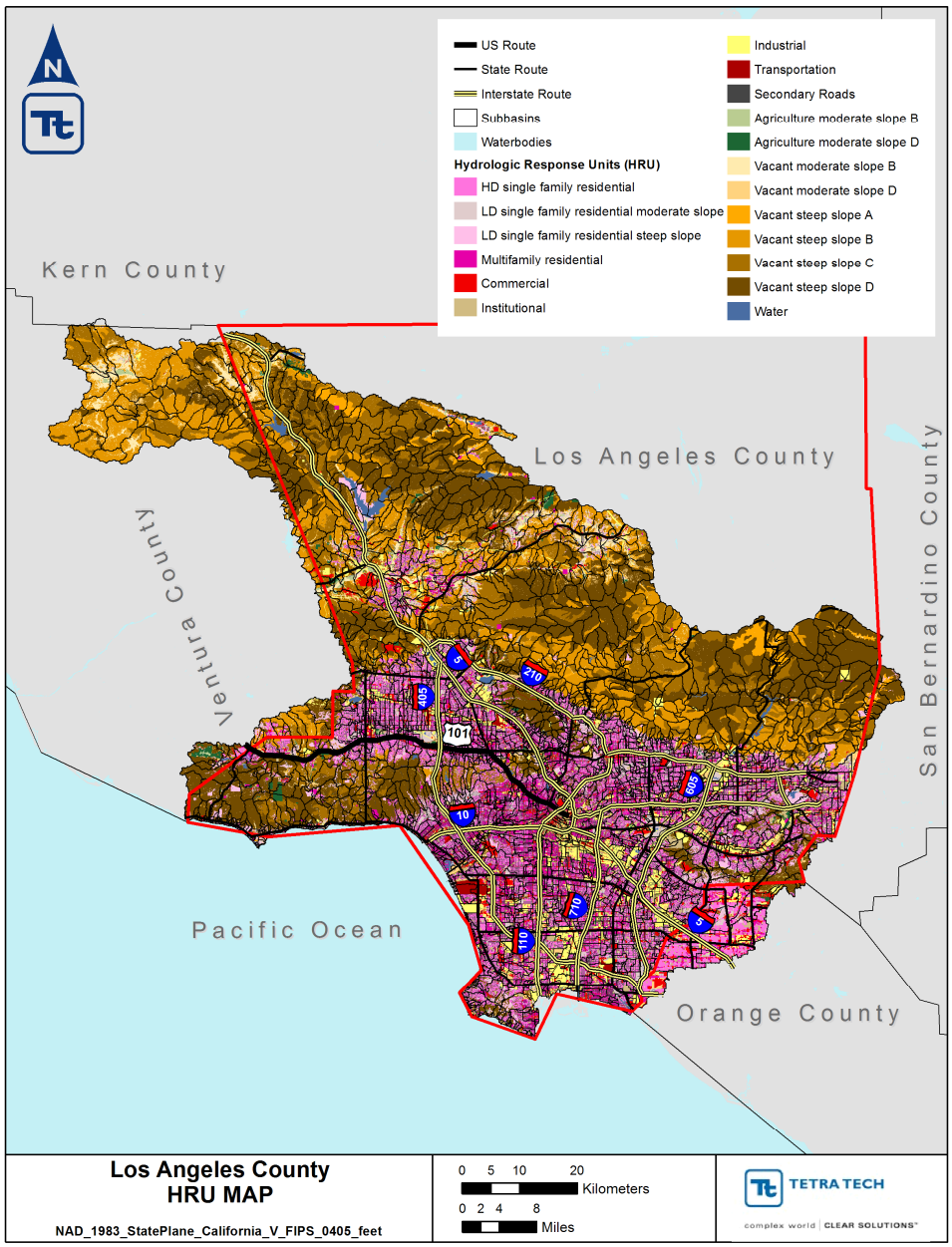

Implementing Source Water Protection Programs in a Texas

Camille W. Sowells, P.E., BCEE, Camp Dresser & McKee, Inc.
Christina Petersen, Ph.D., Camp Dresser & McKee, Inc.
Gordon McCurry, P.G., Camp Dresser & McKee, Inc.
Alexandria Doody, Camp Dresser & McKee, Inc.
Sean Ables, P.G., Texas Commission on Environmental Quality

TOPIC: 7th Symposium on Groundwater Hydrology, Quality, and Management
SUBTOPIC: Groundwater Quality and Human Health

Abstract

The water that surrounds us - lakes, rivers, streams, and aquifers - makes up our drinking water sources. These source waters can be threatened by a number of potential sources of contamination, such as on-site septic systems, sewer lines, hazardous chemical storage, storm water runoff, and animal wastes. The determination of the potential or risk is a key component of the source water assessment.

The Texas Source Water Assessment and Protection (SWAP) Program was promulgated as part of amendments to the 1996 Safe Drinking Water Act and consists of two fundamental aspects: Assessment and Protection. Source water assessments determine a water supply's susceptibility to contamination. Source water protection is the implementation of management strategies or practices to mitigate or eliminate risks associated with potential sources of contamination (PSOC). The assessments and protection plan are specific to each public water system, its source waters, and areas of concern which may impact source waters.

The objective of this paper is to discuss the innovative methodology used to encourage development of source water protection programs and conduct source water protection activities for selected public water systems using groundwater as the water supply. The methodology includes both technical activities as well as educational and outreach efforts to encourage active participation in the program. This paper will document the process used and present the results of these activities in multiple communities.

Introduction

The Texas Source Water Assessment and Protection (SWAP) Program was promulgated as part of amendments to the 1996 Safe Drinking Water Act and consists of two fundamental aspects: Assessment and Protection. Source water assessments determine a water supply's susceptibility to contamination. Source water protection is the implementation of management strategies or practices to mitigate or eliminate risks associated with potential sources of contamination (PSOC). The assessments and protection plan are specific to each public water system, its source waters, and areas of concern which may impact source waters.

While the Texas Commission on Environmental Quality (TCEQ) has completed assessments in the past for systems, taking action on the information contained in the assessments has been encouraged but ultimately left to the discretion of the water system. Thus, the protection component of the SWAP program is voluntary. One challenge public water systems face is managing competing demands for limited resources. Resources must be allocated to required expenditures and consequently, voluntary programs such as source water protection may not receive high priority nor have high implementation rates.

To address this problem and as part of the Source Water Protection Program, this project – the Source Water Protection Project (Project) was implemented to encourage active participation by public water systems and their customers in implementing effective source water protection programs. The goals of the Project are:

- Reduce the risk of groundwater pumped from public water supply wells of becoming contaminated
- Integrate source water assessments with source water protection activities
- Document Best Management Practice (BMP) approaches to manage PSOCs so the risk of groundwater contamination is reduced
- Demonstrate progress in the number of public water systems implementing source water protection activities.

Methodology

To address the goals of the Project, an approach was developed to engage public water systems and communities in actively participating in the source water protection process. The approach developed included technical as well as public education and outreach components. This approach builds on the existing required components of the SWAP Program by enhancing the public education and involvement facets of the program. The following multi-step process was used:

- Development of a comprehensive public education and outreach program that includes:
    - Development of a source water assessment and protection "brand" to facilitate a recognition and communication of a consistent message.
    - Identification of community "spark plugs", interested and committed individuals to lead local planning teams and to use the SWAP process to encourage stewardship of the groundwater resources in the project area.
    - Coordination of public meetings throughout the process to share information about the benefits of source water protection; obtain information about the community regarding the water supply system and its water quality issues,

PSOCs, and existing wellhead protection efforts; provide updates on the process; and discuss BMP implementation opportunities and challenges.

- Coordination of community outreach and education events

- Determination of groundwater capture zones through the characterization of local aquifer properties and groundwater modeling; in this case using version 3.2.1 of the Wellhead Analytical Element Model (W*h*AEM2000) developed by the US EPA (Kraemer et al, 2007).
- Identification and assessment of PSOCs through office and field investigation techniques.
- Development of an extensive database to facilitate selection and prioritization of BMPs to minimize the risk of contamination within the wellhead protection area using a three step process to identify appropriate BMPs, evaluate BMPs effectiveness using multiple criteria, and prioritize recommended BMP implementation.
- Identification of potential funding mechanisms to assist with BMP implementation.

The approach is presented graphically in Figure 1, beginning with a notice to proceed (NTP) for a given public water supply system.

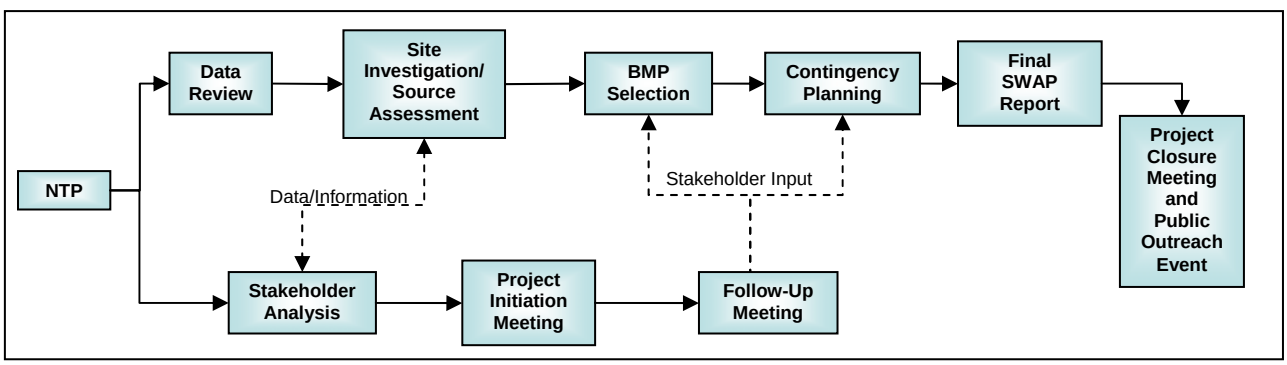

Figure 1 Source Water Protection Project Approach

Data Review

A review of available information for each project area was conducted prior to the project initiation meeting with the system. The review included a list of public water systems; previous source water assessment results, including PWS information, susceptibility ratings for each contaminant for each source; and other available information.

Stakeholder Analysis

In conjunction with data review, the stakeholder analysis of each system was essential to start the consensus building process that will lead to successful source water protection program implementation in each community. The purpose of the stakeholder analysis was to identify a

local planning team that may extend beyond jurisdictional boundaries and use the SWAP process to encourage stewardship of the groundwater resources in the project area.

The stakeholder analysis consists of identifying what activities are taking place in the area of interest, identifying property owners or who is responsible for each activity, and determining which community groups may have an interest or influence in SWAP activities. Because the source water protection program is voluntary, stakeholder identification and motivation is critical to achieving widespread community involvement. Information from the stakeholder analysis was also used to target and personalize the public outreach component of the project and educate, inform and ultimately secure stakeholder participation in the project.

Project Initiation Meeting

A project initiation meeting was held with each public water system. The purpose of the meeting was to introduce the source water assessment and protection program to the community, discuss the project purpose, identify the benefits of proactive source water protection, obtain information about the community and its land uses, answer questions, and obtain the community endorsement to participate in the project. Representatives from the public water supply were invited to attend along with the stakeholders, resources and other interested parties.

Site Investigation/Source Assessment

This task consisted of characterizing local aquifer properties and groundwater supply; conducting a field survey of the water supply system and identifying and assessing potential sources of contamination (PSOCs). Potential sources are widely varied and may range from airplane landing strips to hazardous waste generators to golf courses. Specific tasks included:

- Performing record searches of available data to obtain information such as location of septic tanks and industrial activities.
- Evaluating federal and state databases for potential contamination sources.
- Performing groundwater modeling to determine the wellhead protection area
- Performing field investigations to verify potential source of contamination (PSOC) information.

BMP Evaluation and Selection

Based on data gathered during the source assessment and stakeholder analysis, BMPs were selected to protect the source water supply where evidence of impacts were observed or a significant threat to the aquifer exists. BMP evaluation and selection was based on a prioritized list of potential contaminants, cost, the frequency and peak at which the contaminants may occur, and identification of BMPs which can be implemented and managed by the PWS. In addition, evidence of non-point source pollutant impacts or a threat to the aquifer must be present in order to make BMP recommendations for implementation. BMP selection was coordinated with the local planning team and stakeholders because of the direct economic consequences associated with BMP implementation.

Additional BMP assistance was provided to each participating system. For each BMP selected, additional resources were identified as well as an evaluation of potential funding sources to determine if financial assistance was available. Information regarding each potential funding source including type of funding (grant, loan or other), application deadlines, and other information was provided.

Contingency Planning

As part of the best management practice implementation, a contingency plan was developed for each source water protection area. The goal of the contingency plan is to ensure immediate and long-term protection of the source water supply area. For immediate problems, such as well contamination, the plan identified personnel, testing equipment, protocols (e.g., boil water advisory procedure), notification procedures and methods of containment to isolate pollutants. The plan also identified all key information regarding the water supply system, options for providing alternative water supply and location and capacity of treatment facilities

Outreach Implementation Plan

Implementation of the public education and outreach component of the project is critical to the execution of a successful voluntary SWAP program. Therefore, a comprehensive outreach implementation plan was developed to maximize community participation. The outreach implementation plan consisted of development of a SWAP "Brand," development of promotional materials, implementation of a SWAP website, implementation of a SWAP informational phone line, and coordination public outreach and education events.

The SWAP Logo (as shown in Figure 2) was developed to be included on all SWAP materials. A SWAP website (www.swaptexas.org) was developed and implemented to support the effort to enlist public water system participation in the SWAP program by consolidating source water protection information relevant to public water systems in one easy to access location; providing informative content in an easily navigable manner; providing credibility to outreach efforts; and tracking site usage as a measurement of outreach efforts. Information on the website includes a layman's explanation of source water protection and its implications; links to currently participating public water systems; the SWAP logo, short "success" stories/case studies; links to other relevant information sources, including the TCEQ and EPA SWAP websites. Figure 3 presents a screenshot of the website.



Figure 2. SWAP Logo



Figure 3. SWAP Website

All public information for the project was coordinated to facilitate consensus building, and participation in the project. All mail-outs and promotional materials were structured in user-friendly formats. Meetings were organized as discussions rather than lectures to dispel suspicions and encourage knowledge sharing. Meeting invitations were followed-up with personal phone calls to maximize attendance. Where appropriate, local media and elected officials were notified of meetings and invited to attend.

In addition to the project initiation meeting, a project follow-up meeting and project close-out meeting were conducted to keep the public water systems and their stakeholders involved in the process and informed of the results. The project follow-up meeting was held with each public water system, following the determination of the wellhead protection area, site investigation and BMP evaluation and selection. The purpose of the meeting was to review progress to-date, discuss identified PSOCs, discuss the preliminary selection of BMPs and potential funding sources, obtain system specific information that may affect BMP recommendations, and discuss possible public outreach events. Following the project follow-up meeting, the source water protection report was completed for each system. A final project meeting was conducted to present the report to the system, answer any remaining questions, schedule public outreach events. Each system agreed to participate in a follow-up survey to obtain information on BMP implementation.

Results

So far, eight public water systems have been contacted to participate in the project. At this time, six systems (75%) have agreed to participate. These systems include 26 wells and provide drinking water to over 7,000 customers. For each system the project initiation meeting has been conducted, as well as the groundwater modeling, site investigation, identification of PSOCs, BMP evaluation and selection and project follow-up meeting.

Response to the information provided to the systems and communities has been overwhelmingly positive and throughout the process a number of notable success stories have occurred. One system was able to use the source water protection report and map of the wellhead protection area to prevent a construction debris landfill from being located within the wellhead protection area. For that same system, an abandoned and deteriorated oil rig was removed from a wellhead protection area. In another instance, the project team was able to connect a public water system with a community group specifically interested in funding source water protection activities.

Additional public outreach and education events have been scheduled in three of the six participating systems, and scheduling of additional events is anticipated. The scheduled events include development and distribution of system-specific and PSOC specific information to residents to encourage protection of source water supplies through pollution prevention, participation at a community festival to distribute SWAP information and answer questions.

Based on the information regarding PSOCs within the wellhead protection areas, each system has agreed to implement some of the recommended best management practices. Future actions by each system will include development of the local planning team, investigation of potential funding sources, and implementation of the recommended BMPs. The project team will follow up at 6-months and 1-year time frames to document what BMPs have been implemented.

Conclusions

Effective data analysis and proactive consensus building are the keys to successful source water protection plan implementation. A voluntary source water protection program can be successful in encouraging participation. The development of a comprehensive public outreach and education plan combined with an effective technical approach are the keys to success for this project. Public water systems and their customers are interested in having a proactive role in protecting public water supplies. Technical information provided in a non-threatening, consistent, easy to understand manner provides the catalyst needed for communities to take ownership of protecting public water supplies. The source water protection approach used for this project ultimately resulted in a protection plans that contain practical, protective measures to minimize and prevent undesirable impacts from land use activities on drinking water sources.

References

Kraemer, Stephen R., Henk M. Haitjema, Victor A. Kelson. (2007). Working with W*h*AEM2000. EPA/600/R-05/115l. July 2007. Available for download at http://www.epa.gov/ceampubl/gwater/whaem/index.htm

Keywords

Source water assessment, source water protection, best management practices, groundwater, public outreach and education.

LITHOSTRATIGRAPHY OF NIGERIA-AN OVERVIEW

Kazeem Akorede Shitta
Geotech Nigeria Limited
Klm 8/9 Podo New Garage,
Old lagos bye-pass,Ibadan,Nigeria
E-mail: kazy1424@yahoo.com

ABSTRACT

Nigeria lies very close to the equator (hot country) West coast Africa between latitude 4 N and 14 N degree and longitude 2 E and 15 E degree. The country is located at the Northern end of Eastern branch of west coast of Africa rift system. Nigeria geological set up comprises broadly sedimentary formation and crystalline basement complex, which occur more or less in equal proportion all over the country. The sediment is mainly Upper Cretaceous to recent in age while the basement complex rocks are thought to be Precambrian. The studied area lies between latitude 12.4" and 11.11"W and longitude 13.81" and 14.13" S. The studied area is underlain by Precambrian basement complex of southern western Nigeria .The major rock in the area is charnokite and granite rock. The granite rock which are member of the older granite suite occupy about 65% of the total area .The principal granite is petrographic variety are recognized .The fine grained biotite-granite medium-coarse, non porphyritic biotite -hornblende granite and coarse-porphyritic biotite - hornblende granite. Also three main textural type of Charnokitic rock are also distinguished are coarse grained, massive fine grained and gneissic fine grained .The mode of occurrence of rock is three (1) core of the granite rock as exemplified by study area and few smaller bodies (2) Margin of the granite bodies as seen in Ijare and Uro edemo-idemo Charnokitic bodies and (3) Discrete bodies of the gneissic fine grained Charnokitic rock within the country gneisses as seen in Ilaro and Iju and Emirin village. All the charnokite in the region are dark-greenish to greenish-gray rocks with bluish quartz and greenish feldspar.

INTRODUCTION

Water is known to be a universal solvent. It is also one of the natural resources tapped by man, animals and plants to meet their needs for life sustenance.

The world's water resources include the entire range of natural waters on earth, either in vapour, liquid or solid form. Water is classified as surface water or groundwater. Surface water include rain water collected into rivers, lakes, reservoirs and oceans while groundwater include natural springs, well and boreholes.

Groundwater is commonly understood as water occupying the voids within a geologic stratum, groundwater is free from suspend matter and bacteria. It can be said to be pure, clear and colourless. Groundwater has greater quality than surface water.

About 495,000 children die annually of various diseases due to drinking of water that are not properly safe and sanitize (sea, stream e.t.c.), even as population increases and industries required all over the world, most people generally required about 2.5 litres of water everyday for direct consumption. The average amount of water used domestically each day by every person is about 190 litres (Hamill and Bell, 1986).

Generally, industries require approximately one quarter to one third of the public water supply under normal condition the easiest and most convenient way to meet the public demand for water is to utilize surface water resources, but unfortunately, water such as river, lake, stream e.t.c. are less plentiful than can be imagined. It can be recorded that surface water resources account for less than 2 percent of the world's fresh water.

The latter fresh water available however is unevenly distributed while the sources that are available have been either contaminated or polluted. (Hamill and Bell, 1986).

Groundwater accounts for about 98 percent of the world's fresh water and is fairly evenly distributed throughout the world. It provides a reasonable constant supply which is not completely susceptible to drying up under natural condition unlike surface water (World water balance and water resources of the earth UNECO Copyright 1978).

All over the globe, groundwater has been a very good and important source of water supply. It has been of continuous and tremendous use in irrigation industries and urban centers, as well as in rural communities. It is conveniently available at point of use and possesses excellent quality that requires little or no treatment in most cases.

OCCURRENCE OF GROUND WATER

The concept which explains the ultimate destination of rainwater is the sea either directly through run off or indirectly be infiltration and subsurface flow. A system of water movement in the atmosphere or rainfall, dews, hailstones or snowfalls over land as run off. Vertical and horizontal movement underground as infiltration or subsurface and continuous movement of all forms of water is the hydrogeology cycle. In the atmosphere, water vapours condense and may give rise to precipitation. However, not all this precipitation will reach the ground surface; some are intercepted by vegetation cover or surface of building and other structures and then evaporate back into the atmosphere.

The precipitation that reaches the ground surface may flow in to stream, lake and ocean, where it will either be evaporated or form seepages intruding in to the ground likewise soil moisture and further percolate downward to underline aquifer where it may be held for several years longer.

Groundwater in Nigeria is restricted by the fact that more than half of the country is underlain by crystalline basement rock of pre-cambian era.

The main rock types in this geological terrain include igneous and metamorphic rock such as migmatites and granite gneisses.

Generally in their unaltered form, they are characterized by low porosity and permeability. Porosity in basement rocks is by induction through weathering while secondary permeability induces by tectonic activities which manifest in form of that often act as conduct path facilitating water movement.

In other words, aquiferous zones in the basement terrain include fractured/weathered rocks. The yielding capacity of well, drilled within such rock are always very enormous.

RESEARCH METHODOLOGY.

I. Literature Review: All available geological/hydrological information were collected through the reading of journal, reference seminar paper (Olorunfemi M.O., 1990)
II. Data Gathering: All vertical electrical sounding data were collected from water section of the Federal Ministry of Agriculture and Water Resources Abuja, Wenner array was used in collecting the date.
III. Data Analysis: The data were interpreted by using partial curve matching technique. Computer was then used to interpret the results, from the result obtained geoelectric sections were generated.
IV. Interpretation of Results: Result obtained from each VES station were completed and interpreted in order to determine the best location for groundwater development in the study.

GEOLOGY OF THE STUDY AREA

Akure south Local Government falls within the basement complex region of Nigeria. The studied area lies between latitude 12° 04° and 11° 11° W and 13° 81° and 14°13°. and is underlain by precambian basement complex rocks of South Western Nigeria.

Several part of Africa is underlain by crystalline basement complex rocks. The major types of rocks in Akure are granite rocks and charnokite.

The granite rocks which are member of the older granite suit occupy about 65% of the total area of Akure. Three principal petrographic varieties are recognized, the fine-grained biotite granite, medium to coarse grained, non-porphyritic biotite – hornblende granite and coarse – porphyritic biotite- hornblade granite.

The classification is based largely on the textural characteristics. Also three main textural types of charnockitic rocks are also distinguished in Akure.

These are the coarse-grained variety, massive fine grained and the gneissic fine-grained types. Unlike most of the older granite, the charnokite rocks do not occur in form of smooth rounded boulders and only a few low hills all forming oval to sub-circular and elongated bodies.

The charnockitic rocks appear to have three modes of occurrence in the area, the first occurrence is within what seems to be the 'core' of the granite rock as exemplified by Akure body and few smaller bodies.

The second is along the margins of the granite bodies as seem in Ijare and Uro Edemo-Idemo charnockitic bodies. The first two modes of occurrence are mainly shown by the coarse-grained charnockitic variety. The last mode of occurrence is represented by the discrete bodies of the gneissic fine-grained charnockitic rocks within the country gneisses as seen in Ilara and also near Iju and Emirin villages.

All the charnockitic in the region are dark-greenish to greenish-gray rocks with bluish quartz are greenish feldspars (V. O. Olarewaju, 1997).

HYDROGEOLOGY OF THE STUDY AREA

The major river in Akure in Ondo State is Ero River,this river originates from Igbara Oke road, about 16-18km distance to Akure town.

Osun River is the major source of water runoff in Akure town, there are other smaller rivers such as Owuruwu River which is about 60m distance from Apex Nursery and Primary School, Oba Adesida, which is the Ves location. This river flows to meet Osun River at Akure road, the other rivers such as Otenre River, Omi Atamo, are smaller rivers that serve as runoff in the town; they meet Osun River at a point known as Osun Amon.Osun River flows from the Eastern part to Western part of the town and then flows to Ise town to meet a bigger river called Ogbese in Ondo State.

RESULT AND DISCUSSION

The interpretation of field resistivity data are in terms of resistivities and dept to the bedrock and interfaces across which a strong electrical exists.

The analysis and interpretation of the surveyed data shows four geoelectric layers. These layers are top soil which consists of the various rock types from clayey sand to sandy clay to compact sand. The second is the fresh/highly resistive basement. The fresh basement is characterized by high and infinite resistivity value and could not be contended on for groundwater, but the weathered zone and fractured basement which have lower resistivity value constitute good water zone

GEOELECTRIC SECTION

The quantitative interpretation of the VES data resulted in the production of numbers of geoelectric section. The section provides composite information along lithologic depth, the geoelectric section revealed four subsurface geoelectric layers.

The top layer which consists of (clayey sand and sandy clay) has resistivity value ranging from 70^0hm-m to 580^0hm-m, the maximum layer thickness is 3.0m. The top soil contributes to the development of groundwater, this layer is called the layer of aeration, and the water in this layer is called sub-surface water or zone of aeration. This zone is subdivided into three namely; soil water, intermediate belt and capillary belt.

The water that inf`iltrate into the soil from precipitation and in general ranges to all water present in the sub soil, or (in lithosphere). It may be evaporated from the soil, may be absorbed by plant root (soil water) and then transpired or may percolate downward to groundwater reservoir (intermediate). It occurs in a zone extending from the ground surface to the lower limit of porous water bearing rock formation (capillary) and designated s zone of the rock fracture.

The difference in compaction of the clayey sand is responsible for the variation in the resistivity values.

The resistivity of the second layer (Weathered zone) ranges from 30^ohm-m to 193^ohm-m while the thickness varies between 3m to 15.0m^2. The third layer is the fractured basement which has layer thickness varying from 17.5m – 29m with resistivity value ranging between 90^ohms-m to 240^ohms-m. The layer will be good for groundwater accommodation if the fractures are interconnected and permeable.

The fresh basement which is the fourth layer is characterized by high resistivity value up to 6650^ohm-m. The fresh basement is made up of infinitely resistivity rock in all the stations which form the bedrock.

The rock in this zone is hard, with no permeability and no water bearing. In fresh, non-fractured rock, the porosity is often less than 2%, as a result, run off is high and infiltration rate is very low in this zone.

The geoelectric section shows that the depth to the bedrock varies across the sounding station.

OVERBURDEN LAYER

The thickness of the overburden is an important hydrogeologic consideration in groundwater development in the basement terrain (Ajayi & Hassan 1990, Olorunfemi & Idonigie, 1992). Because water gets into the saturated zone through the overburden , the thickness of the overburden ranges from 23.30m to 36.60m in the study area. The variation in the overburden is due to degree of composition.

WEATHER LAYER

The weathered zone thickness shows the thickness of the weathered layer beneath in all the sounding station established across the study area, with VES 5 having the highest of thickness of about 13m and VES 1 having the lowest with about 2m.deriving from this, the thickness of the weathered layer here has, is sufficient enough for groundwater accumulation and therefore recommended for location of a borehole.

The variation in the weathered layer is due to the degree of weathering.

FRACTURED LAYER

The weathered layer thickness shows the thickness of the fractured layer beneath in all the sounding stations established across the study area, with VES 1 having the higher thickness of about 15m and VES 2 having the lowest with about 1.80m and the variation of this layer is due to degree of fracturing.

VES 5 and VES 1 are the location that will be recommended for groundwater, because they have the highest thickness of both weathered zone and fractured zone respectively which are good for groundwater accumulation.

VES 5 is recommended as priority location for sitting borehole, because it has thick

sequence of both weathered zone and fractured basement, which are good for groundwater accumulation.

If the fractured are interconnected and hence permeable, the thickness of the weathered zone in this section confers advantage on this over others.

The location will be good for optimum groundwater development, because of its availability in the study area; it will also be the only safe source of untreated water in Akure and also the cheapest source of good quality water supply, and its development can take in small crement rather than with relatively large scale financial investment which is the case of dams.

VES 5 has an advantage over VES 1, because the cost of drilling through VES 5 (weathered zone) will be cheaper than drilling through VES 1 which is of harder rock (fractured basement) and more difficult to drill.

VES 1: This location will be good for groundwater development if the fractures in this zone are interconnected and have permeable. The problem with this section is that to drill through fractured basement is very difficult and hard, it can damage the drilling bit.

VES 2: In this location, groundwater yield could be high bit, will not be up to that of (VES 1 and VES 5) so it can not be recommended for groundwater because the dip of the location and also the thickness of the area could affect its yield.

VES 4 will produce minimum groundwater yield, because of its dip and thickness of weathered zone which is small, it ranges between 1.70m to 7.0m.

VES 3: This location has the lowest thickness and the lowest probable groundwater yield, this location could be poor for groundwater yield and it is not recommended because of the thickness and dip as it can be seen in the geoelectric section.

CONCLUSION

The result of a quantitative interpretation of the VES data obtained in a geophysical survey over part of Akure, on a location opposite Apex Nursery and Primary School, Oba Adesida Road, Akure in Ondo State.

The interpreted results obtained from the study area are represented by a geoelectric section which shows the sequence and relationships between the subsurface lithologies.

The weathered layer and the fractured zone have been identified as the aquiferous in the area. The weathered layer is thicker in VES 5 and lowest in VES 1, while the fracture basement is thickest in VES 1. The 2 VES stations have been identified as the most suitable location for groundwater development in the area, with VES 5 being more prolific than others.

REFERENCES

1. Adegoke Anthony O. W. & Ajayi (1988): Groundwater Prospects in Basement Complex Rock of South Western Nigeria. Journal of African Earth Sciences, Vol. 7, No. 1. pp. 227-235.
2. Akinloye (1983):Hydro-geological Investigation or Groundwater Development at Obada Oko, Abeokuta Technical Brink Zones and Company Ltd. Ibadan pp. 10.
3. David L. M. & Ofrey D. (1983): An Indirect Method of Estimating Groundwater Level in Basement Complex Regolith Resources. Vol 1, No. 2, pp 161 – 164.
4. Griffiths O. T. & King R. F. (1981): Applied Geophysical Geophysics for Geologists and Engineers. (The Element of Geophysical Prospecting) 2nd Edition, pp. 1, 88, 105 – 107.
5. Hamill, L. & Bell F. U. (1986): Groundwater Resources Development. Britain Library Cataloguing in Publication Data London. pp. 151 – 158.
6. Jones M. J. (1985): The Western Zone Aquiferous of the Basement Complex Area of African, Quarterly Journal Engineering Geology. pp. 161 – 164.
7. Kelly E. W. (1985): Geoelectric Sounding for Delineating Groundwater Contamination. pp.6.
8. Olorunfemi M. D. & Olayinka A. I. (1992): Alteration of Geoelectric in Okene are and Implication for Borehole Sitting. Journal of Mining and Geology, pp. 403-411.
9. Olorunfemi M. O.(1990): The Hydrogeological Implicationof Topographic Variation with Overburden Thickness in Basement Complex. Area of South Western Nigeria. Journal of Mining and Geology. Vol 26, No. 1.
10. Olorunfemi M. O. & Oloruniwo M. A. (1985): Geoelectric Parameters and Aquifer Characteristics of Some Part of South Western Nigeria. Journal of Mining and Geology.
11. Olorunfemi, M. O. & P.K. Emikanselun (1999): Direct Current Resistivity Sounding for Groundwater Potential in Basement Complex Area of North-Central Nigeria. Journal of Applied Science, Vol. 2, No 1, pp. 31-34.
12. Rahaman M. A. (1976): Review of the Basement Geology of South Western Nigeria in Geology of Nigeria. Elizabithan Publishing Company, Nigeria. pp. 41-58.
13. Schwartz F. W. & M. C. Clymont, G. L. (1977): Application of Surface Resistivity Method Groundwater. pp. 197-200.

Table 1: Summary of Laer Thickness of Resistivities

VES Nunber	Thickness			Resistivities (Ohms-m)				Overburdened Thicknes s EH (M)
L	h1	h2	h3	e1	e2	e3	e4	
1	1.20	2.98	19.08	580	193	613	5400	23.76
2	3.00	8.30	11.10	500	167	2470	6650	22.40
3	1.70	2.55	-	265	80	2565	-	4.25
4	1.15	6.70	-	170	30		-	7.85
5	1.80	14.58	19.58	570	63	594	2660	36.66

Table 2: Resistivity in Sounding Station

VES Station	Thickness Of 1st Layer (m)	Thickness Of 1st Layer (m)	Thickness Of 1st Layer (m)	Depth of Bedrock (m) Overburden Thickness	Weathered Layer Thickness (m)	Resistivity of the Weathered Layer (ohm-m)

1	1.70	2.98	19.08	23.70	19.08	613
2	3.00	8.30	11.10	22.40	11.10	247
3	1.70	2.55	-	4.25	2.55	86
4	1.15	6.70	-	7.85	6.70	30
5	1.80	14.58	19.00	35.38	19.00	594

Town	Location	VES No	Curve Type
AKURE	AKURE, 11, Opposite Apex Nursery and Primary School, Oba Adesida Road, Akure.	1	HA
		2	HA
		3	H
		4	H
		5	HA

Table 3: Classification of VES Curves

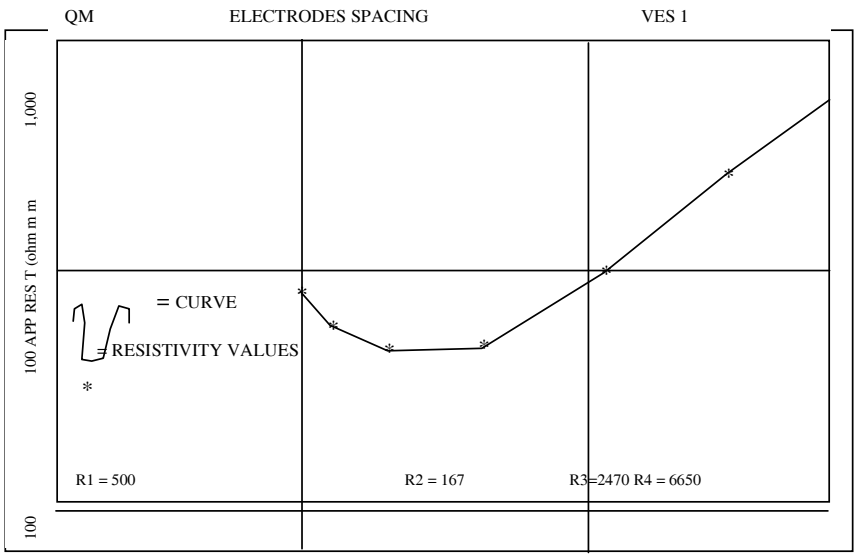

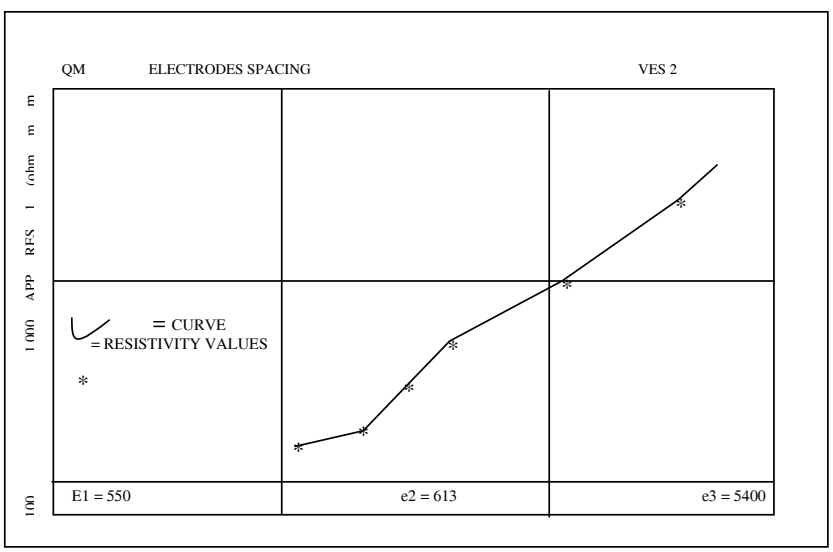

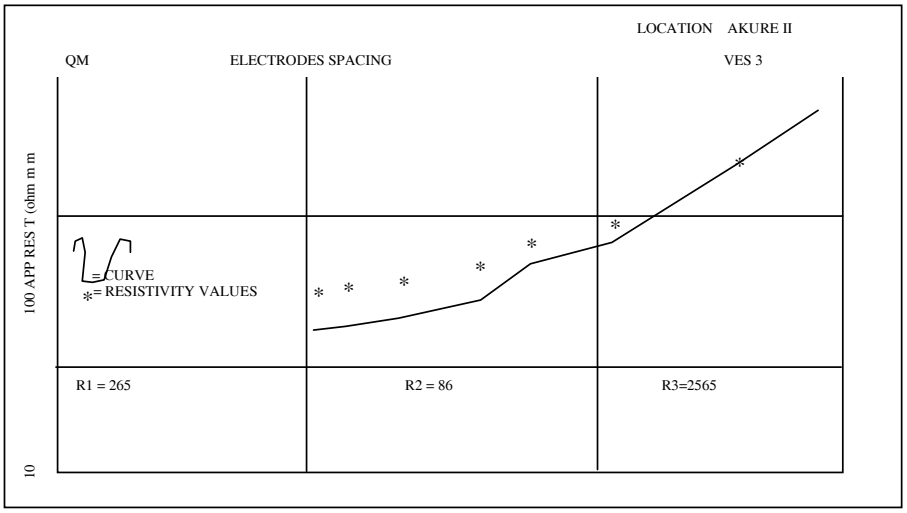
LOCATION AKURE II
QM
ELECTRODES SPACING
VES 3
100 APP RES T (ohm m m
= CURVE
= RESISTIVITY VALUES
R1 = 265
R2 = 86
R3=2565
10

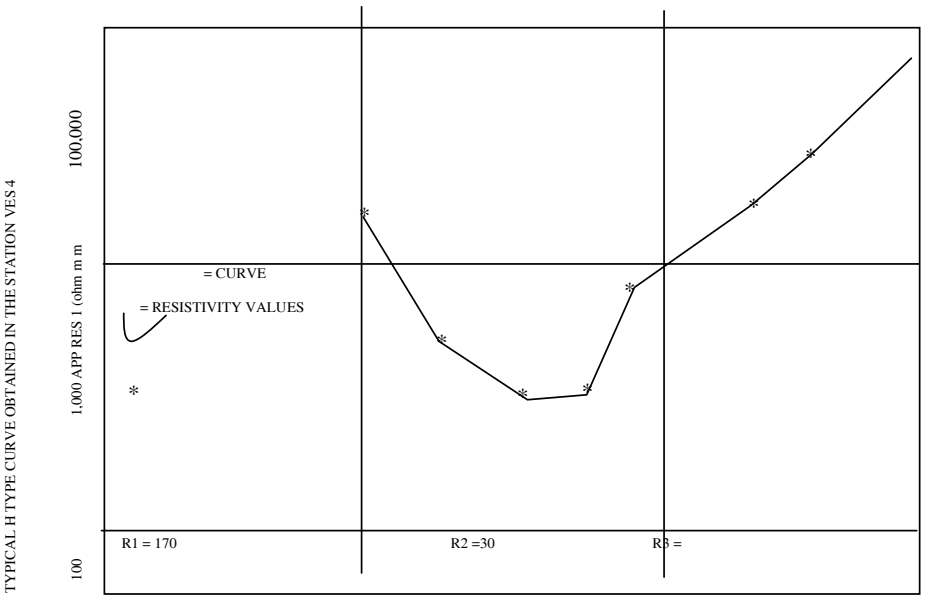
TYPICAL H TYPE CURVE OBTAINED IN THE STATION VES 4
100,000
1,000 APP RES I (ohm m m
= CURVE
= RESISTIVITY VALUES
R1 = 170
R2 =30
R3 =
100

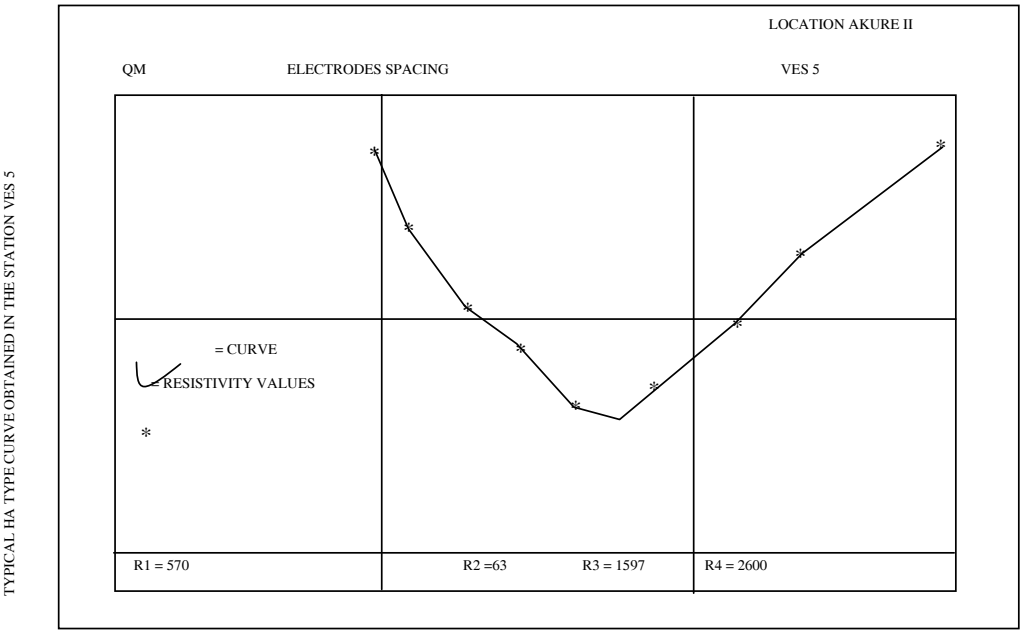
LOCATION AKURE II
QM
ELECTRODES SPACING
VES 5
= CURVE
= RESISTIVITY VALUES
R1 = 570
R2 =63
R3 = 1597
R4 = 2600
TYPICAL HA TYPE CURVE OBTAINED IN THE STATION VES 5

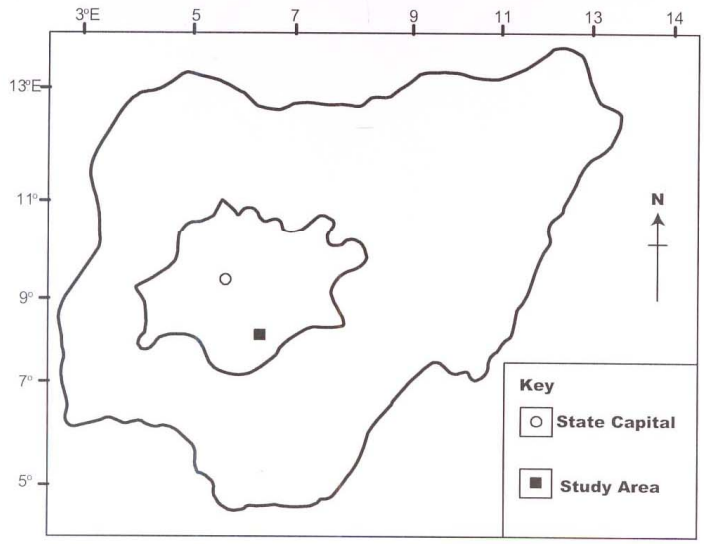

Map of Nigeria showing the Study Area (AKURE) in ONDO State

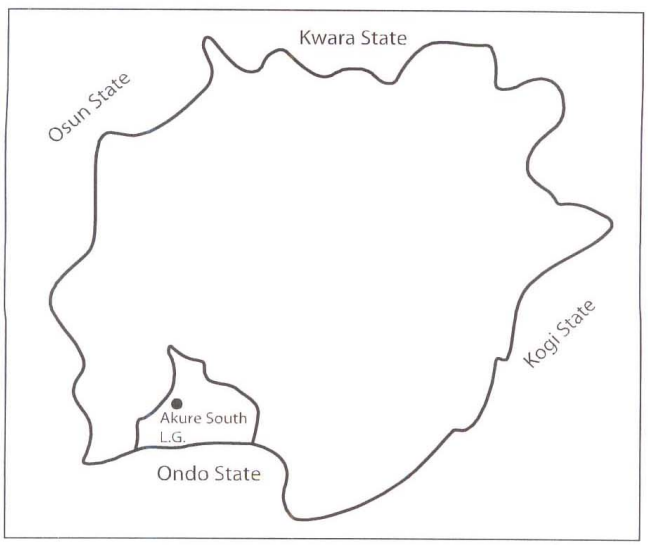

Map of the ONDO State showing (AKURE) Locating the Ives Station

SPECIFIC PROBLEMS RELATED TO PARTIALLY PENETRATING WELLS IN CONFINED AQUIFERS

Ahmad Wagdy, Hany G. Radwan, Sherif M. El-Didy,
Irrigation and Hydraulics Department, Engineering, Cairo University,
Giza, Egypt., Fax. 202 5732949

Abstract

Partial penetration, especially for confined aquifers, may significantly affect the associated well(s) hydraulics due to the incidence of vertical flow in the vicinity of the well. This induces additional head losses, affects the potential pumping rate, and the related peizometeric head distribution around the well. Closed form analytical solution is beyond manual computations due to complicated integrations and summations in addition to dealing with a large number of variables. The main objective of this paper is to provide engineers with a simplified, yet accurate, solution to three specific problems, of common occurrence. Defining the effective aquifer thickness, in case of partial penetration for confined aquifers, is one problem. In case of unknown aquifer thickness, the performed analysis recommends to define the effective thickness as a multiple of the screen length, which in turn, is time dependant. Multiple values of 2, 3, and 4 are found to correspond to pumping periods of 1, 3, and 10 days, regardless of the pumping rate. Determining the optimum screen length for maximum well yield is a second problem. A screen design chart has been prepared while taking into consideration empirically-derived well capacity equation. Detecting the zone of influence of a partially penetrating pumping well is the last studied problem. The peizometric head at any radius can be estimated from proposed influence zone charts that require the pre knowledge of five well and aquifer parameters. All results are postulated based on programming of Hantush equation for partially penetrating wells.

1. Introduction

Partial penetrating wells are of common occurrence incase of unknown aquifer thickness, which causes the flow to have vertical components in the vicinity of the well leading to additional head losses around the well. Figure (1), following Wagdy et al (2009), shows a typical example in a confined aquifer. The differential equation representing the partially penetrating system, Hantush (1957) and Batu, (1998), is as follows:

$$\frac{\partial^2 s}{\partial r^2} + \frac{1}{r}\frac{\partial s}{\partial r} + a^2 \frac{\partial^2 s}{\partial z^2} = \frac{S}{T}\frac{\partial s}{\partial t} \qquad (1)$$

Where:

$$a^2 = \frac{K_z}{K_r}\ , \quad T = K_r b \quad , \ S = S_S b \qquad (2)$$

s : Drawdown at distance r (L) r : Distance from the well (L)
b : Thickness of aquifer (L) S : Storage Coefficient.
T : Transmissivity of the aquifer ($L^2 T^{-1}$) S_s : Specific Storage (L^{-1})
K_r, K_z : Horizontal and vertical hydraulic conductivity of aquifer (LT^{-1})

The solution of Equation (1) for confined aquifer is given by Hantush, (1961, 1964), (Batu, 1998) as follows:

$$s = \frac{Q}{4\pi T}\left\{W(u) + f\left(u, \frac{ar}{b}, \frac{d}{b}, \frac{L}{b}, \frac{z}{b}\right)\right\} \quad (3)$$

Where:-

$$f\left(u, \frac{ar}{b}, \frac{d}{b}, \frac{L}{b}, \frac{z}{b}\right) = \frac{2b}{\pi(L-d)} \sum_{n=1}^{\infty} \frac{1}{n}\left[\sin\left(\frac{n\pi L}{b}\right) - \sin\left(\frac{n\pi d}{b}\right)\cos\left(\frac{n\pi z}{b}\right) W(u, X_n)\right] \quad (4)$$

$$X_n = \frac{n\pi a r}{b} \quad , \quad W(u) = \int_u^{\infty} \frac{e^{-y}}{y} dy \quad (5)$$

$W(u)$: Theis well function.

The first part in Equations (3) represents the case of fully penetrating well, while the term represents the effect of partial penetration.

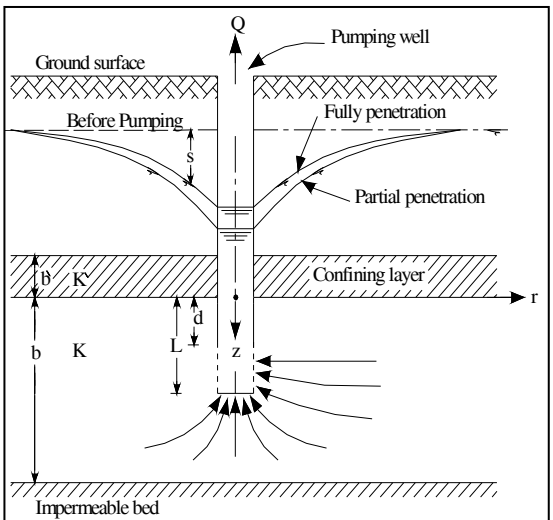

Figure (1): Flow Field for a Partially Penetrating Well in a Confined Aquifer.

2. Effective Aquifer Thickness

In many dewatering processes in the field, the thickness of the aquifer may be unlimited (too large). Common practice, considers the thickness of the aquifer equals 2.5 times of the screen length. Beyond this limit, the effect of the thickness may be neglected as shown in Figure (2). To study the effect of aquifer thickness, the term (b) in Equation (2) must be isolated. This problem will be studied for fine, medium, and coarse sand. The values of (K, S_S) for these soil types will be determined in the following sections.

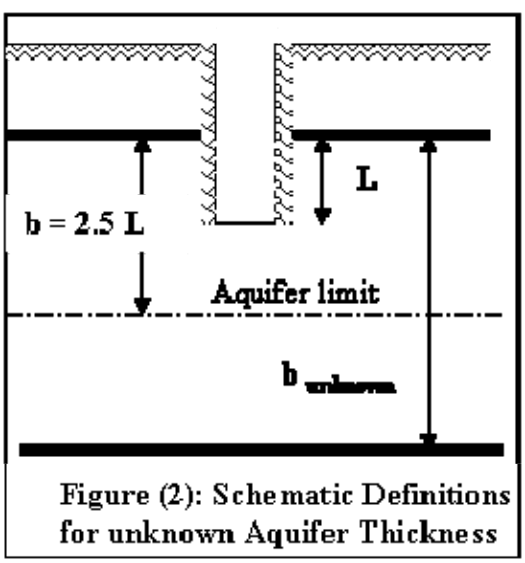

Figure (2): Schematic Definitions for unknown Aquifer Thickness

2.1 Specific Storage (S_S) of sand.

The specific storage is given by (Batu, 1998) as :

$$S_s = \gamma(\alpha + n\beta) \quad (6)$$

Where

γ : Specific weight of water.

α : Compressibility of the aquifer skeleton ($1/(ML^{-1}T^{-2})$.

n : Porosity.

β : Compressibility of water ($1/(ML^{-1}T^{-2})$.

The compressibility of aquifer skeleton (α) depends on the elasticity of the aquifer:

$$\alpha = \frac{1}{E_S} \tag{7}$$

Where E_S is the modulus of elasticity of the solid skeleton. The factor ($\gamma n \beta$) of Equation (6) gives the fraction of storage derived from expansion of water, while the product ($\gamma \alpha$) gives the fraction derived from compression of aquifer (Batu, 1998).

The average void ratio for fine, medium, and coarse sand are 0.62, 0.59, 0.55, respectively. By using the previous values of void ratio for each soil type, the values of modulus of elasticity, will be 23500, 39300, 39300 KN/m^2 for fine, medium, and coarse sand, respectively. The values of n, γ, β,and α=(1/E_S), can be used to calculate the specific storage (S_S), by substituting in Equation (6) as shown in Table (1).

Table (1): Specific Storage (S_S) for Types of Sand Soils.

Soil type	Specific storage (S_S) m^{-1}
Fine sand	4.1939×10^{-4}
Medium sand	2.5138×10^{-4}
Coarse sand	2.5138×10^{-4}

2.2 Horizontal Hydraulic Conductivity (K_r) of sand.

The properties of soil, which affect on groundwater flow are specific storage (S_S), and hydraulic conductivity (k). Ranges of hydraulic conductivity values for unconsolidated sediments are presented in Table (2), following Batu(1998).

Table (2): Arithmetic Mean Average Hydraulic Conductivity K_{av} of Porous materials.

Material	K_{av} (cm/s)	K_{av} (m/d)
Sand (fine)	2.28×10^{-3}	1.96
Sand (medium)	165×10^{-2}	14.3
Sand (coarse)	5.20×10^{-2}	44.93
Gravel	4.03×10^{-1}	348.19

2.3 Hantush's equation in a dimensionless form .

In most common processes in field, the screen extends from the top of aquifer, i.e. d =0, and all measurements occurring at z =0, therefore Equations (3, and 4) will reduce to:

$$s = \frac{Q}{4\pi T}\left\{W(u) + f\left(u, \frac{ar}{b}, \frac{L}{b}\right)\right\} \tag{8}$$

Where

$$f\left(u, \frac{ar}{b}, \frac{L}{b}\right) = \frac{2b}{\pi L}\sum_{n=1}^{\infty}\frac{1}{n}\sin\left(\frac{n\pi L}{b}\right) W\left(u, X_n\right) \tag{9}$$

New parameters, will be defined as follows:-

$$x = \frac{b}{L},\quad y = \frac{r}{L},\quad v = \frac{L^2 S_S}{K t},\quad W^* = \frac{s K L}{Q} \tag{10}$$

By using the previous dimensionless relations, the parameters in Equation (3) can be expressed as follows:-

$$u = \frac{y^2 v}{4} = \frac{r^2 l^2 S_S}{4 l^2 k t} = \frac{r^2 S_S}{4kt}\frac{b}{b} = \frac{r^2 S}{4Tt} \tag{11}$$

$$\frac{ar}{b} = \frac{ay}{x} = \frac{arl}{lb},\quad \frac{l}{b} = \frac{1}{x} \tag{12}$$

Then, Equation (8) will take the form:-

$$W^* = \frac{1}{4\pi x}\left\{ W\left(\frac{y^2 v}{4}\right) + f\left(\frac{y^2 v}{4}, \frac{ay}{x}, \frac{1}{x}\right)\right\} \tag{13}$$

To study the problem of effective aquifer thickness, nominal screen lengths of (L) = 20, 40, 60, 80, 100m will be used, and the common values for well radius r_W = 6, 7, 8 inch.

2.4 Detection of Effective Aquifer Thickness.

This section deals with the effect of aquifer thickness (b) on the drawdown. According to Equation (13), the aquifer thickness (b) is included in the parameter (x), and the drawdown is included in the parameter (W^*). The following curves for each soil type are prepared for variable distances from well; y = (r / L). Each soil type will be discussed separately by using the corresponding values of (S_S), and (K). For the same screen length (L) the only remaining variable in (v) ratio will be the time (t). Thus, (v) will varied by considering: 1.0 min < time < 20 days, after initiation of pumping.

(a) Fine Sand Soil.

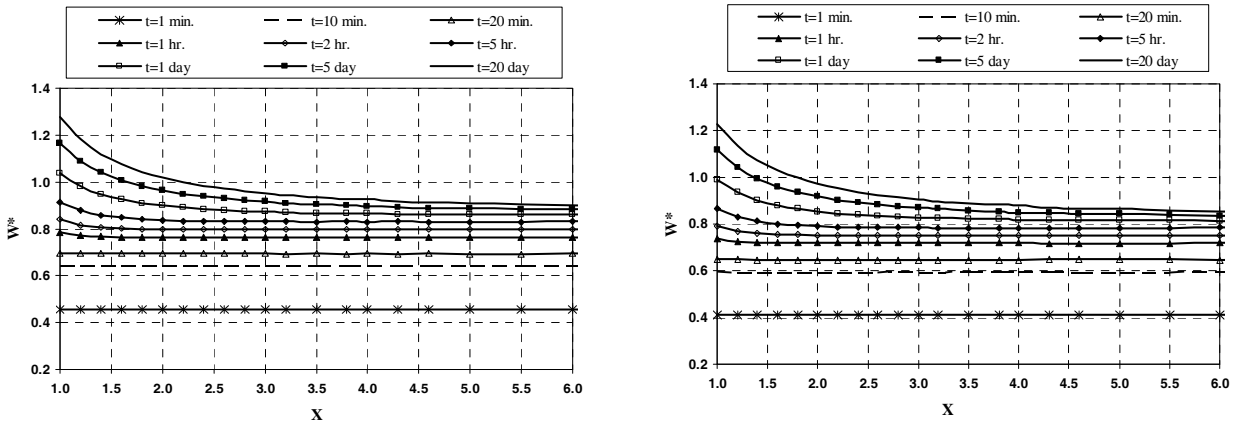

(a) (b)

Figure(3): Detection of the Effective Aquifer Thickness, for Fine Sand at L=20 m. (a) r_w = 6 inch, (b) r_w = 8 inch

Figure (3) shows that, there is no significant influence for well radii. Thus, analysis will proceed for the case of r_w = 6 inch, and screen lengths of 40, and 100 m.

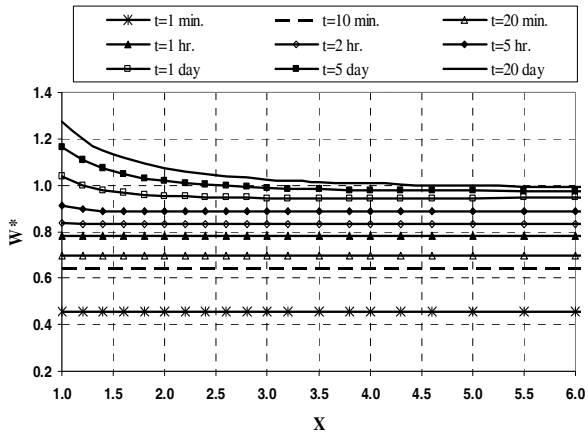

(a) L = 40 m

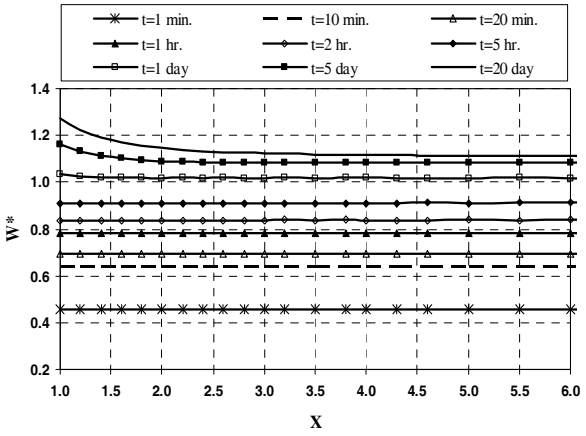

(b) L = 100 m

Figure(4): Detection of the Effective Aquifer Thickness, for Fine Sand at r_w= 6 inch.

(b) Medium Sand Soil.

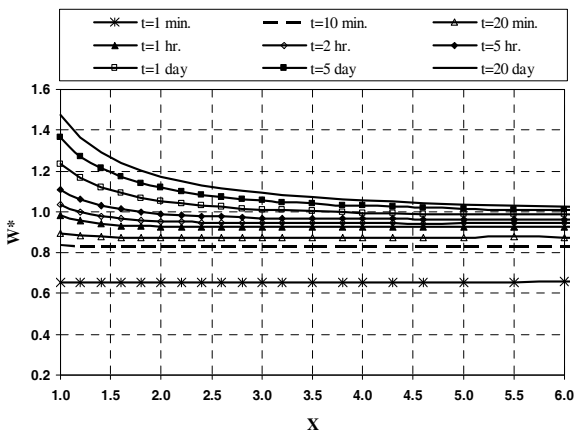

(a) L = 40 m

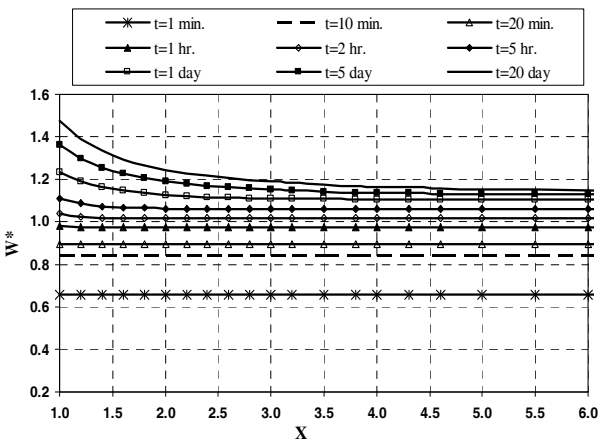

(b) L = 100 m

Figure (5): Detection of the Effective Aquifer Thickness, for Medium Sand at r_w= 6 inch.

(c) Coarse Sand Soil.

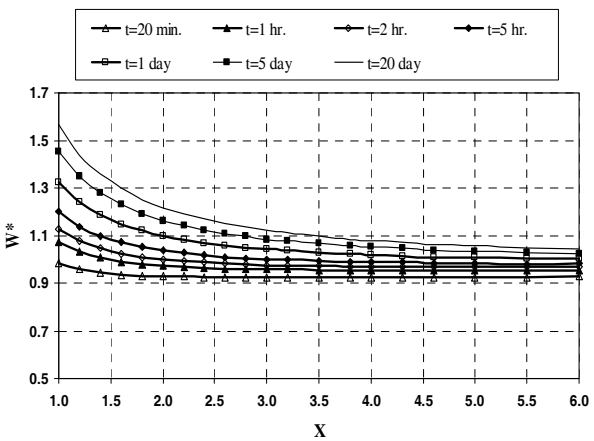

(a) L = 40 m

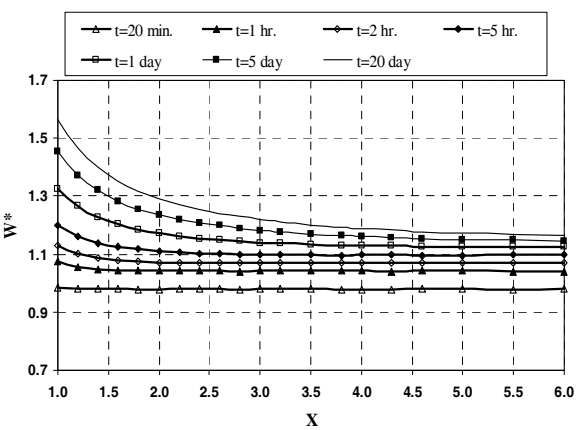

(b) L = 100 m

Figure (6): Detection of the Effective Aquifer Thickness, for Coarse Sand at r_w= 6 inch.

From Figures (4, 5, and 6), the following points can be concluded:-

(1) For the first 20 minutes of pumping, flow is derived from the aquifer in the vicinity of the screen as represented by horizontal lines. This means that, the well may be literally considered as if fully penetrating the layer adjacent to the screen only.

(2) For the same value of penetration ratio (1/x), as time increases, the well is affecting larger part of the aquifer. The values of W^* increases which means that, drawdown increases beyond hypothetical full penetration case (x = 1.0).

(3) For the same screen length, as the thickness of the aquifer increases, the drawdown will increase beyond the case of full penetration.

(4) A limiting, time dependant, effective value exists beyond which the aquifer thickness has no additional influence on drawdown. These are as follows:

$$b = \begin{cases} 2.5\,L & t \le 1.0 \quad day \\ 3.0\,L & 1.0 \le t \le 3.0 \quad days \\ 4.0\,L & 3.0 \le t \le 10.0 \quad days. \end{cases} \tag{14}$$

Aquifer extent is gradually reflected at the well as time passes. The common practice of setting b =2.5L is only acceptable for pumping (recovery) tests lasting less than 24 hours. Should the latter extend beyond 1-day, values from equation (14) are recommended to avoid misleading drawdowns.

(5) For the same screen length and penetration ratio, the drawdown of fine sand will be greater than medium sand which in turn will be greater than coarse sand. According to Equation (10), the following relation may be obtained:

$$s \,\alpha\, W^* \,\alpha \left(\frac{1}{K}\right) \tag{15}$$

2.4 Ratio of the increase in drawdown due to partial penetration.

The values of W* for any penetration ratio (1/x) are drawn in Figures (3 to 6) during detection of effective aquifer thickness. These data will be used for each soil type to determine the increase in drawdown due to partial penetration using :

$$\frac{s_p}{s_f} = \left[\frac{W^*_P}{W^*_f}\right]\left[\frac{b}{L}\right] = \left[\frac{W^*_P}{W^*_f}\right] X \tag{16}$$

The following figures (7, 8, and 9) for the three types of soils, are drawn between (s_p/s_f) and x, for the case of r_w =6 inch. Some interesting points need to be highlighted:

(1) The relation between the ratio of partial penetration drawdown to full penetration drawdown s_p/s_f, and inverse penetration ratio x for the same pumping rate, is linear. The dependence of s_p/s_f on pumping time is insignificant during the first hour of the pumping. However, a recovery in drawdown ratio s_p/s_f of up to 30% may occur at a 10% penetrating well (L/b = 0.1), but after 20 days of operation! (due to enhanced aquifer contribution)

(2) The maximum drawdown ratio s_p/s_f is equal to the ratio (b/L) during the first few minutes after initiation of pumping, then decreases with time.

(3) The variation in the range of the drawdown ratio s_p/s_f at any given penetration ratio is more pronounced for short screens wells (L = 40m) as compared to longer screens (L = 100 m). The effect of soil type is more pronounced at prolonged pumping periods, where s_p/s_f decreases as soil gets coarser.

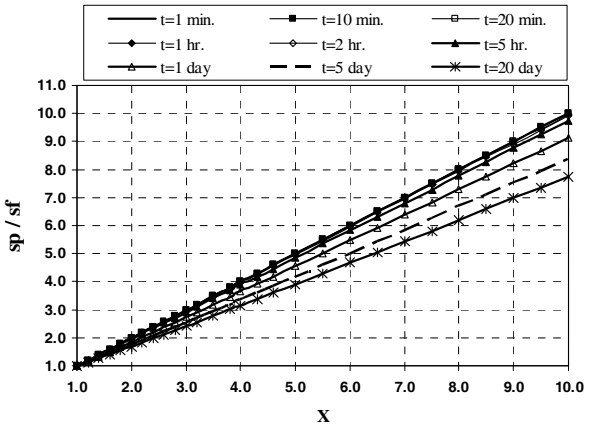

(a) L = 40 m

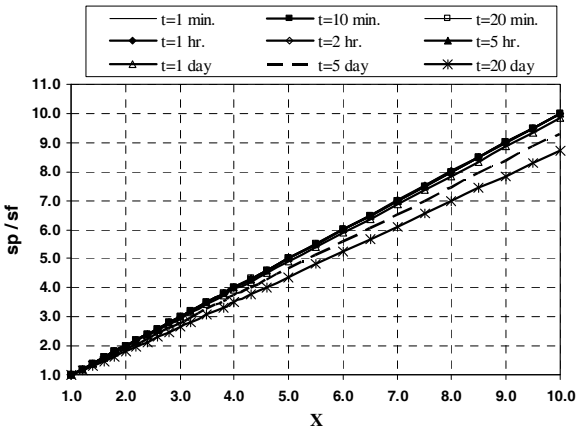

(b) L = 100 m

Figure (7): The ratio of increase in drawdown due to partial penetration, for Fine Sand at r_w= 6 inch.

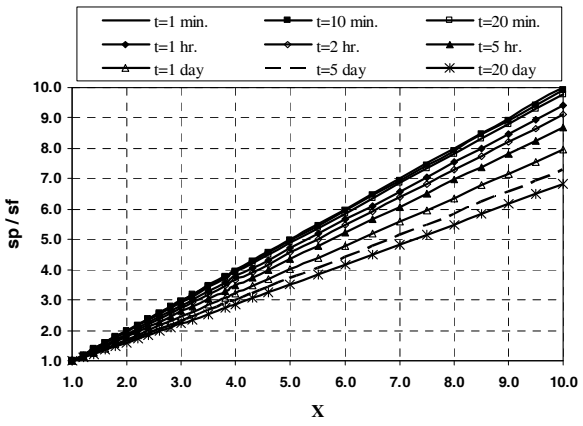

(a) L = 40 m

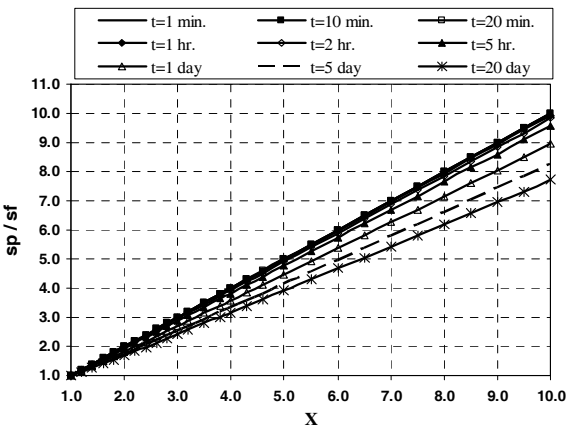

(b) L = 100 m

Figure (8): The ratio of increase in drawdown due to partial penetration, for Medium Sand at r_w= 6 inch.

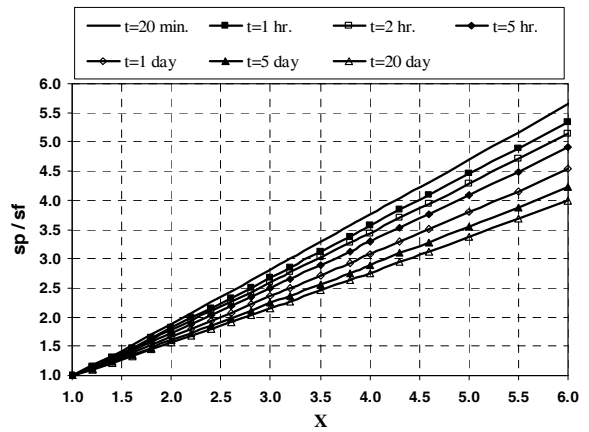

(a) L = 40 m

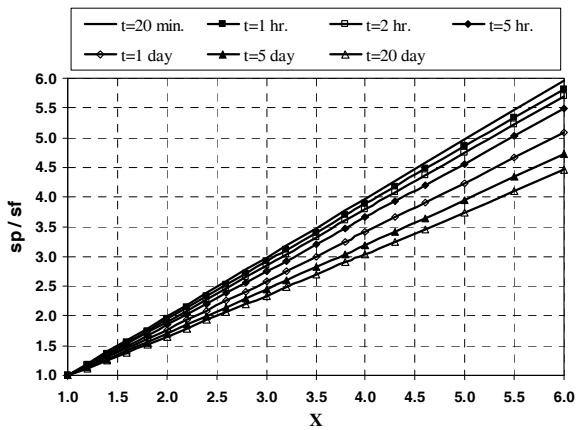

(b) L = 100 m

Figure (9): The ratio of increase in drawdown due to partial penetration, for Coarse Sand at r_w= 6 inch.

2.5 Reduction in the yield due to partial penetration.

For the same drawdown at the well face, the well yield falls beyond that under full penetration. The following relation can be used to determine the ratio between the discharge from partially to fully penetrating, as follows:-

$$\frac{Q_p}{Q_f} = \left[\frac{W^*_f}{W^*_P}\right]\left[\frac{L}{b}\right] = \left[\frac{W^*_f}{W^*_P}\right]\frac{1}{X} \qquad (17)$$

The following figures (10 to 12) for the three types of soils, are drawn between the ratio (Q_P /$Q_{f)}$) , and the ratio x for case of r_w =6 inch.

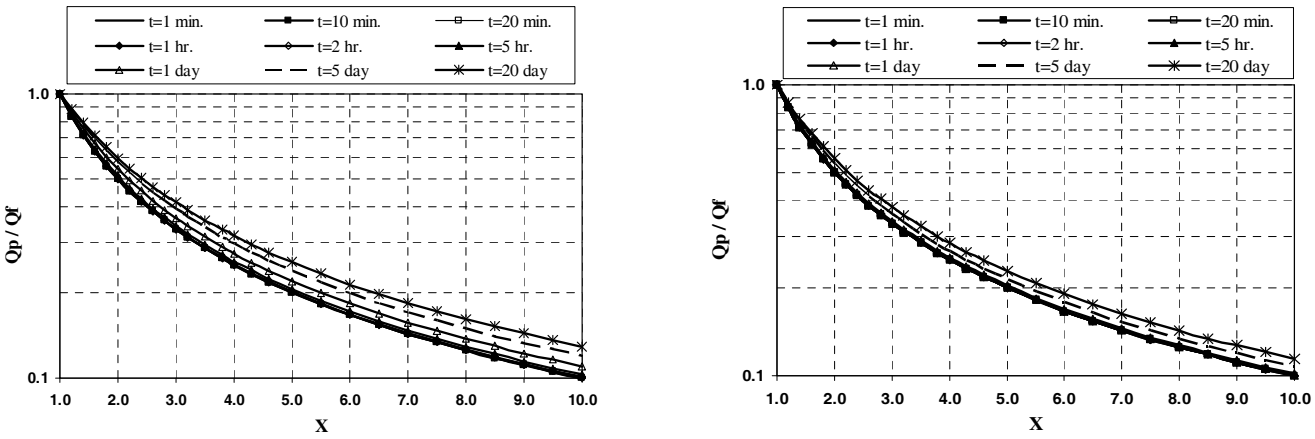

(a) (b)

Figure (10): The ratio of decrease in discharge due to partial penetration, for Fine Sand at r_w= 6 inch.
(a) L = 40 m, (b) L = 100 m

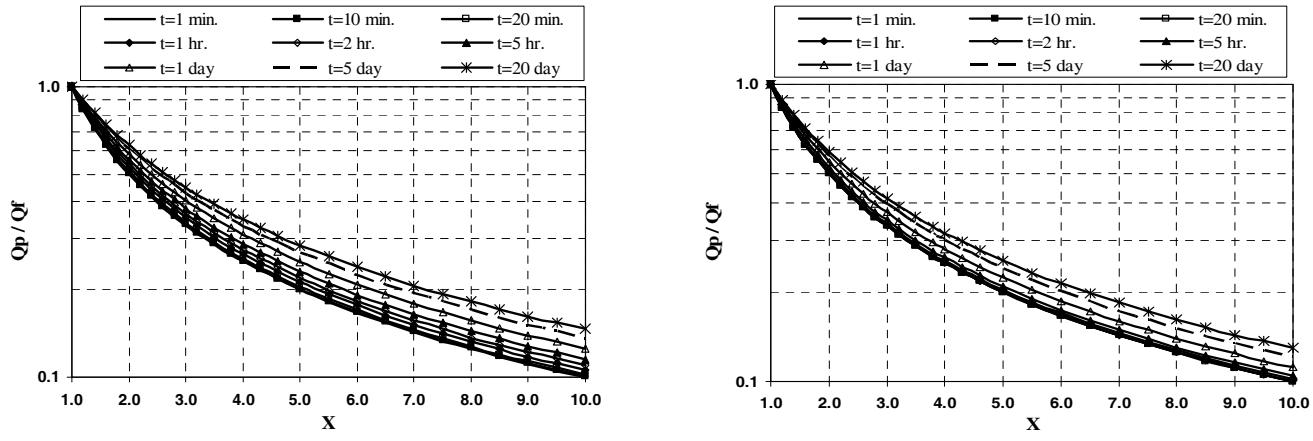

(a) (b)

Figure (11): The ratio of decrease in discharge due to partial penetration, for Medium Sand at r_w= 6 inch.
(a) L = 40 m, (b) L = 100 m

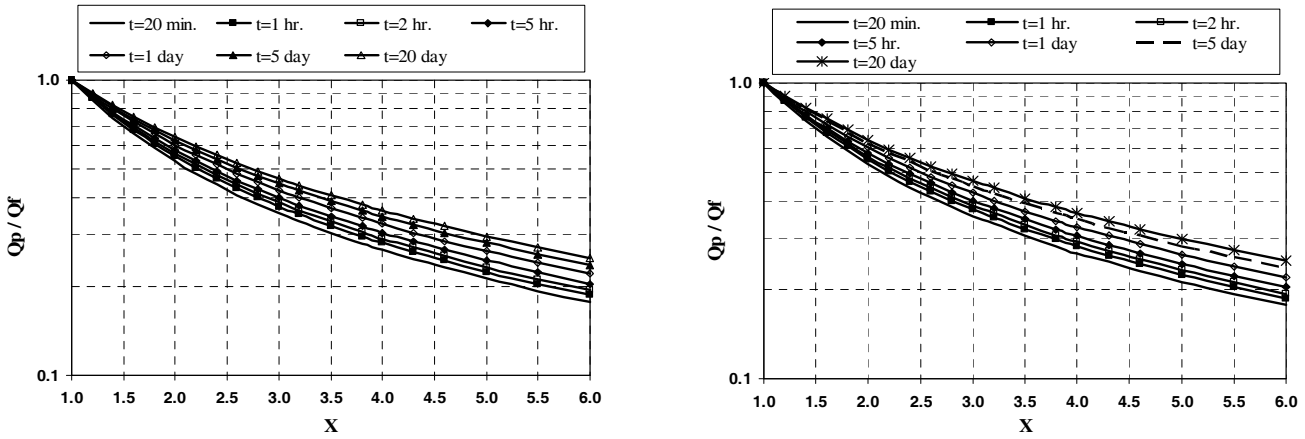

(a) (b)

Figure (12): The ratio of decrease in discharge due to partial penetration, for Coarse Sand at r_w= 6 inch.
(a) L = 40 m, (b) L = 100 m

From Figures (10, 11, and 12), the following points can be concluded:

(1) Ratio of partial to full well yield $\boldsymbol{Q_p/Q_f}$ increases gradually with time.
(2) Higher ratios of $\boldsymbol{Q_p/Q_f}$ happen in short screen wells.

3. Optimum screen length for maximum well yield from a confined aquifer of unknown thickness

When the aquifer thickness is not known, the following empirical equation of well capacity of confined aquifer can be used, following Jumikis (1971):

$$Q_{\max.} = \frac{2\pi r_f l_f \sqrt{K}}{15} \tag{18}$$

Where: Q_{max} : Capacity of confined aquifer (L^3/T), l_f : Length of filter (L)

K : Hydraulic Conductivity (L/T), r_f : Outer radius of filter (L).

Length of the filter is commonly used as the distance from groundwater level to the end of the well. The filter consists of two parts; first, the length between the groundwater level and the top of the aquifer which is variable from case to another and the second is the screen length which is required. Equation (18) can be rewritten in another form by getting the aquifer's capacity per filter's length as follows:-

$$\frac{Q_{\max.}}{l_f} = \frac{2\pi r_f \sqrt{K}}{15} \tag{19}$$

Hantush's Equation (13) can be used to determine the maximum well yield related to each screen length for unlimited aquifer thickness. According to Equation (14) the effect of the aquifer thickness can be neglected after three times of screen length, yet, the aquifer thickness is taken equivalent to twenty times the screen length (x = 20) to ensure that the aquifer is very large, and the drawdown is constant. Hantush's equation is applied to the three types of sand (fine, medium, and coarse), at r_w =6 inch as shown in Figure (13). Curves in Figure (14) are to be used to determine the optimum screen length for a given well yield or determining the well yield for a given screen length

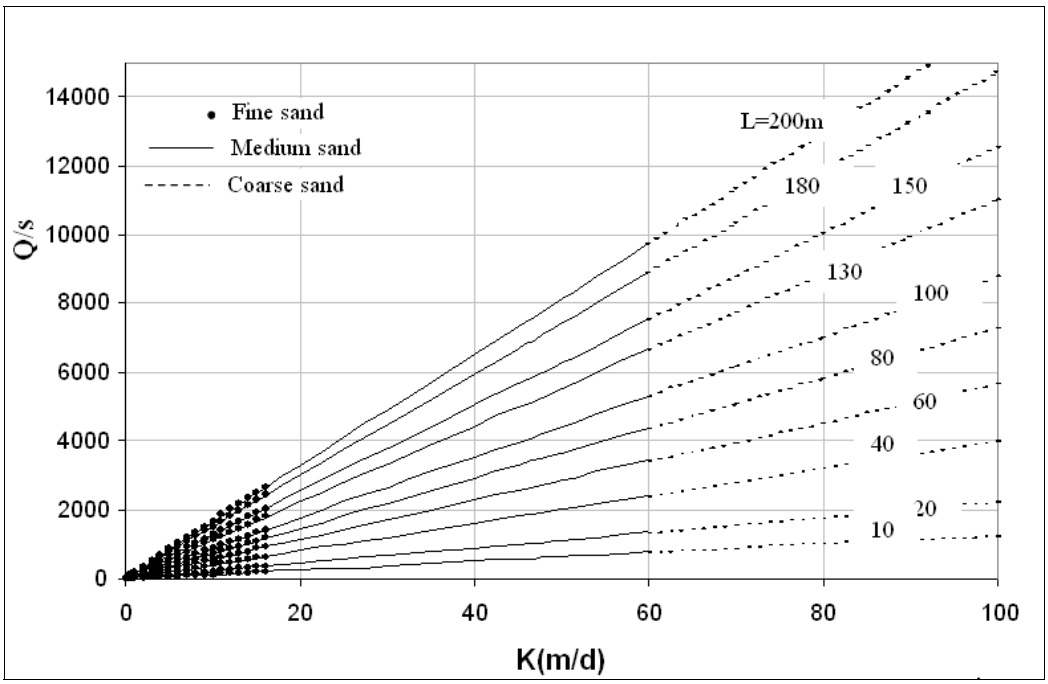

Figure (13): Variation of specific yield (Q/s) with hydraulic conductivity at variable screen lengths for three types of sands, r_w =6 in

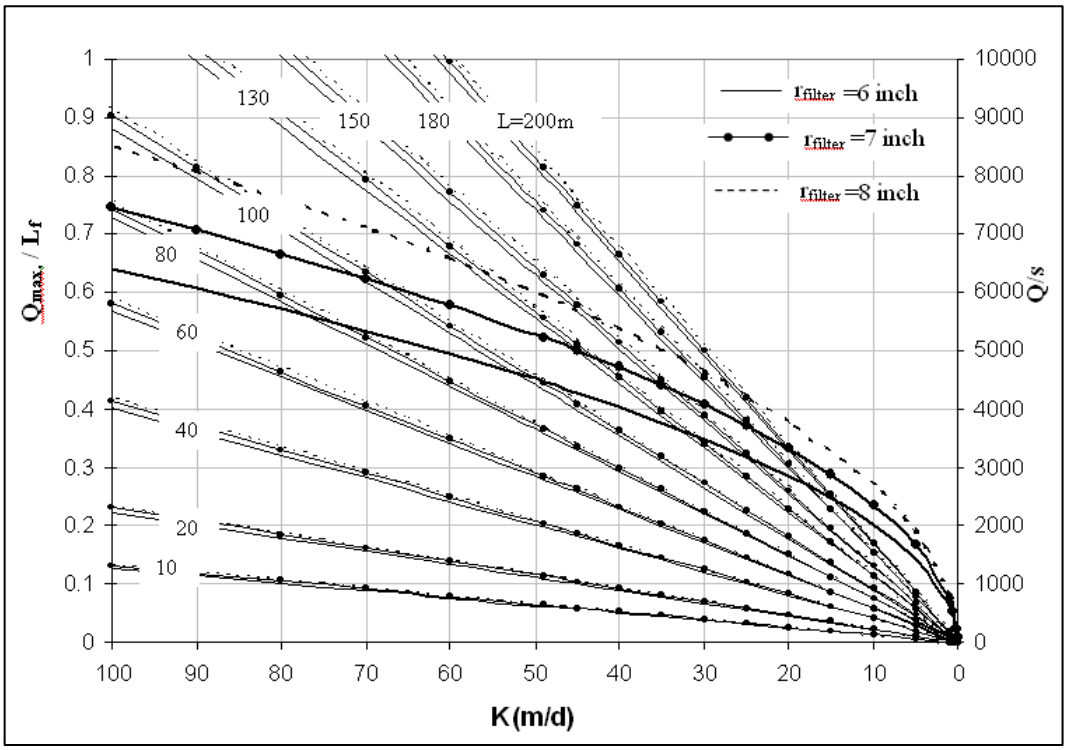

Figure (14): Detection of screen length for extracting maximum well yield from unknown confined aquifer thickness, using Analytical Solution for Hantush Equation (lines), and the Empirical Equation (curves)

4. Radius of influence for partially penetrating well in a confined aquifer at Steady state case

The general equation for a confined aquifer for partially penetrating well is represented by Equation (3). For small values of (u), u < 0.01 (steady state case) Theis equation can be approximated by Equation (-0.5772 –ln (u)) due to approximation of Cooper and Jacob. Equation (3) will be applied between two points, at the face of the well, and at the radius of influence (d/b =z/b =0.0), resulting into:

$$\frac{(s_w - s_r)K}{Q} = \left\{ \frac{1}{2\pi b} \ln\left(\frac{r}{r_w}\right) + \frac{1}{\pi^2 L} \sum_{n=1}^{\infty} \frac{1}{n} \sin\left(\frac{n\pi L}{b}\right) \left[K_o\left(\frac{n\pi a r_w}{b}\right) - K_o\left(\frac{n\pi a r}{b}\right) \right] \right\} \quad (20)$$

The right hand side of Equation (20) is solved using the MATLAB-based program, and the results are shown in Figures (15, and 16) for the two values of r_w (6 in, and 8 in)

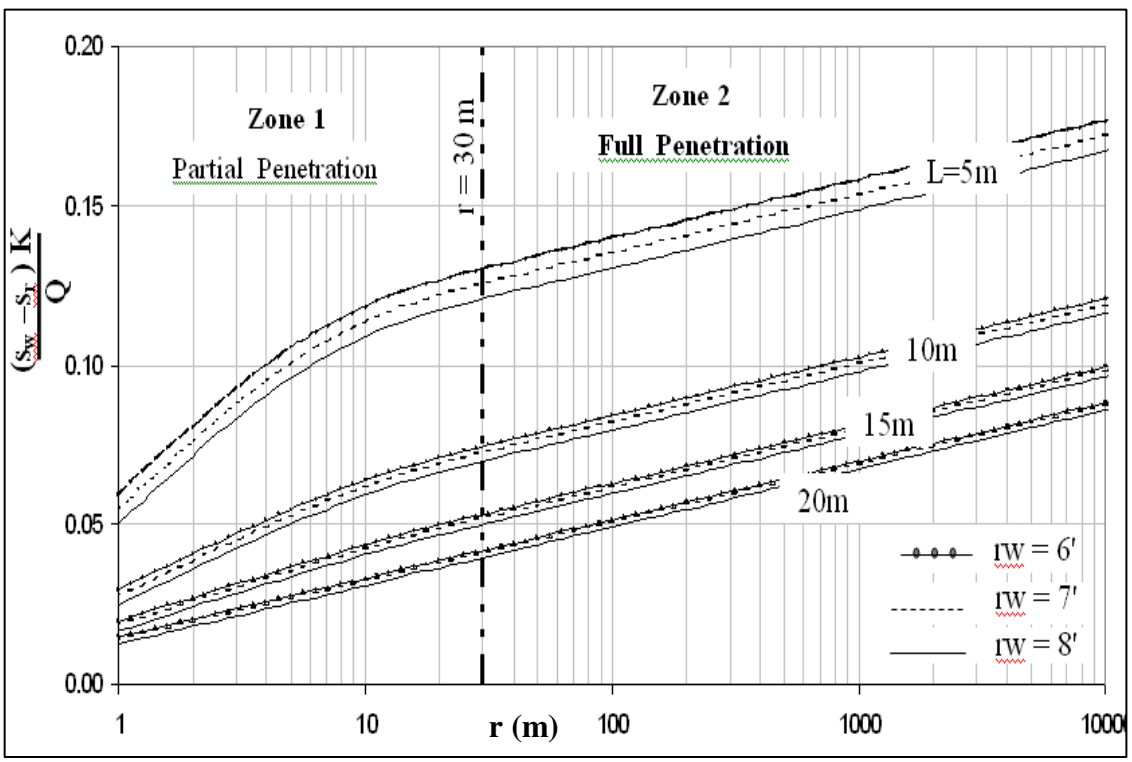

Figure (15): Relation between drawdown at any distance and properties of the Aquifer for partial penetration at b=20 m (confined, steady state).

The provided figures are recommended for calculating the following :

(1) Radius of influence by putting (s_r= 0.0) .
(2) The drawdown at any distance from a well.
(3) The distance at which the drawdown equal a certain value.

As shown from figures (15, 16), two zones exist; (i) The full penetration zone, which has straight parallel lines, and (ii) The partial penetration Zone. The point which separates between these two zones is at a radius close to one and half times of the aquifer thickness which confirms neglecting partial penetration effects for $(ar/b) \geq 1.5$ Furthermore, additional curves are provided by Radwan (2006).

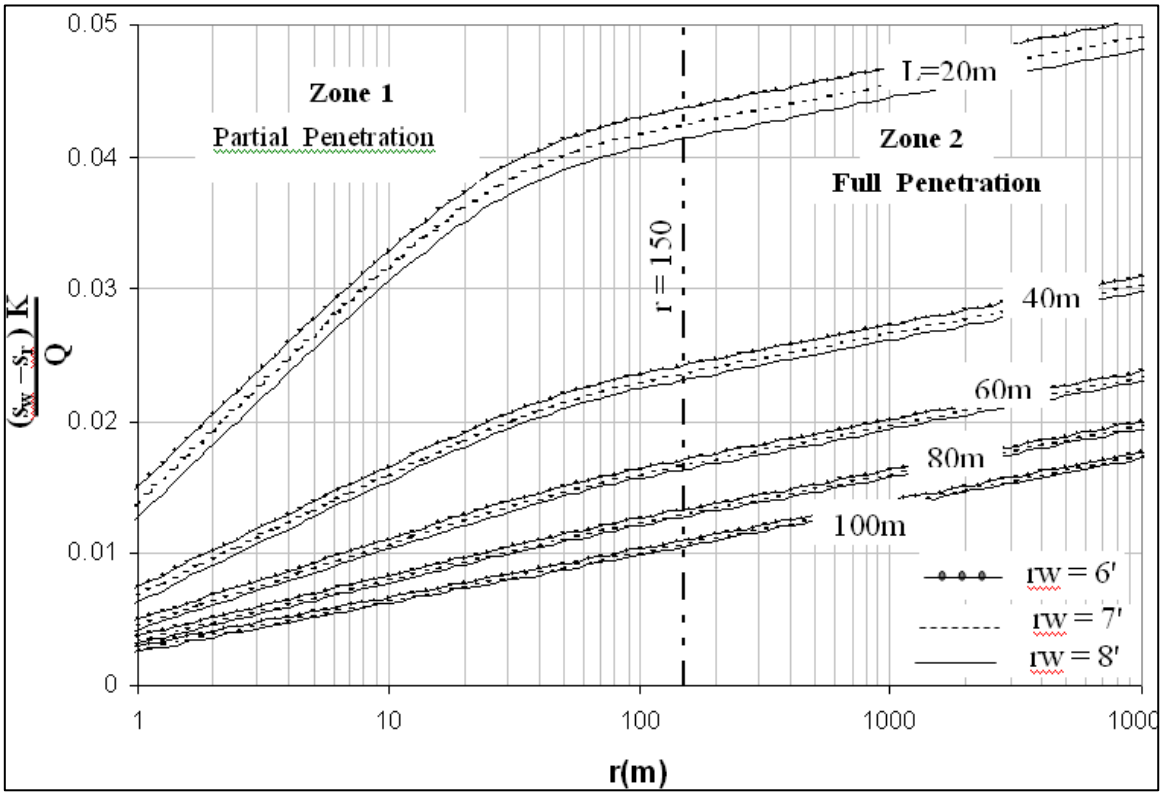

Figure (16): Relation between Drawdown at any Distance and Properties of Confined Aquifer for Partial Penetration, b=100 m (steady state)

4. Conclusion

In this work, the effect of partial penetration on three field problems for confined aquifers have been studied. First, the effective aquifer thickness is proved to be dependent on the pumping time. The commonly applied value of two and half times of the screen length, is only valid for pumping times less than 24 hours. Specific storage of three types of sand soils are calculated. Generally conditions are gradually enhanced with advance of pumping time for patial penetrating wells. Second, a chart, figure (14) is recommended for selection of optimum screen length to extract maximum well yield, taking into consideration the empirical equation of the aquifer capacity. Finally, influence zone charts are prepared for determining the radius of influence or the drawdown at any distance from a fully or partially penetrating well for steady state case, in confined aquifer.

References

Batu V., 1998 " *Aquifer Hydraulics*", A comprehensive guide to Hydrogeologic Data Analysis , Wiley – Inter Science Publication , New York , February 1998.

Braja M. Das., 1983 " Advanced Soil Mechanics " , The university of Texas at El Paso., Hemisphere publishing corporation, Washington, New York, London, 1983.

Hantush, M.S., 1961 " *Drawdown Around a partially Penetrating well*", Journal of the Hydraulics Division. American Society of Civil Engineers, vol. 87, No. 7, pp. 83-98, July, 1961.

Hantush, M.S., 1964 "*Hydraulics of Wells*", Advanced in Hydroscience, edited by Ven Tel Chew, Academic Press, New York, pp. 281-442, 1964.

Radwan, H. 2006 "*Developing an Analytical Program for Solving the Analytical Equations of Groundwater for fully / Partially Penetrating Wells using MATLAB Program*" Masters Thesis, Irrigation and Hydraulics Department, Engineering, Cairo University, 2006.

Jumikis A.R.,1971 "*Foundation Engineering*", Rutgers University,The State University of New Jersey, 1971.

Wagdy, A., Radwan, H., El-Didy, S. 2009 "*Tool for Estimation of Additional Drawdown Due to Partially Penetrating Wells in Confined and Semi-Confined Aquifers*" World Environmental and Water Resources Congress 2009, Great Rivers: protecting the quality of life and bio-diversity, while supporting development and growth critically important for a sustainable future, Kansas City, Missouri, May 2009.

TOOL FOR ESTIMATION OF ADDITIONAL DRAWDOWN DUE TO PARTIALLY PENETRATING WELLS IN CONFINED AND SEMI-CONFINED AQUIFERS

Ahmad Wagdy, Hany G. Radwan, Sherif M. El-Didy,
Irrigation and Hydraulics Department, Engineering, Cairo University,
Giza, Egypt., Fax. 202 5732949

Abstract

This paper presents a simplified approach for estimating the additional drawdown due to partially penetrating wells in confined and semi-confined aquifers. Hantush's Equation usually provides acceptable representation of the associated flow field, should this equation be properly solved. An interactive MATLAB-based computational program has been developed and verified to provide the analytical solution for the later equation. Results are projected as standard design curves which can be used to determine the total and additional drawdown due to partial penetration for semi-confined and confined aquifers, respectively. Empirical formulae, commonly used to calculate the additional drawdown in case of steady state flow for confined aquifers are also discussed, and compared with the analytical solution, showing significant differences in many cases. A proposed design chart for steady flow in confined aquifers, along with two families of curves; one for steady flow in leaky aquifers and the other for transient conditions, are thus recommended for well design purposes.

1. Introduction

Partially penetrating wells are first addressed by *Hantush* 1957. Figure (1) shows schematically a partially penetrating well in a semi-confined aquifer in which the screen interval is located at any place along the aquifer thickness (Batu, 1998). The differential equation representing this system is as follows:

$$\frac{\partial^2 s}{\partial r^2}+\frac{1}{r}\frac{\partial s}{\partial r}+a^2\frac{\partial^2 s}{\partial z^2}-\frac{K'}{Tb'}s=\frac{S}{T}\frac{\partial s}{\partial t} \qquad (1)$$

Where:

$$a^2=\frac{K_z}{K_r},\quad T=K_r b \qquad (2)$$

s : Drawdown at distance r (L).
r : Distance from the well (L).
b : Thickness of aquifer (L).
S : Storage Coefficient.
T : Transmissivity ($L^2 T^{-1}$).
b' : Thickness of confining layer (L).
K' : Hydraulic conductivity of confining layer (LT^{-1}).
K_r, K_z: Horizontal & vertical hydraulic conductivity of aquifer (LT^{-1}).

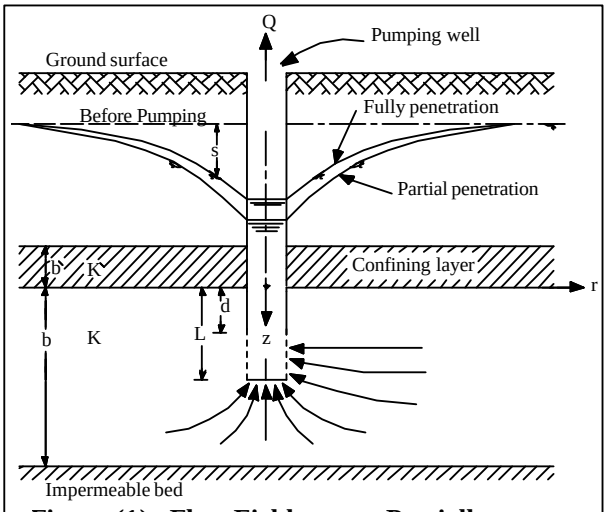

Figure (1): Flow Field near a Partially Penetrating Well in a Semi-Confined Aquifer.

1.1 Semi - Confined Aquifer. (Unsteady state).

Solution of Equation (1), for semi-confined aquifers is given by Hantush (1964), Batu (1998), and Reed (1980) as:

$$s = \frac{Q}{4p\,T}\left\{W\left(u,\frac{r}{B}\right) + f\left(u,\frac{ar}{b},\frac{r}{B},\frac{d}{b},\frac{L}{b},\frac{z}{b}\right)\right\} \quad (3)$$

Where:

$$f\left(u,\frac{ar}{b},\frac{r}{B},\frac{d}{b},\frac{L}{b},\frac{z}{b}\right) = \frac{2b}{p(L-d)}\sum_{n=1}^{\infty}\frac{1}{n}\left[\sin\left(\frac{np\,L}{b}\right)-\sin\left(\frac{np\,d}{b}\right)\right]\cos\left(\frac{np\,z}{b}\right)W(u,K_n) \quad (4)$$

$$K_n = \sqrt{\left(\left(\frac{r}{B}\right)^2+\left(\frac{npar}{b}\right)^2\right)},\quad B^2 = \frac{bb'K}{K'},\quad u = \frac{r^2S}{4T\,t}$$

$$W\left(u,\frac{r}{B}\right) = \int_u^{\infty}\frac{1}{y}\exp\left(-y-\frac{r^2}{4B^2y}\right)dy \qquad \text{Hantush well function.} \quad (5)$$

1.2 Confined Aquifer (Unsteady state).

The solution of Equation (1) for confined aquifer is given by Hantush (1961, 1964) by Letting K` equal zero, as follows (Hantush, 1961), (Batu, 1998):

$$s = \frac{Q}{4p\,T}\left\{W(u) + f\left(u,\frac{ar}{b},\frac{d}{b},\frac{L}{b},\frac{z}{b}\right)\right\} \quad (6)$$

Where:-

$$f\left(u,\frac{ar}{b},\frac{d}{b},\frac{L}{b},\frac{z}{b}\right) = \frac{2b}{p(L-d)}\sum_{n=1}^{\infty}\frac{1}{n}\left[\sin\left(\frac{np\,L}{b}\right)-\sin\left(\frac{np\,d}{b}\right)\right]\cos\left(\frac{np\,z}{b}\right)W(u,X_n) \quad (7)$$

$$X_n = \frac{np\,a\,r}{b},\quad W(u) = \int_u^{\infty}\frac{e^{-y}}{y}dy,\quad W(u)\text{: Theis well function.} \quad (8)$$

The first part in Equations (3, 6) represents the case of fully penetrating well, Hantush well function, and Theis well function, respectively, while the second part represents the effect of partially penetrating well.

2. Partial Penetration for Semi Confined Aquifers

The partial penetration term, containing integration and summation functions, is programmed using Matlab program, (Radwan 2007), and the results are shown in the following sections.

2.1 Steady State, Total Drawdown for Semi-Confined Aquifer due to Partial Penetration

Steady state case will be reached by letting (u) approach zero in equation (3), then

$$W\left(u,\frac{r}{B}\right) = W\left(0,\frac{r}{B}\right) = 2K_o\left(\frac{r}{B}\right) \quad (9)$$

$$W(u,K_n) = W(0,K_n) = 2K_o(K_n) \quad (10)$$

Equations (3, 4) for partial penetration, steady state, semi-confined aquifer become:

$$s = \frac{Q}{4pT}\left\{2K_o\left(\frac{r}{B}\right) + f\left(\frac{ar}{b}, \frac{r}{B}, \frac{L}{b}, \frac{d}{b}\right)\right\} = \frac{Q}{4pT}SD \qquad (11)$$

Where:

$$f\left(\frac{ar}{b}, \frac{r}{B}, \frac{L}{b}, \frac{d}{b}\right) = \frac{4b}{p\,(L-d)}\sum_{n=1}^{\infty}\frac{1}{n}\left[\sin\left(\frac{np\ L}{b}\right) - \sin\left(\frac{np\ d}{b}\right)\right]K_o\left(K_n\right) \qquad (12)$$

SD, the dimensionless drawdown in Equation (11), is a function of four dimensionless parameters (ar/b, r/B, L/b, d/b). General standard curves will be developed to calculate the total drawdown. First, all curves will be drawn at (L/b =1.0) (full penetration) for various ratios of (ar/b, r/B, d/b), then the effect of partially penetration will be included as a ratio of the fully penetrating well (F), for the same ratios of (d/b), where:

$$F = \frac{SD_{Partial-penetration}}{SD_{Full-penetration}} = \frac{s_{Partial-penetration}}{s_{Full-penetration}} \qquad (13)$$

2.1.1 Standard Curves for Fully Penetrating Well $\left(\frac{L}{b} = 1.0\right)$

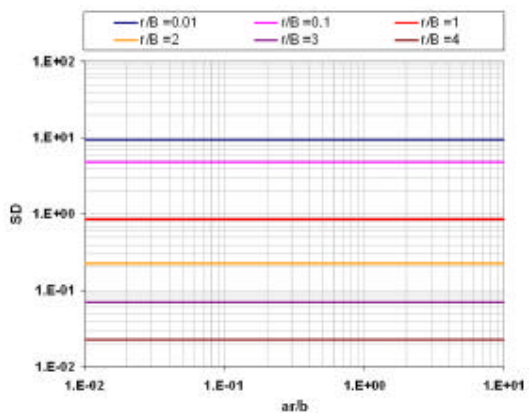

Figure(2-a): SD values for full penetration , steady state in semi -confined aquifer at (d/b)=0.0

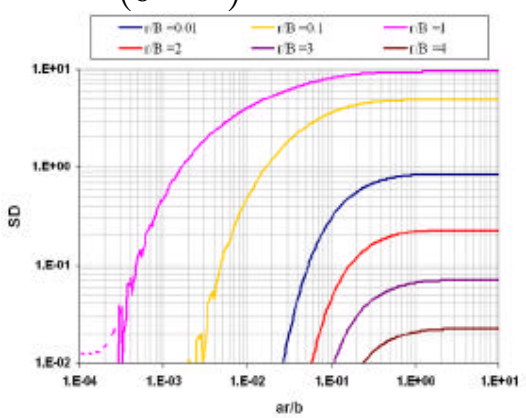

Figure(2-b): SD values for full penetration ,steady state in semi- confined aquifer at(d/b)=0.1

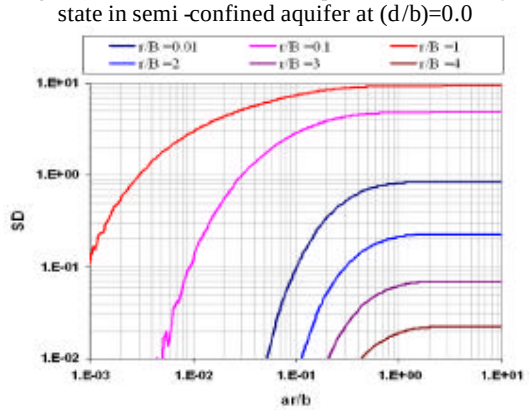

Figure(2-c): SD values for full penetration , steady state in semi -confined aquifer at (d/b)=0.2

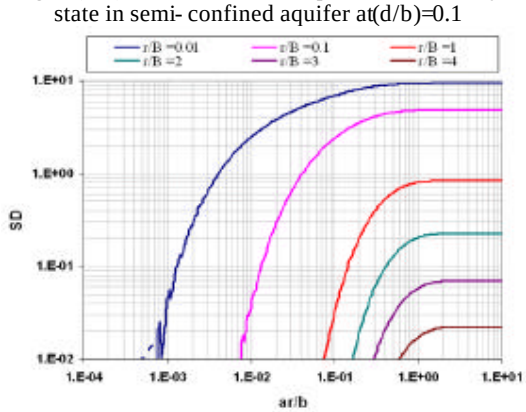

Figure(2-d): SD values for full penetration ,steady state in semi-confined aquifer at(d/b)=0.3

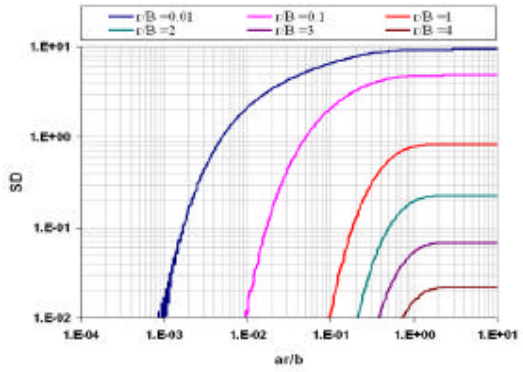

Figure(2-e): SD values for full penetration , steady state in semi- confined aquifer at (d/b)=0.4

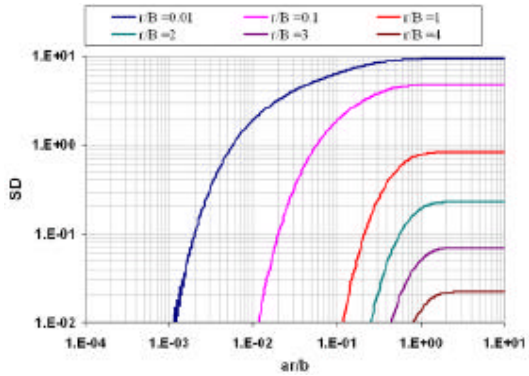

Figure(2-f): SD values for full penetration ,steady state in semi -confined aquifer at (d/b)=0.5

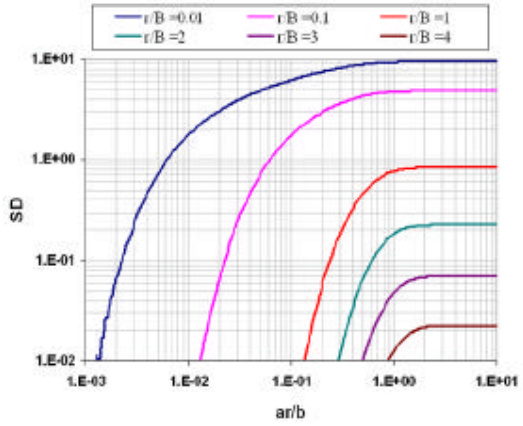

Figure(2-g): SD values for full penetration , steady state in semi- confined aquifer at (d/b)=0.6

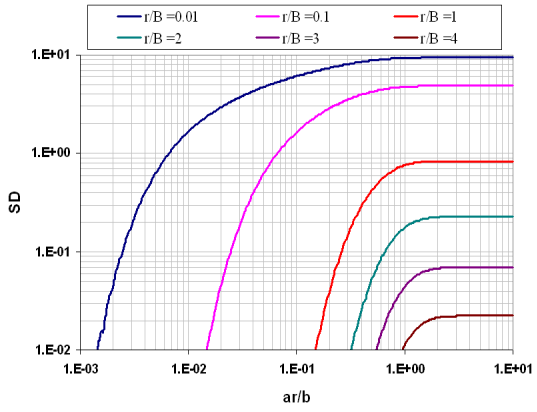

Figure(2-h): SD values for full penetration , steady state in semi -confined aquifer at (d/b)=0.7

At full penetration, extending screen wells, the drawdown will depend on the distance from the well (r) through the ratio $[K_o(r/B)]$ ***not*** the ratio (ar/b), as shown by horizontal lines in figure (2.a). Moreover, the incremental effects of partial penetration on drawdown are restricted to a limiting value of (ar/b), marked by the horizontal part of the individual curves in figures (2.b – 2.h).

2.1.2 Standard Curves for Partially Penetrating Wells L/b [1] 1

Partial penetration effects on drawdown at any distance from the well (r) are illustrated by a family of curves, which are divided into groups as per specific screen ratios (d/b), penetration ratios (L/b), and using nominal ratios of (r/B) = 0.01, 0.1, 1.0, 2.0, 3.0, 4.0.

Figures (3.a to 4.f) reveal a factor F > 1, implying an additional drawdown in case of partial penetration as compared to full penetration case extracting the same discharge. The latter is due to an increase in the velocity of the flow, and accordingly head losses, following the reduction in flow area due to partial penetration. Furthermore, increase of screen length, significantly decreases the drawdown for the same solid part, (d/b) ratio. Moreover, the additional drawdown at any partial penetration ratio decreases as the hydraulic conductivity of confining layer increases (i.e. as r/B decreases).

(a) Group of (d/b) =0.0

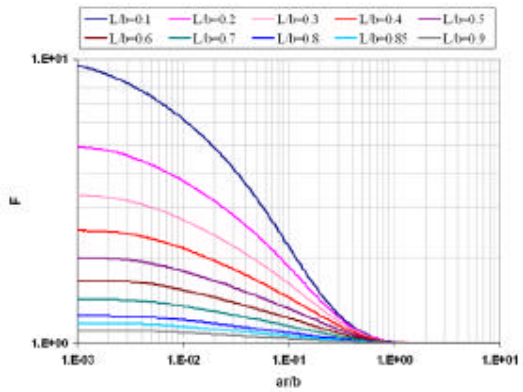

Figure (3-a): The ratio of drawdown of partially to fully penetrating well (F) at (r/ B) =0.01, (d/b) =0.0

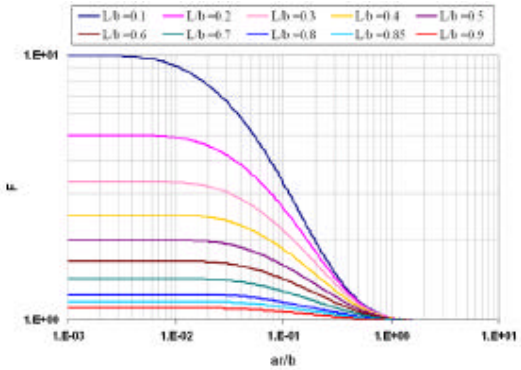

Figure (3-b): The ratio of drawdown of partially to fully penetrating well (F) at (r/ B) =0. 1, (d/b) =0.0

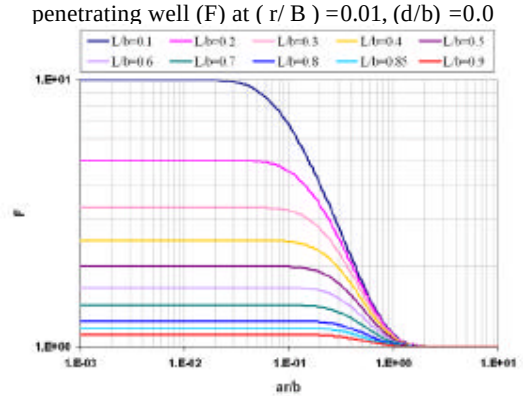

Figure (3-c): The ratio of drawdown of partially to fully penetrating well (F) at (r/ B) =1.0, (d/b) =0.0

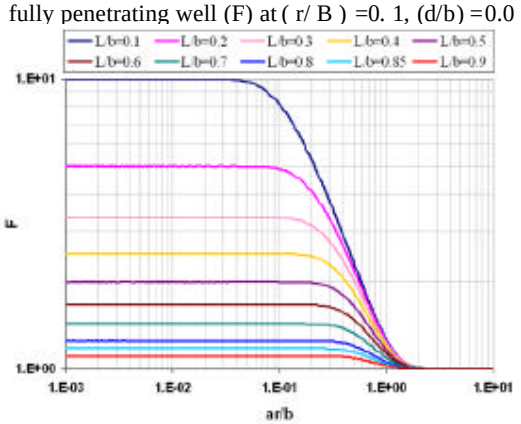

Figure (3-d): The ratio of drawdown of partially to fully penetrating well (F) at (r/ B) =2.0, (d/b) =0.0

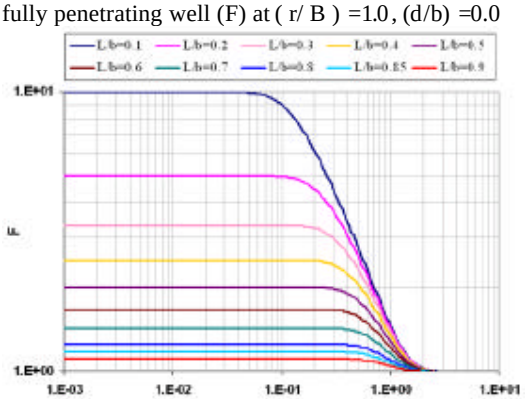

Figure (3-e): The ratio of drawdown of partially to fully penetrating well (F) at (r/ B) =3.0, (d/b) =0.0

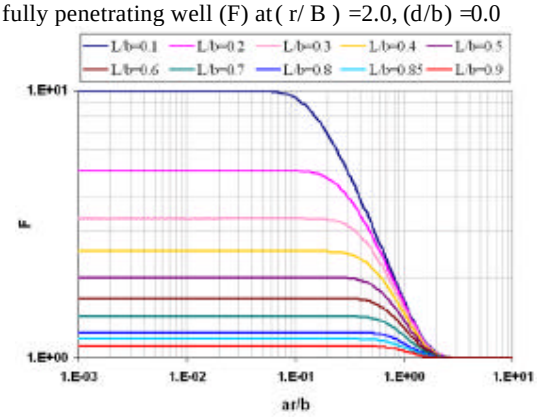

Figure (3-f): The ratio of drawdown of partially to fully penetrating well (F) at (r/ B) =4.0, (d/b) =0.0

(b) Group of (d/b) =0.1 .

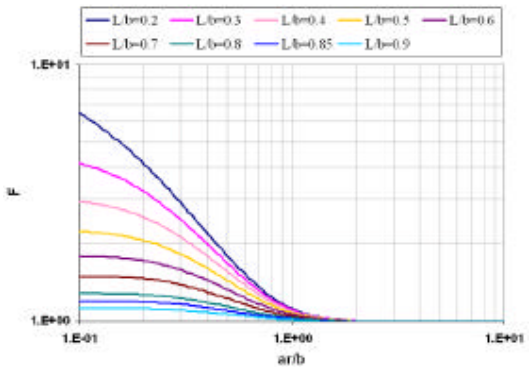

Figure (4-a): The ratio of drawdown of partially to fully penetrating well (F) at (r/ B) =0.01, (d/b)= 0.1

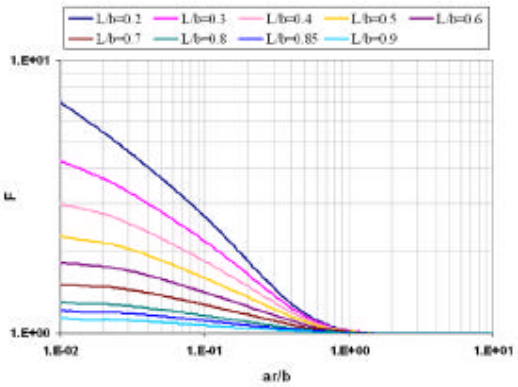

Figure (4-b): The ratio of drawdown of partially to fully penetrating well (F) at(r/ B) =0.1, (d/b) = 0.1

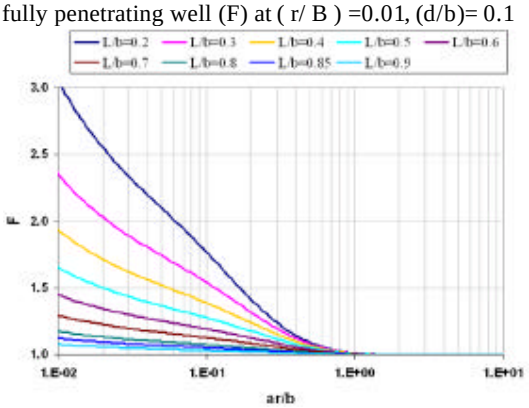

Figure (4-c): The ratio of drawdown of partially to fully penetrating well (F) at(r/ B) =1.0, (d/b) =0.1

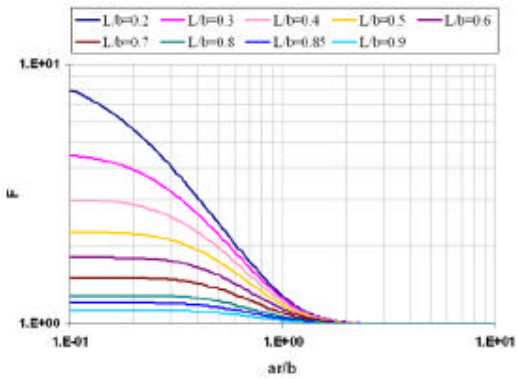

Figure (4-d): The ratio of drawdown of partially to fully penetrating well (F) at (r/ B) =2.0, (d/b) =0.1

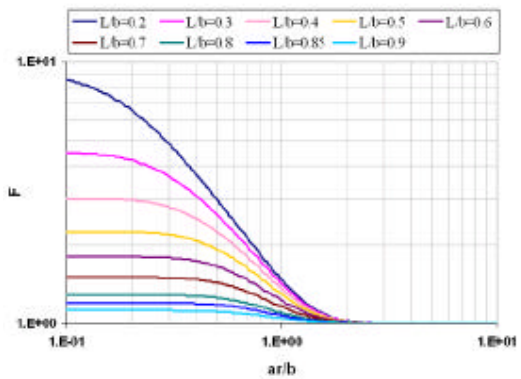

Figure (4-e): The ratio of drawdown of partially to fully penetrating well (F) at(r/ B) =3.0, (d/b) =0.1

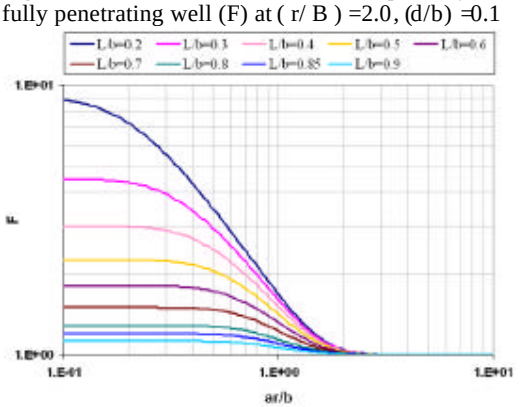

Figure (4-f): The ratio of drawdown of partially to fully penetrating well (F) at(r/ B) =4.0, (d/b) =0.1

The following procedures are recommended to estimate the effect of partial penetration:
Step(1): The well is fully penetrating; (i) compute the ratios (d/b), (ar/b), (r/B), (ii) get the dimensionless drawdown, SD, using figures (2.a to 2.h), for different ratios of (d/b), additional combinations are available at Radwan (2007), (iii) apply Equation (11), to get the drawdown due to full penetration (s_{full}).

Step(2): The well is partially penetrating; (iv) choose the required (d/b) group, then select the suitable ratio of (r/B), then get the factor (F) using figures (3.a to 4.f). (v) drawdown due to partial penetration ($s_{partial}$) finally becomes: ($s_{partial}$) = (s_{full}) * F

The effect of partial penetration may be neglected for two cases. First case follows the common practice, i.e. at the ratio (**ar/b > 1.5**) as illustrated in the former family of curves (where beyond this distance the flow field is similar to that of full penetration). Secondly, when partial penetration ratio is greater than or equal to 80% (l/b = 0.8).

3. Partial Penetration in Confined Aquifers

Several formulae are composed for predicting the additional drawdown due to partial penetration in confined aquifers. Their accuracy will be checked versus the analytical solution proposed in this work as design charts.

3.1 Steady State Flow; Visocky Formula.

Visocky (1970) solved the infinite series and an integral of exponential functions of Hantush's Equation (7), for a limited numbers of parameters and gave an expression for the additional drawdown as follows (Bouwer,1978), (Sternberg, 1973) :

$$s_{wp} = \frac{Q}{4pT}\left(\ln\frac{2.25Tt}{r^2S} + 2s_p\right) \qquad (14)$$

Where $\mathbf{s_{wp}}$ is the drawdown at the well. The first part in Equation (14) refers to Theis's Equation for fully penetrating well under the simplification of Cooper and Jacob (1946) for u < 0.01. The term ($\mathbf{2s_p}$) refers to the additional drawdown due to partial penetration. ($\mathbf{s_p}$) is given by Figure (5), prepared by Sternberg (1973), as dependant on the ratio of (L_e/b) where $\mathbf{L_e}$ is the screened length of the aquifer, but Hantush's Equation (6) depends on the ratios (d/b), and (L/b). The relation between L_e, (d/b), and (L/b) is that L_e=(L/b)-(d/b) as shown in Figure (6). By comparing Equation (14) and Hantush's Equation (6), the values of $2s_p$ should be equal the values of f{(L/b),(d/b),(ar/b)}.

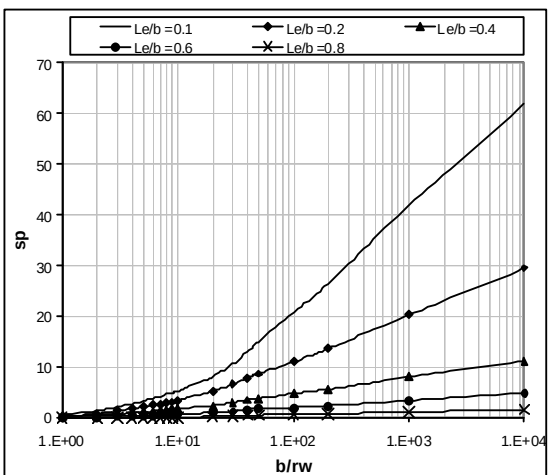

Figure (5): Graph of s_p versus b/r_w for Different Values of L_e/b

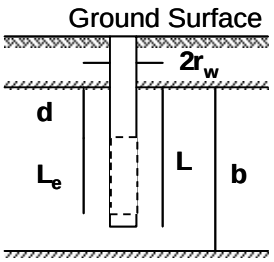

Figure (6): Partial Penetration Parameters

Figure (7) shows the values of f{(L/b),(d/b),(ar/b)} for (d/b)=0, for a homogeneous aquifer (a=1.0) which are prepared using the Matlab-based program. Figure (7) presents the results of an accurate analytical solution of Hantush equation and is recommended as a tool for estimating ***additional*** drawdown in confined,

homogeneous aquifers and fully extending well screen, (d/b)=0.0 which are features of common occurance.

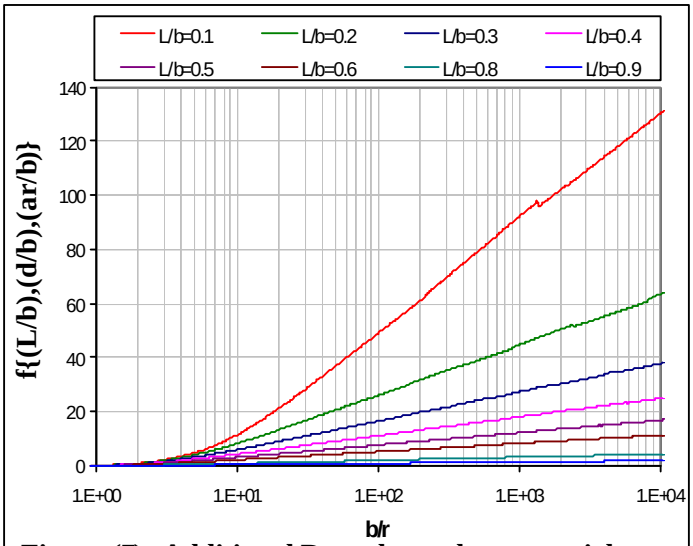

Figure (7): Additional Drawdown due to partial Penetration in Confined Aquifers at (d/b)=0, (a =1.0) for various ratios of (L/b)
Ds = f{(L/b),(d/b),(ar/b)}Q/(4pT)

The comparison between Sternberg curve and the analytical solution for Hantush equation is shown in Figure (8). This figure shows that Visocky formula, although following the same trends, yet is not accurate enough to predict the additional drawdown.

3.2 Netherlands Formula.

Netherlands generated a formula to predict the additional drawdown at the *well face* as follows (Huisman, 1972):

$$\Delta s = \frac{Q}{2\pi T}\frac{1-P}{P}\ln\frac{ah}{r_o} \qquad (15)$$

Where a is a function of the amount of penetration P= (h/b), and the amount of eccentricity (e) =(k/b) where k is the distance between the mid point of the screen and mid point of the aquifer as shown in Figure (9).

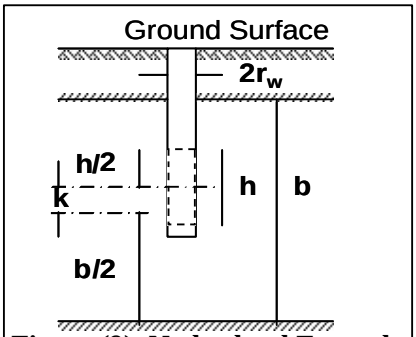

Figure (9): Netherland Formula Parameters

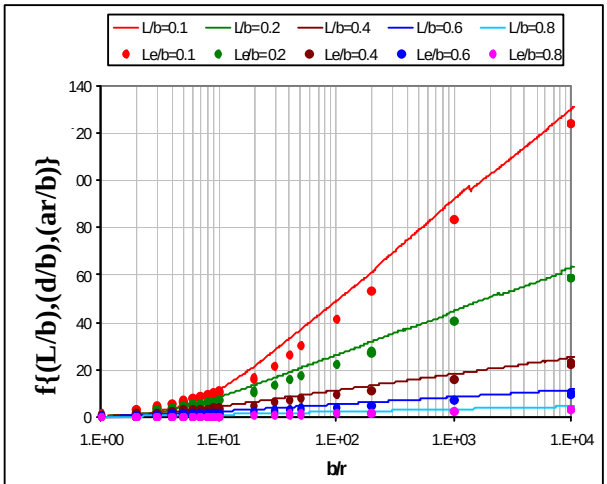

Figure (8): Comparison between Visocky's Equation (Points) and Analytical Solution (Lines) at (d/b)=0, (a=1.0)

The value of a as function of these parameters is given in **Table (1),** (Huisman, 1972).

Table (1): Values of *a* as function of e and P for Netherland Formula (Huisman, 1972).

	e = 0	0.05	0.1	0.15	0.20	0.25	0.30	0.35	0.40	0.45
p = 0.1	0.54	0.54	0.55	0.55	0.56	0.57	0.59	0.61	0.67	1.09
0.2	0.44	0.44	0.45	0.46	0.47	0.49	0.52	0.59	0.89	
0.3	0.37	0.37	0.38	0.39	0.41	0.43	0.50	0.74		
0.4	0.31	0.31	0.32	0.34	0.36	0.42	0.62			
0.5	0.25	0.26	0.27	0.29	0.34	0.51				
0.6	0.21	0.21	0.23	0.27	0.41					
0.7	0.16	0.17	0.20	0.32						
0.8	0.11	0.13	0.22							
0.9	0.06	0.12								

Netherlands Equation also deals with the ratio of screened aquifer or penetration ratio (P) =(h/b) similar to L_e in Visocky's formula, which depends on the position of the screen. The relation between P, (d/b), and (L/b) is that P=(L/b)-(d/b).

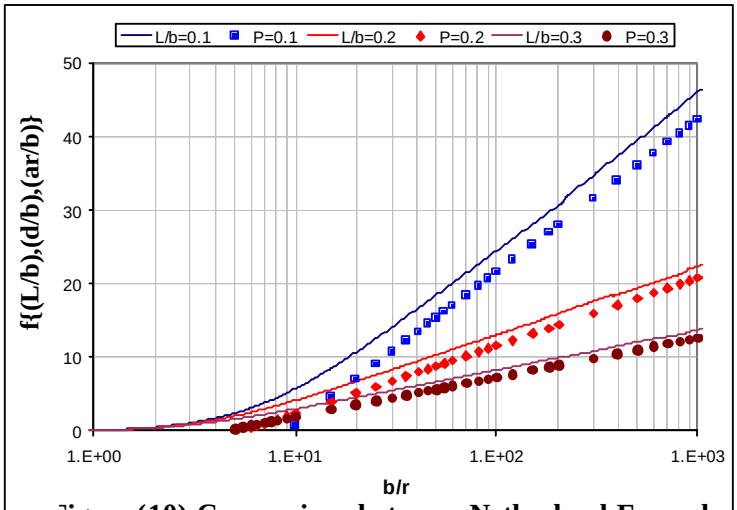

Figure (10): Comparison between Netherland Formula (Points) and Analytical Solution (Lines) at (d/b)=0, (a=1.0)

Comparison between the analytical solution of Hantush equation as proposed by Figure (7), and the half values from the former at (d/b)=0.0, and (a=1.0) is shown in Figure (10). Significant differences exist between the analytical solution and Netherlands formula. Equation (15) has a drawback of neglecting the values of Δs at (b/r) < 1.0, similar to Visocky's formula, whereas Figure (10) shows that, for every penetration ratio (P), Δs is neglected at a different ratio of (b/r).

4. Transient Flow Predictors

This section presents a group of curves for the second term of Equation (6) which concerned with the additional drawdown. Each curve has a certain ratio of (ar/b) beginning from ($1e^{-8}$) to (1.6) to determine the limit of partial penetration's effect. Only ratios of (ar/b) = $1e^{-8}$, 0.1, 1.0, 1.6 will be presented as examples. These curves are specific for the common case of (d/b) = 0.0, and homogenous aquifer (a = 1.0).

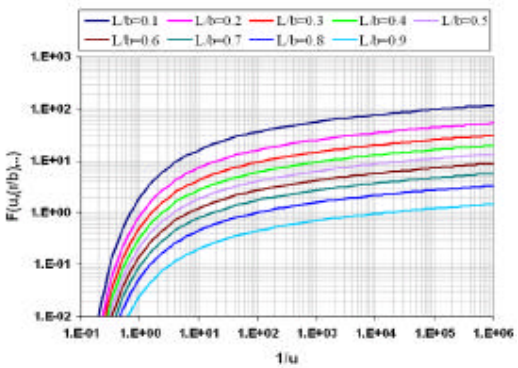

Figure (11-a): Values of f{u,(ar/b),(d/b),(L/b)} in Confined aquifer at {(d/b=0.0),(a=1.0)}, and (ar/b)=1e-8

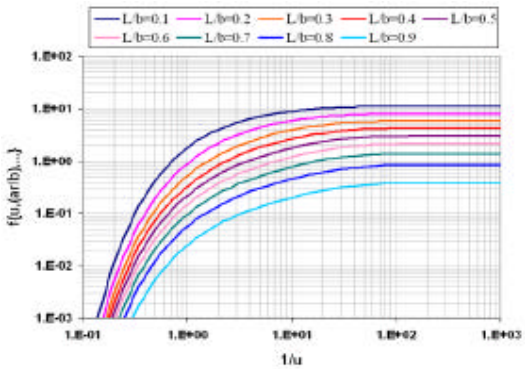

Figure (11-b): Values of f{u,(ar/b),(d/b),(L/b)} in Confined aquifer at {(d/b=0.0),(a=1.0)}, and (ar/b)=0.1

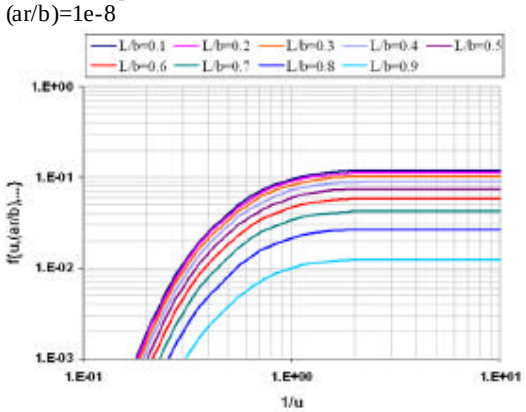

Figure (11-c): Values of f{u,(ar/b),(d/b),(L/b)} in Confined aquifer at {(d/b=0.0),(a=1.0)}, and (ar/b)=1.0

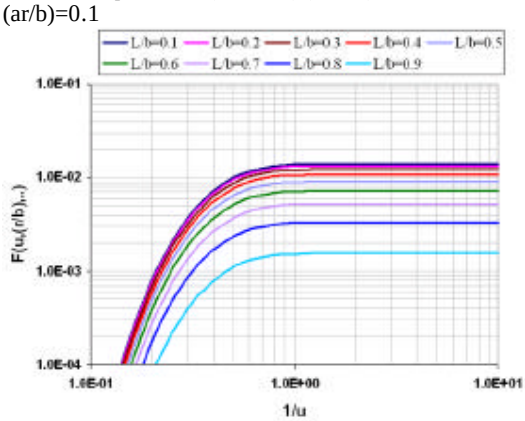

Figure (11-d): Values of f{u,(ar/b),(d/b),(L/b)} in Confined aquifer at {(d/b=0.0),(a=1.0)}, and (ar/b)=1.6

The previous figures are recommended for determining the additional drawdown term due to partial penetration at any distance from the well, and at any time. It is clear from the figures that, the term of additional drawdown may be neglected beyond the ratio of $(ar/b > 1.5)$ which confirms what has been mentioned earlier.

5. Conclusion

An interactive MATLAB-based computational program has been developed and verified to provide the analytical solution Hantush equation to quantify the effects of partial penetration for confined or semi-confined aquifers. A family of curves, figures (2.a to 4.f), have been prepared for semi-confined aquifers to predict the total drawdown due to partial penetration in case of steady state flow. Empirical formulae commonly used to calculate the additional drawdown due to partial penetration in case of steady state flow for confined aquifer are discussed and compared with the analytical solution Several errors, associated with empirical formulae are encountered. A design curve, figure (7), is thus recommended for design purposes. General curves (figs 11.a to 11.d) also are prepared based on Hantush's equation by using the analytical program, to

predict the additional drawdown due to partial penetration in case of unsteady state flow.

References

Batu V., 1998 " *Aquifer Hydraulics*", A comprehensive guide to Hydrogeologic Data Analysis , Wiley – Inter Science Publication , New York , February 1998.

Bouwer H., 1978 "*Groundwater Hydrology* ", Mc Graw-Hill Series in Water Resources and Environmental Engineering, London , 1978.

Hantush, M.S., 1961 " *Drawdown Around a partially Penetrating well*", Journal of the Hydraulics Division. American Society of Civil Engineers, vol. 87, No. 7, pp. 83-98, July, 1961.

Hantush, M.S., 1964 "*Hydraulics of Wells*", Advanced in Hydroscience, edited by Ven Tel Chew, Academic Press, New York, pp. 281-442, 1964.

Huisman, L., 1972 *"Groundwater Recovery"*, University of Technology, Delft, Netherlands,1972.

Radwan, H. 2006 *"Developing an Analytical Program for Solving the Analytical Equations of Groundwater for fully / Partially Penetrating Wells using MATLAB Program"* Masters Thesis, Irrigation and Hydraulics Department, Engineering, Cairo University, 2006.

Reed J.E , 1980 " *Type Curves For Selected Problems of Flow to Wells in Confined Aquifers"*, Geological Survey, United States Government Printing Office, 1980.

Sternberg, Y. M., 1973 "*Efficiency of partially penetrating wells*", Groundwater 11(3): 5-8, 1973.

A NOVEL APPROACH TO GROUNDWATER MODEL DEVELOPMENT

Thomas D. Krom[1] and Richard Lane[2]

[1]Touch Water Ltd., P.O. Box 143, Lincoln, Christchurch, New Zealand; email: touchwater@gmail.com
[2]Applied Research New Zealand Ltd., St. Elmo Courts, Hereford St., Christchurch, New Zealand

ABSTRACT

The hydrogeologic conceptual model is a key source of uncertainty in predictions of groundwater flow. The data used to develop the hydrogeologic conceptual model include geologic sample descriptions, interpretations of geophysical data, geochemical information et al. Frequently there is insufficient information to fully describe the hydrogeology without considerable interpretation from an expert. Existing methods for capturing this knowledge rely on the manual interpretation of hydrogeological structures. This procedure is time consuming, difficult to update and also makes it difficult to maintain alternative interpretations of the hydrogeology.

We show how hydrogeological models can be created from the 3 and 4-dimensional data sets using Radial Basis Function (RBF) models. We develop RBF models for the components in a hydrogeological model: aquifers, aquitards, boundaries, drains, and rivers. This approach has significant advantages. Firstly, the models are consistent with the known data and can be automatically updated when new data comes to hand. Secondly, the models can be influenced by both the choice of high level parameters such as anisotropy while maintaining consistency with the data. Thirdly, the user can add manual interpretations (trends or a priori information) that are maintained separately from measurements, but are then merged in the model building process to produce a model consistent with both measured and interpreted data. Once created, the model can be isosurfaced or gridded at any resolution or fitted to any mesh, a process that provides a flexible interface to flow simulators.

The methodology will be demonstrated on data from New Zealand and Denmark.

INTRODUCTION

There is an increased focus on the development of groundwater models and addressing the uncertainty that is inherent when a system is underdetermined to the degree seen in groundwater systems. A number of works show that the uncertainty associated with developing the geological model, or hydrogeological conceptual model, is a fundamental source of uncertainty in the predictions from groundwater models (Poeter 2007; Stauffer 2005). Since, uncertainty is guaranteed in a groundwater model, it is imperative to develop groundwater models in a manner that clearly exposes the uncertainty by using methods that allow this uncertainty to be explored. This, in part, can be done by applying parameter estimation (optimization)

methods such as advocated by Moore and Doherty (2006). However, those methods are not well suited to geological interpretations.

The data used to develop the hydrogeologic conceptual model includes geologic sample descriptions, interpretations of geophysical data; geochemical information et al. Existing methods for capturing knowledge from these data sets rely on manual interpretation of hydrogeological structures. This procedure is time consuming, difficult to update and reproduce as well as make it difficult to maintain alternative interpretations of the hydrogeology. Our method provides both intuitive tools to aide in capturing knowledge from data as well as separating the interpretation from data.

Radial Basis Functions's (RBF's) have been previously applied in groundwater modeling (Li et al. 2003; Shafieifar et al. 2007). We apply RBF's to develop hydrogeological models from 3 and 4-dimensional data sets processed using our knowledge capture methods. The RBF's are used to model the components of the hydrogeological system: aquifers, aquitards, boundaries, drains, and rivers based on data.

This approach has significant advantages. Firstly, the models are consistent with the known data and can be automatically updated when new data comes to hand. Secondly, the models can be influenced by both the choice of high level parameters such as anisotropy while maintaining consistency with the data. Thirdly, the user can add manual interpretations (trends or a priori information) that are maintained separately from measurements, but are then merged in the model building process to produce a model consistent with both measured and interpreted data. Once created, the model can be iso-surfaced or gridded at any resolution or fitted to any mesh, a process that provides a flexible interface to flow simulators.

The methodology will be demonstrated on data sets from New Zealand and Denmark.

METHOD

The general approach of the method is presented, then Radial Basis Functions which underpin the method are described, and finally the implementation of the method is presented.

The foundation of the method is the concept of a grid free conceptual model. This is based on a set of fundamental ideas:

- Intuitive knowledge capture from data,
- Data driven equations (RBF's) to describe individual elements of the hydrogeologic system, and
- The ability to carry out logical operations on the elements of the hydrogeologic system as well as a priori knowledge about the system.

Method overview

The general application of the method is shown in the Figure 1. The key elements of the method are the development of representations (equations) for data, (e.g. geology, topography, etc.) and a priori knowledge (e.g. structural trends). This concept can be extended to all input for model development. Special logical operators exist for geological conditions, such as erosion surfaces, so that the inter-relation of formations can be explicitly defined. Finally, state information can be added to the model in order to complete the description needed to carry out a flow simulation. This paper focuses on the stages up to and including models for formations.

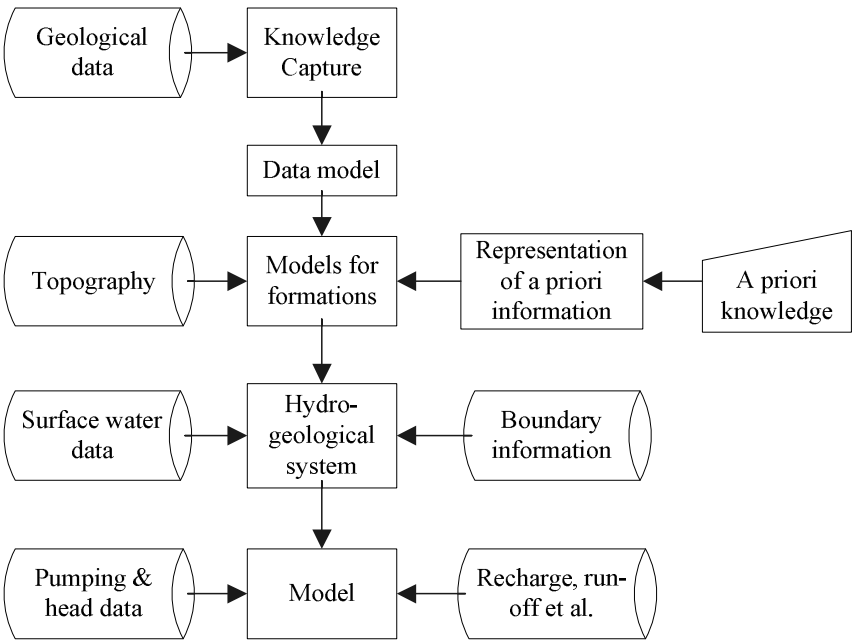

Figure 1. Flow chart for developing a groundwater model using the proposed method.

To walk through the development process:

1. A data set, say lithological well logs, is selected,
2. Grouping of formations according to hydrogeologic behavior leads to contact points that describe the contact between hydrogeologic units.
3. RBF's are fitted to these sets of points, and can be visualized.
4. A priori knowledge, or other data (e.g. dip and strike) are combined with the appropriate RBF's; which results in a description of contact surfaces
5. Formation contacts are arranged in chronological order and the relation to over- and under lying formations is provided (e.g. non-conformal relations).
6. Boundaries are added to the system description, and
7. A solid geometrical model, as RBF's, is produced for the hydrogeological system.

Surface water system features (e.g. rivers, drains, etc.) can be processed in a similar manner. As the topography is represented by an equation, elements are controlled to ensure they lie on the surface, flow down-hill and other error checking. Exterior boundary conditions are processed in a similar manner. State data is also maintained in the system, and is processed to produce input to the groundwater model.

There is in principle no limit to how information can be combined to form a hydrogeologic element, for example formations can be described by a combination of well log information, geophysical data and (hydro-) geochemical information.

Radial Basis Functions

The equations used to represent hydrogeological system elements are developed by fitting RBF's to the data set. RBF's are well established set of methods used in scattered data interpolation, signal processing and artificial intelligence methods. RBFs are real valued functions defined as:

$$y(x) = \sum_{i=1}^{N} w_i \, \phi(\|\boldsymbol{x} - \boldsymbol{c}_i\|),$$

Where, c is the ith center, $\boldsymbol{x}$ is locations in space (or space-time), w is a weight and function ϕ can be any one of a number of functions but typically is either, gaussian, quadratic, or a type of spline function. We apply a polyharmonic (thin-plate) splines function for ϕ. The key factor in the application of a RBF is the determining the weights w_i associated with centers $\boldsymbol{c}_i$, which is a straight forward optimization problem.

Implementation

The methodology is implemented into a unique computer aided modeling environment. The environment has a complete suite of tools for all of the tasks delineated in Figure 1. A prime goal in the implementation of the method is to develop an intuitive user interface. Furthermore, advanced graphics are included in the interface in order that the significance of choices on the resulting hydrogeological model.

CASE STUDIES

Two case studies are presented: a layered aquifer system from New Zealand and a till-outwash complex that overlies a chalk aquifer from Denmark. The focus of these two case studies is to demonstrate the transparency of developing the hydrogeologic frame work in the proposed manner as well as the ability to quickly develop and compare alternative conceptual models for the hydrogeology.

New Zealand Aquifer System

The aquifer system was deposited as a series of alluvial deposits from an area that is being uplifted due the pacific plate being subducted under the Tasman plate, interbedding these alluvial deposits are near shore marine and estuary fine grained sediments. In other words a classic progressive-regressive sedimentary sequence bordered to the South by a volcanic massif.

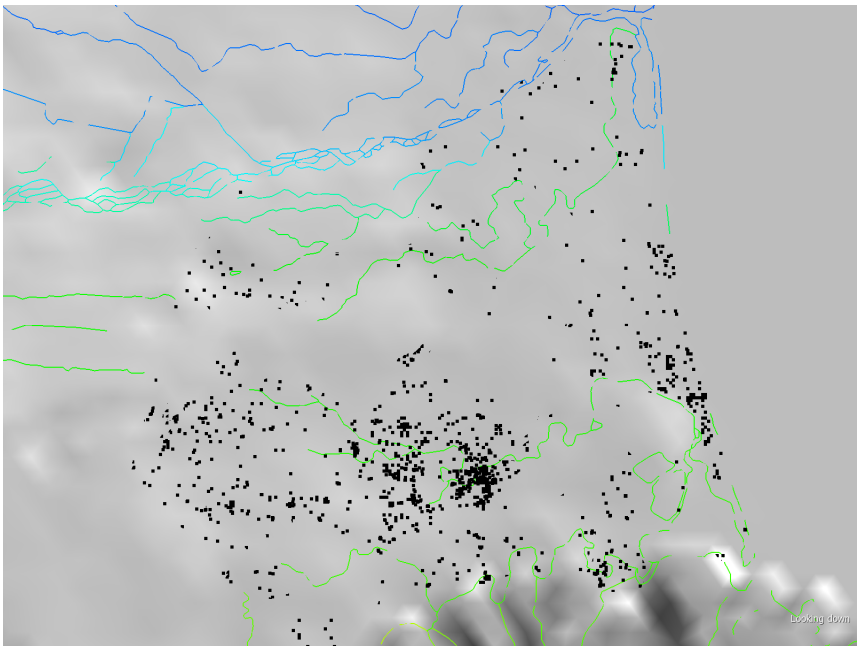

Figure 2. Distribution of wells for the New Zealand case study.

Data. The data for the development of the hydrogeologic framework are 2271 well logs of varying depth. In addition to the well logs there is a digital elevation model, GIS themes for surface water bodies, and time series data for groundwater recovery and water levels. The distribution of wells is shown in Figure 2.

Table 1. Hydrogeology for the New Zealand aquifer system.

Formation	Type	Chronology
Springston	Aquifer	Youngest
Christchurch	Aquitard	
Riccarton	Aquifer	
Bromeley	Aquitard	
Littleton	Aquifer	
Heathcote	Aquitard	
Burwood	Aquifer	
Shirley	Aquitard	
Wainono	Aquifer	
Aquifer 5	Aquifer	Oldest

There are 8 formations that need to be represented in the hydrogeological model (Table 1). A problem lies in how the interpretation of the well logs has been recorded; for example the Littleton fm. is normally denoted “LI”, but in the record one can find not only LI, but LI?, LI-1, LI-2, etc. This problem extends to the other formations as well. The knowledge capture approach we develop aides the hydrogeologist by first presenting all these variations as a group, but then providing tools that allows them to “drag and drop” into a re-classification of the data (Figure 3). Then contact points for the extremes of the group can be extracted (Figure 4).

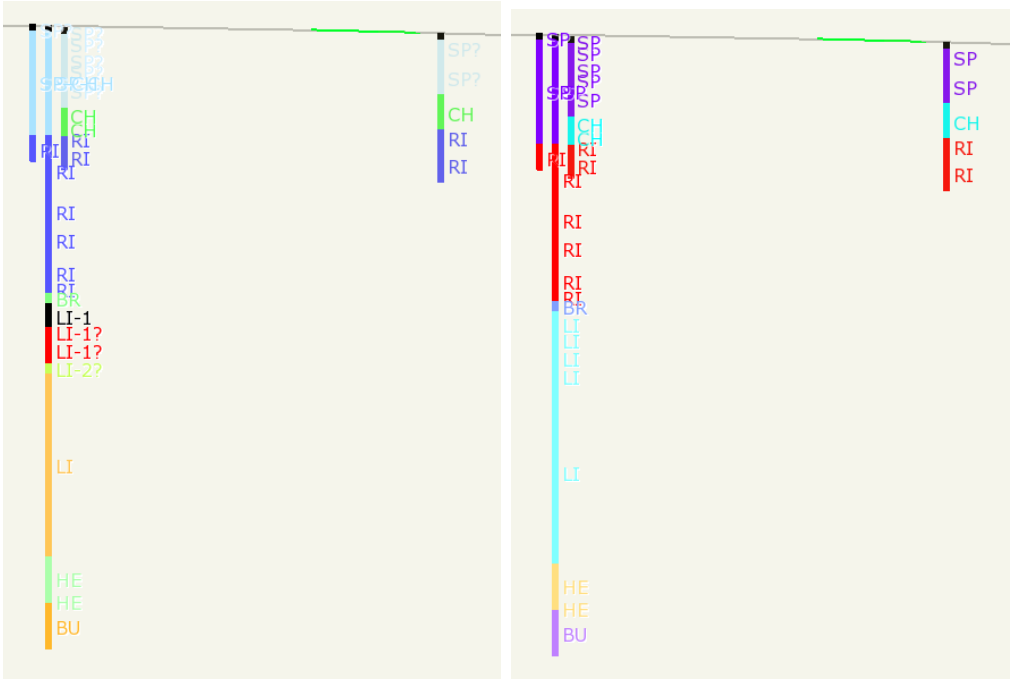

Figure 3. Well logs before (left) and after (right) applying knowledge capture tools. Note the simpler geology in the deep well on the right hand figure.

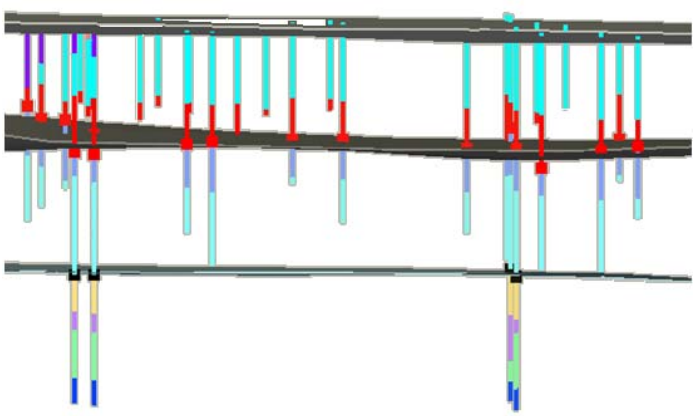

Figure 4. Well logs in 3D after processing, contact selection and 2 fitted surfaces.

Surfaces are modeled by RBF's through the contact points (Figure 4). A series of contacts surfaces are modeled that describe the hydrogeological sequence (Table 1); and used to define the hydrogeologic formations as solid volumes (Figure 5).

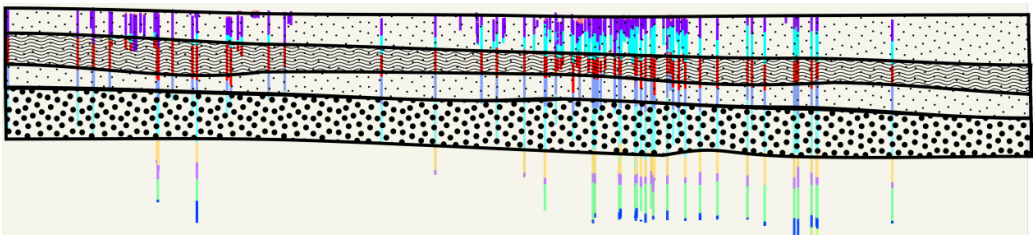

Figure 5. Cross-section of the hydrogeology developed by the complete process.

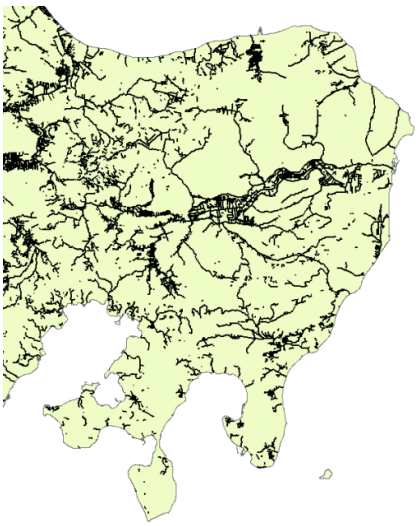

Figure 6. Map of Djursland, note this is a peninsula, the land area show is roughly 40 km wide.

Djursland Aquifer System

In Djursland, Denmark (Figure 6) there was deposited a series of glacial and postglacial sediments on top of an erosion surface which consists of chalk. The glacial sediments have been partially reworked by subsequent glaciations and Quaternary sedimentation. The result is a far more complex geological setting than what is seen in the previous example. Here we have non-layered geology (till complex) resting on an erosion surface (Table 2). The main hydrogeologic issue in the region is quality degradation due to nitrates.

Table 2. Hydrogeology for the Djursland aquifer system.

Formation	Environment	Type	Chronology
Postglacial sediments	various	mainly aquitards	youngest
Till	Glacial	Aquitard	same
Sands and gravels	Glacial	Aquifer	age
Erosion surface			
Chalk	Marine	Aquifer	Oldest

Data. The data for the development of the hydrogeologic framework are 3851 well logs of varying depth. In addition to the well logs there is a digital elevation model and groundwater chemistry data. It is very time consuming if one is to group formations by hand for 3851 well logs, though one can learn by inspecting cross-sections and from experience, which formations are hydrogeologically similar. Our knowledge extraction process quickly resolves the hydrogeological formations at the site.

The hydrogeologic problem is to define sand and gravel aquifers and specifically identify where there is good groundwater protection, i.e. thick tills overlying sand and chalk. The upper 10 – 30 meters of the chalk is a fractured aquifer, regardless of the type of chalk. The geology is simplified into hydrogeological formations in the following manner: tills and silts and other fine grain sediments form one hydrogeologic formation; while sands and gravel form a second formation; finally chalk formations are placed into a 3rd formation. The surface between chalk and the other formations is defined as an erosion surface

.

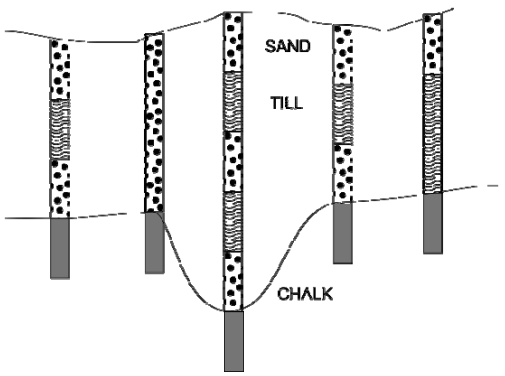

Figure 7. Conceptual problem in the Djurs hydrogeology.

Figure 7 shows the conceptual problem that is solved in the Djursland hydrogeology; that is we have a non-layered system overlying a layered system. The proposed method is ideal to addressing this type of problem because the RBF based model is not constrained to a layered system.

Another problem that needed to be addressed here is that as Djursland is a peninsula, there are no wells to the north and south. This causes a problem with the chalk surface as most interpolation routines will result in the chalk being exposed in the fjords north and south of Djursland. However, the addition of dip points just off shore for the erosion surface "forces" the chalk surface deeper, as we know is the case from wells north of the fjord.

Figure 8 shows the result of the modeling exercise for Djursland where we see a very heterogeneous system overlying the chalk surface.

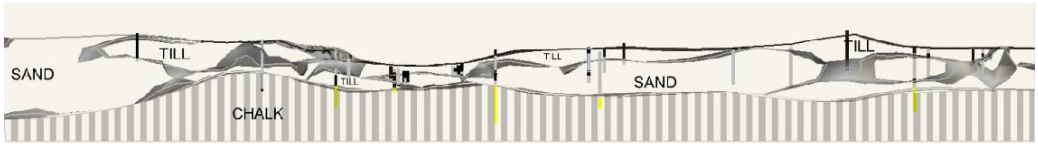

Figure 8. Cross/section modeled using the proposed RBF approach.

CONCLUSIONS

We have presented a methodology that can be applied to develop hydrogeological models in complex hydrogeological systems. We believe the method shows advantages in extracting knowledge from the data and developing grid free hydrogeological models. The method also shows advantages in clearly indicating knowledge that comes from data versus expert opinion/a priori knowledge.

A significant part of the advantage with the method is how it is employed in the implementation and is experienced carrying out the work flow in developing a hydrogeological model as well as in the collaboration between the geologist and hydrogeologist. This is difficult to demonstrate in a technical article.

The method was illustrated for 2 examples: one from New Zealand and another from Denmark. The Danish example shows advantages in modeling non-layered aquifer systems.

REFERENCES

Li, J., Chen, Y., and Pepper, D. (2003). "Radial basis function method for 1-D and 2-D groundwater contaminant transport modeling." *Computational Mechanics*, 32(1-2), 10-15.

Moore, C., and Doherty, J. (2006). "The cost of uniqueness in groundwater model calibration." *Advances in Water Resources*, 29(4), 605-623.

Poeter, E. (2007). "‘‘All Models are Wrong, How Do We Know Which are Useful?’’—Looking Back at the 2006 Darcy Lecture Tour." *Ground Water*, 45(4), 390–391.

Shafieifar, M., Kholghi, M., and Hoorfar, A. (2007). "Comparison of efficiency of radial basis function and finite difference methods for groundwater flow modeling." *Geophysical Research Abstracts*, 9(07798).

Stauffer, F. (2005). "Uncertainty Estimation of Pathlines in Ground Water Models." *Ground Water*, 43(6), 843-849.

Groundwater Mixing using Pulsed Dipole Injection/Extraction Wells

C. R. Radabaugh[1], D. C. Mays[2], and R. M. Neupauer[3]

[1]Graduate Student, University of Colorado Denver, Department of Civil Engineering, Campus Box 113, PO Box 173364, Denver, CO 80217-3364; email: cristyn.radabaugh@ucdenver.edu
[2]Assistant Professor, University of Colorado Denver, Department of Civil Engineering, Campus Box 113, PO Box 173364, Denver, CO 80217-3364, (303) 352-3933; email: david.mays@ucdenver.edu
[3]Assistant Professor, University of Colorado at Boulder, Department of Civil, Environmental, and Architectural Engineering, 428 UCB, ECOT 441, Boulder, CO 80309-0428; email: roseanna.neupauer@colorado.edu

Abstract

Mixing is notoriously difficult in groundwater aquifers, because the Reynolds number is very small. This can limit site remediation, and inducing mixing within the groundwater aquifer could speed the chemical processes or otherwise reduce the amount of time needed to meet site remediation goals. A recent analytical model suggests that mixing in groundwater aquifers may be achieved through pulsed dipole injection and extraction from groundwater wells. Building on past work, this study uses MODFLOW, a finite-difference groundwater flow model code developed by the U.S. Geological Survey, to simulate the flow of groundwater and the movement of particles within a two-dimensional confined aquifer. The analysis shows the effects of pulsing the wells, modifying the frequency of pulsing, and changing the lag time between pulses. Mixing within the groundwater aquifer is shown graphically through the pathlines of the particles and quantified using Lyapunov exponents to determine if the flow is chaotic based on the positions and paths of particles within the aquifer. The model indicates that the pulsed dipole injection/extraction leads to increased mixing within the aquifer.

Introduction

Accelerated mixing in contaminated groundwater aquifers could reduce the required remediation time. Some groundwater remediation methods rely on the injection of chemicals, microbes, or carbon sources into the aquifer to enhance or encourage degradation. This process typically involves injection at one or more wells and the extraction of groundwater at downstream wells. For this type of in-situ remediation to be successful, it is important that the substances introduced into the aquifer spread throughout the region of concern. Unfortunately, the injected substance is likely to travel in the more conductive paths of the aquifer, leading to non-uniform mixing of the injected substance throughout the zone of intended remediation.

Several reports have demonstrated the potential for mixing in laminar flows, which are categorized under the heading of "chaotic advection" (Aref 2002). In this process, mixing occurs when the separation distance between fluid particles increases exponentially with time, which is the signature of chaotic flow. Jones and Aref (1988) analyzed mixing during pulsed injection/extraction in dipole flow, and Stremler et al. (2004) reported that pulsed injection/extraction improved mixing in microarray analysis used in biology research. Two recent studies have explored applications of chaotic advection to aquifers during injection and extraction. Sposito (2006) modeled sequential injection and extraction from a pair of wells. Bagtzoglou and Oates (2007) modeled mixing in groundwater by a system of three wells with random flow assignments. Both Sposito (2006) and Bagtzoglou and Oates (2007) focused on pulsed injection and extraction in two-dimensional, confined, homogeneous aquifers and reinjected the extracted groundwater back into the aquifer thereby forming a closed system. Sposito (2006) assumed steady-state flow during each stress period, and used a first-out-first-in particle reinjection scheme. Bagtzoglou and Oates (2007) did not specify whether their simulation was steady-state or transient during each stress period, and did not specify their reinjection scheme, but they did account for dispersion with a random walk model and for turbulent mixing in the wells. This research indicated that chaotic flow occurs, based on exponential growth of particle separation distance with time.

The present study places Sposito's (2006) conceptual model in the framework of a numerical groundwater model in order to address the following questions: (1) Can mixing be achieved just by pulsed flow, regardless of the reinjection scheme? (2) Will the predicted mixing change significantly after considering an inter-cycle recovery period in which no pumping occurs? (3) How will heterogeneity in the hydraulic conductivity affect the predicted mixing?

This paper reports on the first of these questions. Specifically, we investigate the degree of mixing resulting from pulsed dipole injection/extraction during a single pass from the injection well to the extraction well.

Methods

MODFLOW, a numerical finite difference code developed by the U.S. Geological Survey (Harbaugh et al. 2000), was used to model the flow associated with injection and extraction from a single-layer confined aquifer. In this study, MODFLOW was implemented within PMWIN (Chiang 2005). The model is a single layer, 1500 meter by 1500 meter square divided into 10,000 evenly spaced grid blocks that are 15 meters wide and 15 meters tall. Figure 1 shows a model schematic. The 10-meter thick fully-saturated confined aquifer had an initial hydraulic head of 200 meters throughout the entire model domain. The model includes one fully penetrating injection well and one fully penetrating extraction well located 345 m apart. In these preliminary tests, the model was run as a series of transient simulations corresponding to alternating injection and extraction cycles, with pumping time T = 1 d, and recovery time R = 0 d (Figure 2). The injection and extraction rates are 1.5 m^3/s. The

model was run for six stress periods in all simulations. In order to focus on mixing processes within the pulsed aquifer flow, rather than the recirculation piping, reinjection was not modeled.

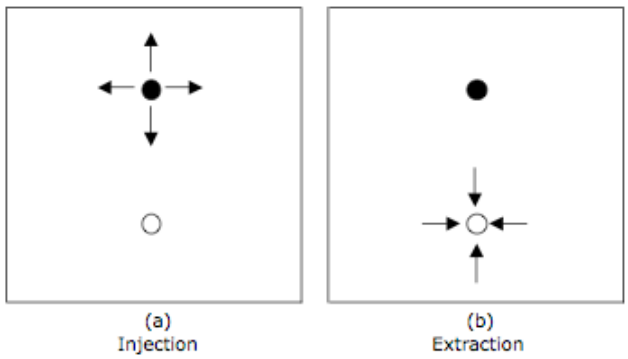

Figure 1. Schematic of pulsed dipole injection/extraction wells. Filled circles denote injection wells; open circles denote extraction wells; and arrows denote flow directions.

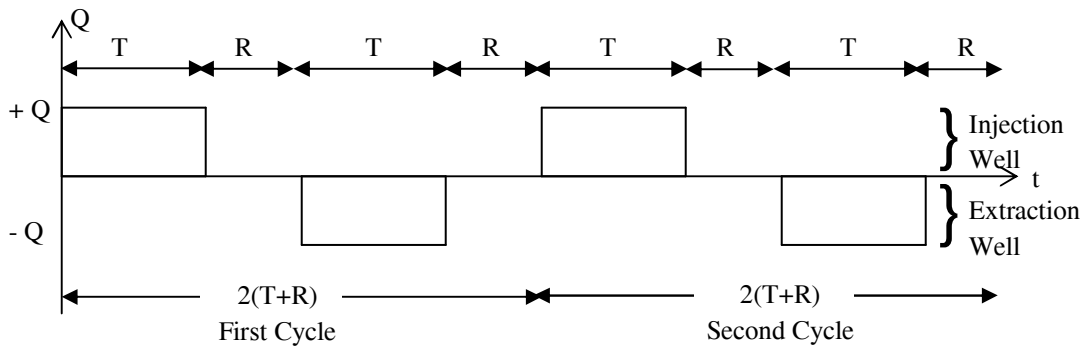

Figure 2. Plot of injection rate vs. time for two injection/extraction cycles. Each cycle comprises an injection period of length T, followed by a recovery period of length R, followed by an extraction period of length T, and a recovery period of length R for a total cycle duration of 2(T + R). Q is the injection rate and –Q is the extraction rate.

Preliminary Results

Particles within the modeled aquifer were then tracked using MODPATH (Pollock 1994), again implemented with PMWIN. Seventy-two particles, located five degrees apart, were started in a circle within the injection well grid block at t = 0. Figure 3 presents the particle locations and their pathlines through time. The pathlines of the particles do not cross.

However, a second simulation considered an additional 72 particles injected at t = T/2. In this case, pathlines did cross (Figure 4).

Initial results indicate that the pathlines of particles injected simultaneously do not cross during the injection and extraction pumping simulation, but when additional

particles are injected midway through the injection periods, the pathlines of the particles do cross. The crossing pathlines indicate that pulsed dipole injection/extraction produces mixing within the aquifer.

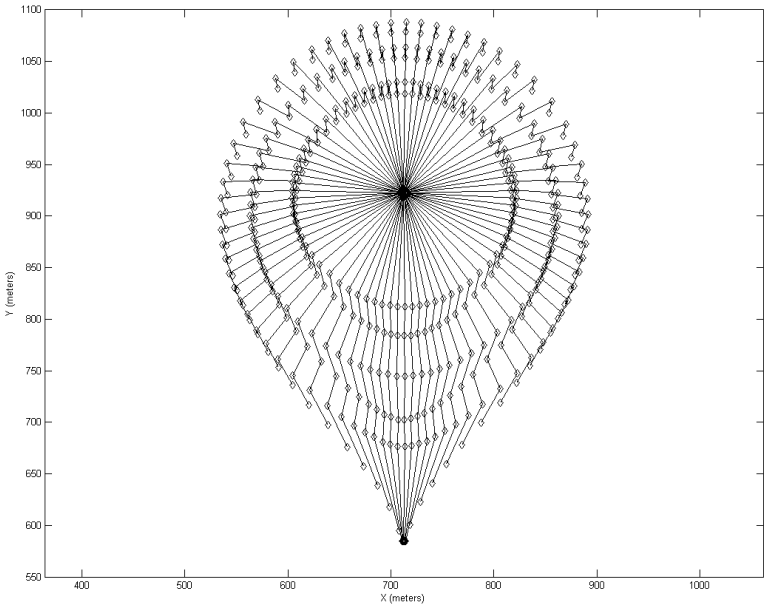

Figure 3. Pathlines for 72 particles injected at t = 0. Recovery time, R, is 0. Particles are shown by open diamonds initially and at the end of each injection or extraction period.

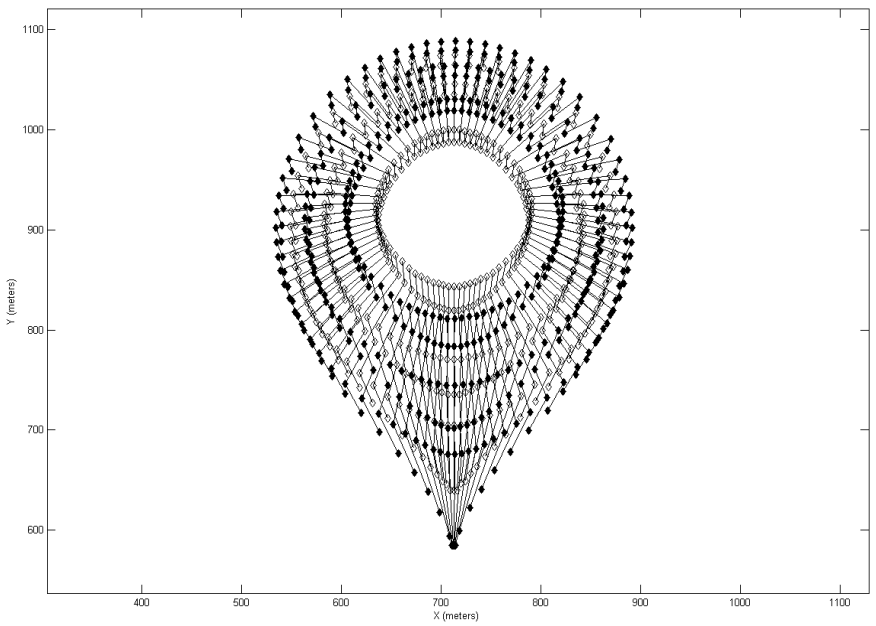

Figure 4. Pathlines for 72 particles injected at t = 0 (closed diamonds), as in Figure 3, with an additional 72 particles injected at t = T/2 (open diamonds). Recovery time, R, is 0. For clarity, the initial positions of the particles have been omitted.

References

Aref, H. (2002). "The development of chaotic advection." *Phys. Fluids*, 14(4), 1315-1325.

Bagtzoglou, A. C. and Oates, P. M. (2007). "Chaotic advection and enhanced groundwater remediation." *Journal of Materials in Civil Engineering*, 19(1), 75-82.

Chiang, W. H. (2005). *3D-Groundwater Modeling with PMWIN*, 2 Ed., Springer, New York, NY.

Sposito, G. (2006). "Chaotic solute advection by unsteady groundwater flow." *Water Resour. Res*., 42, W06D03.

Jones, S. W. and Aref, H. (1988). "Chaotic advection in pulsed source-sink systems." *Phys. Fluids,* 31(3), 469-485.

Harbaugh, A.W., Banta, E.R., Hill, M.C., and McDonald, M.G. (2000). "MODFLOW-2000, the U.S. Geological Survey modular ground-water model -- User guide to modularization concepts and the Ground-Water Flow Process." U.S. Geological Survey Open-File Report 00-92.

Pollock, D.W. (1994). "User's Guide for MODPATH/MODPATH-PLOT, Version 3: A particle tracking post-processing package for MODFLOW, the U.S. Geological Survey finite-difference ground-water flow model." U.S. Geological Survey Open-File Report 94-464.

Stremler, M. A., Haselton, F. R., and Aref, H. (2004). "Designing for chaos: application of chaotic advection at the microscale." *Phil. Trans. R. Soc. Lond.,* 362(1818), 1019-1036.

A Critical Realization Identification Method Based on Pareto Dominance Analysis

J. Wang[1], J. Guan[2], and M.M. Aral[3]

[1]ENVIRON International Corporation, 214 Carnegie Center, Princeton, NJ 08540; PH (609) 243-9853; email: jwang@environcorp.com
[2]Multimedia Environmental Simulations Laboratory, School of Civil and Environmental Engineering, Georgia Institute of Technology, Atlanta, GA 30332; PH (404) 385-2833; email: jguan@ce.gatech.edu
[3]Multimedia Environmental Simulations Laboratory, School of Civil and Environmental Engineering, Georgia Institute of Technology, Atlanta, GA 30332; PH (404) 894-2243; FAX (404) 894-5111; email: maral@ce.gatech.edu

ABSTRACT

Stochastic optimization has been frequently applied to groundwater management problems that involve uncertainties associated with hydrogeologic parameters. In this approach, a series of realizations are used to identify the optimal solution. However, this approach can be computationally intensive, especially for field-scale problems. To alleviate the computational burden associated with these types of stochastic optimization problems, a quantitative procedure identified as Pareto Dominance based Critical Realization Identification (PDCRI) method is developed to screen out the realizations that are most critical to the optimization results prior to the initiation of the optimization calculations. The criticalness of a hydrogeologic parameter realization on the solution is described by its Criticalness Index (CI) value, which is calculated based on a Pareto Dominance analysis. The PDCRI was applied to a hypothetical example to demonstrate its performance. The results show that the PDCRI approach can significantly improve computational efficiency without loss of reliability in optimal solutions and can also be used in other stochastic optimization problems such as optimal remediation system design or groundwater quality monitoring system design under parameter uncertainties.

1. INTRODUCTION

Uncertainties associated with the hydrogeologic input data of groundwater flow and contaminant fate-and-transport models may produce significant uncertainties in the simulation results which involve contaminant concentration and arrival time on the concentration at a point (the time for contaminant concentration to reach a certain level at the exposure point). This can seriously impact the reliability of the related epidemiologic studies. A reliable epidemiologic study sometimes may require the evaluation of extreme contaminant arrival times at an exposure point under multi-

parameter uncertainties. A possible solution to this problem is stochastic optimization.

Stochastic optimization has become a very important research area in recent years. In comparison with a deterministic optimization, a stochastic optimization considers some or all of the system input parameters as stochastic or uncertain variables [*Bakr et al.*, 2003]. The statistical method is a major approach for the solution of stochastic optimization problems. It generates a set of equally probable realizations according to the probabilistic distribution of uncertain parameters using statistical techniques to represent the effect of uncertainties. Its basic idea is that the more realizations a solution complies with, the more robust the outcome will be. This approach has been widely applied to groundwater quality management problems with uncertainties [*Aly and Peralta*, 1999; *Bau and Mayer*, 2006; *Chan*, 1994; *Hilton and Culver*, 2005; *Mantoglou and Kourakos*, 2007; *Mylopoulos et al.*, 1999; *Smalley et al.*, 2000; *Wagner and Gorelick*, 1989; *Wagner et al.*, 1992].

Usually, the reliability of the stochastic optimization results improves as the number of realizations used in the optimization process increases due to better representation of parameter uncertainties with increased number of realizations. However, this reliability improvement is associated with significant increase in computational cost, especially for field-scale problems. The previous studies on the subject have shown that although each realization is equally probable during a stochastic optimization, the effects they have on the final optimization results can be quite different – only a few realizations are really critical to the final results, which are thereby called "critical realizations" [*Mantoglou and Kourakos*, 2007; *Ranjithan et al.*, 1993]. Apparently, the application of only a few critical realizations in the optimization process instead of the whole set of realizations can dramatically improve the computational efficiency while maintaining a desired reliability level.

In *Ranjithan et al.* [1993], the critical realizations were used to improve the computational efficiency for optimal remediation design where uncertainty associated with the hydraulic conductivity parameter was considered. The level of criticalness of each realization, which was determined by the spatial distribution and the degree of variation of the hydraulic conductivity values, was identified using the pattern classification capability of neural networks. While the authors have demonstrated the reliability and efficiency of the optimal remediation design using critical realizations, this work only considered the uncertainty associated with the hydraulic conductivities. The pattern classification technique restricts the application of this method to problems with uncertain parameters showing no clear patterns, such as pumping schedule, or problems with multiple uncertain parameters. Furthermore, training of neural networks may be quite computationally intensive, and may potentially lower the efficiency of this method.

In the optimal pump-and-treat system design methodology developed by *Mantoglou and Kourakos* [2007], the objective function values of the realizations under various remediation policies were evaluated and ranked. The critical realizations were then

selected based on their ranks. Application of this method to an example problem shows that a few critical realizations could retain a comparable reliability level in optimal remediation design while reducing the computational demand significantly. However, the authors also considered the hydraulic conductivity to be the only uncertain variable.

In this study, a quantitative procedure named Pareto Dominance based Critical Realization Identification (PDCRI) was developed to screen out critical realizations under multi-parameter uncertainties by using Pareto dominance analysis, so that evaluation of extreme contaminant arrival times can be accomplished in an efficient manner – by optimization using the few critical realizations in stead of a large number of equally likely realizations can significantly reduce the computational demand while maintaining a similar level of reliability. The effectiveness and reliability of PDCRI was then illustrated by using a hypothetical example.

2. METHODOLOGY OF PDCRI

The Pareto Dominance based Critical Realization Identification (PDCRI) is a procedure that uses Pareto dominance analysis to identify critical realizations for stochastic optimization problems with single or multiple parameter uncertainties. Prior to description of the detailed procure, a few terms used in PDCRI are explained as they are defined in this study.

Realization. A realization is a set of uncertain parameters that are generated for one contaminant transport simulation. Realizations are usually generated from the probabilistic model of uncertain parameters using statistical techniques.

Critical realization. Critical realizations are realizations that can yield the extreme contaminant arrival times with high reliabilities.

Scenario. A scenario is usually a set of decision variables of the related optimization problem. For this study, a scenario stands for a pumping schedule.

Objective. Objective is the system response to a realization and a scenario. The objective in this study is the contaminant concentration at the exposure point.

Reliability. The reliability of a realization is defined as the probability that the extreme arrival time derived from a realization is the closest overall extreme arrival time considering parameter uncertainties.

Pareto dominance. The Pareto dominance is one of the key notions in multi-objective optimization problems [*Voorneveld*, 2003]. Considering two real n-dimensional vectors $\{x\}$ and $\{y\}$, if all the coordinates of vector $\{x\}$ are equal or better than the coordinates of vector $\{y\}$, with at least one coordinate being strictly better, then vector $\{x\}$ is said to Pareto dominate vector $\{y\}$, and vector $\{y\}$ is dominated by vector $\{x\}$ [*Voorneveld*, 2003]. Figure 1 illustrates the Pareto dominance in a two-objective optimization problem, where x_1 and x_3 dominate x_2, or

say x_2 is dominated by x_1 and x_3, but x_1 and x_3 are not dominated by each other. In a PDCRI application, the criticalness of a realization is evaluated by Pareto dominance analysis.

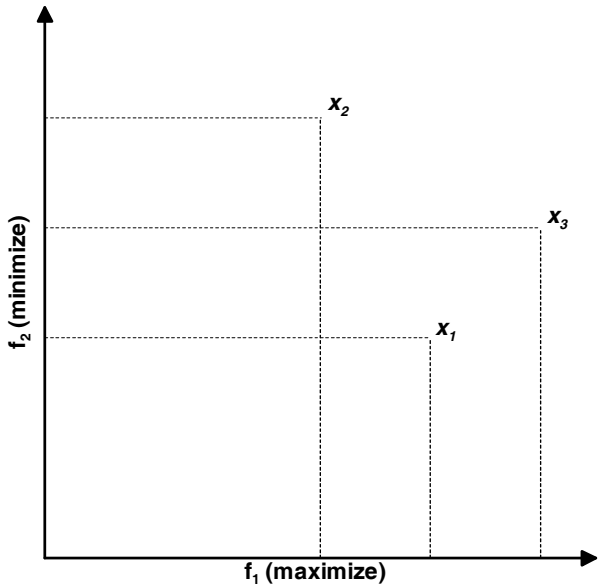

Figure 1. Illustration of Pareto dominance

The working procedure of PDCRI is illustrated in Figure 2. In the first step, a large set of equally probable realizations are generated based on the given probability distributions of uncertain parameters. Several pumping schedules (i.e., scenarios) are also randomly generated according to pumping capacities of the candidate wells. The objective value with regard to each realization under each scenario is then evaluated by using groundwater flow and contaminant transport simulation models. Assuming that n realizations and m scenarios are generated during a PDCRI application, a total number of $m \times n$ groundwater flow and contaminant transport simulations will be conducted. By using objective values obtained from the simulations, an objective vector will be formed for each realization, which consists of m objective values.



Figure 2. Flowchart of PDCRI

After the n objective vectors are obtained, a Pareto dominance analysis is conducted on these objective vectors to determine the number of times that each objective vector dominates and is dominated with respect to other objective vectors. According to the Pareto dominance analysis results, a quantitative index identified as Criticalness Index (CI) can be calculated to indicate the criticalness of a realization. The values of CI vary between 0 and 1. A realization with CI = 1 is the most critical one, and a realization with CI = 0 is the least critical one.

After the CI value for each realization is obtained, the critical realizations can be picked up for the optimization process according to CI values and reliability requirement of the related stochastic optimization problem. As can be seen in later discussions, the reliability of a realization is very close to its CI value when the CI value is close 1. In other words, if the optimization result for a stochastic optimization problem is obtained by using a critical realization with CI=α, then the probability for the result to be the "true" optimal is very close to α. Therefore, if a stochastic optimization problem desires optimal solution with a possibility of at least α, realizations with CI values of α or higher should be chosen as critical realizations.

3. DEMONSTRATION OF PDCRI APPLICATION AND DISCUSSION

To demonstrate the effectiveness and reliability of PDCRI, a hypothetical application with uncertain hydraulic conductivities was created. As shown in Figure 3, the unconfined aquifer is bounded by no-flow boundaries to its North and South. The east and west boundaries are constant head boundaries with heads of 36 feet and 40 feet, respectively. The dimensions of the site are 2,700 feet × 2,000 feet × 50 feet, which is simulated using 270 columns, 200 rows, and 1 layer in MODFLOW and MT3DMS. Each cell has the same size of 10 feet × 10 feet × 50 feet. For the groundwater flow and contaminant transport simulations, each month is simulated as one stress period. Starting from time zero, contaminant is released to the aquifer from node (100, 70) at a constant rate of 100 g/day. As indicated in Figure 3, the contaminant is then collected by the candidate wells with a pumping capacity of 3,000 ft^3/day in each well at a total water supply of 7,000 ft^3/day. The goal of the example problem is to evaluate the earliest contaminant maximum contaminant level (MCL, 20 ppb for the example contaminant) arrival time in the discharged water based on hydraulic conductivity uncertainties. The various hydraulic conductivity distributions were generated using FIELDGEN [*Doherty*, 2007]. One example realization of the hydraulic conductivity distributions is shown in Figure 3. Other properties of the site and the contaminant used in this example are given in Table 1.

For an accurate evaluation of the reliability of stochastic optimization using critical realizations, the probability distribution of the earliest MCL arrival times under hydraulic conductivity uncertainties were pre-obtained using Monte Carlo Simulation (MCS). During the MCS, the earliest MCL arrival times for 1,100 realizations were obtained via optimization. The cumulative probability distribution of these earliest contaminant MCL arrival times is very close to that of a theoretical normal distribution with mean of 8.505 stress periods and standard deviation of 0.277 stress periods, which is therefore taken as the "true" distribution of the earliest MCL arrival times.

To demonstrate the performance of PDCRI, another 1,000 realizations were generated for the example problem. For each realization, the contaminant concentrations in the discharge at the end of stress period 5 under 10 different pumping schedules (scenarios) were evaluated and then used for CI calculations as discussed below.

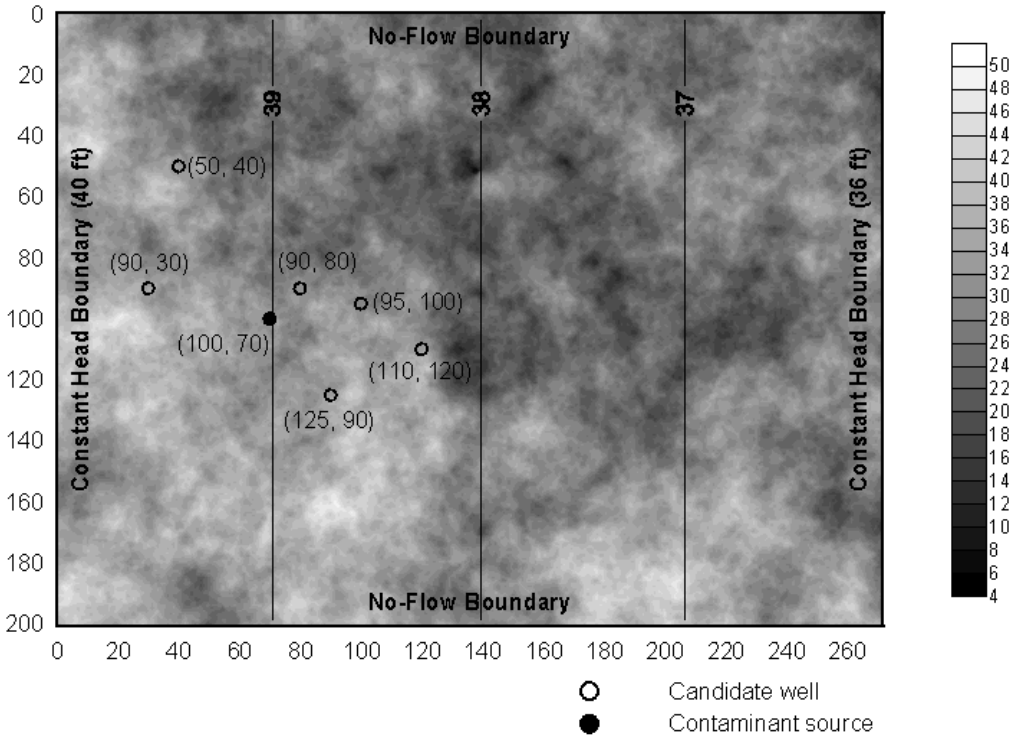

Figure 3. The candidate well locations, contaminant source, hydraulic conductivity and initial head distributions for the example problem (hydraulic conductivity unit: ft/day, head unit: ft)

Table 1. Values of parameters used in the example problem

Parameter	Value
Aquifer thickness	50 ft
Aquifer specific yield	0.05
Effective porosity	0.2
Longitudinal dispersivity	25 ft
Horizontal transverse dispersivity	2.5 ft
Vertical transverse dispersivity	0.25 ft
Diffusion coefficient	8.5×10^{-4} ft^2/day
Soil bulk density	7.7112×10^{4} g/ft^3
Distribution coefficient	5.0×10^{-6} ft^3/g
Contaminant first order reaction rate	5.0×10^{-4} 1/day

In our study, the CI values under 10 scenarios were calculated for various numbers of realizations to examine the reliability of the critical realizations with regard to the total number of realizations used in PDCRI. The obtained CI value and reliability of each realization are plotted in Figure 4 for cases with 10, 100, and 1,000 realizations, respectively. It can be seen from Figure 4 that as the CI value of a realization approaches 1, the reliability of the realization is quite close to its CI value. The higher is the CI value of a realization, the higher is the probability that the realization can yield the earliest MCL arrival time, which demonstrates the effectiveness of criticalness indication using CI.

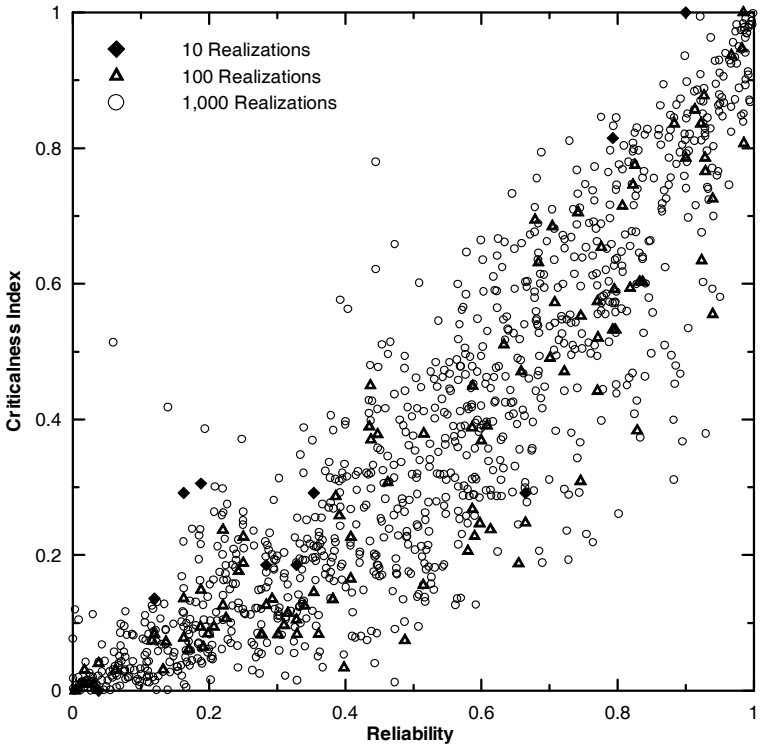

Figure 4. Criticalness Indexes vs. reliabilities of realizations used in PDCRI

4. SUMMARY

Uncertainties associated with the input data of groundwater flow and contaminant fate-and-transport models may produce significant uncertainties in the simulation results such as contaminant concentration and the arrival times, which in turn may seriously impact the reliability of the related epidemiologic studies. Therefore, a reliable epidemiologic study requires the evaluation of extreme contaminant arrival times under multi-parameter uncertainties.

Stochastic optimization, in which a number of equally likely realizations are used to represent parameter uncertainties, has been applied to solve this type of problems. Typically, the reliability improves as more realizations are used. However, the associated high computational cost restricts its application, especially for field-scale problems. To improve the computational efficiency, a few critical realizations are frequently selected to replace the large set of realizations, thus the computational requirement can be reduced to a small fraction of the original one. Several critical realization identification methods have been proposed and applied for optimal remediation design problems under hydraulic conductivity uncertainties.

In this paper, a critical realization identification procedure identified as Pareto Dominance based Critical Realization Identification (PDCRI) was developed. PDCRI can efficiently screen out critical realizations under single or multiple parameter

uncertainties. A quantitative term called Criticalness Index (CI), which is calculated based on multi-objective Pareto dominance analysis, was defined to represent the criticalness of a realization.

The effectiveness and reliabilities of the critical realizations obtained by using PDCRI were tested using a hypothetical example. Optimization results indicate that application of critical realizations in stochastic optimization problems can significantly improve the computational efficiency while maintaining a similar reliability.

REFERENCES:

Aly, A.H., and Peralta, R.C. (1999). "Optimal Design of Aquifer Cleanup Systems under Uncertainty Using a Neural Network and a Genetic Algorithm." *Water Resour. Res.*, *35*(8), 2523-2532.

Bakr, M.I., te Stroet, C.B.M., and Meijerink, A. (2003). "Stochastic Groundwater Quality Management: Role of Spatial Variability and Conditioning." *Water Resour. Res.*, *39*(4), -.

Bau, D.A., and Mayer, A.S. (2006). "Stochastic Management of Pump-and-Treat Strategies Using Surrogate Functions." *Adv. Water Resour.*, *29*(12), 1901-1917.

Chan, N. (1994). "Partial Infeasibility Method for Chance-Constrained Aquifer Management." *J. Water Res. Pl.-ASCE*, *120*(1), 70-89.

Hilton, A.B.C., and Culver, T.B. (2005). "Groundwater Remediation Design under Uncertainty Using Genetic Algorithms." *J. Water Res. Pl.-ASCE*, *131*(1), 25-34.

Mantoglou, A., and Kourakos, G. (2007). "Optimal Groundwater Remediation under Uncertainty Using Multi-Objective Optimization." *Water Resour. Manag.*, *21*(5), 835-847.

Mylopoulos, Y.A., Theodosiou, N., and Mylopoulos, N.A. (1999). "A Stochastic Optimization Approach in the Design of an Aquifer Remediation under Hydrogeologic Uncertainty." *Water Resour. Manag.*, *13*(5), 335-351.

Ranjithan, S., Eheart, J.W., and Garrett, J.H. (1993). "Neural Network Based Screening for Groundwater Reclamation under Uncertainty." *Water Resour. Res.*, *29*(3), 563-574.

Smalley, J.B., Minsker, B.S., and Goldberg, D.E. (2000). "Risk-Based in Situ Bioremediation Design Using a Noisy Genetic Algorithm." *Water Resour. Res.*, *36*(10), 3043-3052.

Voorneveld, M. (2003). "Characterization of Pareto Dominance." *Oper. Res. Lett.*, *31*(1), 7-11.

Wagner, B.J., and Gorelick, S.M. (1989). "Reliable Aquifer Remediation in the Presence of Spatially-Variable Hydraulic Conductivity - from Data to Design." *Water Resour. Res.*, *25*(10), 2211-2225.

Wagner, J.M., Shamir, U., and Nemati, H.R. (1992). "Groundwater Quality Management under Uncertainty - Stochastic-Programming Approaches and the Value of Information." *Water Resour. Res.*, *28*(5), 1233-1246.

Combining rule-based fuzzy model with GIS to predict groundwater vulnerability to contamination

Dhundi R. Pathak*[1] S.M. ASCE, Akira Hiratsuka[1], Isao Awata[1], and Luonan Chen[1]

[1]Graduate School of Engineering, Osaka Sangyo University, 3-1-1 Nakagaito, Daito, Osaka 574-8530, Japan, *corresponding author; e-mail: drpathak@ymail.com

Abstract

The groundwater is the major natural resources for drinking and other various purposes; however, it is under threat of degradation of its quality from concentrated and/or dispersed sources of contamination in urban area of developing countries. Therefore, contamination of groundwater has become a major concern of decision makers and water managers involved with the management of water quantity and quality and their relationship to human health in recent years. Since, groundwater monitoring and mathematical modeling is very costly in regional scale vulnerability assessment, one frequently used water quality protection strategy is to develop contamination potential maps of groundwater, and then prioritize those wells located in the potentially highly contaminated areas for testing of contaminants. However, generation of contamination potential maps is not an easy task due to lack of sufficient hydrogeologic database and inherent uncertainty. This procedure is usually carried out using GIS based overlay index method and process based model. DRASTIC model, a popular index method is used to assess groundwater vulnerability over the large geographical areas on the basis of general hydrogeological knowledge of the contaminant transport in aquifer media. DRASTIC index uses linear model to calculate the vulnerability index and the factors that influence the groundwater vulnerability must be divided into ranges and then be given ratings. This system is unable to describe a continuous transition from the easiest to be polluted to the most difficult to be polluted that is fuzzy nature of the groundwater vulnerability to contamination. Therefore, this paper aims to estimate the risk of an aquifer to be polluted from concentrated and/or dispersed sources which applies the ability of the fuzzy ruled-based system to cope with the modeling of a nonlinear system and presentation of the output of the fuzzy system in the framework of GIS. This may be possible to describe this concept with a set of linguistics rules in the form of "IF-THEN". This paper presents the fuzzy inference system benefiting from fuzzy engine and expert knowledge-based DRASTIC parameters for nonlinear mapping of the intrinsic groundwater vulnerability concept. The developed fuzzy model is applied to a shallow aquifer of Kathmandu Valley, Nepal and the result is compared with that of the DRASTIC model. This methodology has potential for facilitating groundwater vulnerability modeling at a regional scale and can be used for other regions, especially in the case of data scarcity, however, would require incorporation of appropriate input parameters and rule base suitable for the region.

Introduction

Groundwater is a globally important, valuable and renewable natural resource of water supply due to its relatively low susceptibility to contamination in comparison to surface water and its large storage capacity. However, it is under threat of degradation both by inappropriate use and by contamination, especially in haphazard urbanized area of developing countries, like Nepal. Generally, the deterioration of groundwater quality from concentrated and/or dispersed sources of contamination is mainly due to the high growth of population, unplanned growth of cities, and excessive use of fertilizers and pesticides in agriculture land, poor sewage and septic system as well as disposal of the untreated wastewater both from household and industrial activities. Therefore, contamination of groundwater has become a major concern of planners, decision makers and water managers involved with the management of water quantity and quality and their relationship to human health in recent years. In recognition of the need for effective and efficient methods for protecting ground water resources from future contamination, scientists and resource managers have sought to develop techniques for predicting which areas are more likely than others to become contaminated as a result of activities at or near the land surface (NRC 1993). This concept has been widely termed to groundwater vulnerability to contamination. It is the sensitivity of groundwater quality to an imposed contaminant load, which is determined by the intrinsic characteristics of the aquifer. To quantify aquifer vulnerability, one frequently used method is to develop contamination potential maps of groundwater, and then prioritize those wells located in the potentially highly contaminated areas for testing of contaminants. The contamination potential map is the subdivision of the area into several hydrogeological units with different levels of vulnerability, which shows the distribution of highly vulnerable areas, in which pollution is very common because contaminants can reach the groundwater within a very short time. The contamination of groundwater, however is a widespread problem and requires huge investments for remediation. Therefore, it is important to identify which aquifer systems and hydrogeological settings are most vulnerable to contamination prior to implementing groundwater monitoring and remediation programs in large geographical areas. In this context, this study aims to develop groundwater vulnerability map to identify the aquifer's inherent capacity to become contaminated benefiting from fuzzy knowledge and hydrogeological parameters in the frameworks of GIS.

In fact, groundwater monitoring and mathematical modeling is very costly in regional scale vulnerability assessment, which employs sets of extensive field measured data. In this context, the quite conceptual method like generalized knowledge base (GKB) approach may be appropriate in which decision is made on the basis of general hydrogeological knowledge of the contaminant transport in aquifer media (Afshar et al. 2007). In order to tackle the groundwater pollution and to protect its quality in a more scientific and efficient way, many different method based on GKB approach have been developed to evaluate the groundwater vulnerability to pollution such as GOD method (Foster et al. 1987); DRASTIC (Aller et al. 1987); SINTACS (Vrba and Zaporozec 1994), benefiting from the powerful

spatial analysis capability of GIS. The most typical and popular method based on GKB approach is the DRASTIC method, developed by the United States Environmental Protection Agency (EPA) (Aller et al. 1987). Because of its simple and easy to understand characteristics, this method has been adopted in the various part of world (Barber et al. 1994; Lynch et al. 1997; Babiker et al. 2005; Rahman 2008). This method is often modified to better address local issues or better represent a local hydrogeologic setting (Merchant 1994). Further, different researchers modified this methodology for mapping the intrinsic vulnerability of aquifers to better represent a local hydrogeological setting (Zhang 1996; Denny et al. 2007; Gomezdelcampo and Dickerson 2008). Recently, this popular GIS based overlay index method was introduced in Nepal to estimate the aquifer vulnerability to contamination in shallow aquifer of Kathmandu Valley (Pathak et al. 2008). Sensitivity analysis was also utilized to evaluate the relative importance of model parameters and then revised their weights to better address the local hydrogeological and terrain characteristics of Kathmandu.

Although, DRASTIC is one of the most widely used generalized knowledge base method to evaluate groundwater vulnerability, it is unable to describe a continuous transition from the easiest to be polluted to the most difficult to be polluted that is fuzzy nature of the groundwater vulnerability to contamination. Therefore, this paper aims to estimate the risk of an aquifer to be polluted from concentrated and/or dispersed sources which applies the ability of the fuzzy ruled-based system to cope with the modeling of a nonlinear system and presentation of the output of the fuzzy system in the framework of GIS. This may be possible to describe this concept with a set of linguistics rules in the form of "IF-THEN". First introduced by Zadeh (1965), fuzzy logic and fuzzy set theory have been extensively used in ambiguity and uncertainty modeling in decision making. The basic concept in fuzzy logic is quite simple; statements are not only "true" or "false" but also represents the degree of truth or degree of falseness for each input. Fuzzy sets are characterized by membership functions. Several approaches have been used to apply fuzzy set theory to groundwater vulnerability to contamination problems, including fuzzy pattern recognition and optimization technique (Zhou et al. 1999; Chen and Fu 2003), fuzzy rule-based systems (Dixon et al. 2005; Afshar et al. 2007). Afshar et al. (2007) proposed the rule base fuzzy system based on DRASTIC knowledge to evaluate the groundwater vulnerability. To illustrate the performance of the developed model, a hypothetical hydrogeological setting was assumed and results were compared with that of DRASTIC model. However, the previous studies lack to incorporate the fuzzy inference system for mapping the output of actual aquifer systems in geographical scale utilizing the powerful spatial and visual capability of GIS. This paper presents fuzzy rule based model which is developed to incorporate the non linear mapping of intrinsic groundwater concept benefiting from hydrogeological parameters used in DRASTIC method to assess groundwater vulnerability of shallow aquifer of Kathmandu, Nepal. Moreover, the developed model is validated with the result of DRASTIC methodology.

Groundwater vulnerability mapping

Study area

The total area of Valley for the study is about 350 square kilometers as shown as Figure 1, which consists of gentle hills and flat lands at elevations of 1300-1400 meters. Average annual precipitation in the Kathmandu Valley is around 1400 millimeters, about 80% of which falls in the monsoon period during June and July. Within the valley, municipal and other water supplies depend on monsoon rains and the stream and groundwater systems fed by this precipitation. Surface runoff is high during the monsoon and recharge to the shallow aquifers occurs mostly along the basin margins, directly from precipitation and by supply from many small rivers. However, recharge to the deeper aquifers is considered to be limited, due to the presence of clay beds that significantly restrict downward percolation. Because the Kathmandu Valley is a closed basin with gentle slopes toward the centre, groundwater flow is assumed to be slow, particularly in the deeper aquifers. The surface of the Kathmandu Valley is almost flat but it has buried bedrock surface with irregular shapes and high relief. The depth of the Precambrian bedrock from the ground surface ranges from tens of meters to more than 500 meters. The thick quaternary deposits consist of lacustrine and fluvial deposits, which have been eroded, however the original thickness of the deposits is unknown. Based on the engineering and environmental geological map of Kathmandu Valley (Shrestha et al. 1998), the geological setting of Kathmandu Valley with different formations is shown in Figure 2. The brief description of each formation is presented elsewhere (Pathak et al. 2008).

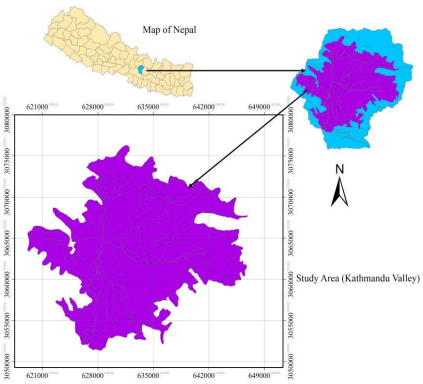

Figure 1. Location map of study area

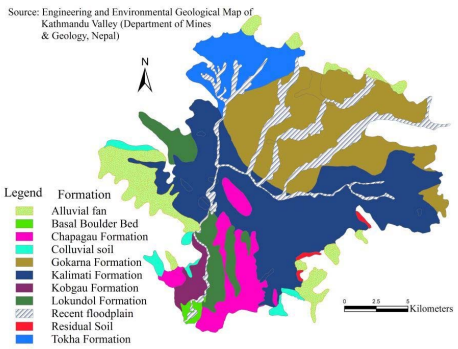

Figure 2. Geological formation map of Valley

DRASTIC and Fuzzy Inference System

Overlay and index methods, such as DRASTIC, are relatively easy to implement and require little data, but the result can be questioned because these methods rely more on the judgment of the analyst than on the actual hydrogeological processes (Frind et al. 2006). Gogu et al. (2003) reported that different overlay and index

methods like DRASTIC applied to same hydrogeological system can generate dramatically dissimilar results. Despite these criticisms due to the lack of proper validation, this method has been adopted worldwide for evaluation of aquifer vulnerability. DRASTIC index uses linear model to calculate the final vulnerability index using the following Equation:

$$VI = D_r D_w + R_r R_w + A_r A_w + S_r S_w + T_r T_w + I_r I_w + C_r C_w \quad (1)$$

The DRASTIC acronym stands for the seven hydrogeological parameters; depth to water, recharge, aquifer media, soil type, topography (slope), impact on the vadose zone media and hydraulic conductivity of the aquifer and the subscripts r and w denote the rating and the weight respectively. DRASTIC elected to use weight for each parameter based on its relative significance contributing to the pollution potential (depth to groundwater = 5; net recharge = 4; aquifer media = 3; soil type = 2; topography = 1; impact on vadose zone = 5; and hydraulic conductivity = 3) and rating value between 1 and 10 to each parameter, except R which ranges between 1 and 9 is given depending on local hydrogeological settings. Once the DRASTIC index has been computed, it is possible to identify areas, which are more likely to be susceptible to groundwater contamination relative to others. The higher the DRASTIC index, the greater is the groundwater pollution potential. In this method, the nature of the vulnerability is taken into account by dividing the values of each affecting factor into ranges and then giving to rating value to each range. However, it should be noted that if a factor value can be measured numerically, unlike the function of DRASTIC index, the fuzzy system generates a continuous vulnerability function by changing any subspace of input to the fuzzy system, which may be considered as pronounced advantage over DRASTIC method.

Fuzzy inference is the process of formulating the mapping from a given input to an output using fuzzy logic that employs the rules upon which decisions are made. A fuzzy rule based model is comprised of fuzzification of input variables, application of fuzzy operator in the antecedent, implication from antecedent to the consequent, aggregation of the consequents across the rules, and defuzzication (Figure 3). Due to the unavailability of soil attenuation type at the required scale over the entire aquifer system and the absence of spatially complete data for hydraulic conductivity, impact on vadose zone and hydraulic conductivity were excluded from DRASTIC system. Each data layer except impact on vadose zone and hydraulic conductivity was generated and/or obtained from its original source as a point, line, or polygon layer. Then, all parameters contributing to groundwater vulnerability were converted from vector (point, line, or polygon) to raster (grid) using the GIS. In raster layer, space is subdivided into discrete cells with required resolution. In this work, all five input parameters for the DRASTIC and fuzzy inference system are generated in five separate raster layers of 500 m x 500 m grid resolution. The detail of acquisition the individual data layers and method of generating input parameters were reported in earlier work (Pathak et al. 2008). The proposed fuzzy rule based model with five inputs, one output and 243 rules is shown in Figure 4. Each input domain was divided into three subdomains and output domain divided into five subdomains. The

rules were of the form "if D (depth to groundwater) is L (low) and R (recharge) is H (high) and A (aquifer media) is H (high) and S (soil type) is H (high) and T (topography) is L (low) then VI (vulnerability index) is VH (very high)," where D, R, A, S, T, and VI are linguistic variables while VH, H, and L are their linguistic values. Trapezoidal membership function, a minimum Mamdani inference and a central defuzzification method are used.

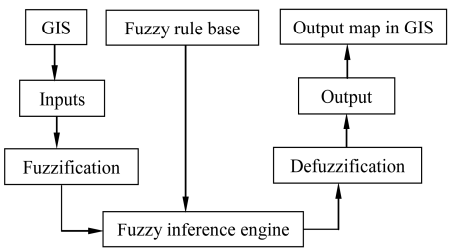

Figure 3. General structure of Fuzzy rule based system

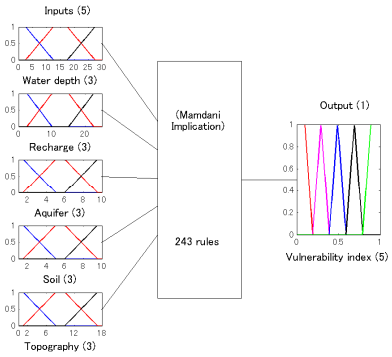

Figure 4. Proposed fuzzy rule based model

Results and discussion

Comparison of DRASTIC and Fuzzy index

The modeled results should however validate from field observations which is quite difficult and expensive in large geographical area. Hence, this study validates the model's performance by comparing the results with those of DRASTIC index. Output of DRASTIC method is first normalized to be able to compare with output of fuzzy rule based model. To compare the output of the fuzzy model with DRASTIC index, vulnerability variation resulting from fuzzy and DRASTIC model with respect to any single input variable, making other parameters constant, is computed taking the characteristics of selected hydrogeological settings of the study area. The characteristics of the five factors of the selected hydrogeological setting used for comparison study are shown in Table 1.

Table 1. Characteristics of selected hydrogeological unit to compare output of Fuzzy and DRASTIC model

Factors	Range	Rating	Weight	Normalized weight
D	4.6 - 9.1m	7	5	0.217
R	178 - 254 mm	8	4	0.174
A	Sand & Gravel	8	3	0.13
S	Sand	8	2	0.087
T	0 - 2 %	10	1	0.043

The comparison between outputs of two models indicates that the fuzzy system

has continuous nature with respect to input factors and unveils two upper and lower bound whereas the output of DRASTIC has a discrete nature as shown as Figures 5(a–c).

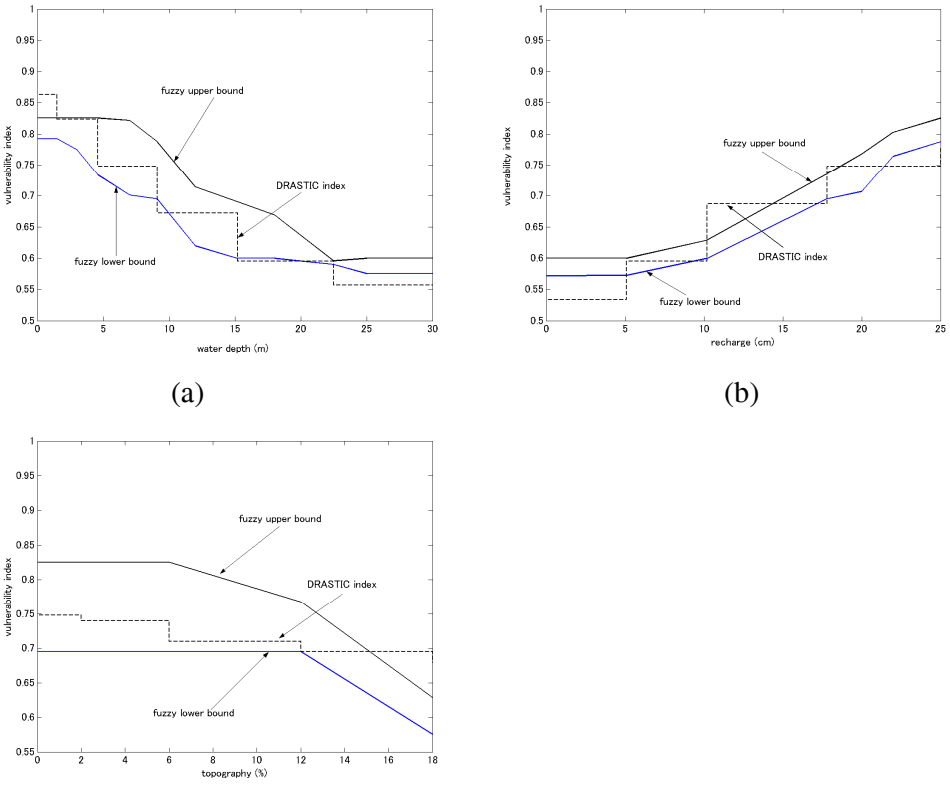

Figure 5. Vulnerability variation of (a) water depth in fuzzy and DRASTIC models; (b) recharge in fuzzy and DRASTIC models; and (c) topography in fuzzy and DRASTIC models

Application and validation

The proposed fuzzy rule based model is a decision making model which benefits from expert's knowledge hence its validation is vital. Validation of any groundwater vulnerability models based on general hydrogeological knowledge is quite difficult with field measured contaminants information in any aquifer systems due to the qualitative nature of vulnerability and inherent uncertainty. Since input parameters and knowledge base are derived from the DRASTIC system, similar results expected from both fuzzy and DRASTIC model. Hence, to demonstrate the performance of proposed fuzzy rule based model, it is applied to shallow groundwater aquifer of Kathmandu, Nepal to evaluate the intrinsic vulnerability and then output is compared with normalized index obtained from DRASTIC method. All input parameters that pertinent to groundwater vulnerability to contamination were converted to raster layer of 500 m x 500 m grid resolution using GIS. Based on defined raster layer, the

input matrix in any fuzzy subsystem is a 48 x 53 matrix covering study area. The vulnerability index in the fuzzy model is computed in each pixel of the study area. Ultimately, the output of fuzzy model is mapped utilizing the powerful spatial and visual capability of GIS (Figure 6). Output map of fuzzy vulnerability index has been compared with output map of DRASTIC method, which is presented in Figure 7. The difference of two outputs is plotted in Figure 8, which indicates that both map follow the same trends, however, the main difference is that fuzzy model has a continuous nature whereas the output of the DRASTIC has a discrete nature.

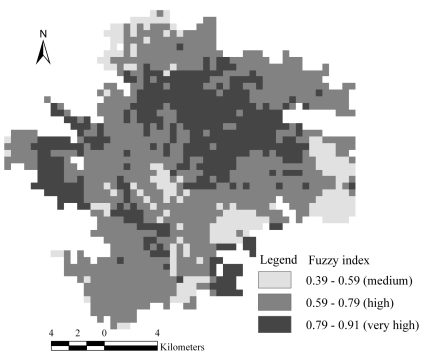

Figure 6. Vulnerability mapping of study area based on fuzzy rule based system.

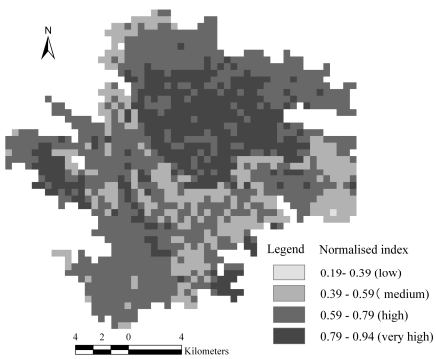

Figure 7. Vulnerability mapping of study area using DRASTIC method

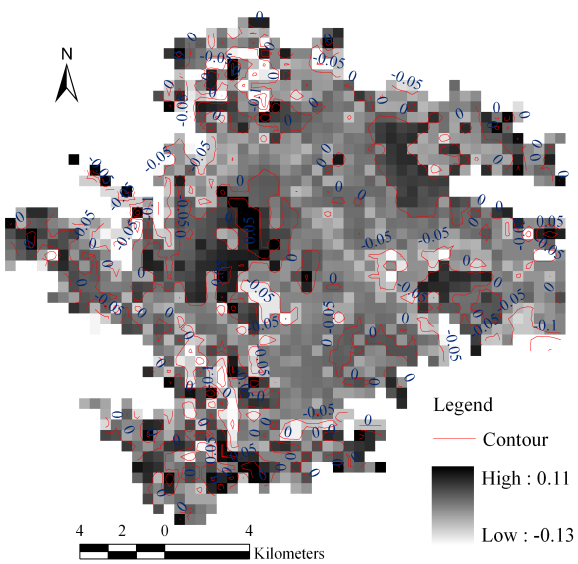

Figure 8. Differences between fuzzy and normalized DRAST index in study region.

Conclusion

The groundwater vulnerability map has developed to identify the aquifer's inherent capacity to become contaminated benefiting from fuzzy knowledge and some hydrogeological parameters that pertinent to groundwater contamination in the frameworks of GIS. A fuzzy rule based model has been proposed to incorporate the non linear mapping of intrinsic groundwater concept benefiting from some environmental and hydrogeological parameters used in DRASTIC method. A comparison between the output of fuzzy rule based model and the output from DRASTIC method was accomplished. The ability of fuzzy model to produce continuous vulnerability function in assessing groundwater vulnerability in the case of data scarcity of the study area may be considered as a pronounced advantage over index method like DRASTIC. It is recognized that the approach adopted to produce the vulnerability index was limited by the availability of data. However, in areas with limited data, this index provides important objective information that could be used for decision making. The developed fuzzy model has potential for facilitating groundwater vulnerability modeling at a regional scale and can be used for other regions, especially in the case of data scarcity, but, would require incorporation of appropriate input parameters and rule base suitable for the region.

REFERENCES

Afshar, A., Marino, M. A., Ebtehaj, M., and Moosavi, J. (2007). "Rule-based fuzzy system for assessing groundwater vulnerability." *Journal of Environmental Engineering,* ASCE, 133(5), 532-540.

Aller, L., Bennet, T., Lehr, H. J., Petty, J. R., and Hackett, G. (1987). "DRASTIC; A standardized system for evaluating groundwater pollution potential using hydrogeologic settings."*USEPA-600/2- 87-035,* 622 pp.

Babiker, I. S., Mohammed, A. A. M., Hiyama, T., and Kato, K. (2005). "A GIS-based DRASTIC model for assessing aquifer vulnerability in Kakamigahara Heights, Gifu Prefecture, central Japan." *Science of the Total Environment,* 345(1-3), 127–140.

Barber, C., Bates, L. E., Barron, R., and Allison, H. (1994). "Comparison of standardized and region-specific methods assessment of the vulnerability of groundwater to pollution: a case study in an agricultural catchment." *Proceedings of 25th IAH Congress Water Down Under*, Melbourne, Australia.

Chen, S. Y., and Fu, G. T. (2003). "A DRASTIC fuzzy pattern recognition methodology for groundwater vulnerability evaluation." *Hydrological Science Journal*, 48(2), 211-220.

Denny, S. C., Allen, D. M., and Journeay, J. M. (2007). "DRASTIC-Fm: a modified vulnerability mapping method for structurally controlled aquifers in the southern Gulf Islands, British Columbia, Canada." *Hydrogeology Journal*, 15(3), 483-493.

Dixon, B. (2005). "Groundwater vulnerability mapping: A GIS and fuzzy rule based integrated tool." *Applied Geography*, 25(4), 327-347.

Frind, E. O., Molson, J. W., and Rudolph, D. L. (2006). "Well vulnerability: A

quantitative approach for source water protection." *Ground Water*, 44(5), 732-742.

Foster, S. S. D. (1987). "Fundamental concepts in aquifer vulnerability, pollution risk and protection strategy." *Proceedings and information/TNO committee on hydrological research,* 38, 36-86.

Gogu, R. C., Hallet, V., and Dassargues, A. (2003). "Comparison of aquifer vulnerability assessment techniques, application to the Neblon river basin (Belgium)." *Environmental Geology*, 44(8), 881-892.

Gomezdelcampo, E., and Dickerson, J. R. (2008). "A modified DRASTIC model for Siting Confined Animal Feeding Operations in Williams County, Ohio, USA." *Environmental Geology*, 55(8), 1821-1832.

Lynch, S. D., Reynders, A. G., and Schulze, R. E. (1997). "A DRASTIC approach to groundwater vulnerability in South Africa." *South African Journal of Science*, 93(2), 59–65.

Merchant, J. W. (1994). "GIS-based groundwater Pollution hazard assessment: A critical review of the DRASTIC model." *Photogrammetry Engineering & Remote Sensing,* 60(9), 1117-1127.

National Research Council (NRC) (1993). "Ground water vulnerability assessment: Contamination potential under conditions of uncertainty." National Academy Press, Washington, DC.

Pathak, D. R., Hiratsuka, A., Awata, I., and Chen, L. (2008). "Groundwater vulnerability assessment in shallow aquifer of Kathmandu Valley using GIS-based DRASTIC model." *Environmental Geology, DOI: 10.1007/s00254-008-1432-8*.

Rahman, A. (2008). "A GIS based DRASTIC model for assessing groundwater vulnerability in shallow aquifer in Aligarh, India." *Applied Geography*, 28(1), 32-53.

Shrestha, O. M., Koirala, A., Karmacharya, S. L., Pradhananga, U. B., Pradhan, P. M., Karmacharya, R., Hanisch, J., Kerntke, M., Joshi, P. R., Steiner, L., Busch, K., Jnwali, B. M., Maske, N. D., Tuladhar, G. B., and Kaphle, K. P. (1998). "Engineering and environmental geological map of Kathmandu Valley." scale 1:50000. Department of Mines and Geology, Nepal.

Vrba, J., and Zaporozec, A. (1994). „Guidebook on mapping groundwater vulnerability." *International contributions to hydrology*. Heinz Heise, Hannover, 16, 131 pp.

Zadeh, L. A. (1965). "Fuzzy sets." *Journal of Information and Control,* 8(3), 338-353.

Zhang, R., Hamerlinck, J. D., Gloss, S. P., Munn, L. (1996). "Determination of nonpoint-source pollution using GIS and numerical models." *Journal of Environmental Quality,* 25(3), 411-418.

Zhou, H. C., Wang, G. L., Yang, Q. (1999). "A multiobjective fuzzy pattern recognition model for assessing groundwater vulnerability based on DRASTIC system." *Hydrological Science Journal*, 44(4), 611-618.

Evaluation of Alternative Geospatial Models using Image Ranking and Machine Learning: An Application in Shallow Groundwater Recharge and Discharge

Yu-Feng Lin[1], Peter Bajcsy[2], Alex Yahja[2] and Chulyun Kim[2]

[1]Illinois State Water Survey/Institute of Natural Resource Sustainability, University of Illinois at Urbana-Champaign, 2204 Griffith Dr., Champaign, IL 61820; PH (217) 333-0235; email: yflin@illinois.edu
[2]National Center for Supercomputing Applications, University of Illinois at Urbana-Champaign, 1205 West Clark Street, Urbana, IL 61801; PH (217) 265-5387; email: pbajcsy@ncsa.uiuc.edu

Abstract:

This paper addresses the problem of accurate estimation of geospatial models from a set of groundwater recharge and discharge maps and from auxiliary remote sensing and terrestrial raster measurements. The motivation for our work is driven by the cost of field measurements, and by the limitations of currently available physics-based modeling techniques that do not include all relevant variables and allow accurate predictions only at coarse spatial scales. The goal is to improve our understanding of the underlying physical phenomena and increase the accuracy of geospatial models—with a combination of remote sensing, field measurements and physics-based modeling. Our approach is to process a set of recharge and discharge maps generated from interpolated sparse field measurements using existing physics-based models, and identify the recharge and discharge map that would be the most suitable for extracting a set of rules between the auxiliary variables of interest and the recharge and discharge map labels. We implemented this approach by ranking recharge and discharge maps using information entropy and mutual information criteria, and then by deriving a set of rules using a machine learning technique, such as the decision tree method. The novelty of our work is in developing a general framework for building geospatial models with the ultimate goal of minimizing cost and maximizing model accuracy. The framework is demonstrated for groundwater recharge and discharge rate models but could be applied to other similar studies, for instance, to understanding hypoxia based on physics-based models and remotely sensed variables. Furthermore, our key

contribution is in designing a ranking method for recharge and discharge maps that allows us to analyze multiple plausible recharge and discharge maps with a different number of zones. This JAVA based software package, Spatial Pattern To Learn (SP2Learn), is designed to be user-friendly and universal utilities for pattern learning to improve model predictions from sparse measurements by computer-assisted integration of spatially dense geospatial image data and machine learning of model dependencies. The reliability indices from SP2Learn will improve the traditionally subjective approach to initiating conceptual models by providing objectively quantifiable conceptual bases for further probabilistic and uncertainty analyses. This new approach has been tested using the dataset from Buena Vista Groundwater Basin, a thoroughly understood system in the Central Sand Plains of Wisconsin. This project was supported by the National Center for Supercomputing Applications - Faculty Fellows Program and the Illinois Water Supply Planning Project.

URL: http://www.sws.uiuc.edu/gws/sware/

Extended Abstract:

There is a large class of problems where the complexity of the underlying phenomena is overwhelming and therefore physics-/chemistry-/biology-based modeling is limited in its accuracy of predictions. The accuracy is typically limited due to (1) the unavoidable uncertainty of direct and indirect measurements feeding complex models, (2) the high cost of measurements collected at sufficient sampling frequency in space, time and variable dimensions, (3) the insufficient computational resources to process all input measurements and execute complex models to make accurate predictions, (4) the lack of scalability of existing models coming from unsatisfied approximations/conditions of the models and/or implementations not utilizing computational resources, and (5) the simplifications in modeling, for instance, by using only a sub-set of variables relevant to predicting the underlying phenomena. This work is motivated by seeking approaches to overcome the accuracy limitations of modeling of complex phenomena.

The class of problems described above occurs in applications coming from the Earth Science domain, although, similar problems concerned with improving modeling accuracy might be

found in other domains. The applications from Earth Sciences would include prediction of precipitation, estimation of recharge/discharge rates from various indirect measurements, predictions of algal biomass in rivers or hypoxia along coasts, or simulations of optimal sewage networks. For instance, estimation of groundwater recharge and discharge (R/D) rates from a set of point geospatial measurements of hydraulic conductivity, bedrock elevation and water table elevation can be based on multiple existing physics-based models, such as MODFLOW , PEST and PRO-GRADE. These models might not generate predictions at fine geospatial scale because the model assumptions have not been met. In this case, exploring the data-driven rules between additional variables such as water proximity, topographic slope or soil type, could also lead to accuracy and model improvement.

Approaches to solving the above class of problems vary. In general, each specific application is decomposed according to multiple sources of accuracy limitations. Each cause of accuracy limitation is tackled separately and then all partial improvements are combined. It is apparent that predicting complex phenomena accurately becomes not only a modeling effort (decoupling and linking model components into a workflow) but also an optimization effort. Optimization is needed for finding the 'best' combination of theoretical models, model parameters, input products, and implementations of theoretical models, as well as for accessing computational resources for executing the models and obtaining predictions. Furthermore, all these modeling and optimization operations require human interactions with intermediate prediction results. Many times, the best predictions are decided based on considerations and tacit knowledge of a scientist or a group of scientists investigating complex phenomena.

The objective of our work is to design a computer-assisted optimization and exploratory framework enabling improvements of modeling accuracy. This work presents a framework for accurate geospatial modeling using image ranking and machine learning. The framework involves the support of optimizations and explorations, and aims at extracting tacit knowledge of domain experts. It could be also viewed as an informatics workflow with a hybrid modeling approach, where physics-based modeling and data-driven modeling approaches are combined. The novelty of our work is in designing a methodology for ranking and extracting relationships, as well as in developing a general framework for building accurate geospatial models. This

quantitative and systematic approach has bridged the gap between the traditional subjective approaches for initiating conceptual models and advanced stochastic and uncertainty analysis.

We will demonstrate how to improve our understanding of R/D pattern by incorporating auxiliary variables, ranking variables for relationship extraction and extracting variable relationships. We used the physics-based R/D rate model that takes field measurements of hydrologic conductivity, water table level and bedrock elevation. In our framework, we explored the accuracy improvements when several image de-noising techniques with a decision tree machine learning technique were employed, and several remote sensing and terrestrial raster measurements were used, for example, topographic slope, soil type and proximity to water bodies. For the specific application, the ranking approach in SP2Learn provides quantifiable reliability indices of R/D maps which enable hydrogeologists to recognize R/D patterns and compare R/D estimations with a more objective approach. In addition, the machine learning process also summarizes the rules and provides the capability of recommending a new optimal R/D pattern. The rules provide the insights of special parameter correlations of each individual study site which were not available to the expert and objective measures such as the confidence of each rule and the description length of the decision tree are given to help the experts make decision. The experts have now the capability to apply those correlations interactively in SP2Learn in order to improve the maps in more systematic and reliable approach.

Our work led to a prototype solution called Spatial Pattern To Learn which is available for free download at http://isda.ncsa.uiuc.edu/Sp2Learn/.

Implementation of the sustainable development concept in the field of groundwater management

C. Schöpfer[1]

[1] Christoph Schöpfer, PhD of Civil Engineering, Bjoernsen Consulting Engineers GmbH, Maria Trost 3, D-56070 Koblenz; PH (+49) 261 8851-260; FAX (+49) 261 8851-336; email: c.schoepfer@bjoernsen.de

ABSTRACT

Sustainable development is defined by the Brundtland Commission as a *"development that meets the needs of the present without compromising the ability of future generations to meet their own needs".*

Unfortunately, in the public discussion sustainability is often equated with ecology and an intact environment, which doesn't meet this definition. Examinations of sustainability have shown that it has to be put in a context of three partly competing goals: ecology, economy and social affairs. These goals can be described by the so-called sustainability triangle, in which those solutions that reach a balance among all three goals are sustainable.

The approach of sustainable development is being applied more and more often in groundwater management. Development and use of the decision system are presented for two large and intensively used groundwater systems with regards to the water supply. These are a multi-layered aquifer of unconsolidated rock and an aquifer of consolidated rock.

EU WATER FRAMEWORK DIRECTIVE AND THE TERM SUSTAINABILITY

At the beginning of the 1990s, the European Commission developed the idea of a standardized water protection guidelines intended to secure the quality and quantity of water. The **EU Water Framework Directive** (European Parliament and the Council of the European Union 2000) went into effect in December 2000, harmonizing European laws for the protection of all bodies of water. The guidelines contain three major, new elements:

- Detailed specifications were introduced to make the management of water bodies transparent.
- Furthermore, economic criteria, such as using efficient measures to ensure water prices are cost-effective and including environmental and resource-

related costs, play central roles in water management.
- Finally, early public involvement would be permitted in all decision making processes.

The specifications set out in the EU Water Framework Directive represented a fundamental shift for European water policies. The duty to protect water is integrated in all policy areas and the responsibility of society and private enterprises in terms of water protection was heightened. The EU Water Framework Directive, therefore, met the definition for the principle of sustainability (see Figure 1).

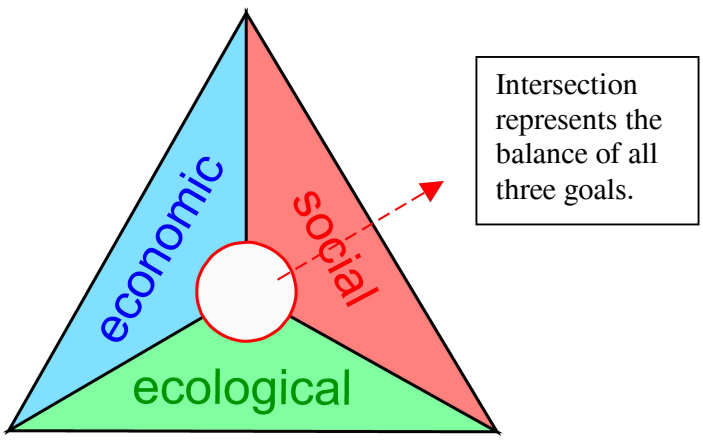

Figure 1. Sustainability triangle.

UNCONSOLIDATED ROCK CASE STUDY RHINE-NECKAR-REGION

The **Rhine-Neckar-Region** is one of the most densely populated areas in Germany (location see Figure 2) and spreads across an area of 1,400 km². Drinking and industrial water is taken from the Oberrheingraben's accumulation of unconsolidated material, which in places is several hundred meters thick, at an annual rate of 160 million m³. In particular, the drinking water supply is taken out of the deeper aquifers for quality reasons. The location of the water extraction, the hydrogeology (especially the composition and location of intermediate layers) and the interaction with surface water (especially the seepage from larger surface waters due to water extraction) influence the upper aquifer.

For the area of the Rhine-Neckar-Region that is located on the east bank of the Rhine, the state of Baden-Württemberg has developed criteria that help evaluate the sustainability of groundwater management (RP Karlsruhe 2003). The study was conducted because of the demands associated with a high degree of groundwater extraction due to the Rhine-Neckar-Region's intense water use among the local population and industry.

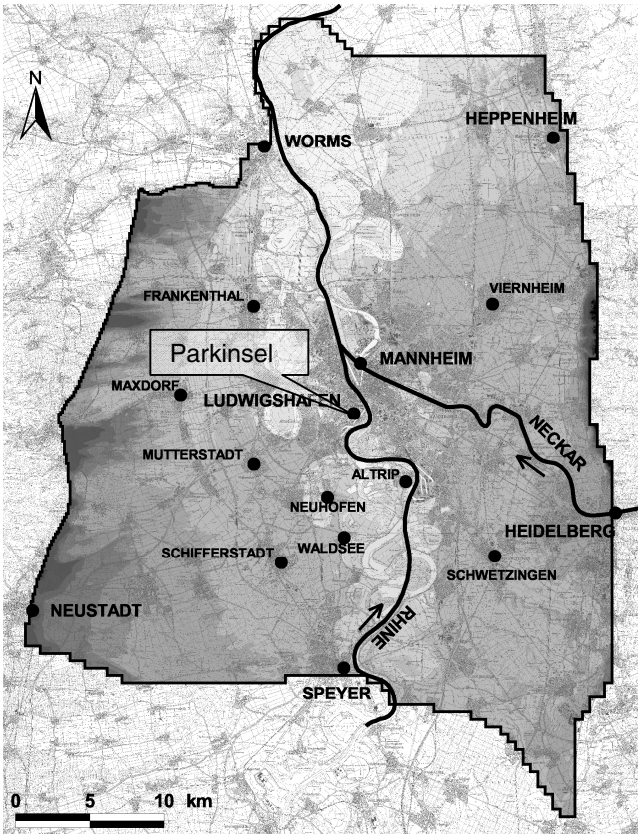

Figure 2. Model area Rhine-Neckar-Region and location of the water extraction point "Parkinsel".

The area of the Rhine-Neckar-Region located on the west bank of the Rhine belongs to the state Rhineland-Palatinate. The groundwater situation is characterized by high groundwater extraction, large-scale contamination in the upper aquifer (OGWL) and an increased risk of contaminant movement from the upper into the middle aquifer (MGWL). Here, the OGWL is not especially thick, making large-scale groundwater extraction impossible. Only in some areas parallel to the Rhine, can larger quantities of groundwater be extracted due to a thicker OGWL. For this reason, groundwater for drinking water supply and industry has for years been extracted in the deeper aquifers (MGWL and UGWL).

In Rhineland-Palatinate, a sustainable groundwater management system was required. The goal of the project's examinations was the **development of an evaluation method** that enables the comparison and evaluation of the requested solution with its alternatives in terms of sustainability in a water rights proposal. The base used for the project was a groundwater model setup to examine different management alternatives.

The developed evaluation method was derived from a cost-benefit analysis. The different effects of groundwater management were evaluated in a quantitative manner, in which single valuations were aggregated and were given different weights. A span of 50 years was defined as the period under observation. This period meets the lifespan of waterworks, and a prognosis of costs and demands is not possible for longer periods of time.

The **main goal is the sustainable management of groundwater**. In this case, the maximum number of points given is 90, which is the sum of the number of points of the three sub-goals. According to the sustainability triangle, the goal "sustainable groundwater management" is distinguished into the three sub-goals of ecology, economy and social affairs. All three sub-goals are given equal weight with a maximal number of points of 30. Figure 3 gives an overview over the different goals and sub-goals.

Target-level 1 to 4						
1	G	2	G	3	G	4	G
Sustainable Groundwater Management	90	1.Ecological	30	Groundwater quality	24	Contaminant movement to MGWL	8
						Contaminant movement to UGWL	8
						Amount of contaminants in deeper aquifers	8
				Interaction with groundwater-dependent ecosystems	6		
		2.Economic	30	Actual costs of drinking water	6		
				Actual costs of process water	6		
				Cost of a groundwater remediation / securing	6		
				Mobilization of contaminant potentials	6		
				Effort for groundwater regulation due to high groundwater levels	6		
		3.Social	30	Conflicts of interest with other types of land use	30	Conflicts of interest with agriculture	10
						Conflicts of interest with industry and trade	10
						Conflicts of interest with habitation and leisure	10

Figure 3. Overview of the goals, criteria and weights "G".

The sub-goal **ecology** includes the two sub-goals "groundwater quality" and "interaction with groundwater-dependent ecosystems". The sub-goal "groundwater quality" is weighted considerably higher with 24 points because of its high importance in groundwater management. Also, the natural protection areas make up only a small part to the total area studied.

The sub-goal **economy** is composed of 5 sub-goals, which represent the economic impact of changes in groundwater management. These are the actual costs of drinking water and process water, the cost of a possible groundwater remediation or securing, the mobilization of contaminant potentials as well as the effort for groundwater regulation due to high groundwater levels. Attention should be paid to the fact that within the sub-goal economy it's not distinguished between measures and costs. The five sub-goals are evaluated equally with 6 points.

The sub-goal **social affairs** covers the conflicts of interest that arise when the water extraction's catchment area is also used for other types of land use. This sub-goal is divided into three areas of importance: conflicts of interest with agriculture, industry and trade, and with habitation and leisure. All these types of land use can impact the groundwater if located in the catchment area.

To **distribute the points**, the following approach was chosen:
- A quantifiable factor was chosen for each criterion that had to be evaluated.
- The alternative with the worst factor is given 0 points.
- The alternative with the best factor is given the maximal number of points.
- In between, for each given factor the points are linearly interpolated.

The implementation of the developed evaluation method is shown on the basis of the **water extraction point "Parkinsel"** of the Technical Works Ludwigshafen AG (see Figure 2 for location). The extraction of groundwater is carried out mainly in the intermediate aquifer (MGWL). Close to the extraction point, a gallery of protection wells in the MGWL helps to keep away contaminants from a nearby contaminated site.

The following alternatives are examined using the evaluation method:
- Reference alternative: extraction of groundwater in the MGWL (7.5 Mio. m³ annually)
- Alternative 1: relocation of the extraction point into the UGWL to protect the extraction with an additional dilution and the aquitards functioning as a barrier
- Alternative 2: relocation of the extraction point into the OGWL to minimize the inflow of contaminated groundwater due to the high proportions of bank filtrate

In all the alternatives, protection wells continue to be operated to stop the contaminant spread from a nearby contaminated site.

The analysis and evaluation of the points according to the above method results in 54 points for the reference alternative, 58 points for alternative 1 and 55 points for alternative 2. The results are very close, even though the relocation in the UGWL is more sustainable than the reference alternative and the relocation in the OGWL. However, the three sub-goals show very different results.

In regards to the sub-goal ecology, the reference alternative is considerably more sustainable than both relocations into the OGWL or the UGWL. For example, a

relocation of extraction point in the OGWL would lead to damage of the population of old trees on the "Parkinsel" due to the lowering of the groundwater table. These trees are parts of a landscape conservation area, which give this alternative very few points for the ecology sub-goal.

For the economy sub-goal, the relocation of extraction point into the UGWL is considerably more sustainable than both the reference alternative and the relocation in the OGWL. For the last two, an adjustment of water treatment would be necessary.

For the social affairs sub-goal, the relocation of extraction point into the OGWL is considerably more sustainable than relocation into the UGWL or the reference alternative. This can be explained by the very small catchment area that results from an extraction in the OGWL (see Figure 4).

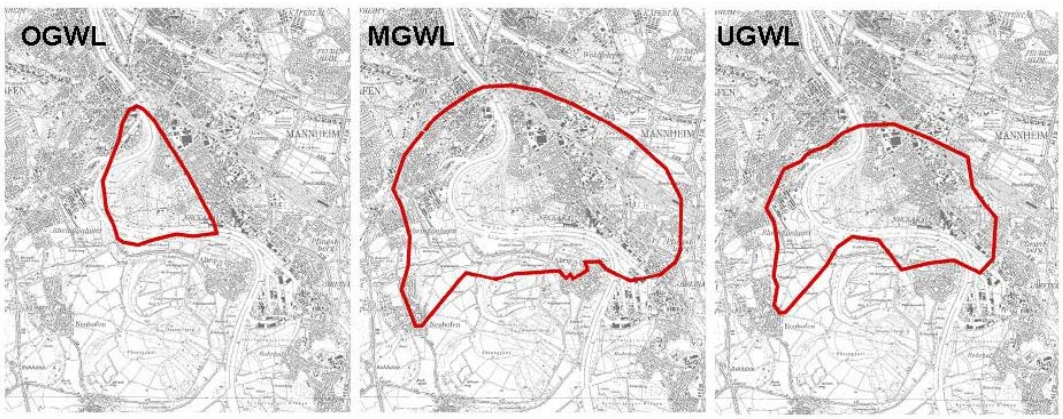

Figure 4. Borders of the catchment area of the water extraction point "Parkinsel" resulting at an extraction in the different aquifers.

CONSOLIDATED ROCK CASE STUDY IN LUXEMBOURG

Luxembourg's water supply demands are mainly met by springs and wells in the uncovered Luxembourg Sandstone. The springs, however, deliver only small amounts of water in times of little precipitation. There is also a potential hazard to water quality in areas where the aquifer of consolidated rock is not covered. For these reasons, new extraction wells are planned to be built in areas where the Luxembourg Sandstone is covered. The extractions are intended to improve the security of the water supply as water demand increases. Figure 5 shows wide fractures in the Luxembourg Sandstone.

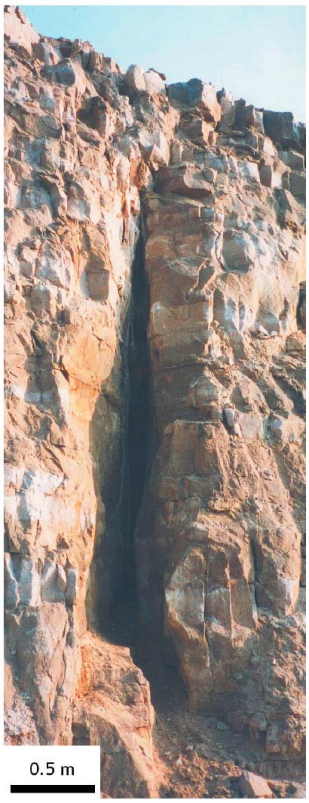

Figure 5. A wide fracture in the Luxembourg Sandstone.

The area under investigation spans the entire range of the Luxembourg Sandstone and extends 15 km west and 10 km south of the state of Luxembourg's borders and spreads across an area of 900 km² (Figure 6).

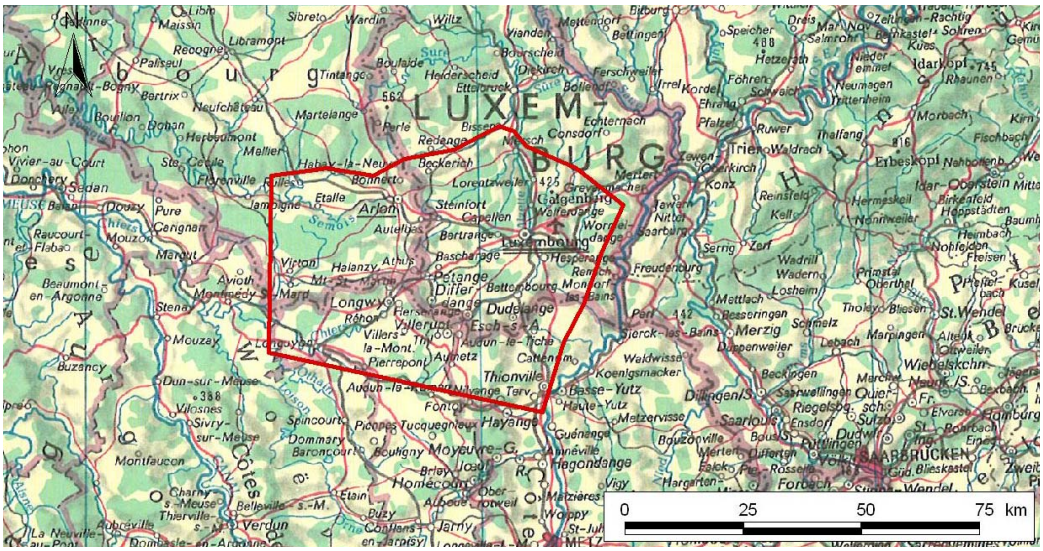

Figure 6. Area of investigation in Luxembourg case study.

The area under investigation lies within the range of the bay of Trier's sedimentation area. In geo-hydraulic terms, there are two aquifers, which, for the most part, are separated with intermediary aquitards. For this reason, the groundwater model was divided into three layers. The first model layer represents the Quaternary period, the second model layer the clays of the Lias geologic period. The third model layer represents the Luxembourg Sandstone, which forms an aquifer that is about 70 m to 80 m thick and can reach a maximum thickness of 100 m. Figure 7 shows how the geology was entered into the groundwater model.

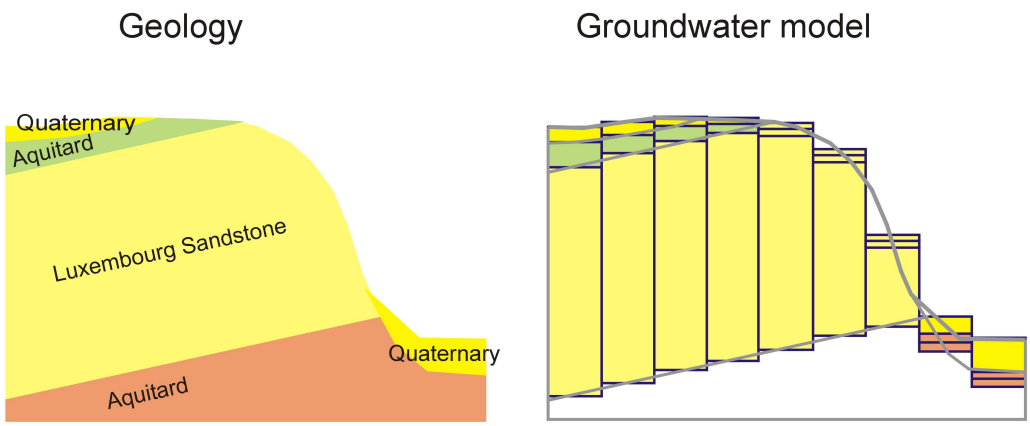

Figure 7. Implementation of the geology in the layers of the numerical groundwater model.

In the model area, approximately 4.5 million m³ of water are extracted annually from the Luxembourg Sandstone. However, the water rights are considerably higher. Furthermore, numerous springs are used for water supply. These springs extract about 9.6 million m³ of water per year.

The **groundwater situation** is substantially influenced by the water extractions. For example, the "Weyler" groundwater measurement point shows a drop in groundwater level of 2 m since 1990 (Figure 8). The overall trend of a falling groundwater level, without a substantial rise of the groundwater level in times of high precipitation, can be interpreted as an indication of the emptying of the Luxembourg Sandstone water storage in this area.

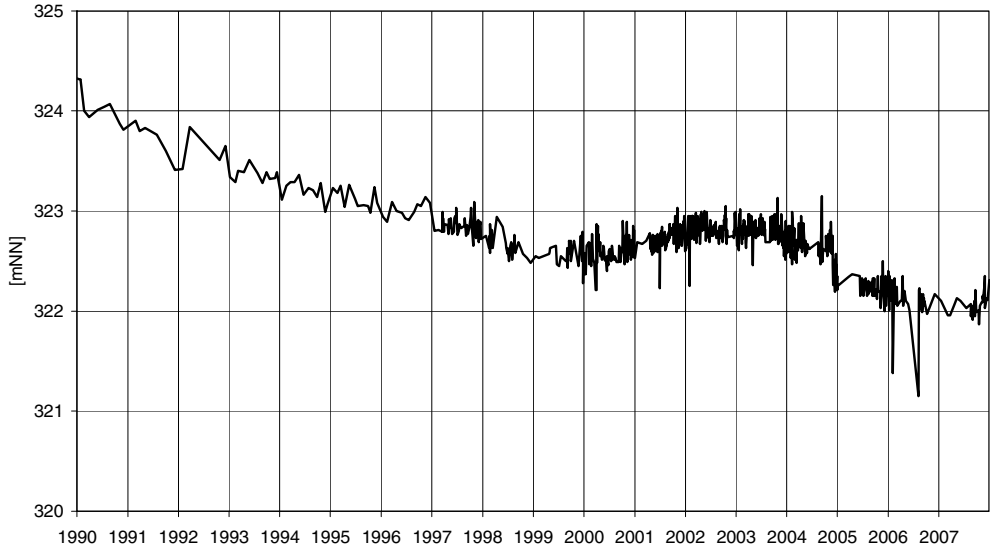

Figure 8. Groundwater hydrograph at the Weyler measurement point.

Another example of the obvious effects the extractions have on the groundwater situation is seen in the groundwater hydrograph at the well SH-15-4, which is located on the model's eastern edge. After very high amounts of groundwater were pumped in 1991, and despite little extraction, three years were required to reach the static level of 1990 (Figure 9).

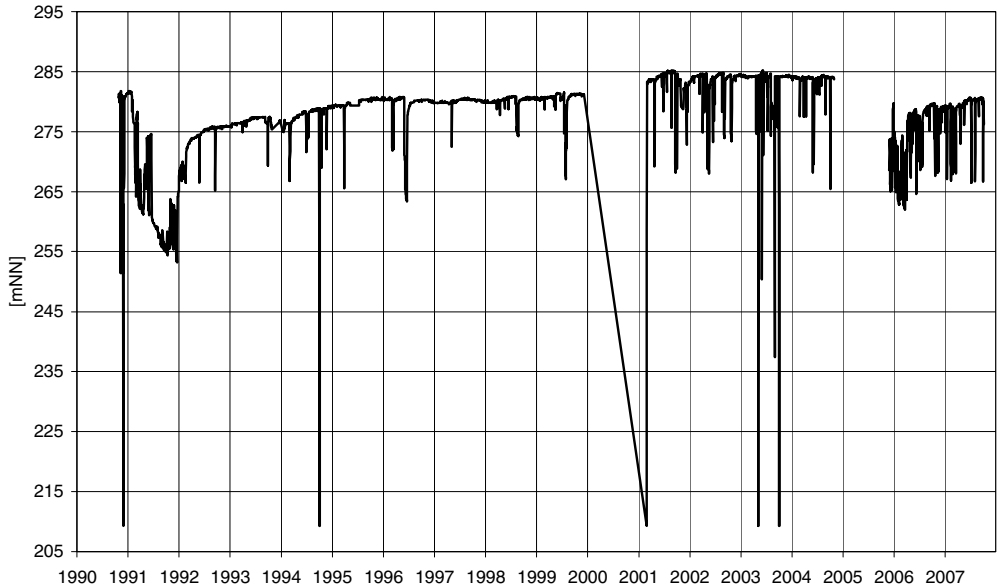

Figure 9. Groundwater hydrograph at well SH-15-4.

These measurements show that, in addition to quality problems, there are also problems regarding the amount of groundwater in aquifers of consolidated rock. The country of Luxembourg currently intends to secure the drinking water supply on its own. In addition to groundwater extractions, a water reservoir dam on the Sauer River provides Luxembourg with drinking water. In light of the rising number of inhabitants and the risks involved using surface water for drinking water, a management plan is designed for the Luxembourg Sandstone. The plan is intended to show, how much groundwater can be extracted with wells in the short and intermediate-term without harming the delivery of the springs. Short-term extractions imply periods ranging from a couple of weeks to as long as six months, and must provide enough water to make up for the complete loss of water from the reservoir for this amount of time. For these time intervals, ideal positions for the extraction wells are to be found, allowing for an operation that doesn't harm the delivery of water from the springs. The evaluation method described in the previous chapter is used and modified for the Luxembourg management plan.

CONCLUSIONS

The statements above show that a sustainable groundwater management system has to include the goals ecology, economy and social affairs. Since water demands and technical means of treating water can change quickly, the period of observation should be chosen according to the service life of the investments (chosen approach: 50 years). Under the given basic conditions, management alternatives can be found to be sustainable in the individual case, but differ from the superior goals of a sustainable water management system. The implementation of the developed evaluation method assumes that various alternatives with the same target achievement can be defined for the case under evaluation.

LITERATURE

European Parliament and the Council of the European Union (2000): Directive 2000/60/EC of the European Parliament and of the Council of 23 October 2000 establishing a framework for Community action in the field of water policy.

RP Karlsruhe (2003): Evaluation of groundwater management in terms of it's sustainability in the cities of Mannheim and Heidelberg and in the Rhine-Neckar-Region, March 2003.
http://www.rp.baden-wuerttemberg.de/servlet/PB/menu/ 1112012/index.html.

Projecting Future Groundwater Availability for Power Generation Plant Licensing

G.A. Day[1] and C. Krambis, Jr[2]

[1]Bechtel Power Corporation, 5275 Westview Drive, Frederick, MD, 21703-8306, USA; PH (301) 228-8917; FAX (240) 379-2818; email: gaday@bechtel.com
[2]Schnabel Engineering, 2020 Avon Court, Suite 15, Charlottesville, VA 22902, USA; PH (434) 975-3200; FAX (434) 975-3233; email: ckrambis@schnabel-eng.com

ABSTRACT

Water sustainability is becoming an issue throughout the United States where population and environmental concerns intensify the competition among municipal, agriculture, industrial, and power generation demands. The demand for groundwater has increased beyond its primary historical uses of agriculture and water supply. Viewed as a problem of sustainability, the long-term challenge for water supplies and regulatory agencies is to maintain steady growth and living standards without compromising the ability of future generations to meet their own needs. Water resource planners must now account for increased power generation needs for a new generation of nuclear power plants that will compete with other demands that typically comprise the existing water availability projections. Planners typically project future groundwater availability using elusive concepts of sustainable yield, safe yield, optimal yield, and consensus yield. These water use projections, resources availability, and allocations are becoming increasingly under scrutiny as demands stretch the available resources and as water consumption decisions are weighed in public policy debates. In this paper, case studies from proposed plant expansions are evaluated for their consideration of groundwater availability.

INTRODUCTION

As surface water allocation within the United States became increasingly expended, reliance upon groundwater to meet the increasing demands of new development (public supply and agricultural irrigation) surged from about 25 percent to about 40 percent since 1950 (Reilly and others, 2008). This has lead to aquifer depletion, groundwater quality deterioration, and land subsidence in many parts of the country, and has prompted states to regulate groundwater withdrawals in an effort to protect the resource and the environment from the effects of over allocation. Planners generally have adopted a conventional “safe yield” approach to manage and regulate the resource, yet depletions still occur. Most regulations and availability estimates are rarely based upon principles of capture described by Theis (1940) and expounded by so many other hydrologists. Two case studies are discussed to illustrate the concepts of safe yield and sustainability, and how management, regulations, and

availability estimates are established and the implication to the federal licensing application process to construct and operate new nuclear power generation facilities.

NUCLEAR ELECTRICAL POWER GENERATING PLANTS

The U.S. Nuclear Regulatory Commission (NRC) licensed and regulates 104 operating nuclear power reactors in the United States. These reactors supply about 20 percent of the nation's electricity (Figure 1) (US NRC, 2009). Nearly all have been operating for 10 years or more. About half have been operating in excess of 20 years while some have or are undergoing license renewal to extend their operating life by an additional 20 years. In addition to the operating power reactors, there are 16 power reactor sites being decommissioned (Taylor and Day, 2007).

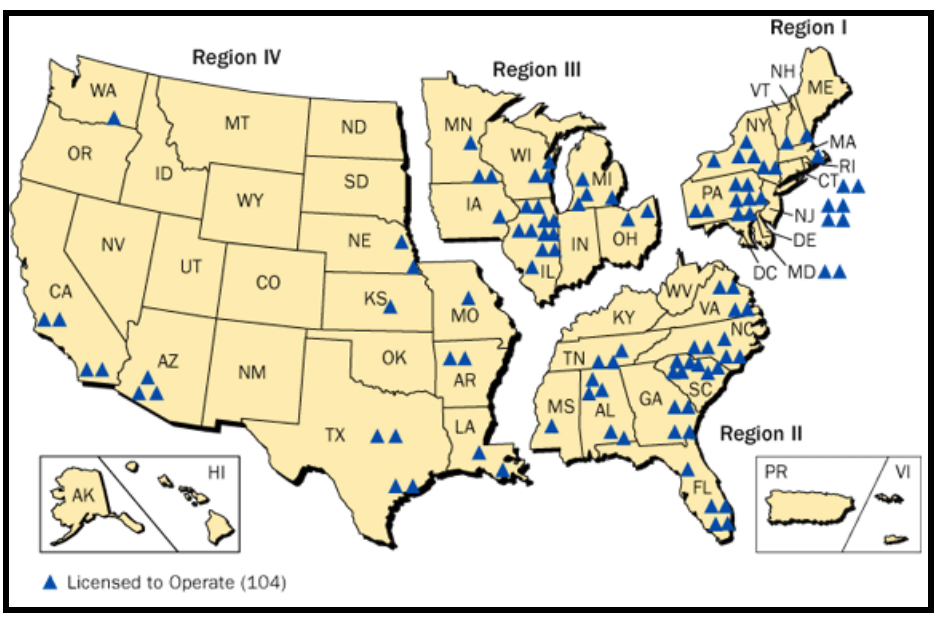

Figure 1. Location of commercial nuclear power reactors in the United States

There has been renewed interest on the part of the electrical utilities to license and construct new power reactors in the United States. This new interest is the result of the reliability and profitability of the current nuclear fleet, a streamlined licensing process that reduces the financial risk to applicants, anticipated growth in the demand for electricity, increased public acceptance of nuclear power, and recent changes to the United States energy policy that promote energy independence as well as reductions in greenhouse gas emissions (Taylor and Day, 2007). Currently, there are 21 new power reactor sites that have initiated or plan to initiate the licensing process (US NRC, 2009). The first of the new generation of power reactors is expected to begin operation in 2015.

This recent surge to submit Combined License (COL) applications to build and operate new nuclear electric power generating plants will require an evaluation of the water resources. Although most electric power generation plants obtain their cooling

water from surface water supplies, their potable, sanitary, fire suppression, and make-up water is typically withdrawn from groundwater. The NRC will question the availability and sustainability of both surface water and groundwater supplies to the plants, as well as the expected environmental impacts by proposed plant withdrawals not only during the construction phase but throughout the operating lifespan. Identifying the long term sustainability of these resources will include an evaluation of plant water demands, water resource availability, and projected future water use allocations. Ultimately, the NRC's concern lies in the possible loss of bonds and plant shut down if projected water availability is later found not to be obtainable throughout the plant's lifetime. Viewed as a problem of sustainability, the long-term challenge for water suppliers and regulatory agencies is to maintain steady growth and living standards without compromising the ability of future generations to meet their own needs (Barker, 2007).

CONCEPT OF GROUNDWATER AVAILABILITY, SAFE YIELD AND SUSTAINABILITY

During the COL application process and the subsequent NRC review, the applicant must evaluate not just the plant's impact to these water resources but future impact (use) projections to the resource, including drought cycles, environmental interactions, and the local or state regulatory controls to protect and provide the water resources. The applicant must determine if the groundwater resources are sustainable through the life of the project. Sustainability is evaluated through hydrogeologic investigations and interpretations, and most importantly, an understanding of the local or state regulatory agencies' water allocation policies and projections.

Planners who project future groundwater availability have used the now elusive concept of safe yield originally defined in 1915 as "the limit to the quantity of water which can be withdrawn regularly and permanently without dangerous depletions of the storage reserve" (Domenico and Schwartz, 1990). The definition has evolved over the years as the volume of water that can be withdrawn annually from an aquifer without exceeding average annual recharge, violating water rights, creating uneconomic conditions for water use, or creates undesirable side effects such as subsidence or saline water intrusion (Neuendorf and others, 2005). As Domenico and Schwartz (1990) state "in practice, safe yield has no unique or constant value, its value at any time depending of the spacing and location of the wells and their influence on the dynamic of interchange between ground water and other elements of the hydrologic cycle". Since the early 1950s researchers have suggested abandoning the term because of its indefiniteness. Sustainability gained popularity in the late 1980s but suffers from a similar lack of definability.

Use of safe yield as a de facto basis to establish availability contrasts with published opinions from hydrologists who argue that average annual recharge (natural recharge) is based on a steady-state, predevelopment condition and is not suitable for a dynamic system. Natural recharge-based safe yield provides only a single numerical value that does not consider transient conditions such as non-steady pumping, increased

withdrawals, seasonal trends, or droughts. Whereas the concept of sustainable groundwater availability can vary not only from one place to another, but also from one time to another as policy, socioeconomic, environmental and climatological conditions change. Groundwater resources can suffer under the misconception that groundwater allocation decisions based on the belief that safe yield projections are sustainable.

The interchangeability of the two terms, safe yield and sustainability, has been questioned by hydrologists. Safe yield is generally considered to be applicable to supply, economics, water quality, and legal rights, whereas sustainability is applied to a broader concept revolving around the complex interdependence of the resource, the environment, and society (Seward, 2006). Groundwater availability has been defined simply as "the amount of water available for use" whereas safe yield and sustainable yield concepts are methods to quantify availability (Mace and others, 2001 and 2006). To help clarify the concept of a safe and/or sustainable yield, other terms have been brought forth, but the nuances of these terms appear to be based on a researcher's philosophy of how to incorporate human needs, policy, law, and management. Eloquently stated; "sustainability, like safe yield, is a value-laden concept and one that in many respects is in the eye of the beholder" (Alley and Leake, 2004).

In defining sustainable safe yield, leading researchers refer to a publication (Theis, 1940) as a starting point, but differ on their interpretation of the role natural recharge has in regards to deriving a sustainable safe yield. One position claims that natural recharge is irrelevant (Bredehoeft, 1997 and 2002), whereas another position defends its use for modern numerical models used to quantify sustainable yields (Kalf and Woolley, 2005 and Sophocleous, 1998 and 2004). Additionally, some argue that emphasizing a scientific approach over a policy/managerial approach to deriving a sustainable safe yield is unrealistic (Mace and others, 2006 and Seward, 2006). From such arguments, two schools of thought in defining safe and sustainable yield have emerged; one takes a scientific approach whereas the other favors subjective, value-laden principles to determine sustainability (Seward, 2006). Despite the conflicting views researchers have formulating a definition and method for evaluating sustainable safe yield, most researchers and planners do agree that modern numerical groundwater models play a large role in defining and quantifying sustainable yield.

GROUNDWATER AVAILABILITY AND ALLOCATION PROJECTIONS

At a federal level, the Sole Source Aquifer (SSA) Program, which is authorized by the Safe Drinking Water Act, allows for protection when a community is dependent on a single source of drinking water. Once a SSA is designated, proposed federal financially-assisted projects that have the potential to contaminate the aquifer are subject to federal review. However, the SSA designation provides only limited federal protection of groundwater (US EPA, 2009).

At state and local levels, groundwater resources are appropriated according to laws and institutions that usually control water use through a permitting process.

Depending on the jurisdiction, and the requested allotment, the applicant may be required to provide a hydrogeologic impact evaluation. In some areas the rule of capture still exits, allowing landowners to capture the water beneath their property.

Case studies from two COL applications in different areas of the country are discussed to present how consideration of groundwater availability is evaluated during COL applications.

Case Study - Texas

An existing electric power generation facility in Texas has submitted a COL application to construct a new two-unit nuclear power generation plant. The existing units obtain cooling water from surface water, while groundwater is withdrawn from a deep aquifer that also supplies most of the potable water to the surrounding area. Operation of the new units would require a two-fold increase in the groundwater presently used by the existing units but would remain within the permitted groundwater allocations held by the utility at this plant.

The NRC's review of this COL application resulted in several follow-up questions that request a description of the sustainable groundwater resource concept (e.g., safe yield or available groundwater resource) and an analysis of current and future sustainable groundwater availability projections throughout the plant's life span. As part of the requested analysis, the utility was asked to quantify the expected impacts from the plant's increased groundwater withdrawal to the regional groundwater resource. The following is a description of the evaluation that followed.

In Texas, surface water belongs to the state, while in general, groundwater is governed by the rule of capture, which grants the landowners the right to capture available groundwater beneath their property regardless of the effects that pumping may have on neighboring wells (Lesikar and others, 2006). In many parts of the state, more groundwater is being used than is being replenished. As a result of these concerns, the Texas Legislature passed laws to encourage the establishments of Groundwater Conservation Districts (GCDs) to develop and implement comprehensive management plans that conserve and protect groundwater resources while protecting the rights of private landowners. The GCD is required to estimate the amount of groundwater available, the amount being used, the amount of recharge, and project water supply and demand. The GCD must address water supply needs in a way that will not conflict with the approved regional water plan that uses groundwater availability data acceptable to the Texas Water Development Board (TWDB). Some GCDs within a common Groundwater Management Area (GMA) may opt to plan jointly. The Texas Supreme Court reserves the right to change groundwater law if the existing laws do not adequately protect the groundwater resources (Lesikar and others, 2006).

Many methods have been used in the past to estimate groundwater availability in Texas. The TWDB has defined groundwater availability as "…the effective recharge

plus the amount of water that can be recovered annually from storage over a specified planning period without causing irreversible harm such as land-surface subsidence or water-quality deterioration" (Mace and others, 2001), and has estimated groundwater availability using average recharge, recharge with storage changes, both recharge approaches with limitations to prevent water-quality deterioration, land-subsidence, or other undesired effects, and systematic depletion (Muller and Price, 1979).

The Regional Water Planning Groups (RWPG) within Texas have also provided groundwater availability estimates using various recharge and systematic depletion approaches, a specific criterion approach – such as subsidence or recharge, or in some cases the TWDB or other outside agent (Mace and others, 2001). These estimates were used by GCD to permit pumping limits. Where there is no GCD, the rule of capture exists. However, the differing approaches and definitions of groundwater availability often produced conflicting results for the same aquifer, and generated uncertainty and mistrust among some RWPG's (Mace and others, 2001). The variety of water planning approaches in use and the conflicting results prompted the RWPG's to request the TWDB develop a standard for estimating groundwater availability (Mace and others, 2001).

In an effort to provide a standard, it has been recommended that the TWDB reject the concept of safe yield and optimal yield in favor of consensus yield (Mace and others, 2001) – an optimal yield that emphasizes policy and stakeholder input – based on the belief that groundwater scientists alone cannot estimate groundwater availability and numerical groundwater availability models are the best tools to use to help estimate groundwater availability. While such criteria are noteworthy, consensus yield may place too much emphasis on stakeholders' involvement over science. One researcher concludes that individuals or groups cannot selfishly allocate groundwater as if it was dam storage because the physics of groundwater flow through a porous media will not allow it (Kalf and Woolley, 2005).

Groundwater availability estimation methods and the planning authority roles in Texas changed following the passing of House Bill 1763 in 2005. This bill requires joint planning among GCD's within a GMA to determine "desired future conditions" of aquifers, including those where rule of capture still pervades (Mace and others, 2006). Each GCD is scheduled to submit to the TWDB in 2010 a "desired future conditions" plan detailing quantitative conditions (e.g., water levels, stream flows) for their respective aquifer in the future based on its planned use (Mace and others, 2006). As part of this process, the TWDB stresses the use of its Groundwater Availability Models (GAM) to estimate the quantitative "desired future conditions". Using the "desired future conditions", the TWDB calculates "managed available groundwater" volumes for use by RWPGs in their future regional water plans and by the GCD's in their groundwater management plans and permitted withdrawal amounts (Mace and others, 2006). In the areas where rule of capture still pervades, if a water user requires state funding to complete a project, they would have to accept an allocation amount given to them by the RWPG.

In the Texas case study, the site had a permit to obtain the groundwater required for plant operations but a detailed review of groundwater sustainability and water use projections was still required. We found that one GCD used values established by the RWPG, while simultaneously declaring the values should be used with caution because they are unscientific and further evaluations are needed. Because Texas groundwater law is continually changing (Jarvis and Campana, 2008) the ability to present an accurate availability scenario is difficult. Ultimately, the TWDB oversees all management plans and sets the "managed available groundwater" volumes to be implemented by the GCD and RWPG.

Case Study - Maryland

An existing electric power generation facility in Maryland has submitted an application to construct a new nuclear power generation plant. The existing units at this facility obtain cooling water from a nearby bay and groundwater use needs from aquifers that supply most of the potable water to the surrounding area. The proposed new unit would also obtain cooling water from the bay. However, options for potable water use by the proposed unit include: increase the plant's existing groundwater allocation, develop a source in a deeper aquifer, and/or desalinization. An evaluation was performed to determine groundwater availability and permit requirements during the COL application.

In Maryland, decades of unchecked pumping within the Atlantic Coastal Plain has led to a decline of groundwater levels, which, if left unchecked, could affect the long-term sustainability of the resource, affect the natural discharge to sensitive streams and estuaries, and increase salinization of the aquifer systems (Shedlock and others, 2007). Groundwater withdrawals are managed by the Maryland Department of Environment (MDE) through the Water Supply Program (WSP), a permitting process aimed to prevent the regional water levels from declining below 80 percent of the aquifer's available drawdown. However, the WSP currently does not have the adequate tools to make science-based groundwater management and permitting decisions (Shedlock and others, 2007).

The Maryland Geologic Survey (MGS) conducts modeling efforts that simulate water-level trends to 2030 in various Coastal Plain aquifers in order to better manage the resource. However, no comprehensive scientifically based method or tool has been devised to provide WSP with a better management system. In response to this, the Advisory Committee on the Management and Protection of the State's Water Resources recommended in a 2004 report that a comprehensive study of the sustainability of the Maryland Coast Plain aquifer system be undertaken. The MGS and the U.S. Geological Survey (USGS) developed a "science plan" that provides new scientific data, and data management and analysis tools for the WSP to use for future groundwater allocations. As part of this plan, a comprehensive review and update of the hydrostratigraphic framework of the Atlantic Coastal Plain of Maryland, Delaware, and several counties of Virginia will be performed primarily for a new modeling effort. The first part of this effort involves development of a regional

numerical groundwater flow model. The second part of the model involves an optimization model that is incorporated with the flow model. These models will be used to optimize conditions based on various management goals to produce optimal locations, pumping rates, and pumping periods of supply wells to better manage the aquifer system with respect to long-term sustainability of the resource (Shedlock and others, 2007). Results of model runs will be evaluated by scientists, resource managers, and decision-makers from both scientific and socioeconomic viewpoints (Shedlock and others, 2007). Implementation of this new tool is scheduled for 2013.

In the Maryland study, the review of existing state groundwater models, water demand projections, and the current water allocation process allowed the utility to rank and prioritize the plant's water supply options. This approach is still under development and will require approval from local, state, and federal agencies. The approach and water use allocation requests are expected to be finalized prior to the state's implementation of the optimization groundwater models.

CONCLUSION

In the case of COL applications, it can be difficult to provide groundwater availability and projections to the NRC that are independent from those set by state and local regulatory authorities and therefore, an understanding is required to determine the difference between "sustainable yield", "safe yield", and "groundwater availability" and how such terms relate to the actual availability evaluations conducted by state and local governments. The issues described in this paper are not unique to Texas and Maryland, but emphasize the stress placed on the nation's water resources and the pressure on water use planners to allocate the resources while addressing changing political, socioeconomic and environmental conditions.

For many researchers and planners, policy is considered to be paramount in determining how much and to whom the groundwater resource is allocated. As one researcher stated, "We cannot use a natural system without altering it" (Sophocleous, 1997). Texas is employing GAMs to allocate groundwater in sensitive areas, and Maryland plans to use a comprehensive modeling system to optimize its permitted withdrawal amounts and points. However, if the results of such modeling efforts are not adhered to because of social economics or politics; the effort of quantifying sustainable yield may remain biased.

REFERENCES

Alley, W.M., and Leake, S.A. (2004). *The journey from safe yield to sustainability*. Ground Water, v. 42, no. 1, 5 p.

Barker, B. (2007). *Running Dry At The Power Plant*. Electric Power Research Institute (EPRI) Journal, Summer 2007, p.26-35, also available online at http://www.epri.com

Bredehoeft, J. (1997). *Safe yield and the water budget myth*. Ground Water, v. 35, no. 6, p. 929.

Bredehoeft, J. (2002). *The Water Budget Myth Revisited: Why Hydrogeologists Model*. Ground Water, v. 40, no. 4, p. 340-345.

Domenico, P.A., and Schwartz, F.W. (1990). *Physical and Chemical Hydrogeology*. John Wiley & Sons, Inc., New York, p. 202-205.

Jarvis, T., and Campana, M.E. (2008). *The Sociotechnological Aspects of Nonrenewable Ground Water Resources: Half-Empty, Half-Full, Top-Down, Bottom-up, and Some Paths Forward*. Conference Summary, NGWA International Conference on Nonrenewable Ground Water Resources; Portland, Oregon.

Kalf, F.R.P., and Woolley, D.R. (2005). *Applicability and methodology of sustainable yield determination in groundwater systems*. Hydrogeology Journal, Volume 13, Number 1; Springer Berlin/Heidelberg, p. 295-312, also available online at http://www.kalfandassociates.com.au/Suspaper.pdf

Lesikar, B., Kaiser, R., and Silvy, V. (2006). *Questions about Groundwater Conservation Districts in Texas*. Texas Water Resources Institute, SR 2002-036, Texas A&M System, also available online at http://twri.tamu.edu

Mace, R.E., Mullican, W.F. III, and Way, T.S. (2001). *Estimating Groundwater Availability in Texas*. TWDB, Austin, Texas, 15 p.

Mace, R.E., Petrossian, R., Bradley, R., and Mullican, W.F. III (2006). *A Streetcar Named Desired Future Conditions: The New Groundwater Availability for Texas*. Chapter 3.1, 7th Annual The Changing Face of Water Rights in Texas, Texas Water Development Board, Austin, Texas, 23 p.

Muller, D.A., and Price, R.D. (1979). *Ground-Water Availability in Texas - Estimates and Projections through 2030*. Report 238, Texas Department of Water Resources, Austin, Texas, 77 p.

Neuendorf, K.K.E., Mehl, J.P. Jr, and Jackson, J.A. (2005). *Glossary Of Geology,* Fifth Edition. American Geological Institute, Alexandria, Virginia, p 567-568.

Reilly, T.E., Dennehy, K.F., Alley, W.M., and Cunningham, W.L. (2008). *Ground-Water Availability in the United States*. U.S. Geological Survey Circular 1323, 70 p., also available online at *http://pubs.usgs.gov/circ/1323/*

Seward, P., Xu, Y., and Brendonck, L. (2006). *Sustainable groundwater use, the capture principle, and adaptive management*. Water SA, Vol. 32, No. 4, p. 473-482.

Shedlock, R.J., Bolton, D.W., Cleaves, E.T., Gerhart, J.M., and Nardi, M.R. (2007). *A science plan for a comprehensive regional assessment of the Atlantic Coastal Plain Aquifer System in Maryland*. Open-File Report 2007-1205, U.S. Geological Survey, Reston, Virginia; prepared in cooperation with the Maryland Geological Survey and the Maryland Department of the Environment.

Sophocleous, M. (1997). *Editorial: Managing water resources systems: why "safe yield" is not sustainable*. Ground Water, v. 35, no. 4, p. 561.

Sophocleous, M. (1998). *On the elusive concept of safe yield and the response of interconnected stream-aquifer systems to development*; Chapter 2, Perspectives on sustainable development of water resources in Kansas. Kansas Geological Survey Bulletin 239, p. 61-85.

Sophocleous, M. (2004). *Discussion of Papers*. Ground Water v. 42, no. 4.

Taylor, S.W., and Day, G.A. (2007). *Radioactive contamination of groundwater at nuclear power plants: Incorporating lessons learned at existing and future facilities*. Proc. 6th International Groundwater Quality Conference, Fremantle, Western Australia, IAHS Press, 2008.

Theis, C.V. (1940). *The source of water derived from wells: essential factors controlling the response of an aquifer to development*. Civil Engineering 10 (5), 277–280.

U.S. EPA (2009). *Sole Source Aquifers*. United States Environmental Protection Agency, http://cfpub.epa.gov/safewater/sourcewater/sourcewater.cfm?action=SSA >(Jan. 17, 2009).

US NRC (2009). *Nuclear Reactor Program.* United States Nuclear Regulator Commission, http://www.nrc.gov/reactors.html. >(Jan. 17, 2009).

Simulation of Subsurface Water Flow by Galerkin Finite Element Method in Dhaka City Aquifer

Shikha Rahman[1*] and Mohammad A. Bhuiyan[2]

[1]Assistant Professor, Department of Civil and Environmental Engineering, One Grand Avenue, California Polytechnic State University at San Luis Obispo, CA 93407; Ph: 805-756-9875; Fax: 805-756-3332; email: rahman@calpoly.edu *Corresponding Author

[2]Professor, Department of Water Resources Engineering, Bangladesh University of Engineering and Technology, Dhaka 1000, Bangladesh; Ph: 9665650-80/7561; Fax: 8802-8613026; email: mbhuiyan@wre.buet.ac.bd

Abstract

A two-dimensional mathematical model has been developed using Galerkin finite element method for simulation of transient saturated-unsaturated groundwater flow in multi-aquifer system with window based, menu-driven, user friendly interface to provide on screen input data interpretation, to guide user through steps of data processing , and to generate reports and graphs from output results. The model is able to handle combined and system-dependent boundary conditions that can be used in practical situation of groundwater flow in the complex hydrogeological conditions of a country like Bangladesh in general and particularly for Dhaka City. Due to less complexity in two-dimensional simulation and the availability of Graphical User Interface (GUI) the model is easier to use and time efficient.

1. Introduction

Groundwater modeling in Bangladesh needs special attention in addition to the usual obstacles such as irregular geometry, boundary conditions, temporal and spatial variation of aquifer characteristics and excitations. During monsoon aquifers are replenished directly from the precipitation-infiltration process due to the accumulated standing water over the submerged lands, the occurrence and distribution of which vary with time. Also the rivers fed the aquifers naturally, or in induced way when heavy pumping near the river occurs, particularly in densely populated urban areas like Dhaka city. In Dhaka the huge demand for drinking and sanitation purposes is exclusively (95% of total abstraction) fulfilled by the groundwater abstractions through approximately six hundred deep tube wells. The unprecedented growth rate of Dhaka City both caused the Dhaka Water Supply and Sewerage Authority (DWASA) to increase the production of drinking water supply by more than six times since the sixties but still the supply is far lagging behind the demand. As a result, beneath Dhaka City, water levels in the aquifers have fallen steadily over the last decades in response of ever increasing abstraction (MPO, 1987). Thus the groundwater resource evaluation, prediction and management bear much attention at this time in Bangladesh.

The present study is devoted to develop a two-dimensional groundwater model that can handle a situation like Dhaka City. Galerkin finite element method is used to develop a two-dimensional numerical algorithm for treating saturated and

unsaturated flows simultaneously. With a view to make the model more user friendly and efficient in operation a Graphical User Interface (GUI) is designed to handle the user input, reporting the output and graph generation.

2. Literature Review

Finite element techniques to two-dimensional saturated-unsaturated flow problems were applied by several researchers. Among them are *Neuman* (1973), *Neuman et. al.* (1974), *Reeves and Duguid* (1976), *Bruch* (1977), *Frind et. al.* (1977). In all of these studies nonlinearities were treated using standard Picard solution algorithm and the models were developed by Galerkin finite element method. To deal with wider range of field conditions, an improved Picard algorithm and a Newton-Raphson algorithm were used by *Huyakorn et. al*. (1984). *Cooley* (1983) used somewhat different sub-domain finite element method in combination with Newton-Raphson and strongly implicit procedure. *Allen and Murphy* (1986) introduced a finite element collocation technique for solving variably saturated flow in two space dimensions. The scheme used a mass-conservative formulation of Richards' equation as the basis for the finite difference time stepping method. *Panday et. al.* (1993) discussed recent advances in finite element modeling techniques for variably saturated flow problems. Although till now, a large number of numerical models in the finite element method have been developed, the number of models handling real problems is very few.

3. Status of Groundwater Modeling in Bangladesh

In Bangladesh several groundwater modeling exercises have been undertaken which can be classified as Single Cell models, Multiple Single Cell models and Multiple Cell Integrated Finite-difference models (MPO, 1987). The first groundwater model used in Bangladesh is in 1977 under BADC/IDA Tubewell Project. The BWDB/ UNDP (1984) water balance study also modeled the groundwater components. From 1983 to 1986, MPO designed a groundwater evaluation program within the National Water Plan (NWP) preparation schedule (MPO, 1987, 1991). RMP/ Montogomery in 1980 developed a finite-difference groundwater model, known as Parsons' model, for DWASA to assess the impact of additional groundwater abstraction from the aquifer systems in Dhaka city region (DWASA, 1991). In 1986 Solomon and Chidley used a United States Geographical Survey (USGS) model to assess the groundwater resources of Dhaka City (MPO, 1987, 1991). Lastly in 1991, the Dhaka region groundwater and subsidence model study, using integrated finite-difference method, was carried out for assessing the impact of proposed installation of 50 new and 10 replacement tubewells (DWASA, 1991). All of the mentioned studies used finite difference models and no finite element model was applied in the major groundwater studies of Bangladesh.

4. Methodology

Galerkin finite element method is used to develop a two-dimensional numerical algorithm for subsurface flow by solving the governing flow equation – the Richards equation (1931). A two-dimensional isothermal Darcian flow of water is considered, in a variably saturated rigid porous medium, assuming that the air phase plays an

insignificant role in the liquid flow process. A modified form of the van Genuchten's (1985) closed-form functions as proposed by Vogel and Cislerova (1988) is used to identify soil moisture characteristics in unsaturated zone.

The Richards' flow equation is obtained by combining Darcy's law with continuity equation, which gives

$$\frac{\partial}{\partial x_i}(K_{ij}\frac{\partial \phi}{\partial x_i}) = \frac{\partial \theta}{\partial t} + S \tag{1}$$

For a two-dimensional vertical soil profile, with the hydraulic conductivity decomposed, it reads:

$$\frac{\partial \theta}{\partial t} = \frac{\partial}{\partial x_i}\left[\mathrm{K}\left(\mathrm{K}_{ij}^{A}\frac{\partial h}{\partial x_j} + \mathrm{K}_{iz}^{A} \right)\right] - S \tag{2}$$

where θ (dimensionless) is the volumetric moisture content, h [L] is the pressure head, S[T^{-1}] is a sink term, x_i (i=1,2)[L] are the spatial coordinates, t [T] is the time, K^A_{ij} (dimensionless) are components of the anisotropy tensor K^A, and K [LT^{-1}] is a scalar unsaturated hydraulic conductivity function given by

$$K(h, x, z) = K_s(x, z)\, K_r(h, x, z) \tag{3}$$

where K_r (dimensionless) is the relative hydraulic conductivity and K_s is the saturated hydraulic conductivity. The anisotropy tensor K^A_{ij} in equation (2) is used to account for the direction-dependent hydraulic conductivity of the porous medium. The diagonal entries of K^A_{ij} equal one and the off-diagonal entries zero for an isotropic medium.

According to the Galerkin method, the approximate or trial solution in terms of pressure head $h(x, z)$ at any given time t can be expressed as a series summation of the products of the nodal pressure heads, h_n, and the associated nodal basis functions $U_e\xi_n^e(\mathrm{x}, \mathrm{z})$:

$$\begin{aligned}\hat{h}(x,z,t) &= \sum_{n=1}^{N} h_n(t) U_e \xi_n^e(x,z); \qquad n = 1,2,.....,N \\ &= \sum_{n=1}^{N} h_n(t)\phi_n(x_i)\end{aligned} \tag{4}$$

The values of h_n must be determined so as to satisfy the initial and boundary conditions of the problem together with the orthogonality requirement:

$$\sum_e \int_{\Omega^e} L(\hat{h})\xi_n^e d\Omega = 0; \qquad n = 1,2,.....,N \tag{5}$$

where Ω^e is the interior of e and L is differential operator of the governing flow equation.

The flow domain is sub-divided into a network of triangular elements with the corners of the triangles as nodes. The spatial discretization transforms the continuous partial differential equation into semidiscrete system of ordinary differential equations, which can be written in a matrix form as

$$[A_{nm}]\{h_m\} + F_{nm}\frac{d\{\theta_m\}}{dt} = \{Q_n\} - \{B_n\} - \{D_n\}; \qquad n, m = 1,2,.....,N \tag{6}$$

in which the elements of the matrices are

$$A_{nm} = \sum_e KK_{ij}^A \int_{\Omega^e} \frac{\partial \xi_n^e}{\partial x_i} \frac{\partial \xi_m^e}{\partial x_j} d\Omega \quad (7a)$$

$$F_{nm} = \delta_{nm} \sum_e \int_{\Omega^e} \xi_n^e d\Omega \quad (7b)$$

$$Q_n = -\sum_e \int_{\Gamma^e} \xi_n^e q d\Gamma \quad (7c)$$

$$B_n = \sum_e KK_{iz}^A \int_{\Omega^e} \frac{\partial \xi_n^e}{\partial x_i} d\Omega \quad (7d)$$

$$D_n = \sum_e \int_{\Omega^e} S \xi_n^e d\Omega \quad (7e)$$

A fully implicit finite difference scheme is used for time discretization and special treatment of the time derivative term is given to ensure mass conservation at each time step as proposed by Celia et al. (1990). An implicit (backward) finite difference scheme is used for both saturated and unsaturated conditions:

$$[F]\frac{\{\theta\}_{j+1} - \{\theta\}_j}{\Delta t_j} + [A]_{j+1}\{h\}_{j+1} = \{Q\}_{j+1} - \{B\}_{j+1} - \{D\}_{j+1} \quad (8)$$

where $(j+1)$ denotes the current time level at which the solution is being considered, j refers to the previous time level, and $\Delta t_j = t_{j+1} - t_j$. The above equation represents the final set of algebraic equations to be solved. Since the coefficients θ, A, B and D are functions of the dependent variable h, the set of equations is generally highly nonlinear. These equations are linearized by Picard iteration scheme and then solved by Gaussian elimination to find the unknown values.

Prior to solving the set of equations proper boundary conditions – system independent Dirichlet, Neuman and Mixed type boundary conditions and system dependent atmospheric and seepage face boundary conditions are incorporated in the model. The input data required to run the model are the material information, nodal information and the atmospheric information.

5. Application of the Model to a Dhaka City Aquifer

During the development and modifications of the different features of the model a number of familiar published problems (Simunek et. al.,1992) have been used to verify the algorithm. After satisfactory performance of all the cases, a real situation in the Dhaka City is simulated to analyze the model behavior.

The study area is located within the north central region of Bangladesh bounded by the rivers Jamuna, Ganges, Meghna and Old Brahmaputra. The study area is bounded by Tongi khal on the north, Buriganga on the west, Balu River on the east and by the District boundary on the south (Fig. 1). The model area covers approximately 320 km^2 and has been selected to cover DWASA's supply area and adjacent areas influenced by the groundwater abstraction. The ground elevation of Dhaka metropolitan area varies from 1m to 8m PWD (Public Works Department) sloping gradually from north to south with the average ground elevation of 4.5 m PWD.



Figure 1. Location of the Study Area

The average yearly rainfall in the study area is 2000 to 2200 mm based on the period April 1976 to March 1997. The long term mean for Dhaka city is 2040 mm per annum (MPO, 1987). Most of the annual rainfall, 80 to 90 percent, falls during the monsoon season from May to September (EPC, 1991). Temperature ranges from lows of about 10°C at night during December and January to daytime highs of over 35°C during April and May (EPC, 1991). Average monthly potential evapotranspiration of Dhaka City ranges from about 2.87 mm/day in January to about 6.25 mm/day in April with a yearly total of 1500 mm. During the monsoon season mean daily values are about 4.8 mm/day (EPC, 1991).

Lithological data of 66 discrete boreholes from Bangladesh Water Development Board (BWDB) have been used to describe the geology in the model. Thirty six of those are located in the Dhaka Metropolitan area. Borehole logs clearly show that the deposits underlying Dhaka are alluvial, heterogeneous and a certain degree of conceptualization is required to derive an operational model. Despite the occurrence of several interbedded layers it is possible to identify at least four major geological units: Upper aquitard (clay and silt), Upper aquifer (fine to medium sand), Lower aquitard (clay and silt), and Lower aquifer (medium to coarse sand).

DWASA have defined the saturated hydraulic conductivity of different zones of Dhaka region from a correlation between the results of pumping tests and lithological profiles. A distributed transmissivity map (Hossain, 1997) based on a number of aquifer tests carried out by DWASA shows transmissivity values in the range of 300-1200 m^2/day. Taking into account the saturated thickness of the layer, horizontal hydraulic conductivity and storage coefficient are calculated and subsequently interpolated to cover the entire model area. The vertical permeabilities are derived from the horizontal permeabilities by assigning (K_h/K_v) a value of anisotropy. Based on the mean anisotropic ratio evaluated by British Geological

Survey (BGS, 1998), ratio of 2.5 for the lower aquifer is adopted. For accurate characterization of the unsaturated soil behavior, a set of field data is required for moisture content, soil water suction and unsaturated hydraulic conductivity. But in the present study in absence of such field data a set of arbitrary fitting parameters is taken.

Observation well data indicates continually increasing abstraction caused the water levels in the Dhaka city aquifer to fall steadily over the last decades and have reached a maximum of over 20 to 25 meters in some areas. A total of 27 observation wells in and around the model area are available, out of which 11 are located within Dhaka City (Fig. 2). The groundwater level of Dhaka City exhibits a large fluctuation between monsoon and the dry season. The groundwater level is declining at a rate of approximately 1.2 m/yr. in Dhaka City. The declination rate is higher in Sabujbagh area (DHA019, DHA020) which is about 1.7 m/yr (DWASA, 1998). This may be due to the installation of deep tube wells (DTW) to keep pace with the rapid expansion of the residential areas. The lowest groundwater level was found in South Basabo (DHA020) which is about -26m PWD. The highest level was found in Maniknagar (DHA013) which is about -14m PWD. Both were found in the year 1996-97. The falling rate of water table is increasing gradually which indicates an alarming situation.



Figure 2. Location of Observation Wells

Based on the available input data the model area has been discretized into 500m grid squares in the horizontal plan. The total number of elements is 1263 and nodes are 1295. The west, east and north of the model area are bounded by the vertical planes passing through the axes of the Buriganga River, Balu river and Tongi khal respectively. As in the city side abstraction is enormously higher than the opposite side of the river obviously a high gradient towards the city from the opposite side of the river prevails. It is assumed that the river is hydraulically connected with the soil layers below its bed. Thus a time dependent Dirichlet boundary condition is imposed on west, east and north boundaries of the study area. No distinct natural condition exists along off-river boundary, i. e., the south boundary of the model area. An artificial time dependent Dirichlet boundary condition is imposed based on the observation well data and their interpolation values in the intermediate nodes. Except boundaries all other internal nodes are treated with atmospheric boundary condition.

Atmospheric data (mean daily precipitation and evaporation) (Fig. 3) and river water level data are collected from the central database of the Surface Water Modeling Center (SWMC) and BWDB. Daily rainfall data are collected for station R009 within the study area. Pan evaporation data for the period has been extracted from the E13 station. The piezometric and abstraction data for the area are collected from DWASA. There are 459 DTWs around the study area of which nearly 220 are located within the study area. A national DEM, based on 500m grid elevation data surveyed during 1960-64, is available covering most of Bangladesh. Dhaka metropolitan area as part of the FAP8A (1991) study, has been utilized.

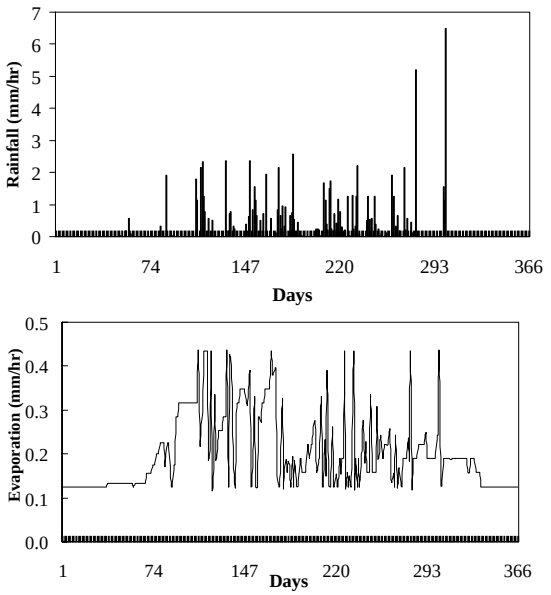

Figure 3. Hydrometeorological Input Data for the Study area for the year 1996

In Dhaka City the groundwater level in general is not affected by annual variations as the impermeable urbanized areas prevent any significant recharge by infiltration. Variations of up to 2m are, however, found for DHA009 at some points and for DHA010, DHA012 and DHA013 at one point each. The absence of annual variations is found both in observations and in simulations. The time series show a steady decrease as a response to increased abstraction in the area in general. The rate of decrease is in general captured very well by the model (DHA001, DHA005, DHA009, DHA011, DHA014, DHA019 and DHA020) while it is slightly underestimated in DHA010, DHA012, DHA013 and DHA021. A comparison between simulated and observed heads inside the study area is shown in Fig. 4.

Given the constraints in data the model calibration is satisfactory. The model is capable of simulating a correct average level and a correct rate of decline in groundwater levels. If more time is spent a closer fit between simulation and observation can be achieved, but more important an effort should be made to verify and complete the input data. After fulfilling the calibration requirement the water balance of the domain is shown in Table 1 for the time period January, 1996 to December, 1996.

Table 1 : Simulated Water Balance for the Model Area, 1996

Components	Volume (m^3)
Abstraction	2652.71×10^6
Atmospheric face (cumulative outward)	$^*1685.14 \times 10^6$
Rainfall	3597.52×10^6
Atmospheric face (cumulative inward)	255.92×10^6
Recharge	1610×10^6
Return flow from water supply	795.8×10^6

*Value indicates loss of water from the surface when no ponding of the surface exists, i. e., evaporation loss from the ponding water instantaneously after heavy precipitation is excluded.

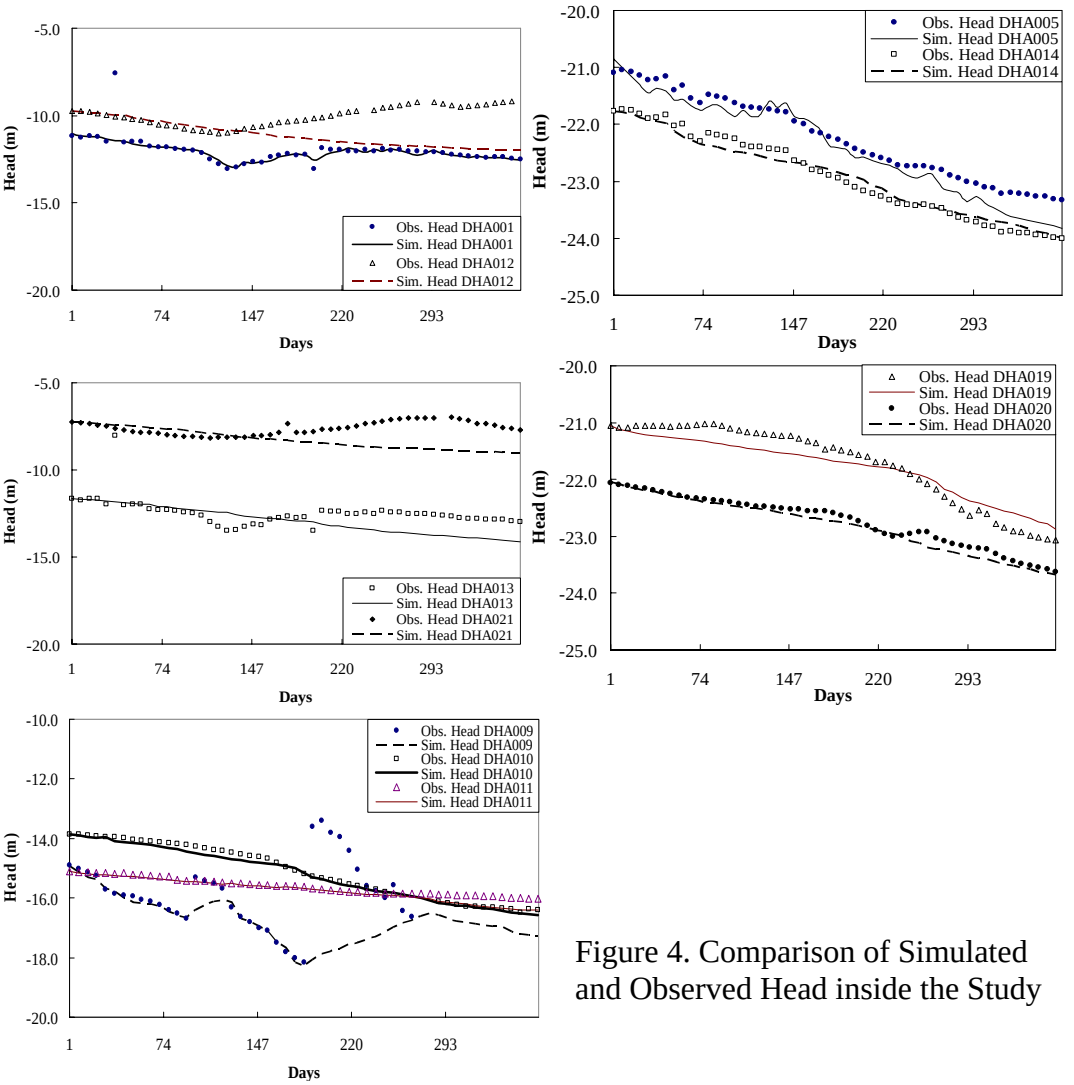

Figure 4. Comparison of Simulated and Observed Head inside the Study

The abstraction of water is mainly compensated in the domain by the boundary flow from the riverside, not only contributed from the river itself but from the high water table of the surrounding area. The volume of water entered to the soil domain from the direct precipitation is only 9.65 percent of the abstraction volume. Most part of the precipitation gets evaporated and lost by surface runoff due to the low hydraulic conductivity of the aquifer.

6. Graphical User Interface (GUI)

A GUI is designed and implemented using Object Oriented Programming language Visual Basic that makes the Fortran program operable in the 32-bit faster windows environment. Selected input and output windows are presented in Figures 5, 6 and 7.

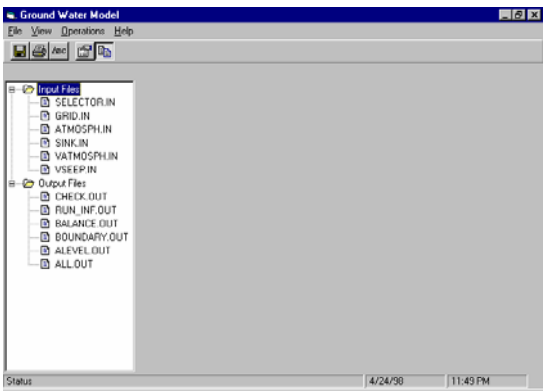

Figure 7. Interface Window that Triggers Different Function depending on User Event

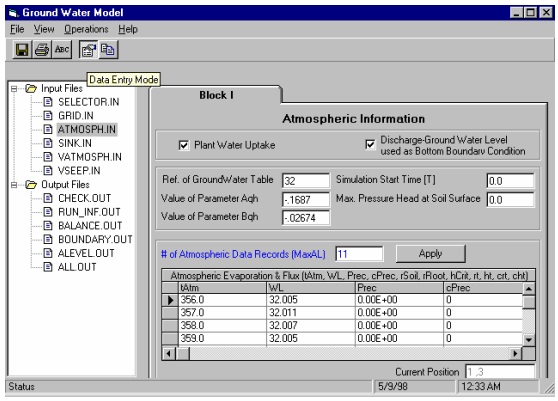

Figure 8. Input of Atmospheric Information in ATMOSPH.IN

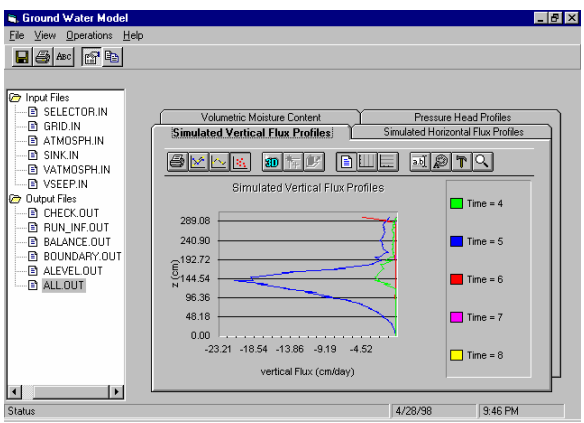

Figure 9. Simulated Vertical Flux Profiles for Selected Days

7. Conclusions

Different features incorporated in the model have been verified by simulating a number of published schematized problems. The model responses in simulating a complex real hydrogeological situation of a real city (Dhaka, Bangladesh) aquifer are reported. The boundary conditions of the domain are derived from the river water level and piezometric level data. Model calibration of the parameters has been performed under this study as well. Simulated water balance components identify the river effect as the most dominating recharge mechanism of the area, which contributes around sixty percent of the total volume of abstraction. Urban recharge (taken 30% of the total abstraction) also contributes to the abstraction volume of the area. The results of simulation show that the approach is fruitful and can be used for detailed study of the groundwater status of densely populated and growing cities like the Dhaka City in future.

The program is proved to work well but have a disadvantage of being associated with the time step of the atmospheric input data, which is usually one day. Shorter and/or automatically set time step for the atmospheric input data, as well as for the boundary-condition subroutines, is therefore recommended. A need has been also identified for yet more flexible treatment of combined and system-dependent boundary conditions (e.g. a combination of the variable atmospheric boundary condition with the variable seepage-face one) and for the coupling of the present model with a two-dimensional model of surface runoff in a flood plain.

References

Allen, M. B., Murphy, C. L., 1986: A finite element collocation method for variable saturated flow in two space dimensions. Water Resources Research 22: 1537-1542.

BWDB/ UNDP, Water Balance Studies, Bangladesh, April, 1984.
Bruch, J. C., Jr., Zyvoloski, 1974: Solution of vertical unsaturated flow of soil water. Soil Sci. 116: 417-422.
British Geological Survey, 1998: Groundwater Studies for Arsenic Contamination in Bangladesh, Mott Macdonald Ltd., UK.
Celia, M. A. Bouloutas, E. T., Zarba, R. L., 1990: A general mass-conservative numerical solution for the unsaturated flow equation. Water Resources Research 26 (7): 1483-1496.
DWASA, February 1991: Dhaka region Groundwater and Subsidence Project, Draft final report.
DWASA, June, 1998: Fourth Dhaka Water Supply Project, Draft Final Report, Groundwater Modeling, Vol. 4.
Engineering and Planning Consultants (EPC), May 1991: Dhaka Region Groundwater and Subsidence Study, Final Report, Vol. 2.
Flood Action Plan (FAP) 8A, 1991: Master Plan Study for Greater Dhaka Protection Project, Japan International Cooperation Agency, Dhaka.
Frind, E. O., and Verge, M. J., 1978: Three-dimensional modeling of groundwater flow systems. Water Resour. Res., 14(3): 844-856.
Hossain, M. I., October, 1997: Evaluation of Aquifer characteristics of Dhaka City using Pumped Well Data, M. E. Thesis, Department of Water Resources Engg., BUET.
Huyakorn, P. S., Thomas, S.D., Thompson, B. M., 1984: Techniques for making finite elements competitive in modeling flow in variably saturated porous media. Water Resources Research 20: 1099-1115.
Master Plan Organization (MPO), June, 1987: The groundwater resource and its availability for development, Technical Report No. 5.
Master Plan Organization (MPO), May, 1991: National WATER Plan Project Phase-II, Simulation Model Report, Vol. III, Groundwater Models.
Panday, S., Huyakorn, P. S., Therrien, R., and Nichols, R. L., 1993: Improved three-dimensional finite element techniques for field simulation of variably saturated flow and transport. J. Contaminant Hydrol., 12, 3-33.
Reeves, M., Duguid, J. O., 1975: water movement through saturated-unsaturated porous media, a finite element Galerkin model. Oak Ridge Natl. Lab., Oak Ridge, Calif., ORNL-4927, 232 pp., cited after Gureghaian (1981).
Richards, L. A., 1931: Capillary conduction of liquids through porous mediums, Physics 1: 318-333.
Simunek, J., Vogel, T. Van Genuchten, M. Th., 1992: The SWMS_2D code for simulating water flow and solute transport in two-dimensional variably saturated media. Version 1.1 Research Report No. 126, January 1992, U. S. Salinity Laboratory, Agricultural Research Service, U. S. Department of Agriculture, Riverside, CA, USA, 169 p.
Van Genuchten, M. Th., 1980: A closed-form equation for predicting the hydraulic conductivity of unsaturated soils. Soil Sci. Soc. Am., J. 44: 892-898.
Vogel, T., Cislerova M., 1988: On the reliability of unsaturated hydraulic conductivity calculated from the moisture retention curve. Transport in Porous Media 3: 1-15.

A Methodology to Reconstruct Groundwater Contamination History with Limited Field Data[1]

Jiabao Guan[2], Morris L. Maslia[3], and Mustafa M. Aral[4]

Abstract

A health risk assessment of exposure to contaminants in drinking water frequently requires reconstructing the groundwater contamination history in aquifers. The development of groundwater flow and contaminant fate and transport models used in such an analysis is time-consuming and expensive. Therefore, new approaches need to be explored to reconstruct groundwater contamination history that may reduce the time and expense of the traditional numerical modeling approaches.

An ongoing health study at U.S. Marine Corps Base Camp Lejeune, North Carolina, will determine if an association exists between exposure to contaminated drinking water and birth defects and childhood cancers in children born to women who were pregnant while living at the base during the period 1968–1985. For this study, there are no field data on groundwater contamination at water-supply wells prior to 1985. Limited contaminant concentration data at several observation wells are available during and after 1992 when remedial investigations of the contaminated aquifers began. To assist the epidemiological study in determining historical exposure scenarios, groundwater contaminant history needs to be reconstructed at base housing areas. Interpreting the mathematical models that are used in the analysis of groundwater flow and contaminant fate and transport and using the field data available on contaminant levels, a linear control model is proposed for the purpose of reconstructing the historical exposure to contaminated groundwater. The control model includes two matrices: (i) the first matrix describes the system behavior of the contaminant movement in aquifers in a natural environment and, (ii) the second matrix reflects the effect of pumping operations on contaminant concentrations. In the control model, the system matrix is recognized by using the least-squares method and the effect of pumping operations is determined by using an optimization method and an improved genetic algorithm when solving for matrix coefficients. To test the proposed methodology and to demonstrate the effectiveness of the model and proposed algorithm, the Tarawa Terrace base housing area of Camp Lejeune, which has been modeled in detail, is chosen. Computational results show that the model proposed herein can be used as a screening method to recover

[1] The findings and conclusions in this paper are those of the authors and do not necessarily represent the views of the Agency for Toxic Substances and Disease Registry or the U.S. Department of Health and Human Services.

[2] Senior Research Engineer, Multimedia Environmental Simulations Laboratory, School of Civil and Environmental Engineering, Georgia Institute of Technology, Atlanta, Georgia 30332, jg79@ce.gatech.edu.

[3] Research Environmental Engineer, Agency for Toxic Substances and Diseases Registry, Centers for Disease Control and Prevention, Atlanta, Georgia 30341, mmaslia@cdc.gov.

[4] Director, Multimedia Environmental Simulations Laboratory, School of Civil and Environmental Engineering, Georgia Institute of Technology, Atlanta, Georgia 30332, mustafa.aral@ce.gatech.edu.

groundwater contamination history with reasonable accuracy considering the lack of data that may exist at many sites.

Key words: control model, least square method, genetic algorithm, groundwater contamination.

Introduction

An ongoing health study at U.S. Marine Corps Base Camp Lejeune, North Carolina (Figure 1), will determine if an association exists between exposure to contaminated drinking water and birth defects and childhood cancers in children born to women who were pregnant while living at the base during the period 1968–1985. In this situation there are no field data on groundwater contamination at water-supply wells prior to 1994. Limited contaminant concentration data at several observation wells are available after during and after 1992 when remedial investigations of the contaminated aquifers began. To assist the epidemiological study in determining historical exposure scenarios, groundwater contaminant history needs to be reconstructed at base housing areas. The traditional approach used to solve this problem is to develop groundwater flow and contaminant fate and transport models and then to apply them to a study area to obtain the contaminant concentration distribution in time and space. However, determining and calibrating model parameters, such as aquifer hydraulic conductivity distributions and boundary conditions, is time-consuming and expensive. Therefore, new approaches need to be explored to reconstruct groundwater contamination history. These new approaches should reduce the time and expense of the traditional numerical modeling approaches. In this paper, a linear control model is proposed to reconstruct the contamination history at the site. The control model consists of two linear parts: the first part describes the system behavior of contaminant movement in aquifers in a natural environment and the second part reflects the effect of pumping operations on contaminant concentrations. Both are expressed as matrices that are separately identified using optimization methods based on the available concentration records and pumping-schedule data. The Tarawa Terrace base housing area of Camp Lejeune which has been modeled in detail (*Maslia et al.* 2007), is used to demonstrate the effectiveness of the model and proposed algorithm described herein.

Control Model

Groundwater resources within the Hadnot Point base housing area at Camp Lejeune were contaminated by leaking landfills for more than 40 years. Contaminated water-supply wells ceased operations during 1994, but contaminant sources were not removed or remediated at the time. Pumping data for water-supply wells prior to 1994 are available, but there are no water-quality records. Some concentration data are available after 1994. For generality, it is assumed that the study period spans from the starting time t_0 to the terminal time T_f and t_a is the time at which the water-supply wells stopped operating. In the study domain there are n locations (water-supply and observation wells) where concentration distributions during the period $[t_a, T_f]$ are recorded, and m water-supply wells whose pumping rates are known within the period $[t_0, t_a]$. For consistency with control systems, the concentrations at observation wells are represented by the vector $X(t)$, denoted as $X(t) = [x_1(t), x_2(t), \ldots, x_n(t)]^T$, and the pumping rates at water-supply wells by $U(t)$, denoted as $U(t) = [u_1(t), u_2(t), \ldots, u_m(t)]^T$, where $x_i(t)$ is the concentration at location i in time t, $u_j(t)$ is the pumping rate at water-supply well j in time t. The concentration states at observation wells can be determined by the system behavior of the contaminant movement in aquifers in a natural environment and the effect of pumping operations. Therefore, the concentration states in the aquifer system can be approximately described by a discrete linear system state equation as

$$\begin{cases} X(k+1) = \mathbf{A}X(k) + \mathbf{B}U(k) \\ X(t_0) = X_0 \end{cases} \tag{1}$$

where $\boldsymbol{A}$ is the $n \times n$ matrix associated with aquifer parameters including contaminant source characteristics, $\boldsymbol{B}$ is the $n \times m$ matrix associated with pumping rates, X_0 is the initial concentration vector at observation wells —it is zero in general—and k is the time step or time stress period. In the model, the matrices $\boldsymbol{A}$ and $\boldsymbol{B}$ are unknown and require being identified using existing recorded data such as time series data of concentrations at observation wells and pumping rates at pumping wells. Once both matrices are identified, Equation (1) can be used to reconstruct the contaminant distribution in time and space.

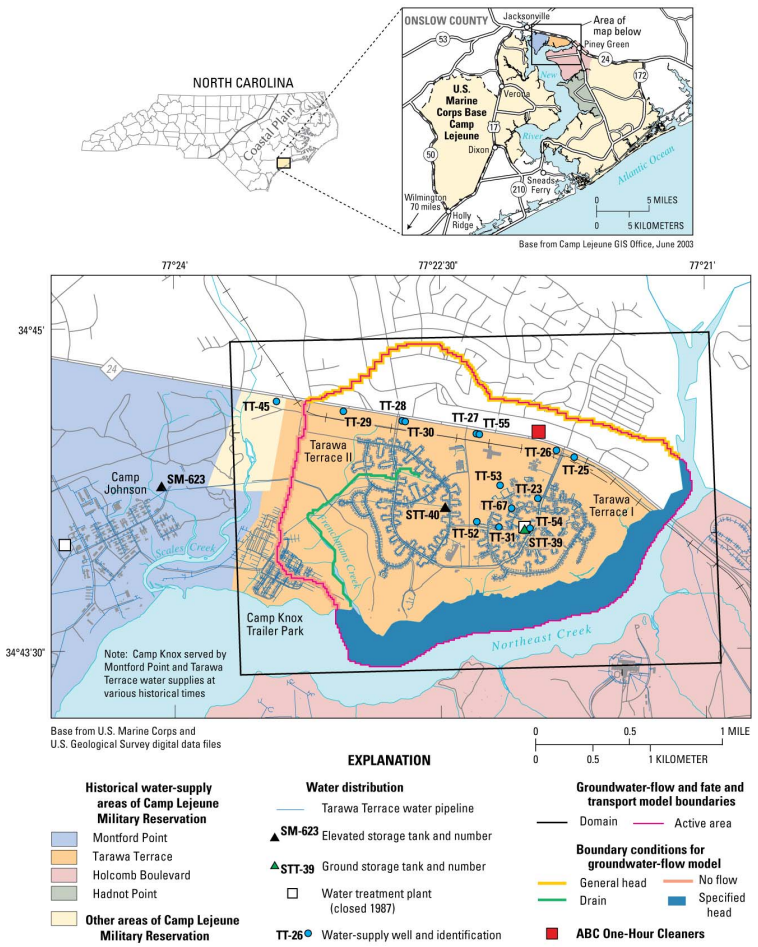

Figure 1. Water-supply areas, groundwater-flow modeling area, and water-supply facilities used for historical reconstruction analyses at Camp Lejeune.

Solution Algorithms

In order to reconstruct contamination history, the system equation described above needs to be recognized, i.e., matrices $\boldsymbol{A}$ and $\boldsymbol{B}$ need to be identified. Based on available data, both matrices $\boldsymbol{A}$ and $\boldsymbol{B}$ can be obtained using a two-step procedure.

Step 1: Since the pumping wells cease operation after t_a, the system states at observation sites depends on just the concentrations at previous time stress period. $\boldsymbol{A}$ can be identified by using the least-squares method based on the concentration data within $[t_a, T_f]$ (*Björck,* 1996).

Step 2: The concentration data are not available during $[t_0, t_a]$ and need to be reconstructed, the least square method cannot be used to estimate matrix $\boldsymbol{B}$. However, it is obvious that concentrations at t_a are both initial concentration distributions during $[t_a, T_f]$ and also a consequence of pumping operations during $[t_0, t_a]$. In some sites there are some additional internal concentration data points during $[t_0, t_a]$. Taking advantage of these concentration data together with the pumping rate data, the estimation of matrix $\boldsymbol{B}$ can be formulated as an optimization problem that finds the matrix $\boldsymbol{B}$ by minimizing the total error between the estimated and observed concentrations at t_a as well as internal data points. The optimization model is then solved by using a genetic algorithm (*Holland*, 1975, *Guan et al*., 2007).

Numerical Applications

In this paper, the Tarawa Terrace base housing area at Camp Lejeune is used as an example to demonstrate the effectiveness of the model and proposed algorithm. The Tarawa Terrace housing area at the Camp Lejeune was constructed during 1951. Drinking water, supplied to the family housing, was contaminated with volatile organic compounds (VOCs), mostly with tetrachloroethylene (PCE) and its degradation by-products. The contamination was linked to the release of PCE from the ABC One-Hour Cleaners (Figure 1) into the groundwater system (*Faye and Green*, 2007; *Jang and Aral*, 2007; *Maslia et al*., 2007). To assist the epidemiological study (*Jang and Aral*, 2007; *Maslia et al*., 2007), detailed groundwater-flow and contaminant fate and transport models in the area were developed by the Agency for Toxic Substances and Disease Registry (ATSDR) and the Georgia Institute of Technology, Multimedia Environmental Simulations Laboratory (*Maslia et al*., 2007; *Jang and Aral*, 2007). The groundwater system at Tarawa Terrace and vicinity was modeled as 12 aquifer layers (*Jang and Aral,* 2007). Fourteen water-supply wells supplied drinking water to the base housing area from the underlying aquifer system (Figure 1). Water-supply wells, TT-26, TT-53 and TT-67 significantly impacted contaminant spreading toward the base housing area. For verification purpose, the calibrated simulation models developed for the ATSDR study are used to calculate contaminant concentration distributions within the study domain. Aquifer parameters, boundary conditions, source characteristics used in the current study (this paper) are exactly same as those used in *Jang and Aral* (2007). The simulation period is from January 1951 through December 1994 and consists of 528 monthly stress periods. To demonstrate the effectiveness of the methodology proposed herein, three Tarawa Terrace water-supply wells—TT-26, TT-53, and TT-67—are selected to operate during 408 monthly stress periods (from January 1951 to December 1984) using pumping schedules described in *Jang and Aral* (2007). Also, it is assumed that pumping operations cease after stress period 408. Five nodes around the contaminant plume are used to test the model, which are nodes 102570, 103438, 103860 (TT-26), 104066 and 104892 in the 7th layer and are closed to the contaminant source ABC Cleaners.

The resulting PCE concentration distributions at the aforementioned nodes are shown in Figure 2. The concentrations from stress period 408 to 528 (December 1984–December 1987) are used to identify system matrix ***A*** using the least-squares method. For identification of the coefficients of the matrix ***B***, two cases are presented. In case 1, only concentration data at stress period 408 (December 1984) are used and in case 2, 8 additional internal concentration data points from stress periods 1–408 are available and this concentration data along with the data at stress period 408 are used together. The PCE concentration distributions at five observation sites for cases 1 and 2, reconstructed using the identified system equation (1), are shown in Figures 3 and 4, respectively. In these figures, a solid line represents the reconstructed concentration distribution and a dashed line represents the measured concentration.

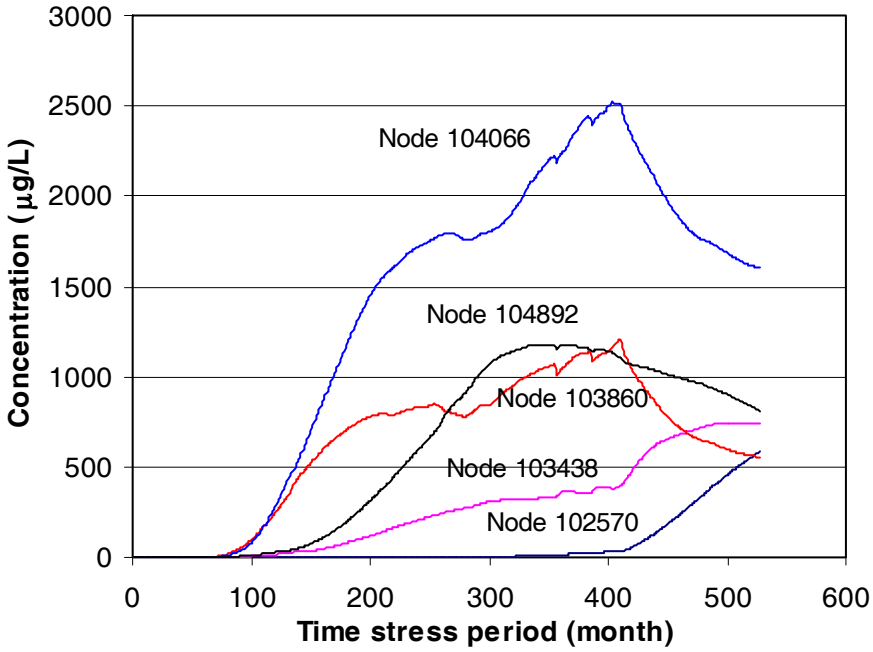

Figure 2. Resulting PCE concentration distributions in five nodes.

Results shown in Figure 3 (case 1, without additional internal data points), clearly show that the concentrations at stress period 408 are nearly identical to "measured" values. Overall, concentration distributions at observation nodes show good recovery, although some errors occur the estimation. Comparing each individual observation site, the concentrations at Node 104892 are best recovered. The maximum concentrations at Nodes 103860 and 104066 contain relatively large error compared to "measured" data. Considering the limited data availability, these results are encouraging and could be used with confidence for the epidemiological study.

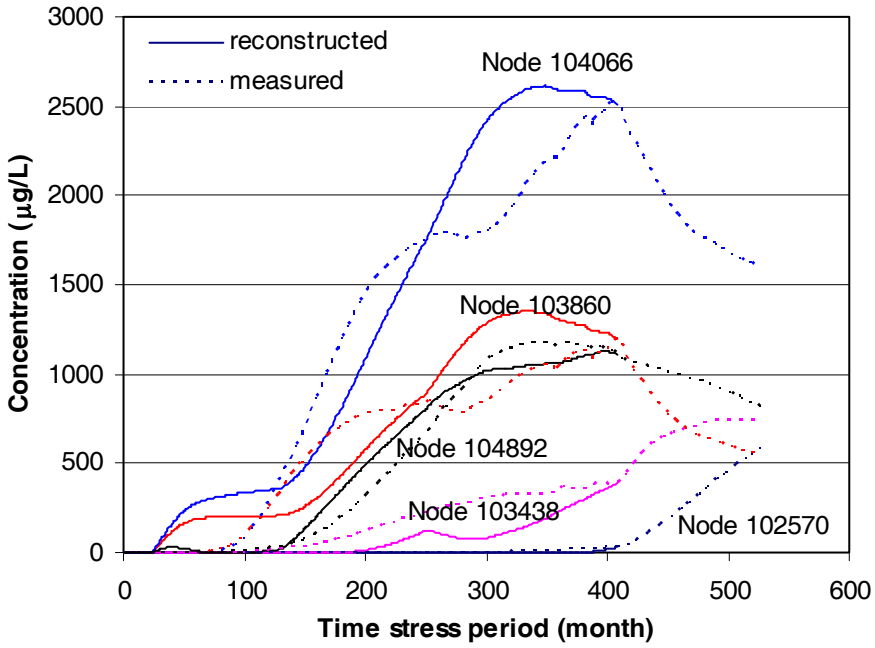

Figure 3. Concentration distributions recovered in case 1 (Without internal data points).

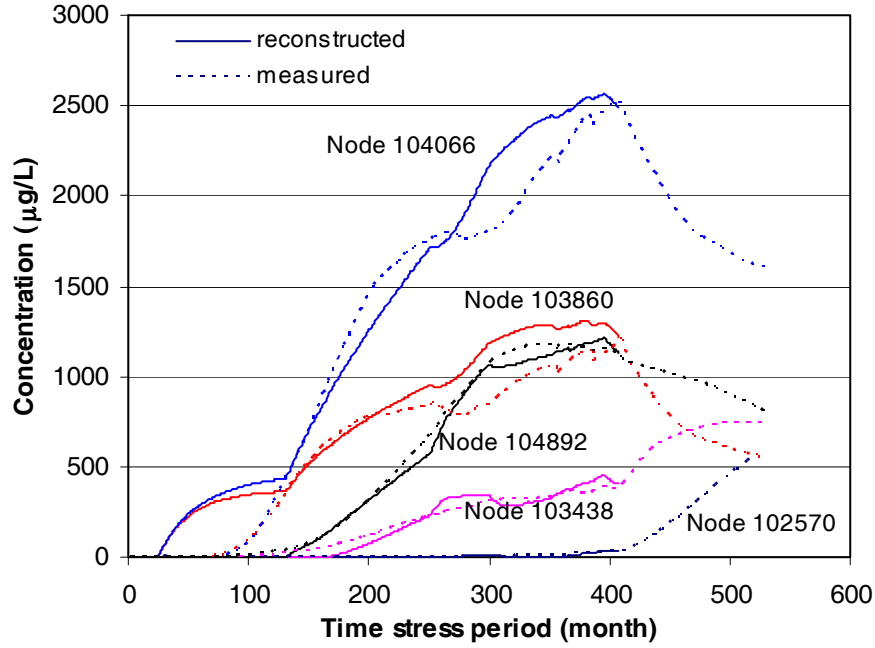

Figure 4. Concentration distributions recovered in Case 2 (With additional 8 internal data points).

If additional internal contaminant concentration data within stress periods 1–408 are available, the estimation accuracy may provide significant improvement. This is demonstrated in case 2 with the addition of 8 "measured" concentration data points within stress periods 1–408. For this scenario (case 2), calculation of the objective function value in optimization includes the additional internal concentrations in estimating coefficients of matrix $\boldsymbol{B}$. Comparing results shown in Figure 4 to those shown in Figure 3 indicates that concentrations distributions at all observation sites in Figure 4 (Case 2, 8 additional data points) are more closely reconstructed.

Conclusions

In this study a linear discrete system state equation is proposed to approximately describe the aquifer system in order to reconstruct the contamination history in the study domain. Compared to costly and time consuming groundwater-flow and contaminant fate and transport model development and calibration, the methodology proposed herein solely requires some measured concentration data at observation wells and water-supply well operation schedules to identify system and pumping effect matrices. The system and pumping effect matrices are determined by the least-squares method and a genetic algorithm, respectively. In this paper, the Tarawa Terrace base housing Camp Lejeune is used as an example to demonstrate the effectiveness of the proposed model and algorithm. The concentration distributions at the observation wells reconstructed from the control model provide a reasonable estimate of accuracy. This probably implies that the proposed model and algorithms provide an effective screening method for reconstructing groundwater contamination history when there are limited or missing historical contaminant concentration data.

References

Faye, R.E. and Green, J.W. Jr., 2007. Analyses of groundwater flow, contaminant fate and transport, and distribution of drinking water at Tarawa Terrace and vicinity, U.S. Marine Corps Base Camp Lejeune, North Carolina: Historical reconstruction and present-day conditions—Chapter E: Occurrence of contaminants in Groundwater. Agency of Toxic Substances and Disease Registry, Atlanta, GA. [cited 2009 January 23]; Available from http://www.atsdr.cdc.gov/sites/lejeune/index.html.

Guan, Jiabao, Kentel, Elcin, and Aral, Mustafa M. (2007). Genetic Algorithm for Constrained Optimization Models and Its Application in Groundwater Resources Management, Journal of Water Resources Planning and Management, Vol. 134(1), pp 64-72.

Björck, Àke, Numerical methods for least squares problems, Philadephia: SIA, c1996, 408p.

Holland, J.H. (1975). Adaptation in natural and artificial systems, University of Michigan Press, Ann Arbor, Mich., 183.

Jang, W. and Aral, M.M., 2007. Simulation of three-dimensional multi-species, multi-phase mass transport of tetrachloroethylene (PCE) and associated degradation by-products. Atlanta, GA: Multimedia Environmental Simulation Laboratory (MESL), School of Civil and Environmental Engineering, Georgia Institute of Technology, Report No.: MESL-02-07.

Maslia, M.L., Sautner, J.B., Faye, R.E., Suárez-Soto, R.J., Aral, M.M., Grayman, W.M., Jang, W., Wang, J., Bove, F.J., Ruckart, P.Z., Valenzuela, C., Green, J.W. Jr., and Krueger, A.L., 2007. Analyses of groundwater flow, contaminant fate and transport, and distribution of drinking water at Tarawa Terrace and vicinity, U.S. Marine Corps Base Camp Lejeune, North Carolina: Historical reconstruction and present-day conditions—Chapter A: Summary of Findings. Agency of Toxic Substances and Disease Registry, Atlanta, GA. [cited 2009 January 23]; Available from http://www.atsdr.cdc.gov/sites/lejeune/index.html.

A Tale of Two Cities –Source Water Protection Case Studies for Systems in Rural Settings

Tina Petersen, PhD. – Camp Dresser & McKee Inc.
Camille W. Sowells, P.E., BCEE – Camp Dresser & McKee Inc.
Gordon McCurry, Ph.D., P.G. – Camp Dresser & McKee Inc.
Alexandra Doody – Camp Dresser & McKee Inc.
Claudia Krug – Camp Dresser & McKee Inc.
Sean Ables, P.G. –Texas Commission on Environmental Quality

TOPIC: 7th Symposium on Groundwater Hydrology, Quality, and Management
SUBTOPIC: Groundwater Quality and Human Health

Abstract

Rural public water supply systems represent the majority of systems in the U.S. Challenges facing the public water supply systems include documented water quality issues such as the presence of coliform bacteria and nitrate and urbanization resulting from development projects in the area. Strategies for dealing with these challenges can vary widely. This paper will present two case studies from a source water protection project being conducted in Central Texas. Both systems are privately owned, rural water system managed by a water supply corporation. Differences between the two systems arise in the populations they serve, with one being a community water system and the other being a non-community system serving a campground. The paper highlights the unique differences between the two systems in terms of implementation of protection measures as well as funding opportunities.

Introduction

Drinking water contamination in source water is a major issue across the nation, from lead contamination in Washington, D.C., Cryptosporidium contamination in Milwaukee to nitrate contamination in rural communities. While the implementation of the Safe Drinking Water Act has resulted in superior drinking water quality in many parts of our country, much room for improvement still exists.

One program US EPA has developed to prevent pollution of groundwater that serves as a source of drinking water for local communities is Source Water Assessment and Protection program. This program provides an opportunity to protect water sources by actively engaging in pollution prevention and engaging the local communities and water systems. Source water protection is a priority for the US EPA and for many states across the nation that have assumed primacy on implementing the program, including Texas (TCEQ, 1999).

This paper will present two case studies from a source water protection project being conducted in Central Texas: one rural system managed by a water supply corporation and the other a private owner/operator system for a campground. The paper will highlight the unique differences between the two systems in terms of potential sources of contamination (PSOCs) as well as implementation of protection measures and funding opportunities.

System #1 - Rural System Managed by a Water Supply Corporation

Water System Description

The first rural public water supply system serves a small city comprised of approximately 1,000 individuals located south of medium sized city in Caldwell County Texas. The system is a water supply corporation (WSC) and managed by a board of directors. Day to day operations are supervised by a WSC General Manager. The water supply serves a rural town with a population of 953 but also provides drinking water for some unincorporated portions of the county as well. Land uses in the community consist primarily of agricultural and residential lands. A small portion of the community consists of commercial land use.

Currently the system serves 860 active connections using two operational public supply wells to withdraw water from the San Marcos alluvium, an unconfined alluvial aquifer under the influence of surface water. The water is treated using a membrane process that injects the waste from the treatment process back into the aquifer via underground injection.

High levels of nitrates and atrazine have been detected in the source water in the past several years. These concentrations have been above the maximum contaminant limit and customers of the system are concerned about their water quality. Additionally, the system has also seen a number of source water samples test positive for total coliform.

Capture Zone Modeling

An early step in the project was to identify the land area that may pose a risk of contamination to a public water supply well. This land area is called a wellhead protection area (WHPA). Modeling to establish the WHPA was conducted using the Wellhead Analytic Element Model (WhAEM2000), a groundwater flow model distributed by the US EPA.

Modeling for this system took into account effects of hydrologic features such as rivers, recharge into the aquifer, aquifer properties, regional groundwater flow, and the effect of pumping of the city's public water supply wells on groundwater flow. The resulting WHPA covers approximately 2,000 acres across two counties, much of it

unincorporated. It is important to note that the WHPA for this system extends beyond its service area.

Potential Contaminant Source Inventory

After developing a WHPA, an inventory of potential sources of groundwater contamination was performed within the WHPA. A search of available environmental regulatory agency databases was conducted for the supply wells, adjoining properties and surrounding properties within a two-mile search radius. Following the database review, representatives from the study team performed a site visit to observe the condition of the existing system wells, identify potential sources of contamination (PSOCs).

The database searches and field inventory identified the potential sources of contamination shown in **Table 2** within the WHPA. Key PSOCs identified in the survey include septic tanks, abandoned water wells, two cemeteries, seven gravel mines, and two petroleum storage tanks. Field visits were limited to observations made using public right of ways; the field team did not enter private property. Therefore, not all PSOCs could be field verified.

Management Strategy

Potential sources of contamination should be managed to minimize the risks of ground water quality degradation within the WHPA. This can be accomplished by developing and implementing best management practices (BMPs) for the PSOCs.
BMPs were recommended for each of the potential sources of contamination described in **Table 1**above. In addition, non-PSOC specific management strategies were identified as well. A summary of the BMPs for this system are provided in **Table 2**.

Septic systems are considered a priority PSOC to address, because improperly maintained septic tanks may contribute to nitrate and coliform contamination of the water supply source water. The large number of septic systems in the WHPA may contribute to source water contamination for various reasons including improper location of the system, poor design, faulty construction, incorrect operation, and poor or no maintenance of the system. Another high priority BMP is investigating and establishing the extent of chemical usage at the two cemeteries in the WHPA. Herbicide and fertilizer use at cemeteries may contribute to source water contamination if improperly applied. Finally, education and outreach BMPs were also recommended for abandoned water wells and chemical using businesses.

PSOC	Quantity	Quantity Field Verified
Abandoned Landfills	2	2
Active/Abandoned Mines	7*	0
Abandoned Water Wells	2	2
Petroleum Storage Tank	2	2
Cemeteries	2	2
Chemical Storage	1	1
Class 5 Injection Well	1	1
Septic Tanks	200**	11
Cotton Gin	1	1
Grain Elevator	2	2
Auto Repair, Sales, Salvage and/or Towing	2	2
Wood Preserving	1	1
• Mines were located on private property and not accessible to the field team **Quantity estimated based on information provided by water supply system personnel		

Table 1
Summary of Potential Sources of Contamination for Rural Community Water System #1

PSOC	Recommended BMPs
Septic System	■ Develop a program to educate homeowners and businesses on septic system maintenance. ■ Provide information from this report to the city to encourage promulgation of a septic system maintenance ordinance. ■ Work with TCEQ and county staff to determine whether septic system inspections are current systems located within the WHPA and coordinate activities to undertake those inspections.
Cemeteries	■ Determine the status of cemetery maintenance. The system staff will contact the owners to determine if chemicals are used or stored on-site. ■ Discuss the SWAP program with cemetery owners and review maintenance activities with them to determine if herbicides and pesticides are being applied in correct amounts. Distribute educational material if applicable.
Abandoned Water Wells	■ Contact the owner, Texas Water Development Board and/or Texas Department of Licensing and Regulation to have wells capped or plugged.

Table 2
Best management practices for Rural Community Water System #1

Chemical using businesses	■ Determine the status of chemical usage. The system staff will contact the businesses to determine if chemicals are used or stored on-site as part of standard business practices. ■ Discuss the SWAP program with business owners. If chemicals are used or stored on-site, distribute applicable literature to the owner/operator.
Other Management Strategies	■ Identify a source water protection coordinator to be the main point of contact and act as a liaison and facilitate source water protection related communication with the city. ■ Form a local planning committee to work on source water protection activities, such as maintaining records of PSOCs and reviewing land use changes.

Table 2 continued
Best management practices for Rural Community Water System #1

Because implementing source water protection in Texas is voluntary and the water system has limited funding and no jurisdictional control over most issues as a water supply corporation, the BMPs listed in **Table 2** are focused on working with the local city and educating home owners. This makes implementing the program extremely challenging for the system. Community involvement and commitment to the Source Water Protection program is the key for success. Therefore, the study team also recommended establishing a local planning committee and source water protection coordinator to champion the program.

Funding opportunities

Adequate resources are needed for a water system to implement their Source Water Protection program. To support these efforts, the regulating agency, the Texas Commission on Environmental Quality (TCEQ) has provided assistance for one outreach event for each water supply system that has agreed to participate in a special Source Water Protection program. The outreach event requested by this system is to staff a booth at the community's Fourth of July celebration. The booth will have brochures and promotional items to educate and encourage residents to protect their source water.

Other funding sources, however, may also be available to a water system to support further implementation activities. The study team performed a search of applicable funding sources for source water protection activities. **Table 3** presents the funding assistance opportunities that were identified for the rural community's recommended BMPs. These funding sources are provided primarily by federal and state government programs focused on drinking water infrastructure. Some of these funding

BMP	BMP Implementation	Funding Availability	Funding Type
Septic Systems – Public Education	System staff	Y	Grants/Loans
Cap Abandoned Wells	Owner of Well	Y	Grants
Local Planning Committee	System staff	Y	Grant
Monitoring Plan	System staff	Y	Grants/Loans

Table 3
Funding Assistance Opportunities for Rural Community Water System #1

mechanisms would require the water system to work in cooperation with a nearby city to apply for funds. There is limited funding available from a nonprofit organization for developing a local planning committee, if the system cooperates with the City to apply for funding.

System #2 – Privately Managed Transient System at Campground

Water System Description

The second rural public water supply system serves a campground in Hays County, Texas. The campground supplies drinking water primarily to a transient (i.e., non-residential) population of recreational visitors, where peak times of use occur on weekends of the summer months. The campground contains 27 sites for recreational vehicles, 35 camping sites, an office, and public bathrooms and showers. In addition to the campground, the area also contains picnic areas, low-density rural residential housing, and undeveloped natural forest. The system is a privately managed system by a single owner who has a full-time operator on staff to handle day-to-day operations of the system.

The campground has one operational well and one emergency well and serves approximately 100 individuals at any given time. Both wells draw from the Trinity alluvial aquifer. The system has several documented problems with coliform bacteria.

Capture zone modeling was completed using the same approach as that for the rural community system. The resulting WHPA covers approximately 700 acres in a single county, all of it unincorporated.

Potential Contaminant Source Inventory

After developing a WHPA, an inventory of potential sources of groundwater contamination was performed within the WHPA. The database searches and field inventory identified the potential sources of contamination shown in **Table 4** within the

PSOC	Quantity	Quantity Field Verified
Septic Tanks	20**	4
Chemical Storage – Elevated Petroleum Storage	1	1
Chemical Storage – Drums, Small Containers	1	1
Water Well	19*	17
* Some water wells could not be located without entering private property and thus were not accessible to the field team **Quantity estimated using county septic system records		

Table 4
Summary of Potential Sources of Contamination for Rural System #2

WHPA. Few PSOCs were identified for this system but include septic tanks, chemical storage, and active water wells. Field visits were limited to observations made using public right of ways; the field team did not enter private property so not all PSOCs could be field verified.

Management Strategy

In conjunction with input from the water system, BMPs were recommended for each of the potential sources of contamination described in **Table 4** above along with general management strategies. A summary of the BMPs for this rural system is provided in **Table 5**.

PSOC	Recommended BMPs
Septic System	■ Continue to perform routine inspection and maintenance on the septic system located at the campground and maintain documentation of inspection and maintenance activities. ■ Educate homeowners in nearby subdivision on septic system maintenance. ■ Work with TCEQ and county staff to determine whether septic system inspections are current for systems located within the WHPA
Chemical Storage	■ Send a mail-out brochure or discuss with elevated storage tank owner the potential risks of petroleum storage tanks. Ask for regular inspections (quarterly or semi-annually) of tank and ground for signs of leaks. ■ Distribute an informational brochure on proper care of propane tanks to all campers when they register at the front office.

Table 5
Best management practices for Campground

Water Wells	■ Outreach to water well users in the subdivision near the campground should be performed and include education on regular well maintenance as well as proper procedures for capping wells that are no longer in use.
Other Management Strategies	■ Continue routine inspection and maintenance of public drinking water wells and maintain records of all inspection and maintenance activities; ■ Exercise care in disinfecting the source water to ensure that residual is maintained through distribution system; ■ Maintain and update records of potential sources of contamination within the WHPA on a routine basis. This includes a review of land use changes and potential sources of contamination.

Table 5 continued
Best management practices for Campground

The BMPs in **Table 5** describe management strategies to address the PSOCs in the WHPA. Septic systems are considered a priority PSOC to address, because improperly maintained septic tanks may contribute to coliform contamination of the water supply source waters. Septic systems, which are located at the campground itself and at neighboring homes, were considered to require BMPs most urgently because improperly maintained septic tanks may contribute to coliform contamination. Storage of chemicals for fuel, such as diesel, gasoline, or propane, either through elevated storage tanks or individual propane canisters, was another PSOC noted in the campground WHPA. The individual propane canisters are used by individual campers. BMPs for these PSOCs focus on education.

Management strategies within the WHPA are directed at all potential sources of contamination within the WHPA boundary. The WHPA is composed entirely of unincorporated areas and thus there is no city to provide jurisdictional support. In addition, septic system inspections are performed by the State in this area. Because this is a private water system supporting a transient population, there is limited opportunity for creating a source water protection planning committee. Therefore, the non-PSOC management strategies focus on drinking water supply well maintenance and record keeping tasks.

Funding opportunities

Funding for the implementation of source water protection activities at private water systems is minimal. The only readily available funding source for private systems is from the Texas Water Development Board through their Drinking Water State Revolving Fund. TCEQ, however, does provide an outreach activity at no cost to the system because of their involvement with the Source Water Protection program that

The outreach event requested by this system is to write and produce an educational brochure which will be handed out to all campers when they enter the campground. The brochure will discuss source water protection and recommend some simple BMPs that campers and RV owners can undertake while staying at the campground. These will focus on managing trash, chemicals, propane canisters, as well as gray water handling.

Discussion

Preliminary findings from investigations suggest that that the rural community water system (system #1) has a diverse set of potential contaminants of concern (PSOCs) while the campground PSOCs at system #2 are primarily related to septic systems, chemical storage and water wells. This difference in PSOCs is a result of the more diverse land uses found in the vicinity of small rural system.

Comparison of Best Management Practices

The BMPs for the system #1 included on a variety of PSOCs, including septic systems, cemeteries, businesses that use chemicals and abandoned water wells. This reflects the land use of the area with residential, agricultural, and commercial land. The campground system (#2), however, was located in a region that has low density residential housing and undeveloped natural forested areas and consequently had many fewer PSOCs, consisting only of septic systems, water wells, and different types of chemical storage.

The BMPs recommended for septic systems warrant an especially close look between the two systems. BMPs in both communities focus on education and outreach. The differences between the two, however, result from the jurisdictional authorities. In the rural community water system (system #1), the recommended BMPs include greater enforcement of existing regulations through inspection by regulatory agencies, and promulgation of septic system maintenance ordinances by the nearby city that has some jurisdictional authority over the WHPA for this system. The community system is afforded these options because of potential teaming with a neighboring town. The WHPA for system #2, on the other hand, is located in an entirely unincorporated area. Therefore, the BMP options are limited to increased maintenance of its own wastewater treatment system. It is important to note that neither water system has the direct ability to impose requirements to septic systems as the Texas Source Water Protection program is voluntary and does not have any enforcement ability.

Comparison of Funding Opportunities

The funding opportunities for the two water systems also exhibited differences. The community water system (system #1) has a greater breadth of opportunities available to

it as a result of potential partnerships with the local city and its status as a water supply corporation. The designation as a water supply corporation affords the system access to several Texas Water Development Fund financial assistance programs, such as the Rural Water Assistance Fund, Clean Water State Revolving Fund. Additionally, the opportunity to team with the city, a political subdivision, provides access to certain federal government programs, such as the Office of Rural Community affairs. The campground, on the other hand, is a private system and thus has very limited funding opportunities as a result of their private status and inability to team with other political subdivisions.

Giving priority to community systems may be intended to help a larger number of individuals, but this is not necessarily true in call cases. The campground serves several thousand customers over the course of a year, merely for a shorter period of time, but exposure to degraded water poses on equally serious health risk.

Conclusions

These findings suggest that community water systems face different challenges than privately owned transient systems. These disparities result from the differences in land uses patterns and associated contaminants that could reach the supply wells, and in funding availability. At the same time, some potential sources of contamination are consistent between the two, such as the presence of potentially failing septic systems. There are no simple solutions to the water quality issues facing either system due to limited funding. Both systems must undertake a dedicated public education and outreach effort to meet the challenges they face.

References:

TCEQ, 1999. Source Water Assessment and Protection Program Strategy. http://www.tceq.state.tx.us/files/txswap.pdf_4291348.pdfAccessed September 8, 2008.

Keywords:

source water protection, source water assessment, best management practices, groundwater.

Quantifying the spread of Arsenic Contamination in Groundwater of the Brahmaputra Floodplains, Assam, India: A Threat to Public Health of the Region

C. Mahanta[1], N. Pathak[2], R. Choudhury[1], P. Borah[1], W.Alam[1]

[1]Department of Civil Engineering, Indian Institute of Technology Guwahati, 781039; PH (91) 0361-2582407; FAX (91) 0361-2690762; email: mahanta_iit@yahoo.com

[2]Department of Civil and Environmental Engineering, University of Wisconsin Madison, 1261 Engineering Hall, 1415 Engineering Drive, Madison, WI 53706 PH (1) 608-554-0361; email: pathak2@wisc.edu

ABSTRACT

Arsenic contamination in groundwater in many countries, including India, has become an issue of global concern. After a relatively recent discovery of arsenic in the upper Brahmaputra floodplains, a Rapid Assessment Program for drinking water in Assam state of India covering all the districts was conducted. The study revealed presence of arsenic beyond permissible limit of 50 ppb in 72 blocks out of 192 blocks spread over 22 districts. A three phase analysis procedure adopted in this study yielded consistent results, showing good analytical performances for a large scale study. Of total 1726 samples spread across 18 districts, a major percentage of samples indicated concentration range of 60 to 150 ppb, emphasizing the need to take up intensive arsenic based research and to develop technologies and water management strategies to provide arsenic free drinking water in the region.

INTRODUCTION

Groundwater arsenic contamination and its impact is one of the most burning issues of global concern. Processes of arsenic mobilization from its source to groundwater are mainly either natural or anthropogenic. Among the anthropogenic causes, activities resulting in discharge of untreated industrial, effluents from metallurgical operations, ceramic, dye and pesticides manufacturing industries, petroleum refinery etc. into water sources are the prime causes of increased arsenic levels in surface and groundwater. However, as regards the geogenic causes, it is ubiquitous in the natural environment. In nature, there are 150 species of As bearing minerals, however, only 3 of them, i.e., As sulphide or Realgar (As_2S_2), as tri-sulphide or orpiment (As_2S_3) and Arsenopyrite or ferrous As sulphide ($FeAsS_2$) are considered as As ore because the amount of As is higher in these three compounds (Harvey, 2006). The main ores of arsenic are Arsenopyrite, Orpiment, Realgar and Arsenopalledenite and is present in nature as iron arsenate, iron sulphate, and in calcareous soils as calcareous arsenolite.
In general, the presence of arsenic depends on the hydro-chemical characteristics of groundwater aquifers, presence of oxidized/ reduced mineral phases and arsenic rich solid phases (Moore et al, 1988; Huang et al, 1994), and they occur principally in the form of inorganic or organic compounds, with arsenite (more toxic form) and

arsenates (less toxic form) constituting the inorganic compounds (WHO Guidelines for Drinking Water Quality,2004). Arsenic can occur in the environment in four different oxidation states (-3, 0, +3, +5) but in natural waters it is mostly found in the inorganic form as oxyanions of trivalent arsenite, As (+3) or pentavelent arsenate, As (+5). In the natural waters of pH ranging from 5 to 9, the predominant species of arsenic are $H_2AsO_4^-$ (lower pH) and $HAsO_4^{-2}$ (higher pH) in +5 (Arsenate state), which is more common in aerobic surface water and H_3AsO_3 in +3 (Arsenite) state, which can be found in anaerobic groundwater (Panthi et al, 2006).

Arsenic contamination in drinking water is a public health issue worldwide. The catastrophic health problems caused due to consumption of arsenic affected water in Bangladesh and West Bengal, India have been in the front page and mass media for more than a decade, the problem being described as the "greatest mass poisoning in history". A total of 9 districts in West Bengal, India with a population of 42.7 million and 42 districts in Bangladesh with a population of 79.9 million have arsenic levels in groundwater above the permissible limits of 50 g/L (Uttam K. et al, 2000). Elevated levels of Arsenic have also been reported in water supplies of communities in Argentina, Austria, Brazil, Canada, China, Ghana, Greece, Hungary, Iceland, India, Japan, Korea, Malaysia, Region Lagunera (Torreon, Mexico), Inner Mongolia, Nepal, Romania, Taiwan, Vitenam, Zimbabwe, and the U.S., with the worst sufferings of the people being reported Bangladesh, West Bengal in India, Inner Mongolia and Xin-Xiang Provinces of People's Republic of China and Taiwan in order of their magnitude. Numerous scientific papers (Ahmed et al., 2005, Ahmed et al., 2004, Horneman et al., 2004, Zheng et al., 2004, Nan Green et al., 2003 , Harvey et al., 2002, Fazal et al ., 2001a, Fazal et al., 2001b, Karimk, 2000, Kamal and Karim, 2000, Begum and Karim, 2000, Hossain et al., 2000, Adel, 2000, Bridge and Husain, 1999, Bridge and Husain, 2000a, Bridge and Husain , 2000b; Karim and Badruzzamann, 1999; Chowdhury et al., 1999, Kamal et al., 1999, Nickson et al., 1998, Nickson et al., 2000, Khalequzzaman, 1999, Ullah, 1998 and Karim et al., 1997) and many organizations have implemented different Arsenic programs and revealed the extent and severity of the problem.

The arsenic contamination in groundwater of northeastern region of India (Assam, Tripura, Manipur, Arunachal Pradesh and Nagaland), the largest storehouse of replenishing freshwater, has been reported by Singh (2004); with maximum arsenic concentration being observed in Johrat, Dhemaji, Golaghat and Lakhimpur districts in the state of Assam; West Tripura, Dhalai and North Tripura districts in the state of Tripura; Thuobal in Manipur; Dibang Valley in Arunachal Pradesh and Mokokchung and Mon districts in the state of Nagaland. Although there have been no clinical manifestations of Arsenicosis in the region (UNESCO, 2005) there could be a likelihood where such manifestation can occur due to the consumption of arsenic contaminated water; because natural springs and dug wells are the only cost effective and viable means of fulfilling the water needs for the people dwelling in this region. Arsenic interferes with a number of essential physiological activities, including the actions of enzymes, essential cations and transcriptional events in cells; including cancer of the skin, kidney, lung and bladder as well as other diseases of the skin,

neurological and cardiovascular system. It is in fact classified as a Class 1 human carcinogen by the USEPA.

Studies around the globe have well documented the impacts that arsenic enriched water has caused to the people in Bangladesh and West Bengal, India (Bhattacharya et al, 1997; Chowdhury, T. R., et al; Chowdhury, U.K. et al, 2000a, b; Chakraborti et al; 2002, 2003, 2004). Recent studies by Chakraborti et al (2004) and Mukherjee et al (2006) has shown that the As occurrence in this region is of geogenic origin and as the sedimentological history of the Brahmaputra valley in Assam is similar to that in Bangladesh, it is thought that the problem would be of similar nature in Assam. With the alarming threat to the people in these areas, it has become utmost important to carry out studies pertaining to the source, distribution, and the magnitude of the problem and thereby provide appropriate means and raise community awareness about the health problems related to chronic As exposure. The aim here is to report the first region-wide picture of arsenic concentrations in groundwater of Brahmaputra valley and to compile and evaluate these analytical results. This information can then be used for a number of purposes, from protection of human health to gaining a better understanding of arsenic geochemistry in regional groundwater.

STUDY AREA

Situated between latitude of 24° - 28° N and longitude of 90° - 96° E, Assam, the landmark state marks the gateway to the northeastern part of India, with three distinct physical units, the Brahmaputra valley in the north along with its vast floodplains, the Barak valley in the narrow protruding south and the hilly region separating the two valleys. With a total of 23 districts - Nalbari, Barpeta, Bongaigaon, Darrang, Dhemaji, Dhubri, Dibrugarh, Goalpara, Lakhimpur, Karbi Anglong, (in the northern bank of the Brahmaputra Floodplain) Nagaon, Sivsagar, Sonitpur, Tinsukia, Golaghat, Jorhat, Karimganj, Kokrajar, Morigaon, Kamrup (in the southern bank of the Brahmaputra Floodplain), Hailakandi, Karimganj, Cachar, North Cachar Hills (in the Barak Valley) and its 192 blocks, it forms an integral part of the Brahmaputra floodplain. With a total length of about 2,900 kms and a drainage basin covering an area of 1.6×10^6 sq. km, the Brahmaputra is the fifth largest river in terms of average discharge at mouth, and a flow of 19,830 m^3s^{-1} (Goswami 1985). The Brahmaputra Basin in Assam is confined by the eastern Himalayas in the north and east, the Patkai and Naga Hills on the northeast and Mikir Hills and Shillong Plateau in the south. The oldest (Precambrian) rocks are exposed in the Shillong Plateau and Mikir Hills and on the northern side the alluvial plains of Assam abuts against the Shiwalik ridge of the Himalayas, which are in turn overlain by highly tectonized Paleozoic sediments. Further on the southeastern part of the alluvial plain the Tertiary rock sequence occurs in Naga and Patkai hills which are overlain by the Quaternary sediments (Older Alluvium). The Recent sediments in the Brahmaputra Valley were deposited as alluvial fan and floodplain sediments of the Brahmaputra and its several tributaries (Evans, 1932 and Mathur and Evans, 1964). Figure 1 shows the study area under consideration including the districts of Assam state in India.

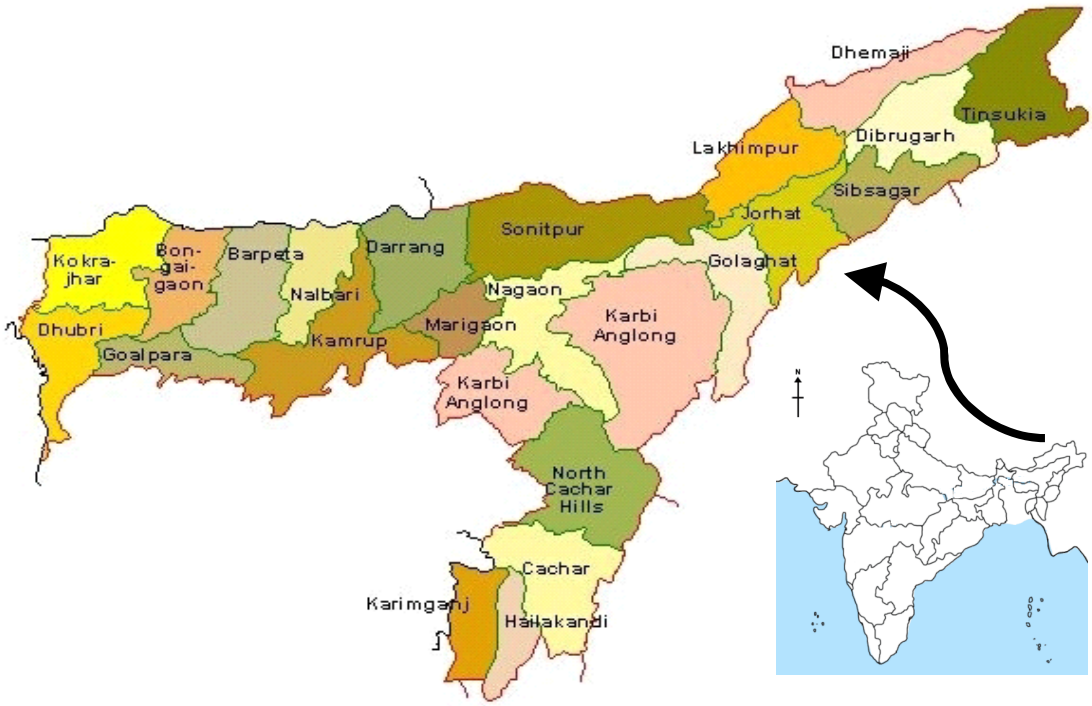

Figure 1. Map of the study area showing different districts of Assam, India

MATERIALS AND METHODS

The project is a joint effort by the United Nations Children's Fund (UNICEF) and Public Health Engineering Department (PHED) of Assam, in collaboration with Indian Institute of Technology (IIT), Guwahati, to study the arsenic problem in Assam, India. A total of around 5,729 samples, from 192 blocks spread across 22 districts were tested for the presence of arsenic. Concentration of arsenic in groundwater sources were determined by a three phase analysis - at the sampling site using an Arsenator, then analyzing 10% of the random samples and all samples showing concentrations of more than 40 ppb using the UV-1 Spectrophotometer (using wavelength of 550 nm and a band width of 2.0 mm) and finally 10% of the samples tested in UV-1 were tested using the Atomic Absorption Spectrophotometer (AAS) for confirmatory test. The Hydride generator method for arsenic analysis in the Atomic Absorption Spectrophotometer (HG-AAS) was used for this.

Water samples from PHED installed tube wells were collected at 200 ml sampling bottles with liner and screw caps and 1 ml dilute Nitric acid or Hydrochloric acid in the ratio 1:1 was added to maintain the pH below 2 and to prevent precipitation of iron and co-precipitation of arsenic. Prior to sample collection the tube wells were pumped for 10 minutes to remove any stagnant water from the water tanks to ensure that only fresh water samples were collected.

RESULTS AND DISCUSSION

A previous study conducted by the current authors including the Bongaigaon and Darrang districts of Assam, India indicated a high risk of groundwater arsenic contamination (Mahanta et al. 2008). During that study out of 50 sampled groundwater wells 15 wells indicated an arsenic concentration above the national drinking standard of 50 µg/l, and 33 had concentrations above the WHO guideline of 10 µg/l. However, no distinct depths/zones, sedimentological features or water chemistry were identified to produce arsenic enriched groundwater. After the initial, reports of excess arsenic in groundwater in Dhubri, Karimganj, and Dhemaji districts by the PHED, Assam a Rapid Assessment of water quality for arsenic and fluoride was conducted by PHED with support from UNICEF. Extensive sampling was done at different locations around the state to understand the source, spread and mobilization mechanism of As in groundwater of the region. The test results of district wise sampling for As and the affected blocks are shown in Table 1.

Table 1. Test results of district wise samples with Arsenic in groundwater and the affected blocks as found during the Rapid Assessment by PHED in 2005

District Name	Distribution of samples having presence of As at different levels (mg/l)			Number of affected blocks
	< 0.01	0.01-<0.05	> 0.05	
Tinsukia	219	1	-	Nil
Cachar	81	68	59	7
Jorhat	104	96	24	6
Barpeta	102	21	7	5
Karimganj	600	150	61	06
Dibrugarh	212	04	-	NIL
Sivasagar	119	72	15	03
Hailakandi	103	45	11	04
Goalpara	131	11	3	2
Dhubri	284	130	21	06
Sonitpur	187	34	06	03
Nalbari	109	25	14	05
Golaghat	171	67	30	05
Morigaon	229	40	02	01
Lakhimpur	159	50	09	05
Darrang	153	92	09	04
Dhemaji	328	128	83	05
Bongaigaon	79	15	06	03
Kokrajhar	239	06	_	NIL
Kamrup	221	39	01	01
Nagaon	258	55	01	01
Karbi Anglong	126	02	_	NIL
Total	4216	1151	362	72

A total of 5,729 samples, from 192 blocks spread across 22 districts were tested for the presence of arsenic. The test results indicated that 72 blocks out of the total 192 blocks were reported to have arsenic beyond the permissible limits of 50 ppb. This implies a grave risk to the public health of the region. With the excess use of groundwater for drinking and irrigation purposes, weathering would increase with the downward groundwater flow. So far no signs of arsenicosis have been documented in Assam. However, there is scope for research why this is so. Sand filters are extensively used in Assam and are used to reduce the wide spread high iron content from water. This seem to reduce the As content too through adsorption and co-precipitation. Arsenic rich water is also partly avoided since the drillers seek water low in iron, which often also has low arsenic content.

District wise categorization of samples for different concentration ranges for a total number of 1738 samples with the Atomic Absorption Spectrophotometer (AAS) shows major percentage of samples falling in the concentration range of (60-100) ppb and (100-150) ppb, while for three districts (Kamrup, Morigaon and Nagaon, located in the southern bank of the Brahmaputra floodplain) the percentage of samples in the concentration range of (0-40) ppb were found to be much higher. The district wise categorizations of the samples under the different concentration ranges are shown in figure 2 (a, b). Concentrations of more than 300 ppb are also observed in 9 districts although the percentage of samples occurring in this category is very low, with the highest percentage of 4% in Jorhat in the Southern bank and Cachar in the Barak Valley.

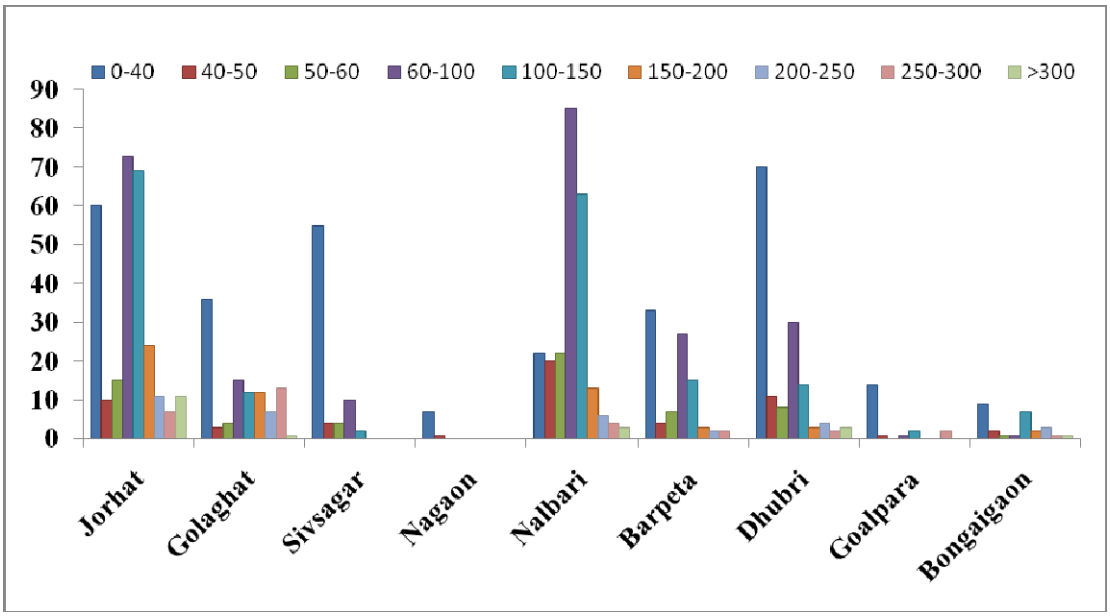

Figure (2a): District wise categorization of samples under particular range (in ppb) after analysis with AAS

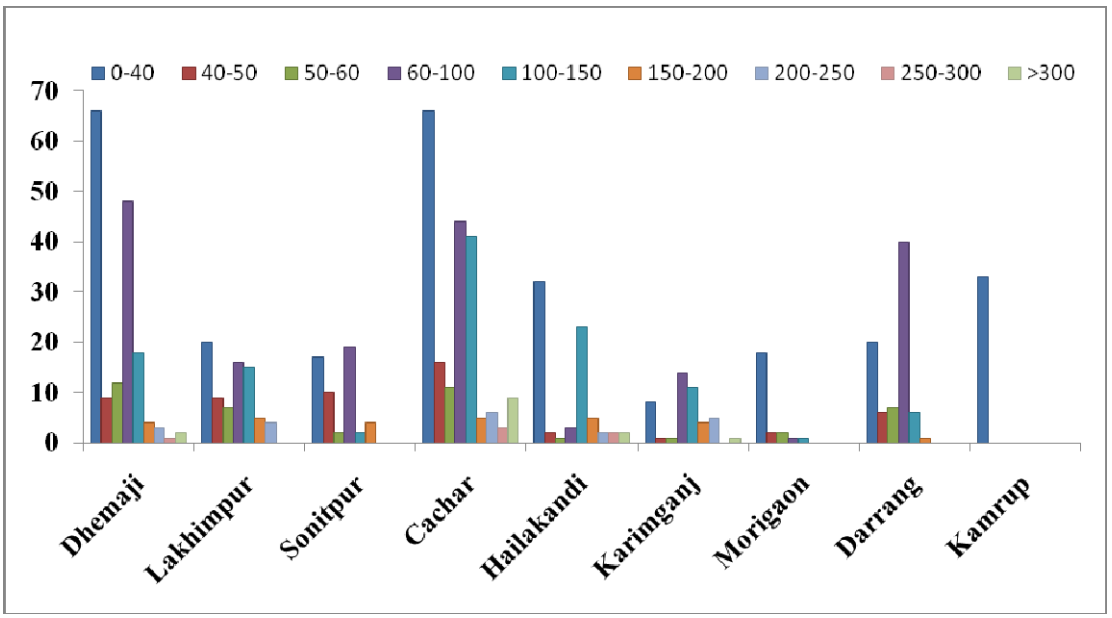

Figure (2b): District wise categorization of samples under particular range (in ppb) after analysis with AAS

The Brahmaputra floodplain bears a close similarity to the hydro- geologic set up of the floodplains in Bangladesh. Therefore, the occurrence of arsenic concentration above the permissible limit of 50 ppb is not unexpected. The locations in this study where the percentage of occurrence of arsenic concentration within the ranges of (60-100) ppb and (100-150) ppb are higher are on or very close to the floodplains. These areas are mainly composed of the recent alluvium, and studies (Smedley, 2005) have shown that most of the areas with arsenic contamination are of Quaternary age. Studies have indicated that the vast tract of Indo-Gangetic alluvium extending further to the west and the Brahmaputra alluvium, both have elevated concentrations of As in wells placed in the late Quaternary and Holocene aquifers. Arsenic released during the weathering of sulphide minerals is generally adsorbed onto the surface of iron oxyhydroxides that precipitated under oxidizing conditions generally prevailing during the deposition of the Holocene sediments. Recent research have also established that bed rock geology also plays an important role (Grosz et al, 2004) and the rapid erosion associated with active tectonics (e.g. the Himalayas) or glacial expedited Holocene weathering of Arsenic bearing minerals also contributes to the enrichment of arsenic in the groundwater (Saunders et al, 2005). A large local variations in As concentrations are probably due to the heterogeneity of the sediments and the resulting variations in redox conditions as well as possible remobilization due to periodic seismic events.

CONCLUSIONS

From the three phase study based on analysis with three instruments i.e. Arsenator, UV Spectrophotometer and AAS, the following can be concluded:

- The Arsenic enrichment in groundwater of some of the affected districts reflects concentration range much above the permissible limit of 50 ppb, suggesting the region to be seriously affected with arsenic contamination.
- The variation in concentration in different districts is probably due to heterogeneity of the sediments and their diverse location in the floodplain.
- Source is mainly considered to be geogenic, as the floodplain is composed of recent alluviums which are generally proved source of arsenic contamination and since there is limited arsenic contributing anthropogenic sources.
- Although no case of arsenicosis has been documented so far in the region, research based studies needs to be taken up to develop technological and remedial measures that best fit the region, to provide safe water to the people in the region.
- The success of the current three tier methodology suggests that this approach can be an effective tool for similar study to be taken up in other arsenic affected areas so far the agreement of the analytical instruments are concerned.

Reference

Adel, M.M. Arsenification: Searching for an Alternative Theory. The Daily Star of Bangladesh. *April (2000).*

Ahmed, K.M., Huq, I., Naidu, R. Extent and severity of arsenic poisoning in Bangladesh. In: Naidu, R. (Ed.), Managing Arsenic in Environment from Soil to Human Health. CSIRO Publication, in press. *(2005).*

Ahmed,K.M., Bhattacharya,P., Hasan, M.A., Akhter,S.H., Alam,S.M.M., Bhuyian, M.A.H., Imam, M.B., Khan, A.A. and Sracek,O. Arsenic enrichment in groundwater of the alluvial aquifers in Bangladesh: an overview, *Appl. Geochem. 19 (2004), pp. 181–200.*

Begum, Z.R. and Karim, M.M. Arsenic groundwater contamination of Bangladesh: community participation in groundwater resources management, Proceedings of 93rd Annual Meeting of Air and Waste Management Association Salt Lake, UT, USA, *18–22 June (2000), pp. 1–10*.

Bhattacharya, P., Chatterjee, D. & Jacks, G. Occurrence of arsenic contaminated groundwater in alluvial aquifers from Delta Plains, Eastern India: Options for safe drinking water supply. *Int. Jour. Water Res. Dev.,* (1997),13(1), pp.79-92.

Bridge, T.E. and Husain,M.T. Groundwater arsenic poisoning and a solution to the arsenic disaster in Bangladesh, *Presented at the ICBEN Conference at Dhaka* Bangladesh, 14 January, The Daily Star of Bangladesh, *21 January 2000 (2000).*

Bridge, T.E., Husain, M.T. Clean Healthy Water for Bangladesh—An Emergency Supply is Desperately Needed to Protect the People from the Arsenic Disaster. *(2000a).*

Bridge, T.E., Husain, M.T. The Increased Draw Down and Recharge in Groundwater Aquifers and Their Relationship to the Arsenic Problem in Bangladesh. *(1999)*

Chakraborti D., Mukherjee S.C., Pati S., Sengupta M.K., Rahman M.M., Chowdhury U.K., Arsenic groundwater contamination in Middle Ganga Plain, Bihar, India: a future danger, *Environ. Health Perspect.* 111 (2003) (9), pp. 1194–1201.

Chakraborti D., Sengupta M.K., Rahman M.M., Ahamed S., Chowdhury U.K., Mukherjee S.C, Groundwater arsenic contamination and its health effects in the Ganga–Meghna–Brahmaputra plain, *J. Environ. Monit.* 6 (2004), pp. 74–83.

Chakraborti, D., Rahman, M.M., Paul, K., Chowdhury, U.K., Sengupta, M.K., Lodh, D., Chanda, C.R., Saha, K.C. and Mukherjee, S.C. Arsenic calamity in the Indian Subcontinent: what lessons have been learned? *Talanta* 58 (2002), pp. 3–22.

Chowdhury U K., Biswas B. K., Roy Chowdhury T., Samanta G., Mandal B.K, Basu G.C., Chanda C.R., Lodh D., Saha K.C., Mukherjee S.K., Roy S., Kabir S.,Quazi Quamruzzaman, Chakraborti D. "Groundwater Arsenic Contamination in Bangladesh and West Bengal, India." *Environmental Health Perspectives* 108(2000), pp.393-397

Chowdhury, T.R. Basu, G.K., Mandal, B.K., Samanta, G., Chowdhury, U.K., Chanda, C.R., Lodh, D., Lal Roy, S., Saha, K.C and Roy, S. As poisoning in the Ganges delta, *Nature 401 (1999), pp. 545–546.*

Evans P., Tertiary successions in Assam, *Trans. Min., Geol. Metall. Inst. India* 27 (1932) (155 pp.)

Fazal, M.A., Kawachi, T., Ichion,E. Validity of the latest research findings on causes of groundwater Arsenic contamination in Bangladesh, *Water Int. 26 (2001) (2), pp. 380–389.*

Fazal,M.A., Kawachi, T. Ichion,E. Extent and severity of groundwater Arsenic contamination in Bangladesh, *Water Int. 26 (2001) (3), pp. 370–379.*

Geen, A.V., Zheng, Y., Versteeg, R., Stute, M., Horneman, A., Dhar, R., Steckler, M., Gelman, A., Small, C., Ahsan, H., Graziano, J.H., Hussain, I., Ahmed, K.M. Spatial variability of arsenic in 6000 tube wells in a 25 km^2 area of Bangladesh. *Water Resour. Res. 39 (5), 1140, doi:10.1029/2002wr001617. (2003).*

Goswami D.C., Brahmaputra River, Assam, India: physiography, basin denudation and channel aggradation, *Water Resour. Res.* 21 (1985), pp. 959–978

Grosz A.E., Grossman J.N., Garrett R., Friske P., Smith D.B., Darnley A.G. , Eric Vowinkel E., A preliminary geochemical map for arsenic in surficial materials of Canada and the United States, *Appl. Geochem.* 19 (2004), pp. 257–260.

Harvey C.F. , Swartz C.H., A.B.M. Badruzzaman, N. Keon-Blute, W. Yu, M.A. Ali, J. Jay, R. Beckie, V. Nidan, D. Brabander, P.M. Oates, K.N. Ashfaque, S. Islam, H.F. Hemond and M.F. Ahmed, Arsenic mobility and groundwater extraction in Bangladesh, *Science* 298 (2002), pp. 1602–1606.

Harvey, C.F., Swartz, C.H., Badruzzaman, A.B.M., Keon-Blute, N., Yu, W., Ali, M.A., Jay, J., Beckie, R., Nidan,V., Brabander, D., Oates, P.M., Ashfaque,K.N.,

Horneman,A., Geen, A.V., Kent, D.V., Mathe, P.E., Zheng, Y., Dhar, R.K., O'Connell, S., Hoque, M.A., Aziz, Z., Shamsudduha, M., Seddique, A.A. and Ahmed, K.M. Decoupling of As and Fe release to Bangladesh groundwater under reducing conditions Part I: evidence from sediment profile, *Geochim. Cosmochim. 68 (2004), pp. 3459–3473.*

Hossain M.F. "Arsenic contamination in Bangladesh - An overview". *Agriculture Ecosystem & Environment,* (2006) 113 (1-4), pp. 1–16.

Hossain, A., Rabbi, M.F., Abid, A.R. and Sadek,S. Arsenic problem in groundwater, a growing threat to public health in Bangladesh: an overall perspective and management modeling approaches. In: *K. Sato and Y. Iwasa,* Editors, *Proceedings of the International Symposium 2000 on Groundwater* Saitama, *Japan, 7–17 May (2000), pp. 473–474.*

Huang Y.C., Batchelor B , Koseoglu S.S, Cross-flow surfactant-based ultrafiltration of heavy-metals from waste streams, *Sep. Sci. Technol.* 29 (1994), pp. 1979–1998.

Kamal, M.M., Hansen, A.M. and Badruzzaman, A.B.M. Assessment of pollution of the river Buriganga, Bangladesh, using a water quality model, *Water Sci. Technol. 40 (1999) (2), pp. 129–136.*

Kamal, M.R. and Karim, M.M. GIS application for monitoring Arsenic groundwater

contamination exposure in Bangladesh. In: K. Sato and Y. Iwasa, Editors, *Proceedings of the International Symposium on Groundwater Saitama, Japan, 7–9 May (2000), pp. 55–60.*

Karim, M.A., Komori, Y. and Alam, M. Subsurface arsenic occurrence and depth of contamination in Bangladesh, *J. Environ. Chem. 7 (1997) (4), pp. 783–792*.

Karim, M.M. Arsenic in groundwater and health problem in Bangladesh, *J. Water Res. 34 (2000) (1), pp. 304–310.*

Karim, M.R and Badruzzaman, A.B.M. Modeling of nutrient transport and dissolved oxygen in the water column in river system, *Pollut. Res. 18 (1999) (3), pp. 195–206.*

Khalequzzaman, M. Looking to Heavens for Safe Water. The Daily Star Newspaper of Bangladesh, *24 September. (1999)*

Mahanta C., Nayanjyoti Pathak, Prosun Bhattacharya,Gustav Enmark and Daniel Nordborg Source, distribution and release mechanisms of Arsenic in the groundwater of Assam floodplains of Northeast India*, Proceedings at World Water and Environmental Resources Congress of EWRI/ASCE 2008* Honolulu, Hawaii, May 12-16, (2008)

Mathur L.P. and Evans P., Oil in India Int. Geol. Cong. 22nd Session, India, New Delhi (1964) (85 pp.).

Moore, J.N., Ficklin W.H., Johns C. Partitioning of arsenic and metals in reducing sulfidic sediments. *Environmental Science and Technology* 22 (1988),pp. 432-437.

Mukherjee A.B., Bhattacharya P., Jacks G., Banerjee D.M., Ramanathan A.L., Mahanta C., Groundwater arsenic contamination in India: extent and severity. In: R. Naidu, E. Smith, G. Owens, P. Bhattacharya and P. Nadebaum, Editors, *Managing arsenic in the environment: from soil to human health*, CSIRO Publishing, Melbourne (2006), pp. 533–594.

Nickson, R.T., McArthur, J., Burgess, W., Ahmed, K.M., Ravenscroft, P., Rahman, M. Arsenic poisoning in Bangladesh groundwater, *Nature 395 (1998), pp. 338–339.*

Nickson,R.T., McArthur, J., Burgess, W., Ravenscroft, P., Burgess, W.G. and Ahmed, K.M. Mechanism of As release to groundwater Bangladesh and West Bengal, *Appl. Geochem.* 15 (2000), pp. *403–413*.

P. Smedley, Arsenic occurrence in groundwater in South and East Asia: scale, causes and mitigation, *Towards a more effective operational response volume I, environment and social unit South Asian Region, Water and Sanitation Program-WSP*, World Bank (2005), pp. 17–80.

Panthi S.R., Sharma S., Mishra A.K. Recent status of arsenic contamination in groundwater of Nepal — a review, *Kathmandu University J Sci Eng Technol* II (1) (2006), pp. 1–11.

Saunders JA, Lee MK, Uddin A, Mohammad S, Wilkin RT, Fayek M, Korte N.E, Natural arsenic contamination of Holocene alluvial aquifers by linked tectonic, weathering, and microbial processes. Geochem Geophys Geosyst 6(2005), pp.1–7.

Singh A.K, Arsenic contamination in the groundwater of North Eastern India. In: Proceedings on national seminar on hydrology, Roorkee, (2004).

Ullah, S.M, Arsenic contamination of groundwater and irrigated soil of Bangladesh, *International Conferences on As Pollution of Groundwater in Bangladesh: Causes Effects and Remedies* Dhaka Community Hospital, Dhaka, Bangladesh, *8–12 February (1998).*

UNESCO (2005), Enmark G and Nordborg D, Arsenic in the groundwater of the Brahmaputra Floodplains, Assam, India- Source, distribution and release mechanisms ,2007.

Zheng, Y., Stute,M., Geen,A. V., Gavrieli, I., Dhar, R., Simpson, H.J., Schlosser, P., and Ahmed,K.M. Redox control of arsenic mobilization in Bangladesh groundwater, *Appl. Geochem. 19 (2004), pp. 201–214.*

Vadose Zone Transport of Nitrate in the Sierra Pelona Groundwater Basin, Agua Dulce, California

Claudia T. Krug[1] and Zbigniew Kabala[2]

[1]Camp, Dresser, and McKee, Inc., 125 South Wacker Drive, Suite 600, Chicago, IL 60606, phone: (312) 346-5000, email: krugct@cdm.com
[2]Department of Civil and Environmental Engineering, Duke University, 121 Hudson Hall, Durham, NC, 27708, phone: (919) 660-5200, email: zbigniew.kabala@duke.edu

ABSTRACT

Using data from previous studies about nitrate contamination in Agua Dulce, CA and the numerical modeling program HYDRUS-1D, nitrate transport in the vadose zone associated with septic system discharges was evaluated. Thirty-six modeling scenarios were assessed and the results analyzed. With soil borings less than 6 m deep, steady state nitrate transport within the system is reached within 200 days, while steady state is not reached with the deeper boring within 500 days. The modeling results show that the nitrate concentration plume is less than the maximum contaminant level (MCL) of 10 mg/L within 1.3 m below the septic leachfield in all scenarios. The analysis of the fully-mixed tank scenario clearly shows that nitrate concentrations in groundwater are of greater concern during drought conditions. These findings help explain the pattern of nitrate concentrations observed in the aquifer system in this region.

I. Introduction

Septic systems service approximately 23 percent of homes in the United States [*EPA*, 2002], primarily in suburban and rural areas. In some areas entire communities are serviced by septic systems, forming areas with high septic system densities. Communities that have septic systems also often use private wells as their drinking water supply source rather than a public water supply. This leads to public concern regarding the drinking water quality, as septic system effluent recharges groundwater, and private wells can potentially extract contaminated water. Older or poorly designed septic systems can surcharge effluent to the ground surface or readily transport contaminants to the groundwater [*Bouma*, 1975], thus increasing the risks of adverse health effects due to elevated contaminant levels.

Nitrogen is one of the contaminants about which there is the most public concern as it can cause accelerated eutrophication in open water bodies [*Beal et al.*, 2005] and can negatively affect human health. Because of these concerns, the United States Environmental Protection Agency (EPA) established the regulatory limit for nitrate in drinking water, known as the maximum contaminant level (MCL), at 10 mg/L (measured as NO_3-N).

Although nitrate occurs naturally in many environments, anthropogenic activity also increases nitrate levels in groundwater. Point and diffuse sources such as agricultural areas, livestock manure, and septic systems are some of the most common anthropogenic sources of nitrate. Factors that influence the effect of septic systems on groundwater include the density of septic systems, lot size, soil type, depth to groundwater, location of drinking water wells, local groundwater recharge, and hydraulic conductivity [*Beal et al.*, 2005; *EPA*, 2002]. Numerical models can be used to evaluate how contaminants such as nitrogen travel through the vadose zone between the septic leachfield and groundwater. The model HYDRUS-1D (Simunek et al. 2005) has been used to model water movement through unsaturated soil [*Pang et al.*, 2006; *Hu et al.*, 2007; *Ndiaye et al.*, 2006; *Pachepsky et al*, 2006] and can be applied to simulate nitrate transport.

Increased levels of nitrate in the Sierra Pelona Groundwater Basin near Agua Dulce, located near Los Angeles, CA were detected in drinking water from private wells since the early 1980s. Through various research investigations into the source of the nitrate contamination, the private domestic septic systems in this rural area faced additional scrutiny. Could the septic systems be the cause of the increased nitrate levels? Additional investigations were undertaken in the mid-1990s, and the need for a public wastewater treatment plant was hotly debated at town meetings.

The proposal to build a wastewater treatment plant and associated sewer system was eventually defeated by the community in 1996 due to concerns over cost and questions about the source of the nitrate. This paper uses site-specific soil data from previous investigations and the HYDRUS-1D computer program to numerically model water and nitrate in the vadose zone, and assesses whether the reasoning behind the community's decision was sound.

II. Site Information

Agua Dulce is a relatively rural area despite its close proximity to Los Angeles. It covers approximately 44.5 km^2 and all homes are served by on-site private septic systems and private drinking water wells. Nitrate levels in groundwater have been a contentious and sensitive topic in Agua Dulce for many years.

Agua Dulce has an arid, Mediterranean climate [*Bailey*, 1966] in the foothills of the San Gabriel Mountains. This area, known as the Sierra Pelona Valley, is underlain by two groundwater source regions. The groundwater in the south-central part of the watershed comes from an alluvial aquifer which is greater than 50 m thick. This is the most densely populated section of the watershed and is shown on Figure 1 between the Mint Canyon fault and the Elkhorn fault. In the higher elevations, there is either no alluvium or the alluvium is above the groundwater table; in these areas groundwater develops in fractures in the underlying crystalline rock. Groundwater is recharged throughout the watershed primarily through rainfall percolation following rainstorms and irrigation [*Williams et al.*, 1998a].

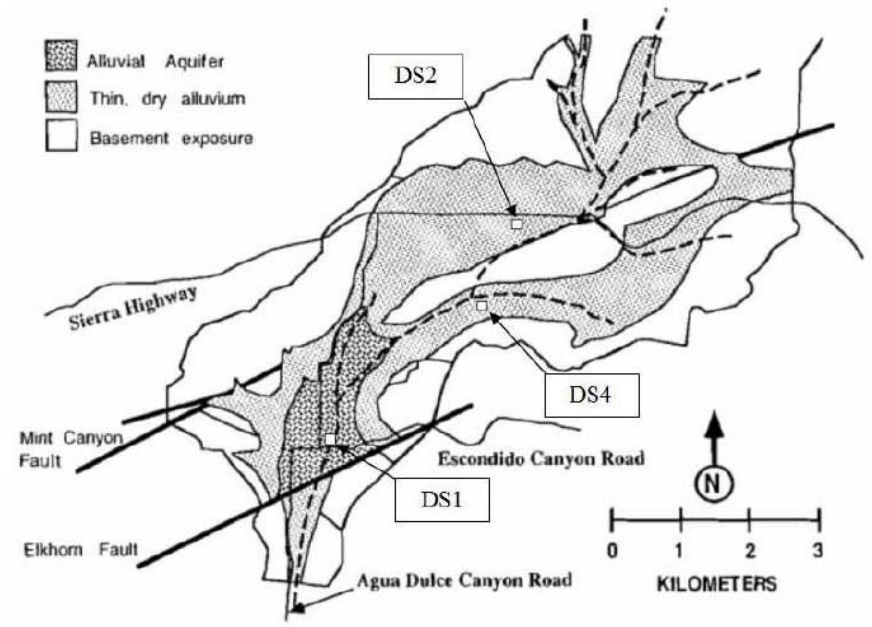

Figure 1: Hydrogeologic map of Agua Dulce with drill site locations

As part of the UCR study, soil borings were advanced at four sites in 1993 and 1994, representing the various land uses in the Sierra Pelona Valley. The groundwater table below Drill Site 1 (DS1) is shallow, and nitrate concentrations are known to be moderate to high, most likely due to anthropogenic influences since the area has been residential for many years. Groundwater at Drill Site 2 (DS2) has high nitrate concentrations. Groundwater beneath this site has been produced from fractured granitic bedrock beneath the thin alluvium of the Agua Dulce Canyon. This area is low density residential. Drill Site 4 (DS4) is located in an area with an alluviual aquifer and a thick vadose zone. The area was previously used for agricultural and animal pens and does not currently have any residential use. Locations of DS1, DS2, and DS4 are shown on Figure 1.

Soil profiles from DS1, DS2, and DS4 were evaluated as part of this research. Several soil borings were advanced at each drill site, and one boring from each drill site was investigated further. Using the soil boring designations from the UCR report, these three borings are labeled #1.4 (from DS1), #2.3 (from DS2), and #4.3 (from DS4).

a. Previous Work

Los Angeles County began evaluating the quantity of nitrates in groundwater in the 1980s. Investigations were done into the source and solution of the nitrate levels by James M. Montgomery Consulting Engineers (1982), the Agua Dulce Ad Hoc Committee (1983), and CH2M Hill (1989). Researchers at the University of California at Riverside (UCR) further investigated the area in the mid-90s [*UCR*, 1996; *Williams et al.*, 1998a; *Williams et al.*, 1998b]. The report by J.M. Montgomery assessed groundwater resources in the Agua Dulce and Mint Canyon drainage basin [*Montgomery*, 1982] and included sampling 17 wells for water quality parameters. The Agua Dulce Ad Hoc Committee [1983] followed up on the Montgomery report

and analyzed water samples from 32 wells. CH2M Hill [1989] investigated the groundwater conditions in the area and determined through its sampling of 84 wells that nitrate levels exceeded the drinking water standards in a significant number of wells, which they concluded to be due to the use of septic systems. Following the release of the CH2M Hill report, the results were questioned by residents as it was believed that the report did not evaluate all potential nitrate sources. Because of these doubts, UCR was asked to evaluate the situation further.

The researchers from UCR set out to evaluate the nitrate conditions and groundwater quality in Agua Dulce, identify and quantify the potential sources of nitrate to groundwater, and propose measures to reduce nitrate concentrations in groundwater. Wells were sampled in three separate events by UCR in 1992-93 for a total of 400 samples in addition to three sampling events conducted in the 1980's. Wells with high concentrations of nitrate were found to be randomly distributed throughout the watershed, but were primarily those which were pumping water from fractured bedrock. Table 1 summarizes sampling dates, number of wells sampled, nitrate concentrations, and percentage of wells above the MCL from the six sampling rounds conducted for this region.

Report	Sampling Date	Number of wells sampled	Range (mg/L)	Mean (mg/L)	% above MCL
Montgomery	1982	17	0.2-43	6.9	24%
Agua Dulce Ad Hoc Comm	1983	32	0.98-12.3	3.8	6%
CH2M Hill	1988	84		5.8	24%
UCR	1992	235	<0.1-37.4	5.6	33%
UCR	Spring 1993	92	<0.1-44.7	9.96	34%
UCR	Fall 1993	73	<0.1-33.0	8.2	26%

Table 1: Groundwater Sampling Results and Percentage of Samples above the Maximum Contaminant Level (MCL)

As part of the UCR study, Williams et al. [1998a] evaluated nitrogen isotopic compositions to determine the sources of nitrogen in the Sierra Pelona Valley groundwater samples. Following sampling and isotope analysis of groundwater, surface rocks, soils, and shallow soil profiles, they ascertained that anthropogenic sources such as human and animal waste contribute greater than half of the nitrate in the groundwater and were the primary source of nitrate in the approximately 40 percent of the drinking water wells that are routinely above regulatory limits.

Williams et al. [1998b] also delineated the spatial and temporal nitrate variations in order to determine contamination sources and patterns. Contamination was revealed to be in three major patterns: (i) high nitrate concentrations in isolated wells, affected by localized NO_3 sources, (ii) high nitrate concentrations in a cluster of wells, and (iii) moderate yet consistent nitrate concentrations documented in a large area of the groundwater region. Most of the isolated wells with the high nitrate concentrations were located in fractured basement-rock aquifer regions. Clusters of contaminated

wells occurred mostly in the north-central region of the watershed and contamination is most likely due to stormwater runoff flowing over natural soil and rock containing nitrate. The regional contamination occurred in the south-central section of the watershed in the vicinity of the alluvial aquifer region, as depicted on Figure 1. The majority of the nitrate concentrations in this region were between 5-10 mg/L, and no concentrations were below 2 mg/L. Williams et al. [1998b] determined through pattern analysis that septic waste was more likely to be the cause than animal wastes in this region. These results aligned with the results from Williams et al. [1998a] and presented a unified picture of the nitrate contamination in Agua Dulce.

Williams et al. [1998b] were able to see the effect of rainfall on nitrate concentrations. The large amounts of precipitation in the winter of 1992-93 caused the nitrate to quickly be transported to the groundwater and diluted. The sudden contaminant transport was speculated to have several causes: direct recharge through fractures in the bedrock, direct recharge through faulty septic systems and/or wells, and/or recharge to the aquifer which raises the groundwater level and dissolves nitrates in the capillary and vadose regions above the dry climate water table.

b. Objectives

Previous studies evaluating nitrate contamination in the Sierra Pelona Watershed have determined that domestic septic systems are one of the primary causes of the contamination and help explain its spatial variations. However, numerical modeling of the nitrates and groundwater in the vadose zone between the septic systems to the groundwater has not been completed so the previous conclusions could be considered somewhat inferential. Using site-specific soil data from the previous investigations and the HYDRUS-1D computer program to numerically model water and nitrates in the vadose zone, this research assesses whether or not nitrate-impacted leachate from septic systems reach groundwater and what the likely concentrations would be. This study focuses on the area of Agua Dulce where the vadose zone exists and will not address areas of Agua Dulce where there is fractured rock.

III. Methodology

Water flow and contaminant transport through porous media is a three-dimensional process. However, the modeling efforts for this study were limited to a 1-dimensional representation of transport vertically through the vadose zone given the limited data that was available, the access of computing capabilities, and the knowledge that horizontal flow in the vadose zone is generally less pronounced than vertical flow.

The HYDRUS-1D Software Package was used to simulate water and nitrate movement in one dimension through unsaturated soil given model parameters and boundary conditions [*Simunek et al.*, 2005]. HYDRUS-1D is based on the computer code for HYDRUS, which numerically solves Richards Equation for saturated-unsaturated water flow and numerically approximates the convection-dispersion equation for solute transport using standard Galerkin-type linear finite element schemes. A mass balance equation is also included where the mass of nitrogen going

in from the precipitation and septic system equals the mass of nitrogen exiting the system.

Model simulations were conducted for the three soil profiles described previously. Model inputs were estimated from previous reports and soil investigations as well as from values reported in the literature. The upper boundary conditions for Richards Equation were set as constant flux equal to the regional precipitation rate for a given scenario and estimates of average domestic septic flow rates. The lower boundary condition for water flow was set as a constant pressure head of zero, representative of fully saturated conditions, since the groundwater table was considered to be at the bottom of each soil profile. The upper boundary conditions for the solute concentration were set as constant flux.

Initial conditions for the pressure head were prescribed as linearly distributed along the soil profile. Two pressure head scenarios were run: one representing a dry surface and one representing hydrostatic equilibrium (set as the negative value of the depth of the soil boring). The initial solute concentration throughout the system was set to zero to represent nitrate-free groundwater and a soil system with no existing nitrate impacts.

Three different precipitation cases were considered to represent the range of possible leaching rates and dilution effects: the median precipitation, the driest year on record, and the wettest year on record [*UCR*, 1996]. To account for the fact that the simulations were run in only one dimension, additional simulations were run using a larger surface area for the septic system leachfield. A larger leachfield area was used to simulate that septic loading was uniformly distributed through the area it would reach to the groundwater depth. The smallest leachfield surface area is the most conservative (upper bound) estimate, and the surface areas ranged from 92 m^2 to 507 m^2. Simulations were run for 500 days in order to aim for a steady-state condition.

Analysis of a fully-mixed tank model was used to determine the cumulative effect of septic effluent on the groundwater in the alluvial aquifer region of Agua Dulce. This was done using a mass balance approach which accounts for the background nitrate concentration and the groundwater flow rate flowing into Agua Dulce aquifer, the concentration and flow rate of the precipitation, the septic effluent nitrate concentration and the septic flow rate, and the nitrate concentration and groundwater flow rate leaving Agua Dulce.

IV. Results and Discussion

a. Septic system nitrate transport modeling

Thirty-six different scenarios were modeled using HYDRUS-1D, twelve for each of three drill sites evaluated (at soil borings #1.4, #2.3, and #4.3). Parameter input values for each soil boring and soil layer are shown in Table 2. The UCR report provided the necessary soil parameters, including θ_s, the saturated water content, and K, the unsaturated hydraulic conductivity. Septic effluent flow was taken to be 1.136 m^3/day in all scenarios.

Drill Hole	Layer	Depth (m)	θ_s	K (m/d)
#1.4	Layer I	surface to 1.2 m	0.52	0.191
	Layer II	1.2 m to 3.2 m	0.36	0.263
	Layer III	3.2 m to 4.8 m	0.46	0.172
	groundwater at 4.8 m below grade			
#2.3	Layer I	surface to 0.6 m	0.36	2.263
	Layer II	0.6 m to 1.8 m	0.34	0.335
	Layer III	1.8 m to 3.9 m	0.34	2.494
	Layer IV	3.9 m to 5.4 m	0.31	0.36
	unsaturated region below 5.4 m: fractured crystalline basement			
#4.3	Layer I	surface to 1.5 m	0.34	0.429
	Layer II	1.5 m to 2.7 m	0.34	3.48
	Layer III	2.7 m to 17.2 m	0.3	0.065
	no groundwater reached to 17.2 m below grade			

Table 2: HYDRUS-1D parameter input values for each soil boring and soil layer

For each drill site, three precipitation scenarios were run: low, average, and high precipitation. For each precipitation scenario, two pressure head scenarios were run: one representing a dry surface and one representing hydrostatic equilibrium. In addition, for each pressure head scenario, two effective leachfield area scenarios were run: the actual leachfield area and an adjusted leachfield area.

The modeling results indicate that the simulated nitrate concentration plume would reach groundwater (defined as the nitrate concentration at the bottom of the soil profile greater than zero) within 100 days at soil borings #1.4 and #2.3 when groundwater is at 3.8 m below the leachfield and 4.4 m below the leachfield, respectively, primarily due to the shallow depth of the soil borings. Steady state was not reached within 500 days for soil boring #4.3, with a depth of 17.2 m.

Results showed that soil borings representative of a historically residential site in the alluvial aquifer (boring #1.4) and in an area with historically high natural nitrate underlain by thin, dry alluvium (boring #2.3) have higher nitrate concentration levels entering groundwater than simulations representative of primarily agricultural area also underlain by thin, dry alluvium (boring #4.3). Since nitrate concentration plumes were evaluated for only three soil borings, conclusions about the site usage versus nitrate concentration were unable to be drawn. It was clear that as precipitation amounts increase, the nitrate is diluted and concentrations at groundwater are lower. Larger leachfield areas were shown to yield lower nitrate concentrations since the initial nitrate concentration is dispersed over a larger area. Model runs showed that the effect of the pressure head on nitrate concentrations reaching groundwater was minimal.

Based on average values for nitrate concentration in septic effluent as given by the EPA (2002), along with our model results, we can deduce that the nitrate

concentration plume is below the MCL within 1.3 m below the leachfield. This is useful information for regulators looking to establish an offset distance between groundwater and the bottom of the leachfield.

b. Fully-Mixed Tank Model

The lowest bound on the sampling range from the UCR data sampling was used for the background nitrate concentration and the average number of septic systems located in the alluvial aquifer region of Agua Dulce was estimated. Using the EPA estimates for gallons discharged per day per septic system, and the average nitrate concentration for the effluent, a fully mixed-tank model was used to calculate the nitrate concentration leaving the populated area of Agua Dulce. Soil input parameters were based on UCR data, and the regional minimum, maximum, and average precipitation amounts were used. Based on these assumptions and methods, the nitrate concentrations leaving Agua Dulce range from 0.50 mg/L to 11.6 mg/L.

The worst case scenario with the highest concentrations under these conditions is given the very low value of hydraulic conductivity that occurs due to low soil moisture conditions in times of drought. This condition replicates nitrate concentrations around 5 mg/L, half of the MCL. Since the hydraulic conductivity values are based on soil borings in the vadose zone only, these results are estimates only until more testing is undertaken to determine more specific values throughout the depth of the entire alluvial aquifer. However, these results indicate that nitrate concentrations of water percolating into groundwater (and therefore drinking water) are of greater concern during drought conditions.

Despite the heavy rains in the winter of 1992, nitrate concentrations varied only slightly [*Williams et al.*, 1996b]. In order to investigate this finding an additional series of model simulations were undertaken. The hydraulic conductivity value from the bottom of soil boring #1.4 along with estimates of the hydraulic gradient and a range of precipitation values were used. The findings of these simulations suggest that when the annual precipitation is between 11 and 24 cm/yr (median rainfall is 21 cm/yr), the nitrate concentration leaving the region is between 5 and 10 mg/L. When there is less than 11 cm of annual precipitation, the nitrate concentration leaving the region is greater than 10 mg/L.

V. Conclusions

Using data from previous soil borings collected in Agua Dulce, CA and the numerical modeling program HYDRUS-1D, nitrate transport through the vadose zone was evaluated. Thirty-six modeling scenarios were assessed and the results analyzed. The following are the results of the modeling efforts:

- With shallower soil borings (less than 6 m below grade), steady state nitrate transport within the system is reached within 200 days, while steady state is not reached with the deeper boring (approximately 17 m below grade) within 500 days. However, the steady state for this boring is expected to be reached within approximately 1000 days. By examining steady state solutions, we can determine how the system will behave in the future.

- The modeling results show that the nitrate concentration plume is less than the maximum contaminant level (MCL) of 10 mg/L within 1.3 m below the septic leachfield in all scenarios.
- The analysis of the fully-mixed tank model shows that nitrate concentrations in groundwater are of greater concern during drought conditions. Care should be taken when the precipitation is less than 17 cm/yr. Under these circumstances, nitrate concentrations leaving the Agua Dulce region are high enough that residents should consider using bottled water as their drinking water source, although nitrate-rich water is acceptable for showering and laundry uses.

Based on these results, the decision to keep the town on septic systems and not build a wastewater treatment plant and associated sewer system seems to have been a sound decision. Although the septic systems in town are contributing to the groundwater contamination beneath Agua Dulce it is only under extreme drought conditions that the septic system leachate would cause the high concentrations observed in the groundwater sampling events in the early 1990s. This shows that natural nitrate sources also contribute quite a bit to the groundwater, which is likely what is putting the groundwater nitrate concentrations in this region over the MCL.

In order to limit the amount of nitrate transported to groundwater from septic systems, it is recommended that all septic systems in the Sierra Pelona Valley be inspected regularly (for example, when homes change owners), and replaced when they are no longer optimally performing. Particularly important in the Agua Dulce area is septic system density. By increasing the number of septic systems, the nitrogen loading of the groundwater will increase. No increase in settlement density should be allowed.

BIBLIOGRAPHY

Agua Dulce Ad Hoc Committee (1983), A study of water quality, quantity and usage, Report to Agua Dulce Town Council, Agua Dulce, California.

Bailey, H.P. (1966), *The climate of southern California*, University of California Press, Berkeley, California.

Beal, C.D., E.A. Gardner, and N.W. Menzies (2005), Process, performance, and pollution potential: A review of septic tank-soil absorption systems, *Australian Journal of Soil Research*, 43, 781-802.

Bouma, J. (1975), Unsaturated Flow During Soil Treatment of Septic Tank Effluent, *Journal of Environmental Engineering*, 101, 742-981.

CH2M Hill (1988), Phase II: States I, II, III, Agua Dulce Hydrogeologic Investigation, Final reports to County of Los Angeles, Department of Public Works.

EPA (2002), On-Site Wastewater Treatment Systems Manual, Washington, DC.

Hu, K., R. White, D. Chen, B. Li, W. Li (2007), Stochastic simulation of water drainage at the field scale and its application to irrigation management, *Agricultural Water Management,* 89, 123-130.

Montgomery, J.M. (Consulting Engineers Inc.) (1982), Phase I Agua Dulce/Mint Canyon Hydrogeologic Investigation, Report to County of Los Angeles, Board of Supervisors.

Ndiaye, B., J. Molenat, V. Hallaire, C. Gascuel, Y. Hamon (2007), Effects of agricultural practices on hydraulic properties and water movement in soils in Brittany (France), Soil & Tillage Research, 93, 251-263.

Pachepsky, Y., A. Guber, D. Jacques, J. Simunek, M.T. Van Genuchten, T. Nicholson, R. Cady (2006), Information content and complexity of simulated soil water fluxes, Geoderma, 134, 253-266.

Pang, L., C. Nokes, J. Simunek, H. Kikkert, and R. Hector (2006), Modeling the Impact of Clustered Septic Tank Systems on Groundwater Quality, *Vadose Zone Journal*, 5, 599-609.

Simunek, J., M. T. van Genuchten, and M. Sejna (2005), The HYDRUS-1D Software Package for Simulating the One-Dimensional Movement of Water, Heat, and Multiple Solutes in Variably-Saturated Media. Version 3.0. Department of Environmental Sciences, University of California Riverside, Riverside, California.

University of California Riverside (1996), A.E. Williams, L.J. Lund, and Z. Kabala, Investigation of Nitrate Contamination in the Sierra Pelona Groundwater Basin Agua Dulce, Final Report.

Vanguard News (1996-1997), www.vanguardnews.com.

Vanguard News (1996), http://www.vanguardnews.com/adtc/Water/adtcwr.htm. Viewed 28 Nov 2007.

Williams, A.E., L.J. Lund, J.A. Johnson, and Z.J. Kabala (1998a), Natural and Anthropogenic Nitrate Contamination of Groundwater in a Rural Community, California, *Environmental Science and Technology*, 21(1), 32-39.

Williams, A.E., J.A. Johnson, L.J. Lund, and Z.J. Kabala (1998b), Spatial and Temporal Variations in Nitrate Contamination of a Rural Aquifer, California, *J. Environmental Quality*, 27, 1147-1157.

Exploring the potential of nonlinear and non-equilibrium alcohol partitioning for assessment of DNAPL source zone architecture

Rhiannon E. Ervin and C. Andrew Ramsburg

Department of Civil and Environmental Engineering, Tufts University, 200 College Ave., Room 113 Anderson Hall, Medford, MA 02155; PH (617) 627-3211; FAX (617) 627-3994; email: andrew.ramsburg@tufts.edu

Abstract

Recent research highlights the importance of quantifying the relationship between dense nonaqueous phase liquid (DNAPL) spatial distribution, source strength and source longevity. Since acquiring knowledge of the precise distribution of DNAPL saturations (also known as the DNAPL architecture) may be impracticable (technically or economically), attention is being placed on understanding the key features of the DNAPL architecture that control contaminant mass discharge. Examples of metrics describing DNAPL architecture include reactive travel times, spatial moments of the DNAPL mass, and ratios of DNAPL mass present in ganglia to that present in pools. While other metrics may yet be advanced, the utility of any source zone architecture metric as a site management tool requires that the metric be readily quantifiable. Partitioning tracers are one tool that may permit interrogation of DNAPL architecture. Traditional use of partitioning interwell tracer tests, however, provides an estimate of DNAPL saturation that is integrated over the flow path of the tracer. While helpful in estimating overall saturations or total mass of DNAPL, few interwell tracer tests are designed to provide the spatial resolution required to assess DNAPL architecture. Here we explore the use of partitioning tracers under the conditions of nonlinear and non-equilibrium transport, with the longer-term goal of estimating DNAPL architecture in localized portions of a source zone. Initial efforts were directed toward elucidating liquid-liquid equilibria of 2-octanol, a common partitioning alcohol, in a system comprising water and TCE-NAPL. Results illustrate the importance of assessing tracer partitioning over a wide range of concentrations. Column experiments were conducted in a sandy medium to explore limitations to tracer transport with both the aqueous phase and a uniformly entrapped nonaqueous phase. These preliminary results suggest nonlinear and non-equilibrium partitioning may be exploited to assess DNAPL source zone architecture.

Introduction

In 1993, the EPA concluded that approximately 60% of all National Priority List sites have high likelihood of dense nonaqueous phase liquid (DNAPL) contamination (U.S. EPA, 1993). In the intervening years, relatively few of these source zones, the region containing DNAPL as well as sorbed phase, have reached site closure (National Research Council, 2005). Low water solubilities give chlorinated solvents the potential to remain in the subsurface for decades, resulting in prolonged groundwater contamination. However, aqueous solubilities of chlorinated solvents are orders of magnitude higher than aqueous concentrations known to be harmful to human health (Pankow and Cherry, 1996). Consequently, the dissolved

phase plumes emanating from DNAPL source zones pose risks to human and environmental health.

Upon release, dense organic liquids migrate downward through the subsurface. During this process, DNAPL is entrapped by capillary forces in pores and pools in regions of permeability contrast (Pankow and Cherry, 1996). The term "architecture" is often used to describe the spatial distribution of DNAPL within a source zone. The technical and economic impracticability of determining the exact DNAPL architecture has focused efforts on developing metrics that link DNAPL architecture and contaminant discharge (Christ et al., 2006; Fure et al., 2006; Stroo et al., 2003). Examples of metrics describing DNAPL architecture include reactive travel times (e.g., Jawitz et al., 2005), spatial moments of the DNAPL mass (e.g., Moreno-Barbero and Illangasekare, 2005), and ganglia to pool (GTP) mass ratio (e.g., Christ et al., 2006). Recognition that no treatment can provide complete contaminant removal necessitates an ability to quantify the benefits of partial mass removal (Stroo et al., 2003; Abriola, 2005; Christ et al., 2006). A number studies indicate that reductions in source zone mass may lead to lower downgradient, dissolved-phase concentrations and shorter source longevity (Soga et al., 2004; Christ et al., 2005; Jawitz et al., 2005; Suchomel and Pennell, 2006; Brooks et al., 2008; Kaye et al., 2008). Yet for aggressive source zone treatments to be effective, some knowledge of the amount and distribution of the DNAPL in the source zone is necessary (Christ et al., 2005). Based upon these reports, model upscaling is now incorporating DNAPL architecture metrics (Falta et al., 2005; Moreno-Barbero and Illangasekare, 2005; Park and Parker, 2005; Christ et al., 2006) illustrating the need for these (or other forthcoming metrics) to be reliably quantified.

It is well established that partitioning tracers can be employed to characterize DNAPL source zones (Jin et al., 1995; Annable et al., 1998; Brooks et al., 2002; Meinardus et al., 2002). Use of these tracers involves passing a pulse of partitioning and non-partitioning tracers through a source zone. Analysis of the resulting breakthrough curves permits estimation of an overall DNAPL saturation – one that is averaged along the tracer flow path. Partitioning tracer tests can be conducted using any number of hydraulic designs (Brooks et al., 2002), though assessment of DNAPL architecture requires high resolution (temporal and spatial) sampling. An alternative approach is to obtain estimates of average DNAPL saturation though the use of push-pull tests (Istok et al., 2002). Push-pull tests involve pumping tracers into the subsurface during the "push" phase, and then reversing the flow ("pull" phase) to recover the tracers from the same well.

Objectives

Analysis of partitioning tracer tests commonly assumes linear, equilibrium partitioning. Many partitioning tracers, however, have been observed to exhibit nonlinear or non-equilibrium partitioning (e.g., Wise et al., 1999; Wilson et al., 2000; Moreno-Barbero and Illangasekare, 2006). It is hypothesized that push-pull tests may be designed to quantify local DNAPL architecture metrics such as GTP by exploiting non-idealities in tracer partitioning. Testing this hypothesis requires a thorough understanding of tracer partitioning under both equilibrium and non-equilibrium conditions. Therefore, the specific objective of this work is to evaluate the liquid-

liquid equilibrium (LLE) and non-equilibrium transport of 2-octanol (a representative partitioning tracer).

Materials and Methods

Materials. ACS grade tricholoethene (density-1.46 g/mL, aqueous solubility-1100 mg/L), obtained from Sigma Aldrich, was used as the representative NAPL throughout all experiments. When used in column experiments, the TCE was dyed with 10^{-4} M Oil-Red-O (Alfa Aesar) for visualization purposes. Previous work has shown that the addition of Oil-Red-O at this concentration does not significantly affect the relevant physical properties of the NAPL (Taylor et al., 2001). 2-octanol (density-0.82 g/mL, aqueous solubility-1120 mg/L) was obtained from Arcos Organics (97% purity) and used as the partitioning tracer. HPLC grade isopropanol was received from Sigma Aldrich and used for sample dilution. All aqueous phase solutions were made using water obtained from a Millipore A-10 filtration system (resistivity > 18.1 MΩ*cm). Columns were packed with a 45-50 fraction obtained by sieving Ottawa Federal Fine sand (US Silica). All non-partitioning tracer tests were conducted with 0.01 M solutions of ACS grade sodium bromide and sodium chloride (Fischer Chemical).

Batch Methods. Previous studies have employed one or two points to measure partition coefficients for tracers, but evidence suggests some tracers exhibit nonlinear partitioning (Wise et al., 1999). Thus, LLE batch experiments were conducted over a wide concentration range to more accurately quantify the partition coefficient of 2-octanol in the TCE-water-2-octanol ternary system. Various compositions of 2-octanol, water and TCE were added to 35 mL borosilicate glass centrifuge tubes. Each selected composition was created in tripilicate. Centrifuge tubes were then placed on oscillating shakers (LabQuake) located within a controlled temperature room (Harris Environmental), and allowed to mix for 72 hr at 22.0±0.1°C. Previous experiments suggest 72 hr is sufficient for these systems to reach equilibrium. After equilibration, the tubes were centrifuged at 1500 rpm and 22 °C for 10 min (Beckman Coulter Avanti J-25). After centrifugation, the aqueous and organic phases were carefully separated using disposable glass pipettes. Samples of each phase were subsequently prepared for compositional analysis and density measurements (see analytical methods).

Column Methods. Mass exchange kinetics for the 2-octanol tracer and residual TCE system were studied using 1-D column experiments. The 45-50 sieve fraction of Federal Fine Ottawa sand was dry packed in a Chromaflex glass column having a diameter of 4.8 cm. Upon saturation of the porous medium with the aqueous phase, a non-reactive tracer test was conducted using 0.01 M Br^-. Following the completion of the first tracer test, the aqueous phase was displaced by TCE-NAPL. After obtaining a maximum TCE-NAPL saturation (as evidenced by the absence of water in the column effluent), a residual entrapped saturation of TCE-NAPL was obtained by displacing the mobile NAPL with water. After establishing a residual NAPL saturation, 0.01 M Br^- was used to conduct a second tracer test. Following the preparation of the column, an aqueous solution containing the desired concentration

of 2-octanol was introduced to the column at a flow rate of 2.2 mL/min for approximately 10 pore volumes. The flow rate and packed length were selected to promote non-equilibrium conditions so that partitioning kinetics could be quantified. After the pulse of 2-octanol solution, the column influent was switched to Milli-Q water. Effluent samples were collected throughout the duration of the experiment using an automated fraction collector. Fractions were subsequently sampled and analyzed following the methods described below.

Analytical Methods. Aqueous phase samples collected for 2-octanol and TCE analysis were diluted (~20x) using Milli-Q water and isopropanol (IPA), respectively. NAPL samples collected for 2-octanol and TCE analyses were diluted (~10x) using IPA. NAPL samples collected for water content analysis were not diluted. Concentrations of 2-octanol and TCE in both the aqueous and NAPL phases were quantified using a Hewlet Packard 6890 Gas Chromatograph (GC) equipped with a DB-5 column and flame ionization detector. A five-point calibration curve was obtained on each day of use and checked using a calibration standard every 20 samples. Sample dilutions were prepared in triplicate, with each diluted sample quantified using duplicate injections. Effluent samples from the column experiment were also quantified using duplicate injections. The water content in each NAPL sample was quantified in triplicate using a Mettler Toledo DL38 Karl Fischer Titrator. Prior to each day of use the titrator was calibrated with an AquaStar 1% water standard. Calibration was checked with the water standard at least every ten samples. Density of the NAPL phase was measured in triplicate with a 2.5 mL glass pycnometer that was calibrated with water prior to each use. Effluent samples from the tracer tests were quantified for chloride and bromide concentration using a Dionex ICS-2000 Ion Chromatograph (IC) equipped with an AS-11 column. The instrument was calibrated with a six-point standard curve every fifteen samples.

Results & Discussion

While 2-octanol partitioning data are available from previous studies, most of these data lie within a narrow concentration range at the lower end of possible aqueous phase concentrations (Dwarakanath and Pope, 1998; Young et al., 1999; Brooks et al., 2002; Ramsburg et al., 2005; Thal et al., 2007). In many instances, 2-octanol partitioning data were used to generate partition coefficients at a particular aqueous phase concentration. The resulting partition coefficients are then often assumed to be constant over a wide range of aqueous phase concentrations. Many alcohols, however, exhibit nonlinear partitioning due to their ability to hydrogen bond in both phases (e.g., Wise et al., 1999). Analysis of batch data confirms that 2-octanol exhibits nonlinear partitioning in two-liquid system comprising water, TCE and 2-octanol. For aqueous phase concentrations below 300 mg/L, the partitioning of 2-octanol may be approximated as linear and thus described with a partition coefficient of 338 L_{aq}/L_{NAPL}. Note that this value is between the previously reported values (for the TCE, water, 2-octanol system) of 226 and 389 (Dwarakanath and Pope, 1998; Thal et al., 2007). Above an aqueous phase concentration of 300 mg/L the partition coefficient of 2-octanol increases six-fold, demonstrating the nonlinearity of the partitioning. This increase in 2-octanol affinity for the organic

phase above aqueous concentrations of 300 mg/L indicates that a single valued partition coefficient cannot be employed to accurately describe all possible aqueous phase concentrations of 2-octanol. To accurately describe the 2-octanol distribution in this ternary system, more sophisticated techniques (e.g., UNIQUAC modeling) are required.

LLE data were used to design two column experiments in which the kinetics of tracer mass transfer were examined. To explore the effect of the varying partitioning coefficient, experiments were conducted at two different 2-octanol concentrations. The influent concentrations of 2-octanol for Column 1 and Column 2 were 370 mg/L and 657 mg/L, respectively. Column parameters for each experiment are shown in Table 1.

Table 1. Column Parameters

Column	Influent 2-octanol Concentration (mg/L)	Pore Volume (mL)	Length (cm)	Porosity	TCE-NAPL Saturation
1	370	27	3.6	0.40	20.0%
2	657	28	3.7	0.41	18.5%

The two distinct BTCs resulting from these column experiments are shown in Figure 1. Both BTCs exhibit characteristics of nonequilibrium behavior - a rapid increase in concentration over the duration of the influent pulse, and a long tail thereafter. Visual assessment of the BTCs is made difficult by the competing influences of influent concentration and NAPL saturation. NAPL saturations are difficult to replicate due to the hysteretic nature of the capillary pressure-saturation relationships governing the entrapment process.

To explore the mass transfer kinetics in more detail, a dual diffusion model was employed. The model was based on that developed by Rasmuson and Neretnieks (1980), with minor modifications for use in NAPL-water systems (Adams et al., 2007). The dual diffusion model was coupled with an aqueous phase mass transfer coefficient estimated using data from Powers et al. (1992). Model predictions employing independently determined column parameters failed to capture the shape and maximum C/C_0 value of the BTCs (Figure 1). Consequently, the model was visually fit to the data by adjusting NAPL saturation. The best visual fit, as seen in Figure 1, required NAPL saturations of 2.0% and 1.4% for Columns 1 and 2, respectively. While these model fits capture the general shapes of the BTCs, the fitted saturations are not consistent with experimental observations of NAPL saturation. One possibility for this discrepancy in saturation may relate to of the presence of a surface resistance to 2-octanol partitioning, which was not present within the model. Current efforts are focused on exploring this possibility.

Results from equilibrium batch experiments demonstrate that the partitioning of 2-octanol between TCE and water may be approximated as linear at low aqueous concentrations (<300 mg/L), though the linear assumption fails to describe partitioning data over the larger range of aqueous concentrations. Observations of a linear range in the partitioning of 2-octanol indicate that traditional partitioning tracer tests can be designed to avoid influence of the nonlinearity in the partition coefficient.

In addition, the multistep nature of the equilibrium partitioning data offers potential for novel chemical perturbations that may enhance DNAPL source zone characterization. The long term objective of this research is to determine whether a partitioning tracer approach can be developed to distinguish high and low saturation regions through exploitation of nonlinear and non-equilibrium partitioning. Results from our initial column experiments demonstrate the effects of the nonlinear partitioning and suggest the need for revised descriptions of mass exchange in systems comprising TCE-NAPL for 2-octanol, and water. Current efforts are focused on resolving the 2-octanol partitioning kinetics, characterizing additional tracers, and exploring tracer response from non-uniform NAPL saturations.

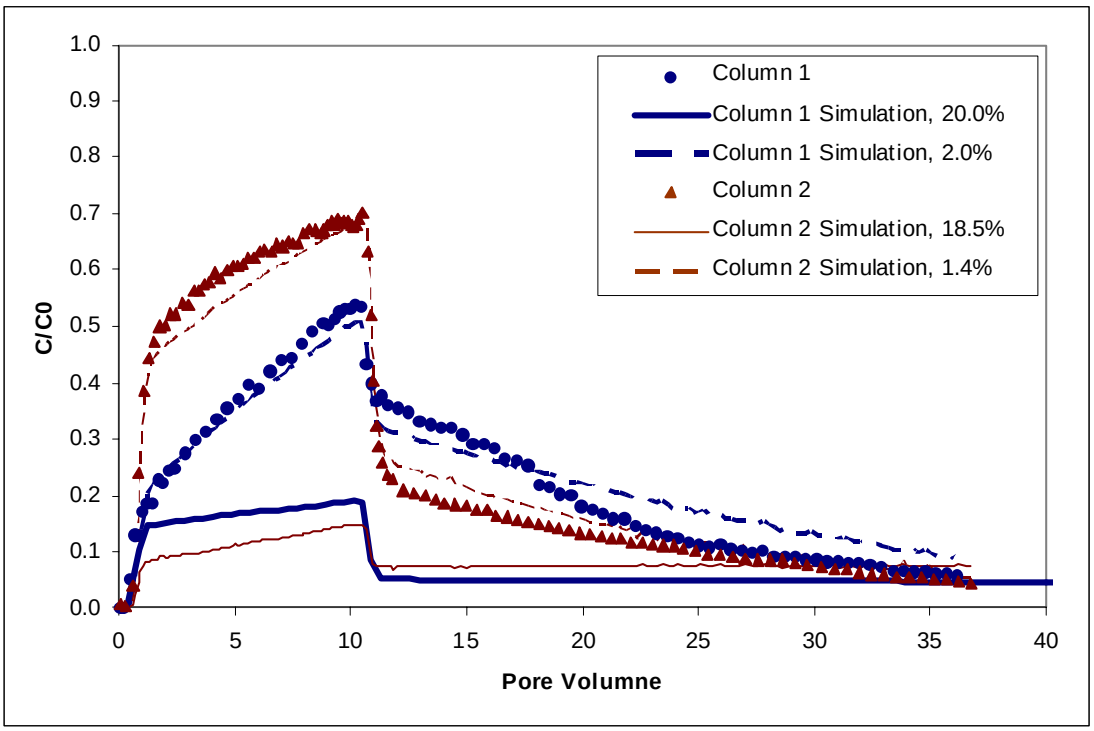

Figure 1. Breakthrough curves (symbols) and model predictions (solid lines) for the laboratory-determined saturations of 20.0% and 18.5% for Columns 1 and 2, respectively. Also shown are visual best fit simulations (dashed lines) at 2.0% saturation (Column 1) and 1.4% (Column 2).

Acknowledgements

The authors gratefully acknowledge Dr. John Christ (U.S. Air Force Academy) and Mr. Ali Boroumand (Tufts University) for supplying the model used herein. Funding for this research was received from the Strategic Environmental Research & Development Program under Project ER-1612. The content of this paper does not necessarily represent the views of the agency and has not been subject to agency review.

References

Abriola, L.M. 2005. Contaminant source zones: remediation or perpetual stewardship? *Environmental Health Perspectives,* 113(7):438-439.

Adams, J., S.R. Douglas, C.A. Ramsburg, and J.A. Christ. Modeling cis-Dichloroethene Partitioning in Tetrachloroethene-NAPL using Intra-Aggregate Diffusion Sorption Models. *American Geophysical Union Fall Meeting*, December 2007, paper number H23D-1618, San Francisco, CA. 10-14.

Annable, M.D., P.S.C. Rao, K. Hatfield, W.D Graham, and C.G. Enfield. 1998a. Partitioning tracers for measuring residual NAPL: Field-scale test results. *Journal of Environmental Engineering*, June, 498-503.

Brooks, M.C., M.D. Annable, P.S.C. Rao, K. Hatfield, J.W. Jawitz, W.R. Wise, A. L. Wood, C. G. Enfield. 2002. Controlled release, blind tests of DNAPL characterization using partitioning tracers. *Journal of Contaminant Hydrology*, 59: 187-210.

Brooks, M.C., A.L. Wood, M.D. Annable, K. Hatfield, J. Cho, C. Holbert, P.S.C. Rao, C.G. Enfield, K. Lynch, and R.E. Smith. 2008. Changes in contaminant mass discharge from DNAPL source mass depletion: Evaluation at two field sites. *Journal of Contaminant Hydrology*, 102:140-153.

Christ, J.A., C.A. Ramsburg, K.D. Pennell, and L.M. Abriola. 2006. Estimating mass discharge from DNAPL source zones using upscaled mass transfer coefficients: An evaluation using multiphase numerical simulations. *Water Resources Research*, 42, W11420, doi:10.1029/2006WR004886

Christ, J.A., C.A. Ramsburg, L.M. Abriola, K.D. Pennell and F.E. Löffler. 2005. Coupling aggressive mass removal with microbial reductive dechlorination for remediation of DNAPL source zones: A review and assessment. *Environmental Health Perspectives*, 113(4): 465-477.

Dwarakanath V. and G.A. Pope. 1998. New approach for estimating alcohol partition coefficients between nonaqueous phase liquids and water, *Environmental Science and Technology,* 32:1662–1666.

Falta, R.W., P.S. Roa and N. Basu. 2005. Assessing the impacts of partial mass depletion in DNAPL source zones I. Analytical modeling of source strength functions and plume response. *Journal of Contaminant Hydrology,* 81:125-147.

Fure, A.D, J.W. Jawitz, and M.D. Annable. 2006. DNAPL source depletion: Linking architecture and flux response. *Journal of Contaminant Hydrology,* 85:118-140.

Istok, J.D., J.A. Field, M.H. Schroth, B.M. Davis, and V. Dwarakanath. 2002. Single-well "push-pull" partitioning tracer test for NAPL detection in the subsurface. *Environmental Science and Technology*, 36(12): 2708-2716.

Jawitz, J. W., A. D. Fure, G. G. Demmy, S. Berglund, and P. S. C. Rao. 2005. Groundwater contaminant flux reduction resulting from nonaqueous phase liquid mass reduction. *Water Resources Research,* 41, W10408, doi:10.1029/2004WR003825.

Jin, M., M. Delshad, V. Dwarakanath, D.C. McKinney, G.A. Pope, K. Sepehrnoori, C.E. Tilburg, and R.E. Jackson. 1995. Partitioning tracer test for detection, estimation and remediation performance assessment of subsurface nonaqueous phase liquids. *Water Resources Research,* 31(5): 1201-1211.

Kaye, A.J., J. Cho, N.B. Basu, X. Chen, M.D. Annable, and J.W. Jawitz. Laboratory investigation of flux reduction from dense non-aqueous phase liquids (DNAPL) partial source zone remediation by enhanced dissolution. 2008. *Journal of Contaminant Hydrology,* 102:17-28.

Meinardus, H.W., Dwarakanath, V., Ewing, J., Hirasaki, G.J., Jackson, R.E., Jin, M., Ginn, J.S., Londergan, J.T., Miller, C.A., and G.A. Pope. 2002. Performance assessment of NAPL remediation in heterogeneous alluvium, *Journal of Contaminant Hydrology*, 54:173-193.

Moreno-Barbero, E. and T.H. Illangasekare. 2005. Simulation and performance assessment of partitioning tracer tests in heterogenous aquifers. *Environmental Engineering and Geoscience*, XI(4):395-404.

Moreno-Barbero, E. and T.H. Illangasekare. 2006. Influence of dense nonaqueous phase liquid pool morphology on the performance of partitioning tracer tests: Evaluation of the equilibrium assumption. *Water Resources Research,* 42(4): Art. No. W04408

National Research Council. 2005. *Contaminants in the Subsurface: Source Zone Assessment and Remediation*. Washington, D.C: National Academic Press

Pankow, J.F. and J.A. Cherry. 1996. *Dense Chlorinated Solvents and Other DNAPLs in Groundwater*. Portland: Waterloo Press

Park, E. and J.C. Parker. 2005. Evaluation of an upscaled model for DNAPL dissolution kinetics in heterogeneous aquifers. *Advances in Water Resources*, 28: 1280-1291.

Powers, S.E, L.M. Abriola and W.J. Webber Jr. 1992. An experimental investigation of nonaqueous phase liquid dissolution in saturated subsurface systems: steady state mass transfer rates. *Water Resources Reseach*, 28(10):2691-2705.

Ramsburg, C.A., K.D. Pennell, L.M. Abriola, G. Daniels, C.D. Drummond, M. Gamache, H-L Hsu, E.A. Petrovskis, K.M. Rathfelder, J.L. Ryder, and T. P. Yavaraski. 2005. Pilot-scale demonstration of surfactant-enhanced PCE solubilization at the Bachman Road site. 2. System operation and evaluation. *Environmental Science and Technology*, 39: 1791-1801.

Rasmuson, A. and I. Neretnieks. 1980. Exact solution of a model for diffusion in particles and longitudinal dispersion in packed beds. *AIChE Journal,* 26(4):686-690.

Soga, K., J.W.E. Page, and T.H. Illangasekare. 2004. A review of NAPL source zone remediation efficiency and the mass flux approach. *Journal of Hazardous Materials*, 110:13-27.

Stroo, H.F., Unger, M., Ward, C.H., Kavanaugh, M.C., Vogel, C., Leeson, A., Marqusee, J.A, Smith, B.P. 2003. Remediating chlorinated solvent source zones. *Environmental Science and Technology,* 37(11):224A-230A.

Suchomel, E.J. and K.D. Pennell. 2006. Reductions in contaminant mass discharge following partial mass removal from DNAPL source zones. *Environmental Science and Technology*, 40(19):6110-6116.

Taylor, T.P., K.D. Pennell, L.M. Abriola, and J.H. Dane. 2001. Surfactant enhanced recovery of tetrachloroethylene from a porous medium containing low permeability lenses: 1. Experimental. *Journal of Contaminant Hydrology*. 48:325-350.

Thal Jr., A.E., Knox, R.C., Sabatini, D.A. 2007. Estimating Partition Coefficients of Tracers, *Ground Water Monitoring and Remediation,* 27(4):135-142.

Willson, C.S., O. Pau, J.A. Pedit, and C.T. Miller. 2000. Mass transfer limitation effects on partitioning tracer tests. *Journal of Contaminant Hydrology*, 45: 79-97.

Wise, W.R., D. Dai, D., E.A. Fitzpatrick, L.W. Evans, P.S.C. Rao, and M.D. Annable. 1999. Nonaqueous phase liquid characterization via partitioning tracer tests: A modified Langmuir relation to describe partitioning nonlinearities. *Journal of Contaminant Hydrology,* 36: 153-165.

U.S. Environmental Protection Agency, Office of Solid Waste and Emergency Response. 1993 Evaluation of the Likelihood of DNAPL Presence at NPL Sites, National Results; *EPA 540R-93-073*; Washington, D.C.

Young, C.M., R.E. Jackson, M. Jin, J.T. Londergan, P.E. Mariner, G.A. Pope, F.J. Anderson and T. Houk. 1999. Characterization of a TCE DNAPL zone in alluvium by partitioning tracers, *Ground Water Monitoring and Remediation,* 19(1): 84-94.

Solute Flux Rate Uncertainty Evaluation at a Monitored Boundary

David E. Langseth, Sc.D., P.E., D. WRE

Gradient Corporation, 20 University Road, Cambridge, MA, 02138; PH (617) 395-5000; FAX (617) 395-5001; email: dlangseth@gradientcorp.com

Abstract

Limitations on data collection density, aggregated spatial and temporal modeling scales, and variations in time can lead to substantial uncertainty in estimated ground water and solute flux rates. Difficulties associated with quantitative characterization of uncertainty often lead to use of conservative assumptions in management decision-making processes, which can lead to non-optimal resource management. This poster describes a computational method for estimating solute flux rate uncertainty at a monitored boundary that can be programmed on an ordinary spreadsheet application and discusses parameter estimation approaches. This method produces results comparable to those produced by Monte Carlo simulation under a reasonable range of assumptions. Two alternative conceptual models at the monitored boundary can be used, one in which the entire area of interest is treated in an integrated manner and the other in which the area of interest is segmented into zones. This poster addresses only the segmented approach. Case study results not shown here indicate that the conceptual model choice has an impact on the analysis results. Use of uncertainty analysis to evaluate likelihood of exceeding target impacts on receiving waters is also illustrated.

Introduction

Estimation of the solute flux rate across a specified boundary is commonly needed. Example boundaries include property boundaries and natural boundaries such as a ground water/surface water interface. A series of monitoring wells is often installed along or near the boundary of interest. Under steady- or quasi steady-state conditions, measured parameters in the monitoring wells along the boundary of interest, combined with other site data, can be used in relatively simple equations to estimate the solute flux rate. The equation simplicity, however, belies the parameter uncertainty and variability. Available data are essentially always sparse with respect to the total area of interest, measured data such as hydraulic conductivity and solute concentration measurements are uncertain, and some conditions, such as the gradient, flow direction, and solute concentrations can change in time. The manner in and degree to which the uncertainty and variability are characterized can have a substantial impact on flux rate characterization and hence on decision-making. For example, in performing human health risk assessments, it is common to use the 95th percentile upper confidence limit on the estimated mean concentration to represent the reasonable maximum concentration at a location (USEPA December 1989). Higher variance in the estimated concentration can, therefore, lead to higher estimates of the reasonable maximum value.

This document presents a computationally simply method for estimating the solute flux rate uncertainty at a monitored boundary that can be easily programmed on a spreadsheet, hopefully helping to address the need for a greater selection of simple and user-friendly stochastic approaches available to hydrogeology practitioners that was noted by Freeze (2004) and Neuman (2004).

Method Description

The one dimensional flux rate in the direction of ground water flow may be approximated as: $F = -CKiA$, where F [MT^{-1}] is the flux rate over area A [L^2], C [ML^{-3}] is the dissolved solute concentration, K [LT^{-1}] is the hydraulic conductivity and i [-] is the hydraulic gradient. For independent variables, the expected value of F ($\overline{F}$) is the product of the expected values of each parameter equals $\overline{F} = -\overline{CAiK} = -\overline{C}\,\overline{A}\,\overline{i}\,\overline{K}$ (Benjamin and Cornell 1970). For independent variables, the coefficient of variation for F (CV_F) is given by:

$$CV_F^2 = CV_C^2 + CV_K^2 + CV_i^2 + CV_A^2 +$$
$$CV_C^2CV_K^2 + CV_C^2CV_i^2 + CV_C^2CV_A^2 + CV_K^2CV_i^2 + CV_K^2CV_A^2 + CV_i^2CV_A^2 +$$
$$CV_C^2CV_K^2CV_i^2 + CV_C^2CV_K^2CV_A^2 + CV_C^2CV_i^2CV_A^2 + CV_K^2CV_i^2CV_A^2 +$$
$$CV_C^2CV_K^2CV_i^2CV_A^2$$

Consider the situation of a property with known ground water contamination and a series of downgradient perimeter monitoring wells, as illustrated in Figure 1. Total solute flux rate across the property boundary may be estimated by either using representative parameters over the entire cross-sectional area of interest (integrated approach) or dividing the total flow cross sectional area into zones, each represented by one or more of the monitoring wells (segmented approach). In general, as the site conditions become more heterogeneous or as spatial trends become more prominent, it becomes more appropriate to divide the flux computation into zones, with each zone ideally representing relatively homogeneous conditions. The integrated and segmented approaches will not in general produce the same results. This poster describes only the segmented approach.

For the segmented approach the total flux is the sum of the flux in each zone, $F = \sum_{i=1}^{n} a_i F_i$, and the mean and variance of the total flux rate are given by Benjamin and Cornell (1970) as $\overline{F} = \sum_{i=1}^{n} a_i \overline{F}_i$ and $\sigma_F^2 = \sum_{i=1}^{n} a_i^2 \sigma_{F_i}^2 + 2\sum_{i=1}^{n}\sum_{j=i+1}^{n} a_i a_j Cov\left[F_i, F_j\right]$, where $\sigma_F^2\left[M^2T^{-2}\right]$ is the variance. The coefficients a_i would commonly all equal 1, but could take other values if, for example, they represented unit conversion factors from the individual zone computations to the total flux rate statement.

Care must be taken to distinguish between variances for point values and variances of a mean over an area or time. The appropriate variance term will often be the variance of the mean value for the area to be evaluated, not the variance of the point values (Jacobson et al. 2002), which is given by Benjamin and Cornell (1970) as

$$\sigma_{\bar{X}}^2 = \frac{\sigma_X^2}{n} + \frac{2}{n^2}\sum_{i=1}^{n}\sum_{j=i+1}^{n} Cov\left[X_i, X_j\right]$$

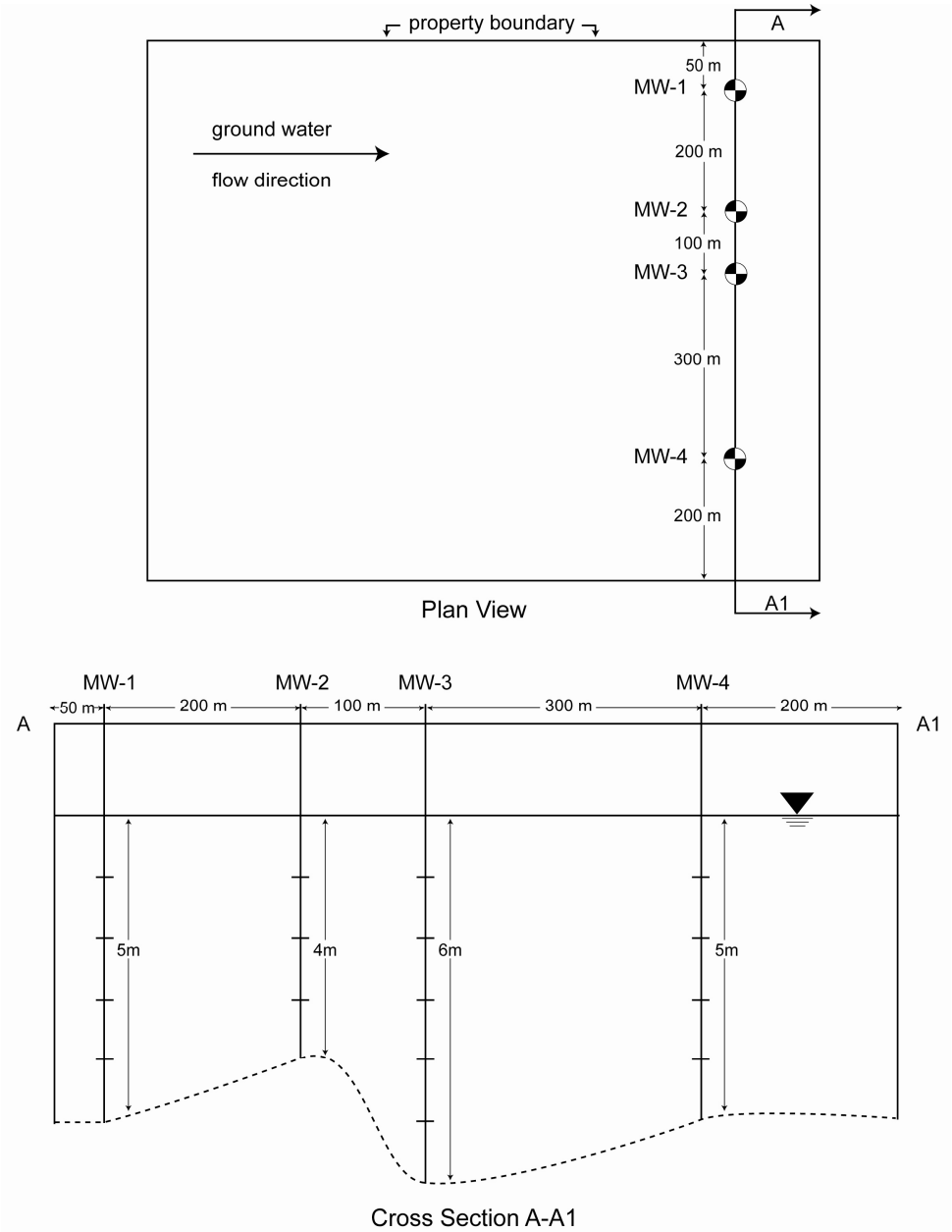

Figure 1: Boundary Monitoring Well Example Schematic

Example Calculation and Parameter Estimation

Table 1 provides hypothetical data of the type that would typically be developed for a monitored boundary as shown in Figure 1. These values represent point estimates at a given time.

Table 1 Example Measured Parameter Values

Well	C [ug/L]	K [cm/s]	Gradient [-]	Saturated Thickness [m]
MW-1	50	4.6E-04	-0.02	5
MW-2	80	2.3E-03	-0.04	4
MW-3	30	1.2E-03	-0.03	6
MW-4	100	1.2E-04	-0.05	5

Estimation of the uncertainty and variability for each of these parameters is discussed below.

Concentration (C): A specific solute, benzene, is specified in this example because measurement error in chemical analysis is compound specific. For benzene measurement error using method 624, Table 6 in 40 CFR 136, app. A, gives the equation for single analyst total variability as $\sigma_r^{'} = 0.26\overline{X} - 1.74$ and the equation for variability including different analysts and laboratories as $\sigma^{'} = 0.25\overline{X} - 1.33$, where $\overline{X}$ is the average recovery for the true concentration, C, all in µg/L. Recovery can be evaluated from site-specific data. Alternatively, recovery in the study used to develop the above equations was characterized as $\overline{X}' = 0.93C + 2.00$.

The measured concentrations were taken as the most likely values of the true concentrations for each zone and were not corrected for recovery in this example. Variance due to measurement error was represented as σ' calculated using $\overline{X}'$. For this sample calculation, the potential mean concentration variability over time in each zone was assumed to range from 0.5 to 1.5 times the measured value. The standard deviation was estimated by dividing this range by 6.

Hydraulic Conductivity (K): Hydraulic conductivity variability in space, after removal of impacts due to trends or correlation in space, has been demonstrated to often follow a lognormal probability distribution (Freeze 1975, de Marsily 1986, Sudicky 1986, Hess et al. 1992), though some data sets that follow a normal distribution have been reported (Vieira et al. 1981). For situations like this example in which the number of site-specific K measurement is small, a-priori information about the shape and magnitude of $\sigma^2_{\ln K}$ can be used to help estimate model parameters. Based on the studies cited above, the probability distribution of K

values was assumed to be lognormal. For the segmented approach, $\sigma^2_{\ln K}$ within each zone was assumed to equal 1, a common value based on data in the citations above, and the median value for each zone ($\breve{K}$) was assumed equal to the measured value in the zone. With only one measurement, the variance of the point values and zonal mean are the same. $\overline{K}$ in each zone was then computed using $\overline{K} = \breve{K} \exp\left(\frac{\sigma^2_{\ln K}}{2}\right)$ (Benjamin and Cornell 1970).

Gradient (i): Mean gradient values in each zone were assumed to range from 0.5 to 1.5 times the Table 1 values in each zone. The standard deviation was estimated by dividing this range by 6. Variance due to measurement error was assumed negligible.

Cross-Sectional Area (A): Variance of the cross-sectional flow area represented by each zone was evaluated by assuming that the horizontal distance represented by each well was known with little uncertainty, but the saturated depth of the aquifer was known with certainty only at the well location. The measured value at the well was taken as the most likely value for each zone and variability for the mean saturated depth in each zone was estimated by assuming that the variance of the point values within each zone was equal to the variance of the point values over the whole area of interest. With only one measurement in each zone, the variance of the mean value for the zone was then equal to the point value variance.

Monte Carlo Simulation

For the MCS, the probability distributions of concentration, gradient, and saturated thickness were represented in two ways: normal distributions with mean and variance as described above, truncated at 0, and uniform distributions ranging $\pm 3\sigma$ around the means. The probability distribution of hydraulic conductivity was represented as a lognormal distribution with mean and variance equal to the values described above. 10,000 realizations were used in each MCS. Figure 2 shows the MCS results using normal distributions for concentration, gradient, and saturated thickness.

Results and Discussion

In order to use the estimated statistics to quantify the flux rate probability distribution, the shape of the distribution must be known or assumed. Results from MCS with both normal and uniform distributions for C, i, and A indicate that the flux rate variation generally follows a distribution that is approximately lognormal. A lognormal distribution for F is consistent with flux being a product of several variables and the parameter with the highest coefficient of variation, K, being lognormally distributed.

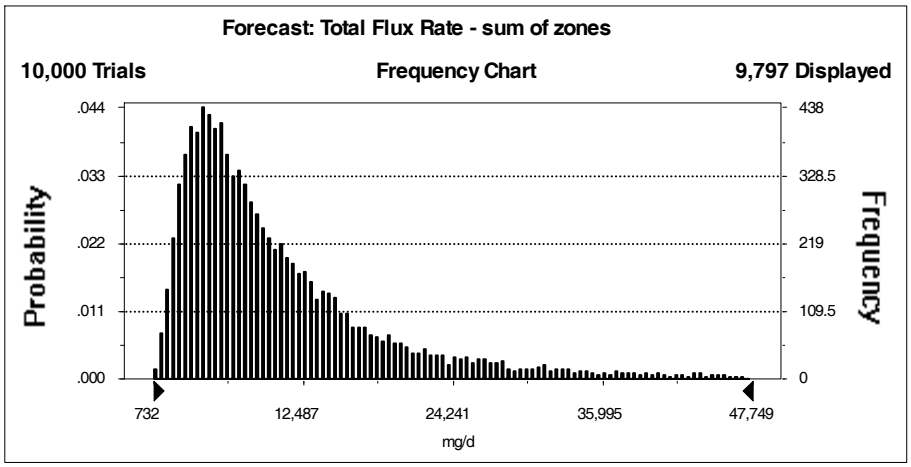

Figure 2: Monte Carlo Simulation Results for Flux Rate

Figure 3 shows flux rate probability distributions from the MCS simulation results using normal (N) and uniform (U) probability distributions for the parameters. As expected, the variance is higher when using uniform probability distributions. Based on the MCS results, the statistics of F computed using the direct calculation approach were applied to a lognormal distribution and are also shown on Figure 3.

Figure 3 shows that the direct computation results are nearly identical to the MCS results. In the absence of having performed the MCS simulation, we would not have known whether lognormality of the flux rate distribution was a reasonable assumption, but equipped with that information, and applying the calculated statistics to the lognormal probability distribution, the direct calculation approach produces a comparable result.

Example Application

Consider the case of contaminated ground water discharging to a stream. The stream has been determined to have a certain capacity to receive the contaminant load from the site, based on dilution or other factors such as volatilization or degradation, without exceeding relevant criteria. Capacity, however, is often a random variable, as it will generally depend at least on the flow rate in the river and perhaps on other variables. In the situation where the capacity depends primarily on the flow rate, and the relationship is linear, the capacity will often follow an approximately lognormal distribution.

The probability that the solute load from the ground water will exceed the river capacity is of interest. The difference between the capacity (C) and load (L) is commonly called a safety margin $SM = C - L$ (Freeze et al. 1990). The system is considered to fail when C is less than L, or when SM is less than zero. If the SM is normally distributed, regardless of the distributions for C and L, the failure

probability is given by Chow *et al*. (1988) as $\overline{R} = F_Z\left(\frac{-1}{CV_{SM}}\right)$, where $F_Z(z)$ is the standard normal cumulative distribution function of z.

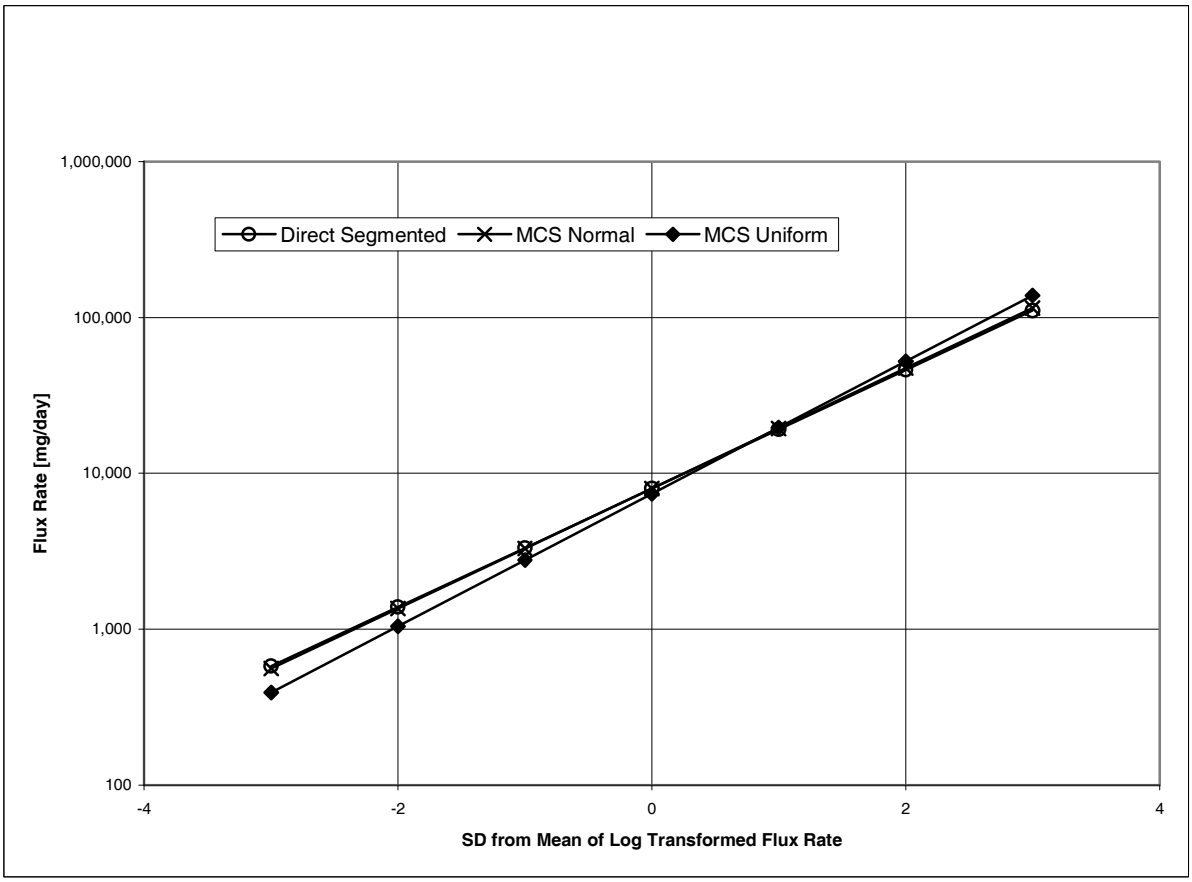

Figure 3: Direct Calculation and MCS Results

Alternatively, if C and L are lognormally distributed and independent, the failure probability in terms of the safety factor, SF = C/L, being less than 1 is given by Chow *et al*. (1988) as $\overline{R} = F_z\left(\frac{-\ln\left[\frac{\overline{C}}{\overline{L}}\left(\frac{1+CV_L^2}{1+CV_C^2}\right)^{0.5}\right]}{\left\{\ln\left[\left(1+CV_C^2\right)\left(1+CV_L^2\right)\right]\right\}^{0.5}}\right)$

Consider a situation in which the load has a mean of 10,000 mg/d with a standard deviation of 12,500 mg/d and the river capacity has been determined to have a mean of 25,000 mg/d with standard deviation also of 12,500 mg/d. Figure 4 shows the probability density functions for the load and capacity. MCS was used to evaluate the safety margin and safety factor assuming all parameters are independent and

characterizing load (flux rate) and capacity using lognormal distributions. Visual evaluation of MCS results for this situation (not shown here) indicates that the safety margin distribution is approximately normal, while the safety factor distribution is approximately lognormal.

The failure risk computed from MCS was 0.12 for both the SM and SF. The failure risk computed using the SM equation above was 0.20, higher than computed using MCS, and using the SF equation above was 0.12, the same as computed using MCS.

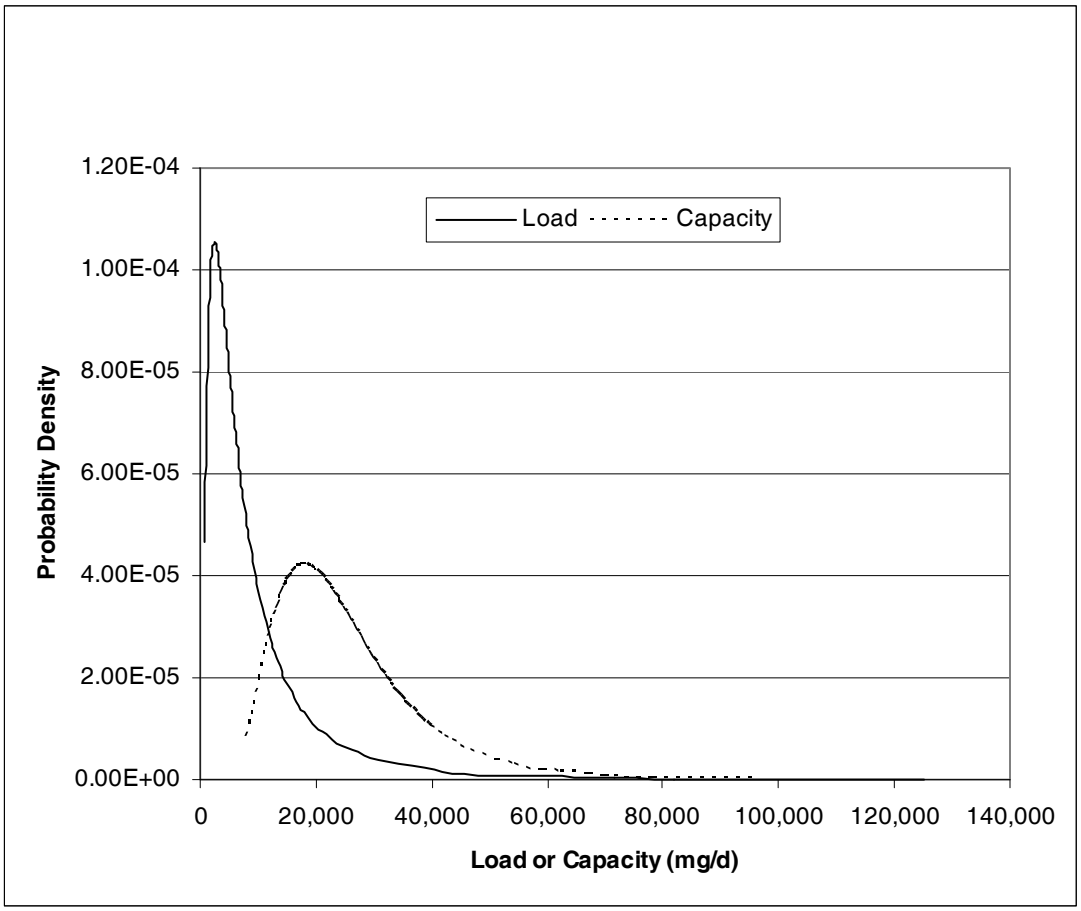

Figure 4: Example Load and Capacity Probability Density Functions

Summary and Conclusions

Application of simple relationships for the moments of linear functions of random variables to issues of ground water solute flux at a monitored cross-section, and associated parameter estimation, has been demonstrated. These relationships may be solved analytically on a spreadsheet. Through comparison with MCS, these simple methods have been shown to produce reasonably accurate results over a range of conditions, with the most comparable results being produced when all the parameters may be considered independent (the impacts of correlation have not been presented here). The principal limitations of the direct calculation method are

related to the inability of the direct method to define the shape of the resultant probability distribution or fully simulate the impact of correlations among the parameter values. Both theory and the MCS simulations, however, indicate that the flux rate has a lognormal distribution. Correlation can be addressed using MCS and partially addressed using expansions of the methods discussed here.

When considering uncertainty in the ground water solute flux rate and receiving water body capacity simultaneously, direct equations for failure risk produce results comparable to those produced by MCS in the absence of correlation between the load and capacity. Direct safety factor calculation in the Example Application produced results almost identical to those from MCS, while the failure risk computed directly from the safety margin approach in the Example Application was somewhat higher. For many situations where ground water discharges to rivers, capacity and load can be expected to be independent of each other and both lognormally distributed, matching the assumptions under which the safety factor equation was developed.

References

Benjamin, J. R., and C. A. Cornell. 1970. Probability, Statistics, and Design for Civil Engineers. McGraw-Hill Book Company, New York.

Chow, V. T., D. R. Maidment, and L. W. Mays. 1988. Applied Hydrology. McGraw-Hill, Inc., New York.

de Marsily, G. 1986. Quantitative Hydrogeology: Groundwater Hydrology for Engineers, 1st edition. Academic Press, San Diego, CA.

Freeze, R. A. 1975. A stochastic-conceptual analysis of one-dimensional groundwater flow in nonuniform homogeneous media. Water Resources Research **11**:725-741.

Freeze, R. A. 2004. The role of stochastic hydrogeological modeling in real-world engineering applications. Stochastic Environmental Research and Risk Assessment **18**:286-289.

Freeze, R. A., J. Massman, L. Smith, T. Sperling, and B. James. 1990. Hydrogeologic Decision Analysis: 1. Framework. Ground Water **28**:738-766.

Hess, K. M., S. H. Wolf, and M. A. Celia. 1992. Large-Scale Natural Gradient Tracer Test in Sand and Gravel, Cape Cod, Massachusetts 3. Hydraulic Conductivity Variability and Calculated Macrodispersivities. Water Resources Research **28**:2011-2027.

Jacobson, E., R. Andricevic, and J. Morrice. 2002. Probabilistic Capture Zone Delineation Based on an Analytic Solution. Ground Water **40**:85-95.

Neuman, S. P. 2004. Stochastic groundwater models in practice. Stochastic Environmental Research and Risk Assessment **18**:268-270.

Sudicky, E. A. 1986. A natural gradient experiment on solute transport in a sand aquifer: Spatial variability of hydraulic conductivity and its role in the dispersion process. Water Resources Research **22**:2069-2082.

USEPA. December 1989. Risk Assessment Guidance for Superfund Volume I: Human Health Evaluation Manual (Part A). *in* O. o. E. a. R. Response, editor.

Vieira, S. R., D. R. Nielsen, and J. W. Biggar. 1981. Spatial variability of field-measured infiltration rate. Soil Sci. Soc. Am. J. **45**:1040-1048.

AN ANALYTICAL SOLUTE TRANSPORT MODEL FOR IN-SITU ESTIMATION OF RETARDATION

Gustavious Paul Williams[1] and David Tomasko[2]

[1]Department of Civil and Environmental Engineering, 368 Clyde Building, Brigham Young University, Provo, UT 84602; email: gus.williams@byu.edu

[2]Environmental Science Division, Argonne National Laboratory, 9600 South Cass Ave, Argonne, IL 60439; email: dtomasko@anl.gov

ABSTRACT

This paper presents an analytical model for evaluating a contaminant's in-situ retardation coefficient from concentration data obtained from an extraction well in a region of initially uniform contamination. Effective retardation estimates are required to effectively evaluate contaminant transport. This estimate often relies on literature values for the distribution coefficient, K_d, and site-specific estimates for effective porosity, bulk density, and chemical composition of the porous medium. When more accuracy is required, column or field studies may be performed to define a contaminant breakthrough curve which is used to determine retardation. These data can, in many instances, be difficult and expensive to obtain and interpret. In practice, in-situ retardation coefficients have been frequently evaluated using the results of injection well data and analytical solutions to the governing transport equation in radial coordinates or multi-dimensional numerical modeling of the transport equation using data from extraction wells.

This study presents a solution and method to use extraction well data and the in-situ contaminant, rather than injection well data and an introduced tracer. Since the solution is based on extraction well data, no tracers or chemicals need to be injected into an aquifer and data from potential remediation wells can be used to obtain these values. In addition to the solution, an integral solution to the instantaneous concentration at the extraction well is presented which allows retardation estimates to be made using only extraction well data and not requiring an observation well. The solution method presented is a numerical inversion of a Laplace transform solution using the Stehfest algorithm to provide non-dimensional results in real time and space.

INTRODUCTION

This paper presents an analytical model for evaluating a contaminant's in-situ retardation coefficient from concentration data obtained from observations wells or an extraction well in a region of initially uniform contamination. An in-situ retardation estimate is required to effectively evaluate contaminant transport. In practice, this estimate often relies on literature values for the distribution coefficient, K_d, and site-specific estimates for effective porosity, bulk density, and chemical composition of the porous medium to calculate retardation. When more accuracy is required, column or field studies are performed to define a contaminant breakthrough curve to determine the contaminant's retardation. These data can, in many instances, be difficult and expensive to obtain and interpret. In practice, in-situ retardation coefficients have been frequently evaluated using the results of injection well data and analytical solutions to the governing transport equation in radial coordinates (Hoopes and Harleman 1967; Tang and Babu 1979; Pickens et al. 1981; and Chen 1985, 1986), or multi-dimensional numerical modeling of the transport equation fitted to field data. This study presents a solution and method to use extraction well data and the in-situ contaminant, rather than injection well data and an introduced tracer to establish in-situ retardation values.

While undergoing transport through a porous medium, a dissolved contaminant often travels at a velocity less than that of the groundwater because of interactions between the contaminant and the solid matrix. The ratio of the relative velocities between the groundwater and dissolved contaminant can be described as the effective retardation; the larger the retardation, the smaller the velocity of the contaminant compared to the groundwater velocity (Freeze and Cheery 1979). That is,

$$V_c = \frac{V_{gw}}{R} \qquad (1)$$

where R is the retardation coefficient, V_c is the velocity of the center of mass of the contaminant plume, and V_{gw} is the average groundwater velocity.

The average groundwater velocity, V_{gw}, is obtained from the Darcy velocity, $V_d = K\nabla h$, by the following relationship:

$$V_{gw} = \frac{K\nabla h}{\phi} \quad or \quad V_{gw}\frac{V_d}{\phi} \qquad (2)$$

where K is the hydraulic conductivity of the porous medium, ϕ is the effective porosity of the porous medium, and ∇h is the hydraulic gradient of the fluid in the porous medium (Freeze and Cherry 1979).

Assuming fast, reversible reactions of the contaminant with the solid matrix, the retardation coefficient, R, in Equation 1 can be written:

$$R = 1 + \rho_b \frac{K_d}{\phi} \qquad (3)$$

where K_d is the distribution coefficient for the contaminant in contact with the solid matrix and ρ_b is the bulk density of the porous medium (Freeze and Cherry 1979). K_d depends on both the contaminant and the physical and chemical makeup of the porous media and is therefore site specific.

This paper presents an analytical solution to estimate *R*, from field extraction and observation wells or even a single extract well located in the plume. The solution relies on a unique boundary condition, a zero contaminant concentration at the edge of the well bore. While this boundary condition allows a useful mathematical solution, it may not accurately represent actual field conditions. This issue is discussed in this paper.

MATHEMATICAL MODEL

This section presents the mathematical description of the model including the governing equations, initial and boundary conditions, various assumptions, the resulting solution, and solution methods.

The equation describing time-dependent, radial flow with dispersion in a porous medium (Ogata 1970) can be written:

$$R\frac{\partial C}{\partial t} = \frac{1}{r}\frac{\partial\left(rD_r\frac{\partial C}{\partial r}\right)}{\partial r} - V_{gw}\frac{\partial C}{\partial r} \qquad (4)$$

Where *C* is the contaminant concentration, *D* is the dispersion coefficient, *r* is the radial coordinate, *R* is the retardation coefficient, and *t* is time.

The steady-state seepage velocity, V_{gw}, at any radius r in Equation 4 is obtained from the continuity equation:

$$V_{gw} = \frac{Q}{2\pi b r \phi} \qquad (5)$$

Where *b* is the thickness of the homogeneous, isotropic, infinite horizontal porous medium and *Q* is the constant rate of groundwater extraction.

For this paper we set $A = \frac{Q}{2\pi b\phi}$ so that $V = \frac{A}{r}$ is the seepage velocity or V_{gw}. From this point in the paper we will drop the subscript for conciseness.

Dispersion in the aquifer is assumed to follow the functional form presented by Bear (1972):

$$D = \alpha V \qquad (6)$$

Where α is the dispersivity. Because mass transfer by diffusion is small relative to advection, it is assumed to be included in the dispersion term (Freeze and Cheery 1979). The dispersivity in Equation

6 is taken to be scale-dependent (Lallemand-Barres and Peaudecerf 1978), i.e., $\alpha = 0.1L$ where *L* is the separation distance from the extraction well to some point of interest in the aquifer.

In terms of the previously defined symbols, the velocity-dependent dispersion coefficient can be written:

$$D = \alpha V \quad or \quad D = \frac{\alpha A}{r} \qquad (7)$$

To solve Equation 4, initial and boundary conditions are required. For this model, the initial contaminant concentration in the aquifer is assumed to be equal to C_0, $\{C(r,0) = C_0\}$ as the radius *r* approaches infinity, the concentration is assumed to be finite and equal to C_0, $\{C(\infty,t) = C_0\}$, and at the radius of the effective well bore, r_w, the concentration is assumed to go to zero instantaneously and stay at that value for all future time $\{C(r_w,t) = 0\}$ (Luckner and Schestakow 1991). These boundary and initial conditions allow a solution, but may not be exactly honored at actual sites.

By substituting Equations 5 and 6 into Equation 4, and making the following substitutions; $c = \frac{C}{C_0}$, $a = \frac{r_w}{\alpha}$, $\tau = \frac{\alpha A t}{R r_w^3}$, and $\bar{r} = \frac{r}{r_w}$, equation 4 can be rewritten in dimensionless form as:

$$\frac{\partial c}{\partial \tau} = \frac{1}{\bar{r}} \frac{\partial^2 c}{\partial \bar{r}^2} - \frac{a}{\bar{r}} \frac{\partial c}{\partial \bar{r}} \qquad (8)$$

Transforming Equation 13 to Laplace space (Hildebrand 1976) and using the initial boundary condition gives the following non-homogeneous, ordinary differential equation:

$$S\bar{c} - 1 = \frac{1}{\bar{r}} \frac{d^2\bar{c}}{d\bar{r}^2} - \frac{a}{\bar{r}} \frac{d\bar{c}}{d\bar{r}} \qquad (9)$$

where S is the Laplace variable and $\bar{c}$ is the dimensionless contaminant concentration in Laplace space.

The solution to Equation 9 can be found by using the method of undetermined coefficients (Kreyszig 1967). With this method, the general solution to the equation is the sum of the solution to the homogeneous portion of the equation and a particular solution that incorporates the non-homogeneity.

The homogeneous part of Equation 9:

$$S\bar{c} = \frac{1}{\bar{r}} \frac{d^2\bar{c}}{d\bar{r}^2} - \frac{a}{\bar{r}} \frac{d\bar{c}}{d\bar{r}} \qquad (10)$$

was solved using the computer package Mathematica version 3 (Wolfram 1996) which yields:

$$\bar{c} = c_1 e^{\frac{a}{2}(\bar{r}-1)} Ai\left[\left(\bar{r} + \frac{a^2}{4S}\right)S^{1/3}\right] + c_2 e^{\frac{a}{2}(\bar{r}-1)} Bi\left[\left(\bar{r} + \frac{a^2}{4S}\right)S^{1/3}\right] \qquad (11)$$

The simplest solution to the particular portion of Equation 9 is:

$$\bar{c} = \frac{1}{S} \qquad (12)$$

Using Equations 11 and 12, the general solution to Equation 9 can be written as:

$$\bar{c} = \frac{1}{S} + c_1 e^{\frac{a}{2}(\bar{r}-1)} Ai\left[\left(\bar{r} + \frac{a^2}{4S}\right)S^{1/3}\right] + c_2 e^{\frac{a}{2}(\bar{r}-1)} Bi\left[\left(\bar{r} + \frac{a^2}{4S}\right)S^{1/3}\right] \qquad (13)$$

Where *Ai* and *Bi* are Airy functions (modified Bessel functions of order 1/3) where *Ai(z)* tends to zero for large *z* while *Bi(z)* increases without bound, and c_1 and c_2 are constants.

To proceed we invoke the two boundary conditions. For the first boundary condition, the concentration is assumed to stay finite as $\bar{r}$ approaches infinity. For this case, since *Bi(z)* increases without bound, the constant c_2 in Equation 18 must equal zero, eliminating the second term.

$$c_2 = 0 \qquad (14)$$

The second boundary condition requires that the concentration be equal to zero for $\bar{r}$ equal to 1.0. To satisfy this condition, the constant c_1 in Equation 18 must have the value:

$$c_1 = \frac{-1}{S} \frac{1}{Ai\left[\left(1 + \frac{a^2}{4S}\right)S^{1/3}\right]} \qquad (15)$$

Using Equations 13, 14, and 15, the solution to Equation 9 can be written as:

$$\bar{c}(S) = \frac{1}{S} - \frac{\left(e^{\frac{a}{2}(r-1)}\right) Ai\left[\left(\bar{r} + \frac{a^2}{4S}\right)S^{1/3}\right]}{S\, Ai\left[\left(1 + \frac{a^2}{4S}\right)S^{1/3}\right]} \qquad (16)$$

Although a closed-form solution to the inversion of Equation 15 to real space is possible, the resulting integrals are difficult to evaluate, as indicated in the solution for an injection well presented by Tang and Babu (1979). To simplify the procedure for converting the concentrations in Laplace space to real space, we use the Stehfest algorithm (Stehfest 1970a and 1970b). The Stehfest algorithm replaces the *S* in Equation 21 with:

$$S = \frac{i\ln(2)}{\tau} \qquad (17)$$

and an approximate solution to the contaminant concentration in real dimensionless time and space is found using a numerical inverse Laplace transform with the expression:

$$C(\tau) = \frac{\ln(2)}{\tau}\sum_{i=1}^{N} V_i \bar{c}\left(\frac{i\ln(2)}{\tau}\right) \qquad (18)$$

where N determines the accuracy of the approximation (an even machine-dependent value, typically between 10 and 18), and the values for V_i are constants that depend on N in the following manner:

$$V_i = (-1)^{\frac{N}{2}+i} \sum_{k=\frac{i+1}{2}}^{\min\left(\frac{N}{2},i\right)} \frac{k^{\frac{N}{2}}(2k)!}{\left(N/2-k\right)!\,k!\,(k-1)!(i-k)!(2k-i)!} \qquad (19)$$

In carrying out the inversion of Equation 16, values of the Airy function were obtained from Amos (1983, 1985, and 1986) as implemented in Matlab (Mathworks 2008).

Estimating Retardation

Contaminant concentrations in the porous medium can be computed as a function of K_d, time, and radial distance from an extraction well by the numerical inversion of Equation 16 and used to determine the in-situ retardation coefficient by matching field measured values to computed values with K_d as the independent variable. This assumes that the initial and boundary conditions in the field are approximated by the assumptions used in this solution. In general, the initial condition of a uniform concentration and the assumption of a constant concentration at infinity are applicable for the scale of most field tests, where the concentration is limited in extent, but the effects from the boundaries are not evident near the well for typical testing time periods.

The second boundary condition is more problematic and may not be approximated at field sites.

Summary

This paper presented the development of a model for estimating the instantaneous concentration of a contaminant in an extraction well located in an initially uniform contaminant distribution. The radial transport equation with velocity-dependent dispersion solution was computed with the Stehfest algorithm to invert the Laplace space function to a dimensionless concentration in real space.

REFERENCES

Abramowitz, M. and I.A. Stegun, 1972, *Handbook of Mathematical Functions with Formulas, Graphs, and Mathematical Tables*, John Wiley and Sons, New York City, New York.

Amos, D.E., 1983, *Computation of Bessel Functions of Complex Argument and Large Order*, SAND83-0643, Sandia National Laboratories, Albuquerque, New Mexico, May.

Amos, D.E., 1985, *A Subroutine Package for Bessel Functions of a Complex Argument and Nonnegative Order*, SAND85-1018, Sandia National Laboratories, Albuquerque, New Mexico, May.

Amos, D.E., 1986, A Portable Package for Bessel Functions of a Complex Argument and Nonnegative Order, *Transactions of Mathematical Software*.

Bear, J., 1972, *Dynamics of Fluids in Porous Media*, American Elsevier Publishing Company, New York City, New York.

Chen, C.S, 1985, Analytical and Approximate Solutions to Radial Dispersion From An Injection Well to a Geological Unit With Simultaneous Diffusion Into Adjacent Strata, *Water Resources Research*, Vol. 21, No. 8, p1069-1076.

Chen, C.S, 1986, Solutions for Radionuclide Transport From an Injection Well Into a Single Fracture in a Porous Formation, *Water Resources Research*, Vol. 22, No. 4, p508-518.

Freeze, R.A. and J.A. Cherry, 1979, *Groundwater*, Prentice-Hall, Inc., Englewood Cliffs, New Jersey.

Hildebrand, F.B., 1976, *Advanced Calculus for Applications*, Prentice-Hall, Inc., Englewood Cliffs, New Jersey.

Hoopes, J.A. and D.R.F. Harleman, 1967, Dispersion in Radial Flow from a Recharge Well, *Journal of Geophysical Research*, Vol. 72, No. 14, p3595-3607.

Lallemand-Barres, A. and P. Peaudecerf, 1978, *Recherche des Relations entre a Valuer de la Dispersivite Macroscopique d'un Milieu Aquifere, Ses Autres Caracteristiques et les Conditions de Mesure*, Bulletin Bureau Geologique Minieres, 4-1978:277-284.

Luckner, L. and W.M. Schestakow, 1991, *Migration Processes in the Soil and Groundwater Zone*, Lewis Publishers, Chelsea, Michigan.

The MathWorks Inc. 2008, *MATLAB Reference Manual*, Prime Park Way, Natick MA

Ogata, A., 1970, *Theory of Dispersion in a Granular Medium*, U.S. Geological Survey Professional Paper, 411-I.

Pickens, J.F., R.E. Jackson, and K.J. Inch, 1981, Measurement of Distribution Coefficients Using a Radial Injection Dual-Tracer Test, *Water Resources Research*, Vol. 17, No. 3, p529-544.

Stehfest, H., 1970a, Algorithm 368, Numerical Inversion of Laplace Transforms, *Communications of the Association for Computing Machinery*, 13(1):47-49.

Stehfest, H., 1970b, Remark on Algorithm 368, Numerical Inversion of Laplace Transforms, Communications of the Association for Computing Machinery, 13(10):624.

Tang, D.H. and D.K. Babu, 1979, Analytical Solution of a Velocity Dependent Dispersion Problem, Water Resources Research, Vol. 15, No. 6, p1471-1478.

Assessing Postulated Accidental Releases of Radioactive Liquid Effluents from Nuclear Power Plants

S.W. Taylor,[1] G.A. Day,[2] A.N. Findikakis,[3] G.A. McLane,[2] and L.E. Young[2]

[1] Bechtel Corporation, 5275 Westview Drive, Frederick, MD 21703-8306; PH (301) 228-7657; FAX (240) 379-2914; email: swtaylor@bechtel.com
[2] Bechtel Power Corporation, 5275 Westview Drive, Frederick, MD 21703-8306
[3] Bechtel Systems and Infrastructure, Inc., P.O. Box 193965, San Francisco, CA 94119-3965

ABSTRACT

Licensing of commercial nuclear power reactors requires an assessment of a postulated accidental release of radioactive liquid effluent in ground and surface waters to demonstrate that the dose to an individual member of the public does not exceed regulatory limits. The radioactive liquid effluent with the highest potential exposure consequences to offsite water users is associated with the liquid waste management system and is comprised of a mixture of fission and activation products with a wide range of half-lives. The liquid effluent containing tanks postulated to fail are located below ground such that a liquid release would enter the groundwater and then be subject to groundwater transport offsite with radionuclide concentrations being attenuated by the processes of radioactive decay, adsorption, and dispersion. Evaluations of these postulated releases have been completed and included in the license applications for 17 new nuclear power reactor sites. Results of these analyses indicate that groundwater travel times vary widely from site to site and that groundwater to surface water pathways are present for many of the sites. Comparisons of predicted radionuclide concentrations at offsite receptor locations to regulatory limits indicate compliance with the dose limits for an individual member of the public, with tritium having the potential for the greatest dose contribution.

INTRODUCTION

Recently, there has been renewed interest on the part of the electrical utilities in licensing new nuclear power reactor in the United States. This interest has been stimulated by a streamlined licensing process that reduces the financial risk to applicants, anticipated growth in the demand for electricity, increased public acceptance of nuclear power, and recent changes to United States energy policy that promote energy independence as well as reductions in greenhouse gas emissions. Currently, there are 21 new power reactor sites planned, with 17 having submitted license applications to the U.S. Nuclear Regulatory Commission (NRC), which regulates the construction and operation of commercial nuclear power plants in the United States. The 17 sites are located primarily in the Central and Eastern United

States; 15 are adjacent to existing reactors and 2 are greenfield sites. Current license application are based on one of five reactor technologies, which include Areva's EPR™, General Electric's Advanced Boiling Water Reactor (ABWR) and Economic Simplified Boiling Water Reactor (ESBWR), Mitsubishi's U.S. Advanced Pressurized Water Reactor (US-APWR), and Westinghouse's AP1000™. These reactors are standardized Generation III designs, as classified by the U.S. Department of Energy, that are in various stages of design certification by the NRC. Table 1 summarizes the sites, locations, and technologies for which licenses applications have been submitted.

Table 1. Current License Applications for New Nuclear Power Reactors.

Site	Location	Technology
Bell Bend Unit 1	Luzerne County, PA	EPR
Bellefonte Units 3 & 4	Jackson County, AL	AP1000
Callaway Unit 2	Callaway County, MO	EPR
Calvert Cliffs Unit 3	Calvert County, MD	EPR
Comanche Peak Units 3 & 4	Somervell County, TX	US-APWR
Fermi Unit 3	Monroe County, MI	ESBWR
Grand Gulf Unit 3	Claiborne County, MS	ESBWR
Levy County Units 1 & 2	Levy County, FL	AP1000
Nine Mile Point Unit 3	Oswego, NY	EPR
North Anna Unit 3	Louisa County, VA	ESBWR
River Bend Unit 3	St. Francisville, LA	ESBWR
Shearon Harris Unit 2 & 3	Wake County, NC	AP1000
South Texas Project Units 3 & 4	Matagorda County, TX	ABWR
Victoria County Station Units 1 & 2	Victoria County, TX	ESBWR
Virgil C. Summer Units 2 & 3	Fairfield County, SC	AP1000
Vogtle Units 3 & 4	Burke County, GA	AP1000

Nuclear power plants, like any other complex industrial facility, utilize substances that, if released to the environment, could result in adverse impacts to human health. In the case of a nuclear power plant, the primary substances of concern include radioactive isotopes generated as fission or activation products. Outside of safety-related containment facilities, the highest liquid phase inventories of these radioactive isotopes generally occur in the Liquid Waste Management System (LWMS) of a nuclear power plant. A typical LWMS includes tanks, piping, pumps, valves, filters, demineralizers, and any additional equipment necessary to process and treat liquid wastes and route them to the point of discharge from the system. As part of the nuclear power plant licensing process, applicants are required to demonstrate that an accidental release of radioactive liquid effluent from a LWMS to the groundwater would not result in a radiation dose to a member of the public in excess of the Federal limit. Assessing a hypothetical, accidental liquid release for a particular site involves data collection efforts needed to characterize the site geology, establish site-specific hydrogeologic properties, and develop conceptual transport models. The radioactive source term, which may include a large number of radionuclides, must also be defined. Transport modeling is then used to estimate radionuclide concentrations in the groundwater, or surface water receiving groundwater discharge, that a member of the public could potentially ingest. Predicted concentrations are then compared against Federal limits, considering dose contributions from multiple radionuclides and radioactive progeny, to determine regulatory compliance.

This paper describes the process of assessing postulated accidental releases of radioactive liquid effluents from nuclear power plants. Regulatory requirements and associated guidance documents are summarized. Radioactive source terms from the different reactor types are described in terms of location, inventory, and radionuclide properties. An overview of the hydrogeologic site characterization activities required to support an accidental liquid release assessment is provided. Reactive transport modeling approaches used to support an accidental release analysis are described. Finally, accidental release analysis results included in current license applications are presented and discussed.

REGULATORY REQUIREMENTS

Radiation dose limits for members of the public from the operation of a nuclear power plant are established in 10 CFR Part 20. In particular, 10 CFR 20.1302 indicates that compliance with the dose limit for liquid releases may be established by demonstrating that (i) the annual average concentrations of radioactive material released in liquid effluents at the boundary of the unrestricted area do not exceed the values specified in Table 2, Column 2 of Appendix B to 10 CFR Part 20; and (ii) the annual dose from external sources to an individual continuously present in an unrestricted area does not exceed 50 mrem. Note that the concentration values given in Table 2, Column 2 of Appendix B are equivalent to the radionuclide concentrations which, if ingested over the course of a year, would produce an annual dose of 50 mrem assuming that an individual ingests water at a rate of 2 L/d.

To assist applicants in preparing license applications for nuclear power plants, the NRC has issued Regulatory Guide 1.206 (NRC, 2007a). Section C.I.2.4.13 of this guidance document is relevant to accidental releases of radioactive liquid effluents and indicates that the applicant should describe the ability of the ground and surface water environment to delay, disperse, dilute, or concentrate liquid effluents, as related to existing or potential future water users. Regulatory Guide 1.206 also indicates that the bases used to determine dilution factors, dispersion coefficients, flow velocities, travel times, adsorption, and pathways of liquid contaminants should be discussed and references to the locations and water users as well as release points be provided.

To provide NRC staff guidance in reviewing license applications for nuclear power plants, the NRC has published NUREG-0800 (NRC, 2007b). In particular, Section 2.4.13, Accidental Releases of Radioactive Liquid Effluents in Ground and Surface Waters, directs NRC staff to: (a) use best current practices to analyze groundwater transport of radioactive liquid effluents; (b) consider sufficient alternate conceptual models to bound the hydrogeologic conditions that define the transport of radioactive liquid effluents; (c) identify the bounding set of plausible pathways that may result in the worst-case contamination; and (d) establish radionuclide transport characteristics from on-site measurements. Also of interest is Branch Technical Position (BTP) 11-6, Postulated Radioactive Releases Due to Liquid-containing Tank Failures. This document provides guidance on developing the radioactive source term to ensure that the highest potential radioactive material inventory is selected among the expected types of liquid waste streams processed by the LWMS. Specifically, this document requires that the radionuclides selected for the radioactive source term and

total inventory should include those that have the highest potential exposure consequences to users of water resources, including long-lived fission and activation products and environmentally mobile radionuclides. BTP 11-6 further prescribes that the radionuclide inventory for the LWMS tank assumed to fail is based on 80% of volume capacity of the tank. BTP 11-6 also indicates that the evaluation of a LWMS tank failure consider the impact on the nearest potable water supply, and the use of water for direct human consumption or indirectly through animals (livestock watering), crops (agricultural irrigation), and food processing (water as an ingredient).

RADIOACTIVE SOURCE TERM

The radioactive source term needed to evaluate the potential dose consequences to individual members of the public from a postulated LWMS tank failure is dependent on the reactor technology adopted for a given site. Radioactive source terms, to be used for assessing a LWMS tank failure, have been identified by the reactor manufacturers based on the criteria provided in BTP 11-6. Table 2 summarizes the characteristics of these source terms for the AP1000, EPR and ESBWR, including physical data on the tank that would have the highest potential exposure consequences, if it were to fail, and the radiological characteristics of the tank's contents.

Table 2. Radioactive Source Terms for Current Reactor Technologies.

Characteristic	AP1000	EPR	ESBWR
Controlling tank	Effluent holdup tank	Reactor coolant storage tank	Equipment drain collection tank
Location	Auxiliary building	Auxiliary building	Radwaste building
Capacity (m^3)	140	115	106
Floor elevation (m bgs)	10.2	9.6	14.0
Radionuclides in mixture	56	60	60
Initial activity (Ci)	476	785	39.8
Activity after 2-y decay (Ci)	111	144	9.17
Radionuclides exceeding individual ECLs after 2-y decay (in descending order of ECL exceedance)	Cs-137, Cs-134, H-3, Co-60, Sr-90, Mn-54, Ag-110m, Ce-144, Fe-55	Cs-134, Cs-137, H-3, Co-60, Sr-90, Zn-65, Mn-54, Ru-106, Fe-55, Ce-144	Cs-137, Co-60, Zn-65, Sr-90, Cs-134, Fe-55, Ru-106, Mn-54, Ce-144, H-3, Ag-110m

A review of the information in Table 2 indicates that the controlling tanks for the source terms are of similar capacity as well as in location relative to site grade. Each tank is located well below grade at depths ranging from 9.6 to 14.0 m below ground surface (bgs) such that a postulated accidental release from a tank failure would occur in the subsurface. At these depths, the source term for each of the designs could be below the water table at many sites in the Central and Eastern United States where new nuclear power plants are being considered.

The radiological data included in Table 2 indicate that each source term represents a mixture of a relatively large number of isotopes, with up to 60 isotopes present. Each isotope has a unique half-live for radioactive decay, while isotopes of a common element have unique transport characteristics in terms of adsorption. In addition, some isotopes may produce progeny that can have significant dose consequences themselves and must be considered in the accidental release analysis.

The total initial activities of the source term, based on 80% of the controlling tank capacity, vary significantly across the reactor technologies, with the ESBWR having the least activity and the EPR having the greatest activity. The half-lives of the isotopes in the source terms are highly variable and range from 30 seconds for Rh-106 to 15.7 million years for I-129. Because the time scales for groundwater transport are relatively large, the short-lived radionuclides in the source term will decay to levels such that they have no impact on demonstrating regulatory compliance. As a measure of the short-lived radionuclide content, each radionuclide was decayed for a two-year period, a representative groundwater travel time, and the total activity determined for each source term. Results summarized in Table 2 indicate that when compared to the total initial activity, only about 20% of the initial source term activity is expected to participate in the assessment of 10 CFR 20.1302 compliance. Comparing the resulting individual radionuclide concentrations against the Effluent Concentration Limits (ECLs) specified in Table 2, Column 2 of Appendix B to 10 CFR Part 20, the radionuclides expected to be important in an accidental release analysis can be identified. The results provided in Table 2 indicate that these radionuclides are similar across the three source terms with the common radionuclides including, in order of decreasing half-life, the following: Cs-137, Sr-90, H-3, Co-60, Fe-55, Cs-134, Mn-54, and Ce-144.

SITE CHARACTERIZATION

In order to assess the dose consequences of a postulated LWMS tank failure on an individual member of the public, a thorough understanding of the geologic and hydrogeologic site characteristics is required, both conceptually and quantitatively. In fact, 10 CFR 100.20(c)(3) requires that factors important to hydrological radionuclide transport be obtained from on-site measurements. Site characterization efforts must be sufficient to: (a) identify the most likely conceptual model for the site along with alternative conceptual models; (b) establish bounding subsurface pathways from the point of release to the nearest potable water supply in an unrestricted area; and (c) define the radionuclide transport characteristics of the groundwater environment. While a complete description of the required site characterization activities is beyond the scope of this paper, the following overview is provided.

Site characterization efforts involve drilling and sampling geotechnical boreholes, and field and laboratory testing for the purpose of defining the stratigraphy as well as determining the geotechnical and transport properties of the subsurface materials. Typically about 100 boreholes per reactor are required to sufficiently define the subsurface conditions for the systems, structures, and components that comprise a nuclear power plant. Observation wells are installed in a subset of the boreholes and completed in the hydrogeologic units of interest. Ideally, observation wells are located such that synoptic measurements yield reliable distributions of piezometric head from which groundwater flow directions and pathways may be inferred. Following installation, slug tests are performed in observation wells to provide estimates of hydraulic conductivity. Pump tests are also typically conducted to define the hydraulic characteristics of the hydrogeologic units of interest. These field and laboratory testing efforts provide on-site measurements of hydraulic

conductivity, total and effective porosity, bulk density, and radionuclide distribution coefficients. Observation wells are then monitored to determine the seasonal variation in piezometric head elevations. These piezometric head data are used to develop piezometric surfaces from which hydraulic gradients can be estimated and groundwater flow paths can be identified.

Groundwater flow models are often used to integrate the large amounts of field and laboratory data described above. Groundwater models provide additional value in that once they are developed and calibrated for pre-construction conditions, they can be used predict post-construction groundwater conditions. This is particularly important for a nuclear power plant because the large foundations may extend below the water table and locally alter the hydrogeologic characteristics. Also, the groundwater recharge characteristics may be altered over relatively large areas with changes in land cover and grading of the site. With these post-construction changes represented and site-specific hydrogeological characteristics represented, the groundwater model can then be used to identify the groundwater pathways for an accidental release of radioactive liquid and associated receptors, and provide a best estimate of the groundwater travel time.

ACCIDENTAL RELEASE ANALYSIS

With the source term, groundwater pathways, and transport characteristics defined, the accidental release analysis becomes a simple matter of performing reactive transport modeling to predict the radionuclide concentrations in the nearest potable water supply in an unrestricted area. Figure 1a depicts a simple conceptual model in which liquid effluent is released from a failed LWMS tank to a water table aquifer with subsequent saturated zone transport to the site boundary. Although each of the current reactor designs incorporate engineered features to mitigate a release (e.g., level alarms, collection sumps, steel and concrete barriers), usually no credit is taken for these features in preventing a release the groundwater environment. At the site boundary, outside of which is considered an unrestricted area, it is hypothesized that an individual member of the public installs a well and ingests water supplied from the well. Figure 1b illustrates the case in which liquid effluent released to the groundwater discharges to surface water within the restricted area, which then discharges offsite to the unrestricted area. In this case, it is assumed that an individual member of the public installs an intake and ingests water supplied from the intake.

A variety of reactive transport modeling approaches can be used to predict radionuclide concentrations at the site boundary, ranging from simple analytical models that consider radioactive decay alone to multi-dimensional numerical models that mechanistically represent all key transport processes. As a rule of thumb, it is desirable to use the simplest model with the fewest parameters in conjunction with conservative assumptions to demonstrate compliance. Because several radionuclides in the source terms produce radioactive progeny that must accounted for, the reactive transport model should normally represent these decay chain sequences. The simplest model that represents these sequences, but ignores hydrodynamic dispersion and retardation, is given by Kennedy and Strenge (1992). Use of this model accounts for advection only, but has the advantage of requiring only one transport parameter, the

groundwater travel time, which can be estimated from on-site measurements of hydraulic conductivity, hydraulic gradient, effective porosity, and groundwater travel distance. A groundwater flow model, used as part of the site characterization effort, can also be used to estimate the groundwater travel time.

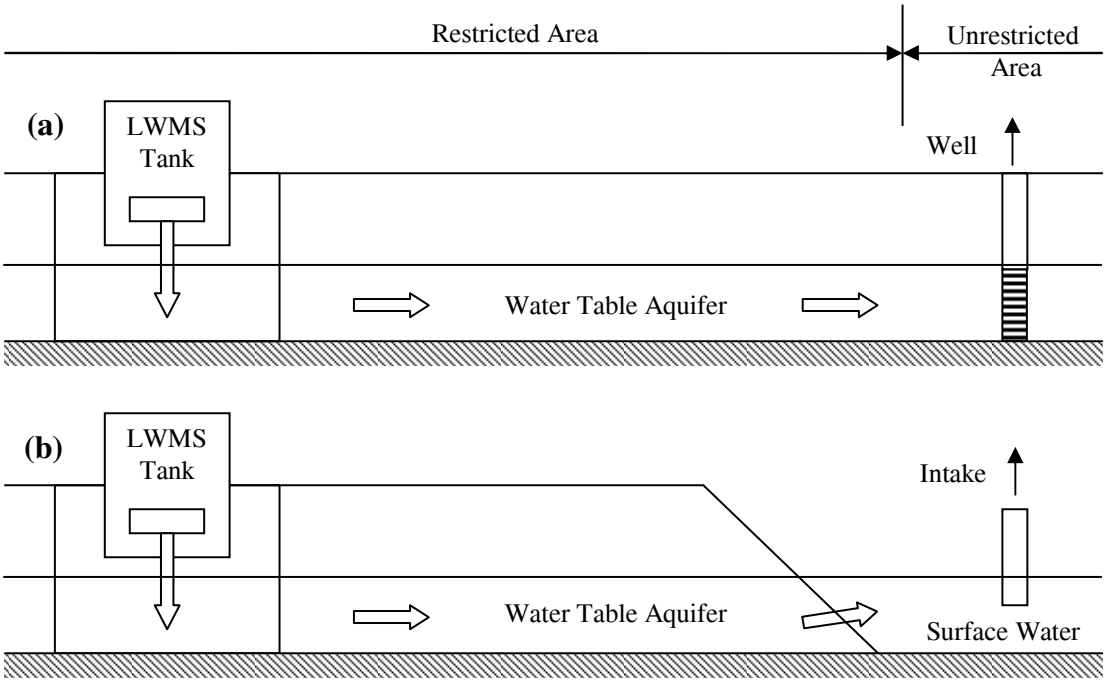

Figure 1. Conceptual Models for an Accidental Release of Liquid Effluent.

If accounting of retardation and hydrodynamic dispersion is needed to further attenuate radionuclide concentrations to demonstrate compliance, a more complex model would be required along with additional parameters needed to represent these processes. Javandel et al. (1984) provide one-dimensional analytical solutions for advective-dispersive-reactive solute transport that can be applied. Use of these solutions requires definition of the groundwater velocity, coefficient of longitudinal hydrodynamic dispersion, and retardation factor. These solutions do not consider decay chain sequences and are applicable only for radionuclides that undergo simple decay. Fortunately, this is the case for most, but not all radionuclides that have the greatest impact on regulatory compliance (i.e., H-3, Mn-54, Fe-55, Co-60, Cs-134, Cs-137, and Ce-144). Note that Sr-90, common to all radioactive sources, produces progeny that may require modeling. Note also that Np-239, present in the source term for the ESBWR, rapidly decays to Pu-239 and can impact compliance. In these cases, Srinivasan and Clement (2008) provide one-dimensional analytical solutions that can be used to model the decay chain sequences.

A complex hydrogeological setting may necessitate the use of a numerical flow and transport model to represent the relevant flow and transport phenomena. Commonly used codes that consider multi-species reactive transport and are capable of modeling radioactive decay chain sequences include RT3D (Clement, 1997) and MT3DMS (Zheng and Wang, 1999). The obvious advantage of numerical models is

their ability to more accurately represent complex hydrogeologic systems. The primary disadvantage is that the data needed to fully define the spatial variability in formation properties and boundary conditions are usually not available, which can introduce uncertainty into the model predictions.

In some cases groundwater contaminated with radioactive liquid effluent may discharge to the surface and mix with uncontaminated surface water before reaching the unrestricted area. In such cases estimating the radionuclide concentrations at the point of compliance should account for dilution of the groundwater discharge in the surface water.

Once radionuclide concentrations are determined for the unrestricted area, they can be compared against the ECLs given in Table 2, Column 2 of Appendix B to 10 CFR Part 20 to assess regulatory compliance. Because the source term consists of a radionuclide mixture and because the individual ECLs correspond to annual dose of 50 mrem, it is necessary to apply the unity rule to ensure that the dose contributions from all radionuclides present, when summed, do not exceed the 50 mrem limit. The unity rule may be expressed as

$$\sum_{i=1}^{n} \frac{C_i}{ECL_i} \leq 1$$

where: C_i is the concentration of the ith radionuclide at the point of compliance; ECL_i is the effluent concentration limit for the ith radionuclide; and n is the number of radionuclides in the mixture. Provided that the unity rule is satisfied, compliance with the requirements of 10 CFR 20.1302 is demonstrated. Note that the left hand side of the unity rule equation is time dependent because the radionuclides in the mixture are retarded by varying degrees and would arrive at the point of compliance at different points in time.

RESULTS AND DISCUSSION OF CURRENT ASSESSMENTS

The analyses described above have been completed for 17 reactor sites and included in license applications submitted to the NRC. The complete applications are available online at http://www.nrc.gov/reactors/new-reactors/col.html. The accidental release assessments are included in Part 2, Final Safety Analysis Report, Section 2.4.13. Table 3 summarizes the groundwater travel times, surface water dilution factors (as applicable), sums of fractions (left-hand-side of unity rule), radionuclides having the greatest dose contributions, and methodologies used for reactive transport analysis. Groundwater travel time was selected as a representative site characteristic because: (a) travel time effectively integrates many of the important hydrogeologic properties (i.e., hydraulic conductivity, hydraulic gradient, effective porosity, groundwater travel distance) into a single parameter; and (b) travel time determines the amount of radionuclide attenuation due to radioactive decay. The surface water dilution factor was included because groundwater to surface water pathways are present at many of the sites, and dilution in surface water plays an important role in reducing radionuclide concentrations.

Table 3. Results of Accidental Release Assessments.

Site	Travel Time (y)	Dilution Factor	Sum of Fractions	Primary Radionuclides	Reactive Transport Methodology
Bell Bend	0.56	4.75E-06	4.70E-03	H-3	Kennedy and Strenge (1992)
Bellefonte	2.33	-	4.92E-02	H-3	Yu et al. (2007)
Callaway	3020	-	2.48E-01	I-129	Kennedy and Strenge (1992)
Calvert Cliffs	4.02	5.09E-04	4.29E-01	H-3	Kennedy and Strenge (1992)
Comanche Peak	-	-	2.20E-01	Cs-134, Cs-137	Assumed diluted in 1.7E+8 m^3 of water and 1-y decay
Grand Gulf	NA	-	7.93E-02	Zn-65	Yu et al. (2007)
Levy Co.	68	-	6.41E-03	H-3	Codell and Duguid (1983)
Nine Mile	21.5	1.43E-03	8.70E-01	H-3	Kennedy and Strenge (1992)
North Anna	5.03	1.02E-03	2.26E-01	Sr-90	Kennedy and Strenge (1992)
River Bend	2.63	-	1.69E-02	Ru-106, Mn-54, Ce-144, Sr-90, Y-90, H-3	Yu et al. (2007)
Harris	2.3	NA	1.40E-01	H-3	Codell and Duguid (1983)
South Texas	123	-	1.00E-02	H-3	Kennedy and Strenge (1992)
Victoria Co.	25.7	-	6.28E-01	H-3	Javandel et al. (1984)
Summer	17.4	1.34E-06	5.32E-04	H-3	Kennedy and Strenge (1992)
Vogtle	6.7	8.30E-05	5.80E-02	H-3	Kennedy and Strenge (1992)
Lee	NA	NA	2.44E-02	H-3	Yu et al. (2007)

Results in Table 3 indicate that the groundwater travel times vary widely, ranging from 0.56 to 3020 years and having a median value of 6.7 years. Groundwater to surface water pathways are present at 8 of 15 sites, with dilution factors ranging in magnitude from 10^{-3} to 10^{-6}. The sum of fractions for all sites is less than unity, suggesting that all sites meet 10 CFR 20.1302 requirements. Based on the magnitude of the dilution factors, it should be noted that compliance may not have been achieved without relying on surface water dilution. Results in Table 3 further indicate that H-3 has the greatest contribution to the sum of fractions at 11 of 16 sites, and is generally the primary radionuclide of interest. This occurs because: (a) initial H-3 concentrations are large relative to its ECL for the AP1000 and EPR technologies; (b) the 12.35-year half-live for H-3 is long relative to many of the site groundwater travel times; and (c) H-3, when integrated into a water molecule, does not undergo adsorption or retardation. In terms of methods used for reactive transport modeling, solutions derived from Kennedy and Strenge (1992) were applied at 8 of the sites, RESRAD-OFFSITE (Yu et al., 2007) was used at 4 of the sites, the solution given by Codell and Duguid (1983) was applied at 2 sites, and the one-dimensional solution given by Javandel et al. (1984) was used at one site.

For the Comanche Peak site, no site-specific accidental release assessment was performed. Instead, the applicant cited the generic assessment included in the US-APWR's Design Control Document, which assumes dilution of the released liquid in 1.7×10^8 m^3 of water prior to reaching the location of the potable water supply and one year of radioactive decay. Therefore, no site-specific travel time or dilution factor is reported for this site. In the Fermi license application, the applicant assumed that ESBWR design features would preclude an accidental release, citing

guidance provided in BTP 11-6 (NRC, 2007b). No assessment was therefore completed for this site.

SUMMARY AND CONCLUSIONS

The licensing of nuclear power reactors requires an assessment of a postulated accidental release of radioactive liquid effluent in ground and surface waters to demonstrate that the dose to an individual member of the public does not exceed regulatory limits. The assessment process requires definition of a radioactive source term, characterization of hydrological transport properties, and reactive transport modeling to predict radionuclide concentrations in water supplies accessible by the public. Seventeen assessments have been completed to date. The liquid effluent containing tanks postulated to fail are located below ground such that the liquid release would enter the groundwater and then be subject to groundwater transport offsite with concentrations being attenuated by the processes of radioactive decay, adsorption, and dispersion. Groundwater travel times vary widely from site to site and groundwater to surface water pathways are present for many of the sites. Comparing predicted concentrations to Federal limits indicates regulatory compliance at all sites.

REFERENCES

Clement, T.P. (1997). "RT3D - A Modular Computer Code for Simulating Reactive Multi-species Transport in 3-Dimensional Groundwater Aquifers." Battelle Pacific Northwest National Laboratory Research Report, PNNL-SA-28967.

Codell, R.B., and Duguid, J. D. (1983). "Radiological Assessment – A Textbook on Environmental Dose Analysis." NUREG/CR-3332.

Javandel, I., Doughty, C., and Tsang, C-F (1984). *Groundwater Transport: Handbook of Mathematical Models, Water Resources Monograph 10*, American Geophysical Union.

Kennedy, W.E., and Strenge, D.L. (1992). "Residual Radioactive Contamination from Decommissioning." NUREG/CR-5512, Volume 1, Pacific Northwest Laboratory.

Srinivasan, V. and Clement, T.P. (2008). Analytical solutions for sequentially coupled one-dimensional reactive transport problems – Part I: Mathematical Derivations, *Advances in Water Resources*, v. 31(2), P. 203-218.

U.S. Nuclear Regulatory Commission (2007a). "Combined License Applications for Nuclear Power Plants." Regulatory Guide 1.206.

U.S. Nuclear Regulatory Commission (2007b). "Standard Review Plan for the Review of Safety Analysis Reports for Nuclear Power Plants." NUREG-0800.

Zheng, Chunmiao, and P. Patrick Wang (1999). "MT3DMS, A Modular Three-dimensional Multi-species Transport Model for Simulation of Advection, Dispersion and Chemical Reactions of Contaminants in Groundwater Systems; Documentation and User's Guide." U.S. Army Engineer Research and Development Center Contract Report SERDP-99-1, Vicksburg, MS.

Yu et al. (2007). "User's Manual for RESRAD-OFFSITE, Version 2." NUREG/CR-6937.

MODELING OF CHLORINATED VOCs TRANSPORT UNDER DUAL BIOREACTIONS

Wonyong Jang and Mustafa M. Aral
Multimedia Environmental Simulation Laboratory, School of Civil and Environmental Engineering, Georgia Institute of Technology, Atlanta, GA, USA

ABSTRACT

Once chlorinated volatile organic compounds (CVOCs) are released into the subsurface they are spread out through the porous soil matrix by complicated processes such as advection, dispersion, and sorption. CVOCs can be also biodegraded by indigenous microorganism via aerobic and anaerobic bioreactions, which generate distinct benign or harmful by-products. Heterogeneous subsurface characteristics and non-uniform distribution and consumption of oxygen in the subsurface may allow the dual bioreactions to coexist within a representative subsurface volume (RSV). The portion of each bioreaction within a RSV will depend on multiple factors such as oxygen, contaminant, and microorganism levels. Oxygen can be supplied into the contaminated zone through the dispersive and advective transport of oxygen in gas phase as well as the flow of the groundwater containing dissolved oxygen. As the dual bioreactions are coupled with multiple fluid flows (groundwater and gas) and multispecies transport, the analysis of the bioreactions is very complicated. However, the enhanced understanding of the dual bioreactions of CVOCs is required in accurately predicting the fate and transport of CVOCs at the contaminated sites.

This study numerically investigates: the effects of dual bioreactions on the fate and transport of CVOCs in the variably saturated zone; and, the temporal and spatial evolution of bioreaction zones in the domain. Trichloroethylene is selected as a primary contaminant, and its sequential aerobic/anaerobic bioreactions are considered.

INTRODUCTION

Soil and groundwater contamination is often initiated by an accidental spill or leakage of chlorinated volatile organic compounds (CVOCs), such as trichloroethylene (TCE) and dichloroethylenes (DCEs), in the form of a non-aqueous phase liquid (NAPL). Leaked NAPL CVOCs volatilize into soil gas, dissolve into water, and absorb onto soil in multi-phase subsurface environments. They often become a long-lasting contaminant source, contributing to subsurface pollution, which may cause ecological and/or human health risks. The transport of the contaminants in the subsurface is a combined outcome of complicated processes such as advection, dispersion, sorption, and chemical and biological transformations. Among those multiple processes, biological transformation of CVOCs can play an important role in converting the toxic contaminant into daughter toxic contaminants or into benign chemicals within the aerobic-anaerobic subsurface environment.

Biological degradation of CVOCs depends on many physicochemical and biological parameters such as oxygen, carbon-sources, and indigenous microorganisms. And the bioprocesses of CVOCs are typically divided into three

main groups: dehalogenation, cometabolism, and oxidation for growth under anaerobic or aerobic conditions (Figure 1). Under anaerobic conditions, TCE can be biologically transformed by sequential reductive dechlorination: TCE ⇒ dichloroethylenes (DCEs) ⇒ vinyl chloride (VC)⇒ Ethene (Figure 1). Under aerobic conditions, however, CVOCs can be biologically degraded via cometabolic processes, which usually don't generate harmful byproducts.

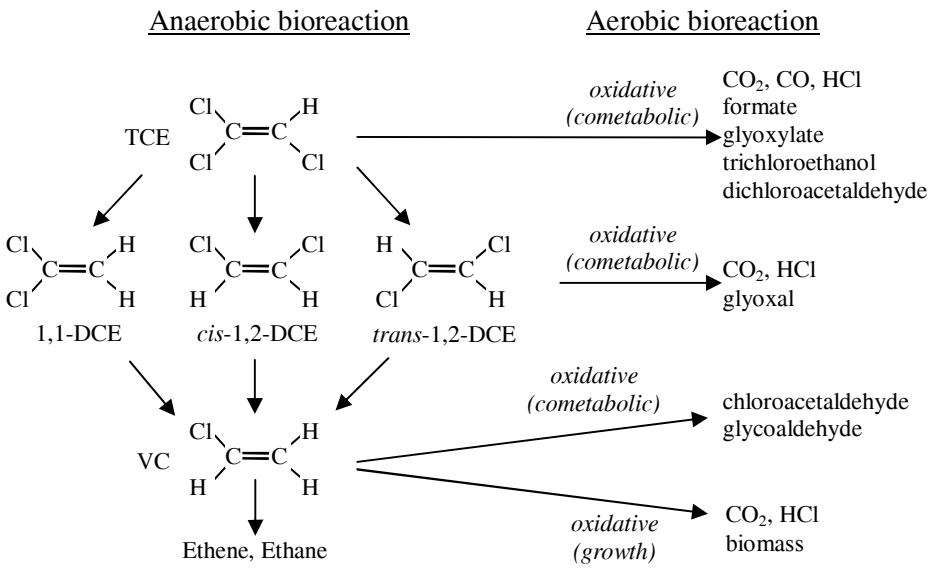

Figure 1. Anaerobic/aerobic degradation of CVOCs.

The aerobic and anaerobic biotransformation of CVOCs has been reported at contaminated sites (Hinchee et al. 1995; Lenczewski et al. 2003). At TCE-contaminated sites, DCEs and VC were also detected within both water and gas phases in the unsaturated zone as well as within the water in the saturated zone (Maslia et al. 2007). These occurrences are due to anaerobic biotransformation and partitioning processes of the contaminants (Lorah and Olsen 1999; Wiedemeier 1998). In addition to anaerobic bioreactions of CVOCs, aerobic bioreactions of DCEs and VC have been also documented at contaminated sites, especially at the aerobic fringe of contaminant plumes (Clement et al. 2000; Lenczewski et al. 2003). It is important to note that the anaerobic and aerobic bioreactions of CVOCs, coexisting at contaminated sites, generate totally different byproducts (Figure 1), resulting in distinct environmental effects. Thus, a well-defined classification of target sites into co-existent aerobic or anaerobic regions is very important in accurately predicting the fate and transport of parent and daughter contaminants.

The subsurface is highly heterogeneous in terms of hydro-geological, physical, chemical, and biological conditions. Considering the heterogeneities, such as rate-limited dispersion of oxygen through porous media and locally distinct utilization of oxygen, we could expect three-types of bioreaction blocks: pure aerobic block, pure anaerobic block, and aerobic-anaerobic-mixed block. The last block refers to a representative subsurface element, in which both aerobic and anaerobic bioreactions occur simultaneously. The concentration and distribution of oxygen in

the subsurface system result from complicated interrelationships between oxygen supply and consumption. Oxygen can be transported into the ground via air circulation between the atmosphere and the subsurface mostly in the unsaturated zone or induced oxygen supply in air sparging (Jang and Aral 2007a; 2009). Aerobic biological processes consume oxygen as an electron acceptor, resulting in the reduction of oxygen concentration.

The purpose of this study is to investigate the aerobic-anaerobic biological transformation of CVOCs and their fate and transport in the subsurface. We focus on the evolution of aerobic and anaerobic bioreaction zones and the development of contaminant plumes under the dual biodegradation of the contaminants. Among CVOCs, TCE is selected as a primary NAPL contaminant. Sequential dehalogenation and cometabolism of contaminants are considered as biological processes in anaerobic and aerobic subsurface environments.

MATHEMATICAL FORMULATION AND NUMERICAL METHOD

The groundwater system considered here consists of groundwater, soil gas, solid soil, and nonaqueous phase liquid (NAPL) TCE. The NAPL TCE is only present in a TCE source area and is assumed to be immobile. The groundwater and soil gas are mobile here, leading to two-phase flow (multiphase flow) in the subsurface system. Contaminant migration occurs along with the flows of groundwater and soil gas.

Flow Equation of Groundwater and Gas: The governing equation for multiphase flow can be written as (Jang and Aral 2007b)

$$\frac{\partial\left(\phi s_f \rho_f\right)}{\partial t} = \nabla \cdot \left[\frac{\rho_f k_m k_{rf}}{\mu_f} \left(\nabla P_f + \rho_f g \nabla z \right) \right] + I_f + Q_f; \quad f = g, w \tag{1}$$

where the subscript f represents the mobile fluids (g: gas and w: water), ϕ is the porosity, s is fluid saturation, ρ is fluid density (ML^{-3}), μ is the dynamic viscosity ($ML^{-1}T^{-1}$), k_r is relative permeability, k_m is the intrinsic permeability tensor for the soil media (L^2), P is the fluid pressure ($ML^{-1}T^{-2}$), g is the gravitational constant (LT^{-2}), z is elevation (L), I_f indicates a sink/source term for the gas phase due to the partitioning processes of contaminants between phases ($ML^{-3}T^{-1}$), and Q is a sink/source ($ML^{-3}T^{-1}$).

Contaminant Fate and Transport Equation: The transport equation of multiple contaminants in the water and gas phases can be written as

$$\frac{\partial\left(\phi s_f C_f^i\right)}{\partial t} = \nabla\left(\phi s_f D_f^i \nabla C_f^i\right) - \nabla\left(q_f C_f^i\right) + I_{f,MT}^i + I_{f,BT}^i \tag{2}$$

where the superscript i and the subscript f represent indexes for chemical species and fluid phases, respectively; C is a concentration of contaminants in each phase (ML^{-3}); D and q are the dispersion tensor (L^2T^{-1}) and Darcy flux (LT^{-1}), respectively; and, I_{MT} and I_{BT} indicate inter-phase mass transfer of contaminants and biotransformation ($ML^{-3}T^{-1}$), respectively. Applying first-order relationships in describing the

dissolution, volatilization, and water-gas partitioning processes for contaminants, the mass transfer terms for the water and the gas phases can be written as,

$$I^i_{w,MT} = \phi s_w \lambda^i_D \left(C^i_{we} - C^i_w\right) + \phi s_g \lambda^i_H \left(C^i_g - H^i C^i_w\right) \quad (3)$$

$$I^i_{g,MT} = \phi s_g \lambda^i_V \left(C^i_{ge} - C^i_g\right) - \phi s_g \lambda^i_H \left(C^i_g - H^i C^i_w\right) \quad (4)$$

where λ_D, λ_V and λ_H are the first-order mass transfer coefficients (T^{-1}) for NAPL/water, NAPL/gas and water/gas phases, respectively; C_{we} and C_{ge} are the maximum contaminant concentrations in water and gas phases, respectively; and, H is a dimensionless Henry's law coefficient. Biological transformations under anaerobic and aerobic conditions, as shown in Figure 1, yield different byproducts. The biological processes of TCE considered herein are listed in Table 1. Among the three isomers of DCEs, cDCE is chosen as the representative of the isomers.

Table 1. Simplified anaerobic and aerobic biotransformation of TCE.

Reaction	Kinetics
• Anaerobic dehalogenation without inhibition or with sequential inhibition. TCE → cDCE → VC	• First-order • Michaelis-Menten
• Aerobic biodegradation. TCE, cDCE, VC → (Oxygen and microbes) → CO_2, H_2O, HCl	• First-order • Michaelis-Menten
• No bioreaction due to lack of carbon sources and/or microorganisms.	None

The bioreaction kinetics of contaminants is very important in designing a bioremediation system, and is also required as components of fate and transport models (Alvarez-Cohen and Speitel 2001). Due to the complexities of biological processes of contaminants, however, it is almost impossible to entirely understand and express all biological reaction mechanism and kinetics. In numerical applications, Michaelis-Menten (or Monod) and first-order kinetics are often used to express reductive dechlorination and cometabolic biodegradation reactions of chlorinated hydrocarbons (Alvarez-Cohen and Speitel 2001; Clement et al. 2000; Haston and McCarty 1999; Schmidt et al. 1985; Wiedemeier 1998). The two kinetics are used herein to delineate co-existing aerobic-anaerobic bioreactions of CVOCs (Table 1). Michaelis-Menten model are (Pavlostathis and Prytula 2000):

$$r_b = -\frac{k' C}{K_S + C} \quad (5)$$

where r_b is the rate of bioreactions ($ML^{-3}T^{-1}$); $k' = kX$ is the maximum bioreaction rate (MT^{-1}); k is the maximum specific rate of substrate degradation ($M_{substrate}\ M^{-1}_{cell}\ T^{-1}$); C is the chemical concentration (ML^{-3}); X is the active microbial concentration (ML^{-3}); K_S is the half-saturation constant for the substrate (ML^{-3}). A first-order model can be written as:

$$r_b = -k_1 C \tag{6}$$

where k_1 is the first-order reaction coefficient (T^{-1}). The biological processes can be expressed:

$$I^i_{w,BT,Anaerobic} = \phi s_w \varepsilon r^{i-1}_{b,Anaerobic} - \phi s_w \varepsilon r^i_{B,Anaerobic} \quad \text{for anaerobic bioreaction} \tag{7}$$

$$I^i_{w,BT,Aerobic} = -\phi s_w (1-\varepsilon) r^i_{B,Aerobic} \quad \text{for aerobic bioreaction} \tag{8}$$

where ε is a ratio of an anaerobic bioreaction to all bio-reaction within a soil matrix.

A three-dimensional Galerkin-finite-element-based numerical model, TechFlowMP (Jang and Aral 2005) is used to solve the multiphase flow and contaminant transport equations. Globally-continuous Darcy velocity estimation process, which was proposed by Yeh (1981), is applied here to improve the accuracy and also to overcome the discontinuity problems in calculating flow velocities.

MODEL APPLICATION

A two-dimensional unconfined aquifer with dimensions of (200 m × 16 m) in (x, y) directions, shown in Figure 2, is used to investigate the plume evolution of TCE, cDCE, and VC under aerobic and anaerobic biotransformation and density-driven advection of the gas phase. TCE in NAPL as a primary contaminant is introduced to the unsaturated zone and resides in the pore spaces as an immobilized contaminant source. The TCE residual is set to NAPL saturation of 0.1 at the source zone.

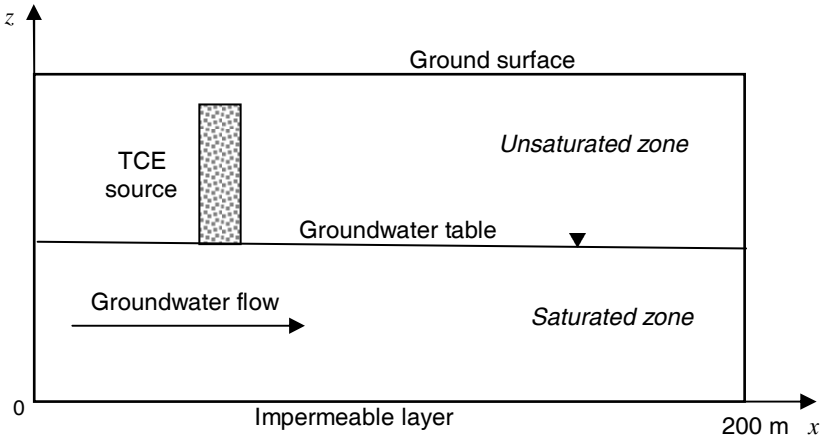

Figure 2. A modeling domain for dual biotransformation of CVOCs.

Initial concentrations of TCE, cDCE, and VC in gas, water, and solid soil phases are set to zero within the domain. As boundary conditions at the ground surface, infiltration for water phase, and constant atmospheric pressure for gas phase are applied. For contaminant transport in gas phase, the ground surface is set to a stagnant boundary layer of 0.3 m thickness. The parameters of a soil medium used here are: k_m=1.0×10^{-10} m^2 and Porosity ϕ=0.35. First-order rate coefficients for dissolution, water-gas partitioning, and volatilization are 1.0 d^{-1}.

Three scenarios are considered here to examine the effect of dual biological reactions on contaminant transport in the subsurface system:

- Case I: Single anaerobic biotransformation can occur in the whole modeling domain. No aerobic bioprocess is assumed.
- Case II: Dual bioreactions. Both anaerobic and aerobic bioreactions coexist in the domain.
- Case II: No bioreaction

EXPECTED RESULTS

The co-existence concept of aerobic and anaerobic bioreactions is implemented in analyzing the transport of multiple CVOCs within the flow of gas and groundwater in the subsurface. In this study, we expect to present the following outcomes:

- the effects of dual bioreactions on the fate and transport of CVOCs in the variably saturated zone;
- the temporal and spatial evolution of bioreaction zones in the domain; and
- the variation in the concentrations of oxygen and other nutrients in the subsurface domain.

The bioreactivity for both aerobic and anaerobic processes can be evaluated according to the distribution and availability of carbon sources for microorganisms. Under the consideration of no, single, and/or simulataneous-multiple bioreactions of CVOCs, more accurate fate and transport of both parent and daughter contaminants could be predicted, which will enhance our understanding of natural attenuation processes at contaminated sites. The temporal and spatial concentration distributions of the contaminants could be used in identifying highest-contamination regions and in assessing potential human health risk due to the toxicity effects.

REFERENCE

Alvarez-Cohen, L., and Speitel, G. E. (2001). "Kinetics of aerobic cometabolism of chlorinated solvents." *Biodegradation*, 12(2), 105-126.

Clement, T. P., Johnson, C. D., Sun, Y. W., Klecka, G. M., and Bartlett, C. (2000). "Natural attenuation of chlorinated ethene compounds: model development and field-scale application at the Dover site." *Journal of Contaminant Hydrology*, 42(2-4), 113-140.

Haston, Z. C., and McCarty, P. L. (1999). "Chlorinated ethene half-velocity coefficients (K-s) for reductive dehalogenation." *Environmental Science & Technology*, 33(2), 223-226.

Hinchee, R. E., Wilson, J. T., and Downey, D. C. (1995). *Intrinsic bioremediation*, Battelle Press, Columbus.

Jang, W., and Aral, M. M. (2005). "Three-dimensional Multiphase Flow and Multi-species Transport Model, TechFlowMP." *Report No. MESL-02-05*, Multimedia Environmental Simulations Laboratory, School of Civil and Environmental Engineering, Georgia Institute of Technology, Atlanta, GA.

Jang, W., and Aral, M. M. (2007a). "Density-driven transport of volatile organic compounds and its impact on contaminated groundwater plume evolution." *Transport in Porous Media*, 67(3), 353-374

Jang, W., and Aral, M. M. (2007b). "Effect of Biotransformation on Multispecies Plume Evolution and Natural Attenuation." *Transport in Porous Media*, DOI : 10.1007/s11242-007-9145-0 (In press).

Jang, W., and Aral, M. M. (2009). " Multiphase Flow Fields in In-situ Air Sparging and its Effect on Remediation." *Transport in Porous Media*, 76(1), 99-119.

Lenczewski, M., Jardine, P., McKay, L., and Layton, A. (2003). "Natural attenuation of trichloroethylene in fractured shale bedrock." *Journal of Contaminant Hydrology*, 64(3-4), 151-168.

Lorah, M. M., and Olsen, L. D. (1999). "Natural attenuation of chlorinated volatile organic compounds in a freshwater tidal wetland: Field evidence of anaerobic biodegradation." *Water Resources Research*, 35(12), 3811-3827.

Maslia, M. L., Sautner, J. B., Faye, R. E., Suárez-Soto, R. J., Aral, M. M., Grayman, W. M., Jang, W., Wang, J., Bove, F. J., Ruckart, P. Z., Valenzuela, C., Green, J. W. J., and Krueger, A. L. (2007). "Analyses of groundwater flow, contaminant fate and transport, and distribution of drinking water at Tarawa Terrace and vicinity, U.S. Marine Corps Base Camp Lejeune, North Carolina: Historical reconstruction and present-day conditions—Executive Summary. Agency of Toxic Substances and Disease Registry, Atlanta, GA. In press."

Pavlostathis, S. G., and Prytula, M. T. (2000). "Kinetics of the sequential microbial reductive dechlorination of hexachlorobenzene." *Environmental Science & Technology*, 34(18), 4001-4009.

Schmidt, S. K., Simkins, S., and Alexander, M. (1985). "Models for the Kinetics of Biodegradation of Organic-Compounds Not Supporting Growth." *Applied and Environmental Microbiology*, 50(2), 323-331.

Wiedemeier, T. H. (1998). *Technical protocol for evaluating natural attenuation of chlorinated solvents in ground water*, National Risk Management Research Laboratory Office of Research and Development, Cincinnati, Ohio.

Yeh, G. T. (1981). "On the computation of Darcian velocity and mass balance in the finite-element modeling of groundwater-flow." *Water Resources Research*, 17(5), 1529-1534.

Reaction Rates in a Transport System with Both Kinetic and Equilibrium Reactions

Gour-Tsyh (George) Yeh[1] and Yilin Fang [2]

[1]Dept. of Civil and Environ. Eng., Univ. of Central Florida, Orlando, FL 32816-2450 PH (407) 823-2317; FAX (407) 823-3315; email: gyeh@mail.ucf
[2]Pacific Northwest National Lab, P.O. Box 999, MS K9-36, Richland, WA 99352 PH (509) 372-4051; email: yilin.fang@pnl.gov

Abstract

The argument of what is the rate of an equilibrium reaction in a transport system is very controversial. It has been argued that the rate of an equilibrium reaction "can be mathematically abstracted as infinity" for the convenience of decoupling equilibrium reactions from kinetic reactions. It has also been argued that the rate of an equilibrium reaction is indefinite. This controversy should not have been aroused at all since, by definition, an equilibrium reaction should not have been associated with a rate per se. We can associate a rate to an equilibrium reaction only if we treat it as an extremely fast kinetic reaction. Then it is legitimate to ask what its rate is. For an extremely fast reaction, its forward and backward rates are asymptotically tending to infinity. The question is then what is its net rate? To answer this question, it is necessary to understand the interplay between transport and reactions. Transport processes and kinetic reactions try to alter the concentrations at each time and at each point of the computational domain. The rates of equilibrium reactions are those rates which are "necessary" to assure that the thermodynamic equations remain fulfilled, i.e., the solution of the concentration field remains on the manifold defined by thermodynamic equations. With this definition of the rates of equilibrium reactions, we can calculate the posteriori equilibrium rates using a subset of decomposed transport equations after all species concentrations are solved. Thus the rate of a fast equilibrium reaction is finite and definite. On the other hand, rates of kinetic reactions require either proposition of reaction pathways or empirical rate equations. Two example problems are used to demonstrate how consistent sets of governing equations are employed to simulate rates of asymptotic kinetic reactions or fast/equilibrium reactions.

1. Introduction

Groundwater has always played an important role in human's history and groundwater contamination has been attracting intensive investigations since the mid 1980's. Contaminants in the water environment undergo changes in concentration resulting from physical, chemical, and/or biological processes, and a capability to understand and model these processes is at the core of water-quality management

(Chin, 2000). Accurate tools for reliable prediction of contaminant migration and transformation are necessary to support the task. Consideration of equilibrium chemistry, kinetic chemistry, and hydrologic transport and the interaction between fluid flow and reactive transport is necessary to be able to reflect the complexity of many real systems. For example, solid phase reactions including precipitation and dissolution can potentially plug pores or open fractures reducing matrix diffusion and promoting rapid flow through fractures.

The development of mechanistically-based reactive chemical transport models has exploded in the last two decades (Yeh and Tripathi, 1989, 1990; Nienhuis et al., 1991; Engesgaard and Kipp, 1992; Šimunnek and Squares, 1994; Chilakapati, A. 1995; Steefel and Yabusaki, 1996; Lichtner and Seith, 1996; Steefel and Van Cappellen, 1998; Tebes-Stevens et al., 1998; Nitao, 1998; Parkhurst and Appelo, 1999; Mann, 2000; Bacon et al., 2000; Steefel, 2001; Yeh et al., 2001; Xu et al., 2003; Yeh et al., 2004a, 2004b; Yang et al., 2008). These numerical reactive transport models have had varied scopes. Many models have coupled simulation of transport with equilibrium geochemistry (e.g. Miller and Benson, 1983; Cederberg et al., 1985; Hostetler and Erikson, 1989; Narasimhan et al., 1986; Liu and Narasimhan, 1989; Griffioen, 1993; Yeh and Tripathi, 1991; Cheng, 1995; Parkhurst, 1995). Some models couple transport with kinetic geochemistry for certain geochemical processes like precipitation-dissolution (e.g. Lichtner, 1996; Steefel and Yabusaki, 1996; Suarez and Šimunnek, 1996) or adsorption (e.g. Theis et al., 1982, Lensing et al., 1994). General reactive transport models capable of handling a complete suite of geochemical reaction processes (aqueous complexation, adsorption, precipitation-dissolution, acid-base, and reduction-oxidation phenomena) and allow any individual reaction for any of these geochemical processes to be handled as either equilibrium or kinetic as appropriate for the system being considered have emerged since the late 1990's and early 2000's (e.g., Yeh et al., 1996; Bacon et al., 2000; Steefel, 2001; Steefel, CRUNCH; Yeh et al., 2001; Xu et al.,2003). A number of models combine the ability to simulate transport with microbial growth and biodegradation reactions but do not encompass inorganic geochemistry (e.g. Widdowson et al., 1988; Kindred and Celia, 1989; Taylor and Jaffee, 1990; Wood et al., 1994; Dykaar and Kitandidis, 1996). Work in reactive transport modeling has been done to couple microbially mediated and at least some purely geochemical processes with transport. Marzel et al. (1994) includes microbial reactions and equilibrium aqueous geochemical speciation. Rittman and Van Briessen (1996) couple equilibrium aqueous complexation and kinetic adsorption with microbiological degradation. Hunter et al. (1998) couple one-dimensional transport with microbial and geochemical reactions for a suite of reactions involving major redox and acid-base pair species. Smith and Jaffee (1998) couple one-dimensional transport with equilibrium speciation and kinetic biogeochemical reactions affecting trace metal transport. Coupled specific microbiological and generic geochemical processes have also been developed (Salvage and Yeh, 1998; Yeh et al. 1998). Chilakapathi (1995) provides significant flexibility in handling any type of kinetic biogeochemical reaction coupled with transport, representing equilibrium processes as fast reversible kinetic reactions, but requires problem specific modifications to the code for new simulations to be run. Recently, these types of reaction-based paradigms capable of simulating any number

of reactions incarnating both geochemical and biological processes have gained popularities and implemented in a number of codes (e.g., Yeh et al. 2004a, 2004b; Kräutle and Knabner, 2005, 2006; Zhang et al. 2007).

This paper describes the development and application of the latest versions of HYDROGEOCHEM (Yeh et al. 2008a, 2008b), a mechanistically-based numerical model for simulation of coupled fluid flow, thermal transport, and reactive chemical transport in variably saturated porous and fractured media. These latest versions are a slight modification of the previous versions. A concept of defining reaction rates of fast reactions is proposed, which makes the modeling of mixed fast/equilibrium and slow/kinetic reactions consistent. The argument of what is the rate for an equilibrium reaction is very controversial. It has been argued that the rate of an equilibrium reaction "can be mathematically abstracted as infinity" for the convenience of decoupling equilibrium reactions from kinetic reactions (Fang et al., 2003). It has also been argued that the rate of an equilibrium reaction is indefinite (Lichtner, 1996). This controversy should not have been aroused at all since, by definition, an equilibrium reaction should not have been associated with a rate per se. We can associate a rate to an equilibrium reaction only if we treat it as a fast kinetic reaction. When we treat an equilibrium reaction as a fast kinetic reaction, then "the rate of an equilibrium reaction is the rate which is 'necessary' to assure that the corresponding thermodynamic equation remains fulfilled." With this definition of equilibrium reactions, we can make posteriori calculation of the rates of equilibrium reactions after all species concentrations are solved. Furthermore, with this definition, all equilibrium reactions must be linearly independent so the system of governing equations is exactly determined. Two example problems are used to demonstrate how consistent sets of governing equations are employed to simulate rates of asymptotic kinetic reactions or fast/equilibrium reactions. For kinetic reactions, both reaction-pathway and empirical approaches to calculate their rates are discussed.

2. Governing Equations of Reactive Transport

The reactive transport equation of any species can be derived based on the conservation law of material mass stating that the rate of mass change is due to biogeochemical reactions (Yeh, 2000)

$$\sum_{i\in\{M\}} \mu_{ik}\hat{C}_i \quad \Leftrightarrow \quad \sum_{i\in\{M\}} \nu_{ik}\hat{C}_i, \;\; k\in\{N\} \tag{1}$$

and advective-dispersive transport as

$$\frac{\partial(\theta C_i)}{\partial t} = \iota_i L(C_i) + \theta \sum_{k\in\{N\}} (\nu_{ik} - \mu_{ik}) R_k, \;\; i\in\{M\} \tag{2}$$

in which

$$L(C_i) = -\nabla\cdot(\mathbf{V}C_i) + \nabla\cdot[\theta\mathbf{D}\cdot\nabla C_i] \tag{3}$$

where μ_{ik} is the reaction stoichiometry of the i-th species in the k-th reaction associated with the reactants; $\hat{C}_i$ is the chemical formula of the i-th species; ν_{ik} is the

reaction stoichiometry of the *i*-th species in the k-th reaction associated with the products; $\{N\}=\{1,2,...,N\}$ in which N is the number of reactions; θ is the effective moisture content (L^3/L^3); C_i is the concentration of the *i*-th species in unit of chemical mass per water volume [M/L^3]; t is the time (T); ι_i is an indicator, $\iota_i=1$ if C_i is a mobile species, $\iota_i=0$ if C_i is an immobile species; L is the advection-dispersion transport operator; R_k is the rate of the *k*-th reaction in chemical mass per water volume per unit time [$M/L^3/T$]; $\{M\}=\{1,2,...,M\}$ in which M is the number of species; **V** is the Darcy's velocity of groundwater (L/T); and **D** is the dispersion coefficient tensor [L^2/T]. In the summation on the right-hand-side of Equation (1), $\nu_{ik}=0$ if $\hat{C}_i$ is not a product of the *k*-th reaction and $\mu_{ik}=0$ if $\hat{C}_i$ is not a reactant of the *k*-th reaction.

Initial conditions for every immobile species must be prescribed. No boundary condition is needed for any immobile species. On the other hand, for every mobile species, in addition to initial conditions, boundary conditions must be specified. Four types of boundary conditions are taken into account, including Dirichlet, variable (inflow-outflow), Cauchy, and Neumann (Yeh et al., 2004a, 2004b).

There are $M+N$ unknowns (M $C_i's$ and N $R_k's$) but only M equations in Equation (1). The system needs to be closed. Let us assume that there are N_E fast/equilibrium reactions (which must be all linearly independent) and N_K slow/kinetic reactions, i.e., $N=N_E+N_K$, where N_E and N_K are the number of equilibrium/fast reactions and kinetic/slow reactions, respectively. For N_K reactions, a rate equation can be formulated for each reaction as

$$R_k=f_k,\ k\in\{N_K\} \tag{4}$$

where $f_k=f_k\left(C_i:i\in\{M\}\right)$ is an explicit function of M $C_i's$ that represents the rate equation of the *k -th* reaction and $\{N_K\}\subset\{N\}$ is the set index of kinetic reactions having N_K members. Substitution of Eq. (4) into Eq. (1) yields

$$\frac{\partial(\theta C_i)}{\partial t}=\iota_i L(C_i)+\theta\sum_{k\in\{N_K\}}(\nu_{ik}-\mu_{ik})f_k+\theta\sum_{k\in\{N_E\}}(\nu_{ik}-\mu_{ik})R_k,\ i\in\{M\} \tag{5}$$

where $\{N_E\}\subset\{N\}$ is the set index of equilibrium/fast reactions having N_E members.

Equation (5) still involves more unknowns (M $C_i's$ and N_E $R_k's$) than the number of equations (M). To close the system, for every equilibrium reaction, thermodynamic approaches are used where a consistent algebraic equation, for example a mass action equation, can be used to describe the corresponding fast/equilibrium reaction as

$$F_k\left(C_i : i \in \{M\}\right) = 0,\ e.g.\ \beta_k^E - \prod_{i \in M} \left(C_i\right)^{\nu_{ik}} / \prod_{i \in M} \left(C_i\right)^{\mu_{ik}} = 0,\ \ k \in \{N_E\} \qquad (6)$$

where $F_k\left(C_i : i \in \{M\}\right) = 0$ is a nonlinear algebraic equation and β_k^E is the modified equilibrium constant of the *k -th* equilibrium reaction (Yeh and Tripathi, 1989). Equations (5) and (6) constitute a system of M nonlinear transport equations and N_E nonlinear algebraic equations for M $C_i's$ and N_E $R_k's$ of unknowns. Simultaneous solutions of this system of M reactive transport equations and N_E nonlinear algebraic equations over the entire domain of interest would demand excessive computational time and computer storage (Yeh and Tripathi, 1989) even with today's computer capacities.

3. Decomposition of Reactive Transport Equations

Decoupling of the N_E $R_k's$ unknowns from the M $C_i's$ unknowns can be made via the Gauss-Jordan reduction of reaction networks (Chilakapati, et al., 1998; Fang, 2003; Kräutle and Knabner, 2007). Performing matrix decomposition of the reaction matrix in Eq. (5), we can reduce it into two subsets of equations as described below.

1) $M - N_E$ transport-equations for $M - N_E$ reaction extents

$$\frac{\partial \theta E_i}{\partial t} = L\left(E_i^m\right) + \theta \sum_{j \in \{N_K\}} D_{ij} f_j,\ i \in \{M - N_E\} \text{ in which } E_i = \sum_{j \in \{M\}} a_{ij} C_j \qquad (7)$$

where E_i is the *i-th* reaction extent [M/L^3]; E_i^m is the portion of E_i , which contains the linear combination of only mobile species; D_{ij} is an element of decomposed reaction matrix; $\{M - N_E\} \subset \{M\}$ having $(M - N_E)$ members is a subset of $\{M\}$; and a_{ij} is the element of a $M \times M$ matrix resulted from the matrix decomposition of a unit matrix and it represents the coefficient of the linear combination of θC_j in E_i.

2) N_E rate-equations for N_E fast/equilibrium reactions

$$\theta D_{ik} R_k = \frac{\partial \theta E_i}{\partial t} - L\left(E_i^m\right) - \theta \sum_{j \in \{N_k\}} D_{ij} f_j,\ k \in \{N_E\},\ i \in \{M_E\} \qquad (8)$$

where D_{ik} is an element of decomposed reaction matrix corresponding to a linearly independent equilibrium reaction; E_i , the *i-th* reaction extent, shall be called an equilibrium variable since it corresponds to a linearly independent equilibrium reaction; and $\{M_E\}$, having M_E $(= M - N_E)$ members, is a subset of $\{M\}$

Before proceed further, several comments are in order here. Firstly, instead of solving M nonlinear reactive transport equations in Equation (5) and N_E nonlinear

algebraic equations in Equation (6) simultaneously, one solves $(M - N_E)$ nonlinear reactive transport equations in Equation (7) one by one for $(M - N_E)$ reaction extents, $E_i's$. Having obtained these variables, $(M - N_E)$ $E_i's$ over the domain, one then solves $(M - N_E)$ linear algebraic equations of Equation (9) and N_E nonlinear algebraic equations for M species concentrations, $C_i's$, at the discretized domain of interest point by point

$$\sum_{\ell \in \{M\}} a_{i\ell} C_\ell = E_i, \quad i \in \{M - N_E\}; \quad F_k\left(C_\ell : \ell \in \{M\}\right) = 0, \quad k \in \{N_E\} \tag{9}$$

Secondly, the argument of what is the rate for an equilibrium reaction is very controversial. It has been argued that the rate of an equilibrium reaction "can be mathematically abstracted as infinity" for the convenience of decoupling equilibrium reactions from kinetic reactions (Fang et al., 2003). It has also been argued that the rate of an equilibrium reaction is indefinite (Lichtner, 1996). This controversy should not have been aroused at all since, by definition, an equilibrium reaction should not have been associated with a rate per se. We can associate a rate to an equilibrium reaction only if we treat it as a fast kinetic reaction. When we treat an equilibrium reaction as a fast kinetic reaction, then "the rate of an equilibrium reaction is that rate which is 'necessary' to assure that the corresponding thermodynamic equation remains fulfilled." With this definition of equilibrium reactions, we can posteriori calculate the N_E rates of N_E equilibrium reactions with Equation (8) after all species concentrations are solved.

4. Numerical Methods

Ideally, one would like to use a numerical approach that is accurate, efficient, and robust. Depending on the specific problem at hand, different numerical approaches may be more or less suitable. For research applications, accuracy is the primary requirement, because one does not want to distort physics due to numerical errors. On the other hand, for large field-scale problems, efficiency and robustness are primary concerns as long as accuracy remains within the bounds of uncertainty associated with model parameters. Thus, to provide accuracy for research applications and efficiency and robustness for practical applications, three coupling strategies (Yeh et al., 2006 and Hammond et al., 2005) were investigated to deal with reactive chemistry. They are: (1) a fully-implicit scheme, (2) a mixed predictor-corrector/operator-splitting method, and (3) an operator-splitting method. For each time-step, we first solve the advective-dispersive transport equations with or without reaction terms. We then solve the reactive chemical system node-by-node to yield concentrations of all species. Details of these coupling strategies can be found elsewhere (Yeh et al., 1996).

Five numerical methods are investigated for solution of the advective-dispersive transport equations (Yeh et al., 2006). Method 1, the finite element methods (FEM) is applied to the conservative form of the transport equations. Method 2, the FEM is

applied to the advective form of the transport equations. Method 3, the modified Lagrangian-Eulerian (LE) approach is applied to the Lagrangian form of the transport equations. Method 4, the LE approach is applied to all interior and downstream boundary nodes while the FEM is applied to the conservative form of the transport equations for the upstream flux boundaries. Method 5, the LE approach is applied to all interior and downstream boundary nodes while the FEM is applied to the advective form of the transport equations for upstream flux boundaries.

In the Lagrangian-Eulerian approaches, there are two computational steps. The first step is to compute the Lagrangian concentration with particle tracking methods dealing with the advection term, and the second step is to compute the final concentration with finite element method dealing with all other terms in the transport equation (Yeh, 1990).

5. Demonstration Examples

Example 1: This example is used to demonstrate the need of species switching in dealing with stiff reactive system under transport and to illustrate the computation of fast/equilibrium rates. It involves the transient simulation of advection-dispersion and equilibrium complexation/precipitation reactions in a domain having a size of 10 dm x 5,000 dm. The domain consists of three heterogeneous zones and is discretized with 200 equal size elements, a moisture content of 0.3, a constant flow field of 155.5 dm/day, and a longitudinal dispersivity of 150 dm (Figure 1). The chemical reactions are shown in Table 1. The network consists of 24 reactions (20 aqueous complexation and four precipitation-dissolution reactions) involving 30 species excluding the species H_2O(aq).

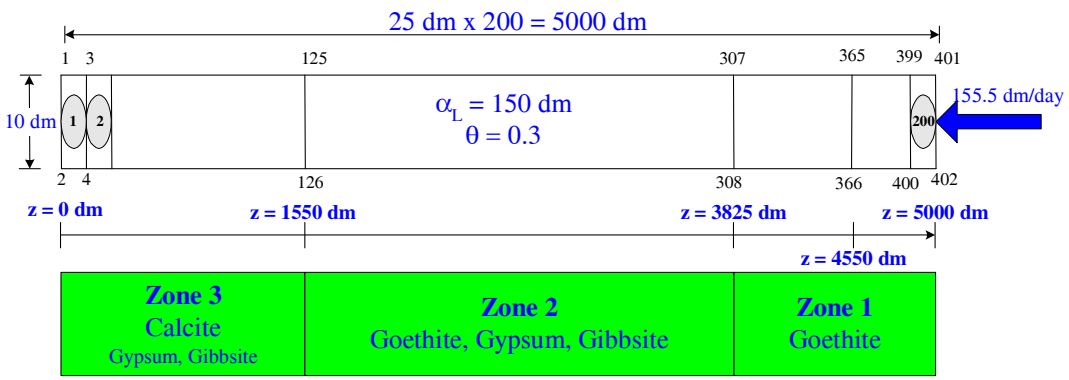

Figure 1 Problem domain and discretization Example 1

Table 1 Reaction Network for Example 1

Reaction	Number	Parameter
Aqueous Complex Reaction		
$H_2O(aq) \leftrightarrow H^+ + OH^-$	(R1)	$LogK_e$= -14.00
$Fe^{3+} + H_2O \leftrightarrow H^+ + FeOH^{2+}$	(R2)	$LogK_e$ = -2.19
$Fe^{3+} + 2H_2O \leftrightarrow 2H^+ + Fe(OH)_2^+$	(R3)	$LogK_e$ = -5.67
$Fe^{3+} + 3H_2O \leftrightarrow 3H^+ + Fe(OH)_3$ (aq)	(R4)	$LogK_e$ = -12.56
$Fe^{3+} + 4H_2O \leftrightarrow 4H^+ + Fe(OH)_4^-$	(R5)	$LogK_e$ = -21.60
$Al^{3+} + H_2O \leftrightarrow H^+ + AlOH^{2+}$	(R6)	$LogK_e$ = -5.00
$Al^{3+} + 2H_2O \leftrightarrow 2H^+ + Al(OH)_2^+$	(R7)	$LogK_e$ = -10.20
$Al^{3+} + 4H_2O \leftrightarrow 4H^+ + Al(OH)_4^-$	(R8)	$LogK_e$ = -23.00
$Al^{3+} + 3H_2O \leftrightarrow 3H^+ + Al(OH)_3$ (aq)	(R9)	$LogK_e$ = -17.20
$H^+ + CO_3^{2-} \leftrightarrow HCO_3^-$	(R10)	$LogK_e$ = 10.33
$2H^+ + CO_3^{2-} \leftrightarrow H_2CO_3$	(R11)	$LogK_e$ = 16.68
$Ca^{2+} + CO_3^{2-} \leftrightarrow CaCO_3$ (aq)	(R12)	$LogK_e$ = 3.22
$Ca^{2+} + H^+ + CO_3^{2-} \leftrightarrow CaHCO_3^+$	(R13)	$LogK_e$ = 11.44
$H^+ + SO_4^{2-} \leftrightarrow HSO_4^-$	(R14)	$LogK_e$ = 1.99
$Ca^{2+} + SO_4^{2-} \leftrightarrow CaSO_4$ (aq)	(R15)	$LogK_e$ = 2.30
$Al^{3+} + SO_4^{2-} \leftrightarrow AlSO_4^+$	(R16)	$LogK_e$ = 3.50
$Al^{3+} + 2SO_4^{2-} \leftrightarrow Al(SO_4)_2^-$	(R17)	$LogK_e$ = 5.00
$Fe^{3+} + SO_4^{2-} \leftrightarrow FeSO_4^+$	(R18)	$LogK_e$ = 4.04
$Fe^{3+} + 2SO_4^{2-} \leftrightarrow Fe(SO_4)_2^-$	(R19)	$LogK_e$ = 5.42
$Na^+ + SO_4^{2-} \leftrightarrow NaSO_4^-$	(R20)	$LogK_e$ = 0.07
Precipitation/Dissolution Reactions		
$Ca^{2+} + CO_3^{2-} \leftrightarrow CaCO_3$ (s)	(R21)	$LogK_e$ = 8.48
$Al^{3+} + 3H_2O \leftrightarrow 3H^+ + Al(OH)_3$ (s)	(R22)	$LogK_e$ = -9.11
$Fe^{3+} + 3H_2O \leftrightarrow 3H^+ + Fe(OH)_3$ (s)	(R23)	$LogK_e$ = -4.89
$Ca^{2+} + SO_4^{2-} \leftrightarrow CaSO_4$ (s)	(R24)	$LogK_e$ = 4.58

Table 2 shows the distributions of the initial total concentrations of each component in the domain. Variable boundary conditions with the incoming dissolved concentrations as listed in Table 3 are assigned on the right (nodes 401 and 402) and left (nodes 1 and 2) sides (Figure 1). On the top and bottom sides, zero flux is imposed. A constant time step size of 0.025 day is used for 400 time steps resulting in a total simulation time of 10 days.

To start the simulation, the preprocessor in HYDROGEOCHEM (Yeh et al., 2008a) automatically choose Ca^{2+}, CO_3^{2-}, Al^{3+}, SO_4^{2-}, H^+, Fe^{3+}, and Na^+ as 7 components. Without using the species switching, the simulation will stop at node 299 while checking the mass balance of the Al^{3+} component during the first precipitation cycle at the first nonlinear iteration (between solving solute transport and chemical reaction) of the first time step. To resolve this mass non-balance error, the species switching was applied to re-run this example. From the output file, the species switching was performed for nodes 299 and 300 during the first precipitation cycle at the first and second nonlinear iterations of the first time step, and for nodes

301 and 302 during the first precipitation cycle at the first through seventh nonlinear iterations of the first time step. The aqueous complexed species $Al(OH)_4^-$ was selected by the pre-processor in HYDROGEOCHEM (Yeh et al., 2008a) to replace Al^{3+} as the new component for all these switches. With the species switching to overcome this mass non-balance error, all 400 time steps of the simulation were successfully achieved.

Table 2 Initial Conditions for Example 1

Total Con. (M)	**Sub-Region**			
	$0 \le z < 1{,}550$	$1{,}550 \le z < 3{,}825$	$3{,}825 \le z < 4{,}550$	$4{,}550 \le z < 5{,}000$
$[Ca^{2+}]$	9.2500×10^{-1}	6.3500×10^{-1}	9.6700×10^{-3}	7.4854×10^{-3}
$[CO_3^{2-}]$	9.5500×10^{-1}	6.3600×10^{-1}	1.0000×10^{-4}	1.0000×10^{-4}
$[Al^{3+}]$	4.2622×10^{-5}	4.2622×10^{-5}	1.2400×10^{-2}	4.0000×10^{-2}
$[SO_4^{2-}]$	2.4288×10^{-2}	2.4288×10^{-2}	1.3300×10^{-1}	2.0000×10^{-1}
$[H^+]$	2.0447×10^{-2}	2.0447×10^{-2}	-1.2660×10^{-1}	-3.4516×10^{-3}
$[Fe^{3+}]$	1.2350×10^{-5}	1.2350×10^{-5}	3.7066×10^{-2}	3.2589×10^{-2}
$[Na^+]$	2.3518×10^{-2}	2.3518×10^{-2}	9.4648×10^{-2}	1.4000×10^{-1}

Table 3 Incoming Species Concentrations for Variable Boundary Conditions

Unit: M	t = 0 day	t = 2.5 day	t = 2.6 day	t = 120 day
(Ca^{2+})	7.4854×10^{-3}	7.4854×10^{-3}	3.94×10^{-3}	3.94×10^{-3}
(CO_3^{2-})	1.0×10^{-4}	1.0×10^{-4}	2.5×10^{-3}	2.5×10^{-3}
(Al^{3+})	4.0×10^{-2}	4.0×10^{-2}	9.3077×10^{-9}	9.3077×10^{-9}
(SO_4^{2-})	2.0×10^{-1}	2.0×10^{-1}	4.4424×10^{-3}	4.4424×10^{-3}
(H^+)	1.7071×10^{-3}	1.7071×10^{-3}	2.7628×10^{-3}	2.7628×10^{-3}
(Fe^{3+})	2.093×10^{-3}	2.093×10^{-3}	3.0788×10^{-7}	3.0788×10^{-7}
(Na^+)	1.4×10^{-1}	1.4×10^{-1}	2.3518×10^{-2}	2.3518×10^{-2}

The spatial-temporal distributions of total analytical, total precipitated concentrations of all seven components were reported elsewhere (Yeh et al., 2004a). The concentration evolutions of four precipitated species were also discussed. The interactions between transport and reactions governing the reactive transport processes were well addressed (Yeh et al., 2004a). Here only new results on the rates of all 24 fast reactions are presented. Figures 2 through 6 depict rates of 20 complexation reactions. Reaction (R10) has the highest rate while Reaction (R4) has the lowest rate. Figure 7 depicts the rate of four precipitation-dissolution reactions. It is seen that Reactions (R21) and (R24) have the highest precipitation-dissolution rates and Reaction 23 has the slowest rate. It is clear that all 24 reaction rates are finite and definite and both are time and space dependent under the transport system.

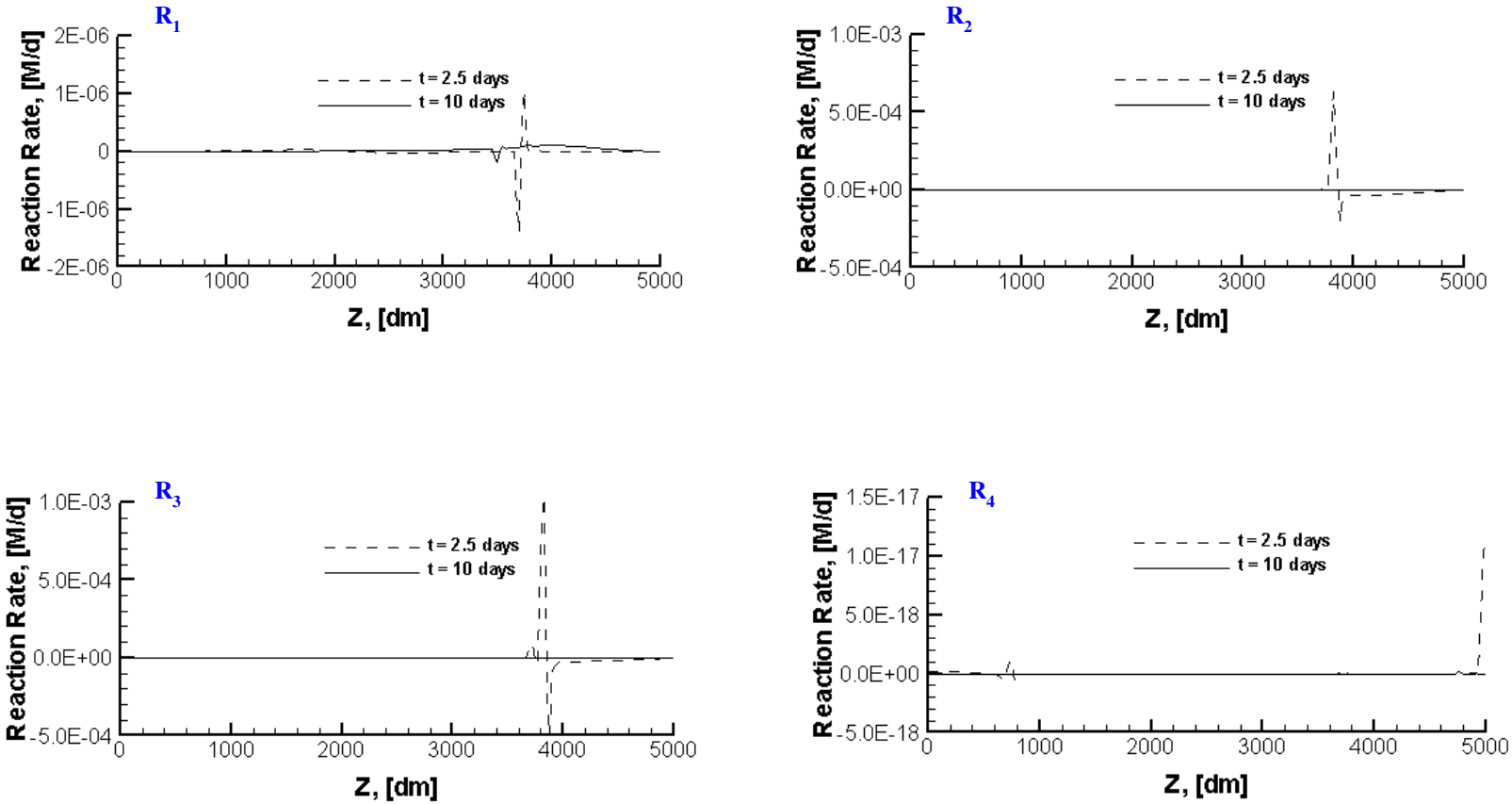

Figure 2 Reaction Rates of Reactions (R1) through (R4) for Example 1

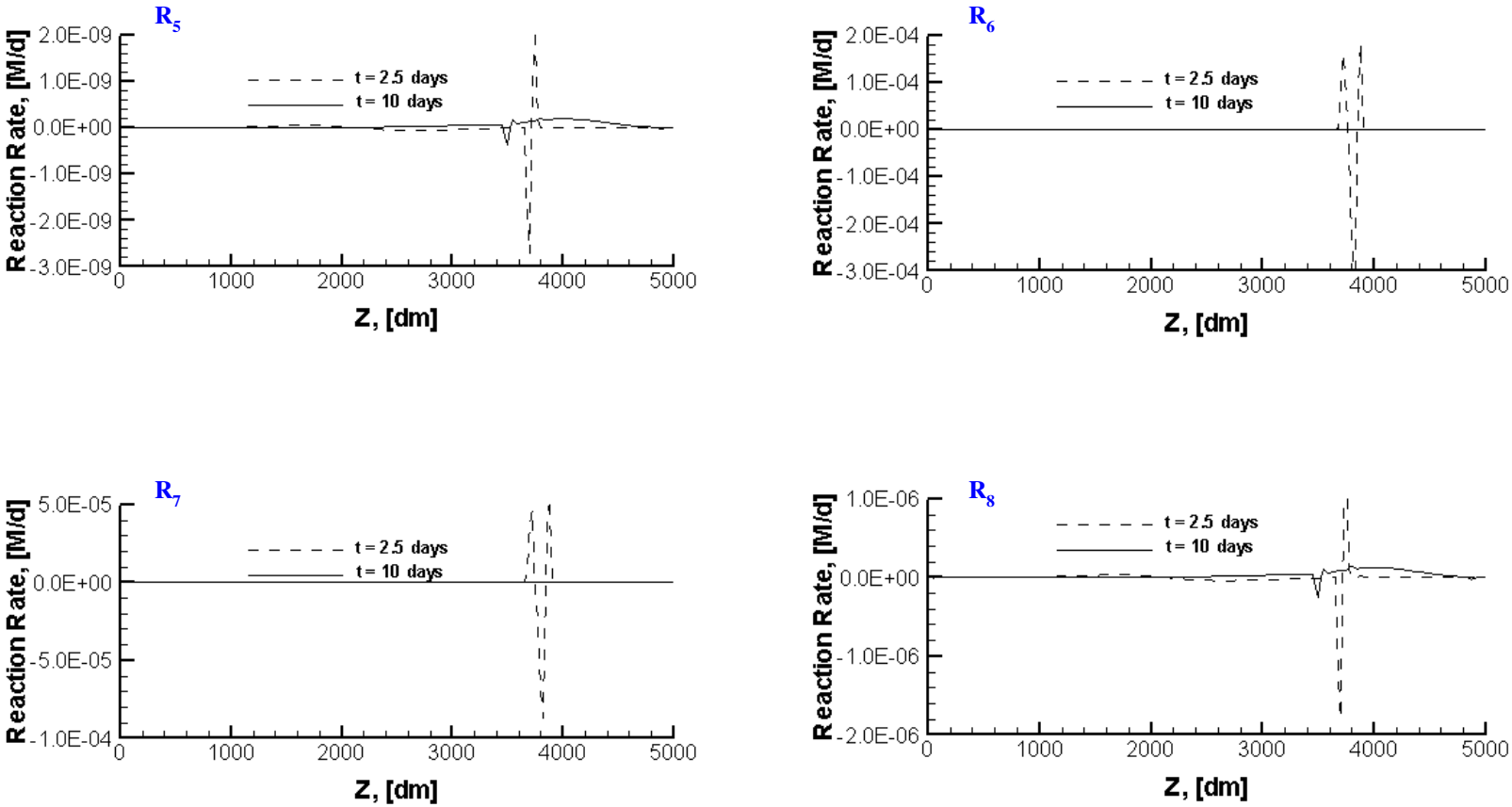

Figure 3 Reaction Rates of Reactions (R5) through (R8) for Example 1

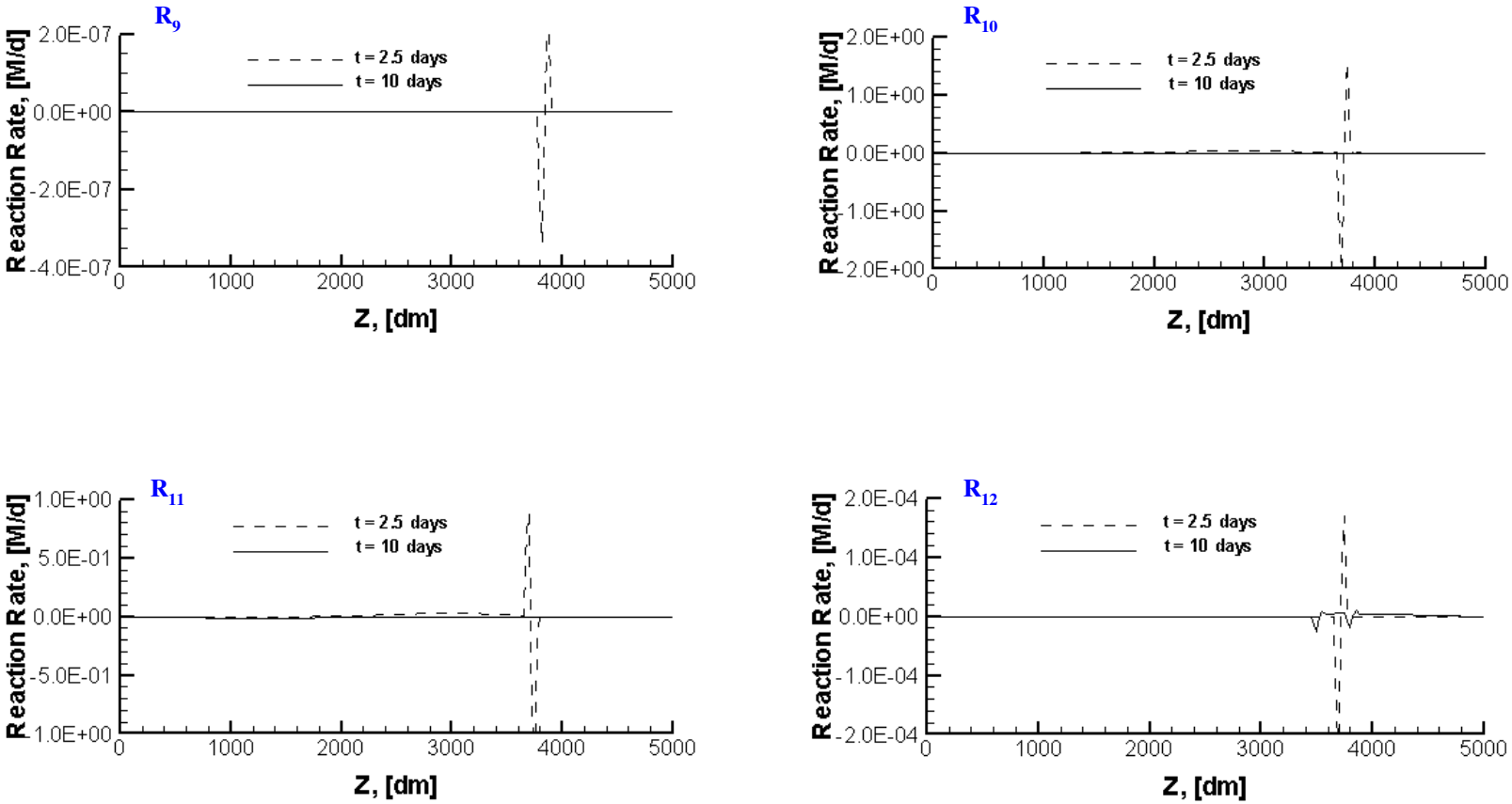

Figure 4 Reaction Rates of Reactions (R9) through (R12) for Example 1

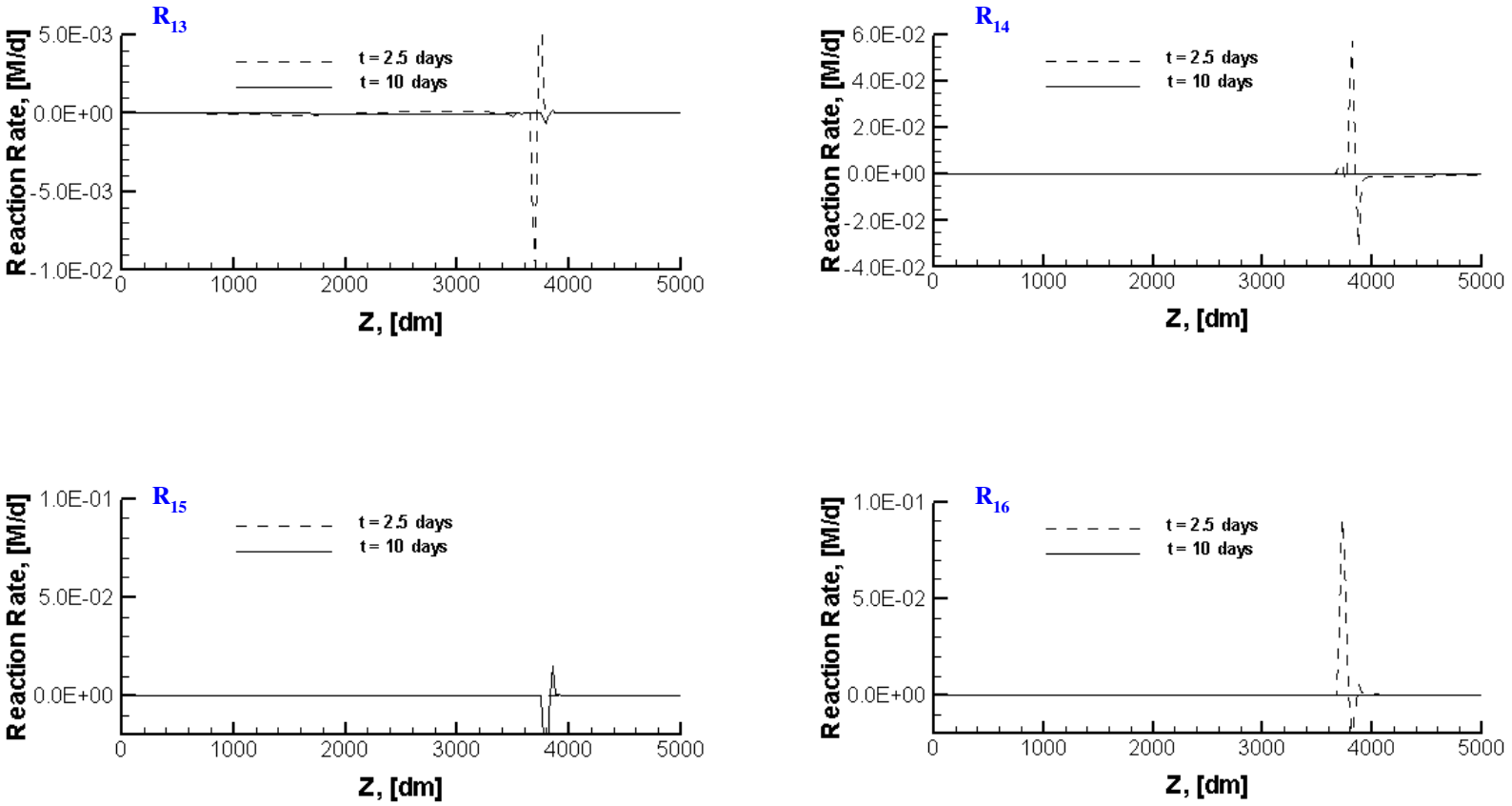

Figure 5 Reaction Rates of Reactions (R13) through (R16) for Example 1

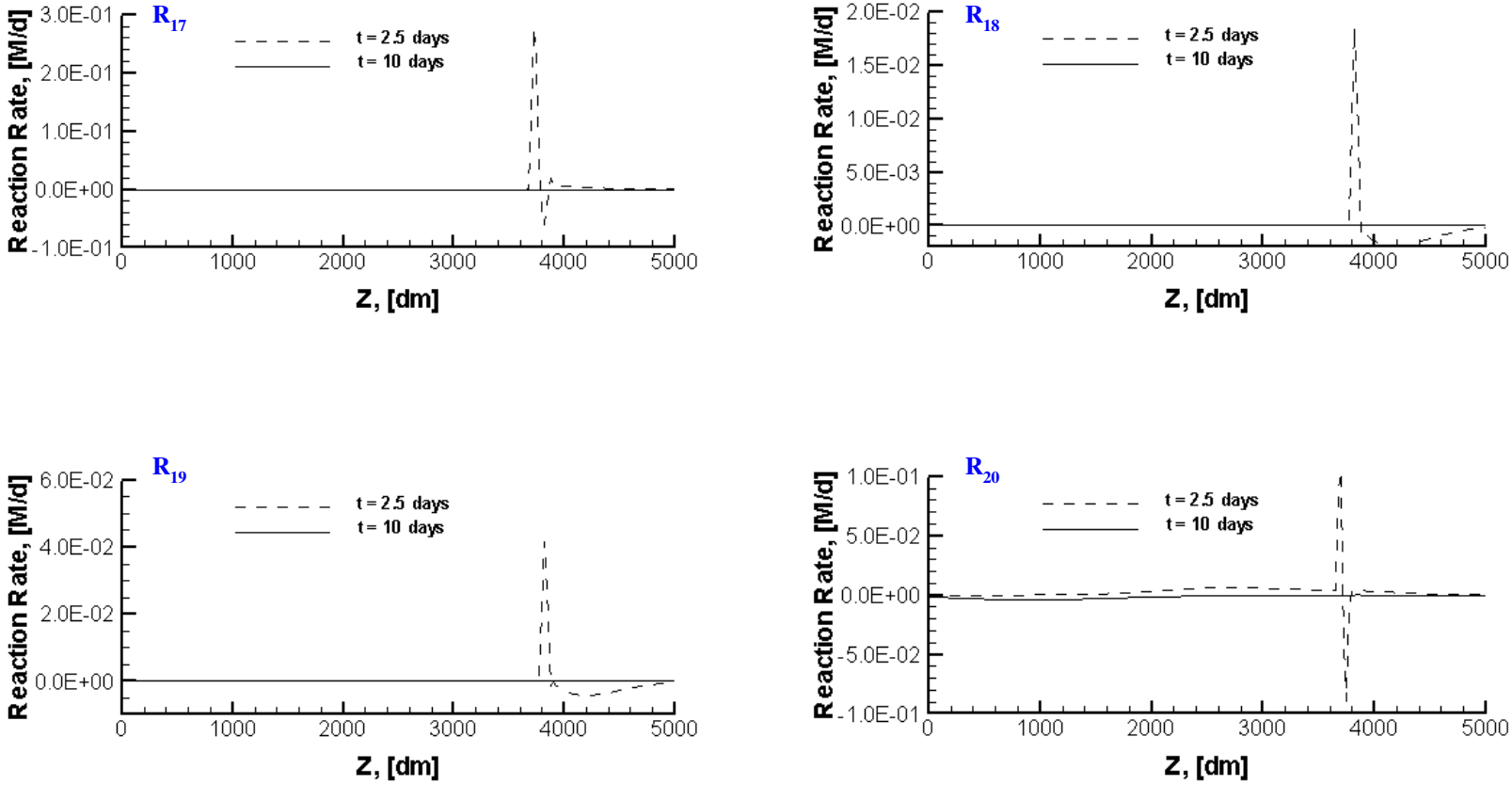

Figure 6 Reaction Rates of Reactions (R17) through (R20) for Example 1

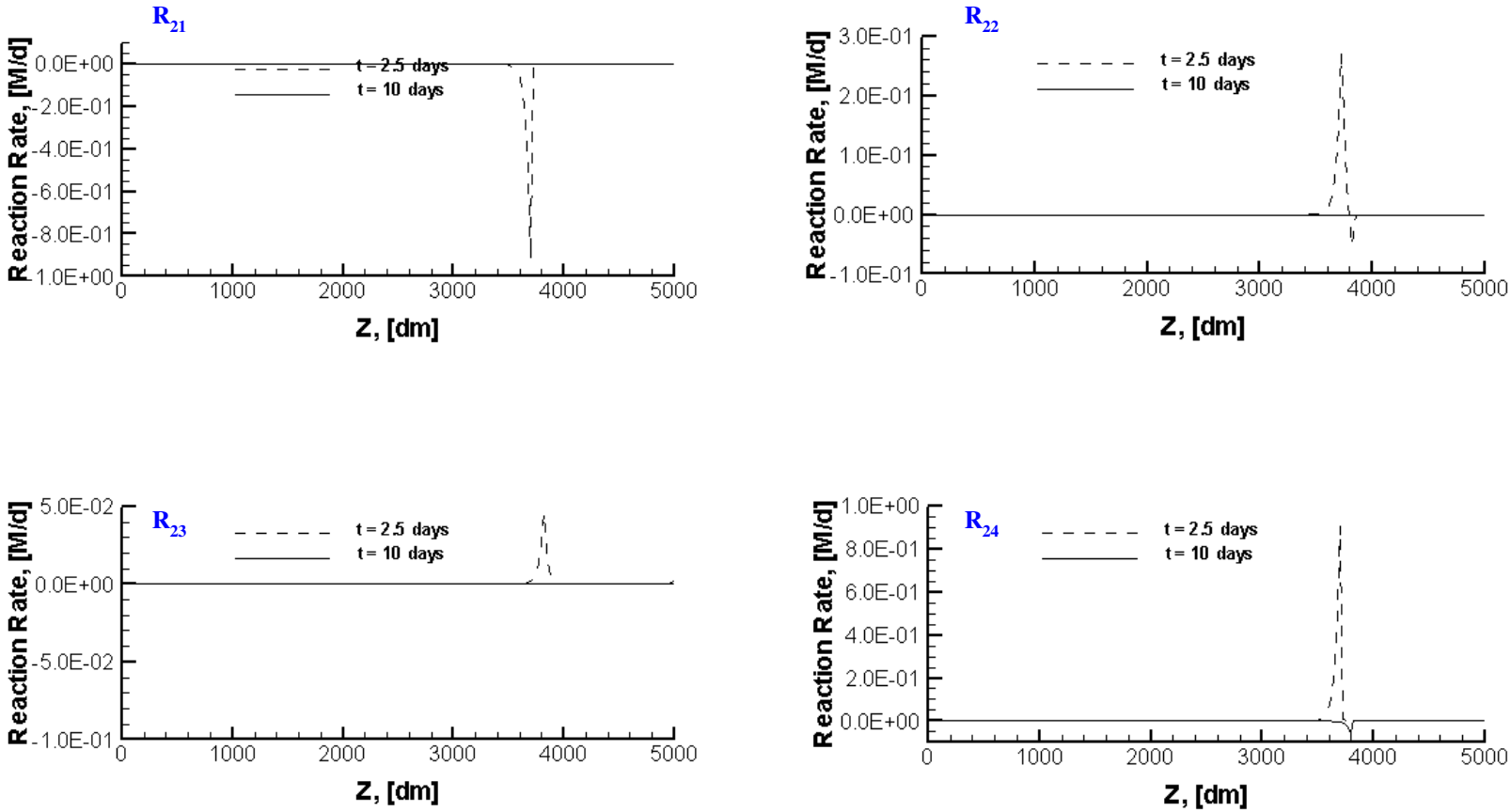

Figure 7 Reaction Rates of Reactions (R21) through (R24) for Example 1

Example 2: This example involves steady flow and transient reactive transport within a regular region with size 200 dm × 200 dm × 100 dm. The simulation region is discretized into 20 × 20 × 10 = 4,000 elements connected at 21 × 21 × 11 = 4,851 nodes. Each element has the same size of 10 × 10 × 10 = 1,000 dm^3.

The flow boundary conditions are given as: no flux is imposed on the left (x = 0), on the back (y = 200 dm), and at the bottom (z = 0) sides of the region; pressure head is assumed to vary from zero at z = 30 dm to 30 dm at the bottom (z = 0) on the right (x = 200 dm) and front (y = 0) sides; variable boundary conditions are applied elsewhere (Figure 8). Ponding depth is assumed zero for all variable boundary surfaces. The incoming fluxes of variable boundary are assumed to be 1 dm/day for the top surface and zero for the front and right sides above the water surface. The steady-state solution is to be sought. A pre-initial condition is set as h = 30 - z, which means the pre-initial water table is located at z = 30 dm.

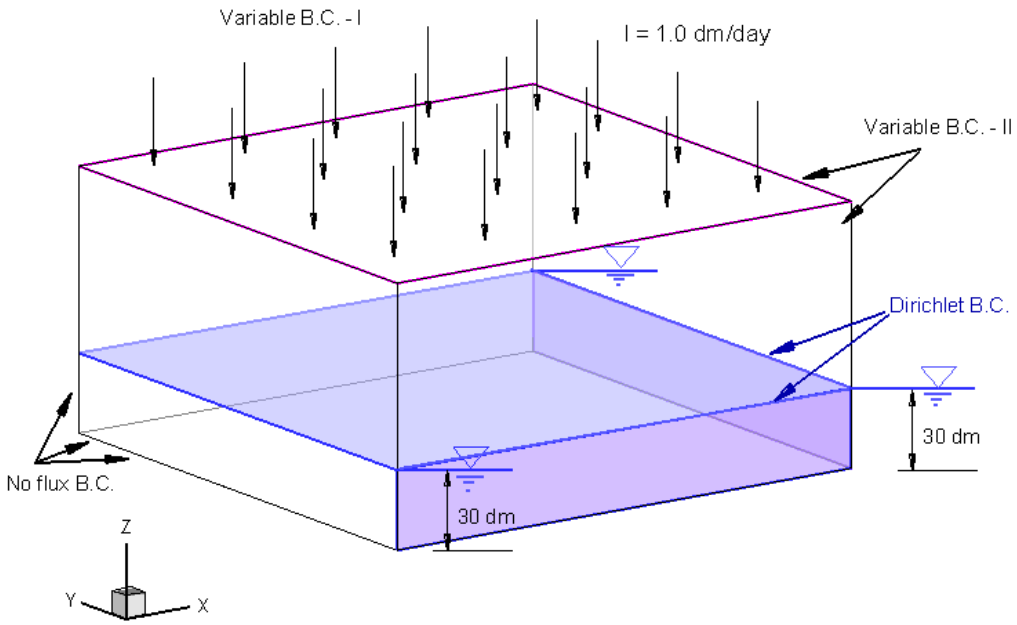

Figure 8 Problem domain and boundary conditions for Example 2 (unit: dm)

The problem domain contains one type of material. The material has the saturated hydraulic conductivities of $K_{xx} = K_{yy} = K_{zz} = 1$ dm/day and $K_{xy} = K_{xz} = K_{yz} = 0$ dm/day. The unsaturated characteristic hydraulic properties of the material are given as

$$\theta = \theta_r + (\theta_s - \theta_r)\frac{A}{A + |h - h_a|^B} \quad \text{and} \quad K_r = \left(\frac{\theta - \theta_r}{\theta_s - \theta_r}\right)^n \tag{9}$$

where $h_a = 0$ m, A = 1,000 m^2, B = 2, $\theta_s = 0.25$, and $\theta_r = 0.05$ are the parameters used to compute the water content and n = 2 is the parameter to compute the relative hydraulic conductivity.

The steady-state pressure head contours and the velocity fields are plotted in Figure 9 along a 2-D cross-section (x=0) of the domain.

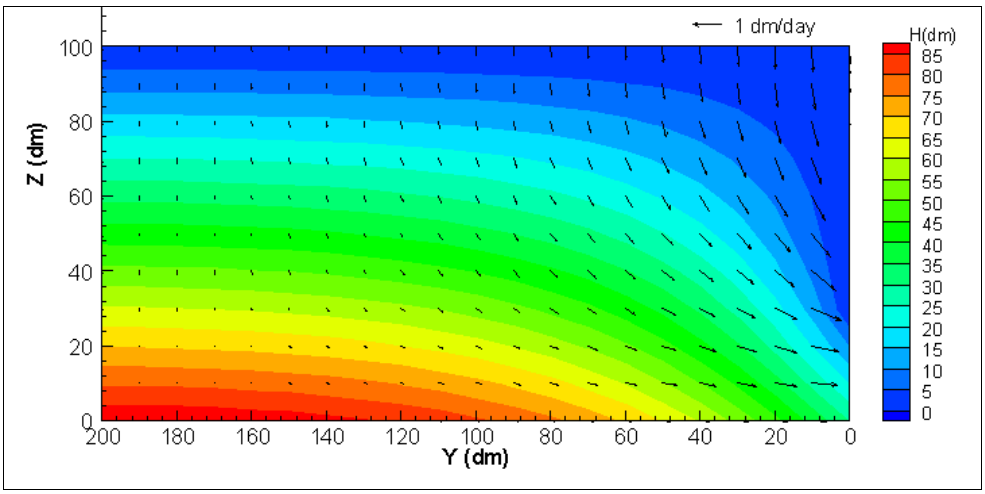

Figure 9 Steady-state velocity and pressure distribution along cross-section x = 0

Given the flow fields, transient reactive transport is simulated. The types of boundary condition are described in Figure 10. No flux is imposed on the left (x = 0), on the back (y = 200 dm), and on the bottom (z = 0) sides of the region. Dirichlet boundary is located on the top surface of the domain within 0 dm < x < 90 dm and 130 dm < y < 150 dm. Variable B.C-I is imposed on the top surface excluding the domain of Dirichlet boundary. Variable B.C-II is specified on the right side (x = 200 dm) and front side (y = 0).

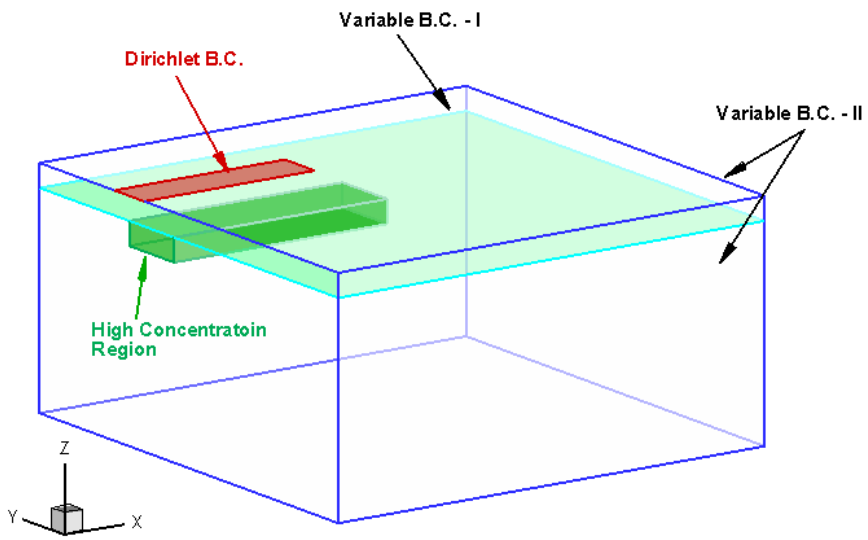

Figure 10 Boundary conditions and a high initial concentration region

For reactive transport simulations, the system of adsorption-dissolution reactions affecting the distribution and stability of Co(II)-EDTA in Fe-oxide coated sand (Szecsödy et al., 1994) is adopted here. To make the model more general, two ion-

exchange reactions (one fast reaction and one slow reaction) are appended. As a result, the reaction network consists of a total of 33 reactions involving 42 species (30 aqueous complexes, 8 adsorbed species, 3 ion-exchanged species, and one mineral) as shown in Table 4 (Yeh et al., 2004b).

Table 4 Reaction Network for Example 2

Reaction	**No**	**parameter**
Mineral Dissolution and Surface Site Formation Reactions		
$Fe(OH)_{3(s)} \rightarrow Fe^{3+} - 3\ H^+$	(R1)	$k_1^f = 0.05$
$Fe(OH)_{3(s)} \leftrightarrow FeOH$	(R2)	*
Aqueous Complexation Reactions		
$CoEDTA^{2-} \leftrightarrow Co^{2+} + EDTA^{4-}$	(R3)	$Logk_3^f = 2.03$ $Log\ k_3^b = 20.00$
$Ca^{2+} + EDTA^{4-} \leftrightarrow CaEDTA^2$	(R4)	$Log\ K_4^e = 12.32$
$H^+ + EDTA^{4-} + Ca^{2+} \leftrightarrow CaHEDTA^-$	(R5)	$Log\ K_5^e = 15.93$
$Ca^{2+} \leftrightarrow H^+ + Ca(OH)^+$	(R6)	$LogK_6^e = -12.60$
$Fe^{3+} + EDTA^{4-} \leftrightarrow FeEDTA^-$	(R7)	$Log\ k_7^f = 25.$, $Log\ k_7^b = -2.57$
$Fe^{3+} + H^+ + EDTA^{4-} \leftrightarrow FeHEDTA$	(R8)	$Log\ K_8^e = 29.08$
$Fe^{3+} + EDTA^{4-} \leftrightarrow H^+ + FeEDTA(OH)^{2-}$	(R9)	$Log\ K_9^e = 19.65$
$Fe^{3+} + EDTA^{4-} \leftrightarrow 2H^+ + FeEDTA(OH)_2^3$	(R10)	$LogK_{10}^e = -36.30$
$Fe^{3+} \leftrightarrow H^+ + Fe(OH)^{2+}$	(R11)	$LogK_{11}^e = -2.19$
$Fe^{3+} \leftrightarrow 2H^+ + Fe(OH)_2$	(R12)	$LogK_{12}^e = -5.67$
$Fe^{3+} \leftrightarrow 3H^+ + Fe(OH)_3$	(R13)	$LogK_{13}^e = -13.60$
$Fe^{3+} \leftrightarrow 4H^+ + Fe(OH)_4$	(R14)	$LogK_{14}^e = -21.60$
$2Fe^{3+} \leftrightarrow 2H^+ + Fe_2(OH)_2^{4+}$	(R15)	$LogK_{15}^e = -2.95$
$H^+ + Co^{2+} + EDTA^{4-} \leftrightarrow CoHEDTA^-$	(R16)	$LogK_{16}^e = 21.40$
$Co^{2+} \leftrightarrow H^+ + Co(OH)^+$	(R17)	$LogK_{17}^e = -9.67$
$Co^{2+} \leftrightarrow 2H^+ + Co(OH)_2$	(R18)	$LogK_{18}^e = -18.76$
$Co^{2+} \leftrightarrow 3H^+ + Co(OH)_3$	(R19)	$LogK_{19}^e = -32.23$
$H^+ + EDTA^{4-} \leftrightarrow HEDTA^{3-}$	(R20)	$LogK_{20}^e = 11.03$
$2H^+ + EDTA^{4-} \leftrightarrow H_2EDTA^{2-}$	(R21)	$LogK_{21}^e = 17.78$

$3H^+ + EDTA^{4-} \leftrightarrow H_3EDTA^-$	(R22)	$LogK_{22}^e = 20.89$
$4H^+ + EDTA^{4-} \leftrightarrow H_4EDTA$	(R23)	$LogK_{23}^e = 23.10$
$H^+ + OH^- \leftrightarrow H_2O^{\&}$	(R24)	$LogK_{24}^e = 14.00$
Adsorption-Desorption Reactions		
$FeOH \leftrightarrow FeO^- + H^+$	(R25)	$LogK_{25}^e = -11.60$
$FeOH + H^+ \leftrightarrow FeOH_2^+$	(R26)	$Log\ K_{26}^e = 5.60$
$FeOH + 3H^+ + EDTA^{4-} \leftrightarrow FeOH_2\text{-}H_2EDTA^-$	(R27)	$LogK_{27}^e = 30.48$
$FeOH + Fe^{3+} + H^+ + EDTA^{4-} \leftrightarrow FeOH_2\text{-}FeEDTA$	(R28)	$Logk_{28}^f = 40.00$, $Log\ k_{28}^b = 2.37$
$FeOH + H^+ + Co^{2+} + EDTA^{4-} \leftrightarrow FeOH_2\text{-}CoEDTA^-$	(R29)	$Logk_{29}^f = 30.00$, $Log\ k_{29}^b = 1.51$
$FeOH - H^+ + Co^{2+} \leftrightarrow FeO\text{-}Co^+$	(R30)	$Logk_{30}^f = -0.99$, $Log\ k_{30}^b = 1.70$
$FeOH + H^+ + Ca^{2+} + EDTA^{4-} \leftrightarrow FeOH_2\text{-}CaEDTA^-$	(R31)	$Log\ k_{31}^f = 25.0$ $Log\ k_{31}^b = 1.19$
Ion-Exchange Reactions		
$Mg^{2+} + 2\ \overline{Na^+} \leftrightarrow \overline{Mg^{2+}} + 2Na^+$	(R32)	$Logk_{32}^f = -0.75$, $Log\ k_{32}^b = -0.5$
$Ca^{2+} + 2\ \overline{Na^+} \leftrightarrow \overline{Ca^{2+}} + 2Na^+$	(R33)	$Log\ k_{33}^e = 0.6$

* $\frac{S_A N_s}{N_A} M_{mineral}[M] = [S_1] + [S_2] + [S_3] + [S_4] + [S_5] + [S_6] + [S_7] + [S_8]$ This users' specified equation is modified from Stumm and Morgan, 1996, in which S_A is the unit surface area ($m^2\ g^{-1}$) of mineral, N_S is the surface site density (mol sites m^{-2}), N_A is Avogadro's number (mol sites per mol), $M_{mineral}$ is the molecular weight of mineral

&The species H_2O can be decoupled from the system if its activity is assumed 1.0.

The reaction network in Table 4 is complex involving both kinetic and equilibrium reactions in every type of reactions (aqueous complexation, adsorption-desorption, and ion-exchange). Initially, the metal-hydroxide mineral $Fe(OH)_3(s)$ becomes solubilized and produces two aqueous species Fe^{3+} and H^+ through an irreversible reaction [Reaction (R1) in Table 4]. In addition, adsorbing sites, FeOH, are formed on the surface of the mineral $Fe(OH)_3(s)$ [Reaction (R2)]. The surface site commonly undergoes ionization reactions upon contact with water [Reactions (R25) and (R26)]. Species $CoEDTA^{2-}$ dissolves into Co^{2+} and $EDTA^{4-}$ [Reaction (R3)]. Then Co^{2+}, $EDTA^{4-}$, Ca^{2+}, and Fe^{3+} react to form various complexed species [Reactions (R4) through (R23)]. In turn, some of these complexed species are adsorbed on the surface of mineral $Fe(OH)_3(s)$ [Reactions (R27) through (R31)]. In addition, three ions (Ca^{2+}, Mg^{2+} and Na^+) are involved in ion exchange reactions to form three ion-exchanged species ($\overline{Ca^{2+}}$, $\overline{Mg^{2+}}$, and $\overline{Na^+}$)in the reaction system [Reactions (R32) and (R33)].

The reacting system involves a total of 41 species, excluding the species H_2O whose activity is set as 1.0, 25 equilibrium reactions ($N_E = 25$) and 8 kinetic reactions ($N_K = 8$). The preprocessor in HYDROGEOCHEM performs a formal matrix decomposition of the reaction network (Fang et al., 2003) and automatically set up 25 nonlinear algebraic equations and 16 nonlinear transport equations for reaction extents (Yeh et al., 2004b). Out of these 16 reaction extents, five involved only immobile species; thus, instead of solving 29 nonlinear transport equations for 29 aqueous species, one has to solve only 11 nonlinear transport equations for 11 reaction extents each of which involved both mobile and immobile species.

For numerical simulations, the initial conditions are listed in Table 5 for the species whose concentration is not zero. Low initial concentrations are given in the entire domain, except for a small region $[0 \le x \le 100, 110 \le y \le 140, 80 \le z \le 90]$which has high initial concentrations (Figure 10). The species concentrations with non-zero values on the boundaries are listed in Table 6.

Table 5 Initial conditions for reactive chemical transport for Example 2

Species	High Concentration Region	Low Concentration Region
Ca^{2+}	1.0e-5	1.0e-5
Fe^{3+}	1.0e-7	1.0e-7
Co^{2+}	1.0e-5	1.0e-5
H^{+}	3.0e-5	1.0e-5
$EDTA^{4-}$	1.0e-5	1.0e-5
$FeEDTA^{-}$	1.0e-5	1.0e-5
$Fe(OH)_3(s)$	2.0e-5	1.0e-7
$CoEDTA^{2-}$	1.0e-6	1.0e-7
Mg^{2+}	1.0e-5	1.0e-5
Na^{+}	1.0e-4	1.0e-5
$\overline{Mg^{2+}}$	1.4e-4	1.0e-5
$\overline{Na^{+}}$	7.0e-4	1.0e-5
$\overline{Ca^{2+}}$	1.5e-4	1.0e-5

Note: The unit for species concentration is mole/dm^3.

Table 6 Boundary conditions for reactive chemical transport for Example 2

Species	Dirichlet B.C	Variable B.C-I	Variable B.C-II
Ca^{2+}	1.0e-3	1.0e-5	0
Fe^{3+}	1.0e-7	1.0e-7	0
Co^{2+}	1.0e-5	1.0e-5	0
H^{+}	1.0e-5	1.0e-5	0
$EDTA^{4-}$	1.0e-3	1.0e-5	0
$FeEDTA^{-}$	1.0e-5	1.0e-5	0
$CoEDTA^{2-}$	1.0e-3	1.0e-7	0
Mg^{2+}	1.0e-5	1.0e-5	0
Na^{+}	1.0e-4	1.0e-5	0

Note: The unit for species concentration is mole/dm^3.

For transient simulations, a time step size of 2 days is used and a total 100 time-step transient simulation is performed in this example. The concentration evolutions of all 41 species were obtained elsewhere (Yeh et al., 2004b). Here only new results on selective equilibrium and kinetic rates are given (Figure 11). The transport and reaction processes governing the spatial-temporal distributions of the mineral [$Fe(OH)_{3(s)}$], surface site [Fe(OH)], and three aqueous species [Fe^{3+}, $EDTA^{4-}$, and $FeEDTA^{-}$] were addressed. The slope of $Fe(OH)_{3(s)}$-versus-time curve was shown almost constant (Yeh et al., 2004b). Under a batch system, this slope should be the sum of rates of Reactions (R1) and (R2) [Eq R1 + k R1 in Figure 11]. It is seen that the rate, R_1 or Eq R1, plus the rate, R_2 or k R1, are clearly not constant due to complicated interactions between transport and reactions. Furthermore, it is seen that the kinetic rates are not necessarily smaller than the equilibrium rates.

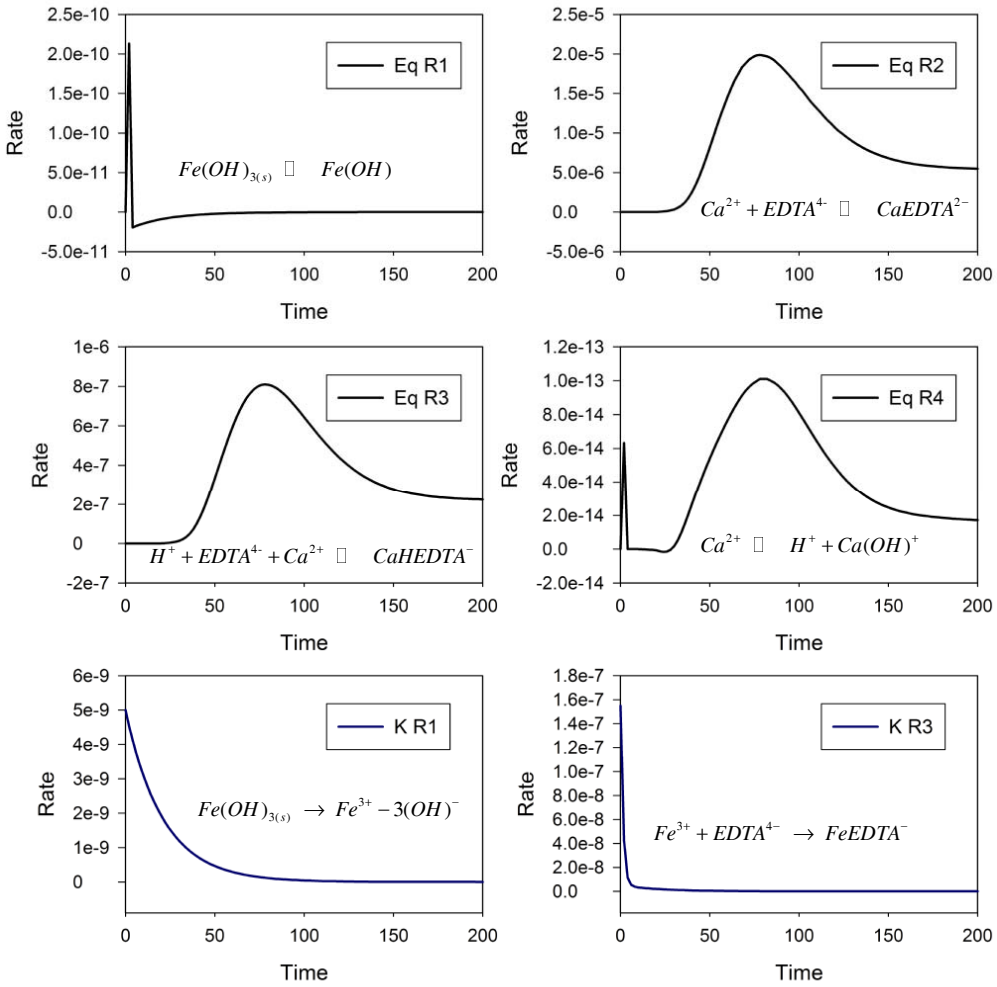

Figure 11 Rates of Selective Reactions at x = 30, y = 120, z = 30

Summary and Conclusion

This paper communicates the development of a mechanistically-based coupled fluid flow and reactive chemical transport model including both fast and slow reactions in variably saturated media. A new concept to define rates of fast/equilibrium reactions is proposed. The rates of equilibrium reactions are those rates which are "necessary" to assure that the thermodynamic equations remain fulfilled, i.e., the solution of the concentration field remains on the manifold defined by thermodynamic equations. With this definition of the rates of equilibrium reactions are finite and definite. They depend on not just the chemical reaction itself, but also on transport processes. The theoretical bases and numerical techniques of the model were summarized and two example problems were presented. The first example focused on a complicated but realistic advective-dispersive-reactive transport problem. It exemplified the need of species switching scheme to solve stiff geochemical equilibrium problems. It also highlighted that consistent, finite, and definite rates of all fast/equilibrium reactions can be obtained. The second example was a reactive transport problem of a comprehensive reaction network in three dimensions. It demonstrated the design capability of the model to simulate the interplay of transport and reactions in the adsorption-dissolution Co(II)-EDTA in Fe-oxide coated sand. It also showed that rates of slow/kinetic reactions are not necessarily smaller than those of fast/equilibrium reactions.

Acknowledgments

The work is supported in part by the U.S. Department of Energy under Grant DE-FG02-04ER63916 with University of Central Florida.

References

Bacon, D. H., M. D. White, and B. P. McGrail, 2000. Subsurface Transport Over Reactive Multiphases (STORM): A General, Coupled, Nonisothermal Multiphase Flow, Reactive Transport, and Porous Medium Alternation Simulator, Version 2, User's Guide. PNNL-13108. Pacific Northwest national Laboratory, Richland, WA 99352

Cederberg, G. A., R. L. Street, and J. O. Leckie, 1985. A Groundwater Mass Transport and Equilibrium Chemistry Model for Multicomponent Systems. Water Resources Research, 21: 1095-1104.

Cheng, H. P., 1995. Development and Application of a Three-Dimensional Finite Element Model of Subsurface Flow, Heat Transfer, and Reactive Chemical Transport. Ph.D. Thesis, Department of Civil and Environmental Engineering, The Pennsylvania State University. University Park, PA.

Chilakapati, A. 1995. RAFT: A Simulator for ReActive Flow and Transport Groundwater Contaminants. PNL Report 10636 (124 pp.)

Chilakapati, A., T. Ginn and J. Szecsody, 1998. An analysis of complex reaction networks in groundwater modeling. Water Resources Research, 34(7): 1767-1780.

Chin, D.A., 2000. Water-Resources Engineering. Prentice Hall Inc.

Dykaar, B. D. and P. K. Kitanidis, 1996. Macrotransport of a Biologically Reacting Solute through Porous Media. Water Resources Research, 32 (2): 307-320.

Engesgaard, P. and K. L. Kipp, 1992. A geochemical transport model for redox-controlled movement of mineral fronts in groundwater flow systems: A case of nitrate removal by oxidation of pyrite. Water Resour. Res. 20(10):2829-2843, 1992.

Fang, Y., Yeh, G.T., and Burgos, W.D., 2003. A New Paradigm to Model Reaction-Based Biogeochemical Processes. Water Resources Res, 39(4), 1083-1108.

Fang, Y., 2003. Reactive Chemical Transport under Multiphase System. Ph.D. Dissertation. Dept. of Civil and Environmental Engineering, The Pennsylvania State University, University Park, PA.

Griffioen, J., 1993. Multicomponent Cation Exchange Including Alkalinization-Acidification Following Flow Through a Sandy Sediment. Water Resources Research, 29(9):3005-3019.

Hammond, G. E., A. J. Valocchi, and P. C. Lichtner, 2005. Application of Jacobian-free Newton–Krylov with physics-based preconditioning to biogeochemical transport. Advances in Water Resources 28, 359–376. Steefel, C. I. and P. Van Cappellen (Guest Editors), 1998. Special Issue: Reactive Transport Modeling of Natural Systems. Journal of Hydrology, 209 (1-4): 1-388.

Hostetler, J. C. and R. L. Erickson, 1989. FASTCHEM Package 5. Report EA-5870-CCM, Electric Power Research Institute.

Hunter, K. S., Y. Wang, and P. Van Cappellen, 1998. Kinetic modeling of microbially-driven redox chemistry of subsurface environments: coupling transport, microbial metabolism and geochemistry. Journal of Hydrology 209:53-80.

Kindred, J. S. and M. A. Celia, 1989. Contaminant Transport and Biodegradation 2. Conceptual Model and Test Simulations. Water Resources Research, 25 (6): 1149-1159.

Kräutle S. and P. Knabner, 2005. A new numerical reduction scheme for fully coupled multicomponent transport-reaction problems in porous media, Water Resour. Res., 41, W09414.

Kräutle, S. and P. Knabner, 2006. A reduction scheme for coupled multicomponent transport-reaction problems in porous media: Generalization to problems with heterogeneous equilibrium reactions. Water Resour. Res. (In press).

Lensing, H. J., M. Voyt, and B. Herrling, 1994. Modeling of Biologically Mediated Redox Processes in the Subsurface. Journal of Hydrology, 159: 125-143.

Lichner, P. C. and M. S. Seith, 1996. User's Manual for MULTIFLO: Part II MULTIFLO 1.0 and GEM 1.0, Multicomponent-multiphase reactive transport model. CNWRA 96-019, Center for Nuclear Waste Regulatory Analyses, San Antonio, Texas.

Lichtner, P. C., 1996. Continuum Formulation of Multicomponent-Multiphase Reactive Transport. In: P. C. Lichtner, C. I. Steefel, and E. H. Oelkers (Editors),

Reactive Transport in Porous Media, Reviews in Mineralogy, Volume 34. Mineralogical Society of America, Washington, D.C., pp. 1-79.

Liu, C. W. and T. Narasimhan, 1989. Redox-controlled Multiple Species Reactive Transport, 1. Model Development. Water Resources Research, 25:869-882.

Mann U., 2000. New design formulation of chemical reactors with multiple reactions: I. basic concepts. Chemical Engineering Science 55(5), 991-1008.

Marzel, P., A. Seco, J. Ferrer, and C. Gambaldón, 1994. Modeling Multiple Reactive Solute Transport with Adsorption Under Equilibrium and Nonequilibrium Conditions. Advances in Water Resources, 17: 363-374.

Miller, C. W. and L. V. Benson, 1983. Simulation of Solute Transport in a Chemically Reactive Heterogeneous System: Model Development and Application. Water Resources Research, 19: 381-391.

Narasimhan, T. N., A. F. White, and T. Tokunaga, 1986. Groundwater contamination from an inactive uranium mill tailings pile: 2. Application of a dynamic mixing model. Water Resources Research, 22(13):1820-1834.

Nienhuis, P., C.A.T. Appelo, and A Willemsen, 1991. Program PHREEQM: Modified from PHREEQE for use in mixing cell flow tube. Free University, Amsterdam, The Netherlands, 1991.

Nitao, J. J., 1998. Reference Manual for the USNT Flow and Transport Code Version 2.0, Lawrence Livermore National Laboratory, Livermore, CA Report UCRL-MA-130651. Lawrence Livermore National Laboratory, Lawrence, CA.

Parkhurst, D. L., 1995. User's Guide to PHREEQC, A Computer Model for Speciation, Reaction-Path, Advective-Dispersive Transport and Inverse Geochemical Calculations. U.S. Geological Survey, Water Resources Investigations Report 95-4227.

Parkhurst, D.L. and Appelo, C.J., 1999. User's guide to PHREEQC (version 2)--A computer program for speciation, batch-reaction, one-dimensional transport, and inverse geochemical calculations. U.S.Geological Survey Water-Resources Investigations Report 99-4259 (312 pp).

Rittmann, B. E. and J. M. VanBriesen, 1996. Microbiological Processes in Reactive Modeling. In: P. C. Lichtner, C. I. Steefel, and E. H. Oelkers (Editors), Reactive Transport in Porous Media, Reviews in Mineralogy, Volume 34. Mineralogical Society of America, Washington, D.C., pp. 311-334.

Salvage, K. M. and G. T. Yeh, 1998. Development and application of a numerical model of kinetic and equilibrium microbiological and geochemical reactions (BIOKEMOD). J. of Hydrology. 209:27-52.

Simunnek J. and D. L. Squares, 1994. Two-dimensional model for variably saturated porous media with major ion chemistry. Water Resour. Res. 30(4):1115-1133, 1994.

Smith, S. L. and P. R. Jaffee, 1998. Modeling the Transport and Reaction of Trace Metals in Water Saturated Soils and Sediments. Water Resources Research, 34 (11):3135-3147.

Steefel, C.I. and S. B. Yabusaki, 1996. OS3D/GIMRT, Software for Modeling Multi-Component-Multidimensional Reactive Transport, User's Manual and Programmer's Guide. PNL-11166, Pacific Northwest Laboratory, Richland, WA (55 pp.).

Steefel, C. I. and P. Van Cappellen (Guest Editors), 1998. Special Issue: Reactive Transport Modeling of Natural Systems. Journal of Hydrology, 209 (1-4): 1-388.

Steefel, C. I., 2001. GIMRT, version 1.2: Software for modeling multicomponent, multidimensional reactive transport. User's Guide, UCRL-MA-143182. Livermore, California: Lawrence Livermore National Laboratory

Steefel, C. I., CRUNCH. A Computer Program for Multicomponent Reactive Transport in Porous Media. http://www-esd.lbl.gov/ESD staff/steefel/WebCrunch.htm

Suarez, D. and J. Šimunnek, 1996. Solute Transport Modeling Under Variably Saturated Water Flow Conditions. In: P. C. Lichtner, C. I. Steefel, and E. H. Oelkers (Editors), Reactive Transport in Porous Media, Reviews in Mineralogy, Volume 34. Mineralogical Society of America, Washington, D.C., pp. 229-268.

Szecsödy, J. E., J. M. Zachara, and P. Bruckhart, 1994. Adsorption-dissolution reactions affecting the distribution and stability of Co(II)-EDTA in Fe-oxide coated sand. Environmental Science and Technology, 28:1706-1716.

Taylor, S. W. and P. R. Jaffee, 1990. Substrate and Biomass Transport in a Porous Medium. Water Resources Research, 26 (9): 2181-2194.

Tebes-Stevens, C., Valocchi A.J., VanBriesen, J.M., and Rittmann, B.E., 1998. Multicomponent transport with coupled geochemical and microbiological reactions: model description and example simulations. Journal of Hydrology, 209: 8-26.

Theis, T. L., D. J. Kirkner, and A. A. Jennings, 1982. Multi-Solute Subsurface Transport Modeling for Energy Solid Wastes. Tech. Progress Rept. C00-10253-3, Department of Civil Engineering, University of Notre Dame, Norte Dame, IN.

Widdowson, M. A., F. J. Molz, and L. D. Benefield, 1988. A Numerical Transport Model for Oxygen- and Nitrate-Based Respiration Linked to Substrate and Nutrient Availability in Porous Media. Water Resources Research, 24 (9): 1553-1565.

Wood, B. D., C. N. Dawson, J. E. Szecsody, and G. P. Streile, 1994. Modeling Contaminant Transport and Biodegradation in a Layered Porous Media System. Water Resources Research, 30 (6): 1833-1845.

Xu, T., E. Sonnenthal, N. Spycher, and Pruess, 2003. TOUGHREACT User's Guide: A Simulation Program for Non-Isothermal Multiphase Reactive Geochemical Transport in Variably Saturated Geologic Media. Earth Sciences Division, Lawrence Berkeley National Laboratory, University of California, Berkeley, CA 94720, April 2003.

Yang, C., J. Samper, and L. Montenegro, 2008. CORE2D V4: A Code for water flow, heat and solute transport and geochemical reactions: Simulations of chemical interactions of clays and concrete. International Workshop 'Modelling Reactive Transport in Porous Media' Strassbourg, France, Januray 21-24, 2008.

Yeh, G. T. and V. S. Tripathi, 1989. A Critical Evaluation of Recent Developments in Hydrogeochemical Transport Models of Reactive Multichemical Components. Water Resources Research, 25 (1): 93-108.

Yeh, G. T. and V. S. Tripathi, 1990. HYDROGEOCHEM: A Coupled Model of HYDROlogical Transport and GEOCHEMical Equilibrium of Multi component Systems, ORNL 6371, Oak Ridge National Laboratory, Oak Ridge, TN. 37831

Yeh, G. T. and V. S. Tripathi, 1991. A model for simulating transport of reactive multispecies components: Model development and demonstration. Water Resour. Res. Vol. 27, No. 12, 3075-3094

Yeh, G. T., K. Salvage, and W. H. Choi. 1996. Reactive Multispecies-Multicomponent Chemical Transport Controlled by both Equilibrium and Kinetic Reactions. Proc. XI-th Int. Conf. on Numerical Methods in Water Resources, Cancun, Mexico, July 22-26, 1996. p. 585-592

Yeh, G. T., K. M. Salvage, J. P. Gwo, J. M. Zachara, and J. E. Szecsody, 1998. HYDROBIOGEOCHEM: A Coupled Model of Hydrologic Transport and Mixed Biogeochemical Kinetic/Equilibrium Reactions in Saturated-Unsaturated Media. ORNL/TM-13668. Oak Ridge National Laboratory, Oak Ridge, TN 37831-6285.

Yeh, G.T., 2000. Computational Subsurface Hydrology Reactions, Transport, and Fate of Chemicals and Microbes. Kluwer Academic Publishers

Yeh, G. T., M. D. Siegel, and M. H. Li, 2001. Numerical modeling of coupled fluid flows and reactive transport including fast and slow chemical reactions. J. Contam. Hydrol. 47, 379-390

Yeh, G. T., J. T. Sun, P. M. Jardine, W. D. Burger, Y. L. Fang, M. H. Li, and M. D. Siegel, 2004a. HYDROGEOCHEM 4.0: HYDROGEOCHEM 4.0: A Coupled Model of Fluid Flow, Thermal Transport, and HYDROGEOCHEMical Transport through Saturated-Unsaturated Media: Version 4.0. ORNL/TM-2004/103, Oak Ridge National Laboratory, Oak Ridge, TN 37831.

Yeh, G. T., J. T. Sun, P. M. Jardine, W. D. Burger, Y. L. Fang, M. H. Li, and M. D. Siegel, 2004b. HYDROGEOCHEM 5.0: A Three-Dimensional Model of Coupled Fluid Flow, Thermal Transport, and HYDROGEOCHEMical Transport through Variably Saturated Conditions - Version 5.0. ORNL/TM-2004/107, Oak Ridge National Laboratory, Oak Ridge, TN 37831.

Yeh, G. T., G. B. Huang, F. Zhang, H. P. Cheng, and H. C. Lin, 2006. WASH123D: A Numerical Model of Flow, Thermal Transport, and Salinity, Sediment, and Water Quality Transport in WAterSHed Systems of 1-D Stream-River Network, 2-D Overland Regime, and 3-D Subsurface Media. A Technical Report Submitted To EPA. Dept. of Civil and Environmental Engineering, University of Central Florida, Orlando, FL 32816

Yeh, G. T., Y. Li, P. M. Jardine, W. D. Burger, Y. L. Fang, M. H. Li, and M. D. Siegel, 2008a. HYDROGEOCHEM 4.5: A Coupled Model of Fluid Flow, Thermal Transport, and HYDROGEOCHEMical Transport through Saturated Unsaturated Media Version 4.1. Dept. of Civil and Environ. Engineering, University of Central Florida, 4000 Central Florid Blvd, Orlando, FL 32816

Yeh, G. T., J. T. Sun, P. M. Jardine, W. D. Burger, Y. L. Fang, M. H. Li, and M. D. Siegel, 2008b. HYDROGEOCHEM 5.5: A Three Dimensional Model of Coupled Fluid Flow, Thermal Transport, and HYDROGEOCHEMical Transport through Variably Saturated Conditions Version 5.1. Dept. of Civil and Environ. Engineering., University of Central Florida, 4000 Central Florid Blvd, Orlando, FL 32816

Zhang, F., G. T. Yeh, J. C. Parker, S. C. Brooks, M. N., Pace, Y. J. Kim, and P. M. Jardine, 2007. A reaction-based paradigm to model three-dimensional reactive chemical transport in groundwater. J. Contaminant Hydrology. Volume 93, 10-32

Comparative Study of Two Standard Septic Tank Drain fields Using Different Sand with Recirculation for Nutrient Removal

Ni-Bin Chang, Marty Wanielista, Fahim Hossian, Zhemin Xuan,
and Ammarin Daranpob

Department of Civil, Environmental, and Construction Engineering,
University of Central Florida, Orlando, Florida, USA

ABSTRACT

On-site Wastewater Treatment System (OWTS) using a septic tank followed by a recirculating sand filter (RSF) with effluent discharged to an unlined standard drain field is a typical performance-based treatment facility for nutrient removal. The type of effluent distribution in the standard drain field systems include gravity systems, low pressure dosed systems, drip irrigation systems, etc. The standard drain field that is constructed by a series of parallel, underground, perforated pipes allows the septic tank effluent to percolate into the surrounding soil in the vadose (unsaturated) zone where most of the residual nutrients may be assimilated. The inclusion of RSF may improve the nitrification to some extent so as to promote denitrification in the drain field. With such design, most residual nutrients in wastewater are expected to be consumed as the wastewater passes through the soil. This author's aim of this paper is to present the effectivenss of RSF and a comparative study with these two different drain field sands for nutrient removal in vadose zone. They include astatula sand (i.e., citrus grove sand) and washed building sand, popular in Central Florida for drain field use. The use of a gene identification method is novel in supporting the biological removal. Research findings show that the performance of washed building sand and the astatula sand in terms of ultimate nutrient removal is about the same. Because astatula sand is less costly it can possibly be considered for replacement of the more expensive washed building sand.

INTRODUCTION

When urban regions gradually expand due to regional development, centralized sewage collection, treatment, and disposal is often unavailable for both geographic and economic reasons. Thus, decentralized or on-site wastewater treatment systems (OWTS) may be necessary to protect public health. Septic tank system was developed in 1860 in France by John Mouras (Crites and Tchobanoglous, 1998). After that it has changed in many aspects of design strategy to give the present shape. Septic tank makes its way in the USA and some part of Africa by British navy around 1883 (Crites and Tchobanoglous, 1998). Later on, septic tank system becomes very common in both developed and developing countries. More than 25 million homes, or 25 percent of the U.S. population, use onsite wastewater treatment systems to meet their wastewater treatment and disposal needs (USEPA, 2002). According to USEPA, about 33% of new septic systems are constructed each year (USEPA, 2003).

On average, medium strength (i.e. 460.00 L/capita*day) untreated domestic wastewater has 40.00 mg/L of total nitrogen (TN), 25.00 mg/L of ammonia (NH_3-N), 720.00 mg/L of total solids (TS), 190.00 mg/L of biochemical oxygen demand (BOD_5), 7.00 mg/L of total phosphorus (TP) and 90.00 mg/L of oil and grease (Metcalf and Eddy, 2003; WEF and ASCE, 2005). As a consequence, nationwide, wastewater effluent from OWTS can represent a large fraction of nutrient loads to groundwater aquifers causing negative impact on drinking water quality and ecosystem integrity. This is due to the presence of phosphorus and nitrogen compounds that are the most frequent measurements to indicate nutrient loadings in natural and build environments. Hence, on-site wastewater effluent disposal has contributed significant adverse impacts to the dynamics of the natural environment. Traditional septic tank system is still not efficient to remove nutrient from wastewater to meet the Clean Water Act (CWA) goals (USEPA, 2003). The aim of this paper is to present a passive OWTS technology that is designed to promote both nitrification and denitrification on one hand and exhibit how the use of different types of sand popular in Florida in standard drain field ends up differing performance of denitrification on the other hand. Supplementary to the routine monitoring and measurement of the nutrient parameters, real-time polymerase chain reaction**,** also called quantitative real time polymerase chain reaction (Q-PCR/qPCR), was used to evaluate the nitrogen removal effect of media by quantifying the ammonia-oxidizing bacteria (AOB), nitrite-oxidizing bacteria (NOB) and denitrifying bacteria in the drain fields.

MATERIALS AND METHODS

System Configuration

The OWTS test center at University of Central Florida (UCF) is sponsored by Florida Department of Environmental Protection (FDEP) with guidance from the state Department of Health (DOH) and is designed for systematic evaluation of nutrients removal, which includes four treatment trains. The system presented in this paper consists of a septic tank followed by a recirculating sand filter (RSF), with effluent discharged to two unlined conventional gravity drain fields in parallel equally, called standard drain fields hereafter, filled with washed building sand and citrus grove (i.e., astatula sand) sand, respectively. The wastewater source for the test center is the 15-person BPW Scholarship House (a female dormitory at UCF campus), which contains a kitchen and living quarters. The wastewater is pumped to a 5.10 m^3 (1,350 gallon) septic tank from where the effluents are divided into different final disposal alternatives.

Figure 1(a) shows the schematic of such a treatment process that elucidates a typical septic tank system with enhanced nitrification and denitrification by using a RSF (EPA, 1999). The influent of wastewater contains some dissolved oxygen so it can trigger the nitrification in the septic tank at first and in the RSF later on because of the full exposure of the effluent to the air. On the other hand, the area between sludge and scum can be completely anaerobic with time so it is possible to support denitrification process in the septic tank (Bounds, 1997). Figure 1(b) illustrates the rationale via the use of RSF to promote the nitrification. A schematic diagram of system layout is shown in Figure 2.

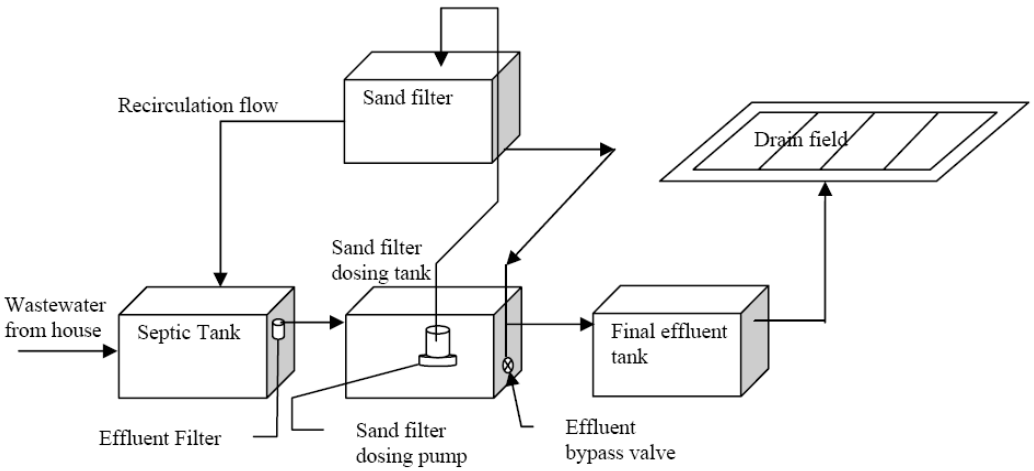

(a) A typical septic system configuration

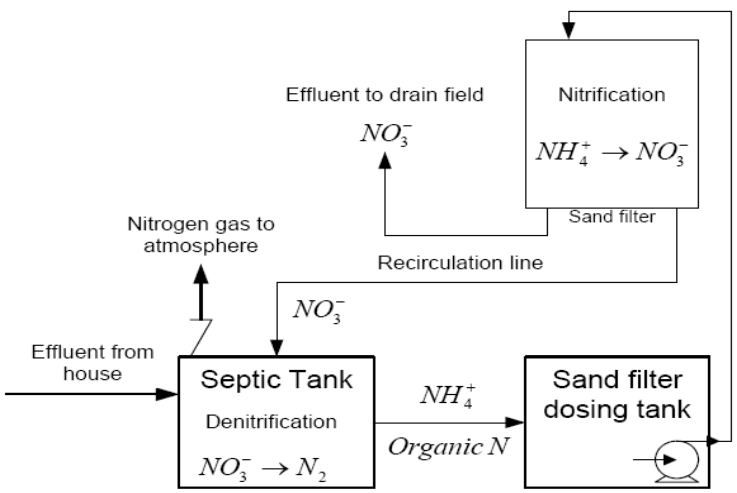

(b) Nitrification and denitrification in a septic tank system

Figure 1: A layout of an effluent filter and a gravel filled drain field (Chang et al., 2007; Venhuizen, 1998)

The tank with a capacity of 5,110.30 liters (i.e. 1,350 gallons) receives the sewage from 15-person BPW scholarship house. A Hydraulic Retention Time (HRT) of 24 hours is assumed in the septic tank. The tank then discharges the sewage to a dosing tank. The dosing tank sends the flow into two directions: one part is going to the distribution tank as feed-forward flow and the other three parts are going to the recirculation sand filter (RSF) as recycled flow. So the recycling ratio is about 3:1. RSF has a depth of about 1.22 meter (i.e. 4 ft) and it is filled with filter media up to 1.067 meter (i.e. 3.5 ft). RSF has three layers: top layer is a gravel layer, middle layer is a sand layer with a depth of 0.61 meter (i.e. 2 ft) and the bottom layer is a gravel layer with depth 0.3048 meter (i.e. 1 ft). The capacity of the sand filter tank is about 3,974.68 liters (i.e. 1,050 gallons). RSF has received frequent dosing at a rate of every 1 hour from the dosing tank. It is found in literature that multiple dosing is very effective to increase the removal efficiency

(USEPA, 1980). The recycled flow from RSF goes to the septic tank and mixes with the fresh sewage flow that promotes further denitrification.

From distribution tank, the wastewater goes to the two drain fields in equal volume. So each drain field may receive about 50% of the total flow from dosing tank. The size of each drain field is about 6.096 m x 4.57 m x 1.22 m (i.e. 20 ft x 15 ft x 4 ft). One of the drain fields is filled with astatula sand and the other drain field is filled with washed building sand. Each drain field is filled with native soil on the top with 0.61 meter in depth and the remaining 0.61 meter is filled by astatula sand or washed building sand, respectively. Astatula sand is used without any pretreatment and the washed buildingsand is washed to make it free from all impurities. These two types of sands are generally available in Florida. Astatula sand has a permeability of 25 cm/min and washed building sand has a permeability of 40 cm/min. Washed building sand is frequently used by contractors in drain field though. Astatula sand is selected as our laboratory experiment shows that this type of sand has the potential capability to remove nutrient.

To sample the infiltrate and proceed with water quality monitoring in vadose zone, three lysimeters (i.e., Soil Moisture Equipment Corporation) are installed in each of the two standard drain fields. The lysimeter is equipment that can collect water from unsaturated or vadose zone by a porcelain cup. The water from a lysimeter is collected by using a vacuum pump. The lycimeters are placed over three different depths: one is at a depth of 20.32 cm (i.e. 8 inches), another one is at a depth of 40.64 cm (i.e. 16 inches) and the other one is at a depth of 60.96 cm (i.e. 24 inches).

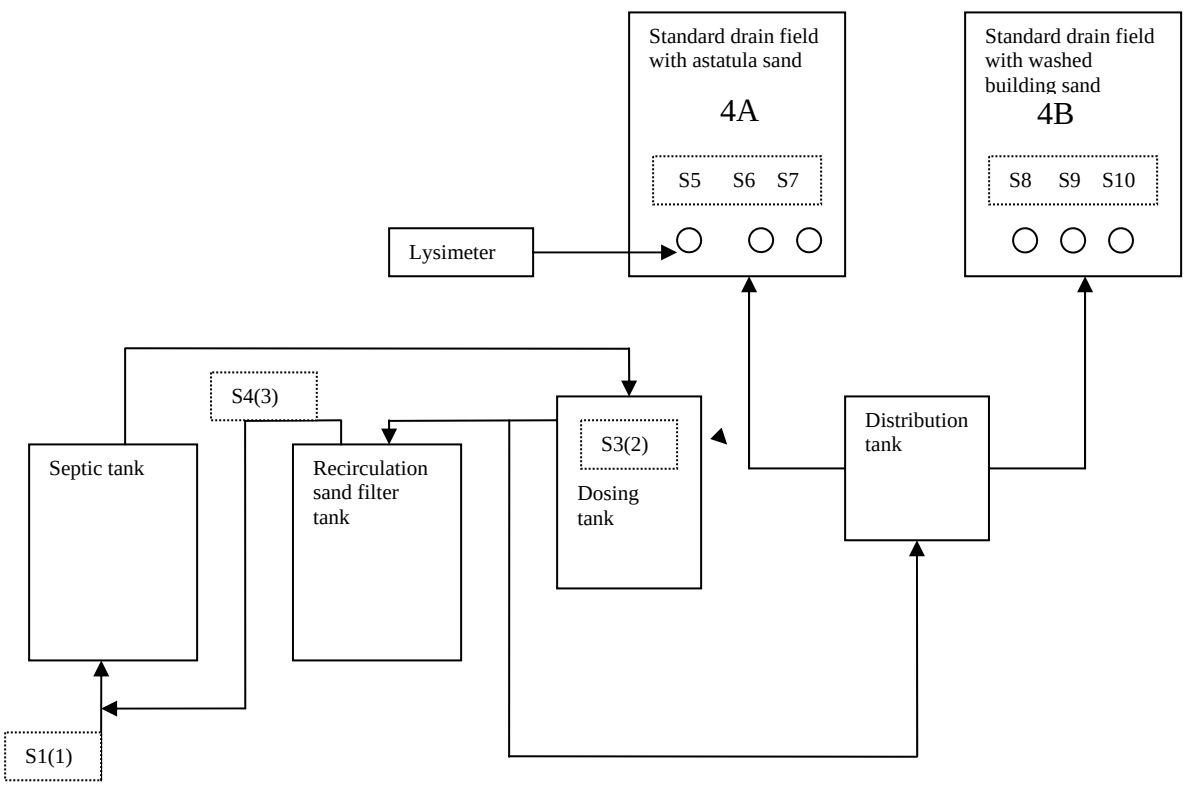

Figure 2. System layout of the OWTS that consists of a septic tank, a dosing tank, a sand-filtered circulation tank, a distributing tank, and two parallel drain fields

There are about 9 sampling points shown in Figure 2 denoted from S1 to S10. Points from S5 to S10 provide samples that were collected from lysimeter directly. S5, S6 and S7 sampling points are located at drain field filled with astatula sand. S8, S9 and S10 sampling points are drain field filled with at washed building sand. Composite sampling method is applied for sample collection (i.e., Composite sample is a mixture of samples collected at different time period and made one representative sample for chemical analysis and can save significant amount of analysis cost as only one sample is analyzed rather than samples collected in different time period.) Samples are collected biweekly in the morning (i.e. from 6:00 to 8:00 AM), in the afternoon (i.e. from 11:00 AM to 1:00 PM) and in the evening (i.e. from 5:00 to 7:00 PM). Major nutrients of concern include ammonia, NO_X-N (i.e. the sum of nitrate and nitrite), NO_2^--N, TN, soluble reactive phosphorus (SRP), TP, fecal coliform and E. coli. All the samples were analyzed by a certified laboratory - Environmental Research & Design Inc. (ERD) in Orlando, Florida. The groundwater nutrient concentrations were also observed in this project. For this purpose, 17 monitoring wells are constructed around the study site as shown in Figure 3. The monitoring wells are divided into two groups: 1) monitoring wells used to observe the effect of drain field and 2) monitoring wells used to observe the effect of whole system including wetlands and B&G drain field system. M1 to M8 are monitoring wells for the first group and MW1 to MW8 are wells for the second groups. All the wells are about 3.048 meter (i.e. 10 feet) deep. The groundwater depth of each well was monitored once in every week and nutrient concentration is analyzed bi-weekly.

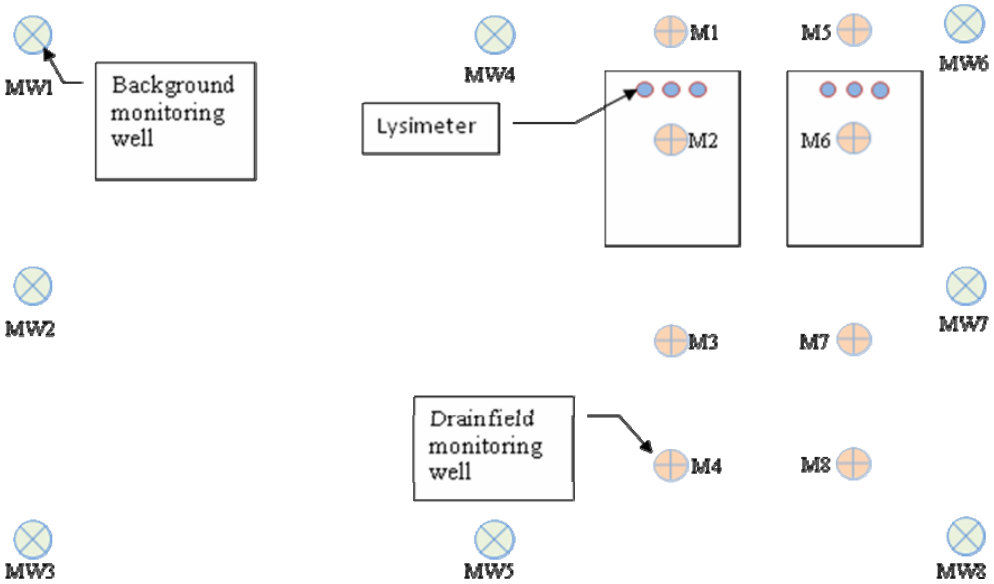

Figure 3: Figure shows the approximate location of groundwater monitoring well

Sampling and Chemical Analysis

A list of methods used to determine the concentrations of these chemicals is shown in Table 1 for reference. Quality assurance and quality control was conducted for each constitute in a sample set. To measure precision, duplicate samples are analyzed to produce a relative percent difference (RPD) between the two measurements. The

accuracy of the measurements is determined by spiking a sample with a known concentration of the parameter and calculating the percent recovery.

Table1: Column study water quality parameters and methods

Parameter	Method	Range*
Nitrates + Nitrites	Hach method 8192	0.01-0.50 mg/L NO_3^-N
Nitrites	Hach method 8507	0.002-0.30 mg/L NO_2^-N
Ammonia	Hach method 8155	0.01-0.50 mg/L NH_3-N
Total Nitrogen	Hach Method 10071	0.5-25.0 mg/L N
Reactive/Orthophosphate	Hach method 8048	0.02-2.50 mg/L PO_4^{3-}
Total phosphorus	Hach method 8190	0.06 to 3.50 mg/L PO_4^{3-}

*Note: In some cases samples were diluted with DI water to fall within this range.

Microbiological Assessment

As mentioned above that the middle layer of the RSF has a depth of 0.61 meter (i.e. 2 ft), sand samples were collected from the top (i.e. 0 ft, Sample No., R1), midpoint (i.e. 1 ft, Sample No., R2) and bottom (i.e. 2 ft, Sample No., R3) of the middle layer of RSF respectively for quantifying the ammonia-oxidizing bacteria (AOB) and nitrite-oxidizing bacteria (NOB) to simulate a profile of microbial activity in regard to the nitrification effect. As part of the total nitrogen removal in this whole wastewater treatment system, the dinitrification effect of soil profile along the flow path was also measured by quantifying the dinitrifier in both drain fields. Three samples were collected from each drain fields at different depth with the same principle. The first was collected at the depth of the bottom of shallowest lysimeter installed (i.e. 20.32 cm (8 inches) deep in sand layer, denoted as Sample No., W1 or A1. The deepest, denoted as Sample No., W3 or A3, was close to the groundwater table. The other one was collected in between: about 1.8 m (6ft) deep from the surface of the ground, denoted as Sample No., W2 or A2. All 9 samples were collected into 1.5mL microcentrifuge tubes, transported at 4 °C and kept at -20 °C until use.

DNA from the sample was extracted in duplicate by using a SoilMaster® DNA Extraction Kit (EPICENTRE) and following the accessory direction. 50 mg of the sample instead of 100 mg was weighed out into the 1.5mL microcentrifuge tube to decrease the effects of enzymatic inhibitors. The extracted DNA was finally resuspended in 300 μL TE Buffer. Real-time PCR quantification was performed on the Stepone® (Applied Biosystems) to amplify the *amoA* gene from the AOB, *NSR* gene from NOB and *nirK* gene from dinitrifier respectively. The target genes are in direct proportion of the number of bacteria. The PCR mixture was prepared in a total volume of 25 μL using 12.5 μL of the SYBR Green PCR Master Mix kit (combines SYBR Green 1 Dye, AmpliTaq Gold® DNA Polymerase, dNTPs with dUTP, Passive Reference 1, and optimized buffer components, Applied Biosystems), 10uM of each primer, standard DNA or extracted DNA from samples and DEPC water to complete the 25 μL volume (Table 2).

Table 3 shows the sequence of the used primes. For generating the standard curves for real-time PCR, Plasmid carrying the target DNA was extracted with a PureLink™ Quick Plasmid Miniprep Kit (Invitrogen), and the plasmid DNA concentration (ng/μL) was measured with spectrophotometer (NanoDrop™ 1000). Since

the sequences of the vector and PCR insert are known, we calculated the copy numbers of *amoA,* NSR and nirK directly from the concentration of extracted plasmid DNA. The standard DNA from plasmid DNA was prepared for tenfold serial dilution, and each of them was quantified in triplicate. Standard curves were obtained by plotting Ct (threshold cycle) as a function of log of the copy number of target DNA. The copy number can be obtained by the known mass concentration of standard DNA and molecular mass of the target gene.

Table 2: The composition of PCR mixture for different genes to be amplified (unit: μL)

	amoA	NSR	nirK
SYBR Green	12.5	12.5	12.5
Primer	1.5	1.5	1
Standard DNA or template DNA	2	2	1
DEPC water	9	9	10.5
Total	25	25	25

Table 3: The oligonucleotide sequences of the primers.

Ammonium monooxygenase (*amoA*)	amoA-1F GGGGTTTCTACTGGTGGT	Rotthauwe et al. (1997)
	amoA-2R CCCCTCKGSAAAGCCTTCTTC	
16S rRNA Nitrospira sp. (*NSR*)	NSR 1113F CCTGCTTTCAGTTGCTACCG	Dionisi, et al (2004)
	NSR 1264R GTTTGCAGCGCTTTGTACCG	
Nitrite reductase (*nirK*)	nirK 876 ATYGGCGGVAYGGCGA	Braker, et al (1998)
	nirK 1040 GCCTCGATCAGRTTRTGGTT	

The PCR protocol for *amoA* quantification was as follows: 2 min at 50°C, 10 min at 95°C, and then 40 cycles consisting of 30 s at 95°C, 45 min at 55°C, and 30 s at 72°C (Okano et al. 2004). PCR amplification for *NSR* consisted of 2 min at 50 °C, 10 min at 95 °C, 35 cycles at 95°C for 15 s, 63 °C for 30 s (Harms et al. 2003). The conditions for *nirK* real-time PCR were 120 s at 50 °C, 900 s at 95 °C afterwards six touchdown cycles were performed: 15 s at 95 °C for denaturation, 30 s at 63 °C for annealing, 30 s at 72°C for extension and 30 s at 80 °C for a final data acquisition step. The annealing temperature was progressively decreased by 1 °C down to 58 °C. Finally, a last cycle with an annealing temperature of 58 °C was repeated 40 times (Henry, et al. 2004).

RESULTS AND DISCUSSION

Standard Drain field Performance for Nutrient Removal

Nutrient concentration is very high in influent wastewater. In microbiological process, ammonia and nitrite can be converted to nitrate through nitrification process and nitrate can be converted to nitrogen gas through denitrification process. Concentration at different point is shown in Table 4. It is found that both ammonia and NO_x-N concentrations decreased in sand filter and drain fields showing that both nitrification and denitrification were present in the drain fields. The RSF can achieve about 99.53% ammonia removal. But at the same time, RSF filter was also removing about 84.31% of

NO_x-N. So it can be concluded that RSF can support both nitrification and denitrification process. In fact, the top layer of RSF may support the nitrification process and the bottom layer the denitrification process. To prove this, we need to use the RT-PCR analysis.

Ammonia and NO_X-N removal can be further removed in drain field with washed building sand. The average concentration of ammonia in astatula drain field and washed building sand drain field is about 0.071 mg/L (i.e. average of S5, S6 and S7) and 0.027 mg/L (i.e. average of S8, S9 and S10), respectively. So the removal efficiency is about 99.83% and 99.93%, respectively. NO_x-N removal in astatula sand and washed building sand drain field is about 82.35% and 93.13%, respectively. Effluent TN concentration is lower than the influent TN concentration. TN removal in astatual sand drain field is about 84.57% and 84.54% in washed building drain field. Denitrifiers may use oxygen rather than nitrate if no anaerobic condition is created. Denitrification may be started in a slow pace or no anaerobic condition is created in the sand filter and continues in both drain fields. It is possible that anaerobic condition may be available in ground at higher depth. In our project the depth of drain field is only 1.219 meter. Sand cannot remove nitrate and nitrite by adsorption. Nitrate, nitrite and sand all are negatively charged and when they come close to each other, they repel due to same charge (Kim et al., 2000).

For phosphorus removal, washed building sand drain field performed well. Average removal efficiency of SRP in the astatula sand drain field and washed building sand drain field is about 47.84% and 56.63%, respectively. TP removal is about 70.83% in astatula sand drain field and 71.20% washed building sand drain field. RSF has played an important role for removing phosphorus species too. About 44.60% of SRP and 70.50% TP is removed by RSF. After the operation of RSF, the phosphorus concentration increased or remained unchanged. It might be due to the feed-forward flow from dosing tank to the drain field as dosing tank has higher phosphorus concentration. So RSF performance for phosphorus removal is almost valueless in this feed-forward flow pathway. Phosphorus can be removed by chemical reaction with minerals present in the sand drain fields or adsorption by clay particles present in the sand. Figure 4 summarizes the variations of pathway in terms of nutrient removal. Table 5 summarizes the nutrient removal efficiencies over all constituents of interest.

Table 4: The nutrient concentrations at different sampling points

Sample description	NH_3-N in mg/L	NO_X-N in mg/L	TN in mg/L	SRP in mg/L	TP in mg/L
S1	42.140	0.102	46.110	4.918	9.891
S3	6.398	0.005	8.318	3.122	3.802
S4	0.199	0.016	7.329	2.725	2.918
S5	0.056	0.005	4.737	2.815	2.989
S6	0.048	0.005	6.674	2.591	2.771
S7	0.110	0.044	9.931	2.289	2.897
S8	0.006	0.011	4.128	2.273	2.430
S9	0.032	0.005	11.579	2.054	2.214
S10	0.044	0.005	5.667	2.072	3.907

Microorganism concentration in influent is very high. Fecal coliform concentration is about $412*10^3$ cfu/100 mL and E. coli concentration is about $214*10^3$ cfu/100 mL (i.e., CFU means colony forming unit.) The concentration is much lower in the drain fields and washed building sand drain field performs better for microorganism removal. Both the drain fields have achieved about 99.99% removal efficiency though. Average E. Coli concentration in astatula sand drain field and washed building sand drain field is about <1 cfu/100 mL and <1 cfu/100 mL, respectively. Average fecal coliform concentration in the astatula sand drain field and washed building sand drain field is about <1 cfu/100 mL and <1 cfu/100 mL, respectively.

Table 5: Summary of nutrient removal efficiency from influent to drain field

Description	NH_3-N (%)	NO_X-N (%)	TN (%)	SRP (%)	TP (%)
astatula sand	99.83	82.35	84.57	47.84	70.82
washed buildingsand	99.93	93.13	84.54	56.62	71.18

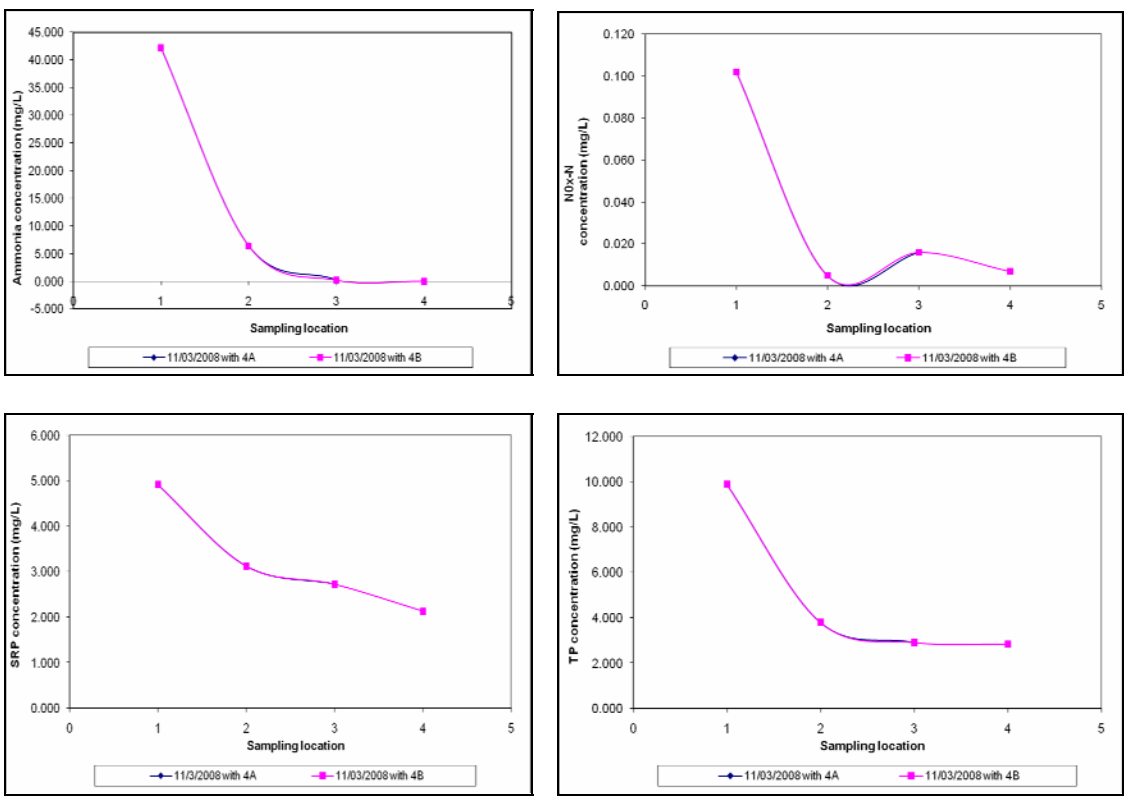

Figure 4: The variations of pathway in terms of nutrient removal

Microbiological Assessment

The standard DNA from plasmid DNA was prepared for tenfold serial dilution (from 10^1 gene copies/uL to 10^5 gene copies/uL), and each of them was quantified in triplicate. Stepone^{TM} V1.0 software (Applied Biosystems) was used to process and ananysis the data. Standard curves were obtained by plotting Ct (threshold cycle) as a function of log of the copy number of target DNA (Table 6).

Table 6: The quantity of different target gene in samples and standard curves used.

Target gene	Sample NO.	gene copy number g^{-1} sample	Standard Curves			
			Slope	Y-Intercept	R^2	Dilution range, gene copies/uL
amoA	R1	4.1×10^{9}	-3.452	49.153	0.989	$10^{5} – 10^{9}$
	R2	3.3×10^{8}				
	R3	1.8×10^{9}				
NSR	R1	9.8×10^{4}	-3.249	32.652	0.995	$10^{1} – 10^{5}$
	R2	1.6×10^{4}				
	R3	1.5×10^{4}				
nirK	W1	1.4×10^{4}	-3.489	36.369	0.984	$10^{1} – 10^{5}$
	A1	UD				
	W2	9.5×10^{4}				
	A2	1.6×10^{5}				
	W3	UD				
	A3	UD				

UD: Under detection limit (which is about 6000 gene copy number g^{-1} sample)

Ammonium oxidation is the first stage of nitrification. The function of autotrophic AOB is to convert ammonium to nitrite within aerobic condition. As the Figure 5(a) shown below, the top sample has highest quantity of AOB with the most oxygen exposure. The amoA gene copy number per gram sample supposed to decrease with the depth. The reason why the bottom sample has more AOB than the midpoint sample may be that there is still some oxygen remaining between the coarse particles in gravel layer. Thus, the midpoint sample has the least amount of AOB rather than bottom sample.

Nitrite oxidation is the other stage of nitrification process. Autotrophic nitrite-oxidizing bacteria convert nitrite to nitrate within aerobic condition. Figure 5(b) below shows that the top sample has highest quantity of NOB in similar principle. From the Table 4, about 40% of NH_3-N had not been removed and flowed out of the outlet of the RSF. The limited concentration of nitrite produced by AOB made the number of NOB keep almost the same at middlepoint and bottom of RSF.

Seen from the Figure 6 above, the *nirK* gene copy numbers per gram sample showed a trend for higher values with the increase of depth. And the *nirK* gene copy numbers per gram of the sample close to the water table reduced to zero approximately. Oxygen content in soil decreased with depth, which is the main reason why *nirK* gene copy number per gram sample increased with depth. The dissolved oxygen in groundwater and reduction of organic matter may cause the reduction of denitrifying bacteria number in sample close to groundwater table abruptly. In addition, the number of denitrifier in washed buliding sand is more than that in astatula sand. However, NO_X-N removal in astatula sand drain field is as good as that in washed building sand drain field. As discussed in previous subsection, the anaerobic condition probably has not been created thoroughly during the initial test run of the treatment system. The nitrification may be started in the drain fields but denitrification had not fully started yet. This implies that the number of denitrifiers has not represented the process of denitrification yet.

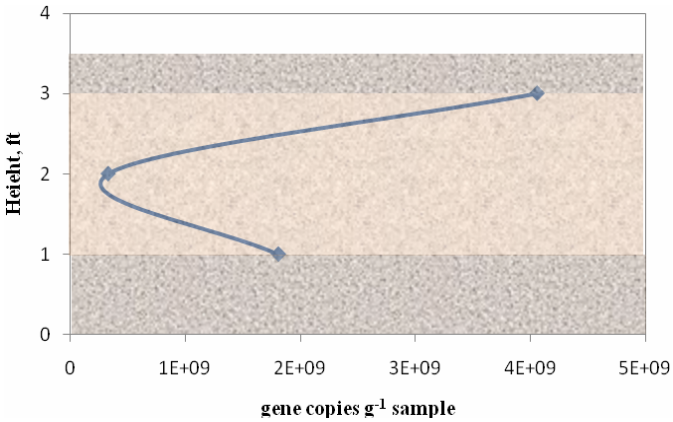

(a) The amoA gene copy number v.s. depth of the real-time PCR

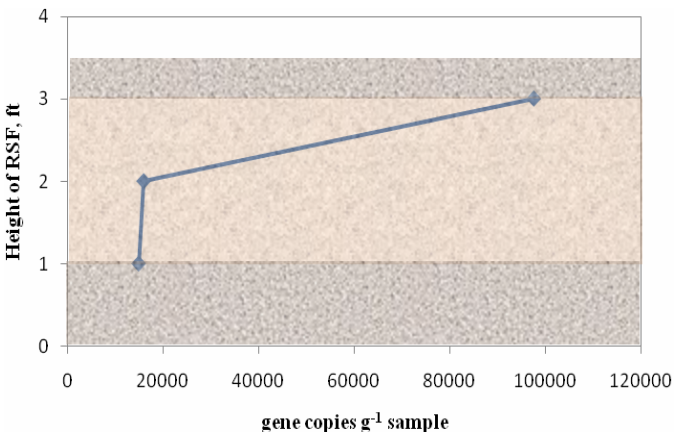

(b) The NSR gene copy number v.s. depth of the real-time PCR

Figure 5: Changing AOB and NOB v.s. depth in RSF

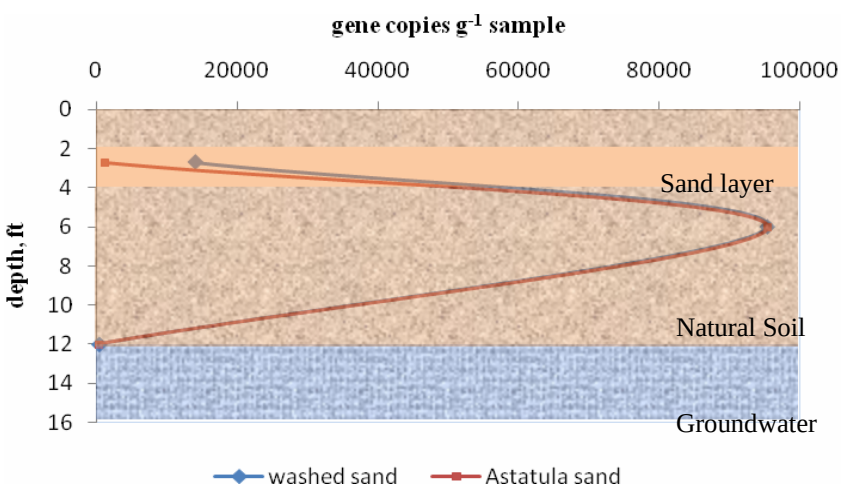

Figure 6: The nirK gene copy number v.s. depth of drain field using the real-time PCR

Groundwater Monitoring

Groundwater elevation data is shown in Figure 7. The groundwater was flowing towards south-west direction indicated by an arrow sign. Nutrient concentration in groundwater was analyzed and found that the concentration was varying widely. Ammonia concentration varied from maximum 7.870 mg/L at M7 to minimum 0.153 mg/L at MW2. The distance between these two wells is about 45.87 meter. NO_X-N concentration was maximum 2.233 mg/L at MW2 to minimum 0.005 mg/L at M4 at a distance of 37.340 mg/L. Both NO_X-N and NO_2-N concentration in groundwater was within the USEPA given guidelines. Note that USEPA recommended maximum NO_3^--N concentration is 10.00 mg/L and NO_2^--N concentration is 1.000 mg/L (USEPA, 1988). It indicated that denitrification rate may increase with increasing depth. It is logical because less oxygen was present at larger depth and more nitrate was available for denitrifiers. Maximum TN concentration was 9.610 mg/L at M7 and minimum TN was 1.300 mg/L at MW8 within a distance of 37.83 meter. Maximum SRP concentration in groundwater was about 0.900 mg/L at MW6 and TP concentration was about 1.76 mg/L at MW7. This phosphorus concentration may not be harmful for groundwater as it is for surface water. Yet, drinking water should contain some phosphorus for teeth and bone formation in human body. National Academy of Science (NAS) recommended about 700 mg of phosphorus per day. Number of E. coli was about <1 cfu/100 mL in all the wells. Maximum fecal coliform concentration was 57 cfu/100 mL at well M8. These microorganisms concentration had also decreased with higher depth. So it can be said that soil in this area was very effective to remove nutrient and harmful microorganisms.

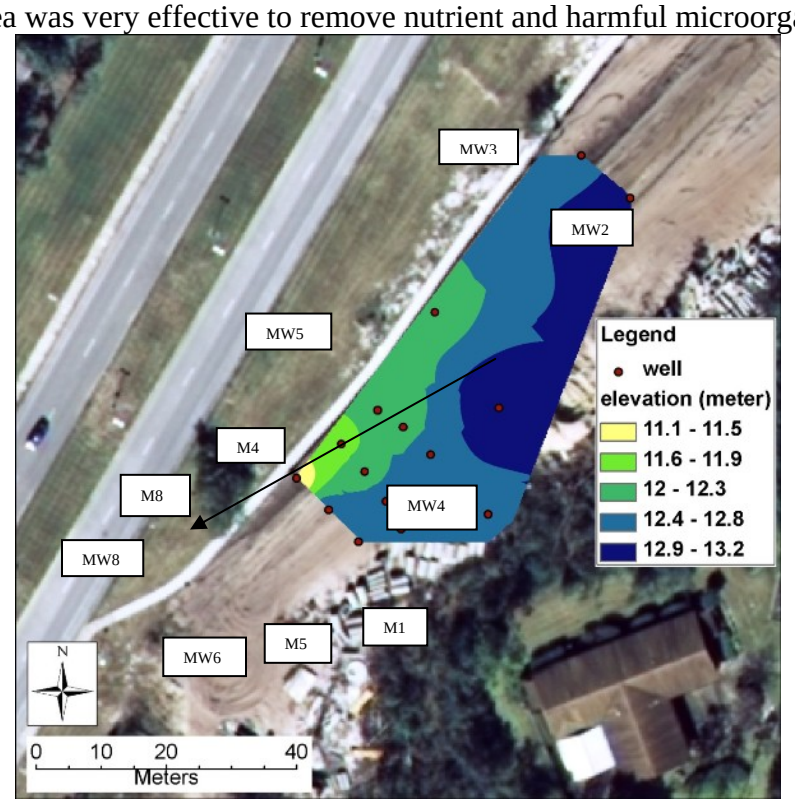

Figure 7: The groundwater table at different groundwater monitoring well at the test site. The arrow sign shows the direction of groundwater flow

CONCLUSIONS

Removal of nutrient by RSF and drain field is basically a combination of physicochemical and microbiological processes. NO_X-N removal efficiency in washed building sand drain field is slightly better than that in astatula sand drain field. In all cases, the ammonia and NOx-N concentration meet the USEPA regulation. While the above said system was removing significant amount of ammonia, it was not removing substantial amount nitrate. In any circumstance, groundwater sample analysis supports that NO_X-N and NO_2-N concentrations are within safe limit according to the USEPA requirement. Phosphorus removal is not high enough in the system. But it would most likely not have a negative affect on groundwater quality. Research findings suggested that phosphorus removal can be enhanced possibly by adsorption, chemical reaction or ion exchange if the sand has more clay and mineral particles. Sorption using a tire crumb mix being investigated at the University OWTS test center is proved effective phosphorus removal too. Due to the cost effectiveness concern, astatula sand may be used to replace the costly washed building sand in the future.

ACKNOWLEDGEMENT

The authors are grateful for the financial support from the Florida Department of Environmental Protection (FDEP) provided through the Watershed Restoration Program's Urban BMP Research and Development Grant.

REFERENCES

Braker G., Fesefeldt A., and Witzel K. P., (1998) Development of PCR primer systems for amplification of nitrite reductase genes (*nirK* and *nirS*) to detect denitrifying bacteria in environmental samples, *Applied and Environmental Microbiology* Vol.64, 3769–3775

Bounds, T.R., (1997), Design and performance of septic tanks, American Society for Testing and Materials, Philadelphia, USA.

Chang, N.B.; Wanielista, M. P.; and Makkeasorn, A. (2007), Innovative design of Low Impact Development in support of Green Building initiative, *Environmental Informatics Archives*, 5, page: 66-85.

Crites, R. and Tchobanoglous, G., (1998), Small and decentralized wastewater management systems, *McGraw Hill publishing*, New York, USA.

Dionisi, H.M., Layton, A.C., Harms, G., Gregory, I.R., Robinson, K.G., Sayler, G.S., (2002). Quantification of Nitrosomonas oligotropha-like ammonia-oxidizing bacteria and Nitrospira spp. from full-scale wastewater treatment plants by competitive PCR. *Applied and Environmental Microbiology*, 68, 245-253.

Harms, G., Layton, A. C., Dionisi, H. M., Gregory, I. R., Garrett, V. M., Hawkins, S. A., Robinson, K.G., and Sayler, G. S., (2003) Real-Time PCR quantification of nitrifying bacteria in a municipal wastewater treatment plant, *Environmental Science and Technology*. 37, 343-351.

Henry, S., Baudoin, E., López-Gutiérrez, J. C., Martin-Laurent, F., Brauman, A., and Philippot, L. (2004) Quantification of denitrifying bacteria in soils by nirK gene targeted real-time PCR. *Journal of Microbiological Methods*, 59, 327– 335.

Kim, H., Seagren, E. A., and Davis A. P. (2000). Engineering Bioretention for Removal of Nitrate from Storm water Runoff, in WEFTEC 2000 Conference Proceedings on CDROM Research Symposium, Nitrogen Removal, Session 19, Anaheim CA, October, 2000.

Okano, Y., Hristova, K. R., Leutenegger, C. M., Jackson, L. E., Denison, R. F., Gebreyesus, B., Lebauer, D., and Scow, K. M. (2004), Application of real-time PCR to study effects of ammonium on population size of ammonia-oxidizing bacteria in soil, *Applied and Environmental Microbiology*, 70(2), 1008-1016.

Rotthauwe, J.H., Boer, W., Liesack W., (1997). The ammonia monoxygenase structural gene *amoA* as a functional marker: molecular fine scale analyses of natural ammonia oxidizing populations. *Applied and Environmental Microbiology*, 63, 4704-4712.

U.S. Environmental Protection Agency (USEPA) (1980). Design manual: onsite wastewater treatment and disposal systems, EPA625/1-80-012, *Office of Research and Development*, Washing ton DC, USA.

U.S. Environmental Protection Agency (USEPA) (1988), Design manual-constructed wetlands and aquatic plant systems for municipal wastewater treatment, EPA/525/1-88/022, US Environmental Protection Agency, Center for Environmental Research Information, Cincinnati, OH, USA.

U.S. Environmental Protection Agency (USEPA) (1999). Decentralized Systems Technology Fact Sheet Recirculating Sand Filters, Office of Water, Washing ton DC, USA.

U.S. Environmental Protection Agency (USEPA) (2002). *USEPA Onsite Wastewater Treatment Systems Manual*, EPA/625/R-00/008, Office of Research and Development, Washing ton DC, USA.

U.S. Environmental Protection Agency (USEPA) (2003), Decentralized approaches to wastewater treatment, Office of wastewater management, USA.

Venhuizen, D., (1998), Sand filter/Drip irrigation systems solve water resources problems, in proceedings of the Eighth National Symposium on Individual and Small Community Sewage systems, American Society of Agricultural Engineers, St. Joseph, USA

Environmental Impacts on Surface Water and Groundwater for Expanding Urban Water Supply Capacity Using Stone Quarries

Xing Fang[1], Ni-Bin Chang[2], Ming-Kuo Lee[3], and Lorraine Wolf[4]

[1] Ph.D., P.E., D.WRE, Associate Professor, Department of Civil Engineering, Auburn University, Auburn, Alabama 36849-5337; Phone (334) 844-8778; Fax (334) 844-6290; email: xing.fang@auburn.edu

[2] Ph.D., P.E., D.WRE, Professor, Department of Civil, Environmental and Construction Engineering, University of Central Florida, Orlando, Florida 32816-2450, Phone (407) 823-1375 Fax (407) 823-3315; email: nchang@mail.ucf.edu

[3] Ph.D., Professor, Department of Geology and Geography, Auburn University, Auburn, Alabama 36849-5305, Phone (334) 844-4898; Fax (334) 844-4486; email: leeming@auburn.edu

[4] Ph.D., Professor, Department of Geology and Geography, Auburn University, Auburn, Alabama 36849-5305, Phone (334) 844-4878; Fax (334) 844-4486; email: wolflor@auburn.edu

Abstract

Global climate change and its related impacts on water supply are universally recognized. In the past few years, drought impacts affecting big metropolitan water supplies alone have plagued Maryland and the Chesapeake Bay in 2001 through 2002, Lake Mead in Las Vegas in 2000 through 2004, the Peace River and Lake Okeechobee in South Florida in 2006, and Lake Lanier in Atlanta in 2007 that especially affected the water resources distribution in three states - Alabama, Florida, and Georgia. One group of unnatural sites, namely crushed stone quarries, holds promise for expanding the reservoir capacity in water supply systems. Inspired by the past and future trend of global change and the need to generate adaptive water resources management strategies, this study develops the conceptual and numerical framework of a spatial decision support system for evaluating the feasibility of water supply development using abandoned and active stone quarries. Whether or not a particular abandoned or active quarry can be used as a water supply reservoir depends on many different factors. Some important factors are the size of a quarry and the volume of water that can be stored, the location of a quarry and its distance to the city or community that needs water supply, the source of water that can be diverted into a quarry, surface runoff input from watershed to quarry, evaporative loss of water in quarry, and groundwater input to quarry. Water storage and recharge in the aquifers must be achieved with caution since water quality may be changed by biogeochemical reactions with aquifer materials. We demonstrate in two cases that mixing of recharge water and groundwater of different hydrochemistry may dissolve certain minerals while allow others to precipitate in the aquifers. A quarry reservoir can become thermal stratification during summer if it is deep enough, and the stratification can lead to oxygen depletion in the bottom waters, and then it may require hypolimnetic oxygenation (aeration) to improve water quality. A lake water quality model is used to examine water quality dynamics in different types of stone quarry reservoirs under different climate and watershed input scenarios.

Introduction

Global climate change and air temperature increase due to rising atmospheric concentrations of carbon dioxide and other green house gases can lead to an increase of water loss by evaporation (Stefan et al. 1998). One model (Burke et al. 2006) suggests that "if global warming–related precipitation changes continue apace, the percentage of the Earth's surface in severe drought could rise from the current 3% to 30% by 2100". "We can project that there is going to be competition for water in the future. We want to take a look over the horizon and see what kind of procedures and innovative approaches we need to make sure we don't end up in water wars" (Manuel 2008). Provision of an adequate quantity of water has been a matter of concern since the beginning of civilization. The average daily per capita water consumption in American cities varies from 130 to 2000 liters (35 to 530 gallons) (McGhee and Steel 1991). The National Academy of Engineering in USA has developed 14 grand challenges for engineering, and one of them is to provide access of clean water: "The world's water supplies are facing new threats; affordable, advanced technologies could make a difference for millions of people around the world." The first common practice for solving the shortage of water is to develop and implement various polices and efforts to conserving water. These conservation practices can be very effective for short periods. Yet the development of sources and/or storage of water supply that can carry a community through extended periods of low streamflow are needed for a long-term solution to the threat of droughts, climate change, and population growth. The source for water supply includes groundwater and surface water supplies. The surface water supplies require the construction of impoundments (storage reservoirs) to meet demand during periods of low river flow. Inspired by the past and future trend of global change and the need to generate adaptive water resources management strategies, the final objective of this study is to develop a spatial decision support system (Chang and Chang 2002) - a robust, efficient, mechanistically-based, integrated decision support tool – for evaluating the feasibility of water supply development using abandoned and active stone quarries. In this writing, we develop a conceptual and numerical framework for understanding, quantifying, and modeling key attributes and criteria that affect development of stone quarries as water-supply reservoirs.

In the recent years the Southeast of United States suddenly finds itself the most rain-starved region of the country. The U.S. Drought Monitor on May 13, 2008 (Figure 1) shows that about 18% of the Southeast remains either in severe or extreme drought even after most of the region had 10 to 12 inches of rain in the previous three months. Although there currently is no immediate public health threat posed by the southeastern drought, it does pose significant challenge and struggle to policy makers and utility companies or authorities to maintain an adequate supply of potable water. At a time when there is a need for more water-supply reservoirs, one may find that the supply of natural sites is quite limited. Most economically attractive and environmentally acceptable natural sites for storage reservoir development in USA have already been developed. "One group of unnatural sites, namely crushed stone quarries holds some promise for expanding reservoir capacity" (Moreau 2007).

Aggregates are natural materials mined either from gravel pits or from quarries. Generally, "pits" produce sands and gravels and "quarries" produce crushed hard rocks. Crushed-stone mining includes four possible important components: stripping, excavation, processing, and trucking. Major rock types processed by the crushed stone industry include limestone, granite, dolomite, sandstone, and quartzite. Most of quarry mines were dug below the local groundwater table, sometimes exceeding 1,000 feet beneath the ground surface. A quarry

lake forms and develops over time when groundwater, surface water and other post-mining drainage accumulates inside an inactive (abandoned) open quarry after dewatering stops. One example of quarry lakes is shown in Figure 1. Recently, some of quarry lakes are created for water storage sites and filled by diverting water from nearby rivers, streams, and reservoirs when contributions from groundwater and surface runoff are limited (Moreau 2007). Whether or not surface runoff or groundwater flow from surrounding watersheds can provide adequate source water during wet seasons for the quarry reservoir is one of the limiting factors for the inclusion of a quarry for integrative water supply development. Another consideration is that diverting water from a nearby stream to a quarry must satisfy aquatic habitat and in-stream flow requirements to maintain a healthy ecosystem downstream of the diverting point.

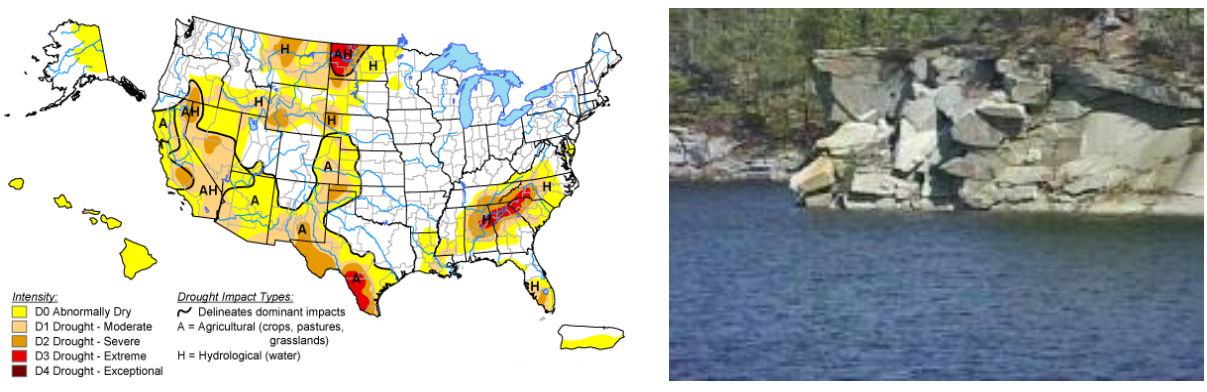

Figure 1. U.S. Drought Monitor for May 13, 2008 (from National Drought Mitigation Center, University of Nebraska – Lincoln) (left panel) and an abandoned quarry in Wake County, North Carolina (right panel).

Feasibility of Using Stone Quarries as Water Supply Reservoirs

Most of drinking water in the Southeast is stored in man-made reservoirs, such as Falls Lake and Lake Jordan for the city of Durham in North Carolina. Water supply systems are "sociotechnical" systems with strong links to society (Grigg 1996). For instance, the Southeast drought has already had not only serious economic consequences (losses of more than $1.3 billion in 2007), but also political consequences, pitting downstream and upstream users (i.e., three states) against one another. Potential climate change and cyclical droughts pose threats to water supplies for many cities in the United States. In addition to water conservation practices, it is important and necessary to examine feasibility and possibility to develop new sources and/or storage of water supply, and this could be an essential alternative in the long-run to solve the problem of shortage in water supply. The USGS Mineral Industry Surveys show that there are 3,358 active quarries for crushed stone production and there are numerous abandoned or inactive quarries in the United States. "What is the feasibility of using active and abandoned quarries for water supply development and solving current and future water supply crisis?" is a question that has yet to be studied holistically. "Abandoned quarries have been largely overlooked as storage sites until recently" as stated by Dr. David H. Moreau, Director of the Water Resources Research Institute of The University of North Carolina. It is worth to mention that some abandoned quarries work better than others for storing water. Any site, according to Dr. Moreau, would need to be examined for contamination that could threaten public health. Another factor to consider is the cost of moving water from the quarry to treatment plants and distribution pipes.

Whether or not a particular abandoned or active quarry can be used as a water supply reservoir depends on many different factors involving water resources, geological, public health, socioeconomic and environmental impacts. Some important factors are the size (volume) of a quarry (affecting how much water can be stored), the location of a quarry and its distance to the city or community that needs water supply, the source of water that can be diverted into a quarry, surface runoff input from surrounding watersheds to quarry, groundwater input to quarry, evaporative loss of water in quarry, etc. To face the future challenge, water supply planning requires us not only to identify abandoned quarries that can be possibly developed as storage reservoirs in the near future but also to consider and identify active quarries for long-term future development, especially in kart regions (covering nearly 25% area of the contiguous USA) where the hydrogeological environment is challenging. In the Southeast the karst geology might strongly affect the decision making process of using stone quarries as alternative water storage.

Impacts of Surface Water and Groundwater on Stone Quarry

In considering the planning, design, and expansion of a water supply system, many competing issues must be addressed and the competing demands must be balanced within the legal and administrative framework (Maidment 1993). Modifications to the water supply system also depend on the extent to which the alternative stone quarries are integrated into the community's existing water resources systems. Regional precipitation variation and extreme drought events are important to water supply development for the fast growing urban regions. Surface runoff input to a quarry lake depends on watershed size surrounding the lake, geological conditions, and regional precipitation variation. Using the lake as outlet, contributing watershed can be delineated from contour maps, field surveys, aerial photographs, and the digital elevation models. If the contributing watershed area to the lake is limited, then surface runoff to fill the lake will be limited. Rainfall is the driven force and the key controlling parameter on surface water input to a quarry lake. Figure 2 shows variations of mean annual precipitin over the contiguous U.S. from 1971 to 2000, and annual precipitation is on the order of 120 cm or more in the Southeast United Sates, but annual evaporation loss from shallow lakes and reservoirs in the area is also high on the order to 100 cm (from Figure 6.1, Viessman and Lewis 2002). The map allows us to examine regional precipitation variations at any site with stone quarry for potential water supply development. Projection of future climate scenarios such as the third generation coupled global climate model from the Canadian Climate Centre for Climate Modeling Analysis (CCCma) and from the Hadley Centre Coupled Model in the United Kingdom can provide us potential change on future precipitation for the study.

Investigation groundwater hydrology of quarry lakes

For potential quarry lake sites in karst regions, it is important to identify land-use risks using geophysical imaging and hydrological field studies. Imaging the subsurface structure of quarry sites and related geologic features such as fractures, solution-generated conduits, and evolving sinkholes is of both practical and academic interest. These geologic features serve to increase the hydraulic conductivity, either as sources of stored water or as preferential pathways for groundwater flow. The use of geophysical methods for imaging void features has demonstrated success; previous research projects have used such methods as electrical resistivity and ground-penetrating radar for this purpose (Carpenter et al. 1998; Kruse et al. 2006). Multielectrode systems allow for true 3-D inversion of the acquired electrical data; however, it is essential that the survey and measurement design be targeted to the scale of the features expected at each

potential quarry lake site. Geophysical imaging methods provide an effective means to locate and characterize important shallow geologic features that may control hydrological transport. For example, the presence of low-permeability layers below the quarry can restrict the leakage of water. The presence of impervious aquitard layers stratigraphically above and surrounding the quarry, however, may retard the artificial recharge process. In cases where such confining layers are absent, water can percolate down-dip in the direction of hydraulic gradient and recharge the underlying aquifers or deep-seated fractured zone. Knowledge of water-table depths not only provide constraints for geophysical data interpretation and hydrological modeling, but also mark the presence of areas with high hydrologic conductivity as characterized by troughs and low hydraulic gradients below the water table. Superimposing these data on a discharge hydrograph provides insight into the internal structure and transportation characteristics of the aquifer (Ryan and Meiman 1996). Multiple-well aquifer pumping tests (Tiedeman and Hsieh 2001) can also be conducted near the quarry sites. For example, a pressure transducer can be used to record the head changes during a pumping test over time. This aquifer test can reveal the degree of hydraulic connection between boreholes and yield valuable insights into the hydrological characteristics of rocks surrounding the quarry. The relation of measured drawdown to distance from the pumped well can be compared to that theoretically observed during radial flow in an aquifer, as predicted by the Theis solution (Viessman and Lewis 2002). The hydraulic conductivity calculated for both the highly conductive and less-conductive parts of the rock represent high-conduit clusters and low-conduit matrix, respectively. These field experiments allow the assessment of water-level change in response to quarry water replenishment; such data are important for recharge operation and water resources management. Both the hydrological and geophysical measurements are geared toward understanding how the geologic features of each candidate site might affect its suitability as a water-supply reservoir.

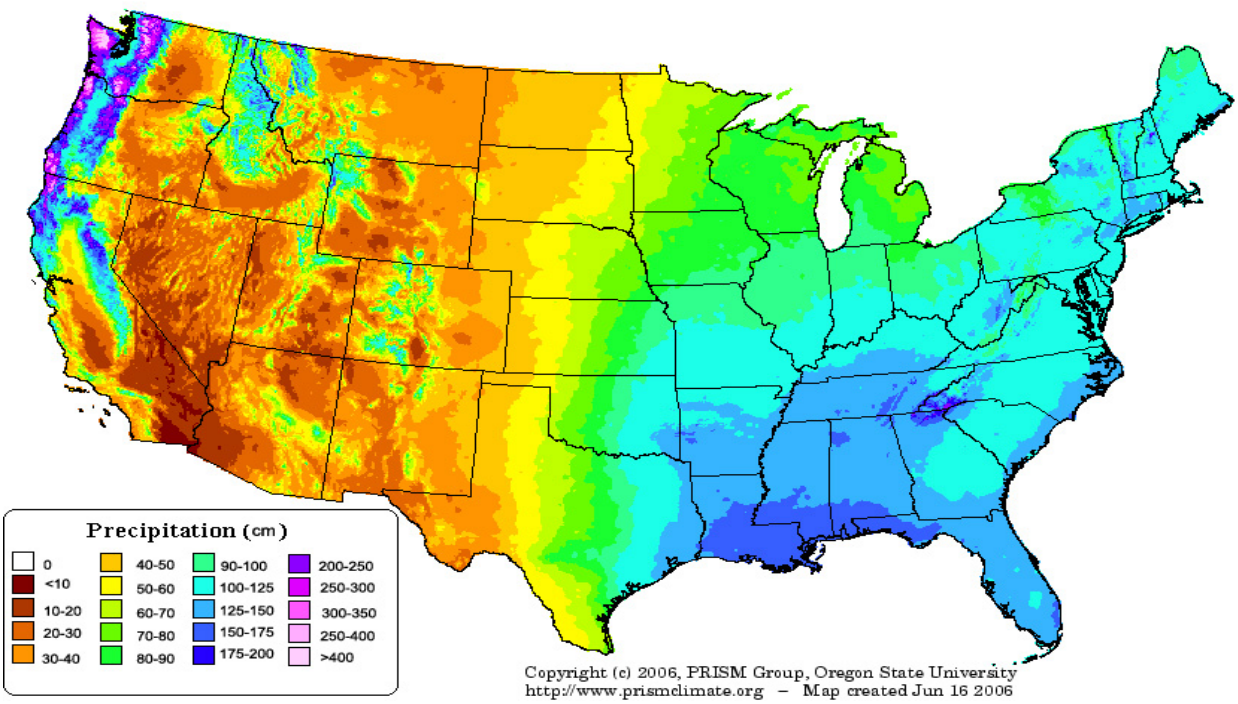

Figure 2. Mean annual precipitation in millimeters by climate divisions, 1971-2000 (Courtesy from Oregon State University).

Investigation of environmental impacts for quarry lakes

In order to evaluate stone quarries development as water supply reservoirs, models for surface-water, unsaturated zone, groundwater, and watershed should be integrated to quantify water budgets and geochemical evolution and consequences for quarry reservoirs under different environmental scenarios. The following discussion show possibility to integrate a watershed model (TOPMODEL), geo-environmental model (FRACFLOW), and lake-water-quality model (MINLAKE96) to assess and characterize stone quarry and its watershed for sustainable water supply development.

Watershed Modeling Analysis: A quarry under feasibility study for water supply serves as outlets or pour points of the surrounding watersheds that can be simulated by TOPMODEL, directing it to connect the simulation domain for a lake water quality model - MINLAKE96 (Fang and Stefan 1996). TOPMODEL is a distributed hydrological model and can use a GIS interface (e.g., ArcMap) for the analysis and manipulation of spatial data (i.e., digital elevation topography, spatial distributions of soil characteristics such as hydraulic conductivity, depth to bedrock, depth of AB soil horizon, and field capacity). Although the model was first developed by Beven and Kirkby (1979), the latest version reflects the current understanding of how precipitation moves over and through watersheds to become streamflow (Wolock 1993). The model is designed to simulate hydrological fluxes of water (infiltration-excess overland flow, saturation overland flow, infiltration, exfiltration, subsurface flow, evapotranspiration, and channel routing) through a watershed and simulates the variable-source-area concept for streamflow generation. The algorithm may assess explicit groundwater/surface-water interactions by predicting the movement of the water table, which determines whether saturated land-surface areas may have the potential to produce saturation overland flow. It uses time series of precipitation and air temperature as part of model input, making it a suitable platform to examine climatic and drought scenarios on water budget for quarry development. Consequently, TOPMODEL has been used in a variety of water resources engineering studies, such as topographic effects on streamflow (Kirkby 1986) and water quality (Wolock et al. 1990), and effects of climate change on hydrological processes (Wolock and Hornberger 1991). Since it is a module-based modeling system with publicly available FORTRAN source code, it can be coupled with other modeling components and systems, such as the lake/reservoir water quality model MINLAKE96 (Fang and Stefan 1996). The hydrographs generated by TOPMODEL at daily time steps are therefore compatible for model integration with a daily-time water quality model of lakes (MINLAKE96, coded in FORTRAN) and assess water balances for a targeted watershed for water quarry development.

Lake Modeling Analysis: A verified, process-oriented, unsteady and one-dimensional (vertical) year-round lake water quality model (MINLAKE96) was used to study impact of global climate change on water temperature, dissolved oxygen (DO), and fish habitat for small lakes in the contiguous U.S. (Stefan et al. 1998). This model is a good candidate to simulate the continuous change of lake stratification and water quality in response to weather (precipitation), inflow, outflow, and exchange processes at the sediment interface, and inlake processes. The water quality parameters that can be modeled after model enhancements include temperature, up to three forms of algae (expressed as chlorophyll-a), available phosphorus, ammonia, nitrate-nitrite, detritus as biochemical oxygen demand, zooplankton, inorganic suspended sediment, and dissolved oxygen. The depth profile of water temperature is computed from a balance between incoming heat from solar and long-wave radiation and the outflow of heat through convection, evaporation, and back radiation. Water loss through evaporation and input from precipitation are

included in the model. MINLAKE96 can simulate daily lake water temperature and DO profiles in a continuous mode for multiple years. Thermal stratification in a quarry reservoir is modeled first before it models transport and fate of contaminants in the quarry. The model requires dividing a lake (quarry reservoir) into a series of well-mixed horizontal water layers and including a sediment layer below (Fang and Stefan 1996).

Stratification characteristics of water temperature and dissolved oxygen in a hypothetic stone quarry lake are simulated using MINLAKE96. The lake simulated has a surface area of 1.7 km^2 (420.1 acre), maximum depth of 24 m (78.7 ft), and lake volume of 1.25 x 10^7 m^3 (3,302.3 MG). Based on the lake volume, this hypothetic lake has similar size as the second stone quarry that the Orange Water and Sewer Authority in North Carolina purchased for future water supply (Moreau 2007). Water temperature and dissolved oxygen concentrations from 1961 to 1995 (more recent weather data can be obtained from NOAA) were simulated using weather data at Raleigh, NC. The numerical simulation model for daily DO profiles in a lake solves the one-dimensional, unsteady transport equation. The vertical DO profiles in the lake are computed from a balance between oxygen sources (surface reaeration and photosynthesis) and oxygen sinks (sedimentary oxygen demand, biochemical oxygen demand, and plant respiration). Oxygen production is related to chlorophyll-a concentration and limitation of available light determined by Haldane kinetics. In the model chlorophyll-a is specified by a mean annual value and a function that calculates typical seasonal chlorophyll cycles based on observation data from 56 lakes or reservoirs in Europe and North American (Marshall and Peter 1989). In the model, the oxygen transfers through the water surface (reaeration) during the open water season is used as an oxygen source or sink term in the topmost water (surface) layer of the lake, and surface oxygen transfer coefficient is calculated as a function of wind speed.

Figure 3 shows simulated time series of dissolved oxygen concentration at five different depths from the water surface under 1979 weather conditions, and simulated results for other years are similar to patterns given in Fig. 3. The lake geometry ratio $A_s^{0.25}/H_{max}$ (where A_s is the surface area in m^2, and H_{max} is the maximum lake depth in m) is equal to 1.5 for this quarry, and this indicates that the lake is strongly stratification during summer (Stefan et al., 1998). Figure 3 does clearly show strong stratification in dissolved oxygen concentration from early spring to later fall, and more or less well mixed for winter months (November to February). It does have weak inverse stratification on dissolved oxygen (due to biochemical and sediment oxygen demand) during winter months. The lake was assumed to be an eutrophic lake with mean annual chlorophyll-a concentration of 15 µg/l and Secchi depth of 1.2 m, and this condition could be resulted from rich nutrient inputs draining from surrounding watersheds. Simulated results for eutrophic lake are shown in the top panel of Figure 3. Starting from early May, dissolved oxygen concentrations at the lake bottom become zero; and anoxic condition last for six months. Even the lake becomes anoxic from 6.5 m depth to the lake bottom in June up to the middle August. Anoxic condition in the large portion of the lake volume will have profound impacts on lake ecosystem and dynamics of many other water quality parameters in the lake. It may require hypolimnetic aeration to improve water quality before it can be used as the source of water supply. The presence of high levels of nitrate in drinking water appears to be the cause of methemoglobinemia or “blue babies”, and this disease primarily affects infants less than 6 months old. Under anaerobic condition the nitrate can be reduced to nitrite and the nitrite converted to free nitrogen by the process of denitrification, and therefore, with some parts of lake volume with anoxic condition could avoid public health problem with nitrate toxicity. If the lake is assumed to be an oligotrophic lake (poor nutrient inputs) with less biochemical oxygen

demand and lower chlorophyll-a concentration (2 µg/l), the lake will not have any volume with anoxic condition as shown in bottom panel of Figure 3 for comparison.

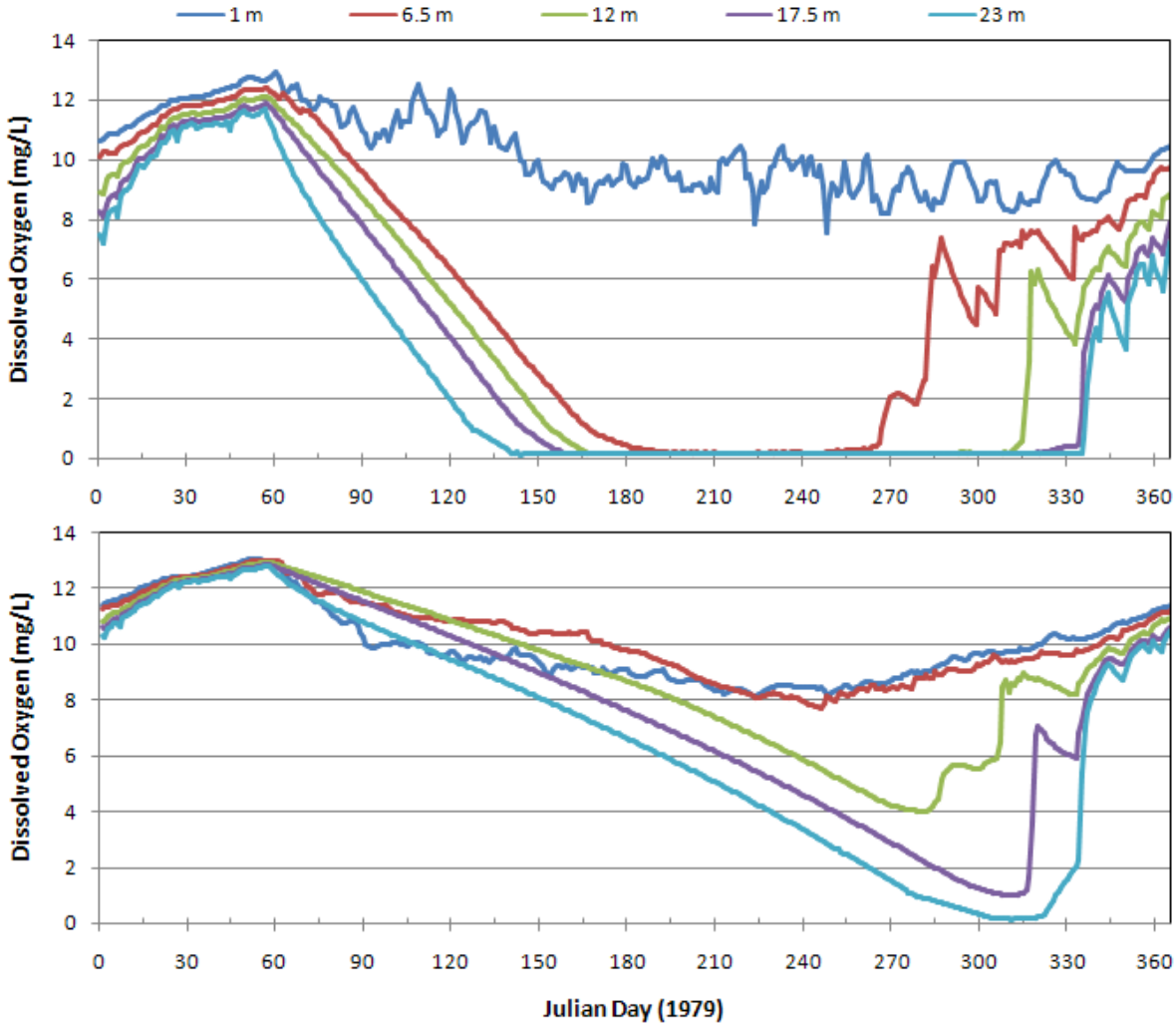

Figure 3. Simulated time series of dissolved oxygen concentration at five depths for a 24-m deep **eutrophic** (top panel) and **oligotrophic** (bottom panel) hypothetic lakes in Raleigh, NC.

Geo-environmental Modeling Analysis: Water storage and recharge in the aquifers must be achieved with caution since water quality may be changed by biogeochemical reactions with aquifer materials. Recharge water may be warmer or cooler than native groundwater and it may dissolve certain minerals while allow others to precipitate. This is because of the temperature-dependent retrograde and prograde solubility of carbonates and sulfates versus silicates mineral groups, respectively. A successful operation of artificial recharge in a quarry requires a more comprehensive understanding of the changes in groundwater flow, storage, and chemical conditions. When surface water is diverted for artificial recharge in quarries, it may or may not be in thermal, redox, or chemical equilibrium with minerals in quarry rocks. In this study we demonstrate the use of a geochemical model, Geochemist's Workbench (Bethke 2008) as a part of the SDSS to investigate the chemical states of surface water and groundwater and quantify how injected water may cause dissolution or precipitation minerals in the quarries. Moreover,

typical fractured rocks consist of confining units and water bearing units that permit the rapid transport of water through connected fractures and conduits (National Research Council 2001; White 2006). We have developed a computer software, FRACFLOW (Lee and Wolf 1998), to simulate such flow characteristics and hydraulic head distribution in fractured/karst rocks bounded by constant-head streams or lakes. This model can be integrated with the watershed and lake models to account for the impact of karst geology on the quarry reuse.

The numerical tools described above can be integrated to address science questions related to (1) chemical interactions among surface water, groundwater, and quarry or aquifer materials; (2) pathogen fate and transport from possible sources in nearby watersheds if the quarry is included; and (3) hydrological loading and storage capacity of the quarry under different geologic conditions. These considerations can be synthesized to generate index values reflecting the feasibility of the sustainable development of water supply with each candidate site for final decision making. One case study is given below to demonstrate geo-environmental analysis. Artificial recharge, storage, and recovery can augment water supply during peak summer seasons or periods of extended drought. One option is to bring river water into the quarries or aquifers during the high-flow and low-demand seasons, the water stored in recharged aquifers can be withdrawn to meet demands during drought. The injected surface water, however, may not be chemically or thermally compatible with the native groundwater and hosting aquifer minerals during recharge conditions. This case study uses Geochemist's Workbench to simulate the geochemical consequences of mixing of surface water and groundwater in the limestone aquifers of Florida and Nevada. Water mixing in limestone aquifers may cause calcite ($CaCO_3$) precipitation that would affect artificial recharge and storage operations or reduce permeability of near-by pumping wells. In the Florida Panhandle area, excess groundwater withdrawals near the coastal areas have forced many municipal supply wells to be abandoned due to saltwater intrusion (McCartha et al. 2003). In the Las Vegas Valley, water demands due to rapid population growth have exceeded the city water system's producing capability from the Paleozoic carbonate aquifers and valley-filled sediments (Katzer and Brothers 1988). Both areas are using artificial recharge and recovery as an option to augment water supply.

In the model, a packet containing 1 kg of Ca-Mg-HCO_3 type Floridian groundwater maintains equilibrium with calcite and dolomite in the aquifer. We used the chemical analyses of PCB1 well in the Panama City Beach area to set the fluid's initial compositions (Table 1). A second type of surface water recharges and mixes into the first fluid packet in a mass ratio of 10:1. The calculation used the surface water chemical data collected from the Appalachicola-Chattahoochee-Flint (ACF) River basin (station ID 023358694, Table 1). As the fluids mix over the course of reaction path modeling, any minerals that become supersatured precipitate. The modeling results indicate that calcite remains undersaturated during mixing and its precipitation does not occur (Figure 4). By contrast, the recharge of Colorado River water into Paleozoic carbonate aquifers in the Las Vegas Valley can lead to significant calcite supersaturation and precipitation (Figure 4). Chemical analyses for well 11A and the injected Colorado River water are shown in Table 1. These waters are more concentrated and have higher calcium and bicarbonate concentrations than those in the Florida Panhandle study area. The geochemical modeling can determine whether mixing of surface water with groundwater may cause significant calcite precipitation under different physio-chemical conditions. The water manager can use the model as a tool to find a site with minimum potential of calcite precipitation that would reduce aquifer permeability.

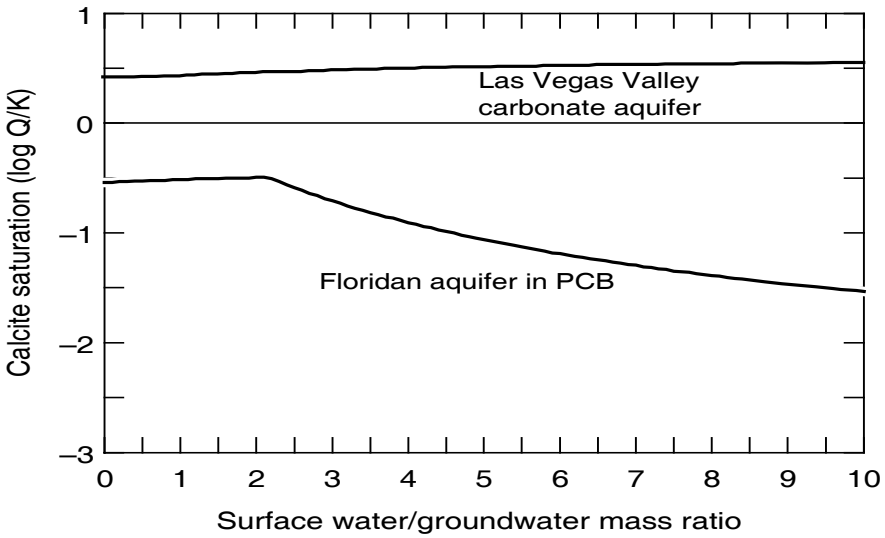

Figure 4. Results of mixing surface water with carbonate groundwater in the Panama City Beach (PCB) and Las Vegas Valley areas. The diagram shows how the saturation index (log Q/K) of calcite varies with mixing ratio of surface water versus groundwater.

Table 1. Major ion compositions (in mg/kg) of surface water and groundwater used in computer simulations of mineral oxidation and fluid mixing reactions

Sample	ACF River[1]	PCB 1[2]	Colorado River[3]	Las Vegas 11A[4]
Alkalinity (HCO_3^-)	15	190	140	224
Ca	4.7	62	86	53.5
Mg	1.2	49	22	26.8
Cl	2.9	196	104	4.8
K	2.5	4.3	3.9	3.8
Na	5.3	104	109	7.1
SO4	5.7	13	311	68
pH	6.6	7.6	8.2	7.8

[1]. Station ID 023358649, http://ga.water.usgs.gov/nawqa/tables/swlusbwc.maj.html
[2]. Panama City Beach groundwater well #1, McCartha (2002)
[3]. Colorado River water in Lake Mead (Katzer and Brothers, 1989)
[4]. Groundwater from Paleozoic limestone (Katzer and Brothers, 1989)

Future Development of Spatial Decision Support System

Our long-term plan is to combine data collection, model integration, field investigation, and decision support tool development from five subject areas relating to the environmental, water resources, geological, public health, and socioeconomic factors that influence the way in which water utility move in the decision making process. The study is to pursue a systematic approach (Change et al., 2008) in order to see interrelationships rather than a misleading cause-effect chain and to use a wealth of modeling and sensing outputs and measurements to examine the process of change rather than simply analyzing snapshots of data for evaluating the feasibility of using stone quarries for sustainable water supply development.

Conclusions

This study has identified potential problems of global climate change and cyclical droughts to water supply in growing urban regions. Inspired by the past and future trend of global change and the need to generate adaptive water resources management strategies, this study has developed the conceptual and numerical framework for future development of a spatial decision support system in order to evaluate the feasibility of water supply development using abandoned and active stone quarries. We used Geochemist's Workbench to demonstrate biogeochemical reactions in two different aquifers, and the necessity to carefully examine chemical equilibrium and mineral precipitation and dissolution reactions in artificial recharge and storage operations for potential stone quarries as water supply development. The field study such as pumping tests and geophysical images can be important in determining key groundwater hydraulic parameters and locating and characterizing shallow geologic features that are important to stone quarry development in karst regions. A deep quarry reservoir can become thermally stratified during summer, and the stratification can lead to oxygen depletion in the bottom waters, thus requiring hypolimnetic oxygenation (aeration) to improve water quality. The water quality model MINLAKE96 was used to examine a hypothetical deep lake in Raleigh, North Carolina, under eutrophic and oligotrophic conditions. Eutrophic lake with rich nutrient input from surrounding watersheds results in long-period of anoxic conditions in hypolimnion during summer. In this study, the conceptual and numerical framework is developed for understanding, quantifying, and modeling key attributes and criteria that affect developing stone quarry as water-supply reservoirs. These consider geological, environmental, public health, water resources, and socioeconomic impacts.

References

Bethke, C. M. (2008). *Geochemical and biogeochemical reaction modeling*, Cambridge University Press, 543.

Beven, K. J., and Kirkby, M. J. (1979). "A physically based, variable contributing area model of basin hydrology." *Hydrological Sciences Bulletin*, 24, 43-69.

Burke, E. J., Brown, S. J., and Christidis, N. (2006). "Modeling the recent evolution of global drought and projections for the twenty-first century with the Hadley centre climate model." *Journal of Hydrometeorology*, 7(5), 1113-1125.

Carpenter, P. J., Doll, W. E., and Kaufmann, R. D. (1998). "Geophysical character of buried sinkholes on the Oak Ridge Reservation, Tennessee." *Journal of Environmental and Engineering Geophysics*, 3, 133-146.

Chang, Y. C. and Chang, N. B., 2002. "The design of a web-based decision support system for the sustainable management of an urban river system." *Water Science and Technology*, 46(6), 131-139.

Chang, N. B., Parvathinathan, G., and Breeden, J. B., 2008a. Combining GIS with fuzzy multiple attribute decision making for landfill setting in a fast growing urban region. *Journal of Environmental Management*, 87, 139–153.

Fang, X., and Stefan, H. G. (1996). "Development and validation of the water quality model MINLAKE96 with winter data." Project Report 390, St. Anthony Falls Laboratory, University of Minnesota, Minneapolis, MN.

Grigg, N. S. (1996). *Water resources management : principles, regulations, and cases*, McGraw-Hill, New York, NY, 540.

Katzer, T., and Brothers, K. (1989). "Artificial recharge in Las Vegas valley, Clark county, Nevada." *Ground Water*, 27, 50-56.

Kirkby, M. (1986). "A runoff simulation model based on hillslope topography." *Scale problems in hydrology*, V. K. Gupta, I. Rodriguez-Iturbe, and E. F. Wood, eds., Dordrecht D. Reidel Publ. Co., 39-56.

Kruse, S., Grasmueck, M., Weiss, M., and Viggiano, D. (2006). " Sinkhole structure imaging in covered Karst terrain." *Geophysical Research Letters*, *33*.

Lee, M. K., and Wolf, L. W. (1998). " Analysis of fluid pressure propagation in heterogeneous rocks: Implications for hydrologically-induced earthquakes." *Geophysical Research Letters*, 25, 2329-2332.

Maidment, D. R. (1993). *Handbook of Hydrology*, McGraw-Hill, Inc., New York, NY.

Manuel, J. (2008). "Drought in the southeast: lessons for water management." *Environmental Health Perspectives*, 116(4), 168-171.

Marshall, C. T., and Peter, R. H. (1989). "General patterns in the seasonal development of chlorophyll a for temperate lakes." *Limnology Oceanography*, 34(5), 856-867.

McCartha, J., and Lee, M. K. (2003). "Water-rock interaction and groundwater flow of the Upper Floridian aquifer in Bay County and surrounding areas, Florida." *Proceeding MODFLOW and More 2003*, Sept. 16-19, v. 1, 433-437, Colorado School of Mines.

McGhee, T. J., and Steel, E. W. (1991). *Water supply and sewerage*, 6th Ed., McGraw-Hill series in water resources and environmental engineering, McGraw-Hill, New York, NY, 602.

Moreau, D. H. (2007). "Off-stream storage: an option for augmenting public water supplies." *WRRI NEWS (Number 356, March-April 2007), Director's Forum,*, Water Resources Research Institute of The University of North Carolina, Raleigh, NC 27695-7912.

National Research Council. (2001). "Conceptual models of flow and transport in the fractured vadose zone." National Academy Press, Washington, D.C., 374.

Ryan, M., and Meiman, J. (1996). " An examination of short-term variation in water quality at a karst spring in Kentucky." *Ground Water*, 34, 23-30.

Stefan, H. G., Fang, X., and Hondzo, M. (1998). "Simulated climate change effects on year-round water temperatures in temperate zone lakes." *Climatic Change*, 40, 547-576.

Tiedeman, C. R., and Hsieh, P. A. (2001). "Assessing an open-well aquifer test in fractured crystalline rock." *Ground Water*, 39, 68-78.

Viessman, W., and Lewis, G. L. (2002). *Introduction to hydrology*, 5th Ed., Pearson Education, Upper Saddle, N.J., 612.

White, W. B. (2006). "Fifty years of karst hydrology and hydrogeology: 1953-2003." *Geol. Soc. America Special Paper 404*, 139-152.

Wolock, D. M., Hornberger, G. M., and Musgrove, T. J. (1990). "Topographic effects on flow path and surface water chemistry of the Llyn Brianne catchments in Wales." *Journal of Hydrology*, 115, 243-259.

Wolock, D. M., and Hornberger, G. M. (1991). "Hydrological effects of changes in atmospheric carbon dioxide levels." *Journal of Forecasting*, 10, 105-116.

Wolock, D. M. (1993). "Simulating the variable-source-area concept of streamflow generation with the watershed model TOPMODEL." USGS Water-Resources Investigations Report 93-4124, Lawrence, Kansas.

Groundwater Baseflow Sourced from Miocene Rocks and Residuals Carries Elevated Selenium into Southern California Streams

Barry Hibbs[1], Mercedes Merino[2], Rachel Andrus[2]
Wynee Hu[2], and Anna Doro-on[3]

[1]Professor and [2]Graduate Research Assistants, Department of Geological Sciences, California State University, Los Angeles; Los Angeles, CA 90032 (323) 343-2414; FAX (323) 343-2435; e-mail: bhibbs@calstatela.edu

[3]Senior Project Engineer, EPD Consultants Inc., 411 N. Harbor Blvd., Ste 304, San Pedro, CA 90731

ABSTRACT

The geochemical patterns of nitrate and selenium exhibit spatial variability within the shallow aquifer of San Diego Creek Watershed, Orange County California. The surface streams in the watershed are fed primarily by groundwater baseflow from the shallow aquifer. A new area was investigated in the watershed in 2004 and 2005 near "Santa Ana Delhi Channel." A covariate relationship is shown in the groundwater data collected near Santa Ana Delhi Channel for selenium, nitrate, and salinity. Despite wide scatter of data, there is a clear positive correlation shown between selenium and nitrate concentrations, and a negative correlation between nitrate/specific conductance and selenium/specific conductance.

A possible set of hypotheses for the correlative relationships between selenium, nitrate, and salinity are as follows: (1) Geologic history plays an important role in controlling selenium content in the shallow aquifer, and selenium may originate from upland marine shales of Miocene age. (2) A historic marsh in low lying swampy areas of the watershed acted as a sink for selenium in runoff waters. (3) Draining the marsh in the late 1800s changed prevailing hydrologic and geochemical structure of the land, essentially converting this selenium sink to a selenium source whereby infiltrating precipitation and shallow groundwater leaches selenium from the historic marsh deposits. Selenium-rich groundwater contributes substantial flow to surface streams via groundwater seepage and springs. (4) Oxidation of selenium by nitrate produces a positive correlation between high nitrate and high selenium. (5) Groundwaters with highest salinity in the local areas near Santa Ana Delhi Channel are sourced from lower permeability alkali soils that were never planted to crops, and nitrogen fertilizer was not used on these soils. These fine textured soils were not leached as effectively historically, and retained more salt

during leaching, so crops were not planted there. As a result, low selenium, high salinity, low nitrate correlations are observed in areas with saline soils; and high selenium, low salinity, high nitrate correlations are observed in the lower salinity areas where agriculture was practiced.

INTRODUCTION

Study Area and Problem Statement. The San Diego Creek Watershed covers approximately 112 square miles in Orange County, California. Regional streams drain headwaters from the Santa Ana Mountains in the north and northeast and the San Joaquin Hills in the southeast. These waters drain ultimately into Upper Newport Bay, one of the last remaining coastal estuaries of southern California (Hibbs and Lee, 2000).

Before 1890, waters draining from the highlands collected in the central low-lying part of the watershed creating a wetland environment known as the "Swamp of the Frogs" Marsh (Trimble, 2003). Wetlands existed where the water table was at ground surface, creating an area where water-logged soils prevented land development. In the late part of the nineteenth century, part of this swamp was drained to make way for the expansion of ranching and agriculture (Trimble, 2003). By dredging channels to drain the marsh, the water table was effectively lowered by several feet so that today a shallow groundwater system exists above deeper regional aquifers.

Previous research found high levels of selenium in the shallow groundwaters flowing within the boundary of the historic Swamp of the Frogs Marsh (Hibbs and Lee, 2000). Geologic history plays an important role in controlling selenium content in the now shallow aquifer. Selenium may originate from upland marine shales of Miocene age (Tracy, 1990). Hibbs and Lee (2000) proposed that the historic marsh acted as a sink for selenium derived from weathering and erosion of upland marine shales. Draining the marsh changed prevailing hydrologic and geochemical structure of the land, essentially converting this selenium sink to a selenium source whereby infiltrating precipitation and shallow groundwaters leach selenium from the historic marsh deposits. Selenium in reduced forms are usually low solubility species, while selenium in oxidized form is highly soluble and moves freely in oxidizing groundwater. Once selenium is oxidized, the selenium-bearing aquifer contributes substantial flow and selenium loading to surface streams in the watershed via groundwater baseflow (Hibbs and Lee, 2000; Meixner and others, 2004).

High levels of selenium in surface water have been linked to birth defects and increased mortality of fish and waterfowl (Frankenberger, 1998). Aquatic life forms depend on regional streams and on the principle drainage feature of the catchment, Upper Newport Bay. Habitats in San Diego Creek Watershed and in Upper Newport Bay could potentially suffer adverse impacts from this naturally occurring source of selenium.

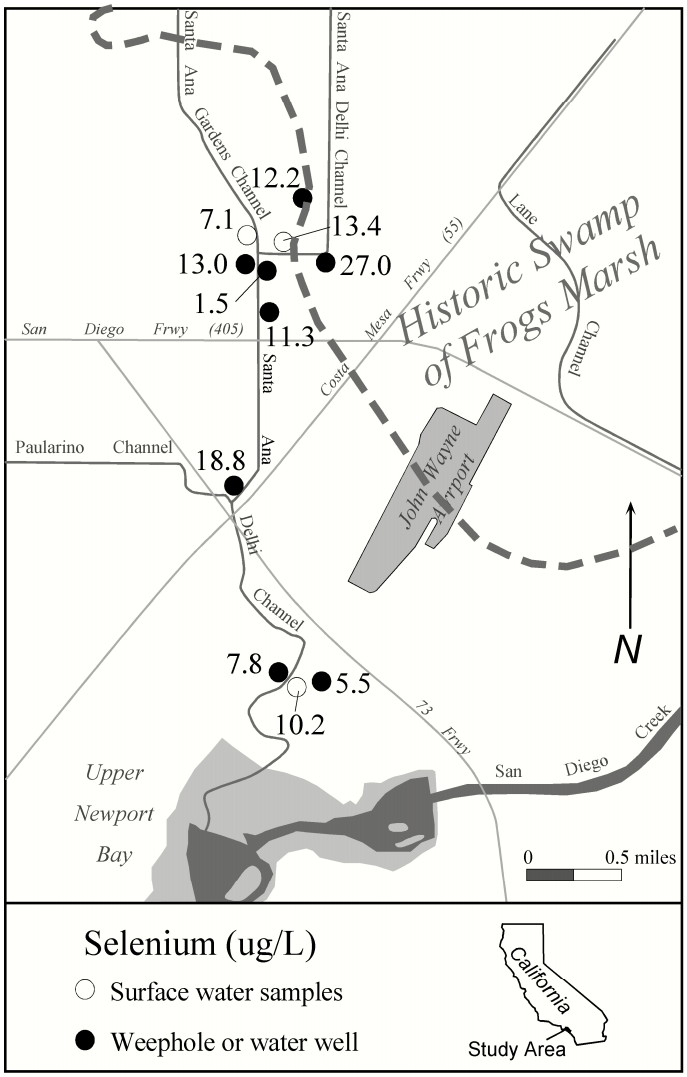

Figure 1. Location of study area in the vicinity of Santa Ana Gardens Channel and Santa Ana Delhi Channel. Results of sampling in Santa Ana Delhi and Santa Ana Gardens Channel showing selenium concentrations in springs, shallow water wells, and surface flows, January 2004.

Land Use History of the Study Area. Three factors placed constraints on specific types of historic agricultural development of the land that was previously occupied by the Swamp of the Frogs Marsh: 1) poor drainage of heavy, fine textured soils; 2) high salinity and high alkali content of soils; and, 3) shallow depth to the water table. The soils of the watershed formed due to historic drainage features of the catchment, where coarser grained materials formed along the flood plains of the ancestral San Diego Creek and other washes, and finer-grained material formed in the central, low-lying part of the watershed.

Considerable effort was made in the early 1900s to improve the poorly drained, alkali lands and increase their productiveness. Additional lowering of the water table did much toward reducing salt concentration, while irrigation water, natural rainfall, and in some instances overflow waters assisted in leaching away some of the alkali (Eckmann, 1919). As a result, crops were eventually put into production in areas close to and even within the area once occupied by the historic marsh. Both synthetic fertilizer and animal manures were subsequently added to regions above and near the outer margins of the Swamp of the Frogs Marsh.

Purpose of Study. The purpose of this sub-study is to determine if groundwater baseflow conditions dominate near Santa Ana Delhi Channel, and to determine the extent to which loading of selenium, nitrate, and other constituents occurs as a result of groundwater seepage. Previous investigations by Hibbs and Lee (2000) and Meixner and others (2004) did not include detailed investigations of Santa Ana Delhi Channel, and vicinity (Figure 1). It is important to determine the relationship between surface water and groundwater in this part of the watershed to determine concentrations of selenium and other hydrochemical parameters. Therefore, we investigated Santa Ana Delhi Channel in January 2004 and March 2005. The work supplements our knowledge of selenium and nitrate in shallow groundwater in San Diego Creek Watershed. This information is expected to help policy-makers to mitigate the effects of these chemical species in the surface waters and groundwater of the watershed.

METHODS

Surface and groundwater samples collected from the Santa Ana Delhi Channel area were analyzed for index parameters, general minerals, selenium, other select trace elements, and nitrate. Field parameters were measured by two field instruments; a Yellow Springs Instrument-63 (YSI-63) gave readings for pH, temperature, temperature-compensated electrical conductivity (EC), and salinity while a YSI-550A gave readings for dissolved oxygen (DO). In addition to field parameters, a number of water samples were collected at each site depending on the types of chemical analyses required. All groundwater samples were collected in triple-rinsed HDPE or LDPE bottles. Aliquots were separated and preserved within twenty-four hours of collection for various chemical analyses. Filtration was performed using 0.45 μm polycarbonate filter paper.

Samples collected for anion analysis were filtered and kept refrigerated below a temperature of 4˚C. Samples to be analyzed for dissolved selenium and cations were filtered and acidified to less than pH 2 with nitric acid (HNO_3) then kept refrigerated (< 4˚C). Anion analysis was conducted by ion chromatography in the Hydrogeology Laboratory at California State University-Los Angeles. Cation analysis was performed by the Soil Water and Plant Laboratory at the University of Arizona. Analysis of total dissolved selenium was conducted by hydride generation atomic absorption (HG-AA) following the

method described by Zhang and others (1999) at the University of California-Riverside.

RESULTS

Our investigation discovered a number of groundwater flows (springs and adjacent shallow wells) along several portions of Santa Ana Delhi Channel (Figures 1 and 2). Electrical conductivity measurements and analysis of general minerals indicates that surface flows were definitively composed of groundwater baseflow. Groundwater contains moderate to small amounts of selenium relative to concentrations observed in other parts of the watershed (Figure 1). With respect to surface flows, selenium is highest in Santa Ana Delhi Channel above the confluence with Santa Ana Gardens Channel (13.4 ug/L Se) and is lowest in Santa Ana Gardens Channel (7.1 ug/L Se) (Figure 1).

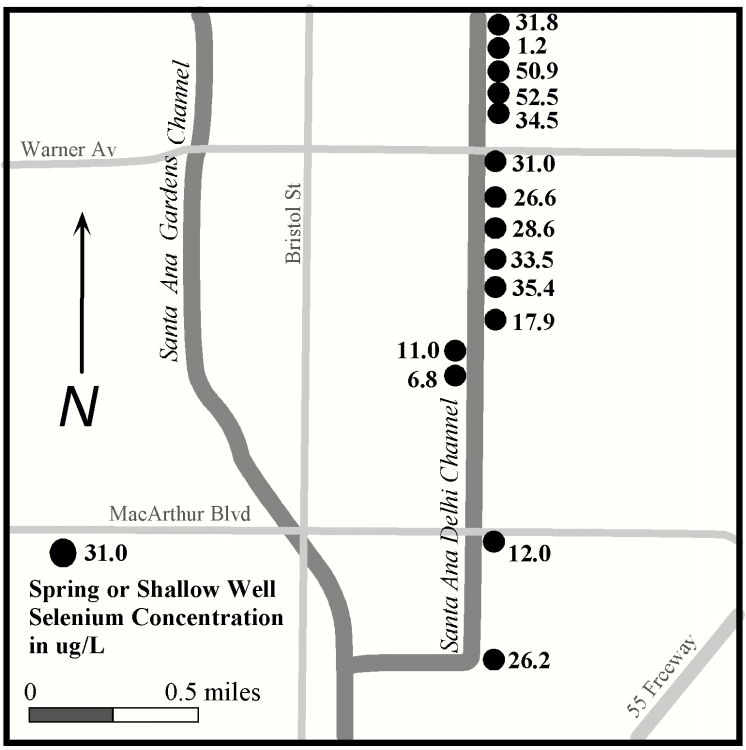

Figure 2. Shallow groundwater data near Santa Ana Delhi Channel showing sampling points at water wells and springs with selenium data, March 2005. All 15 sampling points lie within the historic Swamp of the Frogs Marsh area (see Figure 1).

The portion of Santa Ana Delhi Channel upstream of the groundwater data point "27 ug/L" flows entirely within the boundaries of the historic Swamp of the Frogs Marsh (Figure 1). Therefore, the research team investigated the upstream parts of this channel more intensively in March 2005. This was done

to test apriori predictions of high selenium concentrations in the upper part of Santa Ana Delhi Channel (Figure 1). Data collected from Santa Ana Delhi Channel included 15 new samples, all collected within the historic marsh boundaries. Most samples show moderate to moderately high concentrations of selenium in groundwater (25 to 55 ug/L Se; Figure 2). A few samples are well below 25 ug/L Se however. Selenium is generally lowest in samples collected closest to MacArthur Blvd (Figure 2). One groundwater sample contained only 1.2 ug/L Se. This sample also contained a non-detect concentration of nitrate (<0.5 mg/L NO3-N) and a very high salinity value (9260 uS/cm) (Figures 3, 4 and 5). Previous analysis showed that highly saline ground waters (>10,000 uS/cm) seldom contain high concentrations of selenium (<15 ug/L Se), even within the historic Swamp of the Frogs Marsh region (Meixner and others, 2004). The data suggests that nitrate may be correlated to elevated selenium in groundwater.

DISCUSSION

A covariate relationship is shown for selenium, nitrate, and salinity in groundwaters from Santa Ana Delhi Channel (Figures 3, 4 and 5). Despite wide scatter, there is a clear positive correlation between selenium and nitrate concentrations, and a negative correlation between nitrate/specific conductance and selenium/specific conductance. A possible set of hypotheses for the correlative relationships between selenium, nitrate, and salinity (specific conductance) is as follows:

- Oxidation of selenium by nitrate produces a positive correlation between high nitrate and high selenium. The higher the nitrate concentration, the higher the selenium concentration. Though nitrate is consumed in the oxidation/reduction process, nitrate does not diminish substantially in Santa Ana Delhi Channel due to the stoichiometric relationships between ppb (ug/L) concentrations of selenium, and ppm (mg/L) concentrations of nitrate. This results in a positive correlation between selenium and nitrate (Figure 3).

- Groundwater with highest salinity in the local areas near Santa Ana Delhi Channel near MacArthur Blvd are sourced from lower permeability alkali soils (clays, clayey silts). Fine textured soils were not leached as effectively historically, and retained more salt during leaching. Leaching of salts was important when the alkali soils of the Swamp of the Frogs Marsh region were developed for eventual crop agriculture (1890 to 1960). Leaching was first accomplished simply by draining the water table to allow livestock grazing. Leaching occurred naturally by rainfall infiltration and by percolation of overland flows. Later, as soils started to be leached of salts naturally, alkali resistant crops were planted and irrigated, which increased the rate of leaching. The finer textured, poorly drained soils that were never completely

leached of salts (and were never planted substantially to agriculture) contain organics that consume nitrate (reducing conditions), retain ammonium, and respond to leaching sluggishly. This set of conditions may create an inverse correlation between salinity and nitrate in the data set (Figure 4).

• A low selenium, high salinity, low nitrate correlation is consequently observed in the data set (Figures 3, 4, and 5). The soils with high salinity may contain selenium. However, without the presence of abundant nitrate to oxidize selenium from soils, the selenium concentration remains low in shallow groundwater beneath the soils that are leached by rain or by applied water. High selenium, low salinity, high nitrate correlations are observed in the more permeable, salinity poor areas where agriculture was practiced (Figures 3, 4, and 5). Thus, nitrate availability sourced from agriculture may be a likely factor in selenium mobility.

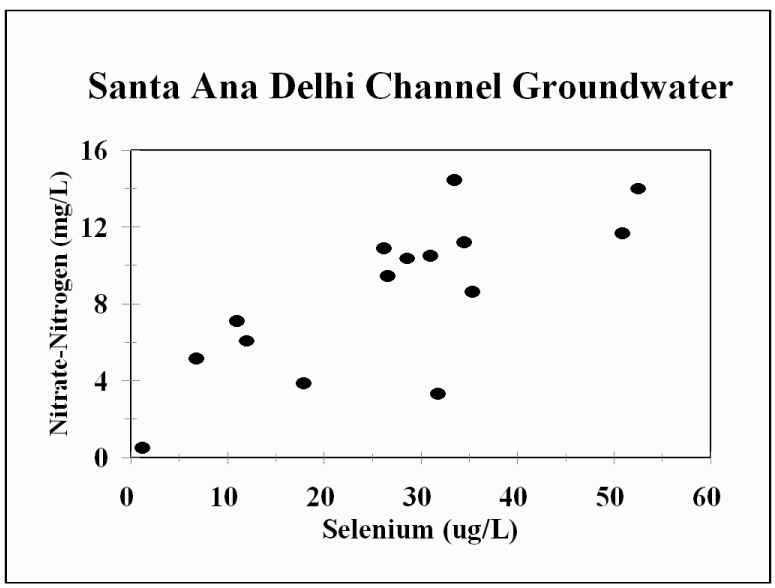

Figure 3. Santa Ana Delhi Channel area shallow groundwater data, showing a positive correlation between selenium and nitrate.

Wright (1999) found that selenium can be oxidized by nitrate from irrigation on Cretaceous marine shale. Dissolved selenium concentrations are positively correlated with dissolved nitrate concentrations in both surface water and ground water samples from irrigated areas in Wright's study area. Theoretical calculations done by Wright (1990) for the oxidation of selenium show favorable Gibbs free energies for the oxidation of selenium by nitrate, indicating nitrate can act as an electron acceptor for the oxidation of selenium. Laboratory batch experiments with selenium-bearing shale and zero-dissolved-oxygen water containing nitrate showed increased selenium concentrations over time with increased nitrate concentrations (Wright, 1990). Wright concluded

that careful management of nitrogen-fertilizer applications in Cretaceous shale settings might help to control the oxidation and mobilization of selenium into surface water and groundwater. If nitrate oxidizes bound forms of selenium in the soils of San Diego Creek Watershed as we postulate, the same type of nitrogen management practices might prove fruitful in the watershed.

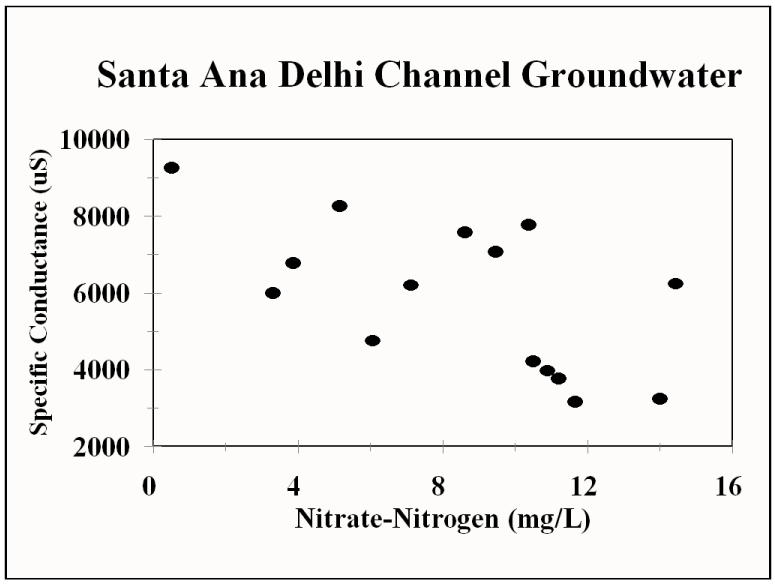

Figure 4. Santa Ana Delhi Channel area shallow groundwater data, showing a negative correlation between nitrate and specific conductance.

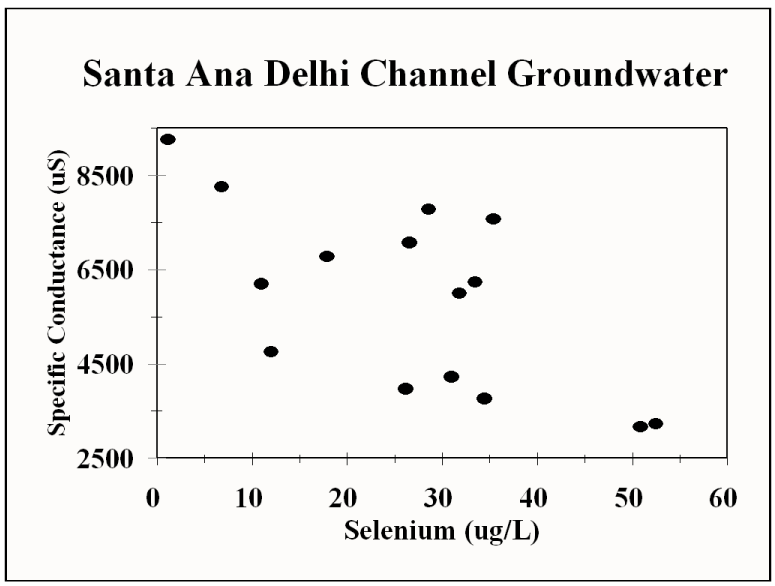

Figure 5. Santa Ana Delhi Channel shallow groundwater data, showing a negative correlation between specific conductance and selenium.

CONCLUSION

We do not exclude oxidation of reduced forms of selenium by dissolved oxygen as a process to explain high selenium in shallow groundwater. This common process was first suggested as the dominant factor by Hibbs and Lee (2000). However, we feel that nitrate is probably as important as dissolved oxygen as an oxidant of reduced forms of selenium. This is because dissolved oxygen is often depleted to suboxic concentrations (<0.3 mg/L) during aquifer recharge through organic rich topsoils and aquifer matrix. We believe dissolved oxygen and nitrate act together to raise oxidation potential in shallow groundwater and both help to oxidize reduced forms of selenium. When dissolved oxygen is near depletion, nitrate continues to keep oxidation potential high. If our hypotheses are correct, and if nitrate continues to be added to the shallow aquifer via application of nitrogen to urban landscapes (by household application, treated wastewater, etc.); or if substantial amount of nitrate is left over in soils from the historical period of agriculture in the region, the selenium in soils could be mobilized by nitrate in greater concentrations than would naturally occur.

Further work is needed in several areas. Selenium speciation work, application of nitrogen and selenium isotopes, and collection and analysis of soil samples are all needed to test these hypotheses. Soil sequential extraction work and geochemical modeling are also recommended.

REFERENCES

Eckmann, E.C., Strahorn, A.T., Holmes, L.C., and Guernsey, J.E. (1919). *Soil survey of the Anaheim area, California*: U.S. Department of Agriculture, Advance Sheets-Field Operations of the Bureau of Soils, 1916.

Frankenberger, W.T. (1998). *Environmental Chemistry of Selenium*. Marcel Dekker, Inc., New York.

Hibbs, B., and M. Lee. (2000). *Sources of Selenium in the San Diego Creek Watershed, Orange County, California.* Defend the Bay & California Urban Environmental Research and Education Center.

Meixner, T.. Hibbs, B., Sjolin, J., and Walker, J. (2004). *Sources of selenium, arsenic, and nutrients in the Newport Bay Watershed*: Contract report prepared for the Santa Ana Regional Water Quality Control Board.

Tracy, J.E., J.D. Oster, R.J. Beaver. (1990). Selenium in the southern coast range of California: well waters, mapped geological units, and related elements. *Journal of Environmental Quality.* Vol. 19(1): 46-50.

Trimble, S.W. (2003). Historical hydrographic and hydrologic changes in the San Diego Creek Watershed, Newport Bay, California. *Journal of Historical Geology*. Vol. 29: 422-444.

Wright, W.G. (1999). Oxidation and Mobilization of Selenium by Nitrate in Irrigation Drainage. *Journal of Environmental Quality*. Vol. 28(4): 1182-1187.

Zhang, Y.Q., J.N. Moore, and W.T. Frankenberger, Jr. (1999). Speciation of soluble selenium in agricultural drainage waters and aqueous soil–sediment extracts using hydride generation atomic absorption spectrometry. *Environmental Science and Technol*ogy, Vol. 33: 1652–1656.

Investigating the Temperature Effects on Nutrient Removal in Green Soprtion Media

Ni-Bin Chang, Marty Wanielista, Devan Henderson, and Ammarin Daranpob

Department of Civil and Environmental Engineering, University of Central Florida, Orlando, Florida, USA

ABSTRACT

High nitrogen and phosphorus concentrations in stormwater runoff, contaminated groundwater, landfill leachate, and domestic and industrial wastewater effluents have negatively impacted the drinking water quality in many regions. The use of filter media, such as tire crumb, sawdust, sand, clay, zeolite, sulfur, limestone, etc., to get better removal efficiencies of nutrients has been the focus in the planning and design of green infrastructure. These material mixes mainly promote the adsorption/absorption and precipitation of orthophosphate in physicochemical process and the transformation of ammonia, nitrite, and nitrate via oxidation and reduction reactions in the microbiological process. However, temperature changes affect nutrient removal efficiencies in both natural and engineered systems. This paper aims to explore the filtration kinetics of selected filter media for nutrient removal at various temperatures to improve their application potential in all weather conditions. Constitutes of concern include ammonia, nitrite, nitrate, total nitrogen, and orthophosphate. Such a kinetics study leads to investigate the capabilities of comparing a natural soil with soil augmentations in regard to removing nutrients under a range of initial concentrations at three different temperatures (i.e., 28°C, 23°C, and 10° C). Significant differences of removal efficiencies associated with these prespecified temperatures were statistically confirmed by ANOVA analyses.

INTRODUCTION

Before 1995, much work was devoted to research for the removal of nutrients primarily with the sand filter method. For this reason, different types of sand filter methods had been developed like: 1) the Washington D.C. sand filter method, 2) the Delaware sand filter design and 3) the Austin sand filter (USEPA, 1999). The removal efficiency of the Delaware sand filter is Total Suspended Solids (TSS) 70.20%, Total Phosphorus (TP) 71.10%, ammonia nitrogen (NH_3-N) 67.00% and Total Kjeldahl nitrogen (TKN) 59.90% (Bell et al., 1995). Recent development shows that removal of ammonia, nitrite, nitrate, and phosphorus can be enhanced by mixing different sorption media, such as sawdust, tire crumb, sand, clay, zeolite, sulfur, and/or limestone, etc., with natural soil (Kim et al., 2000; Clark et al., 2001; Jokela et al., 2002; Hsieh and Davis, 2005). Appropriate media mix in this research is deemed as a kind of multifunctional material or functionalized sorption media that may be used in both natural and built environments to improve the existing physicochemical and microbiological processes for

nutrient removal (Chang et al, 2008). Such media mix has the "green" implications because of the inclusion of some recycled materials, such as tire crumb and sawdust, as part of the recipe to promote the treatment efficiency and effectiveness (Chang et al, 2008). From engineering standpoint, with the aid of such green sorption media, nutrients in the water bodies can be reduced or even mostly removed by enhanced absorption/adsorption, nitrification/denitrification and other chemical reactions, such as precipitation and ion exchange (Hossain et al., 2008).

The adsorption, absorption, ion exchange, and precipitation reactions are actually intertwined with physicochemical and microbiological processes in porous media intermittently. Pollutants removed by the adsorption process in the "green sorption media" may subsequently desorb. Two important biochemical transformation processes are the nitrification and denitrification that occur at the same time as the adsorption, absorption, ion exchange, and precipitation reactions move on. They result in the transformation of ammonia, nitrite, and nitrate via oxidation and reduction reactions in the microbiological process. In short, nitrification is a microbiologically mediated process that occurs under aerobic conditions, resulting in the formation of nitrate whereas denitrification is a microbiologically mediated process but occurs under anoxic or anaerobic conditions, resulting in the formation of gaseous forms of nitrogen. In reduction-oxidation chemistry, however, nitrification is a process in which ammonium is oxidized via nitrifiers and denitrification is a process in which nitrate is reduced to nitrogen gas via denitrifiers. However, nitrifiers can grow best in a temperature range of 35^0C to 42^0C (Rittmann, 2000; USEPA, 1993) and denitrifiers can work well in a range of 10^0C to 25^0C.

The integrated impact of temperature changes on both physicochemical and microbiological processes remains unknown when removing nutrient in these soprtion media mixes. This paper aims to explore how the filtration kinetics of selected filter media for nutrient removal is affected by various temperatures leading to improve the application potential of green sorption media in all weather conditions. It starts with a through literature review followed by the material characterization of a selected sorption media, and a laboratory column study that was conducted to simulate a wastewater/stormwater treatment unit with saturated media conditions. Such a filtration kinetics study may lead to a comparison to investigate the capabilities of comparing a natural soil with soil augmentations in regard to remove nitrogen and phosphorus associated with a range of initial nutrient concentrations at three different temperatures (i.e., 28°C, 23°C, and 10° C).

MATERIALS AND METHODS

Column Design and Setup

The columns were designed to simulate field environments with saturated conditions. By using three columns, it is possible to test the performance of two mixes as compared with a control. The control column is filled with natural soil from the Hunters Trace Pond in Ocala, Florida. The soil was sun dried and sieved with a #10 sieve to remove vegetation, rocks, and large particles. The selected two media recipes are Media Mix 1 consisting of 50% fine sand, 30% tire crumb, 20% sawdust by weight and Media

Mix 2 consisting of 50% fine sand, 25% sawdust, 15% tire crumb, 10% limestone by weight based on a multicriteria decision making (MCDM) analysis (Henderson, 2008)..

The clear Plexiglas columns have an inside diameter of 14.7 cm (5.8 inches) and are 91.4 cm (3.0 feet) in length. The bottom of each column contains a filter with three inches of fish tank rocks to prevent the media and soil mixes from exiting the columns and clogging the tubes. These columns were secured onto a constructed wooded frame with straps. Two ports were installed in each column to take core samples at different heights and hydraulic retention times (HRT). In addition to the ports, the water was sampled from the bottom of each column. The gaps surrounding the ports were sealed with Rectorsell 5 and Plumbing Amazing Goop. One peristaltic pump with peristaltic tubing was used to pump water from three, five gallon reservoirs into each of the columns. A fourth reservoir was used to maintain saturated conditions by connecting the column outlet tubing at a height equal to the desired water level inside the columns. Figure 1 shows the schematic of the column setup.

The HRT for the columns was calculated by using the following equations into a MathCAD file so that any changes in parameters can be quickly adjusted. The contributing parameters include porosity (n), column inside diameter (d_{column}), and the height above sampling port (h). First, the volume ($V_{media(h)}$) was calculated using the following equation.

$$V_{media}(h) := \left[\frac{\pi \cdot \left(d_{column}\right)^2}{4} \cdot h \right] \cdot n \tag{1}$$

Then using this volume and the desired HRT at the bottom of the column, the flow rate (Q) for the pump was calculated.

$$Q := \frac{V_{media3}}{\theta_3} = \cdot \frac{mL}{min} \tag{2}$$

Lastly, by using this flow rate the HRT for each port (θ) can be calculated.

$$\theta_1 := \frac{V_{media1}}{Q} = \cdot min \tag{3}$$

The columns were placed in a room capable of setting a constant temperature for two of the temperatures and a refrigerator for the lowest temperature. This design would allow for the testing of the media mixes at various constant temperatures to determine the temperature impacts on filtration kinetics.

Column Analysis

The pond water wais first augmented with KNO_3 and HK_2PO_4 to pre-selected ranges and then pumped from each of the reservoirs through the columns. The concentration ranges were employed to validate the kinetics. Water samples were taken from three locations of each column; port 1, port 2 and port 3 (i.e., the bottom of

column). These samples were then tested for variations of nitrogen and phosphorus. A summary of these methods is listed Table 1.

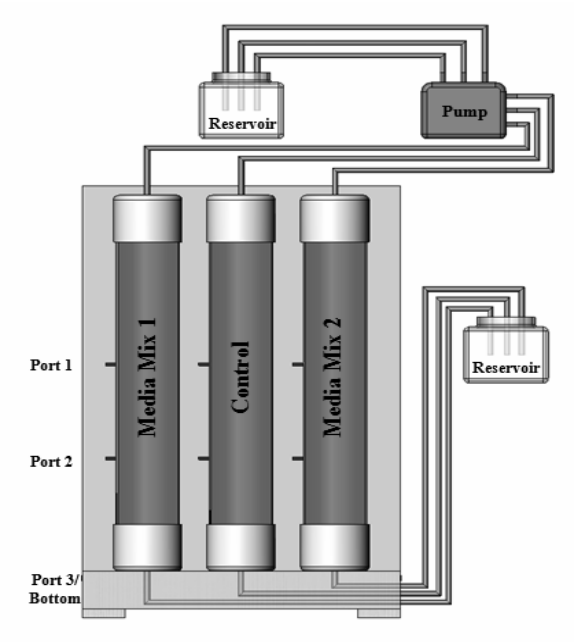

Figure 1: The schematic of Column Design

When the rate of the equation is unknown, as in this experiment, other methods for determining the rate constant can be employed. This type of analysis is often referred to as determining the rate constant from the integrated rate law. The integrated rate law involves integrating the rate law and arranging the equation in terms of the linear equation of a line (Equations 4-6). The definitions of the variables are [C] is the final concentration of the reactant, $[C_0]$ is the initial concentration of the reactant, k is the rate constant, and t stands for time.

Table 1: Column Study Water Quality Parameters and Methods

Parameter	**Method**	**Range***
pH	Fisher Scientific Accumet portable AP61 pH meter	pH units
Dissolved Oxygen	YSI Model 58 DO Meter	
Nitrates + Nitrites	Hach method 8192	0.01-0.50 mg/L NO_3^-N
Nitrites	Hach method 8507	0.002-0.30 mg/L NO_2^-N
Ammonia	Hach method 8155	0.01-0.50 mg/L NH_3-N
Total Nitrogen	Hach Method 10071	0.5-25.0 mg/L N
Reactive/Orthophosphate	Hach method 8048	0.02-2.50 mg/L PO_4^{3-}

*Note: In some cases samples were diluted with DI water to fall within this range.

$$\text{Zero Order: } [C] = -kt \quad (4)$$

$$1^{st} \text{ Order: } Ln[C] = -kt + ln[C_o] \quad (5)$$

$$2^{nd} \text{ Order: } 1/[C] = kt + 1/[C_o] \quad (6)$$

This type of analysis was applied to the columns in an attempt to describe the removal in terms of zero, first, or second order kinetics. The concentrations, inverse concentrations, and natural log of concentrations are plotted versus the retention time to show the removals as low order kinetic functions. A linear regression was performed to each condition and the mean squared error was calculated to justify the best fit. To investigate the actual values for the reaction rate, the differential rate law equations was used.

Temperature Correction Factor Model was applied to biological processes that have small temperature variations. The variables in the Temperature Correction Factor Model are defined as rate constant at temperature T (k_T), the rate constant at 20°C (k_{20}), the temperature correction factor (θ), and temperature in °C (T). A temperature range of around 20°C was used as the reference temperature. Three different temperatures (i.e., 28°C, 23°C, and 10° C) were considered for temperature effects.

$$k_T = k_{20}\theta^{(T-T_{20})} \quad (7)$$

RESULTS AND DISCUSSION

Column Analysis

A comparison of the nitrate removal for the columns at a specific temperature was constructed utilizing an average of the removals at the bottom of the columns for all doses Table 2. From this table it is easy to distinguish how the media mixtures reacted to the change in temperature in terms of nitrate removal. All of the columns achieve their highest removal at 28°C. The nitrate performance increased with temperature. Media Mix 1 and 2 had similar increases; with approximately 10% increase from 10°C to 23°C and then a 15% increase from 23°C to 28°C. The Control column experienced a 12% increase for the first temperature gap and 25% increase between the higher temperatures. Media Mix 1 has the best removals of all three columns for 23°C, 25°C and 28°C with 69.7%, 79.7%, and 95.3% respectively. Media Mix 1 has the highest nitrate removal for all of the experiments with 95.3% nitrate removal. Overall, Media Mix 2 is the best on average.

Table 2: Nitrate Removal Comparison between Temperature and Column (Final Port Comparison)

NO_3^--N	Temp. 1 10° C	Temp. 2 23° C	Temp. 3 28° C
Control Case	8.0%	20.9%	45.8%
Media Mix 1	69.7%	79.7%	95.3%
Media Mix 2	63.2%	77.9%	93.6%

A comparison of the orthophosphate removal for the columns at a specific temperature was also constructed utilizing an average of the removals at the bottom of the columns for all doses Table 3. From this table it is easy to distinguish how the media mixtures reacted to the change in temperature in terms of orthophosphate removal. The

columns all achieved the highest orthophosphate removal at different temperatures; the Control, Media Mix 1, and Media Mix 2 at 10° C, 23° C, and 28° C, respectively. However, the difference between the highest and second highest removals for the Control was only 1%. The highest overall orthophosphate removal was achieved by Media Mix 2 at 28° C. The Control column outperformed the Media Mixes for 10° C and 23° C and came in at a fairly close second for 28°C. Overall, Media Mix 2 and Control are the best equivalently.

Table 3: Orthophosphate Removal Comparison between Temperature and Column (Final Port Comparison)

OP (PO_4^{3-}-P)	Temp 1 10° C	Temp 2 23° C	Temp 3 28° C
Control Case	84.8%	80.0%	72.1%
Media Mix 1	38.5%	63.3%	59.9%
Media Mix 2	58.8%	67.4%	85.5%

ANOVA Analysis

In order to determine the effect of temperature, dose, and media mixture have on the removal efficiency which is statistically valid, the two-way ANOVA analysis was conducted for each dose and nutrient. The removal efficiencies from the bottom of each column were used to standardize the data for comparison. These efficiencies were inserted into SAS® software and a two-way ANOVA was executed. Removal efficiency and media were designated as the main effects in the ANOVA model. The assumed alpha value for all of the computations was 0.1, providing 90% confidence. The assumptions associated with performance of an ANOVA test; independence, normal distributions, and equal variance were considered and the following results were obtained from this analysis. The samples were assumed to be independent since the columns are contained environments and the water travels through each one individually with no interaction. The normal assumption was assumed since only three data points for each combination were taken and thus a reliable normality test can not be performed. Lastly, statistical analysis has shown that the requirement of equal variance does not have a significant effect on the outcome of an ANOVA analysis, due to the robustness of the F distribution under unequal variance conditions when the sample sizes are the same (Neter, 1974 and Rogan, 1977).

From the ANOVA analysis, the change from low to high concentrations seemed to have an effect on the nitrate and orhtophosphorus removals. In terms of nitrate, the ANOVA for low concentration and high concentration had the same results in terms of columns, but there were differences between the low and high concentrations in terms of temperature. This might show that the lower concentration range was near the equilibrium for the microbes. The difference in efficiency for the columns between the temperatures is interesting. Since there is seemingly no difference between 10°C and 23 C°C for the columns, it is assumed that this is the lower range for the microbial activity

and removals were dictated by sorption. The difference between 23°C and 28°C would indicate that there was biological activity along with sorption. The differences between the media mixes could be due to the sorption capacity, ability to provide carbon source for denitrification, and ability to provide an ideal environment for the microbes to attach and thrive.

Filtration Kinetics Analysis

Table 4 shows an example of one of the best runs for material mix 2 column, species, and temperature. An average of all of the R^2 values at each temperature were compared; the highest R^2 values across all three temperatures was taken to be the best model for the overall reaction order (Table 5). Once the reaction order was determined, the rate constants could be calculated. The rate constant for each temperature is equal to the slope of the linear regression of the removals for the selected order. The averages of all rate constants were then computed for each temperature (Tables 6-7).

Table 4: Example Linear Regression Equations for the Media Mix 2 Column

Temp.	Species	Initial Concentration (mg/L)	Zero Order		1st Order		2nd Order	
			Equation	R^2	Equation	R^2	Equation	R^2
10	Nitrate	8	0.06x + 8.3	0.96	-0.03x + 3.1	0.88	0.08x + -0.8	0.65
		25	-0.071x + 24	0.97	-0.004x + 3.2	0.99	0.0002x + 0.04	0.99
	Orthophosphate	3.7	-0.008x + 3.7	0.94	-0.0023x + 1.3	0.91	0.001x + 0.26	0.87
		6.4	0.03x + 6.4	0.98	-0.012x + 2	0.85	0.006x + 0.02	0.84
23	Nitrate	7.2	-0.03x + 5.8	0.75	-0.008x + 1.8	0.91	0.003x + 0.16	0.99
		31.2	-0.18x + 0.33	0.97	0.0098x + 3.6	0.95	0.0006x + 0.02	0.89
	Orthophosphate	2.3	-0.008x + 1.9	0.73	-0.007x + 0.62	0.57	0.008x + 0.66	0.34
		3	-0.014x + 0.14	0.89	-0.008x + 1.1	0.94	0.005x + 0.3	0.91
28	Nitrate	13	-0.09x + 12	0.96	-0.033x + 3.1	0.88	0.06x -1.8	0.65
		25	-0.07 + 24	0.97	-0.004x + 3.2	0.99	0.0002x +0.04	0.99
	Orthophosphate	3.7	-0.0083x + 3.7	0.94	-0.0029x +1.34	0.91	-.001x + 0.256	0.87
		6.2	-0.034x + 6.4	0.98	-.012x + 2.0	0.95	0.006x + .02	0.84

Table 5: Average R^2 Values for Each Temperature for Media Mix 2

Media Mix 2	Nitrate			Orthophosphate		
	10°C	23°C	28°C	10°C	23°C	28°C
Zero	0.69	***0.84***	***0.62***	***0.81***	0.69	0.73
1st	***0.69***	0.82	0.60	0.78	***0.70***	***0.79***
2nd	0.56	0.73	0.59	0.72	0.60	0.77

Table 6: Average Nitrate Kinetic Rate Constants

k	10°C	23°C	28°C
Control (Zero Order)	0.014	0.007	0.03
Media Mix 1 (1st Order)	0.012	0.017	0.05
Media Mix 2 (Zero Order)	0.047	0.076	0.07

Table 7: Average Orthophosphate Kinetic Rate Constants

k	10°C	23°C	28°C
Control (Zero Order)	0.04	0.02	0.02
Media Mix 1 (2nd Order)	0.001	0.02	0.004
Media Mix 2 (1st Order)	0.08	0.01	0.01

Finally, the specific temperature conversion factors (θ) for the Media Mixes can be calculated by plugging in the values for the rate constants and their corresponding temperatures). The temperature conversion factor value was solved for with all three possible permutations and then an average of these produces the modeled value for θ (Tables 8-9). The permutations in the table below are found by taking the kinetic constants found in Tables 38 and 39 above. The values of 1, 2, and 3 stand for the temperatures 10°C, 23°C, and 28°C, respectively, along with the kinetic values associated with those temperatures. For example, θ_{12} was found using the k values for 10°C and 23°C and plugging in 10°C and 23°C for the temperature. Average temperature correction factors were calculated due to smaller variations in magnitude when compared with the Arrhenius Model.

Table 38: Temperature Conversion Constants (θ)

NO_3^--N	Control	Media Mix 1	Media Mix 2
θ_{12}	0.95	1.02	1.04
θ_{13}	1.04	1.07	1.02
θ_{23}	1.30	1.22	0.98
θ_{avg}	***1.10***	***1.11***	***1.01***

Table 39: Temperature Conversion Constant (θ)

OP (PO_4^{3-}-P)	Control	Media Mix 1	Media Mix 2
θ_{12}	0.93	1.28	0.84
θ_{13}	0.97	1.08	0.91
θ_{23}	1.07	0.69	1.11
θ_{avg}	***0.99***	***1.02***	***0.95***

CONCLUSIONS

The selected two media recipes were Media Mix 1 consisting of 50% fine sand, 30% tire crumb, 20% sawdust by weight and Media Mix 2 consisting of 50% fine sand, 25% sawdust, 15% tire crumb, 10% limestone by weight. The control for this study was taken from Hunter's Trace Pond in Ocala, Florida. The best media mixes to select were complicated by the unexpected nutrient addition by some of the media. After taking all aspects into account, the best media for both nitrate and orthophosphate removal was

Media Mix 2 in this study. Yet the best column for nitrate removal for all temperatures is Media Mix 1. Selection of the best media in terms of orthophosphate was less straightforward. The Control Column had the best average removals at 10°C and 23°C. However, in terms of the media performance, Media Mix 1 outperforms Mix 2 for two of the temperatures; although Media Mix 2 does have the highest individual occurrence of orthophosphate removal of all the mixes for all of the temperatures.

The kinetic rates would be helpful in determining the retention time required for the Media Mixes to achieve the best removals. Using this information, along with the media characterization information and desired removals, the depth of media that would be recommended for pilot studies in a retention pond or other high nutrient concentration application could be calculated. The results of this research are limited to the specific media and specific composition of the media mixes eventually selected. The three temperatures selected for this study were accommodated to span the Floridian climate. Data were collected during controlled laboratory experimentation; natural conditions could potentially cause some deviations. Future applications may support use in bioswales, bioinfiltration ponds, pervious pavement, and green roof in the context of Low Impact Development (LID).

REFERENCES

Bell, W., Stokes, L., Gavan, L. J., and Nguyen, T. N. (1995). Assessment of the pollutant removal efficiency of Delaware Sand filter BMPs, City of Alexandria, Department of Transportation and Environmental Services, Alexandria, VA, USA.

Chang, N. B., Wanielista, M., and Hossain, F., (2008). The use of filter media for nutrient removal in natural and built environments: problems, perspectives, and challenges. *Critical Reviews in Environmental Science and Technology*, in review.

Clark, S.; Pitt, R.; Brown, D. (2001). Effect of anaerobiosis on filter media pollutant retention, Presented at the Engineering Foundation and the American Society of Civil Engineers Conference on Information & monitoring needs for evaluating the mitigation effects of BMPs, Snowmass, CO.

Henderson, E. D. (2008). A Kinetics Study of Selected Filtration Media for Nutrient Removal at Various Temperatures, Master's Thesis, UCF, Orlando Florida.

Hsieh, C. H. and Davis, A. P. (2005). Evaluation and optimization of bioretention media for treatment of urban storm water runoff. *Journal of Environmental Engineering, ASCE*, 131(11), 1521-1531.

Hossain, F.; Chang, N. B.; Wanielista, M. (2008). Developing functionalized filter media for nutrient removal in stormwater dry ponds: physicochemical assessment. *Water Air and Soil Pollution*, in review.

Jokela, C. H. Y., Kettunen, R. H., Sormunen, K. M., and Rintala, J. A., (2002), Biological nitrogen removal from municipal landfill leachate: low-cost nitrification in biofilters and laboratory scale in-site denitrification, *Water Research*, 36, 4079-4087.

Kim, H., Seagren, E. A., and Davis, A. P. (2000). Engineering Bioretention for Removal of Nitrate from Storm water Runoff, in WEFTEC 2000 Conference Proceedings on CDROM Research Symposium, Nitrogen Removal, Session 19, Anaheim CA, USA.

Neter, J. and Wasserman, W. (1974). Applied Linear Statistical Models: Regression, Analysis of Variance, and Experimental Designs. Richard D. Irwin, Inc. Homewood Il.

Rittmann, B., McCarty, P. L., McCarty, P., (2000). Environmental Biotechnology: Principles and applications, 2nd edition, *McGraw-Hill Science Engineering*, July, 472.

Rogan, R. C.; Keselman, H. J. (1977). Is the ANOVA F-Test robust to variance heterogeneity when sample sizes are equal?: an investigation via a coefficient of variation. *American Educational Research Journal*, 14(4): 493.

United States Environmental Protection Agency (USEPA) (1993). Nitrogen control manual, EPA-625/R-93-010, Office of research and development, U.S. Environmental Protection Agency, Washington, D.C., USA.

United State Environmental Protection Agency (USEPA), (1999), Storm water technology fact sheet sand filters, EPA 832-F-99-007.

Nutrient and Pathogen Removal with an Innovative Passive Underground Drainfield for On-site Wastewater Treatment

Ni-Bin Chang, Marty Wanielista, Ammarin Daranpob, Fahim Hossian, and Zhemin Xuan

Department of Civil, Environmental, and Construction Engineering, University of Central Florida, Orlando, Florida, USA

ABSTRACT

When urban regions gradually expand due to regional development, centralized sewage collection, treatment, and disposal is often unavailable for both geographic and economic reasons. As a consequence, about a quarter of the residences in the United States relied on decentralized treatment of wastewater. Household wastewater contains high concentration of nutrients (mainly nitrogen and phosphorus), disease-causing organisms and viruses, and some toxic chemicals. Nation wide, wastewater effluent from on-site wastewater treatment (OWTS) can represent a large fraction of nutrient loads to groundwater aquifers. Phosphorus and nitrogen compounds are the most frequent measurements to indicate nutrient loadings. Some aquifers may discharge into springs or other surface waters adversely affecting public health. Hence, on-site wastewater effluent disposal has contributed significant adverse impacts to the dynamics of the natural environment. Nowadays, due to widespread septic tank failure, scientists, engineers, and manufacturers in the wastewater treatment industry have developed a wide range of alternative passive technologies designed to address increasing hydraulic loads, energy saving requirement, and water contamination by nutrients and pathogens in OWTS. This paper aims to present an innovative design of the underground drainfield with soil amendments (sorption media) in a pilot septic tank system. The new system located at the OWTS test center, University of Central Florida (UCF) was tested and proved cost-effective in the initial test run in fall 2008.

INTRODUCTION

Onsite sewage contains organic matter (biochemical oxygen demand), suspended solids, nutrients, and some pathogens, which can cause a number of diseases through ingestion or physical contact. Those water-related diseases include shigellosis, salmonellosis, typhoid fever, and infectious hepatitis (Katzenelson et al., 1976). More than 25 million homes, or 25 percent of the U.S. population, use onsite wastewater treatment systems to meet their wastewater treatment and disposal needs (USEPA, 2002). The most common type of onsite wastewater treatment plant ("mini treatment plant") is the septic system. When properly constructed and maintained, the septic systems can provide years of safe, reliable, cost-effective service.

A septic system consists of four main components. The first component is a home's indoor plumbing, which is a system of drains and pipes located inside a home in

charge of transporting wastewater outside to the next major component, the septic tank. The septic tank is normally an underground, watertight container, made of concrete, fiberglass, or other durable material, which provides primary wastewater treatment. In the septic tank, solids settle to the bottom of the tank and partially decompose by naturally occurring bacteria resulting in a layer of soaps, greases and scum float on top of the liquid wastewater. There is a need to periodically remove the floating scum and submerged solids accumulated in the tank. The liquid wastewater between the floating and settled solids has to be discharged from the septic tank to the next major component of a septic system, the drainfield. The standard drainfield that is constructed by a series of parallel, underground, perforated pipes allows the septic tank effluent to percolate into the surrounding soil in the vadose (unsaturated) zone where most of the residual nutrients may be assimilated. Through various physical, chemical, and biological processes, most bacteria, viruses and nutrients in wastewater are expected to be consumed as the wastewater passes through the soil. The type of effluent distribution in the standard drainfield systems include gravity systems, low pressure dosed systems, drip irrigation systems, etc. and some of them require having an additional pump.

Nutrients such as ammonia, nitrite, nitrate, and phosphorus are common contaminants in the water bodies all over the world, as well the emerging contaminants that affect aquatic ecosystems. All these nutrients have direct and indirect acute and chronic harmful outcome for human beings and ecosystems. Ammonia is an important compound in freshwater ecosystems. It can stimulate phytoplankton growth, exhibit toxicity to aquatic biota, and exert an oxygen demand in surface waters (Beutel, 2006). Hence, primarily due to the limited nitrogen-removal treatment capabilities of conventional septic systems, their density of use in a watershed can produce adverse and undesired aquatic resource impact through accelerated eutrophication. Besides, unionized ammonia is very toxic for salmonid and non-salmonid fish species (Tarazona et al., 2008). Fish mortality, health and reproduction can be hampered by the presence of minute amount of ammonia-N (Servizi and Gordon 2005). Nitrate is more toxic than nitrite and can cause human health problems such as liver damage and even cancers (Gabel et al, 1982; Huang et al., 1998). Nitrate can also bind with hemoglobin and create a situation of oxygen deficiency in an infant's body called methemoglobinemia (Kim-Shapiro et al., 2005). Nitrite, however, can react with amines chemically or enzymatically to form nitrosamines that are very strong carcinogens (Sawyer et al., 2003).

In addition, wastewater also carries different kinds of microorganisms such as bacteria like Escherichia coli and Salmonella typhi, protozoa like Cryptosporidium parvum and Giardia lamblia, helminthes and viruses like hepatitis A virus. Concentration of total coliform is about 10^{7}-10^{9} no./100 mL, fecal coliform is about 10^{4}-10^{6} no./100 mL, Cryptosporidium parvum oocysts is about 10^{-1}-10^{1} no./100 mL and Giardia lamblia cysts is about 10^{-1}-10^{2} no./100 mL in a medium strength wastewater (Metcalf and Eddy, 2003; WEF and ASCE, 2005). Oocysts and cysts are spore phase that will help to survive for a long time for certain microorganisms. These entire microorganisms are responsible for different kinds of diseases like diarrhea, jaundice, food poisoning, dysentery and nausea (Metcalf and Eddy, 2003; WEF and ASCE, 2005). If these diseases are not controlled properly, they may cause harmful effect on health even death due to domestic sewerage pollution.

As a consequence, nutrient and pathogen removal is very important for the sustainability of the aquatic ecosystem and environment. There are many ways for homeowners with septic systems to minimize the potential nutrient impacts that on-site wastewater treatment (OWTS) may have on the environment. Yet early codes did not consider the complex interrelationships among nutrient impacts, soil conditions, wastewater characteristics, biological mechanisms and climate, or geoclimatic differences that might be big in vastly different regions. At present, there is a need for promoting enhanced nitrogen removal in septic systems, as well as a better understanding of nitrogen removal behavior of the septic system effluent plume as it passes through soil to a receiving water body. In general, passive technologies might be advantageous due to their cost effectiveness, system reliability, and low maintenance requirement. This triggers an acute need to perform a thorough technology comparison, screening, and prioritization.

To reduce organic and nitrogen impacts, an aerobic treatment unit (ATU) may be used to treat wastewater prior to ground discharge, typically by adding aeration to promote decomposition of organic matter, reduce pathogens, and transform nutrients. Basic ATU designs include suspended growth systems, fixed-film systems, and integrated fixed film and suspended growth systems (USEPA, 2005). All three types usually have a septic tank ahead of them that removes the large solids and provides some protection to the ATU. Yet passive treatment and disposal systems, which do not use aerator pumps and include no more than one effluent dosing pump, are relatively new (Chang et al., 2007). Passive OWTS is defined by the Florida Department of Health (FDOH) as a type of onsite sewage treatment and disposal system that excludes the use of aerator pumps and includes no more than one effluent dosing pump with mechanical and moving parts and uses a reactive media to assist in nitrogen removal. Reactive media are materials that effluent from a septic tank or pretreatment device passes through prior to reaching the groundwater. This may include but are not limited to soil, saw dust, zeolites, tire crumbs, vegetative removal, sulfur, spodosols, or other media. Hence, a new generation of performance-based, passive (as opposed to conventional) OWTS to effectively remove septic tank effluent nutrients and protect public health and the environment in a cost-effective manner will need to be devised and implemented with innovation. For example, some technologies use a reactive media to assist in nitrogen removal. Saw dust and other wood products, zeolites, tire crumbs, vegetation, sulfur, spodosols, etc. have been suggested or used as such possible treatment media (Chang et al., 2008a). These systems with new materials and methods will require increased focus on system performance, pollutant transport and fate, resulting environmental impacts, and an integration of the planning, design, siting, installation, maintenance, and management functions. Cost effectiveness, system reliability, and proper management become the major concerns in applications. The author's aim of this paper is to present an innovative design of the underground Drainfield with soil amendments (sorption media) in a pilot septic tank system. In the initial test runs, the new system located at the OWTS test center at UCF has been tested and proved cost-effective..

MATERIALS AND METHODS

The development of performance-based passive on-site wastewater treatment systems (i.e., septic tank) for nutrient removal becomes an engineering challenge in the context of sustainability concern. Initial candidates listed for "Passive Nitrogen Removal Technologies" may include but are not limited to: 1) nitrification process: single pass media filters and recirculating media filters; 2) denitrification process: autotrophic versus heterotrophic condition with singles pass or two-stage process; 3) Drainfield modification: autotrophic versus heterotrophic condition; and 4) groundwater treatment (permeable reactive barrier): autotrophic versus heterotrophic condition. During operation, they require no energy and minimal maintenance, thus the use of the word passive. New generation of material mixes with pollution prevention and control potential used for the selective removal of dissolved nutrient species in wastewaters have received a renewed interest recently. This impact led to this invention that had been directed towards developing a new generation of functionalized sorption media with a unique hydraulic pattern for improving the nutrient and pathogen removal in the B&G drainfield which is one of the three treatment trains at the UCF OWTS test center.

System Configuration

With such understanding, the UCF OWTS test center, sponsored by Florida Department of Environmental Protection (FDEP) with technical support of Florida Department of Health (FDOH) and designed for evaluation of nutrients removal on campus, includes (see Figure 1): 1) a septic tank followed by a recirculating sand filter (RSF), with effluent discharged to an unlined conventional gravity drainfield, called standard drainfield hereafter, filled with washed builder's sand; 2) a septic tank followed by a recirculating sand filter (RSF), with effluent discharged to a unlined standard drainfield filled with citrus grove (i.e., astatula sand) sand; 3) a septic tank followed by a subsurface flow (SSF) wetland system; and 4) a septic tank with effluent discharged to a lined underground drainfield (Black & Gold™ (B&G) nugget drainfield), called B&G drainfield hereafter, to allow for soil substitution. Different sorption media for pollution control may be configured into the vegetative unit in the SSF system and the underground drainfield.

The wastewater source for the test center is the 15-person BPW Scholarship House (a female dormitory at UCF campus), which contains a kitchen and living quarters. The wastewater is pumped to 3.78 m^3 (1,000 gallon) and 5.10 m^3 (1,350 gallon) septic tanks from where the effluents are divided into different final disposal alternatives. While the former one handle both B&G drainfield (Figure 2a) and wetland system (Figure 2b), the latter one handles both standard drainfields (Figure 2c). A dosing tank is connected to one septic tank for handling the collected effluent from treatment processes 3) and 4). The pump and pipe arrangement delivers an average of 0.75 m^3/day (200 gpd) to each of the four drainfield systems.

Environmental Monitoring Network

There are two sets of monitoring wells at UCF Test Center, eight drainfield monitoring wells and eight background monitoring wells (Figure1). The eight drainfield monitoring wells are located near the two standard drainfields to monitor the water quality of the groundwater up-gradient, immediate, and down gradient of each standard

drainfield. The eight background wells are located along the perimeter of the test site to monitor the flow regime and the water quality underground. The background monitoring wells (MW1-MW8) were sampled once in a month. The drainfield monitoring wells were sampled on a biweekly basis for monitoring their water quality.

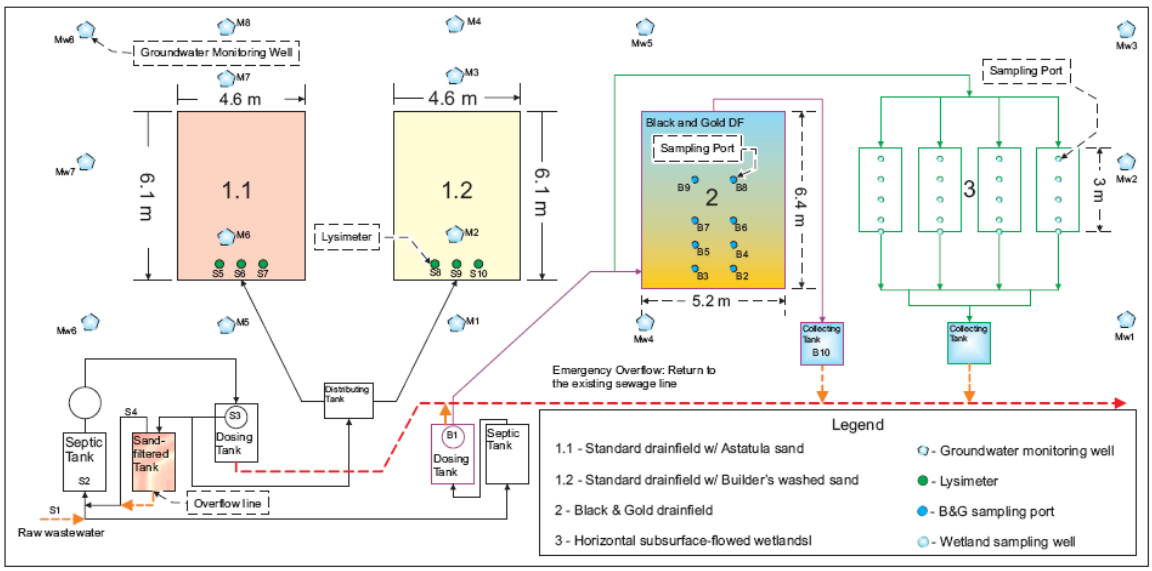

Figure 1. System layout of the UCF Test Center. The first OWTS train consists of a septic tank, a dosing tank, a sand-filtered circulation tank, a distributing tank, and two parallel drainfields. The two drainfields have different infiltration sands, Astatula and Wash Builder's Sand. Three lysimeters are installed at three levels at the header of each drainfield. The three levels of lysimeters are 8", 16", and 24" below the infiltrate surface.



(a) B&G underground Drainfield (b) Subsurface wetland Drainfield (c) Standard Drainfield

Figure 2: Photographs of conventional and passive drainfields at UCF Test Center

B&G Drainfield

In fact, engineered, functionalized, and natural sorption media can be used to treat stormwater runoff, wastewater effluents, groundwater flows, landfill leachates and sources of drinking water for nutrient removal via physicochemical and microbiological processes (Chang et al., 2008b). They include but are not limited to sawdust, peat, compost, zeolite, wheat straw, newspaper, sand, limestone, expanded clay, wood chips, wood fibers, mulch, glass, ash, pumice, bentonite, tire crumbs, expanded shale, oyster shell, and soy meal hull (Chang et al., 2008b). This approach has "green" implications because of the inclusion of recycled material as part of the material mixture promoting treatment efficiency and cost-effectiveness (Chang et al., 2008b). The choice of material

mixes depend on the desired length of service, residence time during an operating cycle, and pollutants in the wastewater. The projected uses of the media are for soil amendments in the B&G drainfield in this paper for on-site wastewater systems filled with the proposed media in a manner that may foster an anaerobic or anoxic environment saturated. The appropriate arrangement of piping system for correct dosing along with the optimal sizing of the anoxic environment with adequate partition eventually sustain the functionality of these functionalized sorption media in the passive drainfields (Wanielista et al., 2008). However, comparative studies are required to prove the advantageous features of passive treatment technologies within all treatment trains at the test center.

With the aid of green sorption media, the objective of this paper is to present the basic functionality of the B&G drainfield filled with a unique recipe of green sorption media to remove both nutrients and pathogens. It leads to develop an innovative passive underground drainfield that is highly sustainable to fit in any landscape and built environment on one hand, and highly applicable in dealing with any type of septic tank systems on the other hand (Wanielista et al., 2008). Figure 3 shows the schematic of the B&G drainfield.

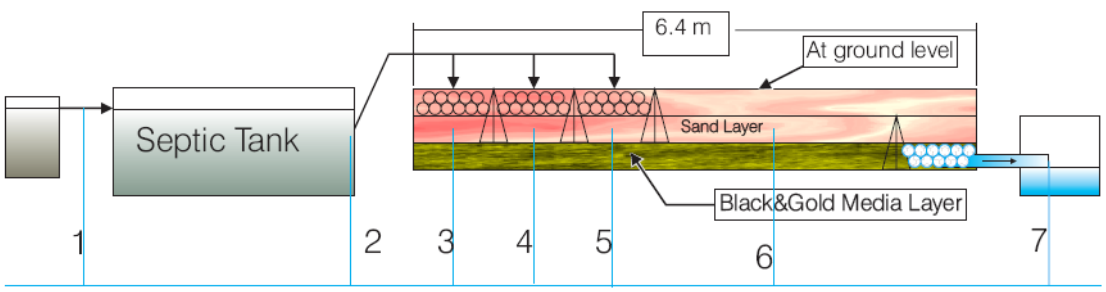

Figure 3. Schematic of the B&G Drainfield (Wanielista et al., 2008).

Reaction Mechanism

The adsorption, absorption, ion exchange, and precipitation processes are actually intertwined with the overall physicochemical process. Some nutrients, such as phosphorus, removed by inorganic media are likely a sorption/precipitation complex. The distinction between adsorption and precipitation is the nature of the chemical bond forming between the pollutant and sorption media. Yet the attraction of sorption surface between the pollutant and the sorption media causes the pollutants to leave the aqueous solution and simply adhere to the sorption media. In the context of using various green sorption media for nutrient removal, it might appear that sorption is followed by precipitation or occurs at the same time in the same physicochemical process. Within the microbiological process, if there are organic sources in the wastewater streams, hydrolysis converts particulate organic nitrogen (N) to soluble organic N, and ammonification in turn releases ammonia into the water bodies. In addition to ammonification, important biochemical transformation processes include nitrification and denitrification. They result in the transformation of nitrogen between ammonia, nitrite, and nitrate forms via oxidation and reduction reactions in microbiological processes. In the presence of ammonia-oxidizing bacteria (AOB) and oxygen in the aerobic environment, ammonium is converted to nitrite (NO_2^-) and nitrite-oxidizing bacteria (NOB) convert nitrite to nitrate (NO_3^-) continuously. Collectively these two reactions are

called nitrification. Conversely, denitrification is an anaerobic respiration process using nitrate as a final electron acceptor with the presence of appropriate electron donors, resulting in the stepwise reduction of NO_3^- to NO_2^-, nitric oxide (NO), nitrous oxide (N_2O), and nitrogen gas (N_2). Denitrification also requires the presence of an electron donor, which may commonly include organic carbon, iron, manganese, or sulfur, to make the reduction happen. As long as the hydraulic retention time (HRT) is long enough, microbe-mineral or sorption media interface can be initiated for either or both nitrification and denitrification process. In our case, sawdust is used as electron donors. The two steps of ammonia oxidation can be summarized as below in equations 1 and 2 (Metcalf and Eddy, 2003),

$$2NH_4^+ + 3O_2 \rightarrow 2NO_2^- + 4H^+ + 2H_2O \quad (1)$$

$$2NO_2^- + O_2 \rightarrow 2NO_3^- \quad (2)$$

And the denitrification of wastewater is shown in equation 3 (Metcalf and Eddy, 2003),

$$C_{10}H_{19}O_3N + 10NO_3^- \rightarrow 5N_2 + 10CO_2 + 3H_2O + NH_3 + 10OH^- \quad (3)$$

Sampling and Analysis

Seven process steps and sampling points within the B&G drainfield system can be identified by Figure 3. Steps 3, 4, and 5 have two media layers; the sand and the B&G layers. B&G thickness is 30.48 cm (12 inches) which contain 68% sand, 7% sawdust, and 25% tire crumb by volume. The sand layer is astatula sand with thickness of 60.96 cm (24 inches) from the ground surface. The PTI pipe is installed for equal distribution of influent. The B&G drainfield was monitored continuously for eight weeks in late 2008. Three sampling campaigns were completed during early Oct., early Nov., and mid Nov. Samples were analyzed by the Environmental Research and Design (ERD), a certified laboratory in Orlando, Florida, for the water quality analysis. Only two datasets addressing the water quality conditions on Oct. 14th and Nov. 5th 2008, were presented in this paper. The initial concentrations of the sewerage can be seen in Table 1 below.

Table 1(a) Initial concentrations of basic parameters

	ALK	Turb	TSS	VSS	BOD_5	$CBOD_5$
Unit	mg/l	NTU	mg/l	mg/l	mg/l	mg/l
Influent (S1)	293.0	123.0	175.0	154.0	31.3	31.2

Table 1(b) Initial concentrations of nitrogen parameters (unit: μg/l)

	NH_3	NO_x-N*	Nitrite	Particulate N		Dissolved Organic N	Total N
Influent (S1)	32,864.0	11.0	8.0	3,760.0		9,635.0	46,270.0

* NO_x-N = NO_2^--N+ NO_3^--N

Table 1(c) Initial concentrations of phosphorus constitutes (unit: μg/l)

	SRP	Dissolved P	Particulate P	Dissolved Organic P	Total P
Influent (S1)	4,928.0	32.0	2,240.0	4,960.0	7,200.0

RESULTS AND DISCUSSION

Nutrient Removal

Figure 4 presents the water quality analysis of the October 14th, 2008 samples. To examine the comparative advantage, the blue bars show the total removal efficiencies of the combination of septic tank and the B&G drainfield whereas the red bars present the removal efficiencies of the B&G drainfield only. If a blue bar is higher than a red bar, removals occurred in both the septic tank and the B&G drainfield. If a red bar is higher than a blue bar, an increase occurred in the septic tank and a removal occurred in the B&G drainfield. For example, by comparing the nitrite removal efficiencies of the total (blue bar) and the B&G drainfield (red bar), the overall removal (blue bar) is less (shorter) than the red bar, and thus the nitrite concentration increases in the septic tank, and nitrite is removed in the B&G drainfield. Overall, this set of data revealed that the B&G drainfield performed very well (see Figure 4) in terms of nutrient and pathogen removal across all relevant species. Nitrate and Nitrite measured at the effluent were less than 2 ppb and 5 ppb (parts per billion), respectively, which are far lower than the USEPA Maximum Contaminant Levels (MCLs) published in the National Primary Drinking Water Regulations (NPDWR or primary standards) at 10,000 ppb and 1,000 ppb, respectively. More than 96 percents of Total Phosphorus was removed. The removal efficiency of $CBOD_5$ and Ammonia was above 90 percents. Turbidity was 30 percent higher than the USEPA MCL standard; however, the primary cause of high turbidity is suspected to be the sawdust mixed in the media. Preliminary tests in the UCF laboratory suggested that the negative effect of sawdust will slowly decrease over time.

The second dataset collected on November 5th, 2008 showed that the performance of the B&G drainfield had improved over time (see Figure 5). Total Nitrogen removal efficiency increased from 58% (October 14th, 2008) to 85% (November 5th, 2008). Total Phosphorus removal stayed above 98%. Fecal Coli and E. Coli removal efficiencies are above 99.9% (below 1 cfu in the effluent samples). The second dataset also confirmed that a smooth nitrification-denitrification process occurred in the B&G drainfield system. Most ammonia conversion occurred mainly in the sand layer of the B&G drainfield, and the nitrate and nitrite conversions occurred in the B&G layer of the B&G drainfield where denitrification plays an important role.

In Figure 6, it also shows that most ammonia was removed in the process steps 3, 4, and 5 at the sand layer (shallow layer); while the nitrate and nitrite were added in the B&G layer (bottom layer) of the same process steps. Figure 6 also revealed the conversion from ammonia to nitrate and nitrite in the B&G drainfield has been successful. Figures 7 and 8 proved that the B&G drainfield not only removes the nutrient but also filters the pathogens especially in the B&G layer of the B&G drainfield.

CONCLUSIONS

This paper presents our initial effort of test run of the B&G drainfield, aiming to demonstrate a new generation performance-based cost-effective passive OWTS technology with sustainability implications. Sampling campaign was conducted in the fall 2008 to support our observations that such a new passive OWTS technology can remove both nutrient and E-coli several more orders of magnitude stringent than required by the

current regulation (MCLs). Overall, more than 85% and 96% of Total Nitrogen and Phosphorus were removed, respectively. The removal efficiency of $CBOD_5$ and Ammonia was also above 90 percents.

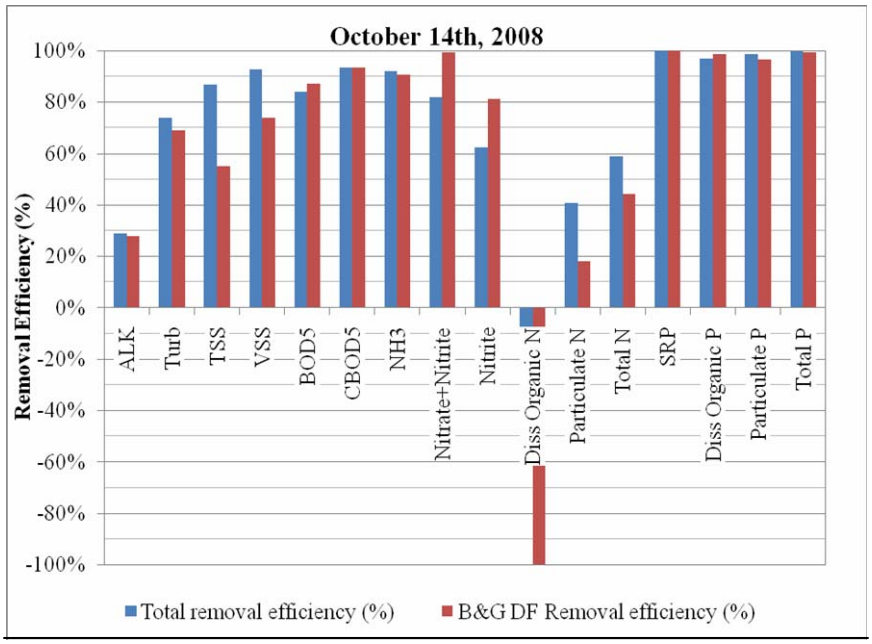

Figure 4. Total removal efficiencies of the Septic Tank and B&G Drainfield (blue bars) compared to the Black and Gold Drainfield only removal efficiencies (red bars). If the blue bar is less in a positive direction than the red bar, it means that the septic tank effluent increases in concentration relative to the input.

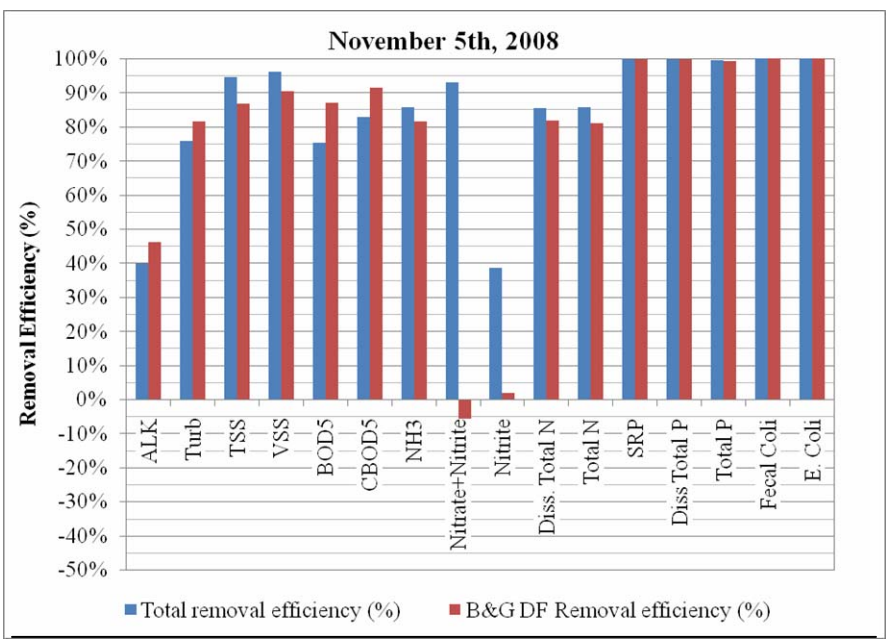

Figure 5. Removal efficiencies of the November 5th, 2008 dataset are presented an improved overall performance of the B&G Drainfield.

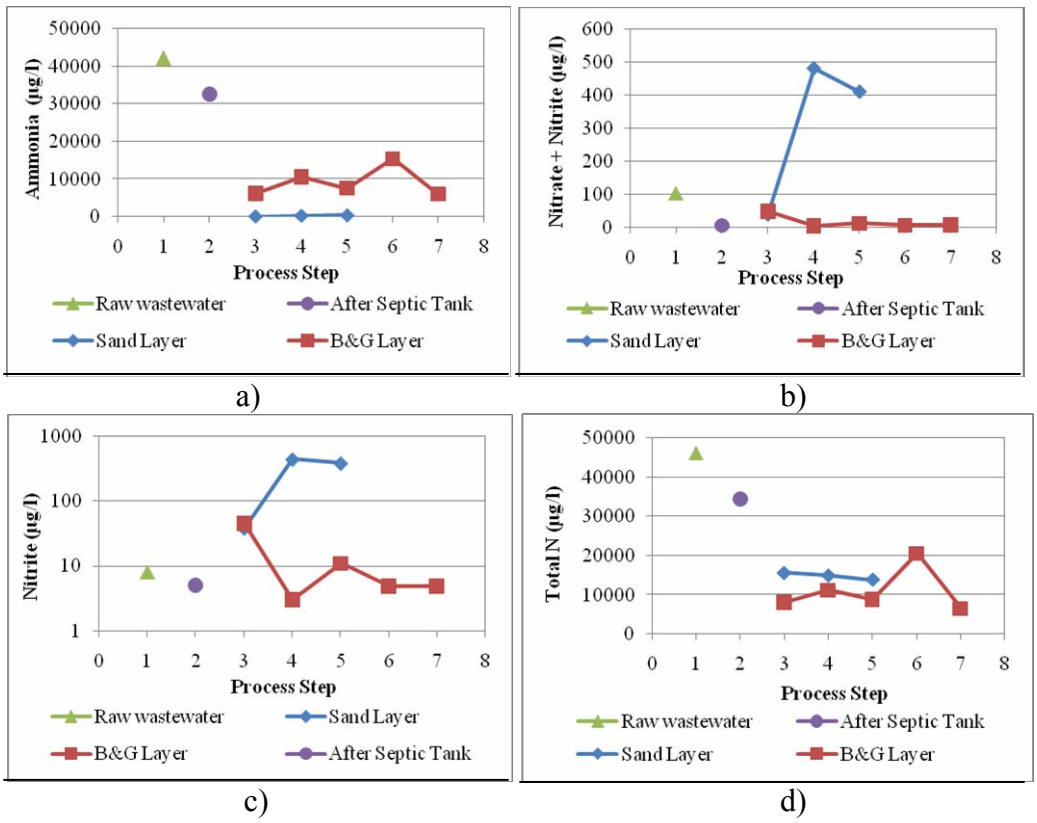

Figure 6. Concentrations of Ammonia, Nitrate, Nitrite, and Total Nitrogen in B&G System.

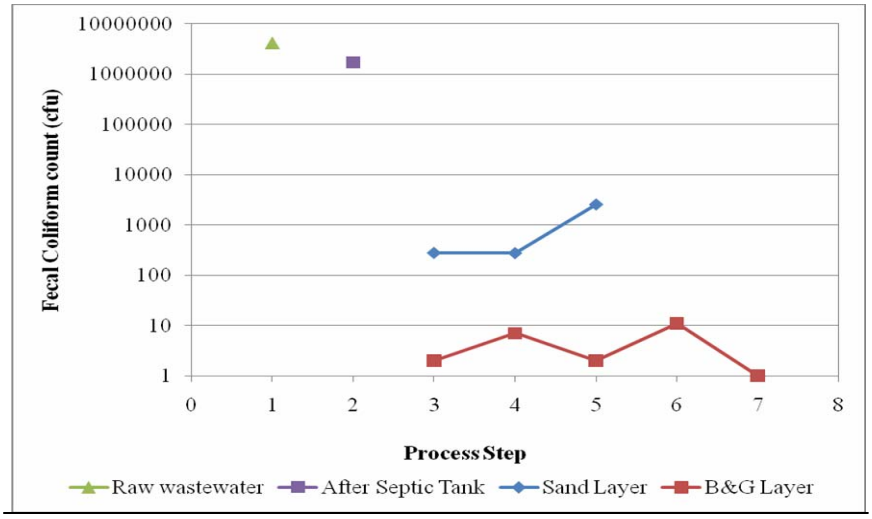

Figure 7. Fecal Coliform Counts after the wastewater has passed through the B&G Drainfield. The average count at the effluent was less than 1 cfu for the two datasets.

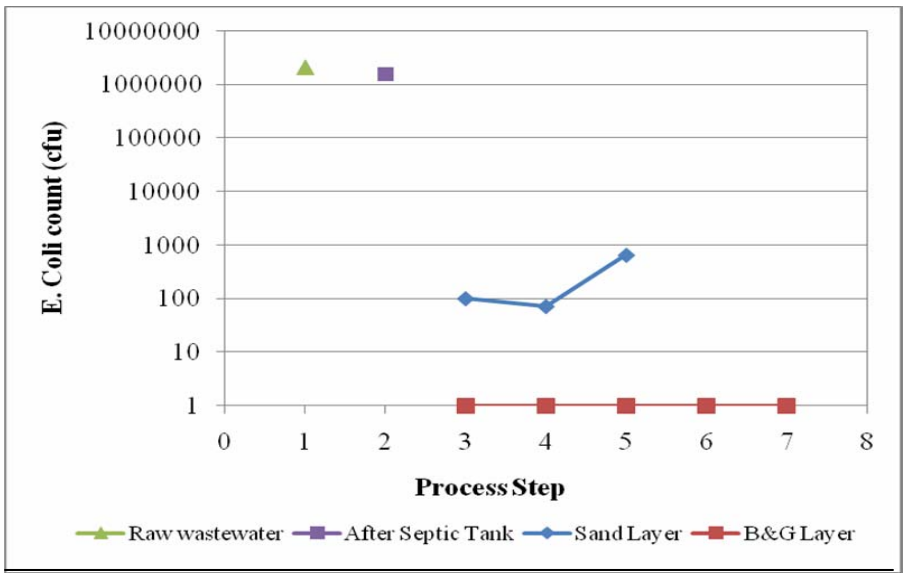

Figure 8. E. Coli Counts in the B&G Drainfield System

Such advancement, however, would be ultimately justified by environmental economics, including direct and indirect costs and benefits, which have been viewed as important information for decision making (Etnier et al., 2000). Besides, the estimation of direct and indirect costs should also be associated with various risk-reduction strategies and methods of risk assessment for decision making. For the design of sustainable neighborhoods, more advanced and adaptive materials, biomaterials, and enabling or multifunctional engineering materials with co-treatment capacities are needed to remove more pollutants, such as heavy metal, pesticides etc., simultaneously. With risk management options at the individual home or community level that are practical, acceptable, and cost effective, the passive OWTS and source separation alternatives may be further integrated based on their comparative advantages.

ACKNOWLEDGEMENT

The authors are grateful for the financial support from the Florida Department of Environmental Protection (FDEP) provided through the Watershed Restoration Program's Urban BMP Research and Development Grant.

REFERENCES

Beutel, M. W. (2006). Inhibition of ammonia release from anoxic profundal sediments in lakes using hypolimnetic oxygenation. *Ecological Engineering*, 28(3), 271-279.

Chang, N. B., Wanielista, M., and Makkeasorn, A. (2007). Innovative Design of Stormwater and On-site Wastewater Treatment Systems in Support of Green Building Initiative. Proceedings of 6th International Conference on Environmental Informatics, November 21-23, 2007, Bangkok, Thailand.

Chang, N. B., Wanielista, M., Shah, T. B., Hossain, F., and Xuan Z. (2008a). Characterizing Green Sorption Media in Vadose Zone to Improve Nutrient

Removal of Septic Tank Drainfields. *Journal of Environmental Quality*, in review.

Chang, N. B., Wanielista, M., and Hossain, F. (2008b). The use of filter media for nutrient removal in natural and built environments: problems, perspectives, and challenges. *Critical Reviews in Environmental Science and Technology*, in review.

Etnier, C., Nelson, V., and Pinkham, R., 2000. Economics of decentralized Wastewater Treatment Systems: Direct and Indirect Costs and Benefits. Department of Agricultural Engineering, Agricultural University of Norway, Norway.

Gabel, B., Kozicki, R., Lahl, U., Podbielski, A., Stachel, B., and Struss, S. (1982). Pollution of drinking water with nitrate. *Chemosphere*, 11, pp- 1147-1154.

Huang, C. P., Wang, H. W., and Chiu, P. C. (1998). Nitrate reduction by metallic iron, *Water Research*, 32(8), 2257-2264.

Katzenelson, E., Buium, I., and Shuval, H. I. (1976). Risk of communicable disease infection associated with wastewater irrigation in agricultural settlements. *Science*, 1976 Nov 26; 194.

Kim-Shapiro, D. B., Gladwin, M. T., Patel, R. P., and Hogg, N. (2005). The reaction between nitrite and hemoglobin: the role of nitrite in hemoglobin-mediated hypoxic vasodilation. *Journal of Inorganic Biochemistry*, 99(1), 237-246.

Metcalf and Eddy (2003). Wastewater engineering: treatment and reuse, 4th edition, McGraw Hill Publishing, New York, USA.

Sawyer, C. N., McCarty, P. L., and Parkin, G. F. (2003). *Chemistry for Environmental Engineering Science*, McGraw-Hill, New York, USA, Fifth Edition.

Servizi, J. A. and Gordon, R. W. (2005). Acute lethal toxicity of ammonia and suspended sediment mixtures to chinook salmon (*Oncorhynchus tshawytscha*). Bulletin *of Environmental Contamination and Toxicology*, 44(4), 650-656

Tarazona, J. V., Munoz, M. J., Ortiz, J. A., Nunez, M. O., and Camargo, J. A. (2008). Fish mortality due to acute ammonia exposure. *Aquaculture Research*, 18(2), 167-172.

U.S. Environmental Protection Agency (USEPA) (2002). *USEPA Onsite Wastewater Treatment Systems Manual*, EPA/625/R-00/008, Office of Research and Development, Washing ton DC, USA.

U.S. Environmental Protection Agency (USEPA) (2005). *Handbook for Management of Onsite and Clustered (Decentralized) Wastewater Treatment Systems*. , EPA832-B-05-001, Office of Research and Development, Washing ton DC, USA.

Wanielista, M., Chang, N. B., and Makkeasorn, A. (2008). Provisional Patent: "Passive Underground Drainfield for Septic Tank Nutrient Removal Using Special Functionalized Green Filtration Media. Atty. Docket No: UCF-663.

Water Environment Federation (WEF) and American Society of Civil Engineers (ASCE) (2005). Biological nutrient removal (BNR) operation in wastewater treatment plants, Manual of practice no. 30, *WEF press and McGraw Hill Publishing*, USA

Selection and Prioritization of Best Management Practices for Potential Sources of Contamination in a Wellhead Protection Area

Tina Petersen, Ph.D., Camp Dresser & McKee, Inc.
Camille W. Sowells, P.E., BCEE, Camp Dresser & McKee, Inc.
Gordon McCurry, Ph.D., P.G., Camp Dresser & McKee, Inc.
Alexandria Doody, Camp Dresser & McKee, Inc.
Sean Ables, P.G., Texas Commission on Environmental Quality

Abstract

Implementing best management practices (BMPs) is one of the key outcomes of a successful Source Water Protection program. BMPs are activities that can be implemented to reduce the risk of adverse future impacts to a public water supply. They can include structural activities such as building additional containment around storage vessels and nonstructural activities such as implementing land use restrictions.

The objective of this paper is to discuss a new and innovative approach to evaluate, select and prioritize BMPs for multiple public water supply systems in Texas. For this project, a database prioritization and selection tool was developed and used to assist in screening BMPs for multiple public water systems in Texas. The BMP selection process included a three-tiered screening process that is described in detail. This tool differs from previous US EPA approaches in that it is streamlined and can be applied efficiently for multiple systems.

Introduction

Best management practices (BMPs) are activities that can reduce the risk of adverse future impacts to a public water supply. These can include structural activities such as building additional containment around storage vessels and nonstructural activities such as implementing land use restrictions. Implementing BMPs is one of the key outcomes of a successful Source Water Protection (SWP) program. [it would be appropriate to briefly describe here what the SWP program is, who administers it, who it applies to, etc] Source Water Protection functions as a component of the Texas Source Water Assessment and Protection (SWAP) Program which functions to implement management strategies to mitigate or eliminate risks associated with potential sources of contamination (PSOCs). Public drinking water supply systems are the focus of the program and the responsibility for implementation lies with the systems and any local coordinators they may designate.

BMPs were selected to help protect the source water supply. Typically multiple BMPs are employed to mitigate the risk from a particular potential source of contamination (PSOC). BMP effectiveness may vary according to site-specific conditions. In addition, a single BMP can control several sources of contamination. A cost effective BMP

strategy may involve a combination of BMPs strategically selected and located to balance the risk of a contaminant's impact and the cost of BMP implementation.

The US EPA (1991) developed an approach to identifying best management practices for groundwater systems that relies on ranking threats to groundwater supplies by potential sources of contamination (PSOC). This approach, however, is quite cumbersome because of the high level of detail required for the assessment and the treatment of each PSOC threat individually.

For this project, a database prioritization and selection tool was developed and used to assist in screening BMPs for multiple public water systems in Texas. The BMP selection process included a three-tiered screening process . This tool differs from previous US EPA approaches in that it is streamlined and can be applied efficiently for multiple systems. Compared to the EPA (1991) approach which requires numerous worksheets and focuses on prioritizing PSOCs, this tool requires just two forms for each PSOC and focuses on prioritizing their associated BMPs rather than PSOCs. A brief summary of the process is presented below.

First, for each water system, a list of PSOCs is developed from office and field investigations within a defined wellhead protection area and entered into the database. The water system PSOCs are screened against a comprehensive listing of BMPs, which is based in part on the Texas Commission on Environmental Quality's "Draft BMP Guidance Manual" (PBS&J, 2006). The initial screening database query creates a table of appropriate BMPS that are applicable to the system PSOCs.

Next, a ranking system within the database was developed to help users further screen BMPs and assess the relative risks associated each PSOC. The approach included evaluating and ranking each BMP giving consideration to the following criteria:

- effectiveness in eliminating contamination;
- addresses known water quality concerns;
- entity who will be implementing the BMP (the system, the owner of the PSOC);
- ease of implementation;
- operations impact;
- funding availability; and
- cost.

Users assess each BMP identified for each PSOC and assign rankings, generally high, medium or low. After ranking all BMPs, the database can be queried to compile a report of rankings and generate a draft list of prioritized recommended BMPs for each public water system.

Finally, BMP selection is coordinated with the local planning team and stakeholders for each public water system because of the direct economic consequences associated with BMP implementation. Additional considerations discussed with the local planning team and stakeholders included public acceptance, impacts and effects on other programs, availability of funding assistance and compatibility with overall goals. A proposed timeline for BMP implementation was developed for each public water system.

Database Development

To evaluate and prioritize selection of BMPs for multiple public water systems, a database was envisioned to easily document and streamline the process. The purpose of the database is to:

- Store a comprehensive listing of potential sources of contamination and the BMPs associated with them.
- Allow entry of water system specific information, including information on each PSOC in the wellhead protection area.
- Allow evaluation and prioritization of BMPs for each system, based on established criteria and site specific PSOCs.

The comprehensive list of PSOC's and associated BMP's was based in part on the Texas Commission on Environmental Quality's "Draft BMP Guidance Manual" (PBS&J, 2006). Additional BMP's were added based on previous project experience. Forms were developed to allow entry of data related to each water system, and it's PSOC's. Finally, a tiered evaluation process was developed to quickly and consistently evaluate each BMP available for use with each PSOC. A detailed description of the evaluation process follows.

BMP Evaluation and Prioritization

Following completion of the initial data gathering, wellhead protection area delineation, site specific research and field data collection activities, a better understanding of potential sources of contamination (PSOCs) to the groundwater supply will emerge. This information is used to undertake the preliminary BMP evaluation and selection.

Upon opening the database, users are given a menu of options to choose from as reflected in Figure 1. To begin BMP evaluation the Tier 1 BMP evaluation is selected.

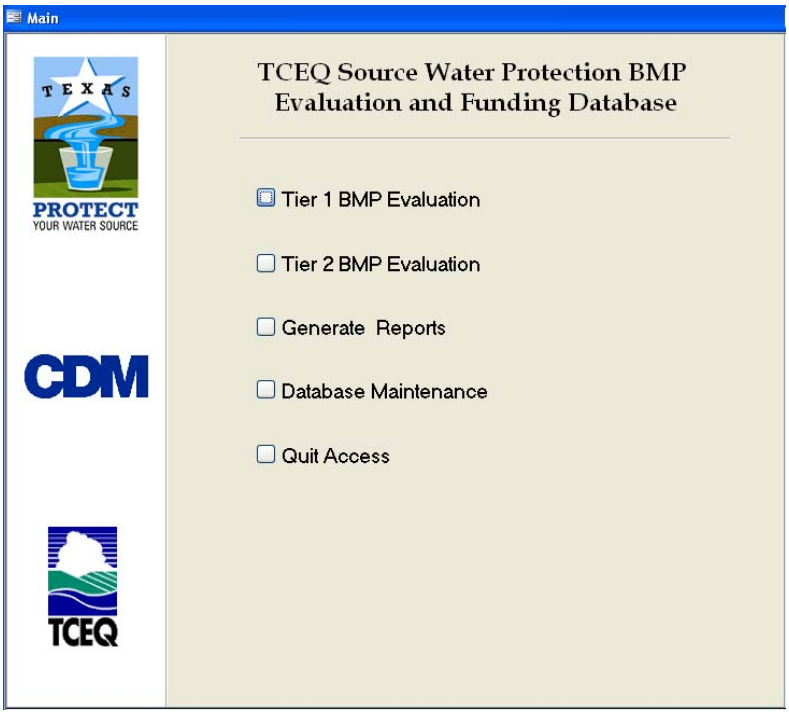

Figure 1. SWAP Database Menu

Tier 1 BMP Evaluation

The initial Tier 1 evaluation consists of reviewing each BMP available for each PSOC identified in the wellhead protection area. The initial review is to determine the applicability of the BMP for the specific PSOC identified. **Figure 2** presents a graphic of the form used in the database to perform this evaluation. As shown in the figure, page 1 of the form includes the public water supply (PWS) Identification Number, and description of the PSOC being evaluated, and the list of BMPs which may be applicable. Page 2 of the form (**Figure 3**) includes additional information or clarifying remarks made by the field team during the site investigation. Page 3 of the form (**Figure 4**) includes information on the types of contaminants associated with the PSOC. Only those BMP's deemed applicable move forward to the Tier 2 Evaluation process.

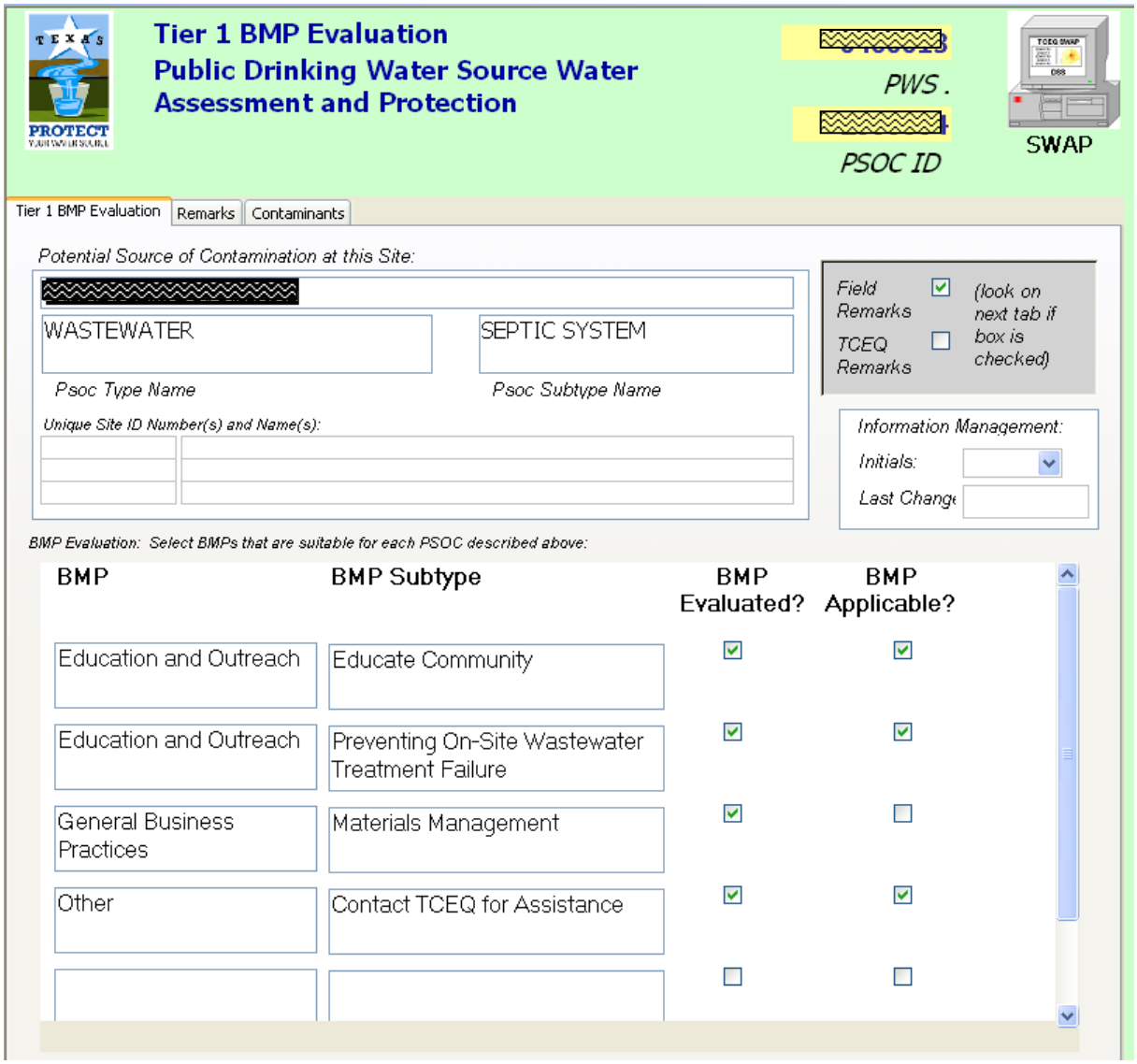

Figure 2. Page 1 of Tier 1 BMP Evaluation

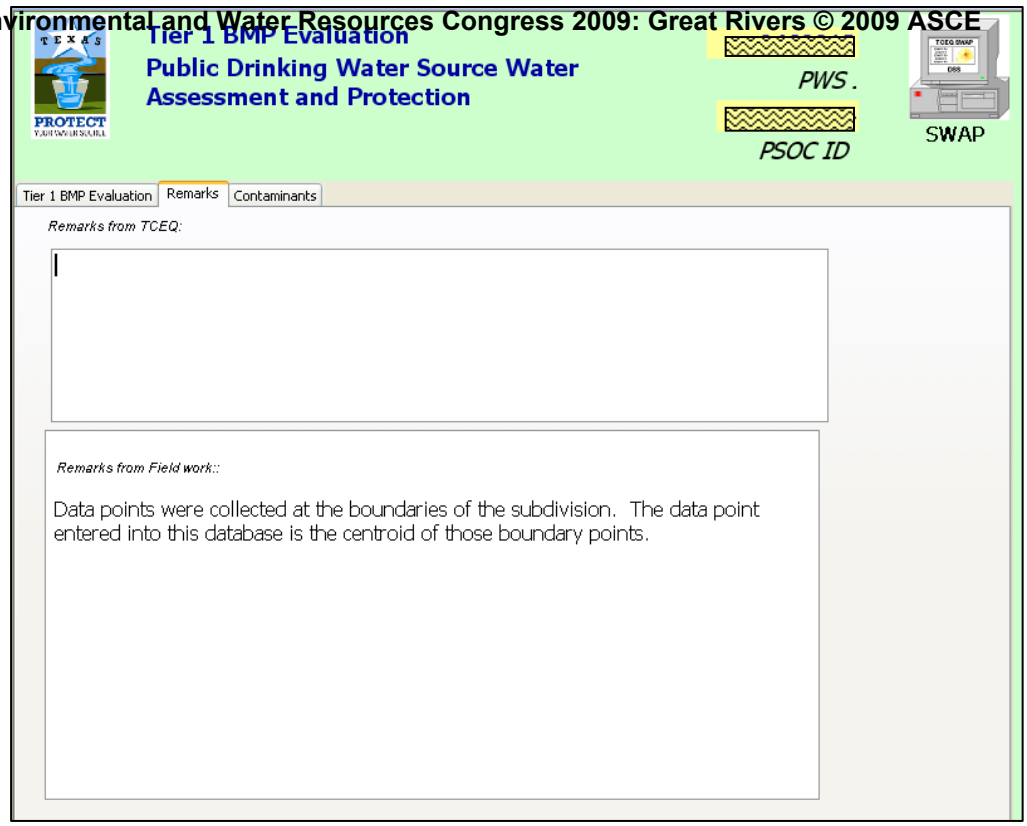

Figure 3. Page 2 of Tier 1 BMP Evaluation

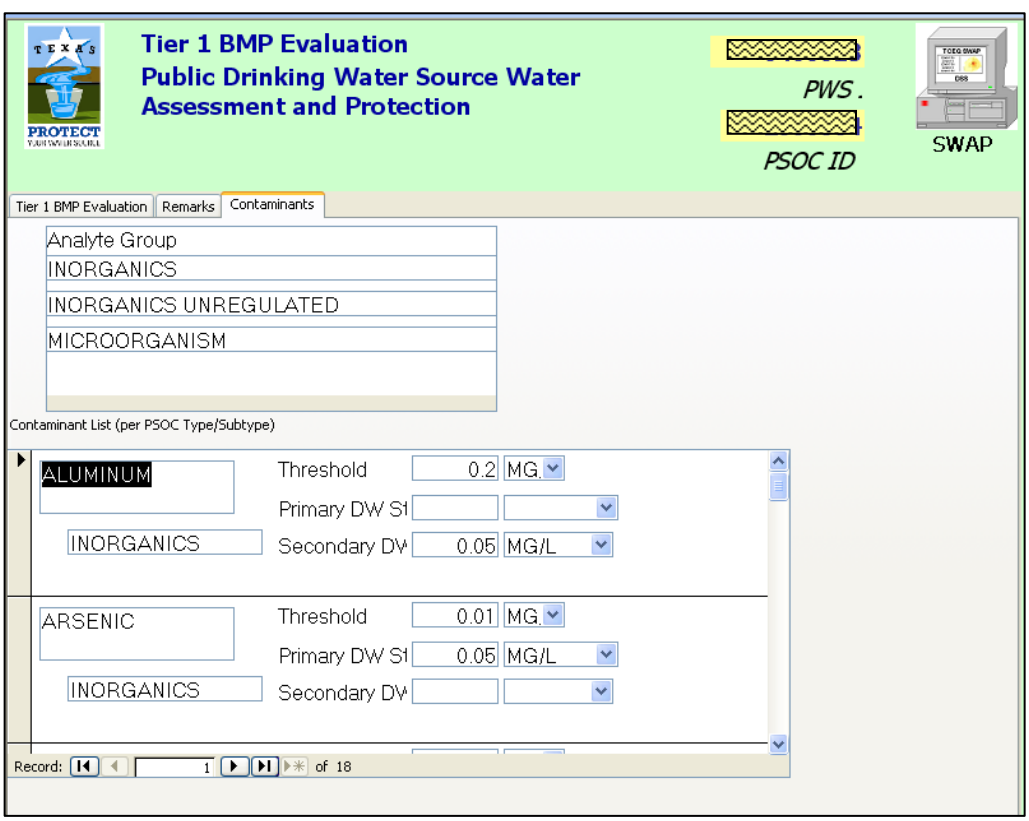

Figure 4. Page 3 of Tier 1 BMP Evaluation

Tier 2 BMP Evaluation

The Tier 2 Evaluation portion of the database is designed to help users further screen BMPs. The approach included evaluating and ranking each BMP giving consideration answering the following questions:

- Does this BMP address an existing water quality concern?
- Will this BMP be effective in elimination or reducing the risk of contamination?
- Who is required to implement this BMP?
- How easy is this BMP to implement?
- What impact on PWS operations will implementing this BMP have?
- What is the relative cost of this BMP?
- Is funding available to assist with implementation of this BMP?

Users assess each BMP identified for each PSOC and assign rankings, generally high, medium or low. The database also links to photos of each PSOC taken during the site investigation portion of the project. After ranking all BMPs, the database is queried to compile a report of rankings and generate a draft list of prioritized recommended BMPs for each public water system. The recommended BMPs then are compiled and presented in the SWP report for the PWS. Figure 5 presents the Tier 2 Evaluation form.

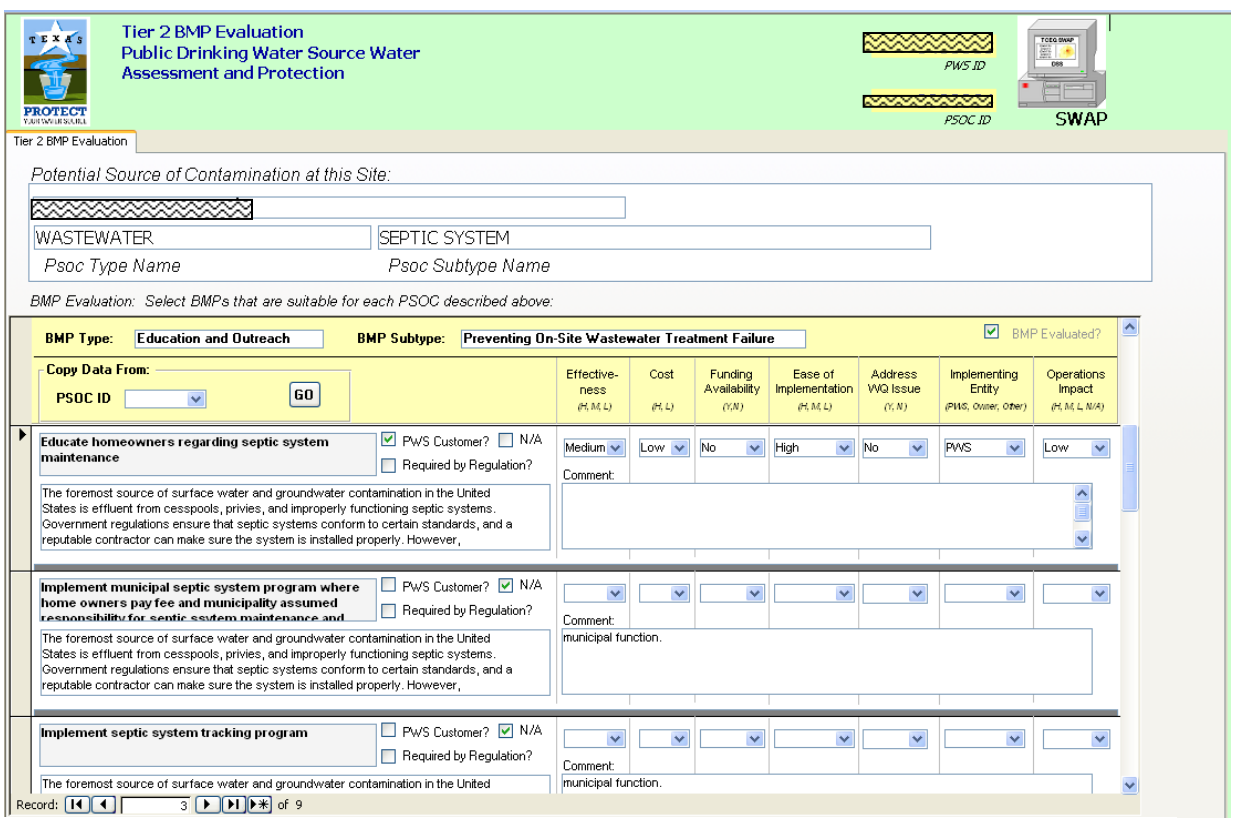

Figure 5. Tier 2 BMP Evaluation Form

Tier 3 BMP Evaluation

The Tier 3 Evaluation is the Project Follow-Up Meeting that is conducted with the public water system and interested local stakeholders. The purpose of the meeting is to keep the system informed of progress to date and obtaining consensus on the recommended BMPs. Meeting objectives include:

- Conveying the groundwater modeling results and the defined wellhead protection area.
- Discussing any known water quality problems or contamination incidents.
- Reviewing the PSOCs located in the wellhead protection area.
- Discussing BMPs recommended to address the PSOCs in the wellhead protection area.

This meeting is essential to obtain system and stakeholder buy-in on the recommended BMPs. Because the local stakeholders will be relied on to implement many of the BMPs and due to the direct economic impacts associated with BMP implementation, stakeholder input and anticipated level of engagement in the process is factored into the BMP selection and evaluation.

Results

The result of this project is a new and innovative approach to evaluate, select and prioritize BMPs for multiple public water supply systems in Texas. This user-friendly, menu-driven database is designed to allow users to efficiently compile, manage and evaluate large amounts of data associated with multiple PSOCs and multiple public water systems. The prioritization report is shown in **Figure 6**. The report provides a total score to each BMP which is used to rank the potential BMPs.

The ranking system places highest priority on those BMPs that can have a direct impact on PSOCs affecting drinking water quality and consequently human health. That focus is consistent with the priority setting approach used by EPA (1991). Use of the Tier 1 and Tier 2 evaluations, however, avoids the need to complete numerous source, wellhead, contaminant, and transport worksheets to yield a final risk score.

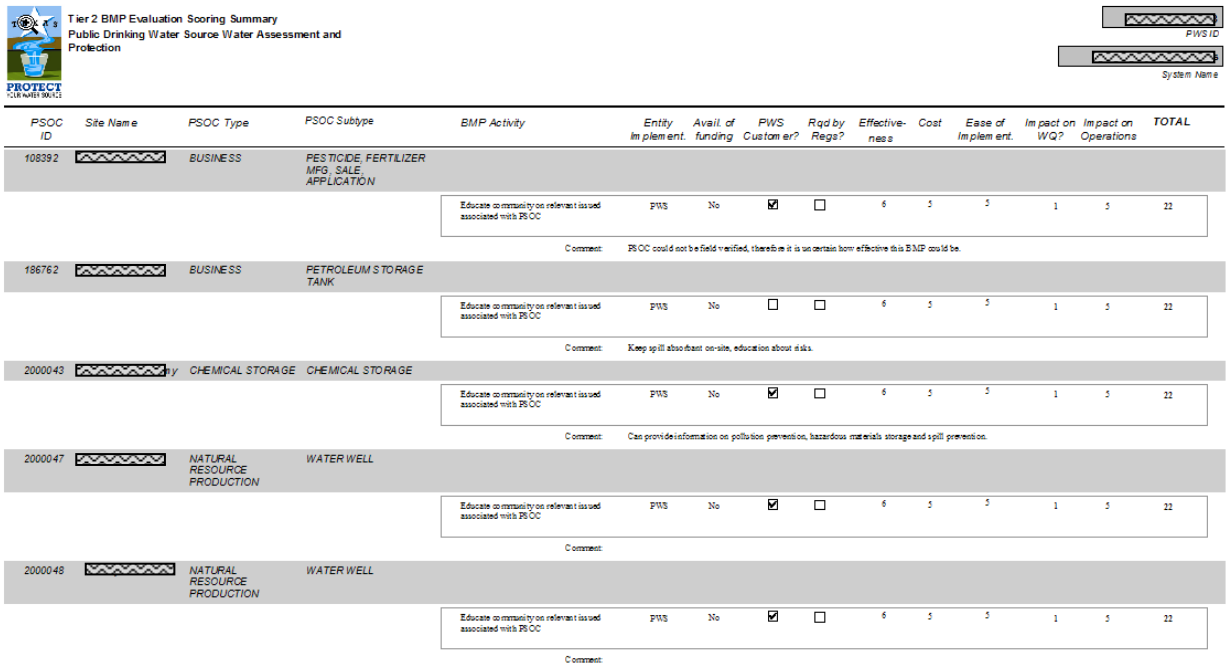

Tier 2 BMP Evaluation Scoring Summary
Public Drinking Water Source Water Assessment and Protection

PWS ID

System Name

PSOC ID	Site Name	PSOC Type	PSOC Subtype	BMP Activity	Entity Implement.	Avail. of funding	PWS Customer?	Rqd by Regs?	Effectiveness	Cost	Ease of Implement.	Impact on WQ?	Impact on Operations	TOTAL
108392		BUSINESS	PESTICIDE, FERTILIZER MFG, SALE, APPLICATION											
				Educate community on relevant issued associated with PSOC	PWS	No	☑	☐	6	5	5	1	5	22
				Comment: PSOC could not be field verified, therefore it is uncertain how effective this BMP could be.										
186762		BUSINESS	PETROLEUM STORAGE TANK											
				Educate community on relevant issued associated with PSOC	PWS	No	☐	☐	6	5	5	1	5	22
				Comment: Keep spill absorbant on-site, education about risks.										
2000043		CHEMICAL STORAGE	CHEMICAL STORAGE											
				Educate community on relevant issued associated with PSOC	PWS	No	☑	☐	6	5	5	1	5	22
				Comment: Can provide information on pollution prevention, hazardous materials storage and spill prevention.										
2000047		NATURAL RESOURCE PRODUCTION	WATER WELL											
				Educate community on relevant issued associated with PSOC	PWS	No	☑	☐	6	5	5	1	5	22
				Comment:										
2000048		NATURAL RESOURCE PRODUCTION	WATER WELL											
				Educate community on relevant issued associated with PSOC	PWS	No	☑	☐	6	5	5	1	5	22
				Comment:										

Figure 6. Tier 2 BMP Results Report

Conclusions

The goal of any source water protection is to take action by implementing BMPs to protect drinking water supply. The database and BMP selection process developed for public water supply systems in Texas focuses on key information that will impact BMP implementation, such as existing water quality issues, funding availability, and who will ultimately implement the BMPs. Consideration of these factors will ultimately allow systems to move to implementation more quickly than previous US EPA approaches, and consequently, will result in a higher level of implementation.

References

US EPA (1991). "Managing Ground Water Contamination Sources in Wellhead Protection Areas: A Priority Setting Approach." US EPA, Washington, D.C. 570/9-91-023.

PBS&J (2006). "Draft BMP Guidance Document" Prepared for TCEQ, Austin, TX.

Keywords

Best management practices, wellhead protection area, source water assessment, source water protection, BMP selection, BMP prioritization, decision making, groundwater.

Controlling Salt-Water Intrusion to Environmental Sensitive Areas due to the Construction of the Rio Anton Ruiz Flood Control Project

By

David Weston and Rafael Velez
Jacksonville District – US Army Corps of Engineers

A. ABSTRACT

The Rio Anton Ruiz Flood Control Project was authorized to reduce flood damages to the coastal communities of Punta Santiago, Verde Mar and Villa Palmira, near Humacao, Puerto Rico. Flood damages used to impact those communities throughout the year until the authorized flood control project was built. Historically, flooding occurred when runoff from the mountains within the watershed would flow into a large upland lagoon and then flooded those communities before reaching the Caribbean Sea. The authorized flood control project protected those communities from flooding by the lagoon with a large levee system and a series of canals to the sea. Since the completion of the authorized flood control project in 2001 there have been major impacts to the lagoon and a surrounding environment due to salt water intrusion. Some of the primary impacts have affected Humacao Wildlife Refuge, which has the last major remnant Pterocarpus Forest on the Island of Puerto Rico. That species of tree is endangered and has a low saltwater tolerance, thus requires mainly freshwater to survive. The lagoon has some fish and other plant species such as mangroves that rely on both fresh and saltwater. Therefore, a series of saltwater intrusion measures were developed and constructed to limit the amounts of saltwater that impact the lagoon and the Pterocarpus Forest as a result of the some of the constructed features from the authorized flood control project. This paper will show how the flood control project was developed, illustrate the some of the project oversights and project dynamics that caused the saltwater intrusion problem, and then explain how saltwater intrusion measures were developed with unique construction measures that were required for installation in environmentally sensitive areas.

B. INTRODUCTION

The Rio Anton Ruiz Flood Control Project is located on the southeast coast of Puerto Rico. The Rio Anton Ruiz Project was developed and authorized as a flood control project to reduce flood damages to the coastal communities of Punta Santiago, Verde Mar and Villa Palmira, near Humacao, Puerto Rico. Flood damages used to impact those communities. Historical flooding occurred when runoff from the mountains within the watershed would flow into a large upland freshwater lagoon (Mandri Lagoon) and forested swamp, then flooded those communities before reaching the Caribbean Sea. The authorized flood control project protects those communities from flooding with a large levee system and a series of canals to the ocean.

Since the completion of the authorized flood control project in 2001 there have been major impacts to the freshwater lagoon and a surrounding environment due to salt water intrusion. Some of the primary impacts have affected Humacao Wildlife Refuge, which has the last major remnant Pterocarpus Forest on the Island of Puerto Rico. That species of tree is endangered and has a low saltwater tolerance, thus requires mainly freshwater to survive and since the completion of the project a vast amount of trees have died due to the saltwater intrusion. Additionally, the biodiversity within the lagoon has changed to a point where some other species of plant, such as mangroves that rely on both fresh and saltwater and fish have evolved since the completion of the flood control project in 2001. Therefore, in order to preserve the approximately 650 acre site of Pterocarpus Forest and preserve some of the biodiversity both the freshwater and saltwater fauna and flora, a series of saltwater intrusion measures were developed and constructed to limit the amounts of saltwater that impact the lagoon and the Pterocarpus Forest.

C. WATERSHED DESCRIPTION

The Rio Anton Ruiz watershed is located on the eastern coast of Puerto Rico with the headwaters originating in the steep mountains near the El Yunque Rainforest. The drainage area map is shown on Figure 1.

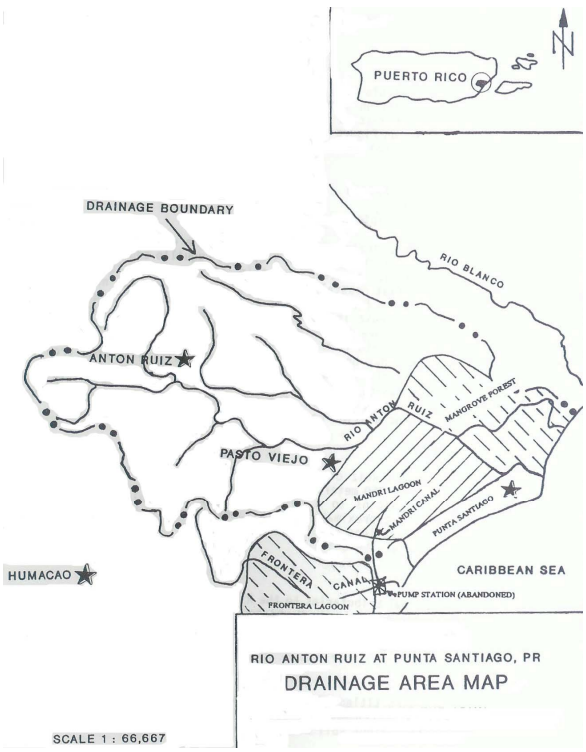

Figure 1

Rainfall will collect into steep mountain streams, then flow in a southeasterly direction across a flat coastal plain before flowing into the Mandri Lagoon. There is a large forest that is thick with primarily freshwater flora such as the Pterocarpus and certain types of Mangroves located within the coastal plain adjacent to the Mandri Lagoon. The Rio Anton Ruiz and Boca Prieta channels are the only outlets for the Rio Anton Ruiz drainage basin. The Mandri Lagoon and low coastal flood plain serve as detention areas during floods and the communities (e.g. Punta Santiago, etc.) at the coast are the main populated areas within in the watershed.

D. HYDROLOGY AND HYDRAULICS

Historically the coastal areas have experienced frequent flooding, which can happen at anytime during the year. The most serious flooding occurs when the runoff from the mountains exceeds the detention capacity of the lagoon and floods the low coastal areas in and around Punta Santiago.

1. Hydrology

The hydrology for the project area was developed with a limited amount of data. Using the US Geological Survey (USGS) quadrangle topographic maps with a scale of 1 to 20,000, the drainage basin was delineated and subdivided into five subbasins as shown on Figure 2.

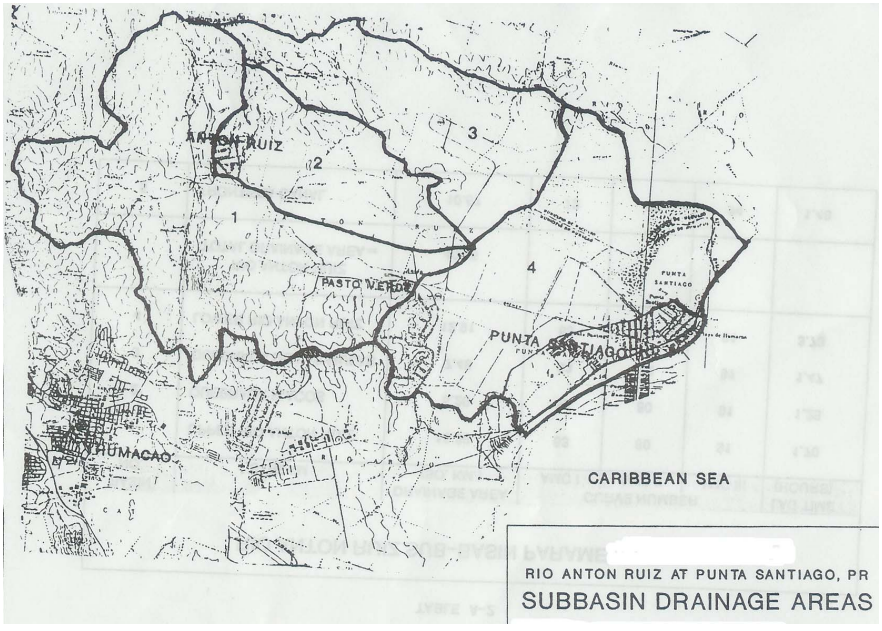

Figure 2

The USGS operates several rain gages near the basin and the National Weather Service (NWS) Technical Paper No. 42 (TP-42) shows generalized estimates of rainfall depth-

frequency data for the area. Contained in the report are the isopluvial maps of precipitation contours for selected frequencies. Table 1 shows the average point rainfalls that were developed for the study area after the adjustments for aerial distribution were applied.

TABLE 1
RAINFALL FOR RIO ANTON RUIZ BASIN
FOR VARIOUS FREQUENCIES AND DURATIONS

Percent Chance Storm	Rainfall in mm						
	Duration in Hours						
	0.25	1	2	3	6	12	24
50	39	70	85	94	110	133	155
20	52	90	114	126	152	185	217
10	61	103	132	148	180	221	260
4	72	119	157	177	217	269	316
2	81	132	176	199	246	306	361
1	89	144	195	221	276	345	408
SPF	89	144	229	290	406	470	540

The Standard Project Storm (SPS) is defined as the most severe flood-producing rainfall depth-area-duration relationship and isohyetal pattern of any storm that is considered reasonably characteristic of the region. The Probable Maximum Precipitation (PMP) is defined as the greatest depth of precipitation for a given duration that is physically possible over a given size storm area at a particular geographical location at a certain time of the year. The SPS was assumed to be 50 percent of the PMP to determine the Standard Project Flood (SPF) for this project study.

The US Army Corps of Engineers (USACE) Hydrologic Engineering Center (HEC) "HEC-1 Flood Hydrograph Package" computer program was used to calculate the runoff volumes and peak discharges for several frequencies. HEC-1 estimates surface runoff resulting from synthetic or observed storm events. The rainfall-runoff relationship for this study was computed by the Soil Conservation Service (SCS) curve number methodology. The SCS method calculates losses from curve numbers which are related to soil types, land uses, and antecedent moisture conditions. Table 2 shows the subbasin parameters that were developed for each of the subbasins.

TABLE 2 - RIO ANTON RUIZ SUBBASIN PARAMETERS

Subbasin No.	Drainage Area (km^2)	Curve Number			Lag Time (Hr)
		AMC I	AMC II	AMC III	
1	15.36	63	80	91	1.70
2	5.20	63	80	91	1.28
3	7.48	63	80	91	1.47
4	12.91	63	80	91	3.73
5	10.57	72	86	94	1.48

Note: Lag times were computed for each basin using the following Kirpich Formula:

$$Lag = 0.0013L^{1.155} / H^{0.385}$$

Where:

Lag = Lag time in hours

L = Length of basin in feet

H = Fall elevation of basin in feet

2. Hydraulics

The original project hydraulic models were developed and compared to Hurricane Donna which according to USGS data was close to 37 year storm event. During that event the rainfall exceeded 371 millimeters for 24 hours and caused major flooding within the project area.

USACE models were developed in the hydraulic analyses of the project. The following USACE numerical models were used: "DWOPER - Dynamic Wave Routing Model", "HEC-2 Water Surface Profiles" model, "HEC-6 Scour and Depositions in Rivers and Reservoirs", "HEC-River Analysis System" (HEC-RAS), and "ACES – Automated Coastal Engineering System" model. These models were used to design the levee protection system, which accounted for wind wave forces generated in the lagoon, as well as the interior and exterior channels. "HEC-6 Scour and Depositions in Rivers and Reservoirs" model was used to analyze the channel scour performance at the coastal outlets.

The levee was designed for an SPF event with stone revetment at the toe. Additional toe protection was provided by vegetation located near the toe of the levee to break up any waves generated on the lagoon side of the levee.

The interior drainage system was designed for a 10 year event and would drain the interior flooded area through two outlets, one at the coast through the existing Boca Prieta outlet and the other outlet would drain into the diversion channel through a culvert structure and into the existing Rio Anton Ruiz outlet. The original design of the proposed diversion channel was to have an invert elevation of -1.5 meters, NGVD, a bottom with of 6 meters, and a 1 vertical to 5 horizontal side slope, which was designed to be close to the conveyance capacity of of the existing Boca Prieta outlet It was anticipated the Rio Anton Ruiz and Boca Prieta outlets at the Caribbean Sea would periodically close and under frequent storm events (5 year or less) these outlets would open due to rainfall runoff.

E. FLOOD CONTROL PROJECT

The project levee is approximately 11,870 feet long and protects those communities along the coastline from SPF flooding from the upland lagoon. The culvert that drains

into the diversion channel consists of 3 – 1.83 m corrugated metal pipes with flap gates. This structure provides an additional outlet for the interior drainage system in the event that the existing Boca Prieta outlet is closed. The diversion channel conveys flows from the lagoon to the sea through the existing Rio Anton Ruiz outlet. The flood control project was completed in June 2001 and is shown on Figure 3.



Figure 3

1. Project Performance

Since the projects completion there has been no flooding from the Mandri Lagoon. All of the runoff from the uplands goes through the Rio Anton Ruiz outlet, however, the outlet does not close as originally anticipated. There has been no damage to the levees due to wave action but there has been a significant amount of Red Mangrove growth along the toe of the levee. Boca Prieta has not opened since the completion of the project and the interior drainage is more dependant on the performance of the culvert structure to drain the interior flooded areas.

F. SALT WATER INTRUSION

Approximately four years after the completion of the flood control project it was noted that there were significant impacts to the Mandri Lagoon and the adjacent forest. Salinity data was gathered by the Department of Natural and Environmental Resources (DNER) in Puerto Rico and are shown on Figures 4, 5 and 6. That data indicates that the salinity levels have more than quadrupled within the Mandri Lagoon since the completion of the flood control project.

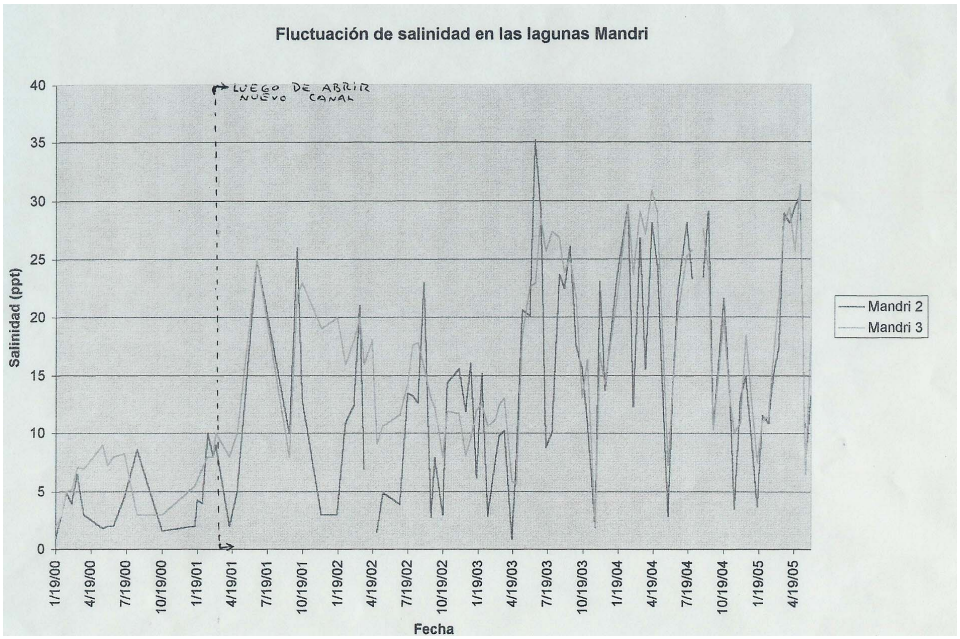

Figure 4

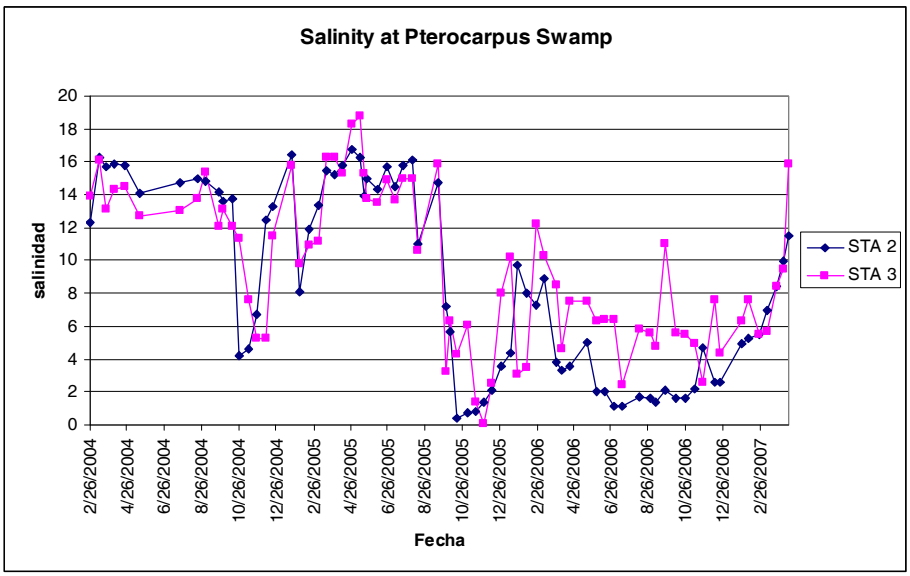

Figure 5

1. Environmental Impacts

The Mandri Lagoon is about 2 meter deep and has a surface area of about 1,237 acres. Historically, the lagoon had low salinity levels, which promoted the growth of Black and White Mangroves, However, due to the much higher salinity levels there has been a significant amount of Red Mangroves that have grown along the edges of the lagoon. The increase of this type of mangrove is consistent with the data shown and as a result there has been a decrease in the white and black mangroves.

It was determined that the cause of the increase in salinity levels in the lagoon were due to the increased capacity of the diversion channel, which were built much larger than originally anticipated. Due to the fill requirement for the levee construction the bottom width of the diversion channel was increased to approximately 24.4 meters, which is approximately four times larger than the originally proposed channel. Additionally, the channel dredged 1 to 2 meters deeper than the invert elevations at the Mandri Lagoon and Rio Anton outlet. Therefore, it was determined that the increased capacity of the diversion channel would allow significantly more water to flow through Rio Anton Ruiz outlet and into Mandri Lagoon. The channel velocities were such that sedimentation would only occur during a limited amount of time throughout the tidal cycle and according to the on-site DNER staff, the Rio Anton Ruiz outlet at the sea had not closed since before the project in 2001.

Additionally, the saltwater intrusion had an adverse effect on a 1400 acre forest, which has about 650 acres of Pterocarpus trees along the Rio Anton Ruiz channel. It was apparent that since the Rio Anton Ruiz outlet had been open for extended periods of time the saltwater had flowed 1,000 to 1,500 meters inland, which was well within the limits of the freshwater forested swamp. Additionally prior to the constructed flood control project, it was personally noted that in 1998 shortly after Hurricane Georges, the Rio Anton Ruiz outlet had not opened but the Boca Prieta outlet was opened due to the storm water runoff from Mandri Lagoon draining to the Caribbean Sea through the Boca Prieta outlet.

2. Salt Water Intrusion Measures (SWIM)

Comparing the data with the areas affected by saltwater it was determined that two SWIM plugs would be better than one for several reasons. The main reason for installing two plugs was the Mandri Lagoon did not have many Pterocarpus trees but did have a vast amount of mangroves. The Rio Anton Ruiz River had a significant amount of Pterocarpus trees that were affected by the saltwater intrusion. These SWIM plugs were temporary measures and additional salinity monitoring would be required to determine the best permanent measure by installing two plugs both system would be independent of each other. Figure 6 shows the locations of the SWIM plugs and the two primary salinity monitoring sites (Mandri 2 and Mandri 3).



Figure 5

The elevations of the plugs were based on closest NOAA tide gage, which was located at Roosevelt Roads approximately 6 km from the site. The elevations of the plugs were set to Mean Low Water (MLW) for several reasons. Based on the historic data there was no desire to completely eliminate the saltwater, only to limit saltwater intrusion to a level of near 5 parts per thousand (ppt). Also DNER staff needed to navigate to the salinity gages, thus the would have to push their small boats over the plug sites.

3. Performance of the Salt Water Intrusion Measures (SWIM) Plugs

The temporary SWIM plugs were installed at the end of March 2007. They were constructed of high-density polyethylene bags that were armored with riprap on upstream and downstream sides to resist damage during storm discharges. The bags have a high tensile strength and could be used for bridging, which facilitated the construction process and as a result the work was completed within a two week time period. These plugs are also durable and UV resistant.

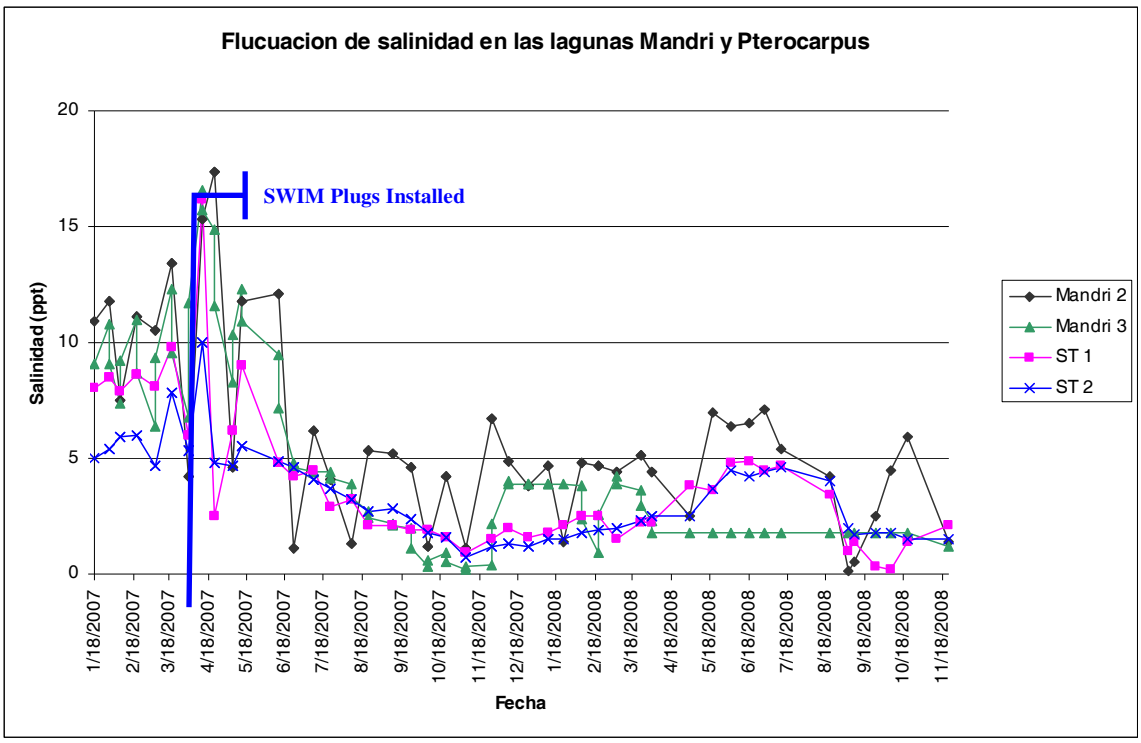

Figure 6

Figure 6 shows the data from the salinity gages in the lagoon and the Rio Anton Ruiz River. The data shows that the salinity levels are much lower now and that could be attributed to the plugs and rainfall. However, it is uncertain as to how well the Pterocarpus trees will respond to the decrease in saltwater.

G. CONCLUSION

It is envisioned that if the SWIM plugs can maintain salinity levels well below 5 ppt then the temporary SWIM plugs may soon developed into a permanent measure. However, if the salinity is such that the levels are reduced enough to promote a reforestation of the Pterocarpus trees, then the height of the SWIM plugs may need to be raised to a point where no saltwater will be permitted at the boundaries of the Pterocarpus forest.

There is a level of uncertainty associated with the data gathered to date because it does not describe the conditions of the Rio Anton Ruiz outlet at the Caribbean Sea. Some of the data has shown that the outlet may have closed since the construction of the plug but it is not noted within the data. It was anticipated that all of the information will be compared to local rain gages that are near the project in order to help develop a better correlation and understanding the physical conditions that affect the Rio Anton Ruiz outlet. However, if there is little to no data on conditions of this outlet, then it will only increase the securitization of the correlations derived from available data.

As a lesson learned from this project, the tools to analyze the potential effects over excavating the diversion channel were developed but not readily available. Additionally, we do not always see some potential project flaws due to the need to help others in an immediate manner and as a result it could cause irrevocable damage to the environment in which we live. In this case, we hope that we have sufficiently stopped the saltwater intrusion into the Pterocarpus forest but it may take a long time until the Pterocarpus trees grows back to the level that existed before the flood control project.

H. ACKNOWLEDGEMENT

We would like to acknowledge Nelson Colon for providing biological expertise. Also Jimmy Matthews P.E. for providing technical assistance the design and installation of the SWIM measures and V. Danuskodi P.E., Ph. D. for hydrological analysis to develop the proposed project. Finally, the Project Manager, Cynthia Perez and DNER for making this project happen in an expedited manner.

I. REFERENCES

Hydrologic Engineering Center. 1990. "HEC-1 Flood Hydrograph Package – User's Manual," U.S. Army Corps of Engineers Hydrologic Engineering Center, Davis California.

Hydrologic Engineering Center. 1991. "HEC-2 Water Surface Profiles – User's Manual," U.S. Army Corps of Engineers Hydrologic Engineering Center, Davis California.

Hydrologic Engineering Center. 1993. "HEC-6 Scour and Depositions in Rivers and Reservoirs – User's Manual," U.S. Army Corps of Engineers Hydrologic Engineering Center, Davis California.

Hydrologic Engineering Center. 2002. "HEC-River Analysis System – User's Manual," version 3.1, U.S. Army Corps of Engineers Hydrologic Engineering Center, Davis California.

Jacksonville District. 2007. "Rio Anton Ruiz at Humacao, Puerto Rico OMRR&R Manual," U.S. Army Corps of Engineers, Jacksonville, Florida.

Jacksonville District. 1993. "Rio Anton Ruiz at Humacao, Puerto Rico Final Detailed Design and Environmental Assessment," U.S. Army Corps of Engineers, Jacksonville, Florida.

U.S. Army Corps of Engineers. 1991. "Engineering and Design – Hydraulic Design of Flood Control Channels," EM 1110-2-1601, U.S. Army Corps of Engineers, Washington D.C.

Estimating Groundwater Seepages to St. Lucie Estuary

Gour-Tsyh Yeh[1], Jae-Young Lee[2], Gordon Hu[3], and Detong Sun[4]

[1]Dept. Of Civil and Environ. Eng., University of Central Florida, Orlando, FL 32816
PH: (407) 823-2317 FAX: (407) 823-3315 Email: gyeh@mail.ucf.edu
[2]Dept. Of Civil and Environ. Eng., University of Central Florida, Orlando, FL 32816
PH: (407) 823-3019 FAX: (407) 823-3315 Email: jylee@mail.ucf.edu
[3]South Florida Water Management District, West Palm Beach, FL 3340
PH: (561) 682-6442 FAX: (561)682-6442 Email: ghu@sfwmd.gov
[4]South Florida Water Management District, West Palm Beach, FL 3340
PH: (561) 682-6442 FAX: (561)682-2242 Email: dsun@sfwmd.gov

Abstract

In this paper, four analytical models describing hydraulic interaction of stream-aquifer systems were applied to St Lucie Estuary (SLE) River Estuaries. These are analytical solutions for: (1) flow from a finite aquifer to a canal, (2) flow from an infinite aquifer to a canal, (3) the linearized Laplace system in a seepage surface, and (4) potential flow through stratified unconfined aquifers. Input data for analytical solutions were obtained from monitoring wells and river stages at seepage-meter sites. Four transects in the study area are available: Club Med, Harbour Ridge, Lutz/MacMillan, and Pendarvis Cove located in the St. Lucie River. The analytical models were first calibrated with seepage meter measurements and then used to estimate of groundwater discharges into St. Lucie River. From this process, analytical relationships between the seepage rate and river stages and/or groundwater tables were established to predict the seasonal and monthly variation in groundwater seepage into SLE. It was found the seepage rate estimations by analytical models agreed well with measured data for some cases but only fair for some other cases. This is not unexpected because analytical solutions have some inherently simplified assumptions, which may be more valid for some cases than the others. From analytical calculations, it is possible to predict approximate seepage rates in the study domain when the assumptions underlying these analytical models are valid. The finite and infinite aquifer models and the linearized Laplace method are good for sites Pendarvis Cove and Lutz/MacMillian, but fair for the other two sites. The stratified unconfined aquifer model gave similarly good agreements with measurements at three sites but poorly at the Club Med site. None of the analytical models presented here can fit the data at this site. To give better estimates at all sites numerical modeling that couple river hydraulics and groundwater flow involving less simplifications of and assumptions for the system may have to be adapted.

1 Introduction

In order to manage the freshwater inflows to the St. Lucie estuary (SLE) more effectively for the benefit of the ecosystem, it is necessary to quantify the influence of freshwater inflow on salinity and other conditions. Past studies indicated groundwater seepage into the SLE is a significant part of freshwater inflow into the system. The quantity of groundwater seepage needs to be put into consideration for water management and ecosystem protection.

During dry seasons or a drought, groundwater input to the estuary is a more significant part of the total freshwater inflow in terms of percentage. Therefore it is a critical parameter for system operation and water reservation during dry seasons or a drought. An accurate quantification of the groundwater input to the system will also lead to more cost effective planning and project design as well as system operation.

The amount of groundwater seepage to the estuary has been the focus of several studies. Seepage meters were deployed to take measurements of groundwater seepage rate. A salinity model was used to "back calculate" the amount of groundwater seepage into the system during a dry period (Morris, 1987). The results of these studies vary and some were not sufficiently documented.

In recent years, South Florida Water Management District (SFWMD) staff has conducted field measurements at several locations in the St. Lucie Estuary and the Indian River Lagoon (IRL). The preliminary analysis has generated valuable information about the process and an estimate of the average seepage rate into the system. It is necessary to continue the analysis of the dataset obtained and use the information to predict the seasonal changes in groundwater seepage into the system.

In this paper, groundwater seepage into the St Lucie Estuary (SLE) was estimated with four analytical models using data obtained by SFWMD. Input data for analytical solutions were obtained from monitoring wells and stream stages at seepage-meter sites. Four transect sites in the study area are available: Club Med, Harbour Ridge, Lutz/MacMillan, and Pendarvis Cove located in the St. Lucie River. Analytical models were first calibrated with seepage meter measurements and then used to estimate of groundwater discharges into the St. Lucie River. Input data included aquifer properties, groundwater levels, and river stages in the study area. From this process, analytical relationships between the seepage rate and groundwater table or stream stage as time series data were established to predict the seasonal and monthly variation in groundwater seepage into the SLE.

2 Description of Four Analytical Models

Analytical solutions to the groundwater flow equation were used to derive hydraulic relationship of stream-aquifer systems with assumptions and simplifications. These solutions analyze subsurface drainage process based on aquifer properties and predict responses of aquifers to various stream stages. In this paper, four analytical solutions describing hydraulic interaction of stream-aquifer systems were applied to SLE system. The analytical solutions presented here are: Model No. 1 - flow from a finite aquifer to a river, Model No. 2 - flow from an infinite aquifer to a river, Model No 3 - 2D linearized solution for a seepage surface, Model No 4 - Potential flow

through stratified unconfined aquifers, and Model No 5 - flow through stratified confined aquifers.

Model No 1 - Transient Flow to Canal from Finite Unconfined Aquifers. Figure 1 depicts unsteady flows to a constant level river from finite unconfined horizontal aquifers. The approximating governing equation for the one-dimensional unconfined aquifers is

$$\frac{S_y}{K\hbar}\frac{\partial h^2}{\partial t} = \frac{\partial^2 h^2}{\partial x^2} \tag{1}$$

where S_y is the specific yield of the aquifer, K is the hydraulic conductivity of the aquifer [L/T], $\hbar$ could be h_o for small time t and could be $(h_r + h_o)/2$ for large time t [L], t is the time [T], h is the water table [L], and x is the distance from the river [L].

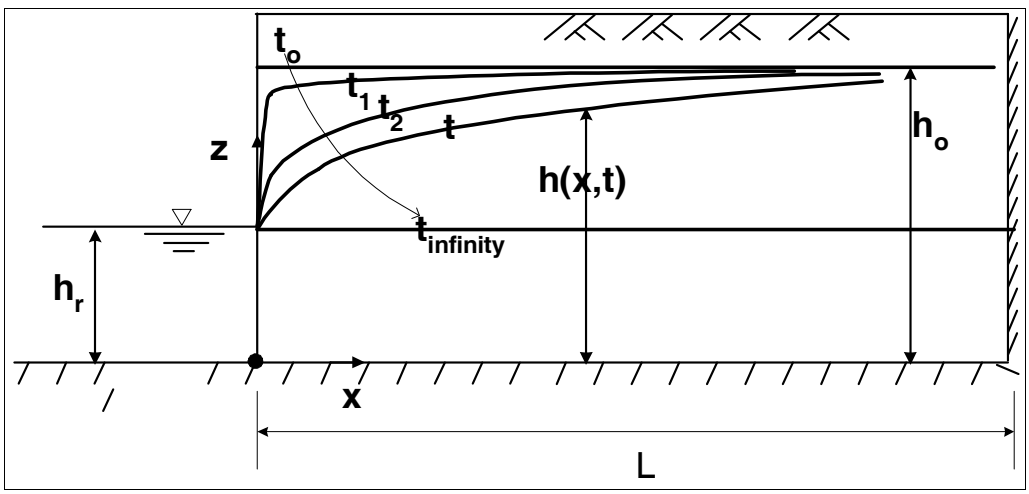

Figure 1 Finite Unconfined Horizontal Aquifer Problems

The initial and boundary conditions for the problem are specified as follows

$$h(x,0) = h_o;\ \ h(0,t) = h_r;\ \ -Kh(L,t)\frac{\partial h(L,t)}{\partial x} = 0 \tag{2}$$

where h_o is the initial water table [L], h_r is the river elevation [L], and L is the width of the aquifer [L]. Steady state condition in the aquifer after infinite time is $h(x,\infty) = h_r$.

The solution for the head h and the aquifer discharge U are:

$$h^2 = h_r^{\,2} + \frac{4(h_o^{\,2} - h_r^2)}{\pi}\sum_{n=1,3,5,\ldots}\frac{1}{n}\sin(\frac{n\pi x}{2L})e^{-\frac{n^2\pi^2\alpha^2}{4L^2}t} \tag{3}$$

and

$$U = -\frac{2(h_o^2 - h_r^2)}{L} K \sum_{n=1,3,5,\ldots} e^{-\frac{n^2\pi^2\alpha^2}{4L^2}t} \tag{4}$$

where $\alpha^2 = \hbar K / S_y$ in which S_y is the specified yield. Equation (4) is valid only when h_r are constant. The well head can be taken as the initial head, $h_o = h_{well}$ if the well is located far away from the river and its head is not affected by the river head.

Model No 2 - Transient Flow to River from Infinite Unconfined Aquifers. The governing equation and initial and boundary conditions are the same as for Model No 1, except for that the boundary condition at $x = L$ should be replaced by

$$h(\infty, t) = h_o \tag{5}$$

The solution for the head h and the aquifer discharge U for this problem are

$$h^2 = h_r^2 + \left(h_o^2 - h_r^2\right) erf\left(\frac{x}{2\alpha\sqrt{t}}\right) \tag{6}$$

and

$$U = -K\left(h_o^2 - h_r^2\right)\frac{1}{\alpha\sqrt{\pi t}} \tag{7}$$

where $\alpha^2 = \hbar K / S_y$ which S_y is the specified yield. As in Model No 1, the initial head can be taken as the well head, i.e., $h_o = h_{well}$, when the well is located far away from the river such that its head is not affected by the river head.

Model No 3 – Two-Dimensional Linearized Model for Seepage Surface. Transient drainage of an aquifer underlying a horizontal impervious layer can be described by the Laplace equation in saturated flow theory (Szilagyi, 2003). Figure 2 depicts the flow system in a two-dimensional domain. The governing equation for this two-dimensional flow in a saturated porous medium was described by the Laplace equation (Van de Giesen et al., 1994)

$$\frac{\partial^2 H(x,z,t)}{\partial x^2} + \frac{\partial^2 H(x,z,t)}{\partial z^2} = 0 \tag{8}$$

where H is the total hydraulic head, x and z are the horizontal and vertical coordinates, and t is time. The above equation is subjected to the following initial and boundary conditions:

$$H(x,z,0) = h_o;\ \ H(0,z,t) = h_r,\ \text{t} > 0;\ \ \frac{\partial H(x,0,t)}{\partial z} = 0;\ \ \frac{\partial H(L,z,t)}{\partial x} = 0 \tag{9}$$

$H(x,z,t) = z = h(x,t)$ at the free furace

where L is the aquifer width, h_o is the initial flat equilibrium water level in the river and in the aquifer, h_r is the value to which the initial water level in the river falls instantaneously (Fig. 2), and h is the phreatic surface, a function of distance from the river and of time as described by the following equation:

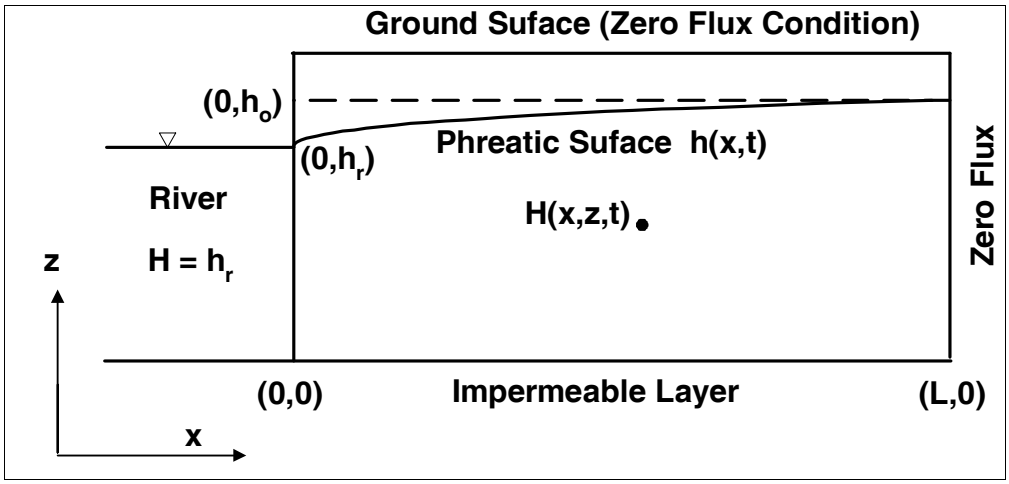

Figure 2 The River-Aquifer System with Full Penetration

$$f\frac{\partial h}{\partial t} = K_s\left(\frac{\partial H}{\partial x}\frac{\partial h}{\partial x} - \frac{\partial H}{\partial z}\right)\Bigg|_{z=h(x,t)} \tag{10}$$

where f is the drainable porosity or specific yield of the aquifer and K_s is the saturated hydraulic conductivity, both assumed to be constant in time. The Laplace equation, Eq. (8), can be solved analytically (Van de Giesen et al., 1994) if Equation (10) is linearized, which implies that the changes in the phreatic surface elevation are small compared to the characteristic depth(h_r), of the saturated zone, then the boundary condition on the phreatic surface is given by the following linear partial differential equation

$$f\frac{\partial h}{\partial t} = -K_s\frac{\partial h}{\partial z} \tag{11}$$

The aquifer discharge, U, to the river ($x = 0$) in the problem is defined by the following equation,

$$U(t) = -\frac{4(h_o - h_r)k_{sat}}{\pi}\sum_{n=1,3,5,\ldots}^{\infty}\frac{1}{n}\tanh\left(\frac{n\pi h_r}{L}\right)\cdot\exp\left(-\frac{K_s}{f}\tanh\left(\frac{n\pi h_r}{L}\right)\frac{n\pi}{L}t\right) \tag{12}$$

which contains parameters: K_s, f, L, h_r ,and h_o, where h_o is initial head that can be taken as the well head, i.e., $h_o = h_{well}$, if the well is located far way from the river

and its head is not affected by the river head. Equation (12) describes aquifer drainage for a fully penetrating river when both h_o and h_r are constant.

Model No 4 - Potential Flow through Stratified Unconfined Aquifers. Analytical models are available for conditions where hydraulic parameters change in the vertical direction, but remain uniform along the horizontal plane. These models provide an alternative that is sometimes useful compared to the general reliance on numerical simulation models such as MODFLOW (McDonald and Harbough, 1988), FEMWATER (Yeh, 1999) and FEWA (Yeh, 1999), WASH123D (Yeh et al., 2006), etc. Figure 3 shows the cross-section forflow in a stratified unconfined aquifer.

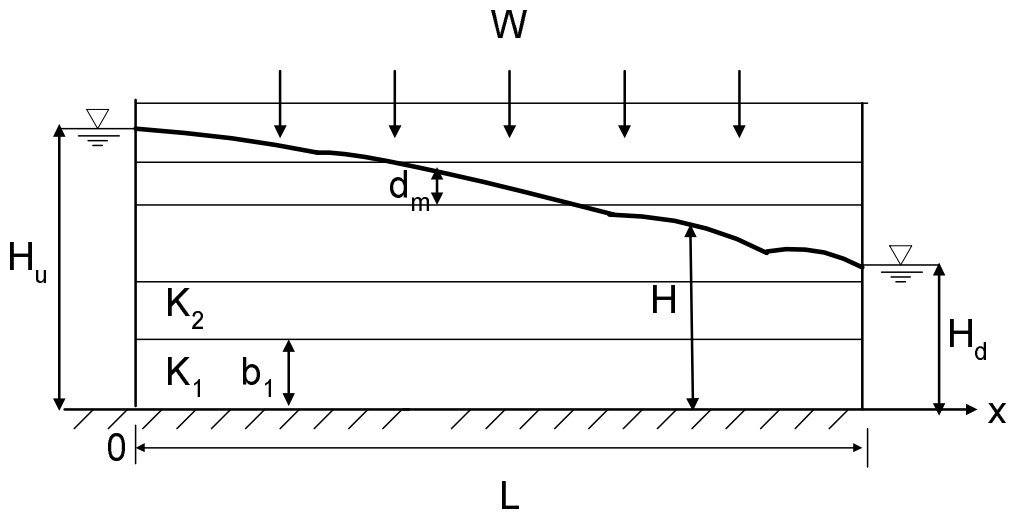

Figure 3 Steady State Flow in Stratified Unconfined Aquifers

Girinskii (1946) has shown that so long as the flow is essentially horizontal, then a potential function can be defined for stratified aquifers which generalize the saturated thickness used for homogeneous unconfined aquifers (also see Bear, 1972). The primary assumption is that the energy losses associated with vertical flow are negligible, which implies that the Dupuit-Forchheimer assumptions apply. For our present purposes, a potential function is one whose gradient gives the aquifer flux. This potential function was defined by Girinskii (1946) and thus is called Girinskii potential function Φ

$$\Phi = \int_0^H (H - z) K(z) dz \tag{13}$$

The continuity equation for flow in stratified unconfined aquifers subject to rainfall rate W is given in terms of the Girinskii potential function as

$$\frac{d^2\Phi}{dx^2} + W = 0 \tag{14}$$

The boundary conditions for the given system are specified as follows

$$\Phi = \Phi_u \text{ at } x = 0 \text{ and } \Phi = \Phi_d \text{ at } x = L \tag{15}$$

in which Φ_u and Φ_d are related to H_u and H_d, respectively, through Equation (13).

The analytical solution of the system described by Equations (14) and (15), is given as follows

$$\Phi(x) = \Phi_u + \left(\Phi_u - \Phi_d\right)\frac{x}{L} + \frac{Wx}{2}\left(L - x\right) \tag{16}$$

The aquifer flux is given by

$$U(x) = -\frac{d\Phi}{dx} = \frac{\left(\Phi_u - \Phi_d\right)}{L} - \frac{WL}{2} + Wx \tag{17}$$

so that

$$U_u = \frac{\left(\Phi_u - \Phi_d\right)}{L} - \frac{WL}{2} \quad \text{and} \quad U_d = \frac{\left(\Phi_u - \Phi_d\right)}{L} + \frac{WL}{2} \tag{18}$$

Equation (18) provides a working equation to calculate seepage rates given the aquifer information (K_1, b_1, K_2, b_2, .., K_n, b_n), upstream and downstream boundary conditions H_d and H_u, and the rainfall rate, W. Given a H, Equation (13) is integrated to yield the following working equation for calculating Φ

$$\begin{aligned}\Phi = H\left(\sum_{i=1}^{m-1} K_i b_i + K_m d_m\right) - \frac{b_1^2}{2}\left(K_1 - K_2\right) - \frac{\left(b_1 + b_2\right)^2}{2}\left(K_2 - K_3\right) - \ldots \\ - \frac{\left(b_1 + b_2 + \ldots + b_{m-1}\right)^2}{2}\left(K_{m-1} - K_m\right) - \frac{K_m H^2}{2}\end{aligned} \tag{19}$$

3 Estimation of Seepage Rate into SLE

The hydrologic data for seepage measurement site was prepared to calculate groundwater seepage by analytical solutions mentioned in Section 1. Four sites of seepage measurement in the St. Lucie River were located as shown in Figure 4 (SLLT: Lutz/MacMillian, SLPD: Pendarvis Cove, SLHR: Harbour Ridge, SLCM: Club Med). The required hydrologic data include monitoring river stage and well stage data. Available 2002-2004 time series data were used to match seepage measurements for the 2002-2003 period for the calibration at monitoring sites. In addition, hydraulic conductivity data for study area were prepared to input analytical solution. To simplify, hydraulic conductivity data was normalized by Box-Cox transformation method over St. Lucie and Martin County.

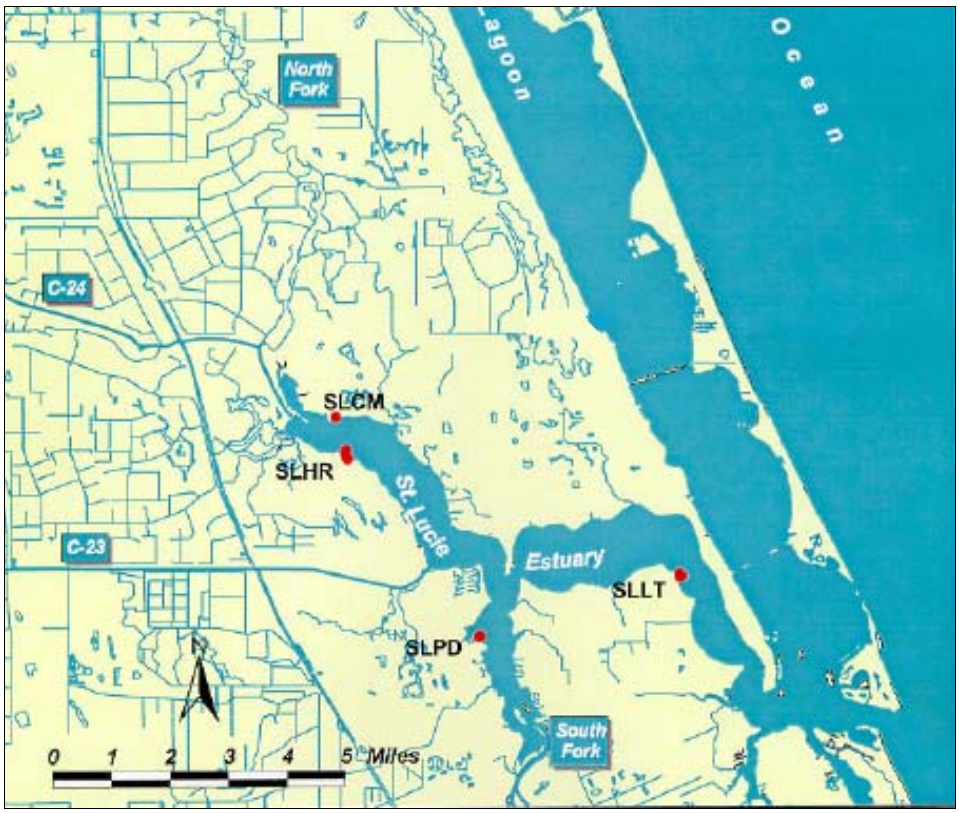

Figure 4 Location of the Seepage Measurement

On every monitoring site, seepage rates (cm/sec) were estimated based on river stage, water table, and/or recharge rate using four analytical models. The daily seepage rate into the SLE were calculated and compared with mean transect seepage for monitoring sites (Belanger et. al. 1998) having several stations of seepage meter. The gaging daily data of corresponding sites have missing or incorrect data. Therefore we selected data period that has available river stage and well stage data in the study domain (DBHYDRO, SFWMD). The stream stage and groundwater table data during 08/01/2002 – 09/25/2004 were used as input to analytical models.

Four analytical models are applied to St. Lucie River watershed to estimate seepage rates using hydrologic and aquifer data from the database (Morris, 1987). Calibrated aquifer parameters of the study area, used in four analytical models, are shown in Table 1.

For the finite aquifer (Model No 1) and the 2D linearized solution model (Model No. 3), the daily water level from the monitoring well is used as an initial condition, h_o . The boundary condition was specified by the river stage, h_r .. The other boundary condition is flux equal to zero at a distance L far away from the river. This distance can be estimated using $L = 1.5\sqrt{\frac{0.5K(h_r + h_{well})t_d}{S_y}}$, where K is the hydraulic conductivity, S_y is the specific yield, and t_d is the duration time of simulations.

Table 1 Calibrated parameters used in analytical models

Parameters	Monitoring sites and available values			
	SLPD	SLLT	SLCM	SLHR
Hydraulic conductivity (K_h : ft/day)	0.3 – 1200.0	0.08 - 520.0	0.001 – 6.0	0.002 – 16.0
Storativity (s)	0.0009	0.0009	0.0001-0.0003	0.0001-0.0003
Specific yield (s_y)	0.20	0.10	0.10	0.20
Thickness of Aquifer (b : ft)	11.0	16.0	11.0	11.0
Width of Finite Aquifer (L : ft)	71 – 85	50 – 80	8 - 13	1 – 2
Width of Stratified Aquifer (L' : ft)	10	267	229	772
Amplitude (η) for the wave propagation model (ft)	2.0	2.0	1.5	1.5
Leakage Rate (W : ft/day)	0.00778	0.00639	0.0	0.0

In the semi-infinite aquifer (Model No 3), water level at the monitoring well is adopted as the initial conditions, h_o. Water level at the gage station in the river, h_r, was specified as boundary condition.

For the stratified unconfined aquifer model (Model No. 4), the measurement head at the monitoring well was used as upstream boundary condition, H_u. The water stage at the gage station in the river was used as downstream boundary condition, H_d. The aquifer with, L, is the distance between the gage station in the river and monitoring well in the aquifer. From MODFLOW input data, the river channel depth is very shallow compared to total aquifer thickness. Therefore, the aquifer information such as hydraulic conductivity has uniform distribution along the vertical direction. The leakage rate data was obtained from recharge data in the MODFLOW input data set.

The estimated seepage rates by four analytical solutions were presented for four sites in Figures 5 through 20. In all figures, the positive values denote seepage from aquifers to the river while the negative values denote discharge from the river to aquifers.

For the Pendarvis Cove site, the seepage rates computed by the finite aquifer model ranged from -1.853×10^{-4} cm/sec to 3.202×10^{-4} cm/day (Figure 5). The seepage for semi-infinite aquifer was obtained from -2.345×10^{-4} cm/sec to 4.053×10^{-4} cm/sec (Figures 9). The seepage rates computed by 2D linearization ranged from -1.637×10^{-4} cm/sec to 3.809×10^{-4} cm/sec (Figure 13). The result of stratified unconfined and confined aquifer ranged from -2.507×10^{-4} cm/sec to 3.564×10^{-4} cm/sec and from -3.618×10^{-4} cm/sec to 5.829×10^{-4} cm/sec (Figure 17) Each of the four analytical model results was compared with the measurement data from seepage meter sites. These figures show that all analytic models have a good agreement with seepage measurement data during the study period.

At the Lutz/Mac Millian site, the finite and infinite aquifer models calculated the seepage rates ranging from -2.067×10^{-5} to 5.494×10^{-4} cm/sec and from -2.616×10^{-5} cm/sec to 6.954×10^{-5} cm/sec, respectively (Figures 6 and 10, respectively). The 2D linearization results ranged from -3.894×10^{-5} cm/sec to 2.214×10^{-4} cm/sec (Figure 14). The seepage rates for stratified unconfined problem give result of -8.580×10^{-6} to 8.866×10^{-5} cm/sec (Figure 18). All four models yielded reasonably good agreements with observation seepage flux measured.

For the Club Med site, the finite and infinite aquifer models generated seepage ranges of -1.840×10^{-8} to 1.103×10^{-5} cm/sec and -2.388×10^{-7} cm/sec to 1.509×10^{-5}, respectively (Figures 7 and 11, respectively). In addition, The 2D linearization method rendered seepage rates of -1.238×10^{-7} to 7.211×10^{-6} cm/sec (Figure 15). The seepage rate for stratified unconfined aquifer was obtained -1.582×10^{-7} to 1.063×10^{-5} cm/sec (Figure 19). None of the models can reproduce the measurement data to within a reasonably accuracy.

In the Harbour Ridge site, the finite aquifer model, semi-infinite aquifer model, 2D linearization method, and stratified unconfined models computed seepage rates in the range of 5.355×10^{-6} to 1.806×10^{-5} cm/sec, 4.792×10^{-6} to 1.617×10^{-5}, 4.809×10^{-6} to 1.523×10^{-5} cm/sec, and 2.282×10^{-6} to 8.924×10^{-6} cm/sec, respectively (Figures 8, 12, 16, and 20, respectively). The stratified model gave good agreements with the measurements at this site except for one data point. All other models performed poorly. It is also noted that all models predict only seepages (i.e. without recharge) in this most upstream site

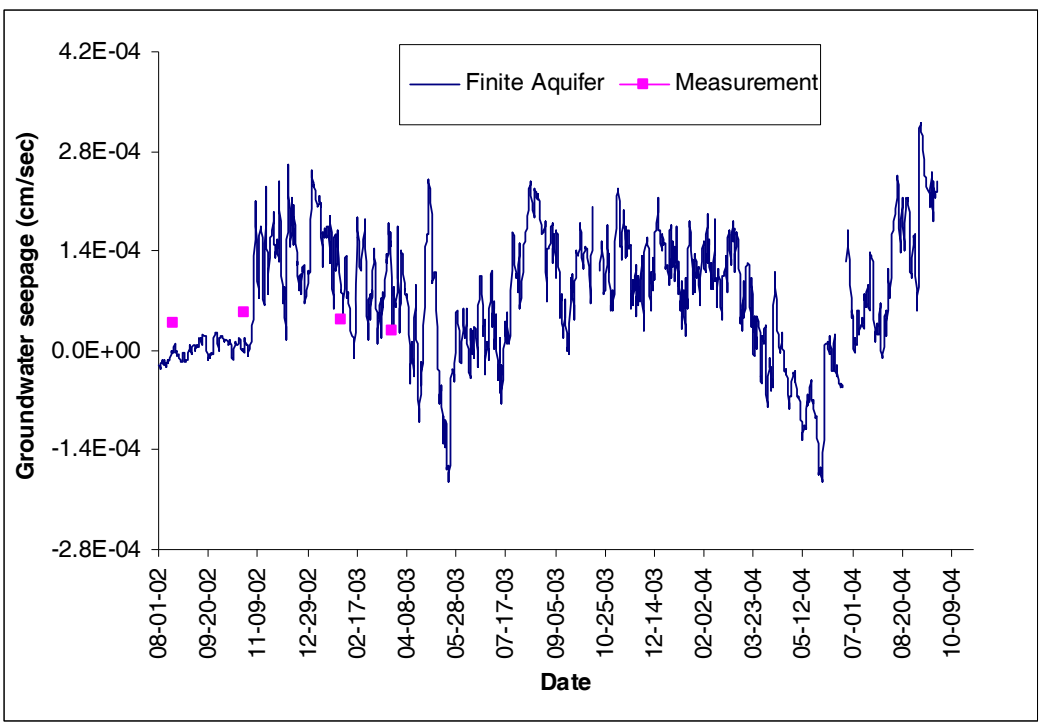

Figure 5 Seepage rates using the Finite Aquifer Model in Pendarvis Cove site

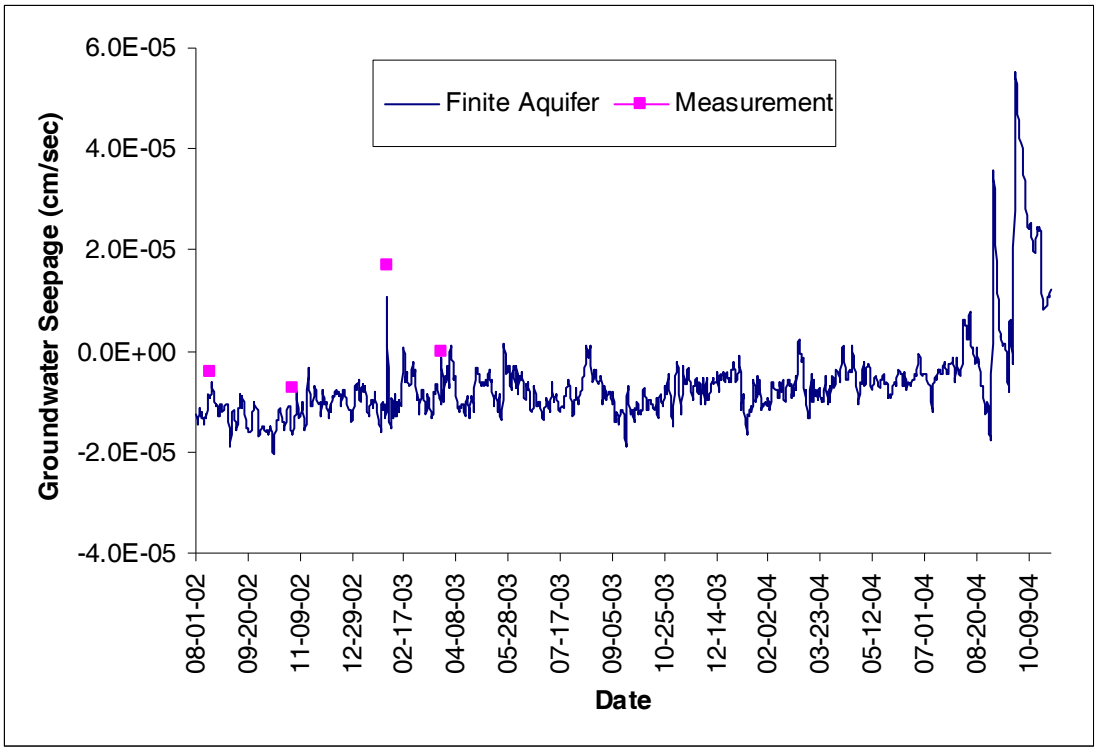

Figure 6 Seepage rates using the Finite Aquifer Model in Lutz/MacMillian site

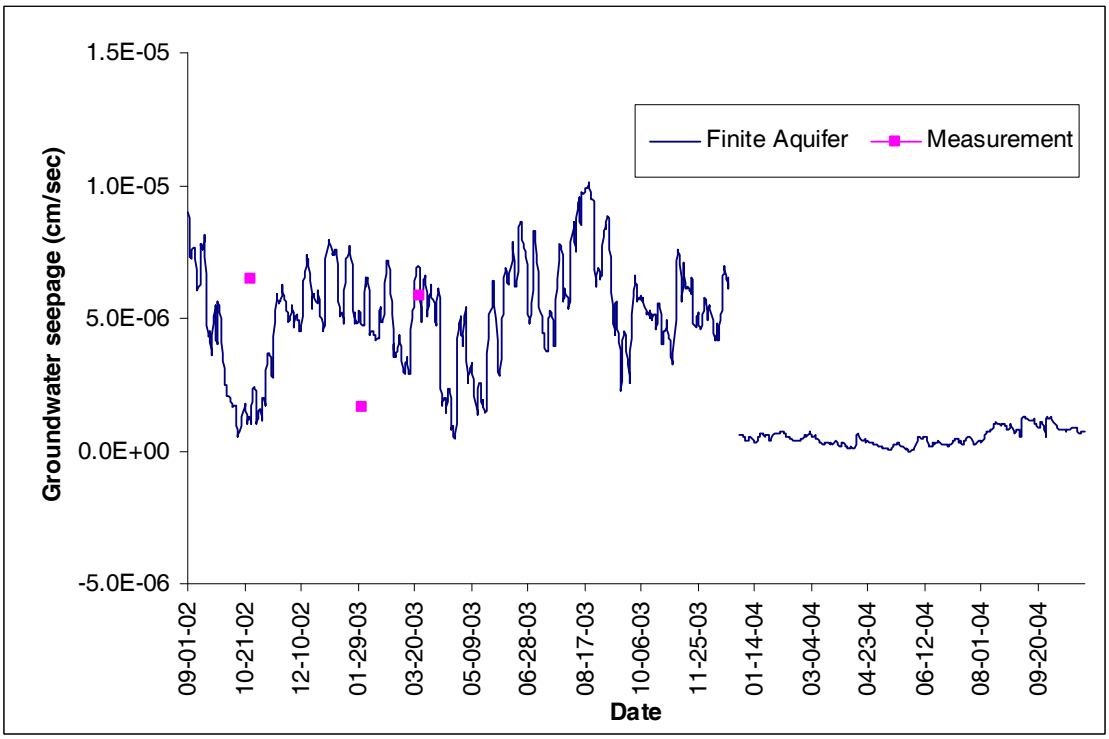

Figure 7 Seepage rates using the Finite Aquifer Model in Club Med site

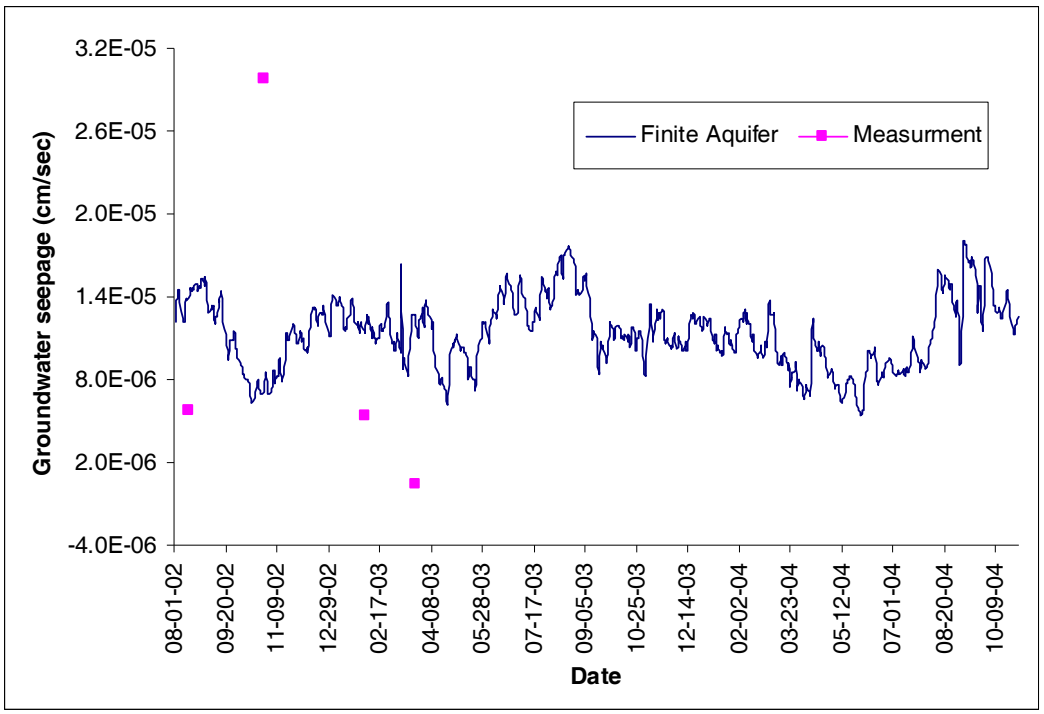

Figure 8 Seepage rates using the Finite Aquifer Model in Harbour Ridge site

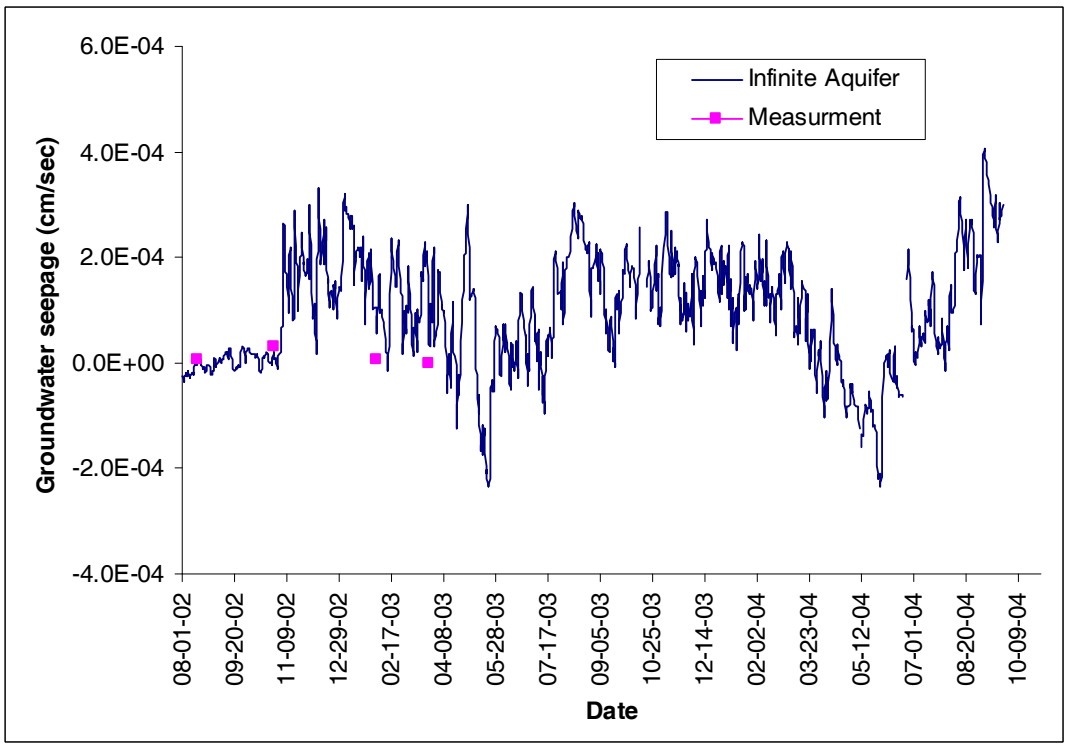

Figure 9 Seepage rates using Infinite Aquifer Model in Pendarvis Cove site

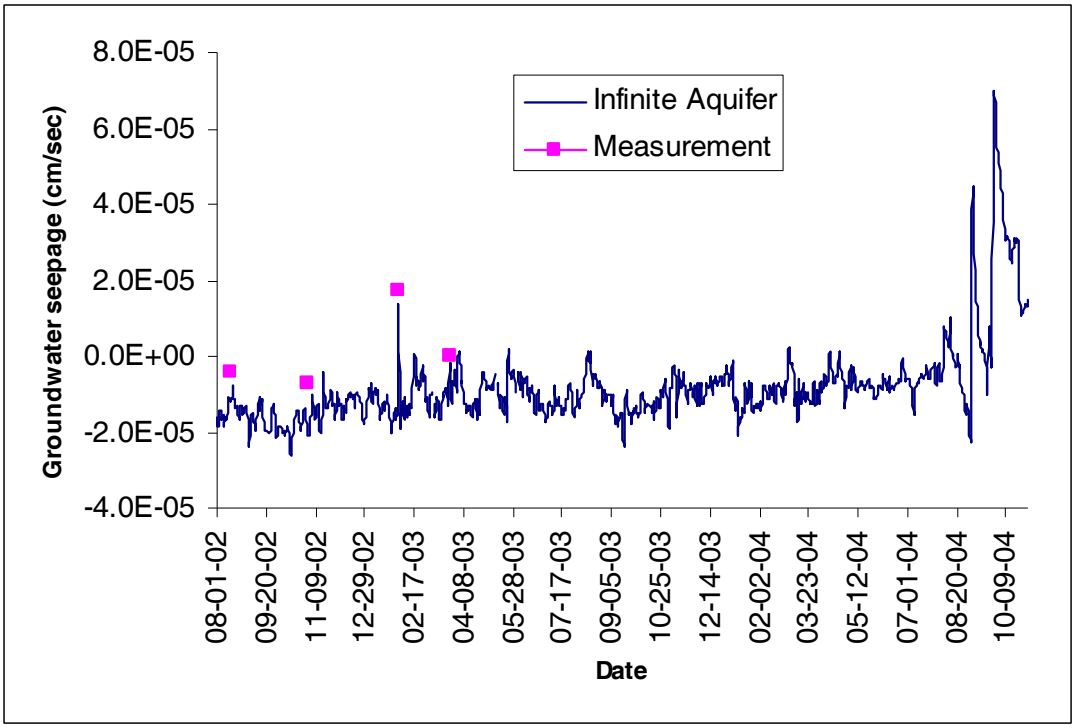

Figure 10 Seepage rates using Infinite Aquifer Model in Lutz/MacMillian site

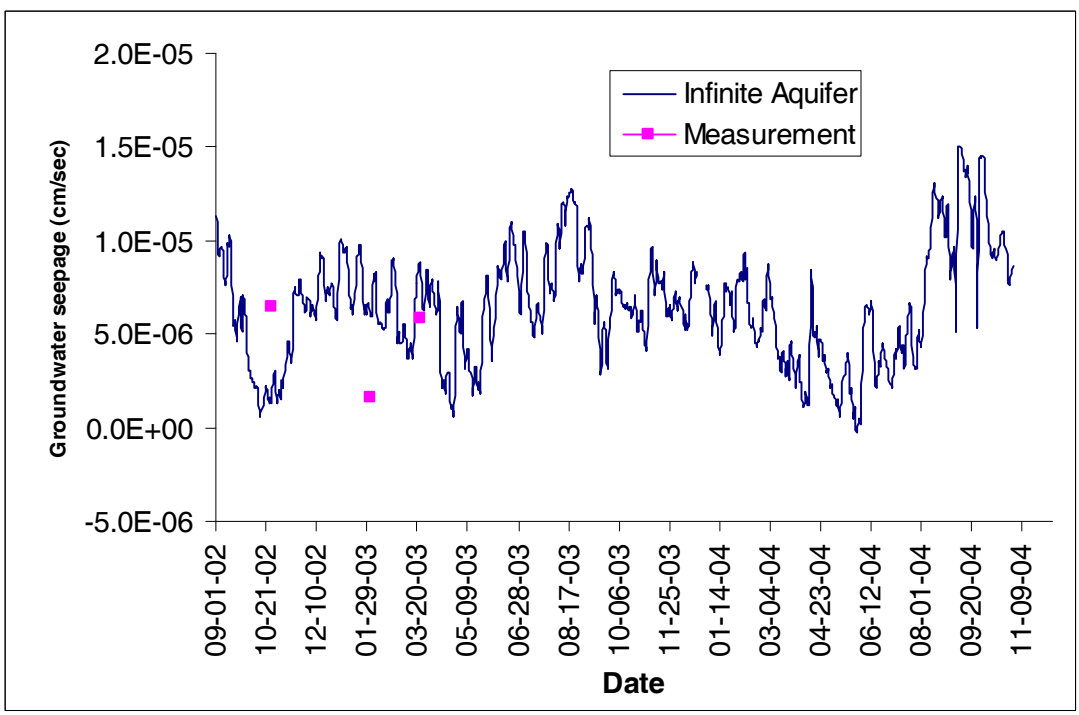

Figure 11 Seepage rates using Infinite Aquifer Model in Club Med site

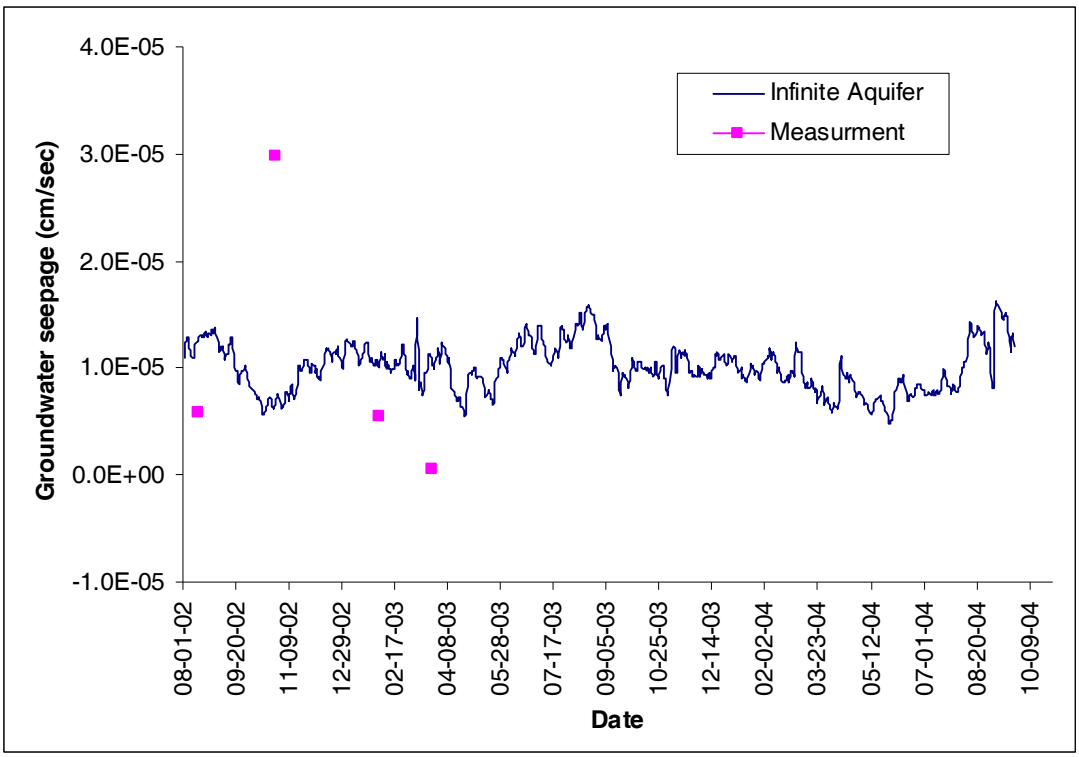

Figure 12 Seepage rates using Infinite Aquifer Model in Harbour Ridge site

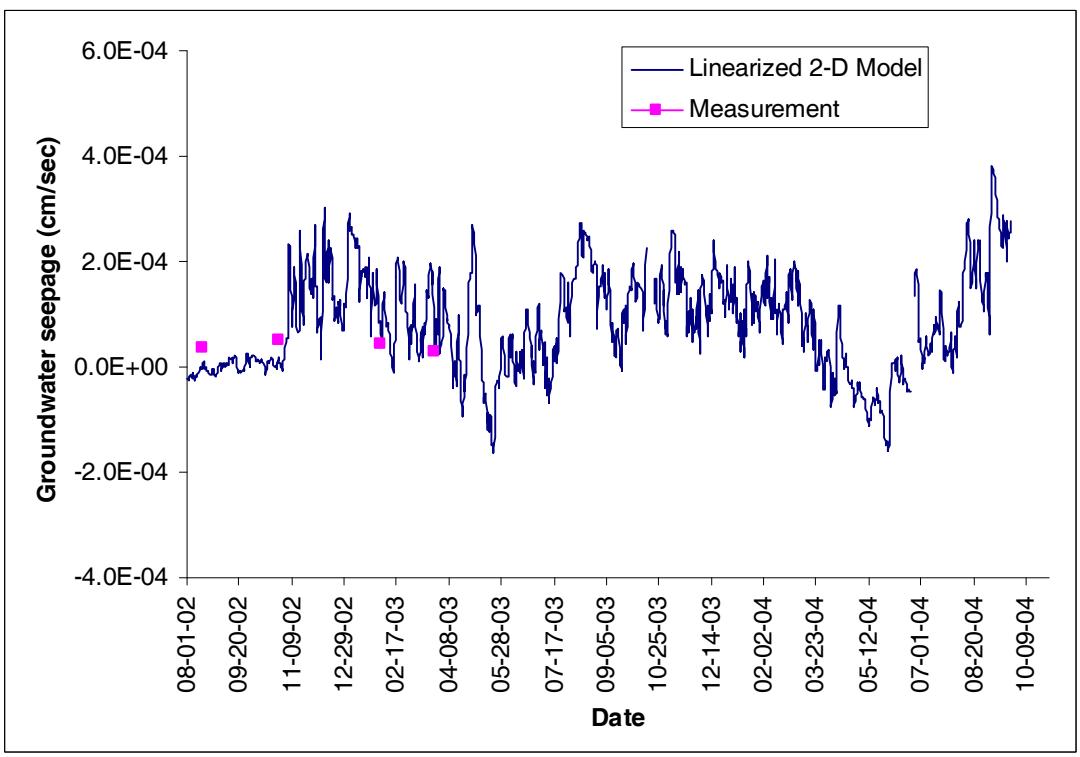

Figure 13 Seepage rates using the Linearized 2D Model in Pendarvis Cove site

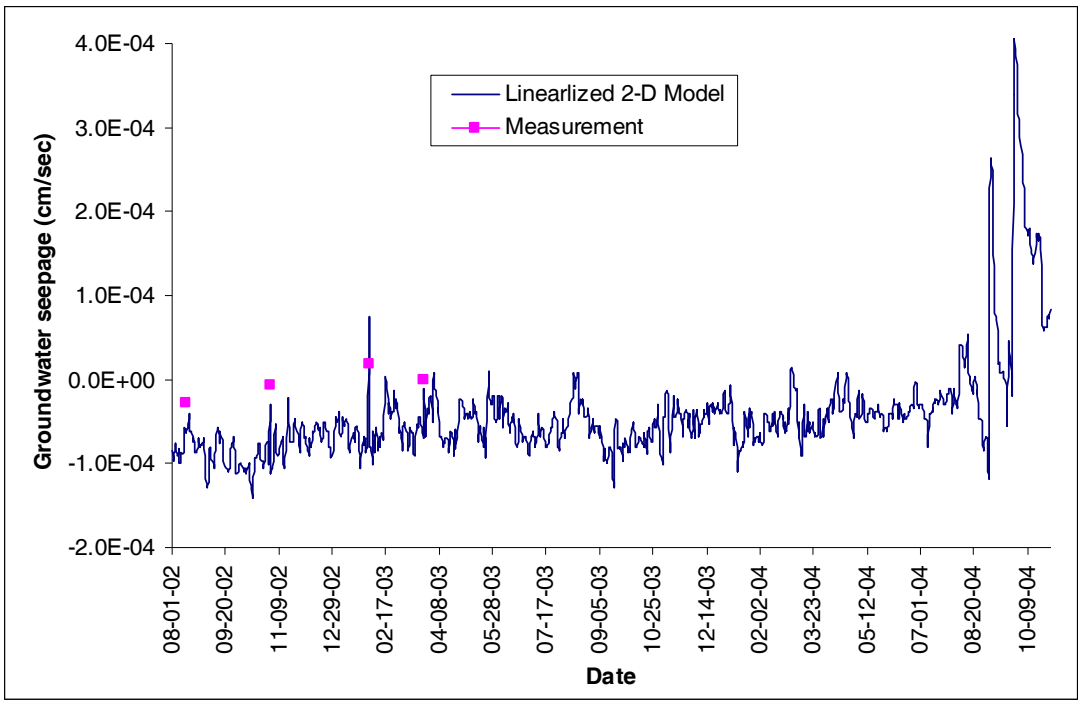

Figure 14 Seepage rates using the Linearized 2D Model in Lutz/MacMillian

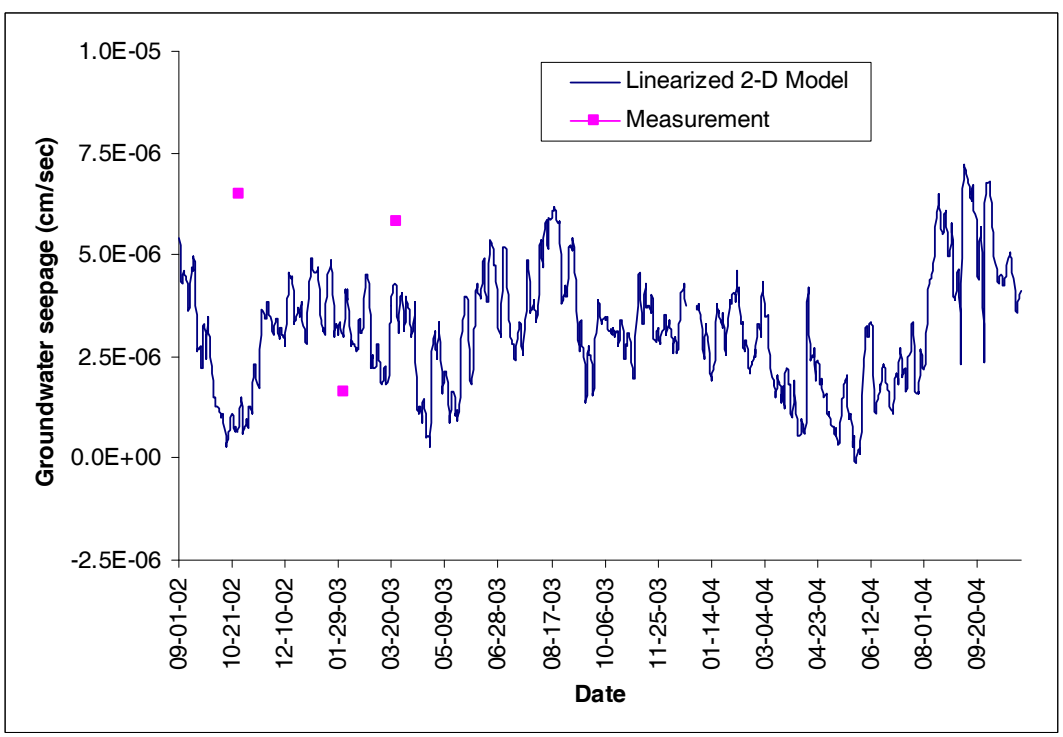

Figure 15 Seepage rates using the Linearized 2D Model in Club Med site

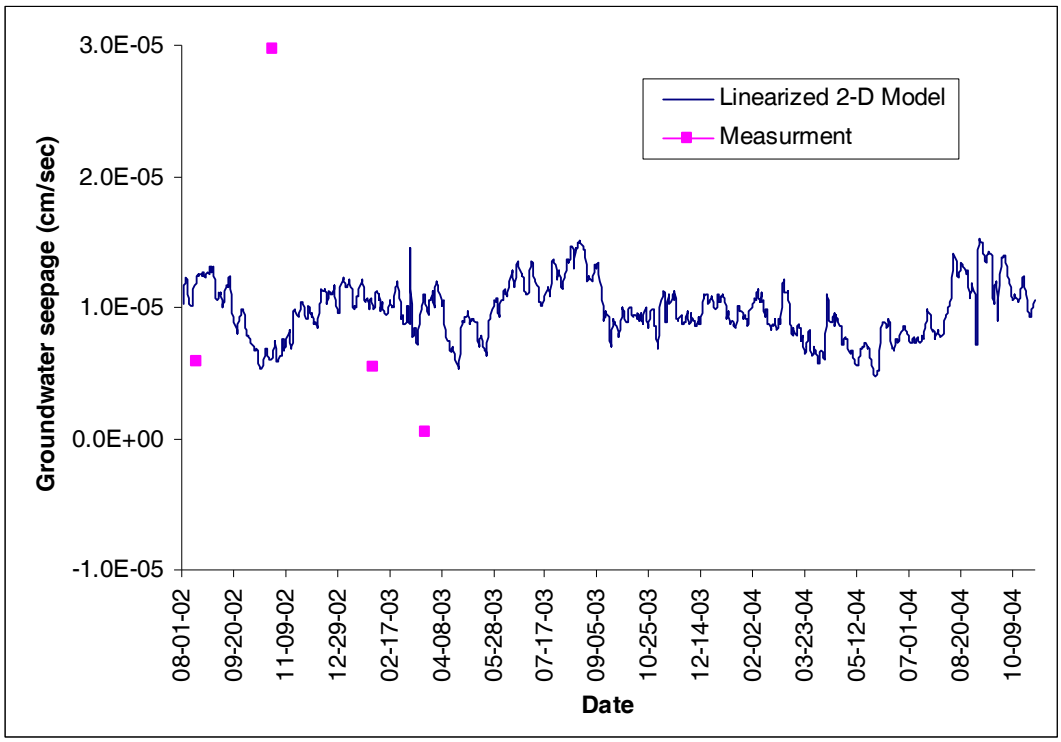

Figure 16 Seepage rates using the Linearized 2D Model in Harbour Ridge site

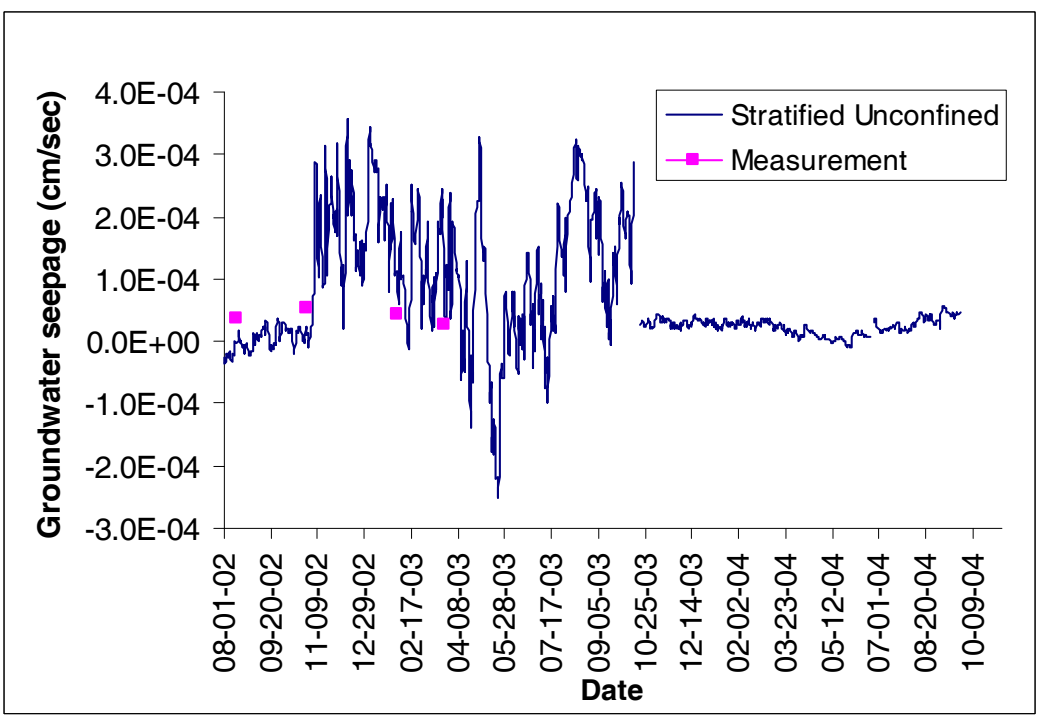

Figure 17 Seepage rates using the Stratified Model in Pendarvis Cove site

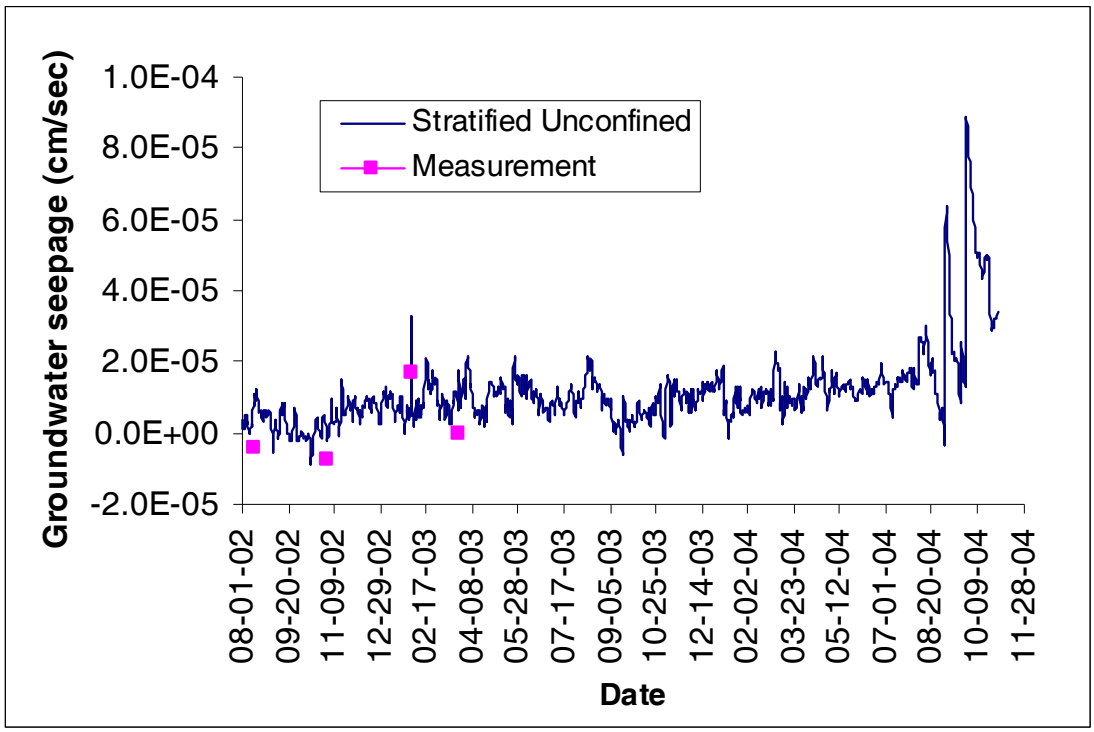

Figure 18 Seepage rates using the Stratified Model in Lutz/MacMillian

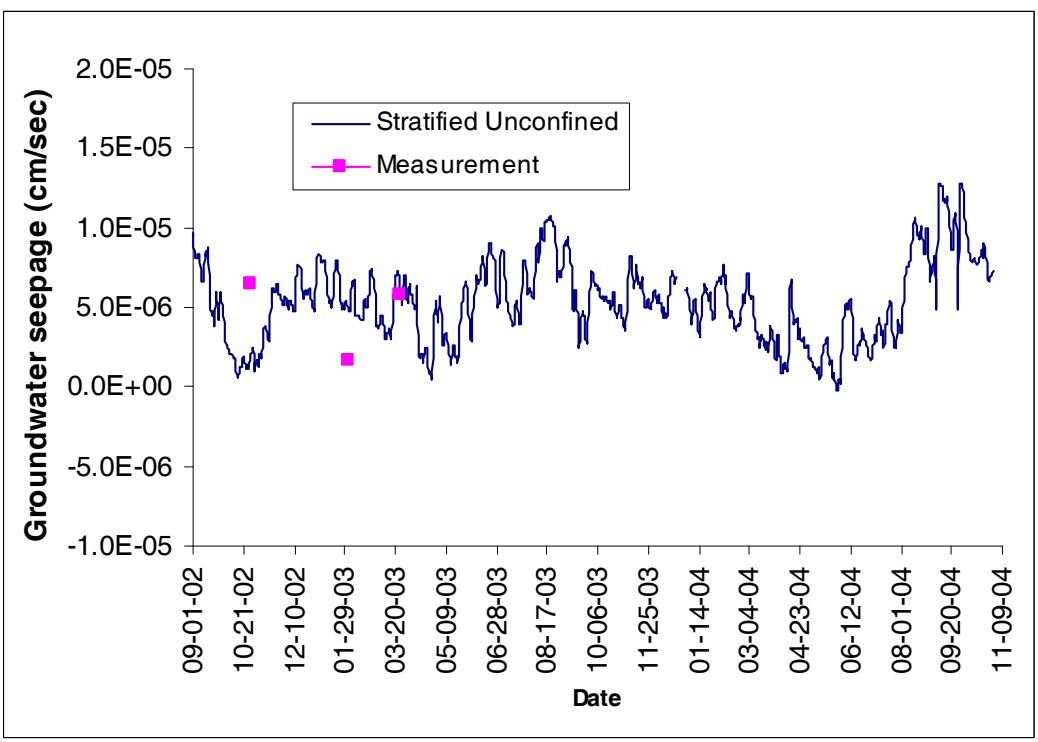

Figure 19 Seepage rates using the Stratified Model in Club Med site

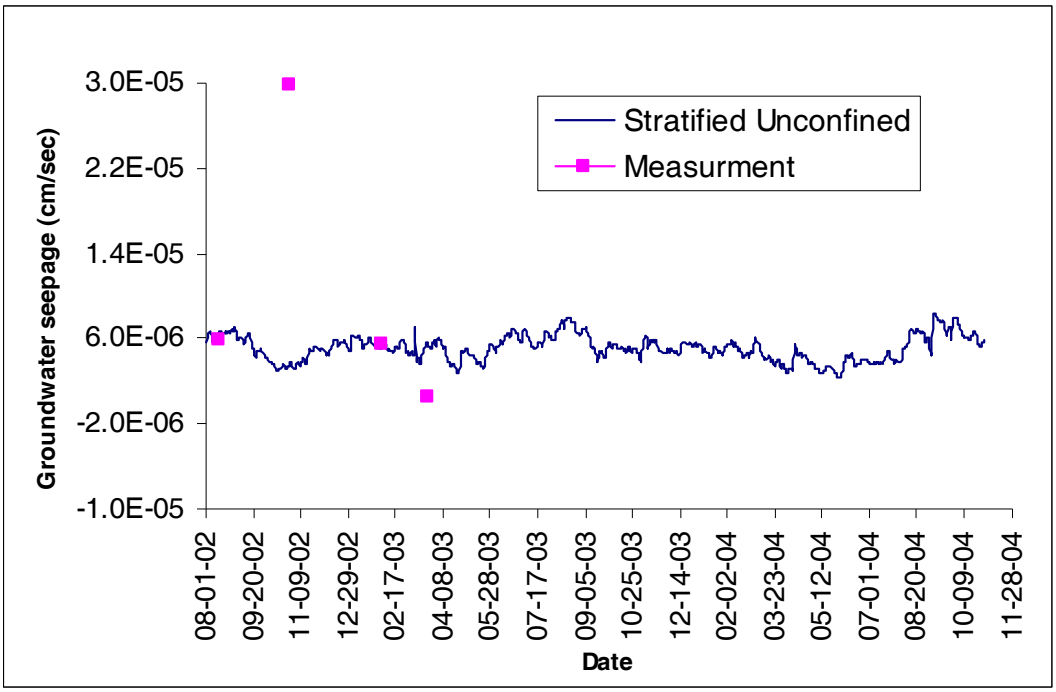

Figure 20 Seepage rates using the Stratified Model in Harbour Ridge site

4 Evaluations of Analytical Modeling of Seepages

From Section 3, it was found the seepage rates estimation by analytical models agreed well with measured data for some cases but only fair for some other cases. This is not unexpected because analytical solutions have some inherently simplified assumptions, which may be more valid for some cases than the others. From Figures 5 through 20, it is seen that the finite and infinite aquifer models and the 2D Linearization method are good for sites Pendarvis Cove and Lutz/MacMillian, but fair for the other two sites. The stratified unconfined model gave good agreements with measurements at three sites but poorly at the Harbour Ridge site. None of the analytical models presented here can fit the data at this site. It is possible to predict approximate seepage rates or seepage amount in the study domain using the analytical models when the assumptions underlying these models are valid.

Acknowledge

Research is supported by South Florida Water Management District under Contract PO # 4500022934 and 4500030897 with University of Central Florida.

References

Bear, J., Dynamics of Fluids in Porous Media, Elsevier, New York, 1972.

Belanger, T. V. and Heck, H. H., Gefvert, C. and Krupa, S., Seepage meter program for St. Lucie River and Indian River Lagoon. *South Florida Water Management District. C-11835*, 2003.

Girinskii, N. K., 1946. Generalization of Some Solutions for Wells to More Complicated Natural Conditions (in Russian). Dokl. A. N. United States S. R. No. 3, 54, 1946.

McDonald, J. M. and A. W. Harbaugh, 1988. A Modular Three-Dimensional Finite Difference Groundwater Flow Model. Techniques of Water Resources Investigations of the United States Geological Survey, Book 6, 586 p., 1988.

Morris, F. R., 1987. Modeling of hydrodynamics and salinity in the St. Lucie Estuary. South Florida Water Management District, Technical Publication 87.

Szilagyi, J. S., Sensitivity Analysis of Aquifer Parameter Estimations based on the Laplace Equation with Linearized Boundary Conditions, *Water Resources Research,* Vol.39, No.6, 1156, 2003.

Van de Giesen, N.C., Parlange, J.Y., and Steenhuis, T.S., Transient Flow to Open Drain: Comparison of Linearized Solutions with and without the Dupuit Assumption. *Water Resources Research,* Vol.30, No.11, 3033-3039, 1994.

Yeh, G. T., 1999. Computational Subsurface Hydrology Fluid Flows. Kluwer Academic Publishers. 277 pages.

Yeh, G. T., G. Husng, H. P. Cheng, F. Zhang, H. C. Lin, E. Edris, and D. Richards, 2005. A First principle, Physics based Watershed Model: WASH123D. Chapter 9 in Watershed Models (V. P. Singh and D. K. Frevert, ed.), CRC Press LLC, 6000 Broken Sound Parkway, NW, (Suite 300) Boca Raton, FL 33487, USA. pp. 211-244.

Analytical-Numerical Solution for Seepage along an Earth Canal Disconnected from the Shallow Aquifer

Yi Liu[1] **and Zhuping Sheng**[1]

[1]Texas AgriLife Research and Extension Center at El Paso, Texas A&M University System, 1380 A&M Circle, El Paso, TX 79927; PH (915) 859-9111; Fax (915) 859-1078; email: yiliu@ag.tamu.edu; z-sheng@tamu.edu

ABSTRACT

To have a better understanding of seepage from the canal beds, authors developed a new infiltration method to analyze seepage beneath canal beds during ponding tests. This is distinct from Green-Ampt method for infiltration on a uniform unsaturated zone and with a constant head in a ponding area. An analytical-numerical equation was derived to represent the seepage flow based on Darcy's law and Romos' method. Five ponding tests conducted on the selected sections of Franklin Canal in El Paso, Texas were analyzed using the proposed methods. The comparison between analytical solution and other ponding test observation indicated that analytical-numerical solution gives a good approximation of seepage losses. The annual canal seepage losses vary spatially depending on hydraulic conditions in the canal, ranging from 86,245~299,467 m^3/km for low flow in the canal, to 177,184~564,875 m^3/km for high flow, which provide a great potential for water conservation.

INTRODUCTION

Ponding test is one of field methods to identify canal seepage loss (Rohwer and Stout, 1948; Warnick, 1951; Worstell, 1976; Kuo, 1982; Sheng et al., 2003; Alam and Bhutta, 2004; Kahlown and Kemper, 2004; Leigh and Fipps, 2004a, 2004b). Vedernikov (1934) derived a first closed-form solution to the problem of seepage form canals of various shapes with water table at infinite depth. Muskat (1946), Polubarinova-Kochina (1962), and Harr (1962) studied seepage losses by using mathematical analysis for triangular and trapezoidal canals. Bouwer (1978) presented solution for canal seepage for various depths and shapes of the canals and of positions of groundwater table in three types of soil conditions: high hydraulic conductivity; low hydraulic conductivity; and the hydraulic conductivity in which the thin layer of sediment below the canal is much lower than the underlying soil. Jeppson (1968) presented a solution for seepage from channels through layered porous mediums by using the method of finite differences. He considered the layers with different permeability and each layer is to be anisotropic condition with different ratios of horizontal to vertical permeability, but the interface between the two layers restricted to being horizontal. For transient seepage of canal, Collis-George and Smiles (1963) got a solution for a rectangular channel and Bouwer (1969) got a plot in terms of dimensionless factors A_w / W_s^2 and Kt / fW_s. The terms A_s, W_s, K, t, and f represent the wetted soil area, the width of the surface water, soil hydraulic conductivity, time and the fillable pore-space fraction of the soil, respectively.

The assumptions for each theoretical study above are: 1. soil behavior is homogeneous and isotropic; 2. ground water is infinitely deep; 3. flow is laminar, thus obey Darcy's law; 4. capillary fringes are negligible; 5. groundwater table is 100% saturated and above the table is 0% saturated; and 6. canal water depth is constant. It should be pointed out, however, that canal water head is usually free falling for ponding test (Sheng, 2003; Leigh and Fipps, 2004a, 2004b). Few theoretical solutions have been found for canal ponding tests with free falling head in literature. Even Green-Ampt (1911) equation also ignores the depth of surface water for infiltration. In this study, the authors presented a new method to assess seepage losses for a trapezoidal shaped canal based on Darcy's law and Romos' method. Five ponding tests conducted at four sites along the Franklin Canal in El Paso, Texas (Sheng et al., 2003) were used to demonstrate applications of the new method.

METHODOLODY

The trapezoidal shaped canal is shown in Figure 1. The canal bed soil with lower hydraulic conductivity K_1 is assumed to be saturated and the seepage flow through the saturated bed soil is assumed to be vertical during ponding test after the canal bed and side banks are wetted for over 48 hours (Sheng, et al, 2003). The wetting front is assumed to be fixed on the interface of the fine bed soil and its underlying sand layer. Let h_c represent the capillary pressure head on the wetting front; h_0 and $h(t)$ represent the initial and any time water depths, respectively, of the canal for the ponding test; b represents the width of the canal bed; d represents the thickness of the canal bed top soil with the lower hydraulic conductivity K_1. Water table is assumed to be deep enough without hydraulic connection with the canal. At the time t, the water volume change rate for a unit length of canal can be written as $(b + 2h/\tan(\alpha))dh/dt$; and the seepage rate through the canal bed and bank soil can be written as $-K_1(h + d - h_c)b/(b + 2h/\tan(\alpha))[1/d + 2\ln((h + d)/d)/\tan(\alpha)]$ based on Darcy's law. The above volume water change rate of the canal is equal to the seepage rate based on water mass balance, so we can have the free falling head rate of the canal as following

$$f \equiv \frac{dh}{dt} = -\frac{K_1(h + d - h_c)b}{b + 2h/\tan(\alpha)}\left[\frac{1}{d} + \frac{2\ln(1 + h/d)}{\tan(\alpha)}\right] \quad (1)$$

with $h(0) = h_0$. Equation (1) is one kind of initial value problem with an autonomous function of h. Ramos (2007) developed a non-standard explicit integration scheme for the initial-value problem. A numerical solution for equation (1) can be written as following based on Ramos (2007)

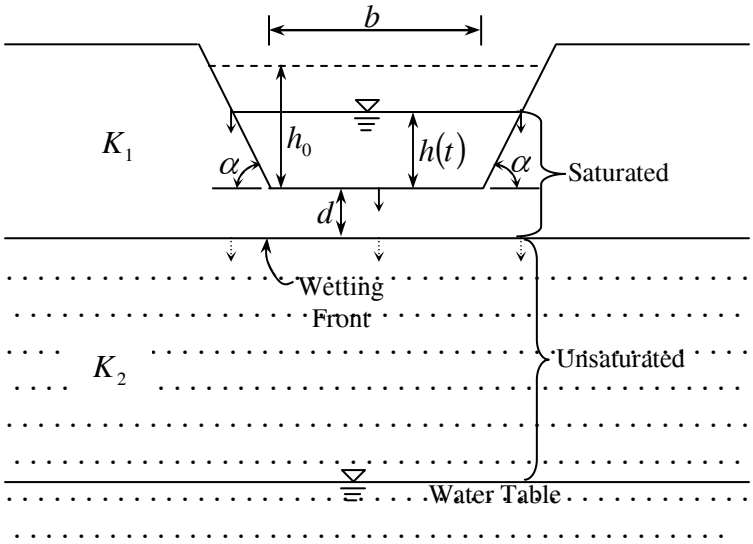

Figure 1. Geometry and symbols for trapezoidal cannels in soil underlain by permeable material: a. The top soil with lower hydraulic conductivity (K_1) below the cannel is homogeneous and underlain by material of much higher hydraulic conductivity (K_2); b. The water table is below the top of this permeable layer which acts as a drainage layer for seepage water.

$$h_{n+1} = h_n + \frac{2 f_n \Delta t}{2 - j_n \Delta t} \tag{2}$$

where h_n represents an approximation of $h(t_n)$ with $t_n = n\Delta t$, Δt is the time step size, and $j_n \equiv \partial f / \partial h(h_n)$. j can be obtained through the derivative of equation (1) with respect to h as following

$$j \equiv \frac{\partial f}{\partial h} = -K_1 \frac{(c_1 h + c_2)\ln(d+h) - 4bdh^2 + c_3 h + c_4}{4\tan(\alpha)h^3 + 4(d^2 + bd\tan\alpha)h^2 + c_5 h + b^2 d^2 \tan^2\alpha} \tag{3}$$

where $c_1 = 4bd^2 - (4bh_c + 2b^2\tan\alpha)d$;

$c_2 = 4bd^3 - (4bh_c + 2b^2\tan\alpha)d^2$;

$c_3 = [(2b^3\tan\alpha + 4bh_c)d - 4bd^2]\ln d - 4bd^2 + (4bh_c - 2b^2\tan\alpha + 2b\tan\alpha)d - 2bh_c\tan\alpha - b^2\tan^2\alpha$;

$c_4 = [(2b^2\tan\alpha + 4bh_c)d^2 - 4bd^3]\ln d + 2(1-b)bd^2\tan\alpha + [2(1-b)bh_c\tan\alpha - b^2\tan^2\alpha]d$; and

$c_5 = \tan\alpha(4d + b\tan\alpha)bd$.

When α is $\pi/2$, the canal shape becomes rectangular. For a rectangular canal, an analytic solution for equation (1) were obtained as following

$$h = (h_0 + d - h_c)e^{-\frac{K_1}{d}t} - d + h_c \tag{4}$$

Figure 2 shows the numerical free falling water depth solution in equation (2) with ponding time for a trapezoidal canal and the analytical solution in equation (4) for a rectangular canal. The good match between equations (4) and numerical results in Figure 3 for $\alpha = 90^\circ$ demonstrated that Ramos' numerical solution works very well.

From equation (1), the seepage rate per unit canal length, $F(h)$, for trapezoidal canals can be calculated using following equation (5):

$$F(h) = (b + 2h/\tan\alpha)\frac{dh}{dt} = -K_1(h + d - h_c)b\left[\frac{1}{d} + \frac{2\ln(1 + h/d)}{\tan(\alpha)}\right] \tag{5}$$

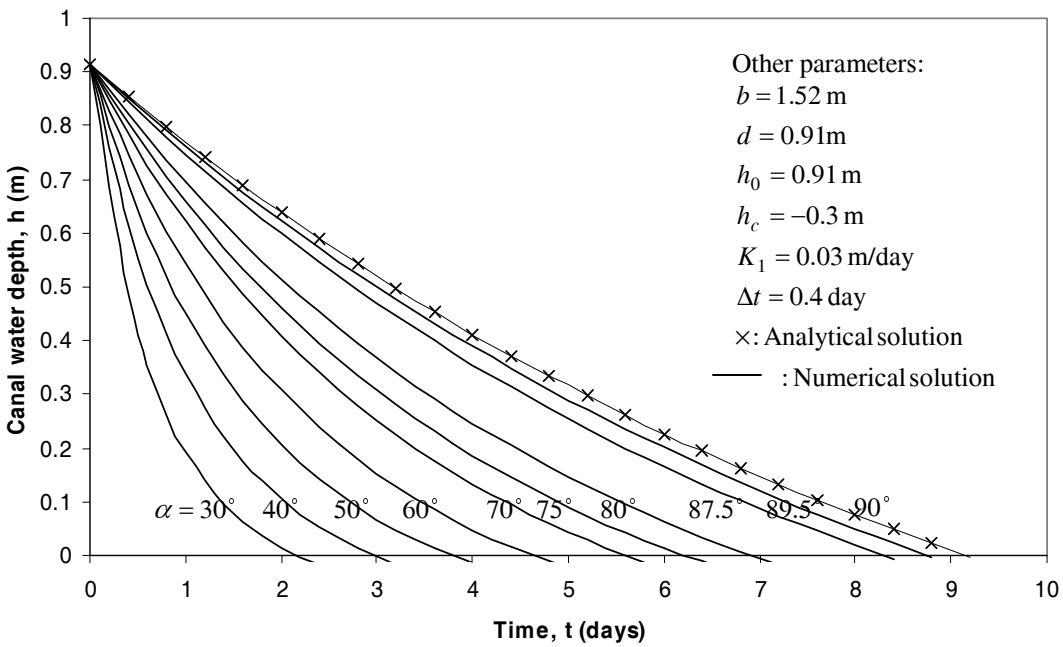

Figure 2. Free falling water depth with ponding time for a trapezoidal canal with different side bank slopes

PARAMETER ANAYSIS OF PONDING TESTS

Five ponding tests were conducted to determine seepage losses from Franklin Canal in the El Paso Country Water Improvement District No. 1, Texas (Sheng et al.,

2003). The top soil in El Paso farm land usually consists of clay or loam with a varying depth of 0.3 to 1 m. This fine top soil mantles the upper unconfined Rio Grande alluvium aquifer with a depth of up to 600 m consisting of fine- to medium-grained sand with interbedded lenses of clay, silt, gravel and caliche (Sheng and Devere, 2005). The canal bed and bank consist of the top soil with lower hydraulic conductivity. Groundwater table in our ponding test area is 15 to 37 m below land surface. The sand between the bottom of the canal bed soil and the water table can be considered to be unsaturated while the bed soil is saturated by seepage. The wetting front with a capillary pressure is assumed to be fixed on the interface of the fine bed soil and its underlying sand layer. This lower permeable canal bed soil controls the canal seepage.

In order to determine parameters that affect seepage losses the equation (2) is employed to inversely analyze ponding test data using parameter estimation software PEST (Doherty, 2002). The values of parameters, d, K_1, and h_c for five ponding tests along Franklin Canal were estimated. The canal bed soil thickness was found to be almost 0.3 m for Sites 1, 2, and 3, and almost 0.9 m for Site 4 (Table 1), respectively.

Table 1. Canal ponding parameter estimation results

Ponding location	Slope $(\tan\alpha)$	Bed width, b (m)	Initial water depth, h_0 (m)	PEST estimation			
				Bed soil thickness, d (m)	Hydraulic conductivity of the bed soil, K_1 (m/day)	Wetting front capillary pressure head, h_c (m)	Average matching error, %
Site 1	0.523	6.68	0.28	0.31	0.0122	-0.09	1.9
Site 2	0.450	3.96	0.36	0.31	0.0147	-0.10	10.4
Site 3 (1st)	0.662	9.72	0.64	0.30	0.00384	-0.08	0.1
Site 3 (2nd)			0.77	0.31	0.00451	-0.09	0.4
Site 4	0.710	10.12	0.39	0.88	0.020	-0.39	5.3

The average error (see Table 1) of the simulated canal water depth to its observed (see Figure 3) is 1.9 to 10.4%. The hydraulic conductivity of the canal bed soil was found to be 0.012, 0.015, 0.004, and 0.02 m/day for Sites 1, 2, 3, and 4, respectively. According to hydraulic conductivity value ranges from Green-Ampt infiltration for different kinds of soil (Rawls et al., 1983; Rawls et al., 1993), the canal bed soil may be categorized as silty clay at Sites 1 and 2, clay at Site 3, and sandy clay at Site 4, respectively. The lab value of the hydraulic conductivity for the underlying material-sandy loam or fine sand is in range of 2.3 to 9.4 m/day. The hydraulic conductivity value of the canal bed soil is 2 to 3 orders of magnitude less than its underlying sandy loam or fine sand material. The wetting front capillary pressure on the bottom of the thin canal bed soil was found to be almost -0.1 m for Sites 1, 2, and 3, and -0.4 m for Site 4, respectively. It means that there exists a vadose zone below the bottom of the saturated canal bed soil during ponding test.

This further proves that the canal bed fine soil layer controls the seepage of the canal water to its underlying phreatic aquifer when the canal is hydraulically disconnected with water table or ground water.

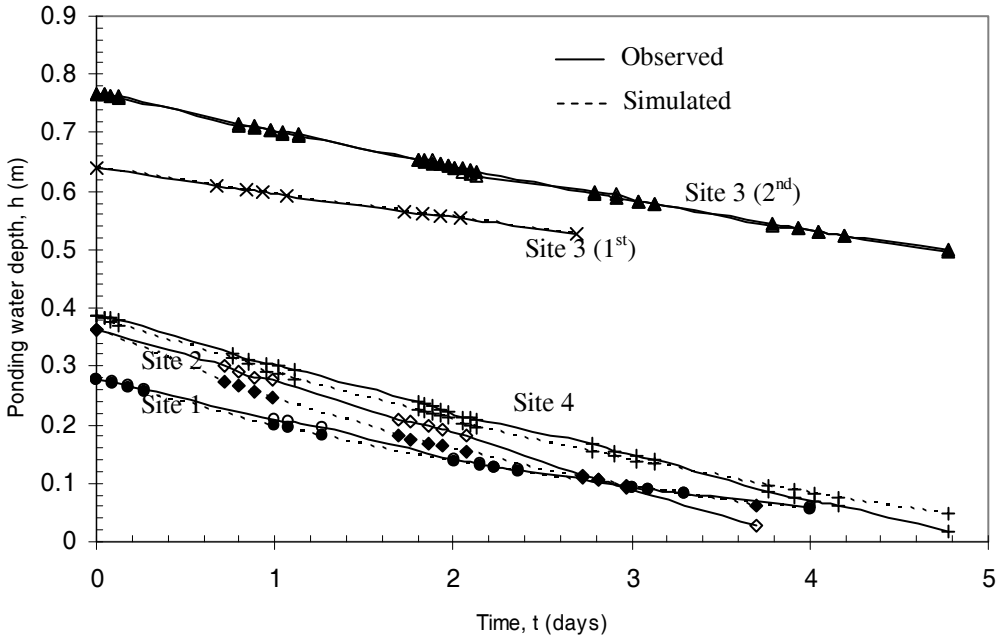

Figure 3. Observed ponding water depth compared to its simulated results along the Franklin Canal in El Paso, TX

POTENTIAL FOR WATER CONSERVATION

Once parameters are determined, one can use equation (5) to estimate seepage losses under different conditions. The Franklin Canal water seepage loss rate with canal water depth were estimated and shown in Figure 4. The seepage loss of the canal at Site 4 is the largest among the four sites because high hydraulic conductivity of its bed and its large bed width, while the seepage loss of the canal at Site 3 is the lowest because its low hydraulic conductivity. Lining canal to decrease canal bed material hydraulic conductivity is the first choice for improvement of water delivery efficiency (water savings or reduction in water diversions for a given level of surface water diversion, Sheng et al., 2003). The annual canal seepage losses vary spatially depending on hydraulic conditions in the canal, ranging from 86,245~299,467 m^3/km for 0.62-meter water depth in the canal, to 177,184~564,875 m^3/km for 1.23-meter water depth (Table 2). If we assume 80% of seepage losses as shown in Table 2 can be saved, then it is anticipated that approximately 451,900 m^3/km can be saved during the irrigation season if the canal is operated at a high capacity at site 4. On the other hand, if the canal is operated at a low water capacity, less water conservation potential of approximately 239,574 m^3/km is anticipated at site 4. At site 3, much lower water conservation potential is anticipated, ranging from 141,747 m^3/km for high flow and 68,996 m^3/km for low flow. Canal beds and hydrological condition in the canal control potential for water conservation.

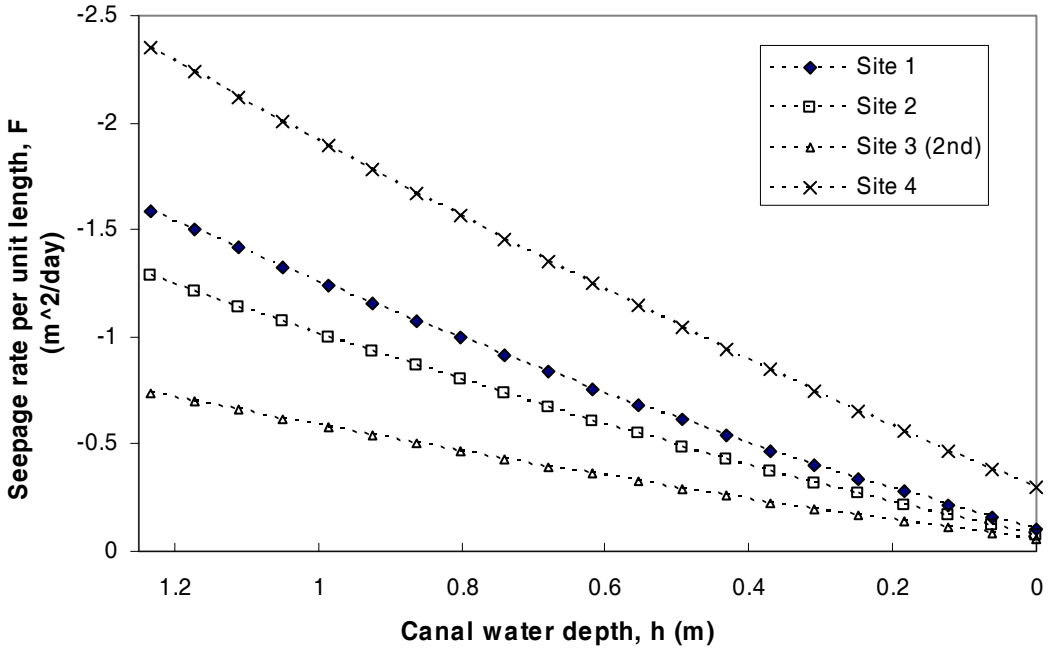

Figure 4. Canal seepage loss rate with canal water depth

Table 2. Canal seepage loss rate

Canal location	Canal water seepage loss rate			
	Canal water depth (m)			
	1.23		0.62	
	m^3/m/day	m^3/km /irrigation season	m^3/m/day	m^3/km /irrigation season
Site 1	1.6	381,333	0.8	182,388
Site 2	1.3	308,145	0.6	146,129
Site 3 (2nd)	0.7	177,184	0.4	86,245
Site 4	2.3	564,875	1.2	299,467

CONCLUSION

A conceptual model for trapezoidal canals in low permeable soil underlain by high permeable material is proposed. Water table is assumed to be deep enough without hydraulic connection with the canal. It is assumed in this model that seepage flow is vertical and laminar after the canal soil is wetted and saturated for over 48 hours.

A numerical solution presented in this paper can be used to determine values of canal bed soil parameters such as hydraulic conductivity, thickness and capillary pressure head on the wetting front from the ponding test. After the parameter values are obtained from ponding tests, an analytical solution is employed to calculate canal seepage loss with variable water depth in canal.

Five ponding tests at four sites along the Franklin Canal were analyzed by coupling the numerical solution for free falling water depth in canal with inverse

model PEST (Parameter Estimation). The hydraulic conductivity of the canal bed soil was found to be 0.012, 0.015, 0.004, and 0.02 m/day for Sites 1, 2, 3, and 4, respectively. The thickness of the bed soil was found to be almost 0.3 m for Sites 1, 2, and 3, and 0.9 m for Site 4. The wetting front capillary pressure head was found to be almost -0.1 m for Sites 1, 2, and 3, and -0.4 m for Site 4.

Franklin Canal seepage loss was evaluated for the four sites using obtained parameter values from the ponding tests. The annual canal seepage losses vary spatially depending on hydraulic conditions in the canal, ranging from 86,245~299,467 m^3/km for 0.62-meter water depth in the canal, to 177,184~564,875 m^3/km for 1.23-meter water depth. There is a great potential to conserve water by lining canals, ranging from 68,996 m^3/km at a low flow condition of site 3, to 451,900 m^3/km at a high flow condition at site 4 for one irrigation season.

ACKNOWLEDGEMENT

The paper is based on the work, in part, supported by the Rio Grande Basin Initiative, which is administrated by Texas Water Resources Institute and sponsored by the Cooperative State Research, Education, and Extension Service, U.S. Department of Agriculture, under Agreement Numbers 2008-34461-19061. The study was also supported by Texas Water Resources Institute and U.S. Bureau of Reclamation. The authors also thank Mrs. Nicole Kyger for her help in preparing figures and map.

REFERENCES

Alam, M.M. and M.N. Bhutta (2004). "Comparative evaluation of canal seepage investigation techniques." *Agricultural Water Management*, 66, 65-76.

Bouwer, H. (1969)). "Theory of seepage from open channels." In *Advances in Hydroscience*, vol. 5, V.T. Chow (ed.), Academic Press, Inc., New York, 121-172.

Bouwer, H. (1978). "Groundwater Hydrology." McGraw-Hill Book Company, New York.

Collis-George, N., and D.E. Smiles (1963). "A study of some aspects of the hydrology of some irrigated soils of western New-South Wales." *J. Soil Res.*, 1, 17-27.

Doherty, J. (200). "PEST model-independent parameter estimation." *Watermark Numerical Computing.*

Harr, M.E. (1962). "Groundwater and seepage." McGraw-Hill Book Company, New York.

Hunt, B.W. (1972). "Seepage from shallow open channel." *Journal of the Hydraulics Division*, Proceedings of the American Society of Civil Engineers, 779-785.

Green, W.H., and G.A. Ampt (1911). "Studies on soil physics, Part I, The flow of air and water through soils." *J. Agric. Sci.*, 4(1), 1-24.

Jeppson, R.W. (1968). "Seepage from channels through layered porous medium." *Water Resources Research*, 2(2), 435-445.

Kahlown, M.A. and W.D. Kemper (2004). "Seepage losses as affected by condition and composition of channel banks." *Agricultural Water Management*, 65, 145-153.

Kuo, R.H. (1982). "Seepage from irrigation canals in Messila Valley, New Mexico." *Doctoral dissertation*, New Mexico State University, NM.

Leigh, E. and G. Fipps (2004a). "Seepage loss test results: the main canal valley municipal utility district No.2." Irrigation Technology Center, Texas A&M University System.

Leigh, E. and G. Fipps (2004b). "Seepage loss test results: seepage and total losses secondary canals 13, 16, and 19 Donna Irrigation District Hidalgo County No.1." Irrigation Technology Center, Texas A&M University System.

Muskat, M. (1937). "The flow of homogeneous fluids through porous media." McGraw-Hill Book Company, New York, 1937, reprinted by J.W. Edwards, Publisher, Inc., Ann Arbor in 1946.

Polubarinova-Kochina, P.Y. (1962). "Theory of groundwater movement". (Translated from the Russian by J.M. Roger Dewiest), Princeton University Press, Princeton, New Jersey.

Rawls, W.J., D.L. Brakensiek, and N. Miller (1983). "Green-Ampt infiltration parameters from soil data." *J. Hydraulic Div., ASCE*, 109(1), 62-70.

Rawls, W.J., L.R. Ahuja, D.L. Brakensiek, and A. Shirmohammadi (1993). "Infiltration and soil water movement." *Handbook of hydrology*, D.R. Maidment, ed., Ch. 5, McGraw-Hill, New York.

Romos, H. (2007). "A non-standard explicit integration scheme for initial-value problems." *Applied Mathematics and Computation*, 189, 710-718.

Rohwer, C., and O.V.P. Stout (1948). "Seepage losses from irrigation canals." *Colorado Agricultural Experiment Station Technical Bulletin* 38.

Sheng, Z., J.P. King, L.S. Aristizabal, and J. Davis (2003). "Assessment of water conservation by lining canals in the Paso Del Norte Region: the Franklin Canal case study." *World Environmental and Water Resources Conference, Environmental and Water Resources Institute*, ASCE, Philadelphia, PA.

Sheng, Z., and J. Devere (2005). "Understanding and managing the stressed Mexico-USA transboundary Hueco bolson aquifer in the El paso del Norte region as a complex system." *Hydrogeology journal* 13:813-825, DOI 10.1007/s10040-0451-8.

Subramanya, K., M.R. Madhav, and G.C. Mishra (1973). "Studies on seepage from canals with partial lining." *Journal of the Hydraulics Division*, (12), 2333-2351.

Warnick, C.C. (1951). "Methods of measuring seepage loss in irrigation canals." Engineering Experiment Station, Bulletin 8.

Worstell, R.V. (1976). "Estimating seepage losses from canal system." *Journal of the Irrigation and Drainage Division*, 137-147.

Vedernikov, V.V. (1934). "Seepage from channels." See also Versicherungen aus Kanalen, Wasserkraft and Wasserwirtschaft, nos. 11, 12, and 13.

Hydrogeologic Investigation for New Water Supply for Water District No. 1 of Johnson County, Kansas

J.W. Henson[1], T. Schrempp[2], M.B. Horsley[3], and K.L. Hahn[4]

[1]Black & Veatch, 8400 Ward Parkway, Kansas City, MO 64114; PH (913) 458-3410; FAX (913) 458-3518; email: hensonj@bv.com
[2]Water District No. 1 of Johnson County, Kansas, 7601 Holliday Drive Kansas City, KS 66106; PH (913) 895-5820; email: tschrempp@waterone.org
[3]Black & Veatch, 8400 Ward Parkway, Kansas City, MO 64114; PH (913) 458-3197; FAX (913) 458-3518; email: horsleymb@bv.com
[4]Black & Veatch, 8400 Ward Parkway, Kansas City, MO 64114; PH (913) 458-3213; FAX (913) 458-3518; email: hahnk@bv.com

ABSTRACT

Water District No. 1 of Johnson County, Kansas (WaterOne) is constructing their Phase V-A Expansion. The expansion program began with an evaluation of the best source of supply to meet their growing needs.

The water supply evaluation included the investigation of horizontal collector wells, which would provide a reliable, high quality supply. A large number of test borings and pumping tests were conducted in the alluvial valleys of the Kansas and Missouri Rivers west of the Kansas City metropolitan area. The results of the testing were used to develop alternative wellfield scenarios. Life-cycle costs were developed, and this information was used to select the most favorable alternative for WaterOne.

PURPOSE OF PROJECT

Water District No. 1 of Johnson County, Kansas (WaterOne) provides drinking water to a population of approximately 400,000 in the Kansas City metropolitan area. The population of the service area has grown significantly and is projected to continue growing. To meet the demands from the expanding service area population, WaterOne identified the need to construct a new water treatment plant and source of supply with a projected long-term capacity of 150 mgd. The expansion program began with an evaluation of the best source of supply.

WaterOne has chosen to implement horizontal collector wells for the first 60 mgd of their expansion. Several factors drove that decision including the following:

- Water pumped from a collector well has relatively consistent water quality and temperature compared to surface water, and it is easier to treat than surface water.
- The water level in the Missouri River has declined over the years due to riverbed degradation.

- Expansion of a collector well supply can be phased more easily than a surface water supply allowing WaterOne to defer costs.

INIITIAL EXPLORATION

Exploration to determine potential locations for horizontal collector wells began with a series of test holes drilled into the alluvium of the Missouri River north of WaterOne's service area. A series of seven borings were drilled and short-term low capacity pumping tests were conducted along a one- mile stretch of the river alluvium.

The borings encountered bedrock approximately 90 to 99 feet below grade. Generally, the top 15 to 20 feet of the formation is sandy silt. From a depth of 20 feet to approximately 55 feet, the aquifer consists of coarse sands. Below 55 feet, the aquifer is very coarse consisting of gravels and sands. Based on the short term pumping tests, estimates of transmissivity were made. Transmissivity is an indication of the ease with which water moves through an aquifer. The estimated range of transmissivity was 300,000 gpd/ft to 650,000 gpd//ft, indicating a highly productive aquifer. Based on the initial results a more detailed aquifer test was conducted.

AQUIFER TESTING

In June of 2005, a detailed aquifer test was performed for Water One north of Wolcott, Kansas, on newly acquired property adjacent to the Missouri River just upstream of River Mile 385. The purpose of the test was to determine the quantity and quality of water that can be obtained at the site by a new horizontal collector well and to help estimate the amount of water that can be obtained by additional future collector wells across the site.

Using the results of the borings and initial testing conducted in 2003, it was determined that the site conditions were favorable for large capacity horizontal collector wells and worthy of additional, more detailed aquifer testing. In 2005, Water One purchased approximately 182 acres. The acquired property set the limits for the detailed aquifer test performed in June 2005. It was decided to perform the aquifer test in the northwest corner of the acquired property, near the location of a test boring from 2003 which indicated some of the best aquifer conditions across the site.

The aquifer test consisted of installing four new observation wells surrounding a new test production well. The test production well was pumped at a constant rate of approximately 1400 gpm for 48 hours, and groundwater level readings were taken from the surrounding observation wells. The Missouri River level was also monitored during the test. The results of the aquifer test indicate that a horizontal collector well at this location should be able to produce up to 17 mgd in the winter and up to 26 mgd in the summer. The aquifer was shown to have a good hydraulic connection with the Missouri River at this location. Upon construction and testing of the first horizontal collector well, coarser aquifer material with higher

transmissivity was encountered than at the location of the nearby aquifer test. Initial yields of as much as 30 mgd are expected from this collector well, which will allow the construction of the second collector well to be deferred by two years.

The results of the aquifer test also provide an initial indication of potential capacities of additional horizontal collector wells in the area, assuming aquifer conditions and the connection of the aquifer with the river are similar in other locations across the site. It is estimated that four collector wells spaced at least 1000 feet apart across the site should be able to maintain the targeted 60 mgd of groundwater supply over a 50-year design life, factoring in loss in well production due to future riverbed degradation and routine lateral maintenance to control the normal loss in well capacity due to natural plugging of the lateral screens.

Over time, wells typically lose capacity due to clogging of the lateral screens and adjacent aquifer. This clogging is primarily the result of migration of fines, chemical precipitation, and bacterial growth. The rate of screen plugging and subsequent loss of efficiency within a horizontal collector well is generally much lower than a typical vertical well as the design entrance and approach velocities are much lower.

In this setting, well capacity will also likely diminish over time because the bed of the Missouri River is degrading. Over the last 70 years, the level of the Missouri River at Kansas City has declined by an average of about 8 feet under low to average flows. The reduction in water level also causes a reduction in saturated thickness of the aquifer and corresponding loss in available drawdown in the well. Over the course of 50 years, it is estimated that the yield of a collector well may be reduced by about 15% if the rate of decline in water levels in the Missouri River continues.

The above resulted in the following assumptions for estimating collector well and wellfield capacity over the 50-year planning period.

- Loss of well capacity, including river degradation is 6% after 3 years and 3% per year thereafter.
- Well redevelopment is performed at the frequency necessary to maintain the desired total system yield of 60 mgd.
- 90% of the previous well capacity is regained each time a well is redeveloped.
- 95 % of the previous well capacity is regained when new laterals are installed.

Based on these assumptions, each well will have its laterals replaced once and will require 10 well redevelopments. This indicates that four collector wells with average capacity of 15 mgd are adequate to reliably produce 60 mgd over the 50-year planning period.

RAW WATER QUALITY

Groundwater quality testing was also performed in 2005 to determine both the water quality at the location of the aquifer test and the water quality between the newly acquired property and the industrial area located to the west. A comprehensive groundwater sample was collected at the end of the detailed aquifer test. This sample was analyzed for the following parameters:

- General chemistry (including such parameters as pH, hardness, alkalinity, etc.).
- Metals.
- Microbiology.
- Radionuclides.
- Disinfection byproducts.
- Volatile and semi-volatile organic chemicals.
- Viruses.
- Asbestos, dioxin, foaming agents.
- Dissolved gases.

No man-made organic chemicals were detected in this groundwater sample. The parameters of interest from a treatment standpoint for this groundwater sample are provided in Table 1.

This groundwater sample was collected after only 48 hours of pumping at approximately 1400 gpm. A future collector well at this site will be pumped nearly 10 times this rate for much longer periods of time and will induce a much larger percentage of surface water. Therefore, the raw water quality being pumped by the collector well is expected to change somewhat over time. Table 2 shows how the raw collector well water quality has changed over time for another nearby well.

Table 1. Selected Laboratory Results for Groundwater Sample

Parameter	Result	Units	Regulatory Maximum Contaminant Limit (MCL)
Iron	8.7	mg/L	0.3 (Secondary MCL)
Manganese	1200	ug/L	50 (Secondary MCL)
pH	6.99	pH units	6.5 to 8.5
Dissolved solids	600	mg/L	500 (Secondary MCL)
Turbidity	84	NTU	-
Total alkalinity	510	mg/L as CaCO3	-
Total hardness	500	mg/L as CaCO3	-

Based on the above characteristics, a softening process has been chosen to reduce mineral concentrations to a level WaterOne's customers are accustomed to.

The concentration of iron in the nearby raw collector well water has decreased significantly over the past five years. The concentrations of dissolved solids, total hardness, and total alkalinity have slowly decreased roughly 10 to 15 percent since startup of their collector well. The concentrations of these parameters tend to go up slightly in the cold winter months when the collector well pumps a higher percentage of groundwater because of the higher river water viscosity and lower Missouri River stages. The concentration of barium has decreased by about 40 percent over time for the nearby well. The concentration of manganese, however, has remained above 400 ug/L since startup. Similar long-term changes to raw water quality may occur at the WaterOne collector well site.

Table 2. Comparison to Nearby Collector Well Water Quality

Parameter	Units	Water One Test Result[1] (6/23/2005)	Nearby Startup[2]	Nearby Long-term[2] (4 years after startup)	Regulatory Maximum Contaminant Limit (MCL)
Iron	mg/L	8.7	4.4	0.4	0.3*
Manganese	ug/L	1200	480	580	50*
pH	pH units	6.99	7.33	7.36	6.5 to 8.5
Dissolved solids	mg/L	600	525	437	500*
Turbidity	NTU	84	13	NA	-
Total alkalinity	mg/L as CaCO3	510	212	198	-
Total hardness	mg/L as CaCO3	500	301	262	-

[1] Groundwater sample collected at test well
[2] Sample taken from plant influent
*Secondary maximum contaminant limit (SMCL)

Total dissolved gases in the groundwater were measured in the field at the same time the comprehensive sample was collected. The total dissolved gas pressure in the groundwater was slightly higher than that of barometric pressure, with a measured saturation of 106.5 percent. Such minimal over-saturation is not expected to significantly affect any treatment process. The measured dissolved oxygen concentration was low (approximately 0.33 mg/L) compared to the saturation concentration of 10 mg/L for fresh water at this temperature. The free carbon dioxide concentration was approximately 155 mg/L as measured by the total dissolved gases monitor and 110 mg/L as calculated from the pH and alkalinity data.

Historic pH and alkalinity data taken from the nearby collector well, indicate that the carbon dioxide concentration in the raw water pumped by their collector well is super-saturated. The concentration appears to peak approximately December of each year. This may be the result of a greater percentage of groundwater and reduced influence of surface water. There has however been an overall trend of reduced free

carbon dioxide concentration over time from approximately 40 mg/L to 10 mg/L over five years.

Based on the data from the nearby well, the carbon dioxide concentration at the WaterOne site is expected to decline over time. Two treatment alternatives are available for the removal of the excess free carbon dioxide: 1) air stripping and 2) reaction with caustic chemicals. Carbon dioxide can be removed from water through air stripping reasonably well and new designs eliminate the concerns over the potential for water to form scale in the aerator and potential biological fouling caused by the high iron concentration.

Without air stripping, additional lime would be required to remove the excess carbon dioxide. The lime added for this purpose would not accomplish any softening. Nearly 200 mg/L of lime would be required to remove 155 mg/L of free carbon dioxide and bring the solution to an equilibrium carbon dioxide concentration of 5 mg/L. This will result in nearly doubling the required lime dosage to treat the water. Additionally, 2.3 mg/L of additional calcium carbonate solids are generated for each part of free carbon dioxide removed, resulting in a substantial increase in solids.

Based on the free carbon dioxide levels, induced draft aeration was implemented at the new water treatment plant Aeration will help to offset the cost of additional lime and solids. For lime softening plants, when raw water free carbon dioxide concentrations exceed 20-25 mg/L, aeration is a cost effective solution.

INDUSTRIAL ACTIVITY

There is an existing industrial area consisting of grain elevators and above-ground tanks located approximately one half mile to the west of the newly acquired property. Products such as liquid calcium chloride, liquid asphalt, sulfuric acid, diesel fuel, liquid propane gas, molasses, coconut oil, gasoline, and methyl ester have historically been stored or handled at the site. It was decided to collect several screening groundwater samples to the west of the collector well site to determine if there is any contamination in the area from the industrial area. A small drilling rig called a “Geoprobe” was mobilized to the site, and two small diameter test wells were drilled. The first test well was drilled through the sands and gravels to a depth of 90 feet where bedrock was encountered. A groundwater sample was collected from the bottom of this test well and submitted to the laboratory for analysis of volatile organic chemicals. Adjacent this test well, another test well was drilled to a depth of 20 feet, which was just below the groundwater table. A groundwater sample was collected from this test well and submitted to the laboratory for analysis of volatile organic chemicals, semi-volatile organic chemicals, and metals.

The results of the laboratory analysis showed no detection of organic chemicals from either sample. Various metals were detected in the shallow sample at rather high concentrations. It was believed that the detection of some of the metals

was caused by soil particles in the unfiltered groundwater sample collected from the Geoprobe.

Later in 2005 during the Environmental Site Assessment activities at the site, it was revealed that there was a barge unloading facility operated to the west of the proposed collector well site for several years in the 1970s reportedly for storage and transport of oil products. Because of this finding and the interference of the first metals analysis by the soil particles, another set of geoprobe samples were collected. A shallow groundwater sample was collected at the western end of the site and both a shallow and deep groundwater sample were collected at the eastern end of the site.

The shallow samples were tested for metals, pesticides and industrial chemicals, PCBs, and other volatile and semivolatile organics. The deep sample was tested for pesticides and industrial chemicals, PCBs, and other volatile and semivolatile organics. The raw groundwater was filtered in the field prior to collection to reduce the amount of sediment in the samples. None of the metals concentrations were above the primary drinking water MCLs. Only iron and manganese were above the secondary MCLs.

The only organic chemical that was detected was in the deep geoprobe sample collected at the eastern site. Di(2-ethylhexyl)phthalate was detected at a concentration of 0.7 ug/L, which is just above the minimum detection limit of 0.6 ug/L for the laboratory apparatus and is below the primary drinking water MCL of 6 ug/L. The laboratory indicated that this detection of di(2-ethylhexyl)phthalate is suspect because their quality control procedures indicated that the laboratory equipment may have been reading high during the analysis. This compound is also found in plastic products and may have been introduced in the laboratory by such items as bottles or gloves at such a low concentration.

CONCLUSION

WaterOne has successfully implemented the first horizontal collector well with a yield greater than originally projected. The water treatment plant is under construction and expected to be on-line in 2009. These are the first steps in ensuring a long-term reliable water supply for its customers for the next 50 years.

A Heuristic Algorithm for Optimal Alignment and Matching of Borehole Stratigraphy

Gustavious P Williams, Norman Jones, and Jeffrey Handy

ABSTRACT

This paper presents an heuristic algorithm, Auto-Align Boreholes (AAB), that computes near-optimal stratigraphy sequences from borehole horizons to define subsurface geology in a computationally efficient manner. Matching horizons across boreholes is not trivial and problem complexity grows exponentially with the number of horizons and boreholes. Our algorithm is based on the Smith and Watermen algorithm used in gene sequencing with modifications.

Our algorithm computes a near optimal alignment between the horizons, subject to constraints. Matching horizons to develop subsurface models has traditionally been done manually, but for large sets of boreholes, manually selecting the horizons becomes difficult. Other methods exist to compute optimal sequences but they become computationally infeasible for even moderate numbers of boreholes.

The optimal alignment problem can be solved exactly by a multiple sequence alignment distance matrix (an exhaustive search method) but is computationally infeasible for even moderate-sized borehole sets. The literature presents other approaches such as dendrographic algorithms and genetic algorithms. Dendrographic method computational requirements vary with the number of borehole pairs squared (or cubed) and the results depend on the order in which sequences are paired. Genetic algorithms must be run many times to ensure that the solution found is not a local minimum (of which there many) and requires a long runtime if the number of boreholes is relatively large.

The AAB algorithm was implemented in the Groundwater Modeling System (GMS), a subsurface pre- and post processing system developed by the United States Army Corps of Engineers. The GMS system can compute and present the borehole horizon information to generate subsurface stratigraphic models.

1. Introduction

This paper presents a new heuristic algorithm, Auto-Align Boreholes (AAB), that computes near-optimal stratigraphy sequence alignments among borehole horizons to define subsurface geology layers and structures. A horizon is a geologic layer boundary and defines the top of the layer. Matching a horizon across numerous boreholes is not a trivial problem since there are many potential matches and the problem complexity grows rapidly with the number of horizons and boreholes (Robinson 1975).

The algorithm presented in this paper computes a near optimal alignment between the horizons, subject to constraints and can be used to develop fence diagrams or more complete subsurface volume models (Lemon and Jones 2003; Fugal 2005). Matching horizons to develop these subsurface models has traditionally been done manually (Lemon and Jones, 2003), but for large sets of boreholes, manually selecting the horizons becomes difficult (Fugal, 2005). Methods exist to compute an optimal sequence, based on the imposed constraints, but this approach quickly becomes computationally infeasible (Smith and Waterman 1980, Waterman and Raymond 1987, Fugal 2005). The AAB algorithm provides an automated means to assign horizons to borehole material interfaces in a computationally efficient, realistic manner.

The AAB algorithm for computing horizon alignments among boreholes presented in this paper was implemented in the Groundwater Modeling System (GMS), a subsurface pre- and post processing system developed by the United States Army Corps of Engineers (USACE) (Jones *et al*., 2002). The GMS system is an integrated pre- and post-processing system for groundwater flow and contaminant transport models and can present the borehole horizon information to users who can use it to generate subsurface stratigraphic models (Jones *et al*., 2002; Lemon and Jones 2003).

1.1 Historic Work

Sequencing of stratigraphic logs and matching layers among boreholes has traditionally relied on a geologist or practitioner to visually connect the material interfaces (horizons) in the boreholes to each other to define a material horizon (Robinson 1975). To support this manual approach early computational work, such as Robinson's (1975), focused on methods to transform borehole and well log data to better present sequences to the practitioners for manual matching.

There was significant work on computational methods for automatically sequencing proteins that mainly occurred in the biological sciences where there was a need for sequencing the genome and other data. These sequences were developed from overlapping or correlated strands of proteins that are analogous to soil layers in a borehole. Smith and Watermen (1980) extended this biological work to the geology problem and presented a dynamic programming technique (SW) to use the data from several boreholes to develop a single optimal stratigraphy for use in geochronology. Waterman and Raymond (1987) extended the SW technique to deal with the problem of gaps and added differing weighting methods to the earlier approach. The AAB algorithm presented in this paper is based on the SW technique.

Tipper (1988) provides a detailed history of this field in a review and annotated bibliography on quantitative geologic stratigraphic correlation that includes over 400 citations detailing the quantitative work done in the field up to that point

1.2 AAB Algorithm Overview

The AAB algorithm computes a set of connections between the horizons at each borehole to define the boundaries of the geologic units in the subsurface. This is done by matching stratigraphy horizons found on multiple boreholes to each other, subject to constraints that maximizes the number of common horizons connected between boreholes and minimizes the slope between the horizon locations on adjacent boreholes. The optimization problem is solved heuristically, which does not guarantee optimality.

The optimal alignment for a borehole alignment problem can be solved exactly by tracing a two dimensional multiple sequence alignment (MSA) distance matrix (Smith and Waterman 1980) which is an exhaustive search that determines the optimal solution based on the given constraints. However, the MSA approach using distance matrices cannot be used for even moderate-sized sets of boreholes due to the large number of traces required to create the distance matrix. For example, if one hundred boreholes with a geometric average length of eight segments (or horizons) were used, it would require 8^{100} or $2.04*10^{90}$ traces within the distance matrix to determine the optimal alignment, with each trace requiring several computer operations (Fugal 2005). This number of calculations is intractable with the computational resources available today.

The literature presents several approaches to the computational issues associated with MSA problem such as dendrographic algorithms (Do *et al.*, 2005) and genetic algorithms (Yokoyama et al. 2001). Dendrographic algorithms align only two or three sequences at a time; then align two or three pairs of sequences together; then two or three groups of sequences until the entire borehole set is aligned. With this method the computational requirements vary proportionally to the number of pairs squared (or cubed) rather than exponentially as with the exhaustive method (Do *et al*., 2005). The primary difficulty with this method is the optimality of the results depend greatly on the order in which sequences are paired. Various methods have been derived for optimizing the order in which sequences are paired within these algorithms—many of which appear to be very promising (Do et al., 2005).

Genetic algorithms have also explored (Yokoyama et al., 2001). However, a genetic algorithm must be run many times to ensure that the solution found is not a local minimum within the solution space which requires a long runtime if the number of boreholes is relatively large (Yokoyama *et al.*, 2001).

The AAB algorithm we developed provides a method to compute a near optimal alignment between boreholes in a computationally efficient manner. Our algorithm is based on the Smith and Watermen algorithm MSA approach (1980) with modifications and additions to address various issues.

The AAB algorithm differs from the globally optimal MSA method by performing the alignment in stages based on the calculation of only a portion of the distance matrix. This results in near-optimal solution that may not be globally optimal. The AAB algorithm follows a stepwise path through the matrix until an entire alignment is computed. Because only one path—or a few—is considered, this method seems to have the same weakness as the dendrographic and genetic algorithm methods. However, the AAB algorithm does not rely on predictive pairing of sequences, as with the dendrographic method, and it is always progressive, and therefore can be more time efficient than the genetic algorithm approach.

2. Algorithm Development

The AAB algorithm solves two main issues found with the SW approach, the computational complexity and the fact that using gap minimization as the only constraint often results in alignments that are not geologically practical (Fugal 2006).

To develop the heuristic AAB algorithm, we modified the distance matrix approach (Smith and Waterman, 1980; Needleman and Wunsh, 1970) with the addition of a slope constraint to address the geological issues and used heuristic search methods to address the computational issues. This section presents the traditional MSA approach and the AAB modifications.

2.1 Traditional MSA distance matrix

The simplest MSA distance matrix formulation finds the longest common subsequence of two sequences. The algorithm written for matrix of two dimensions is (Smith and Waterman, 1980):

$$d_{ij} = \begin{cases} m_i = m_j & \min(d_{i-1,j-1}, \quad d_{i,j-1}+1, \quad d_{i-1,j}+1) \\ m_i \neq m_j & \min(d_{i,j-1}+1, \quad d_{i-1,j}+1) \end{cases} \qquad \textbf{Eq 1}$$

Where: d is the distance (optimization value for $cell_{i,j}$)
m_i and m_j are sequence segments on sequences 1 and 2 respectively

Equation 1 generates a complete distance matrix that defines every possible set of alignments between two boreholes. In this matrix, the calculated cell value, d_{ij}, is the minimum number of gaps that could exist in an alignment between the two boreholes starting at the origin (upper left corner) and continuing to the point represented by the cell.

After computing the distance matrix, the optimal alignment is found by starting at the corner of the matrix where *i* and *j* are at their maximum and performing a recursion to define the alignment. The recursion moves from the current chosen cell to the next by examining the values used to calculate the current cell and selects the cell from this set with the minimum value. The trace is selected from the cells used to define each cell value which is calculated using the cells above or to the left of itself (Equation 1). By picking the minimum of these cell values, we select the trace which defines the optimal alignment by minimizing the number of gaps in this formulation. In the Figure 1 pseudo

code representation, the *trace* vector, is a list of cells which define the optimal alignment. If the values in two or more cells are equal, the solution is ambiguous. Either selection with result in a trace-back that is equally valid. For convenience, the algorithm simply chooses one.

Start
    l = 0
    select trace(l) = cell($d_{m,n}$)
    l = 1
    Do until cell is $d_{0,0}$
        select trace(l) = min { cell($d_{m-1,n}$), cell($d_{m,n-1}$), cell($d_{m-1,n-1}$)
        Cell($d_{m,n}$) = cell(trace(l)
        l = l +1
    EndDo
End

Figure 1 Pseudo code to compute the optimal trace from a distance matrix.

2.2 Slope Constraint

The traditional DMA approach described above gives results which are not always geologically likely. To better match the physical geologic constraints, we modified the traditional DMA approach by adding stratigraphy slope as a second constraint which better mathematically represents the physical constraints on the problem. The slope is defined as the elevation difference between the two connected horizons divided by the distance between the boreholes.

Equation 2 is the modified distance matrix equation with the addition of this constraint.

$$d_{ij} = h \cdot S_{ij} + \begin{cases} m_i = m_j & \min(d_{i-1,j} + g,\ d_{i,j-1} + g,\ d_{i-1,j-1}) \\ m_i \neq m_j & \min(d_{i-1,j} + g,\ d_{i,j-1} + g) \end{cases} \qquad \textbf{Eq 2}$$

Where:

d = distance (optimization) value for $cell_{ij}$
m_i and m_j = $material_i$ on borehole 1 and $material_j$ on borehole 2, respectively
S_{ij} = slope between material segments m_i and m_j
g = gap weight
h = slope weight

The two weighting factors are used to adjust the relative impact of slope and gap constraint violation in the alignment optimization. The addition of this additional constraint significantly improves the geologic representation of the resulting alignment (Fugal 2006).

2.3 Optimality function

The function be minimized by the *Auto-align boreholes* algorithm includes the number of gaps in the alignment and the slope of the connecting horizons is calculated according to Equation 3.

$$Error = w_G \sum_{i=0}^{n} \left(N - H_i\right) + w_S S \qquad \textbf{Eq 3}$$

Where :

S = slope error given in Equation 4,
N = number of horizons in the borehole set
H_i = number of horizons on borehole$_i$
w_G and w_S = weights given to the gap error and slope error, respectively.

In order to obtain the total slope error, borehole adjacency is determined by performing an adjusted Delaunay triangulation where a normal Delaunay triangulation is performed and then adjusted so that all existing cross sections in the model are honored and thin exterior triangles are deleted. Boreholes are then paired with each adjacent borehole as determined by the triangulation. The slope error for each of these borehole pairs is then calculated and summed to give the total slope error according to Equation 4.

$$S = \sum_{i=0}^{N} \left[abs\left(\frac{\left(a_0 - a_i\right) - \left(b_0 - b_i\right)}{d \cdot N \cdot S_0} \right) \right] \qquad \textbf{Eq 4}$$

Where:

S = Weighted slope error
a_0 and b_0 = base elevation for boreholes a and b respectively
a_i and b_i = elevation of horizon pair i in boreholes a and b respectively
d = distance between boreholes a and b
N = number of horizon pairs
S_0 = average horizon slope.

The variables a_0 and b_0 depend on whether the user wishes to compare slope to a level surface ($a_0 = b_0 = 0$) or the ground surface elevation. The average horizon slope is a user defined parameter that normalizes the slope error to an expected horizon slope.

3. Conclusions

The primary result of the creation of this algorithms is that reasonable stratigraphy models can now be created in a matter of minutes rather than in hours or days. For most finite element analysis projects, multiple models must be tested in order to obtain a stable model and informative results. The process of creating such models will likely be greatly facilitated by the implementation of this project.

This AAB algorithm has been shown to be very successful in almost every borehole case tested. Whereas the time requirements for this algorithm increase exponentially when

increasing the number of horizons considered per lift, using the default value for this parameter allows the algorithm to be completed in a relatively small amount of time.

The primary benefit of this new method of creating three dimensional stratigraphy models is not that it returns better results than could be obtained any other way, but that it gives good results faster than any other method.

4. References

Lemon, A.L., & Jones, N.L., "Building solid models from boreholes and user-defined cross-sections," Computers and Geosciences, Vol. 29, No. 5, June, 2003, pp 547-555.

Do, C. B., Mahabhaskyam, M.S.P., Brudno, M. & Batzoglou, S., "Probabilistic consistency-based multiple sequence alignment" Genome Research, Vol. 15, 2005, pp 330-340.

Smith, T. F. & Waterman, M. S., "New stratigraphy correlation techniques" Journal of Geology, Vol. 88, No. 4, 1980, pp 451-457.

Needleman, S.B. & Wunsch, C.D., "A general method applicable to the search for similarities in the amino acid sequence of two proteins." Journal of Molecular Biology, Vol. 48, 1970, 443-453

Notredame, C. & Higgins, D. G., "SAGA: sequence alignment by genetic algorithm" Nucleic Acids Research, Vol. 24, 1996, pp 1515-1524.

Thompson J.D., Higgins D.G., Gibson T.J., "CLUSTAL W: improving the sensitivity of progressive multiple sequence alignment through sequence weighting, position-specific gap penalties and weight matrix choice" Nucleic Acids Research, Vol. 22, 1994, pp 4673-4680

Jones, Norman L., Trevor J. Budge, Alan K. Zundel, Alan M. Lemon, "Generating MODFLOW grids from boundary-representation solid models," *Ground Water*, Vol. 40, No. 2, March-April 2002, pp. 194-200.

Fugal, Adam *A New Automated Approach To Three-Dimensional Soil Stratigraphy Modeling* Master's Thesis, submitted to the Department of Civil and Environmental Engineering, Brigham Young University, Provo, UT, April, 2005

Tipper, J.C. "Techniques for quantitative stratigraphic correlation: a review and annotated bibliography" *Geological Magazine* vol. 125, No. 5, 1988, pp 475-494.

Robinson, J.E. “Transforms to Enhance Correlation of Mechanical Well Logs” *Mathematical Geology*, Vol 7, No. 4, 1975. pp. 323-334.

Watermen, Michael S., and Robert Raymond, Jr. “The Match Game: New Stratigraphic Correlation Algorithms” *Mathematical Geology*, Vol 19, No. 2, 1987 pp 109-127

Epstein, David A., *Efficient Algorithms for Sequence Analysis With Concave and Convex Gap Costs* Ph.D. Dissertation submitted to the Graduate School of Arts and Sciences, Columbia University, New York, New York, 1989.

Saddler, Peter M. “Quantitative Biostratigraphy – Achieving Finer Resolution in Global Correlation” *Annual Reviews of Earth Planet Science* 2004 No. 32 pp 187-213

Olea, Ricardo A. and Robert J. Sampson *User’s Manual For CORRELATOR Version 5.2* Kansas Geological Survey, Mathematical Geology Section, Lawrence, Kansas, May 2003

Composite Analysis of Test-Well and Observation-Well Data during Constant-Head Test

Yen-Ju Chen[1] and Hund-Der Yeh[2]

[1] Ph. D. student, Institute of Environmental Engineering, National Chiao Tung University, 75 Po-Ai Street, Hsinchu 30039, Taiwan; e-mail: yenju.ev92g@nctu.edu.tw

[2] Professor, Institute of Environmental Engineering, National Chiao Tung University, 75 Po-Ai Street, Hsinchu 30039, Taiwan; PH: 886-3-5731910; e-mail: hdyeh@mail.nctu.edu.tw

ABSTRACT

A constant-head test, keeping the buildup or drawdown constant in the test well, is aimed at determining the aquifer parameters. A skin zone around the wellbore due to well drilling or completion has diverse property to the aquifer. Five parameters including the transmissivities and storage coefficients for each of the skin and aquifer zones and the outer radius of the skin zone are determined via the simulated annealing approach to describe the flow system with a finite-thickness skin. Estimated results indicate that analyzing the single-well responses, i.e., test-well flow rate and observation-well drawdown data separately, is insufficient for obtaining accurate estimates for skin and aquifer parameters. Analysis of specific drawdown in an observation well gives biased results in the negative-skin case. The skin and aquifer parameters appear to be accurately determined when the flow-rate and drawdown data are analyzed sequentially or simultaneously.

INTRODUCTION

In a constant-head test (CHT), the buildup or drawdown in the test well is kept constant throughout the test. The transient flow rate at the test well or dispensable buildup/ (drawdown) in an observation well is measured for site characterization. Jacob and Lohman (1952) derived the flow-rate solution for a CHT conducted on a fully penetrating well in a confined aquifer. They showed that the aquifer transmissivity and storage coefficient can be estimated by analyzing the large-time specific drawdown data (i.e., drawdown divided by flow rate) measured in the test well. Mishra and Guyonnet (1992) analyzed the specific drawdown in the

observation well to determine the aquifer parameters. Hiller and Levy (1994) showed that only the hydraulic diffusivity can be determined if drawdown data from an observation well is adopted in the analysis. A skin zone around the wellbore with diverse properties to the aquifer may exist after well drilling or completion. The skin can be classified into two categories: a positive skin having a smaller value of transmissivity than the aquifer zone while a negative skin having a larger one. Figure 1 represents a CHT operated in a confined aquifer with a skin zone around the test well. The analytical solutions for flow rate at the test well and drawdown in an observation well considering the skin effect were developed by Yang and Yeh (2002) and Yang and Yeh (2006), respectively.

This paper aims to show the most reliable ways in the parameter estimation from the analyses of various CHT data sets. The analyses are classified into two categories based on the well number. First, the single-well CHT responses being analyzed include the wellbore flow rate at the test well and drawdown in an observation well. Next, the multi-well responses are analyzed in three ways: interpreting the specific drawdown data in an observation well, examining the flow-rate and drawdown data in two stages, and analyzing the flow-rate and drawdown data simultaneously. The CHT is assumed to be conducted on a fully penetrating well in a confined aquifer with a finite thickness skin. The parameter estimation is achieved using the simulated annealing (SA) approach. The results of this work could provide instructive information in the analysis of the skin-affected CHT data.

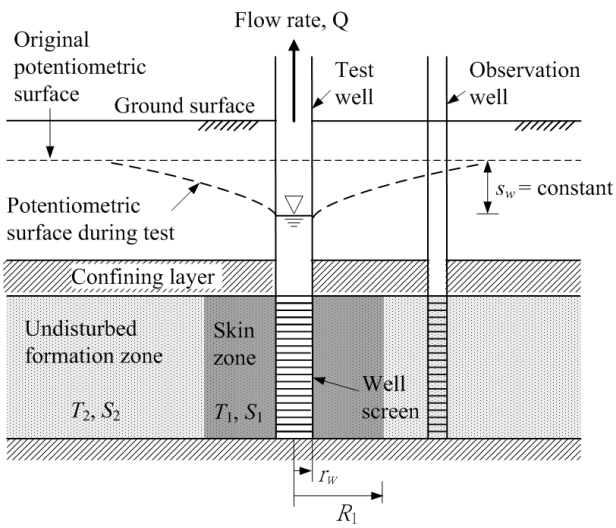

Figure 1. Schematic representation of skin-affected CHT in a confined aquifer.

METHODOLOGY

CHT solution. Yang and Yeh (2002) gave the flow-rate solution in the Laplace domain when the CHT conducted on a fully penetrating well in a confined aquifer with a finite thickness skin as

$$\overline{Q}(p) = \frac{2\pi r_w T_1 s_w q_1 [\Phi_1 I_1(q_1 r_w) + \Phi_2 K_1(q_1 r_w)]}{p[\Phi_2 K_0(q_1 r_w) - \Phi_1 I_0(q_1 r_w)]} \tag{1}$$

and the drawdown solutions as

$$\overline{s}_1(r, p) = \frac{s_w [\Phi_1 I_0(q_1 r) - \Phi_2 K_0(q_1 r)]}{p[\Phi_1 I_0(q_1 r_w) - \Phi_2 K_0(q_1 r_w)]} \tag{2}$$

and

$$\overline{s}_2(r, p) = \frac{s_w [\Phi_1 I_0(q_1 R_1) - \Phi_2 K_0(q_1 R_1)] K_0(q_2 r)}{p[\Phi_1 I_0(q_1 r_w) K_0(q_2 R_1) - \Phi_2 K_0(q_1 r_w) K_0(q_2 R_1)]} \tag{3}$$

with notations Φ_1 and Φ_2 respectively defined as

$$\Phi_1 = \sqrt{\frac{S_2 T_2}{S_1 T_1}} K_0(q_1 R_1) K_1(q_2 R_1) - K_1(q_1 R_1) K_0(q_2 R_1) \tag{4}$$

and

$$\Phi_2 = \sqrt{\frac{S_2 T_2}{S_1 T_1}} I_0(q_1 R_1) K_1(q_2 R_1) + I_1(q_1 R_1) K_0(q_2 R_1) \tag{5}$$

where $\overline{Q}$ is the flow rate across the wellbore in the Laplace domain; $\overline{s}_1$ and $\overline{s}_2$ describe the drawdown responses in the skin and aquifer zones, respectively; p is the Laplace variable; r denotes the location of the observation well; r_w is the radius of well; s_w is the constant drawdown maintained at the well during the test; T and S are the transmissivity and storage coefficient with the subscripts 1 and 2 representing the skin and aquifer zone, respectively; R_1 is the radial distance from centerline of well to outer boundary of skin zone; $q_1 = \sqrt{pS_1 / T_1}$; $q_2 = \sqrt{pS_2 / T_2}$; I_0 and K_0 are the zero-order modified Bessel functions of the first and second kinds, respectively; and I_1 and K_1 are the first-order modified Bessel functions of the first and second kinds, respectively.

Parameter estimation method. Analysis of a specific CHT data set, e.g., flow-rate data or drawdown data, was formulated as a single-objective problem with the objective function defined as the minimum sum of squared residuals. If both

flow-rate and drawdown data are fitted simultaneously to their solutions during the parameter estimation, a simple extension on objective function that combined the weighted sums of squares for both responses will be applied. The weight implemented on the flow-rate component of sum of squares has the unit in day^2/m^4. SA algorithm, which was chosen to find the least value of the sum of squares, was similar to that described in Yeh and Chen (2007).

ANALYSES AND DISCUSSION

Assume a CHT was conducted in a silty confined aquifer. The fully penetrating well with 0.2-m diameter was maintained with a constant drawdown of 3 m during the test. The observation well was located at 1.2 m away from the test well. The hypothetical aquifers have parameters T_1 = 0.05 m^2/d and T_2 = 1.0 m^2/d for positive-skin cases, T_1 = 1.0 m^2/d and T_2 = 0.05 m^2/d for negative-skin cases, $S_1 = S_2 = 10^{-4}$, and R_1 = 0.8 m. The analyzed data of flow rate in the test well and drawdown at the observation well were respectively generated using Eqs. (1) and (3). The estimated results of skin and aquifer parameters using various data sets for positive-skin and negative-skin cases were listed in Table 1.

Analyses of single-well response. The analyses of single-well CHT responses include the wellbore flow rate at the test well and drawdown in an observation well being analyzed separately. Table 1 reveals that analysis of wellbore flow-rate data for the positive-skin case results in fairly good estimates for T_1, S_1 and R_1 but biased estimates for T_2 and S_2. As for the negative-skin case, all the estimated parameter values are close to the target values. However, since we may not know the skin type *a priori*, the estimates for the aquifer parameters are unconvinced via examining wellbore flow-rate data. For both positive- and negative-skin cases, analyses of drawdown data show accurate estimates for R_1 yet significant deviations for T_1, T_2, S_1 and S_2. In short, the analyses of drawdown data are incapable of accurately estimating the skin and aquifer parameters.

Analyses of multi-well responses. Three ways concerning the analyses of multi-well responses were considered. The first one analyzed the specific drawdown data in an observation well. Next, we fixed the skin parameters at the values obtained from the previous flow-rate data analysis and then determined the aquifer parameters only via the analysis of drawdown data. Finally, the flow-rate

and drawdown data were simultaneously fitted to their solutions using a weighted multi-objective optimization.

Table 1. Estimated skin and aquifer parameters using different sets of data.

Data sets being analyzed	Skin parameters			Aquifer parameters	
	T_1 (m^2/d)	S_1	R_1 (m)	T_2 (m^2/d)	S_2
Positive-skin cases					
Target value	**0.05**	**1.00×10^{-4}**	**0.8**	**1.0**	**1.00×10^{-4}**
Flow rate only	0.050	1.02×10^{-4}	0.819	0.718	9.91×10^{-4}
Drawdown only	0.345	6.88×10^{-4}	0.799	6.840	7.11×10^{-4}
Specific drawdown	0.048	1.09×10^{-4}	0.742	0.987	1.03×10^{-4}
Flow rate and drawdown[1]	0.050	1.02×10^{-4}	0.819	0.999	9.22×10^{-5}
Flow rate and drawdown[2]	0.050	1.02×10^{-4}	0.788	0.994	1.01×10^{-4}
Negative-skin cases					
Target value	**1.0**	**1.00×10^{-4}**	**0.8**	**0.05**	**1.00×10^{-4}**
Flow rate only	1.002	9.93×10^{-5}	0.803	0.050	9.85×10^{-5}
Drawdown only	9.389	9.50×10^{-4}	0.801	0.478	9.52×10^{-4}
Specific drawdown	7.525	7.09×10^{-4}	0.454	0.055	7.05×10^{-5}
Flow rate and drawdown[1]	1.002	9.93×10^{-5}	0.803	0.051	1.03×10^{-4}
Flow rate and drawdown[2]	0.999	1.00×10^{-4}	0.800	0.050	9.97×10^{-5}

[1] Flow-rate data is first used to determine the skin parameters (T_1, S_1, and R_1); drawdown data is then applied to determine the aquifer parameters (T_2 and S_2).

[2] Flow-rate and drawdown data are fitted to their solutions simultaneously; the weight applied on the flow-rate component of the objective function is 0.01 day^2/m^4.

The drawdown in the test well keeps constant during a CHT. Therefore, the estimated results for the five parameters from the analysis of specific drawdown response in the test well should be the same as those of flow-rate data. The specific drawdown data in an observation well were produced by the data generated using Eq. (1) divided by those generated using Eq. (3). The estimated parameter values for the positive-skin case, as indicated in Table 1, are fairly close to their target ones. However, for the negative-skin case, significant deviations are found in the estimations of skin parameters T_1, S_1 and R_1.

A two-stage analysis was applied to improve the accuracy of skin and aquifer parameter estimates. In the first stage, the three skin parameters were obtained from the single-well analysis of wellbore flow-rate data, since they reveal acceptable

estimates in both positive- and negative-skin cases based on the results of previous analysis. The values of skin parameters were fixed in the succeeding analysis. In the second stage, the drawdown data were applied to estimate the remaining aquifer parameters. Table 1 shows that the two-stage analyses significantly improve the estimated results for aquifer parameters. However, this method should be taken carefully because it serves only if the skin parameters had been correctly estimated.

The last analysis was achieved by fitting the flow-rate and drawdown data simultaneously to their solutions. The parameter estimation criterion was carried out by the weighted multi-objective function. Figure 2 demonstrates the estimated results for the cases using different magnitudes of weights on the flow-rate (w_1) and drawdown (w_2) components. The case of $w_1 = 0$ and $w_2 = 1$ represents the analysis of drawdown data only, which gives poor estimates on T_1, T_2, S_1 and S_2 for both positive- and negative-skin cases. For the cases of w_2 keeps one, Figures 2a and 2b reveal that even a small value of w_1 (e.g., $w_1 = 10^{-4}$ day^2/m^4) could significantly improve the estimated results for the positive- and negative-skin cases, respectively. On the other hand, the case of $w_1 = 1$ day^2/m^4 and $w_2 = 0$ represents the analysis of flow-rate data only, which obtains biased estimates on T_2 and S_2 but accurate estimates on the five parameters for the positive- and negative-skin cases, respectively. For the cases of w_1 keeps unique, the utilization of $w_2 = 10^{-4}$ during the composite analysis seems slightly improve the estimated results. However, it is suggested that, for positive-skin case, the value of w_2 is equal to or larger than 10^{-3} being used for further improving the estimated results. In fact, the flow-rate and drawdown data have the accuracy on the order of 10^{-2} m^3/day and 10^{-3} m, respectively. If the predicted flow-rate and drawdown data generated from the five estimated parameters are well fitted to their observed ones, the square sums for the flow-rate and drawdown components should be on the order of 10^{-4} m^3/day and 10^{-6} m, respectively. Therefore, in Table 1, the weight applied on the flow-rate component in the multi-objective function was chosen to be 0.01 day^2/m^4, so that the two objectives, i.e., the total sums of squared residuals, were balanced with the same unit and order. Table 1 reveals the estimated results for skin and aquifer parameters are in good agreements with their target values for both positive- and negative-skin cases. In short, composite analysis of flow-rate and drawdown data is highly recommended for obtaining accurate estimates of skin and aquifer parameters as long as the weights are carefully chosen.

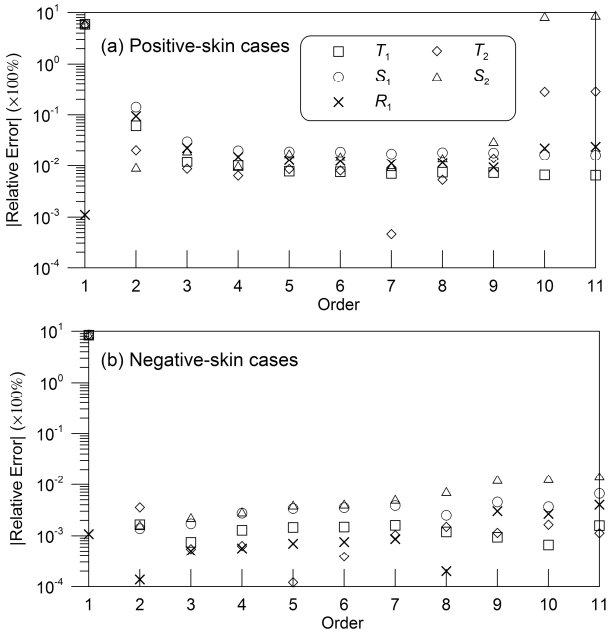

Order	1	2	3	4	5	6	7	8	9	10	11
w_1 (day^2/m^4)	0	10^{-4}	10^{-3}	10^{-2}	0.1	1	1	1	1	1	1
w_2	1	1	1	1	1	1	0.1	10^{-2}	10^{-3}	10^{-4}	0

Figure 2. Absolute relative error plots for the five parameters with respect to various weights applied on the flow-rate (w_1) and drawdown (w_2) data in the composite analyses for (a) positive-skin and (b) negative-skin cases.

CONCLUSION

Two types of CHT analyses were considered, which were classified according to the analyses of well responses being conducted in a single or multiple wells. The analyzed results lead to the following conclusions. In the analyses of single-well responses, the use of flow-rate data yielded accurate estimates for skin parameters but might produce less reliable estimates for aquifer parameters. Next, the analyses of drawdown data were hard to obtain precise estimates for skin and aquifer parameters. In the analyses of multi-well responses, it seemed possible to obtain accurate aquifer parameters using the specific drawdown data when the CHT had the skin effect. In addition, the skin and aquifer parameters appeared to be determined accurately when both the flow-rate and drawdown data were employed in the two-stage analysis. Finally, simultaneous analyzing the flow-rate and drawdown data can obtain the most accurate estimates for all the five parameters if the weights in the objective function were carefully chosen. Therefore, it is highly

recommended to analyze the flow-rate and drawdown data simultaneously.

REFERENCES

Hiller, C.K., and Levy, B.S. (1994). "Estimation of aquifer diffusivity from analysis of constant-head pumping test data." *Ground Water*, 32(1), 47-52.

Jacob, C.E., and Lohman, S.W. (1952). "Nonsteady flow to a well of constant drawdown in an extensive aquifer." *Trans. Am. Geophys. Union.*, 33(4), 559-569.

Mishra, S., and Guyonnet. D. (1992). "Analysis of observation-well response during constant-head testing." *Ground Water*, 30(4), 523-528.

Yang, S.Y., and Yeh, H.D. (2002). "Solution for flow rates across the wellbore in a two-zone confined aquifer." *J. Hydraul. Eng.*, 128(2), 175-183.

Yang, S.Y., and Yeh, H.D. (2006). "A novel analytical solution for constant-head test in a patchy aquifer." *Int. J. Numer. Anal. Methods Geomech.*, 30(12), 1213-1230.

Yeh, H.D., and Chen Y.J. (2007). "Determination of skin and aquifer parameters for a slug test with wellbore-skin effect." *J. Hydrol.*, 342(3-4), 283-294.

Wavelet Analysis of Characteristic Length Scales of Permeability in Stationary and Non-Stationary Porous Media

X. Qi[1] and R. M. Neupauer[2]

[1]Department of Civil Engineering, University of Virginia, P.O. Box 400742, Charlottesville, VA 22904-4742; email: xq6v@virginia.edu
[2]Department of Civil, Environmental, and Architectural Engineering, University of Colorado, UCB 428, Boulder, CO 80309 USA; PH (303) 492-6274; FAX (303) 492-7317; email: neupauer@colorado.edu

ABSTRACT

Heterogeneity of aquifer permeability has a significant influence on the transport of solutes; therefore accurate characterization of aquifer heterogeneity is needed to reliably predict the behavior of solutes. A critical characteristic of heterogeneity is the characteristic length scale that is a measure of the distance over which property values are correlated. We use two-dimensional continuous wavelet analysis to identify characteristic length scales of permeability in stationary and non-stationary porous media. We show that the global and local wavelet energy spectra are the appropriate measures to characterize length scales in stationary and non-stationary permeability fields, respectively. We demonstrate its effectiveness in identifying the characteristic length scales of two-dimensional synthetic permeability data.

INTRODUCTION

Flow and transport through porous media are affected by the heterogeneity of aquifer properties such as permeability. Permeability heterogeneity causes local velocity variations that enhance the dispersion of solutes migrating through the aquifer. Laboratory and field data have shown that both heterogeneity and dispersivity are scale-dependent (Gelhar, 1986; Silliman and Simpson, 1987; Tidwell and Wilson, 1999, 2000). In this paper, we use wavelet analysis to characterize dominant scales of permeability heterogeneity.

Wavelet analysis has recently been used to characterize spatial variability in geophysical systems. Spedding et al. (1992) used two-dimensional wavelets to obtain a scale-space decomposition of surface waves generated by unsteady winds. Kumar and Foufoula-Georgiou (1993) used wavelet transforms to decompose spatial rainfall fields into large-scale (mean behavior) and small-scale (fluctuations) features, and segregated components having characteristic features at different scales. Li and Loehle (1995) used wavelet analysis to identify scales of dominant structures in permeability of alluvial fan deposits in Nevada. Sahimi (2001) and Sahimi and

Hashemi (2001) used wavelet analysis of synthetic and real porosity data to identify the spatial distribution of rock fractures. Frantziskonis (2002) presented a wavelet analysis approach for characterizing scales of one-dimensional transects of porous material properties. Qi and Neupauer (2008) used a related method for identifying dominant scales in one-dimensional, stationary random fields.

Wavelet analysis has also been used to characterize dominant orientations in some geophysical systems. Kumar and Foufoula-Georgiou (1993) used wavelet transforms to isolate directional information to show the anisotropic behavior of rainfall intensity fluctuations. Kumar (1995) used a wavelet transform technique to analyze scale space anisotropy of spatial rainfall fields. Gaillot et al. (1997, 1999) used wavelet analysis to identify size, shape, and orientation in rock fabrics by identifying orientations of distinct boundaries between the mineral and the rock matrix. In a porous medium, permeability can vary gradually, without any distinct boundaries between regions. Neupauer et al. (2006) and Watkins et al. (2009) used a fully-anisotropic Morlet wavelet to demonstrate that wavelet analysis can be used to identify characteristic length scales and orientations in periodic statistically-heterogeneous permeability field.

In this paper, we present wavelet analysis as a method to identify characteristic length scales of permeability in stationary and non-stationary porous media. In the next section, we introduce wavelet analysis. In subsequent sections, we present a wavelet approach for analyzing characteristic length scales in stationary and non-stationary porous media.

BACKGROUND

Wavelet analysis involves the integral transform of a random space function (e.g., a permeability field), with a wavelet as the kernel. A wavelet is a zero-mean function that is non-zero over a finite region. In this work, we use the two-dimensional Mexican hat wavelet given by

$$\psi(\mathbf{x}) = \frac{1}{\sqrt{2\pi}}\left(2 - \mathbf{x}\cdot\mathbf{x}\right)\mathrm{e}^{-\mathbf{x}\cdot\mathbf{x}/2} \quad , \tag{1}$$

where $\mathbf{x} = (x,y)$ is a vector of spatial coordinates. Figure 1a shows a plot of the Mexican hat wavelet. The wavelet transform of a two-dimensional, zero-mean anisotropic function, $f(\mathbf{x})$, is given by

$$W_f(a,\mathbf{b},\theta,\Lambda) = \frac{\sqrt{\Lambda}}{a}\int_{-\infty}^{\infty} f(\mathbf{x})\psi^*\left(\frac{1}{a}\left[\mathbf{ACx}-\mathbf{b}\right]\right)d\mathbf{x} \quad , \tag{2}$$

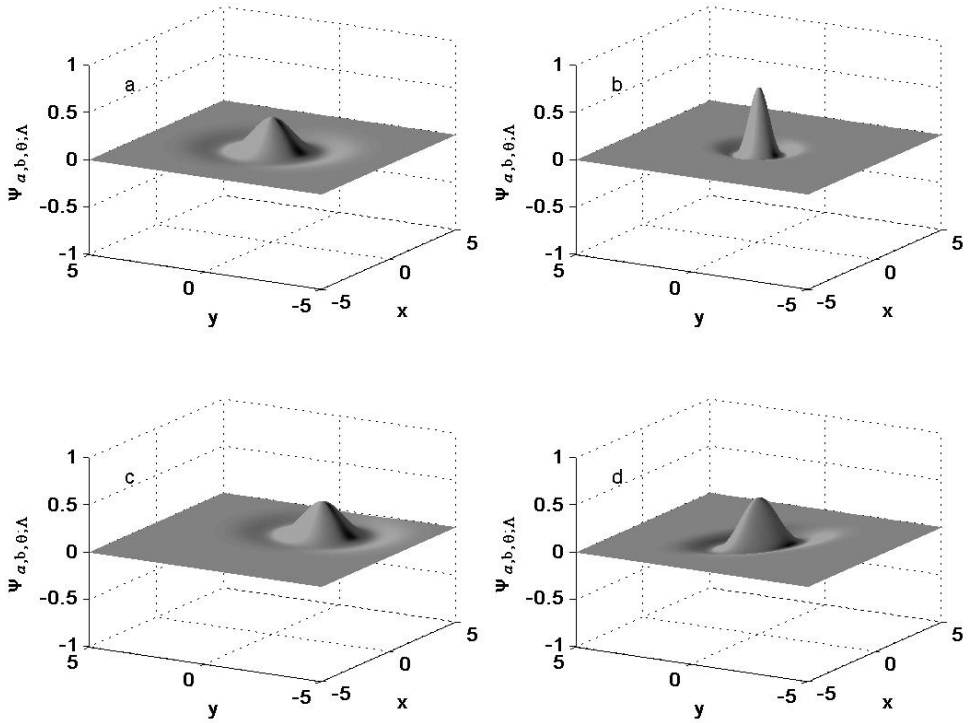

Figure 1. Mexican hat wavelet. (a) Standard wavelet. (b) Scaled wavelet with a = 0.5. (c) Shifted wavelet with (b_x,b_y) = (2,-1). (d) Anisotropic rotated wavelet with θ = -30° and Λ = 2.

where $W_f(a,\mathbf{b},\theta,\Lambda)$ is the wavelet coefficient, a is a scale parameter, $\mathbf{b} = (b_x,b_y)$ is a shift parameter, the asterisk denotes complex conjugate, **C** and **A** are rotation and anisotropy matrices, respectively, given by

$$\mathbf{C} = \begin{bmatrix} \cos\theta & \sin\theta \\ -\sin\theta & \cos\theta \end{bmatrix} \qquad \mathbf{A} = \begin{bmatrix} 1 & 0 \\ 0 & \Lambda \end{bmatrix} \tag{3}$$

where θ is the orientation of the wavelet (defined as positive in the counterclockwise direction with θ = 0° in the +x direction), and Λ is the anisotropy ratio defined as the ratio of the length of the wavelet in the θ direction to the length of the wavelet in the direction perpendicular to θ. Figure 1b-d shows plots of scaled, shifted, and rotated wavelets, respectively.

To analyze a function using wavelet analysis, the wavelet transform in (2) is performed for a range of scales a, shifts **b**, orientations θ, and anisotropy ratios Λ, producing a five-dimensional wavelet coefficient (one scale dimension, two shift dimensions, one orientation dimension, and one anisotropy dimension). The wavelet

coefficients can be used to identify dominant features of the function $f(\mathbf{x})$, including the characteristic length scale. The characteristic length scale of $f(\mathbf{x})$ is related to the wavelet scale a at which a measure of the wavelet coefficient attains its maximum. The appropriate measure to use to determine the characteristic length scale depends on the character of the function.

WAVELET ANALYSIS OF STATIONARY RANDOM FIELDS

For periodic functions, the wavelet spectrum $|W_f(a,\mathbf{b},\theta,\Lambda)\ W_f{}^*(a,\mathbf{b},\theta,\Lambda)|$ can be used to identify the characteristic length scale at each position (e.g., Neupauer et al., 2006; Watkins et al., 2009). For each position $\mathbf{x} = \mathbf{b}$, the magnitude of the wavelet spectrum is relatively large at the wavelet scale a that is dominant at that position.

For random fields, the function $f(\mathbf{x})$ contains randomness; therefore the wavelet coefficients from (2) and the wavelet spectrum also contain randomness. For stationary random fields, the statistical properties of the random field do not vary in space; therefore the characteristic length scale is uniform throughout the random field. In the context of wavelet analysis, stationarity implies that the wavelet spectrum is independent of position $\mathbf{b}$. In other words, a single wavelet scale should be dominant throughout the entire $\mathbf{b}$ domain. In actuality, because of the randomness in $f(\mathbf{x})$, the wavelet spectrum does vary in the $\mathbf{b}$ domain.

Instead of using the wavelet spectrum to identify the characteristic length scales of stationary random fields, we use a measure related to the expected value of the wavelet spectrum. Qi and Neupauer (2008) and Qi (2008) showed that the global wavelet energy spectrum (GWES) is the appropriate measure for identifying characteristic length scales of stationary random fields. For a two-dimensional anisotropic random field $f(\mathbf{x})$, the GWES is defined as (Qi and Neupauer, 2009)

$$E(a,\theta,\Lambda) = \frac{\Lambda}{a^2}\left\langle \left| W_f(a,\mathbf{b},\theta,\Lambda)\right|^2 \right\rangle \tag{4}$$

where $E(a,\ \theta,\ \Lambda)$ is the global wavelet energy spectrum, the angle brackets denote expected value, and $|\ |^2$ denotes the L_2 norm. For a stationary random field, the spatial average of the wavelet spectrum (averaged over the $\mathbf{b}$ domain) is identical to the average wavelet spectrum based on many realizations of the random field; thus the GWES can be evaluated as

$$E(a,\theta,\Lambda) = \frac{\Lambda}{a^2}\left\langle \left| W_f(a,\mathbf{b},\theta,\Lambda)\right|^2 \right\rangle = \frac{\Lambda}{a^2 A}\int_{\mathbf{b}} \left| W_f(a,\mathbf{b},\theta,\Lambda)\right|^2 \, d\mathbf{b} \tag{5}$$

where A is the area of the spatial domain. The GWES is a three-dimensional function, with dimensions of scale, orientation, and anisotropy. If the principal directions of anisotropy are known, the wavelet transform can be performed for just

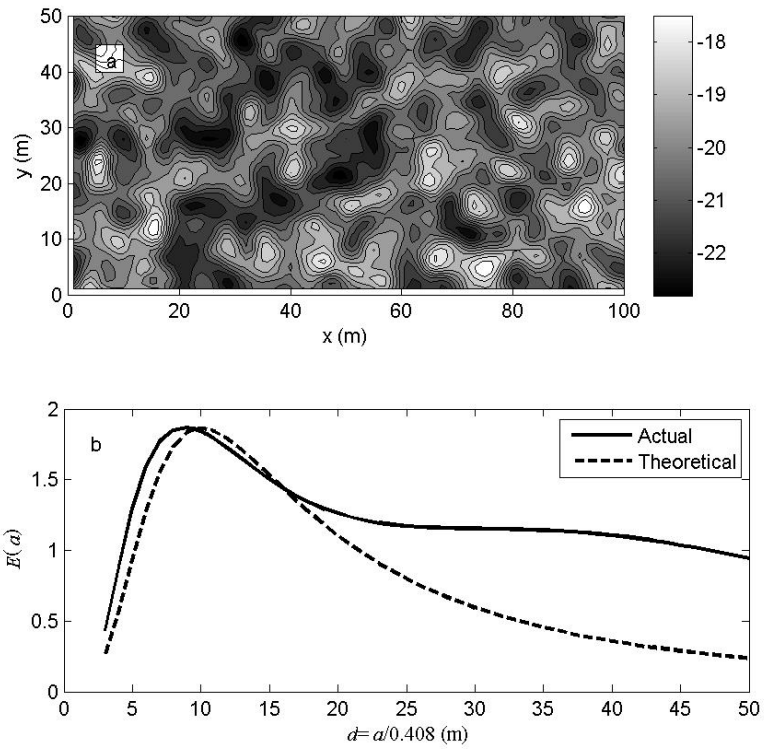

Figure 2. (a) Random field with Gaussian covariance with correlation length of 10 m. (b) GWES of random field.

the principal directions, and the GWES is essentially a two-dimensional function. For an isotropic random field, the statistical properties do not depend on orientation, so the wavelet transform must only be performed for a range of scales, with $\theta = 0^o$ and $\Lambda = 1$; thus the GWES is reduced to a function only of wavelet scale a. Let a_{max} be the wavelet scale at which the GWES attains its maximum. Qi (2008) has shown that the relationship between the characteristic length scale d of the random field and a_{max} depends on the dimensionality of the random field, the wavelet used in the analysis, and on the covariance structure of the random field. For a two-dimensional random field with Gaussian covariance, $a_{max}/d = 0.408$ when wavelet analysis is performed using the Mexican hat wavelet (Qi, 2008).

As an example, consider the two dimensional random permeability field shown in Figure 2a. This random field was generated using sequential Gaussian simulation from the GSLIB software package (Deutsch and Journel, 1992). It has an isotropic Gaussian covariance with a correlation length of 10 m and a spatial discretization of 1m. We performed wavelet analysis using (2) using $\theta = 0^o$ and $\Lambda = 1$ for this isotropic random field, and we used the resulting wavelet coefficients in (5) to calculate the GWES, which is shown in Figure 2b (solid line), where the horizontal axis is the length scale $d = a/0.408$, accounting for the relationship between wavelet scale and length scale. The GWES has a single peak that occurs at $d = 9$ m,

indicating that the characteristic length scale of the random field is approximately 9 m. Recall that this random field was generated with a correlation length of 10 m. Due to randomness, however, the correlation length is not exactly 10 m. Here, through wavelet analysis, we show that the correlation length is slightly smaller. For comparison, Figure 2b also shows the theoretical GWES (dotted line) for a random field with Gaussian covariance with correlation length of 10 m (see Qi (2008) for derivation). The GWES for this random field (solid line) is shifted slightly to the left relative to the theoretical GWES, indicating that the actual correlation length of the random field is slightly smaller than the theoretical correlation length.

WAVELET ANALYSIS OF NON-STATIONARY RANDOM FIELDS

For non-stationary random fields, the characteristic length scales may vary with position **b**; therefore the spatial average of the wavelet spectrum over the **b** domain is not identical to the expected value of the wavelet spectrum. In this situation, the second equality in (5) does not hold.

For non-stationary random fields, a more appropriate wavelet measure is the local wavelet energy spectrum, $E^*(a,\mathbf{b},\theta,\Lambda)$ (LWES), defined as (Farge, 1992)

$$E^*(a,\mathbf{b},\theta,\Lambda) = \frac{\Lambda}{a^2}\left|W_f(a,\mathbf{b},\theta,\Lambda)\right|^2 \tag{6}$$

for a two-dimensional function $f(\mathbf{x})$. Comparison of (5) and (6) shows that the GWES is the spatial average of the LWES.

We used sequential Gaussian simulation (Deutsch and Journel, 1992) to create a zonally-stationary random field with exponential covariance with correlation length of 100 m for $x < 1000$ m, and correlation length of 10 m for $x > 1000$ m (labeled Zone A and Zone B, respectively, in Figure 3a). The LWES of this random field is shown in Figure 3b, where the vertical axis is the length scale $d = a/0.42$. The denominator 0.42 is the ratio of wavelet scale to characteristic length scale for a one-dimensional random field with exponential covariance analyzed with a Mexican hat wavelet (Qi and Neupauer, 2008). The LWES has several isolated subregions with high magnitudes which represent subregions where the random field has strong spatial correlation. The characteristic length scale in those subregions is the scale d at which the LWES attains a local maximum. In Zone A, the characteristic length scales are around 100 m; while in Zone B, the characteristic length scales are around 10 m. Because of randomness in the random field, the LWES is not uniform within each zone. The average LWES for 1000 realizations of the random field (Figure 3c) shows a more uniform result, with the peak value of the LWES occurring at $d = 100$ m throughout most of Zone A, except at the edges; and the peak value of the LWES occurring at $d = 10$ m throughout Zone B except at the boundaries.

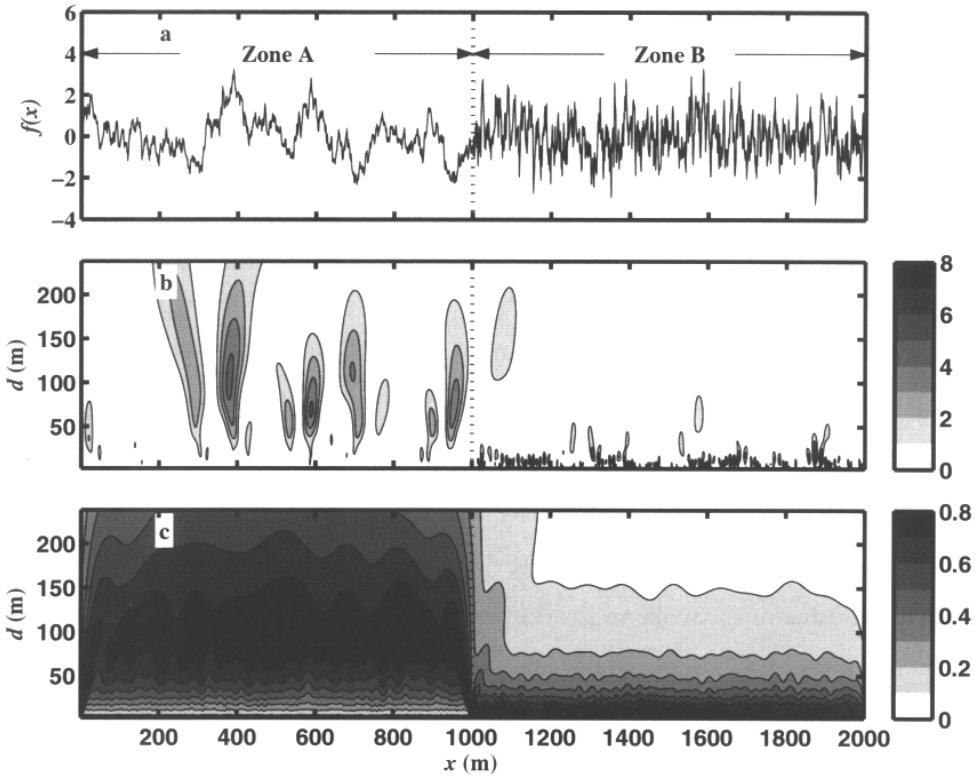

Figure 3. (a) Zonally-stationary random field. (b) LWES of random field. (c) average LWES over 100 realizations of random field. (from Qi, 2008).

CONCLUSIONS

Wavelet analysis can be used to identify characteristic length scales of permeability in statistically stationary and non-stationary porous media. For stationary random fields, the global wavelet energy spectrum has a single peak at a wavelet scale that corresponds to the characteristic length scale of the random field. For non-stationary random fields, the local wavelet energy spectrum must be used. It has local maxima at wavelets scales that correspond to characteristic lengths scales within a subregion of the random field that exhibits strong spatial correlation.

ACKNOWLEDGEMENTS

This work was funded by grants from the National Science Foundation under Grants EAR-0237702 and EAR-0520995.

REFERENCES

Deutsch, C.V., and Journel, A.G. (1992). *GSLIB: Geostatistical Software Library and User's Guide*, Oxford University Press, New York.

Farge, M. (1992). "Wavelet transforms and their applications to turbulence." *Annual Review of Fluid Mechanics,* 24, 395-457.

Frantziskonis, G. (2002). "Wavelet-based analysis of multiscale phenomena: Application to material porosity and identification of dominant scales." *Probabilistic Engineering Mechanics*, 17, 349-357.

Gaillot, P., Darrozes, J., and de Saint Blanquat, M. (1997). "The normalized optimized anisotropic wavelet coefficient (NOAWC) method: An image processing tool for multi-scale analysis of rock fabric." *Geophysical Research Letters,* 24(14), 1819-1822.

Gaillot, P., Darrozes, J., and Bouchez, J.-L. (1999). "Wavelet transforms: a future of rock fabric analysis?" *Journal of Structural Geology,* 21, 1615-1621.

Gelhar, L.W. (1986). "Stochastic subsurface hydrology from theory to applications." *Water Resources Research*, 22(9), 135S-145S

Kumar, P. (1995). "A wavelet based methodology for scale-space anisotropic analysis." *Geophysical Research Letters,* 22(20), 2777-2780.

Kumar, P., and Foufoula-Georgiou, E. (1993). "A multicomponent decomposition of spatial rainfall fields, 1, Segregation of large- and small-scale features using wavelet transforms." *Water Resources Research*, 29(8), 2515-2532.

Li, B.-L. and Loehle, C. (1995). "Wavelet analysis of multiscale permeabilities in the subsurface." *Geophysical Research Letters,* 22(23), 3123-3126.

Neupauer, R.M., Powell, K.L., Qi, X., Lee, D.H., and Villhauer, D.A. (2006). "Characterization of permeability anisotropy using wavelet analysis." *Water Resources Research*, 42, W07419, doi:10.1029/2005WR004364.

Neupauer, R.M. and Powell, K.L. (2005). "A fully-anisotropic Morlet wavelet to identify dominant orientations in a porous medium." *Computers & Geosciences*, in press.

Qi, X. (2008). Wavelet analysis of characteristic length scales of heterogeneous porous media, Ph.D. dissertation, University of Virginia, Charlottesville, Virginia.

Qi, X. and Neupauer, R.M. (2008). "Wavelet analysis of dominant scales of heterogeneous porous media." *Water Resources Research*, 44, W09406, doi:10.1029/2006WR005720.

Qi, X. and Neupauer, R.M. (2009). "Wavelet analysis of characteristic length scales of permeability in two-dimensional stationary porous media." in preparation.

Sahimi, M. (2001). "Characterization and modeling of oil reservoirs and groundwater aquifers: application of wavelet transformation." *Granular Matter*, 3, 3-14.

Sahimi, M. and Hashemi, M. (2001). "Wavelet identification of the spatial distribution of fractures." *Geophysical Research Letters*, 28(4), 611-614.

Silliman, S.E., and Simpson, E.S. (1987). "Laboratory evidence of the scale effect in dispersion of solutes in porous media." *Water Resources Research*, 23(8), 1667-1673.

Spedding, G.R., Browand, F.K., Huang, N.E., and Long, S.R. (1992). "A 2-D

complex wavelet analysis of an unsteady wind-generated surface wave field." *Dynamics of Atmospheres and Oceans*, 20, 55-77.

Tidwell, V.C. and Wilson, J.L. (1999). "Permeability upscaling measured on a block of Berea sandstone: Results and interpretations." *Water Resources Research*, 35(11), 3375-3387.

Tidwell, V.C. and Wilson, J.L. (2000). "Heterogeneity, permeability patterns, and permeability upscaling: Physical characterization of a block of Massillon sandstone exhibiting nested scales of heterogeneity." *SPE Reservoir Evaluation and Engineering*, 3(4), 283-291.

Watkins, L.P., Neupauer, R.M., and Compo, G.P. (2009). "Wavelet analysis and filtering to identify dominant orientations of permeability anisotropy." *Mathematical Geosciences,* in review.

Framing the design process in an undergraduate environmental engineering class

Deb O'Bannon[1], F.ASCE and Tom Kimes[2]

[1]Department of Civil and Mechanical Engineering, University of Missouri-Kansas City, 5100 Rockhill Road, Kansas City MO 64110; PH (816)235-1287; FAX (816)235-1260; email: obannond@umkc.edu
[2]HDR Engineering, Inc. 4435 Main Street, Suite 1000, Kansas City MO 64111; PH (816)360-2737; FAX (816)360-2777; email: tkimes@hdrinc.com

ABSTRACT

The environmental engineering core class at the University of Missouri-Kansas City has introduced a broader definition of "design" to the undergraduate students, and framed the open-ended work they produce in a design life-cycle, which is represented graphically.

STRUCTURE OF CLASS

The basic environmental engineering class at the University of Missouri-Kansas City focuses on water plant and wastewater treatment plant processes. In an effort to include more open-ended design project in the curriculum several years, the following format was established.

1. The class was divided into groups of three or four students.
2. Several different client town/cities were distributed to the groups. Variables include: town size/flow, soft or hard drinking water source, high or low dilution into receiving water (freshwater).
3. Four different designs are produced for the client town.
    a. Laboratory design
    b. Water plant design
    c. Wasteload allocation
    d. Wastewater treatment plant design

The variety of client types help educate students on plant designs different from those they visit on field trips in the class.

AMBIGUITY OF "DESIGN"

Discussions with an advisory board member revealed that when the faculty talks about "design" in engineering classes, we might imply very different steps in the overall design cycle. A graphic was created to differentiate various stages within a project to communicate

it to the students (see Figure 1).

Figure 1: Design process with environmental class indicated.

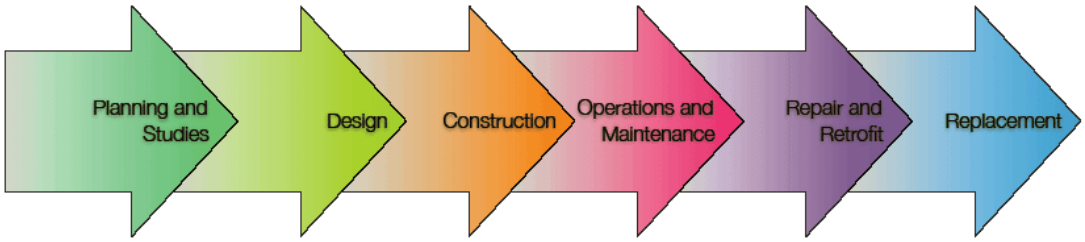

Water/Wastewater

The graphic was printed in large format and posted several prominent places around the department.A modification of the student designs in the environmental engineering class now include a debriefing by professionals who can explain what comes next in the design sequence. The environmental engineering class produces brief planning reports, but are not specifying equipment or dealing with site topography. The professionals who now participate in the conceptual design review are

- architect, who share architectural plans for similar projects,
- water plant designer, who shares the blueprint set for a water plant,
- water quality modeler, who shares actual wasteload allocation efforts, and
- wastewater treatment plant designer, who shares portions of a blueprint set for a wastewater treatment plant.

HOW THE CURRICULA WORKS WITH THE DESIGN GRAPHIC

The required courses were evaluated by the faculty to show where they fit in the design sequence. The civil engineering courses are shown in Figure 2, and the mechanical engineering courses are shown in Figure 3.

Figure 2: CE Required Courses (CE342=Env. Eng; CE355=Water Resources; CE481=Traffic; ME111=freshman design; CE323=Concrete Design; CE422=Steel Design; CE412=senior design)

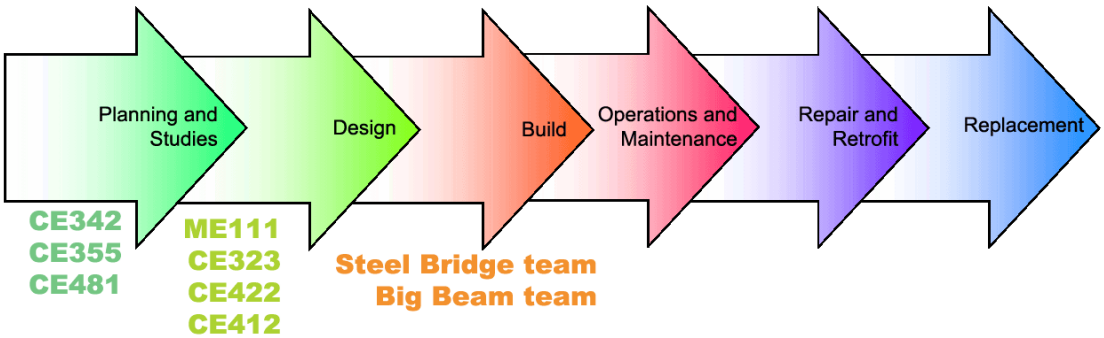

Figure 3: ME Required Classes (ME111=freshman design; ME306=; ME360=thermal systems design; ME440=heating&air conditioning; ME451 =power plant design; ME496=senior design)

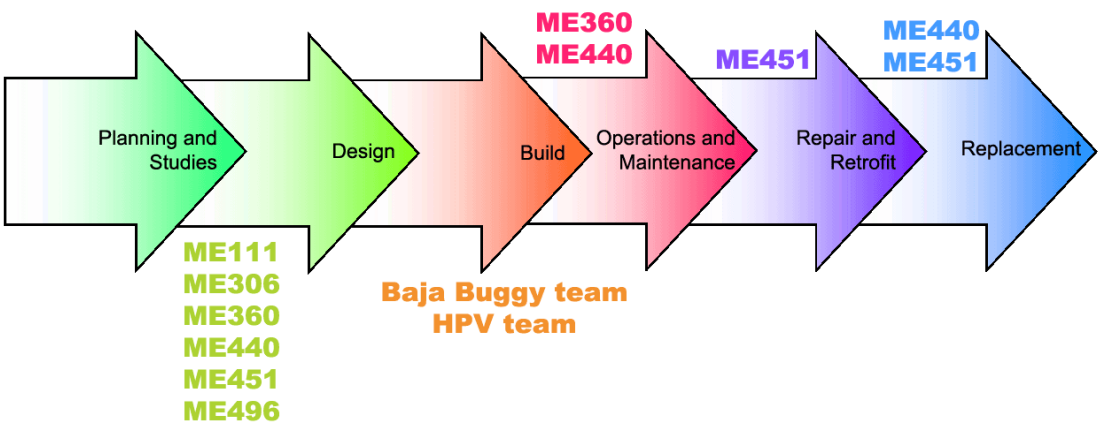

CONCLUSION

The mechanical engineering curriculum presently does a better job of introducing students to the concepts of operations and maintenance, repair and replacement than the current civil engineering curriculum. The recent addition of construction engineering faculty will add the components of O&M and replacement into the civil engineering curriculum.

Integrating Design Heuristics in an Environmental Engineering Course

Kathleen M. Leonard

ASCE Fellow, Professor, Department of Civil and Environmental Engineering,
University of Alabama in Huntsville, Huntsville, AL 35899-0001;
PH (256) 824-6423; FAX (256) 824-6724; email: leonard@eng.uah.edu

ABSTRACT

Although design courses are mandatory requirements for all accredited engineering schools in the United States, in many cases these courses have become a technical exercise with little integration of management and innovation. As a result, current engineering educational strategies produce technicians lacking the advanced critical thinking and management skills required in the 21st century business environment. This paper presents a first approach to integrating modules on design heuristics into a mid-level environmental engineering design course. The goal is to facilitate students' skills in both understanding the mechanics of design and gain practice in research oriented design.

INTRODUCTION

Like most engineering schools, the University of Alabama in Huntsville (UA Huntsville), has several upper-level design courses that draw on technical knowledge accumulated during the students' academic career (while also fulfilling ABET requirements). At this point in their academic careers students are usually competent in integrating the technical tools, but have limitations associated with managerial skills and follow-through in design. In the past several years UA Huntsville has been aided in addressing these limitations by local civil engineering practitioners coming into the classroom as lecturers on topics such as "budgeting a project" and "resume writing skills."

Recently there has been discussion about the limitations of engineering education [Beder, Bordogna]. For example, the National Research Council (NRC) recommends that the engineering education system needs to become more flexible and adaptable to the changing needs of society [NRC]. We, as educators, are adept at traditional lecturing and assigning closed-ended problems. However, recent findings note that

students need to learn by doing, and that creative design skills can be sharpened if exercised. Unfortunately, towards the end of their academic careers students are usually competent in basic science, math and engineering knowledge, but have limitations in integrating these skills with solving a practical problem. One of the issues is novel idea generation. There are many different reasons for this problem. One explanation could simply be that civil engineering students do not have sufficient practice in open-ended problem solving. It may also be that engineering students get the subconscious message that there is only one way to solve problems from their early technical courses.

APPROACH

The environmental engineering curriculum at UA Huntsville includes an environmental engineering design class required of all majors. The design problems are "real-world" projects posed by local civil engineering companies and government agencies. The problem-solving heuristic used in this course is taken from Fogler and LeBLanc composed of five steps: define the problem, generate solutions, decide on a course of action, implement the solution and evaluate the solution. Several interactive classroom exercises were used to introduce problem-solving techniques such as brainstorming and Osborne's checklist. Next, they were introduced to decision analysis tools to assess solutions based on a list of performance objectives and design constraints. The students have to integrate ethics and cost analysis into the final design report and present their findings to the class with monthly research reports.

The project assigned to the students motivates students to use all levels of Bloom's Taxonomy for cognitive domain: integrating (1) knowledge to (2) comprehension through (3) application, (4) analysis: (5) synthesis, and (6) evaluation. A primary objective is to provide the Civil Engineering student with hands-on application of the principles of design and an opportunity for creativity.

The strategy of the course is to produce students who know "how to find out" and "how to examine and evaluate evidence." The following criteria were used in selecting the design problems:

- The design problems are "real" problems proposed by local clients, engineers and researchers.
- Each problem must have an experimental component that could be completed in the semester
- The students were introduced to performing research of refereed literature and technical data.
- The team must compile an experimental plan prior to any lab work
- The team must submit and verify weekly time sheets.

The approach in this study was to use the entire class to brainstorm ideas to solve each design problem. Then each individual two person team must research at least

three different alternatives and use a decision analysis technique to decide on the optimum solution. Each team is required to research, develop and then perform a bench-scale laboratory experiment to prove feasibility. Similarly, the concept of cooperative learning, an instructional method that involves people working in teams to achieve a common goal, was demonstrated by team teaching as documented by NRC.

Each team gives a final oral presentation to local professionals for twenty-five percent of their grade. It must incorporate the team objectives, approach to solving the design problem, all alternatives considered, their decision matrix, and laboratory results. This gives them practice with both oral and communication e benefits of this lecture extend throughout their college coursework for the presentations they will be required to make in most of their subsequent civil engineering classes.

RESULTS

The course has been offered for ten years since its inception in 1998. The students rate the class using a standard "instructor evaluation form" at the end of each semester. This course has consistently received high marks (over 95% agreement) for teaching methods and quality of instruction. Students are surveyed at graduation and mention that this course helped them become aware of that innovation is an important component of design. The course fits into the novel approach in the Civil Engineering department to incorporate design into all levels of the undergraduate curriculum.

CONCLUSIONS

Because engineers will be challenged to fulfill professional expectations within the twenty-first century, the educational system will have to adjust to meet these demands. As proposed in this paper, the utility of learning the art of design alongside hands on implementation can develop a more innovative engineer. The cooperation between the engineering professor and professionals also serves as a role model for teamwork and mutual appreciation.

ACKNOWLEDGEMENTS

The author would like to thank the professionals who suggested and supported this course. The study would not have been possible without the CE 458/558 design students who gave their energy and innovation to their projects.

REFERENCES

Beder, S., (1999) Beyond Technicalities: Expanding Engineering Thinking," *J. of Prof. Issues in Engrg. Educ. And Prac.*, 125(1), 12-18.

Bloom, B. S., Engelhart, M. D., Furst, E. J., Hill, W. H., and Krathwohl, D. R., (1956) *Taxonomy of Educational objectives: The Classification of Educational Objectives. Handbook I: Cognitive Domain*, David McKay, New York.

Bordogna, J, (1998) "Tomorrow's Civil Systems Engineer – The Master Integrator," *J. of Prof. Issues in Engrg. Educ. And Prac.*, 124(2), 48-50.

Fogler, H. S. LeBlanc,S. Strategies for Creative Problem Solving, 2nd ed Prentice Hall, 2008.

National Research Council: Board on Engineering Education, (1995) *Engineering Education: Designing an Adaptive System*, National Academy Press.

Non-traditional University Research Partners that Facilitate Service Learning and Graduate Research for Sustainable Development

M. A. Trotz[1], H.E. Muga[1], L.D. Phillips[1], D. Yeh[1], A. Stuart[2], and J.R. Mihelcic[1]

[1]Department of Civil and Environmental Engineering, University of South Florida, 4202 East Fowler Avenue, ENB118, Tampa FL 33620; PH (813) 974-3172; FAX (813) 974-9106; email: matrotz@eng.usf.edu
[2]Department of Environmental & Occupational Health, and Department of Civil & Environmental Engineering University of South Florida, 13201 Bruce B. Downs Blvd, MDC-56, Tampa, FL 33612; PH (813) 974-6632; email: astuart@hsc.usf.edu

Abstract
Goal 7 of the Millennium Development Goals addresses the need for safe water, sanitation, and hygiene by aiming to halve the proportion of people without access to safe water and adequate sanitation from 1990 benchmarks by 2015. One key for successfully integrating university research with global development is to develop strategic partnerships with non-traditional academic partners that have a strong community presence. Here we use several case studies to demonstrate how these partnerships are integrated with graduate education and research to develop sustainable solutions for global problems.

The Master's International Program in Civil & Environmental Engineering at the University of South Florida (USF) provides students with an opportunity to combine their graduate education with service in the U.S. Peace Corps as water/sanitation engineers and an overseas research component. Key features are a 6-credit research thesis and a 9-credit, three course sequence in: 1) global public health assessment, 2) applied anthropology, and 3) sustainable engineering technology. Students may also incorporate with their degree a new graduate certificate in Water, Health, and Sustainability.

An interdisciplinary graduate course allows students to investigate concepts of sustainability and research methods using a case study focus that focuses on mercury in the Tampa Bay area and a contrasting field based experience in Guyana. Students identify and integrate research approaches across disciplines, implement population surveying methods, and apply simple systems modeling. An NSF research project situated in Bolivia allows undergraduate and doctoral graduate students to work with a non-government organization and rural community water committees to research issues of water supply, water scarcity, sanitation, and watershed management. The Kiran C. Patel Center for Global solutions at USF also supports activities in this like the facilitation of graduate exchange training exercises with UNESCO-IHE students.

Introduction

The National Science Board views international Science and Engineering (S&E) partnerships for research and education as essential for maintaining U.S. competitiveness in the 21st century given the impact of September 11th on intellectual

exchanges across U.S. borders, the shift in leadership due to globalization, and the global nature of challenges like climate change and the spread of HIV (National Science Board, 2008). Successful international S&E partnerships contribute to economic development, capacity building of civil society, elevation of women and underrepresented groups, and productive, socially responsible solutions to global S&E problems (National Science Board, 2008). The United Nations Millennium Development Goals (MDGs) present examples of real challenges that today's graduate must be prepared to solve around the world and provide motivation for integrating international experiences with engineering education (United Nations, 2000; UN Millennium Project, 2005). For example, Goal 7 of the MDGs addresses the need for safe water, sanitation, and hygiene by aiming to halve the proportion of people without access to safe water and adequate sanitation from 1990 benchmarks by 2015. These targets present technological and socio-political challenges (Zimmerman et al., 2008) and to meet them, more non-traditional partnerships and funding mechanisms are emerging that include non-governmental and civic organizations (Hokanson et al., 2006; Mihelcic, et al., 2005, 2006). One key for successfully integrating university research with global development is to develop strategic partnerships with non-traditional academic partners that have a strong community presence.

This paper presents four case studies (Table 1) to demonstrate how these non-traditional partnerships are currently integrated with university level education (undergraduate and graduate) and research to develop sustainable solutions for global problems.

Table 1: Summary of the case studies discussed in this paper.

Case	Non-Traditional Academic Partner	BS	MS	Ph.D.
1. Master's International Program (MIP)	Peace Corps, local community organizations, local government		X	
2. Interdisciplinary Graduate Course with International Field Experience	WWF-Guianas, local NGOs		X	X
3. Bolivia Research Experience and Capstone Design	Local NGOs and community groups	X		X
4. UNESCO-IHE	Dr. Kiran C. Patel Center for Global Solutions, UNESCO-IHE		X	X

Case 1: Master's International Program (MIP)

The Master's International Program (MIP) in Civil & Environmental Engineering at the University of South Florida (USF) provides students with an opportunity to

combine their graduate education with service in the U.S. Peace Corps as water/sanitation engineers in a developing country. Through the program students learn: 1) to interact with the disciplines of public health, applied anthropology and sustainability, 2) to integrate a health and human dimension into engineering, 3) to apply appropriate and sustainable technology and correctly balance the dynamic between society, economy, and the environment, 4) to protect the environment while serving neighbors and humankind, and 5) the critical role engineering can play in the eradication of global poverty and hunger; improving global health; promoting gender equality; facilitating sustainable development, appropriate technology, and beneficial infrastructure; and promoting change that is environmentally and socially just (see http://cee.eng.usf.edu/peacecorps).

There are two program options at USF: a 30-credit M.S. Degree in Civil Engineering and Environmental Engineering which requires a first degree in engineering that is ABET accredited and a 30-credit Master of Science in Engineering Science – Environmental Engineering which is open to any student and does not require make up course work if the first degree is in math or science. For both degrees, 24 credits are taken on campus (4 classes per semester) and 6 are thesis research associated with a project identified and executed while a student serves in the Peace Corps. Eighteen of the 24 credits taken on campus must be in the Civil and Environmental engineering school and students must complete a 9-credit, three course sequence in: 1) global public health assessment, 2) applied anthropology, and 3) sustainable engineering technology. The curriculum includes 15 credits of electives to be suited to the student's area of interest (i.e., environmental, green engineering/sustainability, water resources and quality, transportation planning, structural, materials, geotechnical).

The program is also open to students without an engineering undergraduate degree who would earn a master's in Environmental Engineering Science and to students wishing to pursue a doctoral degree. Students may also incorporate with their degree a new 16-credit graduate certificate in Water, Health, and Sustainability that is intended for public health professionals, humanitarian aid providers, engineers and other planners, or anyone with an interest in addressing critical shortages and health problems associated with inadequate and unsanitary water throughout the world.

MIP students work on a wide variety of projects while serving as engineers with the Peace Corps which are detailed elsewhere (Mihelcic, 2004). Assignments range from the village to larger regional scale and typically consist of assisting communities on issues related to water supply and treatment, wastewater collection and treatment, water resources management, solid waste management, and public health education. Students get involved in all aspects of a engineering project, including surveying, financing, design, material selection, scheduling, construction, billing, worker supervision, and issues of operation and maintenance. Students work closely with public health professionals, assist in the creation and training of community water boards, and work on broader sustainability issues that impact residents of their host country. Under the supervision of a faculty advisor at USF students design their

research thesis which is presented at the end of their field placement. Table 2 lists examples of research derived from the MIP.

Table 2: Examples of research directly derived from, or that involved Master's International Students.

Examples of Research directly derived from Master's International Students
1.Post, J.L. and J.R. Mihelcic "Waste Reduction Strategies for Improved Management of Household Solid Waste in Jamaica," *International Journal of Environment and Waste Management*, in press, 2008.
2.McConville, J.R., and J.R. Mihelcic, "Adapting Life Cycle Thinking Tools to Evaluate Project Sustainability in International Water and Sanitation Development Work," *Environmental Engineering Science*, 24(7):937-948, 2007.
3.Ahrens, B.T. and J.R. Mihelcic, "Making Wastewater Construction Projects Sustainable in Urban, Rural, and Peri-Urban Areas," *Journal of Engineering for Sustainable Development: Energy, Environment, Health*, 1(1):13-32, 2006.
4.Fry, L, J.R. Mihelcic, D.W. Watkins, Jr., "Improving Public Health by Improving Water Supply: Results from Springbox Projects in Cameroon," *Journal of Engineering for Sustainable Development: Energy, Environment, Health*, 1(1):33-42, 2006.
5.Mehl, J., J. Kaiser, D. Hurtado, R. Izurieta, J.R. Mihelcic, "Pathogen Destruction and Aerobic Decomposition in Composting Latrines: Study of Fundamental Mechanisms and User Operation in Rural Panama," in preparation, 2009.
6.Owens, E., J.R. Mihelcic, and Q. Zhang "Solid Waste Material Flow Analysis in a Small Island State Nation," *in preparation,* 2009.
Examples of Research that involved Master's International students or was indirectly motivated by the experience
1.Troschinetz, A.M. and J.R. Mihelcic, "Sustainable Recycling of Municipal Solid Waste in Developing Countries, " *Waste Management,* 29(2):915-923, 2009.
2.Fry, L.M., J.R. Mihelcic, D.W. Watkins, "Water and Non-Water-Related Challenges of Achieving Global Sanitation Coverage," *Environmental Science & Technology*, 42(4): 4298 - 4304, 2008.
3.Cowden, J.R., D.W. Watkins, J.R. Mihelcic, "Stochastic Rainfall Modeling in West Africa: Parsimonious Approaches for Domestic Rainwater Harvesting Assessment," *Journal of Hydrology,* in press, 2008.
4.Hokanson, D. R., Q. Zhang, J. R. Cowden, A. M. Troschinetz, J. R. Mihelcic, and D. M. Johnson, "Challenges to Implementing Drinking Water Technologies in Developing World Countries," *Environmental Engineer: Applied Research and Practice*, Vol. I, Winter, 2007, in Environmental Engineer, the Magazine of the American Academy of Environmental Engineers, 43(1):31-38, 2007.
5.Mihelcic, J.R. J.B. Zimmerman, A. Ramaswami, "Integrating Developed and Developing World Knowledge into Global Discussions and Strategies for Sustainability. Part 1: Science and Technology," Environmental Science & Technology, 41(10):3415-3421, 2007.
6.Mihelcic, J.R., T.D. Eatmon, Jr., R.A. Harris, H.E. Muga, "Engineering Sustainable Construction Materials for the Developing World: A Meta-discipline Approach to Engineering Education," *International Journal of Engineering Education*, 23(6):1116-11125, 2007.

The USF MIP program started in fall 2008 and builds on a previous program initiated in 1997 by Dr. Mihelcic. Major differences in the new program are: requirements for students to take global public health and applied anthropology coursework, a thesis requirement, and the ability to accommodate students without an ABET-accredited first degree who do not wish to perform the entire make up course requirements.

To date 38 students have graduated from the program, of which, 42% of graduates have been female and 11% have been under-represented minorities. 11% of graduates have worked overseas for a non-governmental organization and 17% of graduates have begun doctoral studies. Another 25% of the graduates have worked after graduate for large municipality or the federal government. 32% have become fluent in Spanish, 24% in French, and the remaining students have learned languages such as Bambara, Bislama, Timorese, Palaun, and Patois. To date every student who has left for their Peace Corps assignment (after at least one year on campus) has completed their M.S. degree. Peace Corps graduates have preferential hiring by the U.S. government; therefore this program might be a good fit for engineers who want to work for the Environmental Protection Agency, Interior Department, Forest Service, Army Corps, or Indian Health Services.

Case 2: Interdisciplinary Graduate Course with International Field Experience
In 2006 the USF graduate school awarded interdisciplinary grants for graduate education and research that promoted Sustainable Healthy Communities. A focal area was water and faculty from across the university were invited to a "speed meeting" session where they interacted with each other for 2 minutes at a time to identify potential projects and partners for the grant competition. One of the funded projects, "Understanding and promoting sustainability related to mercury exposures through integrated research, graduate education, and community involvement" introduced two new 3-credit graduate level courses at USF through the departments of Civil and Environmental Engineering, Geography and the College of Public Health. These interdisciplinary courses allow students to investigate concepts of sustainability and research methods using a case study focus on mercury in the Tampa Bay area and a contrasting field based experience in Guyana. Students identify and integrate research approaches across disciplines, implement population surveying methods, conduct environmental sampling and analyses and apply simple systems modeling. The course is team taught and the first part was offered in the spring of 2008 to five students, three of whom are also funded for graduate research on the project. The second course is also being team taught in spring 2009 to ten students including the three research supported graduate students who took the first course.

The second course, Sustainability Concepts and Methods: Mercury in Guyana, includes a field experience in Guyana, South America for one week over the spring break period. By the end of the course students should be able to: 1) discuss and evaluate definitions of sustainability, 2) discuss developing country perspectives on

sustainability, 3) discuss aspects of the developing country context that affect and shape projects with sustainability goals, 4) identify and integrate sustainability research approaches (and/or experts) across disciplines, 5) apply Hg environmental sampling, population surveying, and systems modeling methods, and 6) discuss the value (and limitations) of the above methods from both scientific and social perspectives.

The field site was chosen based on existing partnerships between one of the PIs and entities in Guyana involved in small scale gold mines and mercury use that include Non Governmental Organizations (NGO) and the University of Guyana. Mercury is a global pollutant and the second largest user of mercury is small scale gold mining, especially prevalent in developing countries like Guyana. WWF-Guianas is leading efforts in Guyana, Suriname and French Guiana (the Guianas) to reduce the use of mercury in small scale gold mining through research, education and training programs and one of the PIs (Dr. Trotz) has already worked with them on projects that also involve faculty from the Environmental Studies Unit at the University of Guyana. Since 2005, three doctoral students have been recruited to USF's engineering school from the University of Guyana and two are currently taking this course. These students lead discussions on local culture and customs and share relevant experiences on the class topics to prepare the class for the field trip.

In addition to working in an active mining area, the students will also visit a biodiversity conservation reserve, Iwokrama (www.iwokrama.org), where illegal mining impacts livelihood of indigenous populations along the area's periphery. In developing countries like Guyana where democracy and governance remain focal points for agencies like USAID, partnerships with NGOs and civic organizations are crucial and seen as essential for local development (Trotz, 2008). USF's International Study Abroad program will provide administrative support in organizing this field experience and opportunities exist for converting it into a study abroad program that is self funded in the future through student fees.

Case 3: Bolivia Research Experience and International Capstone Design Course

An NSF research project situated in Bolivia allows undergraduate and doctoral graduate students to work with a non-government organization and rural community water committees to research issues of water supply, water scarcity, sanitation, and watershed management. The project objectives are:

1) Pairing undergraduate and experienced graduate students who have a demonstrated interest in issues of sustainable development.
2) Integrating the research experience into education initiatives that are focused on sustainable development.
3) Ensuring the research experience focuses on appropriate technology (defined here as the use of materials and technology that are culturally, economically, and socially suitable to the area in which they are implemented).
4) Using an operational model for sustainable development that is a global partnership, so students understand how to integrate and transfer the best and

most appropriate knowledge, methodologies, techniques, and practices between the developed and developing worlds.
5) Partnering with both a Bolivian University and nongovernmental organization to ensure students learn the importance of making research socially relevant.
6) Engaging women and underrepresented minorities in science and technology research that has a focus on sustainability.

This NSF research program pairs 3 U.S. undergraduate and 3 graduate students enrolled at either USF or MTU who have a demonstrated interest in issues of sustainable development with 6 ecological engineering students and faculty from the Universidad Tecnològica Boliviana (La Paz), and staff from a non-governmental organization. Students must be majoring in engineering, applied anthropology, or public health. M.S. students with a complimentary skill set are considered, however, doctoral students are preferred. Since 2007 students have conducted research in the small rural Bolivian communities of Palos Blancos, Sapecho, and San Antonio (located NE of La Paz near the Rio Beni River where the Andes begin to meet the Amazon) on topics related to: water supply and treatment, how communities select improvements in sanitation technology, the impact that land use has on water supply, and issues of willingness to pay and public health. Research ublications to date from Bolivia research project are: Fuchs et al. (2008), Fry et al. (2008), and Muga et al. (2009).

Understanding of written and spoken Spanish is required of all students. One modification to the program in Year 2 was that students completed a 1 to 2 week language and culture immersion in Bolivia prior to the start of their one month assignment. Students are housed with student families of the Bolivian student participants. In the first two years, there were 14 U.S. student participants, 12 were female. The third year will have participation from students in engineering, health, and applied anthropology. Graduate students will also be drawn from USF programs that allow students to obtain a dual graduate degree in environmental engineering, global public health, and applied anthropology.

The International Capstone Design (ICD) class allows students to obtain university capstone credit for working on engineering projects in the developing world (Phillips et al., 2004, 2007). The goal of International Capstone Design (ICD) is to provide students a service-learning design experience situated in the developing world so they can explore the technical, economical and social implications of engineering design and construction. Integration of the U.S. Accreditation Board for Engineering and Technology (ABET) accreditation criterion throughout the design experience is crucial to this activity. Practitioner involvement and affiliation with international partners has been a key to the success of the classes to gaining experience similar to that gained during the initial year on the job (Knox et al., 1998; Boschetto-Sandoval et al., 2007).

ICD is a 6-credit major design experience that may be used as a technical elective. The ICD course is structured to emulate the business of a design/build firm in

industry, since the student will likely find themselves in this work environment, within 6-12 months after the class experience. Students form a "design team," of 3-4 students; each team working on a different design project, just as in industry. Student work abroad requires 40 hours of volunteer construction work to learn local tools, materials and techniques. The remainder of time is spent gathering data from the local "clients," conduction topographical surveys, water and soil testing, and gathering other design data. Students return to campus to complete their actual project designs. The most important aspect of the course is that students experience the evolution of a project from conception through preparation of an engineering report which analyzes feasibility of various design options and then completion of final design drawings and specifications. Typical projects include water distribution, wastewater treatment, storm water management, solid waste, as well as roadway or structural design. Relationships built over the last 10 years allow students to work with local governments and NGO's for "real" design projects, benefiting "real" people. Once complete, student designs are transmitted to the international "clients or benefactors."

Due to the number and variety of design projects, industry mentorship is included both abroad and on campus, coaching the students on project delivery and procedures as well as the technical concepts. The mentors are either seasoned professional engineers or recent graduates working towards professional registration who have participated in the program. US professionals as well as local engineering and business professionals serve as in-country mentors.

The USF ICD program is beginning in Spring 2009, and is a relocation of the International Senior Design program formerly of Michigan Technological University. That program was created by Linda Phillips in 2000 and is co-directed by Dennis Magolan. To date 167 students have taken the "international senior design experience" in 15 offerings in either the Dominican Republic or Bolivia. Ownership of the student design projects is so great that 20% of the students have returned to act as in-country mentors, paying their way as the students do. Of the 20%, 40% have returned to mentor more than once.

Case 4: UNESCO-IHE partnership

The University of South Florida launched the Dr. Kiran C. Patel Center for Global Solutions on May 20, 2005. Potable Water and Sanitation, Sustainable Activities, and Urbanization and Migration are the three areas of specialization of the center which has played a crucial role in forging international partnerships for USF faculty to build research and education programs. Two examples of support that are discussed below include observation of the meetings of the UN Secretary General's Advisory Board on Water and Sanitation and facilitation of graduate exchange training exercises with UNESCO-IHE students.

The UNESCO-IHE Institute for Water Education (http://www.unesco-ihe.org/) in Delft, Netherlands formally signed a Memorandum of Understanding with USF in 2007 to develop collaborative educational and research programs. IHE carries out

research, education and capacity building activities in the fields of water, environment and infrastructure, and is the largest water education facility in the world. IHE offers graduate programs (MSc and PhD) related to water science, engineering and management and its students are recruited from around the world with high percentages from Asia and Africa. The USF-IHE partnership (only one of its kind in the US) stemmed from interactions between IHE and USF faculty who work closely with the Patel Center as faculty advisory board members and research fellows, and has led to faculty visits at both institutions, IHE student visits to USF and proposal submittals. While visiting IHE, USF faculty have participated in symposia, site visits and a course on Dutch water management.

For the past two years, the Patel Center, in collaboration with Florida Earth Foundation, hosted a group of IHE MSc students during their 3rd and 4th annual visit to south Florida. Their two day visit of the Tampa Bay area was hosted by Dr. Thomas Crisman from Biology (theme of water resources and wetland ecology) in 2007 and Dr. Daniel Yeh from Civil & Environmental Engineering (theme of Tampa Bay water infrastructure) in 2008. Several USF students from Dr. Yeh's class on Millennium Development Goals also accompanied the IHE students on the two-day visit. A NSF proposal was recently submitted for USF students to conduct summer research at IHE.

Conclusion

The programs discussed above are a part of a larger portfolio of efforts being undertaken at the College level to make more sustainable, international experiences for faculty and students (Thomas et al., 2008). In addition, these case studies align strategically with national goals that have documented the rapid social, political, economic, and environmental changes occurring in the world and associated implications for engineering education, research, practice, and importantly, the economic competitiveness of our Nation (see for example, the National Academy of Engineering in Educating the Engineer of 2020, and the American Society of Civil Engineers in 2025 Vision for Civil Engineering).

Acknowledgements

The authors wish to acknowledge the U.S. Peace Corps, NSF for support of the Sustainable Development Research Experience in Bolivia *under Grant No. 0623558*, and the University of South Florida Graduate School for support under the Sustainable Healthy Communities Initiative.

References

Boschetto-Sandoval, S., C. Sandoval, and Phillips, L. (2007) Pilot Collaboration and Program Development: Engineering Senior Design and Spanish for Cross-Disciplinary Literacy, Proceedings American Society of Engineering Annual Conference & Exposition, June 23-28, Honolulu, HI, 2007.

Fuchs, V.J. and Mihelcic, J. R. (2006) "Engineering Education for International Sustainability: Curriculum Design under the Sustainable Futures Model,"

Proceedings of 5th Annual ASEE Global Colloquium on Engrg Educ., Rio de Janeiro, Brazil, October 9-12, 2006.

Fuchs, V.J., L.M. Fry, and Mihelcic, J.R. (2008) "Delivering Sustainable Waste Infrastructure in an Urbanizing World," Proceedings of the Third International Conference on Sustainability Engineering and Science, Auckland, New Zealand, December 9-12, 2008.

Fry, L.M., Mihelcic, J. R., Watkins, D. W., Reents, N. (2008) "Assessment of change drivers affecting the sustainability of gravity fed water supply in the Alto Beni watershed of Bolivia," American Geophysical Union Fall Meeting, December 15-19, 2008

Hokanson, D.R., Phillips, L.D., and Mihelcic, J. R. (2006) Educating Engineers in the Sustainable Futures Model with a Global Perspective: Education, Research and Diversity Initiatives, International Journal of Engineering Education, Sustainability.

Knox, R. C., Sabatini, D. A., Hughes, D. E., Lambert, R.; and Ketner, R. (1998) Teaching engineering design with practitioner supervision: a case study. Journal of Professional Issues in Engineering Education and Practice. 124(4), 105-109.

Mihelcic, J.R. (2004) "Educating the Future's Water Professional," Water Environment Technology, 16(9):86-92.

Mihelcic, J.R. and Hokanson, D. R. (2005) "Educational Solutions: For a more Sustainable Future," in Environmental Solutions, Eds: NL Nemerow and FJ Agardy, Elsevier, pg. 25-58.

Mihelcic, J.R., Phillips, L.D., Watkins Jr., D.W. (2006) "Integrating a Global Perspective into Education & Research: Engineering International Sustainable Development", Environmental Engineering Science, 23(3) 426-438.

Muga, H.E., J.R. Mihelcic, N. Reents, S. Morales, "Treatment Performance of Wastewater Lagoons in South Yungas Province of Bolivia," World Environmental & Water Resources Congress, Kansas City, May 17-21, 2009.

National Science Board (2008) International Science and Engineering Partnerships: A Priority for U.S. Foreign Policy and Our Nation's Innovation Enterprise. http://www.nsf.gov/pubs/2008/nsb084/nsb084.pdf

Phillips, L. D., Mihelcic, J. R., and Paddock, M. (2004) How academic programs can be integrated into EWB-USA activities. Engineers Without Borders–USA 2004 National Conference. Denver, CO.

Phillips, L. D., M. Brady, and Jousma, K. (2007) Interdisciplinary International Senior Design: How Service Learning Projects in Developing Countries Support ABET Accreditation, Proceedings American Society of Engineering Annual Conference & Exposition, June 23-28, Honolulu, HI.

Selna, M.W., H.T. Glaser, R.R. Trussell, G.R. Chan, M. Sullivan, "Declining Enrollment has Water and Wastewater Professionals Concerned," Proceedings of the 79nd Annual Water Environment Federation Conference & Exposition, 2006.

Thomas, S., Trotz, M. A., Alcantar, N., and Perez, R. (2008) International Partnering to Sustain Engineering Innovation. Proceedings of the 7th ASEE Global Colloquium on Engineering Education, Cape Town, South Africa, October 19–23, 2008.

Trotz, M. A. (2008) Diaspora Communities and Sustainable Urban Development: Lessons from Floods in Guyana. Proceedings of NZSSES Conference: Blueprints for Sustainable Infrastructure, Auckland, New Zealand, December 9-12, 2008.

United Nations (2000) United Nations Millennium Declaration. Resolution adopted by the General Assembly. A/RES/55/2. http://www.un.org/millennium/declaration/ares552e.pdf

UN Millennium Project (2005) Investing in Development: A Practical Plan to Achieve the Millennium Development Goals. New York. http://www.unmillenniumproject.org/reports/fullreport.htm

Zimmerman, J.B., J.R. Mihelcic, Smith, J. A. (2008) Global Stressors on Water Quality and Quantity: Sustainability, Technology Selection, and Governance in a Dynamic World. Environmental Science & Technology, 42(4):4247-4254.

A decision support system for beneficial use of national dam water resources in Swaziland

J.I. Matondo[1] and K. M. Msibi[2]

ABSTRACT

The Government of Swaziland has undertaken the development of water storage and distribution facilities as a process towards overcoming the unevenly distribution of the water resource. However, the current water storage facilities with a total capacity of 720.9×10^6 m^3 can not meet the water demand which stands at 1795×10^6 m^3 annually. The overall objective of this project was to develop an optimum and sustainable decision support tool for water allocation and rationing options for national water reservoirs.

A Decision Support System (DSS) is defined as a user-oriented computer system which supports decision-makers in addressing unstructured problems. The rationing mode in the developed DSS was used to distribute the available stored water at the beginning of April in order to arrive at a priori predetermined reservoir storage level at the end of October. The DSS has three major components and that is the model input, modeling options and outputs screens. The model input component comprises of technical data (inflow, reservoir level, intended % volume at end of October and allowed lowest rationing %), and policy data (uniform rationing or differential rationing). The modeling options comprise of commands to determine optimum rationing %, provide % rationing and observed dam response and imposed rationing %. The output of the DSS comprises of the optimal rationing (%), monthly reservoir volume from April to end of October as well as a graphical representation of the reservoir response and the final recommendation.

The results of the DSS with a starting reservoir level at 15m at the beginning of April and a 10% reservoir level at the end of October, is that there is no need for rationing (that is the water demand for all uses are met) and the reservoir level stands at around 29% at the end of October. The results of the DSS with a starting reservoir at 6m at the beginning of April is that the rationing is 46% for all uses in order to arrive at a 10% reservoir storage level at the end of October is not recommended. This is because, with 54% deficit, there is a danger of crops to wilt beyond recovery. The final DSS recommendation starting with a reservoir level at 6m at the beginning of April is irrigation rationing at 60% (i.e. 40% water deficit) combined with a reduction of 14% of the hectares of irrigated fields. The Nyetane dam was used as a pilot reservoir in the development of the DSS. The developed DSS with all the relevant input data can be used to allocate water efficiently in other reservoirs in the country.

Keywords: Beneficial, Decision support system, Optimum, Rationing, Sustainable use

[1] University of Swaziland P/Bag Kwaluseni, Swaziland
[2] Water Resources Branch, Ministry of Natural resources and Energy, Mbabane Swaziland

BACKGROUND

The Kingdom of Swaziland, is situated in South Eastern Africa between latitude 25° and 28° South and between longitudes 31° and 32° East. It lies some 48 to 225 kilometers inland of the Indian Ocean littoral and hence physically land locked. The country has a total surface area of 17,360 km^2 and therefore, is the smallest country in the southern hemisphere.

There are four distinct physiographic regions within the country namely: highveld, middleveld, lowveld and lubombo, which are clearly distinguished by elevation and relief (Murdoch, 1970). The highveld and upper middleveld are characterized by a Cwb climate. The lower middleveld and lubombo range have a Cwa climate whilst the western and eastern lowveld have a Bsh climate (Murdoch, 1970). Mean annual rainfall ranges from about 1500 millimetres in the highveld to less than 500 millimetres in the southern lowveld.

The water sources in Swaziland are mainly surface waters (rivers, reservoirs), ground water and atmospheric moisture. Figure 1 shows the major drainage basins of Swaziland namely: Komati, Usutu, Mbuluzi, Ngwavuma, Lomati, Pongola and Lubombo. The Komati and Usutu rivers both originate in South Africa while the rest of the basins originate within Swaziland. It should also be noted that all the rivers in Swaziland are international rivers and therefore, the development and management of the surface water resources must be undertaken in collaboration with the other riparian states namely: South Africa and Mozambique.

There are ten big dams in Swaziland which are greater than 5 million cubic metres (MCM). The existing infrastructure is not sufficient to carter for the whole country and currently the lowveld region continues to suffer from drought related problems. The challenge to the government remains that of constructing water storage and distribution facilities and transfers it to areas of acute water shortage. Water resources management is posing a complex challenge due to the increasing competing and conflicting water uses amongst different sectors and also due to population increase which puts pressure on the natural resources.

The overall objective of this project is to develop an optimum and sustainable utilization decision support tool for water allocation and rationing options for national water reservoirs. The specific objectives of this project were. (i) To develop different scenarios for optimal utilization to meet conflicting and competing dam water needs. (ii) To develop a decision support tool for competing dam water requirements, to help in the prioritization of allocations and rationing in times of scarcity i.e. during droughty years.

LITERATURE REVIEW

It has been established by scholars that water resources management problems are more complex world wide (Simonovic, 2000; Wurbs, 1998; Singh, 1995). Population growth, climate variability, regulatory requirements, temporal and spatial scales, socio- economic and environmental considerations, competing and conflicting water uses and transboundary considerations all of these contribute to the complexity of water resources management problems.

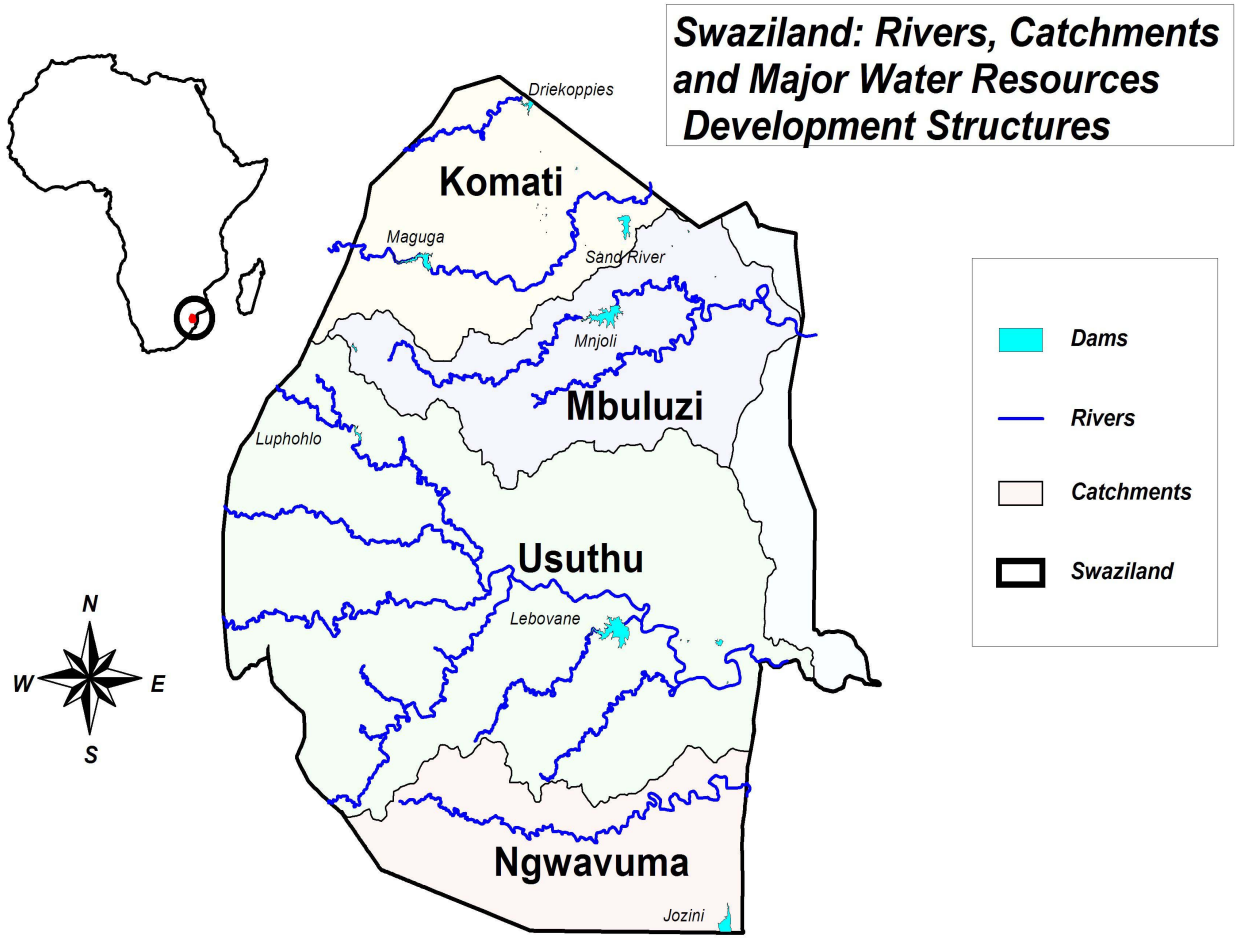

Figure 1. Map of Swaziland showing the major drainage basins and location of existing water storage facilities

The literature on water resources management is rich with Integrated Water Resources Management models that have tended to focus either on understanding how water flows through a watershed in response to hydrologic events or on allocating the water that becomes available among competing and conflicting water uses. Examples of such models are: The US department of Agriculture's Soil Water Assessment Tool (SWART , Arnold and Allen, 1993); RiverWare™ DSS (Zagona et al., 2001); The USA Geological Survey's Modular Modelling System (Leavesley et al., 1996); The US Army Corp of Engineers, HEC-ResSim (USACE, 2003) etc. The SWAT model includes sophisticated physical hydrologic watershed modules that describe, rainfall-runoff processes, irrigated agriculture process, and point and non-point watershed dynamics but with a relatively simple reservoir operation module. The RiverWare™ DSS is a hydrologic and hydraulics operations model, which can be used to develop multi-objectives simulations and optimizations of river and reservoir systems. The HEC-ResSim is a reservoir simulation model that can describe operating rules such as release requirements and constraints, hydropower requirements, multiple reservoir operations etc. All the above water management models require prescribed flows from other models.

Decision Support Systems (DSS) are a specific class of computerized information system that supports business and organizational decision-making activities. A properly designed DSS is an interactive software-based system intended to help decision makers compile useful information from raw data, documents, personal knowledge, and/or business models to identify and solve problems and make decisions. A Decision support system was used in California USA to handle conflict between two groups who have on-demand water management for irrigation, drinking water and hydropower generation (Rajasekaram and Nandalal (2005). Gu and Tang (2000) developed a Water Resources Management Decision Support System to unify the objective world, organization and human factors during intervention. Karamouz *et. al*, (2005) developed a multi-criterion decision making (MCDM) that utilized an analytical hierarchy process which enabled decision makers to incorporate the priority of different objectives in obtaining optimal reservoir operating policies. Both economic and MCDM utility functions are implemented and coupled with deterministic and stochastic optimization models. The DSS was applied to the largest surface water resources system in Iran (the Dez and Karoon river-reservoir system).

METHODOLOGY

Data collection

The information that was required for carrying out this project is: Dam characteristics, hydro meteorological data, water use data, irrigation water requirement, area under irrigation for each crop, and net financial income.

Dam characteristics:

The information that characterize, a dam is the reservoir water level, the corresponding surface area and volume. This information is available from the dam designs and was obtained from the Ministry of Agriculture and Cooperatives which constructed the Nyetane dam. This information was used to compute the evaporation and seepage water losses from the reservoir which are both a function of the reservoir water level. The reservoir level at the beginning of April was used in the Dam height surface area and volume relationship by interpolation to get the corresponding reservoir surface area and volume. The reservoir levels and corresponding surface area and volume were input to the DSS where all the computations are carried out. The dam level was also used to calculate the water seepage losses from the reservoir. The reservoir volume and the volume of seepage losses are used in the water balance equation.

Hydro meteorological data

The hydro-meteorological data needed in this project are: reservoir inflows, temperature, and evaporation values. There is no hydrometric station along Nyetane river and therefore, rainfall runoff modelling was used to establish the monthly inflows into the Nyetane dam. Air temperature and evaporation data was obtained from the department of meteorology. The air temperature and pan evaporation data was required for the computation of water losses from the reservoir through evaporation. The following relationship was used in the computation of evaporation loss from the reservoir:

$$E_t = e_t . A\left(\frac{V_t + V_{t+1}}{2}\right)$$

Where E_t is the total reservoir evaporation for month t, e_t is the evaporation index for month t (which is obtained from the pan evaporation values), A is the reservoir surface area which is a function of the reservoir volume in month t and t+1 (this is usually the reservoir volume at the begining of month t and the reservoir volume at the beginning of month t+1, which is equal to the reservoir volume at the end of month t).

Water use data

The water use data for domestic was obtained from the Rural Water Supply Board while the water use for livestock and irrigation was obtained from the Ministry of Agriculture and Cooperatives. Water use for industry was obtained from the Swaziland Water and Sewage Corporation while water use for hydropower was obtained from the Ministry of Natural Resources and Energy. It should be noted here that water use for hydro power generation is non-consumptive use. That is water can be used to generate hydro power and for other uses down stream. This information was input to the water balance computations in the DSS.

Irrigation water requirement per hectare.

The irrigation water requirement for sugar cane, maize, cotton, vegetables and fruits was obtained from the literature review material. The expression to estimate the crop water consumptive use is as follows:

$$ETc = ETr * Kc \quad \text{(mm/day)}$$

Where ETc is the crop water consumptive use, ETr is the potential evapotranspiration for a reference crop and Kc is the crop coefficient. Crop coefficient values have been established experimentally for different crops and in this study the crop was assumed to be at full canopy cover. Therefore, the crop water requirement as a volume per hectare was obtained when the ETc was multiplied by the area and in this case the hectare. This information was input to the DSS for computing the water demand abstraction.

Area under irrigation.

The area under irrigation for the different crops was obtained from the stakeholders who are irrigating using the water from the Nyetane reservoir. This information is necessary in quantifying the water demand and therefore, the required water abstraction from the reservoir in each month. This information was input to the DSS.

Net financial income

The gross income, input costs and net income per hectare for each crop was obtained from SWADE. This information was required in the DSS for the determination of the returns (net benefits) for the acreage under irrigation for the corresponding optimum water rationing (%).

All the information required for running the Decision Support System (DSS) is presented in Appendix A. All the other calculations are carried out within the DSS (the rationing component).

Development of Scenarios for reservoir operation

The major objective of reservoir operation (post contract problem) is the maximization of net benefits due to water releases for the different uses. This problem is set as follows:

$$Maximize \quad b_w.Q_t + b_p.P \tag{1}$$

$$Subject \quad to$$

$$V_{i+1} = V_i + I_i + R_i - Q_i - E_i \frac{V_i + V_{i+1}}{2} \tag{2}$$

The water release Q_t is the sum of all the water demand for all the activities during month t. The above relationship was used in the DSS in the water rationing process which is carried out from month t = 1,…, 7 (which is from April to October). This is because the water rationing procedure is carried out during the winter months to ensure that the reservoir is used efficiently. Secondly the rain season has been observed to have shifted to the beginning of November that is there is a delay in the onset of the rain season instead of starting at the beginning of October it has currently been observed to start in early November.

The scenarios that were considered are those based on the occurrence of drought recurrance interval such as one in five years, one in ten years etc. The average and wet year conditions are also scenarios for consideration when operating the reservoir. However, it should be noted that the wet year scenario is not of a problem because the water demand is expected to be met and should give the maximum net benefits.

Reservoir starting and ending levels were considered as scenarios in the management of the dam waters and they are linked to the frequency of droughts. This is because if the reservoir is full at the beginning of the season and operated to meet the water demand for the whole season and end up with a low reservoir level (depending on the inflows during the season) then the reservoir is not well operated. Thus, starting the next season with such a low reservoir level gives a high risk for the farmers, and that they might get severe losses. Therefore, the DSS was used to find optimal starting and ending reservoir levels for the different drought scenarios explained above.

Conceptualization of the DSS

Important characteristics of a Decision Support System (DSS) for sustainable water resources management include flexibility for tackling various 'what-if?' scenarios, the facilitation of problem identification and solving by analytical tools enabling the end-user to manage, analyse and present information, and interaction and ease of use to involve the stakeholders into the management process themselves [Simonovic and Bender 1996]. Integrated water resources management comprises numerous complex and unstructured management problems including a geographical component. Resolving ill-structured problems, however, can be achieved by disaggregating them into a series of structured components, each of which tackled with its unique set of tools [Reitsma 1996], and integrated into a comprehensive framework system.

According to Wurbs (1998), the concept of Decision Support Systems became popular during the 1980s in the water manahgement community, as well as in business, engineering and other profeesional fields (Wurbs, 1998). Wurbs, 1998 defines decision support system as a user-oriented computer system which supports decision-makers in addressing unstructured problems. Decision support systems include a collection of software packages and hardware. The decision support system might include data management software, watershed runoff, stream hydraulics, and reservoir system operation models, a computer platform with peripheral hardware devices and an automated real time stream flow and rainfall data collection system.

There are basically two distinct elements of the DSS, namely; *Rationing and Allocation* decision support tools. Ming-Yen Tu *et. al*, (2003) developed a mixed integer linear programming (MILP) model that considers simultaneously both the traditional reservoir rule curves and the hedging rules to manage and operate a multireservoir system. During normal periods of operation when inflows are plentiful, this optimization model efficiently distributes the available stored water from different reservoirs to meet the planned demands imposed by the competing users. However, during periods of drought, and/or when anticipating a drought the planned demand can not be fully met and a water shortage occurs. To minimize the impact of drought, the hedging rule was used to effectively reduce the ongoing water supply to balance with the target storage requirement.

As explained earlier Swaziland receives rainfall during the summer months with very little rain during the winter months. In fact the Lowveld region where the Nyentane reservoir is located does not receive any rainfall during the winter months and has been experiencing drought related problems since 2001 to date. Therefore, the approach by Ming-Yen Tu et. al (2003) was used in the developed DSS. The rationing mode in the DSS was used to distribute the available stored water at the beginning of April in order to arrive at reservoir target levels at the end of October which were determined a priori.

The water resources from the Nyetane dam is used for agricultural activities (sugar cane, citrus fruits, vegetables, and livestock) and domestic. All crops get the required water demand when there is enough water. Rationing is done to all crops and other uses during years with water scarcity.

The current situation in the country under irrigated agriculture is that the growing of sugarcane is a continuous process. That is come the rain season a farmer will have sugarcane fields at different growth stages. Therefore, the problem of water allocation among different crops can not be carried out in the usual way using optimization techniques. Therefore, the approach in this study was to rank the crops according to their net income per hectare. All other crops except dry maize have a high net income per hectare than sugarcane. Therefore, under water scarcity situations the hectrage under sugarcane will be reduced in order to make the available resource enough for part of the sugarcane field and other crops.

Since only a single reservoir site was used to pilot the DSS, a good framework was developed that could be expanded to cover other reservoirs and other scenarios. Figure 2. below illustrates the developed Decision Support System.

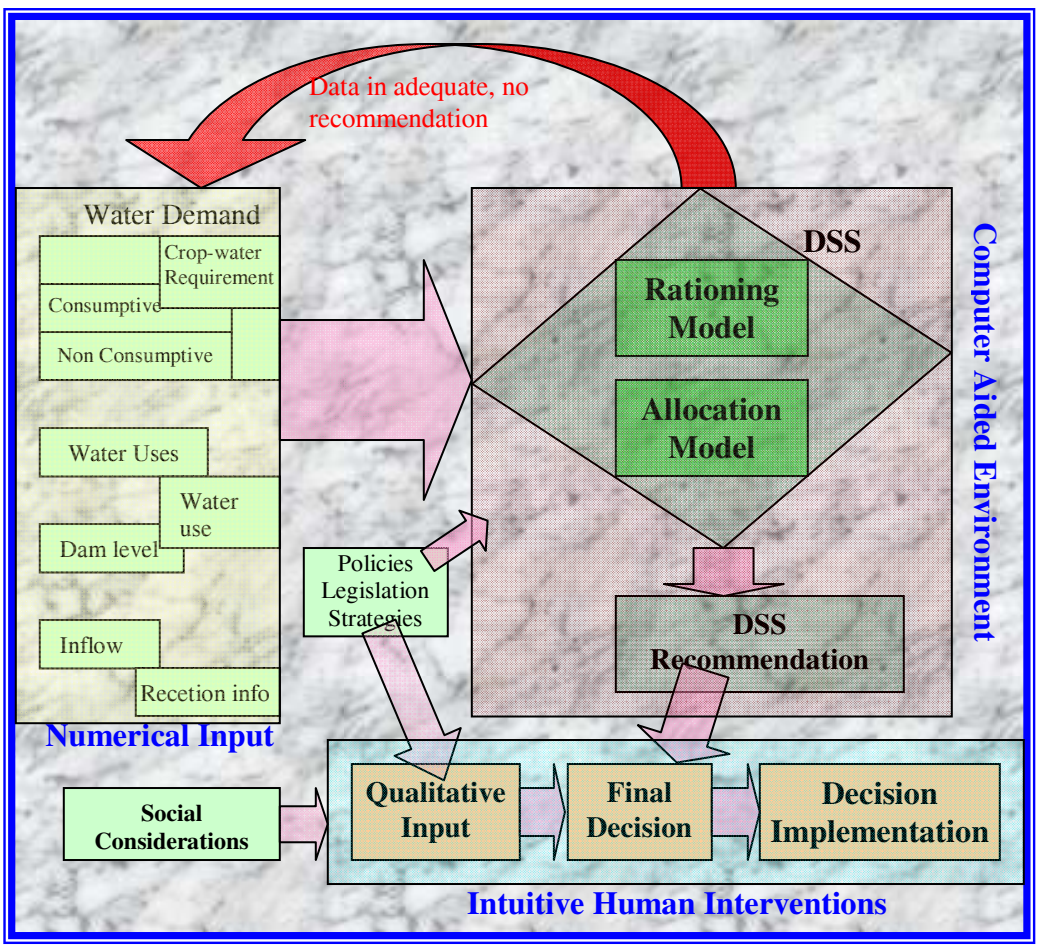

Figure 2: A diagram showing the DSS layout and components

Computational procedure in the DSS

The water balance equation was used in the computational processes in the DSS and is presented below:

$$Q_{t+1} = V_t + I_t - Q_t - Q_l - e\left(\frac{V_t + V_{t+1}}{2}\right) \quad (3)$$

The reservoir level at the beginning of April was used to determine the corresponding reservoir volume using the Dam level, surface area and volume relationship through an interpolation procedure. The inflow for the months from April to October is computed using the following equation:

$$I_{t+1} = I_t \rho^{k(t+1)} \quad (4)$$

Where I_{t+1} is the inflow at time t+1 and k is the groundwater recession constant and ρ is the natural log.

This is because the inflow into the reservoir during the winter months is due to ground water contribution and is recession flow. Q_l is the water loss in the reservoir through seepage and percolation which is computed as a function of the Dam level. Q_t is the total water abstraction for month t (irrigation, domestic, livestock, industrial etc.). The water abstraction is obtained from the water use tables. The water abstraction for each month is subjected to a water rationing iteration process in the DSS using the water balance equation from the beginning of April to the end of October.

Given the reservoir level at the beginning of April, the target reservoir level at the end of October, uniform rationing or differential rationing and the lowest allowed rationing (%), the DSS performs an iteration procedure from April to October to determine the optimal rationing (%). The rationing in this study is the % of the total water demand for that month. That is if the optimal rationing is 90% it means that a 10% water deficit is incurred for all the crops during that month.

RESULTS AND DISCUSSION

The developed DSS has three major components and that is the model input, modeling options and outputs. The model input component comprises of technical data (inflow, reservoir level, intended % volume at end of October and allowed lowest rationing %), and policy data (uniform rationing or differential rationing). The modeling options comprise of commands to determine optimum rationing %, provide % rationing and observed dam response and imposed rationing %. The output of the DSS comprises of the optimal rationing (%), monthly reservoir volume from April to end of October as well as a graphical representation of the reservoir response and the final recommendation.

The DSS is started by inputting the reservoir level at the beginning of April, the intended end of October reservoir volume (%) and the allowed lowest rationing (%). The policy data input is either uniform rationing or differential rationing. When differential rationing is selected two boxes become active at the bottom requesting to input the % of irrigation rationing and the % of rationing the other water uses and then click finish, modeling option and the compute buttons to activate the iterations in the DSS.

The starting reservoir level at the beginning of April is a function of climate and the previous history in the catchment (i.e the rainfall distribution during the previous rain season (October to march). That is during wet years, the reservoir level at the beginning of April is expected to be at maximum supply level and during dry years, the reservoir level at the beginning of April is expected to lie between minimum and maximum supply levels.

A sample output results for the developed DSS are presented in Figures 3 to 4. It can be seen from Figure 3 that with a starting reservoir level at 15m at the beginning of April, there is no need for rationing and the reservoir level stands at around 29% at the end of October. Figure 4 shows the DSS results with a starting reservoir level at 8m at the beginning of April and with uniform rationing the DSS recommends a 63% rationing for all water uses (that is a 37% deficit is incurred by all uses) in order to end up with a reservoir level at 10% at the end of October. Figure 5 shows the results of the DSS with reservoir level in April at 8m but with uniform imposed rationing of 80%. The DSS recommendation is that the imposed rationing of 80% is not recommended (because the reservoir storage is 0 at the end of October) and that a more stringent rationing should be used or to choose the optimization option. Figure 6 presents the results of the DSS with a reservoir at 6m at the beginning of April with uniform rationing. The DSS recommendation is that of rationing at 46% for all uses in order to end up with 10% reservoir storage at the end of October is not recommended. This is because, with 54% deficit, there is a danger of crops to wilt beyond recovery. The final DSS recommendation is irrigation rationing at 60% combined with a reduction of 14% of the hectares of irrigated fields.

CONCLUSIONS AND RECOMMEMNDATIONS

A Decision Support System (DSS) tool has been developed with the use of input information from Nyetane Dam as a pilot reservoir. The Developed DSS can be used to give optimal rationing given the starting reservoir level at the beginning of April and a priori reservoir level at the end of October. The corresponding hectares for the different crops that were irrigated in the season and net benefits can also be obtained. Input data from any other reservoir can be used in the developed DSS for optimal rationing of water resources for that dam.

It is recommended that the developed DSS be implemented in the rationing of the water resources of the Nyetane dam in order to establish the output results of the model in real time operation. This information can then be used to evaluate the sensitivity of the DSS and effects of the water deficits in relation to crop yield can also be analysed.

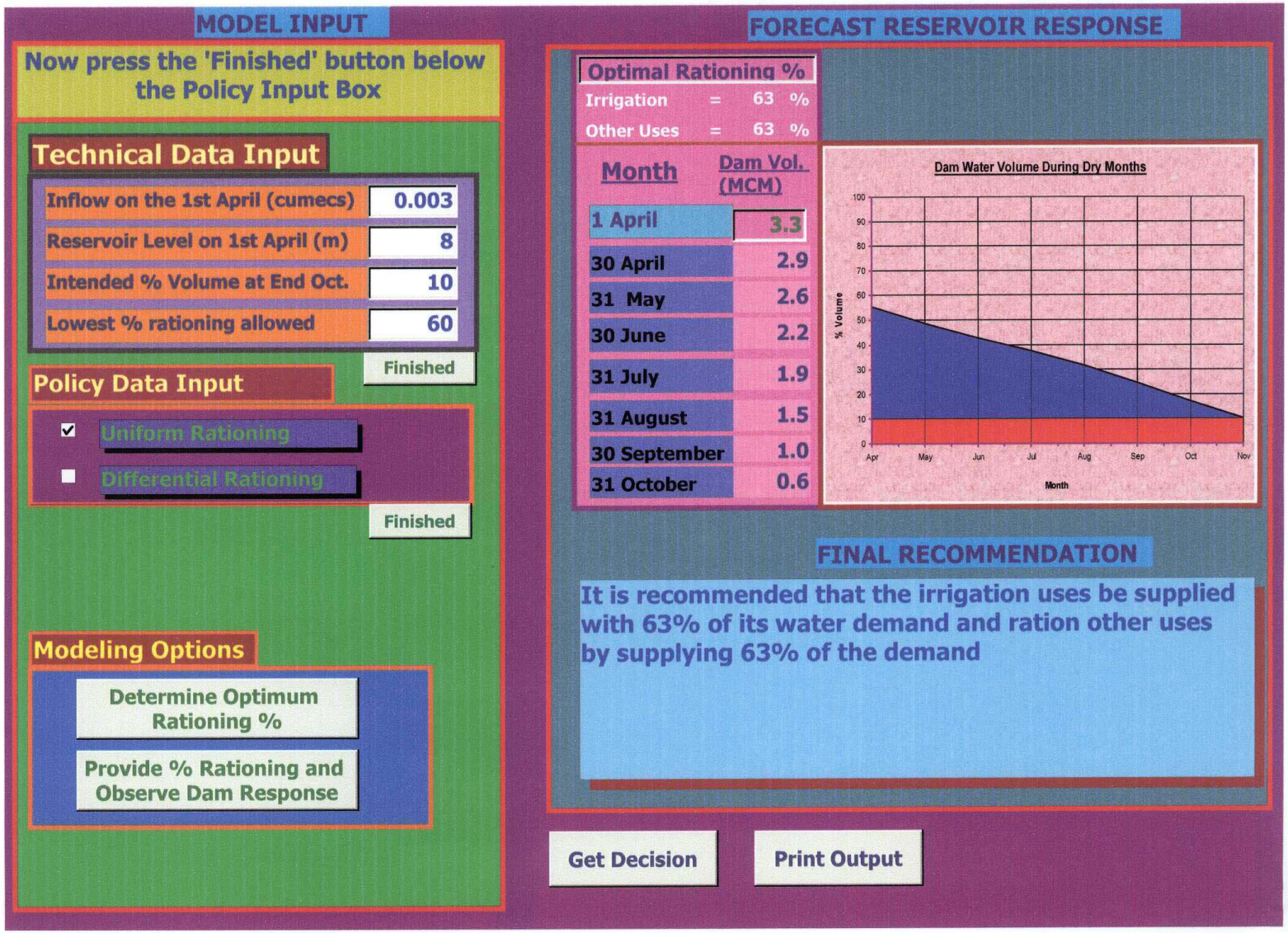

Figure 3: DSS results with starting reservoir level in April at 8m and 10% reservoir level at the end of October

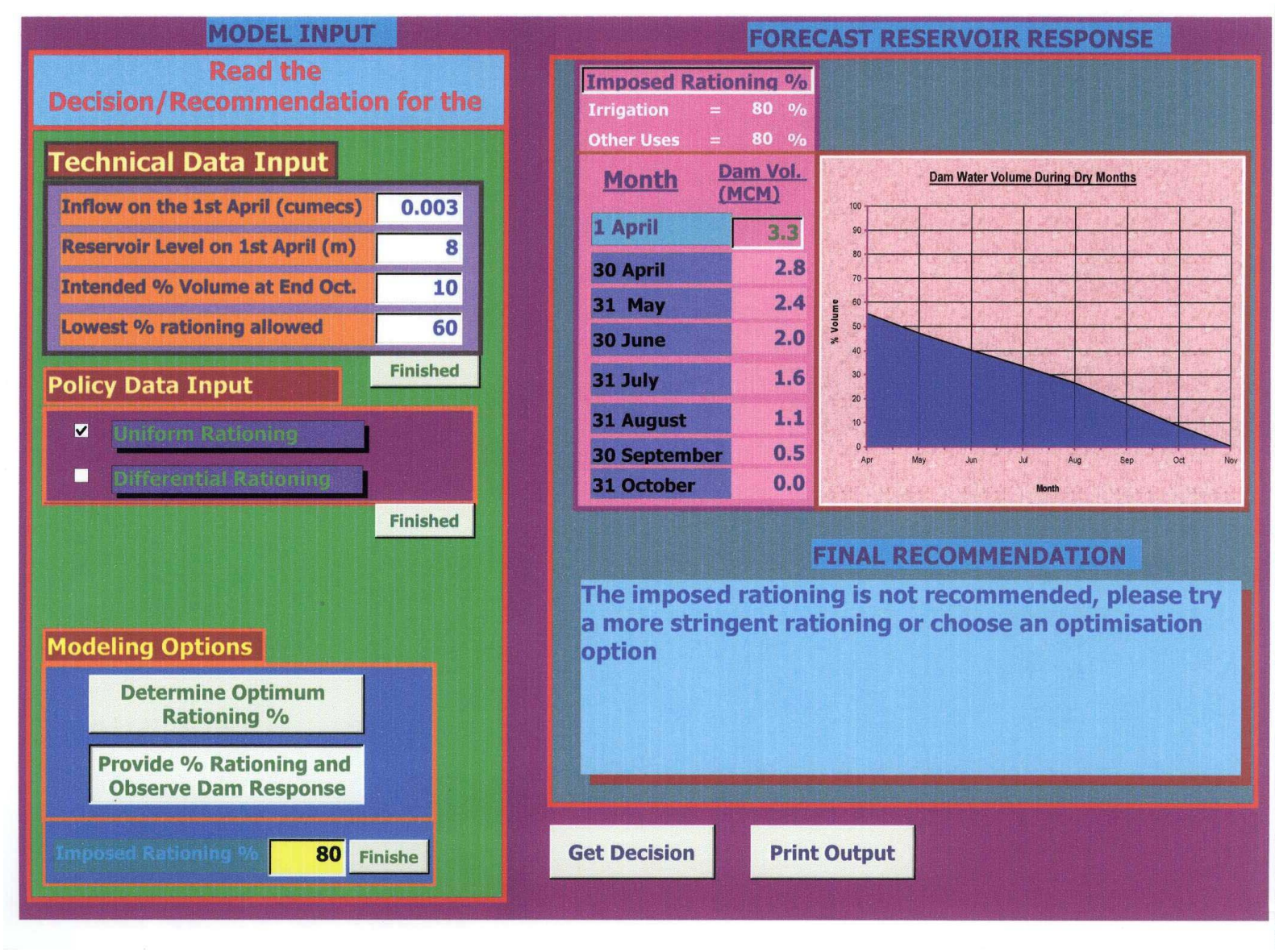

Figure 4: DSS results with starting reservoir level in April at 8m and 10% reservoir level at the end of October

REFERENCES

1. Arnold, J. and P. Allen. 1993. A comprehensive surface-ground-water flow model. Journal of Hydrology 142: 47-69

2. Bellman, R.E., 1957. Dynamic Programming, Princeton University Press, Princeton, New Jersey
3. Bellman, R.E. and S.E. Dreyfus. , 1962. Applied Dynamic Programming, Princeton University Press, Princeton, New Jersey
4. Dreyfus, S.E. and A.M. Law. 1977. The Art and Theory of Dynamic Programming, Academic Press, New York,
5. Jifa Gu and Xijin Tang 2000. Designing a water resources management Decision Support system: An application of the WSR approach. Journal of Systematic Practice and Action Research, Vol. 13, No. 1 February, 2000.
6. Karamouz M., B. Zahraie and S. Araghinejad, 2005. Decision support system for monthly operation of hydropower reservoirs: A case study. Journal of Computing in Civl Engineering, Vol. 19, No. 2 April 2005.
7. Leavesley, G.H., S.L. Markstrom, M.S. Brewer, and R.J. Viger 1996. The modular modelling system (MMS) – The physical process and modelling component of a database-centered decision support system for water and power management. Water, Air, and Soil Pollution 90: 3003-11.
8. Murdoch, G. (1970). Soils and land capability of Swaziland. Swaziland Ministry of Agriculture, Mbabane.

9. Ming-Yen Tu, Nien-Sheng Hsu and W.W. –G Yeh, 2003. Optimization of reservoir management and operation with hedging rules. Journal of Water Resources Planning and Management, Vol. 129, No. 6 November/December 2005, pp. 410-419.
10. Rakasekaram V. and K.D.W. Nandalal, 2005. Decision support system for reservoir water management conflict resolution. Journal of Water Resources Planning and Management, Vol. 131, No. 2 March/April 2003, pp. 86-97.
11. Singh, V.P. (ed). 1995. "Computer models of watershed hydrology" Water resources publications, Littleton, Colorado.

12. US Army Corps of Engineers (USACE). 2003. Hydrologic Engineering Center HEC-ResSim, Reservoir System Simulation User's Manual Version 2.0 CPD-82. Davis, CA
13. Wurbs, R.A. 1998. "Dissemination of Generalized Water Resources Models in the United States." *Water Internation, Vol.23*, No.3.
14. Zagona, E., T. Fulp, R. Shane, T. Magee, and H. Goranflo. 2001. RiverWare: A Generalized tool for Complex Reservoir System Modeling. Journal of the American Water Resources Association 37, No. 4: 913-2

ASSESSMENT OF COMBINED HYDROSEEDING AND COCONET REINFORCEMENT TO CONTROL SOIL EROSION

Mervin M. Cereno[1],

[1] Professor, School of Civil Engineering and Environmental and Sanitary Engineering, Mapua Institute of Technology, Intramuros, Manila, Philippines; PH (+632) 2475000 loc 5200; FAX (+632) 247500 loc 5201; email: mmcereno@mapua.edu.ph; mmcereno@yahoo.com

Abstract: At present, the use of inert materials such as concrete and steel had always been relied as for slope stabilization and soil erosion. The widespread of these materials as stone riprap and concrete are now abridged due to its high cost. It is therefore encourage that the use of alternatives such as planting of grass or vegetation along the slopes is the most sensible form of soil erosion control. However, the use of these methods was not much taken into practice which does not account its efficacy for soil stabilization.

In this study, the researchers' premise is to congregate information that may be significant to evaluate the performance of Hydroseeding with Coconet in controlling soil erosion and ensuring its suitability and applicability in the protection of the slopes. A representative slope had been constructed and tested at 65º taking an account from the 71.56º of the maximum slope with a 10% factor of safety for both hydroseeding and coconet. A rainfall simulation study was conducted in order to assess the effectiveness of combined Hydroseeding with Coconet against surface run-off to control soil erosion. Performance of Hydroseeding with Coconet were assessed which gave progress to where the soil erosion was to be reduced or controlled. Results from the experiment were expected to give the desired data and outputs to the researchers which should show that combined Hydroseeding and Coconet representative slope yields to control soil erosion and protect the slope.

Keywords: Hydroseeding, Coconet, Soil Erosion, Rainfall Simulation, Slope Protection

1.0 INTRODUCTION

Soil erosion, which is caused by water, wind and gravity, is a worldwide problem that threatens an important and non-renewable resource the farmland that is suitable for cultivation. To be able to take actions to this problem, an effective and economical method must be taken as a solution. One method that can be considered is Hydroseeding with combined Coconet. The use of combination of hydroseeding and coconet is cheap and time saving because it requires low-cost-maintenance and less effort. These advantages prove that it can be an effective and economical solution to soil erosion. Hydroseeding is another method of ground re-vegetation to stabilize bare surface to prevent soil erosion. The method calls for the use of cellulose mulch material mix with a tackifier acting as a binder. The cellulose fiber mulch, together with the grass seeds, fertilizer and water are mixed inside the tank of a hydroseeding machine to form into consistent and homogeneous slurry and then hydraulically sprayed to the ground. When sprayed the cellulose fiber mulch together with the fertilizer and the grass seed will act as an absorbent mat, holding enough moisture to allow proper germination of the grass seeds and at the same time performing a tenacious blanket cover to the soil surface even before the grass seeds germination to prevent soil erosion. The cementitious geobinder forms a permeable is non toxic cementitious binder that safely holds the grass seeds uniformly in place, prevents surface erosion and water evaporation in the soil. The cellulose fiber mulch which is biodegradable and will in time revert back to organic matter and assist in the vigorous establishment of the grass ground cover. The hydroseeding slope protection was constructed in the Subic-Clark-Tarlac Expressway Project to showcase the effectiveness of this method in protecting the slope after passing all the required and necessary tests based from the unpublished study of Bases Development Conversion Development Authority Report on the Result of Vegetation Cover Growth for Clay Slope Protection Works of Package 2 SCTEX, 2006, Clark, Angeles City, Pampanga, Philippines.

1.1 Statement of the Problem

The study would like to address the effectiveness of the combined Hydroseeding and Coconet to slope protection on how it will withstand the slope surface, either Hydroseeding or Coconet alone.

Hydroseeding is an innovative method designed for slope protection which is introduced in the Philippines in Subic-Clark-Tarlac Expressway Project. Since it is new in the engineering industry, there was only limited information about the said method. Tests to assess this method were barely made by private construction companies making the data exclusive for the company use.

1.2 Objectives of the Study

The objective of the study is to assess the performance of combined Hydroseeding and Coconet against soil erosion through means of determining the erosion rate from the laboratory test. From the 21-day period, assessment of the vegetative cover during its development growth period shall be done. Results from this experiment shall promulgate the method of combined Hydroseeding and Coconet as an alternative slope protection.

1.3 Significance of the Study

This study gives a comprehensible understanding on hydroseeding with Coconet significant to control soil erosion. Assessment of the properties and its physical behavior of hydroseeding were also determined. Through the test made, the researchers were able to seek new knowledge and announce the effectiveness of Hydroseeding with Coconet as an alternative slope protection.

1.4 Scope and Limitation

The study covers the assessment of the effectiveness of the combined Hydroseeding and Coconet against soil erosion. The study is an outdoor experiment which considers the natural factor such as wind and sunlight. The study of the factors from the outdoor was neglected due to this study which merely focused on the ability to control soil erosion. Transportation of the specimens to the laboratory was by means of a forklift neglecting the level of disturbance. To minimize the disturbance of soil, the test specimens were transported carefully. A fine grained material soil which is silt and clay with a 65º of slope and rainfall intensity rate of 120 mm / hr was used for consistency of the study. An intensity rate of 120mm/hr was used which is the maximum rate of rain happens in the Philippines over 100 yrs. This is based from the records of Flood and Control and Sabo Engineering Center, Department of Public Works and Highways, Technical Standards And Guidelines for Planning and Design, Vol. IV: Natural Slope Failure Countermeasure, 2002, FCSEC DPWH, Philippines.
Other condition prior to the study such as landslide was not included in the study.

2.0 REVIEW OF RELATED LITERATURE AND STUDIES

2.1 Soil Erosion

Effectiveness of coir-based rolled erosion control system in reducing sediment transport from hill slope; Sutherland, R. and Ziegler, A.; 2007, University of Hawaii, Hawaii, USA

2.2 Hydroseeding

Report on the result of Vegetation Cover Growth for Clay Slope Protection Works of Package 2 Subic-Clark-Tarlac Expressway, Bases Conversion Development Authority (BCDA), 2006



Slope Protection at the portion of Subic-Clark-Tarlac Expressway

2.4 Bench Scale Laboratory Test

Standard Index Test Method for the Determination of Unvegetated Rollled Erosion Control Product (RECP) Ability to Protect Soil From Rain Splash and Associated Run-Off Under Bench Scale Conditions

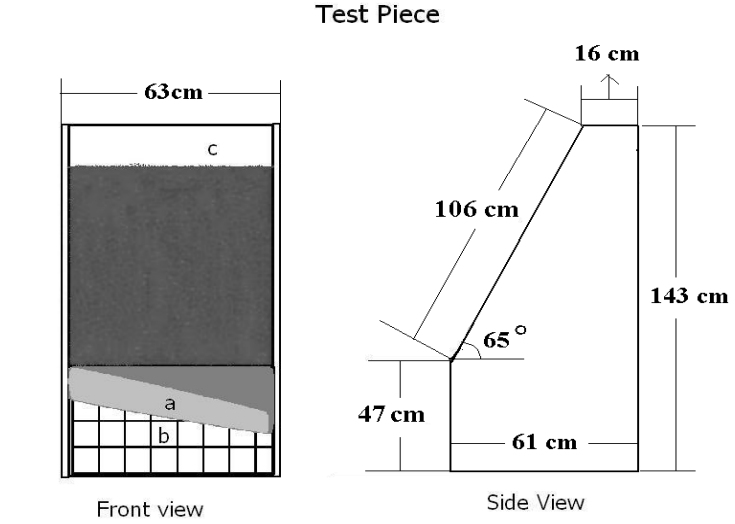

2.3 Coconets

Use of Coconut Geonets, Department of Public Works and Highways – Bureau of Research and Standards, 2005

2.5 Rainfall Simulation

This test method establishes the guidelines, requirements and procedures for evaluating the combination of Hydroseeding and Coconet to protect soils from rainsplash-induced erosion. This test method utilizes small-scale testing procedures, rather than full-scale simulation, and may not be indicative of conditions typically found on sites

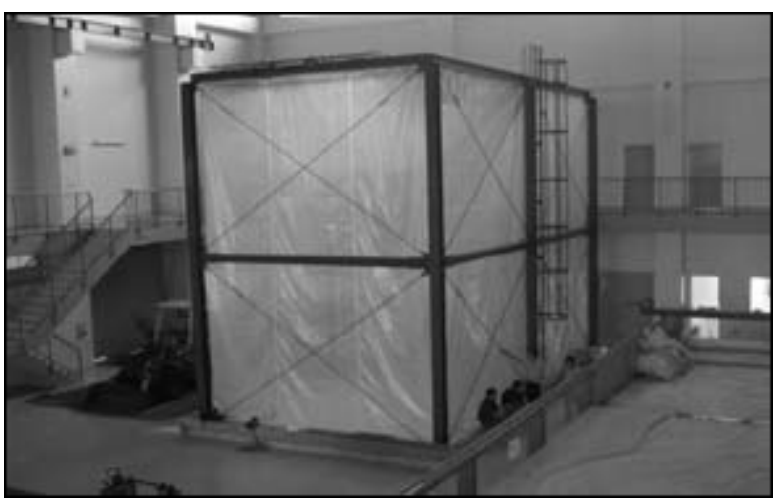

Rainfall Apparatus

2.0 METHODOLOGY

The assessment of the effectiveness of the combination of Hydroseeding and Coconet to control soil erosion were done by comparing its performance to the performance of the bare soil in terms of surface runoff. Soil cores consisting of containers with bare soil and 21 day old soil with hydroseeding and coconet reinforcement were exposed in rainfall simulation. Each specimen had three representations soil core to gather accurate data. The rainfall intensity used in study is 120 mm/hr. The amount of soil and water splashed out by runoff from the containers were collected and weighed. The collections of runoff were done for every 10 minutes for 5 trials, which is equivalent to 50 minutes. Soil sediments were filtered and air dried for 24 hours then weighed using weighing balance sensitive to 0.001 gram. The weight soil sediment per trial was recorded for computation.

In order to assess the effectiveness of the combination of Hydroseeding with Coconet as reinforcement to control soil erosion, the researchers used the performance indicator as suggested by Sutherland, R. and Ziegler, A. in his study in Effectiveness of Coir-Based Rolled Erosion Control System in Reducing Sediment Transport from Hillslope. The following indicators were used:

Sediment Concentration which states the mass of sediments collected over the volume of water collected.

$$Sediment\ Concentration\ \left(\frac{g}{L}\right) \equiv \frac{Mass\ \text{of Sediments Collected (g)}}{Volume\ \text{of Water Collected (L)}}$$

Sediment Yield which states the mass of the sediments collected over the area of the plot and duration of Runoff Collection.

$$\text{Sediment Yield}\ \left(\frac{g}{m^2 h}\right) = \frac{\text{Mass of Sediment Collected (g)}}{\text{Area of the Plot } (m^2) \text{ x Duration of Runoff Collection (h)}}$$

Effectiveness Against Soil Erosion which states the difference between the sediment yield of bare soil and Hydroseeding and Coconet reinforcement over the sediment yield of bare soil.

$$\text{Effectiveness Against Soil Erosion (\%)} = \frac{\text{Bare Sediment Yield}\ \left(\frac{g}{m^2 h}\right) - \text{Sediment of Hydroseeding and Coconet Reinforcement}\ \left(\frac{g}{m^2 h}\right)}{\text{Bare Sediment Yield}\ \left(\frac{g}{m^2 h}\right)} \text{ x } 100$$

4.0 RESULTS and ANALYSIS

Table 1: Total Sediment Concentration and Sediment Yield

Experiment	*Sediment Concentration (g/L)*	*Sediment Yield (g/m^2h)*
Bare Soil	21.49 ± 28.26	563.95 ± 2457.47
Hydroseeding with Coconet	1.56 ± 11.57	5.72 ± 143.77

Table 1 compares the sediment concentration and sediment yield of bare soil and hydroseeding with coconet reinforcement. From the numerical value indicated above, it shows that the Hydroseeding with Coconet reinforcement lessen the mass of the soil eroded.

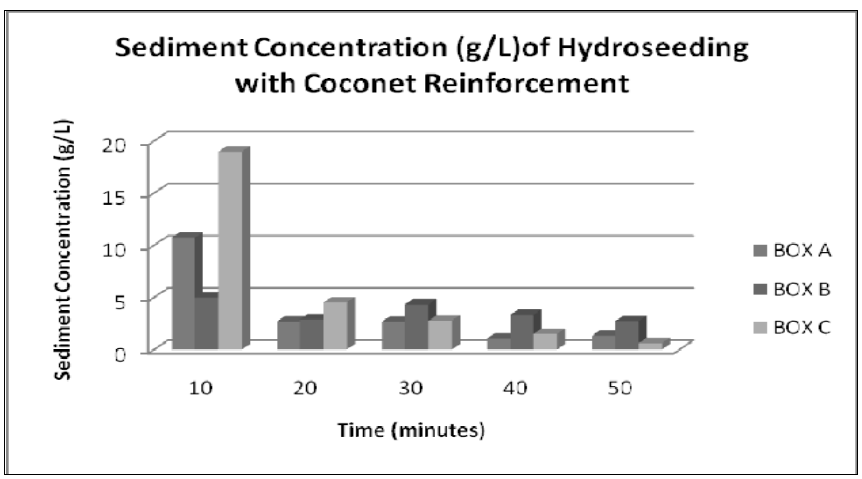

Figure 1: Sediment Concentration (g/L) for Hydroseeding with Coconet Reinforcement

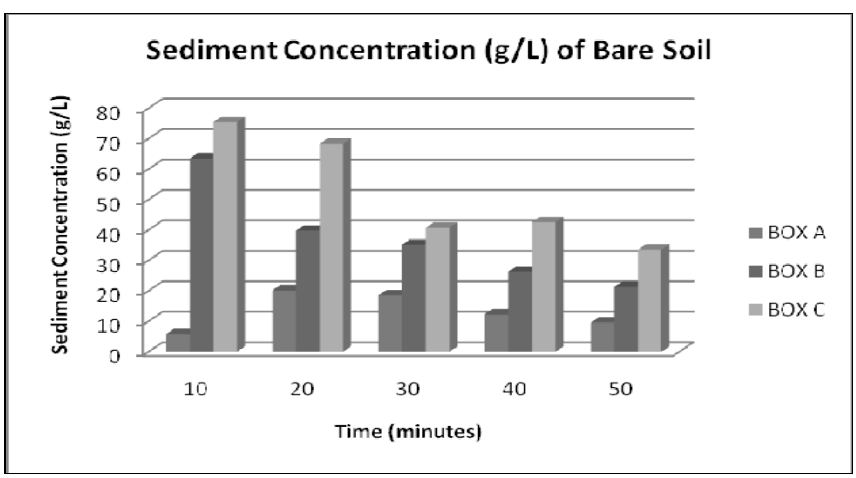

Figure 2: Sediment Concentration (g/L) for Bare Soil

Table 2: Effectiveness of Hydroseeding and Coconet Reinforcement versus Bare Soil against Soil Erosion

Time(mins)	Bare Soil versus Hydroseeding with Coconet (%)
0	0
10	94.15
20	97.95
30	98.4
40	99.01
50	98.99
Average	**97.7**

Table 2 determines the effectiveness of the applied hydroseeding with coconet reinforcement to control against soil erosion. According to the Effectiveness against Soil Erosion Formula, the greater the percentage computed the effective the Hydroseeding with Coconet reinforcement. From the Table 2, it shows that ninety-seven point seven percent (97.7%) of soil erosion was prevented by using hydroseeding with coconet reinforcement. Thus, the hydroseeding and coconet reinforcement is an effective soil erosion control instrument.

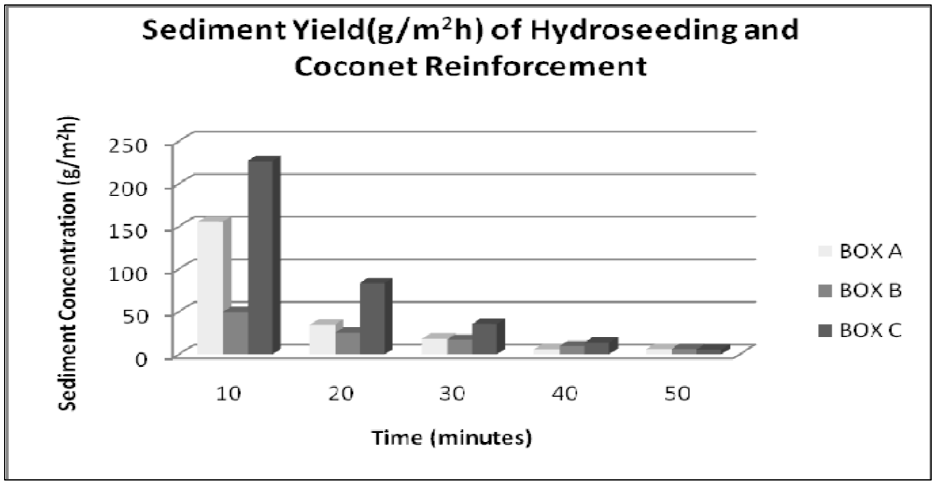

Figure 3: Sediment Yield (g/m^2h) for Hydroseeding with Coconet Reinforcement

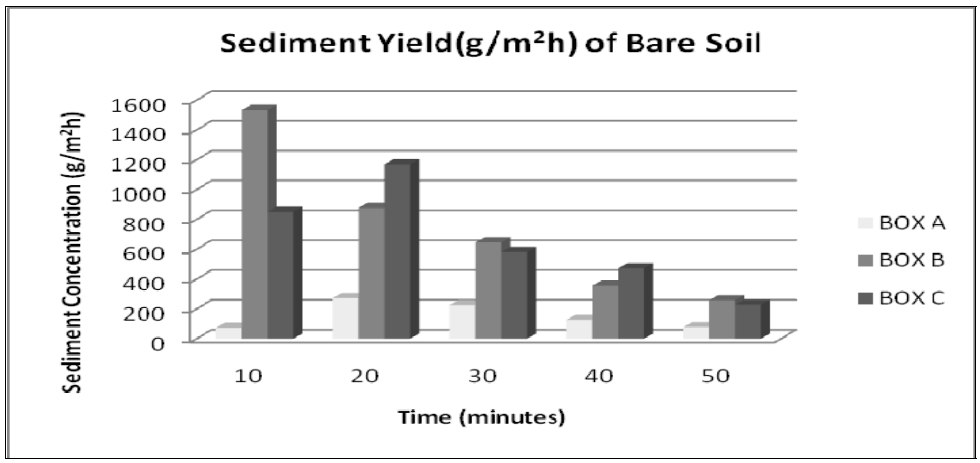

Figure 4: Sediment Sediment Yield (g/m^2h) for Bare Soil



Figure 5: The temporary grass seeds will germinate in forty-eight (48) hours after spraying and planting seedbed.



Figure 6: Grass grown by 110mm after 21 days

5.0 CONCLUSION and RECOMMENDATION

5.1 Conclusion

Results of actual laboratory experiments that were conducted with the use of the Department of Public Works and Highways Artificial Rainfall Simulation Apparatus showed that the use of the combination of Hydroseeding and Coconet reinforcement is effective in controlling soil erosion. From the results of the experiment, it shows that ninety-seven point seven percent (97.7%) of the soil was controlled from erosion given that the used slope is 65 degrees. It overcomes the threshold value of effectiveness of 80% defined from Sutherland, R. and Ziegler, A. in his study in Effectiveness of Coir-Based Rolled Erosion Control System in Reducing Sediment Transport from Hillslope. The researchers concluded that some of the discrepancies occur in the data results were from the calibration of rainfall apparatus.

5.2 Recommendation

The researchers suggests that if similar research(es) will be made in the future, adjustments on the proportions or mixtures of materials shall be given much attention and due consideration on other natural factors such as wind and sunlight. It has been noted by the researchers during the experiment that the slope may collapse easily when the saturation happens. Moreover, the researchers also suggest to use a lesser steep slope in the process, which is actually lower than 65 degrees.

The researchers have recommended taking note of the following basic steps in the application of hydroseeding with coconet:

1. Develop Hydroseeding product formulations and application procedures that will be compatible with current equipment and application methods at a given condition.
2. Take note of the right proportions of the required materials
3. Consider carefully the substitute or alternatives in case of non-availability of natural factors such as sunlight, etc., during the laboratory tests or experiments.
4. Evaluate and field test the various formulations using industry standard application equipment.
5. Conduct laboratory tests on the Hydroseeding and conventional hydroseed products for erosion control capabilities.
6. Conduct laboratory tests for water holding capacity, geobinder and other necessary organic materials, maturity of the materials after planting, water or moisture content, and the chemical and physical characteristics of the materials for Hydroseeding.
7. Develop cost analysis and cost comparisons between this method and other slope protection methods.

REFERENCES:

Sutherland, R. and Ziegler, A.; Effectiveness of coir-based rolled erosion control system in reducing sediment transport from Hillslope; 2007, University of Hawaii, Hawaii, USA

Harlan C. Carrascal, Clayton H. Bergado I, and Ma. Doreen E. Candelaria under Dr. Maria Antonia N. Tanchuling. "Slope Suitability of Coco-fiber Geotextile (Cocomat) for Soil Erosion Control" .Department of Civil Engineering, University of the Philippines.

Bases Conversion Development Authority Report on the Result of Vegetation Cover Growth for Clay Slope Protection Works of Package 2 SCTEP, 2006, BCDA, Clark Angeles City Pampanga – Unpublished

Department of Public Works and Highways, Bureau of Research and Standards, Use of Coconut Geonets to Protect River Banks and Prevent Soil Erosion, 2005, DPWH (BRS), Quezon City, Philippines – Unpublished

Standard Index Test Method for the Determination of Unvegetated Rollled Erosion Control Product (RECP) Ability to Protect Soil From Rain Splash and Associated Run-Off Under Bench Scale Conditions, 2003, US. Available on: www.ectc.org/source_docs/2005/testmethod2.pdf

Flood Control and Sabo Engineering Center, Department of Public Works and Highways, Technical Standards And Guidelines for Planning and Design, Vol. IV: Natural Slope Failure Countermeasure, 2002, FCSEC DPWH, Philippines

Designing Effective Rainfall Harvesting Systems in Developing Areas of Sub-Saharan Africa

Emmanuel U. Nzewi, PhD, PE, M. ASCE
emmanuel@engr.subr.edu

Department of Civil & Environmental Engineering
Suite 321 Pinchback Building
Southern University and A&M College
Baton Rouge, LA 70813

Abstract

This paper examines the design of rainfall-harvesting schemes that could be implemented to improve the availability of water in certain developing regions of sub-Saharan Africa. The focus of the paper is on the evaluation of rainfall distribution patterns in parts of Sub-Saharan Africa. Rainfall harvesting is a sustainable water supply alternative in the developing, as well as in the developed countries of the world. In the developed regions domestic rainfall harvesting is primarily a means for supplementing other sources of water (usually for non-potable water uses). This paper also highlights the activities of non-governmental organizations in the development and implementation of in-country (location specific) appropriate technologies for water supply. These groups fund and implement small projects which solve basic water and environmental engineering problems in small communities in developing areas. Usually the goal is to use in-country appropriate technologies to formulate innovative solutions to problems. In a recent study, the National Research Council, identified integrated water management as a high priority development requirement in its list of emerging technologies that would benefit farmers in Sub-Saharan Africa and South Asia. The study also stressed the need to address water shortage and access to water resources in Sub-Saharan Africa. Furthermore, the World Health Organization (WHO) estimates that the number of people without access to water services will increase from 300 million (in 2003) to 400 million by the year 2020. This paper will also provide an overview of the water resources inventory and distribution in Sub-Saharan Africa to emphasize the need for small-scale, community based water supply alternatives for developing areas in this region. The paper focuses on implementable solutions particularly tailored for the region. These solutions are termed "location-appropriate" and therefore employ locally available resources, whenever possible, to achieve solutions that are cost-effective, sustainable and efficient. It addresses the need to analyze the temporal and spatial variation of precipitation in the design of viable rainfall harvesting systems.

Introduction

Rainwater or rainfall harvesting is the collection and storage of rainfall from roofs or surface catchments for later use. A rainwater harvesting system may include a means for water treatment when the water is used for drinking or cooking. Rainwater harvesting includes processes whereby runoff can be collected and stored for usually non-potable water requirements and/or for irrigation. If potable water requirements are to be met, then some measure of water treatment is necessary.

This study is part of an effort to identify and outline effective solutions to basic water problems faced by peoples and communities in developing areas of the world. The localized solutions identified provide strategies and remedies with the potential of achieving sustained reliable water supply. With respect to domestic rainfall harvesting, any solutions must consider the prevailing climatic factors, cost, locally available materials, scale and any similar factors that might enhance or impede successful implementation of a solution. Domestic rainfall harvesting may be differentiated from communal systems where several families are served from a common water source.

According Nzewi and Luster-Teasley (2008), Nnadi (2004) and Nzewi (2004) several acute water problems have been identified in developing regions. They are: water scarcity, poor drinking water quality (and water borne diseases), roadway drainage and runoff management, surface water pollution, improper dumping of untreated wastewater and solid waste into streams and the flood plain, depletion of groundwater sources, and mismanagement of reservoir systems. This paper highlights one of these problems – water resource availability.

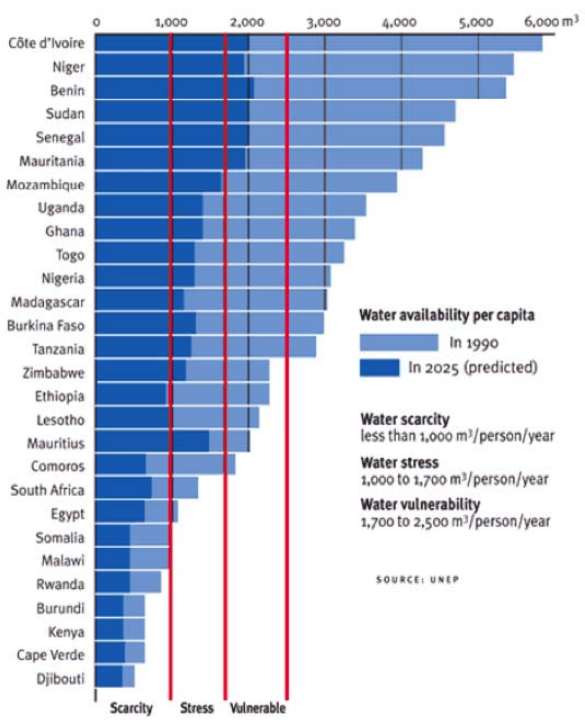

Figure 1 Water availability (m^3/person/year) in Africa in 1990 with 2025 projections.

Furthermore, based on the 1998 United Nations Medium Population Projections, 2.8 billion people in 48 countries will face water stress or scarcity conditions by 2025 (See Figure 1). Some of the countries in this list are in West Asia, Sub-Saharan Africa (Northern and Southern) and in the Middle East. It has been estimated that by 2050 (projected population 9.4 billion), as many as 54 countries with a combined population of about 4 billion may face water stress or scarcity.

Except for Asia, Africa has the highest average population growth in the world, approaching 13 percent of overall world population. This growth could increase percentage of Africa's population relative to the world to about 20

(Source: http://www.sahims.net)

percent ($1/5^{th}$) by 2050, according to the Population Reference Bureau. Significant population growth means more demand for water, which exacerbates the water situation since the continent is already suffering from water scarcity. Africa is the second largest inhabited continent but has only the fifth highest volume of water reserves available. There is therefore a need to increase available water, manage and conserve water resources in Africa.

Sub-Saharan Africa

Figure 2 and Figure 3, below, provide the annual rainfall distribution and list the major rivers in the African continent, respectively. It can be seen that the northernmost (corresponding to the regions around the Sahara desert) and southernmost (western portion) areas are arid. Sub-Saharan African encompasses the Sahel -- a series of countries across the northern part of the continent that are immediately south of the desert – to the southern tip of the continent. The climate is quite diverse ranging from topical humid (around the mid-section of the continent) to arid. A large portion of Sub-Saharan Africa (S-SA) is influenced by the monsoon season. As shown in Figure 3, 12 major rivers drain the area including the Nile river. In the humid (wetter) regions, there is an interconnection between the surface and groundwaters. This is not the case in the arid regions where the groundwater and surface waters are not connected and therefore the recharge of groundwater depends on rainfall. Additionally, base flow is relatively low in rivers in arid regions while evaporation is significantly higher (NAS, 2008). With respect to the distribution of water resources in S-SA, in the Sahel, water resources are limited and spatially unevenly available. As Figure 3 shows, the Nile River drains through basins in the eastern part of the Sahel. West S-SA is served by many rivers including the Niger, Senegal, Volta, Lake Chad and Benue (not listed in Figure 3). The Gulf of Guinea in the west includes the Niger (which drains in the Gulf) where there is a tropical climate highly influence by the monsoon. One fourth of the region's water resources may be found in this region. In comparison, east of the Gulf, is the humid tropical climate of central Africa. Central S-SA is served by the Congo and Ooguue Rivers – and includes almost 50% of the region's water resources. The climate ranges from semi-arid to tropical humid in eastern S-SA and as stated previously the major river here in the Nile. However, the region also boasts of the largest lake in the continent – the Lake Victoria. Finally, the southern region of S-SA has a diverse climate ranging from arid (south southwest) to sub-tropical humid. The Rivers: Zambezi, Limpopo, Orange; and inland lakes: Malawi and Tanganyika, serve the region. Comparatively, available water resources are less abundant in this region. Interestingly, therefore,

eastern and southern S-SA make up only about 25% of the continent's water resources.

Africa (and essentially S-SA) is populated by about 13% (about 905 million) of the world's inhabitants, and the total renewable water resource is approximately 5000 m^3/year/capita. Since S-SA is comparatively sparely populated (on the average), there is adequate (average) renewable water resource per capita even in countries in the Sahel. This is not true in densely populated countries like Nigeria. On the other hand, however the water is not always readily accessible to the population. Herein lies the problem in the region.

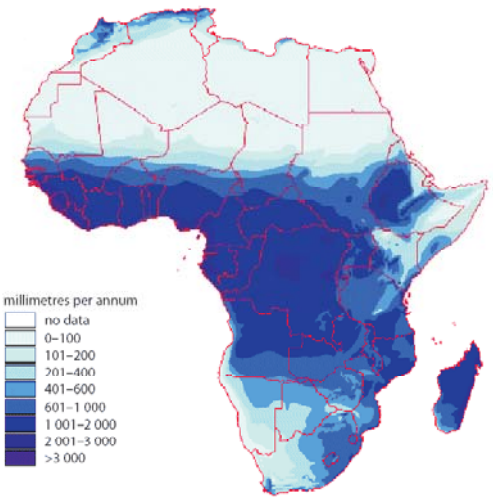

Figure 2 Annual Rainfall Distribution in Africa (Source: FAO/Agrymet)

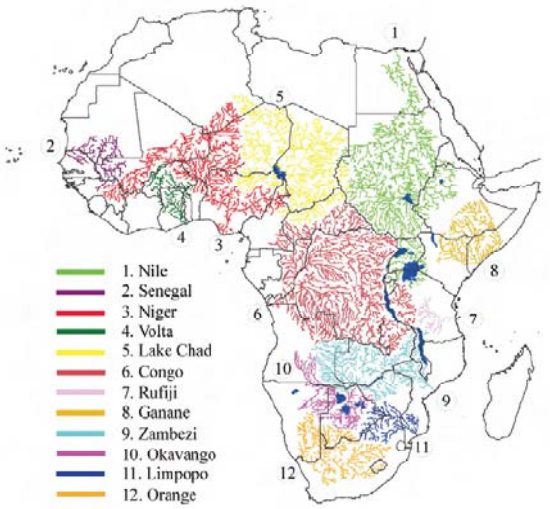

Figure 3 Major Rivers of Africa (Source: NAS, 2008)

Poverty and access to water seem to go hand-in-hand in many African countries, especially in rural areas as shown the relationship between rainfall and GDP for Ethiopia in Figure 4. Those without access to water must travel to find water sources, and the time spent doing this prevents them from improving their own standards of living. Often the quality of life of a rural area can be improved with the simple addition of a well or other source of water that provides clean water. Studies have been able to directly link access to water and poverty.

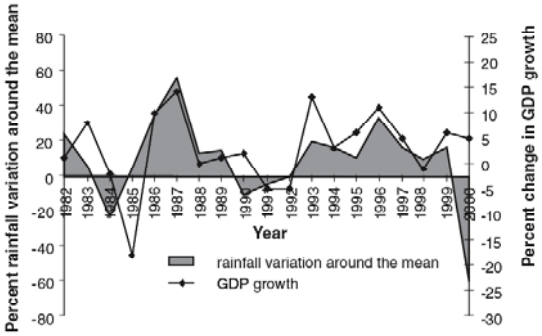

Figure 4 Rainfall Variation Around Mean and Gross Domestic Product in Ethiopia 1982-2000 (Source: NAS, 2008)

Impact of Non-Governmental and Private Groups

In the past, private and non-governmental have embarked on projects designed to alleviate the suffering, disease and poverty in developing regions of the world. Many of these projects have been successful while some have sometimes made the problem worse because the solutions did not adequately consider important factors such as sustainability and the unique cultural tendencies of the peoples involved. The failure of some of these systems resulted in the re-evaluation of solution strategies and provided a knowledge base for what does not work as well. More recently, perhaps in the last 10 years, there has been an increasing crescendo of more effective projects because the approach has shifted to become more location-specific, sustainable methods that employ "green technologies" instead. The term "green technologies" refers to the application of design strategies that minimize the degradation of the environment while making use of renewable resources in their design and implementation. Several organizations have championed this approach but there are two notable ones that are making significant impacts around the globe, but particularly in Sub-Saharan Africa: Engineers Without Borders (particularly United States of America) and WaterAid (United Kingdom)

Engineers Without Borders-USA (EWB-USA) describes itself as follows: "A non-profit humanitarian organization established to partner with developing communities worldwide in order to improve their quality of life. This partnership involves the implementation of sustainable engineering projects while involving and training internationally responsible engineers and engineering students." It has both professional and student-led chapters all over the United States of America. It has established itself in the business of implementing "green" solutions mainly through volunteers in the solution of a wide range of problems that go beyond water supply and sanitation. In fact, many universities have established chapters that sometimes work on a wide array of projects --- year round. Documented projects include: bore-hole (groundwater well) and water distribution system for a small community and local elementary school in Ghana, West Africa; A small hydropower plant and distribution system to benefit villages in India; a reactor that produces biodiesel fuel from oils containing large quantities of fatty acids; a sustainable water development program for a rural community in Nigeria, West Africa; a handheld bleach generator that can disinfect drinking water --- to list a few. EWB-USA has been so impactful that the news about the organization and its activities have been featured several times the American Society of Civil Engineers news in the past year. This is extremely important because the technologies that are being developed and implemented are highly successful and these programs can be easily extended to solve problems, perhaps with minor adaptations, in many communities in Sub-Saharan Africa (S-SA). The goal of this research is to device a means for collecting and disseminating information about "green" water development technologies that can be implemented in S-SA. First, the projects that fall under rainfall harvesting (and water treatment) will be addressed. The goal is not to re-invent the wheel, as the saying goes, but to determine what solutions already exist, catalog them and provide

a resources clearinghouse for disseminating and facilitating location-specific solutions.





Figure 5 Engineers Without Borders Project in Ghana: Water Distribution System

WaterAid (United Kingdom) – describes itself as **"**an international charity whose mission is to overcome poverty by enabling the world's poorest people to gain access to safe water, sanitation and hygiene education." "WaterAid enables the world's poorest people to gain access to safe water, sanitation and hygiene education. These basic human rights underpin health, education and livelihoods and form the first, essential step in overcoming poverty." WaterAid has projects along these lines in 17 countries located in Africa, Asia and the Pacific Region. WaterAid works with local partners so that local issues and conditions are brought to the fore, to provide skills, training and support, in the development of sustainable projects that meet community needs. In S-SA, WaterAid has current projects (sometimes multiple) in: Burkina Faso, Ethiopia, Ghana, Malawi, Mali, Mozambique, Nigeria, Tanzania, Uganda and Zambia.

The importance of the foregoing discussion is to identify established organizations that are at work in Sub-Saharan Africa. The need is great in the region because of population shifts toward urban areas and population growth. In addition, there may be complexities related to shifting rainfall patterns due to changing (whether short or long term) climate shifts. One of the objectives of this paper is to propose strategies that could help in addressing the problem of water availability and access in rural communities in S-SA.

Rainfall Harvesting

Rainfall harvesting can be an attractive water supply alternative because it can be easily integrated into existing water supply systems. Furthermore, it is an environmentally superior to other methods of water supply and an effective means for readily increasing available water resources. The cost of the infrastructure for domestic rainfall harvesting is comparatively lower than for other methods. Rainwater harvesting has the following environmental benefits: (a) reduced storm water volume and peak discharge rate; (b) reduction in urban flooding; (c) reduction in the amount of sewerage diverted to sewage water treatment systems; (d) increased groundwater recharge; and (e) minimal use of energy for pumping.

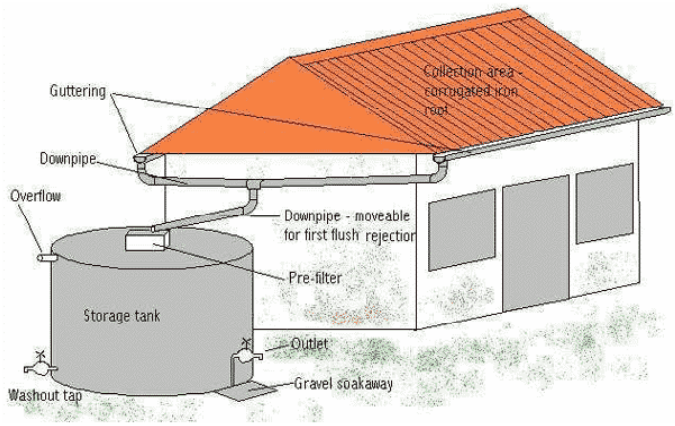

Figure 6 Rooftop Catchment For Rainwater Harvesting
[Courtesy of DTU -- www.eng.warwick.ac.uk/dtu/index.htm]

Several countries in both the developed and under-developed countries that already practice some form of rainwater harvesting; however, it is mostly used for non-potable water. These include, but are not limited to: South Africa, Kenya, Zimbabwe, Ethiopia, China and United States. In the under-developed world, rainwater harvesting can be divided into micro-catchments and macro-catchments. Micro-catchments are specially contoured areas with slopes and berms designed to increase the runoff from rain and concentrate it in a planting basin where it infiltrates and is effectively "stored" in the soil profile. The water is available to plants but protected from evaporation. There are three basic types of microcatchment systems: contour bench terraces, runoff strips and micro-watersheds. Runoff strips and contour bench terraces are best suited for agriculture as they require extensive mechanical re-shaping of the surrounding terrain and create regular patterns which are inconsistent with a natural landscape. Micro-watershed systems are more appropriate for revegetation. These include mound, strip and basin collectors.

Another method of rainfall harvesting is from rooftop catchments. This method is practiced in the developed world but not widely used in the developing world due to the lack of design and implementation knowledge; however it can be implemented in under-developed regions to help ease tension on their water resources. The system consists of three basic elements; a collection area, a conveyance system and a storage area. The collection area would be the roof; the conveyance system would consist of gutters and pipes to transport the collected water to the storage system which is basically a storage tank. In order to maintain the cleanliness of the system, gutters and pipes have to be cleaned periodically. Figure 1 below shows a diagram of a rooftop catchment water harvesting system.

Drinking water is an important requirement for human life, although, it only accounts for a small fraction of total human comsumptive use. Domestic water consumption is highly influenced by the "ease" with which it can be obtained.

Usually, a family that has ready access to water, tends to use more water than a family that has travel far to fetch water (Thomas, 1998).

Rainfall harvesting has been practiced in areas where conditions have been favorable or conditions for other means of water supply have been less desirable. The most expensive component of the RH system is because the storage tank of a system must be large enough to smooth-out both short-term and long-term fluctuations in available rainfall. The tank tends to be large and it is usually impractical to use one that is not well constructed. Most buildings already have a roof thus very little cost if any is incurred in retooling the roof for rainfall harvesting. In areas where rainwater harvesting is currently practiced on a significant scale, it is done out of necessity rather than due to a commitment to autonomy like in China, Rural East Africa and Singapore (Thomas, 1998).

The sizing of the storage tank is a very important design element in development of an effective water harvesting system. There are several web-accessible computer programs for accomplishing this task. Furthermore, for a given location, there is a limit to the amount of water that can be collected via rainfall harvesting. In sizing a storage tank the following information is normally required: household size, water use requirements, water availabilty (rainfall records – including distribution) (DTU 2001).

Rainwater Harvesting in Sub-Sahara Africa

Rainfall varies temporarily and spatially. The rainfall records for several countries in Sub-Saharan Africa were obtained and analyzed. Table 1 shows the monthly average rainfall for two countries: Nigeria and Angola. These sets were chosen to highlight differences in tropical humid and semi-arid climates and temporal variation over the months of the year. The data represents the average monthly rainfall between 1931 and 1960as reported by the National Climatic Data Center in the USA. Full dataset cannot be presented here due to space constraints. The data were obtained for Senegal, Ghana, Gambia, Nigeria, Togo, Mali, Burkina Faso, Cameroon, Republic of Congo and Angola. The sample for the 2 selected countries is provided in Table 1.

In Table 2, the average annual rainfall for all the reporting cities (for each country) have been provided. Table 2 shows a wide range of average annual rainfall values. The average of the annual rainfall values in Table 2 is of 40.7 inches, with a range of 40.1 inches and a standard deviation of 14.1 inches. For rainfall harvesting applications, while the average annual rainfall rate for a country may be used as a regional planning guide, the rainfall values for a city (or a geographic location) should be used in the design of any rainfall harvesting system.

Table 1 Monthly Rainfall [inches] in Selected Cities by Country

NIGERIA

	Jan	Feb	Mar	Apr	May	Jun	Jul	Aug	Sep	Oct	Nov	Dec	Total
Enugu	0.7	1.1	2.6	5.9	10.4	11.4	7.6	6.7	12.8	9.8	2.1	0.5	71.6
Kaduna	0.0	0.1	0.5	2.5	5.9	7.1	8.5	11.9	10.6	2.9	0.1	0.0	50.1
Lagos	1.1	1.8	4.0	5.9	10.6	18.1	11.0	2.5	5.5	8.1	2.7	1.0	72.3
Maiduguri	0.0	0.0	0.0	0.3	1.6	2.7	7.1	8.7	4.2	0.7	0.0	0.0	25.3

ANGOLA

	Jan	Feb	Mar	Apr	May	Jun	Jul	Aug	Sep	Oct	Nov	Dec	Total
Cangamba	8.9	7.4	6.8	1.8	0.1	0.0	0.0	0.2	0.2	1.6	5.1	8.5	40.6
Huambo	8.7	7.8	9.8	5.7	0.4	0.0	0.0	0.0	0.6	5.5	9.6	8.9	57.0
Luanda	1.0	1.4	3.0	4.6	0.5	0.0	0.0	0.0	0.1	0.2	1.1	0.8	12.7
Namibe	0.3	0.4	0.7	0.5	0.0	0.0	0.0	0.0	0.0	0.0	0.1	0.1	2.1

In addition, the temporal variation of rainfall is also important because it can be an factor in the determination of the size of the storage tank. For a system to be effective, the storage must be enough to handle both the short-term and long-term variability in rainfall. Furthermore, for enough water to be collected, the roof area must be adequate to concentrate a large enough volume of water.

Table 2 Average Annual Rainfall by Country (1930 – 1961)

Country	Average Rainfall [in]
Angola	28.1
Burkina Faso	40.8
Cameroon	59.2
Congo	54.9
Gambia	51.0
Ghana	41.8
Mali	19.1
Nigeria	54.8
Senegal	25.8
Togo	31.0

Figure 7, below presents the spatial distribution of rainfall in a country. The purpose is to highlight the in-country variation of rainfall of rainfall. It shows that it is vitally important to determine the rainfall patterns at a particular location rather than using average values determined for the country as whole. A case in point is Nigeria where there's a marked difference between Lagos and Maidugri. In the design of a rainfall harvesting system, it is therefore crucial to study the local rainfall patterns closely so that an effective design can be provided. In addition, since many areas in Sub-Saharan Africa are affected by the monsoon, it is equally important to consider the seasonality of precipitation in the areas.

As a follow up to this study, the rainfall patterns for the entire region will be analyzed and categorized to identify areas that have common/functionally similar patterns. This will help to identify areas that should follow "regionally" developed design guidelines. The purpose is to minimize the effort required to design the systems by "reusing" design "patterns" so as to reduce the effort in providing effective systems. Hopefully simple charts (the goal) will be provided whereby a chart-driven approach that locals can easily use to design an build there systems. The goal of this approach is to empower the local communities –as much as possible so that they play a very active role in providing the solutions themselves. Furthermore, as the activities of Engineers Without Borders and WaterAid expand, best practices will emerge and the methods can be cataloged and disseminated to aid local governments or local communities in generating their own solutions.

Spatial and Temporal Variation of Rainfall In Selected Countries

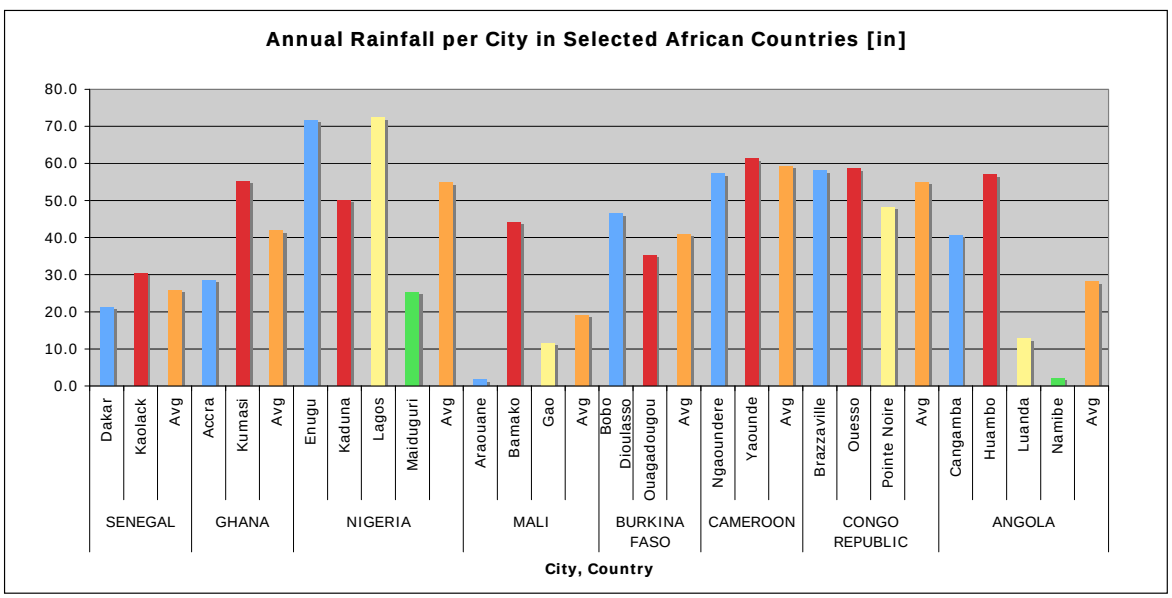

Figure 7 - Spatial Variation of Rainfall within Selected Countries Studied

To design a rainwater harvesting to meet the average demand of 50 liter/day/capita (according to Cowden et al, 2006) the per capita roof area available (**A** [m^2]), the roof runoff coefficient (**C** – a generally accepted value is 0.8, according to Cowden, et al, 2006) must be taken account as well as the expected rainfall amount over a period a time. Average per capita roof sizes (2 – 20 m^2) vary widely and for that reason, a relationship between $\mathbf{S_d}$ and **A** has been developed to aid in determining the viability of a system. The amount of water (liter/day/capita) that can be provided by the rainwater harvesting system is given by:

$$S_d = CAR_k$$

where, R_k is a rainfall coefficient = annual rainfall (mm) divided by 365.

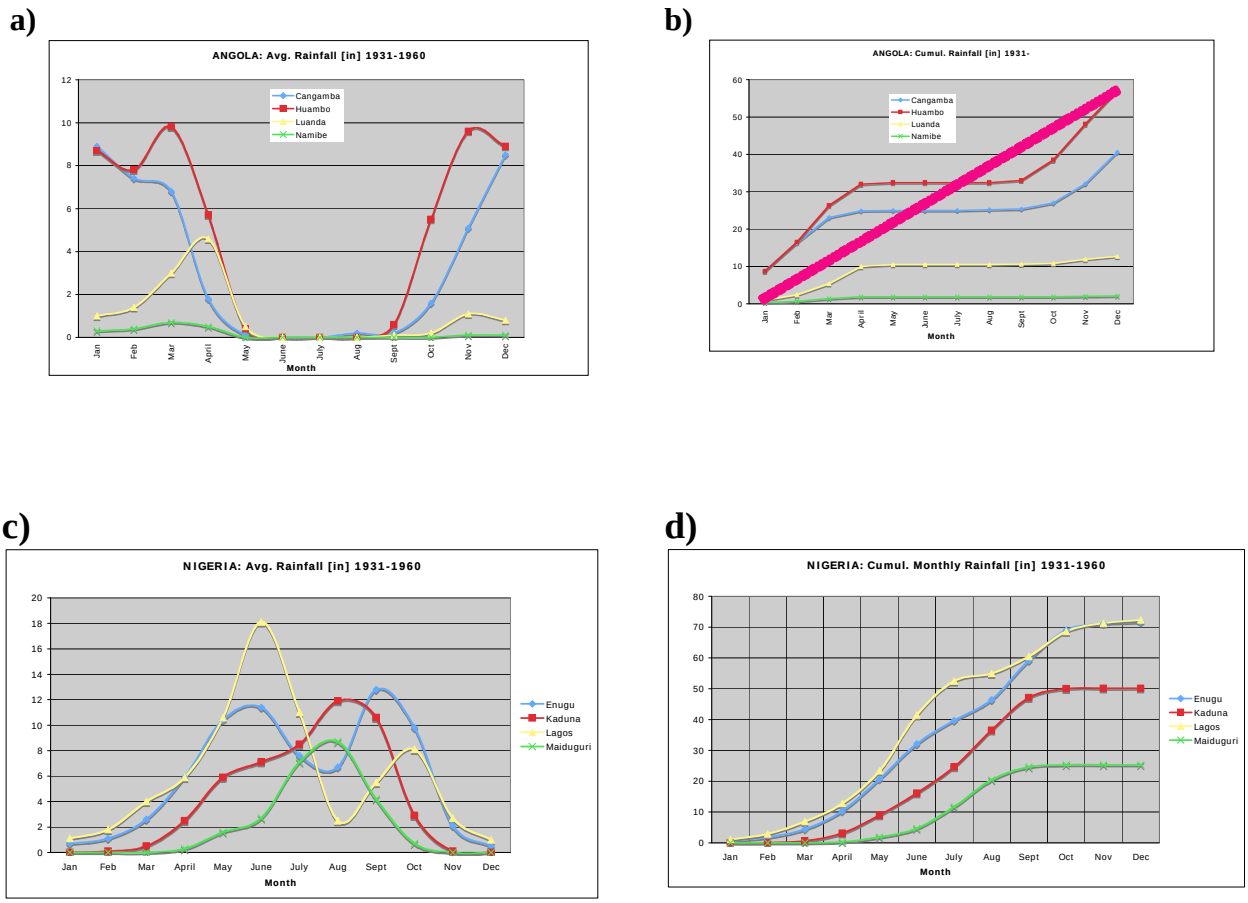

Figure 8 – Monthly Average Rainfall [in] (a, c) and Cumulative Rainfall [in] (b,d) for Selected Cities: Nigeria and Angola

It should be emphasized that in regions where most of the rainfall is concentrated during a few months of the year, much of the rainwater collection (and storage) must occur during those wet months and therefore storage and managed release for future use is necessary. The following presents the water demand/supply scenario for one country (Nigeria).

In Figure 8, the variation of rainfall is captured by evaluation the distribution during the year. It can be seen from Figure 8 (a,c) the difference between the rainfall patterns for Nigeria and Angola. While the cumulative values are not very different the periods over which a large percentage of the rainfall can be captured differs in length and in timing. Thus the design of storage components must be adjusted to reflect these differences.

References

Cowden, J. R., Mihelcic, J. R. and Watkins D. W. (2006), "Domestic Rainwater Harvesting Assessment to Improve Water Supply and Health in Africa's Urban Slums," Proceedings of the 2006 World Environmental and Water Resources Congress, May 21-25, 2006, Omaha, Nebraska.

Development Technology Unit (DTU) (2001), "Recommendations for designing, rainwater Harvesting system tanks. Domestic Roofwater Harvesting Research Program," O-DEV Contract No. ERB IC18 CT98 027, Milestone A6: Report A4, January 2001.

National Research Council, "Emerging Technologies to Benefit Farmers in Sub-Saharan Africa and South Asia, National Academy of Sciences, The National Academies Press, Washington, D.C., 2008.

Nnadi, Fidelia N., "Source Pollution Abatement and Best Management Practices (BMPs)," Proceedings, 7th Africa-USA International Conference on Manufacturing Technology: Connecting Africa to Global Manufacturing, Port Harcourt, Nigeria, July 12-14, 2004.

Nzewi, Emmanuel U., "Managing Water Resources Systems for Sustainable Development in Nigeria," Proceedings, 7th Africa-USA International Conference on Manufacturing Technology: Connecting Africa to Global Manufacturing, Port Harcourt, Nigeria, July 12-14, 2004.

Nzewi, E. U., and Luster-Teasley, S, "Effective Rainwater Harvesting Schemes for Sub-Saharan West Africa, Proceedings, 2008 ASCE Environmental and Water Resources Institute (EWRI) Water Congress, Honolulu, HI, May 2008

Thomas, T. (1998). "Domestic water supply using rainwater harvesting." *Building Research and Information*. 26, 2, 94-101.

Innovative Design at Lake Lenexa

Scott R. Brand, P.E.[1] and Tom A. Jacobs, P.E.[2]

[1]Geotechnical Engineer; Black & Veatch Corporation; 8400 Ward Parkway, Kansas City, Missouri 64114; brandsr@bv.com
[2] Stormwater Engineer; City of Lenexa, Kansas; 12350 West 87th St. Parkway, Lenexa, Kansas 66215-2882; tomajacobs@ci.lenexa.ks.us

ABSTRACT

As new dams get built closer to the public in existing neighborhoods and towns, the Public, through public participation workshops and events are asking for more amenities in the form of parks, recreational facilities, and education seminars be implemented to increase voter satisfaction. The public is also asking for more aesthetic designs if they can be proven cost-effective at providing an appealing element to new dams. Lake Lenexa was designed and built around the idea of providing for basic dam functions such as flood control, enhanced water quality, recreation but also to provide an inviting community focal point for the residents to visit and enjoy; truly interact with the dam. The residential setting became the impetus for a bigger vision emphasizing bold architecture and aesthetics. Innovative design techniques were implemented to capture the architectural elements of the dam.

Extensive architectural elements were incorporated into the dam design including MSE retaining walls, Use of CKD (Cement Kiln Dust), cantilevered spillway bridge, trellis, and a wide variety of landscape architecture.

Water quality enhancements were achieved through the use of wetland treatment cells on the upstream tributaries of the reservoir. In addition, several stream restoration projects were completed for the area.

The overall project includes the development of three wetlands; trails; recreational and park amenities; and a future amphitheater. Three miles of trails connect the lake to surrounding neighborhoods. The architecturally unique dam and "one of a kind" spillway were designed to symbolize the water cycle as water moves from nature into the urban environment and the back to nature. A pedestrian bridge that spans the spillway offers visitors a good view of cascading pools and a fountain.

INTRODUCTION

Lake Lenexa is under construction upstream of the existing Whispering Hills housing development in Lenexa, Kansas, a suburb of Kansas City, with a population of approximately 45,000 residents.

Lake Lenexa is on the western side of Lenexa. The primary roads bordering the site include State Highway 10 to the south, State Highway 7 to the west, 83rd Street to the north, and Woodland Avenue to the east (Figure 1).



Figure 1. Lake Lenexa Location

As an integral part of the city's Rain to Recreation program, Lake Lenexa was designed to reduce flooding for downstream developments, improve water quality, provide recreational opportunities, and preserve critical habitat.

Initial Studies

The purpose of the Coon Creek Watershed Study was to develop a plan for stormwater management tailored specifically for the watershed. The major items studied in the watershed were recent flooding and projected flooding potential after the watershed was developed, hydrologic and hydraulic modeling, water quality concerns, stream stability evaluations, and recreational opportunities.

Initial studies included the following to support permitting activities: determination of jurisdictional wetlands, endangered species, cultural resources, and preparation of mitigation plans for affected areas.

The proposed project included the following: retention lake, four upstream wetland treatment cells for water quality enhancement, and stream restoration projects along the upper reaches of Coon Creek. The project involved a unique solution to the problems within the watershed, while adhering to the Rain to Recreation requirements.

Community Involvement

With the proximity to existing neighborhoods, community involvement was a key requirement of the project. The city of Lenexa solicited community involvement and comments at all stages of the project through public events, workshops and meetings, planning "Input and Review Sessions," newsletters, Web sites and interactive email.

Through these events, the city and Black & Veatch determined how to increase the benefit to the local community by developing stream restoration projects along the upstream reaches of Coon Creek, fish and wildlife habitat, wetland areas in the upper reaches of the reservoir, hiking trails, and park and recreational facilities. Figure 2 details the recreational facilities planned for the park surrounding the reservoir.

Preliminary Design and Aesthetics

Initial design concepts for the dam included the use of roller compacted concrete (RCC) for the main dam and spillway components. However, geotechnical investigations showed potential sources of silts, clays, and weathered shale in the reservoir area that could be used for an embankment dam.

Geotechnical studies were performed to determine the soil and rock zones along the proposed dam alignment, the leakage in the rock zones, available borrow sources and properties, foundation materials, and abutment rock conditions. Additional studies included geological mapping of the abutments and reservoir areas. These studies indicated that the upper portions of the dam abutments consisted of limestone and shale units; the lower stratigraphy consisted of a thick shale layer underlying the reservoir area. Limestone outcrops were visible along the reservoir fringe, generally above the normal water level, except for the Frisbie Limestone (Figure 3).

The geotechnical investigations included soil and rock coring, water pressure testing of rock, installation of piezometers to monitor water levels, seismic refraction testing along the dam alignment, test pits to determine potential borrow sources, and laboratory testing of soil and rock samples to support the design activities.

Initial dam design included an analysis for a central core embankment with an internal chimney drain and blanket drains to control seepage through the embankment. Initial design also included slope stability analyses, seepage analyses, settlement analyses, and drilled pier design for the spillway bridge supports. Figure 4 shows a typical section through the embankment.

The spillway design included the Kansas requirement to pass the 0.4 Probable Maximum Flood (PMF) flows through the spillway with a minimum 3 feet of freeboard. The middle portion of the ogee spillway was designed to pass the 100 year storm event, and the entire spillway was designed to pass flows up to the 0.4 PMF (Figure 5).

Because of the urban location of the project, aesthetics played an integral role in the architectural design of the dam and its components. Elements in the design included a curved dam alignment, ogee spillway, unusual architectural spillway features, spillway bridge (cantilevered section with a separate viewing canopy), spillway steps, curvilinear spillway walls, spout structure, landscaping plans, recreational trails, and the stilling basin design. Figure 6 shows a plan of the dam alignment. Figure 7 shows a close-up of the lower spillway step details. Figure 8 shows details of the upper basin and the low flow channel.

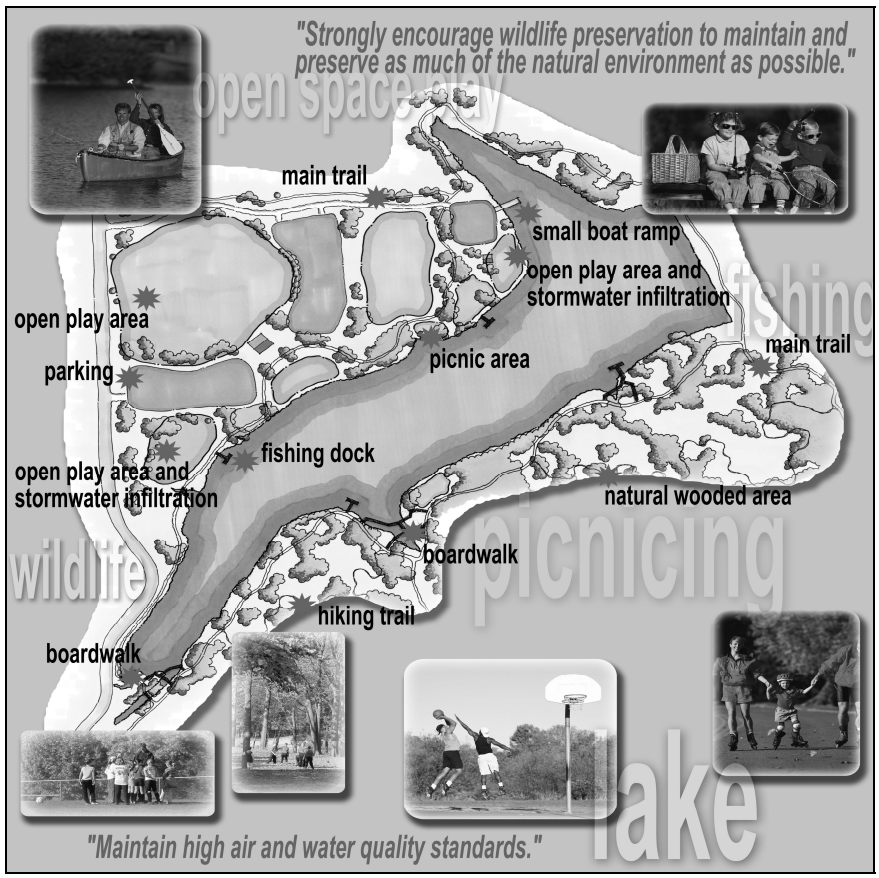

Figure 2. Recreation Components

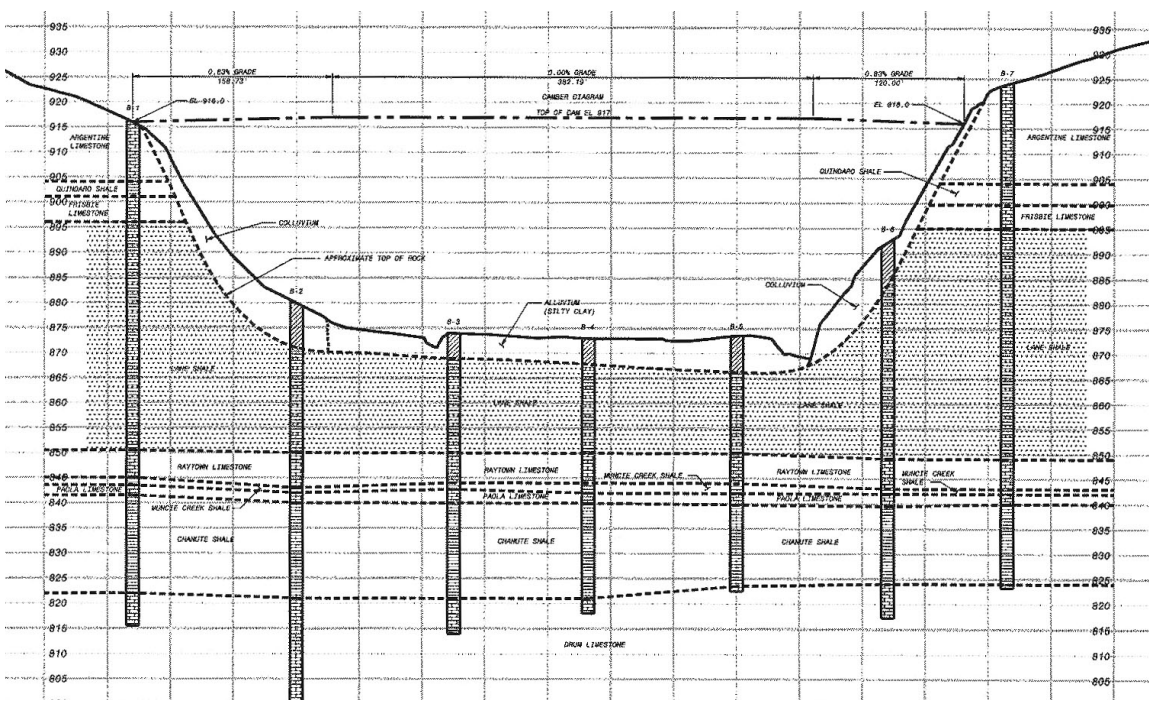

Figure 3. Geologic Cross Section at Dam

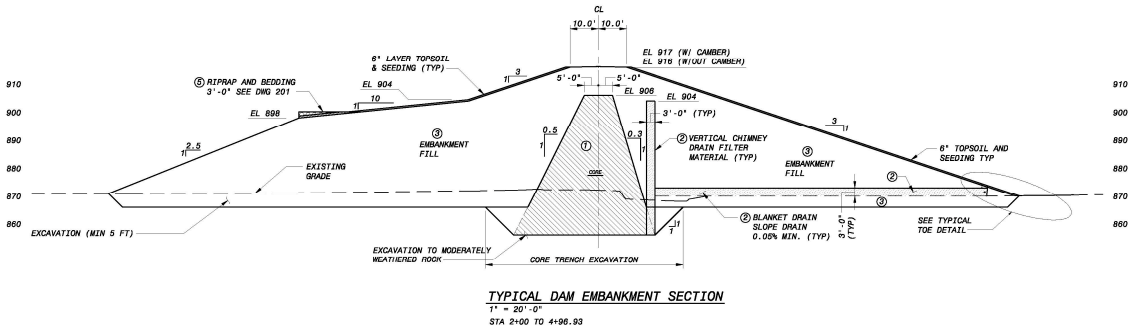

Figure 4. Typical Embankment Section

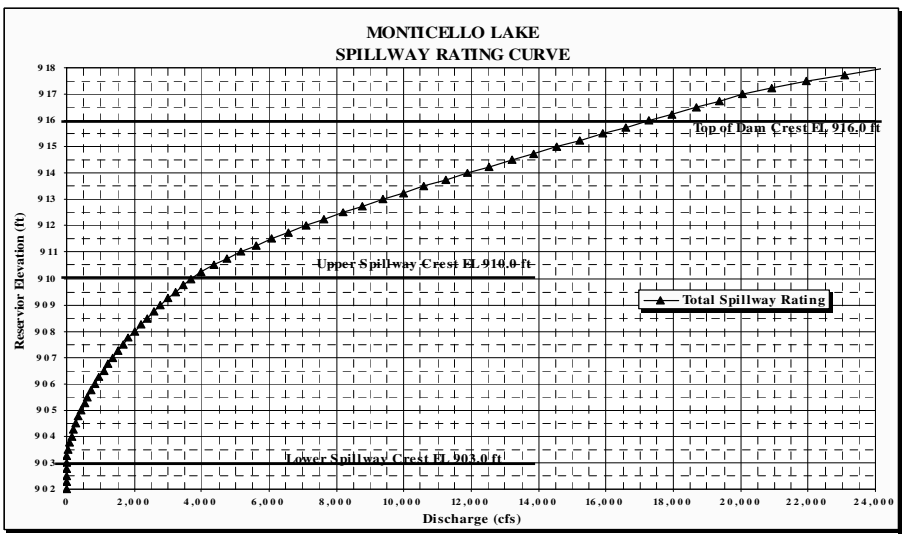

Figure 5. Spillway Rating Curve

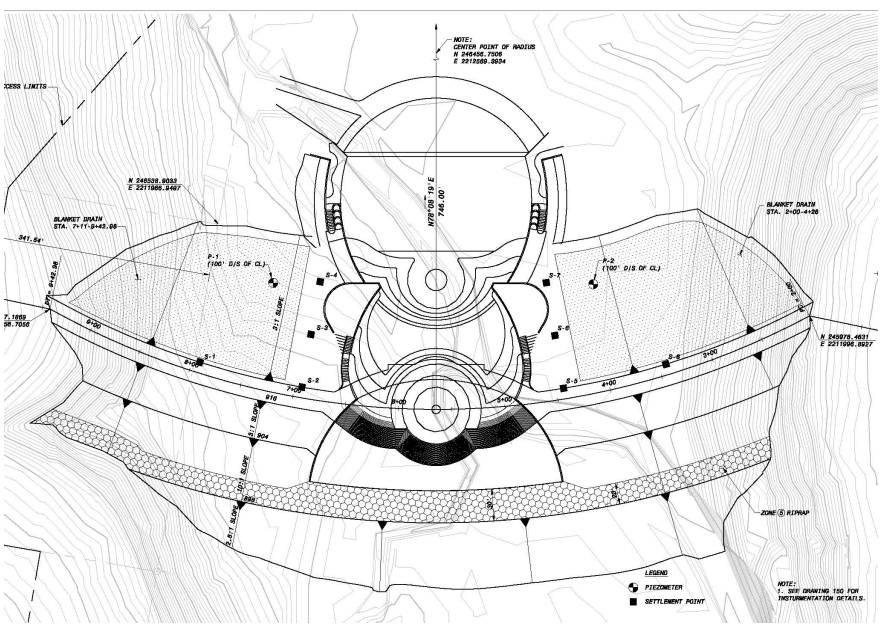

Figure 6. Dam Plan

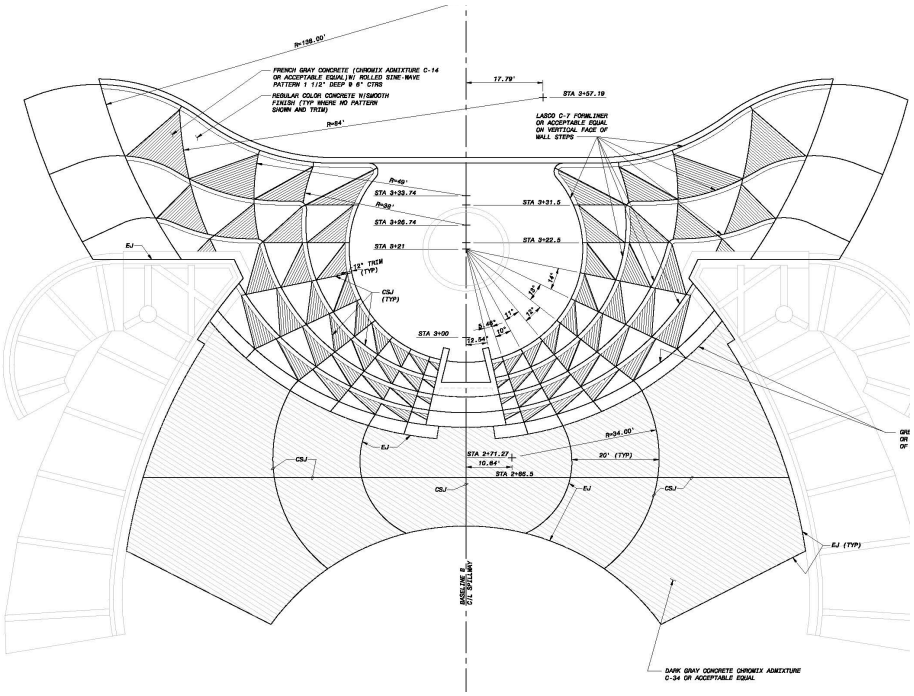

Figure 7. Lower Spillway Step Details and Middle Basin

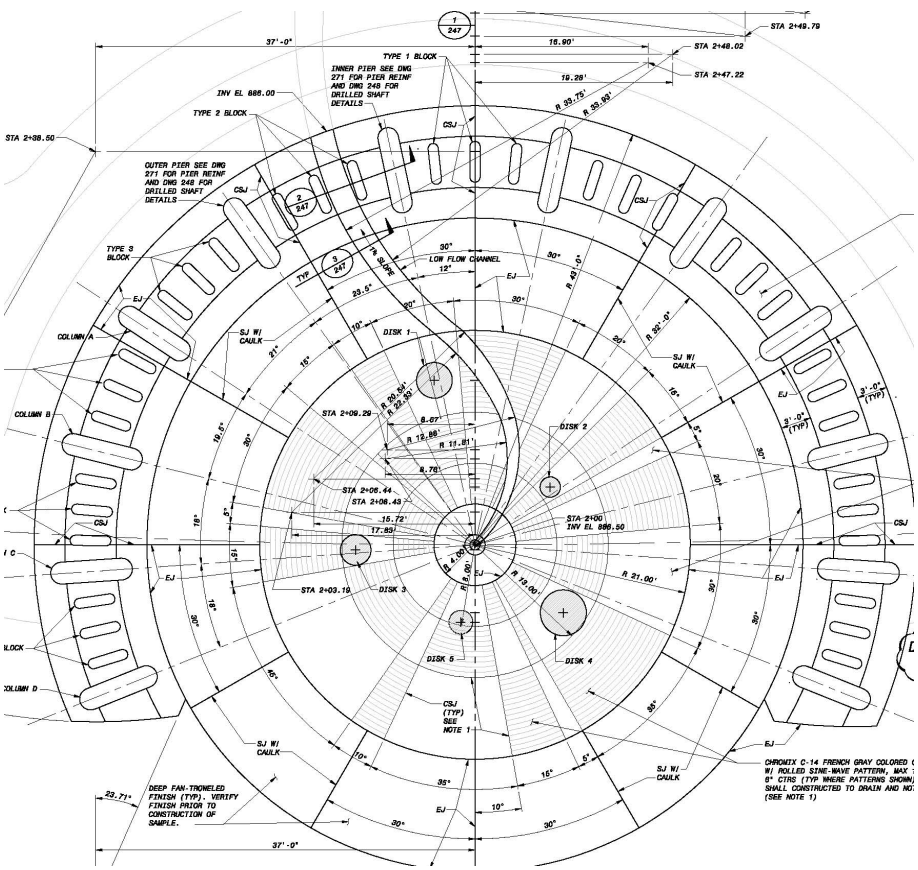

Figure 8. Upper Basin Details

Park facilities surrounding the dam and reservoir include a pavilion for community events, boat ramps and fishing docks, viewing areas, boardwalk and elevated bridges, wetlands, playgrounds, recreational trails, and outdoor classroom areas on the downstream side of the dam (refer to Figure 2).

Final Design/VE Workshop

The original spillway design included high retaining walls that formed the spillway training walls. These retaining walls were counterfort walls designed to withstand high bearing pressures and were a relatively rigid system. Adequate bearing capacity and differential settlement of the walls were design issues.

A VE workshop that included the Owner, Consultant, and Contractor explored cost-effective means to implement the architectural elements of the spillway. The workshop examined several options: various retaining wall systems in lieu of the counterfort walls, alternate materials for stable foundations for the spillway structures and structural slabs, options for providing a positive seepage cutoff under the spillway, options for spillway bridge systems, and changes to the landscaping requirements.

The VE workshop decided to use MSE retaining wall systems to form the high spillway walls and CKD to mix with the onsite borrow silts and clays to provide support for the spillway structures and slabs. Both items are innovative for use on a dam and reservoir project.

Typically, MSE walls are used for road and bridge projects. The decision to use MSE walls provided some valuable benefits: lower installed cost, a flexible wall system that could undergo some settlement, lower bearing pressures at the toe of the wall, ability to accommodate multiple curves in spillway design, and ability to provide a "Fractured Fin" pattern similar to the panels originally envisioned for the spillway walls. The project architect expressed concerns about the overall visual appearance of the walls because of the horizontal and vertical wall joints in the precast panels. However, the benefits outweighed this minor consideration.

CKD material produced by the cement industry is analogous to fly ash from the coal power industry. A mix design testing program demonstrated that the CKD material, mixed with silts and clays, was capable of reaching design strengths of 300 psi. CKD provided a high strength material to support all the spillway structures, including the spillway walls, spillway slabs, and ogee spillway. The onsite borrow clays mixed with the CKD provided a low permeability material that reduced the potential for seepage under the thin spillway slabs and potential uplift on the slabs.

Dam and Spillway Construction

Construction began in the summer of 2004 with general clearing and grubbing of the reservoir and dam areas. Subsequent work included excavation of the dam foundation and core trench areas and field testing of the CKD materials. The core trench

for the dam foundation was excavated into the hard and competent Lane Shale. Water pressure testing showed this material to be tight with no leakage, which provided a good seepage cutoff into the foundation below the dam.

Onsite mix testing of the CKD materials was performed using various proportions of the kiln dust to provide an optimum mixture to meet the strength requirements. Mixing methods, proportions of the materials, and placement procedures were determined during the field testing program. During the actual placement of the CKD materials, samples of mixed CKD materials from behind the mixing equipment were taken to the laboratory and cured under various temperature and curing durations to determine the compressive strength gain of the mixtures with time. Figure 9 shows some of the strength relationships observed from the testing.

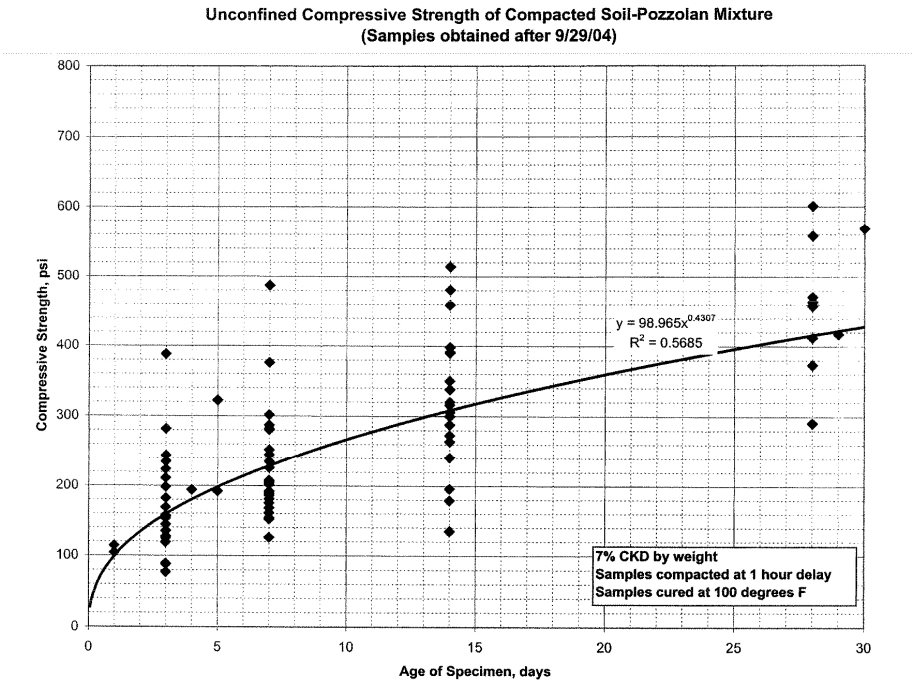

Figure 9. CKD Strength Test Results from Field Samples

Once the weathered materials had been excavated from the spillway area, the CKD materials were placed by mixing the borrow silts and clays with 7 percent kiln dust. The materials were mixed in place with a pulverizer and a water truck operating in tandem. Samples of the mixture were taken to the laboratory daily to create samples for the strength testing (Figure 10).

The MSE walls that formed the spillway training walls and the stilling basin walls were delivered to the site as precast interlocking units. A concrete footing was laid at the base of each wall section to provide a level surface to begin wall placement. As the walls were erected, stainless steel strips were placed to anchor the precast units. Geogrid materials were placed along the joints in the panels to prevent potential movement of fines from the aggregate backfill (Figure 11).



Figure 10. Mixing of CKD with Borrow Materials



Figure 11. MSE Wall Construction

All spillway slabs and walls within the spillway area were underlain and backfilled with the CKD materials. Once a section of the slab was poured and forms stripped, the walls were backfilled with CKD up to the next spillway step elevation.

The spillway bridge is one of the most interesting architectural elements of the project. It consists of a curved concrete section spanning the spillway just downstream of the ogee spillway and upper basin areas. The bridge has cantilevered supports that rely on drilled piers socketed into the underlying bedrock (Figure 12). Figures 13 to 15 show construction photos of the various components of the main spillway.

Grouting of the dam abutments was used on the upper portions of the abutments, primarily within the upper limestone units. A two pattern of grout holes was used on the north and south abutments to seal up the limestone units within the abutments.



Figure 12. Spillway Bridge Supports

Construction Schedule

The project is in the final phase of construction; the dam and spillway are scheduled to be completed in the spring of 2006. Structures will be substantially complete by the end of 2005. Only final grading and landscaping work on the dam remain to be completed. Work on the accompanying park facilities is scheduled to be completed in 2006.

SUMMARY

Through an innovative use of MSE walls and CKD materials, Lake Lenexa was built to combine the contrasting requirements of architecture and engineering to provide a valuable new addition to the city of Lenexa's park system.

Final Construction Photos



Figure 13. North Spillway Walls, Center Spout, and Steps



Figure 14. Lower Stilling Basin



Figure 15. Spillway Upper Basin

PRODUCTION OF DRINKING WATER FROM LAKE WATER SOURCES WITH A NANOFILTER MEMBRANE TO PREVENT THE FORMATION OF DISINFECTION BYPRODUCTS

Rajib Sinha, P.E.[1], Anita Anderson, P.E.[2], Craig Patterson, P.E.[3], and David Pearson[4]

[1]Shaw Environmental and Infrastructure, Inc, 5050 Section Avenue, Cincinnati, OH 45212; Rajib.Sinha@shawgrp.com
[2]Minnesota Department of Health, 320 W. 2nd Street Room 703, Duluth, Minnesota 55802; anita.c.anderson@state.mn.us
[3]U.S. Environmental Protection Agency, 26 W. Martin Luther King Blvd, Cincinnati, OH 45268; Patterson.Craig@epa.gov
[4]ITT Corporation, 227 S. Division Street, Zelienople, PA 16063, david.pearson@itt.com

ABSTRACT

Small community systems that use surface water as a source of drinking water are frequently faced with elevated levels of naturally-occurring organic matter (NOM) that are not removed by conventional filtration methods. These residual levels of NOM may combine with chlorine used for disinfection and create disinfection byproducts (DBPs) potentially in excess of the regulatory limit for various DBPs. Frequently, additional treatment for removal of these DBPs is necessary to avoid non-compliance with the requirements of the Safe Drinking Water Act (SDWA). The formation of DBPs can be prevented by removing NOM, which acts as a precursor to DBP formation. This paper presents the results of field tests conducted on lake water using a nanofilter membrane, incorporating a method for cleaning the membrane using a foam ball. The system uses a tubular membrane with the ends connected to effectively form a single, long, membrane. The lake water is fed into the inside of the membrane tube and the filtrate is forced out, through the membrane into the membrane housing outlet. Using a timer, a foam ball is periodically passed through the inside of the membrane by reversing the flow direction. This foam ball serves to remove accumulated organic matter capable of fouling the membrane surface. This organic matter is flushed to drain as the foam ball passes through the inside of the tube. The system can be operated with the membrane reject water recycled to the system inlet or in a dead-end mode where no membrane reject water is produced until the system is foam ball cleaned. Tests were conducted in both modes of operation. The system requires no pretreatment of the feed water other than a coarse (3mm) screen to prevent large solids from entering the system. The effectiveness of the system in producing drinking water was gauged by measuring the turbidity, color, and particle counts of the system inlet and outlet. Tests were also performed using the aerobic spore *Bacillus subtilis* (*B. subtilis*) as a surrogate for bacteria removal.

Notice: Any opinions expressed in this article are those of the author(s) and do not, necessarily, reflect the official positions and policies of the EPA. Any mention of products or trade names does not constitute recommendation for use by EPA. This document has been reviewed in accordance with EPA's peer and administrative review policies and approved for publication.

INTRODUCTION

The Water Supply and Water Resources Division (WSWRD) of the U. S. Environmental Protection Agency's (EPA's) National Risk Management Research Laboratory (NRMRL) has been conducting tests on small drinking water treatment systems since 1997 in response to the 1996 Reauthorization of the Safe Drinking Water Act (SDWA). The SDWA established standards for drinking water systems and required EPA to assess treatment technologies for small systems serving fewer than 10,000 people. Initial tests were focused on packaged bag and cartridge filtration systems. Subsequently, the program has been expanded to test a variety of filtration systems for the removal of turbidity, chemical contaminants, and microbial contaminants.

Small community systems that use surface water, such as lakes, as a source of drinking water are frequently faced with elevated levels of color and naturally-occurring organic matter (NOM) that are not removed by conventional filtration methods. The organic matter can also serve as a precursor to the formation of disinfection byproducts (DBPs). This paper presents the results of field tests conducted in August 2008 on the Fyne Technology system, which is a membrane-based filtration unit that incorporates hollow fiber nanofiltration membranes for the removal of turbidity, bacteria, color and organic matter from lake water. The membranes are periodically cleaned by a foam ball that removes accumulated organic matter from the membrane surface. The system tested is manufactured by ITT Corporation (Zelienople, PA). The tests were conducted at a field site in Ely, Minnesota, in collaboration with the Minnesota Department of Health (MDH). The results of the tests were compared to the standards for bag filters presented in the Long Term 2 Enhanced Surface Water Treatment Rule (LT2ESWTR) which requires a >3.0 log reduction of *Cryptosporidium* and a turbidity of <0.3 Nephelometric Turbidity Unit (NTU).

SYSTEM DESCRIPTION

The Fyne Process refers to a family of treatment systems offered by ITT Corporation that were originally developed in the United Kingdom to treat waters with high concentrations of organic materials. The Fyne Process can remove both microbial contaminants and reduce the organic content, thus reducing the potential to form DBPs and is well suited for small water systems with a typical capacity to produce 10 to 15 gallons per minute (gpm) of treated water per day. Its small footprint and modular construction makes the Fyne Process ideal for many small communities that must treat water containing high concentrations of organic compounds.

One unique aspect of the Fyne Process is the use of an automated foam ball cleaning process to remove accumulated filter cake and organic and inorganic foulants. In this process, a small foam ball is forced through the tubular filtration elements via water pressure flowing in the opposite direction of normal flow. The foam ball scours the tubular membrane surface, removing the accumulated foulants. "Filter-catchers" (small, perforated plates installed in the module inlet and outlet lines) retain the foam

balls in the system. The cleaning frequency is adjustable and the entire process is fully automated.

Figure 1 shows a process flow diagram for the Fyne Process pilot skid that was tested at the Ely, MN field site. This unit was fitted with two modules constructed of ABS plastic. One module contained the PCI Membrane type ES404 while the other module contained the PCI Membrane type CA2PF. The ES404 has a molecular weight cutoff (MWCO) of approximately 4,000 daltons and is referred to as "Membrane 1" in this paper. The CA2PF has a MWCO of approximately 2,000 daltons and is referred to as "Membrane 2" in this paper. Each module was 3 feet long and contained thirty-six individual, ½-inch diameter, membrane tubes. The 36 membrane tubes were fed in series through the module with U-Bends linking one tube with the next. The maximum operating pressure of the module was 175 pounds per square inch (psi) at 70°F. Figures 2, 3, and 4 show various features of the system.

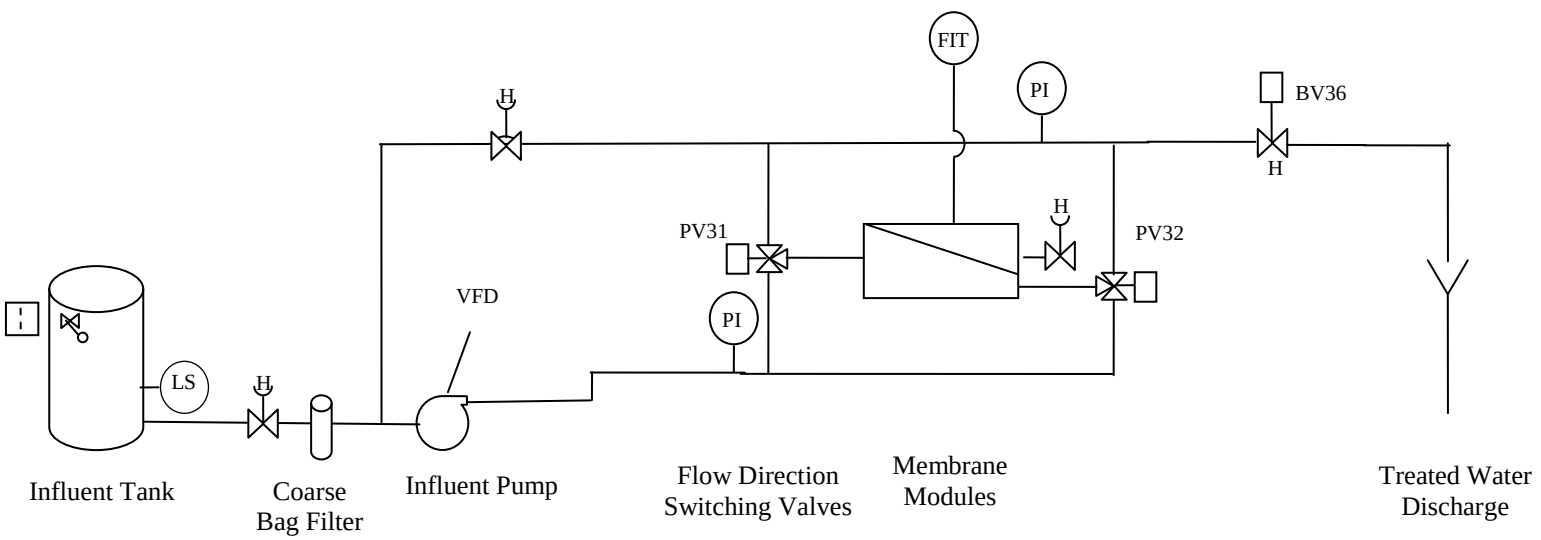

Figure 1. Process Flow Diagram for Fyne Technology System

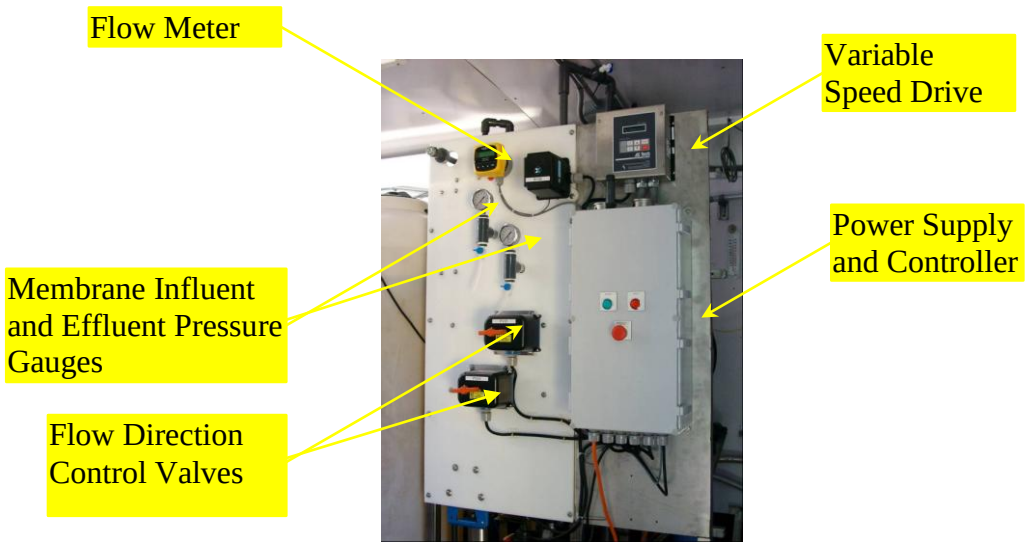

Figure 2. Fyne Technology System Control Panel



Figure 3. Fyne Technology System Influent

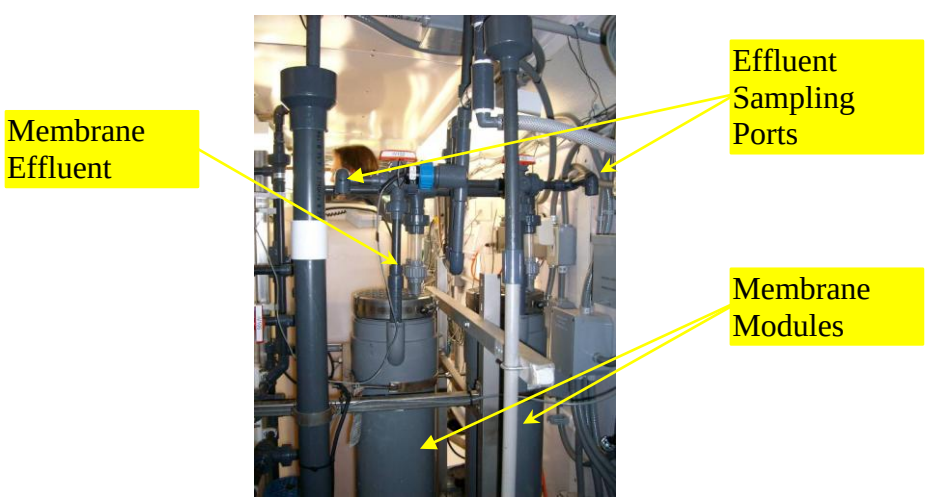

Figure 4. Fyne Technology System Effluent

TEST PROCEDURES AND SAMPLING TECHNIQUES

The Fyne Technology system was evaluated for the ability to remove color and turbidity. The American Public Health Association (APHA) Platinum-Cobalt (Pt-Co) standard method for apparent color was used to measure color removal. Turbidity was measured in NTU. Each membrane module of the Fyne Technology system was sampled and evaluated separately. The color and turbidity of the influent lake water was tested as received and there were no attempts made to modify the influent turbidity levels.

For evaluating specific bacteria removal performance, both systems were challenged with the soil-based aerobic spore *Bacillus Subtilis* (*B. subtilis*). *B. subtilis* was also used as a potential surrogate for *Cryptosporidium*. All samples collected were grab samples. For these challenges, a suspension of the *B. subtilis* spores was prepared by adding 1 mL of *B. subtilis* stock to 500 mL of 0.01% Tween-20 in a 1-L glass beaker. The 500 mL suspension and an additional 500 mL rinseate were added to the influent stream of each system tested, using a peristaltic pump. The total injection time ranged from 15 minutes to about 60 minutes depending on the test conducted. Samples were collected in 100 ml polypropylene containers that were pre-sterilized and contained sodium thiosulfate preservative in tablet form (Fisher Cat No. 09-730-91). The sample bottles were refrigerated to 4±2°C immediately after collection and shipped on ice. The samples were shipped to the EPA Test & Evaluation (T&E) Facility in Cincinnati, OH. All samples were kept in the refrigerator at the T&E Facility until analysis. The *B. subtilis* analysis was performed in accordance with the T&E SOP 021.00.R0, which is based on Method 9215D in Standard Methods for the Examination of Water and Wastewater.

TEST RESULTS

The following test runs were conducted on the Fyne Technology system to evaluate the removal of *B. subtilis*:

Test 1 – Fyne Technology System in Recycle Mode
Test 2 – Fyne Technology System in Recycle Mode (Replicate of Test 1)
Test 3 – Fyne Technology System in Dead End Mode
Test 4 – Fyne Technology System in Dead End Mode (Replicate of Test 3)

The sequencing of the test runs above was designed to allow the systems to undergo a cleaning cycling and flush to remove any residual *B. subtilis*.

Test 1 – Fyne Technology System in Recycle Mode

Table 1 presents the *B. subtilis* analytical results for Test 1 on the Fyne Technology system. For this test, the *B. Subtilis* was injected into the system approximately 10 minutes prior to the T0 sample (which was collected when permeate was observed to discharge from the system). Injection was completed just before the T5 samples were taken (followed by a chaser solution of Tween-20 for another 15 minutes). The system accidentally went into the foam ball cleaning mode immediately after the T30 samples had been collected. T60 samples were collected after the system was restarted. The average log removal for Membrane 1 was 6.34 and that for Membrane 2 was 5.88.

Table 1. *B. subtilis* Analytical Results for Test 1 - Fyne Technology System in Recycle Mode

Sampling Time (min)	No. Cells/100 ml			Log Removal	
	IN	Out 1	Out 2	Membrane 1	Membrane 2
T0	TMTC*	0	275	N/A	N/A
T5	7.2×10^6	0	0	6.85	6.85
T15	7.6×10^6	0	10	6.88	5.88
T15Dup	7.3×10^6	20	0	5.56	6.86
T30	7.9×10^6	0	20	6.89	5.60
T60	3.4×10^5	0	20	5.53	4.23

* TMTC – Too Many to Count

Test 2 – Fyne Technology in Recycle Mode

Table 2 presents the *B. subtilis* analytical results for Test 2. For this test, the injection was completed just as the T0 sample was being collected. The average log removal for Membrane 1 was 6.89 and that for Membrane 2 was 5.96.

Table 2. *B. subtilis* Analytical Results for Test 2 - Fyne Technology System in Recycle Mode

Sampling Time (min)	No. Cells/100 ml			Log Removal	
	IN	Out 1	Out 2	Membrane 1	Membrane 2
T0	TMTC*	0	30	-	-
T5	8.8×10^6	0	30	6.94	5.47
T15	7.6×10^6	0	10	6.88	5.88
T15Dup	8.2×10^6	0	20	6.91	5.61
T30	7.4×10^6	0	0	6.86	6.86
T60	TMTC	0	0	-	-

* TMTC – Too Many to Count

Test 3 – Fyne Technology System in Deadend Mode

Table 3 presents the *B. subtilis* analytical results for Test 3 on the Fyne Technology system. The *B. subtilis* injection for this test was started approximately 10 minutes prior to collecting the T0 sample and completed 5 minutes before the T30 sample (over 40 minutes). The chaser solution was injected for another 25 minutes. The average log removal during this test for Membrane 1 was 4.94 and that for Membrane 2 was 5.25.

Table 3. *B. subtilis* Analytical Results for Test 3 - Fyne Technology System in Deadend Mode

Sampling Time (min)	No. Cells/100 ml			Log Removal	
	IN	Out 1	Out 2	Membrane 1	Membrane 2
T0	1.4×10^6	0	0	6.15	6.15
T5	1.0×10^5	0	200	5.00	2.70
T15	2.5×10^6	0	0	6.40	6.40
T15Dup	8.0×10^4	0	0	4.90	4.90
T30	8.0×10^5	100	0	3.90	5.90
T60	2.8×10^5	160	0	3.24	5.45

Test 4 – Fyne Technology System in Deadend Mode

Table 4 presents the *B. subtilis* analytical results for Test 4 on the Fyne Technology system. The *B. subtilis* injection for this test was started approximately 10 minutes prior to collecting the T0 sample and completed at the time of collection of the T30 sample (over 40 minutes). The chaser solution was started 7 minutes prior to collection of the final sample. The average log removal during this test was 5.66 for both Membrane 1 and Membrane 2.

Table 4. *B. subtilis* Analytical Results for Test 4 - Fyne Technology System in Deadend Mode

Sampling Time (min)	No. Cells/100 ml			Log Removal	
	IN	Out 1	Out 2	Membrane 1	Membrane 2
T0	3.6×10^5	0	0	5.56	5.56
T5	1.9×10^6	0	0	6.28	6.28
T15	3.6×10^5	0	0	5.56	5.56
T15Dup	3.1×10^6	0	0	6.49	6.49
T30	3.0×10^5	0	0	5.48	5.48
T60	4.0×10^4	0	0	4.60	4.60

Raw Water Sample

To confirm that there were negligible *B. subtilis* spores in the lake water (influent), a sample of the raw lake water was analyzed. The results of analysis on two lake water samples (Sample 1 – 0 cells/mL; Sample 2 – 0.2 cells/mL) confirmed that there was negligible *B. subtilis* in the lake water.

Particle Count Removal Data

While the *B. subtilis* challenge tests were used to demonstrate removal by the system, particle counts were measured as an indirect indicator of system performance. Data was collected for the two Fyne Technology system membranes on the removal of particles in the 2 micron (µm) and the 3 µm range, the same size range as that of *B. subtilis* and *Cryptosporidium*. The influent water had an average particle count of about 3,500 over both size ranges. Membrane 1 of the Fyne Technology system produced effluent with an average particle count of 14, representing a 99.6% removal. Membrane 2 of the Fyne Technology system produced an effluent with an average particle count of 17, representing a 99.5% removal. The particle count data was measured using a portable counter which generally gives a higher count than an on-line counter.

Turbidity and Color Removal Data

Specific field tests were not conducted to evaluate the removal of turbidity and color by the two systems tested. However, MDH collected this information on an ongoing basis for the two membranes comprising the Fyne Technology system. The average influent turbidity was 2.18 NTU and the average effluent turbidity for the Fyne Technology system Membrane 1 was 0.17 NTU and that for Membrane 2 was 0.18 NTU. Color was spectrophotometrically measured in terms of the APHA color index. The color index of the influent water was 85.5 while the color index of the effluent from the Fyne Technology system Membrane 1 was 1.28 and from Membrane 2 was 11.5 (for reference, the APHA color index for distilled water is 0). The conductivity of the influent water was 57 milliSiemens per cm (mS/cm) while that for the effluent from the Fyne Technology system Membrane 1 and Membrane 2 was 44.68 mS/cm and 47.32 mS/cm, respectively.

CONCLUSIONS

The performance of the Fyne Technology System confirmed the ability of membrane-based systems in removing bacteria from source water. The effluent from the Fyne Technology System showed nearly 6 to 7 log removal of *B. subtilis* in the recycle mode for both the membrane modules tested in the recycle mode. Membrane 1 (ES404 membrane with a MWCO of approximately 4,000 daltons) showed slightly better overall removal than Membrane 2 (CA2PF membrane with a MWCO of approximately 2,000 daltons). Both membranes showed nearly identical performance for *B. subtilis* removal when tested in the dead-end mode. As suggested in the literature, removal of *B. subtilis* in filtration systems is a conservative indicator of *Cryptosporidium* (Muhammad, et al, 2008). Thus, this removal performance satisfies the LT2ESWTR requirement of >3.0 log reduction for *Cryptosporidium* (U.S. EPA, 2006). The system also performed favorably when compared to the reduction

requirements of 6 log removal for bacteria presented in the "Guide Standard and Protocol for Microbiological Water Purifiers" (EPA, 1987).

Both membranes also showed nearly identical performance in turbidity removal producing water with an average effluent turbidity of 0.17 NTU when treating lake water with an average influent turbidity of 2.18 NTU (representing 92% removal of turbidity). This satisfies the LT2ESWTR requirement of <0.3 NTU effluent turbidity.

However, Membrane 1 showed significantly better performance in color removal by producing water with an average effluent color of 1.28 units PtCo color compared to Membrane 2 which produced water with an average effluent color of 11.5 APHA. Finally, both membranes showed approximately 99.5% removal efficiency for particles in the 2 µm and 3 µm size ranges (the size range for *B. subtilis* and *Cryptosporidium*).

Of significant note is that the system requires no pretreatment of the feed water other than a coarse (3mm) screen to prevent large solids from entering the system. The system is self-cleaning and the concentrated water can be discharged back to the lake water source.

REFERENCES

Muhammad, N, Sinha, R., Krishnan, E.R., Piao, H., Patterson, C. L., Cotruvo, J., Cumberland, S.L., Nero, V.P. Delandra, C. Evaluating Surrogates for Cryptosporidium Removal in Point of Use Systems. Jour. AWWA, 100(12), 98- 107.

U.S. EPA (2006). The Long-Term 2 Enhanced Surface Water Treatment Rule (LT2ESWTR) Implementation Guidance, EPA 816-F-06-005, Washington D.C., USA.

U.S. EPA (1987). Guide Standard and Protocol for Microbiological Water Purifiers, OPP Task Report.

Rainwater Harvesting Experiences In The Humid Southeast USA

Matthew Jones, E.I., Ph.D.[1], William F. Hunt, PE, Ph.D.[2], and Jason Wright, PE[3]

[1] Department of Biological and Agricultural Engineering, North Carolina State University, Box 7625, Raleigh, NC 27695; email: Matthew_Jones@ncsu.edu
[2] Department of Biological and Agricultural Engineering, North Carolina State University, Box 7625, Raleigh, NC 27695; email: Bill_Hunt@ncsu.edu
[3] Department of Biological and Agricultural Engineering, North Carolina State University, Box 7625, Raleigh, NC 27695; email: Jason_Wright@ncsu.edu

Abstract

Due to recent concerns over the environmental impact of stormwater runoff and increased water demands, interest in rainwater harvesting systems as an innovative stormwater treatment practice has developed in humid, well developed regions, such as the southeastern United States. Rainwater harvesting systems are designed to capture runoff from rooftops. The captured water can be used as an alternative to municipal or well water for non-potable applications. The water can be used for irrigation, vehicle washing, toilet flushing, and other non-potable uses. Harvested water can potentially be used for potable uses with proper treatment. Water harvesting systems can reduce peak flows and pollutant loads as well as conserve valuable resources. In order to better understand the anticipated usage and reliability of rainwater harvesting systems in the southeastern United States, a monitoring study was conducted at 5 rainwater harvesting systems in North Carolina, measuring cistern water levels and rainfall. Harvested water was used for a variety of applications including vehicle washing, irrigation, and toilet flushing. In order for water harvesting to be a viable solution for stormwater management the harvested water must be used between storm events. The system must be drained as much as possible to provide storage and peak flow mitigation for the next storm event. Results of the monitoring study showed that the rainwater harvesting systems were typically underutilized. Water usage was most consistent at the location where harvested rainwater was used to flush a toilet; however, the water level within the cistern only dropped below 80% of capacity on one occasion during the 30 month monitoring period. Research showed that the harvested water may require a dedicated use for water harvesting to be an effective stormwater management tool.

Introduction

Throughout history, countless innovative techniques have been developed to collect water for consumption, irrigation, and many other purposes. One of these techniques, rainwater harvesting, is the practice of capturing stormwater runoff, typically from a rooftop, and storing it in a cistern for later use. Historical evidence suggests that sophisticated rainwater collection systems were built before 3,000 BC in Jordan (AbdelKhaleq and Alhaj Ahmed, 2007). Although historically used in areas where water supply was limited by climate or infrastructure, the practice of rainwater harvesting has recently been used in humid and well developed regions in response to

increased water demands and public awareness of the environmental impacts of stormwater runoff.

While water supply is often the primary concern in arid regions or locations where water supply infrastructure is lacking, implementation of rainwater systems in humid, well developed regions offers a unique set of benefits and challenges. There are a number of water uses around a household or business that do not require potable water, such as irrigation, vehicle washing, and toilet flushing. Despite the fact that treatment is not necessary, potable water is typically used to meet these demands because it is often readily available. When potable water is used to meet these demands, chemicals, energy, and money are effectively wasted in treating and distributing the water. This treatment can result in increased infrastructure demands as well as increased costs for the water user. Because there is an economic and environmental benefit of using harvested rainwater for non-potable uses, maintaining an adequate water supply is important, although not as critical in the southeastern United States as other areas since municipal water supplies are generally prevalent. Another advantage of harvested rainwater use in the southeastern United States is that harvested rainwater can often be used to meet water demands when restrictions are placed on potable water use, which is a common practice during times of drought. Due to water restrictions, residents have sought alternative sources of water such as rainwater harvesting systems. This increased interest was exemplified when a rainwater harvesting website hosted by the authors received over 2,000 unique visitors over the span of three days when a local news channel in Raleigh, NC, broadcast information on rainwater harvesting systems. Due to the availability of 55-gallon (208 liter) barrels used to transport and store a variety of industrial products, many homeowners have modified these barrels to capture rooftop runoff in what are commonly referred to as rain barrels.

In some configurations, rainwater harvesting systems can capture a substantial portion of the runoff volume leaving a rooftop during a storm event. When this water is subsequently used for irrigation and infiltrates into the ground, rainwater harvesting can serve as a low impact development (LID) practice. Rainwater cisterns can be particularly effective at capturing the most polluted runoff near the beginning of a storm, commonly referred to as the first flush. During the beginning of a storm event, pollutant concentrations are highest as contaminants are washed from the impervious surface (Zobrist et al., 2000). First flush depths vary based upon a variety of factors, but are often associated with the first 2.5 cm of rainfall in North Carolina. Although rainwater harvesting systems may capture the first flush runoff, the pollutant removal mechanisms employed by a rainwater harvesting system differ substantially from other stormwater best management practices (BMPs). In a conventional stormwater BMP, sedimentation, filtration, vegetative uptake, and microbial processes remove pollutants from runoff flows. In a rainwater harvesting system, pollutant removal within the cistern is minimal, with small amounts of sedimentation and microbial activity. Pollutant removal in a rainwater harvesting system is associated with the use of the harvested rainwater. For example, when rainwater is used to flush toilets, pollutants would be removed by a wastewater treatment plant or septic system. When used for irrigation, pollutants would be removed by plant uptake, filtration, and microbial processes within the soil. As interest in rainwater harvesting increases

within humid regions containing well developed water supply infrastructures, it is important to understand the function of these systems in this relatively recent application.

Methods

A monitoring study was conducted at five rainwater harvesting systems located within North Carolina. The rainwater harvesting systems were located in Craven County, the city of Raleigh, the city of Kinston, Holden Beach, and the city of Fayetteville. At each site, rainfall depths were monitored by tipping bucket rain gauges with a resolution of 0.25 mm and located within 100 m of each cistern installation. Pressure water level data loggers, manufactured by Infinities USA, were used to record water levels on a one hour interval at the Kinston and Craven County locations. A pulley-float stage monitor recorded water levels on a 15 minute interval at the Raleigh location. A pressure water level data logger on a half hour interval, manufactured by Global Water, was used to record water levels in Fayetteville.

In Raleigh, NC, (35°48'37.45"N, 78°42'54.21"W) a 5,300 liter cistern collected water from a 204 m² rooftop and the water was used to flush a toilet at a nature education center. The cistern constituted the primary water supply to the toilet and municipal water was only supplied when the cistern was depleted of rainwater, which did not occur during the study period. During the study period, there were no fixtures installed to supply water from the cistern for any uses other than flushing the toilet. The Raleigh rainwater harvesting system was monitored from June of 2005 through January of 2008.

In Craven County, NC, (35° 8'34.94"N, 77° 9'31.87"W) a 167 m² section of rooftop contributed water to an 11,350 liter cistern and was used to irrigate gardens around the facility. A formal irrigation schedule was not established and water was used when deemed necessary by the building's occupants. Water could be withdrawn from the Craven County cistern using either a gravity fed faucet located at the base of the cistern or a pump supplied faucet located adjacent to the cistern. Faucets connected to the municipal water supply were available at several locations around the perimeter of the building. The Craven County cistern was monitored from May of 2005 through August of 2006.

A 19,680 liter cistern in Kinston, NC, (35°13'44.97"N, 77°36'49.97"W) collected water from a 406 m² section of rooftop, with the collected water used to wash vehicles. The harvested rainwater was pumped to a faucet at a vehicle washing station where signs clearly indicated that the faucet was supplied by rainwater. Within the same vehicle washing station, there were several faucets connected to the municipal water supply. Typically, pressure washers were used at the washing station to clean large commercial vehicles. The Kinston rainwater harvesting system was monitored from June of 2005 through August of 2006.

In Holden Beach, NC (an unused septic tank approximately 5,680 liters was used to collect runoff from a 78.5 m^2 roof top. The tank was fitted with a 186 Watt pump so that the homeowner could use the rain water to water vegetation in her garden and greenhouse. Because of the capacity of the pump the homeowner was restricted to a single spray irrigation system or hand watering.

Results and Discussion

Of the rainwater cisterns involved in this study, the most consistent usage was observed at the Raleigh, NC location. Because there were no other toilets in the vicinity and the rainwater harvesting system served as the only water supply to the facility's toilet, cistern water levels were largely governed by the number of people using the facility. Despite regular usage, the volume of water stored in the cistern only fell below 80% of capacity on one occasion during the monitoring period (Figure 1). Even during a historic drought beginning during the summer of 2007, the cistern maintained an adequate water supply. While the reliable water supply was beneficial, the ability of the rainwater system to capture runoff volume from the rooftop was greatly reduced. The majority of rainfall events resulted in overflow from the rainwater cistern located at this site. Monitoring of the rainwater harvesting system began before the facility was open to the public and educational programs and other functions that would use the facility were under development during the course of the study, which resulted in substantial variations in the number of building occupants. Beginning in February of 2008, workers at this facility installed faucets that were supplied by the cistern to use for irrigation around the property in an effort to better utilize the rainwater supply available.

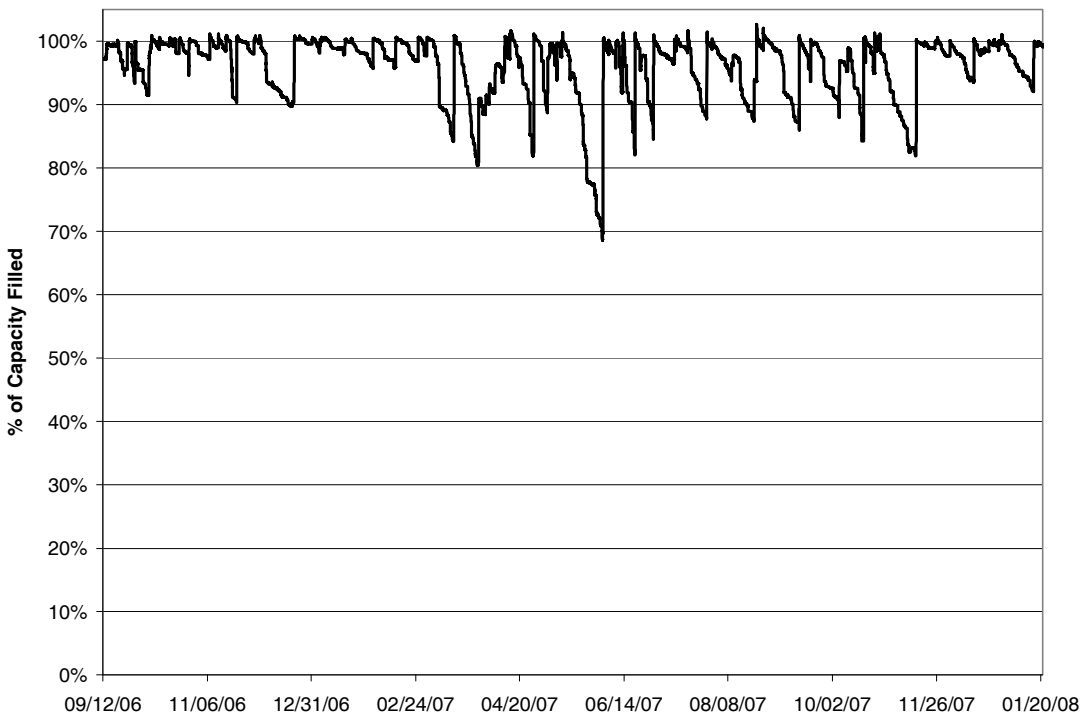

Figure 1. Percentage of cistern capacity filled by runoff storage at the Raleigh location

At the Craven County location, water use from the rainwater cistern was infrequent, with only 7 major uses occurring during the course of the monitoring study (Figure 1). Despite the infrequent water use, usage volumes were substantial. The largest of these uses depleted nearly 70% of the cistern's capacity; however, the fact that water levels decreased consistently over the course of several days suggests that the cistern may have been intentionally drained (Figure 2). Even with infrequent

usage, the volume of water stored in the cistern sometimes took several weeks or months to reach capacity. Part of the reason for the slow recharge is that a first flush diverter installed at this location prevented the initial runoff during a storm from entering the cistern. Limited usage during 2006 suggests that the cistern was used to hand water plants around the property and not used for large scale irrigation. Due to concerns over the cisterns appearance, the system was located on the opposite side of the building from the gardens it was originally intended to irrigate, which likely had substantial impacts on usage volume and frequency.

At the Kinston location, rainwater usage was minimal, with the cistern maintaining at least 80% of its capacity for the duration of the study (Figure 2). Observations at the site confirmed that water demand intended for the rainwater harvesting system was being supplied by municipal water. Vehicles were primarily washed with handheld pressure washers attached to the municipal water supply with water from the rainwater harvesting system used to meet small water demands. After better educating the facility workers on the use of the rainwater harvesting system in early 2006, rainwater usage increased. Even with this increased usage, the cistern remained near capacity, since municipal water was still used for much of the vehicle washing.

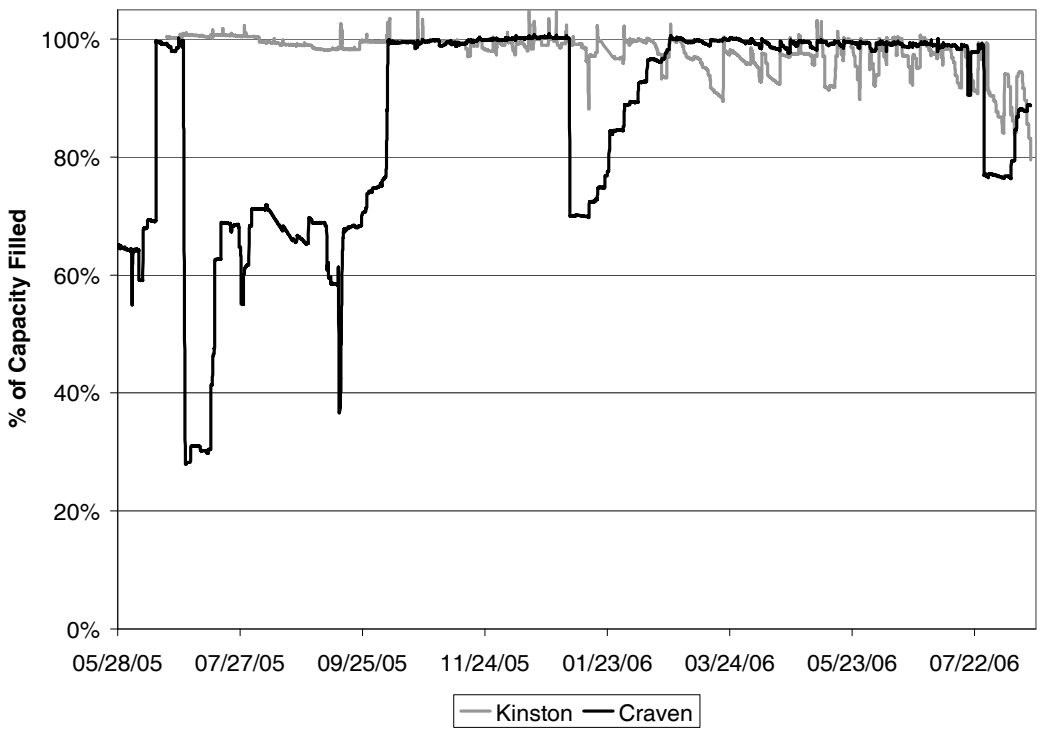

Figure 2. Percentage of cistern capacity filled at Kinston and Craven County sites

The irrigation demand for the Holden Beach water harvesting system was low, preventing the tank from completely emptying. Irrigation demand was lowest in February when 113 liters of water was used from the 5680 liter tank and highest in April when 6132 liters was used. The high demand in the summer was able to reduce the volume in the tank to approximately 20% on one occasion and 30% on two occasions (Figure 3). The prime factor in lowering the tanks internal water level,

however, was a crack in the tank 63.5 cm above the bottom of the tank that allowed the water to infiltrate into the surrounding soil until the water level in the tank was reduced to 63.5 cm. The presence of the rack proved to be in inadvertent benefit. Perhaps future designs for water harvesting systems should include intended "leaks" from the cistern, especially in lower water demand applications. This improved the performance of the Holden Beach system allowing more rooftop runoff to be captured due to the increase in storage volume. Irrigation demand was lowest in the winter months causing available storage to be less during that time with the capacity dropping below 60% on one occasion.

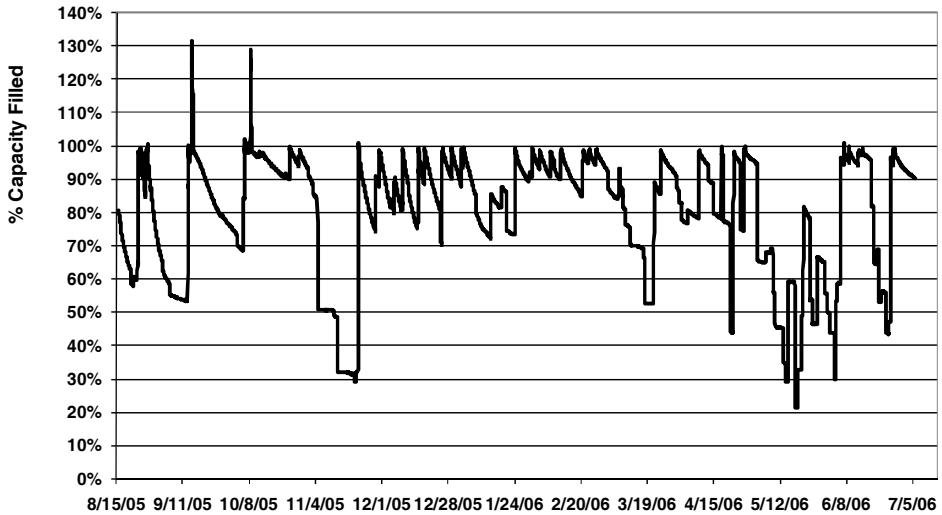

Figure 3: Percentage of cistern capacity filled by rooftop runoff at the Holden Beach location

Conclusion

Results of the monitoring study indicated that rainwater harvesting systems were consistently underutilized. Minimal usage of the captured rainwater greatly diminishes runoff volume reduction and economic benefits of a rainwater harvesting system. It is possible that with better education on the uses of captured rainwater and implementation of automatic usage systems, rainwater harvesting can be used as an effective LID tool in the southeastern United States. Rainwater harvesting systems that incorporate infiltration appear to be a viable design option.

When installing rainwater harvesting systems, knowledge of the anticipated water usage is imperative to ensure that an appropriately sized cistern is used. Because municipal water supplies generally provide a reliable backup to harvested rainwater, rainwater harvesting systems can be used to meet a variety of water needs, supplying substantial water volumes when properly designed. With increased planning, public awareness, and education, rainwater harvesting systems should serve as valuable tools in reducing the demand on municipal water supplies and the negative impacts associated with urban stormwater runoff at the same time.

Acknowledgements

This research was funded in part by the North Carolina Department of Environment and Natural Resources (NCDENR), Division of Water Quality. The authors would like to thank Charlie Humphrey and Dwane Jones of NC State University for their assistance and support throughout this project.

References

AbdelKhaleq, R.A. and Alhaj Ahmed, I. (2007). Rainwater harvesting in ancient civilizations in Jordan. *Water Science & Technology: Water Supply*, **7**(1), 85-93.

Coombes, P.J. and Barry, M.E. (2007). The effect of selection of time steps and average assumptions on the continuous simulation of rainwater harvesting strategies. *Water Science and Technology*, **55**(4), 125-133.

Guo, Y. And Baetz, B.W. (2007). Sizing of Rainwater Storage Units for Green Building Applications. *Journal of Hydrologic Engineering*, **12**(2), 197-205.

Zobrist, J., Muller, S.R., Ammann, A., Bucheli, T.D., Mottier, V., Ochs, M., Schoenenberger, R., Eugster, J., and Boller, M. (2000). Quality of Roof Runoff for Groundwater Infiltration. *Water Research*, **34**(5), 1455-1462.

Deployable Decentralized Biofilm System to Degrade Organic Carbon, Nutrients and Benzene from Wastewater

Dong Chen[1], Che-Jen Lin[1], R. Gavin Jones[2], Sehul Patel[1], Rachelle Smith[2], Thomas G. Chasteen[3], Micheal Radi[1], Sabin Holland[2], Scott A.Waisner[4], Jeffery L. Davis[4]

[1] Department of Civil Engineering, Lamar University, Beaumont, TX 77710-0024; PH (409) 880-8447; FAX (409) 880-8121; email: dchen@my.lamar.edu
[2] Texas Research Institute for Environmental Studies, Sam Houston State University, Huntsville, TX 77340
[3] Department of Chemistry, Sam Houston State University, Huntsville, TX 77341
[4] Environmental Laboratory, U.S. Army Engineer Research and Development Center, 3909 Halls Ferry Rd., Vicksburg, MS 39180

Abstract

Decentralized wastewater treatment systems are of great importance to protect the environment and people's health in the areas without centralized treatment system. Utilizing laboratory cultivated inoculating microorganisms (suborder *Corynebacterineae* including *Agrobacterium sp.* and *Gordonia sp.*) in logarithmic growth stage, a deployable aqueous aerobic bioreactor (DAAB) system was developed for decentralized wastewater treatment. The system is flexible, deployable in a standard shipping container, quick to start, and capable of removing organic carbon, phosphorus and benzene from wastewater. Experimental results indicated that the inoculated consortium had a faster COD removal rate than sewage-born microorganisms during the startup of the system. During the startup period, the removal of total phosphorus in the aeration tank followed a pseudo first-order kinetics (R^2 = 0.90) with a rate constant of 0.027 hr^{-1}. The *Agrobacterium sp.* are likely responsible for the removal of phosphorus from wastewater. No ammonia removal was found in the aeration tank during the startup phase. After the system was in continuous operation with an average flow rate of 11.4 L/min, the removal efficiency of BOD_5 and total suspended solids (TSS) was 83±32% and 84±9%, respectively. The relative large standard deviation of the removal efficiencies is likely due to the small equalization capacity of a small treatment system to resist the variations of the incoming wastewater quality and shock loads. As an important supplement to the pilot studies, laboratorial tests by headspace analysis showed that the *Gordonia sp.* were able to degrade benzene from wastewater. After 26 hours, more significant biodegradation of benzene was found in sessile form (57±8%) than in planktonic form (25±11%) with minimal glucose. However, no benzene degradation was found in sessile form when no glucose was provided. The result suggested that the *Gordonia sp.* could not utilize benzene as the sole carbon and energy source.

Keywords: Decentralized wastewater treatment, biofilm, phosphorus, benzene, *Agrobacterium sp.*, *Gordonia sp.*

1. Introduction

Natural disasters such as hurricanes, tornadoes, floods and earthquakes can cause significant damages of civil infrastructures including municipal wastewater treatment facilities. When the treatment systems fail, human health and environmental quality are at risk. In addition, there are situations in which centralized wastewater treatment facilities are not available or unpractical, such as remote sites or small communities. Consequently, there is a need for technologies that can be rapidly moved into affected areas and put in operation to minimize the impacts or the damages and to provide support for the residents. Compared to centralized treatment system, decentralized systems appear to offer a number of potential advantages, such as flexibility, portability, quick response, easy operation, segregation of wastewater at source, and compatibility with local demands for wastewater reuse.

Although decentralized wastewater treatment systems are essential parts to protect the environment and human health and to support the sustainable development of the society, systematic studies of such systems are rather scarce [van Voorthuizen et al., 1995; Devi and Dahiya, 2008; Massoud et al., 2009; Butler and MacCormick, 2002]. As a result, the advantages and virtual potentials of decentralized wastewater treatment systems have not been explored significantly. Because of the challenges from the emergent situations such as post-disaster scenarios, the decentralized wastewater treatment system has to be well designed and capable of purifying both domestic and potentially recalcitrant and hazardous industrial wastewaters. Among various kinds of industrial wastes, the contaminants from gasoline are of special interests. The environmental pollution of gasoline is caused by accidental spills, leakage from storage tank, or improper disposal. Natural disasters may exacerbate the pollution of gasoline. As one of the major hurricane suffering areas, the US coast of Gulf of Mexico accumulates large amounts of oil exploration and refinery facilities. Therefore, the major aromatic constituent of gasoline, such as benzene is selected as the target industrial pollutant in this study, because benzene is one of compounds with a high water solubility relative to aliphatic constituents of gasoline [Deeb et al., 2001] and accounts for one of the major gasoline components that are found in the water-soluble fraction [Saeed and Mutairi, 1999]. Consequently, benzene is a common contaminant present in the waste stream in combination with the domestic wastewater. In addition, benzene has significant adverse health effects and environmental concerns. It is listed as a category A carcinogen according to USEPA.

In light of these challenges, a deployable aqueous aerobic bioreactor (DAAB) system has been developed utilizing laboratory cultivated microorganisms that are in logarithmic growth stage for a quick start of the treatment system; since seeding sludge is not always available near the treatment site. The whole system is designed to be deployable. It can be transported in a single C-130 aircraft or a 40-foot ISO container or trailer. For easy operation and simplification of the system, attached growth of biofilm was preferred over the suspended activated sludge system, because no sludge recycle is required. In addition, attached growth (sessile) system showed the advantage for fast degradation of benzene over suspended growth (planktonic) system as discovered in this study. In the DAAB, a hydrophobic plastic mesh medium was provided for the attached growth of biofilm. The microbes of suborder *Corynebacterineae* were carefully selected for primary irreversible adhesion to

medium, while others are selected for intercellular adhesion. Specifically, the suborder *Corynebacterineae* is comprised of seven microbes including well known genera, i.e., *Gordonia sp.*, *Caulobacter vibrioides*, *Enterobacter cloacae*, *Agrobacterium sp.*, *Bacillus subtilus*, *Pseudomonas putida* and *Pseudomonas stutzeri*. Among *Corynebacterineae*, the *Agrobacterium sp.* are able to remove phosphorus (Merzouki et al., 1999; de-Bashana and Bashan, 2004), while the *Gordonia sp.* possess the ability to degrade xenobiotics and industrial pollutants (Arenskotter et al., 2004). Many of the isolates of *Gordonia* have been derived from industrially influenced habitats and wastewater treatment systems (Arenskotter et al., 2004).

This study combined the pilot-scale tests to evaluate the overall performance of the system and bench-scale tests to elucidate the biodegradation of the hazardous compound. The main objectives of this study were (1) to explore the organic carbon (BOD and COD) degradation efficiency and TSS removal in the DAAB system; (2) to investigate the potential of nitrogen and phosphorus removal in the DAAB system; (3) to study the microbiological degradation of benzene.

2. Materials and Methodologies

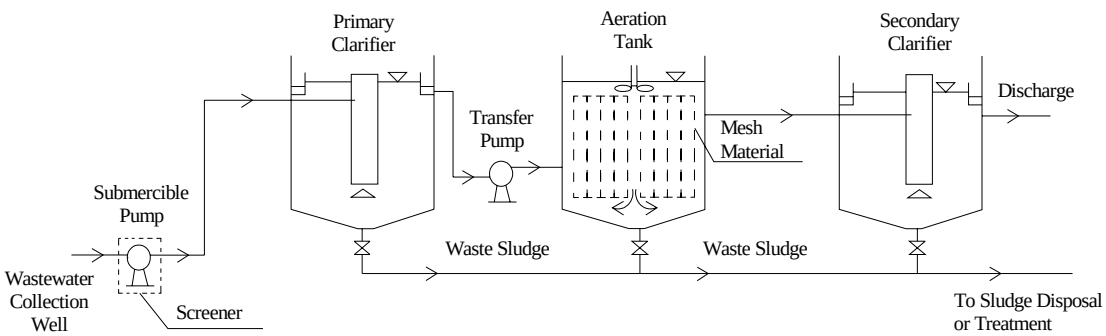

Figure 1. Diagram of the DAAB system.

2.1 The DAAB system

The basic DAAB system consists of a wastewater feed system, a primary sedimentation tank, an aeration tank, and a secondary sedimentation tank, as shown in Figure 1. Each tank was an oval cylinder with a dimension of about 2.4 (L) × 1.9 (W) × 2.0 m (H). The net volume of each tank was about 6.9 m^3. A transfer pump between the primary sedimentation tank and the aeration tank was equipped in order to provide a flexibility of the flow routing for varied topographies of the treatment sites. In this study, the transfer pump intermittently fed the aeration tank from the primary clarifier. The pump was running for about 5 minutes for every 20 minutes. In the aeration tank, the biomass is supported by a composite plastic mesh media to maximize the surface area of biomass. In contrast to conventional aerobic biofilm process (e.g., trickling filters and rotary biological contactors), fine air bubbles are provided through a patented aerator at the surface of the aeration tank for maintaining the desirable dissolved oxygen (DO) concentrations. The fine bubbles significantly increased the oxygen transfer efficiency due to the great surface-to-volume ratio and a long retention time of the air bubbles. In general, the DAAB system was mainly an attached growth system in a compact configuration that potentially provides efficient treatment of wastewater. Depending on the quantity and type of wastewater to be

treated, a DAAB system can consist of four to eight tanks in parallel or in serial fashions.

2.2 Wastewater sample analyses

Grab samples were taken from the DAAB treatment system, transported to the laboratory and analyzed typically within an hour for BOD_5 and total suspended solids (TSS) examinations according to the Standard Methods of USEPA. For COD, ammonia, and total phosphorus measurements, the samples were acidified by sulfuric acid to pH 2 and stored in refrigerator at 4 ºC following the Standard Methods of USEPA. An onsite analytical probe of the Quanta Water Quality Monitoring System (Hydrolab Corporation, Austin, TX) was used for DO, pH, turbidity, conductivity, and temperature measurements. Ammonia and total phosphorus were examined spectrometrically by using QuikChem 8500 Flow Inject Analysis (Lachat Instruments, Loveland, CO).

2.3 Benzene degradation experiments

*Cultures and media***.** Stock cultures of the *Gordonia sp*. (ATCC# BAA-558) were maintained in yeast extract glucose (10 g of Dextrose and 10 g of yeast extract per liter of distilled water) at 30 °C and 200 rpm for seven (7) days. Evaluation of benzene degradation was performed by inoculating cultures into either a minimal glucose media (5.0 g of dextrose, 6.0 g of Na_2HPO_4, 3.0 g of KH_2PO_4, 1.0 g of NH_4Cl, 0.5 g of NaCl, 0.12 g $MgSO_4$, and 0.01 g $CaCl_2$ per liter of distilled water) or into a minimal media supplemented with benzene (Fisher: B411-1 ≥99.0% reagent grade) as the sole carbon and energy source (87 mg/L C_6H_6, 6.0 g of Na_2HPO_4, 3.0 g of KH_2PO_4, 1.0 g of NH_4Cl, 0.5 g of NaCl, 0.12 g $MgSO_4$, and 0.01 g $CaCl_2$ per liter of distilled water). All media were autoclaved at 121 °C for 30 minutes. Benzene was added to the media after the autoclave cycle.

*Benzene degradation by planktonic (substratum-free) cultures***.** Experiments were designed to examine the capabilities of the *Gordonia sp.* to degrade benzene in the presence of a carbon source, as well as the ability of the *Gordonia sp.* to utilize benzene as the sole carbon source. A 100 mL aliquot of the medium previously described was transferred to the headspace analysis apparatus, described by Stalder et al. (1995), in a sterile laminar flow hood. A one milliliter aliquot of the seven-day stock culture was then transferred into either a minimal glucose media or into a minimal media supplemented with benzene as the sole carbon source. *Gordonia* cultures inoculated into the minimal glucose medium were incubated at 30 °C and 200 rpm for 24 hours in the headspace analysis apparatus prior to introducing benzene. The initial concentration of benzene added was 87 mg/L. For the experiments evaluating the ability of the *Gordonia sp.* to utilize benzene as the sole carbon source, a one milliliter aliquot of the seven-day stock culture was simultaneously added to the headspace analysis apparatus with benzene and incubated at 30 °C and 200 rpm. The initial concentration of benzene added was also 87 mg/L. The initial pH and DO before the addition of benzene was 6.1±0.2 and 1.9±0.6 mg/L, respectively.

Benzene degradation by sessile cultures. Examinations of the capabilities of the *Gordonia sp.* to degrade benzene adhered to a substratum were also performed. The steps were same as the descriptions of the planktonic test except that an autoclaved (at 134 °C for 30 minutes) hydrophobic polyethylene surface (5.1×5.1 cm) was initially placed in the solution of the headspace analysis apparatus before the tests. The initial pH and DO before the addition of benzene was 6.1±0.2 and 1.9±0.6 mg/L, respectively.

Examination of benzene. Benzene concentrations were determined by headspace analysis. The preliminary study indicated that the biodegradation activity of the *Gordonia* was below the rate of mass transfer between the gas and aqueous phases for benzene (Lincoff and Gossett, 1984; Peng and Wan, 1997; Prenafeta-Boldú et al., 2002). Therefore, the examination of benzene concentration in gas phase was used to indirectly reflect its aqueous phase concentration (Lincoff and Gossett, 1984). Samples of the headspace gas (1 mL) were withdrawn from the culture bottles using a Series A-2 gas tight syringe (Alltech, Nicholasville, KY) and were analyzed by a Hewlett-Packard 5890 gas chromatography equipped with a 5972 mass spectrometry and an Agilent DB-624 capillary column, 30m × 0.25 mm × 1.4 µm. The injector and detector temperatures were 250 °C and 280 °C, respectively. The initial oven temperature was programmed for 5 minutes at 35 °C then followed by a ramp of 10 °C/min to 126 °C for a total time of 14.10 minutes. All sample injections were made in the splitless mode. The carrier gas was He with a flow rate of 1 mL/min. Calibration curve was done with external standards.

3. Results and Discussions

3.1 System starting up

The system was fed on-site with municipal wastewater from Beaumont, TX directly from the raw wastewater well after the bar screen. The wastewater is mainly composed of domestic wastewater with a small portion of oil refinery wastewater. The general characteristics of the raw wastewater are listed in Table 1. As can be seen, the organic strength of the wastewater was 176±57 mg/L in BOD_5 and 365±128 mg/L in COD. The TSS level was 280±167 mg/L.

Table 1. The general characteristics of the raw wastewater treated by the DAAB system.

BOD_5 (mg/L)	COD (mg/L)	TSS (mg/L)	pH	Turbidity (NTU)	Conductivity (ms/cm)	DO (mg/L)	Temperature (°C)
176±57	365±128	280±167	7.1±1.0	137±46	0.8±0.1	0.3±0.2	15~28

As mentioned earlier, one of the key strengths of the DAAB system is quick startup, because seeding sludge might be difficult to find near the treatment site, especially during post-disaster scenarios. In this research, the degradation of COD from wastewater was compared with or without the inoculation consortium. The experiments were performed in the aeration tank in a completely mixed batch reaction mode. The aeration was kept on during the duration of the experiment. The plastic mesh media in the aeration tank had been pre-cleaned and dried before filling up the municipal wastewater in the aeration tank. The experiments started shortly after the

tank had been filled and well mixed with or without the inoculation consortium. The dosage of each type of the microbes was about 10^{12} counts based on the average of eight examinations. After that, the initial COD concentration of the mixed solution was measured as 183 mg/L and 223 mg/L for the inoculated and controlled test, respectively. DO was around 8 mg/L, pH was around 8.0, and the temperature was about 17 °C.

As shown in Figure 2, after seven hours of the reaction, 68% decrease of COD was observed with inoculation consortium compared to 58% reduction of COD without inoculation consortium. The inoculation of the seven microbes enhanced the COD removal by 10%. However, it was a little surprised to see that the COD removal (58%) without artificial inoculation was pretty significant. Two possible reasons might contribute to the COD degradation without inoculation. First, the plastic mesh media were hydrophobic and had a porous but compact arrangement inside the aeration tank. Consequently, the media might adsorb dissolved organics and catch particulate organic (and inorganic) matters from the wastewater with time. Second, the sewage-born microorganisms might become active and utilize dissolved organics from wastewater under the aeration condition.

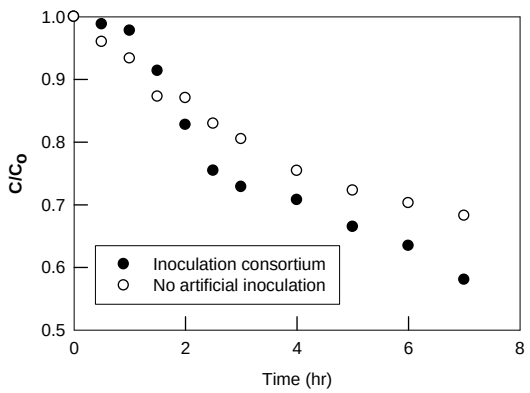

Figure 2. Comparison of COD removal in the batch reaction mode with or without inoculation consortium during initial startup of the DAAB system.

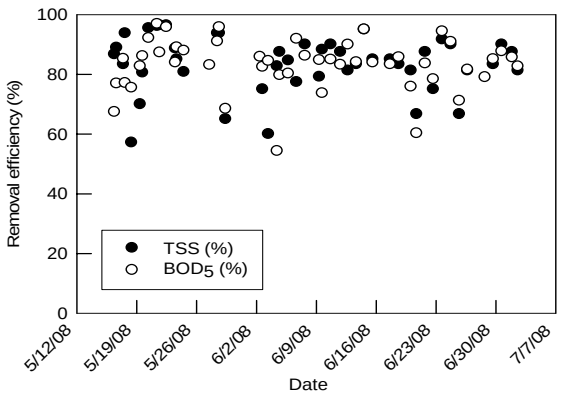

Figure 3. BOD_5 and TSS removal efficiency in the DAAB system.

3.2 BOD_5 and TSS removal

After the system had been started, we examined the treatment efficiency of the DAAB system for BOD_5 and TSS removal. In this set of experiments, the treatment performance was evaluated in continuous operation with an average flow rate of 11.4 L/min (i.e., 3 GPM). DO was 5.4±0.5 mg/L in the aeration tank. As shown in Figure 3, the BOD_5 removal efficiency of the DAAB system was 83±32%. For TSS, the removal efficiency was 84±9%. The effluent BOD_5 and TSS of the system was 28±13 and 42±32 mg/L, respectively. This means the average 30-day BOD_5 of the DAAB effluent met the US national standard for secondary treatment (i.e., 30 mg/L), while TSS was higher than the average 30-day national standard (i.e., 30 mg/L). In future work, a multi-media filtration is planed to be added to further polish the quality of the secondary effluent and to provide an option for wastewater reuse. The relative large variation of the treatment efficiencies is likely due to the fact that a small system like

the DAAB has a minute buffer capacity to absorb and equalize the fluctuations of the incoming wastewater quality and shock loads.

3.3 Ammonia and total phosphorous removal

The DAAB process is typically used to provide wastewater treatment prior to discharging to a receiving water body. To prevent eutrophication of the water body, nutrient, especially phosphorus removal is desired; because phosphorus is a limiting nutrient in most freshwater systems (Tchobanoglous et al., 2003). Therefore, the system needed to be carefully designed and operated to provide a high quality of the effluent. Accordingly, the removal of ammonia and total phosphorus was investigated during the startup period of the system, because the DAAB consortium was more dominated in this period. The experimental results shown in Figure 4 were obtained under a completely mixed batch reaction mode in the aeration tank of the DAAB system. In the batch reaction, the initial BOD_5 was 106 mg/L. DO was around 8 mg/L, pH was around 7.4, and the temperature was 18 °C. As can be seen, the degradation of ammonia was insignificant. During the duration of the batch test, the ammonia concentration in wastewater was constantly around 16.5 mg/L. In contrast, significant degradation of total phosphorus was observed. The total phosphorus concentration decreased from 93.0 initially to 33.1 μg/L after 33.5 hours. The degradation of total phosphorus followed a pseudo first-order reaction (R^2 = 0.90). The reaction rate constant was 0.027 hr^{-1}.

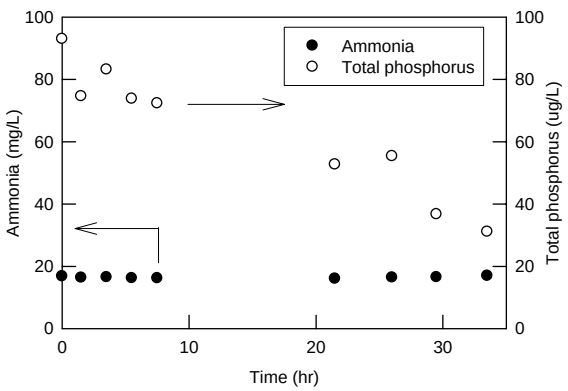

Figure 4. Ammonia and total phosphorous removal in the batch reaction mode during initial startup of the DAAB system.

The usual forms of phosphorus found in wastewater include the orthophosphate, polyphosphate, and organic phosphate. Biological phosphorus removal from wastewater is based on the activity of phosphorus-accumulating organisms (PAOs). In the anaerobic phase, PAOs take up readily biodegradable organic carbon substrates and store them as polyhydroxyalkanoates (PHAs) (Lee et al., 2001). The energy to this anaerobic process is derived from the hydrolysis of intracelluar polyphosphate and the glycolysis of glycogen followed by the release of ortho-phosphate to the bulk liquid (Mino et al., 1987; Okada and Sudo, 1986). In the subsequent aerobic phase, PAOs use the PHAs for generating energy for growth, glycogen synthesis, and phosphate uptake, where the PAOs take up phosphate more than released during the anaerobic phase (Lee et al., 2001).

Among the inoculation microbes used in the DAAB system, the *Agrobacterium sp.* are found responsible for the removal of total phosphorus from wastewater. *Agrobacterium sp.* are PAOs (Merzouki et al., 1999; de-Bashana and Bashan, 2004), which may utilize and store phosphorus inside the cells from wastewater. When the *Agrobacterium sp.* were dosed into the aeration tank from the oxygen-starvation condition (the microbes had been in pellet form), it started to grow and took up phosphate. In addition, it is also possible that total phosphorus could be partially removed through adsorption of organics and attachment of particulates from wastewater onto the plastic mesh media inside the aeration tank. However, compared Figure 4 to Figure 2, the removal rate of total phosphorus (22% removal in 7.5 hours) is much less than COD (32% removal in 7 hours). This fact suggests that biological removal of phosphorus played a role in the DAAB system.

Although there was not a separate anaerobic tank in the DAAB system, the biofilm system was spatially heterogeneous, providing spaces for both, aerobic and anaerobic processes (Gieseke et al., 2002). The biofilm of the DAAB system was exposed to varied DO levels as the transfer pump intermittently fed the aeration tank from the primary clarifier, which had a low DO of 0.3±0.2 mg/L. Once the biofilm was fully developed, the possible anaerobic zones inside the biofilm enabled the completeness of the two-stage cycle for biological phosphorus removal. Consistently, phosphorus removal was reported in attached growth system (Watanabe et al., 1995; Pastorelli et al., 1999; Morgenroth and Wilderer, 1999; Gieseke et al., 2002). After the DAAB system reached steady state and was in the continuous operation mode with an average flow rate of 11.4 L/min, DO in the aeration tank was 5.4±0.5 mg/L, a 43±25% removal efficiency of the total phosphorus was observed.

Nitrogen in municipal wastewater is mostly in the form of ammonium (NH_4^+) and organic nitrogenous compounds (amino acids, amino sugars and proteins) that together are reported as Total Kjeldahl nitrogen (TKN) (Tchobanoglous et al., 2003). Nitrogen can be biologically removed from wastewater by first oxidizing it to nitrate (nitrification by nitroso- and nitro-bacteria) then reducing it to nitrogen gas (denitrification by denitrifying bacteria). The results shown in Figure 4 indicated there was little ammonia removal in the aeration tank, simply because none of the seven inoculation microorganisms had a function of nitrification. In addition, ammonia has a small molecule and is highly soluble in wastewater, which is unlikely to be adsorbed onto the plastic mesh media. Moreover, considering the incoming sewage-born bacteria, nitroso- and nitro-bacteria grow much more slowly than heterotrophic bacteria. Especially in an attached growth system, nitroso- and nitro-bacteria can be easily outcompeted by heterotrophic bacteria when BOD level is not sufficiently low, because the heterotrophic bacteria have a higher biomass yield and thus can dominate the surface area of fixed-film systems over nitrifying organisms (Tchobanoglous et al., 2003). Consequently, nitroso- and nitro-bacteria were slow to grow in the treatment process. However, with the growth and accumulation of sewage-born microorganisms inside the treatment process, nitrification and denitrification might become possible with time.

As is evident from the description above, the DAAB system using the inoculation consortium was effective to remove BOD_5 and total phosphorus from wastewater. In a separate pilot study of industrial wastewater (Sam Houston State

University, 2006), the DAAB system achieved about 10% reduction of aromatic compounds, when the concentration of the influent contaminants was around 1 µg/L. However, the pilot tests were conducted in a very complex chemical system that was designed to include all possible influences and to evaluate the overall performance of the treatment system under real world conditions. The pilot study has less controlled experimental conditions (e.g., volatilization loss, adsorption and photolysis) and may bring environmental concerns if hazardous compounds are artificially introduced into the system. As a result, bench-scale tests were conducted to provide a more controlled environment that could be used to formulate a mechanistic understanding of the microbiological degradation of industrial and hazardous contaminants, such as benzene.

3.4 Biodegradation of benzene

In a preliminary study of the microbiological degradation of benzene by the seven inoculated consortium, the *Gordonia sp.* were the most active microbe to reduce benzene from the solution. Consequently, the *Gordonia sp.* were chosen to determine its capability to degrade benzene in laboratorial cultures. The bioremediation of benzene was investigated using a substratum with or without glucose minimal media and comparing that process to cultures without substratum.

3.4.1. Benzene degradation by planktonic with glucose minimal media

The results of biodegradation of benzene by the *Gordonia* in planktonic form (without a substratum) over a 26 hour time course are shown in Figure 5. The headspace was initially analyzed 20 minutes after 87 mg/L benzene was introduced to the glucose minimal media and bacteria and subsequently every few hours. The initial headspace concentration of benzene was about 15 mg/L. The concentration of benzene in the headspace after 26 hours decreased to 71±7%. This means there was a 29±7% reduction in the benzene concentration in live *Gordonia* cultures. The abiotic control, consisting of benzene and media only, exhibited a benzene reduction of 4±11% after 26 hours. Consequently, the net biodegradation of benzene by the *Gordonia* in planktonic form was 25±11%.

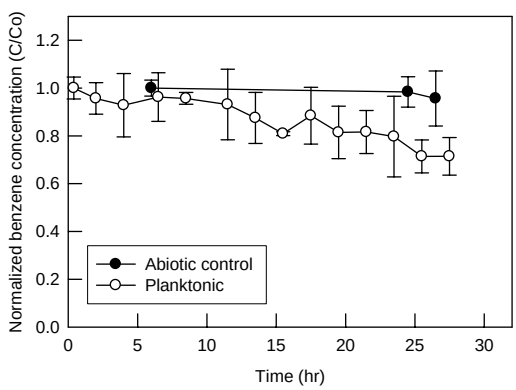

Figure 5. Degradation of benzene by the *Gordonia sp.* in planktonic form with glucose minimal media. The tests were performed in quadruplicates.

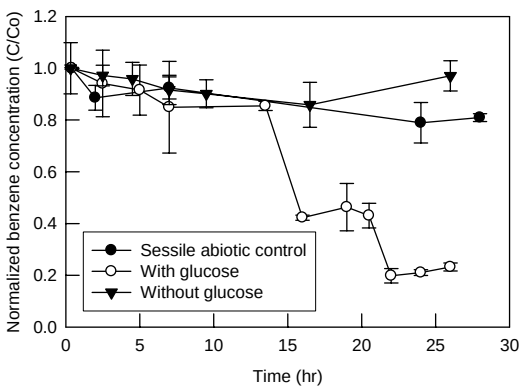

Figure 6. Degradation of benzene by the *Gordonia sp.* in sessile form with or without glucose minimal media. The tests were performed in quadruplicates.

3.4.2. Benzene degradation by sessile cultures

Figure 6 shows the degradation of benzene by the *Gordonia sp.* in sessile form from another quadruplicate study. The headspace was analyzed 20 minutes after 87 mg/L benzene was added to the glucose minimal media, substrate, and bacteria; the initial concentration of benzene was about 15 mg/L. The headspace benzene concentration decreased to 23±2% after 26 hours in that live shaking culture, a 77±2% reduction in the benzene concentration. In the abiotic control, consisting of benzene, substrate and media, benzene concentration decreased to 80±8%. The net biodegradation of benzene concentration in the headspace was 57±8%. The results are summarized in Table 2.

Table 2. Degradation of benzene by the *Gordonia sp.* in planktonic or sessile form with or without glucose studied by headspace analysis.

	Planktonic form		Sessile form		
Percent of the remaining benzene concentration (C/C_0) in the headspace after 26 hours (%)	Abiotic control	With minimal glucose	Abiotic control	With minimal glucose	Without glucose
	96±11	71±7	80±8	23±2	97±6
Net percentage removal after 26 hours (%)		25±11		57±8	0±8

Comparing the biodegradation of benzene by planktonic to sessile culture, it was evident that sessile culture provided much higher removal efficiency of benzene than planktonic culture. Cellular adhesion to a substratum is a critical function for many microorganisms and can be achieved by the use of fibrils or polymers (van Loosdrecht et al., 1990). Sessile organisms exhibit higher rates of uptake for many compounds when compared to planktonic organisms as well as also exhibit a higher rate of mineralization of organic carbon (Kirchman, 1983; Friedrich et al, 1999). Moreover, it is believed cellular adhesion by the *Gordonia* is mediated through the use of mycolic acids, which have also been shown to confer resistance to chemical injury, which makes the organisms of particular interest for utilization in biotechnological approaches for the treatment of industrial pollution (Kacem et al., 2004; Sokolovska et al., 2003). The results obtained in this study indicated the advantage of attached growth system over suspended activated sludge for degradation of hazardous compounds like benzene.

In addition to glucose minimal media, the bioremediation of benzene as the sole carbon and energy source was investigated (see Figure 6). The results indicated that benzene reduction was almost zero after 26 hours. This result reveled that the *Gordonia* were not active at all and could not utilize benzene as the sole carbon and energy source.

Acknowledgement

This study is supported by the Engineer Research and Development Center of the US Army Corps of Engineers under a subcontract issued by the Sam Houston State University (Project No: W912HZ-07-2-0010).

References

Arenskotter, M., Broker, D., and Steinbuchel, A. (2004). "Biology of the Metabolically Diverse Genus Gordonia." *Appl. Environ. Microbiol.*, 70, 3195-3204.

de-Bashan, L.E., and Bashan, Y. (2004). "Recent advances in removing phosphorus from wastewater and its future use as fertilizer (1997–2003)." *Wat. Res.*, 38, 4222-4246.

Butler, R., and MacCormick, T. (2002). "Opportunities for decentralized treatment, sewer mining and effluent re-use." *Desalination*, 103(1-3), 273-283.

Deeb, R.A., Hu, H.Y., Hanson, J.R., Scow, K.M., and Cohen, L.A. (2001). "Substrate interactions in BTEX and MTBE mixtures by an MTBE-degrading isolate." *Environ. Sci. Technol.*, 35(2), 312-317.

Devi, R., and Dahiya, R.P. (2008). "COD and BOD removal from domestic wastewater generated in decentralised sectors." *Bioresource Technology*, 99(2), 344-349.

Friedrich, U., Schallenberg, M., and Holliger, C. (1999). "Perlagic bacteria-particle interactions and community-specific growth rates in four lakes along a trophic gradient." *Microbial Ecology*, 37, 49-61.

Gieseke, A., Arnz, P., Amann, R., and Schramm, A. (2002). "Simultaneous P and N removal in a sequencing batch biofilm reactor: insights from reactor- and microscale investigations." *Wat. Res.*, 36, 501-509.

Kacem, R., Sousa-D'Auria, C.D., Tropis, M., Chami, M., Gounon P., Leblon,G., Houssin, C., and Daffe, M. (2004). "Importance of mycoloyltransferases on the physiology of *Corynebacterium glutamicum*." *Microbiology*, 150, 73-84.

Kirchman, D. (1983). "The production of bacteria attached to particles suspended in a freshwater pond." *Limnology and Oceanography*, 28, 858-872.

Lee, D.S., Jeon, C.O., and Park, J.M. (2001). "Biological nitrogen removal with enhanced phosphate uptake in a sequencing batch reactor using single sludge system." *Wat. Res.*, 35(16), 3968-3976.

van Loosdrecht, M., Lyklema, J., Norde, W., and Zehnder, A. (1990). "Influence of interfaces on microbial activity." *Microbiological Reviews*, 54, 75-87.

Lincoff, A.H., and Gossett, J.M. (1984). "The determination of Henry's constant for volatile organics by equilibrium partitioning in closed systems." *Gas transfer at water surfaces*, D. Reidel, Dordrecht, Holland, pp 17-25.

Massoud, M.A., Tarhini, A., and Nasr, J.A. (2009). "Decentralized approaches to wastewater treatment and management: applicability in developing countries." *J. Environ. Manag.*, 90, 652–659.

Merzouki, M., Delgenes, J.-P., Bernet, N., Moletta, R., and Benlemlih, M. (1999). "Polyphosphate-accumulating and denitrifying bacteria isolated from anaerobic-anoxic and anaerobic–aerobic sequencing batch reactors." *Curr. Microbiol.*, 38, 9–17.

Mino T., Arun V., Tsuzuki Y., and Matsuo T. (1987). "Effect of phosphorus accumulation on acetate metabolism in the biological phosphours removal process." Proceedings of the IAWPRC international conference on biological phosphate removal from wastewaters, Rome. *Adv. Water Pollut. Cont.*, Pergamon Press, Oxford, pp 27–38.

Morgenroth E., and Wilderer P.A. (1999). "Controlled biomass removal: the key parameter to achieve enhanced biological phosphorus removal in biofilm systems." *Wat. Sci. Tech.*, 39(7), 33–40.

Okada, M., and Sudo, R. (1986). "Performance of sequencing batch reactor activated sludge processes for simultaneous removal of nitrogen, phosphorus and BOD as applied to small community sewage treatment." *Wat. Sci. Tech.*, 18(7-8), 363–370.

Pastorelli, G., Canziani, R., Pedrazzi, L., and Rozzi, A. (1999). "Phosphorus and nitrogen removal in moving-bed sequencing batch biofilm reactors." *Wat. Sci. Technol.*, 40(4–5), 169–176.

Peng, J., and Wan, A. (1997). "Measurement of Henry's constants of high-volatility organic compounds using a headspace autosampler." *Environ. Sci. Technol.*, 31(10), 2998-3003.

Prenafeta-Boldú, F.X., Vervoort, J., Grotenhuis, J.T.C., and van Groenestijn, J.W. (2002). "Substrate interactions during the biodegradation of benzene, toluene, ethylbenzene, and xylene (BTEX) hydrocarbons by the fungus *Cladophialophora* sp. strain T1." *Appl. Environ. Microbiol.*, 68(6), 2660–2665.

Saeed, T., and Aultairi, M.Al. (1999). "Chemical composition of the water-soluble fraction of the leaded gasolines in seawater." *Environ. Int.*, 25, 117-129.

Sam Houston State University (2006). *Development and Evaluation of Environmental Technologies*. Master report to Air Force Institute for Operational Health, contract no: F41624-02-2-9000, Huntsville, Texas.

Sokolovska, I., Rozenberg, R., Riez, C., Rouxhet,P.G., Agathos S.N., and Wattiau, P. (2003). "Carbon source-induced modification in the mycolic acid content and cell wall permeability of *Rhodococcus erythropolis* E1." *Appl. Environ Microbiol.*, 69, 7019-7027.

Stalder, V., Bernard, N., Hanselmann, K., Bachofen, R., and Chasteen T. (1995). "A method of repeated sampling of static headspace above anaerobic bacterial cultures with fluorine-induced chemiluminescence detection." *Analytica Chimica Acta.*, 303, 91-97.

Tchobanoglous, G., Burton, F.L., and Stensel, H.D. (2003). *Wastewater Engineering: Treatment and Reuse*. 4th edition. Metcalf & Eddy, Inc., McGraw Hill, New York, Ch 2 & 7.

van Voorthuizen, E.M., Zwijnenburg, A., and Wessling, M. (1995). "Nutrient removal by NF and RO membranes in a decentralized sanitation system." *Wat. Res.*, 39, 3657-3667.

Watanabe, Y., Okabe, S., Hirata, K., and Masuda, S. (1995). "Simultaneous removal of organic materials and nitrogen by microaerobic biofilms." *Wat. Sci. Technol.*, 31(1), 195–203.

Development of Slow-release Chemical Oxidation Methods for Environmental Remediation

Stephanie Luster-Teasley, PhD and Patrick Onochie

North Carolina A&T State University, Department of Civil, Architectural, Agricultural and Environmental Engineering, Greensboro, NC 27411

Abstract

Chemical oxidation (chemox) is an emerging method used for treating subsurface water and soil. In chemox, highly reactive liquids or gases are injected into a contaminated zone where the oxidants rapidly react to oxidize and breakdown subsurface contaminants to less toxic byproducts. Examples of oxidants used in chemox include ozone gas, Fenton's Reagent, and crystalline permanganate or persulfate dissolved in water. Despite the effectiveness of chemical oxidation, there are drawbacks to current chemox technologies. These drawbacks include the need (1) to inject very strong gases or copious volumes of chemox liquids into the ground, (2) to reapply the oxidants into the subsurface to fully clean sites due to side reactions occurring with natural organic matter or plugging of the subsurface system with chemox precipitates, (3) to prevent explosion hazards caused by the rapid reactions, and (4) to protect workers from the health and safety hazards associated with use of these chemicals. A novel approach to improving chemical oxidation treatment is to develop slow-release, or controlled release systems, to deliver chemical oxidants for water and soil remediation. This paper addresses the development of slow-release oxidant prototypes which are able to delay the release of a chemical oxidants which can be used for various applications in water treatment.

1.0 Introduction

Controlled release (CR) methods to deliver drugs and chemicals are increasingly being employed for various fields such as surgery, pharmacology, agriculture[(Akelah 1996; Al-Zahrani 2000; Kakoulides and Valkanas 1994; Mogul et al. 1996; Quaglia et al. 2001; Segal 1991; Shaviv et al. 2003; Vert 2005)]. Examples of CR designs in the pharmaceutical industry include small non-toxic devices implanted under the skin and biodegradable CR polymers implanted in humans subjects [(Bruck 1990; Ding and Liu 1998; Kohn 1996; Lenz and Marchessault 2005; Nair and Laurencin 2006; Segal 1991; Uhrich 1999)]. In agriculture, CR biodegradable polymers and waxes are used for insecticide, fungicide and pesticide applications [(Akelah 1996; Al-Zahrani 2000; Mogul et al. 1996; Quaglia et al. 2001)]. Despite extensive medical and agricultural research for controlled release systems using environmentally benign and biodegradable polymers, few studies have investigated implementing these methods for environmental engineering applications. Several researchers have developed controlled release systems for soil and water remediation using clay, waxes, gels, and waxy polymers. Examples include slow release oxygen polymers for bioremediation, phosphate buffer encapsulation for polymers for pH control during denitrification of groundwater and sediment, alginate gel for Fenton photochemical oxidation, and

encapsulation of bacterial cells [(Brewster 1995; Gates et al. 1995; Kang et al. 2004; Ross et al. 2005; Schwartz 2005)].

Exploring the ability to use biodegradable polymers featuring controlled release capabilities for environmental remediation and treatment is an emerging concept. Like medical and agricultural systems, many environmental engineering treatments rely on mass transfer and delivery of chemicals. Fundamental research of CR applications for environmental protection, decontamination, and remediation therefore merits investigation. CR technologies can extend treatment methods for soil and water remediation. The existing body of literature for biodegradable polymers focuses on seeking affordable replacements for non-degradable, synthetic plastics and methods to increase physical properties such as tensile strength for the packaging industry [(Kaplan et al. 1993; Mayer and Kaplan 1993; Vert 2005)]. For environmental engineering applications, however, the benefit of using polymers which naturally degrade to deliver treatment chemicals provides a method for in-situ remediation that would not need to be removed after treatment is completed.

Chemical oxidants are highly reactive, non-selective chemicals that generate hydroxyl radicals able to degrade environmental contaminants. In current chemical oxidation methods, highly reactive liquids or gases are injected into a contaminated zone. Chemical oxidants rapidly react to oxidize and breakdown subsurface contaminants to less toxic byproducts. Examples of oxidants used in chemox include ozone gas, Fenton's Reagent and crystalline permanganate or persulfate dissolved in water. Despite the effectiveness of chemical oxidation, there are drawbacks to current chemox technologies. These drawbacks include the need (1) to inject very strong gases or copious volumes of chemox liquids into the ground, (2) to reapply the oxidants into the subsurface to fully clean sites due to side reactions occurring with natural organic matter or plugging of the subsurface system with chemox precipitates, (3) to prevent explosion hazards caused by the rapid reactions, and (4) to protect workers from the health and safety hazards associated with use of these chemicals.

The development of a controlled release delivery system for oxidants from a degradable shell has several advantages: (1) it stabilizes the solid oxidants for emplacement in soil, sediment or subsurface applications. The placement may vary from ones that form permeable reactive barriers, packing in a series of wells where contaminated water will flow past the pellets for remediation, packing in a reactor for a pump and treat system, emplacement in sediment or surface water, or augured into soil. (2) It reduces the need for maintenance associated with the gaseous and liquid oxidants. (3) It reduces the dangers associated with handling the oxidant by workers. (4) It extends the release of an oxidant without the need to re-inject the gas or liquid solutions. Therefore this new method has the potential to effectively extend the ability to provide chemox treatment in a fashion similar to using biodegradable medical implants to deliver drug formulations in the body to provide controlled and extended release of their active components.

This research focuses on the development of controlled release with the chemical oxidant potassium permanganate. Potassium permanganate is a purple crystalline oxidant that can be used to remediate trichloroethylene and was selected as the initial target oxidant for prototype development [(Kang et al. 2004; Ross et al. 2005; Schwartz 2005)]. Several researchers have investigated the ability to

encapsulate potassium permanganate for slow release remediation using waxes and chlorine based polymers[(Kang et al. 2004; Ross et al. 2005; Schwartz 2005)]. In the present work, several biodegradable polymers and polymer blends were investigated for their potential to produce slow release $KMnO_4$ for extended periods of time. These prototypes ranged in diameter size from 0.3-0.5 cm solid pellets capable of releasing $KMnO_4$ for over one month duration. This article presents the preliminary laboratory research conducted to produce encapsulated $KMnO_4$ using biodegradable polymers and examining the feasibility of this technology. A second prototype using an alternative "green" oxidant was explored and demonstrates the ability to remediate pathogenic material. This paper will summarize the results for the $KMnO_4$ development and discuss preliminary findings for using alternative oxidants for encapsulation.

2.0 Materials

Certified ACS $KMnO_4$ (Fisher Chemical, Fair Lawn, NJ) was encapsulated in a blend of inert biodegradable polymers. Due to legal constraints, the biodegradable polymers selected for the prototype design will not be disclosed in this article. The structures, henceforth referred to as controlled-release biodegradable polymers (CRBP), Polymer A (a hydrophobic biodegradable polymer), and Polymer B (a hydrophilic biodegradable polymer) were formed into 0.3-0.5 cm in size solid pellets capable of controlled-release of the oxidant. The polymer blends for Polymer A and Polymer B were designed based on three design mechanisms. These mechanisms include: type 1 – Polymer erosion of the CRBP, type 2 - diffusion controlled, and type 3 – combined control. In a type 1 polymer erosion based system, the polymer had a higher capability of dissolving in water to release $KMnO_4$. The type 2 diffusion controlled system was designed for a higher capability for the $KMnO_4$ to diffuse through the shell into water. The type 3 combined control is a combination of type 1 and type 2 systems. Potassium permanganate concentrations in solution were measured using a Spectronic Spectrophotometer at 525 nm wavelength. Trichloroethylene concentrations were analyzed using a HP 5890 Series II gas chromatograph with a flame ionization detector (GC/FID) and a capillary column (J&W Scientific DB-624, 0.53 mm id x 30 m length).

3.0 Results and Discussion

Prototype development was based on three criteria: (1) polymer shell compatibility with the oxidant, (2) the ability for diffusion of the oxidant through the shell boundary, and (3) the ability to form pellet structures feasible for use as fill material for a permeable reactive barrier or in a reactor system. Prototypes with various diffusion and erosion rates were investigated using batch studies with aqueous media. Studies were conducted to evaluate the prototype reaction with the encapsulated oxidant, release of the oxidant from the polymer, and remediation of 500 ppm trichloroethylene in batch reactors. Criteria for biodegradable polymer selection included the compatibility with the selected oxidant, the ability to form solid pellet structures ranging in size less than 0.3-0.5 cm, and the ability of the polymer to degrade or dissolve to release the oxidant. $KMnO_4$ was tested for reactivity with the biodegradable polymers and polymer blends. One concern for shell

material is to ensure the oxidant was not reactive with the polymer. If the $KMnO_4$ is reactive with the shell, visible evidence would be a brown discoloration caused by manganese oxide formation or visible degradation of the shell material. To determine the stability, $KMnO_4$ was encapsulated in biodegradable polymer shells and mounted on a glass slides. Photos at 40x and 100x were taken of the pellets using a digital microscope to observe any reactions or discoloration of the shell. Little to no reactivity was observed between the polymer material and the $KMnO_4$ demonstrating the shell is inert and able to stabilize the oxidant.

3.1 Release Studies for Encapsulated $KMNO_4$

Biphasic $KMnO_4$ release was observed from the encapsulated oxidant pellets. This is consistent with the observations seen in previous studies using wax and chlorinated polymers [(Kang et al. 2004; Ross et al. 2005)]. A rapid release of $KMnO_4$ occurred during the initial 1 – 3 days followed by a controlled and slower release of $KMnO_4$. Oxidant release was delayed by increasing the ratio of hydrophobic Polymer A to hydrophilic polymer B in the polymer blend. Prototype blends were identified as PAB-50, PAB-60, PAB-90, and PAB-100 contained 50%, 60%, 90%, and 100% of Polymer A to Polymer B, respectively. Therefore PAB-50 represented a 1:1 ratio of Polymer A to Polymer B. PAB-50 was observed to release $KMnO_4$ at a faster rate than PAB-60, PAB-90 and PAB-100. PAB-60 and PAB-90 appeared to exhibit similar release rates for $KMnO_4$ with PAB-90 releasing the oxidant slower during the first 20-minutes. PAB-100 demonstrated the slowest release of the oxidant. Homogenous mixing of the polymers and oxidant proved to be important to ensure diffusion of the oxidant from the shell at a controlled rate because the hydrophilic polymer will readily dissolve in water leaving pores in the hydrophobic shell. For example, an excess amount of hydrophilic polymer on the pellet surface led to rapid diffusion of the oxidant from the polymer. Pellets designed with only the hydrophobic polymer demonstrated the slowest rate of oxidant diffusion.

The diffusion based prototypes containing Polymer A proved to be the most effective $KMnO_4$ delivery without the formation of MnO_2 precipitates. The erosion based prototypes with Polymer B formed manganese oxide precipitates. The diffusion based and the combined prototypes were determined to be more feasible for long-term release of the oxidant subsurface. The prototypes with a higher ratio of Polymer B produced MnO_2 precipitate which decreased in formation as the ratio of Polymer A polymer increased in the pellet design. Because manganese oxide is a precipitate known to inhibit the ability to use $KMnO_4$ for trichloroethylene remediation, the PAB-100 prototype was evaluated for the media replacement, continuous release, and TCE remediation studies.

3.2 Replacement Media Study

In the replacement media study, PAB-100 prototypes containing 2% and 20% $KMnO_4$ by mass to polymer ratio were encapsulated in the polymer shell. In batch reactor bottles, 50 ml of DI water and 0.5 g of prototype pellets were sealed and stored for 3 – 4 days at 28°C and in the dark. After 3 – 4 days, the $KMnO_4$ concentration was measured using a Spectronic Spectrometer at 525 nm wavelength.

Following the $KMnO_4$ concentration measurement, the pellets and bottles were rinsed with DI water three times and 50 ml of fresh DI water was added to the bottles with the same pellets. This process was then repeated by storing the reaction bottles for another 3 – 4 days and a $KMnO_4$ measurement was performed. This replacement media study was designed to measure the steady-state release rate of $KMnO_4$ prototypes.

The prototypes demonstrated an initial rapid release of the oxidant followed by a slower, steady state release (Figures 1a and 1b). The 2% prototype exhausted the encapsulated $KMnO_4$ diffusing from the shell within 44 days. The 20% $KMnO_4$ structures however had not exhausted the oxidant within the 44 day period of the experiment.

3.3 Continuous Release Study

In the continuous release studies, PAB-100 prototypes containing 2% and 20% $KMnO_4$ by mass to polymer ratio were encapsulated in the polymer shell. A mass of 0.5 g of pellets were added to 50 ml of DI water in reaction bottles. Measurements for $KMnO_4$ were conducted every 3 – 4 days using a Spectronic Spectrometer at 525 nm wavelength. Following the measurements, the prototypes and the liquid sample were returned the bottles, capped, and stored for another 3 – 4 days at 28°C in the dark before the next measurement. In the continuous batch study, $KMnO_4$ release was observed to extend over a 46- 48 day period where 2% and 20% $KMnO_4$ by mass in polymer prototypes were measured for $KMnO_4$ concentration in water (Figure 2a and 2b).

Future studies to evaluate $KMnO_4$ release will entail optimizing the concentration of $KMnO_4$ (greater than 20% by mass) that can be encapsulated in the polymer structures and reducing the biphasic release observed in the prototypes. Additionally, alternative hydrophobic and hydrophilic polymer blends will be investigated. The surface area of the polymer structures can be enhanced using various shapes and geometries such as cylinder columns, saddles, or hollow tubes.

3.4 Reaction with Trichloroethylene

The prototypes demonstrated the ability to degrade trichloroethylene (TCE) in a batch system. The TCE contaminated water (500 ppm) was added to 25 ml serum bottles with 0.5 g of either the 2%, 20%, or 60% $KMnO_4$ prototypes. The bottles were overfilled and capped to prevent headspace air from being sealed in the bottle. This ensured all TCE would be dissolved in the liquid phase without the need to analyze headspace gas. TCE concentrations were analyzed using a HP 5890 Series II gas chromatograph with a flame ionization detector (GC/FID) and a capillary column (J&W Scientific DB-624, 0.53 mm i.d. x 30 mm length). Measurements were conducted every seven minutes for a total of 77 minutes. Trichloroethylene degradation for the 2% pellets reached 50% removal after 70 minutes while the 20% pellets reached 50% removal of TCE within 47 minutes. The TCE concentration reached 50% reduction in the 60% KMnO4 prototypes within 13 minutes however there was a large formation of MnO_2 (Figure 3). The TCE and $KMnO_4$ reaction demonstrated first order kinetics which is consistent with literature [(Schnarr et al. 1998)].

3.5 Challenges for $KMnO_4$ slow release remediation

There may be several factors that restrict the controlled release system. These factors include the quantity of potassium permanganate that will diffuse from the system, the production of MnO_2, and reaction efficiency may be limited. Prototype design and determination of an adequate quantity of pellets to remediate contaminants should help overcome these challenges. CRBP can overcome the need to inject copious amounts of liquid $KMnO_4$ into the subsurface which is the common practiced currently used for $KMnO_4$ and TCE remediation. Literature reports one of the limiting factors for chemical oxidation methods is the formation of precipitates that will "clog" the soil particles and reduce the effectiveness of transporting chemox liquids subsurface [(Siegrist et al. 1999a; Siegrist et al. 1965; Siegrist et al. 1999b)]. The formation of MnO_2 precipitates which, is also a significant problem for traditional $KMnO_4$ remediation, still remains an important consideration and potential challenge to overcome for CRBP remediation.

4.0 Future Work

Our future work for using chemical oxidants encapsulated in biodegradable polymers will include exploring alternative chemicals for encapsulation and investigating alternative hydrophobic and hydrophilic polymer blends to control degradation rates for the polymer/chemical pellets. We will continue investigate optimization of the chemical to polymer ratio, controlling and modeling chemical diffusion from polymer shells, encapsulation methods (i.e. micro-based and nano-based), and structure geometry. In particular, we are interested in exploring the use of alternative oxidants for treatment of environmental contaminants including various groundwater contaminants, pathogens, and pesticides. Our research efforts have progressed to investigating one alternative oxidant capable of reducing concentrations of pathogens in water. Release studies using the PAB-100 polymer demonstrate the ability to release the alternative oxidant for sustained periods of time. This work appears to be promising and will help promote future efforts in exploring controlled release technologies for environmental remediation.

Acknowledgements

We would like to thank our funding sources NSF Small Grants for Exploratory Research (SGER Grant #0640035) and NSF Broadening Participation in Engineering (BRIGE Grant # 0831631). We would also like to thank Dr. Vestel Shirley, John Carver, and Bryce Holmes in the North Carolina A&T State University Analytical Chemistry Lab for their assistance with this research.

REFERENCES

Akelah, A. (1996). "Novel utilizations of conventional agrochemicals by controlled release formulations." *Materials Science and Engineering*, C(4), 83-98.

Al-Zahrani, S. M. (2000). "Utilization of Polyethylene and Paraffin Waxes as Controlled Delivery Systems for Different Fertilizers." *Industrial Engineering Chemistry Research*, 39(2), 367-371.

Brewster, M. A. G. G. O., JD Redman; KA Sander. (1995). "Observed migration of a controlled DNAPL release by geophysical methods." *Groundwater*, 33(6), 977-987.

Bruck, S. D. (1990). "Leachable components in polymeric medical implants and disposables. A brief critical review." *Medical Progress Through Technology*, 16(3), 131-143.

Ding, J., and Liu, G. (1998). "Water-Soluble Hollow Nanospheres as Potential Drug Carriers." *Journal of Physics and Chemistry B*, 102(31), 6107-6113.

Gates, D. D., Siegrist, R. L., and Cline, S. R. "Chemical oxidation of contaminants in clay or sandy soil." Pittsburgh, PA, USA, 582-588.

Kakoulides, E. P., and Valkanas, G. N. (1994). "Modified Rosin-Paraffin Wax Resings as Controlled Delivery Systems for Fertilizers. Fabrication Parameters Governing Fertilizer Release in Water." *Industrial Engineering Chemistry Research*, 33(6), 1623-1630.

Kang, N., Hua, I., and Rao, P. S. (2004). "Production and Characterization of Encapsulated Potassium Permanganate for Sustained Release as an In-Situ Oxidant." *Industrial Engineering Chemistry Research*, 43(17), 5187-5193.

Kaplan, D. L., Mayer, J. M., Ball, D., McCassie, J., Allen, A. L., and Stenhouse, P. (1993). "Fundamentals of Biodegradable Polymers." Biodegradable Polymers and Packaging, C. Ching, D. L. Kaplan, and E. L. Thomas, eds., Technomic Publishing Company, Inc., Lancaster, PA, 1 - 42.

Kohn, J. "Overview of the use of polymers in medical application as illustrated by the design, characterization, and application of tyrosine-derived polymers." Brookfield, CT, USA, 103-110.

Lenz, R. W., and Marchessault, R. (2005). "Bacterial Polyesters: Biosynthesis, Biodegradable Plastics and Biotechnology." *Biomacromolecules*, 6(1), 1-8.

Mayer, J. M., and Kaplan, D. L. (1993). "Biodegradable Materials and PAckaging - Environmental Test Methods and Needs." Biodegradable Polymers and Packaging, C. Ching, D. L. Kaplan, and E. L. Thomas, eds., Technomic Publishing Company, Lancaster, 233-245.

Mogul, M. G., Akin, H., Harirci, N., Trantolo, D. J., Gresser, J. D., and Wise, D. L. (1996). "Controlled Release of biologically active agents for the purposes of Agricultural Crop Management." *Resources, Conservation and Recycling*, 16, 289-320.

Nair, L. S., and Laurencin, C. T. (2006). "Polymers as biomaterials for tissue engineering and controlled drug delivery." Tissue Engineering I: Scaffold Systems for Tissue Engineering, Springer-Verlag Berlin, Berlin, 47-90.

Quaglia, F., Barbato, F., De Rosa, G., Granata, E., Miro, A., and La Rotonda, M. I. (2001). "Reduction of the Environmental Impact of Pesticides: Waxy Microspheres Encapsulating the Insecticide Carbaryl." *Journal of Agricultural Food Chemistry*, 49(10), 4808-4812.

Ross, C., Murdoch, L. C., Freedman, D. L., and Siegrist, R. L. (2005). "Characteristics of potassium permanganate encapsulated in polymer." *Journal of Environmental Engineering*, 131(8), 1203-1211.

Schnarr, M., Truax, C., Farquhar, G., Hood, E., Gonullu, T., and Stickney, B. (1998). "Laboratory and controlled field experiments using Potassium Permagnanate

to remediate trichloroethylene an dperchloroethylene DNAPLs in porous media." *Journal of Contaminant Hydrology*, 29, 205-224.

Schwartz. (2005). "Modeling of Potassium Permanganate encapsulated in wax."

Segal, M. (1991). "Patches, Pumps, and Timed Release: New Ways to Deliver Drugs." *FDA Consumer*, 25(8), 13-15.

Shaviv, A., Raban, S., and Zaidel, E. (2003). "Modeling Controlled Nutrient Release from Polymer Coated Fertilizers: Diffusion Release from Singe Granules." *Environmental Science and Technology*, 37(10), 2251-2256.

Siegrist, R., Lowe, K. S., Murdoch, L. C., Case, T. L., and Pickering, D. A. (1999a). "In-Situ Oxidation by Fracture Emplaced Reactive Solids." *Journal of Environmental Engineering*, 429-440.

Siegrist, R., Urynowicz, M. A., West, O. R., Crimi, M. L., and Lowe, K. S. (1965). *Principles and Practices of In-Situ Chemical Oxidation Using Permanganate*, Battelle Press, Columbus, OH.

Siegrist, R. L., Lowe, K. S., Murdoch, L. C., Case, T. L., and Pickering, D. A. (1999b). "In situ oxidation by fracture emplaced reactive solids." *Journal of Environmental Engineering*, 125(5), 429-440.

Uhrich, K. (1999). "Polymeric Systems for Controlled Drug Release." *Chemical Reviews*, 99(11), 3181-3198.

Vert, M. (2005). "Aliphatic Polyesters: Great Degradable Polymers that Cannot Do Everything." *Biomacromolecules*, 6(2), 538-546.

Figure 1(a). Release of $KMnO_4$ from the 2% $KMnO_4$ by mass prototype for water media replaced every 3 – 4 days to determine a steady state release from the pellets. (b) Release of $KMnO_4$ from the 20% $KMnO_4$ by mass prototype for water media replaced every 3 – 4 days to determine a steady state release from the pellets

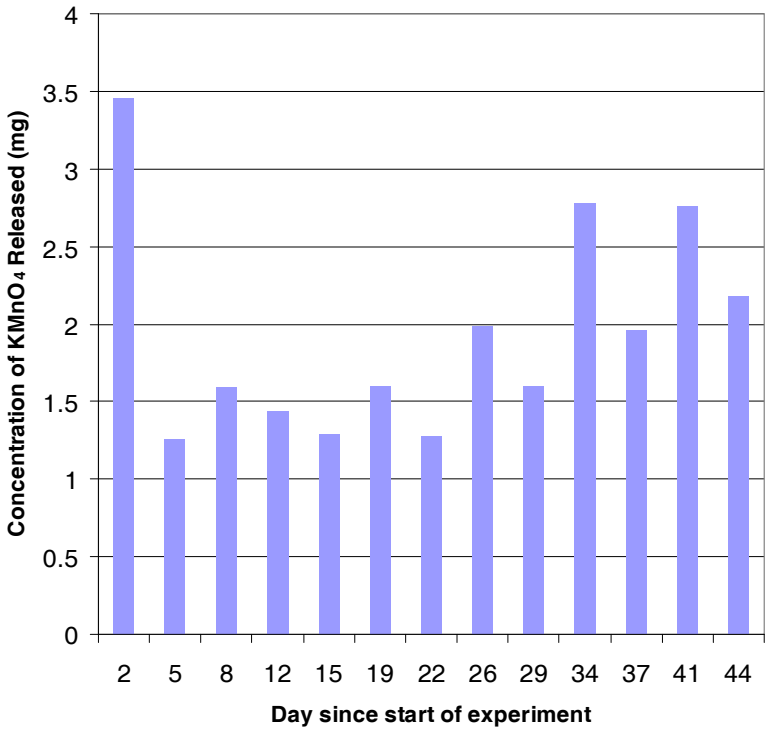

(a)

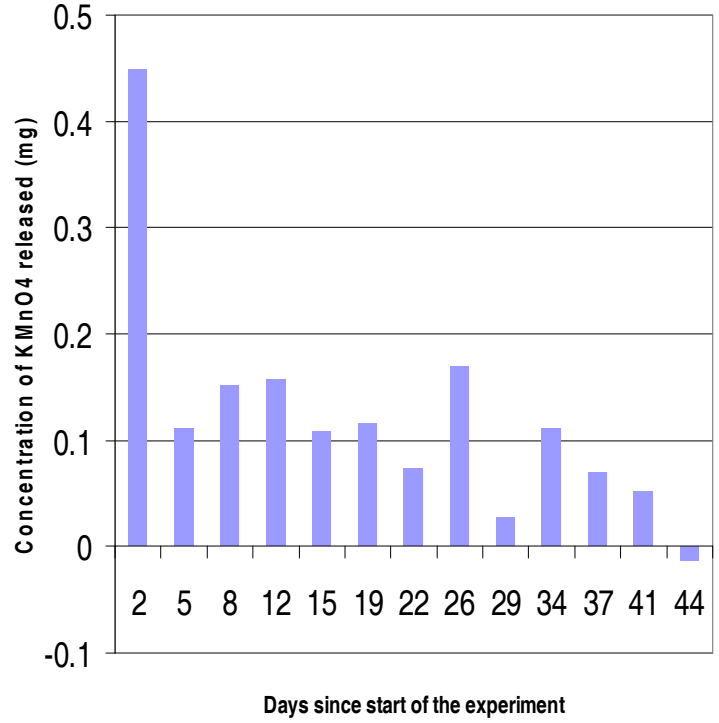

(b)

Figure2. (a) KMnO4 concentration released from the 2% $KMnO_4$ by mass prototype over a 47 day period. (b) $KMnO_4$ concentration released from the 20% $KMnO_4$ by mass prototype over a 47 day period.

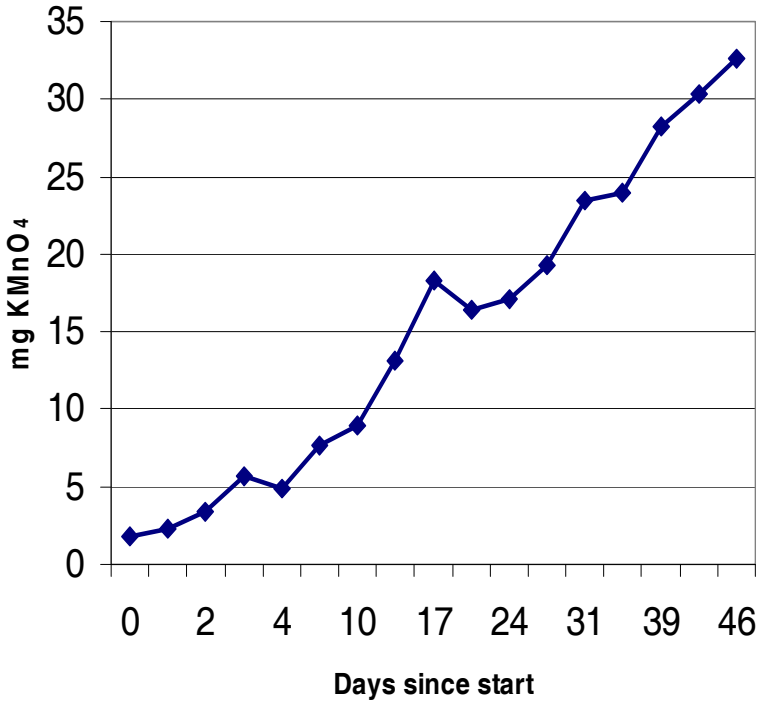

(a)

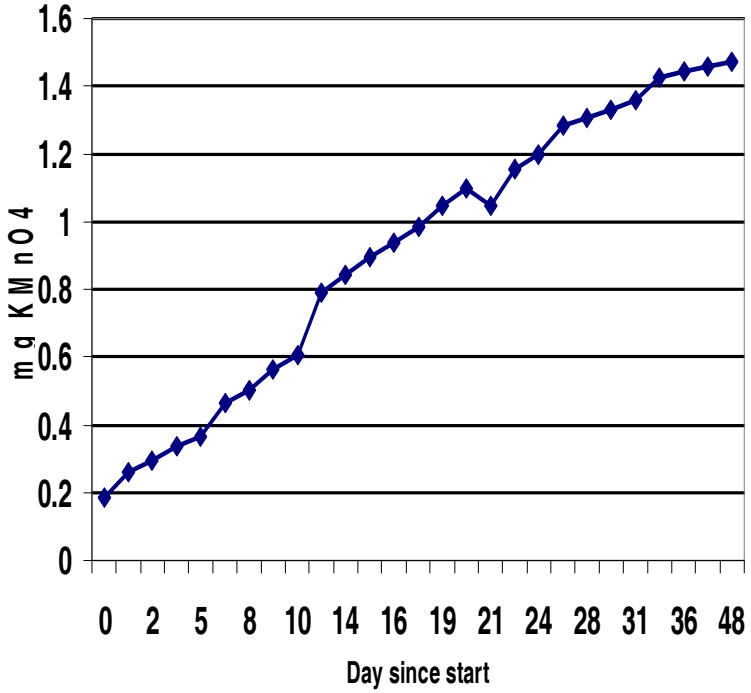

(b)

Figure 3. TCE degradation by $KMnO_4$ released from the 2% (solid line) and 20% (dotted line with triangles) $KMnO_4$ by mass prototype; 60% KMnO4 by mass (dotted line with x)

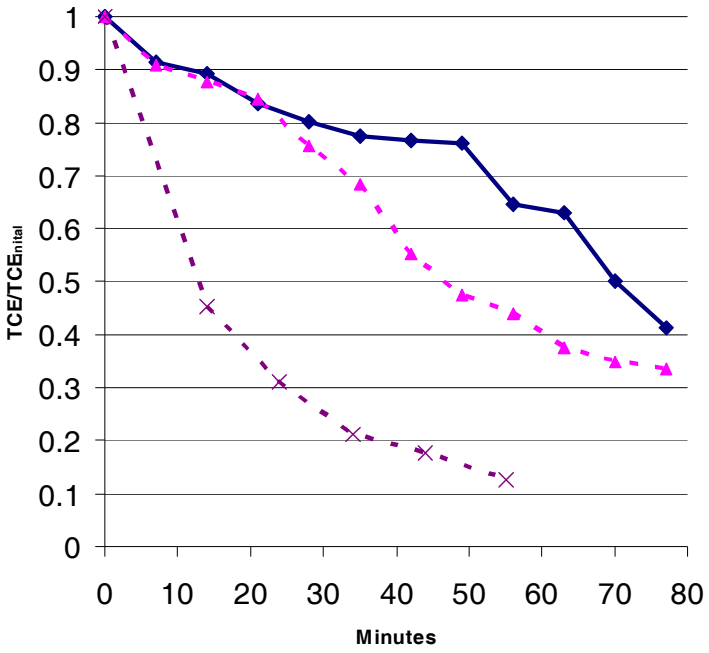

Peracetic acid as an alternative disinfection technology for wet weather sewer overflows

Coyle, E.[1], P.E., L. Ormsbee[2], P.E., P.H. Ph.D., D.WRE, F.ASCE

[1]Environmental Engineer, Kentucky Water Resources Research Institute, 233 Mining and Minerals Resource Building, University of Kentucky, Lexington, Kentucky 40506-0107, (859) 257-8005, email:eecyole@juno.com; [2]Director, Kentucky Water Resources Research Institute, 233 Mining and Minerals Resource Building, University of Kentucky, Lexington, Kentucky 40506-0107, (859) 257-6329, email: lormsbee@engr.uky.edu

Abstract

Combined Sewer Overflows (CSOs) continue to be a significant source of wet weather flows (WWFs). Traditional technologies exist to address wet weather overflows but are many times cost prohibitive, can yield toxic by-products and in areas of older infrastructure, space for facilities to treat overflows is often limited if available at all. As such more cost effective technologies, requiring less space and producing less harmful by-products are currently being explored. One such possibility for alternative high-rate disinfection has been investigated using peracetic acid. The decomposition of peracetic acid results in only the non-toxic by-products of oxygen, methane, carbon dioxide and water, and the disinfection reaction occurs in a short contact time and with a high kill rate. Thus, this technology can prove not only valuable where space is limited, but is also extremely environmentally sound.

Introduction

Since the passage of the Clean Water Act (CWA) in 1972, the nation has spent considerable fiscal resources in an attempt to clean up the country's waterways. Following the passage of the Act, the initial focus of policy makers was on improving the treatment capacity and efficiency of the nation's wastewater treatment plants. Since that time, additional focus has been placed on addressing other sources of contamination such as non-point source runoff and intermittent discharges from wet weather flows (WWFs). In 1994, a coordinate attempt was made to address the problem with combined sewer flows through the development of nine-minimum controls and a subsequent long term control plan (USFR, 1994; USEPA 1995).

Rain induced wet weather flows (WWFs) consist of combined sewer overflows (CSOs), sanitary sewer overflows (SSOs) and stormwater (SW), all of which introduce pathogens to the surface waters when discharged. These waterborne pathogens consist of disease-causing bacteria, viruses, and protozoa. When people come into contact with the contaminated water, these pathogens can be transmitted resulting in severe problems of the digestive system, which can be life-threatening to the very young, very old, or those with damaged immune systems. In 2004 it was estimated that between 3,000 to 6,000 illnesses are caused nationwide on an annual level due to WWFs (EPA, 2004).

Combined sewer systems serve approximately 746 communities containing about 40 million people. Within these communities there are estimated to be around 9,348 CSO outfalls that are regulated by 828 NPDES permits. Most communities with combined sewer systems are located in the Northeast in the Pacific Northwest regions as well as in the Ohio and Missouri River valleys. In the state of Kentucky, there are currently 17 CSO communities with a total of 297 CSOs. The majority of these are associated with Louisville, Kentucky and the Northern County Sanitation District No.1 (see Figure 1 and Table 1).

EPA has estimated that approximately 850 billion gallons of untreated wastewater and stormwater are discharged from these outfalls (EPA, 2004). As of 2002, over $6 billion dollars had been expended in addressing these issues. At that time, it was estimated that an additional $50 billion dollars would have to be spent to achieve an 85% volume reduction of the existing CSOs.

Table 1. List of CSO communities in Kentucky

Community	KPDES Permit	# CSOs	Population Served
Louisville - MSD	KY0022411	115	430,000
N.KY Sanitation Dist. #1	KY0021466	74	335,000
Owensboro	KY0020095	8	54,000
Frankfort	KY0022861	15	50,611
Paducah	KY0022799	11	34,500
Ashland	Ky0022373	8	30,000
Henderson	KY0020711	14	29,500
Pikeville	KY0025291	3	10,000
Pineville	KY0024058	3	9,111
Maysville	KY0020257	11	8,950
Prestonsburg	KY0027413	1	4,800
Catlettsburg	KY0035467	17	4,100
Morganfield	KY0021440	2	3,850
Harlan	KY0026093	1	3,786
Worthington	KY0022926	3	2,168
Vanceburg	KY0021512	5	2,038
Loyall	KY0026115	6	1,332

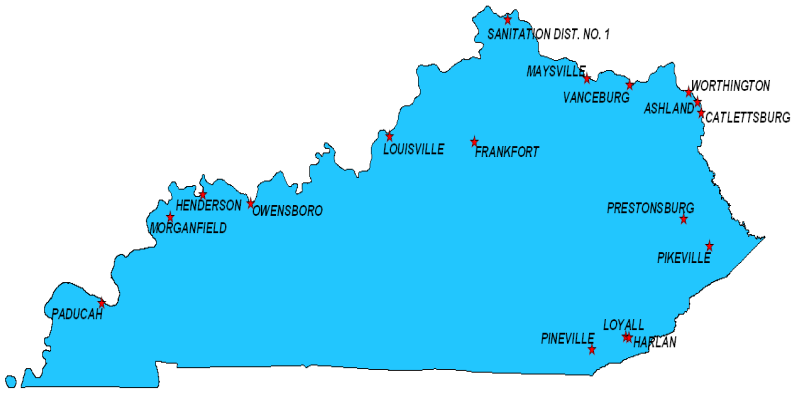

Figure 1. Map of CSO communities in Kentucky

Unlike traditional wastewater treatment plants, the quality and quantity of WWFs can vary significantly within minutes, as well as within hours, days, months and seasons (Wojtenko, et al., 2001) For example, after dry periods, a phenomenon referred to as the "first-flush" occurs during wet weather events, in which build up from the watershed or build up in the collection system, or both, are flushed from the watershed and system into the surface waters. This "flush" into the surface waters is much more concentrated with pollutants than flows that have been diluted throughout the wet weather event after the watershed and collection system have effectively been "rinsed off" by rain water. Another example is seen during the spring and summer seasons of high vegetative growth, when less runoff is introduced to the surface waters and collection system as opposed to more dormant fall and winter seasons when the volume of stormwater runoff is higher and of different character. In addition, the composition of WWF also varies from community to community depending on the characteristics of the individual discharges to the system. As such, not only do flow rate, volume and quality of WWFs vary temporally, they vary with location on a system by system, watershed by watershed basis.

The variation in quality can be seen in the range of constituents for "typical" WWFs. These ranges can be approximated from an examination of data from various sewer districts such as the Louisville Metropolitan Sewer District and Cincinnati Ohio WWF data (see Table 2 below).

Table 2: Representative WWF constituents

Constituents	Maximum	Average/Median	Minimum
E coli (col/100 mL)	10,000,000	501,187	31,623
TN (mg/L)	13	5.1	2.25
TP (mg/L)	2.5	1.5	0.5
TSS (mg/L)	500	150	45
COD (mg/L)	500	100	0
pH (SU)	6.5	7	7.5

As can be seen, the range of values varies depending on the constituent. It is also worth noting that the constituents do no vary directly with each other. Just because one constituent is on the high end of the range does not imply that others will be and vice versa. Due to the independent and highly variable nature of each of the WWF constituents, as well as the temporal and spatial variability of WWFs in general, the disinfection of WWFs is uniquely challenging.

Wet Weather Flow Technologies

The major technologies for addressing wet weather discharges can be grouped into five major categories: 1) operation and maintenance, 2) collection system controls, 3) storage facilities, 4) source reduction through low-impact development techniques, and 5) treatment technologies. This paper will be focusing on treatment or disinfection technologies.

Chlorine is the most commonly used wastewater disinfectant but as early as 1969, alternatives to the chlorination of wastewater were desired due to the costs and hazards involved in transportation, storage and operation, particularly in highly populous areas (Elwood, 1970). In addition, heightened public concern regarding the use of chlorine compounds which produce toxic, mutagenic and carcinogenic by-products has stimulated the desire for alternative disinfectants (Veschetti, et al, 2003). Thus, alternatives to chlorine disinfection are being sought due to the growing concern over safety in handling gaseous chlorine and possible toxic side effects of treatment with chlorine.

According to the USEPA guidance document, "Combined Sewer Overflow Control", methods that are generally referred to as high rate disinfection achieve "…high bacterial kills at lower contact times, using increased mixing intensity, increased disinfectant dosage, chemicals having a higher oxidation rate than chlorine, or a combination thereof" (USEPA, 1993). The guidance further indicates that an acceptable reduction in bacteria concentration of at least 4 log kills should be achieved at detention times less than the conventional values of 15 to 30 minutes. Further, "an ideal disinfection system should guarantee the maximum efficiency in pathogenic microorganism removal without generating toxic and undesirable by-products" (Veschetti, et al., 2003). Thus, alternative disinfectants for WWFs should meet the above criteria, however a 10 minute contact time is now often achieved with many of the leading alternatives.

In 1999, EPA published several publications addressing the issue of treatment of CSO discharges. These included publications for chlorine disinfection (USEPA, 1999a) and for alternative disinfectants (USEPA, 1999b). Potential alternatives include: 1) chlorine dioxide, 2) ozonation, 3) ultraviolet (UV) radiation, 4) electron beam irradiation, and 5) peracetic acid (PAA). This paper will investigate the potential effectiveness of PAA as applied to wastewater discharges from the Town Branch Treatment Plant in Lexington, Kentucky.

Peracetic Acid

PPA (CH_3COOOH) is a very strong oxidant having a oxidation capacity of 1.81 v. The equilibrium chemistry is shown in Figure 2. PAA is produced by combining acetic acid, hydrogen peroxide, and water. Sulfuric acid is typically used as a catalyst for the reaction. PPA residuals appear to be non-toxic and are readily biodegradable in receiving waters. The disinfection rate associated with PPA has also been found to be very rapid which provides an added incentive for application to WWFs.

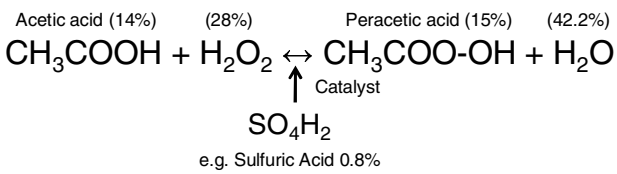

Figure 2: Equilibrium Chemistry for Peracetic Acid

Disinfection Studies

The potential application of PPA for use as a rapid disinfectant was tested using wastewater after primary treatment from the Lexington Town Branch treatment plant. The efficiency of the PPA was measured using Ecoli concentrations ranging from strong (> 1 million MPN/100 ml), moderate (> 100,000 MPN/100 ml, and weak (< 100,000 MPN/100 ml). For each strength, different combinations of contact time (i.e. 2, 5 and 10 minutes) and PPA concentration (i.e. 5, 10, and 15 mg/L) were evaluated.

Strong Wastewaters

Figures 3 and 4 show the disinfection efficiency of peracetic acid for water quality representative of strong WWFs with Ecoli concentrations ranging from approximately 1,000,000 to 2,500,000 MPN/100 ml. It can be seen that secondary water quality standards of 1,000 cols/100 ml is met with 10 - 15 mg/l of PAA up to 2,500,000 MPN/100 ml and that primary water quality standards of 100 col/100 ml is met with 15 mg/l up to 1,000,000 MPN/100 ml. With an increased dose of PAA higher initial concentrations were also brought down to primary water quality standards as show in figure 5. One of the more interesting things to note from each of these figures is that at the 10 and 15 mg/l peracetic acid dosages, the majority of the kill occurs in the first 5 minutes regardless of the initial concentration.

Moderate Wastewaters

Figures 5 through 8 show results from moderate strength WWFs. The primary water quality standard of 100 cols/100 ml is met consistently with the 10 and 15 mg/l doses and achieved or very closely approached with 5 mg/l. It is worth noting that at a contact time of 2 minutes, this standard is met with the 15 mg/l dose and that again, the majority of the disinfection occurs within the first 5 minutes (if not the first two) with the higher dosages. Finally, if a 10 minute contact time is desired such that less peracetic acid is used, it appears that 5 mg/l or a dose slightly higher would achieve primary water quality standards. All doses met secondary water quality standards of 1,000 cols/100 ml.

Weak Wastewater

Figure 9 shows results from an experiment with a weak WWF. As with the moderate strength WWF results, all three doses achieve primary and secondary water quality standards and the majority of the disinfection occurs within the first 5 minutes of treatment.

Conclusions

This study has demonstrated that PPA can be used as an effective disinfectant for WWFs as measured against discharges from an actual wastewater system. In addition to providing disinfection at a rapid rated, PAA requires no post treatment, since the chemical breaks down into harmless by-products.

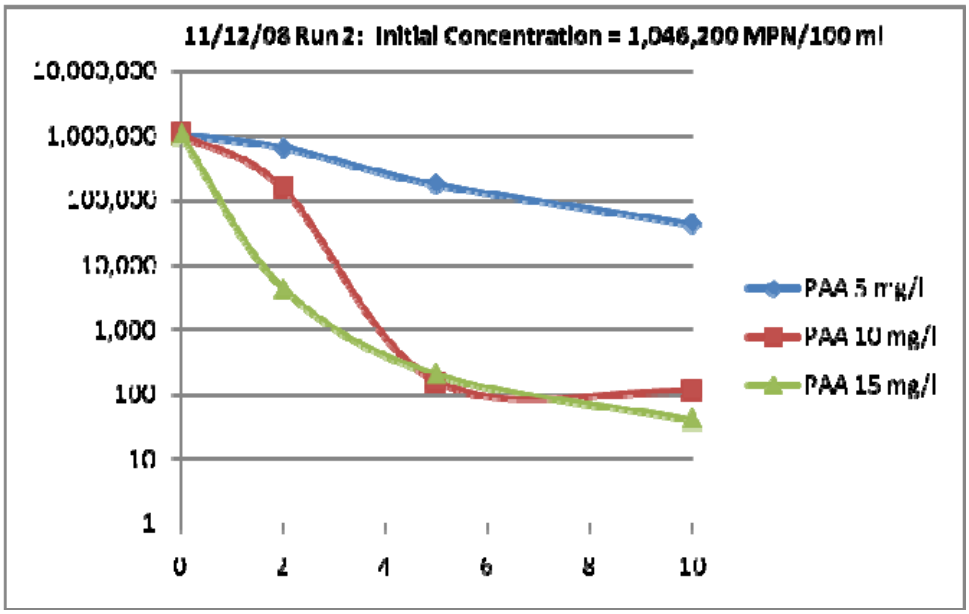

Figure 3: Ecoli Concentration (MPN/100 ml) vs. Contact Time (minutes) 11/12/08 - Run 2 with Initial Ecoli Concentration of 1,046,200 MPN/100 ml

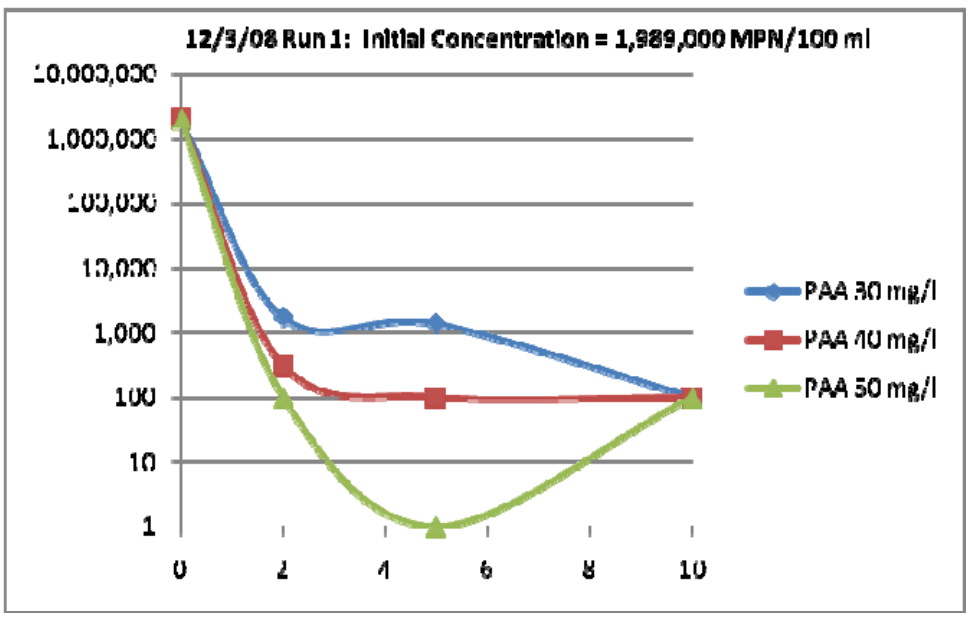

Figure 4: Ecoli Concentration (MPN/100 ml) vs. Contact Time (minutes) 12/3/08 - Run 1 with Initial Ecoli Concentration of 1,989,000 MPN/100 ml

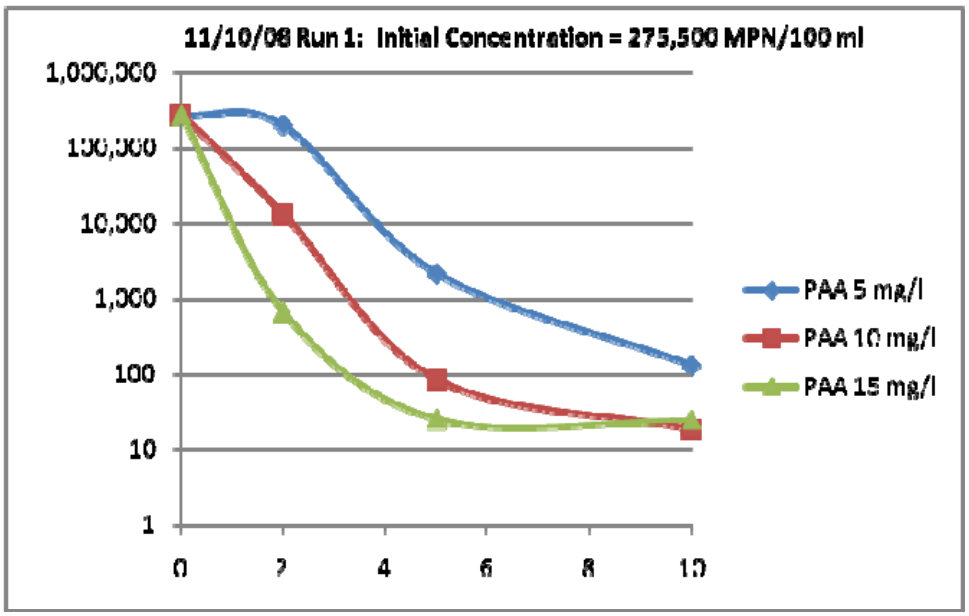

Figure 5: Ecoli Concentration (MPN/100 ml) vs. Contact Time (minutes) 11/10/08 - Run 1 with Initial Ecoli Concentration of 275,500 MPN/100 ml

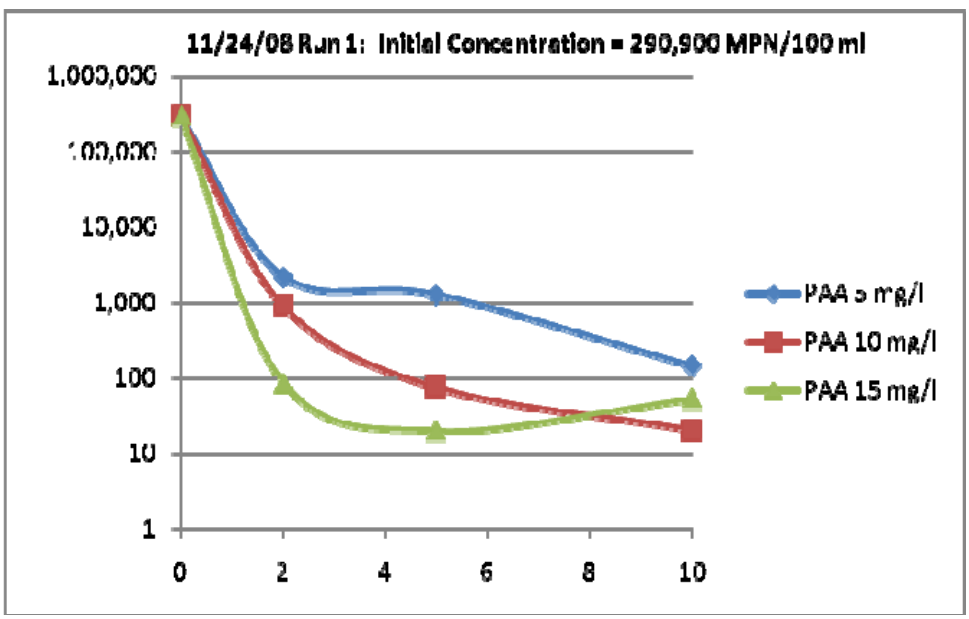

Figure 6: Ecoli Concentration (MPN/100 ml) vs. Contact Time (minutes) 11/24/08 - Run 1 with Initial Ecoli Concentration of 290,900 MPN/100 ml

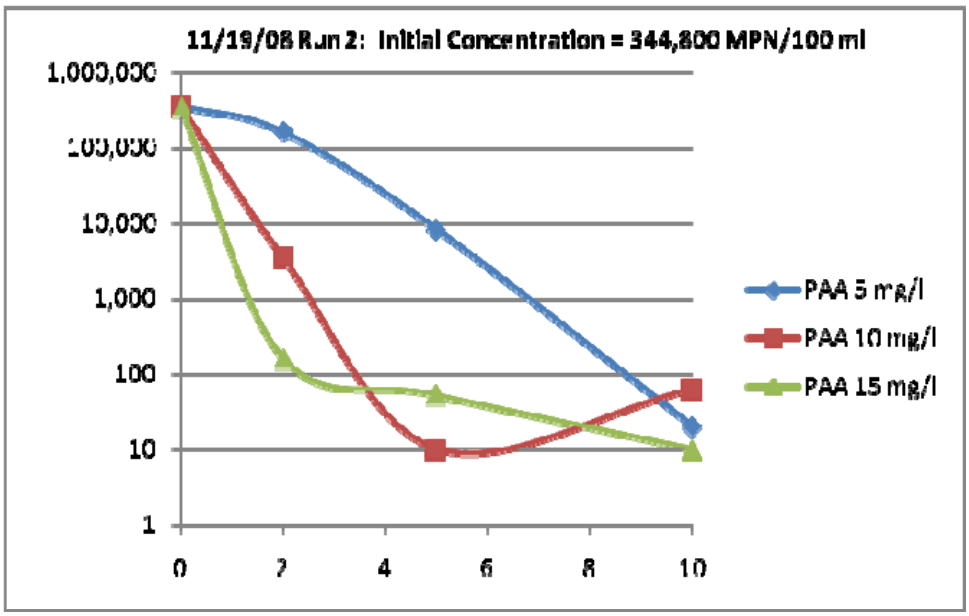

Figure 7: Ecoli Concentration (MPN/100 ml) vs. Contact Time (minutes) 11/19/08 - Run 2 with Initial Ecoli Concentration of 344,800 MPN/100 ml

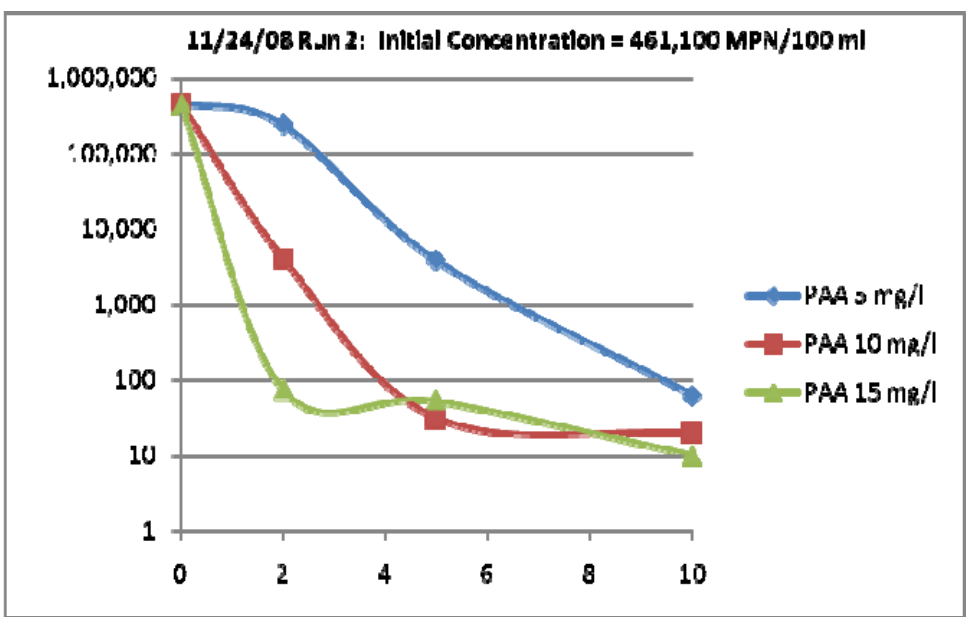

Figure 8: Ecoli Concentration (MPN/100 ml) vs. Contact Time (minutes) 11/24/08 - Run 2 with Initial Ecoli Concentration of 461,100 MPN/100 ml

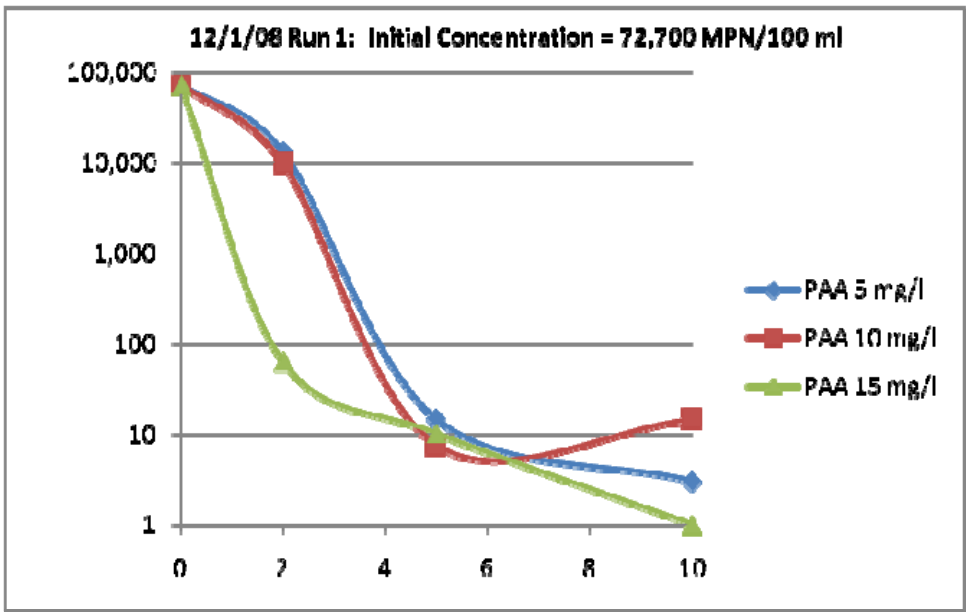

Figure 9: Ecoli Concentration (MPN/100 ml) vs. Contact Time (minutes) 12/1/08 - Run 1 with Initial Ecoli Concentration of 72,700 MPN/100 ml

References

Elwood J.R., R.A. Isaac and M. Weiss. (1970). "Alternate methods of wastewater disinfection". *ASCE Conference Proceeding Paper. National Specialty Conference on Disinfection.* 189-201.

USEPA. (1993). Office of Research and Development. *Combined Sewer Overflow Control*. Washington, DC, USA. [EPA 625-R-93-007]

USEPA. (1994). Office of Research and Development. *Combined Sewer Overflows: Guidance for Nine Minimum Controls*. Washington, DC, USA. [EPA 832-B-95-003]

USEPA. (1999a). Office of Water. *Combined sewer overflow technology fact sheet: Disinfection – Chlorination*. Washington, DC, USA. [EPA 832-F-99-021].

USEPA. (1999b). Office of Water. *Combined sewer overflow technology fact sheet: alternative disinfection methods*. Washington, DC, USA. [EPA 832-F-99-033].

USEPA. (2004). Office of Research and Development. *Report to Congress: Impacts and Control of CSOs and SSOs.* Washington, DC, USA. [EPA 833-R-04-001]

USFR. (1994). "Environmental Protection Agency Combined Sewer Overflow (CSO) Control Policy; Notice", *United States Federal Register*, Tuesday, April 19, 1994

Veschetti E., D. Cutilli, L. Bonadonna, R. Briancesco, C. Martini, G. Cecchini, P. Anastasi and M. Ottaviani. (2003). "Pilot-plant comparative study of peracetic acid and sodium hypochlorite wastewater disinfection". *Water Research*. 37(1):78-94.

Wojtenko I., M.K. Stinson and R. Field. (2001). "Challenges of combined sewer overflow disinfection by ultraviolet light irradiation". *Critical Reviews in Environmental Science and Technology*. 31(3):223-239.

Recycling of multiple waste streams for transportation fuel production via algae cultivation at wastewater treatment plants

Patrick J. Dunlap, Department of Civil Engineering, North Dakota State University
Andrew R. Shaw, Black & Veatch

Abstract

Increasing oil prices have led to recent initiatives to find domestic and renewable sources of transportation fuels. The cultivation of algae for biofuels production offers a uniquely sustainable option to utilize both greenhouse gases and wastewater as a valuable commodity. Algal cells contain lipids which can be converted to biodiesel by the same processes already used for other feedstocks. The most striking advantage over other feedstocks is the potential of algae; with theoretical production per area much higher than the currently favored feedstocks. Also as a non-food crop it will not have an effect on global food prices. Furthermore; the non-oil components of the algae cell also have value, such as cellulose which has the potential to be used for ethanol or methane production. With these advantages in mind, the steady flow of water and nutrients from a wastewater treatment plant presents an opportunity for effluent to be used in algae cultivation. The necessary carbon source could be supplied through a synergistic relationship with coal fired power plants needing to sequester greenhouse gases or as carbon from onsite anaerobic digesters. In any case, the coupling of a wastewater treatment plant with an algae cultivation system offers many exciting opportunities, such as low energy nutrient removal, valuable commodity production, and abatement of greenhouse gases. This paper reviews the current technologies and methods in algae for biofuels production, and suggests the feasibility of their future application to wastewater treatment plants.

Why Algae?

In recent years the push toward alternative and environmentally friendly transportation fuels has been highly visible. Policies, such as the former administration's policy of producing 132 billion liters (35 billion gallons) of ethanol by 2017 and 227 billion liters (60 billion gallons) of ethanol by 2030 (Sciences, 2007), and the funding and subsidies which have come about as a result of these and similar policies have led to immense growth in the biofuels industry in recent years. However, concerns have been raised about the actual versus the perceived impact of corn ethanol and other alternative fuel sources. For example the European Environmental Agency recently recommended that the current EU goal of 10% of transportation fuels being biofuels by 2020 be suspended over their concerns about net greenhouse gas abatement, natural resource utilization, and rainforest destruction; calling the goal "an experiment, whose unintended effects are difficult to predict and difficult to control" (Committee, 2008). It is also possible that biofuels production has been partially responsible for upsetting global food prices; leading to the ethical question should we really be treating food crops as a fuel commodity with the poorer citizens of the world impacted most?

In response to the push for increased alternative fuels production, microalgae has emerged in the public eye as a promising alternative. Serious research into microalgae cultivation for varied production purposes has been taking place for more

than three decades. What makes microalgae unique from other forms of biomass is its ability to convert solar energy so efficiently. Even the most conservative estimates say algae will produce about 20 times more biodiesel per area than soy, for example. Under optimized conditions algae can achieve energy conversion efficiencies much greater than other plant life resulting in a higher yield of fuel per land area. Unfortunately, application and realization of these yields has proven more elusive than theoretical figures might indicate. Algae can also be grown on land not suitable for the growth of other crops and with alternative water sources such as municipal and industrial wastewater, sea water, and saline aquifers. In addition, algae is not a food crop and will not have the impact on global food prices which have been associated with other biofuel feedstock options.

The purpose of this paper is to give an overview of current algae-biofuel technology. Some basics of algae cultivation and the history of its research will also be presented. Major hurdles will be summarized as well as commonly accepted strategies for overcoming those hurdles. Potential applications will be presented, along with their impact on wastewater treatment and water resources.

Basics

The term microalgae refers to microscopic unicellular algae species. It is a very general term for a very diverse group of more than 20,000 species which phycologists - those who study algae - even disagree on how to classify (Vymazal, 1995). Most of the interest has gone to a couple of well understood and promising groups such as members of the green algae genera Chlorella, Botryococcus, and Dunaliella; and the cyanobacteria genus Spirulina. (Benemann J. R., 2003) For practical purposes the major requirements for algal growth are Carbon, Nitrogen, Phosphorus, and water; though other macronutrients and micronutrients are required as well (Vymazal, 1995). pH, temperature, salinity, and insolation are also important factors in algal growth.

In a simplified view the constituents of algal biomass are cellulose, lipids, and proteins. This is significant as all components of the algae cell can be utilized, though traditionally the emphasis has been on maximizing the lipid fraction for increased biodiesel production. The lipids produced by algae are mostly triglycerides and through the process of transesterification can be simply converted to biodiesel as is done with the oil from other feedstocks.

Microalgae cultivation can be separated into two basic methods: open and closed systems. Each system has its own distinct advantages and disadvantages, with research still being performed on both. Open ponds (see Figure 1) have the advantage of being economical, scalable, and to some extant proven, as current commercial algae production for food, animal feed, pharmaceutical, and industrial applications utilize open pond systems. Even though they are more economical, the cost which these systems operate at is still prohibitively expensive for fuel. The disadvantages of the open ponds lay in their exposure to the atmosphere; making these systems susceptible to fluctuations in temperature, changes in salinity due to rain events and evaporation, and invasions by unwanted native species of algae.

Closed systems (see Figure 2) are commonly referred to photobioreactors (PBRs), and compared with open ponds are a relatively new addition to algae cultivation methods. They come in many different configurations, including hanging bags, horizontal and vertical arrays of plastic tubes, and even helix shaped. The advantage is that greater control can be exercised allowing the algae to approach theoretical photosynthetic efficiency, while the disadvantage is the prohibitive costs of the PBRs. It is also worth mentioning that in most concepts both open ponds and closed PBRs use CO_2 diffused through the water to supply a plentiful carbon source for the microalgae. This is necessary to achieve the high productivities commonly reported.

History

Early research into the culturing of algae saw potential for algae to provide a high protein and inexpensive food. Just as now, there was a lot of talk in the 1950s and 60s about algae saving the world, from food not fuel shortages. In the 1970s the Department of Energy (DOE) became interested in microalgae and first funded research for the low energy treatment of wastewater and the anaerobic digestion of the resulting biomass for biogas and ultimately energy production. (Benemann J. R., 2003)

In 1978 the DOE formed the Aquatic Species Program (ASP), which was focused on the cultivation of microalgae for biofuels production in open ponds fed by CO_2 from coal power plants. The ASP was in existence until 1996 and during that time it made many important breakthroughs, which today are considered by many to be the seminal work on the subject. The primary foci of the ASP were on selecting appropriate microalgae strains which were resilient to environmental variation and had high lipid content; increasing the lipid fraction of the individual algae cells; and the operation of open pond facilities to study algae production rates and CO_2 uptake levels (Sheehan, Dunahay, Benemann, & Roessler, 1998).

The 1990s also saw major research in Japan on the hardware of microalgae culturing. Closed photobioreactors were investigated as a means for CO_2 capture and synthesis of higher value co-products. The program was discontinued due to the high cost of these PBRs.

Early in this decade a member of the Aquatic Species Program named John Benemann published "Biofixation of CO_2 and Greenhouse Gas Abatement with Microalgae – Technology Roadmap" the purpose being to provide a guide for R&D which could produce applicable technologies within a decade (Benemann J. R., 2003).

In recent years research into microalgae for biodiesel production has taken a new direction. Government funding is still providing for research, but "clean tech" venture capital and petroleum industry wealth have become major sources as well. Within the last five years more that 50 venture capital companies have started in various areas of the algae-derived production chain; including algae biotechnology, open pond and closed PBR cultivation systems, and algae oil processing. Petroleum companies such as Shell and Chevron have staked claims and have partnered with some of the venture capital companies. Shell is working on an algae oil pilot facility

in Hawaii, and chevron has received funding from the Defense Advanced Research Projects Agency (DARPA) for the researching production of jet fuel from algae. In addition Honeywell, Airbus, and Boeing are other companies who have invested in algae technology.

With this recent research has come a lot of hype in the media, mostly spurred on by the new venture capital companies giving highly bloated figures on productivities, and claiming that algae will be running all our cars in a couple of years. For example in an article from CNN.com in 2008 the CEO of an algae oil startup company claimed that algae is about 50% oil and 0.4 hectares (one acre) of land used to grow algae can produce 380,000 liters (100,000 gallons) of biodiesel per year (Walton M, 2008). The first fact is wrong except under extreme circumstances and the second is actually thermodynamically impossible, but it was still published with no factual rebuttal of any kind. Naturally these sort of sensational stories recently have led to a much needed interest in algae, but with an overly enthusiastic optimism. A personnel favorite of the authors came on a recent American Airlines flight where the in-flight magazine contained an article on algae oil titled, "One Word: ~~Plastics~~ Algae" (Millar, 2008). This suggests the line from the 1967 film The Graduate and compares the venture capital-fueled world of algae oil today to the money to be made in the then emerging plastics industry.

Hurdles

Despite the recent influx of money coming at algae technology research and development, there are still obstacles to overcome. Like most new technologies, in the end it comes down to economic analysis. Algae did not become the food of the future because it could not be made competitive with other crop foods, and the Aquatic Species Program concluded that productivities needed to be higher and fossil fuels prices higher for the idea to work. If the profit from cultivating algae on a mass scale can be made significantly greater than the expenses while remaining socially and environmentally acceptable we will start to see algae oil facilities.

In order to achieve this economic viability, methods need to be found to decrease algae production costs and increase yields while developing new profitable ways to use the algae and the associated process. First it is necessary to analyze ways to keep production costs to a minimum. To achieve this, the open pond system currently appears to be the only feasible option. Millions of dollars of research was discontinued when the Japanese algae programs determined PBRs to be too expensive even for high value products (Benemann J. R., 2003). In 2007 an independent case study by Dr. Krassen Dimitrov used basic thermodynamic principles and conservative economical estimates to determine that a particular algae clean tech company's PBRs would not be competitive with fossil fuels unless crude prices reached $800/barrel (Dimitrov, 2007). John Benemenn from the ASP, a foremost expert on algae cultivation believes that PBRs are too expensive but could serve a role in inoculum production to seed the open ponds (Benemann J. R., 2003). In this way PBRs and open ponds could work together to overcome their individual inherent defects. The bulk of the growth could take place in the inexpensive ponds while changes in environmental conditions are buffered and invasive algae are kept

from taking over by a steady concentrated supply of the desired algae cultivated in a PBR. In addition to this, algae strain selection and genetic engineering could improve the efficiency of ponds in the future.

Another place where there is room for improvement is the optimization of the growth process in the ponds. While the necessary components to grow algae are straightforward, raw ingredients alone do not always constitute the desired recipe. Too many or too few nutrients can have a negative impact on growth, as can pH, temperature, or salinity if they are out of range. If the algae concentration is too high, the increased turbidity will block sunlight and slow the growth of more algae. Also, many see wastewater treatment as an advantageous co-process and if achieving a high quality wastewater effluent is another goal then controlling the process will become even more complex.

For the harvesting of microalgae; flocculation and sedimentation, centrifugation, microscreening, and flotation are all potential methods. Traditionally more energy intensive processes such as centrifugation have been used, and further research in this area could greatly impact microalgae biomass production economy. For example, bioflocculation is a process by which algae cells naturally form readily settling flocs under the right conditions. Flotation also seems to make sense as microalgae are already slightly buoyant due to oil content and if strains with higher amounts of oil are used flotation could be most effective.

Co-Products

Even with optimistic efficiencies and yield projections, the economic feasibility of algae to biofuels remains uncertain. It is popular belief that the best application of this process might lie in co-products and processes which can be produced and coupled with mass algae cultivation. At a WEFTEC 2008 algae committee meeting the idea of co-products and co-processes was a recurring theme. Likewise, this is one of the focuses of Benemann's 2003 roadmap, in which he states that current research should focus on the successes of past programs; such as the DOE's previous research into coupling with wastewater treatment and the production of high value co-products as was done in Japan and more recently by American private companies (Benemann J. R., 2003). Algae biomass and the process by which it is grown offer multiple opportunities to produce higher value products and receive greenhouse gas abatement credits. In this and the following section some of the co-products and co-processes which could create alternative income streams for algae cultivation are discussed.

There are several types of biofuels which can be produced from algae biomass, such as methane, biodiesel, ethanol, hydrocarbon chains, and hydrogen (Benemann J. R., 2003). The best known is biodiesel which simply requires the extraction of the lipid content and processing in the same way as with other feedstocks. The processing method is well established, but the costs associated with lipid extraction are high and more efficient methods are needed. A second biofuel option is to produce ethanol through fermentation of the algae's cellulose. Cellulosic ethanol is currently a hotly studied topic outside of algae research. If breakthroughs are made in this area it will also be a major breakthrough for algae oil research leading to a valuable co-product

to offset microalgae's expensive cultivation. A third biofuel production option is to anaerobically digest the remaining biomass for the production of methane (Benemann et al, 1977). The methane can be easily burned to produce electricity for the facility to help offset the high costs of the processes. This practice is applied at many wastewater treatment plants for their biosolids handling, and has been taken a step further at the wastewater treatment plant of Sunnyvale California where algae biomass used for treatment is harvested and anaerobically digested to produce biogas and ultimately electricity (Benemann J. R., 2003).

Other non-biofuel products include bioplastics which are potentially of higher value than fuels. Though this is still being researched they are currently seeing limited use in Europe and Japan. Algae oil and bioplastics technology each show great promise for the other's future viability. In addition unused biomass can also be sold as animal feed, and the nutrients which were absorbed by the algae can be reclaimed and recycled back to the algae ponds as needed or processed into a fertilizer.

Co-Processes

Another financial justification for algae cultivation comes from coupling it with other processes thereby increasing the efficiency of both. Some of the most promising of these appear to be wastewater treatment and CO_2 sequestration. The concept of growing algae as part of a wastewater treatment process has been around for decades. The most common method is shallow mixed ponds, termed high rate ponds, already used in many locations around the world such as the Sunnyvale Facility mentioned above. In high rate ponds raw wastewater is cleaned by a synergistic relationship between bacterial biomass and algae. Bacteria decompose the incoming organic matter releasing CO_2, Nitrogen, and Phosphorus; and form more bacterial biomass. With energy from sunlight the algae is able to use these components for the formation of more algal biomass and produce more oxygen to be used again by the bacteria (see Figures 3&4). The advantage of this over the conventional activated sludge process is in its energy efficiency, as aeration of the water is not necessary. The tradeoff is a much increased footprint as the surface area exposed to the sun now determines the power input into the system. In natural systems, phosphorus is usually the limiting element in algal growth, but in municipal wastewater it is usually carbon, and because of this limitation high rate ponds usually achieve 80-90% soluble BOD removal, 20-70% N removal, and 10-50% P removal (Lundquist & Benemann, 2007). When the purpose of the process becomes not only wastewater treatment, but also algae biomass production it is advantageous to increase algal production to its maximum, making the limiting factor the amount of sunlight. When CO_2 is diffused through the water to make up for the carbon deficiency, higher levels of treatment can be achieved at much lower costs than conventional nutrient removal systems (Lundquist & Benemann, 2007).

The greenhouse gas abatement potential of algae cultivation is also substantial. By the production of biofuels or improvements in energy efficiency GHGs which would otherwise have been released from fossil fuels are abated. Likewise; fertilizers have a very large carbon footprint associated with them but if they are produced as a byproduct of another process then they abate greenhouse gases. Lundquist estimates

an abatement potential of 455 kg of CO_2 per million liters (1.9 tons of CO_2 per million gallons) of wastewater treated. According to his research, coupling microalgae cultivation with wastewater treatment processes enhanced by CO_2 sequestration makes an economical impact which could lead to near term application for algae cultivation (Lundquist & Benemann, 2007).

Limitations

While algae technology shows a lot of promise there are some limitations to its application at larger scales. Technological and economical hurdles, as previously discussed can be solved on a more general level, but resource availability issues must be addressed for each individual site. The first and most obvious limitation is climatic; maximum solar radiation and high temperatures are desired for obvious reasons. Also, because of the large footprint needed for algae growth, land availability becomes a limitation as well, especially when attempting to couple the process with a wastewater treatment facility. There also is the issue of CO_2 supply. Ideally algae production facilities will be built near a coal fired power plant or some other industrial source of CO_2. If in the future serious legislation is passed regulating GHG emissions then it could become necessary for CO_2 emitting industries to transport and sequester their emissions making this less of an issue. This would however be extremely costly for such an industry to do.

Perhaps the most significant limitation to algae cultivation on the kind of scale needed to offset our nation's use of fossil fuels is the water resources required. For example, if we assume a very optimistic 94 m^3/hectare·yr (10,000 gal/acre·yr) production of biodiesel from algae and a conservative 1270 mm/year (50 inches/year) evaporation from the sunny areas where growth will take place, then to offset the 151 billion liters (40 billion gallons) of diesel used for transportation per year in the US the loss of water just due to evaporation would be almost 21,000 gigaliters/year (17 million acre·ft/year). Though this is not a problem in the near future; it shows the great impact that algae cultivation could have on water resources, and this is definitely something to be kept in mind in an age of water scarcity. In each site the water resources will need to be secured. In some instances wastewater will not be enough and alternatives such as saline aquifers and ocean water will need to be considered.

Because of these limitations, large scale algae cultivation will be only a niche application in the near future, being used successfully only where there is the appropriate intersection of land, water, solar radiation, and CO_2. This is will be the case unless either algae biofuels production proves itself very profitable at economies of scale or the government makes a concerted effort to utilize algae to limit oil imports. If either of these occurs then the infrastructure investment which is necessary might be paid for by petroleum companies, a US government agency, or some combination.

Conclusion

In summation the biofuels from algae cultivation shows incredible potential and advantages over other feedstocks currently used for fuel production, though the

technology has not yet been proven economical. If, however, production hurdles can be overcome, co-products and processes can be incorporated, and fossil fuels prices and security continue to be uncertain; then economic viability could be reached. Several technological advances and policy changes are indicators of this; such as cellulosic ethanol, biopolymer usage, and legislative policies toward greenhouse gas abatement. If massive scale cultivation becomes economical anywhere, it is likely to first occur at wastewater treatment plants due to the advantageous coupling of the two processes. However algae cultivation on the scale which would have an impact on our current imports of fuels is unlikely and would require either a very profitable situation or large government investment. This is due to infrastructure investment which would be necessary to supply the resources to the available land. Most opinions bring up a very vague figure of at least 10 years before algae could be driving our cars because no one really knows. Algae biodiesel could find niche applications where it is viable before this, but it is likely that long term production will fall short of optimistic hyperbole.

Works Cited

Benemann, J. R. (2003). Final Report - Biofixation of CO2 and Greenhouse Gas Abatement with Microalgae - Technology Roadmap.

Benemann, J. R., Koopman, B. L., Weissman, J. C., Eisenber, D. M., & Goebel, P. (1977). Energy Producation with Microalgae. Nature , 19-23.

Committee, E. S. (2008, April 10). Suspend 10 percent biofuels target, says EEA's scientific advisory body. Retrieved January 22, 2009, from European Environmental Agency.

Dimitrov, K. (2007, March). GreenFuel Technologies: A Case Study for Industrial Photosynthetic Energy Capture. Retrieved January 22, 2009, from nanostring.net: http://www.nanostring.net/Algae/CaseStudy.pdf

Lundquist, T., & Benemann, J. (2007, March 23). Using CO2 & Algae to Treat Wastewater and Produce Biofuel Feedstock. First Western Forum on Water & Energy Sustainability, UCSB, Santa Barbara, CA.

Millar, H. (2008, December 15). One Word: ~~Plastics~~ Algae. American Way Magazine, December 2008.

Sciences, T. N. (2007). Water Implications of Biofuels Production in the United States. Washington, D.C.: National Academic Press.

Sheehan, J., Dunahay, T., Benemann, J., & Roessler, P. (1998). A Look Back at the U.S. Deartment of Energy's Aquatic Species Program--Biodiesel from Algae. Golden, CO: National Renewable Energy Laboratory.

Vymazal, J. (1995). Algae and Element Cycling in Wetlands. Boca Raton: Lewis Publishers.

Walton, M. (2008, April 1). Algae: 'The ultimate in renewable energy'. Retrieved January 20, 2009, from CNN.com: http://www.cnn.com/2008/TECH/science/04/01/algae.oil/index.html



Figure 1 – Open Ponds cultivating algae in Ashkelon Israel



Figure 2 – Closed system algae cultivation by Valcent Products™

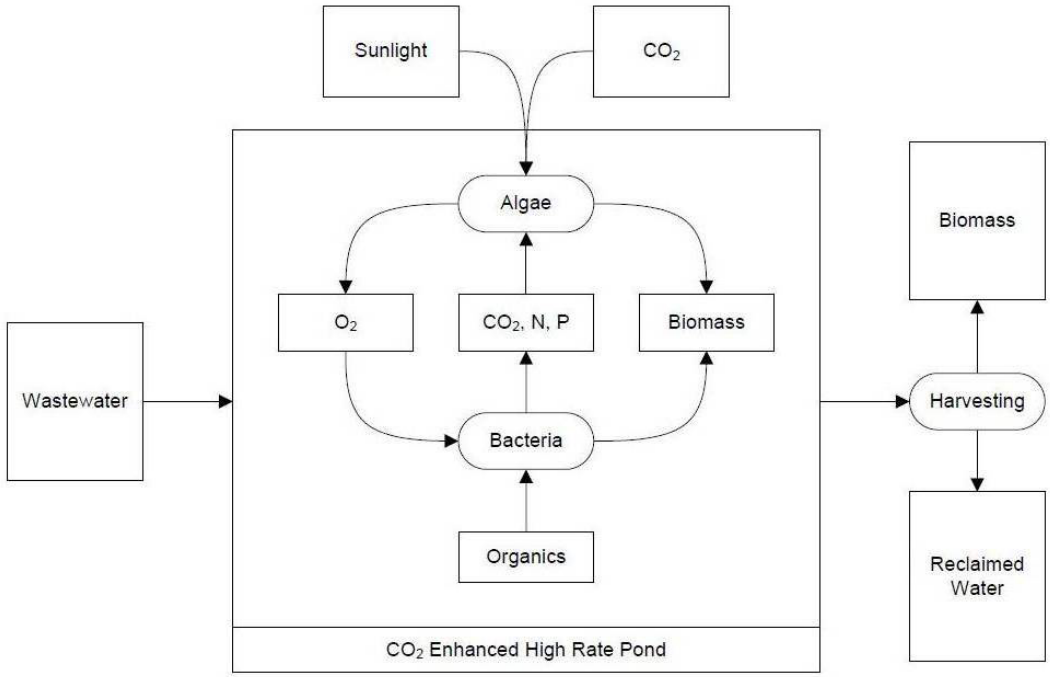

Figure 3 – Algae Cultivation Coupled with a Wastewater Treatment Process

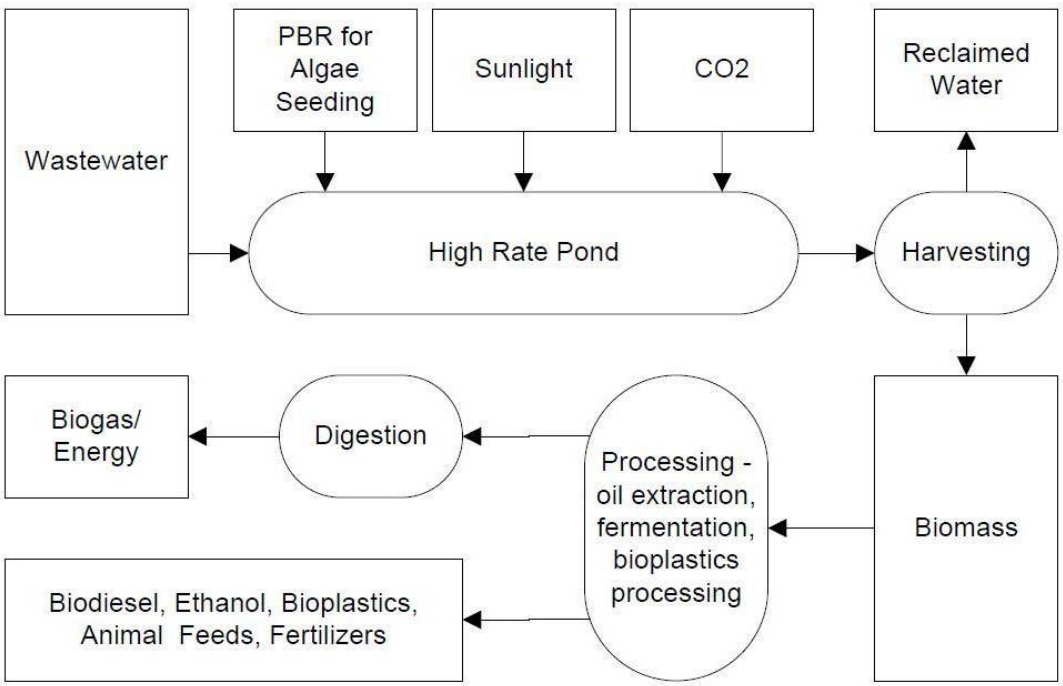

Figure 4 – Potential for Co-Products and Co-Processes in Algae Cultivation

DEVELOPMENT OF A COMMUNITY WATER SECURITY FILTRATION SYSTEM USING COMPOSITE CARTRIDGES

Nur Muhammad, Ph.D., P.E., Rajib Sinha, P.E., E. Radha Krishnan, P.E.[1]
Craig L. Patterson, P.E., Roy C. Haught[2]
Harold H. Harms, Rick Seville[3]

[1]Shaw Environmental and Infrastructure, Inc., 5050 Section Avenue, Cincinnati, OH 45212; Nur.Muhammad@shawgrp.com, Rajib.Sinha@shawgrp.com, Radha.Krishnan@shawgrp.com
[2]U.S. Environmental Protection Agency, 26 W. Martin Luther King Blvd, Cincinnati, OH 45268, Patterson.Craig@epa.gov, Haught.Roy@epa.gov
[3]Harmsco Filtration Products, 7169 N. 49th Terrace, West Palm Beach, FL 33407, rseville@harmsco.com, hharms@harmsco.com

ABSTRACT

Under a Cooperative Research and Development Agreement (CRADA) established between the U.S. Environmental Protection Agency (EPA) and Harmsco, Inc., a prototype Community Water Security Filtration System for drinking water treatment using composite cartridges is being developed and tested at the EPA's Test & Evaluation (T&E) Facility in Cincinnati, Ohio. The filtration system incorporates a composite cartridge that combines physical pre-filtration with carbon adsorption and a cyst-rated final filter for removal of turbidity, specific chemical compounds, and some biological oocysts. The composite cartridge is then followed by ultraviolet (UV) light to provide short wave UV disinfection. The housing is constructed with a tangential inlet that induces a centrifugal motion to the water which aids filtratiom. The research has focused on optimizing the filtration media and housing configuration by testing the system using various biological surrogates and chemical compounds as contaminants. The current system configuration consists of a housing with two chambers; the upper chamber contains 8 (eight) composite cartridges for filtration, while the lower chamber contains six UV lamps for disinfection. Electrodes have been installed between the internal cartridge basket and the housing wall to provide an experimental electroseparation process to enhance particulate and pathogen removal and to determine if there is any pathogen cell disruption. Results of developmental tests conducted on single cartridges to optimize the composite cartridge media configuration show complete removal of Polystyrene Latex (PSL) beads (used as a non-biological surrogate for *Cryptosporidium)* which satisfies the Long Term 2 Enhanced Surface Water Treatment Rule (LT2ESWTR) requirement of >3.0 log reduction of *Cryptosporidium*. Results of tests conducted on the 8-chamber full-scale unit show almost complete removal of MS2 bacteriophage as a surrogate for enteric virus satisfying the LT2ESWTR requirement of a 4-log reduction for viruses.

Notice: Any opinions expressed in this article are those of the author(s) and do not, necessarily, reflect the official positions and policies of the EPA. Any mention of

products or trade names does not constitute recommendation for use by EPA. This document has been reviewed in accordance with EPA's peer and administrative review policies and approved for publication.

INTRODUCTION

The Water Supply and Water Resources Division (WSWRD) of the U.S. Environmental Protection Agency's (EPA's) National Risk Management Research Laboratory (NRMRL) has been conducting research on small drinking water systems since 1997 in response to the 1996 reauthorization of the Safe Drinking Water Act (SDWA) that established standards for drinking water systems and required EPA to assess treatment technologies relevant to small systems serving fewer than 10,000 people. The events of September 11, 2001, have further emphasized the need to develop water security appliances to remove physical, biological and chemical contaminants, resulting from deliberate or accidental contamination of the drinking water supply. Harmsco Filtration Products (Harmsco), based in North Palm Beach, FL, has developed a system combining physical filtration, adsorption and UV disinfection. Under a Cooperative Research and Development Agreement (CRADA) established between EPA and Harmsco, EPA guided and evaluated a multi-layer prototype cartridge at 15 gpm for whole-house water treatment at the EPA Test & Evaluation (T&E) Facility in Cincinnati, Ohio. The evaluation was conducted by Shaw Environmental, Inc. under a contract with EPA-NRMRL. The system showed effective performance in removing turbidity, *Cryptosporidium* size particles (2 - 5 µm), *E.coli*, 3.0 µm PSL beads (a non-biological surrogate of *Cryptosporidium*). The system also exhibited adequate removal of *B. subtilis* spores, but did not perform adequately in removing male-specific 2 (MS2) bacteriophage (a surrogate for enteric virus) (Muhammad, *et al*., 2008). The system showed effective performance in removing chlorine, diazinon and trihalomethanes (THMs) and adequate performance in removing methyl-tert-butyl-ether (MTBE) and haloacetic acids (HAAs) (Muhammad, *et al*., 2008). Based on the performance of the whole-house water treatment system, a larger system with multiple cartridges has been developed to provide filtration at a rate of about 100 gpm, suitable to meet the needs of a small community. The cartridges being developed for the larger system incorporate a different media to provide enhanced filtration. The system also included a UV system with higher wattage and electrodes to experiment with an electroseparation stage to potentially improve the microbial removal capability of the system. The results of tests conducted to date on the community filtration unit are summarized in this article.

SYSTEM DESCRIPTION

Figure 1 shows a cutaway cross-sectional diagram of a whole-house multi-layer single cartridge and the direction of water flow in the cartridge. The composite cartridge filter media is constructed in three layers surrounding a hollow core. The outer filter media is an anti-microbial, pleated, pre-filter designed for the removal of particles and sediment. The second filter layer consists of an extruded activated carbon core to adsorb chemicals (including disinfection by-products) and to improve

taste. The final filtration stage is a submicron, pleated filter media which is also anti-microbial. Figure 2 shows the community system housing and setup at the T&E Facility. The filter system housing consists of an upper chamber that houses eight composite cartridges and a lower chamber that functions as a UV sterilization chamber. The hollow core in each composite filter fits over a downspout that connects the cartridge filter housing to the lower UV chamber. The cartridge filter uses two O-rings to establish a seal between each cartridge and the associated downspout to prevent bypassing of the cartridge. Electrodes have been installed between the internal cartridge basket and the housing wall to provide an experimental electroseparation stage to enhance particulate and pathogen removal.

Water enters the upper chamber tangentially and flows rotationally between the electrode and the outer filter housing, rising upward and then through the composite cartridge filters. The housing is constructed with a tangential inlet that induces a centrifugal motion which aids filtration. Once the influent water has passed through all the filtration stages of the composite cartridge filters, it enters the complex UV reactor through each downspout. After UV treatment, the finished water exits the system housing. Figure 3 shows a cut-away view of the configuration of cartridges in the community filter system, while Figure 4 shows the star-shaped arrangement of the UV lights in the disinfection chamber of the Small Community Unit.

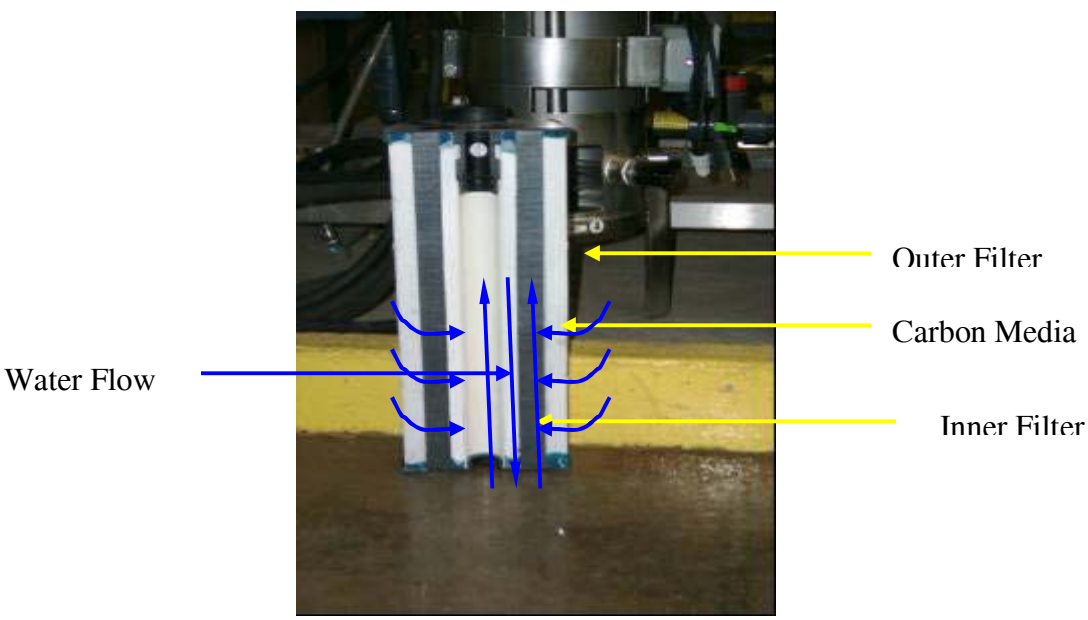

Figure 1: Multi-layer Cartridge and Direction of Flow

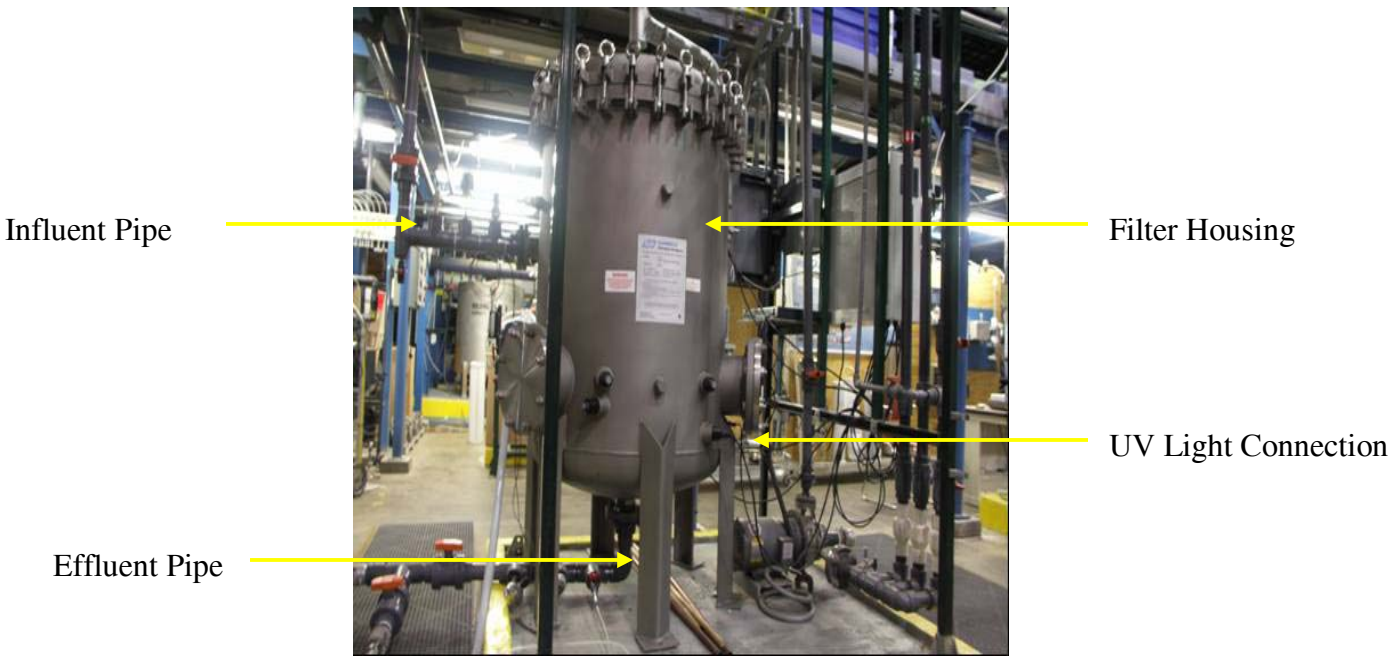

Figure 2. Small Community Filter Setup at T&E Facility

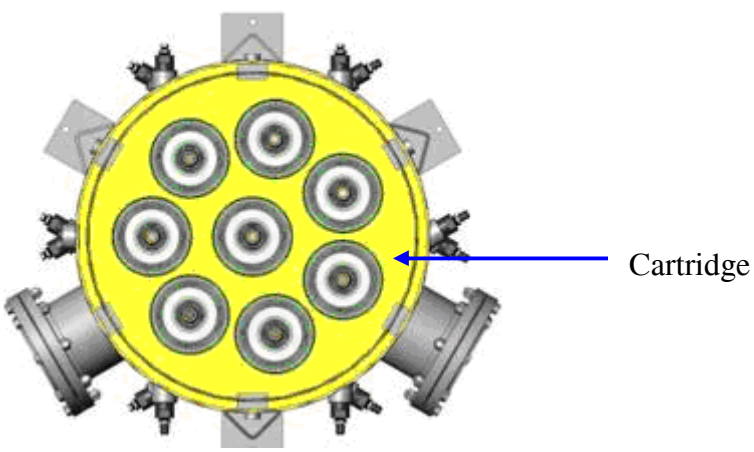

Figure 3. Cut-away View of Cartridges in the Small Community Filter

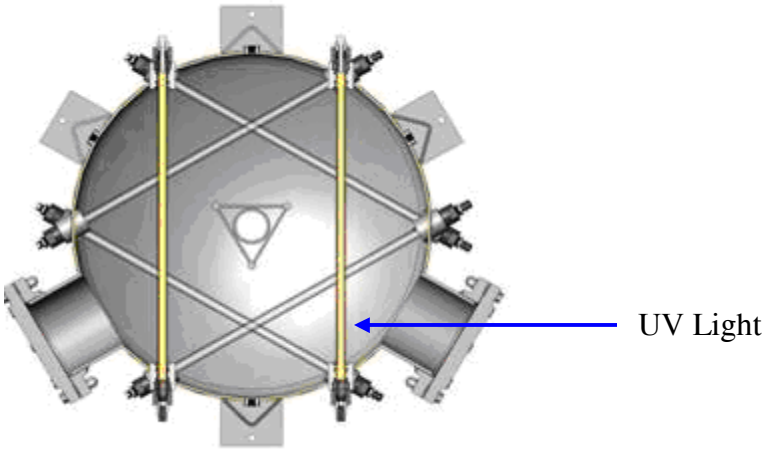

Figure 4. Cut-away View of Complex UV Chamber of the Small Community Filter

EXPERIMENTAL/ANALYTICAL METHODS AND MATERIALS

Evaluation and development of the small community filter system have to date included tests conducted to establish the construction configuration of the cartridges (i.e., the specific media type to be used in the various layers) and the efficacy of the complex UV disinfection using the unique, star-shaped configuration of the UV lamps in the lower disinfection chamber. A test stand was prepared and installed at the cartridge manufacturing location in West Palm Beach, FL to allow for rapid evaluation of various cartridge configurations in order to establish the media with the greatest likelihood of success when scaled up for use in the larger community filter. These experimental challenges were conducted using 3 µm PSL beads.

Concurrently, tests were conducted at the T&E Facility using MS2 bacteriophage to establish the degree of disinfection achieved by the UV lights in the system. The results of these tests could then be compared to collimated beam studies conducted on the same batch of MS2 bacteriophage to enable calculation of an effective UV dosage in the system.

Bench Scale PSL Bead Tests at Manufacturing Location

PSL beads in the size range of *Cryptosporidium* (3.0 µm) have been described by several researchers (Emelko & Huck, 2004; Li *et al*., 1997) as a suitable non-biological surrogate. To establish the cartridge construction configuration, seven small cartridges were manufactured using different proprietary media configurations and challenged with 3.0 µm PSL beads. Figures 5 and 6 shows the seven cartridges and the small cartridge housing used in these developmental tests. Each cartridge was tested individually, and, for each test, a stock solution of PSL beads was prepared using 0.01% Tween-20 that was added to a 14-gallon supply water tank to achieve a

final concentration of ≈ 10^5 PSL beads/100 mL. The water from the supply tank containing the beads was pumped through the cartridges at 6 gallons per minute (gpm) and influent and effluent samples (250 mL) were collected 2 minutes after the start of the test. At the conclusion of each test, the cartridge being tested was removed and the test stand was flushed for several minutes with another cartridge in place to remove any residual PSL beads from the system. A new test cartridge was then placed in the system and the system was operated for approximately 15 minutes prior to placing the PSL beads stock solution in the 14-gallon supply tank to initiate the test on that cartridge.

The PSL beads samples shipped to the T&E Facility and were analyzed following U.S. EPA Method 1622 (U.S. EPA 2001a). Log removal values were calculated comparing the influent and effluent bead concentrations.



Figure 5. Cartridges Used for Establishing Media Configuration



Figure 6. Small Housing Used for Establishing Media Configuration

MS2 Bacteriophage Challenges

MS2 bacteriophage, described as a surrogate for pathogenic enteric viruses (Harrington *et al*., 2003), was used in this study to challenge the system to evaluate the performance of the system in removing viruses. The challenge tests were conducted on the community filter at two flow rates – 50 gpm and 100 gpm – using dechlorinated potable water. MS2 bacteriophage stock with cell concentration of ≈ 10^9 /mL was procured from BioVir Laboratory (Benecia, CA). The MS2 bacteriophage stock was mixed with 500 mL of 0.01% Tween-20 in a glass beaker to provide a stock solution which, when injected into the feed water stream to the community water filter system, would yield a target influent cell concentration of ≈ 10^5 /100 mL. The 500-mL MS2 suspension was injected into the influent stream of the filtration unit using a peristaltic pump. At the completion of injection, an additional 500 mL of 0.01% Tween-20 was injected into the feed stream to rinse out any residual MS2 in the beaker and feed tubing. The total injection time for the suspension and the rinseate was approximately 60 minutes. Grab samples (100 mL) from the influent and effluent stream were collected at 0 (T0), 5 (T5), 10 (T10), 20 (T20), 30 (T30) and 60 (T60) minutes after the start of the injection. The MS2 bacteriophage samples were analyzed using U.S. EPA Method 1602 (U.S. EPA, 2001b). Log removal values were calculated comparing the influent and effluent MS2 bacteriophage concentrations.

RESULTS AND DISCUSSIONS

Bench Scale PSL Bead Tests Results

Table 1 shows the results of the PSL bead tests conducted with the test stand at the Harmsco manufacturing location to establish the media configuration. The results show complete removal of PSL beads by all seven cartridges, and, the calculated log removal value (based on the influent concentration) ranged from 4.0 and 4.9. This removal performance satisfies the LT2ESWTR requirement of >3.0 log reduction for *Cryptosporidium* (U.S. EPA, 2006). Since all seven cartridges demonstrated complete removal of PSL beads in these preliminary tests, focus on the construction of the cartridges can be placed on the cost and ease of manufacturing.

Table 1. Results of PSL Bead Tests Conducted on the Test Stand for Establishing Media Configuration

Test ID	PSL bead Conc/250 mL		Log Removal	Avg. Log Removal
	Influent	Effluent		
Cartridge 1				
1	3.34×10^4	0	4.52	4.00
2	2.50×10^3	0	3.46	
Cartridge 2				
3	1.33×10^4	0	4.12	4.32
4	3.34×10^4	0	4.52	
Cartridge 3				
5	5.00×10^4	0	4.70	4.64
6	3.75×10^4	0	4.57	
Cartridge 4				
7	5.00×10^4	0	4.70	4.90
8	1.22×10^5	0	5.10	
Cartridge 5				
9	8.50×10^4	0	4.93	4.84
10	5.58×10^4	0	4.78	
Cartridge 6				
11	4.50×10^4	0	4.65	4.81
12	9.41×10^4	0	4.97	
Cartridge 7				
13	5.16×10^4	0	4.71	4.68
14	4.34×10^4	0	4.64	

Tables 2 shows the results of MS2 bacteriophage challenges conducted on the community filter at 50 gpm and 100 gpm. The community filter achieved almost complete removal of MS2 bacteriophage at both flow rates, with an average log removal of 4.15. The performance of the community filter satisfied the LT2ESWTR requirement of 4.0 log removal of virus (U.S. EPA, 2006).

Table 2. Results of MS2 Bacteriophage Challenges Conducted on the Community Filter System

Sample ID	No. Cells/100 mL		Log Removal	Average Log Removal
	IN	OUT		
Challenge 1 – 50 gpm				
T0	N/A[a]	N/A[a]	N/A[a]	4.11
T5	1.5×10^4	2	3.88	
T10	3.4×10^4	2	4.23	
T20	1.7×10^4	1	4.23	
T30	1.2×10^4	1	4.10	
T60	2.0×10^3	0	3.30[b]	
Challenge 2 – 50 gpm				
T0	0	0	N/A[a]	4.38
T5	2.8×10^4	2	4.14	
T10	4.7×10^5	7	4.82	
T20	5.2×10^4	2	4.41	
T30	5.7×10^4	2	4.45	
T60	3.6×10^4	3	4.10	
Challenge 5 – 50 gpm				
T0	0	0	N/A	3.88
T5	6.0×10^3	0	3.78	
T10	8.0×10^3	0	3.90	
T20	7.0×10^3	0	3.85	
T30	9.0×10^3	0	3.95	
T60	8.0×10^2	0	2.90[b]	
Challenge 3 – 100 gpm				
T0	0	0	N/A[a]	4.34
T5	1.3×10^4	2	3.81	
T10	4.5×10^4	1	4.65	
T20	5.1×10^4	2	4.40	
T30	3.2×10^4	1	4.51	
T60	2.0×10^3	1	3.30[b]	
Challenge 4 – 100 gpm				
T0	0	0	N/A[a]	4.00
T5	1.7×10^4	3	3.75	
T10	3.7×10^4	4	4.00	
T20	3.2×10^4	2	4.20	
T30	3.2×10^4	4	3.90	
T60	2.0×10^3	1	3.30[b]	

a – Not Available
b - Not considered for average performance evaluation due to low influent concentration

Figure 7 shows the UV dose response graph of the MS2 bacteriophage stock obtained from the results of collimated beam test conducted by BioVir Laboratory. The UV intensity, corresponding to 4.14 log reduction by the community filter, is 90 mJ/cm^2. The UV dosage is independent of flow rate and, therefore, independent of residence time in the system.

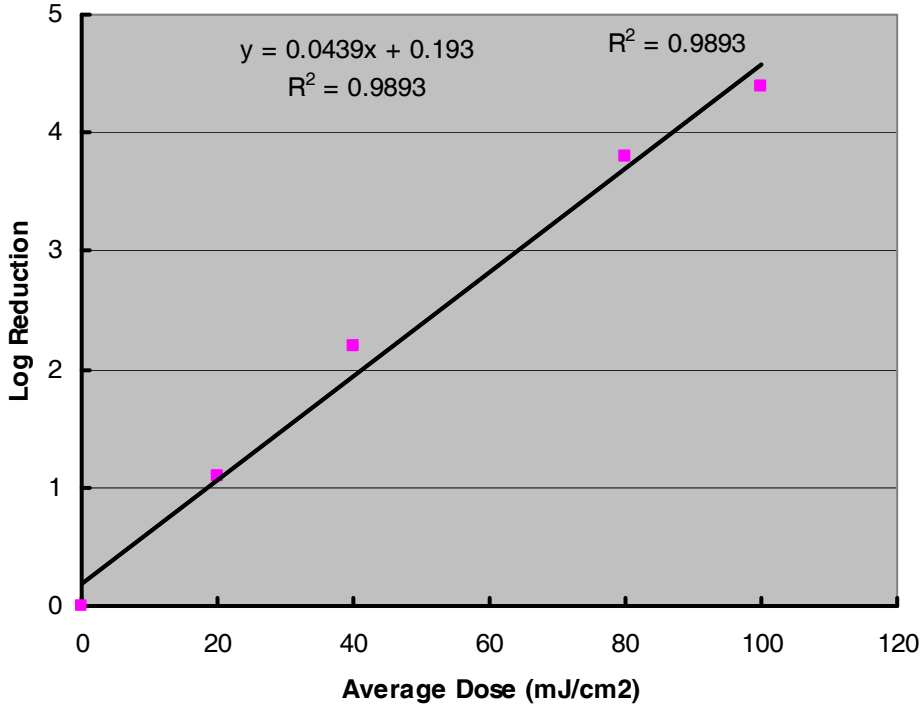

Figure 7. UV Dose Response Graph for MS2 Bacteriophage Stock

CONCLUSIONS

The test stand established at the manufacturer's location to perform preliminary tests provides a rapid and cost-effective methodology to establish cartridge configurations that can be selected for scale-up to the larger community filter system. On the basis of these tests, all the cartridges have shown equal removal performance for PSL beads indicating that other factors, such as ease of manufacturing, cost of materials, and pressure-drop development tests, should be used as the criteria for final cartridge selection. These efforts are currently ongoing and the final cartridge configuration will be tested in the near future on the community filter system to evaluate the removal of chemicals, such as mercury, tetracycline, triclosan and estradiol in addition to turbidity and cysts removal.

The UV intensity of the unit, based on the inactivation of MS2 bacteriophage, is 90 mJ/cm^2 which has been shown to be independent of residence time in this system. Additional MS2 tests are planned to evaluate whether the experimental

electroseparation provisions in the unit would enhance the system performance for removal of turbidity and MS bacteriophage.

REFERENCES

Emelko, M.B. and Huck, P.M. (2004). Microspheres as Surrogates for *Cryptosporidium* Filtration. *Jour. AWWA*, **96**(3), 94 -105.

Harrington, W.G., Xagoraraki, I., Assavasilavasukul, P. and Standridge, J.H. (2003). Effect of Filtration Conditions on Removal of waterborne Pathogens. *Jour. AWWA*, **95**(12), 95 - 104.

Li, S.Y., Goodrich, J.A., Owens, J.H., Willeke, G.E., Schaefer III, F.W. and Clark, R.M. (1997). Reliability of Surrogates for Determining *Cryptosporidium* Removal. *Jour. AWWA*, **89**(5), 90 - 99.

Muhammad, N., Sinha, R., Krishnan, R., Patterson, C. L., Haught, R. C, Harms, H. and Seville, R. (2008). Development of a water security filtration system for whole-house water supply. In *Proceedings of 2008 Environmental and Water Resources Institute (EWRI) Congress*, Honolulu, Hawaii.

U.S. EPA (2006). The Long-Term 2 Enhanced Surface Water Treatment Rule (LT2ESWTR) Implementation Guidance, EPA 816-F-06-005, Washington D.C., USA.

U.S. EPA (2001a). Method 1622: *Cryptosporidium* in Water by Filtration/IMS/FA, Washington D.C., U.S.A.

U.S. EPA (2001b). Method 1602 for Detection and Enumeration of *MS2 Bacteriophage* in Drinking Water, Washington D.C., U.S.A.

Evaluation of a UV/Ozone Treatment Process for Removal of MTBE in Groundwater Supplies in New Mexico

Craig Patterson[1], Fernando Cadena[2], Rajib Sinha[3], Dzung Kim Ngo-Kidd[4], Abbas Ghassemi[2], and E. Radha Krishnan[3]

1. Craig Patterson, P.E., U.S. EPA (M.S. T&E), 26 W. Martin Luther King Drive, Cincinnati, Ohio 45268, patterson.craig@epg.gov.

2. Fernando Cadena, Ph.D., P.E., Visiting Faculty Researcher, P.O. Box 30001, MSC WERC, New Mexico State University, Las Cruces, NM 88003-8001, fcadena@nmsu.edu.

2. Abbas Ghassemi, Ph.D., P.O. Box 30001, MSC WERC, New Mexico State University, Las Cruces, NM 88003-8001, aghassem@nmsu.edu.

3. Rajib Sinha, P.E., Shaw Environmental, Inc., 5050 Section Avenue, Cincinnati, OH 45212, rajib.sinha@shawgrp.com.

3. Radha Krishnan, P.E., Shaw Environmental, Inc., 5050 Section Avenue, Cincinnati, OH 45212, rajib.sinha@shawgrp.com.

4. Kim Ngo Kidd, USEPA REGION VI (6WQ-SD), 1445 Ross Avenue, Suite 1200, Dallas, TX 75202-2733, ngo.kim@epa.gov.

ABSTRACT

EPA's Office of Research and Development is funding pilot-scale studies on MTBE contaminated groundwater using UV/ozone treatment technology (254 nm UV, 5.8 mg/L ozone). The pilot-scale treatment system consists of a GW well pump, a feed tank, a pretreatment system (water softener with iron reduction), a low-pressure UV/ozone treatment system, and GAC post treatment. Treatability studies have been conducted by graduate students at New Mexico State University to determine the effectiveness of UV/ozone treatment on well water contaminated by underground plumes of MTBE and other volatile organic compounds.

NMSU found UV/ozone treatment to be highly effective for removing MTBE and MTBE byproducts in groundwater. The MTBE concentrations after treatment were significantly lower (0.4-7.7 µg/L) as compared to the initial influent concentrations (127-251 µg/L). However, acetone was formed during oxidation of MTBE. Future field studies are planned to investigate the impact of enhanced ozone/medium-pressure UV on MTBE and MTBE byproduct removal and alternative technologies for acetone removal.

KEYWORDS: Ozone, UV, Treatment, MTBE, Groundwater

DISCLAIMER

The U.S. Environmental Protection Agency, through its Office of Research and Development, funded and managed, or partially funded and collaborated in, the research described herein. It has been subjected to the Agency's peer and administrative review and has been approved for external publication. Any opinions expressed in this paper are those of the author (s) and do not necessarily reflect the views of the Agency, therefore, no official endorsement should be inferred. Any mention of trade names or commercial products does not constitute endorsement or recommendation for use.

BACKGROUND

MTBE was first used in the United States in the late 1970s to enhance octane levels when the use of lead in gasoline was discontinued. MTBE helps gasoline burn more cleanly and reduces emissions of carbon monoxide and organic compounds into the air. Because it mixes readily with gasoline, has low production costs, and a high octane rating, MTBE became the oxygenate of choice for most gasoline producers facing State and Federal mandates (Clean Air Act 1990) to produce less-polluting gasoline (1).

The widespread use of MTBE in gasoline led to the contamination of both surface and ground waters in the U.S.. MTBE contamination is found in soils and groundwater wells near leaking underground storage tanks (UST), and in reservoirs used for public water supplies. MTBE is soluble in water and makes its way into drinking water wells more quickly than other chemicals in gasoline like Benzene, Toluene, Ethylbenzene, and Xylene (BTEX). MTBE is 30 times more soluble than benzene in water (2).

MTBE is classified as a possible human carcinogen and has a pungent taste and smell. MTBE is on the U.S. EPA's Contaminant Candidate List (CCL) of contaminants to be regulated (3). The EPA has issued a drinking water advisory of 20 to 40 µg/L (4), however, some States have established State levels that are lower. For instance, Texas established 15 µg/L MTBE as a target level used for cleanup after a fuel spill occurred in Lake Tawakoni (March 2000), a drinking water supply for North Texas (5). MTBE is currently listed on the CCL as a contaminant in need of both occurrence and research priorities (including health research, treatment research, and analytical methods research).

Occurrence of MTBE in Drinking Water Supplies

According to a 2001 United States Geological Survey (USGS) study (6), of 954 community water systems (CWS) sampled in the U.S., 0.5% of the systems contained MTBE levels at $\geq$5 µg/L. If we extrapolate this percentage to the 160,000 public water systems (PWS) in the United States, then roughly 800 PWS are likely to have MTBE contamination at levels $\geq$5 µg/L. The number of affected water systems may increase with time, as plumes from leaking gasoline-underground storage tanks begin to reach more groundwater systems (7). Private wells are also affected, although they are not currently regulated under the Safe Drinking Water Act.

Another nationwide USGS study (8) conducted in 1995 found concentrations of MTBE in urban and agricultural wells to be in the range of 0.2 to 23,000 µg/L. In Dallas/Fort Worth, Texas, 5 of 17 wells tested positive for MTBE and in Albuquerque, New Mexico 1 of 24 wells tested positive. The USGS study also looked at the frequency of

occurrence of MTBE in groundwater wells and found that MTBE was the second most commonly detected volatile organic compound (VOC) after chloroform. Of the wells tested, 28% had chloroform contamination followed by 27% with MTBE contamination. Additional VOCs found were tetrachloroethene 18%; trichloroethene 10%; cis-1,2 dichloroethene 7%; 1,1-dichloroethane 5%; and benzene 5%. These harmful VOCs can also be removed by advanced oxidation process (AOP) technologies.

Treatment Technologies and Cost

According to two new studies by the American Water Works Association and the Association of Metropolitan Water Agencies (9), the estimated cost to remove MTBE from public drinking water systems is in the range of $25-$85 billion. The California MTBE Partnership of 2000 determined that it would cost between $1 to $11 million dollars per well. These clean-up costs (capital and operation and maintenance costs), were determined using GAC adsorption over 30 years with influent MTBE levels of 200 µg/L and non-detect effluent levels.

Small water systems typically choose granular activated carbon (GAC) because it is the more affordable treatment technology. It makes sense for a small water system to purchase a small drum of GAC and pay for replenishing and processing of the carbon. For large groundwater systems, air stripping, granular activated carbon (GAC), and resin adsorbents are all capable of removing MTBE from the water supply (10).

It would not be cost effective for a small system producing only 10,000 gallons of water per day to purchase an air stripper intended to produce a million gallons of water per day. At MTBE concentrations of greater than 300 µg/L, air stripping becomes more economically feasible than alternative treatment technologies. However, much more air is required to oxidize MTBE at low concentrations in water and off-gas treatment adds significantly to the cost (2).

A low cost alternative for MTBE treatment in small systems utilizes an AOP technology that combines ultraviolet radiation (UV) with ozonation for oxidation of MTBE and MTBE byproducts from water as listed in Table 1.

MTBE Byproducts	Abbreviation	Formula
Methyl-tert butyl ether	MTBE	$CH_3OC(CH_3)_3$
t-butyl formate	TBF	$C_5H_{10}O_2$
t-butyl alcohol	TBA	$(CH_3)_3COH$
Isopropyl alcohol	IPA	$(CH_3)_2CHOH$
Acetone	Ac	$(CH_3)_2CO$
Methyl acetate	Mac	CH_3COOCH_3
Carbon Dioxide	CO_2	CO_2

Table 1. MTBE and MTBE byproducts

Benefits of UV/ozone treatment include low operating cost and destruction of MTBE and MTBE byproducts reducing residual handling costs. Both the UV light and ozone generation require minimal use of electricity for small drinking water systems.

INTRODUCTION

The EPA Water Quality Management Branch in Cincinnati, Ohio began evaluating pilot-scale studies by testing and evaluating MTBE and MTBE byproduct destruction using three oxidant combinations: hydrogen peroxide/ozone, ultraviolet irradiation (UV)/ozone, and UV/ozone/hydrogen peroxide. Pilot-scale studies conducted on dechlorinated Cincinnati tap water spiked with 300 µg/L MTBE showed that UV/ozone treatment removed 98% of the MTBE from tap water (at 254 nm UV, 5.8 mg/L dissolved ozone). The studies were setup to simulate real-world conditions at small groundwater systems (3 gallons/minute flow at 20 degrees C).

FIELD STUDIES

EPA, Shaw E&I, Inc., New Mexico State University (NMSU) and Souder and Miller Associates conducted MTBE treatability studies on contaminated groundwater combining low-pressure UV and ozonation technologies. A research trailer was customized with a well pump, a 110-gallon feed tank, a pretreatment system (water softener with iron reduction), and a UV/ozone treatment system as shown in Figure 1.



Figure 1. EPA research trailer with UV/ozone pilot unit and water softener

NMSU and Souder and Miller Associates approached the local community and owners of wells in Roswell, NM to request groundwater for these research studies. NMSU received approval to remove MTBE contaminated groundwater from the owners of Brewer Station 1 in Roswell as shown in Figure 2. After filling fourteen 5-gallon water containers, the groundwater was transported to NMSU in Las Cruces, NM to conduct the research studies. The groundwater containers had high levels of MTBE (ranging from 15 to 40 mg/L) that were diluted to less than 300 µg/L MTBE with uncontaminated groundwater for the treatability studies.



Figure 2. Removing groundwater for MTBE treatability studies

The UV/ozone pilot unit shown in Figure 3 was operated continuously to process ten 110-gallon batches of MTBE-contaminated groundwater. Flow rates of 1, 2, and 3 gallons per minute with corresponding contact times of 3, 1.5, and 1 minute were tested at recycle ratios of between 2.9 and 8.5 in the UV/ozone pilot unit. Samples were taken at time 0, 30, 60, 90 and 120 minutes. Daily operation and maintenance requirements were recorded and influent/effluent samples were analyzed as defined in the Quality Assurance Project Plan. The UV/ozone system cost, reliability, and ease of operation were documented during the treatability study (11). Treatability study average removal efficiency results are summarized in Table 2.



Figure 3. UV/ozone pilot-unit and GAC Drum

	MTBE	TBA	TBF	Ac	IPA	MAc
Influent	182	129	ND	3	7	ND
Effluent	2.3	25.4	0.2	85.9	1.7	0.9
% Efficiency	99	80	-	-	76	-

Table 2. Average removal efficiency of MTBE and MTBE byproducts

CONCLUSIONS

From the research conducted on low pressure UV light in combination with ozone, EPA and NMSU found that optimum treatment efficiencies were about 99% for MTBE and 80% for TBA with contact times between 1 and 3 minutes. The main organic oxidation byproduct was acetone increasing from 3 to 86 µg/L.

Because UV/ozone treatment destroys MTBE through oxidation, it does not require hazardous transport for processing. There is no need for chemical additives and processing of adsorbed contaminants when compared to GAC. Another consideration when selecting a drinking water treatment technology for MTBE is the disinfection capability of UV/ozone treatment to destroy organics and microbial pathogens simultaneously. Proper engineering controls for ozone emissions and UV radiation are necessary during operation of UV/ozone treatment systems to ensure worker health and safety.

PROJECT IMPACTS

VOC contamination of ground and surface waters is an on-going concern for environmental regulators. The project demonstrated the effectiveness of UV/ozone treatment for small groundwater systems. The project verified that AOP technologies, such as UV/ozone, are simple, affordable, readily available treatment alternatives for small groundwater systems affected by MTBE contamination.

Effective treatment technologies for VOCs in groundwater benefit the State primacy agencies and the Public. For instance, New Mexico drinking water supply is comprised of 95% groundwater systems that serve 85% of the population (1.8 million people). Texas drinking water supply is comprised of 80% groundwater systems that serve 6.4 million people daily (11). In both States, a majority of the groundwater wells are small drinking water systems that need affordable treatment technologies. Alternative treatment processes are vital for arid States such as New Mexico, which have on-going drought issues and desperately need clean water sources.

EPA, Shaw E&I, Inc, and NMSU plan to conduct additional studies to improve MTBE and MTBE byproduct oxidation with enhanced ozone/medium pressure UV lamps. Future studies will also address the formation and removal of acetone in water.

ACKNOWLEDGEMENTS

Field sample collection was carried out by Mr. David Ennis with Souder Miller, Inc under supervision of Mr. Craig Shapard with the New Mexico Environment Department. Experimental design, implementation and field analyses were coordinated by Ms. Maritza Macias-Corral, a graduate student in the Civil Engineering Department at NMSU. Dr. Bill Boyle with the Soil, Water and Air Testing Laboratory at NMSU performed the analytical work (11).

REFERENCES

1. United States Environmental Protection Agency (US EPA) Office of Water. *MTBE Fact Sheet 1 Overview,* EPA 510-F-97-014, January 1998.

2. United States Environmental Protection Agency (US EPA) Office of Solid Waste and Emergency Response, " MTBE Fact Sheet #2 –Remediation of MTBE Contaminated Soil and Groundwater", EPA 510-F-97-015, January 1998.

3. United States Environmental Protection Agency (US EPA) Office of Water. *The Drinking Water Contaminant Candidate List – The Source of Priority Contaminants for the Drinking Water Program,* EPA 815-F-05-001, February 2005.

4. United States Environmental Protection Agency (US EPA) Office of Water. *Drinking Water Advisory - Health Effects Analysis on Methyl tertiary-Butyl Ether*, EPA 822-F-97-008, December 1997.

5. Freese and Nichols, Inc. for the Sabine River Authority (SRA) of Texas. *Summary Report of MTBE Contamination in Lake Tawakoni From Gasoline Pipeline Rupture,* SRA00230, December 4, 2000: 14-21.

6. Clawges, R., Rowe, B., and Zogorski, J. *National Survey of MTBE and Other VOCs in Community Drinking Water Sources,* United States Geological Survey (USGS) National Water Quality Assessment Program. FS-064-01, October 2001.

7. Thomson, J.A., and McKinley, J.W. "MTBE Occurrence in Surface and Groundwater", Contaminated Soil Sediment and Water, July-August 2002: 16-19.

8. United States Geological Survey (USGS) National Water Quality Assessment Program. *Occurrence of Gasoline Additive MTBE in Shallow Groundwater in Urban and Agricultural Areas,* FS-114-95, March 1995.

9. American Water Works Association (AWWA) Water Utility Council . *Two Updated MTBE Contamination Cost Analyses Pin MTBE Clean Up Costs,* June 21, 2005. Retrieved September 2, 2005, from http://www.awwa.org/Communications/news/index.cfm?ArticleID=459

10. United States Environmental Protection Agency (US EPA) Office of Water, *MTBE in Drinking Water,* Retrieved August 31, 2005, from http://www.epa.gov/safewater/mtbe.html.

11. Cadena, F., Sinha, R., and Patterson, C., "Evaluation of an Advanced Oxidation Process for the Removal of Gasoline Spills," 40th Summit on Industrial Ecology and Integral Sanitation of the Valencia Basin in Valencia, Venezuela, June 20-22, 2007.

Removal of Waterborne Particles by Electrofiltration

J. Murphy*, Y. Li, R. Ehrhard[1], K. Carns[2], C. Patterson[3], R. Krishnan and R. Sinha[4]

[1]Department of Energy, Environmental and Chemical Engineering, Washington University in St. Louis,1 Brookings Drive, St. Louis, MO 63130
[2]Global Energy Partners, LLC, P.O. Box 2080, Oakhurst, CA 93644
[3]U.S. Environmental Protection Agency,Office of Research and Development, National Risk Management Research Laboratory, 26 West Martin Luther King Drive, Cincinnati, OH 45268
[4]Shaw Environmental, Inc., 5050 Section Avenue, Cincinnati, OH 45212

* To whom correspondence should be addressed (jmurphy@wustl.edu)

ABSTRACT

A pilot-scale evaluation to assess the application of direct current to a rapid sand filter (termed "electrofiltration") verified the theoretical effectiveness of electrofiltration in enhancing the performance of conventional filtration within a water treatment facility. The efforts which are described in this paper were based on prior bench-scale assessments of the electrofiltration process. The analysis, combined with the theory used to describe the phenomenon, was used to design and construct the pilot filter using sand from existing filters in the filtration plant. The filter was tested using effluent from a presedimentation basin, at influent turbidities typically around 30 nephlometric turbidity units (NTU). Initial tests verify that electrofiltration can improve the performance of a filter in terms of both particle removal and turbidity reduction. Results from the preliminary analyses and future plans are presented.

Introduction

Effective removal of waterborne particles is an essential issue in the drinking water treatment process. The particle removal mechanisms can be classified as gravity separation (sedimentation or flotation) and filtration. In order to enhance the removal efficiency, chemical additives, such as iron or aluminum salts and polymers, are widely utilized to eliminate the negative charges carried by particles in nature. After charge neutralization, these particles are ready to attach to each other or to other surfaces to form larger settleable particles, called flocs, which are easier to settle or be removed in the following filtration process (AWWA, 1997).

Chemical additives are essential to enhancing particle removal efficiency, but they result in solids residuals which must be disposed. The expense associated with residuals transport and ultimate disposal can be significant. One of the potential alternative methods to achieve filtration without the addition of chemicals is electrofiltration, where an external electric field inside of the filtration layer is applied to enhance the particle removal. The application of electric field on particle removal is widely applied in air-particle systems, such as electrostatic precipitators. However, in the liquid-particle system, it has received much less attention.

The electrofiltration process is presented schematically in Figure 1. In the electrofiltration process, charge neutralization is not necessary to enhance the particle removal efficiency; thus, the dose of chemical additives can be minimized, resulting in less sludge generation.

Electrofiltration can potentially benefit drinking water treatment plants either through direct filtration, where the need for coagulants could be minimized, or in conventional treatment to reduce coagulation needs and residuals formation.

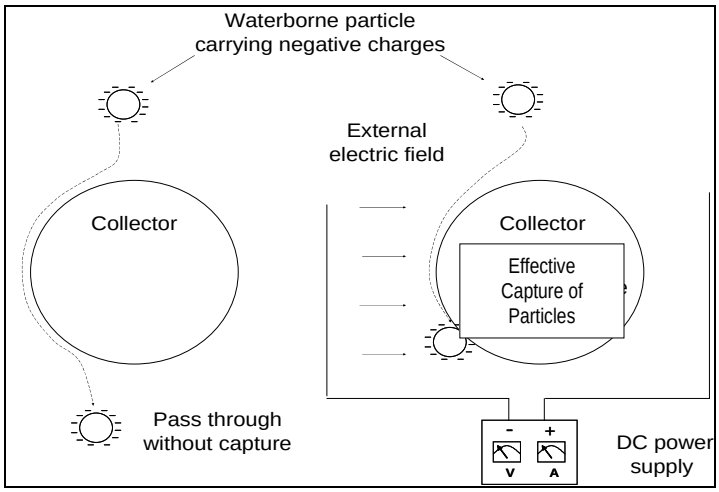

Figure 1. Schematic diagram of the particle motion with and without external electric field.

Electrofiltration has been utilized in the process of cake filtration, sludge dewatering and removal of particles in low ionic strength aqueous suspension (Lockhart, 1983, Ptasinski and Kerkhof, 1992, Zhang et al., 2000). Theoretical analysis regarding the beneficial effect of electrofiltration has been reported in the literature (Judd and Solt, 1989, Kulkarni et al., 2005). Bench-scale experiments conducted at Washington University (Kulkarni et al., 2005) using an external DC electric field applied on a cylindrical filter column resulted in significant improvement in the removal of test particles (kaoline and polystyrene latex beads) and the *Cryptosporidium* oocysts in three different types of media.

The results of the bench-scale analyses, while encouraging, were difficult to extrapolate to full-scale implementation. Thus, our team launched an effort to evaluate the efficacy of electrofiltration on a pilot-scale at a local water treatment plant. These experiments were conducted at the City of St. Louis Howard Bend Water Treatment Plant, in St. Louis, Missouri. The filtration media in the pilot filters was identical to that used by the full-scale facility. In addition, water applied to the filter was obtained from either the settled water basins, or the presedimentation basin, as described below.

Evolution of Experimental Setup

The initial efforts at scale-up followed the approach by Kulkarni et al. (2005). A cylindrical filter with a diameter of one foot was used in the tests. A single electrode was positioned in the center of the filter and the cathode was a solid sheet of stainless steel positioned around the inside wall of the filter. The distance between the anode and cathode was approximately six inches.

Initial pilot evaluations were conducted on-site using water from the full-scale plant's filter influent, (i.e. coagulated and settled but prior to filtration). Typically, this water had turbidity measurements less than 2 NTU. The pilot filter initial results showed that electrofiltration had little impact on the either the particle size removal or turbidity removal. In fact, initial results suggested that electrofiltration had a negative impact on filtered water quality, as shown on Table 1.

The research team assessed this performance and determined that two potential problems with the experimental setup contributed to the poor performance. First, it was determined that because the water applied to the electrofilter had already been coagulated using chemical additives, charged particles within the water had already been neutralized. Second, a mathematical analysis of the spacing between the anode and cathode revealed that the gap between the electrodes was too large to have much impact on particles passing through the filter, and the applied voltage was unnecessarily high.

Table 1. Results from initial electrofilter assessment

Test	Applied Voltage, V	Influent Turbidity, NTU	Filtered Water Turbidity, NTU	
			Control Filter	Electrofilter
1	0	4.80	0.50	0.94
2	20	5.94	0.27	1.23
3	40	5.69	0.29	0.76
4	60	6.31	0.30	0.77

Experimental Setup and Methods

The experimental design was revised to address those problems identified in the initial experimental setup. The schematic diagram of the reconfigured pilot-scale unit is shown in Figure 2. Twelve stainless steel mesh electrodes (12 in. × 24 in.) are embedded in the sand filter with 1 inch spacing. The electrodes are alternatively connected to the positive and negative output of a power supply. A water tank located on the top of the frame was utilized as a reservoir to maintain a constant hydraulic head, approximately 3 feet of water, to the sand filter.

Influent to the pilot unit is recieved from the water plant's pre-sedimentation basin, where settled water turbidity is typically 15 to 30 NTU. The filtered water (filter effluent) passes through a flow meter, which monitors both the flow rate and the total flow, and is then discharged to drain. During the interval of the runs reported in this study, the sand filter is backwashed by tap water to remove the captured particles.

The experimental plan on Table 2 presents the test conditions for the five tests. Only limited results are presented in this paper, as experiments with the test apparatus are continuing at this time. The first three tests (Tests 1 through 3) aimed to prove the effectiveness of the revised experimental set-up on filtration performance. For each of these first three tests, the influent flow rate was held constant while the power was turned on and off so that the enhancement due to the electric field can be determined. The filter

was backwashed in between each power on and off cycle. The fourth test sought to assess the impact of filter loading rate on electrofilter performance. The fifth test explored the effect of electrode voltage while maintaining a constant influent flow rate, in order to determine the applied voltage with the best efficacy. For all the tests, both influent and effluent samples were collected and analyzed in terms of turbidity, zeta potential, and particle counts.

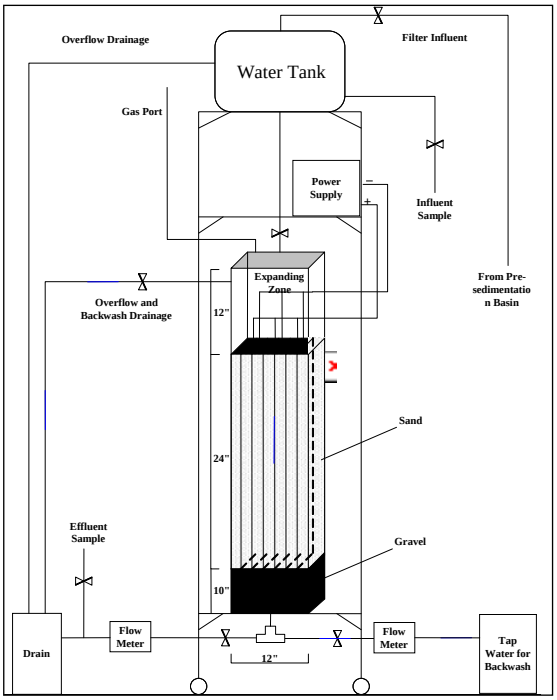

Figure 2. Schematic diagram of the pilot-scale electrofiltration setup

Table 2. Experimental plan

Test	Flow rate, Q (gal/min-ft^2)	Applied Voltage, U (V)	Description
1	0.6	$0 \leftrightarrow 8$	Power on and off alternatively
2	0.6	$0 \leftrightarrow 16$	Power on and off alternatively
3	1.2	$0 \leftrightarrow 24$	Power on and off alternatively
4	$0.6 \rightarrow 0.9 \rightarrow 1.2$	16	Consecutively increasing the flow rate
5	1.2	$0 \rightarrow 8 \rightarrow 12 \rightarrow 16$	Consecutively increasing the voltage

RESULTS AND DISCUSSION

Table 3 summarizes turbidity and zeta potential data for samples of river water and pre-sedimentation basin water. The turbidity of river water varied significantly from test to test, mainly due to weather changes. The treatment plant draws water from the Missouri River, which is notorious for rapid and large fluctuations in turbidity, along with other water quality parameters. Changes to the turbidity of the pre-sedimentation basin water,

and thus the water applied to the pilot filter, corresponds with fluctuations in river water quality; in general, the turbidity of the applied pilot filter water was about one order of magnitude lower than turbidity of the river water. On the other hand, the zeta potential did not vary much from test to test, and it only decreased slightly from the river water to the pre-sedimentation basin water. Since zeta potential is a critical parameter representing the surface change of waterborne particles, a higher value of zeta potential normally corresponds to a higher efficiency of electrofiltration.

Table 3. Summary of measured turbidity and zeta potential

Water Sample	Turbidity (NTU)				Zeta Potential (mV)		
	Test 1	Test 2	Test 3	Test 4	Test 1	Test 2	Test 4
River water	53	233	115	481	-16.5	-18.3	–
Pre-sedimentation basin water	12	32	12	37	-15.9	-17.1	-18.6

Proof-of-Concept Tests

The results of Tests 1 to 3 are shown in Table 4. The results clearly demonstrate that applying a voltage to the electrodes further reduced the turbidity and particle count of the effluent. The particle counts were reduced to approximately 59%, 62%, and 55% of the level without power, respectively. More importantly, most of the particle removal occurs with the smallest particles (2–4 μm). This is more clearly observed by comparing the particle size distributions of the effluent with or without power for a typical run, as shown in Figure 3. Thus, the results suggest that the electrofiltration process may be effective in targeting the removal of waterborne pathogens (e.g. *Cryptosporidium*) because most of pathogens are in the size range (2-4 μm) where electrofiltration works best.

Table 4. Electrofiltration results from proof-of-concept tests

Test	Water Sample	Turbidity (NTU)	Particle Count (#/ml)	2 - 4 μm (#/ml)	> 4 μm (#/ml)
Test 1	Influent	12.4	41638	34298	7340
	Effluent (0V)	0.66	2789	2385	404
	Effluent (8V)	0.47	1645	1348	297
Test 2	Influent	32.2	54968	37123	17845
	Effluent (0V)	8.25	2466	2002	464
	Effluent (16V)	5.05	1539	1253	286
Test 3	Influent	12	31787	22097	9690
	Effluent (0V)	0.97	2024	1438	586
	Effluent (24V)	0.95	1118	848	270

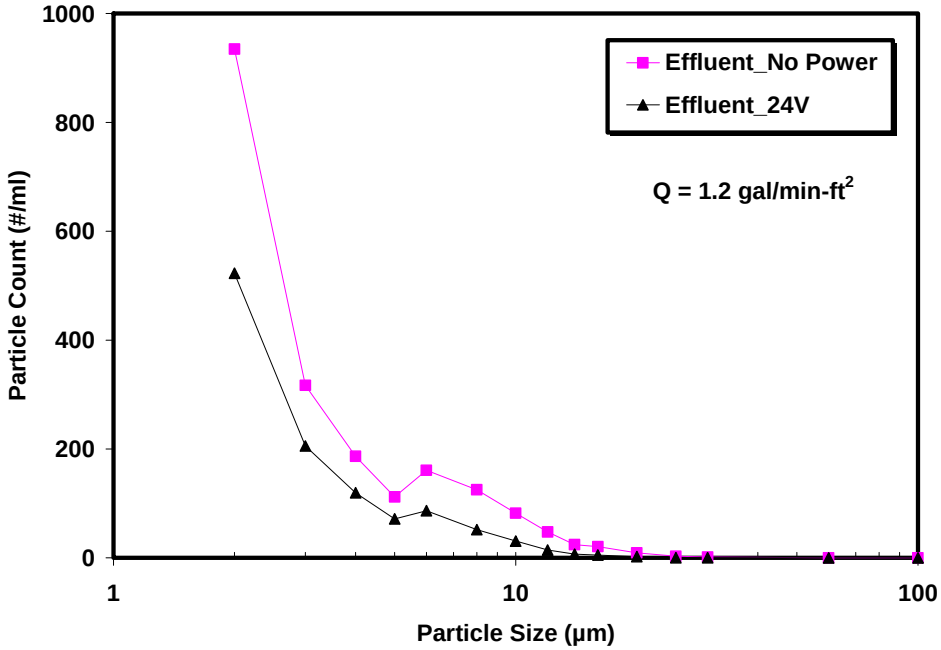

Figure 3. Comparison of particle size distributions of the effluent with or without an electric field for a typical run.

Effect of Filtration Flow Rate

One run was conducted to assess the impact of filter loading rate on electrofilter performance. During this run, no power was applied and the filter was operated at a steady-state filter loading rate of 1.2 gpm/ft^2. Filter power was set at 16 V until steady-state conditions were established, and then the filter loading rate was dropped from the initial rate to 0.9 gpm/ft^2, and finally to 0.6 gpm/ft^2. Further, the impact of applying power to the unit was demonstrated by turning off the power once steady-state is reached at the lowest applied power setting. The impact of flow rate on turbidity and particle removal is shown on Figure 4.

With data from only one run, a statistical comparison is not possible. Figure 4 shows that turbidity removal and particle removal improves as filter loading rate decreases during electrofiltraiton (applied voltage of 16 V). Further, both turbidity removal and particle removal decline once the power is turned off.

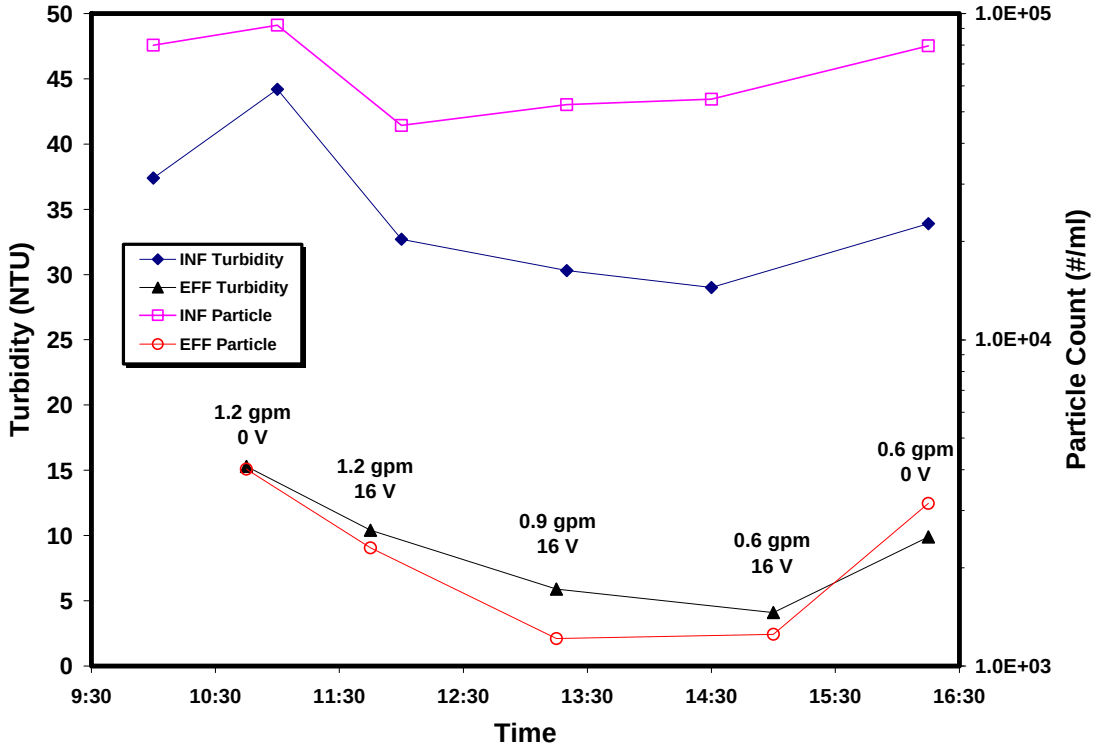

Figure 4. Effect of filter loading rate on electrofiltration

Effect of Electrode Voltage

Figure 5 shows the effect of electrode voltage on electrofiltration, while the filtration loading rate was maintained at 1.2 gpm/ ft^2. As shown in Figure 5, the power was off at the beginning and the end; during the test, the electrode voltage was increased from 8 V to 16 V in 4 V increments. Unfortunately, influent turbidity increased during the testing period; thus, it is not possible to make firm conclusions about filter performance. However, the effluent at 0 V at both the beginning and the end of the test had much higher values of turbidity and particle count than the corresponding values in the 8 to 16 V range. Thus, it is clear that the applied voltage enhanced the particle removal compared to the power off condition.

Estimate of Energy Consumption for Electrofiltration

The energy consumption of electrofiltration can be estimated from the voltage and amperage data recorded by the power supply. Table 5 lists the energy consumption at different applied voltages, based on a flow rate of 1.2 gal/min-ft^2. As the voltage increases, the energy consumption increases as a square function of voltage. The energy consumption at 16 V approaches the edge of economical consideration for practical applications. Based on the results on Figure 5, the particle removal efficiency at 16 V did

not improve significantly compared to 12 V. Hence, a range of 8 to 12 V may be the most cost-effective range for full-scale practice.

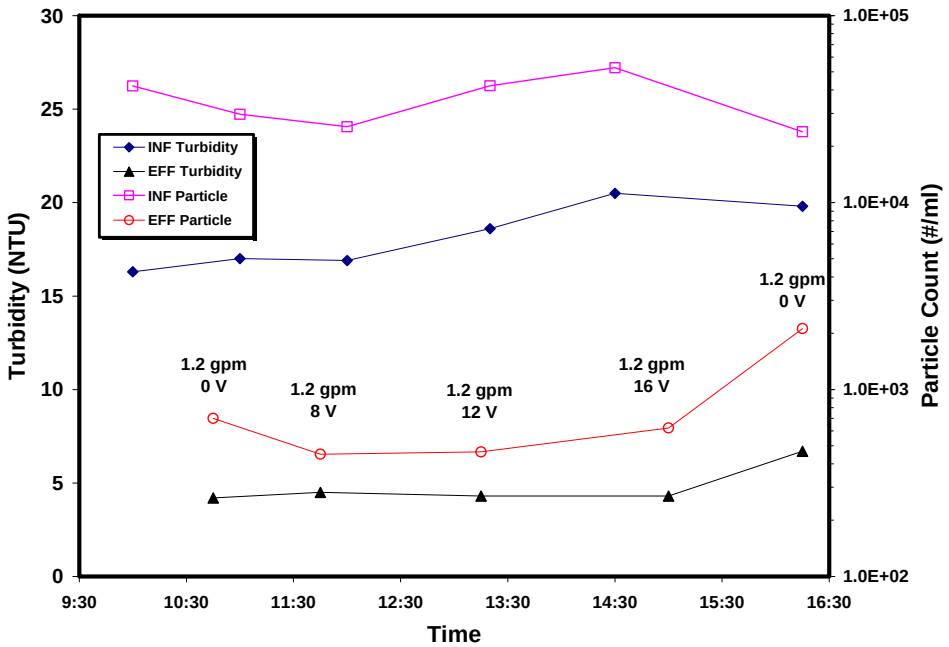

Figure 5. Effect of electrode voltage on electrofiltration.

Table 5. Estimated energy consumption for electrofiltration

Voltage (V)	Current (A)	Power (W)	Energy Consumption (kWh/Mgal)
8	3.4	27.2	378
12	6.2	74.4	1033
16	8.2	131.2	1822
24	14	336	4667

CONCLUSIONS AND FUTURE WORK

The current pilot-scale electrofiltration unit, equipped with vertical mesh electrodes embedded in a sand filter, has demonstrated its effectiveness in removal of waterborne particles. Both the turbidity and the particle count of the filter effluent were reduced when a voltage was applied across the electrodes, compared to the results with power off. When the electrofilter was operated at 8 V, the particle removal efficiency reached 97.2%, compared to 95.5% when the power was off. A separate theoretical analysis, along with prior work by others, has shown that conventional filtration processes often cannot reliably remove very small particles (< 4 μm). This study suggests that the electrofiltration technology can enhance the capture of such small particles. Future work

will focus on optimizing the applied voltage and filter loading rates. Based on the results described in this paper, an operating voltage range of approximately 8 V will be used in future work. Further, water from the presedimentation basin will be diluted in order to achieve an incoming water turbidity of approximately 5 NTU, while maintaining zeta potential at or below -10 mV.

Acknowledgments

This work was sponsored by the U.S. Environmental Protection Agency's (EPA) National Risk Management Research Laboratory (NRMRL) through a Work Assignment under Contract No. EP-C-04-034, with Shaw Environmental, Inc. The authors want to express their sincere gratitude for the capable assistance of staff at the City of St. Louis Howard Bend water treatment facility.

Disclaimer

Any opinion expressed in this report are those of the authors and do not necessarily reflect the official positions and policies of EPA. Any mention of products or trade names does not constitute recommendation for use by EPA.

References:

AWWA (1997) Water Treatment Plant Design, McGraw-Hill Professional.

Genc, A. and Tosun, I. (2002) Experimental studies on the effect of electrode configuration in electrofiltration. Separation Science and Technology 37(13), 3053-3064.

Judd, S.J. and Solt, G.S. (1989) Filtration of Aqueous Suspensions through Fibrous Media under the Influence of an Electric-Field. Colloids and Surfaces 39(1-3), 189-206.

Kulkarni, P., Dutari, G., Weingeist, D., Adin, A., Haught, R. and Biswas, P. (2005) Capture of water-borne colloids in granular beds using external electric fields: improving removal of Cryptosporidium parvum. Water Research 39(6), 1047-1060.

Lockhart, N.C. (1983) Electroosmotic dewatering of clays. III Influence of clay type, exchangable cations and electrode materials. Colloids and Surfaces 6, 253-269.

Ptasinski, K.J. and Kerkhof, P. (1992) Electric-Field Driven Separations - Phenomena and Applications. Separation Science and Technology 27(8-9), 995-1021.

Yao, K., Habibian, M. and O'melia, C. (1971) Water and waste-water filtration: concepts and applications. Environmental Science & Technology 5(11), 1105-1112.

Zhang, S., Tan, R.B.H., Neoh, K.G. and Tien, C. (2000) Electrofiltration of aqueous suspensions. Journal of Colloid and Interface Science 228(2), 393-404.

Water Distribution Optimization: Taking SCADA One Step Forward

Chuck Weber[1] and Simon Bunn[2]

[1]Superintendent of Operations, WaterOne, 7601 Holliday Drive, Kansas City, USA, 66106; PH (913) 895-5821; FAX (913) 895-1828; email: cweber@waterone.org
[2]Chief Technical Officer, Derceto Ltd, PO Box 6114 Wellesley Street, Auckland, New Zealand, 1141; PH +64.9.373.7100; FAX +64.9.373.7101; email: sbunn@derceto.com

ABSTRACT

Implementation of sophisticated SCADA systems in the water industry has given plant operators unprecedented capability to monitor and control all aspects of water production and distribution from a centralized control center. Sophisticated utilities recognize that SCADA need not be composed of one or more isolated "islands of automation" but can and should be a single system operating on a Wide Area Network, and integrated into their enterprise wide information technology system. The next logical step following implementation of a SCADA system is to leverage off this investment using state of the art software to allow predictive as opposed to reactive control of the water system. Resulting benefits can include improving water quality through reduced water age, minimizing energy costs and improved system operations without compromising operational reliability.

WaterOne, a quasi-municipal agency that provides water to more than 400,000 people, implemented an off-the-shelf software solution provided by Derceto Limited that achieved significant results in a very short amount of time. Using the software, WaterOne was able to save over $1 million in electrical costs in the first 18 months of operation, reduce greenhouse gas emissions by 4,800 tons/year, identify areas where further savings can be made, and streamline operation of its water treatment plant.

BACKGROUND

The control rooms of the 1950's through the 1970's were mainly filled with large panels full of gauges, chart recorders, alarm lights, and buttons driven directly from instruments and motor control centers. Commercial computers were large and expensive and even though some mini-computers such as PDP-11s were available their use was limited. Data from the gauges were recorder by chart recorders or sometimes by operators on paper. With the addition of Remote Terminal Units (RTUs) operating over radio links in the 1980's these systems enabled effective real time control of distributed systems from a single location. However, evaluating historical data was cumbersome and automating complex controls was difficult. Figure 1 shows a typical control room from this era.

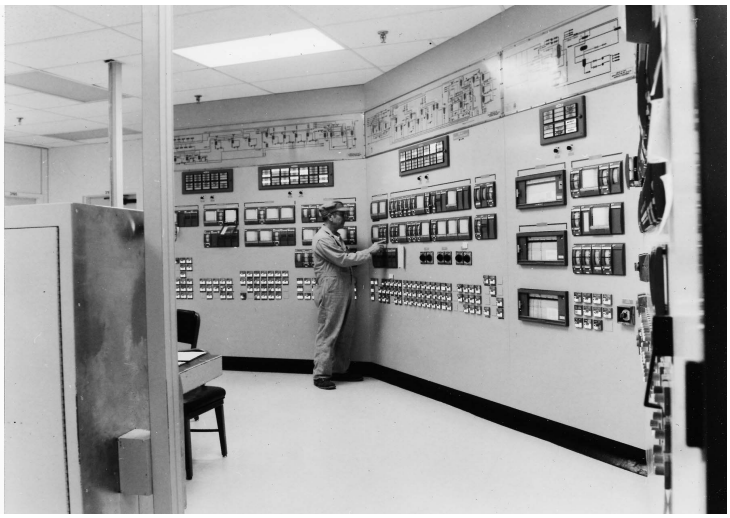

Figure 1. 1950's Control Room

With the introduction of Programmable Logic Controllers (PLCs) mixed automated and manual systems began to appear in the late 1970's. Efficiencies were gained in automation using computerized systems that piggy backed on the newly introduced Personal Computer (PC). The 1980's saw the advent of Supervisory Control and Data Acquisition (SCADA) systems. Automation of control and calculations as well as computerized storage of data brought efficiency to a much higher level. Large historical databases and smart instruments arrived in the 1990's, enabling integration with other business data to allow automated reporting of key performance and control indicators. This resulted in more timely and effective decision making and automation of complex control decisions. Figure 2 shows how large amounts of information flow from multiple plants to a common collection point where it is evaluated and boiled down by computer and delivered to decision makers in a timely and relevant manner.

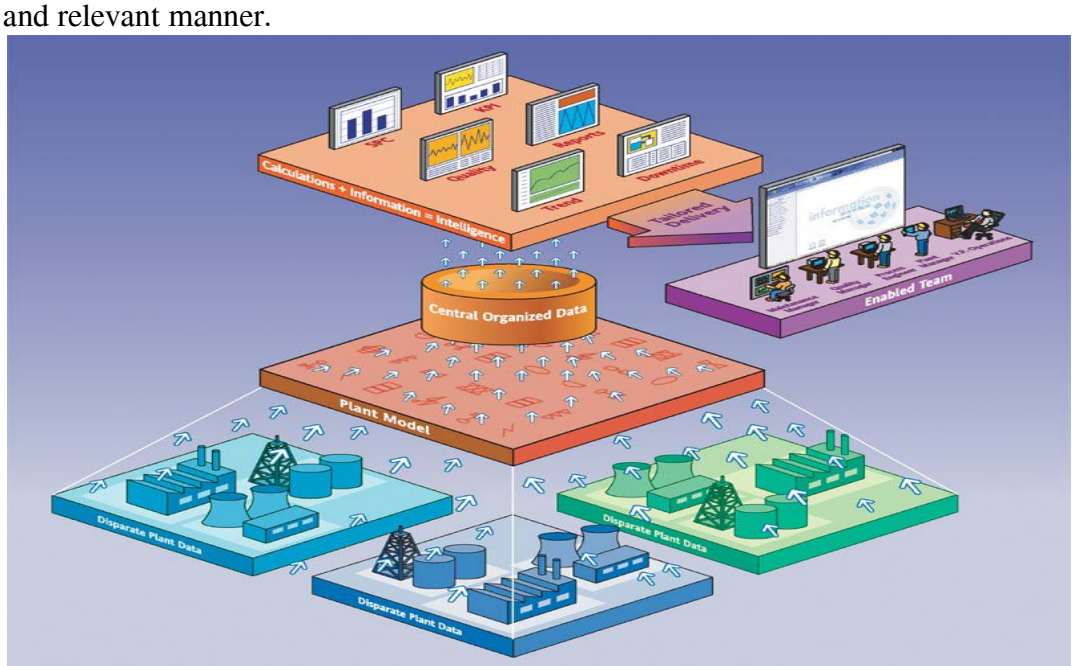

Figure 2. Information Flow

Figure 3 shows a typical modern control room. This control room is located at WaterOne. It was installed in 1991 and last upgraded in 2006. Derceto's Aquadapt software has takes the modern SCADA system one step farther by evaluating data gathered by the SCADA system, selecting the most cost efficient pumps to use in real time and then controlling pumps through the SCADA system. An understanding of WaterOne's system, energy use, and electricity supply tariffs is necessary to understand how Aquadapt software takes advantage of SCADA to achieve energy and cost savings.

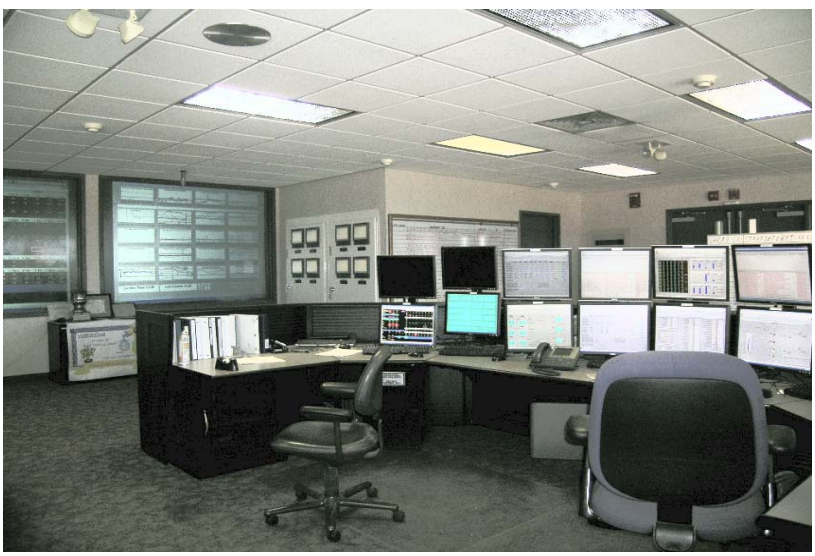

Figure 3. Modern Control Room

WaterOne is a quasi-municipal agency that provides water to more than 400,000 people. It serves residential and commercial accounts in 16 cities in the Johnson County area, has nearly 3,000 miles of transmission and distribution mains, covers a service area of more than 270 square miles, and a treatment capacity of 180 million gallons per day.

Over 84 pumps at 15 different pumping stations are used to deliver water from the rivers through the treatment process and distribution system to the service connections. There are two electric utilities with very different tariff structures serving these pump stations. With this many variables and constantly changing water system demand and other operational parameters, it's easy to see how difficult minimizing energy cost can be without using optimization software with SCADA.

Minimizing energy costs is a good strategic goal, as it is nationally one of the highest costs in producing the "next gallon of water." "The more than 60,000 water systems and 15,000 wastewater systems in the United States are among the country's largest energy consumers, using about 75 billion kWh/yr nationally – 3 percent of annual U.S. electricity consumption *(Palo Alto: 1999).*"

In 2005, WaterOne spent approximately 6.2 million dollars per year on electricity. Ninety-six percent of the electricity purchased is used to pump water. If even a modest 10% reduction was achieved, WaterOne could realize an annual savings $600,000 or more. This was the driver to investigate whether or not WaterOne's pump operations could be optimized with Aquadapt to achieve a reduction in energy costs. Current pump schedules, operational constraints, and electricity tariff structures were the key considerations in determining possible savings through optimization.

ENERGY TARIFFS

The tariffs have two main components, energy used in kilowatt-hours (kWh) and demand in kilowatt (kW). These are measured and priced separately. In the case of WaterOne the key controllable cost is the peak electricity demand occurring in any 30 minute period within a daily window of time set by the electricity supplier. Figure 4 illustrates a good car analogy for kWh and kW. The speed of the car is analogous to the instantaneous demand in kW and the odometer reading is analogous to accumulating use of electricity measured in kWh.

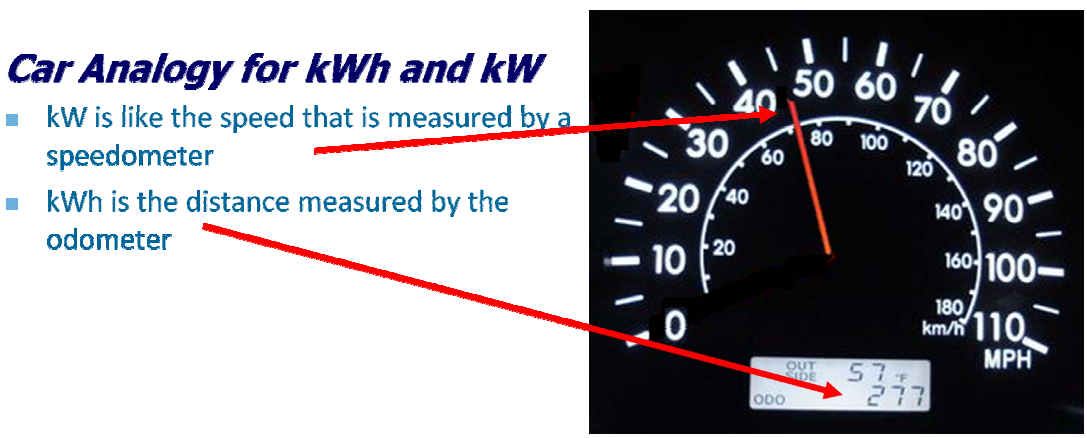

Figure 4. Car Analogy for Tariff Components

WaterOne's distribution system pump stations are primarily served by Kansas City Power & Light (KCP&L). Kansas City Power & Light has a flat kWH tariff and a flat demand charge (kW) that applies 24 hours a day 365 days a year. While this is easy to measure and bill it provides no incentive for load management. There are no options for time-of-use or real-time pricing. The last KCP&L tariff structure changes were made 10 years ago.

WaterOne's source water supply, treatment plant, and transmission pumping stations are served by the Board of Public Utilities (BPU) which also has a flat kWh tariff that applies 24 hours a day 365 days a year. The Board of Public Utilities demand charge however only applies 10 hours a day during weekdays. Demand charges are based on monthly peaks. Winter demand charges are billed as 70% of the highest summer peak, or the actual peak, whichever is greater. For WaterOne the summer peak is substantially more than winter peak and hence the 70% clause always applies and not

the actual monthly peak. This dominant summer peak means that essentially a 12 month ratchet clause applies to our single highest 15 minute period during summer.

There is therefore scope to make savings on the BPU tariff by controlling the summer peak load, although the smallest transgression for 30 minutes could eliminate an entire year's savings. It appears that the electricity market in Kansas is unlikely to change or deregulate any time soon.

DERCETO SOLUTION

Many attempts have been made to control a water utilities electrical load in response to water demand and electricity tariffs. While at first this might seem straight forward, solving the hydraulic equations with all the operational and electrical tariff variables is numerically impossible for all but the smallest systems. For example a water utility with only 11 pumps wanting an hourly schedule for a single day would have 2.96×10^{79} possible schedules to evaluate, which coincidentally is the same value currently accepted as the likely number of atoms in the universe. Given the numeric impossibility of solving this by brute force the following techniques have been attempted:

1. Localized optimization at each pump station using profiling or time triggers
2. Expert Systems using cascading rules
3. Advanced techniques using Genetic Algorithms
4. Multi-Objective Polynomial Systems (MOPS)
5. Dynamic Programming and Stochastic analysis

In order to solve the problem, these techniques still require a considerable amount of assumptions and relaxation of critical rules such as not overflowing or emptying storage tanks, both unacceptable to a modern water utility. The Derceto company felt the market was waiting for an off-the-shelf solution.

To meet this market demand, Derceto developed a "customized off-the-shelf" (COTS) software tool which works online and in real-time to reduce the costs of treated water distribution. Derceto's 'Aquadapt' software generates optimized pump and valve schedules on half hour boundaries for the next 24 to 48 hours with the goal to minimize distribution costs guided primarily by electricity tariffs. Direct connection to the SCADA system provides live data, which is then used by the Aquadapt system to enable it to choose the lowest cost scheduling solution for water production and distribution without breaching constraints These schedules are then automatically output directly to control pumps and valves, again via the SCADA system.

The optimization software calculates the minimum cost solution from the multitude of possible pump schedule combinations to meet the day's evolving demand while maintaining defined constraints such as water turnover and storage requirements. In the case of WaterOne the summer diurnal demand pattern can vary enormously day

to day, and even during the day based on weather and rainfall. Schedules created at the start of the day can have little relevance later on if the weather changes. The Aquadapt software generates a new optimized solution every half an hour as it adapts to changing conditions. The Aquadapt software also automates the entire water distribution process, providing consistent and reliable operation 24 hours a day.

WATERONE IMPLEMENTATION

The Aquadapt software runs on a pair of standard rack mounted server PCs. All user access is via thin client Windows applications running on the WaterOne Wide-Area Network (WAN). Figure 5 is a screen shot of one such application, the standard operator interface at WaterOne called the 'Operator Panel'.

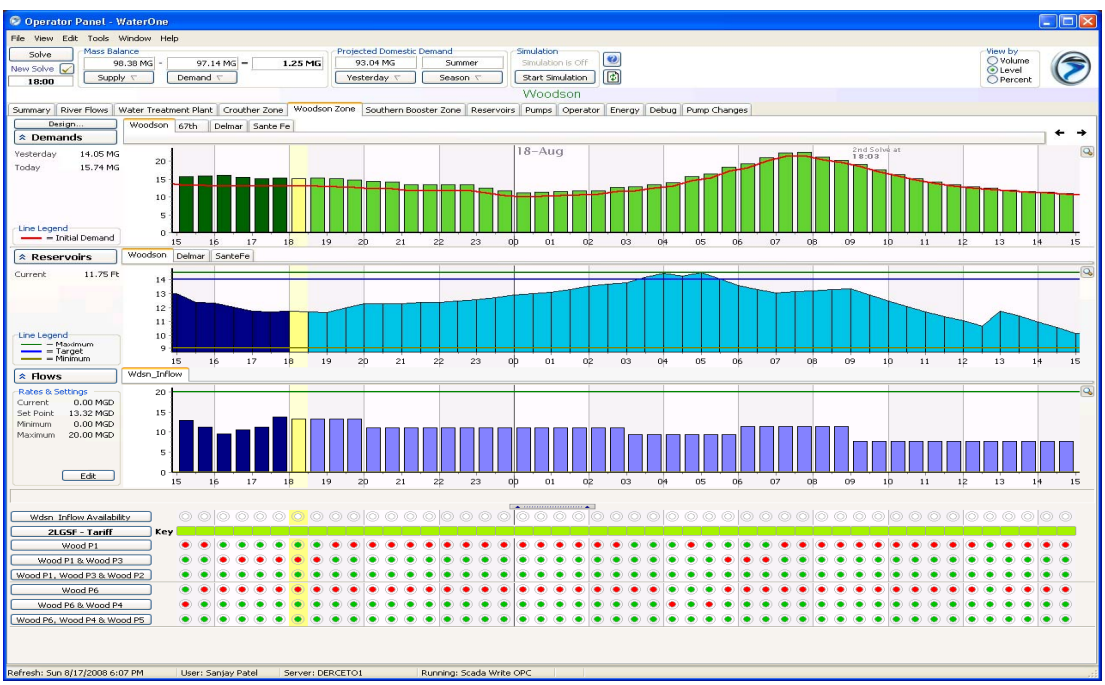

Figure 5. Derceto Aquadapt Operator Panel

This is a screenshot for a single pressure zone, and there are many similar pages for each of the other zones as well pages for the treatment plants, raw water sources, energy reporting data and miscellaneous supporting data. The top of the screen in Figure 5 reports summary information such as total system demand and supply, the time of the last update as well as access to operator inputs such as changing seasons or manually overriding setpoints. The Aquadapt software seeks to balance the supply and demand starting with the projected demand and then applying seasonal demand patterns for each zone with variations for weekday and weekends. The upper green graph in Figure 5 shows the actual and projected demand for water for this pressure zone for a 24 hour period. The yellow bar is the current time, with everything to the left of the bar being history and everything to the right being projected. The middle

portion shows reservoir levels and flows in half-hour increments for the next 24 hours. The bottom portion shows pump schedules for each pump in half-hour increments, with in WaterOnes standard red meaning ON and green means OFF.

PROJECT MANAGEMENT AND PERFORMANCE AUDITING

WaterOne started a three phase implementation of the Derceto Aquadapt software in June 2004. The timeline for the phases are as follows:

- Phase 1 - Feasibility Study - June 2004 to August 2004
- Phase 2 - Detailed Design - September 2004 to April 2005
- Phase 3 - Configuration and Testing - July 2005 to Mar 2006
  - Delivery, Implementation and Site Testing - April/May 2006

The feasibility Study determined that WaterOne could achieve $500,000 annual savings from peak demand reduction and lowest cost source selection. In particular, by reducing electrical demand at the facilities supplied by BPU during the hours of 10:00 a.m. and 8:00 p.m. on weekdays, WaterOne can lower the demand charge.

In order to accomplish the electrical demand reduction, WaterOne would need to vary its treatment plant production by as much as 100 MGD during each 24 hour period, increasing the flow as much as possible during night time hours and cutting back as much as possible between 10:00 a.m. and 8:00 p.m. on weekdays. This approach is contrary to conventional wisdom and operator training which desires to keep the treatment plant flow as steady as possible to prevent upsets in the treatment process.

WaterOne decided to proceed with the Detailed Design to investigate further whether or not changes to the operation of the treatment process could be made to accommodate the large flow swings, without adversely impacting treatment processes and water quality, and fine-tune savings estimates. The results of the Detailed Design showed that an annual savings of $810,000 could be achieved by shifting demand, the payback for implementing the changes would be less than 2 years, and that minimal hardware and equipment changes were necessary for integration with the SCADA system.

Implementation timing was critical to getting the 2 year payback. The software needed to be installed by May 2006 which is the beginning of the summer season for the BPU electrical demand. Otherwise the majority of the savings would be lost for 2006/07. The Derceto software was installed by and running effectively in May 2006.

WaterOne created and maintained an audit tool to measure savings on a monthly basis. The tool used a step function to determine, based historical data, what the

demand in kW would have been without Derceto software and compared it to the actual demand incurred when using the Derceto software. The difference was considered to be the monthly savings achieved with the Derceto software. Four years of historical data was used to develop a relationship between demand in kW and treatment plant flow in MGD. This approach to monitoring the savings allowed for changes in tariff in future years to be normalized in the evaluation.

RESULTS

Derceto helped WaterOne achieve a 20% electrical demand reduction resulting in a $90,000 savings that very first month. Figure 6 shows estimated daily demand reductions for the first month.

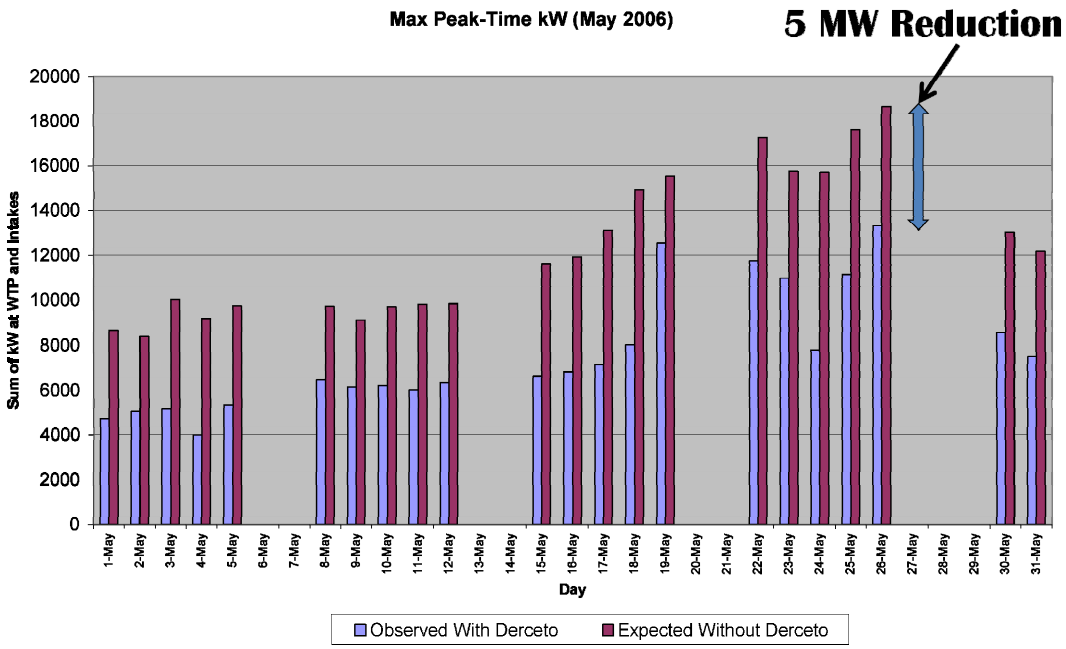

Figure 6. Electrical Peak Demand Reduction May 2006

Using the software, WaterOne was able to save over $1 million in electrical costs in the first 18 months of operation, reduce greenhouse gas emissions by 4,800 tons/year, identify areas where further savings can be made, and streamline operation of its water treatment plant. The reduction in energy use was so dramatic that BPU double checked their electric meters to make sure they were working properly and called WaterOne to verify that we had actually reduced our usage that much.

Operational changes were necessary to accommodate the flow swings that lead to the savings. The operators were involved from the very beginning to help ease the cultural change and shift in operating strategies. Before installing the software, Operators tested alternative ways to make the large flow swings and work out any

bugs and gain confidence that the new way of operating would work. Ongoing training and product enhancements have lead to even greater efficiencies and smoother operations. Although not required, some electric valve operators were installed to help with the flow swings. This minimal cost enhancement increased operator acceptance and more than paid for itself in manpower savings and efficiencies. Operators have gained so much confidence in their abilities to handle the flow changes that they have pushed the flow swings to a greater amount than originally anticipated and are achieving even greater energy savings.

WaterOne is currently using the Derceto Aquadapt software to evaluate energy savings by increasing distribution system storage and other system modifications.

CONCLUSIONS

The considerable investment in a Scada system is often hard to justify financially, but it is an essential tool. Utilization of the data and interfaces presented by a Scada system in areas such as planning and operations optimization can provide additional financial benefits. Even in an energy market that looked unfriendly to energy optimization, significant benefits were achieved.

Buying advanced software "off-the-shelf" reduces risk. Use robust systems to measure the benefits to avoid doubt. Operators need to be involved from start to finish; they know the treatment and distribution systems best. This is just one example of taking SCADA one step forward. Keep an eye on costs and benefits of integrating SCADA in other areas to best serve your customers.

REFERENCES

Electric Power Research Institute, Energy Audit Manual for Water/Wastewater Facilities, (Palo Alto: 1999), Executive Summary.

ARC Population and Employment Allocation Disaggregator - A Simple GIS-based Tool for Parcel-Scale Population Projection

Stephen Bourne, PE [1], Mike Alexander, AICP [2], and Wei Wang [2]

[1]PBS&J, 2198 Goodwood Blvd, Smyrna, GA 30080; PH (404) 895-0753; FAX (770) 426-5316; email: sfbourne@pbsj.com
[2] Atlanta Regional Commission, 20 Courtland St., NE, Atlanta, GA, 30303; PH (404) 463-3100; FAX (404) 463-3205; email: MAlexander@atlantaregional.com, WWang@atlantaregional.com

ABSTRACT

Continued development of urban areas requires careful planning to ensure adequate resources are provided for growing industry and population while sustaining a healthy environment. This paper will discuss the on-going development of a GIS-based software tool, developed by the Atlanta Regional Commission (ARC), for projecting future development of the Atlanta Metropolitan Region. With this tool, the ARC can model growth of projected populations at fine scales, and thereby estimate future demands for transportation infrastructure, water, and other utilities.

The Atlanta metropolitan area is a 22-county region in the northwest corner of Georgia, with a burgeoning population of approximately 5 million. By land area, Atlanta is the fastest growing city in the world with some of the highest commute times in the United States. Continued development strains Atlanta's resources more and more. The ARC is dedicated to unifying the region's collective resources to prepare for a prosperous future. It does so through professional planning initiatives, the provision of objective information and the involvement of the community in collaborative partnerships.

To help adequately plan for future growth, the ARC has developed the ARC Population and Employment Allocation Disaggregation tool, an ESRI ArcMAP extension. The tool employs a two-step disaggregation procedure. Starting with a single region-wide population and employment projection (2000-2050) provided by a Regional Economic Models, INC (REMI) model, the tool first disaggregates this projection to large planning regions called super-districts. The ARC then adjusts the planning level projections manually to match their expectation for growth – and those of Atlanta's stakeholder community; city governments, developers, etc. The tool then disaggregates the superdistrict-scale projections to parcel scale by using map-based factors such as major roads and expressway ramps to estimate likelihood of development and allocating new growth to the most likely areas first. When the projection is at parcel scale, statistics for demands on the travel and utility networks can be calculated and used in forecasting future travel demands on the transportation system. The tool also provides a calibration procedure that compares modeled growth to actual growth and finds the set of model parameters that minimizes differences between the two.

INTRODUCTION

Continued development of urban areas requires careful planning to ensure adequate resources are available for growing industry and population while sustaining a healthy environment. This paper will discuss the on-going development of a GIS-based software tool, developed by the Atlanta Regional Commission (ARC), for projecting future development of the Atlanta Metropolitan Region. With this tool, the ARC can model growth of projected populations and employment at fine scales, and thereby estimate future demands for transportation infrastructure, water, and other utilities.

The Atlanta metropolitan area is a 20-county region in the northwest corner of Georgia, with a burgeoning population of approximately 5 million. By land area, Atlanta is the fastest growing city in the world with some of the highest commute times in the United States. Continued development strains Atlanta's resources more and more. The ARC is the municipal planning organization (MPO) dedicated to unifying the region's collective resources to prepare for a prosperous future. It does so through professional planning initiatives, the provision of objective information and the involvement of the community in collaborative partnerships.

This paper will discuss on-going development of the ARC Population and Employment Allocation Disaggregator tool in two sections, 1) algorithm description, and 2) technology description.

ALGORITHM DESCRIPTION

Step One: Disaggregation from Region-wide to Superdistrict scale.

The first disaggregation step starts with a regional projection provided by the ARCs Regional Economic Models, Inc (REMI) model, which includes 1) projections for 18 employment sectors, based on the North American Industry Classification System (NAICS) categories, and 2) projections for population by age, where there are 17 age categories. The NAICS employment projections are disaggregated to the 78 superdistricts by forcing the distribution of jobs across the superdistricts to follow the distribution observed in the base year – the first year of the time horizon.

The REMI model provides population projections as 17 population-by-age categories, which are first aggregated to a total population projection. To translate population into land use, the total population is translated to household size/income groups, where there are 6 household sizes (size is number of people in the household) and 4 income categories – giving a total of 24 household size/income categories. The households are also distributed across the superdistricts according to observed distributions in the base year.

Interactive Adjustment of Superdistrict-scale Projections

Once the tool has disaggregated the REMI projections to the superdistrict scale, users can make adjustments to the projections using the tool. The need for manual adjustments comes from 1) the tool assumes the base year distribution of jobs and housing will remain constant at the superdistrict scale over the projection time horizon, which may not be true, and 2) often, the ARC planners and the local stakeholders have accurate information about how development will occur in the short-range horizon (0-10 years) and medium-range horizon (10 -20 years). By allowing for manual adjustments, the tool can ingest this information. In the process, the tool can be used to build consensus on superdistrict-scale growth over the time horizon and can therefore raise confidence in ARC projections.

Of course, REMI-based regional totals of jobs and households – also know as control totals - must be matched. Manually adjusting projections will result in either a net increase or decrease in the total regional number of households or jobs. To conserve the control totals, the tool implements a re-balancing algorithm, which evaluates the total number of jobs or households moved by the user to a superdistrict and then compensates by removing a weighted fraction of jobs or households from the remaining superdistricts such that the total removed equals the total re-allocated.

Step Two: Disaggregation from Superdistrict to Parcel Scale

Once superdistrict scale disaggregation has been completed and approved, the second step of the algorithm is to further disaggregate projected growth to the parcel scale. At this point, the analysis becomes raster-based. In a year-by-year loop, the algorithm allocates projected growth first to employment land uses and then residential land-uses, emulating the actual development process, in which available land is occupied progressively over time. Figure 1 shows a schematic of how the algorithm proceeds through step two of the calculation.

The priority for allocation of new growth is driven by likelihood of development, which is evaluated for each raster cell according to a linear combination of map-based factors. For example, for a given scenario, the user might specify that commercial land use is most likely to develop in close proximity to interstate ramps, major roads, and in neighborhoods where commercial land use already exists. By bringing in map layers of interstates and major roads, the tool can evaluate a likelihood of development raster – called an L-raster. This L raster is calculated as the weighted sum of three rasters: 1) proximity to the closest major road, 2) proximity to closest freeway ramp, and 3) density of commercial land use in a neighborhood of raster cells around each grid cell. Figure 2 shows an example of an L-raster calculation for commercial landuse. The L-raster is the figure on the far right. Areas in blue represent the highest likelihood areas for commercial development to occur. New growth will be allocated to these areas first.

Each map factor is associated with a weight, which gives the importance of one factor relative to the other factors. The weights must add up to 1.0, and can be set by the

user. The choice of map factors and their associated weights is decided by the user, making the tool flexible for doing what-if scenarios and identifying the set of factors that are most influential to new growth – see the calibration section of this paper for more detail.

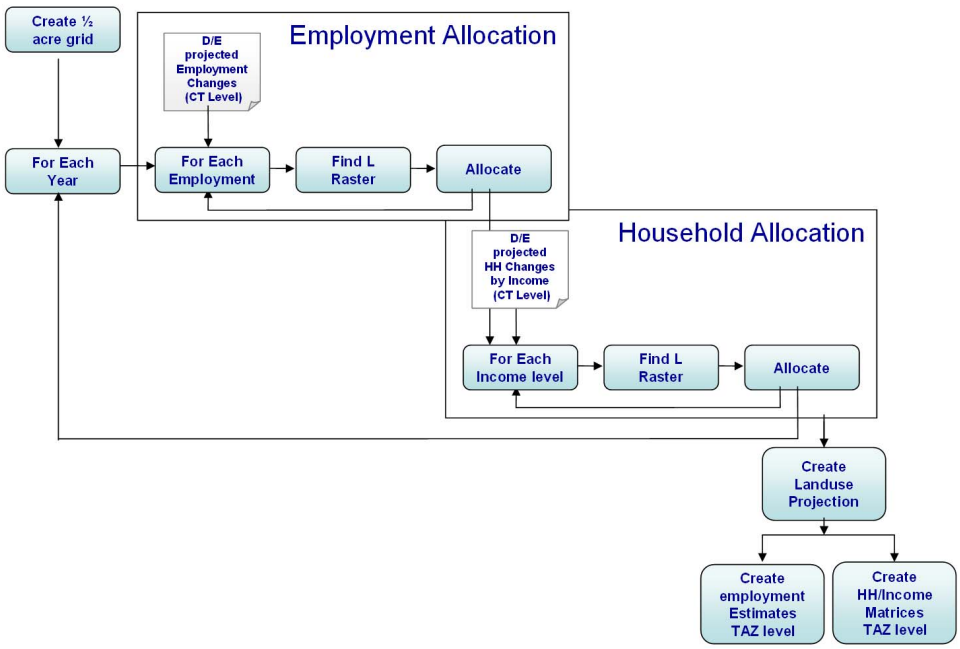

Figure 1: Schematic of Algorithm for Growth Modeling.

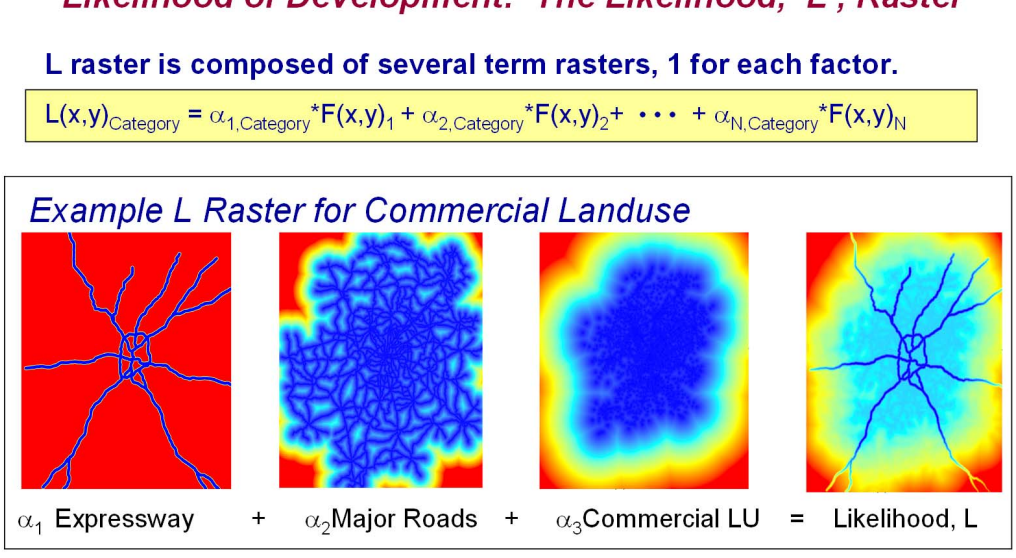

Figure 2: The L-Raster defines the likelihood of commercial or residential development at any given location by creating a weighted sum of user specified factors.

Translation from Employment and Households to Landuse

The superdistrict scale projections come in the form of numbers of new jobs and numbers of new households. As the algorithm allocates new growth by changing land use from vacant to developed, a suitable method for translating employment and households to land use is required. Using an ultimate build-out density map layer, the tool has an estimate at each location of the maximum density of jobs and households. The tool multiplies the number of new jobs or new households for any given year by the ultimate build-out density to arrive at a total number of acres required to contain the jobs or households.

Choosing the Raster Cell Size

In step two, the algorithm is converted from a vector-based to a raster-based calculation, where the vector-based shapes are converted to a grid. Using a raster-based approach is necessary because allocation during the second step must emulate the actual development process, where typically a developer will purchase and divide a large parcel into smaller ones and then develop multiple small parcels at a time in each given year. Converting to a raster-based analysis allows the algorithm to subdivide large parcels into smaller pseudo-parcels, in the form of raster grid cells.

An important aspect of converting to raster-based calculation is to choose the grid cell size of the rasters so that emulated development matches reality. Figure 3 shows the result of an analysis that found the size of actual changes in land use from 1999 to 2001. The rationale for the analysis is that changes in the land use polygons from year to year represent new development. We can set the grid cell size of the raster to match the most likely size of these changes. The implication is that 1) the growth modeling will be more accurate, as the chunks of land allocated to new development will match typical development, and 2) the calculation will proceed more quickly, as the basic grid cell size will be much larger than a single parcel.

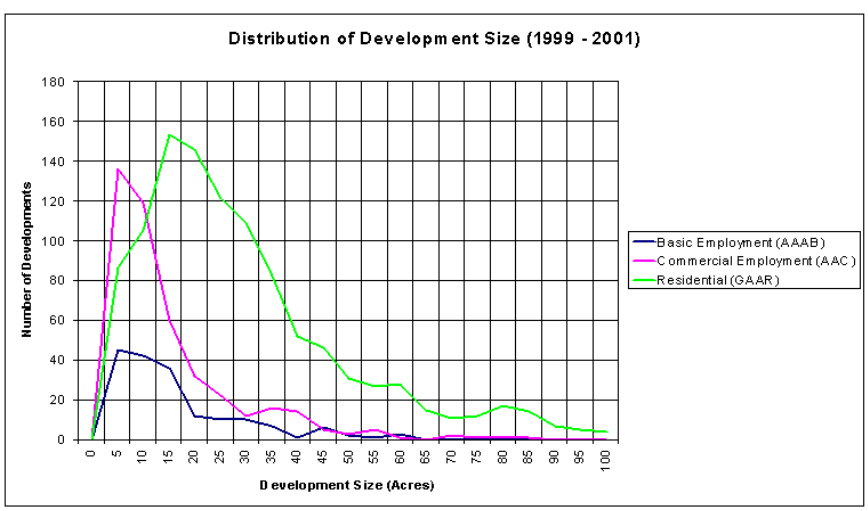

Figure 3: Distribution of Actual Landuse changes from 1999-2001.

For basic and commercial employment and residential landuse polygons, the difference in polygon sizes was calculated by essentially subtracting the 2001 polygons from the 1999 polygons. The distribution of the size of the changes was charted. From the Figure 3 on the preceeding page, we can see that for residential land use, the most likely size of new development is around 15-20 acres. Smaller average sizes for basic and commercial employment land use are found, 5-10 acres respectively. The grid cells size can be specified by the user in the ARC Population Disaggregation tool. The typical size used in our calculations has ranged from 500 ft (5.7 acres) to 1000 ft (23 acres).

Calculating Travel Demand Statistics

Once the algorithm has completed the two-step disaggregation process, a post-processing step is required to evaluate travel demand statistics for use in the ARC's travel demand model. The travel demand model requires employment and population estimates at the traffic analysis zone (TAZ) scale. The U.S. Census defines a TAZ as a special-purpose geographic entity delineated by state and local transportation officials for tabulating traffic related data from the decennial census, especially journey-to-work and place-of-work statistics. In the 13-county Atlanta metropolitan area, there are 1767 TAZs, with an average size of 1688 acres.

The tool calculates TAZ-scale totals for employment and households by income by translating the projected land use in each TAZ back to the NAICS employment and 24 category household size/income categories, ensuring that the distribution of jobs and housing matches that of the superdistrict.

Similar methods for aggregation of results to find demands for water, electricity, gas, and other resources can be added to the tool in the future.

Scenario-based Growth Modeling

In addition to the basic input data (map layers, REMI input, etc.), the user must specify the following to complete a run of the algorithm.

1. The time horizon of the analysis
2. The adjustments to superdistrict-scale projections
3. The map factors that influence development at the parcel scale for basic employment, commercial employment, and residential land uses.
4. The weights for the influential map factors

Collectively, this set of user specifications can be called a growth scenario. The ARC uses the tool to create multiple scenarios and compare the results. The intent can be to evaluate sensitivities to a certain map factor (eg. the effect of major roads), the effect of changing superdistrict scale projections to implement higher growth trends in one area versus another (eg. west Gwinnett County growing faster than east Gwinnett), and so on.

Calibration

An important question to answer in the course of growth modeling is whether the map factors chosen to define likelihood of development, and their respective weights, are reasonable. The tool implements a calibration algorithm to answer this question. The calibration process essentially consists of progressively adjusting weights of the factors until the difference in modeled and actual growth during an historic period is minimized.

The calibration algorithm requires a start year land use layer and end year land use layer. It calculates actual changes in land use by first converting the land use layers to raster form and then evaluating the number of grid cells that changed from vacant land to developed land. Then, the calibration procedure creates a set of possible weights for each map factor and runs the superdistrict to parcel scale disaggregation for every combination of those weights, evaluating the difference in modeled real land use change for each weight set.

The scale at which the comparison is made is dependent on the application. Currently, the comparison of actual and modeled growth occurs at the TAZ-scale, as the tool is being used for travel demand modeling. That is, the distribution of actual and modeled land use change is calculated for each TAZ. The region-wide comparison is made by finding the sum of squared errors (SSE) (ie. sum of differences between modeled and actual land use change) across all the TAZs for each of the three land use categories.

Simplex-based Calibration

The calibration method described above, where all combinations of possible weights are tested, is called the brute force method. Given it takes approximately 5 minutes to run a single growth modeling scenario on the ARC workstations, if there are as little as 3 map factors and the weight range is discretized into [0, 0.2, 0.4, 0.6, 0.8, 1.0], or six possible values, the number of runs of the scenario would equal $6^3 = 216$, which would require 18 hours to run. Given many more factors would normally be influential, and a finer discretization is preferred, a method for more quickly identifying the best set of weights is required.

The simplex calibration method is used to more quickly arrive at the best set of weights. Figure 4 illustrates the procedure. In the figure, 3 map factors are under consideration. The surface in the figure represents all the possible sets of weights that can be evaluated. Each black point on the surface represents a single set of weights. A triangle of neighboring points on the surface is called a simplex. First, the procedure evaluates the SSE for the 10, 8, 9 simplex. Point 10 - [0,1,0] results in the worst match between actual and modeled land use (largest SSE). The procedure then “flips” the triangle about the axis created by points 8 and 9, so that a new simplex is created of points 8, 9, and 6, and the SSE for point 6 is evaluated. The largest SSE is found to be point 9 for this simplex, and the triangle is again flipped to

make a new simplex of points 8, 6, and 7. The procedure continues until a simplex is found where there is no option to flip the simplex triangle and get a lower SSE. The point with the lowest SSE is thus identified as the best possible set of weights.

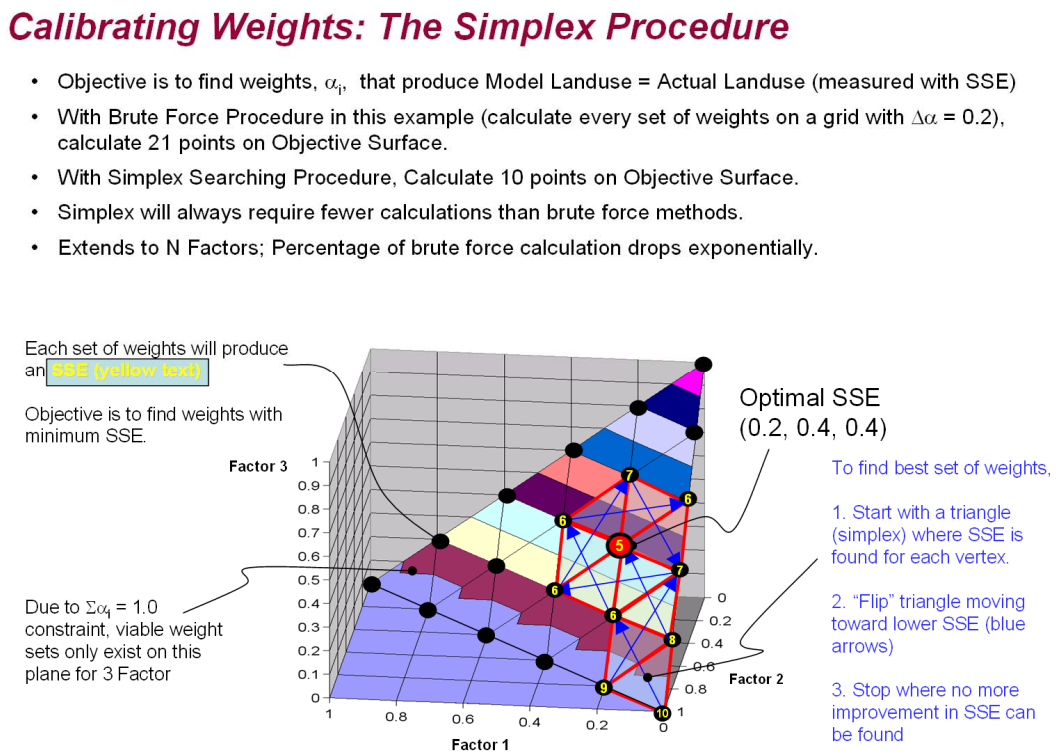

Figure 4: The simplex calibration procedure.

The simplex procedure reduces the calculation time substantially; savings increase as the number of map factors increases and the discretization of the weights becomes finer. A concern with using the simplex method is entering local minima in the SSE surface and not finding the global minimum as a result. To counter this, the algorithm is started from multiple simplexes. Moreover, once a minimum is found in the surface, the procedure "jumps" out of the minimum by moving randomly to a neighboring simplex and re-starting the search from this new point.

The calibration procedure is a powerful way of understanding which map factors are important in terms of new growth and which can be left out of the analysis. Moreover, the procedure provides some insight into the relative importance of each map factor. Finally, the calibration procedure provides some indication of how accurate the super-district to parcel scale disaggregation actually is. By comparing modeled growth to real growth, the ARC can understand how close these can actually come to projecting growth accurately, and conversely how much of the growth is not explainable with the growth model.

TECHNOLOGY DESCRIPTION

The ARC Population Disaggregation tool was created as an ESRI ArcMap 9.2 extension, so that it would work with the standard GIS platform used at ARC, the

platform the majority of ARC staff are trained in and use on a regular basis. Figure 5 shows a screen shot of the tool. The major components of the tool are a windows explorer-like tree that describes the growth scenario and allows the user to enter inputs and run the model, a context-sensitive information panel in the center of the screen that responds to the user clicking nodes in tree with information about the node and options for what you can do with the node, and a map on the far right. The map is the standard ArcMap map, and can be manipulated just as the standard map can.

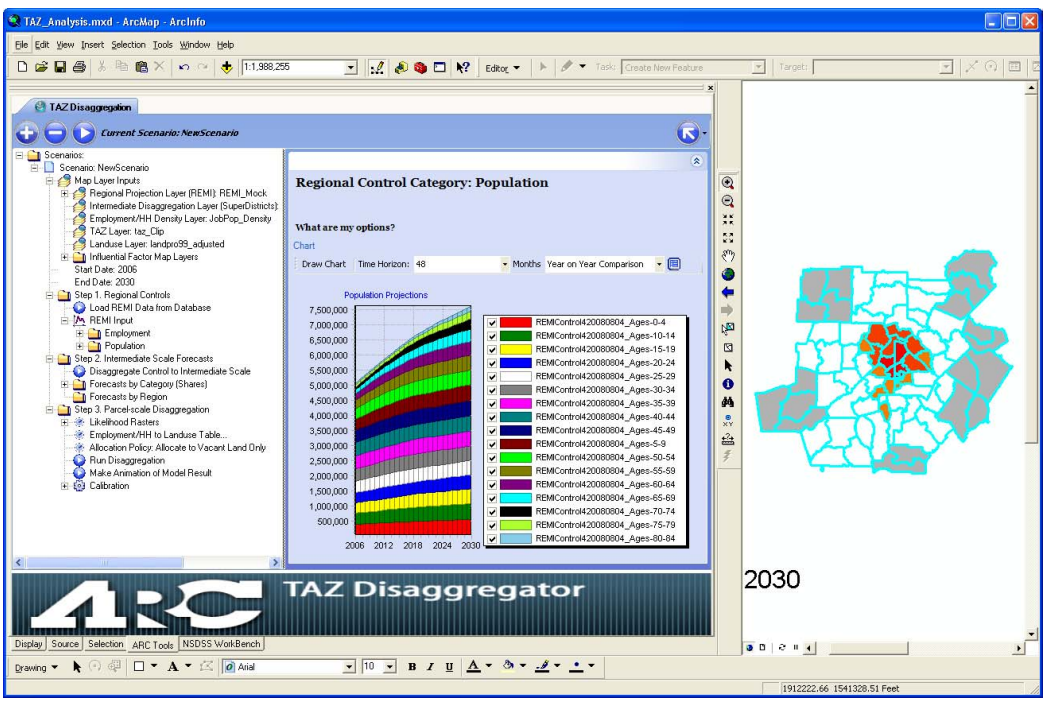

Figure 5: Screen shot of the ARC Population Disaggregator Tool.

Figure 6 shows a screenshot of the tree for a growth scenario. The tree is broken into four major sections 1) map layer inputs, 2) Step 1: Regional Controls, 3) Step 2: disaggregating from regional scale to superdistrict scale, and 4) Step 3: disaggregating from superdistrict scale to parcel scale. The user can create scenarios by clicking the scenarios folder at the top of the tree and clicking the "+" button on the toolbar. Once scenario is created, the user specifies which layers in the map should be considered the map layers to be used in the analysis (REMI layer, superdistrict layer, TAZ layer, etc.) and specifies the collection of map factor layers. The user can also enter the start and end date of the time horizon in this section of the tree.

Once the input data has been specified, the user can load the control data into the tool by clicking on the ***Load REMI Data from database*** node in the tree and choosing the load data option in the information panel. REMI data for the employment and population categories is loaded for the specified time horizon and can be charted as stacked time series charts (see figure 5). In step 2, the user then disaggregates the

regional control time series to the super districts. The results are displayed in a table in the information panel by category and by superdistrict. The user can adjust the projections directly within these tables, or they can select the superdistricts on the map and adjust the projections up or down.

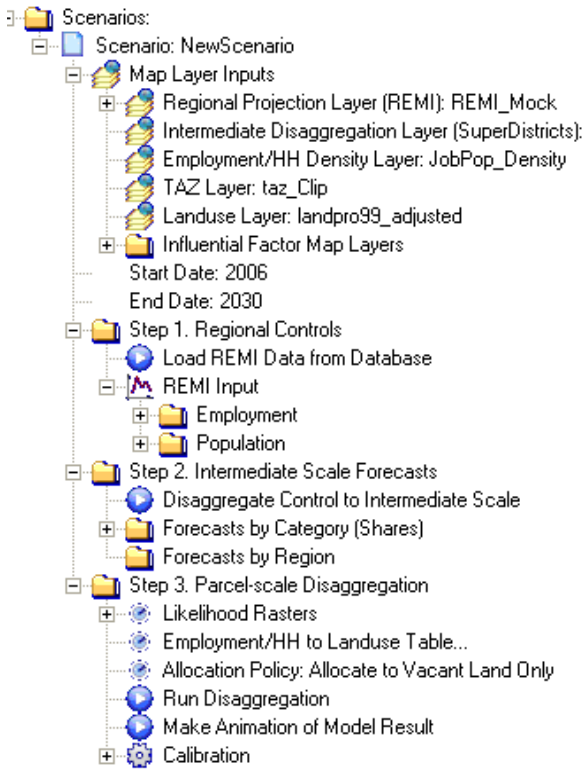

Figure 6: Scenarios for Growth Modeling are created in the Tree.

Finally, the user can run the disaggregation to parcel scale using step 3 in the tree. The user can set the weights for each factor in this part of the tree and set other modeling parameters. This disaggregation step is the most computationally intensive part of the algorithm and takes roughly 5 minutes on ARC workstations. The calibration procedure can also be run from this part of the tree if the user desires. Finally, an option for creating an .avi animation of the growth over the projection time horizon is included.

CONCLUSION

The ARC Population and Employment Allocation Disaggregation Tool is a powerful and flexible tool for GIS-based population projection. Using a combination of disaggregation steps that focus on 1) including the stakeholders in the projection process to build consensus, and 2) increasing accuracy in the modeling exercise through expert advice and calibration to historical pattern, the tool provides new insight into growth patterns in the Atlanta Metropolitan region.

How to Build a Broadly Useable GIS Toolset for Estuary Analysis.

Stephen Bourne[1], Sandra Fox[2] and Palmer Kinser[2]

[1]Post, Buckley, Schuh & Jernigan, 5665 New Northside Drive, Atlanta, GA, 30328
PH (404)895-0753 email: sfbourne@pbsj.com
[2]St. Johns River Water Management District, 4049 Reid Street, Palatka, FL, 32177
PH (386) 329-4535 (Fox) and 329-4339 (Kinser), FAX (386) 329-4329
email:sfox@sjrwmd.com and pkinser@sjrwmd.com

ABSTRACT

Assessment of the health of coastal systems is difficult due to complex geomorphology, hydrodynamics and biogeochemistry. Traditionally, this assessment is tackled with commensurately complex supercomputer–based modeling tools. While these technologies provide useful results, their computational and financial expense renders them unavailable to most coastal professionals. In a pioneer effort to provide a more accessible method of analysis, a GIS-based database of spatial and temporal data that describe the environment, and an accompanying ESRI ArcMap-based toolset, together enabling the creation of a "virtual estuary", were developed for the St. Johns River Water Management District (SJRWMD) in northeast Florida.

The project was envisioned to be developed in a two-phase process. The first, or "Alpha," phase produced a prototype version, designed by a team composed of academic, government, and industry representatives. To ensure adequate and focused progress, the prototype was designed to tackle a single – but multi-disciplinary – problem using the virtual estuary, assessment of water quality. As of the writing of this paper, the Alpha phase of development has been completed. The second, or "Beta," phase (in planning) will put the prototype to the test to tackle several more diverse estuarine analysis problems. In the Beta phase, more institutions will be included to ensure a broad set of problems will be tackled, and to build the user community.

This paper will describe the collaborative committee-based process of project development used in the Alpha phase. The project team was composed of three parts: 1) a project management component – the SJRWMD staff, 2) a research and development component – the consulting water resources software developer, and 3) a design component – the steering committee. The development process consisted of 1) problem identification – assessing the region of influence for water quality sampled in an estuary, 2) a brainstorming session to form an initial set of requirements for what the toolset should do, 3) literature review – to synthesize the state of knowledge on estuary science and methodologies for estuary analysis, 4) rapid development of a prototype, 5) a brainstorming session to reflect on the first prototype and specify more detailed direction for development, 6) final development

of the prototype, and 7) documentation of the development process, the prototype solution, and lessons learned.

Critical decisions in the development process were 1) using nationally-recognized, vetted technologies such as Arc Hydro (Maidment, 2002) as building blocks for the technological solution, 2) ensuring the toolset was a GIS-based workbench for estuarine scientists (who will most likely not be GIS experts) to do simple analysis of estuaries from simple bulk parameter estimation to applying simple analytical models, 3) using brainstorming sessions to synthesize diverse opinions into a cohesive design and to reveal synergies between the experts that lead to novel ideas for tool development, and 4) using rapidly developed prototypes to provide the experts a concrete – and easily modifiable - model of their evolving, communal, design.

INTRODUCTION

Climate change, development pressures and other threats to coastal systems necessitate the continued efforts of environmental professionals to better understand and model these important systems. Relying solely on the most technologically advanced super-computer based models (e.g. Cerco, 2000) leaves most coastal professionals out of the active analytical process due to the financial and computational requirements of these models. Taking advantage of the continuing advancements being made in geographic information systems (GIS), and the nearly ubiquitous nature of this technology, a novel approach to coastal analysis using GIS was sponsored by the St. Johns River Water Management District (SJRWMD) in 2007. This paper will discuss the development of a GIS-based database of spatial and temporal data that describe the estuarine environment and an accompanying ESRI ArcMap-based toolset that together create a "virtual estuary" enabling simple analysis of estuary bulk properties and dynamics.

METHODS

Two-phase project development. An undertaking such as this would be doomed to failure if it was limited to a short project life cycle or if its scope was too broad at the outset. The complex geomorphology, hydrodynamics and biogeochemistry of coastal and estuarine systems suggest multiple potential applications in GIS. SJRWMD's interest in expanding its Arc Hydro water quality assessment application to coastal areas presented an opportunity to apply a progressive approach with a GIS solution. Any solution, let alone a simple one, to this expressed need would not be accomplished without an open mind for a creative solution, expertise in a broad spectrum of scientific and engineering disciplines and proper development timing. Although it was important to keep a broad-range vision in mind throughout, the project was best served with a two-phase development design. The first or "Alpha" phase was to address one coastal problem, preferably from a multi-disciplinary

standpoint to produce a prototype of the GIS solution. At the conclusion of an extensive QAQC process, the second or "Beta" phase will expand the prototype to several more diverse estuarine or coastal problems. During the Beta phase, the user community is expected to expand as more applications are developed.

Collaborative project development. Collaboration provides an efficient use of available knowledge and can result in novel ideas for development when diverse areas of expertise are represented in the collaborating team. Projects similar to the one described herein, ideally, are collaborative in nature – a consultant having been hired by an agency implies at least a working group of two. Add the agency's internal project management hierarchy and the group grows in number but not necessarily in active participation in the project development. What was intended was to invite a diverse group of interested parties from a variety of backgrounds beyond the ordinary agency work group to work on a creative solution for the project. Imposing structure on the collaborative process was essential to focus progress. For this project, the structure took two forms: division of the project team into specific task-groups and a unique project work plan that facilitated the collaborative process.

Task groups. To develop the GIS-based virtual estuary and toolset for SJRWMD, experts in estuarine science and engineering from academic institutions (University of Florida, University of Texas), a non-profit environmental agency (The Nature Conservancy), federal agencies (USGS, USACE) as well as from SJRWMD and PBS&J (the consulting water resources software developer), were invited to participate in the development and review of the new tool. The project team was composed of three parts: 1) a project management component – (SJRWMD staff), 2) a research and development component – (the consulting water resources software developer), and 3) a design component – the steering committee, which comprised the spectrum of experts and provided advice on design and reviewed the prototype. Individual roles necessarily overlapped but this clearly defined approach to task definition helped to clarify appropriate action during the project cycle.

Work plan. The development process or work plan consisted of 1) problem identification, 2) a brainstorming session to form an initial set of requirements for what the toolset should do, 3) literature review – to synthesize the state of knowledge on estuary science and methodologies for estuary analysis, 4) rapid development of a prototype, 5) a second brainstorming session to reflect on the first prototype and specify more detailed direction for development, 6) final development of the prototype, and 7) documentation of the development process, the prototype solution, and lessons learned. Figure 1 displays the process.

Step 1) Problem identification: By necessity, problem definition was preceded by the creation of the Statement of Work and its internal review by SJRWMD as indicated in Figure 1. This was the work of the "project management component" described above. Problem identification was undertaken by the research and

development component of the project team, assisted as needed by SJRWMD staff. Full discussion of the development of the problem identification process is beyond the scope of this paper and is fully presented in the project documentation (PBS&J 2007a, 2007b). In short, the expressed need of SJRWMD for an extension of Arc Hydro functionality to coastal and estuarine areas for water quality assessment required conceptual development to arrive at the problem to be addressed in the project. Simply stated, the standard view of "drainage to a point" fundamental to Arc Hydro does not work well in estuaries because of the influence of the tides. Water and pollutants can come from multiple sources as shown in Figure 2, the physical model of the estuary. The goal of the project was to create a prototype GIS-based tool to assess the region of influence for water quality sampled in an estuary. In order to do that the project team realized that the creation of a virtual estuary within GIS was a necessary first step.

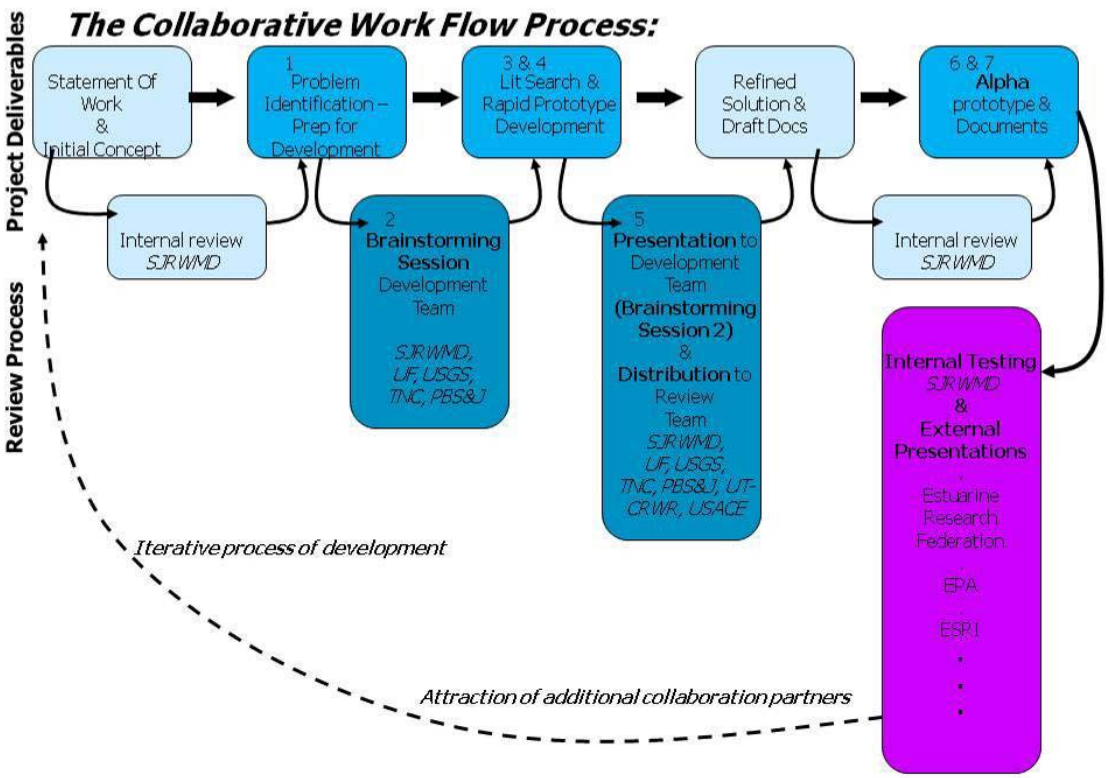

Figure 1. The collaborative work plan. *The seven key elements of the development process displayed in work flow format.*

Step 2) Brainstorming session 1*:* Once the team of estuarine science and engineering experts was assembled, and each member had an opportunity to review the project Statement of Work, an initial brainstorming session was convened in order to form an initial set of requirements for what the toolset should do. This first brainstorming session provided additional background to refine the problem definition and helped to

set the direction for project development. Available data for analysis was inventoried at this session, which led to the choice of a pilot estuary. Additionally, the major direction for the full literature review was determined, and a realistic plan for tool development was created. Lastly the high-level goals for an ideal GIS-based estuary analysis tool were set. The project team decided that the tool should be able to:

- Integrate data from multiple sources,
- Work with the existing district-wide Arc Hydro geodatabase,
- Allow creation of "virtual estuaries" in ArcMap,
- Estimate estuarine bulk parameters such as volume and flushing time, and
- Facilitate development and integration of other models into the same framework.

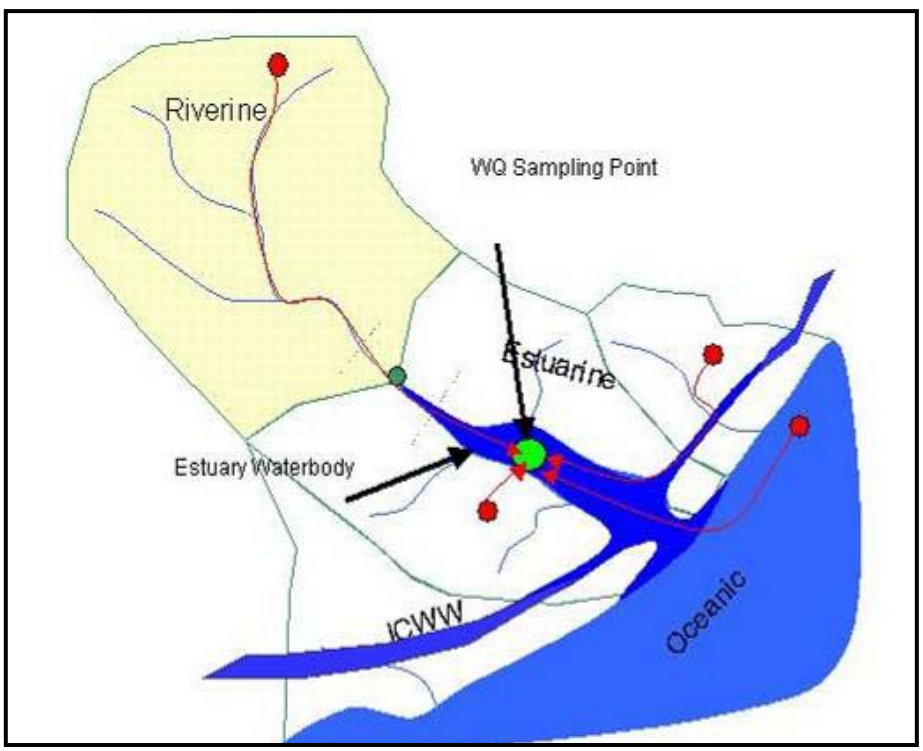

Figure 2. The estuary physical model: *A representation of the water quality assessment problem. The green dot represents the location of a water quality monitoring site. The red dots represent the various sources for pollutants that could travel to the site. ICWW = Intracoastal Waterway.*

These goals were kept high-level to provide only general direction. The goals did not detail how the tool should be designed – it's look and feel and underlying technologies – because the creative process was deemed best left to the research and development component that could forge ahead under the review committee's general direction. The research and development component envisioned that the toolset would be a GIS-based workbench specifically aimed for estuarine scientists (who will

most likely not be GIS experts) to use on their own to do simple analysis of estuaries from simple bulk parameter estimation to applying simple analytical models. Thus, the user interface and functional operation within the GIS were designed to be exceptionally "user friendly".

***Step 3) Literature review*:** Undertaken to synthesize the state of knowledge on estuary science and methodologies for estuary analysis, the literature review was extensive. The full literature review is included in the project documentation (PBS&J, 2007a). Because water quality in an estuary is influenced by the processes delivering pollutants to the estuary and the ability of the estuary to flush out the pollutants, the literature review focused on the following:

1) Methods for estimating estuarine properties, especially their geomorphology, hydrodynamics, and sediment transport properties,
2) Quantification of estuary properties and their relevance to water quality modeling on an estuary-by-estuary basis,
3) Water quality modeling approaches, their data needs, and which are pertinent to SJRWMD, and
4) Previous GIS-based approaches to water resource and environmental analysis.

Step 4) Rapid prototype development: The design approach for this project was based on a standard rapid prototype-based approach provided by PBS&J. Rapid prototype development as a component of GIS-based solution development comes from "rapid application development", a software development methodology, which involves iterative development and the construction of prototypes. The prototyping techniques are intended to accelerate software systems development, particularly important when technology is rapidly evolving. This approach has been implemented with success in several water resources technology software development projects around the country (Bourne et al, 2006; PBS&J, 2006). The rapid prototype concept is particularly helpful for driving creation of new software because it provides a functional version of the software very early in the project life cycle. The prototype can be used, scrutinized, and altered by representatives of the software's user base. This results in a much clearer picture of what is to be developed in the final solution, reduces misconceptions in scope definition, and enables the development of heavily used software.

Step 5) Brainstorming session 2: The second brainstorming session was intended to reflect on the first prototype and specify more detailed direction for development. The availability of the prototype was a key factor in the success of the second brainstorming session, by providing a tangible element to fuel discussions. The participants had something to view rather than just a description or a blueprint.

Step 6) Final prototype development: Refinements were made to the prototype following the second brainstorming session. These were subsequently reviewed by

the project management component (Figure 1). The resulting prototype tool is described in detail in Fox et al. (2008). The tool requires ArcMap at the full ArcInfo license, and both Spatial Analyst and 3-D Analyst extensions. Additionally, the tool creates an environment where data from diverse sources can be synthesized.

Step 7) Documentation: The literature review, committee recommendations, and eventual prototype solution design were documented (PBS&J 2007a; 2007b); the documentation was reviewed by the committee and approved.

CONCLUSIONS

The total number of participants in the original development team from the various agencies, academic institutions and industry was seventeen; additional reviews of prototype tool function and documents were provided by several others. A total of eight institutions were represented (SJRWMD, University of Florida, The Nature Conservancy, USGS, University of Texas, USACE, PBS&J and EPA). The respectable level of interest in participation at the outset of the Alpha stage suggested a need for an alternative to the complex supercomputer based approach to estuarine and coastal analysis. The collaborative development process, task groups and brainstorming-session infused work plan, resulted in a unique prototype GIS-based estuarine analytical toolset that has been described elsewhere (Fox et al., 2008). Opportunities for Beta development are being sought.

Several of the steps in the development process were not unique to this effort. Problem identification, literature reviews and documentation are standards in proper project management. It is worth noting here that the literature review was extensive, indicating the breadth of the effort to essentially use GIS in a way that hasn't been done before. In addition to the Conceptual Approach (PBS&J, 2007a) and the Requirements and Specifications (PBS&J, 2007b) documents that were previously mentioned, a Software User Manual was also provided (PBS&J, 2007c).

Unique to this process was the use of rapid prototype development and collaborative brainstorming sessions in the project development pathway. The prototype provided a central focus for the second brainstorming session, fostering a strong collaborative environment. It aided the development team to verify the requirements and to formally refine the data and process models. The brainstorming sessions were characterized by lively discussions that could have continued for an extended time had limits not been in place within the project management cycle. The second brainstorming session brought consensus on several important fronts (method of estuary polygon delineation, bulk parameter calculations, etc.) and furthered the discussion, although failing to reach accord on one issue (water quality modeling approach). The lack of agreement on the issue of water quality modeling underscored the requirement that the tool be designed to facilitate a wide variety of modeling approaches. However, the project timeline only allowed a single modeling

approach (multiple linear regression) for the initial development phase, although the entire project team recognized that a more sophisticated approach would ultimately be required, a fitting task for continued development. The brainstorming sessions facilitated discussions on a variety of subjects ranging from the various definitions of an estuary to the most effective way to do analytical modeling of water quality. These discussions were regarded by many as the best part of the development process, because they helped to clarify the review committee's recommendations on creation of the most useful tool. This benefited both the software developer, as well as the members of the committee itself.

Critical decisions in the development process were

1) Using nationally-recognized, vetted technologies such as Arc Hydro (Maidment, 2002) as building blocks for the technological solution,
2) Ensuring the toolset was a GIS-based workbench for estuarine scientists (who will most likely not be GIS experts) to do simple analysis of estuaries from simple bulk parameter estimation to applying simple analytical models,
3) Using brainstorming sessions to synthesize diverse opinions into a cohesive design and to reveal synergies between the experts that lead to novel ideas for tool development, and
4) Using rapidly developed prototypes to provide the experts a concrete – and easily modifiable - model of their evolving, communal, design.

REFERENCES

Bourne, S., S. Fleming, R. Laura, C. Absher and J. Hampson. (2006). Gwinnett-ArcHydro: Setting the Foundation for Integrated Water Resources Decision Support. *Proceedings from the American Water Resources Association 2006 Spring Specialty Conference for GIS and Water Resources*, Houston, Texas, May 8 – 10, 2006.

Cerco, C. (2000). Chesapeake Bay Eutrophication Model. In Hobbie, J. E. (ed) *Estuarine science: A synthetic approach to research and practice*. Island Press, Washington, D.C.

Fox S., S. Bourne, C. Montague, A. Ceric and P. Kinser (2008). ACES: Building a GIS-based Analytical Framework for Coastal and Estuarine Study. *Proceedings from the American Water Resources Association 2008 Spring Specialty Conference for GIS and Water Resources*, San Mateo, California, March 17 –19, 2008.

Maidment, D. R., ed. (2002). *Arc Hydro: GIS for Water Resources*. ESRI Press, Redlands, CA.

PBS&J (2006). SJRWMD Arc Hydro Tools Requirements, Specifications, User Work Flow, and Future Recommendations Tampa, FL

PBS&J (2007a). ACES: Analytical Framework for Coastal and Estuarine Study, Part 1: Conceptual Approach. Tampa, FL

PBS&J (2007b). ACES: Analytical Framework for Coastal and Estuarine Study, Part 2: Requirements and Specifications for Software Solution Development. Tampa, FL

PBS&J (2007c). ACES: Analytical Framework for Coastal and Estuarine Study: Software User Manual. Tampa, FL.

Predicting CSOs for Real Time Decision Support

D.J. Hill[1], B. Minsker[2], A. Schmidt[2]

[1] National Center for Supercomputing Applications, University of Illinois, Urbana, IL, USA 61820; PH (217) 244-0076; FAX (217) 244-7396; email: djhill1@ncsa.uiuc.edu
[2] Department of Civil and Environmental Engineering, University of Illinois, Urbana, IL, USA 61820; email: <minsker, aschmidt>@illinois.edu

ABSTRACT

This paper presents a novel data-driven method for modeling combined sewer overflows (CSOs) in real-time. This method treats CSO event generation as a threshold process that is triggered by increasingly intense rainfall events, and predicts the likelihood of a CSO given input conditions using a Bayesian network. The fusion of relevant data from multiple agencies into a unified data stream in real time is described, and a hierarchical modeling strategy is proposed that will facilitate the exploration of the causes of CSOs and direct research into the adaptive management of combined sewer systems using the Chicago wastewater system as a case study.

INTRODUCTION

In many municipalities, the wastewater infrastructure is divided into two systems, one that conveys municipal and industrial wastewaters (i.e. sanitary sewers) and one that conveys stormwater runoff (i.e. storm sewers). However, 746 communities located in 32 states, including many of the nation's largest cities, have combined sewer systems (CSSs) that rely on a common infrastructure to convey all wastewater [EPA 2004]. Precipitation events, in particular, cause critical loading of the wastewater infrastructure resulting in sewer "overflow" events (i.e. events where wastewater is discharged untreated into the environment in order to relieve pressure within the sewer system). From the 9,348 regulated combined sewer overflow (CSO) outfalls in the United States, the EPA estimates that about 850 billion gallons of untreated wastewater and storm water are released as CSOs each year [EPA 2004].

Recently, because of the health affects associated with the discharge of untreated wastewater by CSOs, there has been an interest in adaptive management of CSS. Such management, however, will rely on an understanding of the causes of CSOs throughout a CSS and the ability to forecast their occurrence. In CSSs, wastewater from a particular region is routed to a CSO connecting structure. Using an analogy to watersheds, the region drained to a CSO connecting structure is referred to as a sewershed. Wastewater entering this connecting structure can be either routed to the wastewater treatment facility (WWTF) via a sewer interceptor, or discharged, untreated directly into the environment as a CSO as shown in Figure 1. Fundamentally, CSOs occur when wastewater enters the CSO connecting structure more quickly than it can be leave via the interceptor; however, while this condition is overwhelmingly the result of intense precipitation [EPA 2004], the infrastructure-

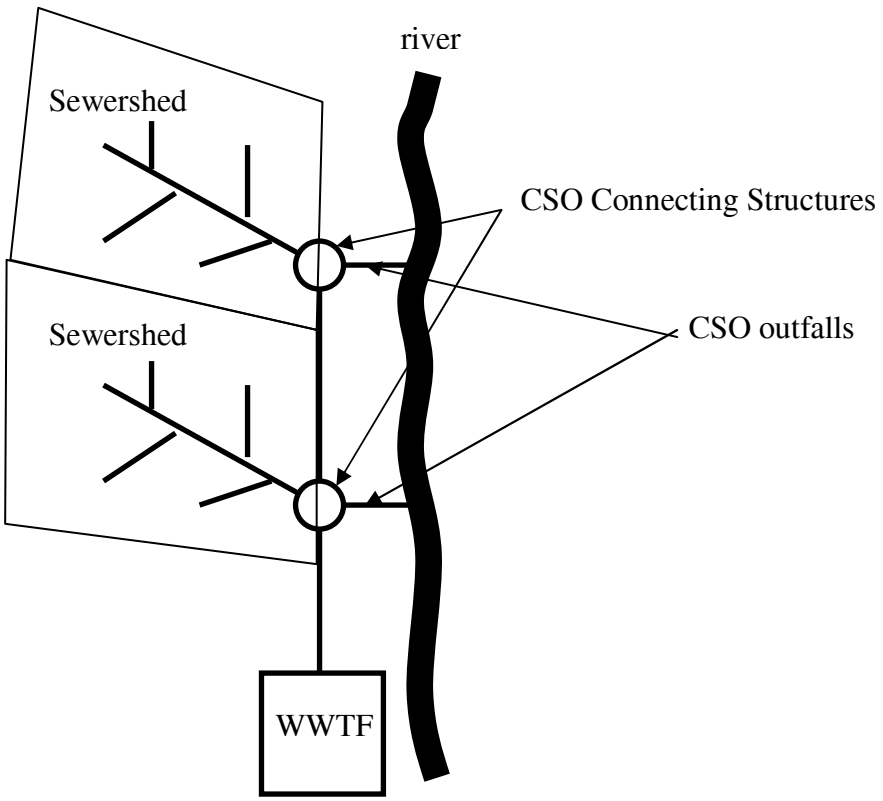

Figure 1. Diagram of a combined sewer system showing two sewersheds (A and B) that are connected to the same wastewater treatment facility (WWTF).

related causes of CSOs in a particular sewershed are often unknown, and likely to vary spatially (i.e., between sewersheds) and temporally.

This study will use modeling of CSOs to explore the causes of CSOs and to direct research into the adaptive management of CSSs using the Chicago wastewater system as a case study. Traditionally, CSOs models have employed complex physics-based flow routing models (e.g. Rouault et al. [2008]). Unfortunately, many such models cannot accurately represent the effects of special hydraulic structures (especially CSO connecting structures); resulting in significant uncertainties in their predictions [Garcia-Salas & Chocat 2006]. Additionally, as is the case in Chicago, CSO data needed to calibrate these models are often unavailable. For these reasons, this study employs a novel approach to CSO modeling that treats the CSO connecting structure as a low pass filter that transmits the stormwater from low and moderate intensity storms to the WWTP, while stormwater from more intense storms is only partially routed to the WWTP with the remainder being discharged as a CSO. This conceptual model, referred to as threshold filtering, has been successfully applied to other hydrologic systems in which behaviors are triggered by increasingly extreme conditions, such as rainfall-runoff modeling [Struthers et al 2007a and 2007b] and flooding [Kusumastuti et al. 2008]. Threshold filtering will be used to derive three increasingly complex models of CSO generation. In the first-order model, CSOs will be modeled as the result of locally intense (i.e., sewershed-scale) storms. The second-order model will extend the first-order model by adding global (i.e., CSS-scale) sewer loading to the first-order model, and the third-order model will extend the second-order model by adding time dynamics. The first- and second-order models will be

implemented using Bayesian Networks (BNs), and the third-order model will be implemented using a Dynamic Bayesian Network (DBN). This hierarchal modeling strategy will facilitate inquiry regarding the relative importance of spatial scale of influence (local vs. global), location (i.e. is the CSO generation process space invariant), and time (i.e. is the CSO generating process time invariant).

CASE STUDY

The Chicago wastewater system will be used to drive the derivation of the CSO models as well as a testbed to use these models to explore the causes of CSOs. In the 1970's Chicago began construction on one of the largest civil engineering projects ever undertaken—the Tunnel and Reservoir Plan (TARP). The TARP system, whose completion is anticipated in 2019, consists of over 100 miles of underground tunnels connecting several reservoirs which can be used during wet weather events to store excess wastewater until it can be treated and discharged into the Chicago waterways system. Phase I of TARP, which consists of the tunnels and structures tying TARP to the sewer system was completed in 2005 and provides over 2 billion gallons of storage. When Phase II is completed, the reservoirs will further increase the capacity of the TARP system by 15.6 billion gallons.

The goal of the completed TARP system is to drastically reduce the volume of untreated wastewater that is discharged into the environment by CSOs. However, observations since the completion of Phase I indicate that despite the currently available storage CSOs still occur at times when storage is available within the TARP system. For example, on Aug 23, 2007, a storm passed over Chicago dropping 1.9 inches of rain in 7.5 hours. The storm resulted in significant flooding in the Chicago area, 189 CSO events and forced the reversal of the North Branch of the Chicago river (a last-resort management decision, which had not been used for 5 years prior), however, at the conclusion of this storm, there was still approximately 500 million gallons (25%) of storage still available in TARP. Events such as this suggest that local behaviors, such as locally heavy rains or bottlenecks in the conveyance of wastewater may result in CSOs. Spatio-temporal analysis of CSO events from Nov. 2004–Dec. 2007 identified a subset of the Chicago sewersheds that generated significantly more CSO events than average. While many of these "critical" sewersheds are clustered in the northeastern region of the system, they are not spatially contiguous and are interspersed with non-critical sewersheds. This observation suggests that CSOs in the critical sewersheds are more influenced by local factors (e.g. local infrastructure differences or locally intense storms) than by system-wide sewer loading. In addition to a moderate seasonal trend, the spatio-temporal analysis also revealed distinct time periods in which CSOs were more likely to occur throughout the Chicago system, which tend to correspond with periods of unusually large quantities of precipitation. This result indicates the importance of precipitation variability to the generation of CSOs.

METHODS

The partitioning of stormwater runoff from a sewershed between sewer conveyance, storage, and overflow can be viewed as a hierarchy of threshold processes that are triggered by increasingly severe precipitation events. The first threshold corresponds to the storm intensity necessary to require the use of

wastewater storage, while the second threshold corresponds to the storm intensity necessary to trigger a CSO. Thus, during light precipitation events, all the stormwater can be conveyed to the WWTF via the sewer network. During moderate storms the system becomes conveyance limited and the wastewater that cannot be conveyed to the WWTF must be stored (if storage is available) until the conveyance limitation is lifted. Finally, during severe storms, the system is both conveyance and storage limited, thus, excess wastewater must be discharged as a CSO. While continuously valued properties (e.g. volume) can be attributed to a CSO, the overflow itself is a discrete temporal event (i.e. it has a well-defined beginning and end).

The models developed in this study predict whether or not the intensity of a given storm exceeds the CSO triggering threshold. Because of the variability in the processes that govern the generation and routing of wastewater through the sewer network, the threshold that triggers CSO events is uncertain. For this reason, it makes sense to model CSO events probabilistically. The probability that a CSO event occurs given the conditions described by a vector of random variables X can be calculated using Bayes' Theorem as

$$\mathrm{P}(CSO \mid X) = \frac{\mathrm{P}(X \mid CSO)\mathrm{P}(CSO)}{\mathrm{P}(X)} \tag{1}$$

where $\mathrm{P}(\cdots)$ indicates the (conditional) probability density function and CSO is a Boolean (yes/no) variable that indicates whether or not a CSO occurs. Thus, given a realization of $X = X'$, whether or not a CSO occurs can be predicted by determining if the likelihood that a CSO occurs (CSO=yes) is greater or less than the likelihood that a CSO does not occur (CSO=no) given X'. This can be expressed mathematically as

$$\arg\max_{CSO} \mathrm{P}(CSO \mid X = X') \tag{2}$$

BNs are graphical models that represent a set of variables and their dependencies as directed acyclic graphs, whose nodes represent the variables and whose arcs represent the conditional dependencies among them. The graphical structure of the BN facilitates Bayesian inference (i.e. solving Equation 2).

Creating a model of the form shown in Equation 2 requires a historical record of precipitation, TARP storage, and whether or not a CSO occurred. Since these data are measured at different spatial and temporal frequencies, it is first necessary to fuse these data (i.e. combine the diverse data sets into a unified data set that has a consistent spatial and temporal resolution). Because the models will be used for real-time forecasting, the fusion process must be automated to continuously process new data as it is collected. This study uses custom transformations that are implemented as a workflow within a semantically enhanced digital watershed to continuously fuse the data. These transformations define virtual sensors, as discussed by Liu et al. [2008], and result in new streams of data that can be used as input to the model or for updating the model parameters.

Historical records of the amount of water in the TARP storage and CSO events from 2004 through 2007 were provided by the MWRD. The storage data are encoded as a time series with irregular frequency, while the CSO data are encoded as event data (i.e. for every CSO event, a start and stop time was recorded). These data are fused to create a time series with uniform 10-minute intervals. The fusion process

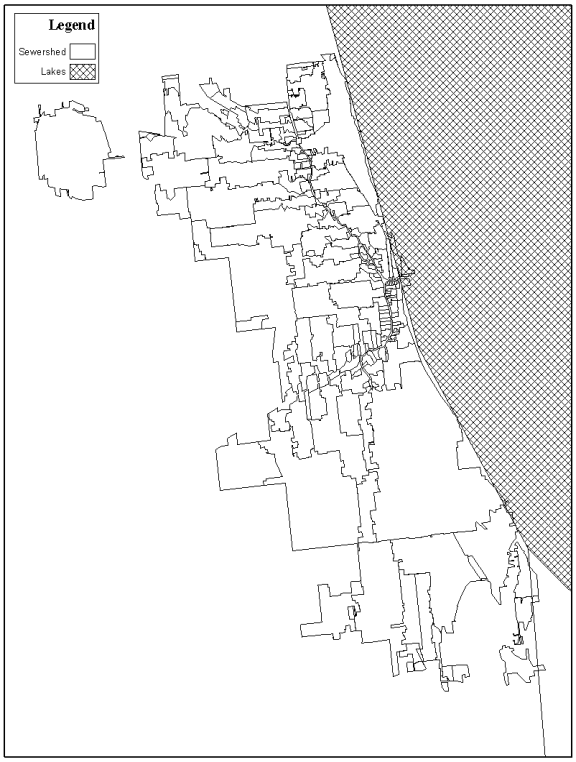

Figure 2: TARP sewersheds.

involved defining the discrete points to fall every 10 minutes starting at midnight (i.e. 00:00, 00:10, 00:20, etc.) and interpolating the CSO and storage records to these points.

The average rainfall rate over each sewershed was estimated using weather radar data from the Next Generation Weather Radar (NEXRAD) system, since, like many other cities [Vieux and Vieux 2005, Sempere-Torres et al. 1999], Chicago does not have a rain gauge network that is dense enough resolve the spatial heterogeneity of rainfall at the sewershed scale. Because no high level radar product (e.g. Level III or MPE) exists that can provide precipitation measurements at the space (~1 km^2) and time (~10 minutes) scales required for the CSO models developed in this study [Smith et al. 2007], NEXRAD Level II data are used. These data are the base reflectivity measurements made by the radar at irregular intervals (5, 6, or 10 minutes between scans), depending on the current operating mode of the radar [Fulton et al. 1998]. These data are georeferenced using a polar grid centered at the radar.

The City of Chicago occupies an area of approximately 525 km^2, which is subdivided into roughly 200 sewersheds that range in size from approximately 0.5 to approximately 70 km^2 as shown in Figure 2. The boundaries of the TARP sewersheds that drain the City of Chicago have been delineated by the Chicago Department of Water through analysis of the sewer network and field studies. These boundary data are encoded and georeferenced as vector polygons in Keyhole Markup Language (KML).

Integrating the NEXRAD and sewershed boundary data to determine the timeseries of spatially averaged rainfall for each sewershed requires several steps. First, a local grid is defined that discretizes the City of Chicago into 0.5x0.5 km

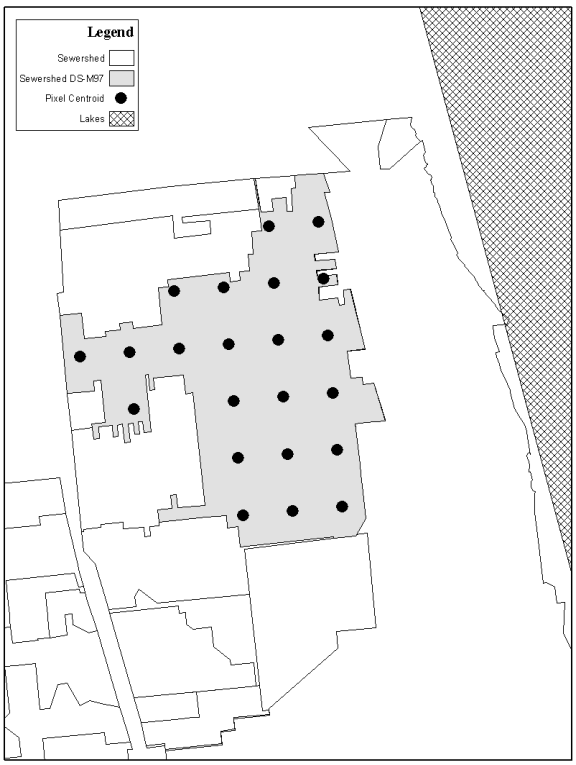

Figure 3: Centroids of the 0.5x0.5 km pixels within TARP sewershed DS-M97

pixels and is georeferenced using the same East-North-Up coordinate as the NEXRAD data. The pixel size for this grid was selected because Vieux and Farafalla [1996] noted that this resolution was sufficient to fill a rectangular grid from NEXRAD level II data. The average reflectivity of each pixel is then calculated using an inverse-distance-squared weighting technique suggested by Smith et al. [2007]. Then the polygon vertices of each sewershed are converted from World Geodetic System 1984 coordinates (used by KML) to the East-North-Up coordinates of the local grid, and a polygon filling algorithm is used to determine which pixels fall inside each sewershed. This algorithm parses the rows of the grid in South to North order once for each polygon, identifying the columns in each row through which an arc of the polygon passes. Assuming that the polygon falls completely within the grid, then processing the list of columns in East to West order quickly reveals the pixels that fall inside the polygon. The sewershed average reflectivity is calculated by averaging the reflectivity of the pixels falling in the sewershed polygon. For example, Figure 3 shows the 5.3 km^2 sewershed that drains into TARP dropshaft DS-M97 and the centroids of the 22 grid pixels that are used to calculate its average rainfall. The sewershed average reflectivity at each radar scan time *t* are then converted to rainfall rate in mm/hr using the standard convective rainfall-reflectivity equation [NWS-ROC 2003].

$$Z = 300R^{1.4} \tag{6}$$

where Z is the reflectivity and R is the rainfall rate. Finally, the sewershed average rainfall rate is averaged over 10 minute intervals to create a timeseries with a regular frequency.

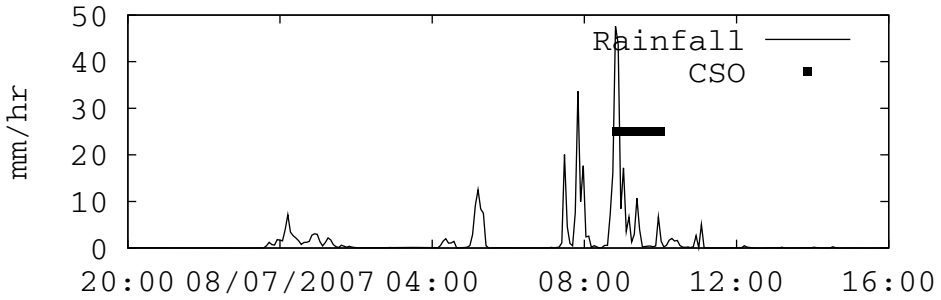

Figure 4: Fused CSO event and rainfall rate data from TARP sewershed DS-M97.

Figure 4 illustrates the result of fusing the CSO event and NEXRAD radar data. This figure shows a 24 hour window of the integrated CSO event and sewershed average rainfall timeseries for the sewershed that drains into TARP dropshaft DS-M97. During this window, there are 3 discrete storms, two low intensity storms that produce no CSOs, and one high intensity storm that results in a CSO event that lasts approximately 1 hour. This CSO event begins roughly halfway through the third storm (at about 9:00am) and is concurrent with the highest intensity rainfall peak in the storm of approximately 45 mm/hr.

The fused rainfall, CSO, and TARP storage timeseries will be divided into discrete storms using the criterion set up by the National Weather Service to define how much rain falls during a particular storm [Fulton et al. 1998]: storms are divided by periods longer than 1 hour where no rain falls. For example, if rain falls continuously from 10:00 until 10:30 and from 11:10 until 13:00 these rainfall events will be associated with the same storm. On the other hand, if rain falls continuously from 10:00 until 10:30 and from 11:35 until 13:00, these rainfall events will be defined as two separate storms. These data will be used to create three increasingly complex models of CSO generation as described in the remainder of this section.

First-Order Model: The first-order model assumes that causes of CSO events in a sewershed are well-described by the local (sewershed-scale) intensity of storms. Thus, the model does not resolve the effects of the storm in other sewersheds that may result in overwhelming the global sewer conveyance and/or storage capacity. These assumptions are valid if the causes of CSOs in a particular sewershed are only loosely dependent on the global system behavior (i.e. sewershed-scale factors drive CSO events), and success of the model to predict CSOs in a particular sewershed will indicate that global management strategies will be unsuccessful at alleviating CSOs in that sewershed, and local management should be pursued.

To characterize the intensity of sewershed-scale storm events the following properties are used: storm average rainfall rate over the sewershed i, storm duration t_r, and inter-storm period t_b. The average rainfall rate and the storm duration indicate the volume of wastewater generated within the sewershed, while the inter-storm period indicates the conditions of the sewer network prior to the storm, which is especially important when the local sewer system is capable of storing large volumes of wastewater.

As discussed so far, the BN model can predict whether or not a storm with characteristic variable values i', t_r', and t_b' will produce CSOs. However, it is often desired to know when a CSO event begins and how long it lasts. If it is assumed that a storm's behavior (i.e. rainfall rate and persistence) in the future is independent of the storm characteristic variables, the storm can be addressed incrementally. That is to say, a given storm S that lasts from time t_0 to time t_S can be decomposed into sub-storms where sub-storm s_t has duration t_0 to t and $0 < t \leq t_S$. Since the storm characteristic variable t_b is dependent only on the conditions leading up to the storm, it will be the same for all sub-storms s_t of storm S, and since the characteristic variables i, t_r only depend on the storm conditions up to and including time t, the BN model can be used at any time during a storm to predict the probability of a CSO occurring at time t during a storm using the incremental values of i, t_r calculated over the duration of the sub-storm s_t.

Second-Order Model: The second-order model builds on the local, first-order model by adding the effects of global storm intensity and global sewer system storage in TARP. This model assumes that global storm intensity only affects the CSO generating process in a particular watershed through the filling of the TARP storage. The volume of remaining storage in TARP will be represented by the variable S, and sewer system-scale storms will be characterized using the variables I and T_r, the average rainfall rate and storm duration over the entire sewer system, respectively. A variable representing the sewer system-scale inter-storm period is not necessary, because the TARP storage variable S provides the antecedent conditions of the sewer system.

Like the first-order model, the second-order model can be applied incrementally to a storm event (if it is assumed that a storm's future behavior is independent of the storm characteristic variables) to determine when a CSO event is likely to begin and how long it will last.

Third-Order Model: The first- and second-order models explore the spatial-scale of influence of the CSO generating processes. The first-order model includes only sewershed-scale processes, while the second-order model includes both sewershed and sewer-system-scale processes. These models can also be applied incrementally during a storm to investigate the temporal region during a storm where CSOs are likely to occur if it is assumed that the future behavior of CSO generating processes are independent of their previous behavior. This may not be a reasonable assumption. For example, if a CSO event occurs at time t, it may be more likely to continue at time $t+\Delta t$ than if a CSO event does not occur at time t. For this reason, the third-order model adds temporal dependencies to the second-order model. Since this model can explicitly represent the temporal dependencies in the system, it can be compared with the second-order model applied incrementally during a storm to test the assumption that the future behavior of CSO generating processes are independent of their previous behavior, which allows the second- (and first-) order model to be applied incrementally.

CONCLUSION

Modeling CSO events is important for understanding the causes of CSOs and for providing decision support to reduce their occurrence. This paper proposes the real-time fusion of heterogeneous data streams for inclusion in the modeling process and a hierarchal modeling strategy that will facilitate inquiry regarding the relative importance of spatial scale of influence (local vs. global), location (i.e. is the CSO generation process space invariant), and time (i.e. is the CSO generating process time invariant). At the conference we plan to present the results of this modeling effort and address the following questions:

How important are global factors in predicting CSOs? The first-order model assumes that CSOs are driven by the intensity (over the sewershed) of storms. Thus, it does not explicitly resolve the effects of the storm on other sewershed, which may result in reducing the conveyance capacity of the sewer system and/or filling the TARP storage. Thus, if the first-order model performs well at predicting the CSO within the sewer system, it will suggest that the global factors are less important than the local factors and that strategies to reduce CSO occurrence should be focused at the sewershed scale. On the other hand, if the second-order model performs significantly better than the first-order model, it would suggest that global factors are important to the generation of CSOs within a sewershed.

Are the CSO generating processes space invariant? After selecting the necessary model complexity (i.e. first-, second-, or third-order) the model parameters can be evaluated across many sewersheds. If the distributions of the random variables in the BN model are not significantly different between sewersheds, this will imply that the CSO generating processes are space-invariant. Thus, one model can be used to predict CSO events in all sewersheds. This is unlikely to be the case, however, it may be likely that sewersheds can be grouped into a small number of clusters in which the CSO generating processes are the same (i.e. the same model can predict CSO events in all the sewersheds in one cluster). Then by comparing and contrasting the sewersheds within and between clusters, it may be possible to determine the underlying features that make these sewersheds similar.

ACKNOWLEDGEMENTS

The authors would like to thank the Metropolitan Water Reclamation District of Greater Chicago and the City of Chicago, who provided data on the Chicago sewer system. This study was funded Adaptive Environmental Sensing and Information Systems (AESIS) initiative, which is supported by the University of Illinois at Urbana-Champaign Vice Chancellor for Research (VCR), the National Center for Supercomputing Applications (NCSA), and the Department of Civil and Environmental Engineering (CEE).

REFERENCES

EPA (2004), Report to Congress on Impacts and Control of Combined Sewer Overflows and Sanitary Sewer Overflows (Report No. EPA 833-R-04-001), Environmental Protection Agency.

Fulton, R.A., Breidenbach, J.P., Seo, D.-J., and Miller, D. (1998), "The WSR-88D rainfall algorithm," Weather and Forecasting, Vol. 13 (June), pp 377-395.

Garcia-Salas J.C. and Chocat, B. (2006), "Assessment of uncertainties in the modelling of CSOs," Water Science and Technology, Vol.54, No. 6-7, pp 247-254.

Kusumastuti, D.I., Sivapalan, M., Struthers, I., Reynolds, D.A., Murray, K., and Turlach, B.A. (2008), "Thresholds in the storm response of a catchment-lake system and the occurrence and magnitude of lake overflows: Implications for flood frequency," Water Resources Research, Vol. 44.

Liu, Y., Hill, D.J., Abdelzaher, T., Heo, J., Choi, J., Minsker, B., and Fazio, D. (2008), Virtual sensor–powered spatiotemporal aggregation and transformation: A case study analyzing near-real-time NEXRAD and precipitation gauge data in a digital watershed. Proc. Environmental Information Management Conference.

NWS-ROC (2003), Operator Handbook Guidance on Adaptable Parameters Doppler Meteorological Radar WSR-88D Handbook, Vol. 4, RPG, National Weather Service Radar Operations Center, Norman, Oklahoma.

Rouault, P., Schroeder, K., Pawlowsky-Reusing, E., and Reimer, E. (2008), "Consideration of online rainfall measurements and nowcasting for RTC of the combined sewage system," Water Science and Technology, Vol. 57, No. 11, pp 1799-1804.

Sempere-Torres, D., Corral, C., Raso, J., and Malgrat, P. (1999), "Use of weather radar for combined sewer overflows monitoring and control," Journal of Environmental Engineering, (April), pp 372-380.

Smith, J.A., Baeck, M.L., Meirdiercks, K.L., Miller, A.J., and Krajewski, W.F. (2007), "Radar rainfall estimation for flash flood forecasting in small urban watersheds," Advances in Water Resources, Vol. 30, pp 2087-2097.

Struthers, I., Hinz, C., and Sivapalan, M. (2007b), "Conceptual examination of climate-soil controls upon rainfall partitioning in an open-fractured soil II: Response to a population of storms," Advances in Water Resources, Vol. 30, pp 518-527.

Struthers, I., Sivaplan, M., and Hinz, C. (2007a), "Conceptual examination of climate-soil controls upon rainfall partitioning in an open-fractured soil I: Single storm response," Advances in Water Resources, Vol. 30, pp 505-517.

Vieux, B.E. and Farafalla, N.S. 1996. Temporal and Spatial Aggregation of NEXRAD Rainfall Estimates on Distributed Storm Runoff Simulation. Proc. The Third International Conference/Workshop on Integrating GIS and Environmental Modeling, National Center for Geographical Information and Analysis.

Vieux, B.E. and Vieux, J.E. (2005), "Statistical evaluation of a radar rainfall system for sewer system management," Atmospheric Research, Vol. 77, pp 322-336.

Protocol Considerations to Improve the Reliability of Data Collection in a Radio Telemetry System

Daniel Lasorso[1], Dr Patrick Garrett[2], Craig L. Patterson[3]

1. University of Cincinnati Department of Electrical Engineering, 814 Rhodes Hall Cincinnati OH 45221, PH (513) 569-7213; FAX (513) 569-7052; email: lasorsdv@email.uc.edu

2. University of Cincinnati Department of Electrical Engineering, 814 Rhodes Hall Cincinnati OH 45221, Associate Professor, PH (513) 556-4751; FAX (513) 556-7326; email: patrick.garrett@uc.edu

3. U. S. Environmental Protection Agency, ORD/NRMRL/WSWRD, 26 W. Martin Luther King Drive, Cincinnati, OH 45268; PH (513) 487-2805; FAX (513) 569-7052; email: patterson.craig@epa.gov

Abstract

In collaboration with Clermont County, the U.S. EPA's Office of Research and Development is developing watershed-wide load and transport models to account for stream processes at the Experimental Stream Facility (ESF) in Milford, Ohio. To better understand environmental stressors in stream flow and the structure and function of stream ecosystems, researchers are establishing continuous water quality monitoring stations along the Lower East Fork River and its tributaries. River and stream water quality are being automatically monitored and recorded every few minutes for: temperature, pH, dissolved oxygen, conductivity, stream flows (light levels, temperature and humidity), weather conditions (rainfall, solar radiation, temperature, humidity and barometric pressure) using remote sensors and weather stations. To transfer water quality data back to the ESF, high frequency data linking is being investigated for reliably and cost effectiveness.

EPA and the University of Cincinnati are examining the existing data telemetry software and suggesting a change in transmission protocol. The new protocol offers two important features: a built in CRC-16 for error correction and the ability to use the station as a digital repeater. Use of a protocol with a CRC will yield many benefits; the quality of transmitted data will be improved thus allowing the system to utilize higher baud rates, which translates into shorter transmission times and power savings. Use of the new protocol does incur additional packet length to accommodate addressing and the CRC as well as additional computational effort to validate incoming data by computing the CRC, so a comparison of protocols is merited. Also discussed are the benefits of 'digipeating' – by allowing each station to act as an addressable repeater transmissions can be broadcast over several hops to extend the range beyond simplex distance with the ultimate goal of meeting the 50 mile specification, though this is subject to the additional considerations of station density and use of directional antennas. Because each station is given a unique address there are possibilities for routing and redundancy in future projects

Keywords: Telemetry, Radio, AX.25 Protocol, Watershed Monitoring

Background

In 2007, Paul Dorsey prototyped a communications system that retrieved telemetry data from a sonde via FM radio in the High Frequency (HF) band [1]. This system allowed an operator with a terminal at the ESF station to remotely access equipment installed at the Shayler Crossing test site, approximately 4.7 miles away as the bird flies. Figure 1 shows that this 4.7 mile link traverses a variety of terrain and land use types, which present insurmountable obstacles to conventional "line of sight" systems, but can be overcome in the HF bands.

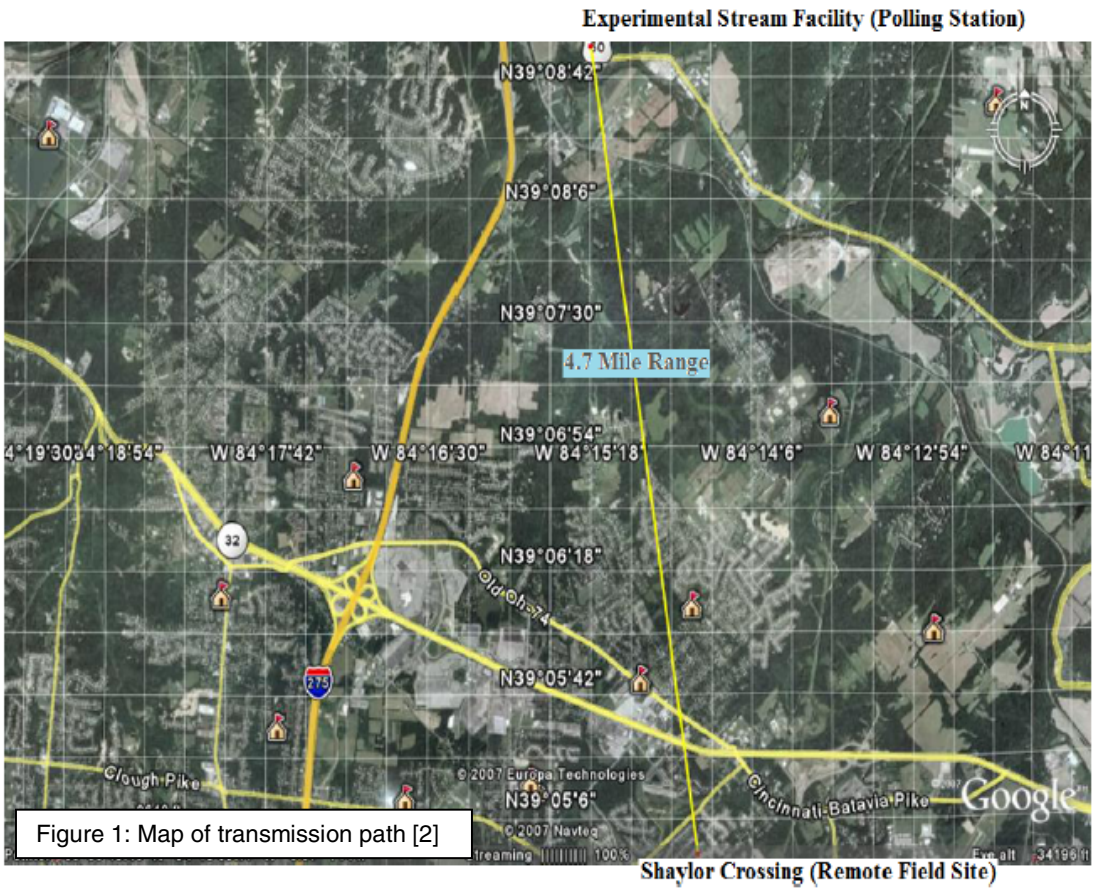

Figure 1: Map of transmission path [2]

This accomplishment is significant for several reasons; first, providing access the sonde data from the computer room means that operators would not have to travel to the site to collect it, thus saving time, vehicle costs – it is a 20 mile round trip, and reducing the risk of accidents associated with field operations [1]. Second, it eliminates the need for leased infrastructure. Third, it opens up the possibility for real time monitoring of data. Lastly, with some programming, it allows data to be collected automatically by a computer and analyzed or used as input into models.

Paul Dorsey was succeeded by Thuy Dang, who studied problems with the reliability of radio wave propagation in the system and determined that "with weak signals, the [Single Side Band

(SSB)] system will provide an intelligible signal where the FM system fails" [3]. By switching to SSB modulation, Dang reduced the system bandwidth and demonstrated performance increases over FM [3]. He also presented a MacroScheduler program that automated the data collection process.

Technical Details

Both endpoints of the system communicate using the RS232 protocol, so the equipment is selected around this. The first piece of equipment in the system is the KWM9612+ Terminal Node Controller (TNC), a modem designed to be used in a wireless environment. This device encodes the RS232 binary levels into an audio range Frequency Shift Key (FSK) signal with frequency components at 1300 and 2100 Hz. The FSK signal is input to the modulator stage of the Icom IC-746Pro radio so that it may be transmitted. The receiving station operates in reverse: the radio frequency FSK signal is brought down to audio frequencies by the receiving IC-476Pro and output to the TNC, where it is converted back to RS232 data. For intra-site communication, a Maxstream spread spectrum radio may be used when the required RS232 cable run would be too long or inconvenient. Figure 2 shows where each component fits into the larger system.

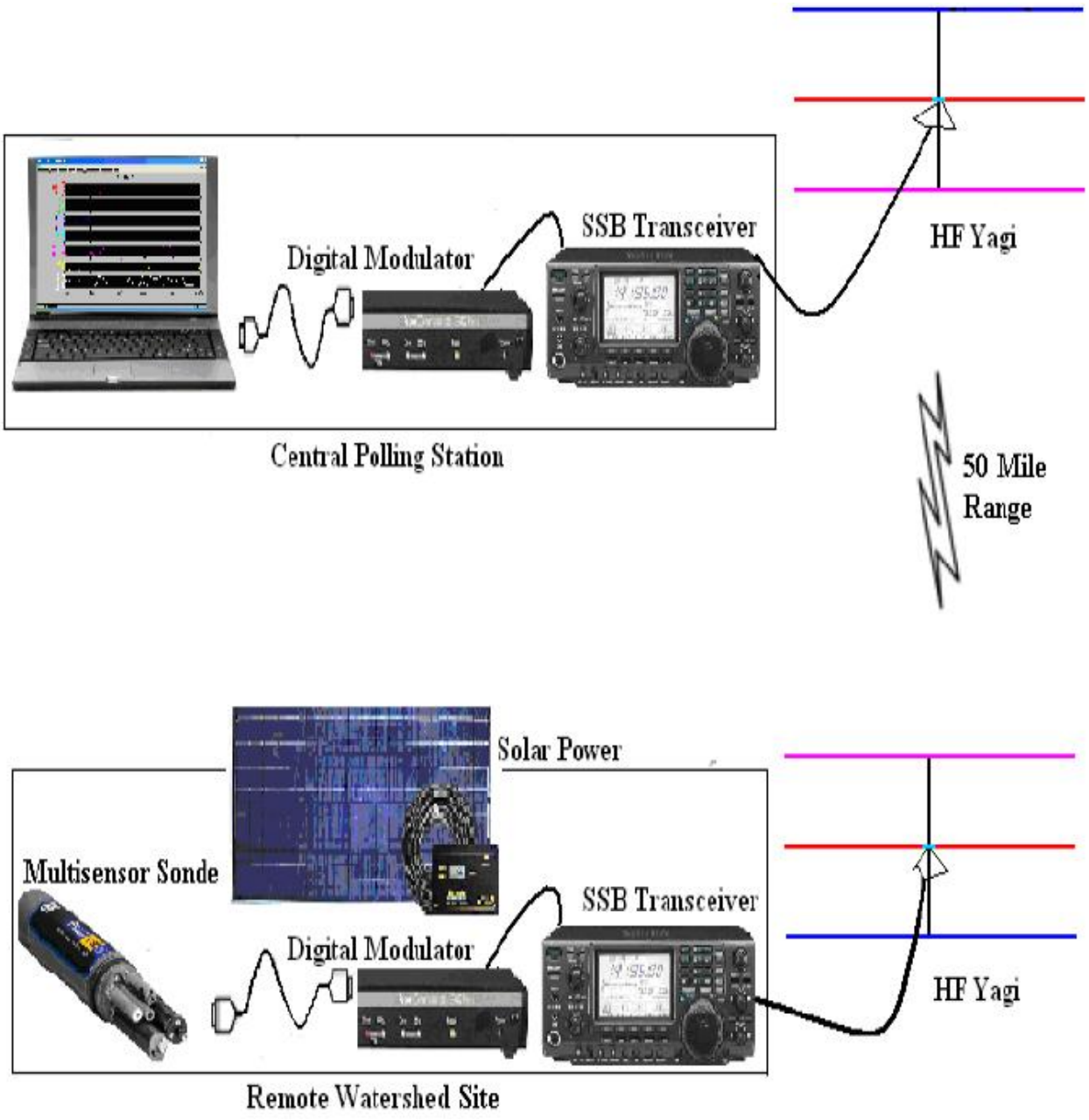

Figure 2: System Components [3]

In the original system, the TNCs are configured to use the Line Substitution (LINESUB) mode, which simply adds a start and end character to each packet before transmitting it [4]. It leaves addressing, error checking, and receipt of confirmation to the application. The TNC offers several other modes as well as support for the AX.25 packet radio standard.

Making Improvements

Reliability is the driving issue behind this set of improvements to the project. When using LINESUB mode, there is no guarantee of data accuracy; to reduce the occurrence of data corruption the baud rate had to be reduced to 300 bps, but even then, errors are fairly common. This issue is not discussed by Dorsey or Dang as the focus of their work on prototyping the radio link, however, in the configurations provided by Dang in Appendex C [3] the baud rate for transmission (HBAUD) is set to 300 bps.

Even so, the system did not work well enough to be relied upon for an unsupervised daily data transfer. The AX.25 protocol provides a CRC-16 check to ensure that data received is identical to data transmitted as well as a mechanism for retransmission when an error occurs [4]. With an error correction scheme in place, it becomes possible to increase the baud rate of the channel. The eventual goal is to reach the TNC's maximum data rate of 38400 bps, which is well over the sonde's maximum baud rate of 19200 bps, but will help to compensate for any additional overhead imposed by the AX.25 protocol.

Metrics of System Performance

Three variables are presented as good measures of system performance in this study: Power Consumption, Execution Time, and Data Integrity. The definition of these aspects of the system and the reasoning behind our interest in them is discussed in this section.

Power Consumption is crucial in a solar/battery powered system. Battery Capacity is measured in Amp-Hours (AH), but Watt-Hours (WH) present a more accurate picture of usage because they also considers the battery's voltage, which drops as its capacity is depleted and when the battery is under extreme load. For this study, both measurements are recorded, but Watt-Hours are considered the primary metric.

Execution Time affects several aspects of the system. A fast execution time means that the equipment is in operation for shorter periods of time, which will extend its useful life. It will also reduce the duty cycle of the battery, allowing it more time to charge.

Data Integrity is arguably the most important element of system performance. At best, bad data will lead to data entry problems and misleading models and trends. At worst, bad data can crash databases when unexpected control characters show up in unsterilized input. Most importantly, the system's usefulness is reduced if the data is unreliable.

Test Procedure to Determine System Performance

Three experimental variables will affect system performance over a given link: the program used to operate the system, the TNC mode (AX.25 or LINESUB), and the baud rate. To obtain an

accurate picture of how these factors affect performance, four configurations of the system have been tested with the parameters noted in Table 1. In each configuration, an identical data set of 277 measurements was retrieved, representing around 20KB of data or approximately one day's worth of samples. This test was executed 3 times for each Configuration to ensure representative sample data. The Program column shows which program was used to retrieve the sonde data; the Macro Scheduler program presented by Dang [3] or the AutoIt program that has been developed for this study. The TNC Mode column shows whether AX.25 or LINESUB mode was used in the run.

Table 1

	Program	TNC Mode	Baud
Configuration 1 (Baseline)	Macro Scheduler [3]	LINESUB	300
Configuration 2	AutoIt	LINESUB	300
Configuration 3	AutoIt	AX.25	300
Configuration 4 (Final)	AutoIt	AX.25	1200

Configuration 1 is the system demonstrated by Dang [3] and provides a baseline that can be used to measure changes in system performance; it is the control group. Configurations 2 and 3 are tested as lemmas: Configuration 2 is used to compare the performance of the programs and Configuration 3 shows that a cost is incurred by changing to a more complicated protocol. Configuration 4 tests the hypothesis that a net performance gain will occur when the baud rate is increased in spite of performance decreases in the previous Configurations.

A WU100 DC wattmeter/power analyzer, shown in Figure 3, is used to measure the power consumed by the system. When this device is installed in the system it continuously measures several variables: Source Voltage, Current, and Wattage. It also keeps track of Minimum (sag) voltage, Peak Amperage, Amp hours (current consumption), and Watt Hours (power consumption).

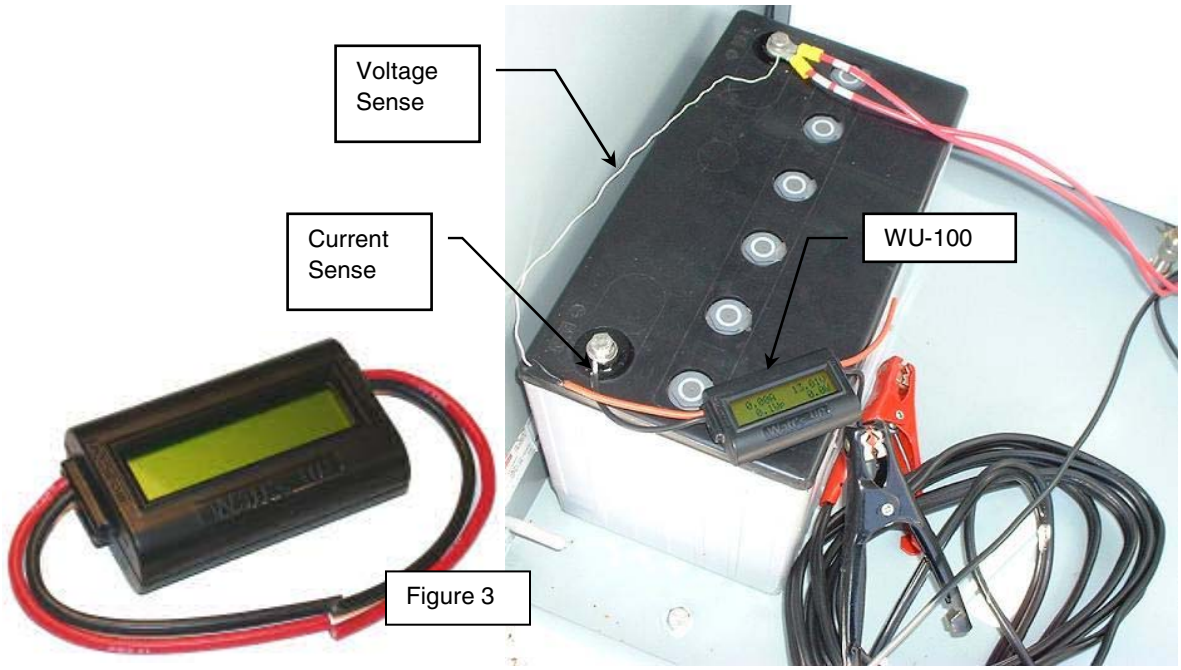

Left-most image courtesy of www.rc-electronics-usa.com

The two sets of leads on the WU100 are connected to the positive and negative sides of the Source and Load, though the three wire connection described later is preferred because it provides more accurate readings by removing the nominal power required by the meter from the measurement.

To install the WU100, as shown Figure 4, the negative lead to the system is disconnected from the battery and attached to the WU100 Load side negative lead. The WU100 Source side negative lead is then attached to the battery's negative terminal. This arrangement allows current to flow through the WU100's sensing element so that it may be measured. Next, the Source side positive lead from the WU100 is connected to the battery's positive terminal, allowing voltage to be measured. Note that the system is not disconnected from the battery's positive terminal and the WU100's Load side positive lead is left unconnected.

Power Test Setup

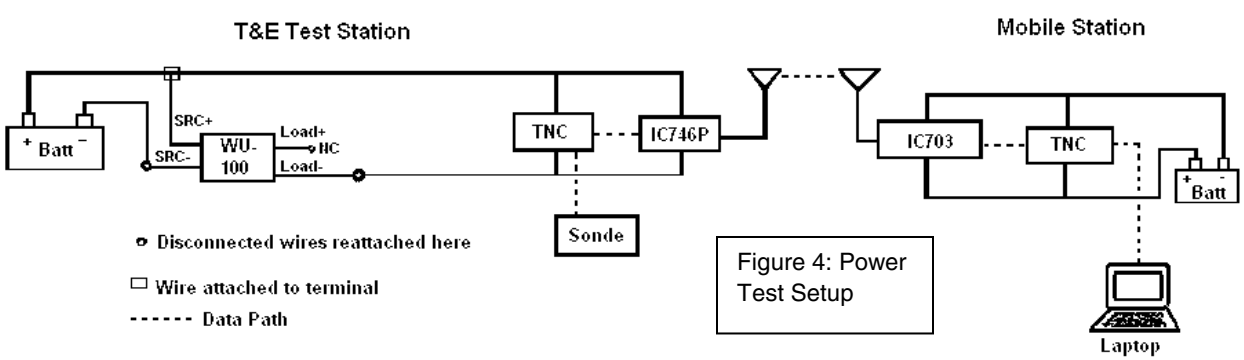

Figure 4: Power Test Setup

Execution time is determined using Microsoft's "timeit" utility available in the Windows Resource Tool Kit. The command to be timed is given to timeit as input and the elapsed time is output along with several other operating system related variables. Input and output for Configuration 2 are shown in Figure 5.

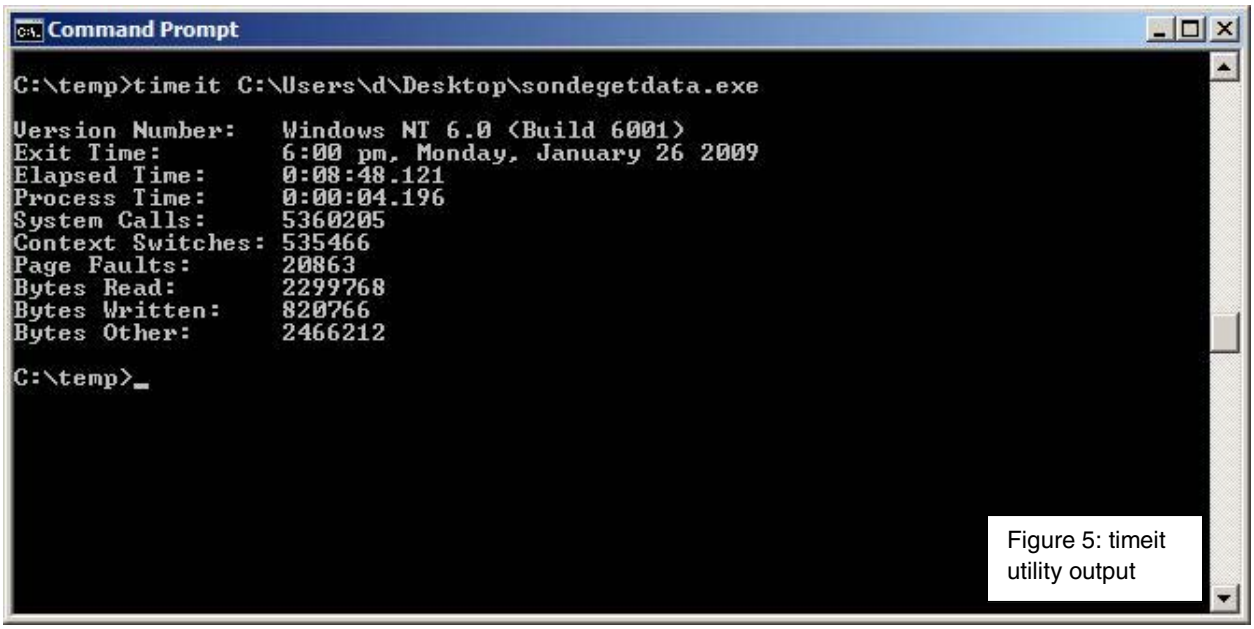

Figure 5: timeit utility output

Data Integrity is paramount to this study, but measuring it is often difficult and subjective. For this test several error types are discussed in the results section and their presence or absence in the retrieved data is used to measure its quality.

Results: Power and Time

The results of the 12 metered tests are shown in Table 2 and Graph 1; note that the error bars in Graph 1 represent 2 standard deviations (95%). The values for Watt Hours, Amp Hours, and Execution Time are the mean of the data collected from the 3 test runs of each configuration.

Table 2

	Watt Hours	Standard Deviation	Amp Hours	Standard Deviation	Execution Time (mm:ss)	Standard Deviation
Configuration 1	12.9	.6	1.04	.05	9:39.160	0.196
Configuration 2	13.8	.1	1.13	.01	9:00.195	10.542
Configuration 3	15.5	.1	1.27	.01	13:57.833	15.470
Configuration 4	5.6	.1	0.45	< .01	6:59.522	2.886

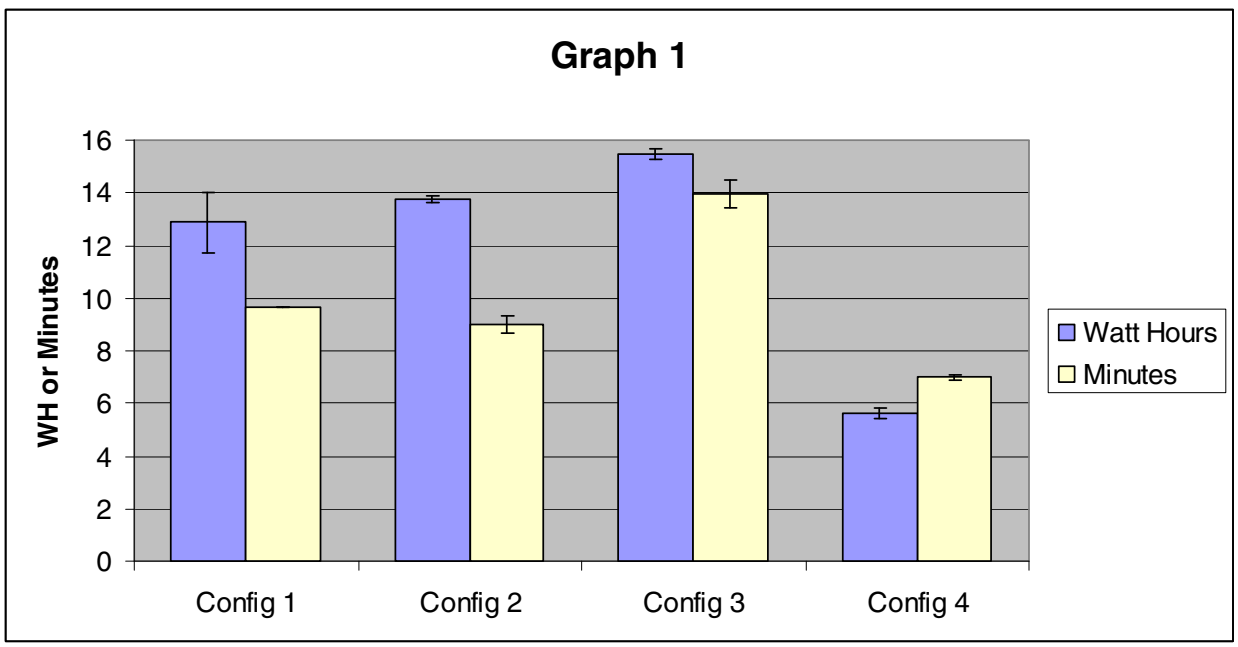

Configuration 1, the system presented by Dang [3], shows very little variation in execution time. This is because MacroScheduler program performs minimal menu navigations and uses hard coded delays. Subsequent Configurations show more variability because the AutoIt program is able to determine when a transmission ends and begins the next one immediately. Configuration 2 executes in a shorter period of time for this reason; however, it uses more power because the program interacts more with the sonde's menu system, thereby sending and receiving more data. Comparing Configurations 1 and 2 shows that there is a power cost incurred by using a more complex program, but a savings in execution time has already been realized.

Appreciable degradation in both Power Consumption and Execution Time occur when the AX.25 protocol is implemented in Configuration 3. Additional power is used because transmitted data also includes meta-data required by the protocol and the TNCs are now required to make further transmissions for handshaking and packet acknowledgement. The AutoIt program must impose additionally delays when recognizing the end of a transmission as it now receives data in large packets instead of one byte at a time. This results in long Execution Times. However, the system now quite robust: it can detect errors in data, request that a bad packet be retransmitted, and it can interpret responses from the sonde.

In Configuration 4, the benefits of the added robustness are realized when the baud rate is increased. The higher baud rate means that it takes less airtime to transmit the same amount of data, resulting in savings in both power and time. The system consumes substantially less power: less than half of the power used by Configuration 1 and slightly more than a third of the power in Configuration 3. Execution Time has also been cut in half from Configuration 3.

Results: Data Integrity

Table 3 shows the types of problems encountered in the system presented by Dang [3]: Bit Errors, Sync Error Output, Missing Headers, and Incomplete Transfers. Figure 6 shows typical data integrity errors that occur during transmission. The red circles show where bit errors that occurred during transmission caused a space character (0x20) to become an “&” (0x26) and a “5” (0x35) to become a “-” (0x2D). It can also be seen that a synchronization error occurred near the end of the data transfer and caused the rest of the data to become non-printable characters (Sync Error Output). Runs 1 and 2 are also both missing the data header as well as some data (Missing Header error); an example of this error is shown in Figure 7.

Table 3

	Bit Errors	Sync Error Output	Missing Header	Incomplete Transfer
Configuration 1	Yes	Yes	Yes	Yes
Configuration 2	Yes	Not Displayed	Yes	Yes
Configuration 3	No	No	No	Yes
Configuration 4	No	No	No	Yes

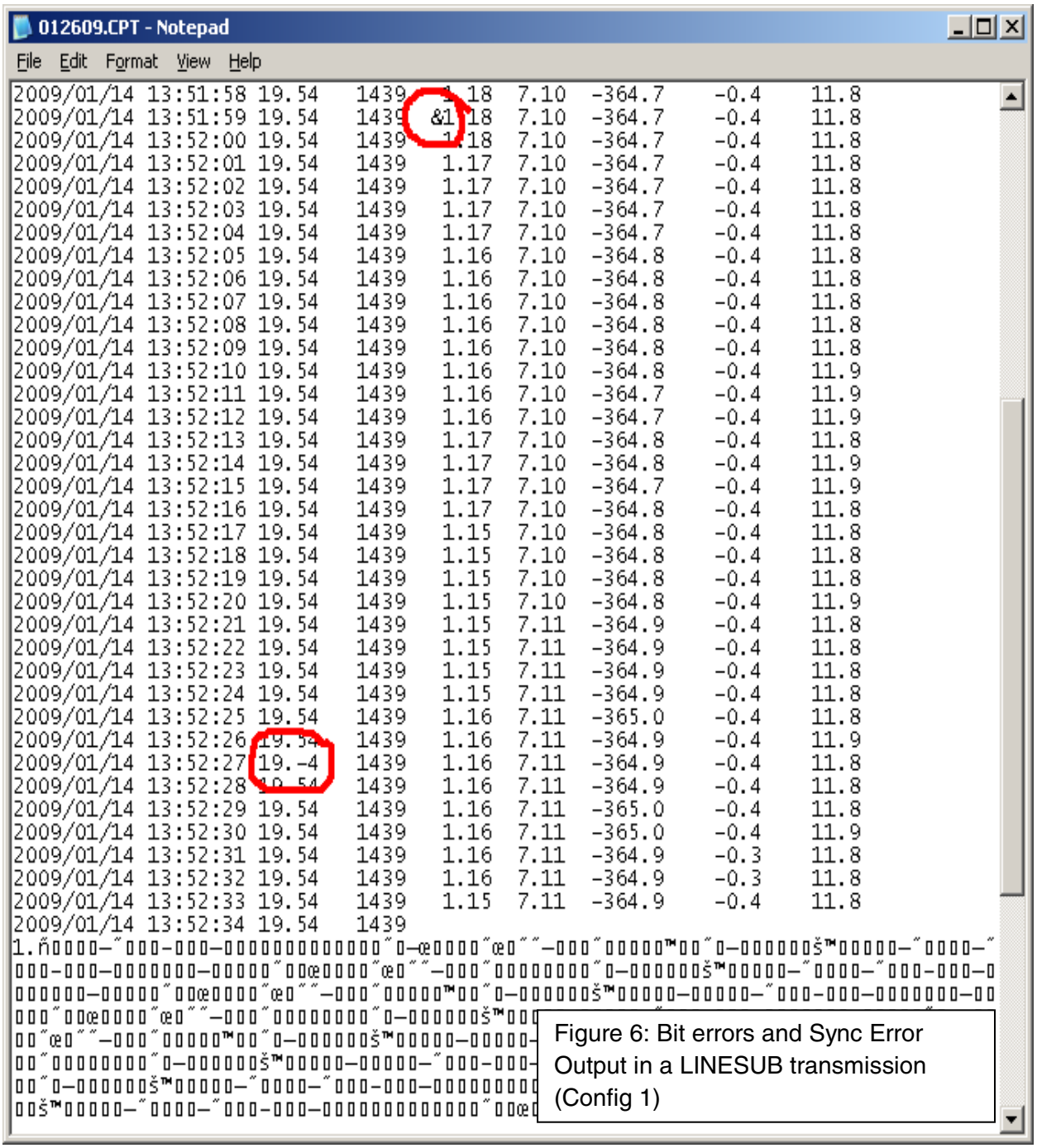

Figure 6: Bit errors and Sync Error Output in a LINESUB transmission (Config 1)

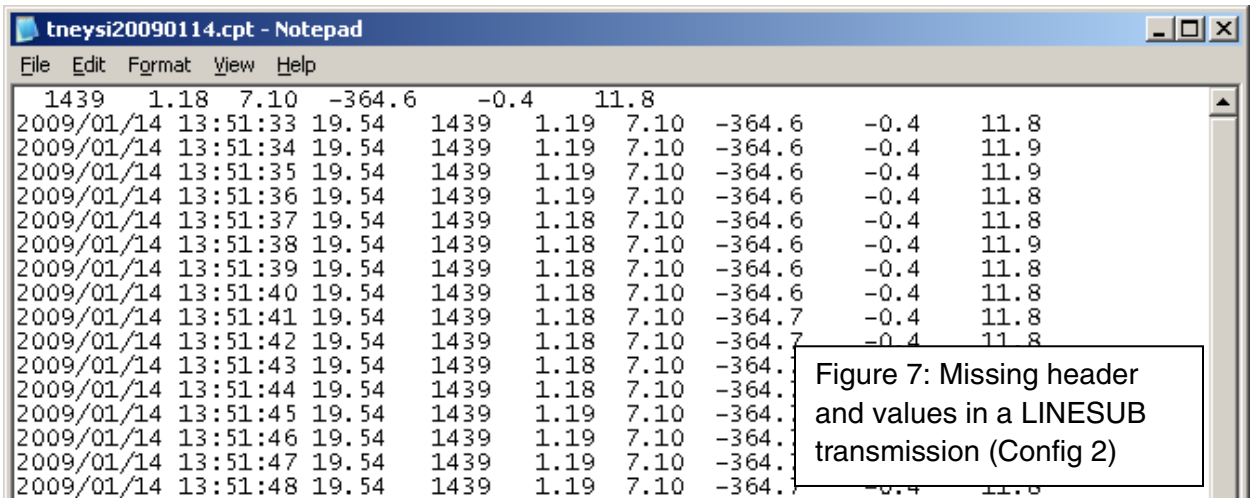

Figure 7: Missing header and values in a LINESUB transmission (Config 2)

It can be seen from Table 3 that switching to the AX.25 protocol (Configurations 3 and 4) eliminated the problems of Bit Errors and Missing Headers. The issue of Sync Error Output is more complex: the ComDebug application is used by AutoIt to communicate with the serial port in Configurations 2-4, while the EcoWatch application is used by MacroScheduler in Configuration 1. The ComDebug application used in Configurations 2-4 may not actually display the Sync Error Output. While this does remove the symptom, it does not solve the problem. However, Configurations 3 and 4 use packetized data with a CRC to ensure the integrity of the content; any packet containing erroneous non-printable characters would be dropped by the receiving TNC and retransmitted, which would prevent this type of error rather than obscuring it. Moreover, there is no reason that changing the supervisory program, the only difference between Configuration 1 and Configuration 2 (refer to Table 1), should prevent a Sync Error Output Error – especially since Configuration 1 exhibited this type of error.

This leaves the question of the Incomplete Transfers. An interesting phenomenon occurs in the in Configurations 3 and 4: all 3 runs of each Configuration produced files that were exactly the same length; Figure 8 shows that Configuration 3 yields files that are all 4356 bytes in size, while Configuration 4 results in files of exactly 7044 bytes. This suggests that the transmissions terminate predictably after the same number of bytes.

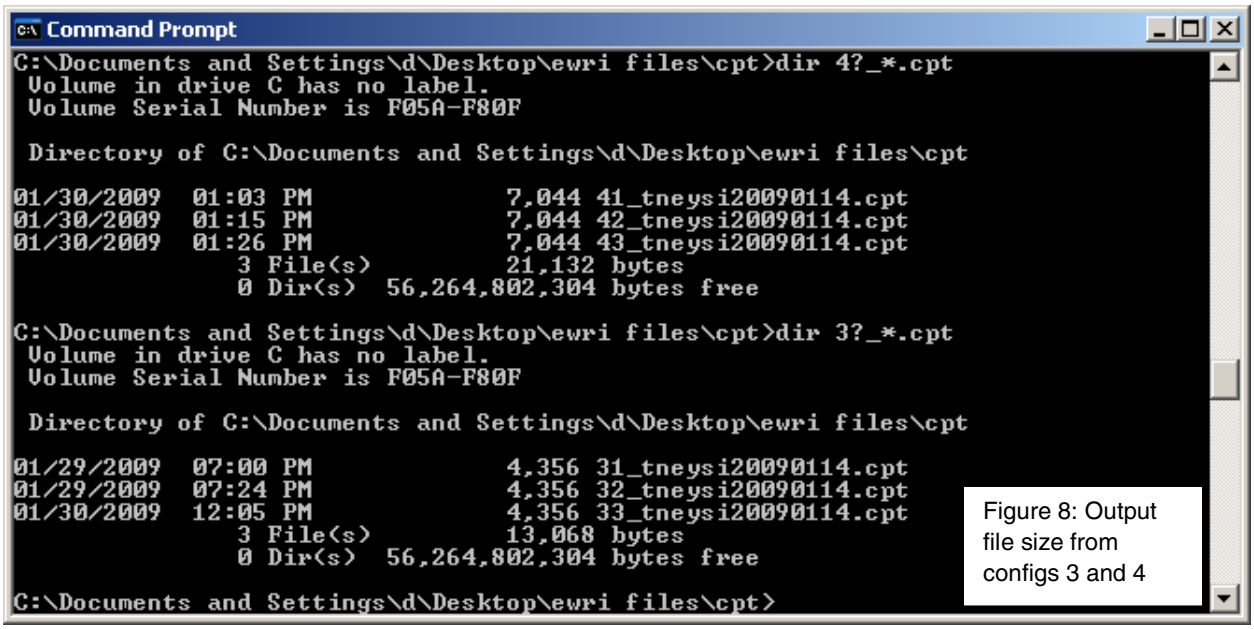

Figure 8: Output file size from configs 3 and 4

A possible explanation for this phenomenon could be that data is bottlenecking into the transferring TNC's receive buffer. The sonde is currently configured to expect a data rate of 9600 bps, which matches up with the 9600 bps setting on the digital side of the TNC (ABAUD setting). However, the modulated side of the TNC was set to either 300 bps or 1200 bps (HBAUD setting) for radio transmission. This creates a situation where the TNC is receiving data to send faster than it can send it, which may be causing either the sonde or the TNC to run out of buffer space and lose unsent data. Further testing is required to validate this hypothesis.

Recommendations

This study has shown that it is possible to attain substantial power and time savings while eliminating several types of transmission errors by adjusting system components for robustness and increasing the baud rate. The next step is to increase the baud rate further in order to realize even greater performance gains. The KWM9612+ TNC has a high speed port that allows baud rates in the range of 4800-38400 bps. Ideally, data could be retrieved hourly (or even more frequently) if the Execution Time and Power Consumption can be reduced far enough. Unfortunately, preliminary attempts to interface this port to the IC746Pro radio have been unsuccessful, but effort will continue in this area.

The issue of Incomplete File Transfers merits further investigation. It is possible that some research into the baud rate and flow control between the systems may yield a solution to this problem. Failing that, data can be retrieved in several smaller transfers instead of one large transfer.

Implementing the AX.25 protocol allows the system to take advantage of several features offered by the KWM9612+ TNC. The TNC offers remote access, repeating, and routing capabilities and all of these deserve consideration. Remote access allows an authorized user to change settings on a remote TNC; this is a useful capability for a central station to have and has been used extensively during testing. Repeating allows a station to pass along a message from another station. Some testing of the repeating capabilities of the TNCs has taken place, but how this capability can be applied for a topological advantage should be given consideration; astute placement of equipment may allow one station to monitor several sites instead of having one station per site. The TNC offers routing and networking features as well, which will become invaluable as the system expands from several stations to potentially several hundred or more.

Caveats

In practice, no test can be perfectly representative of any system and the procedures presented in this study are no exception, though every effort has been taken to assure that they are as accurate as possible. This section is provided for the sake of full disclosure and describes the shortcomings of the study.

The Autoit and MacroScheduler programs have both been modified so that they do not delete the dataset after they have saved it. This assures that each Run is conducted against the exact same data. However, it does mean that each program executes a few less commands and therefore runs shorter and consumes less power. This is mitigated by the fact that the data transfer is the biggest power consumer and takes the longest.

In the field, a pair of Maxstream XTend short range transceivers are used to send data between the sonde and the equipment cabinet. They have been excluded from this study because they are not part of the HF radio link; in practice they consume very little power (1W compared to the ICOM's 100W) and function at a very high baud rate, so their impact is likely negligible.

A smaller 33 AH battery had to be used instead of the normal 93 AH battery. This battery is not capable of sourcing as much current as the 93 AH unit. As a result, the power level of the IC-746Pro was reduced from the 100W used in the field to a level that the battery was able to handle by means of the RF Gain knob. Every effort was made to use the maximum possible transmission power at which the data could be intelligibly transmitted, in order to replicate field conditions.

The test was conducted between the station at The Test and Evaluation Facility and a mobile station in my car. Because walking between the station and my car takes time and the equipment is left running, the power consumed by the idle equipment appears in the metered results. To compensate, I timed 2 minutes on my Timex Atlantis wristwatch between resetting the power meter and executing the program and 2 minutes between the end of execution and the final reading. Thus, each metered result included 4 minutes of idle time. The idle equipment consumes 8.0 WH or .648 AH over the course of 20 minutes, which is divided by 5 to obtain a 4 minute average of 1.6 WH or .127 AH. The calculated 4 minute average was subtracted from each test result prior to calculating the mean and standard deviation values shown in the results section. This does not affect the measurement of execution time, which is the exact time the process was running as recorded by the timeit utility on the computer.

References

[1] Dorsey, P., Patterson, C., Garrett, P., and Haught, R., "Watershed Monitoring Using a Non Line of Sight Data Telemetry System," EWRI World Water Congress, Tampa Bay, Florida, May 16, 2007.

[2] Dorsey, P., "Watershed Sensor Network Non-Line-Of-Sight Data Telemetry System", Masters Thesis, University of Cincinnati, June 2007.

[3] Dang, T. P., "Watershed Security Remote Sensor Data Telemetry System", Masters Thesis, University of Cincinnati, June 2008.

[4] Kantronics KPC-9612 Plus User's Guide, 14830 West 117th Street, Olathe, Kansas 66062, 2003.

Visualizing hydrologic drought information on the web using state-of-the-art geospatial mapping technology

Jae Ryu[1] Mark Svoboda[2] and Jane Okalebo[3]

[1]National Drought Mitigation Center, School of Natural Resources, University of Nebraska, P.O. Box 830988, Lincoln, NE, 68583-0988; PH (402) 472-1483; FAX (402) 472-2946; email: jryu2@unl.edu
[2]National Drought Mitigation Center, School of Natural Resources, University of Nebraska, P.O. Box 830988, Lincoln, NE, 68583-0988; PH (402) 472-8238; FAX (402) 472-2946; email: msvoboda2@unl.edu
[3]School of Natural Resources, University of Nebraska, P.O. Box 830988, Lincoln, NE, 68583-0988; PH (402) 472-6707; FAX (402) 472-2946; email: jane.okalebo@gmail.com

ABSTRACT

Recent advances in web technologies, such as those used by Google Maps (http://maps.google.com), have facilitated the development of more interactive geospatial mapping technologies. The technology behind these mapping tools is known as Asynchronous JavaScript and XML (AJAX), which is aimed at more stable functionality, fast interactivity between servers and clients, and cost-effective data exchanges between the servers behind the scenes. Although Google Maps takes full advantage of this recent technology, there are still many restrictions in terms of customization, source modification, and licensing issues. We propose to use ka-Map (http://ka-map.maptools.org/), which is a very powerful tool for customizing user components such as graphical user interfaces (GUI). Ka-Map can be coupled with MapServer (http://mapserver.gis.umn.edu/), which was developed at the University of Minnesota. Since both ka-Map and MapServer are open source web-mapping technologies that are compliant with Open Geospatial Consortium (OGC) standards, application of these tools for water resources management is of great interest.

INTRODUCTION

A geographic information system (GIS) provides a spatial framework to support decisions for the intelligent use of water resources. These days, applications of GIS are crucial in the sense that many water-related issues and man-made environmental problems can be analyzed and resolved through geospatial data analysis. For instance, many wise environmental decisions, such as how best to manage water resources in regional watersheds, involves geography and advanced geospatial web mapping to better disseminate information, manage resources, and respond to emergencies caused by extreme hydrologic events (e.g. flood and drought) and other cases (e.g. water-borne disease).

Many studies have been done to better manage water resources using GIS technologies from spatial analysis in modeling framework to web-based visualization over the internet (ESRI 2009). Web-based GIS applications, in particular, have grown

substantially over the past few decades. Thanks to advanced computer technologies and enriched GIS datasets, the field of geographic information continues to grow.

Web application platforms such as Google Maps/Earth are showing seamless performance by providing interactive maps to communicate our everyday activities around the world. These tools and technologies help us to improve our understanding of the environment, natural disasters, geopolitical complications, human activities and changes in natural resources. For hydrologic database management applications, the Consortium of Universities for the Advancement of Hydrologic Science, Inc. (CAUAHSI- http://www.cuahsi.org/) Hydrologic Information System (HIS) project has been initiated to facilitate data accessibility and visualize geographically distributed hydrologic data sources through the universities' alliances. The goal of CAUAHSI-HIS is to bring all water resource data, including precipitation, streamflow, water quality, and ground water levels together into a service-oriented architecture through "web services", known as specialized machine-to-machine communications via internet protocols (Maidment 2008). Such efforts are extremely important in providing seamless service for the widest variety of water data available to the research community and public domains. Hydrologic ontology defined in geospatial databases can be utilized to translate water observations data from various formats (e.g. text, excel, binary) into a single format compatible with an internet friendly hierarchical data structure (e.g. eXtensible Markup Language (XML)) that can be stored effectively (Maidment 2008). The water data discovery and acquisition system, called HydroSeek (http://www.hydroseek.org), is a good example of a geospatial database available on the internet.

In this paper, we propose to use ka-Map to visualize hydrologic drought information across the country. One major advantage of this tool is that all analysis output and dynamic maps of hydrologic information through data processing can be displayed efficiently on the web through an OpenGIS framework. Additionally, many different image formats of the maps (as users create them on their web browsers) are made available, including png, gif, tiff, and pdf formats Such visualization and customized maps are very useful for integrating and assimilating environmental datasets into digital watersheds along with other real-time data collections, including satellite-based remote sensing and/or automated wireless data networks. Additionally, local decision makers responsible for hydrologic event response plans and management can easily identify the spatial extent of areas vulnerable to upcoming hydrologic events, especially drought.

DATA ASSIMILATION

The United States Geological Survey (USGS) maintains 1,659 unregulated gauge stations, known as the Hydro-Climatic Data Network (HCDN) across the country to provide naturalized streamflow data for research activities related to climate change and other subjects (http://pubs.usgs.gov/wri/wri934076/1st_page.html). Records of unregulated streamflow (i.e., natural streamflow, as opposed to streams with upstream diversions or dam operations) are important in understanding the effects of hydrologic drought on regional water resources. A total of 1,009 unregulated gauge stations, a subset of 1,659 stations, were utilized for this study to visualize hydrologic drought information across the country. Selection criteria for streamflow gauge stations and data assimilation processes were determined based on a data quality assurance test. First, daily streamflow

data was downloaded from the USGS website (http://waterdata.usgs.gov/nwis/sw). Time horizons of the daily streamflow data was taken from as early as 1845 to the year 2005 and saved in text format, and then additional test was conducted to maintain data integrity. For instance, some stations that had duplicate records of streamflow within several unnecessary columns and whole segments of data missing were eliminated.

VISUALIZATION TECHNOLOGY

Open source based web-mapping platforms such as MapServer are commonly used by many water scientists wanting to publish maps online. Although MapServer is well suited for interactive web-mapping, MapServer alone is not able to accomplish a set of advanced actions such as enhancing robust and stable interactions between servers and clients. AJAX supports the functions of MapServer and is based on open standards, which means this technology is less dependent on any established or specific operating system and/or commercial software. The main advantage of AJAX is that it is very fast and reduces the time spent in (processing time) redrawing dynamic maps requested by the client within a web browser. AJAX accomplishes faster data processing by manipulating data via specific requests (e.g., event handling) rather than reading the entire page on the web. This high-speed mapping technology drives developers to integrate AJAX applications into web services. Figure 1 represents an integrated system of dynamic mapping technology within an open-source platform, including MapServer, geospatial database, and ka-map utilizing AJAX technology.

MapServer

Mapserver, an open source development environment, is widely used to implement web-based GIS solutions around the world since it was originally developed at the University of Minnesota (UMN) in collaboration with the National Aeronautics and Space Administration (NASA) and the Minnesota Department of Natural Resources (MNDNR). Although MapServer is not a full-featured GIS system, MapServer can visualize various formats of GIS data (e.g., images, raster, and vector data) through an internet gateway. Additionally, MapServer allows users to create and manage map files, which characterize individual map layers including data source, legend, scale, and metadata. In this project, MapServer will be enhanced to produce integrated maps along with drought prediction outputs as follows. First, all metadata will be customized to help the end users. A customization of metadata will help reduce the time required for map caching as it predefines analysis settings such as the queryable field, hyperlink information, color setting, and layer description. Second, the system should be able to operate conjunctively with the geospatial database to provide reliable web services in terms of time and quality. These components will enhance the dynamic mapping system through GIS technology, and help local decision makers identify the spatial extents of potential droughts via customized views.

Geospatial Database, PostGIS

A reliable geospatial database is another important key element in accomplishing the goals of this project. PostGIS (http://postgis.refractions.net/) is a tool used to support geographic objects within PostgreSQL (http://www.postgresql.org/), a powerful open-source relational database system. PostGIS enables the PostgreSQL server to be used as a

backend spatial database for geographic information systems (GIS), such as ESRI's ArcSDE and Oracle's spatial extension. PostGIS is also developed in an open-source environment so that it complies with Open-Source Geospatial Consortium (OGC) standards. Currently, PostGIS supports various geospatial data formats as well as data validations associated with geological coordinate systems. PostGIS can be used by implementing SQL routines to visualize the results via MapServer so that the interactive dynamic maps will be made available much faster over high-speed broadband internet connections.

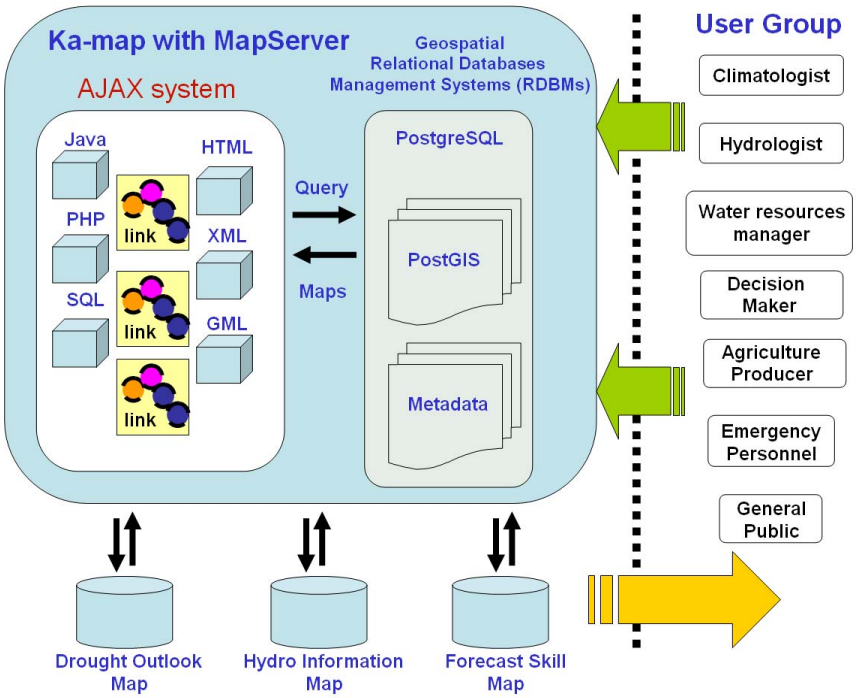

Figure 1. Integrating MapServer into ka-map utilizing AJAX technology

Ka-Map with AJAX technology

As an open source package, ka-Map will also be integrated with MapServer. Normally, a map is created by MapServer through map files (e.g., mymapfile.map) and then is made available on the web in cached form through ka-Map. Basic processing of these integrations is conducted through a simple cycle. MapServer is in charge of creating maps, and it waits for requests from users via a graphic user interface (GUI) in ka-Map. When a request is initiated by the user, both MapServer and ka-Map work together to generate and present new maps on the web. But when many duplicate requests are presented, only ka-Map is working on caching and redrawing the maps; MapServer sits idle and waits for the next batch of new calls. Traditionally, this process is done by a series of subsequent protocols including mouse clicks and/or zooming in, and then waiting for the entire map image, and waiting again for the web browser to publish maps, whereas the integration with ka-Map splits maps into several pieces when first requested and stores them on the server, then retrieves the map later for the user. This simplified cycle leverages system enhancements by improving the performance of the web browsers. Moreover, AJAX technologies facilitate the level of interactivity between servers and

clients, pre-rendering by caching the tile images stored in the server, and saving time by accelerating smooth panning and zooming.

DEMONSTRATION

For testing and demonstration purposes, we developed a mock-up to visualize raw geographic data (e.g. vector, raster, and coverage) on web-based GIS services (Web Service). Advantages of this service provide interactive communication tools between Web Service and end-users that require customizing geophysics applications. Figure 2 and Figure 3 show the main page of the mock-up and a sample of client's web service request, respectively. For instance, users can request the map for the area of interest to identify USGS gauge stations for further information. The graphical user interface (GUI) main page shown in Figure 2 allows the user to change the map sizes from the drop-down lists or enables them to zoom in or zoom out by clicking zooming tools built in ka-Map.

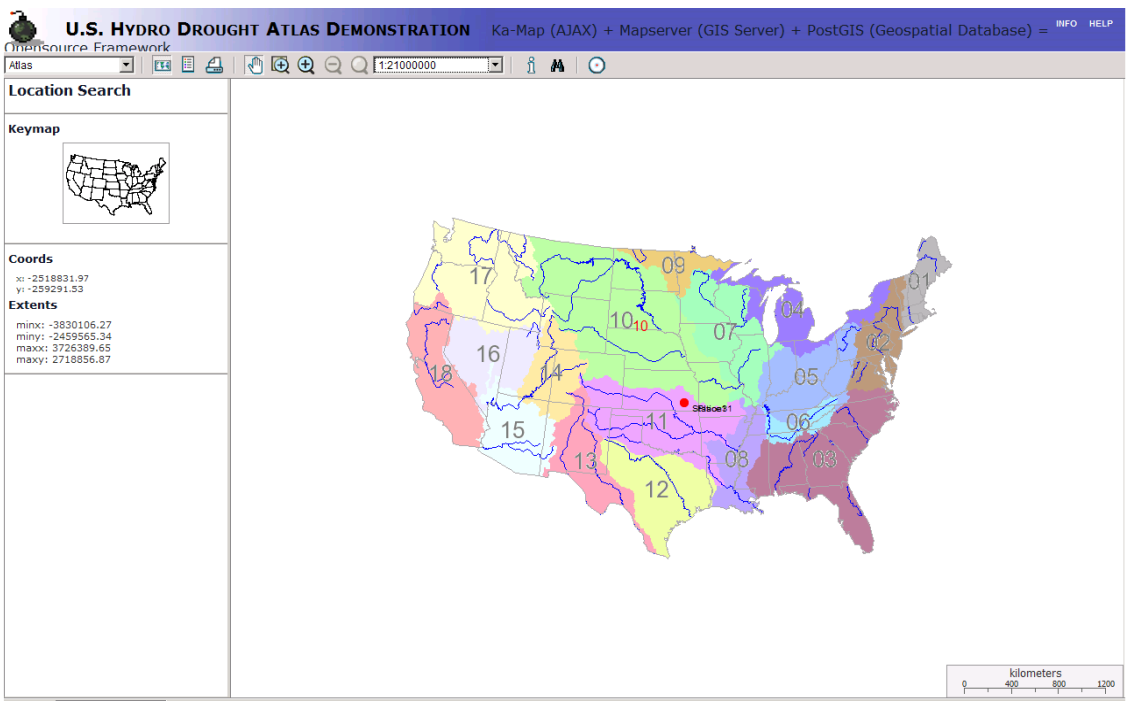

Figure 2: Main page with web-based GIS services. The color ramp in the main frame represents a total of 18 watersheds in the conterminous U.S.

The red circle on the left panel in Figure 3 indicates that the user has identified two USGS streamflow gage stations for further investigation.

Future Work

We created a mock-up of a web-based GIS service for data visualization to end-users using state-of-the-art geospatial mapping technologies, including AJAX and PostGIS. All these services comply with OGC standards so that many potential deployments to multi-disciplinary research activities are expected. The initial development activity is part of the first stage of an ongoing U.S. Drought Atlas project underway at the National Drought Mitigation Center (NDMC). A number of

improvements and enhancements are needed to pursue seamless Web Services for NDMC clientele. These activities may include: 1) stabilizing robust web service architecture in combination with geospatial database, PostGIS, to manage high volumes of geospatial datasets (e.g. raster, satellite images); 2) integrating current Web Services with other services, such as Web Map Service (WMS 2009) and Web Feature Service (WFS 2009); and 3) improving the GUI to better communicate and understand service availability and accessibility for advanced users, and seeking further information (e.g. metadata) for their research interests.

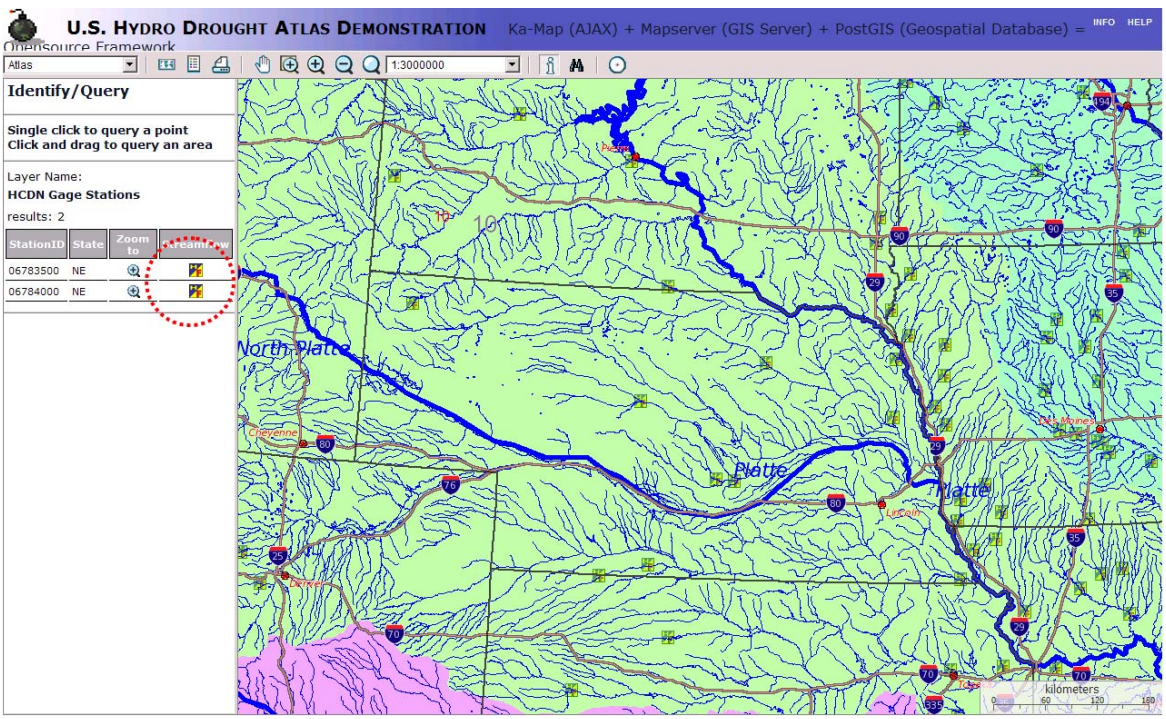

Figure 3: Web Services are customized for the client's view.

Acknowledgement. Support from the Risk Management Agency within the United States Department of Agriculture is gratefully acknowledged.

References

ESRI. (2009). "Arcnews." *ESRI, Winter 2008/2009*.

Maidment, D. R. (2008). "Bringing water data together." *Journal of Water Resources Planning and Management*, 134(2), 95-202.

WFS. (2009). "Web feature service." *Open Geospatial Consortium, Inc.*, <http://www.opengeospatial.org/standards/wfs>(Jan. 7, 2009).

WMS. (2009). "Web map service." *Open Geospatial Consortium, Inc.*, <http://www.opengeospatial.org/standards/wms>(Jan. 7, 2009).

"Let it Rain" - Gage-Adjusted Radar Rainfall (GARR) Data for Peachtree Creek Sewer Basin Modeling

Alberto Bechara, P.E.[1], Jim Moffitt[2], Vahe Kokorian, P.E.[1], Rasheed Ahmad, Ph.D., P.E. [1]

[1] City of Atlanta , Department of Watershed Management, 230 Peachtree Street , Suite 500, Atlanta GA 30303; PH (404) 979-6999; email: abechara@atlantaga.gov
[2] OneRain Inc., 1531 Skyway Drive Unit D, Longmont, CO 80504; PH (303) 774-2033; email: jim.moffitt@onerain.com

Abstract

Sewer hydraulic models are developed to reveal and simulate problem areas in sewer system networks. During model development precipitation input data, typically from rain gages, are applied and system parameters are adjusted until the calibrated model output matches the collected system flow meter data. The calibrated model is later used to evaluate problem areas and identify solutions to the system's deficiencies in order to comply with regulatory requirements, which are met by eliminating surcharge and overflow locations within the sewer system.

Calibration of the sewer system is only as accurate as its input rain data, so it should be a priority to use the best rain data attainable. While rain gages can be accurate and precise, they can only provide data at discrete points, resulting in low spatial resolution and ambiguity regarding how much rain has fallen in between gages. Installing denser networks of rain gages can help improve the spatial resolution of the gage data, but is expensive in terms of equipment fees, installation, and maintenance. For this reason, the City of Atlanta initiated a pilot program which uses a technique called Gage-Adjusted Radar Rainfall (GARR). GARR datasets are produced by taking regional NEXRAD radar data and calibrating them with co-located rain gages. GARR combines the high spatial and temporal resolution of radar with the volumetric accuracy of rain gages.

The study compared the hydraulic models that were developed using a GARR dataset, and a dataset consisting of rain gages only. Both datasets used information from 30 "tipping-bucket" rain gages from March 2001. The GARR analysis incorporated NEXRAD radar data on a 2x2 km grid, with a 15-minute sample rate. Correlations between the two precipitation measurement systems were strong. Rainfall timing was well matched. Incorporating the gage volumes resulted in lowering the radar rainfall estimated by 20%. The sewer hydraulic modeling results showed that the Flow (Q), Velocity (V) and Depth (d) response to the flow meter data matched more closely when GARR data is used as compared to the conventional rain gage data.

Because rainfall is the input variable with the largest impact on modeling sewer systems, it is also essential information for determining rehabilitation efforts and system upsizing. By using the GARR process to enhance real time rainfall data, the City of Atlanta will create more accurate models, attain a better representation of

storm frequency, intensity, duration, and improve future forecasting capabilities. Using GARR techniques will achieve a more accurate hydraulic sewer model, and better quantify inflows from storm events and their impacts on the system.

Introduction

Prior to 1915, the 19 square miles that comprised the City of Atlanta, and what is now the core downtown area, utilized a combined sewer system. As the City grew to its present total area of 132 square miles, the trend changed to a separate storm and sanitary collection system. The First Amended Consent Decree (FACD) imposed on the City of Atlanta since 1999 mandates the elimination of all unpermitted discharges and sanitary sewer overflows to achieve compliance with National Pollutant Discharge Elimination System (NPDES) permits. To accomplish this goal a Rainfall and Flow monitoring Plan were initiated to identify excessive infiltration and Inflow and to quantify peak flow factors for the macro system (Interceptor and Trunk) in a sanitary sewer model that would evolve through the years to include the micro system which will include outfalls and its tributaries. The model was deemed essential to assist in the development of operational procedures that may optimize system capacity, as well as to evaluate the impact of proposed system improvements. The rainfall plan is comprised of 32 rain gages operated by a consultant at strategic locations throughout the 10 city sewer basins, and an additional 16 rain gages operated by the City of Atlanta at Wastewater Treatment Facilities (WWTF) and Combined Sewer Overflow (CSO) facilities. The strength of a rain gage network is its ability to consistently estimate rain falling on a number of discrete points. Its weakness is the network's inability to estimate rain falling between the gages. Sewer hydraulic models are developed to reveal and simulate problem areas in sewer system networks. During model development precipitation input data, typically from rain gages, are applied and system parameters are adjusted until the calibrated model output matches the collected system flow meter data. The calibrated model is later used to evaluate problem areas and identify solutions to the system's deficiencies in order to comply with regulatory requirements, which are met by eliminating surcharge and overflow locations within the sewer system.

One of the main input data for a good calibrated model is rain data, so it should be a priority to use the best rain data attainable. While rain gages can be accurate and precise, they can only provide data at discrete points, resulting in low spatial resolution and ambiguity regarding how much rain has fallen in between gages. Installing denser networks of rain gages can help improve the spatial resolution of the gage data, but is expensive in terms of equipment fees, installation, and maintenance. For this reason, the City of Atlanta initiated a pilot program which uses a technique called Gage-Adjusted Radar Rainfall (GARR). GARR datasets are produced by taking regional NEXRAD radar data and calibrating them with co-located rain gages. GARR combines the high spatial and temporal resolution of radar with the volumetric accuracy of rain gages.

The study compared the hydraulic models output from March 3 2001 storm that were developed using a GARR dataset, and a dataset consisting of rain gages only.

Background

Currently, the City is served by approximately 1900 miles of sewer mains (15% combined and 85% separated). All sewage flow within the City is treated by three wastewater treatment facilities, to serve a population of 1.6 million approximately with a total average daily flow of 182 MGD. In addition to the flow produced within the City, there are six adjoining jurisdictions contributing flow to the City of Atlanta sewer system that comprise 45% of the total flow.

The City of Atlanta is divided into 260 sewersheds that join to form ten sewer basins. As defined by the First Amended Consent Decree (FACD) a Sewer basin contains all portions of the wastewater collection and transmission systems tributary to a trunk sewer entering a WWTP. The following ten sewer basins are separate from each other, but some of them are hydraulically-linked at the treatment plant: 1) Camp Creek (CMC); 2) Intrenchment Creek (INC); 3) Long Island (LIC); 4) Nancy Creek (NCR); 5) Peachtree Creek (PTC); 6) Proctor Creek (PRC); 7) Sandy Creek (SDC); 8) South River (SRV); 9) Sugar Creek (SGC) and 10) Utoy Creek (UTC).

Consent Decree Root

The FACD mandates the elimination of all unpermitted discharges and sanitary sewer overflows to achieve compliance with NPDES permits. This is accomplished through a number of plans under sections VIII.C.1, VIII.C.2. and VII.B.8.D of the FACD.

One plan is the System-wide Flow and Rainfall Monitoring Plan whose purpose is identifying excessive infiltration and inflow (I/I), quantifying peak flow factors, establishing sewer group priorities, and serves as a data source for hydraulic and hydrologic modeling. The City has submitted this plan to EPA/ GA EPD (Environmental Protection Division.)

To fulfill the requirements of the FACD, ADS Environmental Services was contracted in 1999 to install and maintain flow meters and rain gages, process and analyze the meter data and prepare monthly reports. Thirty-two 32 rain gages (tipping bucket) were installed throughout the City to provide a comprehensive network for establishing a rainfall record. Originally the selection of the preliminary rain gage locations uses a “circle of influence” methodology. Most rain gages are located at existing City owned /operated facilities such as libraries, fire stations, public schools, police stations, etc. These locations provide several favorable items such as ease of access, security, ease of connection to existing telephone lines and proximity to proposed flow monitoring locations.

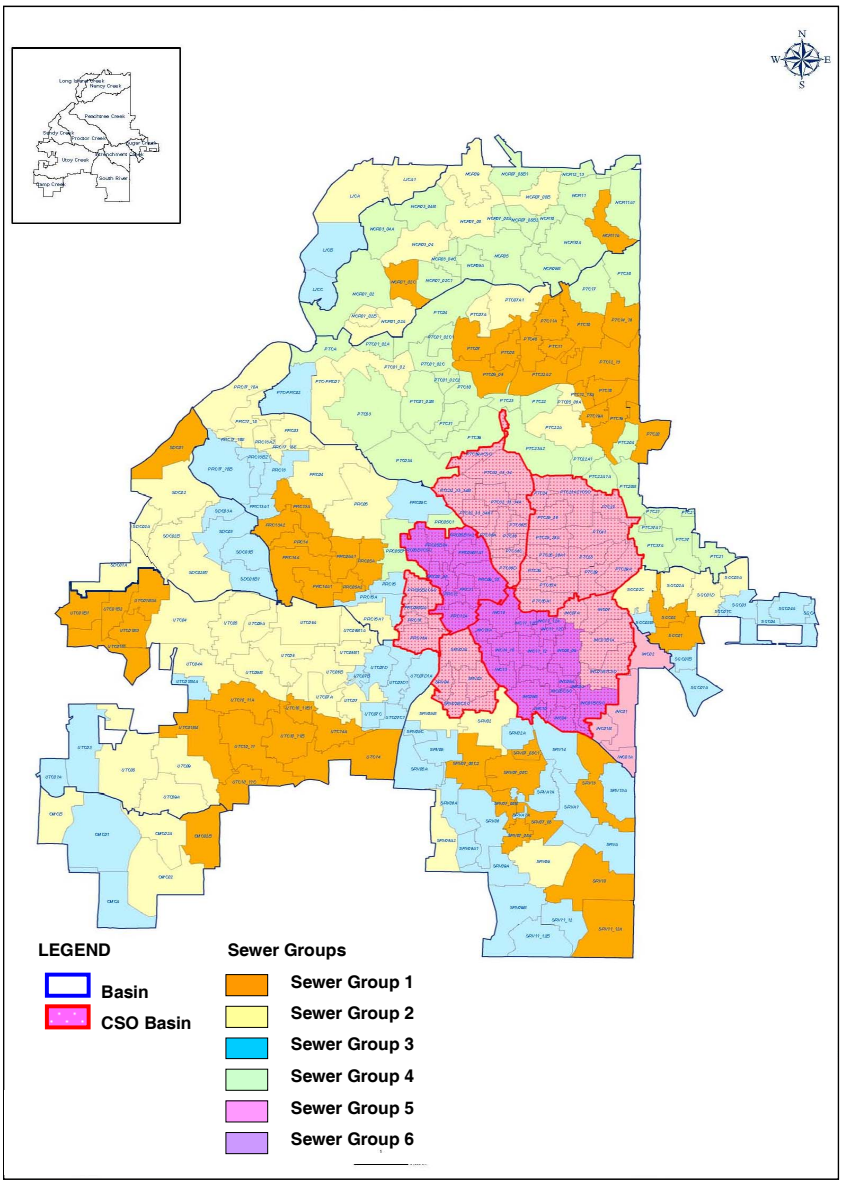

Figure 1. Prioritization plan by sewer groups.

The need for a comprehensive hydraulic model was realized early in the consent decree process through the requirement of a System-wide Hydraulic Modeling Plan. The model was deemed essential to assist in the development of operational procedures that may optimize system capacity, as well as to evaluate the impact of proposed system improvements. This plan is responsible for selecting the modeling software to be used and establishing the modeling approach, data verification, calibration methodology, performance and overall sensitivity. Infoworks CS (IWCS) is the current modeling software that the city uses.

As with other modeling software packages, IWCS dynamically simulates the flow within a sewer system by iteratively calculating flows in each pipe segment until it

converges on a solution at a predetermined tolerance such as (0.01 MGD) for flow and (0.01 ft.) for Depth. As all models, it is heavily dependant on the physical characteristics of the system including pipe diameter, length and slope, network connectivity, manhole coordinates, inverts and ground elevations, as well as sewer facility configuration such as Wastewater Treatment Plant, CSO facilities and Pump stations.

Modeling Approach

Due to the immediate need for a hydraulic model, the City's modeling approach consisted of a three step process to obtain the physical asset data. Initially, in 2000, a macro model was built for only the large trunk and interceptor sewers (i.e. greater than 24-inch in diameter). This basic model provided the City with an initial capacity assessment of the system. Following that over the next four years, one sewer group per year and all major outfalls (greater than 12-inch diameter) were added as defined in the Prioritization Plan. The criteria for the initial prioritization of the Sewer Groups took account of ten items that related to:

1) Frequency of Overflows,
2) Severity of Rainfall Dependent Infiltration/Inflow (RDI/I),
3) Risk to Surface Waters (Creeks),
4) Impact Failure,
5) Status of Ongoing Rehabilitation or Renewal,
6) Available Capacity in Sewers,
7) Judgment of Sewer Operation & Maintenance Division,
8) Relative Impact of RDI/I from Jurisdiction Outside the City's Control,
9) Proposed Development Intensity and
10) Location of Sewer Within the Combined System as shown in Figure 2.

Lastly, all sewer lines 8-inch and above are currently being added resulting from Sanitary Survey Evaluation System (SSES) work that began in July 2002 and is an ongoing task. The end result is a comprehensive model for the City.

Calibration

Once the physical attributes have been received from SSES and a model is built, the model network is loaded to simulate dry weather flow. As population and trade flow data (Commercial/Industrial) is not readily available, an average dry weather flow (ADWF) is obtained from meter data pertaining to the sewershed. The ADWF is then distributed throughout the model and loaded onto manholes. Diurnal patterns that vary according to the time of day were developed and applied to dry weather flows based on flow data gathered from the meters. The diurnal profiles are derived from the flow meter data. Approximately seven days of ADWF are needed for calibration. For dry weather calibrations, a 10% margin of error is allowed on the total volume and peak flow. To meet this performance tolerance, base flow loading and/or the diurnal profile may be adjusted to match measured flow data.

Wet Weather Flow (WWF) calibration is achieved by comparing peak flows, velocity and depth of metered data with a model's simulated results. Wet weather parameters, such as contributing runoff area, slope and width of drainage sub-catchments, are adjusted until an acceptable correlation between simulation results and metered data is achieved for at least three recorded storm events. Calibration storm events have the following desirable characteristics:

- Antecedent conditions - preferably 5 dry days preceding the rainfall event.
- Total rainfall depth – 1-inch to 2-inch total depth. Larger storms (>2-inch) may produce manhole overflows within the model simulation results. This simulated flood volume loss will not be reflected in the measured flow meter data. Smaller storms (< 1-inch) do not adequately mimic the effects of a design storm.
- Season of event – Spring storms are preferable due to their tendency to be larger in volume and duration.
- For wet weather calibration, a 20% margin of error is allowed.

Rain Data for Modeling

InfoWorks CS (IWCS), the modeling software used by the City, has a very flexible and effective way of handling rainfall data input into the model. The software has two basic methods for assigning rainfall input data. The first method is the conventional method that the city has been using and requires to geographically locate all discrete rain gages within a rainfall boundary area and identifying them with a profile number. The software then creates Thiessen polygon regions and assigns rainfall to the sub-catchments within that region. The disadvantage of this method is that when there are missing rain gage data, as is common with rain gage networks, there are no input data for the entire corresponding region defined by the Thiessen polygon.

The second method uses regions or polygons defined by the modeler to identify the different rainfall profile boundaries. The software can use multiple rainfall and regions provided that each rainfall profile is associated with a corresponding rain gage boundary region. For this study we decided to use the sewershed boundaries within the Peachtree Sewer Basin and assigned rainfall profiles corresponding to each sewershed boundary region as shown in Figure 2. Figure 2 shows both boundary regions for Thiessen and Radar Rain polygons. The GIS shape file was then created from the sewershed boundaries. These boundary regions were then supplied to OneRain, Inc. and the corresponding profile were populated with the GARR rainfall data. IWCS had a limitation in using regions defined by the sewershed polygons with multiple vertices, so the regions GIS shape file was manually adjusted using simplified polygons to cover each sewershed area. Since the rainfall input data were developed from the GARR data, the sewershed regions had rainfall estimates for every time step of the simulation.

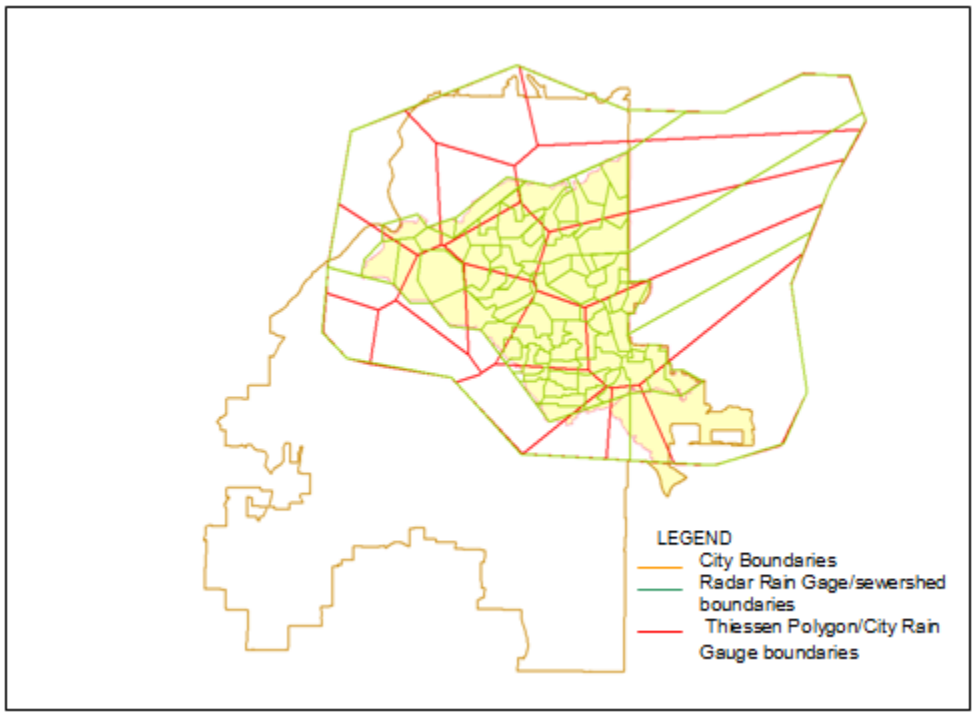

Figure 2. Comparison between Thiessen and Radar Rain Polygons for the Peach Creek Study Area.

Gage-adjusted Radar Rainfall Estimates

The GARR analysis incorporated NEXRAD radar data on a 2x2 km grid, with a 15-minute sample rate. Each radar image is a composite prepared using data from all National Weather Service WSR-88D radars covering the study area. The study area was based on the extents of the Atlanta city limits and what rain gages were available in and around that area. This area consisted of 783 2x2 radar pixels (29 rows and 27 columns) bounded approximately on the west by –84.6654° W longitude, on the east by –84.1491° W longitude, on the north by 34.0120° N latitude, and on the south by 33.4910° N latitude. A combination of 5-minute and 15-minute rain gage data for the study area were provided by the City.

The rain gage data were reviewed and checked for quality using several steps. First, six gages that failed to report rainfall for the entire study period were removed from the analysis. The next step was to divide the study period into separate rainfall events. Then scatter-plots were generated that compare the event gage volumes with their co-located unadjusted (raw) radar pixel rainfall estimate. Using these scatter-plots, under- and over-reporting gages tend to stand out from the rest of the group. During this step, the gages that recorded no rainfall and were paired with a radar pixel that did measure rainfall were removed from that period of the analysis. Figure 3 presents the scatter-plot comparing gage and (unadjusted) radar accumulations for the March 3-4, 2001 event. Gages circled in red indicate non-reporting gages and gages that appear to be under- or over-reporting for this event.

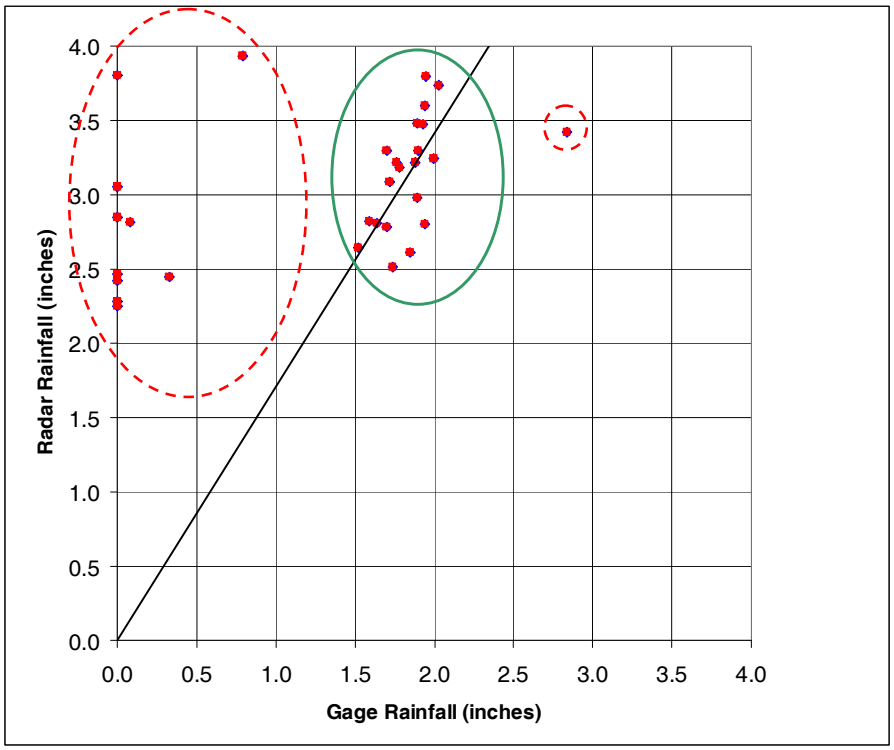

Figure 3. Comparing gage and radar accumulations for March 3-4, 2001 event. Suspect gages in dotted red circles required further investigation.

OneRain has developed tools to assist in the removal of these radar artifacts. However, initial analysis of the local Atlanta radar mosaic for March 2001 indicated that little filtering was required. For this pilot project, there was a much smaller number of discontinuities than typically exists. However, if further analysis is performed, a longer record of radar will be examined to determine necessary filtering. For this pilot study the only radar filtering performed was the removal of radar 'noise' or scatter that is common in raw radar. This noise in raw radar will appear as isolated short-term (usually less than 2 or 3 time-steps), stationary patterns that occur during times of no rainfall. Less than 0.4% of the 2784 radar frames required this type of filtering.

After the gages are checked and raw radar data has been filtered, comparisons and integration with gage data begins. A time-series was generated to compare each gage's data with its co-located radar pixel. At each pixel containing a gage location, an event gage/radar (G/R) ratio was computed by dividing the gage's measurement by the radar's during each event. Next, a Kriging-based interpolation technique was used to determine the appropriate geometry and distance-weighted G/R ratio for every other pixel in the domain. The G/R ratios were then multiplied by the filtered radar dataset for each time period during the study to determine the gage-adjusted radar rainfall amounts. This process was repeated for each event during the study period.

Figure 4 presents a block diagram description of the spatially variable gage-adjusted radar rainfall process.

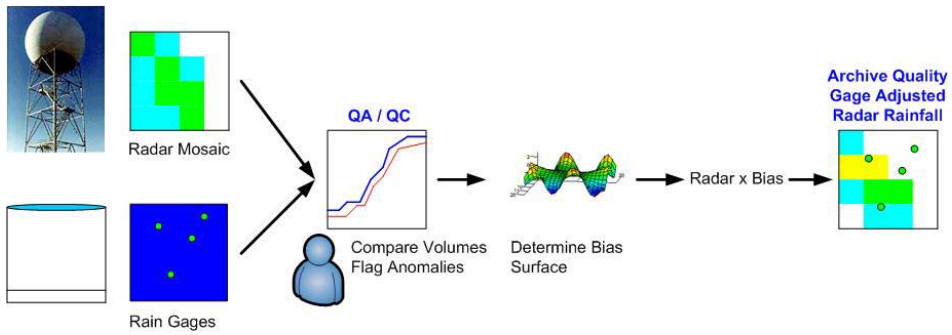

Figure 4. Block diagram depicting spatially variable gage adjustment process.

Gage-adjusted Radar Rainfall Results

Figure 5 shows the total rainfall accumulation across the City of Atlanta, study area for March 3-4, 2001. (This event became the focus of modeling results presented later in this paper.) For the entire study period, the central southern edge of the study area received the most rainfall. Pixel 15, counting from the bottom left of the image, along the southern study area boundary, received a gage-adjusted estimate of 12.0 inches of rainfall. The unadjusted radar estimates for that same pixel was 15.1 inches. Table 1 presents the ten highest rainfall intensities for time periods ranging from 15 minutes to 24 hours (start times are in UTC). The ten most intense 15-minute accumulations all occurred on March 12. The ten most intense one day totals occurred across four different days: March 3, March 11, March 12 and March 14.

Figure 6 shows the result of the gage-adjusted radar rainfall adjustment procedure. A G/R ratio was determined for each pixel and for each storm period before being multiplied by all of the raw radar rainfall estimates during those time steps. The result is a gage-adjusted radar rainfall dataset that matches the volume and timing of the rain gage network, but includes the spatial information from the radar. The Gages line shows the average accumulated rainfall for the gages with valid rainfall data and the Radar line shows the average accumulated rainfall from the radar pixels over the valid rain gages. The AdjRadar line shows the average gage-adjusted radar rainfall estimates for the pixels at the rain gages. In this figure, the AdjRadar line nearly matches the Gages line, indicating a good match between the rain gage and the gage-adjusted radar rainfall datasets. Overall, the gage-adjusted radar rainfall estimates were approximately 20% lower than the unadjusted radar estimates.

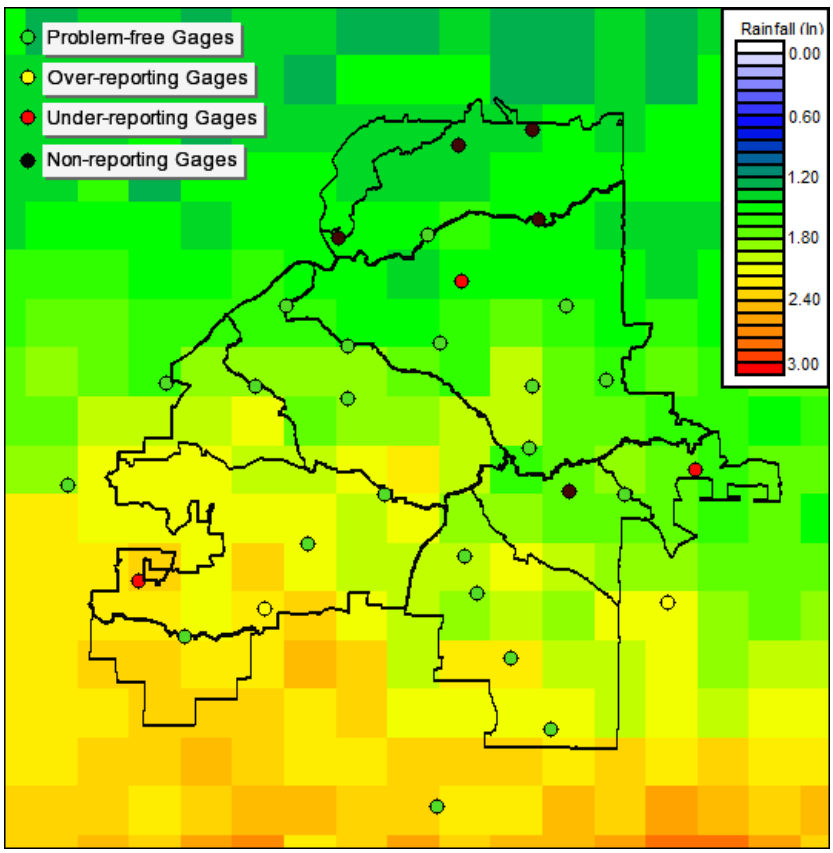

Figure 5. Gage-Adjusted Radar Rainfall estimates for March 3-4, 2001.

Table 1. Top ten rainfall intensities.

15-Minute Accumulations		1-Hour Accumulations		3-Hour Accumulations	
Start	Inches	Start	Inches	Start	Inches
3/12/2001 14:00	0.377	3/12/2001 13:45	1.128	3/4/2001 0:45	1.674
3/12/2001 14:15	0.324	3/12/2001 13:45	1.127	3/4/2001 0:30	1.669
3/12/2001 14:15	0.324	3/12/2001 13:30	1.117	3/4/2001 1:15	1.651
3/12/2001 14:00	0.324	3/12/2001 13:45	1.062	3/4/2001 0:30	1.596
3/12/2001 14:00	0.324	3/12/2001 13:45	1.061	3/4/2001 0:30	1.560
3/12/2001 14:00	0.324	3/12/2001 13:45	1.057	3/4/2001 0:30	1.521
3/12/2001 14:15	0.324	3/12/2001 13:45	1.026	3/4/2001 1:00	1.518
3/12/2001 14:00	0.324	3/12/2001 13:45	1.024	3/4/2001 1:00	1.515
3/12/2001 14:00	0.324	3/12/2001 13:30	0.983	3/4/2001 0:30	1.511
3/12/2001 14:00	0.323	3/12/2001 13:30	0.983	3/4/2001 1:00	1.502
6-Hour Accumulations		**12-Hour Accumulations**		**24-Hour Accumulations**	
Start	Inches	Start	Inches	Start	Inches
3/15/2001 2:00	2.054	3/12/2001 11:30	2.853	3/12/2001 0:00	2.911
3/15/2001 3:00	2.003	3/12/2001 11:15	2.834	3/11/2001 23:15	2.892
3/3/2001 22:15	1.994	3/14/2001 22:45	2.765	3/12/2001 0:00	2.787
3/15/2001 3:15	1.991	3/14/2001 22:45	2.753	3/14/2001 13:15	2.779
3/15/2001 3:00	1.985	3/12/2001 11:15	2.723	3/11/2001 23:00	2.773
3/15/2001 3:00	1.977	3/12/2001 11:15	2.703	3/14/2001 10:45	2.767
3/15/2001 3:15	1.972	3/12/2001 11:00	2.691	3/11/2001 22:30	2.764
3/3/2001 22:15	1.969	3/12/2001 11:30	2.684	3/11/2001 23:15	2.759
3/15/2001 2:15	1.966	3/12/2001 10:30	2.676	3/3/2001 5:00	2.738
3/3/2001 22:30	1.952	3/14/2001 22:45	2.669	3/12/2001 0:00	2.720

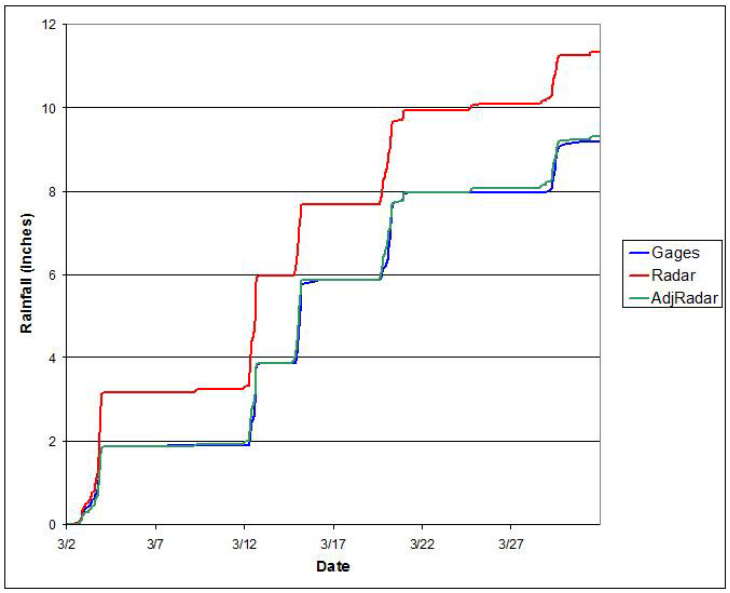

Figure 6. Average gage, raw radar, and gage-adjusted radar rainfall accumulation plot for March 2-30, 2001.

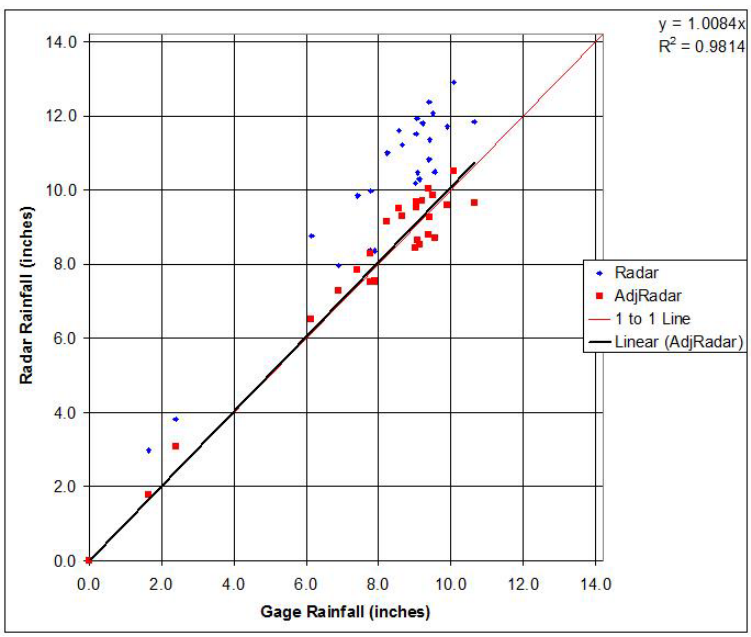

Figure 7. Scatter-plot of radar and gage-adjusted radar rainfall totals versus gage rainfall for each gage for March 2-30, 2001.

Figure 7 shows the scatter-plot of total rainfall measured at the gages compared to the radar and adjusted radar rainfall estimates at the pixels over the rain gages for March 2-30, 2001. If the gage and gage-adjusted radar rainfall estimates were identical, all points would lie on the 45-degree best fit line. However, due to scaling issues, measuring errors, natural variability, and other uncertainties, these values will not always match. Nevertheless, the gage-adjusted radar rainfall data are expected to

cluster around the 45-degree line. In summary, correlations between the two precipitation measurement systems were strong. Rainfall timing was well matched. Incorporating the gage volumes resulted in lowering the radar rainfall estimated by 20%.

Model Results

As stated earlier the current sewer modeling method is based on Thiessen Polygon distribution of rain gage boundaries that correspond to individual rain gages. When data for an individual rain gage is missing, the entire modeling results for the corresponding sewershed region is affected. An example of missing rain gage data occurred during the March 3-4 2001 rain event where flowmeter data were available. The total rainfall for the 38 hour event during this storm is around 2.8 inches with a frequency of less than 1 year and a maximum intensity of 1.15 in/hr. As mentioned earlier, in order to calibrate a sewershed, three (3) rain events with corresponding flowmeter data are required.

The GARR rainfall data were imported into each corresponding sewershed region profile of the Peachtree Creek Basin in the IWCS model. The rainfall profile was then used to run a simulation of sewershed PTC07A1 and calibrate it against the available flowmeter data. Figure 8 shows the simulation results for the flow from the model with the GARR calibrated input data and the Thiessen Polygon rain gage data. Both rainfall datasets are plotted versus the observed flow meter data for the period from 3/2/2001 to 3/4/2001.

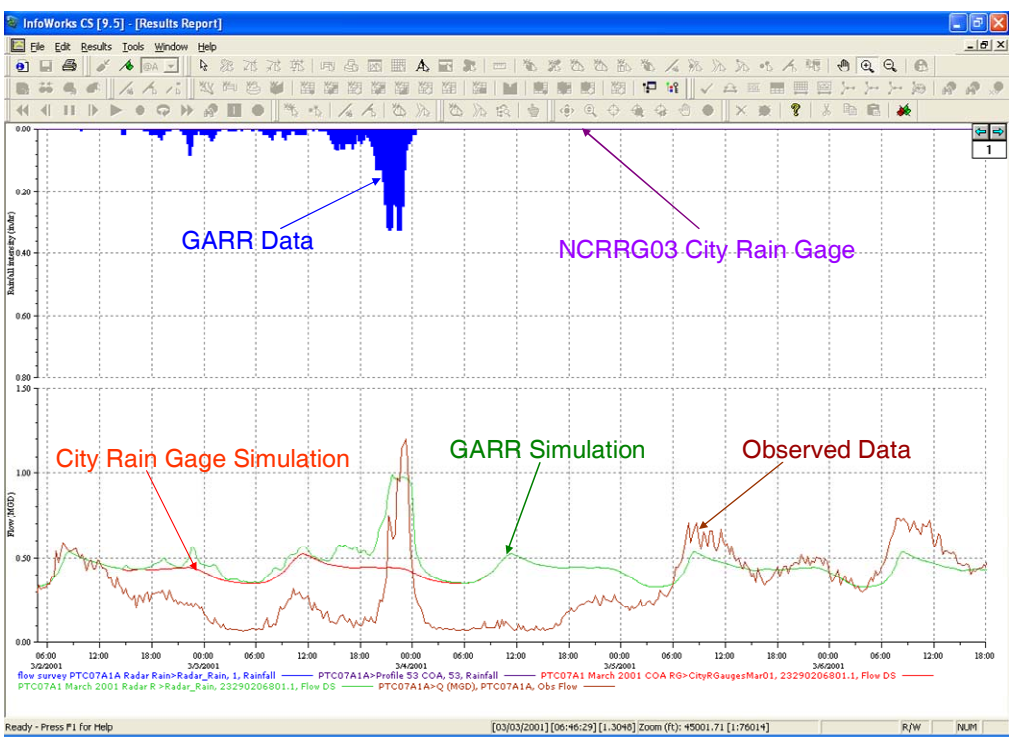

Figure 8. Comparing model results.

With the Thiessen Polygon method, modeling results for the sewershed were entirely dependent on rain data from the sewershed's single gage which recorded no data for the event. Therefore, the model could not be calibrated for the event. In contrast, the GARR rain data enabled us to populate the same storm event for that sewershed and to verify the model response to the observed ones.

Conclusion-Lessons Learned

GARR has made it possible to calibrate the sewer system model during periods when data from individual gages were unavailable. In addition, GARR rainfall datasets provide vastly improved spatial distribution of model input and more detailed characterization of rainfall events. This capability will become more and more critical as the City refines and adds detail to their system model.

This GARR Pilot Study provided valuable feedback on the quality of the gage data collection system. The system correlated well with the radar system and suggests that its data could provide the gage data foundation for additional historical analysis.

The success of this historical GARR analysis indicates it is good candidate for transitioning to a real-time application of GARR. Real-time GARR analysis uses a more simple algorithm called "uniform adjustment", which is based on the average gage/radar ratio over the preceding hour. Although spatially variable gage/radar ratios are not used, uniformly adjusted radar still integrates the spatial resolution of radar with the volume accuracy of rain gages. Real-time GARR, particularly when published on the web in real-time, can be a powerful tool for sewer system operations during rainfall events.

Another option for the City of Atlanta system is to implement gage-adjusted radar forecasting. Radar forecasting is typically based on the McGill Algorithm of Precipitation by LaGrangrian Extrapolation (MAPLE). MAPLE incorporates the past 90 minutes of radar movement to extrapolate the growth, decay, direction and speed of existing precipitation cells. MAPLE also attempts to determine the transition between rain, freezing rain, and snow. Once MAPLE forecasts are obtained, the gage/radar ratio over the preceding hour is applied to the data in order to calculate the forecasted GARR estimate. Forecasted GARR would better enable the ability to predict spills and flooding areas in the storm sewer system.

Rainfall is the input variable with the largest impact on modeling sewer systems. Its information is essential for determining rehabilitation efforts and system upsizing. By using the GARR process to enhance rainfall input data, the City of Atlanta will create more accurate models, attain a better representation of storm frequency, intensity, duration, and potentially improve future forecasting capabilities. By using GARR techniques, inflows from storm events and the resulting impacts will be better quantified.

Adaptive Long-Term Monitoring at BP Environmental Restoration Sites

Matthew Zavislak[1], John Dustman[2], Dennis Beckmann[3]

[1] Summit Envirosolutions, Inc., 1217 Bandana Blvd. N, St. Paul, MN 55108; PH (651) 644-8080; email: jdustman@summite.com, mzavislak@summite.com

[2] Remediation Engineering and Technology, BP Corp., North America; PH (281) 366-6982; email: dennis.beckmann@bp.com

Abstract

In partnership with BP, Summit Envirosolutions, Inc. has developed a unique set of software tools for reducing costs and improving effectiveness of long-term monitoring (LTM) through adaptive assessment to achieve remediation goals.

There are four components which comprise the software toolset. The first component, EPIPHINY®, is a database platform which gives the user the ability to quickly import and analyze analytical sampling data. The second, ModelBuilder™, creates and visualizes geostatistical models of spatial and temporal data, and identifies areas of significant data uncertainty which may benefit from additional sampling. The third, SampleOptimizer™, identifies redundant sampling locations and frequencies in historical data in preparation for future sampling events. SampleTracker™, the fourth component, enables users to create time-dependent site-wide remediation targets (e.g., expected reductions in mass) or well-specific targets (e.g., expected concentration trends) and to evaluate new data relative to those targets, as well as providing automated alerts of unexpected deviations.

This paper presents the long-term monitoring optimization (LTMO) results for two BP case study sites. The results are presented in the form of tradeoff curves associated with competing objectives: 1) minimizing the number of sampling locations; and 2) minimizing the maximum interpolation errors at all sampling locations which were recommended to be removed, as well as comparative visualizations showing the site concentrations before and after optimization.

1.0 Introduction

Routine long-term monitoring (LTM) is a significant component of overall operating expenditures at many private and public sector environmental restoration sites, with some estimating it as 30% of the average overall restoration project budget [ASCE 2003]. These costs not only include the cost of sample collection and laboratory analysis, but also the associated data management, data analysis, and reporting which is needed.

Numerous approaches to long-term monitoring optimization (LTMO) have been developed to optimize the selection of future samples to be taken in the next sampling round, in order to minimize the costs for sample collection and laboratory analysis [see ASCE 2003]. However, SampleOptimizer™ is unique in that it is the only approach which performs true mathematical optimization by utilizing a multi-objective genetic algorithm. Further, EPIPHINY® and SampleTracker™ enable their users to lower their data management, analysis, and reporting costs through automated importing, querying, and reporting modules.

This paper gives describes the technologies which comprise EPIPHINY®, SampleOptimizer™, and SampleTracker™, and presents the results of several case study analyses using these tools.

2.0 Technology Description

Experience indicates that the single largest component of data analysis budgets is usually putting the data into a form that can be analyzed. The environmental data industry still lacks a unified "data dictionary"; therefore, data formats differ between analytical laboratories, field equipment, and internet sources. The use of Microsoft® Excel® is currently the predominant repository of environmental data and is primarily used to prepare tables of data for reports.

2.1 EPIPHINY®

EPIPHINY® represents a new approach to "handshake" disparate data sources into a common database format. Import routines, data sets, and query results can all be saved and shared amongst EPIPHINY® users. Its powerful I/O algorithms can import and export data to and from text documents, spreadsheets, several database formats, as well as shape file formats utilized by ESRI ArcGIS®. The software provides robust data normalization and validation, parameter and location grouping, graphing, cross-tab table generation, intuitive interfaces for SampleOptimizer™ and SampleTracker™.

2.2 ModelBuilder™ and SampleOptimizer™

Both ModelBuilder™ and SampleOptimizer™ utilize algorithms from Data to Knowledge (D2K), a data analysis and optimization package created at the National Center for Supercomputer Applications (NCSA) at the University of Illinois [Welge et al. 2003]. ModelBuilder™ and SampleOptimizer™ were built to be powerful and customizable, yet their configuration is automatable and is thus easily accessible to everyday users.

As previously mentioned, SampleOptimizer™ employs a multi-objective genetic algorithm called NSGA-II, proposed by Deb (2002), to generate an optimal set of solutions between various competing objectives. This set of optimal solutions is known as a tradeoff curve or Pareto frontier. The advantage of using genetic algorithms to solve multi-objective problems is that the entire Pareto frontier can be generated in a single computational run. Figure 1, below, shows a set of snapshots of the Pareto frontier as developed by the software.

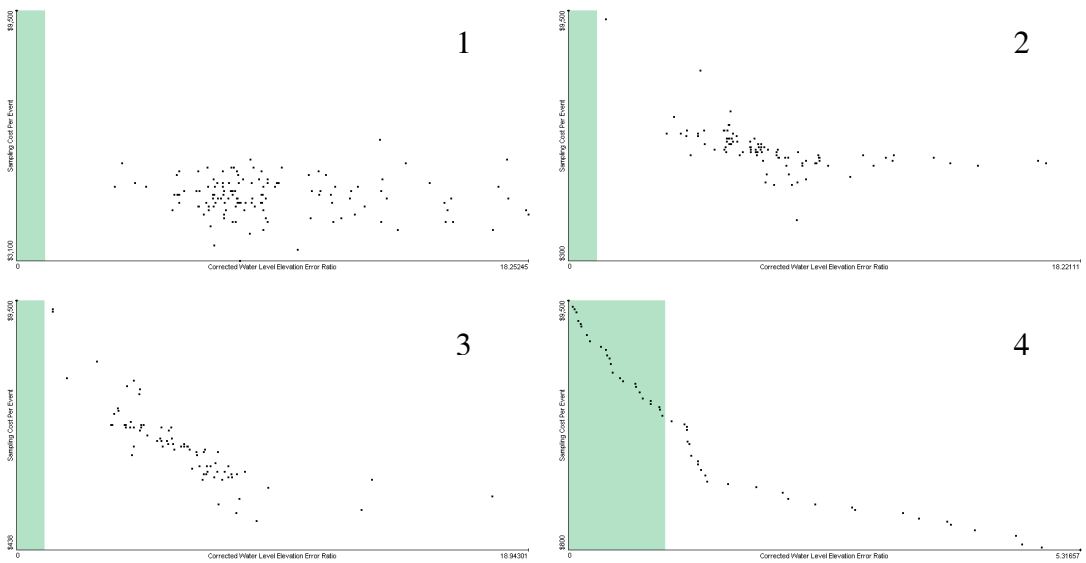

Figure 1: Progression of Pareto Frontier (shown chronologically, from 1 to 4)
The shaded areas highlight designs which fulfill the user defined accuracy objective.

ModelBuilder™ is a software module which assists the user in selecting a suitable interpolation model to use with their site data in SampleOptimizer™. In contrast to other interpolating packages which are strictly manually-configurable (such as ESRI® ArcView® Spatial Analyst), ModelBuilder™ automatically suggests a set of interpolation model parameters which are relevant to the site data. For example, when Ordinary Kriging is chosen as the interpolator, ModelBuilder™ suggests the values to be used for the theoretical variogram (nugget, spherical term, linear term).

After the model parameters have been chosen, ModelBuilder™ creates site visualizations which are easily customized to the user's choice of labels, symbols, and ranges. ModelBuilder™ also has the ability to calculate a mass metric value (based on summing the interpolated concentration values) for a site which can be inputted into SampleTracker™ for monitoring along with the values at individual sampling locations. Lastly, ModelBuilder™ has the ability to generate visualization maps of model and data uncertainty which can be used qualitatively utilized during site analysis to help decide if and where to site new sampling locations (see Figure 2, below). These uncertainty maps are created through a multi-step leave-one-out cross validation mechanism which is automated, and yet can be customized if needed.

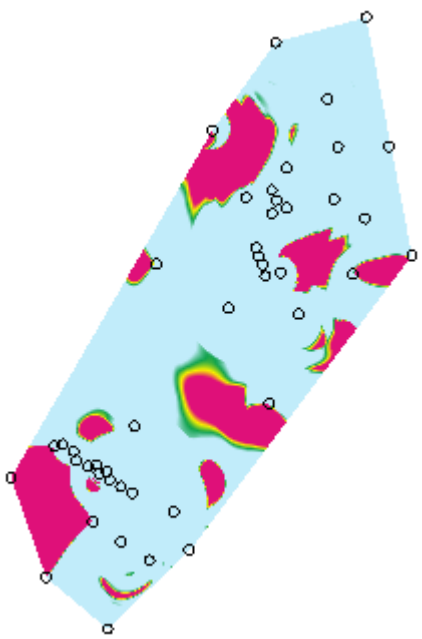

Figure 2: Example Relative Uncertainty Analysis Visualization
High relative uncertainty areas are highlighted in magenta.

2.3 SampleTracker™

SampleTracker™ is a complimentary application to both EPIPHINY® and SampleOptimizer™ which is designed to review current monitoring data against historical data and identify cases where current data deviates from expectations which are based on the historical dataset. These expectations are formulated in the form of bounds, which represent a statistical estimate of the range of values that might be expected in a specific sampling event, based on the historical data at that location.

Any current data value which is outside the bounds range for that location is reported to the user as being out-of-bounds (see Figure 3, below). Like ModelBuilder™ and SampleOptimizer™, SampleTracker™ makes configuration recommendations based on the site data which can be optionally customized by the user.

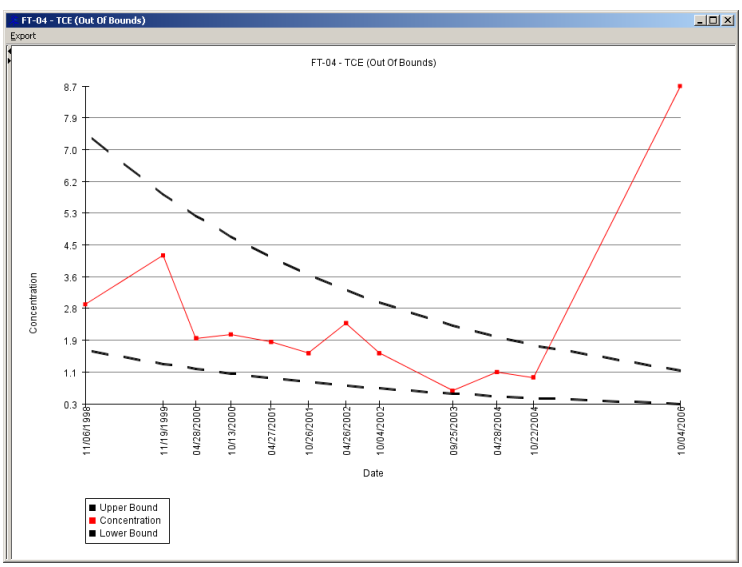

Figure 3: Example Unexpected Data Alert

4.0 Methodology

As with any data analysis tool, the quality of the analysis is dependent on the quality of the data. The spatial analysis of data generally requires basic information such as the geographic coordinates of the sampling location, the elevation of the sampling location (or, in the case of a monitoring well, the screened interval), and a result of analysis or measurement. The results of analysis using SampleOptimizer™ will be dependent on the level of understanding of the site conceptual model; it is generally not prudent to optimize data that are combined from multiple groundwater flow systems that are not hydraulically connected.

It is important to note that sampling at a site will usually be ultimately determined via discussions with the relevant stake holders, including any applicable regulatory bodies, and the results we provide here are the first step towards implementing a new sampling plan.

5.0 Results

5.1 Site 1 – Groundwater Elevation Sampling; Spatial Analysis

The site is sampled frequently during the year -- locations are regularly sampled at least quarterly; some locations have irregular additional sampling taking place on a monthly basis, and sometimes even more frequently. This site's geology is more complex, with a large recharge basin approximately half a mile off site, and active pumping taking place in the part of the site.

For this analysis, site data was first imported from two Microsoft® Access® database files into EPIPHINY®. One database contained the sampling results, and the other contained the well information (coordinates, depths, etc.). The import process was very straightforward and took approximately half an hour.

Next, after brief consultation with site personnel, a representative two-day sampling event in April 2008 which included 95 sampling locations was chosen to be the focus of the optimization. After about an hour of computation, the software presented the Pareto Frontier shown in Figure 4.

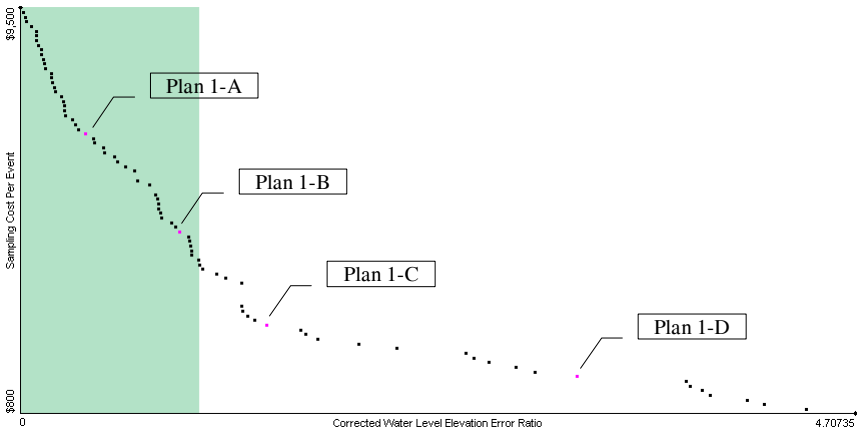

Figure 4: Site 1 Pareto Frontier

Next, various sampling plans in the Pareto Frontier were considered, and the four plans highlighted above were chosen for further consideration. Plume visualizations for each plan were created by ModelBuilder™, and are presented below in Figure 5.

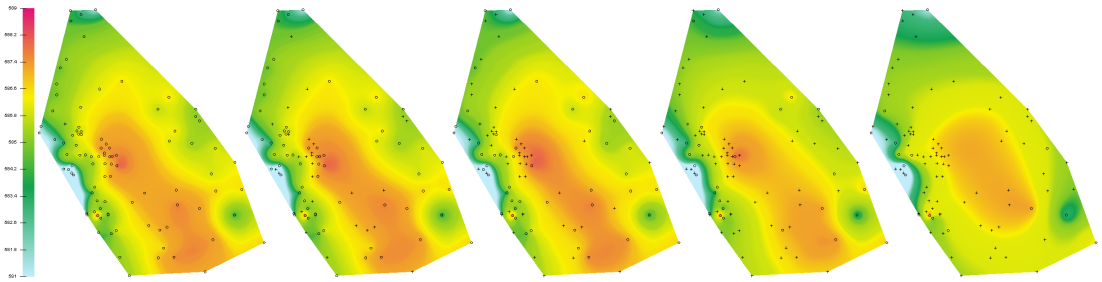

Figure 5: Selections from Site 1 Pareto Frontier
(From Left to Right: All 95 locations, Plan 1-A, Plan 1-B, Plan 1-C, Plan 1-D)

After viewing the plume visualizations, Plan 1-C was selected for proposal to the site team for consideration in future sampling events, since it offered very high savings in the number of samples taken (51%) while maintaining an excellent amount of useful information.

5.2 Site 2 – Benzene Sampling; Spatio-Temporal Analysis

This site uses regular semi-annual sampling, with approximately 50 samples per event and has an overall simple hydrogeology. There is no active pumping at the site, and there is a gradual hydraulic gradient present from the north east to the south west.

As with the previous site, the site data needed to first be imported from its native format. The data proved to require some basic reformatting in Excel®, but after less than an hour of formatting work, the data was ready to be imported into EPIPHINY®.

Once in EPIPHINY®, the data was queried and studied, and benzene was determined to likely be the driving COC at the site because of its levels relative to its USEPA MCL. After brief consultation with members of the site team, optimization of both the choice of sampling location as well as sampling frequency (called spatio-temporal optimization) was decided as the appropriate method. As a result, the seven most recent sampling events from 2005 through early 2008 were queried, and their data was easily exported into SamplingOptimizer™.

For Site 2, a novel approach for spatio-temporal analysis was chosen as an experiment. First, individual spatial optimizations were performed for each of the chosen sampling events. Next, a plan which was felt to represent an appropriate tradeoff between useful information and sampling cost was selected for each event. Next, the seven optimized sampling plans were tabulated in a spreadsheet, and analyzed as a group. After careful consideration, two most recent sampling events were weighted most heavily in deciding which frequency to recommend to the project team for consideration (see Table 1 for an example).

Plan #	464	71	1690	527	930	190	334	
Well ID	**Q1 2005**	**Q3 2005**	**Q2 2006**	**Q4 2006**	**Q2 2007**	**Q4 2007**	**Q2 2008**	**Recommended Frequency**
SW-2	On	On	On	On	On	Off	Off	Off
SWP-24	Off	Off	Off	Off	Off	Off	Off	Off
SW-8	Off	On	Off	Off	Off	Off	On	Annual
SW-14	On	Off	Off	Off	On	Off	On	Annual
SW-1	On	On	On	On	On	On	On	Semi-annual
SW-3	On	On	On	Off	On	On	On	Semi-annual
Sampling Reduction	34%	37%	40%	26%	33%	28%	20%	27%

Table 1: Example Frequency Analysis for Site 2
(Abbreviated for space consideration)

To check the results of the analysis, the proposed plan was visualized for the most recent sampling event (see Figure 6). While the amount of sampling reduction for this example (27%) is less than at Site 1, each sample at Site 2 is more costly to take since each one must be sent to a lab for analysis, and therefore such a sampling reduction would likely be worthwhile.

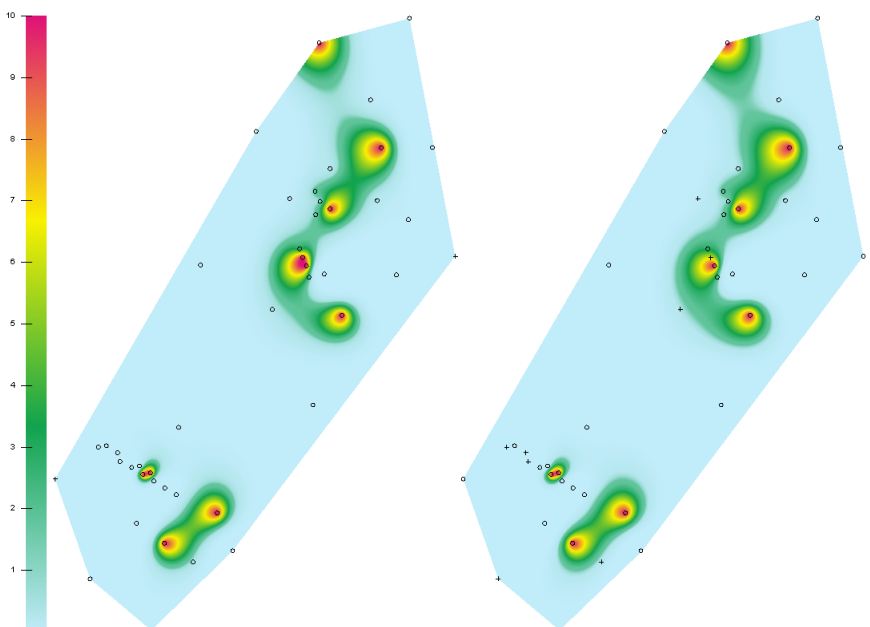

Figure 6: Site 2 Optimization (Q2 2008)
(Left - Before, Right - After)

6.0 Conclusions

At both sites, the use of the software tools was a success. EPIPHINY® was able to quickly and easily import site data, and made it easy for the user to export data to SampleOptimizer™. SampleOptimizer™ proved intuitive to use and found significant levels of potential sampling redundancy at both sites. Both of these sites will continue to be studied and future work will include results from using SampleTracker™.

References

Deb, K., et al., A Fast and Elitist Multiobjective Genetic Algorithm: NSGA-II, *IEEE Trans. Evol. Computation*, 6(2), 182-197, 2002.

ASCE Task Committee on the State of the Art in Long-Term Groundwater Monitoring Design, *Long-Term Groundwater Monitoring: The State of the Art*, ed. by B.S. Minsker, American Society of Civil Engineers, Reston, VA, 2003.

Welge, M., L. Auvil, A. Shirk, C. Bushell, P. Bajcsy, D. Cai, T. Redman, D. Clutter, R. Aydt, and D. Tcheng, *Data to Knowledge (D2K)* An Automated Learning Group Report, National Center for Supercomputing applications, University of Illinois at Urbana-Champaign, 2003. Available at http://alg.ncsa.uiuc.edu.

Application of Radio Frequency Tracers to Individual and Group Particle Displacement Within a Laboratory

T.J. Lauth[(1)], A. N. Papanicolaou[(2)]

(1) Graduate Research Assistant, IIHR-Hydroscience and Engineering, Department of Civil and Environmental Engineering, The University of Iowa, Iowa City, IA 52242, E-mail: timothy-lauth@uiowa.edu.

(2) Associate Professor, Robert and Virginia Faculty Fellow in Engineering, IIHR-Hydroscience and Engineering, Department of Civil and Environmental Engineering, The University of Iowa, Iowa City, IA 52242, E-mail: apapanic@engineering.uiowa.edu.

Abstract

Multiple approaches (shear stress, discharge, stream power, etc.) have been developed for describing the rate of bedload movement, each with a means of being calculated in the field. One current approach relies on the mean virtual velocity of individual sediment particles. Virtual velocity is determined by dividing the displacement length of a particle by the sum of the rest and displacement times. The focus of this research is the application of a Radio Frequency Identification (RFID) system as a means to monitor individual and group particle displacement and rest times necessary for calculating the virtual velocity, so that the bedload transport rate can be predicted. An RFID system consists of programmed transponders and a corresponding reader that communicate using radio waves. This communication provides the ability to track individual particles with embedded transponders. By setting customized antennas in the flume to act as gateways, communication between the antennas and particles traveling over a known distance provides the time between antennas, allowing for the calculation of the 1-D virtual velocity. To develop this system, multiple obstacles needed to be overcome. Past RFID research has shown that transponder orientation and transponder signal collision can present large problems to the application of RFID technology to sediment transport research. These two problems have been accounted for by: 1) using particles consisting of two transponders oriented perpendicularly to each other, and by 2) using transponders that have anti-collision signal capabilities. The use of anti-collision capable transponders also provides the capability of tracking the flux of a group of particles. Tracking a group of particles allows for correction due to the flow field and the possibility of hiding. Cameras and image analysis tools will be used for confirmation of results.

Introduction

Many relationships exist for equating a quantifiable parameter to the rate of movement of bed material in a gravel bed stream to provide for future bedload rate prediction. One of the most popular parameters used for this prediction is the Shields parameter, a non-dimensionalized form of the critical shear stress (Shields, 1936). This shear stress value is commonly calculated using an erosion flume, where conditions (such as slope, flow depth, etc.) on a bed test section can be changed until incipient motion is achieved. Discharge is a second commonly used variable for predicting bedload rate (Schloklitsch, 1934), and can be measured using an acoustic doppler velocimeter along with surveying equipment to determine channel geometry. A third means of relating to bedload transport rate is stream power (Bagnold, 1966), which requires the same equipment as discharge to calculate. More recently, the virtual velocity of a particle has been used to develop such a relationship to account for the random nature of particle movement. The virtual velocity is given as the distance traveled by a particle divided by time the flow was capable of moving a particle of that size. The use of the total time flow capable of moving a given particle size instead of just the movement time for that particle accounts for the random aspect of particle movement (Haschenburger and Church, 1998); that for non-fully mobile beds, particles randomly experience periods of movement and rest dependent on localized flow conditions.

Due to its emphasis on individual particle movement, the use of virtual velocity as the independent variable requires a tracing technique for quantitative measurement. In the past, the painting of individual particles or groups of particles was widely used for tracing but the burial and hiding of particles during events strong enough for movement have often led to a low recovery rate. Low recovery rates result in an over-representation of the results of the located particles (in many cases, leading to an over-prediction of movement due to the loss of buried particles). In an attempt to increase the rate of recovery, many researchers have switched to tracing techniques that do not require a line-of-sight for discovery. One such technique is the use of particles equipped with radio transponders, as part of a radio frequency identification system.

Radio frequency identification technology is commonly considered to have first been developed during World War II, as a means identifying friendly aircraft. The technology then did not significantly further develop until the 1960s and 1970s, during which it started to be used for its most common application today, inventory tracking and supply management. The main mechanism for communication between a transponder (the combination of transponder and receiver, also commonly called a tag) and an antenna in an RFID system is the transmission of radio waves at a set frequency. The transponder consists of a small antenna, circuit for holding information, and capacitor that is charged when in the presence of the antenna's electromagnetic field. The reader acts to translate the radio waves received from the antenna in to a form usable by the operator and to send control signals to the antenna for transmission as radio waves to facilitate communication with transponder. For most applications of RFID technology near water and metal (both highly present in this research), the communication frequency used is 125 kHz, which has a longer wavelength than other RFID frequencies and thus does not get absorbed as easily by the two materials.

RFID technology has many benefits that make it well-suited for use as a particle-tracing tool: 1) particle communication is not dependent on sight for discovery, making detection during an event possible, 2) radio communication is possible through most bed materials, so detection of buried particles is possible, 3) the cost of individual particles is small, so, although recovery rate

can be very high, loss is not a serious limiting factor, 4) distance between particle and antenna does not matter as long as the particle is within the antenna's electromagnetic field, 5) the possibility of unique codes for each particle make individual particle tracing possible, 6) depending on the antenna configuration, particle detection can be treated as LaGrangian (i.e. finding each particle in the field) or Eulerian (i.e. each particle passing a set detection point).

Objectives

Prior RFID research in the field of sediment transport has focused on the issues of development of RFID as a tracer (Ergenzinger, Schmidt, & Busskamp,1989), use to measure step length and travel path (Habersack, 2001), and particle tracing in coastal environments (i.e. the transition from gravel to sand)(Allan, Hart, & Tranquili, 2006). The goal of this research is to present RFID as a tool for the prediction of bedload transport rates by using the virtual velocity of particles. Having a transponder-equipped particle move through a set up with multiple antennas spaced at known intervals could potentially yield time and reach-specific virtual velocity values. These specific virtual velocity values can allow a more precise calculation of the bedload rates. As opposed to real-time measurements, the use of RFID technology for tracing has largely been limited to gathering one final measurement after a particle-mobilizing event has concluded and the reach has drained. In this research, communication between the antenna and particle is only possible when the particle passes through the antenna coil. This setup provides the ability to determine, for the first time, the bedload transport rate in quasi-real-time without removing the particle from the system or visual tracking. However, due to the current limitations of RFID technology, the testing will be limited to the calculation of 1D virtual velocity values. 2D virtual velocity values will be gathered using video analysis and used for comparison.

Methodology

The experiments will be carried out in a 21.1 m long flume, with a 0.7m wide by 0.55 m high cross-section (Papanicolaou and Kramer, 2005). A simulated gravel bed consisting of five layers of 19 mm marbles packed in the densest possible configuration has been carefully placed in the bed in the flume (Papanicolaou and Schuyler, 2003). The necessary development length for a rough bed has been taken into consideration, with the test section located 10.9 m from the flume's entrance. For the test section, the top layer of marble-packed bed is made up of opaque white marbles, as to better contrast with the painted particles. The flow will be monitored by an electronic flow meter and controlled using two pumps with digital speed controls. Flow depth will be maintained using the flume's tailgate and exit rods to restrict the flow at the of the flume.

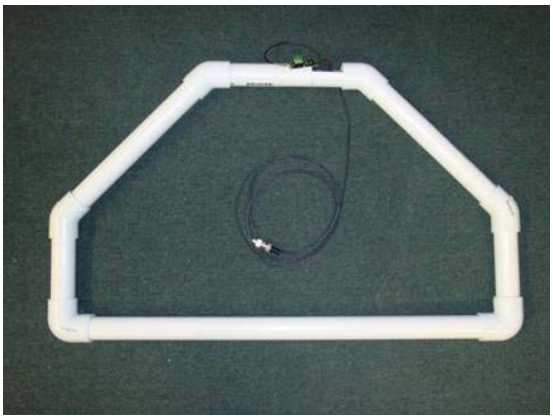

Fig 1. Antenna for RFID Reader

The RFID equipment located in and around the test section of the flume consists of four antennas, a reader, a computer, and 50 particles. The computer will be running a custom-built program developed using LabView software as a base. As a particle passes a given antenna, the program will display the identification code of the transponders in communication, the number of the antenna the transponders are in contact with, and the time of contact, all of which will be written into a text file for logging. The four antennas have been designed to fit within the cross-sectional dimensions of flume as well as be waterproof to a point safely above testing depth to avoid contact of the tuning electronics with the flowing water. These four antennas are connected back to the reader by means of a multiplexer and cable. Placing antennas as a cross-sectional gateway for the particles to travel through has not been tried before for RFID use in sediment transport research, but has been done in RFID research involved with fish tracking. The antennas will be oriented parallel to the cross-section of the flume to allow for detection of the particles as they roll through the antenna coil (providing quasi-real-time tracking of the particle).



Fig 2. Glass casing for transponders

Each test particle is made up of a glass case and two transponders. The glass cases were made from 25.4 mm glass marbles annealed to reduce the chance of cracking and then with the transponder holes drilled out. With the case prepared, two transponders programmed with unique identification codes were placed in the glass case, sealed in with outdoor silicone, and the whole particles were spray painted for easy numerical identification while testing.

To complete the experimental setup, three cameras have been placed around the flume to record both the plan and profile movement of particles through the test section. Two of the cameras will view the tests from the side through the flume's glass walls, and the third remote-controlled camera is mounted overhead to capture the plan view movement. Each camera has been connected to a computer for digital storage and analysis of video. To help ensure clear

video footage is captured, the flume wall opposite the profile-view cameras has been blacked out, and additional lights have been placed around the flume to remove shadows.

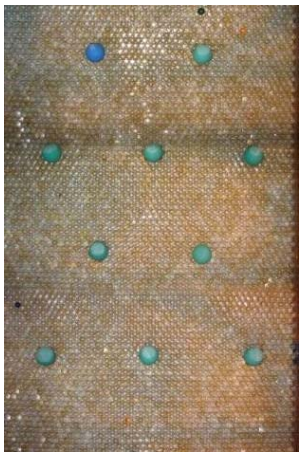

Fig 3. Potential Grid for 10-Particle Organized Test

Three feeding configurations are to be considered for the experimental tests, namely: 1) individual particles, 2) a 10-particle group organized upstream of the section corresponding at 2% packing density, and 3) a 10-particle group with no organization upstream of the section. The individual particles will be fed upstream of the test section using a feeder pipe designed to standardize release, provide for a quick release, and minimize flow disruption. The organized 10-particle group of tests is being run to account for the flow field within the flume. The non-organized 10-particle group of tests will be run to account for the hiding effect that will occur when particles start to group. Each group of tests will be run for a standard set of flow levels and flume slopes.

Discussion of RFID Complications, Solutions, & Expected Results

Prior research has revealed two serious impediments to the wider application of RFID technology to sediment transport: 1. Transponder orientation's significant effect on communication range between transponder and antenna, and 2. Signal collision due to multiple transponders in the antenna's electromagnetic field. These two impediments dictated the selection of the RFID system. Past experiments (Lauth & Papanicolaou, 2008) have indicated that particle orientation can have transponder orientation lead to nearly a 50% reduction in communication distance; unpublished trial tests put the reduction at closer to an order of magnitude. The reduction in signal strength is due to non-optimal direction of the tag antenna. With one of the main benefits of RFID particle tracking being the ability to detect and account for buried particles, the significant communication reduction could possibly lead to an over-reporting of buried particles as lost particles. To account for the effect of transponder orientation on particle communication, the transponders within the particle have been oriented perpendicularly to each other. While using two transponders in each particle will not guarantee at least one ideal orientation for communication, the potential loss in communication ability will be partially accounted for by the rotation of the particle while moving.

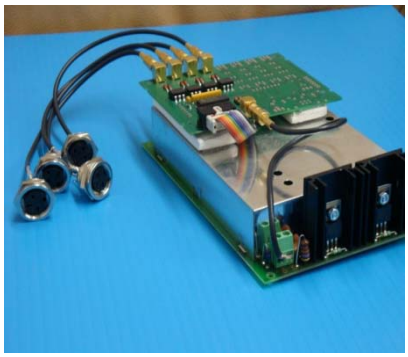

Fig 4. Uncased RFID Reader with Multiplexer

Previous testing with a RFID system has indicated that communication is not possible between an antenna and multiple tags. Because the reader does not have a system to distinguish a priority to which tag should be read when multiple are in the electromagnetic field, the reader fails to correctly identify any transponder, leading to communication failure (a condition known as signal collision). This problem can be solved in one of two ways, either by controlling transponder movement as to remove the chance of two transponders both being within the field at the same time, or by utilizing a system whose transponders and reader have an algorithm for assigning priority for transponder reading. Given the desire to use a two-transponder particle for testing, this research relies on a reader and transponders equipped with a priority algorithm.

One final impediment to RFID research not mentioned thus far in the sediment transport literature is the large effect that background electromagnetic interference can have on communication distance. A large component of RFID sediment transport research has taken place in natural streams and rivers (Nichols, 2002, Habersack, 2003, Lamarre, MacVicars, and Roy, 2005), many times in environments with little modern influence. However, the equipment developed for field research often requires development and initial testing in laboratory environments. These environments are at risk for background electromagnetic interference caused by poorly shielded electronics or electronics that emit irregular electromagnetic pulses (one prominent example is a digital flow controller). Such interference can be hard or expensive to detect, and may be systemic to the laboratory's power lines. This problem can be solved by removing the interference source, properly shielding the work environment (through use of a Faraday cage), or by using a reader that can filter out background interference. For this research, a reader with a filter was employed with attempts made to lessen the impact of interference sources.

The expectation for this research is that the transponders for each particle will communicate with each antenna the particle rolls through as the particle travels down the test section with each communication recorded. The timestamps from successive antenna passes along with the known distance between antennas will provide the 1D virtual velocity. Because the calculation of the virtual velocity will only be 1D, video files from the plan view camera will be analyzed using tracking software to determine the 2D virtual velocity for comparison. A recognized limitation of the current experimentation is that the packed simulated gravel bed will not allow for burial.

The use of RFIDs will potentially provide a finer resolution for the calculation of virtual velocity and thus bedload transport. These calculations could be made in real-time instead of after event. Furthermore, automation is possible where previously a large time dedication by a field researcher was required.

References

Allan, J.C., Hart, R., and Tranquili, J.V. (2006). "The Use of Passive Integrated Transponder (PIT) Tags to Trace Cobble Transport in a Mixed Sand-and-Gravel Beach on the High-Energy Oregon Coast, USA". *Marine Geology*, **232**, 63-86.

Bagnold, R.A. (1966). "An Approach to the Sediment Transport Problem from General Physics." *US Geological Survey Professional Paper*, **422-I**

Ergenzinger, P., Schmidt K.H., and Busskamp, R. (1989). "The Pebble Transmitter System (PETS): First Results of a Technique for Studying Coarse Material Erosion, Transport and Deposition". *Zeitschrift f˙ur Geomorphologie N.F.* **33**, 503–508.

Habersack, H.M. (2001). "Radio Tracking Gravel Particles in a Large Braided River in New Zealand: a Field Test of the Stochastic Theory of Bed Load Transport Proposed by Einstein." *Hydrological Processes*. **15**, 377-391.

Habersack, H.M. (2003). "Use of Radio-Tracking Techniques in Bed Load Transport Investigations." *Erosion and Sediment Transport Measurement in Rivers: Technological and Methodological Advances* (Proceedings on the Oslo Workshop, June 2002). IAHS Publication 283. 172-180.

Haschenburger, J. and Church, C. (1998). "Bed Material Transport Estimated from the Virtual Velocity of Sediment." *Earth Surface Processes and Landforms*, **23**, 791-808.

Lamarre, H., MacVicar, B., and Roy, A.G. (2005). "Using Passive Integrated Transponder (PIT) Tags to Investigate Sediment Transport in Gravel-Bed Rivers." *Journal of Sedimentary Research*, **75,** 736-741.

Lauth, T.J. and Papanicolaou, A.N. (2008). "Experimental/Feasibility Study of Radio Frequency Tracers for Monitoring Sediment Transport and Scour Around Bridges"

Nichols, M.H. (2002). "Tracking Large Particle Movement with Passive Radio Transponders in Ephemeral, Alluvial Channels." *Hydraulic Measurements and Experimental Methods*, 171-176.

Papanicolaou, A. and Kramer, C. The Role of Relative Submergence On Cluster Microtopography And Bedload Predictions In Mountain Streams. Published at the International Symposium, IAHR, River, Coastal, and Estuarine Morphodynamics, October, 2005, Illinois, p. 1083-1087

Papanicolaou, A.N. and Schuyler, A. (2003). Effects of Sediment Specific Gravity on Cluster-Bedform Evolution; An Experimental Study, *Journal of Engineering Mechanics, ASCE,* vol. 129, No. 10, p. 1206.

Shields, A. (1936). "Application of Similarity Principles and Turbulence Research to Bed-Load Movement." *California Institute of Technology Publication No. 167*, Soil Conservation Surface, Pasadena, Calif.

Schoklitsch, A. (1934). "Der geschiebetrieb und die geschiebefracht [Bedload Transport and Bedload Movement]", *Wasserkraft Wasserwirtschaft*, **4** 1-7.

Cost-effective automated water quality monitoring systems providing high-resolution data in near real-time

Rob Ellison MS[1], Mike Cook PhD[2]

[1]YSI, Integrated Systems & Services, 13 Atlantis Dr., Marion MA 02378, PH (508) 468-8612, e-mail: rellison@ysi.com
[2]YSI, Environmental Monitoring Systems, 9940 Summers Ridge Rd, San Diego, CA 92121, PH: (858) 546-8327, e-mail: mcook@ysi.com

ABSTRACT

Automated monitoring systems are providing near real-time data at very high spatial and temporal resolution at a fraction of the cost of sampling programs. Significant improvements have been made in regards to reliability, maintenance intervals and ease-of-use that are making autonomous technologies the most cost-effective means of environmental monitoring. Data will be presented on the effectiveness of an automated vertical profiling system and a low-cost, autonomous underwater vehicle (AUV) used to transport a water quality monitoring package through a water column. Data from several case studies in drinking water reservoirs and natural environments throughout the world will be shown. Particular focus will be on the cost benefits of the vertical profiler in drinking water reservoirs and the AUV in environmental mapping applications. The profiling system provides near real-time data throughout the water column for a number of key water quality parameters such as temperature, algae biomass, turbidity, and dissolved oxygen. The data are being used to optimize water treatment and react to events, resulting in significant cost savings and providing better quality water. The AUV is used for a variety of water quality and bottom mapping applications. Monitoring agencies and consulting firms are using the system to provide very high-resolution data for point source and non-point source mapping, side-scan sonar surveys, and environmental impact projects at a fraction of the cost of current methods.

INTRODUCTION

The pressures on research groups, monitoring agencies and the private sector to expand and improve environmental data collection with limited resources have never been greater. At the same time an increased understanding of the high variability in natural systems (temporal and spatial) requires data to be collected at a higher resolution. Real-time monitoring of water quality offers a number of advantages over periodic spot sampling. The primary benefit is improved accuracy of the data and lower operating costs. As more real-time data is collected at shorter and shorter intervals, users are detecting greater and greater variation in natural environments, temporally and spatially. These variations are important to understand the environment, identify baseline conditions and thus recognize when conditions stray from baseline.

The evolution of field sensing equipment has resulted in increasing volumes of data with a decreasing level of effort. Manual monitoring in the field often involves vehicles, boats, multiple technical personnel, fuel and requires a significant amount of labor to collect a relatively small amount of data. In some cases the data resolution does

not provide information on daily variations and often misses events such as algae blooms, storms or natural disasters. Fixed-point continuous monitoring stations such as data buoys offer high temporal resolution data and larger sensor payload capacity, but from only one fixed depth. Automated vertical profiling platforms offer high temporal and spatial (vertical) resolution and can monitor in near-real time the dynamics of a water column which allows user to monitor dynamics and events on relevant time scales. These systems are able to track short- and long-term natural cycles and trends and in some cases forecast events (algae blooms), monitor events and the impact and recovery of events.

Autonomous mapping vehicles provide spatial coverage of water quality at unprecedented resolutions, allowing users to map water bodies and develop improved understandings of the dynamics of the system. They are also capable of bathymetric mapping that can be used to map bottom type, calculate water volume, and visualize bottom features. Due to the limitations of spot sampling and the growing importance of collecting environmental data at environmentally relevant time and spatial scales, YSI has developed two new autonomous water quality platforms which allow for detailed unmanned monitoring. Figure 1 presents results from the Vertical Profiler and the AUV.

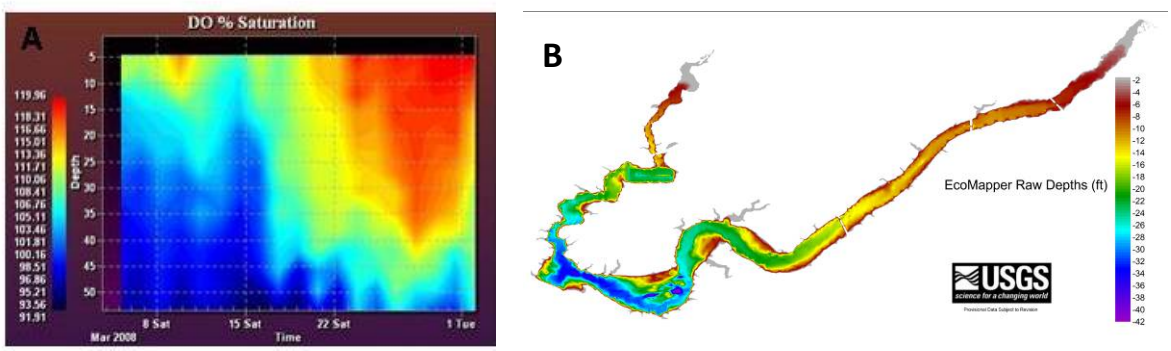

Figure 1. Two types of time-series data from (A) the Vertical Profiler showing variations in dissolved oxygen within a column of water over time and (B) an AUV mapping of depth of a lake.

Technological developments in the areas of in-situ sensors, data telemetry, and automated platforms have resulted in significant increases in system reliability and significant reductions in the cost of ownership. In regards to in-situ sensors, reliability has improved from new and more robust sensing methods, such as optical dissolved oxygen, as well as improved antifouling techniques that extend maintenance intervals thus reducing the cost of ownership. Data telemetry systems have evolved to plug-and-play systems that can post data to the web within minutes and requires no internal support, and monitoring platforms have developed to provide extremely high spatial and temporal resolution that would be extremely expensive or impossible to duplicate with other sampling modes.

This paper will focus on two automated platforms that are providing researchers, consultants and monitoring groups with tools to generate exceptionally high-resolution data that would have been cost prohibitive or impossible using more manual methods. The first platform is an automated vertical profiling system that provides water quality times-series data in near real-time throughout a water column. The systems are mounted

to fixed structures or to floating platforms and can be used in a variety of aquatic environments. The second platform is an autonomous underwater vehicle (AUV) designed specifically for water quality and bathymetric mapping. The vehicle collects data at 1 Hz as it moves horizontally and vertically through a water body at speeds of 1 to 4 knots. Both systems operate autonomously to carry a water quality sensor suite. The profiling system provides a time-series data set from multiple depths within a column of water. The system has been designed for extended maintenance intervals to maintain an affordable operating cost. The AUV runs missions on pre-programmed routes collecting data at a rate of 1 Hz. This allows an operator to map water bodies with 100% coverage. The autonomous operation of both systems results in a low cost of operation and high-resolution data.

AUTOMATED VERTICAL PROFILER

The Automated Vertical Profiler is a rugged monitoring platform that transports a YSI multiparameter water quality sonde through a water column at a user-defined interval. The system is capable of collecting water quality data in up to 100 m of freshwater or seawater. **Figure 2** presents a schematic of the Profiler. The water quality sonde is connected to a remote-controlled winch that raises and lowers the sonde to preprogrammed levels to collect vertical profile water quality data. The sonde is capable of measuring temperature, conductivity, salinity, specific conductance, dissolved oxygen, depth, pH, ORP, turbidity, algae biomass and blue-green algae biomass. A meteorological suite can also be installed. Considering the capabilities, there are a wide range of applications for the profiler including drinking water reservoir monitoring to improve treatment efficiency as well as lake/estuary/near coastal continuous monitoring.

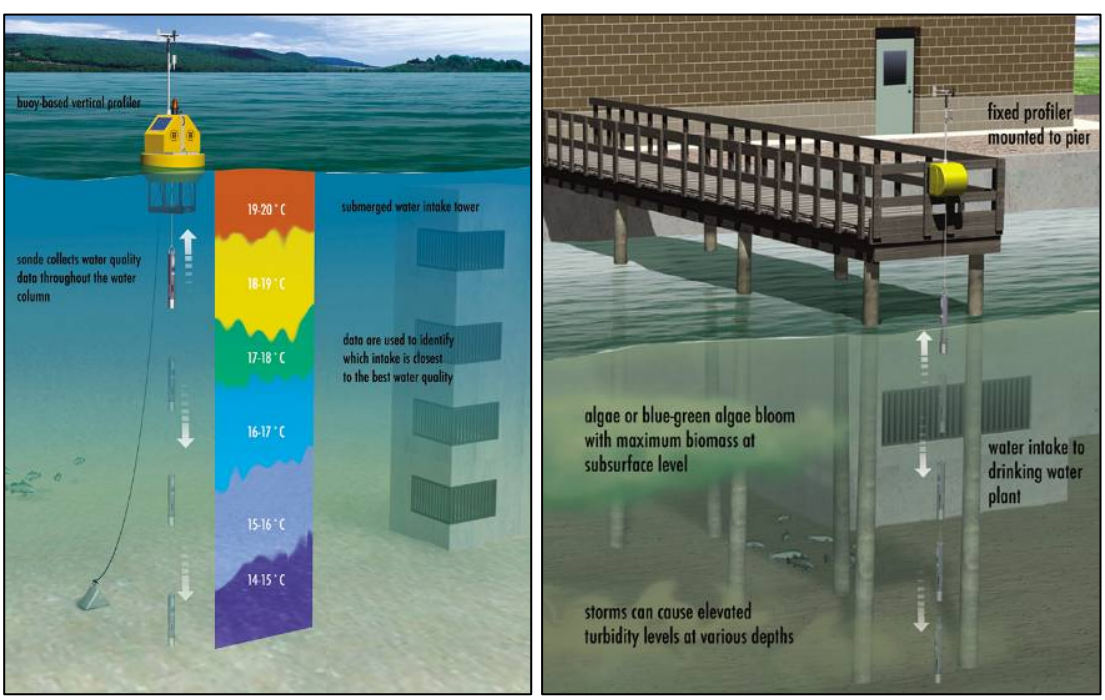

Figure 2 Schematic of the Vertical Profiler System installed near water intakes for drinking water plants; LEFT graphic of a profiling system mounted to a floating platform. RIGHT graphic of a profiling system mounted to a fixed platform such as a piling,

Of particular interest in recent years have been problems caused by blue-green algae (aka cyanobacteria) in drinking water reservoirs, often triggered by increased nutrient loading in watersheds. Blue-green algae are responsible for producing compounds (geosmin & MIB) that cause taste and odor problems in drinking water and in some cases producing toxins that can contaminate drinking water supplies. Planktonic algae, including blue-green algae, move throughout the water column and biomass in constant flux. The profiling systems allow plant operators to track total algae and blue-green algae biomass in near real-time in addition to other water quality parameters that can often stimulate an algae bloom or be impacted by algae growth such as temperature, dissolved oxygen, conductivity and pH. In reservoirs that have multiple water intakes to the plant, operators use the profiler data to identify the intakes with the best water quality thus increasing filter run-times, reducing chemical use and the likelihood of poor drinking water quality and customer complaints.

An important drinking water reservoir for the Raleigh, North Carolina area is Falls Lake. This lake serves 450,000 people and has been impacted by blue-green algae blooms for many years with blue-green algae making up to 75-95% of the algae population in the summer months (Werblow, 2008). A team at the Center for Applied Aquatic Ecology at North Carolina State University, working closely with the plant operators, has installed and maintained a continuous monitoring system for the past five years. The system is providing valuable data on blue-green algae dynamics during floods, droughts and storm events and saving the treatment plant operators money while improving water quality. The system is composed of multiple vertical profiling systems that profile the water column every 3 hours at 0.5 m depth intervals. The profiles are able to identify the chlorophyll maximum that guides where the optimal intake depths should be. The system also tracks algae blooms that can come and go with days or weeks and would likely be missed by manual sampling schemes. The profiler data are posted to a website (see Figure 3) that can be accessed by the public, researchers and plant operators to see the latest water quality information (www.ncsu.edu/wq).

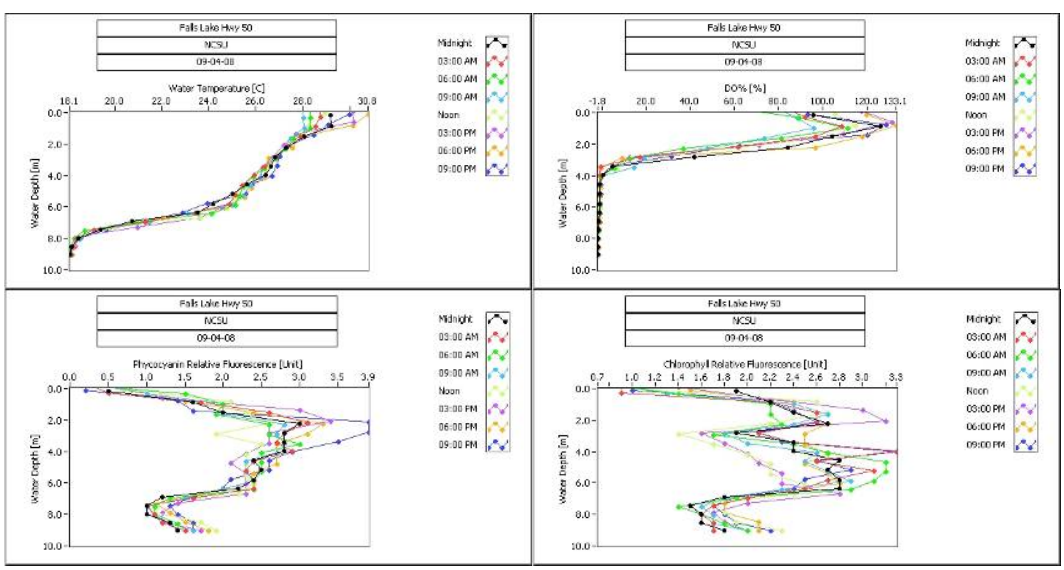

FIGURE 3: Examples of the daily profiler data posted to the web from Falls Lake. Graphs (from L to R, T to B) of temperature, dissolved oxygen, chlorophyll and blue-green algae.

A vertical profiling system offers significant cost savings. For plant operators, the near real-time data allows them to choose water intakes with the lowest blue-green algae biomass and therefore use less treatment chemicals, such as powdered activated carbon, needed for water with high blue-green algae biomass. In fact, plant operators have indicated that the cost of one fixed profiling system was less than the cost of one-week supply of PAC to treat high algae concentration. In other source water applications that use oxygenation systems, vertical profilers can result in significant power savings by providing continuous data on the dissolved oxygen levels and stratification. Profiler users in California have reported up to 50% savings in power consumption when the profilers have been installed. For researchers and monitoring groups, the price of the data is far less than using more manual methods.

AUTONOMOUS UNDERWATER VEHICLE

The EcoMapper™ AUV is a small, person-deployable environmental mapping vehicle that can operate in depths of <1 m and run for more than 8 hours on a single battery charge. These capabilities are coupled with a large sensor suite that requires only one field technician to deploy from shore, significantly lowering the operating costs. The data set that the vehicle is capable of collecting would be extremely challenging or impossible to collect from a boat or research vessel due to the EcoMapper's undulation and shallow depth capabilities and maneuverability. The EcoMapper has been designed to be an environmental mapping work horse capable of routine use in freshwater and near-coastal environments. The user loads pre-programmed mapping missions into the vehicle and the vehicle will operate completely autonomously to map an area, allowing the operator to conduct more technical work in the field.

The physical design allows for easy deployment from shore by one person. All external components on the vehicle can be easily replaced or installed in the field with the exception of the side-scan sonar. The external replaceable components include the water quality sensors, handle and balance assembly, vehicle antennae, control planes, propeller and cowling. This provides a more reliable system that can be repaired or re-configured in the field, saving the user valuable time and money.

The water quality sensors are located in the bow and are protected by the sensor guard. The field-replaceable water quality sensors suite (sensor payload is identical to the Vertical Profiler) is integrated into a sensor bulkhead which allows the user to add or remove sensors easily, providing a flexible payload that can be easily configured for a specific study. The EcoMapper antennae includes a GPS antennae, a charging plug for the internal lithium-ion power supply, optional cell phone and long-range radio antennas, and a series of LEDs that provide visibility to the vehicle while on the surface and indicate vehicle power and battery charging status. The four fins or control planes are field-replaceable as is the two-bladed prop and cowling. Figure presents a drawing of the EcoMapper.

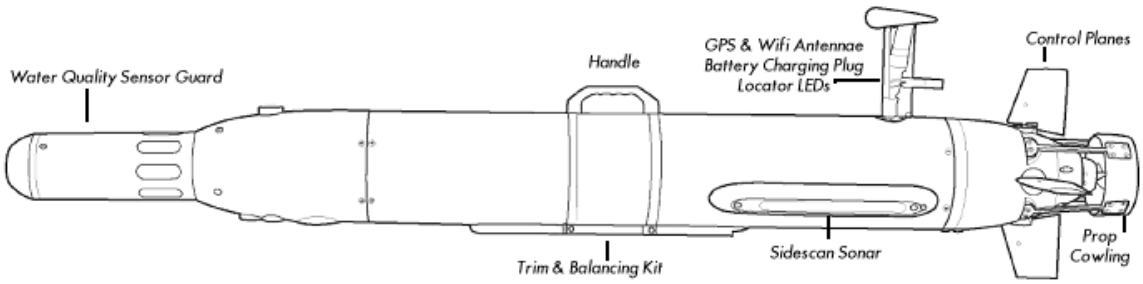

Figure 4. Technical drawing of the EcoMapper vehicle

Vehicle Specifications

Below is a list of technical specifications for the AUV. The AUV provides a flexible platform for water quality monitoring and hydrographic surveying. Options provide users the ability to monitor various water quality parameters as well as the ability to incorporate various bathymetry options making the AUV a valuable tool for lakes, reservoirs, estuaries and shallow coastal operations.

Dimensions: Length: 60.1 inches (152.65 cm);
Diameter: 5.8 inches (14.73 cm)
Weight (air): 45 lbs (20.41 kg)
Energy: 600 W-Hrs of rechargeable Lithium-Ion batteries (>300 cycles)
Endurance: 8 hours at speed of 2.5 knots (battery configuration dependent)
Speed Range: 1 - 4 knots
Control: Four independent control planes
External Connection: Data - wireless 802.11g Ethernet (up to 200m comm. distance)
Navigation: Dead reckoning via GPS (when on the surface)
Tracking: Internal data log (with programmable resolution)
Sensors: Conductivity, Temperature, Depth, height from bottom, 3-axis digital compass
Onboard Electronics: Low power X86 processor, 80 GB drive (data collection)
Software: Windows XP Embedded, GUI-based Navigation Suite
Communication: 2.4 GHz radio link (when on the surface)
Additional Options: Water Quality Sensors: Optical Dissolved Oxygen, Turbidity, Chlorophyll Fluorescence, Blue-green Algae Fluorescence, pH, ORP, Side-Scan Sonar: Imagenex 330 kHz or 330 / 800 kHz, DVL
Security System: Safety Tow Float

The EcoMapper is designed for fast deployment and ease-of-use and VectorMap mission planning software is a key feature to this capability. The software is loaded onto the user's PC and accepts a variety of geo-referenced map formats. The software allows the user to draw a mission directly on the map or image. For each leg of a mission, the user will program the location, vehicle speed, depth from surface or height from bottom or undulate between the two points, and which sensors to activate and log. Once a mission is created, a mission plan file is formed and transferred to the EcoMapper by loading it onto the UVC vehicle control software.

Communication with the vehicle is established via a Wi-Fi connection. The Wi-Fi antennae is located within the EcoMapper antennae and transmits a signal to the EcoMapper Communications Box, which is accessed by a wireless enabled PC or handheld device. The Communications Box is comprised of a rechargeable lithium-ion power supply, modem and Wi-Fi antenna. By running Windows™ Remote Desktop on a laptop or Pocket PC, the user can access the on-board computer and run the UVC vehicle control software. UVC is used to load missions, check diagnostics, transfer data and ~~to~~ take manual control of the vehicle when it is on the surface and within Wi-Fi range. After all vehicle missions, the EcoMapper creates a .log file. This file can be opened in mission planning software and overlaid onto the mission file to observe the vehicle's actual course.

Vehicle navigation occurs through the use of GPS position fixes at a series of surface waypoints. Between surface waypoints the vehicle 'dead-reckons' when it dives below the surface. If the vehicle is pushed off course between waypoints, the vehicle will detect this and travel back to the intended waypoint before continuing its mission. In areas with strong currents, more surface waypoints are required to keep the vehicle on course. An optional Doppler Velocity Log (DVL) will be available in the near future and will allow for very accurate sub-surface navigation in a range of conditions.

The EcoMapper has several safety features to minimize vehicle damage or loss in the case of unforeseen events. Internal detectors can detect a leak into the vehicle which will trigger the vehicle to surface and abort the mission. A series of safety rules are available to program vehicle behavior under specified circumstances such as; no forward progress, diving below specified depth, low power level, and mission length longer than specified time. A location pinger is standard in the event that the vehicle does not surface and a safety tow body is available that includes a large inflation device, depth sensor, additional pinger and control electronics if the AUV loses power and becomes stuck. A cell phone located in the vehicle can be used to track the vehicle when it is on the surface.

The EcoMapper has been deployed in a variety of environments over the past two years ranging from coastal to in-land waters and reservoirs to estuaries. In 2008 YSI worked with an agency in Illinois that required high-resolution water quality data at varying depths. The demonstration was conducted in one day and the purpose was only to demonstrate the EcoMapper's capabilities and not to conduct a scientific study. The EcoMapper mission was developed on site and required approximately 30 minutes to program and transfer to the vehicle. The site was a 4,900 acre lake surrounded by a recreation area that is a popular destination for fishing, water skiing, swimming, hiking and picnicking. The land and lake are owned by a power company that operates a nuclear power station in the area. The power station produces 1,043 net megawatts (electricity for ~1 million homes) and uses the lake to cool the plant's thermal discharge.

The lake is currently on the EPA's 303(d) list of impaired waters and classified as eutrophic. Sources of pollution are primarily agriculture, shoreline erosion and urban run off/sewers. There are currently no TMDLs reported for this water body and the source of impairment is listed as unknown. Groups monitoring the lake and the power company were both interested in the EcoMapper to autonomously produce high-resolution thermal and bathymetry maps of the lake in order to evaluate the lake's capacity to accept the thermal discharge and to study the ecological impacts of the discharge. Past thermal mapping was conducted through the use of aircraft and IR cameras, which provided a thermal map of the surface only. A preliminary mapping of the area around the power plant's thermal outfall was performed. The mission was 4 hours and 45 minutes with the

first half on the surface at a speed of 2 knots and the second half at 4 feet below the surface at a speed of 4 knots. The mission length was 11.1 miles.

Figure 5 shows some of the data collected. Image A displays the mission developed for the thermal outfall, where the dots indicate waypoints and the lines indicate the planned mission. Image B presents water depth, while Image C displays the water surface temperature with the thermal outfall evident from the hot water distribution. Image D shows subsurface temperature collected from 4 feet below the water surface. A clear difference in temperature distribution is seen between the surface (Image C) and subsurface data (Image D). Image E presents dissolved oxygen data at the surface while Image F highlights chlorophyll fluorescence at the surface. A clear pattern of lower algae biomass near the thermal outfall and increasing biomass away from the outfall was observed.

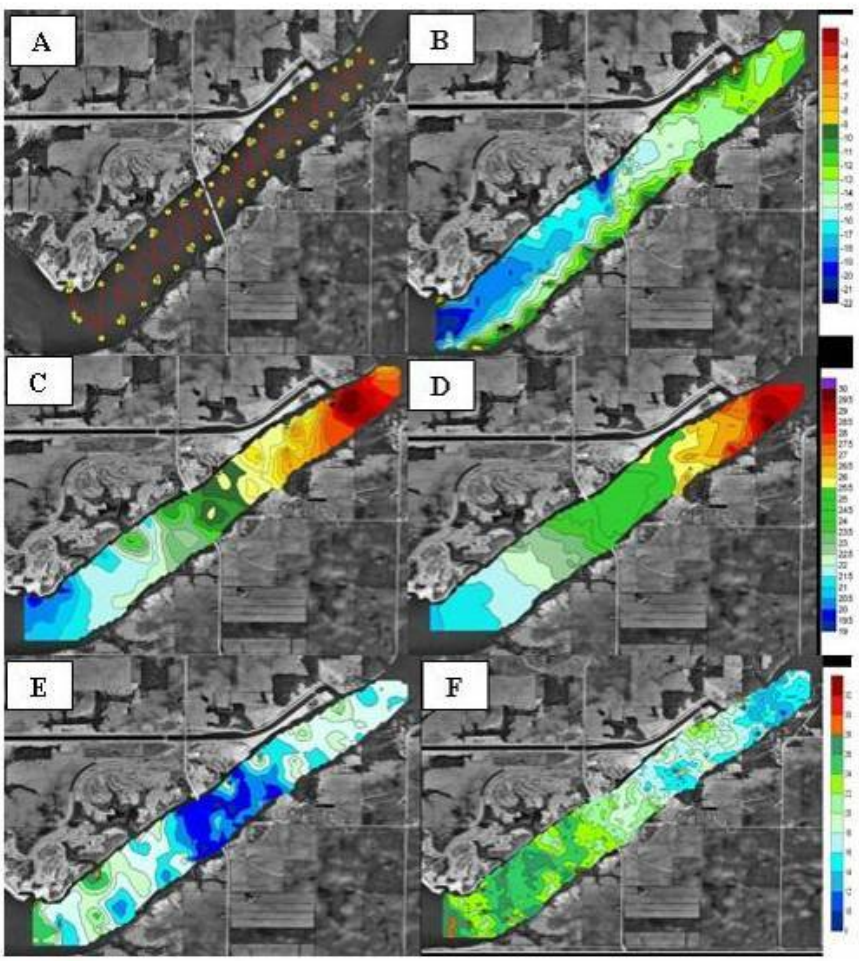

Figure 3. Test results from EcoMapper survey in a cooling lake

The second case study displays the potential of the EcoMapper for bottom mapping applications. The vehicle provides an exceptionally stable platform for side-scan sonar studies when it is navigated below the water surface. A lake was chosen as a test site for bottom mapping applications, where the EcoMapper was tasked with mapping a submerged aggregate plant. Charts of the location of the plant were made available and

the EcoMapper mission was planned to navigate approximately 5 m above the site (FIGURE 4). Two missions were planned; the initial mission was used for target location and the second mission was used for a more detailed target mapping. Within one day the EcoMapper was able to lock in on the target and map the submerged plant. Image A presents an original photo of the old aggregate plant at the bottom of the lake; metal structures that remain today can be observed in the photo. Image B displays a geo-referenced technical drawing of the plant; the purple lines are contour lines, while the orange lines and dots represent the AUV mission. Image C presents side-scan sonar images from the AUV mission; it can be observed from the data collected that there is an old grate present for aggregate sorting, as well as the concrete walls and steel girders from the aggregate plant. Lines indicating plant walls are wavy due to the navigation of the AUV.

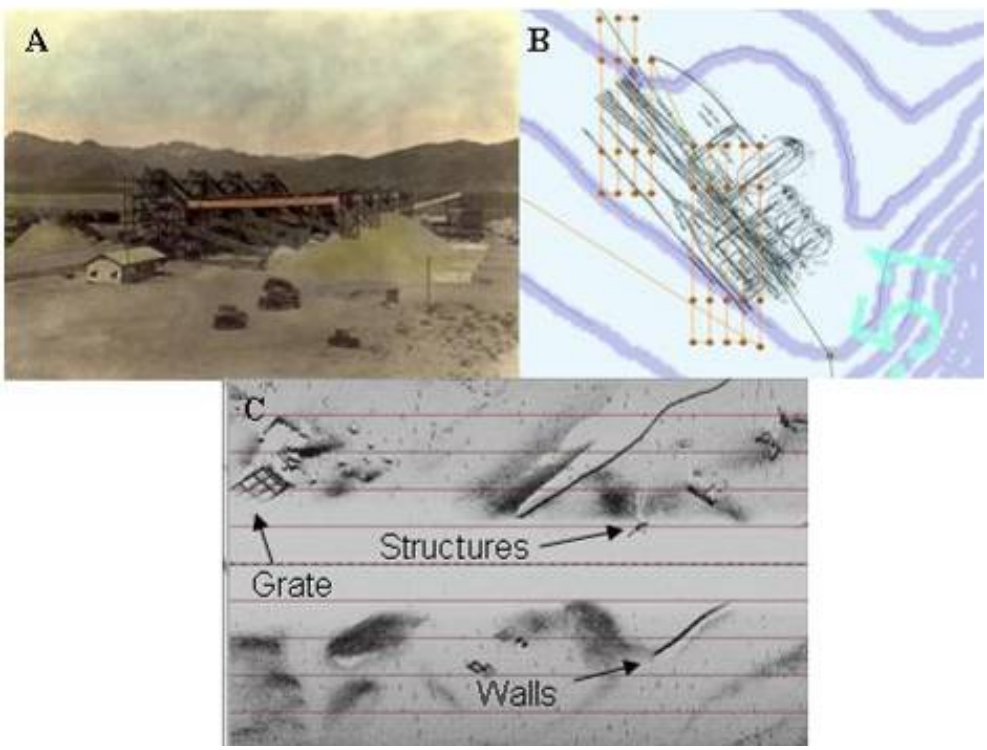

Figure 4. Side-scan sonar data from submerged aggregate plant in Lake Mead, NV

The EcoMapper AUV is a cost-effective platform for applications that require high-resolution spatial mapping of water quality. Applications for which the vehicle is well designed include baseline environmental monitoring, hypoxic zone mapping, algae bloom tracking, source water mapping and volume measurement, shallow water mapping, point-source studies, dye tracer studies, temperature and stratification studies, rapid response, environmental impact studies, and port and harbor security. In addition the EcoMapper can provide accurate bathymetry mapping with the depth standard and optional side-scan sonar package.

CONCLUSIONS

Both autonomous environmental monitoring systems presented here are capable of producing unique, high-resolution data that would be exceptionally difficult to generate with more manual methods. The Vertical Profiler provides a long-term time-series data set with important insight into the vertical dynamics of water body. The system is designed for continuous use with infrequent maintenance visits and remote troubleshooting capabilities. Given the size and cost, an EcoMapper provides a platform to efficiently collect three-dimensional data that were previously unattainable or cost- and time-prohibitive to operations personnel and scientists alike. EcoMapper missions can be run with only one person from shore and more technically demanding work can be completed while the vehicle is collecting data. In addition, the EcoMapper is designed for frequent use and can be deployed daily with rapid mission planning, fast battery re-charge, and field-replaceable sensors. Groups tasked with environmental monitoring or mapping should evaluate the cost of ownership and operation of field sensors and monitoring platforms carefully and consider how the use of autonomous systems such as those discussed here can provide high-resolution data at low operating costs.

REFERENCES

Curtin, T., Bellingham, J., Catipovic, J., and Webb, D. (1993).Autonomous Oceanographic Sampling Networks. *Oceanography* 16(3):86-94.

Curtin, T., Crimmins, D., Curcio, J., Benjamin, M., and Roper, C. (2005). Autonomous Underwater Vehicles: Trends and Transformations. *MTS* 39(3):65-75.

Werblow, S. (2008). Vertical Profiling Safeguards Drinking Water and Sheds Light on Cyanobacteria. *AWWA Journal* 100(9): 48-52.

South Florida Water Control System Tracker: Real-time Water Budgeting for Pragmatic Water Control Operations

Leslie Gowdish, Ph.D.[1], Stephen Bourne, P.E. [1], Lakin Flowers[2], Ken Stewart, Ph.D. [2], Jack Hampson[1]

[1]*Post Buckley, Schuh & Jernigan, Inc. 5300 W. Cypress St., Tampa, FL, 33607*
[2]*SFWMD, P.O. Box 24680, West Palm Beach, FL 33416*

Abstract

The South Florida Water Management District (SFWMD), one of five water management districts in Florida, is responsible for regional flood control, water supply and water quality protection as well as ecosystem restoration in the Southern portion of Florida. The SFWMD is partitioned into water control systems (WCS). Analogous to watersheds in that vertical fluxes of water enter through rain and exit through evapotranspiration, the WCSs differ in that they have control structures to regulate horizontal flux through a system of canals. Efficient control of these structures ensures that SFWMD's multiple water resources objectives are met. SFWMD is currently building an operations decision support system (ODSS) for control of its water-control systems. A possible source of information for the ODSS is a water-budget-based real-time assessment of WCS system state, which is implemented as the WCS Tracker application.

The WCS Tracker application is a computer software solution that comprises 1) an extension to ESRI's ArcMap software, 2) an enterprise geo-database, and 3) a windows service for real-time calculation. Through a SCADA system, the WCS Tracker application receives real-time measurements of gage and radar-based rainfall, gage-based evapotranspiration, and flow and stage measurement of the WCS control structures. By way of various interpolation schemes, this input is re-analyzed into a regular time interval and used in a water budget equation to evaluate the storage of water in the water control system. This storage term is an indicator of oncoming overland flow and thus provides advanced warning to aid in control structure decisions.

The WCS Tracker has been developed over three year-long phases in 2005, 2006, and 2007. Over the first three phases, the WCS Tracker application was transformed from a research proof of concept, to a raw prototype, to a matured workbench that allows operators to create and configure new WCSs, calibrate them with historical data, enroll them in real-time services, and explore their water budget model results.

The current phase of the WCS Tracker (2008) focuses on integration into the SFWMD enterprise through technology and knowledge transfer. First, the WCS Tracker will be enhanced to provide direct access to historical data from SFWMD's DBHydro database. DBHydro represents the best store of meteorological and hydrological information for calibration of WCS water balance models. A fast and user-friendly means of accessing this data directly from the WCS Tracker tools is essential for ongoing water budget modeling. Second, the WCS Tracker will be made more accessible to SFWMD operations and research staff by migrating the application to SFWMD's Citrix environment. Third, the WCS Tracker will be stabilized and tested for quality assurance. Lastly, the WCS Tracker will be thoroughly introduced to SFWMD operators through one-on-one training workshops. Through these workshops, the WCS Tracker will be refined based on operator preferences to ensure comfort with the tool and successful acceptance by its users.

Introduction

The South Florida Water Management District (SFWMD), one of five water management districts in Florida, is responsible for regional flood control, water supply and water quality protection as well as ecosystem restoration in the Southern portion of Florida. The SFWMD is partitioned into 168 water control systems (WCS) that are managed by the Operations and Management group. Analogous to watersheds in that vertical fluxes of water enter through rain and exit through evapotranspiration, the WCSs differ in that they have control structures, such as pumps, gates and weirs, to regulate horizontal flux through a system of canals. Efficient control of these structures ensures that SFWMD's multiple water resources objectives are met.

The Operations division of SFWMD is charged with controlling the structures at the outlets and inlets of the WCSs to avoid flood damage and to ensure the highest available water supply during drought. As part of meeting its charge, the Operations division is building the operational decision support system (ODSS). A possible source of information for the ODSS is a water-budget-based real-time assessment of WCS system state, which is implemented as the WCS Tracker application. The WCS Tracker does nowcasting of the storage of water in the WCSs. Nowcasting is real-time modeling of the WCSs to determine current WCS system state.

The WCS Tracker has been developed over three year-long phases in 2005, 2006, and 2007. During this first phase, the Arc Hydro Enhanced Database (AHED) was developed by the SFWMD information technology department as the GIS database of record for the District. This GIS enterprise database is based on the basic Arc Hydro design, but extends the design for the purposes of providing the business groups at SFWMD with a useful framework for production of tools like the WCS Tracker. It was determined in the first phase that the AHED database would provide the geo-spatial foundation for the WCS Tracker.

In the second phase, the alpha version of the WCS Tracker was developed and installed on O&M machines. With this operational version of the WCS Tracker, real-time calculations of the water budget models for the pilot area commenced. A new database, specifically intended for operational purposes called OpHydro was built. The OpHydro schema design started with replicating the Arc Hydro Enhanced Database (AHED) schema. The schema was then extended to add data structures for real-time water budget modeling. The addition of supporting data structures to store time-series facilitated the use of OpHydro as a unifying spatial platform that could store data from the SCADA OASys system, IMS, and the DBHYDRO databases.

The third phase of development matured the WCS Tracker to a workbench that allows operators to create and configure new WCSs, enroll them in real-time services, and explore their water budget model results. Additionally, it provided a more accurate water budget calculation procedure, an optimization-based means of calibrating WCSs with historical data from the District's DBHydro database, and an enhanced user experience through user friendly interface design, animation of recent rainfall and storage data, and enhanced time series processing capabilities.

This paper will describe the current phase of the WCS Tracker (2008) which focuses on integration into the SFWMD enterprise through technology and knowledge transfer. First, the WCS Tracker will be enhanced to provide direct access to historical data from SFWMD's DBHydro database. DBHydro represents the best store of meteorological and hydrological information for calibrating WCS water balance models. A fast and user-friendly means of accessing this data directly from the WCS Tracker tools is essential for ongoing water budget modeling. Second, the WCS Tracker will be made more accessible to SFWMD operations and research staff by migrating the application to SFWMD's Citrix environment. Third, the WCS Tracker will be stabilized and tested for quality assurance. Lastly, the WCS Tracker will be thoroughly introduced to SFWMD operators through one-on-one training workshops. Through these workshops, the WCS Tracker will be refined based on operator preferences to ensure comfort with the tool and successful acceptance by its users.

WCS Tracker Application

A WCS is composed of a land portion on which overland flow occurs and a water portion, which may be composed of natural rivers and lakes or man-made canals. The land portion is known as the water control catchment (WCC). The water portion is known as the water control unit (WCU). Figure 1 schematically illustrates a WCS.

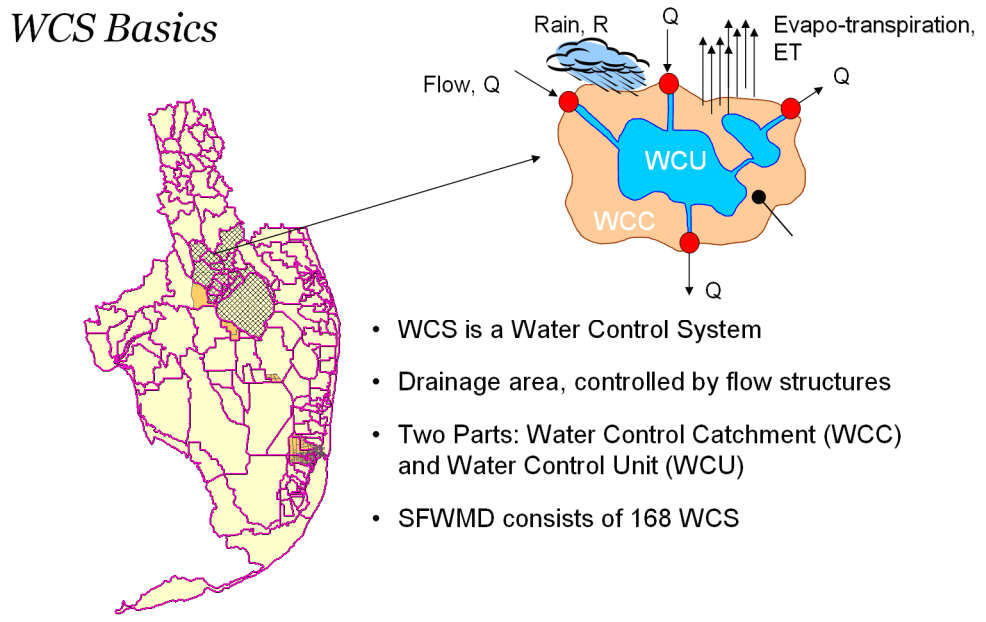

Figure 1. The basic WCS contains two regions, the terrestrial water control catchment (WCC) and the water conveying water control unit (WCU).

A water budget can be applied to each WCS by deriving a water budget equation for the WCC and WCU separately and then subtracting the two equations to produce a single, solvable, water budget equation. The remainder term of the final water budget equation is equivalent to the storage within the WCC plus an additive error term:

$$S_{wcc}(t) = (R_{wcc}(t) - ET_{wcc}(t))A_{wcc} + (R_{wcu}(t) - ET_{wcu}(t))A_{wcu} + Q_s(t)\Delta t - S_{wcu}(t) + S_{wcu}(t-1) + S_{wcc}(t-1) + \varepsilon$$

where

S	=	Storage volume (l^3)
R	=	Rainfall accumulation during interval $\triangle$t (l)
ET	=	Evapotranspiration accumulation during interval $\triangle$t (l)
A	=	Area (l^2)
Qs	=	Flow through Control Structures (l^3/t)

The WCS Tracker application is a computer software solution that comprises 1) an extension to ESRI's ArcMap software, 2) an enterprise geo-database, and 3) a windows service for real-time calculation. Through the SFWMD supervisory control and data acquisition (SCADA) system, the WCS Tracker application receives real-time measurements of gage and radar-based rainfall, gage-based evapotranspiration, and flow and stage measurement of the WCS control structures. By way of various interpolation schemes, this input is re-analyzed into a regular time interval and used in the water budget equation above to evaluate the storage of water in the water

control system. This storage term is an indicator of oncoming overland flow and thus provides advanced warning to aid in control structure decisions.

The workbench for the WCS Tracker application is shown in Figure 2. The extension is embedded into the ArcMap software as a contents view control. A windows-explorer like tree, called the WCS Tree, is the central control. This tree provides an organized hierarchical view of the WCS(s) currently selected. As the user selects nodes in the tree, contextual information and options about the node are presented in the informational panels (see figure 2). The map and chart present cartographic depictions and time series depictions of the WCS respectively and are driven by selection of nodes in the tree that apply to the WCS and its inventory of time series.

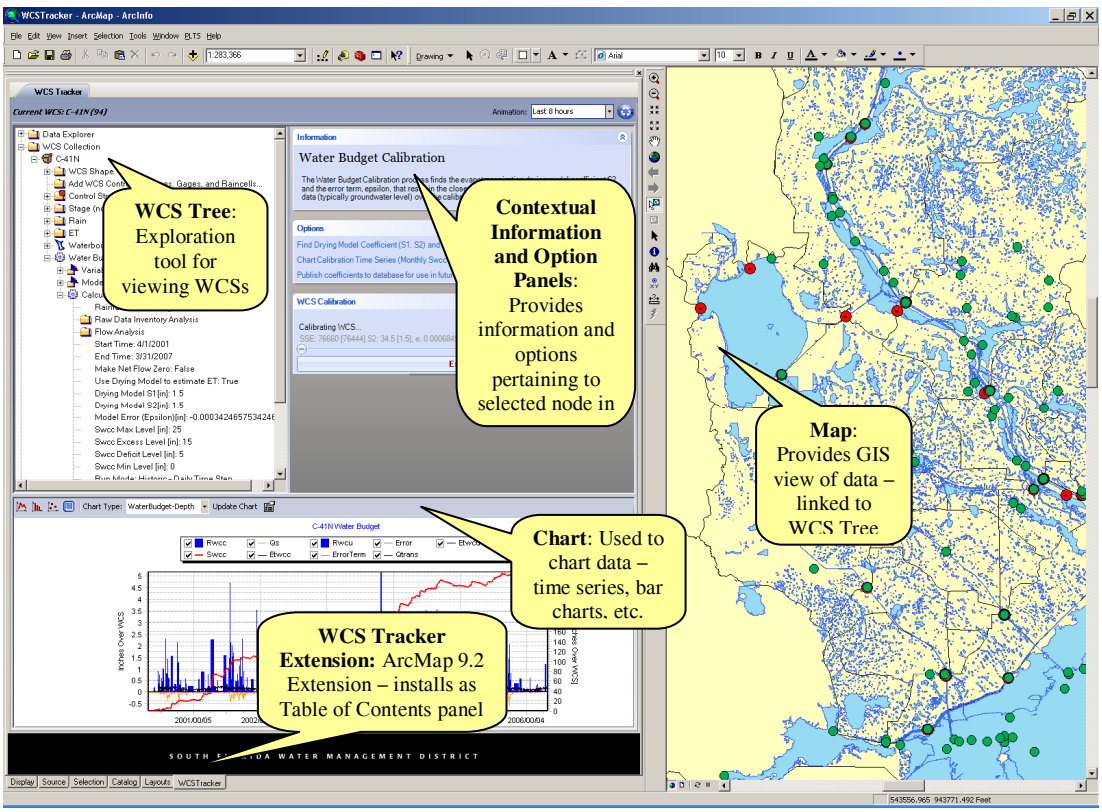

Figure 2. WCS Tracker workbench within ESRI's ArcMap.

WCS Tracker Phase IV (2008)

The current phase of the WCS Tracker (2008) focuses on integration into the SFWMD enterprise through technology and knowledge transfer. This was accomplished by 1) providing direct access to historical data from SFWMD's DBHydro database, 2) deploying the application to SFWMD's Citrix environment; 3) on-going stabilization and testing, and 4) on-site comprehensive training workshops.

Access to DBHydro Database

The introduction of the ability to calibrate and configure WCSs has underscored a need for automated access from the WCS Tracker to sources of historical data. Previously, data for calibration was collected manually from SFWMD's DBHydro database and imported to the OpHydro database. The DBHydro database represents the best store of meteorological and hydrological information available for use in WCS historical calibration. A fast and user-friendly means of accessing this data directly from the WCS Tracker tools was deemed essential for ongoing WCS modeling.

During the current phase, a functional component was developed for direct access to the DBHydro database from the WCS Tracker user interface enabling SFWMD users the ability to explore, visualize, and download any data within DBHydro. From a user's perspective, the WCS Tracker interface will allow them the ability to select a monitoring point or structure and desired variable: stage, rain, ET or flow. The WCS Tracker GUI will then display a list of all DBKeys that fit the user's requirements. DBKeys are unique identification keys for every time series stored in the DBHydro database. The user can then select a DBKey and the time series data will be charted. If the user desires, they can associate DBKeys with monitoring points or control structures in the OpHydro database. By associating the DBKey with the monitoring point/structure it can now be used for calibration purposes.

Access to the DBHydro database is accomplished through activating stored procedures contained in the OpHydro database. These stored procedures in turn execute procedures in the DBHydro database for retrieving DBKeys and their time series. Figure 3 shows the processes for: 1) searching for data in DBHydro; 2) accessing historic time series data for specified DBKey from DBHydro; and 3) storing the time series data to OpHydro through the WCS Tracker interface.

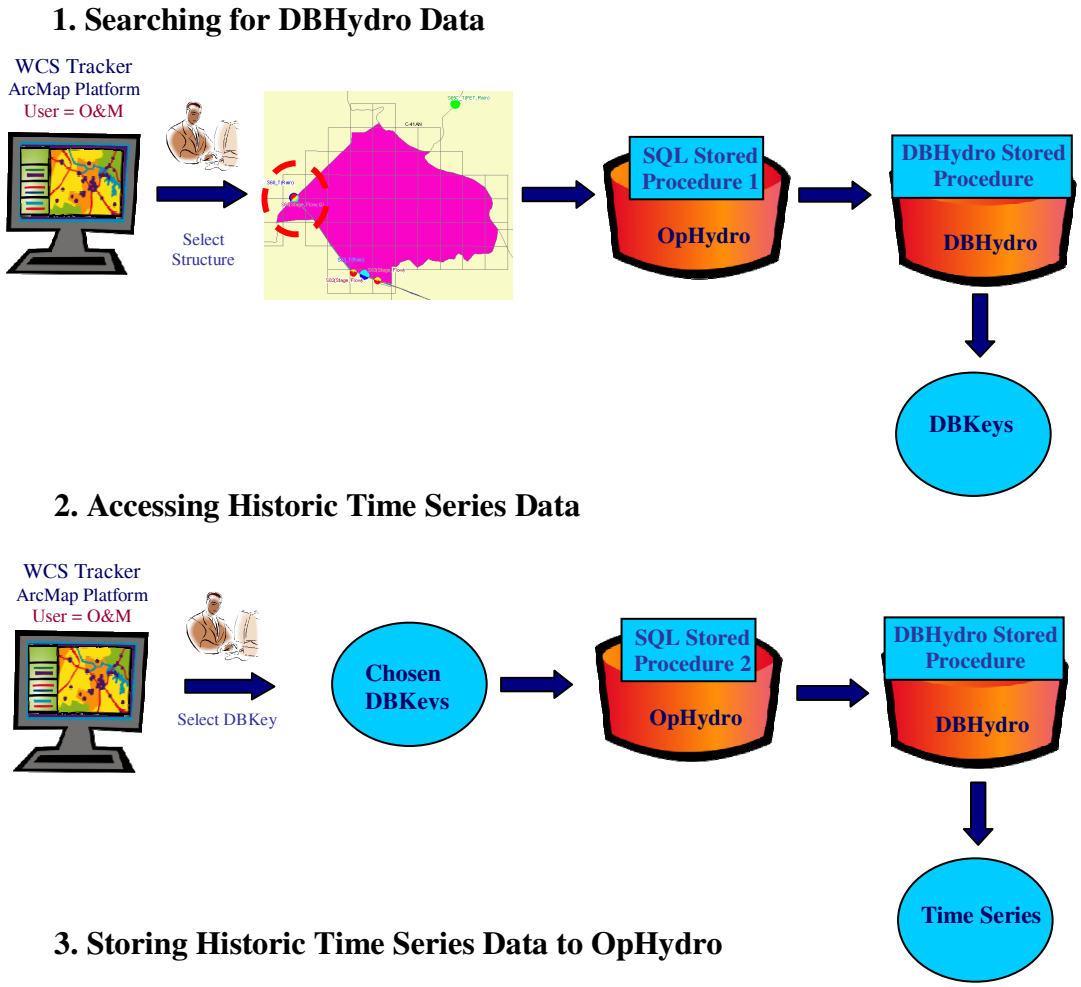

Figure 3. Schematic showing the three processes for: searching for DBHdyro data; accessing historic time series data for specified DBKey from DBHydro; and storing the time series data to OpHydro through the WCS Tracker interface.

Migration to Citrix Environment

Building the WCS Tracker user base is essential. Previously, the WCS Tracker application needed to be installed on each user's computer. Since the application is an extension of ESRI's ArcMap, ArcMap must also be installed on each computer. This limited the number of users that could access the WCS Tracker application. In this phase, the application has been made more accessible to SFWMD operations and research staff by migrating the application to SFWMD's Citrix environment. The Citrix environment allows multiple users to log on and run applications in separate, protected sessions on a single server without having them installed on their local hard drive. Since the application resides on a single server, it allows for an easier, faster and more reliable deployment, maintenance and upgrade, in addition to providing mass availability.

In order for the WCS Tracker application to successfully run on SFWMD's Citrix environment several coding conventions were required. The most significant requirement was that the application could not be coded to read or write to a specific drive. In addition, the SFWMD protocol for Citrix migration required a multi-stage process of development and testing on several servers prior to full deployment to the Citrix environment to ensure minimal conflicts with other Citrix environment applications. The greatest challenge in successfully migrating the WCS Tracker to the Citrix environment was how to handle multi-user access and editing of the same database, OpHydro. This was accomplished by enforcing through the WCS Tracker tool a single-editor policy, where only one editing session can be opened on the OpHydro database at a time.

Testing and Stabilization for Quality Assurance

Testing was conducted through-out the current phase to ensure that any application and architecture modifications were functional and stabilized for quality assurance. This consisted of integration testing of a series of use cases to ensure that each functional requirement of the application is performing as it is supposed to. Each use case was described in a table that listed the functionality, the actor, the flow of events, any alternative flow of events, pre-conditions, post-conditions and user interface components. Table 1 provides an example of a use case for searching for DBHydro data within WCS Tracker.

Table 1. Example integration test for searching for DBHydro data within the WCS Tracker application

Use Case:	**Search for DBHydro Data**
Description:	User searches for historic data in DBHydro database. WCS Tracker displays a list of historic time series data based on proximity to monitoring point/structure of interest and parameter of interest.
Actors:	Operator

Flow of Events:	1. User clicks on a monitoring point under the Data Explorer node in WCS Tree 2. User selects the *Rain* parameter from the drop down menu in the Time Series Explorer panel 3. User clicks the *Find DBHydro data close to this monitoring point* contextual option 4. A list of available historic time series data close to the monitoring point from DBHydro appears within the Time Series Explorer panel
Alternative Flow of Events:	1a. User clicks on a control structure under the Data Explorer node in the WCS Tree 2a. User selects the *Flow* parameter from the drop down menu in the Time Series Explorer panel 2b. User selects the *Stage* parameter from the drop down menu in the Time Series Explorer panel 2c. User selects the *ET* parameter from the drop down menu in the Time Series Explorer panel 3a. User clicks the *Find DBHydro data close to this control structure* contextual option 4a. A list of available historic time series data close to the control structure from DBHydro appears within the Time Series Explorer panel
Pre-conditions:	Valid ArcMap MXD is open with OpHydro databases set. User has searched for existing data in OpHydro database.
Post-conditions:	
U.I. Components	WCS Tracker Tab. WCS Tree with contextual options and nodes for Data Explorer.

Training Workshops

The addition of the direct link with the DBHydro database from the WCS Tracker interface and the deployment of the application to SFWMD's Citrix environment during the current phase brought the WCS Tracker tools to a point where they could be used widely by the operators at the District. Therefore, a comprehensive on-site training program was developed to encourage full adoption of the tool in day-to-day usage.

The training workshop was conducted to demonstrate the application, validate its stability, resolve issues, and train SFWMD staff on the application's use. Training was done with the O&M water management team to demonstrate functionality through pre-defined usage scenarios that string together functionalities in a manner resembling everyday use. The workshop occurred over two days during morning sessions. Any application stability issues and additional refinements identified during the morning sessions were addressed in the afternoons in preparation for the next day

of the workshop. We have found great success with this kind of intense workshop in the past with other development projects. The result of the workshop is a refined tool that works exactly how the water managers expect.

Conclusions

The WCS Tracker is a real-time water budget application for assessing the current state of a Water Control System (WCS) within SFWMD. The WCS Tracker has been developed over four year-long phases in 2005, 2006, 2007 and 2008. Over the first three phases, the WCS Tracker application was transformed from a research proof of concept, to a raw prototype, to a matured workbench that allows operators to create and configure new WCSs, calibrate them with historical data, enroll them in real-time services, and explore their water budget model results. Over the last and current phase, the WCS Tracker application has undergone further enhancements by providing direct access to the DBHydro database, SFWMD's best store of historic data. In addition, the application has been migrated to SFWMD's Citrix environment allowing increased accessibility to users. Testing was conducted throughout the phase for quality assurance and to ensure a stable and functional application. Lastly, a comprehensive one-on-one training workshop provided technology and knowledge transfer to SFWMD users. Building the WCS Tracker user base is essential for continued development of the application. In the future, more hands on training workshops will be crucial to the successful transfer of the WCS Tracker application to SFWMD's Operations and Management group.

Coordinating and implementing a graduate course on interdisciplinary modeling for water-related issues

Laurel Saito,[1] M. ASCE

[1] Graduate Program of Hydrologic Sciences, University of Nevada Reno, Mail Stop 186, 1664 N. Virginia Street, Reno, NV 89557; PH (775) 784-1921; Fax (775) 784-4583; email: lsaito@cabnr.unr.edu

ABSTRACT

The science and management of water-related issues is inherently interdisciplinary, involving hydrology, atmospheric science, water quality, geochemistry, sociology, economics, environmental science, and ecology. Although these issues are increasingly being addressed in an interdisciplinary manner, education and training in interdisciplinary approaches in higher education face challenges that include: engaging faculty from different disciplines to teach a course, attracting students from different disciplines to participate in a course, and finding effective teaching approaches that work for diverse academic backgrounds. A graduate-level course on interdisciplinary modeling for water-related issues was recently offered by 17 faculty from three institutions with an overall objective of *engaging interdisciplinary discourse in modeling aquatic ecosystems*. Students were introduced to models available in different disciplines and how such models might be applied together to address water-related issues, and issues in implementing interdisciplinary approaches. Students also worked in interdisciplinary teams to apply interdisciplinary modeling approaches. This presentation describes the development, implementation, and outcomes of the course, including some of the challenges, rewards, and lessons learned.

INTRODUCTION

The science and management of water-related issues is inherently interdisciplinary, involving hydrology, atmospheric science, water quality, geochemistry, sociology, economics, environmental science, and ecology. Models are useful tools for addressing water-related issues, but there are many challenges in implementing interdisciplinary modeling approaches (Saito et al. 2007). A primary challenge that this paper addresses is the need for education and training in interdisciplinary approaches (Nicolsen et al. 2002; USGS 1999). Education and training in interdisciplinary approaches in higher education face challenges that include: engaging faculty from different disciplines to teach a course, attracting students from different disciplines to participate in a course, and finding effective teaching approaches that work for diverse academic backgrounds. In 2005, a workshop funded by the National Science Foundation was held to develop a curriculum for a graduate-level course on interdisciplinary modeling for aquatic ecosystems. The outcomes of that workshop were extremely positive (Saito et al. 2007) and led to the first course offering in July 2008, as described in this paper.

COURSE DESCRIPTION

After the workshop in 2005, faculty from the University of Nevada Reno (UNR) and the University of California at Davis (UCD) worked together to provide an offering of a graduate course on interdisciplinary modeling that could be attended jointly by students from UNR and UCD. This offering occurred in Summer 2008 at the Tahoe Center for Environmental Science (TCES), a facility located between the two campuses in which both universities have office and meeting space. There was a lead coordinator at each university, seven co-instructors, and eight guest lecturers from UNR, UCD, and the Desert Research Institute (DRI) who participated in teaching the course. The course was held 8 hours each day for 15 days (a three-week period), and generally followed a format of lectures in the morning, followed by related laboratory exercises in the afternoon. Students worked in teams of four to complete an interdisciplinary modeling project that was started in the second week of the course. There was one field trip to learn more about the topics of the interdisciplinary modeling projects. A wiki was used to allow continual updates of the course website with materials from lectures and exercises and to share data for the projects. Topics covered ranged from disciplinary approaches such as watershed modeling, algal modeling, economic modeling, and atmospheric modeling, to issues with interdisciplinary modeling such as modeling uncertainty and issues of scale. Some case studies of interdisciplinary modeling projects were also presented.

OUTCOMES

Although eight students from UNR participated in the course, no students from UCD participated. The students in the course were graduate students in economics, political science, hydrology, environmental science, and ecology. Thus, despite the small class size, there was great diversity in the backgrounds of the students. Faculty were very impressed with the modeling projects, not only because of the amount of work completed in such a short period of time, but also because of the innovation and creativity used to approach the projects. Student evaluations of the course were overwhelmingly positive. Students especially liked being exposed to so many different disciplines during one class, using the wiki as an instructional tool, and the interdisciplinary modeling project.

CHALLENGES, REWARDS, AND LESSONS LEARNED

A number of challenges were involved in implementing the course, including finding faculty willing to participate in such a course for little or no compensation or course credit, finding students to participate in the course from diverse disciplinary backgrounds to enable interdisciplinary dialogue and interaction during the course, and coordinating and designing the lectures and exercises among diverse faculty. Despite the extra effort required to implement the course, the rewards for faculty included the opportunity to see lectures and exercises from other disciplines and opportunities for interaction among themselves to discuss research and possible collaborations. The students gained valuable skills in interdisciplinary communication

and dialogue, as well as an appreciation of the amount of resources available to them from other disciplines in water-related modeling. Among the many lessons learned was the need for adequate housing when the course is offered far from campus, which was especially true for potential UCD students. In addition, one student was taking the course pass/fail, which affected group interactions in her modeling group. In the future, students will not be allowed to take the course pass/fail so that all students are invested in doing the interdisciplinary modeling project.

REFERENCES:

Nicolson, C.R., Starfield, A.M., Kofinas, G.P., and Kruse, J.A. (2002). "Ten heuristics for interdisciplinary modeling projects." *Ecosystems*, 5, 376-384.

Saito, L., Segale, H.M., DeAngelis, D.L., and Jenkins, S. (2007). "Developing an interdisciplinary curriculum framework for aquatic ecosystem modeling." *Journal of College Science Teaching*, 37, 2, 46-52.

[USGS] US Geological Survey. (1999). *Summary report of the workshop on enhancing integrated science*. Available at http://www.usgs.gov/integrated_science/.

Experiences Teaching a Multi-Disciplinary Course

Daniel P. Loucks

School of Civil and Environmental Engineering, Cornell University, Ithaca, NY 14853
PH (607) 255-4896; FAX (607) 255 9004: email: Loucks@cornell.edu

ABSTRACT

Cornell University offers a two-year professional masters degree program in public administration. This program attracts participants who have had work experience and interests in furthering their careers in consulting and in government and non-governmental organizations, mostly dealing with economic development, public finance, and environmental protection. They are an incredibly bright and interesting group of individuals (for example one recent student had 17 years of experience managing the Indian railroad!) but typically they have not had much training in quantitative methods, and specifically model building and use. In fact many will almost do anything to avoid such work. We who plan courses for these individuals have decided that their academic program should include at least three courses in quantitative analyses, including the use of statistics and systems analysis methods. I offer one of these courses that focuses on the art and science of building and solving models to aid in the identification and evaluation of alternative plans or policies for addressing public policy issues and problems.

INTRODUCTION

Public System Modeling is a course designed for students enrolled in our professional master's degree program offered by Cornell University's Institute for Public Affairs. Students who are admitted to this program come from many different disciplinary backgrounds, but few have the training in mathematics and physics that engineers typically have. Few have had statistics, probability, calculus, or even the economics that would be ideal prerequisites for this course in public systems modeling. And few if any are really interested in getting such a background. The faculty of CIPA believes some background and experience in the use of simulation and optimization modeling should be a requirement of the master's degree program. Many CIPA alumni tell us the organizations they work for use such methods applied to economic development, financial planning, and environmental resources management. So, the challenge is how to offer these subjects in model building and use an effective way without taking too much of the available time students have for the study of all the courses they want to take during their two years at Cornell.

COURSE CONTENT

The course is designed to be an introduction to the art model building and use, especially related to public sector planning and management issues. This includes environmental policy issues as well as other public sector problems in administration, management and development. The course introduces for the first time to many students the quantitative systems approach for identifying, evaluating and estimating the physical, economic, environmental, and social impacts of decisions planners and managers are asked to make when addressing specific issues of concern. The problems examined in this course are not likely to be those any of the students will address after graduation, but are designed to help individuals develop the skills of building and using quantitative models to address and analyze problems. Students call this a puzzle solving course. By the end of this one-semester course students should feel competent in the development and use of computational and modeling tools for generating information useful to those making decisions typically addressed by public administrators and policy makers.

The quantitative methods introduced in this course include various deterministic and probabilistic optimization and simulation approaches and models, and decision analysis. They require some knowledge of differential calculus useful in economic analyses. Multi-objective modeling approaches for generating efficient tradeoffs among different system performance criteria are also introduced. All of the quantitative mathematical methods involving calculus, statistics, probability theory and systems engineering or operations research are at the level of undergraduate introductory courses in those subject areas. The aim of all of this 'modeling technology' is to facilitate the identification and evaluation of the impacts of alternative courses of action and the communication of that information in ways that result in more informed decision making.

The public sector ‘puzzles’ examined in this course include, but are not limited to, those involving public health, air and water quality, military strategies, timber and water yield management in watersheds, transportation planning, location of public facilities, privatization of public utilities, environmental economics, enhancing police and fire services, public infrastructure expansion and maintenance policies and urban development. Benefit-cost analyses and an introduction to engineering economics are also included.

The course involves the use of several computer software packages, none of which require computer programming. Yet interestingly, students have more trouble understanding how to construct flow diagrams that outline some search procedure, for example, than learning how to perform a Monte Carlo simulation.

Homework exercises are assigned and students are encouraged to, work on them with others in the class. The end-of-course project is a team effort, but each member of each team is graded based on the team's work and the recommendations of others in the team. This is intended to simulate a typical consulting experience where teams consisting of professionals often from different disciplines are assigned to address a problem. The course includes one test to evaluate how much each individual has learned in the course without outside help. A teaching assistant provides considerable outside class time help to those who desire it.

STUDENT RESPONSES

Just how well is this course working? Perhaps one measure of this is the end-of-course responses provided by the students. Each year almost everyone cites the enormous work load and time spent on the homework exercises, yet at the same time they comment on how enjoyable and valuable the course has been for them. The teaching assistants I've had have been critical to the degree of success this course has had. Being available when students want help considerably contributes to how they feel about the course.

Clearly I've learned in my some 40 years of teaching here and elsewhere that at least I can't please everyone all the time, and perhaps some never. On the positive side a sampling of comments from this past Fall semester's course include:

> "The course succeeded in bringing a mathematical subject to mostly non-mathematical students, in a rapid fashion, using well chosen examples and carefully using the essential math tools without overburdening them with excessive rigor.
>
> The course itself is very useful for anyone interested in policy planning. The subject matter is very strong, teaching some very helpful and dynamic modeling concepts.
>
> The homeworks assigned were drawn from real-life situations and were very applicable to my academic requirements as a Public Administrative student.
>
> The course content is very useful, and it seems to be helpful when taking other courses such as economics or finance.
>
> The group work was helpful in that it taught us to work well in a group.

On the negative side a sampling of comments from the same class of students included:

> "Too many methods to learn. I need more time and easier exercises to digest them.
>
> It'd be helpful to have real world application in mind or more of a big picture, rather than just seemingly random problems on the homework, especially since most of the class is comprised of policy-minded people and not science-based people.
>
> Even as someone with a background in advanced calculus and statistics, homework exercises still took me a VERY long time to complete, even with added help.
>
> The lectures for me were not very helpful. First of all, the time of the class was too early, from 8:00 am to 10:00am. For such an intense and difficult course, it was hard being so attentive so early in the morning.
>
> I really liked the course content, but I think it could have been explained better.

> There were too many assignments. Instead of weekly assignments, bi-monthly assignments would've been better. It would have given us more time to concentrate on and understand each assignment better.
>
> The course is more valuable for students with a good mathematics background, hence graduate level math or calculus should be made a pre-requisite for the course."

DISCUSSION

Many multidisciplinary courses are taught by a team of professors, each a specialist in his or her discipline. In this Public Systems Modeling course I pretend I know something about a wide variety of public policy issues but clearly I do not have any in-depth knowledge of all of them. (But I'm learning!) Obviously I can and should improve my teaching methods and style and student comments are perhaps a useful guide for learning what needs improving. Yet the dilemma is that students with different backgrounds require different amounts of time and instruction to learn what is being taught. In this situation it is not possible to require all students to take prerequisite courses in various disciplines to prepare them to take a course like this. Cornell offers a web-based course covering some of the fundamentals of mathematics and statistics the summer before students arrive at Cornell, and encourages CIPA applicants to take it if they feel the need for it and have the opportunity to take it. In any case we can not assume everyone in the class will have had those subjects. Many who have had calculus and statistics early in their academic careers, claim that by the time they become CIPA students they have forgotten them. What this generally leads to is more outside class time devoted to helping those having weaker backgrounds.

I also teach a junior undergraduate engineering class and a graduate engineering class at Cornell. While it is dangerous to generalize, and there are exceptions, I have to say that my experience in front of CIPA students seems much more enjoyable than when I'm in front of engineering students – those in my own discipline! CIPA students ask more questions in class and argue more with me. They talk more. They make me think. I learn something from them that I don't when students are very quiet and not interacting with me. Perhaps by the time I see those engineering students in my classes they are exhausted from all the chemistry, physics and engineering pounded into them that diminishes the creativity and curiosity they came to Cornell with. They also typically have not had the work experiences that CIPA students have. In my view this says something about the advantages of a more liberal education and perhaps some job experience prior to entering a graduate program to get a degree in engineering. See for example the papers on water resources education in the Special issue of Journal of Contemporary Water Research and Education on *A Creative Critique of U.S. Water Education* (Issue 139, June, 2008).

CONCLUSION

I've described a public systems modeling course I teach to students enrolled in a professional master's degree in public administration. These students have had a variety

of work experiences and were trained in a variety of disciplines. The multi-disciplinary interactions among these students as they struggle together to develop and apply analytical models as aids for analyzing a wide variety of public policy problems or issues are probably the most educational aspects of this course. They know they benefit from this experience, probably because they know how such tools and approaches together with different disciplinary inputs could have benefited them in the jobs they had prior to coming to Cornell.

The challenge of course is just how best to provide and enrich this learning experience. Hopefully the discussion that this talk motivates will provide all of us some ideas we can explore that could improve the effectiveness of not only this course but other multi-disciplinary courses as well.

Water Resources in Sudan: Enhancing Rainfall Harvesting Methods for Water Supply

S. Mohamed-Ali[1], S. Luster-Teasley, PhD[1], and E. Nzewi, PhD, PE[2]

[1]North Carolina A&T State University, Department of Civil, Architectural, Agricultural and Environmental Engineering, 1601 E Market Street, Greensboro, NC 27411

[2]Southern University and A&M College, Department of Civil & Environmental Engineering, Suite 321 Pinchback Building, Baton Rouge, LA 70813

Abstract

In Sudan, the climate ranges from arid in the north and northwest to wet-and-dry tropical weather in the southwest. In semi-arid zones in Sudan such as West region, safe drinking water is rare. In particular, areas in North Darfur and South Kordofan States rely on groundwater supply (wells) or water storage methods called *hafir* or earth dams for their water supply. *Hafir* are small lakes constructed in low lying areas to allow water to be stored during rainfall events. Improved water supply methods, to provide adequate water quality and water supply, are acutely needed for this region. Rainfall collection is one of water sources in Sudan and rainwater harvesting (RWH) methods can be implemented to improve the production of crops and livestock in the region. In Sudan, rainfall decreases from south to north, the annual average varying from 120 cm (47 in) in the south to less than 10 cm (4 in) in the north. Agricultural production and domestic water needs would be very difficult to sustain without the use of locally viable rainwater harvesting techniques to enhance water supply; and the reduction of water demand by water conservation. In North Darfur, where the rainfall is concentrated over short periods of time, rainwater harvesting techniques have been developed for various types of water collection schemes by implementing domestic rain water harvesting.

The potential to greatly improve water supply and water quality in Sudan exists. This can be achieved by designing and implementing modified rainwater harvesting methods from the United States and other regions that may be applicable in Sudan. This paper presents the water supply problems in Sudan and proposes RWH solutions tailored for the region. It also includes strategies for improving current RWH methods that are being used in developing regions.

Introduction

Sudan is the largest country in Africa covering a total area of 2,505,813 square kilometers. It is divided into nine regional boundaries which are Northern, Eastern, Darfur, Khartoum, Kordofan, Central, Upper Nile, Bahr El Ghazal, and Equatoria (Figure 1 and Figure 2). In Sudan, the climate ranges from arid in the north and northwest region to wet-and-dry tropical weather in the south and southwest region. Table 1 provides a summary of the rainfall zones and average rainfall for Sudan regions and states.

The desert regions of the Northern, Eastern, and Western regional boundaries

include the northern border of the Northern State, Nile State, Red Sea State, Kordofan and Darfur which experience an average of 0 – 75 mm of rain during two to three months of the year. The southern portion of this region ranges from semi-desert to sandy, low-rainfall savannah with 75 – 400 mm of rainfall. Agricultural production starts in semi-arid zone which includes the southern state borders of the Nile, Northern, and Red Sea and the northern border of Kassala. The states included in the sandy low-rainfall savannah include Khartoum, the south borders for Kassala, and the north border of Gedaref.

The Western regional boundary of Sudan encompasses Darfur (i.e. Northern Darfur, Western Darfur, and Southern Darfur) and Kordofan (i.e. Northern Kordofan and Southern Kordofan). In this region the average rainfall is from 0 to 900 mm and the region is classified as an arid desert to high savannah rainfall zone. The arid, or desert, rainfall zone includes Northern Darfur and Northern Kordofan. The semi-arid rainfall zone of Western Darfur additionally has a water supply from Jabal Marrah Mountain. In Northern and Western Darfur water is acquired from small water pools called *wadis* water sources that will become dry during the winter months. An isolated region in the northwest region of Northern Darfur called the *jizzu* experiences sufficient winter rainfall in January and February to support animal grazing. The sandy, low-rainfall savannah in the Western regional boundary averages between 300 to 400 mm of rainfall within a three to four month rainy season. This rainfall zone extends across the middle of the Western Regional Boundary states such as Western Darfur, Western Kordofan, and the southern borders Northern Darfur and Northern Kordofan. During the rainy season, Southern Darfur, and Southern Kordofan is covered by grass known as *goz*.

The Central Clay Plains regional boundaries of Sudan can be divided into the northeast central clay plains region and the southern clay plains region. The central clay plains include the Central and Upper Nile Regional Boundaries which include Gedaref, Sennar, White Nile, Blue Nile, Upper Nile and Jonglai state. The states located in this region are classified as a clayey, low-rainfall savannah. The southern clay plains region range from clayey, high-rainfall savannah to tropical rainfall zones and include the south border of Southern Darfur, Bahr El-Ghazal and Equatoria Regional Boundaries. The rainfall ranges between 1000 and 1 500 mm and the rainy period between seven to eight months in duration.

Water collection methods in Sudan

Water resources in Sudan are significantly impacted by the regional climate, access to water sources, and rainwater harvesting opportunities. For example, major cities in Sudan are primarily located near the banks of the Nile River due to the adequate water resource while Sudanese villages are primarily located in semi-desert and savannah area and have limited access to water. People who live with limited access to water resources support their water needs by living nomadic lives and travel to find water sources, living in villages but travel extended distances to transport water back to the villages, or use community water harvesting methods such as hafirs or earth dams.

Hafirs and earth dams represent two traditional, low cost water harvesting methods currently used in the western and eastern regions of Sudan. In the semi-arid

zone the rainfall is concentrated over short periods of time that people in this region try to collect the water by making local reservoirs known as hafir (Figure 3). In Sudan the 'hafir' is the primary RWH method used to store runoff water during the rainy season and the collected water is stored for use during the winter months. The hafir is a natural or manmade (hand or machine) deep catchment area with an approximate 3.5 m average depth. The hafir is recharged with water through manmade canals. The hafir's water is used by the community, farmers, nomads, and animals. To prevent sediment, solid materials and silt from entering the collected water, a trap is built before the inlet pipe. This trap is a deep trough to clear water by leaving the silt and solid materials at the base and tapped off the water in the top to the hafir by the inlet pipe.



Figure 3: The Azagarfa hafir in Darfur

Earth dams, or check dams, are built in a stream of a narrow valley or across a gully or riverbed with length range from 50m to 1000m (Figure 4 and Figure 5). The slow moving water through the dams allows for storage of this water. Dam designs may also include spillways, sluice gates, channels and embankments to allow control of the water .



Figure 4: The Asagarfa Earth dam (Source: Practical Action Sudan)



Figure 5: Um Baronga Earth Dam (Source: Practical Action Sudan)

Methodology

Limited written resources, such as journal articles, are available regarding water sustainability in Sudan. Therefore, to obtain information regarding RWH, representatives from Sudanese based water action groups were contacted by phone and by e-mail in Sudan and the United Stated. The representatives were interviewed to discuss water sustainability in the Sudan, to explain current RWH methods, and were asked to provide documentation or photos about the methods. The North Carolina Department of Environment and Natural Resources (NCDENR) and the Division of Water Quality (DWQ) "Technical Guidance: Storm water Treatment Credit for Rainwater Harvesting Systems" provides a resource for developing RWH system. Using this guidance document, a **rooftop rainwater harvesting** system was

designed for use in the Sudan with some modifications to meet the needs of Sudanese people.

Interviews

Mr. Hashim Altayeb, the **Quality Assurance Manager** (Practical Action Organization-Sudan), was interviewed by phone. He was able to provide background information for RWH methods in Sudan, photos, and discuss the feasibility of improving RWH methods. Mr. Mohamed Saleh Farah, **Senior Programs Practical** (Practical Action Organization-Sudan), was interviewed by phone and discussed the problems specifically related to implementing RWH methods in Sudan such as climate, resources, and economic feasibility.

Plan Development

The potential to greatly improve water supply and water quality in Sudan exists. This can be achieved by designing and implementing modified rainwater harvesting methods from the United States and other regions that may be applicable in Sudan. Based on the information provided by Practical Action Organization – Sudan and the NCDENR guidance document, a RWH system was designed to address four goals:

1) Generalizing the idea and the concept of RWH methods for Sudan to the people in all regions to collect clean rainwater.

2) Help people in western Sudan (Darfur and Kordofan), eastern Sudan and southern Sudan by designing rainwater harvesting modifications for public buildings (i.e. schools, government buildings) thus creating a central rooftop RWH system in each village.

3) If implementing rooftop methods in Sudan, local Sudan developers need to be educated about RWH methods that can be used to increase water collection. Additionally builders from developed countries interested in helping improve water resources in third world countries must consider the economic and resource limitations in countries such as Sudan.

Results: Proposed Design

In the United States, rooftop RWH methods are used to collect water for non-potable water systems such as vehicle washing and toilet flushing. In Sudan however where potable water supply is the primary concern, a RWH system combined with a water treatment systems would be necessary to collect water which would be safe to use for drinking, cooking, and daily water without the threat of illness. Based on the climate, local Sudanese resources, economic feasibility, and architectural design for Sudanese homes, rooftop RWH systems are feasible for water collection in Sudan. Rooftop systems would need to be modified to meet the needs the Sudanese cities or villages. Figure 6 provides and example of a basic rainwater harvesting system design developed by the NCDENR.

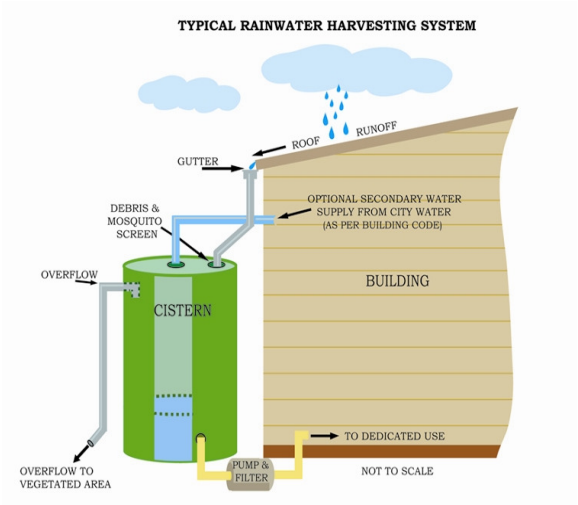

Figure 6: Schematic of a rainwater harvesting system (Source: NCDENR)

Sudanese Resources

One of the main purposes of this paper is to recommend methods for RWH systems which could be used in all the Sudanese houses and in various Sudanese regions feasible for RWH systems. Due to limited resources in the Sudan, materials used for the RWH system would need to be very simple, inexpensive, and a resource available within the village or country. Most Sudanese families will possess basic materials such as plastic barrels, mesh, pipes, and filtration material such as sand and rocks. Supplies that would be readily accessible in Sudan which could be used for a RWH system include:

1- **Plastic Barrel:** The Plastic barrel is the above ground that holds the rainwater The plastic barrels are available in the most of Sudanese houses because families will collect and store extra water supplied by the city in barrels in case of water rationing or limited water supply from the city.
2- **Roof Surface**: Suitable surface such as metal or clay/wood surface with slope.
3- **Pipe (gutter):** Install a gutter system along the roof edge to convey the rainwater from the roof to the cistern or plastic barrel to another pipe fixed at the end of the sloped pipe to the cistern or plastic barrel.
4- **Small piece of mesh**: It has a circular shape and fixed at the entrance of the rain water pipe in the roof to filter the rainfall water from leaves, coarse dirt or any others solid materials that may come with water from roof.
5- Filtration System: A small, slow sand filtration system can be built by filling a plastic barrel with pebbles and coarse sand to filter water from the small pieces of materials that may not filter using only mesh.
6- **Water Purification**: Sudanese currently use two methods for water treatment. These include Aluminum Sulfate, called shub, and a regional plant called Morina oleifera.
7- **Tap:** install on the plastic barrel for treated water access.

Modification of Roof Top Rainwater Harvesting System for Sudan's cities

Most of the Sudanese's homes located in cities are made of clay, rocks, or concrete (Figure 7). The roof is sloped to one side to discharge the rainfall water through holes located on the edge of the roof. These holes allow water to drain from the rooftop. A small modification would need to be made to the roof such that a sloped gutter system is installed along the roof edge to help direct rainwater flow for harvesting. Using a sloped pipe, the rain water can be collected from the roof and transported through this pipe to a collection barrel designed to operate like a slow sand filter. The barrels should contain pebbles at the bottom and coarse sand on the top to filter the collected water. Filtered water can be stored in a separate barrel. This water can then be filtered a second time and boiled before using for cooking and drinking.



Figure 7: Photo of typical Home in Sudanese city

Modification of Roof Top Rainwater Harvesting System for Sudan villages

In the poorer villages in Sudan such as Amdrosa, Nur Alhuda and Omar teina (western Sudan) most homes will be made with thatched roofs and homes that would not be able to support the addition of a metal roof (Figure 8). The cost of replacing the roof with concrete or metal-like material may prove to be too costly for villagers to pay for individual home systems. Therefore a centralized, RWH rooftop system or "Water Center" would help the entire village collect and store the daily water needed. The roof of the RWH building would need to be cleaned and maintained especially during the rainy months from April to December. Before diverting the rain water into the storage tank or open well/bore, a slow sand filter would be needed to treat the water. At the individual homes, this water would then be used after a final filtering step and boiling before using for cooking and drinking.

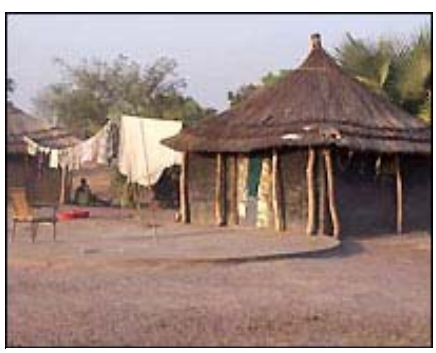

Figure 8: Photo of home in Sudanese Village

In the sandy areas of Sudan where water percolation occurs such as in the Western Region (e.g. Darfur and Kordofan), rainwater from the roof can be diverted to shallow recharge structures such as percolation pits, recharge trenches, and shallow/small recharge wells. In the clay area such as Eastern Region (e.g. Gerdef and Kassala) where the soil is impervious, rainwater would need to be diverted to the deep recharge structures system such as percolation pit with boreholes, recharge trench with boreholes and deep/large recharge wells. All of these methods would be needed for deep percolation into the underlying sandy layer.

Sudanese Water Treatment

In Sudan water there is a greater need for potable water than palatable water. Sudanese, in both cities and villages, use a native material called ***shub*** to treat collected water. ***Shub*** rocks are traditionally added to collected water to settle sand or any other fine particles. The water is then filtered and boiled. The scientific name for ***shub*** is **Alum** (Aluminum Sulfate $Al_2(SO_4)_3$) and is commonly called filter alum. Additionally, there is a native plant called Moringa oleifera used for water treatment (Figure 9 and 10). Moringa oleifera leaves are used as filter material to treat water. The chemicals released by the leaves are traditionally used in Sudan to treat stomach problems as well as mild forms of malaria. Thus using shub or Moringa oleifera in rainwater harvesting designs provides a low cost, native material to treat water for Sudanese RWH systems.



Figure 9: Moring oleifera plant



Figure 10: Seeds from Moringa Oleifera

Conclusion

The potential to greatly improve water supply and water quality in Sudan exists. This can be achieved by designing and implementing modified rainwater harvesting methods from the United States and other regions that may be applicable in Sudan. The implementation of rooftop collection designs for rainwater harvesting in Sudan cities would be feasible by attaching a gutter system to the roof to help direct rainwater from the roof top for home rainwater harvesting systems. In villages, where homes have thatched roofs due to economics and location, a centralized rainwater harvesting system on a community building, such as a school, could be used for rainwater harvesting. Following rainwater collection by the roof, slow sand filtering the water and treating the collected rainwater using local and native Sudanese resources such as Moringa and shub can provide alternative water for potable use.

RWH therefore can help both individual homes and communities where water supplies are limited or scarce. Currently hafir, earth dams, and wells are the primary methods used to help increase water supplies for the various Sudanese regions. These options however require people to travel to the hafir, earth dam, or well water source. In western and southern Sudan villages, women and girls in the villages are responsible for traveling long distances to water sources to bring back water for drinking, cooking, and washing body and clothes. It is not uncommon for women and children to travel for hours during the day to collect water. The lives of these women can be improved by applying the RWH methods because instead of spending time walking to collect water, women and children could have time for other village tasks and education.

Using creative RWH designs, considering the economic feasibility of a country, and the public need for water, there are many options for exploring sustainable designs to improve the lives of people. Education for RWH methods and

efforts from developed countries to improve water resources in third world countries is important to help improve the lives of people in these regions. As the interest in green technologies and sustainability increases, many of the technologies being using in developed countries have broad based applications that can be applied to many regions in the world.

References

Interviews

1. Mr. Hashin Altayeb, Practical Action Sudan, Block No. 4 street 49, off Pio Yokwan Road Khartoum W; Email hashime@practicalaction.org.sd
2. Mr. Alva Dut, Water for Sudan, Inc. in Rochester, NY, USA; Email salva.dut@waterforsudan.org
3. Mr. Mohamed Saleh Farah, Practical Action Sudan Block No. 4 street 49, off Pio Yokwan Road Khartoum W; Email mohameds@practicalaction.org.sd
4. Mr. Eric Wolvovsky; National Oceanic and Atmospheric Administration (NOAA) 5200 Auth Road Camp Springs, Maryland, USA 20746; Email: Eric.Wolvovsky@noaa.gov

Books

4. Asano, T; Burton, F.; Leverenz, H.; Tsuchihashi, R.; Tchabanoglous, G.; Water Reuse Issue, Technologies, and Applications. Metcalf & Eddy, 2007.
5. Food and Agriculture Organization of the United Nations (FAO); Fertilizer use by crop in the Sudan. First edition, Rome, 2006.

Internet-Pictures and Resources

6. http://www.militaryphotos.net/forums/showthread.php?...
7. South Sudan's unlikely capital By Jonah Fisher BBC News, http://Rumbeknews.bbc.co.uk/1/hi/world/africa/4192133.stm
8. A Khartoum boom, courtesy of China By Vivienne Walt, Fortune, August 6 2007. http://www.militaryphotos.net/forums/showthread.php?...
9. http://practicalaction.org/images/sudan-0053-water.jpg
10. http://www.piroofing.com/templates/System/details.as
11. http://www.greensboronc.gov/departments/Water/watersystem/chemicals.htm
12. http://www.harvesth2o.com/rainwaterstorage.shtml
13. ftp://ftp.fao.org/docrep/fao/009/a0416e/a0416e02.pdf
14. http://www.photius.com/countries/sudan/geography/sudan_geography_geographical_regions.html
15. http://lcweb2.loc.gov/frd/cs/sudan/sd_glos.html#jizzu
16. ftp://ftp.fao.org/docrep/fao/009/a0416e/a0416e02.pdf
17. http://practicalaction.org/practicalanswers/product_info.php?products_id=66
18. http://www.genocidewatch.org/images/Sudan1_Dec_06_Eyewitness_Names_70_Villages_Destroyed_in_Past_Three_Months.pdf
19. http://wateris.wordpress.com/category/sudan/
20. http://www.asia.ru/WishListView/AddWishProduct?produ... (mish in Sudan)
21. http://www.aboutrainwaterharvesting.com/rwh_methods.htm
22. http://www.harvesth2o.com/zilker.shtml
23. http://buy.ecplaza.net/search/1s1nf20sell/moringa_seeds.html
24. http://ersson.sustainabilitylane.com/rainwatr.htm

25. http://www.waterforsudan.org/OurStory.htm
26. http://www.sudan.net/government/admnmap.html
27. http://www.khayma.com/hawaj/shab.htm
28. http://www.twfta.com/cn00156444/showroom_19021.htm
29. http://www.usplastic.com/catalog/product.asp?catalog%5Fname=USPlastic&category%5Fname=25&product%5Fid=292
30. http://www.delange.org/Moringa/Moringa.htm
31. http://www.depha.org/maps/sudan/. Data Exchange Platform For Horn of Africa. GIS Data.

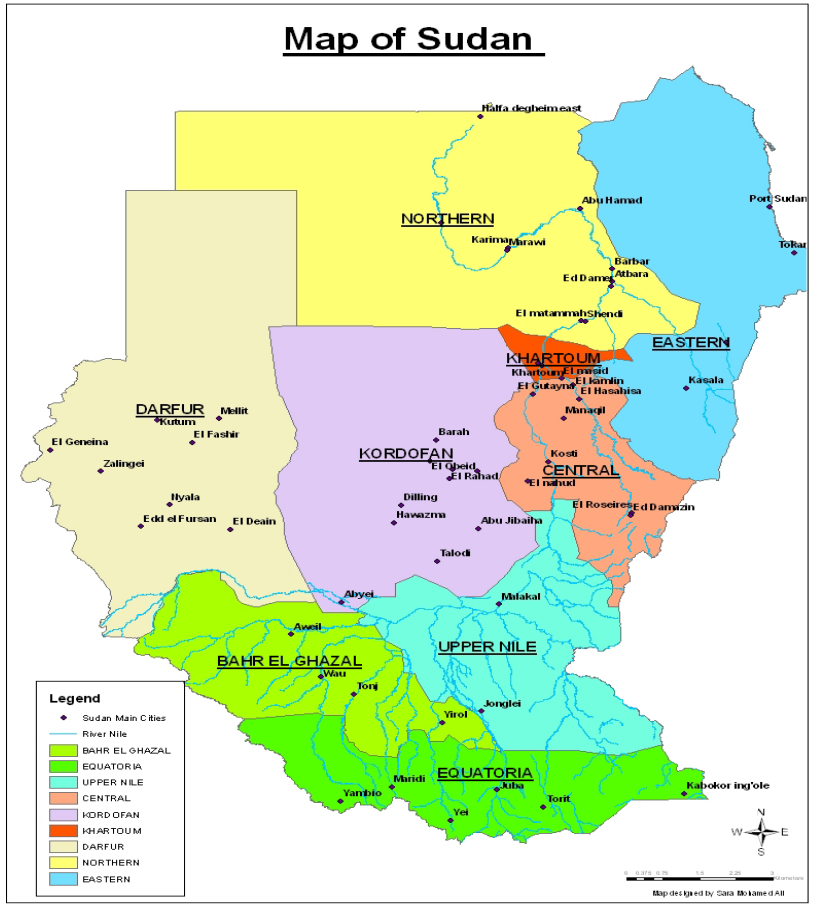

Figure 1. Map of Sudan Regions

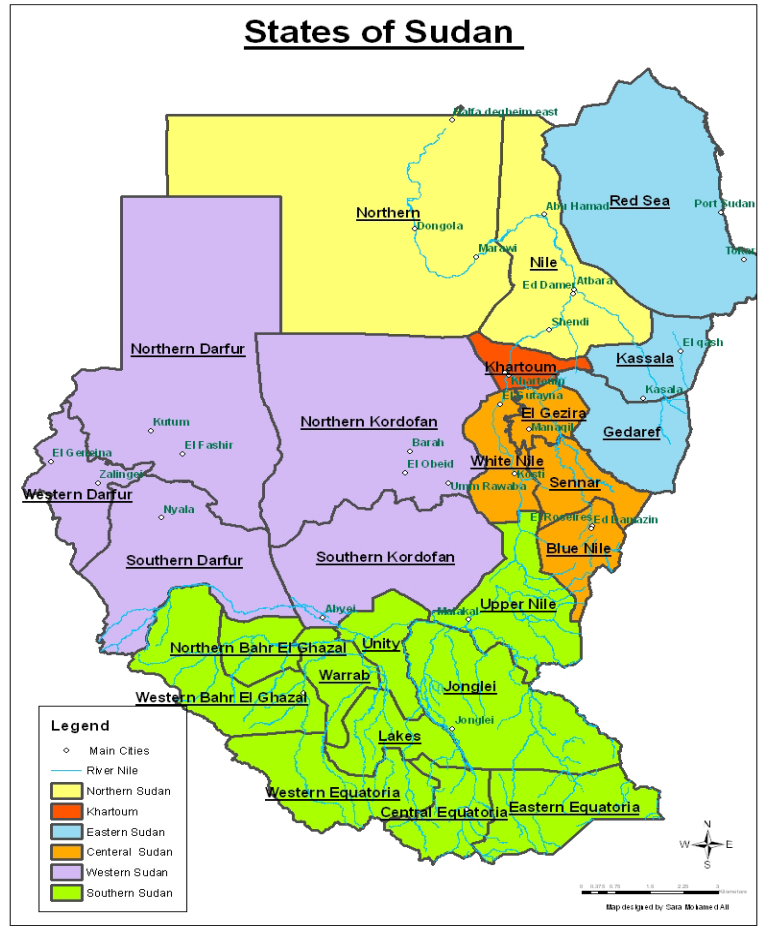

Figure 2. Map of Sudan States

Table 1: Rainfall zones and average rainfall for Sudan Regions and State

Rainfall Zones	Regions	Average rainfall (mm)	RWH Method
Desert	Northern region :North border of Nile State and Northern State	0–75	No RWH used
	Western region: North border of Northern Darfur state; Northwest border of Northern Kordofan		
	Eastern region: Red sea state		
Semi-desert	Northern region: South border of Nile State, South border of Northern State	75–300	Hafir and Earth Dams
	Western region: Middle part of Northern Darfur, North Border of Northern Kordofan		
	Eastern region: Southern border of Red Sea state; North border of Kassala State Central Region: Khartoum		
low-rainfall savannah (sandy)	Eastern region: South border of Kassala state, North border of Gedaref State	300–400	Hafir and Earth Dams
	Western region: Kordofan, southern border of Northern Darfur, central region of Western Darfur		
	Central clay plains region: North border of White Nile and Gezira States		
low-rainfall savannah (clayey)	Eastern region: Gedaref State and Southern border of Kassala State	400–900	Hafir and Earth Dams
	Western region: Southern border of Western Darfur, Southern Darfur, Southern border of Northern Kordofan, and Southern Kordofan		
	Central clay plains region: Southern border of Gezira, Sennar, White Nile, White Nile, Blue Nile, and Upper Nile States		
	Southern region: Jonglei, Northern border of Eastern Equatoria, Lakes, Northern Bahr El-Ghazal; and Western border of Western Bahr El-Ghazal and Unity State		
High-rainfall savannah	Western region: Southern border of Southern Darfur State	900–1300	No RWH used
	Southern region: Southern border of Eastern Equatoria, Bahr El-Jabal, Western Equatoria, and Southern border of Northern Bahr El-Ghazal and Western Bahr El-Ghazal States		
Tropical	Southern region: Far southern border of Western Equatoria and far south border of Central Equatoria	Above 1300	No RWH used

Environment and Water Resources in 2050:
The Challenge for Engineering Education

Jeff R. Wright[1]

[1]Dean of Engineering, School of Engineering, University of California, P.O. Box 2039, Merced, CA 95344; PH (209) 228-4410; email: jwright@eng.ucmerced.edu.

ABSTRACT

The evolution of the field of environmental and water resources engineering over the next half century will both shape and be shaped by, changes in the formal education of tomorrow's technical workforce in this domain. While predicting *anything* 40 years into the future is initially daunting and ultimately humbling, this paper presents a framework for anticipating the changes that will be needed in the way we educate environmental engineers. Particular attention is given to the expectation for new and emerging information and computational technologies, and opportunities and challenges for developing new educational pedagogies.

PERSPECTIVE

Endeavoring to evaluate attempts to predict the future with respect to important societal concerns Princeton physicist Gerard K. O'Neill made the observation that forecasters tend to underestimate the rate of technical change, and overestimate the rate of social change (O'Neill, G.;1981). This appears to be consistent with the rapid pace at which engineering innovation over the past several decades has provided technologies and methodologies that can improve water resources assessment and management, as well as the sluggishness with which widespread incorporation of such advances are mandated for use within comprehensive resource management programs. Slower still is the rate at which this innovation has motivated widespread changes in the undergraduate engineering curriculum.

Within this framework, a number of prognostications from the perspectives of *technological change*, *social change*, and *educational change* are offered describing the challenges and opportunities for water resources professionals and educators between now and 2050.

TECHNOLOGICAL CHANGE

Sustainable Distributed Energy Sources. Recent attention to concerns of energy independence, sustainability, and global warming will drive massive R&D investments in renewable energy sources and dramatically improve distribution and control systems (Sayigh, 2008). This investment will produce cost effective, modular and scalable sources of high quality energy that will enable increasingly reliable

water monitoring, assessment, management and control systems. Improved efficiencies, reliability, and maintainability of these systems will dramatically reduce the overall relative cost of providing sustainable water resources to all sectors. New technologies for energy storage will enable much more efficient load shifting and balancing that will allow enhanced optimization of production and delivery systems.

Ubiquitous Environmental Sensor Technologies. New sensor technologies and methodologies for use are being created at an ever increasing rate (Kanouin, O. and Trankler, H.R.;2004). Advances in modern sensor technology across all spatial and performance scales will continue and accelerate over the next 40 years. Smaller and more efficient sensors will be adaptable to widespread environmental and water resources monitoring systems, and. more readily integrated into physical infrastructure to monitor performance and condition, which will improve service and dramatically reduce the cost of systems maintenance and operation. Sensor networks will become increasingly energy independent and able to collect and transmit data reliably and continuously as needed.

Remote Sensing and Earth Observation. Remote sensing and related earth observation technologies will advance quickly with much higher resolution and reliability. High resolution technologies will enable daily image capture from all populated areas with higher frequency data collection from sensitive or critical areas. Custom image capture perspectives and schedules will be readily available to engineers, scientists, and water authorities. Large scale data storage and central repositories will enable widespread access to these data stores.

Intelligent Visualization and Image Analysis Systems. New and continuously improved intelligent and adaptive systems will be created to perform real time analysis of images and sensor signals. The information from the analysis of these images will be combined seamlessly with data from distributed sensor networks to provide immediate and reliable measurements of the condition and health of environmental and water resource systems. Autonomous learning agents and adaptive systems will form the structure for intelligent scene-driven data analysis algorithms, providing opportunities for the development of more cost effective and responsive early warning systems.

Adaptive Modeling Systems. Modeling will remain an important component of water resources planning and management and environmental engineering (Loucks, 2008). While innovation will continue in the design and development of next generation modeling technologies and methodologies, major advances must be made in the utilization of this innovation. New model applications development environments will emerge rapidly over the coming decades that will enable new opportunities for rapid prototyping of water resources models utilizing fully emerging computing architectures including virtual distributed client-server networks and grid computers. Prototyping will enable rapid integration of state-of-the-art simulation and optimization algorithms as well as inferential algorithms. New gigapixel hardware output display devices such as 3D powerwalls, caves, and other immersive media systems (including networked systems supporting multiple users across space and time) will emerge rapidly enabling exploratory evaluation of complex images for use

by systems managers as well as water resources engineers and scientists (Grant, et.al; 2008). These modeling and systems technologies will expand greatly the rate at which modern shared vision modeling environments can be developed for, and used by, water resources stakeholders.

Commonplace Open Information Management Systems. The interactive access and use of water resources models and data will be facilitated greatly by Open Information Management Systems (OIMS) which will become widely available and commonplace enabled by explosive growth in the development and use of free and open source software. Transparent interfaces for the spectrum of input and output devices will enable systems to be designed and implemented by engineers and administrators without the need for extensive and expensive computational support staffs.

SOCIAL CHANGE

Increased Public Awareness of Water Issues. Expanded pressures on water resources from continued population growth (see Table 1) and environmental pressures will become much more visible to the general public, with growth in size and number of better informed citizens action groups that will hold municipalities and water authorities much more accountable for sharing information and water resources forecasts, and providing regular updates on water related and environmental issues. Daily water reports will become commonplace in print, broadcast and online media, and other public forums.

Increased Public Pressure for Water Sustainability. Because of increased availability of water resources information and the need for improved stewardship of this valuable resource, the society demands for the sustainability of reliable and high quality water sources will be much more visible on the public agenda. The decisions by water agencies and public officials responsible for water resources will be under increased scrutiny because of a larger and better informed citizenry. Water related public expenditures and the stewardship of public infrastructure will be more visible and will provide the basis for citizen choices in public elections.

Table 1. Projected growth and change in U.S. population demographics by 2050:

Year	2005	2050
[1]Population (millions)		
World	**6,426**	**9,309**
United States	**296**	**438**
[2]Shifts in U.S. Racial/ethnic groups		
Foreign-born	12%	19%
White	67%	47%
Hispanic	14%	29%
Black	13%	13%
Asian	5%	9%

[1]U.S. Census Bureau (2008)
[2]Passel and Cohn (2008)

EDUCATIONAL CHANGE

Universal Technical General Education. The perspective on general education by most of our universities is that technical students must have broader backgrounds in the arts, humanities, and the social sciences. While certainly true, in this increasingly technical and complex society it will become increasingly

important for non-technical students to obtain, through their formal education, a deeper understanding of technologies and sciences that impact their lives. This is nowhere more true than in areas of public welfare such as health care, environmental sustainability, and water reliability and quality assurance. Universities will be under increasing pressure to provide technically-based learning experiences to all students, driven by the country's need to attract more K-12 students into technical careers, or careers that involve the management of technology. Stronger and more effective linkages and networks will be created between universities, community colleges, and K-12 institutions to improve the seamless transition of students into career paths that are more compelling for them because of the impact they will have on society.

Technical Workforce Diversification. The next 40 years will experience not only rapid world and U.S. population growth but dramatic demographic shifts (Bergman, 2004; El Nasser, 2008; Passel and Cohn, 2008) as reflected in Table 1. Most dramatically, the U.S. will no longer have a majority Caucasian population in this country, with the fraction of White citizens dropping from 67% to 47% at the same time that the Hispanic population will increase from 14% to 29%. With the Hispanic representation in the current U.S. engineering workforce at less than 5.5% and the current enrollment in engineering undergraduate degree programs at fewer than 3 . 5% of total engineering students (NSF, 2005), increasing Hispanic participation in engineering will be a top priority in the coming decades. Doing so will result in an influx of new talent and important new perspective into the engineering workforce at the time when this is essential for the country. Strong and targeted recruitment pipeline facilitation efforts will emerge nationally, particularly in the U.S. southwest.

Standard 5-year Requirement for Engineering. By 2050 the majority of engineering programs in the U.S., particularly those disciplines that address most directly engineering problems in the public sector (e.g. civil engineering, environmental engineering, etc.) will transition to 5-year programs; many offering streamlined BSE/MS emphasis programs. For water resources and environmental engineering students, this will enable broader exposure to information management and networking communications technologies, modeling and model development tools and techniques, data and database development technologies, and collaboration systems. Valuable internship and co-op experiences will become a formal and required component for most of these programs

Global Learning Communities. Recent interest in the development of national and international learning communities will continue (Smith, et.al.,2004; Palloff and Pratt, 2007) and become commonplace within the engineering community. These collaborations will include educational/research universities at multiple locations working as approriate with leading private sector firms and government organizations. Curricula will become increasingly experiential learning-based, and be configured in a manner that will reduce the overall cost and redundancy of staffing and equipping more narrow, but higher quality programs. Courses will consist of flexible module choices within a connected theme, and will adapt most directly to specialized learning needs rather than teaching needs. The resulting curricula for a particular degree or certification will be offered by the very top faculty and professionals in the area regardless of physical location.

Lifeline Learning. Universities and learning communities will become an increasingly important part of a student's formal professional development throughout one's career. With improved networked communications methodologies and infrastructure, students will be able to remain linked to their formal education continuously and formally. Academic programs will transition from being a foundational experience for formal engineering education to one that is viewed explicitly as part of one's *lifeline learning* (Wright, J.R.; 2000); students will stay "connected" with their learning roots, and will nourish, as well as be nourished by that foundation.

REFERENCES

Bergman, Mike (2004). Census Bureau Projects Tripling of Hispanic and Asian Populations in 50 years; Non-Hispanic Whites may Drop to Half of Total Population. *http://www.census.gov/Press-Release/www/releases/archives/.*

El Nasser, Haya, (2008). U.S. Hispanic Population to Triple by 2050, *USA Today*, February 12.

Grant Wallace, Otto J. Anshus, Peng Bi, Han Chen, Yuqun Chen, Douglas Clark, Perry Cook, Adam Finkelstein, Thomas Funkhouser, Anoop Gupta, Matthew Hibbs, Kai Li, Zhiyan Liu, Rudrajit Samanta, Rahul Sukthankar, and Olga Troyanskaya. (2008) *Tools and Applications for Large-Scale Display Walls.* IEEE Computer Graphics and Applications, July.

Kanouin, O. and Trankler, H.R. (2004). Sensor Technology Advances and Future Trends, Instrumentation and Measurement, IEEE Transactions, 53:6, December, 1497-1501.

Loucks, Daniel P. (2008). Water Resource Management Models. *The Bridge*. National Academy of Engineering: Washington, D.C. Fall.

NSF Engineering Task Force (2005). *The Engineering Workforce: Current State,Issues, and Recommendations Final Report to the Assistant Director of Engineering,* The National Science Foundation, May, 48 pages.

O'Neill, G. (1981). *Year 2081: A Hopeful View of the Human Future*. Simon and Schuster, New York.

Palloff, Rena M., and Pratt, Keith (2007). *Building Online Learning Communities: Effective Strategies for the Virtual Classroom*, Jossey Bass, San Francisco.

Passel and Cohn (2008) *U.S. Population Projections: 2005-2050*, Pew Hispanic Research Center: Social and Demographic Trends, February, 55 pages.

Peterson, Erik R. and Posner, Rachel, (2008). Global Water Futures: a Roadmap for Future U.S. Policy. *Center for Strategic and International Studies*, September.

Sayigh, Ali (ed.) (2008). *Renewable Energy 2008*, Sovereign Publications, London.

Smith, Barbara, MacGregor, Jean, Mathews, Roberta, and Gabelnick, Faith. (2004). *Learning Communities: Reforming Undergraduate Education.* Jossey-Bass, San Francisco.

U.S. Census Bureau (2008). Projections of the Population and Components of Change for the United States: 2010 to 2050. (NP2008-T-1) Population Division, August 14.

Wright, J.R. (2000). Internetworking and Lifeline Leaning, ASCE Journal of Water Resources Planning and Management, Vol. 126, No. 1, January/February.

Environmental and Developmental Risks and Stressors Impacting a 2050 Vision

Walter M. Grayman[1]

[1]W.M. Grayman Consulting Engineer, 321 Ritchie Ave., Cincinnati, OH, 45215,
PH: (513) 761-1722, email: grayman@fuse.net

Abstract

A vision of what our water resources and environment may look like in the year 2050 must consider the increasing risks and stressors facing our planet. Recent papers, reports and books are used as the source and basis for identifying the range of future challenges facing the world's water resources and environment. They reflect domestic and international views from people in government, academia, institutions, and private practice. The issues have been distilled down into the following major issues/topics: (1) Aging infrastructure; (2) Population growth and demographic shifts; (3) Public health; (4) Economic development; (5) Energy use and production; (6) Climate change; (7) Sustainability; (8) Pollution of our environment; (9) Security; and (10) Institutional issues such as public participation, regulations, environmental justice and utility governance. Each of these topics is assessed in terms of their potential impacts on future water resources and environment and the challenges we will face over the next 40 years in fulfilling a shared vision of the environment and water resources in the year 2050.

Keywords
Risk, stressors, future, water resources, environment

BACKGROUND

The EWRI Emerging and Innovative Technology Committee (EITC) recently formed the Environmental/Water Resources Vision 2050 task committee. The specific goals of this task committee are to develop a vision of what the state of our natural and constructed environment and water resources could and should look like in the year 2050, and identify the actions needed now and on into the future to make that state a reality. These actions would include both the technical and policy advancements that need to be made in order to achieve the identified 2050 view. As such, it will serve as a very rough research agenda for the coming 40 years. The task committee will enlist a wide range of experts in the environmental/water resources field in the development of this vision.

Our world and society are dynamic systems that continuously change and evolve. Therefore, an important consideration in the development of future vision is an understanding of the risks and stressors that are and will be facing our planet and society over the coming 40 years.

Several recent papers, reports and books have addressed issues related to trends, risks and stressors that may impact the water resources and environment around the world. These publications serve as a source and basis for identifying the range of future challenges. Following is a partial list of some of the key documents that were reviewed in order to identify the range of trends/risks/stressors that are likely to impact future water resources and environment in the United States and around the world.

- The World's Water 2006-2007: The Biennial Report on Freshwater Resources (Gleick, 2006).
- The United Nations World Water Development Report (UNESCO, 2006).
- AwwaRF Update of Strategic Assessment of Future of Water Utilities: Trend Paper (McGuire and Patrick, 2005; Means et al, 2005).
- TECHNEAU: Trends Regarding Future Risks for Water Supply Systems (Rosen and Lindhe, 2007).
- Sustainable Water management in the City of the Future [SWITCH] (Khatri et al, 2007).
- U.S. Drinking Water Challenges in the Twenty-First Century (Levin et al, 2002).
- Wastewater Management in the 21st Century (Daigger, 2007).
- Integrated Water Management for the 21st Century (Bouwer, 2002).
- Innovative Urban Wet-Weather Flow Management Systems [Sustainability Principles for Urban Infrastructure] (Heaney et al, 2000)

These reports and papers form a diverse set of views on future trends and important issues in the water resources/environmental area. They reflect domestic and international views from people in government, academia, institutions, and private practice with backgrounds in the various areas of water resources and the environment. There are many commonalities and also some subtle differences among the various papers. The issues raised in the papers have been distilled down into the following ten major issues/topics related to our water resources and environment. Each of these topics is examined in greater detail in terms of the major trends and their applicability within the fields of water resources and the environment. However, it is the intersection of the various trends that together present the greatest challenges to the future water resources and environment.

- Aging infrastructure
- Population growth and demographic shifts
- Public health
- Economic development
- Energy use and production

- Climate change
- Sustainability
- Pollution of our environment
- Security
- Institutional issues

SUMMARY OF STRESSORS

Aging infrastructure

The American Society of Civil Engineers (ASCE, 2005) report card on America's comprehensive infrastructure assessed the state and needs of public infrastructures and drew the following conclusions: "$1.6 trillion is needed over a five-year period to bring the nation's infrastructure to a good condition. Establishing a long-term development and maintenance plan must become a national priority." Of the 15 general infrastructure areas, the water resources categories received a grade of either D or D-, marks indicating the failing condition of these infrastructures and the urgency for immediate repair, rehabilitation and replacement.

The estimated direct costs associated with repairing and/or replacing the nation's water resources infrastructure are well documented (USEPA, 2002; USEPA, 2005). The likely implications and impacts of not making needed replacement or repair include:

- Significant and ever increasing operations and maintenance costs
- Increasing drinking water and water pollution violations due to the inability of the infrastructure to function properly
- Inability to meet water use demands
- Health concerns due to contaminants entering into water distribution systems or untreated or improperly treated wastewater discharging into water bodies
- Inability to support future growth and development

Population growth and demographic shifts

Population is a major factor in influencing the quantity of water that is used and the amount of wastewater that is generated and as a result, will impact the balance of water availability and the adequacy of the water resources infrastructure in the future. The United Nations (2004) projects total world population to rise from 6.1 billion in 2000 to a range of 7.4 to 12.8 billion people in year 2050 depending upon differing fertility and life expectancy scenarios with most of the increase occurring in less developed countries. The U.S. Census Bureau's Population Projections Program projects an increase in population in the U.S. from 282 million in 2000 to 420 million in 2050 (U.S. Census Bureau, 2004-2005). They also project a large spatial variation in population increases across the country with the largest increases generally occurring in areas where water use is already the most stressed. Figure 1 shows the projected percentage changes in population by state for the period from 2000 to 2030.

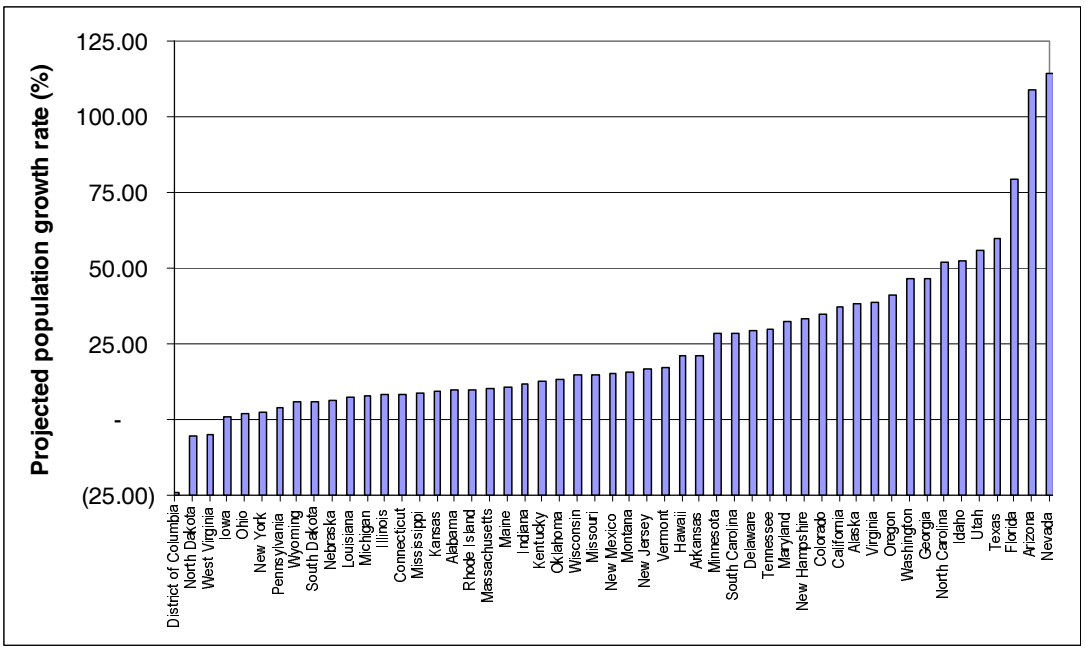

Figure 1. Projected population changes by State for 2000 to 2030

The AwwaRF sponsored futures workshop, included U.S. population and demographic shifts as one of the top ten major trends that will affect how water industry operates in the next 20 years (Means et al, 2005). Specific implications include:

- Communities with burgeoning populations will have to find the resources to fund new facilities while areas with static or shrinking populations face the challenge of diminishing customer base, resulting in a limited rate capacity to replace aging water infrastructure.
- In areas of burgeoning population, utilities will need to consider the contaminant loading from additional human activity and manage this loading to minimize deleterious effects on water quality and treatment.
- Other demographic aspects that may impact water resources management include: an aging customer base, a more educated population, ethnic shifts in population, and increasing income gap

Another demographic change deserving greater attention is the population shift that has resulted and will continue to result in under utilized water infrastructure capacity serving a dwindling customer basis. Examples include rust-belt cities and even a sudden cessation of phenomenal population growth such as in Las Vegas. The nature of the population-induced stress to water infrastructure is different from those with a burgeoning population. Increased water residence time and greater water quality deterioration in drinking water distribution system, for example, has come to the front page of challenges facing water industry. The question of asset management in a dynamic population environment within the service time of a built environment remains unexplored at this stage, and deserves better understandings.

Public health

Public health was the primary driving force in the United States in the 19th and 20th century for the establishment of both public drinking water supplies and municipal sewer systems and treatment plants. As a result of these advances, the most serious waterborne diseases such as cholera and typhoid were virtually eliminated in the United States. However, waterborne infectious disease (WBID) is still a significant concern in the U.S (Levin et al, 2002) and in many of the less developed countries, waterborne disease is still rampant, killing millions of people on an annual basis. Specific public health impacts include:

- The full extent of WBID in the U.S. is not known and current incidence estimates are likely to be several orders of magnitude greater than estimates by the CDC.
- There is emerging evidence that disinfection by-products such as trihalomethanes resulting from chlorination may be carcinogenic and have other possible health effects.
- A multi-barrier approach is needed to address some of the most common waterborne pathogens (e.g., *Giardia, Cryptosporidium*, and some viruses).
- There are trends throughout the world in the emergence and resurgence of diseases including some waterborne diseases. This includes waterborne pathogens that have developed resistance to antibiotics or increased in virulence.

Economic development

Like population increases, economic development generally results in increased (and more spatially concentrated) water usage, increased wastewater production, and more increased stormwater runoff and non point source pollution. Much of this is associated with the urbanization process that generally accompanies economic development. However, there is significant uncertainty in the impacts of future economic development in the United States because of the increasing trends towards globalization, shifts in agricultural water practices, and the possible effects of technological change. Technological change could foster further development that could increase the strain on the water resources infrastructure or, more optimistically, could provide methods for mitigating the impacts of development. Daigger (2007) emphasizes this in his statement that, "further technological developments are crucial to fully and effectively implement new approaches to urban water management that are inherently and significantly more sustainable and that better serve the full range of people irrespective of their economic situation."

Energy use and production

Gleick (2006) observed that there is a strong linkage between the water and energy sectors since water is required to produce and use energy, and energy is used to clean, transport and use water. Most water supply and waste water systems are dependent upon pumping and most water and waste water treatment plant components need sources of energy to perform their functions. According to the Alliance to Save Energy (2002), the water and wastewater sectors are responsible for about 2 to 3% of global energy use. However, in the absence of a comprehensive energy policy for the United

States, there is much uncertainty in the likely impacts of energy on the water resources infrastructure. Some potential impacts include:

- Significantly increased water usage in parts of the country to accommodate agriculture and processing costs associated with bio fuels.
- Increased construction costs due to increased energy costs and petrol-based products such as PVC and HDPE pipes.
- Potential (unknown) impacts of renewable energy methods (wind, solar, hydro power) and increased nuclear power generation.
- Increasing global energy usage and its likely impact on energy availability and cost. This may force water and wastewater utilities to achieve greater energy efficiency in order to offset energy costs.
- Energy shortages may occur with increased frequency and water (and wastewater) systems will need increased capability to switch to alternate or backup energy supplies (Means et al., 2005)
- New energy-intensive treatment technologies may not achieve their expected potential despite their advantages (Means et al., 2005)

Climate change

The area of climate change and the potential impacts of human activities on climate change has been an active area of research, debate and concern for well over a quarter of a century. Modern studies are generally based on mathematical and statistical analyses and a physical understanding of the processes involved in climate change. However, there is still uncertainty in climate change modeling and analysis and most reputable studies attempt to qualitatively or quantitatively assess or express this uncertain. The most recent report issued by the Intergovernmental Panel on Climate Change (IPCC, 2007) concluded that:

- Warming of the climate system is unequivocal, as is now evident from observations of increases in global average air and ocean temperatures, widespread melting of snow and ice, and rising global average sea level
- Most of the observed increase in global average temperatures since the mid-20th century is very likely due to the observed increase in anthropogenic greenhouse gas concentrations.

Some of the potential impacts of climate change on the water resources of the United States are identified by Levin et al (2002), Cromwell et al. (2007), Miller and Yates (2006), and Buchberger et al. (2008) and include:

- Changes in hydrologic cycles shifting the timing, intensity, seasonality and spatial distribution of precipitation
- Perturbation of stressed ecosystems
- Droughts followed by severe weather events can result in more polluted runoff to surface waters and less infiltration to replenish aquifers and could destabilize natural biological controls of pests and pathogens.
- Warmer temperatures of surface water sources may contribute to increased harmful algal blooms resulting in taste, odor and toxic (e.g., cyanobacteria) impacts on water.

- Warmer temperatures and heavy precipitation events may result in increased sediment and non-point source pollutant loadings to watercourses. This may cause higher microbial and nutrient loadings in drinking water supplies and make water treatment more difficult.
- Throughout the U.S., temperature and hydrology changes may result in changes in watershed vegetation and aquatic ecology. Potential impacts of this will be increased wildfires, pest infestations, and reservoir eutrophication.
- Rising sea levels will increase the risk of coastal flooding to wastewater facilities and coupled with lower freshwater base flows will increase salinity in coastal aquifers.
- Heavy precipitation events may result in increased sediment and non-point source pollutant loadings to watercourses. This may make water treatment more difficult.
- The increased variability due to global warming in key parameters affecting water quality and quantity will put a premium on good long-term planning for water and wastewater utilities. Reevaluation of the entire utility portfolio from source to tap with respect to adaptation strategies is needed.

Sustainability

The Brundtland Commission, formally the World Commission on Environment and Development (WCED), was convened by the United Nations in 1983. The Report of the Commission, *Our Common Future*, was published by Oxford University Press in 1987 and contains the following definition for sustainable development, "development that meets the needs of the present without compromising the ability of future generations to meet their own needs" (Bruntland, 1987). It recognizes that land, water, air, and minerals are all essential but finite natural resources that contribute to a healthy planet and society. UNESCO (2006) established a goal to ensure environmental sustainability. The report recognizes that "healthy ecosystems are essential for the maintenance of biodiversity and human wellbeing" and that "we depend upon them for our drinking water, food security and a wide range of environmental goods and services". It sets a target to "integrate the principles of sustainable development into country policies and programmes and reverse the loss of environmental resources". Overextraction of groundwater and depletion of other key resources are other significant examples of non sustainable development.

Pollution of our environment

There are many pathways by which our water resources and environment can be compromised through pollution. These include air pollution, point and non point sources of water pollution, salt water intrusion into existing aquifers, and other related pathways. "Pollution of water bodies alters chemistry and ecology of rivers, lakes and wetlands; greenhouse gas emissions produce dramatic changes in runoff and rainfall patterns" (UNESCO, 2006).

Bouwer (2002) addresses the potential impacts of non point sources on our groundwater resources. "Since almost all liquid fresh water on the planet occurs underground, groundwater will be used more and more and, hence, must be protected against depletion and contamination, especially from nonpoint sources like intensive

agriculture. A significant nonpoint source of groundwater pollution is agriculture, with its use of fertilizer, pesticides, and salt containing irrigation water that contaminate the drainage water as it moves from the root zone to the underlying groundwater. The problem can be expected to get worse in the future as agriculture must intensify (including use of more agricultural chemicals) to keep up with the demands for more food and fiber by increasing populations."

Saltwater intrusion is a natural process that occurs in coastal aquifers, where there is hydraulic connectivity between the aquifer and the seawater. This is a natural process but the rate of saltwater intrusion will increase (or decrease) due to a changing imbalance in the freshwater aquifers and the sea levels. Increasing ground-water withdrawals from these aquifers can cause further lateral and vertical intrusion of surrounding saltwater. Similarly, sea level rises that have been discussed as a potential effect from climate change, can result in increased saltwater intrusion. The impacts of salt water intrusion include more intensive water treatment requirements and/or decreased availability of fresh water for various uses including agriculture.

Security

Water utilities have historically been concerned with security issues such as accidental pollution spills into their raw water source, and vandalism or other criminal activities resulting in damage to equipment. The twenty-first century has brought an increasing concern over intentional acts directed against water and wastewater utilities. These include physical damage to utility facilities and purposeful contamination of the water supply. Means et al (2005) list the following implications to increased security concerns facing the drinking water industry. Most of these also apply to the wastewater area.

- The need for improved physical security has been accepted by drinking water utilities following the September 2001 terrorist activities.
- Utilities now need to examine the nature and capabilities of the real threats faced by the water industry.
- Utilities are becoming increasingly vulnerable to security breaches on information technology systems by both internal and external threats.
- Risk and cost tradeoffs are not well understood by a traditional mindset.
- Utilities will require a sophisticated workforce to understand the risks and use the required tools for responding to these risks.

Institutional issues - Public participation, regulations, environmental justice and utility governance

Gleick (2006) notes that there has been a dramatic change in the way that water decisions are made around the world moving from decisions by a small number of technical or engineering experts to significant involvement by the public. This is only one of several trends in the area of institutional issue that are and will affect the operations and decision-making in the water resources field. Other issues in this area include privatization of water systems, customer expectations concerning the safety and reliability of their water supply, communications of information to water customers, water as a human right, valuation of water, and creative partnerships between water/wastewater utilities and other sectors. Conflicting water resources and

environmental regulations lead to inefficient or insufficient management of the resources.

SUMMARY AND CONCLUSIONS

Our planet and society are not static. There are pressures, risks, and stressors that continually affect and change it. This dynamic behavior must be considered whenever we do future planning so that we are not building a blue print for a situation that will no longer exist. Though there is always uncertainty in the future, an understanding of potential and likely stressors is an essential element in developing a vision for our water resources and environment in the year 2050.

ACKNOWLEDGEMENTS

Much of the information in this paper was derived from an EPA sponsored research project at the University of Cincinnati called the Water Resources Adaptation Program (WRAP). I would like to acknowledge my fellow members of the WRAP team (Steven Buchberger, Robert Clark, and Zhiwei Li) for their insights and contributions and to our EPA Project Officer, Jeffrey Yang, for his vision and technical guidance.

The U.S. Environmental Protection Agency, through its Office of Research and Development, funded and managed, or partially funded and collaborated in, the research described herein. It has been subjected to the Agency's administrative review and has been approved for external publication. Any opinions expressed in this paper are those of the author and do not necessarily reflect the views of the Agency; therefore, no official endorsement should be inferred. Any mention of trade names or commercial products does not constitute endorsement or recommendation for use.

REFERENCES

Alliance to Save Energy. (2002). Taking Advantage of Untapped Energy and Water Efficiency Opportunities in Municipal Water Systems. http://www.watergy.org/resources/publications/watergy.pdf [20/3/2007]

ASCE (2005). http://www.asce.org/reportcard/2005/index.cfm

Bouwer, H. (2002). Integrated water management for the 21st Century: problems and solutions." ASCE Journal of Irrigation & Drainage Engineering 128(4): 193-203.

Bruntland, G. (ed.), (1987). "Our common future: The World Commission on Environment and Development", Oxford, Oxford University Press.

Buchberger, S.G., Clark, R.M. Grayman, W.M., Li, Z., Tong, S., Yang, Y.J. (2008). Impacts of Global Change on Municipal Water Distribution Systems. *Proceedings of 2008 International Symposium on WDSA*, Kruger Park, South Africa.

Cromwell III, J. E., Smith, J. B., and Raucher, R. S. (2007). "No Doubt About Climate Change and Its Implications for Water Suppliers." Journal: American Water Works Association, 99(9), 112-117.

Daigger, G.T. (2007). Wastewater Management in the 21st Century. J. Environmental Engineering , ASCE. 133(7): 671-680.

Gleick, P. (2006). The world's water, 2006-2007: the biennial report on freshwater resources. Island Press, Washington, DC.

Heaney, J.P., Pitt, R., and Field, R. (eds.) (2000). Innovative urban wet-weather flow management systems. EPA-600-R-99-029, Cincinnati, OH. http://www.epa.gov/ORD/NRMRL/pubs/600r99029/600R99029prelim.pdf.

IPCC (2007). Climate Change 2007 - The Physical Science Basis. Contribution of Working Group I to the Fourth Assessment Report of the IPCC. Cambridge University Press, New York.

Khatri, K.B., Vairavamoorthy, K.N., and Pathiran, A. (2007). Inventory of Important Global Change Pressures on Urban Water Systems in the City of the Future. SWITCH, UNESCO-IHE. http://switchurbanwater.lboro.ac.uk/outputs/pdfs/WP4-0_DEL_Milestone_global_change_pressures.pdf

Levin, R. B., Epstein, P. R., Ford, T. E., Harrington, W., Olson, E., and Reichard, E. G. (2002). U.S. Drinking Water Challenges in the Twenty-First Century. Environ.Health Perspect., 110 43-52.

McGuire Environmental Consultants, and Patrick, R. (2005). Update of Strategic Assessment of Future of Water Utilities: Trend Paper. Awwa Research Foundation, Denver, CO.

Means Ill, E. G., Ospina, L., and Patrick, R. (2005). "Ten primary trends and their implications for water utilities." Journal: American Water Works Association, 97(7), 64-77.

Miller, K. A., and Yates, D. N. (2006). Climate change and water resources : a primer for municipal water providers. AWWA Research Foundation, American Water Works Association, IWA Pub., Denver, CO.

Rosén, L., and Lindhe, A. (2007). Trend report – Report on trends regarding future risks. Rep. No. D 1.1.9, Techneau.

UNESCO. (2006). Water a shared responsibility - The United Nations World Water Development Report 2. Rep. No. UN-WATER/WWAP/2006/3, http://unesdoc.unesco.org/images/0014/001444/144409E.pdf

United Nations (2004). World Population to 2300. New York. http://www.un.org/esa/population/publications/longrange2/WorldPop2300final.pdf

U.S. Census Bureau (2004-2005). Population Projections. http://www.census.gov/population/www/projections/popproj.html

U.S. Environmental Protection Agency (2002). *The Clean Water and Drinking Water Infrastructure Gap Analysis*.

U.S. Environmental Protection Agency (2005). Drinking Water Infrastructure Needs Survey and Assessment, Third Report to Congress.

Flood Risk Management Circa 2050

Gerald Galloway[1] PE, PhD, Dist.M.ASCE

[1]Civil and Environmental Engineering, University of Maryland, College Park , MD 20742 and Trustee, ASFPM Foundation; PH (301) 405-1341; FAX(301) 405-2585; email:gegallo@umd.edu

ABSTRACT

Today the United States faces increasing annual flood damages and climate change will only exacerbate this problem. In spite of nearly 73 years of flood control and 41 years of floodplain management, the challenge continues. This paper provides a positive vision of how the floodplain of 2050 might appear if appropriate measures were taken by governments and the public at large in the years ahead. It is based on the output of the 2007 ASFPM (Association of State Floodplain Managers) Foundation Gilbert F. White National Flood Policy Forum that examined this topic.

YEARS OF FLOODS

Floods have been a part of American history. Early Eastern colonists battled overflows from the Delaware River into nearby agricultural lands. Early in the 18th century, the founders of New Orleans initiated levee building to protect the growing city. Over time, as the nation moved to the west, it established its towns and cities alongside rivers, the principal highways for movement of goods and people, and, as the cities grew, the problems of periodic flooding became more evident. By the middle of the 19th century, the federal government began its involvement in attempting to reduce flood losses. Shortly after the turn-of-the-century it had begun to actively assist states and local communities in dealing with the flood challenge. Major floods in 1927 and 1936 caused the Congress to reevaluate the federal role and legislate a national approach to flooding that would drive federal and state efforts for the rest of the 20th century. The Flood Control Act of 1936, in its name, defined the method by which engineers would address flooding-***control*** the waters by keeping them off the land, storing them behind dams, and speeding them to the oceans through channel work and floodways. The 1936 Act and a 1928 Act, targeted at the lower Mississippi Valley, were focused on preventing disasters-no more destructive flooding-and led to the construction of large systems such as the Mississippi River and Tributaries project that protects the lower Mississippi Valley from Cairo Illinois to the Gulf of Mexico against inundation, and the countless smaller projects designed to protect individual communities, agricultural areas, and critical infrastructure.

The environmental movement of the 1960s, coupled with the growing knowledge of the work of the University of Chicago geographer, Gilbert F. White, that focused on adjusting human use of the floodplain as opposed to protecting humans in the floodplain from flooding, began a slowdown in the construction of flood control

structures and a search for alternative approaches- nonstructural methods - to deal with flooding. These methods included land-use controls to prevent unwise development in the floodplain, floodproofing and elevation of structures, acquisition of most frequently flooded lands, use of natural storage of flood waters in upstream wetlands, development of early warning systems to permit evacuation of flood hazard areas, and provision of insurance to those at risk. In 1968, Congress passed the National Flood Insurance Program (NFIP) that has grown to include today over 20,000 communities and over 5.7 million policyholders.

In 1993, the Midwest was devastated by massive flooding that took 38 lives and caused over $16 billion in damages. Because the flooding was extensive-eight Midwestern states-and water remained in homes and on the land in some places for over six months, the nation was exposed through evening news and other media coverage to the devastation and human trauma that resulted from this flood. Calls for action were heard in the Congress and by the Administration and led to a White House study of the causes of the flood and the development of recommendations to deal with future such events. The report, which was issued in 1994, indicated that although the flood was a significant event, floods of that magnitude were natural events and would continue to occur (IFMRC 1994). It pointed out that national flood damages continue to grow and that people and property are at risk across the country. It noted that occupation of the floodplain and attempts to protect those in the floodplain had caused significant environmental damage and threatened ecosystems that provided rich goods and services to both the natural and human environment. It acknowledged that flood control structures had prevented $18 billion in damages during the 1993 flood. The report recommended that, in moving forward with efforts to reduce flood damages, the nation should not only strive to reduce flood losses but also concurrently protect and enhance the natural environment of the floodplain. The report offered a vision for the future of the floodplain that would carefully balance the use of both structural and nonstructural methods to bring about both sustainable use of lands that were already the home for many long settled communities and important for the conduct of commerce, as well as ensuring that the loss of riverine ecosystems was reversed. Although there was some support for action on the recommendations, other national priorities moved on to the scene and the report was soon forgotten.

INTO THE 21ST CENTURY

While non-governmental organizations, such as the Association of State Floodplain Managers, continued to point out the growth in flood losses in the latter half of the 20th century, entreaties for a retrospective look at the national approach generally fell on deaf ears. While the these organizations were unable to promote any detailed examination by the Congress of the flood problem, they were at least able to convince the Congress to support a $1 billion modernization of flood mapping by the NFIP in order to more accurately depict the threat faced by those who live in and near the floodplain.

On August 29, 2005, Hurricane Katrina smashed into the Louisiana-Mississippi Gulf Coast and inflicted massive damages on the people and the built and natural environment of the region. Over 1800 people lost their lives. The costs of property losses, response and recovery operations and insurance claims payouts have not been completely identified but likely will exceed $100 billion. Over 120 mi.² of the wetland buffer that existed between New Orleans and the Gulf were also destroyed by the hurricane. Three and one half years after the hurricane, only 70% of the pre-Katrina population has returned to the region and many parts of the city of New Orleans and the Gulf Coast have yet to be restored or have plans made for their eventual resettlement or reuse. Once again just as it occurred after the 1993 Flood, the outcries about the need to deal with flooding were loud and the promises great. Some initial debate about alternative approaches to the restoration of below-sea level areas of New Orleans (move people out) were quickly seen to be impolitic and the President of the United States appeared in that city with a promise to make " the flood protection system stronger than it has ever been (Bush 2005)." Since 2005, the focus of federal effort in New Orleans has been on restoration of the hurricane protection system (levees, pumps and other structures) to a level that would protect the city against the 100-year (1% annual chance of occurrence) flood event, a level that is far less than the approximately 400-year Katrina storm surge event.

Questions about why levees failed in New Orleans during the hurricane and why the destruction along the Mississippi coast line was so complete did bring calls for investigations, reviews, and studies and did result in Congressional hearings. Two reports by the US Army Corps of Engineers (USACE) dealt with the technical issues surrounding the levee failures as well as the flaws in the decision-making from Washington to New Orleans over the 40 year history of the New Orleans hurricane protection project (IPET 2008; Woolley and Shabman 2007). The IPET report was supplemented by reports from the American Society of Civil Engineers (ASCE 2008) and a blue ribbon panel of the National Research Council (NAE/NRC 2006). The Federal Emergency Management Agency (FEMA) commissioned an Interagency Levee Policy Review Committee (ILP RC 2006) to examine how levees were treated in the NFIP. The net result of the conduct of these studies, together with the attention of ASFPM and the National Association of Flood and Storm Water Management Agencies (NAFSMA), was the identification of the fragile nature of thousands of miles of levees across the entire nation and the need for evaluation of the condition of these levees (a conclusion also reached in the 1994 IFMRC report). This attention eventually led to the passage, in the Water Resources Development Act of 2007, of provisions to establish a national levee safety program (NCLS 2009).

FLOOD RISK MANAGEMENT

In recognition of the gradual shift away from a structural-only approach, during the last decades of the 20th century organizations such as the Federal Emergency Management Agency (FEMA) and the US Army Corps of Engineers (USACE) began to drop use of "flood control" in favor of "flood damage reduction" in describing

activities related to management of the floodplain. But in Europe, the approach was to move even farther away from flood control.

Under flood control, those responsible for reducing damages chose a level of protection for areas in danger based on either an economic analysis that determined that the benefits of providing the protection (flood damages avoided) exceeded the cost of constructing the protection, or a national policy such as "no more floods." Following the disastrous floods in 1953, the government of the Netherlands took action to prevent recurrence of such catastrophic events and eventually established a 10,000-year level of protection for coastal areas (and in 2008, a Delta Commission recommended that the level be increased to 100,000-year protection.) The European Community began however to consider a different approach, flood risk management. Under this approach, the risk to a given area would be defined by examining the probability that the flood might occur, the probability that whatever protection system existed would function as designed, and the consequences should the area actually flood. Establishing a risk-based approach not only identified the level of risk faced by each community but also offered a method of prioritization in carrying out protection efforts. It became clear, using flood risk management, that the risk could be reduced not only by increasing the probability that the protection system would do the job, but also by taking steps within the protected community to reduce its vulnerability to flooding through use of nonstructural methods including the avoidance of development. While Europe moved ahead with this concept, it was not until Katrina, that it began to be examined in any detail in the United States (Galloway 2008). Now, as USACE and FEMA move to deal with post-Katrina flood vulnerability, they have both adopted a flood risk management paradigm.

WHAT ABOUT THE FUTURE?

With flood damages increasing each decade, the population of the nation increasing at a high rate and moving to coastal and riverine areas, and climate change promising an increased potential for flooding even in areas where total rainfall may decrease, it became obvious to the professionals in the floodplain management business that something needed to be done. In 2007, the ASFPM Foundation decided to conduct a Gilbert F. White Flood Policy Forum, the foundation's vehicle for addressing critical issues in floodplain management. The Forum would examine what actions needed to be taken to ensure that by 2050 the flood risk situation found at the start of the 21st century would be mitigated.

In November 2007, the Foundation brought together for two days in Washington 75 national and international flood experts to discuss what the floodplain might look like in 2050 if no action were taken to slow the growth in damages and what it might look like if specific actions were taken to move in the opposite direction. The group quickly agreed that an unchecked 2050 would present the nation significant problems and would threaten the lives and property of those living in and near the floodplain as well as the economic viability of the nation as a whole. They also agreed that if the nation was willing to address the challenges it faced in managing the floodplain,

future damages could be reduced, the ecology of the floodplain could be rejuvenated, and the nation could benefit.

GILBERT WHITE'S THESIS

In defining a broader than structures-only approach to dealing with floods, Gilbert White identified eight adjustments that could be made to floodplain use that would reduce the potential for losses and ensure long-term sustainable use of the riverine environment (White, 1945):

- Elevation. Raising structures above the expected flood level.
- Flood abatement. Using measures "taken outside of stream channels with the effect of reducing the crest of flood flows or changing the debris load for a flood event."
- Flood protection. Using engineering works to minimize the impacts of flooding.
- Emergency measures. In areas already occupied, taking actions to mitigate floods that do occur through temporary evacuation, the adjustment of services, and flood fighting.
- Structural adjustments. Designing buildings and other structures to reduce losses when floods occur.
- Land use. Permanently removing property and services beyond the reach of floods.
- Public relief. Using public grants and direct rehabilitation to relieve the impact of flood losses.
- Insurance. Mitigating the financial effects of flooding on structure owners and businesses through use of insurance.

During the Forum, participants examined the eight methods of adjustment to determine if White's original list was still relevant, and where it was not or where he was not fully useful in the 21st century and what changes might be made to increase its modern utility. They were also asked to identify new adjustments that might be added to White's list to better address the needs of the country in the future.

A SUSTAINABLE 2050 FLOODPLAIN

Not surprisingly, forum participants determined that the adjustments posited by White in 1942 largely remain relevant today. They also identified several areas where new adjustments measures could be added to those developed by White. The Forum participants concluded that, should action be taken in accordance with a suite of adjustment measures, the floodplain of 2050 would be far less dangerous, environmentally more suitable, and overall more sustainable than it would be should no action be taken to deal with the impending challenges.

In a looking forward to 2050 in light of the White adjustments to flooding, participants saw that the more sustainable floodplain would see:

- Land-use in which all states would have comprehensive land-use planning that effectively identified their land and water resources and the natural hazards and that development would be permitted only when there would be no adverse impact on flooding or on the natural and beneficial functions of the floodplain.
- Building and development standards targeted at avoiding new construction in flood prone and residual risk areas behind levees and below dams to reduce the exposure to flood damages. Where structures were built, the nature of their construction would reduce the potential for losses should floods occur. Those who took actions that increased their flood risk would not be rewarded with federal benefits.
- Elevating structures in the floodplain would no longer be considered as the best or even desirable solution since structure surrounded by water pose a risk to both those in the structures and those that must be concerned about the condition of those that occupy the structures.
- All-hazard insurance would be mandatory throughout the United States.
- Structural flood protection would only be used to deal with existing development where no other alternatives existed. The first choice would be nonstructural.
- Emergency measures would be based on robust pre-disaster mitigation activities that took full advantage of the lessons learned in previous flooding events.
- Disaster relief and assistance would be available to all as a backup to other adjustments but the public at large would understand the limits of such relief and assistance.
- Watershed planning would clearly identify the impacts of upstream activities on those downstream and vice versa. Every effort would be made to ensure maximum natural storage of flood waters.

While 21st-century consideration of Gilbert White's eight adjustments would certainly go a long way to ensure that the floodplain of 2050 was more sustainable, the participants also recognized that four additional adjustments should be considered. They believe that the nation must also consider:

- Providing room for rivers and oceans by choosing not to occupy flood prone areas and thus avoiding the hazard as well as precluding unintended adverse impacts on ecosystems. This adjustment would ensure that development would routinely place distance between human occupation of the landscape and rivers and oceans.
- Requiring exercise of personal responsibility by recognizing the hazards that are faced, the risks that are taken in dealing with these hazards and the need to become concerned with the sustainability of the environment.
- Recognizing the geographic interdependence of floodplain activities and taking steps to minimize the impacts of these interdependencies. Damages to one community, business, or industry may have significant economic and social impacts at locations far from the flooded area.

- Ensuring national awareness of the flood hazard and education of the population on flood processes, mitigation and avoidance. Those who are well-educated are far more likely to take appropriate action to reduce their vulnerability to flooding or to totally avoid placing themselves at risk. 21st-century information technology offers the rare opportunity for near real-time distribution of hazard information to the entire population.

Attention the above adjustments would result in a 2050 Floodplain where: "… *in spite of rapidly growing populations and a changing climate, both flood risk and land and water resources are being managed towards more sustainable outcomes. The nation views land and water as precious resources, and therefore protects the natural and beneficial functions of floodplains, wetlands, and coastal areas. Because these areas have been reserved—and in some cases, restored—a maximum amount of natural mitigation of flooding takes place continually. Integrated water management is an accepted practice. All new development is designed and built so that it has no adverse impact on flood levels, sedimentation, erosion, riparian or coastal habitat, or other community-designated values. The market strongly favors sustainable development, which means that floodprone construction rarely occurs. Private and public losses due to floods are indemnified through a government-backed but private system of universal insurance coverage that encourages mitigation. Floodplain management programs are funded from fees charged for development impacts, a highway trust fund, or other secure sources. Risk communication through all levels of government has become advanced enough that local decision making is well informed; policy decisions are based on sound science." (ASFPM Foundation 2008).*

GETTING TO 2050

New approaches don't just happen. Even though flood professionals may strongly endorse modified White-developed adjustments and the addition of other adjustments to deal with the uniqueness of our current situation, these approaches must be understood and accepted by the population at large and they must find their way into clear and holistic public policies that treat land and water is important natural resources/ As the forum report notes, the twin goals of these policies must be "to protect people and property from flooding while also protecting flood prone lands from people." Even with new policies there remains a need for dealing with the nation's fragmented system of water resource management, disaster relief and mitigation. Efforts must be made to eliminate disincentives to correct action, duplication of programs and minimization of costly and time-consuming litigation. Moving to a safe and sustainable 2050 floodplain will require access to accurate and comprehensive data about our natural resources, the hazards we face and integration of these data with the increasingly available data and information about all their aspects of society *(ASFPM Foundation 2008).*

A movement to this better floodplain of 2050 will also require adequate funding to not only with proper siting and construction of future development and removal of

unwise past development, but also with the need to maintain the infrastructure that currently exists and that provides protection for many areas.

The Forum report points out that the circumstances that surround early 21st century development are unique and represent the opportunity for significant change in the way in which we do business. The report concludes with by providing six guidelines that "capsulize the new ways of thinking and operating that will be needed to achieve safe and sustainable relationships with our water resources," and lead to the safe and sustainable floodplain of 2050. These guidelines ask that decision-makers and the public at large to:

- **Make room for rivers, oceans, and adjacent lands.**
- **Reverse perverse incentives in government programs that make it more profitable to act unwisely than to recognize the need for long term safety and sustainability.**
- **Restore and enhance the natural, beneficial functions of riverine and coastal areas.**
- **Generate a renaissance in water resources governance and development of the policies and organization that will support this renaissance.**
- **Identify risks and resources and communicate at public and individual levels.**
- **Assume personal and public responsibility for their actions in the floodplain** *(ASFPM Foundation 2008).*

IMPLICATIONS FOR CIVIL ENGINEERS

According to ASCE's *Vision 2025 (2007)*, "Entrusted by society to create a sustainable world and enhance the global quality of life, civil engineers serve competently, collaboratively, and ethically as master

- planners, designers, constructors, and operators of society's economic and social engine—the built environment;
- stewards of the natural environment and its resources;
- innovators and integrators of ideas and technology across the public, private, and academic sectors;
- managers of risk and uncertainty caused by natural events, accidents, and other threats; and
- leaders in discussions and decisions shaping public environmental and infrastructure policy."

Moving from where we are today in floodplain and flood risk management to the future described above will require civil engineers to live up to the aspirational expectations of *Vision 2025*. Implementation of the modifications of Gilbert White's original adjustments to floodplain use, the suggested new adjustments, and the guidelines proposed in the report on the Gilbert F. White forum will demand from

civil engineers full exercise of the knowledge, skills and attitudes needed to serve the nation in the manner described above. It is important that, as floodplain professionals define a visionary state for 2050, civil engineers are prepared to support this effort and see it through to its fulfillment.

IN SUM

The United States faces major challenges in dealing with flooding. Damages from disastrous floods are on the rise people and property remain at risk. Over the next 40+ years, if action is not taken to deal with the problem, it will grow substantially worse. Climate change, population growth, unbridled development in hazardous areas, and a lack of personal responsibility on the part of individuals subject to flooding will lead to an untenable situation by the middle of the 21st century. Since the federal government became involved with flooding in the early part of the 20th century, it has moved from trying to control the floods to jointly to addressing the problem through use of both structural and nonstructural means and recognizing the need to see flooding as a risk. Gilbert White's seminal work identified what actions could be taken to deal with the flood threat and proposed eight adjustments that have stood the test of time. Those attending the ASFPM Foundation 2007 Forum identified four additional areas where human adjustment might result in even better future conditions. With attention to these opportunities, the American floodplain of the future can be far different than it is today. Civil engineers are at the nexus of this challenge and must, along with their many other responsibilities, take on the challenge of flooding 2050.

ACKNOWLEDGMENTS

The author would like to acknowledge the great efforts of the ASFPM Foundation team that planned and carried out the 2007 Flood Policy Forum, synthesized its results and prepared the report of the Forum: Doug Plascencia, Bruce Baird, Diane Brown, Larry Larson, Dale Lehman, Jackie Monday, and Edward Thomas. Their work made possible this paper.

REFERENCES

American Society of Civil Engineers (ASCE). (2008). The New Orleans Hurricane Protection System: What Went Wrong and Why: A Report by the American Society of Civil Engineers Hurricane Katrina External Review Panel. Reston, VA: ASCE. Available at http://www.asce.org/static/hurricane/whitehouse.cfm

American Society of Civil Engineers, ASCE Steering Committee to Plan a Summit on the Future of the Civil Engineering Profession in 2025 (ASCE). (2007). *The Vision for Civil Engineering in 2025*. Reston VA: ASCE

ASFPM Foundation. (2008). *Floodplain Management 2050*. Report of the 2007 Assembly of the Gilbert F. White National Flood Policy Forum. Madison, WI: ASFPM

Galloway, GE. (2008). Floor risk management in the United States and the impact of Hurricane Katrina. *International Journal of River Basin Management*, 4:6 303-306.

Interagency Floodplain Management Review Committee (IFMRC). (1994). Sharing the Challenge: Floodplain Management into the 21st Century. Report of the Interagency Floodplain Management Review Committee to the Administration Floodplain Management Task Force. Washington, D.C.: U.S. Government Printing Office.

Interagency Levee Policy Review Committee (ILPRC). (2006). The National Levee Challenge: Levees and the FEMA Flood Map Modernization Initiative. Washington: FEMA. Available at http://www.fema.gov/library/viewRecord.do?id=2677

Interagency Performance Evaluation Task Force (IPET). (2008). Final Draft Volume I – Executive Summary and Final Draft Volume VIII Risk and Reliability Report. Available at https://ipet.wes.army.mil/

NAE/NRC (National Academy of Engineering/National Research Council). (2006). Third Report of the National Academy of Engineering/National Research Council Committee on New Orleans Regional Hurricane Protection Projects. Washington: National Academy Press.

National Committee on Levee Safety (NCLS). (2009). *Draft Report to Congress on Recommendations for a National Levee Safety Program*. Washington: US Army Corps of Engineers. Available at http://www.iwr.usace.army.mil/ncls/docs/NCLS-Recommendation-Report_012009_DRAFT.pdf

White, Gilbert F. (1945). Human Adjustment to Floods: A Geographical Approach to the Flood Problem in the United States. *Research Paper No. 29*. Chicago: University of Chicago,

Woolley, Douglas and Leonard Shabman. (2008). Decision-Making Chronology for the Lake Pontchartrain & Vicinity Hurricane Protection Project. Final Report for the Headquarters, U.S. Army Corps of Engineers. Alexandria, VA: Institute for Water Resources, U.S. Army Corps of Engineers.

Working Group for Post-Hurricane Planning for the Louisiana Coast. (2006). *A New Framework for Planning the Future of Coastal Louisiana after the Hurricanes of 2005*. Cambridge, MD: University of Maryland Center for Environmental Science. Available on line at: http://www.umces.edu/la-restore/.A

Urban Stormwater Management in 2050

James P. Heaney[1] **and** John J. Sansalone[2]

[1]**Department of Environmental Engineering Sciences, University of Florida, P.O. Box 116450, Gainesville, FL 32611; PH (352) 392-0841; FAX (352) 392-3076; email: heaney@ufl.edu**
[2] **Department of Environmental Engineering Sciences, University of Florida, P.O. Box 116450, Gainesville, FL 32611; PH (352) 392-0841; FAX (352) 392-3076; email: jsansal@ufl.edu**

ABSTRACT

During the past 40 years, urban stormwater management has evolved from focus on drainage and flood control to inclusion of stormwater quality associated with nonpoint pollution. This paper projects what the urban stormwater field could look like in the year 2050. The projections are based on our best judgments as to the internal and external drivers that are expected to change the field during the next 40 years. Relevant projections by other stormwater groups are reviewed. Anticipated changes include the growing interest in stormwater reuse, on-site control of stormwater using a variety of low impact development alternatives, generation and accretion of recalcitrant residuals, toxics and chemicals as well as changing temporal and spatial phenomena of the urban hydrologic cycle due to changes in climate and patterns of urban settlement. Key expected drivers of changing attitudes are the greatly increasing relative cost of providing water and energy; greater concern about developing more sustainable green materials and infrastructure systems; and technological advances that will allow proactive management of urban stormwater systems using real time control and including source controls.

INTRODUCTION

As early as the 1960's, urban water experts were advocating the need to take an integrated systems view of water supply, wastewater, and stormwater (Heaney et al. 2000). While these investigators were able to scope out the problem, they lacked the essential computational and measurement tools to conduct these evaluations. Since the 1960's, computational power and models such as SWMM, geographical information system (GIS) tools and computational fluid dynamics (CFD) have been coupled with advances in urban water chemistry and particulate measurements, and imaging technology at scales ranging from x-ray tomography to satellite imaging for water chemistry indices to flood depths. This paper focuses on urban stormwater management with the notable exception of flood control that is described in a companion paper by Galloway (2009). A literature review of sustainability concepts and related efforts to forecast future stormwater systems is presented in the next section. Then, methods of analysis are described. Lastly, our forecasted major shifts in stormwater management are presented.

LITERATURE REVIEW

Innovative Urban Water Systems. Heaney et al. (2000) list the following principles for sustainable water infrastructure systems for the 21st century based on a thorough review of the literature on urban water systems:

- Individual urban activities should minimize the external inputs to support their activities at the parcel level. For water supply, import only essential water for high valued uses such as drinking water, cooking, showers and baths. Reuse wastewater and stormwater for less important uses such as lawn watering and toilet flushing. Minimize the demand for water by utilizing less water intensive technologies where possible. For transportation, minimize the generation of impervious areas, especially directly connected impervious areas, for providing traffic flow and parking in low use areas.
- Minimize the external export of residuals from individual parcels and local neighborhoods. For wastewater, export only highly concentrated wastes that need to be treated off-site. Reuse less contaminated wastes such as shower water for lawn watering. For storm water, minimize off-site discharge by encouraging infiltration of less contaminated stormwater and using cisterns or other collection devices to capture and reuse stormwater for lawn watering and toilet flushing.
- Structure the economic evaluation of infrastructure options to maximize the incentive to manage demand by using commodity use charges instead of fixed charges. For stormwater, assess charges based on the cost of providing stormwater quality control for smaller storms and flood control for larger storms. Charges should be based on the imperviousness with higher charges for directly connected imperviousness and the nature of the use of the impervious areas and their pollutant potential. Some charge should be assessed for pervious areas. Credit is now being provided for on-site storage and infiltration. However, the credit needs to be subject to quantifiable system behavior for hydrologic restoration and load management.
- Assess new development for the full cost of providing the infrastructure that it demands, not only within the development, but also external support services.
- Implement policies to make drivers pay the full cost of using personal automobiles through appropriate taxes on gasoline.

Blue Water in Green Cities. Novotny (2006) organized an NSF sponsored workshop on urban water systems of the future. He lists the following nine drivers of the change to more sustainable urban water systems.

1. Population growth and migration
2. Global climate change
3. Land stewardship and ethics
4. Increasing living standard and leisure time
5. Multiple use and overuse of urban waters
6. Change in hydrology
7. Long distance transfer of water and sewage
8. Improved efficiency of wastewater and stormwater runoff treatment
9. Limits have been reached and developing remedies is urgent

The ongoing downturn in the United States and world economy has modified the extent to which Novotny's drivers apply, e.g., our standard of living may be declining. However, this list is still current. Novotny (2006) summarizes the results of an international interdisciplinary workshop of experts that described visionary concepts on how to ensure that cities and their water resources can become more sustainable within the broader concepts of green cities and smart growth. This paradigm will evolve from the concept of the total hydrologic water and mass balance where water supply, stormwater, and wastewater will be considered and managed in a closed loop. The paradigm will include making the landscape hydrologically and ecologically functional. Selected papers from this workshop are presented in Novotny and Brown (2007).

IWA/IAHR Joint Committee on Urban Drainage: An international group of experts affiliated with the IWA/IAHR Joint Committee on Urban Drainage prepared a position paper on current conditions and expected future developments in this field (Marsalek et al. 2007). They discuss the following four future scenarios: 1) Business-as-usual; 2) Privatization; 3) Technocratic; and 4) Green. The Green option is viewed by the authors as synonomous with decentralization of urban water systems in order to maximize the reuse of treated wastewater and stormwater. They correctly caution that these Green approaches have not been implemented on a large scale and significant potential public health issues need to be considered.

EPA Research Plan. US EPA (2007) developed a research plan directed at encouraging innovation and research for water infrastructure for the 21st century. Most of their suggested topics deal with existing infrastructure issues. This plan is somewhat limited by the lack of a federal water agency that can take a holistic view of urban water in general and urban stormwater in particular. For example, US EPA deals with urban stormwater quality issues while the Corps of Engineers is responsible for flood control.

URBAN STORMWATER MODELS, SENSORS AND METHODS

Elliott and Trowsdale (2007) analyze and compare ten simulation models for evaluating urban stormwater systems with emphasis on decentralized systems. Weinstein et al. (2006) show how low impact development systems can be simulated. Heaney and Lee (2006) and Lee et al. (2005) describe a simulation and optimization model for decentralized urban stormwater systems. Modeling decentralized low impact development systems is much more challenging than modeling centralized traditional systems for several reasons including:

- many more controls to analyze, e.g., hundreds of small storage-release systems as opposed to a single neighborhood detention pond;.
- the reliance on infiltration greatly increases the uncertainty regarding performance;
- control can be exercised anywhere in the stormwater systems, thus blurring the distinction between the transport/storage and control elements in the model;
- increased questions regarding liability in the case of system "failures", e.g., allegations that flooding was caused by overland flow from nearby parcels;

- increased complexity regarding the expected water quality changes associated with subsurface phenomena;
- increased complexity from the non-stationary coupling of water chemistry, variably-saturated phenomena and the fate/transformation of chemicals and particulates in such systems;
- by design, decentralized systems are high surface area systems resulting in systems of higher reactivity and therefore greater temporal variability and also spatial variability;
- measurement practices adopted from centralized steady flow wastewater treatment systems; and applied to decentralized systems, or single/multiple unit operations subject to unsteady runoff loadings (Sansalone and Kim 2008).

Present and projected computer hardware and software will allow modeling of these more complex decentralized systems. For example, SWMM and CFD can be coupled and validated to predict the fate of chemicals and particulates whether in centralized or newer decentralized systems once the constitutive properties of the system are known (Kuang et al. 2008). While the hydrologic parameter inputs to such models have developed and matured over the last 50 years, a similar evolution is progressing for rainfall-runoff chemical and particulate phenonema, in particular with respect to coupling unit operation and process concepts (Sansalone 2005). New sensor and more fundamental measurement systems and methods are essential to accurately monitor urban stormwater systems and institute proactive adaptive controls. Experimental urban watersheds with state of the art representative monitoring and modeling are an essential element of selected future systems in order to find the optimal mix of centralized and decentralized systems.

Whether our urban water systems are centralized or decentralized, the complexity and uncertainty of rainfall-runoff relationships requires more progress towards continuous simulation that couple hydrology, chemistry and treatment. Beyond event-based modeling and design load concepts for unit operation and process (UOP) and low impact development systems which still provides heuristic and instructive insights and examinations; the long-term performance and viability of such systems is completely unknown and requires continuous simulation. Longer term assessments also require the coupling of rainfall-runoff relationships with coupled constitutive relationships for chemical, particulate and thermal regimes. For example, is transport of particulate matter a first-order process (a mass-based first-flush) or zero-order process as a function of hydrology (Sheng et al 2008)? Modeling also requires that the signature of a UOP or low impact development system must be generated for rainfall-runoff as well as for chemical, particulate and thermal regimes, recognizing that the signature changes (non-stationary), as these systems age and are not maintained (Kim and Sansalone 2008). While the hydrologic responses of a UOP or low impact development system have been effectively modeled under saturated or unsaturated conditions with existing models, modeling of the hydrodynamic, chemical, particulate and thermal regimes is more complex and not as common. The simple steady-state signature, the more complex event-based signature, or the much more challenging non-stationary signature of a UOP or low impact development system that includes chemical transformation, pollutant re-mobilization and scour can be developed with CFD. CFD is arguably one of the most powerful tools for assessment of UOP and LID systems since the introduction of continuous simulation

modeling. However, as with any powerful tool, CFD has liabilities. CFD requires far more representative data and monitoring than what is currently collected. For example, accurate particle size distribution (PSD), whether monitored in-situ or ex-situ is required. Additionally, CFD requires validation. As we move forward towards 2050 tools such as continuous simulation modeling, SWMM, GIS and CFD modeling will be coupled, providing an even more significant advance for urban water cycle management.

URBAN REUSE AND POLLUTANT INVENTORY

Reuse and urban pollutant inventories will continue to grow as we move toward 2050. Pollutant load inventories in urban control systems (including UOPs and low impact development) can be mobile and leachable while representing an inventory that requires recovery and management. Additionally, pollutant inventory in conventional urban conveyance systems and urban land uses requires recovery, quantification and management; otherwise this load becomes part of the urban water cycle. This is particularly important with respect to stormwater and wastewater reuse as a component of the urban water cycle. As we move toward 2050, source controls and pollutant recovery from urban source areas such as pavement cleaning can make a very demonstrable difference to reduce loads with a commensurate reduction in operation and maintenance requirements for centralized or decentralized systems. Load management is required to reduce phenomena such pollutant leaching from urban load inventories. As our technologies and infrastructure systems are improved to provide treatment, greater quantitative management and credit for such management will need to be provided. Management of such systems is a critical issue for persistent chemicals, in particular metals, which accrete at the aqueous-particulate interface and have a history of ecological impacts in urban civilizations. In addition to metals, modern chemicals include xenobiotic and organic chemicals used in the manufacture of materials from asphalt pavement to plastic water bottles; chemicals that are leached into to the urban water cycle and in some cases directly into the food web (Sansalone 2008).

Management of rainfall-runoff requires recognition that hydrology and chemistry are coupled phenomena in urban environs, and it is only with restoration of the hydrologic cycle and management of the urban water cycle that these cycles will be sustainable at the urban interface. The success or failure of reuse is dependent in large part upon our understanding and application of hydrologic processes and treatment controls as an integral part of the urban water cycle. Water reuse is now a critical and important component of the urban water cycle. This reuse is currently dominated by highly treated wastewater but also includes stormwater in selected urban areas. The need for such reuse will continue to increase. Distributing reuse water makes sense on a volumetric basis; however more attention is required for the chemical and microbiological loadings that are cycled back to urban areas by reuse water; becoming part of the hydrologic and urban water cycles. Persistent chemicals in runoff and runoff residuals include metals, organics, endocrine disrupting compounds (EDCs) and nutrients. Transport and fate are a function of land use, land use activity and infrastructure conditions. Unless reuse runoff is specifically treated for the aqueous fraction of these species, such chemicals have the potential to be redistributed back to the urban environs. The particulate residual fraction

must be separated and also be managed due to the potential of leaching or volatilization of these chemicals. Urban runoff contains pathogens and will require disinfection before reuse. While highly treated wastewater as reuse may have very low gravimetric levels of TSS and BOD_5 and provided with a disinfection residual; concentrations of nutrients, salts, EDCs and emerging contaminants must also be significantly reduced before re-introduction into urban hydrologic cycle. States such as Florida and California lead the nation with respect to reuse on a volumetric basis, and it is a logical extension to extend this leadership to urban chemical cycling management.

FORECASTED CHANGES

Heaney et al. (2000) developed urban water budgets for Denver and New York City to provide a first approximation on the expected utilization of wastewater and stormwater for non-potable purposes. Urban stormwater varies in relative importance because of climatic variability. Water budgets indicated that annual urban runoff was about 20 % of water use for Denver while it was about 100% of water use for New York City (Heaney et al. 2000). However, seasonal shortages can be expected due to timing issues; thus, on-site storage would be needed in most cases. Effective use of soil moisture storage can reduce the need for constructed storage facilities including cisterns, rain barrels, and rooftop storage.

Per capita indoor water use is expected to decline from historical levels of about 70 gallons per capita per day (gpcd) to as low as 40 gpcd with current technology especially high efficiency toilets (Aquacraft 2005). On the other hand, outdoor irrigation usage is increasing in many areas due to larger landscape areas and the use of automatic sprinkling systems that encourages higher application rates. Outdoor water use exceeds indoor water use in many of the warmer, more arid, parts of the country. Outdoor water use also contributes to the peak demands. Virtually all of the indoor water use ends up as wastewater that is treated along with infiltration and inflow (I/I) to the sewers. Thus, wastewater supply including I/I is a fairly steady 80-120 gpcd year round. This wastewater supply can be expected to decrease to 50-75 gpcd due to decreased indoor demand and more effective I/I controls. Irrigation demand decreases as precipitation increases so there is a mismatch between irrigation demand and the available supply of stormwater for reuse as irrigation water. A continuous simulation model can be used to estimate the amount of storage that is needed to provide irrigation water from reuse sources (Asano et al. 2007).

The quantity of stormwater per capita increased dramatically during the 20th century due to (Heaney et al. 2000):

- more automobiles which required more streets and parking and created additional pollutant sources
- larger houses on larger lots that increased runoff quantity and pollutant loads
- Growth of suburbia and much lower population densities
- More contemporary urban area was devoted to parking than to human habitat and commercial activities.
- Low density urbanization generated over three times as much stormwater runoff per family than did pre-automobile land use patterns.

Major trends during the 21st century can be expected to decrease the demand for urban stormwater systems:

- "Green developments" that increase population density and reduce urban sprawl
- Major modifications in our energy policies that increase the relative cost of energy compared to its historically very low costs in the United States (Friedman 2007)
- The reduced demand for more larger homes and landscapes due to changing economic conditions and public attitudes towards sustainable lifestyles
- The availability of advanced modeling and data gathering techniques that will enable the direct measurement of stormwater fluxes throughout the urban area and the resultant ability to implement proactive real time control systems that optimize performance for the entire contributing watershed.

These trends should have a very positive impact on urban water systems in the following ways:

- Higher gasoline costs will reduce the demand for automobile travel that is the largest source of directly connected impervious areas in cities. This will reduce stormwater runoff generation and the associated pollutant loads.
- Higher energy costs will encourage higher density urban development and reverse the trend over the past 50 years towards lower density urban sprawl that has greatly increased urban stormwater generation.
- Higher density urban development will reduce the irrigated area per person and higher energy costs will reduce demands for irrigation water.
- Higher energy costs favor the development of decentralized urban water systems because water distribution and collection systems constitute the majority of the cost of urban water systems.

SUMMARY AND CONCLUSIONS

During the past 40 years, urban stormwater management has evolved from focus on drainage and flood control to inclusion of stormwater quality associated with nonpoint pollution and how the demand for off-site stormwater services can be reduced by on-site management, primarily through infiltration. This paper projects what the urban stormwater field could look like in the year 2050. Recently developed similar projections by other stormwater groups were reviewed. Anticipated changes include the growing interest in stormwater reuse, on-site control of stormwater using a variety of low impact development alternatives, and changing patterns of urban runoff due to changes in climate and patterns of urban settlement. Key expected drivers of changing attitudes are the greatly increasing relative cost of providing water and energy; greater concern about developing more sustainable green systems; and technological advances that will allow proactive management of urban stormwater systems using real time control. Sustainable green systems will also require management of pollutant loads from reuse and active control and management of recalcitrant or toxic residual inventories generated in urban environs and activities. Source controls and green materials can improve the sustainability of such systems.

REFERENCES

Aquacraft, Inc. (2005). *Water and Energy Savings from High Efficiency Fixtures and Appliances in Single Family Homes*. US EPA Combined Retrofit Report.

Asano, T., Burton, F., Leverenz, H., Tsuchihashi, R., and Tchobanoglous, G. (2007). *Water Reuse*. McGraw-Hill, New York, 1570 p.

Elliott, A. and Trowsdale, S. (2007). A review of models for low impact urban stormwater drainage. *Environ. Modeling and Software*, (22), 3, p. 394-405.

Friedman, T. (2008). *Hot, Flat, and Crowded. Why We Need a Green Revolution-and How It Can Renew America*. Farrar, Straus, and Giroux, New York.

Galloway, G. (2009). **Flood risk management circa 2050.** Proc. ASCE-EWRI Water Congress, Kansas City, MO

Heaney, J.P. (2000). Principles of integrated urban water management. Chapter 2 in Heaney, J.P., Pitt, R. and R. Field, Eds. 2000. *Innovative Urban Wet-Weather Flow Management Systems.* EPA-600-R-99-029, Cincinnati, OH.

Heaney, J. (2007). Centralized and decentralized urban water, wastewater and storm water systems. Chapter 15 in Novotny, V. and Brown, P., Eds. *Cities of the Future: Towards Integrated Sustainable Water and Landscape Management*. IWA Publishing, London, p. 237-250.

Heaney, J. and Lee, J. (2006). *Methods for Optimizing Urban Wet-Weather Control Systems.* EPA/600/R-06/034, US EPA. Washington, DC.

Kim J.Y. and Sansalone J.J., "Hydrodynamic Separation of Particulate Matter Transported by Source Area Runoff", *ASCE J. of Environmental Engineering*, 134(11), 912-922, November 2008.

Lee, J., Heaney, J.., and Lai, D. (2005). Optimization of integrated urban wet-weather control strategies. *J. of Water Resources Planning and Mgt.*, Vol. 131, No. 4.

Marsalek, J., Ashley, R., Chocat, B., Matos, M., Rauch, W., Schilling, W. and Urbonas, B. (2007). Urban drainage at cross-roads: Four future scenarios ranging from business-as-usual to sustainability. Chapter 21 in Novotny, V. and Brown, P., Eds. *Cities of the Future: Towards Integrated Sustainable Water and Landscape Management*. IWA Publishing, London, p. 338-356.

Novotny, V. (2006). *Cities of the Future: Creating Blue Water in Green Cities.* Wingspread Workshop Report to NSF, 30 p.

Novotny, V. and Brown, P.Eds. 2007. *Cities of the Future: Towards Integrated Sustainable Water and Landscape Management*. IWA Publishing, 427 p.

Sansalone J., (2005) "A Perspective on the Synthesis of Unit Operations and Process (UOP) Concepts with Hydrologic Control for Rainfall-Runoff", *ASCE J. of Environmental Engineering*, 131(7), 995-998, July (2005)

Sansalone J., (2008) "Rainfall-Runoff Management and the Urban Water Cycle", *Florida Water Resources Journal*, 1(1), 15-18.

Sansalone J., Kuang X., Ranieri, V., (2008) "Permeable Pavement as a Hydraulic and Filtration Interface for Urban Drainage" *ASCE J. of Irrigation and Drainage*, 134(5), 666-674.

Sheng Y, Ying G, Sansalone J., (2008) "Differentiation of transport for particulate and dissolved water chemistry load indices in rainfall-runoff from urban source area watersheds", *J. of Hydrology,* 361(1-2), 144-158.

Shuster, W.D., M.A. Morrison, and R. Webb, R. (2008). Front-loading urban stormwater management for success – a perspective incorporating current studies on the implementation of retrofit low-impact development. *Cities and the Environment* 1(2):article 8, 15 p.

US EPA. (2007). *Innovation and Research for Water Infrastructure for the 21st Century Research Plan*, Edison, NJ

Weinstein, N., Glass, C., Heaney, J.P., Huber, W.C., Jones, P., Kloss, C., Quigley, M., Stephens, K., and Strecker, E. (2006). *Decentralized Stormwater Controls for Urban Retrofit and Combined Sewer Overflow Reduction.* WERF 03-SW-3, Alexandria, VA, 182 p.

Ying G. and Sansalone J., (2008), "Partitioning and granulometric distribution of metal Leachate from urban traffic dry deposition particulate matter subject to acidic rainfall and runoff retention", *Water Research*, 42 (15), 4146-4162.

Urban Water and Wastewater Management in 2050

Glen T. Daigger[1]

[1]CH2M HILL, 9191 South Jamaica Street, Englewood, CO 80112 USA; PH (720) 286-2542; FAX (720) 286-9271; e-mail: gdaigger@ch2m.com

ABSTRACT

Population growth, coupled with increased standards of living and growing resource limitations, is creating water shortages and necessitates changes form the "linear" urban water management approach historically used. Fortunately, evolving approaches and enabling technologies allow integrated 21st century urban water management systems to be assembled which require the removal of much less water from the natural environment, can achieve energy neutrality (no net energy input to the water management system), and provide significant nutrient recovery. They incorporate increased efficiency, use of local water resources, and much greater recovery and recycling. These systems provide further advantages, including easier expansion, reduced urban heat island effects, and dramatically increased urban aesthetics. Our existing "linear" systems can be transformed by aggressively incorporating these modern concepts into new developments and when redevelopment occurs. Education and professional practice must be transformed to break down historical barriers between drinking, storm, and waste water. Economic analysis requires careful consideration of marginal effects.

INTRODUCTION

The current approach to managing water in urban areas has been used for millennia and was codified in modern cities in the late 19th and early 20th century. It is a "linear" system that involves removing large quantities of water from the environment, transporting it often long distances to the urban area, treating it to potable water standards, distributing it to meet all urban water uses (even those for which different water qualities would be more than sufficient), collecting used water for treatment to meet water quality standards, and remote discharge. Likewise, urban stormwater is collected and conveyed out of the urban area. This 20th century approach has been highly successful in meeting its original objective of protecting the public from enteric disease and flooding when the population of the planet was less than 2 Billion people and the population was mostly rural. However, by 2050 the population of the planet will be approaching nearly 10 Billion people, the vast majority will reside in urban areas, and they will be experiencing a significantly elevated standard of living which will place severe strains on the resources of the planet unless current resource consumption patterns are altered (Daigger, 2007a; NRC, 2003). Under these circumstances the current "linear" 20th century urban water and wastewater management systems will no longer be sustainable as it contributes to water stress (the lack of sufficient water supplies to meet human needs), environmental degradation (due to "dehydration" of the environment), excessive

resource consumption, and the dispersal of nutrients into the aquatic environment (Daigger, 2008).

Fortunately alternate urban water and wastewater management approaches are developing which use water much more efficiently (require significantly less water to be abstracted from the environment), use less resources (energy and chemicals), and better manage nutrients (Daigger, 2008, 2007b; Daigger and Crawford, 2007). These new 21st century approaches capture local water resources through techniques such as rainwater harvesting and distributed stormwater management, reduce net water use through use of water conservation and water reclamation and recycling technologies, can become energy neutral by both reducing energy use by distributed urban water management and by extracting energy and heat from the wastewater stream, and recover nutrients. The distribution of potable and non-potable water and separation of wastewater components at the source contribute further to energy and nutrient recovery objectives and offer the potential to significantly improve public health protection. 21st century approaches can also enhance the urban environment by retaining water in the urban landscape and creating natural areas that are not only amenities but also reduce urban heat island effects.

This paper outlines the individual technologies and approaches which form the basis for the 21st century urban water (and wastewater) management systems and demonstrates how they can be integrated into more highly performing systems. The year 2050 is chosen for this analysis for two reasons. First, planning for water management systems must be long-term in nature due to the long life of water management infrastructure. Second, the year 2050 represents an expected plateau in the human population, growing through the first half of the 21st century to reach a global population of approximately 10 billion (450 Million in the US), and remaining at this level through the second half of the 21st century (Daigger, 2007a; UN, 2005).

Transition from the current "stove-piped", "linear" system to a more integrated system will require significant changes to urban infrastructure, urban water management institutions, and professional practice (Daigger, 2008; Daigger and Crawford, 2007). This transition will require integrated action but can be implemented aggressively in areas where new development is occurring and in existing urban areas as redevelopment occurs. Over time both expanding needs can be met and existing urban areas can be transformed into this higher performing approach to urban water and wastewater management. Elements of this transition will be described.

ELEMENTS OF THE 21st CENTURY APPROACH

Table 1 summarizes key approaches and technologies that enable the 21st century approach to urban water management (Daigger, 2008). A wide variety of water conservation technologies are available, and more are expected in the future. Experience in water short areas indicates that application of these technologies can reduce domestic and commercial indoor water use substantially from over 400 L/capita-day to between 120 and 150 L/capita-day. This is the obvious starting point as reduced water use also means significantly reduced used water volumes, which can facilitate added innovations as will be discussed below. Reduced water consumption

means that local water sources can become a higher proportion of the urban water supply. One such source is local rainfall, which can be captured by a wide variety of means and stored in either constructed storage or in local aquifers. Even if the rainwater is not reused, infiltration into the local groundwater by a wide variety of techniques (as illustrated in Table 1) provides a local groundwater source which can replenish local streams and enhance the local environment (Strecker, *et al.*, 2005).

Table 1. Approaches and Technologies Enabling the 21st Century Approach to Urban Water Management.

Approach	Example Enabling Technologies
Water Conservation	Low-Flush Toilets, Low-Volume Showerheads, Washing Machines, Dish Washers, Xeriscape, Drip Irrigation
Distributed Stormwater Management	Rainwater Harvesting, Green Roofs, Porous Pavement, Rain Gardens, Vegetated Strips
Water Reclamation and Reuse	Membrane Bioreactors, Advanced Oxidation, Ultra-violet Disinfection
Source Separation	Dual Distribution Systems, Urine Separating Toilets
Distributed Water Treatment	Membranes, Advanced Oxidation, Ultra-violet Disinfection
Heat Recovery	Heat Pumps
Organic Management for Energy Production	Anaerobic Treatment, Microbial Fuel Cells
Nutrient Recovery	Crystallizers, Struvite and Calcium Phosphate

Water reclamation and reuse produces another local water source which can contribute significantly to meeting urban water needs (Daigger, 2007b). Used water can be treated to meet essentially any quality requirement, including for potable consumption or even for industrial applications requiring ultra-pure water. Table 1 lists some of the technologies which are making this approach cost-effective (Daigger, *et al.*, 2005; Daigger, 2003). An evolving approach is source separation, which recognizes that different water qualities are appropriate for different uses. This general concept has been used for several decades with dual distribution systems where reclaimed water is distributed for urban irrigation. It is now being extended recognizing the small proportion of water which actually needs to meet potable water standards – on the order of 30 to 40 L/capita-day. If the small needed amount of potable water is produced from fresh water sources and non-potable and irrigation water is supplied by rainwater harvesting and water reclamation and reuse, net water removal from the external environment can be reduced by more an order of magnitude. More extensive treatment, perhaps at a more local level to minimize deterioration in the distribution system, can be applied to the small amount of water which must meet potable water standards. This is the concept of distributed water treatment.

Source separation can be extended further to the collection of used water from domestic and commercial sources. Grey water is relatively uncontaminated and, consequently, can be treated without chemicals and with relatively little energy to produce non-potable water that can be used for a variety of sources. Importantly, this

is the largest proportion of domestic and commercial water use. Further separation of black water (feces) from yellow water (urine) segregates the majority of the organic matter (which can be used for energy production) from the majority of the nutrients in the waste stream. Figure 1 illustrates the typical distribution of organic matter (as expressed as five-day biochemical oxygen demand – BOD_5) and nutrients in the domestic waste stream. When it is recognized that the black water (and kitchen waste if it is also combined) represents a relatively small proportion of the waste volume, and yellow water may represent only about 1 L/capita-day, one can see that separation of these waste sources results in not only smaller volumes but much higher concentrations can be processed in different ways. Due to the higher concentration the resulting organic matter stream can be subject to direct anaerobic treatment and the biogas collected for energy production, rather than being subject to aerobic treatment which requires energy. In the future it may be possible to directly produce electricity from the organic matter contained in this waste stream using microbial fuel cells (Logan, *et al.*, 2006). The concentrated yellow water can be separately treated to recover nutrients and to remove pharmaceuticals (which are also concentrated in this stream).

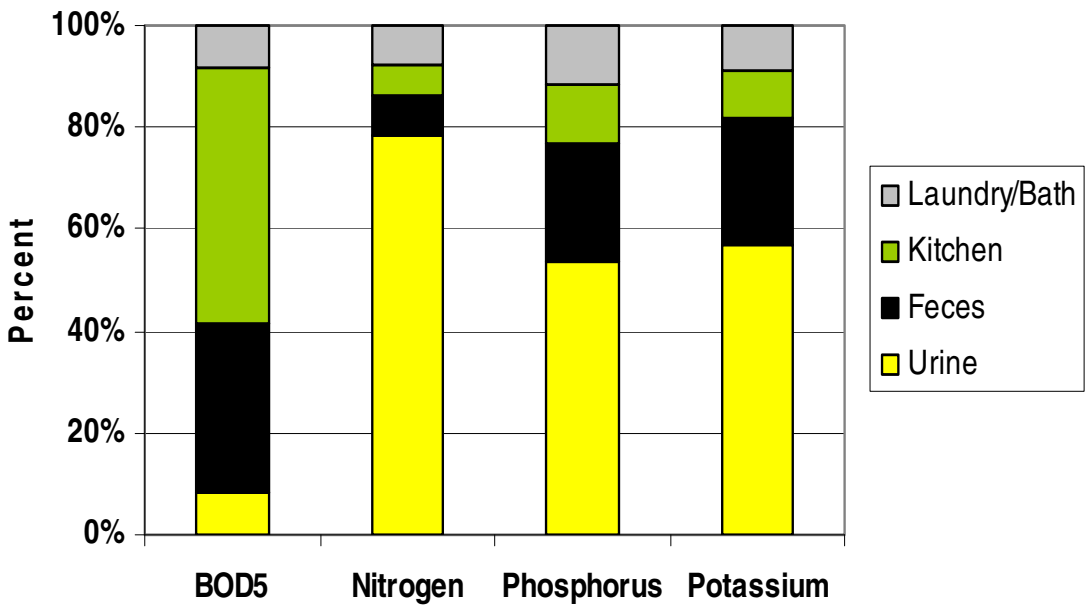

Figure 1. Distribution of Organic Matter and Nutrients in a Typical Domestic Waste Stream (From Henze and Ledin, 2001).

Not only can energy be produced from the organic matter contained in the waste stream, the thermal mass of the water and waste stream can also be used productively. Heat exchangers and heat pumps can be used to extract heat from the waste stream for space heating, and heat can also be rejected to this stream for space cooling as well.

These technologies and approaches represent a significant departure from the traditional linear approach described in the introduction. These elements can be

further combined into integrated systems with further enhanced performance characteristics.

INTEGRATED 21st CENTURY URBAN WATER MANAGEMENT SYSTEMS

When developing integrated urban water, organic matter, and nutrient management systems it is necessary to recognize the appropriate scale for various activities. Development of the stormwater, water treatment, and wastewater reclamation technologies listed in Table 1 allows water management to be accomplished on a more distributed basis. This offers at least two advantages. First, transmission distances (and consequently pumping energy requirements) are minimized when rainwater is captured and reclaimed water is produced closer to its use. Second, production of high quality reclaimed water facilitates extraction of heat from or rejection of heat to the waste stream to meet local needs. At the same time, economical energy production and nutrient recovery from the waste stream requires relatively large quantities of organic matter and nutrients, suggesting that these functions be accomplished on a more centralized basis.

Integrated urban water management systems must also comply with a set of guiding principals and constraints, as summarized in Table 2. The guiding principals help to conceive of systems alternatives, while the constraints must be complied with for any alternative that will perform acceptably on the long-term.

Table 2. Integrated Urban Water Management Systems Guiding Principals and Constraints (From Daigger, 2008).

Guiding Principals	Constraints
Protect and Use Local Water Resources	Maintain Water Balance Under Dry and Wet Conditions
Mimic Local Hydrogeology	Maintain Salt Balance
Provide Multiple Barriers to Protect Public Health	Maintain Nutrient Balance
Minimize Resource Consumption and Maximize Recovery	Collect and Manage Residuals

Figure 2 provides an example integrated 21st century urban water management system intended to use only local water supplies. Potable and non-potable water are supplied separately for the reasons outlined above. Potable water is supplied by local water resources, in this example assumed to be by a potable water aquifer which will provide suitable capacity due to the relatively small amount of potable water required when potable and non-potable needs are met separately. Non-potable water supply is provided by rainwater harvesting and water reclamation and recycling. Non-potable water storage (to balance demand with production) is provided by another local aquifer. Salt build-up is a possibility in a closed system such as this, which can be controlled by the export of brine (produced through reverse osmosis treatment of a portion of the reclaimed water) to a saline water aquifer.

Figure 3 provides an example integrated 21st century urban water management system intended to minimize energy requirements and maximize nutrient recovery. Potable and non-potable water supply is separated, this time to minimize pumping distances

and, consequently, also the pumping energy for potable and non-potable water distribution. Local water supplies (rainwater, grey water wastewater reclamation) are used for non-potable water supply because of the lower resulting energy consumption, as discussed above. Separate collection of black water and yellow water allows the concentrated black water stream to be treated anaerobically for biogas production and for recovery of nutrients from the yellow water stream. The thermal mass of the waste stream is used locally as a heat source for space heating and to reject heat for space cooling, depending on the season.

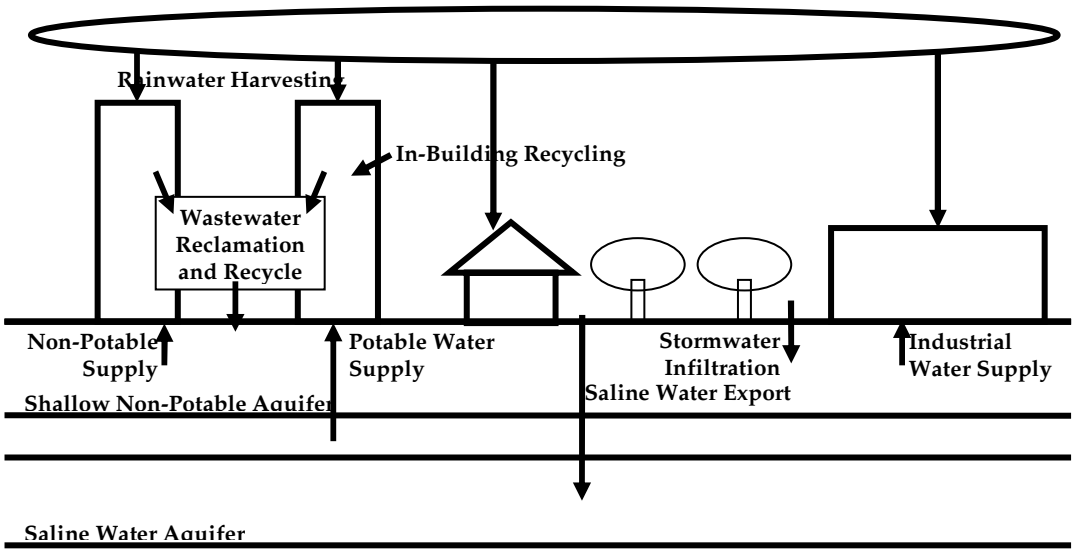

Figure 2. Example 21st Century Urban Water Management System Which Minimizes Net Water Removal From the Environment.

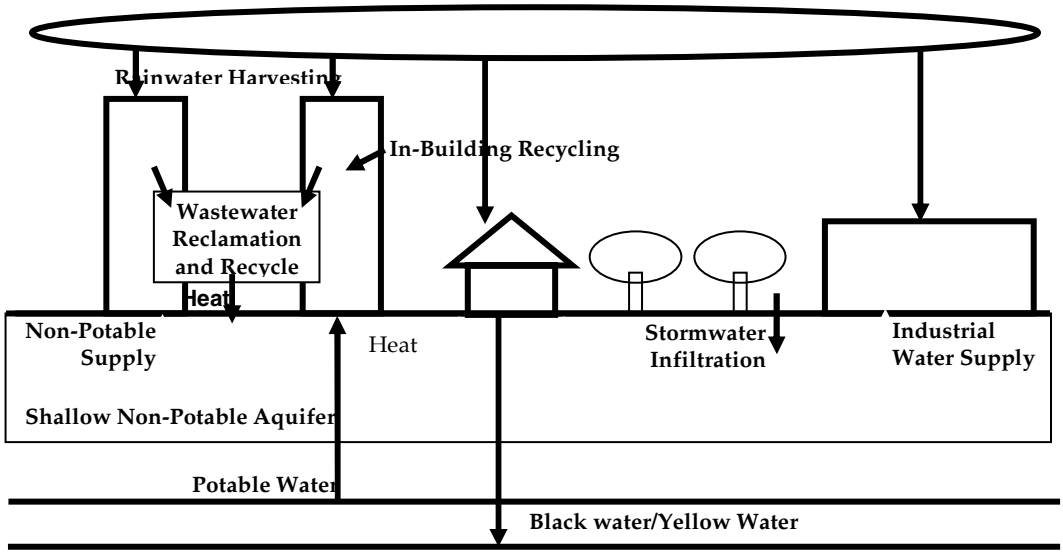

Figure 3. Example 21st Century Urban Water Management System Minimizing Energy Use and Maximizing Nutrient Recovery.

Analysis of systems such as these demonstrates that they can significantly reduce net water use, which makes water available to meet growing needs based on population

and economic growth; to achieve energy neutrality (no net energy input required), and significant nutrient recovery. They provide further benefits to the urban area, including reduced heat island effects (due to the increased vegetated cover) and greatly improved aesthetics. The monetary value of these benefits is often not reflected in cost-benefit analysis, but they are real. These examples are just two of the many possible.

TRANSITION TO 21st CENTURY SYSTEMS

When the high efficiency, closed loop 21st century integrated urban water management systems illustrated above are compared to our current, linear 20th century systems, one may ask "How can we transform our existing systems?". Said another way, what will we do with our "legacy" systems. When phrased in this fashion, the answer becomes obvious as we have significant experience in many contexts dealing with legacy systems and phasing them out while phasing in new generation approaches. We do it by aggressively incorporating 21st century approaches into new developments and also when we redevelop existing urban areas. Recognizing that the US population is expected to grow by 50 percent from the current 300 Million to about 450 Million by 2050, simply incorporating 21st century approaches into new development will result in one-third penetration of the new approaches into the water management infrastructure that will exist in 2050. Recognizing the urgent need for repair and replacement of much of our existing urban water management infrastructure, aggressively incorporating 21st century approaches as this infrastructure is redeveloped will result in significant conversion of our entire infrastructure. The key is to begin now, as it will provide two benefits. One is accelerating the transition from 20th to 21st century approaches which will allow us to capture the benefits of these new approaches as quickly as possible. The second is that aggressively incorporating these approaches will provide the practical knowledge that will allow the "fine tuning" of these new approaches and drive a research and development (R&D) agenda that will lead to their further advancement. The modular nature of 21st century infrastructure is another advantage as it can be easily added and expanded in response to demand and thereby facilitating financing.

Institutional arrangements are certainly a key to accelerating the transition to routine implementation of 21st century approaches (Daigger, 2008; Daigger and Crawford, 2007). In many areas urban drinking water, waste, and stormwater are managed by separate utilities. Even when they are managed by the same utility they are often not managed in an integrated fashion. Examination of the example systems presented above illustrates that this will not be possible in the future as the integrated systems simply consider that "water is water". This may lead some to conclude that integrated 21st century systems can only be implemented when a single utility is responsible for all forms of water within the urban area. Fortunately, numerous examples exist where separate utilities successfully cooperate, indicating that utility reform is not a necessary precursor. In fact, the principal constraint may be the structure of our historic educational approaches and our professional organizations which emphasize the separate management of drinking water, wastewater, and stormwater. Better integrating our approaches to education and expanded cooperation by our professional organizations can create an integrated vision for urban water

management, which can carry into professional practice. This historic division may be the reason that so many utilities with combined responsibilities currently fail to act in an integrated fashion.

Economics are a key to enabling rapid transition to 21st century integrated urban water management approaches (Daigger, 2008; Daigger and Crawford, 2007). There are two important aspects to this. First, the benefits of these integrated approaches can be broad and must be evaluated properly. For example, the cost benefits of options which reduce net water demand (such as water conservation, rainwater harvesting, and water reclamation and reuse) should not be compared to the average cost of delivering potable water. Reduced demand will allow the most expensive water supply option to be retired or implementation of the next most expensive water supply option to be avoided (depending on whether the options being considered will reduce demand or meet growing demand). In other words, the marginal cost, rather than the average cost must be considered in the evaluation. This concept is well known to professionals routinely engaged in evaluating water reclamation and reuse options, but not by water management professionals in general. Multiple benefits can also be generated by these measures – for example a reduction in both water supply and waste management costs – and all of these benefits must be considered in the evaluation. In other words, we must be careful to perform a "global" rather than "local" optimization. We must also include broader benefits such as reductions in heat island affects and reductions in greenhouse gas (GHG) emissions in the overall evaluation.

At the same time, the costs and benefits for various options may not be uniformly distributed between the responsible parties. Such issues can be dealt with through inter-agency or inter-departmental charges. It may also be necessary to change the basis for financing urban water management utilities. In many instances urban drinking water and waste management utilities are financed based on user charges based on the volume of water sold or wastewater generated. Obviously, this penalizes utilities for reducing water use and wastewater generation, steps which are contrary to our general objectives. Moreover, since utility costs do not go down in proportion to the volume of water sold or wastewater processed. This challenge has been faced by many electric utilities and has been solved by at least partially separating the revenue that the electric utility receives from the quantity of electricity it sells. The more enlightened approach compensates electric utilities for causing increased efficiency of electricity use, along with the total amount used. The same approach could be applied to urban water management utilities.

CONCLUSIONS

The traditional, 20th century approach to urban water management may be described as "linear" and involves removing large quantities of water from the environment, transporting it often long distances to the urban area, treating all to potable water standards, distributing it to meet all urban water uses (even those for which different water qualities would be more than sufficient), collecting used water for treatment to meet water quality standards, and remote discharge. While this linear 20th century

approach has successfully protected public health, several factors are creating the need to transform our approach to urban water management, including:

- **Global population** from, from less than 2 Billion in the first half of the 20th century to approximately 10 Billion by 2050 (US population growth from less than 100 Million to approximately 450 Million).
- **Urbanization**, from less than one-third of the total population in the first half of the 20th century to more than half today and to more than two-thirds of the total population by 2050.
- **Increased living standards**, which are necessary to allow global population to stabilize.
- **Resource availability**, from a period of apparently excess resources in the 20th century to resource limitations in the 21st century.

As a result, widespread water stress is developing both globally and within the US.

Fortunately, higher efficiency, closed loop approaches are available which can:

- Dramatically reduce the quantity of water urban areas must remove from the external environment.
- Achieve energy neutrality (i.e., no net energy input required).
- Achieve significant nutrient recovery for reuse.

These 21st century approaches incorporate (1) increased water conservation and efficiency, (2) distributed stormwater management which captures and uses rainfall, (3) source separation, (4) water reclamation and reuse, (5) distributed water treatment, (6) heat recovery, (7) organic management for energy production, and (8) nutrient recovery. To achieve full benefit, these approaches must be developed into integrated urban water management systems where a variety of qualities of water are produced and used and collected for reuse. The transition from linear 20th century to closed loop 21st century approaches can be implemented by aggressively incorporating 21st century approaches into new development and as redevelopment occurs. The modular nature of these technologies facilitates incremental additions in response to growing demand. Changes in professional practice and our educational system are required to develop practitioners capable of developing and implementing these integrated systems. Economics must be carefully examined, often considering marginal cost impacts. Collaboration between utilities will be required, including approaches to financing them.

REFERENCES

Daigger, G. T. (2008) "AEESP lecture – Evolving urban water and residuals management paradigms: Water reclamation and reuse, decentralization, resource recovery." *Proceedings of the 81st Annual Water Environment Federation Technical Exhibition and Conference*, Chicago, IL, CD-ROM, October 18-22, 2008.

Daigger, G.T. (2007) "Wastewater management in the 21st century." *Journal of Environmental Engineering*, **133(7)**, 671-680.

Daigger, G. T. (2007) "Creation of sustainable water resources by water reclamation and reuse." *Proceedings of the 3rd International Conference on Sustainable Water Environment: Integrated Water Resources – New Steps*, Sapporo, Japan, October 24-25, 2007.

Daigger, G. T. and G. V. Crawford (2007) "Enhanced water system security and sustainability by incorporating centralized and decentralized water reclamation and reuse into urban water management systems." *Journal of Environmental Engineering Management*, **17(1)**, 1-10.

Daigger, G. T., B. E. Rittmann, S. Adham, and G. Andreottola (2005) "Are membrane bioreactors ready for widespread application?" *Environmental Science and Technology*, October 1, 2005, 399A-406A.

Daigger, G. T. (2003) "Tools for future success." *Water Environment & Technology*, **15(12)**, 38-45.

Henze, M. and Ledin, A. (2001) Types, Characteristics and Quantities of classic, Combined Domestic Wastewater, in *Decentralised Sanitation and Reuse: Concepts, Systems and Implementation*, Lens, P., Zeeman, G. and Lettinga, G, Ed., IWA Publishing, London.

Logan, B. E., Hamelers, B., Rozendal, R., Schroder, U., Keller, J., Freguia, S., Aelterman, P., Verstraete, W., and Rabaey, K. (2006) Microbial Fuel Cells: Methodology and Technology. *Environment Science and Technology*, **40**(17), 5181-5192.

National Research Council (2003) *Cities Transformed: Demographic Change and its Implications in the Developing World*, The National Academy Press, Washington D.C.

Strecker, E., Huber, W, Heaney, J., Bodine, D., Sansalone, J.,Quigley, M., Leisenring, M., Pankani, D., Thayumanavan, A. (2005) *Critical Assessment of Stormwater Treatment and Control Selection Issues*, 02-SW-1, WERF, Alexandria, VA.

United Nations (2005) *World Population Prospects: The 2004 Revision*, Economic and Social Affairs, United Nations. www.un.org/esa/population/unpop.htm.

Challenges of Managing California's Sacramento-San Joaquin Delta

Jay R. Lund#, Ellen Hanak*, William E. Fleenor#, William A. Bennett#, Richard E. Howitt#, Jeffrey F. Mount#, Peter B. Moyle#
University of California – Davis, Center for Watershed Sciences
* Public Policy Institute of California, San Francisco, CA.

"Once a landscape has been established, its origins are repressed from memory. It takes on the appearance of an 'object' which has been there, outside us, from the start." Karatani Kojin, *Origins of Japanese Literature*, Duke University Press, 1993, p. 34.

The Sacramento–San Joaquin Delta is the hub of California's water supply system and the home of numerous native fish species, five of which already are listed as threatened or endangered. The recent rapid decline of populations of many of these fish species has been followed by court rulings restricting water exports from the Delta, focusing public and political attention on one of California's most important and iconic water controversies.

In our previous report, *Envisioning Futures for the Sacramento–San Joaquin Delta*, we explored the alternatives available for the long-term management of this multifaceted resource. We concluded that change is inevitable for the Delta and that retaining the current policy of exporting large amounts of water through pumps in the southern Delta was both risky and unsustainable. We examined nine long-term strategies for managing the Delta from the perspectives of environmental, economic, and water supply performance.

In this report, we continue the theme of analyzing how the Delta will change in the future and how California can respond to expected changes to meet state economic and environmental objectives. We focus on a central question for long-term Delta policy: Which water management strategies best meet the goals of environmental sustainability and water supply reliability? Many other decisions concerning California's water management, the Delta aquatic environment, and Delta land use depend on the answer to this question. We provide an integrated analysis of these issues in a series of technical appendices and summarize the results and their policy implications in this report. These analyses allow us to arrive at some firm conclusions regarding the desirability of various long-term alternatives for the Delta from a scientific and technical perspective.

Managing the Inevitable

Although the Delta is the focus of growing controversies regarding fish and water supplies, it is also being subjected to major physical forces that are at odds with

current Delta policy. These physical forces are sea level rise, land subsidence, changing runoff patterns, and earthquakes.

The Delta is a product of sea level rise over the last 12,000 years. At the end of the last Ice Age, the current Delta was only a confluence of rivers flowing to a delta outside of the Golden Gate Bridge. As the sea level rose, the Delta began to form as higher tides began to flood the area of confluence about 6,000 years ago. Continuing sea level rise can be seen in the last century of tidal records worldwide and for San Francisco. With climate warming, sea levels and Delta water levels are expected to increase by one to three feet, perhaps more, over the coming century. Without large investments to raise Delta levees, this rise in sea level will cause many levees to fail, pushing seawater into the Delta. Even if the levees could be sustained, sea level rise would increase the salinity of Delta waters.

Land subsidence—or the sinking of Delta islands—began when the marshlands were first diked and drained in the late 1800s and it continues today as the peat soils oxidize and erode. Most islands are below sea level, many by more than 20 feet. Subsidence increases seepage into the islands, raises the likelihood of levee failures, and increases the costs and consequences of catastrophic island flooding.

California's runoff patterns are changing. Over the last 50 years, there has been a shift toward less snow and more rain in the Sierra Nevada mountains. These shifts—probably associated with climate warming—have increased winter inflows to the Delta. Climate models indicate that this trend will continue, with even larger and more frequent floods in the future. The increases in winter flood flows also will increase island flooding.

Earthquakes are probably the greatest unavoidable threat to today's Delta. Several authoritative investigators have concluded that a major earthquake, such as the 1906 San Francisco earthquake, will likely cause the failure of many Delta islands simultaneously, with a two-in-three chance of such an earthquake occurring within the next 30 years. Such failures would directly threaten water supplies and would affect thousands of roads, bridges, homes, and businesses at the same time. The water supply costs of such an event are estimated to be in the tens of billions of dollars. The likelihood and costs of earthquake-related failures increase significantly with sea level rise and land subsidence.

The Delta also faces a powerful biological driver of change—the invasion of aquatic and terrestrial species from all over the world. Today, nonnative species dominate the Delta, threatening the survival of remaining native species, changing the way the ecosystem functions, and making the ecosystem and the services it provides less predictable. Unfortunately, new species continue to arrive at a high rate, adding a new wild card to the management deck every time one becomes established.

These factors alone are sufficient to conclude that the Delta of the future will be very different from the Delta of today and the Delta of the past, regardless of what management and policy actions are taken and what happens to California's environment and economy. Californians cannot go back to the Delta that existed before its marshy tracts were diked and drained; it would require 3.4 billion cubic yards of material to fill subsided islands alone. Nor is it possible to return to the agricultural Delta of early 20th century; the levee upgrade costs are too great, and salinity will intrude farther into Delta waters even with higher levees. This salinity will decrease the productivity of millions of acres of farmland that depend on Delta

waters and will raise water treatment costs and public health risks for the two-thirds of Californians who rely on the Delta as a source of drinking water. Salinity intrusion can be delayed for a time by releasing more fresh water into the Delta, but it cannot be delayed indefinitely. As these changes transform Delta water and landscapes, invasive species will continue to alter the Delta ecosystem.

Even if California could sustain the current Delta against these forces, would it be in the best interests of the state's residents and environment to do so? As found in our earlier report and confirmed by recent events, the current Delta is performing poorly from almost everyone's perspective. Given the potential for catastrophic failure of the system, it is important to examine strategic alternatives for managing the Delta. Although the Delta problem is extremely complex, it is unrealistic to seek solutions to all issues simultaneously. California needs to develop a strategic direction for the Delta before working out all the details of how to get there.

Water Exports: A Central Issue in the Delta

This report focuses on a central question for Delta policy: how to manage Delta water supplies and, in particular, water exports. This question lies at the heart of the wider debates over meeting environmental and economic goals for the Delta. Export policy decisions will drive environmental actions and regulations, determine investments in Delta levees and the ecosystem, and ultimately shape much Delta land use.

In broad terms, there are only four long-term strategies for managing Delta water exports: (1) continue pumping exports through the Delta (the current policy), (2) divert water upstream and convey it around the Delta through a peripheral canal, (3) combine the current through-Delta pumping strategy with a peripheral canal (so-called "dual conveyance" or "dual facility"), and (4) end exports altogether. All Delta water export policies, including those examined in our earlier report, are variants of these four basic strategies. The use of most other tools available to California's water managers to meet water supply needs— including conservation, groundwater and surface storage, transfers, recycling, and desalination—depends significantly on this strategic decision.

A wide range of environmental management tools could improve conditions for the Delta's threatened aquatic life. Reducing or ending the use of the southern Delta pumps could prevent fish entrainment and the altered water flows that harm fish. Increasing the volume of water flowing into the Delta and rebuilding variability in Delta water flows are two strategies for creating a more diverse and beneficial aquatic habitat. Ample opportunities also exist to expand aquatic habitat on the Delta's fringes and within the Delta itself, particularly given the likelihood of island flooding. Methods also are available to improve the design and management of aquatic habitat and to suppress harmful invasive species. The suitability of these tools, and their potential performance, will be significantly affected by the water export strategy employed.

Likewise, many land use, road, rail and other infrastructure decisions in the Delta will largely depend on the state's long-term strategy for Delta water exports. The present strategy of responding to emergencies only as they happen puts California in the position of making Delta policy by default rather than by deliberate consideration of the best long-term alternatives.

Evaluating Strategic Decisions

Because the strategic decision of how to manage water exports is of central importance for so many other management decisions, we focus our analysis on the quantitative comparison and evaluation of the four approaches to exporting water from the Delta. Decisionmaking for other related issues seems likely to become easier once the log-jammed decision on a sustainable long-term Delta export policy is established.

The four alternatives are examined in terms of the two co-equal objectives for the Delta suggested by the governor's Delta Vision Blue Ribbon Task Force: environmental sustainability and water supply reliability. To represent environmental sustainability, we focus on the likelihood of sustaining viable populations of desirable fish species, including native species and others that do well under similar conditions. We assess water supply performance in terms of statewide economic costs and benefits.

To facilitate explicit comparisons among export alternatives, we employ a method known as "decision analysis." This method allows us to explicitly consider a range of possible outcomes, account for major risks and uncertainties, and examine how the water and environmental management system would likely respond to major failures in these alternatives.

For the economic analysis, many aspects of the water export decision can be quantified, making it possible to draw clear comparisons among alternatives. Elements used in the assessment include capital and operating costs, the costs of water shortages, the costs resulting from an extensive Delta levee failure, and the costs of repair after an extensive failure. We also compare alternatives in terms of water quality costs for drinking water treatment and agricultural production. We estimate ranges of answers to reflect the uncertainty in these costs.

The viability of fish populations under different water management alternatives is more difficult to assess. However, California is fortunate to have many experts on the Delta ecosystem and its fishes, and years of studies have improved understanding of these issues. We surveyed a group of experts on the Delta ecosystem to help us understand how each export alternative would likely affect the viability of fish populations. We complemented these results with an analysis of conditions under which different groups of fish species thrive and our own assessment of how Delta fish species would likely be affected by long-term changes in Delta conditions. This allowed us to establish ranges for the likelihood that fish populations would be sustained for each of the four water export alternatives.

In comparing alternatives, we also consider major risks. For example, if a peripheral canal were built and listed fish species did not recover, legal and political actions would be likely to seek reductions in water exports through the canal. Another uncertainty is the timing of an earthquake or flood that will cause an extensive failure of levees in the Delta, disrupting exports that pass through the Delta.

Comparing the Water Export Alternatives

When this information on costs, risks, and likely performance of Delta fish populations is integrated in the decision analysis, it produces estimates of the likely ranges of economic costs and fish population viability for each of the four export management alternatives. A summary of our analysis appears in Figure S.1. Fish population viability estimates are presented for two key Delta species—the delta smelt and fall-

run Chinook salmon. For delta smelt, viability is defined as achieving sufficient recovery to avoid Endangered Species Act restrictions on water exports. For fall-run Chinook salmon, viability is defined as maintaining adequate populations to support commercial and recreational fisheries.

For some alternatives, the range of likely economic performance is quite broad. A dual facility has likely costs as low as $250 million and as high as $1.4 billion per year. For continued through-Delta pumping, the range is even larger, with a low of $550 million and a high of $2 billion per year. These ranges reflect considerable uncertainty. For through–Delta pumping, a major uncertainty is how soon the system will be damaged by a large-scale levee failure. A dual facility would become much more expensive if extensive investments were made to maintain the through-Delta export channels. For fish, the ranges reflect the considerable uncertainties about species performance, depending in part on how carefully the ecosystem components of any Delta alternative are managed, as well as on influences from external sources (i.e., for salmon, the ocean and upper watershed).

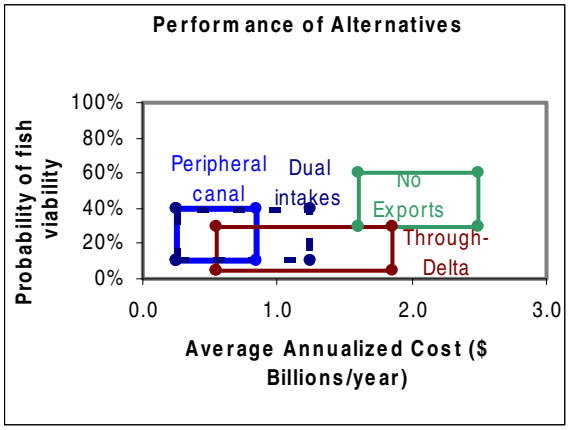

(a) Delta smelt

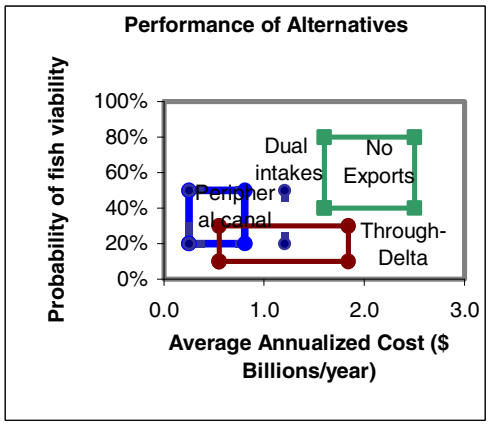

(b) Fall-run Chinook salmon fishery

Figure 1 - Range of costs and fish population viability for Delta export alternatives in 2050

Despite these uncertainties, some clear comparisons emerge. In terms of statewide economic cost, the most likely ordering of alternatives is a peripheral canal (best), followed by dual conveyance, continued through-Delta exports, and, in last place, ending exports. Even if a peripheral canal faced relatively high construction costs (on the order of $10 billion) and could export only 60 percent of current levels because of endangered species restrictions, its total costs would not exceed $1 billion per year. Dual conveyance is potentially more costly than a canal alone, because it will likely entail additional infrastructure costs to continue through-Delta pumping. Dual conveyance costs also could be somewhat higher because the lower water quality pumped from the Delta increases costs for urban and agricultural users.

Several key drivers make continued through-Delta pumping relatively costly. First, by mid-century, the increased salinity of Delta waters imposes water treatment costs on the order of $200 million to $1 billion per year, every year. Second, this alternative requires significant investments, initially to fortify key levees and to improve Delta

channels and, ultimately, to build a peripheral canal when the levee system fails.[1] Third, a catastrophic failure of key levees would cause large one-time costs of $8 billion to $15 billion. The no exports alternative, in contrast, involves considerable costs outside the Delta itself, as water users develop alternative, higher-cost sources and reduce water use, particularly for agriculture in the southern Central Valley. Our estimates assume that water users have time to prepare for an end of exports. The costs would be considerably higher—more like those of a catastrophic failure—if they had no time to prepare.

The most likely ranking of alternatives is quite different for fish viability, with no exports being the best, followed by a peripheral canal and dual conveyance (tied), and continued through-Delta pumping in last place. A broad consensus exists among estuarine experts that ending exports is likely to be best for a range of desirable fish species—ending the harmful entrainment and unnatural flow patterns generated by the southern Delta pumps, as well as providing more water for aquatic habitat. A peripheral canal provides the first two of these benefits; our estimates of fish viability assume that a peripheral canal would be designed and operated to minimize new entrainment problems at the upstream intake. Although in principle dual conveyance offers some additional flexibility for water management, we do not believe that it will have appreciably different outcomes from a canal-only alternative for either delta smelt or salmon. Finally, continued through-Delta pumping is the least beneficial for fish, given the problems of entrainment and disruption created by the southern Delta pumps. Through-Delta pumping also prevents the more flexible management of environmental water flows to increase aquatic habitat variability.

How do the alternatives compare when environmental benefit and economic performance are considered together, as co-equal objectives?

- The peripheral canal and dual conveyance alternatives are very likely to perform better than continued through-Delta export pumping on both objectives. The peripheral canal has a two-thirds chance of outperforming through-Delta pumping; these chances exceed 50 percent with a dual facility. In contrast, through-Delta pumping has less than a 5 percent chance of outperforming the two canal-based alternatives on both co-equal objectives.
- There seems little reason to prefer a dual facility over a peripheral canal. The two alternatives are likely to perform equally from the perspective of desirable fish species, and dual conveyance is likely to be more costly. Nevertheless, for an interim period, it may be valuable to maintain some through-Delta pumping as part of a dual system, to aid water quality for Delta farmers and provide additional flexibility for exports and environmental operations. With time, the through-Delta portion of dual conveyance will probably become less reliable and more expensive as a result of endangered species regulations, sea level rise, and island failures. A dual conveyance alternative with significant investments to support through-Delta pumping is unlikely to be worth the additional costs, given the water quality and environmental risks of through-Delta pumping.

[1] Our analysis finds that a peripheral canal would be built after massive levee failure, because this would be the least expensive response. If, instead, a decision were made to rebuild the failed levees or to end exports, the expected cost of the through-Delta strategy would be higher than the range presented here.

- A clear tradeoff exists between a peripheral canal and dual conveyance and the alternative of ending exports. A peripheral canal and dual conveyance are better in terms of costs to the economy, but ending exports is better for fish. Selecting between these alternatives will require a value judgment. The tradeoff may be easier to make if some of the economic benefits of a canal-based alternative could be used to support enhanced ecosystem investments in the Delta, thereby improving environmental outcomes.

Selecting an export strategy does not, in itself, solve the Delta's problems; it is only a necessary step toward a solution and should provide a framework that improves subsequent decisionmaking. Many technical, regulatory, financial, governance, and policy decisions must accompany the implementation of a long-term strategy. In particular, no matter which export strategy is selected, there will have to be investment in improvements of aquatic habitats within the Delta to increase the likelihood of fish recovery. As indicated by the range of costs and likelihood of restoring fish populations to health, the implementation details will be at least as important as the specific strategy selected.

Policy and Regulatory Implications

Almost a century of Delta regulations, laws, policies, and agreements have revolved around the historical policy of maintaining the Delta as a largely freshwater body and exporting water through the Delta. This situation no longer serves the interests of the state's environment or economy. An institutional framework is required for establishing, operating, regulating, and financing a new Delta strategy. Successful new institutional arrangements are unlikely to emerge from a stakeholder-led process. Large numbers of parties with divergent interests are ill-suited to crafting workable solutions without outside leadership. The governor and the legislature can provide the necessary leadership to make such profound institutional changes to prepare for and manage the Delta of the future.

Conclusions

Our conclusions can be summarized in four broad areas.

1. **Fundamental changes are inevitable in the Delta.** "Restoring the Delta" is an unrealistic notion given the historical changes that have occurred and the immutable forces that will affect the Delta in the decades to come.
   - Sea level rise, earthquakes, continued land subsidence, and higher winter flood flows will increase the frequency and costs of Delta island failures.
   - Maintaining all Delta islands is not cost-effective.
   - The Delta of the future—with large bodies of open water—will significantly differ from the Delta of yesterday or today.
   - California is unprepared for the changes that will occur in the Delta.
2. **The conditions for the Delta's fish can be improved.** Naturally occurring improvements include greater aquatic habitat as islands become permanently flooded. Managed changes in water intakes, water operations, and habitat also can improve conditions for fish but the following issues must be considered:

- Rebuilding large, self-sustaining populations of desirable Delta fish species will require large and carefully designed ecosystem investments.
- More diverse habitat is fundamental to improving conditions for desirable fish species, with greater variability in Delta water flow and salinity as part of this strategy.
- Water export alternatives matter for fish, and the current export alternative is almost certainly the worst for desirable fish species.
- Preventing new invasions of alien species and better control of existing problem invaders are needed to create a more predictable and favorable environment.
- Some species in the Delta are likely to be sustained only with heroic efforts.

3. **For water exports, time favors a peripheral canal and is unfavorable to other alternatives**. Figure S.2 presents a conceptual view of how export alternatives are likely to perform over time and the choices California will face. Water exports are currently declining from historical high levels as a result of court rulings regarding endangered species. Additional species listings are likely to cause further export reductions in the near term. The accumulating effects of land subsidence, sea level rise, worsening floods, and earthquakes will make continuation of through-Delta pumping less reliable and more costly over time but it will leave peripheral canal exports relatively unaffected. However, it will take some time before a peripheral canal can be constructed. How well a dual conveyance alternative ultimately performs will depend on the size of the canal component. If the canal were sufficiently large, it could take an increasing share of exports as through-Delta pumping became less viable. As the figure highlights, the ability of each alternative to support fish populations also significantly affects its ability to support exports.
4. **A peripheral canal is a necessary component of a long-term solution that serves economic and ecosystem objectives co-equally.**
   - Sea level rise will make Delta export pumping increasingly unattractive and eventually infeasible.
   - The long-term water export choice is between building a peripheral canal (which is best for the economy) and ending Delta exports (which is best for fish).
   - A potential compromise is to allocate some of the savings generated by a peripheral canal to enhanced ecosystem investments.
5. **A successful long-term Delta solution will require governance, regulatory, and finance arrangements that allow decisions to be made in a timely way.**
   - To be viable, a peripheral canal or dual conveyance would require effective governance, regulatory, and financing mechanisms.
   - Governance mechanisms can be devised to provide appropriate environmental safeguards for a peripheral canal.
   - Financing mechanisms are available to cover the range of water system needs.
   - It makes economic and environmental sense to involve upstream diverters, as well as users of exported water, in providing more water to the Delta.
   - Establishing these arrangements requires involvement from the legislature and governor.
   - The current regulatory framework is not prepared to deal with the Delta of the future.

Recommendations

The Delta of the future will be very different, and the costs of inaction are high. California needs to prepare for this changed future to direct it more favorably. This means charting a new strategic direction for Delta water management, planning environmental investments from the vantage point of a changing Delta, and developing strategies to manage levee failures. Preparing for the future through governance and regulatory reforms is also essential.

1. **Initiate a planned transition away from through-Delta pumping to other export strategies.**
   Table 1 summarizes the role of the four alternatives in the context of such a transition. Continued through-Delta exports are already demonstrably harmful to the environment, and with time they become unviable for the state's economy. The transition away from through-Delta pumping will occur over time, whether planned for or not. A more expeditious, planned transition would be less susceptible to the rapid, costly changes accompanying earthquakes, floods, and levee failures.

Table 1 - Summary Comparison of Water Export Alternatives

Alternative	Role
Continued through-Delta exports	Increasingly unstable and costly solution
Dual conveyance	Interim solution for transition to peripheral canal
Peripheral canal	Potential to provide both cost-effective water supply and improved fish viability
No exports	Best for fish but most costly to the economy; ultimate outcome without a peripheral canal

2. **The most promising strategy for meeting co-equal long-term state environmental and economic objectives is a peripheral canal. This strategy should include the following elements:**
   - Export water users commit up front to pay for a peripheral canal and water export facilities.
   - Safeguards on the operation of a peripheral canal are provided through governance and ownership institutions rather than by limits on the physical capacity of the canal, to enable better environmental and water supply performance
   - Export water users and upstream diverters commit funds and water to improve the ecosystem. Although upstream diverters have more senior water rights, both groups of users are partially responsible for declines in the Delta ecosystem.
3. **Actively prepare for a changing Delta ecosystem.** Habitat conservation planning needs to consider the effects of sea level rise, climate warming, permanent levee failures, and new invasive species. A rigidly negotiated habitat conservation plan is unlikely to succeed; experimentation and detailed modeling studies to inform a decision-capable governing framework will be needed.

- Ecosystem management should favor diverse habitat and flow conditions for multiple species.
- Hydrodynamic modeling needs to consider sea level rise, permanently flooded islands, and the potential for managing Delta flow patterns to favor desirable fish species.

4. **Move away from levees as the primary means of managing Delta land and water.** Prepare for island failures. Provide major state levee investments only for those Delta islands that have a cost-effective statewide interest; devise mitigation strategies for land owners on other islands.
5. **Develop a new framework for governance and regulation of the Delta.** In addition to developing workable governance and finance institutions for water supply and ecosystem management, policymakers need to anticipate regulating a very different Delta environment.
   - The regulatory consequences of sea level rise and island failures need to be addressed now, so that flexible water management tools are readily available to help California meet its environmental and economic goals,
   - The number, importance, and urgency of problems associated with a Delta transition require a decision-capable governance and regulatory system and one that is at least somewhat more centralized than the current, highly decentralized system. The current governance system is effective at tinkering with the status quo but will likely be ineffective in overseeing any sort of major transition.

Charting the Future for a Changing Delta

The ongoing and increasingly rapid changes in the Delta pose a long-term challenge to California as a whole, as well as to all parties involved in this perennial source of conflict. All parties seeking to achieve the Delta Vision's co-equal objectives of environmental sustainability and water supply reliability have an interest in making a peripheral canal part of a long-term solution for the Delta. This strategy must be embedded in a comprehensive set of actions to improve aquatic environments in the Delta and the greater watersheds of the Sacramento and San Joaquin Rivers. To be viable, a long-term solution must include governance, regulatory, and financial arrangements to ensure that various goals are well served, including water supply, environmental management, and the state's local interests in the Delta. It is unlikely that local and regional stakeholders can negotiate such arrangements on their own in a timely way, given the complexity of the problem and its innumerable stakeholders. Pursuit of a grand consensus solution for the Delta's many issues is likely only to continue the deteriorating status quo. Leadership from the governor and legislature will be needed to create conditions for reasonable governance of the new Delta, with cooperation from local governments and federal agencies that regulate and manage water and land use.

Reference

Lund, J., E. Hanak, W. Fleenor, W. Bennett, R. Howitt, J. Mount, and P. Moyle, *Comparing Futures for the Sacramento-San Joaquin Delta*, Public Policy Institute of California, San Francisco, CA, July 2008.

Characterization of Water Resources and Environmental Disasters

Walter M. Grayman[1]

[1]W.M. Grayman Consulting Engineer, 321 Ritchie Ave., Cincinnati, OH, 45215,
PH: (513) 761-1722, email: grayman@fuse.net

Abstract

When you think about water resources and environmental disasters, some of the recent events that come to mind include Hurricane Katrina, the 2004 Indian Ocean tsunami and the Exxon Valdez oil spill. However, other than concluding that "I know a disaster when I see one", what can we do to better characterize and rank disasters? Some potential criteria include: economic damage, environmental damage, fatalities, reconstruction cost, aesthetic damage, disruption of normal activities, destruction of irreplaceable objects, and long-term or permanent loss of species. This paper explores past water resources/environmental disasters and provides a rough comparison of their impacts in terms of a range of criteria. It also provides a taxonomy of disasters in terms of causes (natural events, human induced), predictability and potential impacts.

Keywords
Disasters, water resources, environment

DEFINITION OF DISASTERS

Following are several definitions of the word "disaster" resulting from a search on the Web:

- A disaster (from Middle French désastre, from Old Italian disastro, from the Greek pejorative prefix dis- bad + aster star) is the impact of a natural or man-made hazard that negatively affects society or environment. http://en.wikipedia.org/wiki/Disaster
- An unexpected natural or man-made catastrophe of substantial extent causing significant physical damage or destruction, loss of life or sometimes permanent change to the natural environment; An unforeseen event causing great loss, upset or unpleasantness of whatever kind. http://en.wiktionary.org/wiki/disaster
- A serious disruption of the functioning of a community or a society causing widespread human, material, economic or environmental losses which exceed the ability of the affected community or society to cope using its own resources. www.adrc.or.jp/publications/terminology/top.htm

- Any occurrence that causes damage, ecological destruction, loss of human lives, or deterioration of health and health services on a scale sufficient to warrant an extraordinary response from outside the affected community area. www.nhtsa.dot.gov/PEOPLE/injury/ems/emstraumasystem03/glossary.htm
- A sudden, unplanned calamitous event, which causes loss and hardship to all or part of an enterprise and thereby significantly impacts its ability to deliver essential services for some period of time. www.state.mn.us/portal/mn/jsp/content.do
- An occurrence, either natural or man made, that causes human suffering and creates human needs that victims cannot alleviate without assistance. http://wps.prenhall.com/chet_langan_preparing_1/0,9681,1613226-content,00.html
- An event that causes major disruption on the economy, society and the environment. Its origin or causes may be directly derived from natural phenomena, i.e. geophysical (as volcanic or seismic events that cause collapse of infrastructure, landslides or liquefaction, etc.) or climatic (as hurricanes, typhoons, tornadoes, major variation in rainfall both in terms of excess or deficit causing drought). Although usually not covered by the methodology, disasters may also have a "human" or anthropic origin as chemical spills, industrial accidents, or voluntarily caused events such as war, terrorist actions, etc. Disaster consequences or damage will always be associated with human intervention before, during and after the event (the "disaster cycle"). http://magic.un.org.mx/www2/desastres-capacitacion/wbi/GLOSSARY.doc

Though each of the definitions differs slightly, there is a rather clear consensus that disasters are natural or human events, usually unexpected, that result in significant impacts in terms of a variety of metrics.

WHAT CONSTITUTES A DISASTER?

Other than concluding that "I know a disaster when I see one", what can we do to better characterize and rank disasters? Obviously, statements such as "my hair is a disaster today" or "that party was a real disaster" are only frivolous uses of the word "disaster". On the other hand, most people would agree that the "Great Flood of 1993" that hit the Upper Mississippi River (Johnson et al., 2004), as described in the following paragraph, constitutes a real water resources disaster.

> "The magnitude and severity of the resulting flood event was overwhelming. The areal extent, intensity, and long duration of the flooding makes this one of the greatest natural disasters ever in the United States. At least 48 people lost their lives as a result of this extreme flood. Over 500 river forecast stations in the Midwest were above flood stage at the same time. Nearly 150 major rivers and tributaries flooded. Banks and channels of many rivers were severely eroded, and sediment was deposited over large areas of the flood plains of the Mississippi, Missouri, and Illinois Rivers. Economic damages approached $20 billion. Levees were broken; farmland, towns, and transportation routes were destroyed; and more than 50,000 homes were damaged or destroyed. Water-quality threats to public health and safety were of paramount concern. These threats included contamination of drinking-

water supplies, disruption of wastewater-treatment plant operations, failure of septic systems, and risks associated with the inundation of facilities that handle hazardous materials."

Water resources/environmental disasters can vary significantly in terms of characteristics, time scale, likelihood and impacts. These topics are discussed in the following sections.

CATEGORIZATION OF DISASTERS

Disasters may be categorized in various dimensions. One way of categorizing disasters is by the cause of the disaster. In broad terms, disasters may be categorized in the following broad classes:

- Natural disasters: Disasters caused by natural events
- Human-induced accidents: Accidental events that are the result of human activities
- Disasters at the intersection between natural and man-induced: Events that are caused in part by natural events and in part by human actions
- Voluntary disasters: Intentional events purposely caused by humans

In some cases, the lines between categories of disasters are fuzzy. For example, a wildfire could be a natural disaster (e.g., caused by lightning), a human accident or an intentional event. Similarly, there is still some debate as to whether climate change is a purely natural event, an accidental by-product of human actions, or an intersection of natural and human actions. Impacts of floods may result from natural precipitation events intersecting with the failure of dams and/or levees. Table 1 lists examples of disasters and a suggested categorization of events into one of the four categories.

Table 1. Types of Disasters

Natural	**Human accidents**	**Natural-human**	**Voluntary**
Hurricane	Infrastructure failure	Flood	War
Tornado	Chemical emission	Drought	Terrorist act
Volcano		Epidemics	
Tsunami		Famine	
Heatwave		Wildfires	
Earthquake		Landslides	
Blizzards		Environmental	
Meteor		Climate change	

In many cases, these categories may be further sub-divided. For example, following is a list of potential categories and examples of environmental disasters (http://en.wikipedia.org/wiki/List_of_environmental_disasters):

- Agricultural (Salinization of the Fertile Crescent)
- Biodiversity (Extinction of American megafauna)
- Coal (Martin County, Kentucky sludge spill)

- Human health (Infectious diseases introduced by Europeans colonizing America)
- Industrial (Minamata, Japan mercury poising)
- Mining (Ok Tedi environmental disaster in Papua, New Guinea)
- Oil industry (Environmental issues in the Niger Delta relating to the oil industry)
- Nuclear (Chernobyl and Three Mile Island accidents)
- Pollution
- Air (The Great Smog of 1948 in London)
- Land (Dust bowl in U.S. and Canada in 1934-1939)
- Water – fresh
- Water - marine (Environmental threats to the Great Barrier Reef)

Another form of categorization relates to the time-scale of the event and resulting impacts. Most disasters involve relatively short timescales (on the order of minutes, hours or days). For example, an earthquake may only last less than a minute and the impacts are largely immediate. Slightly longer timescales are associated with events such as floods which may move through a river basin over a period of days to weeks. Droughts, famine, epidemics and war may occur over and result in impacts spread out over months or years. Climate change could result in impacts over several decades or even centuries.

METRICS FOR EVALUATING DISASTERS

Various metrics can be used to assess and rank the seriousness of disasters. Following is a list of some potential metrics.

- Economic damage
- Environmental damage
- Fatalities
- Reconstruction cost
- Aesthetic damage
- Disruption of normal activities
- Destruction of irreplaceable objects
- Loss of species
- Homelessness
- Illness

Some of these metrics are more amenable to quantification than others. For example, economic damage may be quantified in terms of dollars (losses or reconstruction cost) while environmental damage may be loosely categorized as severe, moderate or low, or in a more quantitative sense by the number of acres or square miles of land or sea that have been impacted. More specific metrics may also be used in evaluating impacts such as the gallons of oil that were spilled.

Examples of different metrics being used to rank disasters are shown in Tables 2 and 3. In Table 2, the top ten deadliest natural disasters are ranked in terms of loss of

human life. In Table 3, hurricanes hitting United States are assessed and ranked by two different metrics, damage (in dollars) and loss of life.

Table 2. Top 10 Deadliest Natural Disasters

Rank	Event	Location	Year	Death toll (estimate)
1	China floods	China	1931	2,000,000 – 4,000,000
2	Yellow River flood	China	1887	900,000 – 2,000,000
3	Shaanxi earthquake	Shaanxi Province, China	1556	830,000 +
4	Bhola cyclone	Bangladesh	1970	500,000
5	India cyclone	India	1839	> 300,000
6	Antioch earthquake	Antioch, Turkey	526	250,000
7	Earthquake/tsunami	Indian Ocean	2004	229,866
8	Tangshan earthquake	Tangsha, China	1976	242,000
9	Haiyuan earthquake	Haiyuan, China	1920	240,000
10	Baqiao dam failure	Henan, China	1975	231,000

Adapted from http://en.wikipedia.org/wiki/List_of_natural_disasters_by_death_toll

Table 3. Top 10 U.S. Hurricanes

	Ranked by Damage			Ranked by Number of Deaths		
Rank	Name	Year	$ Billions	Name	Year	Deaths
1	**Katrina**	2005	200	Galveston	1900	9000
2	Andrew	1992	44	Florida	1928	1800
3	Charley	2004	15	**Katrina**	2005	800
4	Ivan	2004	14	NC to NY	1938	600
5	Hugo	1989	12	Florida	1935	423
6	Agnes	1972	11	Audrey	1957	390
7	Betsy	1965	11	Miami	1926	373
8	Frances	2004	9	Louisiana	1909	350
9	Camille	1969	9	Gulf Coast	1919	287
10	Diane	1955	7	New Orleans	1915	275

Adapted from http://www.epicdisasters.com/

Examination of the two alternative metrics for ranking hurricanes shows that there is only one hurricane (Katrina) that is in the top ten in terms of both metrics. This illustrates the importance of selecting a metric that reflects the specific characteristic of interest. Examination of the two lists also shows that nine out of the ten worst hurricanes in terms of damage occurred in the past 50 years while nine out of ten of the worst hurricanes in terms of deaths occurred over 50 years ago. This certainly suggests a trend in the United States of increasing economic damage and decreasing loss of life from natural disasters.

IMPENDING DISASTERS

In most cases, we cannot accurately predict the time and extent of specific natural or human-induced disasters. However, in many cases we can assign a probability or likelihood of a particular type of disaster at a specific or general location. For example, USGS in cooperation with other agencies issued a report (USGS, 2007) stating that:

- California has more than a 99% chance of having a magnitude 6.7 or larger earthquake within the next 30 years, according to scientists using a new model to determine the probability of big quakes.
- The likelihood of a major quake of magnitude 7.5 or greater in the next 30 years is 46% and such a quake is most likely to occur in the southern half of the state.

The Times-Picayune (the primary New Orleans newspaper) published a five-part series in 2002 (3 years before Hurricane Katrina) containing the following opening paragraph: "It's been almost 40 years since a major hurricane inundated New Orleans. Since Hurricane Betsy's storm surge poured into the city in 1965, our landscape has been sinking and our coastline disappearing. Despite billions of dollars spent on higher levees and flood control, this is no place to be when The Big One inevitably hits (Times-Picayune, June 23, 2002)." This was a sentiment that was widely shared by the water resources and disaster management profession.

Leatherman et al. (2007) discussed the likelihood and consequences of a disaster impacting Lake Okeechobee in Florida as follows: "Lake Okeechobee is a disaster waiting to happen, just like New Orleans when Hurricane Katrina struck in 2005. The dike that is keeping the nation's second largest lake from overflowing the low-lying areas to the south has a high probability of failing during the next major hurricane. It failed back in 1928, when a hurricane whipped up waves and surge that breached the earthen dike, generating an estimated 15-foot high wall of water that drowned 2,500 people. Now there are 40,000 people living in small towns that are in danger during hurricane season".

For many water resources phenomena, events have traditionally been classified probabilistically by their expected frequency. For example, a 100-year flood is expected to occur, on average, once per one hundred years. Many hydrologists are now questioning the true stationarity of such events and, as a result, the probabilistic manner by which extreme events are predicted. Matalas (1998) expressed such concerns in the following statement. "Among the uncertainties affecting the management of water resource systems are those that derive from the lack of knowledge as to how hydrology will unfold in the future, more specifically over the time bound by the economic time horizon. Interest in the hydrologic past is driven in expectation of shedding light on the hydrologic future."

Other potentially disastrous events are largely unpredictable in terms of location, extent or timing, and, in fact, whether they may occur. Following the events of

September 11, 2001, it was widely held that some form of intentional terrorist event would be attempted towards a water or wastewater facility in the United States. Will such an event occur and, if so, when, where, and how? These are all questions that cannot be answered either definitively or even probabilistically. Rare natural events such as collisions between large meteors and the earth, and even more common events such as tsunamis do not lend themselves well to predictability.

SUMMARY AND CONCLUSIONS

Though there are many definitions for the word "disaster", there is a rather clear consensus that disasters are natural or human events, usually unexpected, that result in significant impacts in terms of a variety of metrics. Disasters may be categorized by the cause of the disaster: (a) natural disasters; (b) human-induced accidents; (c) disasters at the intersection between natural and human-induced; and (d) voluntary or intentional disasters. They may also be categorized by their timescale ranging from seconds or minutes (e.g., earthquakes), to hours or days (e.g., floods), to months to years (e.g., drought), or even very long-term such as climate change that may span decades or centuries. Various metrics can be used to assess and rank the seriousness of disasters including: economic damage, fatalities, environmental, ecological or aesthetic damage, and homelessness. Examination of disasters in the U.S. over the past century, suggests a trend of increasing economic damage and decreasing loss of life from natural disasters.

In most cases, we cannot accurately predict the time and extent of specific natural or human-induced disasters. In many cases we can assign a probability or likelihood of a particular type of disaster at a specific or general location. Other potentially disastrous events are largely unpredictable in terms of location, extent or timing, and, in fact, whether they may occur. Planning for disasters should consider both the likelihood of occurrence and the consequences of the events. For those events that have a high probability of occurrence over a relatively short timeframe (i.e., disasters waiting to happen) or even those events with a lower probability but a high consequence if they occur, actions to mitigate or reduce the likelihood of the events are appropriate.

REFERENCES

Johnson, G.P., Holmes, Jr., R.R., and Waite, L.A. (2004). The Great Flood of 1993 on the Upper Mississippi River—10 Years Later. USGS Fact Sheet 2004-3024. http://il.water.usgs.gov/pubs/fs2004-3024.pdf

Leatherman, S.P., Zhang, K., and Xiao, C. (2007). Lake Okeechobee, Florida: The Next Hurricane Disaster? Water Resources Impact, AWRA, 9(6): 5-7.

Matalas, N.C. (1998). Note on the Assumption of Hydrologic Stationarity. Water Resources Update, UCOWR, Issue No. 112.

USGS (2007). The Uniform California Earthquake Rupture Forecast, Version 2 (UCERF 2). USGS Open File Report 2007-1437. http://pubs.usgs.gov/of/2007/1437/

How Reliable is New York City's Water Supply?

Daniel P. Loucks

School of Civil and Environmental Engineering, Cornell University, Ithaca, NY 14853
PH (607) 255-4896; FAX (607) 255-9004; email: DPL3@cornell.edu

ABSTRACT

The New York City water supply system provides drinking water to over 9 million customers. It operates almost entirely by gravity and is delivered to the city via a system of aqueducts and tunnels, some constructed over 100 years ago. Currently the system's safe yield exceeds the demand, but demands are expected to increase, and major system outages are possible, especially in the Delaware water supply aqueduct. NYC receives about 55% of its water supply from the Delaware component of their system. The current leakage from the aqueduct exceeds 40 mgd, and folks living some 700 feet above the tunnel on the surface are seeing new lakes and streams created by that leak. The city is facing a major challenge, how to repair the leaks and not cause a total collapse of the tunnel. This talk will discuss some of those challenges and the possible consequences and options and what is being done about it.

INTRODUCTION

Early Manhattan settlers obtained water from wells, even for fire protection. By 1830 wooden pipe distribution systems were replaced with cast iron pipes As the population of the city increased, the well water became polluted and supply was insufficient. The supply was supplemented by cisterns and water drawn from a few springs in upper Manhattan. This was followed by impounding Croton River water and transporting it to the city via an aqueduct. This aqueduct, known today as the Old Croton Aqueduct, had a capacity of about 90 million gallons per day (mgd) and was placed in service in 1842. In 1883 a commission was formed to build a second aqueduct from the Croton watershed as well as additional storage reservoirs. This aqueduct, known as the New Croton Aqueduct, was placed in service in 1890.

In 1905 the city decided to develop the Catskill region as an additional water source. The Catskill System, included the Ashokan Reservoir and Catskill Aqueduct, was completed in 1915. The remaining development of the Catskill System, involving the construction of the Schoharie Reservoir and Shandaken Tunnel, was completed in 1928.

In May 1931 the Supreme Court of the United States upheld the right of the city to augment its water supply from the headwaters of the Delaware River. Construction of the Delaware System began in March 1937 and was placed in service in stages: The Delaware Aqueduct was completed in 1944, Rondout Reservoir in 1950, Neversink Reservoir in 1954, Pepacton Reservoir in 1955 and Cannonsville Reservoir in 1964.



Figure 1. New York City's Water Supply System (DEP, 1999).

Water for the system is impounded in three upstate reservoir systems which include 19 reservoirs and three controlled lakes with a total storage capacity of approximately 580 billion gallons. The three water collection systems were designed and built with various interconnections to increase flexibility by permitting exchange of water from one to another. This feature mitigates localized droughts and takes advantage of excess water in any of the three watersheds. Approximately 95% of the total water supply is delivered to the consumer by gravity. Only about 5% of the water is regularly pumped to maintain the desired pressure. As a result, operating costs are relatively insensitive to fluctuations in the cost of power. When drought conditions exist, additional pumping is required.

Today New York has one of the world's most robust water systems (Figure 1). Eight million residents in the city, and another one million upriver, daily consume 1.2 billion gallons that flow through a network of reservoirs and aqueducts stretching from the Delaware River watershed to the Connecticut border almost 100 miles to the southeast.

The Croton system in Westchester County, which began providing water in 1842, meets about 10 percent of the city's needs. The Catskill system, built in the first quarter of the 20th century, provides 40 percent. The remaining 50% or 600 million gallons a day also come from the Catskill Mountains, through the Delaware Aqueduct system, which was finished in the 1960s. This system includes the Rondout-West Branch tunnel, completed in 1944 and promised to last at least a century. The Rondout-West Branch tunnel is 45 miles long, 13.5 feet wide, up to 1,200 feet below ground and responsible for transporting half of New York City's water supply from reservoirs in the Catskill Mountains.

Since 1842, there have been no significant interruptions of service other than brief annual shutdowns for the purpose of routine inspections during the period from 1842 to the Civil War. Clearly water supply planning in NYC has been quite foresighted and successful. Today however this record of reliable water supplies is potentially threatened because of leaks in the tunnels (aqueducts) that bring upstream water to the city.

LEAKS IN THE SYSTEM

The city was aware of the extensive leaks in the Rondout-West Branch tunnel 20 years ago. For most of those 20 years it has been leaking over 20 million gallons a day. In 2004 the city's Department of Environmental Protection (DEP) hired consultants to assess the extent of the problem. They discovered the leaks had increased to about 40 million gallons per day. When in 2007 residents of the small community of Wawarsing located above the tunnel reported cracks in building foundations and sinkholes in their yards, mold, wells contaminated with E. coli and basements that flooded even on dry days, the city's Department of Environmental Protection initiated a five-year, $240 million project to prepare to fix the tunnel. The challenges are to keep water flowing through New Yorkers' faucets and prevent tunnel collapse during the repairs. The most immediate job is to fix a valve at the bottom of a 700-foot access shaft so pumps will eventually be able to drain the tunnel, and to ensure that the tunnel does not crack or collapse while it is empty due to the hydrostatic pressure outside the tunnel.

For this, the city has employed deep-sea divers to work 700 feet below the surface in 12-hour shifts, with each diver taking a four-hour turn hacking away at concrete to expose the valve. The story of these divers and what they must do to prepare themselves for this work and what they must go through after their work has been the subject of a number of newspaper articles. These articles are finally informing the public about these leaks and what is being done to reduce if not eliminate them (Belson, 2008; Zale, 2008).

ISSUES AND OPTIONS

NYC's DEP estimates the earliest the city might dewater the tunnel is in two to three years because of all the preparatory work required. As the divers study the underwater pumps, the city is investigating where, how and whether to build a bypass tunnel, and how much to expand the filtration system that will permit lower quality water to be pumped from the Croton system.

Another option is to build another tunnel across the Hudson River connecting the four Delaware system reservoirs to the Catskill reservoirs. This tunnel would be more expensive than a smaller bypass, but would give the city more flexibility by connecting two giant water systems. But building water tunnels can take decades: One known as New York City Tunnel No. 3 was started nearly 40 years ago and is not scheduled for completion until 2015.

The city is not only focusing on supply reliability but also on demand reduction. DEP has been quite successful in reducing the average daily water consumption which in the 1980s was about 200 gallons per person to the current consumption of about 150 gallons per person by repairing leaky pipes and through subsidizing water use conservation measures such as water leak surveys, water saving shower heads and lawn sprinklers, more efficient clothes dryers, and low-flush toilets.

There are a number of other options not yet discussed in the press that are being considered, but one thing is clear, an unplanned failure of the Delaware Aqueduct over an extended time period will result in major shortages of water for the city. Sure, everyone can buy bottled water, and more groundwater can be pumped from aquifers in the area, but each of those options has its negative impacts. And neither will provide much fire protection without an extraordinarily high energy cost. Addressing this issue is not only a challenging engineering problem, it is also a political one. Everyone expects a failure sometime. It's a question of when and how much. Will the city be ready for it?

What ever options are taken to alleviate any unplanned shortfall in water supply as a result of a tunnel failure, the city recognizes those options will have economic, environmental and social impacts that have to be traded off against the risks and consequences of experiencing that shortfall. Clearly these decisions are not going to be easy, but indeed now is the time to think about what should be done before any unplanned event occurs, and then hope there will be enough time to do it before any unplanned event occurs.. With the help of engineering consultants and panels of 'experts' this is exactly what the city is doing. The city hopes it will have the time and resources to be ready for an unplanned event – and indeed create a planned shortfall before an unplanned one occurs.

Standby folks, the story is just beginning.

REFERENCES

Belson, K. (2008), "Plumber's Job on a Giant's Scale: Fixing New York's Drinking Straw," NY Times, Nov. 22, www.nytimes.com/2008/11/23/nyregion/23tunnel.html

DEP, (1999), New York City 1999 Drinking Water Supply and Quality Report, Dept. of Environmental Protection, 10pp. www.nyc.gov/html/dep/pdf/wsstat99.pdf

Zale, Alan, (2008), Deep Sea Living in Underground Tunnels, http://pruned.blogspot.com/2008/12/deep-sea-living-in-underground-tunnels.html

ASSESSING POLLUTANT LOADS AND EVALUATION OF TREATMENT SYSTEMS TO ACHIEVE WATER QUALITY GOALS FOR LAND DEVELOPMENT PROJECTS

Steven D. Trinkaus, P.E., CPESC, CPSWQ, Trinkaus Engineering, Southbury, CT

ABSTRACT:

It is widely acknowledged that all types of land development have some type of impacts on the environment. Most of these impacts adversely affect our environment, such as those from non-point sources, such as storm water discharges. In the past 10-15 years, the adverse impacts on water quality from non-point source pollutants have become very significant. These pollutants have adversely affected our natural and in particular our aquatic environments. Most municipal land use agencies are unaware of the types of pollutants in non-point source runoff and the negative effects that they have on our environment. The commissions are also not aware how various storm water treatment systems remove pollutants associated with non-point source runoff.

The preparation of a pollutant loading analysis is one tool that can be used to not only determine the amount of pollutants associated with development, but how effective the storm water treatment systems are at the removal of the pollutants.

NON-POINT SOURCE POLLUTANTS – WHY THEY MATTER:

Numerous studies have shown that the amount of pollutants discharged from a development site in the storm water is directly related to the extent of the impervious cover. Recent studies by Tom Schueler of the Chesapeake Stormwater Network in the State of Virginia have also shown that the runoff from disturbed soils can also contribute to non-point source runoff. The following is a description of the common pollutants found in non-point source runoff.

Total Suspended Solids:

Total Suspended Solids (TSS) is particles that are dissolved in water. Sources of TSS in the undisturbed environment are silt, decaying plant and animal matter. On a developed site, the sources include soil erosion, sand used for winter sanding operations, atmospheric deposition and debris found on impervious surfaces. TSS is leading cause of turbidity in water bodies. TSS in water bodies block light from reaching aquatic vegetation, with less light in the water, photosynthesis is reduced. As photosynthesis is reduced, less oxygen is produced by the vegetation thus affecting many aquatic species. As dead vegetation decomposes, more oxygen is used in the decomposition process thus further reducing oxygen levels in the water. TSS can also clog gravel substrate in breeding streams, affecting insect larvae and fish eggs.

Nutrients:

Nutrients, such as Total Nitrogen (TN) and Total Phosphorous (TP) in storm water can have adverse impacts on receiving water bodies. While these nutrients are necessary for growth by aquatic plants, excessive levels of these nutrients do cause excessive growth these plants, especially algae. This excessive growth leads to eutrophication of surface waters. Nitrogen is a limiting pollutant in tidal areas, while

Phosphorous is a limiting pollutant in freshwater systems, particularly ponds and lakes. The common sources of TN and TP are the application of inorganic and organic fertilizers for crop production, lawn fertilization and the disposal of waste residues (biosolids, animal manure, and compost). As noted above, decomposition of excessive vegetated growth, leads to lower dissolved oxygen levels in the water. Dissloved Inorganic Nitrogen (DIN) is also a concern in the environment.

Metals:

Common metal pollutants, such as zinc (Zn), copper (Cu) and cadmium (Cd) are highly toxic to aquatic life. These pollutants can not only kill some forms of aquatic life, the metals can bioaccumulate in higher forms of aquatic life. Human beings can be adversely affected by these pollutants thru the consumption of these higher aquatic species. The most common source of metal pollutants is the transportation system. These metals are found in brake linings, vehicle exhaust, tire and engine wear. After they accumulate on impervious surfaces, they are easily washed into the storm drainage with the next rain event, likely attached to TSS particles.

Hydrocarbons:

Vehicles are also the source of hydrocarbon pollutants. Petroleum hydrocarbons (TPH), such as oil and grease are one type. Vehicle exhaust that is deposited on the road surface contributes polycyclic aromatic hydrocarbons (PAHs). PAHs also result from the incomplete burning of fossil fuels and can be deposited by atmospheric deposition on an impervious surface. Both TPH's and PAHs are highly toxic chemicals which attach themselves to sediment particles, which are then washed off the impervious surface during rainfall events. They are not easily removed from the environment.

WATER QUALITY STANDARDS:

Many states have begun to set limits for Total Maximum Daily Loads (TMDLs) for many impaired streams, rivers and lakes from pollutants over time. As defined by the EPA, "a TMDL is a calculation of the maximum amount of a pollutant that a waterbody can receive and still meet water quality standards, and an allocation of that amount to the pollutant's sources." Increased discharges of pollutants will increase the impairment of the waterbody.

Some state agencies have begun to adopt removal goals for various pollutants in storm water. The most common pollutant being regulated is TSS. Due to chemical bonding, particles of other pollutants, such as nutrients, pesticides, bacteria, metals and hydrocarbons become attached to small sediment particles. It has been widely noted in literature that if TSS is being removed by a treatment system, it is extremely likely that the other pollutants are also removed, but this is not always the case. Many municipal land use commissions have difficulty determining if this goal will be met for land development projects.

TYPES OF WATER QUALITY MODELS:

Two very technical water quality models are the SLAMM (Source Loading and Management Model) and the P8 model (Program for Predicting Polluting Particle Passage through Pits, Puddles and Ponds). These two models were developed to

assess pollutant loads from development and to determine the removal efficiencies of treatment facilities. They can be cumbersome for design community to use and are difficult for the regulatory community to evaluate. Both the SLAMM and P8 model requires continuous hourly rainfall and daily air temperature data which is not readily available to the design community. SLAMM is a model used to understand the common sources of urban storm water pollutants and the control of these pollutants. It is based upon actual field observations and must be calibrated prior to use. Both of these models are more difficult to use in many parts of the country, where the necessary input data is not readily available.

There is one model that can be used to easily estimate annual pollutant loads from typical land development projects. This model is the Simple Method as developed by Tom Schueler in 1987. Based upon simple inputs, such as annual rainfall, drainage area, percent impervious cover and pollutant concentration, the annual pollutant load in pounds can be calculated. This equation can be used for all of the typical pollutant associated with land development projects, such as TSS, TN, TP, Zn, Cu, TPH and DIN. The equation can also be used to calculate the pollutant load for a given storm event, such as the 90% storm (a storm which provides 1" of rainfall or less).

THE SIMPLE METHOD:

In 1987, Tom Schueler developed the Simple Method as a way to estimate pollutant loads for various chemical pollutants on an annual basis. The Simple Method requires a small amount of information to be utilized; annual precipitation, pollutant concentrations, percent impervious cover and subwatershed areas. The formula of the Simple Method is as follows:

$L = [(P)(Pj)(Rv)]/12(C)(A)(2.72)$ or reduced to $L = 0.226(P)(Pj)(Rv)(C)(A)$, where

L = Pollutant load in pounds
P = Rainfall depth over desired time period (inches)
Pj = Factor that corrects P for storms that produce no runoff, use Pj = 0.9
Rv = Runoff coefficient, fraction of rainfall that turns to runoff, $Rv = 0.05 + 0.009(I)$
I = Site Impervious coverage (percent)
C = Flow weighted mean concentration of pollutant (mg/l)
A = Area of site (acres)
0.226 = Unit Conversion Factor

The Simple Method provides reasonable estimates of changes in pollutant amounts resulting from different types of development. There are three aspects of the Simple Method that engineers need to keep in mind when using the equation.

1. It only estimates the pollutant load from storm events and does not consider pollutants from baseflow volumes. For large low density residential developments, where I < 5%, up to 75% of the annual runoff volume may be comprised of baseflow, the annual nutrient load associated with the baseflow may be equal to the annual load associated with the development.

2. Its primary usefulness is for calculating and comparing the relative storm water pollutant loads from various development concepts.

3. It provides an estimate of the pollutant loads that are likely close to the "true" but unknown value for a development project.

One area of concern to calculating pollutant loads on annual basis is the fact that neither the engineer nor the land use agencies can evaluate how the annual load is reaching the receiving wetland or waterbody. However, there is a solution to this issue. The Simple Method can also be used to calculate the pollutant load for a particular storm event. If you wanted to calculate the pollutant load for the 1" rainfall event, which comprises approximately 90% of the annual rainfall events, you would simply set P = 1". This will allow the calculated loads to be related to the 1" rainfall event, thus providing the regulatory agency with values that are easier to comprehend.

You can also take the annual load and divide it by the number of annual rainfall events for the area which will yield a pollutant load per storm event. Both these methods will yield a value that is more understandable to local regulatory agencies.

STORM WATER POLLUTANT CONCENTRATIONS:

Concentrations for the various storm water pollutants were originally developed from the studies conducted under the National Urban Runoff Program (NURP) in various parts of the country. Over time, additional research condand overseen by Robert Pitt, P.E., PhD at the University of Alabama; Roger Bannerman at Wisconsin Department of Natural Resources and the Center for Watershed Protection have provided confirmation of many of the NURP numbers, while providing documentation for adjusting pollutant concentrations per different types of land use. The National Stormwater Quality Database (NSQD), Version 1.1 prepared by Alex Maestre and Robert Pitt of the University of Alabama and the Center for Watershed Protection (September 4, 2005) provides pollutant concentrations based upon monitoring data, which was part of the EPA's National Pollutant Discharge Elimination System (NPDES). This study looked and evaluated data from 1992 to 2002 from 3,765 events on 360 sites in 65 communities throughout United States.

Reliable pollutant concentrations are provided for TSS, TN and TP for various types of development in addition to natural ecosystems. For various land uses, the total and disconnected impervious areas are provided. This information is very helpful for the engineer in assessing which pollutant concentration to use for a particular land use practice. The engineer needs to verify that the proposed impervious cover for a project is consistent with the value provided for a given pollutant concentration. The following table is a sample of these concentrations for different types of land use.

Residential	TSS	TP	TN
2-8 units/acre	60 mg/l	0.38 mg/l	2.1 mg/l
8+ units/acre	60 mg/l	0.38 mg/l	2.1mg/l
Commercial	58 mg/l	0.25 mg/l	2.6 mg/l

Industrial	80 mg/l	0.23 mg/l	2.1 mg/l
Paved roads	99 mg/l	0.25 mg/l	2.3 mg/l
Deciduous Forest	90 mg/l	0.1 mg/l	1.5 mg/l

(NSQD, table 55, 56, 58, 60 and 61)

STORM WATER TREATMENT PRACTICES:

There are three major types of storm water treatment practices:

A. Conventional Systems, which includes catch basins, dry detention ponds, stone and vegetated swales, wet ponds and oil/grit separators.

B. Manufactured Systems, such as hydrodynamic separators, underground filter and infiltration systems.

C. Low Impact Development (LID) systems, such as bioretention, extended wet detention ponds, constructed wetlands, gravel wetlands (submerged horizontal flow systems), vegetated filter strips, and surface sand filters.

While some development sites may have limitations for Conventional systems, these same sites are likely able to can accommodate multiple types of LID systems in a treatment train configuration.

POLLUTANT REMOVAL RATES FOR TREATMENT PRACTICES:

In order to address the changes in pollutant loads, engineers have many tools at their disposal to treat the storm water to reduce the pollutant loads. These tools consist of Conventional, Manufactured and Low Impact Development systems noted above. By the application of pollutant removal efficiencies for the different treatment systems, the engineer can demonstrate how effective the storm water treatment system will be at their removal of a given pollutant.

The efficiency of any storm water treatment system is usually provided as a removal efficiency rate, which refers to the change in pollutant load from the inflow to outflow of the treatment system. There are two types of computational methods to determine this removal efficiency, the event mean concentration (EMC) efficiency and mass efficiency.

EMC efficiency gives equal weight to both large and small storm events and averages the incoming and outgoing concentrations for all storm events. The mass efficiency is affected by the volume of water in the system and water losses that may occur within the practice. Examples of water loss in the practice are infiltration and evapotranspiration. This method is based upon a summation of incoming and outgoing loads and is considered a more accurate method than EMC efficiency. The EMC calculation generally results in lower removal rates and thus can be considered to be more conservative in this application.

There are four sources for pollutant removal efficiencies. The first is the International BMP Database (ASCE/EWRI) of October 2007. The BMP Database provides inflow and outflow concentrations for each pollutant considered, from which removal efficiencies can be calculated.

The second and third are the National Pollutant Removal Performance Database for Stormwater Treatment Practices, 2nd Edition (March 200) and Version 3 (September 2007) by the Center for Watershed Protection. While median removal rates are provided for the practices, it is important for the engineer to evaluate the

supporting data for each system. The number of studies conducted for a given treatment system along with whether or not actual pollutant concentrations were measured as part of the study need to be assessed to provide the engineer with a comfort level regarding the published removal rate.

The fourth is the two annual reports from the University of New Hampshire Stormwater Center for 2005 and 2007. Dr. Robert Roseen, P.E. and his colleagues of the University of New Hampshire Storm Water Center (UNHSC) has been generating very impressive data on how Conventional, Manufactured and LID systems function in a northern climatic area. Dr. Roseen's research has shown that those treatment practices associated with LID have much greater removal rates than many of the Conventional and Manufactured systems and that the LID systems work very well during the winter months. His research has also demonstrated that many of the manufactured systems, such as hydrodynamic separators which claim high removal rates of TSS (based upon lab tests) are significantly less efficient at TSS removal in the real world.

The monitoring of Best Management Practices (BMPs) is an emerging field of research and therefore, the number of studies of certain treatment practices is limited at this time.

ASSESSMENT OF POLLUTANT LOADS AND EVALUATION OF REMOVAL EFFICIENCIES:

In order to assess changes in pollutant concentrations, the engineer must first calculate the pollutant loads for the undeveloped site. Even if there is some amount of impervious cover on the site, the engineer needs to assume that the impervious area does not exist and use a natural undisturbed land cover type to calculate pollutant loads for the natural condition.

The most important consideration in the preparation of a pollutant loading analysis for proposed conditions is the use of the appropriate pollutant concentration for the proposed land use. The engineer needs to evaluate the proposed percentage of impervious cover for a given land use to ensure that it is consistent with the pollutant concentration data. If there are substantial differences in the percent impervious cover for a specific land use when compared to a pollutant concentration from the Database, the engineer needs to determine how to account for this change. One way would be to separate out the roadway area from the lots in a residential subdivision. This would allow the engineer to use appropriate pollutant concentrations for each land use.

The following example will demonstrate the analysis and computations necessary in the preparation of a pollutant loading analysis for TSS. The area of concern for water quality issues is the large wetland in the east central portion of the site (right central area in Figure 1 below).

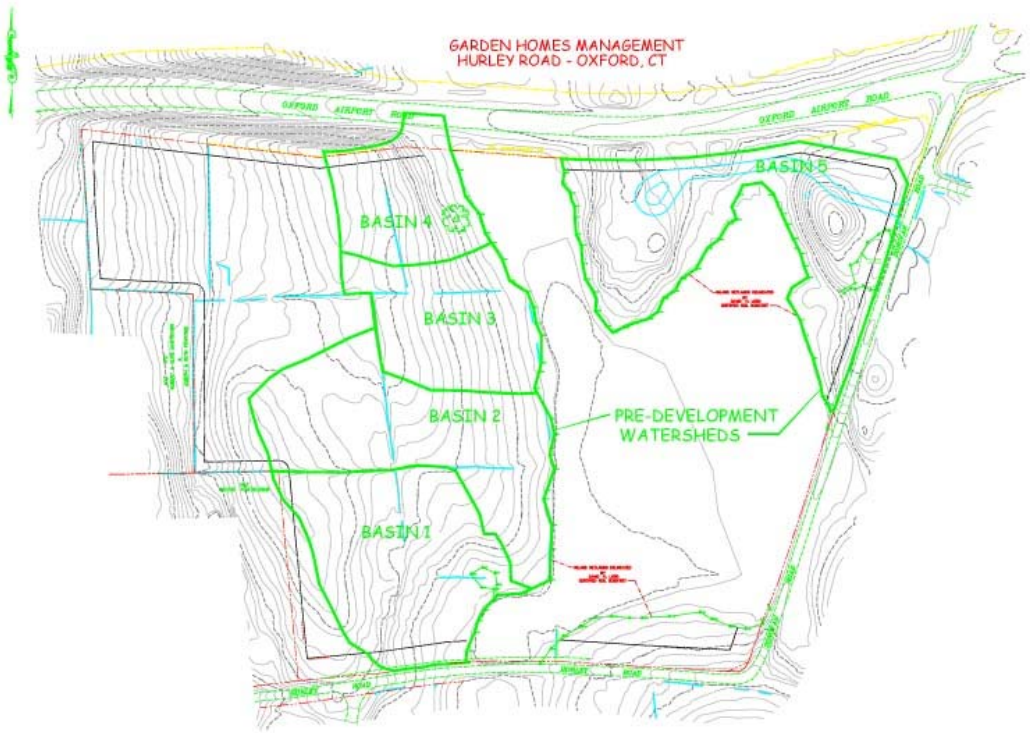

Figure 1- Oxford Commons Existing Conditions

The site is currently vacant and consists of dense meadows/brush areas. That portion of the site tributary to the central wetland area was divided into five watershed areas. Utilizing the Simple Equation, and site specific information for each watershed area, the pollutant loads were calculated for the existing conditions for each watershed area for TSS.

Watershed Area:	Basin 1	Basin 2	Basin 3	Basin 4	Basin 5
Annual Load of TSS (lbs)	179.7	193.3	113.4	91.8	175.3

Total TSS Annual Load for Natural Conditions is 753.5 pounds.

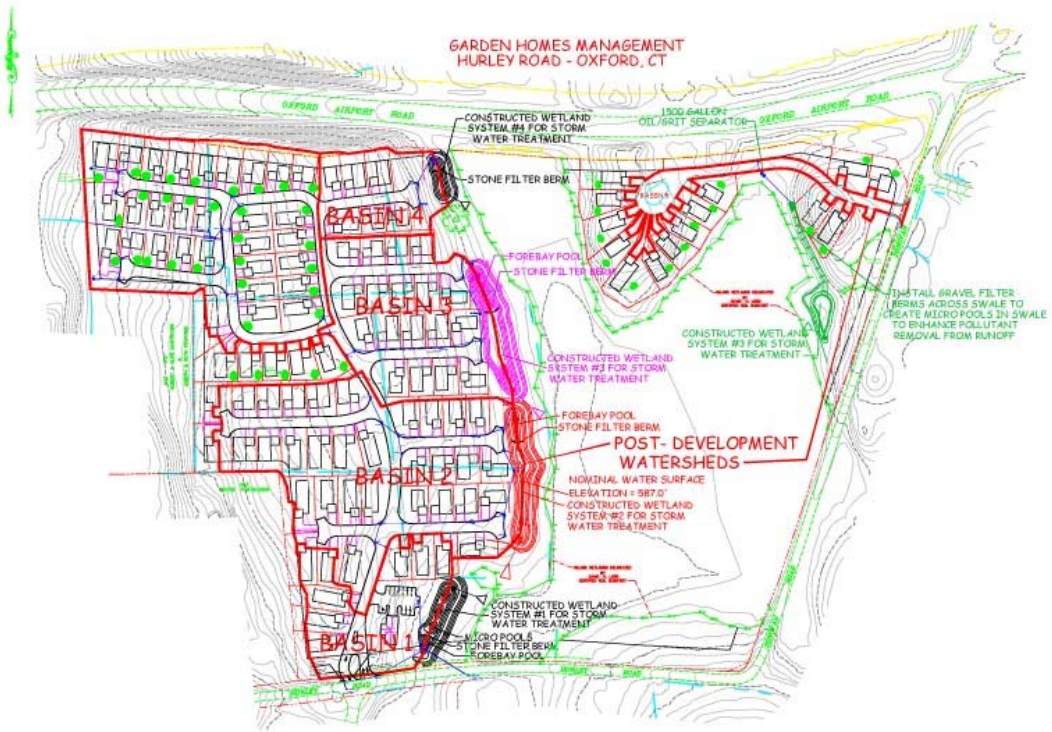

Figure 2 - Oxford Commons Future Conditions

The future conditions on the site will consist of the following land uses: Manufactured housing units on lots which average 7,000 sq.ft. (6 units per acre) accessed by 24' wide paved roads. The watershed boundaries shown in Figure 2 above reflect the proposed site grading.

Pollutant loads were calculated for the future conditions for each watershed area for TSS.

Watershed Area:	Basin 1	Basin 2	Basin 3	Basin 4	Basin 5
Annual Load of TSS (lbs)	576.6	1948.3	1068.2	368.0	672.1
Net Change:	+396.9	+1755.0	+954.8	+276.2	+496.8

Total TSS Annual Load for Future Conditions is 4,636.2 pounds.

You can see that the annual load for TSS substantially increases the site. For Basins #1 through #4 the storm water treatment train consists of the following systems: catch basins with 24" sumps [last CB with 48" sump & hooded outlet], 4' deep forebay at inlet of Extended Detention Ponds (EDP). The runoff from Basin #5 is treated by catch basins with 24" sumps [last CB with 48" sump & hooded outlet], Oil/grit separator, Wet Swale (WS), and Extended Detention Shallow Wetland (EDSW).

The Extended Detention Ponds are long linear, and shallow systems designed to increase the flow time of the runoff within the basin. The Water Quality Volume (WQV) is maintained as a fixed volume within the bottom of the basin. The bottoms of the basins will be planted with native emergent species to enhance the removal of pollutants from the runoff.

The Wet Swale has a minimum base width of 8', along with the installation of gravel filter berms within the swale. The filter berms will create micro pools within the swale, enhancing pollutant removal, reducing flow velocities and allowing infiltration to occur.

The removal rates for TSS for each component of the treatment systems are stated below:

CB with deep sump	EDP	EDSW	WS	Oil/grit separator
25%	80%	69%	1%	0%

Calculate total removal rate for TSS for Basin #1:
Deep catch basin with hooded outlet = 576.6*0.25 = 144.15 lbs.
Extended Detention Pond = (576.6-44.15)*0.80 = 345.96 lbs.
Total TSS removed = 144.15+345.96 = 490.11 lbs or 490.11/576.6 = 85.0%

Calculate total removal rate for TSS for Basin #2:
Deep catch basin with hooded outlet = 1948.3*0.25 = 487.07 lbs.
Extended Detention Pond = (1948.3-487.07)*0.80 = 1168.98 lbs.
Total TSS removed = 487.07+1168.98 = 344.08 lbs or 1656/1948.3 = 85.0%

Calculate total removal rate for TSS for Basin #3:
Deep catch basin with hooded outlet = 1068.2*0.25 = 267.0 lbs.
Extended Detention Pond = (1068.2-267.0)*0.80 = 640.9 lbs.
Total TSS removed = 267.0+640.9 = 907.9 lbs or 907.9/1068.2 = 85.0%

Calculate total removal rate for TSS for Basin #4:
Deep catch basin with hooded outlet = 368.0*0.25 = 92.0 lbs.
Extended Detention Pond = (368-92)*0.80 = 220.8 lbs.
Total TSS removed = 92.0+220.8 = 344.08 lbs or 312.8/368.0 = 85.0%

Calculate total removal rate for TSS for Basin #5:
Deep catch basin with hooded outlet = 672.1*0.25 = 168.0 lbs.
Oil/grit Separator = (672.1-168)*0.0 = 0.0 lbs.
Wet Swale = (672.1-168.0-0)*0.60 = 302.4 lbs.
Extended Detention Shallow Wetland = (672.1-168.0-0-302.4)*0.69 = 139.2 lbs.
Total TSS removed = 168.0+0+302.4+139.2 = 609.6 lbs or 609.6/672.1 = 90.7%

In this case, the goal of 80% removal of TSS at the limit of the delineated inland wetland area would easily be achieved by the storm water treatment practices proposed for this project. Similar analyses can be performed for TP, TN, Zn, Cu and other pollutants of concern.

As you can see multiple treatment practices in series (treatment train) can significantly improve the percent removal of a given pollutant versus a single treatment practice. There are simple ways to increase the pollutant removal efficiency for some treatment systems. As an example, the use of 48" deep sumps and hooded outlets on a catch basin will increase the TSS removal to 25% from 15%.

CONCLUSION:

It can be seen by the application of the Simple Equation and easily obtained site data how a design engineer can evaluate the changes in pollutant amounts and then apply appropriate removal efficiencies to determine whether a land development project will achieve water quality goals.

AUTHOR CONTACT INFORMATION:

Steven David Trinkaus, P.E., CPSEC, CPSWQ; ASC E Member Grade; Trinkaus Engineering, LLC; 114 Hunters Ridge Road; Southbury, Connecticut 06488; Phone: 203-264-4558; Fax: 203-264-4559; email: strinkaus@earthlink.net; Website: http://www.trinkausengineering.com

References:

1. "The Practice of Watershed Protection" by Tom Schueler and Heather Holland published by the Center for Watershed Protection
2. International BMP Database of October 2007 as published by ASCE/EWRI
3. National Pollutant Removal Performance Database for Stormwater Treatment Practices, 2nd Edition (March 200) and Version 3 (September 2007) by the Center for Watershed Protection
4. 2005 and 2007 Annual Reports from the University of New Hampshire Stormwater Center (Dr. Robert Roseen, Director)
5. The National Stormwater Quality Database (NSQD), Version 1.1 prepared by Alex Maestre and Robert Pitt of the University of Alabama and the Center for Watershed Protection (September 4, 2005)

Characterization of a Perchlorate Contaminated Site

Yacoub Najjar, Professor
Kansas State University
2118 Fiedler Hall
Civil Engineering Department
Manhattan, KS 66506
USA
ea4146@ksu.edu

Sam Mryyan
Environmental Compliance Manager
Adjutant General's Department
2800 SW Topeka Blvd.
Topeka, KS 66611
USA
sam.mryyan@us.army.mil

ABSTRACT
Conventional methods of subsurface assessment for remediation or monitoring purposes often involve field sampling and laboratory analyses of soil and water samples for specific contaminants species. Even though these procedures are well established and produce reliable results, they have a number of disadvantages. Among others, they are not measured in real time, and they are sometimes destructive because excavations are needed to obtain soil samples. Furthermore, the sampling and testing processes can be quite laborious and expensive. Various investigations have been carried out to develop alternative, nondestructive methods for such routine measurements. The application of artificial neural networks (ANN) in environmental site characterization has proved to be an effective modeling method for the prediction of migration paths of environmental contaminants. However, the uses of ANN modeling for the migration of explosives-related contaminants (in particular perchlorate) in water and soil, have not been widely reported in the literature. For this reason, this study will explore the potential use of neural network modeling for predicting the amount and distribution of perchlorate at military installations.

Introduction

Testing and training ranges are essential to maintaining the readiness of the armed forces of the United States. Recently, concerns have arisen over potential environmental contamination from residues of energetic materials at impact ranges. Jenkins, et al. (2001) concluded that the current state of knowledge concerning the nature, extent, and fate of contamination is inadequate to ensure sound management of ranges as sustainable resources. The potential for environmental impacts, including contamination of drinking water supplies, mandates that the Department of Defense (DOD) demonstrate responsible management of these facilities in order to continue testing and training activities.

The application of artificial neural networks (ANN) in environmental site characterization has proved to be an effective modeling method for the prediction of migration paths of environmental contaminants (Mryyan & Najjar, 2005; Dowla & Rogers, 1995 and Rizzo et al. 1996). However, the uses of ANN modeling for the migration of explosives-related contaminants (in particular perchlorate) in water and

soil, have not been widely reported in the literature. For this reason, this study will explore the potential use of neural network modeling for predicting the amount and distribution of perchlorate at military installations, specifically the Massachusetts Military Reservation (MMR).

Background of Study Area

MMR is a site that has been associated with military operations for several decades. This site was utilized for many purposes, one of which led to the presence of perchlorate in soil, sediments, surface water, and groundwater. The data used in this study was obtained from this site.

Although the MMR is a large area of land, the area of concern is only 7.4 acres. This site is referred to as Demolition Area One (Demo 1) and is located on Camp Edwards, approximately 2 miles northeast of the Otis Rotary in Bourne, Massachusetts. Demo 1 is located in a natural topographic depression that covers approximately one acre at its base and lies 45 ft below the surrounding grade.

Demo 1 was established in its current location between 1986 and 1989 as a heavy demolition site. Its primary use was for training engineer and explosive ordnance disposal units and for the destruction of various types of unexploded ordnance. Such ordnance (that include perchlorate) included explosive charges of C-4, 2,4,6-trinitrotoluene (TNT), and det-cord with a weight limit of 40 lbs, Bangalore torpedoes, and claymore mines (AMEC, 2001). According to Pennington et al. (2002): In January, 2000, the U.S. Environmental Protection Agency (EPA) Region I issued an Administrative Order for Response Action in the matter of Training Range and Impact Area, Massachusetts Military Reservation to the Massachusetts National Guard. The purpose of the Order was to require the respondents to undertake Rapid Response Actions and Feasibility Studies, Design and Remedial Actions to abate the threat to public health presented by the contamination from past and present activities and sources at and emanating from the (MMR) Training Range and Impact Area.

In 2004, the MMR implemented a program to correct the negative impacts of perchlorate contamination at the Demo 1 site. Two extraction, treatment, and recharge (ETR) systems were installed within the area of contamination. These wells pump the contaminated groundwater out, remove explosives and perchlorate contamination from the water, and then reinject the treated water back into the wells. This is done at a rate of 110 gallons per minute (USACE, 2006). This process continues to date.

Pre-Existing Data

At the start of this research, perchlorate laboratory analysis data were available for the years 2000–2005. The ANN model was developed, tested, and calibrated using the available data from the MMR facility. A total of 459 samples were collected and analyzed at the Demo 1.

In accordance with the Administrative Order for Response Action, the U.S. Army Environmental Center (EC) collected water quality samples at 51 monitoring wells in 33 locations. Site investigations at and down gradient (west) of Demo 1 included the collection of approximately 650 soil samples and the installation of monitoring wells in 33 locations (USACE, 2006). Data from all monitoring wells were utilized in this study. Water quality samples were collected by the EC between August 2000 and December 2005. These samples were analyzed for over 200 compounds to include explosives, volatile organic compounds, semi-volatile organic compounds, pesticides and herbicides, polychlorinated biphenyls (PCBs), polychlorinated naphthalenes, dioxins, and heavy metals.

Model Development

Back-propagation networks were developed using the TR-SEQ1, a three layered ANN training software package developed by Najjar (2001). The purpose of the ANN model is to predict the concentrations of perchlorate at the MMR from appropriate input parameters.

Determination of Appropriate Model Inputs

This section will discuss the process used to determine the selection of input parameters for the ANN models. The determination of the appropriate model inputs is a process that requires a great deal of consideration. Huang (2006) states, "Whereas in physically-based models the necessary input parameters are specified by the equations that describe the physical, chemical, or biological process being simulated, there is no such specification in ANN models." Because of this, it is imperative that there be an adequate amount of relevant input data to train the ANN model.

Based on the available MMR data, backpropagation neural network was chosen as the most-appropriate ANN for developing the site profiling prediction model. The back-propagation approach used by Najjar & Mryyan (2005) and Dowlas & Rogers (1995) has proven successful in past environmental site profiling because of its ability to accurately predict the amount and distribution of environmental contaminants at a given site.

The performance of a network is dependent on the following factors: The number of hidden layers and nodes. For ANN mapping, one hidden layer was used between the input layer and output layer. The number of hidden nodes in the hidden layer was determined by adaptive training

and online monitoring of accuracy measures on the testing datasets. This was done by varying the number of initial hidden nodes, in the hidden layer, until the network was able to best learn the patterns involved in the testing datasets. Fully connected internal structure, where every node in one layer connects to all the nodes in the next layer, was used. (Mryyan and Najjar,2005)

It is worth mentioning that the input domain of the network was determined by a trial and error approach, because there is no reference in the literature that could provide guidance for selection of the inputs. The number and type of nodes in the input layer. Given the MMR data, the following nine potential input parameters were considered:

X east, Y north, Sample depth from sea level (Z), Groundwater elevation (G), Cumulative number of days since 1/1/2000 (T), Cumulative amount of rain since 1/1/2000 (R),Amount of water injected back to groundwater at the Pew Road well (INJ1), Amount of water injected back to groundwater at the Perking Road well 2 (INJ2), and Amount of water injected back to groundwater at the Perking Road well 3 (INJ3)

In order to determine the domain of input parameters for the optimal ANN model, the effect of input parameters on the output and the performance evaluation criteria (statistical accuracy measures and graphical evaluation) are utilized to identify and distinguish the most important parameters that contribute to the best perchlorate prediction. Various training and testing trials, eliminating different input parameters, were conducted in order to identify the most important input parameters. In the initial step, all nine potential input parameters (X, Y, Z, G, T, R, INJ1, INJ2 and INJ3) were used to develop the desired perchlorate prediction model. In the second step, one parameter was eliminated to arrive at eight inputs (X, Y, Z, T, R, INJ1, INJ2 and INJ3. Groundwater (G) was not included. In the final step, seven input parameters were used (X, Y, Z, T, INJ1, INJ2 and INJ3. Rain (R) and groundwater elevations (G) were not included. (See table 1)

Based on previous environmental site profiling knowledge (Mryyan & Najjar, 2005;Mryyan & Najjar, 2006 and Mryyan & Najjar, 2007), input(s) with minimal impact on the accuracy of ANN model prediction were eliminated from the input domain in trial cases. If the statistical accuracy measures were improved by eliminating one input parameter, the effect of eliminating two input parameters at the same time was investigated further. This procedure was repeated until the statistical accuracy measures did not improve by eliminating more input parameters. The purpose of this procedure was to obtain the optimal ANN model—the highest statistical accuracy with the least number of input parameters. In this study, based on the two stages approach, it was

determined that all of the nine potential input parameters (X, Y, G, Z, T, R, INJ1, INJ2 and INJ3) were necessary to accurately predict the amount and the distribution of perchlorate at Demo1. Table 2 to 4 show the statistical accuracy for each of the three trial cases.

Model Training and Testing

In order to obtain the best perchlorate prediction model, the database used for training should represent all possible features and sub-features that the network is required to learn. This study adopted a two-stage training methodology for every ANN model trial structure. In the first stage, the entire database was divided into training, testing and validation sub-databases at the ratio of about 50%: 25% : 25%. The training sub-database contained all the datasets with the maximum or minimum value of each input and output parameter. Using the training and testing datasets for training and testing respectively, the least-error-structure is selected based on the following statistical accuracy measures (Tables 2, 3 and 4): Averaged Squared Error (ASE), Mean Absolute Relative Error (MARE) and Coefficient of determination (R^2) on the testing datasets. Then the network was trained, tested, and validated at its least-error structure with the corresponding sub-databases.

Felker (2005) reported that if the statistical accuracy measures at the least-error structure for training, testing, and validation data sets were found to be comparable, then the second stage of training is not necessary. Otherwise, this indicates that the developed net does not recognize some of the features in the database. In this case, the second stage training was carried out. In the second stage, all datasets in the database were used to re-train the least-error structure identified in stage one. A total of three cases were investigated in order to obtain the optimal ANN model for perchlorate prediction. The optimal ANN structures for all cases are listed in Table 2.

Model Selection

The best model is considered as the one with the highest statistical accuracy. Statistical (MARE, R^2 and ASE) accuracy measures were adopted to select the optimal network models. Tables 2 to 4 show the accuracy measure obtained for each trial case. The statistical accuracy measures, ASE and R^2, were improved by training on all data at its optimal ANN structure (obtained from stage I). It was found that the 7 input case and the 8 input case are comparable, however, the 9 input case outperformed the 7 and the 8 input cases in all other statistical accuracy and graphical measures. It was then decided to select the 9 input case as the optimal ANN model for this study.

In summary, for the MMR perchlorate prediction model, it was determined that the optimal network model contained 9 input parameters,

9 hidden nodes, and 1 output parameter (9-9-1). The corresponding accuracy measures for this network based on stage II training is listed in table 2.

Data Banks

Once the optimal network model was determined to represent the MMR site, the network was used to predict the values of perchlorate contamination at any desired location. The only parameter required in order to provide needed predictions is the input data vector (X, Y, G, Z, T, R, INJ1, INJ2, and INJ3).

The Demo 1 site was divided in the x, y, and z directions using $\Delta x = \Delta y = 25$ ft. The grid system generated in the (x, y) plane produced 4,527 grid points. These coordinates were used for z = -50 ft, -25 ft, 0 ft, 25 ft and 50 ft, generating a total of 22,637 grid points. For each of the generated grid points, the perchlorate concentration values were predicted using the corresponding (x, y, z) coordinates via the optimized 9-9-1 network (Table 2). Predictions were made using data representing one specific date in time. This means that values for the parameters G, Z, R, INJ 1, INJ 2, and INJ3 remained constant for specific time, although z varied for any given x and y coordinate.

Excel Application

Once the ANN model was developed, the optimal network parameters (9-9-1) was used to create an Excel and Visual Basic software program called MMR perchlorate level determination (MMR-PLD). To make the program user-friendly, a graphical user interface (GUI) was developed. To find the perchlorate level at any certain x and y coordinate throughout the Demo 1 site, all the user must do is enter the desired date (t) and desired depth (z). The program will then return the perchlorate level for x,y and z.

Contour Maps

It is often difficult to analyze large amounts of contaminant data in relation to a specific area such as Demo 1. By taking known data and creating a contour map, a visual graph of the study area can be created. This allows for easier interpretation and comparison of given data. For this reason, contour maps of the Demo 1 site were created using version 8 of Surfer® software (2007) to assist in the visualization of perchlorate contamination from years 2000 to 2005. This was done using the results obtained from the 9-9-1 ANN model, as described before.

The contour maps had (x, y) as a variable and (z) as a constant. Figures 4–33 indicate perchlorate concentrations at z = -50 ft, -25 ft, 0 ft, 25 ft and 50 ft for years 2000 to 2005. By creating contour maps for each year and each depth, trends in the concentration of perchlorate

contamination over time and at different depths can be tracked easily. Such images also allow for easy identification of contaminated areas.

In all contour maps (Figures 4 to 33), a red color reflects a high value of perchlorate and a light color represents a low perchlorate value. Consequently, a red color means that a high value of perchlorate concentrations above the regulatory limit of 1 part per billion, and a white color indicates no perchlorate concentration. Color ramp is used between the red and white colors to map intermediate perchlorate concentration values according to scale shown on the figures.

As stated before, 3-D contour maps were generated at depths of -50 ft, -25 ft, 0 ft, 25 ft and 50 ft for the years 2000 to 2005. For the purposes of comparison, these depths will be divided into three categories: below sea level (-50 ft and -25 ft), sea level (0 ft) and above sea level (25 ft and 50 ft).

Before the implementation of the Extraction, Treatment and Recharge (ETR) methods in 2004, high levels of perchlorate were noted in groundwater samples as demonstrated in the contour maps for years 2000 to 2003. This finding is consistent with known natural migration patterns of perchlorate in groundwater. The highest levels of contamination for these years were noted below sea level, as shown in Figures 4–6 and 10–12. At sea level and above, levels of contamination decreased but were still present, as shown in Figures 16–18, 22–24, and 28–30.

With the implementation of the ETR wells, the pattern of perchlorate contamination changes. Groundwater that has been drawn off and treated by the ETR system no longer contains perchlorate. When this treated water is reinjected into the wells, it is reinjected below sea level. This causes a significant decrease in the levels of perchlorate. On the contour maps for 2004 and 2005, at a level 50 ft below sea level (Figures 9 & 9), there is no evidence of perchlorate contamination. At -25 ft, levels of perchlorate contamination begin to increase (Figures 14 & 15), with the greatest amount noted at 25 ft above sea level (Figures 26 & 27).

Concluding Remarks

The ANN-modeling used in this paper demonstrates the neural network's ability to accurately predict perchlorate contamination using multiple variables. When comparing the trends observed using the ANN-generated data and the actual trends identified in the MMR 2006 System Performance Monitoring Report, both agree that perchlorate levels are decreasing due to the use of the ETR systems. This proves that the ETR systems were both effective and necessary for the removal of perchlorate contamination at the Demo 1 site, as demonstrated in the contour maps.

This study has proven that it is possible to utilize backpropagation ANN-modeling to accurately predict groundwater and soil contamination using limited known data. This allows for the study of not only small sites, but larger sites such as the Demo 1 site. By utilizing ANN methodology, more similar in-depth studies can be performed at a lower cost due to the decreased need for sampling data.

REFERENCES

1. AMEC. (2001). Impact Area Groundwater Study Program (IAGWSP) Technical Team Memorandum 01-6, Central Impact Area Groundwater Report (in preparation).AMEC Earth and Environment, Inc., Westford, MA.
2. Dowla, F. U. & Rogers, L. (1995). *Solving problems in environmental engineering and geosciences with artificial neural networks*. The MIT Press.
3. Golden Software, Inc. Surfer User's Guide. (2007).
4. Huang, C. (2006). On the use of the artificial neural network in geo-engineering applications. Doctoral dissertation. Kansas State University School of Civil Engineering. Directed by Dr. Y. Najjar.
5. Mryyan, S.A. and Najjar, Y. M. (2005) "Investigating the Environmental Impact of an Abandon Landfill," Intelligent Engineering system through Artificial Neural Networks, Volume 15. pp. 751-761
6. Mryyan, S.A. and Najjar, Y. M. (2006) "Using Neural Network to Investigate the Environmental Impact of an Abandon Landfill," World Water and Environmental Resources Congress 2006, pp. 250-262. American Society of Civil Engineering.
7. Mryyan, S.A. and Najjar, Y. M. (2007) "Environmental Site Profiling: A Comparative Study" Intelligent Engineering system through Artificial Neural Networks, Volume 17. pp. 61-66
8. Najjar, Y. M. (2001). TR-SEQ1 ANN Training Program. Manhattan.
9. Pennington, J. C., Brannon, J. M. & Mirecki, J. E. (2002). *Distribution and fate of energetics on DOD test and training ranges.* (Technical Report *2* ERDC TR-02-8). U.S. Army Corps of Engineers Washington, DC.
10. Rizzo, D. M., Lillys, T. P. & Doughety, D. E. (1996). Comparisons of site characterization methods using mixed data. In Shackelford, C. D. et al. (Eds.) *Uncertainty in the geological environment: From theory to practice, ASCE geotechnical special publication No. 58*: Vol. 1 (pp. 167–179).

Table 1- Optimal Structure of All Trial Cases

ANN Structure	9 input	8 input	7 input

Initial number of HN	1	2	2
Maximum # of iterations at optimal structure	1000	1000	4000
# of HN at optimal structure	9	8	6

*9 inputs (all Potential parameters included), * 8 inputs (Rain not included), *7 inputs (Rain and Groundwater elevation not included)

Table 2- Network Statistical Accuracy Output for 9 Inputs

9			MARE			R-square			ASE		
Stages	Itr	HN	Training	Testing	Validations	Training	Testing	Validations	Training	Testing	Validations
stage I	1000	9	116	136	NA	0.434	0.63	NA	0.0042	0.0018	NA
stage I	1000	9	116	NA	124	0.434	NA	0.28	0.0042	NA	0.0046
stage II	1000	9	139	NA	NA	0.607	NA	NA	0.0025	NA	NA

Table 3- Network Statistical Accuracy Output for 8 Inputs

8			MARE			R-square			ASE		
Stages	Itr	HN	Training	Testing	Validations	Training	Testing	Validations	Training	Testing	Validations
stage I-A	1000	8	140	138	NA	0.46	0.63	NA	0.004	0.002	NA
stage I-B	1000	8	140	NA	141	0.46	NA	0.39	0.004	NA	0.004
stage II	1000	8	118	NA	NA	0.57	NA	NA	0.003	NA	NA

Table 4- Network Statistical Accuracy Output for 7 Inputs

7			MARE			R-square			ASE		
Stages	Itr	HN	Training	Testing	Validations	Training	Testing	Validations	Training	Testing	Validations
stage I-A	4000	6	149	142	NA	0.502	0.54	NA	0.003	0.0022	NA
stage I-B	4000	6	149	NA	155	0.502	NA	0.302	0.003	NA	0.00476
stage II	4000	6	123	NA	NA	0.503	NA	NA	0.0032	NA	NA

HN: Optimal Hidden Nodes Itr: Iterations
INHN: Initial umber of hidden nodes MARE-tr: Mean Absolute Relative Error Training
R2tr: Coefficient of determination Training MARE-ts: Mean Absolute Relative Error Testing
R2ts: Coefficient of determination Testing

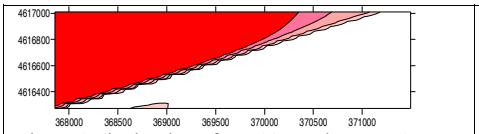

Figure 1-distribution of perchlorate in groundwater in 2000 at Z = -50 ft.

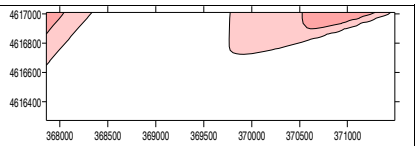

Figure 2 – distribution of perchlorate in groundwater in 2003 at Z = -50 ft.

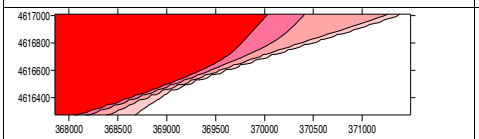

Figure 3- distribution of perchlorate in groundwater in 2001 at Z = -50 ft

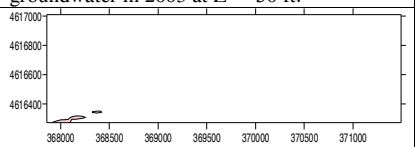

Figure 4- distribution of perchlorate in groundwater in 2004 at Z = -50 ft.

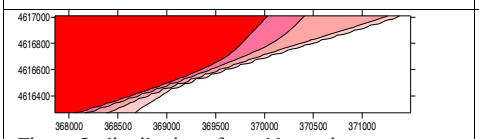

Figure 5- distribution of perchlorate in groundwater- 2002,Z = -50 ft.

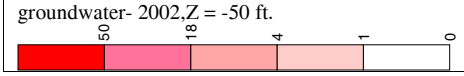

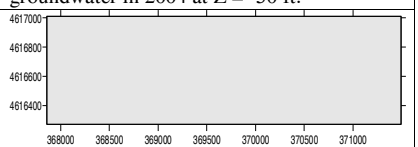

Figure 6- distribution of perchlorate in groundwater-2005,Z = -50 ft.

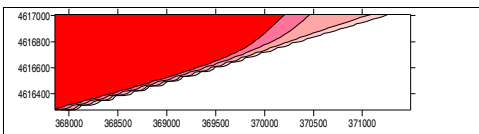

Figure 7- distribution of perchlorate in groundwater in 2000 at Z = -25 ft.

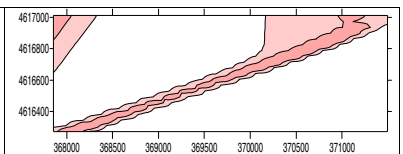

Figure 8- distribution of perchlorate in groundwater in 2003 at Z = -25 ft.

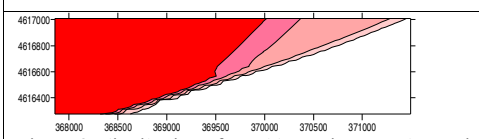

Figure 9- distribution of perchlorate in groundwater in 2001 at Z = -25 ft.

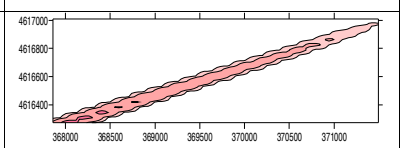

Figure 10- distribution of perchlorate in groundwater in 2004 at Z = -25 ft.

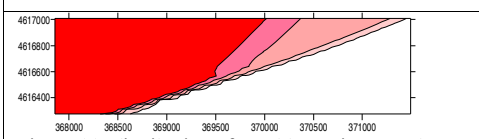

Figure 11- distribution of perchlorate in groundwater in 2002 at Z = -25 ft.

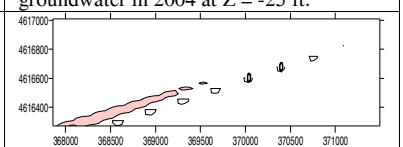

Figure12- distribution of perchlorate in groundwater -2005, Z = -25 ft.

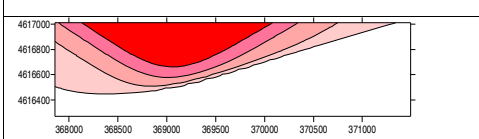

Figure 13- distribution of perchlorate in groundwater in 2000 at Z =0 ft

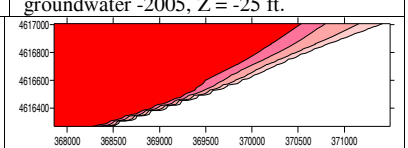

Figure 14- distribution of perchlorate in groundwater in 2001 at Z = 0 ft.

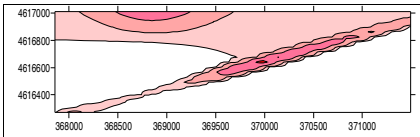

Figure 15- Contour map - distribution of perchlorate in groundwater in 2002 at Z = 0 ft.

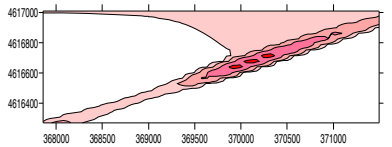

Figure 16- distribution of perchlorate in groundwater in 2003 at Z = 0 ft.

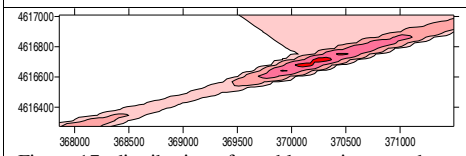

Figure 17- distribution of perchlorate in groundwater in 2004 at Z = 0 ft.

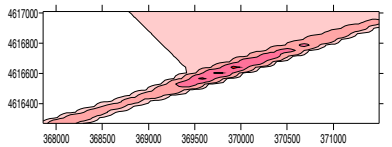

Figure 18- distribution of perchlorate in groundwater in 2005 at Z = 0ft.

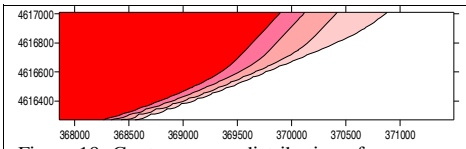

Figure 19- Contour map - distribution of perchlorate in groundwater in 2000 at Z = 25 ft.

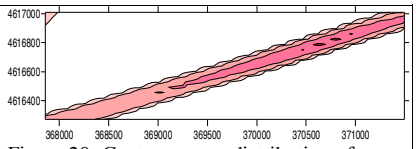

Figure 20- Contour map - distribution of perchlorate in groundwater in 2003 at Z = 25 ft.

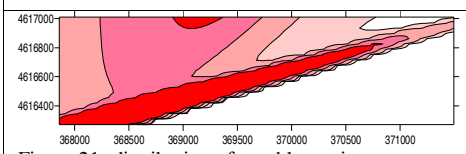

Figure 21- distribution of perchlorate in groundwater in 2001 at Z =25 ft.

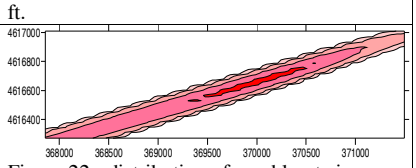

Figure 22-, distribution of perchlorate in groundwater in 2004 at Z =25 ft.

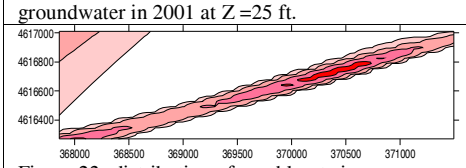

Figure 23- distribution of perchlorate in groundwater in 2002 at Z = 25 ft.

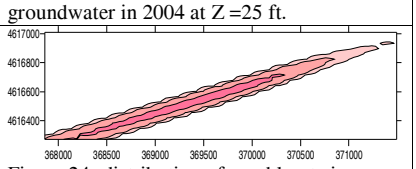

Figure 24- distribution of perchlorate in groundwater in 2005 at Z 25 ft.

Numerical Modeling of Ozonation of Organic Chemicals in Surface Water

Tingting Zhu[1], Yafei Jia[2], Ajit Sadana[3] and Sam S.Y. Wang[4]

[1]Research Scientist, National Center for Computational Hydroscience and Engineering (NCCHE), The University of Mississippi, P.O. Box 5362, University, MS 38677, USA; PH (662)915-3960; FAX (662)915-7796; email: tzhu@ncche.olemiss.edu
[2]Research Professor, NCCHE, The University of Mississippi, P.O. Box 5362, University, MS 38677, USA; PH (662)915-3960; FAX (662)915-7796; email: jia@ncche.olemiss.edu
[3]Professor, Department of Chemical Engineering, The University of Mississippi, P.O. Box 1848, University, MS 38677, USA; PH (662)915-5349; FAX (662)915-7023; email: cmsadana@olemiss.edu
[4]Frederick A.P. Barnard Professor and Director, NCCHE, The University of Mississippi, P.O. Box 5362, University, MS 38677, USA; PH (662)915-3960; FAX (662)915-7796; email: wang@ncche.olemiss.edu

ABSTRACT

Ozonation of organic chemicals generally can result in less toxic and more bio-degradable products. It is proposed to use ozone as a potential decontaminant in case of chemical spill in surface waters. CCHE2D chemical model, a two-dimensional depth-averaged and process-based chemical fate and transport model, was developed for simulating multiple decontamination tests including two-chemical-reaction processes. In this study, toluene decontamination by ozone was selected as an example. Both chemicals' transport, fate and the reactions between these two are all taken into consideration. The model is also used to investigate the effectiveness of decontamination on the water quality by comparing the simulation results of a self-decay case with scenarios of ozonation. The hypothetical case demonstrated the model's capability to represent not only the chemical fate and transport but also the decontamination operations.

INTRODUCTION

Recently, there is a rising awareness of water infrastructure security. Surface water quality can be deteriorated by chemical spill incidents caused by natural or manmade disasters such as extreme flood, transportation accidents, willful dumping, etc. There is an increasing need to assess the environmental impact of the chemical spill incidents and to evaluate the mitigation and control measures to counteract the negative effects. Numerical models have been extensively used as an assessment and evaluation tool. Some examples are the modeling of the chemical spill on the Rhine River in November 1986 (Mossman *et al.*, 1988); the simulation of the long-term impacts of heavy metals or PCBs in both fresh and coastal waters (Thomann et al. 1993, Ji et al., 2002, QEA, 1999).

The CCHE2D chemical model (Zhu et al., 2006) has been developed and validated to simulate chemical fate and transport. It is a two-dimensional depth-integrated and process-based model for simulating advection, dispersion, settling and erosion of sediments, partition between dissolved and particulate phases of chemicals, mass transfer between the water column and sediment bed, and chemical decay through volatilization, photolysis, hydrolysis, and biodegradation, etc. It was integrated with CCHE2D hydrodynamic and sediment transport model (Jia and Wang, 1999; Jia et al., 2002). The model uses a finite element numerical scheme and staggered quadrilateral meshes. It has been developed for simulating free surface flows, sediment/pollutant transport and channel morphological changes. The model has been verified and validated vigorously using analytical solutions, physical model data, and field data.

In this study, the CCHE2D chemical model was extended to simulate the reactions between two chemicals in addition to their individual fate and transport. The purpose of this new development is to study the decontamination measures in case of a chemical spill incident using numerical simulation. The selected study case here is the ozonation of spilled toluene resulted from a hypothetical spill incident.

Toluene (C_7H_8 or $C_6H_5CH_3$) is a common solvent and can be used as additive to gasoline, adhesive and cleaning agent, and as a raw material in the production of benzene and polymers (ATSDR, 1994). By inhalation or ingestion, toluene can cause acute and chronicle health problems, and also poses as a cancer threat (ATSDR, 1994, USEPA, 1999). Toluene is a colorless, flammable, refractive liquid, which is slightly soluble in water (The Merck Index, 1989) with the solubility of 0.47 g/l at 20°C. The Maximum Contaminant Level (MCL) of toluene in drinking water suggested by the USEPA is 1 ppm. Over 100 toluene spill incidents have occured since 2000 (NRC, 2009). One of the major incidents occured in March 1993, when 65,000 gallons of toluene was spilled into the Ohio River.

Ozone has been widely used to reduce the concentration of aromatic organic pollutants such as toluene, benzene, etc., in wastewater and drinking water. The advantage of ozonation is that it generally results in less toxic, more bio-degradable products. Ozone itself decomposes into oxygen if not consumed by the pollutants. In the drinking water industry, the only regulated ozonation by-product in United States (USEPA, 1998) and Europe (EU, 1998) is bromated, which is formed by the ozonation of bromide-containing waters. The reaction products of ozonation of toluene are not well documented in literature. Wibau et al. (1950) reported that formic, acetic, oxalic acids, carbon dioxide and water may be formed in the ozonation of toluene. Recently, Pi et al. (2005) proposed a reaction pathway for the reaction of ozone and some aromatic compounds, including toluene and the products of toluene ozonation would be short chain hydrocarbons, which are more bio-degradable and less toxic than toluene. Hence, it is proposed to use ozone to clean the spilled toluene in a natural water body.

REACTION MECHANISM

In aqueous phase, ozone oxidizes toluene by two major mechanisms (Hoigne and Bader, 1976; Langlais et al., 1991, von Gunten, 2003): one is the direct oxidation

of toluene by ozone molecules; and the other is indirect oxidation by hydroxyl radical reactions. Toluene reacts with ozone in the following form:

$$\eta O_3 + C_6H_5CH_3 \rightarrow \text{products}$$

in which, η is the stoichiometric ratio ranging from 1-2.5 with the maximum measured in the laboratory condition of 5 (Hoigne and Bader, 1983).

Ozonation of toluene occurs by direct and indirect oxidation. The reactions can be written as:

$$-dC/dt = k_T\, C_{ozone}\, C$$

$$-dC_{ozone}/dt = (\eta\, k_T) C_{ozone} C$$

in which, C is the toluene concentration, C_{ozone} is the ozone concentration, and k_T is the overall rate constant.

Kuo and Chen (1996) carried out a traditional ozonation test at pH values varying from 3 to 11 at 25°C. The initial concentration of ozone is from 0.00013 to 0.0002 mol/l (6.24 mg/l to 9.6 mg/l), and toluene concentration varies from 0.0005 – 0.002 mol/l (46 mg/l to 184 mg/l). The overall rate constant ranges from 2.34 l/(M s) to 29.41 l/(M s) (The pH ranges from 3.0 to 9.0). The oxidation kinetics is first-order with respect to the ozone concentration, and the reaction order in toluene varies with pH ranging from 0 to 1 (0 for pH over 10.0; 0.5 for pH between 7.0 and 9.0; and 1 for pH below 5.4). The measured stoichiometric ratio is 1 in their study. The oxidation rate is determined by both the direct and indirect mechanisms in distilled water (initial pH of 5.2-5.4) and other weak acids.

In natural waters, ozone can be consumed not only by the spilled pollutants but also by a lot of organic and inorganic compounds existing in the background. The rate of dissolved ozone consumption can be written as:

$$-dC_{ozone}/dt = wC_{ozone}$$

in which, w is the specific ozone utilization rate, a function of the pH and chemical composition of the water matrix.

Yurteri and Gurol (1988, 1989) did different experiments using synthetic water samples from several rivers and groundwater. Various chemical consumptions have been tested (pH = 6.8 – 9.0; TOC (total organic carbon) 0.3-5.3 mg/l; alkalinity = 10 – 500 mg/l as $CaCO_3$). The temperature was controlled at 20±1°C. The initial ozone concentration was set around 10 mg/l. The experiments were carried out in a headspace-free reactor made of dark glass so that volatilization was limited. The specific ozone utilization rate was found to be

$$\log w = -3.98 + 0.66\text{pH} + 0.61 \log (\text{TOC}) - 0.42 \log(\text{alkalinity}/10)$$

in which, w is in /hr.

GOVERNING EQUATIONS OF THE MODEL

The chemical model simulates the ozonation of toluene by solving three transport equations simultaneously: two for the toluene transport in the water and bed

respectively; and the third for the transport of ozone in the water. The transport equation in the water is written as:

$$\frac{\partial C}{\partial t} + \frac{\partial}{\partial x}(uC) + \frac{\partial}{\partial y}(vC) = \frac{\partial}{\partial x}(E_{xx}\frac{\partial C}{\partial x}) + \frac{\partial}{\partial y}(E_{yy}\frac{\partial C}{\partial y}) + S_k + S_{load}$$

where C is depth-averaged concentration for either ozone or toluene (mg/l); u , v are depth-averaged velocities in x and y direction (m/s), respectively; E_{xx} and E_{yy} are components of dispersion tensor E (m^2/s); S_k is kinetic source term (mg/l/s); and S_{load} is the external loading (mg/l/s).

The kinetic source term for ozone is mainly due to the consumption of toluene and background organic and inorganic compounds:

$$S_{ozone} = wC_{ozone}$$

The kinetic source term for toluene comprises of chemical source/sink due to net settling or eroded sediment flux, vertical diffusion, decay (volatilization and biodegradation) and decomposition by ozonation.

$$S_{toluene} = S_{load} + S_{sed} + S_{v-diff} + S_{decay} + S_{ozonation}$$

where S_{sed} is chemical source/sink due to net settling or eroded sediment flux (mg/l/s); S_{v-diff} is vertical diffusion flux at the water-sediment interface (mg/l/s); and S_{decay} is chemical decay term (mg/l/s).

$$S_{ozonation} = k_T C_{toluene} C_{ozone}$$

It is assumed that the convection and dispersion in bed sediments are negligible. The governing equation for the bed sediments in the conservative form is:

$$\frac{\partial (C_s \times D_{sed})}{\partial t} = S_{load,s} - S_{sed} + S_{v-dif} + S_{decay,s}$$

where C_s is the toluene concentration in bed (mg/l); D_{sed1} is the depth of sediment layer (m); $S_{load,s}$ is the external load to bed (mg/l/s); and $S_{decay,s}$ is the chemical decay rate in the bed (mg/l/s).

SIMULATION OF TOLUENE OZONATION SCENARIO

In this study, a hypothetic toluene spill incident was assumed to occur in a reservior. The reservoir is about 18 km long and 4 km wide with the water depth of about 4 m in the main channel. It was assumed that 270 tons of toluene was spilled into the middle of the reservoir over a period of 12 hours due. In order to clean the spilled toluene, the following numerical ozonation operation procedures were designed:

1. Identify the highest toluene plume in the reservoir, which can be found out using the simulation results of the toluene spill incident.
2. Set up an ozone barrier in the reservoir close to the plume with high concentration of toluene. The ozone barrier shall move at a similar

speed with the traveling velocity of the toluene plume so that when it passes by, toluene can be degraded more efficiently. The traveling velocity of the plume can be estimated from the flow simulation results. The length of the ozone barrier is set about the width of the plume. Two barrier width and two ozone generation capacity were tested in this study, which makes four operations in total.

3. Analyze the efficiency of ozonation using the simulation results of the chemical model. Adjust the location and ozone generation capacity of the ozone barrier if necessary to achieve favorable cleaning effects.

Flow simulation was conducted first to obtain the flow field (flow velocity, water depth, and eddy viscosity). With the input of flow field, the CCHE chemical model was then used to simulate the fate and transport of toluene spill incident, which provides the temporal and spatial toluene concentration in the reservoir and also serves as the background level without ozonation. Finally, four ozonation operations were simulated and analyzed.

Flow Field Simulation

The simulation domain was descretized into a 70 by 174 numerical mesh. Steady flow condition was assumed with the flow discharge at upstream being 120 m^3/s and water surface elevation at downstream 90.25 m. Manning's roughness coefficient was set as 0.025. Mixing length model was used for the turbulence closure. The steady flow was simulated at a time step of 20 seconds using the CCHE2D model. Figure 1 shows the bathymetry of the reservoir, locations of inlet, outlet and toluene spill, and local flow field near the spill site.

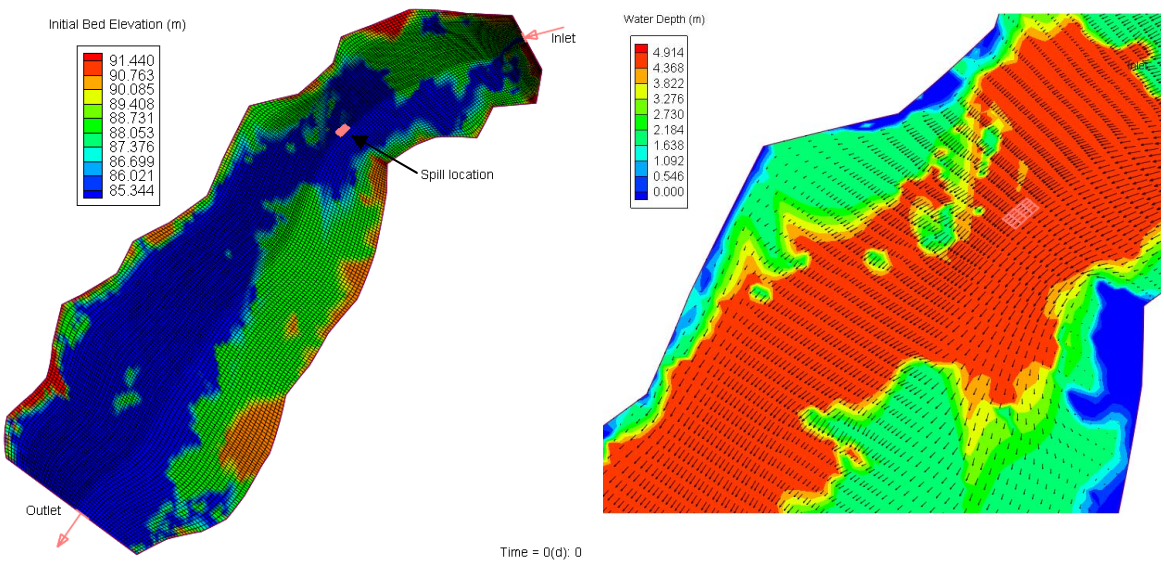

Figure 1 Numerical domain (left) and local flow field (right)

Simulation of Toluene Spill

The hypothetic toluene spill incident was simulated for 10 days. The parameters for simulating toluene decay processes and interaction with sediments are listed in Table 1.

Table 1 Parameters for simulating toluene

Biodegradation rate (s^{-1})	1.30787E-006
Partition coefficient	100
Vertical diffusion (m^2/s)	1E-007
Gas phase transfer rate (m/s)	1E-005
Henry's constant (atm m^3/mol)	0.00664
Suspended sediment concentration (mg/l)	10
Bed porosity	0.4

Toluene concentration still exceeds EPA's MCL at the end of 10 days although due to the decay processes, it has decreased from 298 mg/l (at the end of first day after spill) to 7 mg/l (at the end of 10 days after spill) (shown in Figure 2).

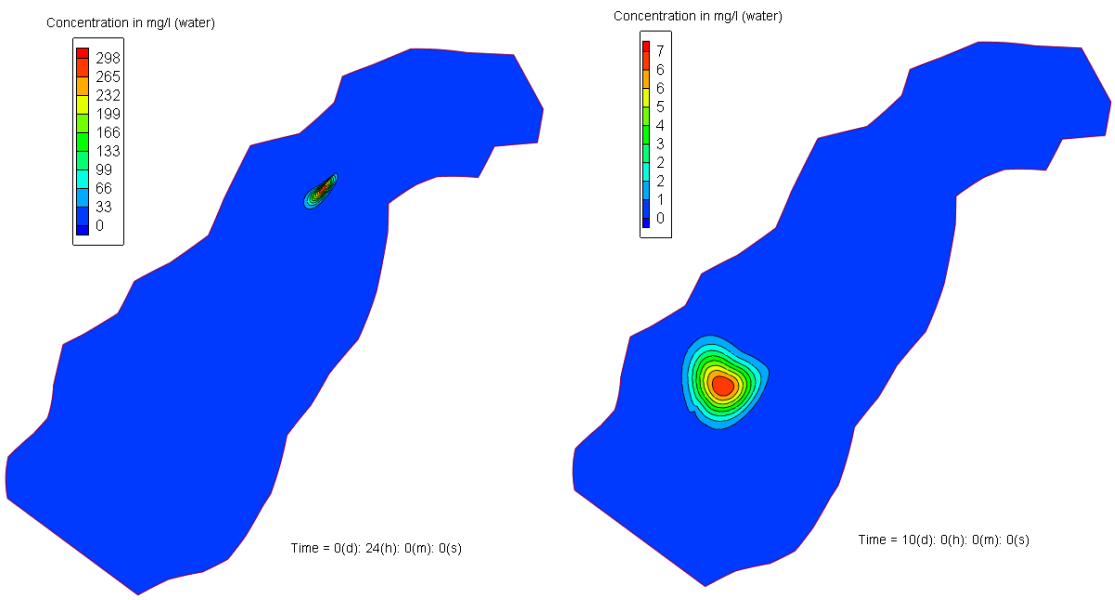

Figure 2 Toluene concentration distributions after the spill

Simulation of Ozonation Options

The hypothetic ozonation was designed to start right after all toluene was spilled into the reservoir, i.e. after 12 hours of the spill. Four options of ozonation barrier were summarized in Table 2. The barrier moves downstream with the tolune plume at an average speed of 0.013 m/s.

Table 2 Ozonation Operation Parameters

Options	1	2	3	4
Barrier width (m)	80	160	80	160
Ozone generation capacity (g/s)	650	650	1650	1650

The reservoir water is neutral with pH value of 7 and it is assumed that during the simulation period the water temperature is at 20°C. To simplify the problem, it is also assumed that the consumption of ozone was mainly by toluene. The overall rate constant of ozonation was set as 0.0002 s^{-1}. The stoichoimetric ratio was set at 1. Four ozonation options were simulated using the same flow, environmental condition, and ozonation rate constant. The simulation results of Option1 and 2 are found to be similar and that's the case for Option 3 and 4, which suggests that ozone generation capacity is the dominant factor to increase the toluene removal rate. Figure 3 shows the toluene concentration distributions at the end of day 3 after the spill. It can be seen that with higher ozone generation capacity, option 3 can clean the spill site faster.

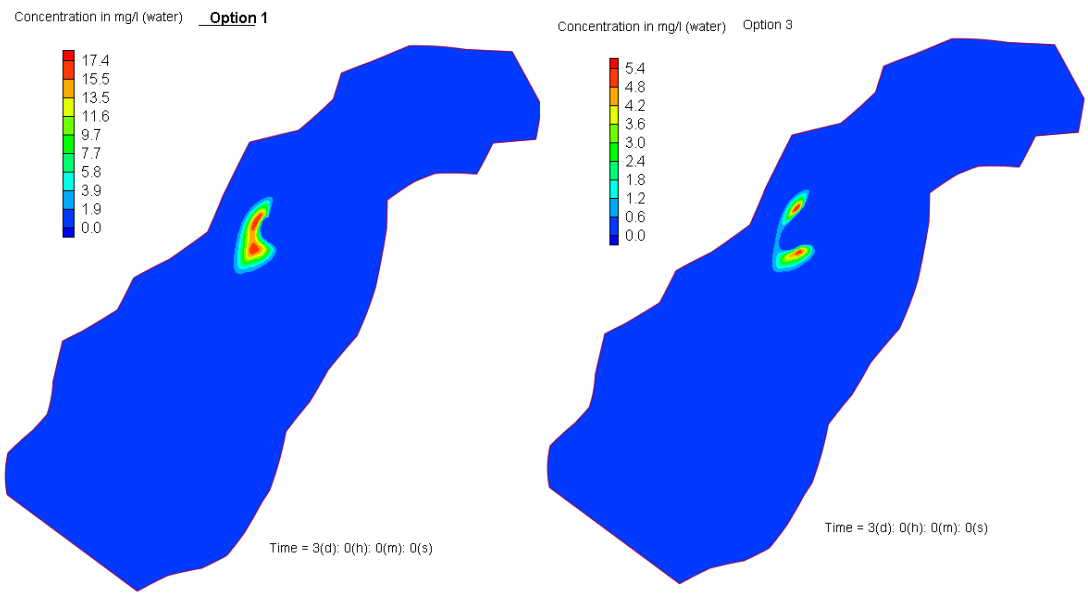

Figure 3 Toluene concentration distributions with ozonation

Total mass of toluene in the reservoir was calculated as the ozonation went on to show the removal rates for each option (Figure 4). Again, Option 1 and 2 has the similar mass reducing pattern, which is also true for Option 3 and 4. In Option 3 and 4, the toluene mass reached zero after 100 hours, while it took about 200 hours in Option 1 and 2.

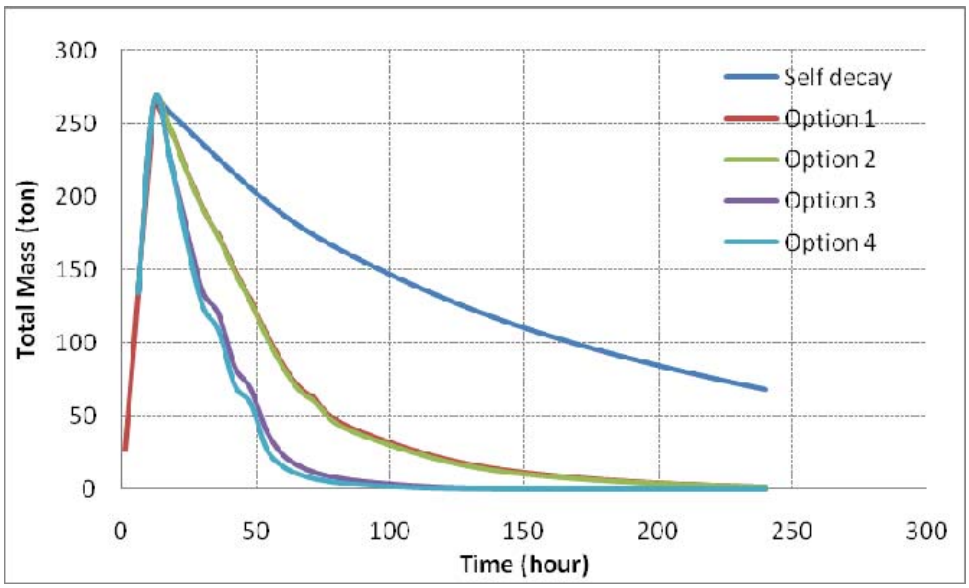

Figure 4 Toluene removal rate of four ozonation options

The water is considered safe if everywhere in the reservoir the toluene concentration is below the MCL (1 ppm). Figure 5 shows the days it took for each option to bring the water back to the safe level. After ten days, the toluene concentration still exceeds the MCL if no ozonation was conducted. Using Options 3 and 4, the water quality can recover the soonest within 5 days.

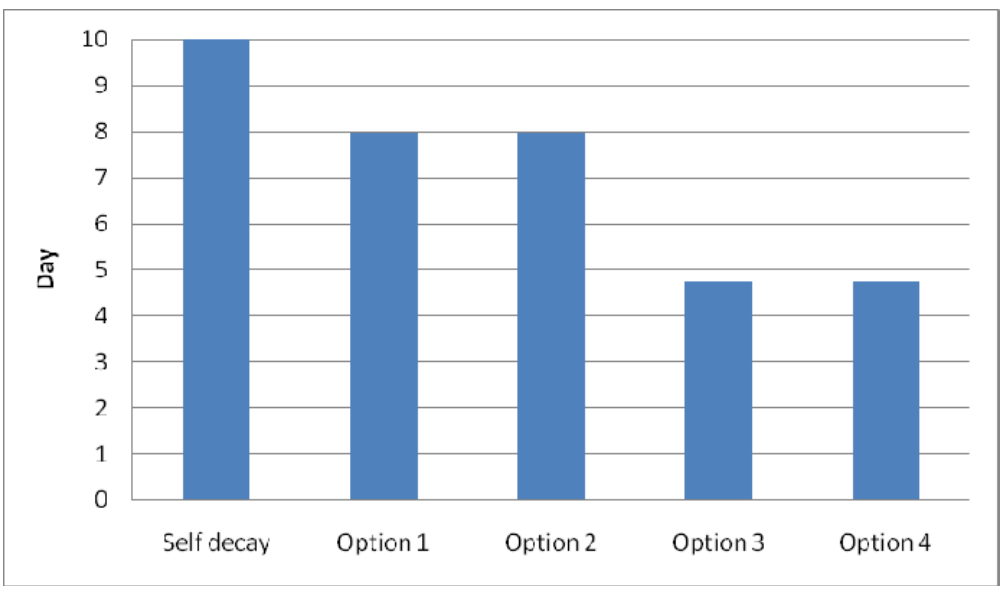

Figure 5 Toluene clean-up time

CONCLUSIONS

A hypothetic toluene spill incident in a reservoir was assumed and the clean-up operations by means of ozonation were designed and simulated using the CCHE chemical decontamination model in this study. The process-based model simulates major decay processes of toluene in the surface waters including ozonation, volatilization, biodegradation and interaction with suspended sediments and bed sediments. As this study emphasizes the simulations of toluene ozonation, the hydraulic condition was simplified as steady flow and the toluene decay processes were represented using those from literature. The spatial and temporal concentration distributions of toluene and ozone were obtained from the simulation results.

The impact of ozonation on toluene distributions can be found by comparing the toluene transport scenarios with or without ozone. With the ozone barrier moving with the toluene plume, the spilled toluene can be decontaminated at least twice as faster compared with that of self decay case. The model is also able to investigate the effectiveness of different ozonation options. It was found through the simulations of four options that the width of ozone barrier has very limited impact on the toluene removal rate. However, the ozone generation capacity plays an important role. With higher ozone generation capacity, the total mass of toluene decreases faster and the reservoir would be cleaned up in about half of the time compared with the lower capacity options.

Although this case study is hypothetical, it demonstrates that the model is a useful initial tool to help design and evaluate clean-up operations. The practical layout of ozone device needs more study in the future taking into account of factors such as device size, device movement, and cost etc. This would further enhance the effective removal of toluene or other contamination removal under consideration.

REFERENCES

Agency for Toxic Substances and Disease Registry (ATSDR). *Toxicological Profile for Toluene* (Update). U.S. Public Health Service, U.S. Department of Health and Human Services, Atlanta, GA. 1994.

EU Official Journal of the European Community L 330: Directive 98/83/EG, 1998.

Hoigne, J., Bader, H. The Role of Hydroxyl Radical Reactions in Ozonation Processes in Aqueous Solutions. *Water Res.* 1976, 10, 377-386.

Hoigne, J., Bader, H. Rate Constants of Reactions of Ozone with Organic and Inorganic Compounds in Water. II: Dissociating Organic Compounds. *Water Res.* 1983, 17, 185-194.

Ji, Z., J.H. Hamrick, and J. Pagenkopf, 2002. Sediment and Metals Modeling in Shallow River. ASCE, *J. of Environ. Eng.,* Vol. 128, No. 2, pp 105-119.

Jia, Y., and S.S.Y., Wang, 1999. Numerical Model for Channel Fow and morphological change studies. ASCE, *Journal of Hydraulic Engineering,* Vol. 125, No. 9, pp 924-933.

Jia, Y., S.S.Y., Wang, and Y. Xu, 2002. Validation and Application of a 2D Model to Channels with Complex Geometry. *International Journal of Computational Engineering Science*, Vol. 3, No. 1 (2002) 57-71. Imperial College Press.

Kuo, C. and Chen, S, 1996. Ozonation and Peroxone Oxidation of Toluene in Aqueous Solutions, *Ind. Eng. Chem. Res.* 1996, 35, 3973-3983.

Langlais, B., Reckhow, D.A., Brink, D.R., Eds. Ozone in Water Treatment – Application and Engineering, Lewis; 1991.

Mossman, D. J., J.L. Schnoor, and W. Stumm, 1988. Predicting the Effects of a Pesticide Release to the Rhine River, *J. Water Pollut. Control Fed.* 1988, 60, 1806-1812.

Pi, Y., Schumacher, J., and Jekel, M. Decomposition of aqueous ozone in the presence of aromatic organic solutes, *Water Res.* 2005, 39, 83-88.

Quantitative Environmental Analysis, LLC, 1999. PCBs in the Upper Hudson River, Volume 2, A model of PCB fate, transport, and bioaccumulation, prepared for General Electric, Albany, New York.

The Merck Index. *An Encyclopedia of Chemicals, Drugs, and Biologicals*. 11th ed. Ed. S. Budavari. Merck and Co. Inc., Rahway, NJ. 1989.

Thomann, R.V., W. Merklin, and B. Wright, 1993. Modeling Cadmium Fate at Superfund Site: Impact of Bioturbation. *J. Environ. Eng.*, 119(3), 424-442.

USEPA Federal Register 1998; 63(241): 69390-69476.

U.S. Environmental Protection Agency. *Integrated Risk Information System (IRIS) on Toluene*. National Center for Environmental Assessment, Office of Research and Development, Washington, DC. 1999.

Von Gunten, U. Ozonation of Drinking Water: Part I. Oxidation Kinetics and Product Formation, *Water Res.* 2003, 37, 1443-1467.

Wibaut, J/P. et al. The Mechanism of the Reaction between Ozone and Aromatic Compounds. *Recueil* 1950, 69, 1355-1362.

Yurteri, C. and Gurol, M.D. Ozone Consumption in Natural Waters: Effects of Background Organic Matter, pH and Carbonate Species, Ozone Science & Engineering, International Ozone Associateion, 1988, Vol. 10, pp.277-290.

Yurteri, C. and Gurol, M.D. Evaluation of Kinetic Parameters for the Ozonation of Organic Microphollutants, *Wat. Sci. Tech.,* Vol. 211, Brington, pp.465-476, 1989.

Zhu, T., Jia, Y. and Wang, S. S.Y., 2004. Environmental Impacts Assessment of Disastrous Chemical Spill Using CCHE2D Model, Proceedings of the International Conference of Hydroscience and Engineering 2006, Philadelphia, PA, USA (CD-ROM).

Simulation of Tehran Air Pollution Using Artificial Neural Networks

1. Ali Yazdanpanahrostami, M.Sc. in Civil and Environmental Engineering, Amirkabir University of Technology (Tehran Polytechnic), Research and Planning Center of Tehran, Tehran Municipality, Tehran, Iran. P.O. Box: 13117/87448, Tel: +98 (911)1539923, Fax: +98 (21)666566250, Email: yazdanpanah@members.asce.org

2. Kabir Rasouli, M.Sc. student, Department of Earth & Ocean Sciences, University of British Columbia (UBC). 6339, Stores Road, Vancouver, BC, Canada, P.C. V6T 1Z4; Tel: +1 (778)928-1265 Email: krasouli@eos.ubc.ca.

Abstract

Air pollution is one of the most important environmental issues of the populated cities, which is seriously threatening human health. This is caused by several factors, such as climo-physiologic characteristics of the region, deficiency of perennial plants, vehicles-mobile pollution sources- and also stationary sources including factories and power plants. Vehicles' gas emission is the major source of air pollution which is related to the type and magnitude of fuel they consume. In comparison, the stationary sources only contribute one fifth of the total pollutant emission.

In this study, the effect of fuel consumption increase on Tehran (Iran's capital) air pollution is evaluated. Obviously, weather patterns have also considerable role on air pollution which are considered in the proposed simulation model. For this purpose, the most effective parameters on Tehran air pollution are identified and selected as the input of simulation model. Then, Artificial Neural Network (ANN) models are chosen due to their efficient power and robustness in identifying the nature of complicated phenomena which air pollution is one of them. Tehran is selected as a case study because of its higher violation to the air pollution standards and being one of the five polluted cities around the world. Results show that the proposed model can be implemented successfully to monitor the air pollution changes and consequently makes it possible for associated managers to develop appropriate policies against the air pollution.

Keywords: Air Pollution, Fuel Consumption, Weather Parameter, Simulation, Artificial Neural Network (ANN), Tehran

1. INTRODUCTION

Today, human because of fundamental changes in world population, technology and industry has more interaction with environment than he had in past. For the first time in human history, more people are living in towns and cities than in rural areas. As a result, the demand for land in and around cities is becoming acute; urban sprawl is re-shaping landscapes and affecting people's quality of life and the environment as never before. Overall consumption, energy use, water use and waste generation go along with a growing number of urban households. Consequently, the huge detrimental human activities influence greatly on environment.

Urban environment, in its general sense, consists of resources, human and processes through which the later can convert the former into products and services. It is a mélange of natural, human-made and socio-economic environments due attention to each of which is required in order to avoid imbalance in the whole. Hence, coordination and interaction between all these three dimensions of environment ought to be aimed in any urban management policy. Today, ever-increasing problems of urban environments, particularly in developing cities, have brought a significant importance to urban management. Human impact on the environment is determined by three main factors: the materials standard of living, the applied technology and the number of people. (Fenger et al, 1998)

Air pollution is one of the challenging outcomes of human impacts and technology growth which is very important because of its direct effect on the health of people, specially in developing cities. Two decades of unparalleled growth have, however, come at a cost. Swelling urban population and increased concentration of industry and automobile traffic in and around cities have resulted in sever air pollution, threatening human health and undermining the productivity of the urban population. (Shah et al, 1997)

The prediction and simulation of air pollution concentrations is not an easy task as it involves non-linear relationships and variables of uncertainty. Several models have been developed and can be classified as either deterministic or empirical models. Deterministic models such as the Urban Airshed Model (UAM) and Canadian Hemispheric and Regional Ozone and NO*x* System (CHRONOS) are Eulerian-based models that require several inputs such as meteorological data, topographical data and emissions inventory. A difficulty encountered with such deterministic models is that emissions from natural and anthropogenic sources, such as industry and traffic, are often uncertain and not normally available. Also, deterministic models are computer intensive. (Mintz et al, 2005)

Ozone (O_3) is one of the main components of photochemical pollution which has become a major concern for public health in recent years. A study conducted in 20 US cities failed to find an association between O_3 concentration and mortality from either all causes, cardiovascular (CV) disease or respiratory disease. In contrast, more recent studies carried out in Hong Kong, Santiago de Chile, and Montreal (Quebec) reported a

significant correlation between O3 concentration and short-term mortality. (Parodia et al, 2005)

In this study, attempts have been made to explore the relationship between Tehran air pollution parameters (Ozone: O_3, Sulfur Oxide: SO_2, Nitrogen Oxide: NO_2, carbon monoxide: CO and particle matters PM) and meteorological variables and fuel consumption to analyze the role of different factors on Tehran air pollution. Having selected appropriate predictors, Artificial Neural Networks (ANN) models are developed. In next section a brief introduction of Tehran air pollution problem is given, then the ANN models used in this research are introduced. Finally, the results are discussed with some details and conclusion is given.

2. TEHRAN AIR POLLUTION

2-1. TEHRAN AT A GLANCE

Tehran, a mega city now, was once a rural area the pleasant and congenial climate and rich nature. In 1775, it was chosen as the capital city. At the beginning of 1921, as a result of the development of urban sights, the foundation of public buildings such as offices and banks could perhaps be credited as the most essential as it transformed Tehran from a traditional town to a modern city. From 1955 to 1962, Tehran turned to the industrial and administrative pole of the country as a result of which a torrent of immigrants flew into the city seeking better life standards. The trend of physical expansion in Tehran which has always been under the pressure of economic, social and political issues, one can infer that its growth has never followed a systematic, well-planned strategy in harmony with its natural capacities.

Today, Tehran metropolitan area is 655 square kilometer and the population is over 8 millions. 22 districts each of which has a municipality work under the supervision of the municipality of Tehran. Figure 1 illustrates a map of Tehran and its 22 districts.

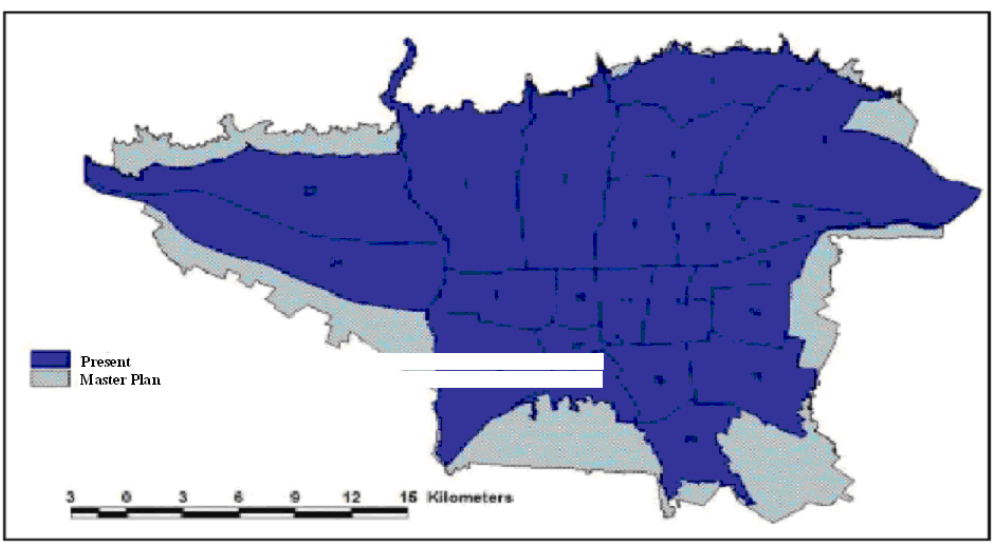

Figure 1. Map of Tehran and its municipality districts

Among all environmental issues of Tehran, air pollution is by far the gravest as it not only smudges the face of the city giving it an ever looking grey sky, but also puts the health of the inhabitants into serious jeopardy. Hence, both people and authorities are extremely concerned about it.

Tehran is located in a deep and valley-like space embraced by mountains from three different angels only allowing wind blows from the south and southwest. In terms of climate, Tehran is considered to be sited in dry Mediterranean zone. The direction of wind blow in the west of Tehran is typically from west to east and in the east from south to north. Being quite a vast city, Tehran has a variety of climates. Since the west of Tehran has a less stable climate and enjoys winds twice as fast as the ones blowing in the east, it is less prone to the effects of pollutants than the east where winds usually blow with a steady pace. Winds are generally supposed to blow faster in the first months of year than in the last ones; however, as mentioned above, this is not the case in the east of Tehran, which might be why its weather is polluted with pollutants in cold months of the year.

2-2. SITUATION OF AIR POLLUTION IN TEHRAN

Density of air pollutants increases during climatic extremes, both in cold and warm months of year, due to certain climatic changes in winter and increase in the amount of fuel consumption in summer. Investigations carried out by Tehran municipality show that in 2004, the number of unhealthy days reaches 108 and in 2006, even though declines to 67 days(Table 1), but was still very critical compared to the once a year occurrence standard released by the Environmental Protection Agency. Figure 2 illustrates the distribution of Tehran air pollution in critical days in a critical and normal day.

Table 1, Tehran air pollution regarding PSI

Year	Good	Moderate	unhealthy	hazardous
2003	10	194	159	2
2004	16	241	108	0
2005	22	251	93	0
2006	29	269	67	0
2007	31	316	18	0
2008	5	310	50	1

2-3. TRANSPORTATION AND IMPACTS ON AIR POLLUTION

Today, there are around 3 million cars traveling in Tehran. The share of transportation in air pollution of Tehran is around 88%. Vehicles manufactured before 2000 specify 70% of the pollution to themselves; whereas the ones entering the market after 2004 only produce 20% of the pollution. 75% of pollution is due to light vehicles while only 21% belongs to motorcycles and only 2% is produced by bus transportation system and the

rest is caused by other sectors. Constant expansion of urban societies and the growth of car manufacturing enterprises urge the need for a proper transportation system which utilizes the latest technological advances. (A report on ecological situation of Tehran, An insight to current trend and future actions, 2008), (Hesami, 2007)

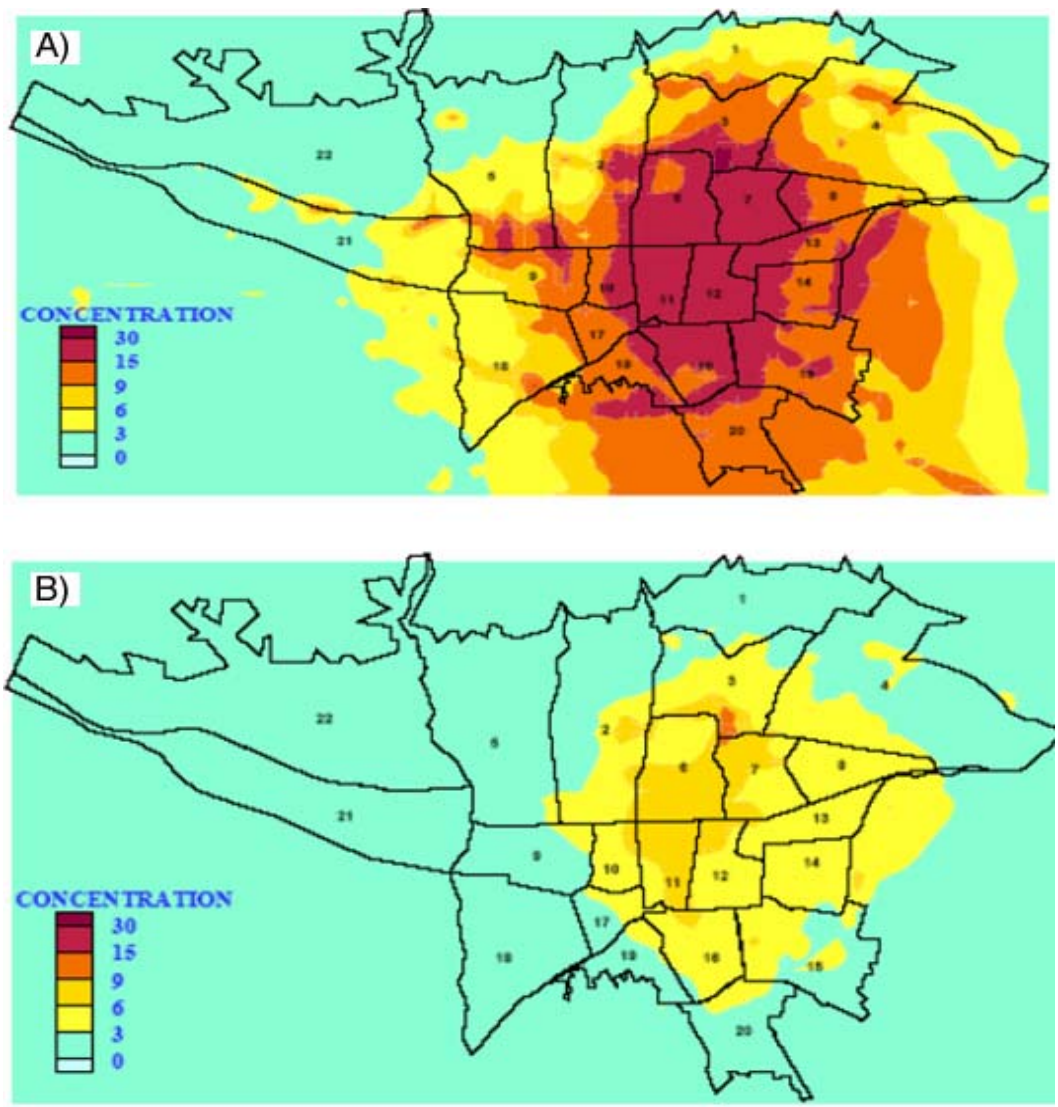

Figure 2. Critical air pollution distribution state in A) a critical day and B) Relatively normal conditions.

There are many air pollution gauges in Tehran operated by Air Quality Control Company of Tehran Municipality in order to monitor the air pollution continuously throughout the year. The air pollution data body used in this study is provided by this center. Meteorological data was collected by Iran Meteorological Organization and Air Quality Control Company of Tehran Municipality.

3- SIMULATION MODEL

3-1- ARTIFICIAL NEURAL NETWORKS

The architecture of ANNs is adapted from biological neural networks, which recognize patterns and learn from their interaction with the environment. Figure 3 shows the components of a typical three-layer feed forward artificial neural network. As shown in this figure, each node j receives incoming signals from every node i in the previous layer. Associated with each incoming signal (x_i) to node j, is a weight (w_{ji}) in order to give a large level of flexibility in the model formulation of the hidden layer that corresponds to the hidden or artificial variables. Since the input-output relation is easy to be computed, the neural network model can be considered as an effective technique in any descriptive or optimization procedure. (Karamouz et al, 2006)

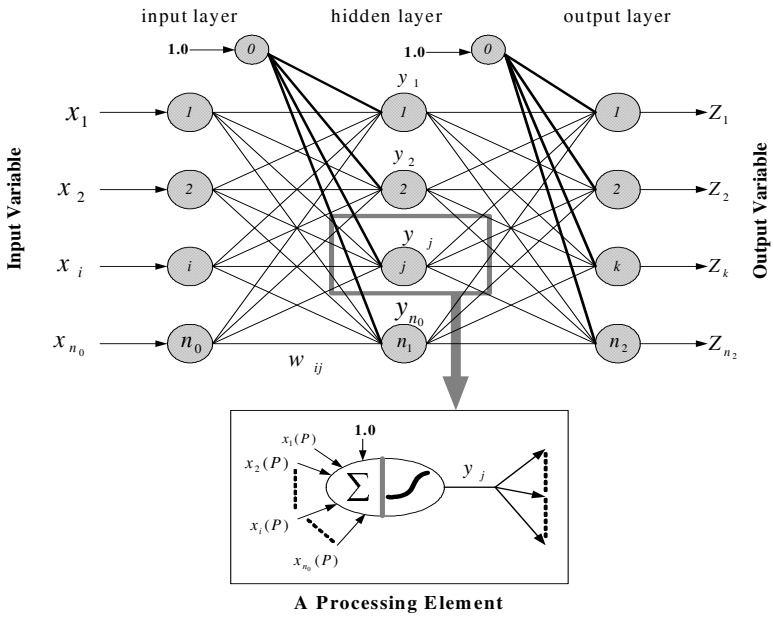

Figure 3. Typical three-layer feed forward artificial neural network (Hsu et al., 1995)

3-2. INPUTS OF SIMULATION MODEL

The relation between monthly records of O3, CO, NO2, PM-10 and SO2 as air pollution indicators and the weather parameters and also fuel consumption has been computed to find the best predictors for the simulation model. We chose average of maximum

relative humidity, average of minimum relative humidity, average of wind speed, monthly sunshine hours and monthly precipitation as the weather parameters which have strong effect on air pollution indicators and benzin, gasoil, kerosene and fueloil as the fuel consumption indicators.

The results of the best correlation obtained for each air pollution indicator are presented in Table 2. As shown, there is a significant relationship between predictors and ozone, one of the most factors of air pollution that seriously affect the health of inhabitants. The NO2 and SO2 indices can also be considered as indicators of Tehran air pollution. We didn't find strong relationship between CO and PM with the predictors in the period of 2001 to 2005.

Table 2: Correlation of each air pollution indicator with weather and fuel consumption indicators

Index	Kerosene	Gasoil	Average of Relative Humidity	Monthly Sunshine Hours	Benzin
O3	0.75	0.65	0.77	0.83	0.56
NO2	0.5	-	-	0.31	0.61
SO2	0.56	-	0.4	-	0.7

3-3. RESULTS OF ANN MODEL

Three different ANN models of Multi-Layer Perceptron Neural Network (MLP), are trained using three sets of data classified in Table 2. In first model, monthly time series of Kerosene, Gasoil, average of relative humidity, sunshine hours, and Benzin are given as inputs and Ozone as model output. In other two models, three of 5 variables are given and NO2 and SO2 are simulated.

In order to find the structure of these models, we have developed MLPs with tansig and Pureline activation functions in hidden and output layers respectively. The number of neurons in hidden layer is selected using cross-validation technique. For this purpose, all 52 set of input and output are divided into 26 chunks. Then, the MLP model is trained 50 set of data and validated by the 2 remaining sets. This is repeated for each of the chunks. The error of calibration and validation are obtained averaging the errors of all 26 trains. These steps are repeated for number of neurons from 2 to 15. Now, there are two errors of calibration and validation for each number of neurons in hidden layer. To quantify the ANNs performance, Root Mean Square Error, RMSE index has been calculated. Table 3 shows the calibration and validation errors for O3, NO2, and SO2 for different number of neurons in hidden layer.

Table 3. Cross-validation results for selecting optimum number of neurons in hidden layer

Neuron	O3			NO2			SO2		
	Err-Calib	Err-Valid	MinMax	Err-Calib	Err-Valid	MinMax	Err-Calib	Err-Valid	MinMax
2	7.15	1.58	7.1	2.83	0.97	2.83	6.94	1.97	6.94
3	7.12	1.78	7.1	2.81	2.53	2.81	6.65	2.04	6.65
4	6.91	4.87	6.9	2.66	1.12	2.66	6.46	8.40	8.40
5	6.78	89.29	89.3	2.60	2.32	2.60	6.32	3.81	6.32
6	6.63	18.49	18.5	2.62	1.92	2.62	6.16	5.60	6.16
7	6.52	15.63	15.6	2.59	5.90	5.90	5.94	17.16	17.16
8	6.44	11.77	11.8	2.49	2.87	2.87	5.90	8.96	8.96
9	6.44	5.43	6.44	2.50	4.02	4.02	5.76	47.41	47.41
10	6.43	4.04	6.43	2.51	7.72	7.72	5.67	8.62	8.62
11	6.43	4.71	6.43	2.49	3.85	3.85	5.70	11.44	11.44
12	6.43	5.90	6.43	2.48	5.52	5.52	5.68	8.54	8.54
13	6.42	6.21	6.42	2.49	3.33	3.33	5.67	15.68	15.68
14	6.43	3.99	6.43	2.48	3.19	3.19	5.67	8.79	8.79
15	6.43	4.77	6.43	2.48	3.30	3.30	5.65	10.02	10.02

To select the optimum number of neurons in hidden layer, we tried Min-Max approach. According to this method, NO2 and SO2 models have 5 and 6 neurons respectively, and in case of O3 following the Min-Max method we should have selected 13 neurons, but since the variation of train error for neuron numbers of greater than 8 is almost the same, we select the number of neuron with small validation error. Therefore, we selected 3 neurons for O3 model (Table 2).

After the selection of model architecture, the models are trained for 80 percent of data and validated by rest of the data. The RMSE error index of 1.97 and 1.37 obtained for validation periods of both O3 and NO2 models with 1000 epochs, respectively. This was 2.56 for SO2 model which obtained with 5000 epochs. Learning rate for all the models is considered 0.001. The time series of observation against the forecast for training and validation periods are given in figures 4 to 6 which show the robustness of the developed models in test period.

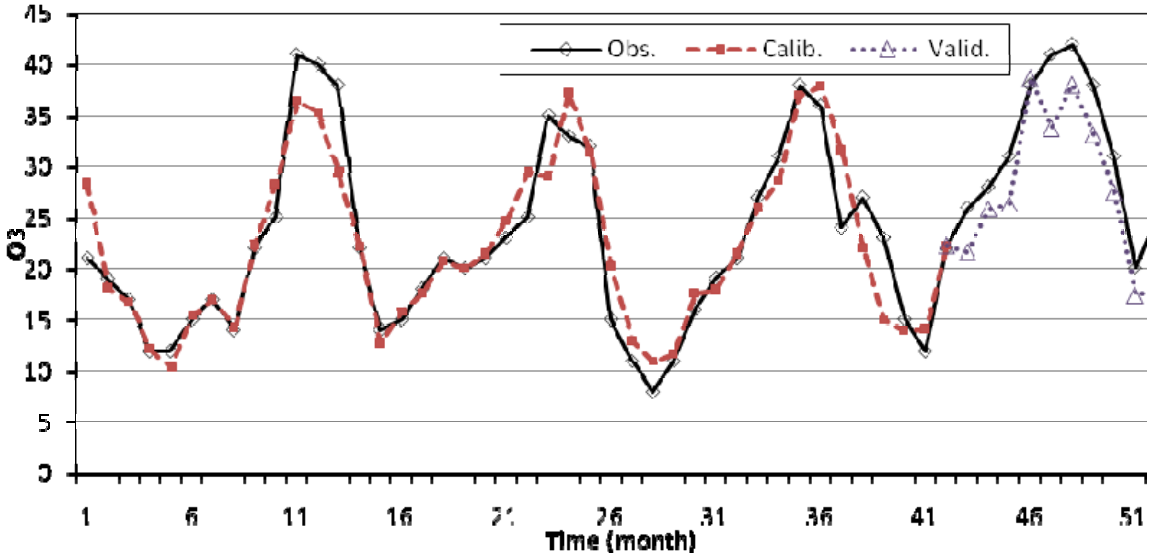

Figure 4. Simulated and observed time series of O3(Sep. 2001-Dec. 2005)

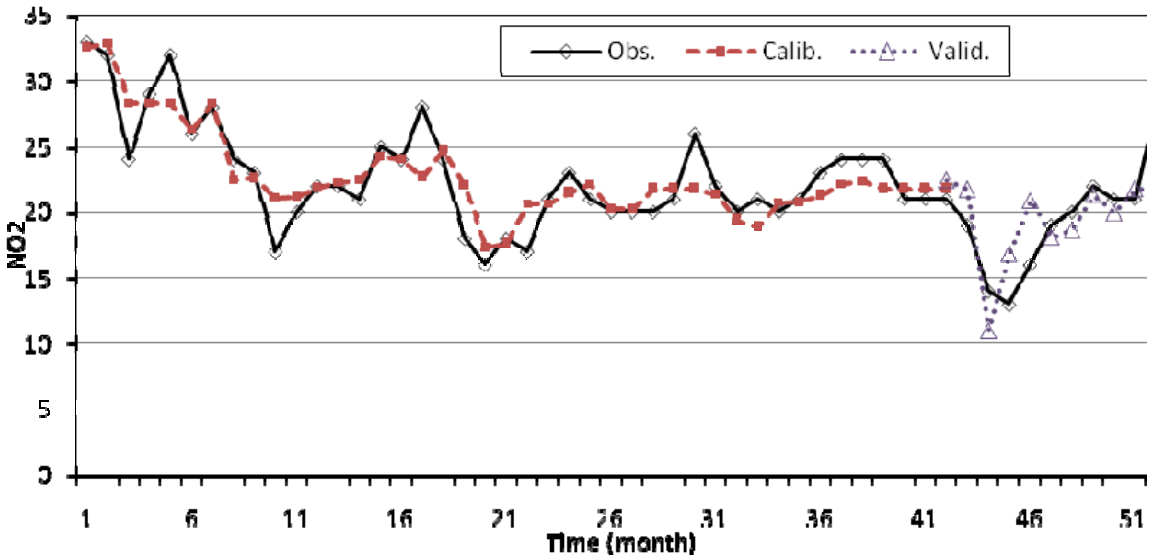

Figure 5. Simulated and observed time series of NO2 (Sep. 2001-Dec. 2005)

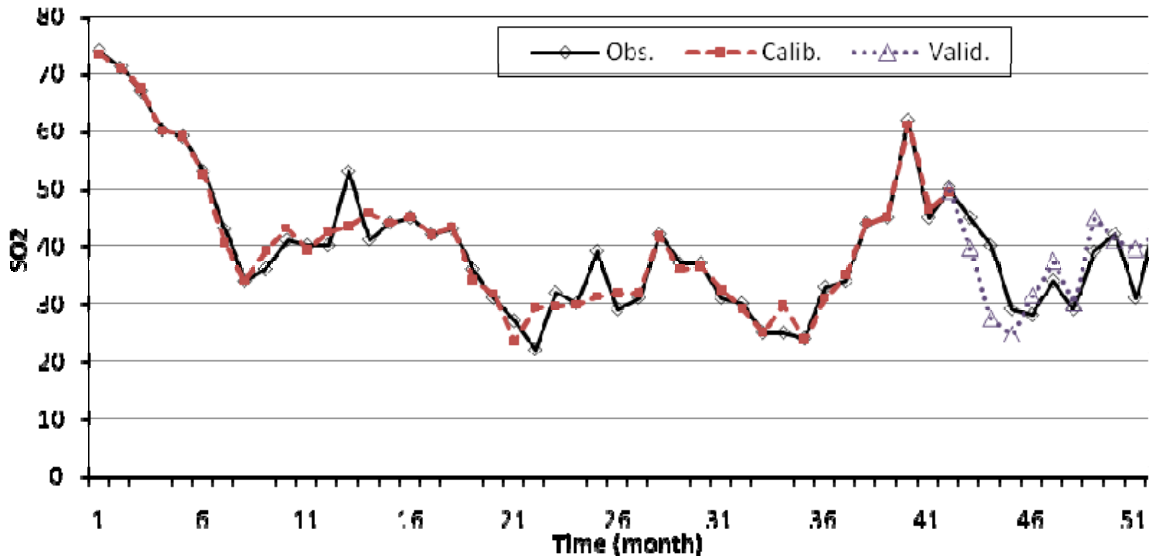

Figure 6. Simulated and observed time series of SO2 (Sep. 2001-Dec. 2005)

4- CONCLUSION

The purpose of this study is to analyze Tehran air pollution problem focusing on impacts of vehicles' portion of pollution and its relation with fuel consumption and weather patterns. For this purpose, the correlations between fuel consumption indicators (benzin, gas oil, kerosene and oil), weather parameters and Tehran air pollution indicators (Ozone, Sulfur Dioxide, Nitrogen Dioxide, Carbon Monoxide and particle matters) have been computed. Five fuel consumption and climate indicators highly correlated with pollution indices have been used as air pollution predictors and as input of three different MLP models. These models are used to simulate Ozone, Sulfur Dioxide, and Nitrogen Dioxide. Results show that even though there is short length of recorded data available, developed models simulate the Tehran air pollution effectively and can be used for making different traffic policies in city in order to reduce the air pollution. Using these models for different cloud coverage, humidity rates and fuel consumption air pollution of Tehran are simulated. Since the climatic variables can be predicted and the fuel consumption of Tehran has some special patterns it is also to predict the air pollution conditions in Tehran in advance and consequently protective policies for its reduction.

5- REFERENCE

Environment and development committee, (2008) "A report on ecological situation of Tehran, An insight to current trend and future actions" Published by the Municipality of Tehran, Tehran, Iran

Fenger, J., Hertel, O. and Pslmgren, F. (1998) "Urban Air Pollution - European Aspects." Kluwer Academic Publishers

Hesami, Z (2007) “Pondering of sustainable development about Tehran air pollution due to transportation” First National Air Pollution Conference, Tehran, Iran,

Hsu, K., Gupta, H. V., Sorooshian, S. (1995). “Artificial neural nerwork modeling of the rainfall-runoff process.” *Water Resources Research*, 31(10), 2517-2530.

Karamouz, M, Yazdanpanah, A., Moridi, A. and Nazif, S. (2006) "Effect of Large Scale Climate Signals on Iran Monsoon Rainfall" *An International Perspective on Environment and Water Resources*, ASCE, EWRI, India

Mintz, R., Young, B. R. and Svrcek, W. Y. (2005) "Fuzzy logic modeling of surface ozone concentrations", *Computers and Chemical Engineering,* 29**,** 2049**–**2059)

Parodia**,** S, Vercellib**,** M., Garroneb, E., Fontanad, V. and Izzotti**,** A. (2005) "Ozone air pollution and daily mortality in Genoa, Italy between 1993 and 1996", *Public Health* 119, 844–850

Shah, J., Nagpal, T. and Brandon, G. J. "Urban Air Quality management strategy in Asia.", *Guidebook of the World Bank*, Washington D.C.

Distributed Power Generation at State Facilities: Economic Analysis of Savings and Carbon Credits

Joel G. Burken[1], A. Curt Elmore[2], Mariesa Crow[3], Will Granich[2], Trenton Blair[4]

Civil, Architectural and Environmental Engineering, Missouri University of Science and Technology, 1401 N Pine Street, Rolla Missouri, 65409
PH (573)-341-6547; FAX (573)-341-4729; Email, Burken@mst.edu
[2]Geological Engineering, Missouri S&T elmoreac@mst.edu, wagr38@mst.edu;
[3]Electrical and Computer Engineering, Missouri S&T, crow@mst.edu ;
[4]Division of Facilities Management, Design & Construction, State Of Missouri, Trent.Blair@oa.mo.gov

ABSTRACT

States own numerous dispersed facilities, many in remote locations. These facilities could be potential locations for renewable energy generation systems, using the power to offset the electricity use at the locations with excess being sold back to the utilities, i.e. the grid. In efforts to initiate renewable energy generation at state facilities, the State of Missouri undertook a study to erect a combined photovoltaic (PV) array and wind turbine renewable energy project at a highway patrol facility. In this study, a new rapid site evaluation for wind power potential was undertaken. The annual energy generation was estimated to be 22,800 kilowatt hours (kWh) (12 month x 1,900 kWh/month). The PV/wind turbine system installed and operational in under five months from project initiation.

Based upon electricity offsets alone, an economic analysis estimated that the wind turbine part of the project would have a payback period of 18 - 25 years. When considering the Carbon Credits (CC) that could be generated, the payback period was reduced. Carbon Credits are largely an unknown and misunderstood commodity. The current trading price of $3 to $4 per CC equivalent is expected to increase to around $12 in the short term, and within the payback period of this project, carbon credits are anticipated to reach $20-30. Carbon Credit finance is still largely an untested market for entities such as a state, and the economics covered in this talk are not easily attained on small projects. This talk will discuss how agglomeration of the small projects could lead to marketing of these credits to help the economic analysis of the individual projects.

INTRODUCTION

At a time when energy costs are escalating and energy security is a concern nationally, renewable energy is clearly a part of the national future. In this future, many entities are looking to enter the energy production efforts, including farmers, private companies, schools and private companies. State institutes are also interested in pursuing renewable energy projects, but the diversity of state facilities and of each individual application, hinders the ease of entering into a renewable energy project for individual facilities. As part of an effort to focus on the siting and implementation

processes, the State of Missouri Division of Facilities Management, Design & Construction teamed with Missouri University of Science and Technology to deploy a small demonstration project. Critical factors in the project planning were rapid sight evaluation and power projections, particularly for the wind project, which was completed using novel methods based on readily available weather data. Small, distributed energy generation systems will be located at various state facilities to primarily offset electricity produced from fossil fuel and not be sited for ideal wind resources, which is done for most wind energy projects. For each small project in dispersed locations, detailed and expensive wind studies that can take months to years to complete are impractical.

In utilizing wind turbines or PV arrays for renewable energy sources, the electricity generated is the primary commodity produced and has the greatest economic value. As a result of future regulatory action on the market valuation of carbon emissions, the costs of fossil fuel generated electricity will almost certainly increase, with many projections suggesting increases of two to three fold, particularly in Missouri where energy is currently very inexpensive. Concurrently, the value of carbon credits and renewable energy credits are projected to increase, offering other revenue streams from the renewable energy sources. The market value of carbon credits in particular is highly volatile. For example, the value of carbon credits (based on offsetting or sequestering one tonne of CO_2) on the European market, climbed to $30 a tonne and then fell to almost 0 within a year. Developing an understanding of these markets and how to capitalize on the economic potential is essential for renewable energy projects as evolution of carbon credit markets is clearly a contributor to the financial feasibility for renewable energy technologies. The sale of carbon credits can be carried out in a variety of methods, including open markets or direct purchase by companies, states or industries. The credits can also be sold to organizations like EcoSecurities, who develops projects and offer guaranteed purchase agreements and builds an agglomerated portfolio to market later. As a whole, carbon credits are an emerging source of income to those generating alternative energy which modestly adds to the economic returns from the project currently and may be a considerable revenue stream in the future.

Site Assessment and Implementation Siting studies which include the collection of wind and/or solar data at candidate locations are routinely performed during feasibility studies for wind and/or solar farms which generate energy for utility company purchase. One of the major challenges associated with installing relatively small renewable energy systems at existing facilities is that the facilities may not be located in areas with high potential for renewable energy (especially wind) generation. A second challenge is that the cost of installing a weather station to measure the available wind and solar resources at the facility location may cost a significant fraction of the renewable energy systems. The annual energy generation was estimated to be 22,800 kWh (12 month x 1,900 kWh/month). The use of non-specific wind velocity data from regional databases may provide reliable wind turbine performance predictions. Details of this methodology are presented in recent

publications on small wind turbine prediction modeling (Elmore and Gallagher, 2009). This methodology will be applied for the project outlined in this paper.

Obtaining an interconnection agreement with the local municipality was also an unexpected hurdle. The local municipality required the interconnection participant to carry liability insurance in order to enter the interconnection agreement. The State of Missouri, however, is self-insured. Both entities, the state and local utility, were cooperative, but the novel aspects of the renewable energy project had not been considered in previous experiences for both state and utility personnel. The interconnection agreement was completed, and the lessons learned on how to address liability issues on this novel project will hopefully aid in future similar projects. The PV and wind turbine selection, installation, and interconnection was completed in roughly five months. The resulting system is described below in Table 1 and shown in Figure 1. Some preliminary lessons learned:

1. Review the local utility interconnection permit because the requirements may vary significantly from utility to utility. For this project there were some unanticipated costs: a PE was required to develop a one line electrical diagram; two shutoff switches (one for the wind and one for the PV) were required on the line from the inverters to the utility connection; and the utility requested approximately $1,000 to install a net meter. These items were not required for similar projects in other jurisdictions.
2. Ask the tenant to participate in the project financially to prevent escalation of installation costs related to potential modifications to the facility. For example, the tenant requested extra grounding of the system and that utilities be installed without cutting a light duty asphalt driveway. These actions were not technically required, and the tenant may not have made such requests if they shared in the costs.
3. The instrumentation vendor needs to provide a statement of qualifications indicating that they have instrumented the exact wind turbine and PV models being installed.
4. The tenant should be prepared for significant public interest.

Table 1. Equipment list along with the manufacturer and model numbers for the project at the Missouri State Highway Patrol Troop I Headquarters.

Item:	Manufacturer:	Model Number:
Solar Panels (x 10)	Sharp	ND-216U2
Solar Panel Inverter	Fronius	Fronius IG 2000
PV Array Ground Mounts	DP&W Corporation	Series DP-LPRGM-TL
Wind Turbine and Guyed Lattice Tower (36.6 m)	Bergey Windpower	Bergey Excel S
Wind Turbine Inverter	Bergey Windpower	Gridtek 10
Anemometer (x3)	Fat Spaniel Technologies	254
Pyranometer	Fat Spaniel Technologies	454
Barometric Pressure Sensor	Met One Instruments Inc.	092
Temperature Probe	Fat Spaniel Technologies	439/259

Renewable Energy Performance Methodology The performance of the photovoltaic (PV) array is currently being monitored using a data feed from Fat Spaniel Technologies. After the solar power is converted in the Frionus IG 2000 inverter, the power produced, in kilowatts (kW), is monitored by the Fronius EZ Card. The data is averaged every minute and posted to the data feed where the results can be viewed. To obtain the daily energy produced, in kilowatt hours (kW-hrs), the daily sum of the minute averages must be calculated. When divided by sixty this converts the power to kW-hrs for that particular day.



Figure 1 Photo of completed wind turbine and PV solar array.

The performance of the wind turbine is currently being monitored using a data feed from Fat Spaniel Technologies. After the wind turbine power is converted in the Gridtek 10 inverter, the power, voltage and current produced are monitored using a current transducer. The minute averages of the power are sent to a data feed, and the voltage and current values are sent to a website produced by Fat Spaniel. The daily energy produced can be calculated by taking the daily sum of the minute averages of the power and dividing by 60.

Carbon Credit Finances Carbon credit trading is currently a voluntary program in the US. As such, there is no single approved methodology for quantifying or exchanging CCs. Numerous methodologies and marketing approaches are available. In all of these methods and approaches, the basic premise for CC generation in renewable energy projects is that the energy is used to offset use of electricity from a fossil fuel source emitting greenhouse gasses (GHG), whereas the renewable energy does not emit GHGs. The protocols used for quantifying the CCs vary in the specific methodologies used to quantify and market GHG emissions mitigated in the project. Three of the most common types of projects for CC quantification, validating, and marketing are listed in Table 2 below.

Table 2 Three common methodologies for carbon credit quantification, validation, and marketing.

CC Methodologies	Summary	Reference
CDM - Clean Development Mechanism	From Kyoto, very complete, widely accepted	CDM 1
CCX – Chicago Climate Exchange	Linked with CCX market, "arbitrary" values	CCX
CCAR – California Climate Action Registry	Newest, limited project types, widely accepted	CCAR

Protocols for Carbon Credit Determination and Verification CDM Protocol is based on standards intended for use with the "Clean Development Mechanism" program from the Kyoto Protocol. CDM protocols are very thorough and transparent, including numerous tools for calculating baseline, additionality, and other important factors that affect a project's quality and market value. CDM standards are available for most types of acceptable GHG reduction or mitigating projects. Verification of a CC project is usually completed by a third party, but can also be done by the aggregator (if it has the technical expertise) or by the trading platform, both of which are usually done for a set fee ($/CCE). As verification processes can be tedious and quite complex for some types of projects, it can also be quite costly. Often the verification can include a new mechanism or methodology for measuring the carbon sequestration or mitigation. Relating this mechanism or methodology to true carbon credits can be brought into question and can be accepted/not accepted under the different protocols. Acceptance by one is not acceptance by all. In the case of mechanical (wind, hydro) or PV electrical generation, the verification is rather straight forward based upon the power generated and the source of electricity that was offset.

Credits that are quantified and verified following CDM protocols are certified emission reduction (CER) credits, each equivalent to one tonne of CO_2. These CERs can be traded and sold, and used by industrialized countries to meet a part of their emission reduction targets under the Kyoto Protocol. If not within the Kyoto framework, the credits are voluntary and do not need to prescribe to the CDM standard. Reductions can be part of a subscribed voluntary program, such as the Chicago Climate Exchange, in which members are legally bound to emissions reduction schedules. The protocols for such programs are terms as a Voluntary Carbon Standard (VCS), seeking to provide a credible but simple set of criteria that will provide integrity. Credits verified using the VCS result in voluntary emission reductions (VERs) that are independently verified and represent real, quantifiable, additional and permanent project-based emission reductions. In a regulatory framework or a cap and trade system, CERs are backed by a recognized framework and institutions, i.e. the UN for the Kyoto Protocol, to ensure that real greenhouse gas emission reductions take place, as well as providing a clear audit trail. In the US, the CCX is established as the largest voluntary market and for the CCX trading, these

VCSs are adequate. CCX standards and protocols are available for most types of emissions reductions or sequestration projects, but can be very specific in nature. CCAR Protocol is the newest of the three protocols available and although it is not as well established, it rapidly becoming accepted. In summary, a "carbon credit" does not always represent the same quantity or assurance of emissions reduction.

Marketing Carbon Credits In a regulatory framework of a cap and trade system, entities are held to emissions levels through the capping process to determine the allowable emissions for each entity (government institute, private company, or industrial facility). Caps can then be met by direct reductions or by buying offsets wherein another entity can show the reduced emissions. Through this mechanism, the most financially advantageous emissions reductions should result. In such a model, the trading is done in an open market to let market pressure determine the monetary value of the emissions reductions. In such a market, all emissions reductions must be 'equal' and thus the rigor of the CERs as noted above. In the Kyoto Protocol framework, the European Climate Exchange (ECX) is the market where the trading of carbon credits takes place. Trading can also occur directly between those supplying the emissions reductions and those needing the credits to meet their cap, but the CERs are still required.

In the voluntary market of the US, there is no set standard. Members of the CCX have voluntarily joined and followed the prescribed reductions schedules of the CCX. Under these schedules, members of Phase I and II have legally committed to reach 6% below their initial baseline from 2003 – 2010 (CCX, 2009). For projects that market VERs, the VCS protocols are adequate and generally used. VERs can also be marketed directly to parties interested in offsetting their carbon emissions, such as business travel. There are many entities marketing emissions reductions directly to 'consumers' (Ecobusinesslinks, 2009). In such cases the consumers buying the offsets may be taken with marketing of such projects of tree plantings, but in reality there may be little or no credibility. In research by the Financial Times, the voluntary carbon credit business was filled with fraudulent activity and lacking verification using approved protocols (Fidler Harvey, 2007). In the same study, the regulated market was noted to hit $68 billion annually by the year 2010. Certainly there is value in carbon credits as this value is expected to increase.

Carbon Credit Values Projections for carbon credits range widely, and will certainly be driven by any cap and trade programs in the US. Many estimates have such legislation appearing in 2011 or 2012. In 2008, the discussion of the Warner Leiberman bill on a proposed cap and trade system in May-June 2008 caused a clear increase in the CCX market to over $7, more than $2 above the previous high, see Figure 2. The bill proposed a cap and trade program in place by 2012 and to curb US emissions by 50% by 2050; however, the bill was not passed by the Senate.

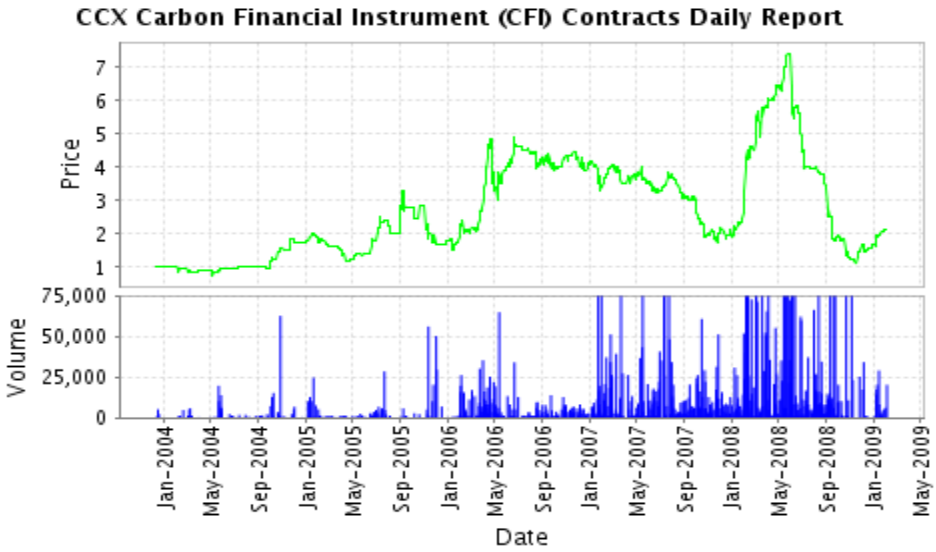

Figure 2 CCX prices for carbon credits showing a high during discussions of the Warner Leiberman bill (CCX.com).

Carbon Credit Revenues for the Troop I Project In this project, the revenue that can be generated over the life of the project will be modeled under a variety of scenarios, where electricity values ranges from 0.02 to 0.14 $/kWh, and where the carbon credit pricing ranges according to the projections shown in Figure 3. These projections were generated in collaborations with personnel at EcoSecurities, a carbon credit brokerage firm, as part of a project on the financial benefit of using livestock waste digestion to produce methane and subsequently electricity (Grover, 2008). Many estimates are that carbon credit prices will initially be listed at $10 – 15 when allocations are initially set, should cap and trade legislation be in place by around 2012. While this is a highly volatile market and not yet well understood, the projections cover almost all scenarios we have investigated, short of no climate change action by the US, or carbon credits hitting the extremes of existing projections, which were above $60.

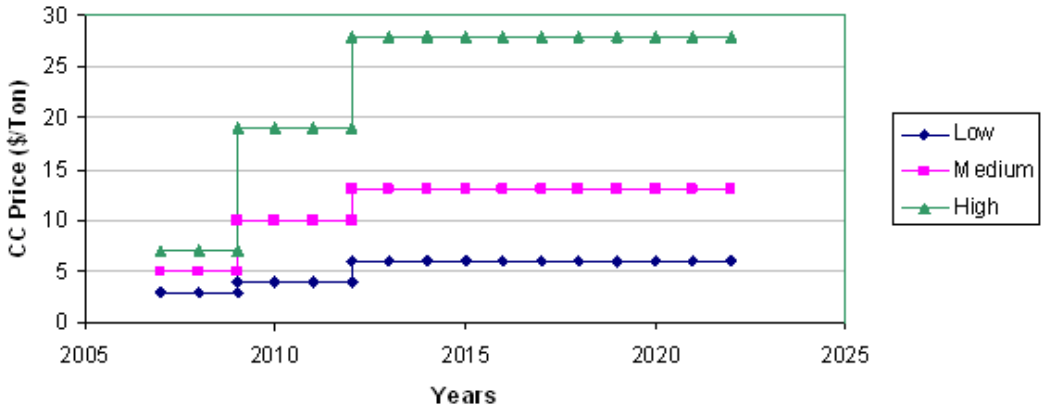

Figure 3 Carbon Credit projection scenarios based upon a variety of actions proposed at the federal and state level. (Grover 2008)

In projecting the carbon credits generated in this project, the CCX emission factors will be utilized (Boyt, 2007). Currently, the emissions factors for this region of the country are 0.68 tonnes CO_2/MWh. Based upon the estimated electricity generation of 22,800 kWh annually, estimates are that approximately 15 tonnes of carbon credits will be generated, representing $100 – $320 annually for the range of carbon emissions anticipated.

The electricity produced is estimated at a value of $1,400 to $2,700 annually for the range of electricity rates expected during the payback period of this project. Overall, electricity offsets represent about 90% of the estimated financial benefit of the renewable energy project. These projections are conservative in estimations and once a reasonable data set of energy production is available (typically 6-12 months), a true evaluation of the carbon credit revenue potential can be fully completed.

ACKNOWLEDGEMENTS

This project was funded by the Missouri Office of Administration Division of Facility Management, Design, and Construction. The authors would like to acknowledge the contributions of may that assisted with this project. Numerous staff at Rolla Municipal Utilities, Missouri State Highway Patrol Troop I headquarters, Missouri S&T were all instrumental in assisting to complete administrative paper trail and physical installation of this system is astonishingly rapid fashion for a project with so many entities involved. We also thank Missouri S&T student Sarah Seigfried for commentary and input on the carbon credit mechanisms.

REFERENCES

Boyk, W, 2007, Advisory 2007-012007 CCX Greenhouse Gas Emission Factors For Direct Emission Sources CCX http://www.chicagoclimateexchange.com/info/advisories/2007/2007-01.pdf (Accessed Jan 2009)

CCAR California Climate Action Registry, 2009, Project Protocols http://www.climateregistry.org/tools/protocols/project-protocols.html (Accessed Jan 2009)

CCX – Chicago Climate Cexhange, 2009 Offsets from Renewable Energy http://www.chicagoclimateexchange.com/content.jsf?id=244 (Accessed Jan 2009)

CDM – Clean Development Mechanism, 2009, Approved Baseline and Monitoring Methodologies, Nations Framework Convention on Climate Change http://cdm.unfccc.int/methodologies/PAmethodologies/approved.html, United (Accessed Jan 2009)

Ecobusinesslinks, 2009, How much does Carbon Offsetting cost? Price survey! http://www.ecobusinesslinks.com/carbon_offset_wind_credits_carbon_reduction.htm (Accessed Jan 2009)

Elmore, A.C. and Gallagher, R. 2009) Using Regional Climate Center Data to Predict Small Wind Turbine Performance, Pract. Periodical of Haz., Toxic, and Radioactive Waste Mgmt. Volume 13, Issue 1, pp. 14-19.

Harvey, F and Fidler, S, 2007, Industry caught in carbon 'smokescreen' Financial Times, April 25, 2007, www.ft.com (Accessed Jan 2009)

DRIVE FOR ZERO NET CARBON IMPACT

Presented By: Jessica Lamb & Ashlynn Horras
In association with Luke Fencl, Courtney Warren, and Sebastian Medina

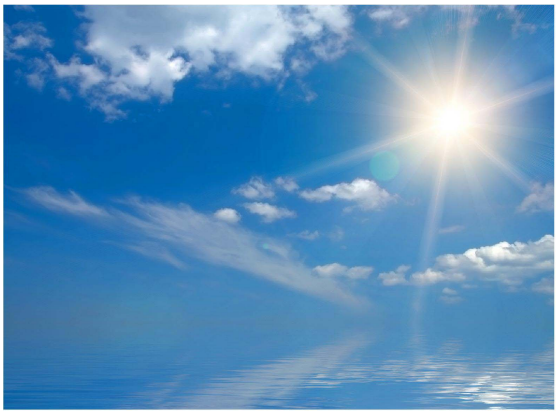

Today we are challenged with increasing concerns over global climate change, dependency on depleting hydrocarbon forms of energy, the growing scarcity of water resources to support quality of life infrastructure, and sustainability of infrastructure development on natural resources under current technologies and practices. Our future depends upon the development and commercialization of technologies in the field of renewable energy sources for cogeneration or combined heat and power (CHP). These renewable sources could include biomass, biogas, synfuels, and solar power.

CONSUMER/GOVERNMENTAL POSITIONS

There is no doubt that the way society views the environment is changing. Seventy-six percent of Americans believe it is important that their electric utility offers power produced from renewable sources. Fifty-six percent felt it was so essential that they would pay a small fee to cover the cost of energy generated from renewable sources. Forty-two percent of Americans can now name at least one form of renewable energy, whereas only 20% of Americans could do this last year.'

An MRA commissioned survey of key clients shows that utilities believe that a cap and trade system and a federal Renewable Portfolio Standards (RPS) mandate are inevitable and the clients are correct.[2] The government will play a major role in how the industry interacts with the environment in the near future. It's nearly certain governmental restrictions on greenhouse gas emissions will become more severe. President Barack Obama proposed a market-based cap and trade system in efforts to reduce greenhouse gas emission significantly by 2050. President Obama aims to reduce greenhouse gas emissions 80% by 2050. This means that in the near future, greenhouse gases such as carbon and methane will actually be worth money — to simply allow them to enter the atmosphere as waste heat will essentially be burning money. However, when these gases are sequestered and used to make a process self sufficient, a profit can be realized. President Obama also campaigned on the promise to invest in a new digital utility grid to accommodate current and future energy requirements as well as incentives for research and development of the next generation of renew-able energy technologies.

Energy in the U.S. costs on average $0.089/kWh in 2008. However, if energy prices rise according to the current trend, electricity could cost nearly $0.50/kWh by 2050, an increase of more than 500%.[3] Natural gas prices follow an even steeper climb. Natural gas prices have more than doubled this decade from $5.77 per 1000 ft^3 at the beginning of 2000 to $13.23 per 1000 ft^3 in May of this year.[4]

With consumers quickly becoming aware of climate change, the increase of oil based energy costs would open the market up for renewables. As soon as gas prices surpass the cost of renewables, the economic drawback would no longer exist. The social and environmental incentives would place green technologies as a high priority.

WHAT IS CHP?

The production of combined heat and power (CHP) uses one source of fuel to generate power and thermal heat— CHP is more efficient and cleaner than utilizing conventional generation.

What differentiates CHP from conventional generation is the use of waste heat. On average, fossil-fueled power plants lose two-thirds of their energy in the form of waste heat. The release of this heat contributes to global warming, caused by gases such as carbon dioxide (C02) and air pollutants like nitrogen oxides (NOx) and sulfur dioxide (S02) being emitted into the air. However, CHP systems implement waste heat recovery technologies to capture large quantities of the heat and, because of this, achieve efficiencies of 60%-80% for producing electrical and thermal energy. This is what makes cogeneration a great application. Instead of releasing waste heat and its intrinsic greenhouse gases, which are likely to have a dollar value soon, the heat is reused to create a sustainable process. The higher efficiencies of CHP systems translates into: lower operating costs, reduced emissions of all pollutants, increased reliability and power quality, and reduced grid congestion and avoided distribution losses.

Because there are many technologies that may be employed to generate CHP, the site-specific efficiency can only be determined once the technologies are installed. The system's efficiency actually depends on the technology used to generate heat and power. However, six commonly installed technologies which provide rather standard ranges of achievable efficiencies are:

- Steam Turbine: 80%
- Diesel Engine: 70-80%
- Natural Gas Engine: 70-80%
- Gas Turbine: 70-75%
- Microturbine: 65-75%
- Fuel Cell: 65-80%

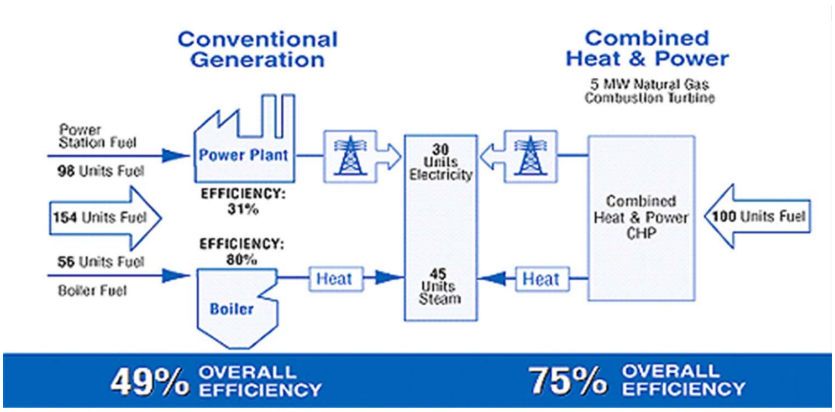

One of the many economic benefits to utilizing CHP is that it can offer stability in opposition to unstable energy prices by allowing the user to supply its own power during times when electricity prices are very high.

CHP & RENEWABLE ENERGY



Wastewater treatment plants have specific needs for heat and power, making them a perfect candidate for CHP. Heat can be used for anaerobic digesters, building heating, and cleaning solutions for membranes. Power is required for pumping, compressed air, blowers, UV treatment, ozone generators, instrumentation, and varying process equipment.

The concept behind cogeneration is to provide reliable, efficient, environmentally responsible energy sources. When looking at renewables, five major categories exist: wind, hydropower, geothermal, solar and biomass. Wind and hydropower lack direct applications of heat, while geothermal would involve specific location requirements.

Waste production must be kept at a minimum, and energy production should be lower than retail cost. Furthermore, contaminants must be eliminated for public health. Our criteria of meeting the Triple Bottom Line led us to focus on biogas, biomass, concentrated solar power, and microbial fuel cells. These produce power along with utilizing waste either in the form of heat or sludge.

BIOGAS

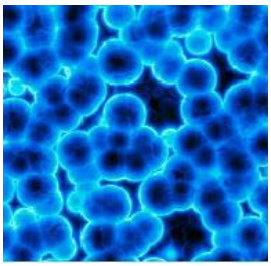

Biogas is a naturally occurring byproduct from wastewater treatment. Microbial organisms break down the organic matter in the water during anaerobic digestion; this process releases biogas. With methane as its main component, biogas has the potential to run in current natural gas engines, making it a prime candidate for renewables and CHP. However, due to the sensitivity of the equipment, contaminants must be removed before combustion. The three main contaminants plaguing biogas usage are carbon dioxide (C02), hydrogen sulfide (H2S), and siloxanes.[5] C02 is the other major gaseous component of biogas. C02 decreases the BTU capacity of the gas, lowering the methane concentration. H2S is highly reactive acid which can corrode and eventually destroy equipment when in contact with moisture. Also, there exists a maximum workplace concentration of H2S of 5 ppm in order to avoid toxic levels. Emerging around 2000 siloxanes are a new contaminant in biogas. Siloxanes oxidize to form silicon dioxide during combustion, creating deposits in piping and engines. When left untreated, siloxanes can damage equipment to the point of needing replacement after a couple of months of usage. Furthermore, if siloxanes were to be added to the CAA's partic-ulate list, the EPA would require cleaning, even with flaring. In order to use in engines, treatment of all three contaminants is suggested. For the possibility of selling back to the natural gas pipeline, all three must be treated.

CLEANING

In keeping with the mission statement, cleaning processes were examined by eco-friendly standards while making sure waste is kept to a minimum. Current treatment options often contain a media which the gas passes through or expensive chemical processes which need to be continually fed. This fails the criteria of waste reducing, considering the media has to be disposed of and replaced on a regular basis. We opted for a biological solution, which eliminates the need for expense chemicals while providing an environmentally responsible solution.



Biogas provides a solution to the rising consumer concern over climate change…

For the treatment of C02, water scrubbing is recommended. This is based on C02 being more soluble in water than methane. The water absorbs the C02, leaving behind a higher concentration of methane.[5] This is a fairly tested treatment option and could be implemented immediately. A biological solution is recommended for H2S. Thiobacillus, a chemtroph, has been found to use carbon and energy produced from the oxidation of H2S to grow new cells.[7] This meets the requirement of a green solution along with minimal waste. However, the technology is untested and in the early stages of development. Investment in research and development is suggested to obtain concrete evidence and implementation requirements. For siloxanes, chilling prior to cleaning is recommended.

Chilling to -40°C removes up to 90% of the siloxanes along with moisture in the gas.[5] This can be achieved through trigeneration, in which excess heat from the engines is used as an absorption chiller by evaporating a refrigerant to create a cool sink. This is CHP at the next level, using heat, instead of intensive electricity consumption, for power. To treat the remaining siloxanes, a molecular sieve by ATF is suggested. A pilot plant of trigeneration combined with a molecular sieve is recommended. Additionally, studies have indicated that siloxanes, like H2S, may be able to be broken down by bacteria.[8] Investment in research and development on the effectiveness of varying bacterium is recommended.

BIOMASS & SYNFUELS



Non-gasified bio-mass as a renewable energy source for cogeneration includes limited options. However, one application for biomass as a renewable CHP source is through a process called fast pyrolysis. The biomass used for fast pyrolysis could include domestic refuse, sludge, wood-chips, or feedstock. This can allow for the reuse of valuable carbon and methane gas to produce another fuel as opposed to flaring and releasing waste heat. Fast pyrolysis is the chemical decomposition of organic material induced by heat in the absence of oxygen. This process is exemplified by its short residence time, usually 0.5 seconds - 2.0 seconds. This is what differentiates pyrolysis from gasification, which has a much longer residence time.

The pyrolysis process will produce combustible gases such as carbon monoxide, hydrogen, methane, and other hydrocarbons. Theses gases will condense to liquid form and will have produced oil/char and contaminated water, which will require particulates to be removed by equipment such as fabric filters or wet scrubbers. The oil from pyrolysis is showing promising signs of being an effective substitute for petroleum. There have been successful demonstrations that show pyrolysis oil can be fired in boilers to produce a suitable amount of steam for the demonstration. As with any emerging technology, there are a few limitations. Due to rapid heating, the biomass must be ground into fine particles and contain extremely low moisture content. Correcting these drawbacks may simply raise the treatment costs at specific sites. Nevertheless, this is an up-and-coming technology that is showing promising signs.

CONCENTRATED SOLAR POWER

Solar technology has long had great public perception. The sun is an infinite and powerful source of energy and has been researched for decades. Concentrated solar power (CSP) works similarly to the photovoltaic cells most people are familiar with. CSP is different in that it concentrates the solar rays using mirrors or lenses to achieve maximum solar efficiency.

There are five main types of CSP listed in the table. The table also includes basic information and specifications for each type to be used for comparison.

After evaluating the specifications of each type of CSP technology, it is clear that two of the five suit the

	Parabolic Trough	Parabolic Dish	Linear Fresnel	Concentrated Photovoltaics	Power Tower
Example		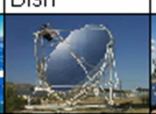			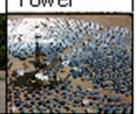
Capital Costs	$4,200/kW	$6,000/kW	$3,400/kW	$7,500/kW	$4,500/kW
Minimum required footprint	580 acres	0.165 acres	900 acres	0.140 acres	520 acres
Power Output	100 MW	25 kW & up	200 MW	25 kW & up	50 MW
Operating Costs	$58/kW/year	$56/kW/year	NA	NA	$56/kW/year
Storage Capabilities	None at small size	None currently	None currently	None currently	6 hours

needs of water or wastewater treatment plants. Water is costly to pump long distances and because of this, treatment plants are located near concentrations of people. Hundreds of acres are simply not available in an urban or suburban area. For that reason, only the Parabolic Dish and Concentrated Photovoltaic (CPV) technologies are suitable. Another benefit of the Parabolic Dish and CPV technologies is that they can be scaled up or down to meet the needs of each unique plant.

Neither of these technologies have been established in a long-term solution. The Parabolic Dish technology needs to be mass-produced, to improve upon reliability issues, and tested with high-wind conditions before it becomes a standard solution with cogeneration. CPV has fewer issues, but still needs to show long-term proof before it is standardized.

Another issue to keep in mind with CSP is that it requires direct sunlight, as opposed to reflected sunlight. Because storage technologies are not currently viable, CSP must be used in conjunction with one or more base load sources. Even so, solar power has the potential to greatly lessen the cost of powering a water treatment plant.

The use of solar power is both environmentally and economically beneficial. The two smaller CSP technologies listed above can provide free energy with little or no maintenance costs, no fuel costs, and no transportation costs after capital investment, in addition, the use of solar energy generates no carbon emissions, a factor that will become pivotal when Carbon Trading becomes a reality.

FUEL CELLS



A fuel cell is an electrochemical conversion device that produces electricity from fuel (on the anode side) and an oxidant (on the cathode side), which react in the presence of an electrolyte. The reactants flow into the cell, and the reaction products flow out of it, while the electrolyte remains within it. Fuel cells can operate virtually continuously as long as the necessary flows are maintained.

This fascinating technology has been around and under research for over 100 years. Chemical fuel cells are extremely expensive due to requiring catalysts to speed up the reaction and increase efficiencies. This catalyst is usually platinum or nickel. Another problem facing chemical fuel cells is extremely high operation temperatures, which eventually damage the device, resulting in constant maintenance.

One type of genuine fuel cell that has long-term potential is the microbial fuel cell (MFC). Unlike other fuel cells, which use hydrogen, methanol or ethanol as a fuel, MFC uses bacteria to generate electricity by converting bio-chemical energy into electrical energy. In other words, microbial fuel cells operate on waste. As the bacteria consume the pollutants, they shed electrons, which flow through a circuit and generate electricity. In the process, pollutants are broken down, with the sole byproduct of clean water.

With constant inquiries done at Penn State, Washington University in St. Louis and Ghen University (Belgium), research groups found varying efficiency results. The device's maximum system power generation depends on the electron donor substrates. In similar MFC systems, 494 mW/m^2 was produced with glucose" and 506 mW/m^2 with acetate[72], but only 305 mW/m^2 was achieved with butyrate", 261 mW/m^2 with swine wastewater", and 146 mW/m^2 with domestic waste-water". However, just like chemical fuel cells, microbial fuel cells could be stacked in order to meet the required operating voltage.

Energy recovery from wastewater is the next step towards sustainability. An MFC would be used in a treatment system as a replacement for the existing energy-demanding bioreactor (such as an activated sludge system), resulting in a net energy-producing system. However, it is not yet clear how to economically scale up an MFC or what the costs would be to replace a conventional system with an MFC-based design. Scale-up and materials issues are the greatest challenges in applying MFCs for wastewater treatment.

In the U.S., approximately 4% of the electricity produced is used for the operation of the whole water and wastewater infrastructure[75]. A treatment system based on an MFC provides a great opportunity to develop the technology, because the substrate is "free" and wastewater must be treated. At a modern treatment plant, the wastewater may contain 9.3 times as much energy as is used to treat it[6].

MFCs represent a promising technology for renewable energy production; their most likely near-term applications are as a method of simultaneous waste-water treatment and electricity production. However, a great amount of research has proved they can be further utilized in other specialized applications as well—for example, as power sources for environmental sensors and environmental bioremediation. With modifications, MFC technologies could find applications ranging from H_2 production to renewable energy production from agricultural biomass.

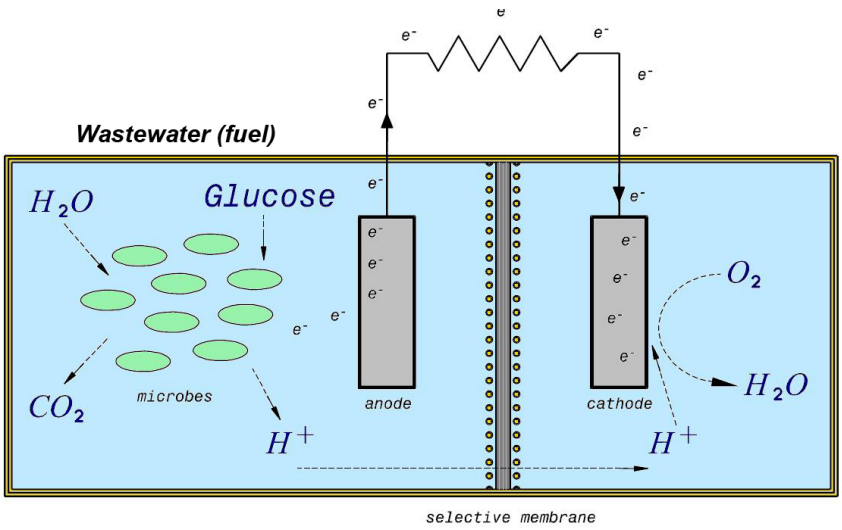

MICROBIAL FUEL CELL

The Penn State research group is now ready to begin the phase of demonstrating pilot-scale prototypes. Even though it is too early to predict the price of this apparatus in commercial applications, MFCs are rapidly evolving technologies that will fascinate scientists and engineers who are challenged with waste technologies and energy production in the coming decades.

REFERENCES

1. "Most Consumers Will Pay More for Renewable Energy." Environmental Leader. 15 Dec 2006. 8 Jul 2008. http://www.environmen-talleader.com/2006/11/15/most-consumers-will-pay-more-for-renewable-energy

2. U.S. Renewable Market Assessment. 28 Jul 2008.

3. "Average Retail Price of Electricity to Ultimate Customers by End-Use Sector." Energy Information Administration. 22 Oct 2007.10 Jul 2008. http://www.eia.doe.gov/cneaf/elec-tricity/epa/epat7p4.html

4. Natural Gas Navigator. Energy Information Administration. 29 Jul 2008.1 Aug 2008. http://tonto.eia.doe.gov/dnav/ng/hist/n3020us 3a.html

5. Efficiency Benefits. U.S. Environmental Protection Agency. 1 Aug 2008.1 Aug 2008. http://www.epa.gov/CHP/basic/efficiency.html

6. Economic Benefits. U.S. Environmental Protection Agency. 1 Aug 2008.1 Aug 2008. http://www.epa.gov/CHP/basic/economics.html

7. Beland, M., Falletta P, Soreanu, G., Syed, M. Removal of Hydrongen Sulfide from Gas Streams Using Biological Processes-A Review. Canadian Biosystems Engineering 48 2.1-2.14.

8. Grumping, R., Hensel, R., Hinrner, A. V,

9. Michalke, K. Microbial Degradation of Octamethylcyclotetrasiloxane. Applied and Environmental Microbiology 65.5 (1999): 2276-2278.

10. Rowan, James. Personal interview. 2 Jul 2008. 10.4.24 Pyrolysis Remediation Technologies

11. Screening Method and Reference Guide 4.0. 3 Jul 2008. http://www.frtr.gov/matrix2/sec-tion4/4-25.html

12. Stoddard, Larry E. Idaho Power Company: Central Station Technology Assessment. 10 Jun2008.

13. Liu, H.; Cheng, S.; Logan, B. E. Production of Electricity from Acetate or Butyrate in a Single Chamber Microbial Fuel Cell. Environ. Sci. Technol. 2005, 39, 658-662.

14. Liu, H.; Logan, B. E. Electricity Generation Using an Air-Cathode Single Chamber Microbial Fuel Cell in the Presence and Absence of a Proton Exchange Membrane. Environ. Sci. Technol. 2004,38, 4040-4046.

15. Min, B.; et al. Electricity Generation from Swine Wastewater Using Microbial Fuel Cells. Water Res. 2005, 39, 4961-4968.

16. Electric Power Research Institute. U.S. Water Consumption for Power Production—The Next Half Century; Water and Sustainability, Vol. 3; 2002; www.epri.com.

17. Shizas, I.; Bagley, D. M. Experimental Determination of Energy Content of Unknown Organics in Municipal Wastewater Streams. J. Energ.Eng. 2004,130,4^53.

Permitting Of Confined Animal Feeding Operations: Issues And Challenges

William F. Ritter[1] P.E., FASCE and S. Rao Chitikela[2] P.E., MASCE

[1]Professor of Bioresources and Civil and Environmental Engineering, Bioresources Engineering Department, University of Delaware, Newark, DE. 19716; PH (302) 831-2468; e-mail: writter@udel.edu
[2] Project Manager, ERM, 350 Eagleview Blvd., Suite 200, Exton, PA. 19341; PH (610) 524-3508; e-mail: rao.chitikela@erm.com

ABSTRACT

EPA implemented new regulations for confined animal feeding operations in 2003. They were revised in 2008 based upon a court decision. Many confined feeding operations above a certain size are required to obtain a NPDES permit under the Clean Water Act. The 40 Code of Federal Regulations Part 122, Section 122.23 describes the permitting requirements for confined animal feeding operations. The paper discusses the main points of the regulations along with some of the challenges in nutrient management planning.

INTRODUCTION

In February of 2003, EPA issued revised Clean Water Act (CWA) permitting requirements and effluent limitations for confined animal feeding operations (CAFOs). These were the first revisions to the CWA for CAFOs since it was passed in 1972. In February 2005, the Second Circuit Court of Appeals issued its decision in the Waterkeeper Alliance versus EPA regarding legal challenges to the 2003 rule. The court directed EPA to remove the requirement for all CAFOs to apply for National Pollutant Discharge Elimination System (NPDES) permits and added requirements for Nutrient Management Plans (NMPs). EPA published rules in June 2006 and March 2008 describing how they would address the Second Circuit Court of Appeals decision (EPA, 2008).

In the 2003 rule, all CAFOs were required to apply for NPDES permits. The revised rule instead requires only those CAFOs that discharge or propose to discharge to apply for a permit. In the discussion of the revised rule, EPA further clarifies how operators should evaluate whether they discharge or propose to discharge. A CAFO owner or operator can determine on a case by case basis as to whether the CAFO does or will discharge from its production area or land application site based upon an objective assessment of the CAFO's design, construction, operation and maintenance. The final rule also provides for a voluntary no discharge certification option for CAFOs that do not discharge or propose to discharge.

The revised rule requires CAFO operators to submit NMPs along with their NPDES permit application. CAFO operators were already required to develop and implement NMPs under the 2003 rule, but they could be done after the NPDES permit was granted. In the new rule EPA removed the provision that allowed new source swine, poultry and veal calf CAFOs to use containment structures designed for a 100-year, 24-hour storm to fulfill the no discharge requirement. Such CAFOs may now meet the no discharge requirement with site-specific best management practice effluent limitations.

CODE OF FEDERAL REGULATIONS APPLIED TO CAFOs

The Title 40 of the Code of Federal Regulations (CFR) is the 'Protection of the Environment' that includes federal requirements of environmental control. The 40 CFR Part 122 provides the requirements of the EPA NPDES permit program and the implementation by various states is conducted through the requirements of 40 CFR Part 123.

The 40 CFR Part 122, Section 122.23 includes the permitting requirements of CAFOs and the 40 CFR Part 412 provides the effluent guidelines and standards of the CAFO point source category agricultural livestock operations. The animal feeding operation (AFO) is defined as "a lot or facility (other than an aquatic animal production facility) where animals (other than aquatic animals) have been, are, or will be stabled or confined and fed or maintained for a total of 45 days or more in any 12-month period, and crops, vegetation, forage growth, or post-harvest residues are not sustained in the normal growing season over any portion of the lot or facility." The CAFO is an AFO defined as large, medium, or small based upon a specified number of animals housed at the operation. The agricultural activities related to CAFOs are included in the Table 1 along with the applicable Standard Industrial Classification (SIC) and North American Industry Classification System (NAICS) codes, and the specified sizes of CAFOs are shown in Table 2.

The standard industrial classification identified in Table 1 is not comprehensive, however, the CAFO facilities must review the rule applicability criteria under the 40 CFR Section 122.23. A CAFO that is not a large or medium size as included in the Table 2 above is designated as a 'small CAFO'. The EPA and/or the states that are delegated by the EPA will review and make the CAFO designations and depending on wastewater or process water pollutants contributing to the impairment of waters of the United States.

A NPDES permit would be required by an owner or operator of a CAFO as defined above that discharges or proposed (or potential) to discharge wastewater from the production or land application area, and are point sources. A factual objective assessment on the CAFO is needed of its design, construction, operation, and maintenance, to see whether a wastewater discharge will be possible. As defined in 40 CFR Section 122.23, a CAFO may be identified for one group of livestock operation but, however, the NPDES requirements will be applicable to all animals and manure, litter, and process wastewater caused by those animals of that confinement. Additionally, the 'land application area' is also defined by the rule as land that could be owned, rented or

leased by the owner or operator for application of manure, litter, or process wastewater from the CAFO. Thus, the owner or operator of the CAFO shall apply for a NPDES permit, or submit a notice of intent to cover their operation under a general permit category if one can be issued by the regulating agency and, if not, a NPDES permit application must be applied and the permit shall be obtained.

Table 1. The regulated CAFO entities and their NAICS and SIC codes as included in 40 CFR Section 122.23 (Federal Register, 2008).

Regulated CAFO Entity	NAICS	SIC
Beef cattle feedlots including veal calves)	112112	0211
Beef cattle ranching and farming	112111	0212
Hogs (Swine)	11221	0213
Sheep and Goats	11241, 11242	0214
General livestock except dairy and poultry	11299	0219
Dairy farms	11212	0241
Broilers, fryers, and roaster chickens	11232	0251
Chicken eggs	11231	0252
Turkey and turkey eggs	11233	0253
Poultry hatcheries	11234	0254
Poultry and eggs	11239	0259
Ducks	11239	0259
Horses and other equines	11292	0272

Table 2. The regulated CAFOs and their defined sizes of operation (GCS, 2009).

CAFO	Large	Medium
Mature dairy cows, whether milked or dry	700	200-699
Veal calves	1,000	300-999
Cattle other than mature dairy cows or veal calves (and is not limited to heifers, steers, bulls, and cow/calf pairs)	1,000	300-999
Swine each weighing 25 kg or more	2,500	750-2,499
Swine each weighing less than 25 kg	10,000	3,000-9,999
Horses	500	150-499
Sheep or lambs	10,000	3,000-9,999
Turkeys	55,000	16,500-54,999
Laying hens or broilers (AFO using a liquid manure handling system)	30,000	9,000-29,999
Chickens (other than laying hens) (AFO using other than a liquid manure handling system)	125,000	37,500-124,999
Laying hens (AFO using other than a liquid manure handling system)	82,000	25,000-81,999
Ducks (AFO using a liquid manure handling system)	5,000	1,500-4,999
Ducks (AFO using other than a liquid manure handling system)	30,000	10,000-29,999

The 'process wastewater' is defined as "water directly or indirectly used in the operation of the AFO for any or all of the following: spillage or overflow from animal or poultry watering systems; washing, cleaning, or flushing pens, barns, manure pits, or other AFO facilities; direct contact swimming, washing, or spray cooling of animals; or dust control. Process wastewater also includes any water which comes into contact with any raw materials, products, or byproducts including manure, litter, feed, milk, eggs, or bedding." The 'production area' is defined as "that part of an AFO that includes the animal confinement area, the manure storage area, the raw materials storage area, and the waste containment areas. The animal confinement area includes but is not limited to open lots, housed lots, feedlots, confinement houses, stall barns, free stall barns, milkrooms, milking centers, cowyards, barnyards, medication pens, walkers, animal walkways, and stables. The manure storage area includes but is not limited to lagoons, runoff ponds, storage sheds, stockpiles, under house or pit storages, liquid impoundments, static piles, and composting piles. The raw materials storage area includes but is not limited to feed silos, silage bunkers, and bedding materials. The waste containment area includes but is not limited to settling basins, and areas within berms and diversions which separate uncontaminated storm water. Also included in the definition of production area is any egg washing or egg processing facility, and any area used in the storage, handling, treatment, or disposal of mortalities."

The NPDES permit application and its contents requirements are included in the 40 CFR Part 122 Section 122.21. The applications of CAFOs must complete the Form 2B, in addition to completion of other required forms and data submission(s). As per the requirements of 40 CFR Section 122.21(i), the application shall contain: name of the owner or operator; facility location and addresses; latitude and longitude of the production area (including the entrance to production area); topographic map showing the location of production area(s); specific data on the number and type of animals; type(s) of containment and storage and total capacity for manure, litter, and process wastewater storage (tons/gallons); total number of acres available for land application of manure, litter, or process wastewater; estimated amounts of manure, litter, and process wastewater generated per year (tons/gallons); estimated amounts of manure, litter, and process wastewater transferred to other persons per year (tons/gallons); and, a certification that a 'nutrient management plan (NMP)' is completed and will be implemented by the effective date of the NPDES permit-issuance (GCS, 2009).

As the NPDES permit application requirements of CAFOs are included in the 40 CFR Section 122.23, the process wastewater effluent guidelines and standards are included in the 40 CFR Part 412 – CAFOs Point Source Category. However, a CAFO that discharges process wastewater to publicly owned treatment works (POTW) will need to comply with the requirements of 40 CFR Part 403 – General Pretreatment Regulations for Existing and New Sources of Pollution. The 40 CFR Part 412, Subparts A, B, C, and D, include the applicable best practicable control technology currently available (BPT), best control technology for conventional pollutants (BCT), best available control technology economically achievable (BAT), new source performance standards (NSPS), and pretreatment standards for new sources (PSNS) to: horses and sheep, ducks, dairy cows and cattle other than veal calves, and swine, poultry, and veal calves, respectively.

The BPT, BAT, and NSPS limitations are applicable to 'large' CAFOs. The 40 CFR Section 412.4 provides the requirements of best management practices (BMPs) for land application of manure and, however, these requirements are applicable to dairy and beef cattle other than veal calves (Subpart C), and swine, poultry, and veal calves (Subpart D) CAFOs (GCS, 2009).

The NMP shall be prepared based on the applicable requirements of 40 CFR Sections 122.42(e) and 412.4(c). The NPDES permit for any CAFO will include a NMP with the BMPs and the operational measurements toward complying with the applicable process wastewater effluent limitations and standards. The permitted CAFOs shall have the NMPs developed and implemented by February 27, 2009. All new CAFOs or CAFOs that apply for a NPDES permit after February 27, 2009, shall have a NMP developed and implemented by the effective date of the permit. The NMP shall be prepared "based on a field-specific assessment of the potential for nitrogen and phosphorus transport from the field and that addresses the form, source, amount, timing, and method of application of nutrients on each field to achieve realistic production goals, while minimizing nitrogen and phosphorus movement to surface waters" (GCS, 2009).

The application rates for manure, litter, and process wastewater applied to land must minimize phosphorus and nitrogen transport to surface waters as per the applicable and identified technical standards, and those technical standards of nutrient management shall include a field-specific assessment of the potential for nitrogen and phosphorus transport, the methodology of nutrient management to comply with the applicable standards, such as multi-year application of phosphorus on fields that will not play a significant role in the phosphorus runoff to surface water, and phased implementation of phosphorus-based nutrient management, etc., as required. The manure, at a minimum, needs to be analyzed once annually for nitrogen and phosphorus content, and the soil analyzed once every five years for phosphorus content. The results of these annual manure and soil analyses need to be used in the determination of manure, litter, and process wastewater land application rates. The equipment used for land application of manure, litter, and process wastewater must periodically be inspected for leaks and as needed. A setback of 30.5 m need to be observed between the manure, litter, and process wastewater land application, and surface waters to possible conduits to surface waters, such as, open tile line intake structures, sinkholes, and agricultural well heads. As an alternative, the CAFO may use a setback of 30.5 m with a 10.7 m wide vegetated buffer, "a narrow, permanent strip of dense perennial vegetation established parallel to the contours of and perpendicular to the dominant slope of the field for the purposes of slowing water runoff, enhancing water infiltration, and minimizing the risk of any potential nutrients or pollutants from leaving the field and reaching surface waters, where applications of manure, litter, or process wastewater are prohibited." However, additionally, if possible, as a compliance alternative, the owner or operator of the CAFO can demonstrate to the regulator that a setback or buffer is not required and the alternative conservation practice or characteristics of the field of land application provides pollutant reductions equivalent or better than the usage of 30.5 m setback (GCS, 2006).

APPLICABLE REQUIREMENTS FOR HORSES, SHEEP, AND DUCK CAFOs

For horses and sheep CAFOs, except for the applicable NPDES stormwater discharge requirements, the existing point sources shall not discharge any process waste to navigable waters. However, the process waste may be discharged to navigable or the U.S. waters via overflows caused by the 10-year, 24-hour rainfall event for the geographic location of CAFO (Ref. 40 CFR Sections 412.12, 412.13, and 412.15) (GCS, 2009).

For ducks, the existing dry and wet lot operations shall comply with the BOD5 and fecal coliform BPT limits of maximum daily of 1.66 kilograms per 1,000 ducks and a maximum monthly average of 0.91 kilogram per 1,000 ducks, and 400 MPN per 100 mL at any time, respectively. As per the NSPS requirement, any new source shall not discharge process wastewaters to U.S. waters; however, the process wastewater may be discharged to navigable or the U.S. waters via overflows caused by the 25-year, 24-hour rainfall event for the geographic location of CAFO (Ref. 40 CFR Section 412.25). The PSNS requirement is that no discharge of process wastewater to a POTW; however, the process wastewater may be discharged to a POTW via overflows caused by the 25-year, 24-hour rainfall event for the geographic location of CAFO (Ref. 40 CFR Section 412.26) (GCS, 2009).

APPLICABLE REQUIREMENTS FOR DAIRY COWS AND CATTLE CAFOs

The BPT limits require the existing point sources of no discharge of manure, litter, or process wastewater to U.S. waters. However, an overflow of manure, litter, or process wastewater may overflow to U.S. waters via the runoff and the direct precipitation from a 25-year, 24-hour rainfall event. But the production area need to be operated as per the additional measures and records maintained under 40 CFR Section 412.37(a) and (b) – *visual daily and weekly inspections* of water lines and stormwater facilities, and manure, litter, and process wastewater impoundments and containment structures; and usage of *depth markers* indicating the minimum capacity necessary to contain the runoff and direct precipitation of the 25-year, 24-hour rainfall event, and 100-year, 24-hour rainfall event in the case of new sources. However, the CAFO can also request 'voluntary alternative performance standards' that could be useful based on site-specific alternative technologies and duly submitting the supporting information (as included in 40 CFR Section 412.31(a)(2)(i)) and for land application areas (40 CFR Section 412.31(b). The applicable BCT and BAT limits of this CAFO production and land application areas are the same as BPT requirements under 40 CFR Sections 412.31(a) and (b). The NSPS requirements of *new sources* are also same as the BPT, BCT, and BAT, except that the applicable discharge limits and permit requirements shall be attained by the effective date of the CAFO NPDES permit. And the new sources commenced between April 14, 1993, and April 14, 2003, must comply with the BPT standards of 40 CFR Sections 412.31(a) and (b), after the completion of compliance period as required by the 40 CFR Section 122.29(d)(1). The 'additional measures' for new sources (if the effluent limits of Swine, Poultry, and Veal Calves NSPS of 40 CFR Section 412.46(a)(1) are applicable) also include 'that all open surface manure storage structures shall include a *depth marker*

indicating the minimum capacity to contain the maximum runoff and direct precipitation with the design storm used for no discharge.' The animal mortalities of the CAFOs shall not be discharged to the liquid manure or process wastewater streams (40 CFR Section 412.37(a)(4)). Additional recordkeeping requirements are applicable for the production and land application areas and the records shall be maintained for five-years from the date of creation (40 CFR Sections 412.37(b) and (c)) (GCS, 2009).

APPLICABLE REQUIREMENTS FOR SWINE, POULTRY, AND VEAL CAFOs

The BPT, BCT, and BAT requirements of existing CAFOs production and land application areas are same as 40 CFR Sections 412.31(a) and (b) and discussed above except that the CAFO shall comply with the limits and requirements by February 27, 2009. The NSPS requirements of new sources are: no discharge of manure, litter, or process wastewater pollutants to U.S. waters; usage of BMP effluent limits based on site-specific evaluations of the entire CAFO production area; proper design and operation of open manure storage for rainy seasons and additional capacities for chronic rainfalls and the land application measures consistent to the NMP; evaluation toward the adequate capacity of the manure storage structure using the recent version of Soil Plant Air Water (SPAW) Hydrology Tool and 100-year local climate data, or usage of an approved technical evaluation based on site-specific data; and the additional measures as included under 40 CFR Sections 412.47(a) and (b) that are discussed in the above section and same as the 40 CFR Section 412.37(a) and (b). The new sources of CAFO land application areas shall comply with the limits and requirements same as BPT. However, the new sources shall comply with the permit limits and requirements from the effective date of the permit. And the new sources commenced between April 14, 1993, and April 14, 2003, must comply with the BPT standards of 40 CFR Sections 412.43(a) and (b), after the completion of compliance period as required by the 40 CFR Section 122.29(d)(1). Moreover, the new sources that are commenced wastewater discharging between April 14, 2003, and January 20, 2009, and have these NSPS applicable requirements shall continue to comply with the requirements for the duration of time as specified in 40 CFR 122.29(d)(1). The additional measures for the new sources are as discussed in the above section (Dairy Cows and cattle other than Veal calves) and as included under the 40 CFR Section 412.37(a) through (c) (GCS, 2009).

The Form 2B of the NPDES permit application is used for applying toward 'permit to discharge wastewater – concentrated animal feeding operations and aquatic animal production facilities.' This Form 2B requires: owner and/or operator and facility contact information; facility status – new or existing; type and number of livestock and operation; generation rates of manure, litter, and process wastewater; land application area, and transfer of waste to other facilities or persons; type of waste containment, storage, and capacity; details and status of the NMP; BMPs to be practiced; and a certification of details by the facility responsible person or official.

The requirements of the preparation and maintenance of a NMP are included in the 40 CFR Part 122 Section 122.42(e). Some of the requirements are new and effective as of December 22, 2008, besides the existing requirements promulgated by 2003 and

modified thereof. The NMP shall have the methodology, such as, the BMPs necessary to comply with the applicable waste discharge limits and standards, in compliance with the 40 CFR Parts 122 and 412 and applicable sections. Primarily, the NMP shall ensure: adequate storage and operation of manure, litter, and process wastewater facilities; proper management of animal mortalities; prevention of any contact of livestock with U.S. waters; proper selection and usage of chemicals and not discharged to manure, litter, or process wastewaters unless those chemicals are designed toward in the waste treatment; observation of buffer zones to control runoff; protocols for testing of the manure, litter, process wastewater, and soil; protocols for proper land application of manure, litter, and process wastewater toward a specific nutrient management practice; requirements of implementation and management of elements of NMP; record keeping requirements including transfer of waste to other parties; annual reporting requirements of CAFOs waste (manure, litter, and process wastewater) generation and land application acreage; certification of the NMP by a certified nutrient management planner; actual crop(s) planted and actual yield(s) for each field, and the amounts of nitrogen and phosphorus taken up by crops, for the previous 12-months; and compliance terms or requirements of the NMP with respect to the CAFOs NPDES permit, such as, land application rates of manure, litter, or process wastewater in a linear or narrative-rate approach. Any changes to the NMP shall be handled through the requirements of 40 CFR Section 122.42(e)(6) (GCS, 2009).

NUTRIENT MANAGEMENT PLANS

CAFOs are required to develop and implement a NMP. Manure is to be applied at rates that meet crop needs while avoiding over application that could lead to water quality degradation. The new regulations require that each field that receives manure be evaluated using a risk assessment method to determine the extent of risk of nitrogen and phosphorus losses from the field. The risk assessment methods vary from state to state. If the risk from phosphorus in runoff is low then manure application rates may be applied at nitrogen based agronomic rates. For phosphorus risk assessment the state may use the phosphorus index, soil phosphorus threshold or soil phosphorus test (Davis, 2003). The phosphorus index considers both transport and source factors. Producers may lower their index by changing manure application method or installing BMPs or changing the feed formulation. If phytase is added to swine or broiler feed the content of the phosphorus in the manure may be reduced from 25 to 30% (Sutton and Humenik, 2003). The soil phosphorus threshold level sets a threshold level for soil test phosphorus above which manure application must be stopped or the application rate is based on crop phosphorus removal rates. Delaware, Maryland and Pennsylvania require manure must be applied at phosphorus crop removal rates if the soil test high or very high in phosphorus. One of the challenges in nutrient management is interpreting the soil phosphorus test because different laboratories use different test methods and different extractants, which will give different results. The soil test phosphorus approach uses the standard fertilizer recommendations found in state agronomy guides for manure application that may generally be obtained through the Cooperative Extension Service. When the phosphorus recommendation is zero either no manure is applied or it is applied at rates that replace crop phosphorus removal.

In some states there is too much manure produced in some areas to be applied at agronomic nitrogen or phosphorus rates. When this happens, the manure has to be transported or alternative uses found for the manure. This problem can occur in certain areas of the Delmarva Peninsula for broiler litter. In response to this problem, both Delaware and Maryland have started programs for relocation of poultry manure. Delaware pays up to $0.11 per 1000 kg per km for raw manure with a cap of $18 per 1000 kg for raw manure and $0.049 per 1000 kg per km for processed manure. In 2007 the average cost was $10.65 per 1000 kg. . In 2001, when the program started 20.7 x 10^6 kg was relocated or went for alternative uses. In 2007, 84.8 x 10^6 kg was relocated or when to alternative uses. The challenge for Delaware and Maryland in a tough economic climate is to find money to pay for the program.

Some of the challenges Oregon (State CAFO Organization, 2009) is facing in their NMP regulations are:

- How do you train staff to review and enforce NMP requirements?
- Do you have an adequate tool to calculate application rates?
- What do you look for in inspections and how much staff time will they take.
- What are the requirements for land application during adverse weather conditions at permitted sites?
- Do you have a tool to determine when and what type of enforcement is appropriate?

FINANCIAL ASSISTANCE

The 2002 and now the 2008 Farm Bill offers several voluntary conservation programs producers can use to help comply with the new CAFO rules (Cohen et al., 2003). The largest program is the Environmental Quality Incentives Program (EQUIP). EQUIP pays up to 75% in cost share funds to assist producers in implementing conservation systems and addressing regulatory requirements. By statue, at least 60% of EQUIP financial assistance funds must be used for livestock and poultry operations. Fifteen states have the Agricultural Management Assistance Program (AMA) including Delaware, Maryland, Pennsylvania and New York. CAFO operators may use AMA funds to develop and implement NMPs. Other programs, such as, the Conservation Reserve Program, Conservation Reserve Enhancement Program, and Wetlands Reserve Program may also support CAFO operators to implement conservation programs.

CONCLUSIONS

In 2003, EPA implemented new permitting regulations for CAFOs. The regulations are meant to be more effective in protecting and restoring water quality than the original regulations implemented under the Clean water Act in the 1970s. Some CAFOs are exempt from obtaining a permit if they can prove they have no discharge. Along with the NPDES permit CAFO operations must also develop NMPs. In many areas land application rates for manure will be based upon phosphorus because the soil tests high in phosphorus or there is a great potential for runoff. Manure application rates based upon

phosphorus crop needs may present problems in some areas to find enough land to apply the manure. In these cases manure must be relocated or alternative uses found for it.

REFERENCES

Cohen, K., Fifueroa, A., Amosson, S. and Almas, L. (2003). "Financial and technical assistance available to CAFO owners and operators." CAFO Fact Sheet #30, Livestock and Poultry Stewardship Curriculum, Midwest Plan Service, Iowa State University, Ames IA.

Davis, J. (2003). "Making decisions about application rates." CAFO Fact Sheet #25, Livestock and Poultry Stewardship Curriculum, Midwest Plan Service, Iowa State University, Ames IA.

Federal Register (USA)(2008). "40 CFR Parts 9, 122, and 412 – Revised National Pollutant Discharge Elimination System Permit Regulation and Effluent Limitations Guidelines for Concentrated Animal Feeding Operations in Response to the Waterkeeper Decision; Final Rule." Vol. 73, No. 225, November 20, 2008.

Global Compliance Solutions (2009). 40 CFR Parts 122 and 412 and associated all rule(s) sections were accessed at www.regscan.com, on 1/18/2009 and 1/19/2009.

State CAFO Organization. (2009). "2007 Oregon CAFO program summary and challenges." http://www.state.cafos.org, (assessed 1?25/09).

Sutton, A., and Humenik, F. (2003). "Technology options to comply with land application rules." CAFO Fact Sheet #24, Livestock and Poultry Stewardship Curriculum, Midwest Plan Service, Iowa State University. Ames IA.

U.S. Environmental Protection Agency (2009a). Form 2B. http://www.epa.gov/npdes/pubs/cafo_fedrgstr_form2b.pdf (accessed 1/19/2009).

U.S. Environmental Protection Agency (2009b). "NPDES Permit Application Forms." http://cfpub2.epa.gov/npdes/doctype.cfm?sort=name&program_id=45&document_type_id=8, (accessed on 1/19/2009).

U.S. Environmental Protection Agency (2008). "Confined animal feeding operations final rulemaking." Fact Sheet, EPA, Washington, DC.

A Comparative Study of Water Quality Indices for Karun River

S.Ali Mojahedi[1] and J. Attari[2]

[1]Expert, Water Resources Planning Department, Ministry of Energy, Valiasar and Neyayesh crossing, Tehran, Iran; email: ali.mojahedi@gmail.com
[2]Assistant Professor, Water Engineering Department, Power and Water University of Technology, P.O. Box 16765-1719, Tehran, Iran; email: attari@pwut.ac.ir

ABSTRACT

Water quality is an important factor for preservation of human life and aquatic ecosystem. In rivers, water quality is affected by the environment, climate condition, seasonal variation, land-use, natural and man-made pollution of watershed. Considering growth of water use for different consumptions and discharge of pollutions in rivers, several water quality parameters are usually monitored along rivers in different periods. However, there is a need to combine results of such measurements in the form of composite indices which are understandable to decision makers and general public. For this purpose, some indices for classification of water quality in rivers have been applied world wide recently. In this paper, two Water Quality Indices (i.e. National Science Foundation of the USA and Council of Ministers of Environment of Canada) were trialed for the case of Karun River system which is the most important river of Iran. These indices were calculated using existing data and their variations have been analyzed and compared in 9 stations, located along the river, for different periods. Results showed that application of these simplified indices was satisfactory for the educational case study and could be replicated for other communities in Iran.

Keywords: Water Quality, River, Water Quality Index, NSF WQI, CCME WQI

INTRODUCTION

Water quality is an important factor for preservation of human life and aquatic ecosystem. Even if water may be available in adequate quantities, its un-suitable quality limits the uses that can be made of it. Although the natural ecosystem is in harmony with natural water quality, any significant changes to water quality will usually be disruptive to the ecosystem (WHO, 1996).

Quality of surface water is affected by the environment, climate condition, seasonal variation, land-use, natural and man-made pollution of watershed. Considering growth of water use for different consumptions (e.g. domestic, agricultural, and industrial) and discharge of wastewaters in rivers, several water quality parameters are usually monitored along rivers in different periods. However, there is a need to combine results of such measurements in the form of composite indices which are understandable to political decision makers, non-technical water mangers and general public (Simoes, et al., 2008).

A number of indexes have been developed to summarize water quality data in an easily expressible and easily understood format (Sanchez, et al., 2007). A water quality index provides a convenient means of summarizing complex water quality data and facilitating its communication to a general audience. Furthermore, it provides a platform for comparison of the water quality among different sites with an ultimate view of classification of water quality in rivers.

National Sanitation Foundation of the USA developed the Water Quality Index (NSFWQI) in 1970. This standard method was used for quantifying and comparing water quality in various parts of that country. This index is the aggregate score of water quality parameters, commonly used by state regulatory agencies to provide general water quality descriptions (excellent, good, average, fair, poor).

The Canadian Council of Ministers of the Environment also developed a Water Quality Index (CCMEWQI).This simple tool has been devised as an alternative for traditional reports on water quality trends which typically consisted of variable-by-variable, water-body-by-water-body statistical summaries (CCME, 2001).

The objective of this paper is to assess the water quality in the Karun River system which is the most important river of Iran. In the absence of any local index, the NSF WQI as well as CCME WQI has been trailed for this purpose in the case study and results were compared with each other.

BACKGROUND & METHODOLOGY

The NSF Water Quality index comprises nine parameters. These are dissolved oxygen (DO), Fecal Coliform, pH, Biochemical Oxygen Demand (BOD), temperature, total phosphate, nitrates, turbidity and total solids. According to score of each parameter, a "Q-Value" is assigned to each parameter from figures or tables of test results. The weighted average of these values is introduced as the NSF WQI. This combined index can vary in the range of 0-100, 0 being "Very bad" and 100 as the "Excellent" (Willkes University , 2009).

The CCME Index incorporates three elements: Scope (F1) - the number of variables not meeting water quality objectives; Frequency (F2) - the number of times these objectives are not met; and Amplitude (F3)- the amount by which the objectives are not met. The CCME WQI is then calculated as:

$$CCME\ \ WQI = 100 - \frac{\sqrt{F_1^{\,2} + F_2^{\,2} + F_3^{\,2}}}{1.732} \tag{1}$$

The index produces a number between 0 (worst water quality) and 100 (best water quality). These numbers are divided into 5 descriptive categories to simplify presentation. The CCME WQI allows the index user to select the objective set on which to compare measured water quality. This is a design feature that increases the versatility of the index considerably but allows for misuse (CCME, 2001).

Table 1. Ranges of Water Quality Classification by NFS and CCME

NSF Water Quality Index		CCME Water Quality Index	
Range	**Quality**	**Range**	**Quality**
90-100	Excellent	95-100	Excellent
70-90	Good	80-94	Good
50-70	Medium	65-79	Fair
25-50	Bad	45-64	Marginal
0-25	Very bad	0-44	Poor

In the absence of any local index, the NSF WQI as well as CCME WQI has been trailed for Karun River System in Iran. Most of the existing data for calculation of these indices were collected form the Khuzestan Water and Power Authority (KWPA) and Iran Water Resources Management Company (IWRMC). A list of water quality parameters for calculation of CCME WQI for Karun River is given in Table 2. The Objectives, mentioned in this Table, were adopted from Krenkel and Novotny (1980).These indices were calculated using existing data and their variations have been analyzed and compared in 9 stations, located along the river, for different periods. For calculation of the CCME WQI, a spread sheet in EXCEL developed by CCME in 2001 was employed.

Table 2. List of water quality parameters for calculation of CCME WQI in Karun River

Parameter	Objective	Sampling Period	Parameter	Objective	Sampling Period
Dissolved Phosphorous Total (mg/L)	0.03	2002 - 2008	Total Lead (mg/L)	0.05	2006 - 2008
pH	6.5< >9	2002 - 2008	Dissolved Iron (mg/L)	1	2006 - 2008
Dissolved Oxygen (mg/L)	5	2002 - 2008	Total Zinc (mg/L)	0.1	2006 - 2008
Dissolved Nitrogen (mg/L)	20	2002 - 2008	Total Dissolved Solids (mg/L)	500	2002 - 2008
Fecal Coliforms No./100ml	200	2004 - 2008	Dissolved Sulphate (mg/L)	250	2002 - 2008
Dissolved Chloride (mg/L)	150	2002 - 2008	Dissolved Sodium (mg/L)	100	2002 - 2008

STUDY AREA

Karun River, located in South West of Iran, is the most important river of the country. Major projects have been constructed or are under construction on this river including five large dams with a total storage capacity of about 13 BCM (IWPCO, KWPA, 2008).

The flow rate of Karun river, measured at Ahwaz station, are 90 m^3/s in low water seasons, 2500 m^3/s high water season and about 5000 m^3/s in maximum floods

(AWWC, 2006). This River suffers from discharge of pollution loads from industrial, agricultural, agro-industrial and domestic sources. Increasing water withdrawal from and wastewater discharge to the river has endangered the aquatic life of this important ecosystem. Furthermore, the drinking and in-stream water quality standards have been violated in many instances. (Karamouz et al., 2008).

The Karun River System consists of Karun River and Dez River. This system feeds Khuzestan plain which is located down stream of Gotvand Dam. Figure 1 depicts the study the area between the Gotvand Dam and Khoramshahr City including 9 water quality monitoring stations (Table 3).

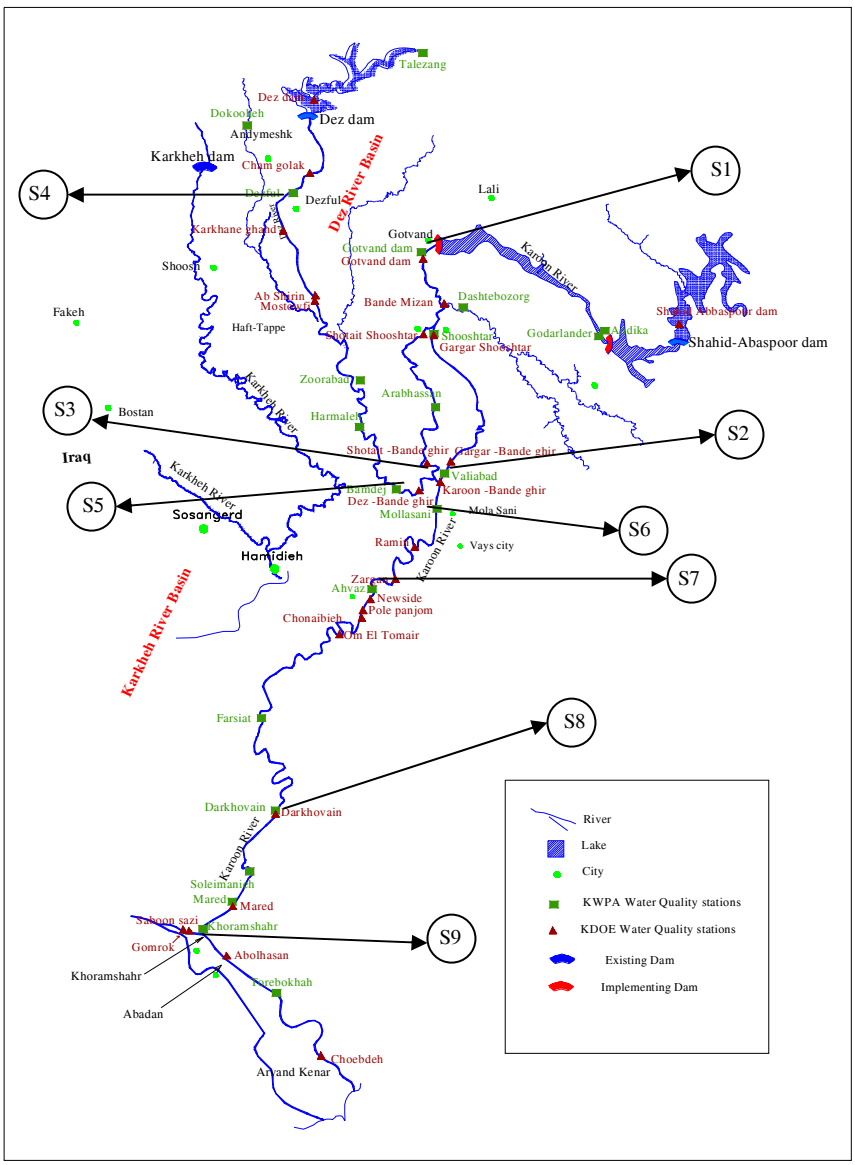

Figure 1. Karun River System (Karamouz et al. , 2008)

Table 3. Water Quality Monitoring Stations along Karun River System

Name of River	Name of Station	Code
Karun	Gotvand Dam	S1
GarGar	Valiabad	S2
Shotait	Bandeghir	S3
Dez	Dezful	S4
Dez	Bamdej	S5
Karun	Mollasani	S6
Karun	Ahvaz	S7
Karun	Darkhovain	S8
Karun	Khoramshahr	S9

RESULTS & DISCUSSION

In the Karun River, BOD, DO, Na, Cl parameters were found to be in an acceptable range, with respect to water quality criteria. The high value of Focal Coliform is an indication of un-treated wastewater discharge to this river. Furthermore, the TDS value is also considerably higher than the water quality criteria. This is attributed mostly to drainage of agricultural return flow and is to an extent stemmed from salinity of parts of the upper watershed.

Figure 2 depicts temporal variation of the CCME water quality index for 9 stations located along the Karun River system. The temporal trend lines of this index are found to be generally similar, despite their locations. Some minor discrepancies are attributed to missing data. Each line shows a rapid decline in the 2nd half of the study period which is classified as "Marginal" and "Poor". This is because of inclusion of heavy metal and Focal Coliform parameters data which has decreased the value of the index. Typically, the Water Quality Index decreased towards the downstream end of the Karun River. The lowest values were observed at Stations 2, 7 and 8 because of some local wastewater discharge and agricultural return flows. The Index at these stations is considered to be in "poor" category according to CCME classification. Further to decline of WQI in 2006-2007, a more rigor policy for the Karun River protection was enforced by the Department of Environment of Iran.

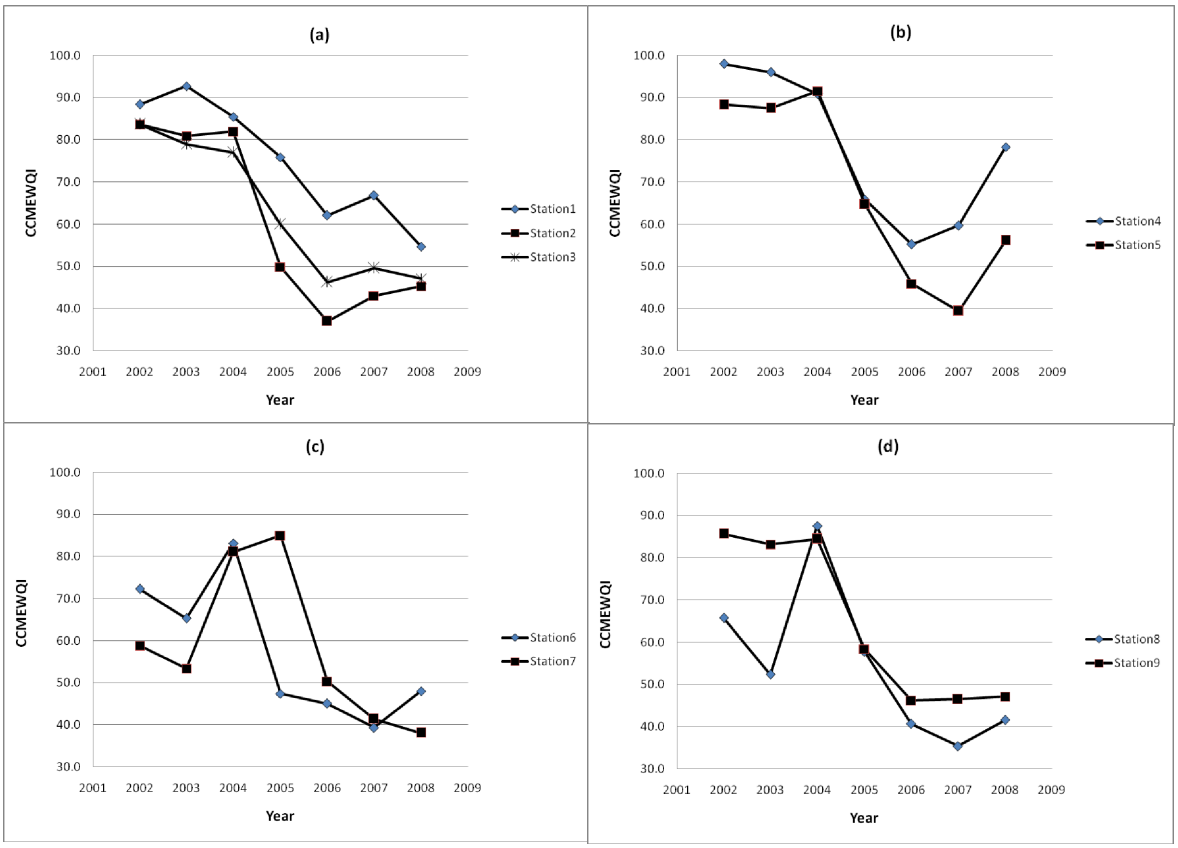

Figure 2. Spatial & temporal variation of CCME WQI for Karun River system

The NSF WQI was also calculated at the 9 stations along the Karun River for 2006-2008 and the results were plotted in Figure 3. This index did not vary significantly and therefore remained in the "Medium" category. A comparison of these results with the CCME WQI at a given station showed lower values for the latter frequently. This difference can be attributed to the fact that NSF WQI does not include heavy metals and divergence of parameters and method of calculation. Therefore, the range of classification of WQI for NSF and CCME differs with each other.

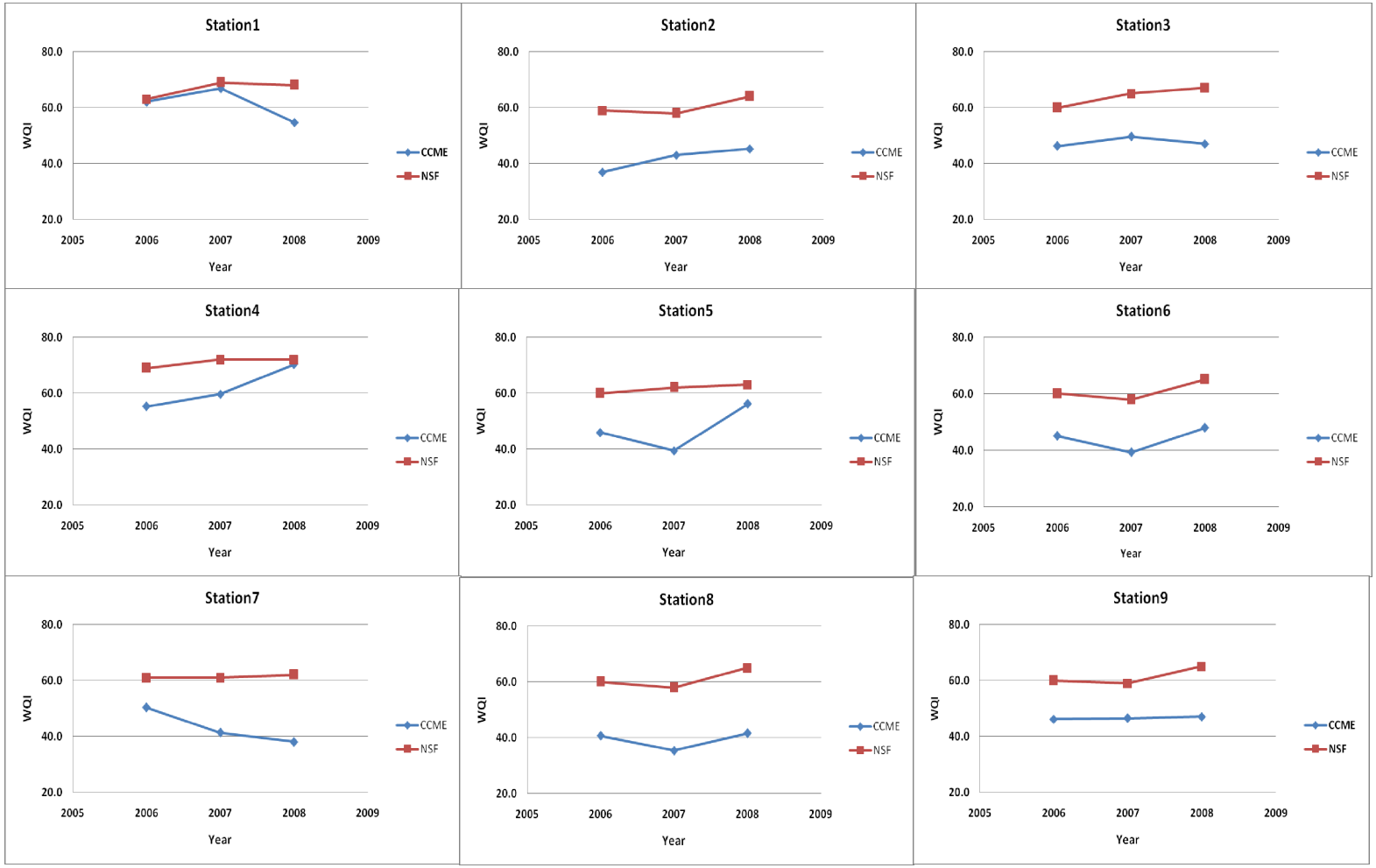

Figure 3. Comparison of NSF WQI and CCME WQI along Karun River syste

CONCULSION

In this paper, two Water Quality Indices (i.e. NSF and CCME) was trialed for the case of Karun River, in the South Western part of Iran. Results showed that:

- In the absence of any local water quality index, application of NSF WQI as well as CCME WQI for the case study in Iran was found satisfactory, despite some differences in environmental protection standards.
- The Karun River was considered in "Medium" category by NSF whereas "Marginal" to "Poor" in CCME classification. Regardless of such a difference, they can be both valid for practical purposes.
- To make the most of such a case study for rivers in Iran, it is useful to develop local bench marks for water quality variables.

ACKNOWLEDGMENTS

The authors are grateful Khuzestan Water and Power Authority (KWPA), as well as and Iran Water Resources Management Company (IWRMC) for providing the water quality data.

REFERENCES

AWWC, (2006). Ahwaz Water and Wastewater Company. http://www.aww.co.ir (1 Jan. 2009).

Canadian Council of Ministers of the Environment (CCME), (2001). "Canadian Water Quality guidelines for the protection of aquatic life." *CCME Water Quality Index 1.0*, User's Manual & Technical Report.

Couillard, D., and Lefebvre Y. (1985). "Analysis of Water Quality Indices.", *J. of Environmental Management,* (21),161-179.

IWPCO, (2008). Iran Water and Power Resources Development Company. http://www.iwpco.ir (1 Jan. 2009).

Karamouz, M., Kerachian, R., Akhbari M. and Hafez B. (2008). "Design of river Water Quality Monitoring Networks: A Case Study.", Environ Model Assess, Springer, DOI 10.1007/s10666-008-9172-4.

Krenkel, P. A. and Novotny, v., (1980), "Water Quality Management", Academic PRESS, New York, NY 10003.

KWPA, (2008). Khuzestan Water and Power Authority. http://www.kwpa.ir (1 Jan. 2009).

Sanchez, E., et al.,(2007), "Use of Water Quality Index and Dissolved Oxygen Deficit as Simple Indicators of Watersheds Pollution", *J. of Ecological Indicators,* (7), 315-328.

Simoes, F. S., et al., (2008), " Water Quality Index as a Simple Indicator of Aquaculture Effects on Aquatic Bodies", *J. of Ecological Indicators,* (8), 476-484.

United Nations Environmental Program (UNEP), (1996). "Water Quality Monitoring-A practical guide to design and implementation of freshwater quality studies

and programs.", Bertram J. Balance R. (Eds.), UNEP/WHO, ISBN 0 419 22320 7.

Willkes University (2009),"Calculating NSF Water Quality Index", Center for Environmental Quality Environmental Engineering and Earth Sciences. http://www.water-research.net/watrqualindex/index.htm (1 Jan. 2009).

BEYOND COMPLIANCE AND TOWARD SUSTAINABILITY: ADVANTAGES OF SYSTEMS ENVIRONMENTAL ENGINEERING

*Oral Saulters[1], Blase Leven[1], Larry Erickson[1], John Pickrell[2], Leslie Jamka[1], Ryan Green[1]

[1]Urban Operations Laboratory, Center for Hazardous Substance Research, Kansas State University, 104 Ward Hall, Manhattan, KS 66506; PH (785) 532-6519; *corresponding author email: osaulter@ksu.edu
[2]Comparative Toxicology Laboratories, Diagnostic Medicine/Pathobiology, Kansas State University, 1800 Denison Avenue, Manhattan, KS 66506; PH (785) 532-4331

ABSTRACT

New technologies are not only critical in supporting military and industrial success, but also play a significant role in advancing sustainable development. With the current global economic challenges, effective tools and partnerships which streamline the design and dissemination of these technologies are more important than ever. Accordingly, the systems environmental engineering approach utilized by the Urban Operations Laboratory (UOL), [comprised of M2 Technologies, Kansas State University, and CABEM Technologies], has facilitated innovative research, training, assessment, and product design for DoD and other stakeholders. Through strategic life-cycle environmental assessments (LCEA); programmatic environment, safety, and occupational health evaluations (PESHE); Health Hazard Assessments; and other proactive studies and reports, UOL has helped foster successful development and deployment of non-lethal technologies. More specifically, these efforts provide a framework for addressing complex environment, safety, and occupational health (ESOH) risks that affect personnel, infrastructure, property, and natural/cultural resources. Integrated analyses (comprehensive and transdisciplinary) involving flexible groups of subject matter experts, are employed in support of public and private collaborations with a focus on inputs, hazards, and constraints. This paper highlights the UOL process which can translate into advantages for a variety of projects (e.g., environmental, water, energy, infrastructure, etc.).

URBAN OPERATIONS LABORATORY

Background

In 1989 Congress appropriated funds to establish the Center for Hazardous Substance Research at Kansas State University, which later spearheaded the formation of the Nonlethal Environmental Evaluation and Remediation (NEER) Consortium in 2001. The successful public-private consortium was subsequently expanded into the UOL to support dynamic military needs through practical environmental assessments, software tool design and development, and innovative technology (product, service, or activity) development. UOL performs environmental analysis for its military partners in accordance with international, federal, state, and local regulations and policies, including: DoDI 5000.02 (Operation of the Defense Acquisition

System) (DoD, 2008), DoD Military Standard MIL-STD-882D (Practice for System Safety) (DoD, 2000), the National Environmental Policy Act (Congress, 1970), and Executive Order 13423 Strengthening Federal Environmental, Energy, and Transportation Management (CEQ, 2007), among others. Further information is available at www.uol.ksu.edu.

Approaches and Tools

Working closely with DoD Integrated Product Teams and the Joint Non-Lethal Weapon Directorate (JNLWD) Human Effects Review Board, UOL provides technical input and assistance throughout the design and development process. Through an iterative approach involving multidisciplinary professionals, including engineers, scientists, toxicologists, safety professionals, legal/regulatory advisors, financial planners, and military analysts, UOL is able to effectively leverage a variety of resources and methods. In addition to the Environmental Knowledge and Assessment Tool (EKAT) (M2 Technologies, 2008), various DoD databases and Environmental Protection Agency (EPA) models are utilized with special attention to green engineering principles. Empirical multimedia sampling and analysis are often performed by the team to supplement available experimental data and simulated and predictive data sets.

Technologies and Capabilities

To date, several innovative technologies, devices, and systems have been successfully evaluated at various phases of acquisition. Given the established user need for these nonlethal technologies and their integration, the capability to assess these systems in the context of unintended human health and ecological impacts is paramount.

U.S. MILITARY AND THE ENVIRONMENT

Transformation

Early in the 19th century, aspects of environmental management were integrated into the American military mission, including the Lewis and Clark Expedition (Corps of Discovery). As military activities, equipment, and facilities became more complex and mechanized, the need for effective natural resource conservation and environmental stewardship emerged. The history of the chemical weapons program illustrates the conundrum of unanticipated consequences (Allen, 1997). In terms of environmental quality and prioritization, there has been a transformative progression from early command and control approaches with regulatory drivers, to more recent preventive measures with overarching sustainability objectives. For example, the Air Force is now actively working to institutionalize sustainability into its design and construction philosophy, requiring military construction (MILCON) capable of achieving the U.S. Green Building Council's Leadership in Energy and Environmental Design (LEED) Silver level of certification (Mesick, 2009). Similarly, in 2008, the Army issued its first sustainability report, which is the first report from any major federal agency to follow the Global Reporting Initiative's sustainability reporting framework (DA, 2008).

Four Focus Areas

Military environmental programs are administered through four primary focus areas: 1) conservation, 2) restoration, 3) compliance, and 4) pollution prevention. The tremendous technical and financial challenges of investigating and remediating historic/legacy contamination sites demonstrate the need for strategies and tools that integrate environmental considerations much earlier in the technology development cycle (DoD, 2002).

ENVIRONMENTAL KNOWLEDGE AND ASSESSMENT

The Environmental Knowledge and Assessment Tool (www.ekat-tool.com) is an automated web-based tool designed by the UOL Consortium to identify, research, and evaluate environmental and pollution prevention options, and safety-related issues for products and systems (Boguski, 2007). Originally a concept jointly developed with the Marine Corps System Command in order to better integrate environmental requirements into the systems acquisition program, to support DODI 5000.2, the tool's features also make it useful to other public and private sector organizations. EKAT is organized to conveniently compile basic information on technical and regulatory requirements and serves as a resource center linking to other references, tools, and databases to assist in research efforts to minimize any unintentional safety and environmental effects associated with product use. Key modules and capabilities of EKAT include the following:

- Environmental screening. The environmental screening feature allows the user to evaluate chemicals or materials for potential environmental compliance and safety and health issues by comparing chemicals to federal environmental regulations and other pertinent lists.
- NEPA Decision Tree. The National Environmental Policy Act (NEPA) module assists military users in meeting federally-mandated requirements to consider environmental and related issues in proposed actions.
- EmisCalc. EmisCalc allows the user to estimate actual air pollutant emissions or calculate the potential emissions for processes using EPA-approved air emission factors from the EPA Factor Information Retrieval database.
- TRACI for EKAT. TRACI for EKAT Tool is a modified version of the EPA software tool, The Reduction and Assessment of Chemical and Other Environmental Impacts (TRACI), which allows the user to evaluate the environmental impact of releases to air and/or water over the lifecycle of a product, helping the individual understand and mitigate future liability.
- PESHE Report Generator. Military users utilize the Programmatic, Environmental Safety and Occupational Health Evaluation (PESHE) module to guide analysis and preparation of the comprehensive ESOH report, as required by the Department of Defense for all programs, in support of DODI 5000.02.
- EKAT Wizard. The EKAT wizard feature is set up in a question and answer format to guide users and help them determine which assessments, tools and other EKAT resources can help best address their requirements.

EKAT contains additional research options, including information resource documents and guides, providing the user with quick access to myriad resources for investigating material

properties, reviewing specific ESOH regulations and databases, finding pollution prevention alternatives, as well as providing links to other Internet resources on topics of interest.

LCEA METHODOLOGY AND APPROACH

Initial Characterization

The first step is to ensure that the team clearly understands the proposed technology concepts, materials and byproducts, and intended uses. Determining potentially applicable regulations and acquiring key data (screening and scoping) are performed with tools such as EKAT. Potential impacts are qualitatively estimated and baseline inventory information is compiled.

Evaluating Impacts

Evaluating the effects or impacts for a proposed action or technology is at the heart of the UOL systems process. Interdisciplinary teams of subject matter experts carefully collect and evaluate theoretical and empirical data to further predict, quantify, and assess any unanticipated impacts. At this stage, information is synthesized to ascertain the level of significance. Preliminary findings and ranking are then analyzed, along with any needed mitigation measures.

Decision-Making

Tentative recommendations are shared with military and technology leaders for preliminary input with respect to selecting the proposed action or technology.

Documentation

Based on proponent feedback, draft reports, such as an LCEA or PESHE, are cooperatively completed. As part of this process, monitoring and oversight plans are incorporated. Programmatic recommendations are completed and used as technical resources for further site-specific/geospatial evaluations and local public involvement. As Figure 1 outlines, the steps are iterative with feedback loops; the concepts are mindfully integrated throughout the system development and procurement life cycle. The acquisition continuum provides several opportunities for both formal and informal environmental analysis, as illustrated in Figure 2, thus contributing to technology maturation while addressing environmental quality.

During initial planning and design, UOL professionals review the capabilities and requirements. ESOH experts are part of the IPT from the beginning. Efforts are initiated on PESHE construction prior to system development and demonstration. Environmental specifications and attributes are an integral part of prototype development. During field testing, data are collected to update and confirm predictions and verify compliance with standards. Considerations for deployment, transportation, and storage activities are carefully implemented. Before fielding and production, formal program assessments are completed. This information is provided to military installations for site-specific analysis. Given the holistic procedure, demilitarization and disposal actions are proactively evaluated to minimize waste generation and

maximize reuse and recycling back into the technology sphere.

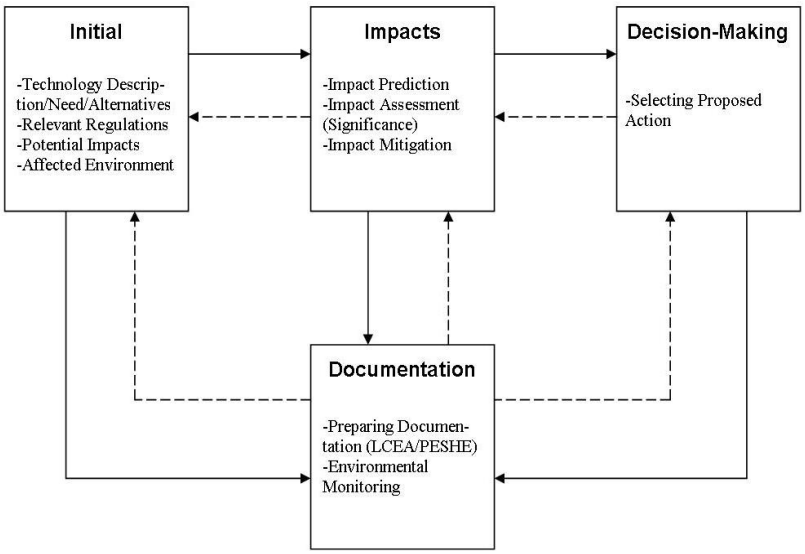

Figure 1. Conceptual Framework for Life-Cycle Environmental Assessment.

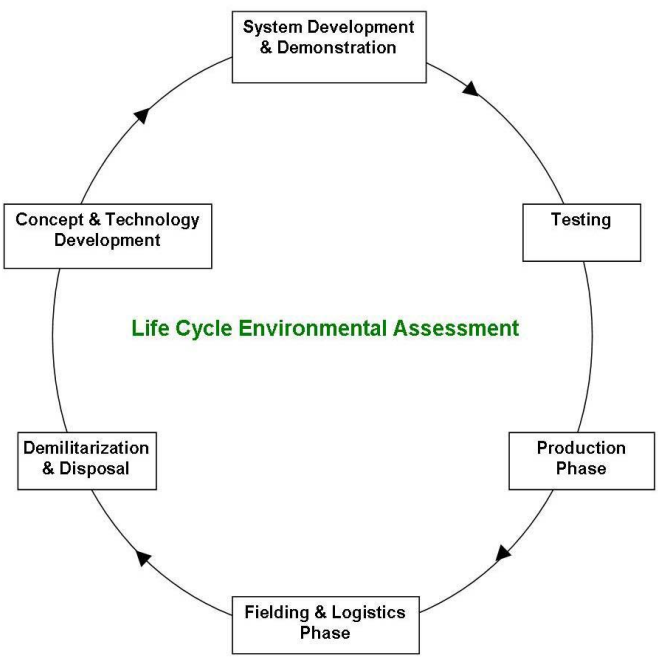

Figure 2. Acquisition Continuum and Integrated Life-Cycle Environmental Assessment.

ENHANCING ENGINEERING OPPORTUNITIES

Given the current economic and energy challenges (e.g., global recession, precarious and emerging markets, geopolitics, climate change, etc.) facing the U.S. and the international community, life-cycle strategies to improve cost and schedule efficiencies, while reducing liabilities are crucial. Many public projects aim merely to achieve regulatory compliance, regretfully missing fecund (sustainability) options, while many privately driven analogs often have even less rigorous macro requirements (limited by near-term profit metrics). However, if myopic perspectives are reframed/enhanced, various emerging as well as more established projects, from concept to implementation and beyond, present lucrative opportunities to use systems-based methodologies and determine fully burdened costs. In particular, pre-operation (strategy and planning, research and development, product/process design); operation (raw material acquisition, manufacturing, transportation, use, waste/emissions, recycling); and post-operation (demobilization, decommissioning, remediation, and restoration) hazards and risks can be addressed. Moreover, technology and policy dimensions can benefit by incorporating these concepts into early tradeoff analysis. By bringing together diverse teams of experts and users/customers for scoping and holistically mapping processes, unintended impacts can be identified for further evaluation and stakeholder engagement/input. This can facilitate technical, regulatory, and social (cross-functional) dialogue; thereby galvanizing empowerment and creative problem-solving for long-term societal needs.

NON-LETHAL TECHNOLOGIES

Background

Prior to 1995, non-lethal technologies had been used primarily in specialty law enforcement applications. The successful utilization by U.S. Marines in 1995, to assist the safe withdrawal of United Nations Peacekeepers in Somalia, served as a pivotal event in establishing the efficacy of their use. The Pentagon issued a policy directive codifying the development and employment responsibilities for non-lethal weapons systems (DoD, 1996). It designated the U.S. Marine Corps as the Executive Agent and provided official definition, "Weapons are explicitly designed and primarily employed so as to incapacitate personnel or materiel, while minimizing fatalities, permanent injury to personnel, and undesired damage to property and the environment." The following year, the DoD Joint Non-Lethal Weapons Program (JNLWP) was created. Asymmetric and decentralized threats have further contributed to the need for these enhanced security capabilities (e.g., crowd control; checkpoint and convey operations; humanitarian relief; etc) (DoD, 2007). Partnering with the JNLWP, UOL has supported the advancement of several non-lethal systems and tools, of which three are highlighted below (UOL, 2008).

Mobility Denial System/Anti-Traction Material

The Mobility Denial System/Anti-Traction Material project is a Marine Corps led program using a water-based slippery gel material which when sprayed on surfaces is designed to preclude and/or minimize access to designated areas by individuals and vehicles. UOL evaluated early formulations and identified potential chemicals of concern. Support activities included developing a geographic information system (GIS) suitability training tool, sampling and analysis, risk assessment, installation consultation, etc. Based on findings, the gel material

was optimized, and personal protective equipment and best management practices were incorporated.

Aroma and Odor Compounds

Aroma and odor compounds are foul-smelling mixtures used for targeted delivery as area clearing mechanisms. UOL identified problematic constituents in formulations and reviewed conventional and novel delivery subsystems for various DoD agencies. Release scenarios were estimated and safe concentrations were calculated to assist technology development, Figure 3 provides an example of a conceptual exposure estimate. Recommendations for payload enhancement, ecotoxicity testing, and controlled release delivery were completed.

Flash-Bang Grenades/Non-Lethal Airburst Munitions

For this joint forces program, early small-arms launch platforms and payloads were assessed by UOL. Based on input, problematic compounds were eliminated, including perchlorate (Saulters, 2006). Improved flash-bang pyrotechnics have been developed as the basis for these versatile systems. Limited field sampling and analysis, in test chambers and ambient conditions, were completed. Innovative metal-based payloads, fuzes, and activators are currently being analyzed. UOL is involved with several variations, including: hand delivered, single shot, and multiple fire applications of this multisensory (light, sound, and heat flux) technology.

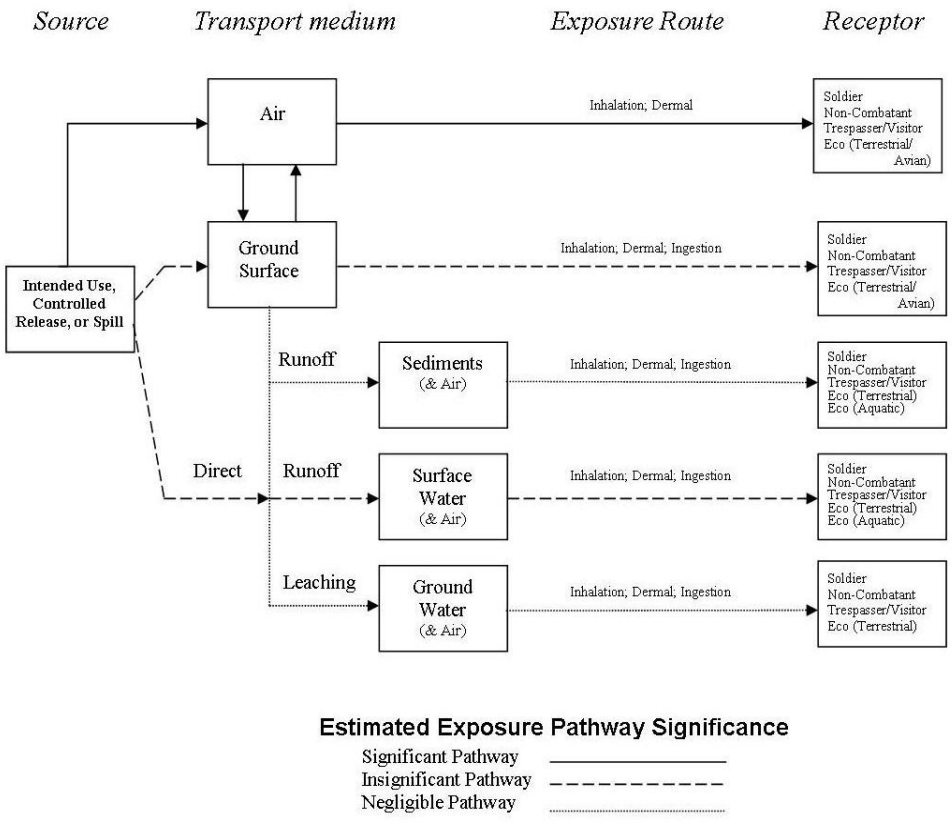

Figure 3. Conceptual Exposure Pathway Estimates for Aroma and Odor Technologies.

CONCLUSIONS

Based on the successful public-private framework followed by UOL, several instructive advantages can be derived.

1) A strong commitment to stewardship and sustainability from organizational leaders contributes to an enduring ethos of quality and dynamic balance (top down).

2) Strategic life-cycle environmental assessments, integrated during systems development and procurement, have been demonstrated to elevate triple bottom line priorities (environment, economics, social) while also driving innovation at the operations level (bottom up).

3) Early partnership and cooperative involvement are essential to effective planning and implementation, utilizing both multidisciplinary teams and robust data tools. These upstream collaborative efforts can lead to improved products and processes, while minimizing unintended environmental and safety consequences (proactive rather than reactive).

4) Efficiencies can be captured by streamlining and leveraging efforts between stakeholder groups with similar objectives, thereby fortuitously breaking barriers, building capacity, and creating synergy. Examples include: joint services testing requirements rather than fragmented redundancy; combined environment, safety, and occupational health data sharing; transdisciplinary research, development, and knowledge dissemination (doing more with less).

Overall, with growing economic, environmental, and energy constraints throughout society, pragmatic approaches to product development and decision-making, such as the UOL methodology are vital.

ACKNOWLEDGEMENTS

This work was partially funded through the award of a contract from the United States Marine Corps Systems Command to M2 Technologies, Inc.

REFERENCES

Allen, D. T., Consoli, F. J., Davis, J. A., Warren, J. L., editors. (1997) "Public policy applications of life-cycle assessment." *Proceedings from the Workshop on Application of Life-Cycle Assessment to Public Policy*; 1995 Aug 14-19; Wintergreen, VA. Pensacola FL: Society of Environmental Toxicology and Chemistry, 138 p.

Boguski, T., Erickson. L. E., Fredkin, J., Green, R., Jamka, L., Norris, G., Vera, L., and Whitely, C. (2007) "Use the Environmental Knowledge and Assessment Tool to Assist with Environmental Management." *Environmental Progress*, 26:251-262.

Council on Environmental Quality (CEQ) (2007), *Instructions for Implementing Executive Order 13423 Strengthening Federal Environmental, Energy, and Transportation Management*, March. http://ofee.gov/eo/eo13423_instructions.pdf

M2 Technologies, Inc., Kansas State University, and CABEM Technologies (2008), *Environmental Knowledge and Assessment Tool*, version 7.506. http://www.ekat-tool.com/DesktopModules/Login.aspx

Mesick, G. (2009) "Air Force Focus on Sustainability." *The Military Engineer (TME), Society of American Military Engineers*; January-February 2009, Volume 101, Number 657, 35.

Saulters, O., Boguski, T., Hutchinson, S., Leven, B., Pickrell, J., Davis, L., Kulakow, P., and Erickson, L. E. (2007) "Perchlorate: An Evaluation and Framework for Stakeholders." *Proceedings of the International Conference on the Future of Agriculture: Science, Stewardship, and Sustainability*; 2006 Aug 7-9; Sacramento, CA. http://www.engg.ksu.edu/CHSR/events/ag/200608/proceed/docs/3-3-2.pdf

U.S. Department of the Army (DA) (2008), Office of the Assistant Secretary of the Army for Installations and the Environment, *Sustainability Report 2007*, September 5.

U.S. Congress (1970), *National Environmental Policy Act*, P.L. 91-190, S. 1075, 91st Congress.

U.S. Department of Defense (DoD) (1996), *Directive 3000.3, Policy for Non-Lethal Weapons*, July 9.

U.S. Department of Defense (DoD) (2000), *Standard Practice for System Safety, MIL-STD-882D*, February 10.

United States Department of Defense (DoD) (2002), *Environmental Restoration Program Annual Report to Congress.*

U.S. Department of Defense (DoD) (2007), *Non-Lethal Weapons Program, Escalation of Force Options*.

U.S. Department of Defense (DoD) (2008), Office of the Under Secretary of Defense for Acquisition, Technology and Logistics (USD(AT&L)). *DoD Instruction 5000.02 Operation of the Defense Acquisition System*, December 2.

Urban Operations Laboratory (UOL) (2008), *Non-Lethal Environmental Evaluation and Remediation Center, 2007 Annual Report*, January.

Environmental Impact of Coffee Processing Effluent on the Ecological Integrity of Rivers found in Gomma woreda of Jimma zone, Ethiopia

Y.K. Kebede[1], F. Assefa[2], and A. Amsalu[3]

[1]Soil and Water Management Research Division, Ethiopian Institute of Agricultural Research, P.O.Box 28019, Addis Ababa, Ethiopia; PH (+251) 112 795437; FAX (+251) 471 111999; email: jaredkassahun@yahoo.com
[2]Biology Department, Addis Ababa University, P.O.Box 1176, Addis Ababa, Ethiopia; PH +251 1 0111239471; FAX (+251) 1111239472; email: asefafasil2003@yahoo.com
[3] Geography and Environmental Studies Department, Addis Ababa University; P.O.BOX 150223, Addis Ababa, Ethiopia; PH +251 1 0111239471; FAX (+251) 1111239472; email: muksitay@yahoo.com

ABSTRACT

The environmental impact generated from coffee processing effluent was assessed by comparing reference sites with downstream locations. The physico-chemical parameters of coffee effluent on average consists of very high amount of BOD (2200mg/l), NO_3 (26.4mg/l), low pH (4.3), and zero DO values. Thus, BOD values as high as 1900mg/l and 1700mg/l were found at the downstream sites of Bore and Fite rivers, respectively. The cluster analysis was effective in clustering the downstream sites of Fite and Bore rivers. Based on the principal component analysis, fresh water loving species of Heptagenidae and Hydropsycidae had higher weighted average for oxygen while pollution tolerant species of Chironomidae and Oligocheata had higher weighted average for BOD. The habitat score of the study sites was in the range of 29% (very poor) up to 84% (excellent). In general, the integrity of most of downstream sites was impacted by the coffee processing activity in the area.

1. INTRODUCTION

Coffee is the most important commodity in the world (Chanakya and Alwis, 2004) and in Ethiopia it is produced on small and large scale farms, which can produce more than 226,971 tons of coffee per annum (CSA, 2005), making Ethiopia the largest coffee producer and exporter in Africa. In addition, the presence of cheap labor market coupled with the high demand for wet processed coffee has increased the number of coffee processing stations in the country.

The process of separating the beans from coffee cherries during wet processing generates enormous volumes of waste material (solid and liquid). These by-products of coffee processing (coffee pulp and processing effluent) result in bad odour in the surrounding areas, breeding of disease vectors, when dumped around the processing

plants and pollution of ground water and surface water bodies through leaching and run-offs, respectively (Mbru *et al*.,1994). In addition, the composition of coffee pulp is organic and mainly contains carbohydrates, proteins, fibres, fat, caffeine, polyphenols, and pectins (Gathua *et al*., 1991). Thus, the decomposition of this organic waste in the rivers makes the water unsuitable for various uses and damages the aquatic ecosystem. However, the lack of the hitherto enforcement of environmental assessment before issuing the permit to the newly established processing stations and failure of monitoring and evaluation activities of the existing processing stations have resulted in the generation of huge amounts of processing by-products around major rivers used for coffee processing in Ethiopia.

Human activities degrade water resources by altering one or more of five principal groups of attributes: water quality, habitat structure, flow regime, energy source and biotic interactions (Karr and Chu, 1999). Therefore, simple chemical monitorings may not detect an integrative health conditions of water environments due to degradations of physical habitat and flow modifications (Judy *et al*., 1984). But, the most direct and effective measure of the integrity of a water body is the status of its living system (Guye *et al*., 2004). Therefore, an effective method for the assessment of ecological integrity must integrate physical and chemical parameters and ecological processes (Harper *et al*., 2000).

The present study is therefore an assessment of the ecological integrity of environmental quality around processing stations using physico-chemical data, macroinvertebrate community structure and qualitative habitat evaluation index (QHEI).

2. MATERIALS AND METHODS

2.1. Study area and location of sampling sites

Gomma woreda (Fig 1) is one of the 13 woredas in Jimma zone (district) known for predominantly growing coffee. It is located 390 km south west of Addis Ababa and about 50 km west of the Jimma city.

Gomma woreda enjoys well distributed annual rainfall. The average annual rainfall (15 years) is 1524 mm (IPMS, 2007). Agroecologically, Gomma woreda is classified as 96% wet midland and 4% lowland. Altitude in Gomma ranges from 1387 to 2870 m.a.s.l (IPMS, 2007). The three dominant soil types in the woreda are Eutric Vertisols, Humic Alisols and Humic Nitosols, of which Nitosols are the most abundant covering about 90% of the woreda. Many perennial rivers exist as a result of the topography, vegetation and rainfall pattern in the woreda (admnistration unit). Cheseche, Kota, Awetu, Urgessa, Fite, Janje, Sunde and Bore rivers are the prominent rivers found in the woreda. The rivers drain to Ghibe/Omo to the east and Dedesa River to the north (ORG, 2003).

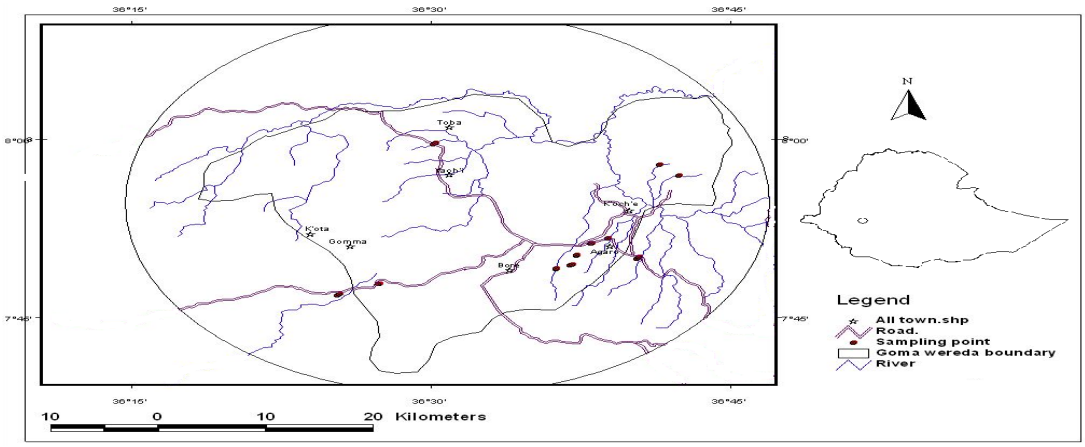

Figure 1. Location of the study area, its rivers, towns, roads and sampling points.

2.2. Water sampling technique

In this work, environmental impact generated from wet coffee processing effluent was conducted by using the technique of comparing upstream reference sites (Control sites without any impact from the effluent and other possible pollutants because of their location above processing stations) and downstream (locations below coffee processing stations which are effluent receivers) locations. Two samples from each site were taken once. Therefore, eleven processing stations (22sampling sites) were used in order to assess the environmental impact arising from these processing stations. Biological and physicochemical river water quality assessment was conducted in November 2007 (peak coffee processing month). Riffle sites of homogenous habitat were chosen (Gerth and Herlihy, 2006) and used for water and macroinvertebrate sampling for physico-chemical and biological analysis. The location of the sampling points at the lower course of the study rivers were placed sufficiently downstream from 50 to 300m below effluent entry points to ensure dispersion of the effluent over a wide cross section of the river.

2.2.1. Water Sampling and analysis

A composite sampling technique was employed to take water samples and samples were taken at three sampling points across the width (Bartram and Balance, 2001). The water samples were collected by inserting the bottles to a 21 to 30 cm depth to the opposite direction of the course of the river flow. The samples were kept in ice boxes and were immediately transported to Environmental Health Laboratory of Jimma University for chemical analysis following the standard methods (APHA, 1998). NO_3-N was determined by Phenoldisulfonic acid method. NH_3+NH_4 by Phenate method, PO_4^{-3}-P by Ascorbic acid method, TDS by Gravimetric standard method and TSS by filtration. BOD_5 (Biological Oxygen Demand) was determined by the Azide modification of the winkler's titrimetric method by determining DO (Dissolved Oxygen) contents of the samples before and after 5 days incubation at 20 ^{0}C. Nutrient analyses were performed in triplicate, and BOD was analyzed in duplicate. In-situ measurements of pH and water temperature were taken using

pH/mV/thermometer (*Model HI 8424*NEW) while DO was measured at the site using dissolved oxygen meter (*Model HI-9143*).

2.2.2. Macroinvertebrate sampling and counting

A triangular D-frame kick net with a 250 μm mesh size was used to collect macroinvertebrate in the riffle site by disturbing the river bed using kicking action over a distance of 10 meters for 3 minutes (Parsons and Norris, 1996). Macroinvertebrate sampling was conducted only once from each riffle sampling sites. After three minutes all the contents of the net were transferred in to a five liter collecting jar. To each jar 70% ethanol was added and transported to Jimma University Environmental Health laboratory for sorting and identification. In the laboratory, the collected samples were transferred into a bowel containing sufficient amount of water, agitated and sieved with 500 μm mesh to discard the mud and retain the macroinvertebrate. This was repeated until all the macroinvertebrates were washed from the mud. The samples were then transferred to wheel trays to easily pick them up using forceps. All macroinvertebrates were sorted and identified using binocular dissecting microscope and identification key (Bouchard, 2004) and assigned to their respective taxonomic levels.

2.3. Habitat survey

The habitat conditions of the sampling sites were assessed using a qualitative habitat evaluation index. Six habitat parameters were used for evaluating QHEI, based on the references widely used (Rankin, 2006). It is composed of six variables: substrate, instream cover, channel morphology, riparian zone and bank erosion, pool/glide and riffle/run quality, and gradient. Each principal parameter was divided into metric components and summed to provide the total QHEI site score of 100.

2.4. Multivariate Statistical Methods

2.4.1. One Way Analysis of Variance

Differences in physicochemical variables among sampling sites were assessed by analyzing one-way analysis of variance (ANOVA) using MSTAT software.

2.4.2. Cluster Analysis

The Bray –Curtis similarity index was used to calculate the distance between sampling sites and single link clustering method was used to cluster sampling sites (Quinn and Keough, 2002). Biodiversity professional® software (1997) was used to construct the cluster.

2.4.3. Principal Component Analysis

Relationships between the environmental and biological data were assessed using canonical multivariate analysis with the software program CANOCO 4.5 (ter Braak and Smilauer, 2002). First, Detrended correspondence analysis (DCA) of square-root transformed taxa abundance, with downweighting of rare taxa, detrending by segments and non-linear rescaling was used to determine the biological turnover, or gradient length, of the species data set. DCA for taxa (species) abundance of the second axis was less than 2, implying that taxa abundance exhibit linear response to environmental gradients (ter Braak and Smilauer, 2002). For this reason, principal component analysis (PCA) was used in the ordination of taxa abundance, environmental variables and sampling sites.

3. RESULT AND DISCUSSION

3.1. Physico-chemical parameters

There was a variation in physicochemical parameters along the course of the rivers and among the rivers (Table 1).

Table 1. Mean Physico-chemical characterstics of water samples of rivers of Jimma zone at locations above and below coffee effluent discharge points with their QHEI values.

Rivers	No.		BOD		DO		pH*		NO_3		QHEI	
	U	L	U*	L*	U	L	U	L	U	L	U	L
Sugo	1	2	1.5	600	5.98	5.98	7.0	7.0	2.51	2.13	27	39
Sunde	3	4	4	330	6.82	6.54	7.1	6.5	2.28	2.51	52	54
Chisech	5	6	1	2.3	6.6	6	6.8	7.3	0.48	1.58	75	75
Songa	7	8	270	150	5.4	5.4	6.7	6.6	1.83	2.05	81	75
Urgessa	9	10	0.8	200	7.64	7.13	7.8	6.9	1.28	2.55	84	78
Janje	11	12	1	600	5.15	6.87	6.7	7.3	1.64	2.09	76	47
Fite	13	14	1.3	1700	7.02	6.35	7.2	6.9	1.43	2.13	83	75
Guracho	15	16	6	5.3	6.15	5.71	6.8	6.7	0.94	1.03	67	59
Funtule	17	18	110	2.5	5.15	3.93	6.7	5.9	1.25	2.50	67	46
Bore	19	20	2.3	1900	6.49	0	6.9	5.8	2.41	2.80	81	59
Chore	21	22	1.9	3.2	6.04	3	7.2	6.5	1.42	1.39	78	79

U*: upstream sites; L*: downstream sites; all units except pH and QHEI are in mg/l.

BOD levels extend from 0.8mg/l at upstream site of Urgessa river to 1900mg/l at downstream sites of Bore river. The BOD values at the downstream sites of Bore and Fite rivers reached to 1900mg/l and 1700mg/l values from 2.3 and 1.3mg/l levels at the upstream sites. These BOD values were close to the average BOD content recorded for the diluted raw effluent (2200mg/l) just before it entered into the river

(Table 2). The high BOD content at the downstream sites of Songa and Urgessa rivers might be partly explained by the high BOD levels of their upstream sites and this might be related to other pollution sources such as erosion from the nearby agricultural fields. Additionally, the BOD values were even higher after the discharge of the effluent into the river which had increased the organic load of the river further.

Janje and Fite rivers that contain high BOD values despite the opposite relationship between DO and BOD (Meyrick, 2005) and these high DO values might be related to the discharge of the rivers that have high potential to dilute the organic effluent entered into the river and a continuous aeration along its way to downstream sites (Giller and Malmqvist, 1998). Nevertheless, the very high BOD content was mainly related to organic enrichment from the coffee processing effluent (Von Enden and Calvert, 2002) and its effect was much more pronounced at the downstream sites of Bore and Fite rivers. In general, most of the downstream sites were impacted from coffee processing effluent so that the average BOD value was 499mg/l which according to Von Enden and Calvert (2002) should be reduced to less than 200mg/l before its entrance to natural water ways.

The upstream DO values of all sampling sites were found to be more than 5mg/l (Table 1). There was a drastic change in DO at the downstream sites at Bore river (0 mg/l), and Chore river (3mg/l) with the decrease of 100%, and 50% of their respective upstream sites. The lowest DO level recorded was 0mg/l at the downstream site of Bore river while the highest was 7.64mg/l at upstream site of Urgessa river. There was a significant variation between DO values of the study sites as expected ($P<0.05$). Therefore, the main ecological effect of organic pollution in a watercourse is the decrease in oxygen content (Murthy *et al*., 2004).

Table 2. Summary of average physical and chemical values for upstream and downstream sites with their statistical values and raw effluents data.

	pH	Temp	BOD	DO	TDS	TSS	NO_3	NH_3
Upstream	7.03	17.68	36.35	6.22	132.27	115.05	1.59	0.33
Downstream	6.74	17.89	499.34	5.17	170.45	91.45	2.07	0.506
Significance	0.02	0.09	0.00	0.00	0.00	0.00	0.16	0.00
Raw Effluent	4.3	-	2200	0	1810	252	26.4	11.9

*Environmental variables with significant P value ($P<0.05$); all units except pH are in mg/l.

A general pattern of NO_3 increment at downstream sites compared the upstream sites was observed during the sampling periods. Similarly, Ammonia concentration (Table 1) increased following the effluent discharge. Although raw coffee wastewater contains 26.4mg/l NO_3, the lowest and highest NO_3 content of the downstream samples were within the range of 0.487 (Chiseche) to 2.547mg/l (Urgessa). A decrease in Nitrogenous pollutants may be associated with flow rate and dilution effects of the river water. Large volume of water has the capacity to reduce BOD and other organic pollutants.

On the basis of QHEI score, the habitat score of the upper streams was in the range of 27% (poor) upto 85% (excellent). Accordingly, the upper stream sampling sites of Chiseche, Songa, Urgessa, Janje, Fite Bore and Chore displayed scores more than 70% and evaluated as excellent. Likewise, the sampling sites at Gurracho, and Funtule were found as good (55-69); whereas Sunde was valued as fair (43-54) and Sugo as poor (32-42). Similarly, the downstream sampling sites of Chiseche, Songa, Urgessa, Fite and Chore were evaluated as excellent. Likewise, the sampling sites at Gurracho and Bore were valued as good; whereas the sampling sites at Sunde, Janje and Funtule were in a fair condition. In addition, the sampling sites at Sugo remained in a poor condition.

In general, the comparison between upstream and downstream sites clearly demonstrated the deterioration of water quality in most downstream sites. As a result, the downstream sites of Janje, Urgessa, Fite and Bore rivers were impaired by the coffee processing activities of the area during the study period. However, the construction of lagoon for the containment of coffee pulp and coffee wastewater around Chiseche rivers and the placement of processing station at a considerable distance from Songa river made these sites relatively unimpacted. A different level of impact was found on the remaining rivers.

3.2. Biological Analysis

3.2.1. Cluster analysis

In order to show the relationship of each cluster to all others and similarity/dissimilarity levels of each cluster, dissimilarity analysis of the macroinvertebrate composition was undertaken in all river sampling sites.

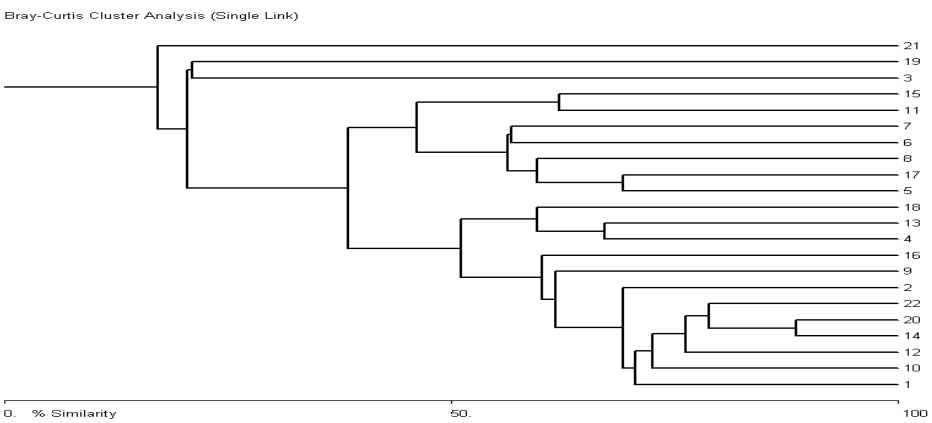

Figure 2. The hierarchical clustering of sampling sites using macroinvertebrate taxa composition

This analysis (Fig. 2) revealed that the highest similarity was found between the downstream sites of Fite (14) and Bore rivers (20) while the lowest similarity was found between the upstream sites of Sugo (1) and Chore rivers (21). In addition, the

downstream sites of Urgessa (30) and Janje (33) rivers were clustered together. These sites were also found to have a similar diversity index.

3.2.3. Principal Component Analysis

Although slight difference was observed for the results of environmental variables and biological indicators to depict the pollution gradient along the river separately, the combination of both were able to clearly define and explain the pollution gradients (Figure 3).

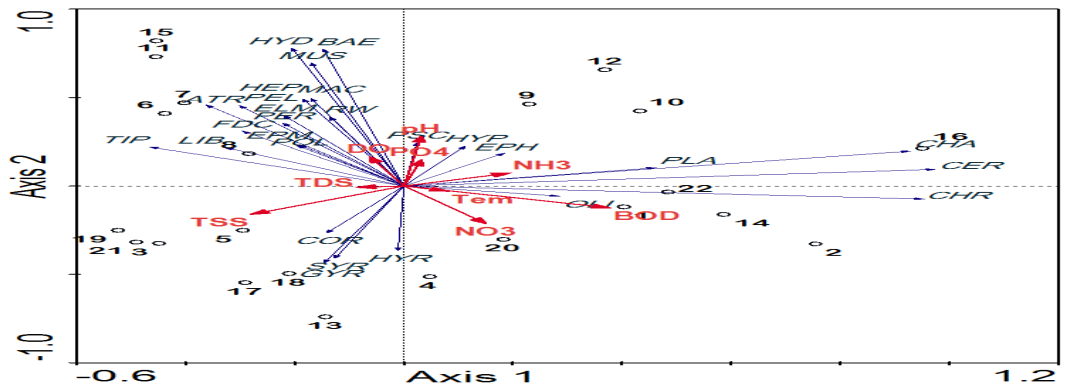

Figure3: PCA triplot of samples, macroinvertebrates and environmental variables based on the first two axes

In the ranking of the projection points, the origin (0, 0) indicates the global average of the variable. (ter Braak and Smilauer, 2002). Therefore, TDS, Temperature and PO_4 did not change much (short arrow length) and hence their influence were minimal as compared to BOD, TSS, NO_3, pH, and DO environmental lines which displayed the maximum rate of change across the diagram. Therefore, variations in macroinvertebrate composition were strongly correlated with these environmental variables.

Although slight difference was observed for the results of environmental variables and biological indicators to depict the pollution gradient along the river separately, the combination of both were able to clearly define and explain the pollution gradients. The high oxygen weighted average for oxygen loving species (Hydropsychidae, Baetidae, Heptagenidae, Perlidae and Psychodidae) is as expected since Heptagenidae is in Ephemeroptera family while Hydropsychidae, Perlidae and Psychodidae are in Trichoptera family. Ephemeroptera, Trichoptera and Plecoptera are considered to be abundant in oxygen rich water very sensitive for pollution and used as a water quality monitoring index in Ethiopia (Worku Legesse, 2000). Therefore sites 8 (Sugo lower), 6 (Chiseche lower), 7 (Songa upper), 11(Janje upper), and 15(Gurracho upper) had higher DO values than the rest sites.

On the contrary organically polluted sites were found to be dominated by pollution tolerant species of Chaoboridae, Oligochaeta, Ceratopogenidae and Chironomidae

taxa and except the taxa of Oligochaeta, all the species are in the Diptera family. The special characteristics of the above mentioned taxa are their ability to flourish in very low oxygen (high BOD) level and dominate the entire site with great abundance (Gallardo *et al*,. 2006). Sites 14 (Fite lower) and 2 (Sugo lower) and 20 (Bore lower) had the highest BOD values than the rest sites. Therefore the species-site-environment PCA triplot diagram clearly discriminated unimpacted sites from the severely impacted ones.

4. CONCLUSION

The results of this study revealed ecological impairment of most of the downstream sites due to the activities of processing stations. Measures of physico-chemical parameters, macroinvertabrate community and QHEI analyses indicated the significance environmental impact around most of wet coffee processing stations. Therefore, the downstream sites of Urgessa, Sugo, Sunde, Janje, Fite and Bore rivers were impaired by the coffee processing activities in the area during the study period. However, the construction of lagoon for the containment of coffee pulp and coffee wastewater around Chiseche rivers and the placement of processing station at a considerable distance from Songa river made these sites relatively unimpacted. A different level of impact was found on the remaining rivers.

5. REFERENCES

APHA, 1998. Standard Methods for Examination of Water and Wastewater, 20th ed. American Public Health Association, American Water Works Association and the Water and Environment Federation, Washington, DC.

Bartram, J., and Balance, R. (Eds.), 2001. Water Quality Wonitoring—A Practical Guide to The Design and Implementation of Freshwater Quality Studies and Monitoring Programmes. Spon Press, London, Published on behalf of UNEP and WHO, pp. 50–87.

Bouchard, R.W., Jr. (2004). Guide to aquatic macroinvertebrates of the upper Midwest water resource center, University of Minnesota, St.Paul, MN.208pp.

Central Statistical Authority (CSA). (2005) .National Statistics Table B3 and B4. Addis Ababa, Ethiopia.

Chanakya, H.N. and A.A.P. De Alwis. (2004). Environmental issues and management in primary coffee processing, Process Safety and Environmental Protection, 82 (B4): 1 – 10

Gallardo, A.C., J.E. Garrish, C.R. Hill, and J.B. Stribiling. (2006). *Biological Assessment of the Cattail Creek and Brighton Dam Watershed,* 61 pp. Tetra Tech Inc., Howard Country, Maryland.

Gathua, B., P. Rantala, and R. Maatta. (1991) Coffee Industry Wastes. Water Science Technology, Vol. 24, No. 1: 53-60

Gerth, W. J., & Herlihy, A. T. (2006). Effect of sampling different habitat types in regional macroinvertebrate bioassessment surveys. *Journal of the North American Benthological Society*, 25(2), 501–512.

Giller, P.S. and B. Malmqvist, (1998). *The biology of streams and rivers*. Oxford

University Press, New York
Guye, B., P. Smailes, and J. Adams. (2004). A water quality index for use with diatoms in the assessment of rivers. Water SA, 309 (4):493-498.
Harper, D.M., J.L. Kemp, B. Vogel, and M.D. Newson. (2000). Towards the assessement of 'ecological integrity' in running waters of the United Kingdom. *Hydrobiologia* **422/423**: 133-142.
Improving Market Success and Productivity (IPMS) of Ethiopian Farmers Project. (2007). Goma Pilot Learning Wereda Diagnosis and program design. www.ipmsethiopia.org/content/files/Documents/PLS-DPD/goma.pdf (Acessed: June,2008).
Judy R. D., P.N. Seeley Jr, T.M. Murray, S.C. Svirsky, M.R. Whitworth, and L.S. Ischinger. (1984). National fisheries Survey. Technical report: initial findings, vol. Washington, DC, USA: United States Fish and Wildlife Service (FWS/OBS-84/06).
Karr, J.R. and E.W. Chu, 1999. Restoring life in running waters: better biological monitoring . Island Press, Washington, D.C.
Mburu, J.K., J.T. Thuo, and R.C. Marder. (1994). The characterization of wastewater from coffee processing factories in Kenya. Kenya Coffee. 59:1757-1763.
Meyrick, S. (2005). Aquatic macroinvertebrates as an indicator of water quality after an incident of organic pollution in the Bourne Stream, Dorset. A S216 Environmental Science, Open University Project.
Murthy, K.V.N., A. D'Sa, and G. Kapur. (2004). An effluent treatment-cum-electricity generation option at coffee estates: is it financially feasible? Draft version. International Energy Initiative, Bangalore.
Oromia Regional government (ORG). (2003). Gomma Aanaa (district) based development programme: Project document Oromia Economic Study Project Office, Addis Ababa, Ethiopia.
Parsons, M. and R.H. Norris (1996). The effect of habitatspecific sampling on biological assessment of water quality using a predictive model. *Freshwater Biology*, **36,** 419–434.
Quinn, G.P. and M.J. Keough. (2002). *Experimental design and data analysis for biologists*. Cambridge University Press, UK.
Rankin, E.T. 2006. Methods for assessing habitat in flowing waters: using the qualitative habitat evaluation index (QHEI). OHIO EPA Technical Bulletin EAS/2006-06-1.
ter Braak, C.J.F. and Smilauer, P. (2002). CANOCO Reference manual and CanocoDraw for windows User's guide: Software for Canonical Community Ordination (Version 4.5). Microcomputer power (Ithaca, NY, USA). 500pp.
Von Enden, J.C. and Calvert, K.C. (2002). Review of Coffee Waste Water Characteristics and Approaches to Treatment. PPP Project, Improvement of Coffee Quality and Sustainability of Coffee Production in Vietnam". German Technical Cooperation Agency (GTZ).
Worku Legesse (2001). Senstivity of biotic indices to natural disturbances. PhD thesis, Departement of Zoology and Animal Ecology, University College Cork, Repuplic of Irland.

How to Save the Second Aral Sea?

Rysbekov Yusup Khai. [1]

[1]Department of Management, Scientific-Information Centre of Interstate Coordination Water Commission of Central Asia, 100187, 100187, Tashkent, B-11, Karasu-4, Uzbekistan PH (99871) 265-1659; FAX (99871; email: yusuprysbekov@icwc-aral.uz

ABSTRACT

In the beginning of 1960s Aral Sea had water area more than 66000 km^2. Now Aral Sea was divided into three Seas, and has the total area 20000 km^2, including Eastern Aral Sea (EAS) - 11000 km^2, Western Aral Sea (WAS) - 5000 km^2, Northern Aral Sea (NAS) - 3300 km^2. Now only NAS (Kazakhstan) has real chances for survival.

Preservation of WAS (Uzbekistan) is impossible without creation of artificial flowing ecosystem "WAS - Amu Darya River delta". There is a line of concomitant factors for benefit for WAS preservation, in comparison with EAS:

- WAS has the large depths, the smaller area and water volume;
- WAS' water have smaller mineralization

The offered proposal has by innovative part the connection of Western part of NAS with WAS, construction of channel NAS-WAS and dam, which will separate WAS from EAS. Idea's realization will be favorable for Kazakhstan also.

INTRODUCTION

Intensive development of irrigation in the Amu Darya River Basin (RB) and Syr Darya RB in 1970-1980s has caused sharp reduction of water level in the Aral Sea, and hope for reception of additional water from Siberia were not justified. According to the available data, average multiyear river flow in the Aral Sea Basin (ASB) in 1911-1960 made about 117 km^3/year, including for Amu Darya RB - 80 km^3, and for Syr Darya RB - 37 km^3. In this period the Aral Sea received on the average about 56 km^3 of water per year, including 42 km^3 from Amu Darya River and 14 km^3 from Syr Darya River.

Next decades sharp decrease of inflow in the Aral Sea is observed: in 1961-1970 it has decreased till 30.0 km^3/year, 1971-1980 - up to 16.7 km^3, 1981-1990 - up to 3.5 km^2, 1991-1999 - till 7.6 km^3/year on the average. In 1980-2001 per separate years waters of Amu Darya and Syr Darya did not reach Aral Sea. Accordingly, sea level has decreased from 53 m (beginning of 1960s) up to 41 m (1985-1986), and 30 m (2001).

In 1985-1986 Aral Sea was divided into Large Aral Sea (LAS) and Northern/Small Aral Sea (NAS), later the LAS was divided into Eastern Aral and Western Aral Seas (EAS and WAS).

In the beginning of 1960s the Aral Sea had water area more than 66000 km^2 (see Figure 1) now total area of three Seas makes less than 20000 km^2: EAS, with gulfs - less than 11000 km^2, WAS - about 5000 km^2, and NAS - about 3300 km^2) (see Figure 2).

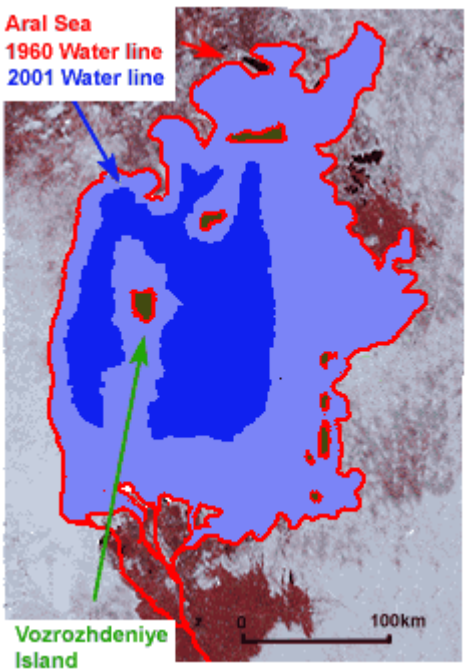

Figure 1. Dynamics of the Aral Sea level for 1960-2001.

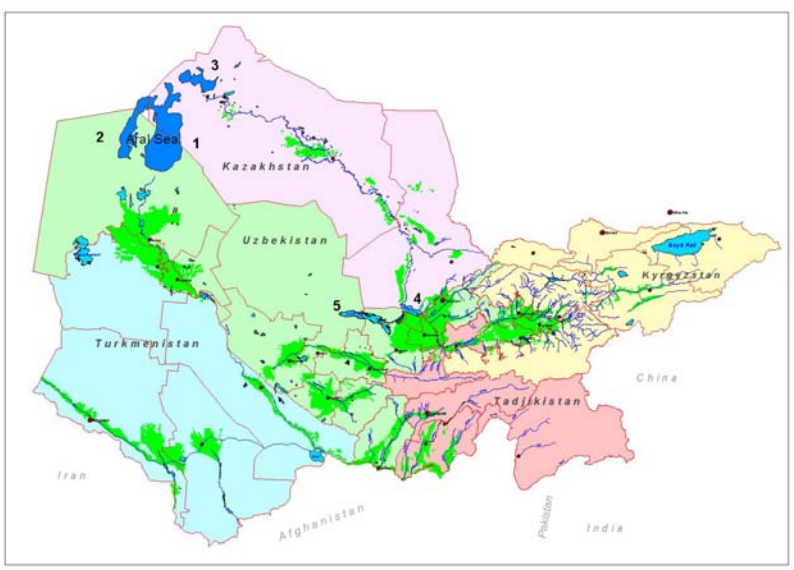

Figure 2. Aral See Basin (1 - Eastern Aral Sea, 2 - Western Aral Sea, 3 - Northern Aral Sea, 4 - Shardara reservoir, 5 - Arnasai Lake ecosystem).

Now, as a result of realization of the appropriate measures by Government of Republic of Kazakhstan (construction of Kokaral dam in the Berg' strait, maintenance of constant inflow in the Sea), only NAS has real chances for survival.

In the whole, the tragedy of the Aral Sea was caused by inept management and ignoring water requirements of the ecosystem. In middle of 1980s the Amu Darya River and Syr Darya River water shortages downstream were recognized by the Soviet Government (by Moscow) as a critical water management situation that was exacerbated by the lack of a unified water management body. As a consequence and according to the appropriate political decisions (1984, 1985, 1986, and 1987) the Basin Water Organizations (BVO) "Syr Darya" and "Amu Darya" were established. These BVOs were responsible for water allocation between the Central Asian states and operation of the associated interstate hydraulic structures. However, it was established that if in the Amu Darya River and the Syr Darya River water availability is higher than estimated, water may be accumulated in the reservoirs, and under very high water, a share of water may be released downstream to the Aral Sea. This was a short-sighted decision and a political mistake, which resulted in aggravating the health of the Aral Sea.

BASIC RESULTS OF THE PREVIOUS RESEARCHES

In last 20 years a line of researches was carried out in the context of saving of the Aral Sea (or its separate parts). The basic accent in them was made on preservation of wetlands of the rivers (Amu Darya and Syr Darya) deltas and separate parts of the Aral Sea (NAS, WAS, EAS) in the limited borders, which would ensure their steady existence. So, according to Nachtnebel P. et al. (2006), Shutter J. and Dukhovny V. (2006) and other sources, the offered ways for preservation of water ecosystems in coastal zone of Aral Sea are reduced to the following basic variants (other variants do not leave for frameworks resulted below):

1. Reduction of total area of Aral Sea (with variants);
2. Reduction of area of Aral Sea, but with NAS' liquidation;
3. Separation of NAS and WAS;
4. Separation of NAS and WAS, at reduction of WAS' area;
5. Preservation of NAS and WAS, at separating of EAS;
6. Preservation of reduced LAS and NAS;
7. Preservation of reduced LAS, but NAS is salty reservoir;
8. Preservation of reduced EAS, but WAS and NAS are salty reservoirs;
9. Preservation of reduced WAS and NAS, but EAS is salty reservoir;
10. WAS exists, EAS is completely separated;
11. EAS exists, WAS is completely separated;
12. EAS and WAS continue to exist in natural condition, without human intervention.

4. Variant # 13. Water of Amu Darya is directed to WAS.

Analysis shows, that most expedient, attractive and possible to realization is the variant №13, which can be accepted for a basis for preservation of WAS.

But this idea, which was offered by Academy of Sciences of Uzbekistan, is not considered as correct by authors of the report under the Project INTAS - 0511 REBASOWS (Nachtnebel P. et al., 2006).

If we shall distract from definition "reduced", and we shall take into account that the task on preservation of NAS is practically solved, variant #13 is close to variants # 5 and # 9. This task (preservation NAS is solved) can be advanced and is put in other plane only, namely - in context of maintenance of national interests of Kazakhstan and Uzbekistan in ecological sphere in future.

OFFERED IDEA AND ITS POSITIVE PRECONDITIONS

Considered in present analysis zone is known under "Southern Prearalie", which includes of Amu Darya River delta in the whole and adjacent with WAS and EAS areas in territory of Uzbekistan. EAS receives waters from Amu Darya River after satisfaction of needs of its delta, which includes system of wetlands and numerous lakes. In turn, WAS receives water only in case of water surplus in EAS (having poured from EAS).

It is necessary to note that Amu Darya River delta and its wetlands not receive always water in quantities, which are sufficient for its steady existence, is especial - in dry years (in particular, in 2000, 2001) and this circumstance complicates management of water ecosystems of river delta and coastal zone. Earlier realized projects in this zone do not give the concrete answer to the question on sustainable management of Amu Darya River delta and coastal zone of WAS and EAS.

In developing situation it is necessary to recognize (Rysbekov Yu., 2006, 2007) that a preservation of WAS is impossible without creation artificial dynamical (flowing) ecosystem "Delta - delta" (in our case - "Delta of Amu Darya River - WAS"). If the problem of WAS' preservation will not be solved, the parameters of water ecosystems in River delta will sharply vary depending on receipt of water (as a whole - dry or wet year), and it is senselessly to reason on their sustainable existence. Offered idea consists in connection of western part of NAS (Kazakhstan) with WAS (Uzbekistan) by means of construction of the artificial channel "NAS - WAS" that will allow:

- To supply a fluidity of water and to reduce of water mineralization of NAS on all to its length (now sea waters mix up badly, as a fresh river water runs into it of its eastern part, while water of western part of NAS has higher mineralization),
- Considerably to expand vital space and to supply more favorable conditions of duplication both residing of freshwater and sea fishes in NAS,
- To exclude dump of river fresh waters (from Syr Darya River) in EAS, which can be used for filling of WAS and improvement of water quality in it.

We shall result while as minimum 3 factors for the benefit of offered variant:

- (1) WAS has the large depths, than EAS. EAS is flat natural depression and has depths 3-4 m. The maximal depths of WAS make more than 40 m,
- (2) WAS' waters have smaller mineralization, than EAS' waters. According to available data, mineralization of WAS waters was stabilized at level of 80-90 g/l (on other data - it has reached 100 g/l). At the same time, mineralization of EAS' waters makes not less, than 140 g/l,
- (3) WAS has smaller area and water volume, than EAS. It will ensure stability of management of the Sea after its restoration.

At acceptance of the decision about preservation of WAS, there are 2 hypothetical routes for construction of the artificial channel to WAS (Rysbekov Yu. and Tillaiev B., 2008), namely:

- Through Sudochie lake - Southern channel,
- Through Lakes Rybachie and Muinak - Northern channel.

Analysis shows that the construction of the Southern channel is preferable from the point of view of technical practicability, smaller financial charges and future efficiency. Thus, in addition 2 factors testify for the benefit of WAS' preservation:

(4) Realization of technical measures (construction of dams etc.) will be cheaper,

(5) Channel from delta of Amu Darya will pass on the route including lake Sudochie - object of the Ramsar the Convention that is one of important factor.

For achievement of offered idea it is necessary to change the approaches to management by coastal zone of WAS and delta of Amu Darya River with purposes of creation of uniform flowing water ecosystem "Delta-Sea".

For this purpose it is necessary to determine:

- Minimal river flow, which will supply a flowing regime for sustainable functioning of new artificial ecosystem.

This water volume can not be used for other needs (irrigation, etc.) in downstream zones of Amu Darya River,

- Optimum quantities of wetlands and lakes in delta of Amu Darya, which necessary and can be saved.

It is necessary resolutely to refuse a number of wetlands (Akushpa etc.), which have few chances for survival, and which parameters do not promote steady management by them in view of an economic efficiency (small areas and depths, high mineralization, low biological productivity, etc.),

- Optimum water level (OWL) in WAS as bases for necessary calculations.

OWL can be determined after acceptance of decision about water limits (requirements) for ecosystem "Delta-Sea". It is possible to accept for base of this water limits the volumes of collector-drainage waters, which are dumped (without benefit) in the EAS, and sanitary water releases to the Amu Darya delta,

- (4) Development of necessary measures on service by ecosystem "Delta-Sea", for maintenance of its functionality

As a rule, it is an operational measures,

- (5) Volumes of bio-efficiency (fish, vegetation etc.)'s restoration.

These volumes will depend from quantity and quality of water, which flows in new ecosystem "Delta-Sea", proceeds on it and accumulates in WAS,

- (6) Volumes of artificial wood landings (area, kinds of vegetation etc.) in adjacent to system "Delta-Sea" areas.

These measures will allow to lower negative pressure on new ecosystem and will promote common improvement of zone,

- (7) Other necessary measures on maintenance of stability of ecosystem "Amu Darya Delta - WAS".

There are following positive preconditions to the offered idea's realization:

- (1) Fresh water surpluses from Syr Darya River very are dumped in the practically dead sea (EAS) through Kokaral water-regulating structure.

So, according to IFAS (International Fund for Aral Saving)'s data, in 2003 mineralization of water, which flow down from NAS to EAS, makes 1.7-1.8 g/l. At the same time, average mineralization of NAS' water is equaled bout 15 g/l. This river water do not improve an ecological condition in EAS, which has water mineralization about 140-150 g/l. Valuable and practically fresh water is dumped in EAS at the sharp water deficiency in Syr Darya RB only with the purposes for safety of Kokaral dam.

- (1.1) Experts will confirm that in EAS is dumped fish with water (direct damage for Kazakh fishermen), most part of which doomed on extinction in EAS,

- (1.2) Volumes of dumped water are huge.

So, in 2003 NAS has received 9.0 km^3 of river water from Syr Darya, from which 7.3 km^3 (more than 80 %) is dumped in EAS. This water volume (7.3 km^3) is enough for irrigation about 700 000 - 800 000 ha.

- (1.3) It is necessary to say that in 2003 the EAS has received about 6.3 km^3 collector-drainage water from Amy Darya part,

- (2) Waters of EAS supersede waters of high mineralization from EAS to WAS, and it worsens quality of EAS' waters. EAS' waters is intensively spent for evaporation (small depths of EAS),

- (3) Fresh river water from Syr Darya is accumulated in the east part of NAS (excepting a river flow from the mouth of Syr Darya to the Kokaral dam), as waters with higher mineralization of NAS' rest (to west) part do not promote an intensive mixing the rather fresh water (mineralization - 1.5-1.8 g/l) and sea salty waters (15-18 g/l) of medial and western part of NAS,

- (3.1) More fresh and easy river water from Syr Darya (in comparison with sea water) is dumped to EAS always. As the consequence, most part of fishes will be to live in the east part of NAS.

Accordingly, the Kokaral dam supports ecological stability and steady fish craft only of small (east) part of NAS. presentations in conference proceedings.

REALIZATION OF IDEA

Realization of proposed idea assumes the complex approach, in view of the stated above rules, in particular:

a) preservation of WAS by means of creation of uniform ecosystem "Delta of Amu Darya - WAS");

b) construction of Southern channel for maintenance of WAS by collector-drainage waters from irrigated lands,

c) construction of the artificial channel "NAS-WAS".

d) construction of dam (Uzbek part) between EAS and WAS, which will separate EAS from WAS.

It is represented to expedient a preservation of WAS' water level on considerably higher marks, than EAS (presumably, the excess should be not less than 6-7 m).

Difference in absolute marks between WAS and EAS will depend on the decision, at what level for preservation of EAS is expedient. Volume of civil works depends on the accepted water level in EAS also. All rest (dam's parameters, hydraulic engineering structures) requires forwarding research and engineering substantiation.

Dam between WAS and EAS should be equipped with water-regulating structures, in particular - for passing of water by higher mineralization from the bottom layers of WAS and for catastrophic dump. In start period it is possible to supersede waters of high mineralization (up to 90-100 g/l) in process of receipt of collector-drainage water of smaller salinity from delta of Amu Darya (5-7 g/l) and NAS (up to 15 g/l), and further it is necessary to adjust and support an acceptable level of water mineralization in WAS. It is represented expedient to provide in system of hydraulic engineering structures an opportunity for construction of pump station for pump out from NAS the strong-salty waters from depths 15-20-30 m for further prospect, and it will promote further desalinization of NAS' water.

The question of use of drying up coastal zone of EAS requires an expert analysis (production of salt, restoration of vegetation - wood planting etc.).

Now WAS and EAS completely have lost such important function as a place for the craft fishes. The following conditions for survival of alive organisms in water environment can be accepted as base for step-by-step revival of fish craft in EAS:

- (1) Separate kinds of seaweed maintain salinity up to 280 g/l, and of microorganisms (bacteria) - from 120 g/l and higher;
- (2) Intervals of salinity from river up to ocean waters are considered as favorable conditions for the majority of alive water organisms.

In particular, salinity of ocean's water makes about 35 g/l on the average, water of the Caspian Sea (excepting rivers' mouths) - 13 g/l. It is wide known that a flounder was delivered from the Caspian in the Aral Sea; the flounder can live and give posterity at water salinity in limits 20-60 g/l.

CONCLUSION

The Aral Sea Basin was quoted by the UN Environmental Program as one of the most staggering disasters of the 20th century, and the Aral Sea region is referred to as an ecological disaster zone on a global scale. Restoration of WAS will doubtless give the positive social-political, socioeconomic and ecological effects. In particular, the economic benefit will be reflected in revival of fish and hunting craft, and a greatest feedback should be from fish-cultivation that positively will have an effect on a socioeconomic situation of the local population of contiguous areas.

Coming back to Figure 2, it should be noted that the preservation of the WAS will allow to solve a line of tasks connected with to operation of Shardara reservoir (Kazakhstan) and Arnasai Lake System (Uzbekistan) (Rysbekov Yu. and Tillaiev B., 2008), which are in of the Syr Darya River Basin. ALS was formed in 1969, when about 22 km^3 of water was dumped in it and this water volume makes more than half of the multi-year water resources of the Syrdarya River Basin.

In last 40 years the Arnasai was used as a receiver of superfluous water with the purposes of protecting the territory of Kazakhstan against high waters, as the Shardara reservoir could not contain the water and the Syrdarya River could not pass water surpluses to the Aral Sea.

Before dividing of the Aral Sea into the Large (LAS) and Small Seas (NAS) water of Amu Darya and Syr Darya flew in one sea, with successful realization of the proposed project they will flow also in one Sea - WAS. But it is already a philosophy.

In 1993 in Kyzyl-Orda the Heads of Central Asia States (CASs) have signed the Agreement, in which they have recognized as general tasks, in particular:

a) "guaranteed maintenance of water submission in the Aral Sea in the volumes allowing to support its reduced, but steady water area at an ecologically acceptable level and preservation thus seas as natural object";

b) "restoration of balance of broken ecosystem…, first of all - in territory of deltas of Amu Darya, Syr Darya and contiguous sites…, creation here the artificial steady landscape complexes".

In this plan, the realization of offered idea answers political will of the Head of CASs to stabilize a situation in the Aral region.

REFERENCES

Nachtnebel P., Dukhovny V., Tashmukhamedov O., Tuchin A.., Vasilyev O. etc (2006). *The rehabilitation of the ecosystem and bioproductivity of the Aral Sea under conditions of water scarcity.* Report INTAS-0511 REBASOWS. Scientific-Information Centre of Interstate Coordination Water Commission of Central Asia. Vienna-Tashkent.

Rysbekov Yu.(2006). *Substantiation of the necessity of creation artificial ecosystem "Amu Darya delta - Western Aral Sea/* Proceedings of the GISIG ITALY ECO-IMAGINE International Conference (Genoa, Italy).

Rysbekov Yu. (2007) *Creation of System "Delta-Sea" as a Basis of Ecosystem Approach to the Management of Large Aral Sea's Coastal Zone.* Proceedings of the International Conference "Coastal Zone, Environment and Sustainable Development, Vulnerability, Adaptation and Beyond (SZESD2k7) (Dehli, India)

Shutter J. and Dukhovny V. (2006). *Integrated Water Resources Management in the Aral Sea Basin with the Purpose of Filling of the Southern Prearalie's water surfaces.* Report NATO SFP 974357, Scientific-Information Centre of Interstate Coordination Water Commission of Central Asia,. Tashkent, Uzbekistan.

Rysbekov Yu. and Tillaiev B. (2008). *About problem of the Aral sea and possible ways of its decision in thesis form or attempt of the concrete answer on eternal Russian question.* Collection of the proceedings "Problems of the Aral sea and Priaralie" Scientific-Information Centre of Interstate Coordination Water Commission of Central Asia. Tashkent, Uzbekistan.

© Rysbekov Yu. Khai. 2009

Air – Borne Heavy Metal Contamination to River Ganga (India)

J. Pandey*, K. Shubhashish & Richa Pandey
Center of Advanced Study in Botany, Banaras Hindu University
Varanasi, India – 221005

ABSTRACT

A two year study was undertaken at Ganges basin of India to evaluate the atmospheric input of six heavy metals to river Ganga. Atmospheric bulk deposition was collected on a fortnightly basis at 8 river sites from April 2006 through March 2008 to determine atmospheric loading of heavy metals to river Ganga. The sampling protocol consisted of bulk collectors placed at 24 locations (3 at each site) selected along a 20 km long tract of river Ganga at Varanasi, India. The atmospheric fluxes of six heavy metals to river Ganga were estimated as (g ha^{-1} y^{-1}) : Cd – 0.56 – 20.15; Cr – 0.34 – 8.87; Cu – 1.63 – 58.17; Ni – 0.21 – 7.32; Pb – 1.80 – 124.00; Zn – 124.15 – 477.18. Atmospheric deposition of all the elements was lowest at Adalpura (site 1) and highest at Rajghat downstream site (site 8) receiving maximum down – wind urban industrial emissions. Zinc alone contributed to more than 68 % of total measured heavy metal input. For season, the atmospheric fluxes were measured highest during winter followed by summer and rainy seasons. Data on heavy metal concentrations in mid – stream water showed significant correlation with their respective values received through atmospheric deposition. Corresponding to the atmospheric deposition, except for Zn, highest concentrations of Cd, Cr, Cu, Ni and Pb in mid – stream were recorded during winter followed by summer and rainy seasons. Concentrations were recorded highest for Zn followed by Ni, Cr, Pb, Cu and Cd. Concentrations of all the heavy metals were high in down – stream sampling locations. Although the concentrations of Cr, Cu and Zn remained well below their maximum admissible concentrations (MAC), more than 80 % of water samples of 7 out of 8 locations sampled, showed Cd, Ni and Pb levels above their respective MAC. Heavy metal loading to mid – stream implicates the adjoining urban agglomeration of Varanasi as the principal emission source area. The atmospheric loading to the river will continue to rise with the completion of Ganga Express highway. This may lead to serious health implications in long – run since Ganga water is also used for drinking purpose by a large population.

Key words : Atmospheric deposition, contamination, Ganga basin, heavy metals, pollution, Varanasi

*Corresponding Author, e – mail : jiten_pandey@rediffmail.com

INTRODUCTION

The solute chemistry of a river depends on a number of processes occurring within its catchment. Some chemical constituents are imported into the river system through weathering and surface run – off. A number of other elements and ions including those of potentially toxic heavy metals are added into the system through surface discharge and atmospheric deposition. The impact of long – range atmospheric transport and deposition of pollutant aerosols on terrestrial environment is well documented from long back, impact of aerially – driven pollutant aerosols on lotic systems have received attention only recently (Thornton and Dise, 1998). Some earlier studies have shown sizable atmospheric input of trace metals to lake systems (Bragazza, 2006). In India, the

data so far available on these lines have been mainly confined to the deposition and effects of acidic components of the atmosphere (Kumar *et al*., 2001). Far less attention has been paid towards atmospheric deposition – linked heavy metal contamination to river systems. During recent years anthropogenic activities have dramatically increased the atmospheric deposition of pollutant elements even in areas far – away from the direct human influence (Pandey and Pandey, 2005). Although the problem of atmospheric deposition of pollutant elements is of global concern, this problem is rapidly rising in developing countries including India due to newly establishing industries coupled with fastened urban growth and lack of efficient control measures (Borbely – Kiss *et al*., 1999; Pandey and Pandey, 2009).

Atmospherically – driven heavy metals have been shown to significantly contaminate soil and dietary vegetables causing a serious risk to human health when plant – based foodstuffs are consumed (Pandey and Pandey, 2009). Furthermore, dietary intake of trace elements depends also on irrigational water use. There exists a strong relationship between the concentrations of trace elements in irrigational water supply and their accumulation in agricultural crops (Sharma *et al*., 2006). Thus, the deposition of heavy metals on water bodies could doubly increase the human intake through food chain as well as through drinking water use. Most of the surface discharge sources contaminate soil and water bodies under limited spatial range, aerial emission which often follows long – range atmospheric transport, contaminate wider range of ecosystems down – wind to emission sources. Furthermore, unlike surface discharge, where stream – flow restricts mid – stream contamination, atmospheric deposition directly adds contaminants on to the water surfaces. Thus, despite all efforts to reduce surface – discharge – linked heavy metal contamination, addition of atmospherically driven toxic metals will continue to contaminate surface water resources even to those water bodies situated away from the emission sources. At a time when a human health has become a global priority, a better understanding of atmospheric deposition – linked heavy metal contamination of fresh water resources seems to have particular significance.

In the present study, an attempt was made to examine the variations in the concentrations of six heavy metals in mid – stream water of Ganga river in relation to their inputs through atmospheric deposition at Varanasi. Recent studies conducted in India have indicated the rising atmospheric transport of trace elements derived from distant sources, variations in the regional deposition patterns of these elements and, their significance with respect to contamination of terrestrial environment including agro – ecosystems (Singh and Agrawal, 2005; Pandey and Pandey, 2009). However, there is a general dearth of studies explicitly addressing the atmospheric transport of potentially toxic heavy metals in Indian river systems and their significant role in contaminating these fresh water resources. This investigation is an effort in this direction with a view to examine the magnitude of contamination of mid – stream Ganga water at Varanasi in relation to atmospheric deposition of some important heavy metals.

MATERIALS AND METHODS

The study area

The present study was conducted at selected sites of Ganga river at Varanasi between April, 2006 to March, 2008. The study area is situated between 25^0 $18^/$ N latitude and 83^0 $1^/$ E longitude in the midst of eastern Gangetic plane at 76.19 meter above msl. Eight sampling locations selected at 20 km long river site for this study

extends from Adalpura to 3 km down – stream of Malviya bridge at Rajghat (Table 1). The climate of the region is tropical monsoonal with dominant westerly winds.

Methods

The bulk atmospheric deposition was collected using bulk samplers which combine the precipitation and dry fallout in the same container. These collection systems were maintained at a height of 2 m and were devised to avoid bird nesting as described in Pandey and Pandey (2009). After collection, samples of atmospheric deposition were acidified with HNO_3 (Merck), filtered and stored in dark at ambient temperature before analysis. Heavy metals in atmospheric particulates were extracted following ternary acid digestion procedure (Allen *et al*., 1986). Mid – stream sub-surface water samples were digested with HNO_3 at 80^0 C (APHA, 1987). The concentrations of Cd, Cr, Cu, Ni, Pb and Zn in digested filtrates were determined with an atomic absorption spectrophotometer (Perkin Elmer model 2130, USA). A quality control has been performed using acidified water blank for checking the contaminations during field collection and during sample treatment in the laboratory.

Effects of sites and seasons were assessed using analysis of variance (ANOVA) following appropriate transformations whenever required. Correlation coefficients (r) were computed to test the linearity of relationships and temporal variability was determined by calculating coefficient of variation (CV) across time.

RESULTS AND DISCUSSION

The bulk atmospheric deposition was observed highest for Zn (124.15 – 477.18 g ha^{-1} y^{-1}) and lowest for Cd (0.56 - 20.15 g ha^{-1} y^{-1}). Atmospheric deposition of Pb (1.80 - 124.00 g ha^{-1} y^{-1}) also remained high. On spatial scale, the atmospheric deposition appeared higher at source oriented sites in comparison to those of the non – source oriented locations, the values being lowest at Adlpr (site 2) and increased almost consistently up to Rjght (site 8). Except for Zn, depositions of all the heavy metals were observed highest during winter (Fig. 1). Seasonal as well as between – site variations in the atmospheric deposition were significant ($p < 0.001$) (Table 2). Atmospheric deposition recorded in this study are, in general, comparable to those observed in earlier studies conducted in other parts of Indian tropics receiving similar atmospheric loadings (Singh and Agrawal, 2005; Pandey and Pandey, 2009).

Heavy metal concentration in mid – stream water showed large differences and followed a trend almost similar to those observed for atmospheric deposition. With few exceptions, concentrations of these metals increased almost consistently down – stream from Adlpr to Rjght (Fig. 2). Concentrations in mid – stream water were recorded maximum for Zn (26.70 – 198.60 µg L^{-1}) and minimum for Cd (ND – 8.60 µg L^{-1}). Similar observations have been made by Eder and Offiong (2002) for Lower Cross River Basin, Southeastern Nigeria. Except for Zn, concentrations were recorded highest during winter (Fig. 2b). For Zn, concentrations were recorded highest during summer (Fig. 2b).

In the present study, the concentrations of Cr (1.50 – 29.60 µg L^{-1}), Cu (2.41 – 18.45 µg L^{-1}) and Zn (26.75 – 198.60 µg L^{-1}) in mid – stream water of all the eight locations were well below their respective maximum admissible concentrations (MAC) of 50, 1000 and 5000 µg L^{-1} (Table 3). However, the concentrations of Cd (ND - 8.60 µg L^{-1}) were found to be greater than its MAC (3.0 µg L^{-1}) in 7 out of 8 locations sampled. Similarly, Pb concentrations (0.28 – 16.80 µg L^{-1}) in 7 out of 8 locations were higher than its MAC of 1.5 µg L^{-1}. Eighty seven percent of total water samples had Pb concentrations

above the MAC of 1.5 µg L^{-1}, while 82 % of the water samples showed Ni in excess of its MAC (20 µg L^{-1}). This may lead to serious health implications since Ganga water is also used for drinking purpose by a large population.

The patterns of spatial variations bear great significance in establishing source – receptor relationships. Site – wise variations of heavy metal concentrations in mid – stream river water as indicated by ANOVA was significant (Table 2). Correlation analysis indicated significant ($p < 0.01$) relationships between mean concentrations of Cd, Cr, Cu, Ni, Pb and Zn in water and their respective rates of aerial deposition (Table 4). Similar observations have been made by Thorton and Dise (1998) in a number of streams in English Lake District of Cumbria. The total aerial metal input which was computed as Cd + Cr + Cu + Ni + Pb + Zn, ranged from 160.12 – 643.35 g ha^{-1} y^{-1} and, with few exceptions, increased almost consistently from site 1 (Adlpr) to site 8 (Rjghtds). These atmospheric fluxes of total metals observed for Ganges although were significantly lower than those observed very earlier for Lake Michigan (Eisenreich, 1980), a corresponding trend in total metal concentration in mid – stream water (34.70 – 336.10 µg L^{-1}) is an indicative of the role of aerially – driven input of heavy metals in mid – stream water contamination. Temporal variability remained higher (cv = 0.123 – 0.336) for mid – stream heavy metal concentration in comparison to that of the atmospheric deposition (cv = 0.115 - 0.326). However, the differences between mean cv values of these two functions were not significant. This further support that the atmospheric deposition is the main contributor to mid – stream water contamination. Low temperature, calm wind and concurrent formation of inversion during winter could restrict dispersal and consequently raise the deposition of atmospheric aerosols. Zinc appeared exception due probably to added atmospheric loading of soil- borne particulates during summer months. Mid – stream heavy metal concentration showed almost similar seasonal pattern. Relatively high concentration of Zn during rainy season could be linked to surface – borne metal added through run – off.

The main sources of these elements into the atmosphere are urban – industrial emissions in adjoining areas (Pandey and Agrawal, 1994). Re - suspension of the land – deposited particulates coupled with predominant westerly winds could further substantiate deposition of heavy metals (Pandey and Pandey, 2009) towards down – wind locations. These inputs are in addition to the urban flushing and surface run – off being added to the river. However, since stream flow restricts cross – stream lateral mixing of surface – fed materials, atmospheric deposition could be considered as the major forcing factor responsible for mid – stream heavy metal contamination of Ganga river. A comparison of Adlpr site with rest of the sampling locations shows that more than 86 % of mid – stream water samples of the latter showed about 1.5 to 36 fold increase in the heavy metal concentrations under the influence of anthropogenic emission sources. Except for Adlpr (site 1), the remaining 7 locations fall into medium to high concentration zones (Eder and Offiong, 2002).

Our observations clearly indicate that Ganga river at Varanasi receive sizably high atmospheric inputs of Cd, Cr, Cu, Pb and Zn. The spatial and temporal patterns of atmospheric deposition strongly implicate the western and north – western periphery of river Ganga at Varanasi as the primary emission sources. Concentrations of these metals in mid – stream water showed significant correlations with their respective inputs through atmospheric depositions. This indicates that the atmospheric deposition is the major

contributor to mid – stream heavy metal contamination of Ganga water at Varanasi. The study suggests that the aerial catchment can sizably contribute to surface water contamination of potentially toxic metals. These observations form the first report on atmospheric deposition – linked mid – stream water contamination of Ganges. Furthermore, more than 82 % of water samples of 7 out of 8 locations sampled at Varanasi showed Cd, Ni and Pb levels above their maximum admissible concentrations. This may lead to serious health implications in long – run since Ganga water is also used for drinking purpose by a large population.

ACKNOWLEDGEMENTS

The authors are thankful to Head, Department of Botany, Banaras Hindu University for laboratory facilities and University Grants Commission (UGC), New Delhi for financial support.

REFERENCES

Allen, S. E., Grimshaw, H. M. and Rowland, A. P. (1986) Chemical analysis. pp. 285 – 344. *In* : P. D. Moore & S. B. Chapman (eds.) *Methods in Plant Ecology*. Blackwell Scientific Publication, Oxford, London.

American Public Health Association (1987) Standard Methods for the Examination of Water and Wastewater. APHA, Washington, DC.

Borbely – Kiss, I., Koltay, E., Szabo, G. Y., Bazo, L. and Tar, K. (1999) Composition and sources of urban and rural atmospheric aerosols in Eastern Hungry. *Journal of Aerosol Science,* 30, 369 – 291.

Bragazza, L. (2006) Heavy metals in bog waters : An alternative way to assess atmospheric precipitation quality ? *Global and PlanetaryChenges,* 53**,** 290 – 298.

Eder, A. and Offiong, O. E. (2002) Evaluation of water quality pollution indices for heavy metal contamination monitoring. A Case study from Akpabuyo – Odukpani area, Lower Cross River Basin (Southeastern Nigeria). *Geojournal,* 57, 295 – 304.

Eisenreich, S. J. (1980) Atmospheric input of trace metals to Lake Michigan. *Water, Air and Soil Pollution*, 13, 287 – 301.

Friedland, A. J., Miller, E. K. (1999) Major elemental cycling in a high elevation Adirondack forest : Patterns and changes, 1986 – 1996. *Ecological Applications,* 9**,** 958 – 967.

Kumar, S., Datta, R., Sinha, S., Kojima, T., Katoh, S. and Mohan, M. (2001) Carbon stock, afforestation and acidic deposition: An analysis of inter – relation with reference to arid areas. *Water, Air, and Soil Pollution,* 130, 1127 – 1132.

Pandey J. and Agrawal, M. (1994) Evaluation of air pollution phytotoxicity in a seasonally dry tropical urban environment using three woody perennials. *The New Phytologist,* 126, 53 – 61.

Pandey, U. and Pandey, J. (2005) The influence of catchment modifications on two fresh water lakes of Udaipur. pp. 256 – 262 In : K. K. S. Bhatia & S. D. Khobragade. (eds.) *Urban Lakes in India* : *Conservation, Management and Rejuvenation* (Part – I), National Institute Hydrology, Roorkee, India.

Pandey, J. and Pandey, U. (2009) Accumulation of heavy metals in dietary vegetables and cultivated soil horizon in organic farming system in relation to atmospheric deposition in a seasonally dry tropical region of India. *Environmental Monitoring and Assessment,* 148 (1), 61 – 74.

Sharma, R. K., Agrawal, M. and Marshall, F. (2006) Heavy metal contamination of soil and vegetables in suburban areas of Varanasi, India. *Ecotoxicology and Environmental Safety,* 66, 258 – 266.

Siegel, F. R. (2002) Environmental geochemistry of potentially toxic metals. Springer – Verlag, Berlin.

Singh, R. K. and Agrawal, M. (2005) Atmospheric deposition around a heavily industrialized area in a seasonally dry tropical environment of India. *Environmental Pollution,* 138**,** 142 – 152.

Thornton, G. J. P. and Dise, N. B. (1998) The influence of catchment characteristics, agricultural activities and atmospheric deposition on the chemistry of small streams in the English Lake District. *The Science of the Total Environment,* 216, 63 – 75.

Table 1. Description of sampling sites.

S. N.	Sampling sites	Site code	Description
1.	Adalpura	Adlpr	2 km upstream to famous Sheetla Mata temple at Adalpura
2.	Bypass upstream	Bypus	2 km upstream to bypass (highway) bridge
3.	Bypass downstream	Bypds	Downstream bypass (highway) bridge
4.	Samne Ghat	Smnght	Near panton bridge connecting to Ramnagar
5.	Assi Ghat	Asght	Near historical Assi Ghat
6.	Dashaswamedh Ghat	Dsmdght	Near historical Dashaswamedh Ghat
7.	Raj Ghat upstream	Rjghtus	Upstream to Malviya bridge
8.	Raj Ghat downstream	Rjghtds	3 km downstream to Malviya bridge

Table 2. F ratio obtained from two – way analysis of variance (ANOVA) for heavy metal concentrations in Ganga water.

Source of variation	Cd	Cr	Cu	Ni	Pb	Zn
Atmospheric deposition						
Site (S)	67.38*	37.11*	34.65*	69.24*	112.26*	39.61*
Season (s)	56.30**	23.60**	31.70**	44.00**	68.90**	21.82**
S × s	42.75**	12.45**	16.27**	23.48**	37.25**	11.70**
River water						
Site (S)	77.36**	23.67**	29.52**	26.56**	78.33**	36.00**
Season (s)	48.81**	16.00**	18.96**	12.26**	42.86**	4.40*
S × s	26.18**	7.60**	95.60**	9.38**	35.60**	3.32*

*$P < 0.01$; **$P < 0.001$

Table 3. Percent of water samples with heavy metals exceeding their respective MAC*

Sampling stations	% water samples > MAC*					
	Cd	Cr	Cu	Ni	Pb	Zn
Adlpr	-	-	-	-	-	-
Bypus	36	-	-	12	68	-
Bypds	68	-	-	68	100	-
Smnght	72	-	-	72	100	-
Asght	100	-	-	100	100	-
Dsmdght	100	-	-	100	100	-
Rjghtus	100	-	-	100	100	-
Rjghtds	100	-	-	100	100	-

*MAC : maximum admissible concentration (Siegel, 2002)

Table 4. Correlation matrix between heavy metal concentration in mid – stream river water and their respective input through atmospheric deposition.

Variable	Cd	Cr	Cu	Ni	Pb	Zn
Cd	0.563**					
Cr	0.361	0.488**				
Cu	0.426*	0.352	0.532**			
Ni	0.218	0.426*	0.361	0.467*		
Pb	0.446*	0.429*	0.426*	0.397	0.572**	
Zn	0.176	0.273	0.328	0.418*	0.245	0.434*

*$P < 0.05$; **$P < 0.01$

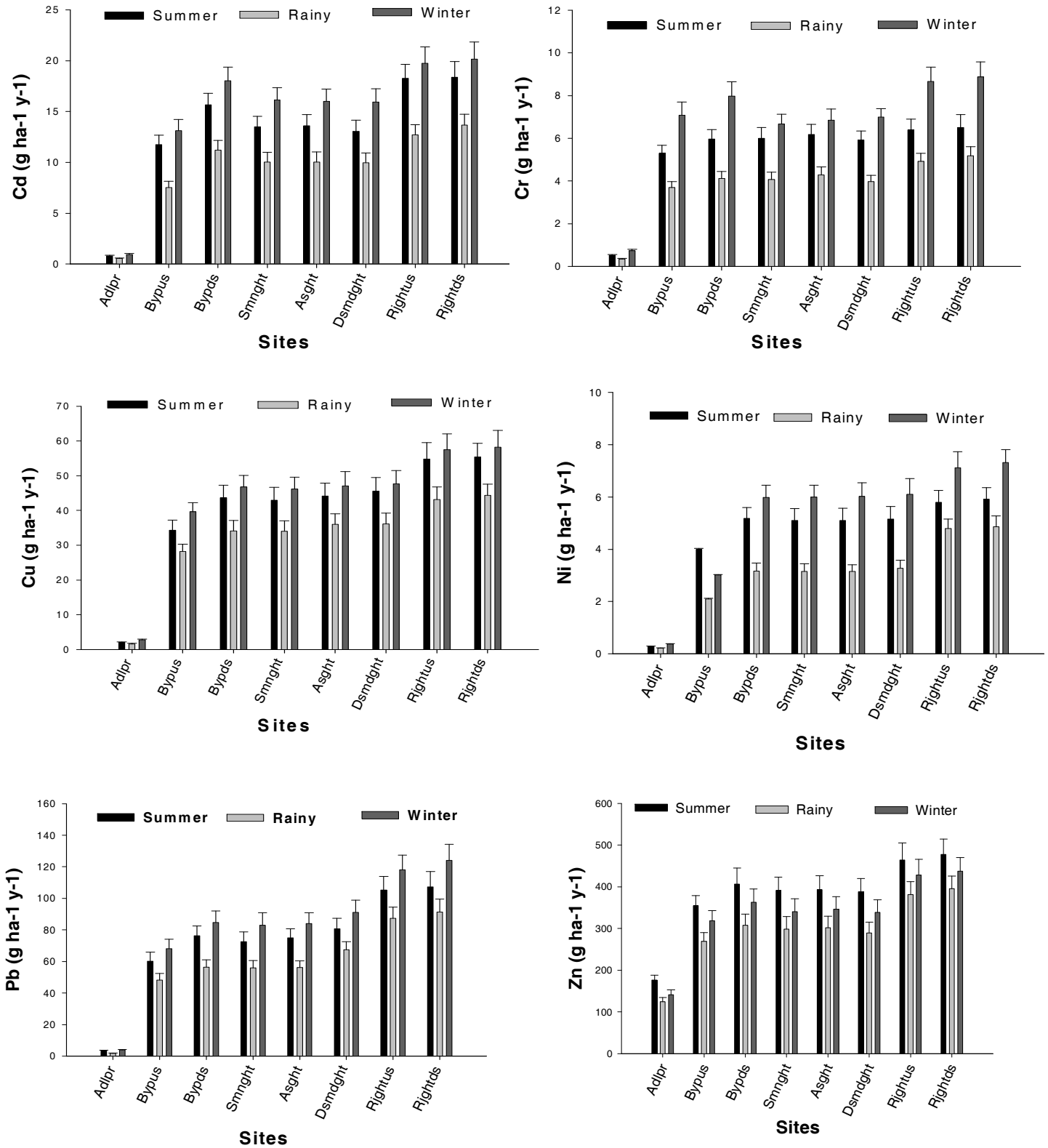

Figure1. Atmospheric deposition of heavy metals at selected river sites of Varanasi. Values are mean (n = 48) ± 1SE

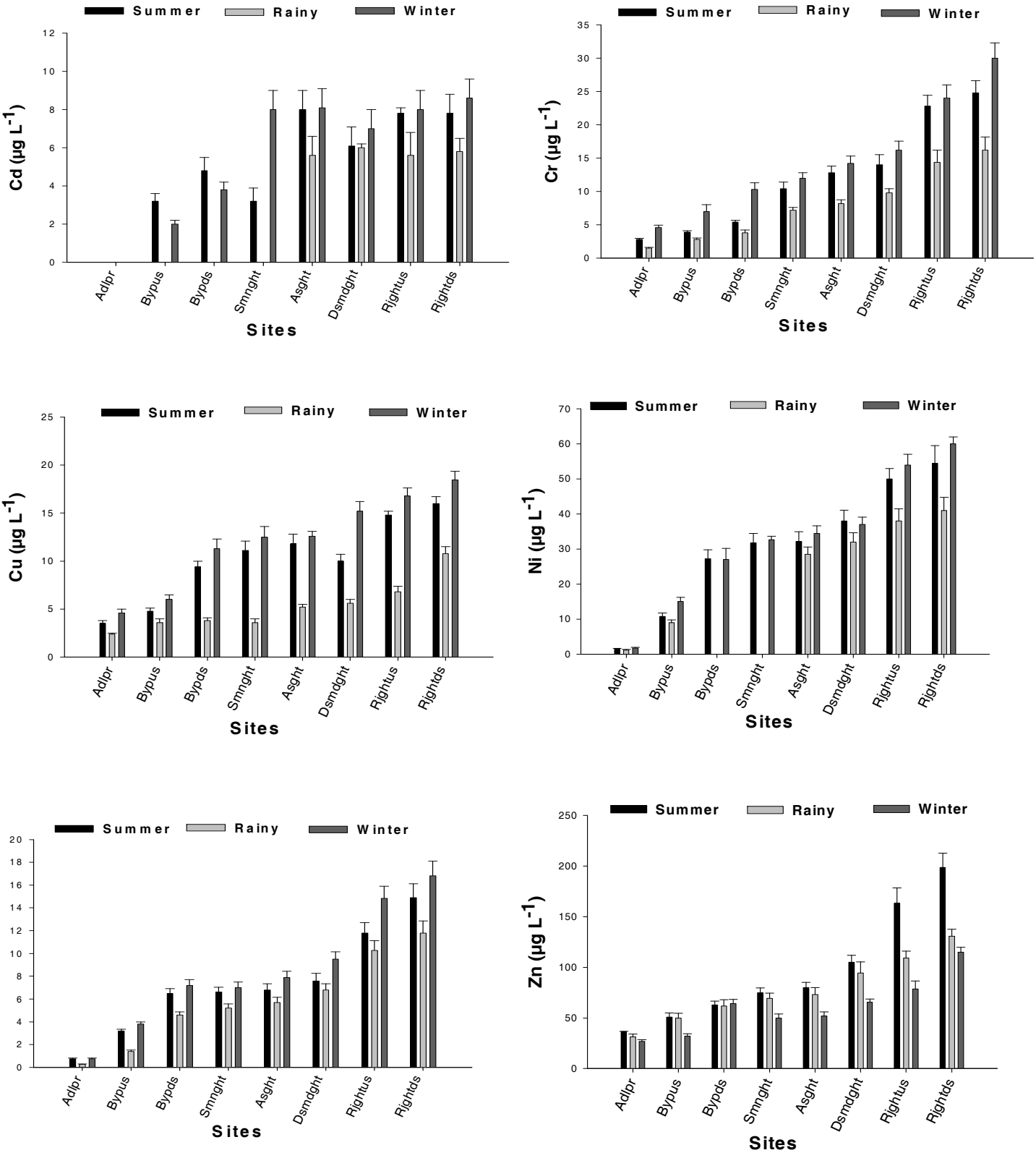

Figure2. Concentrations of heavy metals in mid – stream water of Ganga river at Varanasi. Values are mean (n = 48) ± 1SE. Values not appeared in the figure are below detectable limits

The effect of sewage pollutant of Bandar Imam Petrochemical Company on benthic macrofauna community using biodiversity indices and bioindicators

Taybeh Tabatabaie[1], Fazel Amiri[2] M.B. Nabavi, M.Sh. Fazeli, M.Afkhami [3]

[1] Former Graduate Student of Islamic Azad University Department of Environmental, Research and Science Branch Ahwaz, Iran.
Corresponding Author's : tabatabaie20@yahoo.com

[2] Faculty Member of Islamic Azad University Department of Natural Resources, Bushehr Branch, Iran. famiri@na.iut.ac.ir , famiri@iaubushehr.ac.ir

[3] Assist. Prof. Department of Environmental, Islamic Azad University, Research and Science Branch Ahwaz, Iran.

Abstract

Macrobenthos are an important part of sea-bed fauna which include *Polycheata*, *Decapoda* and *Mollusca*. Some species of this group are considered as biological indicators for aquatic ecosystem. Macrobenthos are mostly inhabitants without migration and they can be used as indexes of ecological crises related to water. In the present research, benthic community structure in Ghanam creek and region of Mossa creek, It is located around B.I.P.C sewage outlet were studied, eight station were selected, and water & sediment samples were collected in two season warm (September) and cold (February). Result of research indicated that station of sewage outlet around had least species and higher organic matter, on the contrary, the station far from petrochemical industry (station located in Ghanam creek) activities had higher species diversity. Also, present study showed that Polychaetes, reference of pollution bioindicators had higher aboundance. Cosequently, macrobenthic biodiversity relation with dissolved oxyqen and percentage of organic matter in the sediment.

Key words: Macrobenthos, Ghanam creek, Dissolved oxygen

1. Introduction

Creeks usually considered as most complex and riches ecosystems in aquaticecosystem, and one of as important zones of environmental. Human activity increased in the ecosystems (example industries settlement or entrance of pollutant sewage of urban, industry or agriculture) to cause destroied these ecosystem, because of high production of organic matter and provide a safety place for varied marines.

Mossa creek is a long canal with high depth, it is a tidal marine in Iran. The creek stretches almost 56 km along the North western of the Persian Gulf. It is connected with Mahshahr port and Shadegan watershed (largest watershed in Iran), width of creek on opening mouth is 37-40 km. Water depth on the west is 80m, and on the East decreased (5-18m). Tidal wave in zone cause to water of creek mixed with Persian Gulf. Change of water quantity within seasons is 4m.

It contains numerous sources of organic pollution including sewage outlet industries. The creek is of immense importance to zone for trading, commercial development and increase petrochemical industries.

However industry location in the area to cause huge volume entrance of industry and non-industry pollutans to this aqua ecosystem. In the present research , environmetal condition in Ghanam greek (reference of unpollution creek) and region of Mossa creek, it is located around Bandar Iman Petrochemical Company(B.I.P.C) sewage outlet (reference of pollution Maximum), were studied.

Previous pollution survey in the Ghanam creek, performed Nabavi and Savari(2002), Mahdi soltani(2007) showed that, this area had moderate pollution load.

The objective of this study is to analyse the relationship between Macrobenthos with physicochemical parameter, percentage of organic matter and gerain sediment analyse (GSA) for determine pollution load.

2. Material and methods

2.1. Site selection

Mossa creek is situated in North western Persian gulf ($30^\circ\ 21'$ until $30^\circ\ 31'$, $48^\circ\ 52'$ until $49^\circ\ 15'$). Bandar Iman Petrochemical located in North of Mossa creek, it is largest petrochemical company in Iran, this area is 450 ha . For the purpose of this study, the eight stations along Mossa creek were selected. Stations 1,2&5 were siuated in the earlier sewage outlet of B.I.P.C, Stations 3&4 located in distance 500m from sewage outlet, and Stations 6,7&8 located in Ghanam creek (Figure.1). The creek was sampled on the 8th September 2007, and 8th February 2008.

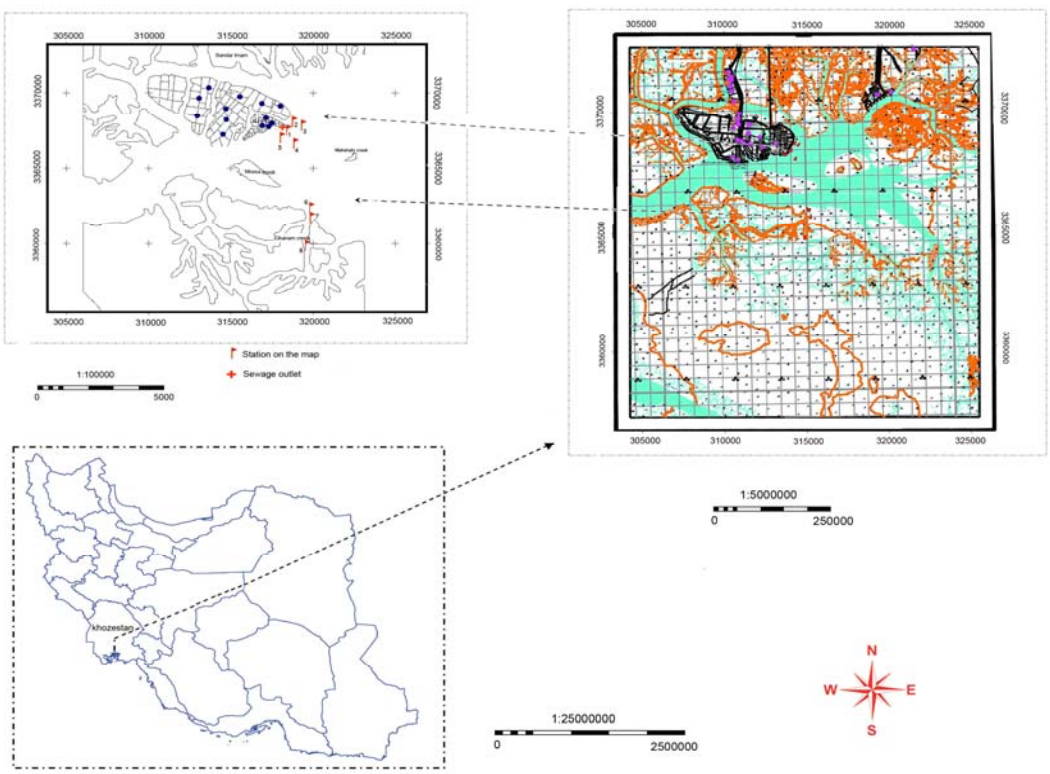

Figure 1. Location of the Mossa creek and B.I.P.C. The sampling stations are indicated.

2.2. Water sampling

Water samples were taken in 3 bottles from each station. Point samples in each satation were determined with GPS. Samples were taken from water near the bottom of the creek with Nansen. The dissolved oxygen (DO) and temperature were measured "insitu" by portable do-meter. pH and Salinity were measured in laboratory.

2.3. Macrobenthos sampling

Four grab amples were collected at eight stations with Van Veen grab of $0.025\,m^2$. Three of the samples were allocated to study the macrobenthic and fourth was used for sediment analysis. Samples for macrobenthos were processed through a sieve with a mesh size of $0.5\,mm$ and the retained fraction was fixed 5% formalin stained with Rose Bengal. Granulometry of the sediment was determined using Buchanan and Kain's method (Bunchanan 8 kain, 1984). The organic content was analysed using Elwakeel riley method.

2.4. Statistical Analysis

The total number of species, the shannon- weaver diversity index(Shannonand Weaver 1963) was calculated for each station by using MVSP (Multiple Variate Statistical Package, 2007) software.Differences between stations were tested with one-way ANOVA and differences between seasons were tested with t-test after verifying normality using the Kolmogorov- Smirnov test (Zar, 1999). Correlation between diversity index and physicochemical parameters were calculated by Spearman test. Compersion between stations, season was performed by Duncan's post hoc test. The affinities among stations, based on the macrofona species, were established trough cluster analysis,using UPGMA(unweighted pair group method using arithmetic averages),(Estacio et al, 1997; Garcia & Gomez, 2005).

3. Results

3.1. Physicochemical parameters

Results of ANOVA showed that no difference between stations for purpose of temperature (p=0.985), PH (p=0.425) and percentage of organic mater (p=0.16); also t-test analysis showed that no difference between seasons based on DO(p=0.435) and percentage of organic matter variables (p=0.378). The statistical analysis indicat that the oxygen dissolved and salinity was different between station ($p \leq 0.05$).The different between pH, temperature and salinity was significant ($p \leq 0.05$). All stations for cold and warm season were dominated by silty-clay (Figure.2 and Figure.3). The cluster analysis approach between stations indicat that the physicochemicaly variables was different near and far from sewage outlet (Figure.4).

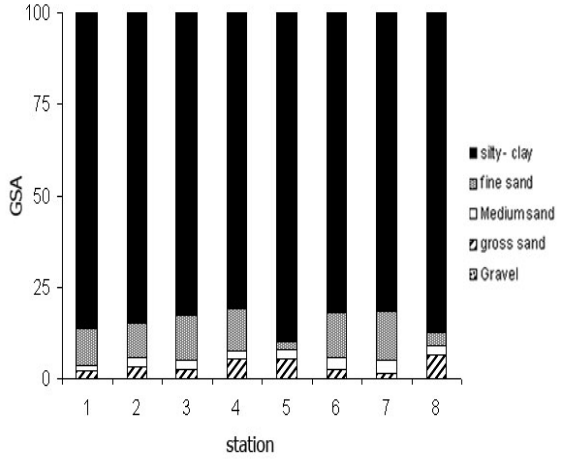

Figureure 2. warm season

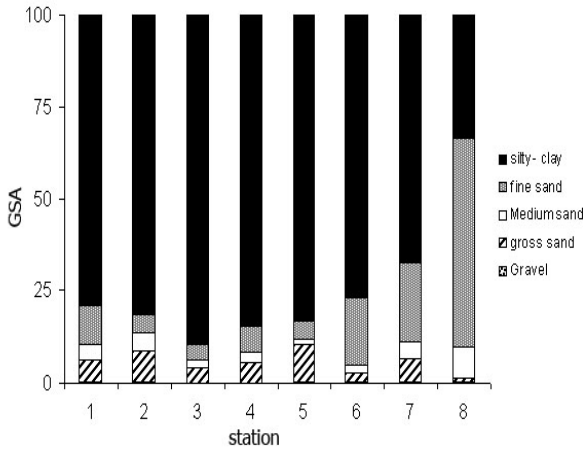

Figureure 3. cold season

Figureure 2. and Figureure 3. Sediment granulometry measured in the eight stations sampled in the warm and cold season.

Spearman analysis gives a correlation of -0.50 between oxygen concentration and organic matter (Figure.5& Figure.6). Also the correlation of 0.55 between changes in the total organic matter and percentages of silty-clay (Figure 7, Figure 8).

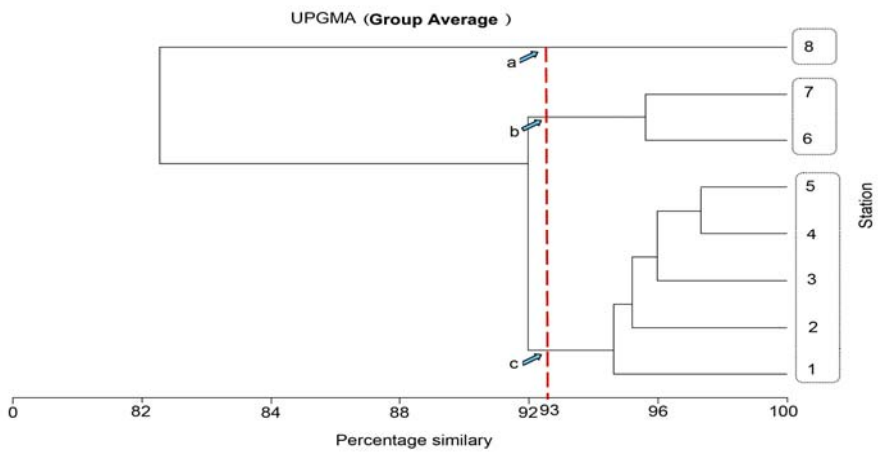

Figure 4. Cluster analysis elaborated using the value of the physicochemical parameters measured in stations.

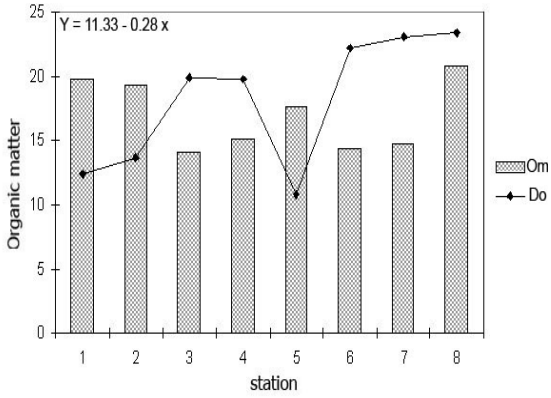

Figure.5. warm season

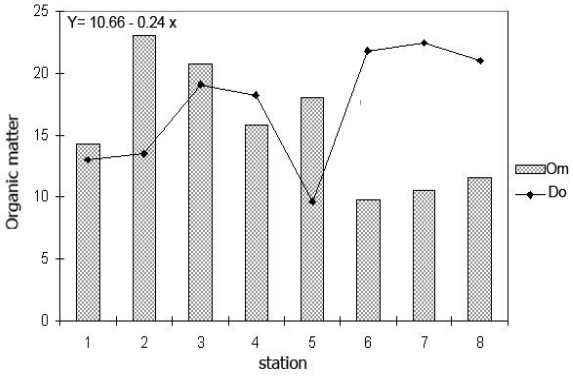

Figure.6. cold season

Figure.5& Figure.6. Comparison between the dissolved oxygen ($\frac{mg}{l}$) and total organic matter (OM) in sediment (%) measured in stations, in the warm and cold season.

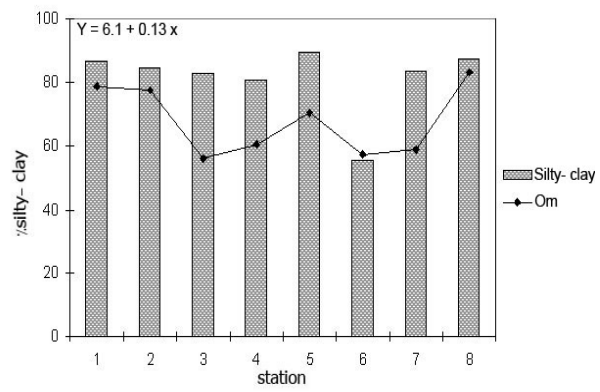

Figure 7. warm season

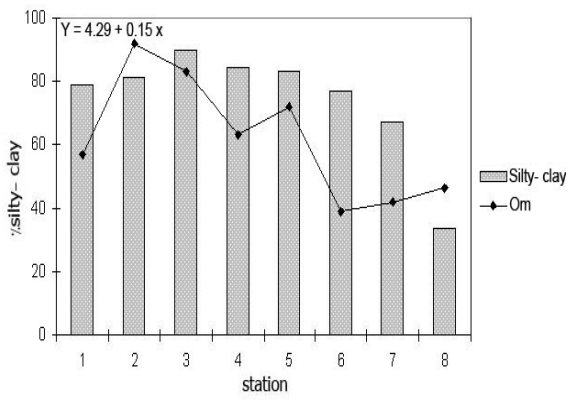

Figure.8. cold season

Figure 7and Figure 8. Comparision between the total organic matter(OM) in sediment (%) and Silty-Clay grains (%) measured in the stations for seasons.

3.2. Macrobenthos

Figure.9 show condition of shanon's index between station. According to statistical analysis , difference between stations was significant($p \leq 0.05$). Cluster analysis based on shanon's index were able to discriminate between stations of near and far from sewage outlet (Figure.10). The polychaetes community was discriminating in the particular conditions (Figure.11, Figure.12).

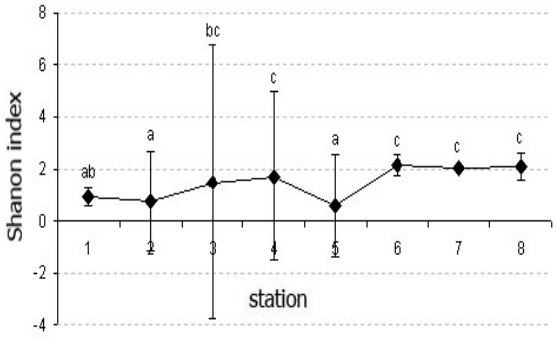

Figure 9. Average of shanon index condition in the station.

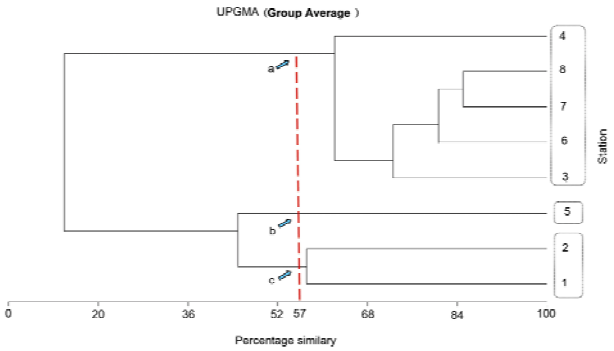

Figure 10. Cluster analysis using the shanon index in each station .

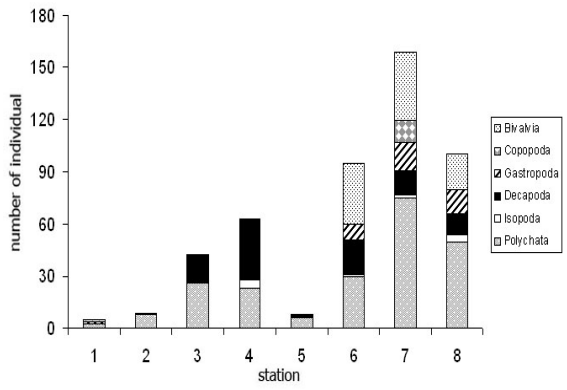

Figure 11. warm season

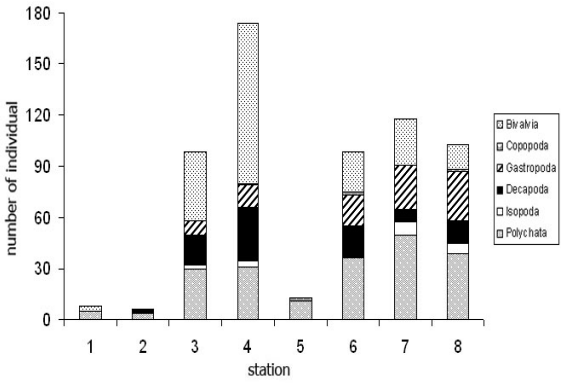

Figure 12. Cold season

Figure 11and Figure 12. Number of individuals in all stations for warm and cold season.

A sperman analysis give a correlation of0.93 between of shanon's index and combination DO (Figure 13 and Figure 14).

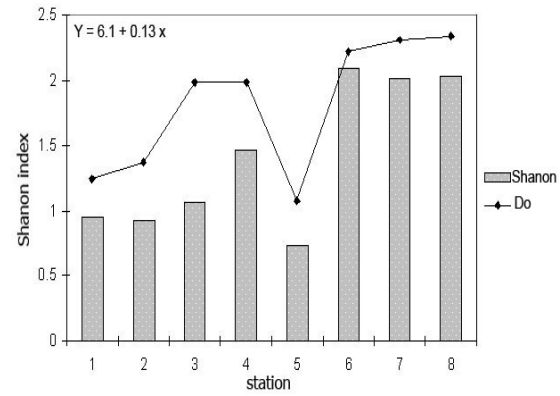

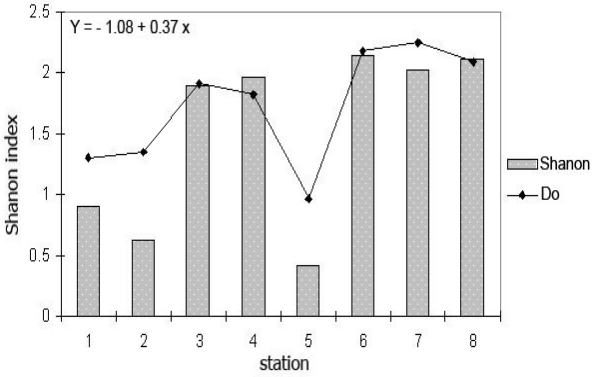

Figure 13 and Figure 14. Relationship between the shanon index and Do(mg^{-1}) showed in the warm and cold season.

4. Discussion

BIPC located near the Mossa creek and enterance sewage outlet in to this aqua ecosystem.Sewage outlet to cause decrease dissolved oxygen, species diversity and increase percentage of organic matter in the neighbouring stations of sewage outlet. Also according to Welch index, near stations sewage outlet to settle in class of high load pollution.

Table 1. Welch index (1992)

Welch index	Class of water quality
3-5	High pollution
1-3	Moderate pollution
<1	Unpollution water

Table 2. Condition of stations acording to Welch index

Class of water quality	Stations
High pollution	**1,2& 5**
Moderate pollution	**3,4,6,7& 8**

The results of this study show that organic pollution value increase in fine grain of sediment. Our results seem to support the review by Susana carvalho etal (2006);(Figure.2 and Figure.3). In the Mossa creek, polychaetes turned out to be the best group to discriminate between all station. In most of the studies, the polychates were refere to marine pollution, especially to the lack of oxygen and usually discriminate among station better than other groups of Macrobenthos (Carvalho etal. 2006, Garcia and Gomes.2005). The results of this research indicated that macrobenthos diversity relate with dissolved oxygen end percentage of organic matter, the present study highlighted zones of high and low pollution impact on the macrobenthic fauna. Generally, Macrobenthos assemblage decrease from the near seawage outlet, with the opposite pattern for dissolved oxygen, which has led to an increase of macrobenthos in the Ghanam creek.

Abu-hilal(1994), Hassan etal(1995) and EL-sammak(2001) established that high level of organic pollution in Dubai creek to cause decrease dissolved oxygen and macrobenthos diversity.Johansson (1997), Flemer(1999) and Wu(2002) to explained that, in response to decreasing oxygen concentration, species richness and diversity both decrease, and the species composition is largely determined by the tolerance to oxygen deficiency. The adverse biological effects on soft bottom communities are mainly due to reduced oxygen content of the water (Saiz-Salinaz, 1997). However, the interpretation of stress due to low dissolved oxygen is difficult because there is a lack of information about oxygen tolerances for most macrobenthic species (Dauer etal, 1993). Consequently, the importance of oxygen in water column and percentage of organic matter in sediment as key factors for macrofaunal assemblage in sediment is well known. Figure.15 summarises possible outcomes under different levels of organic matter and dissolved oxygen.

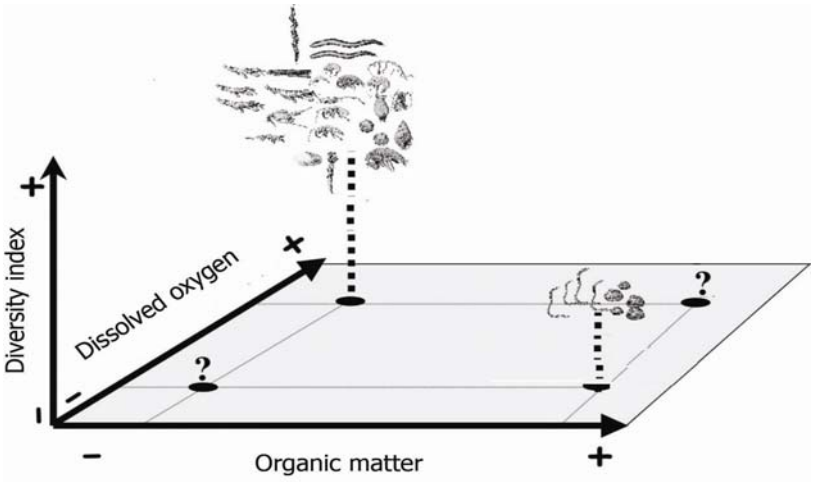

Figureure 15. Schematic model indicating the diversity index under different level of organic matter and dissolved oxygen.

References

1. Abu-Hilal, A. H., Adam, A. B., Banat, I. m., Hassan, E. S., (1994). Sanitary conditions in three creeks in Dubai, Sharjeh and Ajman Emirates on the Arabian Gulf (UAE). Environ. Monit. Assess. 32, pp. 21-36.

2. Buchanan, J. B., Kian, J. M., (1984). Measurment of the physical and chemical environment. In: Holme,N. A. , Meintyre, A. D. , Methods for the study of marine benthos. Blackwell scientific publications, Oxford, pp. 30-50.

3. Dauer, D. M., Luckenbach,M. W., Rodi, A. J., (1993). Abundance biomass comparison : effect of an estuarine

   gradient, anoxic/ hypoxic events and contaminated sediments. Marine Biology 116, pp. 507-518.

4. El-Sammak, A., (2001). Heavy metal pollution in bottom sediment, Dubai, united Arab Emirates. Bull. Environ. Contam. Toxical. 67, pp. 296-303.

5. Estacio, F. J.,Garcia-Adiego, E. M., D. A., Garcia- Gomez, J. C., Daza, J. L., Hortas, F., Gomez-Ariza, J. L.,(1997). Ecological analysis in a polluted area of Algeciras Bay(southern spain): external versus internal out falls and environmental implications. Marine Pollution Bulletin34, pp. 780-793.

6. Flemer, D. A., Kruczynski, W. L., Ruth, B. F., Bundrick, C. M., (1999). The relative influence of hypoxia, anoxcia and associated environmental factors as determinants of macrobenthic community structure in a Northern Gulf of Mexico estuary. Journal of Aquatic Ecosystem stress and Recovery 6, pp. 311-328.

7. Guerra- Garcia, J. M., Garcia- Gomez, J. C., (2005). Oxygen levels versus chemical pollutions: do they have similar influence on macro faunal assemblages? Acase study in a harbour with two opposing entrances, Environmental pollution 2005, 281-291.

8. Hassan, E. S. , Banat, I. M., Abu-Hilal, A. H., (1995). post- gulf war nutrients and microbial assessment for coastal waters of Dubai, Sharjeah, and ajman

Emirates(UAE). Environ. Int. 21(1), pp. 23-32.

9. Johansson, B., (1997). Behavioral response to gradually declining oxygen concentration by Baltic sea macrobenthic crustaceans. Marine Biology 129, pp. 71-78.
10. Kazemi, J., (2002). Study environmental effect of mercury in the Bandar Imam Petrochemical Company sewage on Mossa creek environmental. MSC thesis.
11. Mahdavi Soltani, J., (2007).Comparsion of benthic communities structure in Gazaleh and Ghanam creeks as bioindicators of pollution. MSC thesis.
12. Mojtahedzadeh, Z., (2005). Description of environmental management frame of "AR" and "PX" in Bandar Imam Petrochemical Company. MSC thesis.
13. Nabavi, M.B., Savari,A., (2002). Indices of critical environmental in Mossa creek and improvment methods.Three conference of criticalies environmental.
14. Saiz-Salinaz, J. I.,(1997). Evaluation of adverse biological effects induced by pollution in the Bilbaoo estuary (spain). Environmental Pollution 96, pp. 351-359.
15. Shannon, C. E., Weaner, W., (1963). The mathematical theory of communications . University of Ilinois press. Urbana, pp. 117.
16. Susana Carvalho, Miguel B. Gaspar, Ana Moura, Carlos Vale, Paulo Antunes, Odete Gil, Luis cancela da Fonseca, manuela falcao, (2006). The use marine biotic index AMBI in the assessment of the ecological status of the Obidos lagoon(Portugal). Marine pollution Bulletin.
17. Wu, R. S. S., (2002). Hypoxia:form molecular responses to ecosystem responses. Marine Pollution Bulletin45, pp. 35-45.
18. Zar, J. H., (1999). Biostatistical Analysis (4th ed.), Prentice Hall, Upper Saddle River, NJ.

Enzymatic Treatment of a Modified Food Processing Wastewater

Dr. Anastasia E. M. Chirnside

Anastasia E. M. Chirnside, Assistant Professor, Department of Bioresources Engineering, University of Delaware. 531 South College Ave., Newark, DE 19716-2140. Tel: 302-831-8871, Fax: 302-831-2469, aemc@udel.edu.

Abstract

The wastewater resulting from soy-processing is found to have extremely high amounts of Total Kjeldahl Nitrogen (TKN), Chemical Oxygen Demand (COD) and a high pH. We have developed an attached growth, packed-bed bioreactor (PBR) containing the white rot fungus (WRF), *Phanerochaete chrysosporium*. This fungus secretes enzymes that catalyze oxidation reactions resulting in degradation of recalcitrant compounds. Previous studies utilizing the fungus in the bioreactor found that the high pH of the wastewater caused inhibition of TKN and COD degradation. Adjustment of the wastewater pH before introduction into the bioreactor resulted in a greater reduction of TKN and COD. However, complete degradation did not occur and pH adjustment was required continuously. Thus, we investigated the effectiveness of treating the wastewater with the enzyme culture solution obtained from the reactor instead of utilizing the fungal reactor itself in order to overcome the inhibitory effect of high pH on fungal activity within the reactor.

The inorganic forms of nitrogen found in the pH adjusted wastewater were removed by treatment with both anion and cation exchange columns. Diluted wastewater (10% and 20%) was treated with enzyme solution (5% and 10%) and monitored for changes in TKN and COD for 24 hours. There was little change in pH over time for any of the treatments. The COD dropped 50 – 67% for all treatments over 24 hours. Removal of the inorganic nitrogen within the wastewater before treatment with the enzymes resulted in a greater reduction in COD. There was little change in TKN over time for any of the treatments.

Treating the wastewater with fungal enzymes successfully reduced the COD concentration by approximately 60%. The results indicate that the use of the ligninolytic enzymes of the white rot fungi to degrade soy-processing wastewater could be a viable treatment technology.

Introduction

Soybean hulls are processed into soy flour in a method similar to paper mill production. The wastewater (SHW) resulting from the soy-processing is found to have

extremely high amounts of Total Kjeldahl Nitrogen (TKN), Chemical Oxygen Demand (COD) and a high pH. After conventional aerobic and anaerobic treatment, the SHW still has extremely high concentrations of TKN (300-350 mg/l), COD (4,000-5,000 mg/l) and pH (>8.0) [Cabe, 2002]. The soy flour processing plant has a NPDES permit to discharge wastewater despite its high levels of TKN. The reasoning for this decision is that the nitrogen is in a complex form that is unavailable to the degrading organisms and therefore will not add to the degradation of the surface water quality. However, this assumption may not include consideration of photo-degradation processes that would, in fact, result in nitrogen availability. Developing a BAT that can treat and remove this nitrogen before the wastewater is discharged would be an environmentally safer approach. The overall objective of this project is to investigate possible alternative treatment technologies.

In recent years white rot fungi, specifically *Phanerochaete chrysosporium*, have been found to have the ability to degrade an extremely diverse range of very persistent or toxic environmental pollutants. Studies have shown that the white rot fungus is able to degrade pesticides, polyaromatic hydrocarbons, polychlorinated biphenyls (PCBs), and most halogenated aromatics (Hammel, 1995; Reddy and Mathew, 2001; and Wu and Yumiko, 1996). We have developed an attached growth, packed-bed bioreactor (PBR) containing the white rot fungus (WRF), *Phanerochaete chrysosporium.* This fungus secretes enzymes that catalyze oxidation reactions resulting in degradation of recalcitrant compounds. Previous studies utilizing the fungus in the bioreactor found that the high pH of the wastewater caused inhibition of TKN and COD degradation (Hetrick and Chirnside, 2001). Adjustment of the wastewater pH before introduction into the bioreactor resulted in a greater reduction of TKN and COD. However, complete degradation did not occur and pH adjustment was required continuously.

The objective of this study was to investigate the effectiveness of treating the wastewater with the enzyme culture solution obtained from the reactor instead of utilizing the fungal reactor itself in order to overcome the inhibitory effect of high pH on fungal activity within the reactor. Initially, the inorganic forms of nitrogen found in the wastewater will be removed by treatment with both anion and cation exchange columns. Therefore, there will be no chance that the enzymes will react with the inorganic nitrogen.

Material and Methods

The WRF was grown and placed in the PBR according to methods described by Chirnside (2008). The fungus was fed growth solution in the PBR for 2 months. Then 4 liters of carbon-limited media was fed to the WRF to initiate peroxidase enzyme production. The pH of the wastewater was adjusted to 7.52 utilizing concentrated H_2SO_4.

The lignin peroxidase enzyme (LiP) extracted from the PBR was used for the experiments. The enzyme solution was tested for activity following the procedure outlined in Chirnside (2008). The enzyme assay resulted in a LiP activity of 871.2 U l^{-1} and a manganese peroxidase activity of 849.0 U l^{-1}. Inorganic nitrogen was removed from half of the wastewater using cation and anion exchange columns. The pH was readjusted

to below 7. Two wastewater dilutions (10% and 20%) and 2 enzyme concentrations (5% and 10%) were examined. The diluted wastewater was treated with the enzyme solutions and monitored for changes in TKN, pH, and COD for 24 hours. Sampled times were at 0 hours, 2 hours, 4 hours, 8 hours, and 24 hours. The experiment was done in triplicate.

Results and Discussion

There was little change in pH over time for any of the treatments. The pH of the "no removal" treatments ranged 6.0 and 7.0 and did not change significantly over 24 hours. For the "removal" treatments, the pH ranged between 4.5 and 5.0 with little change over time. When the inorganic nitrogen was removed from the wastewater, addition of the enzyme solution caused a decrease in pH. There was a greater decrease in the treatments receiving the higher enzyme concentration (Figure 1).

Chemical oxygen demand (COD) dropped 50 – 67% for all treatments over 24 hours (Figure 2). The COD for all treatments began between 4750 and 5800 mgL^{-1} and all dropped below 3250 mgL^{-1} over 24 hours. There was a greater reduction in COD in the wastewater that was diluted 20% than that diluted to 10%. Removal of the inorganic nitrogen within the wastewater before treatment with the enzyme solution had little effect on the degradation of COD. For the treatments receiving higher enzyme concentrations, there was a slight increase in COD degradation.

There was little change in Total Kjeldahl Nitrogen (TKN) over time for any of the treatments (Figure 3). There was an increase in TKN for all treatments during the 24-hour incubation period. It was possible that the degradation of COD resulted in the release of NH_3-N, which would have resulted in higher TKN values. There was a greater decrease in TKN for treatments containing the treated wastewater (inorganic N removal). The greatest change was seen in the higher wastewater dilution containing the 10% enzyme solution.

Conclusions

Continuous recycling of pH-adjusted wastewater was an effective treatment for reducing both the TKN and the COD concentration of the soy processing wastewater. The success of the experiment indicates that further research would be advisable. The physical properties of the PBR need to be optimized in order to design a continuous treatment operation that would require little maintenance. Another option that could be investigated is the utilization of a series of bioreactors in which the effluent is pH-adjusted before introduction into the next bioreactor.

Treatment of the wastewater directly with the fungal enzymes had variable success in decreasing the TKN. When the inorganic nitrogen was removed from the wastewater, the solution pH remained equivalent to the pH of the enzyme solution. This would be advantageous to the ligninase enzyme system of the WRF. The presence of inorganic nitrogen and Total Kjeldahl Nitrogen caused the pH of the enzyme treated wastewater to rise slightly but the pH remained at a neutral value.

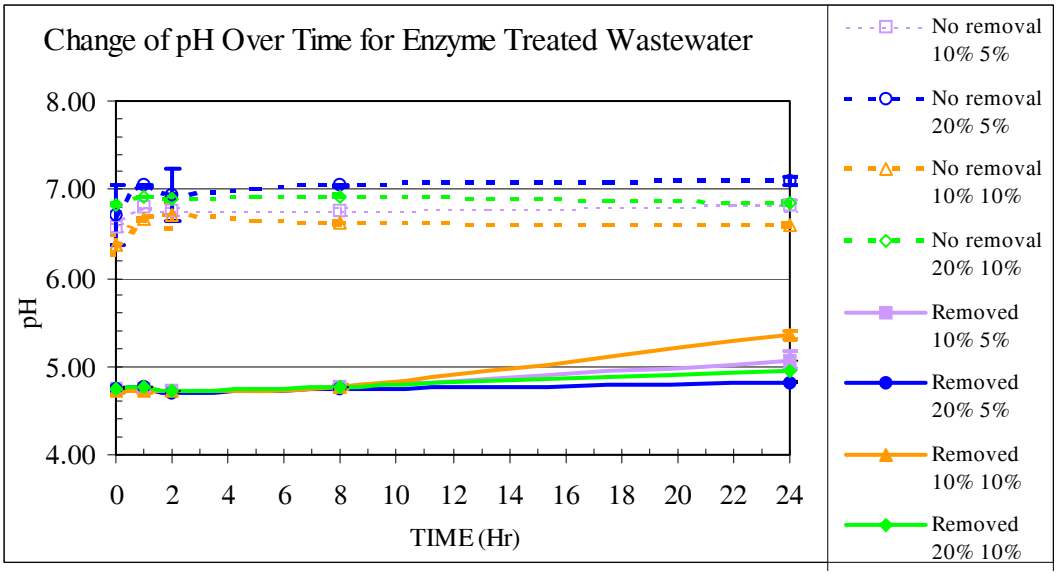

Figure 1. The change in pH over time for the enzyme treated wastewater. The solid curves represent the wastewater that had the inorganic N removed. The first percentage represents the wastewater dilution factor (20 or 10%), while the second percentage represents the enzyme concentration (10 or 5%).

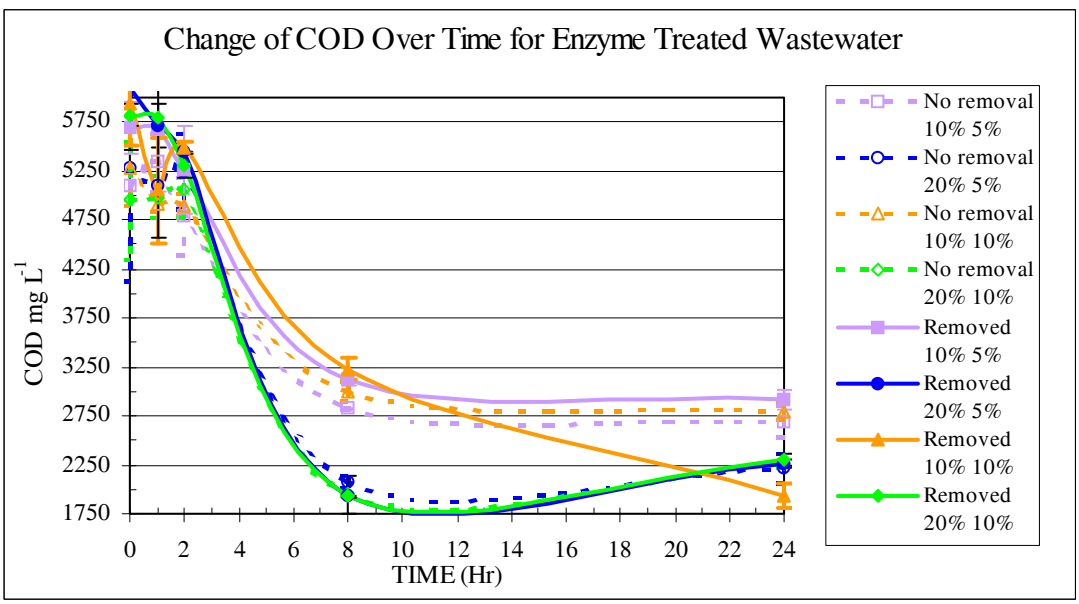

Figure 2. Change in COD over time of wastewater treated with fungal enzymes.

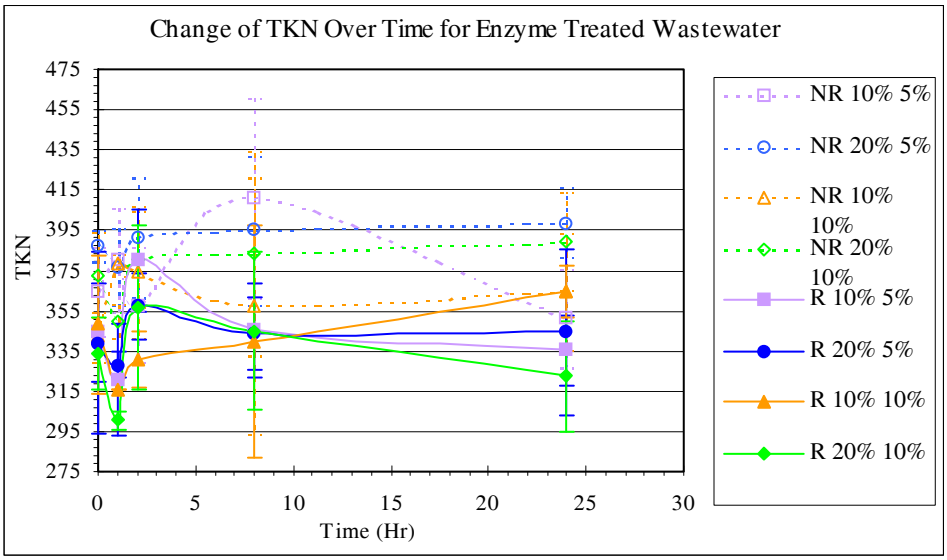

Figure 3. The change in TKN over time of wastewater treated with fungal enzymes.

There was little change in the TKN over time when the wastewater was treated directly with the fungal enzyme solution. However, TKN concentration increased and then decreased during the experiment indicating that chemical reactions were occurring. There was great variability in the TKN concentration during the first few hours of the experiment. Changing the sampling times of the experiment to assess changes during the first 2 to 3 hours may help to explain the decreases and increases in TKN concentration that occurred. The rates of TKN degradation differed among treatments especially during the first few hours. However, it was difficult to assess the trends of the different treatments due to the lack of observations during the first hour or two. Design changes in the experimental set up would provide better data to answer the objectives of this research.

Treating the wastewater with fungal enzymes successfully reduced the COD concentration by approximately 60%. The results indicate that the use of the ligninolytic enzymes of the white rot fungi to degrade soy-processing wastewater could be a viable treatment technology. However, the results also present more questions about the interrelationship between COD degradation and TKN concentration. In order to successfully remove both COD and TKN from the wastewater, a better understanding of the reaction chemistry is needed. Further research in this area would help design a treatment system that could effectively degrade both of these recalcitrant pollutants. Optimization of the PBR to increase both fungal growth and ligninolytic enzyme production is needed in order for this treatment method to become a “best available technology” in the National Pollutant Discharge Elimination System for wastewater discharge control under the Clean Water Act.

References

CABE Associates, Inc. (20020. "Companion Report to the Mexico Farms LLC NPDES Permit Application", January, Dover, DE.

Chirnside, A. E. M. (2008). "Biodegradation of a Food Processing Wastewater Utilizing *Phanerochaete chrysosporium*." *Proc., World Environmental and Water Resources Congress, May 12-16*, 2008, R. W. Babcock, Jr. and R. Walton, eds., Environmental and Water Resources Institute of the American Society of Civil Engineers, Honolulu, Hawaii

Hammel. K.E. (1995). "Organopollutant degradation by ligninolytic fungi." *Microbial transformation and degradation of toxic organic chemicals*, L. Y. Young and C. E. Cernigilia, eds., Wiley-Liss, Inc., New York, 331-346.

Hetrick, J. and A.E.M. Chirnside. (2001). "Biological Treatment of Industrial Wastewater". *Delaware Water Resources Center Student Research Conference Annual Report*. DWRC. Newark, DE.

Wu, F., O. Hiroaki and T. Yumiko. (1996). "Activities of Ligninolytic Enzymes of the White Rot Fungus, *Phanerochaete chrysosporium* and its recalcitrant substance degradability. *Water Science Technology*: 34(7-8): 69-78

The Affect of Municipal Landfill Leachate on the Characterization of Fluid Flow Through Clay

S. Merayyan[1] and A. Hope[2]

[1]Assistant Professor, Department of Civil Engineering, California State University, Sacramento, 6000 J. St., Sacramento, CA 95819-6029; PH (916)278-5349; FAX (916)278-7957; email:merayyan@csus.edu
[2]Project Engineer, RMC Water and Environment, 2001 N. Main St., Suite 400, Walnut Creek, CA 94596; PH (925)627-4100; FAX (925)627-4101; email:ahope@rmcwater.com

Abstract

Federal and state regulations prescribe design requirements for low permeability clay landfill liners based on saturated hydraulic conductivity. The assumption that clay liners are saturated for the duration of their life is a simplification of the true processes at work. The fact that clay liners are compacted to optimum, or just wet of optimum, proves that they are initially subject to unsaturated conditions, and it is well known that liners can remain variably saturated for the duration of their life. While this is appropriate for landfill cover liners, leaching affects may drastically change pore fluid chemistry as water moves through the landfill to the bottom liner. In this study the goal is to determine the affect of modeling two different pore fluids—leachate and water. This research uses an approach that critically assesses how leachate will move through a landfill bottom liner differently than water.

The result of this study is the affect of leachate on the soil-water characteristic curve and a quantitative comparison of how a liner would be expected to perform when permeated with leachate versus water. Samples prepared with leachate resulted in lower water content than samples prepared with water. Both the Van Genuchten and Cory-Brook models fit the data (leachate and water) very well. At higher (400 cm of water) the difference between the leachate samples and water sample became obvious.

Background

Historically solid waste landfills have included natural attenuation and containment landfills. Natural attenuation landfills focused on non-hazardous waste from municipal sources and typically leached into groundwater due to poorly constructed or no liners (Bagachi, 1994). Containment Landfills were developed in the latter half of the twentieth century to accepted wastes from industrial sources in addition to municipal wastes. These landfills used low permeability liners to restrict seepage of leachate to groundwater. As water percolates through the solid wastes, biological materials and chemical constituents are leached into solution as the waste undergoes simultaneous and interrelated biological, chemical, and physical changes (Bagachi, 1994). This solution is referred to as Leachate.

Current practice of sanitary landfill engineering came into play in 1984 with an amendment to the 1976 Resource Conservation and Recovery Act that gave the EPA jurisdiction over landfills (Hickman and Richard, 2000). The EPA responded with the prescriptive Subtitle D that is still referred to today for design specifications. In California landfills are classifies into three categories:

- Class I. Hazardous Waste
- Class II. Designated Waste
- Class III. Municipal Waste

Liners are materials which line the bottom and below grade-sides of a landfill and act as a final barrier to the underlying hydrogeology. Their primary function is to control leachate. Liners collect the landfill infiltration and divert it into leachate collection systems so standing water forms above the liner, forming a hydraulic head. Liners are the final defense for underlying aquifers. Because liners are subject to leachate infiltration, they are the focus of this study.

Covers and liners are multilayered systems with the focus around a low permeability layer. They are made up of three general materials: Geomembrane, geosynthetic clay liner, and compacted clay liners. Often a composite liner is used which utilizes a combination of these materials. Still today clay continues to be an important material in landfill liner design. When clay is used as a hydraulic barrier, field compaction usually occurs at a moisture content wet of optimum. This tends to yield a more oriented or dispersed structure which exhibits a lower hydraulic conductivity. Moisture contents ranging from 2% to 4% above optimum are common (Bagachi, 1994).

Both Federal and California law mandate cover and bottom liner systems for Class I, II, and III. Final Covers are closure and post closure measures which mostly serve to minimize infiltration into the landfill, mitigate erosion, and control gas emissions. Interim covers are spread over the active landfill face in order to control vectors, fire, water infiltration, erosion, and to prevent unsightliness (Dunn and Singh, 1995). Although cover liners are not naturally subjected to leachate seepage, facilities that use leachate recirculation systems will pump leachate from above the bottom liner and redirect it to above the waste layer or to a treatment system where it is removed from the landfill.

Minimum requirements for cover and liner systems are outlined in Titles 40, Part 258 of the Code of Federal Regulations and in Title 27, Chapter 3 of California Code of Regulations. Liners are required to meet minimum standards outlined in Subtitle D of these documents. Liner thickness is usually specified between five to twelve feet of clay, with two feet as the minimum, and hydraulic conductivities are specified in terms of saturated conductivity assuming water as the permeating fluid.

Federal and state regulations prescribe design requirements for low permeability layers based on intrinsic hydraulic conductivity using water as pore fluid. Research has shown that many of the mechanical properties of clay soils are closely related to the water-retention characteristics of the soil mass; and since the latter is a function of the mineralogy, pore fluid chemistry, fabric and structure of the soil mass; any change of the pore fluid chemistry may lead to a removal of the existing bonds and therefore an alteration of the internal equilibrium stability of the soil mass (Raymond et al., 1984).

The current approach to landfill liner design also bypasses an accurate prediction of the rate of water movement through the liner under unsaturated conditions and the assumption that clay liners are saturated for the duration of their life is a simplification of the true process at work. The fact that clay liners are compacted to optimum moisture content, or just wet of optimum, shows that they are initially subject to unsaturated conditions and it is well known that liners can remain variably saturated for the duration of their lives (Bigachi, 1994).

This study seeks to produce a more accurate account of the difference in complex fluid movement processes occurring in municipal landfill liners by accounting for clay-chemical

interactions via the soil-water characteristic relationship (see Figure 1). The purpose is to produce a quantitative one-dimensional comparison of the difference in how leachate and water will be expected to flow through a clay liner. Some of the defining parameters of the SWCC are the saturation water content (θs), irreducible water content (θr), and the air-entry pressure head (Ψ_a).

Figure 1. Soil-water Characteristic Curve (SWCC)

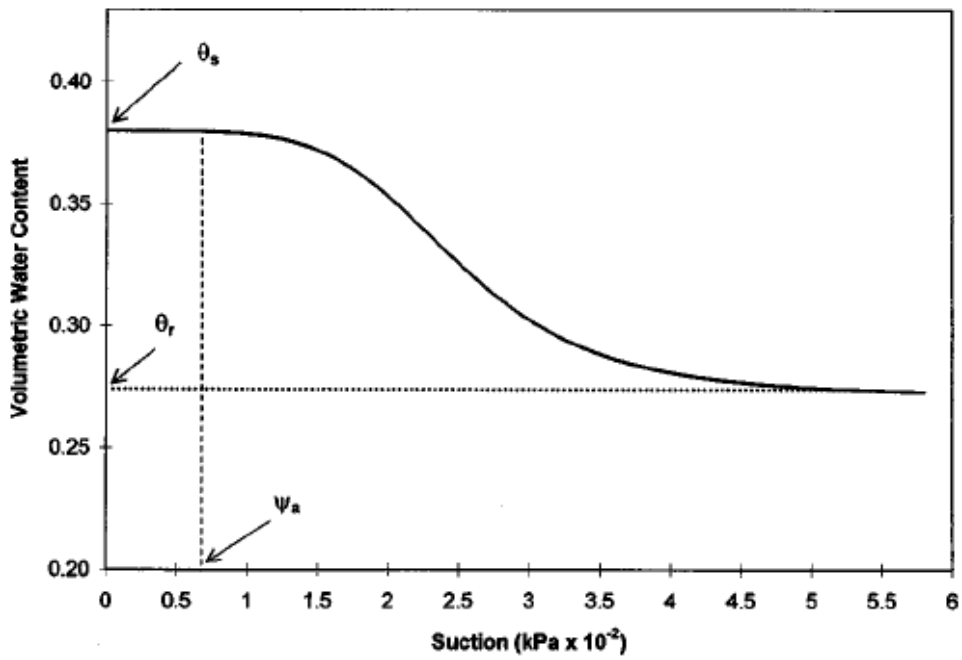

Material and Methodology

Clay

The clay used for this research was sampled from a stockpile currently supplying low permeability clay for the construction of two landfill liners for the Chicago Grade Landfill in the Atascadero-Templeton area of Northern San Luis Obispo County, California. Leachate was sampled from the City of Paso Robles Landfill located just outside of Paso Robles, CA in San Luis Obispo County. This is a Class III waste management facility permitted by the Regional Water Quality Control Board to dispose non-hazardous municipal solid waste.

An initial geotechnical analysis (see Tables 1 & 2) was performed in accordance with ASTM D698, D4318, C127, D70, and D854s on the clay samples to determine their basic properties. This analysis also verified that the samples were representative of the clay used for liner construction by comparing the results with previous geotechnical investigations. Like the one conducted by Hoover and Associates in 2002. In their results showed that the that the hydraulic conductivity measurements in the $1x10^{-8}$ to $1x10^{-7}$ cm/sec range when compacted to 90% relative compaction on the wet side of optimum. The geotechnical report by Hoover & Associates also revealed that the atterberg limits were (LL=40 and PI=14).

Table 1. USCS Classification and Grain Size Distribution

Soil Type	USCS Classification	Grain Size Distribution			
		Gravel	Sand	Silt	Clay
Brown Clay Sample	Sandy-Lean Clay (CL)	8%	28%	13%	51%

Table 2. Standard Compaction Results

Soil Property Index	Value
Standard Proctor Maximum Dry Density	96.6 PCF
Optimum Moisture Content	25.5 %
Liquid Limits	39
Plasticity Index	14
Specific Gravity	2.68

Leachate

Leachate was sampled from the City of Paso Robles Landfill located outside of Paso Robles, CA in San Luis Obispo County. This is a class III waste management facility permitted by the Regional Water Quality Control Board to dispose non-hazardous municipal solid waste. Typical waste types received for disposal are summarized in Table

Table 3: Waste Constituents of Landfill where Leachate was Sampled

Waste Constituent	Percent
Residential Curbside Collection Wastes	21.5%
Commercial Bin Service Discards	40.0%
Roll-Off Box Debris	5.9%
Self-Hauled Wastes	14.9%
City of Paso Robles Waste Debris	2.7%
Sewage Treatment Plant Grit Screenings	0.4%
Mattresses and Sofa's	0.2%

Just less than 5.0 gallons of leachate was sampled from the leachate system that provided recirculation to a closed portion of the landfill. The sample was collected in a 5.0 Gallon HDPE container and was immediately sealed with an air-tight lid. The sample was kept at room temperature (approximately 60°F) and sheltered from any direct natural or artificial light for the duration of laboratory testing. It was beyond the scope of this study to provide analysis of leachate constituents (see table 4); however the March 2003 Detection Monitoring report submitted to the California Regional Water Quality Control Board revealed the following leachate characteristics:

Table 4: March 2003 Leachate Constituents

Analyte	Result (mg/L)
Total Dissolved solids	1240
Chloride	294
Sulfate	91.9
Sodium	246
Barium	0.204
Copper	0.014
Lead	0.026

No volatile organic compounds (VOCs) were detected in the 2003 analysis; however, past reports (January, 1995) have indicated the presence of organic compounds (see table 5):

Table 5: March 2003 VOC Constituents

Analyte	Result (µg/L)
Chloroethane	42
1,1-Dichloroethane	64
Methylene Chloride	350
Tertachloroethane	29
Toluene	23
1,1,1-Trichloroethane	41
Trichlorofloromethane	24
Xylenes	14

Pressure Plate Extractor

For this study the axis translation method was used. This is a simple and effective way to measure soil water characteristic curves.

Hillel (1956) [as discussed in Miller et al., 2002] demonstrated that the pore-water pressure is increased by an amount equal to the increase in the ambient chamber air-pressure. In other words, the soil matric suction remained constant when measured at various ambient pressures.

A Pressure Plate Extractor (PPE) is used to provide ambient pressures above atmospheric. The pressure tank, valves, gages, and ceramic plates were all obtained from Soil Moisture Corporation, in Santa Barbara, a picture of which is provided in Figure 2.

Figure 2. Pressure Plate Extractor and Pressure Regulating Manifold

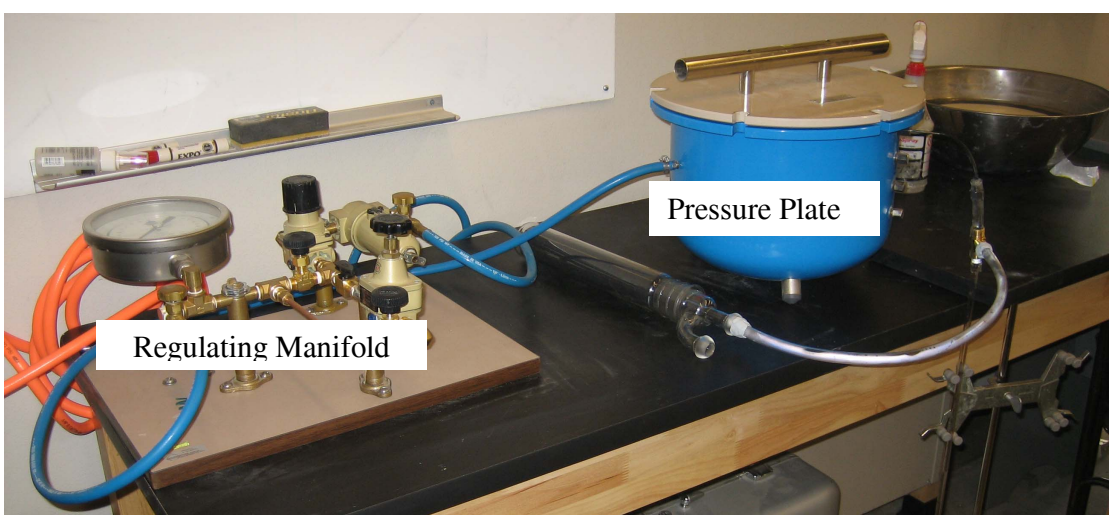

The PPE is capable of imposing matric suctions up to 5.0 Bars. Four ceramic plates, capable of withstanding air-entry values up to 0.5, 1.0, 3.0, and 5.0 Bars are used in this study. The ceramic plates are manufactured with microscopic pores to allow the passage of water. As long as the pressure in the extractor does not exceed the air entry value of the plate, air will not flow through

the pores because of surface tension forces at the gas-liquid interface. The air-entry value is a function of the pore diameter (Soil Moisture Corp 2006).

When the soil is placed on the ceramic plates, and the extractor is pressurized, water will begin to flow from around each of the soil particles and out through the ceramic plate. Equilibrium occurs when the effective curvature of the water films throughout the soil are the same as the pores in the plate (Soil Moisture Corp 2006).

Pressure is supplied to the PPE through an available 120 psi supply line which is controlled with one standard regulator in series with a nullmatic regulator. Together, the two regulators can control a stable pressure supply within 0.5 psi (0.02 Bar) accuracy. The nullmatic regulator has a maximum capacity of 4.0 Bars and must be bypassed beyond this range. The main difference in using this bypass was an increased difficulty in setting the target pressure. Once the target pressure was set, no fluctuations were visible.

In order to determine the affects of leachate on unsaturated fluid movement two samples are prepared—a control utilizing water as the pore fluid and another utilizing leachate. A pressure plate extractor (PPE) is used to indirectly measure changes in matric suction and corresponding water contents to determine the soil-water characteristic relationship. Samples are compacted at 3 to 4% wet of optimum using a standard compaction effort. For each test, twelve samples are carefully cut from the compaction mold, placed into confining rings and then positioned on a ceramic plate in the PPE. The resulting water contents are measured at four imposed matric suctions—0.5, 1.0, 3.0, and 5.0 BARs.

SWCC Functions

Soil water characteristic functions provide mathematical representations of the soil water characteristic curve based on empirical parameters. These functions vary in their ability to describe the curves and their applicability may change depending on the soil properties. This study considered two different characteristic functions.

The Brooks Corey Model [(1964) as discussed in Merayyan, 2001]:

$$\theta(h) = \theta r + \frac{\theta s - \theta r}{\left[(h/\Psi_a)\right]^{\lambda}} \tag{1}$$

where λ is the pore-size distribution index.

The Van Genuchten Model [(1980) as discussed in Merayyan 2001]:

$$\theta(h) = \theta r + \frac{\theta s - \theta r}{\left[1 + (-\alpha h)^n\right]^m} \tag{2}$$

where α is an optimized parameter and is inversely related to the air-entry suction.

Both of these models require parameter optimization in order to uniquely describe a soil. Brooks Corey requires optimization of θ_r, ψ_a, and λ. The Brooks Corey is heavily dependent on λ. Through Kelvin's capillary law, the pore-size distribution index is assumed to be analogous with the slope of the soil-water characteristic curve (Leong and Rahardjo, 1997).

The Van Genuchten model is defined by three parameters, α, n, and m. Each of these parameters is described by Leong and Rahardjo (1997). The parameter α is the pivot point of the

curve; as α increases, the air-entry suction decreases [(Tinjum et. Al, 1997) as discussed in Miller et al., 2002]. The parameter n controls the slope of the SWCC about the pivot point, which occurs at a normalized volumetric water content (Θ) of 0.5, where: $\Theta = (\theta_w-\theta_r)/(\theta_s-\theta_r)$. As n increases, the sloping portion of the curve between ψ_a and the knee (the point of inflection at the lower portion of the curve as it approaches a horizontal position) of the SWCC becomes steeper (Merayyan, 2001). The parameter m rotates the sloping portion of the curve. As m increases, the range of the curve between ψ_a and the knee of the SWCC decreases. The stability of the curve-fitting process is improved by equating the parameter m to 1-(1/n) [(Van Genuchten et al., 1997) as discussed in Merayyan, 2001]. This relationship was adopted for this study.

Excel Solver

Soil Water Characteristic parameter optimization was conducted using Microsoft Excel's Solver routine. Solver is part of a suite of commands which operated within Excel's programming structure. Solver allows the user to find an optimal value for a single cell, called the target cell, by changing the value of other user-specified cells, called adjustable cells. The target cells and the adjustable cells are directly or indirectly related via formulas. Once the constraints relating to iterations, precision, and convergence are inputted, the program will change the values in the adjustable cells to achieve the desired kind of optimization in the target cell, i.e. maximum, minimum, or target value. In this case a SSR method is computed as the desired minimized target. The residuals are computed as the difference between the measured and theoretical volumetric water contents and summed over all equilibrium pressures (i.e. 0.5 Bar, 1 Bar, 3 Bar, 5 Bar). The sum of the square residuals can be calculated as the following:

$$SSR = \sum_{i=1}^{n} w_i \left(\theta_{mi} - \theta_{ci}\right)^2 \quad (3)$$

Solver Setup

All options are selected in a fashion which allows for the best possible precision. The largest values allowed by Solver for iterations and computation time are chosen and the smallest values for precision and tolerance are selected. The default values for all other options are accepted. Table describes the necessary Solver inputs relating to iterations, precision, and convergence.

Table 6: Excel Solver Configuration

User Input	Value
Maximum Computation time	10,000 sec
Iterations	10,000 sec
Precision	0.0000001
Tolerance	0.0000001 %
Convergence	0.0000001
Other Constraints	None

Results

The results of this study are presented in this section. A statistical significance was performed on the experimental data. Further more, the effects of leachate on the Soil Water Characteristic Curve using the Van Genuchten and Brooks Corey Models are presented. This result is discussed in terms of how parameters have affected common properties of the soil water characteristic curve including air-entry suction head.

Statistical Significance

There is an apparent decline in measured equilibrium water contents for samples permeated with leachate. In order to determine if this decline is significant or the result of experimental variability, a two-tailed T-test is conducted on the difference in means for the final measured gravimetric water contents (see table 7). The null hypothesis is no difference exists between the mean water contents for leachate and water at a given equilibrium moisture content. The outcome is that experimental results are significant at the 2.5% level, meaning the probability of measuring a difference similar to what was measured in this study if leachate had no affect on equilibrium water contents is less than 2.5%. The T-test results are summarized in Table .

Table 7: Experimental Data Results

Matric Suction	Water			Leachate			Diff. in Means
	Final Measured Gravimetric Water Content	Variance	Mean	Final Measured Gravimetric Water Content	Variance	Mean	
0.5-Bar	0.2878 0.2883 0.2898	1.055E-06	0.2886	0.2761 0.2807 0.2808	7.305E-06	0.2792	0.0094
1-Bar	0.2692 0.2744 0.2752	1.049E-05	0.2729	0.2692 0.2700 0.2705	4.450E-07	0.2699	0.0031
3-Bar	0.2526 0.2524 0.2525	1.274E-08	0.2525	0.2452 0.2388 0.2429	1.030E-05	0.2423	0.0102
5-Bar	0.2442 0.2414 0.2452	3.868E-06	0.2436	[1]0.2293 0.2268 0.2291	1.934E-06	0.2284	0.0152

Table 8: T-Test Results

Statistical Characteristic	Value
std. deviation	0.004977119
average	0.009465
t-statistic	4.2703
Degrees of Freedom	3
standard error of difference	0.002
two-tailed P value	0.0238

[1] This sample reached equilibrium pressure at 4.92 Bars, .0 Bars.

Optimization Results

The Parameter Optimization process resulted in the soil-water characteristic function parameters given in

Table .

Table 9: Parameter Optimization Results

Soil-Water Characteristic Model	Parameter	Physical Interpretation	Parameter Optimization Results	
Van Genuchten	α (1/cm)	Empirical constant	Water	1.103105
			Leachate	1.129887
	n	Empirical constant	Water	m=1-(1/n)
			Leachate	
Brooks Corey	h_b (cm)	Air-entry value	Water	149.1409
			Leachate	158.9680
	λ	Empirical constant	Water	0.091387
			Leachate	0.109697

Soil Water Characteristic Curve

The following figures present the SWCC for leachate and water based on the results of the parameter optimization process. Figure 3 through Figure **6** show the Van Genuchten and Brooks Corey SWCCs for water and leachate. Both models showed a relatively good fit of the data and a close fit to one another.

Figure 3: Van Genuchten SWCC for Water

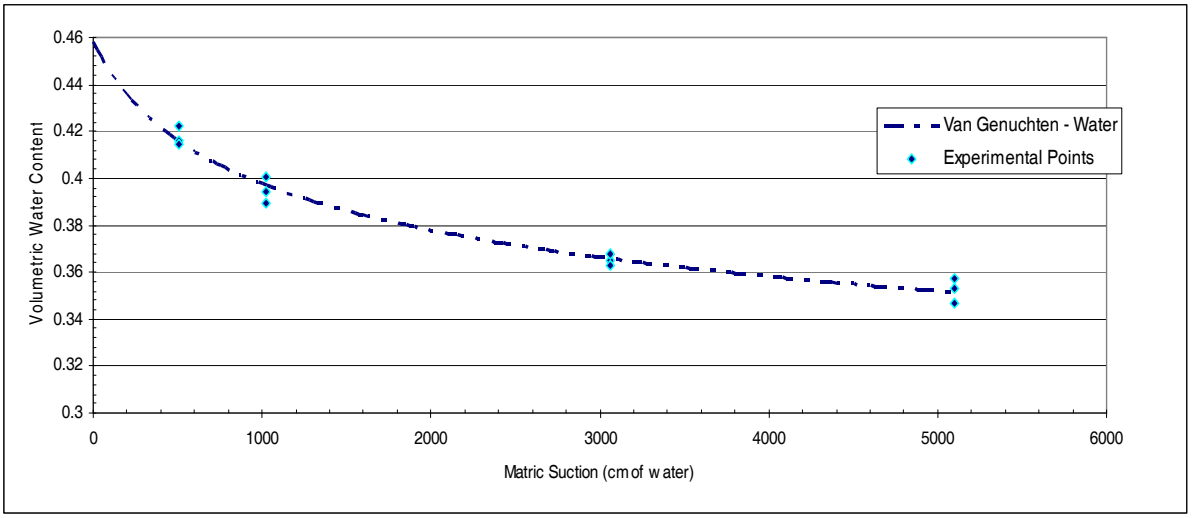

Figure 4: Van Genuchten SWCC for Leachate

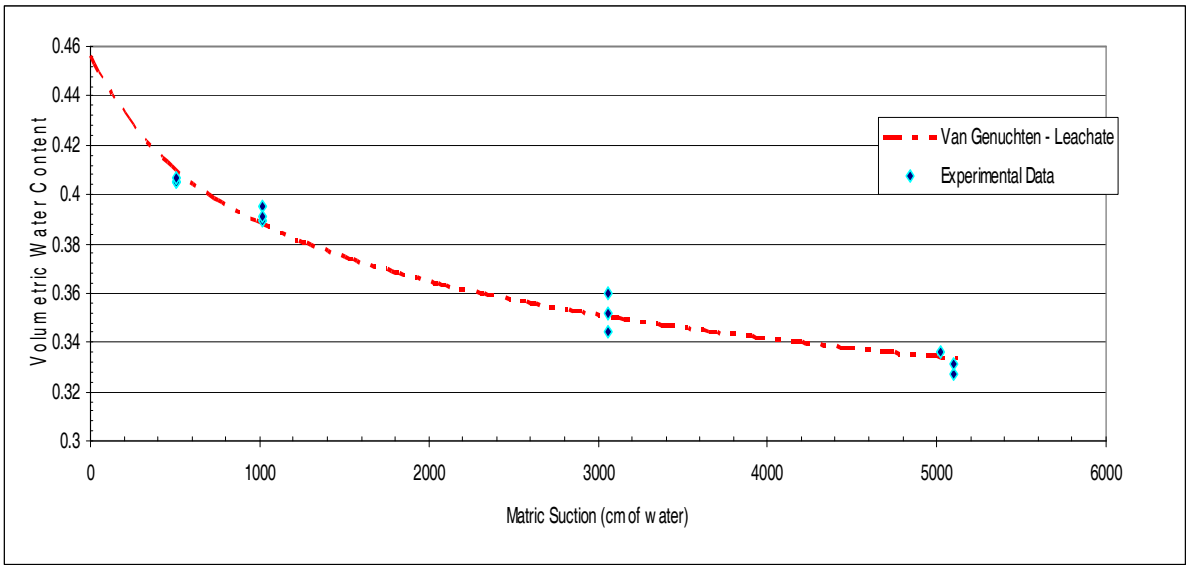

Figure 5: Brooks Corey SWCC for Water

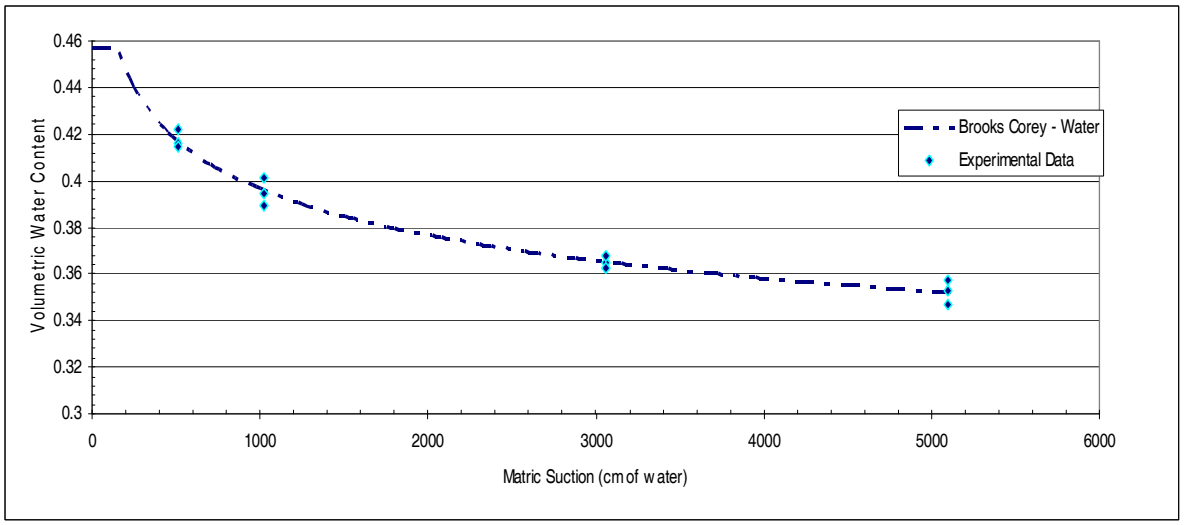

Figure 6: Brooks Corey SWCC for Leachate

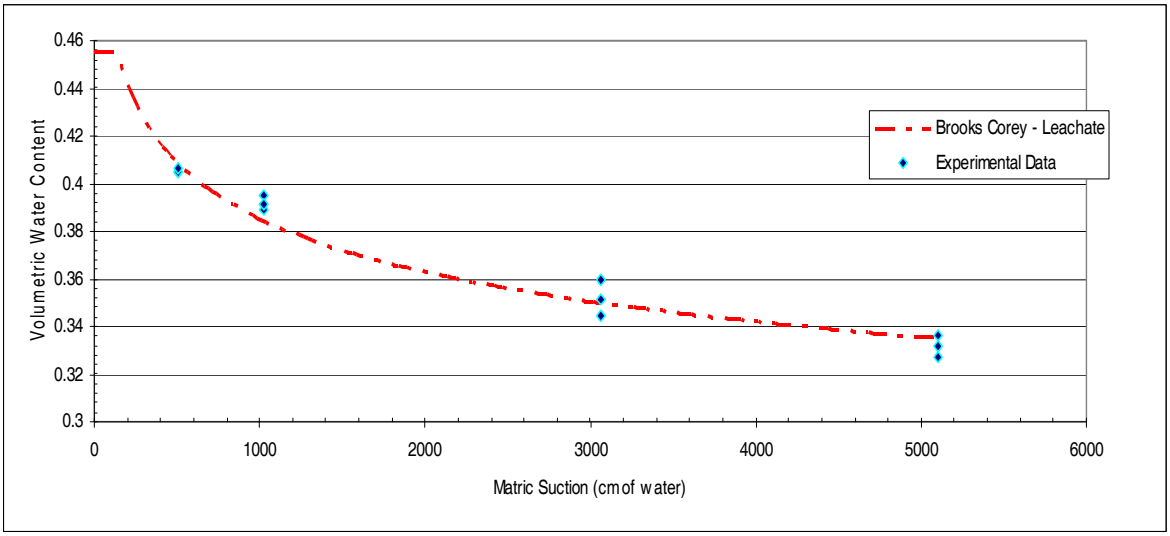

Affects on the SWCC

Leachate has a discernable impact on the soil-water-characteristic curves. For both Van Genuchten (VG) and Brooks Corey (BC) models, the leachate curve fell bellow the water curve. The percent difference between the leachate and water SWCCs is provided in Figure .

Figure 7: Percent Difference between Leachate and Water Volumetric Fluid Contents

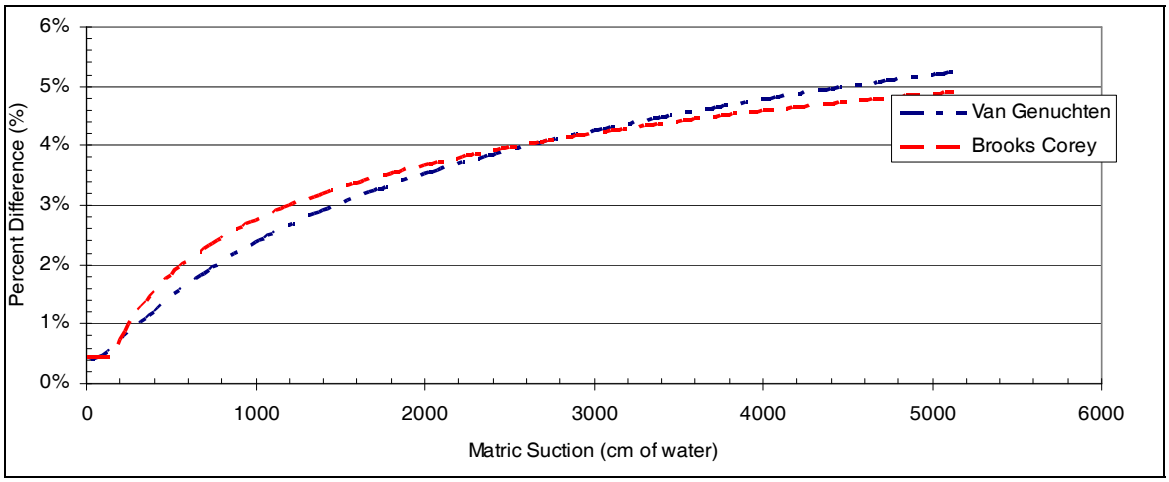

Higher values of matric suction exhibit greater percent differences in computed or theoretical volumetric water contents. The range which is applicable for this study and for

landfill liners in general lies below 2000 cm of suction—this range corresponds to moisture contents at or above optimum which are appropriate for clay liners. For purposes relative to landfill liners, it appears leachate caused as much as a 25% difference in the SWCC.

The affects of leachate on individual characteristics such as air-entry value, steepness, inflection, and rotation are a bit more subtle. The most significant difference between models is how they handle the air-entry portion of the curve (ψ_a), also called the bubbling pressure. Along a drying path, the SWCCs normally remain horizontal at saturated volumetric water content until ψ_a is reached at which point the curve begins to dip downward. While this point is not clearly defined on the Van Genuchten curve, ψ_a is distinctly represented on the BC SWCCs. The VG model depicts the curve as immediately dropping away from saturation as matric suction increases. Although the VG model does not specifically define a variable for ψ_a, the parameter α is commonly associated with the inverse of air-entry portion of the curve. Work by Merayyan et al (2002) has found similar differences in the way the BC and VG models predict the air entry-portion of the curve.

Comparison of the results from the parameter optimization indicates that α decreased by 4.0% when the soil was permeated with leachate, suggesting the air-entry increased. This is consistent to the BC model which indicates leachate increased the air-entry value from 149.1 to 158.0 cm, a 6.4 % increase. The affect on other SWCC parameters are provided in

Table 10.

Table 10: Leachate's Affect on BC and VG Parameters

Model	Parameter	Parameter Optimization Results		% Difference
Van Genuchten	α (1/cm)	Water	0.003901	-4.0%
		Leachate	0.003747	
	n	Water	1.103105	2.4%
		Leachate	1.129887	
Brooks Corey	h_b (cm)	Water	149.1409	6.4%
		Leachate	158.968	
	λ	Water	0.091387	18.2%
		Leachate	0.109697	

The other parameter in the Brooks Corey model is the pore-size distribution index, λ, which showed an 18.2 % decrease indicating a steeper slope about the pivot point. A decrease in the slope controlling parameter in the VG model, *n*, also indicates a steeper slope about the pivot point for the leachate SWCC.

Summary and Conclusions

Municipal landfill leachate and clay which was used in construction of a low permeability liner were used to assess the impacts which leachate could have on the soil-

water-characteristic curve and subsequent flow characteristics. A pressure plate extractor was used in conjunction with the axis-translation technique to produce matric suction vs. water content data. The SWCC's were developed based on PPE data and curve fit to the Van Genuchten and Brooks Corey models using Excel Solver routine for parameter optimization. A numerical analysis was conducted with CHEMFLO-2000 using a finite differences approach to solving Richards Equation for the change in matric suction, unsaturated conductivity, and cumulative flux with respect to time. Because the purpose of this study is to discuss the impacts leachate might have on the SWCC and consequent flow conditions through unsaturated clay as it pertains to landfill liners, every effort was made to model the soil in terms of realistic landfill conditions where feasible. Decisions about modeling inputs such as initial conditions, boundary conditions, and soil column properties are managed to match field conditions.

The study indicates leachate causes a decrease in matric suction for given moisture content and consequently an increase in hydraulic conductivity and cumulative flux through a common landfill clay for both Van Genuchten and Brooks Corey models. The largest difference in predicted matric potentials for water contents between saturation and those appropriate for landfill liner design vary depending on the modeling scenario utilized. On average these differences ranged from zero to 209 cm at saturation (20.5 kPa) for Brooks Corey and 368 cm (36.1 kPa) at saturation for Van Genuchten. Hydraulic conductivities also increased when permeated with leachate. Increases in cumulative flux are mostly dependent on the time lag between when leachate and water begin saturation.

The Brooks Corey and Van Genuchten models handle the air-entry portion of the SWC quite differently and this had a substantial impact of the outcome of hydraulic conductivity versus matric suction relationships. Consequently any predictions of flow conditions which depended on this portion of the curve, below a matric potential of about 200 cm (19.6 kPa) was heavily dependent upon the choice of model. Because the numerical modeling appropriate for landfills depended on this the air-entry portion of the curve, the change in hydraulic conductivity from water to leachate depended on the model. Even though there was a discernable difference in both models, the largest difference was not more than 2.4×10^{-7} cm/hour.

These findings are consistent with historical research detailing how pore fluid chemistry has a definite affect on flow characteristics. The most recent study, published by Ichola & Gaidi (2006) at the same time this study was being conducted, concluded leachate causes an increase in hydraulic conductivity when measured with methods similar to those in this study. Ichola & Gaidi found that even though permeability was influenced by leachate, the increase was not more than 4.32×10^{-5} cm/hour.

A significant original contribution of this study is the use of finite difference model in conjunction with the soil water characteristic curve to determine possible chemical effects leachate may have on landfill performance. Previous studies have used geotechnical methods such as flexible and rigid wall-permeameter tests to analyze these affects. These methods are very different from the soil-water characteristic approach used in this thesis.

Engineering Implications

Current regulations and common landfill liner design practices use a water-saturated permeability approach for specifying liner materials. While this approach utilizes a specification which can be easily tested in the laboratory, it does not represent true conditions in the field. This study has attempted to more closely model field conditions for the time between liner construction and saturation. A complete analysis of how leachate might flow through a landfill liner while also considering the chemical affects by leachate on flow characteristics is a significant contribution of this study. Most previous analysis of chemical pore-fluid interactions and its affects on the soil water characteristic curve or flow characteristics have been in some part different from the unsteady-state approach used in this study (with the exception of the 2006 study by Ichola & Gaidi).

While it has been determined that leachate increases unsaturated permeability, although not more than $1x10^{-7}$ cm/hour, it cannot be concluded that current regulations for liner designs are deficient. From an environmental perspective, specifying intrinsic permeability may be a more conservative approach in specifying permeability characteristics; unsaturated permeability tends to be lower than intrinsic values for clay soils. Better understanding of desiccation cracking, wilting point, and field capacity of materials used for landfill liners and covers might stand to gain from understanding how design criteria might be impacted by changes in pore fluid chemistry. The bottom-line is pore fluid chemistry has a real affect on properties of clayey soils. Engineers should be aware of the limitations invoked by neglecting pore fluid chemistry.

References

Bagachi, A. Design and Construction and Monitoring of Landfills 2nd Edition. New York: 1994

Dunn, Jefferey and Singh, Udai. "Landfill Closures: Environmental Protection and Land Recovery." Geotechnical Special Publication No. 53 (1995).

Hickman, H. Lanier Jr. and Eldredge, Richard W. "A Brief History of Solid Waste Management in the US During the Last 50 Years." MSW Management. 2000. http://www.forester.net/msw_0001_history.html.

Ichola, Alimi and Gaidi, L. "Hydraulic Ocnductivity and Pollutant Dispersion Coefficient Assessment during Leachate Flow in Unsaturated Clay" Geotechnical Special Publication No. 147 Vol 2 (2006) 1547-1558.

Leong, E.C. and Rahrdjo, H. "Permeability Functions for Unsaturated Soils." Journal of Geotechnical and Geoenvironmental Engineering. (1997) 1118-1126.

Merayyan, Saad. "Evaluation of the Unsaturated Hydraulic Functions of Compacted Landfill Clay Liners: Impact on the Predicted Leakage Rates" PhD Dissertation Department of Civil Engineering, Wayne State University , Detroit, Michigan, 2001. Original copy acquired by author.

Miller, Carol J.; Merayyan, Saad; Yesiller, Nazli. "Impact of Soil Type and Compaction Conditions on the Soil-Water Characteristic Curve". Journal of Geotechnical and Geoenvironmental Engineering (2002): 733-742.

Miller, Carol J.; Merayyan, Saad; Yesiller, Nazli. "Unsaturated performance comparison of compacted clay landfill liners". Geotechnical Special Publication No. 99 (2000): 555-568.

Miller, Carol P.; Wright, Steven J. "Predicting Leakage through Clay Landfill Covers." National Conference on Environmental Engineering (1984) 708-710.

Time Series Analysis of Performance Data from Closed Landfills To Forecast Post Closure Monitoring Needs

Banu Sizirici[1] and Berrin Tansel[1]

[1]Civil and Environmental Engineering Department, Florida International University
10555 West Flagler Street, Engineering Center Miami, FL, 33174;
Ph (305)348 2928; e-mail:bsizi001@fiu.edu

Abstract

A landfill is considered functionally stable when it no longer presents an unacceptable threat to human health and the environment. Landfill stability depends on factors which include variables that relate to operations both before and after the closure of a landfill cell. Therefore, post closure period (PCC) decisions should be based on operational factors, design factors and post-closure performance data. The question of appropriate PCC period for landfills requires in-depth case studies focusing on the analysis of the performance data from closed landfills. In this study the performance data from a closed case study landfill was evaluated to forecast the level of stability of a landfill in terms of leachate and gas generation rates and quality .The data was analyzed by time series decomposition technique since seasonality in graphs was identified by regularly spaced peaks and troughs. The data clearly showed the general trend and provided a clear forecast for future planning purposes. Decreasing trends were seen for leachate quantity, landfill gas and methane , chloride, sodium , total dissolved solids, vinyl chloride,1,4-dichlorobenzene, chlorobenzene, xylenes, ethylbenzene, toluene, total BTEX and cis-1,2-dichloroethylene. Increasing trends were seen for iron and bicarbonate. Steady trends were seen for pH, ammonia and benzene. Based on these results, PCC monitoring needs identified for closed case study landfill.

Introduction

Post closure care (PCC) begins when the landfill is closed. PCC duration prescribed by Resource Conservation and Recovery Act (RCRA), Subtitle D is 30 years. The 30-year period can be shortened or extended depending on whether the landfill presents potential threats to human health or the environment or not (Tansel et al., 2007). A landfill is considered functionally stable (once Municipal Solid Waste inside the landfill reaches a functionally stable state) when it no longer presents an unacceptable threat. Currently, there are no specific metrics which can be used for systematic evaluation of relative stability of closed landfills; which, at the same time, allow an objective determination of the adequacy of the 30-year post closure period (Tansel et al., 2008). To forecast PCC monitoring needs include leachate monitoring, groundwater and gas monitoring, final cover maintenance and risk analysis (Vesilind et al., 2001; Reinhart et al., 1997; Tansel et al., 2008). Leachate monitoring should be based on evaluation of leachate quantity and quality trends, and projection of future

trends for parameters of concern. Evaluations of these parameters give the present levels and projection of future concentrations and trends for the parameters of concern overtime. Based on the evaluations, decisions can be made to continue or discontinue the monitoring for determined parameters (Tansel et al., 2008). The purpose of the Landfill Gas (LFG) monitoring is to evaluate whether LFG monitoring can be changed, optimized, reduced or discontinued in terms of the landfill gas production trend overtime.

Prediction of the changes in leachate quantity and quality and landfill gas quantity require quantitative tool. Thus, the monitoring of these parameters with the suitable trend analysis method can make long-term predictions of landfill stability easier. The trend analysis for the landfill components gives an idea to predict the future generation rates. Time series decomposition approach is a quick and easy method of generation a range of parameters to forecast (Worrall et al., 1998). Decomposition has been widely regarded as a successful strategy for the extrapolation of time series in the traditional approach of using mean, seasonality, trend, and error (Armstrong et al., 2004). MacGregor, 2001 showed that decomposition to be beneficial for judgmental forecasting. The purpose of this study is evaluation to forecast the level of stability of a landfill in terms of leachate and landfill gas generation rates.

Materials

In this study the performance data from a closed case study landfill was evaluated to forecast the level of stability of a landfill in terms of leachate and gas generation rates and quality. The case study landfill is located in south Florida, USA which has a subtropical climate. The landfill has been closed since 1987. The case study landfill is partially lined and has vegetative cover. Landfill gas data are available from 2004 to 2008 and are recorded on a monthly basis. Generated Landfill gas is collected by the landfill gas management system and eliminated through an enclosed flare approximately 1 to 1.5 hours per day. The landfill gas composition is shown in Table 1. Leachate quantity data is available from 1989 to 2008 and leachate quantity is monitored on monthly basis. Leachate quality is monitored twice a year (April and September). The monitoring data were available from 2001 to 2006. After 2006, leachate quality was sampled once a year. A total of 46 parameters was monitored. Among these parameters, 28 parameters were non-detected parameters (i.e., always below the detection limit), eight parameters were always above the maximum contaminant limit (MCL) and ten parameters were below the MCL. Table 2 presents the parameters detected in leachate.

Table 1. Landfil gas composition.

Constituent	Percentage in gas
Methane	45%
Oxygen	1.36%
Carbon dioxide	30%

Table 2. The parameters of interest in leachate.

Below MCL	Above MCL
1,4-Dichlorobenzene	Chloride
Chlorobenzene	Bicarbonate
cis-1,2-Dichloroethylene	Sodium
Dichlorodifluoromethane	Ammonium as N
Ethylbenzene	Iron
Methyl-tert-butyl ether (MTBE)	Benzene
Tetrachloroethene	Vinyl Chloride
Toluene	Total Dissolved Solids
Xylenes	
Total BTEX	

Methods

Available leachate quantity and quality data and landfill gas data were plotted as a function of time to identify changes in these parameters to forecast the stability of landfill. At the beginning, data were plotted as a function of time with fitted line regression analysis. But the graphs did not show a clear trend (i.e., decreasing or increasing). The classical regression analysis approach could not be used for most of the data since there were significant seasonal variations in the data. Seasonal effects on the data were identified by regularly spaced peaks and troughs which had a consistent cycle with approximately similar magnitude. Therefore, the data were analyzed by Minitab 15 The time series decomposition method which separates the data into linear and seasonal components, as well as error, and forecasts future trends (Minitab 15, 2005). Time series decomposition approach is a quick and easy method of generation a range of parameters forecast (Worrall et al., 1998). It can be used by either selecting an additive or multiplicative model.

For the additive model, forecasts can be made by the following model:

$$y_t = T_t + S_t + e_t \qquad t = 1, \ldots, n$$

For the multiplicative model, forecasts can be made by the following model:

$$y_t = T_t \times S_t \times e_t \qquad t = 1, \ldots, n$$

where, t : time, y_t : observed data, T_t : trend component, S_t : seasonal component, and e_t : error term.

The additive model assumes that amplitude of both the seasonal and irregular variations in data do not change as the level of the trend rises or falls. The multiplicative model assumes that the amplitude of both the seasonal and irregular variations increase as the level of the trend rises. The data from the case study landfill showed more adequate fit with the multiplicative model with a linear parametric component (T_t). Therefore, time series decomposition with multiplicative model was used for the trend

analyses. The accuracy of the time series analysis can be expressed by mean absolute percentage error (MAPE), mean absolute deviation (MAD), and mean squared deviation (MSD) as shown in Table 3 (Minitab15 StatGuide). Smaller values generally indicate a better fitting model (Armstrong et al., 2004).

Table 3. Methods for determining the accuracy of the time series analysis.

Mean Absolute Percentage Error (MAPE)	Mean Absolute Deviation (MAD)	Mean Squared Deviation (MSD)
Measures the accuracy of fitted time series values as a percentage.	Measures the accuracy of fitted time series values in the same units as the data.	More sensitive measure of an unusually large forecast error than MAD.
$MAPE = \frac{\sum \left\| (y_t - y_t^1)/y_t \right\|}{n} x100$	$MAD = \frac{\sum_{t=1}^{n} \left\| y_t - y_t^1 \right\|}{n}$	$MSD = \frac{\sum_{t=1}^{n} \left\| y_t - y_t^1 \right\|^2}{n}$

* y_t : actual value , y_t^1 : fitted value, n : number of observations, $y_t \neq 0$

Results

Figure 1 shows the leachate generation rate for the 80 months. Leachate quantity data were used from January 2001 to December 2005 (60 month). Leachate quantity samples collected each month showed that leachate quantity has increased during the rainy season and decreased during the dry season. The generated leachate has a decreasing trend. However, when forecasting values were compared the real values, it was seen that forecasting values were significantly smaller than the real values. Leachate generation rates are greatly affected by the type and condition of the in placed cover system and waste materials at the landfill (Akesson et al., 1997).

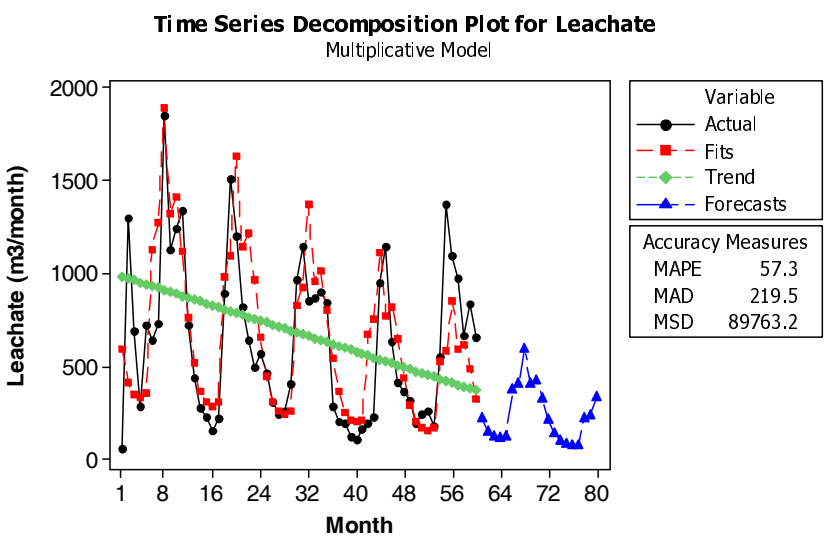

Figure 1. Time series projections leachate generation

Since the case study landfill has vegetative cover, leachate quantity mostly depend on the volume of the infiltrating rainfall and the other weather related event (e.g., hurricanes). Figure 2 presents the predicted monthly gas generation rate for 80 months period. Landfill gas data were used from January 2004 to June 2008 (54 months). The graph did not give the clear correlation but showed that Landfill gas has decreasing trend and in the 80th month LFG generation will be minimum value.

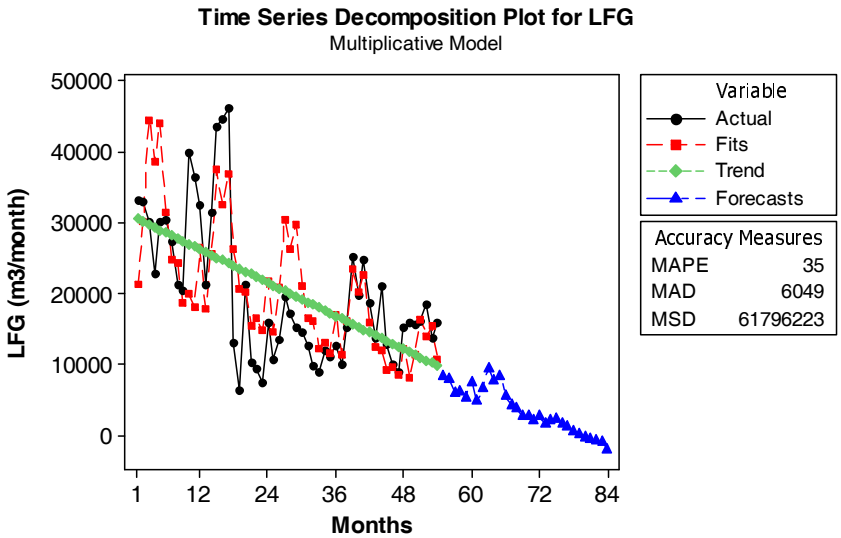

Figure 2. Time series projections of gas generation

Figure 3 presents the methane generation rate for 80 months period. Landfill methane data were used from January 2004 to June 2008 (54 months). The graph shows that methane generation is decreasing overtime.

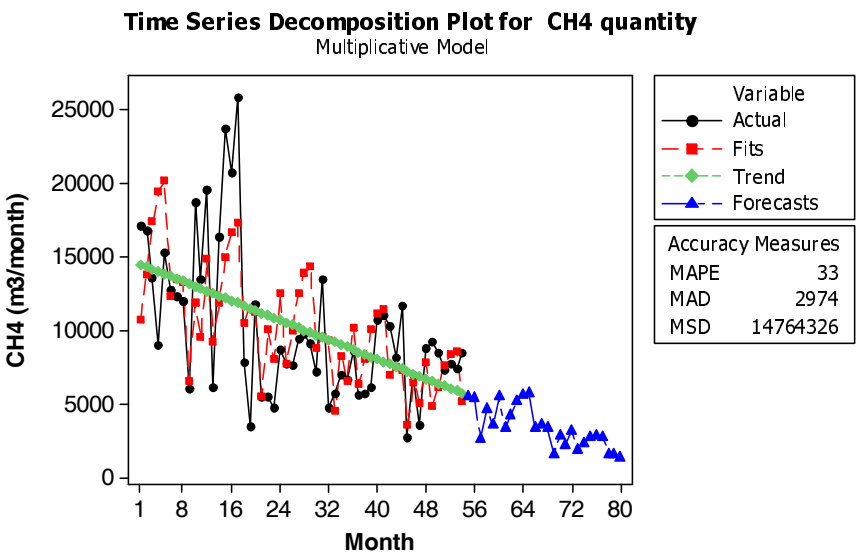

Figure 3. Time series projections of CH_4 generation

Available leachate quality data were plotted as a function of time showed that samples collected at the end of the dry season (April) had high contamination levels; and the samples collected at the end of the rainy season (August) had lower levels due to dilution by infiltrating rain water. Figure 4 presents the chloride levels in leachate. The available data from April 2001 to April 2006 were used. The data after 2006 were not used due to changes in the sampling period. (Leachate samples were collected biannually until 2006. After 2006 the management decided to collect the leachate samples once a year) The graph shows a clear trend that the decomposition model fits adequately except part of the second annual cycle is under predicted. Based on the time series analysis, the chloride concentration would be below the MCL by the year 2023. The major sources of chlorine in MSW are paper and plastics. (U.S. Congress, Office of Technology Assessment. (1989).

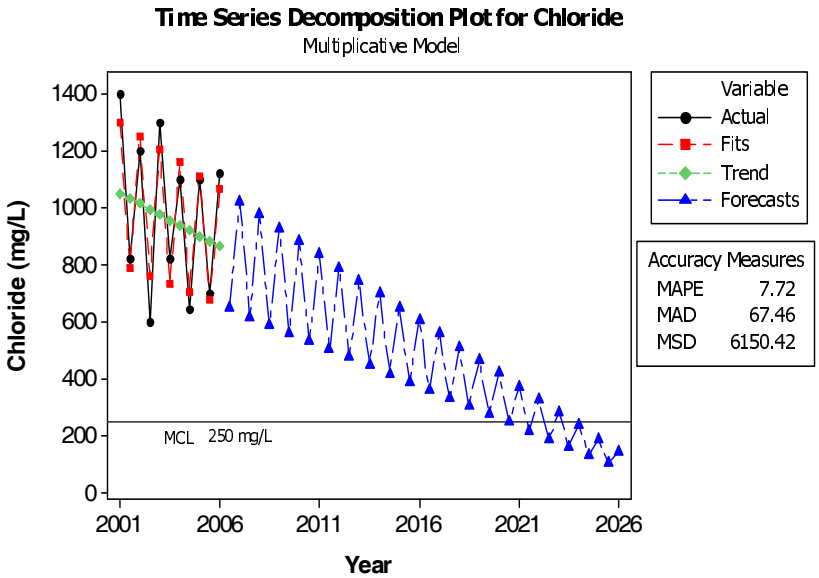

Figure 4. Time series projections of chloride generation

Figure 5 presents the sodium concentrations in leachate. The data were used from April 2001 to April 2006. The data fit fairly well except for the data collected in 2002 September. When the data were examined, it was seen that April 2002 and September 2002 data were exactly the same indicating that maybe September 2002 data were not actually obtained from a field sample. Based on the graph, sodium concentration would be below the MCL by the year 2011. Sodium is probably derived from the dissolution of salts in the waste (Statom et al., 2004)

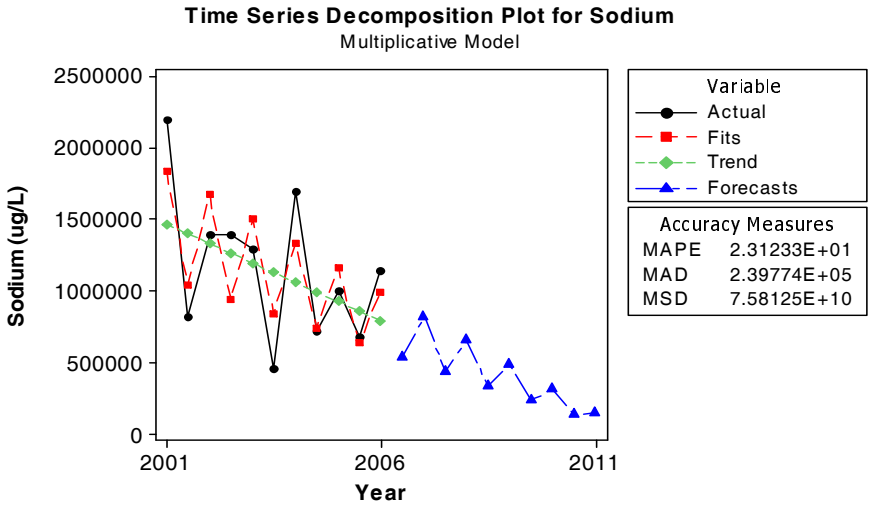

Figure 5. Time series projections of sodium generation

Figure 6 shows the bicarbonate generation in leachate. The data were used from September 2001 to September 2005. Due to the data in April 2006 has enormous value, this period was counted as an outlier. The figure shows that bicarbonate has an increasing trend. When organic content of the waste is decomposes due to the high moisture content, great amount of bicarbonate formed as a by product of bacterial respiration. The other source for bicarbonate could be cap system of landfill. Cover system consists of a two-foot thick limerock cover. As rain falls through the atmosphere, it absorbs carbon dioxide and forms a weak carbonic acid the acidic water slowly dissolve limestone.

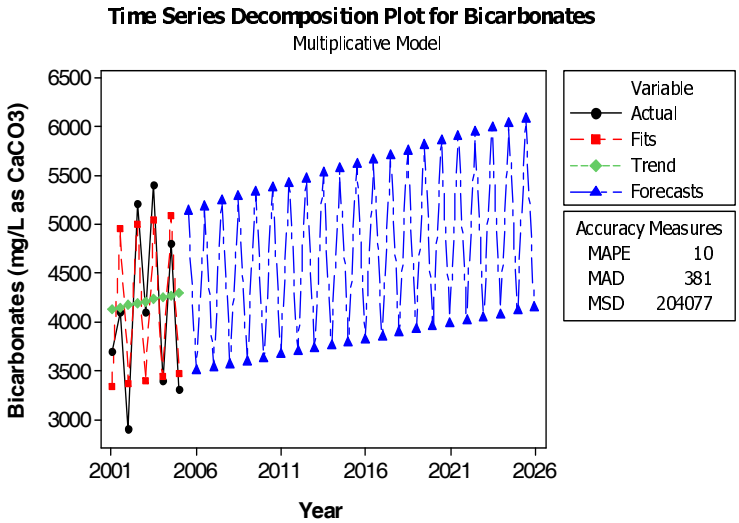

Figure 6. Time series projections of bicorbanate generation

After plotting all common parameters detected in leachate, trends of these parameters were identified. Based on trend analysis result, future level of each parameter was predicted shown in Table 3. The data from case study landfill showed

significant seasonal trends for most of the landfill parameters. The parameters showed seasonal trend better fitted to timer series decomposition method. Decreasing trends were seen for leachate quantity, landfill gas and methane , chloride, sodium , total dissolved solids, vinyl chloride,1,4-Dichlorobenzene, Chlorobenzene,Xylenes, Ethylbenzene, Toluene, Total BTEX, cis-1,2-Dichloroethylene. Increasing trends were seen for iron and bicarbonate. Steady trends were seen for pH, ammonia and benzene.

Table 3. Trends of parameters of interests landfill (Tansel et al., 2008).

Time Series Parameters	Trend	High Value	Low Value	Mean	Comment
Leachate quantity (m^3/month)	Decreasing	1847	54	630	Projections and observations indicate decreasing trend
Landfill gas generation rate m^3/month	Decreasing	54900	7251	22099	Projections and observations indicate decreasing trend
Sodium (mg/L)	Decreasing	2200	460	1150.5	MCL will be reached in 2011
Chloride (mg/L)	Decreasing	1400	600	984.3	MCL will be reached in 2023
Total Dissolved Solid (mg/L)	Decreasing	5800	1300	4030	MCL will be reached in 2031
Iron (µg/L)	Increasing	4400	1400	2935.4	Projections indicates iron has increasing trend
Ammonia as N (mg/L)	Decreasing	3100	16	836.5	Projections indicate decreasing trend, observations indicate steady trend. Projections indicate that level will be close to zero in 2014.
Bicarbonate (mg/L)	Increasing	13300	590	4584.6	Projections indicates bicarbonate has increasing trend
pH	Steady	8	7	7.48	
Vinyl chloride (µg/L)	Decreasing	3	1	1.7	MCL will be reached in 2010
1,4-Dichlorobenzene (µg/L)	Decreasing	12	1	6.98	Already below MCL
Chlorobenzene (µg/L)	Increasing	15	7.3	11.1	Already below MCL. Projections indicate increasing trend, observations indicate steady trend.
Benzene (µg/L)	Decreasing	4	0.18	3.13	Projections show a decreasing trend, observations show a steady trend. Projections show that MCL will be reached in 2030.
Toluene(µg/L)	Decreasing	7.6	1	3.39	Already below MCL
Ethylbenzene(µg/L)	Decreasing	19	3.9	8.98	Already below MCL
Xylenes (µg/L)	Decreasing	28	5.8	13.26	Already below MCL
Total BTEX(µg/L)	Decreasing	51.3	18.6	30.45	Already below MCL

Conclusions

In this study landfill leachate quality and quantity data, landfill gas quantity data, were evaluated to forecast the functional stability of the landfill. For the leachate, the leachate quality and quantity data were analyzed to identify trends. Time series multiplicative decomposition model in general provided an adequate forecast for future planning purposes for the parameters monitored in leachate. Analyses showed that leachate quantity has been decreasing overtime. Plotted leachate parameters data showed significant seasonal variations. A total of 46 parameters have been monitored in case study landfill. Among these parameters, 28 parameters are non-detected parameters (always below detection limit), eight parameters are always above Maximum Concentration Limit (MCL, Chloride, bicarbonate, sodium, ammonium as N, iron, benzene, vinyl chloride and total dissolved solids), and ten parameters are below the MCL (1,4 dichlorobenzene, chlorobenzene, cis-1,2 dichloroethylene, ethylbenzene, dichlorodifluoromethane, methyl-tert-butyl ether, tetrachloroethene, toluene, xylene and total BTEX). Except for iron and bicarbonate, the contaminants in leachate have decreasing trend. The purpose of the evaluation of leachate is to determine whether the leachate management practices may be optimized, reduced or discontinued. As a result of the leachate analysis, the following suggestions were made:

- Significantly reduce or stop the monitoring frequency for non detected parameters,
- Reduce monitoring frequency for parameters consistently below MCL,
- Continue monitoring for parameters above MCL, and
- Refine projections of parameters above MCL as more data become available.

For the landfill gas (LFG) module, generated LFG trend was analyzed overtime. Total landfill gas quantity has been decreasing overtime. Outcomes of landfill gas analysis showed that remaining LFG generation potential is so small. Therefore eliminating active LFG management and converting to a passive venting system is acceptable.

References

Akesson M, Nilsson P (1997). "Seasonal changes of leachate production and quality from test cells." *Journal of Environ Eng.,* 123(9): 892-900.

Armstrong J. S., Collopy, F., Yokum, T. (2004). "Decomposition by causal forces: A procedure for forecasting complex time series." *International Journal of Forecasting,* 21(1): 25-36.

MacGregor, D. G. (2001), "Decomposition for judgmental forecasting and estimation," in J. S. Armstrong (ed.), *Principles of Forecasting*, Kluwer Academic Publishers, Boston, MA.

Minitab 15 StatGuide. Minitab Inc. (2007). *Minitab Statistical Software*, Release 15 for Windows, State College, PA.

Reinhart, D. R., Townsend, T. G. (1997). *Landfill Bioreactor Design & Operation*, Lewis Publishers, Boca Raton, FL.

Statom., R. A., Thyne G. D., McCray, J. E. (2004). "Temporal changes in leachate chemistry of a municipal solid waste landfill cell in Florida." *USA Environmental Geology,* 45(1): 982-991.

Tansel, B., Sizirici B., Reinhart, D.R., Kulkarni A. (2008). *Performance Based Decision System for Determining Post-Closure Care (PCC) Period in Florida Landfills Final Report,* Hinkley Center for Solid and Hazardous Waste Management, Gainesville, FL.

Tansel, B., Reinhart, D.R., Sizirici B., Rayapharapu V.K. (2007). Performance Measures for Comparison of Determining Post Closure Care (PCC) Period in Landfills, *ASCE Conf. Proc*, 10.1061/40927(243)322: 1-10.

U.S. Congress, Office of Technology Assessment. (1989). *Facing America's Trash: What Next for Municipal Solid Waste.* U.S. Government Printing Office, OTA-O-424, Washington, DC.

Vesilind, P.A., Worrell, W., Reinhart, D. (2001). *Solid Waste Engineering*, Brooks/Cole: Pacific Grove, CA.

Worrall, F., Burt., T.P.(1998). "Decomposition of river water nitrate time-series - comparing agricultural and urban signals." *Science of The Total Environment,* 210(11): 153-162.

Using tracers to derive sediment provenance after the occurrence of a 500-year flood in a Midwestern stream

Kevin D. Denn[(1)], A.N. (Thanos) Papanicolaou[(2)], and Christopher G. Wilson[(3)]

[(1)]Graduate Research Assistant, IIHR-Hydroscience and Engineering, Dept. of Civil and Environmental Engineering, University of Iowa, Iowa City, IA, 52242-1585 U.S.A.
phone: +1 319 335 5237; fax: +1 319 335 5238; e-mail: kevin-denn@uiowa.edu

[(2)]Associate Professor, Robert and Virginia Wheeler Faculty Fellow in Engineering, IIHR-Hydroscience and Engineering, Dept. of Civil and Environmental Engineering, University of Iowa, Iowa City, IA, 52242-1585 U.S.A.

[(3)]Post-Doctoral Research Associate, IIHR-Hydroscience and Engineering, Dept. of Civil and Environmental Engineering, University of Iowa, Iowa City, IA, 52242-1585 U.S.A.

ABSTRACT

In June 2008, catastrophic flooding of the Cedar River inundated a large portion of downtown Cedar Rapids, Iowa. As a result, floodwaters deposited a large amount of sediment throughout the city. The sediment origin is of intense scientific and public interest due to the quantity of deposited sediment and the potential presence of persistent organic pollutants (PCBs, chlordanes, and synthetic fragrances) attached to the sediment. The primary objective of this study is to determine the temporal and spatial patterns of deposited sediment. Two potential sediment sources have been identified: the bed of the Cedar River and the channel banks. We hypothesize that sediment from the two sources was distributed heterogeneously throughout the city. Therefore, samples were gathered from the two source areas, as well as from terrestrial areas within and adjacent to the flooded region. We will compare the deposited sediment gathered from the terrestrial areas with the sediment obtained from the source areas using natural biogeochemical tracing techniques. The tracing techniques will include an analysis of radionuclides (e.g., ^{7}Be, ^{210}Pb, ^{137}Cs), stable isotopes ratios (e.g., δ^{15}N and δ^{13}C), and elemental ratios (C/N). This comparison will allow us to determine the provenance of the sediment particles, which will assist us in developing a sediment budget for the segment of the Cedar River that flows through downtown Cedar Rapids. Further, we will identify the key processes affecting sediment delivery and redistribution that occurred during the flood. Sediment dynamics during floods is poorly described in the existing scientific literature. The methods established in this study will provide for engineers and researchers the ability to track the transport of sediments in similar floods.

Keywords: sediment transport, radionuclide, stable isotope ratio, floods

1. INTRODUCTION

Recent investigations into episodic sediment transport processes have utilized biogeochemical tracing techniques as a means to determine erosional and depositional patterns. Primary biogeochemical tracing techniques used in these investigations

have included radionuclides (Blake, Walling, & He, 2002; Palinkas, Nittrouer, Wheatcroft, & Langone, 2005), stable isotope ratios (Fox & Papanicolaou, 2007; Olley, 2002), and elemental ratios (Leithold & Blair, 2001; Middelburg & Nieuwenhuize, 1998). Specifically, the aforementioned biogeochemical tracing techniques can be used to identify sediment transport processes affecting sediment delivery and redistribution during floods.

Radionuclide analysis is a key technique used to trace sediment transport patterns during floods. Some radionuclides are naturally occurring (^{7}Be, ^{210}Pb), while others are anthropogenically produced (^{137}Cs). ^{7}Be ($t_{1/2}$ 53.3 d) is produced as solar radiation interacts with Earth's atmosphere. Resulting atmospheric ^{7}Be is delivered to the surface of the Earth via fallout. ^{210}Pb ($t_{1/2}$ 22.3 y) is produced as a result of decaying ^{226}Ra. As ^{226}Ra, which is found in most soils and rocks, decays, a series of processes eventually lead to the production of excess ^{210}Pb in the atmosphere (Mabit, Benmansour, & Walling, 2008). Excess atmospheric ^{210}Pb is deposited as fallout on the surface of the Earth. ^{137}Cs ($t_{1/2}$ 30.2 y) in the soil is the result of atmospheric nuclear testing that took place from the 1950s to the 1970s. Currently, fallout of ^{137}Cs has fallen below detectible levels, excluding regions near nuclear accidents such as Chernobyl (Ritchie, 2001). The difference between the naturally occurring radionuclides and anthropogenically produced radionuclides is important. Naturally occurring radionuclides are produced and delivered to soil over time regardless of anthropogenic activities, whereas anthropogenically produced radionuclides may or may not be delivered to soil over time as anthropogenic patterns change.

After fallout, the radionuclides are quickly and strongly fixed to surface particles. Redistribution of surface particles (and consequently, radionuclides) throughout a watershed typically occur as a result of physical processes (Mabit, et al., 2008). The attached radionuclides allow researchers to trace sediment transport patterns.

To determine sediment transport patterns, numerous samples must be obtained from regions that were as well as were not affected by floodwater. Samples must be collected from both the inundated regions and the non-flooded (heretofore referred to as reference) regions in order to allow researchers to compare radionuclide activities within each region. This comparison is necessary because radionuclides can be delivered to floodplains via two distinct methods: direct input from atmospheric fallout and accumulation of sediment during depositional periods. Assuming a homogeneous distribution of fallout-delivered radionuclides across the study area, higher radionuclide activity in the inundated floodplain areas relative to reference areas can be assumed to have resulted from depositional processes (Blake, et al., 2002).

Two other key techniques used to trace sediment transport patterns require a determination of stable isotope ratios and an elemental ratio. Stable isotope ratios (δ^{15}N and δ^{13}C) and a C/N elemental ratio have been used to trace sediment throughout a watershed (Fox & Papanicolaou, 2007). The use of these ratios holds strong promise in tracing temporal and spatial patterns of sediment over the course of

a flood. Investigation into the ability of these ratios to trace the patterns of sediment in floodwater, however, is preliminary at this point.

The primary objective of this study is to determine the temporal and spatial patterns of deposited sediment. Specifically, this study will establish methods that will allow engineers and researchers to track the transport of sediment in floods similar to the June 2008 flood of Cedar Rapids. Methods established will incorporate biogeochemical tracing techniques, including an analysis of radionuclides, stable isotopes ratios, and elemental ratios.

2. STUDY AREA DESCRIPTION

Cedar Rapids is divided by the north-south flowing Cedar River (Figure 1, aerial image courtesy of maps.live.com). The western portion of the city is dominated by residential areas. Bordering the eastern bank of the Cedar River is the downtown business district. North of the business district and east of the Cedar River is Cedar Lake. Numerous automobile bridges connect the two sides of the city, with the largest, most upstream being the Interstate-380 bridge.

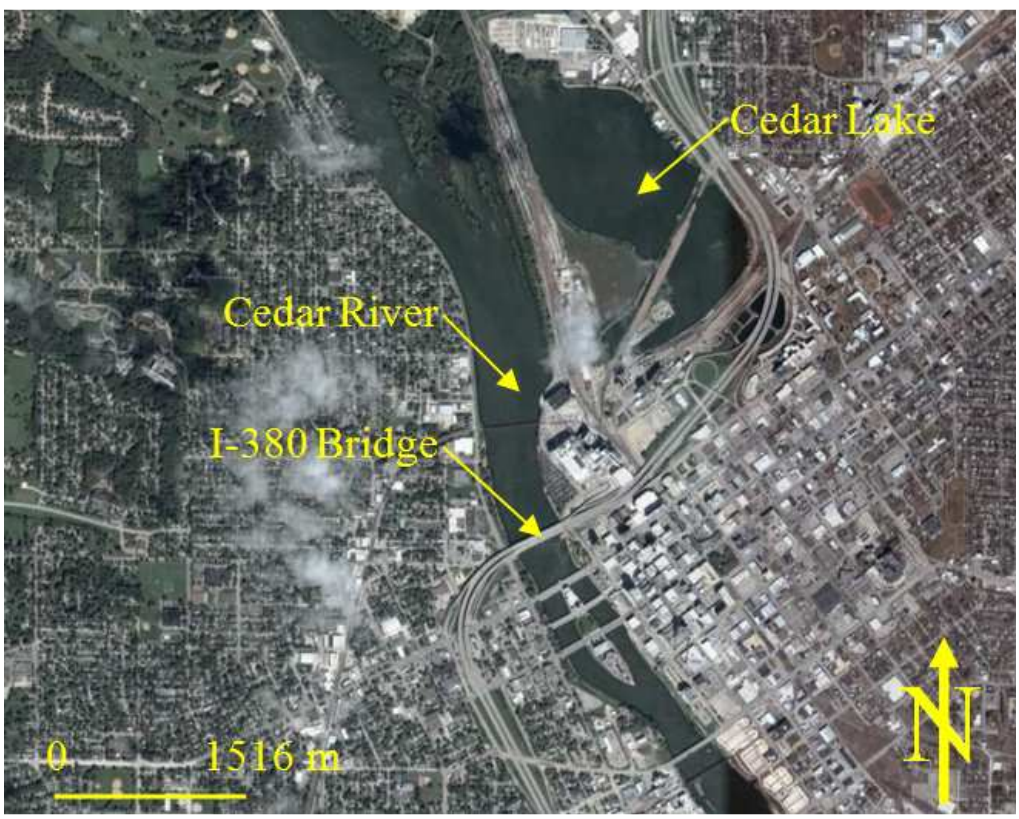

Figure 1: Aerial view of Cedar Rapids during normal flow conditions.

The I-380 bridge is significant to this study due to a gated weir system that was installed beneath the bridge. An aerial view of the bridge and the nine gates is

displayed in Figure 2 (aerial image courtesy of maps.live.com). During the flood, gates 7, 8, and 9 were left closed. As the floodwater reached this obstruction, floodwater velocity was reduced, allowing suspended matter to settle upstream of the gates.

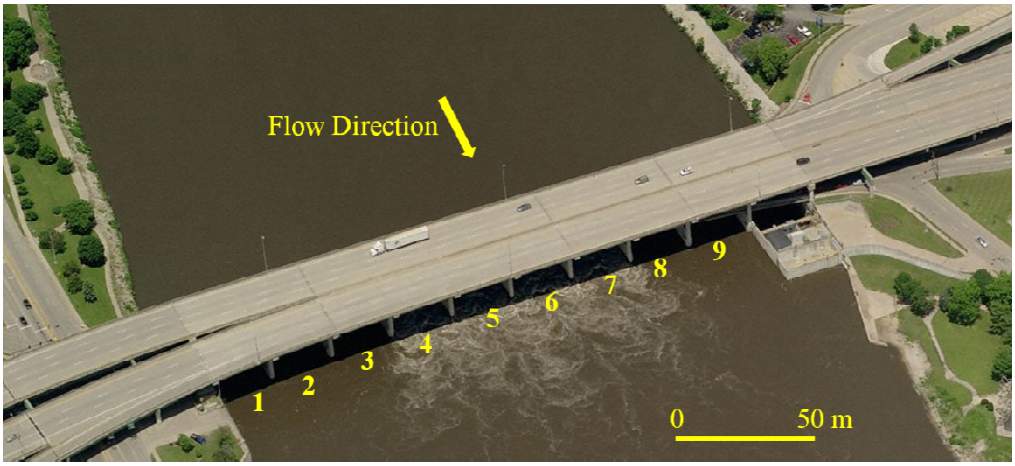

Figure 2: I-380 bridge with gated weir system during normal flow conditions.

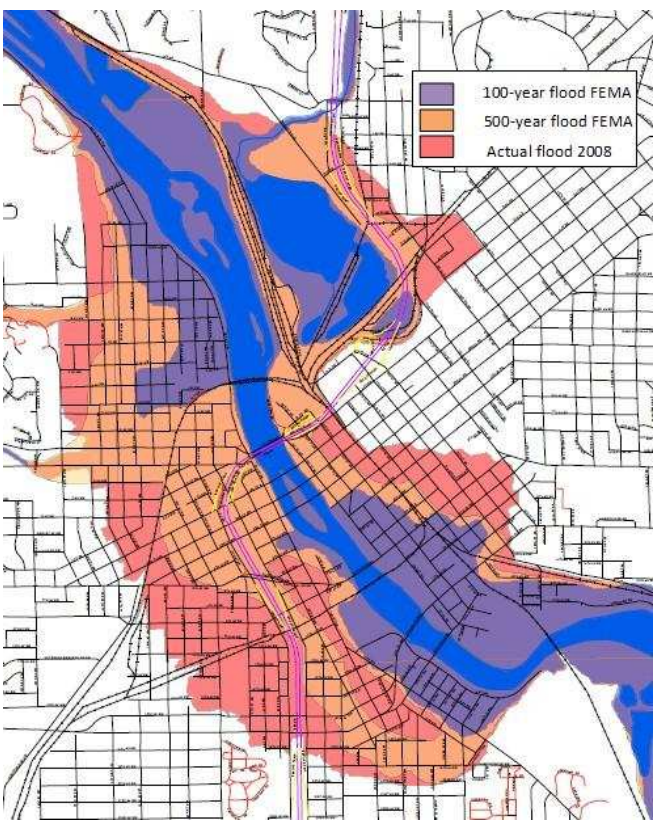

Figure 3: Flood extents.

Figure 3 displays the 100- and 500-year flood boundaries according to the Federal Emergency Management Agency (FEMA) and the recorded flood extents (Corridor Recovery, 2008). In some locations, the recorded flood boundaries are far outside of the 500-year flood border. During the flood, approximately 10 square miles were affected by the floodwaters (Corridor Recovery, 2008). Both residential and commercial areas were within the inundated areas.

3. METHODOLOGY

Source, depositional, and reference samples were gathered to determine the provenance of the sediment particles. Using a systematic procedure, the clay-sized fraction of each sample was isolated. After isolation of the clay-sized fraction, samples were analyzed for biogeochemical tracers.

3.1 SAMPLING

Samples were collected from source and depositional areas after the flooding of Cedar Rapids. Two potential sediment sources were identified: the bed of Cedar Lake and the channel banks. Both 30-cm cores and 5-cm surface samples were collected from the stream banks. On the west bank of the Cedar River, 11 surface samples were obtained and 7 cores were taken. On the east bank, six surface samples were collected and four cores were taken. Upstream of the I-380 bridge (shown in Figure 2), five samples were gathered.

Two depositional areas were identified: the bed of the Cedar River immediately upstream of the I-380 bridge and inundated terrestrial areas. The bed of the Cedar River where the five source samples were obtained can be assumed either a sediment source or a depositional area depending on the location from which the flood is being viewed. If observing the flood upstream of the I-380 bridge, the aforementioned sampling area immediately upstream of the bridge can be assumed a depositional area due to the decreased floodwater velocity at this location relative to the incoming floodwater velocity. However, if viewing the flood downstream of the I-380 bridge, the sampling area can be assumed a sediment source because some sediment was likely suspended at this point as the floodwater passed over the bed sampling location. Therefore, the same five source samples gathered upstream of the I-380 bridge were also used as depositional samples.

Terrestrial samples were collected from the inundated region and reference locations. Outside of the inundated areas, 21 reference samples were collected. Within the inundated terrestrial regions, 235 samples were gathered. These 235 samples are heretofore referred to as ‘terrestrial’ samples.

3.2 LABORATORY PREPARATION OF SEDIMENT SAMPLES

The bulk of the surface area of each sample is contained within the clay-sized fraction (Leithold & Blair, 2001); therefore, the majority of the tracers is also contained

within it. As a result, isolation of the clay-sized fraction of each sample was completed to maximize the radionuclide activity per gram. A systematic process was used to isolate the clay-sized fraction of each sample. First, samples were oven-dried at 60°C. Samples were then lightly crushed with a rolling pin to <2 mm. Sub-samples (approximately 90 g each) were next removed from each sample and disaggregated using a 30.22 g L^{-1} solution of deionized water and sodium hexametaphosphate in a 1 mL to 1 g ratio. The sand-sized fraction of the disaggregated samples was then removed through sieving. The remaining clay- and silt-sized particles were suspended in deionized water after thorough mixing. A settling procedure was then completed utilizing Stokes' Law. The settling time for silt-sized particles (>0.002 mm) to settle 10 cm was determined to be 7 hr, 40 min. After 7 hr, 40 min only clay-sized particles were contained within the top 10 cm of the water column. A slow siphoning of the top 10 cm of the water column allowed for isolation of the clay-sized fraction while minimizing remixing. Two additional repetitions of the mixing, settling, and siphoning processes were completed to ensure removal of the majority of the clay-sized particles. Finally, the siphoned clay-sized fraction solution was oven-dried at 60°C until only solids remained.

3.3 LABORATORY BIOGEOCHEMICAL ANALYSIS

Analysis of the clay-sized fraction was completed for the ^{210}Pb, ^{7}Be, ^{137}Cs, and ^{40}K radionuclides. Gamma ray emissions were detected by a high purity germanium detector that was continuously cooled in a liquid nitrogen bath. Each sample was analyzed for 82800 s. This sample time was chosen because a high counting time (20000 to 80000 s) is required to obtain an acceptable analytical precision of less than ±10% at the 95% confidence level (Mabit, et al., 2008). The gamma ray emissions were converted to a digital signal using a DSPEC jr 2.0 integrated gamma spectrometer. The accuracy of the gamma spectrometer is listed as a change of <±3% of the reference peak from 0 to 50000 counts per s (Ametek, 2008). Using a MAESTRO-32 MCA Emulator, the digital signals were converted to and recorded as radionuclide activity. The radionuclide activity of each sample was standardized by dividing the activity (gamma ray emission counts) of each sample by both the amount of time the sample was analyzed (s) and the mass of the sample (g), yielding units of cts/s/g. Then, the standardized radionuclide activity was corrected back to the date of the flood. From this, the relative radionuclide activity of each sample was determined.

4. RESULTS

Preliminary results indicate that ^{137}Cs and ^{7}Be are the most promising radionuclides to use to trace the temporal and spatial patterns of the sediment. Currently, analysis of the radionuclide activity of 26 terrestrial, 16 reference, and 5 river samples has been completed.

4.1 RELATIVE ACTIVITIES

Relative activities for ^{7}Be and ^{137}Cs were determined for terrestrial, reference, and river samples. The means (μ) and standard deviations (σ) for each of the sample groups are displayed in Table 1.

Table 1: Radionuclide activity means and standard deviations.

	^{7}Be		**^{137}Cs**	
Sample Location	μ	σ	μ	σ
Terrestrial	5.50E-04	3.20E-04	1.46E-02	1.16E-02
Reference	9.40E-04	4.83E-04	1.16E-02	9.08E-03
River	2.46E-03	1.11E-03	4.05E-03	4.76E-04

Analysis of the radionuclide activity means and standard deviations is currently in the preliminary stages. However, a statistical analysis (Student's t-test) was completed on the sample groups to determine the distinctness of each sample group. Assumptions used in the Student's t-test included: 1) normal distribution of the sample sets, 2) independent sample sets, and 3) equal variances within the sample sets. A zero mean difference between the sample sets was specified as the null hypothesis. The p-value was then calculated using two-tailed statistical analyses. A low p-value (<0.10) indicated that the means of the sample sets were distinct with 90 percent confidence. Table 2 displays the results of the Student's t-test.

Table 2: Student's t-test results.

^{7}Be		**^{137}Cs**	
Sample Set Comparison	*p-value*	*Sample Set Comparison*	*p-value*
Reference vs. Terrestrial	0.014	Reference vs. Terrestrial	0.39
Reference vs. River	0.0015	Reference vs. River	0.083
River vs. Terrestrial	0.0000012	River vs. Terrestrial	0.055

As exhibited in Table 2, five of the six sample set comparisons can be considered statistically distinct with 90 percent confidence. The reference versus terrestrial sample set comparison for ^{137}Cs cannot be considered distinct with 90 percent confidence. The five sample set comparisons can be assumed statistically distinct because the low p-values allow for a rejection of the null hypothesis. Because the null hypothesis assumed a zero mean difference between the samples, and because the null hypothesis was rejected for the five sample set comparisons, those five comparisons can be considered statistically distinct.

The radionuclide activities of ^{7}Be and ^{137}Cs were plotted spatially. Figure 4 displays contours of ^{7}Be activities across the sampling area, while Figure 5 exhibits contours of ^{137}Cs activities.

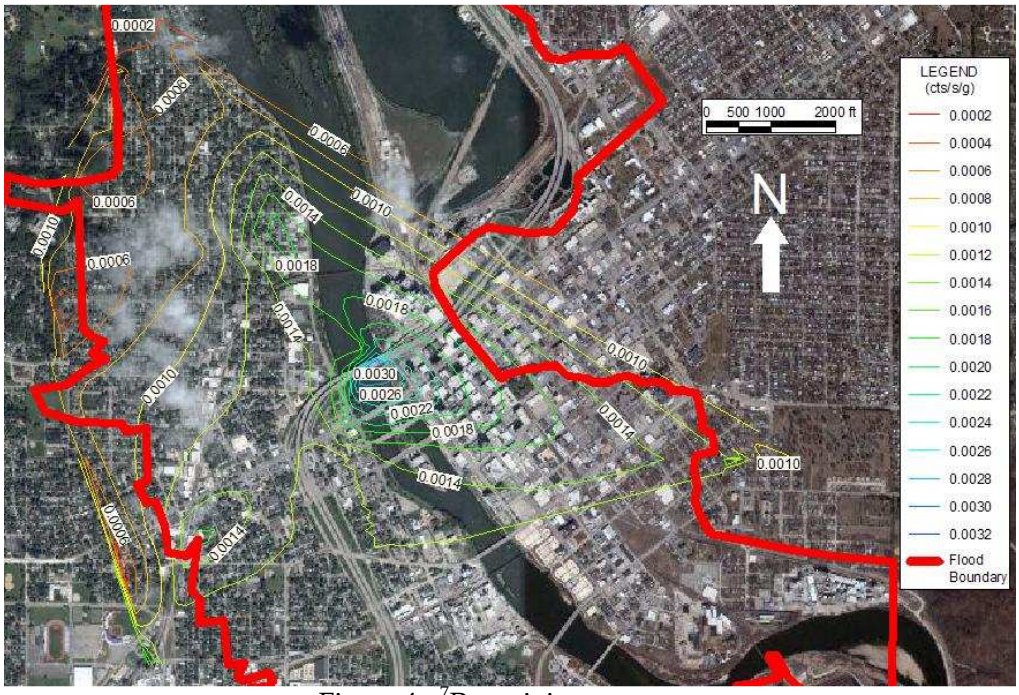

Figure 4: ^{7}Be activity contours.

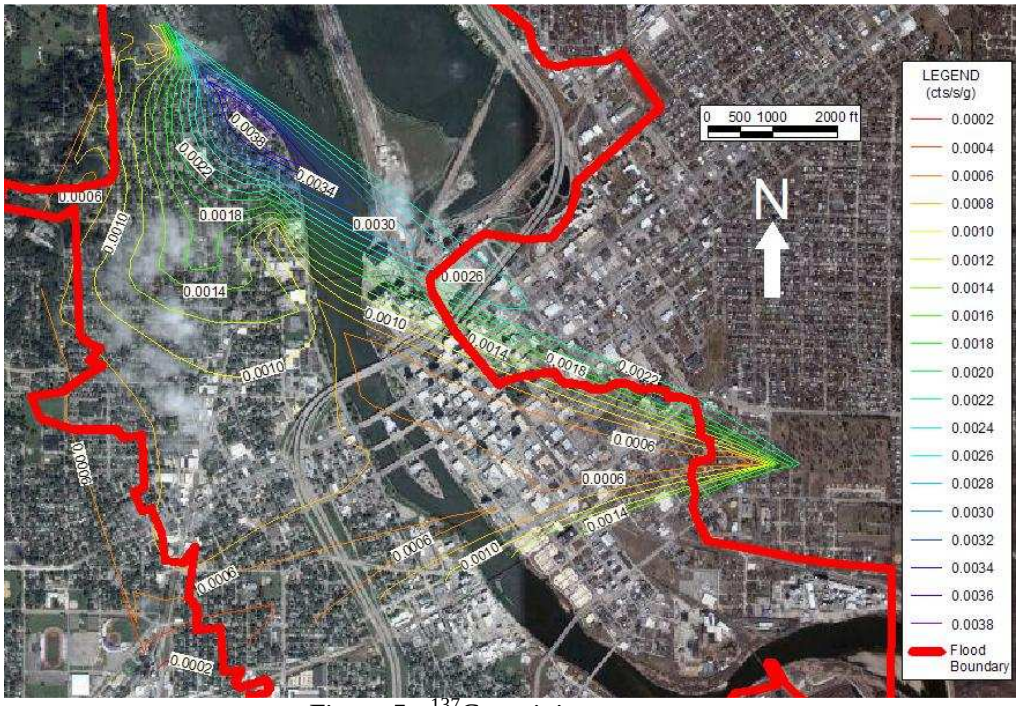

Figure 5: ^{137}Cs activity contours.

As exhibited in Figure 4, the highest activities of ^{7}Be are in the immediate vicinity of the I-380 bridge. Figure 5 displays high activities of ^{137}Cs at the northeastern edge of

the sampling region. In fact, Figure 4 and Figure 5 exhibit opposing trends. Where the activities of ^{7}Be are high, ^{137}Cs activities are low, and vice versa.

Two different conclusions can be drawn from this observation. The first conclusion is that more sediment was deposited in areas enriched in ^{137}Cs. Because ^{137}Cs is no longer being delivered to the soil through atmospheric processes in measurable quantities (Ritchie, 2001), exposure of the source area to the atmosphere is irrelevant. Determination of the ^{137}Cs activities allows for the quantification of erosional and depositional amounts (Mabit, et al., 2008). Therefore, ^{137}Cs can indicate where the majority of the sediment was deposited. Higher activities of ^{137}Cs indicate that more sediment was deposited in areas along the northeastern border of the sampling region.

The second conclusion is that sediment deposited in areas with high activities of ^{7}Be was of surficial origin. Because ^{7}Be is delivered to soil via atmospheric processes, a general source area can be determined. Sampling areas with high activities of ^{7}Be were enriched with deposited material having relatively high ^{7}Be contents. The only source areas with high ^{7}Be contents were surficial areas. Therefore, the sediment deposited near the I-380 bridge was likely of surficial origin. Further analysis of these results complemented with sediment modeling will likely provide further reasoning about the provenance of the deposited sediment.

5. CONCLUSIONS

Biogeochemical tracers have been widely used to trace sediment through watersheds. However, sediment transport processes during floods have been poorly documented in existing scientific literature. The current focus of this study has been to begin to map these processes using radionuclide tracers. ^{137}Cs and ^{7}Be have insofar shown to be the most promising radionuclides based on sample means, standard deviations, statistical analyses, and relative activity contours. Because ^{137}Cs production and fallout has been minimal in recent years, quantification of erosional and depositional amounts can be determined using this radionuclide. ^{7}Be, on the other hand, can provide clues as to the general source area of deposited material. After further analysis of the results, conclusions may be drawn regarding the specific provenance of the deposited material. These conclusions will likely provide to engineers and researchers tools with which to track the transport of sediments in similar floods.

ACKNOWLEDGEMENTS

The authors and principal investigator Papanicolaou would like to acknowledge the student and postdoctoral support provided by Iowa's Multiscale Carbon and Nitrogen Studies (IMCANS): Combining Remote and In-Situ Approaches in Agricultural Landscapes program, and its director, Dr. William Byrd.

REFERENCES

Ametek (2008). DSPEC jr 2.0 Retrieved Jan. 22, 2009

Blake, W. H., Walling, D. E., & He, Q. (2002). Using cosmogenic beryllium-7 as a tracer in sediment budget investigations. *Geografiska Annaler, 84 A*(2), 89-102.

Corridor Recovery (2008). Flood Statistics. *Corridor Recovery*, 2009, from http://www.corridorrecovery.org/stats.asp

Fox, J. F., & Papanicolaou, A. N. (2007). The use of carbon and nitrogen isotopes to study watershed erosion processes. *Journal of the American Water Resources Association, 43*(4), 1047-1064.

Leithold, E. L., & Blair, N. E. (2001). Watershed control on the carbon loading of marine sedimentary particles. *Geochimica et Cosmochimica Acta, 65*(14), 2231-2240.

Mabit, L., Benmansour, M., & Walling, D. E. (2008). Comparative advantages and limitations of the fallout radionuclides Cs-137, Pb-210, and Be-7 for assessing soil erosion and sedimentation. *Journal of Environmental Radioactivity, 99*, 1799-1807.

Middelburg, J. J., & Nieuwenhuize, J. (1998). Carbon and nitrogen stable isotopes in suspended matter and sediments from the Schelde Estuary. *Marine Chemistry, 60*, 217-225.

Olley, J. M. (2002). *Organic carbon supply to a large lowland river and implications for aquatic ecosystems*. Paper presented at the The Structure, Function and Management Implications of Fluvial Sedimentary Systems, Alice Springs, Australia.

Palinkas, C. M., Nittrouer, C. A., Wheatcroft, R. A., & Langone, L. (2005). The use of Be-7 to identify event and seasonal sedimentation near the Po River delta, Adriatic Sea. *Marine Geology, 222-223*, 95-112.

Ritchie, J. C. (2001). *Cesium-137 - An under-used tool for estimating soil erosion rates and patterns*. Paper presented at the Soil Erosion Research for the 21st Century.

Nitrification Inhibition by UVA Photocatalytic TiO_2 nanoparticles: the Role of Reactive Oxygen Species on Nanotoxicity

Okkyoung Choi[1] and Zhiqiang Hu[2]

[1]Department of Civil and Environmental Engineering, University of Missouri, Columbia, MO 65211. PH (573) 882-9141; email: oc7p5@mizzou.edu

[2]Department of Civil and Environmental Engineering, University of Missouri, E2509 Lafferre Hall, Columbia, MO 65211 PH (573) 884-0497; email: huzh@missouri.edu

ABSTRACT

We measured the toxicity of TiO_2 nanoparticles to nitrifying bacteria under ultraviolet conditions. Nitrifying bacteria play an important role of nitrification in wastewater treatment plants. Although there was no inhibitory effect of TiO_2 nanoparticles under ambient light or dark conditions, nitrification inhibition was significantly increased when TiO_2 nanoparticles were exposed to ultraviolet (UV) for 30 minutes. Under UV exposure, both TiO_2 nanoparticles and bulk TiO_2 generated the same amount of reactive oxygen species (ROS) in the cells although TiO_2 nanoparticles were more toxic than the bulk counterpart. While the inhibition was well correlated to intracellular ROS concentration, the ROS correlations were different for the different forms of TiO_2 or for the different nanoparticles (e.g., Ag vs. TiO_2), indicating that ROS is not a good chemical marker of the toxicity of nanoparticles.

INTRODUCTION

TiO_2 nanoparticles are one of the most used nano-materials in nanotechnology enhanced products such as cosmetics, sunscreen, and paint, because they have photocatalytic property to generate reactive oxygen species after light exposure (365 nm, UVA). But little is known on how the exposure of TiO_2 nanoparticles affects wastewater treatment. TiO_2 is semiconductor with bandgap energy 3.2 eV (365nm). Whena shortwave light less than 365nm shines on TiO_2, reactive oxygen species (ROS) are generated by photoelectrochemical mechanisms. The main objective of this work was to evaluate the role of ROS in determining nanotoxicity. Nitrifying bacteria are sensitive to a number of environmental factors such as pH, dissolved oxygen concentration, and temperature, and are therefore susceptible to inhibition in wastewater treatment (Hu et al. 2002). We cultured nitrifying bacteria and measured oxygen uptake rates of nitrifying bacteria treated with commercially available TiO_2 (Anatase). Also we compared the toxicity of nano-Ag and nano-TiO_2 and bulk TiO_2 to better understand the mode of action of nanoparticles.

METHODS AND MATERIALS

TiO_2 nanoparticles (TiO_2 NPs) were purchased in anatase form (Nanostructured & Amorphous Materials Inc, Los Alamos, NM) because of its high efficiency as a photocatalyst. Silver nanoparticles (Ag NPs) were prepared in the laboratory following a previous report (Choi et al. 2008). Transmission Electron Microscopy (TEM, JEOL 1400) was applied under an acceleration voltage of 100 keV for size valication. The toxicity of nanoparticles was evaluated by the oxygen uptake rate changes after adding nanoparticles suspension into a nitrifying culture. The nitrifying bacteria were enriched for more than two years under a continuous system (1day HRT, 20 days SRT, at 25 ± 2 ^oC) and an aliquot of nitrifying culture was used in a batch system for each toxicity test. The rate of dissolved oxygen (DO) decrease was measured during the nitrification process in closed respirometric bottles. Ammonium nitrate was used as the only nitrogen source because the ammonia monooxygenase (AMO, $NH_3 \rightarrow NH_2OH$) was the most sensitive to nanoparticles. A UVA lamp (Blak-Ray Lamp Model UVL-56, 365 nm, 750 μW/cm^2 at 15cm) was used to activate the TiO_2 NPs for 30 mins before each toxicity test. Intracelluar ROS accumulation was measured using fluorescent dyes (dichlorodihydrofluorescein diacetate, Invitrogen, OR, USA). Nanoparticle-treated cultures were distributed 200 μL in each 96-well microplate and the fluorescence was measured using a microreader (VICTOR^3, PerkinElmer, CT, USA) with a 485 nm excitation and a 535 nm emission filter. Increased fluorescence was measured after 30 mins exposure of TiO_2 only or TiO_2 + UVA and normalized as H_2O_2 concentration using standard calibration of H_2O_2 and fluorescence increase.

RESULTS AND DISCUSSION

We found 100 mg/L TiO_2 inhibited only 24.4 (±5.4) % to ammonia oxidation. However, after 30mins UVA exposure, the toxicity of TiO_2 was increased dramatically and it inhibited nitrification by 65.8 (±7.7) % at 1 mg/L TiO_2. We found the toxicity of TiO_2 under UVA was synergistically increased because the toxicity was more than the sum of individual toxicity of UVA (Figure 1) and TiO_2. The toxicity of TiO_2 was linearly increased as increasing UVA exposure time (Figure 1) and TiO_2 concentration (Figure 2). Furthermore, TiO_2 nanoparticles were more toxic to nitrifying bacteria than the bulk TiO_2 (ANOVA, $P< 0.05$) (Figure 2).

However, at the same TiO_2 concentrations, there was no statistical difference of intercellular ROS concentration between the bulk and the commercial nano-TiO_2 (ANOVA, $P< 0.05$, Figure 3). Figure 3 shows the toxicity of TiO_2 was strongly related to intracellular ROS. Without UV exposure, no reactive oxygen species were detected in the nitrifying culture treated with nano-TiO_2 (Figure. 3).

The ROS concentrations corresponded to 100 ~ 310 μM H_2O_2 at 0 ~ 2 mg/L nano-TiO_2 under UVA exposure. These values were ten times larger than the ROS concentrations measured in similar nitrifying culture treated with nano-Ag (1 ~ 20 μM H_2O_2) (Figure 4) (Choi and Hu 2008). Silver nanoparticles generated much less ROS in the cells but show higher degree of inhibition than nano-TiO_2. The relationship of ROS with nano-Ag inhibition could be explained with the saturate model (Choi and Hu 2008). In contrast, a linear relationship (R^2 =0.98) with nano-TiO_2 inhibition was observed (Figure 3). These results suggest that other cytotoxicity mechanisms of nanoparticles are present in addition to intercellular ROS accumulation. It appeared that TiO_2 may inhibit nitrification in wastewater plants when the nitrifiers are exposed to UV light from sunlight.

CONCLUSION

- TiO_2 nanoparticles were activated under UV exposure to generate reactive oxygen species (ROS) that were correlated with nitrification inhibition. There was no inhibition by TiO_2 nanoparticles in the absence of UVA. Compared to nano-TiO_2, bulk TiO_2 generated the same amount of ROS but with lower toxicity.
- Based on the comparison of ROS concentrations from different nanoparticles (e.g., Ag and TiO_2) and different chemical forms (nano-TiO_2 vs. bulk TiO_2), the reactive oxygen species are not a good chemical marker to indicate the toxicity of nanoparticles.

REFERENCES

Choi, O. K., Deng, K., Kim, N. J., Ross, L., and Hu, Z. Q. (2008). "The inhibitory effects of silver nanoparticles, silver ions, and silver chloride colloids on microbial growth." *Water Res.*, 42, 3066-3074.

Choi, O. K., and Hu, Z. Q. (2008). "Size dependent and reactive oxygen species related nanosilver toxicity to nitrifying bacteria." *Environ. Sci. Technol.*, 42, 4583-4588.

Hu, Z. Q., Chandran, K., Grasso, D., and Smets, B. F. (2002). "Effect of nickel and cadmium speciation on nitrification inhibition." *Environ. Sci. Technol.*, 36(14), 3074-3078.

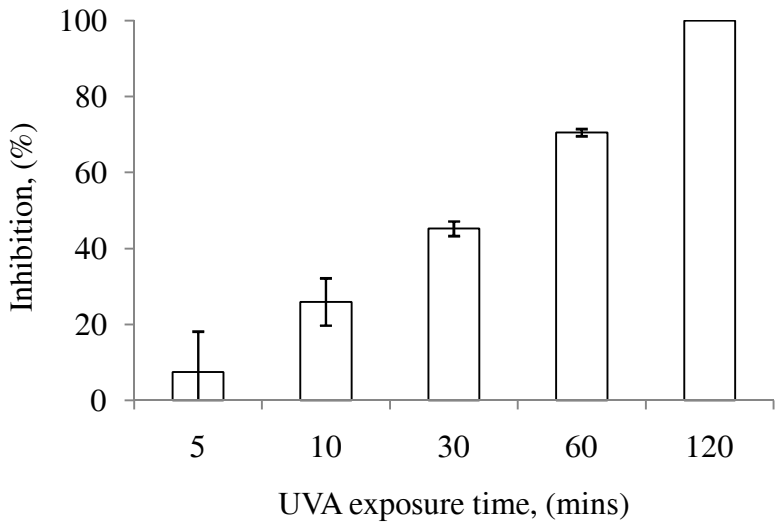

Figure 1. Nitrification inhibition by UV light. The inhibition increased linearly with the exposure time. Error bars indicate one standard deviation of triplicate samples.

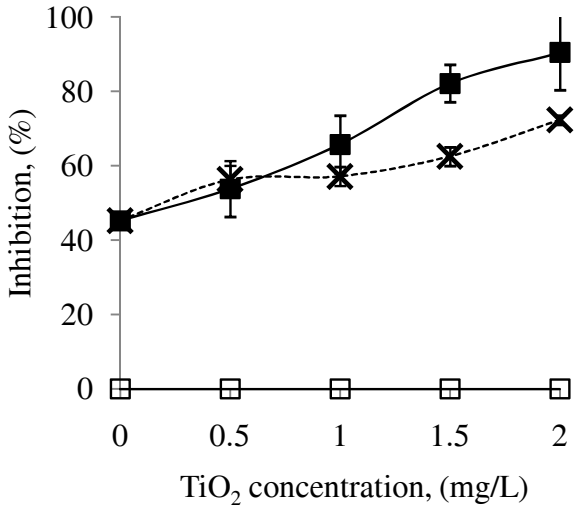

Figure 2. Nitrification inhibition by nano-TiO_2 in the presence (filled symbols) and absence (open symbols) of 30 min UVA exposure. Open squares show no inhibition by nano-TiO_2 in the absence of UVA. For comparison, the inhibition by the bulk TiO_2 (×) in the presence of UV exposure is similar to that by nano-TiO_2 but with less degree. Error bars indicate one standard deviation of triplicate samples.

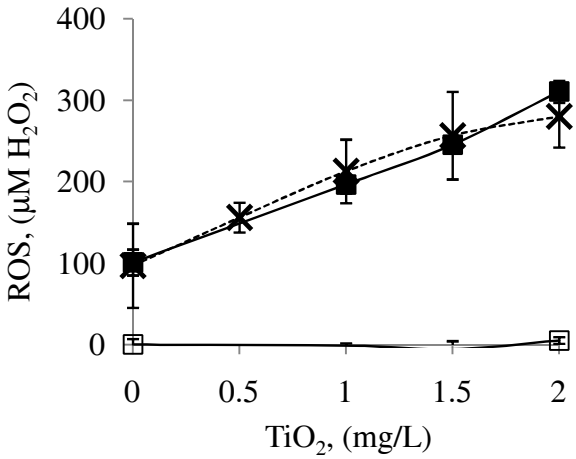

Figure 3. Intercellular reactive oxygen species (ROS) generation in cells treated with TiO_2 nanoparticles (■) and bulk TiO_2 (×) under UVA exposure. Without UV exposure, TiO_2 nanoparticles did not induce intercellular ROS (□). Error bars indicate on standard deviation of five replicates.

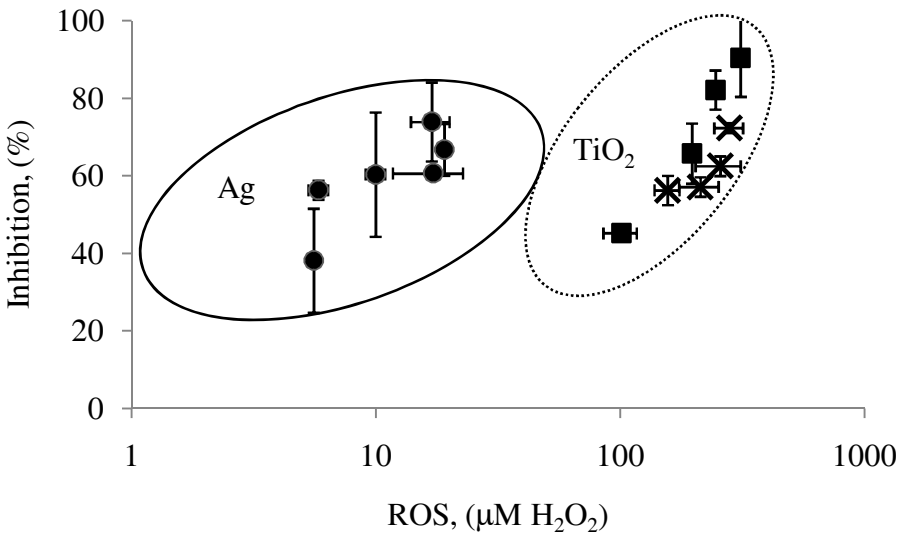

Figure 4. The relationship between the inhibition and ROS concentration. The inhibition was plotted as a function of ROS from samples treated with TiO_2 nanoparticles (■), TiO_2 bulk suspension (×) under UV exposure and Ag nanoparticles (●). Note: the log-scale in X-axis.

The Economic and Environmental Significance of Nonpoint Source Abatement in Large Watersheds

Jamie Lefkowitz[1], Kirk Westphal[2], P.E., Jeffrey Walker[3], and Gary Mercer, P.E.[4]

[1] CDM, Water Resources Division, 50 Hampshire Street, Cambridge, MA 02139, (617)452-6591, email: LefkowitzJ@cdm.com
[2] CDM, Water Resources Division, (617)452-6440, email: WestphalKS@cdm.com
[3] CDM, Water Resources Division, (617)452-6283, email: WalkerJD@cdm.com
[4] CDM, Water Resources Division, (617)452-6238, email: MercerGW@cdm.com

ABSTRACT

Throughout the United States, nonpoint source pollution from stormwater runoff, failing septic tanks and other diverse sources is a significant, often dominant, cause of noncompliance with water quality standards in large watersheds. Even with this knowledge, considerable economic resources are spent on reduction of conventional point source pollution (e.g., wastewater discharges and combined sewer overflows) with little more than a casual understanding of the nonpoint source pollution sources within a large watershed, or of the potential value of dollars spent, as measured by improvements in receiving water quality or designated use attainability. This work shows that quantification of nonpoint sources and their influence on regulatory compliance should be at the forefront of watershed management efforts, not as a replacement for point source abatement, but as a factor worthy of equivalent scientific and economic attention. With this guiding principle, this work illustrates how abatement costs and resulting environmental improvements for both point and nonpoint source controls must be clearly understood and managed together if the fundamental precepts and objectives of the Clean Water Act are to be addressed decisively.

In 2002, the U.S. Army Corps of Engineers initiated the Merrimack River Watershed Assessment Study to address water quality impairments on the Merrimack River. As a result of combined sewer overflows (CSOs) and other point and nonpoint sources, many reaches of the river have been placed on the New Hampshire and Massachusetts 303(d) lists for violations of bacteria water quality standards. The goal of the study was to quantify the relative impacts of point sources and nonpoint sources on water quality, and to compare the economic and environmental value of alternative management strategies. The study blended comprehensive field monitoring with detailed simulation modeling that compared alternative management strategies for watershed-wide pollution abatement. The management strategy which resulted in the greatest value of abatement dollars was a combination of modest treatment upgrades and partial combined sewer separation with modest nonpoint source reduction throughout the watershed. This balanced approach showed more value than scenarios focusing only on long-term CSO control plans and full combined sewer separation, emphasizing the need for a more comprehensive approach to managing sources of pollution as well as the need for more attention on the economic value of nonpoint source abatement alternatives for large watersheds.

STUDY OVERVIEW

A watershed assessment study was conducted for the Merrimack River watershed in southern New Hampshire and northeastern Massachusetts (USACE, 2006). The study included a comprehensive monitoring program, a continuous flow and water quality model, and an analysis of stakeholder-developed alternative pollution management options. Many reaches of the river are listed on NH and MA 303(d) lists for violations of bacterial water quality standards. The sources of these impairments are not readily apparent, as most of the upper watershed consists of forested land and rural communities, with the most downstream reaches flowing through five urban communities before emptying into the Atlantic Ocean: Manchester NH, Nashua NH, Lowell MA, Lawrence MA (Greater Lawrence Sanitary District, GLSD), and Haverhill MA. The five communities, each of which are serviced by aging combined sewer systems, have signed individual consent agreements with the United States Environmental Protection Agency to commit large sums of money to the abatement of combined sewer overflows (CSOs) in accordance with the federal Clean Water Act. Each community is in various stages of development and implementation of CSO Long-Term Control Plans (LTCPs). Since enforcement protocols are specific to individual communities, these plans are being developed in isolation from the rest of the watershed, and even from the other CSO communities along the mainstem. Collectively, these communities may need to spend up to $500 million on CSO control alone to comply with EPA mandates. While there are credible estimates of the bulk bacterial loads discharged from these CSOs each year, the plans were mandated with incomplete understanding of the relative magnitude of these loads with respect to other loads throughout the basin, and more importantly, with no attempts to quantify the expected improvements in river compliance or use attainability.

The CSO communities recognized the need for a comprehensive look at the issue and formed the Merrimack River Basin Community Coalition. The Coalition approached the New England District of the United States Army Corps of Engineers (USACE) for assistance in conducting the multi-jurisdictional watershed assessment. The USACE was able to assist through study authorization provided in Section 729 of WRDA 1986, as amended and entered into a 50-50 cost sharing agreement with the Coalition to perform the Merrimack River Watershed Assessment Study. The study was structured around the following three basic tenets:

1. Pollution abatement should not be limited to local enforcement, as this results in only partial accounting of pollution sources and can ignore the prevailing causal mechanisms within a watershed.
2. Pollution abatement investments should only be made when expected environmental benefits can be well defined, measured, and prioritized.
3. Pollution abatement should be a cooperative process, with local, state, and federal authorities working to ensure the productive allocation of financial resources to restore and protect the nation's natural resources.

This watershed assessment, therefore, has placed the implementation of LTCPs in proper context by asking the question: "What are the *relative* instream impacts

attributable to CSOs and to other sources, and how can watershed restoration be balanced such that investments in LTCPs, wastewater treatment technology, septic system rehabilitation, illicit connection detection and abatement, etc. are commensurate with expected improvements?" In other words, the USACE study helped quantify how much of the documented impairment is attributable to each major identifiable source type (CSOs, wastewater treatment plants, nonpoint sources), and therefore the extent to which alternative abatement strategies are actually likely to help restore the river.

MERRIMACK RIVER WATERSHED

The Merrimack River is formed by the confluence of the Pemigewasset and Winnipesaukee Rivers in Franklin, New Hampshire. The River flows southward for approximately 125 kilometers in New Hampshire; it turns abruptly across the New Hampshire - Massachusetts border and flows in a northeasterly direction for approximately another 80 kilometers before discharging to the Atlantic Ocean at Newburyport, Massachusetts. The final 35 kilometers of the River, downstream of Haverhill, Massachusetts, are tidally influenced. A map of the Merrimack River watershed is shown in Figure 1.

The Merrimack River watershed covers an area of approximately 13,000 square kilometers in New Hampshire (76 percent of the drainage area) and the northeastern portion of Massachusetts (24 percent of the drainage area), making it the fourth largest watershed in New England. It encompasses a variety of terrain and climate conditions, from the mountainous White Mountain region in northern New Hampshire to the estuarine coastal basin of northeastern Massachusetts. Precipitation in the watershed is fairly evenly distributed throughout the year; however temperatures in the basin generally vary widely on an annual basis. A mix of deciduous and evergreen forest, covering approximately 77 percent of the watershed area, dominates the land use in the basin. Urban areas, including residential, industrial, and commercial land uses, make up the second largest land use category, covering approximately 10 percent of the total watershed area.

CONTINUOUS SIMULATION MODELING

A suite of three modeling software packages were used in conjunction with existing CSO models for the five urban centers to create a continuous flow and water quality model for the Merrimack River from Hooksett, NH to Newburyport, MA. The watershed hydrology and nonpoint source loads were modeled using HSPF[1], except for the land areas covered by the individual CSO models for the five major communities, which were developed prior to this study in SWMM[2] and MOUSE[3]. The flows and loads from the watershed model and CSO models were input to the more detailed instream hydraulic and water quality models at the upstream boundary, the confluences of major tributaries, and at diffuse points along the mainstem to account for direct runoff to the channel. SWMM was chosen as the model code for the hydraulics, and WASP[4] was used to simulate water quality in the mainstem

1 Hydrologic Simulation Program FORTRAN, developed by the U.S. Geological Survey
2 Storm Water Management Model, developed by the U.S. Environmental Protection Agency
3 Model for Urban Sewers, developed by DHI
4 Water Quality Simulation Program, developed by the U.S. Environmental Protection Agency

Merrimack River. The models were calibrated to data collected as part of the comprehensive monitoring aspect of the study, which included wet- and dry-weather surveys of flow, mainstem and tributary water quality, and CSO outfalls. Examples of the calibration results from the continuous flow and water quality model are shown in Figure 2.

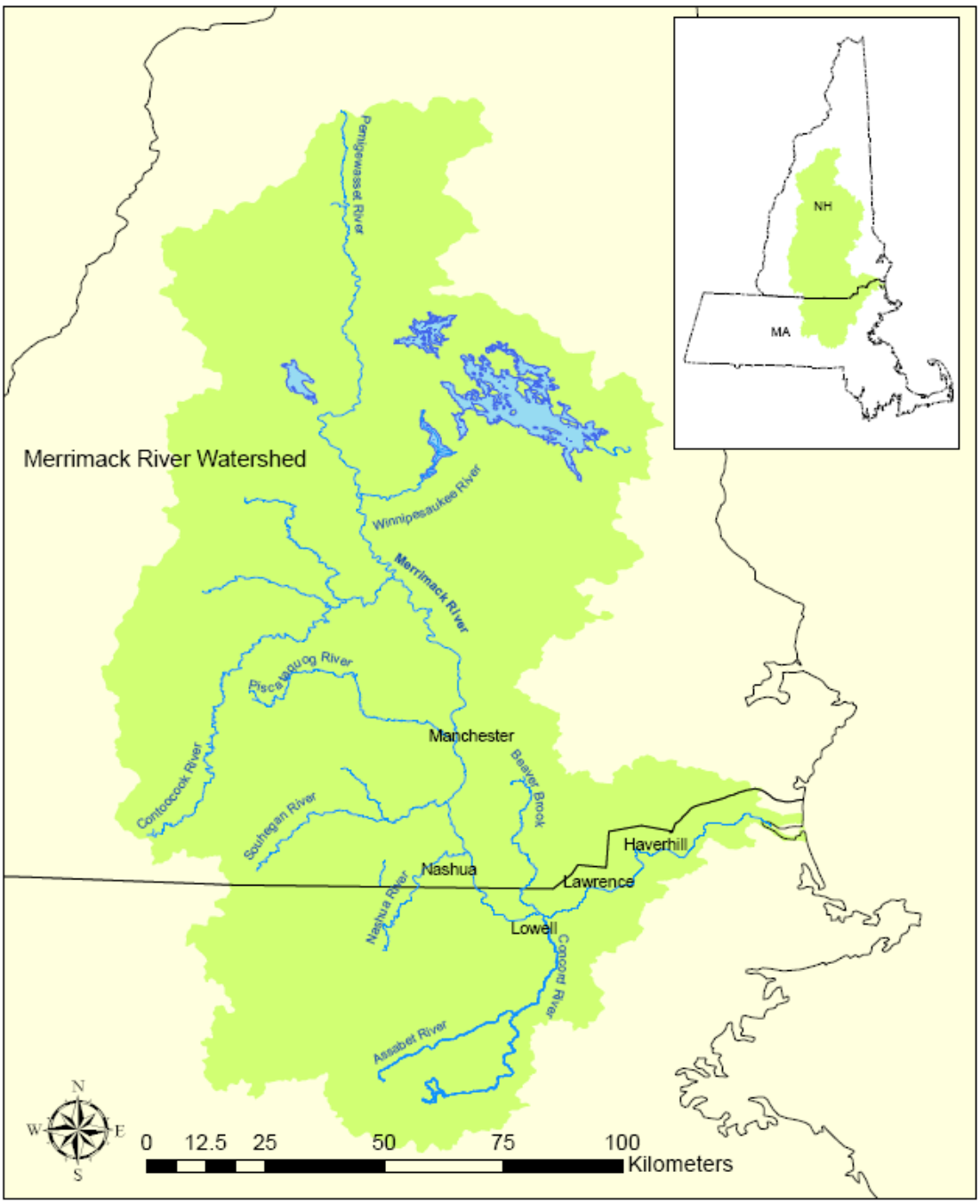

Figure 1: Merrimack River Watershed

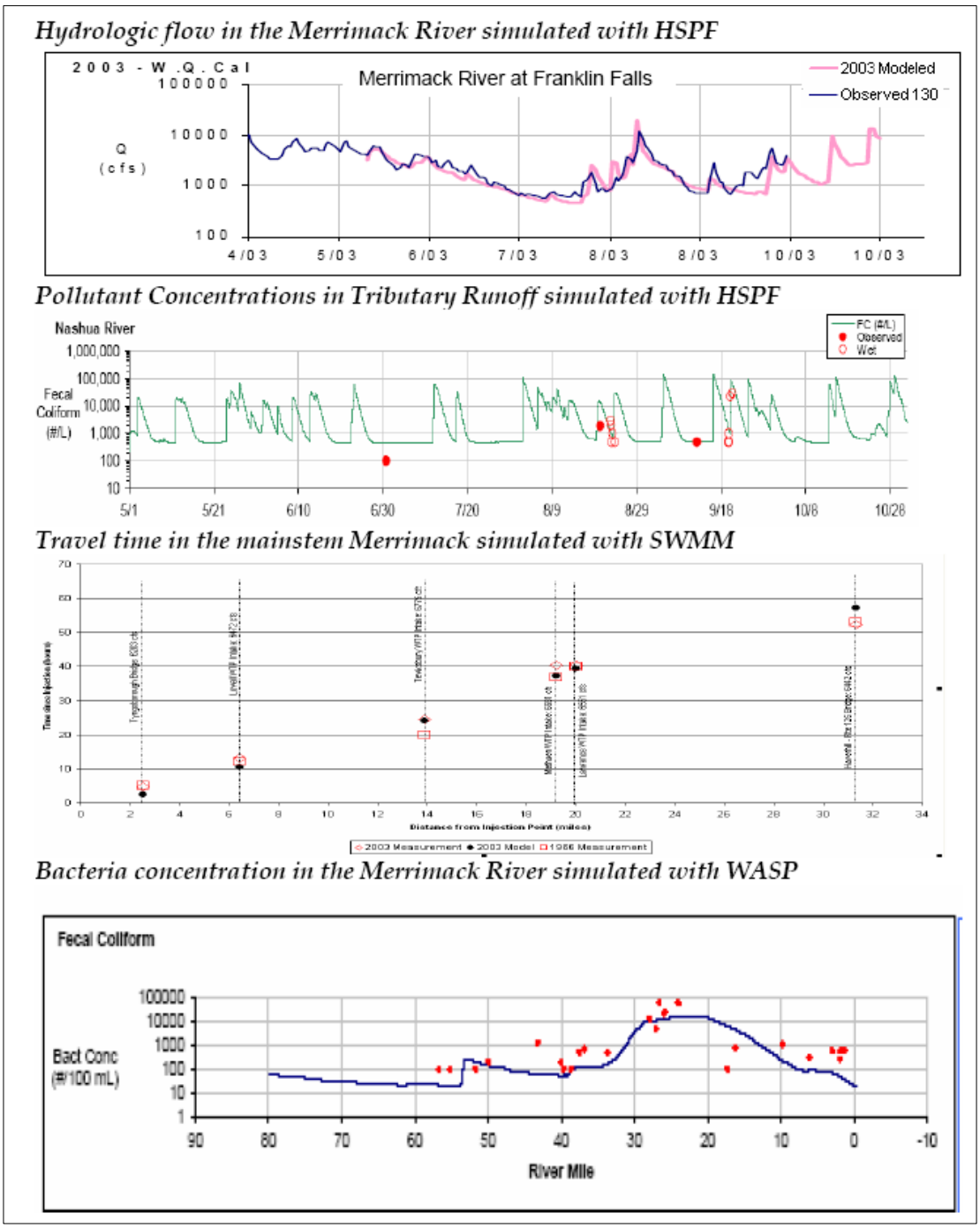

Figure 2: Representative Calibration Results (USACE, 2006)

ANALYSIS OF ALTERNATIVE MANAGEMENT STRATEGIES

Comprehensive water quality monitoring, flow measurement, and dynamic simulation modeling of the watershed were employed to develop qualitative and quantitative understanding of the relative impacts of contributing bacteria sources, the impacts of reducing specific load categories, and the costs associated with abatement. What resulted was a clear indication of the leading causes of non-compliance in this

watershed, and the most cost-effective abatement strategies. Interestingly, since bacteria compliance in Massachusetts and New Hampshire is a time-averaged standard, the leading contributor to noncompliance with standards was *not* the source that contributed the most pollutant load. Details of the monitoring study and the modeling are available through project reports posted on the Army Corps of Engineers Website (www.nae.usace.army.mil/projects). Specific reports include:

- Field Monitoring Report
- Model Development Report
- Phase I Final Report

The field data and models were first employed to test the fundamental hypothesis for this large watershed; that nonpoint sources (NPS) are a significant contributing source of bacteria even though the basin contains five communities with CSO outfalls. The analysis suggested that while the total annual load from combined sewers could be expected to exceed the total load from all other sources, the timing of the loads was critical in assessing compliance with standards and use attainability. Combined sewer overflows, while depositing enormous quantities of untreated bacteria into the river, occur infrequently, only during severe rainstorms. They are usually short in duration (measured in minutes or hours), and unacceptably high concentrations of the bacteria generally disperse and decay within hours or days. Conversely, nonpoint source loads from failing septic systems, wash-off from even modest rain events, illicit sewer connections, etc. occur on a more continuous basis, and while the cumulative contribution may be less than that of CSOs, the constancy of the load renders these sources the leading cause of time-averaged non-compliance and failure to support recreational uses and shellfish harvesting in the river.

Prior to simulating alternative abatement scenarios, stakeholders from local, state, and federal agencies convened to identify the most appropriate ways to measure progress toward compliance with bacteria water quality standards. The group, which included regulatory agencies, non-profit organizations, project sponsors, and research organizations, reached consensus on the most important metric for the river; the number of river miles that could be brought into compliance with each alternative abatement strategy. This metric formed the basis of a fundamental comparison of plans with different focal points, each of which could be associated with economic costs, and through simulation modeling, expected environmental benefits in the form of river miles brought into compliance with state standards for bacteria levels.

To determine expected environmental benefits, alternative abatement plans that focused on specific load types were simulated. CSO abatement, in the form of established short-term and long-term control plans were modeled by linking pre-existing collection system models of the five cities to the watershed and riverine models. The effects of full sewer separation were also modeled, even though this is not part of established control plans (and would have a countering side-effect of increasing urban stormwater loads during all rainstorms). Nonpoint source abatement plans on the scale of a 13,000 square kilometer watershed are more difficult to formulate and simulate, and indeed there is very little precedent for such activity at this scale. Following the intent of EPA's Phase II Stormwater program, though, it was

assumed that the Best Management Practices (BMP's) commonly promoted could, on average, reduce bacteria levels in runoff and baseflow by approximately 20%. This, then, was the benchmark associated with the management strategy for nonpoint source bacteria; a target of 20% reduction throughout the basin. This exercise in no way implies that diffuse loads are so evenly distributed, or that each community or county would require the same level of controls. It simply represented an idealized method of developing a planning-level costs and benefits for a very large and diverse watershed.

Following this assumption, then, was an attempt to estimate order-of-magnitude costs for achieving 20% reductions. It follows that if Phase II BMPs are suggestive of approximately 20% reduction in bacteria (granted, a very heuristic value), that costs associated with Phase II compliance could be related to this reduction, though full compliance generally yields additional improvement in nutrients and other contaminants in addition to bacteria. Again, using heuristic knowledge from representative communities already embarking on Phase II compliance programs in New England, a cost scale was developed and applied, and which will be subsequently examined and tested later in this study. The smallest communities in the Merrimack watershed, with dispersed populations of just a few hundred people, were assigned a theoretical cost of $1 million to comply with Phase II stormwater requirements, while the largest communities, with dense populations of approximately 100,000 were assigned a cost of $5 million. In a watershed with 13,000 square kilometers and nearly 2 million people, this averaged out to roughly $250 per capita, or 37,000 per square kilometer. Spread over ten years, which is a reasonable equivalent planning time for CSO control plan implementation, the analysis predicted a cost of $25 per capita per year to reduce basin-wide NPS bacteria by 20%. Again, these assumptions will be explored further in subsequent sections.

The costs of alternative management programs were then plotted against the number of river miles that the models predicted could revert into compliance as an environmental return on investment. The results are shown in Figure 3, and illustrate the rapidly diminishing returns of exclusive focus on CSO abatement.

The analysis suggests that environmental returns on investment for prioritizing NPS abatement above CSO control at this regulatory juncture would be 4 times higher than continuing purely with CSO abatement and no basin-wide NPS program. Furthermore, it is clear that there is an obvious limit to the improvements that can be attributed to CSO abatement, (in this case, only 16 to 19 of the 130 river kilometers studied, even though the CSO cities and their impacts span the entire 130 kilometers). When municipal budgets are scrutinized more and more heavily due to uncertain economic conditions at all levels of the public and private sectors, it becomes increasingly difficult to justify expenditures with such poor returns. A far more sensible approach would be to shift regulatory focus to NPS reduction on a regional basis, while de-emphasizing continued CSO abatement and phasing it in much more gradually over time (since it does have undeniable benefits using the scale presented herein, as well as other epidemiological benefits which are not considered directly due to the prioritization of stakeholder interests).

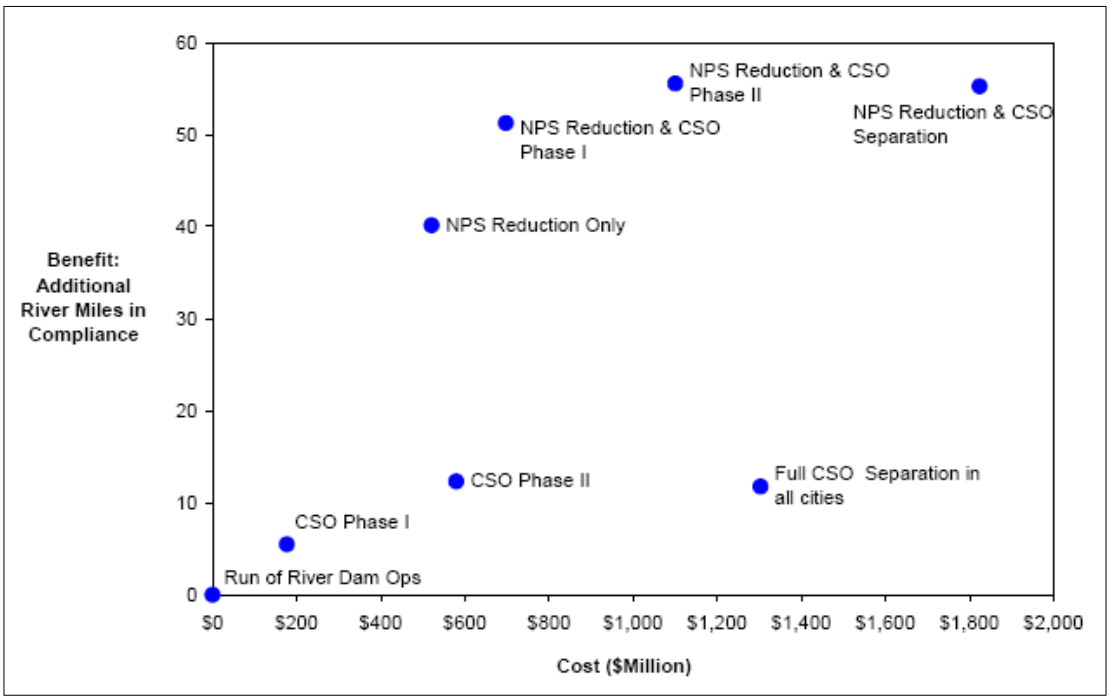

Figure 3: Comparative Value of Alternatives

COMPARISON OF NONPOINT SOURCE ABATEMENT COSTS

There is limited information available on the success, in economic terms, of NPS bacteria pollution abatement programs in large watersheds. The well documented Long Island Sound programs have focused mostly on point source reductions and beach closures rather than the in-stream impacts of NPS bacteria loads. Nonpoint source reductions are a large aspect of the Chesapeake Bay programs, but the major concern in the watershed are nutrients. Despite the lack of documented cases of large scale NPS pollution abatement programs, it is still possible to draw on the successes of small scale programs and apply the same logic to larger watersheds.

Of the many successful NPS abatement programs documented for small watersheds, the majority involve largely agricultural watersheds. However, several have focused on other sources including wildlife and failing private septic systems. In many cases, there are few or no point sources entering these small rivers, so the impairments have necessarily been attributed to NPS. While this is not the case in the Merrimack River watershed, it may be true for the many smaller communities and subbasins. The principle of the value of dollars spent on NPS abatement in small watersheds should also be applicable to large watersheds. A comparison of the balanced watershed management alternative realized by the Merrimack River Watershed Assessment Study and the small scale NPS successes in other watersheds across the country supports the concept that NPS abatement as part of a balanced program for large river basins is most cost effective.

The Coneross Creek watershed is an example of a successful NPS abatement program in a small watershed that had a combination of a few point sources as well as NPS problems resulting in fecal coliform impairments. After a three year program funded

by EPA Section 319 funds, monitoring showed significant improvement in the fecal coliform counts in the creek, to the point of de-listing the waters as impaired (EPA, 2007). The Coneross Creek watershed (200 square kilometers) is part of the larger Savannah River basin which forms the border of South Carolina and Georgia. The watershed encompasses several rural suburban communities, with land uses including forested, agricultural/grassland, and urban (SC DHEC, 2000). Based on county population densities, the Coneross Creek watershed is significantly more rural than the southern portions of the Merrimack River watershed (SOURCE:2000 census). The NPS abatement program, however, focused largely on individual land owners, making a scaling up approach based on population possible.

The NPS abatement program in the Coneross Creek watershed cost a total of $1.1 million over the course of 3 years (EPA, 2007). The program components included public outreach and education, implementation of agricultural best management practices, and reparation of failing septic systems. Based on population estimates of the watershed (U.S. Census, 2000), the project cost was approximately $37 per capita per year. That figure, scaled up based on population, yields an estimate of $74 million per year (or $5,700 per square kilometer) for the entire Merrimack River Watershed, which has a total population of about 2 million people (USACE, 2006).

More generally, the estimated cost of EPA Phase II stormwater programs is $3.75 to $6.00 per capita per year (Reese, 2003). There are significant differences in the watershed characteristics of the Coneross Creek and Merrimack River basins, and the NPS abatement program for the Merrimack would necessarily be much different than that of the Coneross Creek. However, this scaling up exercise gives another model for estimating the potential cost and benefit of including a significant NPS abatement program as part of a balanced watershed management strategy. Figure 4 shows a summary of the various NPS abatement program costs and estimates.

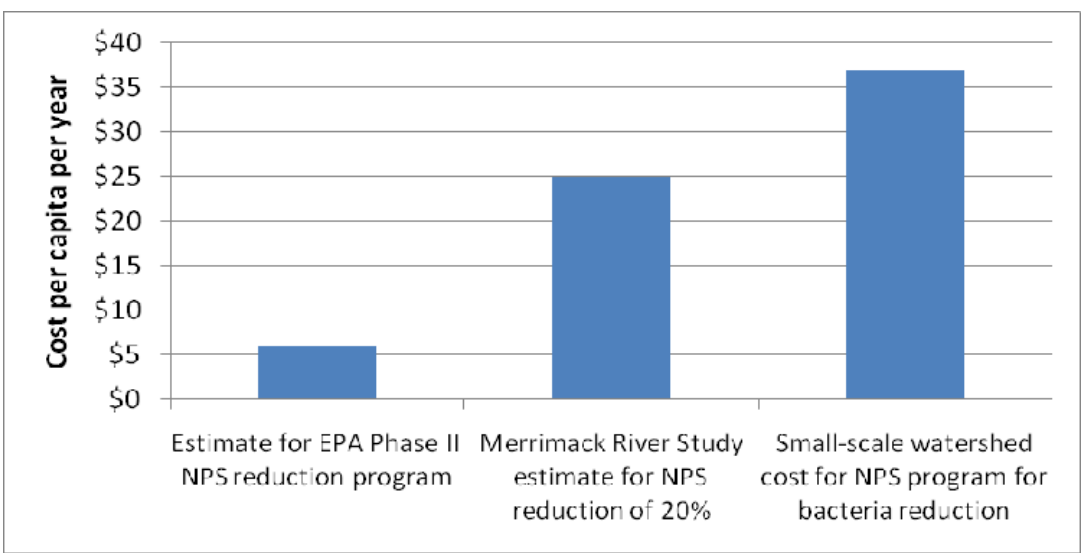

Figure 4: Cost Comparisons for Nonpoint Source Abatement

CONCLUSIONS

The results of the Merrimack River Watershed Assessment Study reveal the importance of a thorough understanding of the impact of nonpoint source pollution in large watersheds with multiple potential causes of noncompliance. Particularly, quantifying the contributions from nonpoint sources and directly comparing alternative management strategies – a spectrum of approaches from point source elimination only (LTCPs), nonpoint source reduction only, and balanced abatement strategies – will lead to a better understanding of the most economical and effective way of bringing a river into compliance. The lack of research and documentation of nonpoint source abatement programs in large watersheds forced an estimation of the cost of such a program for the Merrimack River. Comparisons made with the available information, including the cost of a small-scale successful nonpoint source abatement program and EPA Phase II stormwater program cost estimates, demonstrate that the approximation of $25 per capita per year for 20% reduction in nonpoint source pollution is reasonable. An economical analysis of the management alternatives associated with point and nonpoint source abatement on a watershed scale must include a logical metric for comparison, such as bringing river miles into compliance, to effectively evaluate the options that exist for communities within a large watershed. The Merrimack River study can be used as a benchmark for future pollution management planning in large watersheds throughout the country. Similar studies are highly recommended to build support for the hypothesis that the Merrimack River case is an example of a common situation where the focus of pollution abatement strategies (and funding) in large watersheds lean heavily toward point source reduction, to the exclusion of potentially dominant nonpoint source pollution.

REFERENCES

Reese, Andrew J. (2003) "Funding Phase II Stormwater Programs." *National Conference on Urban Stormwater: Enhancing Programs at the Local Level,* U.S. Environmental Protection Agency.

South Carolina Department of Health and Environmental Control (SC DHEC), Bureau of Water. (2000) *Total Maximum Daily Load (TMDL) Coneross Creek, South Carolina.*

U.S. Army Corps of Engineers New England District. (2006) *Merrimack River Watershed Assessment Study – Phase I Final Report.*

U.S. Army Corps of Engineers New England District. (2006) *Merrimack River Watershed Assessment Study – Monitoring Report.*

U.S. Army Corps of Engineers New England District. (2006) *Merrimack River Watershed Assessment Study – Model Development.*

U.S. Census Bureau. (2000) *Census 2000: South Carolina Profile.*

U.S. Environmental Protection Agency. (2007) "Homeowners and Agricultural Community Reduce Bacteria Levels in Oconee County Watersheds." *Section 319 Nonpoint Source Success Stories.*

The Nitrogen Budget of DRW in the Northeastern China

Chengwei Han[1] and Shiguo Xu[2]

1. Doctoral student, School of Civil and Hydraulic Engineering, Dalian University of Technology, Dalian 116024; China; Tel. +86-411-81609852, email: cwhan@student.dlut.edu.cn

2. Professor, School of Civil and Hydraulic Engineering, Dalian University of Technology, Dalian 116024,China; Tel. +86-411-84707680, email: sgxu@dlut.edu.cn

ABSTRACT

The nitrogen (N) budget is studied to evaluate N inputs and outputs of DHF Reservoir Watershed (DRW), where it is cold semiarid climate in northeastern China. Using the data of 2003 as a typical calculation year, the input of N is quantified from the aspects of atmospheric deposition, fertilizer use, biological fixation, net food and feed input, output of N from ammonia volatilization, denitrification and runoff export, respectively. It is addressed that the atmosphere deposition, fertilizer use and food and feed input dominates more than 90% of the total input. In the output side of N, the ammonia volatilization and denitrification are the main items, which account for 55% of the total N input and 95.1% of the total N output. However runoff N export is 6.49% of the total N input. This is owing to the more water retention time in reservoir for N settling and more sites for denitrification. Over the whole watershed, the budget of N is positive (13.52 kg ha^{-1} yr^{-1}), which results in the N accumulation in landscape and the TN concentration increase in DHF Reservoir.

KEYWORDS*: Nitrogen, Budget, Water quality, Northeastern China*

1. Introduction

Research finds that the input of reactive nitrogen (N) to global cycles have increased dramatically as a result of anthropogenic activities, which would accelerate the N accumulation in landscapes and the N delivery into water bodies (Galloway et al. 2004; Galloway et al. 1995). Total reactive N inputs into the global system have increased from 15.6 Tg yr^{-1} to 139 Tg yr^{-1} between 1890 and 1990 (Galloway and Cowling 2002). As N is a major determinant of water quality, the big increasing of reactive N load will likely cause severe damage to environmental services at local, regional, and global scale.

In order to understand the nitrogen dynamics in the watershed scale, recent studies have constructed N budget, which include N inputs and N outputs. The budget has been well documented at the scale of watershed, which aim at the identification of the fate of N surpluses or in long-term assessment of N fluxes and their respective impact on the environment. Boyer et al. constructed budget describing N inputs and outputs for 16 catchments in the northeastern U.S.A (Boyer et al. 2002). At the same time, Xing and Zhu addressed N budget in the three major rivers in China (Xing and Zhu 2002). N temporal and spatial trends have been investigated by budget (Schaefer and Alber 2007). On the other hand, N budget is used in the environment management, which is developed to evaluation the decreased effect of impoundments on N fluxes(Bosch and

Allan 2008).

In China, there is the largest population in the world. To meet the food and fiber demands of 1.3 billion people, application of N fertilizers has been increasing drastically to 22.20 Tg N in 1995, which is one fourth of the world's total (Liu et al. 2006). There surplus N inputs far exceed N outputs in products shipped out of agricultural ecosystems (Chen et al. 2008). However, There is little knowledge about N budgets in China. Chen et al. developed N budgets in an agricultural watersheds in a warm and humid area of southeast China (Chen et al. 2008). Liu et al. investigate both temporal and spatial changes in the N budgets of Yangtze River basin (Liu et al. 2008). These researches are focused on south or middle of China. Because climate change can result in marked changes in N cycles, these researches are not enough. Now the region of northeastern China , the main foodstuff producing region, has been suffered potential N risk (Sun et al. 2008). For example, The TN concentration of DHF Reservoir Watershed (DRW) , which provides drinking water for the 20 million people in Liaoning province, is increased from 0.98 mg $L^{-1}$to 2.23 mg L^{-1}. However, the sources and the fate of N in the cold semiarid region of the northeastern China are hardly studied.

The objective of this study is to quantify N inputs and outputs for the DRW, a watershed in northeastern China. It mainly focuses on providing a further understanding of the relation between N budget and water quality trend in the cold semiarid catchment. Generally, for a river watershed, 20-26% of the total N inputs in average is exported through runoff (Boyer et al. 2002; Howarth et al. 2006). Due to the decreased effect of reservoir, there will be different relation in the large-scale reservoir. This research on nitrogen-water quality linkages should be broadened to address the issues of N losses and N balance in a watershed-scale.

2. Materials and methods

2.1 Study area

The DRW (518 910 ha) is a mixed land use watershed located in northeastern China. It has three tributaries, which includes Hun River (52.7%), Suzi River (37.1%) and She River (10.2%)(Figure 1.). The annual precipitation varies from 650 mm ~ 800 mm, and 50% of precipitation occurs in July and August. The catchment includes Qinyuan Country, Xinbin Country and Fushun Country. DRW comprises arable land (15.47%), forest (80.26%), wetland (0.82%), water body (2.25%), and residential land (1.20%). The cultivated land and population are shown in Table 1. And the distribution of the land use is shown in Table 2.

Table 1 Cultivated land area and population in DRW

Cultivated land area (ha)			Population (10^3 persons)		
Upland	Paddy field	Total	Rural	Urban	Total
75 586	12 671	87 757	251.2	156.0	407.2

Table 2 Land use in DHF (ha)

Region	Agriculture	Forest	Wetland	Water	Urban	Other	Total Area
Qinyuan Country	10 305	41 782	347	7 416	355	0	212 659
Xinbin Country	33 307	179 577	2 946	1 123	3 940	0	214 365
Fushun Country	36 640	195 128	938	3 155	1 951	2	91 886
Total Area	80 252	416 487	4 231	11 693	6 245	2	518 910

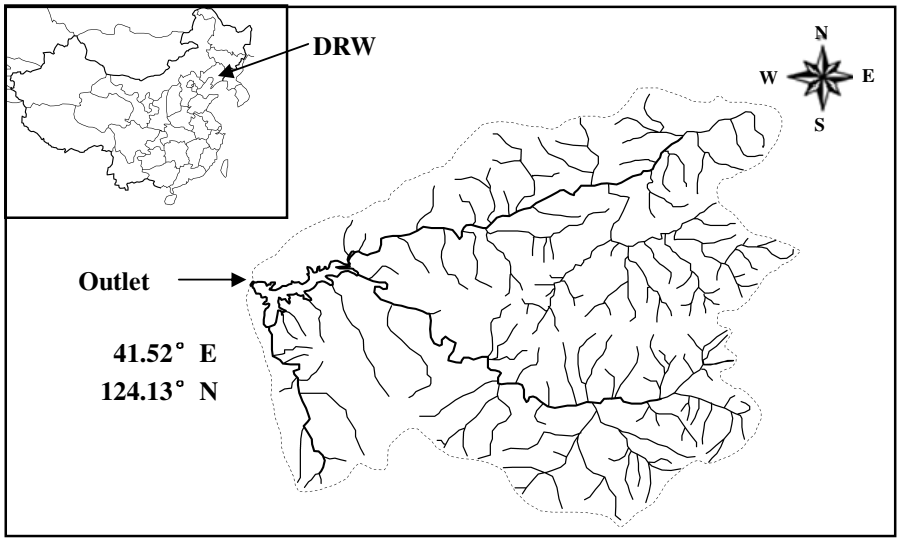

Figure 1 The map of DHF reservoir watershed

In this study, fluxes of N input and output is individually quantified using various approaches and available data: local and national statistical data, digital land cover map, local meteorological and hydrological data, as shown in Table 3. All fluxes are conducted for 2003 to investigate the increasing N concentration in DRW between 2000 and 2005.

Table 3 Basic data used in this study

	Item	Source
Agricultural data	Maize, rice, soybeans, vegetables, N fertilizer	Fushun yearbook Fushun statistical yearbook
Population	Total population, rural population	Fushun yearbook Fushun statistical yearbook
Livestock population	Pigs, cattle, sheep, poultry	Fushun yearbook Fushun statistical yearbook
Land use/cover data	Digital land cover map of China	www.geodata.cn
Hydrological data	Water quantity and quality	Annals of DHF

2.2 Nutrogen budget

The N budget of DRW is studied by the approach described in Boyer's study (Boyer et al. 2002). Mass conservation of N in watershed system can be described as:

$$\triangle S = M_{\text{total}} - X_{\text{total}} \quad (1)$$

Where M_{total} is the mass of total N inputs within the system during a year, X_{total} is the annual mass of total N outputs of the system, $\triangle S$ is the change in the mass of N in the representative year. According to field survey, we constructed the N budget model for DRW that lists the fluxes (inputs and outputs) across the whole watershed, as presented in Figure 2

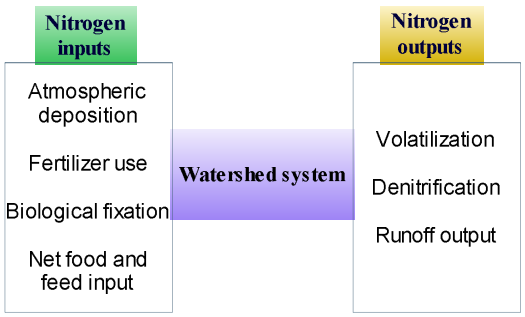

Figure 2 Conceptual diagrams of nitrogen budget

N budget inputs include atmospheric deposition (M_{ad}, which is composed of wet deposition (M_{wd}) and dry deposition (M_{dd})), fertilizer use (M_f), biological fixation (M_{bf}), net food and feed input (M_{ff}). Watershed system consists of soil stock, pool stock, and atmospheric stock. N outputs are composed of volatilization (X_v), denitrification (X_d), runoff export (X_{re}). Due to the large area of DRW, the leaching N loss is assumed to be equal to the return flow to stream flow and reservoir.

2.3 Total N inputs

2.3.1 Fertilizer

The Industrial fixation of nitrogen for the use as fertilizer currently totals approximately 80 Tg a year and represents the largest human contribution of nitrogen to the global cycle. The statistical data of N fertilizer is obtained from the Fushun yearbook and Fushun statistical yearbook. It is assumed that N fertilizers are used equivalently in the arable land. There are about 8 614T N used into DRW in 2003.

2.3.2 Atmospheric deposition

Atmospheric deposition is another main source of N inputs. The N deposition to ecosystems in the absence and presence of human influence increases from 0.5 kg N $ha^{-1}yr^{-1}$ to 10 kg N $ha^{-1}yr^{-1}$ (Galloway et al. 2008). In the DRW, historic data on wet deposition is not available. We used information in the Sanjiang Plain, which is similar in climate and geography with DRW (Sun et al. 2007). Wet TN deposition in the forms of nitrate (NO_y), ammonium (NH_4^+) and organic nitrogen is 7.57 kg ha^{-1} yr^{-1}. In order to estimate the value of dry atmospheric deposition, we employed a proportion of wet deposition N cited from the previous studies. The total N deposition could be quantified by method of Lovett and Lindberg(Johnson and WLindberg 1991)

$$M_{ad} = -0.72+2.07 \cdot M_{wd} \quad (2)$$

2.3.3 Biological fixation

N fixation is estimated by multiplying the area of N-fixing species with literature-derived N fixing rates. Soybeans are the major N fixing crop in DRW, which is accounting for 19% of the N in total crop production. According to the Boyer et al., the fixation rate for soybeans is 96 kg ha^{-1} yr^{-1} (Boyer et al. 2002). In addition, rice land and forest land also could fix N. The fixation rates are 15 kg N ha^{-1} yr^{-1} and 1 kg N ha^{-1} yr^{-1} respectively (Bashkin et al. 2002). Summarized result is shown in Table 4.

Table4. Biological fixation rate in DRW

	Soybeans land	Rice land	Forested land
Fixing rating (kg ha^{-1} yr^{-1})	96[a]	15[b]	1[b]
Area (ha)	5670	6631	416487

Sources: a. Boyer et al 2002; b. Bashkin et al 2002.

2.3.4 Net food and feed input

Both human and animals require food and feed, and these demands are met both by local agriculture and by imports from other regions. Transfer of agricultural products could be important source of N to a watershed. For example, Howarth et al. estimated that the net input of N in food and feed is 28% of total N inputs to the NE U.S. region.

In DRW, human population and livestock populations are obtained from Fushun yearbook and Fushun statistical yearbook. The production and average consumption (urban, rural) of cereal, meat and vegetable are obtained from Fushun statistical yearbook. Animal consumption is estimated by multiplying populations by published annual per capita N consumption rates (Van Horn 1998). The animal consumption rates used in this study are shown in Table 5. According to the Fushun statistical yearbook, the cereal, meat, and vegetable for human food consumption are 95 kg, 29.5 kg 158.2 kg for urban people, 170.94 kg, 27.7 kg and 225.66 kg for rural people.

Table5. Animal N consumption rates (kg animal-1 yr-1)

Animal	Pigs & hogs	Beef cattle	Dairy cattle	Sheep	Poultry
N consumption rates	8.51	66.75	156	5.97	0.13

Source: Van Horn (1998)

2.4 Total N outputs

2.4.1 Ammonium volatilization

Volatilization is a major N loss fluxes. Fertilizer use, confined animal feeding operations, and manure application on fields contribute most to ammonia emission (Goebes et al. 2003). Gaseous N loss rate through fertilizer primarily varies with fertilizer types and application method. Ammonium bicarbonate, urea, and mixed fertilizer are the main N fertilizers applied in the DHF. According to Chen et al, the volatilization losses as a percentage of fertilizers applied: 25% for urea and ammonium nitrate, 18%for other combined fertilizers (Chen 2002).

Human and animal wastes are another source of NH_3 volatilization. A number of emission factors have been proposed for developing ammonia emissions inventories. The emission factor includes the process of animal breed, manure management and application (Battye et al. 2003; Faulkner and Shaw 2008; Xing and Zhu 2002). The emission factors for different animals are listed in Table 6.

Table 6 Emission factors for animals in DHF (kg N hd^{-1} yr^{-1})

Beef cattle[a]	Dairy cattle[a]	Pigs&hogs[a]	Sheep[b]	Poultry[a]	Human[c]
10.71	19.68	4.78	1.34	0.15	0.2

Sources: a. Faulkner and Shaw 2008; b. Battye et al. 2003; c. Xing and Zhu 2002

Forest and wetland also could generate ammonia emission. The ammonia emission factors are selected as 1.2 kg N ha^{-1} $yr^{-1}$and 0.3 kg N ha^{-1} yr^{-1}, which is equal to the factor given by Buowman et al.(Bouwman et al. 1997)

2.4.2 Denitrification

Denitrification is another important N output from natural and human altered systems (Schlesinger 2009). Previous researchers suggest that continental shelf sediments account for the largest portion (44%) of total global denitrification, followed by terrestrial soils (22%) and oceanic oxygen minimum zones (14%). Within watersheds, the amount of land-based denitrified N is generally highest in terrestrial soils, with progressively smaller amounts denitrified in groundwater, rivers, lakes and reservoirs. Seitzinger et al. suggested that denitrification in soil, groundwater, lakes and rives are 10-15 kg N ha^{-1} yr^{-1}, 2.5-5 kg N ha^{-1} yr^{-1} and 0-0.5 kg N ha^{-1} yr^{-1} in northeast of China (Seitzinger et al. 2006). We choose the mean values in the DRW.

2.4.3 Runoff export

In the DRW, The reservoir outlet is the pass of watershed output. Therefore the TN concentration of runoff is relative stable. The average TN concentration at the outlet is 1.54 mgL^{-1} in 2003. The amount of N export in runoff is flow-weighted, and estimated by multiplying measured concentration of TN.

3. Results and discussion

3.1 DHF nitrogen budget

Table 7 shows the values of all variables used for calculating the N budget in DRW in 2003. On the inputs side, atmosphere deposition and N fertilizer application constitute major contributing factors at 14.95 kg N ha^{-1} yr^{-1} and 15.26 kg N ha^{-1} yr^{-1}, or approximately 31.59% and 32.25% of the total N input into the watershed, respectively. The left parts are biological fixation and net food and feed input, which are contribute at 2.4 kg N ha^{-1} yr^{-1} and 9.55 kg N ha^{-1} yr^{-1}. In total, 47.32 kg N ha^{-1} yr^{-1} is imported into the watershed. On the output side, N outputs through ammonium volatilization and denitrification are found to be 9.60 kg N ha^{-1} yr^{-1}, 15.97 kg N ha^{-1} yr^{-1} or 20.29%, 33.75% of total N inputs, respectively. N output from runoff is relatively small at 3.07 or 6.49% of the total N input.

Table 4 N budget of the DRW

	$\triangle S$	M_{total}	M_{ad}	M_f	M_{bf}	M_{ff}	X_{total}	X_v	X_d	X_{re}
DRW (kg N ha^{-1} yr^{-1})	13.52	47.32	14.95	15.26	2.40	9.55	33.80	9.60	15.97	3.07
Percent of N inputs	28.57	100.00	31.59	32.25	5.07	20.18	71.43	20.29	33.75	6.49

The N budget of the DRW is positive, which indicates that there is 13.52 kg N ha^{-1} yr^{-1} entering into DRW. The accumulation of N is due to the input rates of atmospheric deposition, fertilization, and net food and feed input are not matched by output rates in Ammonia volatilization, denitrification and runoff output. N accumulation in the watershed results in TN concentration increasing from 0.98 mg L^{-1} to 2.03 mg L^{-1} in the period from 2000 to 2005.

3.2 Water quality of DHF reservoir

Soil is the major source of N to reservoirs. It plays the most important role in determining N concentration in the reservoir. For the DHF reservoir, the concentration of TN has increased from 0.98 mg L^{-1} to 2.03 mg L^{-1} in the period of 2000-2005. The nitrogen increases are highly correlated with the human generated inputs of nitrogen. These inputs are dominated by fertilizers, atmospheric deposition and net food and feed input. The N budget for the DHF catchment indicates that a lot of N input enters into the DHF Reservoir every year.

As to the relation of N input and water quality, previous research found that the flux of N in large rivers is well explained as a function of the catchment N budget. Boyer et al. and Howarth et al. reported that the runoff typically export about 26% of their total inputs (Boyer et al. 2002; Howarth et al. 2006). The estimated N runoff outputs are not directly comparable to these values (3.07<10.38, which is used in net food and feed input).

Reservoir TN concentration depends on the balance of N inputs into and outputs out of balance as well as the consumption and production by biological processes in the reservoir. Inputs of N for DRW are mainly from watershed soils and atmospheric deposition. Outputs of N include nitrogen lost by outflow from outlets, to the sediment and by denitrification. Research demonstrate that the impoundments could remove N from environment. There are more water retention time in lake for N settling and more sites for effective denitrification (Hillbricht-Ilkowska 1999). N denitrification has been shown to be the primary mechanisms to removing N for reservoir (Stanley and Doyle 2002). Due to the influence of impoundment, the river runoff export only account for 11.4% of total N input (Bosch and Allan 2008). In addition, there are a lot of BMP (vegetation) installation in DRW, which could reduced the N delivery from soil to water (Zhu et al. 2008) .

3.3 Budget uncertainty analysis

Budget approaches differ in how the system is defined, in what fluxes are considered to be internal to the system versus inputs or outputs from the system, and in which fluxes are excluded because they are considered insignificant or highly uncertain. There is also variation in how some fluxes are combined to form net fluxes. Although the budget is constructed with systemic considering and best data available in DRW, there could be unavoidable uncertainty in the N budget associated with N inputs and outputs. Most farmers in the watershed burn rice straw to

ease tillage and control rice stem rot following the harvest of rice. Another component of N loss due to incineration is domestic incineration of wood fuel. In the rural area in the DHF catchment, people still use wood fuel for cooking, which is collected from the nearby fields. Due to the lack of relative data, the N wet deposition obtained from the Sanjiang Plain data will increase the uncertainty in N budget.

4. Conclusions

The major result of this study is that the N budget of DHF reservoir watershed is constructed, where is located in the northeast of China. Taking 2003 as a typical calculation year, the N budget is positive (13.52 kg N ha^{-1} yr^{-1}). It results in the N accumulation in landscape and TN concentration increasing in DHF Reservoir. Furthermore, the research indicates that the atmosphere deposition, fertilizer use and food and feed input dominate more than 90% of the total N input. In the N output side, the ammonia volatilization and denitrification are the main factors, which account for 55% of the total N inputs and 95.1% of the total N outputs. However, the N export in the runoff is only 6.49% of the total N input; this is owing to the more water retention time in reservoir for N settling and the more sites for denitrification. The result of N budget can be used to understand the ecosystem processes and evaluate the N risk in the catchment.

References

Bashkin, V. N., Park, S. U., Choi, M. S., and Lee, C. B. (2002). "Nitrogen budgets for the Republic of Korea and the Yellow Sea region." *Biogeochemistry*, 57(1), 387-403.

Battye, W., Aneja, V. P., and Roelle, P. A. (2003). "Evaluation and improvement of ammonia emissions inventories." *Atmospheric Environment*, 37(27), 3873-3883.

Bosch, N. S., and Allan, J. D. (2008). "The influence of impoundments on nutrient budgets in two catchments of Southeastern Michigan." *Biogeochemistry*, 87(3), 325-338.

Bouwman, A. F., Lee, D. S., Asman, W. A. H., Dentener, F. J., VanderHoek, K. W., and Olivier, J. G. J. (1997). "A global high-resolution emission inventory for ammonia." *Global Biogeochemical Cycles*, 11(4), 561-587.

Boyer, E. W., Goodale, C. L., Jaworsk, N. A., and Howarth, R. W. (2002). "Anthropogenic nitrogen sources and relationships to riverine nitrogen export in the northeastern USA." *Biogeochemistry*, 57(1), 137-169.

Chen, F. (2002). "Agricultural ecology." *Press of China Agricultural University, Beijing*.

Chen, N. W., Hong, H. S., Zhang, L. P., and Cao, W. Z. (2008). "Nitrogen sources and exports in an agricultural watershed in Southeast China." *Biogeochemistry*, 87(2), 169-179.

Faulkner, W. B., and Shaw, B. W. (2008). "Review of ammonia emission factors for United States animal agriculture." *Atmospheric Environment*, 42(27), 6567-6574.

Galloway, J. N., and Cowling, E. B. (2002). "Reactive nitrogen and the world: 200 years of change." *Ambio*, 31(2), 64-71.

Galloway, J. N., Dentener, F. J., Capone, D. G., Boyer, E. W., Howarth, R. W., Seitzinger, S. P., Asner, G. P., Cleveland, C. C., Green, P. A., Holland, E. A., Karl, D. M., Michaels, A. F., Porter, J. H., Townsend, A. R., and Vorosmarty, C. J. (2004). "Nitrogen cycles: past,

present, and future." *Biogeochemistry*, 70(2), 153-226.

Galloway, J. N., Schlesinger, W. H., Levy, H., Michaels, A., and Schnoor, J. L. (1995). "Nitrogen-Fixation - Anthropogenic Enhancement-Environmental Response." *Global Biogeochemical Cycles*, 9(2), 235-252.

Galloway, J. N., Townsend, A. R., Erisman, J. W., Bekunda, M., Cai, Z., Freney, J. R., Martinelli, L. A., Seitzinger, S. P., and Sutton, M. A. (2008). "Transformation of the nitrogen cycle: recent trends, questions, and potential solutions." *Science*, 320(5878), 889-92.

Hillbricht-Ilkowska, A. (1999). "Shallow lakes in lowland river systems: Role in transport and transformations of nutrients and in biological diversity." *Hydrobiologia*, 409, 349-358.

Howarth, R. W., Swaney, D. P., Boyer, E. W., Marino, R., Jaworski, N., and Goodale, C. (2006). "The influence of climate on average nitrogen export from large watersheds in the Northeastern United States." *Biogeochemistry*, 79(1-2), 163-186.

Johnson, D. W., and WLindberg, S. E. (1991). "Atmospheric deposition and forest nutrient cycling." *Ecological series 91. Springer-Verlag, NY.*

Liu, C., Wang, Q. X., and Watanabe, M. (2006). "Nitrogen transported to three Gorges Dam from agro-ecosystems during 1980-2000." *Biogeochemistry*, 81(3), 291-312.

Liu, C., Watanabe, M., and Wang, Q. X. (2008). "Changes in nitrogen budgets and nitrogen use efficiency in the agroecosystems of the Changjiang River basin between 1980 and 2000." *Nutrient Cycling in Agroecosystems*, 80(1), 19-37.

Schaefer, S. C., and Alber, M. (2007). "Temporal and spatial trends in nitrogen and phosphorus inputs to the watershed of the Altamaha River, Georgia, USA." *Biogeochemistry*, 86(3), 231-249.

Schlesinger, W. H. (2009). "On the fate of anthropogenic nitrogen." *PNAS*, 106(1), 203-208.

Seitzinger, S., Harrison, J. A., Bohlke, J. K., Bouwman, A. F., Lowrance, R., Peterson, B., Tobias, C., and Van Drecht, G. (2006). "Denitrification across landscapes and waterscapes: A synthesis." *Ecological Applications*, 16(6), 2064-2090.

Stanley, E. H., and Doyle, M. W. (2002). "A geomorphic perspective on nutrient retention following dam removal." *Bioscience*, 52(8), 693-701.

Sun, B., Shen, R. P., and Bouwman, A. F. (2008). "Surface N balances in agricultural crop production systems in China for the period 1980-2015." *Pedosphere*, 18(3), 304-315.

Sun, Z. G., Liu, J. S., and Wang, J. D. (2007). "Dynamics of nitrogen in the atmospheric wet deposition and its ecological effects in typical wetland ecosystem of Sanjiang plain." *Advances in Water Science*, 18(2), 182.

Van Horn, H. H. (1998). "Factors affecting manure quantity, quality, and use." *Proceedings of the Mid-south Ruminant Nutrition Conference*, 9-20.

Xing, G. X., and Zhu, Z. L. (2002). "Regional nitrogen budgets for China and its major watersheds." *Biogeochemistry*, 57(1), 405-427.

Zhu, Z. X., Nordin, R., and Mazumder, A. (2008). "Soil and vegetation as the determinants of lake nitrogen concentrations in forested watersheds in British Columbia, Canada." *Ecological Indicators*, 8(5), 431-441.

Wastewater Utilities: Are You Ready for Kansas' Nutrient Removal Policy?

Heather Phillips[1], Katie Funderburk[2]

[1]Black & Veatch Corporation, 8400 Ward Parkway, Kansas City, MO 64114; PH (913) 458-3350; FAX (913) 458-3626; email: PhillipsHM@bv.com
[2]Black & Veatch Corporation, 8400 Ward Parkway, Kansas City, MO 64114; PH (913) 458-3147; FAX (913) 458-3802; email: FunderburkKM@bv.com

ABSTRACT

In 2004, the EPA mandated all states to develop Action Plans and nutrient water quality criteria to rehabilitate impaired waters. In accordance with this mandate, the Kansas Department of Health and Environment (KDHE) has developed a nutrient removal policy whereby wastewater treatment plants (WWTP) with capacity greater than 1 mgd must meet technology based biological nutrient removal (BNR) goals to concentrations of 8 mg/L total nitrogen (TN) and 1.5 mg/L total phosphorus (TP). These guidelines were set to achieve the recommended overall nitrogen and phosphorus reduction of 30% for the State's lakes and streams (KDHE Water Bureau, 2004). This total reduction will involve best management practices for non-point sources as well as the previously stated goals for the point source contributors. This paper will discuss the key issues of BNR upgrades in Kansas: (1) capital costs, (2) data collection, (3) staff requirements, (4) operating costs, and (5) sustainability. While other states have established enhanced nutrient removal (ENR) or limit-of-technology (LOT) standards for severely impaired waters, the state of water quality in Kansas enables most utilities to upgrade their systems for BNR goals. This provides essential time for planning, training, and funding, while improving the overall water quality in Kansas.

INTRODUCTION

The Gulf of Mexico contains a hypoxic zone, or area of low dissolved oxygen concentration (< 2 mg/L), also known as the dead zone, that extends up to 125 km offshore and to a depth of 60 m depending on the season (EPA Science Advisory Board, 2007). Both nitrogen and phosphorus are nutrients in wastewater effluents that have been linked to hypoxic conditions in the Gulf of Mexico. The US Environmental Protection Agency (EPA) has been closely monitoring the Dead Zone, and established the Mississippi River/Gulf of Mexico Watershed Nutrient Task Force (or Task Force) in 1997. In 2001, the Task Force, in coordination with the White House Office of Science and Technology Policy, issued the Action Plan for Reducing, Mitigating, and Controlling Hypoxia in the Northern Gulf of Mexico (EPA, 2001). The plan implemented ten management actions, with progress to be assessed every five years.

In response to the Federal Action Plan, KDHE identified 224 impaired stream segments and 187 impaired reservoirs in the river basin and issued a Surface Water Nutrient Reduction Plan in December 2004 as a guide for the State's approach to reducing nutrients (KDHE Bureau of Water, 2004). This plan outlines the regulations for nutrient reduction at Kansas wastewater treatment plants over 1 mgd, since these facilities generate approximately 85 percent of the point-source nitrogen and phosphorus discharges in Kansas. Point sources generate approximately 18 percent of the 51,000 pounds of nitrogen, and 25 percent of the 7,000 pounds of phosphorus leaving the State annually, but are the easiest to monitor and regulate (KDHE Bureau of Water, 2004).

Currently, 18 WWTP throughout the State have nutrient monitoring requirements and goals written into their NPDES permit Schedule of Compliance (Tate, 2008). The goals for each of these plants are the previously stated technology-based BNR limits for nitrogen and phosphorus on an annual average basis. The monitoring of nitrogen and phosphorus is required on a monthly basis for most of the plants in Kansas subject to this requirement. At this time, no limits have been incorporated into any permits, but the limits could be added in the coming years as part permit requirements. Additionally, as part of the permit Schedule of Compliance, the State has required several utilities to conduct feasibility and cost studies for adding BNR treatment to their existing plants.

It is the State's plan that plants larger than 1 mgd be in compliance with the BNR limits within the next 15 years. The WWTP have been placed into five categories based on size, transportation rates, and location, to determine the priority of implementing nutrient reduction plans (KDHE Water Bureau, 2004).

CAPITAL COSTS

Nitrogen and phosphorus can be removed from wastewater to the limits proposed by the State by biological treatment. BNR is a combination of treatment processes that manipulate the treatment environment to allow microbes to remove nitrogen species and phosphorus. To accomplish this, the new or modified treatment trains must be divided into several zones where the operating conditions are controlled to be aerobic, anoxic, or anaerobic.

Biological nitrogen removal occurs in two stages. First, ammonia within the raw wastewater is converted to nitrite and then to nitrate in the oxic portion of the basin, provided that the system is operating at an adequate solids retention time (SRT). Upgrading for nitrification typically involves construction of additional aeration basins and secondary clarifiers. To remove nitrates, mixed liquor recycling pumps must be installed to convey nitrified wastewater to new anoxic zones, where denitrification can take place. Figure 1 is a traditional BNR plant layout.

The biological phosphorus removal process requires the addition of two reaction zones to the traditional BOD removal treatment train. The first is a pre-anoxic zone where RAS is held to remove any remaining dissolved oxygen and nitrate from the RAS stream before it enters the anaerobic zone. The second is an anaerobic zone where RAS and raw wastewater are combined and mixed. The biological phosphorus removal system does not need any special consideration in the aerated oxic portion of the basin other than to ensure that the MLSS is not over-aerated before entering the final clarifier. This oxygen control in the final part of the aeration basin is needed to minimize carryover of oxygen into the RAS stream.

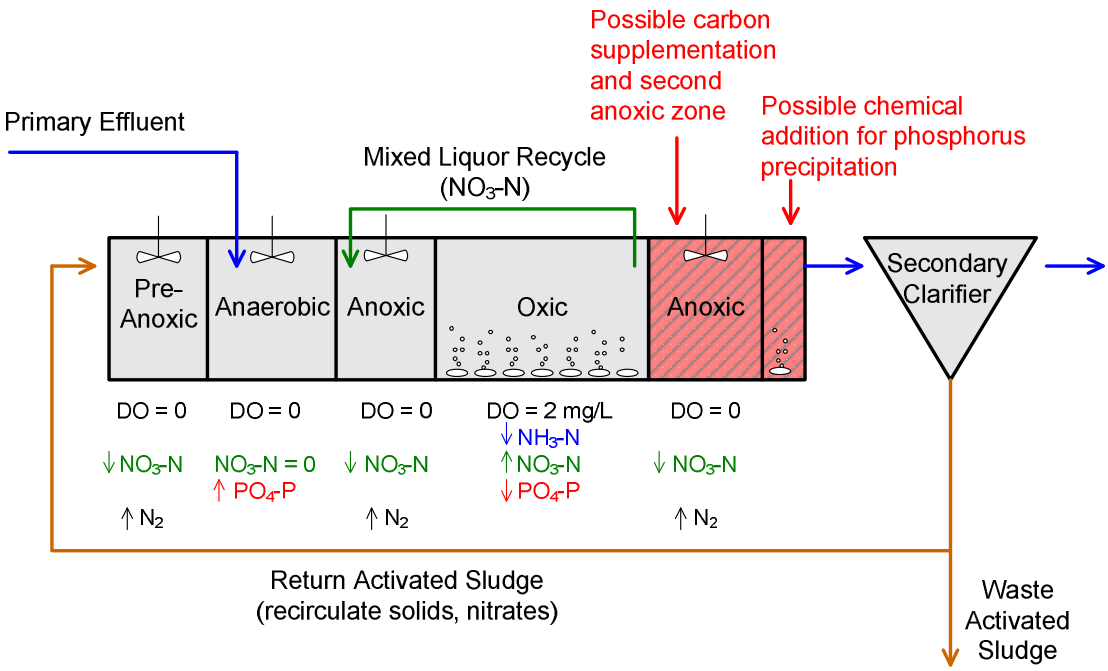

Figure 1: Typical BNR Schematic and Nutrient Transformations

With the volatile costs of steel and concrete, the most cost-effective expansion plans include reuse of existing facilities. To whatever extent possible, utilities should rehabilitate concrete structures as part of their BNR upgrades. Simple upgrades, such as adding baffle walls to create anoxic zones, or replacing clarifier sludge removal mechanisms, offer significant cost advantages over demolition and new construction. Gravity thickeners or sludge storage tanks can be converted into fermenters in some cases, and depending on the plant effluent phosphorus limits, enough volatile fatty acids (VFA) could be fermented onsite to offset the need for purchasing chemicals.

If existing facilities are reused, it is important to consider that most existing liquid trains will need to be derated from their original capacity. To maintain the capacity of the plant and to add biological nutrient removal capabilities, additional trains or facilities may need to be added in conjunction with reuse of existing facilities. This approach is still a more cost-effective than building all new facilities.

Table 1 summarizes recent projects designed and constructed in Kansas to upgrade existing plants to include biological phosphorus removal. For comparison, all of the construction costs are listed in Year 2009 dollars based on the ENR indices. The BNR expansion average cost per mgd is $2,840,000. The variance in this range is due partly to the scope of the expansion, the treatment processes selected, and the condition of the existing facilities.

Table 1. Kansas Wastewater Treatment Plant Expansions

NUTRIENT REMOVAL – WASTEWATER TREATMENT PLANTS												
		Type of Project							Phosphorus Removal		Nitrogen Removal	
Project Location	Year Constructed	Study	Design	Design-Build	Size (mgd)	WWTP Upgrade / Expansion	Construction Cost (millions in 2009 $)	Construction Cost Per MGD (millions in 2009 $)	Biological	Chemical	Nitrification	Denitrification (anoxic zones)
Independence, KS	2001	•		•	3	•	8	2.7	•		•	•
Johnson County, KS (Blue River)	2005	•	•		10.5	•	34.6	3.3	•	•	•	•
Johnson County, KS (ICMB)	2007	•	•		12	•	32.7	2.7	•		•	•
Johnson County (Millcreek)	2006	•	•		14	•	12.2	0.9			•	
Lawrence, KS (Kaw River)	2000	•	•		12.5	•	50.4	4.0			•	
Topeka, KS (North Topeka)	1994	•	•		12	•	43.8	3.6	•		•	

As new and modified treatment facilities are designed and constructed, it is prudent to consider additional facilities that may be required in the future to meet potentially more stringent nutrient removal limits and to reserve sufficient space on the site and within the hydraulic profile of the facility.

DATA COLLECTION

While most plants currently monitor influent and effluent BOD, TSS and possibly ammonia, few plants in the Midwest have sufficient records on nitrate or phosphorus concentrations. Very few plants have records of influent soluble carbon or volatile fatty acids, constituents that drive biological nutrient removal. It is important for facilities to implement additional sampling programs during studies and facility planning efforts, so that the necessary data will be available when plant expansions enter detailed design. Standards have been developed for wastewater characterization (Melcer, 2003), and Figure 2 summarizes the general types of wastewater chemical oxygen demand (COD) and their role in biological nutrient removal.

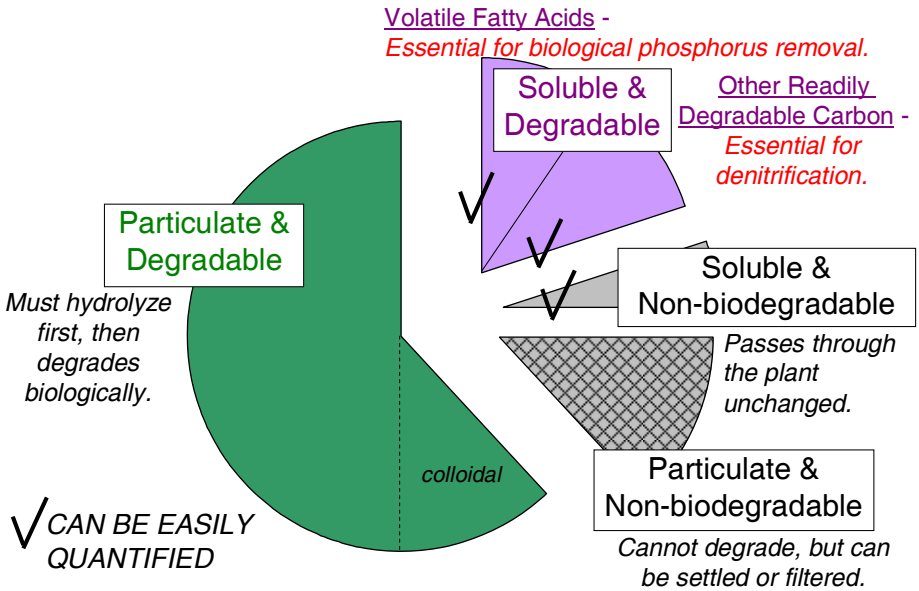

Figure 2: Typical Proportions of Wastewater Chemical Oxygen Demand

It is important to quantify the influent readily biodegradable COD for all BNR facilities. If the influent wastewater characteristics are not susceptible to biological denitrification, the facility may have to be upgraded to provide larger anoxic zones or carbon supplementation. Wastewater denitrification occurs at three well-known rates (Barnard, 1975), and complete denitrification is highly dependent on the available carbon and detention time as shown on Figure 3. If the facility is subject to a total nitrogen (TN) or total inorganic nitrogen (TIN) limit, sampling must also be conducted to quantify the recalcitrant dissolved organic nitrogen, or rDON (Bratby, 2008).

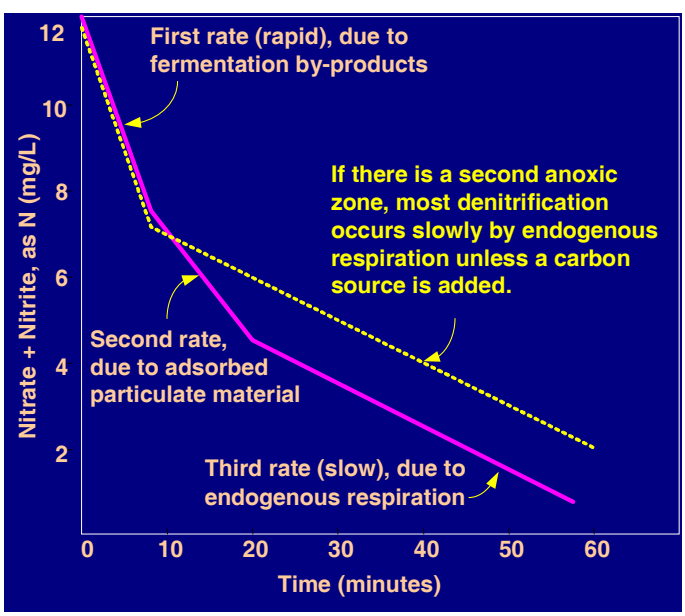

Figure 3 – Three Rates of Denitrification in Wastewater

If the influent wastewater is not amenable to biological phosphorus removal, the facility may require chemical feed facilities for phosphorus precipitation or VFA supplementation. A cost-effective solution may be to construct an on-site fermenter which generates VFA from primary sludge. Johnson County Wastewater is constructing two fermenters as part of its BNR upgrades at the Douglas L. Smith Middle Basin Plant in Overland Park, Kansas. The facility is unique in that it will process sludge from another plant in addition to its own, and the hauled sludge is a source of "imported" nutrients that had to be taken into account the design (Phillips et al, 2006).

STAFF REQUIREMENTS

Biological nutrient removal facilities require careful monitoring of dissolved oxygen; recycle rates; and ammonia, nitrate and phosphorus concentrations. Not only must operators understand the equipment that they work with, but they must also understand the microbiology fundamentals. Utilities must plan for additional training and certification of their current operators as well as for adding new operators, maintenance workers, and laboratory staff. Equipment that requires operation and maintenance at a typical BNR facility is shown on Figure 4. A plant that removes only BOD and TSS would include the oxic zone, clarifier, and RAS and WAS pumps only, with much less sampling and monitoring. In general, when a plant is upgraded for nutrient removal, the utility should plan for at least one additional operator and one additional laboratory technician, and possibly several more positions for larger expansions.

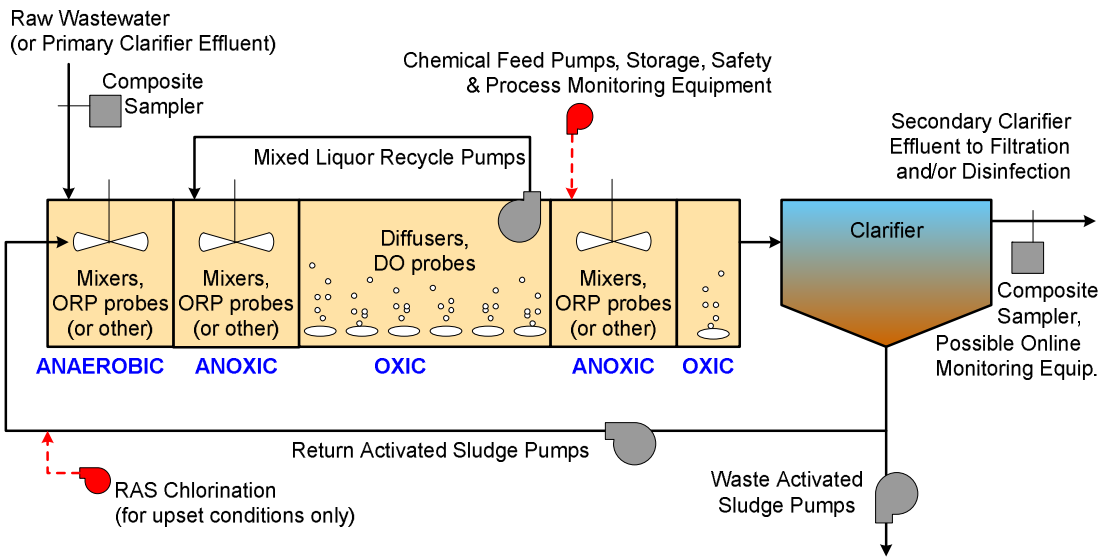

Figure 4: Equipment at a Biological Nutrient Removal Facility

OPERATING COSTS

Upgrading to nitrification can double the amount oxygen needed from that used for an activated sludge process that removes BOD only, which can double the costs of electricity. Anoxic zone mixers and mixed liquor recycle pumps, which must convey two to four times the plant influent flowrate, also add to electricity use. Depending on the level of treatment required, expensive chemicals may be needed to enhance denitrification or phosphorus removal, and utilities must plan for increases in operating costs accordingly.

Biosolids treatment and disposal must also be considered. In general, a plant that nitrifies will produce less biosolids than a plant that removes BOD and TSS only; however, if chemicals are added for phosphorus removal, sludge quantities can increase substantially. Also, when plant expansions reach a certain size (generally 10 mgd) it may be cost-effective to add primary clarification to reduce the number of new aeration tanks to be constructed. This generates new sludge that must be processed, which is typically accomplished by anaerobic digestion. In addition to producing Class A biosolids that can be land-applied, a second benefit of anaerobic digestion is that the methane generated can be harvested to generate electricity and thus reduce electrical costs.

For most households in Kansas, the monthly wastewater bill has traditionally been the lowest utility bill, compared to the gas or electric bills which can be ten or twenty times the monthly cost of a wastewater bill. As utilities expand and upgrade for nutrient removal, and operating costs increase, rate payers can expect a significant increase in monthly bills. Smaller communities will suffer the greatest increases, since there are fewer households in the service area to contribute to the overall operating costs. These increases could range from approximately $200 per month in smaller communities (4,000 or fewer) to $28 dollars per month in communities with 100,000 citizens (KDHE Water Bureau, 2004).

SUSTAINABILITY

In the past, environmental issues have focused on a “cradle to grave” approach by which chemicals, for example, are tracked from their production point to the end user. Today, utilities can benefit from a “cradle to cradle” approach by which energy optimization studies and carbon footprint analyses accompany traditional engineering studies to develop solutions that meet the triple bottom line: economic, environmental and social responsibilities. By looking at the entire picture, utilities can plan responsibly for the future.

A sustainability study must include three components: economic, social, and environmental impacts. Economic impacts can be quantified by determining capital and operating costs through a present worth evaluation. Social impacts can be evaluated with public participation hearings, surveys, and maintaining good communications with regulators, neighboring communities, and invested

stakeholders. The third component of a sustainability study, environmental impacts, is more difficult to evaluate. While there are models that can accurately predict plant effluent quality, there are currently no standard approaches to quantifying or predicting wastewater plant greenhouse gas (GHG) emissions. Extensive carbon footprint studies have been conducted in Australia (Bridle et al., 2008; de Haas et al., 2008) and many expect GHGs to become regulated in the United States in the coming years, so many utilities are changing the way they approach projects.

CONCLUSIONS

Kansas is a small part of the Mississippi/Atchafalaya River Basin (MARB), which covers 31 states and includes 41 percent of the US population; however, KDHE is a leading agency in addressing nutrient control. Point sources are not the largest contributors to the Gulf of Mexico hypoxia, but they are the easiest to monitor and regulate. Many WWTPs in Kansas have already implemented facility improvements to achieve BNR goals of 8 mg/L TN and 1.5 mg/L TP. A sampling of recent projects concluded that capital expenditures ranged from $0.90 to $4.00 per gallon of treated wastewater (based on 2009 dollars). By comparison, "limit of technology" (3 mg/L TN, 0.3 mg/L TP) projects in the Chesapeake Bay area averaged $8.20/GPD based on 2006/2007 dollars (Harper et al., 2008).

Improving water quality through BNR projects will come at a cost to rate-payers, who could expect utility bills to increase by $50 per month, or much more for smaller communities. BNR facilities require much more sampling, monitoring and maintenance and therefore their operating costs are higher than the costs associated with BOD and TSS removal. As a result, states such as Kansas will experience a demand for skilled laboratory technicians and wastewater treatment plant operators who are certified for biological nutrient removal. A disadvantage is that utilities may have trouble filling these open positions, especially with retirements on the rise. Training budgets will have to be expanded in order to keep up with changing nutrient policies and facility upgrades. Adapting to nutrient control policies will not be easy, but with careful planning, Kansas utilities have the opportunity to lead the region in finding sustainable solutions for its communities.

REFERENCES

Barnard, J. L. (1975). "Biological nutrient removal without the addition of chemicals." *Water Res.*, IWA, 9, 485-490.

Bratby, J., Jimenez, J., Parker, D. (2008) "Dissolved organic nitrogen – is it significant, and can it be removed?" *Proceeding of the 81st Annual Water Environment Federation Technical Exhibition and Conference.*

Bridle, T., Shaw, A., Cooper, S., Yap, K.C., Third, K., Domurad, M. (2008) "Estimation of greenhouse gas emissions from wastewater treatment plants. *Proceedings of the IWA World Water Congress*.

de Haas, D., Foley, J., Barr, K. (2008). "Greenhouse gas inventories from WWTPs – the trade-off with nutrient removal." *Proceedings of the 81st Annual Water Environment Federation Technical Exhibition and Conference*

Enivornmental Protection Agency, Science Advisory Board. (2007). *Hypoxia in the Northern Gulf of Mexico*.

Environmental Protection Agency, Mississippi River/Gulf of Mexico Watershed Nutrient Task Force. (2001). *Action Plan for Reducing, Mitigating, and Controlling Hypoxia in the Northern Gulf of Mexico*.

Harper, S. R., Coleman, D., Tobocman, D., Wilkinson, D., Bender, L.-A. (2008). "Analysis of nutrient removal costs in the Chesapeake Bay program and implications for the Mississippi-Atchafalaya River Basin." *Proceedings of the 81st Annual Water Environment Federation Technical Exhibition and Conference*

KDHE Bureau of Water. (2004). "Surface Water Nutrient Reduction Plan." Kansas Department of Health and Environment.

Melcer H., Dold, P., Jones, R.M., Bye, C.M., Takacs, I., Stensel, H.D., Wilson, A.W., Sun, P., Bury, S. (2003). *Methods for Wastewater Characterization in Activated Sludge Modeling. Water Environment Research Foundation Report No. 99-WWF-3*. IWA Publishing and Water Environment Federation.

Phillips, H.M., Scanlan, P., Kobylinski, E. (2006). "Regionalization of biosolids processing: good for biosolids; hard on liquid processing."*Proceedings of the 2006 Residuals and Biosolids Management Conference*, Water Environment Federation.

Tate, M. (2008). "Operating Data for Kansas Plants" *Proceedings of the 2008 Nutrient Reduction Conference*, Kansas Water Environment Association.

Application of Biopile System for the Remediation of Petroleum-hydrocarbon Contaminated Soils

C. M. Kao[1], H. Y. Chien[1], Rao Y. Surampalli[2], W. P. Sung[3]

[1]Institute of Environmental Engineering, National Sun Yat-Sen University, Taiwan, E-mail: jkao@mail.nsysu.edu.tw
[2]U.S. Environmental Protection Agency, Kansas City, Kansas, USA
[3]Department of Landscape Design and Management, National Chin-Yi University of Technology, Taiwan

ABSTRACT

The objective of this study was to assess the potential of applying enhanced bioremediation on the treatment of petroleum-hydrocarbon contaminated soils. Microcosm experiments were conducted to determine the optimal biodegradation conditions. The control factors included oxygen content, nutrient addition, addition of commercially available mixed microbial inocula, addition of wood chips and rice husks (volume ratio = 1:1) as bulking agents, and addition of organic amendments (chicken manures). Results indicate that the supplement of microbial inocula or chicken manures could significantly increase the microbial populations in soils, and thus, enhance the efficiency of total petroleum hydrocarbon (TPH) removal (initial TPH = 5,500 mg/kg). The highest first-order TPH decay rate and removal ratio were approximately 0.015 day^{-1} and 85%, respectively, observed in microcosms containing microbial inocula (mass ratio of soil to inocula = 50:1), nutrient, and bulking agent (volume ratio of soil to bulking agent = 10 to 1) during 155 days of incubation. Results indicate that the first-order TPH decay rates of 0.015 and 0.0142 day^{-1} can be obtained with the addition of microbial inocula and chicken manures, respectively, compared with the decay rate of 0.0069 day^{-1} under intrinsic conditions. Thus, chicken manures have the potential to be used as substitutes of commercial microbial inocula. The decay rate and removal ratio can be further enhanced to 0.0196 day^{-1} and 87%, respectively, with frequent soil shaking and air replacement. Results will be useful in designing an ex-situ soil bioremediation systems (e.g., biopile, landfarming) for practical application.

INTRODUCTION

Accidental releases of petroleum products from above-ground or underground storage tanks (USTs) are one of the most common causes of soils contamination. Among those petroleum products, diesel oil is one of the most widely used fuel oils in society today. Although diesel oil is largely comprised of simple unbranched n-alkanes in the range of C10-C22, it also contains more recalcitrant and less biodegradable petroleum hydrocarbons. Thus, diesel-oil contaminated soils are more difficult to treat compared to more volatile petroleum products (e.g., gasoline). Currently, with the increasing attention towards the environment preservation, biological decontamination has become a valuable alternative to chemical treatments. Bioremediation is an ecologically acceptable technology that uses microorganisms to efficiently degrade pollutants in the environment. Biopile and landfarming systems have been listed as feasible ex situ remedial technologies for the treatment of petroleum-hydrocarbon contaminated soils, especially for soils polluted with less biodegradable and less volatile petroleum product (e.g., diesel oil). Biopiles, also known as biocells and compost piles, are used to reduce concentrations of petroleum products in excavated soils through the processes of biodegradation (US EPA, 2004; Sarkar et al., 2005).

Biopiles are constructed by forming excavated contaminated soils into piles above ground with the aim of enhancing conditions for biodegradation. Landfarming, also known as land treatment or land application, is an above-ground soil remediation technology. Landfarming usually involves spreading excavated contaminated soils in a thin layer on the ground surface and stimulating aerobic microbial activity within the soils through aeration and/or the addition of minerals, nutrients, and moisture. The enhanced microbial activities in both biopile and landfarming systems result in degradation of adsorbed petroleum constituents through microbial degradation. Addition of organic material to the contaminated soils can be beneficial, as it is a source of co-substrates, microorganisms, and nutrients, and ameliorates the structure and water-retaining capacity of the soils. For optimum biopile and landfarming conditions, it is important to know the characteristics of the contaminated soils before the beginning of treatments. Although there are many biopile and landfarming systems for the treatment of petroleum-hydrocarbon contaminated soils, there is a lack of information on the addition of organic materials, bulking agents, microbial inocula on optimizing bioremedial conditions of biopile and landfarming systems for the treatment of diesel-oil contaminated soils. Thus, the primary objective of this study was to assess the potential of enhancing the bioremediation efficiency on the clean up of diesel-oil polluted soils. In this study, microcosm experiment was performed for efficiency evaluation by the nutrient supplementation, addition of commercially available mixed microbial inocula, addition of wood chips and rice husks as bulking agents, and addition of organic materials (chicken manures). Optimal conditions obtained from the study could be used to improve the treatment efficiency of the ex situ soil bioremediation systems (e.g., biopile, landfarming) for the treatment of diesel-oil contaminated soils.

MATERIALS AND METHODS

Construction of microcosms. Microcosms were constructed to evaluate the effectiveness of enhanced bioremediation of diesel oil-contaminated soils under different biodegradation conditions. The six major groups applied in this study included control group (A), nutrient addition group (B), bulking agent addition group (C), commercially available mixed microbial inocula addition group (D), organic material addition group (E), and soil shaking and air replacement group (F). Each microcosm was constructed with 50 mL nutrient medium or deionized (DI) water, certain amount of amendments (bulking agent, mixed microbial inocula, or organic materials), and 150 g of fuel oil-contaminated soils in a 300-mL bottle sealed with Teflon-lined rubber septa. The headspace in each microcosm was approximately 150 mL, and was filled with air. The final mineral medium in each microcosm consisted of (milligram per liter of H_2O) $(NH_4)_2SO_4$, 100; K_2HPO_4, 174; KH_2PO_4, 136; $CaCl_2$, 0.4; $FeCl_3 \cdot 6H_2O$, 0.3; H_3BO4, 0.03; concentrated HCl, 0.25, $MgSO_4 \cdot 7H_2O$, 3; $MnSO_4 \cdot H_2O$, 0.09; and $NaMoO_4 \cdot 2H_2O$, 0.01. The medium solution was autoclaved before use. The initial soil TPH concentrations in microcosm bottles were approximately 5,500 mg/kg. The pH of each microcosm solution was approximately 7.5, and was relatively stable throughout the experiment (varied from 7 to 7.5) (data not shown). In Group A, both live and dead control microcosms were prepared. The live control microcosms only contained diesel-oil contaminated soils and DI water. Dead control bottles contained 250 mg/L $HgCl_2$ and 500 mg/L NaN_3, and soils used for this control group were autoclaved before use. In Group B, nutrient solution instead of DI water was used to evaluate the feasibility of TPH biodegradation enhancement by nutrient addition. In Group C, bulking agents of wood chips and rice husks (volume ratio = 1:1) were mixed with soils to increase the soil permeability. In Group D, commercially available mixed microbial (Oil Gator^{TM}) was added into the microcosms to increase the population TPH degraders. In Group E, organic material (chicken

manure) was added to increase the bacterial populations and organic carbon. In Group F, microcosm shaking (and rotation) and air replacement was provided to simulate the soil tilling and air supplement of landfarming system. Thus, in Group F, the microcosms were opened and shaken (and rotated) for 30 min once a week. After shaking, the microcosm was then sealed for further incubation.

Chemicals and sample analyses. The diesel oil was purchased from Chinese Petroleum Corp. (Taiwan) and used as received. Microcosms were incubated in the dark at 25°C. The microbial inocula used in this study were dry powders consisting of mixed cultures of oil-degrading bacteria, trade name "Oil Gator^{TM}," (Product Service Company, Jackson, Mississippi, USA), which has been approved by US Environmental Protection Agency (US EPA) for field application. Wood chips, rice husks, and chicken manures were collected from a rice mill, a lumber mill, and a chicken farm in southern Taiwan, respectively. Duplicate microcosms were sacrificed at each time point and analyzed for TPH concentrations. The TPH was characterized by the presence of hydrocarbons ranging from C_6 to C_{40} (APHA, 2001; TEPA, 2003). Five grams of soil sample collected from each microcosm was added in a 40-mL vial containing 10 mL of mixture of n-hexane/acetone (v/v, 1:1). The 40-mL vial was shaken for 24 h then spun on a Hettich-Zentrifugen EBA 21 Centrifuge for 30 min at 10,000 rpm. The supernatant was collected and stored until analysis at 4°C in the dark. Analysis of TPH extract was performed using a Hewlett-Packard 6890 gas chromatography (GC) equipped with a flame ionization detector and a DB-1 (HT) capillary column (0.32 mm x 30 m). The injector temperature was 300ºC and the detector temperature was 350ºC. The oven temperature was programmed to increase from 50ºC (5 min) to 350ºC (10 min) at 10ºC/min. Headspace gas sample was collected from each microcosm and analyzed for carbon dioxide and oxygen contents. To account for the bulking agent addition on the determination of soil TPH, the final TPH concentrations in soils were calculated by multiplying the reciprocal of soil percentage in media (soils and bulking agents). Hnu gas analyzer (Model 108) (MA, USA) was used for carbon dioxide and oxygen measurements in the headspace of microcosms.

Microbial enumeration and decay rate calculation. Microbial enumeration was performed for each group of microcosms on selected day to determine the number of total heterotrophs and total anaerobes. Total plate counts were conducted using plate count agar (Difco) to assess the approximate size of the total cultivable heterotrophic bacterial in soil samples using the spread plate method [27]. Prepared plates were incubated at 30ºC for 48 h, then counted for colony forming unit (CFU). The total anaerobes are enumerated using five-tube MPN assay [8]. The total anaerobe tubes contained media and were scored positive based on optical density. The following first-order decay model for soil TPH concentration evaluation was used to determine the first-order decay rates for TPH in the microcosms:

$$C_e = C_0 \exp(-kt) \qquad (1)$$

where C_0 is the initial TPH concentration in soil sample before treatment (mg/kg), C_e is the TPH concentration in soil sample after treatment (mg/kg), k is the temperature-dependent decay rate constant (day^{-1}), and t is the operation period (day). In this study, the treatment efficiency (percentage of TPH removal) was determined using the difference between the initial (day 0) and final (day 155) soil TPH concentrations in microcosms.

RESULTS AND DISCUSSION

Control and nutrient addition groups. Figure 1 shows the variations in soil TPH concentrations in Groups A (A1: live control; A2: dead control) and B (with nutrient

addition). TPH concentrations on Day 0 and Day 155 (the last day of incubation) in each group of microcosm were used to calculate the percentage of TPH removal. Approximately 7.2% of TPH removal was observed in A2 microcosms during the 155-day investigation period. This indicates that physical and chemical reactions had only little contributions on TPH removal in this system. TPH concentrations in A1 dropped from 5,415 to 2,953 mg/L after 155 days of incubation. Results reveal that naturally occurring microorganisms in A1 microcosms were able to degrade 45% of TPH, and caused the decrease in TPH concentrations. The trend of TPH degradation levelled off after approximately 74 to 93 days of operation. Results show that the TPH removal had a good match with the first-order decay model during the first half of the operational period from 0 to 74 days. Because the level off of TPH removal trend was observed after 74 days of operation, the first-order decay rate was calculated from day 0 to day 74. The calculated first-order decay rate for A1 was 0.0069 d^{-1}. The calculated decay rate was close to the decay rates reported in other studies (Wilson and Kolhatkar; Chen et al., 2005; Kao et al., 2005). Results from Group B microcosms show that slight higher TPH removal ratio was observed with nutrient addition. TPH concentrations in Group B microcosms dropped from 5,318 to 2,276 mg/L (Figure 1). This indicates that approximately 57% of TPH was removed after 155 days of operation. Results show that the TPH removal curve matched with the first-order decay model during the first half of the operational period, and the calculated first order decay rate was 0.0111 d^{-1} (calculated from day 0 to day 74). Results reveal that TPH bioremediation rate could be enhanced with nutrient addition. Because site soils contained intrinsic nutrient and bacteria, addition of extra nutrients only caused slight increase in TPH removal rate (Figure 1). Results from Group B microcosms also show that the TPH removal curve levelled off after 74 days of operation. This indicates that nutrient was not a limiting factor of the TPH biodegradation during the later part of incubation. Figure 2 shows the variations in measured oxygen and carbon dioxide contents in the headspace of representative groups of microcosms. Results indicate that the oxygen content dropped from approximately 20.3% on day 0 to 0.2% on day 35, and carbon dioxide content increased from approximately 0.1% on day 0 to 12% on day 35 in A1 microcosms. Similar trends of oxygen and carbon dioxide variations were observed in Group B (data not shown). This reveals that the redox conditions had been changed from aerobic to anaerobic conditions after approximately 35 days of incubation in both A1 and B microcosms. No significant changes of the oxygen and carbon dioxide contents were observed in A2 microcosms, and the observed oxygen and carbon dioxide contents remained at approximately 20 and 0.1%, respectively during the 155 days of incubation (data not shown). This indicates that biodegradation processes did not occur in the kill control group (A2). Results indicate that the total heterotrophs in A1 microcosms increased from 3.2×10^5 CFU/g of soil on day 0 to 8.1×10^5 CFU/g of soil after 30 days of incubation. Slight decrease in the populations of total heterotrophs was observed on days 70 and 155 in A1. This might be due to the fact that more biodegradable organics and oxygen were depleted during the later part of the incubation period. However, the total anaerobes in A1 increased from 5.88×10^2 cell/g of soil on day 0 to 2.8×10^4 cell/g of soil after 30 days of incubation. The populations of total anaerobes increased to 3.3×10^4 and 6.1×10^4 cell/g of soil on days 70 and 155, respectively. This indicates that the oxidation-reduction (redox) conditions in A1 microcosm became more appropriate for the growth of anaerobic microorganisms, and total anaerobes became the dominant microorganisms. The observed variation in microbial population in Group B was similar to Group A1 microcosms. This also indicates that the anaerobic degradation was the dominant biodegradation pattern after the complete consumption of oxygen.

Bulking agent addition groups. Figure 3 shows the variations in soil TPH concentrations in Groups C1 to C4 microcosms (with bulking agent addition). Approximately 74, 69, and 64% of TPH removal were observed in Groups C1, C2, and C3 microcosms, respectively. Thus, TPH removal ratio in Group C1 (volume ratio of soil to bulking agent = 3 to 1) was higher than the TPH removal rates observed from Groups C2 (volume ratio of soil to bulking agent = 5 to 1) and C3 (volume ratio of soil to bulking agent = 10 to 1). This indicates that higher volume ratio of soil to bulking agent caused higher TPH degradation rates. The addition of bulking agents in microcosm would cause the increase in soil permeability, and thus, increase the bioavailability of petroleum hydrocarbons to bacteria under both aerobic and anaerobic conditions. Although the total oxygen amount in microcosm would be the same, more efficient oxygen consumption rate and higher TPH degradation rate would occur in microcosms with bulking agents addition. After the depletion of oxygen, anaerobic biodegradation dominated the degradation processes. Again, bulking agents would increase the bioavailability of petroleum hydrocarbons to anaerobic bacteria in microcosms. Thus, higher percentage of TPH removal was observed in C1 with higher soil to bulking agent ratio after 155 days of operation. Compared with the TPH removal ratio in Group C3, results show that a slight increase in the percentage of TPH removal was observed (67% of TPH removal) in Group C4 (soil to bulking agent ratio = 10 to 1) with nutrient addition (Figure 2). Results reveal that bulking agent addition had more significant effect on TPH degradation than the effect caused by nutrient addition. Results of Groups A, B, and C also indicate that appropriate bulking agent and nutrient addition would enhance the removal of TPH. However, results from the microcosm study also indicate that TPH removal trends in Groups B and C levelled off after approximately 93 days of operation. Most petroleum hydrocarbons are biodegradable under both aerobic and anaerobic conditions. Nevertheless, rates of BTEX biodegradation under aerobic conditions are higher than those under anaerobic conditions. Aerobic bioremediation generally proceeds more quickly than anaerobic bioremediation. Organic compounds are removed more completely under aerobic biodegradation. Petroleum hydrocarbons with less molecular weights, less aromatic rings, and less branched structures are usually more biodegradable and can be biodegraded in the early stage of the biodegradation processes. Thus, more biodegradable hydrocarbons were degraded during the early part of the operational period under aerobic conditions. The less degradable components, which could not be easily degraded by intrinsic bacteria, remained in the soils for a longer period of time before removal. Thus, no significant TPH removal can be observed during the latter operational period (from day 93 to day 155). Results show that TPH decay curve followed a typical first-order degradation pattern. The first-order decay rates for Group C microcosms were calculated from day 0 to the day that the TPH removal was insignificant (day 93). The calculated first-order decay rates for Groups C1, C2, C3, and C4 were 0.0123, 0.0105, 0.0099, 0.01 d^{-1}, respectively. Although the calculated decay rates for all four groups of microcosms were close, results indicate that Group C1 with soil to bulking agent ratio of 3 to 1 had higher decay rate. The variations in oxygen and carbon dioxide contents in the headspace of C1 microcosms are shown in Figure 2. Results show that oxygen content dropped significantly after the start of the incubation (Figure 2), and it dropped to 1% after approximately 30 days of incubation. Thus, the redox conditions of the microcosms shifted from aerobic to anoxic/anaerobic conditions after 30 days. Similar variations in oxygen and carbon dioxide contents in C2 to C4 microcosms were observed (data not shown). The variation of the redox conditions also caused the decrease in TPH removal rate in the latter part of the operation. Results indicate that the total heterotrophs in C1 microcosms increased from 3.2×10^5 CFU/g of soil on day 0 to 4.4×10^6 CFU/g of soil after 30 days of incubation. Slight decrease in the populations of total heterotrophs was observed on days 70 and 155 in C1. This might be due to the fact of oxygen consumption, which inhibited the

growth of total heterotrophs. However, the total anaerobes in D1 increased from 5.88×10^2 cell/g of soils on day 0 to 7.1×10^4 cell/g of soil after 30 days of incubation. This indicates that the redox conditions in Group C1 microcosms became more appropriate for the growth of anaerobic microorganisms, and total anaerobes became the dominant microorganisms after 30 days of operation. Similar trends of microbial growth were observed in Groups C2 to C4 (data not shown). This also indicates that the anaerobic degradation was the dominant biodegradation pattern after the oxygen consumption.

Inocula addition groups. Figure 4 shows the variations in soil TPH concentrations with and without the addition of inocula (Oil Gator™), bulking agent (soil to bulking agent ratio = 10 to 1), and nutrients. Approximately 80, 83, and 85% of TPH removal were observed in Groups D1, D2, and D3 microcosms, respectively. A slight increase in TPH concentration was observed on day 35 due to the effects that some high molecular weight petroleum hydrocarbons were biodegraded and produced byproducts with lower molecular weights, which appeared within the C_6 to C_{40} range. This would also cause the regulation compliance problem at the early stage of soil remediation due to the increase in TPH concentration in soil samples. Although a slight increase in TPH concentrations was also observed in Groups A1, B, and C during the incubation period from days 40 to 50, the increment was not significant (Figure 1). This might be due to the effects that the TPH decay rates in those microcosm groups were only moderate, and thus, the accumulation of degradation byproducts would not cause a significant increase in TPH concentrations. Among Groups D1 to D3 microcosms, results show that the highest TPH degradation rate was observed in Microcosms D3 with nutrient, bulking agent (soil to bulking agent ratio = 10:1), and Oil Gator™ addition. The TPH degradation rate in Group D2 was slightly higher than the rate observed in D1. This indicates that nutrient addition was not an important factor on TPH removal. Oxygen contents in the headspace of D3 microcosms dropped from 21% to 0.1% after approximately 23 days of operation, and thus, the redox conditions of the microcosms shifted from aerobic to anoxic/anaerobic conditions after 23 days. Similar variations in oxygen and carbon dioxide contents in Groups D1 and D2 microcosms were observed (data not shown). The abrupt consumption of oxygen content could be due to the increase in microbial populations caused by the addition of oil Gator™. The variation of the redox conditions also caused the decreased in TPH removal rate in the latter part of the operation. Results indicate that the total heterotrophs in Group D1 microcosms increased from 3.2×10^5 CFU/g of soil on day 0 to 6.2×10^7 CFU/g of soil after 30 days of incubation. Slight decrease in the populations of total heterotrophs was observed on days 70 and 155 in D1. However, the total anaerobes in D3 increased from 5.88×10^2 cell/g of soils on day 0 to 3.2×10^5 cell/g of soil after 30 days of incubation. The populations of total anaerobes increased to 5.7×10^5 and 2.9×10^5 cell/g of soils on days 70 and 155, respectively. This indicates that the redox conditions in D3 microcosm became more appropriate for the growth of anaerobic microorganisms, and total anaerobes became the dominant microorganisms. Similar trends of microbial growth were observed in Groups D1 and D2 (data not shown). This also indicates that the anaerobic degradation was the dominant biodegradation pattern after oxygen consumption. Compared with the results from Groups A, B, and C, addition of Oil Gator™ in Group D could further enhance the TPH removal. Because the applied inocula, Oil Gator™, contained mixed petroleum hydrocarbon degraders, the increased microbial species and populations could increase the TPH degradation rates. Moreover, the inocula also caused the continuous removal of TPH during the later operational period although the decay rates were much lower (Figure 4). Results also show that TPH concentrations in D3 microcosms met the target level of 1,000 mg/kg after 155 days of operation (dropped to 842 mg/kg on day 155). The calculated first-order decay rates for Groups D1, D2, and D3 microcosms were 0.0143,

0.0147, and 0.015 d^{-1}, respectively, from days 0 to 74. The observed oxygen content was less than 0.1% after 23 days of operation in D3 microcosms, which shifted of redox potential from aerobic to anoxic/anaerobic conditions. This also indicates that the anaerobic biodegradation processes were the dominant biodegradation patterns after 23 days.

Organic material addition groups. Figure 5 shows the variations in soil TPH concentrations in Group E microcosms with the addition of organic material (chicken manure) and with or without the bulking agent (soil to bulking agent ratio = 10 to 1) addition. Oxygen contents in the headspace of E2 microcosms dropped from 20.7% to below 0.1% after approximately 23 days, and thus, the redox conditions of the microcosms shifted from aerobic to anoxic/anaerobic conditions after 23 days. Similar variations in oxygen and carbon dioxide contents in E1 microcosms were observed (data not shown). The abrupt consumption of oxygen content could be due to the increase in microbial population caused by the addition of chicken manure. Results show that the total heterotrophs were increased in the early stage of the incubation and decreased after 30 days of operation. This could be due to the addition of chicken manure in the microcosms. The observed total anaerobes in E2 microcosms were increased to 9.2×10^5 cell/g of soil after 30 days of incubation. This might be due to the complete oxygen consumption after 23 days, which caused the decrease in total heterotrophs and increase in total anaerobes. Again, microbial populations in E1 microcosms were similar to the observed populations in E2 microcosms (data not shown). Results also indicate that a slight increase in TPH concentration was observed in the early stage of the operational period from days 15 to 23 (Fig. 4). This might be due to the effects that chicken manure contained some organic carbons, which fell into the diesel oil range (C_6 to C_{40}), and thus, caused the increase in TPH concentrations. Similar to the degradation trends of Group E microcosms, a slight increase in TPH concentration was observed after 35 days of operation. This could be also due to the production of byproducts with low molecular weights, which appeared within the C_6 to C_{40} range. The increase in TPH concentrations in soil samples might cause the regulation compliance problem at the early stage of future field operation. Because most of the organics in chicken manure are biodegradable, TPH concentrations in both E1 and E2 microcosms dropped to below 1,000 mg/kg and met the target level of 1,000 mg/kg after 155 days of operation. Approximately 80% and 82% of TPH removal were observed in Groups E1 and E2 microcosms, respectively. The calculated first-order decay rates for E1 and E2 microcosms were 0.014 and 0.0142 d^{-1}, respectively, from day 0 to day 74. Slightly higher TPH removal rate was observed in Microcosms E2 than the rate observed in E1. This indicates that bulking agent addition in E2 also enhanced the TPH degradation through the effect of increased soil permeability. Results from five groups (A to E) of microcosm study show that chicken manure and Oil Gator™ addition had significant contributions on the improvement of TPH biodegradation. This could be due to the effect that both chicken manure and Oil Gator™ addition increased the microbial species and population in soils. Contaminated soils are often poor in organic matters, and have general low microbial activities. Bioremediation can be enhanced by introducing nutrients and organic matters, and through inoculation of enriched microbial consortia into soil. Chicken manure would serve as the source of co-substrates and nutrients to microorganisms. It might also improve the structure and water-retaining capacity of the soils. Thus, the microbial population and microbial activity would increase after the addition of chicken manure. The diversified microbial species in both chicken manure and Oil Gator™ were able to degrade most of the petroleum hydrocarbons varied from C_6 to C_{40}. Although an increase in TPH concentrations was observed in the early stage of operation, subsequent TPH removal was significant. Results indicate that addition of chicken manure was an appropriate alternative for the addition of commercial available inocula.

Microcosm shaking and air replacement group. Group F was conducted to simulate the soil tilling and air replacement caused by land farming or biopile processes with the addition of organic material (chicken manure) and bulking agent (soil to bulking agent ratio = 10 to 1). Figure 5 shows the variations in soil TPH concentrations in Group F microcosms. Results from the headspace gas analysis show that oxygen content remained high due to the air replacement process (Figure 2). Thus, the redox condition in Group F remained aerobic throughout the experiment. Results from the microbial enumeration also corresponded with the observed oxygen contents in microcosms. Results show that the populations of total heterotrophs remained high and total anaerobes remained low in F microcosms. This could be due to the addition of chicken manure and frequent air replacement of the microcosms. Results show that significant TPH decrease was observed since the beginning of the operation. This indicates that shaking and air replacement could enhance the TPH biodegradation and maintain a high TPH removal efficiency. TPH concentrations in F microcosms dropped from 5,415 to 720 mg/L after 155 days of incubation (approximately 87% of TPH removal), and the calculated first-order decay rate was 0.0196 d^{-1}. Although the final TPH concentration in F was only slightly lower than the observed final TPH concentrations in Groups D2, D3, and E2 microcosms, the calculated decay rate for Group F microcosms was higher. Thus, the incubation time or remediation time can be significantly reduced. Because the microcosms in Group F were opened for air supplement, the mechanism of volatilization might be also the cause of increased degradation efficiency. Results also reveal that air quality monitoring should be performed if landfarming or biopile systems are applied for the remediation of petroleum-hydrocarbon contaminated soils due to the occurrence of volatilization mechanism. Results from the microcosm study indicate that the residual compounds are not easily biodegraded under both aerobic and anaerobic conditions. Thus, more aggressive remedial measures (e.g., chemical oxidation, soil washing) are required if the soil remediation goals are more stringent than the action level (1,000 mg/kg) applied in this study.

CONCLUSIONS

In this study, batch microcosm experiments were conducted to assess the potential of application of enhanced bioremediation processes to clean up diesel-oil contaminated soils. The laboratory microcosm experiments were conducted to determine the optimal biodegradation conditions of diesel-oil hydrocarbons. Conclusions obtained from this study include the following:

(1) Addition of nutrient, commercially available mixed microbial inocula (Oil Gator™), bulking agents, and organic materials (chicken manure) would enhance the efficiency of TPH biodegradation. Higher first-order TPH decay rates were observed in microcosms with the addition of chicken manure (decay rate = 0.0142 day^{-1}) or mixed microbial inocula (decay rate = 0.015 day^{-1}). Thus, chicken manures have the potential to be used as substitutes of commercial microbial inocula. TPH decay rate was only 0.0069 day^{-1} in microcosms under intrinsic conditions.

(2) The TPH decay rate and removal ratio can be further enhanced to 0.0196 day^{-1} and 87%, respectively, with frequent soil shaking and air replacement.

(3) Less TPH removal efficiency was observed in the later stage of the incubation in microcosms without air supplement. This might be due to the following two effects (a) complete oxygen consumption, and (b) the remaining compounds or byproducts might be less biodegradable, which caused the decreased TPH removal rates.

(4) The decreased oxygen and increased carbon dioxide contents in the headspace of microcosms indicate the occurrence of aerobic biodegradation. Moreover, the increased total heterotrophs in the early stage and increased total anaerobes in the later stage of the microcosm study also confirmed the shift of aerobic biodegradation to anaerobic biodegradation pattern when complete oxygen consumption was observed.
(5) Addition of organic materials (chicken manure) would increase the microbial population, and thus, caused the increased TPH removal rate. However, addition of chicken manure would also cause the increase in TPH concentration and regulation compliance problem in the early stage of the operation.

This performance study provides us insight into the characteristics and kinetics of diesel-oil contaminated soils remediation by enhanced bioremediation. These findings would be helpful in designing an ex-situ field-scale bioremediation system (e.g., landfarming or biopile) for practical application.

ACKNOWLEDGEMENTS

This study was funded by National Science Council in Taiwan and Chinese Petroleum Corp., Taiwan. Additional thanks to Dr. K.L. Huang of Chinese Petroleum Corp., Taiwan, and Dr. W.Y. Huang and Ms. Y.L. Kuo of National Sun Yat-Sen University for their assistance throughout this project. The views or opinions expressed in this article are those of the writers and should not be construed as opinions of the U.S. Environmental Protection Agency.

REFERENCES

TEPA (Taiwan Environmental Protection Administration), A research on the determination of the TPHs pollution levels in soil, Technical Report, Taiwan, 2003.

APHA (American Public Health Association), Standard Methods for the Examination of Water and Wastewater, 21th Ed, APHA-AWWA-WEF, Washington, DC, 2001.

Wilson J.T. and R. Kolhatkar, Role of natural attenuation in life cycle of MTBE plumes. J. Environ. Eng. 128 (2002) 876-882.

Chen K.F., C.M. Kao, J.Y. Wang, T.Y. Chen, and C.C. Chien, Natural attenuation of MTBE at two petroleum-hydrocarbon spill sites. J. Hazard. Mater. A125 (2005) 10-16.

Kao C.M., W.Y. Huang, L.J. Chang, H.Y. Chien, and F. Hou, Application of monitored natural attenuation to remediate a petroleum-hydrocarbon spill site. Water Sci. Technol. 53 (2005) 321-328.

Sarkar D., M. Ferguson, R. Datta, and S. Birnbaum, Bioremediation of petroleum hydrocarbons in contaminated soils: Comparison of biosolids addition, carbon supplementation, and monitored natural attenuation. Environ. Pollut. 136 (2005) 187-195.

US EPA, US Environmental Protection Agency, How to Evaluate Alternative Cleanup Technologies for Underground Storage Tank Sites: a Guide for Corrective Action Plan Reviewers. EPA/510/R-04-002, 2004.

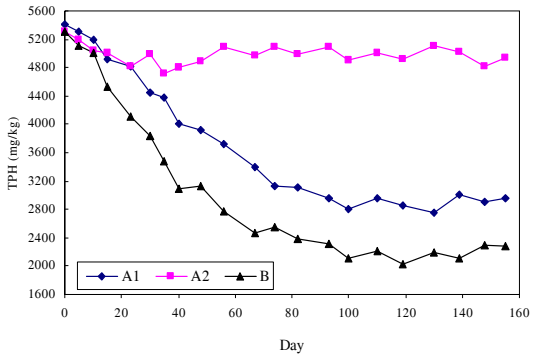

Fig. 1. Variations in soil TPH concentrations in Groups A (A1: live control; A2: dead control) and B (with nutrient addition) microcosms.

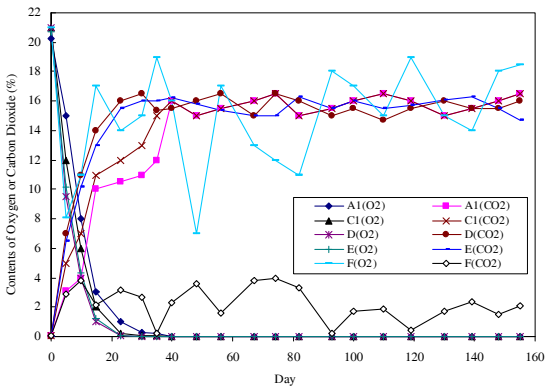

Fig. 2. Variations in measured oxygen and carbon dioxide contents in the headspace of representative groups of microcosms.

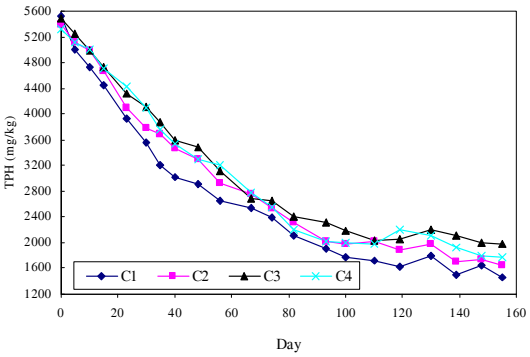

Fig. 3. Variations in soil TPH concentrations in Groups C1 to C4 microcosms (with bulking agent addition).

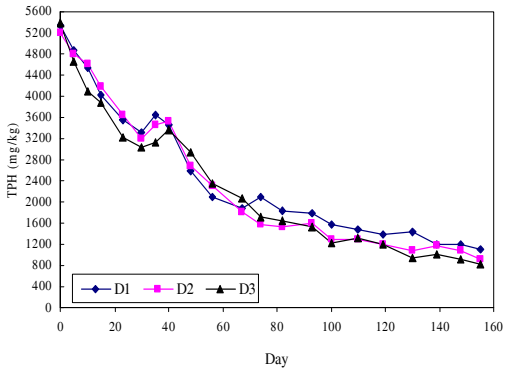

Fig. 4. Variations in soil TPH concentrations in Group D microcosms with and without the addition of inocula (Oil Gator^{TM}), bulking agent (soil to bulking agent ratio = 10 to 1), and nutrients.

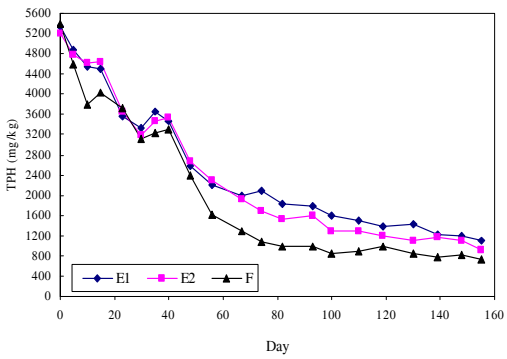

Fig. 5. Variations in soil TPH concentrations in Groups E [with the addition of organic material (chicken manure) and with or without the bulking agent (soil to bulking agent ratio = 10 to 1) addition] and F microcosms [with organic material addition and bulking agent addition with microcosm shaking and air replacement weekly (volume ratio of soil to bulking agent = 10 to 1)].

PEROXIDASE-MEDIATED STABILIZATION OF 2,4-DICHLOROPHENOL IN A MODEL HUMIN-MINERAL GEOMATERIAL

Mónica Palomo[1] and Alok Bhandari[2]

[1]Department of Civil Engineering, California State Polytechnic University, Pomona, CA

[2]Department of Agricultural & Biosystems Engineering, Iowa State University, Ames, IA

Abstract

Enhanced polymerization of phenolic contaminants induced by the application of the enzyme horseradish peroxidase (HRP) has drawn attention of many researchers due to its potential for remediation of contaminated soils. This study utilized 2,4-dichlorophenol (DCP) as a probe solute to evaluate the ability of HRP to stabilize pesticide derivatives in a model humin-mineral geomaterial. The model soil was derived from a natural surface soil treated with alkali to remove humic and fulvic acids. The resulting humin-mineral material had SOM content and chemical characteristics that were different from the parent soil. Sorption of DCP was complete within 24 hrs and most of the sorbed DCP was removed from the geomaterial by water and methanol suggesting weak solute-sorbent interactions. Phase distribution of DCP polymerization products (DPP) also appeared to be complete within 24 hrs, but a significantly higher amount of the solute was stabilized in the presence of HRP. The total extractable solute decreased, and DPP bound residues increased with contact time and initial solute concentration. These results illustrate the potential of utilizing HRP-mediated oxidation for in situ stabilization of pesticide derivatives, such as DCP, in humin-mineral geomaterials representative of soils found below the root zone.

Background

Enhanced polymerization of phenolic contaminants induced by the application of the enzyme horseradish peroxidase (HRP) has drawn attention of many researchers due to its potential for remediation of contaminated soils. Sorption and binding of phenolic contaminants to the humin component of SOM is of interest due to the latter's abundance

in soil, representing up to 50% of soil organic carbon (Kononova, 1966), and due to humin's strong interactions with organic pollutants in the subsurface (Kohl and Rice, 1998). This study utilized 2,4-dichlorophenol (DCP) as a probe solute to evaluate the ability of HRP to stabilize pesticide derivatives in a model humin-mineral geomaterial.

Methodology

The model soil was derived from a natural surface soil (3.2% SOM) treated with alkali to remove humic acid (HA) and fulvic acid (FA). Detailed information about the parent surface soil is provided elsewhere (Lesan and Bhandari, 2003). HA and FA removal required a total of 42 sequential fill-and-withdraw extraction cycles with alkali. The alkali-extracted soil was thereafter conditioned by 10 washes with distilled-deionized water, 10 washes with pH 7 phosphate buffer to neutralize pH, and finally 10 washes with $CaCl_2$. Dried soil material was homogenized and stored in the refrigerator at 1 °C until further use. The alkali extracted soil or humin-mineral (HM) soil contained a total of 1.1 % SOM as humin.

Solute sorption and extraction procedures have been described by Palomo and Bhandari (2005). Water and methanol extractable solute was defined as the "solvent extractable" fraction, which represented the fraction of solute slowly released from soil. Sorption was conducted at five different initial DCP concentrations (ranging from 0.5 to 500 μM) and three contact times (1, 7 and 28 days). Experimental procedures were carried out in absence (DCP only) and presence of HRP. Addition of HRP to the systems induced the formation of dichlorophenol polynmerization products (DPP).

Results and Discussion

The phase distribution of solute between water and the humin-mineral soil was complete within 24 hrs for both DCP and DPP; no significant increase in the levels of sorbed solute was observed beyond 1 day. At all initial solute concentrations, DPP sorption was significantly higher than that observed for DCP only (Figure 1). The solute removed by solvent extraction was reduced upon addition of HRP. Thus, the total solute stabilized was significantly increased when the phenolic polymerization was induced

(Figure 1). At 500 μM, the sorbed mass of DCP and DPP was 602 and 2234 μmole/kg, respectively. While the stabilized mass of DCP and DPP was 11 and 512 μmole/kg, respectively, respectively.

Most of the sorbed DCP was removed from the geomaterial through solvent extractions, suggesting weak solute-sorbent interactions. The total extractable solute decreased, and DPP stabilized residues increased with contact time and initial solute concentration (Figure 2).

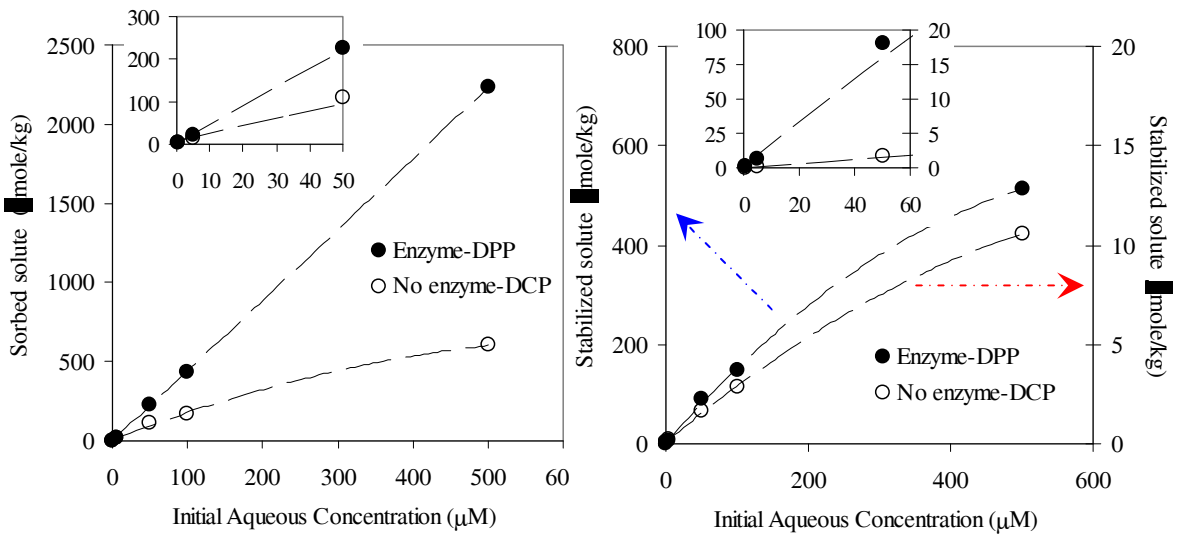

Figure 1- Sorbed (left) and stabilized (right) solute in the absence or presence of enzyme, 7 days of contact time, humin-mineral fraction of agricultural soil.

The utilization of HRP to induce polymerization of DCP was successful and it increased the quantity of mass initially sorbed to the soil. Dichlorophenol polymerization products included precipitated oligomers of DCP, oligomers formed by cross coupling of SOM and DCP, soluble oligomers and sorbed DCP trapped in the soil structure. Solute distribution results showed that, for both DCP and DPP, the extractable fraction decreased and the stabilized residue increased as a function of contact time.

A comparison of the HM sorption results to those obtained for the parent soil (AG) is shown in Figure 2. In the absence of enzyme, significantly more DCP was sorbed to AG (~1089 μmole/kg,) than to HM (~601 μ mole/kg). However, the masses of stabilized residues at the end of the 28 days of contact were comparable (25 and 18 μmole/kg, for AG and HM, respectively). When HRP was added, sorption to AG and HM was 1959 and 2211 μmole/kg, respectively. While the mass of DPP sorbed to HM was higher than the mass sorbed to AG, the amount of DPP stabilized in the soil was slightly higher for AG soil (795 and 636 μmole/kg, for AG and HM, respectively). However, the amount of stabilized chemical was not proportional to the SOM content. Results show high affinity of HM toward DPP, indicating that the chemical characteristics of humin compensate for the reduction of SOM content. These results illustrate the potential of utilizing HRP-mediated oxidation for in situ stabilization of pesticide derivatives, such as DCP, in humin-mineral geomaterials representative of soils found below the root zone.

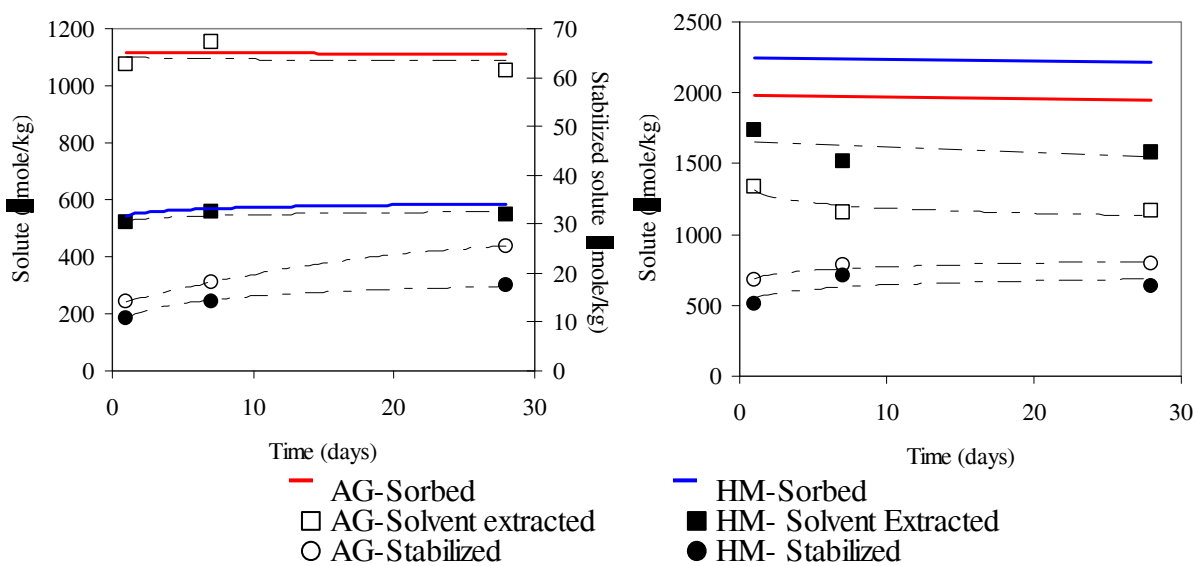

Figure 2- Solute distribution as function of contact time. On the left DCP only (no enzyme added), on the right DPP (enzyme added), C_o=500 μM. Humin-mineral results are in solid symbols, surface soil data in hollow symbols. Solid lines represent the total solute sorbed.

References

Kononova, M. M. (1966). *Soil Organic Matter*. T. A. Nowakowski and A. C. D. Newman (translators). Pergamon Press, Oxford.

Kohl, S. D. and Rice, J. A (1998)." The binding of contaminants to humin: A mass balance". *Chemosphere*, 56:251-261.

Lesan, H.M. and Bhandari, A. (2003) "Atrazine sorption on surface soils: Time-dependent phase distribution and apparent desorption hysteresis." *Water Research*, 37, 1644-1654.

Palomo, M. and Bhandari, A. (2005) "Time-dependent sorption-desorption behavior of 2,4-dichlorophenol and its polymerization products in surface soils". *Environ. Sci. Technol*. 39:2143-2151.

pH variation and its effect on metal concentration during electrokinetics

Ming Xiao[1] PhD, PE, M. ASCE, and Ashleigh D. Love[2], Zheng Teng[3], PhD, PE

Extended Abstract for

the ASCE-EWRI World Environmental & Water Resources Congress 2009 (EWRI09)
Topic: Environmental
Sub-Topic: Soil and Subsurface Remediation

Extended Abstract

Heavy metal contaminated soils pose significant threat to the environment and human health. Electrokinetic remediation is an emerging remedial technology that removes the contaminants from silty or clayey soils by applying an electric potential across contaminated and saturated soils using a pair of electrodes. The anode attracts negatively charged contaminants, and the cathode attracts positively charged contaminants, such as heavy metal ions. When the cationic contaminants reach the cathode, they can be pumped out with the contaminated water and disposed or treated safely. However, the electrokinetics is complicated by the metal precipitation before the metal ions can reach the cathode. This is caused by electrolysis that occurs at both electrodes. At the anode, water is oxidized, releasing oxygen and creating H^+ that results in an acid front moving towards the cathode. At the cathode, hydrogen is evolved and a base front of hydroxyl ions (OH^-) is generated and moves to the anode. The metal ions migrating toward the cathode tend to react with OH^- when they reach the base front to form metal hydroxides, which precipitate from the pore fluid as solid form.

The pH of the pore solution is a dominant variable that appears to control electroosmosis and contaminant migration in clays (Eykholt and Daniel, 1994; Acar and Alshawabkeh, 1996; Reddy et al., 1997). The reactions that are directly regulated by pH include adsorption and desorption, dissolution and precipitation, complexation and speciation (Hicks and Tondorf, 1994). The effectiveness of electrokinetics depends on achieving an acidic pH in the soil such that the metal ions are not adsorbed to soil surface and remain mobile in pore fluid. The experiments by Eykholt (1992) indicated the sharp pH front developed within several days and persisted within the cathode region of the soil throughout the testing period. Since ionic mobility of the hydrogen ion is about 1.8 times that of the hydroxyl ion (Acar and Alshawabkeh, 1993), the acid and base fronts usually

[1] Communicating author: Assistant Professor, Department of Civil and Geomatics Engineering, M/S EE94. California State University, Fresno, California 93740. Phone: (559) 278-7588. Email: mxiao@csufresno.edu
[2] Graduate student and staff engineer, BSK Associates. Fresno, CA.
[3] Engineer, Provost & Pritchard Engineering Group, Inc. 286 W. Cromwell Avenue. Fresno, CA 93711.

meet at regions close to the cathode. For example, Probstein and Hicks (1993) found that the pH jump, which is the sharp increase of pH where the acid and base fronts meet, occurs at 2/3 of the total distance from the anode; and Al-Hamdan and Reddy (2008) observed the pH jump occurred at 0.74 of the total distance from anode. A test by Yu and Neretnieks (1996), however, showed that the pH jump moved to anode in sand, possibly caused by the adsorption of hydrogen ions in the sand.

pH was usually measured longitudinally in laboratory and field tests. Whether and how pH varies with depth is unknown. Meanwhile, variation of metal ion concentrations with depth was reported in the literature. Alshawabhek et al. (2005) observed transverse upward migration of metal ions and an increase in concentrations in the upper few centimeters of the soil; they attributed this phenomenon to the evaporation and upward pore fluid flow. Pilot tests by USAEC (2000) showed a significant increase in metal concentrations of cadmium and chromium as the soil depth decreased from 10ft to 5ft.

This paper reports the experimental work that aims to identify the possible causes of vertical variation of metal ion concentration, such as pH and water content. A sandy clay is spiked with lead chloride ($PbCl_2$). The soil is uniformly compacted and then saturated in a Plexiglas soil box (30cm long, 12.7cm wide, 20cm tall). Electrokinetic geosynthetics (EKG) is used as electrode. EKG is an electrically conductive geosynthetic material and was recently explored in the UK (Jones et al., 2005, 1996; Kalumba and Glendinning, 2006). EKG materials are formed by incorporating conductive elements with the traditional geosynthetics, or the geosynthetics is made of or coated with conductive polymer. Use of EKG has not been reported in the US, and commercial manufacturing of EKG is not available. In this research, graphite rods (2.7mm in diameter) are tired together and bonded to geogrid to serve as electrodes. Graphite is electrically conductive and does not introduce new ions into the soil. The electrodes are connected to a DC power supply, which can supply adjustable voltage from 0 to 100V. Constant-voltage method is used, and the voltage gradient is maintained at 1V/cm. Five perforated tubes are pre-installed in the soil, so that pH probes can be inserted into the tubes to measure the pH in the pore water at different depths, longitudinal locations, and time. A small solid-stem flight auger (0.5inch in diameter) is used to retrieve soil samples during the process of the test, and lead concentrations at different depths, longitudinal locations, and time are measured using the inductively coupled plasma spectroscopy (ICP). The retrieved soil samples are also tested for water content. The results are analyzed to identify possible effects of pH and water content on metal concentration during electrokinetics.

References

Acar, Y.B. and Alshawabkeh, A.N. 1993. Principles of electrokinetic remediation. *Environmental Science and Technology*, 27:2638-2647.

Acar, Y.B. and Alshawabkeh, A.N. 1996. Electrokinetic remediation. I: Pilot-scale tests with lead-spiked kaolinite. *J. Geotechnical Engineering*, 122(3):173-185.

Al-Hamdan, A.Z. and Reddy, K.R. 2008. Electrokinetic remediation modeling incorporating geochemical effects. *J. Geotechnical and Geoenvironmental Engineering*, 134(1):91-105.

Alshawabkeh, A.N., Bricka, R.M, and Gent, D.B. 2005. Pilot-scale electrokinetic cleanup of lead-contaminated soils. *J. Geotechnical and Geoenvironmental engineering*. 131(3):283-291.

Eykholt, G.R. 1992. Driving and complicating features of the electrokinetic treatment of contaminated soils. PhD dissertation, University of Texas at Austin.

Eykholt, G.R. and Daniel, D.E. 1994. Impact of system chemistry on electroosmosis in contaminated soil. *J. Geotechnical Engineering*, 120(5):797-815.

Hicks, R.E., and Tondorf, S. 1994. Electrorestoration of metal contaminated soils. *Environmental Science and Technology*, 28(2):2203-2210.

Jones, C.J.F.P., Lamont-Black, J., Glendinning, S., and Pugh, R.C. 2005. New applications for smart geosynthetics. ASCE Geo-Institute GSP 142. Waste Containment and Remediation, Proceedings of the Geo-Frontiers 2005 Conference, Austin, Texas, January 24-26, 2005.

Kalumba, D. and Glendinning S. 2006. A beach scale model for developing of an integrated in-situ remediation for heavy metals using EKG electrodes. ASCE GSP 148 Advances in Unsaturated Soil, Seepage, and Environmental Geotechnics, Proceedings of GeoShanghai International Conference, Shanghai, China. 6-8 June 2006.

Probstein, R.F. and Hicks, R.E. 1993. Removal of contaminants from soils by electric fields. *Science*, 260:48-503. April 23, 1993.

Reddy, K.R., Parupudi, U.S., Devulapalli, S.N., and Xu, C.Y. 1997. Effects of soil composition on the removal of chromium by electrokinetics. *J. Hazardous Materials*, 55:135-158.

USAEC. 2000. In-situ electrokinetic remediation of metal contaminated soils technology status report. US Army Environmental Center, report number: SFIM-AEC-ET-CR-99022, July 2000.

Yu, J-W., and Neretnieks, I. 1996. Modeling of transport and reaction processes in a porous medium in an electrical field. *Chemical Engineering Science*, 51(19):4355-4368.

Pore-scale Characterization of Residual Non-aqueous Phase Liquids (NAPLs) in Fractional Wettability Porous Media

Riyadh I. Al-Raoush

Department of Civil and Environmental Engineering, Southern University and A&M College, Baton Rouge, LA 70813, Tel: (225) 933-7780, Fax: (225) 771-4320, Email: riyadh@engr.subr.edu

Abstract

The objective of this research was to investigate the impact of wettability of porous media on pore-scale characteristics of residual non-aqueous phase liquids (NAPLs). Synchrotron X-ray microtomography was used to obtain high-resolution 3D images of fractional wettability sand systems. Pore-scale characteristics of NAPL blobs such as volumes, lengths, interfacial areas and shape factors were computed from the 3D images. Four systems of different NAPL-wet mass fractions containing the residual NAPL were imaged and analyzed. In systems comprised of 100%, 50%, 25%, and 0% NAPL-wet mass fractions, residual NAPL saturations were 0.125, 0.067, 0.083, and 0.121; mean blob volumes normalized by the volume of a sphere with mean grain diameter were 0.97, 1.23, 1.93, and 2.39; normalized mean blob interfacial areas were 43.75, 35.86, 34.25, and 30.88 mm^{-1}; and mean sphericity index values were 0.216, 0.262, 0.455, and 0.569, respectively. Findings revealed that spatial variation in the wettability of porous media surfaces has a significant impact on pore-scale characteristics of residual NAPL blobs in saturated porous media systems.

1.0 Introduction

The release of non-aqueous phase liquids (NAPLs), such as gasoline and chlorinated solvents, into the subsurface can lead to groundwater contamination. As NAPLs migrate downward through a porous medium, residual portions are entrapped in the complex void space due to capillary forces and serve as a long-term source of groundwater pollution. Pore-scale characterization of the residual NAPL phase is required for the assessment, design and implementation of an efficient cleanup and remediation strategy.

Different methods have been used for pore-scale characterization of NAPLs in porous media. Main techniques include direct observation of NAPLs in the pore space (Chatzis and Morrow, 1983; Conrad et. al., 1992; Mayer and Miller, 1992; Wardlaw and McKellar, 1985; Powers et. al., 1992), 2D micromodels (Sahloul et. al., 2002; Chomsurin and Werth, 2003) and 3D imaging techniques (Johns and Gladden, 1999; Al-Raoush and Willson, 2005; Culligan et. al., 2006; Goldstein, et. al., 2007).

While these investigations provide valuable insights on the characteristics of NAPLs, they all assume uniform wettability of the porous media (i.e., either water-wet or NAPL-wet systems). In water-wet systems where the solid surfaces are preferentially wetted by water, residual NAPL is entrapped in larger pore bodies as disconnected volumes which range in complexity from simple singlets which occupy single pore bodies to complex ganglia that extend in length to occupy multiple pore bodies.

Spatial variation in wettability is common in natural subsurface systems where a combination of water-wet and NAPL-wet solid surfaces can be found. This type of porous media is called fractional wettability porous media. Variations in wettability of natural subsurface systems occur due to variations of porous media properties such as mineral composition, organic matter distribution, surface roughness and sorption of active agents to the surface of the porous media (Anderson, 1986; Powers and Tamblin, 1995). Spatial variation of wettability has a significant impact on pore-scale distribution and configuration of residual NAPL in subsurface systems, which in turn influences pore-scale displacement mechanisms (McDougall and Sorbie, 1995; Harrold et. al., 2001; Peri and Blunt, 2007) flow (Hui and Blunt, 2000; Jackson et. al., 2003; Karabakal and Bagci, 2004), NAPL-water interfacial area (Bradford and Leij, 1997; Jain, 2003), NAPL dissolution (Bradford and Abriola, 2001; Zhao et. al., 2007), capillary pressure and relative permeability (Masalmeh, 2003; Gladkikh and Bryant, 2006), residual phase saturation (Lackner and Torsaeter, 2006), and infiltration of fluids into porous media (Munehide and Tomokasu, 2008).

The objective of this research was to investigate the impact of fractional wettability of porous media on the characteristics of residual NAPLs. High-resolution 3D mages of different fractional wettability sand systems were obtained using synchrotron X-ray microtomography. Quantification of the morphology and entrapment patterns of residual NAPL was obtained using 3D image processing algorithms.

2.0 Materials and Methods

2.1 Materials

A uniform fine sand of median size (D_{50}=250 μm) was used as the porous medium. A uniform size of grains was selected to eliminate the impact of heterogeneity of the grains while investigating the impact of wettability on the morphology of residual NAPL phase. Immiscible fluids used in the experiment were de-aired water (represents the aqueous phase) and Soltrol 220 (Chevron Philips Chemical Company). Soltrol 220, a mixture of C_{13}-C_{17} hydrocarbons, was used to model organic contaminates since it has properties similar to common hydrocarbon contaminants. Soltrol was doped with Iodononane (10% by mass) to enhance its contrast in the images. After preliminary imaging of the system, it was observed that the contrast of the images was sufficient to extract (i.e., segment) the organic fluid (i.e., Soltrol) in the image without the need to dope the aqueous phase. The density and viscosity of the aqueous solution are 0.97 gm/cm^3 and 1.02 cP, respectively; and for the doped soltrol, 0.78 gm/cm^3 and 4.79 cP, respectively.

Octadecyltrichlorosilane (OTS) (Acros Organics) was used to create NAPL-wet sand system following the procedure presented in (Bradford and Leij, 1996). The procedure is summarized as follows: a solution was created by adding 5% by volume of OTS to ethanol. The solution was then added to untreated sand (i.e., water-wet) until it became completely saturated; the mixture was stirred for several hours. The mixture was rinsed off with ethanol that removed most of the OTS, and then evenly placed in a pan in a vented area to air dry overnight. The remaining mixture was cured in an oven at 100°C for an hour to allow the remaining ethanol to be evaporated. Fractional wettability systems were obtained by combining various mass fractions of untreated and OTS-treated sands. Systems will be designated herein by their percentage of OTS-treated sand (i.e., equivalent NAPL-wet mass fraction). Four different systems containing the residual NAPL were imaged; 100%, 75%, 50%, and 0% OTS-treated mass fraction (i.e., NAPL-wet mass fractions, respectively).

2.2 Creation of residual NAPL saturation

A special cell was fabricated to establish the residual NAPL in the saturated fractional wettability systems and to be mounted in the tomography station for imaging. The cell consisted of a column of polycarbonate connected to aluminum end fittings to allow insertion of tubes to perform drainage and imbibition of fluids. The height of the column was 83.5 mm and the inside diameter was 6.0 mm. Porous polypropylene frits (10 μm) were placed at both aluminum ends of the columns to retain the porous media and to ensure homogenous injection and displacement of the immiscible fluids.

Fractional wettability sand systems were packed under dry conditions to ensure homogenous distribution of sand grains in the column. Approximately 2.0 pore-volumes of de-aired water were injected vertically upward through the column at a constant rate of 2.5 ml/hr using a syringe connected to a Cole-Parmer Series 74900 syringe pump. The doped Soltrol was then injected vertically upward at the same constant flow rate used for the de-aired water. Water was finally flushed through the column to displace the NAPL and create the residual NAPL saturation.

2.3 Microtomography imaging

The systems were imaged using synchrotron X-ray microtomography at the GeoSoilEnviroCARS 13-BM-C beamline at the Advanced Photon Source, Argonne National Laboratory, IL. Image resolution is 7.47 μm/pixel in all 3D directions. To avoid boundary effects on the spatial distribution and configurations of immiscible fluids, scans were obtained approximately at mid portions of the columns. Multiple scans were obtained at different locations of each column to obtain large volumetric images. Image reconstruction was performed using algorithms developed by GSECARS to convert CT attenuation data to 3D volumetric data. Each microtomography scan allowed obtaining an image of 600x600x520 voxels (i.e., cubic domain inside the column to avoid boundary effects), where the third dimension is the vertical dimension. For each system, three different scans were obtained at different vertical locations and then stacked to obtain larger images of size 600x600x1200 which were used in the analysis of residual NAPL characterization.

2.4 Characterization of residual NAPL from 3D images

Volume, interfacial area, lengths and shape factors of NAPL blobs were computed using the algorithms developed in (Al-Raoush and Willson, 2005; Lorensen and Cline, 1987). More details can be found in these references.

3.0 Results and Discussion

Fig. 1 shows an example of NAPL residual blobs obtained from 3D imaging of the 0% OTS system, only a portion of the entire image used in analysis is shown in the figure. The color scheme in the image reflects blob identification where blobs are labelled by distinct numbers (shown as different colors in the image). Porosities obtained from images are 0.331, 0.327, 0.334, and 0.325 for the 100%, 50%, 25%, and 0% OTS-treated systems, respectively. Residual NAPL saturations are 0.125, 0.067, 0.083, and 0.121 for the 100%, 50%, 25%, and 0% OTS-treated systems, respectively. The trend of residual NAPL saturations is similar to the ones reported for fractional wettability systems given in (Morrow, 1975; Powers et. al., 1995) where residual NAPL saturations are less in fractionally wet systems (i.e., 50% and 25% OTS-treated systems in this work) and increase as the systems become more NAPL-wet or water-wet.

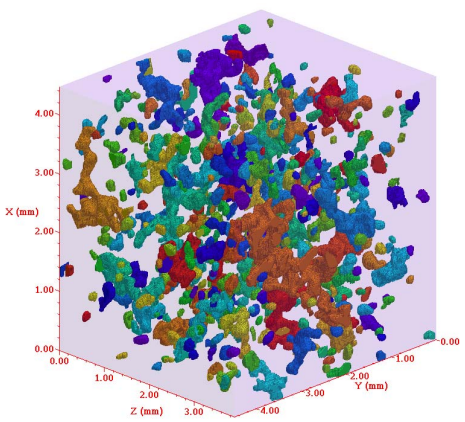

Figure 1: 3D image of residual NAPL extracted from the 0% OTS system.

Fig. 2 shows frequency distributions of blob volumes normalized by the volume of a sphere that has a diameter equivalent to the median grain diameter, D_{50}. In all systems, NAPL blobs vary greatly in size and complexity by orders of magnitude. As can be seen in figure, wettability of the porous medium has a significant impact on sizes of residual NAPL blobs and their distributions in the void space. In the 100%OTS-treated system, blobs have preference for entrapment in small pores, corners, and at contacts of solid surfaces through continuous thin NAPL films. Note that NAPL films are not resolved at the resolution of images in this paper. Therefore, NAPL blobs are distributed in the void space by large numbers with small volumes which makes the total magnitude of residual saturation high. Mean blob volumes normalized by the volume of a sphere with median grain diameter, D_{50}, are 0.97, 1.23, 1.93, and 2.39; and the maximum normalized volumes are 8.81, 13.66, 16.79, and

21.74, for the 100%, 50%, 25%, and 0% OTS-treated systems, respectively. Note that maximum normalized volumes are not shown in the figure to enhance the visualization. A trend of decrease in mean blob volume (i.e., individual blobs) is observed as more fractions of the porous media rendered NAPL-wet indicating that spatial distribution of wettability controls locations and entrapment patterns of residual NAPL blobs. This in turn influences processes such as relative permeability and pressure saturation relations. In a complete NAPL-wet system, the effective permeability to NAPL is much lower than in water-wet systems (at any given saturation) because water in the larger pores hinders the flow of NAPL. This becomes more pronounced as the water saturation increases until the residual NAPL saturation is obtained at higher levels than it would be in a water-wet system. On the other hand, the effective permeability to water is high because residual NAPL is located in the small pores and is coating the larger pores with a thin film which does not affect the flow of water. The relative permeabilities are controlled by the distribution of the fluids in the pores of the void space. The relative permeability of a fluid at any saturation is a function of its mobility, which in turn is a function of capillary size and wettability. The wetting phase has a lower mobility if it is located in the smaller pores and is adhering to the surface of the porous media. However, in a water-wet system, where NAPL occupies the large pores and most of them are coated with a thin water film, NAPL flow occurs through the larger pores where the NAPL is located, water does not exist to impede the flow of NAPL, the NAPL effective permeability, relative to water, is very high. On the other hand, the water effective relative permeability is very low, even when the NAPL saturation are reduced to the residual level**,** because residual NAPL in the large pores remains to effectively block the flow of water.

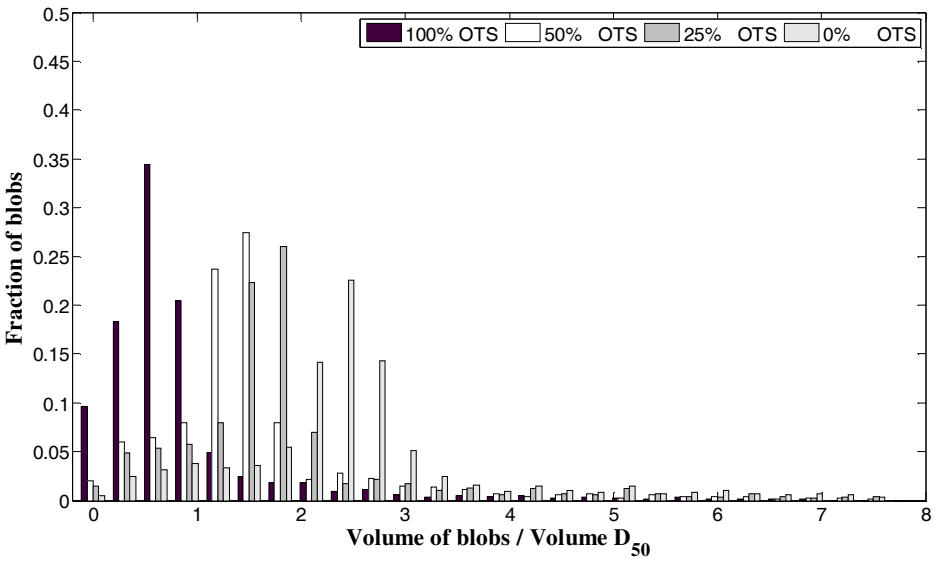

Figure 2: Frequency distributions of blob volumes normalized by the volume of a sphere that has a diameter equivalent to the D_{50} of grains

Fig. 3 shows frequency distributions of blob maximum lengths normalized by the D_{50}. Normalized mean blob lengths are 1.10, 1.45, 1.67, and 1.96; and the maximum normalized lengths are 6.27, 11.31, 10.13, and 15.21, for the 100%, 50%, 25%, and 0% OTS-treated systems, respectively. Note that maximum normalized lengths are not shown in the figure to enhance the visualization These data indicate that as the porous medium comprises more water-wet surfaces, residual NAPL blobs increase in size and length due to the entrapment preferences discussed previously.

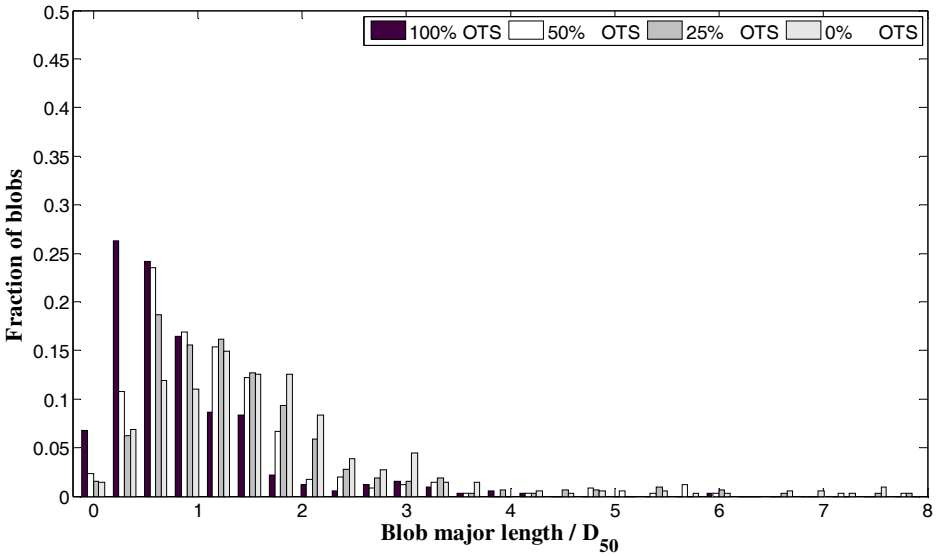

Figure 3: Frequency distributions of blob major lengths normalized by the D_{50} of grains

Fig. 4 shows frequency distributions of NAPL-water interfacial areas normalized by the volume of each blob. Normalized mean blob interfacial areas are 43.75, 35.86, 34.25, and 30.88 mm^{-1}; and the maximum normalized interfacial areas are 112.43, 81.2, 94.78, and 71.90 mm^{-1}, for the 100%, 50%, 25%, and 0% OTS-treated systems, respectively. Note that some maximum values are not shown in the figure to enhance the visualization. Normalized interfacial areas reach the highest mean value in the completely NAPL-wet system (i.e., 100% OTS-treated) and the lowest mean value in the completely water-wet system. The trend of the normalized interfacial areas obtained in this work is similar to the one observed experimentally in (Bradford and Abriola, 2001). This is mainly because blobs tend to decrease in size and assume more spherical shapes as NAPL-wet surfaces increase in the system. This observation becomes apparent as the normalized interfacial area of each individual blob is compared to that of a perfect sphere of equivalent volume; small blobs tend to assume spherical shapes compared to large blobs which usually assume more irregular and branched shapes. This can be seen clearly in Fig. 5 which shows frequency distributions of sphericity index (shape factor) for all systems. Mean sphericity index values are 0.216, 0.262, 0.455, and 0.569; and maximum values are 0.857, 1.507, 1.507, and 1.990, for the 100%, 50%, 25%, and 0% OTS-treated systems,

respectively. Distributions of sphericity index for all systems are consistent with distributions of volumes and lengths provided in Fig.2 and Fig. 3, respectively.

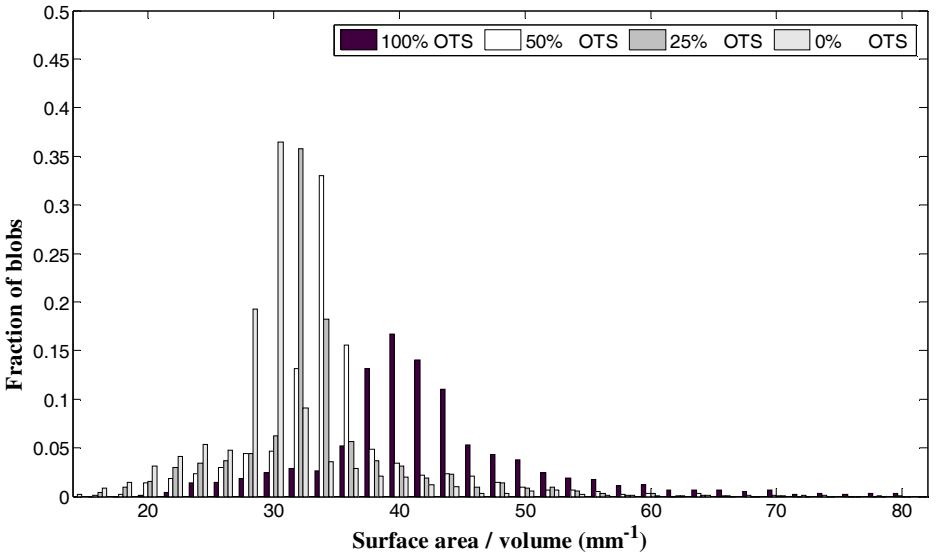

Figure 4: Frequency distributions of NAPL-water interfacial areas normalized by the volume of each blob

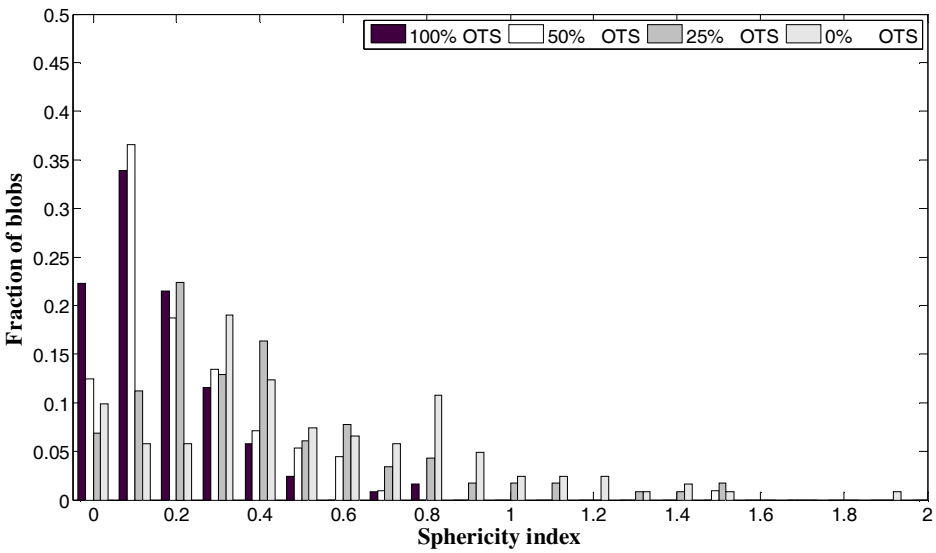

Figure 5: Frequency distributions of sphericity index (shape factor) for all systems

4.0 Conclusions

Findings indicate that spatial variation in wettability of porous media has a significant impact on pore-scale characteristics of residual NAPL blobs in saturated porous media systems. As the porous medium comprises more water-wet surfaces, residual NAPL blobs increase in size and length due to the entrapment at large pore bodies.

Therefore, NAPL-water interfacial areas are smaller in NAPL-wet systems where blobs tend to be more spherical and less branched. Overall residual NAPL saturations are less in fractional wettability systems and increase as the systems become more NAPL-wet or water-wet.

Acknowledgments
This research was performed, in part, at Argonne National Laboratory as a research participant in the FaST Program. The program is administered by Argonne's Division of Educational Programs with funding provided by the U.S. Department of Energy and the National Science Foundation (Contract No. HRD-0310426). The experiment was performed at the GeoSoilEnviroCARS beamline (13-BM-C) at the Advanced Photon Source. GeoSoilEnviroCARS is supported by the National Science Foundation Earth Sciences (EAR-0217473), Department of Energy Geosciences (DE-FG01-94ER14466), and the state of Illinois. Use of the APS was supported by the U.S. Department of Energy, Basic Energy Sciences, Office of Energy Research, under contract No. W-31-109-Eng-38. I would particularly like to thank Maude Johnson, Meagan Pinkney and Lindsey Thomas (Southern University and A&M College), Dr. Mark Rivers and Dr. Peter Eng (GeoSoilEnviroCARS) for their assistance with the imaging portion of this work.

References:

Al-Raoush, R., and Willson. C. S. (2005). "A pore-scale investigation of a multiphase porous media system." *J. Contam. Hydrol.*, *77*, 67-89.

Anderson, W. G. (1986). " Wettability literature survey, 1, Rock/oil/brine interactions and the effects of core handling on wettability." J. Pet. Techno, 38, 1125-1144.

Bradford, S. A., and Leij, F. J. (1996). "Predicting two- and three-fluid capillary pressure-saturation relationships of porous media with fractional wettability." Water Resour.Res., 32(2), 251-259.

Bradford, S. A., and Leij, F. J. (1997). "Estimating interfacial areas for multi-fluid soil systems." J. Contam. Hydrol., 27(1-2), 83-105.

Bradford, S. A., Vendlinski, R. A., and Abriola, L. M. (1999). "The entrapment and long-term dissolution of tetrachloroethylene in fractional wetability porous media." Water Resour. Res., 35(10), 2955-2964.

Bradford, S. A., and Abriola, L. M. (2001). "Dissolution of residual tetrachloroethylene in fractional wettability porous media: incorporation of interfacial area estimates." Water Resour. Res., 27(5), 1183-1195.

Chatzis, I., Morrow, N.R., and Lim, H.T. (1983). "Magnitude and detailed structure of residual oil saturation." Soc. Pet. Eng. J., 311-326.

Chomsurin, C., and Werth, C. J. (2003). "Analysis of pore-scale nonaqueous phase liquid dissolution in etched silicon pore networks." Water Resour. Res., 39, 11, 1-11.

Conrad, S. H., Wilson, J. L., Mason, W. R., and Peplinski, W. J. (1992). "Visualization of residual organic liquid trapped in aquifers." Water Resour. Res., 28, 467-478.

Culligan, K. A., Wildenschild, D., Christensen, B. S. B., Gray, W. G., and Rivers, M. L. (2006). "Pore-scale characteristics of multiphase flow in porous media: A comparison of air-water and oil-water experiments." Adv. Water Resour., 29(2), 227-238.

Gladkikh, M., and Bryant, S. L. (2006). "Influence of wettability on petrophysical properties during imbibition in a random dense packing of equal spheres." J. Pet. Sci. Eng., 52(1-4), 19-34.

Goldstein, L., Prasher, S. O., and Ghoshal, S. (2007). "Three-dimensional visualization and quantification of non-aqueous phase liquid volumes in natural porous media using a medical X-ray Computed Tomography scanner." J. Contam. Hydrol., 93(1-4), 96-110.

Harrold, G., Gooddy, D. C., Lerner, D. N., and Leharne, S. A. (2001). "Wettability changes in trichloroethylene-contaminated sandstone." Environ. Sci. and Technol., 35, 7, 1504-1510.

Hui, M. H., and Blunt, M. J. (2000). "Effect of wettability on three-phase flow in porous media." J. Phys. Chem., B 104, 3833-3845.

Jackson, M. D., Valvatne, P. H., and Blunt, M. J. (2003). "Prediction of wettability variation and its impact on flow using pore- to reservoir-scale simulations." J. Pet. Sci. Eng., 39, 231-246.

Jain, V., Bryant, S., and Sharma, M. (2003). "Influence of wettability and saturation on liquid-liquid interfacial area in porous media." Environ. Sci. and Technol., 37(3), 584-591.

Johns, M. L., and Gladden, L. F. (2001). "Surface-to-volume ratio of ganglia trapped in small-pore systems determined by pulsed–field gradient nuclear magnetic resonance." J. Colloid Interface Sci., 238, 96-104.

Karabakal, U.; Bagci, S. Determination of wettability and its effect on waterflood performance in limestone medium. Energy and Fuels. 2004, 18(2), 438-449.

Lackner, A. S., and Torsaeter, O. (2006). "Effects of pressure and wettability on residual phase saturation in sandstone rock." J. Pet. Sci. Eng., 52(1-4), 237-243.

Lorensen, W. E., and Cline, H. E. (1987). "Marching cubes: a high resolution 3D surface construction algorithm." Comput Graph., 21 (4),163-9.

Masalmeh, S. K. (2003). "The effect of wettability heterogeneity on capillary pressure and relative permeability." J. Pet. Sci. Eng., 39, 399-408.

Mayer, A. S., and Miller, C. T. (1992). "The influence of porous medium characteristics and measurement scale on pore-scale distributions of residual nonaqueous–phase liquids." J. Contam. Hydrol., 11, 189-213.

McDougall, S. R., and Sorbie, K.S. (1995). "The impact of wettability on waterflooding: pore scale simulation." Soc. Pet. Eng. Res. Eng., 10, 208.

Morrow, N. R. (1975). "The effects of surface roughness on contact angle with special reference to petroleum recovery." J. Can. Pet. Technol., 14, 42-53.

Munehide, I., and Tomokasu, F. (2008). "Upward infiltration into porous media as affected by wettability and anionic surfactants." Soil Sci. Soc. America J., 72(3), 741-749.

Peri, M., and Blunt, M. (2005). "Three-dimensional mixed-wet random pore-scale network modeling of two- and three-phase flow in porous media. II. Results Physical Review E - Statistical, Nonlinear, and Soft Matter Physics., 71, 2, 026302-026302.

Powers, S. E., Abriola, L. M., and Weber, W. J. (1992). "An experimental investigation of nonaqueous phase liquid dissolution in saturated subsurface systems: steady state mass transfer." Water Resour. Res, 28(10), 2691-2705.

Powers, S. E., and Tamblin, M. E. (1995). "Wettability of porous media after exposure to synthetic gasolines." J. Contam. Hydrol., 19, 105-125.

Sahloul, N. A., Ioannidis, M. A., and Chatzis, I. (2002). "Dissolution of residual nonaqueous phase liquids in porous media: pore-scale mechanisms and mass transfer rates." Adv. Water Resour., 25, 33-49.

Wardlaw, N. C., and McKellar, M. (1985). "Oil blob populations and mobilization of trapped oil in unconsolidated packs." Can. J. Chem. Eng., 63, 525-531.

Zhao, W. and Ioannidis, M. A. (2007). "Effect of NAPL film stability on the dissolution of residual wetting NAPL in porous media: A pore-scale modeling study." Adv. Water Resour., 30(2), 171-181.

Addressing Contaminated Groundwater and Promoting Environmental Stewardship in Wichita, Kansas – The Gilbert and Mosley Project Story

Paul Anderson, P.E.[1], Shawn Maloney, P.G.[2], and Roger Olsen, Ph.D.[3]

[1] CDM, 9200 Ward Parkway, Suite 500, Kansas City, Missouri, 64114; PH: (816) 444-8270, FX: (816) 444-8232; email: andersonpd@cdm.com
[2] City of Wichita – Department of Environmental Services, 1900 E. 9th Street, Wichita, Kansas, 67214; PH: (316) 268-8351, FX: (316) 268-8390; email: smaloney@wichita.gov
[3] CDM, 555 17th Street, Suite 1100, Denver, Colorado, 80202; PH: (303) 383-2300, FX: (303) 308-3003; email: olsenrl@cdm.com

ABSTRACT

The City of Wichita, Kansas faced a significant environmental challenge when volatile organic compounds impacted a large volume of groundwater extending south of the downtown area to the Arkansas River. This contaminated groundwater posed a threat to human health and the environment and threatened to stagnate economic development as a result of the environmental liability concerns across the project area that encompasses about 3,850 acres and 8,000 parcels of residential, commercial, and industrial properties.

The City, with CDM's assistance, investigated the contaminated groundwater, designed and built a groundwater treatment system to protect human health and the environment, and designed and built the Wichita Area Treatment, Education, and Remediation Center (WATER Center) to provide environmental education resources for the entire Wichita community. The City has turned an environmental liability that threatened human health into an environmental education resource for current and future generations.

1.0 INTRODUCTION

In the early 1990's, the City of Wichita, Kansas (City) faced a significant groundwater contamination issue that consisted primarily of tetrachloroethene (PCE), trichloroethene (TCE), *cis*-1-2-dichloroethene (*cis*-1,2-DCE), and vinyl chloride (VC). Investigative efforts resulted in the delineation of a groundwater plume more than four miles long and a mile-and-a-half wide. This plume of contaminated groundwater extended beneath some 8,000 parcels of land, including more than 550 businesses and hundreds of residential properties. The area was named the Gilbert-Mosley Site (Site) after two streets that intersect near the location at which the contamination was first detected.

The contaminated groundwater threatened human health and the environment, and it also threatened to create significant economic problems. Faced with their own questions of liability, banks immediately stopped lending to business and home buyers in the area.

Unless a solution was developed quickly, the federal government would have most likely classified the Site as a Superfund site, aggravating what already promised to be a long and costly problem. The potential costs quickly added up when projections indicated that if the Site would have entered the Superfund program the property values for the area would decrease by 40% or more, thus creating a financial burden on the taxing entities (city, county, and school district).

The City decided to take the initiative and develop a plan to clean up the Site. A unique partnership between the public and private sectors was established, involving intergovernmental partnerships with local, state, and federal government support, along with participation from the private sector — banks, responsible parties (industry), and the real estate community. The plan's fundamental premise would be the City's acceptance of responsibility for the cleanup of the Gilbert-Mosley Site in exchange for funding commitments from public and private sector partners.

The public funding was established through a new type of tax increment financing (TIF) district in which a decremental type of tax was used to fund the cleanup. This decremental TIF required Kansas State laws to be modified by the legislature. This system allowed the City to maintain property values and use 20% of the 1991 tax value for the Site cleanup. The taxing partners had to agree in order for the funding to be secured. Both the Sedgwick County and USD 259 school district agreed to the decremental TIF in order to prevent a much more significant loss (estimated at 40% or more) of property tax values and tax income.

2.0 SITE HYDROLOGY

Figure 1 shows the location of the Site, the Site boundaries, and the various contamination plumes. The Site is approximately 3,850 acres in size, covers an area approximately 4.4 miles long from north to south, and varies in width from 1.1 to 2.1 miles from west to east. The Site is situated within the Arkansas River floodplain, and the topography of the Site has little relief. The Arkansas River is the most prominent surface water feature and flows towards the south near the western border of the Site and then turns east, south of the Site.

The geology of the Site consists primarily of Arkansas River Valley alluvium and associated terrace deposits overlying the Wellington Formation bedrock. The Wellington Formation is primarily a gray and blue shale of Permian Age. The alluvial sediments consist of interbedded gravels, sands, silts, and clays. The alluvial sediments have a thickness of between 24 and 54 feet and average 30 feet in depth across the Site.

The depth to groundwater across the Site is shallow and in the alluvial aquifer - ranging from 16 to 20 feet across the Site and averaging 18 feet below ground surface. Groundwater levels in the alluvial aquifer fluctuate seasonally and may vary as much as 3 feet, depending on the proximity to the Arkansas River, their flow levels, and the amount of precipitation received. General groundwater flow is to the south, with a gradient

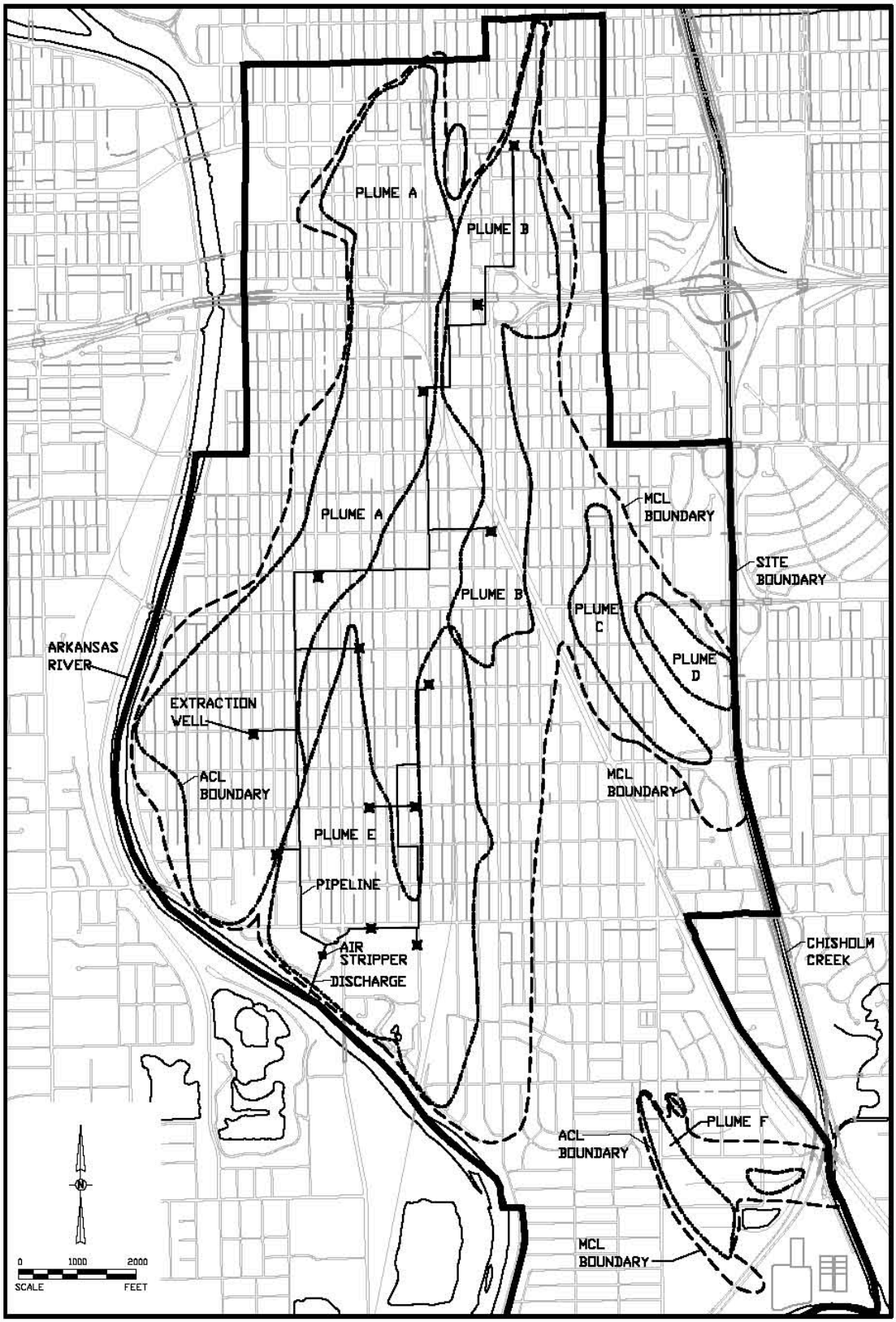

Figure 1: Gilbert-Mosley Site

between 0.0007 and 0.0014 feet/foot across the Site, and the hydraulic conductivity ranges between 380 and 707 feet per day. An average groundwater velocity for the Site, as determined from the calibrated flow model, ranges from 1.2 to 1.7 feet per day.

3.0 INVESTIGATION OF CONTAMINATION

The present boundaries of the Site and the contaminated groundwater plume extents were developed as a result of a series of site investigations that have been conducted privately and by KDHE since 1986. Groundwater contaminated in excess of the maximum contaminant levels (MCLs) covers approximately 2,220 acres, and over 20 sources have been identified. As indicated in Figure 1, six different contaminated groundwater plumes have been identified (Plumes A through F). The City is addressing Plumes A, B, C, and E, and KDHE is addressing Plumes D and F.

Over 5,000 samples of soil, surface water, and groundwater were collected to determine the extent of contamination and to identify source areas. Most of the samples were groundwater collected using direct push (hydraulic) techniques. Throughout most of the plume areas, concentrations of PCE, TCE, and *cis*-1,2-DCE range from 100 to 500 µg/L, and concentrations as high as 19,000 µg/L of PCE and 17,000 µg/L of TCE exist in the groundwater near source areas.

4.0 CORRECTIVE ACTION DECISION

After a public meeting, the Final Corrective Action Decision (CAD), similar to a United States Environmental Protection Agency (USEPA) Record of Decision (ROD) was signed on September 30, 1994. This CAD established the framework for addressing the environmental contamination at the Site.

Among other items, the CAD included the following elements: institutional controls, public education, hydraulic containment, monitoring, source control, and the establishment of alternate cleanup levels. All of these items have been either fully or partially completed by the City, and additional project efforts will continue into the future as appropriate.

4.1 Institutional Controls / Public Education

The City established institutional controls within the defined boundaries of the Site to prohibit the connection of newly-constructed private water wells for private or public drinking water uses. In addition, a public educational program was initiated to discourage the use of groundwater contaminated above the MCLs within the Site.

4.2 Hydraulic Containment

The City installed the Plumes ABE groundwater treatment system to establish hydraulic containment to prevent further migration of the Plumes A, B, and E groundwater. Groundwater contaminated above KDHE's alternate cleanup levels (ACLs – as further

discussed in Section 4.5) is targeted for containment, and any pumped groundwater is treated to below MCLs for the contaminants of concern. The hydraulic containment is anticipated to be terminated once the monitoring efforts indicate that the ACLs have been achieved and sustained over a one-year period. No active remediation is currently being performed at Plume C, and KDHE is responsible for the remediation of the contamination at Plumes D and F.

4.3 Monitoring

The City installed compliance monitoring wells at the zero line (i.e., the area where groundwater contamination was below MCLs) to monitor for the chemicals of concern on a quarterly basis until 2005 and then semi-annual, and the City is currently conducting semi-annual monitoring efforts. Long-term monitoring is anticipated to be required at the compliance and selected monitoring wells for a minimum period of 10 years of annual monitoring following the termination of the hydraulic containment efforts.

4.4 Source Control

The City has initiated investigations and source control activities at certain source areas to investigate and eliminate and/or reduce the toxicity, mobility, and volume of waste/contaminants at the Site. The appropriate future source area control efforts will be determined on an individual basis following source investigations, and source controls have already been implemented at several locations. To date, the City has implemented:

- Two contaminated soil removal projects
- Three air sparging and soil vapor extraction projects
- Three vapor intrusion mitigation systems, and
- The initial design of one electrical resistive heating project for DNAPL

The primary remedial process that the City has utilized for source area controls consists of air sparging and soil vapor extraction. (AS/SVE). The air sparging (AS) process blows compressed air into the groundwater and allows the air to migrate up through the volatile contaminants - thereby allowing the contaminants to enter into the gaseous state.

The soil vapor extraction (SVE) uses a vacuum blower to pull soil gases from the vadose zone above the groundwater out of the ground. The soil gas movement captures the air and volatile contaminants from the AS system and removes volatile contaminants from the soil zone. Typically, the volatile contaminants are below the air-permitting requirements of KDHE and require no off-gas treatment.

4.5 Establishment of Alternate Cleanup Levels

The City proposed ACLs that KDHE approved in the CAD. The ACLs include chemical-specific 10^{-5} excess carcinogenic risk concentrations, or federal MCLs, whichever were greater, to address the uncertainties associated with cumulative risk factors. The federal MCLs, 10^{-5} chemical-specific risk levels, and KDHE's ACLs are summarized in Table 1.

Table 1: Comparison of MCLs and KDHE's ACLs

Contaminant	MCLs (µg/L)	10^{-5} Chemical-Specific Risk Levels (µg/L)	KDHE's ACLs (µg/L)
Tetrachloroethene (PCE)	5	14	14
Trichloroethene (TCE)	5	21	21
1,2-Dichloroethene* (*cis*-1,2-DCE)	70	36.5	70
Vinyl Chloride (VC)	2	0.25	2

* Not a carcinogen (based on a Hazard Index of 1.0).

The plume boundaries based on the MCL and ACL values are shown in Figure 1, and the Plumes ABE groundwater treatment system has been installed to provide hydraulic containment of Plumes A, B, and E. The pumped groundwater is treated to below the MCLs, and the treated effluent is discharged to the nearby Arkansas River under the terms of a National Pollutant Discharge Elimination System (NPDES) permit that was issued by KDHE. The use of the ACLs reduced the total groundwater volume to be treated by an estimated 40 percent and helped to reduce the estimated project cost by approximately $8 million when compared to the initial cost projections.

5.0 DESIGN AND CONSTRUCTION EFFORTS

The CAD established the need for the City to design, construct, and operate a groundwater treatment system to provide hydraulic containment of the contaminated groundwater plumes. The City made the decision to expand the scope of the project to include the construction of extensive environmental education resources to supplement the groundwater treatment system, and these project enhancements resulted in the construction of the Wichita Area Treatment, Education, and Remediation Center (WATER Center). The extensive environmental education components of the project were included to teach current and future generations of schoolchildren and other site visitors about the importance of pollution prevention and environmental stewardship.

In order to expedite the design and construction efforts, three different project phases were established, and a design-build construction approach was selected to accelerate the schedule, allow for greater flexibility and efficiency, and provide the ability to incorporate value-engineering and cost-effectiveness improvements throughout the design and construction efforts. CDM (Wichita, Kansas) was retained as the designer-builder for the project, and Gossen Livingston Associates (Wichita, Kansas) was hired by CDM to provide the architectural design.

The WATER Center is pictured in Figure 2, and the three project phases included the center treatment building (Phase I), the surrounding education building and plaza (Phase II), and numerous site enhancements across the park (Phase III).

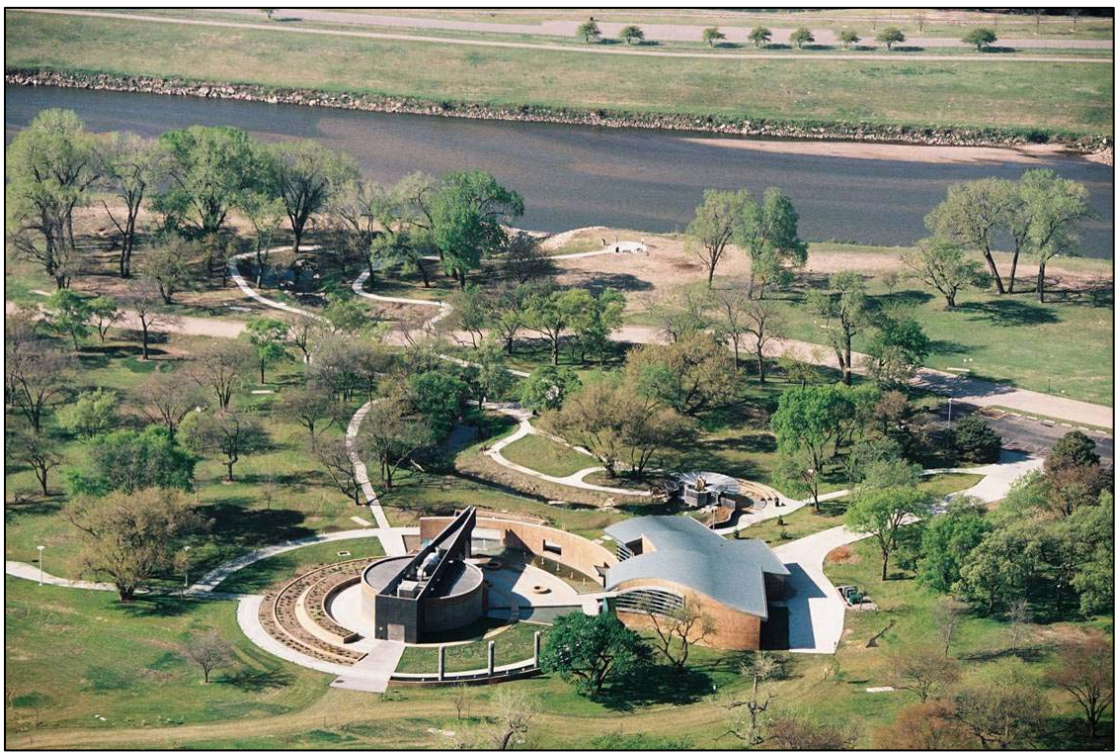

Figure 2. Aerial View of the WATER Center

5.1 Phase I – Groundwater Treatment System and Treatment Building

The Plumes ABE Groundwater Treatment System (Treatment System) consists of 13 extraction wells, 5.3 miles of influent piping, and a hydraulic-venturi air stripper groundwater treatment system. The Treatment System is designed to pump and treat a design flow rate of 860 gallons per minute (1.2 million gallons per day) and a maximum flow rate of 1,095 gpm (1.6 mgd). The approximate locations of the extraction wells, influent piping network, and air stripper are shown on Figure 1.

The 13 extraction wells are 10 inches in diameter and were constructed using stainless steel screens and Schedule 80 PVC casing pipes. The wells were completed with a flush-mount cap, and the total well depths ranged from 28 to 37.5 feet below ground surface. The wells were installed using a reverse-circulation drilling method, and each well was developed to remove sediment from inside the well. Step testing of each well was performed to evaluate the well performance and to determine the local hydrologic characteristics of the aquifer in the immediate vicinity of each well.

To convey the groundwater pumped from the extraction wells to the groundwater treatment building, approximately 28,000 feet of SDR-11 high density polyethylene

(HDPE) piping sections were installed using a horizontal directional drilling technique that minimized disruption and property damage in the residential and commercial areas.

The groundwater treatment building (pictured in Figure 3) is approximately 3,000 sq. ft. in size, and the interior of the treatment building includes a large circular area that contains the groundwater treatment system pumps, hydraulic-venturi treatment heads, control panels, and discharge stacks (pictured in Figure 4). The groundwater treatment system consists of a subsurface concrete tank that is divided into six modules and a clearwell section. Each module includes a transfer pump, two hydraulic-venturi treatment heads, a manifold piping section, transfer hoses, a pressure gauge, and a sample port. These items and other treatment system components were supplied by Hazleton Environmental (Hazleton, Pennsylvania).



Figure 3. Treatment Building



Figure 4. Treatment System

The groundwater flows through each module in series, and the water is progressively treated by the hydraulic-venturi treatment heads through which the water is pumped through spray rings to generate a large amount of surface area for the contaminants to volatilize. The contaminated air flows through the two interior discharge stacks to the discharge fan installed on the roof of the treatment building.

The hydraulic-venturi air stripper treatment system was selected for its compact size, ease of operation and maintenance, and quiet operation—a key consideration given the location of the treatment system in a public park across the street from a residential area. The water flows through the hydraulic-venturi treatment heads aspirate air flows that eliminate the need for large blowers that would create significant noise levels.

The contaminated air is discharged through a discharge fan and stack on the roof of the treatment building, and the contaminant levels contained in the exhaust air are significantly below the threshold level for regulatory permitting. The treated effluent water from the treatment system is discharged to the Arkansas River through either a gravity drain pipe or by the clearwell pump that uses the treated water to supply the fountains, aquarium, fish observatory, meandering creek, and other water feature items.

5.2 Phase II – Environmental Education Building and Plaza Area

The Phase II environmental education building and plaza area are located adjacent to the Phase I treatment building in Herman Hill Park. The 6,300-sq. ft. environmental education building includes an exhibit area with an aquarium (the aquarium uses a single-pass flow of treated water from the treatment system), several offices, public restrooms, a classroom, and a mechanical area. The education building is constructed with concrete walls and a standing-seam metal roof, and the walls and roof are curved to create an architecturally-unique design.

The environmental education building currently includes basic exhibits that are used to teach WATER Center visitors about subjects such as the importance of wetlands, "healthy" versus "unhealthy" aquatic environments, characteristics of native fish species, and other pollution prevention and environmental stewardship topics.

The circular plaza area includes a large number of fountains, terraced landscaped areas, sidewalks, seating elements, specialized lighting features, and a circular concrete arc wall. The plaza area fountains use the treated water from the groundwater treatment system, and this water is also used to supply the overhead discharge from the aqueduct and the water flow that cascades down the poetry water wall on the education building.

6.0 GROUNDWATER TREATMENT SYSTEM OPERATIONS

As of early 2009, the groundwater treatment system had been in nearly continuous operations for over six years and over 2.5 billion gallons of groundwater had been treated. The performance monitoring efforts have indicated that the treated groundwater met the discharge criteria established by the project-specific NPDES discharge permit, and Table 2 provides a sample of the influent and effluent contaminant concentrations during the first six years of operations.

Table 2: Treatment System Influent and Effluent Contaminant Concentrations

Date	Influent (Inflow)				Effluent (Outfall)			
	PCE (µg/L)	TCE (µg/L)	*cis*-1,2-DCE (µg/L)	VC (µg/L)	PCE (µg/L)	TCE (µg/L)	*cis*-1,2-DCE (µg/L)	VC (µg/L)
NPDES	**- - -**	**- - -**	**- - -**	**- - -**	**5**	**5**	**70**	***2***
1/3/2003	110	17	30	1.0	1.8	<1	1.9	<1
3/19/2004	70	13	25	<1	1.2	<1	2.4	<1
3/10/2005	42	9.5	19	<1	<1	<1	1.7	<1
6/28/2006	42	8.9	17	<0.8	<1.1	<0.6	1.1	<0.8
9/20/2007	26	8.4	15	<0.8	<1.1	<0.6	0.7	<0.8
9/24/2008	17	5.5	11	<0.8	<1.1	<0.6	<0.5	<0.8

In addition to the influent and effluent water samples, the sampling efforts for the exhaust air discharge have indicated that the discharge levels have been significantly below the level of regulatory interest and confirmed that an air permit was not required.

7.0 WATER CENTER EDUCATIONAL EFFORTS

City staff have conducted a wide range of on-site and off-site environmental education programming efforts, and the WATER Center has also functioned as a community resource for a wide range of other events.

The on-site programs have included Herman Hill Park site visits by school groups, community organizations of all types (i.e., Big Brothers and Big Sisters, Boy Scouts of America, various nonprofit groups, etc.), and a wide variety of internal City and State of Kansas meetings and events. The off-site programs have included City staff visits to schools, community facilities, and other organizations to present various environmental education programs.

A large number of park visitors have also visited the exterior of the WATER Center and the Herman Hill Park site improvements (plaza area, fish observatory, creek, park shelter, etc.) outside of the open hours of the facility.

In addition to the environmental education programs, the WATER Center has also served as a resource for the entire Wichita community, and the Herman Hill Park facilities have been used for events ranging from the Park Board summer programs to wedding receptions.

8.0 CONCLUSION

The contaminated groundwater in the Gilbert and Mosley Project area posed a significant risk to human health and the environment, and the City faced possible USEPA Superfund intervention in the early 1990s. As a result, real estate development in many areas of the Site ceased due to the contamination and potential environmental liability concerns. The values of thousands of properties were in jeopardy and were projected to decrease 40 percent in value – thus significantly eroding the City's tax base. Through a series of innovative project approaches by the City, many positive benefits have been achieved - including the construction of the WATER Center, restoration of property values throughout the project area, and redevelopment of portions of the Site. In one area of the Site (the Old Town area and warehouse district), over $300 million of commercial development has occurred.

The WATER Center's treatment building, environmental education building, and various site improvements (plaza, fish observatory, creek, rehabilitated park shelter, etc.) will provide environmental education opportunities for current and future generations and will instruct schoolchildren and other site visitors about the importance of pollution prevention and environmental stewardship. The dramatic architecture, water features, and environmental education components combine to make the WATER Center a landmark project and a resource for the entire Wichita community.

Use of In-planta Solid Phase Sampling Devices to Delineate VOC Plumes

Joel Burken, Kendra Waltermire and Emily Sheehan

Civil, Architectural and Environmental Engineering, Missouri University of Science and Technology, 1401 N Pine Street, Rolla Missouri, 65409
PH (573)-341-6547; FAX (573)-341-4729; Email, Burken@mst.edu

ABSTRACT

Plants directly interact with surrounding water, air, and soil, collecting and storing chemicals and elements from the surrounding environment. Two new and innovative sampling methods in which this valuable data can be accessed to replace as well as supplement contaminated-site investigations have been developed. When determining the extent of the plume on a contaminated site, groundwater sampling may be limited due to time, site access, and expense. By using new techniques that place sampling devices inside the trees on site, we can sample trees naturally occurring on a contaminated site or those planted in phytoremediation or redevelopment efforts, evaluate the plume size, and even monitor changes in concentration. These methods will have a minimal footprint and can be accomplished with little materials cost, time, or labor demands. These quick sampling techniques can provide an array of data within a short amount of time to help the efficiency in placement of groundwater monitoring wells, saving time and money as well as undue impact to the ecosystems at hand or personal property.

INTRODUCTION

Tree cores collected from contaminated sites have shown concentrations of VOCs that correlate with the groundwater concentration of VOCs. Previous research has proven that cores can be taken from the tree and analyzed using gas chromatography to determine contamination within the subsurface, particularly for chlorinated solvents (Vroblesky et al. 1999; Larson et al. 2008). The cores are a good qualitative analysis, but the heterogeneity of the cores leaves a range of unpredictability and error. In order to reduce these variables, new methods have been designed. One of the new methods is using a Solid Phase Micro Extraction (SPME) sampler to directly sample the VOC concentration qualitatively in cores. SPME samplers consist of fibers of varying matrixes that have highly absorptive characteristics. SPME samplers passively extract the VOCs through absorption and then the concentration of the sample can be determined by using gas chromatography for analysis (Skaates et al., 2005; Legind et al., 2007). Fibers can also decrease the mobilization costs, site impacts, permanent capital costs and repeat sampling costs. As well, the sensitivity was increased from coring analysis by 20-100 times.

In this research, sampling methods were brought into the trees, rather than taking a small portion of the tree to the laboratory. SPME samplers and a new sampling device called Solid Phase Samplers (SPSs) were placed into trees to show

that they have potential for rapid, improved sampling of trees for groundwater delineations. The following results show there clearly is great potential for this application and the patent-pending technology may greatly increase the accuracy of Phase I site investigations and concurrently decrease costs and damage to property and the environment.

MATERIALS AND METHODS

Field Sampling Using SPME In New Haven, MO, PCE contaminated groundwater has impacted the city water supply and tree-core sampling was critical in delineating the sources on the contamination (Struckhoff et al 2005, Schumacher et al. 2004). On the Kellwood Site (OU2) five trees were cored and then tested using *in-planta* SPME analysis. Cores were collected as previously described (Struckhoff et al 2005, Schumacher et al. 2004) and in the borehole remaining, SPME analysis was conducted using time weighted average (TWA) methods (Koziel and Pawliszyn, 2001), using 100 μm Carboxene SPME fibers supplied by Supelco Analytical (Sigma-Aldrich Co., Bellafonte, Pennsylvania). In TWA analysis, a SPME fiber with a high contaminant affinity is exposed to a sample media with the fiber retracted into the SPME needle for a given period of time. For TWA analysis, the contaminant concentration in the fiber must not be near the equilibrium concentration or the TWA rules of sampling are violated. The fibers were exposed in the trees at the New Haven Kellwood Site (OU2) site for 70 – 75 minutes, capped and transported to the Missouri S&T environmental engineering laboratory for analysis using an Agilent 6890 GC with detection via ECD. Details are presented elsewhere (Sheehan 2009).

SPS development and Testing SPSs were constructed and exposed to a steady concentration of PCE to evaluate absorption rates. SPSs were constructed using polydimethyl silicone (PDMS) tubing cut into sections with mass ~0.5g. Mass was accurately determined and recorded, and each section was placed on a threaded stainless steel screw and secured with a nut, Figure 1. SPSs were placed in methanol for two days and allowed to dry under a hood to remove any contamination from production, shipping and storage. The SPSs were then placed in an incubator for 2 days at 100°C. The tubes were then cooled off and placed into a 100 mL beaker within a 300 mL screw top jar also containing a layer of PDMS oil dosed with PCE/TCE, Figure 2. This controlled the chemical activity (i.e. concentration) in the gas phase at low levels, without depleting the mass via absorption into the SPSs. There was no direct contact of SPSs with PDMS oil containing PCE/TCE. The tubes were placed within the PCE/TCE environment at the same time. To determine the uptake rates, the tubes were removed at varying times: 1 hour, 2 hour, 12 hour, 24 hr/1 day, 2 days, 3 days, 4.25 days, 7 days, 11 days, and 14 days. When a tube was removed from the vial with tweezers, the tube was placed within a 20 mL headspace sampling vial and immediately capped then stored at 4 ˚C. Once all SPSs were removed, they were run at once in a headspace autosampler at 35 ˚C with direct injection to an HP 5890 GC with ECD for detection. The data was plotted over time.

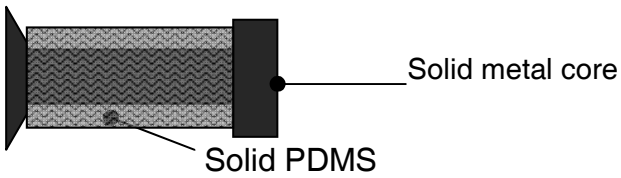

Figure 1: Solid Phase Sampler (SPS) assembly

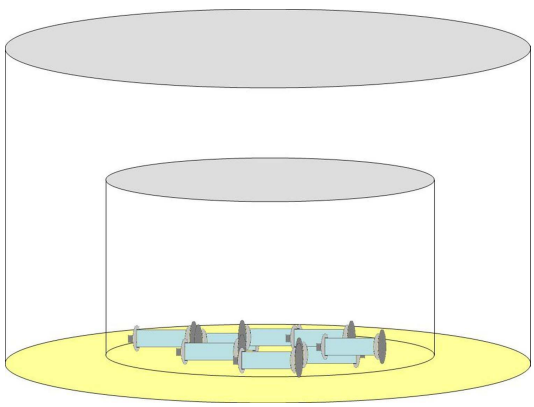

Figure 2: Solid Phase Samplers were placed in an open beaker inside a closed beaker containing PCE and TCE dosed PDMS oil.

Comparison of SPSs Versus Cores

As tree cores are highly variable in their collection and initial evaluation was set to evaluate tree xylem tissue versus the SPSs as a material, surrogate cores were used and constructed by cutting dowel rods at a mass of ~0.5g, diameter 0.4 cm, and the mass of each was recorded. The SPSs and cores were placed in a 100 mL beaker, as noted above, with an added aluminum foil divider placed in the center to separate the cores from the SPSs. The SPSs and cores were exposed for 3 weeks allowing them both to come to equilibrium with the surrounding environment. SPSs and cores were removed using tweezers and placed into separate vials and capped for analysis as noted above.

RESULTS

Field Comparison of *In-planta* SPME Methods and Tree Core Analysis Sampling of trees at the New Haven Kellwood Site (OU2) was conducted on 4 trees known to be in a polluted area that had been previously analyzed and one tree that had been sampled and never shown to contain contaminants (Schumacher et al, 2004). Results of tree core analysis using accepted methods revealed contamination of both TCE and PCE in the trees. Based on peak areas using the same GC methods, the *in-planta*

SPME methods had peak areas from 4 to 230 times higher, with an average increase of 13 times for TCE and 62 times greater for PCE, Table 1. For the one duplicate analysis, the SPME also had a similar variation between the two analyses, 85% vs 91% for TCE and 55% vs 53% for PCE. This analysis shows that SPME *in-planta* analysis has definite potential for providing improved method detection limits with similar variability in analysis. The SPME analysis also has the benefit of potentially rapid analysis. The headspace methods for tree core analysis generally have a 24 hour equilibration period, although recent method development has shown that heating samples can reduce the equilibration period required (Vroblesky, 2008).

Table 1 Comparison of standard tree core analysis and *in-planta* SPME analysis with TWA methods.

Tree #	Cores-TCE	Cores-PCE	SPME-TCE	SPME-PCE
Tree 1	3.8×10^2	2.1×10^4	5.8×10^3	1.2×10^6
Tree 2	6.1×10^2	1.9×10^4	1.7×10^4	4.4×10^6
Tree 3	9.4×10^1	5.2×10^2	5.8×10^2	2.5×10^3
Tree 4a	5.3×10^1	2.8×10^3	3.7×10^2	3.3×10^4
Tree 4b	3.6×10^2	6.2×10^3	4.3×10^3	7.1×10^4
Tree 5	ND	1.4×10^2	ND	7.2×10^3

Sorption Rates for SPSs Results for the absorption rates showed a clear relationship for both PCE and TCE absorption, Figure 3. Absorption as measure by the mass transferred to the SPSs increased rapidly over the first 96 hours and then reached apparent equilibrium at approximately 240 hours, 10 days. Equilibrium was reached if the change was less than 1 % over 72 hours. A simple first order uptake model was applied to each, Equation 1, with a first order uptake coefficient of 0.017 hr^{-1} and 0.024 hr^{-1} for PCE and TCE respectively. The importance of this methodology is to show that the SPS is more sensitive and predictable in the uptake (i.e. absorption). While the sensitivity is beneficial for getting the lowest possible method detection limits, the predictability of the uptake lets short term sampling (24 hours) be extrapolated to actual equilibrium concentrations.

$$A = A_{max} (1\text{-}e^{-kt}) \qquad \text{(Equation 1)}$$

Where A = peak area, A_{max} = peak area at equilibrium, k = 1st order rate coefficient (hr^{-1}), t = time (hours).

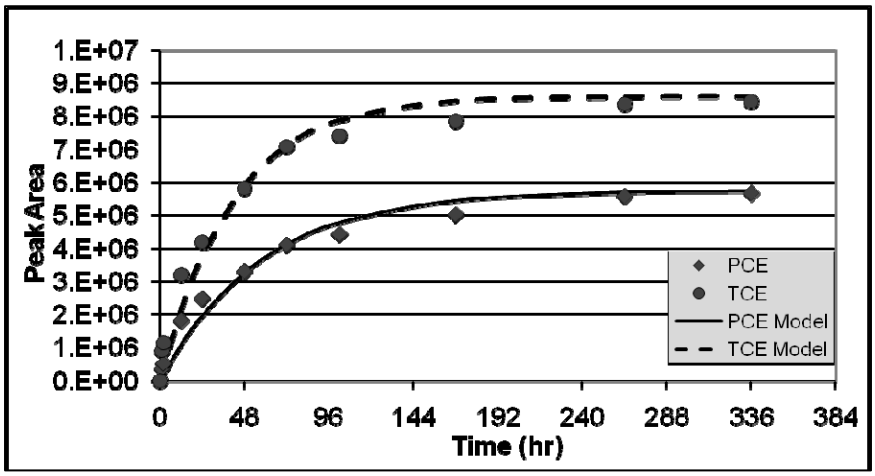

Figure 3: SPS-controlled absorption rate of PCE and TCE, showing equilibrium in approximately 10 days. The absorption followed a 1st order kinetic model.

Comparison of SPS and Core Equilibrium Concentration The equilibrium comparison of cores and SPSs exposed to the same headspace concentration revealed that the SPSs were more sensitive for PCE and had lower variability for both PCE and TCE; while core and headspace analysis was slightly more sensitive for TCE, Figure 4. The SPS peak area response was 98% higher than the core analysis for PCE, whereas the SPS response was 35% lower than the core analysis. The SPSs were more reproducible. The 95% confidence interval was only 0.9% and 0.8% of the mean for SPS analysis of PCE and TCE respectively, where as these values were 2.7% and 2.4 % for the cores analyzed.

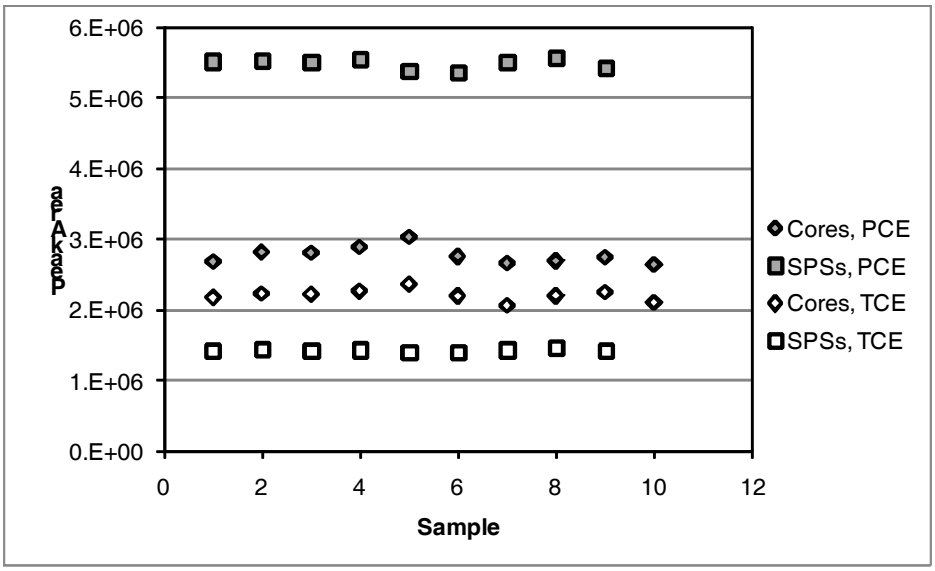

Figure 4: The SPSs and Cores were dosed and analyzed on the GC-ECD headspace autosampler.

CONCLUSION

Using the SPME fibers and SPSs to sample trees in the field appears to have benefits relative to traditional tree coring analyses. These methods may improve the vegetation-sampling approaches that have great benefits for Phase I site assessments and also for monitoring groundwater concentrations at phytoremediation sites. Plant sampling overall has benefits of minimal environmental or property disturbance. Sampling is accomplished with very little materials cost, energy use, or labor demands. As well, with the reproducibility of the SPME fiber and SPSs, groundwater monitoring can be replaced or become more efficient through these methods that are at the very infancy of development. This new approach is patent-pending and appears to have a bright future if optimized further.

ACKNOWLEDGEMENTS

The authors would like to thank Drs. Philipp Mayer and Ulrich Karlson – Goswinkle for their assistance in developing the application of SPME analysis in plants. We also thank Supelco for their support in providing demonstration and discount SPME fibers to test these methods. This work was supported in-part by the OECD Research Fellowship program and the Ministry of the Environment, Ontario, Canada.

REFERENCES

Koziel, J. A., and Pawliszyn, J. (2001). "Air sampling and analysis of volatile organic compounds with solid phase microextraction." *Journal of the Air & Waste Management Association*, 51(2), 173-184.

Larsen, M., Karlson, U., Burken, J. G., Machackova, J., and Trapp, S. (2008). "Using tree core samples to monitor natural attenuation and plume distribution of a PCE contamination." *Environmental Science & Technology*, 42 (5), 1711–1717.

Legind, C. N., Karlson, U., Burken, J. G., Reichenberg, F., and Mayer, P. (2007). "Determining Chemical Activity of (Semi)volatile Compounds by Headspace Solid-Phase Microextraction." *Analytical Chemistry*, 79(7), 2869-2876.

Schumacher, J. G., Struckhoff, G. C., and Burken, J. G. (2004). "Assessment of Subsurface Chlorinated Solvent Contamination Using Tree Cores at the Front Street Site and Former Dry Cleaning Facility at the Riverfront Superfund Site, New Haven Missouri, 1999-2003." *Report 2004-5049*, US Geological Survey.

Sheehan, E. M. (2009). "The Use Of Solid Phase Microextraction Devices For Detection Of Chlorinated Solvents In Vegetative Systems," Missouri University of Science and Technology, Rolla, MO.

Skaates, S. V., Ramaswami, A., and Anderson, A. G. (2005). "Transport and fate of dieldrin in poplar and willow trees analyzed by SPME " *Chemosphere*, 61(1), 85-91.

Struckhoff, G., Burken, J. G., and Schumacher, J. G. (2005). "Phytoremediation of Vadose Zone VOCs." *Environmental Science & Technology.*, 39(6), 1563-1568.

Vroblesky, D. A. (2008). "User's Guide to the Collection and Analysis of Tree Cores to Assess the Distribution of Subsurface Volatile Organic Compounds." U.S. Geological Survey Scientific Investigations Report 2008–5088

Vroblesky, D. A., Neitch, C. T., and Morris, J. T. (1999). "Chlorinated Ethenes from Groundwater in Tree Trunks." *Environmental Science & Technology.*, 33(1), 510-515.

Application of a Mass Balance-Based Subsurface Contaminant Transport Model

Byline: Benjamin W. Johnson, E.I. [1]; Andrew Curtis Elmore, Ph.D., P.E., M.ASCE[2]; Jeffrey D. Cawlfield, Ph.D., P.E. [3]

Author contact information: Geological Engineering, Missouri University of Science & Technology,129 McNutt Hall, Rolla, MO 65409. Telephone (573) 341-6784, Fax (573) 341-6935, email bwj253@mst.edu

Abstract

The definition of contaminant source release is a necessary element of contaminant mass transport simulation in the saturated zone. At many sites the release history is unknown, and there has been a significant body of research to develop inverse models to define finite release histories. Instead of rigorously defining the source history, a mass balance-based approach is tested to explicitly account for uncertainty in equal length rectangular pulse release variables. The approach has been incorporated into a spreadsheet model which uses a one-dimensional solution to the advection dispersion equation. A concentration dataset collected at a Superfund site was used for model calibration and verification. Several synthetic datasets with known input parameters were also used for model calibration and verification. The model provided reasonable results when the source time parameters were assumed to be random, and the results improved when the mass of contaminant in the aquifer was also assumed to be random. However, the improvements came at the cost of degraded calibration parameter values.

Introduction

The classic approach for modeling mass transport in a groundwater system requires initiating the simulation with the release of the contaminant to the system. Thus the conceptual model and subsequent analytical and numerical transport models require characterization of the source location and the source release function. There is a significant body of literature that addresses the identification of groundwater contamination sources as summarized by Michalak and Kitanidis (2004), Sonnenborg, et al. (1996), and Hill and Tiedeman (2007). Some representative works include Domenico and Robins (1985) which developed the extended pulse model to identify unknowns including the source concentration, source dimensions, the time of when the contaminant first entered the groundwater, the position of the center of mass, and the groundwater dispersivities. The authors acknowledged that unique solutions were not likely using field data although the model was useful for placing

[1] Geological Engineering Graduate Student, Missouri University of Science & Technology, 129 McNutt Hall, Rolla, MO 65409. bwj253@mst.edu
[2] Associate Professor of Geological Engineering, Missouri University of Science & Technology, 129 McNutt Hall, Rolla, MO 65409. elmoreac@mst.edu
[3] Professor of Geological Engineering, Missouri University of Science & Technology, 129 McNutt Hall, Rolla, MO 65409. jdc@mst.edu

reasonable bounds on the unknowns. Ala and Domenico (1992) developed a two-dimensional analytical method called the two-well solution to find the unknowns associated with a finite plane source. Skaggs and Kabala (1994) evaluated complex contaminant release histories (that is, releases other than continuous or rectangular pulses) using Tikhonov regularization. One of the conclusions of their work was that plume history could be adequately recovered if dispersion was relatively minor compared to advection even if the concentration measurements contained moderate random errors. A similar conclusion was developed by Alapati and Kabala (2000) who used a non-linear least-squares method without regularization to recover the release history of a source with a known location. Skaggs and Kabala (1998) also provide limitations when developing the release history of a source with observed data. These include the time since the release, which can be better estimated as the actual time since the release decreases. They show that deconvoluting solute transport systems is an ill-posed problem with solutions that improve as the quality of observed data improves. This sensitivity poses a significant issue to pragmatic application of contaminant release history characterization with field datasets.

Elmore (2007) used a concentration data collected using a direct push drill rig to estimate a subset of the source parameters including the time since the source release t_r, the duration of the release t_s, and the concentration of the source C_0, for a rectangular pulse. That work introduced a one dimensional (1D) spreadsheet model that could be used to estimate t_r, and t_s, by manual iteration with C_0 as a dependent variable assuming that the source location was known.

Much of the previous work focused on developing finite definitions of source history. The focus of this paper is to implement an automated deterministic model that provides reasonable solutions to source parameters by verifying the calibration mechanism with synthetic datasets. The approach initially developed in Elmore (2007) will be expanded to develop a mass-balance basis to estimate t_r, t_s, and C_0 using both synthetic and actual site concentration data.

Model Development

The governing equation for mass advection, dispersion, degradation, and sorption in a one-dimensional flow field is

$$R\left(\frac{\partial}{\partial t}C\right) = -v_x \cdot \left(\frac{\partial}{\partial t}C\right) + D_x \cdot \left(\frac{\partial^2}{\partial t^2}C\right) - k \cdot R \cdot C \qquad (1)$$

where C is the solute concentration, t is time, v_x is the average pore water velocity in longitudinal direction of flow, x is longitudinal distance from source, D_x is the longitudinal dispersion coefficient, k is the net degradation rate constant, and R is the retardation factor for linear, equilibrium sorption defined by Spitz and Moreno (1996).

The Van Genuchten and Alves (1982) solution to Equation 1 given a rectangular source release of magnitude C_0 for t_s is based on the assumptions that advection and dispersion occur in a uniform regional flow field with constant ground water velocity and homogeneous, isotropic aquifer properties.

A dependent relationship between the mass release variables C_0 and t_s may be developed using a mass balance approach by assuming that the groundwater plume has constant rectangular dimensions with width W, thickness b, and length, L. Given a constant concentration C_j for each band, which is the arithmetic average of predicted concentrations in band j, the total mass in solution in the aquifer is given by

$$M = n \cdot W \cdot b \left[\sum_{j=1}^{m} \left(C_j \cdot L_j \right) \right] \tag{2}$$

The normalized total mass in the aquifer is defined as

$$M' = \sum_{j=1}^{m} \left(C_j \cdot L_j \right) \tag{3}$$

where

$$M' = \frac{M}{n \cdot W \cdot b}$$

Spitz and Moreno (1996) provide the following equation for the total contaminant mass per unit aquifer volume

$$\Delta M = C \cdot n + C_a \cdot (1 - n) \cdot \rho_s \tag{4}$$

where C_a is the adsorbed concentration measured as mass of contaminant per mass of dry aquifer matrix material and ρ_s is the density of solids in the aquifer. The adsorbed fraction is also related to the dissolved concentration according to the linear adsorption isotherm equation which may be expressed as

$$C_a = C \cdot foc \cdot K_{oc} \tag{5}$$

where foc is the fraction of organic carbon and K_{oc} is the organic carbon adsorption coefficient. Substituting Equation 5 into Equation 4 and incorporating the contaminant retardation factor, R, gives

$$\Delta M = C \cdot n \cdot R \tag{6}$$

The total mass M_T in the aquifer is the product of the rectangular aquifer volume and ΔM which results in

$$M_T = n \cdot R \cdot W \cdot b \cdot \sum_{j=1}^{m} \left(C_j \cdot L_j \right) \tag{7}$$

Thus the normalized total mass in the aquifer at the time that the dissolved concentrations are measured is defined as

$$M'_T = R \cdot \sum_{j=1}^{m} \left(C_j \cdot L_j\right) \quad (8)$$

where

$$M' = \frac{M_T}{n \cdot W \cdot b}$$

The total mass released to the aquifer by a rectangular pulse through a finite plane with a height b and a width W is given by

$$M_T = v_x \cdot n \cdot W \cdot b \cdot t_s \cdot C_0 \quad (9)$$

which can be normalized as

$$M'_T = v_x \cdot t_s \cdot C_0 \quad (10)$$

If there is no mass decay, the total mass in the aquifer estimated at the time that the band concentrations are measured is equal to the total mass released to the aquifer, and Equation 8 can be substituted into Equation 10 and solved for the initial concentration

$$C_0 = \frac{R}{v_x \cdot t_s} \cdot \sum_{j=1}^{m} \left(C_j \cdot L_j\right) \quad (11)$$

Solutions to the 1D form of the governing equations are readily available in spreadsheet form, and several spreadsheet models are available for free download at the U.S. Environmental Protection Agency (USEPA) website. The use of a spreadsheet makes the manipulation of site concentration data to calculate the C_j values relatively trivial, and the model developed by Dawson (1995) incorporating the Van Genuchten and Alves solution was modified to incorporate Equation 11. Following the mass balance approach used to derive Equation 11, two calibration variables are defined as O, the normalized observed mass, and P, the normalized predicted mass, by the following equations

$$O_j = C_j \cdot L_j \quad (12)$$

$$P_j = \Delta x_j \cdot \sum_{i=1}^{m} C_P(x_i, t_r) \quad (13)$$

where C_P is the model predicted concentration at the points $x_1, x_2, \ldots, x_n$ that land within band j, and the points are separated by the distance

$$\Delta x_j = \frac{L_j}{n} \quad (14)$$

where n denotes the total number of predicted concentration points along the entire plume length.
The use of O and P allow the calculation of paired-data calibration parameters such as the Root Square Mean Error ($RMSE$) defined by Spitz and Moreno (1996). When the minimum range of $RMSE$ values varies per simulation in a given domain of t_r and t_s, the $RRMSE$ is useful to facilitate simulation comparison where

$$RRMSE(t_s, t_r) = \frac{RMSE(t_s,t_r)}{\min [RMSE(t_s,t_r)]} \quad (15)$$

where

$RMSE(t_s, t_r)$ = the $RMSE$ of an iteration defined by a coordinate set of t_r and t_s
$\min [RMSE(t_s, t_r)]$ = the smallest $RMSE$ of all t_r and t_s combinations within a simulation's region boundaries of t_r and t_s

Best estimates of t_r and t_s are determined by identifying regions of low $RRMSE$ values through rigorous calibration iterations along set ranges of t_r and t_s. The coordinates of t_r and t_s at which the corresponding $RRMSE$ error is reduced indicate likely estimates of the actual t_r and t_s. The coefficient of determination, the modeling efficiency, the relative percent difference, and the coefficient of residual mass defined by Spitz and Moreno (1996) were also incorporated into model calibration.

Application

The spreadsheet model was applied to a trichloroethylene (TCE) dataset collected at a Nebraska Superfund site which has been the subject of prior groundwater modeling studies including Elmore (2007), Miller and Elmore (2005), and Elmore and DeAngelis (2004). The unconfined aquifer at the site consists of glacio-fluvial sands and gravels where flow occurs through primary porosity and it is reasonable to assume that the Dupuit theory of vertical equipotential lines is valid for the aquifer. The plume area of the aquifer has not historically been subject to large stresses such as irrigation pumping, and the plume is relatively far from flow and head boundaries. Thus the assumption of steady uniform flow necessary to apply the Van Genuchten and Alves solution is reasonable for the subject plume. A direct push groundwater investigation was conducted in 2002 and 2003 to characterize the extent of the TCE contamination. TCE concentrations above the site action level of 5 μg/l were detected in fifty-nine locations which defined an approximately rectangular plume shape with dimensions of 5,000 m by 550 m. One to six samples were collected at different depth intervals at each location, and no data other than TCE concentrations were collected during the investigation. When multiple depth intervals were sampled at a single location, the arithmetic average of the results was assigned to the location to compress the three dimensional transport system into two dimensions. The plume was then divided into equal length bands for analysis. A remedial action well was installed in the approximate center of the plume 2,930 m from the source. The well was sampled several times contemporaneously with the direct push investigation to

provide treatment design data, but the remedial action well data were not used to calculate the statistics of any simulation. Site aquifer testing data were used to characterize the aquifer K as 39 m/d, Elmore and Vandeberg (1997) gave the hydraulic gradient in the area of the subject plume as 0.0023, the site foc average as 0.00028, and the saturated thickness, b, as $24.7\ m$. Mehran et al. (1987) estimated K_{oc} value for TCE as 120 mg/l, and Piskin (1971) estimated the site n_e as 0.145 and n was assumed to be equal to that value. The density of the solids was assumed to be 2.65 g/cm^3 based on the typical value given by Freeze and Cherry (1979). Elmore (2007) found that dispersion was relatively minor compared to advection. The model was best calibrated using $RRMSE$ as the primary calibration parameter by varying t_s and t_r to generate Figures 1a and 3a. As shown on the figures, areas were mapped at values of $RRMSE = 1.1$, and the coordinates of the centroid of the greatest calibration contour overlap area was selected as the best approximations of t_r and t_s.

Results and Discussion

To reiterate the objective, the contaminant transport model discussed in this paper develops estimates of the initial concentration of the contaminant release (C_0), the time since the contaminant was released (t_r), and the time of contaminant source release (t_s). A synthetic transport system provides given contaminant source release history parameters. The synthetic observed datasets in this experiment were expected to accommodate development of the most appropriate model calibration mechanism by producing the highest quality field data without measurement error. Six synthetic datasets with given analytical solutions of $C_0,\ t_r,\ t_s$ were developed by creating a random number generation selector. The selector randomly chose observed data points from a predicted dataset produced by the Van Genuchten and Alves (1982) solution to Equation 1. The sample size of each synthesized observed dataset represented 5-10% of the predicted dataset.

Equal length bands of analysis were superimposed over each synthetic transport system and tested to determine the most appropriate number of analysis bands to achieve the greatest accuracy. Several model calibration simulations with unique numbers of analysis bands were performed for each synthetic dataset. The number of bands overlaid on each synthetic dataset ranged from three to twelve. Several calibration parameters were tested in each simulation and the normalized mass observed and predicted values were best calibrated with $RRMSE$. Figure 1a graphically represents the accuracy of several different band number calibration simulations when using the $RRMSE$ as the calibration parameter. The plume characterizations of simulations with three or less bands resulted in degraded accuracy. The maximum number of bands was determined by ensuring that each band contained at least one synthetic observed datapoint, which typically required a maximum of twelve bands.

Figure 1: a) Synthetic dataset calibration parameter $RRMSE = 1.1$ contours shown with ±5% accuracy region (left). b) Contours are enlarged showing number of bands per simulation with the synthetic dataset (right). Synthetic solution coordinates: $t_s = 16.5\ yr,\ t_r = 20.0\ yr$

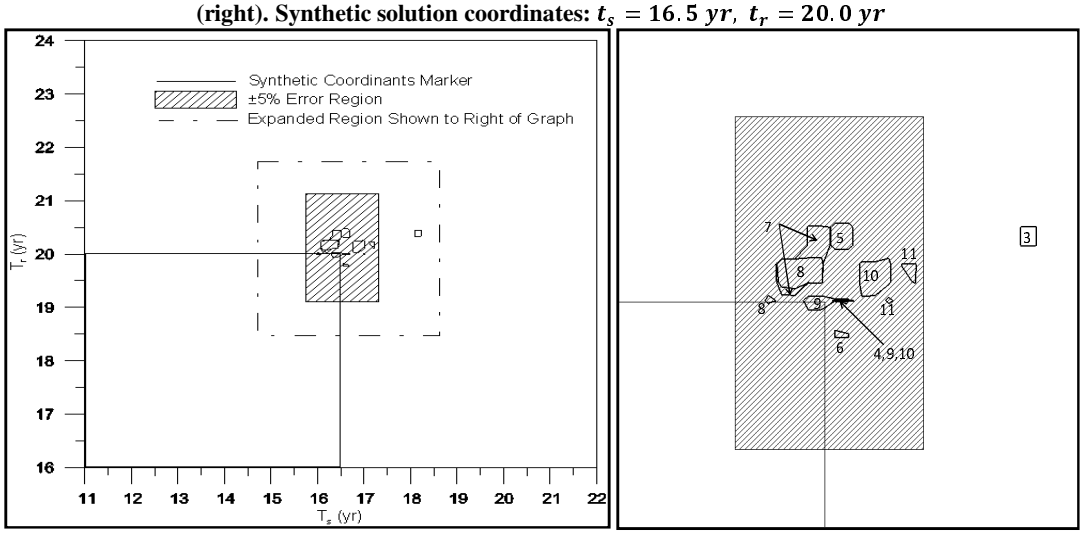

Figure 2: C_0 predictions at synthetic calibration results presented in Figure 2. Synthetic C_0 solution: 4000µg/l

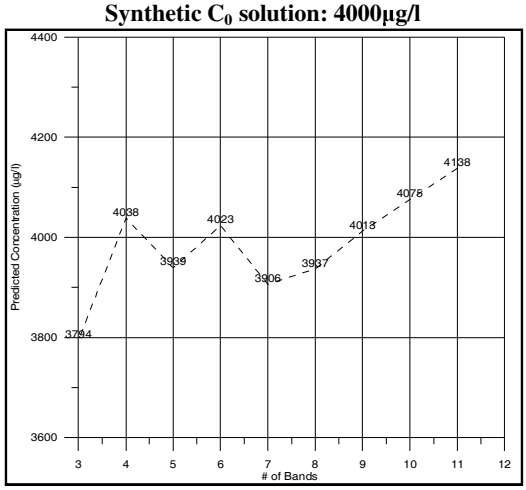

Figure 3: a) Observed field data calibration parameter $RRMSE = 1.1$. The shaded area (with centroid coordinates $t_s = 14.6,\ t_r = 18.7$) marks the contour overlap of equal length band number 3-12 simulations (left). b) C_0 predictions of calibrated observed field data (right).

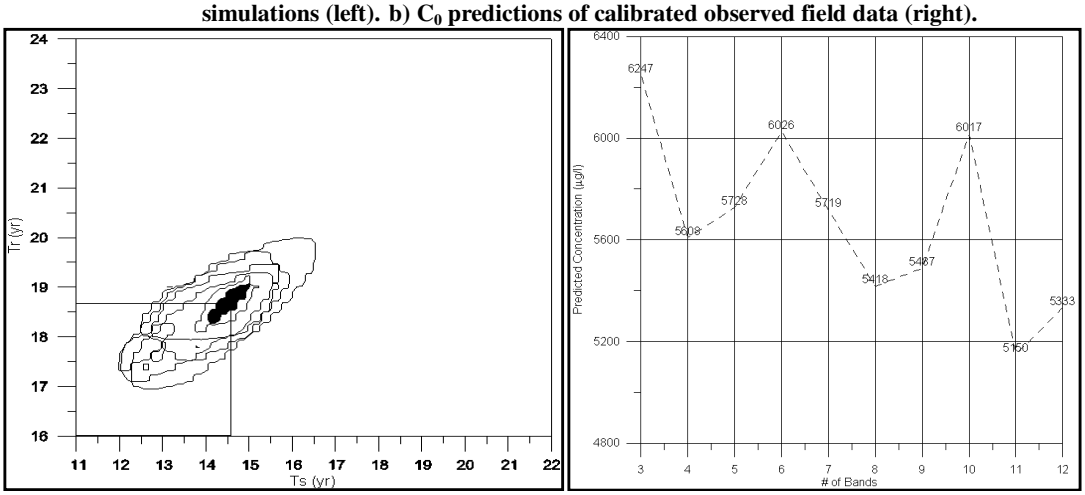

The literature review indicated that it is uncommon for a source history investigation to be applied to field data. For example, a table in Michalak and Kitanidis (2004) lists 14 of 19 inverse modeling applications as having been applied at hypothetical sites. The use of field data creates additional challenges due to the variability of the data compared to hypothetical cases. The sources of the variability may include an unsteady release function, the spatial variability of the aquifer hydrogeology, and concentration measurement error. It is assumed that both the direct push dataset and the well dataset include measurement error and release variability. Furthermore, it would seem reasonable to state that the direct push dataset addresses spatial variability while the well dataset addresses temporal variability. Yet there are inaccuracies associated with these assumptions. While it is convenient to assume that the direct push data represent the TCE concentrations at a single point in time, the data were collected over an approximately 2 year period. Likewise, it is convenient to assume that each time that the well was sampled over the 2 year period; it was pumped so that the resulting capture zone was equally developed to remove an element of spatial variability from the data. However, there were no data collected characterizing the actual extent of capture zone developed during any of the 11 well sampling events. Therefore, both concentration datasets include elements of all of the sources of variability but there is insufficient information available to systematically evaluate the comparability of the concentration datasets. The two concentration datasets are not atypical of those available to practitioners so model verifications have been performed with the explicit acknowledgement that the data may not be perfect in terms of theoretical comparability.

Conclusions

A constant band length likely best represents observed values because the band length is directly proportional to the normalized mass observed. When equal length bands were tested with actual observed values, the $RRMSE = 1.1$ contours became contiguous and consistently overlapped a critical point of interest and were used as an estimates of t_s and t_r. If the adjacent band width, L_j, significantly varies, the normalized mass observed will proportionally vary, which can mask the influence of the observed concentration, C_j, from the calibration parameter $RRMSE$. The synthetic data calibration shown in Figure 2 supports the model's accuracy in estimating the initial concentration, C_0, by ≤5% of the solution, 4000µg/l. Figure 3b shows greater variation of predicted C_0, but the percent variation of the solution suggests reasonable results because no solution varies more than ±10% of the average predicted initial concentration after exclusion of the simulation with three bands of analysis.
The model may appeal to modelers and designers who can rapidly modify the spreadsheets to evaluate concentration time series at various points as well as calculating the potential mass to be treated and the associated treatment costs. The apparent utility of the spreadsheet model should not overshadow the limitations of the underlying 1D model. The 1D model will have limited application based on site-specific hydrogeologic conditions where there is a low potential for multiple or complex contaminant sources. At many sites, the spreadsheet model may provide

preliminary results that may be useful in designing additional data collection efforts or provide the point of departure for more sophisticated multi-dimensional numerical models.

References

Ala, N.K. and Domenico, P.A. (1992). Inverse analytical techniques applied to coincident contaminant distributions at Otis Air Force Base, Massachusetts. *Ground Water*, 30(2), 212-218.

Alapati, S. and Kabala, Z.J. (2000). Recovering the release history of a groundwater contaminant using a non-linear least-squares method. *Hydrol. Process.*, 14, 1003-1016.

Ang, A. and Tang, W (1975). *Probability Concepts in Engineering Planning and Design*. V.1. John Wiley & Sons, Inc., Hoboken, New Jersey.

ASTM. 2002. Standard guide for comparing ground-water flow model simulations to site-specific information, ASTM D 5490-93 (Reapproved 2002).

Dawson, H.E. (1995). *Transport and fate of organic chemicals in soil and groundwater, spreadsheet models SOILCS, SOILSS, SOILUS, TRANS1D*. Colorado School of Mines Office of Special Programs and Continuing Education, Golden, Colorado.

Domenico, P.A. and Robins, G.A. (1985). A new method of contaminant plume analysis. *Ground Water*, 23(4), 476-485.

Elmore, A.C. (2007). Applying a one-dimensional mass transport model using groundwater concentration data. *J. of Environ. Eng.*, 133(4), 372-378.

Elmore, A.C. and DeAngelis, L. (2004). Modeling a groundwater circulation well alternative. *Ground Water Monitoring & Remediation*, 24(1), 66-73.

Elmore, A, C. and Vandeberg, M.A. (1997). Using uncertainty analysis to reduce costs at a pump-and-treat site. *Remediation*, 7(3), 5-21.

Fetter, C.W. (2001), *Applied hydrogeology*, 4th ed., Prentice-Hall, Inc., Upper Saddle River, New Jersey.

Freeze, R.A., and Cherry, J.A. (1979). *Groundwater*. Prentice-Hall, Inc., Upper Saddle River, New Jersey.

Hill, M.C. and Tiedeman, C.R. (2007). *Effective groundwater model calibration with analysis of data, sensitivities, predictions, and uncertainty*. John Wiley & Sons, Inc., Hoboken, New Jersey.

Mehran, M., Olsen, R.L. and Rector, B.M. (1987). Distribution coefficient of trichloroethylene in soil-water systems. *Ground Water*, 25(3), 275-282.

Michalak, A. M., and Kitanidis, P.K. (2004). Estimation of historical groundwater contaminant distribution using the adjoint state method applied to geostatistical inverse modeling. *Water Resources Res.*, 40(W08302).

Miller, G.R. and Elmore, A.C. (2005). Modeling of a groundwater circulation well removal action alternative. *Practice Periodical of Hazardous, Toxic, and Radioactive Waste Management*, 9(2), 122-129.

Piskin, R. (1971). Hydrogeology of the University of Nebraska Field Laboratory at Mead, Nebraska. Ph.D. diss., Department of Geosciences, University of Nebraska, Lincoln.

Skaggs, T.H. and Kabala, Z.J. (1994). Recovering the release history of a groundwater contaminant. *Water Resources Res.*, 30(1), 71-79.

Skaggs, T.H. and Kabala, Z.J. (1998). Recovering the release history of a groundwater contaminant. *Water Resources Res.*, 30(1), 71-79.

Sonnenborg, T.O., Engesgaard, P., and Rosbjerg, D. (1996). Contaminant transport at a waste residue deposit 1. Inverse flow and nonreactive transport modeling. *Water Resources Res.*, 32(4), 925-938.

Spitz, K. and Moreno, J. (1996). *A practical guide to groundwater and solute transport modeling*. John Wiley & Sons, Inc., New York.

Van Genuchten, M. Th. And Alves, W.J. (1982). *Analytical solutions of the one-dimensional convective-dispersive solute transport equation*. Technical Bulletin 161, U.S. Salinity Lab., Agricultural Res. Service, U.S. Dept. of Agriculture, Riverside, California.

Associations of PAHs with Size Fractionated Sediment Particles

Jejal Reddy Bathi[1], Robert Pitt[2] and Shirley E. Clark[3]

Geosyntec Consultants, Santa Barbara, CA – 93101; PH: (805) 897 – 3800; Email: jbathi@geosyntec.Com
[2]Civil, Construction and Environmental Engineering, The University of Alabama, Tuscaloosa, AL 35401; PH: (205) 348 – 0783; Email: rpitt@eng.ua.edu
[3]Penn State Harrisburg, School of Science, Engineering and Technology, Harrisburg Pike, PA – 17507; PH: (717) 948 – 6580; Email: seclark@psu.edu

ABSTRACT

Sediment samples were collected from three different locations and analyzed for selected parameters to study the effects of selected sediment characteristics and contributing source areas on sediment PAHs concentration,. For all cases, the particles in the size range of 180 to 355 µm were most dominant in the sediments. Sediment COD, percent of material weight loss on ignition (material composition analysis) and sediment PAH concentrations showed similar trends of smaller and larger particles associations with higher values than with the intermediate sizes. However, most of the mass of the PAHs were associated with the smaller and intermediate sized particles. Sediments affected by commercial area runoff were found to have higher concentration of PAHs than the sediments affected by non-commercial area runoff.

INTRODUCTION

PAHs are ubiquitous environnemental contaminants and are an example of persistent organic pollutants of environmental concern (Cheung et al. 2006). Prior to the 1800s, the bulk of PAH discharges to the environment were of natural origin, with limited contributions from anthropogenic sources (Metre et al. 2000). There was a shift in the sources of PAH contamination from uncombusted to combusted fossil fuels. The increase in PAH sediment concentrations was coincident with the increase in automobile use and power production, both major consumers of fossil fuels. The magnitude of PAH pollution in runoff depends on the type of contributing source area. Pitt et al. (1999) found the highest runoff PAH concentrations in sheetflow samples from vehicle servicing and parking areas among samples collected from different source areas, with higher concentrations associated with longer interevent periods between rains. Kuklick et al. (1997) observed extreme variability in PAH concentrations, ranging from 33 µg kg^{-1} dry weight in the Edisto River estuary to 9600 µg kg^{-1} dry weight in some areas of urbanized Charleston Harbor showing large effects of urbanization on sediment PAH contamination. The spatial distribution of

PAHs observed by McCready et al. (2000) indicated increased concentrations of PAHs nearer to areas where stormwater enters the Sydney Harbor, Australia.

PAHs in urban runoff can occur in both particulate and soluble forms, although studies have identified the particulate forms as being the most predominant (Hwang and Foster 2006; Pitt et al. 1999). Due to their extremely low solubility and hydrophobic nature, most PAHs are associated primarily with particulate matter. According to Hwang and Foster (2006), particulate-associated PAHs in urban runoff accounts for 68 to 97% of total PAHs in the runoff. The particulate-bound PAHs tended to settle and accumulate in receiving water sediments. Factors that affect the PAH associations with the particulate matter in the aquatic environment include the physical and chemical properties of the specific PAH contaminant, the physical and chemical properties of the aquatic medium, and the physical and chemical properties of the particulate matter. Zhou et al. (1998) observed no correlation between particulate bound PAH concentrations with salinity of samples, while suspended solids concentrations had negative correlations and particulate organic carbon concentrations had positive correlations with particulate bound PAH concentrations They also observed higher concentrations of PAHs with finer particles (generally classified as clay materials, which have large surface areas per unit weight) than with the coarser particles (generally classified as sand particles, which have comparatively less of the organic matter needed for greater PAH sorption). A similar pattern was observed by Aryal et al. (2005), who monitored suspended solids and solid-associated PAHs in Swiss highway runoff for four rain events (samples were only collected during the initial 3 mm of runoff). The concentrations of PAHs in fine fractions (<45μm) were higher than their concentrations in coarse fractions (>45μm). Contributing source areas may also effect the PAHs distribution pattern by solid particle sizes. For example, Guggenberger et al., (1996) noticed homogenous distributions of PAHs by particle sizes in rural soils whereas Muller et al., (2000) observed non-homogeneous distributions of PAHs in urban soils. Recent investigations have also found high PAH concentrations associated with large organic material trapped in stormwater floatable material controls (Rushton 2006), indicating material composition of sediments effects the PAH associations.

This paper describes the measured PAH concentrations on size fractionated sediment particles analyzed using Thermal Desorption analytical methods, PAH trends with respect to selected sediment parameters, and possible major source area effects on sediment PAH pollution. Selected parameters examined for analyzing the trends of PAHs on size fractionated particulate matter included material composition (such as paper debris, organic matter, rubber, or asphalt) and Chemical Oxygen Demand (COD). The sediments affected by residential runoff, commercial area runoff and runoff from residential area with a known history of separate sewer overflows (SSOs) were studied during this research.

MATERIALS AND METHODS

Study Area and Sampling Sediment samples were collected from three different creeks in and around Tuscaloosa and Northport, AL. One sampling area along each of the three creeks was chosen in such a way that the sediment analysis scheme for PAHs represented the sediments affected by different known urban conditions.

One of the sampling areas was along Cribbs Mill Creek, which is an urban creek in Tuscaloosa, AL. The sampling area along the creek was chosen at the downstream end of a few hundred foot long concrete-lined channel in a residential neighborhood. The sediment (bed load) on the concrete channel was therefore mainly affected by the runoff from the surrounding residential areas, with minimal bank erosion material. Another sampling area was along Hunter Creek, which is an urban creek originating in Tuscaloosa County and passes through Northport before joining the Black Warrior River. The sediment at the sampling location was mostly affected by runoff from heavy traffic along McFarland Blvd., commercial areas, and runoff from a trailer park residential area. Physical observations at the site indicated that an outfall from an automobile maintenance shop on the side of the creek directly affected the sediment at the sampling location. The third sampling area was along Carroll's Creek, which starts in Fayette County and joins Lake Tuscaloosa in Tuscaloosa County. The sediment at the sampling location was directly affected by runoff from a high-density residential area on one side of the creek and forested lands on the other side of the creek. The sediment at the sampling point has a history of contamination from sanitary sewage overflows from a separate sewer system (SSOs) in the adjacent residential area (Consent Order NO. 07-139-CWP from the Alabama Department of Environmental Management (ADEM) to the City of Northport, issued in July 2007, there were three SSO incidents during 2006).

All samples were collected in pre-cleaned and autoclaved glass sample bottles using a manual dipper sampler made from polypropylene. The collected sediment samples were dried in aluminum trays at 104°C to remove moisture and then were sieved using a set of stainless-steel sieves with openings of 45, 90, 180, 355, 710, 1400, and 2,800 μm and a mechanical shaker. In addition, large organic material (leaves and other debris) were manually separated from the largest particle fraction and analyzed separately.

Analyses for Material Composition and COD: The material composition of sediments was determined using "Thermal Chromatography" (an expansion of the volatile solids analyses) techniques (Ray 1997). A known amount of sediment sample was placed in a crucible that was heated to higher temperatures, progressively, at set intervals, from 104 to 550°C. After each heating interval, the crucible (with sample) was cooled and weighed in order to determine the percent mass burned off since the last temperature. A heating time of 1 hour at each temperature was maintained to ensure stable weights. Table 1 shows the corresponding temperatures where different material would be combusted. COD analysis of size fractionated sediments was conducted by reactor digestion HACH method 8000.

Analyses for PAHs Concentration: The thermal desorption (TD) sample preparation method uses elevated temperatures as a means to transfer the analytes from solid sample matrices to the gaseous analytical system. This unit was directly attached to the inlet of a gas chromatograph / mass spectrometry (GC/MS) for quantification of PAHs on the size fractionated sediment samples. This TD/GC/MS method was developed and tested for urban creek sediments for PAHs as part of the research activities. The instruments used during this procedure were an

AutoDesorb™ unit (Scientific Instrument Services, Inc. Ringoes, NJ, USA) coupled to a gas chromatograph (Agilent 6890) and a mass spectrograph (Agilent 5973N).

Table 1. Thermal Chromatography Method Parameters

Temperature (°C)	Material lost at these temperatures
Up to 104	Moisture
104 – 240	Paper debris
240 – 365	Leaves and grass
365 – 470	Rubber
470 – 550	Asphalt
Above 550	Remaining material are non-combustible

RESULTS AND DISCUSSION

Sediment Particle Size Distribution: Five samples from each of three creeks were collected and analyzed for particle size distributions (psd). Figure 1 shows the observed psd and box-whisker plots of the particle size ranges observed in the samples. For all cases, the particles in the size range of 180 to 355 µm were dominant. Overall, most of the particles were distributed in the size range of 90 to 710 µm.

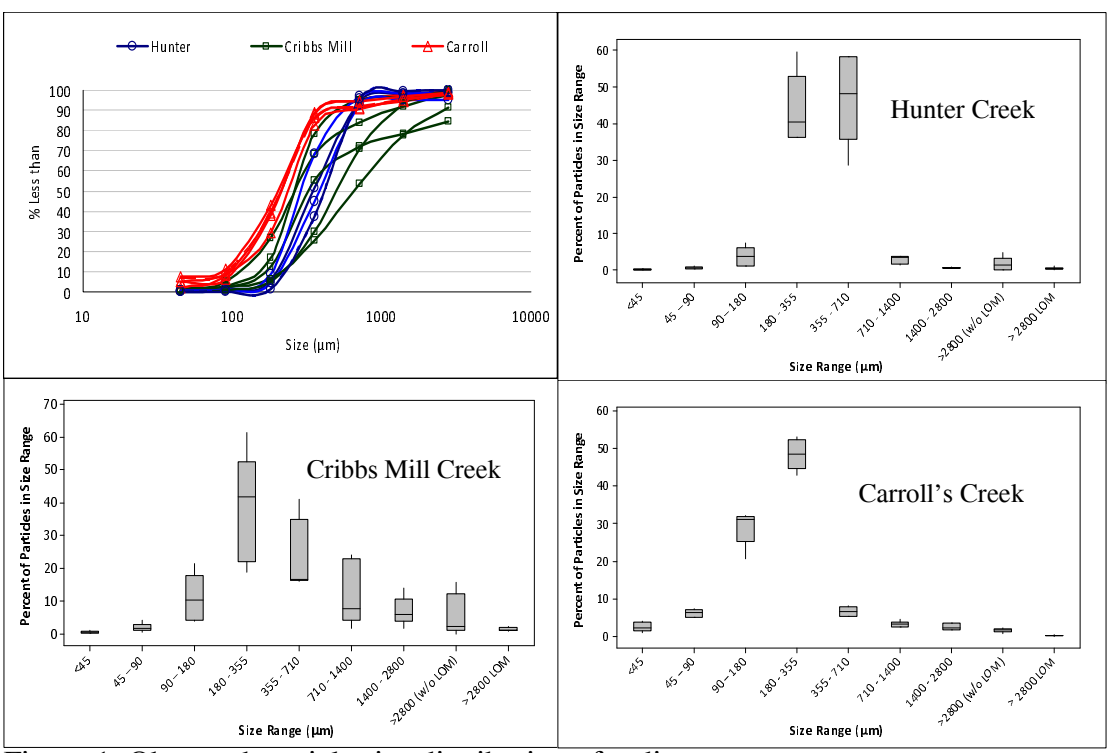

Figure 1. Observed particle size distribution of sediments

Sediment Material Composition and CODs: A composite sediment sample created from the five samples collected at each sampling location was prepared and analyzed for major material composition using thermal chromatography. Table 2 shows the

percentage weight losses observed. Material lost between 240 and 365°C indicates the amount of leaves and grass associated with each particle size that may preferentially sorb PAHs, while material lost between 365 and 550°C indicates rubber and asphalt material that likely have substantial PAH concentrations as part of the component material. Other than for the case of the largest size fraction (> 2800 µm) large organic material (LOM), all other fractions were mostly non-combustible (or non volatile). For the > 2800 µm LOM fraction, most of the material was found to be volatile, and mostly consisted of leaves, grass clippings, etc. The thermal chromatography analyses of sediments indicated that the smaller and larger sediment fractions were associated with a larger volatile content compared to intermediate-sized fractions (Figure 2). The high volatile contents of the large size sediments are caused by presence of relatively large portions of leaf and grass clippings in these sample components.

All sediment fractions of the individual samples were analyzed for COD, as shown in Figure 3. For the >2800µm (LOM only) fraction, the observed CODs for Hunter Creek, Cribbs Mill Creek and Carroll's Creek are 1.6 x 10^{9}, 1.5 x 10^{9} and 1.3 x10^{9} mg/kg respectively. Similar to the total volatile content of sediments, smaller (< 90µm) and larger (> 710µm) size fractions had higher COD concentrations when compared to the intermediate-sized particles. The median COD was found to be associated with particles of about 355µm in size. Log-transformed volatile solids concentrations and associated COD concentrations were strongly linearly related. The regression ANOVA p value was below 0.05 and the response factor (slope term) of the regression was also significant ($p < 0.05$) at 95% C.I.

PAH Content of Size Fractionated Sediment Fractions: Thirteen PAH compounds which were considered to be of most interest due to their potential harmful effects, and which were most abundantly found in earlier stormwater research (Pitt, et. al., 1999), were quantified, with the concentration results shown in Table 4. As shown during the ANOVA analyses, the variations in the PAH concentrations within each size fraction group were smaller than the variations in the concentrations between the size fraction groups. The analytical results showed that, generally, smaller sized and larger sized particles (especially LOMs) were associated with higher concentrations of selected PAHs compared to the medium sized particles (Table 4). This trend is similar to previously reported PAH data (Rushton, 2006). The bimodal distribution of the PAH concentrations was similar to the bimodal distributions observed for volatile content. Prior fugacity modeling by Bathi, et al (2007) showed that PAHs are strongly associated with the organic content of the particulates in aquatic systems. The leaf fractions are therefore found to have the highest concentrations of some of the PAHs because of their higher organic content. Higher concentration of PAHs in the smaller size fractions was also likely associated with their higher organic content

Table 2. Sediment Thermal Chromatography analytical results for material composition (Table 1 shows the likely materials lost for the different temperature ranges)

Size range (µm)	Percentage of weight loss over temperatures range (°C)											
	Cribbs Mill Creek				Hunter Creek				Carroll's Creek			
	105 – 240	240 – 365	365 – 470	470 – 550	105 – 240	240 – 365	365 - 470	470 – 550	105 - 240	240 – 365	365 - 470	470 - 550
<45	3.70	1.85	0.00	1.85	2.23	0.48	0.00	0.34	1.12	0.96	0.94	0.84
45 – 90	0.96	2.88	0.96	0.00	1.24	0.61	0.00	0.44	0.55	0.85	0.48	0.66
90 – 180	0.21	0.85	0.64	0.00	0.37	0.29	0.00	0.15	0.36	0.34	0.41	0.26
180 - 355	0.24	0.85	0.48	0.00	0.40	0.02	0.18	1.56	0.35	0.48	0.32	0.35
355 - 710	0.48	1.69	1.21	0.00	0.24	0.13	0.00	0.26	0.52	0.59	0.51	0.23
710 - 1400	2.57	5.15	3.31	0.00	1.80	2.01	0.71	0.96	1.36	3.47	2.72	1.13
1400 – 2800	3.76	8.65	0.00	6.02	2.65	5.98	2.29	0.71	1.03	4.55	2.50	1.24
>2800 (w/o LOM)	0.84	15.73	0.00	2.81	1.54	2.76	0.65	1.10	0.82	1.04	7.00	0.65
>2800 LOM only	NA*	NA	NA	NA	8.63	42.49	28.33	1.33	20.42	33.46	3.88	0.89

* Not available

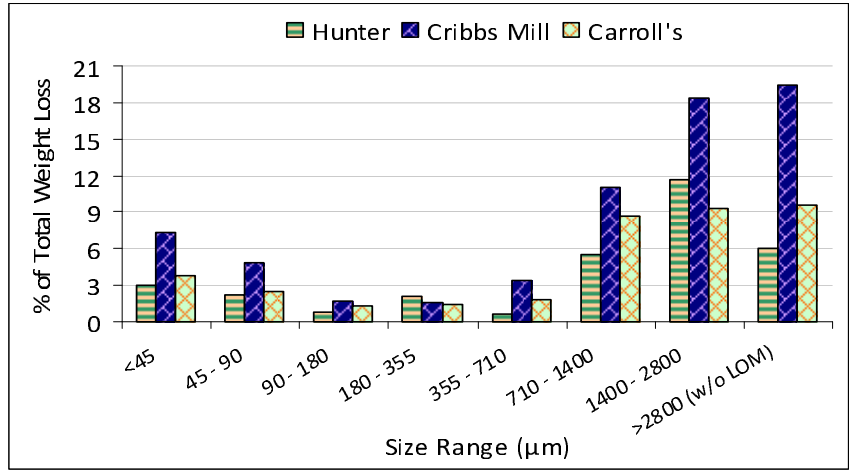

Figure 2. Cumulative weight loss of sediments in Thermal Chromatography over temperature range of 104 – 550 °C

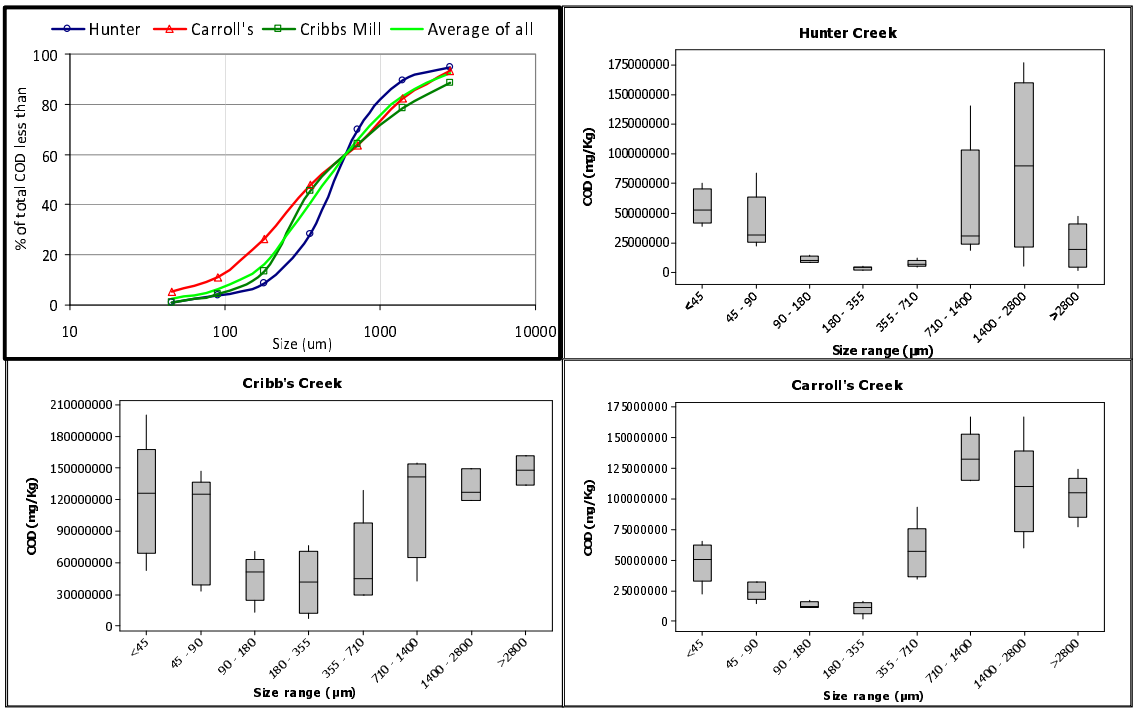

Figure 3. Observed COD of urban creek sediments

and large surface areas of these small particles. Earlier studies by Boehm and Farrington (1984) also found a direct positive relationship between PAH content and the silt/clay fraction of sediments. One-way ANOVA analysis showed significant difference in the analyte concentrations for the different particle sizes ($p < 0.05$). Cluster analyses of the PAH data by particle sizes indicated that for most of the analytes, the >2800µm LOM fraction was a separate group compared to all the other sizes combined (Analyses results are not shown in this paper). Although the smaller (< 90 µm) and larger (> 710 µm) size fractions of the creek sediments were found to contain the highest levels of PAHs, these fractions only represented <1% of the total sediment mass. Therefore, the greatest mass load of the the PAHs was associated with the intermediate sized sediment fractions.

Linear regressions of COD to PAH concentrations on each particle size for each creek showed a significant response factor (slope term) for slightly more than half of the cases tested. When the large-sized LOM samples alone were considered, about 90% of the conditions had significant slope terms, indicating strong linear relations between COD and PAH concentrations. Two-way ANOVA analyses of the PAH concentrations were conducted to investigate the particle size and location as variables. These tests indicated that, except for naphthalene, fluorene, phenanthrene, and indeno(1,2,3-cd)pyrene, all the other PAH analytes were affected by the sediment locations. One-way ANOVA analyses of the concentrations for different particle size ranges comparing the locations showed that for most of the analytes, there were a larger number of significant differences between the creek locations for the smaller particle sizes (<45 and 45 – 90 µm) than for the other sizes (Analyses results are not showed in this paper). Using probability plots and other graphical analyses, Hunter Creek was found to have significantly higher concentrations than the other creeks, especially for the small particle sizes. Hunter Creek sediment had a history of

contamination of hydrocarbons from creek-side businesses that caused the increased PAH concentrations. Cribbs Mill Creek generally had higher PAH concentrations than the sewage-contaminated Carroll's Creek sediments. This might be due to the long lapse in time since the Carroll's Creek sediments were affected by the SSOs (more than a year). The contaminated sediment at Carroll's Creek was either flushed from the contamination site or buried below the surface sampling depth. The Cribbs Mill Creek sampling location was in a long concrete channel with no bank erosion material affecting the sediment concentrations. The concrete lining also had obvious algae growths that may have preferentially sorbed PAHs.

Table 2. Two-Way ANOVA P Values for Analyte Concentrations

PAH	P Value		
	Size	Location	Size*Location
Naphthalene	0.000	0.088	0.116
Fluorene	0.000	0.721	0.481
Phenanthrene	0.000	0.389	0.043
Anthracene	0.000	0.032	0.821
Fluranthene	0.000	0.000	0.000
Pyrene	0.000	0.000	0.000
Benzo(a)anthracene	0.000	0.005	0.002
Chrysene	0.000	0.004	0.000
Benzo(b)flouranthrene	0.000	0.002	0.254
Benzo(a)pyrene	0.004	0.032	0.022
Indeno(1,2,3-cd)pyrene	0.000	0.284	0.250
Dibenz(a,h)anthracene	0.000	0.019	0.002
Benzo(ghi)perylene	0.000	0.041	0.493

Conclusions

Selected characteristics were analyzed for fifteen sediment samples from urban creeks. Sediments were found to be mostly composed of particles in the size range of 90 – 710 μm. The volatile content, COD and PAH content of the sediment particle size fractions had a bimodal distribution, with smaller and larger particles containing relatively higher values then the intermediate particles. The highest concentrations were associated with the LOM fractions. The volatile content and COD of the size fractionated sediments showed strong first order polynomial relationships. The presence of fragmentary plant material in the larger size fractions and the high clay/silt content in the smaller size fractions caused higher PAH concentrations. Positive linear relationships was also seen between PAH and COD content, but was most obvious in the sediment fractions with higher volatile (or COD) content. Sediment samples affected by commercial area runoff were found to have higher PAHs concentration than the samples affected by runoff from non-commercial areas.

Disclaimer: *This material is based upon work supported by the National Science Foundation under Grant No. EPS-0447675. Any opinions, findings, and conclusions or recommendations expressed in this material are those of the author(s) and do not necessarily reflect the views of the National Science Foundation.*

Table 4. Observed PAH content in size fractionated urban stream sediments

PAH	Mean concentration (µg/kg) (standard deviation) for all 15 samples combined								
	< 45 µm	45 – 90 µm	90 – 180 µm	180 – 355 µm	355 – 710 µm	710 - 1400 µm	1400 - 2800 µm	> 2800 µm (w/o LOM)	> 2800 µm LOM
Naphthalene	255 (275)	177(156)	163 (224)	94 (87)	124 (131)	790 (2046)	891(2014)	124 (74)	2637 (2107)
Fluorene	257 (295)	189 (134)	225 (187)	125 (135)	139 (140)	196 (144)	293 (173)	216 (161)	1771 (945)
Phenanthrene	264 (278)	205 (211)	140 (158)	92 (92)	110 (85)	130 (136)	197 (230)	188 (164)	2007 (1422)
Anthracene	354 (397)	288 (273)	261 (253)	152 (150)	182 (182)	366 (314)	491(614)	218 (152)	2255 (1089)
Fluoranthene	650 (868)	624 (753)	345 (372)	202 (242)	247 (336)	259 (237)	237 (197)	191(173)	1520 (902)
Pyrene	653 (738)	519 (548)	412 (577)	175 (174)	240 (405)	207 (153)	192 (122)	172 (129)	2054 (954)
Benzo(a) anthracene	501 (595)	408 (537)	258 (286)	169 (171)	224 (229)	167 (134)	271 (252)	278 (371)	2164 (1045)
Chrysene	591 (618)	602 (689)	363 (363)	202 (199)	273 (268)	190 (125)	296 (242)	171 (130)	1810 (852)
Benzo(b) fluoranthrene	597 (522)	517 (598)	358 (389)	402 (671)	227 (150)	316 (262)	375 (369)	329 (375)	2179 (1425)
Benzo(a)pyrene	1474 (2210)	1524 (3079)	662 (459)	434 (513)	351 (210)	502 (533)	1119 (2086)	392 (255)	2330 (1866)
Indeno(1,2,3-cd) pyrene	787 (544)	657 (538)	942 (794)	258 (187)	332 (189)	576 (774)	706 (917)	357 (424)	1774 (933)
Dibenz(a,h) anthracene	1267 (1864)	787 (1022)	675 (545)	276 (234)	355 (226)	687 (511)	835 (1254)	286 (191)	1492 (775)
Benzo(g,h,i) perylene	706 (686)	465 (451)	591 (691)	199 (226)	174 (116)	551 (567)	396 (299)	348 (229)	2236 (1728)

References:

Aryal, R. K., Furumai, H., Nakajima, F., and Boller, F. (2005). Dynamic behavior of fractional suspended solids and particle bond polycyclic hydrocarbons in highway runoff. *Water Research* 39: 5126-5134.

Bathi, J. R., Pitt. R. (2007) "Fates of Polycyclic Aromatic Hydrocarbons (PAHs) Affect Treatability." World Environmental & Water Resources Congress 2007. ASCE - EWRI. Tampa, FL.

Boehm, P. D., and Farrington, J. W. (1984). Aspects of the polycyclic aromatic hydrocarbon geochemistry of the recent sediments in the Georges Bank region. *Environmental Science and Technology* 18: 840-845.

Cheung, K. C., Leung, H. M., K. Y. Kong, H. M., and Wong, M. H. (2006). Residual levels of DDTs and PAHs in freshwater and marine fish from Hong Kong markets and their health risk assessment. *Chemosphere* 66: 460-468.

Guggenberger, G., Pichler, M., Hartmann, R., and Zech, W. (1996). Polycyclic aromatic hydrocarbons in different forest soils: Mineral horizons. Z. Pflanzenernähr. Bodenk. 159:565–573.

Hwang, H. M., and Foster, G. D. (2006). Characterization of polycyclic aromatic hydrocarbons in urban stormwater runoff flowing into the tidal Anacostia River. *Environmental Pollution* 140: 416-426.

Kuklick. J. R., Siverten, S. K., Sander, M., and Scott. M.I. (1997). Factors influencing polycyclic aromatic hydrocarbon distribution in South Carolina estuarine sediments. *Journal of Experimental Marine Biology and Ecology* 213: 13-29.

McCready, S., Slee, D. J., Birch, G. F., and Taylor, S. E. (2000). The distribution of polycyclic aromatic hydrocarbons in surficial sediments of Sydney Harbour, Australia. *Marine Pollution Bulletin* 40(11): 999-1006.

Metre, V. P. C., Mahler, B. J., and E. T. Furlong. 2000. Urban sprawl leaves its PAH signature. *Environmental Science & Technology* 34(1): 4064-4070.

Müller, S., W. Wilcke, N. Kanchanakool, and W. Zech. (2000). Polycyclic aromatic hydrocarbons (PAHs) and polychlorinated biphenyls (PCBs) in particle-size separate of urban soils in Bangkok, Thailand. Soil Sci. 165:412–419.

Pitt, R., R. Field, M. Lalor, and M. Brown. "Urban Stormwater Toxic Pollutants: Assessment, Sources and Treatability." *Water Environment Research*. Vol. 67, No. 3, pp. 260-275. May/June 1995.

Ray, H. (1997). Street Dirt as a Phosphorus Source in Urban Stormwater. Department of Civil and Environmental Engineering, MSCE, University of Alabama at Birmingham, USA.

Rushton, B. (2006). Broadway outfall stormwater retrofit project, monitoring CDS unit and constructed pond. South Florida Water Management District and City of Temple Terrace, W241. Brooksville, FL.

Zhou, J. L., Fileman, T. W, Evans, S., Donkin,P., Llewllyn, C., W. Readman, J., Mantoura, R.F., and Rowland, S. J. (1998). Fluoranthene and pyrene in the suspended particulate matter and surface sediments of the Humber Estuary, UK. *Marine Pollution Bulltein* 36(8): 587-597.

Sorption and Desorption of Testosterone in Agricultural Soils

Rui Ma[1] and Tian C. Zhang[2]

1. Master student of Department of Civil Engineering, University of Nebraska – Lincoln, Omaha, NE 68106 Phone: 402-554-3565. E-mail: rma@unomaha.edu
2. Professor of Civil Engineering, University of Nebraska – Lincoln, Omaha, NE 68106. Phone: 402-554-3784. Fax: 402-554-3288, E-mail: tzhang1@unl.edu

ABSTRACT

Several studies regarding sorption and dissipation of testosterone in soils have been conducted recently; these studies concluded that the transport of testosterone is limited in the soil/water system. However, this may not explain wide occurrences of testosterone in ground and surface water. In this study, soils from two agricultural fields located in Nebraska, with 3 depths in each location, were utilized to study sorption and desorption of testosterone. The sorption results of batch tests indicated that the Freundlich sorption capacity of the soils ranged from 8.53–38.82 $\mu g^{1-n} mL^n g^{-1}$. The results of desorption experiments indicated that after 3 washes by hormone free distilled water, about 35.14– 102.35 % of the testosterone adsorbed onto the soil in the adsorption tests were desorbed from the soil. Correlations between sorption and soil properties such as cation exchange capacity, surface area, and soil organic matter were investigated. Also, the behavior of sorption and desorption of soils at different depths was compared.

INTRODUCTION

Testosterone is a representative androgenic hormone that can occur artificially or naturally. At a very low concentration level, its wide existence and adverse effects on human and animals have drawn more recent attentions. Agricultural application of manure is an important source of testosterone and other steroid hormones. Hence it is important to understand fate and transport of testosterone in the soil/water system because the presence of testosterone in the environment may pose great impacts on surface and ground water quality.

Recently, several studies have been conducted on sorption, degradation and transport of testosterone in soils. Sorption of testosterone in the soil is believed to be strong. Lee et al. (2003) reported testosterone sorption in sediment and four soils. Sorption of testosterone was believed to reach equilibrium in 24–31 hours. The nonlinear Freundlich sorption coefficient (K_f) in Drummer soil is 59.1 μg^{1-n} mL^n g^{-1} while in other solids sorption was liner with K_d ranging from 4.57 to 27.3 L/kg. Casey et al. (2004) reported maximum K_d values occurred within 5 hours and ranged from 0.5 to 1200 L/kg. Sangsupan et al. (2006) reported that average testosterone K_f values were 26.7 μg^{1-n} mL^n g^{-1} for the 0–10 cm soil depth and 14.0 μg^{1-n} mL^n g^{-1} for the 20–30 cm soil depth. Kim et al. (2007) studied testosterone sorption independent of its

metabolites androstenedione; the K_f values ranged from 228.56 to 3890.45 (μg/kg) $(\mu g/L)^n$. Dissipation of testosterone is rapid according to previous studies. The reported half lives of testosterone are between 8.5 to 21 hours under anaerobic conditions (Lorenzen et al., 2005). These studies have indicated testosterone has a high affinity to the soil and is rapidly degraded to other less potent metabolites. Therefore, researchers have concluded that transport of testosterone is limited in the soil/water system. However, it is difficult to use this conclusion to explain the frequent detections of testosterone in ground and surface water. For example, testosterone has been detected in sediments below a dairy-farm wastewater lagoon to the depth of 45 m reported by Shai A et al. 2008. This observation may be explained by different characteristics in different soils, reversibility of sorption, or other unknown mechanisms that may be related to fate and transport of testosterone.

To fully understand the fate and transport of testosterone in subsurface soils, it is imperative to conduct adsorption and desorption tests with soils at different depths and different properties. The objectives of this study were to conduct: (1) batch sorption tests of testosterone using two agricultural soils, each with 3 different depths and testosterone transformation being inhibited; and (2) desorption tests of testosterone from the same soils after the sorption equilibrium being achieved. This paper presents the results of adsorption isotherms and desorption characteristics that are related to soil properties and soil depth.

MATERIALS AND METHODS

Chemicals and reagents. Testosterone at the highest possible purity (> 98%), methanol and sodium azide were obtained from Sigma-Aldrich (St. Louis, MO). ^{14}C-labeled testosterone was obtained from American Radiolabeled Chemicals (St. Louis, MO). Unlabeled testosterone stock solutions (100 mg/L) was prepared with HPLC grade methanol and was stored in a –20 °C freezer before use; ^{14}C-labeled testosterone series of stock solutions with different activities levels were prepared in solutions of methanol and ultra pure water and were stored in a –4 °C refrigerator.

Soil samples. Soils of 3 depths (0–15.24, 15.24–30.48 and 30.48–60.96 cm) were taken using a steel soil sampling kit (7.6-cm i.d., 80-cm length) driven by a hydro driven probe from an agricultural field in North Platte, NE (NP soil) and Haskell Agricultural Lab in Concord, NE (HAL soil). For each type of the soils, 10 replicates (parallel sub-samples) were taken from locations > 50 cm apart from each other. Once soils arrived at the lab, they were air dried at room temperature and gently passed through a 2-mm sieve. Each soil used in this study was a composite of the ten replicates. Soil properties, such as soil organic matter, cation exchange capacity (CEC), humic matter, metals and soil texture were tested in the Midwest Laboratories (Omaha, NE). The surface area of each soil was tested in the Department of Civil and Environmental Engineering at the University of Virginia.

Sorption and desorption tests. Sorption isotherms were tested in a 10 mL glass centrifuge tube batch reactor (15-415, Kimble, USA). Each batch reactor was loaded with 1 g of the dry soil and 10 mL of ultra pure water containing 0.01 M

$CaCl_2$ and 200 mg/L NaN_3 and then spiked with a combination of unlabeled and ^{14}C-labeled testosterone to form a desired initial testosterone concentration. The glass centrifuge tube batch reactors were sealed with Teflon-lined caps and rotated top to bottom (360°/5 s) for certain time intervals. At the end of the time interval, triplicate reactors were removed and centrifuged. For each reactor an aliquot of 500 μL was taken to test for radioactivity by scintillation counting using a 2500 TR Liquid Scintillation Counter (Packard, Downers Grove, IL). The difference between the initial and final radioactivity in the liquid phase was attributed to sorption of the hormone. Then total testosterone sorbed was calculated by extrapolating the sorption of the labeled testosterone.

Sorption isotherms were tested under 24°C. Six initial testosterone concentrations from 0.003–2 μg/mL were obtained by spiking with both labeled and non labeled testosterone. These concentrations were chosen because they spanned 4 orders of magnitude and represented concentrations of testosterone in manure used for land application. The reactors (triplicates) were then agitated by rotation for 18 hours and then centrifuged at 2000 g for 40 minutes to separate the soil and water. Testosterone adsorbed on the soil was calculated based on mass balance. The Freundlich (eq. 1) and/or Langmuir model were used to fit sorption data:

$$S = K_f C^n \quad (1)$$

where S is the concentration of the hormone adsorbed on the soil (mg g^{-1}); C is the hormone aqueous concentration (mg L^{-1}); n is a measure of sorption isotherm linearity (unitless); and K_f is the Freundlich sorption coefficient (μg^{1-n} mL^n g^{-1}).

After each sorption isotherm test, the liquid phase in the centrifuge tube was poured out from the tube, and then 10 mL hormone free water with 0.01 M $CaCl_2$ and 200 mg/L NaN_3 was introduced into the tube. The tubes were capped and rotated under the same condition as in the sorption isotherm test for 24 hours. After centrifugation, an aliquot of 500 μL was taken to test for radioactivity, and the desorbed testosterone was calculated on the basis of mass balance. The liquid phase in the centrifuge tube was poured out from the tube, and the centrifuge tube was used for the second and then the third desorption test (thus, total 3 cycles were conducted after each adsorption test).

Statistic analysis. Data were tested for significant difference against each other using a Student's T-test for two sample means with unequal variances. For soils sampled at different depths, data were analyzed for significance using a Type 3 Test of Fixed Effects, which is an analysis of variance (F-test) assuming normal populations with different means. Two-tail P values less than 0.05 were considered significant. The statistical test is nominally only testing whether the samples were less than the controls, using a two-tailed test (instead of a one tailed) would effectively double the strength of the test (William P et al., 1992). All statistic analysis is done by EXCEL.

RESULTS AND DISCUSSION

Soil properties. As shown in Table 1, the organic matter content of both the soils decreases with an increase in soil depth. While NP soils contain more sand (30–35%), HAL soils have more clay (20–25%). According to the USDA soil triangle figure, the HAL and NP soils belong to sand silt loam. The CEC ranges from 12.3 to 17.5 meq/100g. Soil metals such as Fe, Cu, Ca and Mg were tested; generally the HAL soil has higher metal content than the NP soil.

Table 1. Selected Soil Properties, Freundlich Parameter K_f and Desorption Percentage (%) as a Function of Soil Depth and Locations.

Properties/ parameters	Depths of HAL Soil (cm)			Depths of NP Soil (cm)		
	0–15.2	15–30.5	30.5–61.0	0–15.2	15–30.5	30.5–61.0
OM[a] (%)	2.2	2	1.3	1.8	1.3	0.7
Clay[b] (%)	20	20	25	12	10	10
Silt (%)	62	65	62	55	60	55
Sand (%)	18	15	13	33	30	35
Total Fe[c]	21	18	11	9	6	4
Total Cu[c]	4.7	4.7	4.5	3.6	3.4	0.9
Total Ca[c]	2131	2733	2826	1856	2115	2290
Total Mg[c]	318	339	358	247	227	221
S_a (m^2/g)[d]	12.61	13.52	17.40	13.37	14.12	13.22
TPV[e] (mL/g)	0.0135	0.0145	0.0183	0.0134	0.0143	0.0133
CEC[f]	13.9	16.9	17.5	12.3	13.2	15.8
K_f[g]	38.82	33.67	32.22	16.47	11.89	9.98
ADP[h] (%)	35.14	39.21	44.34	99.98	90.98	102.35

[a]OM: organic matter. [b]CEC: cation exchange capacity. [c]units = mg/kg. [d]S_a = surface area. [e]TPV = total pore volume. [f]units = meq/100g. [g]units = μg^{1-n} mL^n g^{-1}. [h]ADP = accumulated desorption percentage after three cycles of desorption tests.

Correlations between soil properties and sorption and desorption. The Freundlich sorption coefficient K_f ranges from 8.5293 to 38.8192 μg^{1-n} mL^n g^{-1}. This range is consistent with Lee's results using similar silt loam soil (Drummer soil). Sorption decreases with an increase in soil depth for both the HAL and NP soils. As shown in Table 2, selected soil properties have been correlated with sorption (K_f) and desorption (%). The strength of correlation (R^2) was used to characterize impacts of different properties. Since testosterone has no charge in water during normal pH ranges, the CEC is believed not to relate with sorption. This is verified by $R^2 = 0.1649$ when CEC and K_f are correlated with liner regression with interceptions. However,

the clay, sand, OM (organic matter) content and soil metals are believed to relate with sorption. In a descending order of strength, sorption (K_f) is related to total Fe (R^2 = 0.8647), Mg (R^2 = 0.8592), sand (R^2 = 0.8472, inverse correlation), clay (R^2 = 0.8222), total Cu (R^2 = 0.6765), and organic matter (R^2 = 0.5214). Therefore, these parameters are of utmost importance in determining sorption of testosterone in the soils used in this study. This is consistent with previous studies.

Table 2. Correlation Strength R^2 between Sorption Parameters K_f, Desorption Percentage (%) and Selected Soil Properties.

Soil Properties	Correlation Strength, R^2	
	With K^f (μg^{1-n} mL^n g^{-1})	With Desorption (%)
OM (%)	0.5214	0.384 (inverse)
Clay (%)	0.8222	0.8325 (inverse)
Silt (%)	0.6313	0.8032 (inverse)
Sand (%)	0.8472 (inverse)	0.9341
Surface area (m^2/g)	0.0244	0.0548 (inverse)
Total pore volume (mL/g)	0.1369	0.203 (inverse)
CEC (meq/100g)	0.1649	0.2735 (inverse)
Total Fe (mg/kg)	0.8647	0.7725 (inverse)
Total Cu (mg/kg)	0.6765	0.6348 (inverse)
Total Ca (mg/kg)	0.2457	0.3909 (inverse)
Total Mg (mg/kg)	0.8592	0.8762 (inverse)

Sand is a weak sorptive content for steroid hormone. Partitioning into organic carbon domains of the soil may be the major sorption mechanism as concluded by Casey et al. (2004). The clay content correlates with sorption, presumably due to the testosterone partition onto clay mineral surfaces through hydrophobic interaction with siloxane (–Si–O–Si–) bonds as reported by Van Emmerik et al. (2003). This can also explain why multivalent cations (Mg, Fe) have strong correlation with sorption. Because these cations normally associate with certain clay (Brannon et al. 1997) which may interact with testosterone.

In a descending order of strength, desorption (%) is related to sand content (R^2 = 0.9341), total Mg (R^2 = 0.8762), clay content (R^2 = 0.8325), total Fe (R^2 = 0.7725). Desorption mainly relates with sand content. Sand is a weak sorptive content, the greater the sand content is the larger percentage of sorbed testosterone might come off the soil. Table 2 also shows the inverse relationship between the clay content and organic matter. The interaction between testosterone and soil metals in the sorption step prevents further testosterone desorption, which explains soil metals generally have strong correlation with desorption inversely.

Effects of soil depth on sorption and desorption. As shown in Figure 1, sorption of testosterone decreased with increased depth. The top 15.24-cm soil has the greatest sorption capacity. For the HAL soil, p = 0.0122 for comparison between 0–15.24 cm and 15.24–30.48 cm; p = 0.0187 for between 0–15.24 cm and 30.48–60.96 cm; and p = 0.416 between 15.24–30.48 cm and 30.48–60.96 cm soil. For the NP soil, p = 0.0185 for comparison between 0–15.24 cm and 15.24–30.48 cm; p = 0.00249 for between 0–15.24 cm and 30.48–60.96 cm; and p = 0.105 between 15.24–30.48 cm and 30.48–60.96 cm. All depths are significantly different from each other ($p < 0.05$) regarding sorption. More importantly, topsoils are different from subsurface soils.

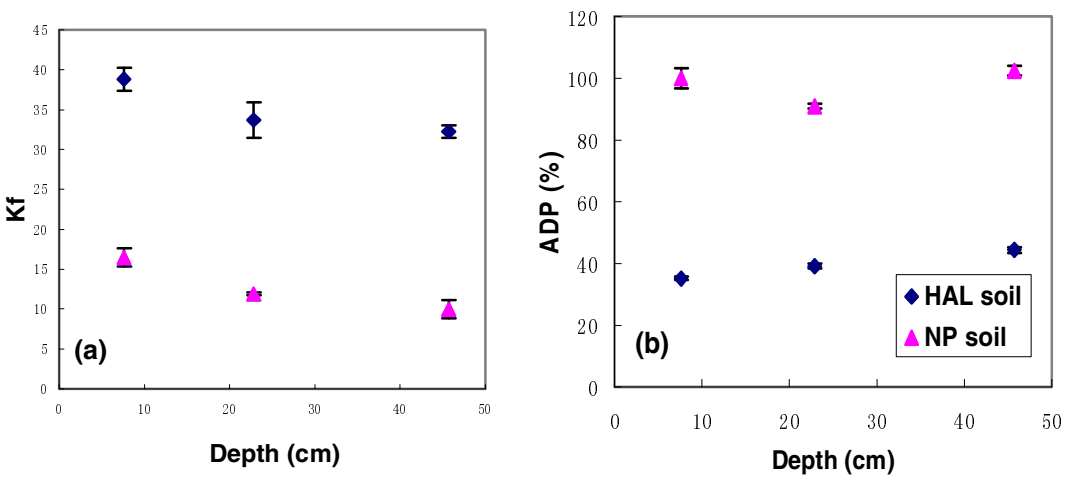

Figure 1. (a) Freundlich sorption parameters K_f of different depths (7.62, 22.86, 45.72 cm) for HAL and NP soils at 24 °C; and (b) accumulated desorption percentage (%) of different depth for HAL and NP soils at 24 °C. Error bars stand for standard deviations (n = 3). ADP stands for accumulated desorption percentage after three cycles of desorption tests.

Desorption percentages significantly increased with the soil depth ($p < 0.05$). For HAL soil, p is 0.0212 for comparison between 0–15.24 cm and 15.24–30.48 cm; p is 0.0087 for between 0–15.24 cm and 30.48–60.96 cm; and p is 0.316 between 15.24–30.48 cm and 30.48–60.96 cm. For NP soil, p is 0.0124 for between 0–15.24 cm and 30.48–60.96 cm; p is 0.127 between 15.24–30.48 cm and 30.48–60.96 cm; and p is 0.221 between 15.24–30.48 cm and 30.48–60.96 cm. This may be because the OM content decreases with increasing depth. A greater OM content is believed to cause stronger binding of testosterone, which leads to less desorption as reported by Hildebrand et al (2006). One exception is between the NP 0–7.62 and 15.24–30.48 cm soil. While the NP 0–15.24 cm soil has a greater OM content than the NP 15.24–

30.48 cm soil, the NP 15.24–30.48 cm soil has a less sand content. Comparison of NP 0–15.24 cm and NP 15.24–30.48 cm desorption data indicates no significant differences (p = 0. 134).

SUMMARY

The sorption of testosterone in this study is comparable with previous studies. However, the desorption experiments that followed adsorption tests indicates a greater potential for sorbed testosterone to come from soils. Also, the organic matter, clay content, sand content and soil metals are important in determining sorption while desorption is mostly related with the sand content, clay content and soil metals. Soil depth posed a remarkable impact on sorption and desorption. Generally, sorption decreases while desorption increases with an increase in soil depth. The findings of this study suggest that it is important to consider soil properties and soil depth when we evaluate fate and transport of testosterone in soil/water systems.

REFERENCES

Brannon, J. M., Myers, T.E. (1997). *Review of Fate and Transport Processes of Explosives*. Technical Report IRRP-97-2, U.S. Army Engineer Waterways Experimental Station. Vicksburg, MS, 1997.

Casey, F.X.M., Hakk, H., Simunek, J., and Larsen, G.L. (2004). "Fate and transport of testosterone in agricultural soils." *Environ. Sci. Technol.*, 38, 790–798.

Hildebrand, C., Londry, K.L., and Farenhorst, A. (2006). "Sorption and desorption of three endocrine disrupters in soils." *J. Environ. Sci. Health, Part B.*, 41, 907–921, 2006.

Kim, I., Yu, Z.Q., Xia, B.H., and Huang, W.L. (2007). "Sorption of male hormones by soils and sediments." *Environ. Toxicol. Chem.*, 26, 264–271.

Lee, L.S., Strock, T.J., Sarmah, A.K., and Rao, P.S.C. (2003). "Sorption and dissipation of testosterone, estrogens, and their primary transformation products in soils and sediment." *Environ. Sci. Technol.,* 37, 4098–4105.

Lorenzen, A., Chapman, R., Hendel, J.G., and Topp, E. (2005). "Persistence and Pathways of Testosterone Dissipation in Agricultural Soil" *J. Environ. Qual.*, 34, 854–860.

Sangsupan, H.A., Radcliffe, D.E., Hartel, P.G., Jenkins, M.B., Vencill, W.K., and Cabrera, M.L. (2006). "Sorption and transport of 17β-estradiol and testosterone in undisturbed soil columns." *J. Environ. Qual.*, 35, 2261–2272.

Shai, A., Ofer, D., Sara, E., Keren C., Irena P., Amit G., Zeev R., Shahar B., Laurence S S. (2008). "Transport of testosterone and estrogen from dairy farm waste lagoons to groundwater." *Environ. Sci. Technol.*, 42, 5521–5526.

Van Emmerik, T., Angove, M.J., Johnson, B.B., Wells, J.D., and Fernandes, M.B. (2003). "Sorption of 17β-estradiol onto selected soil minerals." *J. Colloid Interface Sci.,* 266, 33–39.

William, H P., Brian, P F., Saul, A T., and William T V. (1992). *Numerical Recipes in C: The Art of Scientific Computing*. Cambridge University Press.

A Study on Spatial Distribution of Water Quality And The Behavior of Do Concentration in Tidal Area of Urban Rivers

M. Okabe[1], M. Kawamura[1], T. Kato[2], T. Yamada[2]
[1] *Graduate School of Science and Engineering, Chuo University, Japan;*
[2] *Dept. of Civil Engineering, Chuo University, Japan*
masato_okabe@civil.chuo-u.ac.jp

The aims of these observations are to clarify the urban river water quality in tidal area. This paper explains the spatial distribution of water quality in the tidal area during normal water discharge and the time series of the dissolved oxygen content before and after the flood. This is the basic research to improve water quality.

From the results of the observation, following results are obtained; 1) BOD concentration meets the environmental criteria in Japan. 2) T-N and T-P concentrations rise at the observation points below the discharge points from the water reclamation centers. 3) In the observation during rainfall, the dissolved oxygen saturation decreases from 20% to below 5% at observation point in two hours, and the value recovered after 6 days to recover up. Moreover other observation, dissolved oxygen rises to around 100% in all layers.

Key Words: *Spatial distribution of water quality, Urban river, Tidal area Dissolved oxygen, Field observation,*

1. Introduction

Urban developing around the river has been performed conventionally as not only water resources but also the place of recreation and relaxation for people and space of healing in the world. However in Japan, river development which has very high safety-level for flood disaster has been carried out to secure measures of the flood and storm surge disaster in the high economic growth period As a result, there is great achievement for river improvement but people lost chance to play and luxuriate in the urban river. In recent years, the time comes when we discuss the city and basin that coexist with nature in various plans related to the formation of the country in Japan. Under such situation, it is recognized as a very important problem to improve the water quality and environment in the urban river.

The authors have conventionally conducted many field observation and theoretical development, numerical analysis to ascertain to clarify the state of water quality. For example, the authors[1),2),3)] clarify formation process of the water quality hydrograph that describes water quality change for flooding. We show that the water quality hydrograph is classified into three types and suggest theory of deriving its prediction method from only the law of conservation. Therefore it is possible to track water quality change for flooding in theory. Moreover the authors[4,)] carried out field observations. These observations were about longitudinal distribution and temporal and spatial characteristics of water quality in tidal area of Arakawa River. In conclusion, it is reported that saltwater intrusion in Arakawa River is well-mixed type during spring tide and weakly-mixed type during neap tide and saltwater during neap tide is oxygen depletion. Whereas quantitative estimation that responds to each river because state of water quality shows different circumstances under the basin characteristics and in ordinary water discharge or for flooding. In addition, it is difficult to clarify water quality environment in the river because hydrological and water quality data in the urban river is insufficient.

This paper reports result of three field observations (1. the spatial distribution of water quality in the tidal area in ordinary water discharge, 2. the time series of salinity, the dissolved oxygen and other water qualities before and after the flood, 3. the observation of the salinity intrusion) in the tidal area of Kanda River, Nihombashi River, Sumida River and Arakawa River. Herewith, we clarify the state of water quality in tidal area of urban rivers and this paper is basic research to practice action to clean up water quality.

2. Overview of intended rivers and method of field observation

2.1 Overview of intended rivers

Overview of observation points is shown in Figure 1. Arakawa River has 173km mainstream length and 2940km^2 basin area and we research 21km from river mouse in tidal area of Arakawa River. Sumida River is tributary stream of Arakawa River and the urban river that reaches 100% penetration of sewer system and 80% of its quantity is municipal discharge. Sumida River meets Kanda River and Nihombashi River downstream. Kanda River has 24.6km mainstream length and 105 km^2 basin area and urban river that. Nihombashi River has tributary stream of Kanda river and 4.8km length. Reference point for length of Kanda River and Nihombashi River is reference point of Sumida River in this paper.

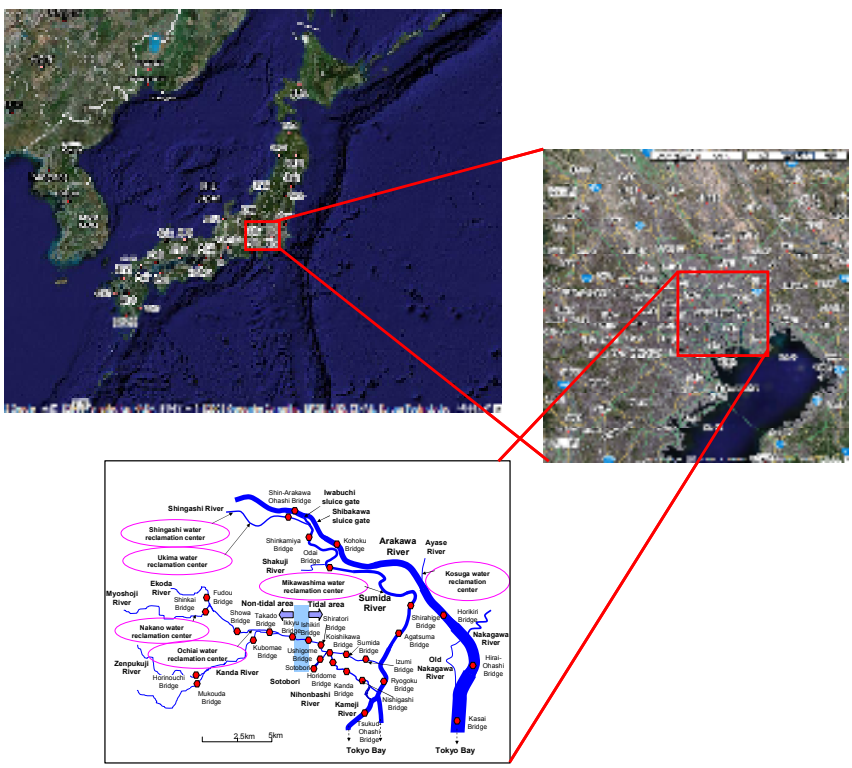

Fig.1 The Overview of Kanda River, Nihombashi River, Sumida River and Arakawa River

2.2. Method of observation

The time series of a tidal level, the rainfall and temperature for three weeks from observation day in normal water discharge are shown in Figure 2. When we obtain water samples, state of water flow is following flow and observation is finished every point before water flow changes reverse. In Sumida River, we moved and obtained water samples by boat and in other rivers; we do it from the bridges. We measure water temperature and salinity and dissolved oxygen(DO) by Multi-Parameter Water Quality Meters(HydroLab) and analysis BOD, total nitrogen(T-N), total phosphorus(T-P), ammonia nitrogen(NH_4 –N) chlorophyl-a and total coliform. BOD and T-P is obtained at three points on vertical direction (surface layer: 30cm from water surface, middle layer: middle depth and bottom layer: 30cm from river bed). Furthermore we practiced continuous measurement (for 107 hours) from 2007 August 28th to September 2nd. We measured the vertical distribution of velocity, dissolved oxygen and salinity to research saltwater intrusion and water environmental quality at Nishigashi point (5.5km from river mouse) in Nihombashi River as shown in Figure 1. We practiced time series measurement at the same point from 2008 May 12th to May 23rd and measured BOD concentration and total coliform obtaining water sample in surface layer and the vertical distribution of flow velocity and dissolved oxygen in a similar way. Workhorse ADCP (Teledyne RD

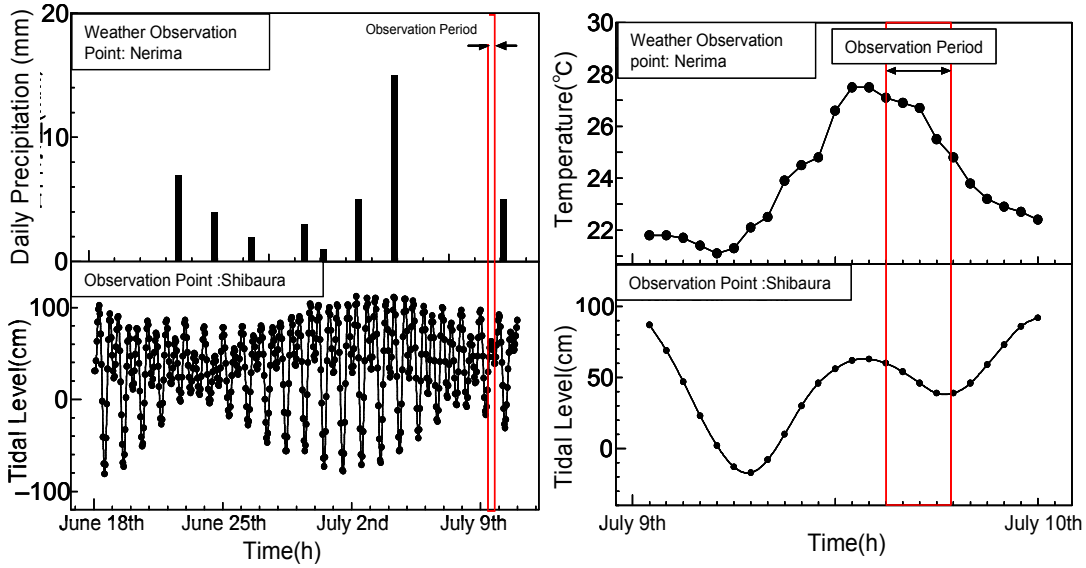

Fig.2 Observing period and time series of Tidal Level , Rainfall and Temperature

Instruments, Inc) was used to measure the vertical distribution of velocity. Dissolved oxygen and salinity were continuously measured at 5 points in the vertical direction (10, 30, 50, 70 and 90 percent of water depth) once every hour.

3. Result of observation of water quality in ordinary water discharge in Nihombashi River, Kanda River, Arakawa River and Sumida River

3.1 Spatial distribution of various water qualities

Obaservation of water quality in ordinary water discharge is practiced in summer and autumn. Result of observation of BOD, T-P, T-N NH_4 –N, total coliform, salinity and dissolved oxygen in Nihombashi River, Kanda River, Arakawa River and Sumida River in autumn is shown in Figure 3. Concentration (except salinity, total coliform and NH_4 –N) which shows red mark in Figure 3 is nonqualified for the environmental criteria of Ministry of the Environment in Japan. Maximum BOD concentration of surface layer is 6.1mg/l at Ushigome Bridge point in Sotobori canal. BOD concentration indicates the value below the environmental criteria (3mg/l) at 80% of the observation points. BOD concentration of bottom layer in Kanda River indicates high value around Sotobori canal point. Max value is 17.0mg/l at 2km upper point from Sotobori Canal and the value decreases in the direction of flowing. Sotobori canal converge 9.5km point from river mouse in Kanda River and Sotobori canal water flow in Kanda River a little bit.

Total phosphorus indicates more than 0.1mg/l at 90% of all observation points and is nonqualified for the environmental criteria. The value of Kanda River and Nihombashi River is higher than Arakawa River and Sumida River and increase on the lower side of flow point from Ochiai water reclamation center (sewage treatment plant). The result of total nitrogen is same result that total phosphorus has but increase on the lower side of flow point from Nakano water reclamation center (above the Nakano water reclamation center). Water volume discharged by Ochiai water reclamation center is almost $2.5m^3/s$ and ordinary flow volume at Ikkyu Bridge in Kanda River is almost $3.2m^3/l$.So almost of flow volume in Kanda River and Nihombashi River is water volume discharged by Ochiai water reclamation center. Ochiai water reclamation center use advanced treatment for BOD and SS though it is important to treat Nitrogen and Phosphorus hereafter.

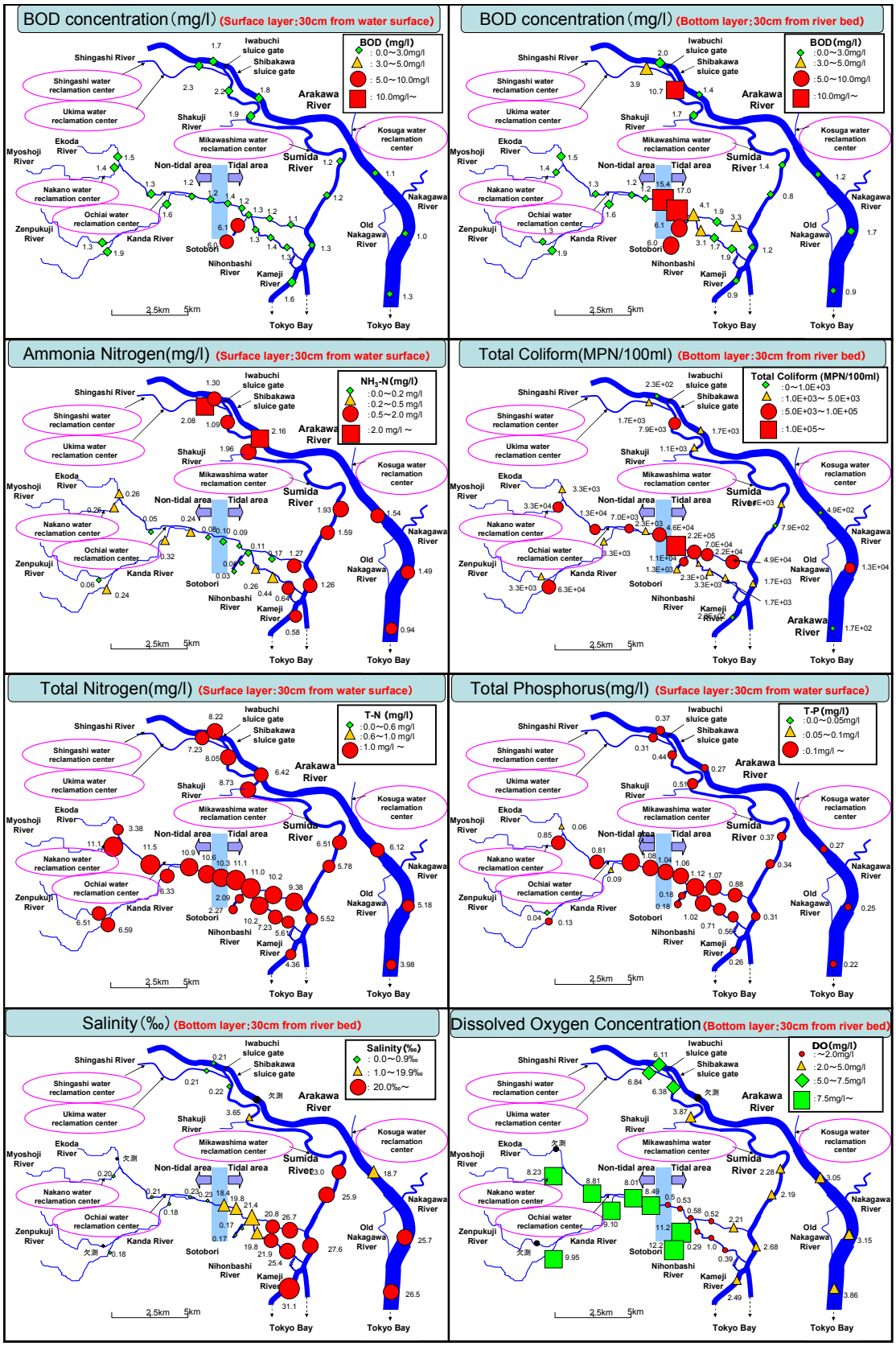

Fig.3 Spatial distribution of water Quality in the tidal area of Kanda River, Nihombashi River, Sumida River and Arakawa River [Date: 16/11/2007]

Ammonia nitrogen in Arakawa River and Sumida River is higher than Kanda River and Nihombashi River and in the following current influence from downstream may remain upper reaches because Maximum value is at end point in Kanda River and Nihombashi River. Total coliform is high in upstream of Kanda River, Sumida River and Arakawa River and decreases in the direction of Tokyo Bay. Total coliform that is used environmental indicator for swimming in river is nonqualified for the environmental criteria and it suggests low of water amenity in the urban river. Salinity (30cm from river bed) intrude to uppermost stream in Kanda River. Dissolved oxygen concentration (30cm from river bed) in Nihombashi River and Kanda River is below 1mg/l and oxygen deficit layer exists in Nihombashi River and Kanda River.

3.2 Longitudinal distribution of various water qualities

Longitudinal distribution of result of water quality observation in autumn is shown in Nihombashi River and Kanda River in Figure 4, Sumidagawa River in Figure 5, Arakawa River in Figure 6. As shown in

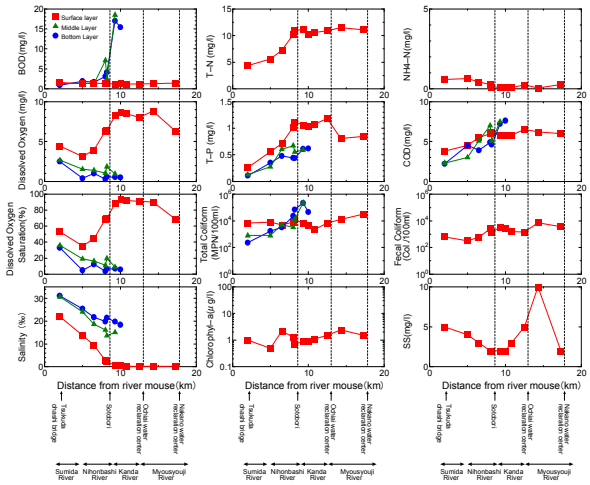

Fig.4 Longitudinal distribution of water Quality in the tidal area of Kanda River and Nihombashi River [Date: 16/11/2007]

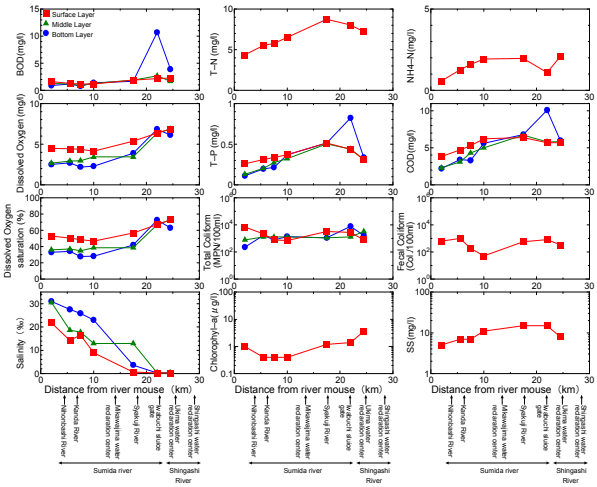

Fig.5 Longitudinal distribution of water Quality in the tidal area of Sumida River [Date: 16/11/2007]

Figure 4, total phosphorus is higher value in surface layer than bottom layer and BOD concentration is higher in bottom layer than surface layer. Total coliform in surface layer hardly changes in vertical direction and in bottom layer indicates high value 2km uppers point from Sotobori canal and decreases in the direction of flowing. Dissolved oxygen in Nihombashi River indicates exceptionally low value and oxygen deficit layer exists in middle and bottom layer in Nihombashi River and Kanda River. As shown in Figure 5, BOD and total phosphorus indicate uniform distribution in vertical direction at many points in Sumida River. While BOD and total phosphorus in Sumida River indicate uniform distribution in vertical direction in Figure 5, total phosphorus in surface layer increases around river mouse. Salinity intrudes to 17km point from river mouse. As shown in Figure 6 BOD and total phosphorus in Arakawa River indicate uniform distribution in vertical direction. The following are shown from the

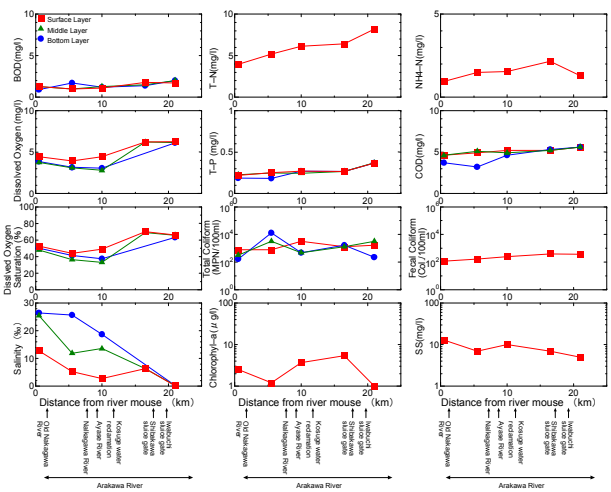

Fig.6 Longitudinal distribution of water Quality in the tidal area of Arakawa River [Date: 16/11/2007]

observation result of spatial distribution of various water quality of showing above. Factors of formation of water quality in Nihombashi River and Kanda River are attributed to influence of treated water from water reclamation center and water from Sotobori canal. We clarify that BOD concentration is high in bottom layer and total phosphorus is high in surface layer. In Sumida River and Arakawa River water quality measured in this observation except Chlorophyl-a around downstream of Shingashi River is high value and decrease in the following. BOD concentration indicates high value in Arakawa River and total phosphorus in Arakawa and BOD concentration in Sumida River show uniform distribution in vertical direction at many points.

4. Characteristic of saltwater intrusion in Nihonbahsi River

Dissolved oxygen showing above in Nihombashi River and Kanda River is exceptionally low value and hypoxic layer on the river bed. To comprehend factors of influx of hypoxic water from Tokyo Bay and formation of river flow on the river bed, we execute observation of characteristic of saltwater intrusion in Nihombashi River.

Continuous change of dissolved oxygen, Salinity and velocity is measured in vertical distribution at Nishigashi Bridge point (5.5km from river mouse) in Nihombashi River between 2007 August 28th and 2007 September 2nd (including spring tide) The authors also measure vertical distribution of dissolved oxygen and salinity in Nihombashi River and Kanda River. Therefore formation of distribution of dissolved oxygen and salinity is difficult around upstream of tidal area in Kanda River and so result of observation at 5.5km point in Nihombashi River is representative result of saltwater intrusion from Tokyo Bay in this paper. Time-series of vertical distribution of dissolved oxygen, salinity, velocity and tidal level is shown in Figure 7. Dissolved oxygen is high value in surface layer and law value on the river bed during falling tide. Salinity is law value in

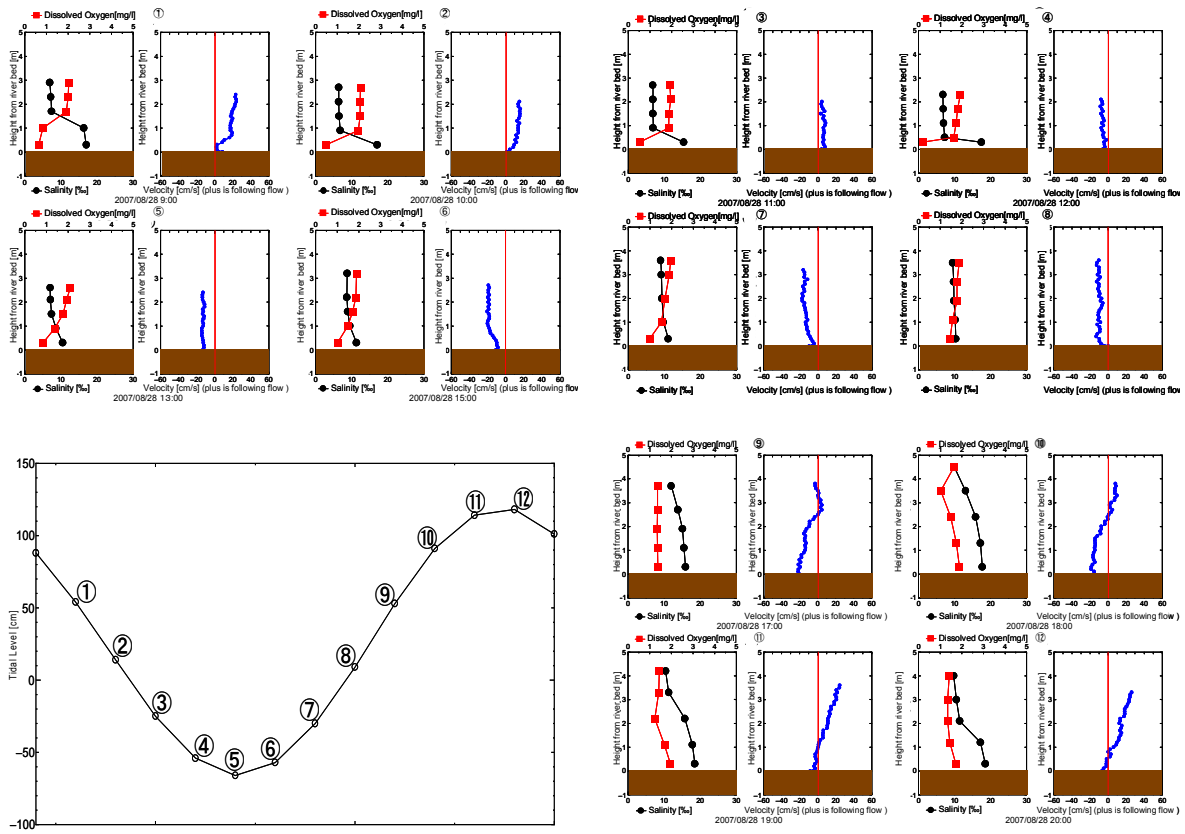

Fig.7 Vertical profile of Dissolved Oxygen Concentration, Salinity, and Velocity and time series of tidal level [Date:28/08-04/09/2007]

surface layer and high value on the river bed. Therefore formation of salinity is weekly-mixed type with double layer. However dissolved oxygen and salinity of surface layer and on the river bed is almost uniform distribution from fall of the tide to flowing tide and saltwater intrude in well-mixed type. Furthermore vertical distribution of velocity, flow on the river bed is little in following flow but it occurs in reverse flow. As mentioned above saltwater intrude in well-mixed type. As shown No.7, 8 and 9 in Figure 7, dissolved oxygen is uniform distribution in vertical direction in reverse flow and higher than in ordinary water discharge. In conclusion, in the phenomenon of hypoxic water on the river bed in Nihombashi River, the flow of the hypoxic water from Tokyo Bay is not a cause. The cause of hypoxic water in Nihombashi River is attributed to continual consumption of oxygen by bottom sediment under formation of flow on the river bed that does not mostly occurs However, it is need to research consumption of oxygen by bottom sediment and verify above consideration

5. Dissolved oxygen saturation and salinity changes during rainfall

Developing sewer system, water environmental quality has been dramatically improved in Nihombashi River and Kanda River while the problem of combined sewer system is that overflow waste water flow to river during rainfall.

It rains in observation in 2007.Total rainfall is 20mm in a couple of hours and maximum hourly rainfall intensity is 10mm/h (AMeDAS Nerima). Figure 8 shows time-series of salinity, dissolved oxygen saturation, tidal level, flow velocity and hourly rainfall intensity . During rainfall, dissolved oxygen saturation rapidly decrease. The cause of dissolved oxygen decrease includes two cases. One case includes that first treatment water from Nakano and Ochiai water reclamation center (sewage treatment plant) or overflow water from sewer system exceed quantity of ordinary discharge (1.6m^3/s in Nihombashi River) to a large degree. It is possible that overflow water from combined sewer system is anaerobic and high concentration of BOD and quantity of flow in Nihombashi River during observation is 42m^3/s (observation value of ADCP)

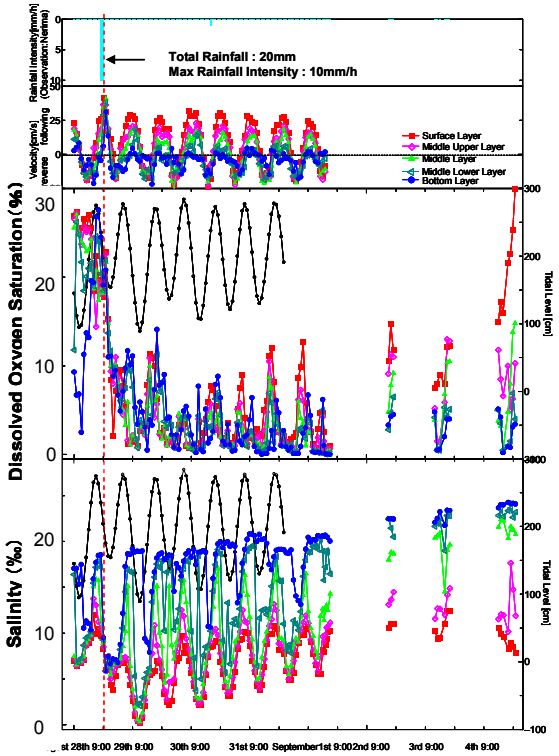

Fig.8 Time series of Velocity, Rainfall, Dissolved Oxygen Saturation and Salinity [Date:28/08-04/09/2007]

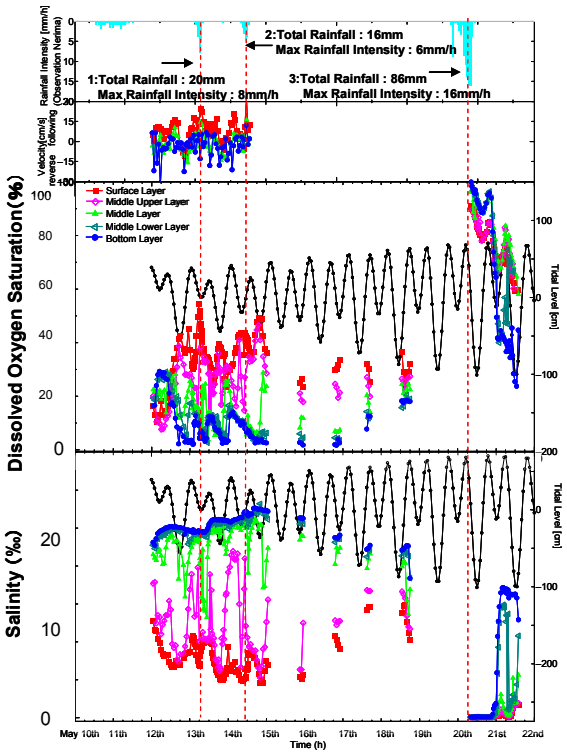

Fig.9 Time series of Velocity, Rainfall, Dissolved Oxygen Saturation and Salinity [Date:12-23/05/2008]

that exceed to a large degree. Therefore it is possible to strongly influence state of water quality. The other cause is attributed to the assumption that particulate matter is kicked up from bottom sediment by rising velocity (nearly 40cm/s) in rainfall and chemical reaction like oxidation or reduction reaction occurs. In addition salinity decreases in all layers for six hours after rainfall. After rainfall, it takes 2days for appearance and odor of river to become normal again before rainfall and 6 hours for salinity to become normal again while 6 days for dissolved oxygen to become normal again. Recovery time of dissolved oxygen is later than salinity. From the observation result, we clarify that it is 6 days that dissolved oxygen becomes normal again from spring tide to neap tide after rainfall.

The Result of observation in 2008 is shown in Figure 9. Its observation conducts from neap tide to spring tide. It rains early in the observation. Total rainfall is 19mm in six hours and maximum hourly rainfall intensity is 8mm/h. Scale of rainfall in observation in 2008 is almost same scale as observation in 2007, but dissolved reduction of oxygen and salinity does not happen in all layers after rainfall. The cause of no reduction in all layers is attributed to no kicking up particulate matter from bottom sediment because of little rising of velocity (10cm/s) on the river bed.

Heavy rain occurred later in the observation. Total rainfall was 86mm in 14 hours and maximum hourly rainfall intensity was 16mm/h. The observation result shows that 5 hours after end of rainfall dissolved oxygen saturation rises 100% and salinity dropped below 1‰. This phenomenon is attributed to the assumption that rainwater flowing in river washed away hypoxic water that existed before heavy rainfall to the downstream. Dissolved oxygen is falling as time goes on and value on the river bed decrease before rain, and value in surface layer also decrease but is higher than before rainfall.

From the observation result, we clarify that below 3 cases occur as variation of dissolved oxygen and salinity after rainfall. 1) When total rainfall is 20mm in a couple of hours and maximum hourly rainfall intensity is 10mm/h, velocity on the river bed rise and dissolved oxygen and salinity fall in all layers. 2) When total rainfall is 19mm in six hours and maximum hourly rainfall intensity is 8mm/h, velocity on the river bed dose not rise and dissolved oxygen and salinity does not change value in all layers. 3) When total rainfall is 86mm in 16 hours and maximum hourly rainfall intensity is 16mm/h, dissolved oxygen rises to around 100% and salinity fall to nearly 0 ‰ in all layers.

6. BOD, total coliform and turbidity during rainfall

The problem in urban river is that overflow waste water from combined sewer system and primary effluent water from sewage treatment plant flow to river during rainfall. To research changing of water quality by the influences, we practice fixed-point observation from 2008 May 12th to 15th. The observation points where BOD, total coliform and turbidity is measured in Kanda River and Nihombashi River during rainfall is shown in Figure 10. As shown in figure, point **A** is 2km below point of flowing from Ochiai water reclamation center, point **B** is 100m below a large exit of storm outfall uppermost stream in tidal area in Kanda River and point **C** is in Nihombashi River, and surface water is obtained at every point. The time-series of BDO, total coliform and rainfall is shown in Figure 11.

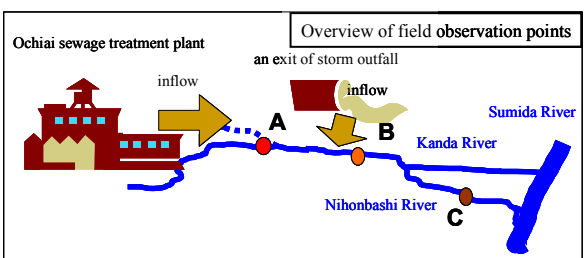

Fig.10 The Overview of observation in Kanda River and Nihombashi River

At point **A** BOD begins to rise three hours later after rainfall and maximum value is 96.0mg/l.But total coliform does not almost change during rainfall. Due to the combined sewer system, discharge in sewer

system flows into Ochiai water reclamation center during heavy rain.When quantity of flow into water reclamation center increase, it changes normal treatment into primary treatment. At this time, water reclamation center does not use advanced treatment for BOD, but treatment for salinity is used as usual. Cause of observation result at point **A** is attributed to discharge of primary treatment.

BOD and total coliform increase during rainfall at point **B**, and maximum value of BOD is 64mg/l and maximum value of total coliform is 1.3×10^8 MPN/100ml. At this time, overflow from the large exit of storm outfall is checked. When the rain grew heavier and the rain water flowed into the combined sewer system, early swollen water in the sewer system flows into water reclamation center. Then the quantity of the flow increases further diluted foul water overflows from the exit of storm outfall to the river. The observation result at point **B** is attributed to this obtaining overflow water in surface layer.

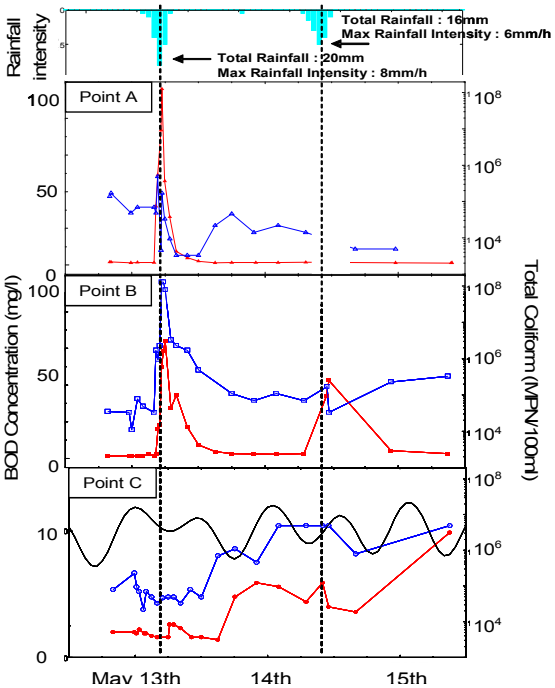

Fig.11 Time series of rainfall, BOD and Total Coliform [Date:12-23/05/2008]

BOD concentration and total coliform at point **C** slowly rise after rainfall. It takes 2 days to rise to maximum value of BOD (10mg/l) after rainfall. This result is attributed to slowly flowing from upstream and retaining water in Niohnbashi River as a tidal river.

Correlation diagram of BOD and turbidity is shown in Figure 12. There strong correlation between BOD and turbidity. If facilities of removing turbidity are set, it is possible to mitigate water pollution in

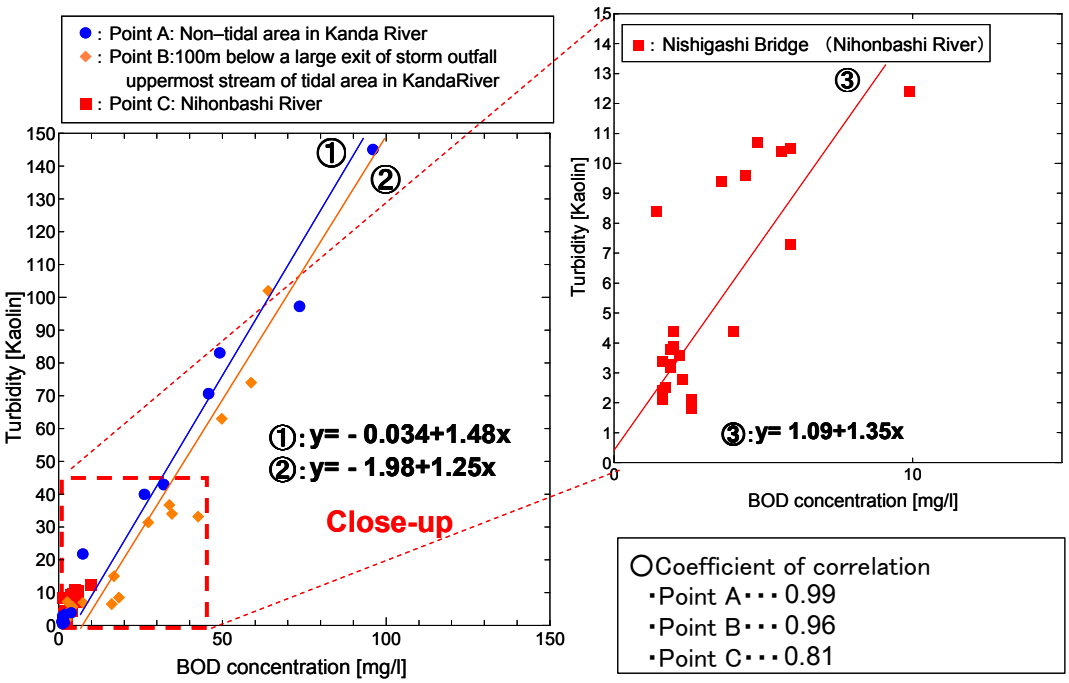

Fig.12 Correlation chart between BOD and Turbidity [Date:12-23/05/2008]

Nihombashi River and Kanda River.

7. Summary of observation result

In this paper, the result of observation of temporal and spatial characteristics of water quality in Nihombashi River, Kanda River, Arakawa River and Sumida River were discussed. Obtained knowledge is shown below.

1) From result of observation in ordinary water discharge. BOD concentration of surface layer indicates the value below the environmental criteria (3mg/l) at 80% of the observation points, but the value of bottom layer in Kanda River indicates high value around Sotobori canal point. Max value is 17.0mg/l at 2km upper point from Sotobori canal and the value decreases in the direction of flowing.
2) Total nitrogen and total phosphorus is nonqualified for the environmental criteria at almost observation points. The value of Kanda River and Nihombashi River is high value on the lower side of flow point from the water reclamation center and the value decreases in the direction of flowing.
3)From result of saltwater intrusion, In Nihombashi River, it is well-mixed type in reverse flow and weekly-mixed type with double layer that dissolved oxygen is high value in surface layer and law value on the river bed in following flow.
4) From the result of time series of water quality, we clarify 3 cases that dissolved oxygen and salinity rapidly fall in all layers and dissolved oxygen and salinity does not change value before rainfall in all layers and dissolved oxygen rises to around 100% and salinity fall to nearly 0‰ in all layers. In addition, it takes 6 days for dissolved oxygen to become normal again from spring tide to neap tide after rainfall.
5) BOD concentration rapidly rises during rainfall and fall after that uppermost stream in tidal area of Kanda River. Total coliform rapidly rises during rainfall and fall after that below the exit of storm outfall. In Nihombashi River, BOD concentration and total coliform slowly rise after rainfall. It takes 2 days to rise to maximum value of BOD (10mg/l).
6) The bed load of Nihombashi River move over regardless of rainfall.

ACKNOWLEDGEMENT

This study is supported by the Institute of Science and Engineering, Chuo University, which is gratefully appreciated.

REFERENCES

[1] Kure, S and Yamada, T, "Studies on formation process of water quality hydrograph in a slope", "*Annual Journal of Hydraulic Engineering*", JSCE, Vol.48(2004.), pp.55-60,(In Japanese)
[2] Kure, S, Ebana, R, Yamada T et al, "A study on formation process of water quality hydrograph in a small basin" "*Annual Journal of Hydraulic Engineering*", Vol.49(2005.), pp.157-162, (In Japanese)
[3] Kure, S, Ebana, R, Yamada T et al, "A study on formation process and estimation method of water quality hydrograph in a small basin", "*Annual Journal of Hydraulic Engineering*", Vol.50(2006), pp.-, (In Japanese)
[4] Motonaga, Y , Dohi M, Yamada T, et al, "Field observation about hydraulic factors influencing water quality in a tidal area of the Ara River", "*Annual Journal of Hydraulic Engineering*" Vol.46(2002), pp.929-934, (In Japanese)

Development of an Amphibian Biotic Index to Evaluate Wetland Health in Northern Missouri

C. D. Shulse[1], R. D. Semlitsch[2], and K. M. Trauth[3]

[1]Missouri Department of Transportation, P.O. Box 1067, Highway 61 South, Hannibal, MO 63401; PH (573) 248-2440; FAX (573) 248-2527; email: Christopher.Shulse@modot.mo.gov
[2]Division of Biological Sciences, 212 Tucker Hall, University of Missouri, Columbia, MO 65211-7400; PH (573) 884-6396; FAX (573) 882-0123; email: SemlitschR@missouri.edu
[3]Department of Civil and Environmental Engineering, E2509 Lafferre Hall, University of Missouri, Columbia, MO 65211-2200; PH (573) 882-5843; FAX (573) 882-4784; email: TrauthK@missouri.edu

ABSTRACT

Most amphibians require suitable wetlands for breeding, oviposition, and juvenile development. Newly metamorphosed juveniles disperse into terrestrial habitat where they spend the majority of their adult lives in undisturbed forest or grassland adjacent to the wetland. Development of new infrastructure can result in wetland draining and habitat fragmentation thereby disrupting necessary life history functions. To ensure the long-term survival of amphibians, it is imperative that developers take into account their conservation needs during project planning and construction of replacement wetlands. In order to assist planners and managers in this effort, we present an index that quantifies the biotic integrity of amphibian populations within constructed wetlands throughout northern Missouri. The index is modeled after Ohio's Amphibian Quality Assessment Index (AQAI) and it incorporates ecological and abundance information for each species inhabiting a wetland. Although refinements will continue, current results indicate this tool can help assess the biological integrity of constructed and natural wetlands. The index can be modified to accommodate regional differences in species' ecology.

INTRODUCTION

The decline of many amphibian species throughout the world is well documented and has received much public attention (Stuart et al. 2004). There are multiple reasons for these declines but habitat loss and alteration is widely perceived as the primary cause (Gardner et al., 2007). Most amphibian species require suitable wetland habitat for breeding and juvenile development. Impaired wetland function at natural sites through alterations in hydrology or the inadequate construction and placement of restored and created wetlands can result in a net loss of habitat necessary for reproduction. Due to their biphasic life cycle, many species also require suitable terrestrial habitat adjacent to the wetland for foraging, hibernation,

aestivation, and shelter. The required amount of land surrounding the wetland is known as "core terrestrial habitat" and it varies in width for each species. However, a distance of 300m from the wetland's edge likely incorporates the needs of most species (Semlitsch and Bodie, 2003; Rittenhouse and Semlitsch, 2007). Additional wetlands in the area, and suitable habitat between them, provide individuals with opportunities for gene exchange and allow for re-colonization of wetlands when local populations crash due to stochastic events. Therefore, destruction, alteration, or fragmentation of the terrestrial core zone can result in habitat loss, disruption of essential life history functions, and population decline even when the aquatic environment is undisturbed.

The goal of federal wetland regulations, and those of some states, is "no-net-loss" of wetlands. However, despite the U.S. Clean Water Act mandating the protection of the physical, chemical, and biological integrity of wetlands, net gains in acreage do not necessarily translate to net gains in ecological function (Semlitsch, 2008). Therefore, replacement wetlands may not adequately compensate ecologically for those lost. For example, although Dahl (2006) found that overall acreage of wetlands in the U.S. increased between 1998 and 2004, most gains were attributed to construction of freshwater ponds that offset the loss of freshwater vegetated wetlands. As the author points out, this trend represents a shift in class and wetland function. Freshwater ponds are not an equivalent replacement for vegetated wetlands. Because many species of wetland plants and animals are dependent upon specific wetland types, replacement wetlands that do not meet their requirements equate to habitat loss regardless of acreage gained.

In order to evaluate the effectiveness of constructed and restored wetlands, it is imperative to examine how they function ecologically. To do this, wetland managers and regulatory authorities need clear performance criteria that are based upon the ecology of wetland inhabitants. While some functional-based wetland assessments rely upon indicators such as energy flow facilitation, nutrient cycling support, and plant or animal community maintenance (Brinson and Rheinhardt, 1996), these assessments often do not contain metrics that incorporate information about the biological components of wetlands (King et al., 2000). Therefore, indexes of biological integrity (IBI's) have been developed that rely upon information about the relative abundance of key indicator species to assess the biotic components of habitats. The first IBI was developed to assess fish communities in small streams in Indiana and Illinois (Karr, 1981). Since its introduction, the original IBI for fish has been modified for use in other regions, ecosystems, and other taxa (Kerans and Karr, 1994; King et al., 2000).

The Ohio Amphibian Index of Biological Integrity (AmphIBI) was developed by the Ohio EPA to create amphibian-based wetland bio-criteria that assesses the extent of wetland disturbance in conjunction with the Ohio Rapid Assessment Method (ORAM version 5.0), an index that categorizes wetlands by type and level of human disturbance (Micacchion, 2002, 2004). Like other IBI's, the AmphIBI uses a set of metrics which are ranked measurements of variables that represent expectations of biological integrity. When the metrics from a wetland are summed, the index provides a "score" that represents the amphibian biotic integrity of the wetland relative to others of the same type. The Ohio AmphIBI is composed of five metrics,

each containing 1 – 10 points, for a total of 50 possible points (see below). The cumulative rating results in better representation of disturbance-based amphibian biotic integrity than the individual metrics separately.

In this paper we introduce a prototype biotic index to assess amphibian assemblages in northern Missouri wetlands. The index is similar to the AQAI in that it is weighted and includes information about each species' sensitivity to disturbance and the number of individuals of each species captured at a site. The index also includes information about each species' range and its abundance throughout Missouri. Our objective is to develop a regionally modifiable, multi-metric amphibian-based biotic index, using the AmphIBI as a template, for Missouri wetlands.

METHODS

We selected 49 constructed wetlands within 26 northern Missouri counties for assessment of amphibian community biotic integrity. Most (37) were within the Central Dissected Till Plains Ecoregion. Eleven were located within the Ozark Highlands Ecoregion and one was slightly within the Osage Plains Ecoregion (Fig. 1). Twenty-nine were "wildlife" or "herp" ponds on Missouri Department of Conservation wildlife areas and 20 were Missouri Department of Transportation compensatory mitigation wetlands. We selected wetlands on public-owned lands that we had permission to access and conduct surveys. For logistical purposes, wetlands were grouped geographically into seven sampling zones, each containing 5 – 9 wetlands. Zone sampling order within each survey period was randomly determined.

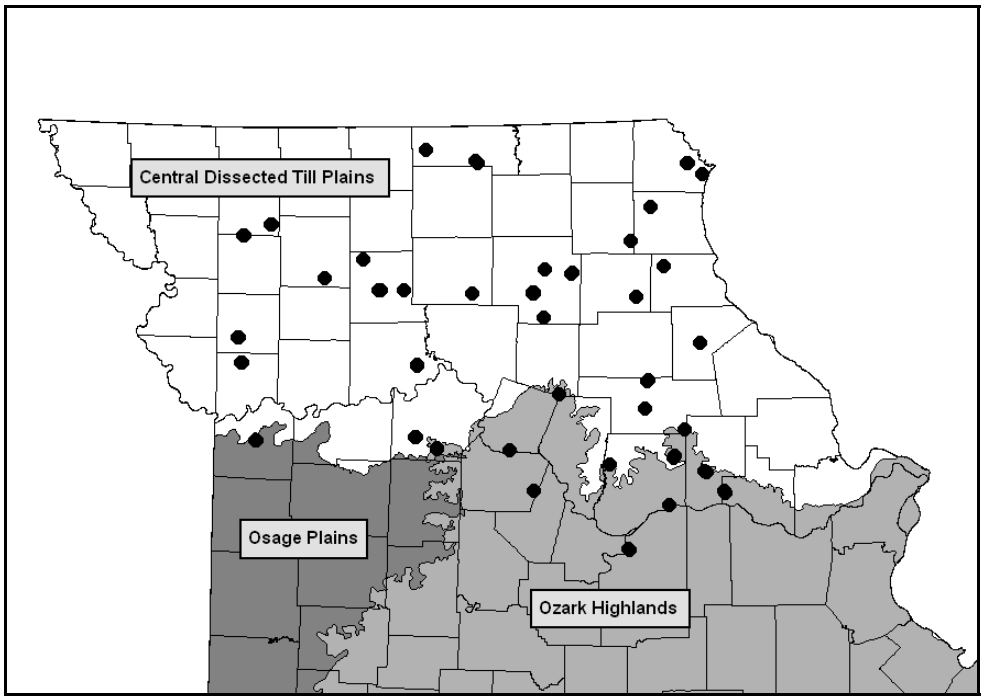

Figure 1. Locations of sampled wetlands. Some dots represent multiple wetlands due to proximity

Amphibian sampling. To increase the probability of detecting breeding adults, eggs, and larvae of most species, amphibian surveys were conducted at each wetland during three time periods in 2006 (March/April, May/June, and July/August). Data from all three periods were pooled. All surveys were conducted during daylight hours. Sampling occurred only if wetlands contained water. Some wetlands contained no standing water during one or more of the sampling periods and therefore data from these sites are based upon one or two surveys.

We used area-constrained dip-netting and commercial minnow traps to capture amphibians and fish. Dip-netting resulted in greater capture frequency of most amphibian species than minnow traps (Shulse and Semlitsch, *unpublished data*) so we used only the dip-net captures in our analyses. Dip-net sweeps were scaled to the size of the wetland (1 sweep/25m² of wetland surface area, 15 sweeps minimum, 200 maximum). Sweeps were ~1.5m long with the net pressed to the bottom of the wetland and dragged toward the sampler. All sweeps were distributed proportionately throughout the different habitats within each wetland. All amphibians and fish were identified in the field and released unharmed at the point of capture. Some amphibians could not be identified reliably to species in the field (leopard frogs, treefrogs, and toads) so individuals within these groups were assigned to three generalized categories (Table 1).

Each amphibian species was assigned a numerical conservation coefficient (CC - Table 1). To obtain these coefficients, amphibian biologists at the University of Missouri discussed the ecology of each species and assigned a score between 1 and 10 for three ecological criteria – sensitivity to disturbance, rarity of the species within Missouri, and range of the species within Missouri. The three scores for each category were averaged to obtain the CC. Higher scores indicate higher conservation priority. The CC's were used to calculate the amphibian conservation index score (ACI) for each wetland. This involves multiplying the number of individuals of each species captured by their respective CC. The result is a subtotal for each species. Subtotals are summed and the total divided by the number of all individuals. This provides the ACI score (range 0 – 9) for the wetland (see example in Table 2).

Table 1. Conservation coefficients for amphibian species captured in Missouri.

Species	Disturbance	Rarity	Range	CC
Acris crepitans	3	1	1	2
Ambystoma opacum	8	10	8	9
Ambystoma maculatum	8	9	8	8
Ambystoma texanum	5	7	6	6
Ambystoma tigrinum	6	10	8	8
***Anaxyrus* – Toad group**	1	3	1	2
***Hyla* – Treefrog group**	5	3	2	3
Leopard frog group	4	4	2	3
Lithobates catesbeianus	1	1	1	1
Lithobates clamitans	2	2	5	3
Nothophthalmus viridescens	8	8	7	8
Pseudacris crucifer	6	7	5	6
Pseudacris triseriata	2	5	5	4

Table 2. Example of amphibian conservation index calculation for a wetland in the Ozark Highlands of Missouri. Adapted from Micacchion, 2002; 2004.

Species	Number of Individuals	CC	Subtotals
Ambystoma opacum	**2**	**8**	**16**
Ambystoma maculatum	**41**	**9**	**369**
Hyla versicolor	**30**	**3**	**90**
Leopard frog complex	**4**	**3**	**12**
Nothophthalmus viridescens	**1**	**8**	**8**
Totals	**78**	**---**	**495**
Biotic Index Score	**6.35**		

Wetland features. To assess the utility of the Ohio AQAI Micacchion (2002) used their values as independent variables in linear regressions with ORAM 5.0 scores as the dependent variable. The Missouri Department of Transportation does not currently employ a metric-based wetland rating system (B. Brooks *pers comm.*). Therefore, we created a trial wetland features index made up of multiple metrics in order to examine the utility of our ACI scores. Although the AQAI, AmphIBI, and ORAM 5.0 are disturbance focused, we were interested in how features relating to the design, placement, and water quality affected amphibian biotic integrity. We measured several features both within the aquatic environment of the wetland and within the 300m terrestrial core zone surrounding each wetland. Features selected are those that have been found to affect amphibian communities from previous investigations. The metrics are: 1) Littoral zone; 2) Fish presence; 3) pH; 4) Depth; 5) Percent undisturbed area with the core zone. The metrics, their scores, and scoring breakpoints are shown in Table 3. Amphibian species richness has been found to be greater in wetlands with shallows (15:1 within-water slopes or less) and that lack predatory fish (Porej and Hetherington, 2005). Steeper slopes (2:1 or 3:1) are commonly observed at farm ponds (Shulse, *pers. obs.*). We therefore used these two extremes in assigning breakpoints and scores. While studies have found that highly acidic conditions can negatively affect amphibians (Dunson and Wyman, 1992; Freda and Dunson, 1985), high pH has also been shown to be detrimental to amphibians (Semlitsch, *unpublished data*). Wetlands in our study were not highly acidic and ranged from 6.2 – 9.79 with median 7.48. We assigned scoring breakpoints so that approximately half of the wetland scores fell on each side of the median. Wetlands with long hydroperiods (>2 yrs) may accumulate large numbers of aquatic macroinvertebrate and fish predators (Semlitsch, 2002). Many amphibian species rely upon temporary wetlands to breed and thus avoid predators associated with permanent water. However, wetlands that are too shallow can dry rapidly resulting in larval death. We found that wetlands we surveyed less than 0.20 meters deep dried in early summer 2006. However, wetlands that were greater than 1 meter deep had stable hydrology. We assigned 0 points to wetlands at both extremes and 10 points to wetlands with intermediate depths. Wetlands between 0.2 and 1m deep tended to dry completely by late summer. The scores for % Undisturbed area of the core zone were chosen to reflect what we perceived to be biologically necessary for amphibian community integrity.

Littoral zone slope and pH were measured at each cardinal direction in the wetlands we sampled. For large wetlands (>0.6 ha) two additional locations were evaluated and all six were spaced evenly around the perimeter. Slopes were calculated by measuring water depth along transects perpendicular to the water's edge at 1m and 3m from the shore. Slope at each location was calculated from the depths and then averaged for each wetland. Measurements of pH were recorded using a Hanna Low-Range Combo Waterproof Tester, and averaged across location and sampling period at each wetland.

Terrestrial core zone analysis. Analyses of land use within the core zone were performed using ArcMap 9.2 GIS software (Environmental Systems Research Institute, 2006). Surveyed wetlands were located on 2006 National Agricultural Imagery Program (NAIP) orthorectified digital aerial photography (2m resolution) and their boundaries were delineated to create a polygon representing each wetland within the GIS. Wetland polygons were overlaid on Missouri Resource Assessment Partnership (MoRAP) Land use and Land cover data (LULC 2005). We performed a buffer analysis of the first 300m radius of terrestrial habitat surrounding each wetland to obtain percentages of each land-use and land-cover type within the area. We summed the percentages of all undisturbed land-use types (grasslands, forest, and deciduous woody/herbaceous mixed, and all wetland types) to obtain a cumulative percentage for this category. The remaining land-use types that represented disturbance were cropland, urban, and impervious surfaces. We did not include a disturbance metric because lower % Undisturbed scores reflected greater disturbance.

Statistical analysis. All analyses were performed in SPSS version 16.0 (SPSS Incorporated, Chicago, Illinois). To examine the relationship between the prototype amphibian biotic index and the wetland features index, we used linear regression with the wetland features index as the dependent variable and the amphibian biotic index values as the independent variable. We also examined the significance of individual metrics within the wetland features index by performing a multiple regression analysis using the generalized linear model feature specifying a normal distribution and log link function in SPSS. In this model, the amphibian biotic index scores were used as the dependent variable and each metric in the wetland features index were independent variables.

Table3. Metric scores and breakpoints for wetland features index.

Metric	Score 0	Score 3	Score 7	Score 10
Littoral Zone Slope	3:1 or steeper	4:1 – 9:1	10:1 – 14:1	15:1 or shallower
Fish Presence	Present	----------	----------	Absent
pH	> 8.00	7.50 – 7.99	7.01 – 7.49	6 – 7
Depth (meters)	0 – 0.19 or > 1	----------	----------	0.2 - 1.0
% Undisturbed	< 45	45 – 59	60 – 84	85 – 100

RESULTS AND DISCUSSION

Figure 2 illustrates the relationship between the ACI values and the trial wetland features index. There is a significant positive relationship between the two variables although the variance explained by the ACI was somewhat moderate (adjusted $R^2 = 32.7\%$). This is very similar to the results presented in Micacchion (2004) (df = 52, F = 26.21, $R^2 = 33.5\%$, p =<0.001). Micacchion's results showed that as disturbance of the wetlands increased, AQAI scores decreased indicating that the amphibian community biotic integrity in their wetlands was negatively associated with the level of human disturbance. While our wetland features index had a metric representing the lack of disturbance in the core zone, and pH and fish presence could be related to disturbance, littoral zone slope and depth represent wetland design features. The results of the multiple regression analysis are shown in Table 4. All five of the metrics had a positive β estimate but only three - Littoral Zone Slope, pH, and % Undisturbed - had 95% confidence intervals that did not include zero, although Depth was close. Therefore, these metrics were most significant in the model examining the relationship between ACI scores and wetland features. The pH metric had a particularly significant effect in the model. This may reflect slightly acidic conditions of the forested wetlands utilized by many species with high CC values. These results underscore the importance of wetland design, aquatic conditions, and wetland placement on the composition of amphibian communities. However, it is important to mention that other metrics based upon other variables (e.g. dissolved oxygen, salinity, distance to nearest wetland, etc.) or higher resolution of our chosen variables (e.g. separating % Undisturbed into its different components) could provide different results and shed light on the details of the relationship. Nevertheless, our intent was solely to create a trial features index with which we could test the utility of our amphibian conservation index.

As previously mentioned, the ACI is similar to Ohio's AQAI. The AQAI is one of five metrics that make up the AmphIBI. The four additional metrics are: 1) disturbance-sensitive species relative abundance; 2) disturbance-tolerant species relative abundance; 3) number of pond breeding salamanders present; 4) presence of the indicator species - spotted salamanders (*Ambystoma maculatum*) or wood frogs (*Lithobates sylvaticus*). When total AmphIBI scores are plotted against ORAM 5.0 scores, the variance explained in the model is improved over the results presented above using only AQAI scores (df = 52, F = 52.61, $R^2 = 50.3\%$, p<0.001, from Michacchion, 2004). The additional four metrics significantly improved model fit. In order to develop a more robust index explaining the relationship between amphibian biotic integrity and wetland quality, we are currently exploring additional metrics to create a multi-metric index similar to the AmphIBI. Preliminary results from a metric representing the relative abundance of species with CC's above 6 have been promising. However, another metric scoring the relative abundance of species with CC's less than 4 has been less clear. This metric worked well in the AmphIBI and there was a clear positive correlation between low ORAM 5.0 scores and the relative abundance of disturbance-tolerant species. The inclusion of non-disturbance based metrics in our rating system may explain why this pattern has not been

observed in our analyses. Amphibians with low CC ratings (leopard frogs, treefrogs, and toads) have been observed to prefer wetlands with shallow littoral zones that lack predatory fish (Porej and Hetherington, 2005; Shulse and Semlitsch, *in prep.*). Their relative abundance in wetlands with high index scores based on these factors could explain this trend.

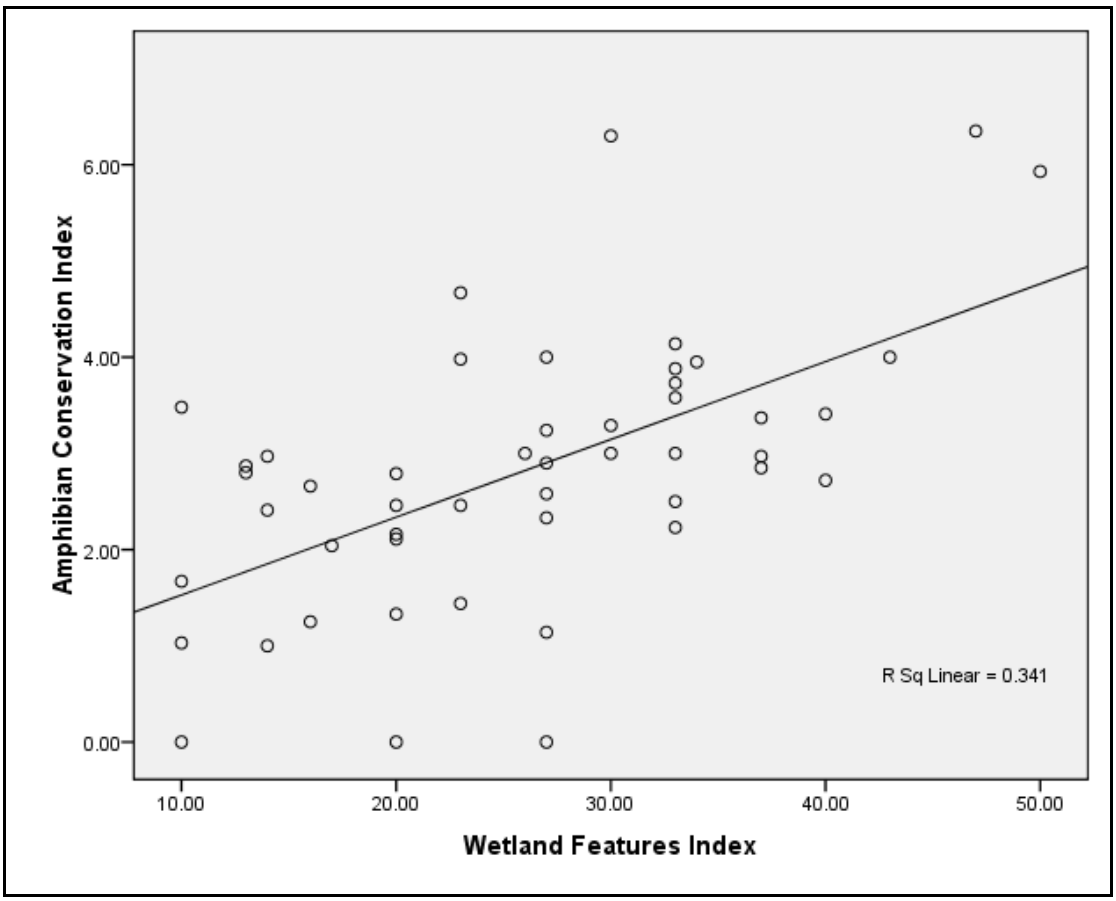

Figure 2. Regression plot of prototype amphibian biotic index vs. trial wetland features index for Missouri. Adjusted $R^2 = 0.327$, df = 47, F = 24.36, p<0.001.

Table 4. β estimates and 95% confidence intervals for metrics in the Missouri wetland features index. ($\chi^2 = 38.17$, df = 5, p<0.001, n = 49).

Metric Score	β	Lower 95% C.I.	Upper 95% C.I.	Sig.
Intercept	0.057	-0.343	0.457	0.779
Littoral Zone Slope	0.044	0.011	0.078	0.010
Fish Presence	0.018	-0.006	0.043	0.138
pH	0.049	0.021	0.077	<0.005
Depth	0.018	-0.001	0.038	0.068
% Undisturbed	0.042	0.009	0.076	0.013

We are also testing a metric that scores the percentage of pond-breeding salamanders based on county records found at each site (Porej et al., 2004). The AmphIBI uses a similar metric; however scores are based upon the absolute number of salamanders recorded at each site. This method would not work well for our index because our wetlands were located in multiple ecoregions within the state and some salamander species did not occur throughout the entire study area. Preliminary results with our percentage-based metric appear promising. The AmphIBI metric using presence of spotted salamanders and wood frogs would not work for a statewide or northern Missouri index because these species have limited distribution north of the Missouri River. As Miccachion (2002, 2004) points out, these species are excellent indicator species for vernal pools in upland forests. We are currently exploring the ecology of northern Missouri amphibian species to determine an appropriate indicator species to use as a metric in the final biotic index.

The AmphIBI is recommended for use only in forest and shrub temporary wetlands (vernal pools) and not for emergent depressional systems (Maccachion, 2002; 2004). This is because amphibian communities of emergent sites show little variation in response to disturbance both within and surrounding the wetlands and therefore these wetlands consistently score low. We saw a similar pattern with many of the mitigation wetlands that were relatively new (< 10 years old) and had high percentages of disturbed land surrounding them. These sites also tended to have higher pH values, probably due to a lack of surrounding forest and leaf litter accumulations. Therefore, these sites are probably inappropriate for many species because they have hostile aquatic and core terrestrial zone environments. Over time, if these sites are allowed to develop a forested canopy, they may provide more suitable habitat. However, this would be most likely only in sites with suitable habitat corridors connecting them to neighboring source populations and with low amounts of disturbance in their terrestrial core zones.

A few additional differences between the ACI and the AQAI merit mention. First, several of the individual coefficient scores differ. This is due primarily to our inclusion of range and rarity information. While treefrogs are somewhat intolerant to disturbance in the terrestrial habitat surrounding their breeding sites (Johnson et al., 2007), they are common and range statewide in Missouri (Johnson, 2000). Therefore, we assigned them a CC of 3 as opposed to the AQAI rating of 5. Conversely, we found spring peepers (*Pseudacris crucifer*) and smallmouth salamanders (*Ambystoma texanum*) to be uncommon and somewhat sensitive to disturbance surrounding their breeding sites. They were therefore rated higher in our index (CC's of 6 as opposed to 2 and 4 respectively in the AQAI). Another difference is sampling methodology. We advocate the use of standardized dip-netting rather than aquatic funnel trapping for amphibian collection. As mentioned, we found that dip-netting resulted in captures of most amphibian species at more sites than funnel trapping. Some species of amphibians with relatively sessile larvae may not be captured effectively in funnel traps that require animal movement. Additionally, 24 hour periods are required to set and collect funnel traps whereas dip-netting can be completed in several hours or less. This eliminates multiple trips to remote wetlands thereby reducing travel and personnel time. Therefore, if standardized techniques and training protocol are followed, dip-netting methods can result in rapid, effective, and economical results.

The results from our study indicate that our prototype biotic index can be used to examine the relationship between amphibian community biotic integrity and features of constructed wetlands in northern Missouri. The index should also be tested at reference natural wetlands; however, we feel that it should perform suitably based on its similarity to the Ohio index. It is probable that multiple indexes will have to be employed, each created for a different region of the state. We will continue to investigate additional parameters for the Amphibian Conservation Index and test its utility with other wetland rating systems.

ACKNOWLEDGEMENTS

The authors wish to thank the staff of the Missouri Department of Transportation, Missouri Department of Conservation, University of Missouri Division of Biological Sciences, and University of Missouri Department of Civil and Environmental Engineering. Special thanks to D. Drake and A. Drayer for dedicated service in the field. This project was funded by a US EPA Region VII Wetland Development Grant CD-98769101-0.

REFERENCES

Brinson, M.M., and Rheinhardt, R. (1996). "The role of reference wetlands in functional assessment and mitigation." Ecological Applications, 6(1):69-76.

Dahl, T.E. (2006). "Status and trends of wetlands in the conterminous United States 1999-2004." U.S. Department of the Interior; Fish and Wildlife Service, Washington, D.C., 112 pp.

Dunson, W.A., and Wyman, R.L., editors. (1992). "Amphibian declines and habitat acidification." Journal of Herpetology, 26:349-352.

Freda, J., and W.A. Dunson. (1985). "Field and laboratory studies of ion balance and growth rates of ranid tadpoles chronically exposed to low pH." Copeia 1985:415-423.

Gardner T.A., Barlow, J. and Peres, C.A. (2007). "Paradox, presumption, and pitfalls in conservation biology: the importance of habitat change for amphibians and reptiles." Biological Conservation, 138:166-179.

Johnson, J.R., Knouft, J.H. and Semlitsch, R.D. (2007). "Sex and seasonal differences in the spatial terrestrial distribution of gray treefrog (*Hyla versicolor*) populations." Biological Conservation, 140:250-258.

Johnson, T.R. (2000). "The Amphibians and Reptiles of Missouri." Missouri Department of Conservation, Jefferson City, Missouri.

Karr, J.R. (1981). "Assessment of biotic integrity using fish communities." Fisheries, 6(6):21-27.

Kerans, B.L. and Karr, J.R. (1994). "A benthic index of biotic integrity (B-IBI) for rivers of the Tennessee Valley." Ecological Applications, 4(4):768-785.

King, R.S., Nunnery, K.T., and Richardson, C.J. (2000) "Macroinvertebrate assemblage response to highway crossings in forested wetlands: implications for biological assessment." Wetlands Ecology and Management, 8: 243-256.

Micacchion, M. (2002). "Amphibian index of biotic integrity (AmphIBI) for wetlands." Final report to U.S. EPA Grant No. CD985875-01, Testing biological metrics and development of wetland assessment techniques using reference sites: Volume 3. Ohio Environmental Protection Agency, Division of Surface Water, Wetland Ecology Unit, Columbus, Ohio.

Micacchion, M. (2004). "Integrated Wetland Assessment Program. Part 7: Amphibian index of biotic integrity (AmphIBI) for Ohio Wetlands." Ohio EPA Technical Report WET/2004-7. Ohio Environmental Protection Agency, Wetland Ecology Group, Division of Surface Water, Columbus, Ohio.

Porej, D., Micacchion, M. and Hetherington, T.E. (2004). "Core terrestrial habitat of local populations of salamanders and wood frogs in agricultural landscapes." Biological Conservation, 120(2004):399-409.

Porej, D. and Hetherington, T.E. (2005). "Designing wetlands for amphibians: the importance of predatory fish and shallow littoral zones in structuring amphibian communities." Wetlands Ecology and Management, 13:445-455.

Rittenhouse, T.A.G. and Semlitsch, R.D. (2007). "Distribution of amphibians in terrestrial habitat surrounding wetlands." Wetlands, 27(1):153-161.

Semlitsch, R.D. (2002). "Critical elements for biologically-based recovery plans of aquatic-breeding amphibians." Conservation Biology, 16(3):619-629.

Semlitsch, R.D. and Bodie, J.R. (2003). "Biological criteria for buffer zones around wetlands and riparian habitats for amphibians and reptiles." Conservation Biology, 17(5):1219-1228.

Semlitsch, R.D. (2008). "Moving wetland mitigation towards conservation banking." National Wetlands Newsletter, 30(5):16.

Stuart, S.N., Chanson, J.S., Cox, N.A., Young, B.E., Rodrigues, A.S.L., Fischman, D.L., and Waller, R.W. (2004). "Status and trends of amphibian declines and extinctions worldwide." Science, 306:1783-1786.

GIS-Based Landscape Parameters for Wetland Evaluation Related to Amphibian Health

Miriam Romero[1], P.E., Kathleen M. Trauth[2], Ph.D., P.E., M.ASCE, Yingkui Li[3], Ph.D., Raymond Semlitsch[4], Ph.D., Christopher D. Shulse[5]

[1]Department of Civil and Environmental Engineering, University of Missouri, E2509 Lafferre Hall, Columbia, MO 65211; Ph (573) 884-7862; email: mrnn7@missouri.edu
[2]Department of Civil and Environmental Engineering, University of Missouri, E2509 Lafferre Hall, Columbia, MO 65211; Ph (573) 882-5843; email: trauthk@missouri.edu
[3]Department of Geography, University of Missouri, 5 Stewart Hall, Columbia, MO 65211; Ph (573) 882-2879; email: liyk@missouri.edu
[4]Biological Science, University of Missouri, 212 Tucker Hall, Columbia, MO 65211; Ph (573) 884-6396; email: semlitschr@missouri.edu
[5]Missouri Department of Transportation Northeast District, PO Box 1067, Hannibal MO 63401; Ph (573) 248-2440; email: christopher.shulse@modot.mo.gov

ABSTRACT

Infrastructure decisions for transportation include where to locate rights-of-way (ROWs) for new transportation routes. These new routes can impact wetlands by replacing them with roadways and by impacting the landscape that supports biodiversity within the wetland. State departments of transportation (DOTs) need guidance for how to evaluate alternative ROWs in light of the potential impact on wetlands. Because a wetland and the surrounding landscape are spatial in nature, they are well-suited to analysis via a geographic information system (GIS). Many landscape parameters can be devised and information layers developed. Meaningful information layers are those that describe the impact that the landscape has on the amphibian life cycle. An interdisciplinary research team from the University of Missouri and the Missouri Department of Transportation (MoDOT) brings the unique perspectives of civil engineering, geography and biological sciences to bear on this problem. At the "micro" scale, amphibian species and abundance have been sampled within 49 constructed wetlands in northern Missouri. These data has been analyzed from the biological perspective to create a habitat quality rating for each wetland, considering that some species are more sensitive to wetland changes, with their presence indicating a higher quality environment. This rating provides the dependent variable, y, for the creation of a regression equation relating landscape parameters to amphibian health, and thus wetland quality, at a "macro" scale. As a first step in developing a regression equation, appropriate GIS variables must be developed. Factors such as land cover, and the presence or absence of roads and streams have been identified as being important to amphibian health. However, one cannot simply utilize layers of land cover, because the important factor is how the amphibians interact with the landscape. This paper focuses on the effort to devise a set of GIS parameters that accurately represent amphibian interactions with the landscape. There

are a number of important requirements for this amphibian-based GIS analysis. . In addition, amphibians first encounter those landscape conditions that are closer to the wetland, so greater importance is associated with nearer features. Because migrating adult or dispersing juvenile amphibians may travel from a wetland in any direction, the analysis must be performed on landscape parameters that occur within discrete "quadrants" or portions of quadrants radiating out from a wetland. In addition, earlier encounters can impact how other features are evaluated, so the context and location of conditions is important, and features must be evaluated from inner to outer locations in a sequential fashion. For example, if an amphibian encounters an interstate highway that constitutes an absolute barrier, then a forested area on the other side of the road has no value because it cannot be used to benefit the amphibians. Lastly, a parameter such as access to water can induce both positive and negative impacts, and the GIS parameter must represent this duality. With appropriate GIS parameters, the regression equation can be developed and used to inform the selection of ROWs to avoid locations that provide important habitat for amphibians.

INTRODUCTION

Wetlands are areas of seasonally, intermittently or permanently waterlogged soil or inundated land. Wetlands are complex, diverse ecosystems which are linked to the landscape surrounding them. The health of wetland is dependent upon the biological, chemical and hydrological processes and the activities occurring within their surroundings.

The amount of wetlands had decreased in the past centuries due to belief that they were worthless lands and because of the increase in the demand for agricultural lands. Approximately 50% of wetlands in the conterminous United States have been drained since European settlement, usually for agricultural usage (Tiner, 1984). The terrestrial habitats surrounding and adjacent to wetlands are critical for the management of natural resources and biodiversity conservation (Semlitsch and Jensen, 2003).

Wetlands are important systems that shelter and sustain a diversity of fauna including invertebrates, water birds, fish and amphibians. Wetlands are places where sediments accumulate, soils and landforms are created, nutrients are recycled and water is purified. Part of the reason that terrestrial habitat adjacent to wetlands are not protected is due to the lack of a clear understanding of the distances from shorelines that are biologically relevant to the wetlands (Semlitsch, 1998).

AMPHIBIANS

Amphibians in the Midwest United States have suffered major loss of habitat due to the conversion of nearly 90% of pre-settlement wetlands to agricultural uses (Dahl 1990). Pond-breeding amphibians require aquatic and terrestrial habitats to complete their lifecycles, and preservation of both habitats is necessary for maintaining local populations. Current wetland regulations focus primarily on aquatic habitats, and criteria to define critical upland habitats and regulations to protect them are often ambiguous or lacking (Porej et al., 2004). Pond-breeding amphibians are an

integral part of wetland ecosystems; however, the replacement or creation of quality amphibian habitat is usually not one of the goals of wetland replacement (Porej et al., 2004).

Semlitsch and Rothermel (2003) proposed the use of stratified criteria that would include three terrestrial zones adjacent to core aquatic and wetlands habitats (Figure 1):

- Aquatic Buffer, the first terrestrial zone (starting from wetland edge), would buffer the core aquatic habitat and protect water resources.
- Core Habitat, the second terrestrial zone (starting from wetland edge), would comprise the core terrestrial habitat defined by semi-aquatic species or species-group use.
- Terrestrial Buffer, the third terrestrial zone (starting from outward edge of second zone), would buffer the core terrestrial habitat from edge effects and surrounding land use practices.

Many species require both aquatic and terrestrial habitats and are limited to areas where there is sufficient moisture for reproduction and survival and access to adjacent terrestrial habitat (Jameson, 1957; Wilbur, 1987; John-Alder and Morrin, 1990; Vos and Stumpel, 1995). Few attempts have been made to model amphibian population dynamics (Halley et al., 1996; Gibbs, 1993) and fewer have been spatially explicit to considered landscape complementation (Vos and Stumpel, 1995). Zanini et al. (2008) stated that increasing urbanization and habitat alteration make it particularly important to find ways to assess the impact of land cover changes on the distribution of natural population.

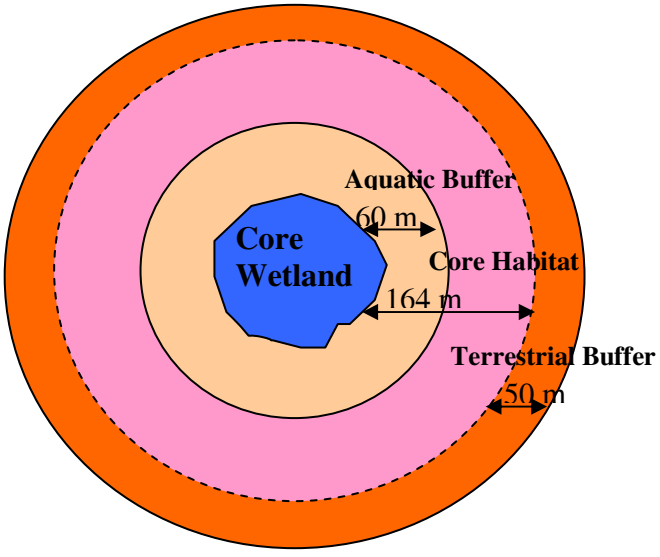

Figure 1. Zones for protection for wetlands (modified from Semlitsch & Rothermel, 2003)

AMPHIBIAN IMPACT AND ANALYSIS

Roads have a huge impact on the environment, with high amphibian mortality caused by traffic being reported in the literature (Ashley and Robinson, 1996; Lodé, 2000; Smith and Dodd, 2003). The researchers stated that the roads represent the most important source of variation in species richness. Similar results were reported in a study of North American salamanders (Porej et al., 2004). Findlay et al. (2000) found that road construction and the associated increase in human presence represents one of the major ways humans transform landscapes. Forman and Deblinger (2000) showed that the significant ecological effects of roads on plants and animals, including amphibians, average 600 m outward from a road.

Relatively few landscape-level studies of amphibian density and movement have been conducted (Houlahan et al., 2000; McGarigal and Cushman, 2002). The majority of the studies have focused on relationships between forest cover and species occurrence, showing positive relationship between amphibian population and area of forest in the surrounding landscape (Dupois and Stevenson, 1999; Trenham and Shaffer, 2005). Knowledge is still quite rudimentary about the population-level implication of habitat area, edge, isolation and road mortality relationship; effective conservation of amphibian population is limited by the lack of specific ecological knowledge and lack of landscape level studies of the effect of habitat loss and fragmentation or movement, survival rate and population dynamics (Cushman, 2006). Law et al. (1991) stated that determining the most relevant physical parameters on a landscape can be used as a basis for decision making and the design of response to specific environmental management challenge.

It is important to develop and implement new methodologies which address broader landscape areas surrounding the wetlands and to analyze the habitat interaction within it. Also, it is important to consider how multiple factors interact across different wetland buffer zones that could affect amphibian population. The present research is an attempt to analyze the interaction between amphibians and landscape conditions in the northern Missouri wetlands.

Roise et al. (2004) stated that the requirements to regulate wetlands (minimize impacts and implement compensatory mitigation) can be quantified and therefore infer that wetland management can be made more efficient through a combination of mathematical programming techniques, a wetlands functional evaluation methodology and information contained within a geographic information system (GIS) model of a landscape.

DATA ACQUISITION/ RESOURCES

A total of 49 wetlands will be analyzed during this study. The locations of the wetlands are shown in Figure 2. ArcGIS 9.2 software will be used to analyze all the wetlands spatially.

- The spatial and GIS wetland location data layer (shapefile) was collected as part of the overall project (Shulse, 2006) which contains information about all the constructed wetlands involved in the research.

- Spatial and GIS data layers necessary (land use/ land cover, streams, roads and topography) are readily accessible through the Center for Applied Research and Environmental Systems (CARES) and the Missouri Spatial Data Information Service (MSDIS) websites. The scales of the GIS data layers obtained are:
  - Land use/ land cover
    - Digital version in raster format obtained from MSDIS (2006) at a scale of 1:24,000.
  - Streams
    - Digital version includes rivers and streams at a scale of 1:24,000.
  - Roads
    - Digital version includes the roads and highways for which MoDOT is responsible.
  - Topography
    - 60 meter digital elevation model (DEM) in raster format from MSDIS.

METHODOLOGY

Missouri amphibian data from forty-nine constructed wetlands in northern Missouri (Figure 2) will be used to develop a regression equation (Eq. 1) which will describe wetland health in terms of the surrounding landscape characteristics. Amphibian data (number of each species in the various lifecycle stages) have been collected and analyzed from the biological perspective to create a habitat quality rating for each wetland (Shulse, 2008). This rating provides the dependent variable, Y, for the development of the regression equation relating landscape parameters to amphibian health. Landscape characteristics that will constitute the independent variables are: roads, streams, forest, landscape position and age of wetland. This model will be expected to increase the effectiveness of constructed wetlands and will decrease the probability of negative effects on the habitat of the wetland due to road constructions.

Once developed, equation 1 can be used to predict or estimate amphibian health under different landscape/ ROW scenarios for decision making. While the independent variables are shown as being represented as X_n, the actual terms may include powers and coefficients, or other functions, applied to the landscape parameters, as shown below:

$$\mathbf{Y=aX_1^b+cX_2^d+eX_3^f+gX_4^h\ldots.} \quad \text{(Eq. 1)}$$

Y=amphibian health, habitat quality rating

X_n=landscape parameters (e.g., roads, streams, forest area, landscape position and age)

a, c, e, g,…= coefficients applied to landscape parameters

b, d, f, h,…= powers to which landscape parameters are raised

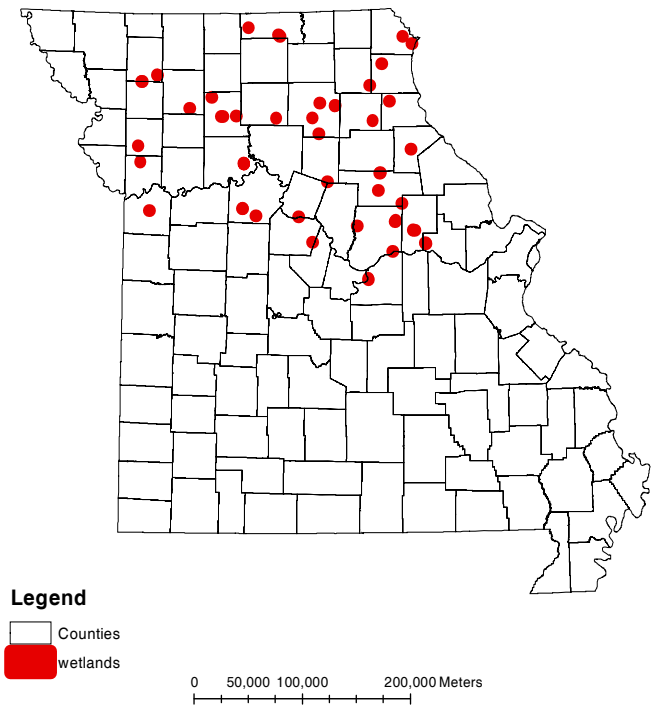

Figure 2. Point locations of compensatory wetlands in the study

SPECIFICATION OF LANDSCAPE PARAMETERS

The specification of features around each wetland will be determined using ArcGIS 9.2. The landscape analysis will consist of circular buffers up to 2.1 kilometers. Rings of 300, 600, 900, 1500 and 2100 meters from the edge of the wetlands will be analyzed. Each wetland will also be divided into quadrants and each wetland will be analyzed independently. Distance from the landscape feature to the wetlands will be an important factor for the prediction of the health of the wetlands. For example, if there is a highway closer to the wetlands area, this may be expected to cause more negative impact to wetlands health than a road that is far away from the wetland area.

The following points summarized the methodology to be used:

I. Landscape parameters

Landscape characteristics that will be used are: road, forest area, streams, landscape position and age. For the features of roads, streams and forest area each ring area will be checked to determine the contribution of each feature to wetlands health. A proximity analysis will be performed by dividing the parameter by the distance of the midpoint of the ring from the centroid of the wetland.

a. Roads
    i. Length of roads in each ring in each quadrant will be measured.
    ii. Both the eastbound and westbound directions of a highway will be measured in order to account for the increase width of such roads.
    iii. The length of road will be divided by the distance from each wetland centroid to the distance of each ring mid-point.
    iv. Independent variable unit will be (length of roads)/ (distance of the wetland centroid to mid-point of the ring).
b. Streams
    i. Length of the streams in each ring in each quadrant will be measured separately for perennial and intermittent streams.
    ii. The length of stream will be divided by the distance from each wetland centroid to the distance of each ring mid-point.
    iii. Perennial streams will be used as a surrogate for the potential presence of fish (possible flood case scenario) and will be expected to have a negative correlation with amphibian health.
    iv. Intermittent streams will be used as a surrogate for amphibian habitat and will be expected to have a positive impact in amphibian's health.
    v. Independent variable unit will be (length of streams)/(distance of the wetland centroid to mid-point of the ring).
c. Forest area
    i. Forest area data will be extracted from land use/land cover data layers.
    ii. Forest area will be determined for each quadrant within each ring for each wetland.
    iii. Independent variable unit will be (area of forest) /(distance of the wetland centroid to mid-point of the ring).
d. Landscape position
    i. DEM, forest area and stream data layers, as well as the digitized wetlands layer will be used determine the landscape position of each wetland.
    ii. A wetland located in an upland position in the landscape would be expected to have less contributing water to support the wetland, but a smaller probability of predatory fish.
    iii. A wetland located in a downslope position in the landscape would be expected to have a greater water contribution from runoff, but a greater probability of predatory fish, which can cause a decrease in the amphibian population.
    iv. The watershed of each wetland will be delineated using ArcGIS 9.2 to define the upland position and the downward position of each wetland.
    v. Independent variable unit will be a normalized value of landscape position.

e. Age of wetland
   i. Age of wetland is an important parameter due to the interactions of amphibians with landscape and the time available for amphibians to colonize the wetlands.
   ii. Independent variable unit will be a normalized value of age of the wetland.

II. Data standardization

a. Data standardization allows the transformation of parameters with various dimensions into dimensionless parameters with values between 0 and 1. This formula can convert numerical data into a standardized scale from 0 to 1.

$S = (X_i - X_{min}) / (X_{max} - X_{min})$, where S is the standardization value for the original value, X_i is the original value, X_{min} is the lowest value and X_{max} is the highest value.

b. Once the parameters are represented in a dimensionless format they can be used in Equation 1.

III. Analysis

a. The initial analysis, to determine the specific forms of the independent variables terms and coefficients will be conducted with the quadrant data summed for each ring. The analysis will consist of examining relations among the standardized landscape characteristic to amphibian abundance. The statistics package, STATA will be used to determine the correlation.

b. Quadrants
   i. Quadrants are important (Figure 3) to check the connectivity between wetlands. If two or more wetlands are near each other, the two wetlands may function as an ecosystem instead of individual wetlands.

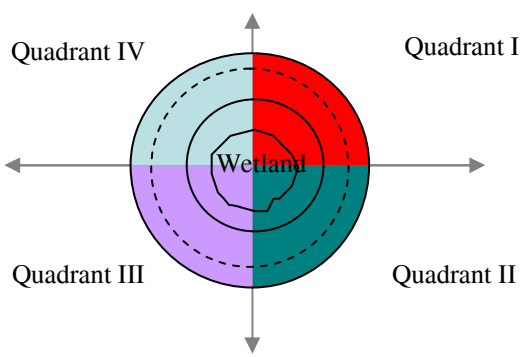

Figure 3. Wetland area divided in 4 different quadrants

   ii. Quadrants are useful to perform directional analysis along a ROW where multiple wetlands could be impacted by ROW selection. They can help in the determination of the intersection of the right-of-way with the functional portions of a wetland.

iii. For individual wetlands located near one another, the amphibian health values will be calculated for each quadrant. In this way, if a wetland will be impacted by road construction, one can determine which quadrant contribute most to amphibian health and thus should be protected and which ones will have less negative impact from future road construction activities.

c. Barriers
   i. A subsequent analysis will evaluate the potential impact of roadways as barriers on the previously determined correlations.
   ii. The analysis will test if roadways eliminate the benefits of forested areas and/or intermittent streams.
   iii. The correlation analysis will be performed as before, except that roads, streams and forest area in quadrants rings and beyond the location of a highway will not be included.

CONCLUSIONS

The goal of this research is to identify landscape characteristics that estimate wetland health in northern Missouri. The model will aid in the development of a rapid wetland assessment tool that could help in the decision making process of a right-of-way, useful for government agencies such as MoDOT and the Missouri Department of Conservation.

Amphibian data will provide the quantitative data to relate to wetland landscape characteristics. The amphibian data will provide the framework for the development of a landscape characteristic model that will predict health of wetlands (based on amphibian data). This methodology will help in the decision making process of the optimum location of a proposed the right-of-way to determine the location that would have the least negative impact on the wetland health.

REFERENCES

Ashley, E.P., and J. T. Robinson. 1996. Road mortality of amphibians, reptiles and other wildlife on the Long Point Causeway, Lake Erie, Ontario.Canadian Field-Naturalist 110: 403-412.

Cushman, Samuel A. 2006. Effects of habitat loss and fragmentation on amphibians: a review and prospectus. Biological conservation. 128(2): 231-240.

Dahl, T. E. 1990. Wetlands: losses in the Unites States 1780's to 1980's. U.S. Fish and Wildlife Service, Washington, D.C.

Dupuis, L.A., and D. Steventon. 1999. Riparian management and the tailed frog in northern coastal forests. Forest Ecology and Management 124, 35-43.

Findlay, C.S. and J Bourdages. 2000. Response time of wetland biodiversity to road construction on adjacent lands. Conservation Biology 14: 86–94.

Gibbs, J. P. 1998. Amphibian movement in response to forest edges, roads, and streambeds in southern New England. Jorunal of Wildlife Management 62: 584-589.

Halley J.M., R. S. Oldham, and J. W. Arntzen. 1996. Predicting the persistence of amphibian population with the help of spatial model. Journal of Applied Ecology 33: 455-470.

Jameson D.L. 1957. Population structure and homing responses in the Pacific tree frog. Copeia: 221–228.

John-Alder H.B., and P. Morrin. 1990. Effects of larval density on jumping ability and stamina in newly metamorphosed *Bufo woodhousii fowleri*. Copeia: 856–860.

Law, A. M., and W. D. Kelton. Simulation modeling and analysis. McGraw-Hill, New York, ed. 2). 1991.

Nuckols, J. R.,M.H. Ward, and L. Jarup. 2004. "Using geographic information systems for exposure assessment in environmental epidemiology studies".Environ Health Perspective 112: 1007-1015.

Porej, D., M. Micacchion, and T. E. Hetherington. 2004. Core terrestrial habitat for conservation of local populations of salamanders and wood frogs in agricultural landscapes. Biological Conservation 120: 399–409.

Semlitsch, R. D. 1998. Biological Delineation of Terrestrial Buffer Zones for Pond-Breeding Salamanders. Conservation Biology 12:1113-1119.

Semlitsch, R. D. and B.B. Rothermel. 2003. A Foundation for Conservation and Management of Amphibians. *Amphibian Conservation*. 2003 Ed., Washington, Smithsonian.

Shulse, C. 2008. EPA Regional Wetlands & Watershed Conference. April 7-11, EPA Region 7, KCI Expo Center, Kansas City, Missouri.

Stanley, S., J. Brown, and S. Grigsby. 2005. Protecting Aquatic Ecosystems: A Guide for Puget Sound Planners to Understand Watershed Processes. Washington State Department of Ecology. Publication #05-06-027. Olympia, WA.

Tiner, R. W., Jr. 1984. Wetlands of the United States: current status and recent trends in U.S. Fish and Wildlife Service, Washington DC, USA.

Vos C.C., and A.H.P. Stumpel. 1995. Comparison of habitat-isolation parameters in relation to fragmented distribution patterns in the tree frog. Landscape Ecology 11: 203–214.

Wilbur H.M. 1987. Regulation of structure in complex systems: experimental temporary pond communities. Ecology 68: 1437–1452.

Zanini F., Klingemann, A., Schlaepfer R., and Benedikt R. Schmidt. (2008). Landscape effects on anuran pond occupancy in an agricultural countryside: barrier-based buffers predict distributions better than circular buffers. Can. J.Zool. 86: 692-699.

The Rush Creek Detention Facility
Planning a Permanent BMP in the Real World

I.M. William Yord, P.E., A.M.,
And C.O. Joe Ennett 2, C. O. Dr. Jerry Richardson M., D.WRE 3

1 Project Manager, Wilson & Company, Inc., Engineers & Architects, 903 East 104th Street, Suite 210, Kansas City Missouri 64110; PH (816) 701-3144; FAX (816) 942-3013; email: William.Yord@wilsonco.com

2 President, Weatherby Lake Improvement Company, 7200 Eastside Drive, Weatherby Lake, Missouri 64152; PH (816) 741-5556; FAX (816) 741-2081; email: office@wlic.org

3 Associate Professor, School of Computing and Engineering, University of Missouri Kansas City, Robert H. Flarsheim Hall 5100 Rockhill Road, Kansas City, MO, 64110; PH (816) 234-1282; FAX (816) 234-1260; email RichardsonJ@umkc.edu

ABSTRACT

Weatherby Lake is one of the cleanest lakes in the State of Missouri. According to test samples of TMDL, phosphorous, heavy metals, and other pollutants, the water quality of Weatherby Lake is comparable to many pristine lakes in Canada. Development upstream of Weatherby Lake in the Platte County area in recent years has threatened the water quality of Weatherby Lake and has prompted action by the Weatherby Lake Improvement Company (WLIC) to take a positive pro-active role in the protection of this natural resource.

INTRODUCTION

Weatherby Lake (Figure 1) is a Class Four City located in Platte County, Missouri. The City was incorporated in 1936 and covers approximately 836 Acres (338.3 Hectares). Weatherby Lake itself is has a total drainage area of 2750 Acres (1112.9 Hectares) and a surface area of approximately 274 Acres (110.9 Hectares) at normal pool level or 33% of the City's land area. The top of the dam is approximately at elevation 890 Feet (271.3 Meters), with a height of 84 Feet (25.6 Meters), a length of 1100 Feet (335.3 Meters), and a maximum pool depth at the dam of approximately 80 Feet (24.4 Meters).(1)

WLIC is responsible for the maintenance of the Lake and its facilities. WLIC and the Missouri Volunteer Lake Program have formed a partnership with a group of 30 local volunteers, also known as the "Stream Team" (Figure 2); which samples influent into the lake and submits those samples to monitor total suspended solids (TSS), Nitrogen, Phosphorous, PH and Chloride. The Stream Team also takes Secchi Disc readings of Weatherby Lake.

In addition to these duties the Stream Team also monitors influent during rain events to determine water quality into Weatherby Lake from the surrounding upstream watershed.



Figure 1; Aerial of Weatherby Lake

In addition to work performed by the Stream Team, monitoring of the facility's inlets and coves is conducted by underwater surveys to determine when dredging may be required. Dredging operations can be extremely costly, time consuming, and disruptive of the use of Weatherby Lake by its residence.

The following is from the Mid-America Association of Conservation District's (MAACD), Missouri Department of Natural Resource's (MDNR) and the Environmental Protection Agency's (EPA) *Urban Conservation Policy Handbook (1998).*

Landowners located downstream of construction sites incur the expense of cleaning up sediment deposits. Accelerated sediment loads reduce the capacity of streams, ponds, and lakes. Direct expenses are incurred when excessive sediment loads must be dredged to restore the capacity of the lake. For example, WLIC, Platte County, Missouri, incurred the expense of dredging the lake to remove sediment. Within five years the same areas had to be dredged again due to construction activities upstream. WLIC spends an average of more than $100,000* annually to maintain the capacity of the lake. This expense includes the dredging operations plus the cost of additional land necessary for sediment disposal. The cost of removing the sediment, transporting it off site and disposing of it averaged over $8 per cubic yard (2).

*According to WLIC officials, approximately 40% of the annual fees collected annually go into a dredging and siltation fund for the maintenance of Weatherby Lake.

According to the Missouri Water Quality Report (Section 305b) dated 2006, Weatherby Lake monitoring data taken by the University of Missouri through 2005 was recorded as shown in Table 1.(3)

Table 1; Trophic Status of Weatherby Lake

Years of Record	SECCHI DEPTH (M)	TOT. PHOS. (µg/L)	TOT. NIT. (µg/L)	CHL-A (µg/L)	Trophic State
3	2-3**	20	403	5	M***

** The Missouri Water Quality Report indicates that the Secchi Depth reading was 2-3 meters. WLIC personnel indicate that this value is actually greater than recorded in Table 1

*** Trophic State: O=Oligotrophic, M=Mesotrophic, E=Eutrophic, HE=Hypereutrophic Unclassified Lake Trophic

Trophic state is an important way to characterize lakes because it relates directly to such factors as lake clarity. Lake clarity is greater in oligotrophic and mesotrophic lakes. Fish production tends to be greater in eutrophic lakes. Very clear water lakes are classified as oligotrophic with little nutrients, sediment, plants, and small populations of fish. Eutrophic lakes are the other end of the spectrum with nutrient rich waters that support larger, more diverse fish and plant populations with poor secchi dish readings.

Weatherby Lake is classified as a mesotrophic lake which lies between oligotrophic and eutrophic lakes; with clear water, submerged plant growth, and medium levels of nutrients. It should be noted that some nutrients in a lake are beneficial; however overproduction of algae that may be caused by overproduction of nutrients into a lake from the watershed may be harmful to the overall health of the facility.

Samples collected by the Stream Team from watercourses upstream of Weatherby Lake have helped determine when increased levels of suspended solids, settleable solids, phosphates, nutrients, and other contaminants in stormwater runoff from the watershed have occurred. (4)



Figure 2; Stream Team Volunteers taking samples at Weatherby Lake

STATEMENT OF THE PROBLEM AND PLAN OF ACTION

Non-source point pollutant loading from commercial development upstream of Weatherby Lake on Rush Creek prompted action by WLIC which was the construction of a regional water quality basin on the tributary downstream of the development activity to help protect Weatherby Lake.

This water regional water quality basin, known as The Rush Creek Detention Facility, presented many technical, non-technical, and permitting problems including;

- Planning
- Ownership
- Operation and Maintenance
- Safety
- Regulatory and legal issues
- Coordination between private and governmental agencies

The most challenging issue was related to permitting the Rush Creek Facility, which was the first of its kind for the Development Services Branch of Kansas City, Missouri. A major hurdle that had to be overcome was how to permit a privately owned Regional Permanent Best Management Practice (BMP) on a public stream. The Rush Creek project set a precedent for future BMP projects.

RUSH CREEK RETENTION AND WATER QUALITY BASIN

The tributary area to the Rush Creek retention facility is approximately 542 Acres (219.3 Hectares). The facility is composed of a fore bay, a 24 foot (7.3 Hectares) high dam, 3.6 Acre-Feet of permanent pool area with a principal spillway that consists of a 12 Feet by 6 Feet Reinforced Concrete Box (RCB) with an inlet equipped with anti-vortex walls, an 18 Inch (0.45 Meters) drawdown pipe and gate valve. The facility also has two 30 foot (9.1 Meters) emergency spillways that were designed for concurrent one-hundred year storm events to meet current APWA and Kansas City criteria. Approximately 1500 Feet (457.2 Meters) of 18 Inch (0.45 Meters) sanitary sewer relocation and a specially designed access road for emergency and maintenance access, to the dam and primary spillways were required for the project (Exhibit A).

PRIVATE OWNERSHIP ON A PUBLIC STREAM

Even though the Rush Creek facility is privately owned, it lies on a public stream, which presented a unique set of challenges for WLIC and Kansas City to overcome. In addition to being permitted through Kansas City, the U.S. Army Corps of Engineers, and the Missouri Department of Natural Resources permits were obtained for its development.

City permitting included the following City departments:

- KCMO Planning and Zoning Department
- KCMO Legal Department
- KCMO Development Services Branch
- KCMO Water Services Division
- KCMO Emergency Services
- KCMO Parks and Recreation Department

Other permits included the following agencies:

- United States Corps of Engineers (USACOE) Kansas City District
- Missouri Department of Natural Resources

The permitting and approval process for the Rush Creek facility took over two years to complete.

A Preliminary Development Plan had to be drafted for the project and submitted to planning and zoning department to gain approval of the City Counsel. Easement dedications for a public street associated with the property on which the facility is located and other easements pertaining to the BMP had to be drafted and executed. These easements ensure ongoing access for the City, protection of the facility, and protection of Rush Creek, if the property were sold.

A "Covenant to Maintain" agreement had to be developed between Kansas City and WLIC to ensure proper ongoing maintenance of the Rush Creek facility. WLIC's attorney and the City's attorney worked on the legal language of the agreement while Wilson & Company worked on the technical issues in the agreement including language for ongoing maintenance and operation of the Rush Creek Facility.

Initially, the 18 Inch (0.45 Meters) interceptor sewer was going to be maintained in place and lined under the facility. During final design, it became clear that moving approximately 1500 Feet (457.2 Meters), of the existing 18 Inch (0.45 Meters) sanitary sewer line around the dam structure was in the best interest of both WLIC and the City for protection of the permanent pool, dam and the sanitary sewer. Plans for this relocation were developed and submitted to Kansas City Water Services Department for approval as part of the Rush Creek project.

The outlet structure for the Rush Creek facility was revised to meet KCMO and APWA requirements. This included adding a second emergency spillway to the dam and re-sizing the primary outlet structure. Wilson & Company worked with Kansas City Water Services Department to include the Rush Creek Facility in the hydraulic basin planning activities on Rush Creek. This facility is designed to accommodate dual 100-year storm events through the emergency spillways with 1 Foot (0.3 Meters) of freeboard. Excavation of a permanent pool area upstream of the primary outlet is sized to accumulate 5 years worth of sediment before dredging is necessary. An 18 Inch (0.45 Meters) drawdown valve is capable of completely draining the facility in approximately 2

hours. A beach analysis was conducted for the facility and an emergency action plan was drafted in conjunction with KCMO Emergency Services and submitted to KCMO and WLIC in case there is ever a breach of the dam. All of the hydraulic data was returned to KCMO Water Services Department to incorporate into their Rush Creek Master Watershed Plan.

Initiation of construction took place on September 8, 2008 which was 6 years after the inception of the plan, which included the following:

- Drafting and acceptance of the Preliminary Development Plan by planning and zoning and the City Counsel
- Drafting the drainage report
- Drafting an emergency management plan
- Plans, specifications and estimates
- Drafting and executing the "Covenant to Maintain" agreement
- Drafting and recording all other easements

CONCLUSONS

Weatherby Lake's citizens continue to be very proactive in maintaining a water quality monitoring program for their facility. A partnership with the Missouri Volunteer Lake Program and this proactive stance provided a baseline for the development of the Rush Creek project and will serve as a guide to help fine tune the operation of the facility as conditions change on Rush Creek.

Even though all parties entered into the Rush Creek Project with best intentions, there were still conflicting technical, legal and political issues that had to be resolved, which included:

- Planning
- Ownership
- Operation and Maintenance
- Safety
- Regulatory and legal issues
- Coordination between private and governmental agencies

The bulk of the work for the Rush Creek Basin was not technical in nature, but legal and political. Since the Rush Creek Detention facility was one of the first regional water quality basins permitted by Development Services, it helped Kansas City start to set a precedent for others to follow for planning and permitting this kind of facility.

The Rush Creek Facility was much larger than most permanent BMPs that will be installed on private property in the coming years. Because of this there was more intense involvement of City staff and departments than there would be for smaller facilities; however, the experiences of the Rush Creek Basin will be multiplied many times over as Kansas City prepares to incorporate these "Green Solutions" into the Combined Sewer Overflow (CSO) program in the coming years.

These Green Solutions in Kansas City will necessitate the use of private property to help mitigate peak discharges associated with wet weather events that contribute to combined sewer overflows. The City is planning on spending five-hundred million dollars out of the two-billion dollar program to install these facilities which amounts to approximately 25% of the CSO infrastructure.

Many of these facilities will end up on private property and will be maintained by private property owners or homeowner associations with their own "Covenant to Maintain" agreements with the City, which may include permanent easements for these facilities.

This will take a private/public partnership not with only one property owner, but many. The City will need to establish a system to efficiently permit, monitor, and possibly maintain this infrastructure in order to make the CSO program effective and viable. The Rush Creek Detention Facility helped set a precedent for others to follow in the future.

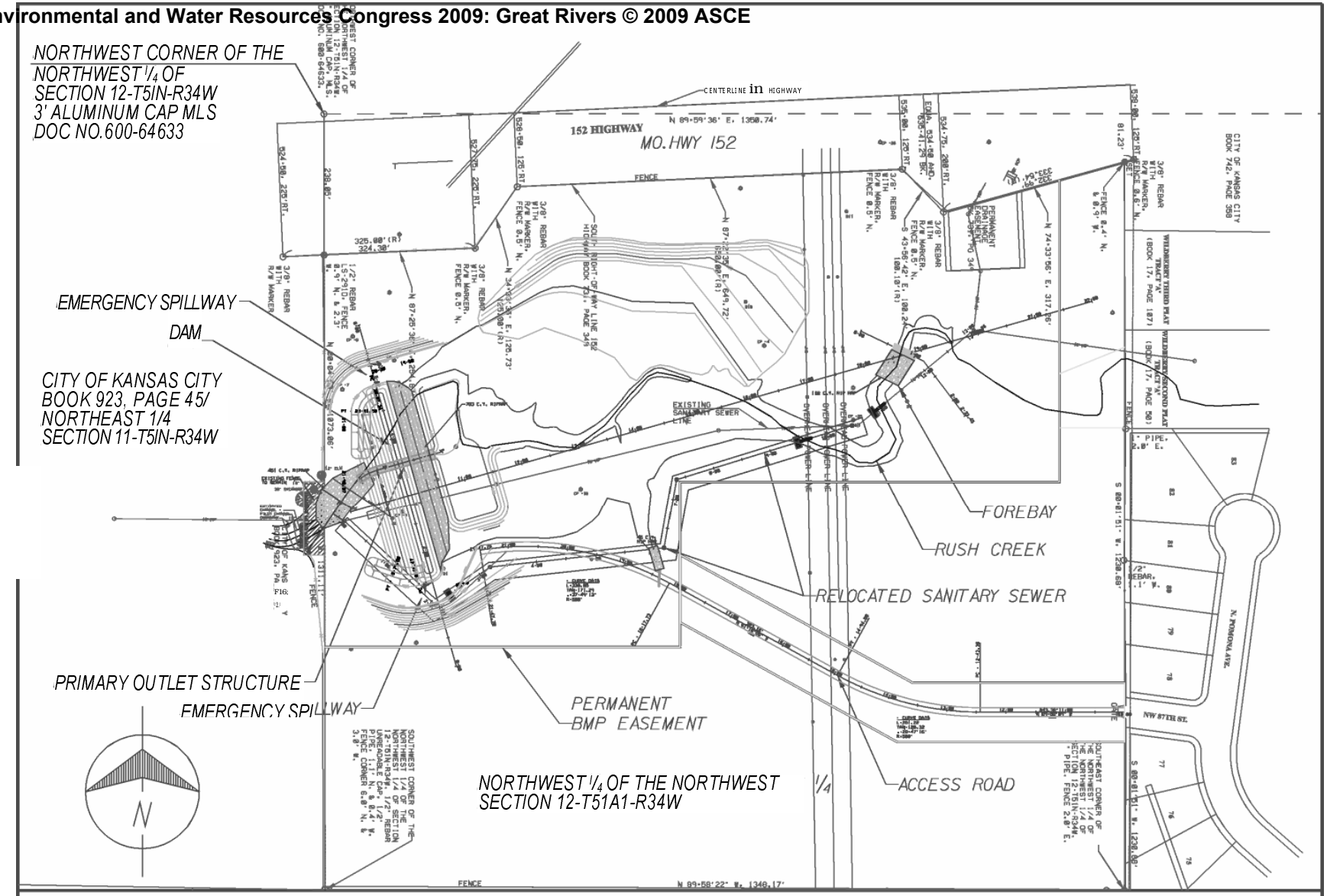

RUSH CREEK DETENTION FACILITY

EXHIBIT A

(1) http://www.dnr.mo.gov/env/wrc/damsft/Crystal_Reports/platte_dams.pdf

(2) Economics of Erosion and Sediment Control, Page 3; Urban Conservation Policy Handbook, EPA Region VII, 1988

(3) Trophic Status, Table 9; page 21 Missouri Water Quality Report (Section 305(b) Report), MDNR, 2006

(4)http://yosemite.epa.gov/water%5Cadopt.nsf/by+State/344C42C05037BAEF85256F9A0080B59F?OpenDocument

General Hydraulic Characteristics of an Open Channel with Narrow Path

M. S. Quimpo[1] and T. Yamada[2]

[1]Graduate School of Civil Engineering, Chuo University, 1-13-27 Kasuga, Bunkyo-ku, Tokyo, Japan, 112-8551; Tel. No. (81) 3-3817-1805; FAX (81) 3-3817-1803; tessquimpo@yahoo.com
[2]Department of Civil Engineering, Faculty of Science and Engineering, Chuo University, 1-13-27 Kasuga, Bunkyo-ku, Tokyo, Japan, 112-8551; Tel. No. (81) 3-3817-1805; FAX (81) 3-3817-1803

ABSTRACT

This study uses laboratory and theoretical experiments considering upstream, narrow and downstream sections of the channel in its normal and inundated state conditions. In a normal state condition, results proved that as the cross-section of a channel decreases, the higher the velocity and maximum water depth occurs. Asymmetry of flow was caused by the occurrence of different velocities and pressures at the exit right and left sides section of a narrow path and was dependent on the initial boundary conditions applied at upstream section of the channel. On the other hand, bank overflow starts to inundate where maximum water depth occurs during the normal state condition then goes to the floodplain upstream side direction. Moreover, Ishikawa's theoretical overflow equation correlates with the laboratory and theoretical results. Understanding the flow characteristics of a channel will allow us to predict and identify the direction and extent of damage in case of flood.

INTRODUCTION

Narrow path form, also known as sudden contraction is one of the natural shapes of a channel. It is known that the form of a channel affects the flow of water in it. At the same time, through erosion and deposition, the flow can also modify the channel shape. Correct measurement of flow characteristics is very essential in the study of the existing states of fluid motion. It is obviously necessary to understand the essential principles of such motion in order to predict with fair certainty what the characteristics of flow, will be under any given conditions (Rouse, 1946).

Previous study says that asymmetrical flow or the so called, Coanda Effect is the fact that the flow becomes asymmetric in spite of symmetric test sections and symmetric inlet and outlet conditions. An increase of velocity near one wall is accompanied with a decrease in pressure, and once a pressure difference is established across the duct, it will maintain the asymmetry of the flow. The choice of one side or the other is dependent on subtle details of the initialization and transient history of the flow.

Appropriate examples of a narrow channel can be found in Fukawa, Tone River and Kitagami River in Japan (**Figs. 1 and 2**). These areas are abundantly populated and are highly susceptible to flooding as it lies in lowlands that are below the flood water level of the river. Although through many years of flood control efforts, the

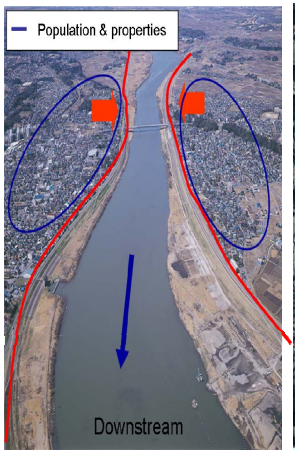

Fig. 1 Tone River

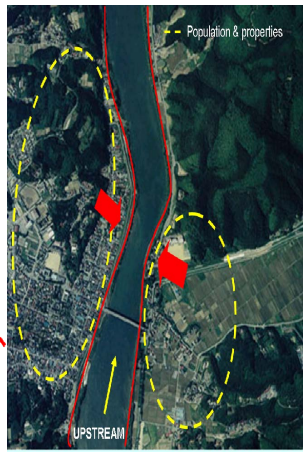

Fig. 2 Kitagami River

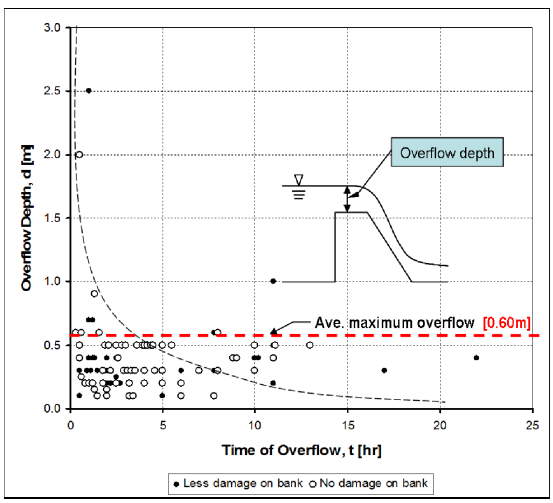

Fig. 4 Maximum Overflow Depth Survey (K.Suga, et. al 1981)

total inundated areas have been reduced, the flood damaged has hardly decreased because population and properties continues to increase in the said area Due to the existence of the same along the narrow channel, widening of the river as flood countermeasure will not be possible.

A survey on the occurrence of maximum overflow depth was conducted to the residents living near the real rivers in Japan and was found that the average maximum overflow depth occurred was approximately 0.60 m. as shown in **Fig. 4.** River banks with less damage and no damage data were considered in the survey (K. Suga et. Al, 1981).

Also, a related theoretical study on overflow was published in determining the maximum overflow depth (Ishikawa, 1982). Its objective was to obtain the overflow water depth profile using the maximum overflow depth equation derived from the continuity and energy conservation momentum equations. Results from this study shows that the maximum overflow depth reach up to 1.35m using the theoretical analysis conducted on real rivers of Japan in 1982. It was based from the ratio of river width, B against height of the bank, H (B/H) parameters and was found applicable if there is a sudden change in river width. However, if there is no significant difference between the channel width and narrow width, it is not clear whether this equation will still be applicable. This theory was found to accurately calculate the maximum height of the overflow from riverbank. Hence, it served as a good working equation to calculate the highest overflow depth.

There are existing structural flood mitigating measures being implemented by Japan's government river administrators. Theories are also in place to determine the maximum overflow depth. This study aims to determine the flow behavior in a narrow open-channel through laboratory experiments using small-scale river model and a theoretical calculation using Ishikawa's theory on bank overflow.

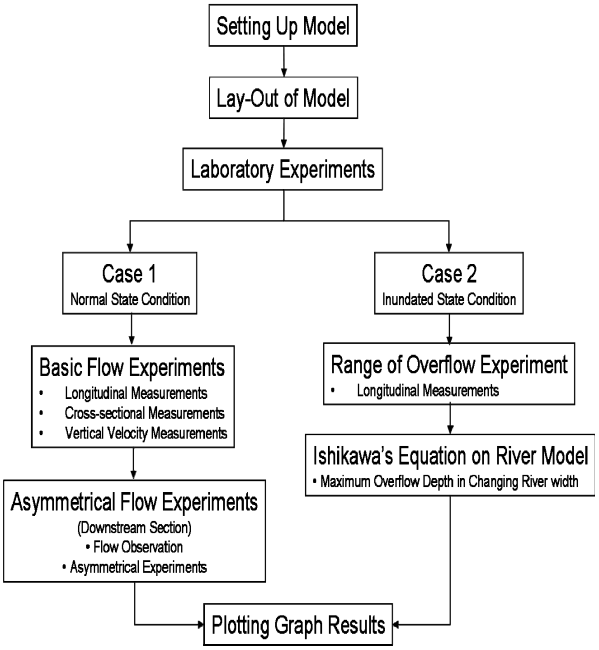

Fig. 5 Methodology Chart

METHODOLOGY

Research procedure

There were two cases conducted in this research: 1) normal state condition and 2) inundated river condition. Case 1 aims to determine the basic flow characteristics of a narrow channel model and investigate occurrence of asymmetrical flow at downstream section through laboratory experiments. On the other hand, case 2 seeks to examine the extent of overflow and behavior of flow using laboratory experiment and theoretical calculation analysis. See methodology chart in **Fig. 5**. River model dimensions and narrow channel model locations were stipulated in **Table 1**.

Table 1: Narrow Path Location

Experiment	Narrow Location (from Upstream)	Diagram
Case 1: Normal State Condition		
I. Basic Flow	7.0 m	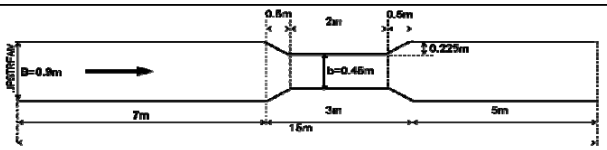
II. Asymmetrical Flow	9.0 m	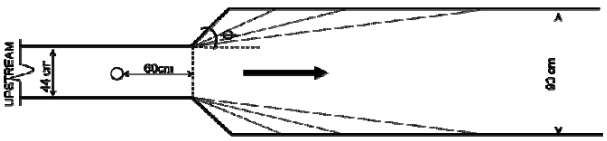
Case 2: Inundated State Condition		
III. Range of Overflow	11.5 m	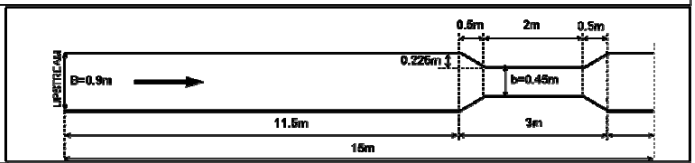
IV. Ishikawa's Overflow Equation	12.1 m	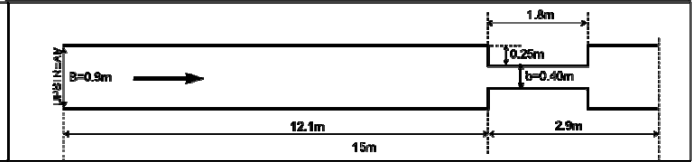

Laboratory experiments on two cases were both performed in a one-sided glass rectangular flume 15 m long, 1.80 m wide and 0.40m deep. It has an adjustable slope of up to a maximum of 1/50 or 30 cm height difference between upstream and downstream sides of the flume. The downstream tailgate was fixed at a certain angle to maintain a steady flow at upstream side of the channel. A 15 kW - 4 pole three phase induction motor pump (HITACHI, Silent Power) is attached to it that supplies discharge of up to 123~124 L/s maximum. Water depth measurements were taken using a point gauge with a reading accuracy of $\pm$1mm. Alternatively, velocities were measured using a 2D-electronic magnetic current meter (KENEK, VM-801H) for case 1-I, which has an adjustable range of 0~200 cm/s and a movable time constant from 0.05~1 sec. On the other hand, for case 1-II, velocities were measured using 3D-electronic magnetic current meter (KENEK, VM-1001RS). With an adjustable range of 0~200 cm/s and a time constant of 0.5~10 secs.

To verify Ishikawa's overflow theory (1982), the third method applied in this research is using his theoretical equation equal to:

$$\delta_2 h_2^{\,2} + \left\{\gamma_2 - \frac{3}{2}(1-b)\right\} h_2 + \frac{3}{2}(1-b)\Delta h + b = 0$$

where: h_2: the maximum overflow water depth; δ_2, γ_2: dimensionless coefficient channel change at the upstream side boundary; b: channel width; and Δh: height difference at upstream and downstream side boundaries as derived in Ishikawa (1982).

River Model Lay-out

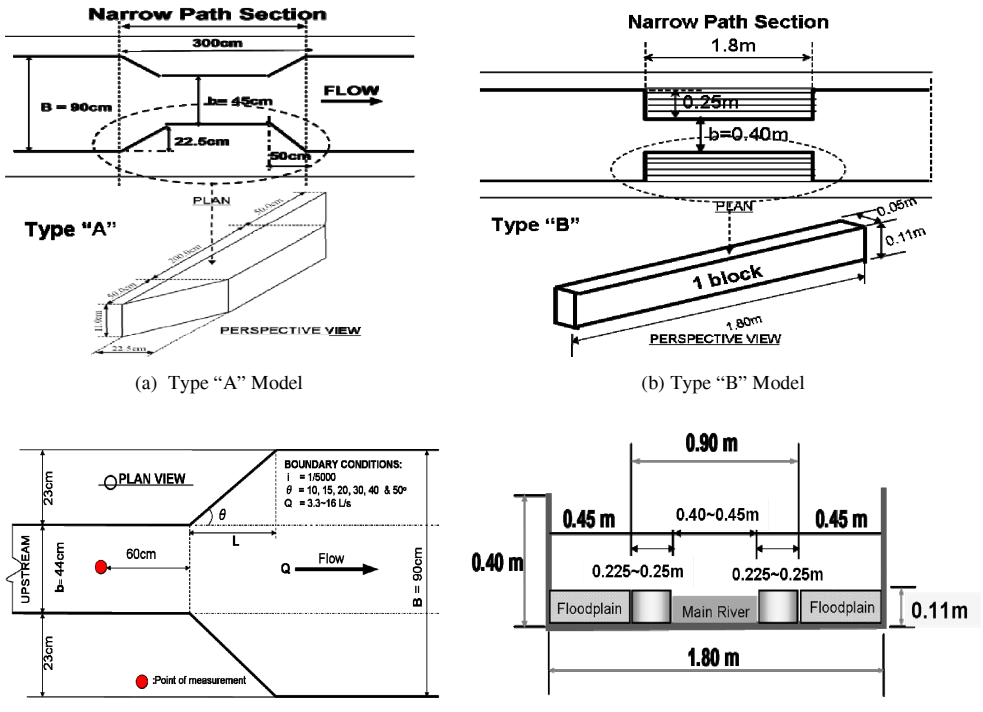

(a) Type "A" Model

(b) Type "B" Model

(c) Type "C" Asymmetrical Model

(d) Cross-Section

Fig. 6 Narrow Path Models Detail

In a rectangular flume, a compound river small scale-model was first constructed that produces a main river that measures 15m long, 0.90m wide and 0.11m deep and floodplains at both sides that measures 15m long, 0.45m wide and 0.11m deep. Then a narrow channel model was laid at each side of the main river. Three different narrow path models were used (**Fig. 6**): (a) Type "A" model for basic flow and range of flow experiments which measures 3m long, 0.225m wide and a depth of 0.11m; (b) Type "B" model for Ishikawa's overflow experiment, composed of blocks which measures 1.8m long, 0.05m wide and 0.11m depth each; and (c) Type "C" model for asymmetrical flow experiments, changing the angle of the narrow exit section as model were used.

Laboratory Experiments

Case 1 - Normal State River

1. Basic Flow Experiment

First, a normal state river condition was conducted. In this case, narrow section was installed 7 m from upstream side of the 15 m flume as stipulated in Table 1-I. River conditions and boundaries were: length equal to 15.0m; flume total width of 1.8m; model width of 0.9m; narrow path width of 0.45m; height of the model equal to 0.11m; and a river slope was set to 1/1000. Also, Manning's number used for the main river was equal to 0.025 $s/m^{1/3}$ and 0.017 $s/m^{1/3}$ for the river bank. Discharge applied at the upper stream boundary, Q was equal to 15L/s constant. Longitudinal, cross-sectional and vertical measurements were conducted in order to acquire velocity distribution and water depth results at each point of measurement. Longitudinal measurements were taken at the middle of the river model. Water depth and velocity were measured at 32 points and 27 points, respectively. On the other hand, cross-sectional velocity measurements were conducted at five (5) cross-sections spaced at an interval of 0.25 m to 0.50 m. Measurements were conducted with 5 points at section 1 to 3; 11 points at section 4; and 9 points at section 5. Widths at each section also vary: sections 1 and 4 equal to 90cm; sections 2 and 4 equal to 67.5cm and section 3 equal to 45cm. While, vertical velocity distribution measurements were conducted at seven (7) sections of the narrow channel with five (5) points of measurements from the bottom of the channel going up to the water surface.

2. Asymmetrical Flow Experiment

This research conducted two (2) experiments. First experiment was merely flow observation experiment. Second experiment on the other hand was conducted to thoroughly identify the asymmetry and symmetry of the flow.

First, an experimental observation was conducted at the downstream section of a narrow channel. River and boundary conditions were : length equal to 15.0m; flume total width of 1.8m; model width of 0.9m; narrow path width of 0.45m; height of the model equal to 0.11m; and a river slope was set to 1/1000. Also, Manning's number used for the main river was equal to 0.025 $s/m^{1/3}$. Discharge applied at the upper stream boundary, Q was equal to 18L/s constant. Blue dye was used to identify the direction and pattern of the flow. First, it was sprayed at the middle section of the channel, and then sprayed randomly without spreading at a specific point. To further

understand the occurrence of this phenomenon, asymmetry laboratory experiments were conducted. The exit section of the narrow model was then changed and adjusted to 10°-50° angles. Furthermore, bed slope was set to 1/5000 and upstream boundary conditions were set to a minimum of 3.3L/s to a maximum of 16L/s.

Case 2 - Inundated River

1. Range of Overflow Experiment (Longitudinal Measurement)

An experiment on an inundated narrow river model measuring the length of inundation was then next conducted. Narrow model section was then transferred near the downstream side, 11.5 m from upstream. River conditions and boundaries for this case were the same as experiment on basic flow characteristics, except for the discharged supplied which was equal to 10 L/s as upstream boundary condition and positioning of the narrow model previously stated.

2. Inundation Width Reduction Experiment (Ishikawa's Overflow Equation)

Different model and method of experiment was conducted for Ishikawa's overflow equation. Ten (10) pcs. - 5cm x 11cm x 180cm wooden blocks were used as narrow path model. They were equally placed (5 blocks) at each bank side to create a narrow path model with an angle of 90°. The narrow blocks were positioned 12.1 m away from upstream section. River conditions and boundaries for this experiment were the same as the aforementioned experiments previously discussed, from model total length, flume total width, model width, narrow width, height, slope to Manning's number. It differs only with the discharged supplied which was equal to 30 L/s as upstream boundary condition, positioning and shape/angle of the narrow model. Each block (from inner) was taken out every after measurement. Measurements were taken 10 times at 7 different narrow widths, measured and then results were averaged. This experiment was conducted to determine the relationship between the width reduction ratios against non-dimensional overflow depth.

RESULTS AND DISCUSSIONS

1. Normal State River

1.1 Longitudinal Measurement

Results in **Fig. 7** shows that water depth fluctuates as it approaches the narrow

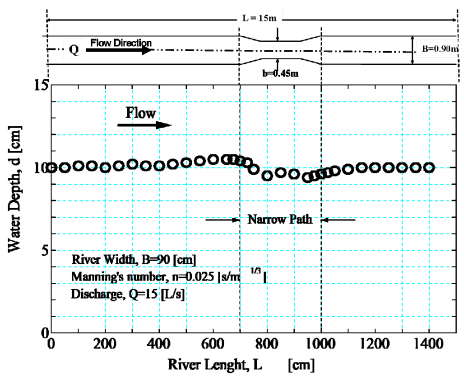

Fig. 7 Water Depth Profile

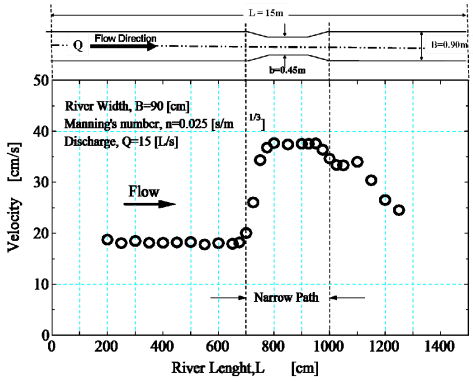

Fig. 8 Velocity Profile

path section of the channel. Then water depth level gradually goes back to its normal depth as it exits the narrow path section.

So with the velocity profile result in **Fig. 8**, velocity abruptly increases as it enters the narrow path section of the channel and gradually decreases as it exits the same. It was also observed that the velocity doubles its value at the narrow path section as compared to its velocity value at upstream section of the channel.

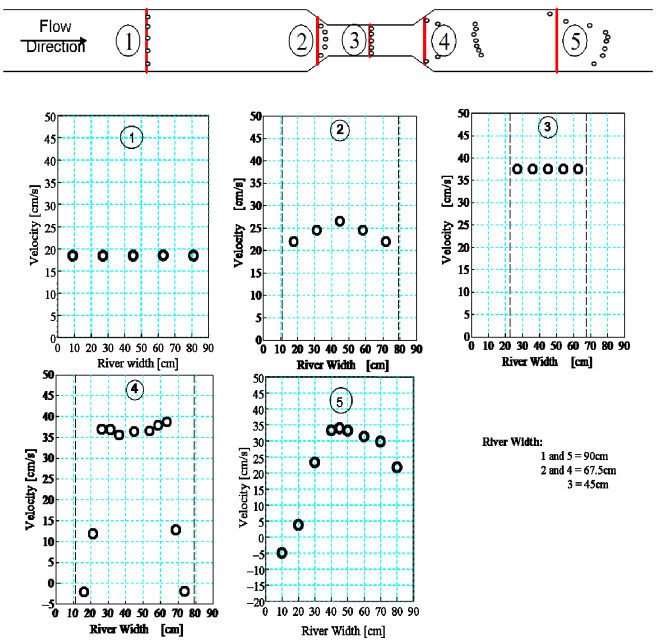

Fig. 9 Cross-Sectional Velocity Profile

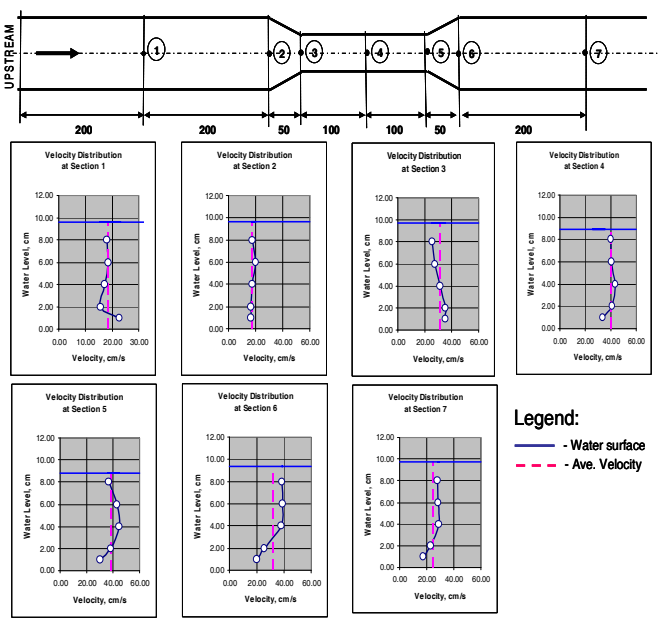

Fig. 10 Vertical Velocity Distribution

1.2 Cross-sectional Measurements

Results are shown in **Fig. 9**. Results show that velocity distributions at sections 1-3 had symmetrical velocity distributions. As observed, as the flow exits a narrow section, velocity distributions becomes asymmetrical as shown in sections 4 and 5.

1.3 Vertical Velocity Distribution

Vertical velocity distribution was conducted to determine how the flow behaves from bottom to the water surface of a narrow channel at the mid-section of the channel (**Fig. 10).** Result shows that at the upstream section of a narrow channel, velocity is not gradually increasing and it only shows almost the same value. Like the cross-sectional experiments results,

maximum velocity occurs at the narrow section of the channel. Velocity distributions at downstream side show that velocity gradually increases as it goes up to the water surface.

1.4 Asymmetrical Flow Experiments

Fig. 11 results show that an asymmetrical flow pattern occurs as the flow exits the narrow path. It was observed that it is when an adverse pressure gradient occurs along the sidewall of the channel.

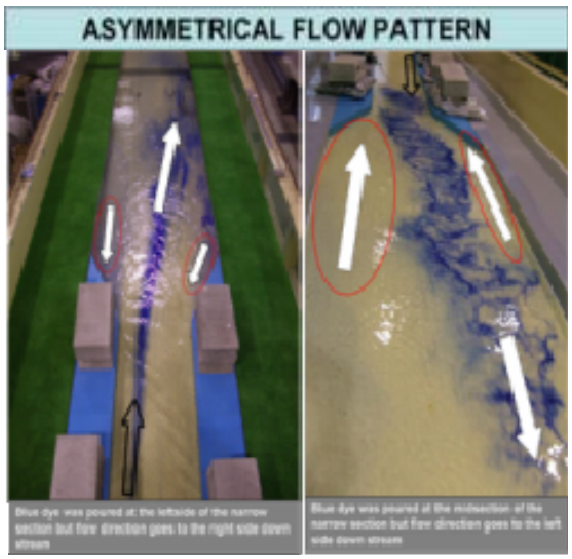

Fig. 11 Asymmetrical Flow Observation

This experiment aims to determine the asymmetry direction of the flow at the exit section of a narrow channel. **Fig. 12** shows the symmetry and asymmetry flow boundaries. Result shows that asymmetry flow to the right mostly occurs at cot θ equal to 5.68. Also, at Froude number, Fr value greater than 1.0 at cot θ value 0.84 and from Fr 1.05 at cot θ value 1.19. On the contrary, asymmetry to the left mostly happens in between Fr value 0.80~1.05 at cot θ value equal to 1.73, 2.75 and 3.73 respectively. Furthermore, symmetry occurs at Fr greater than 0.95.

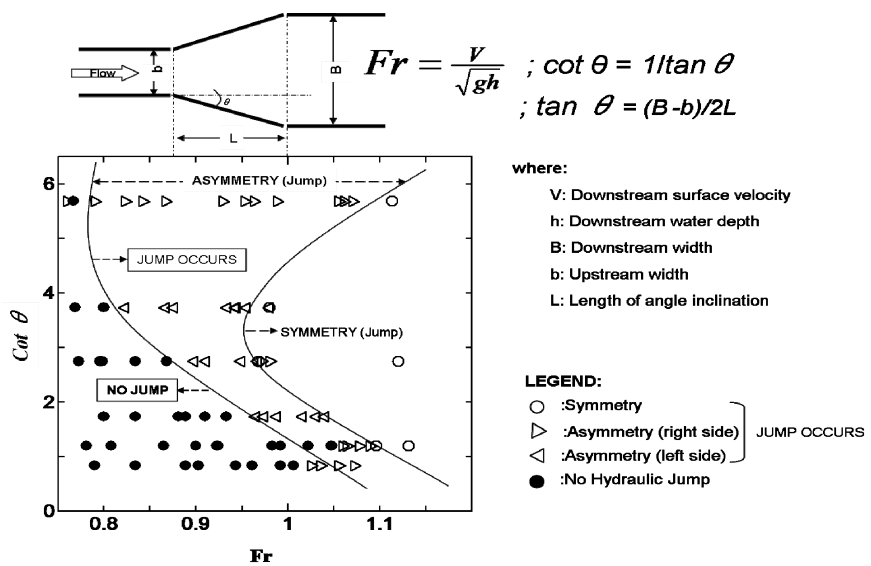

Fig.12 Symmetry and Asymmetry Boundaries

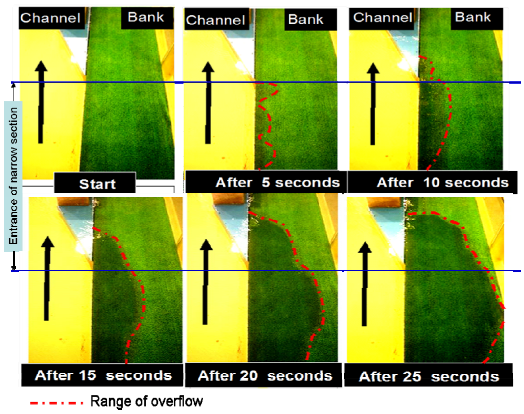

Fig. 13 Longitudinal Range of Bank Overflow

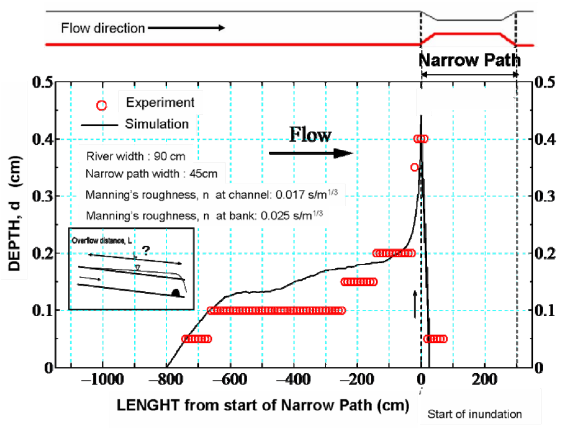

Fig. 14 Cross-Sectional Overflow Distance

2. Inundated River

2.1 Range of Overflow Experiment

Fig. 13 shows Inundation results in longitudinal measurement. Result shows that inundation starts at the upstream approach of the narrow path during the 25 seconds observation. Water starts to inundate from approach section back to upstream side direction.

On the other hand, **Fig. 14** shows that inundation flows back to up to 740cm long from the top of the river bank flowing to upstream direction.

2.2 Comparison to Ishikawas' overflow coefficient

Fig. 15 shows the relationship between the overflow depth and the width reduction ratio. Result shows that the laboratory experiment matches the theoretical line (overflow coefficient, c) equal to 1.0. It also shows that the narrower the width of a channel, the higher the overflow depth.

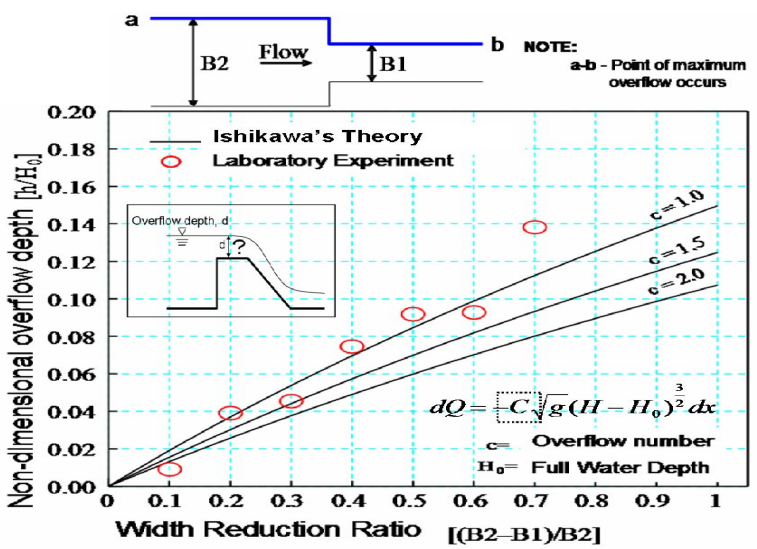

Fig. 15 Overflow Discharge Coefficient Graph

CONCLUSIONS

Case 1

This case shows that as the flow approaches a narrow section of the channel, water depth abruptly increases and as it enters the narrow path, velocity gradually speeds up. Longitudinal and vertical distribution profiles show that the maximum velocity occurs along a narrow section of a channel model. Regardless of the position of the initial pouring of blue dye, flow direction randomly goes to the right or left side of the downstream section of a narrow channel. The observation experiment proves Bernoulli's theorem: "that as the speed of a moving fluid increases, the pressure within that fluid decreases."

Symmetry occurs at Fr greater than 0.95. On the other hand, asymmetry of flow to the right or to the left direction is dependent on the angle inclination of the downstream section of the channel.

Case 2

Inundation starts at the upstream approach section of the narrow path and flows back horizontally to upstream side direction. Based on the results showed with the comparison to Ishikawa's theoretical line in this case, a narrow path falls under overflow coefficient, c equal to 1.0. This study proves that in a sudden contraction/narrow section, Ishikawa's theory was found effective for a sudden contraction channel. Furthermore, it was concluded that using Ishikawa's theoretical calculation can predict a bank overflow depth.

REFERENCES

Negm, A.M. 2001. *Flow Characteristics at Asymmetric Sudden Contraction*. Proc. Of IWTC-VI 2001. Alex. Egypt. March 23-25: 5-19.

H. Rouse, *Elementary Mechanics of Fluids*, 1946

Infrastructure Development Institute-Japan et.al, *Rivers in Japan,* 2006

Homepage, MLIT, Kanto Regional Development Bureau, Keihin River Office

Flood Control Handbook (2004), Japan

K.Suga, T. Ishikawa and T. Kasai, "*The Characteristics of Failure Embankment by Overtopping*", Proceedings of the 25th Japanese Conference on Hydraulics (1981), pp. 355-360.

T. Ishikawa, *"Water Surface Profile of a Flow Decreasing Discharge by Sidewall Overtopping"*, Proceedings of the 26th Japanese Conference on Hydraulics (1982), pp. 417-422.

Yamashita, K., Quimpo, M. Yamada, T. "Water Surface Profile Behavior in an Open-Channel Enlargement", unpublished.

Mathematical Modeling of Bed - Topography Changes at Bridge Abutments

Omer Kose[1] and A.Melih Yanmaz[2]

[1]Assist. Prof., Department of Civil Engineering, Aksaray University, TURKEY, FAX: 90-382-2150592, email:omerkose2000@gmail.com
[2]Prof., Department of Civil Engineering, Middle East Technical University, 06531, Ankara, TURKEY, FAX: 90-312-2107956, email: myanz@metu.edu.tr

ABSTRACT

River bridges are very important elements of transportation systems, failures of which may not only lead to loss of several lives and excessive damages but also various deficiencies including socio-economic factors. Several aspects of bridge failures should be investigated jointly to gather information for scour-resistant design practices. This study specifically focuses on the effect of clear water scouring at vertical-wall abutments on bridge stability. Determination of the time-dependent volume and surface area of scour hole around a vertical-wall abutment would yield relevant information to assess the safety level of the bridge foundation. To this end, temporal variation of geometric features of scour holes around vertical abutments under clear water conditions are examined with reference to an experimental study. Findings of this study would yield some information concerning loss of structural resistance, safe design of footing and sizing and placement details of armoring countermeasures against scouring.

INTRODUCTION

Bridges are subject to various external impacts, such as development of adverse hydraulic conditions during severe floods, disastrous earthquakes, etc., most of which lead to complete failure. Statistical analysis of bridge failures indicate that most frequent cause of bridge failures are attributable to excessive scouring during floods (Shirhole and Holt 1991; Lagasse et al. 1998; and Wardhana and Hadiprioni 2003). Other reasons of failure include overloading, collision and deficiencies in design, construction, material, lack of repair and maintenance, etc (Yanmaz et al. 2007). Bridge failures can lead to loss of several lives and properties, traffic disruption, and deficiencies in various socio-economic conditions. If the reason of bridge failure is not concerned with the structural design and materials, it may originate from lack of hydraulic evaluations, which may also result in pronounced uncertainty in view of bridge stability. New bridges need to be designed to withstand extreme conditions that are likely to occur in the light of lessons learned from past events. On the other hand, existing structures should be monitored periodically on behalf of decision-making for the degree of necessary protective works to be implemented to increase the safety (Yanmaz et al. 2007).

Depending upon the severity of flow conditions, considerable quantities of bed material may be removed from the surrounding of piers and abutments, which leads to loss of structural resistance. Safety margin of the abutment foundation against scouring, which is the difference between the depth of footing and the maximum depth of scour, would decrease during the passage of a severe flood. Hence the resistance, which is the ability of a bridge to withstand external effects would reduce greatly. Assessment of the current safety level of the footing is based on the value of the safety margin as well as geometric characteristics of the bed topography in and around the scour hole. That is why determination of the volume and the surface area of the scour hole around bridge elements is of importance. This study is focused only on the investigation of these aspects around bridge abutments.

The close upstream of a bridge abutment is subject to a strong pressure field. This leads to a three dimensional separation of flow. The primary vortices, which migrate downstream past the abutment, carry significant amount of bed material from the scour hole. Hence the whole vortex structure (primary vortices and wake vortices) scour the loose bed yielding the development of a scour hole around the abutment. Since equilibrium scouring situations are achieved in relatively long durations under clear water conditions, i.e. of the order of several days in a laboratory medium (Melville and Coleman 2000), the corresponding prototype durations may yield relatively long flow durations. That is why the design of bridge foundations on the basis of equilibrium clear water scour depths may give considerably greater values than may occur if the flow is of short duration (Yanmaz and Altinbilek 1991). Therefore, investigation of temporal variation of clear water scour at bridge elements is of importance to estimate the possible extension of the scour hole, which would provide information for safe design of footing and the scour countermeasure to be implemented. The objective of this study is to investigate the geometric characteristics of the instantaneous scour holes around vertical-wall bridge abutments under clear water conditions. To this end, expressions are developed for intantaneous values of volume and surface area of scour holes around vertical-wall abutments.

EXPERIMENTS

Sets of experiments were carried out to investigate the time-dependent variation of scour hole characteristics around vertical-wall abutment models under clear water conditions in a flume 30 m long, 1.25 m wide, and 1.0 m deep with a bed slope of 0.001. Side walls of the flume are made of glass for visual observations. The channel bed material is uniform quartz sand with a median size of D_{50}=1.8 mm. To investigate the effect of abutment size, abutment models made of plexiglas having lengths of L=12.5 cm and 10 cm were tested. Experiments were performed under a constant densimetric particle Froude number of F_d=2.38, which is defined as $u/(\Delta g D_{50})^{0.5}$, where u is the mean approach flow velocity, Δ is the relative density, and g is the gravitational acceleration. Since similar scouring characteristics are expected under different F_d values because of fundamental similarity of all types of local scouring situations, tests performed under a constant value of F_d are found to be representative for the implication of the general scouring trend. In the experiments,

maximum scour depths around the vertical-wall abutments, d_s, are measured against time, t, relative to the initial bed level using a vertical scale attached to the interior of hollow plexiglas abutment with a stick having a small inclined mirror at its end. In the course of experiments, it was observed that the rate of scour development was high in the early stages of the tests. The rate of change of scouring decreased slowly with respect to time. That is why investigation of temporal variation of scour hole characteristics during the principal phase may be of practical interest. Hence, the test duration of an experiment was limited by six hours according to the physical limitations of the laboratory. During this test period, the final equilibrium scour depths were not achieved although the rate of scour reduced to smaller values for all experiments.

Throughout the conduction of the experiments, it was observed that the maximum scour depths occurred around the upstream corner of the abutment. For the determination of time-dependent shapes of scour holes around bridge abutments, experiments were stopped at the end of different test durations; namely 5, 20, 60, 100, and 150 min to determine the contours of the scour holes around abutment models using point gages. Measurements were carried out with respect to the coordinate system given in Figures 1 through 5, which show contours of the bed topography around the abutment with L=12.5 cm obtained at the end of the aforementioned test durations After each run, the bed was flattened to run the experiment with the next duration. An inspection to these figures implies that the upstream side of the abutment is subject to severe scouring where primary vortices dominate scouring action. Contrary to the case of a bridge pier around which symmetrical flow takes place, the rear face of the abutment is subject to considerable accretion in the wake region, which is bounded by the side wall of the channel.

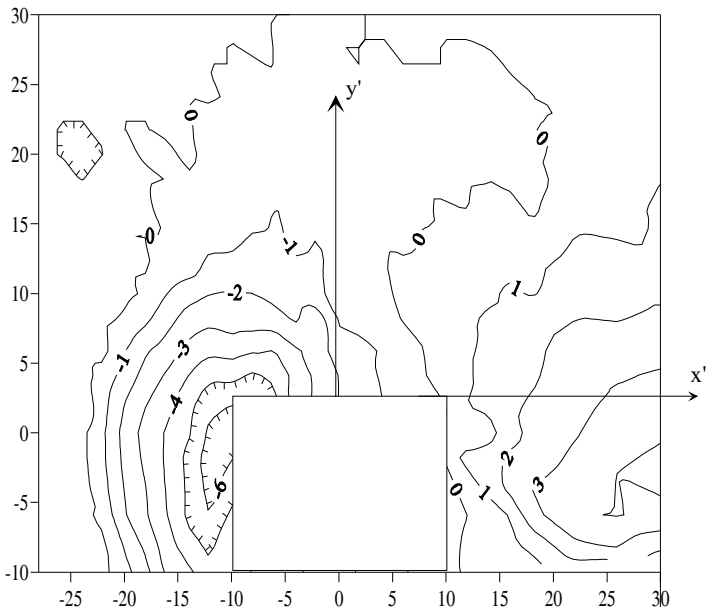

Figure 1. Scour hole contours in cm (L=12.5 cm, t = 5 min)

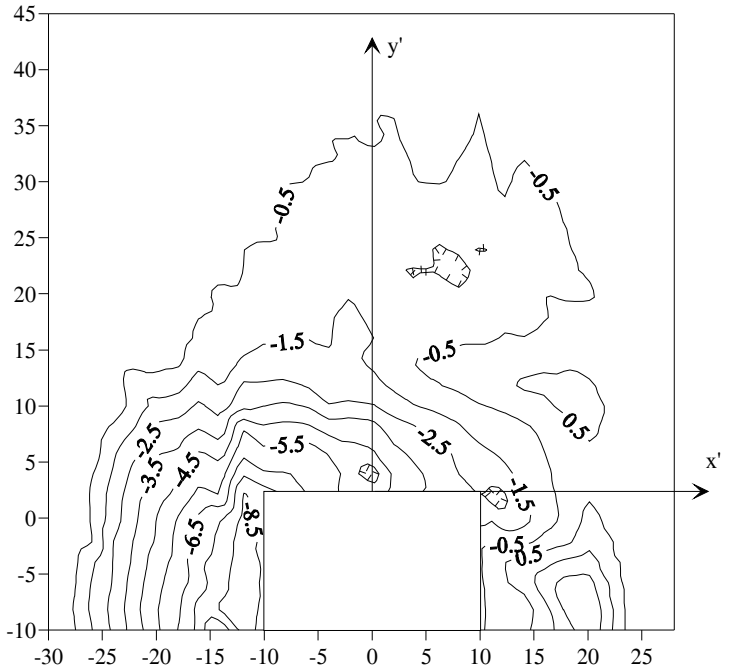

Figure 2. Scour hole contours in cm (L=12.5 cm, t = 20 min).

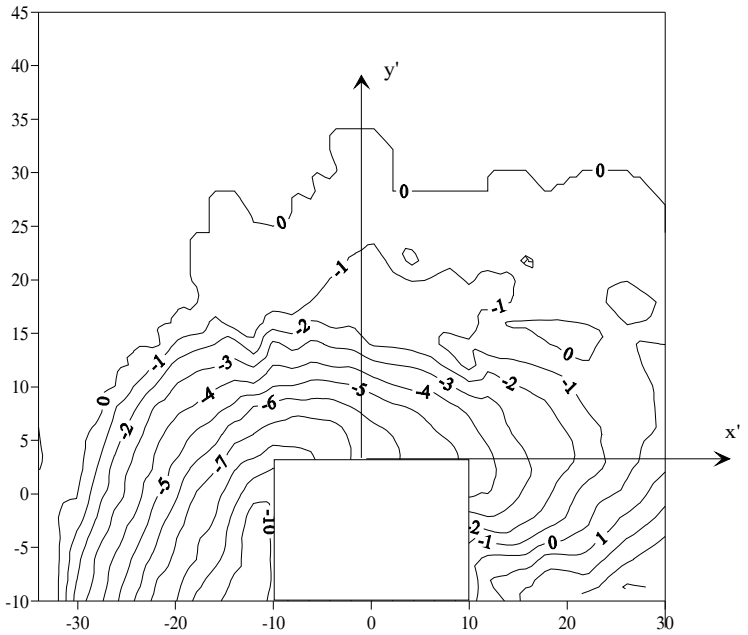

Figure 3. Scour hole contours in cm (L=12.5 cm, t = 60 min).

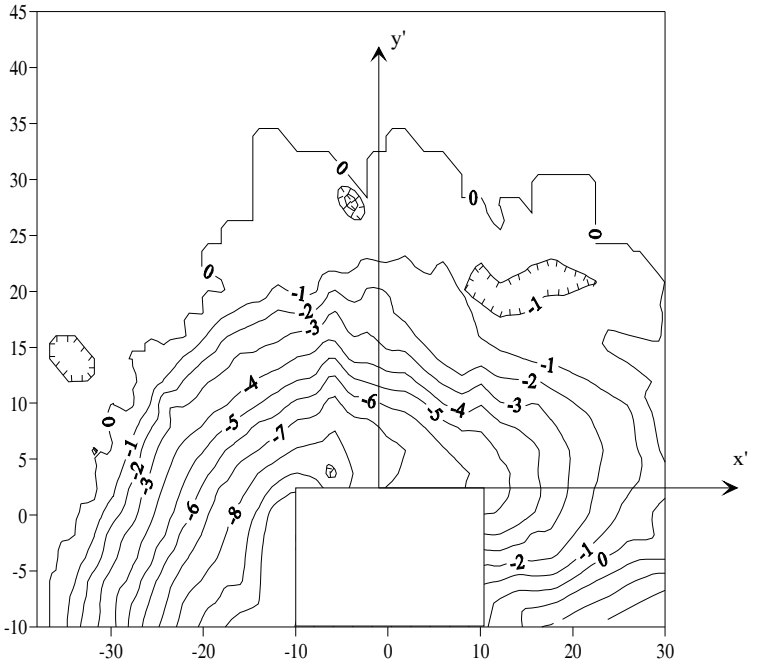

Figure 4. Scour hole contours in cm (L=12.5 cm, t = 100 min)

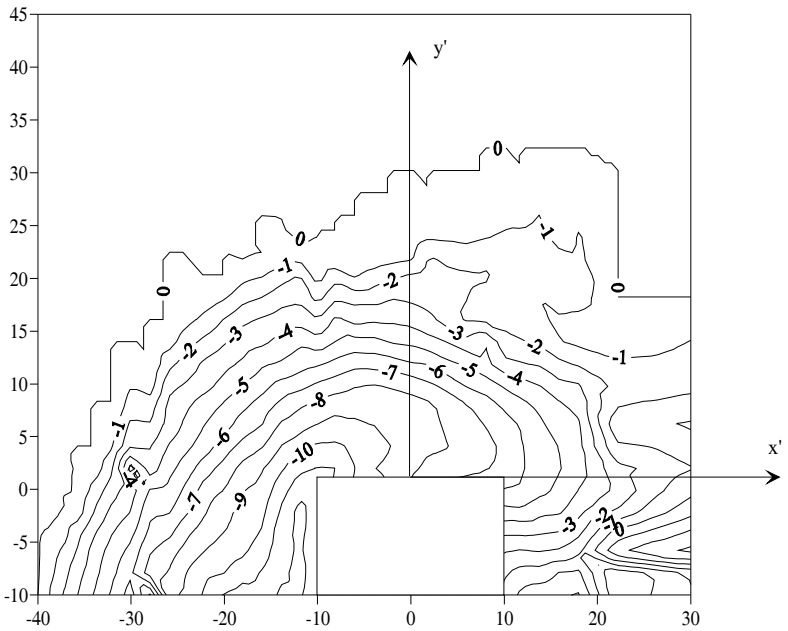

Figure 5. Scour hole contours in cm (L=12.5 cm, 12, t = 150 min).

ANALYSIS OF TEST RESULTS

Kose (2007) developed a semi-empirical model for temporal variation of scour hole around vertical-wall abutments using the results of the aforementioned tests. This model was based on the application of the sediment continuity equation to the scour hole around the abutment. The expression developed for instantaneous volume of the scour hole, V, around a vertical-wall abutment is as follows:

$$\frac{V}{d_s(t)L^2} = \frac{A\alpha}{6}\left(1+S\cot\phi\right)+\frac{B}{3}\left(1+2S\cot\phi+3S^2\cot^2\phi\right)+\frac{C}{3}\left(1+S\cot\phi\right)+ \frac{D}{3}\left(1+2S\cot\phi+S^2\cot^2\phi\right)+\frac{E}{3}-\frac{5\alpha}{6} \quad (1)$$

where $d_s(t)$=instantaneous maximum depth of scour, α=W/L, W=width of abutment, $S=d_s(t)/L$, ϕ=angle of repose of the sediment, $A=\ln\left|\sec(\arctan(2/\alpha))+2/\alpha\right|$, $B=\arctan(2/\alpha)$, $C=\ln\left|\sec(\arctan(E))+E\right|$, $D=\arctan(E)$, and $E=\alpha/2$.

The results of the analysis indicated that the shape of the scour hole remained almost unchanged with respect to time and the side angles of the scour hole, except the rear face of the abutment, was approximately equal to the angle of repose, ϕ, of the sediment. Dey and Barbhuiya (2005) also observed that the upstream scour holes around abutment models of different shapes had a similarity at different times. They concluded that this implied a layer-by-layer scouring process until an equilibrium state was achieved. As a result of this analysis, the volume of the scour hole can be approximated by an inverted semi-cone with a rectangular base having a width, W, and a length, L (Kose 2007). The predictive ability of Equation (1) is checked by the application of a software, which can evaluate the area and volume elements bounded by irregular contours. The volumes obtained from Equation (1) and the software were found to be in relatively good agreement (Kose 2007). The geometric characteristics of the scour holes around vertical-wall abutments can also be expressed with reference to the contours drawn around the abutment models. Using the computed values of instantaneous scour hole volumes obtained from the aforementioned software, the following regression equation with a coefficient of determination of 0.98, is obtained:

$$\frac{V}{d_s(t)L^2} = 1.142T_s^{0.142} \quad (2)$$

where T_s is a dimensionless time parameter, $tD_{50}(\Delta gD_{50})^{0.5}/L^2$, as also previously used by Yanmaz and Altinbilek (1991) and Yanmaz (2006) and t is the time. In a similar way, the temporal variation of the surface area of the scour hole can be expressed by the following equation having a coefficient of determination of 0.960:

$$\frac{A}{WL} = 3.722T_s^{0.182} \quad (3)$$

where A*=A/(WL) with A being the instantaneous surface area of the scour hole. Since Equations (1) and (2) express the dimensionless scour hole volumes, both of them can be used for the practical prototype applications. However, it is obvious that use of Equation (2) is easier. These equations require selection of appropriate design parameters. The length of an abutment is normally dictated by structural and geotechnical requirements. Bed material characteristics in close vicinity to the bridge site are obtained from the collected soil samples, whereas the design time is to be selected according to the hydrological regime of the basin concerned. It should be emphasized herein that the most crucial term is the duration of the design flood. For a conservative design, sufficiently long flow durations, compatible to the local hydrologic conditions of the bridge site concerned, can be taken. Use of Equations (2) and (3) require determination of the scour depth at a vertical-wall abutment corresponding to the design time, which can be obtained using an appropriate equation, such as the one proposed by Oliveto and Hager (2002). They derived the following equation for time-dependent clear water scour depth at vertical-wall abutments

$$\frac{d_s}{L_R} = 0.085\sigma^{-0.5} F_d^{1.5} \log T_d \tag{4}$$

where $L_R=L^{2/3}y^{1/3}$, y=depth of approach flow, σ=geometric standard deviation of particle size distribution, $T_d=t/t_R$, and $t_R=L_R/(\Delta g D_{50})^{0.5}$.

Information obtained from the scouring characteristics at vertical-wall abutments would yield some relevant information for the assessment of the stability of the structure. With the progression of the scour hole, the resistance of the structure to withstand external forces, such as earthquake and flood induced inertia forces, reduces. Assessment of the loss of reduction in the system resistance induced by excessive scouring may dictate the degree of foundation strengthening measures to be implemented. Information concerning the depth, surface area, and volume of the scour hole can also give some clues about the depth and areal extension of the protection zone around the abutment. Within this context, the size of ripraps and the number of armoring layers in the protection area can be found. However, additional experiments need to be conducted to generalize the design details of this armoring countermeasure, which would be the subject of a different future research.

CONCLUSIONS

Topographic characteristics of scour holes around vertical-wall abutments under clear water conditions have been investigated under a densimetric particle Froude number of 2.38. The experiments were carried using abutment lengths of 10 and 12.5 cm in a flume having a quartz sand as the bed material with a median size of 1.8 mm over a bed slope of 0.001. Experiments were stopped at various test durations and the corresponding scour contours around the vertical-wall abutment model were measured. Experimental results implied that the volume of the scour hole around a vertical-wall abutment could be approximated by an inverted semi-cone with a

rectangular base having a width, W, and length, L, which is given by Equation (1). Another volume expression was also obtained based on empirical approach as given in Equation (2). Dimensionless surface area of the scour hole is expressed by Equation (3). Use of Equations (2) and (3) requires determination of the depth of scour, which corresponds to the design duration of the flood. To this end, the equation proposed by Oliveto and Hager (2002) can be used. Findings of this study would provide relevant information to assess the time-dependent loss of resistance of a bridge against excessive scouring. Furthermore, interpretation of the scour hole characteristics would also give information concerning the determination of the areal extension of armoring countermeasures to be implemented around vertical-wall abutments. Additional experiments need to be conducted to generalize the design details of armoring countermeasures at vertical-wall abutments.

Acknowledgements

This research was carried out in Hydraulics Laboratory of the Technical Investigation and Quality Control Department of Turkish State Hydraulics Works, Ankara. The authors are grateful for the support provided by the laboratory staff.

REFERENCES

Dey, S, and Barbhuiya, A. K. (2005). "Time variation of scour at abutments." *J. Hydr. Eng.*, ASCE, 131(1), 11-23.

Kose, O. (2007). *Analytical and experimental investigation of temporal variation of clear water scour depth at bridge abutments*. Ph. D. Thesis, Middle East Technical University, Ankara, Turkey.

Lagasse, P. F, Byars, M. S., and Zevenbergen L. W. (1998). "Bridge scour and stream instability countermeasures." *Proc. International Water Resources Engineering Conference,* ASCE, 1, 5-14.

Melville, B. W., and Coleman S. E. (2000). *Bridge scour*. Colorado: Water Resources Publications.

Oliveto, G., and Hager, W. H. (2002). "Temporal evolution of clear water pier and abutment scour.", *J. Hydr. Eng.*, ASCE, 128(9), 811-820.

Shirhole, A. M, and Holt, R. C. (1991). *Planning for a comprehensive bridge safety program*. Transportation Research Record 1290, Transportation Research Board, National Research Council, Washington, D.C., 1, 39-50.

Wardhana, K., and Hadiprioni, F. C. (2003). "Analysis of recent bridge failures in the United States." *J. Perf. Constr. Fac.*, ASCE, 17(3), 144-150.

Yanmaz, A. M., and Altinbilek, H. D. (1991). "Study of time-dependent local scour around bridge piers." *J. Hydr. Eng.*, ASCE, 117(10), 1247-1268.

Yanmaz, A. M. (2006). "Temporal variation of clear water scour at cylindrical bridge piers." *Canadian J. Civil Eng.*, 33(8), 1098-1102.

Yanmaz, A.M., Caner, A., and Berk, A. (2007). "Renovation of a safety-inspection methodology for river bridges", *J. Perf. Constr. Fac.*, ASCE, Vol.21, No:5, 382-389.

Predicting Rock Scour in an Alluvial River with a One-Dimensional Model

Blair P. Greimann[1], Yong G. Lai[2], and Kuowei Wu[3]

[1] Sedimentation and River Hydraulics, Technical Service Center, Bureau of Reclamation, Denver, CO 80225; PH (303) 445-2563 FAX (303) 445-6351; email: bgreimann@do.usbr.gov
[2] Sedimentation and River Hydraulics, Technical Service Center, Bureau of Reclamation, Denver, CO 80225; PH (303) 445-2560 FAX (303) 445-6351; email: ylai@do.usbr.gov
[3]Water Resources Planning Institute, Water Resources Agency, Wu-Fong, Taichung , Taiwan, R.O.C.; PH: 04-23302980-2331; FAX : 04-23323523; email:kuowei@wrap.gov.tw

ABSTRACT

Taiwan rivers generally have steep slopes, are subject to high flows, have frequent earthquake activity, and have relatively weak bedrock. Bedrock is often exposed and rock scour is an important river process. For example, the river channel downstream of the Shih-Gang on the Tachia River experienced severe rock scour since the Chi-Chi earthquake of 1999 uplifted a portion of the river approximately 10 m. The occurrence of deep rock scour has been a major threat to river infrastructure at many other locations in Taiwan.

In this study, a rock scour model is implemented into a one-dimensional (1D) hydraulic and sediment transport model. The rock scour model has components to predict the potential scour due to direct flow hydraulic forces and scour due to sediment abrasion. The resultant 1D model is capable of simulating the combined effects of rock erosion and alluvial river erosion and deposition. The new model is applied to the Tachia River in the reach affected by the Chi-Chi earthquake in 1999. Findings related to the applicability and limitations of the current rock scour models are reported.

INTRODUCTION

In Taiwan, many alluvial rivers are characterized by the presence and exposure of soft bedrock. The bedrock consists of mainly mudstone and sandstone which are relatively weak (shear strength between 0.5 ~ 25.0 MPa) and subject to substantial erosion during high flows. Once the sediment overlying the bedrock is eroded by the river, the river can begin to erode the bedrock. The scour can damage infrastructure such as bridge piers or diversions founded on the bed rock. To address this significant concern, an extensive research and development program has been set up by the Water Resources Agency of Taiwan. One of the aims is to understand and document the rock scour characteristics such that a predictive model may be formulated.

Rock erosion occurs when water is flowing over bedrock in a fluvial environment. A number of mechanisms are responsible for the erosion of rock. They include hydraulic scour or plucking (plucking of rock fragments by fluid shear stresses), abrasive scour (interaction between rock and moving sediment particles), dissolution, and cavitation. In addition, weathering (chemical or physical) contributes

to the weakening of rock. Dissolution is not a factor within the time scales of interest in this study and velocities are not high enough to cause cavitation.

It is theoretically advantageous to treat different mechanisms separately; however, it is difficult to distinguish the mechanisms in the field. Hydraulic scour can occur without the assistance of sediment particles but many times the flows that can scour bedrock can also carry significant amounts of sediment. Similarly, abrasive scour is strongly dependent on the hydraulic flow characteristics such as shear and turbulence. It is possible that one reach of the river is dominated by hydraulic scour while another by abrasive scour. Or, both mechanisms may operate to erode the rock for some rivers.

In a companion paper "Predicting Rock Scour in an Alluvial River with a Two-Dimensional Model" by Lai et al. a review of rock scour model is presented. In that paper, a two-dimensional (2D) application of the rock scour model is presented. Greimann and Vandeberg (2008) also detailed the development and application of SRH-1D to predict bedrock scour. Here we present a 1D application of the rock scour model. The 2D model can be used for reaches on the order of several kilometers in length and can simulate several years of flow data, but due to computational limitations, cannot be applied to entire rivers or for long term simulations. It is necessary to use a 1D model to calculate large time and spatial scales.

A PROPOSED ROCK EROSION MODEL

We propose that the hydraulic scour and abrasive scour should be modeled separately. Field reconnaissance is recommended to determine whether the study site is hydraulic scour dominant, abrasive scour dominant, or if both play important roles. The proposed combined rock scour rate model takes the following form:

$$E = k_P U \left(\frac{\tau}{\tau_{cri}} - 1 \right)^n + E_a \tag{6}$$

where E is total rock erosion rate; k_P is hydraulic erodibility; U is depth averaged flow velocity; τ is bed shear stress; τ_{cri} is critical shear stress for hydraulic rock scour; n is an empirical exponent; and E_a is abrasive scour rate. In this paper, we are only considering the hydraulic scour of rock. Abrasive scour will be considered in future 1D analysis, and is considered in the companion paper on 2D scour.

The first term on the right hand side of (6) represents the hydraulic scour rate and it is set to be a function of the stream power (τU). The above form has the advantage of being dimensionally consistent as opposed to the dimensional equations used in many existing models such as that of Tomkin et al. (2003). It is also consistent in form to the cohesive sediment transport relationships used in the mobile-bed models. The exponent, n, is assumed to equal 1 as existing data is insufficient to support the use of nonlinear relations. Therefore, two empirical parameters are needed for the hydraulic scour: k_P and τ_{cri}.

Numerical Model Description

The proposed rock erosion model is incorporated into the existing SRH-1D version 2.1, which is a 1D cross section averaged hydraulic and sediment transport mobile bed model for river systems developed at the Bureau of Reclamation (Huang and Greimann, 2008). The model is available for download at: http://www.usbr.gov/pmts/sediment/. The model can simulate steady and unsteady flow, sediment transport, and erosion and deposition. Version 2.1 can now also simulate the effects of bedrock.

Governing equations and numerical methods of SRH-1D are omitted; and only the implementation of the rock erosion model is described here. The bed material beneath the bed surface is divided into a number of sub-layers in the original SRH-1D and they may be spatially distributed. At each cross section, every sub-layer has its own thickness and sediment gradation. A new sub-layer type is added, designated as the "erodible rock", to apply the rock erosion model. If there are granular materials on top of the erodible rock, they are eroded first; if the bedrock is exposed, rock erosion is initiated. The user enters the cross sectional station and elevation points of the bedrock. The bedrock and cross section representation used in SRH-1D is given in Figure 1.

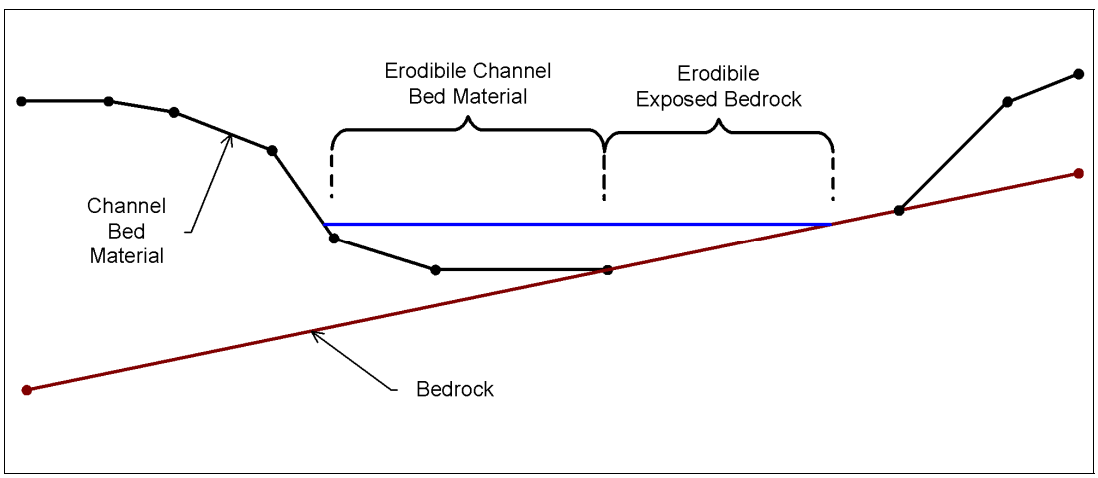

Figure 1. Cross sectional representation of bed rock and alluvial material.

Test and Application of the Rock Erosion Model

The rock erosion model is applied to Tachia River in the reach extending from 10 km upstream of Shih-Gang Dam to the ocean. The Chi-Chi earthquake of 1999 cause approximately 10 m of uplift in the vicinity of the dam. The fault actually passed through the middle of the dam and the North portion of the dam is now 10 m lower than the South portion. The uplift caused by the earthquake and the presence of the dam created a deposition zone upstream of the dam and an erosion zone downstream of the dam. The area near Shih-Gang Dam and the fault line is given in Figure 2. The dam is now repaired but because of the reduction in river slope upstream of the fault, sediment is depositing upstream of the fault line and severe erosion is induced downstream of the fault line. The river profile before and after the earthquake is shown in Figure 3. The displacement caused by the 1999 earthquake,

and the subsequent deposition upstream of the fault line and erosion downstream of the fault line is shown in the figure.

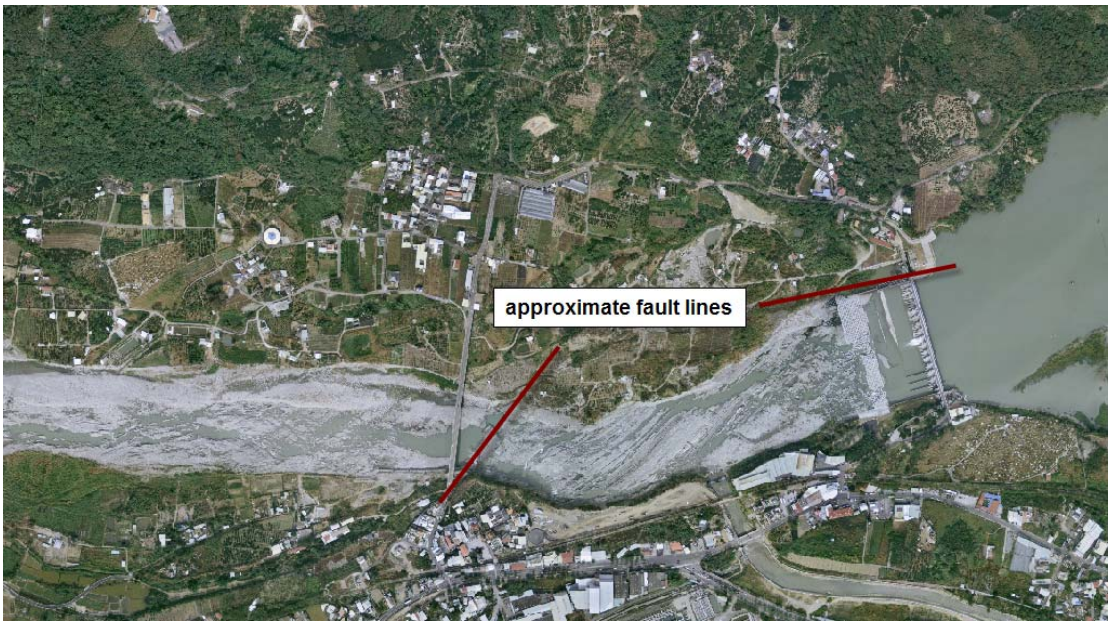

Figure 2. Aerial view of the Tachia River in the vicinity of the Shih-Gang Dam. The fault lines are noted on the figure.

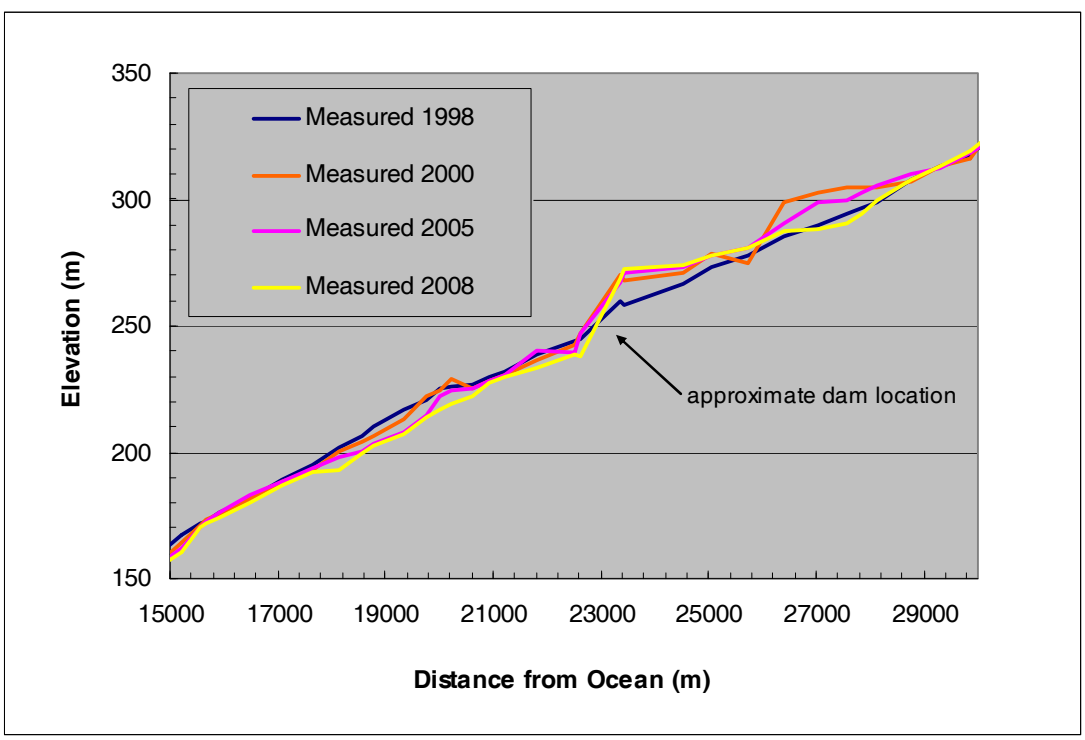

Figure 3. River profile measured at various times. The earthquake occurred in 1999.

The SRH-1D model requires several inputs. They can be divided into hydraulic, sediment and bedrock inputs. The hydraulic inputs include the flow discharge, the cross sectional geometry, and hydraulic roughness parameters. The flow discharge was recorded at Shih-Gang dam and is shown in Figure 4. We simulated the period from 2000 through 2004. There were several large storms during that period and extension erosion downstream of Shih-Gang dam. The flows during that period are given in Figure 4. The flow in the river is extremely variable and the sediment transport and scour are dominated by typhoon events that occur during the summer months. Flows less than 50 cms were ignored. The cross sectional geometry was surveyed by the Taiwan Water Resources Agency in 2000 and 2005. Therefore, it was possible to compare the simulated geometry changes results against measured geometry changes during that period. The hydraulic roughness assumed in the main channel was 0.04. Because of the steep slopes the flow is near critical conditions throughout almost the entire river.

The sediment inputs to the model include the incoming sediment load and the initial bed material gradations. The incoming sediment load was calculated by assuming that the river is at transport capacity at the upstream cross section. This is probably a good assumption because of the tremendous sediment volumes introduced into the upper river as the result of the 1999 earthquake. The initial bed material gradations were taken from several test pits throughout the simulated reach. One interesting feature of the river is that the bed material actually gets coarser in the downstream direction, which is opposite of most rivers. It is likely due to the severe aggradation occurring in the upper watershed due to multiple landslides and also due to the severe erosion occurring in the lower river below Shih-Gang Dam.

Several sediment transport parameters also need to be input, the most important being the formula used to compute the sediment transport capacity. For the simulations shown here, the Parker bedload formula (Parker, 1990) is used in conjunction with the Engelund-Hansen total load formula (Engelund and Hansen, 1972). The Parker equation is used for the gravel sized and larger sediment and the Engelund-Hansen formula is used for the sand sized sediment.

The bedrock geometry input parameters include the bedrock geometry and the erosion rate coefficients. For this paper, we consider only hydraulic scour. The bedrock was assumed to be fully exposed in the reach immediately downstream of the dam for a distance of approximately 3 km. The bedrock erosion coefficients are discussed in the following section.

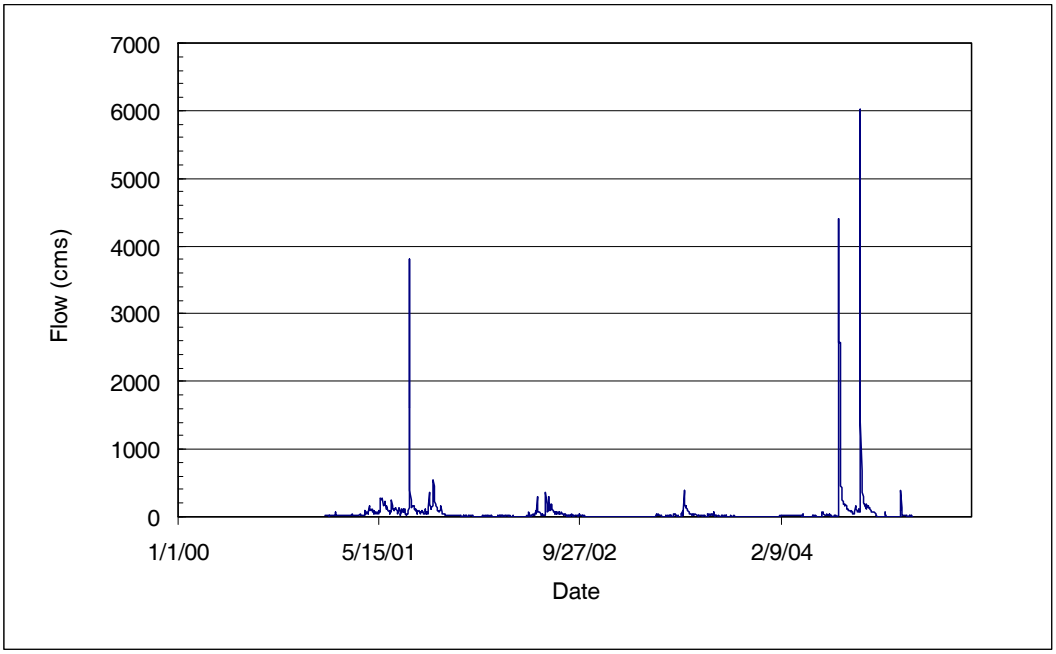

Figure 4. Flow during period of simulation beginning in January 2000 and ending in Dec 2004.

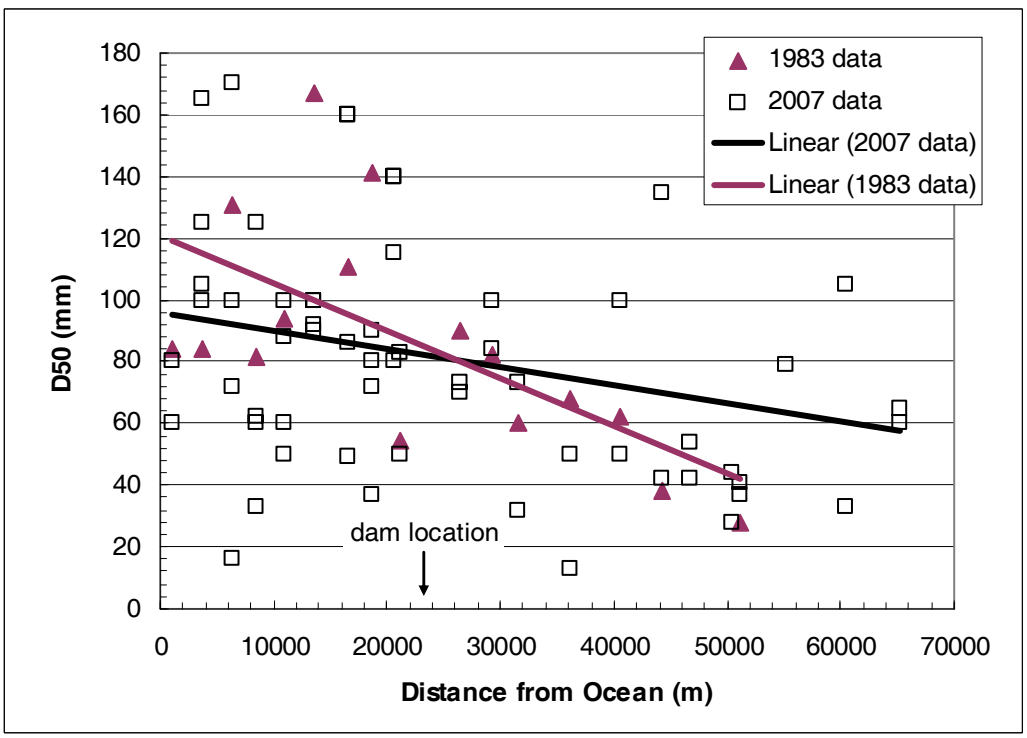

Figure 5. Measured D50 (median diameter) as a function of distance from the ocean. Linear fits to the data are also shown.

RESULTS AND DISCUSSION

We calculated the cases with and without hydraulic rock scour. For the case without hydraulic rock scour, the bedrock was assumed to be not erodible and only the sediment in the river was allowed to erode. For the case of hydraulic rock scour we calibrated the critical scour shear stress, τ_{cri}, and the erosion rate coefficient, k_p. Based upon fits to the erosion data from 2000 to 2005, the calibrated values were τ_{cri} = 200 Pa and k_p = 6E-6. The observed bedrock erosion is within 1 km of the dam and the 1D model including bedrock erosion reproduced the average bed elevation change (Figure 6). The average bed decreased 2m in the location downstream of the dam. The model was not able to reproduce the location and magnitude of local scour, but this is considered beyond the capability of a 1D model. A 2D model would be required to compute the magnitude and location of local scour. The average erosion and deposition patterns of sediment were also reproduced by the model with a few exceptions. Overall, the agreement is considered satisfactory and it was able to reproduce the reaches that were aggrading and degrading. The simulated average bed elevation changes assuming no rock erosion is also shown in Figure 6. The only difference, as expected, is in the area immediately downstream of Shih-Gang dam where the bedrock is exposed.

The measured and computed volume of erosion and deposition is given in Figure 7 for the case of bed rock erosion. There is some bedrock erosion in the reach immediately downstream of the dam. Beyond that bedrock erosion is not significant because it is not exposed or it is considered more resistant to erosion. The computed volumes of total erosion and deposition are in general agreement with the measurements. The volume of bedrock erosion is considerably smaller than the erosion of sediment, but it is significant to the infrastructure located in that reach. As mentioned previously, only hydraulic scour is currently considered. Further tests on the important of abrasive scour will also be considered in future simulations.

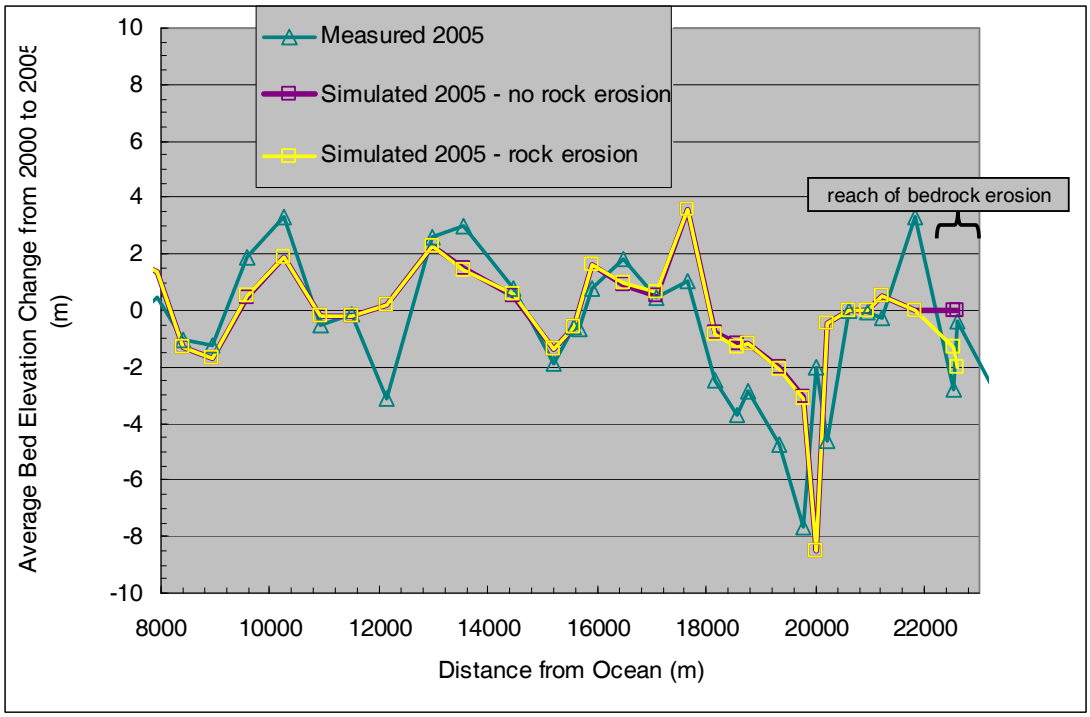

Figure 6. Measured and simulated average bed elevations changes from 2000 to 2005. The model was run with and without rock erosion.

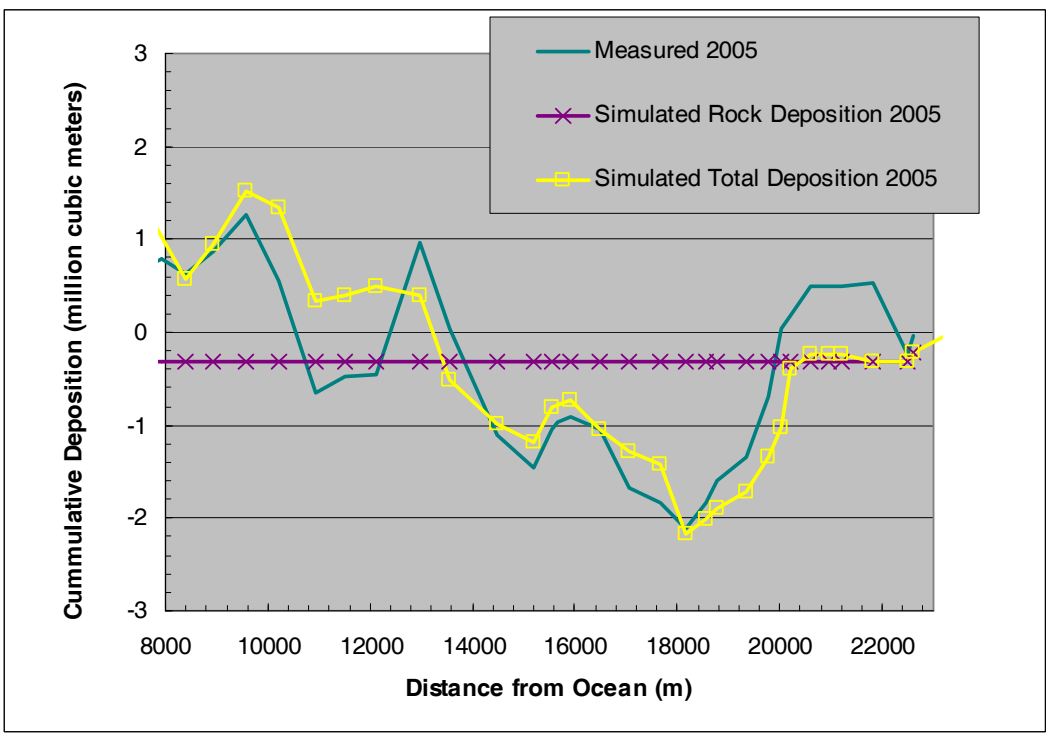

Figure 7. Measured and simulated average bed elevations changes from 2000 to 2005. The model was run with rock erosion.

CONCLUDING REMARKS

A review was conducted for the rock erosion models and a specific rock erosion model is proposed and implemented into an existing 1D model: SRH-1D. The model is then applied to study the erosion downstream of the Shih-Gang Dam on the Tachia River. The following conclusions may be drawn: (1) The presence of rock in the river channel can exert important influences on the erosion and deposition in the river channel, (2) Scour of bedrock can occur under relatively short time scales given the particular conditions in Taiwan, (3) The 1D model can reproduce the average bed elevations changes and the erosion and deposition volumes in the reach, but cannot reproduce the magnitude and location of local scour.

ACKNOWLEDGEMENT

The author would like to acknowledge that the Water Resources Agency of Taiwan has sponsored this study. The project Liaison Officer, Director Chen, Hung-Kwai, and the review committee in Taiwan have provided valuable technical comments. Peer review provided by Jianchun Huang at Reclamation is greatly appreciated.

REFERENCES

Engelund, F., and Hansen, E. (1972). *A monograph on sediment transport in alluvial streams, Teknish Forlag,* Technical Press, Copenhagen, Denmark.

Greimann, B.P., and Vandeberg, M., (2008). Predicting Rock Scour, Technical Report SRH-2008-01, Technical Service Center, Bureau of Reclamation, Denver, CO.

Huang, J., and Greimann, B. (2008). User's Manual for SRH-1D Version 2.1 Sedimentation and River Hydraulics – One Dimension, US Bureau of Reclamation, Technical Service Center, Denver, CO.

Parker, G., (1990). "Surface-Based Bedload Transport Relation for Gravel Rivers," J. Hydraulic Research, 28(4):417-436.

Predicting Rock Scour in an Alluvial River with a Two-Dimensional Model

Yong G. Lai [1], Blair P. Greimann [2] and Kuowei Wu[3]

[1] Sedimentation and River Hydraulics, Technical Service Center, Bureau of Reclamation, Denver, CO 80225; PH (303) 445-2560; FAX (303) 445-6351; email: ylai@do.usbr.gov
[2] Sedimentation and River Hydraulics, Technical Service Center, Bureau of Reclamation, Denver, CO 80225; PH (303) 445-2563; FAX (303) 445-6351; email: bgreiman@do.usbr.gov
[3]Water Resources Planning Institute, Water Resources Agency, Wu-Fong, Taichung , Taiwan, R.O.C.; PH: 04-23302980-2331; FAX : 04-23323523;04-23300392; email:kuowei@wrap.gov.tw

Abstract

Most rivers in Taiwan have a steep slope, subject to high flows, and have relatively weak bedrock. Bedrock is often exposed and rock scour is an important river process. For example, the river channel downstream of the Chi-Chi Weir on the Choshui River experienced up to 10 meters of rock scour since the construction of the weir in 2001. The occurrence of deep rock scour has been a major threat to river infrastructure at many other locations in Taiwan.

In this study, rock scour models are reviewed and a specific rock scour model is proposed. Among rock scour mechanisms, those due to flow hydraulic force and sediment abrasion are considered to be important. The rock scour model is incorporated into an existing two-dimensional (2D) mobile bed model, SRH-2D version 3. The resultant 2D model is capable of simulating the combined effects of rock erosion and alluvial river erosion and deposition. The new model is applied to the river reach at the Chi-Chi Weir in an attempt to test and verify the applicability of the rock scour model. Findings related to the applicability and limitations of the current rock scour models are reported.

Introduction

In Taiwan, many alluvial rivers are characterized by the presence and exposure of soft rocks on the river bed. The bedrock consists of mainly mudstone and sandstone which are relatively weak (shear strength between 0.5 ~ 25.0 MPa) and subject to substantial erosion during high flows. Therefore, soft rock erosion is an important river process in Taiwan. For example, the river channel downstream of the Chi-Chi Weir on the Choshui River experienced up to 10 meters of rock scour since weir construction in 2001.

Rock scour is important to locations where the overlying cobble and gravel river bed has been removed and the relatively weak mudstone or sandstone has been exposed. The large floods that occur in Taiwan wear away the rock, resulting in the erosion of bridge pier foundations, diversion structures, and other infrastructure. To address this significant concern, an extensive research and development program has been set up by the Water Resources Agency of Taiwan. One of the aims is to understand and document the rock scour characteristics such that a predictive model may be formulated.

Tomkin et al. (2003) compared various empirical models for bedrock incision and concluded that they generally cannot explain observed behavior because the current simple empirical approaches do not account for the varying channel capacity in different parts of the river, nor do they account for the distribution of discharge with time. By building a bedrock erosion module into numerical hydraulic and sediment transport models, the variations in channel capacity and specific discharge time series can be explicitly simulated. Therefore, we are

seeking to develop a numerical model which incorporates a rock erosion model and to test and assess the applicability of such models. Such an effort was initiated in 2007 by modifying the one-dimensional (1D) mobile bed sediment model SRH-1D to include the rock erosion model (Greimann and Vandeberg 2008). It was successfully applied to the reach downstream of the Chi-Chi Weir. The new 1D model can now be used to estimate reach averaged rock erosion.

In the current study, a two-dimensional (2D) rock erosion model is developed and tested. The need for a 2D model was recognized during the SRH-1D study, as some erosion areas were observed to be local and exhibit lateral variations. 2D modeling is usually needed for cases where 2D effects are important. Examples include near-field flow zones with in-stream structures such as weirs, diversion dams, release gates, coffer dams, etc.; bends and point bars; perched rivers; and multi-channel systems. 2D models may also be needed if certain hydraulic characteristics are deemed important which include flow recirculation and eddy patterns, lateral variations, overtopped banks and levees, differential flow shears on river banks, and interaction between the main channel, vegetation, and the floodplain.

In the following, a specific rock scour model is developed based on an extensive review, the model is then incorporated into the existing 2D mobile-bed model, SRH-2D version 3, and the model is finally applied to the reach at the Chi-Chi weir.

A Review of Rock Scour Models

Rock erosion occurs when water is flowing over bedrock in a fluvial environment. A number of mechanisms are responsible for the erosion of rock. They include hydraulic scour or plucking (plucking of rock fragments by fluid shear stresses), abrasive scour (interaction between rock and moving sediment particles), dissolution, and cavitation. In addition, weathering (chemical or physical) contributes to the weakening of rock. Only the first two processes are reviewed here since solution is of no interest to this study and cavitation requires extremely high velocity which is probably relevant mainly on spillways and plunge pools.

It is theoretically advantageous to treat different mechanisms separately; but a practically it is difficult to distinguish the mechanisms in the field. Hydraulic scour can occur without the assistance of sediment particles but is influenced by the presence of sediments through particle-rock collision. Similarly, abrasive scour is strongly dependent on the hydraulic flow characteristics such as shear and turbulence. It is possible that one reach of the river is dominated by hydraulic scour while another by abrasive scour. Or, both mechanisms may operate to erode the rock for some rivers.

Clear water alone can cause bedrock scour by instantaneous or progressive failure of closed-end rock joints or by dynamic ejection of single rock blocks (Bollaert and Schleiss 2005). Hydraulic scour is used to refer to this mechanism in this study (plucking is another term used by some researchers). The hydraulic scour erosion rate is normally made a function of flow force; but the selection of the force variable is no easy task. In theory, the instantaneous pressure differentials and shear stresses applied to rocks are the cause of failure rather than a steady applied force (Annandale 2006). This means the instantaneous shear stress or turbulent fluctuations should be used. However, the use of instantaneous quantities is not practical for modeling purposes and average quantities have to be adopted. Therefore, equations relating hydraulic forces to bedrock scour are often empirical in nature.

Several empirical models have been used to estimate reach scale bedrock erosion. Typical methods to compute rock scour rate use the following general equation (Sklar and Deitrich, 2006):

$$E = C\psi^n \tag{1}$$

where E is erosion rate; C is empirical constant representing rock properties; ψ is a flow parameter, e.g. stream power (P) or shear stress (τ); and n is an empirical exponent. The coefficients C and n must be calibrated to each field site and C is a dimensional constant. For example, stream power is used by Seidl and Dietrich (1992), Anderson (1994), and Willett (1999); and average shear stress is used by Howard (1994) and Tucker and Slingerland (1996).

Models based on the excess shear stress are also proposed (e.g. Howard et al. 1994; Tucker and Slingerland, 1997) and it may be expressed as:

$$E = C(\tau - \tau_{cri})^n \tag{2}$$

where τ and τ_{cri} are bed shear stress and critical shear stress, respectively. These models take into account the fact that erosion occurs only after the shear stress exceeds a critical value. Whipple et al. (2000) provided some discussion with regard to the threshold behavior but limited data are available for the critical stress parameterization.

A less empirical methodology was proposed by Annandale (1995, 2006) who used an index method to measure the resistance of rock to motion under a range of hydraulic conditions. Details can be found in Annandale (2006) or Greimann and Vandeburg (2008). Wittler et al. (1998) compared the stream power method of Annandale (2006) with the shear stress based method commonly used in sediment transport analysis. It was shown that the critical stream power method of Annandale (1995, 2006) is closely related to the critical shear stress used for granular materials. Therefore, it should be possible to use the critical shear stress formulation for hydraulic scour instead of the critical stream power.

The presence of sediment particles moving over bedrock is another mechanism to cause erosion due to collisions of particles with exposed bedrock. This mechanism is referred to as abrasive scour in this report. Both bed load and suspended load may contribute to abrasive scour. Most existing rock erosion models empirically incorporate the effect of abrasion into the framework of hydraulic scour as reviewed by Sklar and Dietrich (2006). Extra terms due to effects of grain size, sediment supply, and/or bed cover may be added. Further details are contained in Sklar and Dietrich (2006). These models are very empirical in nature.

A physically based abrasive model due to saltating bed load was developed by Sklar and Dietrich (2004). The bedrock scour rate is expressed as a product of three terms: the average volume of rock detached per particle impact, the rate of particle impacts per unit area per unit time, and the fraction of exposed bedrock. The erosion rate may be expressed as:

$$E_a = \frac{Y}{k_v \sigma_T^2} \frac{w_s^{\,2} q_s}{L_s} F_e \tag{3}$$

where E_a is the abrasive erosion rate due to bed load; w_s is the impact velocity of sediment particles; L_s is the saltation length of sediment particles; q_s is the sediment supply per unit width; Y is the modulus of elasticity of rock; k_v is a rock erodibility parameter; σ_T is the tensile strength of rock; and F_e is the fraction of exposed bedrock. The bedrock parameters σ_T and Y can be measured using laboratory tests of rock cores. Sklar and Dietrich (2004) attempted to

measure the value of k_v directly from laboratory abrasion tests using various rock types. In field situations, it is likely that k_v will be a calibration parameter. Sklar and Dietrich (2004) also provided expressions for w_s and L_s based upon flow and sediment characteristics.

Whipple et al. (2000), however, argue that the bedload saltation may play only a secondary role in abrasive scour on massive, unjointed rocks, and its contribution is mostly due to the plucking (hydraulic) process. Instead it is proposed that abrasion by suspended sediments plays an important role for massive, unjointed rocks. The conclusion that bed load abrasion is less important in larger river systems is supported by a number of field observations (Whipple et al. 2000). Abrasive scour due to suspended sediments was studied by Anderson (1986) and the following erosion rate was proposed:

$$E_a = \frac{S_a \rho_s}{2\rho_r} C U^3 \tag{4}$$

where S_a is the susceptibility of the bedrock to abrasion; ρ_s is sediment density; ρ_r is rock density; C is volumetric suspended sediment concentration; and U is depth-averaged flow velocity.

Recently, a total load abrasive scour model was proposed by Lamb et al. (2008). The bed load abrasive scour model of Sklar and Dietrich (2004) was extended to total load by additionally considering the suspended particle impact. The total load rate equation is expressed as:

$$E_a = \frac{A_1 Y}{k_v \sigma_T^2} \frac{q_t w_s^{\ 3}}{(UH\chi + U_b H_b)} F_e \tag{5}$$

where A_1 is a coefficient representing the fraction of particles impacting the bed; Y is the modulus of elasticity of rock; k_v is a rock erodibility parameter; σ_T is the tensile strength of rock; w_s is the impact velocity of sediment particles; q_t is total sediment supply per unit width; U is depth-averaged flow velocity; U_b is depth-averaged bed load velocity; H is flow depth; H_b is the bed load thickness; χ is an integral relating the suspended flux to U and H; and F_e is the fraction of exposed bedrock. The computational procedure for the impact velocity is complicated. The total load model above is physically based and seems to possess several attractive features. However, we think the model, in its present form, is impractical to be incorporated into a 2D model.

Reviews of existing models have also been carried out by Tomkin et al. (2003) and Sklar and Dietrich (2006). Various methodologies are reviewed to compute rock scour and are classified based upon the mechanism of erosion and whether they include the hydraulic forces, sediment abrasion, and the effect of sediment protecting the rock from scour.

A Proposed Rock Erosion Model

We propose that the hydraulic scour and abrasive scour should be modeled separately, however a combined formula should be developed. Field reconnaissance is recommended to

determine whether the study site is hydraulic scour dominant, abrasive scour dominant, or if both play important roles.

It is proposed that a combined rock scour rate model takes the following form:

$$E = k_P U \left(\frac{\tau}{\tau_{cri}} - 1 \right)^n \left(1 - \frac{c}{c_{tr}} \right) + E_a \tag{6}$$

where E is total rock erosion rate; k_P is hydraulic erodibility; U is depth averaged flow velocity; τ is bed shear stress; τ_{cri} is critical shear stress for hydraulic scour; c and c_{tr} are rock cover thickness and transition thickness, respectively; n is an empirical exponent; and E_a is abrasive scour rate.

The abrasive scour is based on the model of Sklar and Dietrich (2004) which may be replaced by the total load based model similar to Lamb et al. (2008) in the future. In this study, the following model is used:

$$E_a = \frac{0.08 R_b g Y}{k_v \sigma_T^2} q_s \left(\frac{\tau}{\tau_c} - 1 \right)^{-0.5} \left[1 - \left(\frac{u_*}{w_f} \right)^2 \right]^{1.5} F_e \tag{7}$$

where $R_b = \rho_s / \rho - 1$ (ρ_s is sediment density and ρ is water density); g is gravity; k_v is a rock erodibility parameter; Y is the modulus of elasticity of rock; σ_T is the tensile strength of rock; q_s is sediment supply per unit width; w_f is sediment fall velocity; u_* is shear velocity ($\sqrt{\tau/\rho}$); and F_e is the fraction of exposed bedrock.

The first term on the right hand side of (6) represents the hydraulic scour rate and it is set to be a function of the stream power (τU). The above form has the advantage of being dimensionally consistent as opposed to the dimensional equations used in many existing models such as that of Tomkin et al. (2003). It is also consistent in form to the cohesive sediment transport relationships used in the mobile-bed models. The c / c_{tr} term represents the cover effect, and $c_{tr} = 0.1m$ is used as a "critical" thickness above which zero rock erosion is expected. Also, $n = 1$ is used in this study as existing data is insufficient to support the use of nonlinear relations. Therefore, two empirical parameters are needed for the hydraulic scour: k_P and τ_{cri}.

The second term on the right side of (6) is the abrasive model. There are three parameters for abrasive erosion: k_v, Y and σ_T. k_v is a dimensionless parameter representing rock erodibility. It may be estimated in the laboratory as shown by Sklar and Dietrich (2004) or it may have to be calibrated for field applications. Y and σ_T may be measured in the field. Note that the fraction of the exposed bed is represented by F_e in equation (7). It may be the same as the hydraulic scour, i.e., $F_e = 1 - c / c_{tr}$. In the original model, however, $F_e = 1 - q_s / q_t$ is used to represent the fraction of bedrock exposure with q_t the sediment transport capacity per unit width.

It is possible that both hydraulic scour and abrasive scour are important at a particular field site. Under such circumstances, a total of five parameters are needed.

Numerical Model Description

The proposed rock erosion model is incorporated into the existing SRH-2D version 3.0 model, which is a 2D depth-averaged hydraulic and sediment transport mobile bed model for river systems developed at the Bureau of Reclamation. The flow simulation is the same as SRH-2D version 2 (Lai 2008) while its sediment module is based on Greimann et al. (2008). The robustness, accuracy and verification of SRH-2D have been demonstrated and documented by many projects. The flow modeling capability is documented by Lai (2008). Sediment transport modeling details and applications may be found in a number of papers such as Greimann et al. (2008), Lai and Greimann (2007), Lai and Greimann (2008a,b), and a number of project reports (check the following Reclamation website: http://www.usbr.gov/pmts/sediment/).

Governing equations and numerical methods of SRH-2D are omitted; only the implementation of the rock erosion model is described here. The bed material beneath the bed surface is divided into a number of sub-layers in the original SRH-2D and they may be spatially distributed. At each spatial point, every sub-layer has its own thickness and material type represented by granular composition. A new sub-layer material type is added, designated as the "erodible rock", to apply the rock erosion model. If there are granular materials on top of the erodible rock, they are eroded first; if the granular material thickness on top of an erodible rock is reduced below a critical depth, rock erosion would be initiated. The implementation allows the erodible rock to be placed anywhere in the river and located at any depth blow a bed surface. Any number of erodible rock types may be used with each type characterized by its erosion parameters discussed in the above section, "A Proposed Rock Erosion Model".

All governing equations are solved with the finite volume method that guarantees the mass conservation locally and globally. An implicit time marching scheme is used with the arbitrarily shaped unstructured mesh methodology of Lai et al. (2003). A detailed presentation of the numerical method for the flow hydraulics may be found in Lai (2008).

Test and Application of the Rock Erosion Model

The rock erosion model is applied to the river reach downstream of the Chi-Chi Weir on the Choshui River in Taiwan where up to 10 meters of rock scour has been observed since the construction and operation of Chi-Chi Weir in 2001. The calibration study is carried out using survey data from July 2004 to January 2007. Four scenarios are modeled: No-Rock, Hydraulic-Scour, Abrasive-Scour, and Mixed-Scour. The no-rock scenario assumes that the riverbed consists of granular sediment materials only. Results from this scenario would shed light on the role the bedrock plays in erosion control of the channel. The hydraulic-scour scenario assumes that hydraulic scour is the dominant mechanism and abrasive scour is set to zero. The abrasive-scour scenario assumes that abrasive scour is dominant and hydraulic scour is set to zero. Finally, the mixed-scour scenario assumes that both hydraulic and abrasive scours are important.

Solution Domain, Mesh, and Topography: The solution domain and the 2D mesh are displayed in Figure 1. The upstream inlet boundary is located at the Chilu Bridge about 2.06 km upstream of the Chi-Chi Weir and the downstream exit boundary is located at the Mingchu Bridge about 6.7 km downstream of the Weir. The total length of simulated reach is about 8.76 km. The solution domain is wide enough laterally that the domain would fully contain the

highest flow simulated. A 2D mesh was generated which has a total of 10,392 mesh cells. A majority of the cells are quadrilaterals and triangles are used only for mesh zone transition.

Cross sectional survey data were collected in July 2004 and these data are used as the initial bed topography. Another cross sectional survey at the same locations was performed in January 2007 and the data are used for comparison with the model results.

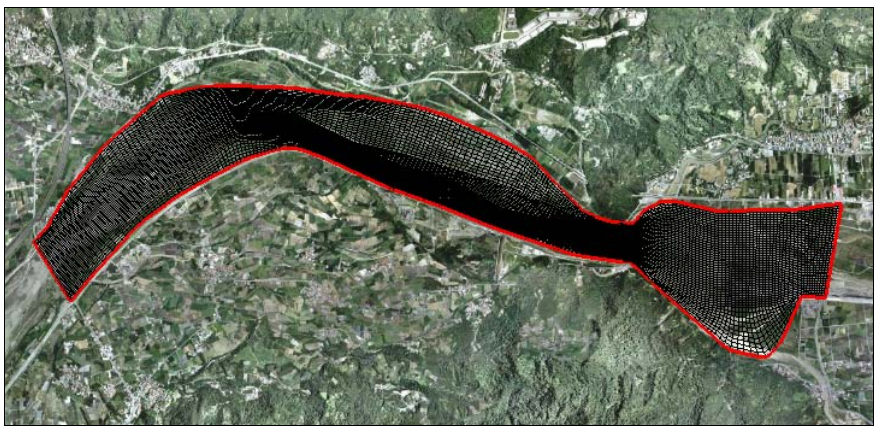

Figure 1. Solution domain and hybrid mesh used.

Representation of Flow Roughness and Bed Gradation: River bed properties, needed as model inputs, include Manning's roughness coefficient and bed sediment gradation. Both may be spatially distributed over the solution domain.

Flow resistance is calculated with the Manning's roughness equation in which the Manning's coefficient (n) is used as one of the model inputs. A constant coefficient of 0.04 is used based on the 2004 bed material analysis carried out by Taiwan engineers.

Bed gradation is spatially distributed according to survey data and a total of 10 zones are used (Figure 2). The first four zones are upstream of the Chi-Chi Weir and were based upon a gradation survey conducted in July 2005. The remaining six zones are downstream of the weir and were based upon a cross-sectional gradation survey conducted in 2004. The sediment size distributions for zones 1 to 8 excluding zone 4 are shown in Figure 3. Zone 4 has very fine materials with 99% of the sediments less than 0.074mm in diameter. Zone 10 represents the non-erodible bed where concrete is present immediately downstream of the weir. Zone 9 represents the erodible bedrock of interest in this study. In zone 9, erodible rock is assumed for all cases except for the no-rock scenario for which the bed material is assumed to be the same as zone 5.

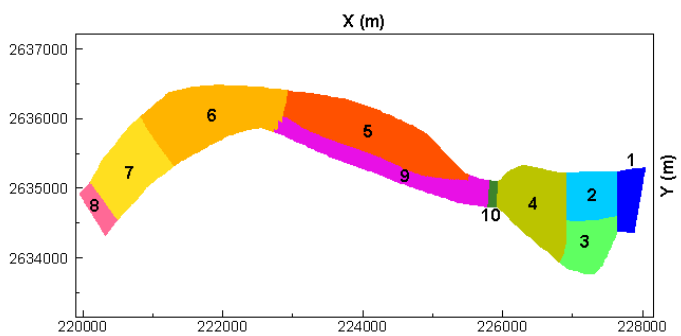

Figure 2. Bed gradation zones used by SRH-2D to bed material distribution

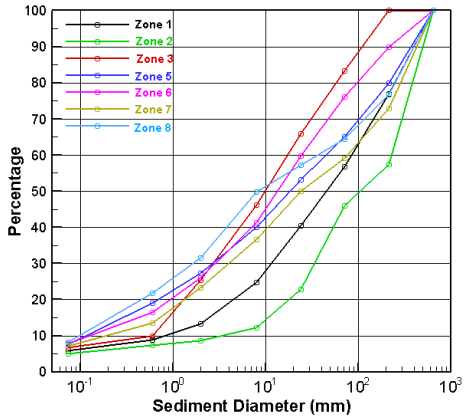

Figure 3. Cumulative sediment size distribution at different zones

Boundary Conditions and Other Sediment Parameters: At the upstream boundary, the flow discharge and sediment supply rate for each size class are needed. A time series flow hydrograph (Figure 4) is specified at the inlet boundary which represents the measured hourly flow data from August 1, 2004 to January 1, 2007. Only discharges above 600 cms are simulated as lower flows will not mobilize the bed sediments appreciably. The upstream sediment supply is set to be the sediment capacity rate.

At the downstream boundary, water surface elevation is specified. The measured rating curve is used to obtain the time variation of the water surface elevation (see Figure 4).

Eight sediment size classes (Table 1) are used to represent the sediments on the river bed and at the inlet. Each size class is transported and modeled individually.

Parker (1990) developed a bedload formula applicable to mixed gravel sediments and it is used to compute the capacity.

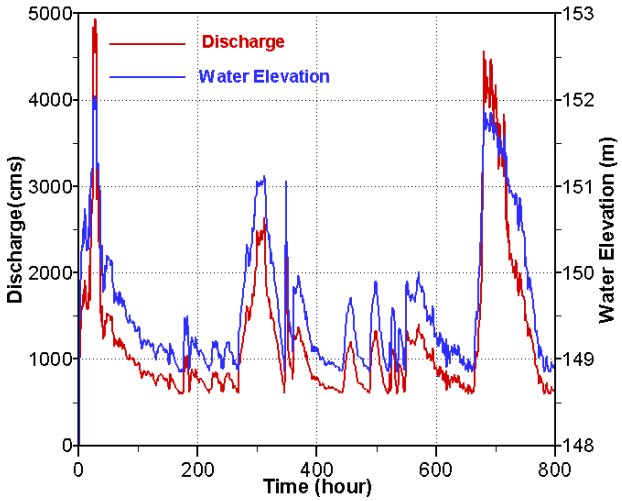

Figure 4. Flow hydrograph at the upstream boundary and water surface elevation at the downstream boundary.

Table 1. Size ranges of each sediment size class

Sediment Size Class	Size Range (mm)
1	0.001 to 0.074
2	0.074 to 0.6
3	0.6 to 2
4	2 to 8
5	8 to 24
6	24 to 72
7	72 to 216
8	216 to 648

Results and Discussion: The no-rock scenario is simulated first assuming that the riverbed in zone 9 consists of granular materials. This scenario, though imaginary, establishes a baseline to anticipate what would happen if no rock is present and helps define the extent to which bedrock controls channel erosion.

The predicted scour depth from July 2004 to January 2007 is shown in Figure 5 in terms of the net bed erosion depth (positive values are for erosion and negative values for deposition). The measured data are shown in Figure 9 where cross-sections (labeled as xs) are also shown for ease of discussion. The model predicts significant erosion for the first 500 meters downstream of the weir. In contrast, there is little erosion based on the measured data. The presence of rock in this short reach helps to stabilize the riverbed. The no-rock scenario modeling predicts erosion up to 4 meters between xs-116 and xs-115, deposition up to 4 meters at xs-114, and erosion between xs-113 and xs-111. The large deposition between xs-115 and xs-113 was not present in the measured data and must be due to the no-rock assumption. The river would reduce the riverbed slope significantly for the first 2.0 km downstream of the weir if there were no rock present. The rock in this reach maintains the bed slope in this reach and there is even an increase in slope due to erosion downstream of xs-116. Erosion pattern after xs-111 is predicted by assuming the bed is covered by granular sediments and the same bed gradations are assumed for all model scenarios. Therefore, results from the no-rock scenario are expected to be similar among all four scenarios simulated. It is seen that the predicted erosion pattern agrees qualitatively with the measured data but differs appreciably in details.

A rock erosion model is needed as demonstrated by the results of no-rock scenario. First, an attempt is made to use only the hydraulic scour model. The two model parameters within the hydraulic scour model are set as: $k_p = 2\times10^{-6}$ and $\tau_{cri} = 250Pa$. The simulated bed erosion pattern is shown in Figure 6. The model correctly predicts little erosion for the first 500 meters downstream of the weir. In comparison with the results of the no-rock scenario, the hydraulic scour model replicates this short reach well. Also, erosion of more than 7 meters is predicted by the hydraulic scour model between xs-116 and xs-114. This is in qualitative agreement with the measured data. However, small bed changes are predicted between xs-114 and xs-111 which is contrary to the data. This may indicate that hydraulic scour is a probable mechanism only for the reach of first 1.5 km downstream of the weir where the most significant erosion was recorded since the construction of the weir. The failure of the model to predict rock scour downstream of xs-114 may be attributed to two possibilities: the erosion mechanism is not due to hydraulic scour or the particular hydraulic model used is deficient. We conjecture that the hydraulic scour

is probably one of the causes for rock erosion at the site but the specific scour model needs to be improved.

Next, a simulation is carried out using only the abrasive-scour model. The model parameter for the erodibility is set as $k_v = 50.0$ while two parameters are $Y = 7.0MPa$ and $\sigma_T = 5.0e^4\ MPa$ based on field estimations. Simulated bed erosion pattern is shown in Figure 7. Similar to the hydraulic scour model, the abrasive model predicts correctly that there is little erosion for the first 500 meters downstream of the weir. The abrasive model predicts that erosion starts from xs-116 and persists downstream on the entire rock bed zone. The results are in agreement with the measured data. Differences between the prediction and measurement lie mainly in the lateral size of the incision. The model predicts rock incision with narrower width than the measured one. The results indicate that abrasive scour could potentially be an important mechanism for the entire reach. However, the quantitative difference in incision width points to a need for improvement. For example, the abrasive model of Sklar and Dietrich (2004) considers only the impact of bed load. It is possible that erosion due to suspended load should also be taken into consideration. It may also be possible that bank erosion is important.

Finally, a simulation is made for the mixed-scour scenario assuming both hydraulic scour and abrasive scours are important. The erosion model parameters are set as follows: $k_p = 1\times10^{-6}$, $\tau_{cri} = 225Pa$, $k_v = 75.0$, $Y = 7.0MPa$, and $\sigma_T = 5.0e4\,MPa$. The simulated bed erosion pattern is shown in Figure 8. As expected, results are a combination of the hydraulic scour and abrasive scour results discussed previously.

Concluding Remarks

A review was conducted for the rock erosion models and a specific rock erosion model is proposed and implemented into an existing 2D model: SRH-2D. The model is then applied to study the erosion downstream of the Chi-Chi Weir. The following conclusions may be drawn:

(1) Rock erosion has to be modeled in order to predict erosion characteristics downstream of the Chi-Chi Weir. If the riverbed is assumed to be covered with only granular sediments found nearby, the model is incapable of replicating the observed erosion pattern.

(2) The widely used stream power based hydraulic scour model predicts the erosion pattern reasonably well for only the first 1.5 km downstream of the weir. Negligible erosion is predicted for the remaining bedrock further downstream, which is contrary to the available data.

(3) The bed load based abrasive scour model of Sklar and Dietrich (2004) provides the best match in results with the measured data. It may suggest that abrasive scour is an important mechanism for the site. Quantitatively, the major difference between the prediction and measurement is that the predicted rock incision width is smaller than the actual. The discrepancy may be attributed to erosion model inaccuracy. It is possible that erosion due to suspended load should be considered or that bank erosion is important.

(4) It is unclear whether a mixed scour model is necessary for the study site. Practically, use of such models should be avoided unless there is clear field evidence supporting their use. More erosion parameters are needed for mixed scour models.

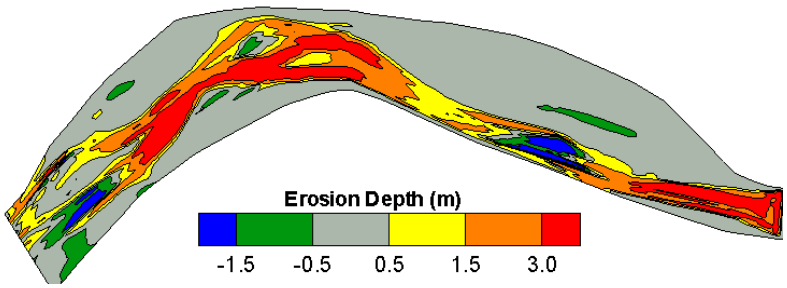

Figure 5. Predicted erosion depth for the no-rock scenario.

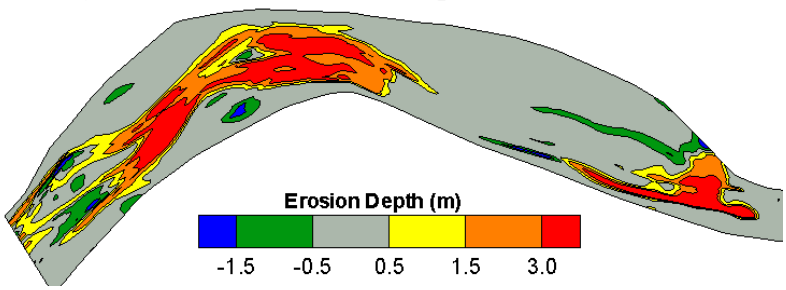

Figure 6. Predicted erosion depth for the hydraulic-scour scenario.

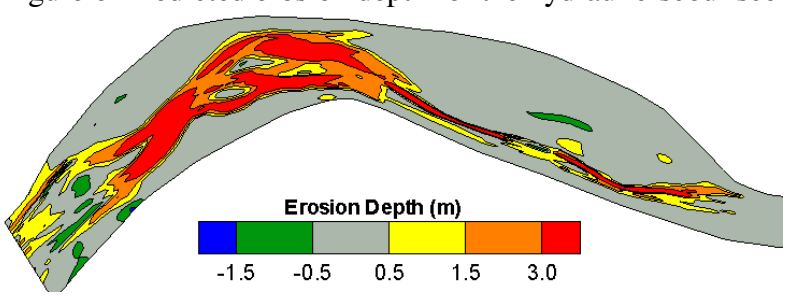

Figure 7. Predicted erosion depth for the abrasive-scour scenario.

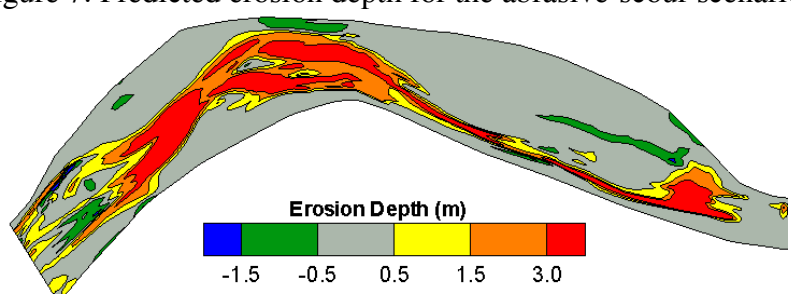

Figure 8. Predicted erosion depth for the mixed-scour scenario.

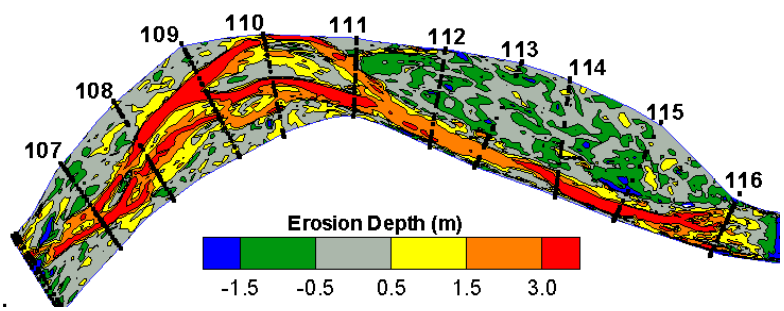

Figure 9. Measured erosion depth (cross-sections are also shown)

Acknowledgement

The author would like to acknowledge that the Water Resources Agency of Taiwan has sponsored this study. The project Liaison Officer, Director Chen, Hung-Kwai, and the review committee in Taiwan have provided valuable technical comments. Peer review provided by Rob Hilldale at Reclamation is greatly appreciated.

References

Anderson, R.S. (1986). "Erosion Profiles due to Particles Entrained by Wind: Application of an Eolian Sediment-Transport Model," Geological Society of America Bulletin, 97, 1270-1278.

Anderson, R.S. (1994). "Evolution of the Santa Cruz Mountains, California, through Tectonic Growth and Geomorphic Decay," J. Geophys. Res., 99, 20,161-20,179.

Annandale, G.W., (1995). "Erodibility," Journal of Hydraulic Research. 43 (4), pp.471-494.

Annandale, G.W., (2006). Scour Technology, Mechanics and Engineering Practice. McGraw Hill, New York.

Bollaert, E.F.R., and A. J. Schleiss (2005). "Physically Based Model for Evaluation of Rock Scour due to High-Velocity Jet Impact," Journal of Hydraulic Engineering, 131(3), pp.153-165.

Greimann, B.P., Lai, Y.G., and Huang, J., (2008). "Two-Dimensional Total Sediment Load Model Equations," J. Hydraulic Engineering, vol.134(8), 1142-1146.

Greimann, B.P., and Vandeberg, M., (2008). Predicting Rock Scour, Technical Report SRH-2008-01, Technical Service Center, Bureau of Reclamation, Denver, CO.

Howard, A.D. (1994). "A Detachment-Limited Model of Drainage Basin Evolution," Water Resour. Res., 30, 2261-2285.

Howard, A.D., Dietrich, W.E., and Seidl, M.A. (1994). "Modeling Fluvial Erosion on Regional to Continental Scales," J. Geophys. Res., 99, 13971-13986.

Lai, Y.G., Weber, L.J., and Patel, V.C. (2003). "Non-hydrostatic three-dimensional method for hydraulic flow simulation - Part I: formulation and verification." J. Hydraulic Engineering, 129(3), 196-205.

Lai, Y.G., and Greimann, B.P. (2007). "Numerical modeling of alternate bar formation downstream of a dike," World Environmental & Water Resources Congress, May 15-19, 2007, Tampa, Florida.

Lai, Y.G. (2008). *SRH-2D Theory and User's Manual version 2.0,* Technical Service Center, Bureau of Reclamation, Denver, CO.

Lai, Y.G., and Greimann, B.P. (2008a). "Predicting contraction scour with a 2D model," World Environmental & Water Resources Congress, May 12-16, 2008, Honolulu, Hawaii.

Lai, Y.G., and Greimann, B.P. (2008b). "Modeling of erosion and deposition at meandering channels," World Environmental & Water Resources Congress, May 12-16, 2008, Honolulu, Hawaii.

Lamb, M.P., Dietrich, W.E., and Sklar, L.S. (2008). "A Modle ofr Fluvial Bedrock Incision by Impacting Suspended and Bed Load Sediment." J. Geophys. Res., 113, F03025.

Parker, G., (1990). "Surface-Based Bedload Transport Relation for Gravel Rivers," J. Hydraulic Research, 28(4):417-436.

Seidl, M.A., and Dietrich, W.E. (1992). "The Problem of Channel Erosion into Bedrock," in Functional Geomorphology, edited by K.H. Schmidt and J. de Poley, Catena Suppl., 23, 101-124.

Sklar, L.S., and Dietrich, W.E. (2004). "A Mechanistic Model for River Incistion into Bedrock by Saltating Bed Load," Water Resources Research, 40:W06301, doi:10.1029/2003WR002496.

Sklar, L.S., and Dietrich, W.E. (2006). "The Role of Sediment in Controlling Steady-State bed Channel Slope: Implications of the Saltation-Abrasion Incision Model," Geomorphology, 82, pp.58-83.

Tomkin, J. H., Brandon, M. T., Pazzaglia, F. J., Barbour, J. R. and Willet, S.D. (2003). "Quantitative Testing of Bedrock Incision Models for the Clearwater River, NW Washington State," Journal of Geophysical Research, 108(B6), 2308, pp.1-19.

Tucker, G.E., and Slingerland, R.L. (1996). "Predicting Sediment Flux from Fold and Thrust Belts," Basin Res., 8, 329-349.

Tucker, G.E., and Slingerland, R.L. (1997). "Drainage Basin Responses to Climate Change," Water Res. Res. 33(8), 2031-2047.

Whipple, K.X., Hancock, G.S., and Anderson, R.S. (2000). "River Incision into Bedrock: Mechanics and Relative Efficacy of Plucking, Abrasion, and Cavitation," Geological Society of America Bulletin 112, 490-503.

Willett, S.D. (1999). "Orogeny and Orography: The Effects of Erosion on the Structure of Mountain Belts," J. Geophys. Res., 104, 28, 957-28, 981.

Wittler, R.J., Annandale, G.W., Ruff, J.F., and Abt, S.R. (1998). "Prototype Validation of Erodibility Index for Scour in Granular Media," American Society of Civil Engineers, Proceedings of the 1998 International Water Resources Engineering Conference, Memphis, Tennessee, August.

3D Numerical Modeling of John Day Lock Tainter Valves

E. Allen Hammack[1] and Richard L. Stockstill[2]

[1]Mechanical Engineer, U.S. Army Engineer Research and Development Center, Coastal and Hydraulics Laboratory, 3909 Halls Ferry Rd., Vicksburg, MS 39180-6199; PH (601) 634-3628; FAX (601) 634-3218; email: Allen.Hammack@usace.army.mil
[2]Research Hydraulic Engineer, U.S. Army Corps of Engineers Engineer Research and Development Center, Coastal and Hydraulics Laboratory, 3909 Halls Ferry Rd., Vicksburg, MS

ABSTRACT

The reverse tainter valves in the culverts at John Day Lock have been failing structurally for the life of the project. Recently, district engineers have decided to redesign these tainter valves to reduce or eliminate cracking and other structural issues. In order to complete this redesign, three-dimensional (3D) simulations were conducted of the flows experienced through the culverts for several valve openings seen during a lock operation. These 3D simulations were performed with the 3D Navier-Stokes module of the numerical code Adaptive Hydraulics (ADH) (http://adh.usace.army.mil/) developed by the U.S. Army Engineer Research and Development Center, Coastal and Hydraulics Laboratory (CHL). This code models the complex 3D flows around hydraulic structures using adaptive meshing techniques on unstructured meshes. The flow variables, pressure and velocity, calculated at each node lying on the surface of the valve were exported for use as boundary conditions for a 3D structural model of the tainter valve.

INTRODUCTION

The John Day Lock is located on the Columbia River. The lock has a chamber that is 26.2 m wide by 205.7 m long and is classified as a very high-lift lock according to U.S. Army Corps of Engineers criteria (EM 1110-2-1604). The John Day Lock has the highest design lift of any lock in North America with a 33.5-m lift at normal pool. The filling and emptying culverts form what is commonly referred to as a split lateral system. Double skin-plated reverse tainter valves control the flow through the culverts. Each 3.7-m-wide by 6.1-m-high wall culvert supplies water to a set of ten manifolds aligned laterally to the lock centerline. The left culvert laterals are located on the upper one-third end of the lock chamber and the right culvert laterals are located in the lower one-third end of the chamber.

The John Day Lock filling system has presented problems since beginning operations in 1968. Prototype tests were conducted in 1973 (Neilson and Pickett, 1986). The prototype investigation was initiated because severe shock waves, vibration, and noise in the lock filling system had been experienced during valve opening. Damage to the filling valve was found in May 1971 and was believed to have resulted from these conditions. The damage consisted of bent skin plates and broken welds in the radial arms and sheared bolts across the top of the valve skin plate. Chanda and Perkins (1974) reported that excessive structural vibration caused failure of monolith joint water stops, damage to valve trunnion arms, and movement of a monolith. Neilson and Pickett (1986) note that the shock waves are not unique at John Day since similar problems have also occurred at the McNary, Ice Harbor, and Lower Monumental Locks. Information obtained at John Day was believed to be applicable to Ice Harbor and Lower Monumental since these locks have nearly identical filling systems and similar troubles during valve opening.

Lock operation produces noise and vibrations during filling. The pounding noise can be reduced by opening the filling valves in stages, so the valve operations have been changed from the design schedule to being operated in a stepped fashion. The two-valve filling operation was recommended by Neilson and Pickett (1986), wherein the valves are operated to one-third open in 40 sec, holding at one-third open for a 300-sec delay, and to fully-open in 80 sec.

Recently, a field inspection report was prepared by North (2006). He reiterated that operation and maintenance of the lock culvert valves have been hindered with problems essentially since completion of construction. Cracks have formed in the steel wrapper plate of the valve members and have been repaired numerous times. A recommendation (North 2006) has been made to replace the tainter valves.

It is generally agreed that before the tainter valves are replaced, an effort should be made to determine the cause of these cracks. CHL performed 3D flow analyses to determine how the structural members interact with the flow. The flow solutions include the pressures on the valve surface and culvert velocities during a lock operation. The computed pressures were to be used as boundary conditions for structural analyses of the current and any proposed valve designs.

NUMERICAL MODEL DESCRIPTION

The numerical flow solver used is the Navier-Stokes module of ADH. This code uses the Reynolds-Averaged Navier-Stokes (RANS) equations, which are the conservation of mass and the conservation of momentum, to calculate the pressure and velocity components throughout the flow domain. Mathematically, these are:

$$\nabla \cdot \boldsymbol{V} = 0$$

and

$$\left(\frac{\partial \boldsymbol{V}}{\partial t}+\boldsymbol{V}\cdot\nabla\boldsymbol{V}\right)-\boldsymbol{g}-\frac{1}{\rho}\nabla\cdot\left(\sigma-\sigma_R\right)=0\,.$$

The RANS equations are written in terms of the mean velocity, $\boldsymbol{V}(\boldsymbol{x}, t)$, and pressure, $p(\boldsymbol{x}, t)$, to reduce the modeling of turbulence to a set of quasi-steady-state equations. The Reynolds stress is used to represent the effect of turbulence on the mean flow. Following the suggestion of Boussinesq, the Reynolds stress tensor is expressed in terms of the strain rate as

$$\sigma_R=-\rho\nu_t\left(\nabla\boldsymbol{V}+\nabla\boldsymbol{V}^T\right).$$

Sufficiently small eddy viscosity has been found to adequately capture macroscopic flow features such as eddies.

GEOMETRY

The flow domain with the major geometric features is shown in Figure 1. The volume consists of a section of culvert beginning immediately downstream of the lock intake and extending thirty hydraulic diameters (137 m total) downstream of an 18.3-m roof transition. Portions of the filling system that do not align with the culvert, including the laterals that would supply flow to the lock chamber, were excluded. At the inflow boundary the culvert is 3.7 x 9.1 m and curves downward 17.1 m over 36.6 m. The culvert is 3.7 m wide and 4.3 m tall at the reverse tainter valve. The tainter valve has a nominal radius of 5.8 m, and the valve well is 3.7 x 6.2 m. The water surface in the valve well is a free surface. Two 4.3 x 0.7-m bulkhead slots, one upstream and one downstream of the valve are included in the model. The downstream bulkhead is capped, while the upstream bulkhead water surface is a free surface.

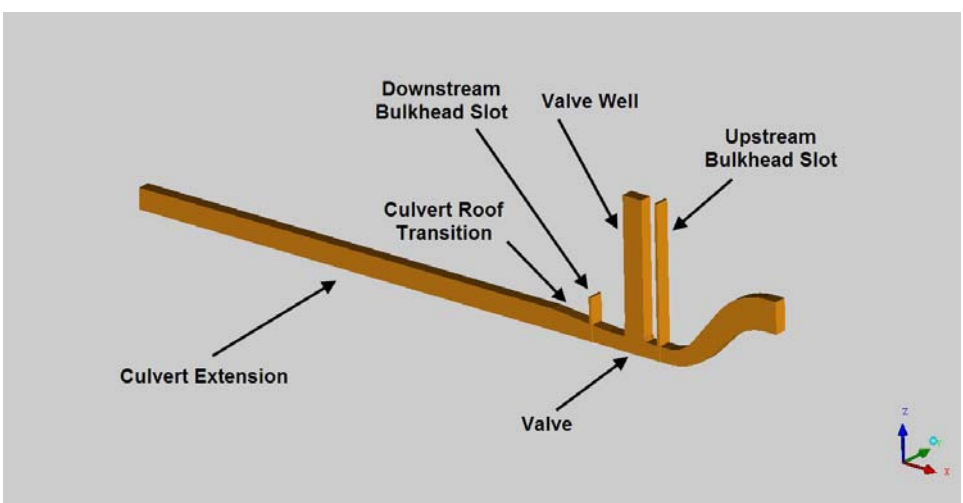

Figure 1. Flow domain.

Six valve openings were chosen for the analyses to represent the valve motion used during a lock-filling operation. Of these – 10, 35, 55, 65, 75, and 90% openings – certain valve openings represent a specific potential problem during a tainter valve operation. The 10% valve opening represents a time where the jet velocity is large and a potential for vibration exists. The 35% valve opening is the location in which the valve is held during normal operating conditions. This is the holding position on the stepped-valve operation schedule that was developed during the field study and adapted as operating procedure. The 55% opening represents the estimated valve opening for the maximum hoist load. Finally, the 90% valve opening represents the estimated opening for maximum variation of the hoist loads.

BOUNDARY CONDITIONS AND MESH DETAILS

The boundary conditions are shown in Figure 2. The model consisted of two flux boundaries – one inflow and one outflow. Hydrostatic pressures corresponding to the desired upper pool (81.7 m) and lower pool (47.2 m) elevations were applied to the inflow and outflow boundaries, respectively. The 34.4-m head differential applied at these boundaries determined the flow through the model. Free-surface boundary conditions were applied to the water surfaces in the upstream bulkhead slot and valve well, so the nodes on these surfaces could move vertically to the elevation corresponding to zero pressure. The water surface of the downstream bulkhead slot was treated as frictionless and stationary. All other model boundaries were specified as no flux boundaries with a uniform friction coefficient representing the surface roughness.

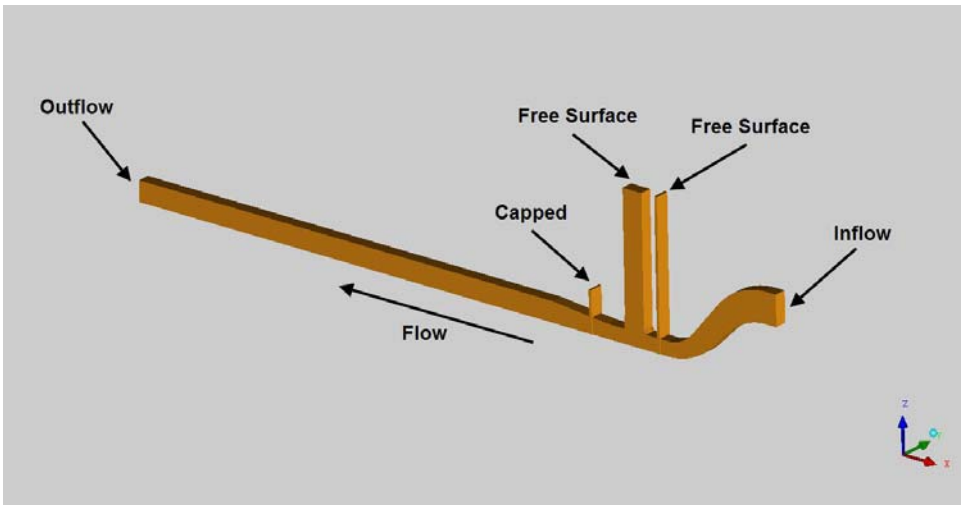

Figure 2. Boundary conditions.

Three-dimensional meshes of the flow volume for each valve opening were constructed from a CAD model using tetrahedral elements. Mesh elements have sides ranging from 13 mm (on the valve surface) to about 0.76 m (far from the valve). The smallest elements were necessary to capture the intricate valve details such as the valve lip, a dominant valve feature in determining flow separation downstream of the valve. In each mesh the valve surface is defined by about 20,000 nodes. Each mesh has between 143,000 and 220,000 nodes and between 706,000 and 1.2 million tetrahedral elements.

RESULTS

Steady-state flow solutions were calculated for each valve position. Table 1 summarizes the flow details from each flow solution. The discharges were calculated by integrating the nodal velocity solutions at the outflow boundary over the entire culvert cross-section. The discharge increases as the valve opening increases because the driving pressures, the hydrostatic pressures on the inflow and outflow boundaries, were constant for each valve position while the flow area underneath the valve opening was increased. The average velocity head of the flow underneath the valve increases as the valve opening is lowered causing the pressure head in the valve well to decrease. This lowering of the average pressure head at the valve well causes the valve well water surface to decrease as the valve is lowered. The maximum velocities occur immediately downstream of the valve lip, with the minimum velocities slightly further downstream.

Table 1. Discharge and water surface solutions for each valve position.

Valve Opening	Discharge (m^3/s)	Valve well WSE (m)	Upstream Bulkhead WSE (m)	Maximum velocity (m/s)
10%	33.4	81.2	81.4	26.2
35%	112.5	78.5	78.8	29.0
55%	200.7	72.4	73.0	30.5
65%	248.2	67.5	68.3	31.1
75%	302.1	61.0	62.0	30.5
90%	387.1	47.4	48.1	29.3

Although the culvert upstream of the valve is short the approach flow to the valve fairly uniform flow. The *x*-component of the flow velocity near the valve is shown in Figure 3. The velocities range from 30 m/s (directed downstream) at the invert to 10 m/s (directed upstream) at the culvert roof. The flow velocity is nearly zero throughout the valve well and bulkheads except for an eddy that forms slightly above the valve.

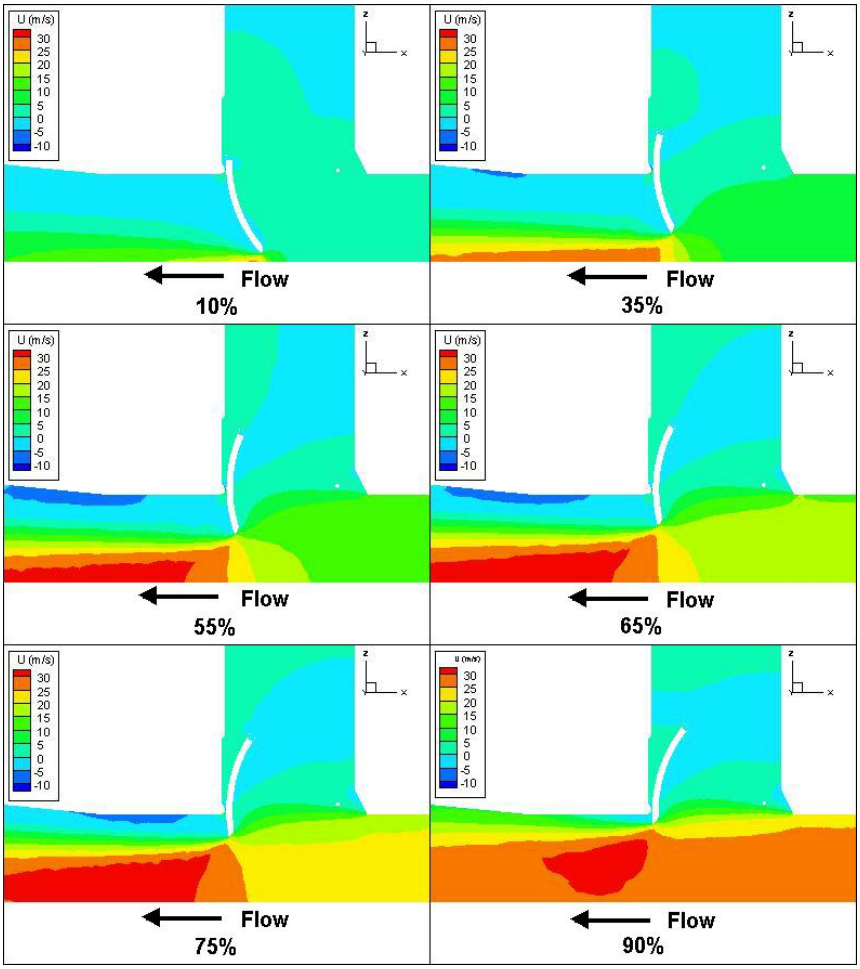

Figure 3. Velocity distribution near the valve.

Each valve opening produces eddies downstream of the valve. These eddies are shown in Figure 4. The largest eddy, caused by the 55% valve opening extends about 70 m downstream of the valve. The smallest eddy, which only extends about 1 m downstream of the valve, is created by the 90% valve opening. Such long eddies indicate that the flow, which separates at the valve lip, does not reattach until well downstream of the culvert roof expansion. Also, the approach flow for the laterals connecting the culvert to the lock chamber is not uniform when these large eddies are present. The only likely exceptions are the flows associated with the 10% and 90% valve openings.

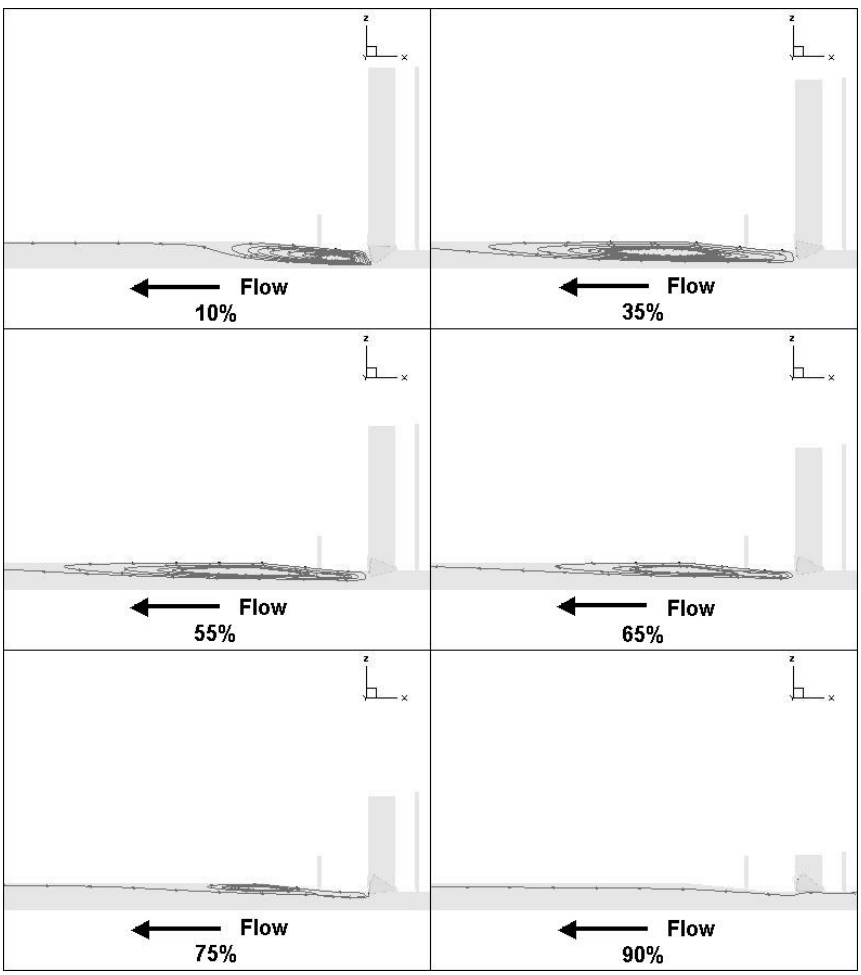

Figure 4. Eddies formed downstream of the valve.

The pressure distributions on the valve surface are shown in Figure 5. The pressures are highest at locations where the velocity near the valve are highest, particularly near the valve seal. The pressure solution was used to determine the pressure boundary conditions for a structural analysis of the entire valve geometry.

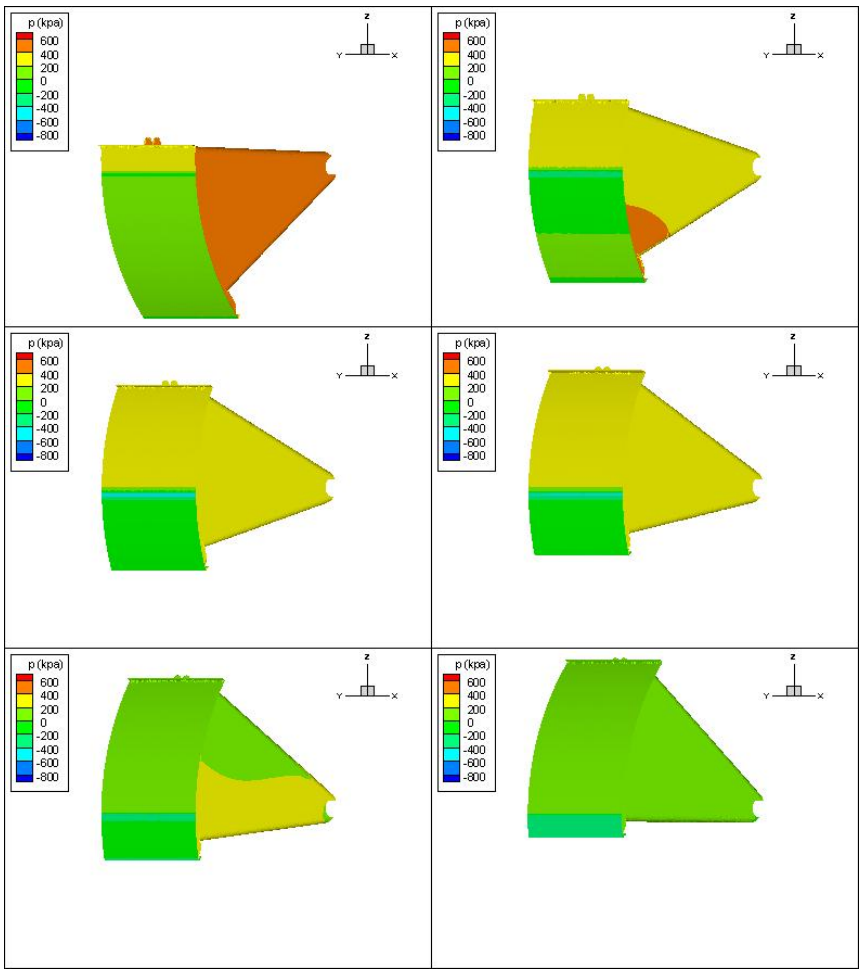

Figure 5. Pressure distribution on the valve surface.

Two different quantities, the discharge coefficient and the valve loss coefficient, were used to validate the flow solutions. Mathematically, these coefficients are

$$C_d = \frac{Q}{bW\sqrt{2gH_L}}$$

and

$$k_v = \frac{H_L}{\frac{v^2}{2g}}.$$

The discharge coefficients and valve loss coefficients are listed in Table 2. These loss coefficients compare well with the general research findings of Pickering (1981).

Table 2. Valve coefficients.

Valve Opening	Discharge coefficient (C_d)	Valve loss coefficient (k_v)
10%	0.83	146.62
35%	0.80	12.30
55%	0.98	3.45
65%	1.08	2.02
75%	1.24	1.16
90%	1.09	1.04

CONCLUSIONS

Pressure and velocity distributions in complex flow regimes, such as in navigation lock culverts, can be accurately calculated using the Navier-Stokes module of ADH. The eddies that form downstream of the valve may disrupt the distribution of flow in the laterals of the real system. The computational method used in this study is useful in situations where time and cost prohibit use of a physical model. The solutions produced in this study were used by Portland District to create loads used to evaluate the current valve structure (particularly the internal structure) and potentially modify the valve design.

The total force acting on the valve can be calculated from the pressure solution by integrating the pressures on the valve surface. The total hydrodynamic force acting on the valve can be couple with the valve weight to determine the uplift force, which can be used in selecting the mechanical components that control the valve movement during lock operation.

ACKNOWLDEGEMENT

The computations described and the results presented were obtained from research sponsored by the U.S. Army Corps of Engineers District, Portland and the Navigation Systems Research Program under the guidance of James E. Clausner, Program Manager. Permission was granted by the Chief of Engineers to publish this information.

LIST OF VARIABLES

$\boldsymbol{x}$ = spatial coordinate, with x and y lying in the horizontal plane and z being in the vertical direction
$\boldsymbol{g}$ = gravitational acceleration
t = time
ρ = fluid density
σ = $-p\mathbf{I} + 2\rho\nu_t\mathbf{s}(\mathbf{V})$
ν = fluid kinematic viscosity
s = $\frac{1}{2}\left(\nabla \boldsymbol{V} + \nabla \boldsymbol{V}^T\right)$
ν_t = fluid eddy viscosity
Q = discharge
b = valve opening height
W = culvert width
H_L = total head loss across the valve (sum of velocity head, pressure head, and elevation head)
v = average flow velocity in the culvert near the valve (3.7 x 4.3 m culvert)

REFERENCES

Chanda, A. J. and Perkins, L.Z. (1974). *Filling and emptying system John Day Lock, Columbia River, Oregon and Washington; hydraulic model investigation*. Technical Report No. 98-1, U.S. Army Engineer Division, North Pacific, Bonneville, Oregon.

Headquarters, US Army Corps of Engineers (2006). *Hydraulic design of navigation locks*. Engineer Manual No. 1110-2-1604, Washington, D.C.

Neilson, F. M. and Pickett, E. B. (1986). *John Day Lock hydraulic prototype tests, Columbia River, Washington*. Draft technical report, Vicksburg, Mississippi: U.S. Army Engineer Waterways Experiment Station.

North, T. (2006). Inspection of the John Day Navigation Lock tainter valves, Memorandum of design, U.S. Army Engineer Portland District, Portland, Oregon.

Pickering, G. A. (1981). *Lock culvert valve loss coefficient*. Technical Report HL-81-10, :U.S Army Engineer Waterways Experiment Station, Vicksburg, Mississippi

A Three-Dimensional Numerical Model for Flow in a Lock Filling System

Richard L. Stockstill, F.ASCE[1] and R. Charlie Berger, F.ASCE[1]

[1]Research Hydraulic Engineer, U.S. Army Engineer Research and Development Center, Coastal and Hydraulics Laboratory, 3909 Halls Ferry Road, Vicksburg, MS 39180-6199.

ABSTRACT

The hydraulic performance of a navigation lock is difficult to evaluate because the unsteady flow is characterized by large variations in pressure and velocity. The lock system contains the interactions of free-surface and pressurized conduit flow. Currently, the filling and emptying system design must be carefully evaluated in a physical model which generally is expensive in terms of both time and money. A numerical model capable of simulating the flow in a navigation lock can provide an economical tool for detailed evaluation of lock systems and components. A flow model of a lock filling and emptying system must be capable of simulating the large- and small-scale flow features found in internal (conduit) flow and free-surface flow within the lock approach and chamber.

This paper describes the development of a complete three-dimensional (3-D) model of a sidewall port lock filling system. The Reynolds Averaged Navier-Stokes equations are used to describe the 3-D flow. The equations are discretized using the Galerkin Least-Squares finite element algorithm on tetrahedral elements with sizes varying over several orders of magnitude. The water-surface location is determined using a moving mesh method. The code is parallelized using Message Passing Interface (MPI) and is capable of adapting the mesh during flow calculations based on error estimations.

The project demonstrates model construction of a lock filling and emptying system that has complicated geometric features including culvert transitions and multi-ported manifolds. Boundary conditions are explained and the applicability of different error estimators is investigated. Computational and hydraulic engineering issues arising from the simulation of a lock filling operation are discussed.

INTRODUCTION

Whether it is new lock construction, rehabilitation of an existing lock, or operational changes to meet modified project objectives, innovative ideas regarding the filling and emptying of locks are being proposed. The problem is that often these ideas fall outside established design guidance. Perhaps some of these ideas, while economically feasible, may not provide the service required for safe navigation through the lock. Currently, the design concept must be carefully evaluated in a physical model, which generally is expensive in terms of both time and money.

A flow solver is being developed to provide an economical means of evaluating the hydraulic performance of a lock culvert system. The Reynolds Averaged Navier-Stokes equations are used to describe the 3-D flow. The equations

are solved using the 3-D Navier-Stokes component of the Adaptive Hydraulics (ADH) (http://adh.usace.army.mil/) code. The equations are discretized using the Galerkin Least-Squares finite element algorithm (Behr and Tezduyar 1994) on tetrahedral elements with sizes often varying over several orders of magnitude. The water-surface location is determined using a moving mesh method that employs space-time finite elements in a manner similar to that presented by Behr (2001). The code is parallelized using MPI and ParMETIS provides efficient mesh portioning. The ADH code is capable of adapting the mesh during flow calculations based on residuals. This automatic mesh refinement ensures suitable resolution in a computationally efficient manner.

NUMERICAL EXAMPLE

An example is provided with simulation of a navigation lock filling operation. The project is Webbers Falls Lock, on the McClellan-Kerr Arkansas River Navigation System about 5 miles (8 km) northwest of Webbers Falls, OK. A typical lock chamber on the Arkansas River is nominally 110 ft (33.5 m) wide by 600 ft (183 m) long. The filling and emptying system is a sidewall port design. A model of the Webbers Falls Lock, which has a 29-ft (8.8-m) lift at normal pools, is shown in Figure 1. It reproduces approximately 500 ft (150 m) of the upstream approach, twin sidewall intake manifolds, the lock chamber, valve wells, sidewall ports and culverts. The culvert system consists of 8-port 7.5-ft (2.29-m) wide by 10-ft (3.05-m) tall intake manifolds on either lock wall from which the flow transitions to 12-ft (3.66 m) by 12-ft (3.66 m) culverts in each wall. Flow is introduced into the lock chamber by 14 ports in each sidewall filling and emptying manifold. Each port is 3.5 ft (1.07 m) tall and has a throat width of 2.54 ft (0.774 m).

Computational Mesh. The initial finite element mesh has 229,090 nodes and 1,126,845 tetrahedral elements. The mesh resolution is illustrated by the surface mesh shown in Figure 2. Details of the mesh resolution at the intakes are shown in Figure 3. A representative sample of the volume mesh is provided in Figure 4, wherein tetrahedral elements are shown on a slice normal to the lock center line from the right wall culvert through a filling and emptying port and into the lock chamber. Figure 4 illustrates the variation in mesh resolution required to describe the geometry. Flow variations are resolved during flow simulations using mesh adaption. The mesh adaption consists of refinement and coarsening. The mesh is not allowed to become coarser than the initial mesh. Therefore, the minimum number of nodes and elements that occur during a simulation are those describing the initial mesh.

Initial and Boundary Conditions. The initial conditions for simulation of a lock filling operation were set with the lock empty and the chamber water surface was set at the lower pool elevation. Zero velocity and hydrostatic pressure were specified at each node. Boundary conditions applied at the inflow consisted of hydrostatic pressure (Dirichlet) and time-varying flux (via natural boundary condition) reproducing a hydrograph. The hydrograph varied linearly increasing from no flow

at the initial time up to the peak discharge of 5,088 cfs (144 cms) at 4 min and then decreasing to zero resulting in a filling time of 10 min.

A no flux boundary condition was applied to all solid boundaries. The free surface within the lock chamber was set as moving boundary while other surface nodes (culvert, intakes, etc.) were fixed boundaries. The nodes within the chamber volume were allowed to move in the vertical direction. Interior nodes moved as a function of surface node displacements. For this example the nodes on a horizontal plane in the lock chamber 6.5 ft (1.98 m) above the floor were fixed (no displacement) thus preserving the complicated geometry of the manifolds.

Conditions at the moving boundary representing the lock chamber water surface were specified as a constant pressure of zero on the nodes and stress-free conditions were enforced on the element faces.

Flow Solutions. The ten minutes of filling operation were simulated using a 5-sec time step. Flow variations within the chamber during filling are shown on Figures 5-7. These pictures show velocity contours at particular times during the simulation. The lock chamber water surface rises from the lower pool (initial conditions) to the upper pool as the lock fills. The jets issuing from the manifolds 1 min after filling started are shown in Figure 8. These velocity contours provide an insightful view of the flow distribution and jet interaction in the culvert manifold and chamber.

Mesh Adaption. Automatic mesh adaption allows the modeler to just focus attention on capturing geometric features when generating a mesh. This is particularly important in modeling hydraulic structures having complicated shapes such as lock filling systems. Mesh refinement required in regions due to flow conditions can be handled with mesh adaption during simulation runs. Adaption is triggered by a residual computed on an elemental basis. Two methods were used to calculate the residual. The first choice is essentially a check on the convergence of continuity. It is the norm of the divergence of the velocity evaluated over an element as shown in Equation 1.

$$\left(\int_{a_e} \left(\frac{\partial u_i}{\partial x_i} \right)^2 da_e \right)^{1/2} A_e \tag{1}$$

Here u_i is the discrete solution of velocity and A_e is the elemental surface area. Tests were conducted to evaluate the appropriateness of the "continuity" residual to indicate regions within the lock model that needed refinement. Residuals were calculated for each time step during a lock filling simulation with no mesh adaption. Values ranged from 0 to 0.00544 cfs over all the time steps. Most of the residual was found near the inflow boundary and in the center of the lock chamber on the chamber floor. Contours of the continuity residual within the sidewall manifolds and the lock chamber at 1 min into the filling operation are shown in the picture on the left of Figure 9. The region near the inflow boundary is where the original mesh is the coarsest. However, one would expect the solutions to be the smoothest in this area and so a coarse mesh might provide adequate resolution.

Another residual indicator was also evaluated. This indicator is related to velocity gradients and was termed the "gradient" indicator. This method of computing error estimation follows that developed by Zienkiewicz and Zhu (1987), which is often referred to as the Z^2 (or Z-Z) method. This method evaluates differences in velocity gradients over the element

$$\left(\int_{v_e} \left(\sigma_{ij}{}^2 \right) dv_e \right)^{1/2} V_e \tag{2}$$

Here σ_{ij} can be thought of as a term of the rate-of-strain tensor

$$\sigma_{ij} = \tfrac{1}{2} \left(\frac{\partial u_i}{\partial x_j} + \frac{\partial u_j}{\partial x_i} \right)^* \tag{3}$$

and V_e is the elemental volume. Again, the velocities are the discrete values. Each tensor term is actually the difference in the gradient obtained from an $L2$ projection of the velocity and that represented with linear basis function, ϕ_i.

$$\left(\frac{\partial u_i}{\partial x_j} \right)^* = \left(\frac{\partial u_i}{\partial x_j} \right)_{L2} - \left(u_i \frac{\partial \phi_i}{\partial x_j} \right) \tag{4}$$

Once more residual values were computed for each time step without mesh adaption. Values ranged from 0 to 0.19986 sec^{-1} over all the time steps. Contours of the residual calculated in this manner at 1 min into the filling operation, are shown in the picture on the right of Figure 9. The residual was found concentrated along the chamber center much like the continuity method found. However, there were regions within the culverts that had measurable values of gradient residual. Closer observation of the residual distribution found that the residual was large in the area of conduit bends (see Figure 10), where the solution is changing the most rapidly (i.e. large gradients).

Both methods may prove to be valuable for automatic mesh refinement. The continuity residual is more useful in regions where the flow is changing directions because the gradient residual will always be large in these areas. However, in an area such as the inflow boundary where the solution is not of interest was purposely made coarse, the gradient method would recognize that the solution there is smooth.

Based on the results shown in Figure 9 and Figure 10, choices of adaption residual triggers were selected. The models were run again with these residual triggers which are listed in

Table **1**. Each simulation employed 4 layers of refinement, two-level Additive Schwarz preconditioning with 4 blocks (see http://adh.usace.army.mil/ for explanation), and were executed using 64 processors on a Cray XT3. The maximum

number of nodes, which occurred near the time of peak discharge, indicates the amount of refinement that was performed by ADH during the lock filling cycles.

Table 1. Mesh adaption results during lock filling. Coarse (initial) mesh had 229,090 nodes and 1,126,845 tetrahedral elements.

Computational Factor	Residual method	
	Continuity	Velocity Gradient
Residual tolerance	0.001 cfs	0.030 sec^{-1}
Maximum number of nodes (rounded to nearest hundred) over all time steps, 4 levels of adaption	258,000	273,500

FUTURE WORK

Additional testing will determine the accuracy of simulating lock culvert flow (pressures, velocity profile, etc.) and lock chamber flow conditions (jet expansion, movement of free surface, etc.). Experiments will be conducted with the different methods of error estimation to determine efficient ways of acquiring accurate solutions with mesh adaption. A means of including the effects of flow control devices such as culvert valves will be added. Representation of moving mechanical equipment such as valves and gates must be added to the code before a full lock model study can be completed. Finally, the capability of modeling a vessel moored in the chamber during locking operations will be developed. A modeling system that accounts for a barge/ship in the lock chamber and that can calculate hawser forces during locking operations will be constructed.

ACKNOWLEDGEMENT

The computations described and the results presented were obtained from research sponsored by the US Army Corps of Engineers Navigation Systems Research Program under the guidance of James E. Clausner, Program Manager. Permission was granted by the Chief of Engineers to publish this information.

REFERENCES

Behr, M. (2001). "Stabilized space-time finite element formulations for free-surface flows." *Communications in Numerical Methods in Engineering*, 17(11), 813-819.

Behr, M. and Tezduyar, T. E. (1994). "Finite element solutions for large-scale flow simulations." *Computer Methods in Applied Mechanics and Engineering*, 112, 3-24.

Zienkiewicz, O. C. and Zhu, J. Z. (1987). "A simple error estimator and adaptive procedure for practical engineering analysis." *International Journal of Numerical Methods in Engineering*, 24, 337-357.

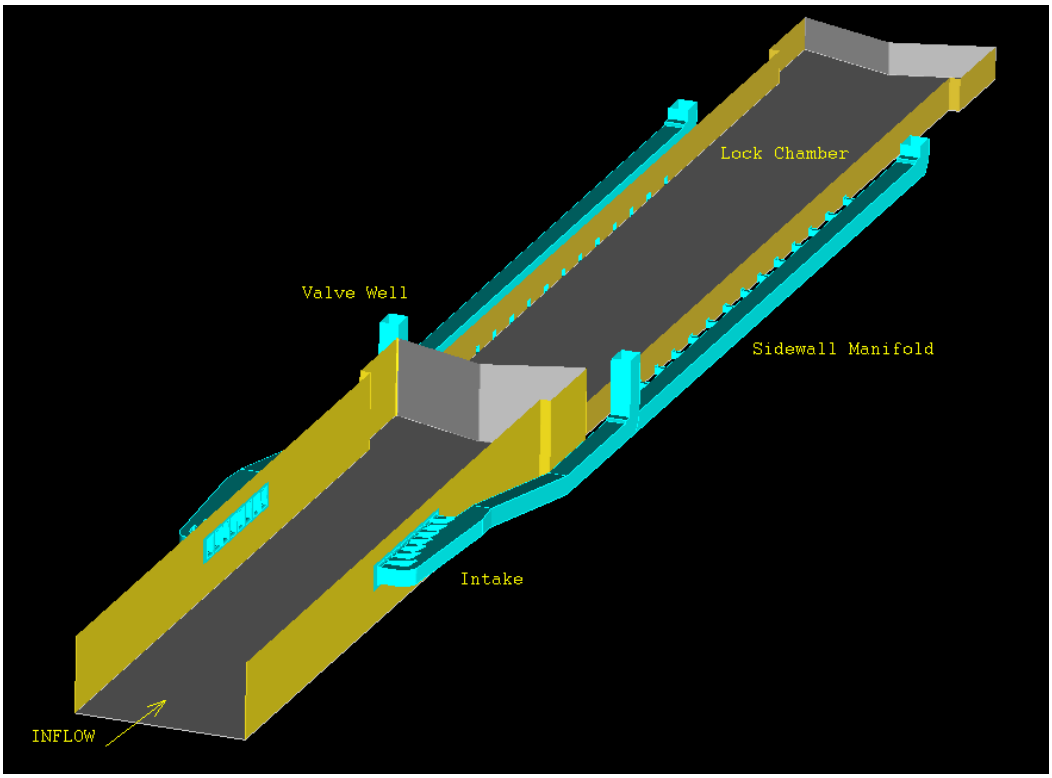

Figure 1. CAD model of Webbers Falls Lock filling system.

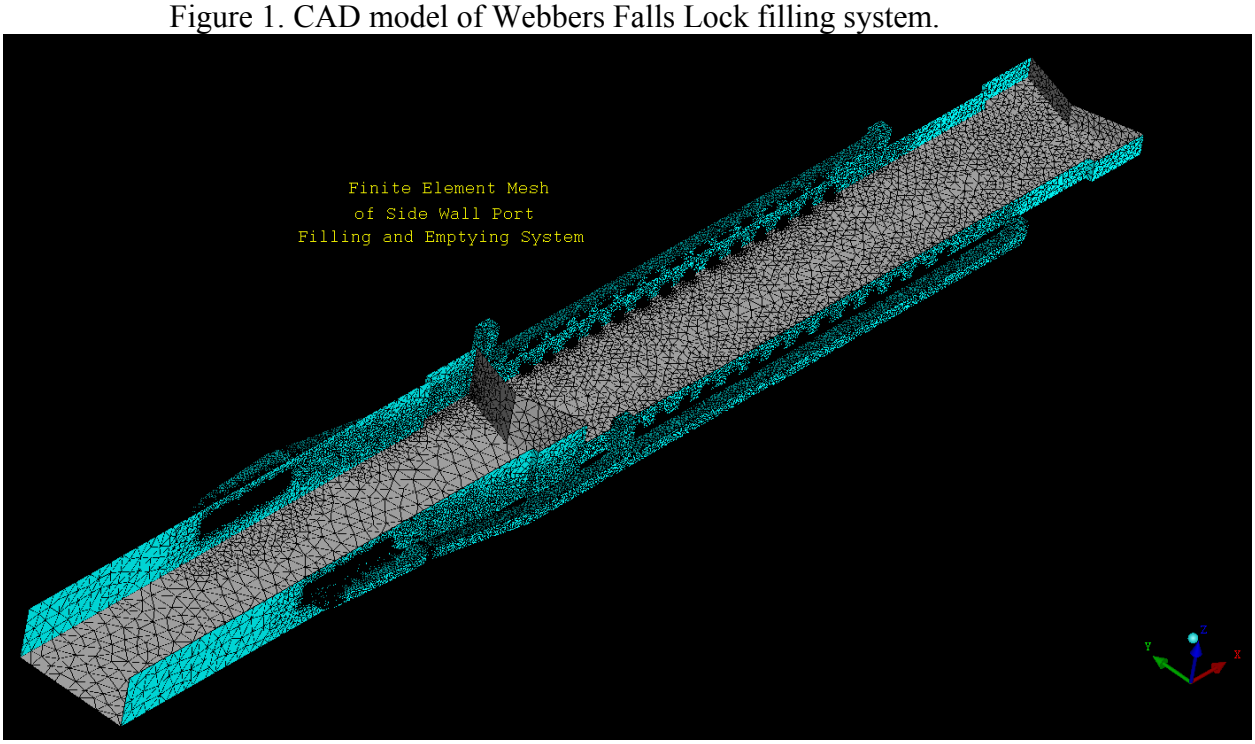

Figure 2. Computational surface mesh of lock filling system with water surface removed (229,090 nodes and 1,126,845 tetrahedral elements).

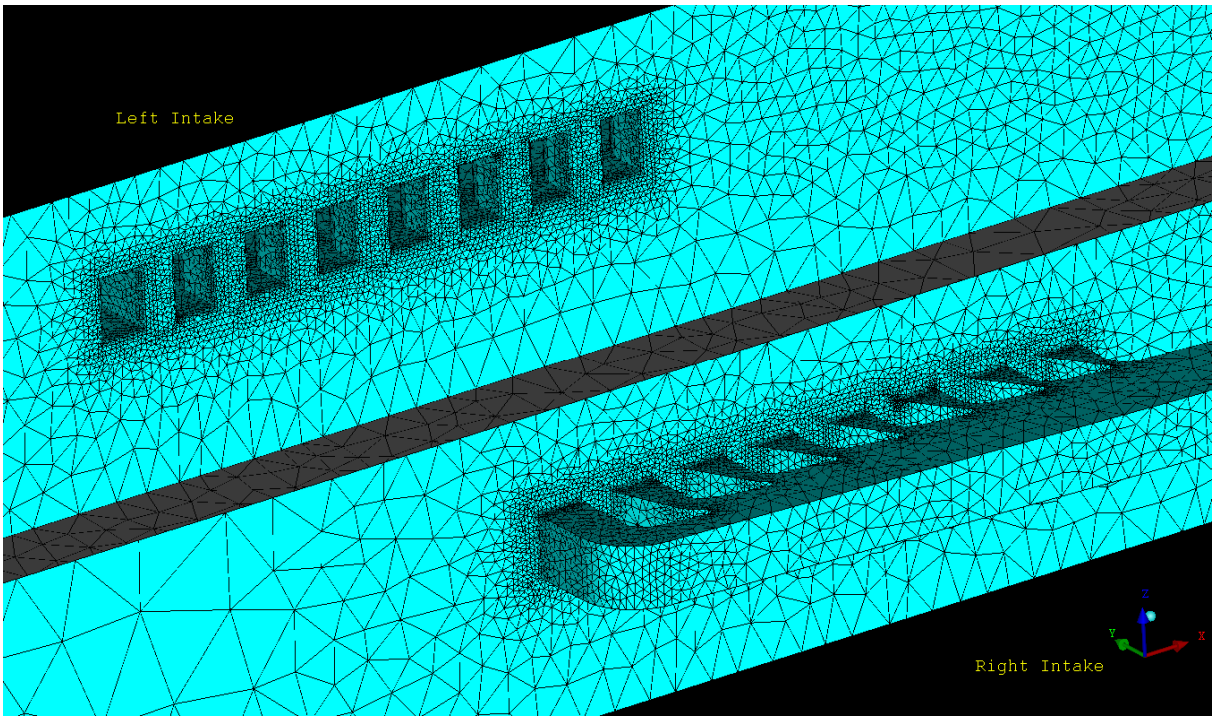

Figure 3. Details of surface mesh at intakes.

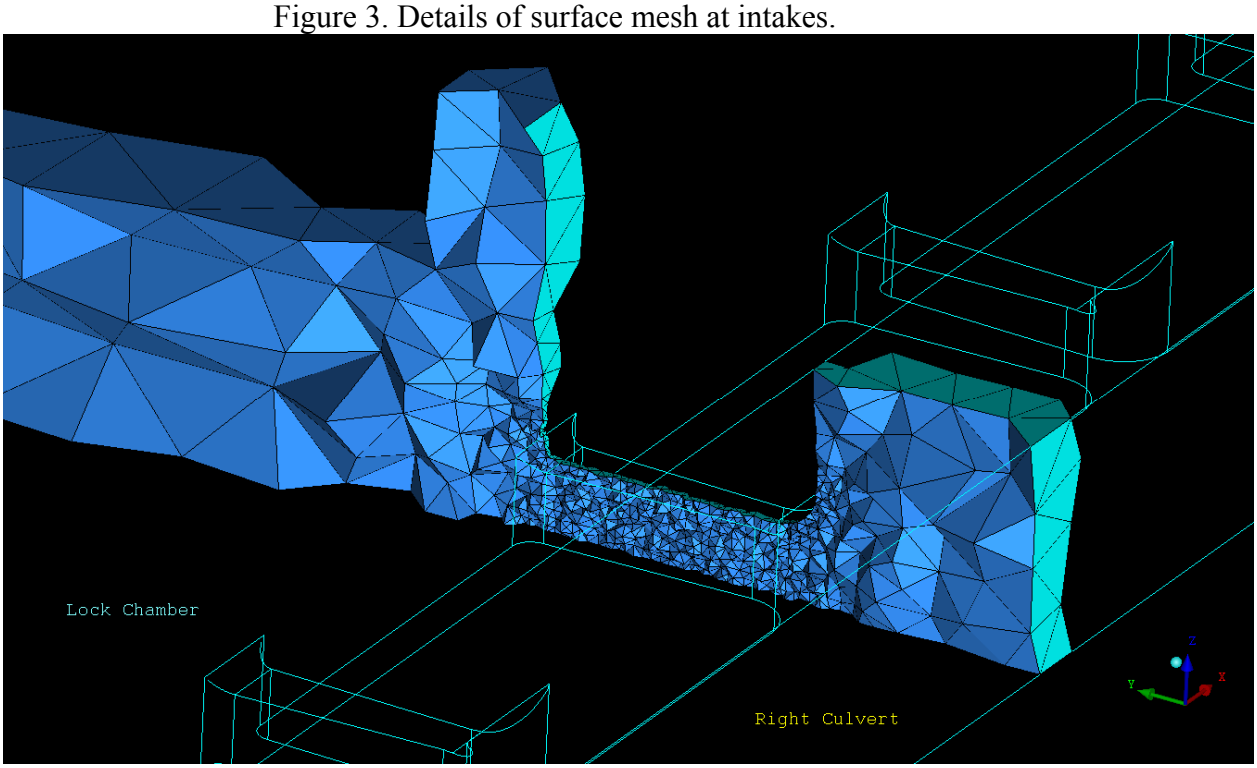

Figure 4. Volume mesh at a section through the right culvert, sidewall port, and lock chamber.

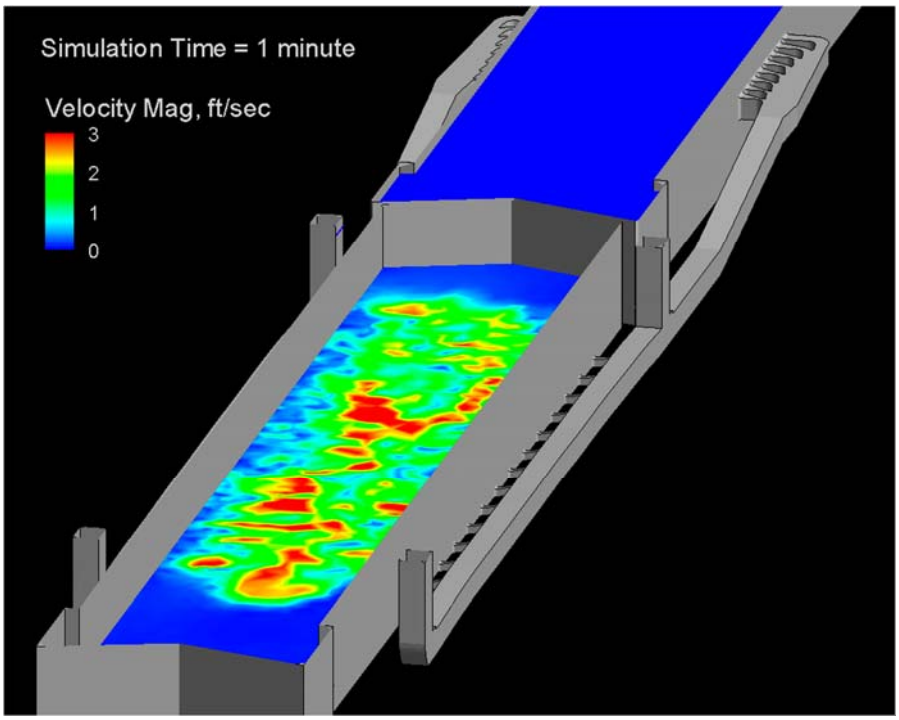

Figure 5. Velocity magnitude contours in the lock chamber 1 min after filling started.

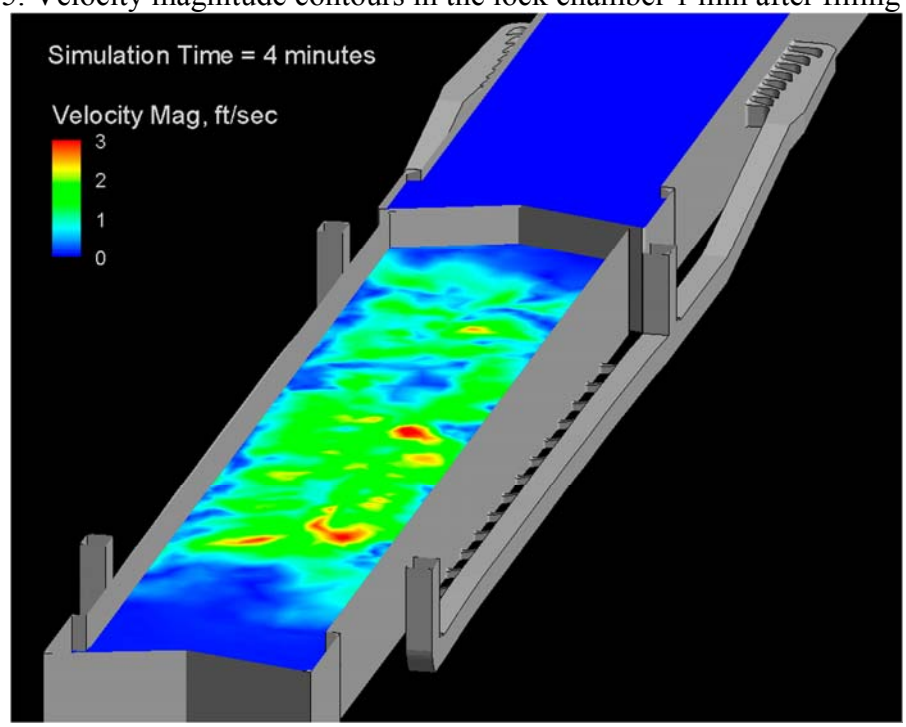

Figure 6. Velocity magnitude contours in the lock chamber 4 min after filling started.

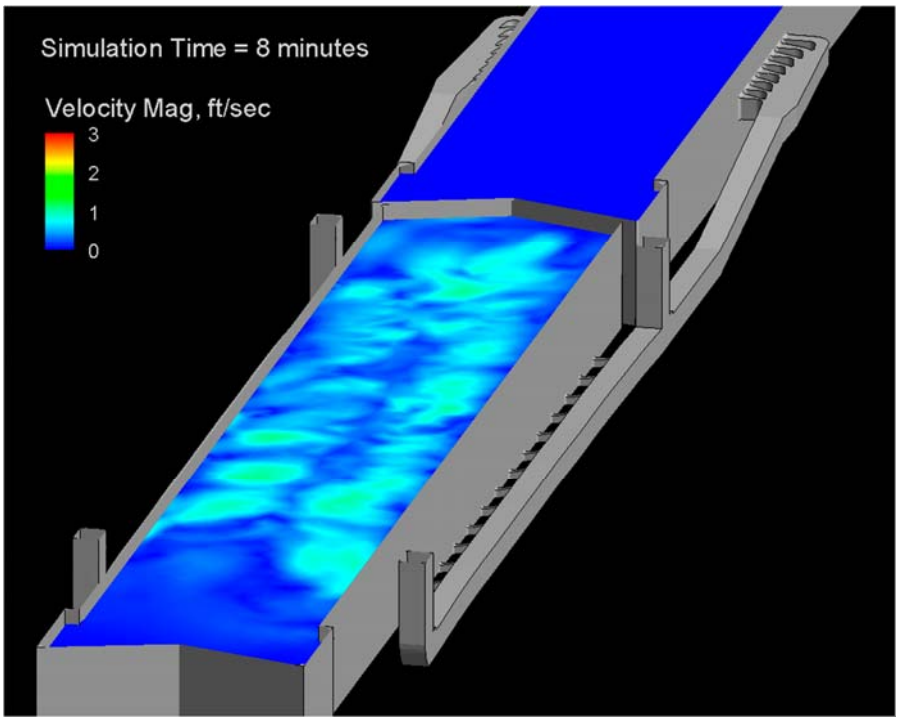

Figure 7. Velocity magnitude contours in the lock chamber 8 min after filling started.

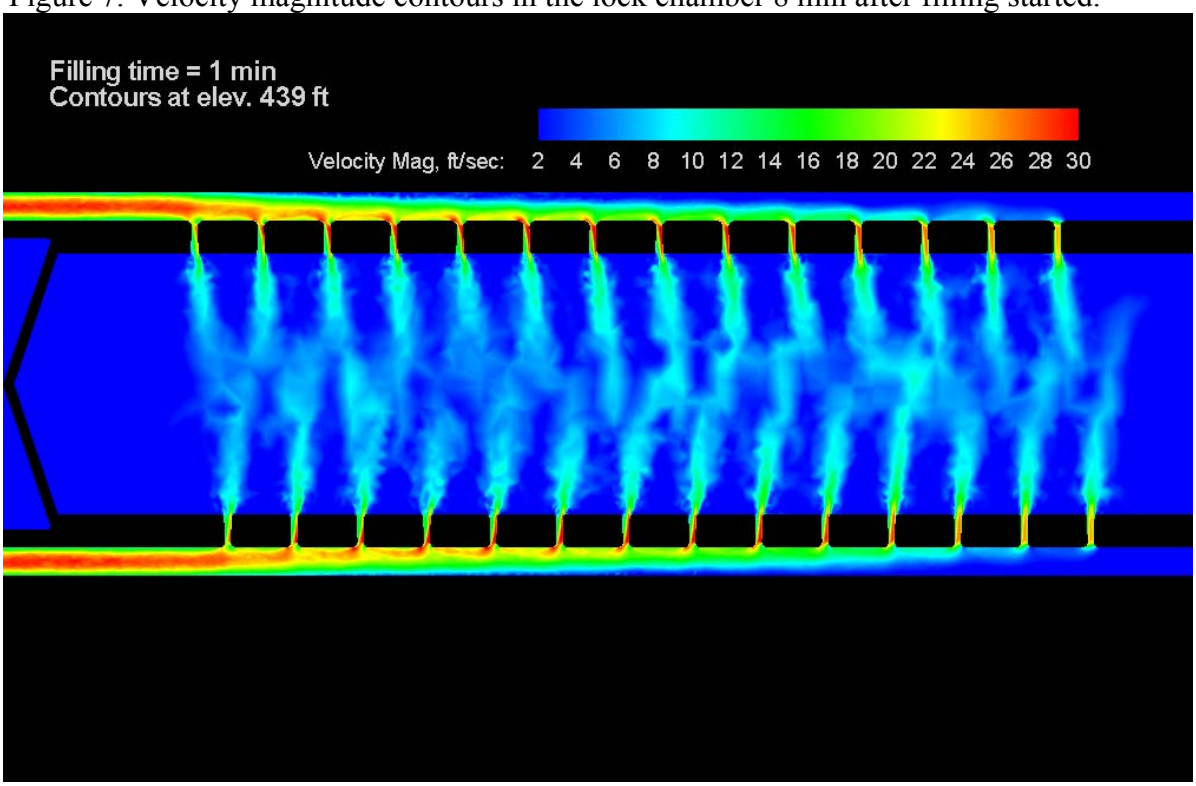

Figure 8. Velocity magnitude contours showing flow in each sidewall manifold and the lock chamber.

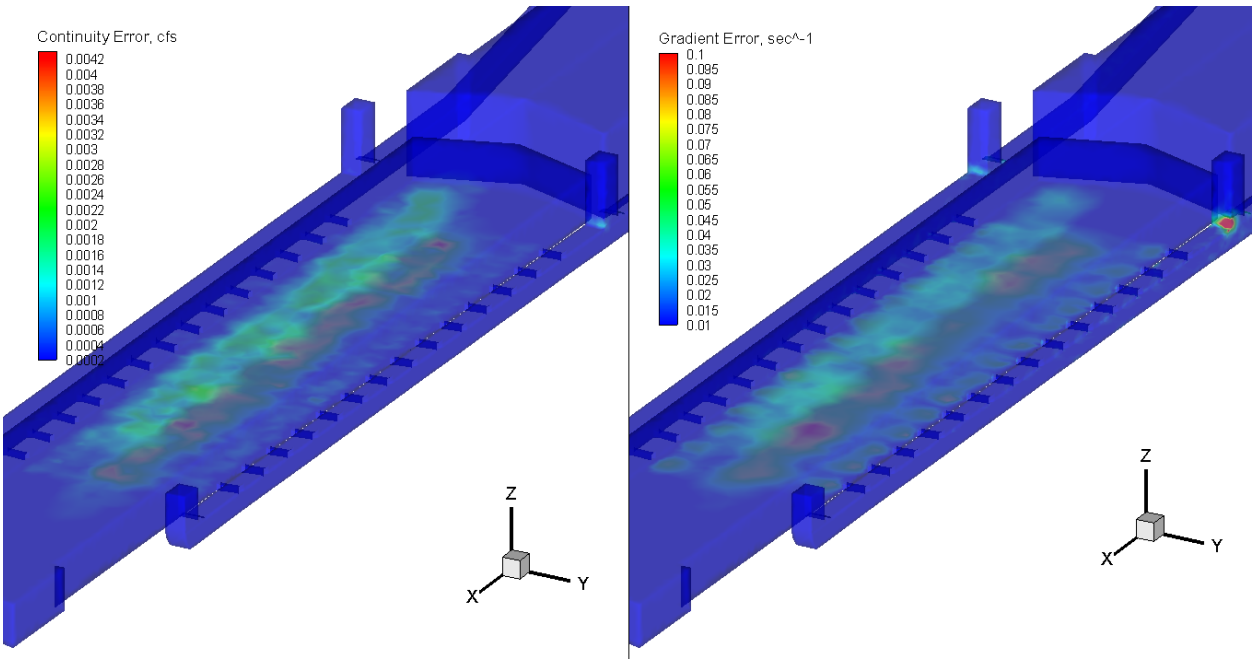

Figure 9. Contours of residual within the sidewall manifolds and the lock chamber 1 min after filling started, continuity method (left) and gradient method (right).

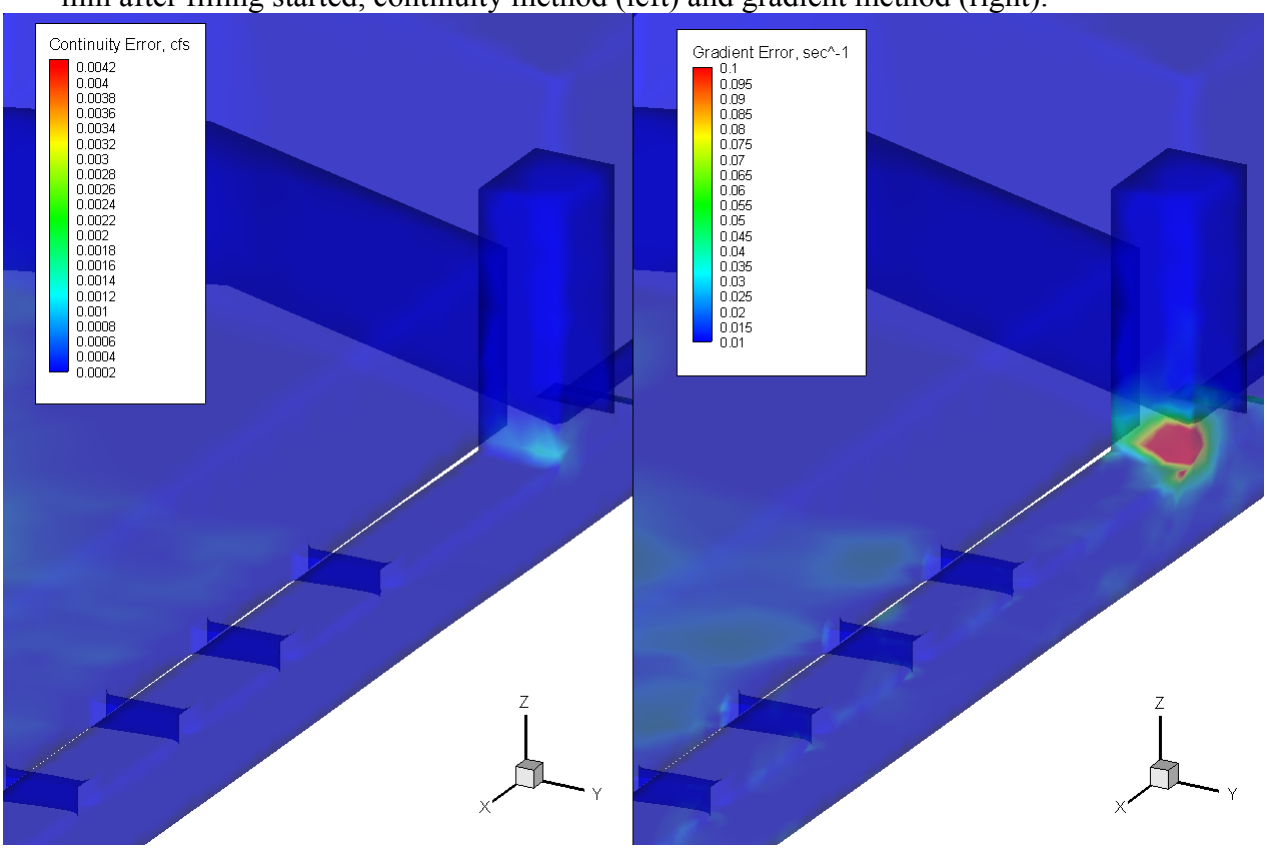

Figure 10. Contours of residual view at the left culvert valve and sidewall manifold 1 min after filling started, continuity method (left) and gradient method (right).

Challenges on Three Dimensional Simulations of Free Surface Flow

Jinwei Qiu[1] and Xing Fang[2]

[1]D.E., Civil Engineer, URS Corporation, 1950 North Stemmons Freeway, Suite 6000, Dallas, Texas 75207; Phone (214) 672-2869; Fax (214) 741-9413; email: jinwei_qiu@urscorp.com

[2] Ph.D., P.E., D.WRE, Associate Professor, Department of Civil Engineering, Auburn University, Auburn, Alabama 36849-5337; Phone (334) 844-8778; Fax (334) 844-6290; email: xing.fang@auburn.edu

Abstract

Unsteady free-surface flow in open channels with or without in-channel structures are very complex. It is a difficult and challenging subject for civil engineering students to fully understand and comprehend. In this study three-dimensional numerical simulations were performed for several case studies of open channel flows and used to demonstrate several aspects of educational challenges of computational hydraulics. FLOW-3D, developed by the Flow Science, Inc., a three-dimensional computational fluid dynamics (CFD) software was utilized as "Virtual Lab" to study these complex flow phenomena. FLOW-3D utilizes a true volume of fluid (TruVOF) method to compute free surface motion and the fractional area/volume obstacle representation (FAVOR) technique to model complex geometric regions. In this study, flow simulations were presented on three case studies in various channel geometry and channel boundary conditions, and the cases include: the flow simulations of flow characteristics in the experimental channels having weirs with different heights in the middle of simulation domain; the flow simulations under complex channel bottom geometry from supercritical flow to subcritical flow with hydraulic jump due to tailwater effects in a laboratory channel; and the flow simulations of flow characteristics in a long river reach with a broad-crested weir located at the middle of the reach. The simulations demonstrate to use basic hydraulic principles to set appropriate boundary conditions, and conduct model comparison and calibration against results from theoretical equations, other numerical models and laboratory measurements. The detailed analyses revealed flow features of the unsteady free-surface flow in open channels under various boundary conditions. The impacts on water surface profile and flow velocities due to in-channel hydraulic structures were discussed. The study demonstrates challenges of computational hydraulics in how students and researchers critically analyze three-dimensional simulation results using basic one- and two-dimensional hydraulic theories and principles.

Introduction

Flow simulation is a common educational and research topic in broad fields such as fluid mechanics, aerodynamics, environmental and civil engineering and so on. Computational Fluid Dynamics (CFD) is a method of simulating a flow process in which standard flow equations such as the Navier-Stokes and continuity equations are discretized and solved for each computational cell in a simulation domain. Using a CFD code is in many ways similar to setting up a laboratory experiment that requires accurate representation of prototype and environment conditions. It is such a currently majority in flow simulation study not only because it is easy in modeling set up and making any change for the model but also for its efforts and money saving. CFD is taught through university graduate curriculum in civil/mechanical/aerospace departments

and through training workshops of CFD software development companies. Three dimensional flow simulations using CFD, especially for free surface flow, are challenge tasks to students and professional practitioners. In this study, we use a three-dimensional CFD software FLOW-3D developed by the Flow Science Inc. to demonstrate some of these challenges.

FLOW-3D solves the following continuity and momentum (Navier-Stokes) equations for the velocity components (*u, v, w*) and pressure as function of time (*t*) in the three dimensional Cartesian (*x, y, z*) or cylindrical (*r,* θ, *z*) coordinate system.

$$V_F \frac{\partial \rho}{\partial t} + \frac{\partial}{\partial x}(\rho u A_x) + R\frac{\partial}{\partial y}(\rho v A_y) + \frac{\partial}{\partial z}(\rho w A_z) + \xi \frac{\rho u A_x}{x} = RDIF + RSOR \qquad (1)$$

$$\frac{\partial u}{\partial t} + \frac{1}{V_F}\left\{uA_x\frac{\partial u}{\partial x} + vA_y R\frac{\partial u}{\partial y} + wA_z\frac{\partial u}{\partial z}\right\} - \xi\frac{A_y v^2}{xV_F} = -\frac{1}{\rho}\frac{\partial p}{\partial x} + G_x + f_x - b_x - \frac{RSOR}{\rho V_F}u$$

$$\frac{\partial v}{\partial t} + \frac{1}{V_F}\left\{uA_x\frac{\partial v}{\partial x} + vA_y R\frac{\partial v}{\partial y} + wA_z\frac{\partial v}{\partial z}\right\} + \xi\frac{A_y uv}{xV_F} = -\frac{1}{\rho}\left(R\frac{\partial p}{\partial y}\right) + G_y + f_y - b_y - \frac{RSOR}{\rho V_F}v$$

$$\frac{\partial w}{\partial t} + \frac{1}{V_F}\left\{uA_x\frac{\partial w}{\partial x} + vA_y R\frac{\partial w}{\partial y} + wA_z\frac{\partial w}{\partial z}\right\} = -\frac{1}{\rho}\frac{\partial p}{\partial z} + G_z + f_z - b_z - \frac{RSOR}{\rho V_F}w \qquad (2)$$

where V_F is the fractional volume open to flow, ρ is the fluid density, *RDIF* is a turbulent diffusion term, and *RSOR* is a mass source term, A_x, A_y, and A_z are the fractional areas open to flow in the *x, y,* and *z* directions, respectively. The coefficient *R* depends on the choice of coordinate system. In these equations, (G_x, G_y, G_z) are body accelerations, (f_x, f_y, f_z) are viscous accelerations, (b_x, b_y, b_z) are flow losses in porous media or across porous baffle plates, and the final terms account for the injection of mass at zero velocity. FLOW-3D can be utilized as "Virtual Lab" to study complex flow problems such as free surface flows. FLOW-3D utilizes a true volume of fluid method (TruVOF) (Hirt and Nichols 1981) to compute free surface motion and the fractional area/volume obstacle representation (FAVOR) technique to model complex geometric regions (Flow Science Inc. 2005). FLOW-3D has been utilized in various civil engineering projects to investigate flow properties (Fang et al. 2007), such as spillway behavior (pressure distributions) (Savage and Johnson 2001), and high-resolution numerical simulation of flow through a highly sinuous river reach (Rodriguez et al. 2004), etc.

Simulations for 2-meter Laboratory Channel

In 2004, Faure, Buil, and Gay published a paper in the Journal of Hydraulic Research, and they used a commercial CFD package CFX (version 4) (CFX Inc. 1997) to develop a three-dimensional model for hydrodynamic and pollutant dispersion simulations for turbulent free-surface flow in open channels. Flow simulations were made with various customizations on how to track free surface and setting appropriate boundary conditions. Here we use FLOW-3D to develop numerical model for Faure's 2-meter laboratory channel (Faure et al. 2004) as a case study demonstrating our point of view. The channel is 2.2 m long (x direction), 0.25 m wide (y direction), 0.35m deep (z direction), and 0.7% slope along x direction (Canal 1 in Faure et al. 2004). Flow in half of the channel is simulated using FLOW-3D due to symmetry, and horizontal channel geometry was developed using FLOW-3D solid modeler. The channel has a flow control structure - a weir at 2.0 m downstream along x direction, and the weir is 0.02 m thick in x direction and 0.09 m high (z direction). In order to simulate effects of wall roughness,

the roughness height of three subcomponents is set as k = 0.001 m for the logarithmic law-of-the-wall turbulent boundary conditions (Flow Science Inc., 2005). The mesh size for the simulation is dx = 0.01 or 0.02 m (2 cm), dy = 0.005 to 0.02 m, and dz = 0.025 m (2.5 cm). The simulation domain covers 2.2 m, 0.125 m, 0.15 m in the x, y, and z directions, respectively. Since the mesh size in the z direction is much smaller than ones in x and y directions, line implicit pressure solver in the z direction is used. The slope of the channel was modeled by setting the gravitational acceleration component in the x direction as 0.06849 m/s^2 that is equivalent to 0.7% slope in the x direction. The gravitational acceleration components in the z and y directions were set as -9.81 and 0.0 m/s^2.

As usually, boundary conditions at the channel wall and bottom were set as the wall boundary, and the top surface of the simulation domain and the channel centerline surface are set as symmetry boundary (zero gradients on flow parameters). The first challenge for the case study is to appropriately set flow boundary conditions at upstream and downstream ends along x direction. For water surface profile simulation in an open channel, the boundary condition is at the downstream end for subcritical flow and at the upstream end for supercritical flow, because the location of the control section in a prismatic channel is generally governed by the state of flow, which in turn is determined by the slope of the channel (Chow 1959). In this case study, the channel has a slope of 0.7% and has a weir between upstream and downstream ends, and this will result the control section at the weir and a M1 water surface profile (Chow 1959; Roberson et al. 1998) approaching to the weir, but FLOW-3D and other CFD software require to set boundary conditions at both upstream and downstream ends of the channel. The second challenge (or a common shortcoming) is to accurately present technical information in technical writing. In the process of simulating flow properties and interpreting their results for Faure's channel, there are two problems encountered: (1) Faure's paper gives a discharge of 0.0036 m^3/s but did not specify clearly that the discharge is for half or full channel width; his numerical model used half of the channel width as simulation domain; (2) The y axis in Faure's Figure 3 (Faure et al. 2004) was labeled as "water depth" instead of "water level". The water level or water surface elevation refers to a specific datum, and for M1 water surface profile, the water depth increases along the flow (x) direction (Chow 1959), while Faure's Figure 3 shows almost horizontal water depth profile, which we think it should be labeled as water level. Several model runs were conducted and results are given below to reveal these challenges.

For this case study, the boundary condition at 2.0 meters downstream of the weir is set as stagnation pressure with fluid height of 9 cm (the same water depth in Figure 2 of Faure's study) or outflow boundary condition (flow leaving the simulation domain). Flow rates in the experimental channel were measured and given by Faure et al. (2004), but flow rates cannot be set as boundary condition for any three-dimensional model. In this case study, two types of upstream boundary conditions, specified velocity and specified pressure were tested using FLOW-3D; the simulated results are compared with the results of Faure's case study. Figure 3 of Faure's paper shows that the inflow water depth at the upstream end of the channel is about 0.126 m when the flow rate is 0.0036 m^3/s. In FLOW-3D model, two average velocities at the upstream cross section were calculated and used for FLOW-3D simulations in order to compare with Faure's simulated water surface elevation: one is 0.114 m/s that will result channel discharge of 0.0036 m^3/s for the whole channel width (0.25 m), another one is 0.228 m/s which will result channel discharge of 0.0036 m^3/s for the half of the channel width (0.125 m). The specified velocity boundary condition at upstream requires to set or specify both velocity and flow depth, but the specified pressure is to set pressure as equivalent fluid height (Flow Science

Inc. 2005). Simulated water surface profiles under different boundary conditions are shown in the Figure 1 including Faure's simulation results (red diamonds). Figure 1 clearly shows the discharge reported by Faure and others is for only the half of the channel width, and reports water surface elevation using the datum at the channel bottom of the upstream end. Simulated water surface elevations reported in Figure 1 are almost horizontal lines after considering (compensating) the channel slope, while simulated water depths (Figure 2) increase along x direction as M1 profile predicts. It is impossible for a horizontal water depth profile to occur as reported by Faure's Figure 3. If the outflow or continuative boundary condition is used at the downstream end, simulated water depth at downstream was very close to the normal depth (Qiu 2008). When the velocity boundary condition was used at upstream and specified pressure at downstream, simulated water level is about 1 cm lower than one with specified pressure at upstream and downstream boundaries (Figure 1). Simulated flow rates with two boundary conditions at three locations (inflow or near upstream boundary, pass at weir and outflow or near downstream boundary) were examined (Qiu 2008). The flow rates with specified velocities at upstream boundary are stable at about 15 sec. and 1800 cm^3/s for half of the channel width. When specified stagnation pressure is used as upstream boundary, the simulated inflow flow rates are not stable even the simulation time is up to 60 sec. and about 1600 cm^3/s. Therefore, when flow rate or discharge is given or known, specified velocity boundary condition should be used, and specified stagnation pressure most likely does not produce the flow rate we need.

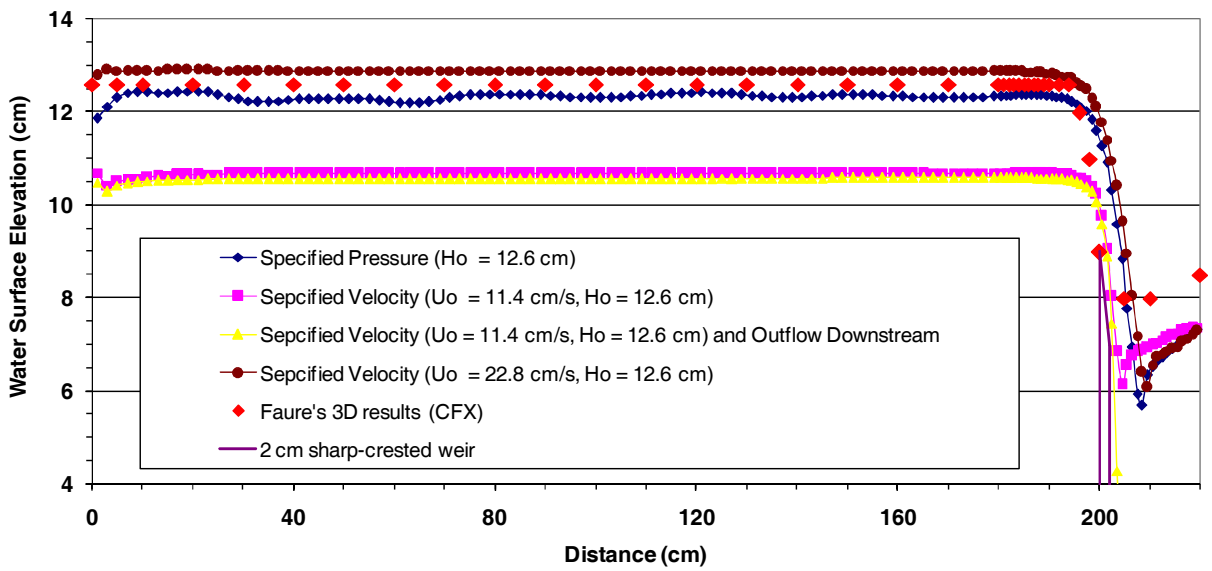

Figure 1. Simulated water surface elevations using FLOW-3D in Faure's Canal 1 with 9 cm high and 2 cm thick weir and 45 degree cut off at the top of the weir under different boundary conditions (dotted lines), and simulated water surface profile using CFX reported by Faure et al. (scatted dots) in 2004.

Because the control section is in the middle of the channel length, two steps are necessary and proposed to set appropriate boundary conditions for the upstream especially the flow depth is complete unknown at the upstream end. The hydraulic theory indicates that the critical flow occurs when flow passes over a weir (Roberson et al. 1998), and computed flow critical depth at the weir using given flow rate allows us to estimate water surface elevation at the weir and the upstream end assuming more or less horizontal M1 profile. When the flow rate is 1800 cm^3/s for

the half channel width, estimated water depth before the weir is about 11.76 cm and projected water depth at upstream end is 10.37 cm (using slope of 0.7% and 200 cm for upstream length) and average velocity of 13.89 cm/s. With projected upstream boundary conditions FLOW-3D run was conducted and water depth profile was smooth except near the upstream end. At the second step we used simulated water depth profile to linearly interpolate or project the water depth at the upstream end as 10.65 cm and mean velocity of 13.52 cm/s. The final runs were executed with updated upstream boundary conditions and give smooth water depth profile along x direction as shown in Figure 2 for three downstream boundary conditions (specified pressure at 9 cm and 5 cm and outflow boundary). These runs indicate that the downstream condition is not the control section for the problem if the flow submergence does not occur or does not impact discharge capacity of the weir. Another two runs setting the upstream fluid heights at 12.6 cm and 14.5 cm (much higher than 10.65 cm) with corresponding velocities to produce 1800 cm^3/s flow rate were conducted to approve the above point of view, and simulated water depth profiles were smooth except short distance near the upstream boundary where sudden/rapid drop on water depths occurred due to acceleration of gravity (Qiu 2008). An additional test run was conducted for discharge of 1800 cm^3/s with 6 cm broad crest rectangular weir using above two step procedures, and simulated smooth water depth profile is also given in Figure 2. The 6 cm broad crest weir pushes the water surface to be about 0.55 cm higher than the one for sharp-crested one under the same discharge, and this test clearly indicates that the control of the water surface profile is at the weir. These testing runs further approve, for this particular case study or physical setting, the control section of the water depth is at the weir and is dependent on inflow rate or how much flow or water is pushed to pass through the weir. Therefore, neither specified mean velocity nor specified fluid height at upstream boundary is the control parameter of the problem instead of the inflow rate (product of velocity, fluid height and channel width) and weir characteristics.

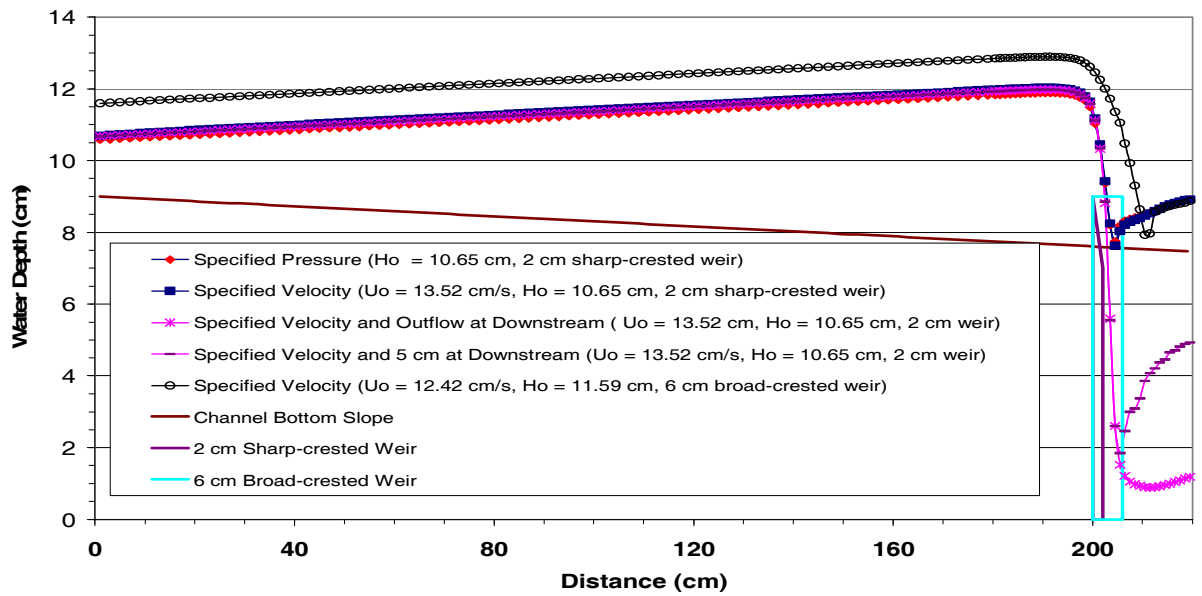

Figure 2. Simulated water depth using FLOW-3D for Canal 1 with 2 cm Sharp Crested Weir (Including 45 Degree Cut at the Top) and 6 cm Broad Crested Weir under Different Boundary Conditions.

Simulations for 4-meter Laboratory Channel

This case study used a 4-meter laboratory channel geometry in Faure's study, and it was named as Canal 2 in Faure's paper. Water depths simulated using CFX and measured in the laboratory for two weir heights are presented in Faure's Figure 2 (a) and (b), respectively. In FLOW-3D model study, channel geometry, mesh size, downstream boundary condition, and initial condition were set in the similar way as for 2-meter channel (Canal 1) presented above. The upstream boundary conditions are based on the flow hydraulic analysis to compute critical depth, water depth at the weir and to project water depth at upstream end, as summarized in Table 1. Figure 3 shows simulated water depths using FLOW-3D model for Canal 2 and simulated water depths match well with measured water depths at three locations (from Faure et al., 2004).

Table 1 Canal 2 flow hydraulic parameter analysis results

Weir height (m)	Channel Discharge (cm^3/s)	Channel critical depth (cm)	Water depth at the upstream of weir (cm)	Interpolated water depth at entrance of channel (cm)	Mean velocity (cm/s)
0.09	7350	7.06	16.06	14.98	39.25
0.12	9900	8.62	20.62	19.95	39.70

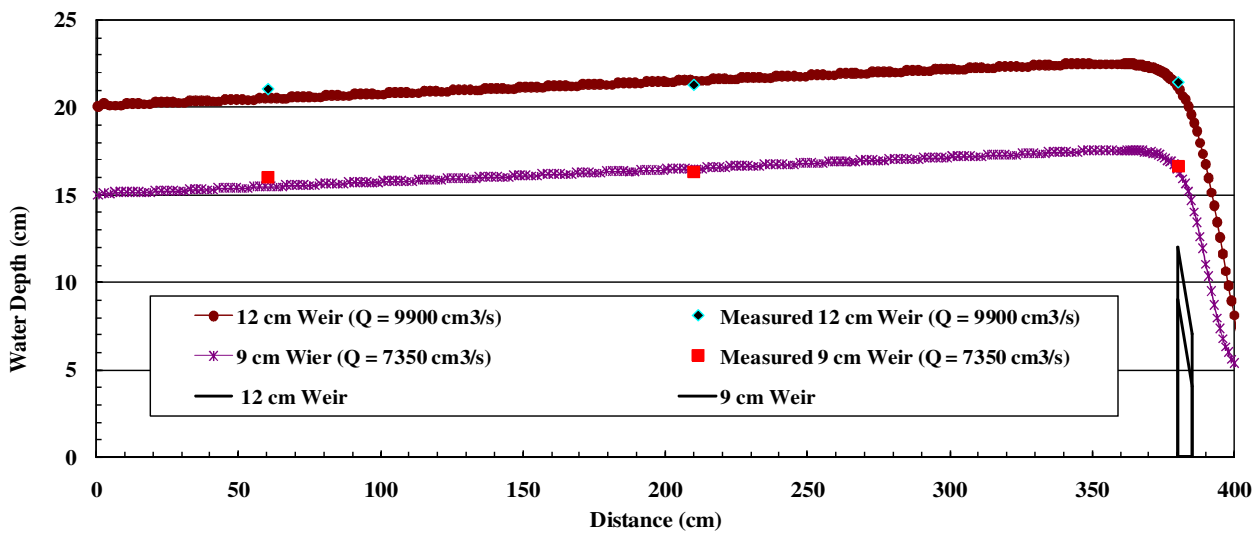

Figure 3. Simulated water depth in Canal 2 with 0.09 m and 0.12 m weirs at 45 degree cut off top of the weir under specified velocity at upstream boundary condition and outflow at downstream boundary condition, and measured points by Faure and Others (scatted dots)

Simulated flow rates were compared with the theoretical discharges of weirs (Roberson et al. 1998) by using the discharge equation for a rectangular weir, and the differences between simulated flow rates by FLOW-3D model and theoretical flow rates are 0.02% for 0.09 m weir and 0.33% for 0.12 m weir (Qiu 2008). The distributions of total velocity magnitude [$V = (u^2 + v^2 + w^2)^{1/2}$] along the water depth at five locations (distances) upstream from the weir in Canal 2 with 0.09 m weir are shown in Figure 4. It can be seen that velocities are different from the theoretical logarithmic profiles at two locations very close to the weir, which indicate that the weir will influence the flow and pressure distributions. The velocity distributions at 21.0 cm, 16.5 cm and 10.5 cm are smooth logarithmic profiles, but the velocity distributions at 0.5 cm and 2.5 cm have much large velocities above the top of weir (depth > 9.0 cm), and these large

velocities indicate water flowing over the weir to downstream due to specified inflow rate. The maximum velocity (occurring just above the weir) at 0.5 cm and 2.5 cm from the weir are 100.66 cm/s and 61.49 cm/s, respectively. At these two locations very near the weir, velocity decreases towards the water surface after it reaches the maximum value. Velocity profiles along z direction at different distances to the weir, along y direction at different water depths, and simulated flow velocity magnitudes in x-z plane were also examined and show that FLOW-3D model is able to capture the flow velocity features under the influence of the weir and simulation results strongly reveal three dimensional flow phenomena near the weir (Qiu 2008).

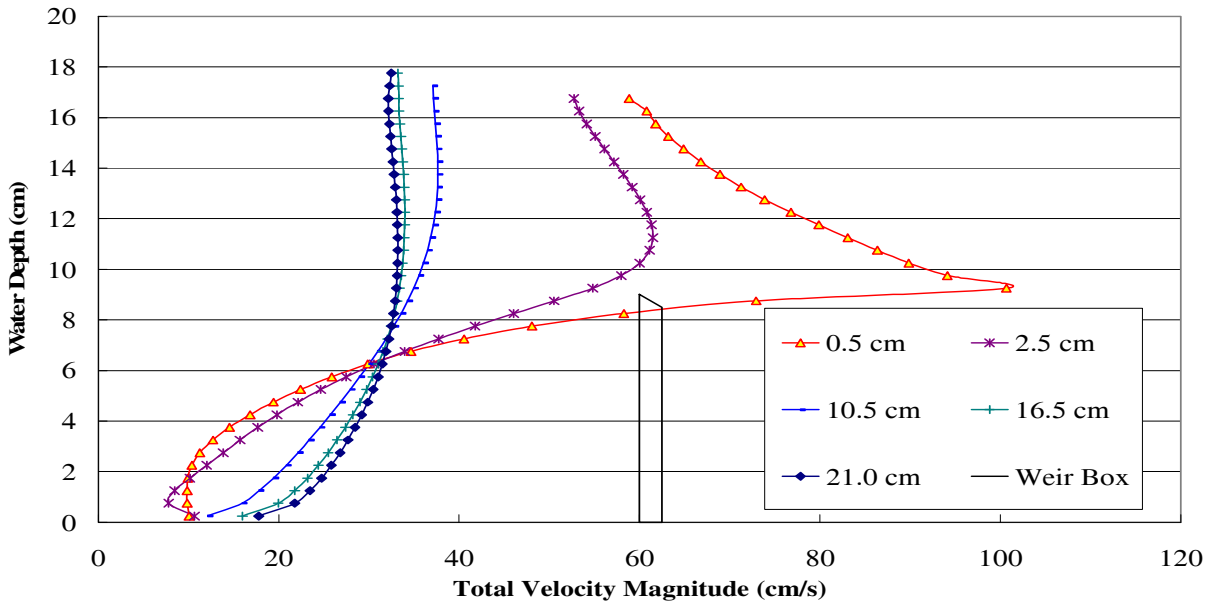

Figure 4. Simulated flow velocities in x-z plane at different distance from the upstream of weir and 2.5 cm from the wall of Canal 2 with 0.09 m weir.

Simulations for Laboratory Channel at Auburn University

Supercritical flows are frequently encountered in hydraulic structures, such as outlets, spillways, chutes, flood-relief canals, and storm water drainage channels (Chow 1959; Stamou et al. 2008). For further exploring FLOW-3D model in simulating such complex hydraulic conditions, such as supercritical flow, subcritical flow, hydraulic jumps, the third model testing is conducted by modeling a laboratory channel geometry build up at Auburn University, which can be used to measure flow hydraulic parameters under different flow boundary conditions, the channel geometry is a compound structure consisting of several kinds of components such as weir, channel (plane and inclined) and rotating tailwater gate (Figure 5). The channel geometry is developed as 7 subcomponents using FLOW-3D's solids modeler. Eight simulation runs are conducted with the same channel geometry but different rotating gate angles that created various tailwater conditions and slightly different inflow boundary conditions. The laboratory channel geometry is total 9.875 ft long in x direction (flow direction) and 1.0 ft wide in y direction (channel width). The channel bottom elevation varies from 0.04 ft to 0.407 ft at different locations. The rotating axis of the gate is set as zero in x and z directions (easy for setting rotation angle), and the channel bottom elevation is 0.083 ft (1 inch) above the rotating axis. The dimensions of each component can be described as: (1) a horizontal channel bottom: dimension of 9.875 x 1.0 x 1.083 ft; (2) a small step block: dimension of 0.167 x 1.0 x 0.04 ft; (3) a well

rounded broad-crested weir: dimension of 0.208 x 1.0 x 0.407 ft; (4) a block with incline plane surface: dimension of 6.042 x 1.0 x (0.04 ~ 0.407) ft, surface slope = 6.22 %; (5) a rotating gate with specified rotating angle: dimension of 0.677 x 1.0 x 0.083 ft. On mesh block (11.4 x 1.0 x 2.5 ft) was used with the mesh size in three directions of dx = 0.05 ft, dy = 0.05 ft, dz = 0.03 - 0.05 ft and having total mesh number of 182400. Specified velocity boundary condition based measured flow rate and fluid height and outflow boundary at the minimum z were used.

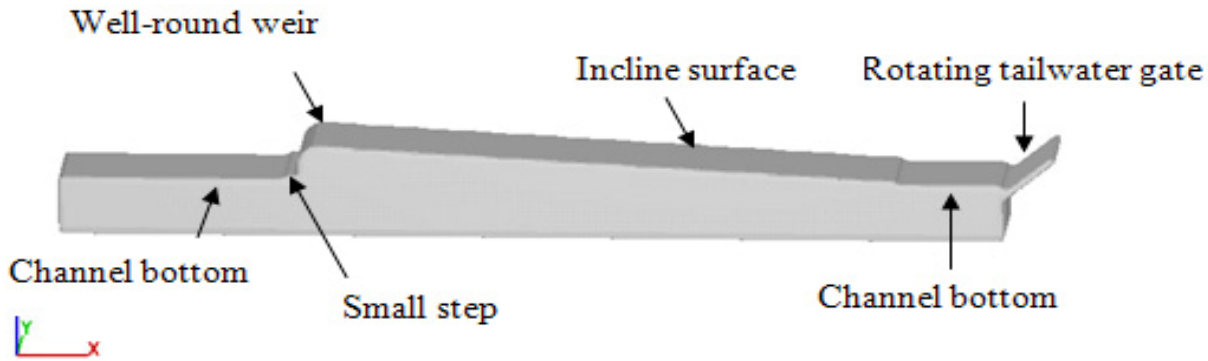

Figure 5. Geometry of FLOW-3D model for laboratory channel at Auburn University (rotating gate angle is 41.42° above the horizontal plane is shown).

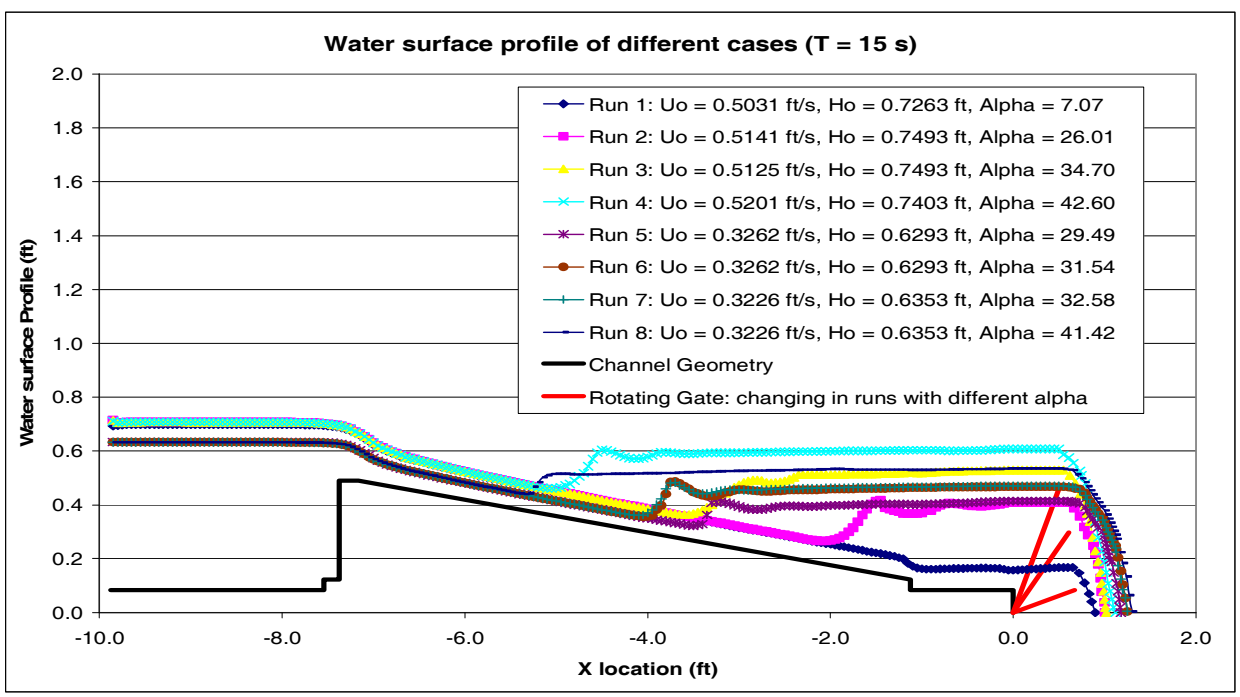

Figure 6. Simulated water surface profiles for Auburn channel under rotating angles.

Figure 6 shows simulated water surface profiles using FLOW-3D model for eight runs with various rotating angles (alpha) and different upstream flow rates. In Figure 6, FLOW-3D only outputs correct water surface profiles before rotating gate ($x < 0$) because FLOW-3D is not able to correctly report fluid height for multiple fluid surfaces. Water surface profiles after $x > 0$ (sharp drop) were manually estimated from 2-D plots with FLOW-3D. Figure 6 very clearly shows differences in water surface profiles among tailwater conditions and successfully simulates from subcritical flow before the step to supercritical flow along inclined channel, and

through hydraulic jump to subcritical flow created by rotating gate. There is no hydraulic jump simulated and observed for run 1 when the gate is almost horizontal. Locations of hydraulic jumps for other runs under influences of different tailwater conditions are clearly showed in Figure 6, and are compared with observed locations in laboratory tests with reasonable agreement (Qiu 2008). Water surface elevations at three fixed locations for all eight tests were measured and compared with FLOW-3D model results (Qiu 2008), and at x = -9.14 ft (0.733 ft downstream of the inflow boundary), the error in fluid height is from 0.73% to -5.53%; and at x = -7.14 ft where it is the highest point of the weir with critical flow condition, the error in fluid height is from 0.88% to -5.72%. At x = -3.77 ft that is a location close to the end of sloping channel bottom, the error in fluid height becomes greater and ranges from 15.54% to -19.88%. Projected location for hydraulic jumps have a relative error from -0.73% to 26.98%; and hydraulic jump location is very sensitive to simulated water surface height at subcritical flow region near the rotating gate (flow control section). In laboratory condition the open space after the rotating gate is not large enough for free fall of flow and the leak of water flow through the gate may result some of the differences between simulated and measured parameters.

Case for River Reach

The last case study is to simulate free-surface flow in a river reach - River 1 in Faure's study (2004) and River 1 with addition of two cylinder culverts through the broad crested weir. The river reach is 400 m long, 40 m wide, 3 m deep, and 0.05% slope. A broad crested weir is located halfway of the reach (x = 200 m) and has a dimension of 4 m thick (in x direction), 40 m wide, and 0.7 m height. The gravitational acceleration component in the x direction as 0.004905 m/s^2 for 0.05% slope. The simulation domain is 400 m x 21 m x 3 m with mesh size of dx = 1 or 2 m, dy = 0.5 - 2 m, and dz = 0.25 m. The geometry of culverts is 0.2 m radius, 4 m long, the central lines of two cylinder culverts are 5 m and 5.8 m in y direction respectively and 0.2 m in z direction. The mesh size is changed to smaller (e.g., dz = 0.1 - 0.25 m) in order to capture the flow features through the culverts. Again water depth was reported in their paper but should be water level, and this effects what boundary conditions can be used for FLOW-3D model and comparison between FLOW-3D's and Faure's results. Simulated water surface profile is very similar to one obtained using CFX by Faure et al. (2004), and the simulated water level at upstream from FLOW-3D model has about 0.15 m difference with CFX model results. Three-dimensional flow characteristics around the broad-crested weir without and with culverts were successfully simulated (Qiu 2008).

Conclusions

Several case studies have been presented to demonstrate that FLOW-3D can be utilized to model the unsteady free-surface flow in experimental channels and a river reach with weir and sluice gates with different boundary conditions. Comparison between simulated and measured flow properties shows reasonable accuracy. The first case study indicates the appropriate boundary condition at upstream for open channel flow study in civil engineering field is using specified velocity and fluid height; and this boundary sets flow rate into the simulation domain. Boundary condition as specified stagnation pressure in turn of fluid height using FLOW-3D does not produce exactly flow rate that the modeler wants or measured in the laboratory and field conditions. In this case study, the control structure is a weir in the middle of simulation domain; and two simulation runs are necessary to accurately define boundary conditions in FLOW-3D.

Simulation runs with sharp-crested and broad-crested weirs demonstrate that the flow capacity of the weirs directly controls upstream fluid height under the same flow rate. It is demonstrated that FLOW-3D can successfully simulate complex open channel flows from supercritical to subcritical with hydraulic jump under the influence of tailwater effects. It is easily to develop the model in FLOW-3D with a rotating tailwater gate at any opening angle. Complex flow simulation from supercritical to subcritical with hydraulic jump is a challenging task for hydraulic engineers, but does not require any customization in FLOW-3D and was simulated with simple boundary condition (specified velocity at upstream) and appropriate representation on channel geometry. The analysis results show that FLOW-3D provides accurate solution for complex open channel flows. This study for river reach indicates that FLOW-3D is able to reveal the complex flow dynamic phenomena near the hydraulic structures, such as flow over weir and through culverts. FLOW-3D can be a powerful vital simulation lab for a study of channel and river reach under various inflow conditions, but there are challenges to students and professional practitioners because it requires in-depth understanding in hydraulic theory and setting appropriate boundary conditions and accurately present the technical information (e.g., water level and water depth profiles).

Acknowledgement

Thanks for Flow Science, Inc. to provide FLOW-3D software with the educational price for university education and research projects.

References

CFX Inc. (1997). "CFX-4.2: Solver." AEA Technology, UK, currently under ANSYS, Inc., (http://www.ansys.com/default.asp).

Chow, V. T. (1959). *Open channel hydraulics*, McGraw Hill, New York.

Fang, X., Jiang, S. D., and Qui, J. W. (2007). "Three dimensional flow simulation in channels and through side weirs." *Proceedings of the Texas Section American Society of Civil Engineers Spring Conference*, April 13, 2007, Taylor, Texas.

Faure, J. B., Buil, N., and Gay, R. (2004). "3-D modeling of unsteady free-surface flow in open channel." *Journal of Hydraulic Research*, 42(3), 263-272.

Flow Science Inc. (2005). "Flow-3D User's Manual (Version 9.0)." Santa Fe, NM 87505.

Hirt, C. W., and Nichols, B. D. (1981). "Volume of Fluid (VOF) method for the dynamics of free boundaries." *Journal of Computational Physics*, 39(1), 201-225.

Qiu, J. (2008). "Gravel transport estimation and flow simulation over low-water stream crossings," Department of Civil Engineering, Lamar University, Beaumont, TX.

Roberson, J. A., Cassidy, J. J., and Chaudhry, M. H. (1998). *Hydraulic engineering*, 2nd Ed., John Wiley & Sons, Inc., New York, NY.

Rodriguez, J. F., Bombardelli, F. A., Garcia, M. H., Frothingham, K. M., Rhoads, B. L., and Abad, J. D. (2004). "High-resolution numerical simulation of flow through a highly sinuous river reach." *Water Resources Management* 18, 177-199.

Savage, B. M., and Johnson, M. C. (2001). "Flow over ogee spillway: Physical and numerical model case study." *Journal of Hydraulic Engineering*, 127(8), 640-650.

Stamou, A. I., Chapsas, D. G., and Christodoulou, G. C. (2008). "3-D numerical modeling of supercritical flow in gradual expansions." *Journal of Hydraulic Research*, 46(3), 402-409.

Comparison of the Princeton Ocean Model and the Regional Ocean Modeling System Hindcasts in the Delaware River and Bay

Richard A. Schmalz, Jr.[1], F. ASCE

Abstract

The National Oceanic and Atmospheric Administration is in the process of developing a nowcast/forecast system for Delaware River and Bay. The Delaware Bay Operational Forecast System (DBOFS) will extend from the head of tide at Trenton, NJ through the Bay entrance out onto the continental shelf and will supplement the Delaware Bay Physical Oceanographic Real Time System (PORTS), which was installed in 2003 to provide observed, real-time water surface elevation, currents, temperature, salinity, and meteorological information. In conjunction with the DBOFS development effort, the Princeton Ocean Model (POM) and the Regional Ocean Modeling System (ROMS) have been applied with a common medium resolution grid in hindcast mode using common forcings to simulate two 15-day periods in March (high river flow) and September (low river flow) 1984. Herein, we compare and contrast the hindcast simulation results versus the National Ocean Service Delaware River and Bay 1984 Circulation Survey measurements of water surface elevation, currents, salinity, and temperature. The effects of a spatially varying bottom friction, subtidal water level forcings at the Chesapeake and Delaware Canal boundary, navigation channel bathymetry, and upriver storage areas on water level, current, and salinity response are considered. In conclusion, plans for further DBOFS development with ROMS using a finer resolution grid are presented.

Introduction

The National Ocean Service (NOS) installed a Physical Oceanographic Real Time System (PORTS) during 2003 to provide water surface elevation, currents at prediction depth (4.7m below MLLW) as well as near-surface and near-bottom temperature and salinity, and meteorological information at the locations shown in Figure 1. To complement the PORTS, a nowcast/forecast system is being developed within the Coastal Ocean Modeling Framework (COMF) as developed by Gross et al. (2006) and further discussed by Aikman et al. (2007). In conjunction with this effort, a Model Evaluation Environment (MEE) as described by Patchen (2007) was constructed

1 Oceanographer, National Oceanic and Atmospheric Administration, National Ocean Service, Coast Survey Development Laboratory, Marine Modeling and Analysis Programs, 1315 East-West Highway, Rm 7824, Silver Spring, Maryland 20910. (301)-713-2809 x104; e-mail: Richard.Schmalz@noaa.gov.

for the Delaware River and Bay based on the NOS 1984-1985 Circulation Data Survey (Klavans et al., 1986; Richardson and Schmalz, 2006). In the context of the Delaware River and Bay Nowcast/Forecast System (DBOFS), the MEE provides additional validation data particularly for currents and density that is not available within the PORTS. The following models were evaluated (Patchen, 2007):

1. Regional Ocean Modeling System (ROMS) as described in Shchepetkin and McWilliams (2005) and Haidvogel et al. (2008).
   On the Internet at: http://www.myroms.org
2. Princeton Ocean Model (POM) as described in Blumberg and Mellor (1987) and Blumberg and Herring (1987).
   On the Internet at: http://www.aos.princeton.edu/WWWPUBLIC/htdocs.pom
3. Finite Volume Coastal Ocean Model (FVCOM) as described in Chen et al. (2006).
   On the Internet at: http://fvcom.smast.umassd.edu/FVCOM/index.html
4. Semi-Implicit Eulerian-Lagrangian Finite Element Model (SELFE) as described in Zhang et al. (2004).
   On the Internet at: http://www.ccalmr.ogi.edu/corie/modeling

Based on the assessment of the MEE results, additional improvement in the water level and current response in the river section above Philadelphia, PA is needed by all of the models to meet the NOS skill requirements (NOS, 1999; Hess et al., 2003). To this end two 15-day periods were selected for further consideration. The first period, 27 March – 10 April, 2004 contained a coastal surge event as well as a high flow event. The second period, 10-24 September, 1984 was dominated by extremely low flow of order 3000 cfs at Trenton, NJ and represented a period of potential salinity intrusion. There also was very little storm activity along the coast and hence the period was dominated by astronomic tides and allowed for an assessment of the tidal response. In this paper, we focus on the first two models and present simulation results for each of these periods in an effort to lead toward improvement. To conclude the paper, we outline further development and testing.

Model Grid and Simulation Setup

The horizontal computational grid for both POM and ROMS, which is 150 (E-W) x 550 (N-S), is shown for the upper Delaware River in Figure 2 and for the lower Delaware River and Bay in Figure 3 with the finest grid resolutions approximately 50 m. Fifteen sigma coordinate levels are used in the vertical with uniform spacings below the surface level in POM, while 10 s coordinate levels are used in ROMS.

To move toward a more standard nowcast/forecast system set-up, the NOS Galveston Bay Operational Nowcast/Forecast System (GBOFS) was emulated but slightly modified using the approach developed during the Long Island Sound Study (LISS). In the LISS, a second section of the grid generation program was used to provide the initial density structure, the SST field at 15 to 30 day intervals, and the salinity and temperature boundary conditions for rivers and the ocean boundary (see Schmalz, 1994). In GBOFS

a ten-step set-up program is used to provide the forcing for each 24 hour nowcast, and for the 30 hour forecast (Schmalz and Richardson, 2002). Within this program, the density structure is updated at the beginning of each nowcast based on the observed PORTS measurements and the sea-surface temperature, salinity and temperature boundary conditions are then persisted over the nowcast/forecast period. Rather than employing this approach, the LISS approach for handling the initial and boundary conditions was used and then steps 6, 7, and 8 in the ten-step nowcast/forecast procedure were eliminated. The remaining steps are used to specify the simulation period (Step 1), generate harmonically reconstructed water surface elevation (Step 2) and currents (Step 3), place the observed data in the appropriate format for the graphics programs (Step 4), produce the subtidal water level signals at Chesapeake City, MD and Cape May, NJ (Step 5), generate the average daily inflows for the 12 rivers (Step 9), and use the Barnes (1973) interpolation from meteorological data at 10 stations (including 2 offshore National Data Buoy Center (NDBC) buoys) to provide the wind and sea-level atmospheric pressure fields. Note the subtidal water level signal at Cape May, NJ was applied to the entire ocean open boundary. Within the present operational NOS nowcast/forecast systems, the approach of applying a measured or forecast coastal subtidal water level to the entire open boundary has been used. In the present case with the open boundary extending to the shelf break this may not be valid. An alternative approach would be to reduce the extent of the grid on the shelf to perhaps the 20 to 50 m contour as used by Celebioglu and Piasecki (2006) or to use a shelf model.

In the MEE, the water level residual at the head of the Chesapeake and Delaware (C&D) canal was considered zero. Here, the water level residual signal at the Chesapeake Bay end of the C&D canal was based on Chesapeake City, MD as determined via a linear regression (bias=0.003, gain=0.784) from the Baltimore, MD water level residual over the four month period July-October, 1984. Monthly root mean square errors (RMSEs) were order 5 cm and storm periods were well produced.

Within the NOS operational nowcast/forecast systems water levels are specified with respect to the MLLW datum at each PORTS station. Within the Galveston Bay Nowcast/Forecast System the model datum is taken as MTL and at each station the tidal epoch adjustment from MTL to MLLW is added to the model prediction. Within the Delaware River and Bay system, two datums are used. Along the coast and within the Bay proper MSL is taken as the model datum, while above Philadelphia, PA mean river level (MRL) is assumed equal to NAVD-1988 and is taken as the model datum.

For the POM simulations, the following revisions to the initial set-up were employed:

1) The C&D canal width was adjusted to its actual channel width of 121.9 m. It was straightened and made one grid cell wide.
2) The United States Army Corps of Engineers (USACOE) project channel depths were specified for the navigation channels from the Bay to Philadelphia, PA from Philadelphia, PA to Newbold, PA and from Newbold, PA to Trenton, NJ.
3) Several upriver marsh areas were specified at depths of order 1 m.

4) SST was specified by using the nearest surface value of the CT moorings and CTD profiles.
5) A spatially varying bottom roughness was incorporated, such that over the continental shelf z_0 = 1 cm, from the Bay entrance to the river mouth z_0 linearly decreases to 0.3 cm, from the river mouth to below the Tacony Bridge, NJ it remains at 0.3 cm, and from there to the head of tide it linearly increases to 1.3 cm.

For the ROMS simulations, the following revisions were employed:

1) The C&D canal width was adjusted to its actual channel width of 121.9 m. It was straightened and made two grid cells wide to accommodate the higher order numerical scheme.
2) The USACOE project channel depths were specified using NOS bathymetric surveys.
3) Upriver marsh areas were not explicitly considered.
4) A full bulk flux formulation was used to provide the surface heat fluxes using the MEE forcing files (Patchen, 2007).
5) A spatially varying quadratic bottom friction coefficient set was used, such that over the continental shelf *rdr* = 0.007, from the Bay entrance to the river mouth *rdr* linearly decreases to 0.005, from the river mouth to the head of tide it linearly increases to 0.009.

High Flow Simulation

Wind speed and direction and atmospheric pressure were produced using Barnes (1973) interpolation at three hour intervals with wind speed and direction root mean square errors (RMSEs) order 2 m/s and 25 ^{o}T, respectively, and sea level atmosphere pressure RMSEs order 1.5 mb. Simulated water levels are compared with observations in Figure 4 at Trenton, NJ and in Table 1 with RMSEs increasing from order 15 cm at the Bay entrance to 25 cm at Philadelphia, PA with a maximum near the head of tide at Trenton, NJ of 37 cm for both models. In this and all subsequent tables, the relative error corresponds to the Willmott et al. (1985) dimensionless (0-1) relative error, with zero representing perfect agreement. Note for the time series plots (Figures 4-6) the indicator of agreement (IND AGMT), equal to one minus the relative error, is given.

Table 1. Water Surface Elevation-MLLW (m) High Flow Hindcast
27 March – April 10, 1984: ROMS Results / POM Results

Station	RMS Error (cm)	Relative Error (-)	Model Mean (cm)	Observed Mean (cm)
Lewes, DE	15/13	0.02/0.02	81/86	86
Cape May, NJ	19/13	0.03/0.01	88/93	93
Indian River, DE	20/22	0.07/0.08	58/62	63
Phila. Pier 11, PA	27/22	0.05/0.03	143/145	133
Trenton, NJ	37/37	0.04/0.04	200/204	191

Current speed and direction model predictions are compared against observations in Tables 2 and 3, respectively. The current strengths at Station 33 and within the river

sections are in reasonable agreement with observations. Current directions are reasonably represented within the Bay and river sections, where the currents are rectilinear. At continental shelf stations 16 and 17 the currents are rotary in nature and both model directions exhibit larger discrepancies from the observations.

Table 2. Current Speed (cm/s) High Flow Hindcast
27 March – April 10, 1984: ROMS Results / POM Results

Station Model Level	RMS Error (cm/s)	Relative Error (-)	Model Mean (cm/s)	Observed Mean (cm/s)
16 Level 6	13.28/12.76	0.49/0.48	7.96/9.82	15.33
17 Level 11	12.27/12.73	0.60/0.59	7.32/14.06	13.34
23 Level 4	16.76/15.28	0.16/0.14	43.12/42.40	40.54
33 Level 4	25.20/19.46	0.22/0.12	58.17/52.19	58.17
50 Level 9	22.65/27.83	0.22/0.38	59.52/46.72	61.78
52 Level 9	16.76/17.99	0.20/0.26	41.37/38.65	47.17

Table 3. Current Direction (^{o}T) High Flow Hindcast
27 March – April 10, 1984: ROMS Results / POM Results

Station Model Level	RMS Error (^{o}T)	Relative Error (-)	Model Mean (^{o}T)	Observed Mean (^{o}T)
16 Level 6	57.77/86.25	0.64/0.78	179.40/194.21	228.85
17 Level 11	113.22/137.58	0.84/0.83	188.76/178.02	215.01
23 Level 4	40.63/31.54	0.05/0.03	234.56/239.16	254.61
33 Level 4	41.86/29.10	0.05/0.02	210.39/219.72	226.66
50 Level 9	48.80/36.06	0.08/0.04	173.56/170.13	176.83
52 Level 9	41.50/30.48	0.06/0.03	154.80/153.85	148.01

The simulated salinities at the corresponding POM model sigma levels (k=1, 15 with 1 representing the near surface) are compared with observations in Table 4. One notes as shown in Figure 5 at Station 33 in the region of large horizontal gradients, that a reasonable RMSE of order 3.0 PSU is achieved. The simulated temperature response is contrasted with observations in Table 5 for both models. With either the SST specification in POM or the bulk heat flux formulation in ROMS, the RMSEs are within order 2 ^{o}C.

Table 4. Salinity (PSU) High Flow Hindcast
27 March – April 10, 1984: ROMS Results / POM Results

Station Model Level	RMS Error (PSU)	Relative Error (-)	Model Mean (PSU)	Observed Mean (PSU)
16 Level 12	0.80/1.05	0.58/0.65	31.87/31.62	32.58
16 Level 8	0.51/0.69	0.56/0.60	31.80/31.60	32.19
16 Level 6	0.64/0.78	0.60/0.59	31.76/31.58	32.28
17 Level 11	0.93/1.01	0.93/0.89	32.97/32.79	33.78
23 Level 4	1.54/1.49	0.45/0.45	25.71/25.33	25.58
33 Level 4	2.97/2.72	0.20/0.17	12.63/12.61	13.14

Table 5. Temperature (°C) High Flow Hindcast
27 March – April 10, 1984: ROMS Results / POM Results

Station Model Level	RMS Error (°C)	Relative Error (-)	Model Mean (°C)	Observed Mean (°C)
16 Level 12	2.16/1.86	0.68/0.69	7.16/6.81	5.01
16 Level 8	2.24/1.82	0.66/0.67	7.29/6.82	5.06
16 Level 6	2.22/1.74	0.65/0.65	7.38/6.83	5.17
17 Level 11	2.19/2.02	0.85/0.85	7.66/7.51	5.51
23 Level 4	0.81/0.73	0.24/0.99	7.19/6.43	6.43
33 Level 4	0.38/1.40	0.04/0.51	6.74/5.71	6.71

Low Flow Simulation

To examine the effect of the above revisions under low flow conditions, the 10-24 September, 1984 period was simulated. Wind speed and direction and atmospheric pressure as produced by the Barnes (1973) interpolation at three hour intervals are compared with hourly observations and are of the same order RMSE as for the high flow period. Note that mean windspeeds are lower than during the high flow period and are quite gentle. Simulated water levels are contrasted with observations in Table 6. RMSEs are generally of the same order as obtained under high flow conditions particularly at Trenton, NJ, where the complete time series is shown in Figure 6. However, one notes at the Bay entrance and at Philadelphia, PA an increase of order 5 cm in RMSE. These results may be improved by reducing the grid extent and specifying the subtidal water level signal nearer the measurement location, but with a loss in the ability to predict the coastal current.

Table 6. Water Surface Elevation-MLLW (m) Low Flow Hindcast
September 10-24, 1984: ROMS Results/ POM Results

Station	RMS Error (cm)	Relative Error (-)	Model Mean (cm)	Observed Mean (cm)
Lewes, DE	18/17	0.04/0.04	71/62	70
Cape May, NJ	21/21	0.04/0.04	80/73	79
Indian River, DE	17/17	0.07/0.07	48/39	47
Ocean City Pier, MD	14/17	0.04/0.06	58/51	61
Phila. Pier 11, PA	27/27	0.05/0.05	113/104	107
Trenton, NJ	35/37	0.04/0.05	132/122	131

In Tables 7 and 8, the current speed and direction comparisons are given. One notes at Station 33 the current speed responses are very similar to those obtained for the high flow hindcast. Note that the current speeds are slightly under-predicted at upriver station 51. Current direction errors are comparable under both high and low flow conditions. In Table

9, the salinity response is compared with observations. At Station 33 in the region of large horizontal salinity gradients both model results are favorable but with POM order 1 PSU closer in agreement with observations. As shown in Table 10, the

Table 7. Current Speed (cm/s) Revised Low Flow Hindcast
September 10-24, 1984: ROMS Results/ POM Results

Station Model Level	RMS Error (cm/s)	Relative Error (-)	Model Mean (cm/s)	Observed Mean (cm/s)
2 Level 8	35.00/22.64	0.57/0.29	40.48/42.16	39.01
16 Level 12	10.35/9.18	0.72/0.65	6.96/6.59	14.38
16 Level 6	7.91/7.55	0.59/0.53	7.39/7.44	9.89
17 Level 6	14.59/12.59	0.58/0.54	7.03/9.66	17.71
18 Level 9	8.25/11.47	0.10/0.24	26.95/25.97	25.18
19 Level 13	14.66/15.92	0.21/0.31	34.81/31.55	28.27
19 Level 5	14.02/22.65	0.09/0.27	46.99/44.74	45.45
22 Level 7	11.15/16.52	0.08/0.20	37.37/32.52	41.69
23 Level 11	18.31/20.50	0.40/0.47	31.24/32.84	17.34
24 Level 8	7.99/14.23	0.10/0.31	28.62/30.66	27.69
25 Level 11	7.04/10.90	0.07/0.22	27.94/23.04	29.22
33 Level 15	19.22/16.06	0.40/0.33	33.72/22.06	29.28
51 Level 5	23.62/27.15	0.28/0.36	48.96/43.12	61.46
154 Level 15	33.53/27.18	0.63/0.57	29.16/10.26	31.47

Table 8. Current Direction (^{o}T) Revised Low Flow Hindcast
September 10-24, 1984: ROMS Results/ POM Results

Station Model Level	RMS Error (^{o}T)	Relative Error (-)	Model Mean (^{o}T)	Observed Mean (^{o}T)
2 Level 8	71.90/46.54	0.14/0.08	223.04/231.70	212.66
16 Level 6	113.91/59.06	0.43/0.30	142.42/159.53	217.85
17 Level 6	89.17/69.50	0.36/0.31	192.56/196.75	230.55
18 Level 9	7.12/17.12	0.00/0.01	223.29/220.75	238.79
19 Level 13	18.40/29.24	0.01/0.02	220.71/232.75	257.01
19 Level 5	22.42/39.79	0.01/0.05	229.33/234.96	247.18
22 Level 7	9.92/17.88	0.00/0.01	227.50/231.26	231.98
23 Level 11	6.07/6.56	0.00/0.00	238.76/240.77	269.80
24 Level 8	45.35/39.07	0.06/0.05	242.35/234.91	245.13
25 Level 11	119.80/120.56	0.87/0.86	107.83/117.22	184.53
33 Level 15	99.29/48.11	0.30/0.07	231.22/225.88	226.26
51 Level 5	30.09/39.65	0.03/0.04	189.95/186.91	194.25
154 Level 15	91.09/99.01	0.31/0.33	165.19/209.43	187.41

temperature responses in both models also compare very well to the observations with POM order 1.0^{o}C lower in RMSE in the lower Bay.

Conclusions, Further Development and Testing

For both 15-day periods, the simulation results for water levels, currents, salinity, and temperature were very similar using either POM or ROMS. Note while the same horizontal grid was used, in the vertical POM uses15 sigma levels while ROMS has 10 s coordinate levels. The third order upstream horizontal advection schemes in ROMS as

Table 9. Salinity (PSU) Revised Low Flow Hindcast
September 10-24, 1984: ROMS Results/ POM Results

Station Model Level	RMS Error (PSU)	Relative Error (-)	Model Mean (PSU)	Observed Mean (PSU)
2 Level 8	0.48/0.40	0.68/0.58	30.04/29.99	30.08
16 Level 12	1.38/1.38	0.93/0.93	31.12/31.08	29.68
16 Level 6	0.27/0.29	0.71/0.78	31.01/31.01	31.15
19 Level 13	0.89/0.41	0.37/0.14	29.20/28.58	28.67
22 Level 7	0.66/1.33	0.12/0.28	26.74/26.28	27.34
23 Level 11	0.76/0.64	0.41/0.45	27.68/27.22	27.44
24 Level 8	0.46/1.11	0.12/0.39	26.41/26.05	26.21
33 Level 15	3.07/2.06	0.56/0.51	19.46/18.01	18.81
154 Level 15	0.65/0.83	0.50/0.71	7.27/6.83	6.59

Table 10. Temperature (^{o}C) Revised Low Flow Hindcast
September 10-24, 1984: ROMS Results/ POM Results

Station Model Level	RMS Error (^{o}C)	Relative Error (-)	Model Mean (^{o}C)	Observed Mean (^{o}C)
2 Level 8	0.63/0.60	0.83/0.81	21.40/20.60	21.04
16 Level 12	1.32/1.19	0.59/0.57	19.15/19.36	20.87
16 Level 6	0.99/0.75	0.78/0.49	21.31/20.48	20.93
19 Level 13	1.56/0.29	0.87/0.60	21.77/20.93	20.67
19 Level 5	1.60/0.34	0.87/0.62	21.79/20.93	20.62
22 Level 7	1.92/0.52	0.87/0.67	22.38/21.22	20.75
23 Level 11	1.24/0.56	0.66/0.80	22.08/21.12	21.20
24 Level 8	2.03/0.61	0.76/0.57	22.46/21.10	20.63
33 Level 15	0.42/0.48	0.72/0.70	23.27/22.85	22.40

opposed to the second order central differencing schemes in POM necessitated an extra day of model spin-up from rest. Both models used the Mellor-Yamada 2.5 level turbulence scheme and employed similar offshore boundary conditions. Both models were run with a 1 second barotropic time step with POM using a 10 second and ROMS a 20 second baroclinic time step. Additional modification of the bottom roughness zones both in value and extent is warranted. Here the bottom friction zones patterned after Walters (1992a; 1992b) were used in both models.

As noted by Johnson et al. (1988) and Galperin and Mellor (1990a; 1990b) a major issue is the representation of the C&D Canal and the river sections above Philadelphia, PA. Within the present grid structure, the C&D Canal is one grid cell wide in POM and two grid cells wide in ROMS. Also order 4 grid cells are employed within the upper river

sections with only 2 grid cells representing the river at Trenton, NJ. The treatment of the change in cross-sectional area with discharge due to the low lying marsh areas is extremely difficult to accomplish within the present grid. A higher resolution grid based on the Delft Hydraulics Laboratory grid generation software has been developed and additional ROMS simulations are being performed.

Acknowledgements

Dr. Frank Aikman provided overall guidance while Mr. Richard C. Patchen directed the MEE Project. Mr. Philip H. Richardson and Mr. Thomas Loeper assisted in the CTD and CT/Current data analysis efforts. Dr. Lyon Lanerolle provided the POM and ROMS grid with initial bathymetry.

References

Aikman III, F., M.S. Vincent, and R.C. Patchen, 2007: "Development and Evolution of Operational Forecast Systems for the Coastal and Estuarine Environment in NOAA's National Ocean Service", *Proceedings of the 10th International Conference on Estuarine and Coastal Modeling, ASCE*, 671-684.

Barnes, S. L., 1973: Mesoscale Objective Map Analysis Using Weighted Time Series Observations, *NOAA Technical Memorandum ERL NSSl-62*, National Severe Storms Laboratory, Norman, OK.

Blumberg, A. F., and G. L. Mellor, 1987: A Description of a Three-Dimensional Coastal Ocean Circulation Model. *Three-Dimensional Coastal Ocean Models*, (ed. Heaps), American Geophysical Union, Washington, DC., 1 - 16.

Blumberg, A. F., and H.J. Herring, 1987: Circulation Modeling using Orthogonal Curvilinear Coordinates, in *Three-Dimensional Models of Marine and Estuarine Dynamics*, (ed. Nihoul and Jamart), Elsevier Oceanography Series, 45, 55-88.

Celebioglu, T.K., and M. Piasecki, 2006: Comparison of Turbulence Models with the use of UnTrim in the Delaware Bay, *Proceedings of the 9th International Conference on Estuarine and Coastal Modeling, ASCE*, 105-122.

Chen, C., R. C. Beardsley, and G. Cowles, 2006: An Unstructured Grid, Finite-Volume Ocean Model (FVCOM) System. Special Issue entitled "Advances in Computational Oceanography", *Oceanography*, vol. 19, No. 1, 78-89.

Galperin, B. and G.L. Mellor, 1990a: A Time-dependent, Three-dimensional Model of the Delaware Bay and River System: Part 1: Description of the Model and Tidal Analysis, *Estuarine, Coastal and Shelf Science*, 31, 231-253.

Galperin, B. and G.L. Mellor, 1990b: A Time-dependent, Three-dimensional Model of the Delaware Bay and River System: Part 2: Three-dimensional Flow Fields and Residual Circulation, *Estuarine, Coastal and Shelf Science*, 31, 255-281.

Gross, T.F, H. Lin, Z. Bronder, M.S. Vincent, 2006: Coastal Ocean Modeling Framework: COMF, *NOAA Technical Report NOS CS 22*, Silver Spring, MD.

Haidvogel, D.P., H. Arango, W.P. Budgell, B.D. Cornuelle, E. Curchister, E. Di Lorenzo, K. Fennel, W. R. Geyer, A. J. Hermann, L. Lanerolle, J. Levin, J. C. McWilliams, A. J. Miller, A. M. Moore, T. M. Powell, A. F. Shchepetkin, C. R. Sherwood, R. P. Signell, John C. Warner, J. Wilkin, 2008: Regional Ocean Forecasting in Terrain-following Coordinates: Model Formulation and Skill Assessment, *Journal of Computational Physics,* 227, 3595-3624.

Hess, K.W., T.F. Gross, R.A. Schmalz, J.G.W. Kelley, F. Aikman, E. Wei, and M.S. Vincent, 2003: NOS Standards for Evaluating Operational Nowcast and Forecast Hydrodynamic Model Systems*, NOAA Technical Report NOS CS 17*, Silver Spring, MD.

Johnson, J.A., L.M. Cohen, L.L. Stahl, and R.C. Patchen, 1988: Final Validation of the Delaware River and Bay Model System, *NOAA Internal Report NOS*, Rockville, MD.

Klavens, A.S., P.J. Stone, and G.A. Stoney, 1984: Delaware River and Bay Circulation Survey: 1984-1985, *NOS Oceanographic Circulation Survey Report No. 9*, Rockville, MD.

NOS, 1999: NOS Procedures for Developing and Implementing Operational Nowcast and Forecast Systems for PORTS, *NOAA Technical Report NOS CO-OPS 0020*, Silver Spring, MD.

Patchen, R.C., 2007: "Establishment of a Delaware Bay Model Evaluation Environment", *Proceedings of the 10th International Conference on Estuarine and Coastal Modeling, ASCE*, 783-818.

Richardson, P.H. and R. A. Schmalz, 2006: Restoration of Delaware River and Bay Circulation Survey, Current Meter and CTD Observations 1984-1985, *NOAA/NOS/CSDL Informal Technical Note No. 5*, Silver Spring, MD.

Schmalz, R. A., 1994: Summary Report, Volume 1: Application and Documentation of the Long Island Sound Three-Dimensional Circulation Model, *NOAA Technical Report NOS OES 003*, Silver Spring, MD.

Schmalz, R. A. and P.H. Richardson, 2002: Evaluation of the NOS Experimental Nowcast/Forecast System for Galveston Bay, *NOAA Technical Report NOS CS 14*, Silver Spring, MD.

Shchepetkin A. F., and J. C. McWilliams, 2005: The Regional Oceanic Modeling System (ROMS): A Split-Explicit, Free-Surface, Topography-Following-Coordinate Oceanic Model, *Ocean Modelling*, 9 (4) 347-404.

Walters, R.A., 1992a: A Study of Salt Transport Processes in Delaware Bay, *Proceedings of the 2nd International Conference on Estuarine and Coastal Modeling, ASCE*, 240-251.

Walters, R.A., 1992b: A 3D, Finite Element Model for Coastal and Estuarine Circulation, *Continental Shelf Research*, 12, 83-102.

Willmott, C. J., S. G. Ackleson, R. E. Davis, J. J. Feddema, K. M. Klink, D.R. Legates, J. O'Donnell, and C. M. Rowe, 1985: Statistics for the evaluation and comparison of models, *Journal of Geophysical Research*, 90, 8995-9005.

Zhang, Y.L., Baptista, A.M., Myers, E.P., 2004. A cross-scale model for 3D baroclinic circulation in estuary–plume–shelf systems: I. Formulation and skill assessment, *Continental Shelf Research,* 24, 2187–2214.



Figure 1. Delaware River and Bay PORTS. Note cu=current meter, wl=water level, wind=wind, at=air temperature, wt=water temperature, ct=conductivity and temperature, baro=barometric pressure, and ag=air gap.

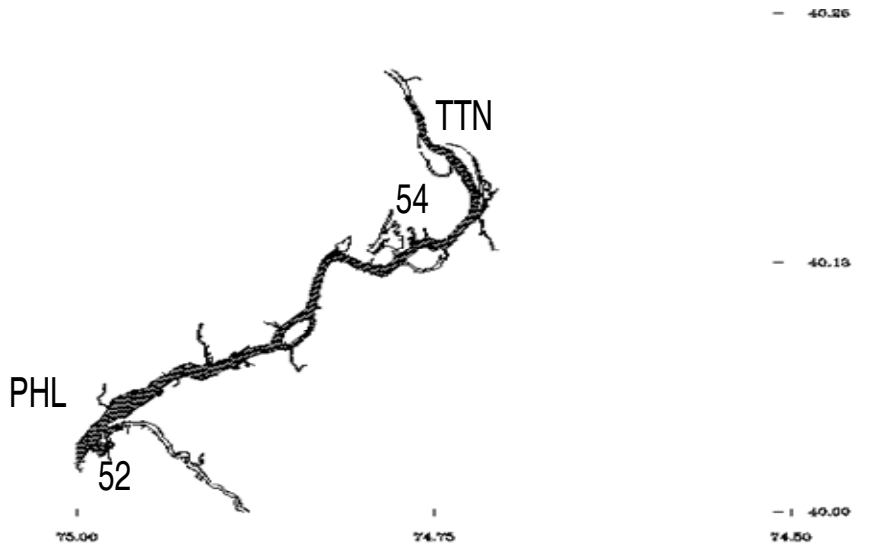

Figure 2. Upper River POM and ROMS grid. Note CTD/Current stations are numbered with Met Stations in text.

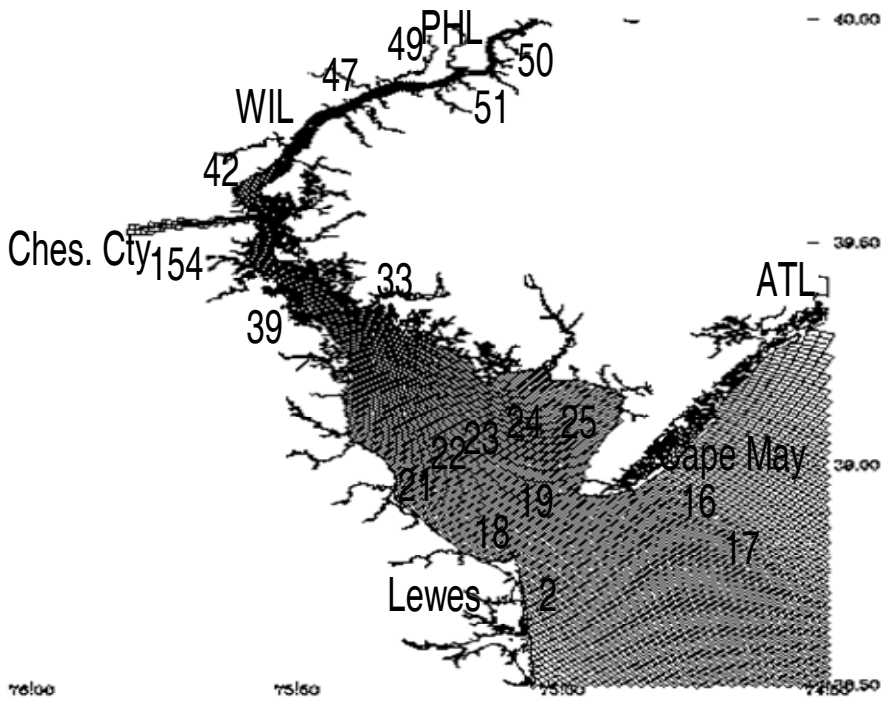

Figure 3. Lower River and Bay POM and ROMS grid. Note Current/CTD stations are numbered, while major cities and Met Stations are in text. Note NBDC buoy 44009 (not shown) is located near the bottom left corner of the map, while NDBC buoy 44012 (not shown) is further to the northeast.

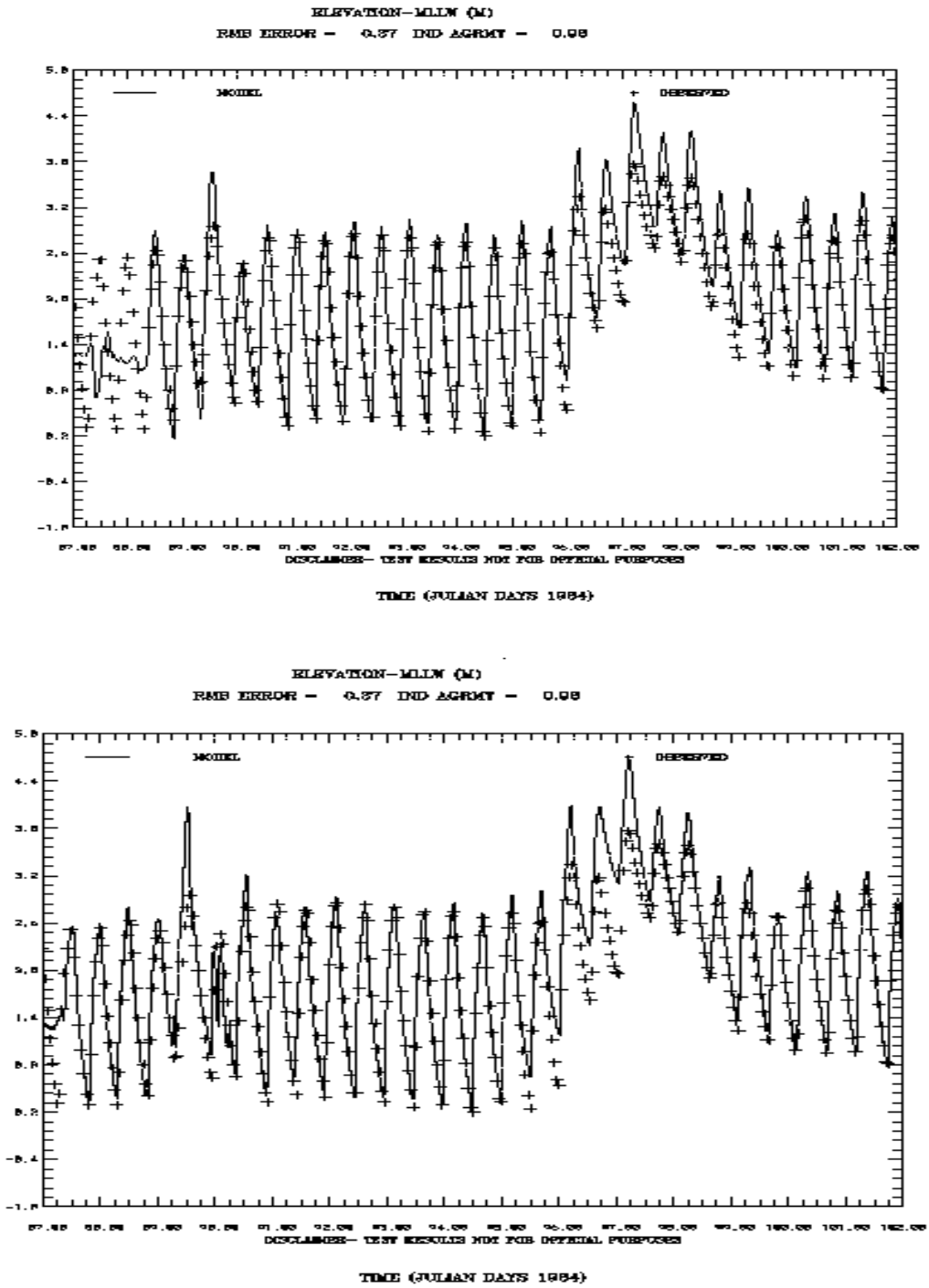

Figure 4. High Flow Hindcast (27 March – 10 April 1984) Water Surface Elevation (m-MLLW) at Trenton, NJ. Top panel: ROMS Hindcast with RMSE=0.37m and IND AGRMT=0.96; Bottom panel: POM Hindcast with RMSE=0.37m and IND AGRMT=0.96. Note observations are at one hour intervals.

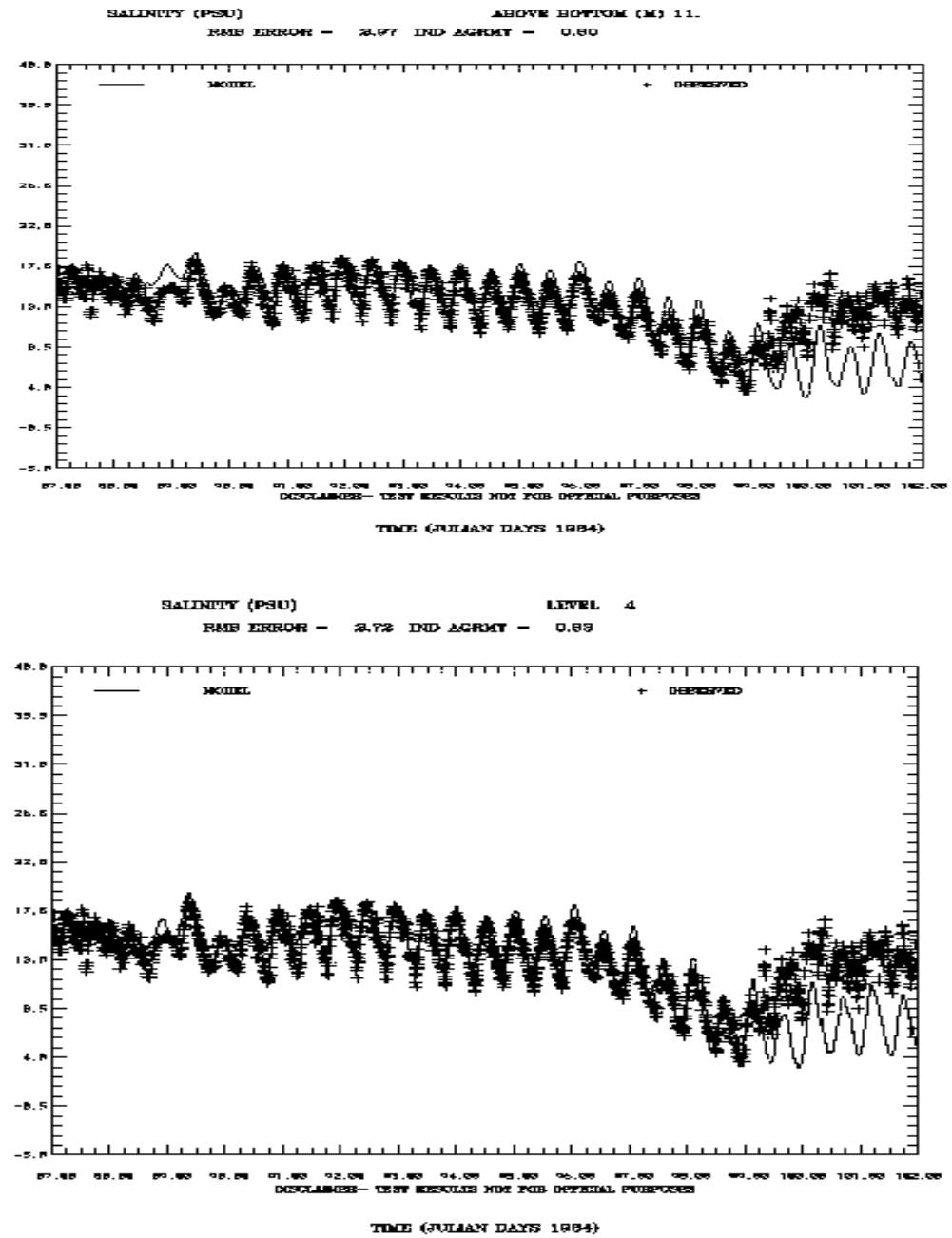

Figure 5. Simulated versus Observed (10 minute) Salinity (PSU) at Station 33 Level 4 at 11m above the bottom. Top panel: ROMS Hindcast with RMSE=2.97 PSU and IND AGRMT=0.80; Bottom panel: POM Hindcast with RMSE=2.72 PSU and IND AGRMT=0.83.

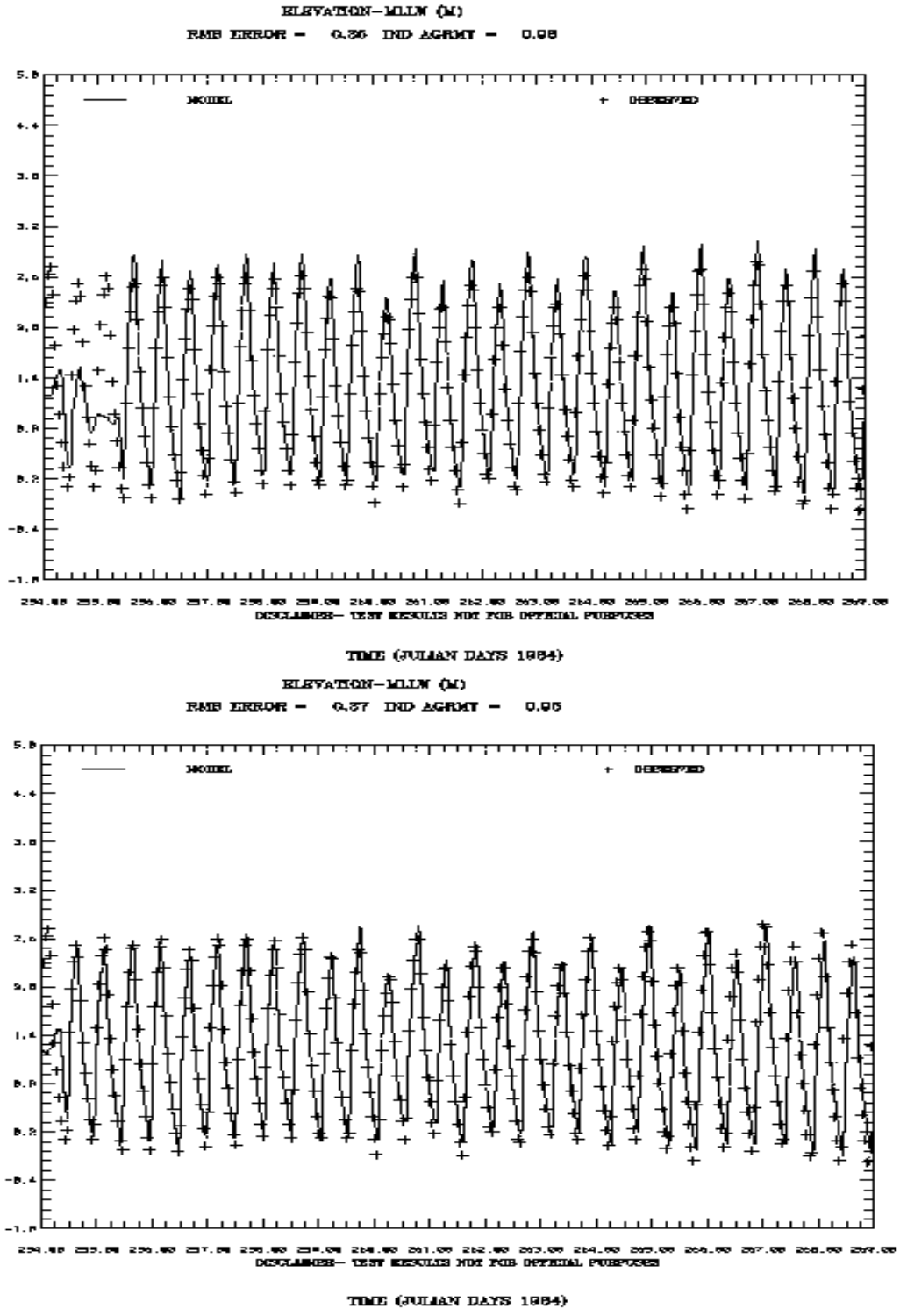

Figure 6. Low Flow Hindcast (10 – 24 September, 1984) Water Surface Elevation (m-MLLW) at Trenton, NJ. Top panel: ROMS Hindcast with RMSE=0.35m and IND AGRMT=0.96; Bottom panel: POM Hindcast with RMSE=0.37m and IND AGRMT=0.95. Note observations are at one hour intervals.

A Process-Based Unsteady Model for Wave-Current-Morphodynamic Changes in Two-Dimensions

S. N. Kuiry[1], Yan Ding[2], and Sam S. Y. Wang[3]

[1] Ph. D., Post Doctoral Research Associate, National Center for Computational Hydroscience and Engineering, The University of Mississippi, University, MS 38677, Email: snkuiry@ncche.olemiss.edu

[2] Ph. D., A. M. ASCE, Research Assistant Professor, National Center for Computational Hydroscience and Engineering, The University of Mississippi, University, MS 38677, Email: ding@ncche.olemiss.edu

[3] Ph.D., P.E., F. ASCE, F.A.P. Barnard Distinguished Professor & Director, National Center for Computational Hydroscience and Engineering, The University of Mississippi, University, MS 38677, Email: wang@ncche.olemiss.edu

Abstract: A process-based two-dimensional model for simulating coastal wave, tide- and wave-induced currents, and coastal morphodynamic change is presented. The integrated model includes three different submodels: (1) wave model, (2) wave-induced current model and (3) sediment transport model. A phase-averaged wave model based on linear wave theory is used to simulate wave transformation, deformation and to calculate radiation stresses. The current model is based on the solution of the conservative form of the nonlinear shallow water equations and effects of the Coriolis force, wind stress, bottom irregularities and short wave-averaged radiation stresses are included. The forward Euler discretization is used for the unsteady term and the convective term is discretized using Godunov-type shock capturing method on non-uniform rectilinear grids. The hydrostatic flux is calculated using an equivalent water depth at each cell interface and the bed slope source term is treated in such a way that exact balance between hydrostatic flux and bed slope source terms is achieved under still water condition. The morphodynamic change is modeled by considering local sediment balance and anisotropic downstream gravitational effect. The three submodels are operated systematically and required parameter values are transferred to the respective submodels. This sequential computations are carried forward in a cyclic order till simulation time reaches to the end time. In order to test the applicability of the model, a severe storm attack on an ideal coast is simulated. The preliminary results show that the developed model can be applied to simulate wave-current-morphodynamic processes in coastal and estuarine zones.

Key words: Coastal inlet flow; Shallow water flow; Wave model; Finite volume method, Morphology.

1 Introduction

In recent years numerical flow models have been increasingly developed and applied to simulate coastal flows and morphological changes due to storm, wave surge or tsunami. Modelling the effects of these extreme events is important for engineering applications and optimum design of coastal structures, sediment management, shoreline protection, maintenance of navigation channel, etc. Such models can be used in a cost effective way comparing to physical model study to refine and optimize designs of coastal structures.

Coastal inlets along barrier islands are used to facilitate exchange of fresh and saline water, navigation and pathway for sediments, nutrients, water-borne materials etc. Such inlets and islands are often attacked by ocean waves, tides and storms, result in significant beach erosion, sediment transport, bed changes of inlet channel and instability of the shoreline. Ding and Wang (2007) and Militello and Kraus (2003) reported that morphodynamic response of an inlet to tides and storm waves can lead to ebb and flood shoals formation, navigation channel refilling, migration of the channel thalweg, skewing of ebb shoals, develop tip shoals, beach erosion, and scour holes inside the inlet and adjacent to the jetty tips. The hydrodynamic and morphodynamic processes associated to these problems may be investigated cheaply using numerical models.

The numerical models for simulating tides and short wave-induced currents as well as short and long term morphological changes must have capabilities to represent short-period waves, long-period tides and nearshore currents with different temporal and spatial scales. Some commercially available models such as MIKE21 (MIKE21 2006; Zyserman and Johnson 2002), DELFT3D (Lesser et al. 2004), SHORECIRC (Svendsen et al. 2003), CMS-M2D (Militello and Kraus 2003; Ding and Wang 2006a) have shown some of these capabilities to deal with flows and morphodynamic changes in coasts. In the present study, the authors have developed a shock-capturing hydrodynamic model to simulate all flow regimes and the new model is coupled with wave and sediment transport models available in the Surface Water Modeling System (SMS). All the three models are executed sequentially and systematically to simulate short waves, wave-induced currents and morphological changes.

The hydrodynamic model was extensively tested (Kuiry et al. 2008; Kuiry et al. 2009) before and hence the integrated model is applied herein to investigate simulation capabilities of severe storm surge, wave-induced currents and subsequently bathymetry changes in a hypothetical costal inlet. The inlet typically represents basic geometry and configuration of a natural inlet with offshore slope, wave and storm forcings. The numerical results correctly reproduce expected trends in hydrodynamic behaviour and morphological changes. Through the preliminary investigation, it can be concluded that the new model can be used to simulate

combined storm and wave-induced currents as well as morphological changes in coastal inlets.

2 Model description

In the present study an integrated model is developed based on the three other submodels (a) wave model, (b) wave-induced current model and (c) sediment transport and morphodynamic change model. The first and third models are readily available in SMS and the second model is developed in this study and integrated with the other models so that all the three models can be operated systematically. Thus the coastal process model uses several differential equations and they are solved in a decoupled way and the necessary values of the parameters are passed from one model to another systematically. The wave model is a phase-averaged model which includes diffraction term in order to represent wave fields in the lee of coastal structures. In the wave-induced depth-averaged current model radiation stresses obtained from the wave model are included so that longshore current can accurately be represented. The cross-shore and longshore sediment transport is calculated by a sediment transport model based on Lund-CIRP total load formulation. The models are briefly described below.

2.1 Wave Model

The CMS-Wave takes into account the effect of an ambient horizontal current or wave behaviour and solves the wave-action balance equation as

$$\frac{\partial\left(v_x N\right)}{\partial x}+\frac{\partial\left(v_y N\right)}{\partial y}+\frac{\partial\left(v_\theta N\right)}{\partial \theta}=\frac{\kappa}{2\sigma}\left[\left(CC_g\cos^2\theta N_y\right)_y-\frac{CC_g}{2}\cos^2\theta N_{yy}\right]-\varepsilon_b N-R \qquad (1)$$

where $N=E(\sigma,\theta)/\sigma$ is the wave-action density to be solved and is a function of frequency σ and direction θ. The spectral wave density $E\left(\sigma,\theta\right)$ represents the wave energy per unit water surface area per frequency interval. In Eq. (1), C, C_g = wave celerity and group velocity, respectively; x, y = horizontal coordinates in two directions; v_x, v_y and v_θ = characteristic velocity with respect to x, y and θ, respectively; N_y, N_{yy} = first and second derivatives with respect to y, respectively; κ = empirical constant representing the intensity of diffraction effect; ε_b = parameterization of wave breaking energy dissipation and R = source terms (e. g., wind forcing, bottom friction loss, nonlinear wave-wave interaction term). The term κ needs to be calibrated and optimized for structures.

The velocity components in Eq. (1) are given by

$$v_x = C_g\cos\theta + u \qquad (2)$$

$$v_y = C_g \sin\theta + v \tag{3}$$

$$v_\theta = \frac{C_g}{C}\left(\sin\theta\frac{\partial C}{\partial x} - \cos\theta\frac{\partial C}{\partial y}\right) \tag{4}$$

where u, v = depth-averaged horizontal current velocity components along x and y directions.

2.2 Wave-induced Current Model

A depth and shortwave averaged forms of the SWE are used for simulating currents induced by tides and waves (Ding and Wang 2006). The governing equations in conservative form can be written as follows:

$$\frac{\partial \mathbf{U}}{\partial t} + \frac{\partial \mathbf{E}(\mathbf{U})}{\partial x} + \frac{\partial \mathbf{G}(\mathbf{U})}{\partial y} = \mathbf{S}(x, y, \mathbf{U}) \tag{5}$$

In which,

$$\mathbf{U} = \begin{bmatrix} H \\ Hu \\ Hv \end{bmatrix}; \quad \mathbf{E} = \begin{bmatrix} Hu \\ Hu^2 + \frac{1}{2}gH^2 \\ Huv \end{bmatrix}; \quad \mathbf{G} = \begin{bmatrix} Hv \\ Huv \\ Hv^2 + \frac{1}{2}gH^2 \end{bmatrix};$$

$$\mathbf{S} = \begin{bmatrix} 0 \\ gH\frac{\partial h}{\partial x} + f(Hv) + \frac{\partial}{\partial x}\left(D_x\frac{\partial(Hu)}{\partial x}\right) + \frac{\partial}{\partial y}\left(D_y\frac{\partial(Hu)}{\partial y}\right) - \tau_{bx} + \tau_{sx} + \tau_{wx} \\ gH\frac{\partial h}{\partial y} - f(Hu) + \frac{\partial}{\partial x}\left(D_x\frac{\partial(Hv)}{\partial x}\right) + \frac{\partial}{\partial y}\left(D_y\frac{\partial(Hv)}{\partial y}\right) - \tau_{by} + \tau_{sy} + \tau_{wy} \end{bmatrix}$$

where $\mathbf{U}$ = vector of conserved variables; $\mathbf{E}$ and $\mathbf{G}$ = convective fluxes in the x- and y-directions, respectively; and $\mathbf{S}$ = source term. In addition, h = still water depth; η = deviation of the water surface from the still water level (Figure 1); $H = (h + \eta)$ = total water depth; u and v = depth-averaged current velocities parallel to the x- and y-directions; g = acceleration due to gravity; f = Coriolis force, $f = 2\omega\sin\varphi$, ω = angular frequency of earth rotation, φ = latitude. The other parameters in the x- and y-directions are: S_{0x} and S_{0y} = bed slopes; D_x and

D_y = diffusion coefficients; τ_{bx} and τ_{by} = bed shear stresses; τ_{sx} and τ_{sy} = wave stresses; τ_{wx} and τ_{wy} = surface wind stresses, respectively.

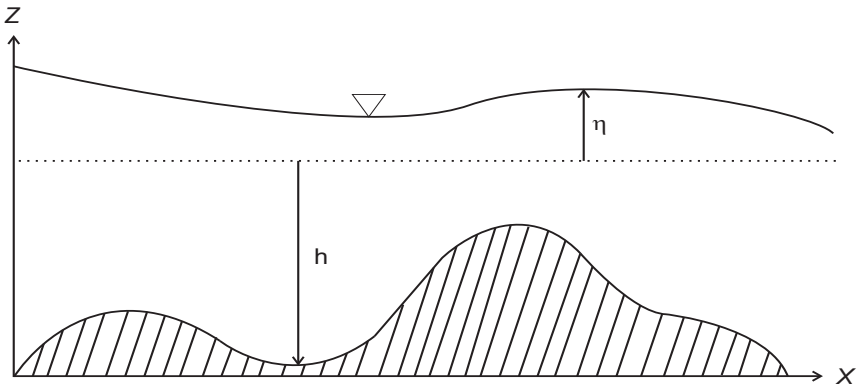

Figure 1: Definition sketch for bed topography, water depth and

2.3 Sediment Transport and Morphodynamic Change Model

The sediment transport model is based on the calculations of sediment transport rates and resultant changes in water depth (bottom elevation) through gradients in transport rates as proposed in Lund-CIRP formulations (Camenen and Larson 2005a, 2005b). Bed level changes are obtained from the sediment continuity equation:

$$\frac{\partial h}{\partial t} = \frac{1}{1-p}\left(\frac{\partial q_{bx}}{\partial x} + \frac{\partial q_{by}}{\partial x} + P - D\right) \tag{6}$$

where q_{bx}, q_{by} = bed load transport rate in the *x*- and *y*-directions, respectively and p = porosity of sediment. The term $\partial q_{bx}/\partial x + \partial q_{by}/\partial y$ represents the bed load component and the term $P - D$ corresponds to the suspended load component. While evaluating the bed changes by Eq. (6), time-averaged transport rates are used ($\overline{q}_{bx}, \overline{q}_{by}$). In this approach, instantaneous transport rates are computed at a time interval of Δt_{sed} and time-averaged transport rates and morphology changes are calculated at a time interval of Δt_{morph}. Also, the bed load components in Eq. (6) are corrected for the slope effect as

$$\overline{q}'_{bx} = \overline{q}_{bx} - D_s \left|\overline{q}_b\right|_x \frac{\partial h}{\partial x} \tag{7}$$

$$\overline{q}'_{by} = \overline{q}_{by} - D_s \left|\overline{q}_b\right|_y \frac{\partial h}{\partial y} \tag{8}$$

where $\overline{q}_b = \sqrt{\overline{q}_{bx}^2 + \overline{q}_{by}^2}$. Finally, Eq. (9) is solved to compute depth changes at the time interval Δt_{morph}.

$$\frac{\partial h}{\partial t} = \frac{1}{1-p}\left(\frac{\partial \overline{q}_{bx}'}{\partial x} + \frac{\partial \overline{q}_{by}'}{\partial x} + \overline{P} - \overline{D} \right) \tag{9}$$

Camenen and Larson (2005a) proposed a general transport formula for bed load under combined effect of wave and current as

$$\frac{q_{bw}}{\sqrt{(s-1)gd_{50}^3}} = a_w \sqrt{\theta_{net}}\,\theta_{cw,m} \exp\left(-b\frac{\theta_{cr}}{\theta_{cw}} \right) \tag{10}$$

$$\frac{q_{bn}}{\sqrt{(s-1)gd_{50}^3}} = a_n \sqrt{\theta_{cn}}\,\theta_{cw,m} \exp\left(-b\frac{\theta_{cr}}{\theta_{cw}} \right) \tag{11}$$

where subscripts *w* and *n* represents wave direction and direction normal to the wave, respectively; d_{50} = median grain diameter; θ_{cr} = critical Shields parameter; s = specific gravity; a_w, a_n and b = empirical constants and $\theta_{cw,m}, \theta_{cw}$ = mean and maximum Shields parameter respectively. The quantities θ_{net} and θ_{cn} represent the net contribution of the shear stress to the transporting velocity during a wave cycle in the direction parallel and normal to the waves, respectively.

The suspended load q_s is computed assuming an exponential concentration profile and a constant velocity over the water column and can be expressed as

$$\mathrm{q}_s = \mathrm{u}\, c_R \frac{\varepsilon}{w_s}\left(1 - e^{-\frac{w_s h}{\varepsilon}} \right) \tag{12}$$

where w_s = sediment settling velocity, c_R = reference concentration and ε = sediment diffusivity (or turbulent mixing coefficient). The transport q_s is considered to be taken place in the direction of current because the waves are assumed to produce a zero net drift and do not contribute to the suspended sediment transport.

3 Solution Methods

In order to simulate coastal hydro and morphological processes, the governing partial differential equations for the three submodels, i.e., the energy balance Eq. (1), the depth- and wave-averaged continuity nentum Eq. (5) and the seabed level

evolution Eq. (9) are solved numerically. The integrated model is developed on a non-uniform rectangular Cartesian coordinate system. Though the wave and morphodynamic change models are used directly from the SMS in the present study, a brief description of solution schemes of the submodels are presented in the following sections.

3.1 Wave Model

The energy balance Eq. (1) is solved by means of parabolic approximation, in which the waves are assumed to have a principal propagation direction from offshore to onshore. Therefore, the computations are carried out line by line from offshore to onshore. The first term of Eq. (1) is discretized by forward difference scheme, second and third terms are discretized by QUICK scheme, diffraction term is discretized by central difference scheme and the source term is obtained by solving algebraic equations. Consequently, Eq. (1) is expressed in a finite difference form and is solved explicitly. The implementation of the numerical scheme is described in detail in Mase (2001) and Mase et al. (2005).

3.2 Hydrodynamic Model

A cell centered finite volume method is used to discretize Eq. (5) over a non-uniform rectangular control volume in a Cartesian grid with the assumption that the dependent variables are represented as piecewise constants. It is useful to rewrite Eq. (5) as

$$\frac{\partial \mathbf{U}}{\partial t} + \nabla \cdot \mathbf{F}\left(\mathbf{U}\right) = \mathbf{S}(x, y, \mathbf{U}) \tag{13}$$

In which, $\mathbf{F} = (\mathbf{E}, \mathbf{G})$ is the flux tensor, in order to introduce integral form of the equations over a fixed control volume Ω:

$$\int_{\Omega} \frac{\partial \mathbf{U}}{\partial t} d\Omega + \int_{\Omega} \left(\nabla \cdot \mathbf{F}\right) d\Omega = \int_{\Omega} \mathbf{S} d\Omega \tag{14}$$

In the 2D approach, a discrete form of Eq. (14) is applied to each cell Ω with dimension $(\Delta x, \Delta y)$ so that the volume integrals represent integrals over the area of the cell and the surface integrals represent the total flux through the cell boundary Γ. Assuming $\mathbf{U}$ as the average value of conservative variables over the volume Ω at a given time, from Eq. (14) and applying Gauss divergence theorem to the second integral, the conservation equation can be written as

$$A \frac{\partial \mathbf{U}}{\partial t} + \int_{\Gamma} \left(\mathbf{F} \cdot \mathbf{n}\right) d\Gamma = A\mathbf{S} \tag{15}$$

where A is the cell area and $\mathbf{n}$ is the unitary outward normal.

A two-dimensional discrete finite volume formulation of system of Eq. (15) with explicit scheme, which applies forward Euler discretization to time derivative, on a non-uniform rectilinear grid with spacing $(\Delta x, \Delta y)$, leads to the inherently conservative method:

$$\mathbf{U}_{i,j}^{n+1} = \mathbf{U}_{i,j}^{n} - \frac{\Delta t}{\Delta x}\left(\mathbf{E}_{i+1/2,j}^{*} - \mathbf{E}_{i-1/2,j}^{*}\right) - \frac{\Delta t}{\Delta y}\left(\mathbf{G}_{i,j+1/2}^{*} - \mathbf{G}_{i,j-1/2}^{*}\right) + \Delta t \mathbf{S}_{i,j} \qquad (16)$$

in which $\mathbf{E}_{i\pm1/2}^{*}, \mathbf{G}_{i\pm1/2}^{*} =$ numerical convective flux functions through the cell interfaces $\Gamma_{i\pm1/2,j}$ and $\Gamma_{i,j\pm1/2}$ (Figure 2) respectively; $\Delta t =$ time step size and $\mathbf{S}_{i,j} =$ a discretization of the source term. In this study Roe's approximate Riemann solver (Roe 1981) is chosen for convective flux computation. The details of the Roe's Riemann solver and its application to two-dimensional shallow water equations may be found in Kuiry et al. (2008). One may refer to Kuiry et al. (2009) for detail discretization of the source term $\mathbf{S}$.

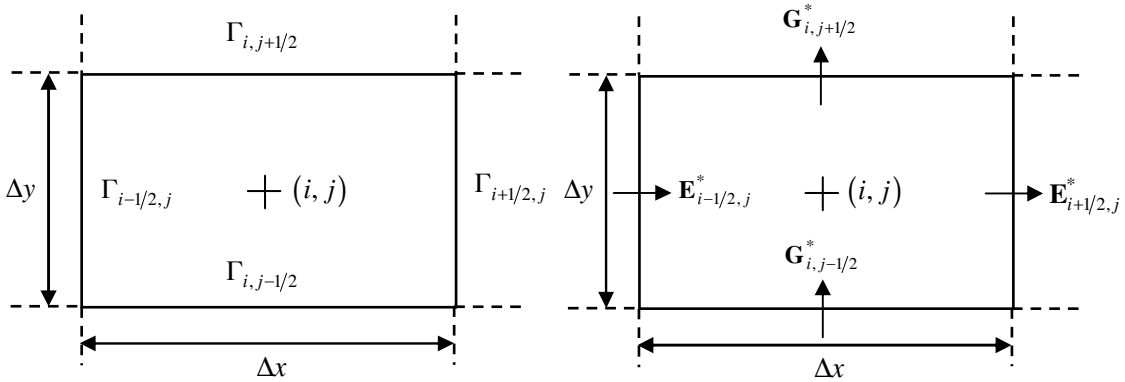

Figure 2: Discretization of a finite volume cell: (a) Interfaces (b) numerical

3.2.1 Balancing of Hydrostatic Flux and Bed Slope Term

The discretization of the bed slope source term for finite volume shallow water flow models has been the subject of numerous recent studies (Nujic 1995; Burguete and García-Navarro 2001; Zhou et al. 2001; Kuiry et al. 2008). In this work, this term is treated in a simple way, which also satisfies a compatibility relation with the hydrostatic flux term. In the absence of flows through the boundaries, the momentum equations reduce to

$$\int_{\Gamma}\left(\frac{1}{2}gH^{2}\right)n_{x}d\Gamma = g\int_{\Omega} H\frac{\partial h}{\partial x}d\Omega \qquad (17)$$

$$\int_{\Gamma}\left(\frac{1}{2}gH^{2}\right)n_{y}d\Gamma = g\int_{\Omega} H\frac{\partial h}{\partial y}d\Omega \qquad (18)$$

This indicates that the sum of the hydrostatic pressure forces on the vertical faces of a cell in a particular direction is numerically equal to the weight component of the water contained within the cell in the same direction. In the discretization procedure, each cell is assumed to be composed of two triangular sub-cells for which bed slopes are calculated and the flow depth in hydrostatic term at each cell face is replaced by an equivalent water depth (Kuiry et al. 2008). Therefore, the bed slope term is expressed as the summation of two source terms for two triangular sub-cells. The discretization technique can be expressed mathematically as:

$$\int_{\Gamma}\left(\frac{1}{2}gH^2\right)\cdot\mathbf{n}d\Gamma=\sum_{m=1}^{NE}\left(\frac{1}{2}gH_{eq}^2\right)\cdot\mathbf{n}\Delta\Gamma_m \tag{19}$$

$$g\int_{\Omega}H\left(\nabla\cdot h\right)d\Omega=g\sum_{s=1}^{2}H_{cs}A_s\mathbf{S}_{0s} \tag{20}$$

where $\Delta\Gamma_m =$ m^{th} edge length; $NE =$ total number of edges in the cell ($NE=4$); $H_{cs} =$ water depth at centroid; $A_s =$ area of the sub-cell; and $\mathbf{S}_{0s} =$ bed slope in the respective coordinate direction of the sth sub-cell. The slope of each triangular sub-cell is computed considering the three vertices lying on a triangular plane (Kuiry et al. 2008). The discretization method described above exactly satisfies Eqs. (17) and (18) under still water condition.

3.2.2 Hydrodynamic Model Stability

The time integration scheme adopted is explicit and must satisfy the stability condition so that no wave resulting at an interface can travel beyond the extent of its stencil. The stability criteria adopted is

$$\Delta t=C_r\min\left[\min\left(\frac{\Delta x}{u+\sqrt{gH}}\right),\min\left(\frac{\Delta y}{v+\sqrt{gH}}\right)\right]_{i,j} \tag{21}$$

where $C_r =$ Courant number between zero and one. In this study $C_r = 0.75$ is used.

3.3 Sediment Transport and Morphodynamic Change Model

In the present study the Lund-CIRP model available in SMS is used to compute bed evolution. In this submodel, the sediment transport properties and transport rates are calculated at the cell centers. After transport rates are calculated by the Lund-CIRP formulae for all the cells in the domain, they are mapped back to the cell faces such that *x*-directed rate is located on the left face center and the *y*-directed rate is located on the bottom face center. These instantaneous transport rates are calculated at the

sediment transport time step Δt_{sed} and instantaneous rates averaged over the morphologic change time step are evaluated at the time step Δt_{morph}. The Eq. (9) is then solved for every cell by means of forward Euler scheme to compute the bed changes over the time period Δt_{morph}. The implementation of the model is explained in Buttolph et al. (2006).

4 Model application

Due to severe storm or hurricane, the flow field in and around of an inlet becomes complex and flow regimes may change from sub- to supercritical. The study of hydraulics of such flow field and morphological changes are important for engineering design of inlet structures. The present model is applied to such an idealized coast with an inlet of 30 m wide. The coast is designed in such a way that it represents the basic geometry, inlet entrance configuration, offshore slope, wave and storm forcings at a medium size inlet. Figure 3 shows the flow domain with bathymetry varying from 30 m at offshore to 3 m deep at the bay. The initial bathymetry does not include any developed flood or ebb shoal and therefore it represents a newly opened coastal inlet.

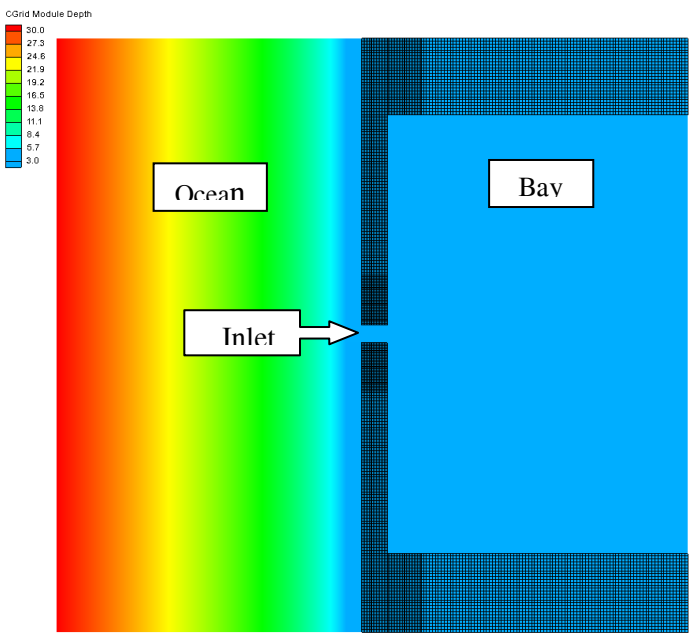

Figure 3: Idealized coast with initial

The wave-current-morphodynamic processes in the inlet are investigated when the inlet is hit by a severe storm at the offshore boundary. A rectangular mesh grid is generated for the flow domain with the help of SMS grid generator with the grid resolution 25 m in the channel and 50 m in the offshore. The three processes are

simulated sequentially by the steering option of the SMS package. An irregular spectral wave with significant wave height $H_s = 3.5$ m, a peak period $T_p = 9$ s, and mean incident angle $= 30^{\circ}$ (JONSWAP spectrum $\gamma = 3.3$) is imposed at the offshore boundary. The storm surge shown in Figure 4 with a peak of 7.0 m is also imposed at the offshore boundary. The other ocean boundaries are specified as free flow boundaries. The radiation stress gradients calculated from the specified wave is held constant throughout the simulation. The uniform grain size in the coast is specified as 0.2 mm. The Lund-CIRP formulations as presented before are used to compute the total sediment transport rate and the bed evolution is calculated using Eq. (10).

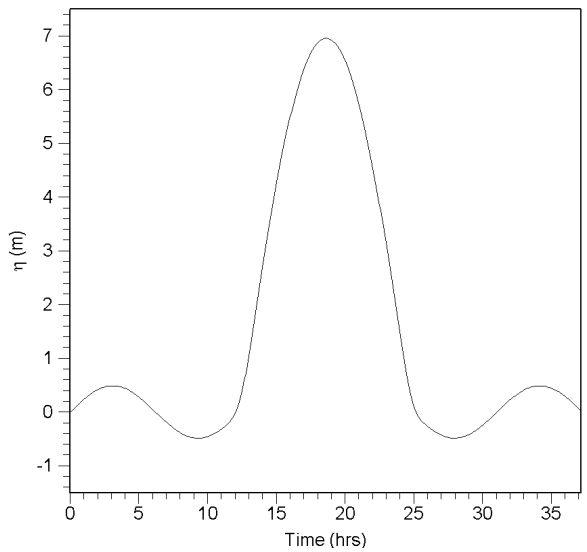

Figure 4: Storm surge imposed at the offshore

The results are reported at two time intervals at 19 hrs and 27 hrs, respectively. At 19 hrs, flood tide passes through the inlet and strong velocities are developed there. Figure 5 shows the morphology changes at 19 hrs and Figure 6 shows the computed bed elevations at the same time interval. The strong velocities cause significant erosion and develop scour hole at the entrance of the inlet and deposition at the bay side. Thus a flood shoal is created in the bay which is frequently observed in a real coastal inlet. Due to the strong flood tide at this time interval, the long shore currents from the south side of the domain also move into the channel while the long shore currents developed in the north side move to the north. At 27 hrs, during the ebb tide, flow passes from the bay to the offshore direction. At this instant, bed erosion takes place at the entrance of ebb tide in the bay side and deposition takes place at the offshore side. Ebb shoals are developed at the offshore due to deposition of the bed materials. It can be observed that the ebb shoals are asymmetric. Such asymmetric shape is expected due to the oblique incident wave which drives the long shore currents to the north. Figure 7 shows the computed bed elevations at 27 hrs. In both the cases, it is observed that significa akes place in and around the inlet.

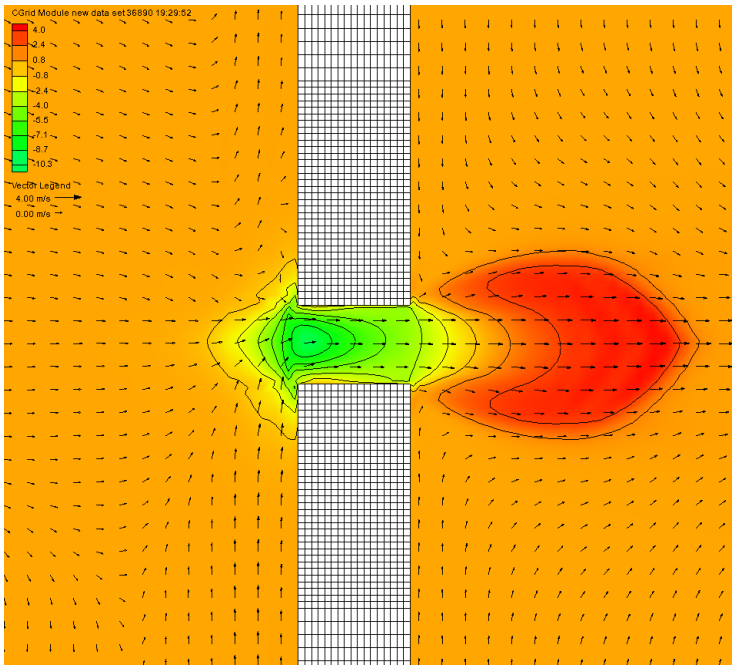

Figure 5: Bed elevation change at t = 19 hrs during flood tide

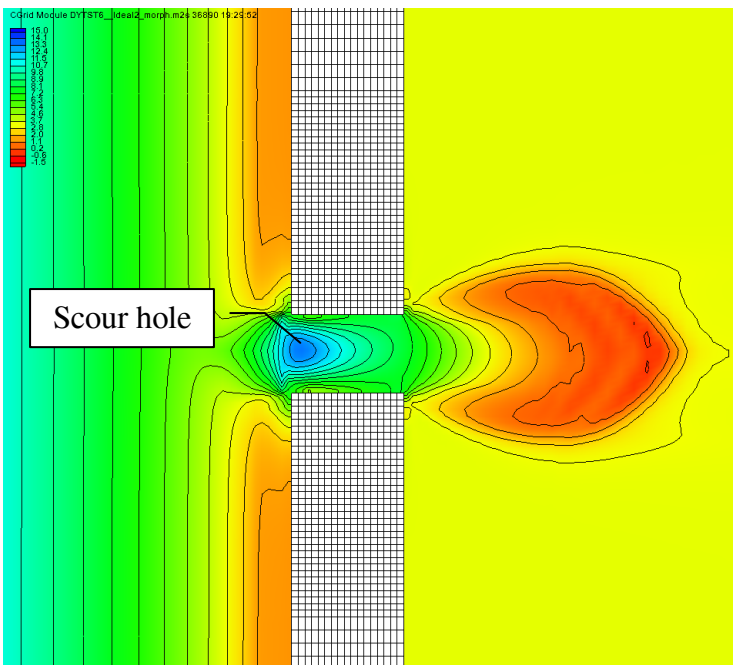

Figure 6: Computed bed elevation at t = 19 hrs during flood tide

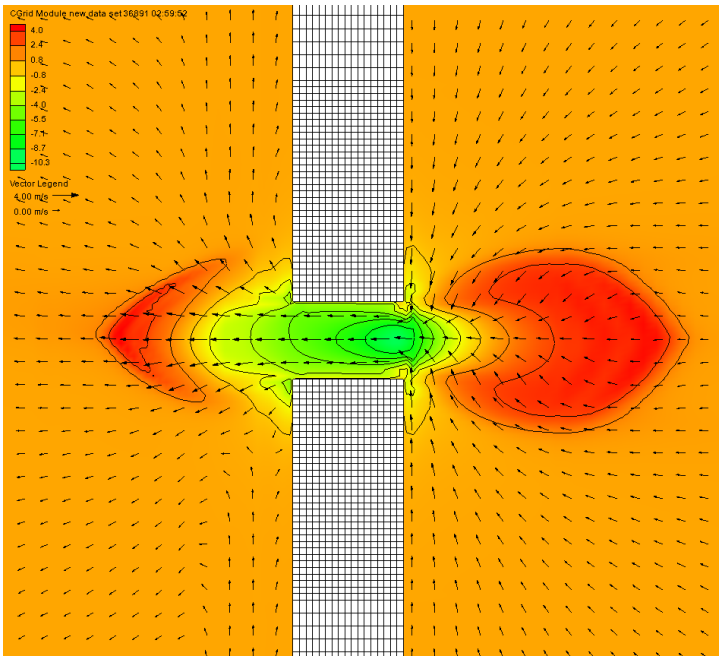

Figure 7: Bed elevation change at t = 27 hrs during ebb tide

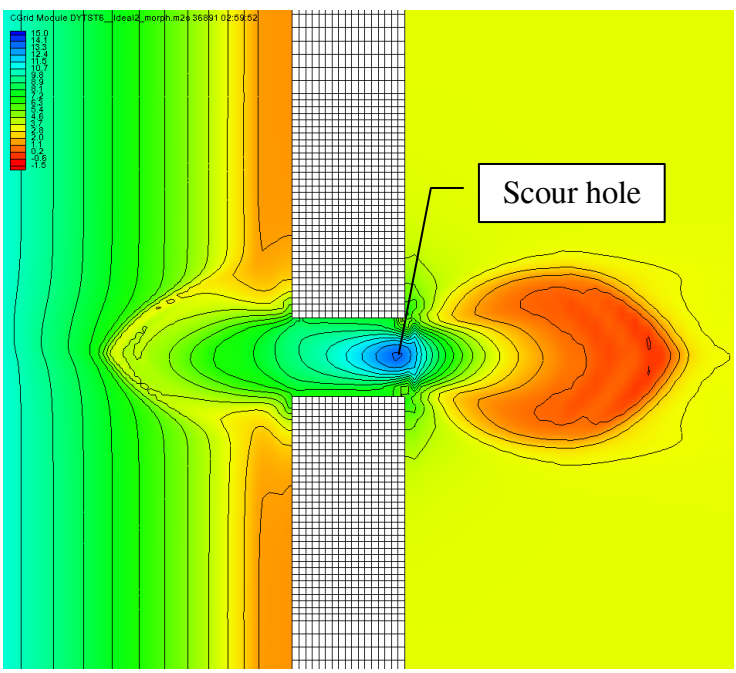

Figure 8: Computed bed elevation at t = 27 hrs during ebb tide

Though the results shown in this study need further investigations to determine the accuracy of the model, it can be stated that the present model can be applied to study wave-current-morphodynamic processes. The shock capturing property of the hydrodynamic model helps to simulate the complex flow scenario in the inlet when attacked by a severe storm.

5 Conclusions

A numerical model for systematic computations of wave-current-morphodynamic processes in two-dimensions is developed. The two-dimensional shallow water equations are solved by shock-capturing finite volume method considering the effects of short wave-averaged radiation stress, wind stress, Coriolis force and strong bottom irregularities. The hydrodynamic model is coupled with the CMS-Wave and morphodynamic models of SMS package in order to simulate wave deformation, transformation and morphological changes in coastal inlets and their adjacent coasts. The applicability of the model is tested by simulating a severe storm surge attacking an idealized coast with an inlet which represents the geometry of a medium size coast. The successful simulation shows that the storm surge causes significant bed erosion, deposition and formation of flood and ebb shoals. The effect of long shore currents is observed especially during the ebb shoal formation in the offshore. The overall results seem to be satisfactory and representative for preliminary investigation of applicability of such a process based numerical model and further study is required to examine the predictive accuracy of the model.

6 Acknowledgements

This work is a product of the research sponsored by the National Center for Computational Hydroscience and Engineering at the University of Mississippi, USA.

7 References

Burguete, J., and García-Navarro, P. (2001). "Efficient construction of high-resolution TVD conservative schemes for equations with source terms: Application to shallow water flows." *Int. J. Numer. Methods Fluids*, 37, 209-248.

Buttolph, A. M., Reed, C. W., Kraus, N. C., Ono, N., Larson, M., Camenen, B., Hanson, H., Wamsley, T., and Zundel, A. K. (2006). Two-dimensional depth-averaged circulation model CMS-M2D: Verson 3.0, report 2, sediment transport and morphology change. Technical Report ERDC/CHL-TR-06-7. U. S. Army Engineer Research and Development Center, Vicksburg, M. S., U. S. A.

Camenen, B., and Larson, M. (2005a). "A bedload sediment transport formula for the nearshore." *Estuarine, Coastal and Shelf Science,* 63, 249-260.

Camenen, B., Larson, M. and Yamashita, T. (2005b), "A suspended load formula for the nearshore" In Proc. 52nd Japanese Coastal Eng. Conf., JSCE, Aomori, Japan,381-385. (in Japanese).

Ding, Y., and Wang, S.S.Y. (2006a). Implementation of an efficient and accurate implicit solution scheme for the IMS-M2D hydrodynamic model. National Center for Computational Hydroscience and Engineering, University of Mississippi, Interim Contract Report for U. S. Army Engineer research and Development Center, Coastal and Hydraulics Laboratory, February 2006.

Ding, Y., and Wang, S.S.Y. (2007). Development of a numerical model for simulating morphodynamic processes driven by tides and waves at coastal inlets. In: Proceeding of the Tenth International Conference on Estuarine and Coastal Modeling Congress 2007, Malcolm L. Spaulding, Editors Newport, Rhode Island, USA, November 5–7, 862-878.

Ding, Y., Wang, S.S.Y. (2006b). Development of a Numerical Model for Simulating Tidal and Wave-Induced Currents in Coastal Inlets, In: Proceeding of the 7th International Conference on Hydroscience and Engineering (ICHE 2006), Sept. 10-13, 2006, Philadelphia (ISBN: 0977447405) (http://idea.library.drexel.edu/handle/1860/1371).

Kuiry, S. N., Ding, Y., and Wang, S. S. Y. (2008). "Development of a two-dimensional shock capturing flow model for coastal barrier breaching". In: Symposium on Numerical Modeling of Coastal Hydrodynamics at the First American Academy of Mechanics (AAM) Conference, June 17-20, New Orleans, LA, USA.

Kuiry, S. N., Ding, Y., and Wang, S. S. Y. (2009). "Two-Dimensional Modelling of Coastal Flows Using Shock-Capturing Finite Volume Method." Communicated to *J. Coast. Eng*.

Kuiry, S. N., Pramanik, K., and Sen, D. J. (2008). "Finite volume model for shallow water equations with improved treatment of source terms." *J. Hydr. Eng*., 134(2), 231-242.

Lesser, G. R., Roelvink, J. A., Van Kester, J. A. T. M., and Stelling, G. S. (2004). "Development and validation of a three-dimensional morphological model." *Coastal Eng.*, 51(8-9), 883-915.

Mase, H. 2001. "Multidirectional random wave transformation model based on energy balance equation." *Coastal Eng*., 43(4):317-337.

Mase, H., H. Amamori, and T. Takayama. 2005a. Wave prediction model in wave-current coexisting field. In: Proceedings 12th Canadian Coastal Conference (CD-ROM).

MIKE 21 (2009). MIKE 21 coastal hydraulics, hydrodynamic module – MIKE 21 HD – basic hydrodynamic module, Danish Hydraulic Institute, < http://www.dhigroup.com/Software/Marine/MIKE21/Details/Hydrodynamics.aspx>, (Jan 15, 2009)

Militello, A., and Kraus, N. C. (2003). Numerical simulation of sediment pathways at an idealized inlet and ebb shoals. In: *Proc. Coastal Sediments 03*, CD-ROM published by Word Scientific Publishing (ISBN 981-238-422-7).

Nujic, M. (1995). "Efficient implementation of non-oscillatory schemes for the computation of free surface flow." *J. Hydraul. Res*., 33(1), 101-111.

Roe, P. L. (1981). "Approximate Riemann solvers, parameter vectors and difference schemes." *J. Comput. Phys.*, 43, 357-372.

Svendsen, I. A., Haas, K., and Zhao, Q. (2003). Quasi-2D nearshore circulation model SHORECIRC – Version 2.0. Technical Report, Center for Applied Coastal Research, University of Delaware, Newark, DE19716.

Zhou, J. G., Causon, D. M., Mingham, C. G., and Ingram, D. M. (2001). "The surface gradient method for the treatment of source terms in the shallow-water equations." *J. Comput. Phys*., 168, 1-25.

Zyserman, J. A., and Johnson, H. K. (2002). "Modelling morphological processes in the vicinity of shore-parallel breakwaters." *Coastal Eng*., 45(3), 261-284.

Simulation of Multilayer Shallow Water Fluid Flow Using Lattice Boltzmann Modeling and High Performance Computing

K. R. Tubbs[1] and F.T-C. Tsai[2]

[1]Donald W. Clayton Graduate Program in Engineering Science, Louisiana State University, 351 Johnston Hall, Baton Rouge, LA, 70803; (225) 578-8937; (225) 268-9529, Email: ktubbs2@lsu.edu
[2]Department of Civil and Environmental Engineering, Louisiana State University, 3418G Patrick F. Taylor Hall, Baton Rouge, LA 70803-6405; PH (225) 578-4246; FAX (225) 578-4945, E-mail: ftsai@lsu.edu

ABSTRACT

A lattice Boltzmann method (LBM) on high performance computing (HPC) environments for three-dimensional shallow water flow fields is developed. Recently, the LBM has become an attractive numerical method to solve various fluid dynamics phenomena. However, LBM has not been extensively applied to shallow water equations. The shallow water equations have wide applications in ocean and hydraulic engineering which can benefit from the advantages of the LBM. The standard LBM for two dimensional shallow water flows is extended to three dimensional flows by solving the multilayer shallow water equations. LBM is an attractive method for solving the multilayered shallow water equations because the extension to a multilayer formulation is straight forward and all simplicities and advantages of the LBM are retained. The performance of the LBM for the multilayer shallow water equations is investigated and optimized in HPC environments. We numerically demonstrate the applicability of the LBM in three dimensional shallow water flows and the LBM performance using OpenMP.

INTRODUCTION

In the last decade, the lattice Boltzmann (LB) method or LBM has become a powerful numerical method for simulating fluid flows (Chen and Doolen 1998). The method is based on statistical physics and models the fluid flow by tracking the evolution of distribution functions of the fluid particles in discrete phase (velocity) space. The essential approach in the LB method lies in the recovery of macroscopic fluid flows from the microscopic flow behavior of the particle movement. The benefits of this description are that the LBM does not involve the solution of global system of equations (locality), which makes it very suitable for parallel computing. Recently, this has become an important feature for numerical methods as high performance computing (HPC) systems are currently being designed to model large scale engineering problems.

The method has been shown to be effective for simulating flows in complicated geometries and implementation on parallel computer architectures (Kandhai et al. 1998). Furthermore, the method has become an alternative to other numerical methods like finite difference, finite element and finite volume methods in

computational fluid dynamics. Due to its attractive feature, recently the LBM has found a wide range of applications including wind-driven ocean circulation (Salmon 1999; Zhong et al. 2006), discontinuous flows with shocks (Zhou et al. 2004; Zhou 2007), and tidal flows on complex geometries with irregular bathymetry (Thömmes et al. 2007). Such practical flow problems of tidal flows in an estuary or coastal regions, rivers, reservoir, and open channel flows are not trivial to simulate since the geometry can be complex and the topography irregular.

In order to take advantage of the shallow water equations while avoiding the drawbacks of the depth averaged models, a multilayer system (Audusse 2005) was adopted in this study. The multilayer shallow water equations have been introduced solved by traditional finite difference, finite element and finite volume methods. Abgrall and Karni (2008) developed relaxation schemes to solve the two-layer shallow water equations. Audusse et al. (2008) extended previous works (Audusse et al. 2006; Audusse and Bristeau 2007) to simulate dam break problems using a finite volume solver.

The objective of this study is to extend the LB formulation to solve the multilayer shallow water equations for three-dimensional shallow water flow problems on irregular boundary geometry and bathymetry. We focus on the application of the multilayer shallow water equations to the problems of wind driven circulation. We implement the LB method on a shared memory HPC system, an IBM p575 in the Center for Computation & Technology, Louisiana State University. In this study, we develop our LB code written in Fortran 90 and parallelized with OpenMP (Chapman and Massaioli 2005) using domain decomposition and cache optimization.

MULTILAYER SHALLOW WATER EQUATION

A multilayer model is based on converting a three-dimensional problem into a number of coupled two-dimensional problems in layers as shown in Figure 1. The governing equations are similar to the traditional shallow water equations with additional terms for the transfer of momentum and mass flux between the layers. This results in the multilayer shallow water equations given as follows:

$$\frac{\partial h^{(\ell)}}{\partial t} + \frac{\partial \left(h^{(\ell)} u_i^{(\ell)} \right)}{\partial x_i} = 0 \tag{1}$$

$$\frac{\partial \left(h^{(\ell)} u_i^{(\ell)} \right)}{\partial t} + \frac{\partial \left(h^{(\ell)} u_i^{(\ell)} u_j^{(\ell)} \right)}{\partial x_j} + \frac{\partial}{\partial x_i} \left(\frac{1}{2} g h^{(\ell)} \sum_{m=1}^{M} h^{(m)} \right) = \nu \left[\frac{\partial^2 \left(h^{(\ell)} u_i^{(\ell)} \right)}{\partial x_j \partial x_j} \right] + F_i^{(\ell)} \tag{2}$$

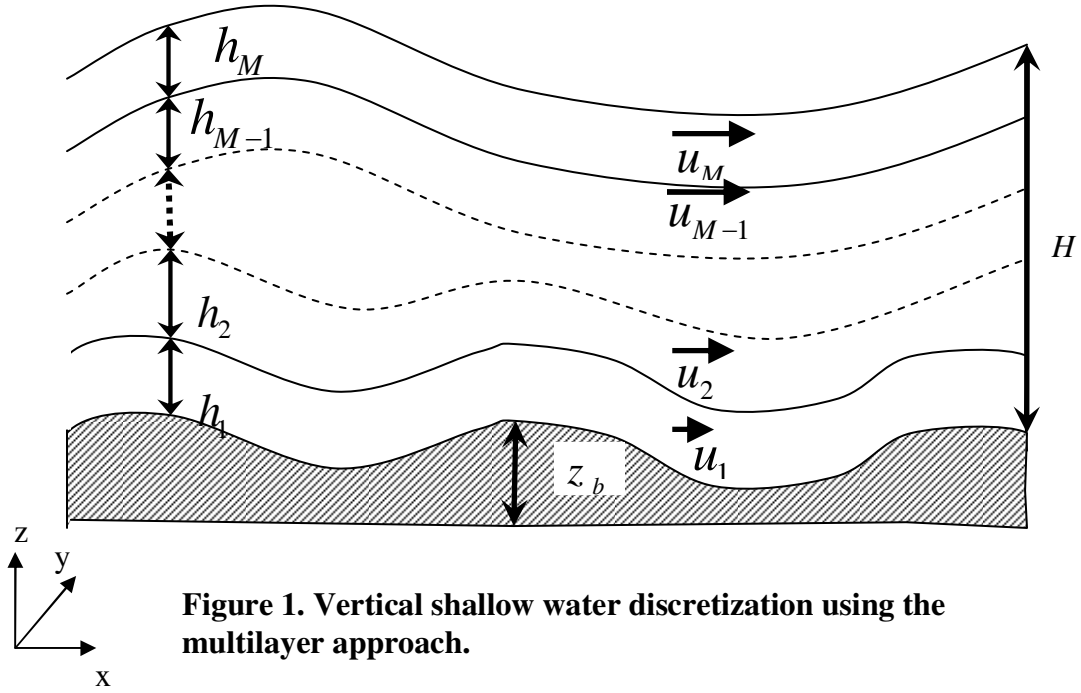

Figure 1. Vertical shallow water discretization using the multilayer approach.

where $h^{(\ell)}$ is the local water height in layer ℓ and $u_i^{(\ell)}$ is the local velocity component in the i direction in layer ℓ, $F_i^{(\ell)}$ is the external force acting on layer ℓ, g is the gravitational acceleration, ν is the dynamic viscosity, x_i is the Cartesian coordinate, and t is time. The external force consists of the wind driven forcing term (only for the top layer), $F_{wi}^{(\ell)}$, the bed slope forcing term, $F_{Pi}^{(\ell)}$, the vertical viscosity term, $F_{\mu i}^{(\ell)}$, and the Coriolis forcing term, $F_{Ci}^{(\ell)}$ as follows

$$F_i^{(\ell)} = F_{wi}^{(\ell)} + F_{Pi}^{(\ell)} + F_{\mu i}^{(\ell)} + F_{Ci}^{(\ell)} \tag{3}$$

$$F_{wi}^{\ell} = \delta_{M\ell} \frac{\rho_a}{\rho_w} C_W u_{Wi} \sqrt{u_{Wi} \cdot u_{Wi}} \tag{4}$$

$$F_{Pi}^{(\ell)} = -g h^{(\ell)} \frac{\partial z_b}{\partial x_i} \tag{5}$$

$$F_{\mu i}^{(\ell)} = -\kappa \delta_{1\ell} u_i^{(\ell)} + 2\mu \left(1 - \delta_{M\ell}\right) \frac{u_i^{(\ell+1)} - u_i^{(\ell)}}{h^{(\ell+1)} - h^{(\ell)}} - 2\mu \left(1 - \delta_{1\ell}\right) \frac{u_i^{(\ell)} - u_i^{(\ell-1)}}{h^{(\ell)} - h^{(\ell-1)}} \tag{6}$$

$$F_{Ci}^{(\ell)} = \begin{cases} f_c h^{(\ell)} u_y, & i = x \\ -f_c h^{(\ell)} u_x, & i = y \end{cases} \tag{7}$$

where $\delta_{1\ell}$ and $\delta_{M\ell}$ are the Kronecker delta function; κ is the bottom friction coefficient, and μ is the interfacial friction coefficient which acts between layers. The water depth is the sum of local water heights of all layers, i.e., $H = \sum_{m=1}^{M} h^{(m)}$.

LATTICE BOLTZMANN METHOD

The LB model is used to solve the shallow water equations for each layer. The LB equation is obtained by integrating the discrete Boltzmann equation:

$$\frac{\partial f_\alpha}{\partial t} + e_{\alpha i}\frac{\partial f_\alpha}{\partial x_i} + F_i\frac{\partial f_\alpha}{\partial e_{\alpha i}} = -\frac{1}{\lambda}\left(f_\alpha - f_\alpha^{eq}\right), \tag{8}$$

for describing dynamics of local particle distribution functions in a discrete velocity field, where f_α is the particle distribution function moving along α direction, f_α^{eq} is the equilibrium distribution function (EDF) along α direction, λ is the relaxation time, $\mathbf{e}_\alpha = \{e_{\alpha i}\}$ is the streaming velocity along α direction, F_i is the external force per unit mass in the shallow water equations, $\left(f_\alpha - f_\alpha^{eq}\right)/\lambda$ is the Bhatnagar-Gross-Krook (BGK) collision operator (Bhatnagar et al. 1954), which represents changes in f_α due to particle collisions. Each direction represents a characteristic direction for the corresponding particle distribution function.

The lattice Boltzmann equation for simulation of Equations (1) - (7) is obtained by integrating Eq. (8) in time along the α direction for each layer as follows:

$$f_\alpha^{(\ell)}\left(\mathbf{x}+\mathbf{e}_\alpha\Delta t, t+\Delta t\right) = f_\alpha^{(\ell)}\left(\mathbf{x},t\right) - \frac{1}{\tau}\left(f_\alpha^{(\ell)}\left(\mathbf{x},t\right) - f_\alpha^{(\ell)eq}\left(\mathbf{x},t\right)\right) + \frac{\Delta t e_{\alpha i}}{6e^2}F_i^{(\ell)}\left(\mathbf{x},t\right) \tag{9}$$

where $\tau = \lambda/\Delta t$ is relaxation time parameter, $e = \Delta x/\Delta t$ the lattice speed, Δx is the lattice size and Δt is the time step.

In each time step, the particle distribution functions arrive to their neighboring nodes at the same time through prescribed lattice connections. Therefore, the streaming velocity $\mathbf{e}_\alpha$ along α direction is determined by the lattice connection and size. In this study, we consider the two dimensional lattice with nine discrete velocities, known as the D2Q9 lattice, shown in Figure 2. The streaming velocity for D2Q9 is

$$\mathbf{e}_\alpha = \begin{cases} (0,0) & \alpha = 0 \\ e\left[\cos\left(\frac{1}{4}(\alpha-1)\pi\right), \sin\left(\frac{1}{4}(\alpha-1)\pi\right)\right], & \alpha = 1,2,3,4 \\ \sqrt{2}e\left[\cos\left(\frac{1}{4}(\alpha-1)\pi\right), \sin\left(\frac{1}{4}(\alpha-1)\pi\right)\right], & \alpha = 5,6,7,8 \end{cases}$$

The water depth and flow velocity for each layer are calculated as the zero and first moments of the distribution functions:

$$h^{(l)} = \sum\nolimits_\alpha f_\alpha^{(l)} \qquad\qquad h^{(l)}u_i^{(l)} = \sum\nolimits_\alpha e_{\alpha i} f_\alpha^{(l)}$$

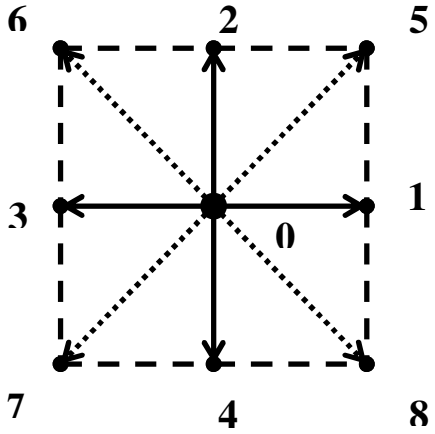

Figure 2. D2Q9 Lattice

The expressions for the EDFs are given by Chen and Doolen (1998):

$$f_\alpha^{(l)eq} = h^{(l)}\omega_\alpha\left(\frac{c_s^2}{e^2}+\frac{\mathbf{u}^{(l)}\cdot\mathbf{e}_\alpha}{e^2}+\frac{3}{2}\frac{\left(\mathbf{u}^{(l)}\cdot\mathbf{e}_\alpha\right)^2}{e^4}-\frac{1}{2}\frac{\mathbf{u}^{(l)}\cdot\mathbf{u}^{(l)}}{e^2}\right) \quad ,\alpha>0$$

$$f_\alpha^{(l)eq} = h^{(l)} - \sum_{\alpha=1}^{8} f_\alpha^{(l)eq}$$

where c_s^2 is known as the squared speed of sound, which in this study is a numerical parameter that relates to the wave celerity. For D2Q9, the weighting coefficients are $\omega_\alpha = 1/3 \quad ,\alpha = 1,2,3,4$ and $\omega_\alpha = 1/12 \quad ,\alpha = 5,6,7,8$.

To ensure that the LB model solves the multilayer shallow water equation with proper LB parameters, the Appendix performs the recovery of the macroscopic differential equation by Chapman-Enskog multi-scale analysis. We obtain $c_S^2 = \frac{1}{2}gH$ and $\nu = \frac{e^2}{3}\Delta t\left(\tau - \frac{1}{2}\right)$.

HIGH PERFORMANCE COMPUTING

OpenMP parallelization is a straightforward extension of serial coding, according to the simple recipe: a) add work distribution directives; b) carefully control variable scoping; c) if needed, choose the most suitable parallel loop scheduling; d) if needed, take care of false sharing of variables among threads. Although this approach works with some very simple codes, most programs parallelized in this way do not scale beyond a small number of processors. (Massaioli and Amati 2002). Often the same codes scale better when parallelized in Message Passing Interface (MPI) on the same symmetric multiprocessing (SMP) system, in spite of the fact that message passing causes memory to memory copies not needed

with shared memory parallelization. A computational advantage of the LBM is that its implementation leads to computational kernels that are very suitable for parallelization in both shared and distributed memory paradigms.

Parallel performance is often evaluated by two factors: parallel speedup, $S = T_1/T_N$, and efficiency, $E = S/N$, where N is the number of threads (processors), T_1 is the computation time for one thread and T_N is the computation time for N threads. Numerical simulations based on domain decomposition with cache optimization using OpenMP were performed. The simulations were run on grids of size $1024\times1024\times5$ for 1000 time steps. Table 1 shows the execution time, speed up and efficiency for explicitly controlled cache optimized implementations. The speed up and efficiency scale up to 16 threads (processors).

Table 1: LBM Performance

Threads	*Execution Time (s)*	*Speed up*	*Efficiency*
1	36.782	1	1
2	17.725	2.00	1.00
4	9.358	3.99	0.98
8	4.876	7.54	0.94
12	3.157	11.65	0.97
16	2.461	14.94	0.93

NUMERICAL RESULTS

We demonstrate the three dimensional multilayer shallow water LBM by simulating wind driven circulation in Lake Pontchartrain, Louisiana; an area of interest to coastal and environmental engineers. Lake Pontchartrain is an estuarine lake in Southeastern Louisiana with a mean depth of $3.8\,m\,(0.5\,m - 5\,m)$ and an area of approximately $1630\,km^2$. The LBM is applied to wind driven circulation to illustrate it its ability to handle irregular bathymetries and boundaries. A constant wind shear stress is applied throughout and a wind speed of $5\,m/s$ in the North West direction is used.

In the LBM formulation, the computational domain is covered by $272\times160\times5$ lattices with $\tau = 0.6$ $\Delta x = 250$ m, $\Delta t = 0.5$ s, and $e = 500\,m/s$. The initial conditions are applied by initializing the distribution functions to an EDF with the initial water depths defined above and velocities equal to zero, i.e. $f_\alpha = f_\alpha^{eq}\left(h = h^{init}, u_x = 0, u_y = 0\right)$. Free slip bounce-back boundary conditions are applied along the borders of the lake. The simulation was run up to time, $t = 20\,hrs$. Figure 3 shows the instantaneous surface velocity field at $t = 20\,hrs$.

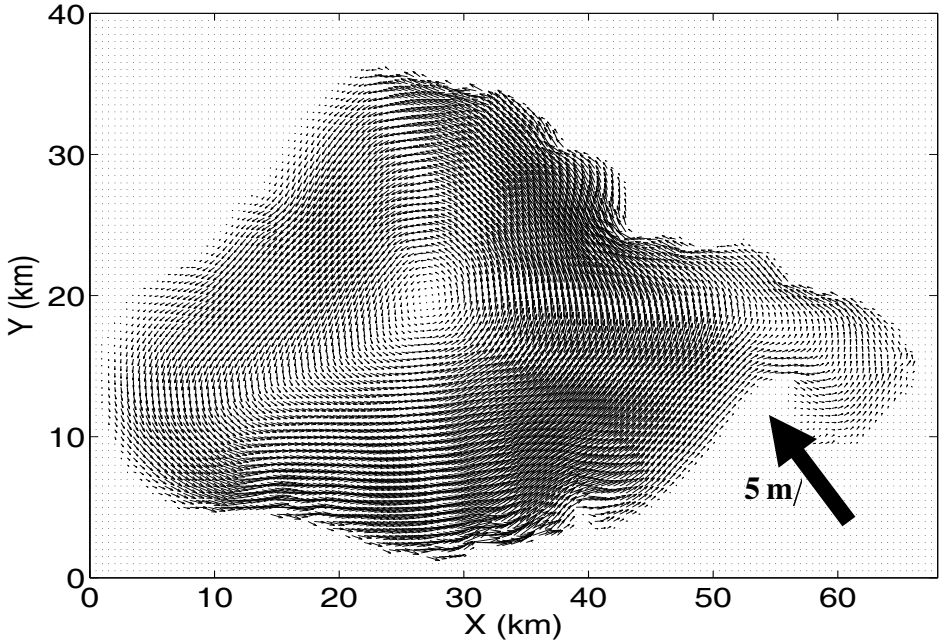

Figure 3. Instantaneous surface velocity field wind driven circulation in Lake Pontchartrain, LA at $t = 20$ hrs

CONCLUSION

The standard LBM for two dimensional shallow water flows is extended to solve the multilayer shallow water equations for three-dimensional shallow water flow problems on irregular boundary geometry and bathymetry. We numerically demonstrate the applicability of the LBM in three dimensional shallow water flows by simulating wind driven circulation in Lake Ponchartrain, LA. The LBM shows promising speedup and efficiency on a shared memory system up to 16 processors using OpenMP.

ACKNOWLEDGEMENTS

This research was supported in part by the National Scientific Foundation under Grant No. 0504507and the Department of the Interior, U.S. Geological Survey under Grant No. 05HQGR0142

REFERENCES

Abgrall, R. and S. Karni (2008). A Relaxation Scheme for the Two-Layer Shallow Water System. Hyperbolic Problems: Theory, Numerics, Applications**:** 135-144.

Audusse, E. (2005). "A multilayer Sainte-Venant model." Discrete and Continuous Dynamical Systems, Series B **5**(2): 189-214.

Audusse, E. and M.-O. Bristeau (2007). "Finite-Volume Solvers for a Multilayer Saint-Venant System." International Journal of Applied Mathematics and Computer Science **17**(3): 311-320.

Audusse, E., M. O. Bristeau and A. Decoene (2006). 3D Free Surface Flows Simulations Using a Multilayer Saint-Venant Model. Comparisons with Navier-Stokes Solutions. Numerical Mathematics and Advanced Applications**:** 181-189.

Audusse, E., M. O. Bristeau and A. Decoene (2008). "Numerical simulations of 3D free surface flows by a multilayer Saint-Venant model." International Journal for Numerical Methods in Fluids **56**(3): 331-350.

Bhatnagar, P. L., E. P. Gross and M. Krook (1954). "A Model for Collision Processes in Gases. I. Small Amplitude Processes in Charged and Neutral One-Component Systems." Physical Review **94**(3): 511.

Chapman, B. M. and F. Massaioli (2005). "OpenMP." Parallel Computing **31**(10-12): 957-959.

Chen, S. and G. D. Doolen (1998). "Lattice Boltzmann method for fluid flows." Annual Review of Fluid Mechanics **30**: 329-364.

Kandhai, D., A. Koponen, A. G. Hoekstra, M. Kataja, J. Timonen and P. M. A. Sloot (1998). "Lattice-Boltzmann hydrodynamics on parallel systems." Computer Physics Communications **111**(1-3): 14-26.

Massaioli, F. and G. Amati (2002). Achieving high performance in a LBM code using OpenMP. Fourth European Workshop on OpenMP, Roma.

Salmon, R. (1999). "The Lattice Boltzmann method as a basis for ocean circulation modeling." Journal of Marine Research **57**: 503-35.

Thömmes, G., M. Seaïd and M. K. Banda (2007). "Lattice Boltzmann methods for shallow water flow applications." International Journal for Numerical Methods in Fluids **55**(7): 673-692.

Zhong, L., S. Feng, D. Lou and S. Gao (2006). "Wind-driven, double-gyre, ocean circulation in a reduced-gravity, 2.5-layer, lattice boltzmann model." Advances in Atmospheric Sciences **23**(4): 561-78.

Zhou, J. G. (2007). "Lattice Boltzmann Simulations of Discontinuous Flows." International Journal of Modern Physics C: Computational Physics & Physical Computation **18**(1): 1-14.

Zhou, J. G., D. M. Causon, C. G. Mingham and D. M. Ingram (2004). "Numerical Prediction of Dam-Break Flows in General Geometries with Complex Bed Topography." Journal of Hydraulic Engineering **130**(4): 332-340.

Two Dimensional Hydraulic Modeling of the Lower Skokomish River

Cassie Klumpp[1]

[1] U.S. Bureau of Reclamation, Sedimentation and River Hydraulic Group, Denver, Colorado, cklumpp@usbr.gov.

ABSTRACT

The Bureau of Reclamation's Sedimentation and River Hydraulics Group SRH-2D model was applied to the lower 10 miles of the Skokomish River, WA. This was in conjunction with a Geomorphic Study of the reach. The river is aggrading and is therefore limited in its ability to convey flood flows. The 2D model was used to identify channel capacity and areas within the reach where overbank flooding occurs. The model was applied to existing conditions in the reach, and may be used in the future for proposed changes to improve channel capacity.

INTRODUCTION

The Skokomish River is located in Washington at the southeastern portion of the Olympic peninsula near the southern extent of the Hood Canal. The river flows east from its headwaters in the Olympic Mountains and descends through narrow gorges to the Skokomish valley. The study area for modeling and geomorphic assessment is contained within the lower 10 miles of the river (see Figure 1).

The objective of the study was to construct a two dimensional (2D) hydraulic model to evaluate the present channel capacity and overbank flooding locations.

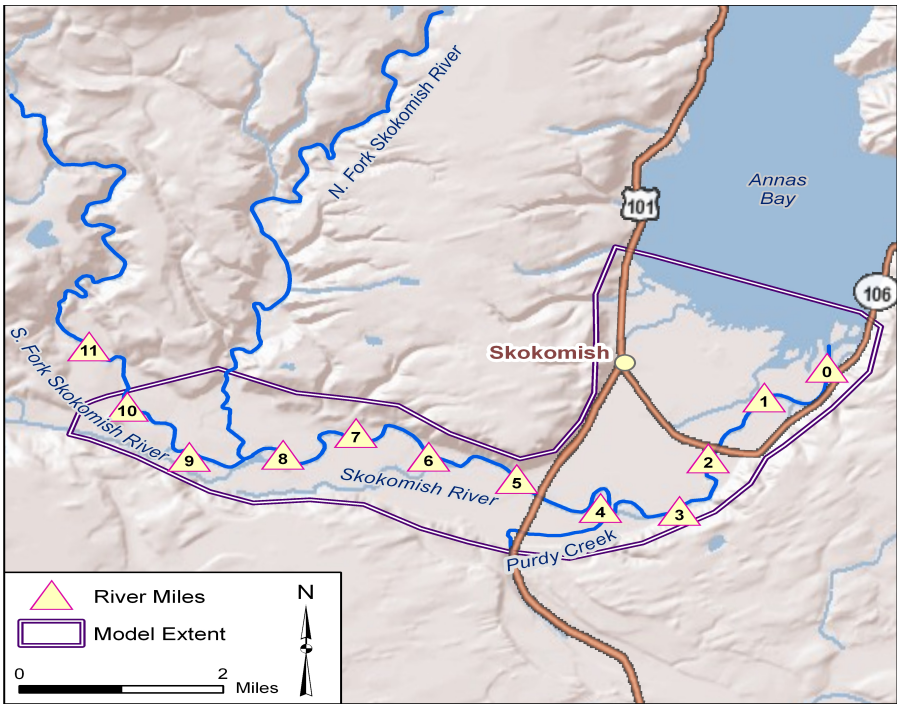

Figure 1-Project Location Map.

MODEL DESCRIPTION

SRH-2D is a 2D hydraulic model for river systems (Lai, 2007). SRH-2D is particularly useful for problems where 2D hydraulic effects are important. Examples include rivers with meander bends, a high level of connectivity with the floodplain, or multiple flow paths with varying elevations and alignments.

SRH-2D has been successfully applied to several Reclamation projects in recent years. The model version utilized in this study assumes static bed topography and, therefore, does not predict vertical incision or aggradation, or lateral migration of the channel through bank erosion. One of the major advantages of the SRH-2D model is the use of the arbitrarily shaped element method used for geometry representation. This unstructured meshing strategy allows for greater flexibility through the development of non-uniform mesh cells that can vary in size and density across the modeled area depending on the detail needed. This approach allows larger areas to be modeled while still preserving an increased density of smaller mesh cells in critical areas where more topographic detail is needed.

HYDROLOGY DATA

The Bureau of Reclamation (England, 2007) conducted a peak flow and flow duration analysis on five gages in the Skokomish basin. The gage utilized for the 2D model was the USGS gage on the Skokomish River at Potlatch (#12059500; Table 1). After 1994, the USGS no longer published peak flows at the Potlatch station for flows where the stage exceeded 15 feet (approximately 4,000 cfs) because the river

flowed out of the main channel. Return flood events were determined at the gage using the Expected Moments Algorithm methodology (England, 2007).

Table 1-Discharges for return period floods based on the USGS reference gage 12059500, Skokomish River near Potlatch, Wa for period of record 1844-2006. Gage has a drainage area 117 square miles, and is located just upstream of the U.S. Highway 101 Bridge.

Annual Exceedance Probability (%)	Return Period (years)	LP-Model Estimate (cfs)	Peak Discharge (cfs) 5 % Confidence Limit	95% Confidence Limit
75	1.33	13,500	11,900	15,000
66.7	1.5	14,900	13,300	16,500
50	2	17,500	15,800	19,300
20	5	23,400	21,300	25,900

MODEL GRID AND TOPOGRAPHY

A Surface Water Modeling System (SMS versions 9.2 and 10.0, Environmental Modeling Systems, 2008) pre-processor was used to generate the mesh. Polygon and triangular elements were used to delineate the unstructured mesh. Polygon boundaries, inside of which the mesh was generated, were initially based on roughness variations. These boundaries were then further sub-divided to allow for proper representation of flow lines, such as in meander bends. The final iteration in creating a surface representation was to increase the mesh cell density in areas where an improved representation of topographic breaks was needed.

The unstructured mesh contains 134,361 rectangular and triangular elements and 116,450 nodes. The mesh generated for the 2D model is shown in Figure 2.

Three different sources were used to obtain elevation values for the mesh:

- 1994 Photogrammetry
  Source: Bell Walker & Associates
  Description: A photogrammetry model was built with a stereoscopic drafting station using GPS registered aerial photography.
- 2002 bare earth Light Detection and Ranging (LiDAR) data
  Source: Puget Sound LiDAR Consortium
  Description: Bare earth LiDAR containing the X,Y,Z values of all the LiDAR returns classified as ground.
- 2007 In-channel ground survey data
  Source: USACE, October 2007

Description: Top of bank-to-top of bank cross section survey from RM 10 to 2.

A Triangular Irregular Network (TIN) was created from either a combination of the photogrammetry data and in channel survey data, or LiDAR data and channel survey data. The survey data was limited to cross-section lines. Additional points were interpolated between cross-sections and used to improve the quality of the TINs. The limitations of the topographic data sets were as follows:

- No survey data was available for the mainstem Skokomish channel just above RM 2.
- Hydraulic controls (riffles) that influence water surface elevation may have been missed if they were not captured by the cross section surveys.
- LiDAR data did not have vegetation removed in the bare earth model in densely vegetated areas.
- Photogrammetry appeared to have less topographic detail than LiDAR in overbank areas.
- Channel survey data for the North Fork, Vance Creek, and Purdy Creek were limited or not available.

A text file was imported into ArcGIS (Esri, 2008) as a point layer. Elevation data were added to the point features by interpolating elevation data from the TIN surface. The elevation data was then inserted back into SMS for input to the 2D hydrodynamic model. A typical example of the mesh topography is shown in Figure 3.

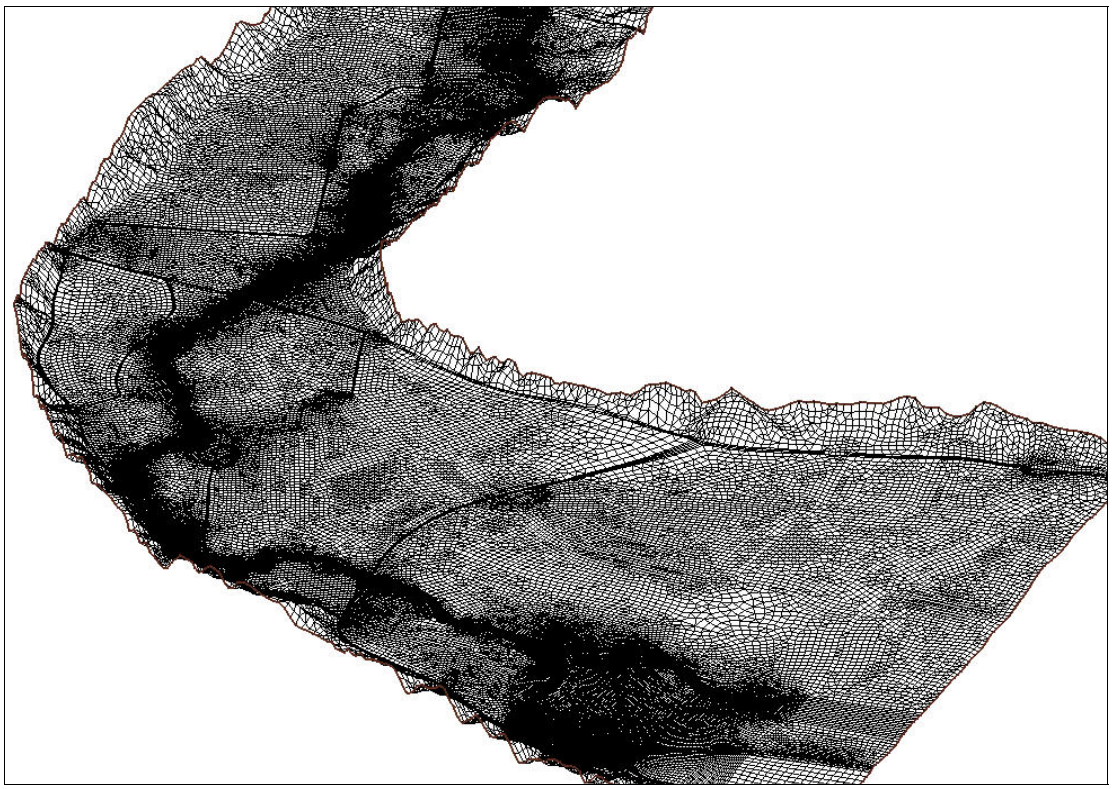

Figure 2-Grid for the lower portion of the model.

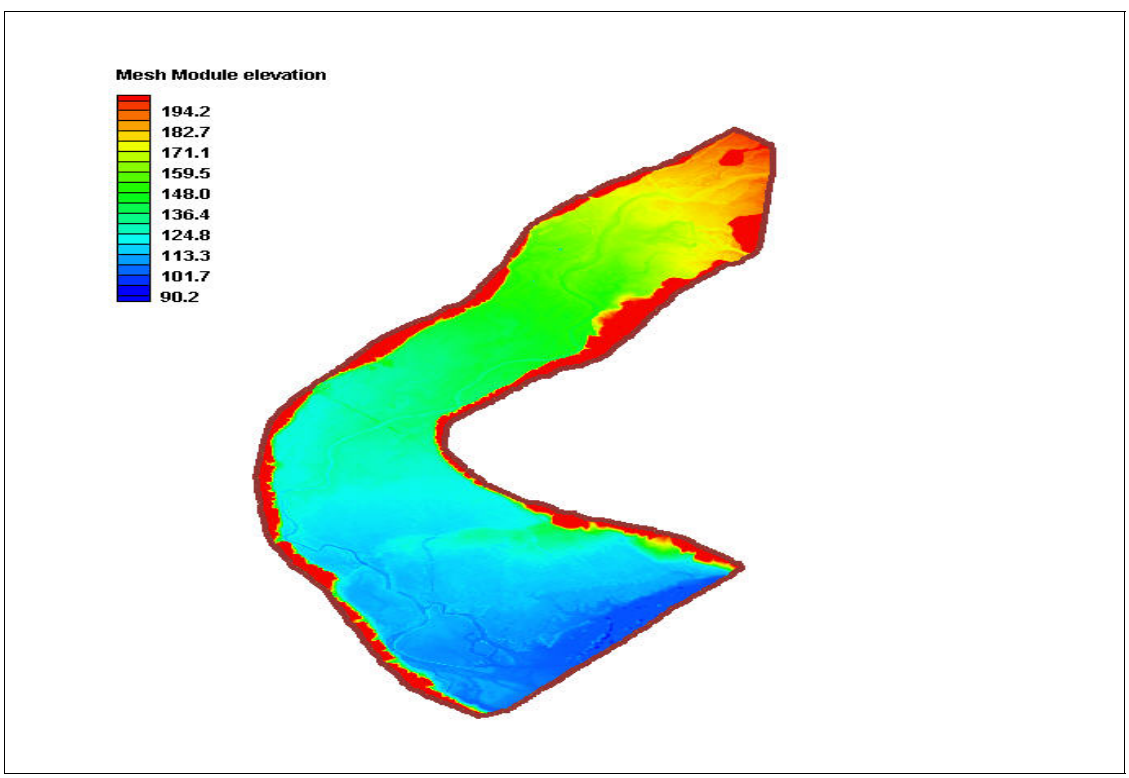

Figure 3-Typical mesh topography.

MODEL VERIFICATION

Comparisons between model results and measured data were made with LiDAR and photogrammetry data sets. The 2D model was calibrated to measured data for both low flow and high flow conditions. Measured low flow water surface elevation data were collected in late July and early August, 2007 (U.S. Army Corps of Engineers, 2007). Flow data during the same time period were based on the USGS gage, Skokomish River near Potlatch. High flow calibrations were based on measured flood data collected by the U.S. Army Corps of Engineers during the December, 2007 event. Manning's n roughness values were varied to validate model predictions. A comparison of measured and predicted data for the December flood are shown in Table 2.

Table 2. Comparison of measured high water surface elevations and model water surface elevations for the December Flood.

Point #	Mile Skok. Valley Rd.	HWM Elevation (feet)	Model WS Elevations (36,000 cfs) (feet)	Model WS Elevations (17,500 cfs) (feet)
20	4.98	80.97	82.0	80.2
14A	3.8	60.54	58.3	57.7
14B	3.8	60.54	59.7	58.6
13A	3.46	54.76	55.8	55.0
13B	3.46	54.76	55.8	54.0
10A	2.95	53.32	53.7	52.9
10B	2.95	53.32	53.7	52.9
8	2.5	47.9	47.0	46.7
4	1.75	41.49	40.7	36.6
3	1.45	36.07	38.0	35.4

MODEL RESULTS

Model simulations began with a dry channel bed. Simulations were continued until the model had reached a near steady state condition. The model was determined to have reached a steady state condition by comparing two model runs (point files as ascii data sets) at different simulation time periods in ARCGIS 9.2 (ESRI, 2008); the two data sets were joined together as shapefiles and velocities and or water depths were compared. The mean sum of the difference in water depths was less than 0.01 feet indicating an equilibrium condition had been reached. This was typically using a 3 second time step and running the model for 400,000 time steps.

One of the primary goals of the modeling was to determine current channel capacity and locations where a flow spills out of the channel. The current channel capacity based on the 2D model LiDAR topography appears to be around 2,000 cfs. The channel capacity for the photogrammetry topography appears to be slightly less than 2,000 cfs (Figure 4). Model results show the majority of the main channel flow losses occur between RM 8 and 5. A significant narrowing of the river occurs at RM 8 and flows have exited the channel here historically. Additional channel losses occur between RM 6 and 5 (at the U. S. Highway 101 Bridge).

High flow results (Figure 5) show significant flow loss from the main channel, especially for the 100-year flood of 36,000 cfs. For the 100 year flood, flows decrease significantly as you go downstream between RM 10 and 8. The channel narrowing at RM 8 affects all of the higher flows. Flows appear to increase between RM 5 and 2 as tributaries bring flows back into the main channel, especially for flows between 12,000 and 36,000 cfs.

The spatial distribution of flow (inundation) is shown in Figures 6-8 for a 6,000 cfs flow event. The majority of this flow remains in the channel until RM 8, when approximately 1,600 cfs leaves the channel on river left leaving approximately 4,500 cfs in the main channel; pinch points and channel narrowing affects flows at RM 8. Most of the flow returns to the channel at RM 7. Flow leaves the channel again before RM 6 and stays outside of the main channel until roughly RM 2. More flow is seen on river right between RM 5 and 6. Channel narrowing and levees are likely affecting the flows just above RM 6.

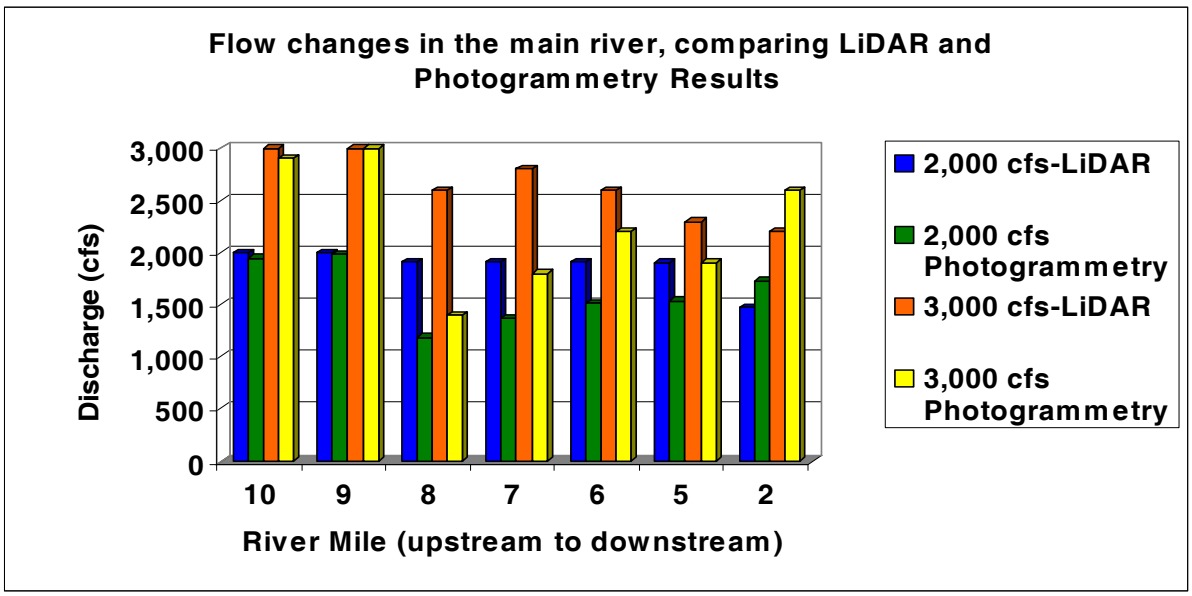

Figure 4-Comparison of in-channel flows for LiDAR and photogrammetry topography.

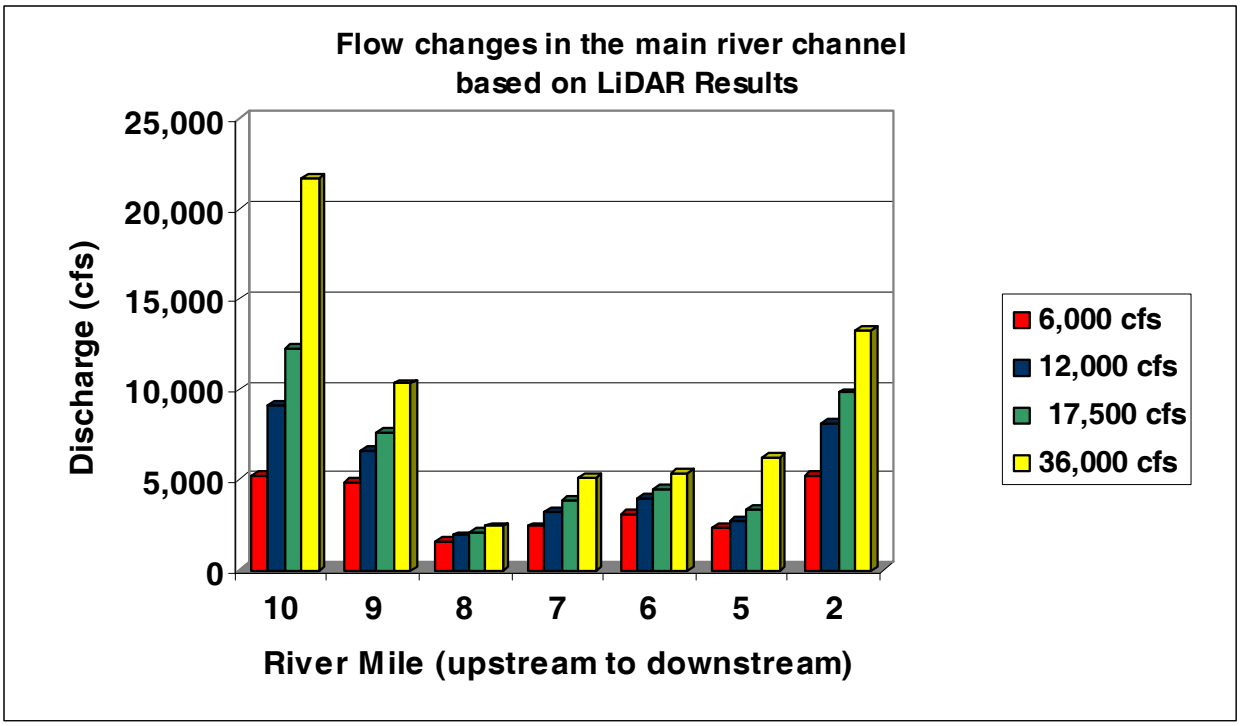

Figure 5- Comparison of in channel discharges for flows ranging between 6,000 and 36,000 cfs.

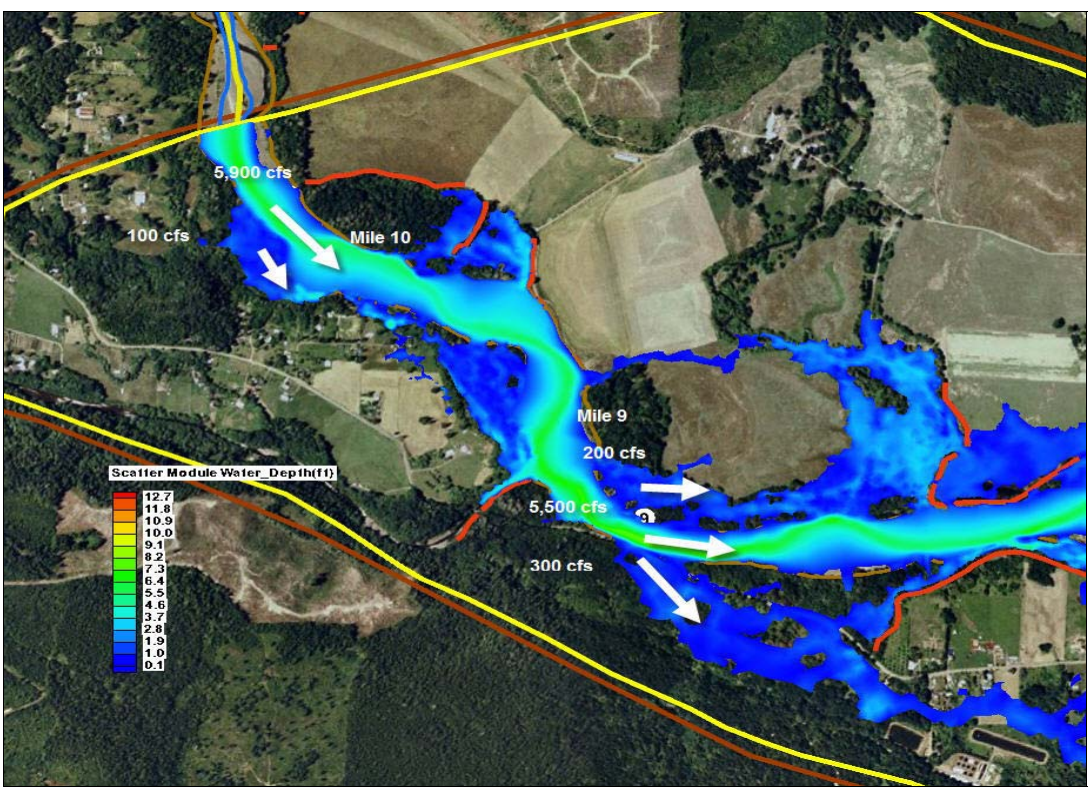

Figure 6- Spatial Distribution of flow for 6,000 cfs near RM 9 and 10.

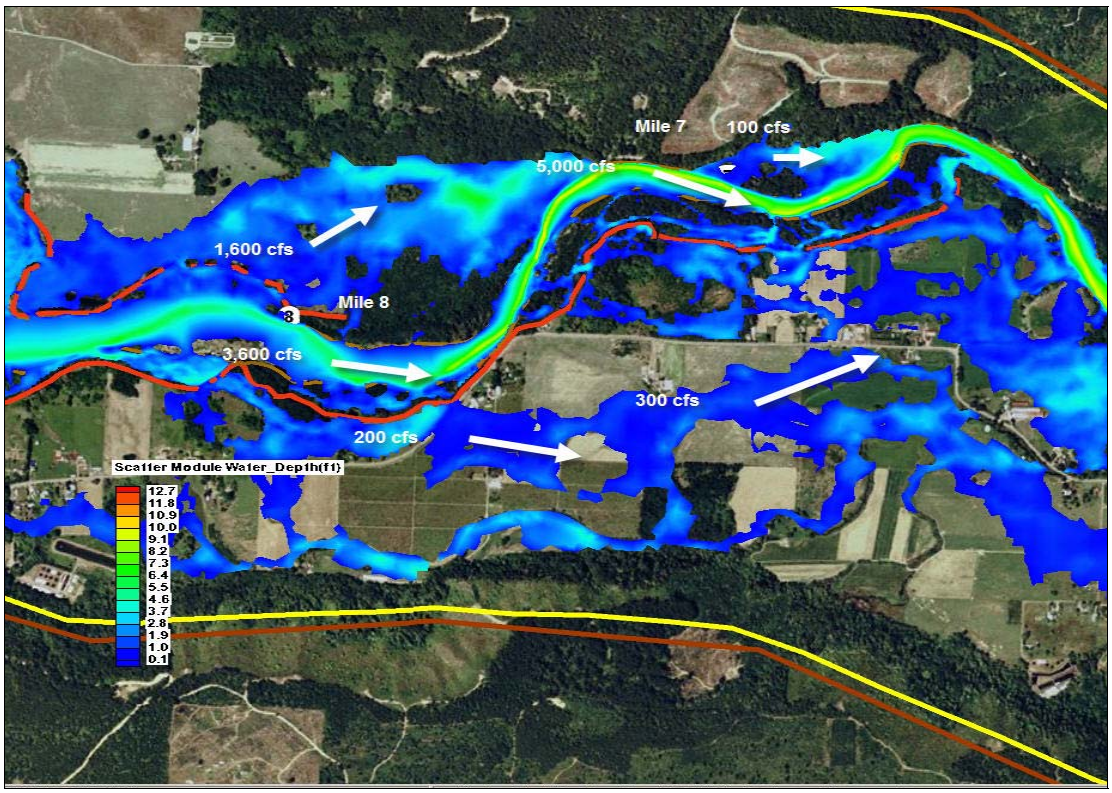

Figure 7-Spatial distribution of flow for 6,000 cfs near RM 7 and 8.

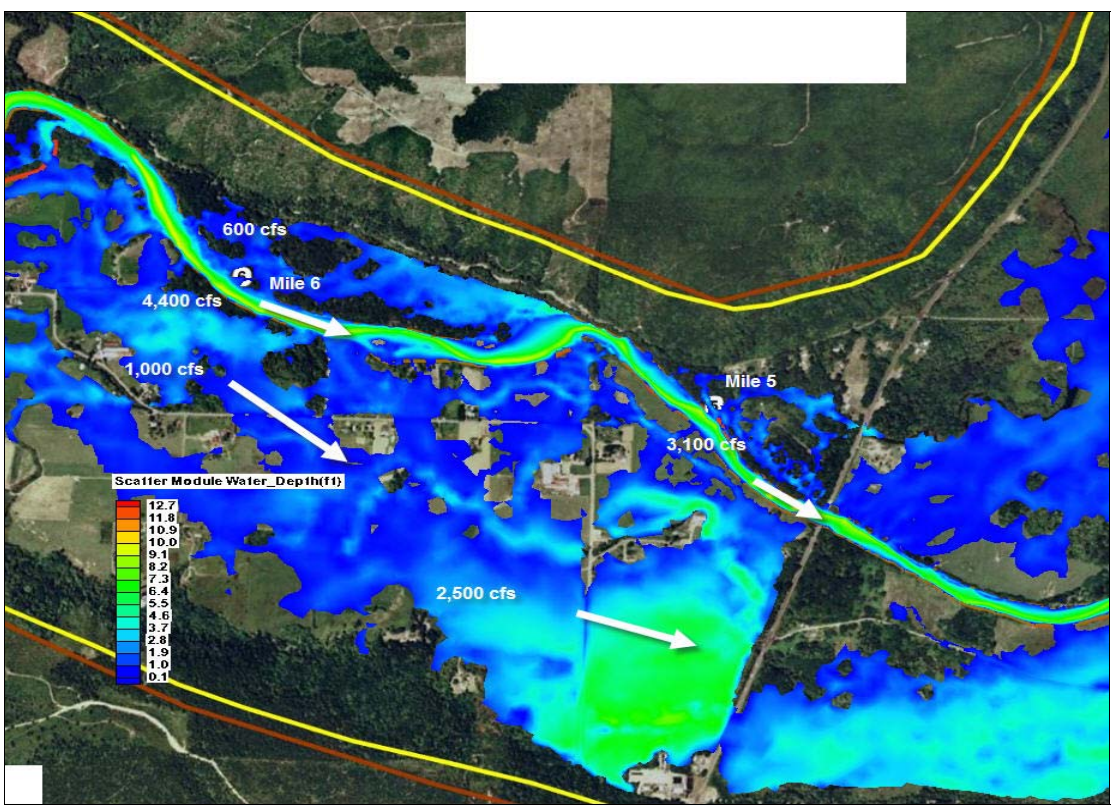

Figure 8- Spatial distribution of flow for 6,000 cfs near RM 5 and 6.

CONCLUSIONS

A two dimensional (2D) hydraulic model was applied to the lower Skokomish River reach in Mason County, WA. The purpose of the model application was to help identify the current channel capacity as well as to locate areas where flow spills out of the main channel. Significant flow exits the channel for discharges greater that 2,000 cfs. Model limitations include the lower reach from RM 2 to 0. Neither the LiDAR nor photogrammetry topography has the correct below water channel elevations. With refinement and collection of additional survey and tidal data, the base model grid can be modified to accommodate more current topography and flows.

The 2D model could be used as a tool to model future conditions including levee setbacks and flow changes for North Fork. The model can simulate a wide range of flows from a low flow of 370 cfs up to the 100-year flood (36,000 cfs). The model was validated in areas where measured data was available for both low and high flows.

REFERENCES

Bell Walker and Associates, 1994, Photogrammetry model from GPS registered aerial photography.

Bountry, Jennifer, Godaire, Jeanne, Klinger, Ralph, Varyu, David and Piety, Lucy, 2007, Skokomish River Geomorphic Study, Mason County, Washington, U.S. Bureau of Reclamation, Denver, Colorado.

Corps of Engineers, 2007, In channel survey data, top of bank to top of bank survey. U.S. Department of the Army, Seattle District.

Environmental Modeling Systems, 2008, SMS Computer Program and Manual, Environmental Modeling Systems, Inc, Utah.

England, John, 2007, Flood Frequency, Flow Duration and Trends, Skokomish Geomorphic Study, Skokomish River, Washington, U.S. Bureau of Reclamation, Denver, Colorado.

ESRI, 2008, ARCGIS 9.2 software, http:/www.esri.com.

Lai, Y.G, 2007, SRH-2D,User's Manual Version 1.1. Bureau of Reclamation, Technical Service Center, Sedimentation and River Hydraulics Group, Denver, CO 80225.

USING COMPUTATIONAL MODEL – ADH TO EVALUATE RELATIONSHIP OF WATER SURFACE ELEVATION TO WING DIKES

Renjie Xia[1]

[1] Ph.D., P.E., Hydraulic Engineer, U.S. Army Corps of Engineers, Rock Island District, Clock Tower Building, P.O. Box 2004, Rock Island, IL 61204, (309) 794-5272, renjie.xia@usace.army.mil

ABSTRACT

The use of hydraulic structures, such as wing dikes, to control flow, increase the channel capacity to carry sediment, and reduce periodic dredging requirements is an important management tool utilized on the Upper Mississippi River. Wing dikes concentrate flow in the navigation channel, control flow into secondary channels, and influence the location of channel erosion and sedimentation. This study modeled the lower portion of Pool 22 of the Mississippi River from river mile 301.2 to 304.2 using the ADaptive Hydraulics (ADH) Modeling System. Alternatives, including no dikes and dikes in the main channel, were compared to evaluate the relationship of water surface elevation to wing dikes for a range of flow conditions. This study showed that (1) construction of new wing dikes initially alters the water surface elevation, but the change is small; (2) for flow discharges less than 160,000 cfs, with decreasing the river flow, the change of water surface elevation due to wing dikes decreases; and (3) for flow discharges greater than 160,000 cfs, with increasing the river flow, the change of water surface elevation due to wing dikes decreases.

ADH MODELING SYSTEM

The ADaptive Hydraulics (ADH) Modeling System, developed and supported by the Coastal and Hydraulics Lab of the Engineer Research and Development Center (ERDC) of the US Army Corps of Engineers (USACE), is a modeling package that can handle both saturated and unsaturated groundwater, overland flow, three dimensional Navier-Stokes flow, and two or three dimensional shallow water problems (ERDC 2006).

ADH is designed to work in conjunction with the Groundwater Modeling System (GMS) and the Surface Water Modeling System (SMS). The major benefits of ADH are: its use of adaptive numerical meshes employed to improve model accuracy without sacrificing efficiency; its use for supercritical flow; its rapid convergence of flows to steady state solutions; and its other features such as wetting and drying, coupled sediment transport, and wind effects (ERDC 2006).

Three files (the mesh file, boundary condition file, and hot star file) are needed to run a model in ADH. The mesh file should be constructed first and can be generated directly and quickly using the two or three dimensional GMS or the two dimensional SMS. ADH uses only triangular elements while GMS and SMS support triangular and quadrilateral elements. The mesh file created from GMS is designated with a .3dm extension while the mesh file created from SMS is designated with a .2dm extension then the user must simply change it to .3dm (ERDC 2006).

Once a mesh file has been constructed, the boundary conditions for the problem and operating parameters for ADH must be specified in the boundary condition file. This file contains a series of control cards, which fall into eight categories: operational parameters controlling the operation, iteration parameters controlling the iterative methods, material properties defining the flow and transport constants for each material, boundary strings defining the interior and surface boundaries of the problem, solution controls specifying the initial/boundary conditions, time controls specifying the time steps, output controls defining the times at which the output is printed, and series defining various parameters (ERDC 2006).

The hot start file is generated to establish the initial conditions of the problem. Initial conditions consist of depths and velocities at all nodes. Field data are often available and used to provide a starting point for many problems. A hot start file is a required part of a model; however, it may be a zero-length file (empty). For simple problems a cold start simulation (initial conditions of `0.0`) may be sufficient. Cold start problems in ADH are handled by leaving the hot-start file blank. If data types are not specified default values will be supplied (ERDC 2006).

ADH simulation provides the velocity and overland head distributions in the flow field. ADH allows the user to calculate the transport of noncohesive or cohesive sediments. The sediment is transported as suspended load and bed load, and ADH provides the bed changes and suspended sediment concentration distribution.

BACKGROUND OF POOL 22

Lock and Dam 22 is a unit of the Inland Waterway Navigation System of the Upper Mississippi River. Pool 22 extends from River Mile (RM) 301.2 at Saverton, Missouri to RM 324.9 at Lock and Dam 21 at Quincy, Illinois.

The main lock is 110 feet wide and 600 feet long with a maximum lift of 10.5 feet. The dam has a total length of 3,084 feet, including a gross length of gated sections (1,024 feet), a non-overflow earth dike section (460 feet) and an overflow earth dam section (1,600 feet). The dam is operated to maintain a minimum pool elevation of 459.5 feet in order to provide a nine-foot navigation channel (USACE 1996).

The average slope of the channel thalweg for the 23.7 river miles in Pool 22 is 0.17 foot per mile. Channel velocities vary from about 2.9 feet per second at normal conditions to about 5.9 feet per second at high flows (USACE 1996).

Dam 22 is operated to allow high water to recede naturally with the dam gates all open until an elevation of 459.5 feet is reached on the lock 22 pool gage; then, with decreasing flows, the dam is operated to maintain the elevation of 459.5 feet on the pool gage for all lower flows.

CASES INVESTIGATED

ADH was used to model the lower portion of Pool 22 from RM 301.2 to RM 304.2. This application demonstrates how ADH handles the two dimensional shallow water problems. The ADH finite element mesh was created based on bathymetric survey data (a set of coordinate

points with elevation Z values) provided by the Operations Division, US Army Corps of Engineers, Rock Island District.

The eddy viscosity was set for a value of 30 (ft^2/s) throughout different flow domains. The Manning's n ranged from 0.025 to 0.027 for the main channel and from 0.032 to 0.04 for aquatic, off-channel areas. The Manning's n for the area immediately downstream of the submersible tainter gates was assigned as 0.055 due to the presence of the stilling basin and large stone on the river bed used to control erosion.

Five flow conditions were investigated in this study (Table 1). The flow discharges of 60,000, 110,000, 162,000, 302,000, and 466,850 cfs represent the very low, low, normal, high, and very high flow (the peak of the great flood of 2008), respectively. For flow discharges less than 160,000 cfs, dam gates are closed to maintain a flat pool of 459.5 feet.

Table 1. Discharges and Water Surface Elevations at Upstream and Downstream Boundaries

	Upstream Boundary at RM 304.2	Downstream Boundary at Dam 22
Case 1	60,000 cfs	459.5 ft
Case 2	110,000 cfs	459.5 ft
Case 3	162,000 cfs	459.7 ft
Case 4	302,000 cfs	468.4 ft
Case 5	466,850 cfs	475.7 ft

The objective of this study is to evaluate the relationship of water surface elevation to wing dikes under various flow and wing dike conditions using ADH.

There are six existing wing dikes within the three-mile long river reach. Due to degradation over time, the elevations of the existing dikes are much lower than the original design elevations (Fig 1). In general, the top elevation of a dike is designed as 456.5 feet or three feet below the flat pool of 459.5 feet. Two conditions were used to test the relationship between the wing dike crest elevations and upstream river levels:

(1) The existing condition - the six wing dikes have elevations lower than 456.5 feet, and
(2) The rehabilitated wing dike condition - the six wing dikes have elevations restored to 456.5 feet (Fig 2).

For each condition, ADH simulation provides flow velocity and water surface elevation at each node, including these nodes (31 points) along the upstream boundary, which is three miles away from the Lock and Dam 22. Then, the cross-sectional average flow velocity and water surface elevation on the upstream boundary are calculated and compared.

PRIMARY RESULTS

The results were summarized in Table 2(a) to 2(e) and Table 3. It should be indicated that the results are primary, and just concluded from Pool 22 of the Upper Mississippi River. Table 2(a) to 2(e) show the changes of flow velocity and water surface elevation at each node along the

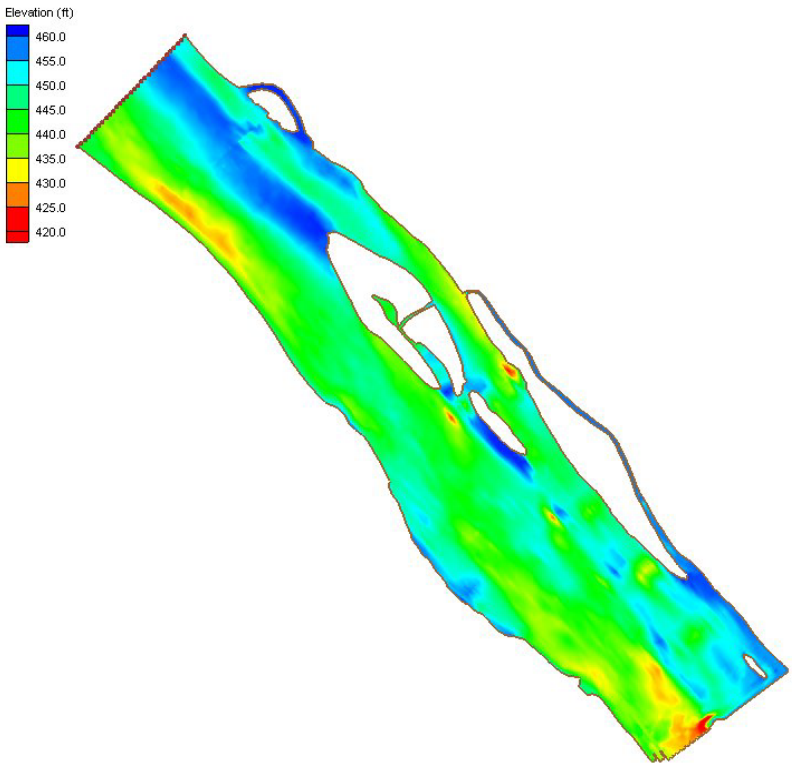

Fig 1 Existing Condition

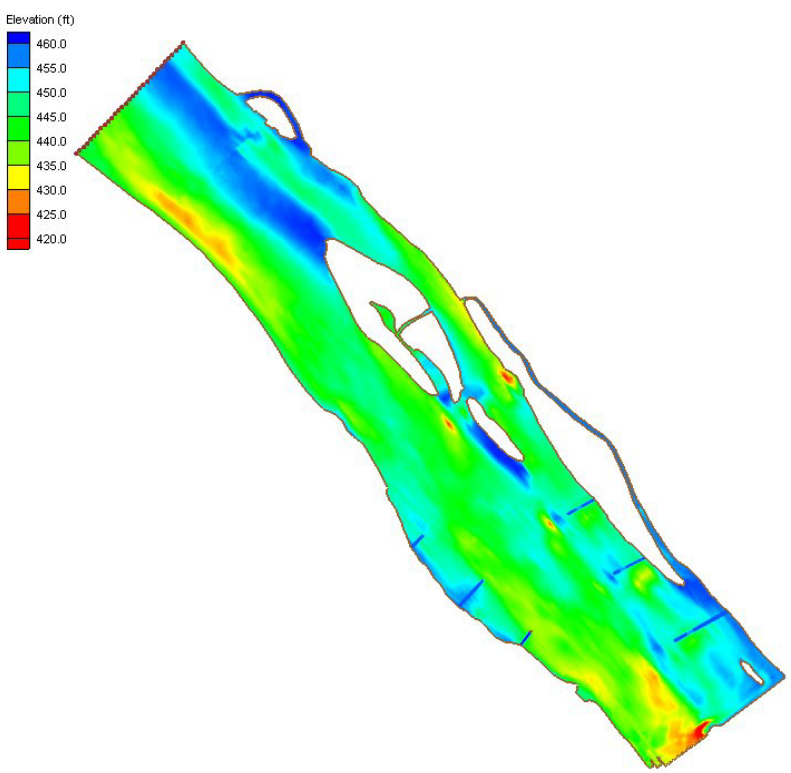

Fig 2 Rehabilitated Wing Dike Condition

Table 2 (a). Changes of Flow Velocity and Water Surface Elevation at Nodes for Existing and Wing Dike Conditions

Node number on upstream boundary	Case 1 - 60,000 cfs & 459.5 ft				
	Existing condition		Wing dike condition		
	Flow velocity (ft/s)	Water surface elevation (ft)	Flow velocity (ft/s)	Water surface elevation (ft)	Change of water surface elevation (ft)
1	1.61	459.80	1.60	459.83	0.03
2	1.46	459.80	1.46	459.82	0.02
3	1.47	459.79	1.47	459.82	0.03
4	1.38	459.78	1.37	459.80	0.02
5	1.53	459.79	1.53	459.81	0.02
6	1.61	459.78	1.61	459.80	0.02
7	1.71	459.78	1.71	459.80	0.02
8	1.79	459.80	1.79	459.82	0.02
9	1.73	459.78	1.73	459.81	0.03
10	1.73	459.79	1.73	459.82	0.03
11	1.73	459.79	1.73	459.81	0.02
12	1.69	459.80	1.68	459.82	0.02
13	1.59	459.80	1.60	459.82	0.02
14	1.48	459.79	1.48	459.81	0.02
15	1.44	459.80	1.44	459.82	0.02
16	1.33	459.79	1.33	459.82	0.03
17	1.17	459.79	1.16	459.82	0.03
18	1.07	459.79	1.07	459.82	0.03
19	0.98	459.79	0.98	459.81	0.02
20	0.87	459.79	0.87	459.81	0.02
21	0.76	459.79	0.76	459.81	0.02
22	0.65	459.79	0.64	459.81	0.02
23	0.55	459.79	0.55	459.81	0.02
24	0.56	459.79	0.56	459.81	0.02
25	0.47	459.78	0.47	459.81	0.03
26	0.60	459.78	0.60	459.80	0.02
27	0.93	459.78	0.93	459.81	0.03
28	0.93	459.78	0.93	459.80	0.02
29	0.88	459.78	0.88	459.80	0.02
30	1.03	459.79	1.03	459.81	0.02
31	1.15	459.80	1.14	459.82	0.02
Average	1.22	459.79	1.22	459.81	0.02

Table 2(b)

Node number on upstream boundary	Case 2 - 110,000 cfs & 459.5 ft				
	Existing condition		Wing dike condition		
	Flow velocity (ft/s)	Water surface elevation (ft)	Flow velocity (ft/s)	Water surface elevation (ft)	Change of water surface elevation (ft)
1	2.55	460.48	2.55	460.54	0.06
2	2.68	460.45	2.66	460.52	0.07
3	2.56	460.43	2.55	460.49	0.06
4	2.45	460.39	2.44	460.46	0.07
5	2.69	460.42	2.67	460.48	0.06
6	2.85	460.39	2.83	460.45	0.06
7	2.97	460.41	2.96	460.47	0.06
8	3.14	460.43	3.12	460.49	0.06
9	3.04	460.41	3.02	460.47	0.06
10	3.06	460.43	3.05	460.49	0.06
11	3.06	460.43	3.04	460.49	0.06
12	2.97	460.44	2.96	460.50	0.06
13	2.81	460.44	2.80	460.50	0.06
14	2.61	460.43	2.59	460.49	0.06
15	2.54	460.44	2.53	460.50	0.06
16	2.35	460.43	2.34	460.50	0.07
17	2.08	460.43	2.08	460.50	0.07
18	1.92	460.43	1.91	460.49	0.06
19	1.77	460.43	1.76	460.49	0.06
20	1.56	460.43	1.56	460.49	0.06
21	1.40	460.42	1.40	460.48	0.06
22	1.19	460.41	1.19	460.47	0.06
23	1.05	460.41	1.04	460.47	0.06
24	1.05	460.42	1.06	460.48	0.06
25	0.91	460.40	0.91	460.47	0.07
26	1.12	460.39	1.12	460.45	0.06
27	1.67	460.41	1.66	460.47	0.06
28	1.64	460.39	1.64	460.46	0.07
29	1.62	460.38	1.62	460.44	0.06
30	1.73	460.42	1.72	460.48	0.06
31	2.10	460.47	2.09	460.53	0.06
Average	2.16	460.42	2.16	460.48	0.06

Table 2(c)

Node number on upstream boundary	Case 3 - 162,000 cfs & 459.7 ft				
	Existing condition		Wing dike condition		
	Flow velocity (ft/s)	Water surface elevation (ft)	Flow velocity (ft/s)	Water surface elevation (ft)	Change of water surface elevation (ft)
1	3.59	461.62	3.56	461.73	0.11
2	3.65	461.58	3.62	461.69	0.11
3	3.49	461.54	3.46	461.66	0.12
4	3.43	461.47	3.41	461.59	0.12
5	3.66	461.51	3.64	461.63	0.12
6	3.87	461.47	3.84	461.59	0.12
7	4.08	461.47	4.05	461.59	0.12
8	4.28	461.53	4.25	461.64	0.11
9	4.17	461.49	4.14	461.61	0.12
10	4.18	461.52	4.14	461.64	0.12
11	4.14	461.53	4.11	461.65	0.12
12	4.04	461.55	4.00	461.67	0.12
13	3.91	461.54	3.89	461.65	0.11
14	3.57	461.54	3.55	461.66	0.12
15	3.52	461.55	3.50	461.67	0.12
16	3.26	461.54	3.24	461.66	0.12
17	2.92	461.53	2.91	461.64	0.11
18	2.71	461.53	2.70	461.64	0.11
19	2.51	461.52	2.50	461.64	0.12
20	2.27	461.52	2.26	461.64	0.12
21	2.03	461.52	2.03	461.63	0.11
22	1.78	461.50	1.77	461.61	0.11
23	1.61	461.49	1.61	461.60	0.11
24	1.61	461.50	1.62	461.62	0.12
25	1.41	461.48	1.41	461.60	0.12
26	1.72	461.45	1.72	461.57	0.12
27	2.33	461.49	2.32	461.61	0.12
28	2.37	461.47	2.37	461.58	0.11
29	2.28	461.45	2.27	461.57	0.12
30	2.56	461.48	2.54	461.60	0.12
31	3.05	461.62	3.03	461.74	0.12
Average	3.03	461.52	3.01	461.63	0.11

Table 2(d)

Node number on upstream boundary	Case 4 - 302,000 cfs & 468.4 ft				
	Existing condition		Wing dike condition		
	Flow velocity (ft/s)	Water surface elevation (ft)	Flow velocity (ft/s)	Water surface elevation (ft)	Change of water surface elevation (ft)
1	4.31	471.00	4.30	471.03	0.03
2	4.28	470.93	4.28	470.97	0.04
3	4.18	470.88	4.18	470.91	0.03
4	4.03	470.83	4.03	470.87	0.04
5	4.38	470.83	4.37	470.86	0.03
6	4.47	470.81	4.46	470.85	0.04
7	4.64	470.81	4.63	470.84	0.03
8	4.84	470.84	4.83	470.87	0.03
9	4.67	470.83	4.66	470.87	0.04
10	4.74	470.85	4.73	470.88	0.03
11	4.70	470.85	4.69	470.89	0.04
12	4.63	470.86	4.63	470.89	0.03
13	4.47	470.87	4.46	470.90	0.03
14	4.24	470.85	4.23	470.89	0.04
15	4.19	470.86	4.19	470.89	0.03
16	3.94	470.86	3.93	470.90	0.04
17	3.73	470.84	3.72	470.87	0.03
18	3.54	470.84	3.54	470.87	0.03
19	3.38	470.84	3.38	470.87	0.03
20	3.22	470.83	3.21	470.87	0.04
21	3.06	470.82	3.06	470.86	0.04
22	2.86	470.81	2.86	470.85	0.04
23	2.74	470.81	2.74	470.84	0.03
24	2.75	470.82	2.75	470.85	0.03
25	2.62	470.80	2.62	470.84	0.04
26	2.78	470.78	2.78	470.81	0.03
27	3.25	470.82	3.25	470.86	0.04
28	3.30	470.79	3.30	470.83	0.04
29	3.22	470.79	3.21	470.83	0.04
30	3.38	470.85	3.36	470.89	0.04
31	3.99	471.02	4.00	471.06	0.04
Average	3.82	470.84	3.82	470.88	0.04

Table 2(e)

Node number on upstream boundary	Case 5 - 466,850 cfs & 475.7 ft				
	Existing condition		Wing dike condition		
	Flow velocity (ft/s)	Water surface elevation (ft)	Flow velocity (ft/s)	Water surface elevation (ft)	Change of water surface elevation (ft)
1	5.02	479.44	5.02	479.46	0.02
2	4.94	479.34	4.93	479.36	0.02
3	4.85	479.27	4.82	479.31	0.04
4	4.71	479.22	4.74	479.23	0.01
5	4.99	479.22	4.99	479.24	0.02
6	5.13	479.18	5.09	479.21	0.03
7	5.23	479.20	5.24	479.21	0.01
8	5.40	479.24	5.40	479.26	0.02
9	5.30	479.20	5.30	479.22	0.02
10	5.31	479.23	5.30	479.25	0.02
11	5.29	479.23	5.28	479.25	0.02
12	5.23	479.23	5.23	479.25	0.02
13	5.05	479.25	5.05	479.27	0.02
14	4.93	479.21	4.92	479.23	0.02
15	4.84	479.23	4.83	479.25	0.02
16	4.60	479.24	4.59	479.26	0.02
17	4.44	479.20	4.44	479.21	0.01
18	4.26	479.21	4.26	479.23	0.02
19	4.10	479.21	4.10	479.23	0.02
20	3.99	479.19	3.99	479.21	0.02
21	3.81	479.20	3.81	479.22	0.02
22	3.68	479.18	3.68	479.20	0.02
23	3.59	479.17	3.58	479.20	0.03
24	3.58	479.19	3.57	479.21	0.02
25	3.48	479.17	3.50	479.19	0.02
26	3.61	479.15	3.56	479.19	0.04
27	3.98	479.21	4.01	479.20	0.01
28	4.04	479.17	4.05	479.19	0.02
29	3.99	479.18	3.98	479.20	0.02
30	4.11	479.26	4.11	479.28	0.02
31	4.75	479.50	4.75	479.52	0.02
Average	4.52	479.23	4.52	479.25	0.02

Table 3. Comparisons of Cross-sectional Average Flow Velocity and Water Surface Elevation between Existing and Wing Dike Conditions

Case condition	Cross-sectional average on upstream boundary				
	Existing condition		Wing dike condition		
	Flow velocity (ft/s)	Water surface elevation (ft)	Flow velocity (ft/s)	Water surface elevation (ft)	Change of water surface elevation (ft)
60k cfs & 459.5 ft	1.22	459.79	1.22	459.81	0.02
110k cfs & 459.5 ft	2.16	460.42	2.16	460.48	0.06
162k cfs & 459.7 ft	3.03	461.52	3.01	461.63	0.11
302k cfs & 468.4 ft	3.82	470.84	3.82	470.88	0.04
467k cfs & 475.7 ft	4.52	479.23	4.52	479.25	0.02

upstream boundary for the cases investigated. Table 3 compares the cross-sectional average flow velocity and water surface elevation along the upstream boundary between the existing and wing dike conditions.

Based upon the results shown in Table 3, the conclusions are:

(1) Construction of new wing dikes alters the water surface elevation, but the change is small.
(2) For flow discharges less than 160,000 cfs, with decreasing the river flow, the change of water surface elevation due to wing dikes decreases.
(3) For flow discharges greater than 160,000 cfs, with increasing the river flow, the change of water surface elevation due to wing dikes decreases.

DISCLAIMER

The views expressed in this article are those of the author and do not reflect the official policy or position of the Department of the Army, Department of Defense, or the U.S. Government.

REFERENCES

ERDC (Engineer Research and Development Center), (2006). "Guidelines for Solving Two Dimensional Shallow Water Problems with the Adaptive Hydraulics (ADH) Modeling System."

USACE (U.S. Army Corps of Engineers), (1996). "Lock and Dam No. 22, Appendix 22." Master Water Control Manual.

ADH = FAST & STABLE 2D FINITE ELEMENT MODEL

Thomas Gambucci[1]

[1] P.E., D.WRE., Hydraulics Engineer, Regional Technical Specialist MVD - Navigation and Flood Control, U.S. Army Corps of Engineers, Rock Island District, Clock Tower Building, P.O. Box 2004, Rock Island, IL 61204, (309) 794-5848, thomas.r.gambucci@usace.army.mil

ABSTRACT

ADH (ADaptive Hydraulics) is the modern, multi-dimensional hydraulic modeling program in development by the Coastal and Hydraulics Laboratory (CHL) of the Corps' Engineering and Research Development Center (ERDC). The model was publicly released in September 2007 but has been used by the Rock Island District (MVR) since January 2006. MVR and other Corps Districts have been successful using ADH for many 2D applications and have found the shallow-water (2-D) module of ADH to be very fast and stable compared to previously used 2D hydraulic programs (RMA2 and HiVel2D). As beta users of the software, MVR had the opportunity to provide feedback to ERDC to help shape the program towards user needs and has assisted in technology transfer to other Corps districts throughout the region by hosting training workshops.

The Navigation and Ecosystem Restoration Program (NESP) is the implementation program for the recommendations contained within the Chief's Report for the Upper Mississippi River and Illinois Waterway System Navigation Study. This presentation will discuss the advantages of ADH and how it was used for the NESP Lock and Dam 22 project. A range of modeling applications were addressed, including: design of approach channel improvements, guardwall porting design for a newly proposed guardwall, design of a fish passage structure through the existing spillway, velocity field calculations during different stages of construction, and the overall effects of sedimentation due to the proposed work. Ongoing modeling activities are evaluating the effects of multiple projects constructed within a river reach to support objectives for both navigation and ecosystem restoration.

ADH MODELING SYSTEM

ADaptive Hydraulics (ADH) Modeling System developed and supported by the Coastal and Hydraulics Lab of Engineer Research and Development Center (ERDC) of US Army Corps of Engineers (USACE) is a software package that can handle both saturated and unsaturated groundwater, overland flow, three dimensional Navier-Stokes flow, and two or three dimensional shallow water problems. ADH is designed to work in conjunction with the Groundwater Modeling System (GMS) and the Surface Water Modeling System (SMS). (ERDC 2006) SMS (the Surface-Water Modeling System) is used to view/create the model mesh and display results for 2D models; GMS (the Ground-Water Modeling System) is used for 3D models.

The major benefits of ADH are its use of grid adaptation during computations that can improve model accuracy, stability and speed. ADH has the ability to make use of multiple processors to

further increase speed. Three files are needed to run a model in ADH: the mesh file (*.3dm), the boundary condition file (*.bc), and the hot start file (*.hot).

Once a mesh file has been constructed, the boundary conditions for the problem and operating parameters for ADH must be specified in the boundary condition file. This file contains a series of one line control cards, which fall into eight categories: operational parameters controlling the operation, iteration parameters controlling the iterative methods, material properties defining the flow and transport constants for each material, boundary strings defining the interior and surface boundaries of the problem, solution controls specifying the initial/boundary conditions, time controls specifying the time steps, output controls defining the times at which the output is printed, and series defining various parameters. (ERDC 2006)

The hot start file is generated to establish the initial conditions of the problem. Initial conditions consist of the depths and velocity components. Field data are often available and used as a starting point for many problems. A hot start file is a required part of a model; however, it may be a zero-length file (empty). For simple problems a cold start simulation (initial conditions of `0.0`) may be sufficient. Cold start problems in ADH are handled by leaving the hot-start file blank. If data types are not specified default values will be supplied (ERDC 2006). It is the experience of MVR that the cold start method is much slower than using a hot start. Time differences were investigated and it was concluded that 2D river models should start with a sloping water surface estimate. Without this estimate a flat pool is assumed and computation times are much higher in order to converge upon a solution. More details of the time difference will be presented later in this paper.

ADH simulation provides the velocity and overland head distributions in the flow field. The public release version (3893) can be found at http://chl.erdc.usace.army.mil/software, under "ADaptive Hydraulics Modeling (ADH)" and "ADH Downloads", and is intended solely for 2D swallow water applications. In a version still under development, multiple-grain sediments can be transported; ADH allows the user to calculate the transport of noncohesive or cohesive sediments. The sediment is transported as suspended load and bed load, and ADH provides the bed changes and suspended sediment concentration distribution. Currently, MVR, MVP and a few other Corps Districts have some experience with sediment ADH and are providing feedback to ERDC.

OLDER 2D FINITE ELEMENT MODELING SYSTEMS

RMA2

RMA2 is a 2D depth averaged hydrodynamic numerical model that computes the water surface elevations and horizontal flow velocities at nodal points of a finite element mesh that represents the river. RMA2 can be used to analyze both steady and unsteady state problems. TABS-MD was the predecessor to the RMA2 program and the names are often used interchangeably. In the past RMA2 was sometimes (erroneously) referred to as SMS, the interface to display mesh/model input and output. To run a hydro analysis, the GFGEN program was typically run first to pre-process the geometry file (mesh), then RMA2 was run to compute the hydrodynamic field. Since the computations of this finite element model are an implicit scheme, they are

performed simultaneously in a matrix form. Various RMA2 compilations were used to limit the matrix size to the number of nodes and elements in the model, which optimizes and improves computation speed. SMS (the Surface-Water Modeling System) is used to view/create the model mesh and display results. For 3D applications GMS (the Ground-Water Modeling System) is used. RMA2 was commonly used by MVR from 1995 to 2005. A common stability problem was the issue of wetting/drying elements. Modelers became experienced with troubleshooting techniques such as adding/refining elements, modifying eddy viscosities and using marsh porosity. RMA2 is no longer used at MVR due to the vast improvements in speed and stability seen with the ADH program.

HIVEL2D

HIVEL2D is a 2D numerical model used to analyze high velocity flow, and it has been adapted for use with both supercritical and/or subcritical flow fields with either lined or natural channels. HIVEL2D is a linear solver so only linear elements are created (no middle/side nodes). Using the command of Linear ↔ Quadratic in SMS, the RMA2 grid with quadratic elements can be easily converted to HIVEL2D grid with only linear elements. HIVEL2D was extended to include guard walls and was used to simulate the flow under and around the guard walls. Thus, HIVEL2D can be used to rapidly evaluate the navigation conditions in lock approaches for various guard wall configurations. HIVEL2D was the predecessor to ADH and it should now be considered obsolete.

CASE STUDY

In 2005 and 2006, the Rock Island District (MVR) developed and calibrated a 2D model of channel flow on the Upper Mississippi River near Saverton, Missouri as part of the Navigation and Ecosystem Restoration Program (NESP). The purpose of the study was to minimize impacts to navigation and the environment due to the proposed addition of a 1,200 ft lock chamber in the auxiliary bay of Lock and Dam 22 along with its associated approach walls. The base condition models formed the basis of comparison to future design alternative models. Future conditions modeling involved the addition of design features such as approach walls, dike fields, and a 1,200 ft lock in the auxiliary bay location. Future model results showed the effects of these design features on the river currents and how these changes might impact navigation. The numerical modeling was performed at the same time as physical navigation modeling at ERDC, and the two models complemented one another in various ways.

For the base condition models, numerical modeling was first performed using RMA2 and HIVEL2D. The HIVEL2D program was used in the pool because it was capable of modeling a proposed ported guardwall, an anticipated future conditions model (see Figure 1). Between each cell in the guardwall is a skirt that partially blocks off flow to eliminate excessive pinning forces upon approaching/exiting tows. HIVEL2D (and ADH) can place a local pressure field (“lid”) on the mesh. RMA2 was used in the tailwater due to higher computation speeds than HIVEL2D and the absence of a ported guardwall. The calibration was completed in December 2006 and base condition models were completed in 2006. Details of the calibration process and the base condition results are given in a study report dated 3/16/06 (Xia and Gambucci, 2006).

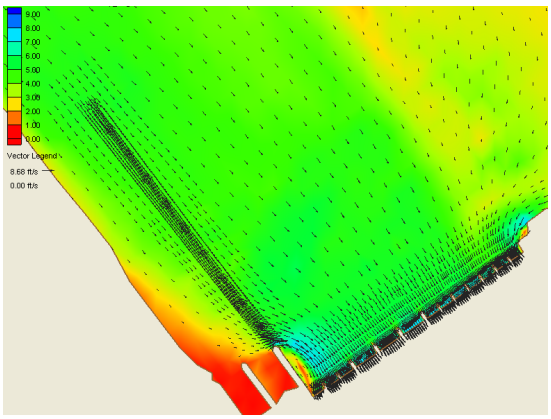

Without Guardwall

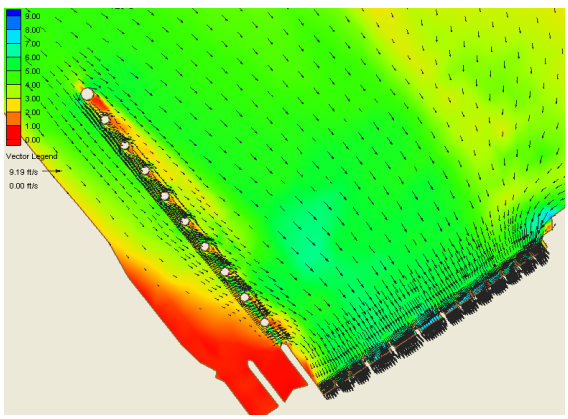

With Guardwall

Figure 1. Vectors of flow velocities (ft/s) near the guardwall area for 162,000 cfs, Pool 22 with and without guardwall cells.

In May of 2006, a new 2D hydraulic finite element solver named "ADaptive Hydraulics (ADH)" became available to MVR and the NESP team through ERDC. A few sample runs were made with ADH on converted RMA2 & HIVEL2D grids and it was evident that the software had great potential to increase computational speed and model stability. For the Lock and Dam 22 study, further runs produced the following speed advantages over the older software:

- RMA2 runs that were taking 2-4 hours of computation time now took 10-20 minutes using ADH.
- HiVel2D runs that were taking 8-12 hours of computation time now took 30-60 minutes using ADH.

Due to these dramatic speed increases, the desire to migrate to ADH was strong; however, testing for accuracy and stability was first conducted before the decision was made.

In June of 2006, a study was performed using ADH with the calibration discharge and comparing results to those of the earlier models RMA2 and HIVEL2D. Several cross sections were analyzed and found to be comparable to the former calibration study results; the results were nearly identical. ADH results were then checked against the Upper Mississippi River Flow Frequency Study (USACE, 2003) profiles for a range of discharges and found to be producing comparable water surface elevation slopes. Once these tests were complete, the decision was made by the NESP team to convert all base condition models to ADH models in both the pool and the tailwater of Lock and Dam 22. This saved computation time and provided direct comparisons to the future conditions models.

There are many techniques within ADH that can be used to save computation time. One of the most beneficial lessons learned has been the use of a sloping water surface hotstart file at the beginning of model calculations rather than using a flat water surface. This applies to 2D models in shallow water riverine environments. When modeling a stretch of river two to three miles

long, a flat surface starting assumption leads to prolonged computation times because the natural water slope can cause an elevation difference of one to two feet from the upstream boundary to the downstream boundary. The difference in starting elevation methodologies was investigated and it was later recommended to always start models with an estimate of the water slope rather than use a flat water surface. Below are some results of the investigation to quantify time saving benefits for the ADH model of Pool 22:

1) Initial timestep of 1 second versus an initial timestep of 2 seconds. Hotstart file based on a flat water elevation assumption with zero initial velocity. ADH run time for these two models was 1 hour 11 minutes and 1 hour 38 minutes.

2) Initial timestep of 10 seconds versus an initial timestep of 100 seconds. Hotstart file based on previous model output (depths and velocities) using 162,000 cfs. This modeling technique uses an initial flow rate of 162,000 cfs that was reduced to 130,000 cfs during the run (at timestep 1000). Run time for these two models was 3 minutes and 16 minutes, a significant improvement over the flat elevation hotstart assumption.

3) The velocity difference (plus or minus 0.5 ft/s) for the flat elevation hotstart model and the sloping elevation hotstart is shown in Figure 2. The sloping elevation came from the last timestep of a previous model run (including depths and velocities). Run time for these two models was 1 hour 11 minutes versus 16 minutes. Figure 2 shows that the difference in velocities is very similar to comparisons 1 & 2 above where only the initial timestep was altered.

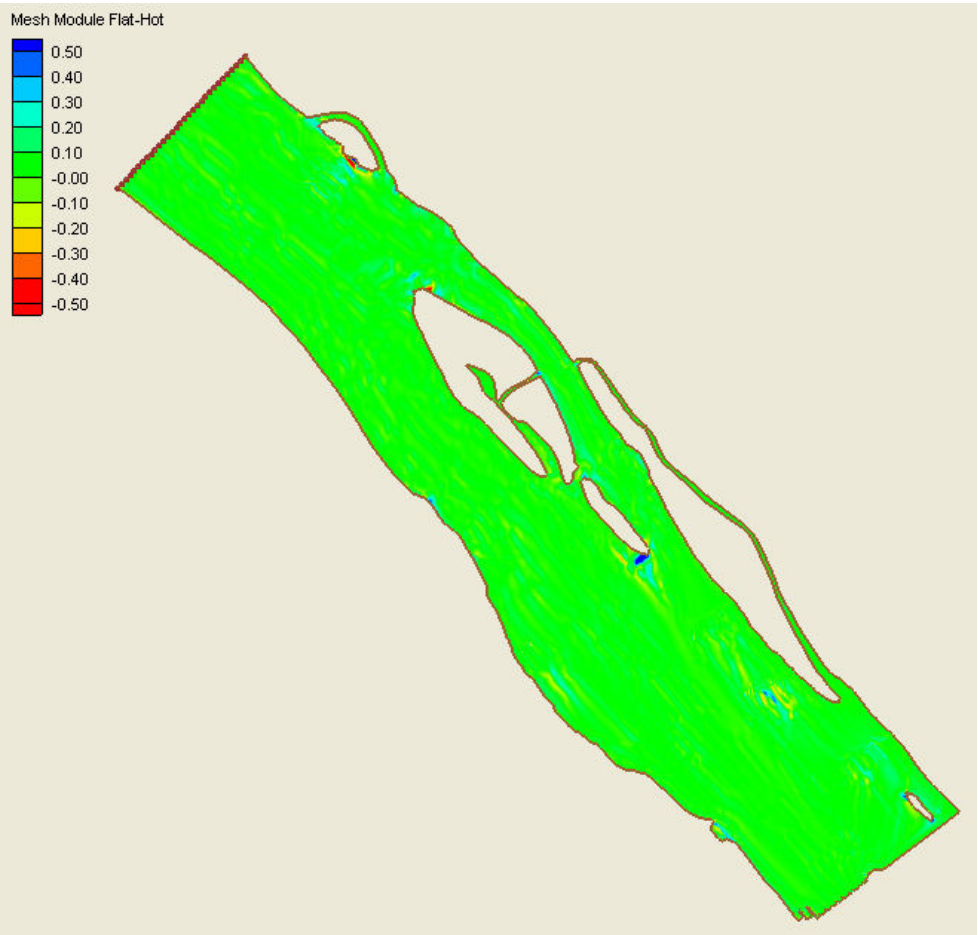

Figure 2. Pool 22 ADH Model Comparison: Velocity difference (plus or minus 0.5 ft/s) between a flat elevation hotstart file and a sloping elevation hotstart file.

Conclusion of sloping hotstart testing:
Starting ADH models with a hotstart file based on a sloping water elevation increases computational speed without changing the accuracy of the solution. The time savings is significant, approximately an hour per model run. This time savings was critical for the success of the construction sequencing modeling of Lock and Dam 22, a study that produced 141 ADH models for the final report (Gambucci, Xia, and Staley, 2008). ADH models should use initial starting conditions based off of a sloping water surface wherever possible in order to save time. A sloping water surface can be done based on an existing model run output files (OHD and OVL files), or if no existing model run exists MVP wrote up a procedure on how to create sloping surface hotstart files. If model output is available, ERDC has a program called "ADH_hot.exe" that allows for easy creation of hotstart files based on existing output files.

From 2006 to present, several Corps districts have used ADH including MVP, MVR, MVS, NWO, and MVN. Many tips and lessons learned have been shared within this initial ADH users group and feedback has been given to ERDC to help improve the program. MVR and MVP have hosted training workshops to facilitate technology transfer to the region with ERDC instructors to explain advanced features such as hydrodynamic vessel effects and sediment transport.

PRIMARY RESULTS

The Rock Island District (MVR) has seen vast improvements in speed and stability by using ADH and is no longer using the older programs RMA2 and HiVel2D for 2D shallow water applications. ADH has the potential to handle many other complex issues such as sediment transport, vessel movement, wind effects, and 3D applications including groundwater. Although the public release version of ADH does not yet support these features, it is recommended that users of RMA2 or HiVel2D make the transition to ADH for 2D shallow water applications. It is very simple to convert RMA2 and HiVel2D meshes into ADH format. The new mesh may be manually refined or modified using SMS, and during ADH computations the automatic grid adaptation of ADH will address areas of the mesh that are unstable.

DISCLAIMER

The views expressed in this article are those of the author and do not reflect the official policy or position of the Department of the Army, Department of Defense, or the U.S. Government.

REFERENCES

USACE (U.S. Army Corps of Engineers), (1996). "Lock and Dam No. 22, Appendix 22." Master Water Control Manual.

ERDC (Engineer Research and Development Center), (2006). "Guidelines for Solving Two Dimensional Shallow Water Problems with the Adaptive Hydraulics (ADH) Modeling System."

USACE CEMVR EC-HH (Xia and Gambucci), (2006). "Numerical Model Calibration and Base Conditions Report", Hydraulic Study of Lock and Dam 22.

USACE (U.S. Army Corps of Engineers), (August 2003). "Upper Mississippi River System Flow Frequency Study", Hydrology & Hydraulics Appendix C, Mississippi River

USACE CEMVR EC-HH (Gambucci, Xia, and Staley), (2008). "Numerical Model Construction Sequencing Report", Hydraulic Study of Lock and Dam 22.

Evaluation of Methods to Reduce Backflows from the Chicago Waterway System to Lake Michigan

Charles S. Melching[1], M. ASCE, and Emre Alp[2]

[1]Associate Professor, Department of Civil and Environmental Engineering, Marquette University, P.O. Box 1881, Milwaukee, WI, 53201-1881, PH (414) 288-6080, FAX (414) 288-7521, email: charles.melching@marquette.edu
[2]Instructor, Department of Environmental Engineering, Middle East Technical University, Ankara 06531, Turkey, email: emrealp@metu.edu.tr

ABSTRACT

A detailed study of seven historic backflow from the Chicago Waterway System (CWS) to Lake Michigan events (including the 2nd and 4th largest since 1965) was done to evaluate changes in waterway operation procedures to determine if backflows could be avoided or reduced in volume. The study applied a dynamic-wave simulation model to the CWS at a 15-minute time step combining measured inflows for the major tributaries, combined sewer overflow (CSO) pump stations, and water reclamation plants with simulated gravity CSO flows computed by the U.S. Army Corps of Engineers. The simulated CSO inflows were confirmed against a detailed mass balance approach for four storms and the peak flows from the two approaches were found to be remarkably similar. It was found that the hydraulic capacity limitations of the Chicago Sanitary and Ship Canal (CSSC) prevented changes in operations at the Lockport Powerhouse and Controlling Works from substantially reducing backflows. The maximum discharge through the CSSC is around 19,500 cfs whereas inflows may peak at 40,000 to 50,000 cfs and flows cannot drain away fast enough to avoid having to allow backflows to Lake Michigan. These backflows cannot be avoided until the reservoirs of the Tunnel and Reservoir Plan (TARP) are completed.

INTRODUCTION

The Chicago Waterway System (CWS) is composed of the Chicago Sanitary and Ship Canal (CSSC), Calumet-Sag Channel, North Shore Channel (NSC), lower portion of the North Branch Chicago River (NBCR), South Branch Chicago River (SBCR), Chicago River Main Stem, and Little Calumet River (North). In total, the CWS is a 76.3 mi branching network of navigable waterways controlled by hydraulic structures in which the majority of flow is treated sewage effluent. The dominant uses of the CWS are for commercial and recreational navigation and for urban drainage, i.e. draining combined sewer overflows (CSOs), stormwater runoff, and treated wastewater from the Chicago area away from Lake Michigan. The Calumet and Chicago River Systems are shown in Figure 1.

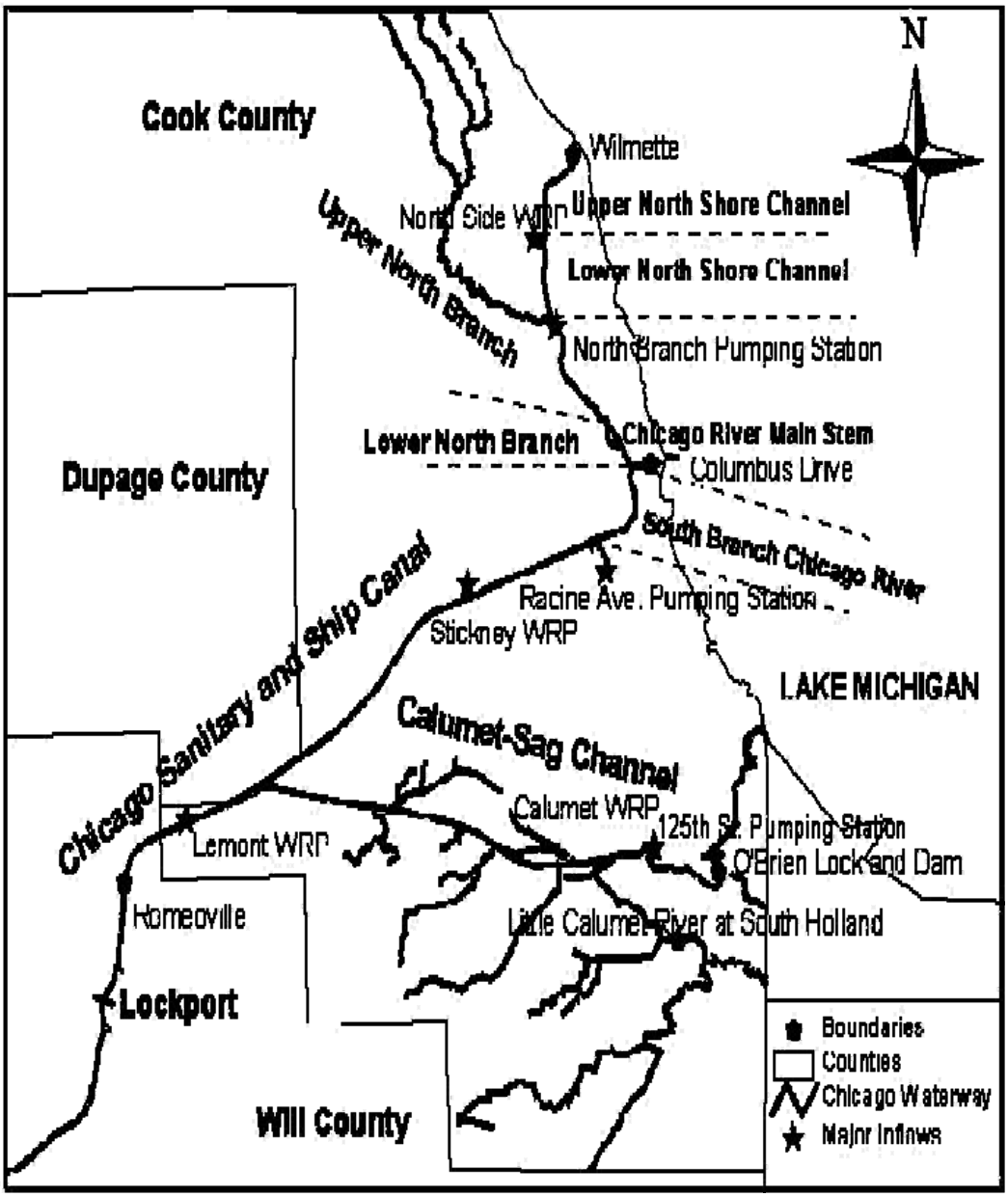

Figure 1. Schematic diagram of the Calumet and the Chicago River Systems.

Minimizing the occurrence of backflows of storm runoff and sewage to Lake Michigan through the lakefront sluice gates and locks is a high priority for the Metropolitan Water Reclamation District of Greater Chicago (MWRDGC). Backflows can potentially affect the water supply of Chicago, the accessibility of beaches to the public, and the general environment of Lake Michigan. Since the O'Brien Lock and Dam were completed in 1965 forty-nine storms have caused the MWRDGC to open the sluice gates or locks at the lakefront and allow water to flow to Lake Michigan. Thirty two of these occurred before 1986 when the first of the Tunnel and Reservoir Plan (TARP) tunnels went on-line for a pre-TARP rate of 1.5 per year and a post-TARP rate of 0.73 per year. The decrease in frequency of

backflows reflects the reduction in flood flows resulting from the TARP tunnels. However, the volumes of the backflows since 1990 have been large with 6 of the 10 largest backflow volumes from 1965 to 2007 occurring since 1990 (Table 1). The objective of this study is to evaluate 7 historic backflow events (1997-2002) to see if changes in operation procedures at the Lockport Powerhouse and Controlling Works can avoid or reduce the volume of backflows.

Table 1. Flow volume of backflow events (in million gallons) from 1990 to 2007.

Date	O'Brien	CRCW	Wilmette	Total
8/23-24/07			224.0	224.0
8/22/02		1296.4	455.4	1751.8
10/13/01			90.7	90.7
8/31/01			75.3	75.3
8/02/01		883.1	139.9	1023.0
6/13/99			9.7	9.7
8/16-17/97		402.0	157.0	559.0
2/20-22/97	1458.0	1947.0	774.0	4179.0
7/17-18/96	1032.0	519.0		1551.0
11/27-28/90	224.0	86.0	154.0	464.0
8/17-18/90			9.5	9.5
5/9-10/90		208.0	289.0	497.0

HYDRAULIC MODEL DESCRIPTION AND VERIFICATION

The DUFLOW (2000) unsteady-flow model for the CWS was calibrated and verified by the Marquette University in 2003. The ability of the model to simulate unsteady flow conditions was demonstrated by comparing the simulation results to measured data for eight different periods between August 1, 1998 and July 31, 1999 (Shrestha and Melching, 2003). Shrestha and Melching (2003) calibrated the model using hourly stage data at three gages operated by the MWRDGC along the CSSC and at the downstream boundary at Romeoville operated by the U.S. Geological Survey (USGS), and using daily flow data collected by the USGS near the Chicago River Controlling Works (CRCW) and O'Brien Lock and Dam upstream boundaries. For the evaluation of the backflow events, the DUFLOW model was extended from Romeoville to the Lockport Controlling Works, LCW, (3 miles downstream from Romeoville and 2.2 miles upstream of the Lockport Power House, LPH, and Lock). The model was run at a 15-min. time step and measured and simulated stage values were compared for a 60-min. time interval. Assumptions, data used, and results are presented in the following subsections.

Measured inflows, outflows, and water-surface elevations. During the study period the USGS operated discharge and stage gages at three primary locations where water is diverted from Lake Michigan into the CWS. These locations are:

i) The Chicago River Main Stem at Columbus Drive (near CRCW)
ii) The Calumet River at the O'Brien Lock and Dam

iii) The North Shore Channel at Maple Avenue (near the Wilmette Pumping Station)

The data from the Chicago River Main Stem at Columbus Drive, the Calumet River at the O'Brien Lock and Dam and the North Shore Channel at Maple Avenue gages were used as the primary flow versus time (5-minute) upstream boundary conditions for the unsteady-flow model. Water-surface elevation versus time data (on a 1-hr basis) from the MWRDGC gage on the CSSC at the LCW were used for the downstream boundary condition.

During the backflow events, MWRDGC estimated the volume of backflows and the USGS measured them with acoustic velocity meter (AVM) gages. It was found that simulations with the volume of backflows estimated by MWRDGC resulted in better water-surface elevation estimates in the CWS than simulations using the USGS measurements. Thus, just during backflow events USGS flows were adjusted to match the MWRDGC backflow volume estimates. This approach is reasonable because the USGS never made discharge measurements during a backflow with which the AVM gages could be properly calibrated at the Lakefront structures (Jim Duncker, USGS, personal commun., 2007).

The data from the USGS gage of the Little Calumet River (South) at South Holland provide a flow versus time upstream boundary condition for the model. Two tributaries to the Calumet-Sag Channel are gaged by the USGS, Tinley Creek near Palos Park and Midlothian Creek at Oak Forest. The USGS gage on the Grand Calumet River at Hohman Avenue at Hammond, IN measures flow on a tributary of the Little Calumet River (North). Flow on the NBCR is measured just upstream of its confluence with the NSC at the USGS gage at Albany Avenue.

Hourly flow data are available from the MWRDGC for the treated effluent discharged to the CWS by each of the three Water Reclamation Plants—North Side, Stickney, and Calumet. In addition, hourly flows discharged to the CWS at three CSO pumping stations—North Branch, Racine Avenue, and 125th Street—were estimated from operation logs and rated pump capacities for these stations.

Estimation of flow for ungaged tributaries and combined sewer overflows. Flows on Midlothian Creek were used to estimate flows on ungaged tributaries on an area-ratio basis as was done in the model calibration (Shrestha and Melching, 2003).

There are nearly 240 CSOs in the modeled portion of the CWS drainage area. Since it is practically difficult to introduce all CSO locations in the modeling, 28 representative CSO locations were identified. In this study, simulated CSO flows were obtained from the U.S. Army Corps of Engineers (Corps), which are calculated on an annual basis in support of the Lake Michigan Diversion Accounting. Detailed discussion of the Corps models (a combination of the Hydrological Simulation Program-Fortran, Special Contributing Area Loading Program, and Tunnel Network Model) is given in Espey et al. (2004). The flow simulations are driven by precipitation data from a network of 25 precipitation gages throughout the Chicago area established by the Corps in 1990.

Channel geometry and roughness coefficient. The channel geometry is represented as a series of 231 measured cross sections. The DUFLOW model uses Chezy's

roughness coefficient, C, to calculate hydraulic resistance. The calibrated C values vary between 6 and 60 and the equivalent Manning's n values range from 0.022 to 0.165. Complete details on the calibrated values of Chezy's C and the equivalent Manning's n value are listed in Table 4.2 of Shrestha and Melching (2003).

Model verification. Although flows in the various branches of the CWS are not measured, water-surface elevation data recorded at different locations were used for calibration and verification of the model. The water-surface elevations recorded at Columbus Drive, O'Brien Lock and Dam, Wilmette, Western Avenue, Willow Springs Road, Southwest Highway, and Sag Junction by the MWRDGC and at Romeoville by the USGS were used for model verification. Details of the calibration and the verification results are given in Alp and Melching (2006), Neugebauer, and Melching (2005), and Shrestha and Melching (2003).

In order to evaluate the backflow events, the DUFLOW model was applied for the following simulation periods:

February 1 - March 30, 1997
August 1 - September 30, 1997
June 1 - June 30, 1999
July 1- November 9, 2001
August 1 – September 23, 2002

As an example of the output, Table 2 lists the statistical analysis for July 1 to November 9, 2001 of the difference between the measured and simulated stages. It can be seen that the errors are below 10 % relative to the depth (where depth is measured from the thalweg of the channel) of the water for all of the values except for simulations at Wilmette and Lawrence Avenue. These high percentages of small errors and close agreement between the simulated and the measured water-surface elevations especially during backflow events at the boundaries indicate an excellent hydraulic verification of the model. Similar results for the other simulation periods are presented in Alp and Melching (2008).

Table 2. Correlation coefficient and percentage of the hourly water-surface elevations for which the error in simulated versus measured elevations relative to the depth of flow (measured from the thalweg of the channel) is less than the specified percentage for July 1, November 9, 2001.

July 1-November 9, 2001		Percentage		
Location	Correlation Coefficient	<±2% of D	<±5% of D	<±10% of D
Wilmette	0.81	0	4	75
Chicago River Controlling Works	0.82	87	99	100
O'Brien Lock and Dam	0.69	97	100	100
Lawrence Avenue (NBCR)	0.65	8	48	83
Western Avenue (CSSC)	0.84	94	99	100
Willow Springs (CSSC)	0.78	97	99	100
Southwest Highway (Cal-Sag)	0.77	84	99	100
Sag Junction	0.80	98	99	100
Romeoville (CSSC)	0.96	95	100	100

EVALUATION OF OPERATION SCHEMES FOR LOCKPORT GATES

Actual operation schemes for the Lockport Gates. Records for 1998-2002 of the opening of the LPH pit gates and LCW sluice gates were obtained from the MWRDGC. These were compared with the measured water-surface elevations at the LCW to establish typical water-surface elevations for various combinations of gate openings. There are 9 LPH pit gates and 7 LCW sluice gates. Comparison of the water-surface elevations at LCW with the various gate openings for the selected storms are detailed in Alp and Melching (2008). The MWRDGC gradually opens the pit gates at the LPH when a larger storm is anticipated and LCW sluice gates are also opened when higher discharges and water-surface elevations are observed. When the 9 LPH pit gates are open, water-surface elevation at the LCW goes down to -5.9 ft CCD on average and when all the gates (LPH and LCW) are open, water-surface elevation goes down to -9.3 ft CCD on average. Different combinations of gate operations result in water-surface elevations ranging from -4 ft CCD to -9.3 ft CCD on average.

Simulation of the Lockport Gate Operation Procedures. Four sets of simulations representing various Lockport gate operation procedures were evaluated and throughout the text some abbreviations explained below are used to describe the simulations:

i) *Before CSO*: Lockport Gates are open 6 to 12 hrs before CSO to bring the water level down to -3, -5, or -7 ft CCD at the LCW and the water level is kept higher than -3 and -4 ft CCD at CRCW and Sag Junction, respectively, as required by navigational regulations. When CSO starts, actual gate operations and LCW water-surface elevations are used. During the backflow event, upstream boundaries are set to zero discharge to see how high the water could rise.

ii) *During CSO*: Gates are open 6 to 12 hrs during CSO event to bring the water level down to -9 ft CCD at the LCW and the water-surface elevation is kept higher than -3 and -4 ft CCD at CRCW and Sag Junction, respectively. Prior to the CSO events, actual gate operations and LCW water-surface elevations are used. During the backflow events, upstream boundaries are set to zero discharge.

iii) *No limit*: Lockport Gates are open 6 to 12 hrs before CSO to bring the water level down to -5, -7, or -9 ft CCD at the LCW without regard to the water-surface elevation limits at CRCW and Sag Junction. When CSO starts, actual gate operations and LCW water-surface elevations are used. During the backflow event, upstream boundaries are set to zero discharge.

iv) *Baseline*: During the backflow events, upstream boundaries are set to zero discharge.

Simulation Results. The results of the *"Before CSO"* simulations reflecting hypothetical gate operations to prevent backflows were compared with the *Baseline* simulations. In these simulations, water-surface elevations were lowered at the LCW while maintaining minimum allowable water-surface elevations at CRCW and Sag

Junction. Outcomes of the simulations show that lowering the water-surface elevations at Lockport to -3 to -5 ft CCD for 6 hours before the CSO event do not provide enough storage for the CSOs in the CWS to prevent backflows. The effect of lowering water-surface elevations at Lockport decreases as locations farther from Lockport are considered with reductions at CRCW ranging from negligible to 0.56 ft and at Wilmette from negligible to 0.43 ft. Even though this practice helps to lower the water-surface elevations in the CWS before the CSO events, the peak water-surface elevations during CSO events are far higher than the levels at which backflows to Lake Michigan are necessary.

In the *"No limit"* simulations, the downstream boundary condition at the LCW was lowered to -5 to -7 ft CCD for an extended 12 hour period before the CSO event and water-surface elevations were allowed to be lower than minimum water-surface elevations limits at CRCW and Sag Junction. Decreases in the peak water-surface elevations of 0.32 to 1.18 ft resulted at Wilmette and decreases on the order of 1.5 ft resulted at CRCW for the events resulting in backflows. However, at both locations peak water-surface elevations were not low enough to prevent backflows to Lake Michigan for all events except October 13, 2001 at Wilmette. Figure 2 shows the water-surface elevation reductions for the *"No limit"* simulations for the August 2, 2001 event, which had the largest decrease at Wilmette among the 7 storms. Similar figures for all storms and scenarios are included in Alp and Melching (2008).

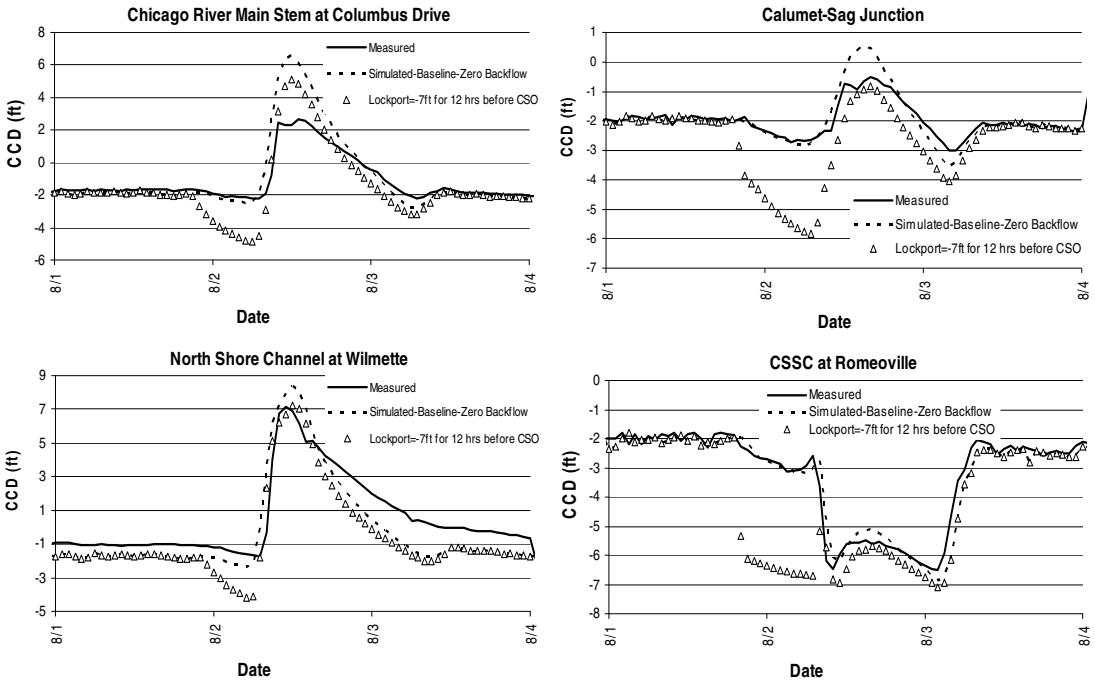

Figure 2. Water-surface elevations at different location in the Chicago Water System for "*No Limit*" simulations for August 1-4, 2001.

In the last set of simulations, water-surface elevations were allowed to go down to -9.0 ft CCD at Lockport to increase the water-surface slope and flow rate in the CSSC just as CSO starts during backflow events. Since, in the actual case (*Baseline*), all Lockport gates were open and water-surface elevations were allowed

to decrease to -9 ft CCD, these simulations resulted in very close peak water-surface elevations to the *Baseline* simulation results.

Inflow-Outflow Comparison. In order to understand the lack of effectiveness of the various simulated changes in gate operations at Lockport in reducing water-surface elevations at the lakefront boundaries, a comparison of the inflows to and outflows from the CWS was done. The measured and estimated inflows were summed on an hourly basis for each backflow event and the summation is compared with the measured outflows at Romeoville in Figure 3 for the August 2, 2001 event. For this event, the peak inflow is nearly 45,000 cubic feet per second (cfs) while the measured peak outflow was 15,479 cfs. This comparison shows that with the inflow being up to 30,000 cfs higher than the outflow for several hours the storage space created by lowering the CWS is quickly filled and the CSSC and/or NSC and NBCR are not capable of draining the CWS fast enough to avoid backflows at the CRCW and Wilmette, respectively, despite changed gate operations at Lockport. Similar results for the other 6 backflow events are shown in Alp and Melching (2008).

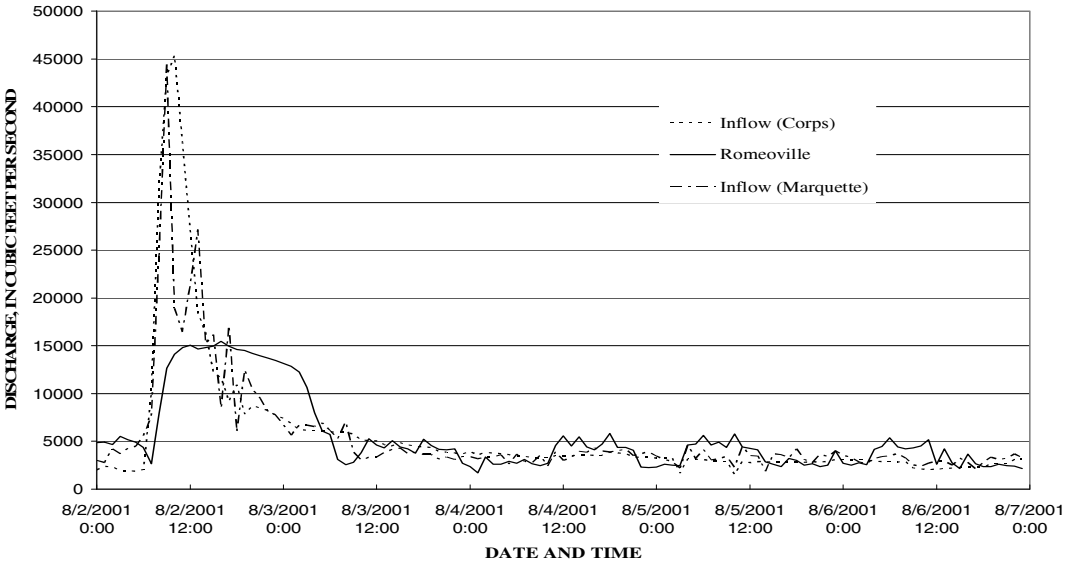

Figure 3. Measured and estimated inflow to the Chicago Waterway System and measured outflow at Romeoville, IL, for August 2 to 6, 2001.

It may be speculated that the inflows estimated by the Corps models are too high, and, thus, the inability of the CWS to drain away high storm flows is overstated in Figure 3. Figure 3 also includes the estimate of total inflows to the CWS based on Marquette University's original estimates of the gravity CSO flows. The Marquette estimates are based on the daily water balance for the CWS and the amount of gravity CSO flow and flow at the lakefront boundaries (where water-surface elevation boundary conditions were used in the original model) needed to match measured water-surface elevations throughout the CWS (Shrestha and Melching, 2003). The peak inflows from the Corps models and Marquette estimates are very close, within 2% for the August 2, 2001 event. The peak flow also was within 2% for the August 31, 2001 event, within 8% for the August 2002 event, and within 18% for the October

2001 event (Alp and Melching, 2008). Differences in volumes are greater, but in general, the agreement between the output of the Corps models and the Marquette estimates is sufficient to conclude that during larger storms the inflows to the CWS overwhelm the drainage ability of the component channels of the CWS.

Measured Water-Surface Elevations. The measured water-surface elevations at different locations on the CWS for the August 2, 2001 event, the second largest backflow event that occurred between 1990 and 2007, are shown in Figure 4 (measured water-surface elevations for the other 6 flow reversal events have similar patterns to those shown in Figure 4). Figure 4 shows that measured water-surface elevations at the locations above Sag Junction are all higher than -2.0 ft CCD even though minimum water-surface elevations at Romeoville and Lockport are around -6 and -9 ft CCD, respectively.

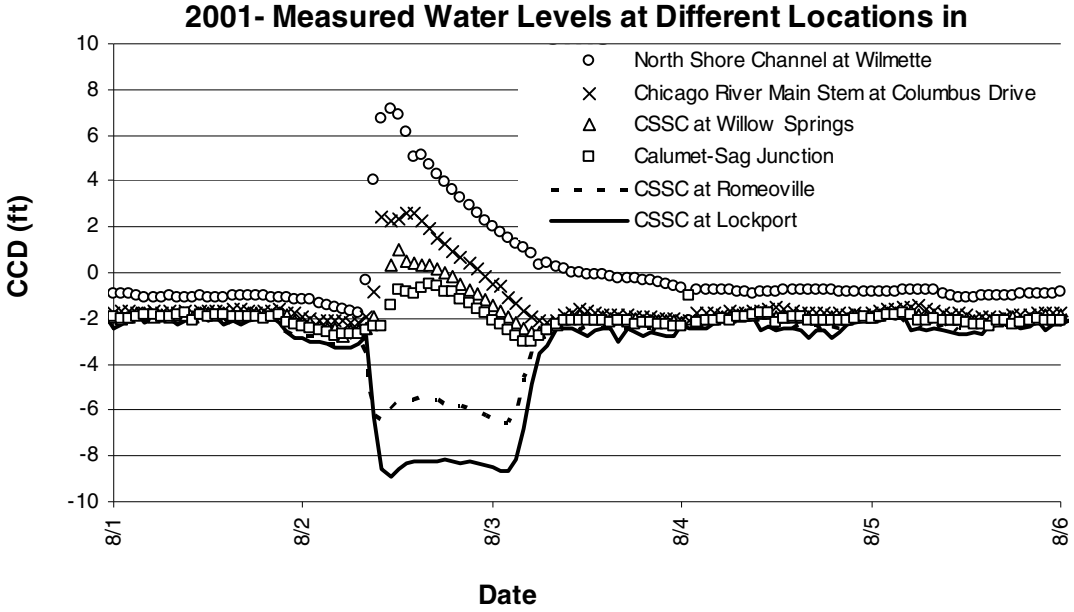

Figure 4. The measured water-surface elevations at different locations in the CWS for the August 2, 2001 backflow event.

For the August 2, 2001 event the maximum difference in water-surface elevation between Wilmette and Columbus Drive (14 mi) is around 5 ft, between Columbus Drive and Sag Junction (23.2 mi) is around 3 ft, and between Sag Junction and the LCW (10.2 mi) is around 8 ft. Thus, a large water-surface slope is present on the CSSC from Sag Junction to the LCW in order for this reach to transport the large storm flows coming from the upstream CSSC and Calumet-Sag Channel. The CSSC was not constructed anticipating the construction of the Calumet-Sag Channel, and the geometry of the CSSC is the same upstream and downstream of Sag Junction. Thus, a two lane highway of water is narrowed to one lane, causing water to back-up each of the two lanes (the upstream CSSC and Calumet-Sag Channel) resulting in low water-surface slopes and flow capacities. Thus, the inability of the CWS to drain high storm flows away from lakefront areas resulting in backflows can be seen in the records of the measured water-surface elevations.

CONCLUSIONS

Changed operations of the gates at Lockport cannot prevent backflows to Lake Michigan because the flow capacity of the CWS is not large enough to drain away high storm flows. These high storm flows quickly fill storage space created by lowering the CWS by opening the gates at Lockport in anticipation of a large storm, and the water-surface elevations at the lakefront rise quickly to flood levels necessitating backflows. It is likely that the MWRDGC's policy of lowering the CWS in anticipation of storms may help avoid backflows for smaller storms, but this possibility was not explicitly evaluated in this study. Finally, there appears to be nothing that the MWRDGC can reasonably do to avoid future backflows until the reservoirs of TARP come on line and the volume of CSO flows is further reduced.

REFERENCES

Alp, E. and Melching, C.S. (2006). "Calibration of a model for simulation of water quality during unsteady flow in the Chicago Waterway System and application to evaluate use attainability analysis remedial actions." *Technical Report 18*, Institute of Urban Environmental Risk Management, Marquette University, Milwaukee, WI. and *Research and Development Department Report No. 2006-84*, Metropolitan Water Reclamation District of Greater Chicago, Chicago, Ill.

Alp, E. and Melching, C.S. (2008). "Evaluation of procedures to prevent flow reversals to Lake Michigan from the Chicago Waterway System," *Technical Report 19*, Institute of Urban Environmental Risk Management, Marquette University, Milwaukee, WI.

DUFLOW, 2000, *DUFLOW for Windows V3.3: DUFLOW Modelling Studio: User's Guide, Reference Guide DUFLOW, and Reference Guide RAM*, EDS/STOWA, Utrecht, The Netherlands.

Espey, W.H., Jr., Melching, C.S., and Mades, D.M., 2004. "Lake Michigan Diversion—Findings of the Fifth Technical Committee for Review of Diversion Flow Measurements and Accounting Procedures," report prepared for the U.S. Army Corps of Engineers, Chicago District, Chicago, Ill.

Neugebauer, A. and Melching, C.S., 2005, "Verification of a continuous water quality model under uncertain storm loads in the Chicago Waterway System," *Technical Report 17*, Institute of Urban Environmental Risk Management, Marquette University, Milwaukee, WI, and Metropolitan Water Reclamation District of Greater Chicago, *Department of Research and Development Report No. 2005-12*, Chicago, IL.

Shrestha, R.L. and Melching, C.S., 2003, "Hydraulic calibration of an unsteady flow model for the Chicago Waterway System," *Technical Report 14*, Institute of Urban Environmental Risk Management, Marquette University, Milwaukee, WI, and Metropolitan Water Reclamation District of Greater Chicago, *Department of Research and Development Report No. 03-18*, Chicago, IL.

Modeling the Evolution of Incised Streams in Hammar Mesopotomian Marsh with emphasis on the Contribution of Tidal Flow in the Filling Requirements

A. H. Alkaabi[1] A. Ramamurthy[2] H.A. Al-Thamiry[3] A.A. Ali[3]

[1]Visiting Professor, Dept. of Building, Civil and Environmental Engineering, Univ. of Concordia, Montreal, CANADA.

[2]Professor, Dept. of Building, Civil and Environmental Engineering, Univ. of Concordia, Montreal, CANADA.

[3]Lecturer, Dept. of Water Resources Engineering, University of Baghdad, IRAQ.

1 Introduction

Tidal flow may contribute significantly in the amount of water to be considered in the restoration of wetlands, particularly when these wetlands were subjected to a drying process and there are shortages in the availability of water coming from highlands. The Mesopotamian marshes (The Iraqi Wetlands) are Al-Hammar Marsh, Al-Huwaiza Marsh, and Central Marshes (Al-Qurna). These marshes were subjected during the last two decades to a drying process for mostly political reasons. The present study concerned with the Al-Hammar Marshes. After the last war in 2003 the aim of the new Iraqi authorities is to restore these marshes and their unique ecosystem. Many studies had been conducted and other still in progress concerning different aspects of the drying process impacts and the identification of the most suitable strategies for this restoration. Although the quality of water available for marshes restoration is of vital importance, the water quantity is also important and essential for the purpose of ecosystem restoration. Some of these studies were concerned directly or indirectly to the availability of water quantity aspects. United Nation Environmental Program (UNEP) and American University Beirut (AUB) (1988) had conducted a study for supporting the environmental management of these marshes. The effects of water deficiency in Tigris and Euphrates Rivers due to Turkish and Syrian water management strategies were investigated indicating the effect of these strategies on water quantity of Tigris and Euphrates Rivers water especially for the restoration of the Mesopotamian Marshes associated with the reduction of flows. UN and the World Bank (2003) had conducted a study of water and sanitation in Iraq, with its relation to marshes restoration process. The study indicates the high TDS values at south of Iraq near the marsh area compared to those values at the Iraqi-Turkish and Iraqi-Syrian borders. The Italian Ministry of the Environmental and Territory and The Free Iraq Foundation (2006) had conducted a hydrological study for an integrated water resources management study in Iraq related to the restoration process. Al-Samarai (1999) had conducted a study of evaluation of the irrigation and drainage projects that had been constructed after the drying process in the marshes area. The UNEP (2003) had conducted a desk study on the environment in Iraq identifying some effects on the marshes environments due to the drying process. The Iraq Foundation (2003) had conducted a study for building a scientific basis for restoration of the Mesopotamian Marshlands. The study

indicate the need of conducting restoration process during high flow periods to flush out the salts and contaminants from the flooded area which means that at the beginning of the restoration process the water salinity going to be high. UNEP (2003) had conducted a progress report of environment in Iraq mentioning some environmental effects of the drying process. The study had concluded that the water quality will get better as the restoration process continued year after year. UNEP (2001) had conducted a study of the Mesopotamian Marshlands a demise of an ecosystem. The study had focused on the different impacts of the drying process on the ecosystem of the marshlands. The US Agency of International Development (2004) had conducted a study of Iraq marshlands restoration program. The part of this study which concerned with water quantity had indicated high shortages in water according to season. AMAR International Charitable Foundation (2003) had conducted a study of the human and environmental aspects of Iraqi Marshlands. The study had also concluded the shortage of water availability.

The main conclusions of reviewing the above mentioned studies are the deficiencies in Tigris and Euphrates Rivers flow. This deficiency has to be considered in the restoration of the Mesopotamian Marshes. The planning target of the new Iraqi authorities and the international environmental agencies is to restore this ecosystem again. The center for restoration of Iraqi marshes (CRIM) is one of the establishments of the ministry of water resources in Iraq. This center is responsible of conducting the studies and the required activities for marshes restoration. The present study was conducted with the corporation of CRIM for the Al-Hammar Marshes and devoted for the study of the Arabian Gulf tidal flow control to contribute to Al-Hammar Marsh. A mathematical model for the flow in this domain was built. HEC-RAS Software (version 3.1.3) and HEC-GeoRAS extension under Arc-View GIS software are adopted in the implementation of this model. The model runs give an estimate of the percentage of water flowing in or out from the marsh. For a full restoration the need of this study is essential.

2 Materials and Methods

Study Site Description

Hammer Marsh is the largest marsh among the Mesopotamian Marshes located on the right side of Euphrates River just before the confluence with Tigris River at Qurna City to form Shat AL-Arab River. The marsh starts from the ends of Euphrates River branches at Nasiriya. These branches are Ghlaiween, Safha, Okeka and Beni-Hassan Rivers, and then downstream Sook AL Sheyukh the AL-Hafara River. Karmet beni-seed and Om-Nakhla Cross Regulators are exist to control the water entering the marsh from these branches. In addition, there are escapes and culverts below AL Nasiriya-Qurna Road to allow Tigris River flow from the Central Marshes at Qurna to Hammar marsh during flood season.

The south petroleum company has executed embankments to protect oil fields. This embankment became a central road connecting north part of Hammer Marsh with the south part at Rumaila. This road has 334 culverts with total length of 4350 m. The design capacity of these culverts is a flood of 100 years return period, which is the same of 1969.

Before drying, in the eightieth of the last century, The Hammar Marsh is part of a complicated interconnected system for water exchange between Tigris, Euphrates, shat AL-Arab Rivers. The branches of Euphrates River are the main feeding sources for Hammar Marsh. The flows of these branches are controlled by several regulators of a fluctuating capacity between 50-500m^3/s. In addition to the above regulators as a feeding control structures, there is also a direct

feeding from the opening through the right embankments of Euphrates River with a capacity of 500m³/s. During the flood season of Tigris River, the water is flowing from Central Marsh to Hammar Marsh through escapes and culverts. These escapes are either a pipe or series of pipes or flow in culverts under bridges. Jehala escape is the largest one with 84 m water way. Sometime the water flow overpasses the road parallel to Euphrates River conveying water from Central Marshes to Hammar Marsh. During flood season, Hammar Marsh becomes a connected lake, while during dry season; it becomes disconnected shallow small lakes.



Figure 1: Location of Study Area

The water depths in these lakes are 0.2-0.5m. In this process, the surface area changes from 3000 km² with 5 km³ flood season storage capacity to a 600 km² with 0.2 km³ storage capacity during dry season.

The accumulated water of Hammar Marsh is discharged as an outflow to Shatt Al-Arab River by Al-Shafi, Al-Ghameej and Garmet Ali Rivers. The Arabian Gulf tidal effect reaches the location of the marsh outlet into Shatt Al-Arab River. The problem is to estimate the amount of water flowing in or out from the marsh during a year.

The drying process of a 90% of the marsh area after 1990 has caused a considerable change in all the topographical features of Hammar Marsh.

Raising Euphrates River shoulders played an important role in the drying of marshes. High level embankments were executed on both sides of Euphrates River with length reaching 94 km in addition to shoulder rising of Ghlaiween, Ekeka and Bani Hassan Rivers. These branches were combined to form assignee channel which meets Euphrates River near Al Fuhood village. This was done to prevent the water from reaching the marsh. Shoulder rising were also executed on several other rivers which have indirect role in the process of the drying operation.

In order to complete the process of drying, Al-Huriya river was executed with maximum discharge of 300m³/sec which draws great part of the Euphrates River flow in Nasiriya to be transported far from Hammar Marsh and discharges in Main Outfall Drain. Basra water supply project which crosses the marsh causes obstruction to the movement of water inside the marsh

The declared goal of this drying process was to obtain agricultural land for operating of about 500,000 donums. This area is distributed between Al-Shafee, Al-Malha and Um-Nakhla Irrigation Projects.

Hydrological Data Analysis

In the present study the hydrologic data is the tool in the evaluation of the existing hydraulic boundary conditions of the study area. The data of precipitation, evaporation and water resources are collected from the Directorates of MOWR records, Meteorological stations records and that available in the literatures and in previous studies.

The rainy seasons in Iraq are from October to May. The months January and February have the maximum rainfall. The analysis of the precipitation data of marshland area for the period (1987-2005), for Nasiriya and Basra governates showed that the average precipitation in Basra for the last 19 years is 144 mm/year, while in Nasiriya is 124mm/year.

The evaporation rates represent the main water losses. The evaporation is effected by air humidity, wind speed and air temperature. Evaporation of the Southern Iraq zone is studied for the last 19 years. The locations of the meteorological stations of Nasiriya are (Lat 31 1, Long 46 14) and Basra station (Lat 30 25, Long 44 50). Moreover the evapo-transpiration, the combined effect of evaporation and water used by plants, must be taken into consideration in the study. The evapo-transpiration has higher values than evaporation only especially in the hot seasons. According to (New Eden Plan, 2006), the monthly evapo-transpiration for Hammar marsh area was calculated using Penman equation with the data of the meteorological stations. The evaporation in Nasiriya is 2874 mm/year, while in Basra is 2253 mm/year. The reason of this difference is the low humidity in Al-Nasiriya. The averaged yearly evaporation is 2563.5 mm, while the averaged evapo-transpiration is 2909.3 mm in the same region. The above figures provide an idea that the evapo-transpiration in study area is 12% higher than the evaporation. So, these values will be considered in the model.

To estimate the required inflow to balance the evaporation in the marsh, the evaporation and precipitation data are used. The required discharge to balance the evaporation for an area of 1000 km^2 in Al-Hammar is about 88m^3/sec.

The main source of water in the Hammer marsh area is Euphrates River. The averaged maximum monthly discharge for the period (1980-1997) is 1429m^3/s, while the averaged minimum monthly discharge for the same period is 71m^3/s.

Garmat Ali River can also be considered as an additional feeder in the restoration of Hammar Marsh through the high tide period of Shat Al-Arab River. Shat Al-Arab River is a tidal river and the tidal effects reach the upstream end of this river. The tidal pattern in the estuary is a mixed type, mainly semi-diurnal; there are two high and low water a day. The tidal period at river estuary is 24.83 hrs. The discharged water into Shatt Al-Arab River is the summation of discharge of Euphrates Tigris in Al-Qurna. Shatt Al-Arab works as a drainage canal for sat water coming from Al-Huwayza marsh and Swaib project area. So, the discharged water into Shatt Al-Arab from Tigris River must be present in the study. The averaged maximum monthly discharge of Tigris River for the period (1980-2004) is 280m^3/s, while the averaged minimum monthly discharge for the same period is 32m^3/s. Exploration the effect of Garmat Ali River in the restoration of Hammar Marsh through the high tide, the stage hydrograph of Shatt Al-Arab River in the nearest station to Garmat Ali River or at the station of available hydrological records is needed. AL Ma'aqal station will be chosen as a boundary condition of Shatt Al-Arab River. The daily two high and two low water levels in Shatt Al-Arab at Ma'aqal in 1997; for example the data of Feb, 1997; as in Table(1).

Table (1) High and Low Water Tides at Ma'aqal; Feb-1997.

	High water		Low water	
Date	Time	Height m	Time	Height m
1-Feb	9:06	1.60	5:21	1.00
	22:02	2.10	16:02	0.80
2-Feb	10:30	1.50	6:36	1.00
	22:55	2.20	16:44	0.90
3-Feb	12:14	1.60	8:02	0.90
	-	-	17:45	1.00
4-	0:03	2.30	9:29	0.80

Feb	14:06	1.70	19:00	1.10
5-Feb	1:11	2.30	10:47	0.80
	15:12	1.90	20:20	1.10
6-Feb	2:09	2.40	11:51	0.80
	16:11	2.00	21:40	1.10
7-Feb	3:00	2.40	12:43	0.70
	17:04	2.00	22:53	1.10
8-Feb	3:52	2.40	13:25	0.80
	17:50	2.10	23:58	1.10
9-Feb	4:42	2.40	14:00	0.80
	18:30	2.20	-	-
10-Feb	5:29	2.40	0:59	1.10
	19:04	2.20	14:28	0.80
11-Feb	6:18	2.30	1:56	1.10
	19:39	2.20	14:54	0.90
12-Feb	7:12	2.20	3:00	1.20
	20:19	2.20	15:20	0.90
13-Feb	8:05	2.00	4:07	1.10
	20:58	2.20	15:44	0.90
14-Feb	9:04	1.80	5:11	1.10
	21:44	2.20	16:12	0.90
15-Feb	10:20	1.60	6:22	1.00
	22:32	2.10	16:47	0.90
16-Feb	12:10	1.50	7:41	0.90
	23:33	2.10	17:37	1.00
17-Feb	13:42	1.50	9:05	0.80
	-	-	18:43	1.10
18-Feb	0:45	2.10	10:22	0.70
	14:49	1.60	19:58	1.20
19-Feb	1:47	2.20	11:17	0.70
	15:38	1.80	21:13	1.20
20-Feb	2:35	2.30	11:58	0.80
	16:22	1.90	22:15	1.30
21-Feb	3:16	2.30	12:32	0.80
	16:59	2.00	23:02	1.20
22-Feb	3:53	2.30	13:00	0.90
	17:30	2.10	23:40	1.20
23-Feb	4:30	2.30	13:27	1.00
	17:57	2.10	-	-
24-Feb	5:03	2.20	0:16	1.20
	18:18	2.10	13:51	1.00
25-Feb	5:38	2.20	0:56	1.20
	18:39	2.20	14:10	1.00
26-Feb	6:13	2.20	1:41	1.20
	19:03	2.20	14:27	1.00
27-Feb	6:49	2.10	2:29	1.20
	19:30	2.20	14:39	1.00
28-Feb	7:23	2.00	3:18	1.20
	20:00	2.20	14:46	1.00

Topographical Data Analysis

The topographical information is consists of two parts; The collected data from different sources and the topographical survey with ground equipments. During the surveying, collected data from different sources are available. The team focus attention towards newly satellite images that providing a scope details of Hammar Marsh, the length and location of channels or rivers, the intersection of the existing rivers or channels with each others, and specifying the location of the existing hydraulic structures. Using the ground equipments, 50 cross sections and 7 profiles are surveyed. The location of the 50 surveyed cross sections is in Al-Hammar marsh inner and outer boundaries with seven longitudinal profiles. 15 cross sections of Shatt Al-Arab River had been collected from MOWR, the Directorate of Gages which have been surveyed in 2006. These cross sections are started from Al-Qurna towards Al-Maqal. Table (2) shows the GPS of the collected cross sections.

Table (2) Location of Shatt Al-Arab River Cross Sections

Section Name	East	North
Sec 1	733240	3432822
Sec 2	736675	3431203
Sec 3	736256	3428553
Sec 4	737905	3423778
Sec 5	740808	3419814
Sec 6	742967	3416669
Sec 7	746129	3411977
Sec 8	750656	3407584
Sec 9	759993	3404755
Sec 10	764771	3392047
Sec 11	765740	3387447
Sec 12	766277	3386570
Sec 13	767431	3385152
Sec 14	768565	3384244
Sec 15	770365	3383385

DEM and Storage Curves

These surveying details are used to create the updated digital elevation model (DEM) concerning the Hammar Marshes. The DEM of Hammar Marsh is shown in Figure 3. With the help of Arc-View software, the updated DEM will provide a powerful background for the analysis, particularly the stage-volume and area-elevation curves of the marsh area within any scenario of inundation. In addition to that, DEM grids are necessary in the construction of the numerical model as a geometric data.

The stage-volume and area-elevation curves are shown in Figures 15 and 16. The increment in surface area due to the water level variation gives good idea about the best required amount of water to inundate a reasonable area of the marsh. From the percentage increment of surface area, water level of 2.7 m AMSL is the goal of our study. This water level will provide storage of 1477milion m^3 with a surface area of 1331 Km^2.

3 Model Results and Discussion

Studying the tidal effect of Shatt Al-Arab on Hammar Marsh through Garmat Ali River needs an estimation of the discharged tidal water into the marsh during the high water tide. A hydrologic routing model and steady / unsteady hydrodynamic circulation model (RMA2) were prepared to analyze flow pattern inside the marsh.

A finite element meshes of about 4000 elements have been developed over an area of 1552 km^2 is shown in Figure 4. The model inlets are presented along the direction of the proposed locations of feeding, the first location is the ends of Um Nakhla project canals, the second location is the main canals of Al-Malha project and the last location is the main two canals of Al-Shafi and Al-Ghumaeech project. The outlet is located near the drying embankment in the south-east part of the marsh near Garmat Ali River. The culverts along Ar Rumailla road are also considered. The meshes are built using an adaptive tessellation technique for triangle elements and a patch technique for rectangular one.

A total number of 80 cross sections were constructed and obtained from the DEM through the Arc-View GIS with HEC- GEO-RAS extension. These cross sections are covering the marsh area with different spacing according to the hydraulic requirements. The hydrologic data of the recent years have been used in the implementation of the hydraulic model. The existing marsh hydraulic structure (Ar Rumaila culverts are taken into Consideration in the model. The boundary conditions are defined as a flow hydrograph in all feeding locations while the downstream boundary condition is considered as a stage hydrograph taken into consideration the tidal effect to investigate the location of stagnant and to estimate the amount of water that may enter from the tidal phenomena with and without a hydraulic structure. The Manning n is to be taken 0.045 for non vegetated portion when the water depth becomes more than 2 m; while it is equal to 0.070 for vegetated areas when the water depth becomes less than 2 m. The value of eddy viscosity affects stability and turbulent fluid characteristics. Ultimately, more than one technique was adapted in the definition of the eddy viscosity number.

Depending on the results of model, a construction of a head regulator on Garmat Ali River with a designed discharge of 500m^3/ sec near the navigation locks on the drying embankment is necessary to control tidal flow, as well as a gated structure in Ar Rumaila road site instead or with the existing 334 pipes. The designed discharge of the structure is 600m^3/sec. The locations of the proposed hydraulic structures are shown in Figure 5.

The effect of tidal wave on discharged water into or out of the marsh without a hydraulic structure at the down stream end is shown in Figure 6. The net inflow water into the marsh is started when water level at Garmat Ali River is higher than 2.1 m. The period of 25 days will provide an extra storage of 64.8 million m^3 within the marsh area during the high water tide. In other words it represents about 15% reduction in the required inflow discharges from all feeders for the purpose of restoration.

The depths of water, inundated areas and velocity trace are shown in figures 7, 8, 9, 10, 11 and 12. The green color in the all figures concerning water depth represents the shallow regions while the blue color represents the deep areas. The velocity circulations are inserted as a hyperlink to explain the locations of stagnant velocities, locations of high velocity and the inundated areas within the marsh. It is worthwhile to notice that the vegetation effects have been taken into consideration in the analysis of flow circulation within the region in terms of short velocity vectors and islands. These figures are repeated for three different discharge scenarios:

- The normal required discharge of 200m3/sec.
- The minimum required discharge of 80m3/sec.
- The maximum Flood discharge of 600m3/sec.

4 Conclusions

1- 15% reduction in the required inflow discharges from all feeders for the purpose of restoration can be acheived.The net inflow water into the marsh is started when water level at Garmat Ali River is higher than 2.1 m. The period of 25 days will provide an extra storage of 64.8 million m^3 within the marsh area during the high water tide.

2- Construction of a head regulator on Garmat Ali River with a designed discharge of $500m^3$/ sec near the navigation locks on the drying embankment is necessary to control tidal flow, as well as a gated structure in Ar Rumaila road site instead or with the existing 334 pipes. The designed discharge of the structure is $600m^3$/sec.

5 References

1. Al-Samari, M. J. “Irrigation and Drainage Projects in Messan, Basra, and Nasiriya”, Ph.D. Thesis, University of Baghdad. Iraq 1999.
2. ”Building a Scientific Basis for Restoration of the Mesopotamian Marshlands”, The Iraq Foundation, 2003.
3. ”Desk Study on the Environment in Iraq”, UNEP, 2003.
4. ”Environment in Iraq: UNEP Progress Report”, 2003.
5. "General Scheme of Water Resources and Land Development in Iraq", Ministry of Irrigation of Iraq. Moscow-Baghdad 1982.
6. “HEC-RAS Manual”, US Army Corps of Engineers, Hydrologic Engineering Center HEC, USA Oct 2002.
7. “HEC Geo-RAS Manual”, US Army Corps of Engineers, Hydrologic Engineering Center, USA Oct 2002.
8. ”Iraq Marshlands Restoration Program”, U.S. Agency for International Development, Iraq 2004.
9. "Mathematical Model of Flow in Hammar Marsh, Restoration of Central Marshes Study Volume V”, AL-Tawasul International Company for Engineering Design and Consultants, CRIM, Baghdad, Iraq 2006.
10. “Meteorological Stations Records of Southern Region of Iraq”, Ministry of Transportation and Communications, 2006.
11. ”The Mesopotamian Marshlands: Demise of an Ecosystem”, UNEP, 2001.

12. "Navigation Study of Euphrates River", SOGREAH Consulting Engineering, Grenoble, France 1986.
13. “NEW EDEN Master Plan for Integrated Water Resources Management in the Marshlands area”, Ministry of Water Resources, Ministry of Environment, Ministry of Municipalities and Public Works which Prepared in cooperation with the Italian Ministry for the environment and Territory and the Free Iraq Foundation, Italy April 2006.
14. SMS Manual, Environmental Modeling Research Laboratory, Brigham Young University, USA, Dec 2003.
15. "Shatt Al-Arab Project", Feasibility report, POL Service and Hydroproject, Basrah, Iraq 1981.
16. “Support for the Environmental Management of the Iraqi Marshes”, UNEP and AUB, Volume II-B, 1988.
17. "The problem of high water levels in Al-Hammar Marsh", Ministry of Irrigation of Iraq, Al-Furat Center1989.
18. "The Study of Al-Hammar Marsh and Shatt Al-Arab River", Ministry of Irrigation of Iraq, Al-Furat Center 1987.
19. "Topographical Surveying, Restoration of Hammar Marshes Study Volume VI", AL-Tawasul International Company for Engineering Design and Consultants, CRIM, Baghdad, Iraq 2006.
20. .”The Iraqi Marshlands: A Human and Environmental Study”, AMAR International Charitable Foundation, Iraq 2003.
21. “Water and Sanitation”, United Nation and World Bank, Working Paper, October 2003.

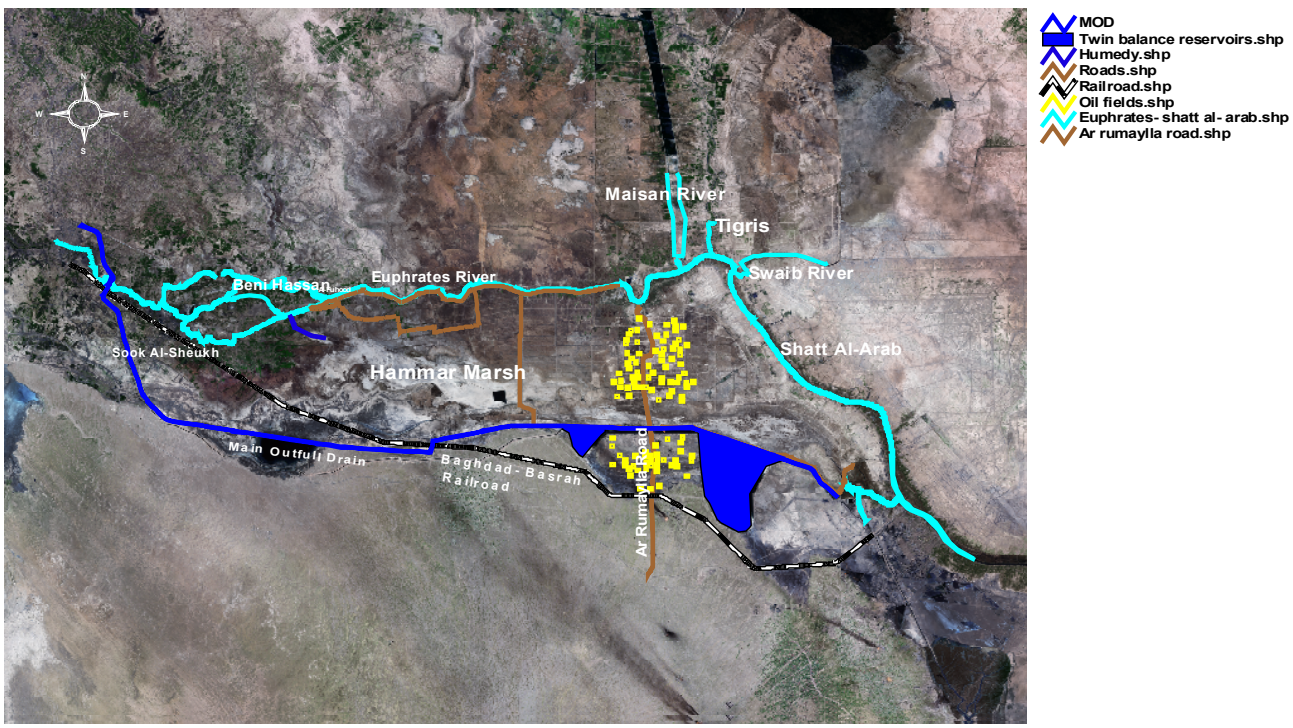

Figure 2: Main Obstructions before 1990

This page intentionally left blank

Numerical Simulations of Coastal Floods and Morphological Changes due to Sea Level Rise and Hazardous Storm

Yan Ding[1], Moustafa Elgohry[2] , and Sam S. Y. Wang[3]
[1]Ph.D., A.M. ASCE, Research Assistant Professor, National Center for Computational Hydroscience and Engineering, The University of Mississippi, University, MS 38677
[2]Graduate Student, Same Institute
[3]Ph.D., P.E., F. ASCE, F.A.P. Barnard Distinguished Professor & Director, Same Institute

ABSTRACT

This paper presents a simulation approach for assessment of the impacts of sea level rise (SLR) on an estuary under complex hydrological conditions such as storm wave, tide, river flood, and sediment transport from rivers to estuary and coast. An integrated coastal/estuarine processes model is used to simulate hydrodynamic and morphodynamic responses to several scenarios of SLR and hazardous storms. Numerical results indicate that this model enables to simulate coastal flooding/inundation, shoreline retreat, and morphological change and respond correctly the interactive impacts of SLR and storms; it is therefore applicable to coastal/estuarine water planning and management for the purpose of flood prevention and erosion protection against the global mean SLR and hazardous storms.

INTRODUCTION

Global mean Sea Level Rise (SLR) is one of the significant impacts of global climate changes since the 20th century. A continued global SLR has been referred by various studies (Gibeaut 2007, Walton Jr. 2007, Williams et al. 2008, Feldman 2008, Gill et al. 2008, Batten 2008). The sea level is not only rising, but also accelerating due to the increasing emission of greenhouse gases, for instance carbon dioxide. Most climate modeling work is based on the increasing rate of SLR. In a more recent study, the Intergovernmental Panel on Climate Change (IPCC) reported that the average global mean sea level rose at an average rate of 1.8 mm per year from 1961 to 2003 and at an average rate of 3.1 mm per year from 1993 to 2003 (IPCC 2007).

Sea level rise may increase the susceptibility of coastal populations and ecosystems through the permanent inundation of low-lying coastal regions, amplification of episodic flooding events, and increased beach erosion and saline intrusion. Ultimately, this may lead to the retreat of millions of people, severe damage to coastal infrastructure and property, and a considerable loss of coastal ecosystems (Nicholls and Lowe 2004). Under a local SLR condition, more frequent extreme hydrological events such as hazardous storms, hurricanes, and high tides may cause more severe damages due to flooding/inundation and coastal erosion than ever on coastal infrastructure, shoreline, wetland, and ecosystem.

SLR will modify hydrodynamic processes and morphological features at coasts and estuaries. Therefore, SLR will change storm wave heights and lengths, and tidal prisms and currents. The magnitude of this effect depends on bathymetries, tide ranges, as well as properties of wave and wind. This effect can be reproduced by using hydrodynamic models provided that the modeling process and parameters are properly based on flow conditions since the modeled conditions represent projected future scenarios beyond the calibrated conditions (ASCE Task Committee on Sea Level Rise and Its Effects on Bays and Estuaries 1992). In addition, SLR may change the morphological equilibrium between the mean sea level and sediment supply which is related to the local bed changes and shoreline relocation (retreat/accretion). The increase in sea level will change not only the coastal landscape due to inundation, but also bedform due to the retreated shores and approaching storm waves; it is therefore important to investigate the changes of hydrodynamic and morphodynamic processes due to both SLR and storms in coastal and estuarine waters for assessment of environmental impacts of SLR in combination with storms, typhoons, or hurricanes.

The study of hypothetical SLR scenarios to assess the SLR-related impacts has been performed in previous studies (CCSP 2008; Cooper et al. 2005). For example, CCSP (2008) used three assumed SLR scenarios (0.3, 0.5, and 1.0 m of SLR by 2100) to evaluate several aspects of SLR impacts for the mid-Atlantic US coast using a range of elevation data sets which have large variations in vertical resolution and horizontal accuracy. Cooper et al. (2005) applied digital elevation models to study the impact of projected sea level rise to the New Jersey coast. They used two relative sea level rise projections, 0.61 meter and 1.22 meter to study what areas could be chronically inundated. The used maps however do not reflect the flooding or inundation that could occur at a precise location. Unfortunately, most of the previous researches have neglected the primary SLR impact on morphological changes due to sediment transport and increased storm waves.

The goal of this study aims to simulate hydrodynamic and morphodynamic responses to SLR and storm by using a two-dimensional coastal hydrodynamic and morphodynamic simulation model, CCHE2D-Coast. This study did not estimate how much the SLR will be; instead, it used different hypothetical local SLR scenarios which are broadly based on recent SLR forecasting studies combined with historical storm as hydrological forcings. In this study, the application of CCHE2D-Coast demonstrated the predictions of the morphological changes in an estuary due to a storm flood event and five hypothetical SLR scenarios.

MODEL DESCRIPTION

CCHE2D-Coast, a coastal/estuarine process model developed in the National Center for Computational Hydroscience and Engineering (NCCHE) has been utilized to assess the impacts of the SLR on coasts and estuaries under combined hydrological conditions such as storm waves, tides, river flood, as well as sediment transport from river reaches to the offshore (Ding and Wang 2007; Ding et al. 2007). This integrated coastal process model is composed of three integrated submodels to simulate waves, tidal and wave-induced currents, and sediment transport and morphological change.

The CCHE2D-Coast wave model enables to simulate irregular wave deformations including refraction, diffraction, wave breaking, etc. The hydrodynamic model is capable of computing tide, wave-induced currents, and wave-current interaction due to different physical forces, for example, tides, waves, river inflow, wind, bottom roughness, and Coriolis force. The morphodynamic process model is to simulate sediment transport and morphological change due to combined waves and currents driven by river flows, tidal flows, and nearshore currents. The integrated model has been built in a developed and well validated simulation package, CCHE2D (Jia et al. 2002). The three submodels can support a non-orthogonal mesh so as to efficiently simulate complex geometry in coastal and estuarine areas. CCHE2D-Coast has been extensively verified and validated by a number of previous studies. One may refer to Ding et al. (2006) and Ding and Wang (2008) for the details of model development and validation.

COMPUTATIONAL DOMAIN AND BOUNDARY CONDITIONS

The study site is a medium-sized estuary, which is located at the west coast of Taiwan Island, and has a river mouth sand bar, two inside islands, and two rivers as shown in Figure 1. The estuary is subjected to various hydrological forcings such as river inflows, waves, tides, winds, etc. The sediments in the estuary can be transported due to river flows, longshore currents, tidal flows, wave breaking, etc. In addition to flooding and inundation, severe morphological changes such as scours at the river mouth, depositions in the tidal river reaches, may take place due to river flood, storm waves and surges.

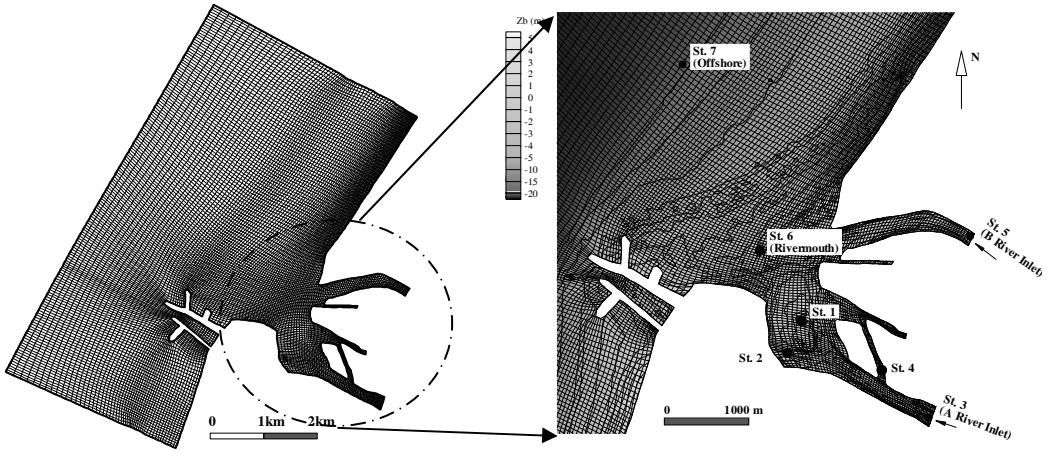

Figure 1. Computational domain and close-up view of the estuary

Possible SLR may cause disastrous flooding and inundation in this area during storm periods due to dense population in the coastal community. In order to examine the impacts of SLR during storms on the estuarine area, a computational domain was set up to cover the investigated estuary (Figure 1). A real storm (typhoon) which attacked this coast during a period from 8/31/2005 to 9/2/2005 was used as the storm event for the study. The storm flood inflows from the two rivers were applied to the

two river inlets as the river inflow boundary conditions. As shown in Figure 2, the two hydrographs at the inlets of the two rivers were produced beforehand by simulating respectively the storm flood flows in the two rivers from far upstream down to the estuary using a one-dimensional river flow model. The peak discharge was 2013.67m^3/s in the river at south and 992.66m^3/s in another river at north, respectively, in which the peak flood in the north river remained two hours of delay in comparison with the one at south.

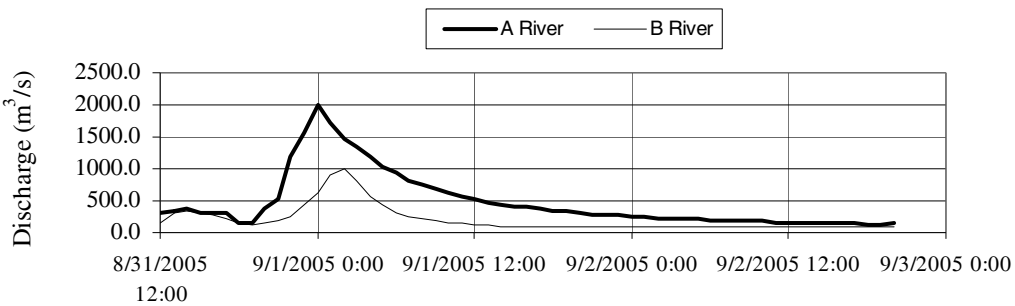

Figure 2. Hydrographs at two river upstream inlets during a storm flood event

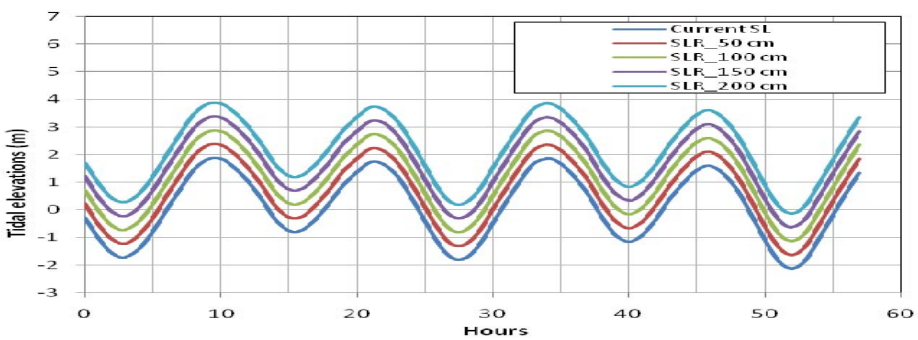

Figure 3. Tidal elevations boundary conditions at offshore

In this study, CCHE2D-Coast was applied to simulate flood flows and morphodynamic processes in the estuary due to the storm event and five hypothetical SLR scenarios (i.e. 0.5, 1.0, 1.5, 2.0 meters, and a case without mean sea level change) to reflect the increases of mean sea level. The mean SLR cases can be considered as the different scenarios of tidal elevations at the open sea. The SLR was added to the measured tidal elevations during the storm period to simulate the tides under the conditions of the SLR. Figure 3 shows five cases for tidal elevations at offshore which were applied to simulate the five different hypothetical SLR scenarios. The boundary conditions of the tidal elevations at offshore over the storm period were produced by computing ocean flows over a much larger regional grid covering the estuary using a two-dimensional ocean flow model. As the boundary conditions of wave model at offshore of the estuary, the wave properties (i.e. significant heights, averaged periods, and mean directions) at offshore were computed by using the SWAN wave model. The obtained significant wave heights varied in the range from 0.5 m to 1.6 m during the flood event. Meanwhile, Figure 4 shows the time series of prevailing wind speed and direction which has been used in this study as surface wind forcing over the estuary. The wind speed varies from 0.3 m/s to 16.4

m/s. Because the complexity and uncertainty of the future evolution of current bathymetry, this study assumed the current bathymetry within the computational domain will not change until the storm event takes place.

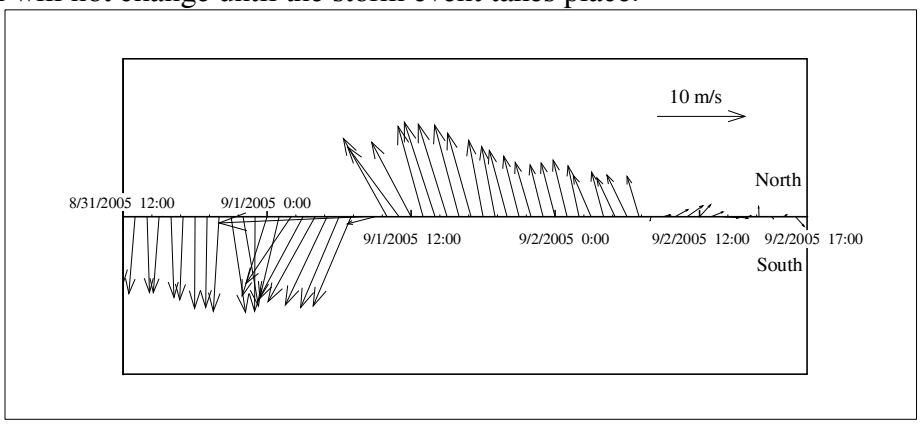

Figure 4. Wind speed and direction over the estuary during the storm event

NUMERICAL RESULTS OF HYDRODYNAMIC AND MORPHOLOGICAL CHANGES

In this section, the computed results of wave, current, sediment transport, and morphological change under the selected SLR scenarios are presented.

Figure 5 shows the distributions of computed wave properties (i.e. significant wave heights and mean directions) at the flood peak under the SLR conditions. Along with the increase of the mean sea level in the estuary from the current sea level (no SLR) to 2-meter SLR, the offshore waves could invade the estuarine area from the river mouth toward the estuarine river reaches. In comparison with the case for the current sea level (Figure 5a), sea level rises from 0.5 m to 2.0 m would promote the invasion of offshore waves inside the estuary for longer periods during the storm event, and further increase the flooding area and change the morphological features in the bay area.

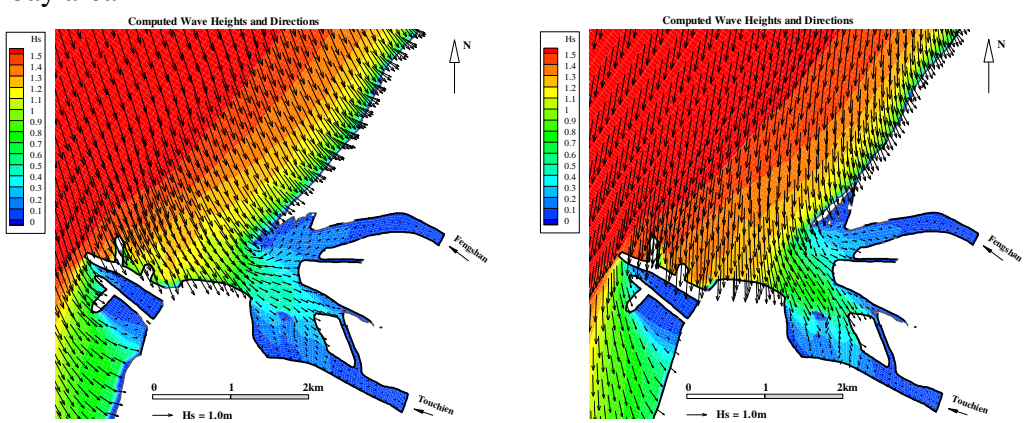

(a) Current sea level (b) SLR = 2.0 m

Figure 5. Comparison of computed wave height and directions at flood peak

Figure 6 shows the comparison of the computed current fields at the flood peak due to different SLR cases over a range from the current sea level to 2.0 m SLR. The results show that there are significant increase in water elevations, offshore water invasion inside the estuary, and widening inundation areas along with the continual increase of SLR. Furthermore, the river mouth bar is increasingly inundated by overflowing waters for longer period.

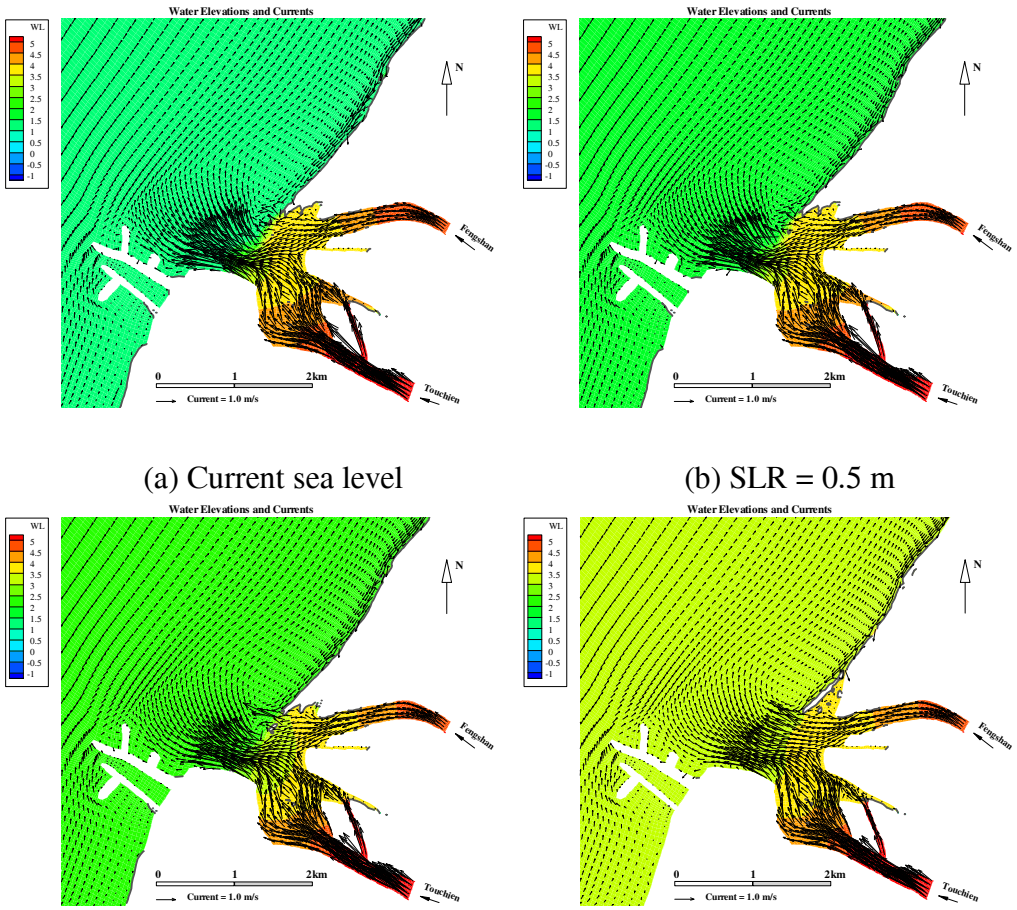

(a) Current sea level (b) SLR = 0.5 m

(c) SLR = 1.0 m (d) SLR = 2.0 m

Figure 6. Comparison of computed water elevations and currents at the flood peak

The differences of water elevations at seven different monitoring stations due to different SLR scenarios have been examined. As shown in Figure 1b, these stations represent offshore, river mouth, three upstream cross sections and two inlet locations. As an example, for only two cases, the time series of water elevations at all stations are plotted in Figure 7. Furthermore, the inter-comparisons of water elevations at four stations under the five SLR scenarios are shown in Figure 8. The following remarks can be summarized from these plots/graphs: (1) there are obvious wet/dry cycle change at all upstream monitoring stations (Stations 1 to 5) due to the continual increase in SLR. For example, by comparing Figures 9a and 9b, the oscillation of water elevations for stations 1 and 2 has been induced due to the increased effect of offshore tidal waves. This effect is spreaded for other upstream stations by continual

increase in SLR as plotted in Figures 9c and 9d. (2) As it can be seen from Figure 10a, there is significant inundation effect at the river mouth bar due to continual increase in SLR and the river mouth area behaves like offshore station after SLR 1.5 m. (3) The upstream river area is more susceptible to the tidal effect as it is shown in Figures 9c, 9d and 10d. For example as shown in Figure 10d for A River inlet, the continual increase in SLR promote the invasion of tidal waves inside the rivers and increase the water elevations.

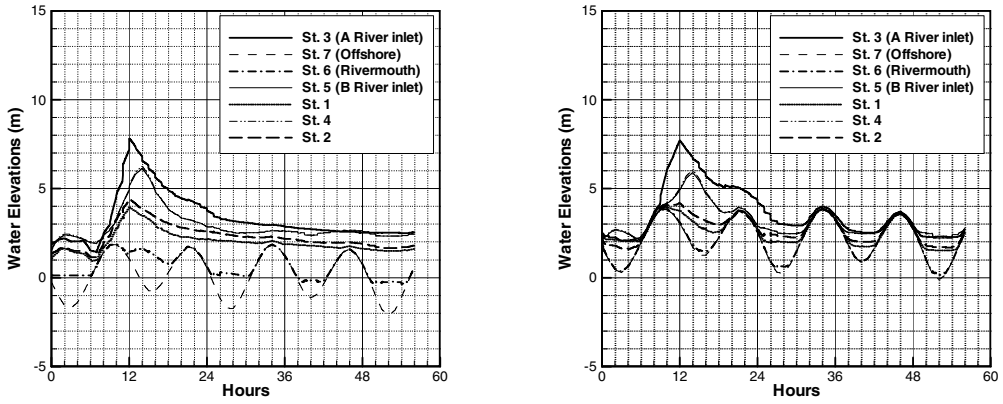

(a) Current sea level (b) SLR = 2.0 m

Figure 7. Comparison of computed water elevation at seven stations due to different SLR scenarios

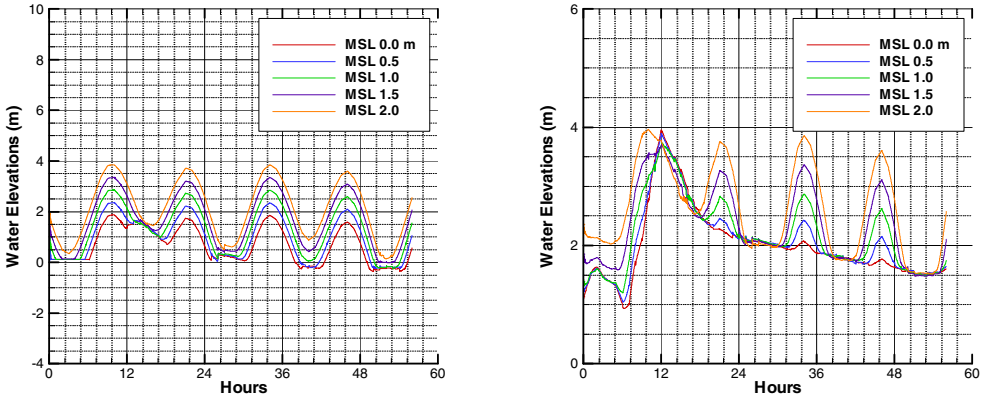

(a) Station 6 (Rivermouth) (b) Station 1

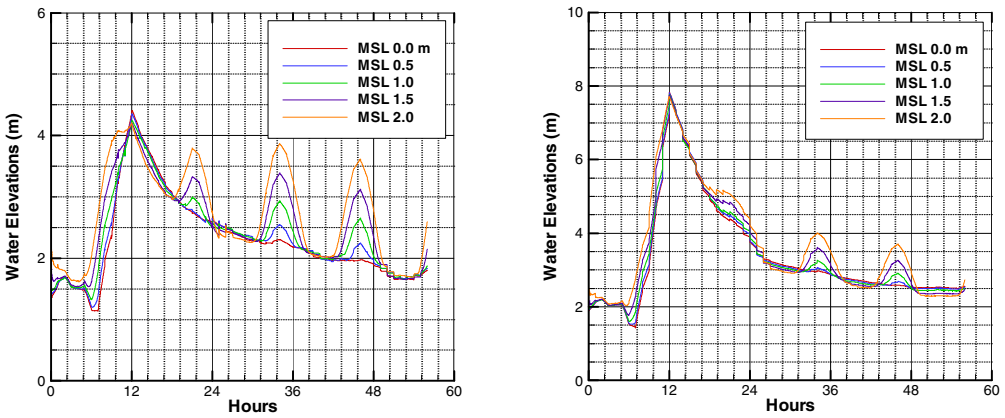

(c) Station 2 (South bank) (d) Station 3

Figure 8. Computed water elevation at different stations

The morphodynamic process is complicated in the investigated estuary due to the existence of the two inside island, which affects the river course and then the erosion/deposition processes. However, the model was effectively able to simulate these processes as depicted in Figure 9, which shows that there are significant changes in erosion/deposition areas due to different SLR. It also shows the gradually reducing areas of deposition in the estuary region for increasing SLR at offshore. This could occur due to the increased sediment transport capacity of flow with continual increase in SLR. The results indicate that with the increasing of SLR, the river mouth bar is increasingly eroded, which consequently will cause a significant landward displacement of the shoreline.

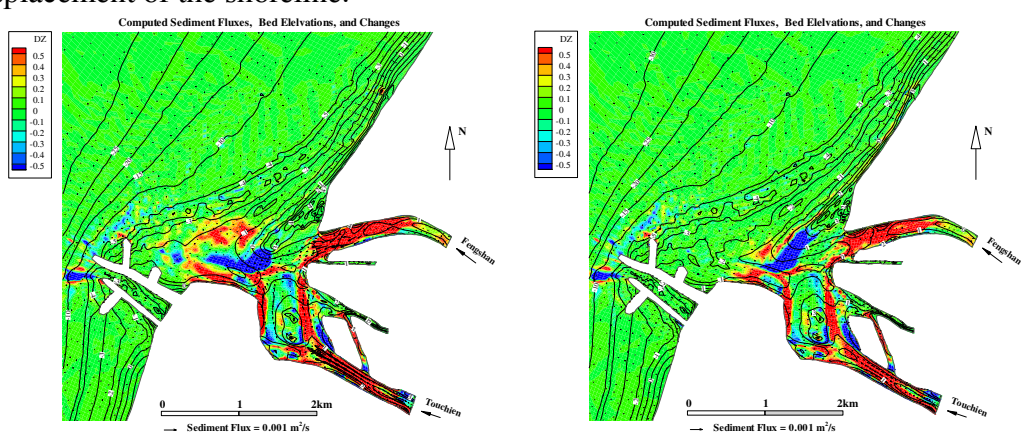

(a) Current sea level (b) SLR = 2.0 m

Figure 9. Comparisons of computed bed changes after the storm flood (The unit of bed change DZ in the legend: m)

CONCLUSIONS

This paper presents a simulation approach for assessment of the impacts of sea level rise (SLR) on an estuary under complex hydrological conditions such as storm wave, tide, river flood, and sediment transport from rivers to estuary and coast. By using the CCHE2D-Coast, the hydrodynamic results show that there are obvious wet/dry cycle changes at all upstream monitoring stations. Furthermore, there is a significant inundation effect at the river mouth bar in case of SLR higher than 1.5m. In addition, the river area is more susceptible to the tidal effect at SLR 0.5m. The morphodynamic results show that there is apparent change in erosion/deposition areas due to SLR. Especially, the river mouth bar is more exposed to be eroded, which consequently could cause landward shoreline retreat due to inundation and waves approaching to inland.

The preliminary test results of the study demonstrate that the CCHE2D-Coast model is able to effectively simulate the complex hydrodynamic and morphodynamic processes in coasts and estuaries under different SLR scenarios. Therefore, the deployed model can be effectively used in coastal regions planning and management to predict the eroded and inundated areas due to the global mean SLR and hazardous storms. The results are promising for future more detailed analysis, which may incorporate land subsidence effects.

ACKNOWLEDGMENT

This work was a product of the research partially sponsored by the National Center for Computational Hydroscience and Engineering at The University of Mississippi. The authors would like to thank Dr. Keh-Chia Yeh for their help to collect the boundary conditions for the study.

REFERENCES

ASCE Task Committee on Sea Level Rise and Its Effects on Bays and Estuaries. (1992). Effects of Sea Level Rise on Bays and Estuaries. Journal of Hydraulic Engineering, ASCE, 118(1), 1-10.

Batten, B. K., Weberg, P., Mampara, M., and Xu, L. (2008). Evaluation of Sea Level Rise from FEMA Flood Insurance Studies: Magnitude and Time-Frames of Relevance. In: Solutions to Coastal Disasters 2008, Ed. By Louise Wallendorf et al., ASCE, Proceeding of Solutions to Coastal Disasters 2008 Conference, April 13-16, Oahu, Hawaii, pp.62-71.

CCSP (U.S. Climate Change Science Program). (2008). Coastal Sensitivity to Sea Level Rise: A Focus on the Mid-Atlantic Region for Synthesis and Assessment Product 4.1. http://www.climatescience.gov/Library/sap/sap4-1/public-review-draft/. <May 16, 2008>.

Cooper, M. J. P., Beevers, M.D., and Oppenheimer, M. (2005). Future sea level rise and the New Jersey coast – Assessing potential impacts and opportunities, Science, Technology and Environmental Policy Program. Woodrow Wilson School of Public and International Affairs, Princeton University, http://www.princeton.edu/~cmi/news/Future%20of%20 Sea%20 Level %20Rise%20and%20the%20New%20Jersey%20Coast.pdf. <Apr.20, 2008>.

Ding, Y., Wang, S. S. Y., and Jia., Y. (2006). Development and validation of a quasi three-dimensional coastal area morphological model. Journal of Waterway, Port, Coastal, and Ocean Engineering, ASCE 132(6), 462-476.

Ding, Y., and Wang, S.S. Y. (2008). Development and application of coastal and estuarine morphological process modeling system, Journal of Coastal Research, Special Issue No. 52, pp127-140.

Ding, Y., Yeh, K.-C., Chen, H.-K., and Wang, S.S.Y. (2007). Simulations of morphodynamic changes due to waves and tides in an estuary using CCHE2D-coast model. World Environmental and Water Resources Congress 2007: Restoring our Natural Habitat, Ed. By K.C. Kabbes, Proceeding of ASCE-EWRI Congress 2007, May 15-19, Tampa, Florida.

Ding, Y., and Wang, S. S. Y. (2008). Numerical simulations of coastal flood and morphological change due to hazardous hydrological conditions at coast and estuary. In: Solutions to Coastal Disasters 2008, Ed. By Louise Wallendorf et al., ASCE, Proceeding of Solutions to Coastal Disasters 2008 Conference, April 13-16, Oahu, Hawaii, pp349-360.

Feldman, R. L. (2008). Recommendations for Responding to Sea Level Rise: Lessons from North Carolina. In: Solutions to Coastal Disasters 2008, Ed. By Louise Wallendorf et al., ASCE, Proceeding of Solutions to Coastal Disasters 2008 Conference, April 13-16, Oahu, Hawaii, pp15-27.

Gibeaut, J. C. (2007). Modeling Future Coastal Wetland Transition Induced by Relative Sea-Level Rise. In: Coastal Sediment'07, Ed. By Nicholas C. Kraus and Julie Dean Rosati, Proceeding, 6th Int. Symposium On Coastal Engineering and Science of Coastal Sediment Process, May 13-17, New Orleans, LA, pp1193-1199.

Gill, R. L., Allen, A. L., Fenstermacher, L. E. and Zervas, C. (2008). Sea Level Trends, Inundation Analysis, and Exceedance Probability: Results and Applications from Long-Term NOAA Tide Stations. In: Solutions to Coastal Disasters 2008, Ed. By Louise Wallendorf et al., ASCE, Proceeding of Solutions to Coastal Disasters 2008 Conference, April 13-16, Oahu, Hawaii, pp50-61.

IPCC (2007). Climate Change 2007: Synthesis Report. Intergovernmental Panel on Climate Change. http://www.ipcc.ch/pdf/assessment-report/ar4/syr/ar4_syr.pdf. <Mar. 31, 2008>.

Jia, Y., Wang, S. S. Y., and Xu, Y. C. (2002). Validation and application of a 2D model to channel with complex geometry. International Journal of Computational Engineering Science 3(1), 57-71.

Nicholls, R.J., and Lowe, J.A. (2004). Benefits of Mitigation of Climate Change for Coastal Areas. Global Environmental Change 14, 229-244.

Walton Jr., T. L. (2007). Projected sea level rise in Florida. Journal of Ocean Engineering 34, 1832-1840.

Williams, S. J., Gutierrez, B. T., Thrieler, E. R., and Pendleton, E. (2008). Geologic Effects and Coastal Vulnerability to Sea-Level Rise, Erosion, and Storms. In: Solutions to Coastal Disasters 2008, Ed. By Louise Wallendorf et al., ASCE, Proceeding of Solutions to Coastal Disasters 2008 Conference, April 13-16, Oahu, Hawaii, pp1-14.

Comparison of HEC-RAS and InfoWorks RS A Case Study in Grand Prairie, Texas

Thomas W. Mountz[1] and Josha Crowley[2]

[1] Managing Engineer, Espey Consultants, Inc., 3809 South Second St., Suite B-300, Austin, TX, 78704; PH (512) 326-5659; email: tmountz@espeyconsultants.com
[2] Project Manager, Espey Consultants, Inc., 3809 South Second St., Suite B-300, Austin, TX, 78704; PH (512) 326-5659; email: jcrowley@espeyconsultants.com

ABSTRACT

The Hydrologic Engineering Center's River Analysis System (HEC- RAS) is a one-dimensional computer model intended to perform hydraulic calculations for a network of open channels. This model is widely available, free of cost and is the most commonly used hydraulic model in the United States. Most HEC-RAS models are steady state. Unsteady flow analysis in HEC-RAS differs in many ways from the traditional steady state analysis. The largest difference involves the ability to input a full hydrograph to analyze the response of the river system to flows (and tailwater conditions) that vary with time.

InfoWorks RS is a hydrologic and hydraulic modeling package by Wallingford Software that is intended to provide a more comprehensive analysis than HEC-RAS. The 2D Module provides detailed surface flooding analysis for overland flows. In addition, the unsteady solution within InfoWorks is reported to be more stable than HEC-RAS. The capabilities of this software package also extend into several areas that HEC-RAS does not; including data management and hydrology calculations inclusive in the model. InfoWorks RS is commonly used in Europe and is being used more frequently in the US in especially complicated modeling and flood forecasting scenarios.

This is a case study on Lower Mountain Creek in Grand Prairie, Texas. The study area is between Mountain Creek Lake and the confluence with the West Fork Trinity River. This area offers many challenges to a traditional HEC-RAS analysis, including relatively flat channel slope, a wide floodplain with split flows through multiple bridge openings, and considerable shallow overbank flooding. A comparison of the results using Steady HEC-RAS, Unsteady HEC-RAS and InfoWorks RS (IWRS) will be presented. The comparison will include not only differences in computational results, but differences in model structure, input requirements, and methodology.

INRODUCTION: LOWER MOUNTAIN CREEK

The flooding risks for Lower Mountain Creek in Grand Prairie, Texas were studied in detail. The hydrologic analysis encompasses the drainage areas of Mountain Creek between Joe Pool Lake Dam and the confluence with the West Fork Trinity River.

The hydraulic analysis of Mountain Creek includes 22,350 linear feet of channel between Mountain Creek Lake Dam and the confluence with West Fork Trinity River. The hydraulic analysis of Thompson's Branch, a tributary to Mountain Creek, includes 4,940 linear feet of channel between Idlewild Street and the confluence with Mountain Creek.

There are three flooding sources in the project area, these are; 1) local flooding, 2) Mountain Creek, and 3) the West Fork Trinity River. Local flooding refers to water falling directly on the area considered or flowing to it on a minor tributary or stream. Mountain Creek flooding refers to water within the main channel and overbanks of Mountain Creek. The West Fork Trinity River can also flood property along Mountain Creek even in the absence of significant flows on Mountain Creek itself.

HISTORY OF HEC-RAS

The US Army Corps of Engineer's (USACE) Hydrologic Engineering Center (HEC) released HEC-2, Water Surface Profiles in 1968. HEC-2 was one of the first open channel hydraulics programs available and could incorporate bridge and culvert analyses and other hydraulics modeling components. HEC released a replacement program in 1995, HEC-RAS (River Analysis System). HEC-RAS incorporated a graphical user interface (GUI) that greatly facilitated input and display of model results. Updates to HEC-RAS are still being actively developed. Among the improvements since the initial version of HEC-RAS are channel modification analysis, mixed-flow capabilities, bridge scour analysis, lateral and inline weir analysis, hydraulic simulation of gated structures, modeling of changes in Manning's "n" in the vertical direction, and geographic information system (GIS) integration capabilities. Full unsteady flow analysis capabilities were integrated in HEC-RAS in 2001.

HEC-HMS (Hydrologic Modeling System) is usually used in conjunction with HEC-RAS to perform the hydrologic computations and determine flow rates and hydrographs used in the hydraulic analysis. HEC-HMS and HEC-RAS have limited GIS capabilities. Two additional programs; HEC-GeoHMS and HEC-GeoRAS are used (in conjunction with ESRI ArcView or ArcMap) to extract GIS data into HEC-RAS or HEC-HMS. For example, HEC-GeoRAS can be used to lay-out and populate the bulk of a HEC-RAS model. The model itself is then fine tuned and the analysis performed within HEC-RAS. The results are then exported back to HEC-GeoRAS to develop floodplains and other visual representations of the analysis results.

STEADY HEC-RAS DETAILS

The Mountain Creek model was created initially using the HEC-2 effective model from the FEMA Flood Insurance Study. Cross-section locations and bridge data were brought into a new HEC-RAS model and then updated with field survey and recent LIDAR topographic data using HEC-GeoRAS. See Figure 1 for the HEC-RAS

model layout. The hydrology was updated in a new HEC-HMS model and flows were applied to specific channel cross-sections.

Conveyance Issues

The Lower Mountain Creek floodplain has been characterized as a "bathtub" because it is relatively flat with a very wide floodplain. As rainfall and runoff increase a large portion of the floodplain is inundated quickly. Flow increases up to and including the 100-year design storm event do not significantly increase the extent of flooding but do increase in depth, hence the "bathtub" analogy. Manning's "n" values for much of the overbanks were set high to account for extensive tree cover in undeveloped areas and for fences and buildings in developed areas

The study area is crossed by three major elevated roadways and one railroad line with two to four bridge openings each. Existing development has blocked or restricted flow access to all but one of the off-channel bridge openings under Jefferson Road and Main Street (Hwy 180). The channel connecting these bridge openings has also been blocked upstream and downstream from direct connection to Mountain Creek; therefore conveyance was restricted on these secondary structures within the HEC-RAS model.

Thompson's Branch

The hydraulic model for Thompson's Branch was created as a separate model and not included in the Mountain Creek flood analysis. The model of this tributary was used primarily to assess the effectiveness of the channel to convey local flows because this area is more severely inundated by the Mountain Creek flood flows perpendicular to the Thompson's Branch channel.

UNSTEADY HEC-RAS DETAILS

Unsteady flow analysis in HEC-RAS differs in many ways from the traditional steady state analysis. The largest difference involves the ability to input a full hydrograph into the model to analyze the response of the river system to flows that vary with time. Additional differences are listed below:

Table 1. Comparison of Steady to Unsteady Solutions

Steady Solution	Unsteady Solution
Energy – profiles computed based on energy losses	Momentum – profiles computed based on sum of forces
Internal energy losses estimated by Manning's and Form Loss equations	External boundary shear represented by Manning's equation
Steady Flow is input (Q=VA) and Inflow = Outflow	Unsteady flow is based on continuity equation (Outflow = Inflow – Storage)

In addition to the computational differences between steady and unsteady HEC-RAS, there are many other differences that require attention when running an unsteady model.

Pilot Channel
A slight modification had to be incorporated into the HEC-RAS geometry to produce a stable unsteady HEC-RAS run. For model stability, a small pilot channel was added to the geometry to guarantee flow in the downstream direction and reduce the effective slope for low flow rates with no impact to maximum calculated water surface elevations.

Flow Locations
The HEC-HMS data was applied to the model differently than for the steady model. It was not appropriate to use the calculated confluence hydrographs within the study reach since these quantities include modified Puls routing information generated by the steady HEC-RAS model. Using these flows would result in double-counting valley storage and over-estimating peak attenuation. Therefore, the individual sub-basin hydrographs within the study reach were added as lateral inflow hydrographs.

Hydraulic Property Tables (HTAB)
The steady HEC-RAS analysis uses the energy equation for an exact hydraulic calculation for each cross section and structure (internal boundary). Due to different requirements of the momentum equation, hydraulic properties are pre-computed for each cross section and structure in the unsteady model. To complete the flow simulation, one must execute the geometry preprocessor to build these rating curves. The Hydraulic Property Table (HTAB) can be viewed for each structure and internal boundary. Any incongruities shown by the HTAB must be resolved prior to attempting the full flow simulation.

Initial Conditions/ Minimum Flow Rate
To avoid sudden changes and computational problems for HEC-RAS, initial conditions must be defined. This is typically represented as a stable flow scenario in the river system prior to the start of the flood simulation desired. The unsteady flow simulation cannot run dry so a minimum flow rate was assumed for the inflow hydrograph at the upstream limit of the model. It is also possible to use the output of a previous simulation to resolve stability problems at the beginning of a run

Time Step
Stability and accuracy can be gained by trying to satisfy the Courant Condition when selecting the computational time step. Generally, a smaller time step will produce a smaller incremental change within the computation and result in a more stable model. For the 1% unsteady model a time step of 20 seconds was selected for a total run of 48 hours.

HEC-RAS RESULTS

The differences between the steady state results and the unsteady results in HEC-RAS were significant. These differences are most likely the cause of different routing techniques. The effects of valley storage and related peak attenuation are accounted for by using modified Puls routing in HEC-HMS in the steady state model and are

calculated by HEC-RAS in the unsteady model. In addition, the unsteady HEC-RAS model shows storage impacts and calculated effects for each individual cross-section, while the steady model is limited to the larger routing reaches as defined within HEC-HMS. The existing condition 1% annual chance event water surface profile was compared to the effective FEMA model results. Generally the results from this study were very similar to the effective model. See Figure 3 for the profile comparison.

HISTORY OF INFOWORKS RS

InfoWorks RS (IWRS) was launched in 2002 with the release of InfoWorks v4.0 as the successor to well established ISIS river modeling software. The first release of InfoWorks RS offered the 1D flow and hydrology simulation capability inside the InfoWorks environment and enhancements included updating the ISIS data model to be geo-referenced; the addition of ground modeling functionality; and the development of an automated flood mapping capability. The GIS functionality of the InfoWorks GUI allowed flood maps to be overlaid on top of ground model data, topographic maps or aerial photography to provide a detailed method of viewing the model results.

Development of InfoWorks v4.5, released during August 2002 saw the inclusion of water quality, sediment transport and PDM conceptual soil moisture runoff model. The ground modeling functionality was enhanced to support both grid based and TIN (Triangular Irregular Networks) based ground models. Most recently, the release of v9.0 has provided a step change to functionality of InfoWorks RS with the inclusion of the InfoWorks 2D module and the HR Breach methods. Representing the flows in 2D provides more detail and accuracy, particularly for local water levels and velocities and is useful for flood damage assessment and analyzing risk from flood inundation. The HR Breach methods allow for simulation of the failure of embankments and dams providing completely integrated 1D, 2D and breach simulation functionality in a single product (single model networks, single data storage, single simulation and single results analysis and post-processing).

INFOWORKS RS DETAILS

InfoWorks RS v.9.0 modeling software is an integrated modeling package that is the equivalent of packaging HEC-HMS, HEC-GeoHMS, HEC-GeoRAS, AND HEC-RAS into one model. It calculates the hydrology and hydraulics from information input and/or developed within the model environment by the user on the GUI interface to integrate with a GIS-based terrain model stored within a common database. One major advantage of IWRS is the ability to generate, for instance, cross-section information, then use it, change it, manipulate it, etc. without impacting the plotting of the data.

Initial Conditions

The model uses a base flow in the steady state condition to generate initial conditions for the full unsteady solution. This is essentially the same as the initial conditions required for the HEC-RAS unsteady model with very similar base flow values. This steady state run is used to solve most of the instability issues that arise as the model begins and because, as in HEC-RAS unsteady, the unsteady model cannot run "dry".

Model Components

The physical components of an IWRS model consist of nodes and links. Nodes are the physical components that include channel sections, flow input, weirs, storage areas, junctions, spill units, etc. The channel sections are generally limited to the stream channel with limited overbanks instead of sections that extend across an entire floodplain as in HEC-RAS. Spill Units are ridge lines or similar flow boundaries (weir, bridge deck, etc.) that will allow "spill" from one node to another. Links are the connections between nodes. All nodes must be linked correctly. The interface includes a validation tool that must be run when changes are made to the nodes and links. This tool allows the user to quickly locate problems and correct them. The model will not "run" until all of the critical validation issues have been corrected. Figure 2 show the IWRS model network.

Importing HEC Model Data

IWRS 9.0 allows the import of data sets from HEC-HMS and HEC-RAS models. One can import rainfall incremental data and/or computed hydrographs. Computed hydrographs can be applied to specific nodes or can, in some cases, be input as lateral flow proportioned across more than one node. One can also import channel cross-section data sets. However, the HEC-RAS bridge details cannot be imported at this time because of significant differences in modeling methodologies.

Bridge Modeling

Bridge modeling methodology is one area, in these users' opinion, that is more user-friendly and accurate in the HEC-RAS model. In IWRS a bridge link applies to the bridge opening only. It can be modeled as one or more arch or rectangular openings between piers or it can be a rectangular opening with the total width and type of piers specified. It will not allow the input of a sloping low chord (bottom of bridge) although it can be reasonable simulated with a series of openings. The bridge deck is a separate node (spill unit) connected to the channel sections with links other than the bridge. The bridge deck or weir if specified must be one elevation. The alternative is to define the deck as the section replacing the underlying ground model points.

Time Step

The steady state event analysis for initial conditions was run using direct input of runoff. The unsteady analysis may be run using either a fixed time step set by the user or an adaptive (variable) time step determined by the program. Use of the adaptive time step reduces some of the instability that may occur in a HEC-RAS unsteady run by allowing the model to test, iterate and determine the most workable solution.

Model Issues

There are only two major issues, at this time, to utilizing IWRS for a flood analysis. The first is that FEMA does not generally accept IWRS as a model for flood map amendments. FEMA will only accept the model if certified by a Cooperating Technical Partner (CTP). The City of Grand Prairie is a CTP thus the impetus for this model and the comparison to the previously completed HEC-RAS model and the cooperation of Wallingford Software in providing this demo copy of the IWRS v.9.0.2 software and limited technical support.

The other disadvantage is the model development learning curve. The differences between modeling with HEC software and InfoWorks are akin to switching between AutoCAD and MicroStation software for drafting. The mentioned drafting programs are different enough that there is a significant learning curve when a long-time user of one switches to drawing with the other. A similar learning curve was found in this comparative analysis with one very notable additional hindrance. The HEC suite of models developed in the US use technical terminology developed here, whereas IWRS, developed in the United Kingdom, uses some different the technical terminology. The confusion found is as basic as a sign that says "WAY OUT" (UK) meaning "EXIT:" (US) or "MIND THE GAP" (UK) instead of "WATCH YOUR STEP" (US). Once the user understands the "language" differences then the model construction becomes more intuitive.

INFOWORKS RS RESULTS

For this preliminary analysis, the IWRS modeling concentrated on the hydraulic analysis using the 1D methodology. The hydrology was input as flood hydrographs previously developed in the HEC-HMS model for Mountain Creek as point and/or lateral nodes approximating the drainge area locations. Cross-sections were imported from HEC-RAS for the existing conditions on Mountain Creek. Overbank length of each section was reduced to limit overbank input in the channel flow and maximize the use of storage areas in the west overbank only because the east side is in the Dallas City Limits and the floodplain extent in there is limited. Figure 2 shows the IWRS model structure.

Unlike the HEC-RAS analysis, the Thompson's Branch channel cross-sections were also imported and modified. A third set of channel sections was developed for the side channel extending from Thompson's Branch to Jefferson Road. This channel was not modeled in HEC-RAS because it is graded from Jefferson Road down to Thompson's Branch (upstream direction for Mountain Creek).

All bridge openings and culverts not located on the main channel of Mountain Creek were input as spill units and/or orifices connecting storage areas and section nodes. Model results are shown on comparative graphs in Figure 3 and Figure 4. Figure 3 shows the 1% (100-year) water surface profiles for each model. The IWRS model shows a substantially lower elevation for any given location. Because this is a preliminary model there may be some additions corrections needed to the offline

structure parameters. Figure 4 shows the calculated maximum flow for each model for Mountain Creek channel sections. This comparison is deceiving because it looks like the IWRS model has "lost" a substantial potion of the flow volume. In the HEC-RAS analyses flow is input to the channel first then apportioned to the overbanks when the channel capacity is exceeded. Because the HEC-RAS sections cover the full extent of the floodplain they include the total volume. The IWRS plot only includes that potion of the event volume carried within each limited channel section. In the model, flow can "spill" to adjacent storage areas depending on water surface elevation. Other flow nodes such as those for Thompson's Branch and/or drainge areas west of the main channel do not reach the Mountain Creek channel until all flow is funneled to it upstream of the IH-30 roadway.

CONCLUSIONS

The previous study on Mountain Creek has already shown the advantage of the HEC-RAS unsteady analysis versus the steady analysis. This paper analyzes those results compared to those modeled by the 1D unsteady results generated by InfoWorks RS 9.0. The preliminary results from IWRS show the potential for more accurate accounting of flow movement and storage outside the main stream channel.

A preliminary analysis of the model results as depicted in Figures 3 and 4 show that the offline bridge openings, especially those under westbound Jefferson Road, may provide more flow capacity than previous anticipated. Greater conveyance through these structures reduces the upstream flood levels and the extent of inundation. Viewing the simulation as it progressed, we noticed that the overbank area located between the railroad line and Main Street (Hwy 180) began to be inundated much earlier in the event than previously thought and was one of the last areas to "dry out" after the rainfall ended. This effect has been corroborated by eye-witness accounts of area flooding.

Despite the learning curve issues we found that the IWRS model does provide an intuitive method to link the various physical features and allow for flow to follow a more "natural" path than may be modeled easily in HEC-RAS. The greatest advantages are the functionality of having all hydrologic, hydraulic, and terrain data in the same database with seamless interaction that allows more rapid analysis, correction, and publishing of results. It appears that the more complex the overbank shallow flooding becomes, the more advantageous IWRS becomes relative to HEC-RAS.

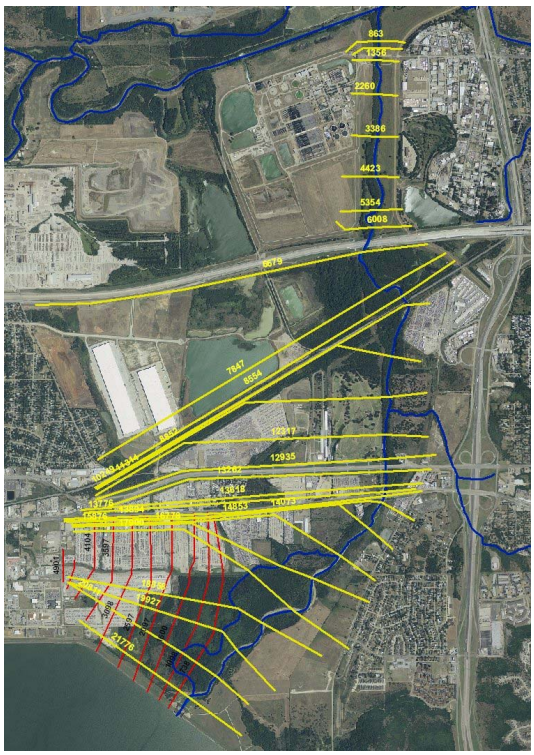

Figure 1: HEC-RAS Model

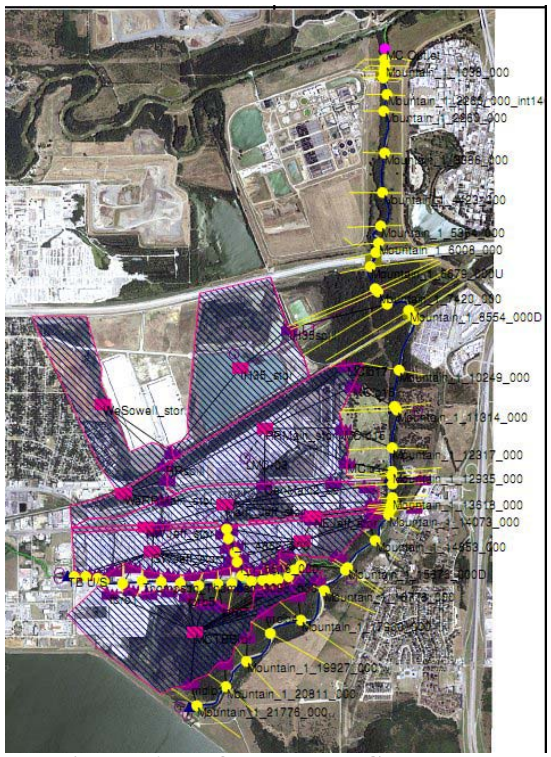

Figure 2: InfoWorks RS Network

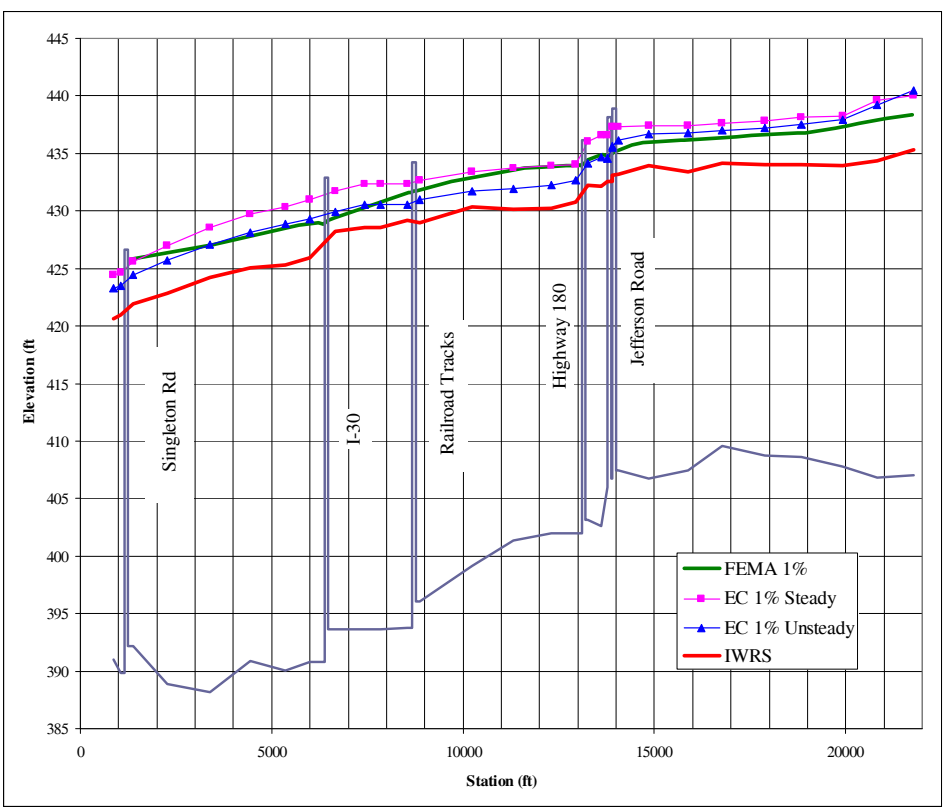

Figure 3: 1% Existing Profile Comparison

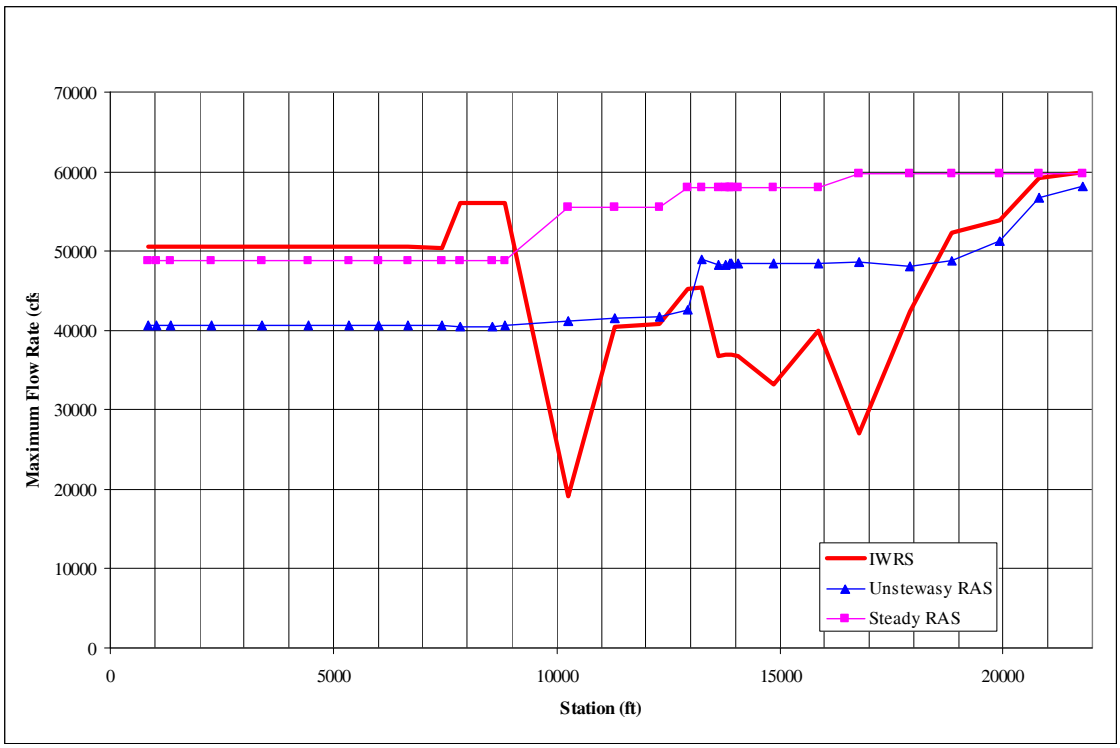

Figure 4: 1% Existing Maximum Flow Comparison

REFERENCES

Haestad Methods, Inc., *Floodplain Modeling Using HEC-RAS*, First Edition http://www.haestad.com/library/

US Army Corps of Engineers, Hydrologic Engineering Center, *HEC-RAS 3.1.3*, May 2005

Vernon R. Bonner, *Unsteady River Modeling Using HEC-RAS*, Bonner Consulting, Carlsbad, CA, 2007

InfoWorks v.9.0.2, *Help Topics, What's New in this/previous Version(s),* Wallingford Software Ltd., Oxfordshire, U.K., July 2008

DIVERSION OF S-4 BASIN DRAINAGE FROM LAKE OKEECHOBEE: HYDRAULIC MODELING OF ALTERNATIVES USING HEC-RAS

Stephanie C. Otis[1] and Gene L. Foster[2]

[1] P.E., Ph.D., M.ASCE, Senior Civil Engineer, Burns & McDonnell Engineering Co., 9400 Ward Parkway, Kansas City, MO 64114-3319; Phone (816) 822-4399; FAX (816) 822-3514; E-mail: sotis@burnsmcd.com
[2] P.E., M.ASCE, Associate Water Resources Engineer, Burns & McDonnell Engineering Co., 9400 Ward Parkway, Kansas City, MO 64114-3319; Phone (816) 822-3167; FAX (816) 822-3514; E-mail: gfoster@burnsmcd.com

ABSTRACT

One of the goals of the current Everglades restoration effort is to reduce the delivery of stormwater runoff to Lake Okeechobee from the drainage basins located south of the lake. The S-4 Basin is one of these drainage basins that has not yet been diverted. An analysis was performed to determine the feasibility of diverting S-4 Basin drainage southward, away from Lake Okeechobee. Unsteady flow hydraulic models of the diversion alternatives were developed using the Corps of Engineers HEC-RAS program. These models are relatively complex with the numerous canals, pump stations, gated culverts and other structures. This paper covers the project background, model setup and the challenges faced by the modelers as well as some of the results obtained through the modeling effort.

INTRODUCTION

The Florida Department of Environmental Protection (FDEP) and the South Florida Water Management District (SFWMD) have established policies that seek to limit the discharge of phosphorus contained in stormwater runoff to Lake Okeechobee. In Florida's 1994 Everglades Forever Act (EFA), several drainage districts located on the south shore of Lake Okeechobee are specifically required to install conveyance systems that would divert at least 80 percent of the drainage historically discharged to the lake southward into one of the SFWMD's primary conveyance canals. Through these canals, this drainage is delivered to one of the existing stormwater treatment areas (STA) for treatment prior to its discharge into the sensitive Everglades ecosystem.

The S-4 Basin is one of the water management basins located along the south shore of Lake Okeechobee, but none of its component drainage districts are required in the EFA to install diversion systems. However, in light of pending regulations that may further limit phosphorus discharges to Lake Okeechobee, it is anticipated that this basin's discharges to the lake may be restricted in the future as well. For this reason, the Everglades Agricultural Area Environmental Protection District (EAAEPD) commissioned the S-4 Basin Feasibility Study to investigate alternatives

to reduce discharges to Lake Okeechobee from the S-4 Basin. This study was co-funded by SFWMD (Burns & McDonnell, 2006, 2008).

The potential diversion of stormwater drainage from the S-4 Basin is complicated by one fundamental constraint: the performance of the existing drainage systems in the S-4 and receiving basin(s) cannot be compromised during flood events. This constraint requires first that any potential diversions into adjacent drainage basins must not cause or exacerbate flooding within these receiving basins. Therefore, the allowable diversion rate into these basins is highly variable depending on the amount of local runoff. Secondly, because the allowable diversion rate from the S-4 Basin can be zero at times, this constraint also requires that any proposed diversions not interfere with the basin's existing drainage system. Therefore, due to the dynamic nature of this constraint it was necessary to model the hydraulics of the primary conveyance canals within the S-4 and receiving basins to assess the potential performance of the various diversion alternatives.

PROJECT HYDRAULIC MODEL

Because of the flat topography, stormwater drainage within south Florida is accomplished primarily through a system of man-made canals with numerous control structures and pump stations. The flow in these canals is very dynamic, with flow reversals and even looped flow common. Therefore, the computer model chosen to simulate the operation of the S-4 and adjacent drainage basins must be capable of simulating these unsteady flow conditions.

At the time this study was initiated, Version 4.0 of the Corps of Engineers River Analysis System (HEC-RAS) was available only as a beta release and the writers were not yet familiar with its new capabilities. Therefore, the first attempts to model the proposed diversion system used a version of the U.S. Environmental Protection Agency's Storm Water Management Model (SWMM). Although this model has many fine features, it is probably better suited for use on enclosed stormwater systems. Even after inclusion of an optional real-time control module, this model's ability to simulate the operation of gated control structures proved to be problematic. Some of these structures have multiple stage triggers that cause them to be opened or closed. In order to simulate these triggers, it was sometimes necessary to introduce dummy structures that operated in series and/or in parallel to the real structure. Because of this complicated model architecture, the SWMM model often had trouble converging to a solution and execution times were excessive.

The hydraulic modeling for this study was eventually switched to HEC-RAS, Version 4.0 after the writers became aware of its new capabilities for control of gated structures. Although the new sediment transport features of Version 4.0 have been widely publicized, the new gate control features are equally significant. In prior HEC-RAS versions, gate control was accomplished by simple stage or flow triggers tied to a single reference location, typically immediately upstream or downstream of the structure. In Version 4.0, gate operations can be controlled using script-style rules that can employ multiple if/else if /else logic structures. These new control rules allowed direct control of a structure's gates given stage or flow conditions at multiple reference locations, which was vital to successfully model the proposed diversion

system. The new gate control rules also allow one to implement seasonal, time of day and other complicated rule sets.

Consistent with the requirements in the EFA for diversions at other drainage districts, the goal of the proposed S-4 Basin diversion system is to divert an average of 80 percent of its historical discharges to Lake Okeechobee. Because of the dynamic nature of these diversions, the diversion efficiency of the alternative diversion schemes was demonstrated by simulating system operations over a 15-year continuous period (water years 1993–2007) using a 5-minute simulation time step.

BASELINE CONDITIONS MODELING

The first modeling task in this study was to estimate baseline conditions. Currently, the S-4 Basin and potential receiving basins for diversions (C-139 and S-3/S-8 basin) are not hydraulically connected. Figure 1 shows the general orientation of these basins and the existing culverts and pump stations that control flow between them. Because these basins are not currently interconnected, the baseline HEC-RAS models for the S-4 Basin and C-139 and S-3/S-8 basins were developed separately.

The S-4 Basin (Figure 2) includes all or part of five special drainage districts (Clewiston Drainage District, Disston Island Conservancy District, East Hendry County Drainage District, South Florida Conservancy District and Sugarland Drainage District) plus a large farm area owned by the U.S. Sugar (Townsite). Drainage from these districts is discharged into the one of the basin's major canals: Clewiston, C-20/21 or LD-1. From these canals, basin drainage is currently discharged to Lake Okeechobee through the S-310 lock or S-4 pump station. Drainage also exits the basin through S-235 culverts into the C-43 Basin.

The C-139 Basin is logically divided into north and south subbasins, which are separated at the G-150 control structure. The northern C-139 subbasin drains into the L-1 Canal and the southern subbasin into the L-2 and L-3 canals. These canals run along the northern and eastern perimeter of the C-139 Basin. Discharges from the northern basin occur at G-136 into the S-3/S-8 Basin and into the southern subbasin at G-150. Southern basin discharge occurs primarily at the four G-342 culverts into STA-5. A planned enlargement of STA-5 will soon be under construction. With this enlargement, a new inflow pump station (G-508) will also be installed. G-406 is a bypass structure that opens only when required flow exceed the capacity of STA-5.

Discharge from the C-139 Basin through G-136 enters the L-1E Canal. This canal connects with the Miami Canal at structure G-212. The Miami Canal is the principal conveyance canal in the S-3/S-8 Basin, connecting Lake Okeechobee at S-3/S-354 with Water Conservation Area 3A (WCA-3A) at the S-8 pump station. The majority of the discharge into the S-3/S-8 Basin is delivered to STA-3/4 for treatment prior to being discharged into WCA-3A.

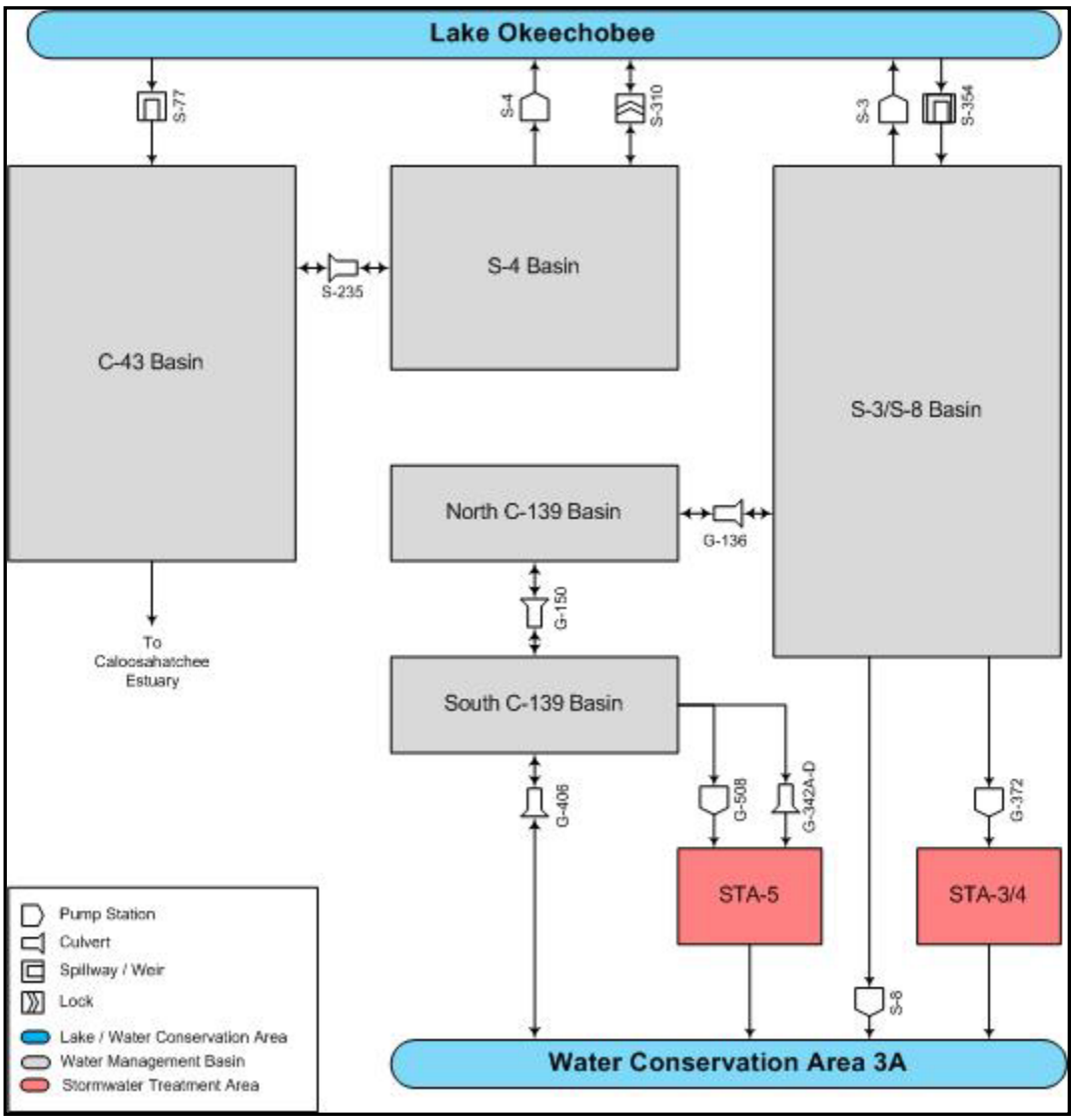

Figure 1: Project Area Schematic

The baseline hydraulic models for these basins include only the major canals in each basin. The numerous secondary canals, laterals and sublaterals in these basins are not represented explicitly in the model. Stormwater runoff from these basins into the primary canal system was treated as a point sources where it occurs as a specific structure or canal confluence or as a uniform inflow when it is distributed over a long canal reach. A dataset derived from historical mean daily flow records was used to define the inflow hydrographs at each of these points.

The boundary conditions used in the HEC-RAS model consist of estimated stage hydrographs at each model domain boundary. These boundaries included Lake Okeechobee stages, tailwater stages in the C-43 Canal below S-235, G-212 tailwater stages in the Miami Canal, stages in STA-5 and G-406 tailwater stages.

Table 1 is a summary of the average annual basin discharges under baseline conditions. This table lists both estimated discharge volumes and the corresponding total phosphorus (TP) loadings.

Table 1: Average Annual Discharge for Baseline Conditions

Basin	Destination	Volume (acre-feet)	TP Load (kg)
S-4	C-43 Canal @ S-235	57,544	16,104
	Lake Okeechobee @ S-310	16,859	4,973
	Lake Okeechobee @ S-4	28,038	7,961
	Total Lake Okeechobee	44,897	12,934
C-139	L-1E Canal @ G-136	17,745	4,688
	STA-5 @ G-342A-D+G-508	162,946	42,389

ALTERNATIVES

Three different diversion alternatives — alternative schemes for delivering S-4 Basin drainage southward — were identified in this study. In addition, two different treatment alternatives were considered (that is, delivery of diverted drainage to STA-5 or to STA-3/4), for a total of six diversion/treatment combinations. The diversion alternatives were numbered 1-3 and the treatment alternatives A or B, so the complete alternatives were named 1A, 1B, 2A, etc.

As an example, Alternative 2A is featured below. Figure 2 is a schematic for this alternative with the new, relocated or modified structures shown in red. In this alternative, S-4 Basin diversions are delivered southward via two new connections. Drainage discharged into the Clewiston Canal is diverted through a southward extension of this canal. This extension requires relocation of pump station EPD-06 (EPD-06A), a new control structure at the confluence of this canal extension and the L-1E Canal (G-136B) and a new divide structure in the L-1E Canal (G-136C). Diversions delivered to this point flow westward into the L-1 Canal and then southward.

Drainage from the Sugarland Drainage District would be delivered directly into the L-1 Canal through a new gated culvert designated G-96A. Stages in the L-1 Canal are often lower than stages to the south in the L-2 Canal so a new pump station is included to lift flow from the L-1 into the L-2 Canal. Without a new G-150A pump station, potential diversion amounts would be severely limited.

MODELING RESULTS

Table 2 compares the average annual discharge volumes for Alternative 2A with those for baseline conditions. As shown, this alternative would reduce Lake Okeechobee discharges by approximately 60 percent. The diversion efficiencies of the other "A" alternatives (1A and 3A) were respectively 51 and 64 percent. Therefore, none of the "A" alternatives were able to achieve diversion efficiencies near the desired 80 percent target.

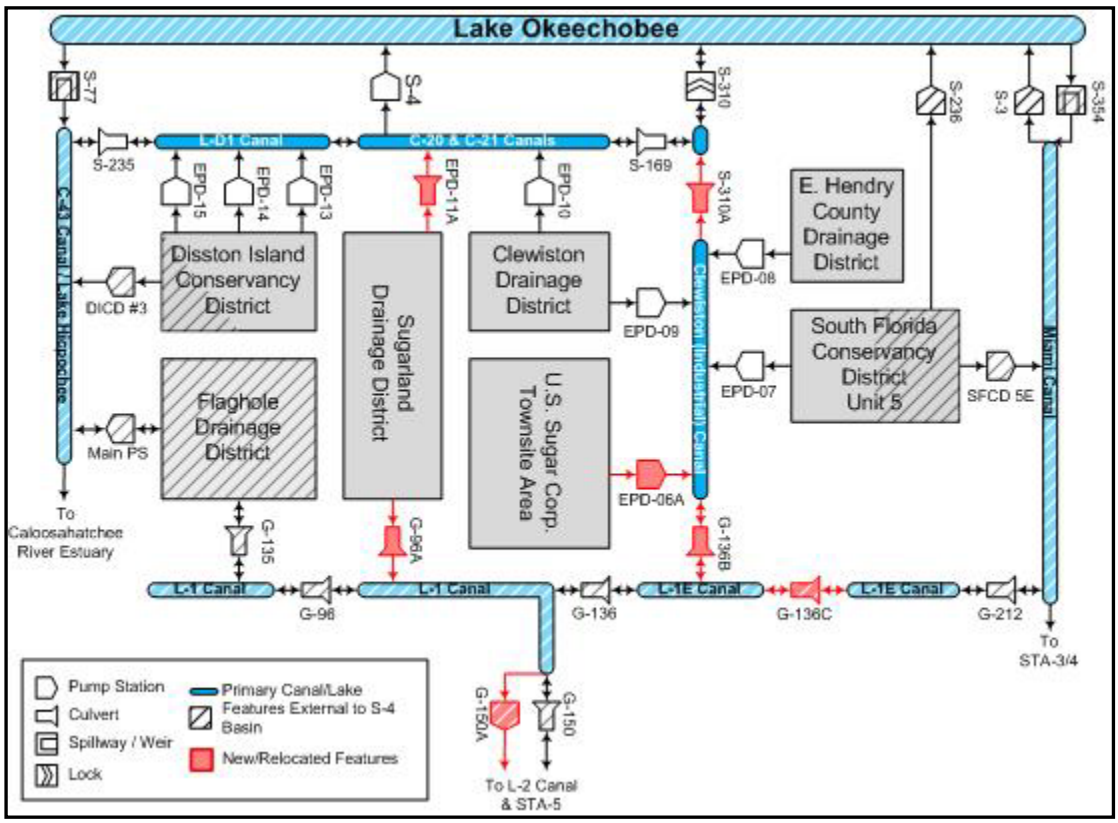

Figure 2: Schematic for Alternative 2A

Table 2: Average Annual Discharge Comparison for Alternative 2A

Basin	Destination	Discharge Volume (acre-feet)		Percent Difference
		Baseline	Alternative 2A	
S-4	C-43 Canal @ S-235	57,544	53,636	-6.8
	Lake Okeechobee @ S-310	16,859	8,103	-51.9
	Lake Okeechobee @ S-4	28,038	9,828	-64.9
	Total Lake Okeechobee	44,897	17,931	-60.0
C-139	L-1E Canal @ G-136	17,745	17,683	-0.3
	STA-5 @ G-342A-D+G-508	162,946	196,493	+20.6

In the "B" alternatives, S-4 Basin diversions are transported eastward in the L-1E Canal to the Miami Canal. From this confluence, these diversions would flow southward in the Miami Canal to STA-3/4. This flow path is less restrictive from a hydraulic perspective than the path required to deliver these diversions to STA-5. The diversion efficiencies for the three "B" alternatives (1B, 2B and 3B) were respectively 81, 85 and 74 percent. However, based on conditions that existed at the start of this study, SFWMD staff stated that there was no surplus treatment capacity at STA-3/4. Therefore, it is possible that additional STA capacity in the S-3/S-8 Basin would be required to accommodate diversions from the S-4 Basin.

USING HEC-RAS 4.0 FOR UNSTEADY FLOW MODELING

To this point, this paper has presented a discussion of the S-4 Basin diversion project and an example of the HEC-RAS hydraulic modeling completed for this project. The balance of this paper will focus on some of the problems and limitations encountered.

Many readers will be familiar with using HEC-RAS, and its predecessor HEC-2, to estimate steady-flow water surface profiles. For those who may be unfamiliar with HEC-RAS, particularly when using unsteady flows, some background information is provided.

HEC-RAS is designed to perform one-dimensional hydraulic calculations for a network of natural or man-made channels. The stream network is defined as one or more stream reaches, with each stream reach in turn represented by a series of stream cross sections. For this project, the unsteady flow capabilities of HEC-RAS were used to simulate the operation of the S-4 Basin system over a 15-year period. In this mode, HEC-RAS routes flow through the system by solving the St. Venant equations for each model time step; this project used five-minute time steps. HEC-RAS is able to route flow through the drainage network, modeling the effects of backwater, flow reversal, surcharging, looped connections, and pressure flow. The model network can also include weirs, gated and ungated culverts, and pump stations that are located in inline or lateral structures. HEC-RAS can also be programmed to operate pump stations and gates using complex logic based on flow rates, velocity, or stages (U.S. Army Corps of Engineers, 2008).

Model Setup

Many of the requirements for setup of the project HEC-RAS models are common to all similar hydraulic models. In the case of this study, there were many proposed canal extensions, canal enlargements and new control structures. Finding optimum sizes for these improvements can be relatively time consuming using an unsteady flow model. In this study, the writers found it useful to start with a steady flow model, with flow rates equal to design maximums to help size these improvements. The benefits of this peak flow analysis were fourfold:

- Obtained a better understanding of the flow characteristics of the existing drainage system, especially in areas of limited geometric information;
- Identified problem areas thus allowing these problem areas to be corrected or avoided (that is, by taking an alternate path);
- Identified potential target stages for the diversions; and
- Facilitated selection of structure type (that is, pump station vs. gated, gravity flow structure) at certain locations.

Initial Conditions

By default, HEC-RAS will determine the initial state of an unsteady flow model (water surface elevations and flows) by finding a steady flow solution to the model using initial flow rates. In an unsteady flow model it is not uncommon for this steady flow solution to fail. These failures were often the most frustrating because HEC-RAS would quit without ever generating any useful results or error messages that could be used for debugging. Under these conditions, it is often necessary to

force HEC-RAS to set startup conditions using an initial conditions file (alternately referred to as a hot start or restart file). This file contains the initial water surface elevations at each cross section within the model.

When specified, HEC-RAS will write a restart file at a specified time (usually after the last model time step), but it is necessary to have a working model first. This is accomplished using a special hot start model. This model will employ the same geometric data as the production model but different model boundary conditions. The typical procedure is to increase the initial water surface elevations at the model boundaries to levels higher than may be physically possible and then gradually reduce these elevations down to the real initial conditions.

Raising the initial water surface elevations effectively drowns out the model, which prevents the most common reason for a model crash, a dry channel. In HEC-RAS, the solver will become unstable and crash if the water surface elevation at any cross section should drop to its invert elevation. If the hot start model should fail, then it is easy to find out when, where and why this occurred. In the HEC-RAS models developed for this study, startup problems were typically caused by one of two conditions: an error in the cross section data or improper gate control logic, which allowed canal stages to fall below target levels. Once a successful hot start model run has been made, the restart file written at the end of this model can be used to specify a valid starting solution for the production model run.

Data Storage System

In an unsteady flow model, HEC-RAS uses the Corps of Engineers' Data Storage System (DSS) for storage of the model input flow and stage hydrographs and storage of model output. DSS was specifically designed for efficient storage and retrieval of regular-interval scientific data (for example, daily streamflow hydrographs or hourly precipitation data). The DSS viewer program (HEC-DSSVue) will export data to or imported data from Microsoft Excel, making this system very user friendly (U.S. Army Corps of Engineers, 2006).

Unfortunately, for the S-4 Basin study the HEC-RAS/DSS interface proved to be problematic. During execution of an unsteady flow model, HEC-RAS writes the model results to a scratch disk file. Once the actual simulation finishes, HEC-RAS launches the DSS Writer program. It appears that this program initializes the specified output DSS file. It was found that this program would tend to crash as the models became more complex (more structures and stream cross sections) and simulation periods increased. This appears to be a limitation of the DSS Writer program only, not a problem with the simulation engine in HEC-RAS or of the DSS file format.

A simple work around was found for the DSS Writer problem, split the entire simulation period into smaller pieces. In this study, a 15-year simulation period was used. It was found that a model run between four and five years long would execute just fine; therefore, each model run was divided into four sets so no single model run was longer than four years. To preserve model states from one model subset to the next, it was necessary to write a hot start file at the end of each model subset (except the final one) and use these hot start files to set the initial conditions for the next subset in series.

With a 15-year simulation period and 5-minute time step, the hydraulic models for this study generated over 1.5 million data points at each structure and cross section. To reduce the magnitude of these data by half, the HEC-RAS models were configured to save the results for every other time step only. This still left a prodigious amount of data to analyze for each model run. This volume was reduced to a manageable level by using the HEC-DSSVue engine to calculate average daily values from the detailed modeling results. This left less than 5,500 daily values for each run, which could be easily manipulated and summarized using Microsoft Excel.

Irrigation Withdrawals

The canals within the S-4 and adjacent water management basins serve not only to carry away excess drainage but also to supply irrigation water during dry periods. There are no explicit records of irrigation withdrawals but the magnitude and timing of these withdrawals were estimated by calculating a daily water balance for each canal reach. These irrigation withdrawals were represented as negative values in the canal inflow hydrographs.

These irrigation withdrawals proved to be problematic at times when the gates at both ends of a canal reach were closed. If these withdrawals were of sufficient magnitude to lower canal stages to or near its invert the unsteady flow solver would often crash. The solution to this problem was fairly straightforward: modify the gate control logic to open a gate slightly if canal stage fall to danger levels.

Lateral Structures

One of the most finicky structures found in HEC-RAS 4.0 were lateral structures. Gated lateral structures were sometimes used to serve a dual purpose: to mimic the flow control provided by a typical inline control structure and to also connect a new canal or lateral to an existing canal reach without splitting the existing canal reach and adding a new junction. Although using lateral structures in place of a true junction made network changes easier, these lateral structures did not always work as planned. In some instances, HEC-RAS did not properly maintain the flow balance across a lateral structure. That is, the flow upstream of the lateral structure less the flow downstream did not always equal the net lateral flow through these structures. The lesson learned here is that it is generally better to take the time to insert a true junction in a model reach to connect to a lateral canal and then place an inline control structure in this canal when necessary rather than using a lateral structure.

Gate Operating Rules

One important lesson learned from the general types of model errors discussed above is that there is value in keeping gate control rules as simple as possible. Of course this goal is not always possible because some of the structures in the S-4 Basin have complex, multi-condition operating criteria. The more complex these operating rules, the more likely it is that there may be unintended conflict with other structures in the system. Often these adverse situations were found only by trial and error.

CONCLUSIONS

HEC-RAS, Version 4.0, proved to be an excellent modeling tool for use in this study and would be similarly applicable to any of the man-made drainage systems common in south Florida and elsewhere. In fact, the new gate operating rule feature added in this latest program version was found to be essential to effectively implement the complicated operating rules required at some structure.

However, the HEC-RAS model is not without some faults. The problem mentioned above with the DSS Writer when modeling complex systems or with long simulation periods is frustrating but not difficult to work around. Another suggested enhancement to the HEC-RAS model would be to implement a rule-based control system for pump stations, similar to that now available for gated structures.

ACKNOWLEDGEMENTS

The writers wish to thank the Everglades Agricultural Area Environmental Protection District for its sponsorship of the S-4 Basin Feasibility Study and the prior S-4 Basin Diversion Study. The S-4 Basin Feasibility Study was also co-funded by the South Florida Water Management District. EAAEPD and SFWMD staff and consultants provided valuable direction and comments that greatly improved the quality of these studies.

REFERENCES

Burns & McDonnell Engineering Co. (2008, September). *S-4 Basin Feasibility Study*. Prepared for Everglades Agricultural Area Environmental Protection District. Kansas City, MO.

Burns & McDonnell Engineering Co. (2006, January). *S-4 Basin Diversion Study*. Prepared for Everglades Agricultural Area Environmental Protection District. Kansas City, MO.

U.S. Army Corps of Engineers. (2006, January). *HEC-DSSVue: HEC Data Storage System Visual Utility Engine*. Hydrologic Engineering Center.

U.S. Army Corps of Engineers. (2008, April). *HEC-RAS 4.0*. Hydrologic Engineering Center.

New Floodplain Delineation Capabilities in HEC-RAS

Cameron T. Ackerman, P.E., D.WRE[1]; Mark R. Jensen[1];
and Gary W. Brunner, P.E.[1]

[1]Hydrologic Engineering Center, Institute for Water Resources, U.S. Army Corps of Engineers, 609 2nd St., Davis, CA 95616; (530) 756-1104; email: cameron.ackerman@usace.army.mil; mark.jensen@usace.army.mil; gary.brunner@usace.army.mil

Abstract

The Hydrologic Engineering Center's River Analysis System (HEC-RAS) is widely used for computing water surface elevations with results processed using GIS to determine inundation extent and flood depths. These floodplain boundary and flood depth results are used to establish flood insurance rate maps, analyze severe flood events, establish emergency action plans, estimate flood damage losses, and evaluate habitat restoration alternatives. New floodplain delineation tools in HEC-RAS provide the capability to develop inundation maps utilizing water surface profile results and a model of the ground surface. This delineation capability allow the modeler to visualize the resulting floodplain directly within HEC-RAS, providing a more efficient environment for hydraulic model refinement than processing results in GIS. The resulting floodplain boundary and flood depths may then be used in other modeling software to evaluate floodplain impacts.

Introduction

The Hydrologic Engineering Center's River Analysis System (HEC-RAS) is widely used for computing water surface elevations for steady-flow profiles and unsteady-flow simulations. Floodplain boundary and flood depth results are used to establish flood insurance rate maps, analyze severe flood events, establish emergency action plans, estimate flood damage losses, and evaluate habitat restoration alternatives. It is commonplace to create these inundation maps using automated methods within GIS (or CADD)-based software; however, this method requires the additional expense of purchasing an external piece of software. Even with such software as HEC-GeoRAS (HEC, 2005), which is designed to work seamlessly with HEC-RAS output with in ArcGIS (ESRI, 2004), the user must acquire the requisite knowledge to use the software.

Working with the Federal Emergency Management Agency and the National Institute for Building Sciences, HEC has to improved the use of HEC-RAS output with HAZUS-MH and developed methods for directly computing inundation maps within the HEC-RAS. The addition of floodplain delineation capabilities provides the modeler with an integrated system for computing geospatial data from simulation results, visualizing

results, and refining model input. Further, inundation boundary and depth data results may then be used in GIS software and combined with additional data to perform additional analysis and map publishing.

HEC-RAS Improvements

Generation of floodplain boundary maps from HEC-RAS simulation results using automated GIS methods began in the mid-1990s with arc macro language (AML) scripts. Previously, scripts had been developed using HEC-2 output. In March 1999, the first GIS interface built specifically to assist HEC-RAS modeling (HEC-GeoRAS) was publicly released (HEC, 1999). HEC-GeoRAS was a simple interface that provided barebones tools to the user for creating geometric data for import and performing floodplain delineation using HEC-RAS output. Over the years, GIS software has greatly improved allowing the once complex, command line arguments to become simple push-button activities. This has allowed the field of river hydraulics field to use significantly improved the tools for creating and evaluating hydraulic models. Complex river networks can be laid out within the GIS and results can be visualized using background data layers to assist the process. The benefits of using a GIS to assist in hydraulic modeling are well known. Today, modelers no longer need to be versed in only river hydraulics and HEC-RAS, they must also be experienced GIS users.

New floodplain delineation tools in HEC-RAS increase the efficiency of analysis and refinement within a single modeling environment. Results are visualized immediately through a RAS interface that plots the underlying geometric data and ground surface.

Geometry Requirements

The new version of HEC-RAS creates two new files for use with the mapping portion of the software. These files are created in an easily readable/parseable extensible markup language (XML) format. HEC-RAS geometry is written in GML (geography markup language), the format supported by the Open Geospatial Consortium (OGC) (http://opengeospatial.org). Currently, the river network, cross sections, bank stations, and storage areas are written for use in mapping. Water surface elevations (and other simulation results) are written to a simple XML file for each cross section. These files may also be used to provide as inputs to other software for floodplain delineation and mapping outside of the HEC-RAS program.

A digital terrain model in form of a grid is required to represent the land surface. Currently, HEC-RAS supports the binary raster floating-point value format. This float format is a non-proprietary format that consists of two files, the binary floating point file (.flt) and the support ASCII header file (.hdr). Many software packages support the import or export of this format. HEC-RAS supports either a single terrain model or multiple terrain tiles that covers the area of interest. New capabilities in HEC-RAS are implemented so that the entire dataset does not have to be read into memory; therefore, there is not a limitation on the size of the terrain model that can be processed. Users, however, are encouraged to use multiple terrain tiles to reduce the extra null space (i.e. no

data cells) where the terrain is not needed for analysis. Individual terrain tiles should be created at the user's discretion to minimize file size and computation times because once loaded into HEC-RAS, the terrain tiles are managed as a single terrain layer within the interface. The HEC-RAS mapping interface is shown in Figure 1 with a tiled terrain, river, cross section, and storage area layers.

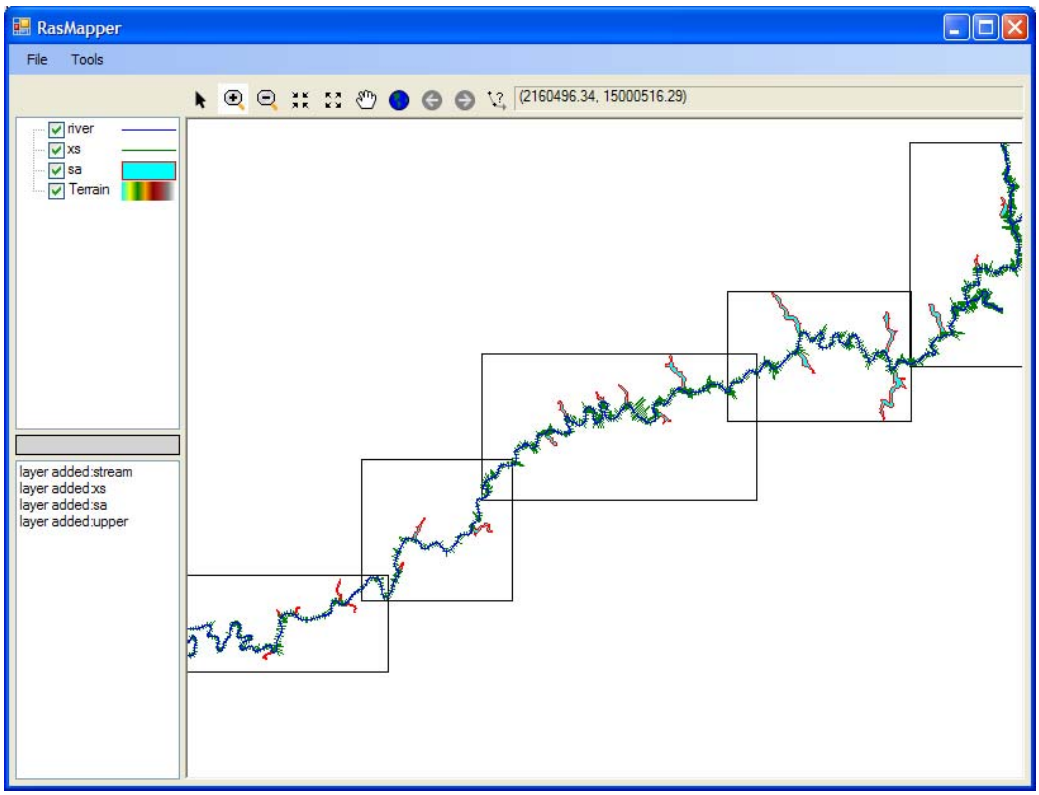

Figure 1. The HEC-RAS mapping interface showing tiled terrain models with model geometry.

Geometric Data Preparation

Geometric data are used to create an interpolation surface for assigning water surface elevations throughout the model area prior to computing the floodplain boundary. The interpolated surface is created for each terrain tile by creating interpolation regions between each set of cross sections based on the cross section layout, location of the bank positions on the cross sections, and the shape of the river centerline. The shape of the river centerline is applied to the bank station locations to create bank lines that approximate the meander of the river channel between cross sections. Closer cross section spacing improves the representation of the channel limits. The shape of the river centerline is also applied to the outer edge of the cross sections to create model bounds that attempt to include the floodplain throughout the bends of river's meander. Interpolation regions are created in areas bounded by cross sections, bank lines, river centerlines, and model limit lines. An example region generated for the area between the river centerline and bank stations is shown in Figure 2.

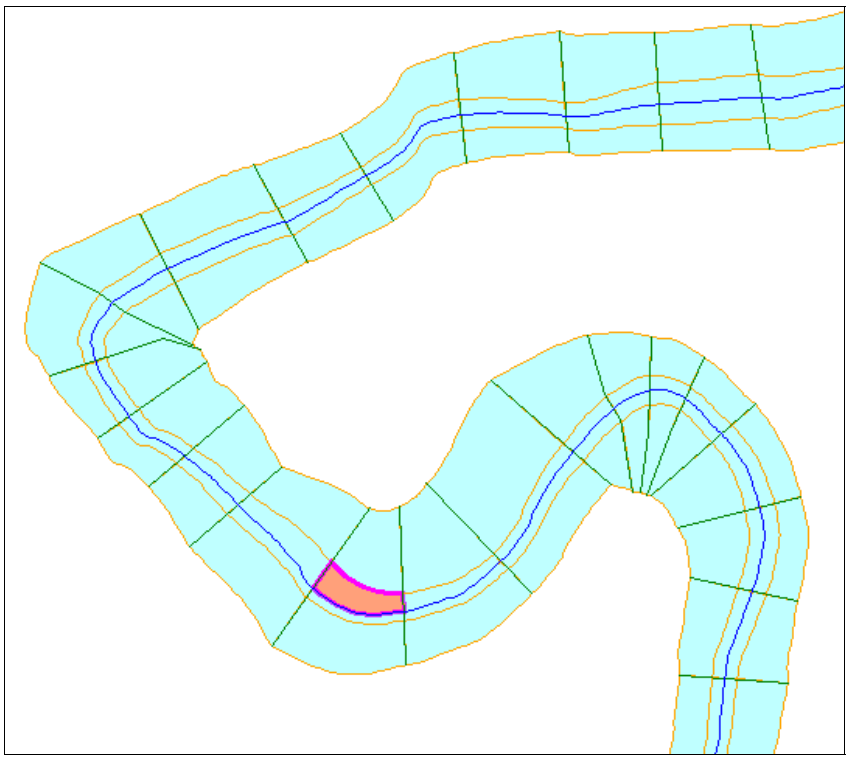

Figure 2. Interpolation regions (example highlighted) are created between cross sections using bank lines and model limit lines based on the shape of the river.

Interpolation regions are used to define boundaries for interpolation of the underlying terrain surface grid. Interpolation of grid-cell values within each region is performed using a nine-point finite-difference approach. Cross-section weighted values (from zero to one) are computed based on cell proximity to bounding cross sections. The surface within the interpolation region is obtained by solving the potential equation. This produces a smooth transition in water surface values from cross section to cross section. Known boundary conditions are provided for cells along each edge of the interpolation region. For edges shared with a cross section, boundary cells are given a value of zero or one; thus the value of a grid cell which is located directly on top of a cross section line is solely influence by that cross section. Along the river line and a bank line, the boundary condition is set based on the distance along the line between the bounding cross sections. Boundary condition values used at the model limit lines are given by setting the slope normal to the bounds to zero.

Results from the interpolation surface are stored to disk to allow for repetitive use during the floodplain delineation process. Not only can the interpolation surface be used for floodplain mapping, it can be used for distributing additional hydraulic parameters computed by RAS such as velocities, water temperature, shear stress, stream power, and ice thickness. The RAS Mapping window allows the user to select the input geometry and output layers to be generated, as shown in Figure 3.

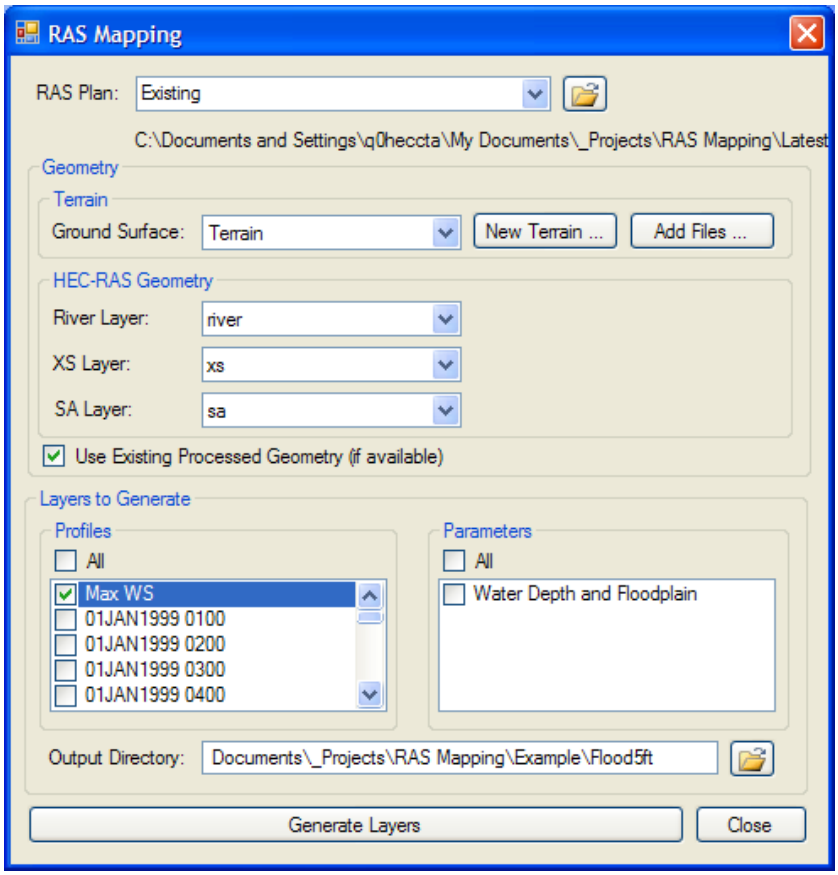

Figure 3. The RAS Mapping window is used to select input and output parameters for processing.

Floodplain Delineation

Once computed, the interpolation surface facilitates efficient mapping of HEC-RAS results at individual cross sections on to the entire model domain. Water surface elevations through the model limits are computed by applying the HEC-RAS water surface elevations results. If storage areas are present, the water surface elevation for the storage area is added to the water surface elevation grid. A flood depth grid is then created by comparing the water surface elevation and ground surface at each grid cell. Depth grids are stored in the binary float format based on the original properties of the underlying terrain grid.

A floodplain boundary polygon is computed by contouring the depth surface at zero depth. A final floodplain boundary is then achieved using a flood fill algorithm to connect the floodplain area. The floodplain boundary polygon is stored in the Shapefile format (ESRI, 1998).

Initial testing on a dataset with 600 million cells took approximately three minutes to compute the cross-section weighted interpolation surface with an additional seven minutes to create the depth grid. In general terms, the tiled terrain dataset covered about 120 river miles and using a 5-foot grid-cell size and took up 2.5 gigabytes of disk space.

Data Visualization

Floodplain delineation results have been added to the RAS mapping interface to assist modelers evaluate the impact of model results spatially. Flood depths and boundaries can be evaluated in the context of the cross section layout to identify areas of discontinuity helpful in model refinement. Development of visualization tools have focused on efficient memory usage. Grids are rendered quickly because only the data visible in the mapping window is loaded, allowing modelers to easily navigate the model area using the available pan and zoom tools. An example inundation map displayed with model geometry is shown in Figure 4.

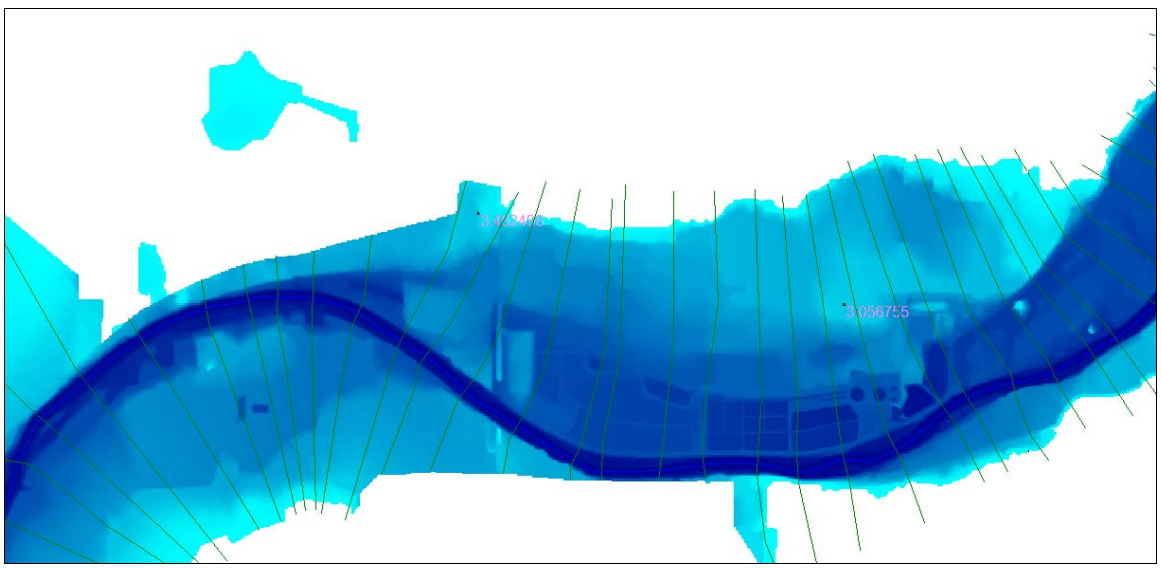

Figure 4. Example RAS display of a flood depth grid overlaid with model geometry.

Summary

The new floodplain delineation capabilities in HEC-RAS do not intend to replace the capabilities of a GIS, but to assist engineers in performing hydraulic analysis in a more integrated environment. Because the delineation tools exist within a single software package, modelers will be able to more efficiently produce hydraulic models and spatial data for use in analysis and mapping. Because the resultant spatial data is stored in published formats, this data is readily accessible for use in related disciplines such as flood damage analysis, ecosystem restoration, flood warning preparedness, and hazard evaluation. Further, the methods implemented by HEC-RAS for handling digital terrain models attempts to manage very large datasets that are being created with the latest remote sensing techniques, by only reading portions of the gridded data as needed.

While these new HEC-RAS mapping tools greatly improve the process of mapping simulation results, there is still progress to be made. Software is rapidly evolving to

include mapping of numerous output variables such as velocities, water temperature, and shear stress. Adding the ability to exclude selected locations of high ground not included in the terrain model, delineating areas outside the bounds of the cross sections that are flooded due to backwater areas, and improving data handling are planned improvements and just a few of many features to be considered.

References

ESRI (1998). *ESRI Shapefile Technical Description, An ESRI White Paper*. Environmental Systems Research Institute, Inc., Redlands, CA. (http://www.esri.com/library/whitepapers/pdfs/shapefile.pdf)

ESRI (2002). *What is ArcGIS?* Environmental Systems Research Institute, Inc., Redlands, CA. (http://www.esri.com/library/whitepapers/pdfs/what_is_arcgis.pdf)

HEC (1999). *HEC-GeoRAS – An extension for support of HEC-RAS using ArcInfo*, CPD-75, March 1999. Hydrologic Engineering Center, Institute for Water Resources, U.S. Corps of Engineers, Davis, CA.

HEC (2005). *HEC-GeoRAS – An extension for support of HEC-RAS using ArcGIS*, CPD-83, September 2005. Hydrologic Engineering Center, Institute for Water Resources, U.S. Corps of Engineers, Davis, CA.

HEC (2008). *HEC-RAS River Analysis System, User's Manual, Version 4.0*, CPD-68, January 2008. Hydrologic Engineering Center, Institute for Water Resources, U.S. Corps of Engineers, Davis, CA

Transitioning NWS Operational Hydraulics Models from FLDWAV to HEC-RAS

Fekadu Moreda[1,2], Angelica Gutierrez[1], Seann Reed[1], Cecile Aschwanden[1,3]

[1]NOAA, National Weather Service, Office of Hydrologic Development, 1325 East-West Highway, Silver Spring, MD 20910; phone: 301-713-0640 x 129; email: Fekadu.moreda@noaa.gov
[2]Riverside Technology, Inc.[3]Wyle Information Systems

Abstract

The NOAA National Weather Service (NWS) Office of Hydrologic Development (OHD) is investigating two approaches to transition NWS operational hydraulic models from FLDWAV to HEC-RAS: (1) transform existing FLDWAV and DWOPER models into HEC-RAS and (2) modify and calibrate existing HEC-RAS models created for a purpose other than real-time forecasting. We evaluated these two approaches in the lower part of the Tar River, NC, and the lower Columbia River, OR. We also developed procedures and utility programs to assist with model conversions. The results are mixed. For the relatively simple Tar River, direct duplication of FLDWAV cross-sections and Manning's roughness specifications within HEC-RAS resulted in similar simulations. Also, a model built with more detailed cross-sections but the same roughness parameters from FLDWAV model could produce comparable simulation with some simple Manning's *n* adjustments. For the lower Columbia, approximate duplication of geometry requires more Manning's *n* adjustments, but still offers a viable pathway toward model conversion. Further work on the lower Columbia model is needed to see whether more precise representation of storage areas will improve results.

Key words: St. Venant Equations, calibration of hydraulics model, Tar River, Columbia River. FLDWAV, HEC-RAS

1 Introduction

In 2007, a team of National Weather Service (NWS) hydrologists reviewed several well-known hydraulic models to identify methods to improve hydraulic modeling capabilities for NWS operational forecasting (NWS, 2007). NWS forecasters currently use Flood Wave Dynamic Model (FLDWAV) and Dynamic Wave Operation (DWOPER) (Fread, 1998) for operational hydraulic modeling. NWS (2007) recommends including the United States Army Corps of Engineers (USACE) Hydrologic Engineering Center-River Analysis System (HEC-RAS) in the operational environment, testing FLDWAV and HEC-RAS on identical data sets, and developing methods to transform FLDWAV models to HEC-RAS. Compared to FLDWAV, the study found that HEC-RAS offers a much more user friendly GUI, better documentation, training, and the option to specify more detailed cross-section and hydraulic structure information. Based on those conclusions, NWS managers have decided to replace FLDWAV and DWOPER with HEC-RAS. This

proposal is based on two basic assumptions: (1) HEC-RAS can provide equivalent functionality capable of replacing existing FLDWAV and DWOPER models (with relatively minor HEC-RAS enhancements), and (2) through collaboration with HEC, it will be more economical to maintain and enhance HEC-RAS alone, rather than independently maintaining HEC-RAS and FLDWAV. Efforts are underway to include the HEC-RAS software in the NWS Community Hydrologic Prediction System (CHPS). CHPS is the software infrastructure intended to replace the NWS River Forecast System (NWSRFS). Because the NWS has defined an aggressive schedule to transition from NWSRFS to CHPS, River Forecast Centers (RFCs) need simple and inexpensive procedures to convert or replace DWOPER and FLDWAV models with HEC-RAS models.

Here we report on investigations into two approaches to meet this need: (1) transform existing FLDWAV and DWOPER models into HEC-RAS and (2) modify and calibrate existing HEC-RAS models created for a purpose other than real-time forecasting (e.g. HEC-RAS models for Federal Emergency Management Agency (FEMA) flood insurance rate maps). In this study, we developed and compared HEC-RAS models for the lower part of the Tar River, NC, and the lower Columbia River, OR, using these two approaches.

During the evaluation, we developed procedures and utility programs to assist with model conversions. Some model conversion challenges included determining equivalent hydraulic representations for cross-section geometry, ineffective areas, bridges, and specifying channel roughness factors. The procedures described here include an expeditious calibration strategy for RFC implementations when needed. This paper presents a subset of finding from a larger, ongoing Office of Hydrologic Development (OHD) project to facilitate the transition from FLDWAV to HEC-RAS. Additional information and a more detailed report can be found at http://www.weather.gov/oh/hrl/hsmb/hydraulics/index.html.

2 Models

2.1 FLDWAV

DWOPER is the initial model developed by Fread (1978). Later, in an effort to combine DWOPER with a stand alone NWS dam break program (DAMBRK), FLDWAV emerged as a comprehensive dynamic hydraulic model that can be used to simulate network of rivers with several hydraulic structures including an option to simulate dam failure or series of dam failures. FLDWAV is being used in day to day forecasting on over two dozen of large rivers over the United States and several rivers elsewhere in the world. The model is based on the implicit finite difference solution of the complete one-dimensional Saint-Venant equations of unsteady flow.

The two basic equations are the continuity and momentum equations 2.1 and 2.2, respectively.

$$\frac{\partial Q}{\partial x} + \frac{\partial s_{co}(A + A_o)}{\partial x} - q = 0 \qquad 2.1$$

$$\frac{\partial (S_m Q)}{\partial t} + \frac{\partial (\beta Q^2 / A)}{\partial x} + gA\left(\frac{\partial h}{\partial x} + S_f + S_e + S_i\right) + L - W_f B = 0 \qquad 2.2$$

Where Q is the flow, h is the water-surface elevation, A is the active cross-sectional area of flow, A_o is the inactive off channel storage area, S_{co} and S_m are sinuosity factors, x is longitudinal distance along the rive channel, t is the time, q is the lateral inflow or outflow, β is the momentum coefficient for velocity distribution, g is the acceleration due to gravity, S_f is the channel flood-plain boundary friction slope, S_e is the expansion-contraction slope, S_i is addition friction slope for viscous fluids and debris flow, B is that active low top width and W_f is the effect of wind resistance on the surface of flow.

Among the slopes that are listed in the above equation, it is important to describe the S_f as it is central to the model parameterization.

$$S_f = \frac{n^2 |Q| Q}{\mu^2 A^2 R^{4/3}} = \frac{|Q| Q}{K^2} \qquad 2.3$$

In Equation 2.3 n is the Manning's n coefficient of frictional resistance, M is a unit conversion factor *1.49* for English units and *1.0* for SI units, R is the hydraulic radius and K is the conveyance. The equations are solved using the well known four-point implicit box finite difference schemes documented by (Fread,1988).

2.2 HEC-RAS

Hydrologic Engineering Center-River Analysis System (HEC-RAS), is an integrated system of software comprised of a graphical user interface (GUI), separate hydraulic analysis component, and data storage management (Brunner, 2002). Though the system has several modules, in this paper we focus only on the unsteady flow simulation.

The unsteady flow model solves essentially the same equations as FLDWAV (Equations 2.1 and 2.2), except that the current version of HEC-RAS does not include the wind effects term, the expansion and contraction slope term (S_e), or the viscous fluid term (S_i). Similar to FLDWAV, HEC-RAS uses a four-point implicit finite difference scheme to generate a set of finite difference equations. However, HEC-RAS solves the finite difference equations using linearization and a sparse matrix linear algebra solver while FLDWAV applies a Newton-Raphson iteration technique to solve the nonlinear equations.

2.3 Major differences between HEC-RAS and FLDWAV

Although the two models solve the same basic hydrodynamic equations, there are many differences in the model parameterization and solution techniques. Our detailed report

will describe these differences. Here we focus on a few major differences that have the biggest impacts on simulations.

Both models include different options to describe the physical characteristics of the system (Gee and Brunner, 2005). For example, FLDWAV represents cross-section geometry using elevation-top width pairs, which results in a symmetric channel for most FLDWAV implementations. HEC-RAS cross sections can be symmetric but are most often irregular to match the natural landscape. Also, FLDWAV and HEC-RAS differ in the methods available to calculate the friction slope S_f. Both FLDWAV and HEC-RAS compute a composite conveyance K in each cross section to solve for S_f, however, the available methods to calculate the composite K differ. Differences in how Manning's n values are specified and differences in the definitions of left and right overbanks result in conveyance differences.

3 Methodology

3.1 Study Areas and Models

Two rivers were used to evaluate differences between FLDWAV and HEC-RAS water level simulations: the lower Tar River in North Carolina and the lower Columbia River which forms the border between Oregon and Washington.

3.1.1 Tar River

Tides influence water levels in the lower Tar River starting form its inlet at Pamlico Sound upstream to USGS Gauge 02083893 at Rock Springs, NC (approximately 30 miles) (Figure 1). Because of the tidal influence, the NWS needs to run dynamic hydraulic models to provide water level forecasts at locations such as Washington and Greenville, NC. Use of a dynamic hydraulic model is also a pre-requisite for eventually providing dynamic flood mapping services.

In this study, we model a single reach of the Tar River between Tarboro and Washington, NC. Riverside Technology (RTi) set-up and calibrated a FLDWAV model for this reach (RTi, 2007). The simulated reach covers of 48 miles with 102 cross-sections spaced at about 0.5 miles on average. RTi derived cross-sections for FLDWAV using cross-section data obtained from the North Carolina Floodplain Mapping Program and originally derived by the North Carolina US Geological Survey (USGS). The model accounts for the impacts of ten bridges. Four of these are modeled explicitly using bridge geometry while the other six are modeled approximately using constricted cross sections along with expansion and contraction coefficients. The parameters used in FLDWAV for the four bridges were used directly in HEC-RAS. However, for those bridges approximated by the expansion and constriction coefficients, we used the cross-sections without coefficients since HEC-RAS does not use these coefficients in the unsteady flow model. The lateral flows were originally generated using a distributed hydrologic model (Koren et al., 2004) on 4-km grid cells but later aggregated into seven inflows. We converted this FLDWAV model to HEC-RAS as described below.

We also took the steady flow HEC-RAS model with more detailed channel geometry developed by the NC USGS and converted it to an unsteady flow model. To cover the same domain as the FLDWAV model, the detailed model was modified to include five additional cross-sections from Grimesland to Washington. The channel geometry for these five sections was duplicated from FLDWAV and the overbank elevations derived from LiDAR elevation data.

The boundary condition and internal calibration/validation points on the Tar River are plotted in Figure 1. The discharge record at the Tarboro site is used as the upstream boundary condition, while the stage record at the Washington gauge is used as the downstream boundary condition. Tar River simulations are run from July 1, 1999, to August 31, 2005. This period includes a wide range of hydrological conditions, with noticeably high stage cases during Hurricanes Floyd (Sept 1999) and Isabel (Sept 2003). All simulations were run at an hourly time step using hourly input data.



Figure 1. Lower Tar River Modeled Reach

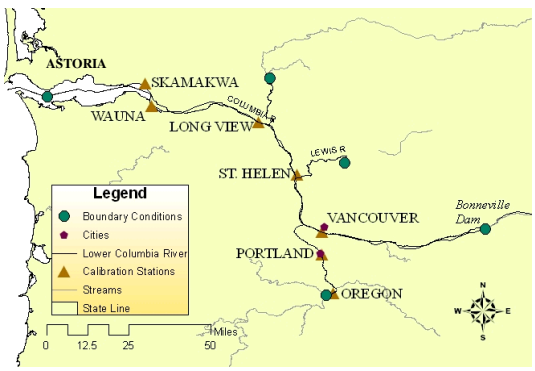

Figure 2. Lower Columbia

3.1.2 Columbia River

The NWS Northwest River Forecast Center operational DWOPER model of the lower Columbia River extends from Bonneville Dam to Astoria, OR (Figure 2). The model includes three major tributaries: the Willamette River, the Cowlitz River, and the Lewis River. The main channel of the lower Columbia River covers 127.5 miles, while the Willamette, Cowlitz, and Lewis segments cover 32 miles, 23 miles, and 19 miles respectively. The main river has 22 cross-sections with an average spacing of 6 miles. The Willamette, Cowlitz, and Lewis have 33, 20, and 26 cross-sections respectively. The boundary condition and internal calibration/validation points on the Columbia River and tributaries are plotted in Figure 2. For the Columbia River, discharge records from Bonneville dam define the upstream boundary condition and tide observations at Astoria, OR, define the downstream condition. Discharge records are also used at the upstream boundaries for the three simulated tributaries. A lateral inflow is applied at the river-mile 114.7 on the Columbia River and a second lateral inflow is applied at the river-mile 25.3 on the Willamette River. These two lateral flows are applied to represent tributaries, which are not modeled as rivers. An internal boundary condition represented as a rating

curve on the Willamette River at Oregon City was used to represent a 50 ft fall. The simulation runs are from Feb 1, 1995 to Feb 28, 1996.

Although NWRFC uses DWOPER for operational runs, we created a nearly identical FLDWAV model of the lower Columbia model as a reference to facilitate study over our year long calibration period. We then created a symmetric HEC-RAS model duplicating the DWOPER/FLDWAV parameterization and model layout.

A HEC-RAS model with more detailed channel geometry for the Columbia River system was obtained from the Hydrologic Engineering Center (HEC). The model was originally developed by the USACE Portland District and later modified by HEC. The initial model contains 604 cross-sections of which 330 describe the lower Columbia River from Bonneville to Astoria, 86 the Willamette River, and 3 the Cowlitz tributary; the remaining 185 are located in distribution channels along the river. There are no bridges specified in the model; however, ineffective areas are specified in 61 river cross-sections.

The detailed HEC-RAS model was modified to cover the exact same domain as the DWOPER and symmetric HEC-RAS models. We extended the Cowlitz tributary and added the Lewis Tributary. These additions used the cross-section information from the symmetric model.

3.2 FLDWAV to HEC-RAS Parameter Conversions

3.2.1 Cross-sections

The representation of the cross-section is different in the FLDWAV and HEC-RAS models. In the FLDWAV models, a river cross-section is approximated by a predefined number of pairs of top width (BS) and elevation (HS). The total number of pairs in FLDWAV (NB) is fixed for a given model and typically five to eight pairs are required to define a cross-section. HEC-RAS represents cross-sections using station-elevation (X-Z) pairs. Figure 3 shows a FLDWAV and HEC-RAS representation of the same cross-section from our Tar River model. The validity of using simplified cross-sections for large river routing has been established (Fread, 1998; Hicks, 1996). The complexity of the channel is fully represented in the detailed cross-section, which may be advantageous in areas where there are flood mapping needs. We compare simulations from the symmetric and detailed cross-section models to assess the added value of having detailed cross-sections for modeling at NWS river forecast points.

In order to represent the symmetric cross-sections of FLDWAV in HEC-RAS, the BS versus HS pairs are translated to station versus elevation. To facilitate the conversion of the cross-sections from FLDWAV to HEC-RAS, we developed a program called *fld2ras*. In addition to converting top width-elevation pairs to station-elevation pairs, *fld2ras* (1) reorders station numbering (if necessary) to be compatible with the HEC-RAS convention to decrease from upstream to downstream, (2) converts distances between cross-sections from miles to feet, (3) assigns default bank station locations required by HEC-RAS, (4) modifies the cross-section shape to account for the FLDWAV AS

parameter (explained below), (5) creates HEC-RAS ineffective areas to approximate FLDWAV ineffective areas defined by the FLDWAV BSS parameter (optional, explained below), and (6) creates a text file formatted for import into HEC-RAS.

An important feature in the FLDWAV/DWOPER model of the lower Columbia River is a parameter that represents the active channel cross-sectional area below the lowest HS elevation. This parameter helps to define the area subject to the deposition and scour processes below the river line, in lieu of using the exact cross section. The parameter is known as *AS*. In HEC-RAS, this *AS* parameter is not available. Therefore to account for the area, at each cross-section, an additional active area is added by assuming a rectangular bottom with same width as the lowest HS value. The depth of the additional area is calculated using *Depth = AS/BS(1).* The elevation of the lowest point is then calculated as *Lowest Elevation= HS(1)- Depth.*

3.2.2 Roughness

The FLDWAV model has the option in which the user can define a stage or flow versus Manning's *n* relationship. Flow is preferred to stage because the calibration of Manning's *n* for different flow levels is relatively straightforward for long reaches, and the geomorphology literature supports the assumption that breaks in channel properties occur at consistent flow levels along a reach. If calibration causes Manning's *n* values to depart from published ranges, the modeler knows to check other parts of the model for errors.

In typical HEC-RAS applications, Manning's *n* values vary horizontally along a cross-section with higher values typically assigned in the floodplain. This can produce a similar effect to the typical FLDWAV application of defining composite Manning's *n* values that tend to increase when high flows reach the floodplain, reflecting the physical presence of brush, trees, or man-made structures in the floodplain. Assigning fixed Manning's *n* values that do not vary with depth or flow can be reasonable for design applications (e.g. when models are calibrated against only single events using high water marks); however, this approach cannot properly represent the physics for unsteady modeling across a range of flows. Therefore, HEC-RAS also provides the option to specify flow roughness factors as a function of flow. Using this feature we reproduce FLDWAV Manning's *n* parameterizations within HEC-RAS. Note that in HEC-RAS 4.0 specification of flow roughness factors is limited to uniform flow increments. Through a Memorandum of Agreement between HEC and NWS, HEC has added the option to define non-uniform flow increments and made this capability available for this study via HEC-RAS 4.0.1 Beta.

Figure 4, shows the FLDWAV Tar River model calibrated Manning's *n* values versus flow for calibration reaches defined in the model. The calibration strategy used to subdivide the reaches and change Manning's values manually or automatically is described by Fread et al. (1986) and RTi (2007).

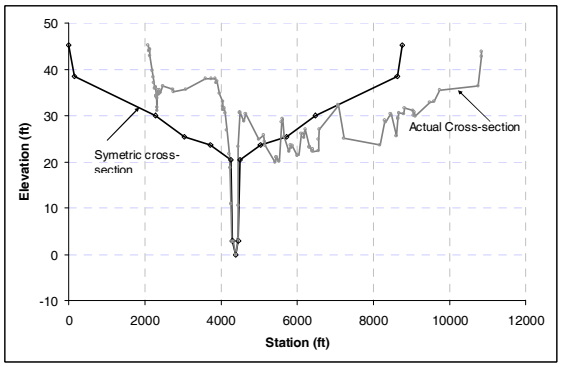

Figure 3. A symmetric and detailed representation of a cross-section of Tar River. While the detailed cross-section is obtained from 105 survey points, the symmetric cross-section is represented by only 16 points which were derived from FLDWAV (eight pairs of top width (BS) and elevation (HS)).

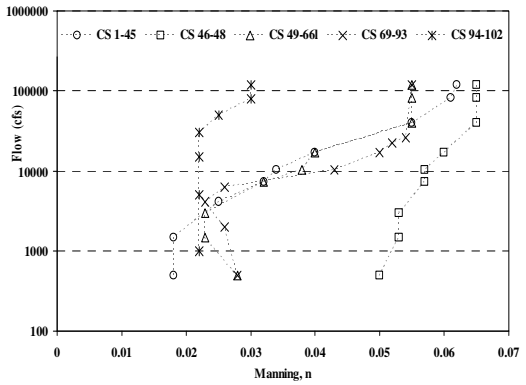

Figure 4. Variation of Manning's *n* versus flow for five cross-section reaches that are designated by the calibration gauges for the Tar River.

3.3 Experiments

For the Tar River we simulated five sets of stages using 1) the FLDWAV model, 2) the HEC-RAS symmetric model with FLDWAV Manning's *n*-flow parameters (SYM), 3) the HEC-RAS detailed model with raw Manning's *n* values from the USGS steady flow analysis (DET_RAW_n), 4) the HEC-RAS detailed model with Manning's *n*-flow parameters from FLDWAV (DET_FLDWAV_n), and 5) the detailed model with calibrated Manning's *n* values (DET_CAL_n).

Similarly, for the Columbia River, we simulated five sets of stages using 1) the FLDWAV model, 2) the HEC-RAS symmetric model with FLDWAV Manning's *n*-flow parameters (SYM), 3) a calibrated version of the HEC-RAS symmetric model (SYM_CAL), 4) the HEC-RAS detailed model with FLDWAV Manning's *n*-flow parameters (DET_FLDWAV_n), and 5) the HEC-RAS detailed model with some additional calibration (DET_CAL_n). In both the Tar and lower Columbia, the calibrated Manning's *n* values were determined through manual calibration by comparing observed and simulated stages at several points along the rivers.

4 Results

Table 1 summarizes statistical results for four validation stations on the Tar River. The FLDWAV and symmetric HEC-RAS model (SYM) exhibit similar overall bias and RMSE and examination of the hydrographs (not shown here) showed acceptable results over all flow ranges. This result was achieved through direct conversion of model geometry and FLDWAV Manning's *n* parameters and no further calibration. We did not attempt further calibration of the HEC-RAS symmetric model, although additional fine tuning can be easily done within HEC-RAS. On the other hand, the detailed HEC-RAS model with raw Manning's *n* values specified for steady state applications

(DET_RAW_n) produced much higher RMSE statistics compared to the other two models. It therefore required more additional work. To achieve a more reasonable result with the detailed model, we first replaced the Manning's *n* values with those from FLDWAV (DET_FLDWAV_n). This yielded some improvements, but additional calibration was necessary to produce acceptable results comparable to those from FLDWAV (DET_CAL_n).

Table 2 summarizes statistical results for the validation stations on the lower Columbia River. For the lower Columbia, direct conversion of model geometry and DWOPER Manning's *n* values did not produce results as satisfactory as those for the Tar River. Although RMSE statistics (SYM) relative to observed stages come close to the FLDWAV results for most stations (the Oregon station is the big exception), examination of the hydrographs (Figure 5) shows that the HEC-RAS symmetric model and FLDWAV simulations deviate substantially from each other. One possible reason for more differences between FLDWAV and HEC-RAS SYM in the lower Columbia compared to the Tar River is that our conversion of the AS parameter is only an approximation. Independent experiments running FLDWAV with and without the AS parameter show that AS values have a very large impact on simulation results (not shown here). Table 2 also shows that some manual calibration effort with the symmetric HEC-RAS model (SYM_CAL compared to SYM) produces improved results at all stations except Portland on the Willamette tributary. We also found that using the detailed model with FLDWAV Manning's *n* parameterizations (DET_FLDWAV_n) provides a good starting point, but some manual calibration produces dramatic improvements (DET_CAL_n). Figure 5 highlights the improvements from calibration in the lower Columbia models both for a station that is highly affected by inflow hydrographs (Vancouver) and for a downstream station dominated more by tides (Wauna).

Table 1 Bias and (RMSE) both in ft (ft) for the Tar River

		HEC-RAS			
Stations	FLDWAV	SYM	DET_RAW_n	DET_FLDWAV_n	DET_CAL_n
Tarboro	.03 (.32)	.04 (.34)	1.71 (2.03)	-0.15 (0.60	0.04 (0.38)
Rcksp	.12 (.51)	.16 (.63)	0.88 (1.20)	-1.13 (1.45)	-0.43 (0.68
Grnvl	.00 (.90)	.36 (1.11)	1.86 (2.30)	-0.55 (1.05)	-0.40 (0.86)
Grim	.16 (.28)	.00 (.22)	1.96 (2.25)	0.00 (0.22)	0.11 (0.24)

* Note that the time period for statistical evaluation is shorter for Rock Springs and Grimesland due to a more limited duration of observed data.

Table 2 Bias and (RMSE) both in (ft) for the Columbia River

		HEC-RAS			
Stations	FLDWAV	SYM	SYM_CAL	DET_FLDWAV_n	DET_CAL_n
Vancouver	0.72 (1.04)	-0.44 (1.06)	-0.17 (0.76)	-054 (1.17)	-0.17 (0.79)
St. Helen	1.12 (1.37)	0.63 (1.08)	0.38 (0.91)	-0.31 (1.11)	0.76 (1.27)
Long View	0.48 (0.87)	0.31 (0.77)	-0.08 (0.62)	-2.21 (2.53)	0.04 (0.85)
Wauna	0.19 (0.84)	0.27 (0.86)	-0.04 (0.80)	-0.61 (1.01)	-0.51 (1.00)
Skamakwa	0.35 (0.85)	0.28 (0.74)	0.14 (0.74)	0.03 (0.69)	-0.00 (0.80)
Oregon	0.77 (1.23)	1.76 (2.27)	0.04 (1.31)	-0.51 (1.09)	-026 (0.80)
Portland	0.57 (0.94)	-0.58 (1.08)	-0.85 (1.24)	-0.51 (1.09)	-025 (0.82)

5 Conclusions and Future Work

We investigated two approaches for replacing FLDWAV models with HEC-RAS models for use in operational forecasting. The first is conversion of existing FLDWAV models and the second is acquisition and modification of HEC-RAS models originally developed for other purposes. Both approaches can save time over building a new model from scratch because they take advantage of cross-section geometry and hydraulic feature data developed by others. The second approach requires more effort than the first because the available model domain and boundary conditions may not exactly match RFC needs, the roughness values assigned for other applications may not be suitable for continuous modeling over a wide range of flows, and the model may not be stable under all flow conditions of interest.

We have developed simple techniques to convert FLDWAV geometry and Manning's *n* parameters from FLDWAV to HEC-RAS models. For the Tar River, there is considerable value in transferring both the FLDWAV geometry and Manning's *n* parameters into HEC-RAS. After this transfer, minimal Manning's *n* adjustments are required to attain equivalent results. In a case when we use more detailed cross-section geometry data in place of FLDWAV geometry, there is still value in using previously calibrated Manning's *n* values. However, considerably more Manning's n adjustments are required. This is true even if the detailed and symmetric models were originally derived from the same elevation data.

For the Columbia River, direct conversion of model geometry and Manning's *n* was not as successful in replicating FLDWAV results. The main difference between the Tar and Columbia models is that the Columbia model includes an *AS* parameter for which there is no direct equivalent in HEC-RAS. Despite this difference, the calibrated Manning's *n* values from FLDWAV provided good initial estimates for further calibration both with the symmetric geometry from FLDWAV and the detailed HEC-RAS model.

In our two case studies, the more detailed models (e.g. more cross-sections, more detailed cross-sections, and more explicitly defined storage areas and structures) did not show substantially improved simulations or provide for easier calibration than the simpler, symmetric models. There are still potential benefits from more detailed models, but use of simpler models makes the most sense until these benefits are proven. More detailed models may be more amenable to accurate flood forecast mapping if the models are properly geo-referenced. With more study, the more detailed lower Columbia model will likely help us to more properly represent off channel storages. It may be that calibrated Manning's *n* values are compensating for physical inaccuracies in the simpler models; however, this would be difficult to prove.

Results from this study suggest that converting FLDWAV models into HEC-RAS is a viable option and likely to be less work than acquiring a more detailed HEC-RAS model from another source and modifying it. Additional work is required to rigorously evaluate stability of the models to make sure models are stable over a range of conditions for

operational needs. The model validations described here were done in simulation mode. Our next step is to validate these models in operational mode and running them side-by-side with the existing operational models. This is particularly important for the lower Columbia where we believe we can still improve the HEC-RAS model.

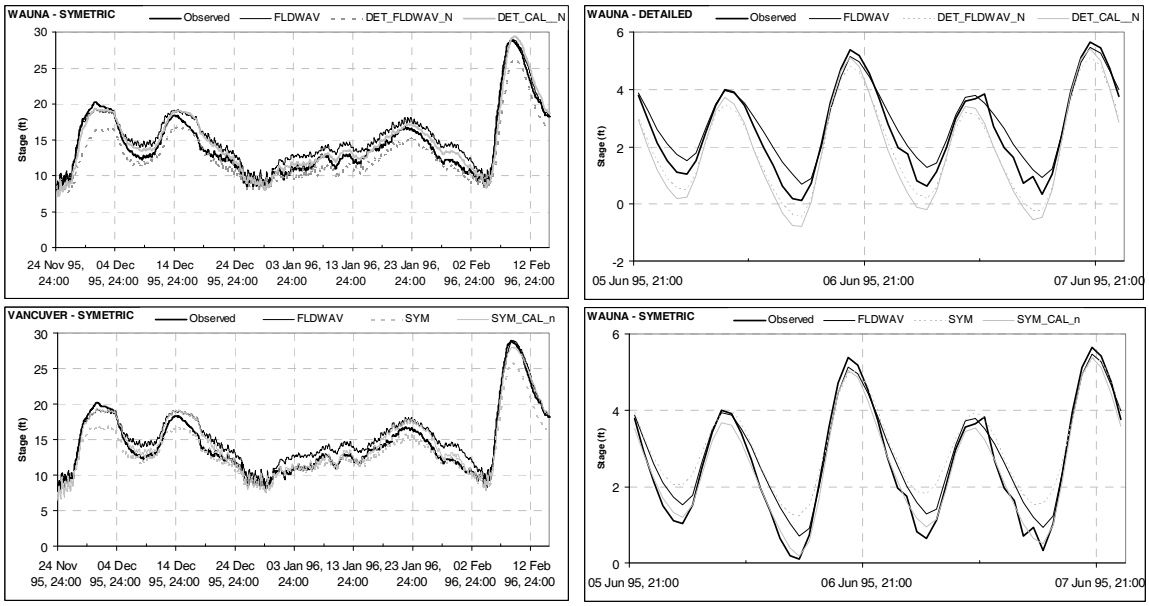

Figure 5 Example of simulated and observed hydrographs for Columbia River at Vancouver and Wauna stations

6 References

Brunner, W. G, 2002, HEC-RAS, River Analysis System Hydraulic Reference Manual. Downloadable http://www.hec.usace.army.mil/software/hec-ras/hecras-download.html

Fread D.L., 1998. NWS FLDWAV model: Theoretical Description, Hydrologic research Laboratory, Office of Hydrology, National Weather Service, NOAA

Fread, D. L., and J.M. Lewis, 1986. Parameter Optimization of Dynamic Routing models. Proceedings of ASCE Conference /H.Y. EE. WW Divis. Long Beach, CA.

Fread, D. and G. Smith, 1978. Calibration Technique for 1-d Unsteady Flow Models. Journal of the Hydraulics Division, ASCE, Vol. 104 No. HY7.

Gee, Michael D. and G. W. Brunner, 2005. Dam break flood routing using HEC-RAS and NWS-FLDWAV, ASCE/EWRI, 2005.

Hicks, F.E, 1996. Hydraulic flood routing with minimal channel data: Peace River Canada. Can.Civ Eng. 23:524-535

Koren, V., Reed, S., Smith, M., Zhang, Z., Seo, D.-J., 2004. Hydrology laboratory research modeling system (HL-RMS) of the US national weather Service. Journal of Hydrology, Vol. 291, 297-318.

National Weather Service, Evaluation of Different Hydraulic Models in Support of National Weather Service Operations, Final Report of the Hydraulic Model Evaluation Team, http://www.weather.gov/oh/rfcdev/docs/Final_Report_EvaluationHydraulicModels.pdf, 2007.

Riverside Technology, Inc., RTi, Calibration for the Lower Tar River Basin, Phase II Task Completion Report, Task 6-0016, submitted to NOAA/NWS/OHD, May 2007.

Numerical simulation of dissolved oxygen concentration in the downstream of Three Georges Dam

Xiangju Cheng[1], Xuewei Chen[1], Yongcan Chen[2]
[1]School of Engineering, Research Center of Ocean Engineering, Sun Yat-sen University, Guangzhou 510275, China
[2]Department of Hydraulic Engineering, Tsinghua University, Beijing 100084, China

Abstract: Strong colliding between the flow discharged from spillway and the water-body in the stilling basin will produce a lot of air bubbles in the downstream of the Three Georges Dam. Bubble mass transfer will be dominant and can cause total dissolved gas (TDG) supersaturation. Elevated TDG levels can have an adverse effect on aquatic organisms in the form of gas bubble trauma (GBT). TDG concentration is changed with distance from the spillway crest and depending on hydraulic and operating conditions. Dissolved oxygen (DO) transport model is developed in this paper and used to simulate the physical processes of gas transfer coupled with the air-water two-phase mixture flow model. Supersaturated DO concentration in the water-body downstream along with distance is successfully calculated during spillage when the water level is 139m in the Three Georges reservoir.
Keywords: bubble interface mass transfer, supersaturated DO concentration, numerical simulation, Three Georges dam.

1. Introduction

Hydropower projects usually have more functions such as flood control, navigation, irrigation and electricity production. However, total dissolved gas will be supersaturated in the water-body of downstream during high flow periods. Suppersaturation of dissolved gas which typically occur between April and September can have an adverse effect on aquatic organisms in the form of gas bubble trauma (GBT). Such trauma is typically exhibited by the formation of gas bubbles within the tissue and circulatory systems of aquatic organisms which may lead to mortality under extreme conditions. According to the observation data provided by the water environmental monitor centre of the Three Gorges project, DO concentrations at the river sites of Dong Yue temple, Huang Lin temple, and Nan Jingguan are over 110% during high flow periods when the water level is 135m or 145m in the Three Georges reservoir [1]. With the increasing of water level in the reservoir, surface and deep gates are spilling at the same time. More and more air bubbles will be produced due to the strong mixing between air and water. TDG levels in the water-body of downstream will be increased even supersaturated. Anadromous fish species such as paddlefish and mullet are important natural resources in the middle reach of Yangtze River. So it is essential to predict the trend of dissolved gas supersaturation during spillage at Three Georges Dam.

The complete process of air entrainment into the water flow and the mass transfer through air bubbles and free-surface have been studied previously by researchers [2, 3]. Earlier works used a material control volume approach to calculate the dissolved gas concentration [4, 5]. Although this approach allowed the calculation of the

depth-averaged dissolved gas at some point downstream of the spillway but the models are unable to predict the most dangerous regions for the fish. Therefore it cannot be used to evaluate different spillway modifications designed to alleviate the supersaturation problem. A recent work by Urban et al [6] calculated the concentration field of dissolved gas downstream of a spillway. One-dimensional mass transport equation for imcompressible flow is used in those models. However, the turbulence kinetic energy and gas void ratio in the equations are estimated from some empirical equations and some depth-averaged values. It can be easily seen that those studies collected at the dams less than 50m height and some specific hydropower projects.

The work presented in this paper is a part of efforts to reduce the impact of hydropower dams on fish in Yangtze River. The air-water two-phase mixture model has been implemented to calculate the values of some important factors such as gas void ratio, turbulence kinetic energy and water flow velocities. Dissolved gas concentration transport equation is used to calculate the concentration distribution of TDG in the liquid phase. The bubble interface mass transfer coefficient is calculated based on Ref. [7]. Due to lack of observed data for the concentration of TDG, the DO concentration is represented to the TDG concentration here. Two-dimensional numerical results are compared with the measured data in the downstream during spillway operations for Three Georges Dam.

2. Mass transfer equations and definitions

DO transport model is obtained using a mass balance of the gas dissolved in the liquid phase in a control volume. The dimensionless DO transport equation reads:

$$\frac{\partial(\rho C)}{\partial t} + \nabla \cdot (\rho \vec{U} C) = \nabla \cdot [\rho(\nu + \frac{\nu_t}{\sigma_t})\nabla C] + \rho S_C \tag{1}$$

where C is DO concentration in a control volume expressed as a percent of saturation concentration, U is the flow velocity, S_c is the DO source due to the overall air transfer from the bubbles to the liquid and from the atmosphere to the liquid, ν is the molecular diffusivity of air in water, ν_t is the turbulence diffusivity of air-water mixture liquid, ρ is the density of air-water mixture, and σ_t is the turbulence Schmidt number.

Considering that the density of air-water two-phase flow is changing with time and space in Eq. (1), Zarrati *et al* [8] took two-phase flow as laminar flow and simulated the flow field of air-water two-phase flow under different values of σ_t. It showed that the simulated results are similar when the value range of σ_t is between 0.5 and 2. So the value of σ_t is between 0.5 and 2 in this paper.

It has been generally recognized that supersaturation is caused by the higher pressures which is exerted on the bubbles in the stilling basin. It makes bubbles have a higher saturation concentration. As large numbers of bubbles travel to various depths, the combined effect of the corresponding pressures has been termed "effective saturation concentration C_{se}", named by Hibbs and Gulliver [9]. There are, however, two types of interfaces available for gas transfer: one is the free surfaces and the other

is the bubble-water interface. The two types of interfaces have different saturation concentrations. The two saturation concentrations S_c can be written as

$$S_C = K_{\mathrm{L,B}} a_{\mathrm{B}} (C_{\mathrm{se}} - C) + K_{\mathrm{L,s}} a_{\mathrm{s}} (C_{\mathrm{s}} - C) \tag{2}$$

where $K_{\mathrm{L,B}}$ is mass transfer rate coefficient across the air bubble interface, $K_{\mathrm{L,s}}$ is the mass transfer rate coefficient across the air-water interface , a_{B} and a_{s} are surface areas of air bubbles and air-water interfaces respectively.

The effective saturation concentration (C_{se}) can be expressed by the increased transfer potential between air bubble and surrounding water under hydrostatic pressure. It is a combination of the atmospheric saturation concentration and the increased transfer potential due to hydrostatic pressure.

$$C_{\mathrm{se}} = C_{\mathrm{s}} (1 + \frac{\gamma d_{\mathrm{eff}}}{p_{\mathrm{atm}}}) \tag{3}$$

where d_{eff} is the effective depth which is experienced by the bubbles, γ is the specific weight of water and p_{atm} is the atmospheric pressure. Hibbs et al [10] found that an effective depth would be function of the specific discharge q. For a very small flow rate, the spillway flow may not penetrate to the stilling basin floor and air bubbles move down to an effective depth. The ability of air bubbles releasing air into water will be decreased. The maximum effective depth can be estimated as 2/3 depth of tailwater. For a large hydraulic structure such as Three Georges dam or Ge Zhouba dam has a 10 m deep or greater stilling basin, so C_{se} will be twice greater than atmosphere saturation.

Due to the strong entrainment of air bubbles, the endured large hydrostatic pressure, and long subsistent time in water of air bubbles, the bubble-water interface transfer is the main source of DO in the downstream. Fumio Takemura et al [7] studied a small spherical bubble rising through stagnant water and the gas-liquid mass transfer coefficient was estimated from observed bubble diameter versus time. Though the results were studied under the Reynolds number of flow less than 100, however, even the Reynolds number is larger enough, and the transfer characterization of air bubble-water interface is nearly unchanged. So based on the results and taken some modification of the equation presented by Fumio Takemura, the numerical equation of air bubble-water interface transfer coefficient in this paper can be expressed as

$$K_{L,B} = \beta \cdot \frac{\nu}{R_b \sqrt{\pi}} \left\{ 1 - \frac{2}{3} \frac{1}{(1 + 0.09 Re^{2/3})^{3/4}} \right\} Pe^{1/2} \tag{4}$$

where R_b is the air bubble diameter, Pe is the Peclet number and equal to $2R_b v_r / D_m$, Re is the Reynolds number and equal to $2R_b \sqrt{2k/3} / \nu_t$, v_r is the air bubble rising velocity and equal to a constant 0.25m/s, k is the turbulence kinetic energy, β is an uncertain constant which is taken to be a calibrated parameter in the present study.

To simplify the model, the air bubble diameters are assumed to be the same in this paper. The air bubble-water interfacial surface area can be expressed as

$$a_B = n \cdot A_g \tag{5}$$

where n is the numerical density of air bubble in water, A_g is the surface area of one air bubble ($=4\pi R_b^2$). According to the definition of gas void ratio, it can be obtained

$$\alpha_a = \frac{V_a}{V_m} = \frac{N}{V_m} V_b = n \cdot \frac{4}{3} \pi R_b^3 \tag{6}$$

where α_a is the gas void ratio in air-water two-phase flow, N is the air bubble number in volume of V_m, V_b is an air bubble volume in which the bubble diameter is R_b. So the air bubble-water interfacial surface area can be expressed as

$$a_B = \frac{3 \cdot \alpha_a}{4\pi R_b^3} \cdot 4\pi R_b^2 = 3\alpha_a / R_b \tag{7}$$

When the aqueous concentration of oxygen is supersaturated, surface mass transfer will decrease the supersaturated DO concentration as time goes on. The transfer is estimated by Cheng [11] combined with the flow velocity and turbulence kinetic energy.

$$K_{L,s} = 0.002436 U^{(-5/3)} k^{(4/3)} \tag{8}$$

where U is the flow velocity, k is the turbulence kinetic energy, and

$$a_s = \frac{A_s}{V_m} \approx \frac{1}{\Delta Z} \tag{9}$$

where A_s is the water surface area, V_m is the surface flow volume, Δz is the surface thickness. Li [12] showed that the difference of computed DO concentration was less than 1% whetherΔz is equal to 0.005m, 0.01m, 0.02m or 0.03m. In this paper, the height of grid cell is about 0.5m, so theΔz is equal to the height of grid cell. The position of the air-water surface of flow over spillway is discussed by Chanson [13]. He considered that the gas void ratio at the air-water free interface is equal to 0.9 can favorably reflect the characteristics of air-water interface.

Hydrodynamics variables (U, ν_t, k, α_a) will be changed as the flow moves downstream. These variables will be calculated for each control volume using the air-water two-phase mixture model and RNG k-ε model. The description of the mixture flow model for air-water two-phase flow and RNG k-ε model is presented in Ref. [14].

3. Numerical method

The mixture model for air-water two-phase flow is solved using commercial flow simulation software Fluent 6.2 and the DO transport model is solved using User Defined Scalars [15]. A six-equation, two-fluid, dispersed turbulence model is constructed. The control-volume-based technique is used to solve the equations. The calculation domain is divided into discrete control volumes by the structured grid. The convective fluxes in the mean volume fraction, momentum and turbulence closure

equations are discretized by employing a conservative, second-order accurate upwind scheme. The pressure-velocity coupling algorithm is the pressure-implicit with splitting of operators (PISO), which is based on the higher degree of the approximate relation between the corrections for pressure and velocity and may also be useful for transient calculations on highly skewed meshes.

4. Application example

The results of the models are compared with field data measured at the Three Georges dam on the Yangtze river. DO data are provided by the water environmental monitor centre in the Three Gorges project construction company.

4.1. Solution domain

The Three Georges Dam has width of 483m spillway with 23 deep gates and 22 surface gates. The elevations of deep gates and surface gates are 90m and 158m respectively. Water discharge takes place in 14 powerhouse existed in the east and north direction respectively. DO concentration is measured in the sections of Dong Yue temple about 2 km far and Huang Lin temple about 12 km far downstream of the spillway when the water level of the Three Georges reservoir is 139m. In this work, 2D simulations are performed in a cross-section which includes the reservoir, spillway of deep gate and stilling basin (shown in Fig.1). The design curves of vertical section of deep spillway are presented in Ref. [15]. Although 3D effects are unavoidable, 2D simulations are less expensive. It should present most of the physical features of the flow in the DO production area. 3D simulations will be performed in the later study.

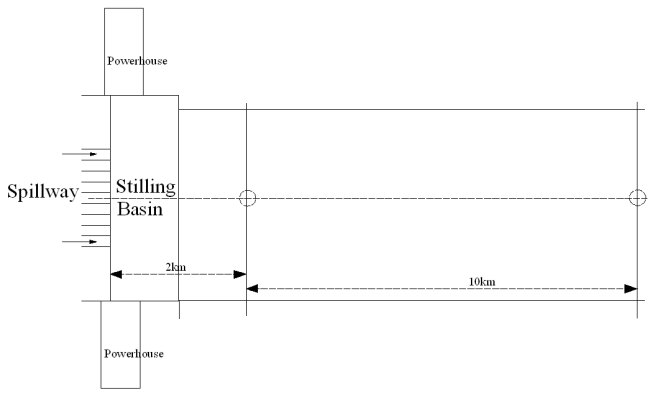

Fig. 1. Spillway of Three Georges dam and the numerical domain downstream of spillway

There are two simulation conditions in the present work. Case 1: Measured time is July 20, 2004. Only 12 deep gates discharged and flow rate is 17200m^3 per second. There are 8 generating electricity sets working and the flow rate is 7100 m^3 per second. Water level is 66.97 m and water depth is about 28 m at the downstream of the Three Georges dam. Water level of Three Georges reservoir is 139 m. Case 2: Measured time is August 23, 2005. Only 20 deep gates discharged and the flow is 30530m^3 per second. There are 13 generating electricity sets working and flow rate is 11447 m^3 per second. Water level is 66.97 m and water depth is about 29 m at the

downstream of the Three Georges dam. Water level of Three Georges reservoir is 139 m.

Non-uniform structured grids are used in the present work. Grid size is about 0.5m where the water jets are falling into water-body of downstream. The grid size is properly coarsened where the air entrainment nearly does not exist in the downstream of river and is about 2 m along with the direction of water flow.

4.2. Boundary conditions

The inlet section consists of the inlet of water on the lower part and the inlet of air on the higher part upstream of the spillway. The water inflow velocity can be calculated according to the discharge and the water depth at the inlet. The air boundary is setting as pressure-inlet conditions on which atmospheric pressure is assumed. Due to the boundary between water and air at the downstream outlet can not be distinguished, it is defined as a pressure boundary or free-flow condition. All of the walls are set as the stationary, non-slip wall. The viscosity layer near to the wall is dealing with as the standard wall function. The initial flow field over the spillway is full of air. Through the time-dependent simulation, the water flows over the spillway and produced air-water two-phase flow.

4.3. Some assumptions

As discussed earlier, the bubble interface mass transfer coefficient is a function of the diameter of the bubble. Meanwhile, DO concentration is affected by the discharge from the powerhouse. Focusing on oxygen transfer, the following assumptions simplify the numerical model in the paper.

(1) The process of gas transfer across the bubble surface and the water surface is the only way by which interfacial mass transfer takes place;

(2) The initial bubble shape is spherical and it retains its original shape during its travel through the water column. The bubbles are single-sized bubbles and the diameter of bubble is 5 mm;

(3) DO concentration in the water discharged from the powerhouse is not changed and equal to the concentration in the reservoir. Taken the discharge from powerhouse into account, DO concentrations of downstream water-body during spillage at the Three Georges Dam may be expressed as

$$C_d^{'} = \frac{C_u Q_1 + C_d Q_2}{Q_1 + Q_2} \tag{10}$$

where C_u is DO concentration at the upstream of the spillway, C_d is DO concentration in the water after discharged from spillway, Q_1 is the flow rate discharged through the powerhouse, Q_2 is the flow rate discharged through the spillway, $C_d^{'}$ is DO concentration at the downstream of the spillway after water is complete mixed between the flow discharged through the spillway and through the powerhouse exits. So the C_d is can be simulated by use of the air-water two-phase mixture model and the DO transport model. Then $C_d^{'}$ can be computed based on the Eq. (10). It is the actual

DO concentration in river. $C_d^{'}$ will be used to compare with the measured DO concentration in this paper.

5. Results and discussion

5.1. Model Calibration

The models were calibrated using field data of DO concentration at the downstream of the water during the spillage at the Three Georges dam. The only coefficient β in Eq. (4) will be determined after the simulated DO concentration is calibrated by the field data.

Fig. 2 compares the DO concentration between model prediction and field data, as a percent of saturation, and the scatter dots are the field data. Field data are measured at the 2 km and 12 km downstream of the Three Georges dam. It can be seen that the two types of results are nearly close to each other and the standard error between simulation and field data is less than 0.5%. Fig. 3 compares model prediction and field data of DO concentrations along with the water depth at 1 km section downstream of Three Georges dam. The scatter dots are the field data. It can be seen that the standard error between simulation predictions and field data is less than 1%. The results show that the model in this paper and the numerical method to simulate supersaturated DO concentration are reasonable and feasible.

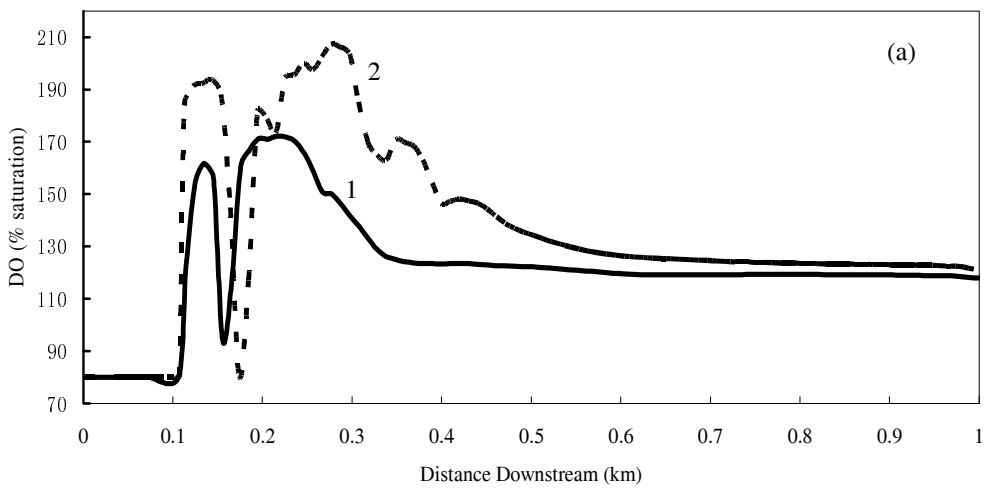

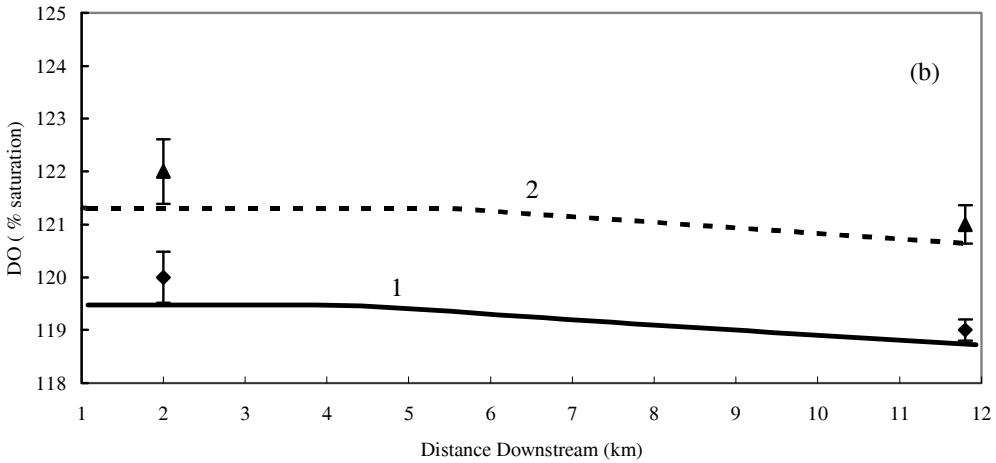

Fig. 2. Model prediction and field data of DO concentration along with the direction of water flow in the downstream of Three Georges Dam. Curves 1 and 2 represent the model prediction data of case 1 and 2, respectively.

For the two flow conditions, the distribution of DO concentrations along with distance is similar to each other. DO concentration in reservoir is nearly 80% of saturation. When water jets impact the water cushion pool, because the impacting time is very short and the water jets haven't mixed with the water cushion pool adequately, the temporary decrease of DO concentration appears. However, with the adequate mixing between the water jets and the downstream water cushion, turbulence, high gas void ratio and hydrostatic pressure lead to rapid transfer through bubble interface and eventually DO concentration reaches a maximum. With the flow tending to stable, water turbulence being weakened and air bubbles being disappeared, DO concentration will be decreased and eventually plateau in the downstream tailwater. The effect of the spillway and stilling basin on transfer process diminishes with distance and the change of DO concentration becomes minimal. It is shown from Fig. 2 that DO concentration is nearly 120% of saturation when flow reaches to 1 km and it remains 119% when flow reaches to 12 km in the case 1. That is to say, DO concentration just dissipates 1% in the range of 11 km. Some field data show that supersaturated DO concentration will decrease 6~8% of saturation in the range of 100 km. The results show again that the model in this paper to simulate supersaturated DO concentration is reasonable. The results also show that once DO concentration is supersaturated in water, it will need fairly long time and distance to recovery to the normal level before super-saturation.

Because the flow rate in case 2 is more than that of in case 1, peak of DO concentration in case 2 is also higher than that of in case 1 and DO concentration along the distance is also higher than that of in case 1.

It is worthwhile to mention that water depth is one of the important factors to affect the supersaturated DO concentration. As seen from Fig. 3, DO concentrations are not obviously being stratified along water depth. There is only 5% of saturation in the

range of 28 m water depth. DO concentrations still remain supersaturated under 28 m. It is maybe that the adequate mixing in the stilling basin can be used to explain this un-stratified phenomenon of DO concentration. Based on the field results, DO concentrations is nearly equal to each other along with the water depth in a section no matter it is at the water surface or at 30m deep under the water surface.

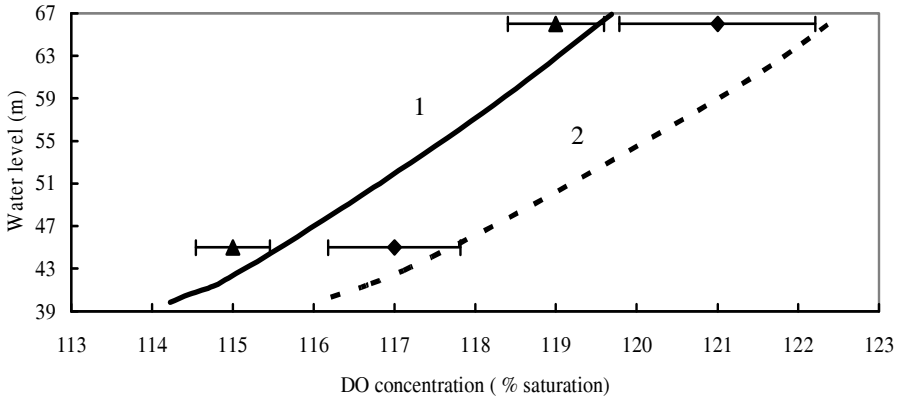

Fig.3. Model prediction and field data of DO concentration along with the water level at 1 km section in the downstream of Three Georges dam. Curves 1 and 2 represent the model prediction data of case 1 and 2, respectively.

5.2. Volumetric mass transfer coefficient of air bubble

Fig. 4 shows the air bubble volumetric mass transfer coefficients in two cases. The values of air bubble volumetric mass transfer coefficients change from 0 to 0.26. Many other authors also studied the volumetric mass transfer coefficients of air bubbles by means of numerical simulation and experiments under different Reynolds number [16, 17]. They found that when the Reynolds number of water flow is between 4000 and 40000, the air bubble volumetric mass transfer coefficients will change from 0 to 0.3. The Reynolds numbers are nearly equal to 30000 at the conditions of the two cases in this paper. The distribution in the volumetric mass transfer coefficients is very similar to that of DO concentration in the downstream of the Three Georges dam. So it is shown that the predicted volumetric mass transfer coefficient of air bubble is available in this paper. In the domain of water jets impacting with the stilling basin, high turbulence produces a lot of air bubbles which increase the air bubble interface area and transfer quantity. So the volumetric mass transfer coefficient reaches to maximum. At the same region, DO concentration reaches to maximum (See Fig. 2). With the flow gradually becomes calm, mass transfer through air bubble surface is decreased along the downstream of the stilling basin due to less air bubbles, lower turbulence, decreased gas void ratios and smaller hydrostatic pressure. Bubble transfer is no longer dominant and the mass transfer coefficient to across the air-water surface interface becomes important in this region. So the DO concentration is increased along with the flow direction due to the mass transfer at air-water surface.

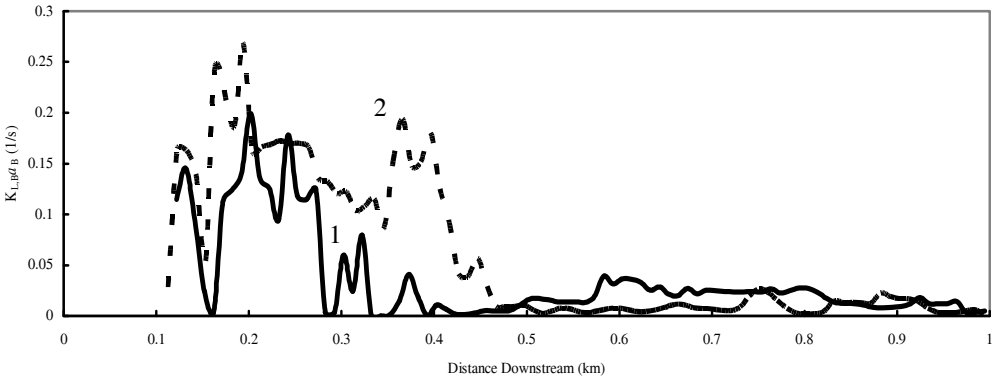

Fig. 4. Air bubble interface mass transfer coefficients downstream of Three Georges dam. Curves 1 and 2 represent the model prediction data of case 1 and 2, respectively.

6. Conclusions

The findings in this paper are summarized as follows:

(i) This study presented a numerical model to predict the DO concentration of the downstream water of the Three Georges dam during spillage. It is based on air-water mixture flow approach and allowed to the computation of the gas source on the DO transport equation. There is a good agreement between the model predictions and field data. In order to study the supersaturated TDG in the downstream of the Three Georges dam, the numerical methods in this paper have a great benefit in practice.

(ii) The numerical results have shown that the dissipating rate of supersaturated DO concentration in water-body is too slow. In the range of 10 km of river, the DO concentration is only 1% decreased. So DO concentration is once supersaturated in river, it will need fairly long time and distance to recovery to the normal level before super-saturation. Consequently, to search a realizable method for decreasing DO concentration is a key scientific problem for protection fish in river.

(iii) It is worthwhile to mention that the presented work is the initial step toward the development multidimensional simulation tools for the analysis of the problem of DO levels in the downstream of spillways. Next step work will consider the effect of air bubble size distribution and bubble number density on DO concentration. Besides the DO, the DN and total dissolved gas are all affect the fish living. So determination of the relationship of these three kinds of concentrations is also the next step work.

Acknowledgements This work was supported by National Natural Science Foundation of China (Grant No. 50609011).

References

[1] CHENG XJ, CHEN YC, LIU N, et al. Supersaturated reaeraion analysis at the Three Gorges reservoir during discharge. Journal of hydroelectric engineering 2005; (6): 62-67 [In Chinese].

[2] Geldert DA, Gulliver JS, Wilhelms SC, Modeling dissolved gas supersaturation below spillway plunge pools. Journal of Hydraulic Engineering 1998; 124(5): 513-521.

[3] Huang HQ. Computational model of total dissolved gas downstream of a spillway, Ph. D Thesis, University of Iowa, USA; 2002, p. 10-80.
[4] Johnson PL, King DL. Prediction of dissolved gas transfer at hydraulic structures. Symp. Reaeration Res. ASCE, New York, NY.
[5] Joseph JO, Gulliver JS. Dissolved gas supersaturation downstream of a spillway II: Computational model. Journal of hydraulic research 2000; 38(2): 151-159.
[6] Urban AL, Gulliver JS, Johnson DW. Modeling total dissolved gas concentration downstream of spillways. Journal of hydraulic engineering 2008; 134 (5): 550-561.
[7] Motarjemi M, Jameson GJ. Mass transfer from very small bubbles-the optimum bubble size for aeration. Chemical engineering science 1978; (33): 1415-1423.
[8] Zarrati AR. Mathematical modeling of air-water mixtures in open channels. Journal of hydraulic research 1994; 32(5): 707-720.
[9] Gulliver JS, Hibbs DE, McDonald JP. Measurement of effective saturation concentration at hydraulic structures. Journal of hydraulic engineering 1997; 123(2): 86-97.
[10] Hibbs DE, Gulliver JS. Prediction of effective saturation concentration at spillway plunge pools. Journal of hydraulic engineering 1997; 123(11): 940-949.
[11] CHENG XJ, LUO L, ZHAO WQ, et al. Study on re-aeration law of water flow over spillway. Journal of Hydrodynamics, Ser. B. 2006; 18(2):231-236.
[12] Li R, Li J, Li KF. Progress in atmospheric reaeration conefficients of turbulent water body. Journal of Environmental Science in Shanghai 2000; 19(4): 176-179 [In Chinese].
[13] Chanson H, Toombes L. Strong interactions between free-surface aeration and turbulence in an open channel flow. Experimental Thermal and Fluid Science 2003; (27):525-535.
[14] CHENG XJ, CHEN YC, LUO L. Numerical simulation of air-water two-phase flow over stepped spillway. Science in China (Ser. E) 2006; 49(6): 674-684.
[15] Zhou S, Zhou Ch, Cai JM, et al. Study on the hydraulics of Three Georges dam Water Control Project. Beijing: water publication; 2006, p. 7-10 [in Chinese].
[16] Kumar MD, Sanyal J, Anupam J. A generalized approach to model oxygen transfer in bioreactors using population balances and computational fluid dynamics. Chenmical engineering science 2005; (60): 213-218.
[17] Wang TF, Wang JF. Numerical simulation of gas-liquid mass transfer in bubble columns with a CFD-PBM coupled model. Chemical engineering science 2007; 62: 7107-7118.
[18] Wilhelms SC, Gulliver JS. Bubbles and waves description of self-aerated spillway flow. Journal of hydraulic research 2005; 43(5): 522-531.

On a Two-Dimensional Temperature Model: Development and Verification

Yong G. Lai [1] and David Mooney[2]

[1] Sedimentation and River Hydraulics Group, Technical Service Center, Bureau of Reclamation, Denver, CO 80225; PH (303) 445-2560; FAX (303) 445-6351; email: ylai@do.usbr.gov

[2] San Joaquin River Restoration Program, Mid-Pacific Region, Bureau of Reclamation, Sacramento, CA 95825; PH (916) 978-5458; email: dmooney@mp.usbr.gov

Abstract

Government regulators on many rivers have specified acceptable temperatures based upon habitat and biological criteria. These temperature thresholds impose constraints on reservoir operations and can limit water deliveries and power generation. Existing tools based on low-order modeling simplify a river to a simple line with limited spatial distribution of inputs and poorly represent physics of the river processes. The limited spatial extents restrict the usefulness of low-order modeling for such features as agricultural returns, gravel pits, groundwater upwelling, side channel activation, and streamside vegetation. It also imposes limitation on fish habitat assessment and reoperation outside the range of the calibration datasets.

This study develops a two-dimensional (2D) temperature module for an existing 2D hydraulic model, SRH-2D version 2. The 2D model incorporates data with both lateral and longitudinal geographic extents rather than lumping results into a point-to-point or uni-directional representation. The objective was to improve the representation of spatial features where low-order models resort to empiricism for a lumped treatment. Better representation of processes leads to increased accuracy and higher confidence.

The SRH-2D temperature model utilizes meterological data as inputs (solar radiation, cloud cover, air temperature, dewpoint temperature and wind speed). Physical processes modeled include solar radiation, terrain and vegetation shade, atmospheric radiation, water back radiation, heat exchange between water and river bed, water surface evaporative and conductive losses.

The model formulation, along with governing and process equations, is discussed first. The model is then tested and verified with simple cases having analytical solutions. The model is finally verified by applying to flows on the McKay Creek downstream of the McKay Dam.

Introduction

Water temperature is a key element for water quality studies and for some cases the most important attribute for stream analysis (Bartholow, 2002). Stream manipulation may lead to changes in water temperature which in turn may affect aquatic systems in many ways. Stream modifications may include reservoir discharge, release temperature, irrigation diversion, riparian shading, channel alteration, thermal loading, etc. Since many rivers have temperature compliance criteria for habitat and biological reasons, understanding of the temperature change due to stream manipulation becomes important. With climate change and growing emphasis on maintaining biological function in addition to water deliveries, the impact of thermal criteria in constraining water operations is expected to increase.

Assessment and prediction of stream manipulation consequences on water temperature for shallow streams are often carried out with numerical temperature models. Example models include SNTEMP (Theurer et al., 1984), SSTEMP (Bartholow, 1990), and ADYN/RQUAL (Hauser and Schohl, 2003), among others. Most existing tools are based on low-order modeling that represent a channel as a line of homogeneous longitudinal elements with limited spatial distribution of inputs. Some physical processes are poorly represented. Limited spatial extent restricts the usefulness of the model by neglecting spatial features such as tributaries and agricultural returns, gravel pits, groundwater upwelling, side channel activation, and streamside vegetation are highly parameterized or not included. The simplified picture of interactions requires inferring or estimating the real processes through conversion to lower order dimensions by the use of a number of empirical parameters used as abstract calibration coefficients. These coefficients increase the difficulty of model usage as well as the uncertainty, because most rivers do not have sufficient data to calibrate the independent effects of different features. Further, coefficients not tied to physical processes do not apply across a broad range of conditions. Predictive capability is limited to circumstances within measured ranges and cannot estimate the impact from changes on how the system operates. Example coefficients include: adjustments for estimates of velocity distributions (travel times) in the main channel, multiple flow paths, lateral inflows (surface or subsurface), and storage areas.

In this presentation, a two-dimensional (2D) temperature module is developed which incorporates geographic extents both laterally and longitudinally. A 2D representation provides a more direct and quantitative estimate of temperature impacts using the same spatially distributed area as is significant for biological characteristics. The developed 2D temperature module is then incorporated into an existing 2D hydraulic flow model, SRH-2D version 2 (Lai, 2008). The SRH-2D flow model is based on SRH-W (Lai, 2006) and has been widely applied by Reclamation and by external institutions. Many restoration projects in recent years apply 2D flow models to assess stream habitat suitability (e.g., Moir and Pasternack, 2008). Therefore, a temperature module would be a valuable addition where temperature is an important water quality element.

2D modeling provides accurate flow hydraulics which eliminates the need for abstract travel time adjustment coefficients and flow routing. When there are multiple flow paths, such as with gravel pits or side channels, flow moves at different speeds

along the different paths and, as a results, heats or cools at different rates. The difference in flow velocities between the river centerline and banks is also captured, eliminating the need to calibrate for cross section averaging. Spatially distributed sources of heat and cooling (ground water, solar, wind, vegetation) are directly transferable to the model and do not require grouping by reach. As a result, the spatially explicit results may show acceptable areas within generally unacceptable conditions and permit compromises where simplified models might indicate temperature violations. A process model can indicate the most critical component of the more critical areas to focus solutions. Grouping and lumping with abstract coefficients obscures the actual steps preventing temperature compliance.

Multi-dimensional tools for temperature modeling of reservoirs and lakes exist, for example, the 2D laterally averaged model CE-QUAL-W2 (Cole and Buchak 1995) and three-dimensional (3D) model U^{2}RANS (Lai et al. 2004). However, they are not applicable to typical streams. 2D laterally averaged reservoir models neglect lateral effects in favor of vertical stratification and are mostly limited to impounded areas; 3D models can accurately simulate temperature but the scale limits application to small areas. This paper focuses on shallow water streams where vertical stratification is negligible and complete vertical mixing is assumed.

Governing Equations and Process Models

The 2D depth-averaged flow equations are based on the assumptions that stream flows are shallow compared to width and the effect of vertical motion is negligible. Details of the equations and their numerical solution procedure may be found in Lai (2008) and are omitted here.

Conservation of thermal energy leads to the 2D depth-averaged temperature equation expressed as:

$$\frac{\partial hT}{\partial t}+\frac{\partial hUT}{\partial x}+\frac{\partial hVT}{\partial y}=\frac{\partial}{\partial x}\left[\frac{h\nu_t}{\sigma_t}\frac{\partial T}{\partial x}\right]+\frac{\partial}{\partial y}\left[\frac{h\nu_t}{\sigma_t}\frac{\partial T}{\partial y}\right]+\frac{\Phi_{net}}{c_w\rho_w}+\frac{q_{sp}}{A_{sp}}(T_{sp}-T) \quad (1)$$

In the above, T is depth averaged water temperature [C], x and y are horizontal Cartesian coordinates [m], t is time [s], h is water depth [m], U and V are depth-averaged velocity components [m/s] in x and y directions, respectively, ν_t is the turbulent viscosity and dispersion [m^2/s], σ_t is the thermal Prandtl number, ρ_w is the water density [kg/m^3], c_w is the specific heat of water [J/kg/C], q_{sp} is the spring water flow rate [m^3/s] into the stream (zero if spring flows out), A_{sp} is the area [m^2] of the spring water inflow, T_{sp} is the spring water temperature [C], and Φ_{net} is the net heat exchange [W/m^2] between water column and its surroundings (through water surface and streambed).

The turbulent eddy viscosity (ν_t) is computed with a turbulence model (Rodi 2003). Two turbulence models may be used in SRH-2D: the depth-averaged parabolic

model or the two-equation k-ε model (Lai 2008). The Prandtl number is computed as follows (Bowie et al. 1985; Fischer et al. 1979; Kim and Chapra 1997):

$$\frac{\nu_t}{\sigma_t} = C_d h u_* \tag{2}$$

where u_* is the bed frictional velocity and C_d is a constant coefficient which may be case dependent.

The net heat flux, Φ_{net}, consists of six contributions as follows:

$$\Phi_{net} = \Phi_{ns} + \Phi_{na} + \Phi_{bed} - \Phi_{br} - \Phi_e - \Phi_c \tag{3}$$

where

Φ_{ns} = net solar radiation entering water surface
Φ_{na} = net atmospheric radiation entering water surface
Φ_{br} = heat loss by back radiation from stream
Φ_e = evaporative heat loss at water surface
Φ_c = conductive heat loss at water surface
Φ_{bed} = heat flux into stream at channel bed

The net solar radiation at a water surface incorporates five thermal processes: extra-terrestrial solar radiation, attenuation due to atmosphere, correction for cloud cover, reflection by water surface, and correction due to terrain and vegetation shade. The processes are described fully in a number of reports and textbooks on hydrology (e.g., Huber and Harleman 1968; Eagleson 1970; Brutsaert 1991).

If measured solar radiation (Φ_{Sm}) at water surface is available, the net solar radiation is computed as (Hauser and Schohl 2003):

$$\Phi_{ns} = \Phi_{Sm} R_S \tag{4}$$

where Φ_{Sm} is measured solar radiation (shade free solar radiation at the water) and R_S is reflection and terrain and vegetation shading factor which is computed by the following equations (Hauser and Schohl 2003):

$$R_S = R_{sm} \quad \text{if } X_n \le B \text{ (shade free)} \tag{5a}$$

$$R_S = 0.2 \quad \text{if } X_n > B + W \text{ (full shade)} \tag{5b}$$

$$R_S = R_{sm}\frac{B + W - X_n}{W} + 0.2\frac{X_n - B}{W} \quad \text{if } B < X_n \le B + W \text{ (partial shade)} \tag{5c}$$

In the above:

$R_{sm} = 1 - a(57.3\alpha)^{-b}$ = shade-free reflection factor (a and b see Table 1)

α = solar altitude in radians
W = width of the stream cross section
B = distance from trees to water edge
$X_n = H_b \cos\beta / \tan\alpha$ = normal distance from trees to shadow edge
H_b = tree/bank height from water surface
$\beta = \left|\theta - \frac{90}{57.3}\right|$ = angle between sun and stream axis normal in radian
$\theta = \left|A_{zs} - \frac{A_{zr}}{57.3}\right|$ = angle between sun and stream axis in radian
A_{zr} = river azimuth, clockwise from north to direction of flow in degree
$\cos(A_{ZS}) = -\frac{\sin(\phi)\sin(\alpha) - \sin(\delta)}{\cos(\phi)\cos(\alpha)}$ = sun azimuth in radian

Table 1. Coefficients of solar radiation reflection

Cloud Cover	a	B
0-0.05	1.18	0.77
0.05 – 0.5	2.20	0.97
0.5 – 0.92	0.95	0.75
0.92 – 1.0	0.35	0.45

The solar altitude (α) is computed, assuming a spherical geometry, as follows (Huber and Harleman, 1968):

$$\sin\alpha = \sin\phi \sin\delta + \cos\phi \cos\delta \cos h \tag{6}$$

where ϕ is site latitude in radians, δ is sun declination (between the sun and equator) in radians, and h is the sun hour angle in radians.

If solar radiation is not measured, it can be computed using semi-empirical relationships. The approach follows Huber and Harleman (1968) is described in detail by Lai et al. (2004).

The net long-wave radiation emitted by the atmosphere is computed as:

$$\Phi_{na} = 5.16432 \cdot 10^{-13}(1 + 0.17C^2)(T_a + 273.16)^6 \tag{7}$$

where $C = (1 - S/S_0)^{3/5}$ is cloud cover and T_a is dry bulb air temperature [C].

The outgoing black-body radiation emitted from the water surface is a function only of the water temperature, and it is given by (Huber and Harleman 1968):

$$\Phi_{br} = \varepsilon_w \sigma (T_w + 273.16)^4 \tag{8}$$

where T_w is water-surface temperature [C], ε_w is emissivity (0.97 by Huber and Harleman 1968 and 0.98 by Tung et al. 2006), and σ is Stefan-Boltzman constant (5.672e-8 W/m^2/K^4).

The evaporative heat loss is computed by:

$$\Phi_{evp} = \rho_w L(a1 + b1W_a)(e_s - e_a) \tag{9}$$

where:

$L = (597 - 0.57T_w) * 4184$ = the latent heat [*J/kg*]

T_w = water temperature in Celsius

a1, b1 = constants: a1=0.0 to 4.0e-9; b1=1.0e-9 to 3.0e-9

$e_a = 2.171 \cdot 10^8 \exp\left[\frac{-4157}{T_d + 239.09}\right]$ = saturation vapor pressure [mb]

T_d = dewpoint temperature in Celsius.

$e_s = \alpha_j + \beta_j T_w$ = saturation vapor pressure [mb] with coefficient in Table 2

Table 2. Coefficients to compute saturation vapor pressure

T	j	αj	βj
0-5	1	6.05	0.522
5-10	2	5.10	0.710
10-15	3	2.65	0.954
15-20	4	-2.04	1.265
20-25	5	-9.94	1.659
25-30	6	-22.29	2.151
30-35	7	-40.63	2.761
35-40	8	-66.90	3.511

The conduction heat loss is:

$$\Phi_{cond} = \rho_w L(a1 + b1W_a) \cdot 0.61 \cdot 10^{-3} P(T_w - T_a) \tag{10}$$

where P is air barometric pressure in mb.

Heat exchange between stream bed and stream water is significant for shallow streams and it consists of two contributions: conduction from bed to stream and net solar radiation entering bed. It is computed by the following expression:

$$\Phi_{bed} = \frac{\kappa_b}{0.5\delta_b}(T_b - T_w) - (1 - A_b)(1 - \beta)\exp[-\eta(D - 0.6)]\Phi_{ns} \tag{11}$$

where κ_b is the thermal conductivity of the streambed bed material, δ_b is the effective bed thickness used for hear conduction computation, T_w is the water temperature, T_b is the effective stream bed temperature which is updated each time step by $T_b = T_b^{old} - \frac{\Phi_{bed}\Delta t}{\rho_b c_b \delta_b}$ with ρ_b and c_b the density and specific heat of the bed materials and Δt is the time step for simulation, A_b is albedo of bed material, β is fraction of solar radiation absorbed in the top 0.6m of surface water, η is extinction coefficient in water [1/m], and D is water depth [m].

Numerical Method

A detailed presentation of the numerical method is omitted here. Basically, the flow equations are solved with the finite volume method that guarantees the mass conservation locally and globally. An implicit time marching scheme is used with the arbitrarily shaped unstructured mesh methodology of Lai (2003). A detailed presentation of the numerical method for the flow hydraulics may be found in Lai (2008). The temperature equation is discretized and solved similar to the momentum equation.

Test and Verification with Cases Having Analytical Solutions

The following three test cases solve the unsteady 1D temperature equation:

$$\frac{\partial T}{\partial t} + \frac{\partial UT}{\partial x} = k(T_{eq} - T) \tag{12}$$

The purpose is to test and verify the implementation and solution of the unsteady temperature equation within SRH-2D. The above equation has the following exact solution:

$$T(t,x) = T_0(t-\tau)e^{-\kappa\tau} + T_{avg}(1-e^{-\kappa\tau}) + \kappa T_\Delta \frac{\cos[\omega(t-\tau)]}{\omega^2+\kappa^2}\left[\omega e^{-\kappa\tau} - \omega\cos(\omega\tau) + \kappa\sin(\omega\tau)\right]$$
$$+ \kappa T_\Delta \frac{\sin[\omega(t-\tau)]}{\omega^2+\kappa^2}\left[-\kappa e^{-\kappa\tau} + \kappa\cos(\omega\tau) + \omega\sin(\omega\tau)\right] \tag{13}$$

In the above, $T_0(t)$ is boundary condition at x=0, κ is a first-order rate constant which is a function of meteorological parameters and water depth, $T_{eq} = T_\Delta \sin\left(\frac{2\pi t}{P_\Delta}\right) + T_{avg}$ is water temperature, $\tau = x/U$, and $\omega = \frac{2\pi}{P_\Delta}$.

The first case has the following parameters: a constant flow velocity of U=1.0 mile/day, a zero equilibrium temperature $T_{eq} = 0$, and a constant coefficient k=0.2/day. A 100 mile straight channel is assumed for SRH-2D modeling. The mesh has 100 mesh cells in the flow direction and 2 cells in the lateral. Initially temperature is 20 Celsius everywhere and the temperature at $x = 0$ is held at 20 Celsius all the time. Simulation is carried out for 50 days with a time step of one hour. The temperature at $x = 100$ miles is compared in Figure 1 between the model solution and the exact solution. A good agreement is obtained for this simple case.

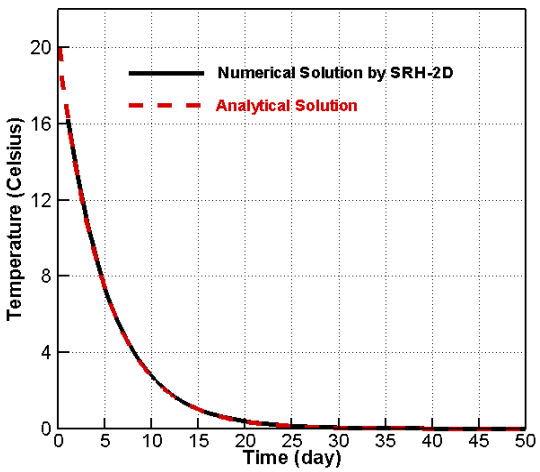

Figure 1. Comparison of temperature at 100-mile location between model and analytical solution for case 1.

Test case 2 has the following parameters: a constant flow velocity of U=1.0 mile/day, a zero equilibrium temperature $T_{eq} = 0$, and k=0.0. A 100-mile straight channel is assumed. The initial temperature is zero everywhere but the temperature at $x = 0$ is changing with time according to $T(x=0) = 10 + 10\sin\left(\frac{2\pi t}{P}\right)$ with the period P = 20 days. The same mesh is used as case 1. The computed temperature at $x = 40$ miles is compared with the exact solution in Figure 2. The computed temperature remains at zero until about day 35. Theoretically, the temperature wave reaches the location at day 40. The discrepancy is due to the numerical diffusion caused by discretization error as zero diffusion is assumed in the analytical Solution.

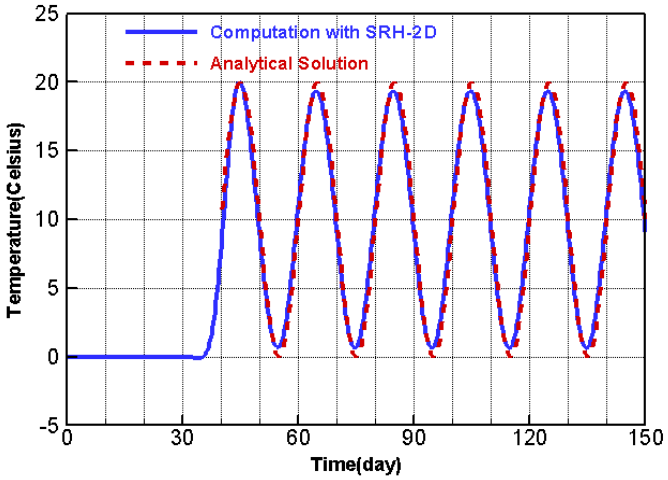

Figure 2. Comparison of simulated temperature and the exact solution at a location of 40 miles for case 2.

Test case 3 has the following parameters: a constant flow velocity of U=1.0 mile/day, $T_{\Delta} = 10$, $T_{avg} = 15$, $P_{\Delta} = 360$, and a constant coefficient k = 0.2/day. A 100-mile straight channel is assumed for SRH-2D modeling. The mesh has 100 or 300 mesh cells in the flow direction and 2 cells in the lateral. Initially temperature is 11.51 Celsius everywhere and the temperature at $x = 0$ is $T_0(t) = 10\sin(\frac{2\pi t}{10}) + 10$. Simulation is carried out for 150 days with a time step of 6 minutes. The temperature at $x = 4.5$ *miles* is compared in Figure 3 between the model solution and the exact solution. A good agreement is obtained.

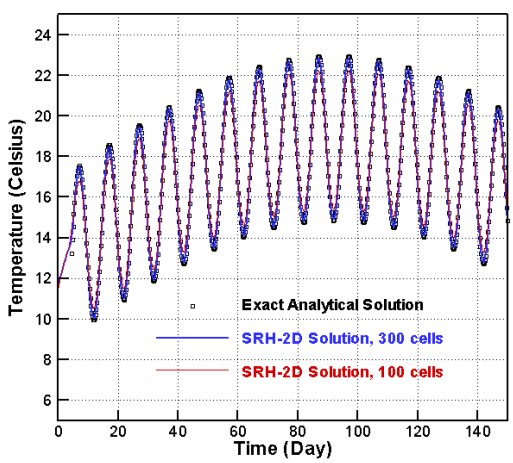

Figure 3. Comparison of simulated temperature and exact solution at channel mile 4.5 for case 3.

Temperature Modeling for the KcKay Dam Tailwater

The SRH-2D temperature model used a river reach downstream of the KcKay Dam for model verification and application. A reach along the McKay Creek and the first 2.57 miles of the Umatilla River has been studied by Bender (2001) with the 1D temperature model ADYN/RQUAL.

Case Description: McKay Dam and Reservoir are located on McKay Creek about 6 miles south of Pendleton, northeast Oregon. Downstream of the dam, the McKay Creek flows into the middle Umatilla River (at about RM 52). The Umatilla River drains into the Columbia River at about Columbia River Mile 289. The 2.57-mile reach of the Umatilla River from the confluence of the Umatilla River and the McKay Creek to the Reith Bridge could be managed to provide a water temperature to benefit the fishery. In particular, the flat slope and pools within the first mile of the Umatilla River downstream of the confluence with McKay Creek provides potential habitat for fish.

Cross-sectional channel survey downstream of the McKay Creek was conducted in March and November 2000 by Reclamation staff. The U.S. Army Corp of Engineers (Walla Walla District Office) provided sparse cross-section data of the Umatilla River collected in 1950. Around 64 cross-sections were assembled by Bender (2001) to carry out the temperature study for a 9-mile reach from McKay Dam to downstream of the Reith Bridge on the Umatilla River. The same cross sectional data are used to construct a 2D model for SRH-2D modeling in this study.

The model simulation starts from midnight July 27, 2000 and continues for 5 days. Temperature measurements at selected locations provide a comparison between model predictions and measured data. Continuous McKay Creek and Umatilla River temperature data were collected by the Umatilla tribes at the following four locations: Scheeler's Bridge (McKay RM 3.7), McKay School Bridge (McKay RM 1.9, Fish Barrier at the confluence (McKay RM 0.0), and Reith Bridge (Umatilla RM -2.57).

Mesh and Model Input Parameters: The simulation domain consists of about 6 miles of McKay Creek downstream of the McKay Dam and 3 miles of Umatilla River downstream of the confluence between McKay Creek and Umatilla River. The developed 2D mesh consists of 4,024 cells with both quadrilateral cells and triangular cells. The topography is interpolated from the cross sectional survey data.

Boundary conditions include water discharge and temperature downstream of the McKay Dam and upstream of the confluence in the Umatilla River. The hourly McKay Dam release discharge and temperature are used as upstream boundary conditions for the modeling period. The discharge downstream of the McKay Dam varies from 242 to 257 cfs and temperature ranges from 8.3 to 9.1 Celsius. The hourly flow, from 40 to 49 cfs, at Pendleton, Oregon is used as the upstream condition of the Umatilla River. The temperature, ranging from 24 to 27 Celsius, at the Umatilla River is based on a synoptic survey taken on July 28, 2000.

Initial conditions of the modeling used a steady state flow discharge of (257 cfs) at midnight of July 27, 2000. The initial temperature varies depending on the location of the cross section from 8.4C downstream of the McKay Dam to 23.0C at the Reith Bridge.

Hourly meteorological data, including cloud cover, air temperature, dewpoint temperature, air pressure and wind speed, are based on the national Weather Service (NWS) data from Pendleton, Oregon; and Agrimet solar radiation data are from Hermiston, Oregon (station HMRO).

Vegetation shade data includes the azimuth angle, tree height, tree distance to water edge at each cross section. They are delineated based on the aerial photo map.

Results and Discussion: Simulation is carried out from midnight of July 27, 2000 and lasts for five days. The simulated temperature is cross-sectionally averaged at five locations where measured temperature is available. Comparisons of the simulated and measured temperature are shown in Figure 4 to Figure 8 at measurement five locations.

It is seen that agreement is favorable for all locations with the maximum difference less than one degree Celsius. This comparison is encouraging as little effort is spent to locally calibrate the model to achieve a good match. Default values are used for most thermal processes and the few parameter values that are calibrated are constant for the entire reach modeled.

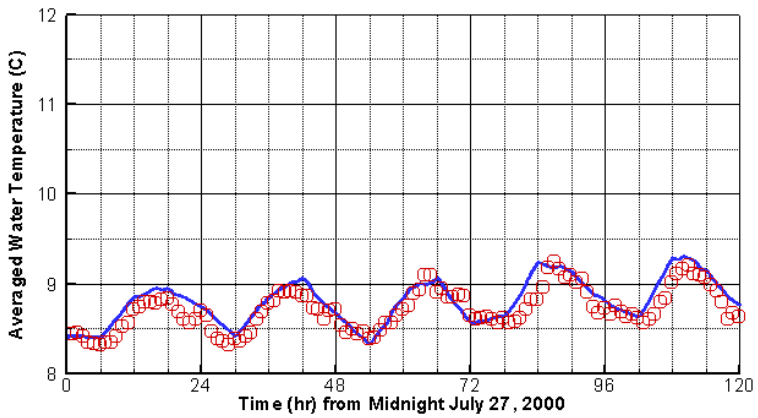

Figure 4. Comparison of temperature near McKay Dam (McKay RM 6.0) from July 28 through August 1, 2000; Solid Line: Simulated; Symbol: Measured

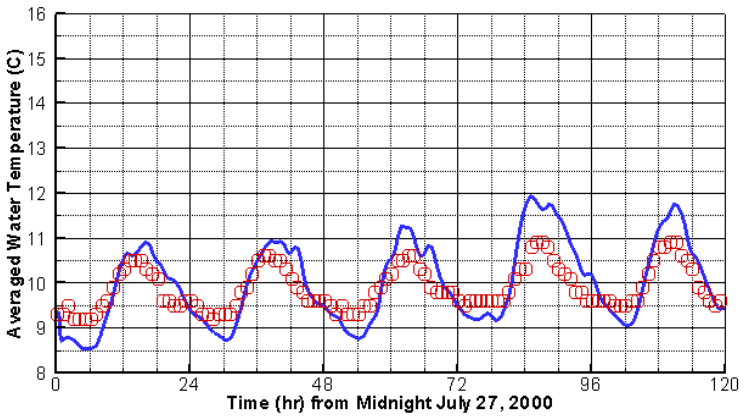

Figure 5. Comparison of temperature at Scheeler's (McKay RM 3.7) from July 28 through August 1, 2000; Solid Line: Simulated; Symbol: Measured

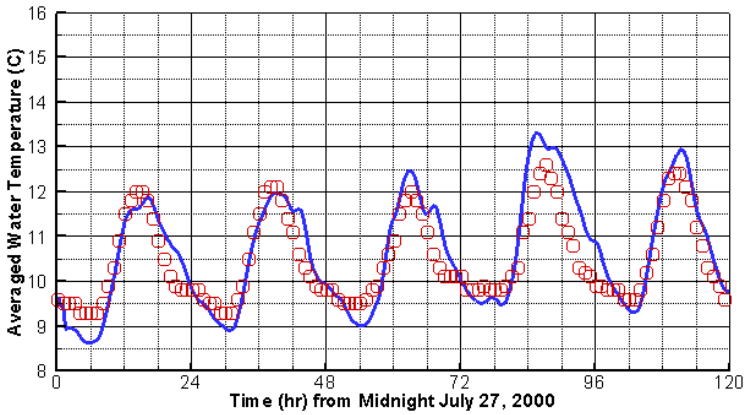

Figure 6. Comparison of temperature at School (McKay RM 1.9) from July 28 through August 1, 2000; Solid Line: Simulated; Symbol: Measured

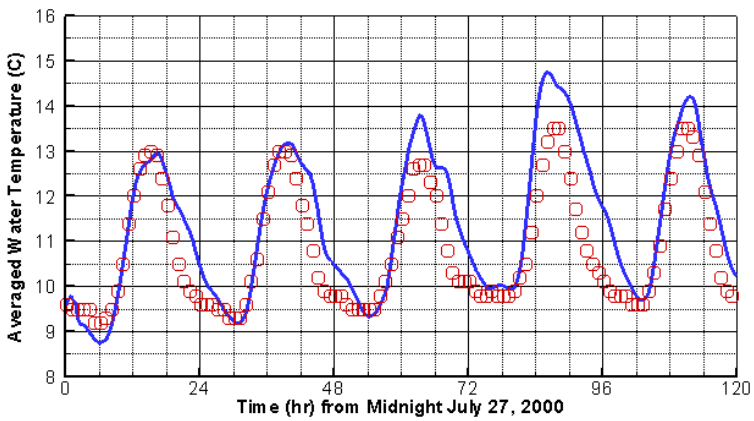

Figure 7. Comparison of temperature at Fish Barrier (McKay RM 0.01) from July 28 through August 1, 2000; Solid Line: Simulated; Symbol: Measured

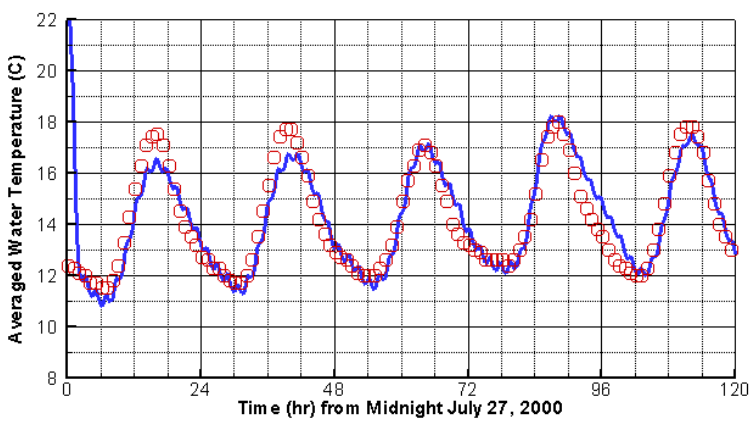

Figure 8. Comparison of temperature at Reith Bridge (RM -2.57) from July 28 through August 1, 2000; Solid Line: Simulated; Symbol: Measured

Concluding Remarks

A 2D depth-averaged temperature module is developed and incorporated into the existing SRH-2D model to simulate both flow hydraulics and diurnal temperature change. Such a model would be useful for habitat modeling, particularly for cases where spatial features such as agricultural returns, gravel pits, groundwater upwelling, side channel activation, and streamside vegetation are present.

Only development, testing, and a verification study are reported. The model is shown to reproduce the cases with exact solutions accurately; the model also matches a 9-mile reach downstream of the McKay Creek Dam in Northeast Oregon. Comparison between the model and the measurement is encouraging. The next step for development will collect lateral measured data on the San Joaquin River to compare against simulated data.

Acknowledgements

This study is partially funded by Reclamation's Science and Technology Program. Technical assistance by and discussion with Merlynn Bender at the Technical Service Center, Bureau of Reclamation are acknowledged, who also provided the data for the McKay Creek case. Peer review by Blair Greimann at the Bureau of Reclamation is appreciated.

References

Bartholow, J. M. (1990). "Stream temperature model," Managing Fisheries and Wildlife on Rangelands Grazed by Livestock: A Guidance and Reference Document for Biologists, Pages IV-20 to IV-47, W.S. Platts (ed.), W.S. Platts and Assoc. for the Nevada Department of Wildlife. December, 1990.

Batholow, J. M. (2002). "Modeling uncertainty: quicksand for water temperature modeling," American Institute of Hydrology Conference on Hydrologic Extremes: Challenges for Science and Management, Portland, OR, October 13-17, 2002.

Bender, M.D. (2001). "Temperature modeling of McKay Dam Tailwater," Project Report, Technical Service Center, Bureau of reclamation.

Bowie, G.L., W. Mills, D. Porcella, C. Campbell, and C. Chamberlin (1985). "Rates, constants, and kinetics of formulation in surface water quality modeling," 2nd edn. Report EPA 600/3-85/040. US Environmental Protection Agency, Athens.

Brutsaert, W. 91991). Evaporation into the Atmosphere, Kluwer Academic Publishers.

Cole, T. M. and E. M. Buchak. (1995). "CE-QUAL-W2: A Two-Dimensional, Laterally Averaged, Hydrodynamic and Water Quality Model, Version 2.0 User Manual," Instruction Report EL-95-1, U.S. Army Corps of Engineers, Washington, DC.

Eagleson, P.S. (1970). Dynamic Hydrology, McGraw-Hill, Inc.

Fischer, H.B., E,J. List, R.C.Y. Koh, J. Imberger, and N.H. Brooks (1979). Mixing in Land and Coastal Waters, Academic Press, New York.

Hauser, G.E. and G.A. Schohl (2003). "River Modeling System v4 – Vol. 2 Technical Reference," Report No. WR28-1-590-164, Tennessee Valley Authority, Norris, Tennessee.

Huber, W.C., and Harleman, D.R.F. (1968). "Laboratory and Analytical Studies of the Thermal Stratification in Reservoirs," Hydrodynamics Laboratory Technical Report No. 112, Department of Civil Engineering, Massachusetts Institute of Technology, Cambridge, Massachusetts, 277 pp.

Kim, K.S. and S.C. Chapra (1997). "Temperature model for highly transient shallow streams," J. Hydraulic Engineering, 123(1), 30-40.

Lai, Y.G., Weber, L.J., and Patel, V.C. (2003). "Non-hydrostatic three-dimensional method for hydraulic flow simulation - Part I: formulation and verification." *ASCE J. Hydraulic Engineering*, 129(3), 196-205.

Lai, Y.G., R. Ettema, A. J. Odgaard, and M. Muste. (2004). "Lake Almanor Cold-Water Feasibility Study: Numerical Model," IIHR Technical Report No. 439, IIHR – Hydroscience & Engineering, College of Engineering, The University of Iowa, Iowa City, Iowa.

Lai, Y.G. (2006). *Theory and User Manual for SRH-W Version 1.1*, Technical Service Center, Bureau of Reclamation, Denver, CO.

Lai, Y.G. (2008). *SRH-2D Theory and User's Manual version 2.0,* Technical Service Center, Bureau of Reclamation, Denver, CO.

Moir, H.J. and G.B. Pasternack. (2008). "Relationships between mesoscale morphological units, stream hydraulics and Chinook salmon spawning habitat on the Lower Yuba River, California," Geomorphology, doi:10.1016/j.geomorph.2008.01.001.

Rodi, W. (1993). "Turbulence models and their application in hydraulics," 3rd Ed., IAHR Monograph, Balkema, Rotterdam, The Netherlands.

Theurer, F.D., K.A. Voos, and W.J. Miller. (1984). "Instream Water Temperature Model," Instream Flow Inf. Paper 16, U.S. Fish and Wildlife Service, FWS/OBS-84/15.

Tung, C.P., T.Y. Lee, and Y.C. Yang. (2006). "Modeling climate-change impacts on stream temperature of Formosan landlocked salmon habitat," Hydrological Processes, 20, 1629-1649.

SIMULATIONS OF AQUACULTURE DISSOLVED WASTE TRANSPORT AND MIXING IN NEAR-COASTAL WATERS

S. K. Venayagamoorthy[1], O. B. Fringer[2,3], J. R. Koseff[2,3] and R. L. Naylor[2,4]

[1] Department of Civil and Environmental Engineering, Campus Delivery 1372, Colorado State University, Fort Collins, CO 80523-1372, USA, PH (970) 491-1915, FAX (970) 491-7727, email: vskaran@colostate.edu, A.M. ASCE.
[2] Environmental Fluid Mechanics Laboratory, Department of Civil and Environmental Engineering, Stanford University, Stanford, California 94305-4020. Emails: fringer@stanford.edu, koseff@stanford.edu
[3] Woods Institute for the Environment, Stanford University, Stanford, CA 94305, USA.
[4] Food Security and Environment Program, Stanford University, Stanford, California 94305-4205. Email: roz@stanford.edu

ABSTRACT

The present study focuses on understanding the transport and fate of dissolved waste from aquaculture pens in near-coastal environments using the hydrodynamic code SUNTANS, which employs unstructured grids to compute flows at very high resolution. We perform simulations of the dissolved waste field and study the effects of different flow conditions (tides and currents) on the evolution of the waste plume. The fish pen causes partial blockage of the flow, leading to the deceleration of the approaching flow and the formation of a downstream wake. Results of the concentration field for an oscillatory flow condition superimposed on a mean current are presented and compared with the concentration resulting from a unidirectional flow field. The simulation results highlight the complex (and different) circulation patterns that occur around a submerged fish pen under oscillatory flow conditions and provide an understanding of the impact of aquaculture fish pens on coastal water quality.

1. INTRODUCTION

The rapid growth of marine aquaculture in the last few years poses a major threat to ocean ecosystems. For example, wastes and nutrient levels from aquaculture pens alter the character of the surrounding ecosystem. A recent comprehensive review on aquaculture by Naylor and Burke (2005) highlights some of the ecological impacts of marine aquaculture. The dispersal of wastes from pens released into the coastal ocean may not necessarily be "Gaussian" (monotonically decreasing from the source in all directions), and 'dilution may not be the solution'. The evidence from previous field and laboratory studies (Crimaldi *et al*., 2002) suggests that waste maybe transported in plumes, which retain their coherence and possess relatively high concentrations over large distances. This pattern of dispersal could result in much

higher concentrations of wastes at certain points on the coastline, even at considerable distances from the source.

In the present study, our focus is to understand the dispersal of dissolved wastes such as nitrogen from an aquaculture pen using high-resolution two-dimensional (in the *x*-*y* horizontal plane) numerical simulations under different time-varying flows. Previous work by others (Chatwin 1975, Smith 1982 and Kay 1997) has shown how strong oscillatory effects dominate the character of the plume over time intervals of several wave periods. However, these studies do not consider the presence of a porous obstacle in the flow field, which has the added complexity of a downstream wake. Our emphasis in this study is to understand the behavior of the plume evolution under oscillatory flow conditions superimposed on a constant mean current compared to the classical spreading that would occur under unidirectional flow conditions in the "near-field" downstream of an aquaculture pen. The layout of this paper is as follows: in Section 2, we briefly discuss the computational approach we employ for this study and provide an overview of the problem set-up. We present results of the dispersion of a continuous pollutant source emanating from an aquaculture pen under unidirectional as well as oscillatory flow conditions in Section 3. We draw our conclusions and provide directions for future work in Section 4.

2. NUMERICAL METHOD AND PROBLEM CONFIGURATION

We employ the SUNTANS code developed by Fringer *et al.* (2006) to perform highly resolved simulations of flow through and around a fish pen in the domain shown in Figure 1, in a water depth of 50 m. SUNTANS is an unstructured, finite-volume, parallel coastal-ocean simulator that solves the incompressible three-dimensional nonhydrostatic Navier-Stokes equations with the Boussinesq approximation. It also solves equations for the free-surface as well as scalar transport of salinity and temperature. This code has been applied to a host of coastal problems and processes such as the generation and evolution of internal waves in Monterey Bay (Jachec *et al*., 2006) and the South China Sea (Zhang and Fringer, 2006) and high-resolution simulations of estuarine hydrodynamics (Wang and Fringer, 2006).

At the boundaries of the domain shown in Figure 1, we impose a velocity field of the form

$$u = U_m + U_t \sin(\omega t), \tag{1}$$

where $U_m \geq 0$ is the amplitude of the mean current; U_t is the amplitude of the sinusoidal tidal component of the flow field with forcing frequency ω; and u is the horizontal (x) velocity component at the boundary. Boundary conditions for the horizontal velocity u are free-slip at the lateral walls. The horizontal component in the y-direction of the velocity field v has no-flux boundary conditions on the lateral walls, and the scalar field has gradient-free boundary condition on all walls. The unstructured mesh has a total of 72,500 cells, with grid refinement near the fish pen as shown in Figure 1. The resolution near the pen is roughly 1 m, while that in the farfield is stretched to 15 m. The fish pen centered at x = 100 m and y = 200 m is cylindrical in shape with a diameter of D = 20 m. A drag law formulation is employed to account for the flow reduction inside the pens and the resulting decrease in

momentum downstream of the pens. This drag formulation is given by a quadratic drag-law on the right-hand side of the *x*- and *y*-momentum equations of the form

$$F_{D,x} = -\frac{pC_D\left(u_x^2 + u_y^2\right)^{1/2}}{D}u_x, \qquad F_{D,y} = -\frac{pC_D\left(u_x^2 + u_y^2\right)^{1/2}}{D}u_y, \tag{2}$$

where C_D=1 is the drag coefficient, u_x and u_y are the easterly and northerly components of the velocity, and p=1 inside of the pens while p=0 outside of the pens. We use a horizontal eddy-viscosity of $\nu_h = 10^{-3}$ m^2 s^{-1}, and a quadratic bottom drag law formulation with a drag coefficient of $C_{D,bottom}$=0.0025. An estimate of the Reynolds number based on a characteristic velocity scale of 0.1 m s^{-1} and the specified values of D = 20 m and $\nu_h = 10^{-3}$ m^2 s^{-1} is Re = 2000. A continuous pollutant (scalar) point source is placed at the pen location as an approximation of the effluent waste discharged from the pen.

An important non-dimensional parameters for the simple model flow problem defined by Eq. (1) is the ratio of the tidal to mean flow given by

$$\eta = \frac{U_t}{U_m}, \tag{2}$$

which compares the amplitude of the oscillatory flow to the amplitude of the mean current and is an important parameter that determines the shape of the contaminant plume (Purnama and Kay 1999). A second important parameter is the non-dimensional tidal excursion lengthscale given by

$$K = \frac{2U_t}{\omega D}, \tag{3}$$

where U_t is the amplitude of the tidal current, ω is the forcing frequency and D is the pen diameter. This represents the ratio of the tidal excursion to the pen diameter and is analogous to the Keulegan-Carpenter number used in wave-structure interaction studies. In this study, we have used $U_t = U_m$ = 0.1 m s^{-1}, which is representative of typical coastal flow current magnitudes.

3. RESULTS AND DISCUSSION

We carried out a series of two-dimensional simulations with a forcing frequency $\omega = 8.73\times10^{-4}$ *rad s*$^{-1}$ corresponding to a wave period of T = 2 hours and a non-dimensional excursion lengthscale K = 11.5. In what follows, we present results for two cases, namely: Unidirectional flow case with U_t / U_m = 0 and an oscillatory plus uniform flow case with U_t / U_m = 1.

3.1 Unidirectional Flow Case

The case of a steady uniform flow past an obstacle such as an isolated cylinder has been studied extensively. Here we consider a similar situation except that the fish pen permits some flow through it. We account for the reduction in momentum in the flow

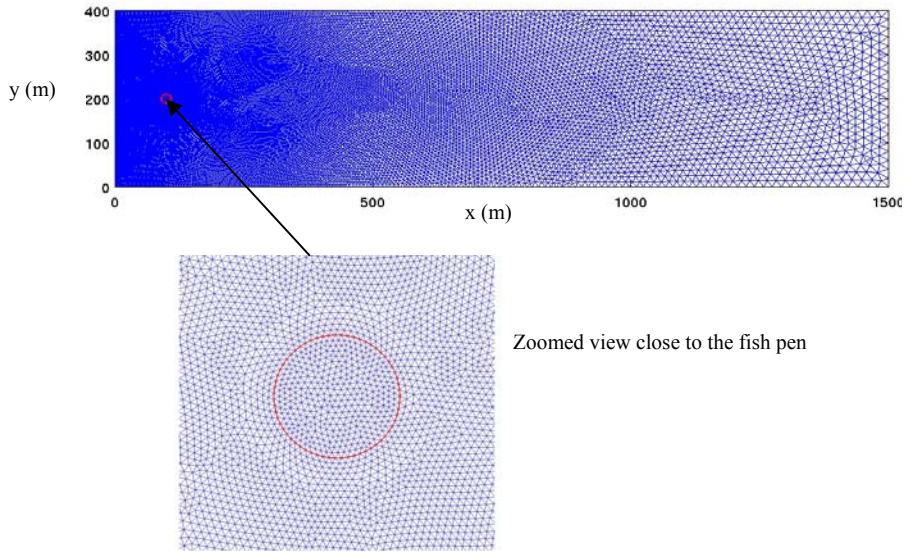

Figure 1. Unstructured computational mesh showing the domain used in the simulations for this study. A velocity described by Eq. (1) is imposed at the left boundary of the domain with frequency $\omega = 8.73 \times 10^{-4}$ *rad* s^{-1} in a depth of d = 50 m.

inside the pen using a drag law formulation with a drag coefficient $C_D = 1$. We further assume that the concentration of the waste discharged is uniform inside the pen based on the justification that mixing occurs within the pen as result of the swimming motion of the fish. We impose a mean current of $U_m = 0.1$ m s^{-1}.

The mixing and transport of a continuous point source collocated within the fish pen is shown in Figure 2 using a time sequence of the concentration field over a time period of nearly three wave periods (with $T = 2$ hours) under uniform flow conditions. Figure 2(a) shows the initial condition at time $t = 0$. As time progresses, the fish pen causes partial blockage of the flow, leading to the deceleration of the approaching flow and the formation of a downstream wake as would be expected. Initially, a recirculation zone with closed streamlines develops just past the fish pen and is termed the primary wake by White and Nepf (2003), as shown in Figure 2 (b), (c) and (d). Eventually the wake becomes unstable resulting in unsteady and periodic vortex shedding (see Figure 2(e) onwards). Further in time, the wake becomes more or less fully developed (Figure 2(l)), thus defining a "mixing zone". Downstream of this mixing zone, it may be expected that far-field mixing governed by simple advection due to the ambient current and turbulent diffusion will control the mixing of the pollutant field.

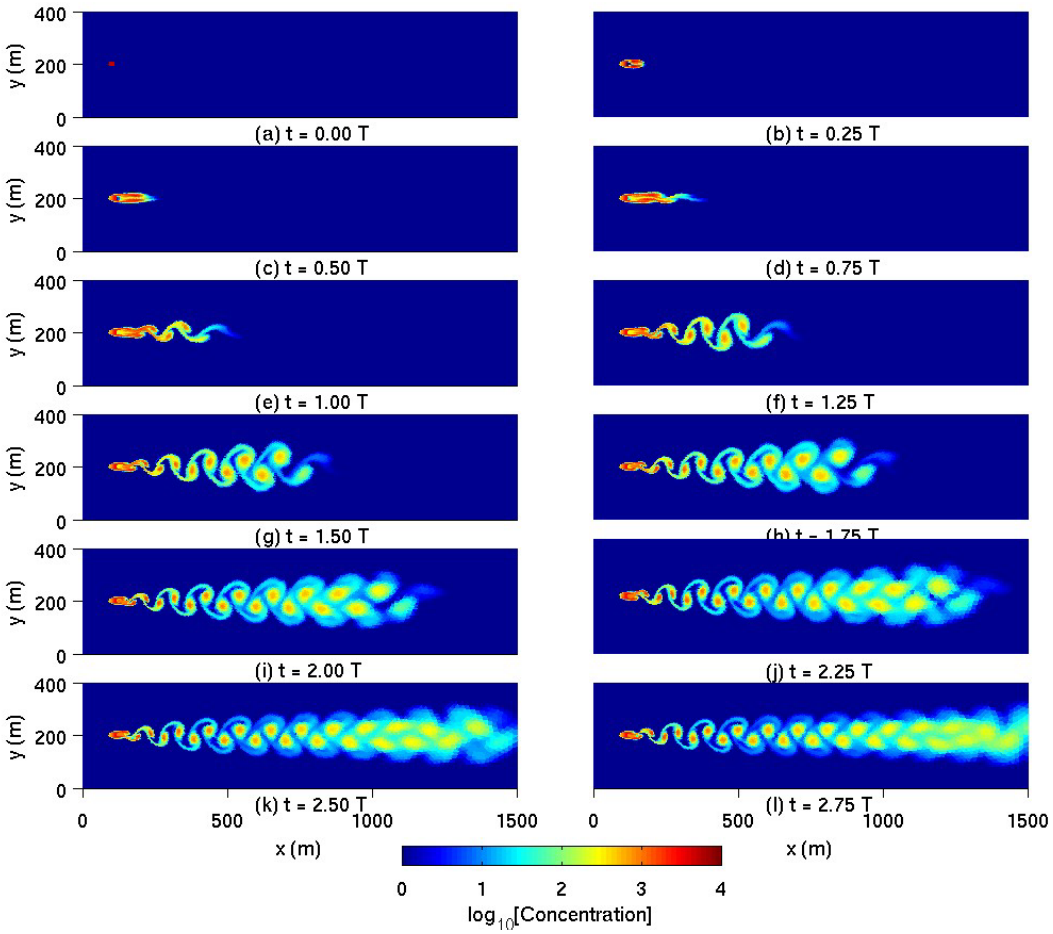

Figure 2. Normalized concentration field (shown in color) for a uniform flow case (U_t/U_m = 0). The continuous point source is located within the perimeter of the fish pen. Time is normalized by the wave period T = 2 hours.

3.2 Oscillatory Plus Uniform Flow Case

Here we consider a case with an oscillatory component in Eq. (1) with magnitude equal to the mean component (i.e. U_t/U_m = 1). All other parameters are exactly the same as for the uniform case discussed in Sec. 3.1. Here, the flow will stagnate at certain points in time when the tidal velocity exactly negates the mean velocity. It should be noted that for U_t/U_m >1, the fluid will reverse direction twice during each tidal cycle and in the special case when U_t/U_m = ∞, the vortex wake created during each half cycle will sweep past the fish pen during each subsequent half cycle (Williamson 1985).

The results for the case U_t/U_m = 1 are shown in Figure 3. When the tidal component is in phase with the mean current, the flow evolves in a similar manner to that of the unidirectional flow case discussed in Sec. 3.1 (see Figure 3 (a) - (c)). Soon after the initial vortex shedding begins, the flow starts to retard as the tidal velocity reverses direction and increases in amplitude. This causes the plume to contract in the longitudinal direction with a simultaneous dispersion in the lateral direction as shown

in Figure 3(d) & (e), and in subsequent wave cycles in Figure 3(h), (j) & (l), respectively. Note how the vortex shedding is also attenuated during this period. This behavior was first described by Chatwin (1975), where he points out that the contaminant cloud appears to be periodically expanding and contracting. The plume is stretched during the period of high flow during the first half tidal cycle and contracts during the second half-cycle (see also Smith 1982). We note that as the extent of the plume reaches the lateral boundaries, the no-flux boundary condition used at these boundaries results in the non-physical longitudinal spreading that is observed as shown in Figure 3(i) and (j).

These results indicate that the mixing and dispersion of the pollutant field under oscillatory flow conditions is very different from the unidirectional flow case and could result in plumes of waste with relatively high concentration occurring at considerable distances from the source.

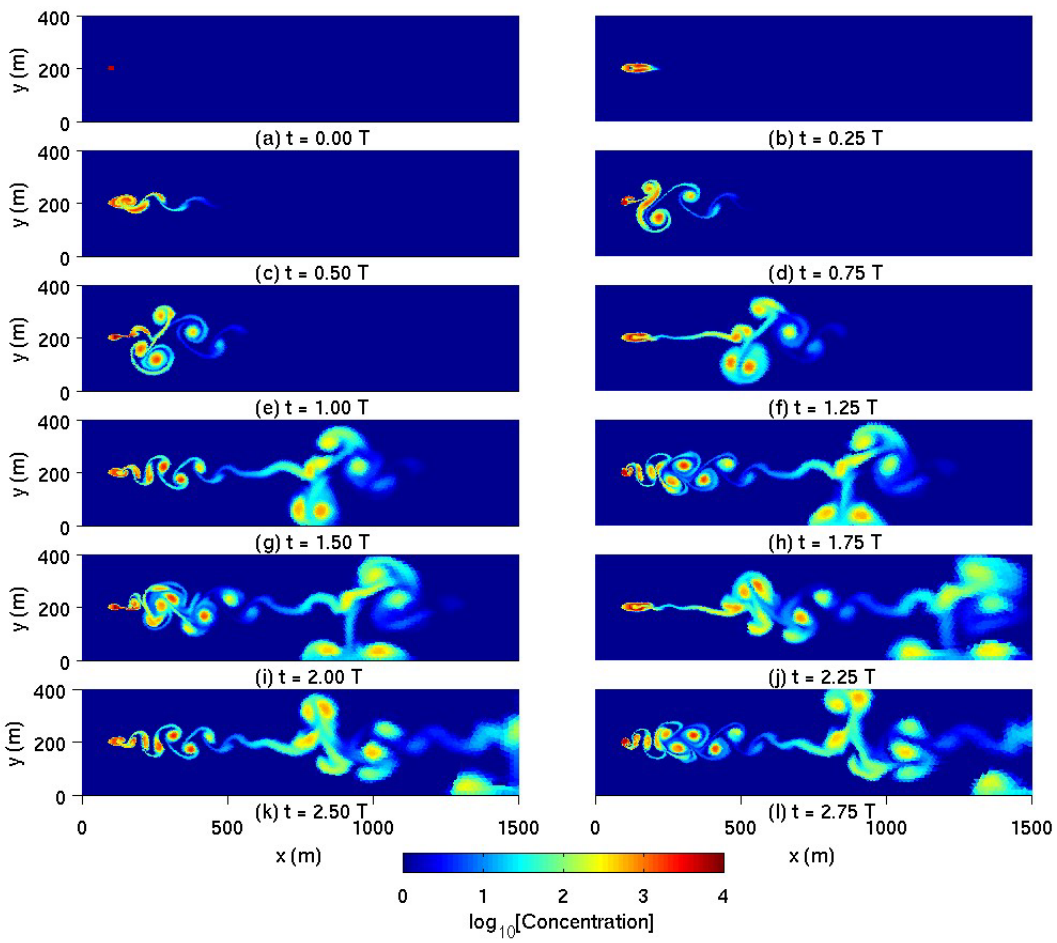

Figure 3. Normalized concentration field (shown in color) for an oscillatory flow case (U_t/U_m = 1). The continuous point source is located within the perimeter of the fish pen. Time is normalized by the wave period T = 2 hours.

4. CONCLUSIONS AND FUTURE WORK

We have presented results from highly resolved two-dimensional numerical simulations of the mixing and transport of a continuous point source of waste from an aquaculture pen. To our knowledge, this is the first detailed numerical study of the evolution of a waste plume downstream of a porous obstacle under oscillatory flow conditions. The emphasis of this study was to highlight the complex and different plume dispersion patterns that occur under such flow conditions, with concentration profiles that are not necessarily Gaussian.

This study is a first step towards understanding the complex three-dimensional flow structure that would occur in the vicinity of aquaculture pens. We are currently carrying out a detailed study to quantify the dependence of the horizontal dispersion coefficient on the two non-dimensional numbers η and K for a wide parameter space using two-dimensional simulations. We are also performing highly-resolved three-dimensional nonhydrostatic simulations to understand the plume structure resulting from the complex flow patterns that occur due to flow separation over and under a submerged aquaculture pen. Further extensions of this study will address the mixing and dispersion of the waste plume from a single aquaculture pen under stratified flow conditions. We will also explore cases with multiple aquaculture pens where we expect the flow field to be significantly modified due to hydrodynamic interference effects. This would be a useful extension of the present work and would provide a basis to examine the issues of spacing of aquaculture pens.

ACKNOWLEDGMENTS

We gratefully acknowledge the support of the Lenfest Ocean Program (Director: Margaret Bowman).

REFERENCES

Chatwin, P. C. (1975). "On the longitudinal dispersion of passive contaminant in an oscillatory flow in tube". *J. Fluid. Mech*. **71**: 513-527.

Crimaldi, J.P., Wiley, M. B. and Koseff. J. R. (2002). "The relationship between mean and instantaneous structure in turbulent passive scalar plumes." *Journal of Turbulence*, **3 (014)** http://stacks.iop.org/JoT/3/014.

Fringer, O. B., M. G. Gerritsen, and R. L. Street. (2006). "An unstructured-grid, finite-volume, nonhydrostatic, parallel coastal ocean simulator." *Ocean Modell*. **14**: 139-173.

Jachec, S. J., Fringer, O. B., Gerritsen, M. G. and Street, R. L. (2006). "Numerical simulation of internal tides and the resulting energetics within Monterey Bay and the surrounding area." *Geophys. Res. Lett*. **33**: doi:10.1029/2006GL026314.

Kay, A. (1997). "Advection-diffusion in reversing and oscillating flows: 2. Flow with multiple reversals." *IMA J. Appl. Math.* **58**, 185-210.

Naylor, R., and Burke. M. (2005). "Aquaculture and ocean resources: Raising tigers of the sea." *Annu. Rev. Environ. Resour*. **30**: 185-218.

Purnama A., and Kay, A. (1999). "Effluent discharge into tidal water: Optimal or economic strategy?" *Environmetrics*. **10**: 601-624.

Smith, R. 1982. "Contaminant dispersion in oscillatory flows." *J. Fluid Mech*. **114**: 379-398.

Wang, B., Fringer, O. B. and Street, R. L. (2006). "Application of an unstructured-grid, finite-volume parallel coastal ocean simulator to the Snohomish River Estuary." *Proceedings of the fifth international workshop on unstructured mesh numerical modelling of coastal, shelf and ocean flows*.

White, B. and Nepf, H. (2003). "Scalar transport in random cylinder arrays at moderate Reynolds number." *J. Fluid Mech.* **487**, 43-79.

Williamson, C. H. K. (1985). "Sinusoidal flow relative to circular cylinders." *J. Fluid Mech.* **155**, 141-174.

Zhang, Z., and Fringer, O. B. (2006). "A Numerical Study of Nonlinear Internal Wave Generation in the Luzon Strait." *Proceedings of the 6th International Symposium on Stratified Flows*, pp 300-305.

The Importance of In-stream Hydraulics in River Water Quality Models: Lessons from the Blackstone River

Jeffrey D. Walker[1], Paula Sturdevant Rees[2] and Thomas K. Walsh[3]

[1] CDM, One Cambridge Place, 50 Hampshire Street, Cambridge, MA 02139
[2] Department of Public Health (Environmental Health Sciences), University of Massachusetts - Amherst, Blasdell House, 310 Hicks Way, Amherst, MA 01003
[3] Upper Blackstone Water Pollution Abatement District, 50 Route 20, Millbury, MA 01527

Abstract

Water quality models of rivers often include three fundamental components: inflows and pollutant loads from point sources and watershed runoff, in-stream hydraulics, and in-stream water quality processes. In many cases, model development focuses mainly on the first and third components, while less attention is given to the in-stream hydraulics. An existing hydrologic model was used as a basis to develop a water quality model of the Blackstone River. Although the original model was calibrated to daily streamflow records, the hydraulics of the model proved to underestimate the travel time of the river. Initial attempts to calibrate the water quality model were unsuccessful since many of the parameter values governing in-stream processes were forced outside of acceptable ranges to compensate for the underestimated travel times.

In order to develop a more robust water quality model, the mainstem of the river was resegmented into a greater number of reaches such that each reach represented a uniform hydraulic profile. The resegmented model resulted in a longer travel time more representative of the actual conditions of the river. Subsequent calibration of the water quality model yielded realistic parameters values, which were within an acceptable range and similar to those used for other rivers in the region. This work illustrates the importance of developing a good hydraulic, and not just hydrologic, representation of a river as the foundation for a water quality model.

Introduction

Water quality models of rivers often include three fundamental components: inflows and pollutant loads from point sources and watershed runoff, in-stream hydraulics, and in-stream water quality processes. In many cases, model development focuses mainly on the first and third components, while less attention is given to the in-stream hydraulics. However, water quality processes (physical, chemical and biological) are closely tied to in-stream hydraulics through the travel time in the river, which is the time it takes on average for a parcel of water to travel down the river

before being discharged to a receiving water body. Rivers that have a short travel time from the headwaters to the outlet are less prone to algal blooms than rivers of similar length that flow more slowly, simply because there is less time for algae to grow. Therefore, the hydraulics of a model, which govern the travel time, are an important control on in-stream water quality processes.

In addition to travel time, simulation of water quality processes is controlled by a set of model parameters. These parameters define the rate at which each process occurs as a function of ambient conditions such as nutrient availability, light, or temperature. Most model parameters are based on some physical, chemical or biological process that can be measured directly in a controlled setting. These measurements define an acceptable range of values for each parameter. In most cases, a model is considered a credible and robust tool for making management decisions when it is an accurate representation of the processes that it is simulating. To achieve this, each parameter value should be within an acceptable range as determined from laboratory experiments or from measurements in similar systems.

During model calibration, the value of each parameter is adjusted until simulated concentrations match those measured in the field. In the case of algae, parameters that govern the growth rate are adjusted until a suitable match between the simulated and observed concentrations of algae (or chlorophyll a) is achieved. If the initial model results produce too little algae, the growth parameter may be increased until the observed concentration of algae is attained. However, since parameters are not explicitly limited to an acceptable range in most models, calibration may result in a parameter value that is outside of its acceptable range. One reason this may occur is if the travel time simulated in the model is too short. Instead of turning up the algae growth parameter, the hydraulics may need to be modified to increase the travel time of the river and allow more time for the algae to grow.

A case study from the Blackstone River in southern New England illustrates the importance of using a good hydraulic model as the basis for the development of a water quality model. Initial efforts to calibrate the dynamic water quality model were unsuccessful due to an inaccurate hydraulic representation of the river, which yielded an underestimated travel time, especially under low flows. In order to achieve an acceptable water quality calibration, the model was resegmented into shorter reaches which improved the travel time and resulted in parameter values that were within acceptable ranges.

Study Overview

The Blackstone River is 77 km (46 miles) long, and runs from Worcester, MA to Narragansett Bay in Providence, RI (Figure 1). Mean annual discharge near the

outlet of the river in Pawtucket, RI is about 24 m^3/s (850 cfs). The watershed is 1,230 km^2 (475 mi^2) in area, with about two thirds of the area in Massachusetts and the rest in Rhode Island. Land use in the watershed is primarily forested (51%) and residential (21%) (Barbaro and Zarriello, 2007).

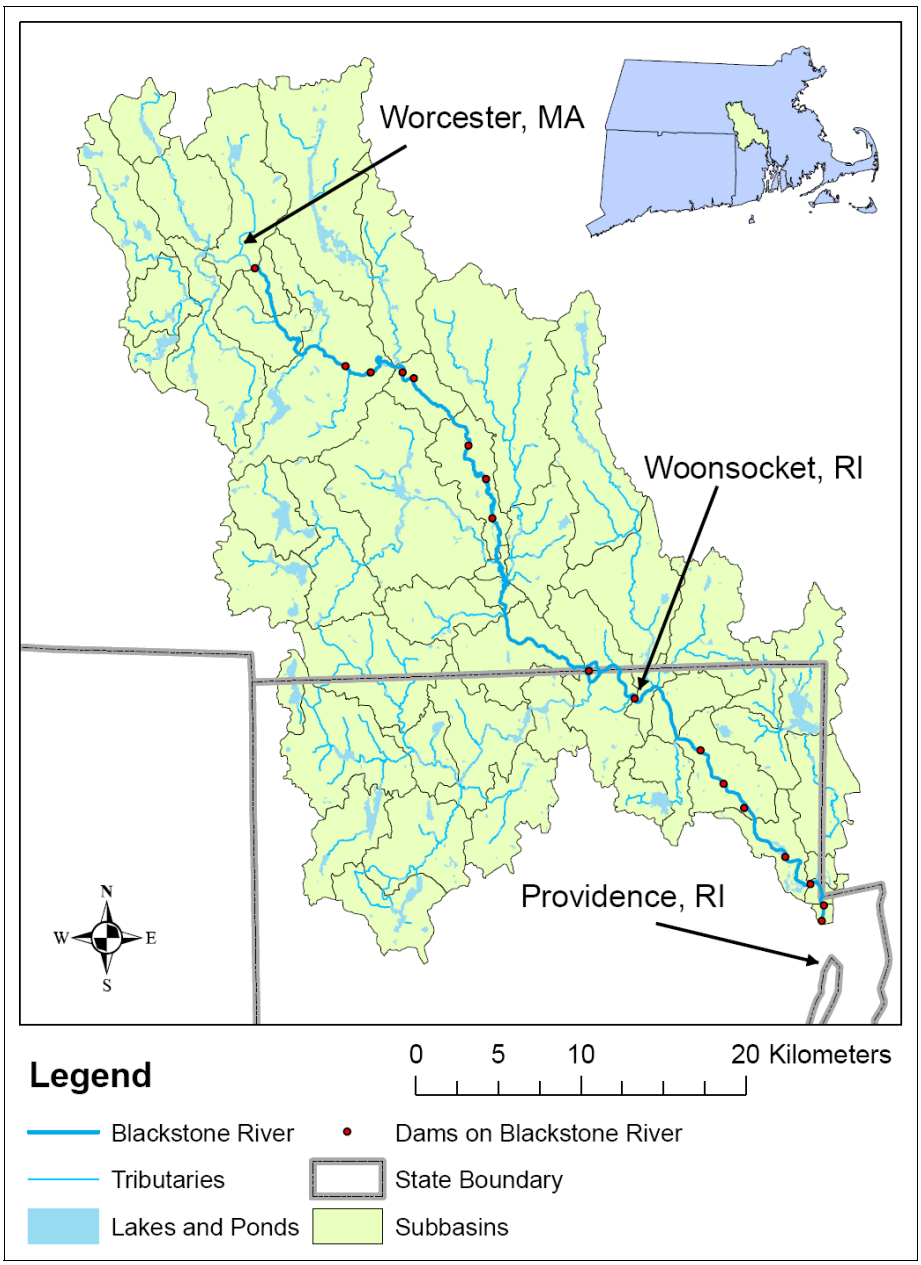

Figure 1. Map of the Blackstone River Watershed.

Throughout the 19th and 20th centuries, dams were constructed along the river to support developing industries, especially textiles. Today, there are 17 dams along the river, which create a series of impoundments from the headwaters to the river outlet. These impoundments lower the velocity of the river and are believed to have significant impacts on the water quality, such as algal blooms and resulting low dissolved oxygen levels.

In 2004, the Upper Blackstone Water Pollution Abatement District (UBWPAD) initiated the Blackstone River Water Quality Assessment to assess the impacts of watershed management strategies on in-stream water quality through a comprehensive field sampling program and the development of a dynamic water quality model. The study was focused on quantifying nutrient loads from point and non-point sources, and evaluating the impacts of various watershed management strategies to reduce nutrient loads to the river. The field sampling program and development of the water quality model were conducted by researchers at the University of Massachusetts in Amherst, MA (UMass Amherst) with technical support and project oversight provided by CDM. The focus of this paper will be on the water quality model development and calibration, for which water quality data from the field sampling program was used.

Model Development

In 2006, the United States Geologic Survey (USGS) developed a rainfall-runoff model to evaluate the impact of water management alternatives on in-stream flows in the Blackstone River (Barbaro and Zarriello, 2007). The model was developed using Hydrologic Simulation Program – FORTRAN (HSPF), which is a widely used tool that is recognized and accepted by regulatory agencies for policy-level decision guidance (Bicknell et al, 2000). This hydrologic model was used as a basis for development of the Blackstone River HSPF water quality model.

In the USGS hydrologic model, the mainstem of the Blackstone River was delineated into 14 reaches, with an additional 36 reaches representing the tributaries to the mainstem. In HSPF, each river reach is simulated as a uniform segment with constant depth, slope and cross-sectional area. Water is routed downstream from one reach to the next based on stage-discharge relationships, which reflect the in-stream hydraulics of the reach.

The original 14 mainstem reaches varied in length from 1.2 – 13.0 km (0.75 – 8.1 miles) with an average length of 5.0 km (3.1 miles). Many of the mainstem reaches included a mix of deep, slow-moving impoundments and shallow, swift riverine segments. While this discretization was suitable to meet the objectives of the hydrologic model, it underestimated the travel time along the river. Travel time is a

major factor controlling water quality processes since it determines, for example, the amount of time during which nutrients in the water are available for algal growth. To improve the travel time simulation, the model was resegmented into more reaches of shorter length such that each reach represented an approximately uniform hydraulic behavior.

An existing Hydrologic Engineering Centers River Analysis System (HEC-RAS) model was used to resegment the HSPF model. The HEC-RAS model was developed by CDM for updating Federal Emergency Management Agency (FEMA) flood plain maps of the watershed and included over 700 cross-sections along the mainstem of the river. Since this model did not include the tributaries to the Blackstone River, the HSPF model resegmentation effort focused only on the mainstem. The HEC-RAS model was used to generate a longitudinal profile of the river that showed the changes in slope and depth, which were used along with the original reach boundaries and locations of dams and tributary inflows to delineate the new reach boundaries. The new reaches were limited to a maximum length of 0.8 km (0.5 miles). Resegmentation increased the number of mainstem reaches from 14 to 110. The resegmented reaches were considered to better represent observed hydraulic variability along the river than those in the original model delineation.

Once the new reaches were defined, the HEC-RAS model was used to simulate the water surface elevations of each reach at the full range of observed flows. The results of these simulations were used to develop the relationship between depth, surface area, volume and outflow that is used for hydraulic routing in each new reach in the resegmented HSPF model. To ensure that resegmentation of the model did not disrupt the hydrologic calibration, the simulated flows of the new model were compared to those of the old model as well as the historical records at the streamflow gages. Statistical comparisons showed that the resegmented model performed slightly better than the original model, likely due to the finer resolution of the river reaches and the improved hydraulics and stage-discharge relationships.

Time of Travel Comparisons

The travel times along the river were compared between the original and resegmented models to evaluate the impact of resegmentation on the river hydraulics at the full range of flows. The greatest difference between the two models occurred at low flows, with the original model predicting a total travel time (from headwaters to outlet) of 3 days and the resegmented model predicting 30 days at the 99% exceedence flow (Figure 2). This change in total travel time was considered more realistic given the length of the river and the observed velocities at low flows. At higher flows, the difference between the two models was less significant with the

original model predicting1.3 days and the resegmented model predicting 2.1 days at the 1% exceedence flow (Figure 3).

Figure 2 shows how the model resegmentation improved the representation of impoundments and their impact on the total travel time of the river under low flows. The slope of the cumulative travel time curve between each reach boundary is related to the residence time of that reach, which is the average time that a parcel of water takes to travel through the reach. The residence time is equal to the reach length divided by the average cross-sectional velocity. Segments with greater residence times have greater slopes in the cumulative travel time curves in Figure 2 since it takes more time for a parcel of water to travel through the segment per unit distance. The steeper segments of the resegmented model curve indicate locations of impoundments, where the residence time is longer due to the restriction of flow by the impounding dam. The cumulative impact of these impoundments increases the total travel time of the river from the headwaters to the outlet. The travel time curve of the original model does not reflect these impoundments as indicated by its approximately constant slope.

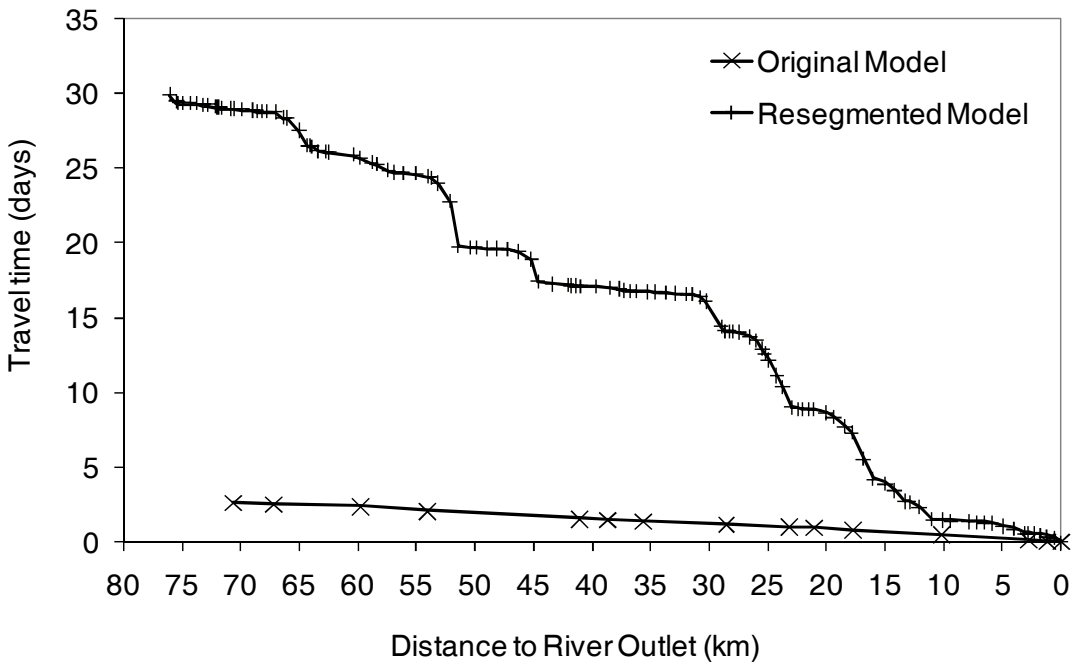

Figure 2. Travel time for original and resegmented models under the 99% exceedence flow. Markers indicate reach boundaries.

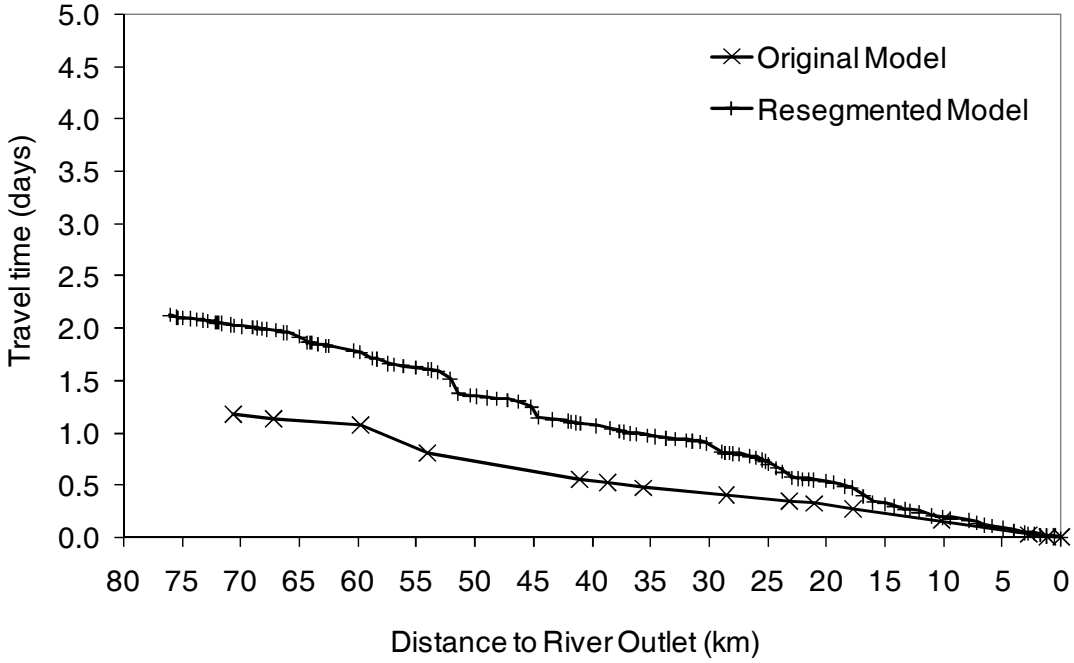

Figure 3. Travel time for original and resegmented models under the 5% exceedence flow. Markers indicate reach boundaries.

Water Quality Calibration

With the improved travel time representation in the resegmented model, the simulation of in-stream water quality processes was more reflective of the actual dynamics of the river (UMass Amherst and CDM, 2008). Prior to resegmentation, initial efforts to calibrate the water quality model required parameter values that varied by reach in order to compensate for the differences in residence time of the reaches. For example, a reach that included a large impoundment required a higher value for the algal growth rate in order to reflect the additional growth observed in that reach, which was in fact due to the increased residence time of the reach and not the biological processes inherent to algae in that reach. Many parameter values were assigned to compensate for the underestimated travel time, and as a result these parameters varied by reach in the model. In reality, most parameters, such as algal growth, do not vary along a river – algae will grow at the same rate in any reach given identical ambient conditions such as light and nutrient availability. Model resegmentation corrected this issue and allowed for the use of global parameter values for most parameters.

Some parameters, such as sediment oxygen demand (SOD), continued to be reach-variable. In reality, these processes do vary by reach since they are determined

by discharge of organic matter upstream. For example, a reach that receives discharge from a wastewater treatment facility would likely have higher SOD due to the high levels of organic matter in treated wastewater. Impoundments are also frequently observed to have higher SOD due to accumulating organic matter in the sediments behind a dam.

In addition to the implementation of global parameter values, resegmentation also resulted in parameter values that were within acceptable ranges. For example, in the initial model calibration, the maximum algal growth rate parameter varied between 1.4 – 10.1 d^{-1}. A review of multiple water quality models suggests that an acceptable range for the maximum algal growth rate is between 1 – 3 d^{-1} based on the EPA's *Rates, Constants, and Kinetics Formulations in Surface Water Quality Modeling* (Bowie et al., 1985). In the resegmented water quality model, the maximum algal growth rate was set globally to 1.9 d^{-1} in all reaches. This value is also similar to those used in models of similar systems in the region. By improving the hydraulics of the model through resegmentation, the in-stream water quality processes were considered more robust for making watershed management decisions.

Conclusions

In river water quality models, in-stream processes are dependent on both model parameter values that define the process rates as well as in-stream hydraulics and resulting travel times. Without a sound hydraulic model to serve as the basis for the water quality model, calibration can result in parameter values that must compensate for unrepresentative travel times in order to match simulated concentrations with those measured in the field. When these values exceed acceptable ranges based on laboratory measurements or experience in other systems, confidence in the accuracy of the model to represent the actual system dynamics is diminished. Development of the Blackstone River water quality model highlights the importance of using an accurate hydraulic model as the basis for developing the water quality model. Future work will include continued calibration of the water quality model and the use of tracer studies to confirm the accuracy of simulated travel times in the model.

References

Barbaro, J.R., and Zarriello, P.J. (2007). *A Precipitation-Runoff Model for the Blackstone River Basin, Massachusetts and Rhode Island*. U.S. Geological Survey Scientific Investigations Report 2006-5213.

Bicknell, B.R., Imhoff, J.C., Kittle, J.L., Jr., Jobes, T.H., and Donigian, A.S., Jr. (2000). *Hydrologic Simulation Program – FORTRAN User's manual for release 12*. Mountain View, CA, AQUA TERRA Consultants.

Bowie, G.L., Mills, W.B., Porcella, D.B., Campbell, C.L., Pagenkopf, J.R., Rupp, G.L., Johnson, K.M., Chan, P.W.H., Gherini, S.A., and Chamberlin, C.E. (1985). *Rates, Constants, and Kinetics Formulations in Surface Water Quality Modeling*. U.S. Environmental Protection Agency Report 600/3-85/040, page 290.

University of Massachusetts Amherst and CDM (UMass Amherst and CDM) (2008). *Blackstone River HSPF Water Quality Model Calibration Report*. Prepared for Upper Blackstone Water Pollution Abatement District.

Inundation Mapping Using Hydraulic Models and GIS: Case Studies of Steady and Unsteady Models on the Tar River, NC

Cécile Aschwanden[1,2], Seann Reed[1], Keren Cepero[3],

[1]NOAA, National Weather Service, Office of Hydrologic Development, 1325 East-West Highway, Silver Spring, MD 20910; phone: 301-713-0640 x192; email: Cecile.Aschwanden@noaa.gov
[2]Wyle Information Systems
[3]North Carolina State University, Dept. of Marine, Earth & Atmospheric Sciences

ABSTRACT

The National Weather Service (NWS) recently began providing static inundation maps at selected river forecast points through the Advanced Hydrologic Prediction Service (AHPS) web pages. Positive feedback has motivated efforts to expand the forecast mapping program. In order to expand this mapping program efficiently and effectively, we need a more objective basis for determining where static forecast mapping is acceptable and where real-time, dynamic forecast mapping is required. With the current static forecast mapping approach, we do not have quantitative guidance specifying how far away from forecast points the maps are valid. This pre-print describes a methodology to develop this type of guidance and better understand sources of forecast mapping uncertainty. For this pre-print, we present limited results from an example case study on the Tar River, NC, comparing water surface profiles generated from steady and unsteady flow hydraulic models. Results that are more comprehensive will be presented at the conference.

INTRODUCTION

The National Weather Service (NWS) recently began providing static inundation maps at selected river forecast points through the Advanced Hydrologic Prediction Service (AHPS) web pages. The static map libraries serve the public by providing information about the approximate extent of flooding associated with river stage forecasts at pre-defined stage increments. Positive feedback has motivated efforts to expand the forecast mapping program. In order to expand this mapping program efficiently while producing accurate maps, we need a more objective basis for determining where static mapping is acceptable and where real-time, dynamic forecast mapping is required. We also need improved verification methods to assure the accuracy of forecast maps and better understanding of the associated uncertainties. Specifically, the static inundation mapping techniques currently used may have limited validity as one moves away from the forecast point where they are calibrated. We expect dynamic forecast mapping techniques to be more accurate and applicable to longer river reaches. Here, we describe a methodology to quantify the errors associated with the static forecast mapping assumptions relative to a more robust dynamic forecast mapping approach. We also plan to look at the impacts of elevation data accuracy on mapping errors. Our first study area is the Tar River, NC, where we compare water surface profiles and inundation maps generated from steady and

unsteady flow hydraulic models. Initial mapping verification efforts are focused on Hurricane Floyd, 1999, due to the availability of unique flood observations.

In this study, we use the US Army Corps of Engineers (USACE) Hydrologic Engineering Center (HEC) -River Analysis System (HEC-RAS) and the HEC-GeoRAS pre- and post-processor. HEC-RAS was used to generate the existing static map libraries and the NWS is working with HEC to include HEC-RAS as an operational forecasting tool in the next generation NWS hydrologic software referred to as the Community Hydrologic Prediction System (CHPS).

BACKGROUND

What static inundation mapping services does the NWS currently provide?

The Advanced Hydrologic Prediction Service (AHPS) currently provides inundation maps for 33 of the 4257 NWS forecast points (http://www.weather.gov/ahps/inundation.php). The AHPS maps are often based on modeling done by Federal Emergency Management Agency (FEMA) mapping contractors. Under the "Inundation Mapping" tab on the web page for a given forecast point, three data type screens are available (Figures 1a-c) for each location.

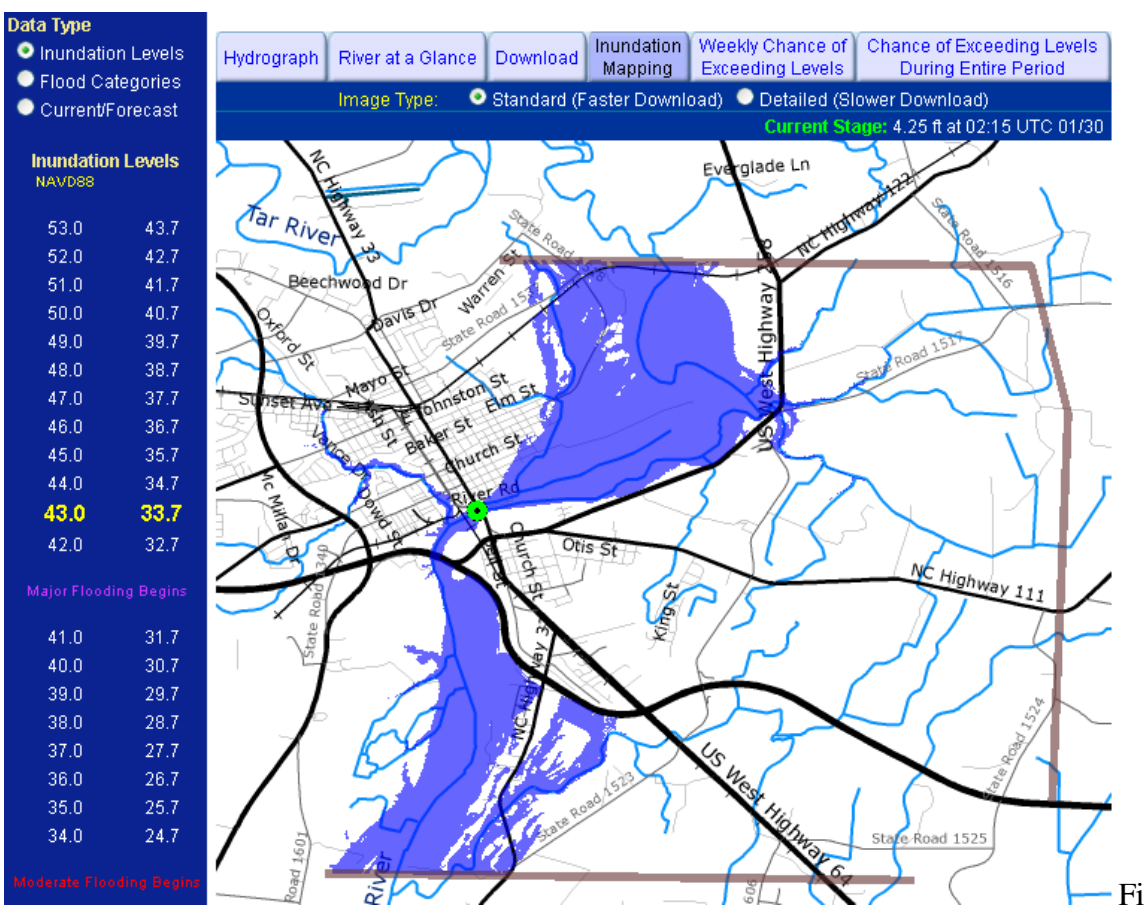

Figure 1a: Inundation levels for the Tar River at Tarboro, NC (TARN7)

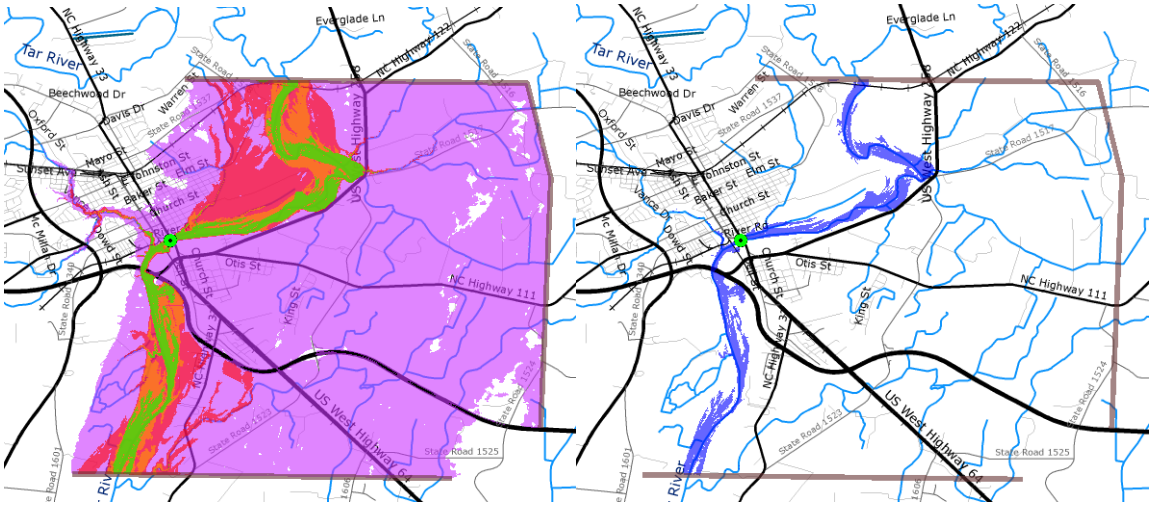

Figure 1b: Flood categories for TARN7 Figure 1c: Current/Forecast for TARN7

Figure 1. (a) The user can mouse-over different stages to see the corresponding inundation levels. (b) The NWS defines the five flood categories "Below Flood Stage" (green), "Action or Near Flood Stage" (yellow), "Minor Flood Stage" (orange), "Moderate Flood Stage" (red) and "Major Flood Stage" (purple) for each river forecast point location. "Action or Near Flood Stage" may coincide with "Minor Flood Stage" depending on each location. (c) Inundation map associated with the most recent forecast stage.

Where available, the 100-year flood, the 500-year flood and the floodway data layers from the Federal Emergency Management Agency (FEMA) can be turned on for reference. The inundation levels stored in the static map library begin at "Action or Near Flood Stage" with one foot increments and end at the historic recorded crest level. The transparency of each layer can be adjusted and basic zooming or panning features exist.

The Current/Forecast Data Type screen (Figure 1c) automatically displays the static map layer that corresponds to the current, maximum forecast stage at a gauge location. Because all of the map layers representing different inundation levels were pre-calculated and are being stored in the map library, computational requirements are minimal and the flood forecast map display changes immediately when a new stage forecast is available.

What techniques are used to create these maps?

One dimensional hydraulic models are used to create water surface profiles and GIS-based post-processors are used with digital terrain data to create inundation maps. Most of the static map libraries are created using steady-state models. Using this approach, modelers will adjust the flow until a profile with the desired stage at the forecast point of interest is reached. This ties a forecast stage to a map layer.

An alternative approach was used to create static maps for the Lower Colorado River in Texas. For the Lower Colorado, profiles corresponding to stages of interest at NWS forecast points were interpolated from profiles developed for FEMA's National Flood Insurance Program (NFIP). The input FEMA profiles correspond to design floods (e.g. 2, 5, 10, 25, 50, 100, and 500 year floods) generated using design storms, hydrologic models, and unsteady HEC-RAS models. Both steady and unsteady approaches to generate static libraries are relatively simple and can leverage data and models from FEMA's National Flood Insurance Program (NFIP).

The hydraulic models generate water surface profiles extending upstream and downstream from forecast points of interest; however, the validity of steady flow modeling diminishes with distance from a forecast point. In the case of the Lower Colorado, the pre-defined profiles generated from unsteady models may also differ from dynamically generated profiles if the real-time conditions do not match the assumed conditions in generating the profiles. The distances upstream and downstream for which these static maps are valid will vary from site to site and have not been rigorously quantified. NWS (2007) suggests only a general guideline to apply models for no more than one to two miles upstream or downstream from the forecast point.

Another limitation of static forecast mapping is that static maps will not be available for stages that exceed the historic flood.

What is dynamic inundation mapping?

Dynamic forecast mapping addresses limitations of static forecast mapping. Dynamic forecast mapping involves re-computing maps based on real-time conditions that may be different from the conditions assumed when creating the static maps. If a NWS River Forecast Center (RFC) runs an unsteady hydraulic model for forecasting, dynamically generated water surface profiles from this model can be used to generate forecast maps that are valid all along a river.

Unsteady hydraulic models, as opposed to hydrologic models, are required to create accurate stage forecasts at locations with looped rating curves (a single stage may correspond to two different flows). Channels with large flood plains and mild slopes often have looped rating curves. For points that have single valued rating curves, hydrologic models can predict flows and a rating curve can convert flows to stages. In both cases, the static maps are tied to a stage rather than a flow and therefore are valid at the forecast point. However, at locations away from the forecast point, deviations between the true water surface profile and the statically mapped profile may occur in either case due to differences in the actual flood wave from the conditions assumed when creating the static maps.

Two drawbacks of dynamic forecast mapping are an increase in the computational requirements and that more human resources are required to quality control model outputs.

METHODOLOGY

Static versus Dynamic Forecast Mapping

In this study, we compare flood maps from a static forecast mapping approach to those from a dynamic forecast mapping approach. To generate example static maps, we run a steady flow model, generate a water surface profile and create a map. We then run an unsteady model for the same reach. From the unsteady model and for the forecast point of interest, we can identify times when the simulated stage matches the stage predicted by the steady model. We output instantaneous profiles at these times, generate maps and compare these maps to those from the steady model.

We used HEC-RAS to generate water surface profiles and HEC-GeoRAS to map the extent of the flooding. HEC-GeoRAS intersects the modeled water surface with digital terrain data to determine the inundated area. HEC-RAS includes both Steady Flow and Unsteady Flow modules. The Steady Flow module computes profiles using the standard-step approach based on the Energy equation and the Unsteady Flow module solves the Saint-Venant Continuity and Momentum equations. The HEC-RAS Steady Flow module uses empirical contraction and expansion coefficients to compute energy losses at contracting and expanding sections. The Unsteady Flow module accounts for expansions and contractions only through changes in cross-sectional flow area through the Momentum equation. This approach cannot account for all the forces caused by large scale eddies that occur with expansions and contractions. Because of this, HEC-RAS Steady Flow elevations will generally be higher than Unsteady Flow results even if the same flows, model geometry, and roughness parameters are being used (Brunner, personal communication).

Here, we wish to isolate the differences between static and dynamic forecast mapping approaches. Therefore, we wish to eliminate any differences in unsteady and steady flow computational techniques. To do this, we generate steady flow results in this study by inputting constant flow time series into the HEC-RAS Unsteady module. Identical channel geometry and roughness parameters are used for both steady and unsteady runs. For the same reason, we do not use the existing maps on the AHPS web site as examples for our steady state runs. Although we are using the same underlying cross-section data, other parameters in our HEC-RAS model are different from those used to create the AHPS maps and, in the case of the North Carolina points, we are using different software to convert the water surface profiles into maps. It will be useful to compare the overall accuracy of the AHPS maps to those we create from our unsteady model but that is not our purpose here.

Study Area

We plan to study several forecast points in North Carolina where static inundation mapping services are already available. Figure 2 shows the NWS forecast locations where static maps are available. Figure 2 also shows the locations of high water marks that were collected by the US Army Corps of Engineers after Hurricane Floyd (USACE,

1999). These data will help in evaluating the quality of our mapping results. To the extent possible, we will also use post-event aerial photography obtained from the U.S. Geological Survey (USGS) Earth Resources Observation and Science (EROS) Center for qualitative verification.

For this pre-print, we present example results near Greenville, North Carolina. To do this, we use an unsteady HEC-RAS model developed for approximately 48 river miles of the Tar River from Tarboro, NC to Washington, NC (area highlighted in red on Figure 2). To build this model, we obtained the cross-section data in HEC-RAS format from the North Carolina USGS via the North Carolina Floodplain Mapping Program. The cross-sections were originally produced from a combination of Light Detection and Ranging (LIDAR) data and USGS field surveys. Moreda et al. (2009, this proceedings) describe this model in more detail, including how the unsteady flow model was calibrated. The calibration period spanned several years, July 1 1999 through August 31 2005. Observed stage data at four observation stations were used in calibration. In the example presented here, we focus on the USGS Station near Greenville, NC and on the flood peak generated during Hurricane Floyd (September, 1999).

The initial HEC-RAS model we obtained was not geo-referenced. To correct this, we imported a geo-referenced river centerline into HEC-RAS to replace the existing straight centerline. In this process, HEC-RAS geo-references all cross sections starting from the upstream boundary following the new river centerline downstream and assuming that all cross sections were originally cut at 90 degree angles. The distance between the cross sections is based on the distances (river miles) entered in the hydraulic model.

NED versus LIDAR Data

Two sources of digital terrain data are available for the Tar River study area. The USGS National Elevation Dataset (NED) is readily available for the whole country and relatively easy to process on a personal computer; however, the data accuracy may be inadequate for flood mapping in some areas (http://ned.usgs.gov/). LIDAR data are more accurate and more precise than the NED data but are not available for the whole country. LIDAR data used in this study are available from the North Carolina Floodplain Mapping Program. We will create inundation maps using both sources of elevation data in this study and compare the results. This will give us some idea as to the importance of collecting more accurate elevation data relative to developing a dynamic forecast mapping capability with the existing lower accuracy data. Another factor to consider is that with the HEC-GeoRAS software, the processing of each map is much more computationally expensive when the LIDAR data are used. This may be alleviated with more efficient mapping algorithms or conversion of the raster LIDAR data into a Triangulated Irregular Network (TIN) format.

RESULTS AND DISCUSSION

Figure 3 shows a simulated rating curve from the unsteady HEC-RAS model at Greenville, NC. This curve was built from hourly simulations spanning July 1, 1999 to

August 31, 2001. The looped section of the curve is comprised of data from the Hurricane Floyd event. At a river stage of 20 ft, the flow can be approximately 36,400 cfs while the flood is rising but 8,000 cfs lower when the flood is falling. Clearly, the flood profile is dynamically changing during the event at moderate to high flood levels. At Greenville, flooding begins at 12 ft, moderate flooding begins at 16 ft, and major flooding begins at 18ft.

During Hurricane Floyd, our calibrated unsteady model simulates the peak stage at Greenville to be 25.9 ft (on September 22, 1999 at 0500z) while the observed stage is 25.8 ft. At this time, the simulated flow from the unsteady model is 65,809 cfs. To emulate the static forecast mapping approach, we used trial and error to identify a constant flow input so that the steady flow model predicts the same stage as the unsteady model. The flow required to produce a matching stage was 64,108 cfs.

We repeated this procedure for a smaller flood peak that occurred on October 25, 1999 at 0900z. For this event, the unsteady model simulated peak was 12.8 ft and the observed stage was 13.1 ft. The simulated flow from the unsteady model was 16,816 cfs at this time. A constant flow of 18,329 cfs was applied in the steady state model to generate a matching stage.

For both of these events, we are interested in the difference between the steady and unsteady water surface profiles as one moves away from the Greenville gauge. Figure 4 shows the water surface profiles predicted for approximately a six mile stretch of river centered on Greenville for the September (3a) and October (3b) events. Note that the unsteady profiles are instantaneous profiles predicted at the peak of the flood. Figure 4a shows that the water surface profiles corresponding to the September peak stage are very similar. This may be because the flood was so large that storage areas that would normally be filled with a steady model but not with an unsteady model are filled up in the unsteady model. The fact that the rating curve (Figure 3) is not looped for the highest stages supports this hypothesis. We would expect greater differences in the profiles if these instantaneous profiles were selected during the rising or falling limbs of the hydrograph.

Figure 4b shows that steady and unsteady water surface profiles differ more for the smaller October event. Here, the unsteady result is also the instantaneous profile at the event peak. In this case, the static forecast mapping approach produces errors up to 0.33 ft for distances within 3 miles of the forecast point and up to 0.25 ft for distances within 2 miles.

Due to last minute changes in our methodology, we were unable to create and compare the inundation maps corresponding to the profiles in Figure 4 for this paper. For this reason, we also do not present our verification results using the high water mark data and aerial photography data at this time. These maps and more results will be presented at the conference. To develop a robust set of results, we plan to create and quantitatively compare similar maps at several forecast points and for several stages.

REFERENCES

Moreda, F., Gutierrez, A., Reed, S., Aschwanden, C., Transitioning NWS Operational Hydraulics Models from FLDWAV to HEC-RAS, ASCE World Environmental and Water Resources Congress, Kansas City, MO, May 17-12 (2009).

NWS, Flood Inundation Map Library Guidelines, Draft Guidelines developed by NOAA's National Weather Service, NOAA's Coastal Services Center, and the United States Geological Survey, June 2, 2008.

USACE, "Hurricane Floyd High Water Inundation Study", May 2000.

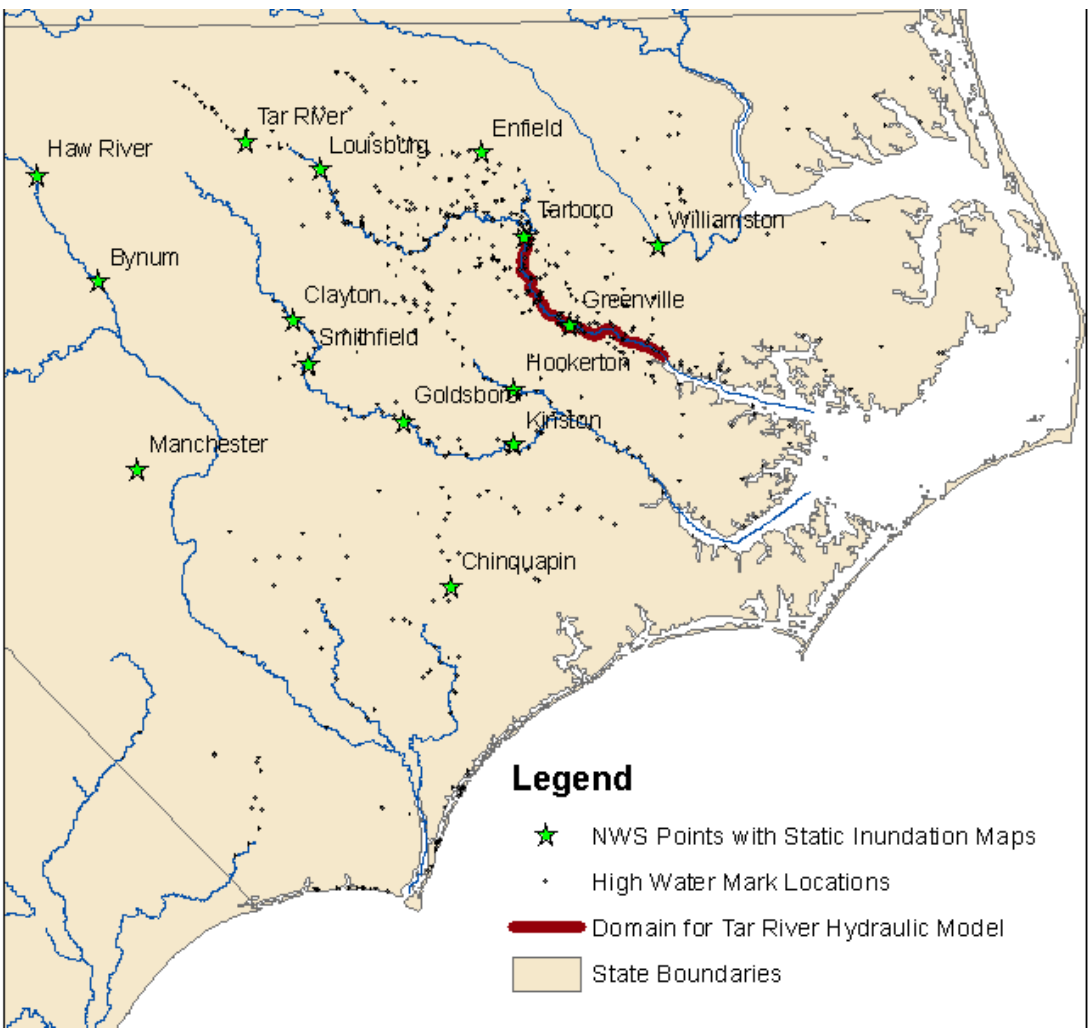

Figure 2. Locations of NWS forecast points with static inundation mapping services in North Carolina. Static forecast maps are available at 15 of the 109 NWS forecast points in North Carolina: Chinquapin (CHIN7), Hookerton (HOKN7), Kinston (KINN7), Greenville (PGVN7), Williamston (WLLN7), Bynum (BYNN7), Clayton (CLYN7), Enfield (EFDN7), Goldsboro (GLDN7), Haw River (HAWN7), Louisburg (LOUN7), Manchester (MANN7), Smithfield (SMFN7), Tarboro (TARN7), and Tar River

(TRVN7). Our initial HEC-RAS model is set up for the Tar River (highlighted in red). High water mark locations from Hurricane Floyd are also shown.

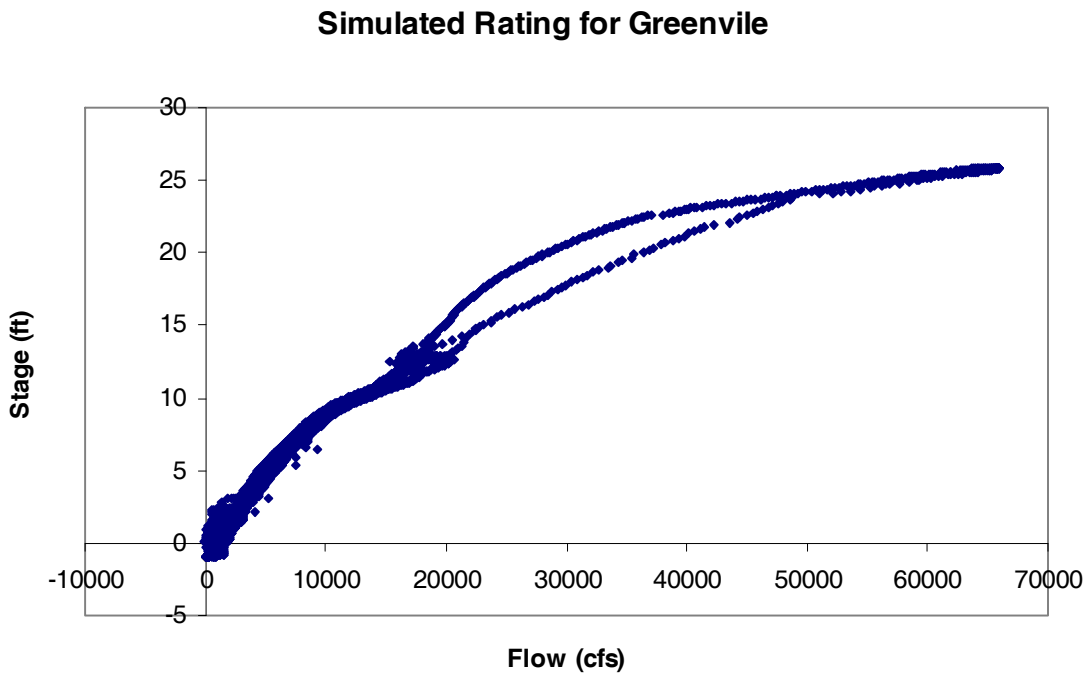

Figure 3. Simulated rating curve for Greenville, NC.

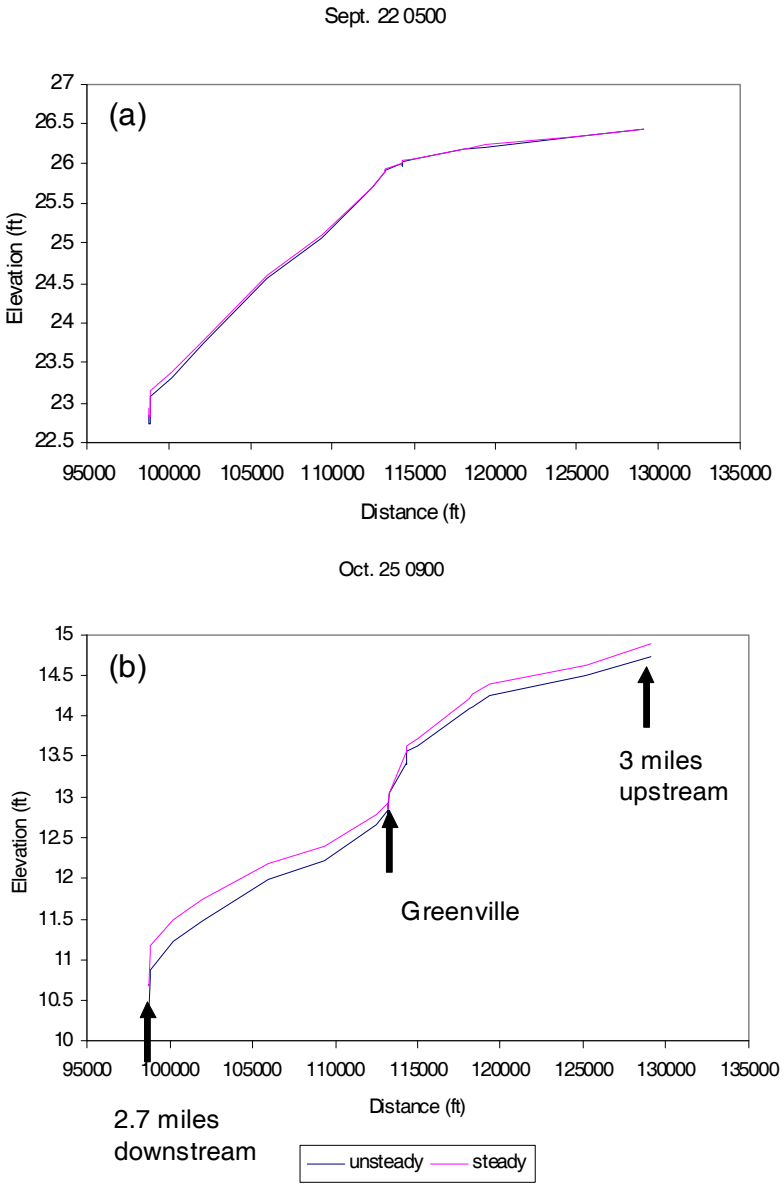

Figure 4. Two sets of water surface profiles generated so that the steady and unsteady model stages at Greenville match. (a) Water surface profiles simulated during the peak of flooding caused by Hurricane Floyd. (b) Water surface profiles for a less severe event during a subsequent month.

PERFORMANCE EVALUATION OF ARTICULATED CONTRETE MATTING (ACM) SPILLWAY AT LAKE ODESSA, IOWA

Thomas Gambucci[1]

[1] P.E., D.WRE., Hydraulics Engineer, Regional Technical Specialist MVD - Navigation and Flood Control, U.S. Army Corps of Engineers, Rock Island District, Clock Tower Building, P.O. Box 2004, Rock Island, IL 61204, (309) 794-5848, thomas.r.gambucci@usace.army.mil

ABSTRACT

Use of Articulated Concrete Matting (ACM) for overflow spillways has great ability to resist high overflow velocities, yet use of ACM for this purpose is rare at the Corps of Engineers. This presentation draws attention to the importance of ACM spillway design to the HH&C community and how it performed at Lake Odessa, Iowa during the Flood of 2008.

Many Environmental Management Projects are protected from flooding by perimeter levees. Typically these levees offer 10-year or 25-year protection and are frequently overtopped causing major damage to levees that can be very expensive to repair following each flood. Levee breaches may also produce adverse impacts on the ecosystems that they are intended to protect. The addition of spillways on perimeter levees can drastically reduce or eliminate overtopping damage to levees. From experience in the Rock Island District, head differences of less than one foot between the exterior and interior water levels will result in insignificant levee damage during overtopping events. A simple but effective spreadsheet technique was used to size the spillways according to this design assumption. The final spillway design made use of articulated concrete matting (ACM) to resist anticipated shear forces versus the more conventional techniques of riprap or concrete spillways. Construction of the spillway was completed in the winter of 2006 by the Corps of Engineers, making the Lake Odessa spillway the first substantial ACM spillway project by the Corps of Engineers. The flood of 2008 overtopped the ACM spillway twice allowing Rock Island District and Resource Agency personnel to monitor water levels. This paper evaluates the performance of the ACM spillway at Lake Odessa and presents lessons learned from the Flood of 2008.

BACKGROUND

The Lake Odessa Wildlife Refuge is located on the Iowa side of the Mississippi River between River Miles (RM) 434.5 and 441.5. It is surrounded by a perimeter levee approximately 8 miles long that was originally built in 1913 by local farmers for flood protection of agricultural land. The levee was enhanced in 1954 including two water control structures for low level water management. Both the inlet and outlet structures were rebuilt following damages sustained by the Flood of 1993. Spillways were added to the project in 2004 and 2006 to allow flood water to fill the interior prior to uncontrolled overtopping of the perimeter levee. Lock and Dam 17 is located at RM 437.1 and ties into the perimeter levee at approximately its mid-point. The Iowa River enters the Mississippi River at RM 434.5, which is just downstream of the refuge. See Figure 1 for an overview of project features.

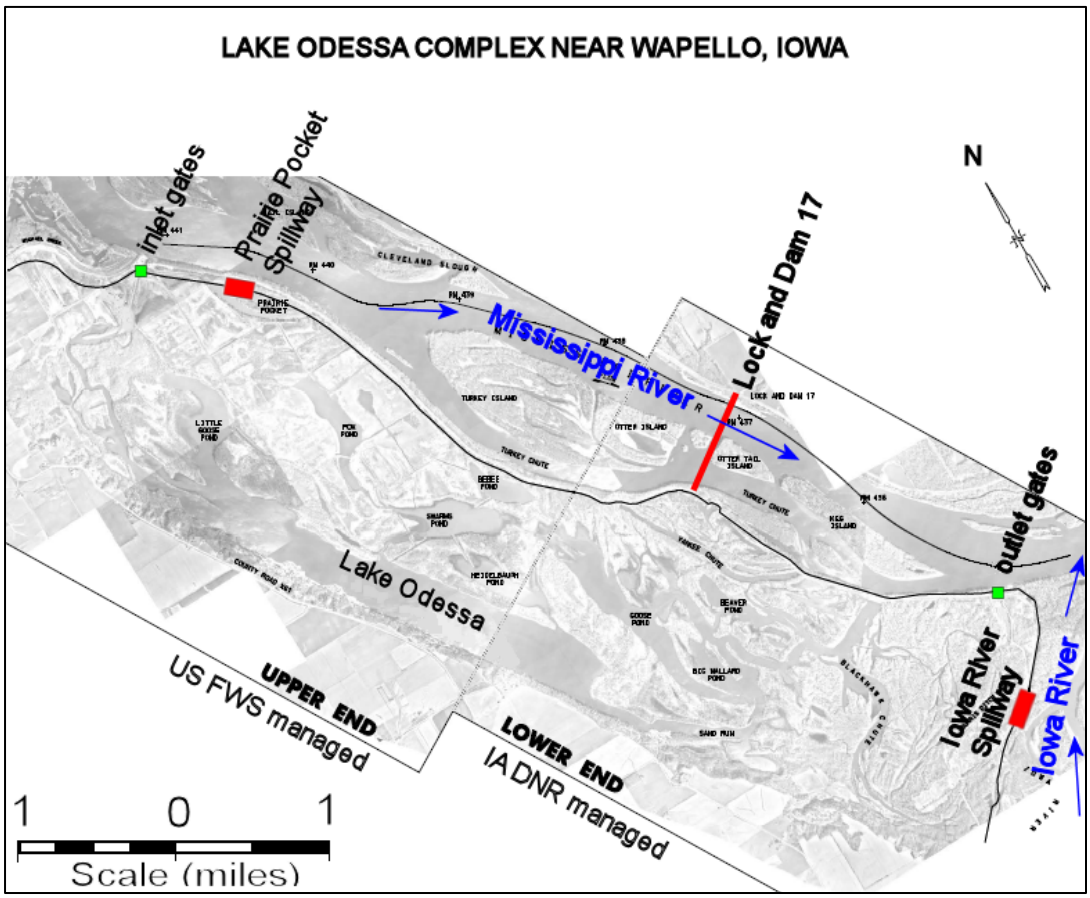

Figure 1. Lake Odessa EMP, Project Overview Map

MANAGEMENT

The U.S. Fish and Wildlife Service (USFWS) manages the levee upstream of RM 438, while the Iowa Department of Natural Resources (IDNR) manages the downstream portion of the levee. Management of the interior is similarly divided by the two agencies. The northern portion of the Lake Odessa complex is part of the U.S. Fish and Wildlife Service (USFWS) Mark Twain National Wildlife Refuge Complex, Port Louisa National Wildlife Refuge, Louisa Division. The Iowa Department of Natural Resources (IDNR) through a cooperative agreement with the USFWS manages the southern portion of the area, the Lake Odessa State Wildlife Management Area. The project area is comprised of a large lake (Lake Odessa), several other backwater bodies of water, wooded land, and open fields, and many archeological sites (DPR 2005).

During non-flood conditions, water enters the refuge through the northern inlet structure in Pool 17, flows through Lake Odessa, and exits through the outlet structure downstream of Lock and Dam 17. During rising waters, these gates are normally closed off to keep the interior at desired water levels; however, when a flood is forecasted, the gates are opened according to an operation plan (DPR 2005, Appendix I Section J) to help fill the interior prior to uncontrolled overtopping of the dam. Based on experience from the Flood of 2008, the gate operation plan has been revised.

SPILLWAY DESIGN

From experience at the Rock Island District, head differences across levees of less than one foot between the exterior and interior water levels result in insignificant or no levee damage. A simple but effective spreadsheet technique was used to size the spillways in order to meet this design assumption. The rate of rise of the Mississippi was chosen to be 0.75 ft per day in the elevation band from the crest of the spillway to the crest of the perimeter levee. This value is very close to the rate of rise experience in the Flood of 1993, but is slower than the rate of rise in both 2001 and 2008 (approx. 1.0 ft/day). The higher rate of rise fills the interior approximately 12 hours faster than the design rate of rise; both rates meet the design criteria of less than one foot of head differential at the time of uncontrolled overtopping. Figure 2 shows the response of interior water levels due to spillway overtopping for various design assumptions.

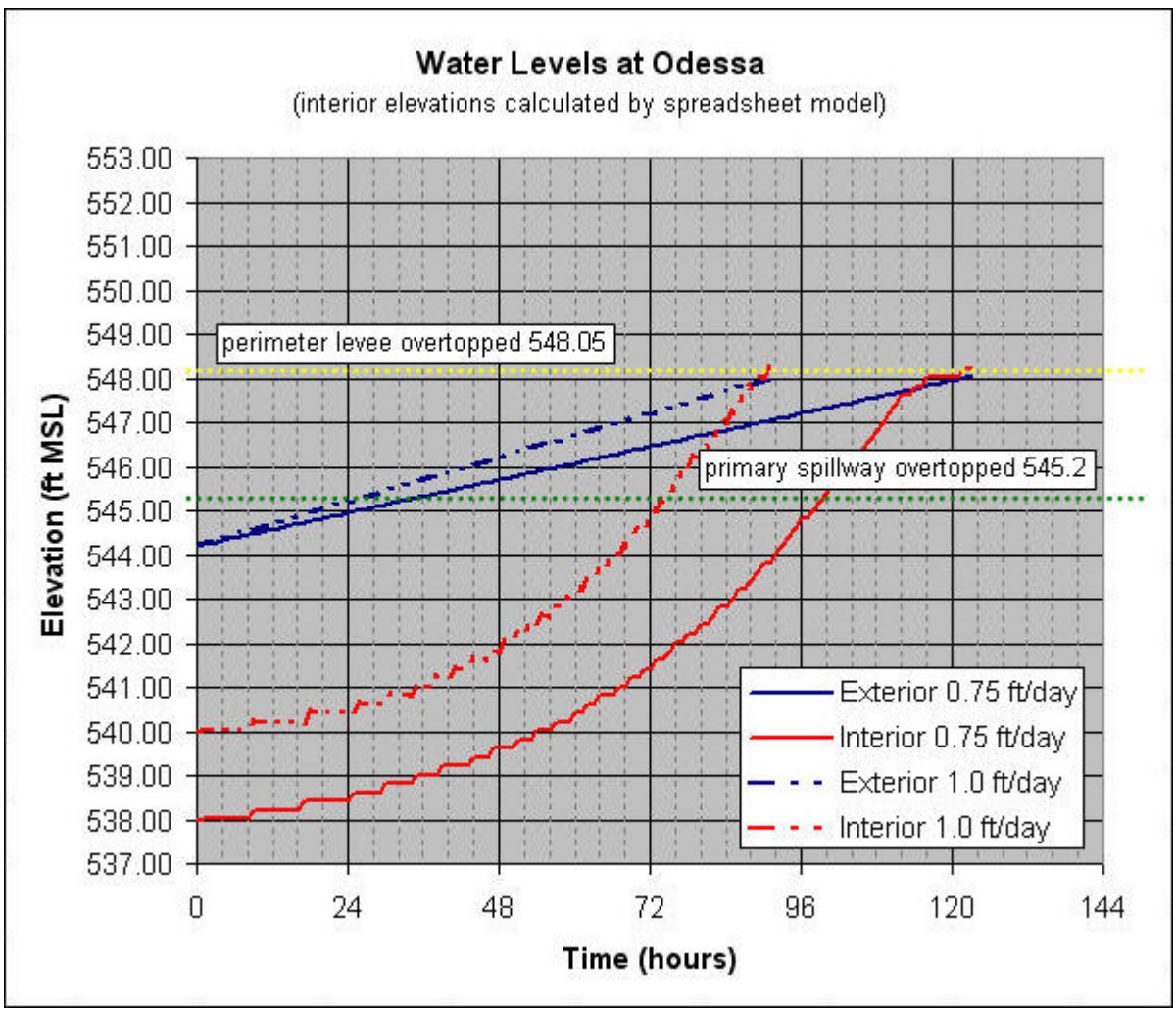

Figure 2. Interior Water Level Response for Final Spillway Design

Final spillway parameters from the analysis are a 1,100-foot long spillway at the downstream end (RM 434.8, the Iowa River Spillway) and a 700-foot long spillway at the upstream location (RM 440.4, the Prairie Pocket Spillway) of the perimeter levee. Crest elevations are 545.2 ft (1912 datum) for the downstream spillway and 545.8 ft (1912 datum) for the upstream spillway. These crest elevations have an estimated risk of overtopping per year of 10% for the downstream spillway (overtops first) and 6% for the upstream spillway. The annual risk of overtopping the perimeter levee is 4% at the downstream location and 2% at the upper end; this sloping (frequency) of the levee is designed to reduce damages by filling of the interior from the lower end. Frequencies are based on the 2003 Mississippi River Flow Frequency study.

An analysis of historical flooding was made in 2003 with the spillway design to investigate if flooding on the Iowa River could overtop the lower spillway without a flood occurring on the Mississippi River. Large flows on the Iowa River typically happen when the Mississippi River stages are also high, but "if the Mississippi River stage were normal, and a very large flood occurred on the Iowa River, there would be adequate flood storage available at the mouth of the Iowa River to reduce flood peaks and avoid overtopping the 545.2 feet (1912 datum) lower spillway crest." (DPR Appendix I) After the historical analysis and DPR were complete, the proposed location of the "lower spillway" was changed from a location near the confluence of the Mississippi River and Iowa River to a location approximately a half mile upstream on the Iowa River tieback levee. This new location was necessary because of archaeological concerns since the old location was located in an area formerly known as Burris City. The new location was adopted but the design crest of the spillway was kept the same due to lack of information about the influence of the Mississippi River upon the water surface slope of the Iowa River.

ARTICULATED CONCRETE MATTING (ACM) SPILLWAY

The spillway design made use of Articulated Concrete Matting (ACM) due to its ability to handle expected shear stresses, its cost relative to traditional (riprap) spillways, and its environmental appeal (it allows vegetation to grow through the matting). The original design head of 7 ft made riprap size too large without special handling and expense; however, smaller riprap was used on the exterior slope to handle outflow from Lake Odessa during flood recession. Construction was completed in the spring of 2007 (Figure 3), making the Iowa River Spillway at Lake Odessa the first substantial ACM spillway for the Corps of Engineers.

The upstream ACM spillway was completed by the USFWS in the winter of 2005 (Figure 4) to assist in filling the interior. It also allows a portion of the Mississippi River to flow through the Lake Odessa Complex during times of flood. This flow establishes a sloped water surface through the interior that reduces head differential (and thus erosion potential) across the levee crest in the upstream-most areas of the perimeter levee.



Figure 3. Iowa River Spillway, 1100-ft long, crest 545.2 ft, River Mile 434.8



Figure 4. Prairie Pocket Spillway, 700-ft long, crest 545.8 ft, River Mile 440.4

THE FLOOD OF 2008

The Flood of 2008 overtopped the Iowa River Spillway on April 27 (Figure 5) and on June 12. As can be seen on Figure 5, the levee adjacent to the spillway is unvegetated and was recently under construction. This was not uncommon elsewhere on the perimeter levee and some areas were lower than design grade. Multiple areas of erosion to the crown of the perimeter levee occurred during the flood, as well as three larger blowouts.



Figure 5. Iowa River Spillway overtopping on April 27, 2008, River Mile 440.4

Prior to the Flood of 2008, a staff gage was established on the interior to monitor rising water levels. The spillway functioned as expected to raise interior water levels according to design; however, due to ongoing levee repair efforts the spillway did not have the full design time (three days) to fill the interior prior to uncontrolled overtopping of the perimeter levee. The low spots in the levee started overtopping two days after the ACM spillway started filling the interior. This led to a greater than 1 ft head difference and erosive forces for more than 24 hours. It is assumed that most of the breaches started forming on April 29, 2008.

Surveys were performed on April 23 and on June 6 to capture the slope of the Iowa River at both a high and low tailwater (Mississippi River) condition near the time of overtopping of the primary ACM spillway (Iowa River Spillway). This data was later used to update the gate operation plan and to modify the design crest of the tieback levee. Survey points are shown in Figure 6 along with levee profiles and a computed historic profile from 1993.

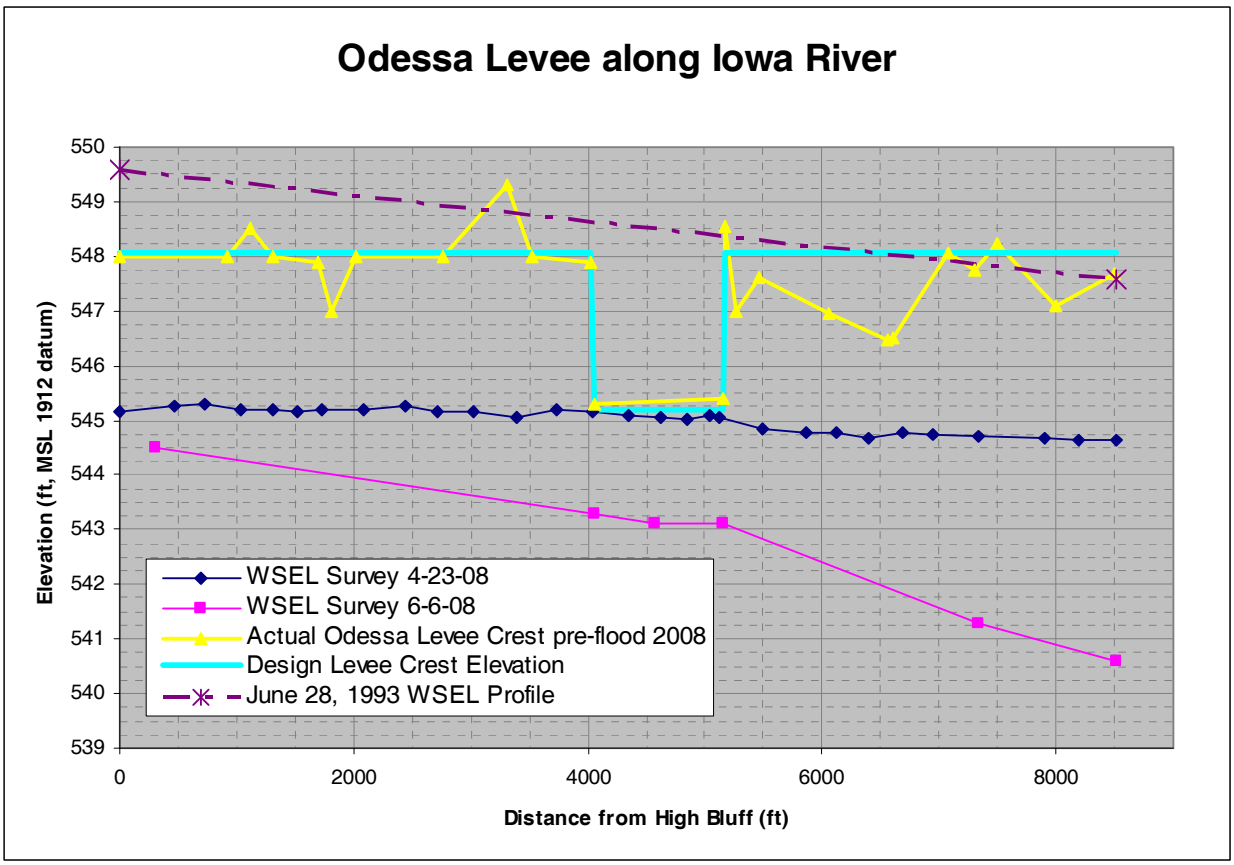

Figure 6. Water Surface and Levee Profiles along the Iowa River Tieback Levee, Lake Odessa

Station "0" in Figure 6 represents the "high bluff" and Station "8000" is near the levee bend where the Iowa River joins the Mississippi River. Based on this survey data, the spillway overtops at a Lock and Dam 17 tailwater stage of 18.5 ft.

Due to the water slope along the Iowa River, the levee at the high bluff is recommended to be raised to elevation 549.5 ft and sloped down to 548.5 ft at the spillway. Sloping the levee in this fashion will help reduce uncontrolled overtopping near the high bluff.
Both ACM spillways functioned well and were not damaged during the Flood of 2008. The Iowa River Spillway did not have vegetation established and the soil was pulled out of the void spaces (See Figure 7). Soil will need to be replaced and seeded in 2009. The extended apron on the spillway is meant to be used as a roadway, and the spaces were filled with crushed stone. This stone was washed out of the spaces during the Flood of 20008 and it is now recommended to replace the stone with vegetated soil. Figure 7 shows the Iowa River Spillway after the first hydrograph peak of the Flood of 2008.



Figure 7. Iowa River Spillway following the Flood of 2008, Lake Odessa

PRIMARY RESULTS

The Articulated Concrete Matting (ACM) spillways at the Lake Odessa Complex performed well during the Flood of 2008. There was no damage to the spillways during the two overtopping events and the size of the Iowa River Spillway allowed interior water levels to rise at the expected rate. The damages that occurred to the perimeter levee in 2008 were located in areas containing unvegetated sand and in areas that were below design grade (or under construction) prior to the flood. ACM should be considered a dependable choice for medium-sized spillways (5-10 ft of head) where the size of traditional riprap design might become prohibitively costly.

While levee damages due to the Flood of 2008 have not yet been calculated, it is assumed that the presence of spillways at the Lake Odessa Complex helped reduce levee damages. During the Flood of 2001, the spillways did not exist and the gated structures could not adequately raise interior water levels prior to overtopping. This gave a much greater head difference at the time of uncontrolled levee overtopping. All of the breaches in 2001 were large levee blowouts that were expensive to repair; most of the breaches in 2008 were small breaches or minor crown erosion. It is expected that damages will be reduced or eliminated after the Lake Odessa perimeter levee is repaired to its design grade and has a well vegetated clay cap along its length.

DISCLAIMER

The views expressed in this article are those of the author and do not reflect the official policy or position of the Department of the Army, Department of Defense, or the U.S. Government.

REFERENCES

USACE (U.S. Army Corps of Engineers), (April 2005). “Lake Odessa Habitat Rehabilitation and Enhancement Project, Definite Project Report (DPR)”

USACE (U.S. Army Corps of Engineers), (August 2003). “Upper Mississippi River System Flow Frequency Study”, Hydrology & Hydraulics Appendix C, Mississippi River

The Development of a Neural-Based Biomarker Forecasting Tool for Classifying Recreational Water Quality

Srinivas Motamarri† and Dominic L. Boccelli‡

Department of Civil and Environmental Engineering, University of Cincinnati, P.O. Box 210071, Cincinnati, OH 45221-0071; FAX (513) 556-2599

†Ph (513) 410-9121; email: srinivasiitr@gmail.com
‡Ph (513) 375-6901; email: dominic.boccelli@uc.edu

Abstract

This study will develop a computational framework capable of rapidly classifying microbial surface water quality for the protection of public health. Three classification tools will be developed using multivariate linear regression (MLR), artificial neural networks (ANN), and linear vector quantization (LVQ). The MLR and ANN approaches first quantify the microbial concentration followed by classification, while the LVQ approach directly classifies the water quality. The algorithms will be applied to microbial and hydrologic data associated with the Charles River Basin using antecedent rainfall over the previous 24 and 168-hrs and lag-1 fecal coliform concentrations as explanatory variables. Preliminary results with the MLR algorithm illustrate very good classification when the observed data is below the appropriate water quality standard (true negative rates $> 95\%$). Unfortunately, the MLR classification approach does not perform as well when the observed data is greater than the standard (true positive rates $\sim 50\%$). Additional studies will be focused on evaluating the architecture and performance of both the ANN and LVQ approaches for classifying the microbial water quality, and the best performing algorithm identified.

1 Introduction

The use of recreational surface waters can pose a public health risk due to elevated pathogens from various point and non-point sources. For over a century, bacterial indicator organisms have been used in the USA to assess the presence of pathogenic organisms in drinking and recreational waters (NRC, 2000). Unfortunately, laboratory analysis of water quality samples, which typically require at least 24 hrs after sampling to provide microbial quantification, eliminates the possibility of providing a rapid response to alert the populous of any potential public health risk.

Data-driven modeling approaches (e.g., linear regression and artificial neural networks) have been developed to provide rapid predictions of microbial quantity. Previous studies (Christensen, Jian, and Ziegler, Christensen et al.; Eleria, 2002;

Eleria and Vogel, 2005; Ferguson et al., 2003) have developed multiple linear regression models to relate bacteria concentrations to explanatory variables for streams and estuaries. Neelakantan et al. (2001) developed an ANN tool to relate peak Cryptosporidium and Giardia concentrations with the other biological, chemical and physical parameters in the surface water. Mas and Ahfeld (2007) compared the performance of ordinary least squares, binary logistic regression methods, and artificial neural networks for the prediction of surface water faecal coliform concentrations in a mixed land-use watershed. These model-based approaches predict the microbial concentrations, which are then used to assign a warning level or classification based on the predicted concentration. Unfortunately, these approaches tend to suffer from high false-negative rates due to uncertainties in predicting high microbial concentrations.

The objective of this study is to develop a forecasting tool based on a neural approach called linear vector quantization (LVQ). LVQ is a class of self-organizing map that seeks to cluster similar sets of explanatory variables based on their desired classification. The advantage of the LVQ approach is that the output of the algorithm is a classification, rather than a concentration, thus potentially removing the uncertainties associated with the prediction step. The performance of the LVQ classification approach will be compared with those based on linear regression and ANN models. The comparison will be performed using the same data and explanatory variables as the model proposed by Eleria and Vogel (2005).

2 Methodology

2.1 *Study Area*

The Charles River Basin, the final nine-mile stretch of river from Watertown Dam to New Charles River Dam in Boston, Massachusetts encompasses a watershed of 36.1 square miles with a population of 500,000. It is one of the most heavily used recreational areas in the country (Eleria, 2002). Even though proper measures were taken by controlling the flows from combined sewer overflows, the public may still be exposed to risk due to pathogens entering the water after hydrologic events (e.g., after a storm) via combined sewer overflows, which is mostly untreated waste, and run-off, which consists of various wastes from impervious surfaces.

Eleria (2002) proposed models for the four flagging monitoring sites (North Beacon Street Bridge in Brighton, Larz Anderson Bridge in Cambridge, Boston University Bridge in Boston, and Longfellow Bridge in Boston) on the Charles River using different combinations of meterological and hydrological explanatory variables. The model developed in this paper is with respect to the Larz Anderson Bridge site.

2.2 *Data Source*

The fecal coliform data (log transformed) and the explanatory variables of antecedent rainfall during the previous 24and 168 hrs, and lag-1 bacteria concentra-

tions are the same as mentioned in Eleria and Vogel (2005). Further information associated with data sources and exploratory analysis can be found in Eleria and Vogel (2005). The original dataset contains 142 samples collected from mid-June through mid-October of 2000-2001. Because bacterial data were not collected every day, the final data set using the lag-1 bacteria concentrations was reduced to 78 samples.

2.3 *Data Classification*

According to the Massachusetts surface water quality standards, fecal coliform bacteria are used as a measure to classify recreational water quality (314 CMR 4.00, 2007). The Charles River is classified as a Class B Warm Water designated as a habitat for fish, other aquatic life and wildlife, and suitable for primary contact recreation, such as swimming, fishing and windsurfing, and secondary contact recreation, such as canoeing, boating etc. For primary contact recreation the geometric mean of fecal coliform bacteria concentration should not be more than 200 colony-forming units (cfu) per 100-mL of the sample. In any case, no more than 10 percent of the samples should exceed 400 cfu/100-mL. For secondary contact recreation, the geometric mean of the fecal coliform bacteria concentration should not be more than 1000 cfu/100-mL and, in any case, no more than 10 percent of the samples should exceed 2000 cfu/100-ml.

2.4 *Multivariate Linear Regression*

2.4.1 *Experimental Design*

The regression coefficients are estimated using the entire data set. The overall performance of the model is evaluated using the mean square error (MSE) and precision in classifying the water quality. The precision is considered using the true negative (TN), true positive (TP), false negative (FN), and false positive (FP) rates. The MATLAB Statistical Toolbox, Version 6, is used to estimate the model coefficients.

2.5 *Artificial Neural Networks – Backpropagation*

2.5.1 *Introduction*

ANN, also referred to as Neural Networks, are a class of computational tools that mimic biological processes of the brain. A neural net consists of a large number of simple processing elements called neurons, units, cells or nodes. Each neuron is connected to other neurons by means of directed communication links, each with an associated weight. The weights represent information being used by the net to solve a problem. Neural nets can be applied to a wide variety of problems, such as storing and recalling data or patterns, classifying patterns, performing general mappings from input patterns to output patterns, grouping similar patterns, or finding solutions to constrained optimization problems. Each neuron has an internal state, called its activation or activity level, which is a function of the inputs received. Typically, a neuron sends an activation signal to

several other neurons. While a neuron can send only one signal at a time, that signal may be broadcast to several other neurons. This leads to neuron layers associated with the inputs and outputs, as well as hidden layers between the two for transforming the input data into the appropriate outputs. The presence of a hidden unit, together with a non linear activation function, gives it the ability to solve more problems that can be solved by a net with only input and output units. On the other hand, it is more difficult to train (i.e., find optimal values for the weights) a net with hidden units. Haykin (1998) can be referred to for a detailed discussion of ANN.

2.5.2 *Experimental Design*

A multi-layer, feed forward network consisting of one input layer, one hidden layer and one output layer was used. The number of nodes in the input layer is fixed by the number of model inputs (i.e three), whereas the number of nodes in the output layer equals the number of model outputs (i.e one). The Tan sigmoidal and linear transfer functions are used in the hidden and output layers. Since there is no accepted rule for the selection of the number of hidden nodes, the number of hidden neurons is decided by simulation experiments. For a range of hidden neurons (3 - 8), ANN models were developed using the leave-one-out method suggested by Haykin (1998). Out of the 78 data samples, one sample is withheld to be used for validation and the ANN weight estimated. Thus, 78 models can be developed for each number of hidden neurons to be evaluated. The range of hidden neurons to be investigated is based on a rule of thumb associated with the number of training samples to the number of connection weights (Masters, 1993). Ultimately, the number of required neurons in the hidden layer are determined based on the overall performance of all models with respect to a particular number of neurons. The MATLAB Neural Network Toolbox, Version 5.0.2 was used to design and implement the network.

2.5.3 *Training*

In this study, the Levenberg-Marquardt optimization method with mean square error as the performance function with a maximum of 1000 epochs is used during training. Prior to training, network interconnections were assigned random initial weights. A technique called early stopping was used during model training to avoid overfitting and subsequent poor generalization (Demuth et al., 2007).

2.6 *Linear Vector Quantization*

LVQ is a pattern classification method in which each output unit represents a particular class or category (several output units should be used for each class). The network contains an input layer, single Kohonen/competitive layer and an output layer. The output layer has many processing elements to translate the information for the competitive layer into the appropriate class. For each class there are a number of grouped processing elements in the Kohonen layer, which learns and classifies with the help of a training set (i.e., supervised learning).

Whenever an input vector is submitted to the network, the euclidian distance from each of the processing elements in the Kohonen layer is determined, and the nearest processing element declared the winner; there will be only one winner for the layer and this element will be "fired." If the wining element is in the expected training class then the weights are modified to draw near to the training vector. If the winning element is not in the expected class, then weights are updated to move away from the training vector. The process is repeated that, in turn, generates one output signifying a particular class found by the network.

2.6.1 *Experimental Design*

As mentioned in the previous section, the LVQ network has a first competitive layer and a second linear layer. The competitive layer learns to classify input vectors in much the same way as the competitive layers of Self-Organizing Maps (Demuth et al., 2007). The linear layer transforms the competitive layer classes into target classifications defined by the user. The number of nodes in the competitive layer plays an important role in classification, and is determined through simulation experiments. A range of neurons (10 - 40) is evaluated and the appropriate number of neurons determined by evaluating the performance based on the error in classification. The MATLAB Neural Network Toolbox, Version 5.0.2 was used to design and implement the network.

2.6.2 *Training*

A target class (1 for not violating a standard and 2 for violating a standard) is predefined for all the input pairs based on the fecal coliform swimming standard (200 cfu/100-mL). Then the network is trained using the LVQ training rule (Demuth et al., 2007). After training, the LVQ net classifies an input vector by assigning it to the same class as the output unit that has the weight vector (reference vector) closest to the input vector. A similar process is repeated for the boating standard (1000 cfu/100-mL). The entire dataset is used for testing to evaluate the ability of the LVQ algorithm to generalize the data set.

3 Results and Discussion

3.1 *Multivariate Linear Regression*

The explanatory variables used are the antecedent rainfall (24 hrs and 168 hrs) and lag-1 fecal coliform bacteria concentrations (log transformed). *Figure 1* illustrates the observed and predicted microbial data from the linear regression model. The regression model has an MSE of 0.2301 and explains 56 percent of the variability in fecal coliform concentration. The performance of the model with respect to both standards is presented in *Table 1* and *Table 2*. Overall, the model performance in classifying water quality with respect to the boating standard (1000 cfu/100-mL) is similar to that of the swimming standard (200 cfu/100-mL). Both standards are correctly identified in over 90% of the samples (TP rates of 94.6% and 98.6% for the 200 and 1000 cfu/100-mL standards, respectively). However, the regression

model has approximately a 50/50 chance of correctly classifying conditions that exceed the standard (TN rates of 54.5% and 50.0% for the 200 and 1000 cfu/100-mL standards, respectively). From Figure 1, the performance of the regression model at low concentrations (approximately 100 cfu/100-mL) is not satisfactory, although the data are generally not misclassified.

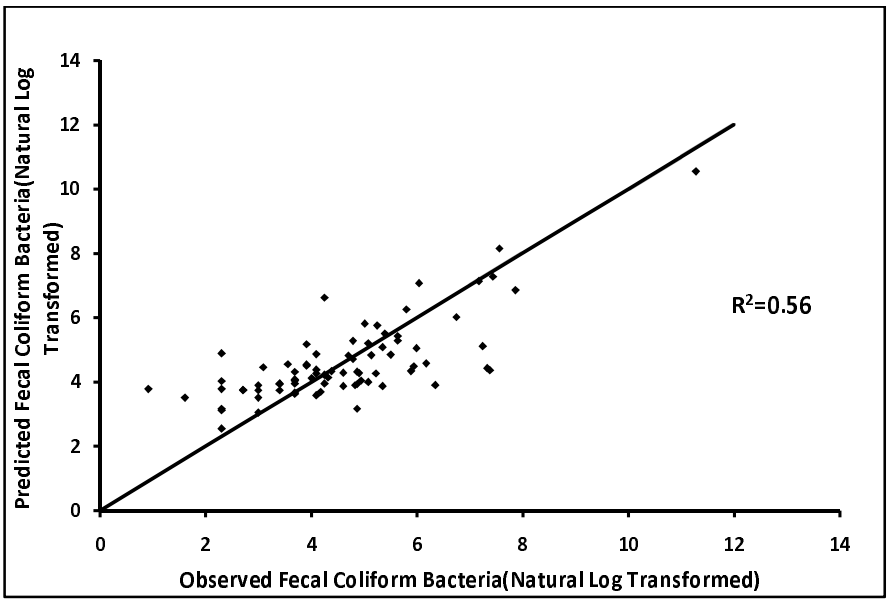

Figure 1: Observed Versus Predicted Fecal Coliform Bacteria Concentrations at Larz Anderson Bridge

Table 1: MLR Model Results (Swimming Standard) - Number of Observations Versus Number of Predictions

		Observed	
		Met Swimming Standard	**Exceeded Swimming Standard**
Predictions	**Met Swimming Standard**	94.64(53)	54.55(12)
	Exceeded Swimming Standard	5.36(3)	45.45(10)

Table 2: MLR Model Results (Boating Standard) - Number of Observations Versus Number of Predictions

		Observed	
		Met Swimming Standard	**Exceeded Swimming Standard**
Predictions	**Met Swimming Standard**	98.57(69)	50(4)
	Exceeded Swimming Standard	1.43(1)	50(4)

4 Summary and Future Work

The present study is intended to develop a tool to classify the recreational water quality in the Charles River Basin using Linear Vector Quantization (LVQ). The performance of the LVQ approach will be compared with the results from multivariate linear regression and artificial neural networks. Bacterial predictions are made using three explanatory variables, antecedent rainfall data from the previous 24 and 168 hrs, and lag-1 bacteria data. The entire data set is used for training and assessment of the individual model architecture to evaluate the ability of each approach to generalize the observed data. The performance of the algorithms will be assessed using the mean square error and the rates associated with correct/incorrect classifications.

The linear regression approach provides similar performance for both the boating and swimming standards. When the bacterial concentrations are below the appropriate standard, the regression model has a high true negative rate. However, when the standards are violated, the regression model has true positive/false negative rates near 50%. The evaluation and development of the artificial neural network and LVQ approaches will continue to be investigated. The performance of these approaches will be compared to the regression analysis and the "best" approach determined.

5 Acknowledgements

This study has been funded by the Ohio Water Resources Research Institute and the US Geological Survey, and their support is greatly appreciated. The authors would also like to thank the Charles River Watershed Association for graciously providing the hydrologic and water quality data used in this study.

References

314 CMR 4.00 (2007). *Massachusetts Surface Water Quality Standards*. Massachusetts Department of Environmental Protection-Division of water Pollution Control.

Christensen, V., X. Jian, and A. Ziegler. Regression analysis and real-time water quality monitoring to estimate constitutent concentrations, loads and yields in the Little Arkansas River, South Central Kansas, 1995-1999. Technical report, US Geological Survey W.

Demuth, H., M. Beals, and M. Hagan (2007). *Neural Network Toolbox User's Guide*. Natick, Massachusetts, USA: The Mathworks, Inc.

Eleria, A. (2002). Forecasting fecal coliform bacteria in the Charles River Basin. Master's thesis, Tufts University, Medford, Massachusetts, USA.

Eleria, A. and R. M. Vogel (2005). Predicting fecal coliform bacteria in the Charles River. *Journal of the American Water Resources Association 41*(5), 1195–1209.

Ferguson, C., A. M. de Roda Husman, M. Altavilla, D. Deere, and N. Ashbolt (2003). Fate and transport of surface water pathogens in watersheds. *Critical Reviews in Environmental Science and Technology 33*(3), 299–361.

Haykin, S. (1998). *Neural Networks*. Englewood Cliffs, New Jersey, USA: Prentice Hall.

Mas, D. M. and D. P. Ahfeld (2007). Comparing artificial neural networks and regression models for predicting faecal coliform concentrations. *Hydrological Sciences 52*(4), 713–731.

Masters, T. (1993). *Practical Neural Network Recipes in C++*. San Diego CA: Academic Press.

Neelakantan, T. R., G. M. Brion, and S. Lingireddy (2001). Neural network modelling of cryptosporidium and giardia concentrations in the Delware River, USA. *Water Science and technology 43*(12), 125–132.

NRC (2000). *Indicators for Waterborne Pathogens*. National Research Council of the National Academics.

Use of Hydraulic Modeling to Develop a Small Dam for the Geum River Reach in Sejong City

Sangman Jeong[1], Christabel Jane Rubio[2], Joo-Heon Lee[3], Leehyung Kim[4], Kwangseob Shin[5]

[1] Professor, Department of Civil and Environmental Engineering, Kongju National University, Cheonan-si, Chungnam-do, 330-717, Republic of Korea, PH: +82-41-521-9300, FAX: +82-41-565-7818, email: smjeong@kongju.ac.kr
[2] Graduate Student, Department of Civil and Environmental Engineering, Kongju National University, PH: +82-41-521-9316, email: cjrubio@kongju.ac.kr
[3] Associate Professor, Department of Civil Engineering, Joongbu University, Kumsan-gun, Chungnam-do, 312-701, Republic of Korea, PH: +82-41-750-6744, email: leejh@joongbu.ac.kr
[4] Assistant Professor, Department of Civil and Environmental Engineering, Kongju National University, PH: +82-41-521-9312, email: leehyung@kongju.ac.kr
[5] Graduate Student, Department of Civil and Environmental Engineering, Kongju National University, PH: +82-41-521-9316, email: ksshin@kongju.ac.kr

Abstract

Currently, building a small dam located 1.16km downstream from Geumnam Bridge is being considered in order to improve the riverine scenery of the site for Sejong City and to create a hydrophilic space. The purpose of this research is to present the appropriate dimensions of a small dam by reviewing the flood control reliability of the Geum River after the small dam is built. To establish this purpose, changes in the flood water level were compared and analyzed by changing the installation height of a small dam using HEC-RAS and FESWMS models. HEC-RAS and FESWMS models were applied to perform the hydraulic analysis of the reach. The results showed that flood control reliability was guaranteed when the installation heights of the small dam were 7 meters and 5 meters using HEC-RAS and FESWMS models respectively. From the FESWMS model, a more accurate result can be developed because the model could provide a two dimensional hydraulic analysis. The results can be used to determine the appropriate dimensions of a small dam for Sejong City.

Introduction

There is a recent increase in the occurrence of floods exceeding the design for hydraulic structures in Korea due to climate change such as global warming. Several types of small dams are installed on many rivers in Korea for various purposes such as water storage, transportation, and flood control. In addition, plans of small dam installation on the rivers within areas where cities will be built have been made to improve riverine scenery and to create hydrophilic spaces.

River barriers such as small dams are major structures affecting water level variation. Significant rise in water level during flood increases the possibility of flooding the surrounding area as a result of water overflowing from riverbanks. Taking this into account, accurate and comprehensive hydraulic analysis of the river dimensions should be completed prior to small dam installation due to uncertainties in rainfall characteristics.

In this research, changes in the characteristics of hydraulic flows due to the small dam, which will be installed on Geum River in Sejong City, were analyzed. To establish this, hydraulic analysis was performed using a one-dimensional model and a two-dimensional model with a 200-year frequency flood design for the target section. The main purpose of this paper is to determine the appropriate size of small dam based on the results of hydraulic analyses contingent upon the installation of small dams.

Background

Study Area

A 10.39km section located in the middle region of the Geum River from Miho stream confluence to Daekyo stream confluence was selected for the hydraulic analysis of the reach after the small dam is built. Building the small dam 1.16km downstream from Geumnam Bridge is being considered in order to improve the riverine scenery of the site for Sejong City and to create a hydrophilic space(Korea Land Corporation, 2007). The Geum River basin, one of the five major rivers in Korea, encompasses a total area of 9,810.4km^2 with a total reach length of 397.79km. Figure 1 illustrates the study section.

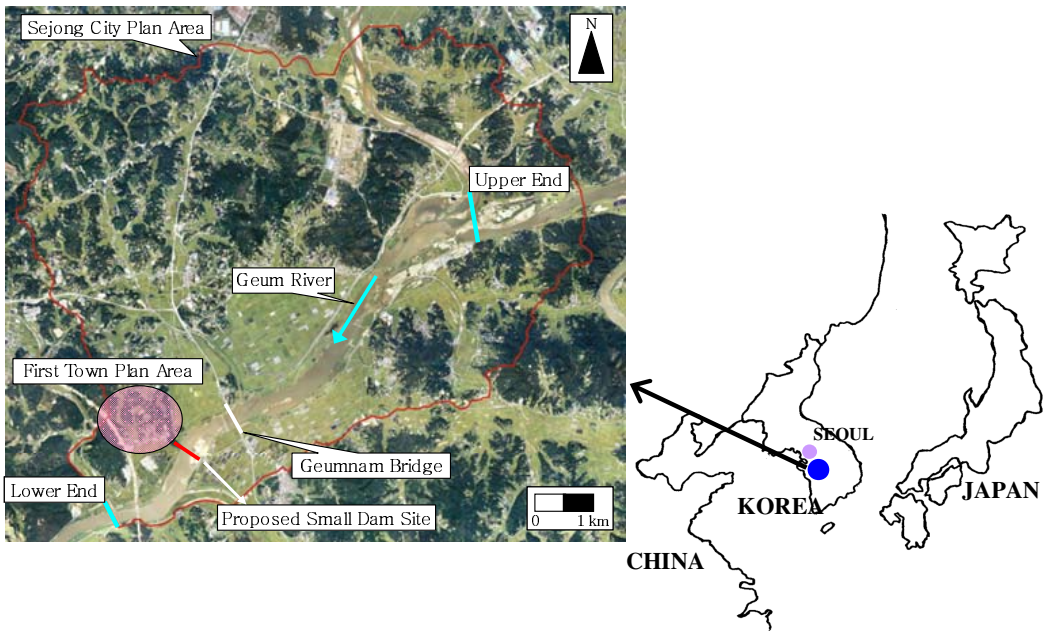

Figure 1. Study section of the Geum River in Sejong City.

Model Description

One-dimensional HEC-RAS and two-dimensional FESWMS were used in order to perform hydraulic analysis for the installation of hydraulic structures. The FESWMS is a model designed by the U. S. Federal Highway Administration in order to simulate flows near road facilities that cross rivers. The FESWMS is an ideal model for simulating flows near one or more than one hydraulic structure. The previous models have not been able to simulate these kinds of flows. Thus, this program is very helpful for analyzing the flows of the complex topography of rivers where river-crossing structures are installed.

Hydraulic Analysis

Changes in flood water level were compared and analyzed by changing the installation height of a small dam using HEC-RAS and FESWMS models. As shown in Table 1, the installation heights of small dam were set into seven scenarios based on the normal water level of the cross section 1.16 km downstream from Geumnam Bridge. Hydraulic analysis for each scenario was then performed. In addition, the results for both one-dimensional and two-dimensional models were compared for each section of the study area and then were analyzed.

Table 1. Height of the small dam for each scenario.

Scenarios	Height(m)	Crest elevation (EL. m)	Remarks
CASE 1	0	6.13	Normal water level (9.66 EL. m)
CASE 2	4	13.66	
CASE 3	5	14.66	
CASE 4	6	15.66	
CASE 5	7	16.66	
CASE 6	8	17.66	
CASE 7	9	18.66	

Input Data

Upstream and downstream boundary conditions, roughness coefficient, contraction coefficient, and expansion coefficient, etc., were used for the HEC-RAS model, whereas upstream and downstream boundary conditions, roughness coefficient, turbulent exchange coefficient, acceleration of gravity, and water temperature, etc., were used for the FESWMS model. Table 2 shows the input data used for the HEC-RAS and FESWMS models.

Table 2. Input data for HEC-RAS and FESWMS.

Models / Parameters	HEC-RAS	FESWMS
Upstream boundary condition (Miho stream confluence)	12,960 m^3/sec	12,960 m^3/sec
Downstream boundary condition (Daekyo stream confluence)	EL. 23.84 m	EL. 23.84 m

Roughness coefficient	0.027	0.027
Contraction coefficient	0.1	-
Expansion coefficient	0.3	-
Turbulent exchange coefficient	-	1,500 N·sec/m^2
Acceleration of gravity	-	9.8 m/sec^2
Water temperature	-	15 ℃

For the upstream boundary condition of both one-dimensional and two-dimensional models, 200-year frequency flood flow at the Miho stream confluence was used. Whereas for the downstream boundary condition, 200-year frequency flood water level at the Daekyo stream confluence was used. Moreover, the roughness coefficient of the target area was determined using the "Geum River Basin Maintenance Plan (by the Ministry of Land, Transport and Maritime Affairs, MLTM, established in 2002)" due to the extensive length of the study reach and data limitation. Since the target area is located between Daecheong Dam in Jojeongji and Ji stream confluence, the roughness coefficient of the said area, as indicated in the MLTM plan, was applied.

The turbulent exchange coefficient needed for the two-dimensional FESWMS was determined through the User's Manual. The turbulent exchange coefficient for regular rivers, with a value of 1,500 N·sec/m^2, was applied(Environmental Modeling Research Laboratory, 2000). Using this coefficient, the simulation results indicated a significant convergence with a stable solution.

Geometry data

The geometry data were developed using the cross sectional and longitudinal section data from the "Geum River Basin Maintenance Plan" (MLTM, 2002) and a digital map with the scale of 1:5,000. Table 3 indicates the geometry data used for the HEC-RAS and FESWMS models.

Table 3. Geometry data for HEC-RAS and FESWMS.

Models / Geometry data	HEC-RAS	FESWMS
Cross section	22 cross sections	-
Cross section lenths(mean)	495 m	-
Nodes	-	9,110
Elements	-	2,498

As illustrated in Figure 2, the geometry data of HEC-RAS was established with a total of 22 cross sections over the entire study reach, and the finite element mesh of FESWMS was organized with a total of 9,110 nodes and a total of 2,498 elements over the whole study section. Figure 3 shows the finite element mesh made over the study section.

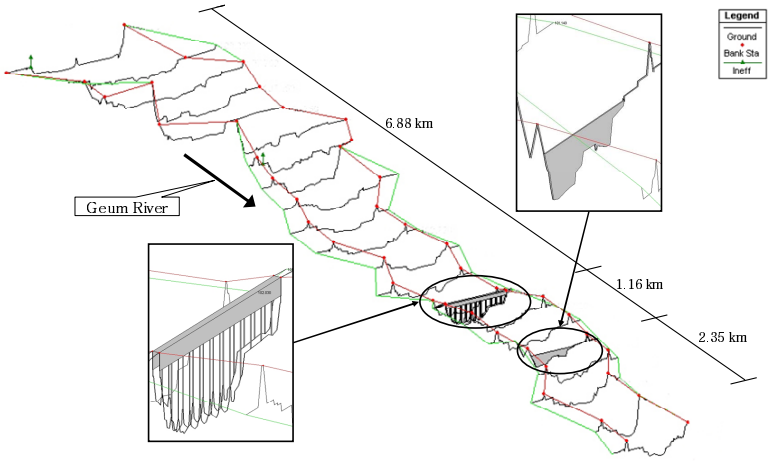

Figure 2. Cross section of the study reach (HEC-RAS model).

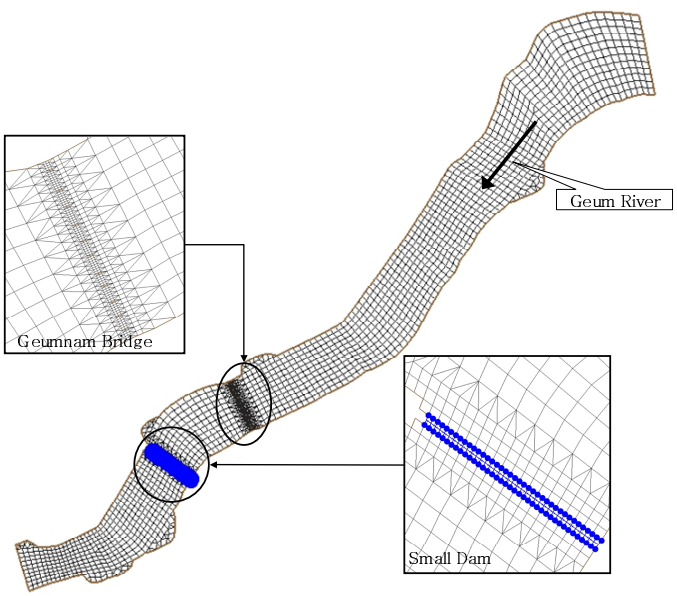

Figure 3. Finite element mesh of the study reach (FESWMS model).

Results and Discussion

Reviewing the Applicability of Models

Since actual water level measured for a 200-year frequency flood is not available, the calculated and measured value cannot be verified. Therefore, the calculated flood water level of the one-dimensional model was compared with that of the two-dimensional model to review the applicability of the models. Consequently, as shown in Table 4, the difference was -0.18m to 0.07m in CASE 1. The percentage of the difference ranged from -0.72% to +0.29%. In CASE 7, a difference ranging from -0.27m to 0.21m was obtained giving a percentage difference from -1.06% to +0.88%. The percentage of difference was observed to be highest in CASE 7. This

indicated that the higher the installation height of the dam, the greater the difference between the calculated values. However, the percentages of the differences were within the range of ±2% in both CASE 1 and CASE 7. Overall, the calculated flood water levels of HEC-RAS and FESWMS were close. The deviation between the calculated values maybe accounted to the difference in parameter and geometry data used for the one-dimensional and two-dimensional model.

Table 4. Flood water level for HEC-RAS and FESWMS model.

Distance from downstream (km)	CASE 1(EL. m)		Difference (%) [(A-B)/A]x100	CASE 7(EL. m)		Difference (%) [(A-B)/A]x100
	HEC-RAS (A)	FESWMS (B)		HEC-RAS (A)	FESWMS (B)	
10.39	25.13	25.27	-0.55	25.55	25.77	-0.85
9.84	25.10	25.22	-0.47	25.53	25.73	-0.77
9.34	25.09	25.21	-0.47	25.52	25.72	-0.78
8.89	25.06	25.20	-0.54	25.49	25.71	-0.85
8.39	24.97	25.12	-0.59	25.41	25.64	-0.90
7.87	24.83	25.01	-0.72	25.29	25.55	-1.03
7.39	24.80	24.97	-0.68	25.25	25.52	-1.06
6.89	24.74	24.87	-0.52	25.20	25.43	-0.91
6.38	24.69	24.81	-0.50	25.16	25.39	-0.90
5.87	24.65	24.77	-0.48	25.12	25.35	-0.91
5.36	24.63	24.76	-0.51	25.11	25.34	-0.92
4.80	24.53	24.65	-0.48	25.02	25.25	-0.90
4.25	24.51	24.64	-0.52	25.00	25.24	-0.96
3.67	24.37	24.52	-0.60	24.88	25.14	-1.03
3.52*	24.34	24.30	+0.16	24.86	24.92	-0.24
3.26	24.34	24.36	-0.08	24.85	25.00	-0.60
2.78	24.31	24.32	-0.02	24.83	24.95	-0.49
2.35**	24.21	24.24	-0.14	24.74	24.81	-0.28
1.92	24.18	24.15	+0.11	24.18	23.97	+0.88
1.37	24.15	24.12	+0.11	24.15	24.17	-0.08
0.57	23.85	23.78	+0.28	23.85	23.78	+0.30
0	23.84	23.77	+0.29	23.84	23.77	+0.29

* Geumnam Bridge cross section
** Small Dam cross section

Results of HEC-RAS model

The developed one-dimensional HEC-RAS model implies that as the installation height of small dam increases, upstream flood water level also increases. Consequently, downstream flood water level for each case was the same. Calculated flood water level of CASES 1 until 5 did not exceed the designed flood water level, suggesting that small dam installation height of these cases are safe from overflowing. On the other hand, calculated water levels for CASES 6 and 7 exceeded the designed flood water level. Therefore, these two cases indicate possibility of water overflowing the small dam. With regards to the flow rate, results indicate that

as the installation height of the small dam increases, the upstream flow rate decreases. Additionally, downstream flow rate for all cases were the same. Figure 4 provides the comparison of flood water levels in each scenario of the one-dimensional HEC-RAS while the comparison of the flow rates is given by Figure 5.

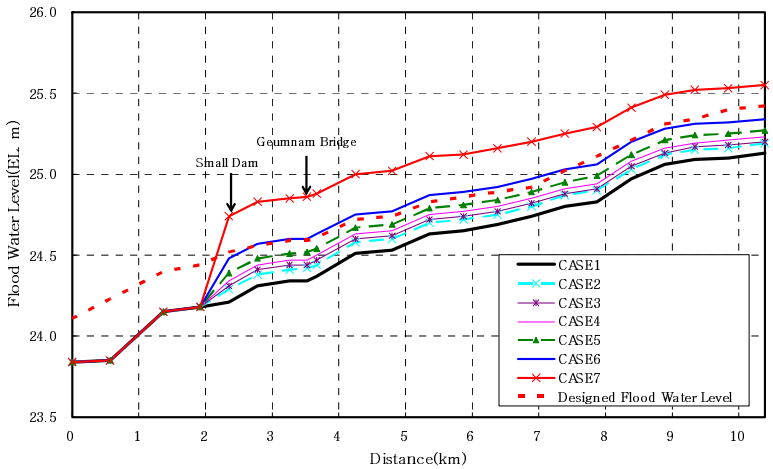

Figure 4. Flood water level for each scenario (HEC-RAS model).

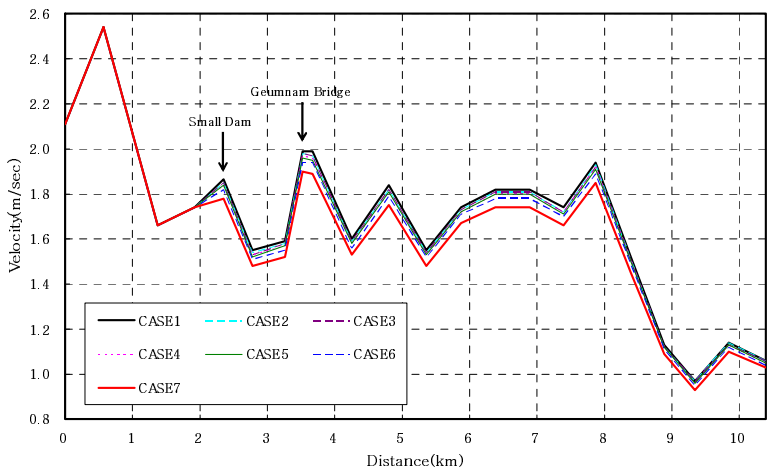

Figure 5. Velocity for each scenario (HEC-RAS model).

Results of FESWMS model

Simulation of the two-dimensional FESWMS model showed that the higher the installation height of the small dam, the higher the upstream flood water level. Downstream flood water levels, on the other hand, have small converging changes. After the convergence, the flood water level remained the same. Calculated flood water levels for CASES 1 to 3 did not exceed the designed flood water level, indicating that these small dams will not overflow. While results of CASE 4 until CASE 7 were higher than the designed flood water level. Thus, allowing water to

overflow during flood. Immediately downstream of the small dam, it can be observed that as the small dam installation height increases, the flood water level decreases. This can be due to the increase in flow rate as the dam is overflown with water.

Considering the flow rates, it is evident that as the installation height of the small dam increases, the upstream flow rate decreases. Moreover, a converging flow rate from the immediate downstream of the small dam is obtained. Consequently, after the convergence, flow rate is almost the same for all cases. Immediately downstream of the small dam, results implies that the higher the installation height of the small dam, the higher the flow rate. The reason for this was that severe flow disturbance occurred downstream due to a larger dam. Figure 6 shows the comparison of flood water levels in each scenario of the two-dimensional FESWMS whereas Figure 7 illustrates the comparison of flow rates.

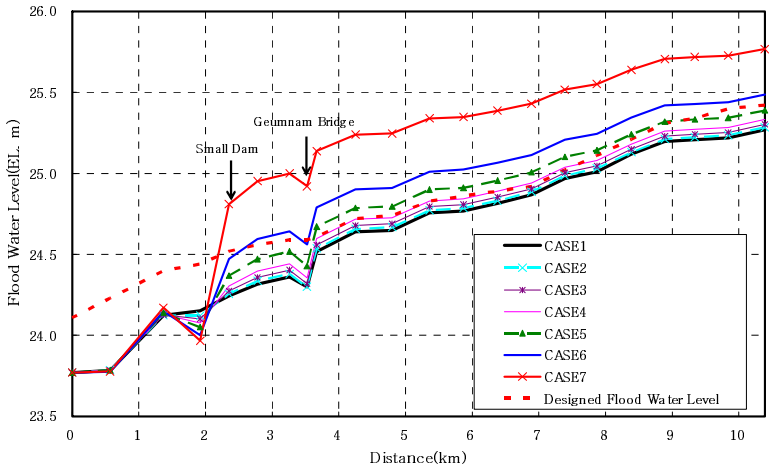

Figure 6. Flood water level for each scenario (FESWMS model).

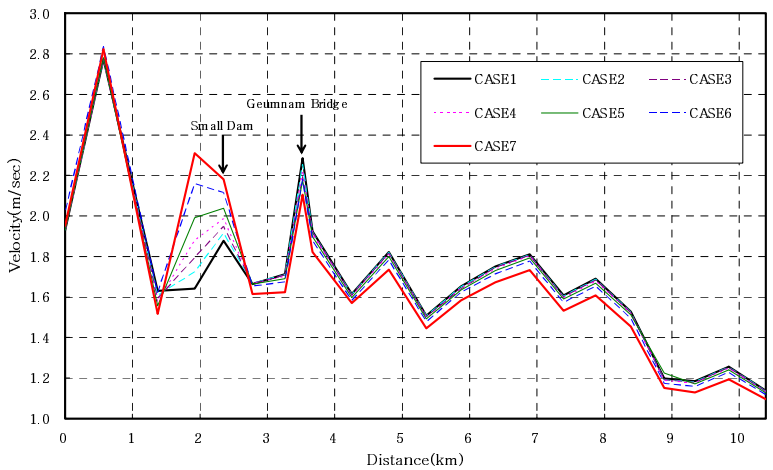

Figure 7. Velocity for each scenario (FESWMS model).

In this research, changes in the flow of the two-dimensional FESWMS in each scenario were analyzed for the section of Geumnam Bridge, where a hydraulic structure existed, and that of the small dam. As for the bridge section, high velocity occurred in between the piers of the bridge. The reason for this was considered to be the decrease in the cross sectional area of flow due to the piers. Figure 8 presents the velocity vector at the section of Geumnam Bridge.

As for changes in flow at the small dam section, results suggest that the small dam installation height is inversely proportional to the upstream flow rate. Downstream, flow rate increased and flow disturbance occurred. In this section also, there was a change in river width located at the bend. The flow rate of the main channel was very different from that of both banks. Specifically, that of the right bank downstream from the small dam, where water flowed backwards. Figure 9 presents the velocity vector for the section of the small dam.

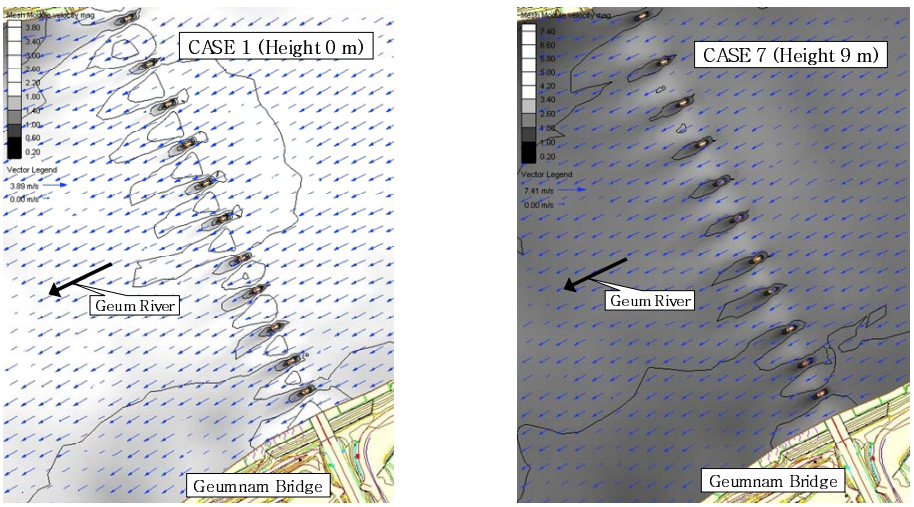

(a) CASE 1 (b) CASE 7

Figure 8. Velocity vector for Geumnam Bridge cross section.

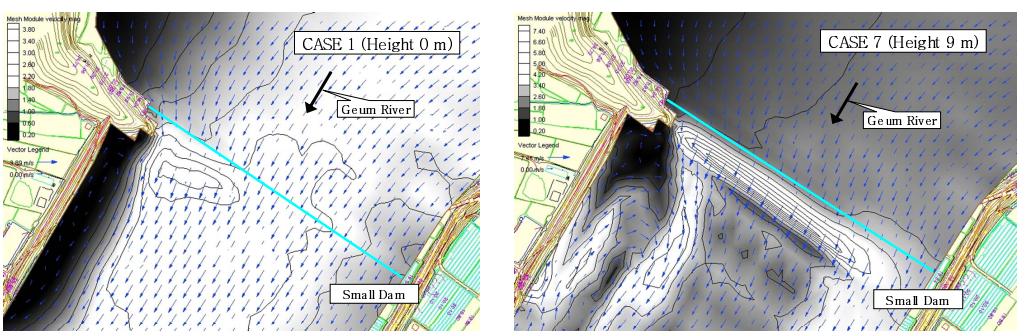

(a) CASE 1 (b) CASE 7

Figure 9. Velocity vector for Small Dam cross section.

Conclusions

In this paper, changes in the characteristics of hydraulic flow on rivers depending on the installation of small dams were analyzed in order to propose the size of a small dam, which was safe from overflowing. As a result of performing hydraulic analysis for each scenario using the one-dimensional and two-dimensional models, the conclusions below were established:

(1) One-dimensional hydraulic analysis results considering the installation of small dams suggested that the designed flood water level was not exceeded in the cases that the small dam is 0m to 7m high. When the height of the small dam was 8m or higher, water will overflow.
(2) Two-dimensional hydraulic analysis results considering on the installation of small dams indicated that the small dams were safe from overflowing with the condition that installation height is between 0m to 5m high. When the height of the small dam was 6m or higher, the small dam will overflow.

Based on the results of one-dimensional and two-dimensional hydraulic analyses, it is concluded that it is appropriate to design the height of small dams at 5m or less in order to be safe from overflowing.

The size of small dam safe from overflowing was proposed by performing hydraulic analysis for rivers contingent upon the installation of small dams. They are expected to be used for determining the sizes of small dams in the future. In addition, validity in terms of water utilization and environment, research shall be reviewed and research shall be made in order to review the effects of small dams.

References

Duan, J.G. and Nanda, S.K. (2006). "Two-dimensional depth-averaged model simulation of suspended sediment concentration distribution in a groyne field". Journal of Hydrology. Vol. 327. pp. 426-437.

Environmental Modeling Research Laboratory(EMRL). (2000). "SMS(SurfaceWater Modeling System) User's Manual". Brigham Young University.

Knight, D.W. and Shiono, K. (1996). River channel and floodplain hydraulics. In: Anderson, M.G., Walling, D.E., Bates, P.D.(Eds), Floodplain Processes. Wiley, Chichester.

Korea Land Corporation(KOLAND). (2007). "Riverbed Change Investigation for the Geum River and Miho Stream of Multifunctional Administrative City". KOLAND.

Ministry of Land, Transport and Maritime Affairs(MLTM). (2002). "Geum River basin management plans". MLTM, DRCMO.

US Army Corps of Engineers(USACE). (2002). HEC-RAS River Analysis System: Hydraulic Reference Manual. US Army Corps of Engineers Hydrologic Engineering Center. Davis, CA.

An Efficient Solution for Water Supply Networks

S. Engin Mendi
University of Arkansas at Little Rock
Department of Computer Science
2801 South University Ave.
Little Rock, AR, 72204
esmendi@ualr.edu

ABSTRACT

In a computer implementation, a water network model is represented by a set of network data (values of parameters) and a set of equations (physical operation of the model). The fundamental model is formulated using the laws of physics. Subsequently, different models can be derived by mathematical manipulation. For water network models three physical laws are employed: flow continuity, head-loss continuity and component equations (head/flow law).

Industry and academia have made a significant investment in the research and development of computer algorithms for the design, modelling and control of water supply networks. The industrial use of many of these algorithms is commonplace and they are complex procedures used to solve systems of equations. Therefore, powerful numerical algorithms used to solve the model equations are crucial in terms of their computational complexity i.e. requirement of average number of iterations for finding a solution with a required accuracy.

Along with physically simplified networks representing certain aspects of reality, neglecting other aspects with a smaller number of components than the original network, effective solution methods for water supply networks become common practice. To do this, first we must form a mathematical model representing the physical system; second, we need to set up an efficient solution implementation which is specific to the equation systems and finally we must visaliuze and post-process the results.

Keywords

Water Supply Networks, Water Distribution Networks, Conjugate Gradient Method

1. INTRODUCTION

A water supply network [6] is a system of engineered hydrologic and hydraulic components, including a raw (untreated) water reservoir (above or below ground) where the water gathers, such as a lake, a river, or groundwater from an underground aquifer; transmission from treatment, through pipes to treated water storage, that may be either elevated or ground level; and distribution through piping/watermains from storage to consumption (at houses, fire hydrants, industrial use points, etc). Figure 1 [2] illustrates an example model of network supplying water to more than 76,000 inhabitants. A conceptual model of a water network can be presented as an input-output system with input and output variables, demand, initial conditions and a mathematical model as shown in Figure 2 [1]. Input variables are source inflows, source heads and initial reservoir levels, output variables are flows in pipes and heads and demands are node outflows representing water consumption. Initial con-



Figure 1: Example model of water supply network

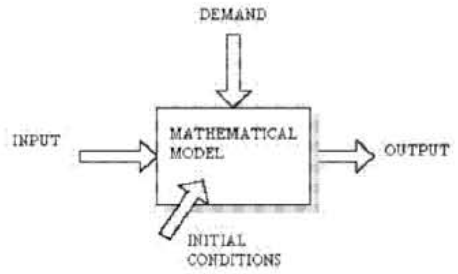

Figure 2: Input-output model (conceptual model) of a water network

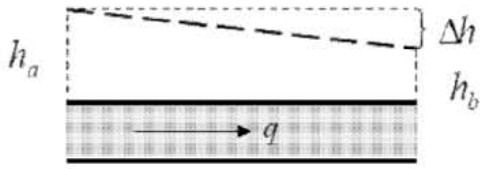

Figure 3: Example of a single tube

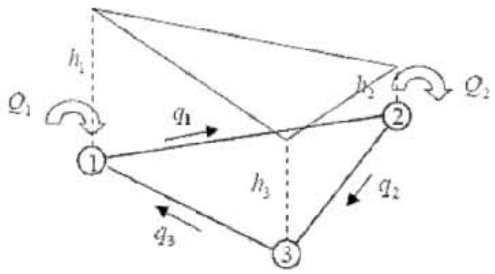

Figure 4: Example of a 3 tube with 3 node

ditions comprise the initial reservoir levels, and finally water network mathematical model is the set of mathematical equations modelling the behaviour of the physical system.

2. ANALYSIS OF THE PHYSICAL PROBLEM

We present the underlying physical problem that can be demonstrated in the example of a single tube, which is flown through by a fluid as shown in Figure 3 [3]. The loss of hydraulic head Δh in the tube depends on the velocity v of the flow:

$$\Delta h = \lambda \frac{l}{d} \frac{v^2}{2g}$$

where l is the length of the tube, d the diameter and $g = 9.81 m/s^2$ the acceleration due to gravity. The factor λ describes the roughness of the tube material, and can be assumed for *laminar* flow as:

$$\lambda = \frac{64}{Re}, \quad Re = \frac{v.d}{\nu} = \frac{v.d}{1.10^{-6}}$$

With $v = \frac{q}{A} = \frac{4.q}{d^2\pi}$ we get:

$$\Rightarrow \quad q = \frac{\pi.g.d^4}{128.\nu.l} \Delta h_i = \frac{\pi.g.d^4}{128.\nu.l} (h_a - h_b)$$

$\frac{\pi.g.d^4}{128.\nu.l}$ is B the permeability of the tube. Finally we get a linear relation between the flow and the difference in hydraulic head:

$$q = B.(h_a - h_b)$$

To demonstrate the procedure calculating the flow distribution in a pipe network, an example with 3 nodes and 3 tubes is shown below Figure 4 [3]: The system must fulfill the constraint that the sum of inflow and outflow has to be 0 in every node:

$$\begin{aligned} q_1 - q_3 - Q_1 &= B_1.(h_1 - h_2) - B_3.(h_3 - h_1) - Q_1 = 0 \\ -q_1 + q_2 + Q_2 &= -B_1.(h_1 - h_2) + B_2.(h_2 - h_3) + Q_2 = 0 \\ -q_2 + q_3 &= -B_2.(h_2 - h_3) + B_3.(h_3 - h_1) = 0 \end{aligned}$$

This leads to a linear equation system:

$$\underline{\underline{B}}\ \underline{h} + \underline{Q} = \underline{0}$$

$$\begin{bmatrix} B_1 + B_3 & -B_1 & -B_3 \\ -B_1 & B_1 + B_2 & -B_2 \\ -B_3 & -B_2 & B_2 + B_3 \end{bmatrix} \begin{bmatrix} h_1 \\ h_2 \\ h_3 \end{bmatrix} + \begin{bmatrix} -Q_1 \\ +Q_2 \\ 0 \end{bmatrix} = \begin{bmatrix} 0 \\ 0 \\ 0 \end{bmatrix}$$

where $\underline{\underline{B}}$ is the global permeability matrix, and $\underline{Q}$ denotes the flow vector. The equation system shown here is singular, i.e. it has no unique solution. This is due to the fact that all formulas are based on the difference in hydraulic head between two nodes, but an absolute height of the system is not specified. Therefore, we have to include such a boundary condition by defining the absolute height of one node (e.g. height of first node $h_1 = 0$). This can be enforced, for example, by setting the off-diagonal entries $B_{1,i}$ and $B_{i,1}$ of the coefficient matrix and the entry Q_1 of the right hand side vector to 0, while setting the diagonal entry $B_{1,1}$ to 1.

3. REQUIREMENT SPECIFICATIONS

3.1 Functional Requirements

To understand the needs of the project, assess feasibility, prevent ambiguity, and reach a valid project, the most important actions to be taken are determination and engineering of the requirements. The most important issues we considered during requirement specifications are:

- To make requirements consistent with the objective of the project.
- To specify requirements at proper level of abstraction.
- To state bounded and unambiguous requirements.
- To prevent conflicting requirements.
- To state technically achievable requirements.

3.1.1 *General Requirements*

The software application calculates the flows in the tubes of a network. The pipe network consists of nodes and tubes between the nodes.

- A node is defined by its coordinates x, y and a flow Q (inflow: $Q<0$; outflow: $Q>0$).
- A tube with diameter d lies between two nodes a, b.

The application should be with the following functionality:

- All input data for the nodes and the tubes is to be read from an ASCII file.
- The resulting fluxes shall be computed.

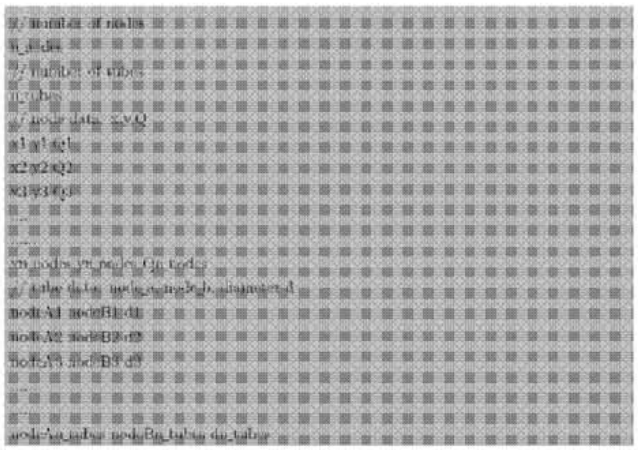

Figure 5: Example of an input file

- Output the results either on screen or in an output file.

The input file containing the network data is divided into three parts:

- The number of nodes and tubes has to be specified.
- The nodes are given with the x-coordinate, the y-coordinate and the amount of inflow/outflow.
- The tubes are given with the start node, the end node and the diameter.

The input file has to be saved as a simple text file. The input file will look like below shown in Figure 5:

3.2 Non-Functional Requirements

3.2.1 Usability

In developing our application, some of the most important issues to be considered are making the user easily adapt the application and learn the application. Considering these aspects, we plan to design the application as simple as possible. The controls will be simple, adjustable and enough for the actions to be taken.

3.2.2 Reliability

The application should be as bug free as possible. All components should work synchronously, so that, any error or problem caused by one of the components should not block other componentsŠ workflow.

3.2.3 Portability

Our application will work on different platforms, such as: Linux and Windows.

3.3 Software Requirements

Our application will work on different operating systems, such as: Windows XP or Linux operating systems.

3.4 Hardware Requirements

Our application will work on a PC having at least Pentium 4 class CPU.

4. DESIGN

4.1 High-Level Design

4.1.1 Class Structure

We present the input data that shall be saved in a class structure given figure below:

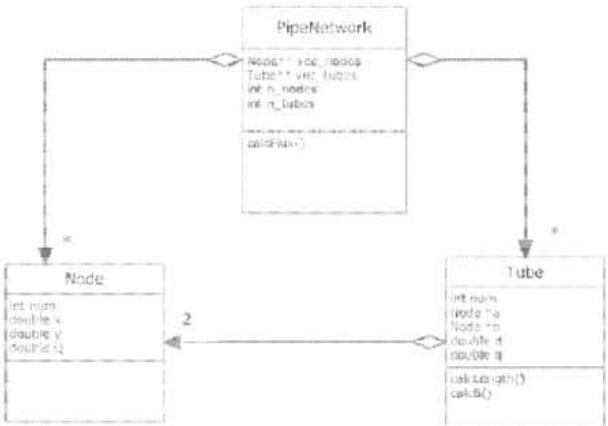

Figure 6: Class Structure

4.1.2 Class Descriptions

The descriptions of the classes are given below:

Node

Usage:

```
Node (int i, double x, double y, double Q):
Creates node i with discharge Q on coordinates
(x, y).
```

Parameters:

```
i:  Index of the node.
x:  X coordinate of the node.
y:  Y coordinate of the node.
Q:  Discharge of the node.
```

Tube

Usage:

```
Tube (int i, node* a, node* b, double q):
Creates tube i with discharge q with a and b nodes.
```

Parameters:

```
i:  Index of the tube.
a:  Start node of the tube.
b:  End node of the tube.
q:  Discharge flowing in the tube.
```

Methods:

```
calcLength():  Calculates the length of the tube.
calcB(double l):  Calculates the permeability of the
tube with length l.
```

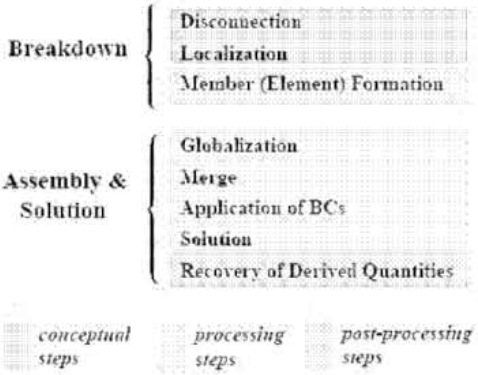

Figure 7: Implementation Steps

PipeNetwork

Usage:
```
PipeNetwork(const char* filename):
Reads the input file.
```

Parameters:
```
filename:  The name of the input file.
```

Methods:
```
calcFlux():  Calculates the flux in each tube.
```

Variables:
```
vec_nodes:  Pointer array which stores the node
information created by Node.
vec_tubes:  Pointer array which stores the tube
information created by Tube.
n_nodes:  Number of nodes.
n_tubes:  Number of tubes.
```

4.2 Low-Level Design

4.2.1 Implementation

The implementation steps of the software, major and minor, are summarized in Figure 7. The two major processing steps are **Breakdown**, followed by **Assembly & Solution**. The first 3 substeps are: *a*) disconnection, *b*) localization and *c*) computation of tube permeability equations. Collectively these form the *breakdown*. The first two are flagged as *conceptual* in Figure 7 because they are not actually programmed as such: they are implicitly carried out through the user-provided problem definition. Processing actually begins at the tube permeability equation forming substep.To carry out the first breakdown step we proceed to *disconnect* or *disassemble* the system into its components in order to effectively deal with a local tube.The first substep in the assembly & solution major step, as shown in Figure 7, is *globalization*. This operation is done tube by tube. It refers the tube permeability equations to the global system so it can be merged into the global permeability. The globalized tube permeability matrices for the network can now be obtained by inserting appropriate local permeability factors and inserting the boundary conditions.

4.2.2 Functional Algorithm

In the following algorithm a framework of the function, which calculates the flux distribution is shown:

PipeNetwork::calcFlux():

- `create the permeability matrix B(n_nodes)`
- ∀ `tubes i:`
  - `get the bounding node numbers n_a, n_b`
  - `calculate the local permeability factor B_i`
  - `assemble B_i to the global permeability matrix:`
    - ◇ `B(n_a,n_a) += B_i ; B(n_b,n_b) += B_i`
    - ◇ `B(n_a,n_a) -= B_i ; B(n_b,n_b) -= B_i`
- `create the flux vector Q(n_nodes)`
- ∀ `nodes i:`
  - `Q(i) += Q_in(i)`
- `insert the boundary condition h(1)=0.0, for (i=2,...,n_nodes):`
  - `set B(i,1) = B(1,i) = 0.0`
  - `set Q(1) = 0.0`
  - `set B(1,1) = 1.0`
- `solve the linear equation system`
- `postprocessing: calculate the flux in every tube,` ∀ `tubes i:`
  - `q_i = B_i*(h_node_a - h_node_b)`

4.2.3 Solution

Because memory efficiency and time consumption are important factors for solving large systems of linear equations, we present the conjugate gradient method (CG) which is an effective method for symmetric positive definite systems. CG is an iterative method minimizing quadratic form of the equation system $Ax = B$.

$$Ax + b = 0, \quad a \in R^{n,n}, \quad \textit{symmetric and positive definite}$$

$$Q(x) := \frac{1}{2} x^T Ax + b^T x \ \rightarrow Min$$

where Q is quadrative form, $\underline{\underline{A}}$ is a matrix and $\underline{x}$ and $\underline{b}$ are vectors. The method [4] proceeds by generating:

- vector sequences of iterates (i.e., successive approximations to the solution),
- residuals corresponding to the iterates, and
- search directions used in updating the iterates and residuals.

Although the length of these sequences can become large, only a small number of vectors needs to be kept in memory. In every iteration of the method, two inner products

are performed in order to compute update scalars that are defined to make the sequences satisfy certain orthogonality conditions. On a symmetric positive definite linear system these conditions imply that the distance to the true solution is minimized in some norm. The iterates $x^{(i)}$ are updated in each iteration by a multiple a_i of the search direction vector $p^{(i)}$:

$$x^{(i)} = x^{(i-1)} + a_i p^{(i)}$$

Correspondingly the residuals $r^{(i)} = b - Ax^{(i)}$ are updated as:

$$r^{(i)} = r^{(i-1)} + a_i q^{(i)}$$

where $q^{(i)} = Ap^{(i)}$. The choice $a_i = \frac{r^{(i-1)^T} r^{(i-1)}}{p^{(i)^T} Ap^{(i)}}$ minimizes $r^{(i)^T} A^{-1} r^{(i)}$ over all possible choices for a. The search directions are updated using the residuals:

$$p^{(i)} = r^{(i)} + \beta_{(i-1)} p^{(i-1)}$$

where the choice $\beta_i = \frac{r^{(i)^T} r^{(i)}}{r^{(i-1)^T} r^{(i-1)}}$ ensures that $p^{(i)}$ and $Ap^{(i-1)}$ (or equivalently $r^{(i)}$ and $r^{(i-1)}$) are orthogonal. In fact, one can show that this choice of $\beta^{(i)}$ makes $p^{(i)}$ and $r^{(i)}$ orthogonal to all previous $Ap^{(j)}$ and $r^{(j)}$ respectively. In the CG, two coupled two-term recurrences are used; one that updates residuals using a search direction vector, and one updating the search direction with a newly computed residual. This makes the CG quite attractive computationally.

Accurate predictions of the convergence of iterative methods are difficult to make, but useful bounds can often be obtained.

The method involves one matrix-vector product, three vector updates, and two inner products per iteration. Some slight computational variants exist that have the same structure. [5] The steps of CG can be summarized as in Figure 8: The pseudocode for the preconditioned conjugate gradient method is given below. It uses a preconditioner M. For $M = 1$, one obtains the unpreconditioned version of the conjugate gradient algorithm. In that case, the algorithm may be further simplified by skipping the "*solve*" line and replacing $z^{(i-1)}$ by $r^{(i-1)}$ and $z^{(0)}$ by $r^{(0)}$.

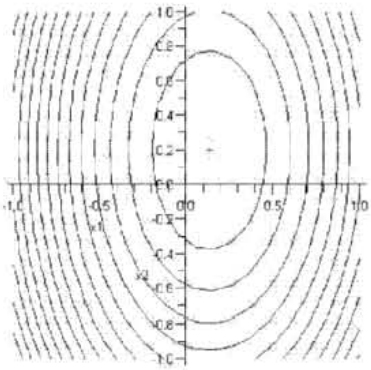

Figure 9: Contours of the quadratic form

Pseudocode:

Compute $r^{(0)} = b - Ax^{(0)}$ for some initial guess $x^{(0)}$
for i = 1, 2, ... do
Solve $Mz^{(i-1)} = r^{(i-1)}$ $\rho^{(i-1)} = r^{(i)^T} z^{(i-1)}$
if $i = 1$ then
$p^{(i)} = z^{(0)}$
else
$\beta_{(i-1)} = \frac{\rho_{(i-1)}}{\rho_{(i-2)}}$
$p^{i} = z^{(i-1)} + \beta_{(i-1)} p^{(i-1)}$
end if
$q^{(i)} = Ap^{(i)}$
$a_i = \frac{\rho_{(i-1)}}{r^{(i)^T} q^{(i)}}$
$x^{(i)} = x^{(i-1)} + a_{(i)} p^{(i)}$
$r^{(i)} = r^{(i-1)} + a_{(i)} q^{(i)}$
Compute convergence; continue if necessary.
end for

Figure 9 and Figure 10 are contours of the quadratic form that each ellipsoidal curve has constant *Q(x)* and graph of the quadratic form *Q(x)* that the minimum point of this surface is the solution to $Ax = B$, respectively, for a simple problem where $\underline{\underline{A}} = \begin{bmatrix} 3 & 0 \\ 0 & 1 \end{bmatrix}$, $\underline{b} = \begin{bmatrix} -0.4 \\ -0.2 \end{bmatrix}$. For this case x will be $\underline{x} = \begin{bmatrix} -0.133333 \\ 0.2 \end{bmatrix}$ Gradient iteration for convergence to the solution and error analysis will respectively be as given in the Figure 11 and Figure 12 for the same simple problem.

5. NUMERICAL EXAMPLE

In this section, a numerical example is presented in order to demonstrate the properties of the proposed project. The main point of this example is to investigate the procedure presented in this report. The topology of example network is depicted in Figure 13. The example has 9 nodes and 12 tubes with inflow at the nodes 1, 3 and 7 and outflow at the node 9 (minus sign designates the inflow and plus sign designates the outflow). All tubes have the same diameter of 0.5m. For the given example model the input file will look like in Figure 14. The solution of this model which calculates the flows in each tube of the network is depicted in Figure 15 (minus sign in the results shows that the flow direction must

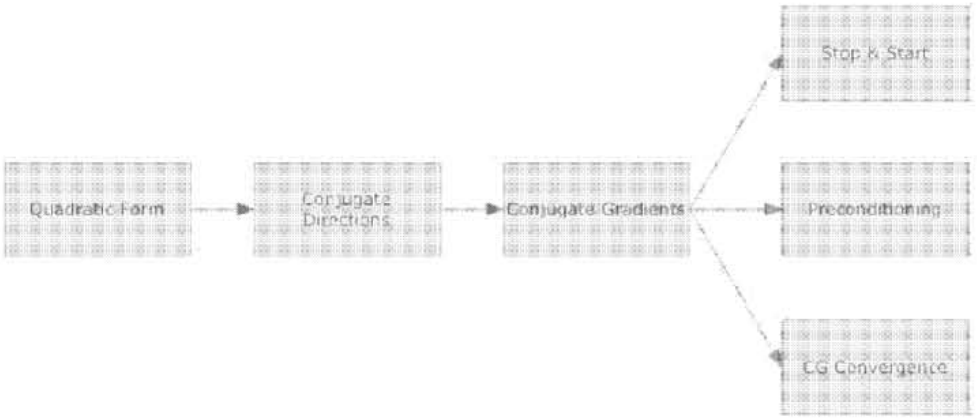

Figure 8: CG Steps

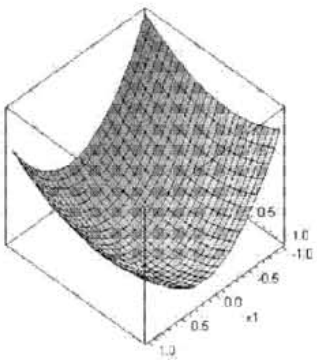

Figure 10: Graph of the quadratic form

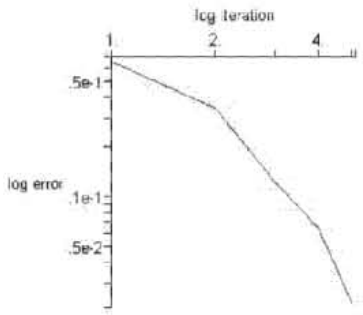

Figure 12: Graph of errors

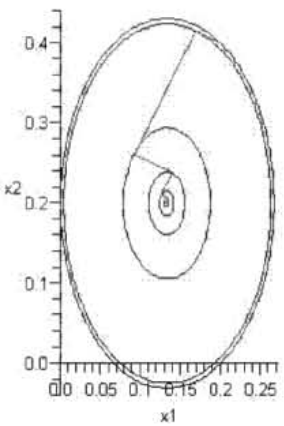

Figure 11: Graph of iterations

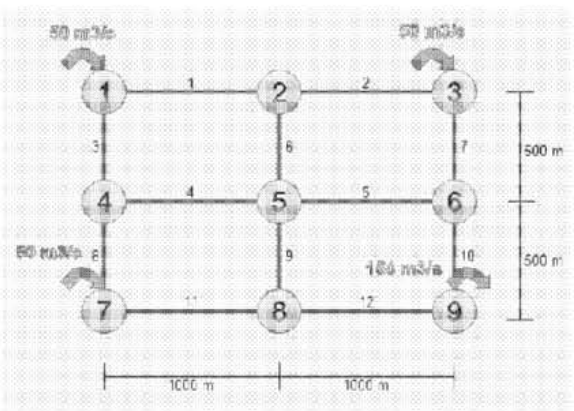

Figure 13: Simplified model of example network

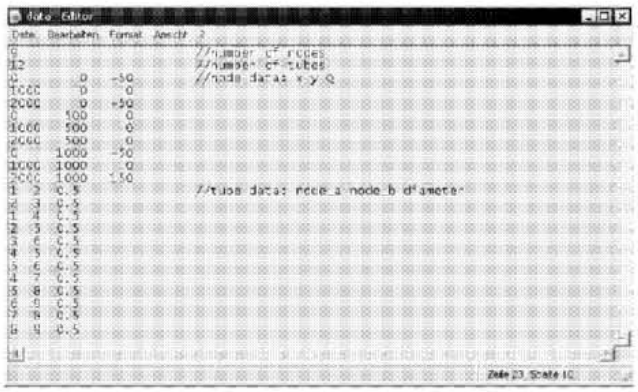

Figure 14: Input file

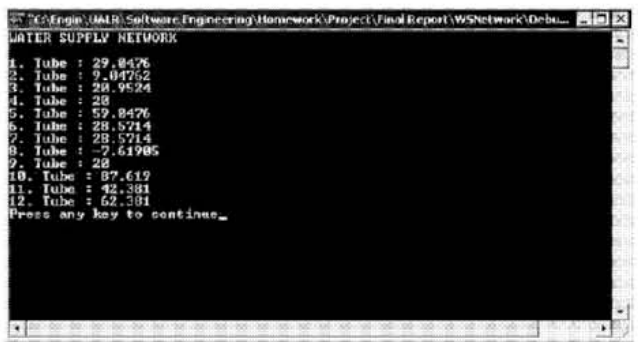

Figure 15: Output results

be opposite of the initial assumed direction. For instance, for the 8th tube, at first, flow direction is considered from node 4 to node 7 in the input file. But as a result it must be the opposite, from node 7 to node 4).

6. CONCLUSION

Type of mathematical model, numerical algorithms used to solve the model equations, initial conditions, computational complexity, form of solution and post-processing requirements for analysing the results can be counted as evaluation criterias for the solution of water supply networks. Additionally, factoring of sparce matrices may be impossible due to limited memory, and will be time-consuming as well; even the backsolving step (like in Gauss Elimination) may be slower than iterative solution. On the other hand, CG is very memory-efficient and run quickly with sparse matrices. Therefore, we present a solution for water networks, meeting all these requirements above.

7. REFERENCES

[1] J. H. Andersen and R. S. Powell. Simulation of water networks containing controlling elements. Journal of Water Resources Planning & Management, 125:162–169, 2003.

[2] P. L. M. Bounds, K. Ulanicka, B. Ulanicki, B. Dacre, and G. Cummings. Optimal scheduling of south-staffordshire water supply system using the finesse package. In Advances in Water Supply Management, 2003.

[3] M. C. Potter, D. C. Wiggert, and M. Hondzo. Mechanics of Fluids. Prentice Hall, 1999.

[4] W. H. Press and S. A. Teukolsky, editors. Numerical Recipes in C++: The Art of Scientific Computing. Cambridge University Press, 2002.

[5] J. R. Shewchuk. An introduction to the conjugate gradient method without the agonizing pain. Technical report, School of Computer Science, Carnegie Mellon University, 1994.

[6] K. Ulanicka, B. Ulanicki, J. P. Rance, B. Coulbeck, R. Powell, and C. Wang. Benchmarks for water networks modelling. In Advances in Water Supply Management, 1998.

Comparison of Mean Flow and Turbulence around Experimental Spur Dike

Jennifer G. Duan[1] and Li He[2]

ABSTRACT

An acoustic Doppler velocimeter was used to measure flow and turbulence around an experimental spur dike in a flat and a scoured bed. Differences of mean velocity, turbulent intensity and Reynolds stresses between these two flow fields were compared and analyzed. Upon the formation of scour hole, mean flow velocities in the downstream and lateral directions were reduced, but increased in the vertical direction. The turbulence intensities (*u'* and *v'*) are much larger, and the vertical component (*w'*) is smaller than that in the flat bed. Bed shear stresses determined from near-bed Reynolds stresses in the scoured bed were smaller than that in the flat bed. These results indicated that local scour has not only significantly reduced bed shear but also contributed to the increase of turbulence intensities in the scouring zone.

INTRODUCTION

Spur dikes are hydraulic engineering structures for preserving the desired water depth, deflecting the main current in the harbor channels and rivers, and protecting river banks. Flow field passing through a spur dike is characterized with the separation of approaching flow in three dimensions (3D) from upstream to the horse shoe vortex downstream of the dike. The complexity of flow field increases as the scour hole develops [9].

Local scour is caused by the erosive forces from flow turbulence acting on the erodible bed in the vicinity of an obstacle or structure placed in a stream, such as a spur dike, a bridge pier. Mean flow and turbulence properties are equally important for sediment entrainment, suspension, transportation, and deposition [4]. The scour mechanism involves two interactive elements, one is 3D unsteady flow field near the boundary, especially turbulent fluctuations and the resultant bed shear stresses; and the other is the morphology of sediment particles on bed surface [4]. The transport of sediment particles in turbulent flows depends on the interactions between the particles and the coherent turbulent structures [7]. Bey et al. [4] found turbulence fluctuations and mean flow features directly influence the scour process.

Mean bed shear stress or near-bed velocity were traditionally used for estimating the rate of sediment transport in well developed boundary layer flows [11]. For flows with developing boundary layers of sufficient non-uniform topography or roughness, sediment transport does not directly correlate to mean flow properties [11]. Researches found near-bed turbulence structure played a significant role in

[1] Assistant Professor, Department of Civil Engineering, University of Arizona, 1209 E. 2nd Street, Tucson, AZ 85721. Email: gduan@email.arizona.edu.

[2] Visiting Scholar, Department of Civil Engineering and Engineering Mechanics, University of Arizona, same address, also formerly, Ph.D. Candidate, State Key Lab of Hydroscience and Engineering, Department of Hydraulic Engineering, Tsinghua University, Beijing, P.R. China.

transporting sediment through a combination of micro-ADV, LDV, PIV and high-speed motion picture photography [11]. Recent measurements found that hydraulic forces acting on various sized sediment particles vary according to bed configurations. Measured turbulent flow field (e.g., turbulence intensities, Reynolds shear stresses) at various azimuthal planes around a 45° wing-wall and vertical-wall abutment concluded that the near-bed Reynolds stresses are more accurate for estimating sediment transport rate [8,9]. Sterk et al. found normal Reynolds stresses ($\rho\overline{u'^2}$ and $\rho\overline{w'^2}$) contributed more than the Reynolds stresses $-\rho\overline{u'w'}$ to sand transported by saltation in two-dimensional flows. Experiments of Nelson et al. [10] and Williams et al. [13] both showed that $-\rho\overline{u'w'}$ poorly correlates to sediment entrainment in turbulent boundary layers, however turbulent bursts by u' and w' components played a significant role in producing shear stresses. Normal stress $\rho\overline{u'^2}$ is a better predictor for the entrainment of coarse sand and gravels than $\rho\overline{w'^2}$ and $-\rho\overline{u'w'}$ in 2D flows because there was a strong positive correlation between the transport rate and near-bed instantaneous streamwise velocity [6,10]. The most effective events that move sediment are those with a large u'. Therefore, sediment flux can increase even when bed shear stress decreases [10] (Nelson et al., 1995). Applying concepts derived from steady uniform flow to non-uniform flows of developing boundary layer are problematic [9,10].

The present experimental study aims to quantify the differences of mean and turbulence flow field between a flat and scoured bed. Turbulent flow passing through an emergent spur dike on a flat and a scoured bed were measured, respectively, by using a SonTek 25-MHz MicroADV. Time histories of velocities in all three spatial dimensions were recorded at cross sections parallel to the dike. These measurements were used to study time-averaged, downstream primary flow and cross-sectional flow properties, as well as turbulence properties (e.g., turbulence intensities) at the upstream and downstream sections of the dike. Impacts of the dike on flow structure include flow convergence, locally increased bed-shear stress and increased turbulence in the vertical, which explains the initiation of local scour and sorting of sediment in the scour hole.

EXPERIMENTAL DATA

Experiment set-up

Experiments were conducted in a 12.8-m-long and 60.8-cm-wide flume located at the St. Anthony Falls Laboratory, University of Minnesota. A valve was used to control discharge. The channel sides are glass walls, and bed slope was 0.0004. Bed surface had a roughness height about 0.4 mm. A 20-cm-long, 4-mm-thick, and 40-cm-height metal plate was installed at 6m downstream of the flume inlet and protruded from the right hand side of the flume to serve as a model dike structure, and it emerged from the water surface during all experimental runs. Two experiments

were performed: firstly channel bed was fixed; secondly, bed surface was covered with a well-sorted sand and gravel mixture having a median grain diameter of 1.59 mm.

A downward looking microADV was used to measure instantaneous velocity field. MicroADV has been commonly used in measuring point-wise 3D velocity fields through recording the Doppler shift produced by targeted material in the flow. The acoustic sensor consisted of one transmitter and three receivers. The receivers are aligned to intersect with the transmit beam at a small sampling volume located about 50 mm from the probe tip. The sample volume is a cylinder of diameter 4.5 mm and height of 5.6 mm. The sampling frequency of the ADV was 25 Hz, with a sampling duration of 1-1.5 minutes in each measuring location. It can measure mean flow velocities from 1 mm/s to 2.5 m/s with an accuracy of $\pm 1\%$ of the measurement range. The microADV was attached to a point gauge fixed on an instrument carriage that was mounted on horizontal steel rails and moved on wheels. The ADV can move along the flume automatically driven by an electric motor, and also manually in the transverse and vertical directions to measure flow velocities at any location near the dike.

Nine cross sections shown in Fig. 1, including three upstream of the dike, one at the dike tip, and five downstream of the dike, were measured. Nine vertical profiles at intervals of 5 cm were measured at each cross section, and each vertical profile had 7–9 points with 1 cm spacing. At each measuring node, about 1,500 instantaneous velocities at three respective directions were recorded. Flow depth was measured at locations where velocity was measured with a laser profiler attached to the instrument carriage. These measurements of velocities and surface elevations were used to determine mean velocities, turbulence intensities, Reynolds stresses, and bed-shear stresses.

Data Processing

In the data analysis, the origin of the Cartesian coordinate is at the upstream side of the dike on the right wall of the initial bed surface elevation, thus the *x* axis is the downstream direction, *y* axis is pointing to the left bank in the transverse direction, and *z* axis is towards the water surface in the vertical. The *z*=0 plane was the flume bottom in the flat bed run, but the initial bed surface in the erodible bed run. The velocity components are denoted as u_j, v_j, and w_j, respectively.

The friction velocity of approaching flow was calculated by fitting the velocity profiles with the logarithmic law. Because of the effects of side wall the maximum mean-velocity $\bar{u}$ occurred slightly below the free surface, indicative of the dip phenomenon [2] when a rectangular channel had a low flow width to depth ratio ($B/H \le 5$) [2]. The shear velocity, u_*, and zero velocity level, z_0, were determined by assuming the von Karman constant is 0.41. Flow is hydraulically rough with $ks = 1.20\ mm$ in the flat-bed runs. Whereas in the erodible bed run, the shear velocity

was $u_* = 5.55\ cm/s$ and the roughness height was $ks = 1.59\ mm$, which was much greater than the thickness of viscous sublayer $\delta = 11.6\frac{\nu}{u_*} = 0.234\ mm$. Therefore, flow in the erodible bed runs was also hydraulically rough. The mean velocity of approaching flow is 59.43 cm/s.

At solid walls, all mean and turbulence velocities and Reynolds stresses are zero. Because of the complex turbulence flow near the dike, this study linearly interpolated these properties at each vertical line. The duration of the experimental run was 48 hours to allow the local scour reach an asymptotic state so that bed surface was completely armored. Contour lines of the scoured depth were shown in Fig.2 in which the zero contour line is the initial bed surface and also the edge of the scouring hole. The total scour volume was 0.0081 m^3. The maximum scour depth is 8.87cm at x=15.4cm, y=25cm.

RESULTS AND DISCUSSION

Mean Velocity

The contour lines of dimensionless time-averaged velocity components $\overline{u}$, $\overline{v}$ and $\overline{w}$ at different cross sections of the flat and scoured bed are shown in Fig.3 (a) and (b), respectively. The distributions of downstream component of mean velocity are similar, but the distributions of lateral and vertical components of mean velocities are very different. In both cases the maximum downstream mean velocity occurred slightly below the free surface [3]. This dip phenomenon is noticable because of the small flow aspect ratio in the present experiments [2]. The small channel aspect ratio together with the presence of free surface induces the secondary flow that dampens the vertical velocity fluctuations [2].

Flow separation begins at the dike tip in both runs, and shifts slightly towards the right bank, and then turns back to the left side wall as shown in Fig.4. The length of flow separation in the asymptotic state is about 3.5 times the dike length, much shorter than that for non-erodible flat bed. Flow reattached immediately at the end of the scour hole. The detached shear layer has nearly zero mean downstream velocity, and coincides with the thalweg of bed surface, especially at sections with $0.5<x/L<3.5$. One can find that the maximum scour depth developed along the path of the detached shear layer where the turbulence intensity is the maximum.

In the scoured bed, the mean velocity component, $\overline{u}$, at the contraction section is about 1.2 times as large as the mean velocity of approaching flow, while in the flat bed, the mean velocity at the contraction is about 1.3 times as that of the approaching flow. This shows that the streamwise component of mean velocity has been reduced after the scour hole is formed as observed by Thompson [12]. In the meantime, the

downstream component of mean velocity near the bed was increased in the primary flow zone and reduced in the recirculation zone where negative velocities (in blue color) as shown in Fig. 3(a). The increase in $\bar{u}$ and the extent of recirculation zone are much larger in the flat bed than that in the scoured bed. However, the mean velocity of recirculating flow is less than 10% of the approaching flow velocity.

The mean downstream velocity, $\bar{u}$, reaches its maximum at the dike section in the scoured bed. The streamwise velocity has been greatly reduced in the scoured zone. At the zone above the initial bed where $z/L>0.0$, the distribution of mean flow velocity is similar to that in the plane bed. Flow contracted at the dike section, and consequently the contour lines of $\bar{u}$ showed the existence of a pronounced skewness in the $\bar{u}$ component. This attributes to the effect of the horse shoe vortex and the associated helicoidal flow around the dike.

In both cases, the transverse component of mean velocity increases as flow approaches to the dike. At the dike section the transverse velocity in the primary flow reaches the maximum near the bed, and it is towards the left bank. The transverse velocity reverses its sign in the flow recirculation zone. The apparent difference in the distribution of $\bar{v}$ is that the maximum $\bar{v}$ in both the primary and the recirculation flows in the flat bed are larger than that in the scoured bed, which implies the reduction of flow intensity as the local scour forms.

The mean vertical velocity, $\bar{w}$, approximately is zero at regions upstream of the dike impacted zone. As flow approaches the dike, the negative values of $\bar{w}$ upstream of the dike corroborate the existence of a strong downward flow in the scoured bed, while the mean vertical flow is upward at the tip of the dike in the flat bed. This phenomenon showed that the helicoidal flow originated at the dike tip in the flat bed has shifted to the upstream after the scour hole was formed. The magnitude of $\bar{w}$ decreases as the helicoidal flow attenuates downstream of the dike. The mean vertical velocity is the maximum at approximately the middle of flow depth and decreases towards both the surface and the bed. At $x/L=5.0$, Fig. 3(a) showed a strong upward flow where hydraulic suction may take place that dislodges bed sediment downstream of the dike. Further downstream $\bar{w}$ diminishes rapidly.

In summary, after the scour hole is formed, the mean downstream velocity was reduced primarily due to the enlarged cross sections. On the other hand, the mean transverse velocity has increased near the bed surface in the scour hole, and the mean vertical velocity reverses its direction towards the flow surface in the scour hole. The

increases in the lateral and vertical mean flow indicated sediment entrainment and transport towards the left bank.

Turbulence Intensity

Reynolds decomposition into mean and fluctuating portions is commonly employed in analyzing turbulence velocity fields [1]. The contour lines of dimensionless turbulence intensities in 3D, symbolized as $\sqrt{\overline{u'^2}}/u_*$, $\sqrt{\overline{v'^2}}/u_*$, $\sqrt{\overline{w'^2}}/u_*$ at different cross sections were shown in Fig.4. In the flat bed, the turbulent intensities in three directions are nearly the same with a similar distribution. Turbulent intensities increase as the distance from the dike increases, while the largest turbulent intensity occurred at the center of each section.

After local scour reaches the asymptote state, the distributions of $\sqrt{\overline{v'^2}}$ and $\sqrt{\overline{w'^2}}$ are very similar to that of $\sqrt{\overline{u'^2}}$. The magnitude of $\sqrt{\overline{v'^2}}$ is larger than that of $\sqrt{\overline{u'^2}}$, and the magnitude of $\sqrt{\overline{w'^2}}$ is smaller than both. The magnitudes of $\sqrt{\overline{v'^2}}$ and $\sqrt{\overline{u'^2}}$ were increased at the dike tip in the scoured bed, but no noticeable increment was observed in the flat bed. At the contraction section, the turbulence intensities are the largest where $\sqrt{\overline{u'^2}}$ has nearly the same magnitude as U_0, while $\sqrt{\overline{v'^2}}$ is 1.65 times U_0. Downstream of the dike, the dimensionless $\sqrt{\overline{u'^2}}/u_*$ is larger than that in the flat bed. The increase of $\sqrt{\overline{v'^2}}$ in the local scour zone is not as apparent as that of $\sqrt{\overline{u'^2}}$. The turbulence intensity, $\sqrt{\overline{w'^2}}$, has increased in the area immediately above the bed upstream of the dike in the scour hole, while there is limited increase near the right-hand side wall in the flat bed. While downstream of the dike, $\sqrt{\overline{w'^2}}$ has increased in the primary flow zone, and reduced in the flow recirculation zone.

CONCLUSIONS

Mean flow and turbulence fields around a spur dike in a flat and scoured bed surface were compared and analyzed. As the scour hole forms, flow separation zone in the lee of the dike was shortened. The mean streamwise velocity has been reduced, but both the lateral and vertical mean velocities are increased. In the meantime the turbulent intensity $\sqrt{\overline{w'^2}}$ near the bed has increased so much that the Reynolds stress $-\rho\overline{u'w'}$ near the bed is less important than the corresponding

turbulent intensity. At the dike section, the transverse mean velocity $\bar{v}$ has also increased due to flow contraction, which is accompanied with a large increase of $\sqrt{\overline{v'^2}}$ and $\sqrt{\overline{u'^2}}$. Downstream of the dike in the primary flow zone, turbulent intensity $\sqrt{\overline{u'^2}}$ has increased more than that of $\sqrt{\overline{v'^2}}$, while the increase in $\sqrt{\overline{w'^2}}$ primarily resides in the recirculation zone.

ACKNOWLEDGEMENTS

The authors are grateful for research funding provided by the Visitor Program of the National Center of Earth Surface Dynamics (NCED) under NSF Award EAR-0120914 and NSF Award EAR-0532691 to the University of Arizona. Mr. Jeff Marr is the NCED Visitor Program Manager. This project is also in collaboration with the State Key Laboratory of Hydroscience and Engineering at Tsinghua Univ.

Reference

[1] Adrian, R. J., Christensen, K. T., and Liu, Z.-C. (2000). "Analysis and interpretation of instantaneous turbulent velocity fields." *Experiments in Fluids*, 29, 275-290.

[2] Balachandar, R., and Bhuiyan, F. (2007). "Higher-order momentums of velocity fluctuations in an open-chanenl flow with large bottom roughness." *J. Hydraul. Eng.*, 133(1), 77-87.

[3] Balachandar, R. and Patel, V. C. (2002). "Rough wall boundary layer on plates in open channels." *J. Hydraul. Eng.*, 128(10), 947-951.

[4] Bey, A., Faruque, M. A. A., and Balachandar, R. (2007). "Two-dimensional scour hole problem: Role of fluid structures." *J. Hydraul. Eng.*, 133(4), 414-430.

[5] Chrisohoides, A., Sotiropoulos, F., and Sturm, T. W. (2003). "Coherent structures in flat-bed abutment flow: computational fluid dynamics simulations and experiments." *J. Hydraul. Engrg.*, 129(3), 177-186.

[6] Clifford, N. J., McClatchey, J., and French, J. R. (1991). "Measurements of turbulence in the benthic boundary layer over a gravel bed and comparison between acoustic measurements and predictions of the bed-load transport of marine gravels." *Sedimentology*, 38, 161-171.

[7] Cuthbertson, A. J. S., and Ervine, D. A. (2005). "Experimental study of fine particle settling in turbulent open channel flows over rough porous beds." *J. Hydraul. Eng.*, 133(8), 905-916.

[8] Dey, S., and Barbhuiya, A. K. (2005). "Time variation of scour at abutments." *J. Hydraul. Eng.*, 131(1), 11-23.

[9] Dey, S., and Barbhuiya, A. K. (2006). "Velocity and turbulent in a scour hole at a vertical-wall abutment." *Flow Measurement and Instrumentation*, 17, 13-21.

[10] Duan, J., He, L., Wang, G. Q., and Fu, X. D. (Submitted). "Turbulent burst around experimental spur dike." *J. of Hydraul. Eng.*, 2008.

[11] Nelson, J. M., Shreve, R. L., Mclean, S. R., and Drake, T. G. (1995). "Role of near-bed turbulence structure in bed load transport and bed form mechanics." *Water Resource Res.*, 31(8), 2071-2086.

[12] Thompson, D. M. (2006). "The role of vortex shedding in the scour of pools." *Advances in Water Resources*, 29, 121-129.

[13] Williams, J. J., Thorne, P. D., and Heathershaw, A. D. (1989). "Comparisons between acoustic measurements and predictions of the bed-load transport of marine gravels." *Sedimentology*, 36, 973-979.

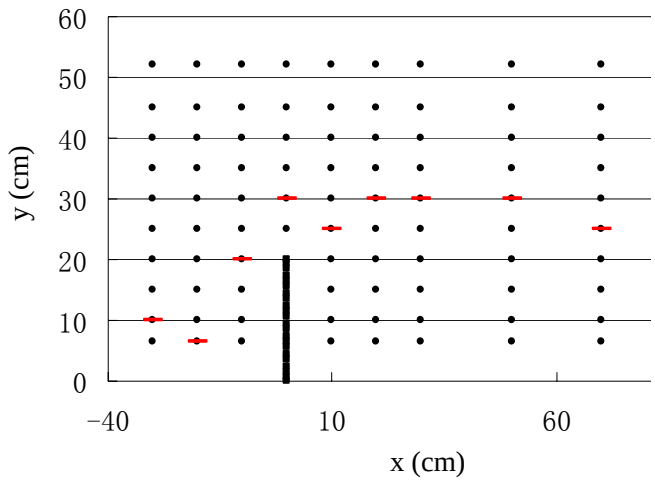

Fig. 1. Plan view of the experimental flume with measurement points denoted with solid dots, and red bars are the locations of thalweg at each cross section

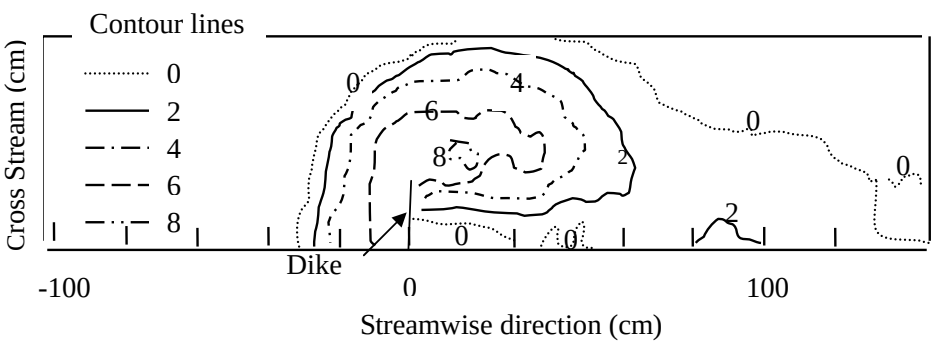

Fig. 2. Contour lines of bed elevation in the scour hole

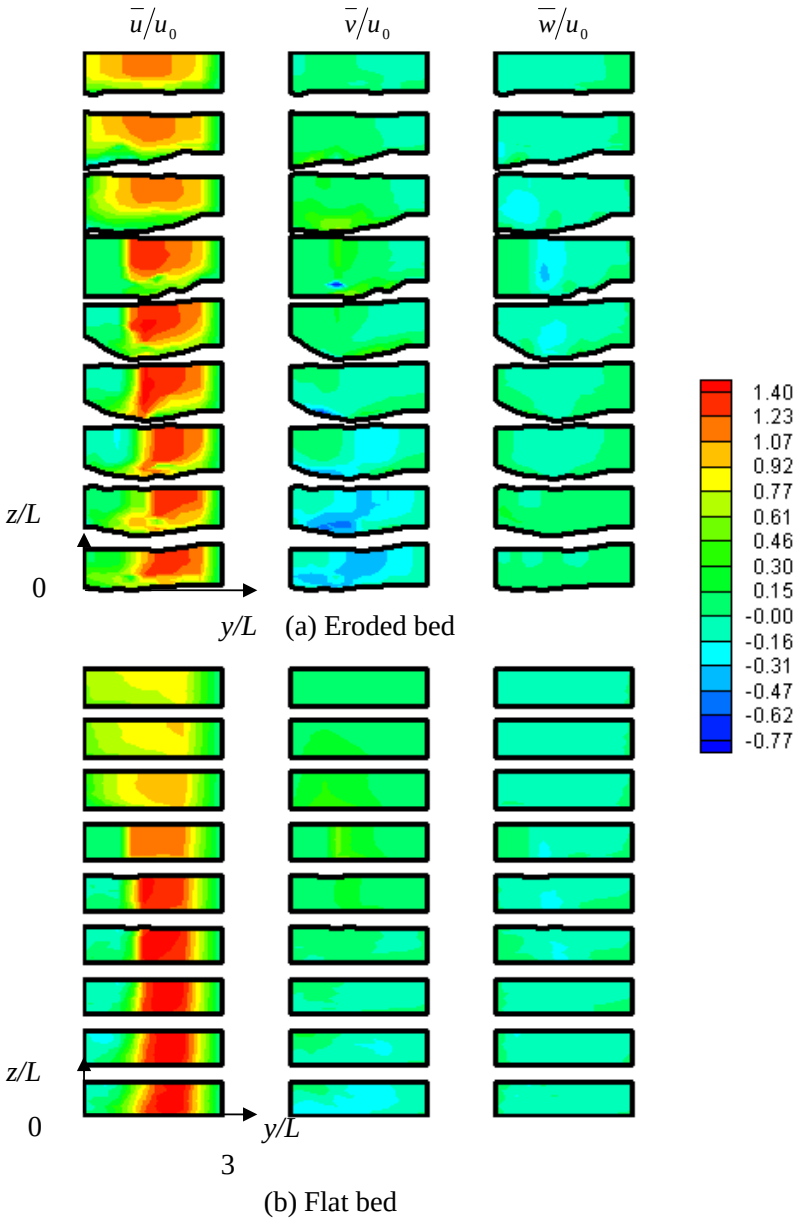

Fig. 3. Distribution of dimensionless mean velocities at cross sections for the scoured and flat bed surfaces ($\bar{u}/u_0$, $\bar{v}/u_0$ and $\bar{w}/u_0$)

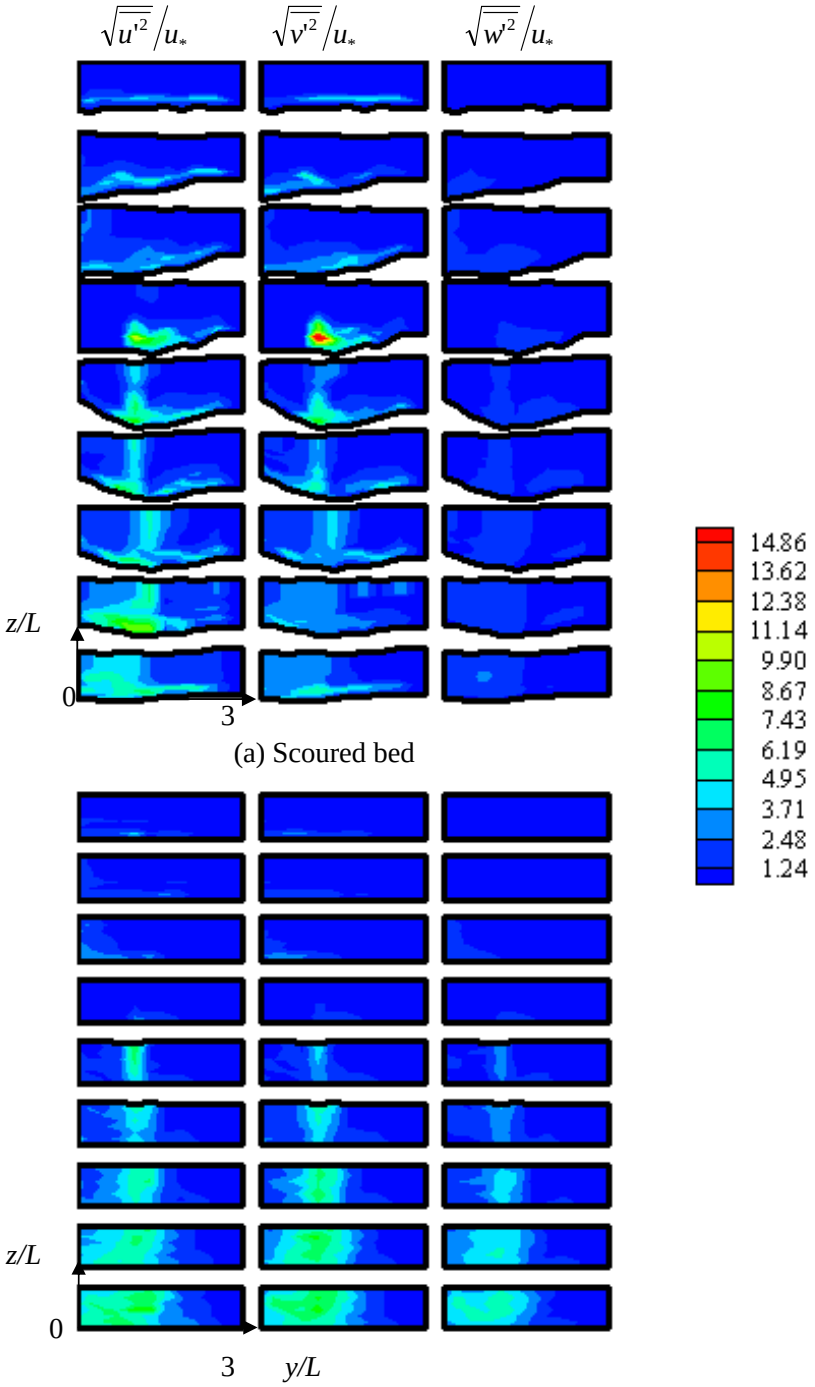

Fig. 4. Distribution of turbulent intensities $\sqrt{\overline{u'^2}}/u_*$, $\sqrt{\overline{v'^2}}/u_*$ and $\sqrt{\overline{w'^2}}/u_*$ at various cross sections for scoured and flat bed surfaces

Measuring Discharge with ADCPs: Inferences from Synthetic Velocity Profiles

Chris R. Rehmann[1], David S. Mueller[2], and Kevin A. Oberg[3]

[1]Department of Civil, Construction, and Environmental Engineering, Iowa State University, 374 Town Engineering Building, Ames, IA 50011; PH (515) 294-1203; FAX (515) 294-8216; email: rehmann@iastate.edu
[2]U.S. Geological Survey, Office of Surface Water, 9818 Bluegrass Parkway, Louisville, KY 40299; PH (502) 493-1935; FAX (502) 493-1909; email: dmueller@usgs.gov
[3]U.S. Geological Survey, Office of Surface Water, 1201 W. University Ave., Suite 100, Urbana, IL 61801-2748; PH (502) 493-1935; FAX (217) 344-0082; email: kaoberg@usgs.gov

ABSTRACT

Synthetic velocity profiles are used to determine guidelines for sampling discharge with acoustic Doppler current profilers (ADCPs). The analysis allows the effects of instrument characteristics, sampling parameters, and properties of the flow to be studied systematically. For mid-section measurements, the averaging time required for a single profile measurement always exceeded the 40 s usually recommended for velocity measurements, and it increased with increasing sample interval and increasing time scale of the large eddies. Similarly, simulations of transect measurements show that discharge error decreases as the number of large eddies sampled increases. The simulations allow sampling criteria that account for the physics of the flow to be developed.

INTRODUCTION

Traditional methods for measuring discharge in rivers include mechanical instruments such as Price AA meters and tracer measurements using salt or dye. Acoustic Doppler current profilers (ADCPs) offer the advantage of increased spatial and temporal resolution of the velocity field, but sampling requirements regarding parameters such as the number of profiles, number of transects, and total measurement duration must be considered for transect measurements, in which velocity is measured as the instrument moves across the river, and mid-section measurements, in which velocity is measured by sampling at several fixed points.

Current practice in the U.S. Geological Survey (USGS) is to average results from four transects except when the flow changes rapidly (Oberg et al. 2005), but as Oberg and Mueller (2007) noted, no research had been done to support that choice of the number of transects. They compiled data from laboratory experiments and field measurements and concluded that the key parameter controlling the measurement uncertainty is the measurement duration rather than the number of transects. From the

data available to them, they suggested collecting at least two transects over a total duration of at least 720 s.

Although a criterion based on the measurement duration captures a key part of the sampling procedure, measurements of discharge also depend on the velocity profile, instrument characteristics, turbulence, and other sampling parameters. The profile of depth-averaged velocity is described by the channel width B, cross-sectional average velocity U, and the shape of the profile. The instrument noise, which will be taken to be Gaussian noise, can be characterized with the standard deviation σ_u. At a minimum, the turbulence must be described by a velocity scale, length scale, and kinematic viscosity ν. For open channel flow, the velocity and length scales of the large eddies can be related to the shear velocity u_* and depth H, respectively. To complement the work of Oberg and Mueller (2007) for transect measurements of discharge and augment it for mid-section measurements, we use synthetic profiles to account for some of these factors and provide guidelines for measuring discharge with ADCPs.

METHODS

The synthetic velocity profiles are constructed as the sum of a mean velocity profile $\bar{u}(y)$, ADCP noise $u_n(y,t)$, and turbulence $u'(y,t)$, where y is the transverse coordinate and t is time. The mean velocity is computed from the theoretical profile developed by Seo and Baek (2004):

$$\frac{\bar{u}(y)}{U} = \frac{\Gamma(\alpha+\beta)}{\Gamma(\alpha)\Gamma(\beta)}\left(\frac{y}{B}\right)^{\alpha-1}\left(1-\frac{y}{B}\right)^{\beta-1} \tag{1}$$

where $\Gamma(z)$ is the gamma function and α and β are parameters. The two parameters α and β determine the skewness and kurtosis of the profile: When $\alpha = \beta$, the skewness is zero; that is, the profile is symmetric about the channel centerline; as α increases in this case, the profile becomes more peaked. When $\alpha \neq \beta$, the profile is skewed; as α increases past β, the peak shifts from one side of the centerline to the other. Typical values of α and β range from 1 to 4.5 (Seo and Baek 2004).

ADCP noise is assumed to follow a normal, or Gaussian, distribution (Stacey et al. 1999)—that is, $u_n = N(0,\sigma_u)$, where $N(\mu_x,\sigma_x)$ is the normal random variable with mean μ_x and standard deviation σ_x. For the simulations using the data in Oberg and Mueller (2007), the standard deviation σ_u was taken to be 1 cm/s for modes 5 and 11, and it varies between 14 and 32 cm/s for mode 1. For mode 12 it varies between 6 and 115 cm/s, with a mean of about 29 cm/s. These values are somewhat larger than the specifications for the RD Instruments Workhorse Rio Grande (RD Instruments 2003).

A synthetic turbulent signal was constructed using an approach like that of García et al. (2005). This approach involves making a velocity signal that has a specified one-dimensional energy spectrum $E_{11}(k_1)$, where k_1 is the wavenumber in the streamwise direction. The spectrum can be computed from a model energy spectrum function $E(k)$, where k is the magnitude of the wavenumber (Pope 2000);

we use a form due to W.C. Reynolds, which rises as k^2 for wavenumbers smaller than some wavenumber k_L, includes an inertial subrange, and has a sharp cutoff at a viscous wavenumber k_v.

Specifying the energy spectrum requires specifying the turbulence Reynolds number $R_T = q^4/(\varepsilon\nu)$, or—given a value of the kinematic viscosity ν—the turbulent kinetic energy $q^2/2$ and ε, the rate of dissipation of turbulent kinetic energy. However, for practical use, these quantities should be related to easily measured or estimated parameters, such as the mean velocity and the depth. Relations from Nezu and Nakagawa (1993) can be used to compute depth-averaged values of turbulent kinetic energy and dissipation in terms of the shear velocity u_* and H:

$$\frac{\bar{q}}{u_*} \approx 2.03 \qquad \text{and} \qquad \frac{\bar{\varepsilon} H}{u_*^3} \approx 8 . \tag{2}$$

The shear velocity can be related to the depth-averaged velocity $\bar{u}$ by assuming a logarithmic velocity profile over a rough bed with equivalent sand grain roughness k_s:

$$u_* = \frac{\kappa \bar{u}}{\ln\left(H / e z_0\right)}, \tag{3}$$

where $z_0 = k_s/30$. The logarithmic dependence of the shear velocity on the relative roughness z_0/H shows that the shear velocity does not depend strongly on k_s.

For mid-section measurements, velocity signals at each point were constructed. Averaging the signals over enough samples and integrating the results across the channel yields the discharge estimate for the case of no turbulence and ADCP noise. Therefore, this procedure was used to determine the number of samples, or the averaging time, required for the average to converge to within 5% of the ultimate value. Because this averaging time itself is a random variable, the calculations were repeated 1000 times to determine a distribution, as well as mean and standard deviation.

For transect measurements, the simulations can help to evaluate and extend the work of Oberg and Mueller (2007), who used many sets of transect measurements collected in the field to recommend sampling criteria. Because the shape of the velocity profile is not given, two cases were considered: one with $\alpha = \beta = 1.25$ and one with $\alpha = \beta = 5$. Sample intervals were taken to be 0.5 s for mode 1, 0.6 s for modes 5 and 11, and 0.7 s for mode 12.

MID-SECTION MEASUREMENTS

Mid-section measurements offer the advantage of resolving the velocity profiles well at particular points. With enough samples, mid-section measurements with ADCPs will provide estimates of discharge that converge to the value obtained with perfectly measured velocity profiles, but that value is subject to the error in measuring the profile at a limited number of points, which can be determined from these simulations. In other words, the uncertainty in discharge caused by ADCP noise

and turbulence can be driven to zero by collecting more samples, but error caused by discretizing the profile will remain.

The simulations allow the averaging time for mid-section measurements to be determined and its dependence on various parameters to be investigated. For the examples given in Figs. 1a and b, averaging times for each profile vary from 50 to about 340 s. These values exceed the 40 s duration recommended for each velocity measurement in a mid-section measurement of discharge (Rantz et al. 1982, p. 141). The histograms of the averaging time, which was taken to be the arithmetic mean of 1000 values, are skewed to high values. For ADCP measurements, the practical implication is that for a particular realization or measurement, the required averaging time can be much larger than the mean from many realizations.

Except at smaller depths, the averaging time increases with increasing depth in both the case with fixed sample interval Δt and varying maximum velocity u_{max} and the case with fixed $u_{\max}$ and varying Δt. The averaging time also increases as the maximum velocity decreases (Fig. 1a). The larger averaging times required for larger depths and smaller velocities result from an increase in the time scale of the largest eddies. In the free surface region of channel flow, the length of the largest eddies scales as the depth H (Nezu and Nakagawa 1993, p. 71). The velocity of the largest eddies scales either with the mean velocity or the shear velocity u_*, which is proportional to the mean velocity. In either case, a relevant time scale can be formulated as $H/\bar{u}$, and therefore, as the time scale of the turbulence increases, the averaging time increases. In other words, the measurement must sample enough large eddies of the flow.

The averaging time increases as the sample interval increases (Fig. 1b). That is, even for measurements with the same large eddy time scale, the sample interval—or equivalently, the number of samples, affects the averaging time. One might expect that if all other parameters are fixed, the number of samples must be some particular value. However, at different depths, the averaging times in Fig. 12b vary by a factor that depends on Δt. The data in Figs. 1a and b can be collapsed somewhat by a dimensionally inhomogeneous expression, and a more satisfying expression that can be generalized is being sought.

TRANSECT MEASUREMENTS

Transect measurements offer the advantage of better spatial resolution. While the usual USGS guidelines for mid-section measurements require 25-30 sections, the transect measurements used in Oberg and Mueller (2007) had between 130 and 1250 points per transect. Therefore, the error in discretizing the velocity profile can be much smaller for transect measurements. The disadvantage is that far fewer samples are collected at each transverse location; the maximum number of transects in the sets compiled by Oberg and Mueller (2007) was 33 for a comparison between the ADCP and a Price AA meter. In normal practice, however, a typical number of transects in a discharge measurement is four.

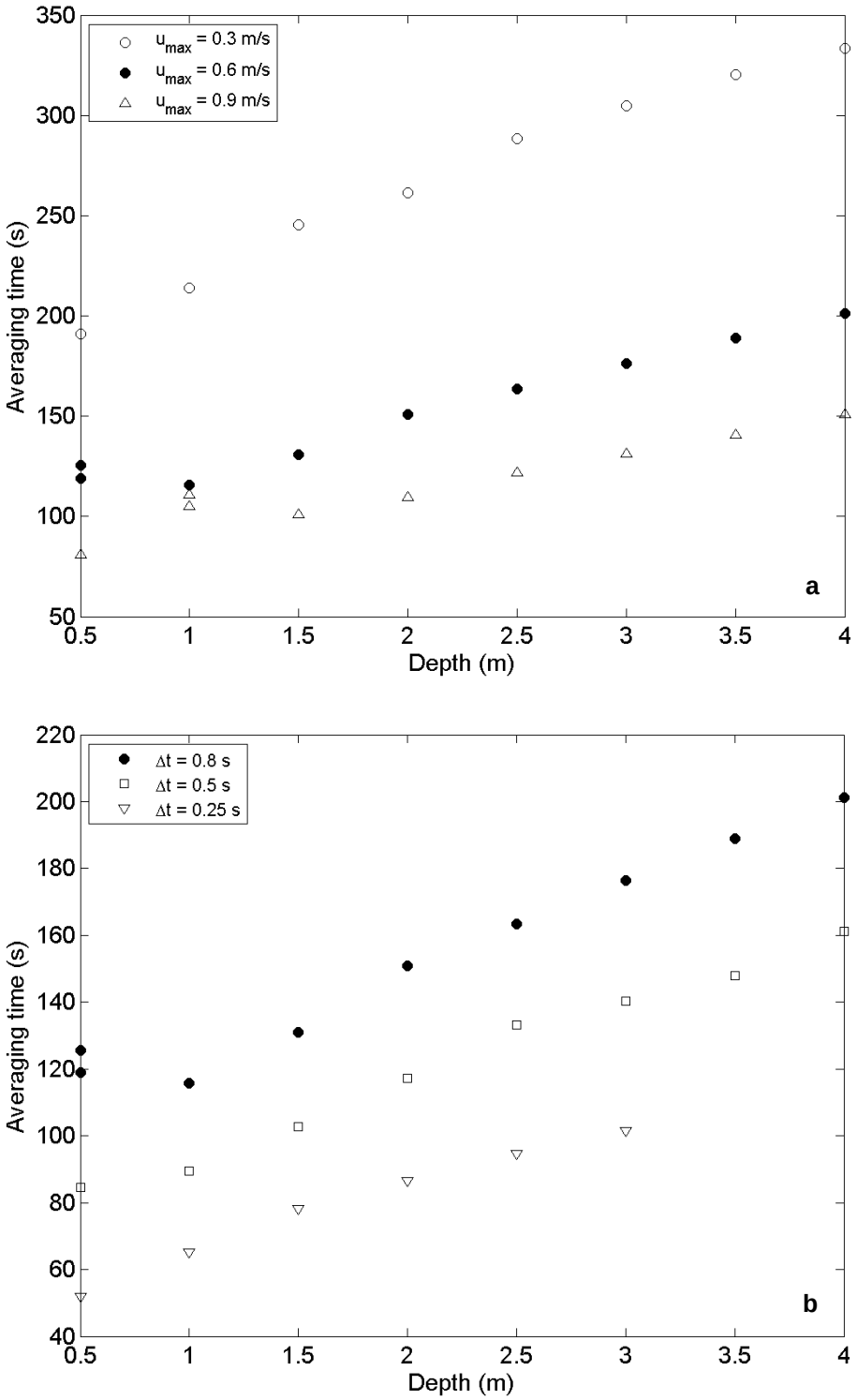

Fig. 1. Averaging time from the simulations of the section-by-section measurements. Each value is an arithmetic average over 1000 realizations. For both cases, $\alpha = \beta = 1.25$, $\sigma_u = 1$ cm/s, $k_s = 1$ mm, and the number of profiles was 10. In (a) the sample interval was set at 0.8 s, and the maximum velocity was varied, while in (b) the maximum velocity was set at 0.6 m/s, and the sample interval was varied.

As in Oberg and Mueller (2007), discharge error decreases with increasing total measurement duration. While the current guidance for discharge measurements specifies the number of transects, the field measurements collected by Oberg and Mueller (2007) showed that measurement duration was more important in determining uncertainty than number of transects. The simulations illustrate also this point (Fig. 2): Simulations with more transects but shorter durations can have larger uncertainty. The spread is smaller for the more uniform velocity profile ($\alpha = \beta =$ 1.25), but in both cases only a few cases with duration greater than the 720 s recommended by Oberg and Mueller (2007) have discharge error greater than 5%.

The discussion of the mid-section measurements and the potential usefulness of a dimensionless formulation suggest that testing other approaches is worthwhile. Two important time scales aside from the overall measurement duration T_s that emerged from the analysis of mid-section measurements were the sample interval and the time scale of the large eddies. Therefore, the discharge error could be analyzed in terms of the total number of samples $T_s/\Delta t$ or the ratio $u_* T_s/H$, which can be interpreted (up to a constant factor) as the number of large eddies sampled. Regarding the latter parameter, the discharge error decreases as $u_* T_s/H$ increases (Fig. 3); that is, as more large turbulent structures are sampled, the estimate of discharge improves. Although small error can occur for values of $u_* T_s/H$, except for three cases, errors do not remain less than 5% until $u_* T_s/H > 20$ when profiles are more uniform ($\alpha = \beta =$ 1.25) and until $u_* T_s/H > 40$ when profiles are less uniform ($\alpha = \beta = 5$).

The advantage of criteria based on total measurement duration or number of samples is that they are simple to apply. A possible disadvantage is that—even though the field data from Oberg and Mueller (2007) covered rivers with wide ranges of drainage areas, widths, depths, and velocities—the criteria might not apply generally. Because the criterion $u_* T_s/H > 40$ was developed from the same set of parameters, it also might not be general. Furthermore, it is more difficult to apply: One must estimate the shear velocity from a force balance for steady, uniform flow, from a logarithmic velocity profile (as in equation 3), or from some other approach. Fortunately, the depth and mean velocity can be estimated from preliminary ADCP measurements in the field, and the shear velocity does not depend strongly on the bed roughness, measured with either k_s or z_0. The key advantage of a criterion based on the value of $u_* T_s/H$ is that it accounts for the physics of the flow being measured. Therefore, it may be more general than a criterion based on measurement duration or the number of samples.

CONCLUSION

Synthetic velocity profiles were used to examine sampling schemes for discharge computed from mid-section measurements and transect measurements. Although field measurements provide the most reliable test of sampling schemes, the simulations allow the effects of some parameters or sampling issues to be isolated and studied systematically. The study of mid-section measurements with ADCP noise and turbulence focused on the time required for the average error to converge to the value in the absence of noise and turbulence; for the parameters considered, the averaging

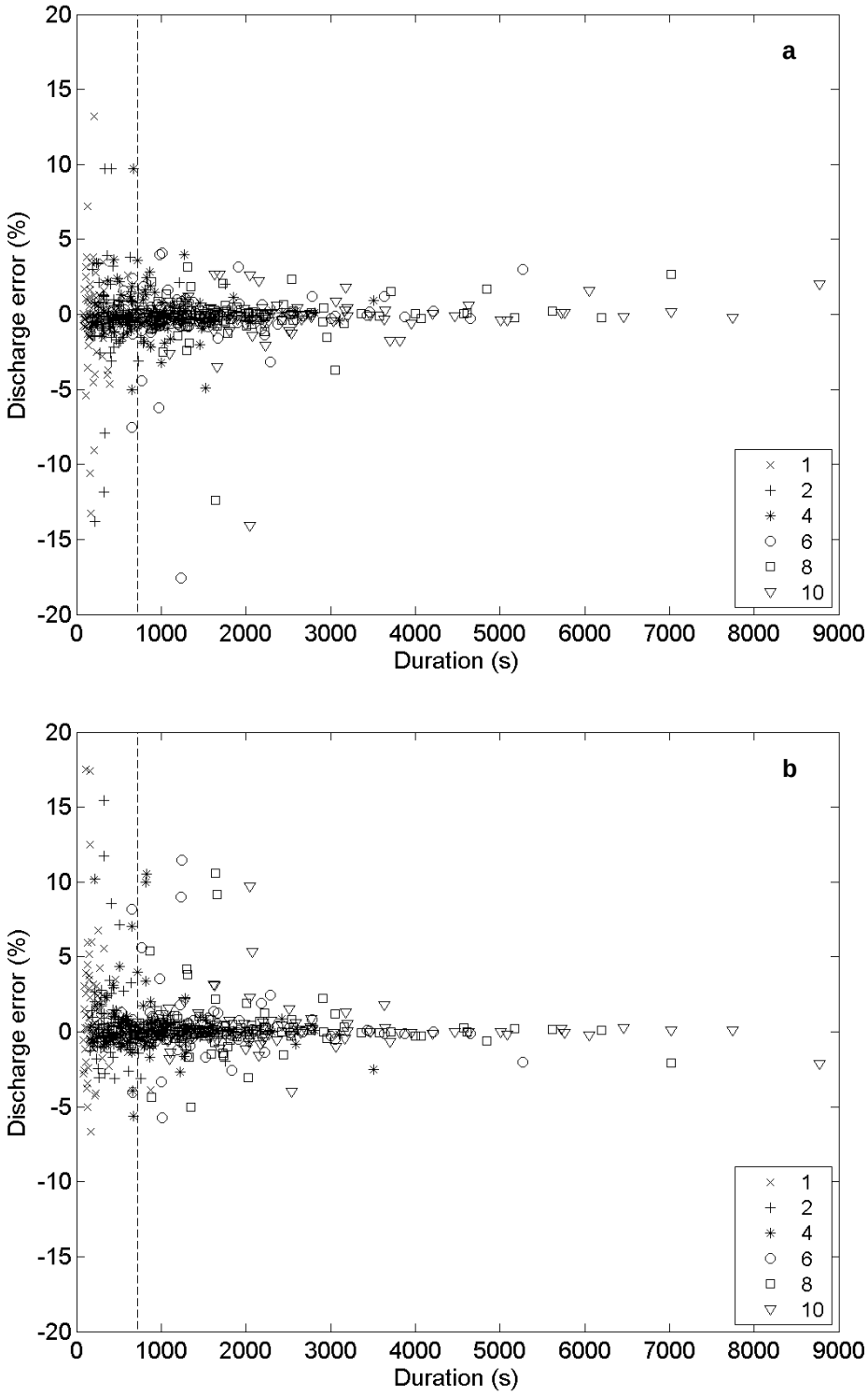

Fig. 2. Effect of measurement duration on discharge error. These plots are analogous to Fig. 5 of Oberg and Mueller (2007): (a) $\alpha = \beta = 1.25$, (b) $\alpha = \beta = 5$. The dashed line is the duration of 720 s recommended by Oberg and Mueller (2007), and the symbols indicate the number of transects in the average.

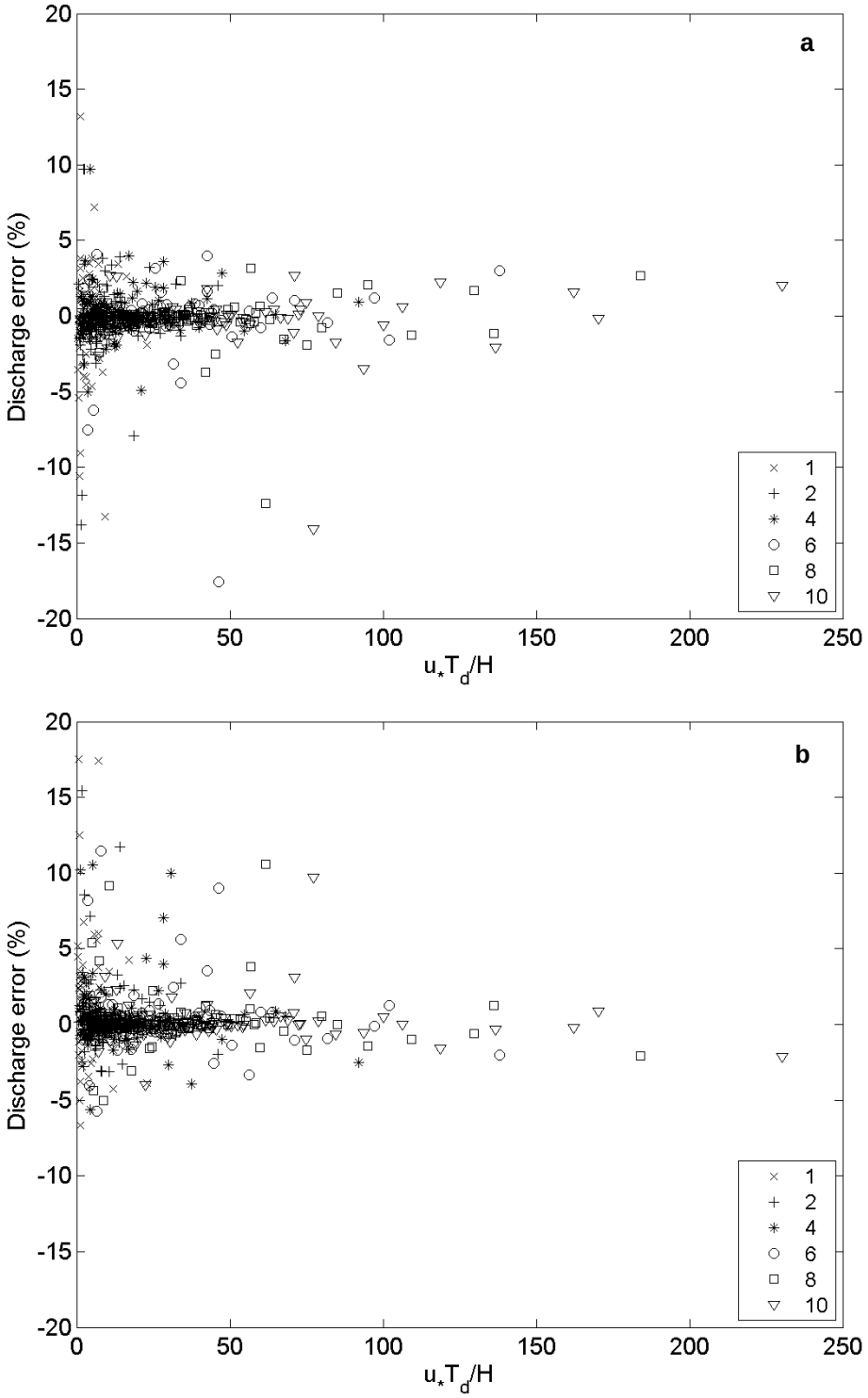

Fig. 3. Effect of the ratio of measurement duration and large eddy time scale on discharge error: (a) $\alpha = \beta = 1.25$, (b) $\alpha = \beta = 5$. The symbols indicate the number of transects in the average.

time required for a single profile measurement always exceeded the 40 s usually recommended for velocity measurements. The averaging time increases as the time scale of the large eddies, which is proportional to H/u_*, increases, and it also increases with sample interval. In general, mid-section measurements must sample enough large eddies of the flow.

Simulations of transect measurements with noise and turbulence complement and extend the analysis of field data by Oberg and Mueller (2007). Calculations mostly support the duration of 720 s recommended by Oberg and Mueller (2007). Also, the discharge error decreases as u_*T_s/H, which is related to the number of large eddies sampled, increases. For the cases simulated, most errors are less than 5% when $u_*T_s/H > 40$. Although the latter criterion requires some effort to apply, its key advantage is that it accounts for the physics of the flow being measured and therefore may be more general than a criterion based on measurement duration or number of samples.

REFERENCES

García, C. M., Cantero, M. I., Niño, Y., and García, M. H. (2005). "Turbulence measurements with acoustic Doppler velocimeters." *J. Hydraul. Eng.*, 131(12), 1062-1073.

Nezu. I, and Nakagawa, H. (1993). *Turbulence in Open-Channel Flows*. IAHR, Balkema, Rotterdam, The Netherlands.

Oberg, K., and Mueller, D. S. (2007). Validation of streamflow measurements made with acoustic Doppler current profilers." *J. Hydraul. Eng.*, 133(12), 1421-1432.

Oberg, K. A., Morlock, S. E., and Caldwell, W. S. (2005). "Quality-assurance plan for discharge measurements using acoustic Doppler current profilers." *U.S. Geological Survey Scientific Investigations Rep. 2005-5183*, Denver.

Pope, S. B. (2000). *Turbulent Flows*. Cambridge University Press, Cambridge, UK.

Rantz, S. E., et al. (1982). "Measurement and computation of streamflow." *U.S. Geological Survey Water-Supply Paper 2175*, Denver.

RD Instruments (2003). *WinRiver User's Guide, USGS Version*. RD Instruments, 957-6096-00 edition.

Seo, I.-W., and Baek, K. O. (2004). "Estimation of the longitudinal dispersion coefficient using the velocity profile in natural streams." *J. Hydraul. Eng.*, 130(3), 227-236.

Stacey, M. T., Monismith, S. G., and Burau, J. R. (1999). "Measurements of Reynolds stress profiles in unstratified tidal flow." *J. Geophys. Res.*, 104(C5), 10933-10949.

STATISTICAL ANALYSIS OF WATER DISTRIBUTION NETWORKS DESIGN USING HARMONY SEARCH

Mora, Daniel[(1)]; Iglesias, Pedro L; Martinez, F.Javier; Fuertes, Vicente S.

[(1)]Centro Multidisciplinar de Modelación de Fluidos, Universidad Politécnica de Valencia, Camino de Vera S/N CP 46022, Valencia (España)
phone: +34 387 9890; fax: +34 96 3877981; e-mail: damome@doctor.upv.es

ABSTRACT

The meta-heuristic techniques are optimization methods that allow the search beyond local minimums, which extends in many occasions the search field, and therefore, the capacity to obtain good solutions. The Harmony Search (HS) is a heuristic technique of optimization used for water distribution networks design.

Initially, the work displays the results of the HS on a water network studied in the literature (network of Hanoi). The results show the kindness of the method. Also is made a statistical analysis of the obtained solutions. This analysis allows verifying the values of the harmony parameters more suitable for the proposed method.

The second part analyzes the influence of harmony parameters in the velocity of the algorithm. The aim is to find the most suitable configuration of the problem, so that good solutions are obtained in the less time.

INTRODUCTION

The design of water distribution networks is extremely complex. It is well-known that when the diameters of the conductions are chosen as decision variables, the restrictions are implied functions of these variables of decision, so the space's region of solutions is a no convex type and the objective function becomes multimodal. Traditionally, water distribution network design, upgrade, or rehabilitation has been based on engineering judgement. Traditionally, water distribution network design, upgrade, or rehabilitation has been based on engineering judgement.

Howewer, in the last three decades a significant amount of research has focused on the optimal design of water distribution networks. Initially, researchers have used linear programming to optimize a design of a pipe network (Alperovits and Shamir, 1977). Later studies applied nonlinear programming to the network design problems. Some examples are Su et al (1987) that used non linear programming to optimize looped pipe networks or Lansey and Mays (1989), whose model was able to simulate pumps, tanks and multiple loading cases.

The application of heuristic techniques of optimization allows the search beyond these local minimums, which generally ample the field search and with it the capacity to obtain better solutions. The evolutionary algorithms are methods of search of solutions that are based in the natural beginning of the evolution. Inside the evolutionary algorithms, we can find Genetic Algorithms (GA), Particle Swarm Optimization (PSO), Ant Colony, Harmony Search (HS) and so on.

Some investigators have compared these techniques to each other (Zecchin et al, 2007), but it is difficult to say that one of them is clearly better than the others.

The Harmony Search Algorithm imitate the process of a band´s improvisation searching the perfect state of "harmony" (Geem, 2001). The Harmony Search has been applied successfully in many optimization problems (Lee, 2004; Mahdavi, 2006). In this case we apply the method to water distribution design, and the final solution will correspond to the combination of diameters that provides the smaller cost in a network. Previous works like those of Geem (2002, 2006) demonstrate the utility of the method for this kind of problems.

In the same way, other authors have tried to do improvements in the original algorithm, increasing the efficiency in the search minimums or in the speed. For example, Omran and Mahdavi (2007) present modifications on the original algorithm (Global-best HS). These modifications try to obtain a more efficient work of the algorithm in continuous and discreet problems.

The aim is to minimize the necessary costs of investment for the implantation of a certain system, starting from the topological layout and the demands and requirements of pressure in the nodes. This cost is associated to a goal function that will be evaluated in each algorithm iteration. Thus, each one of the possible diameters will represent a musical note and each one of the network conductions will be represented by an instrument. The combination of instruments and musical notes will provide a music sheet (solution) in each iteration.

Initially, the work show the kindness of HS method on the network of Hanoi. Also is made a statistical analysis of the obtained solutions. As it is a water network of important size and with a real layout, there is a wide range of solutions obtained with different models of design in the literature, which has allowed us to compare the results of the different models of design.

The statistical analysis of the solutions allows to optimize the HS parameters, so that we can establish the most suitable for the proposed method. A suitable combination of parameters not only provides better results in the cost of the network, but allows to make a smaller number of iterations until reaching the final solution. In this way the influence in the method of the parameters Harmony Memory Size (HMS), Harmony Memoy Considering Rate (HMCR) and Pitch Adjusting Rate is analyzed (PAR).

METHODOLOGY

Most of heuristic techniques are based on the imitation of natural processes. HS tries to imitate the improvisation process of a music band. The process consists of finding every time a better music sheet, which is represented by an objective function that there is to minimize.

The notes of every musical instrument determine the quality of the music sheet and the value of the objective function is the combination from all the musical notes that represent values of the decision variables.

The random character of the method does not guarantee a complete exploration of the space of solutions, nor supposes guarantee to reach a minimum of the objective function. However, the method offers a set of good solutions that try to improve.

In the method each one of the decision variables can have a rank of possible different solutions, which is represented with an alphanumerical variable (music note). The combination of these notes (variables of decision) composes a music sheet, that will be improved in the next iteration (to see figure 1). A music sheet represents a solution to the problem. This solution is constituted by a serial of notes that defines a unique solution of the optimization process

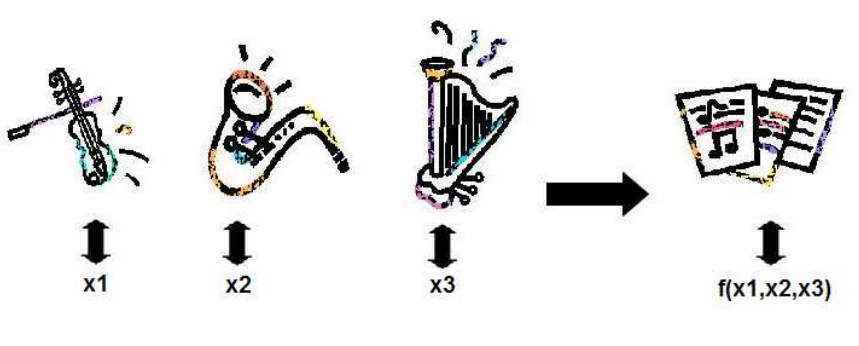

Figure 1. Composition of a music sheet

In the design of water distribution networks, each gene is represented with a number or a letter, that identifies the diameter of each one of the lines. In this paper the only network components that are considered are the pipes, but it is possible incorporate elements as pumps, tanks, valves and reservoirs without invalidating the algorithms.

In order to solve the optimization problem it is necessary to have a discrete set of possible solutions (musical sheet). This set of musical sheets is what also forms the harmony memory size. In HS a generic music sheet X is constituted by an equal number of notes to the number of decision variables (N_{VD}), so that generic sheet i of a memory is defined as a vector of numerical values.

$$X^i = \left\{X_1^i, X_2^i, \ldots, X_{N_{VD}}^i\right\}$$

The characteristic that measures "kindness" or capacity of a certain music sheet's survival regarding the others is known like aptitude. The aptitude of a certain generic sheet is identified through the value that adopts the objective function for the codified solution. In the case of the algorithm proposed for design and extension of distribution networks this objective function is defined as

$$F(X^i) = \sum_{j=1}^{N_{VD}} C_j\left(X_j^i\right) \quad L_j + \lambda \quad \sum_{s=1}^{N_S}\sum_{k=1}^{N_R} \delta_{k,s} \quad \left(H_{min,k} \quad H_{k,s}\right)$$

where C_j is the associated unit cost to the decision variable's value contained in link j of music sheet i; and L_i is the length of conduction of pipe j. Moreover, they are N_R imposed restrictions that must achieve the possible solutions of the problem. These restrictions have been including through a penalty in the total cost of the solution that later affects the aptitude of the music sheet. The restrictions that must be fulfilled are the derived ones to satisfy the restrictions with minimum pressure height ($H_{min,k}$) in each node k. These restrictions must be verified in all the analyzed scenes N_S, that usually are the on-speed operation of the system and its operation under the scene of failure of some of the conductions. The function penalty represents the difference between the

head height of the node k in scene s ($H_{k,s}$) and the required minimum height ($H_{min,k}$). In order to compute this penalty two variables are defined. One of them ($\delta_{k,s}$) is a binary variable that adopts value 1 if $H_{k,s} < H_{min,k}$, and it adopts null value in opposite case. The parameter λ represents a weight function that establishes the penalty's value for not verifying the restrictions of minimum pressure in the nodes. Pressure is considered as a hard constraint, and λ is big enough (10^7) for reject all solutions that violates the constraint.

The proposed method tries the evolution of a random population throught a parallelism similar to the improvisation process of a band in the search of a perfect music sheet. All the parameters of adjustment for HS will be specified from the beginning of the problem. For it an adjustment of three parameters of extreme importance is possible, as they are the harmony memory size (number of musical instruments), the Harmony Memory Considering Rate (HMCR) and the Pitch Adjustment Rate (PAR).

HS works with a sequential form. Thus, once given the value of the different parameters from optimization an assembly of scores is created of random way. Each one of these music sheets is composed by so many notes as variable of decision we have in the problem. A complete musical sheet provides a solution for the problem, with a certain value for the objective function.

The following iteration of the algorithm improvises a new music sheet X^i from the previous, considering HMCR and PAR. HMCR is the probability of choosing one value from the historic values stored in the harmony memory, and (1-HMCR) is the probability of randomly choosing one feasible value not limited to those stored in the harmony memory. An HMCR value of 1 is not recommended because of the possibility that the solution may be improved by values not stored in the harmony memory.

Every component of the new sheet is examined to determine whether it should be pitch-adjusted. This procedure uses the PAR parameter that sets the rate of adjustment for the note X^i_j. PAR is the probability of a note X^i_j changes it value. Thus, if the note is modified, the pitch adjust will be:

$$X^i_j \rightarrow X^i_j \pm \alpha$$

where based on the value of α the X^i_j note will increase (α =1) or will decrease (α=-1).

This way, the harmony memory size will have to be enough in order to guarantee the diversity of solutions, and, in addition, it must grow with the number of music sheet's bits. The main problem that is generated when using high memories is that convergence time of the algorithm is bigger. Therefore it is necessary to reach a commitment solution depending on the approach of the problem.

The following sections analyze the capacity of the proposed HS method to obtain equal or better solutions to the existing ones in the references. It has been analyzed the Hanoi network, determining the minimum cost of design them. Thus, working on the network of Hanoi, the influence of the different parameters has been analyzed on the final solution, dividing the work in two phases: First stage where the best combination of parameters in the obtaining of the minimum cost for the network is analyzed, and one second phase, where the influence of the parameters in the number of iterations is analyzed until reaching the final solution.

APPLICATION EXAMPLE

The analysis of the proposed model has been made on the network of Hanoi (to see Figure 4), propose by Fujiwara and Khang (1990). As it is a water network of important size and with a real layout, there is a wide range of solutions obtained with different models of design in the bibliography, which has allowed us to compare the results of the different models of design.

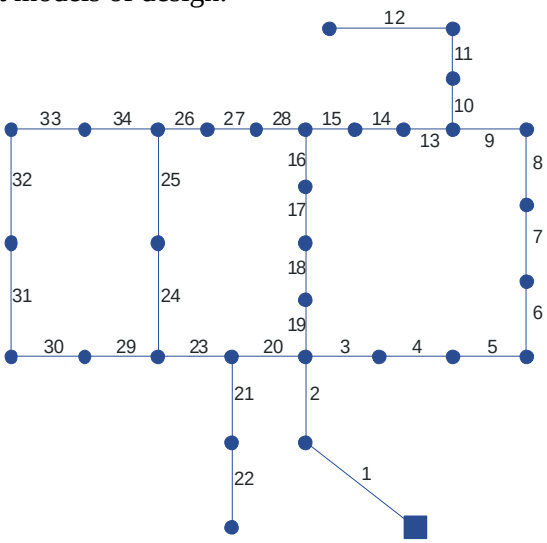

Figure 2. Network of Hanoi.

One of the characteristics that contribute to define the optimal solution of the network is the range of diameters used. For the study we used the original range of the bibliography.

Original range		
Nº Diameter	Diameter (mm)	Cost (um/m)
A	304'8	45'73
B	406'4	70'40
C	508'0	98'39
D	609'6	129'33
E	762'0	180'75
F	1016'0	278'28

Table 1. Range of diameters used for the design of the water distribution network.

The table 2 shows the solution's variation obtained by some researchers, as well as its corresponding total cost.

	Bibliography Solutions			Obtained Solutions			
Líne	Matías[1]	Savic1[2]	Savic2[3]	Sol Genetic[4]	Sol PSO[5]	Sol annealing 2[6]	Sol HS[7]
1	1016	1016	1016	1016	1016	1016	1016
2	1016	1016	1016	1016	1016	1016	1016
3	1016	1016	1016	1016	1016	1016	1016
4	1016	1016	1016	1016	1016	1016	1016
5	1016	1016	1016	1016	1016	1016	1016
6	1016	1016	1016	1016	1016	1016	1016
7	1016	1016	1016	1016	1016	1016	1016

8	1016	1016	1016	1016	1016	1016	1016
9	1016	762	1016	1016	1016	762	1016
10	762	762	762	762	762	762	762
11	609,6	762	609,6	609,6	609,6	762	609,6
12	609,6	609,6	609,6	609,6	609,6	609,6	609,6
13	508	406,4	508	508	508	406,4	508
14	406,4	406,4	406,4	406,4	406,4	406,4	406,4
15	304,8	304,8	304,8	304,8	304,8	304,8	304,8
16	304,8	406,4	304,8	304,8	304,8	304,8	304,8
17	406,4	508	406,4	406,4	406,4	406,4	406,4
18	609,6	609,6	508	609,6	609,6	609,6	609,6
19	609,6	609,6	508	508	508	508	508
20	1016	1016	1016	1016	1016	1016	1016
21	508	508	508	508	508	508	508
22	304,8	304,8	304,8	304,8	304,8	304,8	304,8
23	1016	1016	1016	1016	1016	1016	1016
24	762	762	762	762	762	762	762
25	762	762	762	762	762	762	762
26	508	508	508	508	508	609,6	508
27	304,8	304,8	304,8	304,8	304,8	406,4	304,8
28	304,8	304,8	304,8	304,8	304,8	304,8	304,8
29	406,4	406,4	406,4	406,4	406,4	406,4	406,4
30	304,8	406,4	406,4	304,8	304,8	406,4	304,8
31	304,8	304,8	304,8	304,8	304,8	304,8	304,8
32	406,4	304,8	304,8	406,4	406,4	406,4	406,4
33	406,4	406,4	406,4	406,4	406,4	406,4	406,4
34	609,6	508	508	609,6	609,6	609,6	609,6
Coste (miles um)	**6.093**	**6.187**	**6.073**	**6.081**	**6.081**	**6.125**	**6.081**

(1) Obtained solution by de Matías (2003).
(2) Obtained solution by Savic y Walters (1997).
(3) Obtained solution by Savic (1997), no pressure restrictions acomplished.
(4) Obtained solution with Pseudo Genetic algorithm.
(5) Obtained solution with Particle Swarm Optimization.
(6) Obtained solution with Simulated Snnealing.
(7) Obtained solution with Harmony Search.
Highlighted in grey the diameters that are different from the proposed solution of Savic & Walters, that verifies the restrictions of pressure in the nodes..

Table 2. Comparison of diameters (mm) obtained as solution for the network of Hanoi.

If we rely on the obtained minimum value, we observe that the HS improves those of all his competitors but the one of Savic[2], in terms of the used heuristic method does not fulfill the pressure specifications. HS obtains like minimum cost 6.081 thousands of um. The rest of solutions that shows the table fulfills these specifications, consisting of which all the nodes have a pressure over 30 mca

ANALYSIS OF THE RESULTS

One of the main characteristics of HS is that it works in a random way. The characteristics of the method do not guarantee with certainty the obtaining of the optimal value of the system. In addition, the obtained result can suffer sometimes certain variations. In order to analyze this randomness it is necessary to make statistical analyses that will study the influence that have the different parameters from the HS algorithm proposed in the solution of the analyzed network, with the purpose of optimizing them to increase the probability of obtaining the minimum.

In a first study, the harmony memory size, HMCR and PAR were modified were modified to study the influence of parameters. For it they have been made 54000

simulations altogether. For the calculation of these simulations we use a computer system in parallel with 23 computers AMD Duron to 1400 MHz and 128 MB of ram.

The initial values are the recommended ones by Geem (2001). The harmony memory size go from 15 to 135 individuals, varying the HMCR between 0.88 and 0.92, and PAR between 0.05 and 0.015.

The histogram of figure 3 represents the total of simulations. This graph incorporates the accumulated probability of the obtained solutions. The graph allows to detect the more frequent solutions, as well as to determine the probability of obtaining a given solution better to one given. It is important to consider that the histogram represents the totality of obtained costs, and so they are including all the possible combinations of size of memory, HMCR and pitchrate, those that worse work, reason why it is even logical that the number of values corresponding to the minimum cost is not very high.

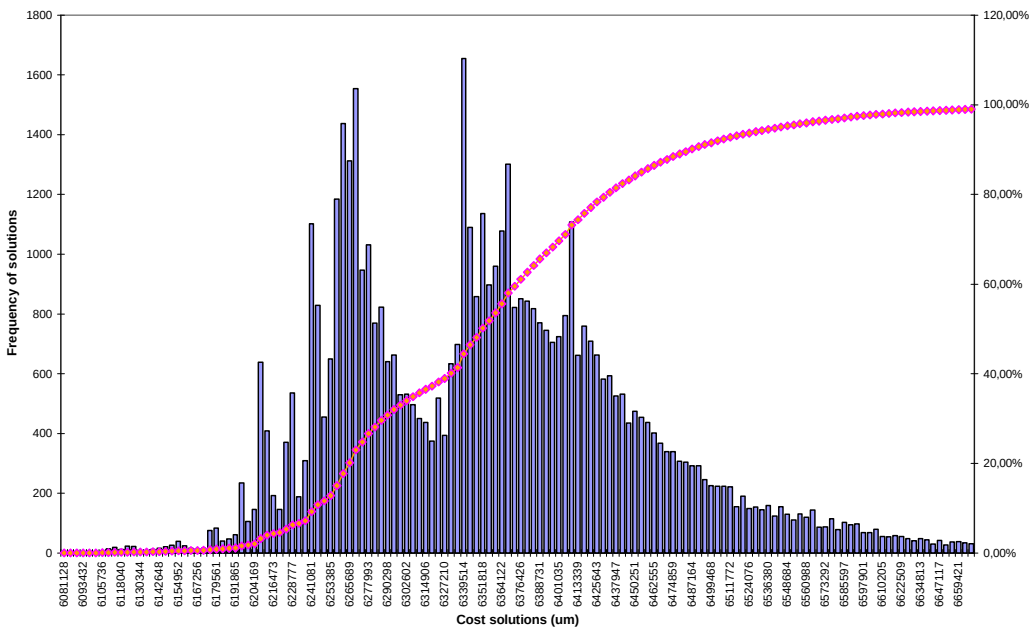

Figure 3. Histogram

In order to determine the influence of the different parameters in the obtaining of the minimum cost value, we adopted the solution corresponding to 6081 thousands of monetary units. This minimum was considered the optimal value of design. The optimal value of design is obtained only four times in the 54000 simulations that were realised. The concept of "good solution" is introduced now. One of the characteristics of the heuristics methods in general is the capacity to obtain not only one single optimal value, but to obtain a set of "good solutions" on the design problem. In this work "good solution" is defined with whose cost is over the minimum cost until in a 3%.

Figure 4 indicates the probability of obtaining a “good solution” for each combination of memory size and HMCR.

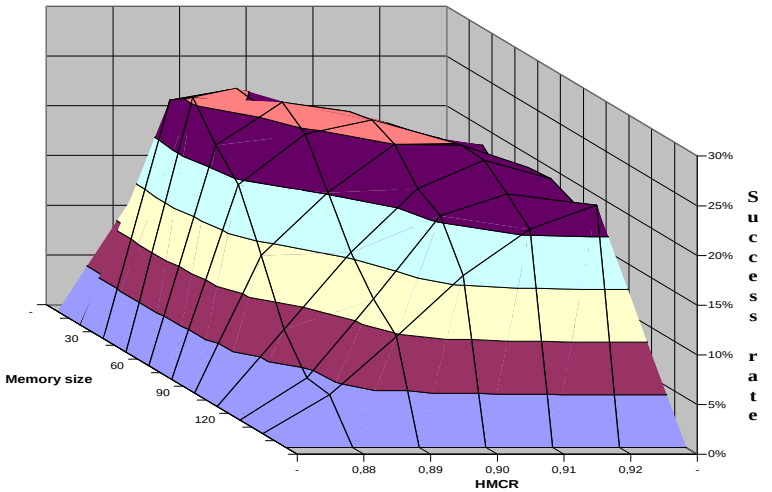

Figure 4. Probability of obtain a “good solution” (Memory Size vs HMCR)

Figure 4 shows that sizes of memory over 45 and below 120 are those that provide better results. In the same way, these memory sizes, combined with values HMCR of 0.89 and 0.90 give rates of success over 25%. This shows the capacity of the method not only to obtain minimum values, but also to obtain with relative frequency values very near the optimal one defined. Thus, Figure 5 indicates the probability of obtaining a “good solution” for each combination of memory size and PAR

Figure 5 shows that the used values of PAR do not have a great influence on the result of the simulation. In the other way, the results confirm that harmony memory size has a great influence in the final result of the simulation, since in the analyzed network sizes of memory between 45 and 90 provide higher probabilities of success.

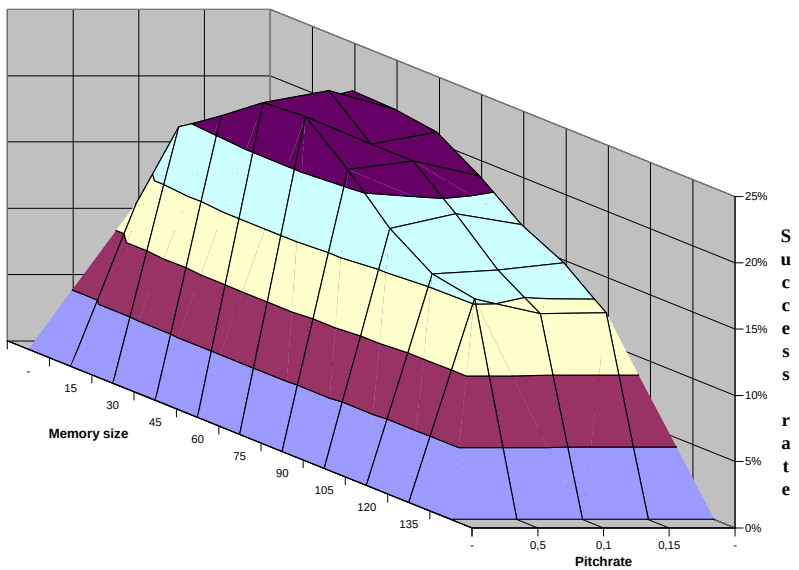

Figure 5. Probability of obtain a “good solution” (Memory Size vs PAR)

Another factor to consider when the optimal parameters of the method are chosen is the speed with which it calculates HS, since to choose values or others it influences in

the number of total iterations that HS makes before reaching the final solution. The graphs 6 and 7 represent the number of iterations that the algorithm realises in each case.

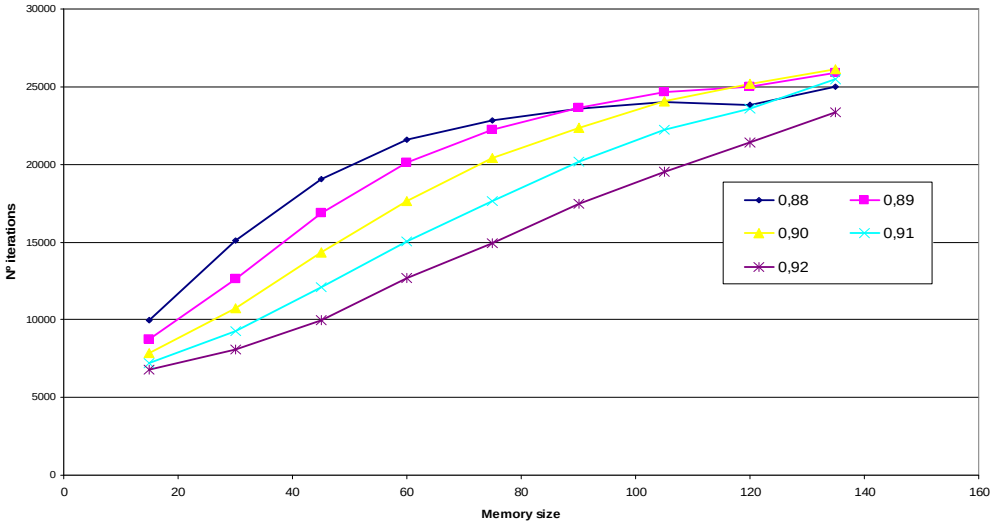

Figure 6. Number of iterations according to HMCR

Figure 6 shows that at the most great is the used size of memory greater number of iterations realise the algorithm before finding the final solution, and so the HS is slower. Thus, higher values of HMCR bring about an increase of the number of realised iterations in every simulation.

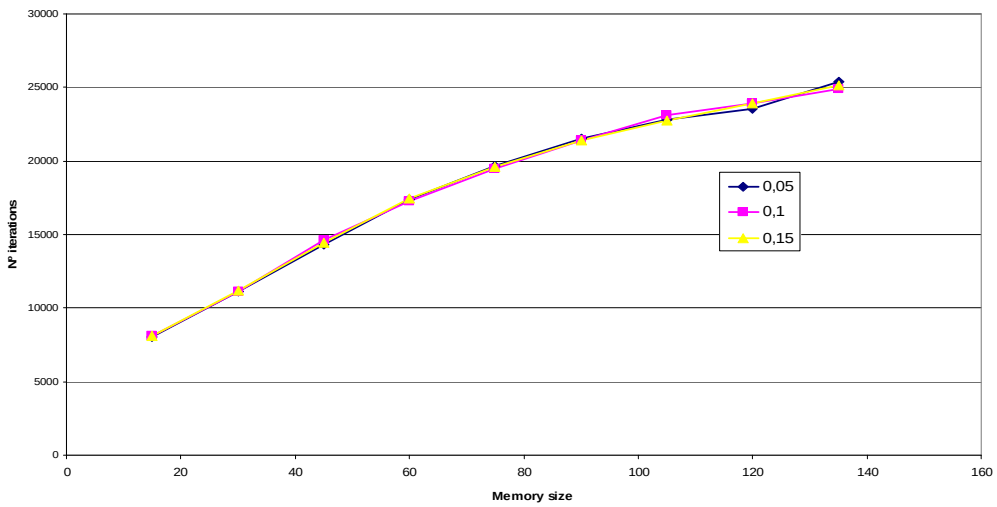

Figure 7. Number of iterations according to pitch rate

Figure 7 confirms the increase of the number of iterations realised by the algorithm when the size of memory is greater. Nevertheless, pitchrate in the studied values have not any type of influence in the number of made iterations, since the three series studied are superposed.

CONCLUSIONS

The economic design in the Water Distribution Networks is of great interest, as it allows us to choose a solution between the different alternatives that verify the imposed hydraulic conditions. In this work, the main objective consists of making the design of a water distribution network, using for it a method based on HS.

The objective of the economic design is to find the minimum cost for the analyzed network. However, it is possible to define the concept of "good solution". The statistical analysis for the different parameters from HS allows to conclude that:

- The size of the memory has a key influence in the obtaining of good solutions, because harmony memory sizes too high or too low make worse the yield of the algorithm.

  Thus, whichever greater is the memory size, greater is the number of iterations that the algorithm realises until finding the minimum, which makes the process slowly.

- For the studied values, PAR does not represent a great influence in the optimization process.

- In the studied network, values around 0.90 HMCR are the most suitable if the objective considers only to obtain good solutions of design. In the other way, whichever minor is HMCR greater number of iterations realises the algorithm, which makes the calculation slowest.

- The results are valid in the network of Hanoi. It is necessary the verification of these hypotheses in other models.

REFERENCES

Alperovits, E; Shamir, U (1977). "Design of Optimal Water Distribution Systems". Water Resource Research, Vol 12, nº 6, 885-900.

Geem, Zong Woo (2001). "Optimal cost design of water distribution networks using harmony search". Environmental Planning and Management Program. John Hopkins University.

Iglesias, P.L; Mora, D; Fuertes, V; Martinez, F.J (2006). "Análisis estadístico de soluciones de diseño de Redes de Abastecimiento de Agua mediante Algoritmos Genéticos". XXII Congreso Latinoamericano de Hidráulica. Ciudad Guayana. Venezuela.

Lansey, K.E; Mays, L.W (1989). "Optimization model for water distribution system design." J. Hydr. Engrg., ASCE, Vol 115, nº 10, 1401-1418.

Lee, K.G; Geem, Z (2005). "A new meta-heuristic algorithm for continuous engineering optimization: harmony search theory and practice". Computer methods in applied mechanics and engineering, 194, pp 3902-3933.

Mahdavi, M; Fesanghary, M; Damangir, E (2007) "An improved harmony search algorithm for solving optimizatin problems". Applied Mathematics and Computation 188, pp 1567-1579.

Matías, A (2003). “Diseño de redes de distribución de agua contemplando la fiabilidad mediante algoritmos genéticos”. Tesis Doctoral – Dpto. Ingeniería Hidráulica y Medio Ambiente. Universidad Politécnica de Valencia

Mora, D; Iglesias, P.L; Fuertes, V; Martinez, F.J (2006). “Metodología para diseño y ampliación de redes de abastecimiento mediante Algoritmos Genéticos”. XII Congreso Internacional de Ingeniería de Proyectos. Valencia. España

Omran, M; Mahdavi, M (2008). “Global-best harmony search”. Applied Mathematics and Computation 198, pp 643-656.

Su, Y.C; Mays, L.W; Duan, N.; Lansey, K.E. (1987). “Reliability-based optimization model for water distribution Systems”. J. Hydr. Engrg., ASCE, Vol 114, nº12, 1539-1556.

Wu, Z, Y; Simpson, A.R (2001). “Competent Genetic-Evolutionay Optimization of Water Distribution Systems”. Journal of Computing in Civil Engineering, April 2001, pp 89-101.

Alternatives Study of Willwood Diversion Dam Siltation Removal in Wyoming, USA

Hui-Ming Shih[1], Chih Ted Yang[2], Patrick F. Horn[3], and Lynn C. Stutzman[4]

[1]Martin/Martin Inc., 12499 W. Colfax Ave., Lakewood, Colorado, USA 80215; PH (303) 431-6100; email: mshih@martinmartin.com
[2]Civil and environmental Engineering, Colorado State University, Fort Collins, Colorado, USA 80523-1372; PH (970) 491-8160; email:ctyang@engr.colostate.edu
[3]Martin/Martin Inc., 12499 W. Colfax Ave., Lakewood, Colorado, USA 80215; PH (303) 431-6100; email: phorn@martinmartin.com
[4]Engineering Associates, 902, 13th Street, Cody, Wyoming, USA 82414; PH (307) 587-4911; email: lynnst@EAEngineers.com

ABSTRACT

Willwood Dam was built in 1924 as a diversion dam for irrigation. It is a run-of-the river reservoir located at a developing point bar in Wyoming, U.S.A. Based on current operating criteria, the release flow is restricted by an allowable turbidity increase of 10 Nephelometric Turbidity Units (NTU) from upstream to downstream of the dam. Currently, two of the three sluice gates have been clogged by siltation. These limited sluicing capacities have increased the sedimentation within the reservoir and the irrigation canal network.

In this study, de-siltation alternatives combining dredging, sluicing, and flushing were recommended to achieve the dam's operation goals and restrict sediment accumulation. Three operation curves and three dredging alternatives were used to evaluate sediment flushing/sluicing performances by using GSTARS 3.01 models. This study presents an efficiency analysis of the de-siltation alternatives, the expected operation life, and recommendations for this dam rehabilitation project.

1. INTRODUCTION

1.1 General Information

Willwood dam is a concrete gravity dam, built in 1924 as a diversion dam for the Shoshone Irrigation Project. The dam is located on the Shoshone River in Park County, Wyoming, USA, as shown in Figure 1. Flow is diverted through the two 5.5 ft by 7.0 ft gates into the Willwood Canal which was initially designed to carry a flow of 320 cfs. The irrigation system covers an area of approximately 12,000 acres in the Willwood Irrigation District (WID).

Willwood Dam has a height of 70 ft, a weir crest length of 271 ft, and a total crest length of 476 ft. The weir crest is at elevation 4499.5 ft. Besides the two diversion gates, the dam has three sluiceways controlled by 3.6 ft by 4.5 ft cast iron sluice gates. The dam is founded on sandstone and partly shale.



Figure 1. Location map of Willwood Dam in Wyoming.

1.2 Fully Filled Siltation

Most upstream sediments have been trapped in the Buffalo Bill Dam. Sediment materials transported between the Buffalo Dam and the Willwood Dam are from channel bed erosion and bank erosion. Willwood Dam is located downstream of a sharp channel bend. A massive fluvial point bar has developed and narrowed the channel width from the left bank. The right bank is predominantly high and vertical rock cliff (Figure 2.a). Currently, only the diversion gates and the north sluice gate can be operated.

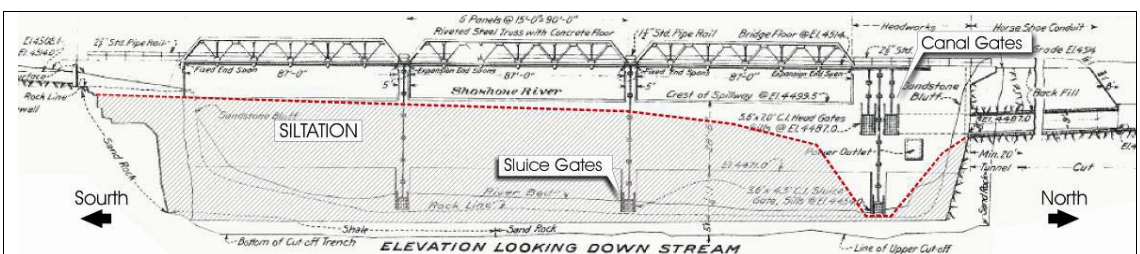

a. Dam face and current siltation

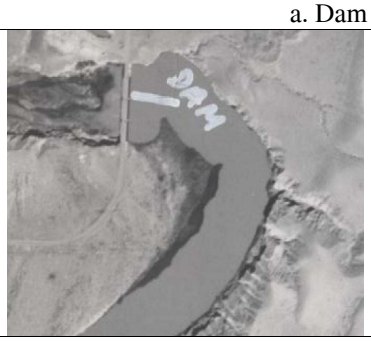

b. July, 1962

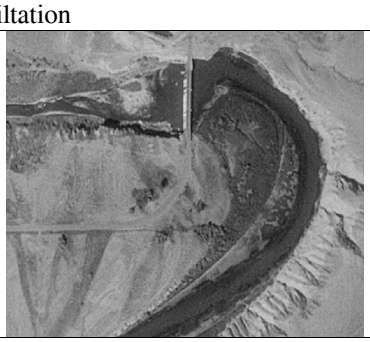

c. September, 1994

Figure 2. Willwood Dam siltation and field pictures

Siltation has nearly filled the dam and blocked the center and south sluice gates. The existing topography indicates that a flushing cone has formed in front of the north gate. Sedimentation is occurring at the toe of the south apron. Aerial photos from 1962 and 1994 (Figures 2.b and c) illustrate the progression of the point bar upstream of the dam. The siltation is impacting the function of the Willwood diversion system and poses a threat to the stability of Willwood Dam.

1.3 Reservoir Desiltation Studies

Building new reservoirs is rather difficult due to the new environmental regulations, high cost of construction, and lack of suitable dam sites. Therefore, techniques for reservoir desiltation have received increasing attention recently (Lai and Shen, 1996).

Some case studies for sediment routing, especially using flushing/sluicing, were done by Zyrjanov (1973) for the Ouchi-Kurgan Reservoir of USSR, Xia and Ren (1980) for the Heisonglin Reservoir of China, Wei (1986), Hong and Chen (1992), and Qian et al (1993) for the Sanmenxia Reservoir of China, Lin (1992), Hu (1995), and Su (1995) on sluicing activities in China, Un Ji (2006) in Korea, and Locher and Wang (1995) at Cowlitz Falls Dam in USA.

Reservoir sluicing and sediment management is often in conflict with water-use management (Brandt 2000, Fan and Jiang 1980). Three approaches, i.e., sluicing, flushing, and dredging can be used to remove reservoir sediments (Lai and Shen, 1996; Atkinson, 1996; and Talebbeydokhti and Naghshineh, 2004). These approaches are defined as (Atkinson, 1996, Morris and Fan, 1997, Brandt, 2000, and Talebbeydokhti and Naghshineh, 2004):

Sluicing: To discharge incoming sediments through the reservoir during high flows with heavy sediment concentrations without necessarily drawing down the water level.

Flushing: To erode and transport reservoir-sediment accumulation through the reservoir with drawing down the water level.

Dredging: To remove the reservoir sediment by mechanical means such as dredging and siphoning.

These methods were employed to evaluate the siltation removal alternatives in Willwood Dam. Desiltation by regulating flow is illustrated in Figure 3 for this study.

The Generalized Sediment Transport model for Alluvial River Simulation version 3.0 (GSTARS3) was developed by US Bureau of Reclamation (USBR) in 2002 (Yang and Simões, 2002). It is a semi-two-dimensional model using stream tubes, and can simulate sediment transport at a channel bend.

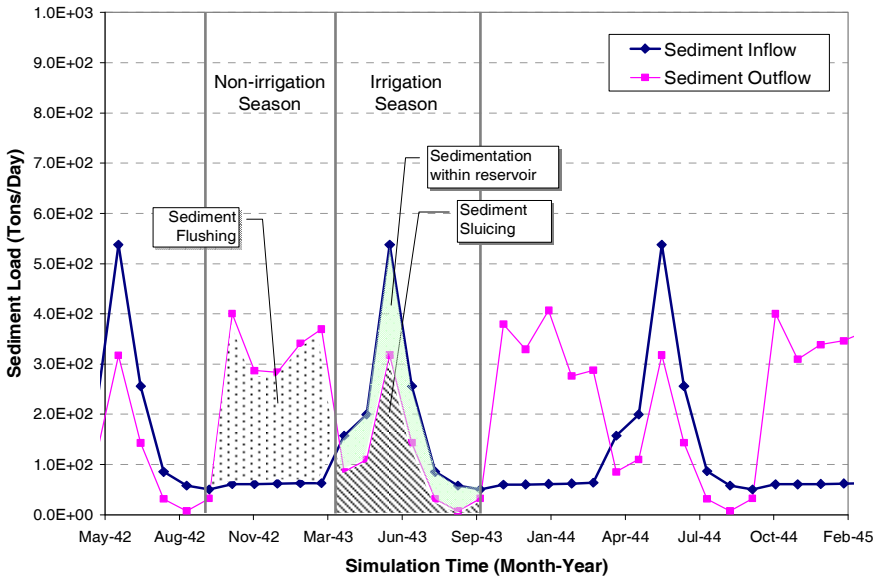

Figure 3. Sediment-graphs of sediment inflow and outflow by regulating flow.

1.4 Study Objectives and Scopes

Reservoir sedimentation has negative impacts on irrigation and environmental demands. Reservoir sediment removal can improve dam stability and dam operation, satisfy irrigation demand, extend dam operation life, optimize dam management and maintenance cost, etc. The scopes of this study are to analyze siltation impacts on dam safety and channel hydraulics; to evaluate the siltation impacts on current dam operations; to provide preliminary alternatives of siltation removal; and to suggest future studies to facilitate the dam rehabilitation project.

2. DAM OPERATION AND SILTATION DEVELOPMENT

The current Willwood Diversion Dam Operating Criteria was revised in 1982. The water level in the pool is maintained between the dam crest elevation of 4,499.5 ft and an elevation 4,500 ft. This is accomplished by first adjusting the irrigation intake gates to obtain the desired canal flow and then adjusting the sluice gates. The water level is maintained by opening the north gate first, then the center gate, and finally the south gate. From hydraulic sediment transport view points, this operation accelerated the point bar development at the left bank.

During the non-irrigation season, the criteria specifies that the water level should be held below the sill bottom of the irrigation canal gates to prevent the damages from ice forming. Since 1982, operations of Willwood Dam have been subject to an agreement executed by Bureau of Reclamation, Wyoming Department of Environmental Quality, and the Willwood Irrigation District. The increase of turbidity is limited to 10 Nephelometric Turbidity Units (NTU). When the increase of turbidity is more than 10 NTU, the sluice gate openings shall immediately be decreased until the increasing turbidity return to the legally allowable level. Consequently, the water level would exceed the canal gate sill, and additional suspended materials would be trapped within the reservoir.

The following comments were taken from Willwood Hydroelectric Project Feasibility Study (Stone & Webster Engineering Corporation, 1982):

> *"However, it is quite likely that this will seriously restrict sluicing as practiced in the past, resulting in a more filled-in reservoir with lower trap efficiency and higher sediment content in the irrigation system."*

The reservoir is almost entirely filled by siltation. Because of this, the Willwood Dam has lost its abilities of performing water level operations, siltation flushing and sluicing, and flow releasing. It cannot comply with the current operating criteria with only one sluice gate. During irrigation seasons, the north gate is completely shut down to refill water in the reservoir. River flows downstream over the dam crest, and a desired irrigation flow is taken from the canal gates. In winter, the water stages are several feet below the dam crest and higher than the top of the canal gates. Due to the high water stage, the sluice gate cannot flush sediment efficiently during winter causing accelerated sediment deposition in the reservoir. A dam inspection was made by the Bureau of Reclamation in 1982 indicated a significant loss of concrete downstream of the north sluice gate due to flow and ice passing over the crest. In order to improve the current conditions and achieve the operating goals, there is a need to increase the sluicing capacity and lower the water level during non-irrigation season.

3. AVAILABLE HISTORICAL DATA AND STATISTICAL ANALYSES

Flow discharges were gauged by U.S. Geological Survey (USGS) and USBR during different time periods. Sediment data were measured by USGS between 1979 and 1982. Flow turbidities were measured by WID between 1982 and 1989. A rating table of the sluice gates was referenced from the Willwood Dam Operating Criteria (1982). These records are explained and analyzed below.

3.1 USGS Flow and Sediment Concentration Data

Flow and sediment data from November 1979 to October 1982 were measured at USGS Gauge Station 06283800 (http://nwis.waterdata.usgs.gov/nwis/). The sediment samples show the measured suspended load and particle size distribution of the suspended material (Figure 4). The average particle size is approximately 0.063 mm which is classified as coarse silt.

The following empirical relationship between discharge and daily suspended load was developed using USGS suspended sediment data with a correlation coefficient of 0.73:

$$Q_s = 0.0015 \cdot Q^{1.7674} \quad (1)$$

where Q_s = total sediment load in tons per day, and Q = flow discharge in cubic feet per second.

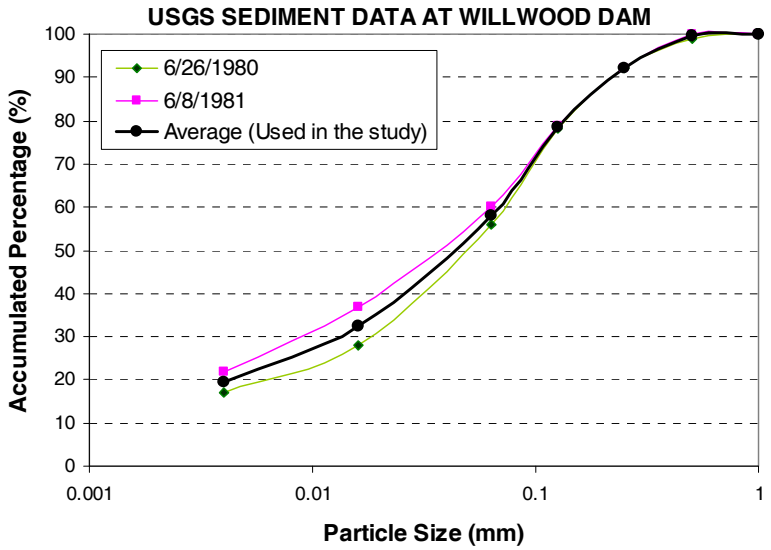

Figure 4. Particle size distribution of suspended material.

3.2 USBR Flow Data and Design Flow

USBR Gauge Station SRWY is located at the Willwood Dam crest and diversion canal to measure flows during irrigation seasons since 1996. The average river inflow is about 732 cfs during irrigation season. In non-irrigation season, river flow is primarily released from upstream Buffalo Bill Dam. According to the report of Willwood Hydroelectric Project (Stone & Webster Engineering Corporation, 1982), the flow in Shoshone River below Heart Mtn. Power Plant is 350 cfs in normal years.

Currently, the water demand for WID already exceeded this initial design capacity. In this study, the canal discharge record from 2005 to 2007 shows that the mean canal flow is about 320 cfs, and a flow of 400 cfs is approximately the maximum irrigation demand of WID. In this study, the monthly mean flows and a design irrigation flow of 400 cfs were used as design inflows during irrigation season. A constant flow of 350cfs was used as stream flow during non-irrigation season. Table 1 shows the monthly design flows used for sediment removal alternative simulations. Using Eq. 1 and monthly flows, sediment inflow of Willwood Dam is approximate 21,616 tons per year.

Table 1. Table of design flow for sediment transport modeling (Unit: cfs)

	Jan	**Feb**	**Mar.**	**Apr.**	**May**	**Jun.**
Canal Flow	0	0	0	400	400	400
Design Inflow	350	350	350	694	793	1386
	Jul.	**Aug.**	**Sep.**	**Oct.**	**Nov.**	**Dec.**
Canal Flow	400	400	400	400	0	0
Design Inflow	913	514	432	400	350	350

3.3 Willwood Irrigation District Flow Turbidity Observation

Generally, flow turbidity is proportional to suspended particles. However, only the flow discharges and NTU at upstream and downstream sampling points had been monitored and recorded without sediment concentration observation from 1982 to

1989. During this period, there are 497 records available. The relationship of flow discharge and NTU was studied and shown in Figure 5. When the release rate is less than 400 cfs, the passing percentage of the increasing NTU of less than 10 is 85%. This flow was used for design released flow during non-irrigation season.

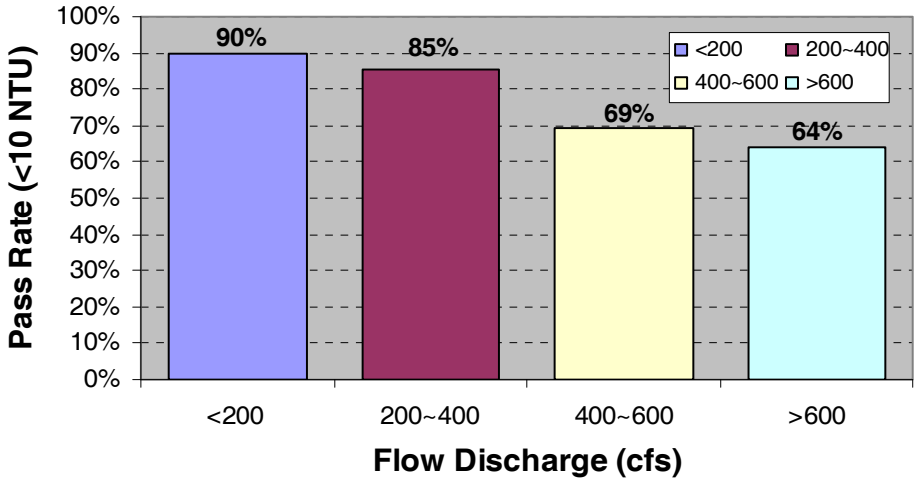

Figure 5. Flow and passing percentage of the increasing NTU's less than 10

3.4 Sluice Gate and Spillway's Rating Curves

3.4.1 Flow-Stage Rating Curve Equation of the Sluice Gates

Based on the flow rating table, on the Willwood Dam Operating Criteria (1982), the following sluice gate rating curve equation is obtained.

$$Q = C \cdot A\sqrt{2gH} \tag{2}$$

$$C = -0.0197 \cdot A + 1 \tag{3}$$

where Q = flow discharge in cfs; C = discharge coefficient; A = gate opening area in ft^2; g = 32.2 ft^2/sec, gravitational acceleration; and H = water depth from gate invert to water surface. Eq. (2) has a correlation coefficient $R^2 = 0.99$.

3.4.2 Flow-Stage Rating Curve Equation of Over-Topping Flow through the Dam Crest

The following standard weir formula is used to estimate the over-topping discharge through the dam crest. The discharge coefficient, C_w, is determined using USBR gauge flow data.

$$Q_{spillway} = C_w L H^{3/2} \tag{4}$$

$$C_w = 0.5619 \cdot \ln(H) + 2.1372 \tag{5}$$

where $Q_{spillway}$ = weir flow discharge in cfs; C_w = discharge coefficient; L = length of the spillway crest in ft; and H = upstream water head above the spillway crest in ft. The regression equations indicate close correlations with observed data with a correlation coefficient $R^2 = 0.70$.

4. PROPOSED DAM OPERATION

4.1 General Operation Constraints and Requirements

First, the sequence of operation of the three gates should be reversed to reduce the point bar development after dredging.

Second, WID requires approximate 55% of the mean daily river flow for irrigation during irrigation season. In order to satisfy all ecological and management objectives, three operation plans are recommended for this study, one for irrigation season and two for non-irrigation season.

Third, in order to reduce the possibility of cavitation or erosion at the gate sills, the sluice gates should remain open at least one foot.

4.2 Proposed Sluicing Plan and Dam Operation Curves

Sluicing can pass high flow with heavy sediment concentration during irrigation season and can also be used to reduce the probability of flow overtopping the spillway. By drawing down the water level, the flushing of sediment can be very effective in removing previous accumulated sediment and also to pass sediment inflow. It will be used during non-irrigation seasons. An efficient dam operation would present the maximum allowable flushing flows and minimum operation costs.

4.2.1 Irrigation Season Operation Curve

The south gate will be raised 1 foot initially when the reservoir water surface exceeds the dam crest. The discharge is approximately 200 cfs under this condition. The water surface should be stabilized at this elevation by adjusting gate opening. The recommended sequence of operations for the three gates and the relationship of flows and water stages are shown by an operating chart in Figure 6. Based on this operating, when released flow is greater than 2,200 cfs, all gates will be completely opened, and consequently, the water stage will exceed the dam crest.

4.2.2 Non-Irrigation Season Operation Curves

According to historical records, mean flow rate of 350 cfs should be maintained during non-irrigation season with a maximum released discharge of 400 cfs through the sluice gates. This would satisfy the limit of increasing 10 NTU. Flow would overtop the spillway crest when it exceeds 400 cfs. Two proposed operation plans were designed for non-irrigation season. The first plan is the normal operation by opening south and center gates. The operation chart is shown in Figure 7. In cases when the increase of NTU exceeds 10, the second plan will be take place using the south gate only. The operating chart is shown in Figure 8. The first plan has higher efficiency for sediment flushing than the second plan. Because of the limit of the increasing 10 NTU, a reduced released flow rate through gates will increase water stage within the reservoir.

Based on the proposed water level operation, the water stage is controlled at elevation 4499.5 during irrigation season, and at the elevation 4479.0 with a flushing discharge of 400 cfs during non-irrigation season. These values were used as the sediment transport model inputs.

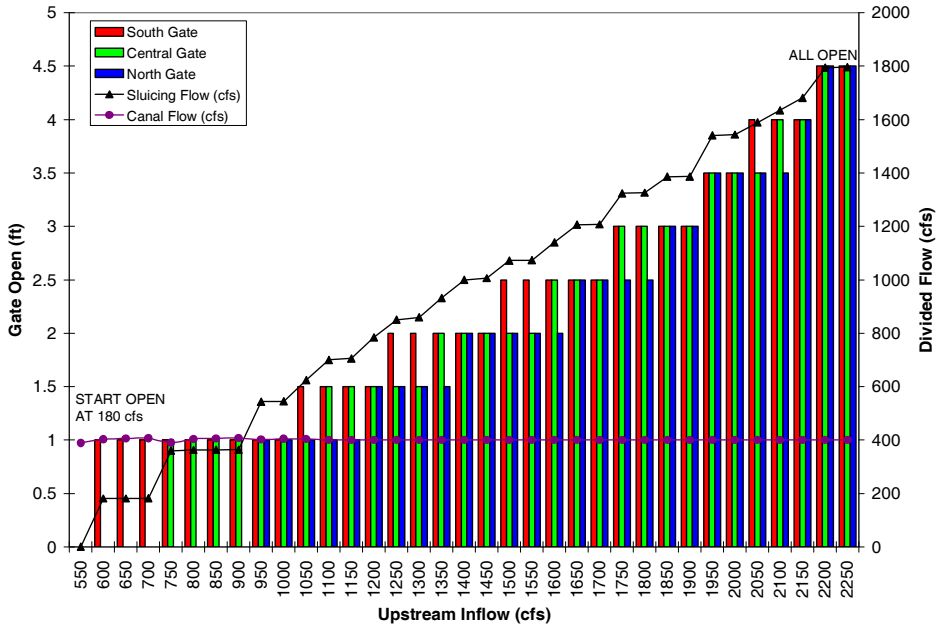

Figure 6. Proposed operation sequences of sluice gates during irrigation season.

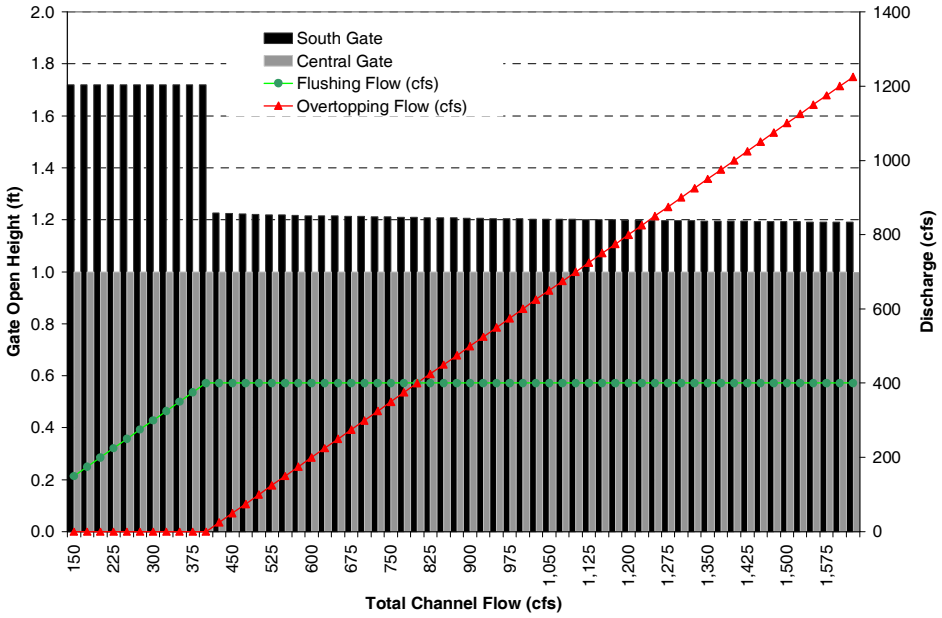

Figure 7. Proposed operation sequences of sluice gates during non-irrigation season (Increasing NTU <10).

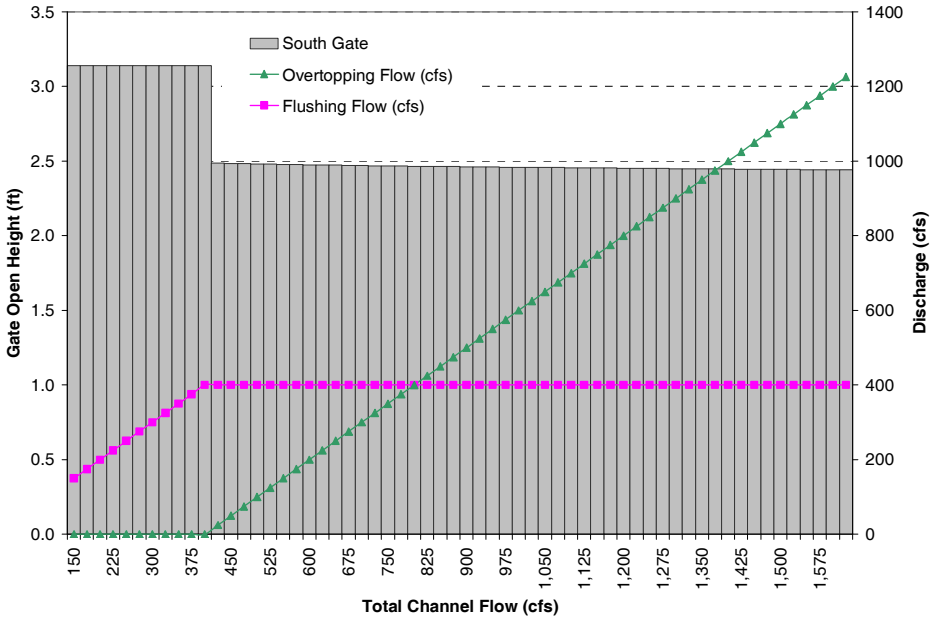

Figure 8. Proposed operation sequences of sluice gates during non-irrigation season (Increasing NTU >10).

5. SILTATION DREDGING ALTERNATIVES

The siltation threat at the upstream face of the dam is one of the primary concerns. For Willwood Dam, sluice gates are the only devise to remove sediment by river flow. Without removing the siltation in front of the clogged sluice gates and replacing sluice gates, Willwood Dam cannot restore its abilities of sediment sluicing and flushing. In order to accomplish the goals of rehabilitation and extend operating life, sediment removal is the first phase of the project. The proposed sediment dredging alternatives are described in the following sections.

5.1 Alternative I. Full Scale Removal

This alternative proposes to rehabilitate the reservoir storage using full scale dredging. It would construct a thalweg slope of 2% connecting the sluice gate invert to the existing channel bottom at the upstream end (Figure 9). Rock banks on both sides of the bank would be exposed in the initial design. Large quantities of sediment will be removed from the existing point bar while maintaining stable bank slopes. This alternative indicates that approximately 365,000 cubic yards of sediment would need to be removed. The rehabilitated reservoir storage would be 211,000 cubic yards at the canal gate sill (EL.= 4,487.0) and 396,000 cubic yards at the dam crest (EL.= 4,499.5). Simulated bed profiles are shown in Figure 9.

5.2 Alternative II. Partial Siltation Removal

The simulated results from Alternative I are used as inputs to a sediment transport model. The simulated results conclude an approximately equilibrium bed elevation of 4,480 will form at the dam in approximate 5 years. According to this equilibrium condition, Alternative II would dredge out sediments in front of the sluice gates and above the elevation of 4,480 ft (Figure 11). This alternative indicates that

approximately 255,000 cubic yards of sediment would need to be removed. The proposed reservoir storage would be 99,900 cubic yards below the canal gate sill and 276,500 cubic yards below the dam crest. After the gates begin sluicing, the reservoir bed condition would reach a balance condition.

5.3 Alternative III. Limited Siltation Removal in Front of Sluice Gates

Alternative III would minimize the dredging cost and replace the clogged sluice gates. This plan would remove minimal amount of siltation in front of the dam (Figure 13). No siltation removal would occur at the current point bar. This alternative indicates that approximately 45,500 cubic yards of sediment would need to be removed. The proposed reservoir storage would be 32,300 cubic yard at the canal gate sill and 90,000 cubic yards at the dam crest.

6. SEDIMENT TRANSPORT AND DESILTATION SIMULATION

Four simulations combining the reservoir routing and the sediment flushing/sluicing routing were used to determine the proposed operating life of Willwood Dam. The first three simulations are to individually use the dredging alternatives with the proposed water level operation. An additional simulation using current water level operating criteria with the full scale dredging plan was estimated to compare with other proposed alternatives. In this study, USBR GSTARS3 was revised and utilized to evaluate the sediment removal performance of each simulation. Routing including the use of sluice gate, operating curves, spillway, and diversion was developed and included into the revised GSTARS 3.01 (Yang and Shih, 2009). Detail procedures and simulation results are described below.

6.1 Model Input and Assumptions

The geometric inputs of three proposed dredging plans were utilized in the sediment transport models. Particle size distribution and resulting sediment rating from Eq. 1 were used for sediment inputs. Upstream conditions incorporate monthly mean flow discharges for river inflows. For downstream conditions, the proposed operation curves and current operating criteria were used for time-related controls of released flows and stage storage. Flow stage and discharge equations for spillway and sluice gate provided hydraulic facility inputs. Flow viscosity was calculated using an average water temperature of 53ºF. To simulate flow and sediment transportation distribution, three stream tubes were applied in the sediment sluicing/flushing modeling. Sluice gates are the only devise used to discharge sediment in the simulations.

The rock foundation of Willwood Dam at an elevation of 4454 feet was used as an erodible limit for modeling purposes. Based on the proposed channel alignment, a radius of 410 ft was used to compute the effects due to the channel bend. The time interval for flow hydraulics modeling is one month based the design monthly flows. The time interval of sediment transport modeling was 15 seconds. Total computed duration was 100 years for determining de-siltation efficiencies and a proposed operating life.

6.1.1 Canal Outlet Gate Rating Curve

A stage-discharge rating curve is required to simulate the WID canal gates. For this study, the following standard orifice equation is used.

$$Q = C \cdot A\sqrt{2gH} \tag{6}$$

where Q = flow discharge in cfs; C = discharge coefficient; A = gate opening area in ft^2; g = 32.2 ft^2/sec, gravitational acceleration; and H = water depth from gate invert to water surface. A discharge coefficient of 0.6 is a commonly suggested value and can be modified by observed data, if needed.

6.1.2 Sediment Transport Simulation

Willwood Dam is a run-of-the-river reservoir and is hydraulically characterized by a river mechanism. Because the sediment particles are mainly silt and sand, the sediment transport equation, revised Ackers and White equation (Wallingford, 1990, and Yang and Simoes, 2002), was used to represent sediment transport capacity within the study reach. It is

$$C_w = A \cdot G\frac{d_s}{h}\left(\frac{V}{u_*}\right)^B\left(\frac{C}{D}-1\right)^E \tag{7}$$

where, C_w = sediment concentration by weight; d_s= particle size; u_* = shear velocity; h= flow depth; G=specific gravity of sediment, and

$$C = \frac{{u_*}^B}{\sqrt{(G-1)gd_s}}\left[\frac{V}{\sqrt{32}\log(10h/d_s)}\right]^{1-B} \tag{8}$$

For 1.0< dimensionless particle diameter, $d_* = \left(\frac{(G-1)g}{\upsilon^2}\right)^{1/3} d_s$ <60,

$$\log A = -3.46 + 2.79\log d_* - 0.98(\log d_*)^2 \tag{9}$$

$$B = 1.0 - 0.56\log d_* \tag{10}$$

$$D = \frac{0.23}{d_*^{0.5}} + 0.14 \tag{11}$$

$$E = \frac{6.83}{d_*} + 1.67 \tag{12}$$

For d_* >60

$$A = 0.025 \tag{13}$$

$$B = 0 \tag{14}$$

$$D = 0.17 \tag{15}$$

$$E = 1.78 \tag{16}$$

6.2 Simulation Results and Comparison

6.2.1 Results of Alternative I: Full Siltation Removal

The simulated profile shown in Figure 9 illustrates that a wedge-shaped deposition and flushing cone would form near the upstream face of the dam. The top elevation of the siltation wedges is approximately 4,478 ft. Figure 10 shows the simulated cross section variations at the channel bend. While siltation is rising, secondary flow effect at the channel bend is becoming more significant. A new cross-sectional pattern within the main channel is formed by cutting into the deposits near the right bank after siltation elevation reaches the drawdown water level. Therefore, the flow during non-irrigation season is the dominant flow for the new channel forming. Consequently, the sediment along the left bank would be accumulating faster than at the right bank. As the cross section narrows, secondary flow will enhance the point bar development at the inner bank. The point bar sedimentation is mainly developed during irrigation season because of a higher operating water level. The channel thalweg will meander closer to the right bank mimicking current conditions.

6.2.2 Results of Alternative II: Partial Siltation Removal

The simulated profile and cross section variations for Alternative II are shown in Figures 11 and 12. A wedge-shaped deposition and flushing cone would form near the upstream face of the dam. Due to secondary flow effect, the simulated cross sections indicate that the channel thalweg would also meander closer to the right bank after siltation elevation reaches the drawdown water level.

Comparison between the Alternatives I and II indicates that Alternative I provides more reservoir storage than Alternative II. With Alternative I, siltation would take approximate 10 years to fill the reservoir volume and reach the elevation of 4,478 ft. In Alternative II, sedimentation would accumulate faster than Alternative I.

6.2.3 Results of Alternative III: Limited Siltation Removal in Front of Sluice Gates

The simulated profiles of for Alternative III are shown in Figures 13. Because the dredged profile cannot provide an efficient slope for sediment flushing, the siltation would raise up to the elevation of approximate 4,491. Refer to Figure 14, the simulated cross sections indicate that the new siltation would deposit on top of the historical siltation. A high and steep flushing corn would appear in front of the dam. These indicate that this alternative might form an unstable bed profile and flush high sediment concentration during non-irrigation season.

Compare to Alternatives I and II, Alternative III does not provide any storage for sedimentation. Based on this alternative, a high concentration flushing would require government permitting or agreements to perform the short duration flushing during non-irrigation season. In addition, there is still a high risk for the new sluice gates to become blocked in the near future.

6.2.4 Results of Simulation Using the Current Operating Criteria with a Full Siltation Removal

The simulated profile and cross section variations are shown in Figures 15 and 16. Because the current operating criteria require higher operating water levels than the proposed, the flow profile hydraulically performs a less sediment flushing efficiency than the proposed water level operation. A higher wedge-shaped deposition and flushing cone would form near the upstream face of the dam. Siltation would be quickly accumulated and reach the canal gate invert in approximate 10 years. The simulated cross sections of 80 year and 100 year are approximately similar with the current siltation in the field. Comparison of the current operating criteria and the proposed reservoir operation, the simulations indicate that using the proposed operation with the proposed dredging alternatives would perform at lower elevations of the siltation top. This indicates that the drawdown water level of sediment flushing is a significant factor for sedimentation geometry within the reservoir.

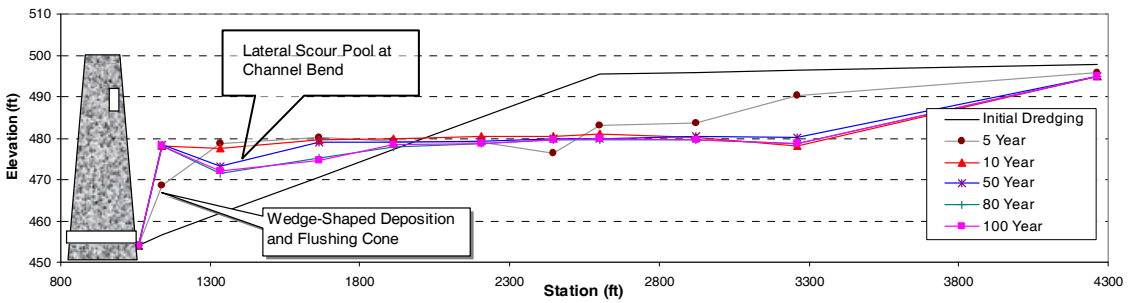

Figure 9. Time series changes of the reservoir bed profile (Alternative I).

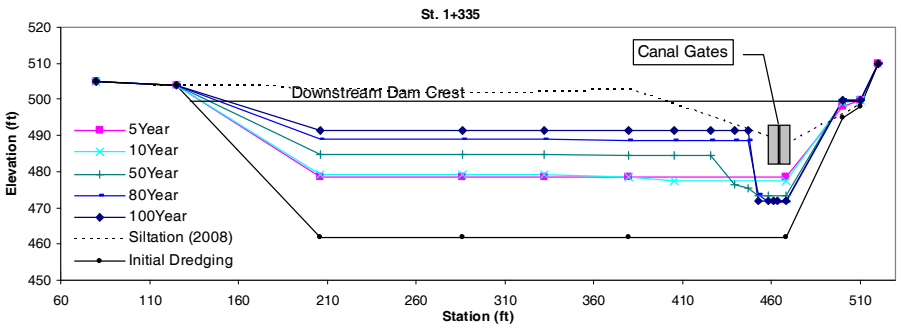

Figure 10. Simulated cross section variations and point bar development at channel bend (Alternative I).

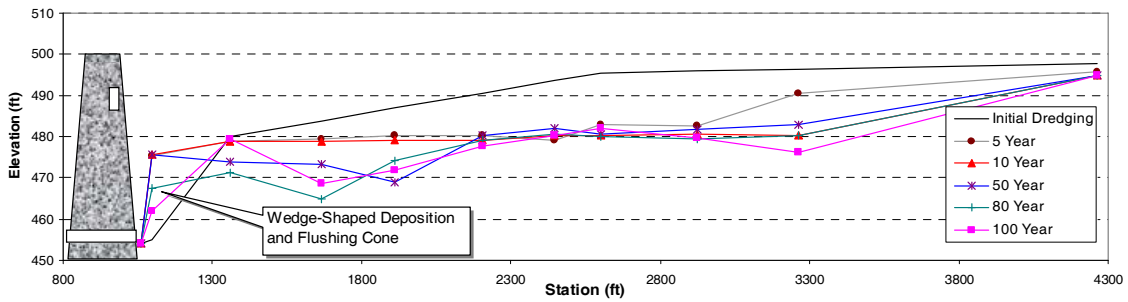

Figure 11. Time series changes of the reservoir bed profile (Alternative II).

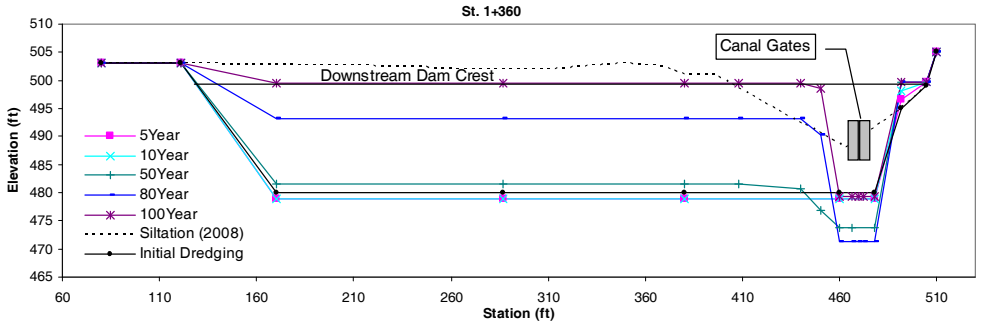

Figure 12. Simulated cross section variations and point bar development at channel bend (Alternative II).

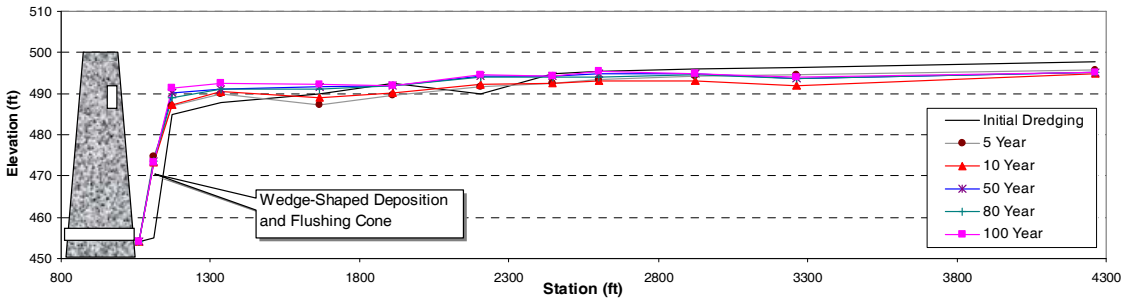

Figure 13. Time series changes of the reservoir bed profile (Alternative III).

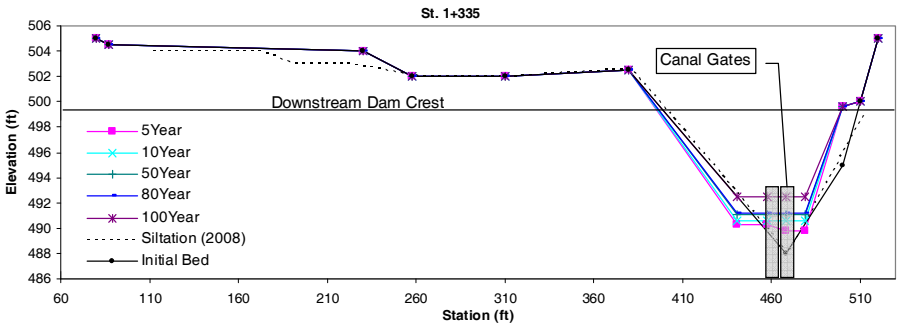

Figure 14. Simulated cross section variations and point bar development at channel bend (Alternative III).

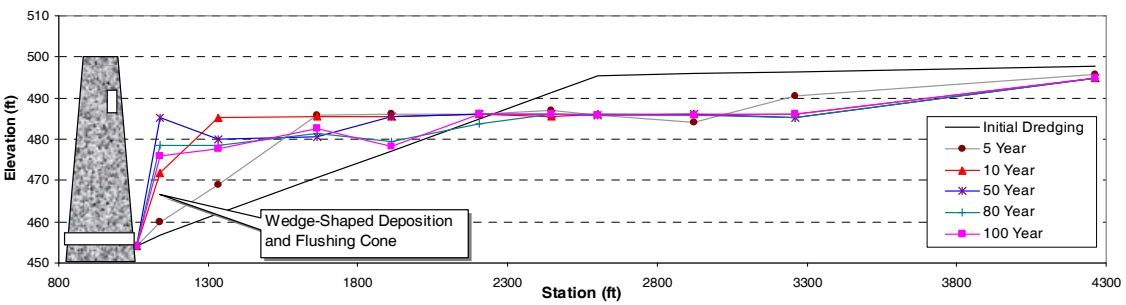

Figure 15. Time series changes of the reservoir bed profile (Using Current Operating Criteria).

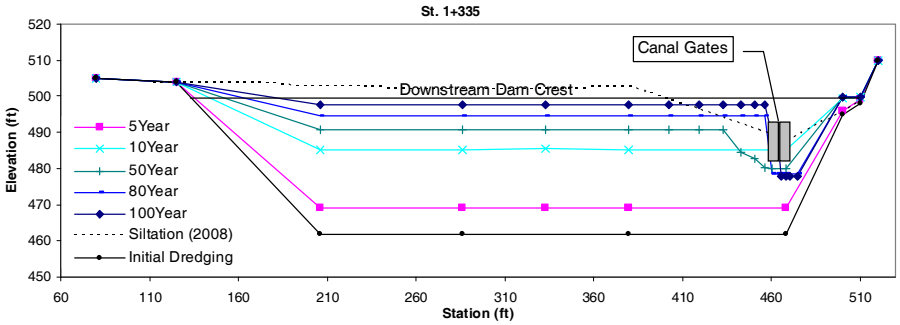

Figure 16. Simulated cross section variations and point bar development at channel bend (Using Current Operating Criteria).

6.2.5 Comparison of desiltating efficiencies

Efficiency of flushing sediment through the reservoir is important in determining the feasibility of flushing operations (Talebbeydokhti and Naghshineh, 2004). With respect to the amount of water usage and the value of flushed sediment, flushing efficiency F_e is defined as (Lai and Shen, 1996, and Brandt, 2000)

$$F_e = \frac{V_{os} - V_{is}}{V_w} \tag{17}$$

where V_{os} = volume of flushed sediment in the time interval Δt; V_{is} = newly-added volume of deposits from the upstream sediment supply in Δt, and V_w = water volume used in Δt. In this study, flushing efficiency of the four cases are estimated over time as shown in Figure 17. The flushing efficiency is approximately less than 0.01% in average because of the constraints of a low flow during the non-irrigation season and the limit of turbidity by increasing 10 NTU. The results indicate that Alternative II with using the proposed reservoir operation appears to be the most efficient de-siltation plan using river flow. The worst efficiency in the first 60 years is the one using the current operating criteria. The flushing efficiency of Alternative III with using the proposed operation would decrease over time and then, become the worst than other plans after 60 years.

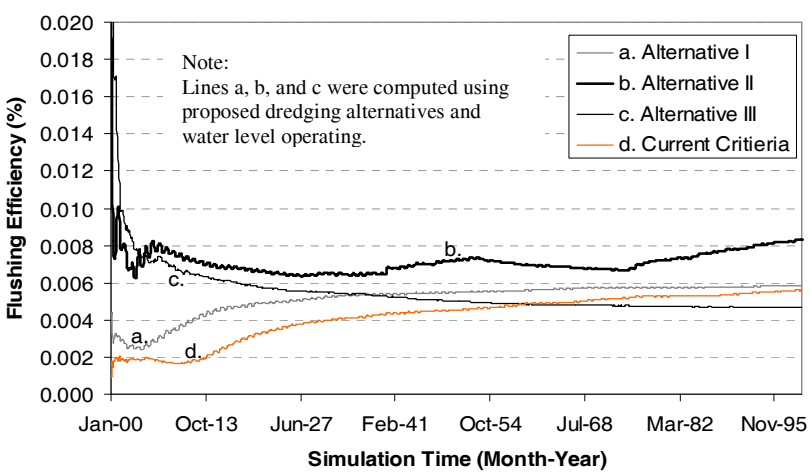

Figure 17. Flushing efficiency v.s. simulation time.

6.3 Proposed Operating Life

The challenge in the evaluation of projects which promote sustainability of reservoirs is to determine realistic reservoir life (Palmieri etal, 1998). Based on the considerations of the proposed dam operation, sediment transport modeling, the general design life of the mechanical equipments, siltation stability, and upstream condition changes, a proposed operating life selecting Alternatives I or II with the proposed reservoir operation is estimated to be at least 50 years.

VII. CONCLUSIONS AND RECOMMENDATIONS

The conclusions and recommendations are described in following sections.

7.1 Conclusions

1. In order to restrict the point-bar development and increase the sediment flushing/sluicing efficiency, a combination of siltation dredging and revising the reservoir operation were recommended to perform a long term operation. According to water turbidity samples, the maximum allowable released flow of 400 cfs should be used in conformity with environmental regulations during non-irrigation season and to optimize sediment sluicing and irrigation during irrigation season. These revisions could result in a better flushing efficiency than the current dam operating criteria and would decrease the expense of regular maintenance.
2. Based on limit information available, GSTARS 3.01 model was used to simulate the processes of sediment transport and siltation sluicing/flushing behind the Willwood Dam as well as simulated the sediment transport at the channel bend by using stream tubes.
3. According to simulations based on the dam operations and siltation dredging alternatives, the proposed reservoir operation and the siltation dredging Alternative II would perform the best flushing efficiency and would provide an estimated operating life of at last 50 years
4. Reservoir operation significantly affects siltation formation in the reservoir. According to simulation results, they indicate that siltation elevation at the upstream face of the dam is mainly dominated by water level drawdown during non-irrigation season.

7.2 Future Phases

To evaluate possible alternatives, operating revisions, study reliability, and expected project goals, the following items need to be addressed to provide a comprehensive study plan for this project: 1. Sediment sampling for sediment transport model revision and calibration based on past-rehabilitation conditions.; 2. Canal gate flow discharge coefficient calibration.; and 3. Dam operating criteria revision.

Acknowledgements

This paper is based partially on work supported by Engineering Associates, Willwood Irrigation District, and Wyoming Water Development Commission, Wyoming, U.S.A. The authors appreciate the supports and cooperation of the irrigation district manager, Tom Walker, and his staff with useful historical information and data. The financial

support provided by Chris Abernathy, Project Manager of the Wyoming Water Development Commission was critical to the study.

Reference

Atkinson, E. (1996). *The feasibility of flushing sediment from reservoirs,* Report OD137, HR Wallingford.

Anders, B. S. (2000). *Reservoir Desiltation by Means of Hydraulic Flushing: Sedimentological and Geomorphological Effects in Reservoirs and Downstream Reaches as* Illustrated by the Cachi Reservoir and the Revenatazon River, Costa Rica, Institute of Geography, Faculty of Science, University of Copenhagen, ISBN 87-87945-36-3.

Fan, J. and Jiang, R. (1980). "On methods for the desiltation of reservoirs." International Seminar of Experts on Reservoir Desiltation, Tunis, 1980, Com 14, p. 17.

Hong, S. and Chen, Z. (1992). "Erosional and depositional changes and their effects during different operation periods at the Sanmenxia Reservoir." Sediment Management, *Proceedings of the 5th International Symposium on River Sedimentation*, Karlsruhe, 1992, University of Karlsruhe, Institute of Hydraulic Structures and Agricultural Engineering, Vol. 2, pp. 943-952.

Hu, C. (1995). "Controlling reservoir sedimentation in China." *Hydropower and Dams*, March, pp. 50-52.

Ji, U. (2006). *NUMERICAL MODEL FOR SEDIMENT FLUSHING AT THE NAKDONG RIVER ESTUARY BARRAGE*, Ph. D. dissertation, Colorado State University in Fort Collins, USA.

Lai, J., S. & Shen, H. W. (1996). "Flushing sediment through reservoirs." *Journal of Hydraulic Research*, 34(2).

Lin, B. (1992). "Watershed and sediment management in China." *Sediment Management, Proceedings of the 5th International Symposium on River Sedimentation*, Karlsruhe, 1992, University of Karlsruhe, Institute of Hydraulic Structures and Agricultural Engineering, Vol. 1, pp. 5-18.

Locher, F.A. and Wang, J.S. (1995). "Operation procedures for sediment bypassing at Cowlitz Falls Dam. Sediment Management and Erosion Control on Water Resources Projects." Fifteenth Annual USCOLD Lecture Series, San Francisco, California, May 15-19, 1995, pp. 75-90.

Morris, G.L. and Fan, J. (1997). *Reservoir Sedimentation Handbook*, McGraw-Hill Professional, ISBN: 978-0070433021

Palmieri, A., Shah, F. and Dinar, A. (1998). "Reservoir sedimentation and the sustainable management of dams." World Congress of Environmental and Resource Economists, Venice.,

Qian, Y., Cheng, X., Fu, C. and Shang, H. (1993). "Influence of the upstream reservoirs on the adjustment of downstream alluvial channel." *International Journal of Sediment Research*, Vol. 8(3), pp. 1-20.

Stone & Webster Engineering Corporation (1982).*Willwood Hydroelectric Project Report on Feasibility Study*, submitted to the Willwood Irrigation District, Willwood Wyoming.

Su, Y. (1995). "Operational mode of the reservoirs in heavily sediment-laden rivers in China." *HYDRA 2000, Proceedings of the XXVIth Congress of the IAHR*,

Volume 4, the Hydraulics of Water Resources and Their Development, London, 11-15 Sep., 1995, J. Gardiner, ed., Thomas Telford Services Ltd, London, pp. 278-283.

Talebbeydokhti, N. and Naghshineh, A. (2004). "Flushing sediment through reservoirs." *Iranian Journal of Science & Technology*, Transaction B, Vol. 28, No. B1, p.119-136.

Wallingford, H. R. (1990). Sediment transport, the Ackers and White theory revised, Report SR237, England.

Wei, Y. (1986). "The silt problem in San Men Gorge Dam and its remodifying project." Journal of Water Resources, Vol. 5(2), pp. 188-192.

Wyoming, Bureau of Reclamation, State of Wyoming Department of Environmental Quality and the Willwood Irrigation District (1982). *Operating Criteria, Willwood Diversion Dam, Shoshone Irrigation Project*.

Xia, M. and Ren, Z. (1980). "Methods of sluicing sediment from Heisonglin Reservoir and its utilization downstream." International Symposium on River Sedimentation, Beijing 1980. Li B., ed., pp. 717-726.

Yang, C. T. and Simões, F. J. M. (2002). *User's Manual for GSTARS3 (Generalized Sediment Transport model for Alluvial River Simulation version 3.*0), U.S. Department of the Interior Bureau of Reclamation, Technical Service Center, Denver, Colorado.

Yang, C. T. and Shih, H. M. (2009). *User's Manual for GSTARS3.01 (Generalized Sediment Transport model for Alluvial River Simulation version 3.01*), Hydroscience and Training Center, Colorado State University, Fort Collins, Colorado.

Zyrjanov, A. G. (1973). "Dynamics of reservoir silting of Ouchi-Kurgan Hydroelectric Station and experience of preventing of sediment siltation." *Hydrotechnical Construction*, No. 1, pp. 32-37

Managing Reservoir Discharge through Accurate Flow Measurement

Bryan J. Heiner[1] and Steven L. Barfuss[2]

[1] Graduate Research Assistant, Utah State University, Department of Civil and Environmental Engineering, Utah Water Research Laboratory, 8200 Old Main Hill, Logan, UT 84322-8200; PH (435) 797-3171; email: bryan.heiner@aggiemail.usu.edu

[2] Research Assistant Professor, Utah State University, Department of Civil and Environmental Engineering, Utah Water Research Laboratory, 8200 Old Main Hill, Logan, UT 84322-8200; PH (435) 797-3214; email: barfuss@engineering.usu.edu

Abstract

Reservoirs store water for many important purposes in today's world, including culinary, irrigation, recreation, and flood control. In order to ensure that this valuable resource is wisely utilized, the discharge from reservoirs must be managed through accurate flow measurement. Unfortunately many reservoirs do not have measurement structures that allow flows to be monitored or accurately managed. It is not uncommon to have reservoir discharge set by historical arbitrary methods, such as opening a valve a certain number of turns on a certain day or keeping downstream river banks or channels at a certain elevation. While historical methods are better than nothing, consistent releases in these cases usually depend on constant reservoir head or stable stream beds.

In cases where reservoir discharge flow measurement equipment is available, special care must be taken to ensure that the flow measurement equipment is properly maintained and the flow measurements are performed correctly. Multiple methods or types of flow measurement are commonly used to measure discharge release from reservoirs. These include but are not limited to rated sections, flumes and weirs for open channel discharge or magnetic and ultrasonic meters for pressurized pipes. This paper discusses various types of measurement errors that are commonly found in field applications and the need for regular calibration and maintenance. The paper also addresses when standard calibrations or discharge rating tables can be used, and when custom calibrations are necessary. Small inaccuracies may appear to be insignificant, but over time can accumulate to large volumes of mismanaged water. Field data is used to demonstrate and contrast both accurate and inaccurate flow measurements and how each affects water users and contributes to reservoir management.

Introduction

Most dry and arid regions of the world deal with problems related to limited water resources. To enable water to be stored and used over time dams are constructed to create water storage reservoirs. Reservoirs were built in large quantities during the mid-twentieth-century, when the United States built a large number of dams on all scales (Nicklow, 2007). Where dams are built to release water over time it is essential that the release of reservoir water be accurately monitored to enable appropriate distribution over the longest available period. Releasing too much or too little water may result in shortages or unexpected losses due to mismanagement. Unfortunately no work has been found by the authors that directly discusses reservoir release and its accuracies. This paper will discuss the types of measurement devices that are available for monitoring reservoir releases, their expected accuracies, and what can be done to correct any inaccuracies.

Measurement Methods

It is not uncommon for reservoirs to have no accurate method to measure the discharge or release from the reservoir. In some cases, historical methods are the only way known to manage the reservoir. From field experience it has been found that one common type of historical reservoir management is to open the low level outlet valve a certain number of turns on a certain day. The same method issued from year to year is passed down from one reservoir operations manager to another. It may even be recorded or written on the wall next to the low level outlet works. Another common method that has been found in the field is to mark a height in the downstream channel and release water according to the depth of flow during a certain period of time. Although historical and habitual methods are better than nothing, great inaccuracies can occur using these approaches and water is easily mismanaged. To help water distributors and reservoir operators manage the release of water, many open channel and closed conduit measurement structures or devices are available. These structures should be designed and built during construction but in necessary, can be added to already existing systems.

Open Channel Measurement Methods –

Open channel measurement structures vary widely depending on specific applications. Even though many open channel measurement devices are available, this section focuses on just rated sections, long throated or ramp flumes, and parshall flumes.

Rated Sections – Rated sections consist of stage height vs. elevation charts or graphs. These charts and graph are site specific and are created using the velocity-area principle (USBR, 2001). Current meters are often used to determine the mean velocity of the channel or stream. The mean velocity is then multiplied by the area of the cross section at the particular stage. Several stages must be completed and combined to form a rating curve for the specific site. Rated sections can be accurate

to +/- 10 percent, but this accuracy often decreases over time unless consistent ratings are performed (USBR, 2001).

Long Throated or Ramp Flumes – These flume types are emerging as a new and efficient open channel flow measurement device because of their simple shapes and ease of install (Bos et al., 1991). Long Throated flumes are typically site specific having unique dimensions and sizes based on channel geometries or design discharges. Long throated flumes often consist of a ramp placed into the bottom of a channel with a staff gauge and stilling well installed upstream to measure head. When properly calibrated long throated flumes can be accurate to +/- 2 percent up to 90 percent submergence (USBR 2001).

Parshall Flumes – Parshall flumes were developed at Colorado State University from 1915-1922 as a simple way to measure discharge in open channels (Cone, 1917; Parshall, 1926; Merkley, 2008). Parshall Flumes consist of a flat sill that is converged to a set throat width that correspondingly forces the water to pass through critical depth. Parshall flume sizes are available from 1 inch to 50 feet, and unlike many other structures geometric similarity does not exist, meaning that a 1-foot flume is not a scaled version of a 20-foot flume. Because of the lack of similarity, each specified flume size has its own calibration and corresponding rating curve. Parshall flumes can be accurate to +/- 3_to_5 percent up to 50 percent submergence on flumes with 3 inch throats or less; and +/- 3_to_5 percent up to 80 percent submergence on flumes with throats greater than 8 ft (USBR, 2001).

Pressurized Conduit Measurement Methods –

Another common method for flow measurement occurs in pressurized conduits. These measurement devices are often installed on the outlet works of the reservoir. Many different devices are available for measuring flow in pressurized conduits. This section focuses on two of the most commonly used devices to monitor reservoir release; magnetic flux and ultrasonic flow meters.

Magnetic Flux Meters – These meters use the principle of Faraday's law of induction to calculate a flow passing through a closed conduit. As a fluid passes through an applied magnetic field an electrical voltage is generated that is directly proportional to the speed of the passing fluid (Repas, 2007). Magnetic Flux meters contain no moving parts and can vary in size from 0.1 to 72 inch. When properly installed and calibrated, magnetic flow meters can be accurate up to +/- 0.25 percent of the upper range flow boundary (Miller, 1996).

Ultrasonic Meters – These meters emit sounds waves that propagate through the fluid and can be installed without intrusion of the flow area. Ultrasonic meters come in two varieties doppler and transit time. Doppler ultrasonic meters send ultrasonic signals across the pipes and measure the frequency change due to the movement of particles in the fluid. Transit time ultrasonic meters send sound waves across the conduit and measure the time difference between the sound waves traveling upstream

compared to those traveling downstream (Miller, 1996). Ultrasonic meters are available from 1 to 108 inch depending on transducers and meter type, and offer accuracies of up to 1_to_5 percent of the upper flow boundary (Miller, 1996).

Open channel and closed conduit flow measurement devices are installed in the stream bed immediately downstream of the reservoir, or the low level outlet works to reservoirs respectively. Unfortunately, flow measurement devices require that design specifications and installation procedures be correctly followed, if not accurate flow measurements are rarely possible. Table 1 below contains a summary of the flow measurement devices discussed in this paper and their specified accuracies if design requirements are met.

Table 1 - Summary of Flow Measurement Devices

Measurement Device	Type	Accuracy
Historical Methods	Either	-
Rated Sections	Open Channel	+/- 10%
Long Throated Flumes	Open Channel	+/- 2%
Parshall Flumes	Open Channel	+/- 3_to_5%
Magnetic Flux Meter	Pressurized Conduit	+/- 0.25%
Ultrasonic Meter	Pressurized Conduit	+/- 1_to_5%

Determining Flow Measurement Accuracies

Flow measurement devices are capable of certain levels of accuracy when installed and operated under specified design conditions. It is uncommon for flow measurement devices located downstream of reservoirs to be installed under ideal conditions because most small to medium sized dams were not initially designed to have flow measurement. Because current water resources have become an item of consistent legal and political discussion, accurate flow measurement on water distribution and reservoir release have become increasingly important in this day and age. Consequently many reservoirs have added flow measurements structures to exiting channels and pipes to provide opportunities for real time flow measurement from the structure. A study conducted at Utah State University, Utah Water Research Laboratory (UWRL) has investigated the accuracies of flow measurement on reservoir releases in Utah. The following describes the methods used to determine the accuracies for open channel and pressurized pipe flow measurements.

Open Channel Flow Measurements –

Where applicable, open channel flow measurements made at thirteen sites in the state of Utah were evaluated by current metering. A pygmy meter and counter attached to a four foot top set rod were generally used unless special equipment was necessary. A cross section was selected perpendicular to the stream or channel flow, and was divided into several sections called verticals. The average velocity in each vertical

section was determined by the six-tenths-depth method, which, as stated by the Water Measurement Manual from the Bureau of Reclamation consists of measuring the velocity at 0.6 of the depth from the water surface. Each vertical section had two or more velocity measurements taken over 40 second intervals for repeatability. Discharge was then calculated at each flow rate using the Mid Section Method (Figure 1), which utilizes the area-velocity principle. The discharge is calculated in each section by multiplying the section's average velocity by the area. Corrections for edge sections are applied and the total discharge is found by summing the discharge in each vertical section (SonTek/YSI, 2007; ISO, 2007; Merkley, 2008; USBR, 2001).

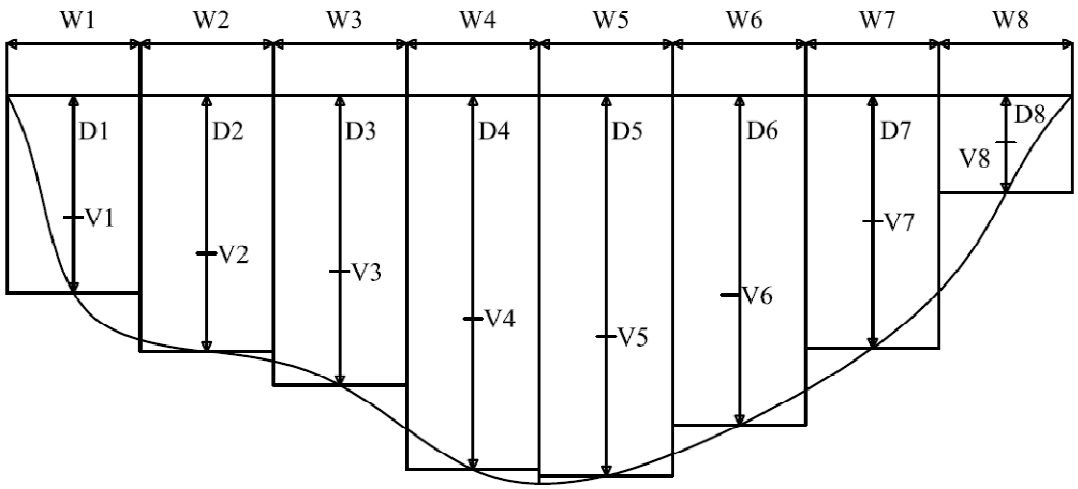

Figure 1 - Mid Section Method Calculations Illustration

Pressured Pipe Flow Measurements –

To evaluate the accuracy of pipe flow measurements at eight sites in the State of Utah, a Fuji Portaflow X ultrasonic meter with FLD-41 transducers was used as a reference meter. The Fuji meter was selected because of its ease of installation, portability, wide range of pipe sizes and accuracy. The reference meter was calibrated at the UWRL, producing output flow to +/- 3% without calibration and +/- 1% after calibration and maintaining less than 0.25% uncertainty. Where available, the Fuji meter was laboratory calibrated on pipes similar to field installation before field testing took place. Laboratory calibrations of the Fuji reference meter were performed on nine sizes of pipe, including: 6, 12, 14, 16, 18, 20, 24, 36, and 42-inch steel. In all cases the reference meter was installed according to manufacturer specifications. Calibrating the reference meter on such a wide range of pipes confirms the accuracy of the meter on possible pipe sizes encountered in the field. Transducers were installed according to the manufacturer's specifications, so that at least 10 diameters of straight pipe were provided both upstream and downstream of the transducer location from the nearest obstructions. This specification ensured that acceptable flow conditions occurred at the reference meter location. Flow and time were logged for each test allowing synchronization of time and flow from each meter.

Discussion of Errors and their Corrections

Flow discharge accuracies from twenty-one reservoirs have been investigated during the UWRL study. Of the twenty-one reservoirs, five used magnetic meters, three used ultrasonic meters, and thirteen used parshall flumes to measure reservoir releases. Each reservoir discharge was determined for accuracy as described previously. Table 2 contains a summary of the results. Of the twenty-one measurement devices that were tested, three of the five magnetic meters, all three ultrasonic meters, and seven of thirteen parshall flumes were not measuring flow to the levels of accuracy that design specifications claim.

In addition to the twenty-one flow measurement structures, many other sites were visited that a calibration were not possible because of dangerous conditions, lack of access to pipe or deep channels, insufficient pipe or upstream channel, or constraints on time. When these conditions existed design specifications were verified as much as possible and discrepancy and possibilities of error were noted. When variable reservoir discharge was possible, multiple flows were calibrated. The minimum and maximum errors are reported in Table 2 columns 3 and 4. In most cases the reservoir release was not able to be adjusted and only one flow rate was checked three times. These values are reported in Table 2 column 5.

Table 2- Summary of Results

Site	Type of	Measured Error		
#	Measurement Device	Min	Max	Average
(1)	(2)	(3)	(4)	(5)
1	Magnetic	-	-	14.29%
2	Magnetic	-	-	-17.14%
3	Magnetic	-	-	1.24%
4	Magnetic	-	-	-2.06%
5	Magnetic	-	-	-3.25%
6	Ultrasonic	-	-	-3.89%
7	Ultrasonic	-	-	6.80%
8	Ultrasonic	-	-	4.21%
9	Parshall	-	-	6.12%
10	Parshall	-	-	2.30%
11	Parshall	-	-	0.98%
12	Parshall	-	-	9.71%
13	Parshall	-	-	3.73%
14	Parshall	-	-	-3.75%
15	Parshall	-	-	-0.44%
16	Parshall	-	-	-1.70%
17	Parshall	-	-	-6.54%
18	Parshall	-	-	5.73%
19	Parshall	2.42%	30.00%	-
20	Parshall	5.00%	12.00%	-
21	Parshall	-12.00%	27.00%	-

Unfortunately, a complete description of the results and problems associated with each individual site is not possible in this document. Accordingly, only a brief overview of findings and possible errors associated with the different measurement devices tested will follow.

Open Channel Measurement Devices –

The following items were found to affect accuracy in open channel measurement devices during this study.

Correct rating – Using the correct rating is essential to rated sections, long throated and parshall flumes. If the incorrect rating is used then substantial errors can occur. Incorrect ratings are often used due to poor record keeping, poor communication, ignorance, and out of date calibrations. Changing channel geometry and upstream flow conditions can also cause ratings to change. For these reasons, rating curves for the measurement structure should be regularly verified.

Correct placement of staff gauge – Most manufacturers specify the correct location of staff gauges and stilling wells for their devices. If the staff gauge or stilling well is located at a different location than specified by the manufacturer, the standard rating will not give accurate flow measurements. For example the correct location for the staff gauge or stilling well on a parshall flume is 2/3A upstream from the throat, where A is defined as the length of the approach section (Parshall, 1926; USBR, 2001). If the staff gauge of stilling well is at a different location, then the associated rating will not be accurate and a calibration of the device will be necessary.

Approach Conditions – Most open channel measurement structures specify sub-critical upstream flow. If approach flows are not sub-critical upstream of the structure or approach flow is skewed due to sediment or debris, accurate head readings are difficult to obtain and the standard rating may not apply. To enable uniform sub-critical flow upstream of the device a settling or stilling basin can be dug upstream to increase the depth and slow velocities; however it is recommended that if the control width is greater than 50 percent of the approach channel, then 10 average approach flow widths of straight unobstructed approach are required. If the control width is less than 50 percent, then 20 control widths of straight unobstructed approach are required (Bos et al., 1991; USBR, 2001). If sediment or debris has been deposited upstream of the structure, removing the sediment prior to a re-calibration of the device is suggested.

Correct Dimensions – Design specification must be followed to obtain accurate flow measurements. This is especially important for parshall flumes which are not geometrically similar. One cause of incorrect geometry arises when installation procedures are not closely monitored and specifications are not checked. This can occur when construction workers are not informed of the importance to have tight

tolerances. When dimensions of field installation do not match standard flume geometries, custom calibrations are necessary.

Submergence – If design submergence levels are exceeded, then corrections must be applied to obtain accurate flow measurements. If submergence corrections are not applied, errors up to 60 percent are possible (USBR, 2007). When submergence criteria has been exceeded it is necessary to use a rating curve created under submerged conditions (USBR, 2001).

Settlement – Many individuals have looked at the effects of settlement in parshall flumes (Abt and Staker, 1990; Abt et al, 1994; Genoves et al, 1993; Apt et al, 1995). The results of these studies apply corrections to settlement of small flumes, and corrections for a combination of settlement and submergence. Settlement of +/- 10 % can amount to 32 percent deviation in flow rate (Abt and Staker, 1990; Genoves et al, 1993). When mixed with submergence, errors can be substantially higher (Abt et al, 1995). Corrections to settlement with and without submergence are available and must be applied in order to achieve accurate flow measurements.

Pressurized Conduit Measurement Devices –

Correct Inside Diameter – One of the largest sources of error for Ultrasonic meter installations is not having the correct pipe material, wall thickness or inside diameter entered into the meter program. Errors often occur because the user does not have an acceptable method for measuring the ID of the pipe or it is incorrectly entered in the device. This is a relatively simple correction to perform if the proper pipe wall thickness measurement equipment is used.

Approach Conditions – All meter manufacturers supply upstream and downstream straight pipe requirements for correct meter installation. Typically, ten diameters of straight unobstructed pipe upstream of the meter provide acceptable flow conditions, although many hydraulic texts suggest 20 diameters. If excessive turbulence and flow disturbances are upstream of the meter, errors in flow will occur. New installations should specify adequate straight pipe for metering. Existing installations may require custom calibrations, with field pipe conditions reproduced in a laboratory.

Cavitation – Cavitation causes excessive levels of vibration and turbulence into pressurized pipe flow and may cause errors to arise in flow measurements. Installing a meter downstream of a pump or control valve often results in large errors.

Correct installation – To enable accurate flow measurements all pipe meters must be installed according to manufacturer's specifications. Many Ultrasonic meter manufacturers specify that transducers be installed on pipe that is free of excessive rust and scaling and in the correct locations to receive strong signal strength. If the installation does not meet manufacturer's specifications, the meters will not measure flow accurately.

Reservoir discharge flow measurement errors may seem small and insignificant, but over time these errors accumulate to large volumes of mismanaged water. For example, site 17 uses a parshall flume to measure reservoir discharge and at the time of the field calibration indicated a -6.54 percent deviation in flow measurement accuracy from the actual flow. This means at the time there was more water being released from the reservoir than the staff gauge reading indicated. For example, if the staff gauge reading indicates 4.71 cfs from the flume (0.55 ft), the actual flow would be 5.03 cfs. Consider a 6 month irrigation season supplied from a 1000 ac-ft reservoir with an average reservoir release of 5 cfs and the error in measurement similar to site 17, the total volume of excess water released would be around 117 ac-ft. At first glance 117 ac-ft doesn't seem substantial, but in actuality the 117 ac-ft of excess water released is over 10 percent of the reservoirs capacity. In comparison, a separate study conducted at the Utah Water Research Laboratory determined the accuracy of reservoir release of a larger reservoir to be around the same as site 17. When the flows were monitored over a single month (July) 2000 ac-ft more water was released than supposed (Barfuss and Jensen, 2007).

Conclusions

In order to ensure that reservoir water is wisely utilized, the discharge from reservoirs must be managed through accurate flow measurement. Both open channel and pressurized pipe measurement devices can accurately measure reservoir releases if proper design criteria are followed. Of twenty-one sites investigated in Utah only 13 were measuring within accuracy levels specified by manufactures and flow measurement manuals. Inaccuracies occur in many field installations because reservoirs were not initially constructed with flow measurements in mind. When existing reservoirs have flow measurement devices installed later, ideal or design specification may not be available and flow measurement devices may need custom calibrations. Other errors were caused from improper installation to lack of maintenance or improper operation. Over time, flow measurement errors can accumulate to large volumes of mismanaged water. Management of reservoir releases is becoming more important today due to the increased need for water resources and the proper management of those resources. If flow measurement devices are properly maintained and corrections are made to structures producing inaccurate results, then flow reservoir management will be improved and less water will be wasted.

References

Abt, Steven R., Genovez, A., and Florentin, B. (1994). "Correction for Settlement in Submerged Parshall Flumes." *J. of Irrigation and Drainage Engineering.*, ASCE, 120(3), pp. 676-682

Abt, Steven R., and Staker, Kenneth J. (1990). "Rating correction for lateral settlement of Parshall Flumes." *J. of irrigation and Drainage Engineering.*, ASCE, 116(6), pp. 797-803.

Apt, Steven R., Florentin, C. Bradley., Genovez, Ana., Ruth, and Bryan C. (1995). "Settlement and Submergence Adjustments for Parshall Flume." *J. of Irrigation and Drainage Engineering.*, ASCE, 121(5), pp. 317-321.

Barfuss, S., and Jensen J. (2007). "Evaluation of Flow Measurement Accuracies at Piute Dam." Utah Water Research Laboratory, Report no. 1795.

Bos, M.G., J.A. Replogle, and A.J. Clemmens. (1991). "Flow Measuring Flumes for Open Channel Systems." *American Society of Agricultural Engineers.* Republication of book by same title, originally by John Wiley and Sons, New York, 1984, pp. 321.

Cone, V.M. (1917). "The Venturi Flume." *J. of Agricultural Reserch*, 9(4), pp. 115-123.

Genoves, A., Abt, S., Florentin, B., and Garton, A. (1993). "Correction for Settlement in a Parshall Flume." *J. of Irrigation and Drainage Engineering*, ASCE, 119(6), pp. 1081-1091.

International Standard, ISO 748. (2007). "Hydrometry measurement of liquid flow in open channels using current meters or floats" 4th edition, Web www.iso.org, Published in Switzerland

Merkley, Gary P. (2008). "Irrigation Conveyance and Control Flow Measurement & Structure Design", Lecture Notes, Class BIE 5300/6300 Utah State University.

Miller, Richard W. (1996). *Flow Measurement Engineering Handbook* Ed. 3, McGraw-Hill, Boston, MA.

Nicklow, John W. (2007). "DAMS" http://www.waterencyclopedia.com/Da-En/Dams.htm, Viewed 10/17/2007.

Parshall, R.L. (1926). "The Improved Venturi Flume." Transactions, ASCE, 89, pp. 841-851

Repas, Robert ed. (2007). "Magnetic Inductive Flowmeters." Machine Design, 79(19), pp. 63-63

SonTek/YSI Inc., YSI incorporated. 2007. *FlowTracker® Handheld ADV® Technical Manual Firmware Version 3.3 Software Version 2.20,* San Diego, CA 92121-3091 USA.

U. S. Department of the Interior, Bureau of Reclamation (USBR). (2001). *Water Measurement Manual* 3rd Edition, U.S. Government Printing Office, Washington, DC.

U. S. Department of the Interior, Bureau of Reclamation (USBR). (2007). *Water Operation and Maintenance Bulletin*, NO. 180, U.S. Government Printing Office, Washington, DC.

Numerical modeling of flushing process in Dez dam reservoir by HR Wallingford method

Ali Khosronejad[1], Afshin Ashrafzadeh[2], Majid Vazifedoust[3]
[1]Assistant Professor of University of Guilan, Rasht, Iran, PO. Box: 1314
[2]Assistant Professor of University of Guilan, Rasht, Iran, PO. Box: 1314
[3]Assistant Professor of University of Guilan, Rasht, Iran, PO. Box: 1314

ABSTRACT

Dez dam is one of the key dams in Iran. It is 203 m high with a reservoir of 2.3 BCM volume. This double arch dam has been constructed in a narrow gorge in 1962, southern west of Iran. It has three irrigation outlets at level of 222.7 m asl, two power intakes at elevation of 270 m asl. No bottom outlet have been designed and installed for Dez dam and consequently the sediment-entering reservoir cannot be evacuated easily. Considering an annual 15.8 million cubic meter sediment inflow into the reservoir, the bed level is increasing about 1.2 meter per year and therefore it is very necessary to take an appropriate measure saving dam reservoir.
One of existing method to save dam reservoir is to flush the sediment out through existing bottom outlets.
In this study, the feasibility and efficiency of pressure and free flow sediment flushing techniques have been studied and some good points are presented. The results of present study shows that the flushing method cannot resolve the sedimentation problem of Dez dam and it must be applied jointly by other methods to save the reservoir from being decommissioned.

INTRODUCTION

In the present study, the Wallingford (Developed by HR Wallingford, UK) model has been applied to Dez dam sedimentation problem to evaluate the efficiency of flushing method solving this problem. 36 different scenarios, for three different case: full desiltation of reservoir (against annual inflow sediment), evacuation of annual deposited inflow sediment by turbidity currents, and releasing the sediment accumulated in the area close to dam annually (within 1000 m distance from dam) are considered and simulated by this simple empirical model. Consequently, 108 different test case has been considered, and the flushing efficiency of all cases are evaluated.
On the basis of HR Wallingford recommendations, as model developer, the results of this model should be interpreted in an appropriate way by a specialist team to avoiding any wrong conclusion. Accordingly, the results will be presented along with related interpretations.

MOST EFFECTIVE PARAMETER AFFECTING THE FLUSHED SEDIMENT

In this study, analysis on various scenarios shows that the most effective parameter of flushing is the water level gradient in reservoir at the beginning and end of flushing. One other effective parameter is the duration of flushing and flow discharge from outlets.

Figure 1 shows the effect of water level gradient on the volume of sediment released from reservoir and figure 2 illustrates the discharge effects on the volume of released sediments.

The water scarcity is notably important for KWPA and therefore just pressure flushing is possible for Dez dam not free flow flushing. In Pressure flushing, during flushing the water level will lowered but free flow through reservoir won't happen and so relatively small amount of sediment will be release and a wedge shape cone will shape just in front of flushing device entrance. The shape of this wedge will soon be stable and outflow water will be clear as well. In free flow flushing, the water level will be drawn down during flushing even till a river shape flow through reservoir to be created. Such shape of flow through reservoir naturally follows by high turbulence flow capable to remove huge amount of sediment from reservoir (in comparison to pressure flushing). This type of flushing will have tremendous impact on environment and also needs huge amount of water to be flushed out of reservoir. Thus, in this report, the flushing meant by pressure flushing not free flow flushing.

BRIEF DESCRIPTION OF MODEL

a basic equation is used in Wallingford model to estimate the sediment discharge from outlets during flushing process. This equation is an empirical relation derived and verified with field data in different countries.

$$Q_S = \psi \frac{Q_f^{1.6} S^{1.2}}{W^{0.6}} \quad (1)$$

Where

ψ : Constant related to sediment type, size and flushing type which is 1600 for this case

Q_f : Flow discharge

S : water level slope during flushing

The output table of Wallingford modeling results (table 1) contains: Column 1 is scenario number, column 2 is flow discharge, column 3 is flushing duration, water level during flushing in column 5 to 7 and maximum sediment released out volume at column 8.

The trap efficiency of Dez dam reservoir by Wallingford model has been estimated 91.2 percent.

OUTPUT TABLE OF WALLINGFORD MODEL

The results of flushing modeling by Wallingford model is presented through a table of results. The main important items in this table to decision making and evaluation of flushing efficiency are column 9 to 14 (see table 1) and the most important one is column 9 in which the *SBR* function is presented. The *SBR* shows the ratio of total output sediment during flushing to annual inflow sediment (during pressure flushing). If *SBR* is greater than 1 then a sustainable solution will achieved by this method otherwise another method should be tried.

By the way, the SBR_d function shows the same concept of *SBR* but for free flow flushing type and is not applicable here.

Based on the previous column results, the feasibility of flushing method for each scenario is interpreted in the end column. In this column, *F, V/H/E* means feasible with very high efficiency; *F, H/E* means feasible with high efficiency; *F, almost E*

means feasible almost efficient; and *N.F* means not efficient and need to find another sustainable way to release entering sediments.

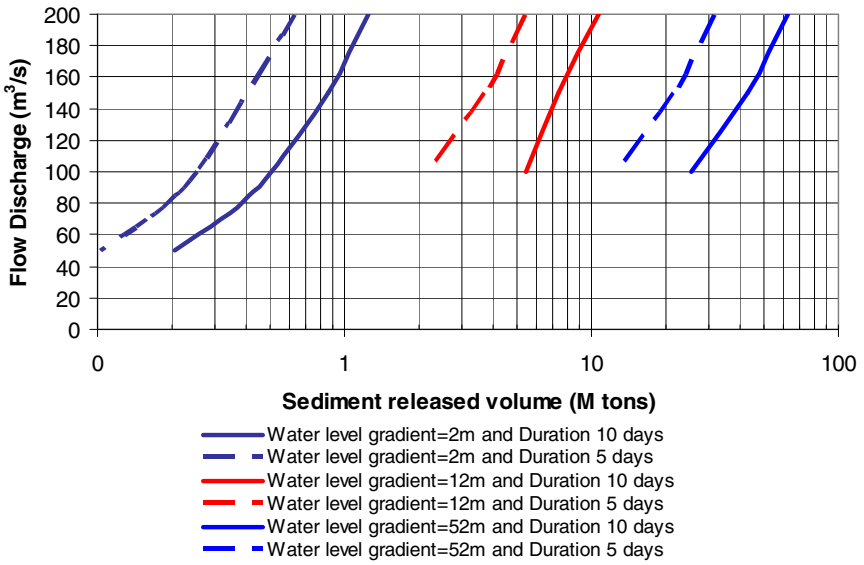

Figure 1. Water level gradient and flushing duration effects on sediment flushed out volume

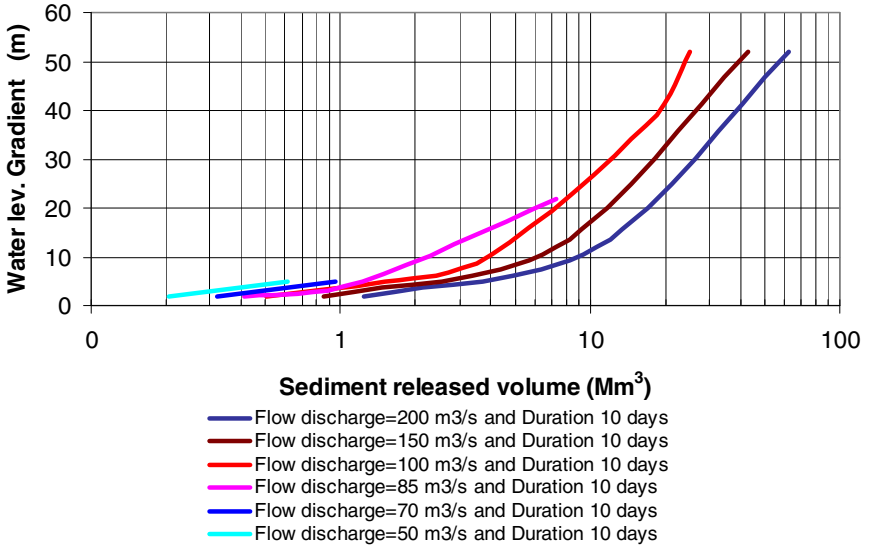

Figure 2. Water level gradient and flushing duration effects on sediment flushed out volume

EVALUATING THE EFFICIENCY OF FLUSHING METHOD TO RELEASE TOTAL INFLOW SEDIMENTS, IN DEZ DAM RESERVOIR

Total inflow sediment into reservoir, on the basis of foregoing studies is some 17,500,000 tons. Based on the results of Wallingford model, the flushing method will be sustainable if the water level gradient is more than 37 meter which requires huge

amount of water to be released and practically impossible. Furthermore lots of other difficulties will rise during flushing with such a 60 km long reservoir. By the way, the results of these cases are shown in the table 1. As it is already mentioned, the obtained results by this model should first be analyzed by experts and then taking into account. The interpretation of this writer is that the flushing method is not capable to solve the Dez reservoir sedimentation problem.

Table 1. Results of Wallingford Model for different scenarios of releasing total annual inflow sediments; SBR >1 efficient, <1 not efficient; F, V/H/E: feasible with very high efficiency, F, H/E: feasible with high efficiency, F: feasible almost efficient, N.F: not efficient, needs another sustainable way to release entering sediments

Scenario N°	Discharge (m^3/sec)	Duration (day)	Mean annual sediment inflow (ton)	Mean water level during flushing (m)	Water gradient (m)	Water level before flushing (m)	Max. sediment released D/S (ton)	SBR	LTCR	DDR	FWR	TWR	SBR_d	Feasibility and efficiency
1	200	10		300	52		62'097'000	**3.89**	0.39	0.29	2.78		32.33	**F, V/H/E**
2	200	5		300	52		31'048'000	**1.94**	0.39	0.29	2.78		16.17	**F, V/H/E**
3	150	10		300	52		42'722'000	**2.68**	0.36	0.29	2.41		20.41	**F, V/H/E**
4	150	5		300	52		21'361'000	**1.34**	0.36	0.29	2.41		10.20	**F, V/H/E**
5	150	5		310	42		16'532'000	**1.04**	0.28	0.23	2.41		10.20	**F, H/E**
6	150	5		320	32		11'929'000	**0.75**	0.2	0.18	2.41		10.20	**N.F**
7	100	5		300	52		12'609'000	**0.79**	0.31	0.29	1.97		5.33	**N.F**
8	100	5		315	37		8'381'000	**0.52**	0.2	0.2	1.97		5.33	**N.F**
9	100	5		340	12		2'170'000	**0.14**	0.06	0.07	1.97		5.33	**N.F**
10	100	10		315	37		16'763'000	**1.05**	0.2	0.2	1.97		10.67	**F, H/E**
11	100	10		332	20		4'006'000	**0.25**	0.1	0.11	1.97		5.33	**N.F**
12	100	10		300	52		25'219'000	**1.58**	0.31	0.29	1.97		10.67	**F, V/H/E**
13	200	10		340	12		10688000	**0.67**	0.08	0.07	2.78		32.33	**N.F**
14	200	5		340	12		5344000	**0.33**	0.08	0.07	2.78		16.17	**N.F**
15	200	10		350	2		1245000	**0.08**	0.01	0.01	2.78		32.33	**N.F**
16	200	5		350	2		622400	**0.04**	0.01	0.01	2.78		16.17	**N.F**
17	150	10		340	12		7353000	**0.46**	0.07	0.07	2.41		20.41	**N.F**
18	150	10		350	2		856400	**0.05**	0.01	0.01	2.41		20.41	**N.F**
19	150	5	17'500'000	340	12	352	3676480	**0.23**	0.07	0.07	2.41	1.61	10.20	**N.F**
20	150	5		350	2		428204	**0.03**	0.01	0.01	2.41		10.20	**N.F**
21	100	10		350	2		505548	**0.03**	0.01	0.01	1.97		10.67	**N.F**
22	100	5		350	2		252774	**0.02**	0.01	0.01	1.97		5.33	**N.F**
23	85	10		350	2		409267	**0.03**	0.01	0.01	1.82		8.22	**N.F**
24	85	5		350	2		204634	**0.01**	0.01	0.01	1.82		4.11	**N.F**
25	70	10		350	2		317973	**0.02**	0.01	0.01	1.65		6.03	**N.F**
26	70	5		350	2		158956	**0.01**	0.01	0.01	1.65		3.01	**N.F**
27	50	10		350	2		205316	**0.01**	0.01	0.01	1.39		3.52	**N.F**
28	50	5		350	2		102658	**0.01**	0.01	0.01	1.39		1.76	**N.F**
29	100	10		347	5		1518000	**0.10**	0.02	0.03	1.97		10.67	**N.F**
30	100	5		347	5		759000	**0.05**	0.02	0.03	1.97		5.33	**N.F**
31	85	10		347	5		1229000	**0.08**	0.02	0.03	1.82		8.22	**N.F**
32	85	5		347	5		614476	**0.04**	0.02	0.03	1.82		4.11	**N.F**
33	70	10		347	5		954812	**0.06**	0.02	0.03	1.65		6.03	**N.F**
34	70	5		347	5		477406	**0.03**	0.02	0.03	1.65		3.01	**N.F**
35	50	10		347	5		616526	**0.04**	0.02	0.03	1.39		3.52	**N.F**
36	50	5		347	5		308263	**0.02**	0.02	0.03	1.39		1.76	**N.F**

EVALUATING THE EFFICIENCY OF FLUSHING METHOD TO RELEASE INFLOW TURBIDITY CURRENT, IN DEZ DAM RESERVOIR

Total inflow sediment into reservoir, on the basis of foregoing studies is some 17,500,000 tons and the fraction related to inflow density currents is estimated by Akcres about 11 to 13 percent of total. Although, the present feasibility study on the

previous data including hydrography maps, bed longitudinal profile, height-surface-volume curve of reservoir shows that the inflow sediment volume by density current is more than 50 percent of total and it is so underestimated by Akcers. Even though one considers the inflow sediment of 11 percent of total for density current, then inflow volume of sediment is about 2,000,000 tons which should be released to have a sustainable solution for dez dam sedimentation. Because, on the basis of present studies sediment coming by turbidity current can only reach the dam area.
By considering the inflow annual sediments equal to this value of 2,000,000 then the table 2 show the results of modeling by Wallingford method. As it shown in the table 2, even in this case the pressure flushing could not create a sustainable solution.

Table 2. Results of Wallingford Model for different scenarios of releasing annual inflow sediments by turbidity currents (11% of total volume); SBR >1 efficient, <1 not efficient; N.F: not efficient, needs another sustainable way to release entering sediments

Scenario N°	Discharge (m^3/sec)	Duration (day)	Mean annual sediment inflow (ton)	Mean water level during flushing (m)	Water gradient (m)	Water level before flushing (m)	Max. sediment released D/S (ton)	SBR	LTCR	DDR	FWR	TWR	SBR_d	Feasibility and efficiency
1	200	10	2'000'000	350	2	352	1'245'000	0.7	-	-	-	-	-	N.F
2	150	10		350	2		856'400	0.5	-	-	-	-	-	N.F
3	150	5		350	2		428'204	0.3	-	-	-	-	-	N.F
4	100	10		350	2		505'548	0.3	-	-	-	-	-	N.F
5	100	5		350	2		252'774	0.2	-	-	-	-	-	N.F
6	85	10		350	2		409'267	0.3	-	-	-	-	-	N.F
7	85	5		350	2		204'634	0.1	-	-	-	-	-	N.F
8	70	10		350	2		317'973	0.2	-	-	-	-	-	N.F
9	70	5		350	2		158'956	0.1	-	-	-	-	-	N.F
10	50	10		350	2		205'316	0.1	-	-	-	-	-	N.F
11	50	5		350	2		102'658	0.1	-	-	-	-	-	N.F
12	100	10		347	5		1'518'000	0.9	-	-	-	-	-	N.F
13	100	5		347	5		759'000	0.5	-	-	-	-	-	N.F
14	85	10		347	5		1'229'000	0.7	-	-	-	-	-	N.F
15	85	5		347	5		614'476	0.4	-	-	-	-	-	N.F
16	70	10		347	5		954'812	0.5	-	-	-	-	-	N.F
17	70	5		347	5		477'406	0.3	-	-	-	-	-	N.F
18	50	10		347	5		616'526	0.4	-	-	-	-	-	N.F
19	50	5		347	5		308'263	0.2	-	-	-	-	-	N.F

EVALUATING THE EFFICIENCY OF FLUSHING METHOD TO RELEASE THE DEPOSITED SEDIMENTS IN THE AREA NEAR DAM (IN 1000 M DISTANCE FROM DAM)

For such a case, the annual sediment volume (coming by density current and depositing near dam) considered to be released is about 250,000 tons (base on the reservoir geometry in the area close to dam, annual rate of bed level rising and the length of interesting area).
The Wallingford model results for this case, in table 3, show that for this case flushing can be a solution and the annually released sediment will be more than what annually will come to the area.
But the important point is that by this strategy, just the sediments near dam will be removed annually and after some years the sediment masses, accumulated right upstream of flushed cone area, will collapse into created wedge cone blocking

flushing tunnel. Then, however it's a temporary solution but, for sure, it's not a sustainable and reliable solution.

Table 3. Results of Wallingford Model for different scenarios of releasing sediments deposited near the dam (within 1000 m); SBR >1 efficient, <1 not efficient; F, V/H/E: feasible with very high efficiency, N.F: not efficient, needs another sustainable way to release entering sediments

Scenario N°	Discharge (m^3/sec)	Duration (day)	Mean annual sediment inflow (ton)	Mean water level during flushing (m)	Water gradient (m)	Water level before flushing (m)	Max. sediment released D/S (ton)	SBR	LTCR	DDR	FWR	TWR	SBR_d	Feasibility and efficiency
1	200	10		300	52		62'097'000	**257.5**	-	-	-	-	-	**F, V/H/E**
2	200	5		300	52		31'048'000	**128.0**	-	-	-	-	-	**F, V/H/E**
3	150	10		300	52		42'722'000	**177.5**	-	-	-	-	-	**F, V/H/E**
4	150	5		300	52		21'361'000	**88.7**	-	-	-	-	-	**F, V/H/E**
5	150	5		310	42		16'532'000	**69.1**	-	-	-	-	-	**F, V/H/E**
6	150	5		320	32		11'929'000	**49.5**	-	-	-	-	-	**F, V/H/E**
7	100	5		300	52		12'609'000	**52.4**	-	-	-	-	-	**F, V/H/E**
8	100	5		315	37		8'381'000	**34.2**	-	-	-	-	-	**F, V/H/E**
9	100	5		340	12		2'170'000	**9.5**	-	-	-	-	-	**F, V/H/E**
10	100	10		315	37		16'763'000	**69.1**						**F, V/H/E**
11	100	10		332	20		4'006'000	**16.7**						**F, V/H/E**
12	100	10		300	52		25'219'000	**104.0**						**F, V/H/E**
13	200	10		340	12		10'688'000	**44.4**						**F, V/H/E**
14	200	5		340	12		5'344'000	**21.8**						**F, V/H/E**
15	200	10		350	2		1'245'000	**5.1**						**F, V/H/E**
16	200	5		350	2		622'400	**2.9**						**F, V/H/E**
17	150	10		340	12		7'353'000	**30.5**						**F, V/H/E**
18	150	10	275'000	350	2	352	856'400	**3.6**						**F, V/H/E**
19	150	5		340	12		3'676'480	**15.3**						**F, V/H/E**
20	150	5		350	2		428'204	**2.2**						**F, V/H/E**
21	100	10		350	2		505'548	**2.2**						**F, V/H/E**
22	100	5		350	2		252'774	**1.5**						**F, V/H/E**
23	85	10		350	2		409'267	**2.2**						**F, V/H/E**
24	85	5		350	2		204'634	**0.7**						**N.F**
25	70	10		350	2		317'973	**1.5**						**F, V/H/E**
26	70	5		350	2		158'956	**0.7**						**N.F**
27	50	10		350	2		205'316	**0.7**						**N.F**
28	50	5		350	2		102'658	**0.7**						**N.F**
29	100	10		347	5		1'518'000	**6.5**						**F, V/H/E**
30	100	5		347	5		759'000	**3.6**	-	-	-	-	-	**F, V/H/E**
31	85	10		347	5		1'229'000	**5.1**	-	-	-	-	-	**F, V/H/E**
32	85	5		347	5		614'476	**2.9**	-	-	-	-	-	**F, V/H/E**
33	70	10		347	5		954'812	**3.6**	-	-	-	-	-	**F, V/H/E**
34	70	5		347	5		477'406	**2.2**	-	-	-	-	-	**F, V/H/E**
35	50	10		347	5		616'526	**2.9**	-	-	-	-	-	**F, V/H/E**
36	50	5		347	5		308'263	**1.5**	-	-	-	-	-	**F, V/H/E**

CONCLUSIONS

In the present study, for three different cases including fully desiltation of reservoir, evacuation of the sediments deposition due to density current and evacuation of sediments deposited in the area close to dam (within 1000 m from dam), flushing process of Dez reservoir has been modeled by a simple empirical model of HR Wallingford. 108 series of modeling cases by Wallingford model have been done and for each the efficiency of flashings was assessed. The below shows the achieved results in brief:

- *Based on the achieved results in this study, the flushing method is not relevant to desilting the incoming annual sediments and it may not lead to a sustainable solution.*
- *Even if, it is assumed that the volume of incoming sediments by turbidity currents into reservoir is about 11% of total incoming sediment (Ackers report for phase I), then the annually deposited sediment (due to density current) may not be release by flushing method completely, neither.*
- *However, by flushing method, it is possible to release the sediment volume deposited in the area close to dam up to 1000 m from dam, but it must be noted that this approach cannot be a sustainable solution and the sediment mass sliding will very soon happen, blocking the flushing devices.*
- *According to all fore mentioned analysis, it is concluded that a combination of turbidity current venting methodology and mild flushing (cleaning the area closer to outlet devices) could produce bring into being a sustainable solution to Dez dam sedimentation crisis.*

REFERENCES

Atkinson, E. 1996. The Feasibility of Flushing Sediment from Reservoir. TDR Project R5839, Rep. OD 137, HR Wallingford

A. Palamieri, F. Shah, G. W. Annandale, A. Dinar, 2003, Reservoir Conservation, Volume I: The RESCOM approach, The International Bank for Reconstruction and Development, The World Bank, Washington DC, USA

S. Kawashima, T. B. Johnrow, G. W. Annandale, F. Shah, 2003, Reservoir Conservation, Volume II: RESCOM model and user manual, The International Bank for Reconstruction and Development, The World Bank, Washington DC, USA

Tamab, "Analyzing Dez dam sediments", Technical Report, Water Resources investigation Centre, Tehran, 1986.

Ackers and Dezab Co., " Dez dam Rehabilitation project", Technical Report, 2003

KWPA , The Dez dam Hydrographic maps, 2007

SIMULATION STUDY FOR MINIMIZING DIURNAL VARIATION OF FLOW IN A HYDROELECTRIC PROJECT TO REDUCE DOWNSTREAM IMPACT

Maya R.Ray[1] Arup Kr. Sarma[2]

[1] Department of Civil Engineering, Indian Institute of Technology Guwahati, 781039, Assam India E-mail address: r.ray@iitg.ernet.in

[2] Department of Civil Engineering, Indian Institute of Technology Guwahati, 781039, Assam India E-mail address: aks@iitg.ernet.in Tel: +91-361-258 2409

ABSTRACT

Hydro-Electric project are generally operated as peaking plant. This induces diurnal variation of flow in the downstreams of the dam even in a run-of-the-river scheme. Lower Subansiri Hydel project, proposed on the Subansiri River of Assam, India, is one of the major Hydel projects of India. Reservoir Simulation Model has been developed with a prime objective to assess extent of flow variation in the downstream of the dam. The simulation study has revealed that during lean period the discharge in the downstrem increases significantly during the peaking hour and the flow discharge become almost zero during the non-operating period. While the high discharge may cause erosion and can create flood like situation, the low discharge may have several adverse impact like increase in pollutant concentration. Scope of adopting structural and non-structural measures for minimizing deviation of flow from its normal condition has been investigated and encouraging result has been found.

INTRODUCTION

The technique to generate hydropower by conversion of mechanical energy into electrical energy is the oldest technique known to the mankind. Though traditional definition of the hydropower is a renewable, non-polluting and environment friendly source of energy, in the present context this definition needs some revision. Hydropower project induces significant ecological disturbances at upstream (u/s) and downstream (d/s) of the dam and therefore, perhaps can no more be considered as a non-polluting and environment friendly source of energy. Though impact of a dam on its upstream could draw attention of planners and researcher, its d/s impacts remained unrecognized, misunderstood and underestimated. Only recently, issue of d/s impact of a hydropower project has been addressed by researchers. The d/s impacts of dams on river biota have been documented since eighties by some of the researchers (e.g., Ward and Stanford (1979), Lillehammer and Saltveit (1984), Petts (1984), Craig and Kemper (1987)). Brookes in 1994 classified these impacts as first and second order impacts. Petts (1980) observed two kinds of impacts; one immediate and obvious and others are gradual and subtle. Environmental, economical and social impact of the dam at d/s has been reported by Word Commission of Dam (2000). Wohl and Rathburn (2003) found that the sediment entering the reservoir creates sediment-depleted conditions at d/s leading to channel adjustment in the form of bank erosion, bed erosion and channel plan form change.

The direct or indirect source of the above mentioned impacts in the d/s of the dam can be due to the high variation of flow rate in d/s caused by the dam operation. Ecological problem caused on river ecosystem due to hydro power project has been pointed out by Maiolini et al. (2005). Riggsbee et al. (2007) presented the impact on d/s of the dam due to dewatering or removal of the impounded water behind the dam. The degree, however, to which any project, especially hydroelectric, affects a river, varies widely. In the present study an attempt has been made to visualize the changed flow scenario at down stream of Lower Subansiri Hydro Electric Project (LSHEP) due to operation of reservoir in order to generate electricity. Objective of the study is to evolve measures to minimize deviation of d/s flow from its natural condition so that environmental impact can be minimized.

Study area: Subansiri Basin

This project is located in the Assam-Arunachal boarder near North Lakhimpur town of Assam. The project area lies in the Lower Subansiri District of Arunachal Pradesh and Dhemaji District of Assam, India. The river Subansiri, originates from the south of the Po Rom peak (Mount Pororu) at an elevation of 5059m in the Tibetan Himalaya. After flowing for 190km through Tibet, it enters India. It continues its journey through the Himalaya of India for 200km and enters into the plains of Assam through a gorge near Gerukamukh. The Subansiri is the largest tributary of the Brahmaputra. Its total length up to confluence of Brahmaputra River is 520km. Its drainage area up to its confluence of the River Brahmaputra is 37, 000sq.km. The river maintains an almost stable course in the hilly terrain but becomes unstable as soon as it enters into the alluvial plains of Assam.

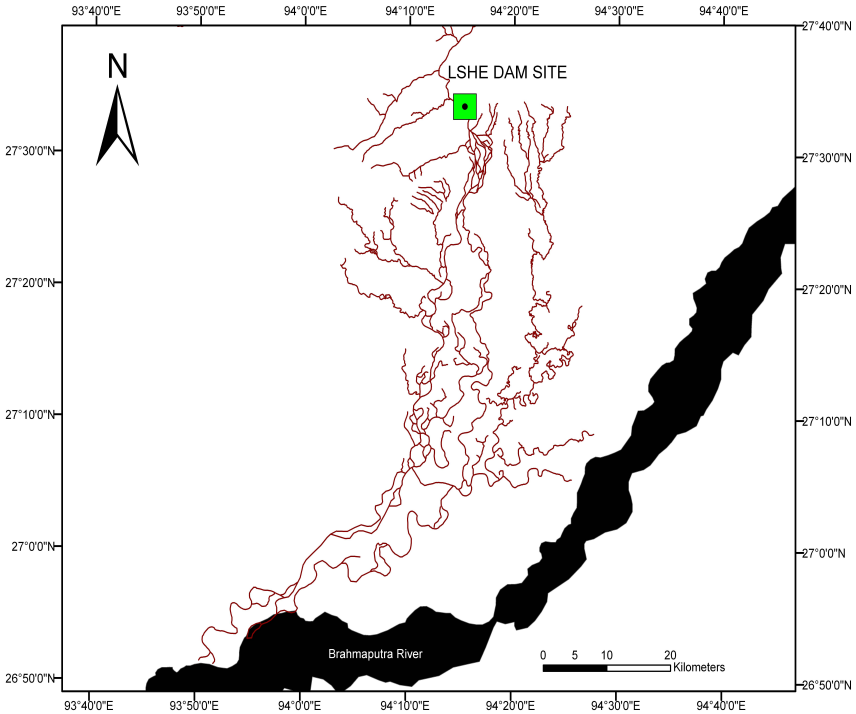

Figure1. Location of Dam Site

RESERVOIR SIMULATION STUDY

To visualize reservoir operation using simulation model is one of the best techniques to foresee the impact of a reservoir on flow scenario on d/s of the dam. According to Warbs (1973), simulation is a process of representing a system with a set of mathematical equations. Simulation, though is not an optimization method, can give optimal or near-optimal solution (Simonovic, 1992). Several simulation models have been discussed in the state of the art review presented by Yeh (1985), Wurbs et al. (1985), and Wurbs (1991). A Reservoir Simulation Model (RSM) has been developed in this study to visualize some important aspects of the River-Reservoir system at any time period. General demand oriented reservoir operating policy is considered to simulate the reservoir operation for twenty years using synthetic stream flow data. Meeting power demand of peak hours generally becomes an objective of a hydropower project in the lean period. This leads to significant diurnal variation at d/s of the dam, which in turn leads to serious ecological problem.

Data used in the development of RSM

Synthetic ten daily stream flows of twenty years provided by National Hydropower Power Corporation (NHPC) have been used as inflow series for the simulation study. Mathematical relationship of Storage-Elevation and Area-Elevation derived from the curve supplied by the NHPC has been used to calculate the reservoir capacity and elevation for each time period. Necessary climatic and reservoir related data were obtained from the NHPC.

Reservoir simulation has been carried out to achieve the following objectives: (1) To visualize changes in the flow scenario at the d/s of LSHEP; (2) To examine scope of flood moderation; and (3) To estimate power production and to analyze pattern of power production.

Development of Reservoir Simulation Model (RSM)

Simulation Algorithm

Following steps has been followed to decide the release at any time period t in the proposed RSM

Available Net Head (H_{nt}) at any time t is calculated based on elevation of reservoir at time t (El_t), elevation of normal tailrace water level (El_{tail}) and head loss due to friction. Head loss of the system can influence power generation considerably. Frictional head loss at time t (h_{ft}) has therefore been computed in this study dynamically based on the actual discharge at time t (Q_{dt}) flowing through the system.

1. Minimum desired release at time t (Rtd) for producing the target power for the peaking hour (*pk*) is calculated

$$R_{td} = Q_{dt} \times 36 \times p_k \div 10^3 \quad (1)$$

2. Maximum possible release at time t (Rtm) for producing the target power round the clock is calculated

$$R_{tm} = Q_{dt} \times 36 \times 24 \div 10^3 \quad (2)$$

3. Actual release is calculated based on the constraints of; (a)Maximum permissible reservoir elevation at that time considering scope of absorbing flood

$$R_{ta} = S_{t-1} + I_t - K_{El} - E_t - R_m \quad (3)$$

Where R_{ta} is available release at time t, S_{t-1} is storage of reservoir at the beginning of time t, I_t is inflow at time t, K_{El} is capacity of reservoir at time t, E_t is evaporation time t, R_m is minimum release provided

(b)Minimum drawdown level

$$R_{ta} = S_{t-1} + I_t - S_d \quad (4)$$

4. New storage at time t (St) at the end of the time period t is calculated based on the release computed in step 4.

$$S_t = S_{t-1} + I_t - R_{ta} - S_p - E_t - R_m \quad (5)$$

Where S_p is spill from the reservoir

5. New reservoir elevation at time t (Elnt) is calculated using storage-Elevation relationship
6. Net head is then calculated taking average of the initial elevation (Elt) at beginning of time period t and the new elevation (Elnt) at end of the time period t, and the entire calculation from step 1 is repeated to obtain the actual discharge in an iterative way (accuracy of 0.0001cumec is considered in this study)
7. Spill at every time is computed
8. Water balance is also checked in all these computation to ensure computational accuracy. After obtaining the actual discharge in step 7, the hours of operation of the turbine, power generated through the turbine (Po) in MW, Total power generated per hour (Poh) in KWh and TDF is calculated.

RESULTS AND DISCUSSION

RSM is used to study three different cases:(I) Reservoir operation with demand oriented standard operating policy (II) Reservoir operation with structural

measures to reduce diurnal variations (III) Reservoir operation to reduce diurnal variations through non structural measures. Detail discussion with necessary figures of the results obtained is give below:

Case-I: Demand oriented standard operating policy

Here reservoir is operated with an objective of generating target power of 2000MW for as many hours as possible without violating the given constraints. Synthetic ten daily stream flow series of 20 years has been used for the purpose. Output of the RSM has revealed that little variation will occur in ten daily total volume of dam released flow as compared to the total flow volume in without dam condition. Figure 2 shows the plot of Inflow series and TDF series for 20 years. To have a close view of these two series, plot of first year of flow is presented in Figure 3.

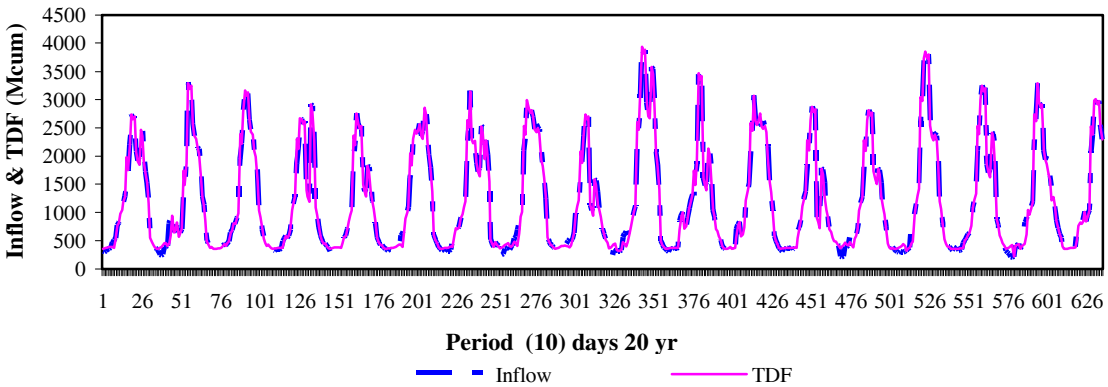

Figure 2. Inflow and TDF series of 20 years10 daily analyses

Figure 3 depicts that the Natural Inflow in ten days and the ten daily TDF after construction of dam are of same order. Visible variation has been observed only in the month of May-June, as the reservoir is drawn down during that period to keep sufficient space for the accommodation of high discharge during monsoon period, which will also provide opportunity of moderating high flood of small duration. It has been observed that though total flow volume in ten days remains more or less same before and after construction of dam, rate of flow in the d/s varies significantly.

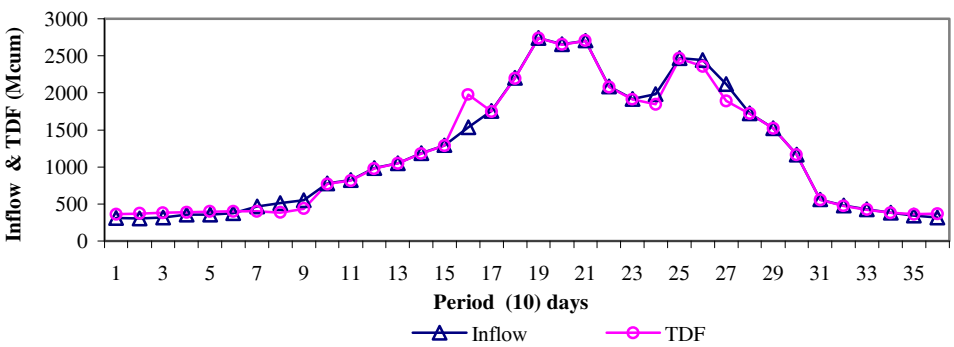

Figure 3. Simulation of the proposed policy for 1st yr

Figure 4 shows the power production series on ten daily bases. Figure 5 show close view of pattern of total power production for through first year. Figure 6 and 7 show the flow situations in d/s of the dam along with the duration of such flow. Average natural flow condition is also plotted in the same figure to have a visual comparison. Figure 7 shows the plot of inflow, turbine discharge, rate of total d/s flow, minimum flow rate at d/s and duration (Hr) of turbine discharge.

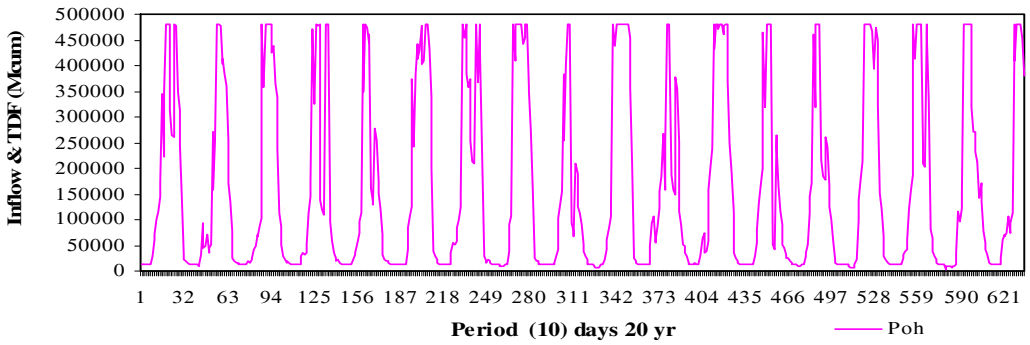

Figure 4. Power-hour series of 20 years for 10 daily analyses

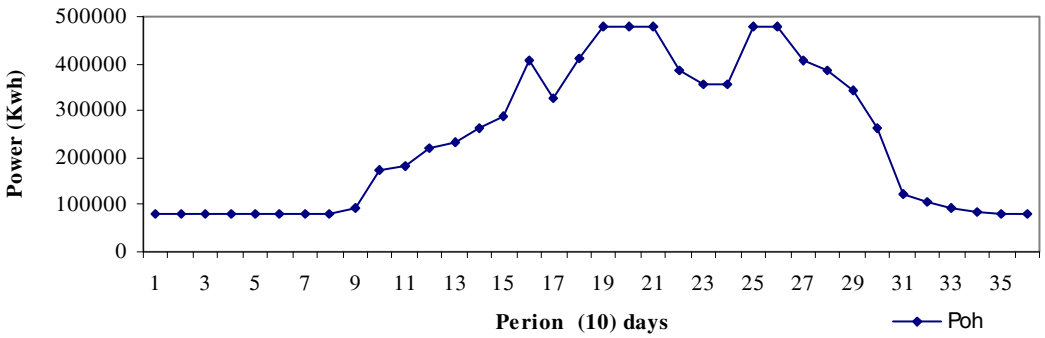

Figure 5. Power production pattern for proposed policy for the 1st yr

From these figure it is clear that the difference in flow rate is quite significant in the lean period, where the maximum out flow rate becomes 2400cumec and minimum flow rate becomes 6cumec, while the average inflow rate in the lean period in natural situation is in the order of 300 to 500cumec. Such diurnal variation in the lean period is of great concern as will cause ecological disturbance at the d/s. Such variation may also induce river bank erosion at d/s.

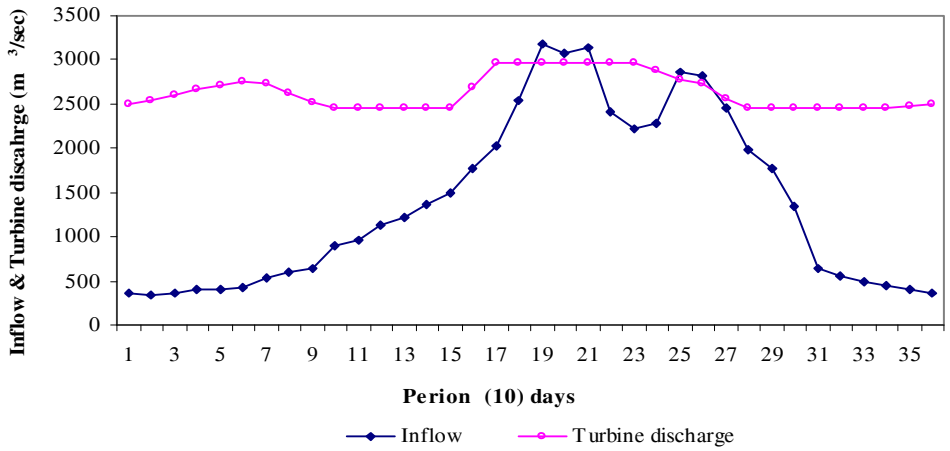

Figure 6. Diurnal variation observed for 1st yr

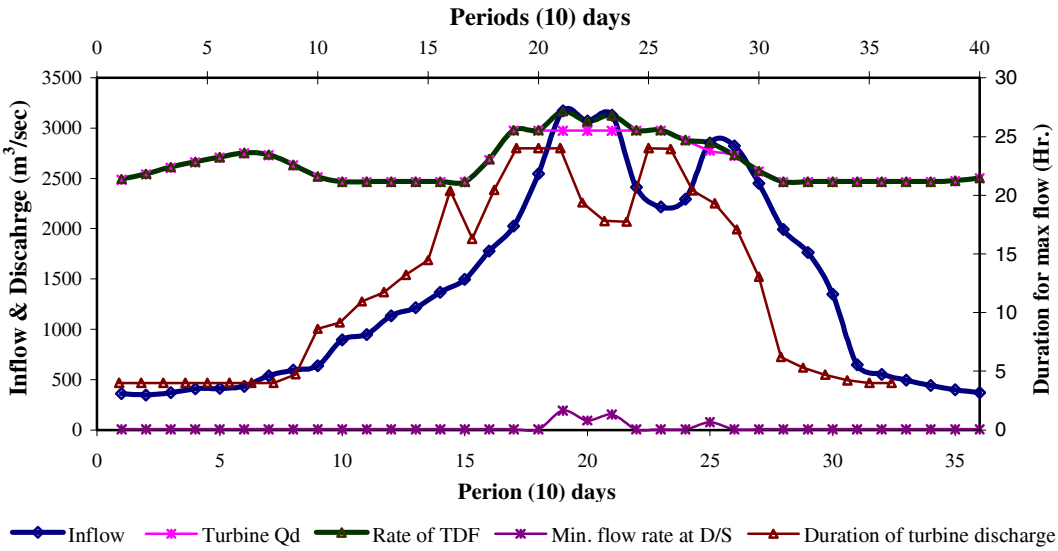

Figure 7. Proposed different concept (structural measure) for 1st yr

To minimize such variation, several measures have been thought about and simulation has been carried out to visualize the effect of such measures. Structural and non-structural measures proposed in this study for minimizing diurnal variation are presented below.

Case –II Policy considering structural measures to reduce diurnal variations

Effect of introducing a small capacity pond in d/s of the reservoir was investigated to explore possibility of minimizing diurnal variation and to analyze its performance. Simulation study has sown that diurnal variation of flow can be significantly minimized by creating a d/s storage of 36MCM. Figure 8. shows the curves showing the ranges within which the d/s flow will vary if a 5m high barrier covering the entire width at 4Km d/s of the dam is placed along with gated marginal embankment, so as to allow flow contribution of small stream during lean period.

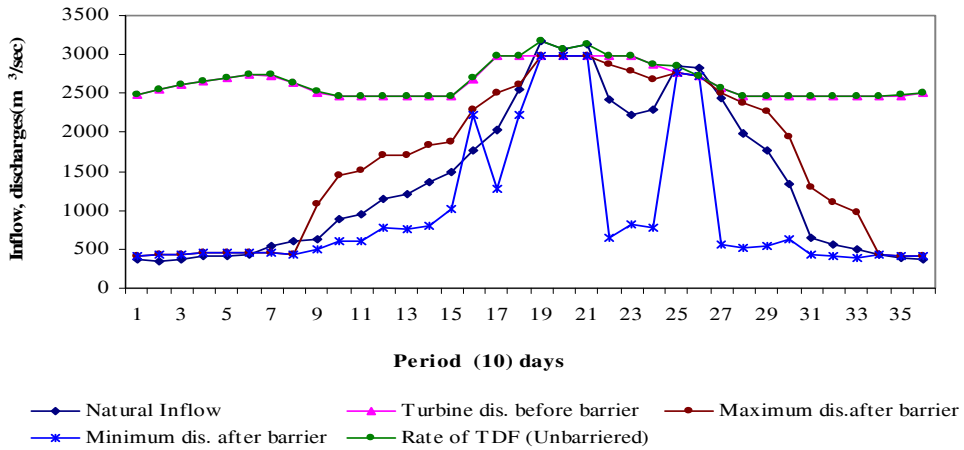

Figure 8. Proposed concept for non structural measure for 1st yr

Case –III Policy considering non structural measures to reduce diurnal variations

Operating one turbine continuously and rest at a time

Another option of providing minimum flow of around 300cumec in the lean period to produce 250MW power continuously by running one turbine for the entire day and to produce 1750MW with the remaining water for the possible period shown in Figure 9. and Figure 10. This will ensure minimum flow of 300cumec throughout the day in the lean period with maximum flow of around 2400cumec for the peaking duration, which will not be less than 2 hours per day even in the lean period.

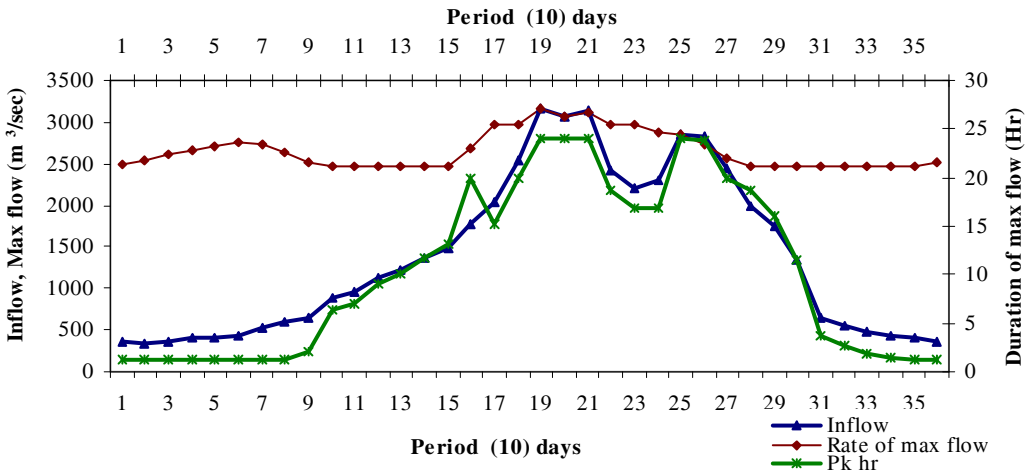

Figure 9. Peaking hour maximum d/s flow and natural inflow rate with one turbine running continuously

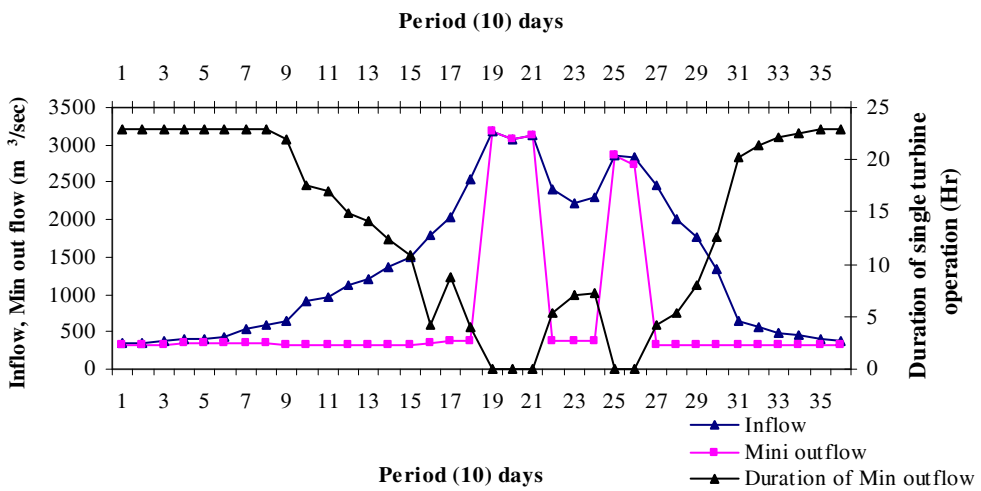

Figure 10. Minimum d/s flows, its duration in a day and natural inflow rate with one turbine running continuously

Operating one turbine continuously and increasing number of turbine one by one

Another option of utilizing the available water by running one turbine continuously and then increasing the number of turbine one by one for maximum possible hours of operation for each of the added turbine. This will restrict maximum rate of flow, of course with a compromise with peaking power. Figure 11. shows the maximum and minimum rate of flow through turbines along with the plot of natural inflow.

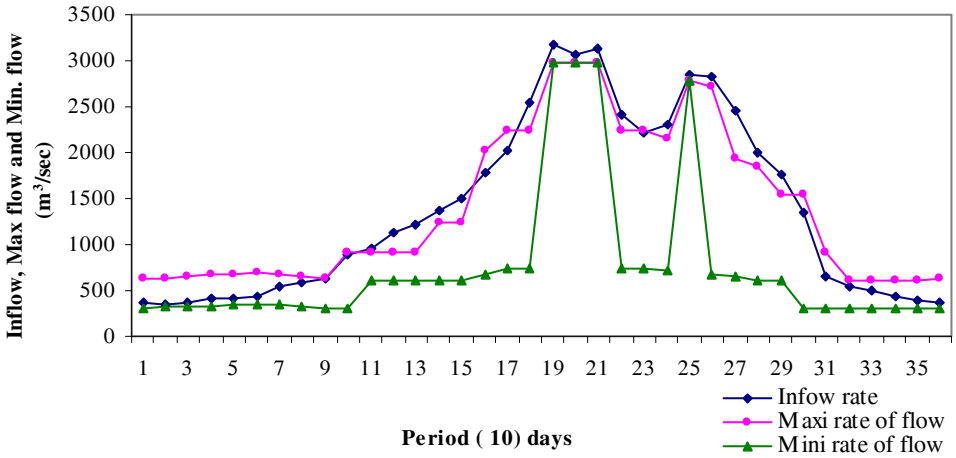

Figure 11. Inflows, Maxi. Turbine Discharge and Min.Turbine discharge for 1st yr

CONCLUSIONS

A reservoir simulation model has been developed to investigate augmented flow scenario d/s of a dam, so that necessary corrective measures can be suggested to minimize d/s environmental impact. The developed simulation model has been applied to the Lower Subansiri Dam, located in the state of Assam and Arunachal Pradesh of India. The simulation study has shown that with the present proposed power production schedule, i.e., with peaking hour of minimum 4hours, flow rate at d/s of the dam will change with a diurnal variation between 6cumec to 2400cumec in the lean period. Natural flow during lean period being in the order of 300cumec, such variations will have adverse effect in the d/s. During flood period diurnal variation induced by the reservoir operation is not that significant and will not create any adverse effect as such. Several alternate operating policy and structural measures have been analyzed to minimize the diurnal variation in the lean period. While implementation of structural measures needs favorable site condition, additional initial investment and running cost, modification of operating policy has been found to be quite convenient. A policy with one turbine running continuously and producing peaking power with the remaining water has been found to be quite convenient. This policy will ensure about 300cumec of flow in the lean period throughout the day of course with a higher discharge of around 2400cumec for a short duration of about 2 hours in the lean period. Another policy of generating power by choosing number turbines to be run based on the available water has also been analyzed. This policy will lead to a flow situation where variation between maximum and minimum flow rate will reduce but the project will not be able to meet the peak demand, as this will lead to almost uniform power production throughout the day.

REFERENCES

Craig, J. E., Kemper J. B. (1987). “Regulated streams: Advances in ecology.” Plenum Press, New York.

Dionne D., Therien, N. (1997). “Minimizing environmental impacts of hydroelectric reservoirs through operational control: a generic approach to reservoirs in northern Quebec.” *Ecological Modeling*, 105(1), 41-63.

Goswami, U., Sarma, J. N., Patgiri, A. D. (1999). "River channel changes of the Subansiri in Assam, India." *Geomorphology*, 30(3), 227-244.
Kannan, K.P., Pillai, N.V. (2002). "Plight of Power Sector in India: Inefficiency, Reform and Political Economy."*Center for Development Studies, Thiruvananthapuram, Kerala, India.*
Lillehammer, A., Saltveit S. J. (1984). "Regulated rivers." *University of Oslo Press*, Oslo,Norway,540.
Maiolini, B., Gumiero, B., Silveri, L. (2005). "The downstream effect of hydropower release in an Alpine glacial stream." American Geophysical Union, Spring Meeting, NB, 33G-01.
Petts, G. E. (1980). "Long-term consequences of upstream impoundment. Environmental Conservation." 7, 325-332.
Petts, G. E. (1984)."Impounded rives. Perspectives for ecological management." Wiley & Sons, Chichester, UK.
Riggsbee, J. A., Julian, J. P., Doyle, M. W. Wetzel R. G. (2007). "Suspended sediment, dissolved organic carbon, and dissolved nitrogen export during the dam removal process." *Water Resources Research,* 43 (W09414), 1-6.
Scudder, T. (1980). "River basin development and local initiative in African savanna environments." *D.R. Harris (ed.) Human Ecology in Savanna Environments*, Academic Press, 383-405.
WAPCOS.(1993). "Morphological Studies of River Brahmaputra." North Eastern Council. Govt. of India, New Delhi, I-1–IX-131.
Ward, J. V., Stanford J. A. (1979). "The ecology of regulated streams." Plenum, New York.
Wohl, E., Rathburn, S. (2003). "Mitigation of sedimentation hazards D/s from reservoirs." *International Journal of Sediment Research*, 18(2), 97-106.
World Commission on Dams (2000). "Downstream Impacts of Large Dams." Thematic Review I.1.
Wurbs, R. A., Tibbets, M. N., Cabezas, L. M., Roy, L. C. (1985). "State-of-the- art review and annotated bibliography of systems analysis techniques applied to reservoir operation." Tech. Rep. 136, Texas Water Resources Institute, College Station, Tex.
Wurbs, R. A. (1991). "Optimization of multiple-purpose reservoir system operations: a review of modeling and analysis approaches." Res. Document No. 34, U.S. Army Corps of Engineers, Hydrologic Engineering Center, Davis, Calif.
Wurbs, R.A. (1993). "Reservoir-system simulation and optimization models." *Journal of Water Resources Planning and Management*, 119(4), 455-472.
Yeh, W. W-G. (1985). "Reservoir management and operations models: A state-of-the- art review." *Water Resources Research*, 21(12), 1797-1818.

Optimal Design and Operation of Fuse-gates Considering Water Loss due to Gates Tilting

Abbas Afshar[1], Zeinab Takbiri[2]

1. Email address : a_afshar@ iust.ac.ir
2. Email address : ze_takbiri@civileng.iust.ac.ir

Abstract: Installation of fuse-gates on free spillways might be a safe and reasonably simple solution to increase reservoir capacity compared with the expensive alternative of dam heightening. This research aims at optimum design of fusegates considering the flood routing process in the reservoir. Owing to the fairly complicated performance of fusegates in flooding condition, its optimum tilting control is a challenging task. The overall expected cost which includes expected cost of water loss and gates replacement as well as the initial gates installation cost is considered as the objective function of the optimization problem. Moreover, an efficient mixed Genetic Algorithm model is utilized to minimize the overall cost. Type of gates, their height and first tilting head are explicitly treated as decision variables. A case example is used to assess the applicability of the proposed optimization scheme. The results indicate that consideration of flood routing could have a significant effect on the optimum design of gates.

Keywords: fusegates; flood routing; genetic algorithm; tilting head; spillway

1. INTRODUCTION

In recent years, with growing the water demand beside the global draught events the world water crisis develops and therefore many alternatives are proposed to cope with this problem. As a practical alternative, one may focus on increasing water supply of existing reservoirs. Dams heightening, dredging the reservoir of existing dams, and gate installation on the existing spillways are some of the possible ways to increase the reservoirs storage.

In 1989 Hydroplus invented fusegate which may be a simple and cost-effective way to increase the water supply capacities of reservoirs as well as spillways capacities depending on the conditions (Falvey and Treille 1995). The fusegates applied on more than 40 dams such as Allan dyke, in France, Beni Amrane dam in Algeria, Black Rock dam in USA, and Terminus dam in USA.

Falvey and Treille (1995) elaborated the discharge characteristics and hydraulics design of fusegates. Chevalier. S, Hydroplus, France (2004), Alla (1996), Jones et al., 1996 discussed about advantages of fusegates in different conditions. Afshar et al., 2003 employed a linear optimization model to minimize the overall cost of gates without considering the replacement cost and effect of installation of fusegates in routing process.

In this study, an efficient Genetic Algorithm model is presented to minimize the total project cost. It includes the expected costs of water loss and replacement cost which is not considered yet, as well as installation and excavation cost under structural, hydraulic, and operational constraints. The type and height of the gates as well as tilting head of first gate are explicitly treated as decision variables. In this proposed model the flood routing affected by installation of fusegate is considered. All gates have an equal height and type. Application of the model to Zarine Roud Dam in Iran, demonstrates applicability and efficiency of the proposed modeling scheme.

2. Hydraulic design of fuse-gates

There are three main components with any fusegate. the water retaining structure, the pressure chamber and the water collecting well. The water retaining element is a concrete or steel structure with a downstream abutment block to prevent the gate sliding. The pressure chamber receives water from water collection well causing an uplift pressure. Collection well ensures that water can enter the chamber when the reservoir water level exceeds the inlet elevation (Falvey and Treille 1995).

When the tilting moment exceeds the stabilizing moment caused by the weight of the fusegate body and water, the fusegate tilts around the downstream edge, imposing water loss and substitution gate replacement cost. The water los initiates when the first fusegate tilts. With tilting the fusegates, they may break and be unusable. Therefore the replacement cost of destroyed fusegates after tilting, should be considered to attain the real expected cost of this project. Because of considering replacement cost, it is important to prevent the tilting of fusegates simultaneously. To control the tilting level of fusegates, the inlet of each gate is set at a different elevation.

Fusegates are commercially available in three standard types designated by ratio of the width of the gates to its height as being wide (W) or narrow (N) and by the tilting range as being low head (LH) or high head (HH) (Falvey and Treille 1995).

Discharge of flood over a non-tilted fusegate may be computed (Rouse 1960) as

$$Q = (2/3)\sqrt{2g}\,C_d L_c h_i^{3/2} \quad (1)$$

where Q = discharge; g = acceleration of gravity; L_c = crest length of the fusegate; and h = difference in the reservoir and the crest elevation of gates; and C_d = the discharge coefficient which is a function of the crest length on the fusegate, and the ratio of h to the total head (depth of flow) over the sill. The best-fit Equation for the discharge coefficient is given by Falvey and Treille (1995):

$$C_d = C_1((h/H) - C_2)^{C_3} \quad (2)$$

where H = height of the fusegate, and C_1, C_2, and C_3 are experimentally determined constants for values of h/H greater than 0.1. The coefficient C_2 is a surface-tension-type term that becomes negligible as the flow depth over the fusegate increases. Discharge coefficients for various types of fusegates are presented in Table 1

Table1. Empirical discharge coefficients for fusegates (Adapted from Falvey and Treille 1995)

Type	c_1	c_2	c_3
WLH(NHL)	0.320 ± 0.004	0.0010	-0.292 ± 0.006
NLH	0.254 ± 0.012	0.0005	-0.319 ± 0.018
WHH	0.315 ± 0.009	0.0375	-0.258 ± 0.005

When water level reaches to a predetermined value and gate tilts, the discharge can be obtained from Equation (2) by letting L_c = the crest length of the fusegate, and C_d = the discharge coefficient for weirs defined as (Rouse, 1960),

$$C_d = 0.611 + 0.075\,(h/P) \quad (3)$$

where P = height of the crest above the upstream approach channel invert elevation. In addition to height and type of gates, the tilting head of each fusegate should be determined for computing the discharge-elevation curve and subsequently outflow hydrograph. It is obvious that with tilting the first gate the whole extra water supply which is saved with fusegates installation is wasted. Furthermore tilting of each gate imposed the replacement cost to the model. Therefore it is important to control the gates tilting with a well managed and planned scheme.

The Figure 3, illustrate a sample inflow and outflow hydrograph for the reservoir with 50 meters wide spillway covered by sixteen fusegates with 3.10 meters width. The peak of entering flood is approximately 4000 cms. It is assumed that all fusegates tilt at

the same time. With tilting all gates at the same time, a significant jump is made in outflow hydrograph that is not desirable.

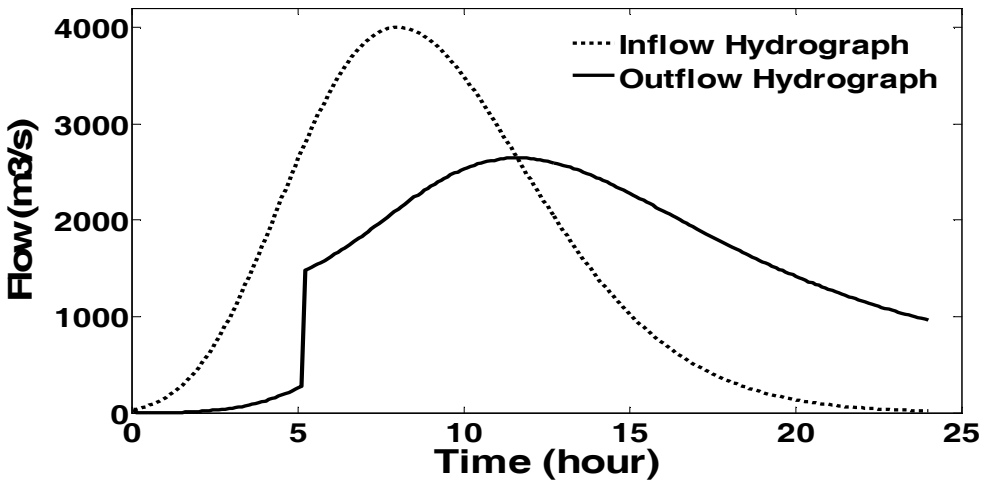

Figure3.a sample Inflow and Outflow Hydrograph of the floods

To avoid a great flood discharging in downstream and high imposed replacement cost of gates, it might be better to prevent the simultaneous tilting of all gates.

3. Optimization model

The total annual expected cost is expressed as

$$TAEC = \sum_{i=1}^{N} [CRF.(CO_{E_i} + CO_{F_i}) + (CO_{W_i} + CO_{RF_i})] \quad (4)$$

In which i refer to the gates number, CO_{E_i} = the excavation cost, CO_{F_i} = fusegate cost, CO_{W_i} = expected annual cost of water loss, CO_{RF_i} = expected annual gate replacement cost, and CRF = capital recovery factor (Peterson 2005)

$$\begin{aligned} CO_{E_i} &= g_e(ED_i) \\ ED &= H - INWL \\ CO_{F_i} &= C_{fuse} \\ CO_{W_i} &= 1/Tr_1 \times V_W \times UCW \\ CO_{RF_i} &= 1/Tr_i \times URC = 1/Tr_i \times g_{Rfuse} \end{aligned} \quad (5)$$

where T = fusegate type, H = fusegate height, h= tilting head, ED = excavation depth, Tr = flood return period associated with tilting head of any gate, Tr_1 = return period for the first tilting, $INWL$ = desired increase in normal water level, V_W = water loss due to gate tilting, UWC = unit water cost, and URC = unit replacement cost.
The objective function is subject to the following physical and operational constraints:

$$\begin{aligned} &Type = NLH \text{ or } WLH \quad \text{for which} \quad 0.3 \le h_i / H \le 0.6 \\ &Type = WHH \quad \text{for which} \quad 0.8 \le h_i / H \le 1.4 \end{aligned} \tag{6}$$

In the propose approach, the tilting head of the first fusegate is treated as decision variable and the tilting heads of other gates are determined as addressed in equation 7.

$$\begin{aligned} &delta = {(h_{\max} - h_{first})}/{(n-1)} \\ &h_1 = h_{first} \qquad h_i = delta + h_{i-1} \\ &if \quad Type = NLH \quad or \quad WLH \quad then \quad \max h = 0.6.\ H \\ &if \quad Type = WLH \quad then \quad \max h = 1.8.\ H \\ &h_{\max} = \max imum \begin{cases} \max h \\ MWL - INWL \end{cases} \end{aligned} \tag{7}$$

where h_{first} = tilting head of the first gate obtained by genetic algorithm, n = number of installed gates, and MWL = maximum water level after routing the design flood before installation of fusegates. In fact the difference between tilting head of the first and last gates are divided into equal increments. Tilting head of a gate is determined as the summation of the fixed increment and the tilting head of the previous gate.
An appropriate version of genetic algorithm is tailored to cope with the combination of the discrete and real-value decision variables of the proposed model. This proposed algorithm is coupled with a simulation model which carries out the routing in the reservoir.

4. Model application

To test the performance of model, Zarineh Rud dam in Iran is used to and its result is present in Fig.6. The Zarineh Rud dam in north-western Iran has 50 meters height and total storage volume of approximately 650 *MCM*. It is desired to increase the total active storage volume by 106MCM, which associates with an increase of 2.35 meter in *NWL*.

The width of the original spillway in Zarineh Rud is 148 meters with spillway design head of 6 meters. Furthermore the maximum design flood with return period of 10000 years has a peak of 5321 cms (Afshar *et al.* 2003).

$$\begin{aligned} &Type = \ NLH: \quad C_{fuse_i} = 0.75 \times 10^5 H_i \ \ dollares \\ &Type = \ WLH: \quad C_{fuse_i} = 1 \times 10^5 H_i \ \ dollares \\ &Type = \ WHH: \quad C_{fuse_i} = 1.25 \times 10^5 H_i \ \ dollares \end{aligned} \tag{8}$$

Replacement cost of a tilted and destructed gate is assumed to be 10 times of the initial installation cost. It is further assumed that one cubic meter of lost water cost 0.5 U.S. dollar, the interest rate, *i* is assumed as 0.1, and the construction period is 24 months.

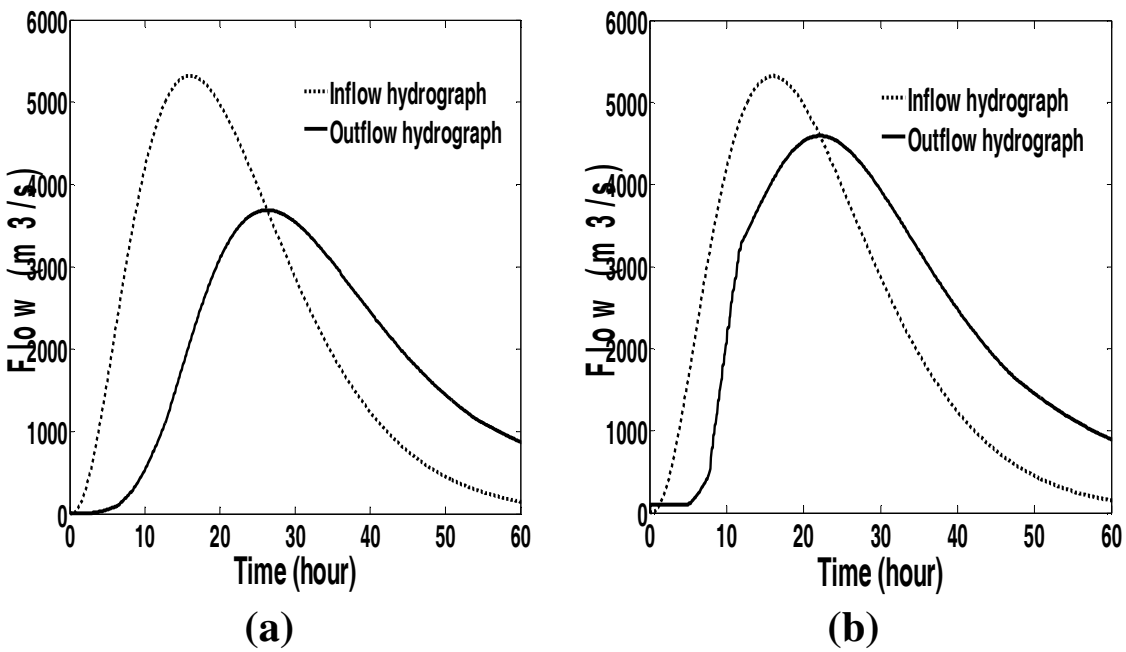

Figure 2.The inflow and outflow hydrograph for design flood (a) when the original spillway used (b) after installation of fusegates

The peak of entering design flood is 5321 cms which reduces to 4593 cms after routing through the reservoir with fusegate installation. Peak outflow before fusegate installation was determined as 3668 cms. The significant difference between these values is made by the jumps affected by tilting the gates step by step, while maintaining the same safety

measures. This figure illustrate that the routing effect in fuse-gated spillways is too important to be ignored. To enhance dam safety, the maximum water level after routing the design flood through the fuse-gated spillway must be known precisely. As presented in Fig.2(b), the maximum water level in fuse-gated spillway may exceed that of original free spillway (i.e., 5.65 m. compared to 5.98 m.). In this case, the gate installation should be modified to confine the maximum water level to that of the initial design.

The proposed simulation-optimization scheme is employed to develop optimal solution to a fairly complex fusegate design for increasing reservoir storage while enhancing dam safety.

A summary of the results of the solution to the model are presented in Table 2.

Table2. The optimum characteristic of selected fusegates

Cost of water units ($)	Height	Type	Number of installed fusegates	Tilting head of first fusegate	Tilting head of last fusegate	Cost of project 10^8 ($)
0.5	3.10 (m)	WLH	30	0.99 (m)	1.86 (m)	7.59

To test the sensitivity of the design to varying input parameters, the proposed simulation-optimization model was employed for different values of water unit cost. The results are presented in Table 3.

Table3. The optimum characteristic of selected fusegates for various costs of water unit

Cost of water units ($)	Height (m)	Type	Number of installed fusegates	Tilting head of first fusegate (m)	Tilting head of last fusegate(m)	Cost of project 10^8 ($)
0.05	3.10	NLH	45	0.93	1.86	7.40
5	3.75	WLH	24	1.50	2.25	8.23
50	4.60	WLH	14	1.60	2.76	9.51
500	4.60	WHH	11	4.10	5.9	10.95

Table 3 shows that with increasing the unit cost of water, the model selects the fusegates with larges heights with reduced tilting heads. Therefore the tall fusegates tilt with larger incoming floods with longer return periods, compared to short gates. According to

Equation 5, the expected cost of lost water decreases with increasing the return period of fusegates design. As the unit cost of water increases the model tries to find the solution with tall gates with relatively larger tilting heads. Although the volume of lost water for high head gates are larger than that of small gates, yet the expected value of lost water may be reduced.

6. Conclusion

An efficient genetic algorithm is used to minimize the overall cost of fusegate project which includes the installation cost and excavation cost as well as expected water loss and replacement cost. A simulation model was applied to computing the outflow hydrographs for any entering flood to reservoir with combination of type, height, and tilting heads of selected fusegates. The effect of installation fusegates on original width of spillway was illustrated in routing process. The results indicated that with installation of fusegates the peak of outflow hydrograph may increase, compared to the original case. Moreover with increasing the unit cost of water the heights of selected fusegates increase to cope with the expected lost water caused by tilting the first fusegate.

References

1. Ait Alla, A (1997), "Achieving economies through innovative spillway design", *Journal of hydropower and dams,* 4(2), 146-149
2. Ait Alla, A., (1996), "The role of fusegates in dam safety", *Journal of hydropower and dams,* 3(6), 67-72
3. Afshar, A., Marino, M.A., and Jalali, M.R., (2003), "Optimum design of fusegates; reconciling dam safety and increasing storage capacity", *Iranian Journal of Science and Technology,*1 (1)
4. Chevalier, S., and Hydroplus, France, (2004), "Fusegates mitigate silting at Beni Amrane reservoir", *Journal of Hydropower and Dams*, Issue 5
5. Jones, S.J. Spencer, D. Rodionov, V.B., Lounatsi, M.E., and Ait Alla, A., (1996), "The reliability of fusegates in ice-affected environments", *Journal of Hydropower and Dams*, Issue 2
6. Falvey, H.T., and Treille, P., (1995), "Hydraulics and design of fusegates, *Journal of Hydraulic Engineering"*, ASCE, 121 (7), 512-518

The Effect of Step Height on Energy Dissipation in Stepped Spillways

S. L. Hunt[1], Ph. D. and E.I.T and K. C. Kadavy, P. E.[2]

[1]Research Hydraulic Engineer, USDA-ARS HERU, 1301 N. Western, Stillwater, OK 74075; PH (405) 624-4135 x222; FAX (405) 624-4136; email: sherry.hunt@ars.usda.gov

[2]Agricultural Engineer, USDA-ARS HERU, 1301 N. Western, Stillwater, OK 74075; PH (405) 624-4135 x 236; email: kem.kadavy@ars.usda.gov

ABSTRACT

A two-dimensional, physical model was constructed to evaluate the energy dissipation on a 4(H):1(V) slope spillway chute. Step heights of 38 mm (1.5 inches) and 76 mm (3.0 inches) were evaluated, and energy losses created by these steps were compared. Model unit discharges ranging from 0.11 $m^3/(s \cdot m)$ (1.2 cfs/ft) to 0.82 $m^3/(s \cdot m)$ (8.9 cfs/ft) were tested. Water surfaces, bed surfaces, velocities, and void fractions in the flow were measured during the tests. The findings from this research show that a relationship developed by Hubert Chanson can be used to determine the inception point for slopes as flat as 4(H):1(V). With increasing step height, the energy losses at similar locations within the spillway chute also increased. The results for energy losses for the 38 mm (1.5 inches) and 76 mm (3.0 inches) steps showed similar linear trends upstream of the inception point, with near zero percent energy loss at the spillway crest to approximately 30% at the inception point. Downstream of the inception point for the two smaller step heights, the results showed a more logarithmic trend from 30% at the inception point or when a normalized length, L/L_{i*}, equals one to 73% when L/L_{i*} equals 3.5. This research is expected to assist engineers with the design of stepped spillways applied on relatively flat embankment dams and the associated stilling basin located at the toe of the spillway.

INTRODUCTION

Many small earthen embankments are faced with hazard classification changes due to urbanized growth within the watershed. Increased infrastructure around an existing dam typically generates more runoff and changes the hydrologic conditions. Often times this creates inadequate spillway capacity for the existing embankment. To bring the dam into compliance with state and federal dam safety laws, rehabilitation of the structure is often necessary. Roller compacted concrete (RCC) stepped spillways are becoming a popular choice in these rehabilitation situations because the spillway capacity can be increased with few or no additional changes to the existing embankment dimensions. RCC stepped spillways are also selected because of the dollars and time saved in the construction of these structures. Yet, design guidelines for RCC stepped spillways applied to small earthen embankments are limited, especially for chute slopes of 2(H):1(V) and flatter. Energy dissipation upstream of the inception point on these flatter sloped stepped spillways are important for determining the size of stilling basin because in many instances air entrainment is not fully developed prior to entering the basin for these small structures.

Stepped spillway research for flatter sloped applications (2(H):1(V) or flatter) has been quite limited, and design guidelines are scarce. Stepped spillways having flatter chute slopes are more typical for rehabilitation projects of existing embankment dams. Model studies can provide insight to engineers faced with designing these structures. Without these studies, the safety and integrity of the stepped spillway designed for these applications may be questioned, and/or it may result in the design engineer being overly conservative, leading to a more expensive project. The United States Department of Agriculture (USDA)-Agricultural Research Service (ARS) Hydraulic Engineering Research Unit (HERU) has focused a fraction of research to stepped spillways applied on existing embankment dams. Air entrainment and energy dissipation in flatter sloped stepped spillways may affect the design of the spillway training walls and the stilling basin differently than steeper stepped spillways. So the USDA-ARS HERU is currently working on a generalized model study to evaluate the effects a 4(H):1(V) slope stepped spillway chute has on the inception point location, the energy dissipation, and velocities for a specified range of flows that are within the skimming flow regime. This paper specifically compares the impact two different step heights have on energy dissipation. This research is expected to assist engineers in the design of these structures.

BACKGROUND

Design engineers have a vested interest in the affects air entrainment and energy dissipation has on the design of stepped spillways and the associated stilling basin applied to embankment dams. In most dam rehabilitations, stepped spillways are placed over the existing earthen embankment; thus, the slope of the spillway is the same as the downstream slope of the dam. Typical slopes for earthen embankments are 2(H):1(V) or flatter, but most of the research to date on stepped spillways has been for chute slopes greater than 2(H):1(V). Strides for improving RCC technology to flatter slope applications are being made.

Rice and Kadavy (1996), Yasuda and Ohtsu (1999), Chanson (2002), Boes and Hager (2003a and 2003b), Hunt and Kadavy (2006, 2007, 2008a, and 2008b), and Felder and Chanson (2008) among others have researched flat-sloped (2(H):1(V) or flatter) stepped spillways. Each has contributed to the engineering of these structures in some fashion. For instance, Rice and Kadavy (1996) along with others have indicated that energy dissipation was significantly more in stepped spillways when compared to smooth spillways of similar design parameters. Chanson (2002) has contributed extensively to the research of stepped spillways by compiling a data base of literature. Chanson's (2002) text on the subject also outlines research he has conducted on scaling effects in stepped spillway modeling, differences in nappe and skimming flow regimes, and development of relationships with regard to inception point location and energy dissipation that occurs in the stepped spillway chute. Boes and Hager (2003a and 2003b) conducted extensive research on air concentration and velocity distributions in stepped spillways, and their work has provide a relationship with regards to identifying the inception point location. It should be noted that the inception point relationships developed and provided by Chanson (1994a and 2002) and Boes and Hager (2003a and 2003b) define the inception point in two different locations. Chanson (1994a and 2002) defines the inception point as the location

where the turbulent boundary layer reaches the free surface whereas Boes and Hager (2003a and 2003b) indicate that the inception point is the location where the air concentration near the chute bed surface is 0.01. Both relationships were primarily developed using steep chute (2(H):1(V) or greater) data, yet Hunt and Kadavy (2006, 2007, 2008a, and 2008b) has found that Chanson's relationship has some applicability to slopes as flat as 4(H):1(V). Hunt and Kadavy (2006, 2007, 2008a, and 2008b) also provide information regarding the determination of energy dissipation both upstream and downstream of the inception point on a 4(H):1(V) stepped chute for a single step height.

The objective of this paper is to compare the effect step height has on the energy dissipation of a 4(H):1(V) stepped spillway, so this paper will summarize data related to velocity, air concentration, and energy loss in stepped spillways. In some cases, fully developed air entrained flow is not achieved in stepped spillways applied to embankment dams because the spillway chute is relatively short. Most energy dissipation data available for stepped chutes are in this highly air entrained zone. Therefore, this research is critical for the design of stepped spillways and their associated stilling basins applied to small embankment dams where this air entrainment may not be developed.

EXPERIMENTAL SET-UP

A two-dimensional (2-D) 1:8 scale model of a stepped spillway was constructed specifically for a study of Renwick Dam in North Dakota. This same model served the purpose for the generalized study on stepped chutes described herein. The primary objectives of the generalized study are to evaluate the inception point, energy losses, and velocities associated with flood flows on flatter sloped stepped spillways. Figure 1 illustrates a schematic of the two-dimensional model used for both the specific and generalized model studies.

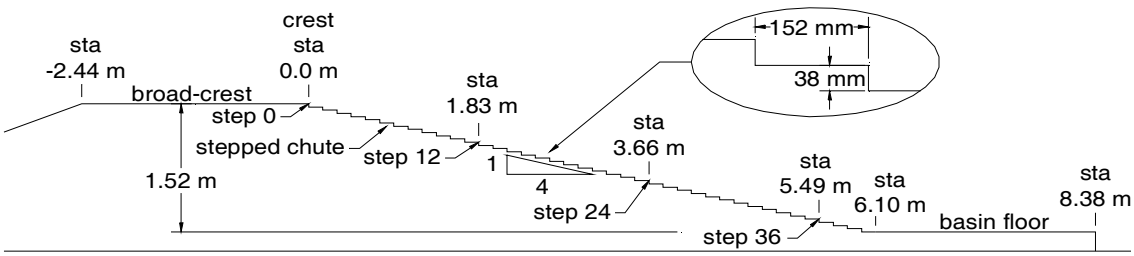

Figure 1. Schematic of stepped spillway model with the 38 mm (1.5 inch) high steps.

The 2-D model was constructed across the full width of a 1.8 m (6 ft) flume. The flume walls are 2.4 m (8 ft) tall, and the spillway model has a vertical drop of 1.5 m (5 ft). Figure 2 illustrates the two-dimensional model as it was originally constructed in the flume. A broad-crested weir served as the entrance conditions to the stepped spillway chute with the downstream edge of the weir corresponding to station 0.0 m (0.0 ft) and step 0. The chute slope was 4(H):1(V). Model step heights of 38 mm (1.5 inches) were originally tested, and later every other step was removed to create a stepped spillway chute with step heights of 76 mm (3.0 inches).

Water surface elevations and velocity measurements were taken throughout testing. Figure 3 illustrates a manually operated point gage attached to a moveable

carriage that was used to measure centerline water and bed surface elevations. Cross-sectional velocity profiles along the broad crested weir were collected with an acoustic Doppler velocimeter (ADV) that was attached to the point gage. The velocities and flow depth measurements at the broad crested weir were used to develop a calibration curve of the flow versus upstream head. The carriage was also used in centerline velocity measurements along the crest section. A second set of rails was attached to the inside of the flume walls and set parallel to the chute slope; thereby, allowing velocity and water surface measurements along the centerline of the chute to be taken perpendicularly to the chute slope. Unit discharges of 0.11, 0.21, 0.28, 0.42, 0.62, 0.82 $m^3/(s \cdot m)$ (1.2, 2.2 3.0, 4.5, 6.6, 8.9 cfs/ft) were tested.



Figure 2. 2-D stepped spillway model with the original 38 mm (1.5 inch) steps.

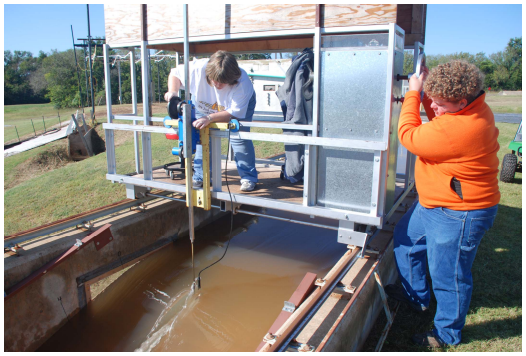

Figure 3. Data collection using a mobile carriage.

Scale effects can be expected when modeling highly air entrained flows when viscous forces and surface tension are not properly accounted for in the modeling. Scale effect is a term used to describe slight distortions that are introduced by ignoring viscous forces and surface tension in highly air entrained flows. Chanson (1994a), Boes and Hager (2003a and 2003b), and Takahashi, et al. (2006) have provided guidance to other researchers on modeling techniques for reducing scale effects associated with air entrained flows. Generally, a scale of 10:1 or larger is an accepted scale for modeling stepped spillways (Chanson, 2002). Boes and Hager (2003a) recommend a minimum Reynolds number of 10^5 and Weber number of 100 to minimize scale effects. Takahashi, et al. (2006) state that the Morton number must be considered to minimize scale effects. Morton's number accounts for both viscous forces and surface tension and is a product of both Reynolds and Weber numbers. For this model study, the Reynolds numbers ranged from 9.6×10^4 to 7.3×10^5, and the Weber numbers ranged from 112 to 234 for unit discharges ranging from 0.11 to 0.82 $m^3/(s \cdot m)$, repectively (Hunt and Kadavy, 2008a and 2008b).

Velocity profiles and flow depths were collected along the centerline of the spillway using three separate measuring devices: 1) an ADV, 2) a pitot tube (PT) coupled with a differential pressure transducer, and 3) a two-tip fiber optical (FO) probe and data acquisition system. Figures 4a, 4b, and 4c show the velocity instrumentation in use during the tests. Each device has a unique range of velocities it captures during operation. The ADV was limited by a maximum velocity of 4.6 m/s (15 ft/s), and it could only be used in non-turbulent flow conditions. The ADV

was primarily used to measure velocities at the broad-crested weir for model calibration. The PT coupled with a pressure transducer captured higher velocities that the ADV could not measure and verified some of the velocity measurements that were collected with the ADV. The two-tip FO probe was used to measure velocities and void fraction (C) in air entrained flows. The two-tip FO probe also allowed a comparison to some of the PT data. In some cases, the PT is not suitable to measure velocities in air entrained flows, but Matos, et al. (2002) reports that a backflushing PT is capable of measuring velocities in air entrained flows if the air concentrations are less than 70%. So to achieve a more accurate velocity measurement in air entrained flows, the PT was backflushed before each measurement to avoid air bubbles in the tube and the lines to the pressure transducer. The void fraction data collected by the FO probe was used to determine the equivalent clear water depth. The equivalent clear water depth is the depth of flow without the presence of air and is relevant to determining the energy loss in the spillway chute.

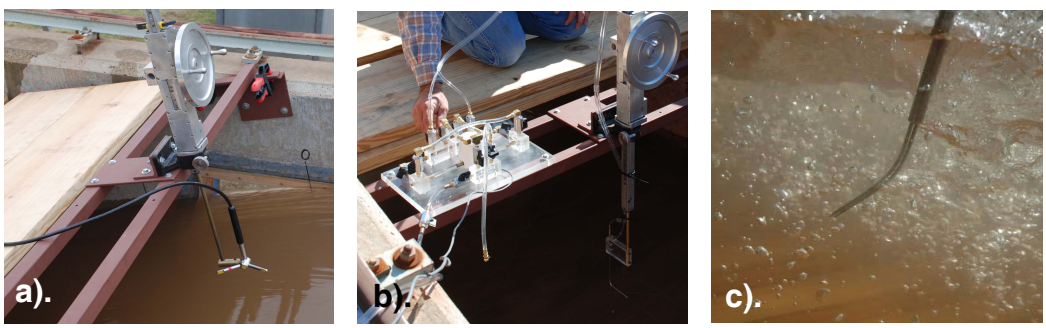

Figure 4. a). ADV flow tracker, b.) Pitot tube with a differential pressure transducer, c.) Two-tipped fiber optic probe.

Velocity profiles were taken normal to the spillway crest surface along the centerline at horizontal stations -2.4, -1.8, -1.2, -0.61, 0.0 m (-8, -6, -4, -2, and 0 ft) with the ADV. Centerline velocities profiles normal to the spillway chute slope were taken at horizontal stations 0.0, 0.61, 1.2, 1.8, 2.4, 3.0, 3.7, 4.3, 4.9, and 5.5 m (0, 2, 4, 6, 8, 10, 12, 14, 16, and 18 ft) with the ADV when applicable, with the PT for all stations along the chute slope, and with the FO probe when air entrainment was present. These horizontal stations correspond to the downstream edge of every fourth step for the stepped spillway having 38 mm (1.5 inch) high steps and every other step for the stepped spillway having 76 mm (3.0 inch) high steps. Figure 1 defines the stations as they relate to the stepped spillway model.

RESULTS AND DISCUSSION

Energy dissipation in a spillway chute is valuable information to the design engineer when it comes to designing the stilling basin. Stepped spillways dissipate a significant amount of energy when compared to traditional smooth chute spillways. Consequently, the stilling basin size for a stepped spillway is traditionally smaller than a stilling basin for a smooth chute spillway if the two spillways are based on similar design parameters.

To determine the energy loss in the spillway chute, velocity must be determined. Figure 5 illustrates typical velocity profiles expected in a stepped spillway. The profiles transition from near uniform at the crest section to a one-sixth

power law distribution near the inception point (Hunt and Kadavy, 2008a; Boes and Hager, 1998; and Chanson, 2000). Figures 6a and 6b present typical depth-velocity and depth-void fraction (C) profiles slightly upstream of the inception point at station 3.05 (10 ft) and downstream of the inception point at station 5.49 m (18 ft) for the stepped spillway having step heights of 38 mm (1.5 inch), respectively. Figures 6a and 6b show both PT and FO data. Air concentrations near the spillway chute bed surface as illustrated in Figure 6a were relatively non-existent and therefore undetectable by the FO probe. The PT was used to capture these velocities. The PT and FO data collected near the inception point yielded similar results with data points clustered closely together. In Figure 6b, distinction between the two profiles are more noticeable, yet the average velocities for the PT and FO data are 3.70 m/s (12.15 ft/s) and 3.69 m/s (12.12 ft/sec), respectively. Based on this outcome, the air concentration in the flow appears small enough that it does not significantly affect the average velocity.

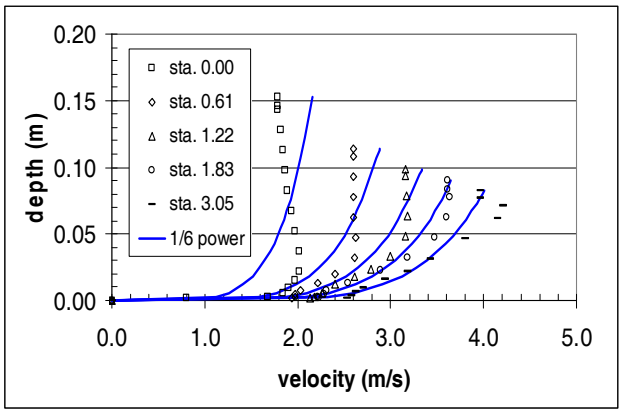

Figure 5. Velocity profiles for a unit discharge of 0.28 $m^3/(s \cdot m)$ (3.0 cfs/ft) transition from a uniform distribution at the crest and approach a one-sixth power law distribution near the inception point.

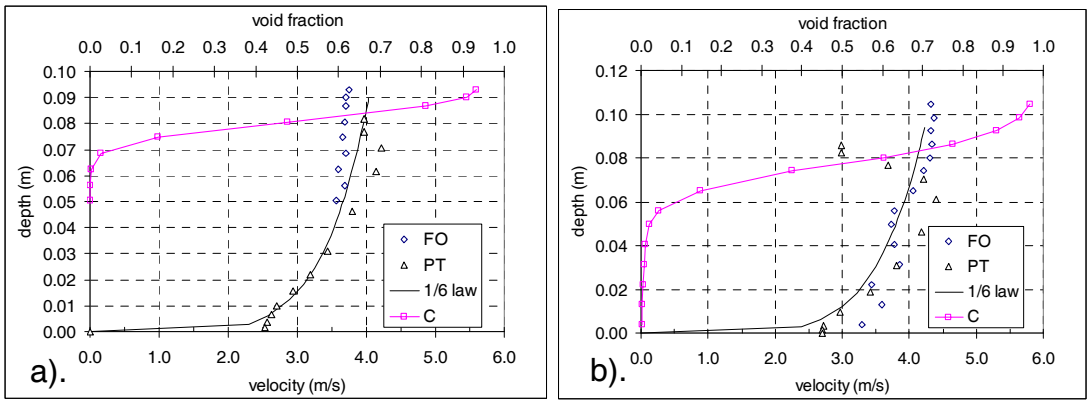

Figure 6. Depth-velocity and depth-void fraction (C) for a unit discharge of 0.28 $m^3/(s \cdot m)$ (3.0 cfs/ft) and a spillway step height of 38 mm (1.5 inches). a). Station 3.05 m (10 ft), b). Station 5.49 m (18 ft).

Figures 6a and 6b also illustrate depth-void fraction profiles. At each station, the void fraction increases in a logarithmic trend. The void fraction data was used to

determine the equivalent clear water depth, y_{cw}, for each station. For air-water flows, Chanson, et al. (2002) defines the equivalent clear water depth as

$$y_{cw} = \int_0^{y_{90}} (1-C) * dy \quad (1)$$

where y_{90} is characteristic depth (m) when the air concentration is 90% and C is air concentration, which is also known as void fraction. Upstream of the inception point, the depth is considered clear water depth because there is no presence of air in the flow. Downstream of the inception point, air is visibly present. Therefore, the equivalent clear water depth downstream of the inception point is the depth of flow with no air present. Figure 7 illustrates the equivalent clear water depth-velocity profile for station 5.49 m (18 ft). When Figure 7 is compared to Figure 6b, the clear water flow depth is less in Figure 7 as compared to the flow depth with air in Figure 6b. The clear water depth is needed to determine the average air concentration in the flow as well as the energy dissipation. As defined by Boes and Hager (2003a), the average air concentration, C_{avg}, in percent is

$$C_{avg} = 1 - \frac{y_{cw}}{y_{90}} * 100 \quad \text{for } \% \quad (2)$$

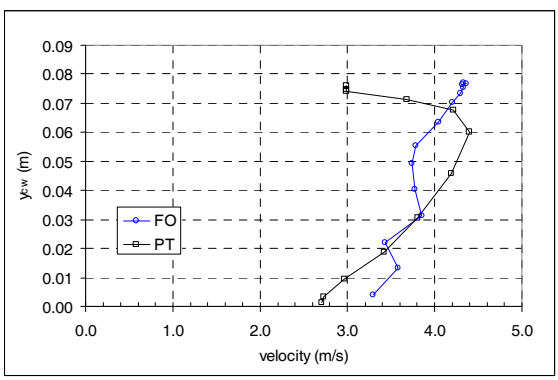

Figure 7. y_{cw}-velocity profiles at station 5.49 m (18 ft) for a q of 0.28 $m^3/(s \cdot m)$ (3.0 cfs/ft) and a stepped spillway with step height equal to 38 mm (1.5 inches).

The average velocity obtained from the velocity profiles was used to determine the relative energy loss on the spillway chute. The average velocity was based on the equivalent clear water depth, y_{cw}, as illustrated in a single example in Figure 7. With the average velocity at each station known, the total energy loss to a given step relative to the step of interest can be determined

$$\Delta H = H_o - H \quad (3)$$

where $H_o = y_o + \frac{V_o^2}{2g}$; $H = y_{cw}\cos\theta + \alpha\frac{V_{cw}^2}{2g}$, V_{cw} = clear water mean velocity; V_o = approach velocity; y_o = approach depth above datum, y_{cw} = clear water flow depth , θ = chute slope, g = gravitational acceleration, and α = energy coefficient. Figure 8 illustrates the energy loss parameters as they relate to the stepped spillway. In many open channel applications where the channel is of regular cross-section with fairly straight alignment, the energy coefficient, α, is assumed to equal one because the effect of nonuniform velocity distribution on the computed velocity head and

momentum is small (Chow, 1959). To determine the effect that the nonuniform velocity distribution has on the computed velocity head and momentum, Equation 4 was used to determine the energy coefficient.

$$\alpha = \frac{\int v^3 dA}{V_{cw}^3} \approx \frac{\sum v^3 \Delta A}{V_{cw}^3 A} \tag{4}$$

where v is the point velocity for an incremental area in the velocity profile, V_{cw} is the mean velocity of the of the equivalent y_{cw}-velocity profile, and A is the total area of the profile. Assuming two-dimensional flow that is uniform across the width, the area, A, is replaced by the equivalent y_{cw}. For both step heights, α ranged from 1.01 to 1.13. This α range is reasonable when compared to values of 1.05 to 1.1 reported by Boes (1999) for fully air entrained flows.

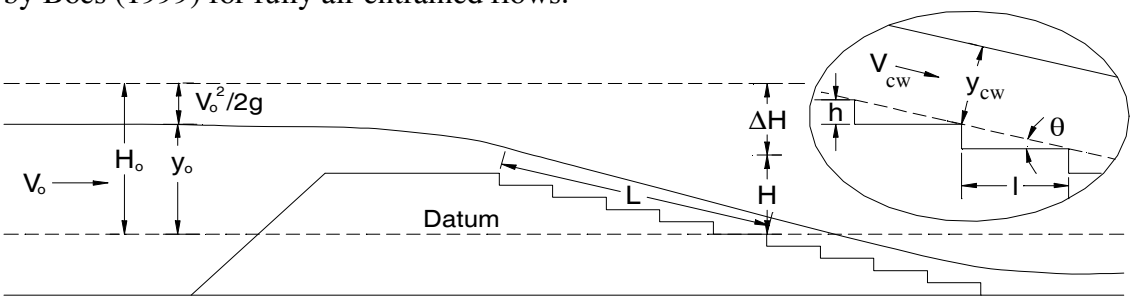

Figure 8. Energy loss parameters as they relate to the stepped spillway.

With the α determined, Equation 3 was used to determine the energy loss in the stepped spillway. Figures 9a and 9b illustrates a comparison of the energy loss for step heights of 38 mm (1.5 inches) and 76 mm (3.0 inches) and unit discharges of 0.11 $m^3/(s \cdot m)$ (1.2 cfs/ft) and 0.82 $m^3/(s \cdot m)$ (8.9 cfs/ft), with respect to horizontal stationing for the spillway. Energy loss increases as the flow descends the spillway chute. Additionally, Figures 9a and 9b illustrate that as the step height increases the energy loss also increases. Figure 9a also shows the inception point locations of 1.4 m (3.6 ft) and 1.1 m (4.6 ft) for the 38 mm (1.5 inch) and 76 mm (3.0 inch) step height chute configurations, respectively; indicating that as step height decreases the inception point moves further downstream for the given discharge. The inception points for Figure 9b are located in the stilling basin, so Figure 9b clearly shows the energy loss is greater for a step height of 76 mm (3.0 inch) upstream of the inception point while Figure 9a undoubtedly illustrates the energy loss is greater for the 76 mm (3.0 inch) steps downstream of the inception point.

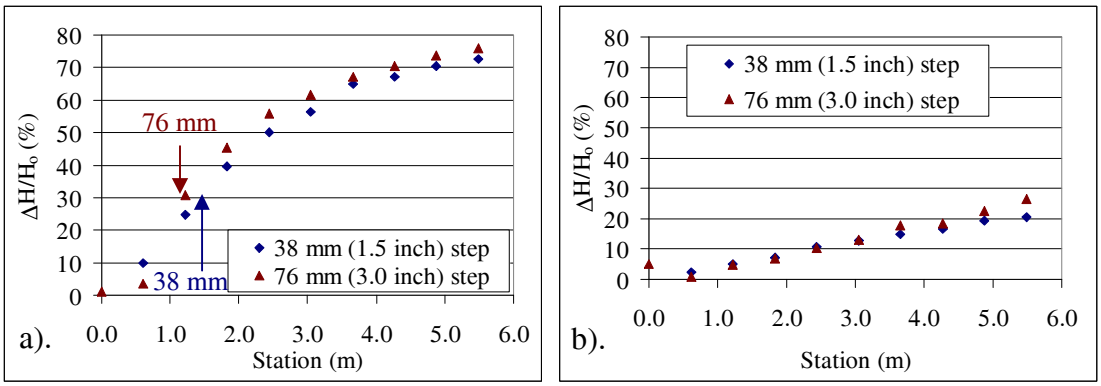

Figure 9. a). Energy loss for 38 mm (1.5 inch) and 76 mm (3.0 inch) step height for a unit discharge of 0.11 $m^3/(s \cdot m)$ (1.2 cfs/ft) versus horizontal stationing with the arrows defining inception point location with regards to step height b). Energy loss for 38 mm (1.5 inch) and 76 mm (3.0 inch) step height for a unit discharge of 0.83 $m^3/(s \cdot m)$ (8.9 cfs/ft) versus horizontal stationing.

Hunt and Kadavy (2008a) further compared the energy loss with respect to the inception point location and reported that the energy loss follows a linear trend upstream of the inception point for a 4(H):1(V) stepped chute with 38 mm (1.5 inch) high steps. The energy loss relationship upstream of the inception point provided by Hunt and Kadavy (2008a) is

$$\frac{\Delta H}{H_o} * 100 = 30 * \frac{L}{L_{i*}} \tag{5}$$

Downstream of the inception point in the same model, Hunt and Kadavy (2008b) reported that the energy loss follows a logarithmic trend, increasing from 30% energy loss at the inception point to approximately 73% for a value of L/L_{i*} of 3.5. Figure 10 illustrates these trends hold with the inclusion of the 76 mm (3.0 inch) step height data and the Salado data from the Rice and Kadavy (1996) study. The Salado data provides additional confirmation that this design information is also applicable for a chute slope of 2.5(H):1(V).

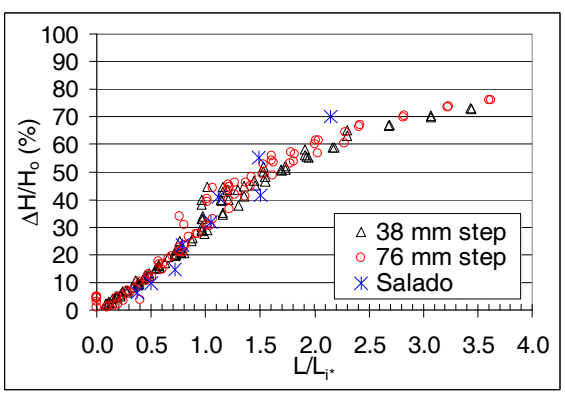

Figure 10. Energy loss versus the normalized length down the spillway chute.

CONCLUSIONS

RCC stepped spillways applied to embankment dams to increase spillway capacity create unique challenges for design engineers. These spillways typically

have flat slopes of 2(H):1(V) or flatter and are relatively short in length when compared to gravity dam stepped spillways. As a result, oftentimes the air entrainment is not fully developed within the spillway chute. Determining the energy loss in the spillway is valuable information for determining the dimensions of the stilling basin. Yet, most literature reports energy losses in the spillway downstream of the inception point where the flow is fully air entrained. In this study, the energy loss through the entire spillway chute is examined with regards to step height and inception point location. Findings show that with increasing step height, the energy losses at similar locations within the spillway chute also increase. Additionally, for a given unit discharge, the inception point location moves further downstream of the crest section as step height decreases. When the energy losses were compared to a normalized length, L/L_{i*}, the energy losses increased linearly from near zero at the spillway crest to 30% at the inception point for both spillway configurations. Downstream of the inception point, the two step height showed that the energy losses increased in a logarithmic trend from 30% at the inception point to approximately 73% when L/L_{i*} equals 3.5. This research is expected to assist engineers with the design of stepped spillways applied to embankment dams.

REFERENCES

Boes, R. M. (1999). "Physical model study on two-phase cascade flow." In *Proc., 28th IAHR Congress*, *Session S1*. Graz, Austria.

Boes, R. M. (2000). "Scale effects in modeling two-phase stepped spillway flow." *Intl. Workshop on Hydraulics of Stepped Spillways,* Zürich, Switzerland, H. E. Minor and W. H. Hager Editors, Balkema Publ., pp. 53-60.

Boes, R. M. and Hager, W. H. (1998). "Fiber-optical experimentation in two-phase Cascade flow." In *Proc. Int. RCC Dams Seminar*, K. Hanson, ed., Denver, Colorado.

Boes, R. M. and W. H. Hager. (2003a). "Two-phase flow characteristics of stepped spillways." *J. of Hydr. Engrg.,* ASCE, 129(9):661-670.

Boes, R. M. and W. H. Hager. (2003b). "Hydraulic design of stepped spillways." *J. of Hydr. Engrg.,* ASCE, 129(9):671-679.

Chanson, H. (1994a). "Hydraulics of skimming flows over stepped channels and spillways." IAHR, *J. Hydr. Res.* 32(3):445-460.

Chanson, H. (2000). "Characteristics of skimming flow over stepped spillways – discussion." *J. of Hydr. Engrg.,* ASCE, 125(4):862-865.

Chanson, H. (2002). *The Hydraulics of Stepped Chutes and Spillways.* Steenwijk, The Netherlands: A. A. Balkema Publishers.

Chow, V. T. 1959. *Open-Channel Hydraulics.* Boston, MA: McGraw-Hill, Book Company, Inc.

Felder, S. and Chanson, H. (2008). "Turbulence and turbulent length and time scales in skimming flows on a stepped spillway. Dynamic similarity, physical modeling and scale effects." Queensland, Australia: The University of Queensland, Division of Civil Engineering.

Gonzalez, C. A. (2005). "An experimental study of free-surface aeration on embankment stepped chutes." PhD Thesis. Queensland, Australia: The University of Queensland, Department of Civil Engineering.

Hunt, S. L., K. C. Kadavy, S. R. Abt, and D. M. Temple. (2006). "Converging RCC stepped spillways." In *the Proc.* 2006 World Environmental and Water Resources Congress, ASCE Conference, Omaha, Nebraska. (CD-ROM).

Hunt, S. L., and K. C. Kadavy. (2007). "Renwick dam RCC stepped spillway research." In *the Proc. Association of State Dam Safety Officials (ASDSO) Annual Meeting*, Austin, Texas. (CD-ROM)

Hunt, S. L. and K. C. Kadavy. (2008a). "Velocities and energy dissipation on a flat-sloped stepped spillway." *In the Proc.* of 2008 American Society of Agriculutral and Biological Engineers (ASABE) Annual International Meeting. Paper No. 084151. St. Joesph, Michigan: ASABE.

Hunt, S. L., and K. C. Kadavy. (2008b). "Energy dissipation on a 4(H):1(V) stepped spillway." In *the Proc. Association of State Dam Safety Officials (ASDSO) 2008 Annual Meeting,* Indian Wells, California. (CD-ROM)

Matos, J., Frizell, K. H., André, S., and Frizell, K. W. (2002). "On performance of velocity measurement techniques in air-water flows." In *the Proc. Hydraulic Measurements and Experimental Methods – 2002*; Estes Park, Colorado; T. L. Wahl, C. A. Pugh, K. A. Oberg, and T. B. Vermeyen, Editors.

Rice, C. E. and K. C. Kadavy. (1996). "Model study of a roller compacted concrete stepped spillway." *J. Hydr. Engrg.*, ASCE, 122(6):92-297.

Takahashi, M., Gonzalez, C. A., and Chanson, H. (2006). "Self-aeration and turbulence in a stepped channel: influence of cavity surface roughness. *International Journal of Multiphase Flow*." 32:1370-1385.

Yasuda, Y. and Ohtsu, I. (1999). "Flow resistance of skimming flow in stepped channels." In *Proc., 28th IAHR Congress*, *Session B14*. Graz, Austria.

The Geneva Dam, IL Hydraulic Roller Problem: Design of a Temporary Steep Riprap Ramp

Yu-Chun Su[1], Ph.D., P.E., CPESC, CPSWQ, CFM;
Loren Wobig[2], P.E., CFM; Brad Winters[3], P.E., CFM; Xin He[4], Ph.D.; and
David T. Williams[5], Ph.D., P.E., D.WRE, F.ASCE, P.H., CPESC

[1]Project Manager, Water Resources, PBS&J; 1250 Wood Branch Park Drive, Suite 300, Houston, TX 77079; PH (281) 493-5100; FAX (281) 493-1047; email: ycsu@pbsj.com
[2]Project Manager, Illinois Department of Natural Resources, Office of Water Resources; One Natural Resources Way, Springfield, Illinois 62702; PH (217) 782-9130; email: loren.wobig@illinois.gov
[3]Project Engineer, Illinois Department of Natural Resources, Office of Water Resources; One Natural Resources Way, Springfield, Illinois 62702; PH (217) 782-9130; email: brad.winters@illinois.gov
[4]Engineer II, Water Resources, PBS&J; 1250 Wood Branch Park Drive, Suite 300, Houston, TX 77079; PH (281) 493-5100; FAX (281) 493-1047; email: xhe@pbsj.com
[5]Senior Technical Advisor, Water Resources, PBS&J; 2032 Lowe St., Suite 202, Fort Collins, CO 80525; PH (619) 823-4778; email: dtwilliams@pbsj.com

ABSTRACT

Run of the river low head dams provide an attractive nuisance since the relatively placid areas downstream of the dam entice people to either swim or canoe/raft/kayak into these areas. To address this public safety issue, the Illinois Department of Natural Resources, Office of Water Resources (IDNR) had been tasked to develop a hydraulic analysis or methodology to define the hydraulic characteristics at the Geneva Dam (on the Fox River near Geneva, IL) spillway and to develop the sizing of a temporary rock ramp on the downstream side of the existing run-of-river dam ogee spillway. The rock ramp was to minimize the existing submerged hydraulic jump "roller" at the site for flow conditions up to a 5-year frequency flow event. The rock ramp would also be stable for up to a 100-year frequency flow condition with a 20-year expected project life until a more permanent solution is developed and implemented.

A temporary rock ramp was proposed and sized to accomplish these criteria for the downstream side of the Geneva dam spillway. Several riprap methods that were applicable to steep slopes were analyzed. To facilitate the computations and to make direct comparisons of the results, a spreadsheet was developed that contained all of the methods and included warnings for applicability of the methods. This paper describes the thought processes, the applicability of single and multi-dimensional computational models for addressing the hydraulic roller problem, and the computations and the development of the steep ramp riprap design spreadsheet.

INTRODUCTION

Run of the river low head dams provide an attractive nuisance since this area, even under quiescent conditions, often contains a submerged hydraulic jump for energy dissipation, resulting in portions of the water traveling downstream, portions boiling to the surface, and other portions flowing back toward the dam. This phenomenon is called a reverse hydraulic roller and entraps people that enter the water, keeps them submerged and causes drowning.

To address this public safety issue, the Illinois Department of Natural Resources, Office of Water Resources (IDNR) had been tasked to develop a hydraulic analysis or methodology to define the hydraulic characteristics at the Geneva Dam (on the Fox River near Geneva, IL) spillway and to develop the sizing of a temporary rock ramp on the downstream side of the existing run-of-river dam ogee spillway. The rock ramp was to minimize the existing submerged hydraulic jump "roller" at the site for flow conditions up to a 5-year frequency flow event. The rock ramp would also be stable for up to a 100-year frequency flow condition with a 20-year expected project life until a more permanent solution is developed and implemented. The basic needs of IDNR to address these issues include:

- Determination of an hydraulic analysis or methodology to define the hydraulic characteristics at the Geneva dam spillway as well as be able to analyze alternatives that could be developed to minimize or alleviate the hydraulic roller problem. It must also be reasonably available (limited cost to purchase and run on existing IDNR office desktop computers) to the Office of Water Resources and reasonably used by Office of Water Resources staff with limited training. This hydraulic analysis or methodology may be applicable to other similar run-of-river dams on the Fox River.

- Development of a hydraulic analysis or methodology to define the hydraulic characteristics at the dam spillway and to support the sizing of a temporary rock ramp on the downstream side of the existing run-of-river dam ogee spillway on the Fox River in Geneva, Illinois.

Figure 1 shows the location of Geneva Dam. Figure 2 shows an aerial image of the area. Figure 3 shows a photo of the dam. Figure 4 shows an illustration of public safety concern related to the roller.

A temporary rock ramp was proposed and sized to accomplish these criteria for the downstream side of the Geneva dam spillway. Several riprap methods that were applicable to steep slopes were analyzed. The riprap methods examined were:

a. U.S. Army Corps of Engineers' (COE) method for steep slopes (from EM 1110-2-1601).
b. Isbash Method, high turbulence (from EM 1110-2-1601).
c. Frizell, Ruff and Mishra method for overtopping flows.

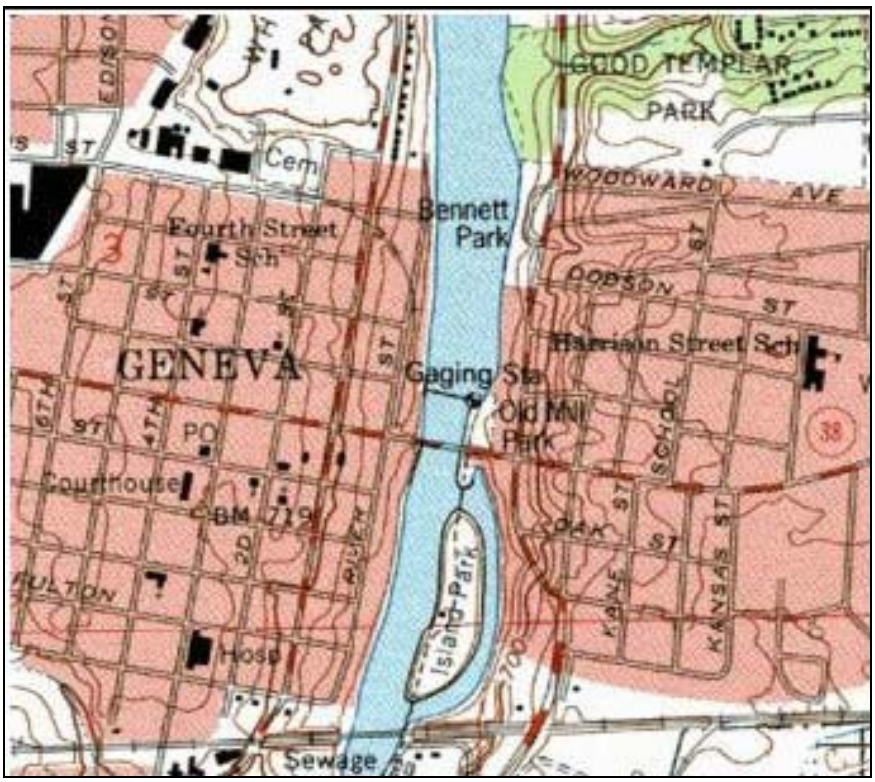

Figure 1. Location of Geneva Dam

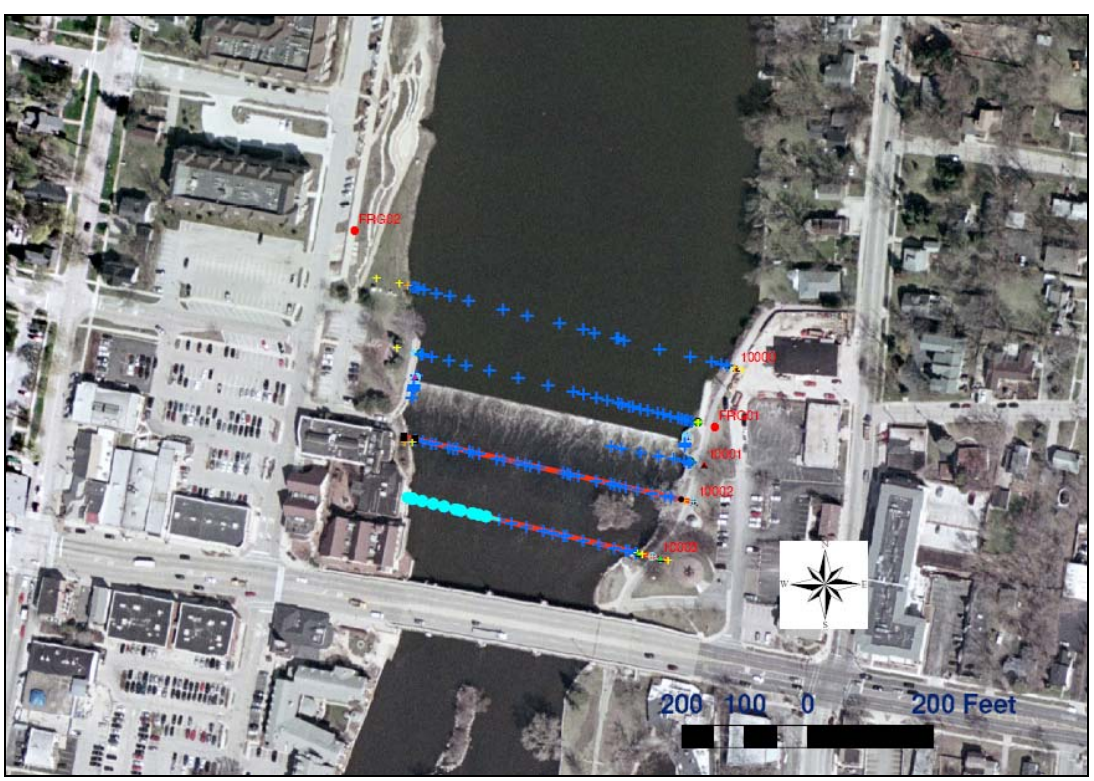

Figure 2. Aerial Image of Geneva Dam Area



Figure 3. Photo of Geneva Dam

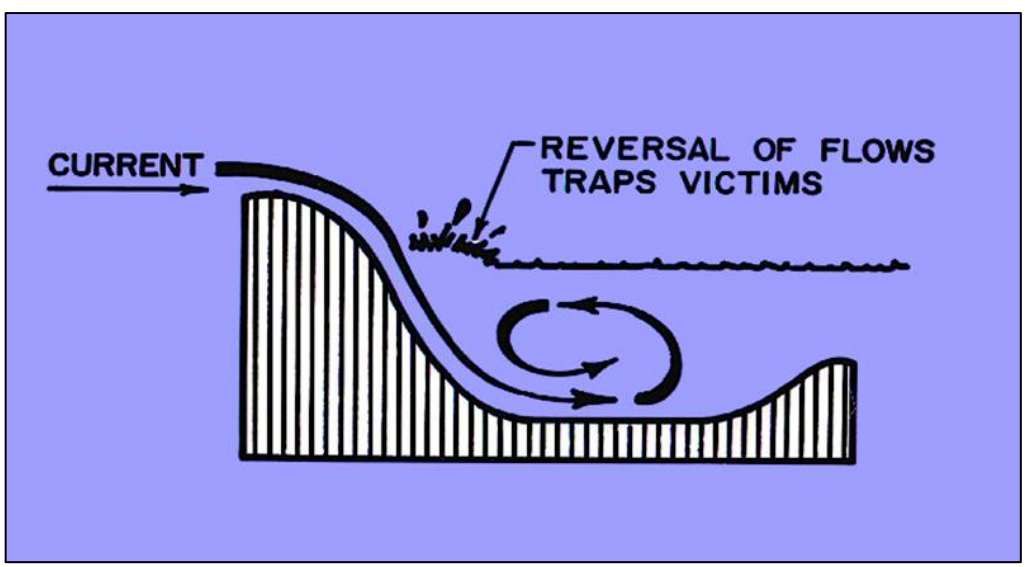

Figure 4. Public Safety Concern of Existing Dam Design

d. Hydraulic Engineering Circular 15, Design of Roadside, Channels with Flexible Linings (HEC-15, FHWA).

To facilitate the computations and to make direct comparisons of the results, a spreadsheet was developed that contained all of the methods and included warnings

for applicability of the methods. This paper describes the thought processes, the applicability of single and multi-dimensional computational models for addressing the hydraulic roller problem, and the computations and development of the steep ramp riprap design spreadsheets.

DATA COLLECTION AND REVIEW

Available data and information were provided by IDNR, including:

- Plan view of survey data available at Geneva Dam;
- Surveyed cross section (parallel to flow) of the Geneva Dam at each dam abutment;
- Four surveyed cross sections of the Fox River in the vicinity of the Geneva Dam (2 cross sections upstream and 2 cross sections downstream of the dam);
- Rating curve for the Geneva Dam;
- Flow frequency data for the Geneva Dam;
- HEC-2 input files for Geneva Dam;
- General description of the Geneva Dam; and
- Representative photos of the Geneva Dam.

Basic information of Geneva Dam includes:

- Type - ogee;
- Material - concrete;
- Weir Length – 134.4 meters (m) or 441 feet (ft);
- Height – 3.96 m (13 ft);
- Spillway elevation – 205.86 m (675.40 ft);
- Length of pool – 3.19 kilometers (km) or 1.98 miles; and
- Area of Pool – 0.36 km^2 (89 acres).

Based on the review of available data provided by IDNR, a technique was recommended to define the hydraulic characteristics at the Geneva dam spillway as well as evaluate possible alternatives to alleviate the hydraulic roller problem. The recommended technique was based upon consideration of availability (limited cost to purchase and run on existing office desktop computers) to IDNR, ability to address the hydraulic conditions for a full range of possible alternatives and use by IDNR engineering staff with limited training and specialized expertise. The technique must be able to, at a minimum, hydraulically (vertical dimension for roller analyses) simulate the following:

a. Structural modifications to the dam weir and apron
    1. Notches
    2. Steps
    3. Apron dimensions, etc.
b. Changes to the weir approach
c. Multiple bypass alternatives
    1. Fish bypass

2. Hydraulic bypass
3. Manual and automated operation of bypasses

Given the complexity of hydrodynamics immediately downstream of a dam and solutions that may include lateral bypasses, two- or even three-dimensional (2D or 3D) model are required to analyze the detailed water velocity distribution in the area. Potential 2D and 3D models that may be suitable for such analysis include: SOBEK, RMA2, FESWMS-FST2DH, HEM2D, HIVEL 2-D, TUFLOW, RMA10, ADCIRC, CH3D-WES, DELFT3D-FLOW, HEM3D, MIKE21/3, GLLVHT, FLUENT, and FLOW-3D. Although dendritic 1D models (such as HEC-RAS) can adequately model simplified bypass conditions, only 2D lateral (horizontal) model are applicable if approach conditions to the bypass are complicated or other multi-dimensional phenomena dominate.

For analysis of the hydraulic roller alone (near field analysis), the FLUENT and FLOW-3D models were recommended. For far field analysis only (for such alternative as bypasses), FESWMS-FST2DH is recommended for mixed flow conditions and if mixed flow is not an issue, RMA2 and FESWMS-FST2DH were recommended. For simulation of the hydraulic roller and far field analyses, a combination of FLUENT or FLOW-3D and RMA2 or FESWMS-FST2DH were recommended. These models do not pass the desktop PC or limited training constraints, so these methods are not recommended for this situation. If the far field conditions are hydraulically simplistic, that portion can be modeled using a 1D model such as HEC-RAS.

DEVELOPMENT OF HYDRAULIC MODEL FOR RIPRAP RAMP DESIGN

An HEC-2 model containing the geometry in the vicinity of Geneva Dam was obtained from IDNR. This geometry was converted to an HEC-RAS model and refinements made to the model. Most of the refinements to the model were made in the area at and near the dam spillway. The HEC-RAS model was then modified to simulate riprap ramp slopes of 5 and 10%. To bracket the possible Manning's n values for the riprap, which depends on its gradation, n values of 0.35 and 0.70 were used for each of the ramp slopes.

The hydrologic conditions include a 5-year frequency flow event for roller minimization, followed by the 10-year, 50-year and the 100-year frequency flow condition for the stability of the rock riprap ramp. Based on the data provided by IDNR, the 100-year flow is 346.88 cubic meters per second (cms) or 12,250 cubic feet per second (cfs). The 5-year flow was estimated to be 192.55 cms (6,800 cfs) by constructing a frequency plot shown in Figure 5 based upon other frequency discharges provided by IDNR.

The developed HEC-RAS model was executed for the following three physical conditions and four discharges:

a. Existing Conditions; 5-year, 10-year, 50-year and 100-year discharges

b. Proposed Riprap Ramp Slope = 0.05; 5-year, 10-year, 50-year and 100-year discharges
c. Proposed Riprap Ramp Slope = 0.10; 5-year, 10-year, 50-year and 100-year discharges

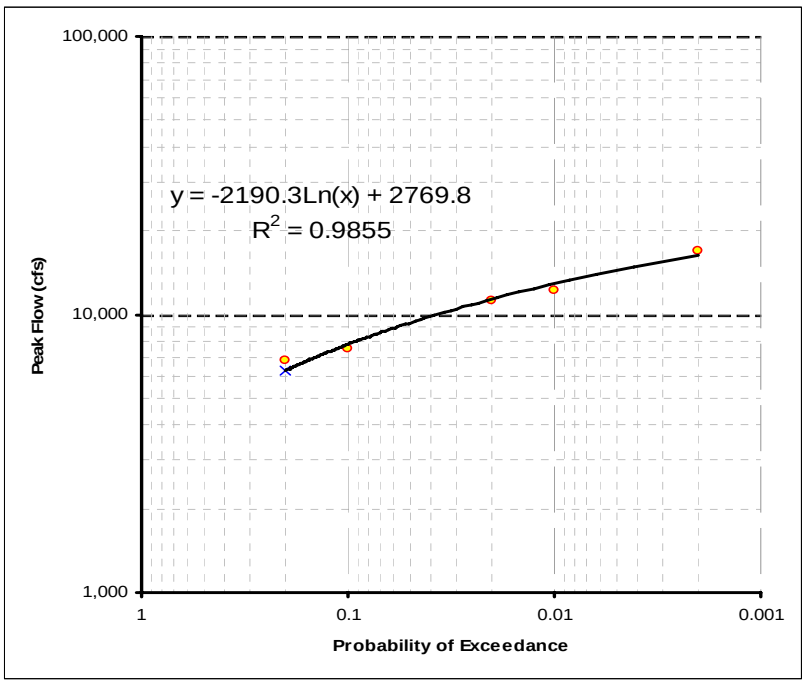

Figure 5. Flow Frequency Plot for Geneva Dam Location

SIZING OF ROCK RIPRAP RAMP

A temporary rock ramp was sized to eliminate, or minimize to a safe level, the existing submerged hydraulic jump "roller" at the site for the specified frequency flow events. The following riprap methods were examined:

a. U.S. Army Corps of Engineers' (COE, 1994) method for steep slopes (from EM 1110-2-1601).
b. Isbash Method, high turbulence (from EM 1110-2-1601).
c. Frizell, Ruff and Mishra method for overtopping flows (1998).
d. Hydraulic Engineering Circular 15, Design of Roadside, Channels with Flexible Linings (HEC-15, FHWA, 2005).

Note that the COE method for steep slopes gives D_{30} for the representative riprap size whereas the others give D_{50}. To make the methods comparable, the D_{30} result was converted to an equivalent D_{50} using the formula $D_{30} = D_{50} (D_{15} / D_{85})^{0.33}$, which is related to the COE gradation method (see EM1110-2-1601). The COE method assumes that the thickness is 1.5 times the D_{100} and the slope can range from 2 to 20%.

The HEC-15 was developed for riprap ramps that have riprap side slopes. Since the riprap design should be based upon the longitudinal slope and not the side slope, the weir side slopes was assumed to be relatively flat. For placement of the riprap on the downstream side of the weir crest, the riprap along the side should be anchored to the concrete sides of the dam. This can be done by extensive grouting or by anchoring large pieces of riprap with rebar that is attached to the concrete walls.

These methods were selected because they have a history of application to steep longitudinal slopes. The inputs to these methods were obtained from the flow data, the results of the HEC-RAS model, and user specified inputs such as the ramp slope. A Microsoft Corporation Excel spreadsheet was developed which included the computations for the four methods mentioned. This spreadsheet can be used for a variety of inputs. Figure 6 shows an illustration of an ogee dam cross section used for riprap volume calculations in the spreadsheet.

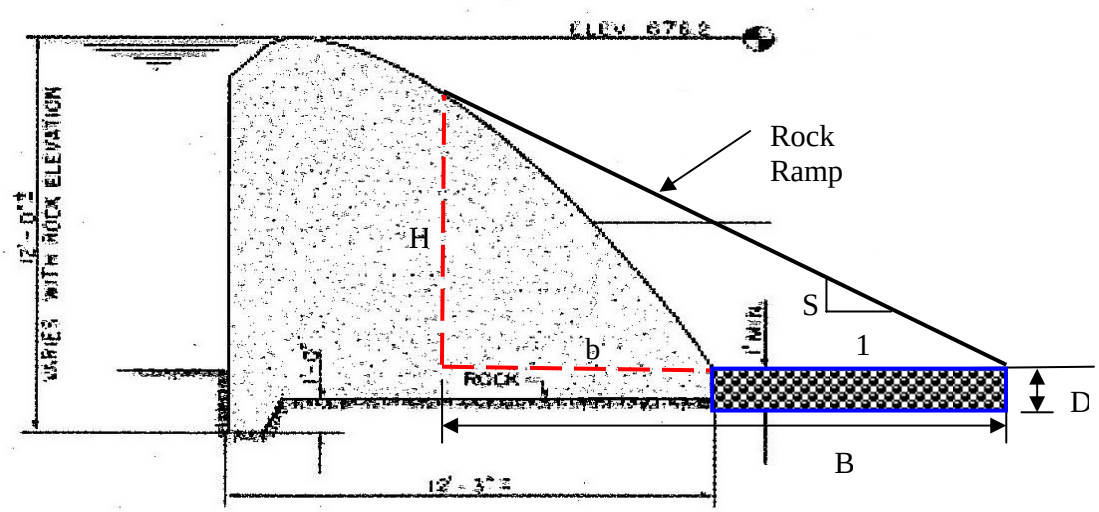

Figure 6. Illustration of Dam Section Used for Riprap Volume Calculations

Table 1 shows the results of the riprap design. The Isbach method results are much higher than the other 3 methods whereas those three methods give remarkably close results. Upon closely examining the Isbach method, it was found that the formula was developed for the construction of dams by depositing rock into running water. If the dumped rock did not slide or roll under that condition, the rock size was considered stable. Obviously this would result in very conservative answers. Because of this, the Isbach method was not recommended.

The next highest results (for a ramp slope of 10%) are from the HEC-15 method but this is not surprising since it uses a safety factor of 1.5. The Frizell et. al. method is the least conservative method for a slope of 10%. In the reference for this method, the unit discharge for the Geneva Dam exceeded those presented in the graph used in determining the D_{50} of the riprap. The COE method shows reasonable results for the full range of ramp slopes and discharges and therefore is recommended for design of the riprap for Geneva Dam.

Table 1. Results of Rock Ramp Design and Riprap Sizing

Return Period (years)	Channel Slope	Manning's n	Methodology				Average D_{50}* (m | ft)
			COE-EM1601-1	COE-EM1601-Isbach	FrizellRuffMishra	FHWA	
			D_{30}* (m | ft)	D_{50} (m | ft)	D_{50} (m | ft)	D_{50} (m | ft)	
5	5%	0.035	0.219 | 0.72	0.680 | 2.23	0.235 | 0.77	0.226 | 0.74	0.351 | 1.15
10			0.235 | 0.77	0.725 | 2.38	0.256 | 0.84	0.232 | 0.76	0.375 | 1.23
50			0.305 | 1.00	0.917 | 3.01	0.271 | 0.89	0.268 | 0.88	0.457 | 1.50
100			0.323 | 1.06	0.960 | 3.15	0.335 | 1.10	0.277 | 0.91	0.491 | 1.61
5		0.070	0.219 | 0.72	0.643 | 2.11	0.235 | 0.77	0.223 | 0.73	0.341 | 1.12
10			0.235 | 0.77	0.658 | 2.16	0.253 | 0.83	0.235 | 0.77	0.357 | 1.17
50			0.305 | 1.00	0.710 | 2.33	0.265 | 0.87	0.280 | 0.92	0.408 | 1.34
100			0.323 | 1.06	0.722 | 2.37	0.329 | 1.08	0.293 | 0.96	0.436 | 1.43
5	10%	0.035	0.320 | 1.05	0.942 | 3.09	0.271 | 0.89	0.381 | 1.25	0.497 | 1.63
10			0.344 | 1.13	0.994 | 3.26	0.296 | 0.97	0.411 | 1.35	0.530 | 1.74
50			0.448 | 1.47	1.192 | 3.91	0.338 | 1.11	0.549 | 1.80	0.655 | 2.15
100			0.475 | 1.56	1.234 | 4.05	0.363 | 1.19	0.585 | 1.92	0.692 | 2.27
5		0.070	0.320 | 1.05	0.643 | 2.11	0.265 | 0.87	0.433 | 1.42	0.433 | 1.42
10			0.344 | 1.13	0.658 | 2.16	0.293 | 0.96	0.469 | 1.54	0.460 | 1.51
50			0.448 | 1.47	0.710 | 2.33	0.326 | 1.07	0.661 | 2.17	0.561 | 1.84
100			0.475 | 1.56	0.722 | 2.37	0.354 | 1.16	0.716 | 2.35	0.591 | 1.94

*Averaging D_{50} includes the conversion of D_{30} to D_{50} using the USACE gradation of $D_{50} = D_{30}/0.82$.

The thickness and gradation of the riprap should be based upon the COE method, which is presented in EM 1110-2-1601, since the recommended method and the COE gradation method uses D_{30} as the basis for design.

Because of the high turbulence, vibration of the riprap would tear filter fabric; therefore, granular filter is recommended. The downstream end of the riprap, as projected from the weir at the design ramp slope, should be buried below the streambed and the burial depth equal to the thickness of the riprap and the filter material. The burial depth of the riprap at the downstream end should be projected horizontally upstream to the weir to define the lower limit of the riprap. Riprap volume can be determined by measuring the projected area of the proposed riprap (including granular filter) and multiplying it by the representative weir length. Note that the riprap immediately downstream of the crest (abutting the crest) can be from 1 to 2 feet below the crest. Cost is hard to estimate because it often depends on the availability of the particular size riprap and market conditions. However, estimates could be made using riprap bids from comparably located projects utilizing the computed riprap volume as described.

CONCLUSIONS

A study was conducted to evaluate and recommend hydraulic models or methodology for the analyses of the hydraulic roller problem at their run-of-the-river dams, in particular, Geneva Dam. A PC based hydraulic model was deemed not feasible to run in this scenario on IDNR desktop computers with limited training. Instead, four riprap methodologies were examined. The COE method for steep slopes was recommended since it did not have the deficiencies of the other methods and produced reasonable results for the full range of slope and discharge conditions. A recommendation using the chosen methodology was also made for the design of temporary riprap ramps to be placed just downstream of the weir crest of the run-of-the-river dams, in particular, Geneva Dam.

REFERENCES

Frizell, K. H., J. F. Ruff and S. Mishra. (1998) *Simplified Design Guidelines for Riprap Subjected to Overtopping Flow*. U.S. Department of Interior, U.S. Bureau of Reclamation, Report ID: PAP-790.

U.S. Army Corps of Engineers, (1994) *Engineering Manuals, EM 1110-2-1601*, 30-Jun-94.

U.S. Department of Transportation, Federal Highway Administration, (2005) "Design of Roadside Channels with Flexible Linings", *Hydraulic Engineering Circular No. 15*, Third Edition, Publication No. FHWA-NHI-05-114, September 2005.

Fish Passage and Abundance around Grade Control Structures on Incised Streams

J. T. Thomas[1], A. N. Papanicolaou[2], C. L. Pierce[3], D. C. Dermisis[2], M. E. Litvan[4], and C. J. Larson[5]

[1]Hungry Canyons Alliance, Golden Hills RC&D Office, P.O. Box 189, Oakland, IA 51560-0189; PH (712) 482-3029; email: john.thomas@rcdnet.net
[2]IIHR - Hydroscience & Engineering, Dept. of Civil and Environmental Engineering, University of Iowa, Iowa City, IA 52242-1585; apapanic@engineering.uiowa.edu, dimitrios-dermisis@uiowa.edu
[3]U.S. Geological Survey, Iowa Cooperative Fish and Wildlife Research Unit, Iowa State University, Ames, IA 50011; cpierce@iastate.edu
[4]Missouri Department of Conservation, Southwest Regional Office, 2630 North Mayfair, Springfield, MO 65803; mary.litvan@mdc.mo.gov
[5]Iowa Department of Natural Resources, 5744 Lewis Road, Lewis, IA 51544; chris.larson@dnr.state.ia.us

ABSTRACT

This paper summarizes research from separate studies of fish passage over weirs (Larson *et al*., 2004; Litvan, 2006; Litvan, *et al*., 2008a-c) and weir hydraulics (Papanicolaou and Dermisis, 2006; Papanicolaou and Dermisis, in press). Channel incision in the deep loess region of western Iowa has caused decreased biodiversity because streams have high sediment loads, altered flow regimes, lost habitat, and lost lateral connectivity with their former floodplains. In-stream grade control structures (GCS) are built to prevent further erosion, protect infrastructure, and reduce sediment loads. However, GCS can have a detrimental impact on fisheries abundance and migration, biodiversity, and longitudinal connectivity. Fish mark-recapture studies were performed on stretches of streams with and without GCS. GCS with vertical or 1:4 (rise/run) downstream slopes did not allow fish migration, but GCS with slopes ≤ 1:15 did. GCS sites were characterized by greater proportions of pool habitat, maximum depths, fish biomass, slightly higher index of biotic integrity (IBI) scores, and greater macroinvertebrate abundance and diversity than non-GCS sites. After modification of three GCS, IBI scores increased and fish species exhibiting truncated distributions before were found throughout the study area. Another study examined the hydraulic performance of GCS to facilitate unimpeded fish passage by determining the mean and turbulent flow characteristics in the vicinity of the GCS via detailed, non-intrusive field tests. Mean flow depth (Y) and velocity (V) atop the GCS were critical for evaluating GCS performance. Turbulent flow measurements illustrated that certain GCS designs cause sudden constrictions which form eddies large enough to disorient fish. GCS with slopes ≤ 1:15 best met the minimum requirements to allow catfish passage of a flow depth of ≥ 0.31 m and a mean flow velocity of ≤ 1.22 m/s.

INTRODUCTION

Channelization of streams and land use changes during the first half of the 20th century caused western Iowa stream channels to become unstable. Coupled with the highly erosive loess soils found in the deep loess region of western Iowa, the channels began to downcut and widen, causing an estimated $1.1 billion in damages to public and private infrastructure (by exposing buried bridge pilings, culvert outlets, utility lines, etc., and increasing their likelihood of failure), loss of farmland, and increased sediment loads (Baumel 1994). Streams that were once merely wetlands or shallow meandering streams are now deep, non-meandering, ditches nearly 9.1 m deep. Obviously, these streams have highly altered flow regimes (Hansen, 1971; Shields *et al*. 1994); channel roughness is lower and flow velocities and discharges are much higher than they once were. These scoured channels have lost much, if not all, of their original habitat; for example, many of these streams are devoid of riffle-pool sequences, except at very low baseflow. Prime fish habitat has been shown to be adversely affected by bed degradation in other studies (Shields *et al*. 1994; Raborn and Schramm 2003). Due to extreme downcutting, many channels have lost lateral connectivity with their former floodplains, except in the most extreme flow discharge events. Many streams are starting to establish a new, much thinner floodplain in the ditch bottom by widening of the channel due to bank failure. Extensive channel erosion has also caused dramatically increased sediment loads. The altered flow regimes, loss of habitat, loss of connectivity, and high sediment loads caused by channel incision has led to decreased biodiversity (Hansen, 1971; Shields *et al*., 1994; Bravard *et al*., 1997; Cooper *et al*., 1997; Shields *et al*., 1998; Raborn and Schramm 2003). Bunn & Arthington (2002) noted that in highly altered environments, invasive species may find it easier to out-compete native species in the new, altered environment. This may explain the abundance of invasive species such as carp in western Iowa streams. At a larger scale, what happens in western Iowa in terms of biodiversity and sediment loading will affect the Missouri and Mississippi Rivers (i.e., decreased dam storage due to siltation) and the Gulf of Mexico (i.e., hypoxia) due to longitudinal connectivity.

The most efficient and affordable way to prevent further channel incision and erosion, protect infrastructure, and reduce sediment loads is to build grade control structures. There are many types of grade control structures (GCS), but important fisheries are found in drainage areas > 7.8 km^2 which are most often controlled with weirs (Fig. 1A-D). Weirs are constructed with steel sheet pile, typically driven into the streambed 6.1 m, with a riprap and concrete grout slope immediately downstream, a riprap stilling basin downstream of the weir slope, and riprap covered banks. Only limestone bedrock is available in western Iowa, and it is found in relatively thin ledges (< 2.4-3.1 m), but due to bedding planes and stratification boulders greater than a 0.77 m^3 are very rare. Riprap also tends to fracture due to freeze/thaw processes and then move under higher flow conditions, so concrete grout is used to lock the riprap in place. Weirs are placed at regular intervals to locally decrease the stream slope and change the stream profile from an erosive steep incline to a stable stair-step pattern. Weirs allow a drop in stream elevation in a controlled setting, prevent further degradation, decrease sediment loads and turbidity, and increase water

quality. GCS have shown to be very economical, with every dollar invested in building a GCS, protecting more than $4.24 in property value and 889 kg of soil.



Figure 1. A) Sheet pile weir with loose riprap slope, originally built at 1:20 (rise/run), but note how rock has moved away from the sheet pile weir (black arrows). B) Sheet pile weir with 1:20 grouted riprap slope. C) Sheet pile weir with 1:4 grouted riprap slope. D) Sheet pile weir with 1:20 fish ladder and steel baffles.

Numerous government agencies affiliated with western Iowa have attempted to halt the process of channel degradation by constructing GCS over the last forty years; more than 750 GCS have been built already in western Iowa. A group of concerned government officials and private landowners formed the Hungry Canyons Alliance (HCA) to provide funding for some of these GCS. Despite these attempts at controlling streambed degradation, the problem is still widespread necessitating the construction of more GCS.

The subjects of streambed degradation, GCS, and the HCA is discussed in much greater detail in an accompanying paper in these proceedings entitled "Fish Passage and Abundance around Grade Control Structures on Incised Streams" by J. Thomas.

In-stream GCS may also increase habitat and flow diversity. The rock rip-rap used to construct GCS adds a unique substrate to the streams of western Iowa that are mostly dominated by silt and sand bottoms. GCS have been shown to affect flow characteristics within a stream, creating slower water above the structure and a scour pool below the structure (Shields *et al*. 1995). These changes in flow and habitat conditions may result in different fish and macroinvertebrate communities near and far away from these structures and increased biological diversity within the stream (Tiemann *et al*. 2004). The modification of local hydraulic conditions may actually

increase habitat for benthic macroinvertebrates during low flow conditions (Gore and Hamilton 1996). Artificial riffles have been shown to support macroinvertebrates at levels similar to natural riffles within the same stream (Ebrahimnezhad and Harper 1997). An increase of macroinvertebrates in stream segments altered by GCS would provide enhanced food resources for nearby fish communities, possibly resulting in improved growth and body condition of fish (Shields *et al*. 1995). Increased depth and substrate types found near GCS may increase diversity, growth, and reproduction potential of fish communities near GCS (Shields and Hoover 1991). Scour holes below GCS may be better fisheries resources than natural scour holes because of habitat stability (Cooper and Knight, 1987). However, some studies have shown that fish communities do not differ between un-altered stream reaches and reaches with GCS (Raborn and Schramm 2003).

Although large dams obviously present obstacles to fish movement, GCS in streams are more serious blockages to fish movement than originally believed (Ovidio & Philippart, 2002) and may limit the longitudinal connectivity of a stream. Streams in western Iowa with GCS tend to have a drainage area of less than 150 km^2. These are warm-water streams where the predominant fish species are channel catfish, flathead chub, creek chub, black bullhead, and yellow bullhead, all of which are not powerful swimmers. Preliminary sampling efforts and angler reports in western Iowa indicated a decline in channel catfish numbers, size and distribution, and species diversity. It is hypothesized that the downstream slope of GCS can be made gentle enough to allow for fish passage. However, the gentler the slope, the more money the GCS cost because of the additional rip-rap needed to create the longer downstream riffle. For example, the cost of a GCS with a 1:20 (rise/run) downstream slope is approximately $40,000 more than the same GCS with a 1:4 downstream slope. The Hungry Canyons Alliance (HCA) and Iowa Department of Natural Resources (DNR) commissioned research to determine the right balance between making GCS ecologically sound while making them inexpensive to build. The purpose of this paper is to review and disseminate the results of this research: two fish sampling studies (Larson *et al*., 2004; Litvan, 2006; Litvan, *et al*., 2008a-c) and one hydraulic (Papanicolaou and Dermisis, 2006; Papanicolaou and Dermisis, in press) study of the effects GCS have on fish passage and abundance. Nowhere in literature has the issue of fish passage been approached from both biologic (mark-recapture) and engineering (hydraulic analysis) viewpoints, making the combination of these studies unique.

METHODS

Fish Sampling Studies

The following methods and results sections dealing with fish sampling studies and GCS are discussed in more detail in Larson *et al*. (2004), Litvan (2006), and Litvan *et al*. (2008a-c). The Iowa Department of Natural Resources (DNR) and Iowa State University sampled fish on streams controlled by GCS through two different sampling studies, but because the methods were the same, they are not differentiated in this methods section. Fish sampling occurred at sites near GCS with different downstream slopes of 1:4, 1:10, 1:15, and 1:20 (rise/run) and at reference sites not near a GCS. Sites near GCS are defined as reaches that extend from the scour pool

below the GCS downstream to a point that is within 40 times the average summer wet width of the stream. Sites not near a GCS are defined as points more than 40 times the average summer wet width of the stream away from a GCS.

Passive gear (hoop nets baited with soy cakes and minnow traps) was used to collect fish for mark/recapture and community analyses during the summer at seven sites, five of which were near GCS. The fourteen hoop nets and fourteen minnow traps (two of each type at each of seven stations) were set for periods of twenty-four hours, four to five days a week. Captured channel catfish, flathead chub, creek chub, black bullhead, and yellow bullhead were measured for length and weight and given a site-specific tag or fin clip and released at the station of capture. All captured fish were inspected for previous fin clips or tags. Marked fish that were recaptured were measured for length and weight, the site of their recapture was noted, and they were given a site-specific fin clip indicating their site of recapture.

Electrofishing equipment was used to collect fish for community analyses and to increase the number of recaptures of marked fish during the fall and spring. A total of 10 sites (five GCS sites and five non-GCS sites which included the seven summer sampling sites) were sampled with a single pass of two backpack electrofishing units for a distance of 280 m (approximately 40 times the average summer wet width of the stream. A block net was placed at the upstream boundary of the electrofishing reach. Target fish species collected were identified, measured for length and weight and inspected for fin clips or tags. A combination of hook and line angling, casting nets, and bank electrofishing techniques were used to sample deep scour pools below GCS that were not accessible with hoop nets or backpack electrofishing methods. Fall and spring sampling periods were scheduled at times corresponding with seasonal migration movements of catfish in order to increase the chance of recapturing marked fish that had moved over GCS. Fish movement over a GCS was evident if a fish marked below a GCS is recaptured at an upstream sampling site or if a fish marked above a GCS is recaptured at a downstream sampling site. Physiochemical measurements including turbidity, dissolved oxygen, pH, canopy coverage, substrate, channel wet width, depth, flow, and water temperature were measured before each sampling event.

The slopes of all GCS were measured to verify that the intended design slope had not decayed due to high-flow events or age. Vertical distance was measured at the sheet pile across the width of the channel. Longitudinal slope was measured using a clinometer from the top of the sheet pile to the end of the GCS and at three shorter intervals within the GCS slope. These measurements were repeated during the spring, summer, and fall throughout the study.

During the summer, macroinvertebrate samples were collected from 20 sites: five sites were at a GCS, five were upstream of a GCS, five were downstream of a GCS, and five sites served as reference sites and more than 1 km away from any GCS. Macroinvertebrates were collected at two randomly chosen gird areas along a 10 m transect. Rocks lying within the predetermined grid spacing were scrubbed by hand, allowing dislodged organisms to flow downstream into a kick net. Washed rocks were placed outside of the sampling quadrant and the remaining substrate was disturbed with a 30 second kick. The two samples taken along the transect were combined and preserved. In the laboratory, macroinvertebrates were counted and

identified to the family level. Macroinvertebrate community structure from each site was evaluated by quantifying the number of taxa present, the number of individuals in each taxon, total macroinvertebrate biomass, and total macroinvertebrate abundance.

An index of biotic integrity (IBI) was used to help determine the status of fish community surveys. Twelve metrics were used to determine each communities IBI score: 1) number of native species; 2) number of sucker species; 3) number of sensitive species; 4) number of benthic invertivores; 5) percentage of total abundance of the top three species; 6) percentage of fish as benthic invertivores; 7) percentage of fish as omnivores; 8) percentage of fish as top carnivores; 9) percentage of fish as lithophilous spawners; 10) percentage of fish assemblage tolerance index; 11) adjusted catch per unit effort; and 12) adjustment for high percentages of deformities, erosions, lesions, and tumors..

Hydraulic Study

The following methods and results sections dealing with a hydraulic study of GCS are discussed in more detail in Papanicolaou and Dermisis (2006) and Papanicolaou and Dermisis (in press). The study was performed by IIHR-Hydroscience & Engineering, The University of Iowa. Twenty-two GCS were selected for determination of hydraulic characteristics: eight riprap weirs (Fig. 1A), ten grouted riprap weirs (Fig. 1B, C), and four fish ladder weirs (baffled and unbaffled) (Fig. 1D). A ground survey was performed for all of these weirs, from which weir slope was determined. The surveys were also used as background information for Acoustic Doppler Velocimeter (ADV) or Large-Scale Particle Image Velocimetry (LSPIV) measurements.

Time-averaged point measurements of mean flow characteristics (water depth and streamwise velocity) were performed during a low flow season for all 22 GCS and repeated during a high flow season for 8 representative GCS. Mean flow measurements of velocity at low flow were made upstream, atop, and downstream of each GCS using an Acoustic Doppler Velocimeter (ADV). An ADV uses a transducer that generates a narrow beam of sound at a known frequency (10MHz). This sound is reflected in all directions in the water. While receivers sample the reflected sound, the ADV measures the change in frequency between the transmitted and received signals which is proportional to the velocity along the bistatic axis of that receiver. Mean flow measurements of velocity at high flow were made upstream, atop, and downstream of each GCS using the Large Scale Particle Image Velocimetry (LSPIV) technique. LSPIV measurements use video equipment to capture the movements of small particles (mulch) as they float on the water surface over a GCS. Froude numbers were calculated to classify different reaches (pool, run, and riffle-glide).

Survey data were combined with the video in an LSPIV software package to calculate the two-dimensional (2-D) velocity field around GCS. Stream discharge was calculated from the combination of the 2D velocity LSPIV data with the 1D vertical velocity ADV data. The discharge was then used for developing stage-discharge equations.

For two GCS (a riprap weir and a baffled fish ladder weir), turbulent flow characteristics were measured at low flow with a high-frequency ADV to determine

instantaneous velocities, turbulent intensities, and Reynolds stresses in three dimensions.

RESULTS

Fish Sampling Studies

The first sampling study showed that the slope of a GCS can impact fish movement. Within a 3 year sampling period, between 10 and 28 percent of recaptured channel catfish and between 15 and 30 percent of recaptured flathead and creek chubs were able to move over GCS with a 1:20 downstream slope. However, within the same 3 year sampling period, no channel catfish and flathead and creek chubs were able to move over GCS with a 1:4 downstream slope. However, extremely low water conditions may have restricted migration behavior regardless of weir design. Species diversity was 1.57 times greater downstream of a 1:4 GCS than upstream.

The second sampling study reinforced the results of the first study. GCS with vertical or 1:4 (rise/run) downstream slopes did not allow fish migration, but GCS with slopes ≤ 1:15 did. GCS sites were characterized by greater proportions of pool habitat, maximum depths, fish biomass, and greater macroinvertebrate abundance and diversity than non-GCS sites. Fish community scores (IBI) were also slightly higher (5%) in stream reaches with GCS versus stream reaches without GCS. 98% of all fish movements over a GCS were in the upstream direction and occurred when streamflow was relatively high. Macroinvertebrate biomass, numerical densities, and diversity were greater in stream reaches with GCS versus stream reaches without GCS. Before modification, only 1% displayed movement over a GCS, but after modification 14.5% of all recaptured catfish, bullheads, and chub showed movement over GCS with 1:15 downstream slopes. After modification of three GCS, IBI scores increased at seven of nine sites and fish species, including channel catfish, which exhibited truncated distributions before modification were found throughout the study area afterwards.

Hydraulic Study

Performance of each GCS was described in terms of meeting the minimum requirements for catfish passage as determined by the Iowa DNR: a minimum flow depth of 0.31 m and a maximum velocity of 1.22 m/s. The best performing GCS had minimum flow depths greater than 0.31 m and maximum velocity requirement of less than 1.22 m/s. The worst performing GCS did not meet either requirement. Without considering drainage area, the best performance was exhibited by low gradient (≤ 1:16 slopes) grouted or riprap weirs and fish ladders with baffles. The worst performing GCS were the high gradient (≥ 1:6) grouted or riprap weirs and fish ladders without baffles.

The limiting factor for fish passage was different depending on GCS drainage area. When the drainage area is less than 51.8 km^2, the best GCS is the low gradient (≤ 1:16 slopes) weirs because flow depth is the limiting factor for fish passage, and low gradient weirs will provide deeper flows than high gradient weirs. When the drainage area is larger than 259 km^2, the best GCS is the low to medium gradient (1:10-1:16 slopes) weirs because maximum velocity is the limiting factor for fish

passage, and low-medium gradient weirs will have slower velocities than high gradient weirs. When the drainage area is between 51.8 and 259 km^2, the best GCS is either a low or medium gradient (≤ 1:10 slopes) weirs because flow depth or maximum velocity are the limiting factors for fish passage.

Measurements where ideal for evaluating the performance of structures at low flow due to the fact low flow conditions persisted throughout the study period; thus, recommendations concerning minimum flow depth requirements may be more accurate than recommendations of maximum velocity requirements because of the low flow conditions. Relations for stage-discharge measurements may not be good predictors for conditions exceeding a recurrence period of 1 year due to the low flow conditions.

Velocities atop GCS were about 10 times greater in magnitude than the upstream approach flow; thus, critical conditions occur over a GCS. Turbulence measurements showed that weirs had lower levels of turbulence compared to fish ladders with baffles; however, stresses on all GCS were ≤ 5.3 N/m^2, which is much less than 1,600 N/m^2 needed to cause fish mortality. Average catfish fork lengths are 0.3 m; turbulent flow measurements illustrated that fish ladders with baffles form eddies 30% larger than the average fork length, which is enough to disorient fish. Fish ladders were observed to often catch debris, probably due to the large quantity of vertical steel sheet pile exposed. Grouted riprap slopes were observed to degrade less quickly and were more resistant to large flow events than riprap slopes.

DISCUSSION AND CONCLUSIONS

These studies describe the effects of GCS have on fish migration and fish and macroinvertebrate abundance and biodiversity. This paper details the results of three studies commissioned to describe the effects of GCS on biota through field sampling (Larson *et al*., 2004; Litvan, 2006; Litvan, *et al*., 2008a-c) and through hydraulic characterization of GCS (Papanicolaou and Dermisis, 2006; Papanicolaou and Dermisis, in press). These studies showed that vertical to steeply sloping (>1:15) GCS will restrict fish migration, whereas gently sloping (<1:15) GCS will allow fish migration; however, extremely low water conditions can restrict migration behavior regardless of weir design. Following modification of weirs to <1:15 slopes, fish community scores (IBI) did not decrease longitudinally along the channel from downstream to upstream, indicating increased longitudinal connectivity. GCS can also have a positive effect on fish and macroinvertebrate communities with respect to increased biota abundance, habitat, and biodiversity compared to stream reaches without GCS. Fish migrating over a GCS will not die due to turbulent stresses because all GCS tested had low enough levels of turbulence. Because fish ladders often catch debris and riprap is not as strong or as resistant to high flows, future GCS should incorporate a grouted riprap slope. Weirs with 15:1 are now recommended for all GCS because they allow fish passage, but are less expensive than 1:20 GCS.

These studies were instrumental in creating design criteria for future GCS to be built in western Iowa that will control channel incision while allowing fish passage and increased longitudinal connectivity. They also showed that engineers and ecologists can cooperatively work together to design GCS that can not only protect streams from the affects of channel incision but can also allow for fish migration,

greater biodiversity, and better longitudinal connectivity of the stream systems in western Iowa.

ACKNOWLEDGEMENTS

Any GCS mentioned in this report were built using Hungry Canyons Alliance (HCA) or USDA Natural Resource Conservation Service (NRCS) Emergency Watershed Protection (EWP) funds. Funding for the Larson *et al*. (2004) study was provided by Iowa DNR Fisheries Bureau. The Litvan (2006) study was funded by the HCA (17%), Iowa DNR Fisheries Bureau (11%), US Geological Survey (22%), US Fish and Wildlife Service (15%), and Iowa State University (35%). The study by Papanicolaou and Dermisis (2006) was funded by the HCA (25%), Iowa DNR Fisheries Bureau (25%), and Iowa DOT Highway Research Board (50%).

REFERENCES

Baumel, C. (1994). "Impact of degrading western Iowa streams on private and public infrastructure costs." *Stream Stabilization in Western Iowa*, Iowa DOT HR-352, Golden Hills Resource Conservation and Development, Oakland, Iowa, 4.1-4.39.

Bravard, J. P., Amoros, C., Pautou, G., Bornette, G., Bournaud, M., Creuzé Des Châtelliers, M., Gibert, J., Peiry, J. L., Perrin, J. F., and Tachet H. (1997). "River incision in south-east France: Morphological phenomena and ecological effects." *Regulated Rivers: Research and Management*, 13, 75–90.

Bunn, S. E., and Arthington A. H. (2002). "Basic principles and ecological consequences of altered flow regimes for aquatic biodiversity." *Environmental Management*, 30(4), 492–507.

Cooper, C. M., and Knight, S. S. (1987). "Fisheries in man-made pools below grade-control structures and in naturally occurring scour holes of unstable streams." *Journal of Soil and Water Conservation,* 42, 370–373.

Cooper, C. M., Testa, S., and Shields, F. D. (1997). "Invertebrate response to physical habitat changes resulting from rehabilitation efforts in an incised unstable stream." *Management of Landscapes Disturbed by Channel Incision*, University of Mississippi, Oxford, MS, pp. 887– 892.

Ebrahimnezhad, M., and Harper, D. M. (1997). "The biological effectiveness of artificial riffles in river rehabilitation." *Aquatic Conservation: Marine and Freshwater Ecosystems*, 7, 187-197.

Gore, J. A., and Hamilton, S. W. (1996). "Comparison of flow-related habitat evaluations downstream of low-head weirs on small and large fluvial ecosystems." *Regulated Rivers: Research and Management*, 12, 459-469.

Hansen, D. R. (1971). "Effects of stream channelization on fishes and bottom fauna in the Little Sioux River, Iowa." *ISWRRI No. 38*, Iowa State Water Resources Research Institute, Ames, Iowa.

Larson, C. J., Atchison, G. J., and Menzel, B. W. (2004). *Annual Progress Report to the Iowa Department of Natural Resources Fisheries Bureau for an Evaluation of Effects of Weirs in Walnut Creek on Fish Abundance and*

Movement, Cold Springs Southwest Regional Office, Iowa Department of Natural Resources.

Litvan, M. E. (2006). *An Evaluation of Effects of Grade Control Structures on Fish Movement and Fish Communities in Turkey Creek, Cass County, IA and Macroinvertebrate Communities in Walnut Creek, Montgomery County, IA*. M.S. Thesis, Iowa State University, Ames, Iowa.

Litvan, M. E., Pierce, C. L., Stewart, T. W., and Larson, C. J. (2008a). "Fish Passage in a Western Iowa Stream Modified by Grade Control Structures." *North American Journal of Fisheries Management*, 28:1384–1397.

Litvan, M. E., Pierce, C. L., Stewart, T. W., and Larson, C. J. (2008b). "Fish Assemblages in a Western Iowa Stream Modified by Grade Control Structures." *North American Journal of Fisheries Management*, 28:1398–1413.

Litvan, M. E., Stewart, T. W., Pierce, C. L., and Larson, C. J. (2008c). "Effects of Grade Control Structures on the Macroinvertebrate Assemblage of an Agriculturally Impacted Stream." *River Research and Applications*, 24: 218–233.

Ovidio, M., and Philippart, J. C. (2002). "The impact of small physical obstacles on upstream movements of six species of fish." *Hydrobiologia*, 483, 55-69.

Papanicolaou, A. N., and Dermisis, D. C. (2006). *Field Investigation of Hydraulic Structures Facilitating Fish Abundance and Passage through Bridges in Western Iowa Streams*, Iowa DOT TR-521, IIHR-Hydroscience & Engineering, University of Iowa, Iowa City, Iowa.

Papanicolaou, A. N., and Dermisis, D. C. (In press). "Fish passage over hydraulic structures in Midwestern Rivers of the USA." *J. River Basin Management*.

Raborn, S. W., and Schramm, H. L. (2003). "Fish assemblage response to recent mitigation of a channelized warmwater stream." *River Research and Applications*, 19, 289-301.

Shields Jr., F. D., and Hoover, J. J. (1991). "Effects of channel restabilization on habitat diversity, Twenty Mile Creek, Mississippi." *Regulated Rivers: Research and Management*, 6, 163-181.

Shields, F. D., Knight, S. S., and Cooper, C. M. (1994). "Effects of channel incision on base flow stream habitats and fishes." *Environmental Management*, 18(1), 43-57.

Shields Jr., F. D., Knight, S. S., and Cooper, C. M. (1995). "Incised stream physical habitat restoration with stone weirs." *Regulated Rivers: Research and Management*, 10, 181-198.

Shields, F. D., Knight, S. S., and Cooper CM. (1998). "Rehabilitation of aquatic habitats in warmwater streams damaged by channel incision in Mississippi." *Hydrobiologia*, 382, 63– 86.

Thomas, J. T. (this volume). "Hungry Canyons Alliance: Streambed Stabilization in Western Iowa."

Tiemann, J. S., Gillette, D. P., Wildhaber, M. L., and Edds, D. R. (2004). "Effects of lowhead dams on riffle-dwelling fishes and macroinvertebrates in a midwestern river." *Transactions of the American Fisheries Society*, 133, 705-717.

Fish passage can be improved by introducing hydraulic refuge. Can the effects be quantified?

Matthew D. Hays[1], Suzanne K. Monk[2,] Trevor P. Hawkes[3], Joseph R. Webb[4], Rollin H. Hotchkiss[5], Mark Belk[6], Russell Rader[7]

1. Undergraduate Research Assistant, Dept. of Civil and Environmental Engineering. 368 Clyde Bldg, Brigham Young University, Provo, UT 84602. Email: cariocahays@gmail.com.
2. Undergraduate Research Assistant, Dept. of Civil and Environmental Engineering. 368 Clyde Bldg, Brigham Young University, Provo, UT 84602. Email: suji.monk@gmail.com.
3. Undergraduate Research Assistant, Dept. of Civil and Environmental Engineering. 368 Clyde Bldg, Brigham Young University, Provo, UT 84602. Email: hawkes.trevor@gmail.com.
4. Undergraduate Research Assistant, Dept. of Civil and Environmental Engineering. 368 Clyde Bldg, Brigham Young University, Provo, UT 84602. Email: joseph.r.webb@gmail.com.
5. Professor, Dept. of Civil and Environmental Engineering. 368 Clyde Bldg, Brigham Young University, Provo, UT 84602. Email: rhh@et.byu.edu.
6. 7. Professors, Dept. of Biology, 401 Widstoe Building, Brigham Young University, Provo, UT 84602. Email: mark_belk@byu.edu; russell_rader@byu.edu

Abstract

Design methods that account for the ability of fish to swim upstream through culverts are based on tests describing how fast and for how long different fish species can swim. These methods are based on an average water velocity but fail to recognize that fish can take advantage of resting places and non-uniform flow in culverts. Culverts that are designed using this average velocity are likely larger than is necessary. Current design methods could be greatly improved by accounting for the non-uniform velocity distributions in culverts, especially those with roughness elements.

In order to better quantify the benefits associated with in-culvert hydraulic refuge, fish tests have been performed in a laboratory flume. This project has focused on one species of fish native to Utah—longnose dace—and the ability to ascend the flume with and without roughness elements—cylinders—in place. Results suggest that the cylinders did allow fish to navigate upstream more successfully than fish attempting to ascend the flume without cylinders at nearly identical average velocities.

It is suggested that further testing be conducted by adapting this protocol to key variables affecting fish passage, producing probability distributions for fish performance applicable to culvert design.

Introduction

Problem Description

Many agencies enforce special design requirements that are meant to abet fish and other organisms attempting to move up or downstream through a culvert. Several categories of culvert design procedures have been defined (Hotchkiss et al. 2007) that account for fish passage.

Most culvert design procedures used when accounting for fish passage use the average velocity in the culvert as a governing design parameter. John T. Beebe points out that the use of the average fluid speed alone does not provide an accurate description of the real interaction between fish and their surroundings, instead suggesting that "the relationship between moving fluid and channel boundary is the most important in smaller streams that are used as habitat by fish (1996)."

Roughness elements, including fish baffles, oversized rock, or other strategically placed objects placed within a culvert drastically alter flow patterns in culverts. Due to a lack of experimental data, however, the effects of roughness elements on fish passage have not been quantified adequately. More testing may allow engineers to more fully understand the differences between the average velocity in a culvert and the local velocity which an individual fish chooses to actually overcome.

A publication by Theodore Castro-Santos (2004) describes an excellent experimental setup used to test fish passage rates and their relation to culvert length and average velocity, as well as valuable discussion of fish swimming behavior. This and similar tests nearly always ignore the effects of roughness elements within the flow.

Fish passage can be measured as the proportion of fish successfully traversing a culvert to those staging an attempt. Treating this proportion as the dependent variable, the number of independent variables affecting fish passage is quite large. The independent variables may be grouped into the following categories: characteristics of fish, characteristics of flow, characteristics of culvert, with a subcategory pertaining to the roughness elements, and characteristics of environment. Many of these are variables are listed below in Table 1.

Some of the variables in Table 1 are easily quantified while others are not. The variables which can be measured in terms of the elementary dimensions of length, mass, and time can be combined in order to reduce the amount of testing necessary to obtain relationships among the many independent parameters. These variables, along with their common symbols and elementary dimensions, are given in Table 2. The Buckingham Pi Theorem has been applied to combine variables into dimensionless ratios.

Table 1. Variables Likely Affecting Fish Passage

Variable	Supporting Source
Fish Characteristics	
Species	
Length or Weight	
Health	
Life Stage	
Flow Characteristics	
Discharge	
Depth	(Cotterell 1998)
Culvert Characteristics	
Length	(Cotterell 1998)
Roughness	(Cotterell 1998)
Inlet Conditions	
Outlet Conditions	
Element Diameter	
Drag Coefficient	
Longitudinal Spacing	
Lateral Spacing	
Environmental Characteristics	
Time of Year	
Time of Day	
Lighting	(Cotterell 1998)
Water Temperature	(Ali 1979)

Table 2. Easily Quantifiable Variables

Variable	Symbol	Elementary Dimensions
Fish Length	L_f	L
Discharge	Q	L^3/T
Depth	y	L
Culvert Length	L_c	L
Element Diameter	D	L
Longitudinal Spacing	L_x	L
Lateral Spacing	L_y	L

Hypothesis

The tests described in this document are expected to show a positive effect of roughness elements on fish passage. Roughness elements placed in an open channel are expected to

correspond to an increase in the percentage of fish passing upstream over a defined distance. Individual fish will likely rest behind cylinders in areas of hydraulic refuge. The tests performed apply specifically to a single species, channel length, and roughness element configuration; however, they provide a better idea of the magnitude of the effects of roughness elements on fish passage, hopefully suggesting that similar tests be performed while altering appropriate variables.

Behavior versus Ability

Fish living in their native environment migrate for various reasons. They may be in search of food, shelter, safety, or a spawning location, among other things. While a laboratory setup may duplicate certain aspects of a natural stream setting, many differences cannot be eliminated. These differences are likely to change fish behavior. It is of paramount importance that results presented here not be applied directly to culvert design procedures without further investigation to the uncertainty due to this key assumption.

In order for a fish to travel upstream through a culvert, it must be physically capable of doing so and must have a motive strong enough for it to expend the necessary energy. These conditions have been described as swimming capacity and attempt rate. Figure 1 illustrates the idea.

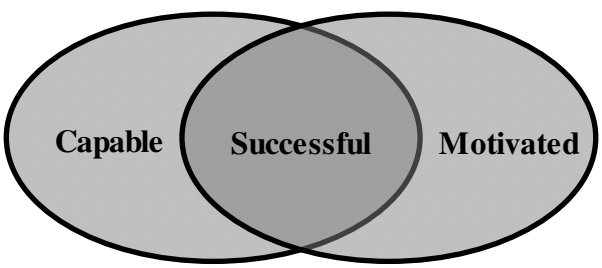

Figure 1. Capacity versus attempt rate.

While fish may be physiologically able to navigate upstream, the right motives for doing so may not be present. On the other hand, motives may be strong enough for a fish to "want" to swim upstream, but the fish may be too small or weak, or the culvert may be too long to allow successful passage. The results in this document do not attempt to differentiate between capacity and attempt rate.

Methods

Test Specimens

Thirty-six specimens of longnose dace were captured from their native stream habitat using an electrofishing device. Captured fish were kept in holding tanks for at least four days before testing began. During this time they were generally fed each day and their tanks were cleaned periodically as needed.

Longnose dace are benthic fish with a long, down-turned snout making them well adapted for life near the bottom of fast-flowing streams. The specimens tested were generally between 5 and 10-cm in total length. A longnose dace is shown in Figure 2 below.



Figure 2. Longnose dace (Helfrich et al. 2005).

Setup

Tests were performed in a rectangular flume with smooth Plexiglas on the bottom and sides. The flume is broken into five sections which were conveniently used as boundaries when monitoring fish movement. Figures 2 and 3 below are elevation and plan views of the flume. Figure 2 includes the locations of cylinders placed in the flume during the experimental setup.

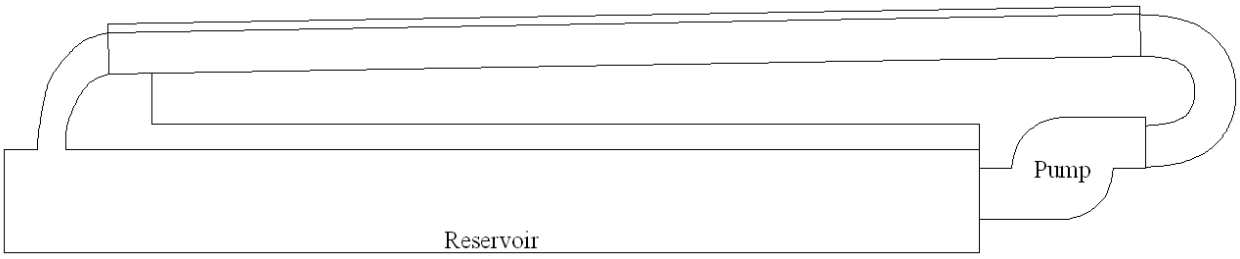

Figure 3. Flume in elevation view.

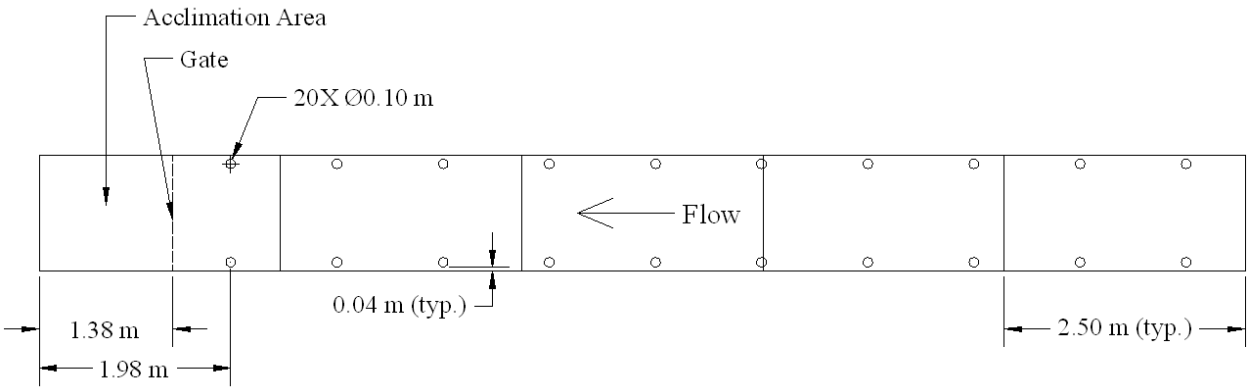

Figure 4. Flume in plan view with cylinders shown.

The acclimation area at the downstream end of the flume is 1.38-m and 1-m wide. The flume is divided into five 2.5-m sections. Within the flume, cylinders with a 10-cm diameter were placed 1-m apart and 5-cm from the flume wall. A boundary curtain was hung around the perimeter of the entire flume. Windows were cut in the curtain on both sides of the flume in order to enable the observer to collect data with minimal disturbance to the fish.

Testing Protocol

Testing included an acclimation period, a test run, and manual motivation. On the date of a test, 6 longnose dace were removed from the holding tank and moved in a bucket to the testing flume. Water from the flume was mixed with water from the holding tank carried in the bucket along with the fish, and the bucket was placed in the flume water for approximately 15 minutes to allow for initial acclimation to flume water conditions. After this 15 minute period, the fish were released into a caged area at the downstream end of the flume, where water speed was maintained such that the fish had little difficulty holding their positions while acclimating. The acclimation period lasted approximately one hour.

Testing and monitoring were performed during the next 80 minutes, during which all observers stayed outside of a boundary curtain to avoid human contact with the fish. The pump frequency and tailgate height were adjusted to attain the desired discharge and depth of flow. Next, the gate holding the fish in the acclimation area was raised, allowing the fish to begin their ascent. At intervals of approximately 10 minutes, fish were counted and their locations marked.

After official testing was completed, an observer entered the boundary curtain to perform an informal manual motivation to determine whether such motivation could stimulate the fish to move upstream. This was done with a small fish net and it was left to the observer to determine how much stimulation should be applied and how to describe any positive or negative affects on fish behavior.

Data forms were created to gather preliminary data. This data includes: type of setup (experimental or control), discharge, channel slope, water temperature, date, times for the beginning of acclimation, beginning of testing, and end of testing and finally, the number of fish tested. A sample data sheet and full protocol are provided in the appendix.

Assumptions

As mentioned in the introduction, native fish habitats are difficult to reproduce in a laboratory. None of the testing described in this report was intended to simulate a natural environment. Instead, any effect associated with differences between nature and the laboratory was assumed to be uniform. Similarly, time in captivity, time of year, time of day, and temperature differences between holding tanks and the flume were kept fairly constant, and any effects on fish behavior were assumed to be uniform.

Results

Data resulting from the tests are displayed below in the following graphs. Fish performance data were collected for groups of six or less individuals in either a control or experimental group. Eighteen fish were placed in the flume for each treatment. Figure 5 shows the relation between tested, attempted, and passed. The definition of these terms follows Figure 5.

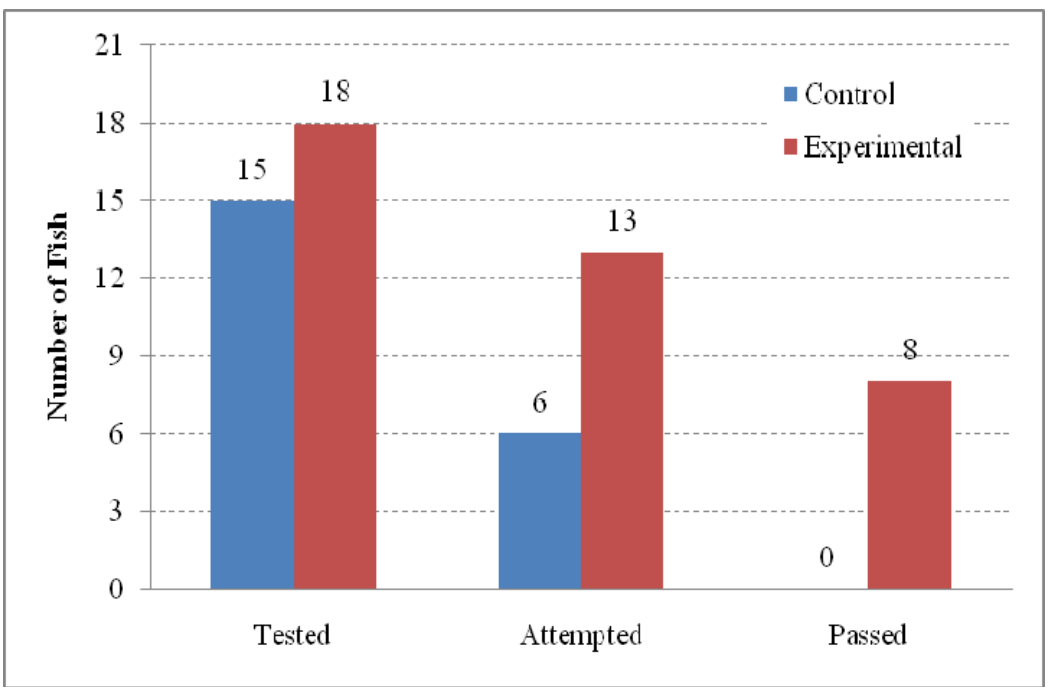

Figure 5. Number of Fish vs. Tested, Attempted, and Passed.

"Tested" is defined as the number of fish in the flume at the end of the acclimation period. "Attempted" is the number of fish that swam past the first section of the flume. "Passed" is the number of fish that made it into the most upstream (fifth) section of the flume. In the control group, 15 fish were tested because three fish failed before the end of the acclimation period. Of these, 6 attempted, and none passed. In the experimental group, 18 were tested, 13 attempted, and 8 passed.

Figure 6 shows the differences between the ratios of passed vs. attempted and passed vs. tested in each of treatment.

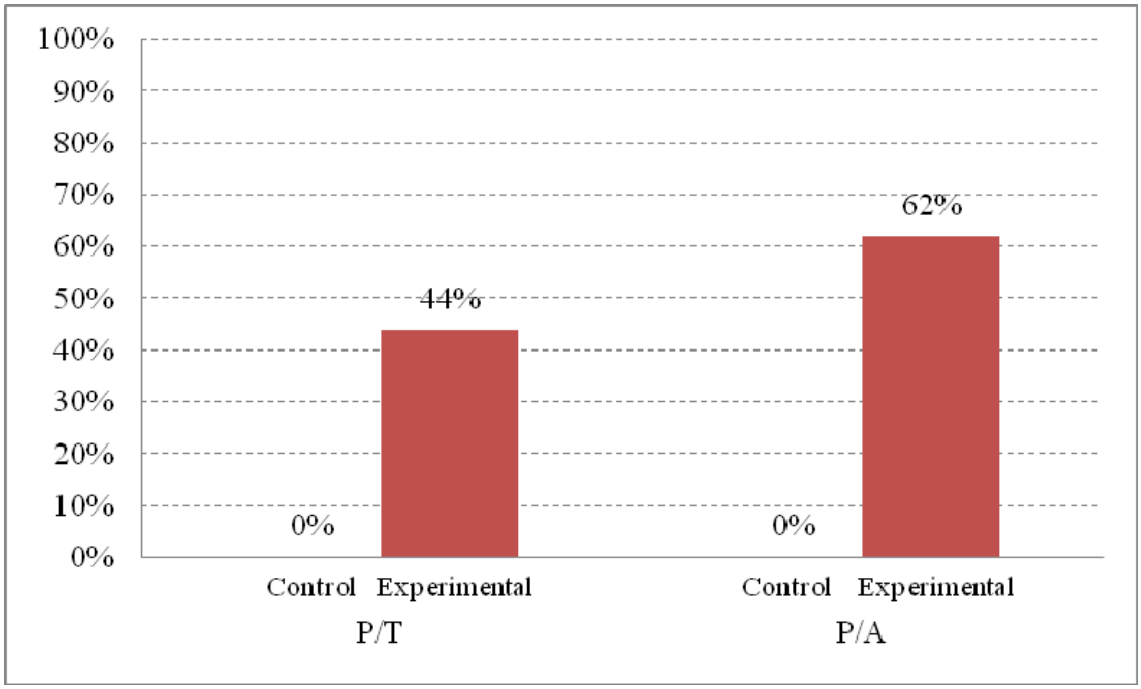

Figure 6. Percentage vs. P/T and P/A. Ratio of Passed vs. Tested and Passed vs. Attempted.

The percentage for each in the control group is 0%. The percentage for P/A in the experimental group is 62% and the percentage for P/T is 44%. In addition to these metrics, fish were observed at various time intervals. In this way, the progress of fish through the flume was observed. Figure 7 shows the number of fish in each section of the flume during given time intervals during the test for the control group. In the control group, none of the fish passed and only six attempted. Figure 8 shows the analogous results for the experimental group.

Eight fish passed in the experimental test and there is a general trend of fish moving towards section five. Only four fish are still in the first section during the last time interval (70-79 min).

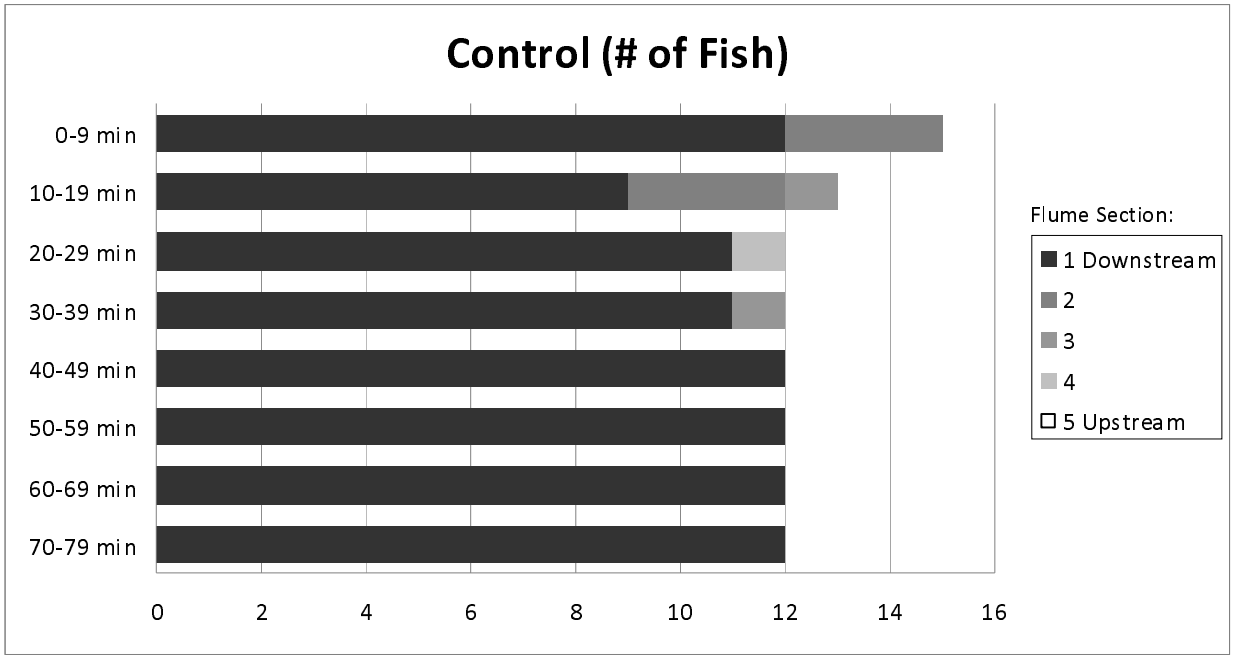

Figure 7. Control: Time vs. Section

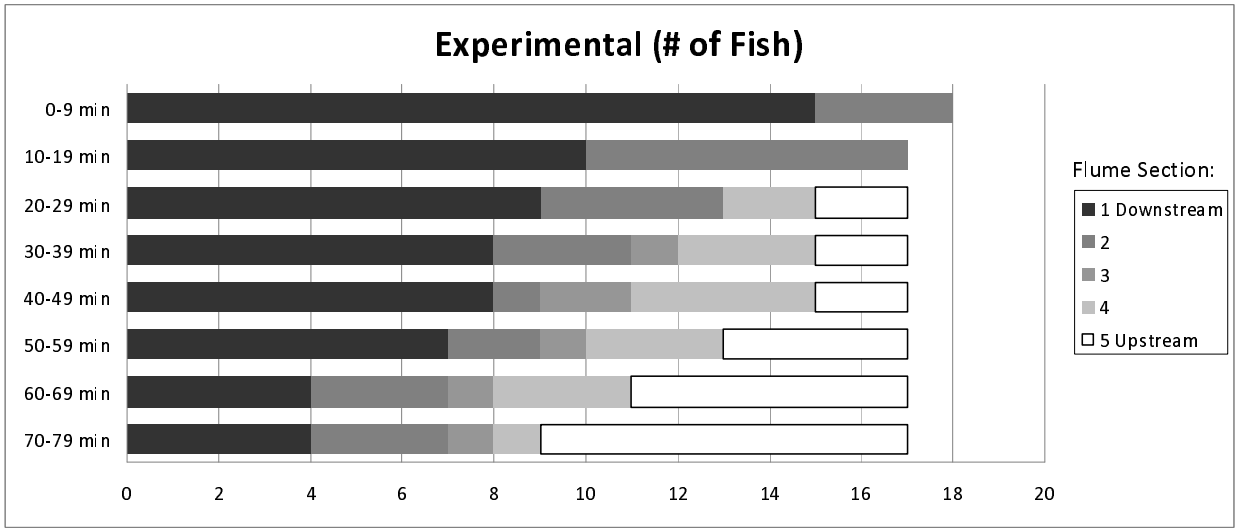

Figure 8. Experimental: Time vs. Section

Discussion

Expectations

As stated in the hypothesis, fish were expected to find refuge behind the cylinders and use this space for resting during their upstream attempt. However, fish were usually observed resting in front of the cylinders. This may be a natural tendency of the fish or it may be an indication that the experimental setup could be modified to increase fish success in navigating up the flume. The longitudinal spacing, lateral spacing, and diameter of the cylinder are variables that could be

changed. A change in the longitudinal spacing would influence the wake zone characteristics of the cylinders and perpetuate these differences downstream. Changing the lateral spacing would change the velocity and turbulence between the cylinder and the wall of the flume. Increasing the diameter of the cylinder would increase the wake zone so there would be a larger rest area behind the cylinder.

Confounding Variables

Time of year, or season, in which fish were captured and tested may be a confounding variable in the results. Informal tests used to determine the final protocol were performed during the summer. In these tests, dace were able to pass without cylinders when tested at 105-cm/s average velocity. However, dace were not able to pass at a similar velocity without cylinders in the fall, which may be due to metabolic changes in the fish between fall and summer. This suggests that fish swimming performance test results may not be representative of fish performance throughout all seasons.

The size of tested fish may be another confounding variable in these results. It was assumed that since the fish were randomly chosen, size would not affect the results. Thus, length and weight was not measured during tests. Nevertheless, bias may have been introduced into the experiment because swimming efficiency does generally increases with fish length (Webb et al. 1984) and the small sample size used in the experiment could have been insufficient to give a good representation of the species as a whole.

Possibly Invalid Assumptions

The following were assumed, but may have actually influenced the results:

- Fish would swim to their maximum capabilities: This may be erroneous since individual fish may not be motivated to swim upstream.
- Fish would all have the same capabilities: This is clearly false; however, it was assumed that by randomly selecting the fish in each group, their capabilities would average out.
- Each group had the same treatment: There is natural variation in each treatment due to human error. In addition, individual differences between the fish in each group may also affect the test results.

More caveats

These results cannot be applied to individuals because they were tested in groups. Social dynamics in fish behavior may result in fish reacting differently when tested individually. Larger test groups and more replications may also be necessary to achieve statistical significance.

Motivation

As discussed in the testing protocol, fish were motivated after the fish were given 80 minutes to swim up the flume. This indicated the existence of a difference between a fish's performance in

a test and its actual capabilities. After motivation, most fish in the test swam further up the flume than they had at any time during the initial 80 minutes. Because the motivation methods were not uniform, no numerical data was analyzed for the effects of physical motivation.

Conclusions

From these results, it can be concluded that cylinders aid in fish passage, when testing fish in groups. The percentage of fish that passed in the experimental tests was much higher than in the control tests. None of the tested fish passed in the control tests, while some fish passed in the control tests with motivation (see Discussion).

These conclusions cannot be applied without considering the difference between behavior and ability (see Introduction), as well as the numerous other elements that could have introduced confounding variables into the results. While common sense would dictate that roughness elements do help fish navigate through a current, the usable, numerical data supporting this is still lacking. A sure basis for revamping culvert construction protocol as suggested in the introduction rests on the gathering of this data.

Recommendations

As the field of research relating to fish passage is still relatively new, many factors affecting fish migration remain arbitrary hypotheses. The practical application of research following protocol similar to those used in this experiment is still in the distant future. In order to help researchers seeking to improve similar research protocol, the authors offer the following recommendations.

Motivation

Motivation of fish, as previously described, is a difficult question facing researchers who are trying to balance resources and results with the authenticity of the fish test environment. In order to show that many fish in the test were swimming well below their physiological capabilities, a step was added to the protocol where after the conclusion of the test period (80 minutes), the fish were encouraged to swim upstream by a small hand held net placed behind them. This was successful to a certain extent; many fish that remained at the starting section of the flume for the entire 80 minutes swam up the flume after the stimulus was applied repeatedly.

The protocol for applying the stimulus and the extent to which fish were encouraged to swim upstream was not standardized, however, rendering the results only useful for further postulating. If further researchers wish to implement a similar method of both volitional and motivated testing, it is recommended that motivation methods be standardized.

Wake region

Previous studies have shown trout using the vortices forming downstream of cylinders as a means of holding position with less energy expenditure (Liao et al. 2003). It was therefore expected that the longnose dace would also position themselves downstream of the cylinders. As discussed earlier, fish in this experiment actually preferred to hold position upstream of the cylinders. Video footage of the experiment suggests that the less turbulent, low velocity area downstream of the cylinders was too small for the fish to use. One fish in particular demonstrated this when it tried to take advantage of the small low velocity region, but it could only do so with its side pressed against the cylinder.

When it maneuvered into a more natural position, with its mouth facing the cylinder and body parallel to the flow, its tail entered the turbulent area of the wake region, and the fish was swept downstream. The authors suggest testing with larger cylinders or different shaped objects, thus enlarging the resting area usable by small fish. It is also recommended that data already gathered on cylinder hydraulics be applied to postulate sizes of cylinders and water velocities that might produce a wake region that would be beneficial to small fish.

Although trout have been shown to use the turbulent vortices (Liao et al. 2003), observations of dace in this experiment suggest that their smaller size may be more conducive to the low velocity area immediately downstream of cylinders.

Also, spacing cylinders more than 5-cm from the side of the flume is recommended because most of the fish had difficulty swimming between the cylinder and the wall of the flume, and some of the fish chose to swim between the cylinders. Increasing this spacing would result in a slower velocity between the cylinder and flume edge, potentially facilitating the fish's movement upstream.

Recommended future testing

Many potential lurking variables could be removed from fish tests using similar protocols. Some of the variables that could be tested and quantified are:

1. Time of day - research suggests that some fish species, even in captivity, tend to migrate at night (Pearson et al. 2005).
2. Time of year – fish behavior in informal testing performed in the summer compared with actual tests done in the fall suggests that longnose dace were far more willing and/or able to swim to the top of the flume in the summer.
3. Duration of captivity before testing – fish observed in captivity shortly after capture tended to regurgitate food and not eat anything for a few days, which could affect their ability and willingness to swim upstream in the flume.
4. Volitional or non-volitional entrance – due to the pre-constructed nature of the flume used in this experiment, an acclimation area inside of the flume was used.

This example of non-volitional entrance into the experimental water flow may introduce stress or other factors that could affect the percentage of fish "passing".

Volitional entrance into the experimental flow section where they are tested has been used in past experiments (Castro-Santos 2004), and could be a method of resolving this dilemma. A measured comparison of this option and the non-volitional method used in this experiment could be useful to future protocol and flume design. The two options are diagrammed below in Figure 10.

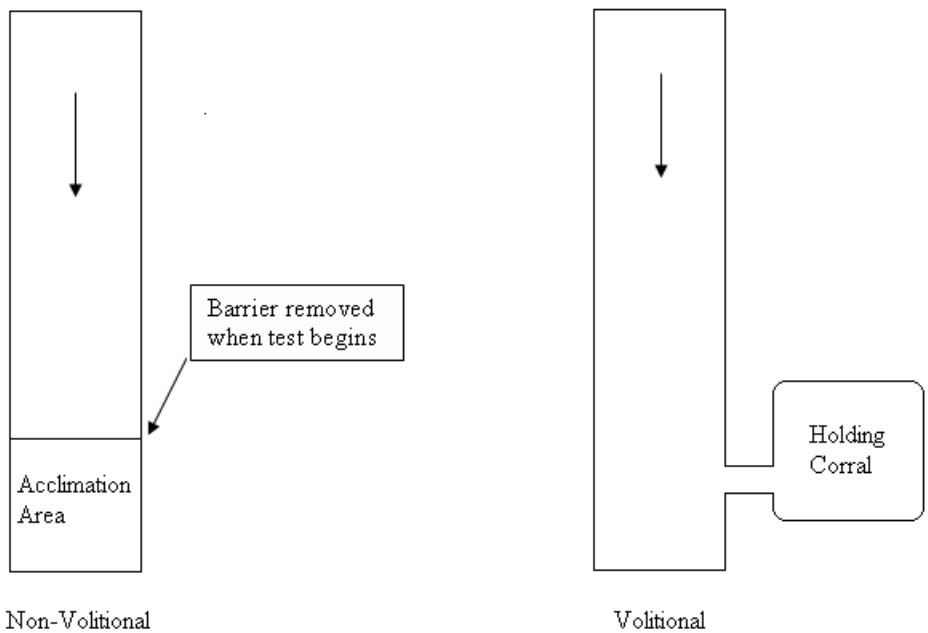

Figure 10. Comparison of acclimation options.

The volitional entrance configuration allows the fish to leave the holding corral and enter the test section at their own will. The non-volitional method keeps the fish in an enclosed partition in the test section until a pre-determined acclimation period is completed, whereupon the barrier holding the fish in is removed and the test begins.

Fish monitoring

Upon examination of the results, it was recognized that because this experimental setup did not allow for monitoring of individuals throughout the test limits the type of conclusions that may be drawn from the tests. Fish tracking systems using radio telemetry could remove this ambiguity, but if funding is an issue, less expensive elastomer tags could be used to identify individual fish by researchers.

Future testing

In order to better understand why the fish generally rested in front of cylinders, a detailed ADV analysis of turbulence and velocity gradients under testing conditions is planned. It is anticipated that these analyses will either demonstrate that: the region downstream of the cylinder was excessively turbulent; the area upstream of the cylinder was ideal for conserving energy; or that a combination of both was the underlying cause of refuge selection.

References

Aedo, J. R. (2008). *Does shape predict performance? An analysis of morphology and swimming performance in great basin fishes.* Unpublished Brigham Young University, Provo, UT.

Ali, M. A. (1979). *Environmental physiology of fishes*, Plenum Press, New York.

Beebe, J. T. (1996). "Fluid Speed Variability and the Importance to Managing Fish Habitat in Rivers." *Regulated Rivers: Research and Management,* 12(1), 63.

Cotterell, E. (1998). *Fish passage in streams, fisheries guidelines for design of stream crossings*. Fisheries Group, Queensland Department of Primary Industries, Brisbane, QLD.

Haro, A., T., Noreika, J., and Odeh, M. (2004). "Swimming performance of upstream migrant fishes in open-channel flow: a new approach to predicting passage through velocity barriers." *Can.J.Fish.Aquat.Sci.,* 61(9), 1590.

Helfrich, L., Newcomb, T., Hallerman, E. & Stein, K. *EFISH: The virtual aquarium.* http://www.cnr.vt.edu/efish/index.html (July 5, 2008)

Hotchkiss, R. H., and Frei, C. M. (2007). "Design for Fish Passage at Roadway-Stream Crossings: Synthesis Report." United States.

Liao, J. C., Beal, D. N., Lauder, G. V., and Triantafyllou, M. S. (2003). "The Karman gait: Novel body kinematics of rainbow trout swimming in a vortex street." *Journal of Experimental Biology*, 206(6), 1059-1073.

Pearson, W., Richmond, M., Johnson, G., Sargeant, S., Mueller, R., Cullinan, V., et al. (2005). *Protocols for evaluation of upstream passage of juvenile salmonids in experimental culvert test bed* No. WA-RD 614.1) Battelle.

Robison, G. E., Mirati, A., & Allen, M. (1999). “Oregon Road/Stream crossing restoration guide.” *Oregon Department of Fish and Wildlife*, http://www.dfw.state.or.us/odfwhtml/infocntrfish/management/oregonrd_stream.pdf (July 1, 2008).

Van Dyke, M. (1982). *An album of fluid motion*. (pp. 31). Stanford, CA: Parabolic Press.

Vogel, S. (1994). Life in velocity gradients. *Life in moving fluids: The physical biology of flow* (pp. 174). Princeton University Press, Princeton, New Jersey.

Webb, P. W., Kostecki, P. T., and Stevens, E. D. (1984). "THE EFFECT OF SIZE AND SWIMMING SPEED ON LOCO MOTOR KINEMATICS OF RAINBOW TROUT SALMO-GAIRDNERI." *Journal of Experimental Biology*, 109, 77-96.

Young, F. D., & Munson, B. R. (2007). *Buckingham pi theorem* (Fourth ed.). John Wiley & Sons, Inc, Hoboken, NJ.

Hydraulic Model Study of Canoe Chute and Fish Passage for the Chicago River North Branch Dam

Jorge D. Abad[1], Andy Waratuke[2], Cristiana Barnas[3], and Marcelo H. Garcia[4]

[1] Postdoctoral research associate, Dept. of Civil and Environmental Engineering, Univ. of Illinois at Urbana-Champaign, 205 N. Mathews Ave., Urbana, IL 61801, abad@illlinois.edu

[2] "Ven Te Chow Hydrosystems" Lab. Manager, Dept. of Civil and Environmental Engineering, Univ. of Illinois at Urbana-Champaign, 205 N. Mathews Ave., Urbana, IL 61801, awaratuk@illlinois.edu

[3] Graduate Research Assistant, Dept. of Civil and Environmental Engineering, Univ. of Illinois at Urbana-Champaign, 205 N. Mathews Ave., Urbana, IL 61801, cbarnas2@illlinois.edu

[4] Chester and Helen Siess Professor, Dept. of Civil and Environmental Engineering, Univ. Illinois at Urbana-Champaign, 205 N. Mathews Ave., Urbana, IL 61801, mhgarcia@illinois.edu

ABSTRACT

The hydrodynamics at two design discharges (85 and 15% exceedence on the flow duration curve) in the vicinity of the existing North Branch Dam are presented. A combination boat chute/fish passage is being designed for integration into the existing dam. The Dutch pool and orifice fishway has been selected for the fishway due to its relatively low flow requirement (on the order of 5 cfs for most operating heads), low velocities in the fishway, and relatively low turbulence in the fishway – all making it a reasonable option for passage of non-anadromous fish in a low-gradient waterway. The details of the hydrodynamics of this structure are being examined with a combination of a physical model study and through the performance Computational Fluid Dynamic (CFD) modeling.

1. CURRENT SCENARIO – CHICAGO NORTH BRANCH DAM

Prior to installing a potential boat chute design within the physical hydraulic model, several case scenarios of the boat chute design will be considered and tested, therefore optimizing its design. Prior to developing a CFD model at prototype scale for the North Branch Dam including any boat chute/fishway design, it is necessary to simulate the current (dam alone) flow structure in the vicinity of the dam to provide a background for future comparisons. Since the aim is to have the boat chute designed and tested to cover a wide range of flow discharges (30 – 223 cfs, corresponding to a flow exceedence of 85% and 15%, respectively), it is important to obtain CFD results for these two flow conditions. Hydrologic data upstream of the dam was obtained from a USGS gaging station 05536105 – North Branch of the Chicago River at Albany Avenue. Flow data for the North Shore Channel upstream of the confluence was obtained for the USGS gaging station 05536101 – North Shore Channel at Wilmette, IL and outfall data from the North Shore Waste Water Treatment Plant operated by MWRDGC.

A three-dimensional model (FLOW3D, Flow Science 2008) CFD models that solves the Navier-Stokes equations together with a model for turbulence (RNG, Yakhot and Smith, 1992), and an interface capturing method (VOF, Hirt and Nichols 1981) is applied to determine the flow

structure for the North Branch Chicago River Dam. The CFD model has been previously applied at several different projects associated with river restoration (Rodriguez et al, 2004; Abad and Garcia, 2005; Abad et al. 2008).

As observed in Figure 1, the computational domain has a reach that extends in the Upper North Branch Chicago River (UNBCR), a reach extending upstream into the North Shore Channel (NSC) and a reach downstream in Lower North Branch Chicago River (LNBCR); therefore suitable boundary conditions at these three boundaries are required. The upstream boundary condition for the UNBCR was determined from a 1-D HEC-RAS model of the upstream reach assuming critical depth at the dam. The HEC-RAS model was calibrated using the USGS gaging station at Albany Street. The Chicago River System downstream of the North Branch Dam is completely controlled by the operation of lock and dam structures located in Wilmette, the Chicago Harbor, and in Lockport and the stages are maintained relatively constant throughout the system. Therefore, a constant stage boundary condition has applied for the LNBCR independent of flow discharge. This stage was determined from the USGS gaging station 05536123 Chicago River at Columbus Drive at Chicago, IL.

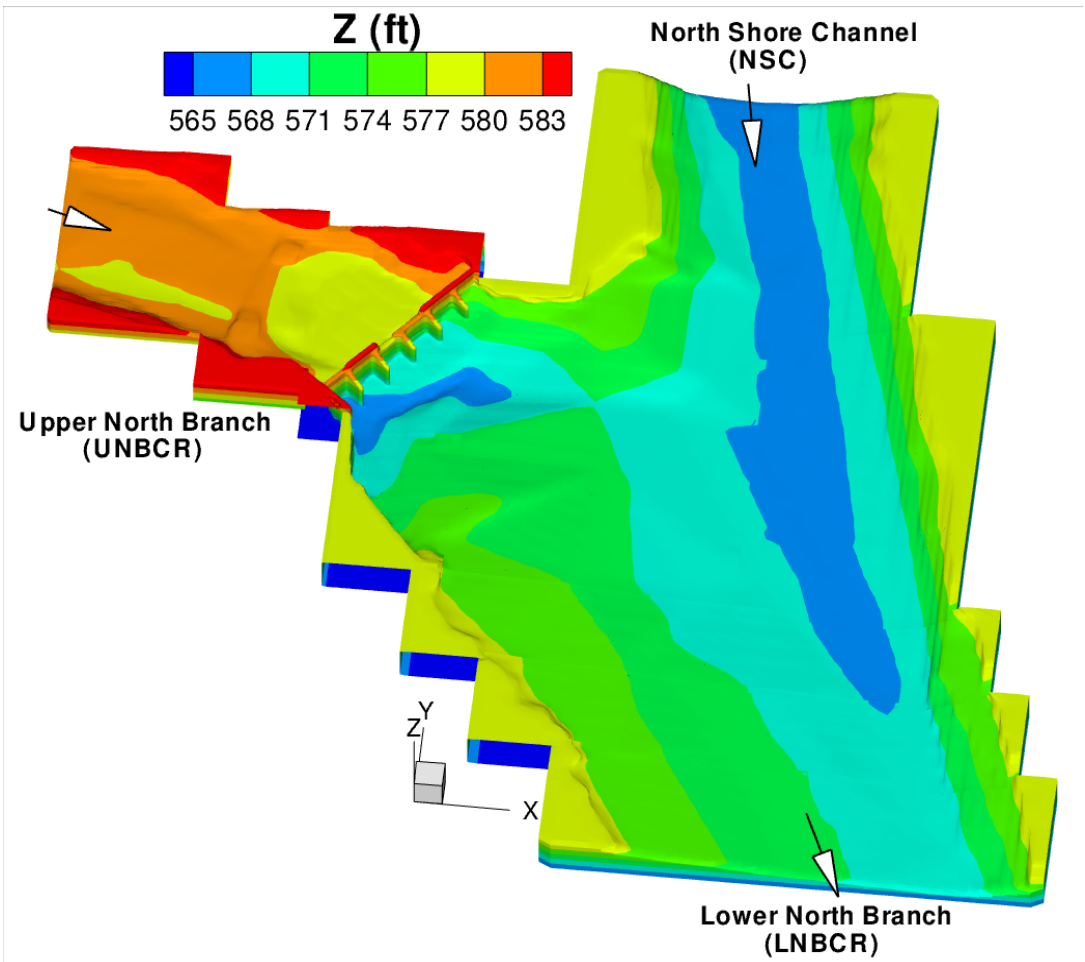

Figure 1. Bed elevation (in ft) of the entire computational domain (using 10 linked-type multiblocks)

Figure 2 shows the water surface elevation (wse) for both design discharges (85% and 15% exceedence). As observed the wse along the North Shore Channel (NSC and LNBCR) is almost constant for both conditions since it is a regulated channel. However, the wse at the UNBCR changes according to the backwater effects exerted by the dam. The control point (for backwater effects) for the 85% exceedence discharge is located upstream of the dam as observed in Figure 2(a), while the control point for the 15% exceedence discharge is given by the dam (Figure 2b).

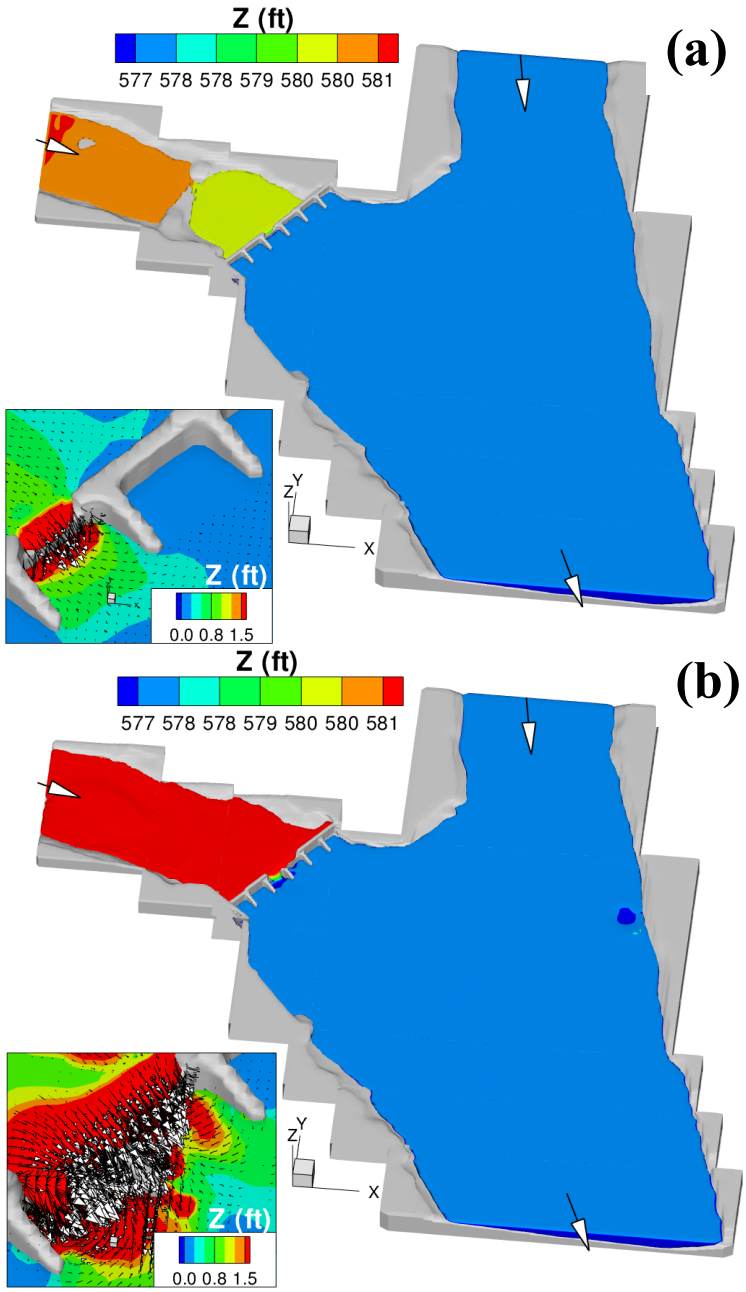

Figure 2. Water surface elevation (ft) for design discharges of (a) 85% exceedence and (b) 15% exceedence

Figure 3 shows the velocity distribution for both design discharges at different elevations (z=572.1 and 576.5 ft). Due to the interaction of NSC and UNBCR channels, there are regions of horizontal recirculation, especially near the downstream part of the dam. The junction serves as expansion for the NSC, therefore the velocities are reduced in this region for both design discharges. Downstream of the junction (around UNBCR), the velocities recover their magnitude as in NSC, demonstrating that the computational domain is good enough to reproduce the effects of the dam and of any future canoe/chute implementation.

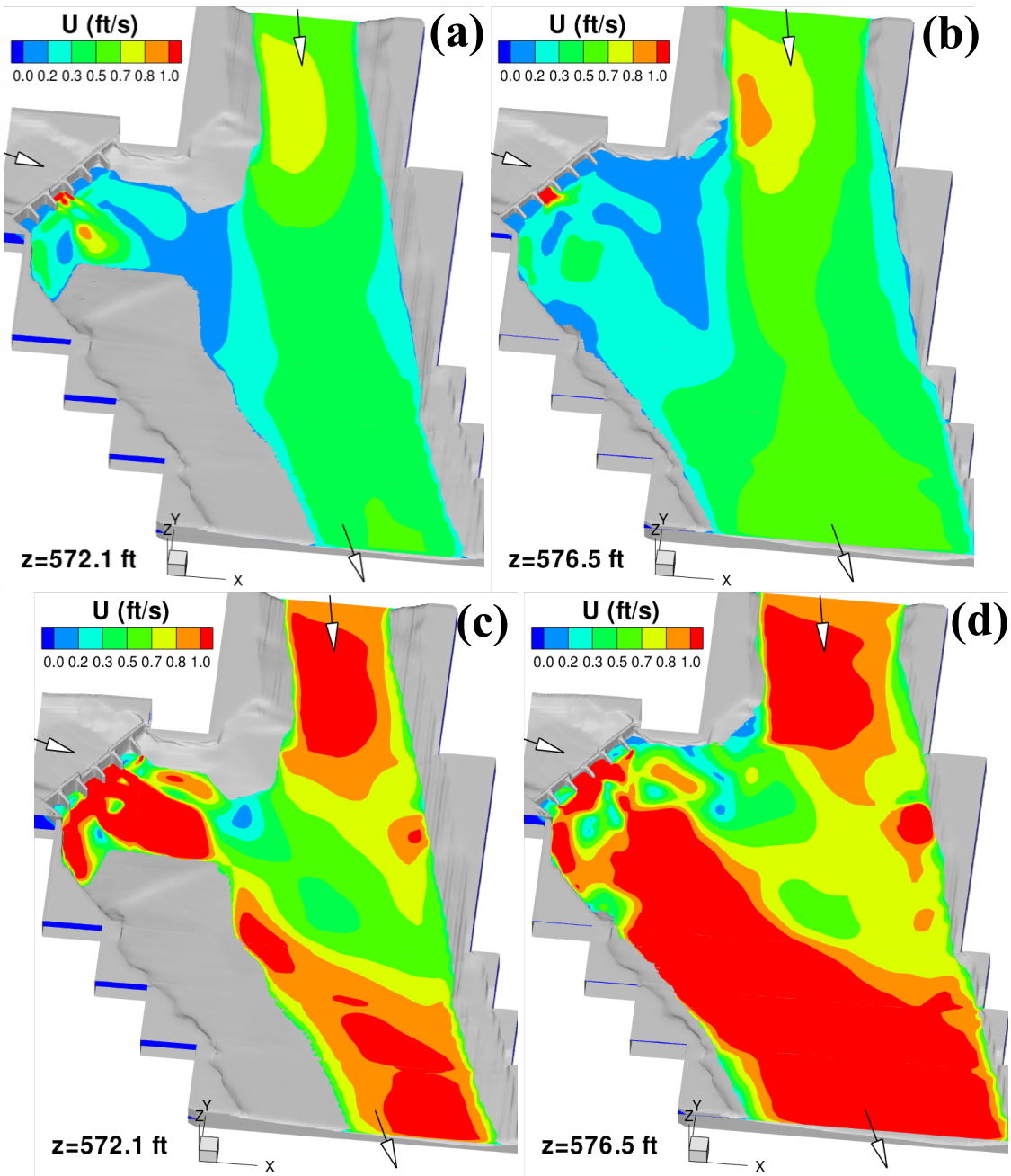

Figure 3. Velocity magnitude for both design discharges at different elevations (a) and (b)85% exceedence, (c) and (d) 15% exceedence

2. TESTING THE ALTERNATIVE: THE DUTCH POOL AND ORIFICE FISHWAY

Boiten and Dommerholt (2006) have presented a methodology (tested against experimental measurements) for the design of the Dutch pool and orifice fishway structure. Figure 4 shows the configuration of the Dutch pool and orifice fishway as used by Boiten and Dommerholt (2006). Herein the upstream and downstream channels are set to have 1.0E-5 of longitudinal slope, while the fishway channel has a longitudinal slope of 0.0625. The present case studies are design under uniform flow conditions, therefore, the upstream and downstream water depth are similar. Several discharges (from 0.057 m^3/s to 0.141 m^3/s) for a range of H=0.5m to H=1.0m are studied. The length and width of each pool are 0.80m and 1.20m respectively. The height and width of each orifice are 0.40m and 0.20m respectively. A total of 8 orifice fishway structures are placed into the channel, being the first orifice located near the right side wall. The design water drop (Δh) between consecutive pools is around 5cm.

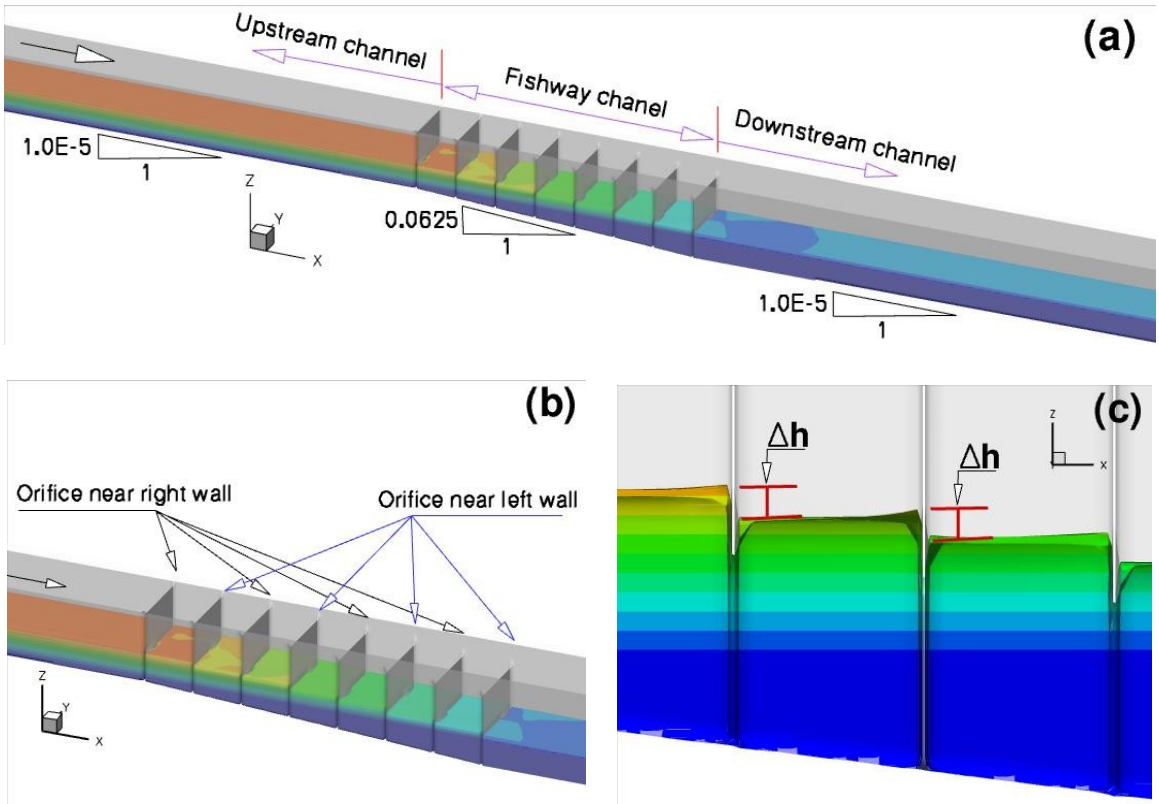

Figure 4. Dutch pool and orifice fishway configuration. (a) 3D view showing upstream, fishway and downstream channels, (b) 3D view showing alternate orifice fishway plates, and (c) Side view showing the difference in water surface elevation at two consecutive pools. The designed water drop elevation is set to 5cm.

Figure 5 shows the comparison of velocity magnitudes at orifice 5. While the agreement is not perfect, it reproduces the averaged velocity magnitude and its distribution. Higher velocities are found near the right lower corner as found in the experiments performed by Boiten and Dommerholt (2006). Currently more simulations are carried out finer meshes in order to improve the agreement and better describe the flow structure though the fishway structures.

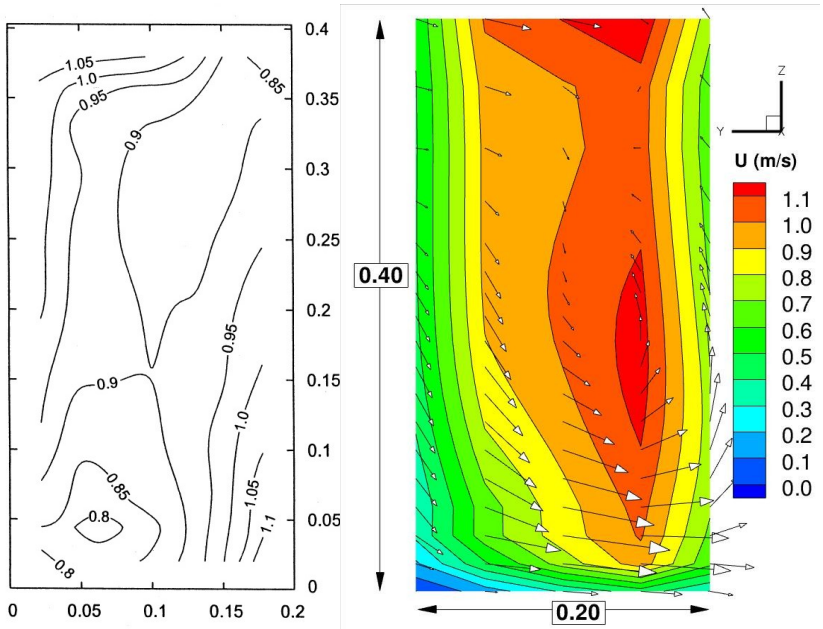

Figure 5. Comparison of measurements (Boiten and Dommerholt, 2006) and modeling results at orifice fishway 5. The water depth is H=1.0m.

Figures 6 and 7 show the plan view of velocity distribution at different elevations (z=0.62m, 0.77m, 0.96m, 1.12m, and 1.30m) for water depths H=0.5m and 0.9m respectively. As expected the velocity magnitudes are increased around the orifice fishway and recirculation cells are created along the pools. Since the orifice are located alternate at both sides, the core of higher velocity magnitude shifts from right to left and so on. The horizontal flow pattern at these different conditions is quite similar.

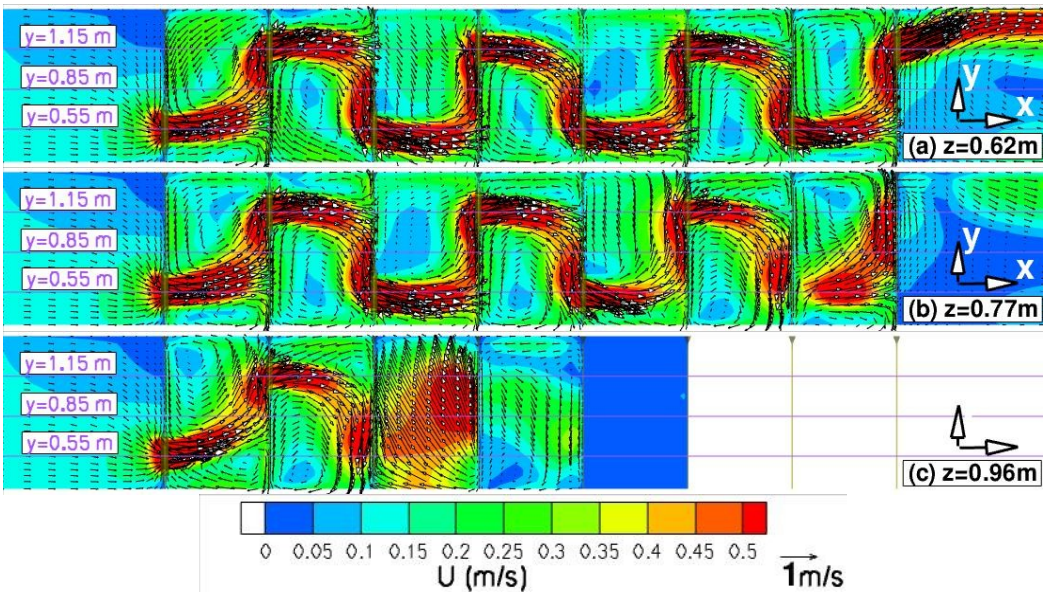

Figure 6. Velocity distribution at (a) z=0.62m, (b) z=0.77m, and (c) z=0.96m for a water depth of H=0.5 m.

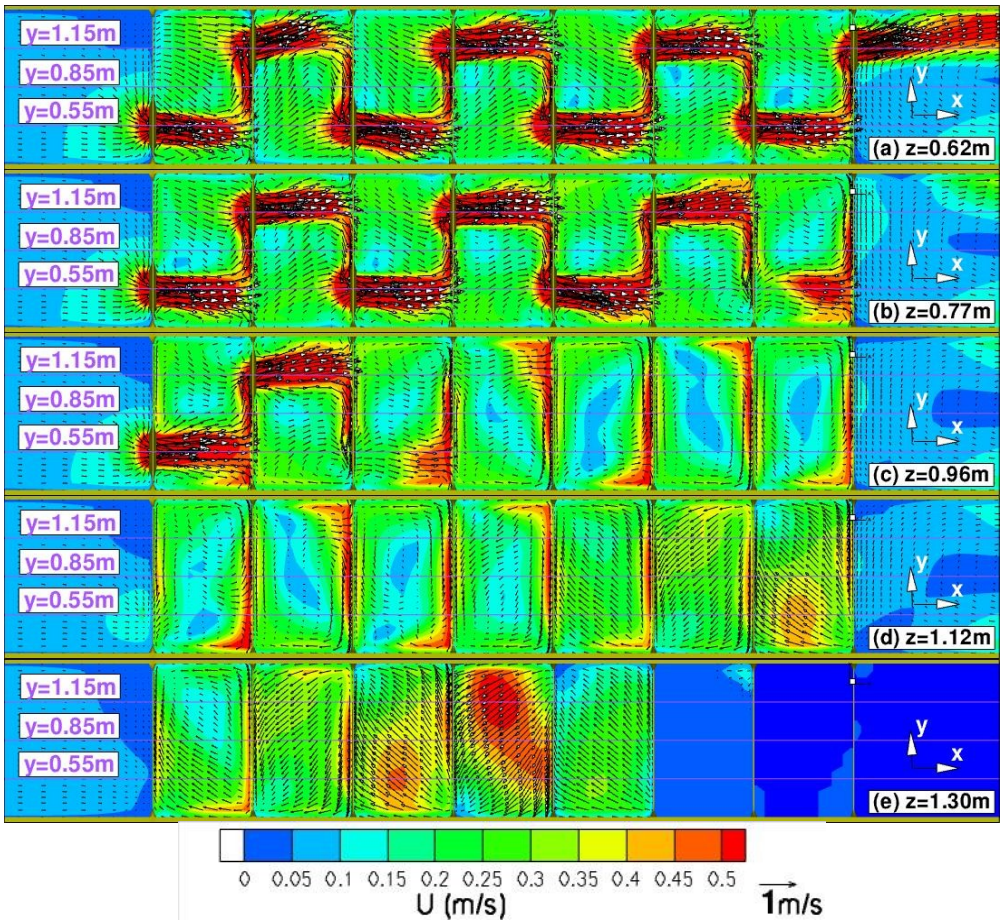

Figure 7. Velocity distribution at (a) z=0.62m, (b) z=0.77m, (c) z=0.96m, (d) z=1.12m, and (e) z=1.30m for a water depth of H=0.9 m.

Figures 8 and 9 show the side view of velocity distribution at different locations along the transversal coordinate (y=0.55m, 0.85m and 1.15m) for water depths H=0.5m and 0.9m respectively. The flow at y=0.85 represents the cross section at the center of the channel, therefore the velocity distribution is quite similar in all pools, while the other longitudinal cross sections (y=0.55m and y=1.15m) represent the location of the orifice, therefore, alternate pools present similar flow pattern. The higher the water depth, H, the higher the vertical velocities along the pools, since the disturbance flow coming out from the orifice is higher and it produces notorious recirculation cells. As designed, the water drop in consecutive pools is around 5cm, therefore, the CFD model was able to capture this macroscopic feature.

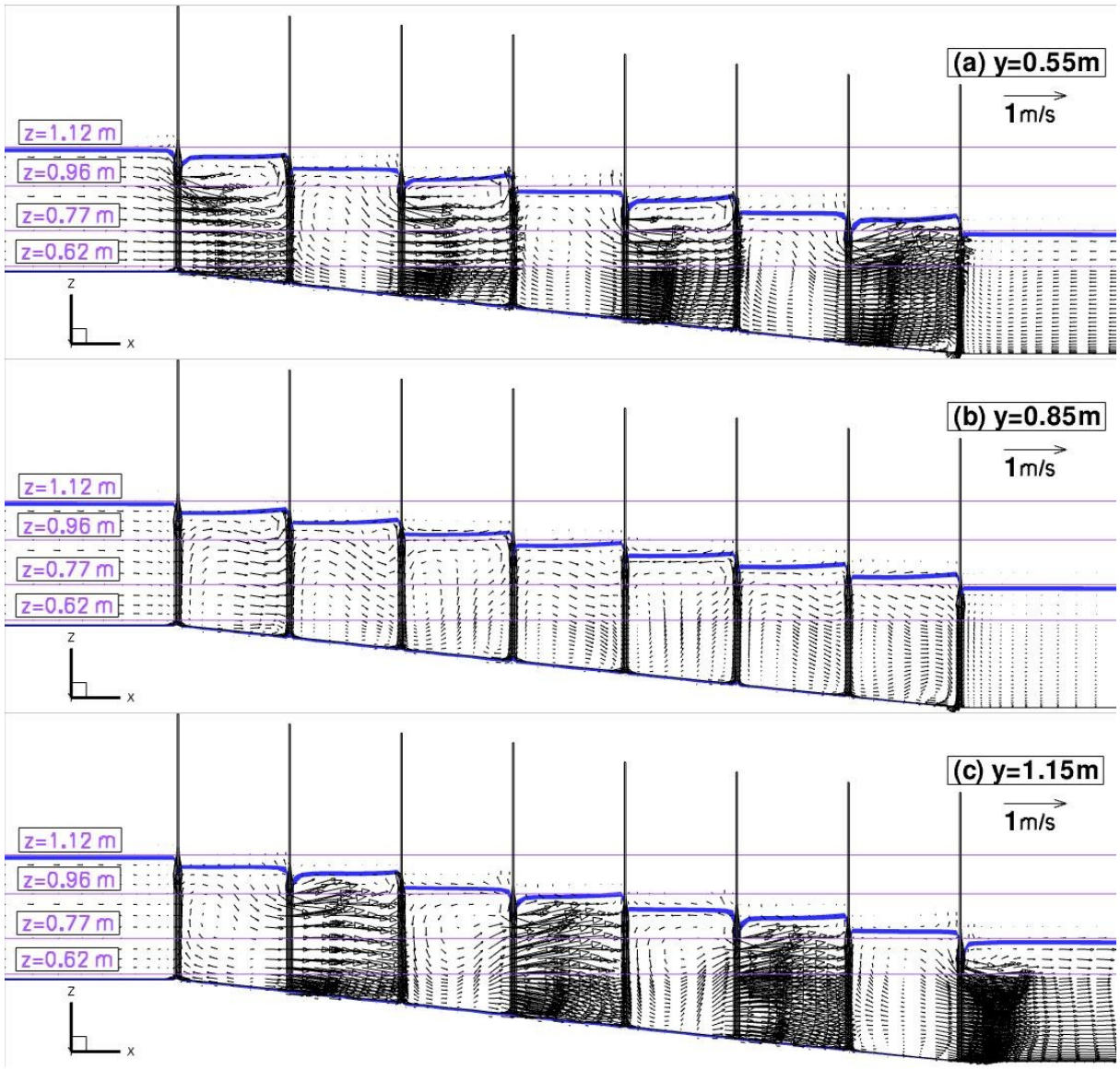

Figure 8. Side view. Velocity distribution at different cross sections along the transversal direction. (a) y=0.55m (orifice location), (b) y=0.85m (channel centerline), and (c) y=1.15 (orifice location). H=0.5 m.

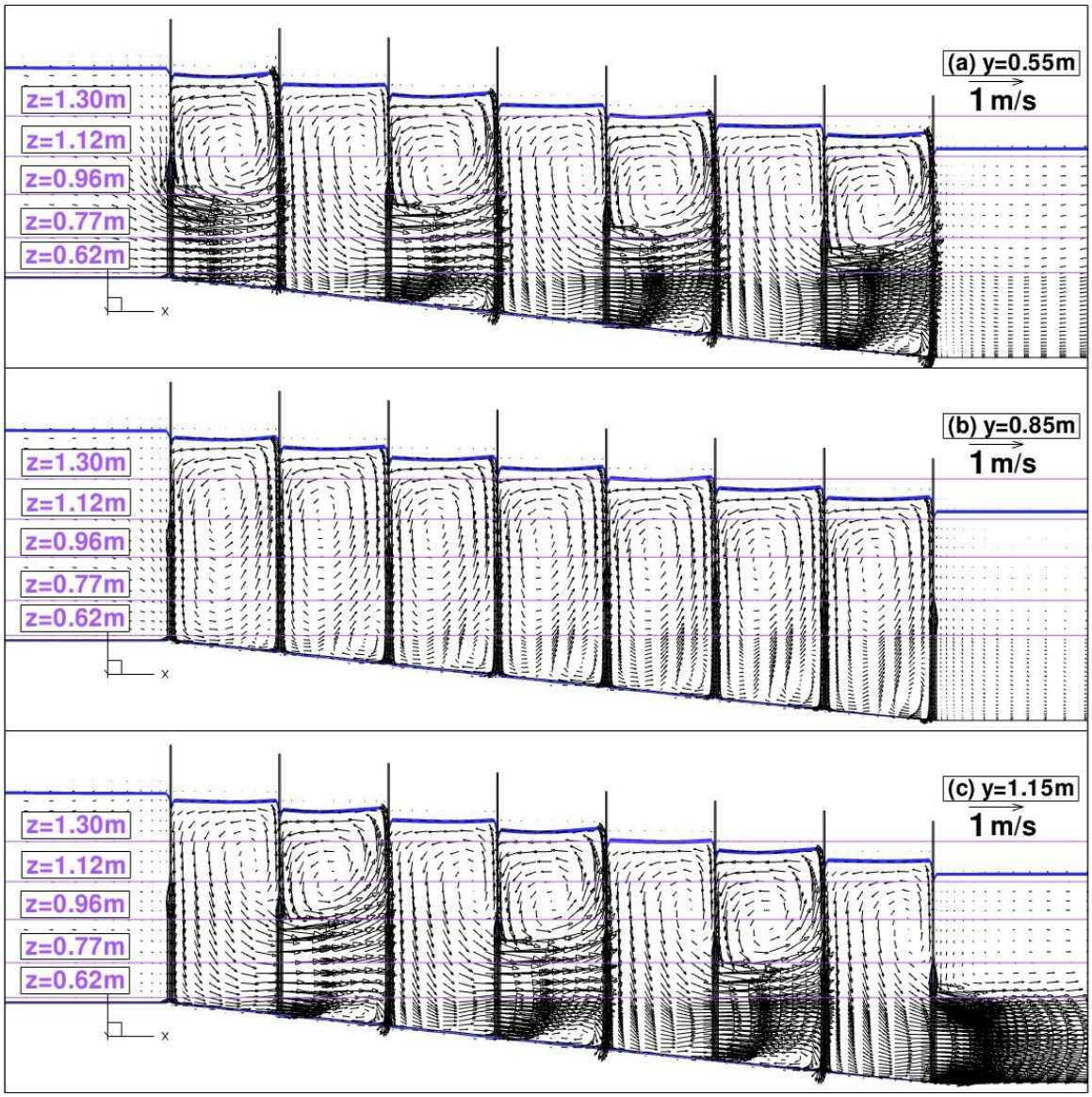

Figure 9.Side view. Velocity distribution at different cross sections along the transversal direction. (a) y=0.55m (orifice location), (b) y=0.85m (channel centerline), and (c) y=1.15 (orifice location). H=0.9 m.

3. PREDICTION OF DESIGNED SCENARIO – CHICAGO NORTH BRANCH DAM + DUTCH POOL AND ORIFICE FISHWAY

The previous sections described the CFD modeling of the current scenario (prototype scale) and the verification of the Dutch pool and orifice fishway. Herein, the objective is to incorporate a boat chute/fishway passage structure in the Chicago North Branch Dam (as shown in Figure 10). Several studies deal with the design of canoe chutes (e.g. Katapodis, C., 1992, Caisley et al. 1999, Caisley and Garcia, 1999, Odeh, 2003). Herein, Caisley et al. (1999) and Caisley and Garcia (1999) are used as designed guidelines.

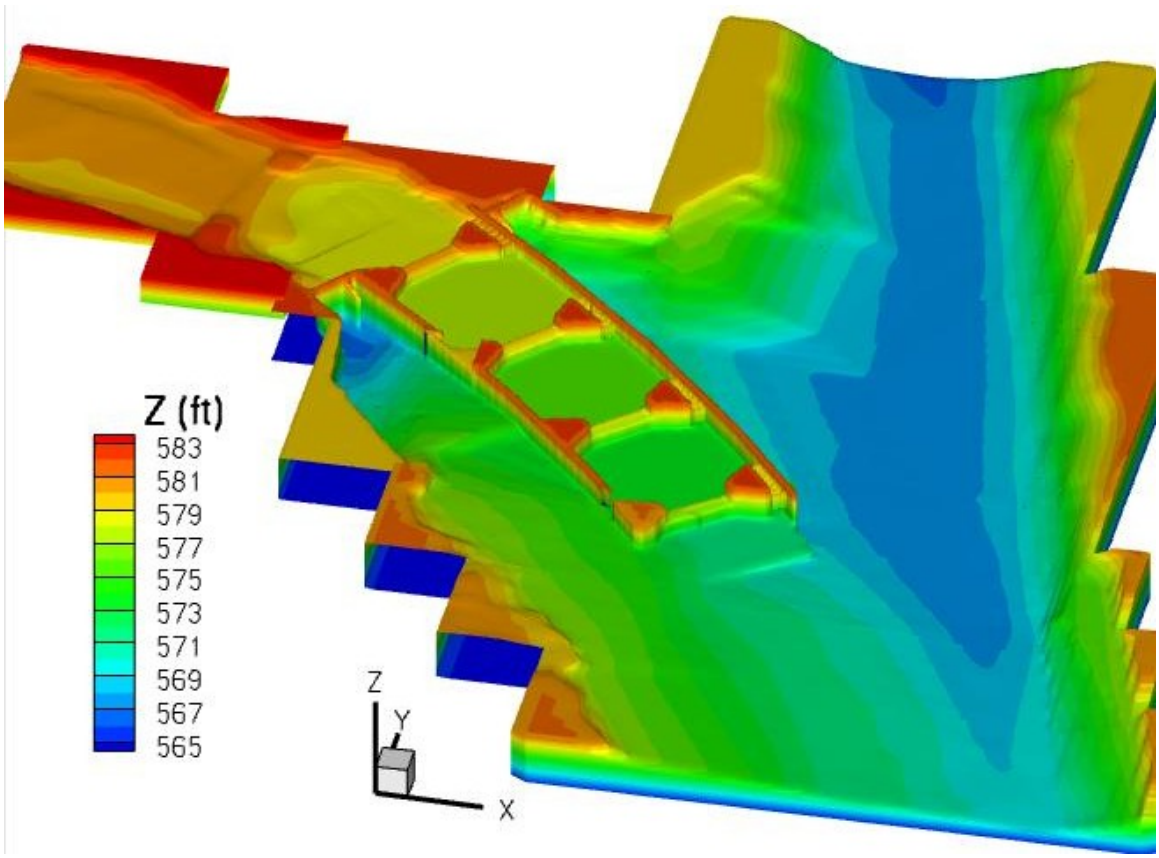

Figure 10.3D view of the computational domain including the Canoe chute and Dutch pool/orifice fishway structure. Colors define the bottom elevation.

Currently the above configuration is being simulated for both design discharges (85% and 15% exceedence) and studied experimentally.

4. REFERENCES

Abad, J. D., Rhoads, B. L., Guneralp, I., García, M. H. (2008) "Flow structure at different stages in a meander-bend with bendway weirs". Journal of Hydraulic Engineering, 138 (8): 1-12.

Abad, J. D. and Garcia, M. H. "Hydrodynamics of Kinoshita-generated meandering bends" (2005). 4th IAHR Symposium on River, Coastal and Estuarine Morphodynamics, University of Illinois, October 4-7.

Boiten, W. and Dommerholt, A. (2006). Standard design of the Dutch pool and orifice fishway. Intl. J. River Basin Management, 4 (3): 219-227.

Caisley, M. E. and Garcia, M. H., (1999). Canoe chutes and fishways for low-head dams: Literature review and design guidelines. Civil Engineering Series, Hydraulic Engineering Series No. 60, ISSN: 0442-1744, Ven Te Chow Hydrosystems Laboratory, Department of Civil and Environmental Engineering, University of Illinois at Urbana-Champaign, 70 p.

Caisley, M. E., Bombardelli, F. A. and Garcia, M. H., (1999). Hydraulic model study of a canoe chute for low-head dams in Illinois. Civil Engineering Series, Hydraulic Engineering Series No. 63, ISSN: 0442-1744, Ven Te Chow Hydrosystems Laboratory, Department of Civil and Environmental Engineering, University of Illinois at Urbana-Champaign, 112 p.

Flow Science Inc., (2009). "Flow3D v. 9.3.1".

Hirt, C. W., and Nichols, B. (1981). "Volume of fluid (VOF) method for the dynamics of free boundaries." J. Comput. Phys., 39, 201–225.

Katapodis, C., (1992). Introduction to fishway design, Department of Fisheries and Oceans, Government of Canada, 70 p.

Odeh, M. (2003). Discharge Rating Equation and Hydraulic Characteristics of Standard Denil Fishways. Journal of Hydraulic Engineering, 129, 5: 341-348.

Rodriguez, J. F., Bombardelli, F. A., García, M. H., Frothingham, K., Rhoads, B. L., Abad, J. D. (2004) "High resolution numerical simulations of flow through a highly sinuous river reach". Water Resources Management, 18: 177-199, Kluwer Academic Publishers.

Yakhot, V., and Smith, L. M. (1992). "The renormalization group, the k-extension and derivation of turbulence models." J. Sci. Comput., 7, 35–61.

Some Findings on Effective discharge Determination for Gravel bed Rivers

Carmen E. Bernedo, P.E., M.ASCE[1]

[1]MWH Americas, Inc., 1801 California St, Suite 2900, Denver, CO 80202; email: carmen.e.bernedo@mwhglobal.com

Abstract

The variability in the effective discharge (Qeff) calculations was assessed and attributed to the flow frequency distribution (FFD) determination, the type of sediment data used in the analysis and the methodology used in the calculation. Improvements to the existing methods for Qeff determination included the use of a Log-Pearson Type III model to represent the FFD in an analytical approach and the use of density frequency distributions to avoid dependence on the class size of histograms, and to replace the concept of frequency of discrete events by frequencies of a continuous variable. A sensitivity analysis by using the analytical approach demonstrate that the use of the suspended sediment load data to infer the bedload transport rates is inappropriate and that FFD with less skew in the data tend to have low values of effective discharge. Qeff for three gravel rivers (*i.e.*, SF Salmon, SF Payette and Boise Rivers) were calculated. Methods used yield to similar results. Effective discharge is reached or exceeded about 6, 17 and 7 days per year for the SF Salmon, SF Payette and Boise River, respectively. The values of effective discharge and bankfull discharge are nearly identical for Boise and Payette River and the effective discharge is 1.2 times the bankfull discharge for Salmon River.This paper will emphasize understanding the basis of the formula or methodology for correct application. Numerical results are presented in comparative tables as well as conclusions.

Background

In this paper, the focus is on assessing the applicability of the effective discharge concept to three gravel bed streams in the Boise and Payette national forests: SF Salmon, SF Payette and Boise. Three different methods will be applied: 1) the traditional method based on the work of Wolman and Miller (1960), 2) the analytical approach of Nash (1994), but improved as it will be explained below and, 3) the method proposed by Emmett and Wolman (2001). The analytical approach of Nash (1994) will be improved by using a more appropriate statistical distribution besides the lognormal proposed by Nash. The methods and results will be compared and their advantages and disadvantages will be determined. Variables that can affect the results of the calculations of effective discharge will be assessed (i.e., number of class intervals/bin size when flow histograms are used, methods for the estimation of the sediment rating curve (Q_s vs. Q) and use of bedload/suspended load sediment data, among others).

Methods used for estimation of effective discharge

For many years, standard practice for effective discharge determination has been based on three main approaches. In the following sections the following notation will be used for each of the approaches to be used:

Method A: The traditional approach based on the flow frequency distribution and the sediment rating curve (Wolman, 1960).

Method B: The analytical approach based on representing the flow frequency distribution with a known statistical distribution and the sediment rating curve represented with a power function (Nash, 1994).

Method C: The approach based on finding the discharge that produces the maximum change in sediment load using the Andrews (1980) definition of effective discharge (Emmett and Wolman, 2001).

From the literature review it is evident that Method A is widely used. Method B is referenced in papers after 1995 but usually produces poor results or results not in good agreement with results of Method A or bankfull discharges. Since Method C is relatively new in comparison with the previous ones (Emmett and Wolman, 2001), no many papers were found that reference it. However, some similar approaches have been used after Andrews (1980) definition of effective discharge. Key references in this study to evaluate approaches used for effective discharge calculation were those published by Wolman and Miller (1960), Andrews (1980), Andrews and Nankervis (1985), Nash (1994), Emmett and Wolman (2001) and Biedenharn (et. al. 2001).

A few typical issues or problems referenced in the literature reviewed include the following:

If a significant proportion of the recorded discharges falls within the first-class interval of the flow distribution, the effective discharge could be significantly underestimated; for example, for streams that display a highly skewed distribution of flow events, like rivers in semi-arid environments, channelized streams, or incised channels (Watson, 2001).

Different criteria used in the selection of number of discharge classes used in the flow frequency distribution histogram (Biedenharn et. al., 2001).

Discontinuous flow frequency distribution histograms that generate an irregular bed material load histogram with outliers that reflect transport associated with individual flood events (Biedenharn et. al., 2001).

The gauging stations at which sediment data are available are located at sites where drainage basins have been impacted by human activities (*i.e.*, continuous changes in land uses) or whose flows are controlled or diverted upstream of the analysis site.

"Scatter pattern" observed in the sediment rating curves. Sediment discharge data not normally distributed and variance not constant with discharge cause differences in the sediment rating equations depending on the procedure used to estimate them (*i.e.*, transformation of data for a linear regression and correction factors to improve the results, non-linear regression estimation and the criteria used to select the model).

Sediment transport measurements taken infrequently and limited to the suspended portion. Suspended transport does not contain the bedload channel material and is more representative of watershed denudation.

Bimodal or multimodal effective discharge histogram. The effective discharge curve is not always a unimodal histogram as Wolman and Miller presented in 1960. Depending on the flow frequency distribution shape and the rating curve equation, the effective discharge curve can have more than one peak. If the multiple peaks are of similar magnitudes, an uncertainty in the selection of the peak (associated with the effective discharge value) is introduced.

In conclusion is that in general, there are three reasons for variability and uncertainty in the effective discharge calculations:

- The flow frequency distribution
- The sediment data used in the analysis
- The methodology used in the calculation

Case Study

Site Description

The study site is composed of three gauged gravel-bed rivers in west-central Idaho, whose drainage areas are within the Boise National Forest and the Payette National Forest. The site is on land administered by the Forest Service. The gage stations selected are:

1. South Fork Salmon River near Krassel Ranger Station, Idaho.
2. Boise River near Twin Springs, Idaho.
3. South Fork Payette River at Lowman, Idaho.

Information used in this report was collected by the USFS at Boise and the USGS (Idaho). The monitoring information was obtained because of the need to understand and describe the sediment-transport capabilities of the rivers to assist in land-use planning efforts of the USFS. Data collected under the direction of the USFS at the three sites include hydraulic geometry, bedload and suspended transport and bedload material characterization by pebble counting. Additional measurements include a survey of the stream reach and pebble counts of the surface substrate. Flows are continuously monitored by the automatic stations of the USGS. None of these site has upstream dams or significant diversions.

South Fork Salmon River near Krassel Ranger Station, ID

The South Fork Salmon River had extensive sedimentation in the early 1960's due to a combination of roads and timber harvesting coupled with very large storms (1955, 1962, 1964 and 1965). By 1965 the USDA Forest Service developed an integrated watershed restoration program concerned with the degradation of the river conditions. Since then this system has been in a recovery phase (Megahan et al. 1980; Platts and Megahan, 1975). A large storm around Jan 1, 1997 generated a lot of new sediment to the system.

In terms of river mechanics, since 1965 the sediment supply was reduced due to a restoration program. Energy available for sediment transport in the river was adequate to remove the excess of sediment in the system.

In 1978 a new Land Management was implemented. One of the challenges of this plan is monitoring to assure that goals are met. The monitoring was designed to be sensitive enough to detect potential problem situations. There were three periods in which sediment transport monitoring was developed, 1984-1986, 1995-1996, 1997. These data were used in the analysis of the effective discharge. Two representative periods (80's and 90's) will help to look at changes in time of streamflow versus sediment transport relationships that could affect the effective discharge estimation.

The study reach is at the Geological Survey (USGS) gage 13310700 (South Fork Salmon River near Krassel Ranger Station, Idaho) in the Payette National Forest. The stream gauging station is approximately 2.25 km downstream from the Krassel Ranger Station at an elevation of about 1,143 m. The drainage area upstream of this location is 852.9 km^2. Average annual streamflow for the period of record is 15.3 m^3/s and bankfull discharge is estimated at 65 m^3/s.

Bedload-transport rates were measured with a Helley-Smith bedload sampler. The three inches sampler was used for all of the SF Salmon River station samples. Suspended sediment was generally sampled at 10 verticals using a depth-integrating sampler. Samplers used included the DH-59, D-49, and D-74 models.

The sediment transport data include 130 measurements of bedload transport and 92 measurements of suspended sediment. Over the range of measured discharges, suspended transport accounts for the majority of the material in transport, with over an order of magnitude greater suspended transport at the lower range of sampled discharges to approximately equal amounts at the highest discharge.

South Fork Payette Station, ID

The study reach is at the Geological Survey (USGS) gage 13235000 (South Fork Payette River at Lowman, Idaho) in the Boise National Forest at an elevation of about1155 m. The drainage area upstream of this location is 1163.7 km^2.

Sediment transport measurements were made by USGS personnel during the spring flows of 1994 and 1995, and 1997. Average annual streamflow for the period of record is 24.4 m^3/s and bankfull discharge is estimated at 85.4 m^3/s.

Bedload-transport rates were measured with a Helley-Smith bedload sampler. The three inches sampler was used for most of the samples on the SF Payette River. The six inches sampler was used for the high flows in 1995. Suspended sediment was generally sampled at 10 verticals using a depth-integrating sampler. Samplers used included the models DH-48 and D-74.

Sediment transport measurements made in 1994 and 1997 include 72 measurements of bedload transport and 37 measurements of suspended sediment transport. Over the range of measured discharges, suspended transport typically accounts for the majority of the material in transport with over an order of magnitude greater suspended transport than bedload transport at the highest discharges and about similar rates between suspended and bedload transport at the lowest discharges during which sediment transport was measured.

Boise River Station, ID

The Boise River originates in the Sawtooth Mountains in Central Idaho as three separate forks that flow in a southwesterly direction. The North Fork and Middle Fork join near Twin Springs and the South Fork discharges into Boise River just above Arrow Rock Dam. The gauge station is located at the Geological Survey (USGS) gage 13185000 (Boise River near Twin Springs) in the Boise National Forest and at an elevation of about 992.4 m. The Boise river watershed to this site, is characterized by mixed forest, grass and brush vegetation in relatively good condition (Love and Benedict, 1948). There appears to be no direct evidence of any significant changes in stream beds in the vicinity of the gauge station.

The drainage area upstream of this location is 2153.8 km^2 and the stream gauging station is approximately 2.9 km upstream from the maximum flow line of Arrowrock Reservoir. The average gradient for the study reach is 0.0038.

Sediment transport measurements were made by USGS personnel predominantly during the spring of 1994, 1995 and 1996 and 1997. During this monitoring program a survey of the stream reach, pebble counts of the surface substrate, and core samples of the subsurface substrate material were carried out.

Bedload-transport rates were measured with a Helley-Smith bedload sampler. The three inches sampler was used for all of the Boise River samples. Suspended sediment was generally sampled at 10 verticals using a depth-integrating sampler. Samplers used for the Boise River were the models DH-59, D-49, D-74, and D-77.

Streamflow has been recorded since March 1911, although prior to October 1, 1965 the station was 0.48 km downstream of the present location. Average and bankfull discharge is estimated at 15.3 m^3/s and 165.2 m^3/s, respectively.

Analyisis and Results

Hydrology

Because the flow discharge patterns are important factors for the effective discharge, a break in the analysis of the Salmon River was done in 1990 to assess possible changes in the value of the effective discharge. However, the selection of the 1990 year to mark the break in the analysis is arbitrary and based on a combination of practical purposes. The mean levels change gradually (due to a cyclic effect) and there are no flow data during 1983-84 and 1987-1988 to analyze changes during the 80's. We can visualize the variation only after 1990. Because flow frequency distributions are critical for the calculation of effective discharge, frequency distributions before and after the adopted break in 1990 were calculated. There are no significant differences between the two periods except for flows lower than 3 m^3/s that are more frequent for the period after 1990.

Lognormal and Log-Pearson Type III models were tested to the data to assess their fits to the empirical frequency density curve. The Log-Pearson Type III models are preferred to fit the data of the Salmon, Payette and Boise Rivers.

Because of the significant skewness in the flow data and the variability of the daily flows, the number of class intervals necessary for an adequate histogram is very large. It would be impractical to use such an interval since scattered effective discharges will occur. As mentioned before, in this case, the use of histograms will ignore important information. A routine was used to analyze the best number of class intervals that could preserve the EFD shape. Because of the skewness of the data, a large number of class intervals is required to preserve the information of the low flows. However, information of the higher flows is missed since some intervals will have frequencies equal to zero. In gravel bed rivers it could be risky to discard information in this range of values since the "effective discharges" will probably be associated with infrequent flows. The number of class intervals selected ranged between 200 and 500 class intervals trying to avoid zero frequencies to analyze the effect of the use of histograms in the effective discharge calculation. Additionally, the approach using an empirical PDF or the relative frequencies obtained from the CDFs avoided the frequencies equal to zero when small width classes are used.

Sediment Transport

Although the sediment transport curves for the gauging stations studied indicate a good log-log relationship between stream discharge and suspended and bedload sediment discharge, there was a fair amount of scatter about the best fit regressions. Bias corrections were done and non-regression estimates were found to assess the sensitivity of the "best curve fit" on the effective discharge calculation.

It is important to notice that sediment rating curves obtained with linear and non linear regression methods have different *"a"* and *"b"* coefficients. It has been shown that the effective discharge is only dependent on the *"b"* coefficient, hence it is expected that different values of these coefficients will lead to different values of effective discharges. The magnitude of this change is evaluated in the effective discharge calculation.

Sediment rating curves for Salmon River data were calculated for the period before and after 1990. Sediment data collected before 1990 were used in combination with flow data collected before 1990 representing the first period of analysis (I). Sediment data collected after 1990

were used in combination with flow data collected after 1990 to represent the second period of analysis (II). In general, it was observed that for the same flows the first period of analysis was associated with greater bedload rates than the second period of analysis. However, the relationship between bedload rates in the first period and second period decreases as flow increases.

Rating curves for suspended sediment data were also estimated for the three sites of study. Where available information allowed separation of the fraction of sand size or larger of the suspended rates, additional curves were developed for these fractions of the suspended sediment. This comparison shows how different rating curve equations are obtained for bedload and suspended sediment, invalidating the suggestions made in past studies about the feasibility of using the sediment load transport information to infer the bedload transport rates or the coefficient *"b"* of the bedload rating curves for the calculation of the effective discharge. Nash (1994) pointed out that poor estimations of the transport function at the highest flows and the extrapolation of the rating curve to higher discharges than these measured can alter the classic form of the effective discharge curves. However, Withing (1999) mentioned that he did not believe these factors were important.

It was observed that the size fractions in motion in the channel were in general smaller than the fractions in the bed. In the three sites analyzed, the D_{50} of the material transported was finer than the D_{50} of the bed-load material. Even though the sediment particle size increases with increase in discharge, most of the bedload transported (caught with the Helly Smith) is sand size in Salmon River and an important portion in Boise and Payette River. Payette River shows a wider range of grain sizes moved from bed material.

The subsurface samples in SF Payette and Boise show that the subsurface layer contains finer material than the surface layer. Finer fractions will be present in the mixture as long as they are shielded by the stable coarser particles. Larger particles will move as soon as the shear stress exceeds the threshold of motion of coarse particles. The grain size distribution of a bar in Boise evidences similar characteristics to those of the grain size distributions of the surface and subsurface samples.

Using the traditional approach (Method A), the results obtained do not indicate a dependence on the "potential" number of class intervals (the ones that statistically can be used allowing a good representation of the EFD) used in the flow frequency distribution. The number of class intervals used was in the range of 200 to 500 for the three sites. However the smaller the number of class intervals the more information hidden in the frequencies and, as a consequence, the low values and high values tend to be under- or over-represented. In sediment load histograms like the one observed for Boise (where the peak is surrounded by other significant sediment loads), care should taken since variations either in the number of bins when method A is applied, or in the *"b"* coefficient, will produce variations in the peak that represent the effective discharge value. In such cases it will be advisable to do a sensitivity analysis to check for the potential "range of effective discharges."

The potential "range of effective discharges" in the effective discharge curves was visualized when the Empirical PDFs were used instead of histograms to represent the flow frequency distributions in the calculations. Although scattered graphs were obtained, by smoothing

these graphs the "competence of effective discharges" (range of potential effective discharges) could be observed. When histograms are used in selecting an arbitrary number of class intervals (*e.g.*, N=25), well defined peaks can be obtained in the effective discharge curve but the potential "range of effective discharges" is missed.

The smaller the discharge range, the more fluctuation in the effective discharge plot in the estimations with Method C. In spite of this pattern, the peak of the plot can be identified, and clear results were obtained when the whole discharge range was divided into 20 to 25 to select the "dQ" to use in the estimation of the slope of the relative accumulative sediment load curve for each historic datum under this range of flows. These results agree with Emmett and Wolman (2001) recommendations of 1/18 discharge range. Effective discharge values by using Method A and C are very similar and as a consequence, so are the recurrence intervals. The advantage of Method C is that we do not have to deal with choosing a good number of class intervals for the histogram.

Effective Discharge is reached or exceeded 6, 17 and 7 days per year for SF Salmon, SF Payette and Boise, respectively. SF Salmon analysis showed a "potential change" in the effective discharge values due to the changes in the availability of coarser material in the bed for transport. This potential change will change the frequency of exceedance from 6 to 4 days per year. These results were obtained based on the EFDs. The values of effective discharge and bankfull discharge are nearly identical for Boise and Payette River and the effective discharge is 1.2 times the bankfull discharge for Salmon River.

Effective discharge calculations were carried out for different *"b"* values obtained with the corrected Linear Regression (LR) and Non Linear Regression (NLR) estimation of the rating curve. It was found that the difference in the effective discharge value obtained was minimal, because the peak in the effective discharge curve (the effective discharge value) was well defined. Boise River did not have a "well defined peak" but a range of competitive effective discharges, so, a change in "*b*" can lead to a significant influence on the effective discharge value.

Results obtained using Method B were lower than those obtained by the other two methods. The reason is that the models, although good for the whole range of flows, did not represent very well the tails of the distribution (high flows). In gravel bed rivers this is important because this is the range of flows where the effective discharge is expected. The models underrepresented the frequencies in this range of flows, causing lower flows to be identified as effective discharges. These results do not invalidate the use of an analytical approach because models that are not "completely perfect" can be used for rivers where threshold conditions are not considerably high. Besides, those models must be used when the EFD is not available or, as in this report, to estimate patterns/sensitivity analysis, etc.

In order to check whether the effective discharge is really responsible for the changes and movement of bedload material, graphs with grain size distribution of bedload transported material (caught in the Helly Smith sampler) and bed material (determined by pebble count) were developed. Flows close to or larger than the bankfull and/or effective discharge contribute to a significant movement of the bed material. In all of the cases it was the sand size material that represented the bulk of the bedload transported.

The similarity in the values of effective and bankfull discharges for the Boise and Payette Rivers shows that the channel is adjusted to the range of discharges that transport the largest sediment load.

Conclusions

Using the analytical approach, a sensitivity analysis was performed to assess the variation of the effective discharge value with changes in the parameters that are involved in its quantification. Unless "a well defined effective discharge" is identified, the effective discharge can vary even with small changes in the parameters involved in the effective discharge calculation.

Sediment rating curves fitted for bedload generally have a larger degree of uncertainty than do curves for suspended sediment. The correlation coefficients are higher for suspended sediment rating curves than for bedload rating curves. For suspended sediment rating curves a logarithmic transformation of the data facilitated a linear regression between the transformed data that provided adequate rating curves (explaining more than 90% of the variability of the data).

Comparison of the bedload rating curves selected for the effective discharge calculation and rating curves obtained for suspended sediment transport showed the difference in the rating curve equations. This result invalidates the suggestions made in past studies (Nash, 1994) about the feasibility of using the suspended sediment load transport data to infer the bedload transport rates or the coefficient "*b*" of the bedload rating curves for the calculation of the effective discharge.

It was observed that the size fractions in motion in the channel were, in general, smaller than the fractions in the bed. In the three sites analyzed, the D_{50} of the material transported was finer than the D_{50} of the bed-load material.

The largest portion of the bedload transported in these gravel bed channels is not in the gravel size, but in the sand size. The sediment samples showed a rather straight cumulative curve (at the sand size) describing the bedload caught with the sampler and a markedly S-shape curve for bedload material. The armour and subarmour layer nearly always have a curve that lies under the bedload caught in the sampler.

In general, the particle size distribution of bedload sediment becomes proportionately coarser as stream discharge increases. Sand contributes (0.5 to 2.0 mm) the major volume of bedload in the three gravel-bed streams studied. However, the major morphological feature of gravel-bed streams is that they are composed of gravel, not the sand that makes up the bulk of the bedload. Records for the Boise and Payette streams showed different patterns from the records for the Salmon stream with respect to the ratios of bedload and suspended rates to discharges. These ratios increased with discharge for the Boise and Payette streams, but decreased with increasing discharge for the Salmon stream.

Using an adequate statistical approach for the selection of the class intervals (based on the EFD), the range of variation in the effective discharge as a function of the class interval size

became very narrow. However, it has been shown that for Method A it is much better to work with the original Empirical PDF or the relative frequencies derived from the empirical CDF than to use histograms. The potential "range of effective discharges" in the effective discharge curves is visualized in this way. Although scattered graphs were obtained, by smoothing these graphs the "competence of effective discharges" could be observed. Method C provided results nearly identical to those obtained with Method A. However, Method B provided results very different from those of Methods A and C. Thus, its use is recommended only when a well-defined flow frequency distribution is not available and/or "theoretical" conclusions need to be described by the proposed models. In fact, if a statistical distribution is good enough to represent the EFD, Method B provides good results.

Effective discharge is reached or exceeded about 6, 17 and 7 days per year for the SF Salmon, SF Payette and Boise, respectively. These results are in good agreement with previous results in the literature about periods of recurrence of effective discharges. The analysis for SF Salmon showed a "potential change" in the effective discharge values due to changes in the availability of coarser material in the bed for transport. This potential change will also change the frequency of occurrence.

Hydraulic geometry equations have been developed for gravel bed rivers and they give reasonable results when large rivers are involved. It has been noticed, however, that results of these equations do not reflect the observations for mountain rivers or steep streams (Chang, 1992). Mountain rivers tend to have flow frequency distributions (from hourly/daily data) that are markedly skewed (due to their characteristic flashy hydrographs). Thus, even though steep, mountain streams may have the same mean flow as streams of lower slopes, the effective discharges will be higher for the mountain rivers. In general, the "equivalence" between two-year floods, mean annual flows, bankfull flow and effective discharges, when applied to hydraulic geometry equations, will not be appropriate when it is known that hydrologic regimes in the sites of study are different from the ones whose source data were used to develop the equations. Hydraulic geometry equations do not take into account the flow regime and/or flow distribution and this may be one of the reasons of the variability between field observations and theoretical results.

Results obtained using the rating curves of the SF Salmon River show that streams similar to SF Salmon River can recover in time if sediment flows into the stream resulting from upland erosion are reduced to levels below the capacity of the stream to flush fines from the system. Because of that, the effective discharge tends to change to a stable value.

From the Analytical approach it is visualized that rivers with the same annual flow availability but with different regimes (*e.g.*, different flow frequency durations) will produce different effective discharges due to the difference in the skewness of the flow frequency distribution graph. The different flow frequency distributions could be associated to different climatic conditions or to different channel gradients.

References

Andrews, E.D., 1980, Effective and Bankfull discharges of streams in the Yampa River Basin, Colorado and Wyoming. Journal of Hydrology 46:311-330.

Andrews, E.D., 1983, Entrainment of gravel from naturally sorted riverbed material, Geological Society of America Bulletin, 94:1225-1231.

Andrews E.D., Nankervis J.M., 1995, Effective Discharge and the design of channel maintenance flows for gravel-bed rivers, *in* natural and Anthropogenic Influences in Fluvial Geomorphology, Costa JE, Miller AJ, Potter KW, Wilcock PR (eds), AGU, Geophysical Monograph 89:151-164.

Ashmore P.E., Day T.J., 1988, Effective Discharge for Suspended Sediment Transport in Streams of the Saskatchewan River Basin, Water Resources Research, 24: 864-870.

Biedenharn D.S., Thorne, CR., Soar, Hey, Watson, 2001, Effective Discharge Calculation Guide, International Journal of Sediment Research, 16 (4): 445-459.

Chang, H.H., 1992, Fluvial Process in River Engineering, Krieger Pub. Co.

Cohn T.A., DeLong L.L., Gilroy E.J., Hirsch R.M., Wells D.K., 1989, Estimating Constituent Loads, Water Resources Research, 25(5): 937-942.

Crawford, C. G., 1991, Estimation of suspended-sediment rating curves and mean suspended-sediment loads, Journal of Hydrology, 129:331-348.

Duan, N., 1983, Smearing estimate: a nonparametric retransformation method, Journal of the American Statistical Association, 78(383):605-610.

Dunne T., Leopold L.B., 1978, Water in Environmental Planning, pp 608-609.

Emmett W. W. and Wolman M. G., 2001, Effective discharge and gravel-bed rivers, Earth Surface Processes and Landforms 26: 1369-1380.

Emmett, W. W., 1999, Quantification of Channel-Maintenance Flows for Gravel-Bed Rivers, pp. 77-84 *in* Wildland Hydrology, American Water Resources Association, TPS-99(3), 536 pp.

Emmett, William W., 1976, Bedload Transport in Two Large, Gravel-Bed Rivers, Idaho and Washington, Third Federal Inter-Agency Sedimentation Conference, Proceedings, Denver, Colorado, March 22-26, 1976, pp. 4-101 to 1-114.

Ferguson, R.I., 1986, River loads underestimated by rating curves: Water Resources Research, 22(1): 74-76.

Knighton, D., 1998, Fluvial Forms and Processes. Arnold. Pub. London. 383 pp.

Leopold L.B., 1992, Sediment size that determines channel morphology, *in* Dynamics Gravel Bed Rivers Billi P, Hey R.D., Thorne CR, Tacconi P (eds) Wiley : Chichester; 297-307.

Love S.K., and Benedict P.C., 1948, Discharge and sediment loads in the Boise River Drainage Basin, Idaho, USGS WS 1048.

Megahan W.F., Platts W.S., and Kulesza B., 1980. River Improves Over Time: South Fork Salmon at Symposium on Watershed Management, 1:380-395, Boise Idaho, July 21-23.

Nash David B., 1994, Effective Sediment-Transporting Discharge from Magnitude-Frequency Analysis, The Journal of Geology, 102: 79-95.

Nordin, F., (1985), The Sediment Load of Rivers, Facets of Hydrology II.

Pickup, G and Warner, R.F., 1976, Effects of hydrologic regime on magnitude and frequency dominant discharge, Journal of Hydrology, 29: 51-75.

Platts William S. and Megahan Walter F., 1975, Time trends in riverbed sediment composition in salmon and steelhead spawning areas: South Fork Salmon river, Idaho.,US Forest Service, Intermountain Forest and Range Experiment Station, Ogden Utah. Fortieth North American Wildlife Conference, Time Trends in Riverbed sediment.

Rosgen, D.,1994, A Classification of Natural Rivers, Cantena, 22:169-199.

Rosgen, D.,1996, Applied river morphology, Wildland Hydrology, Pagosa Springs, Colorado.

Watson, 2001, Stream Restoration Design, Class Notes, Colorado State University.

Whiting P.J., 1999, Sediment-transporting flows in headwater streams, GSA Bulletin, 111(3):450-466.

Williams, R.P., O'Dell, I. and Megahan W., 1989, Hydraulic geometry and sediment data for the South Fork Salmon River, Idaho 1985-86, USGS Open-File Report 89-233. 01961497

Wolman, M.G. and Miller, J.P., 1960. Magnitude and frequency of forces in geomorphic processes, Journal of Geology, 68: 54-74.

Yevjevich, V. M., 1972, Probability and Statistics in Hydrology, Water Resources Publication

Expanded method for filtering submerged objects in echosounder data

Tim D. Osting[1]

[1]Espey Consultants, Inc., 3809 S. 2nd Street, Austin, TX 78704; PH (512) 326-5659; FAX (512) 326-5723; email: tosting@espeyconsultants.com

ABSTRACT

Methods for filtering raw bathymetric field data are useful when developing multi-dimensional hydraulic models for river instream flow studies. Raw field data characterizing a submerged surface may include spikes or irregularities arising from instrument issues (e.g., signal loss, bubbles) or from actual objects (e.g., large woody debris) resting on or above the channel bottom. Identification and filtering of large woody debris (LWD) in single-beam echosounder data has been investigated by others and these concepts can be extended to other submerged objects. An improved application of a median filter approach is presented here that includes a method for varying the filter half-length to account for changes in boat speed.

With improvements to the identification method, typical raw datasets can be used to more effectively locate submerged objects according to size class. When developing a hydraulic model, locating filtered objects aids in identifying areas of bathymetric complexity and calibrating roughness coefficients.

BACKGROUND

Many recent instream flow studies have evaluated aquatic habitat using velocity and depth predictions generated from two-dimensional (2D) hydraulic models (Bowen et al. 2003; Osting et al. 2004; Hardy 2006; BIO-WEST 2008). Development of representative channel bathymetry is necessary for applying aquatic habitat prediction tools across a range of flow; therefore, identification and management of irregularities in inputs can reduce the level of uncertainty. Model bathymetry is potentially the largest source of uncertainty to these models, including uncertainty in the input depth and roughness data as well as uncertainty arising from predictions in areas with sharp vertical gradients (Osting and Hodges 2007).

Where large study sites or deep water prohibits measurement of in-channel bathymetry by conventional means (e.g., total station survey), a boat-mounted marine echosounder allows convenient measurement of depth over a large area. When the echosounder is synchronized with a Global Positioning System (GPS), a typical data set may be comprised of many depth readings per second measured and recorded along the boat path. The boat path, appearing as a line in Figure 1 because of extremely close proximity of each data dot, is designed to provide depth data to suitably characterize the channel bathymetry.

A typical characteristic of raw bathymetric data sets is the existence of irregularities in the data. Some irregularities are caused by erroneous echosounder

readings but others may represent accurate readings of submerged objects, including logs or Large Wood Debris (LWD). To utilize the bathymetric data during development of digital surfaces for modeling, it is desirable to filter the data to remove irregularities. Many filtering options exist, including manual editing, and some filtering methods have been used to both remove erroneous data and identify submerged LWD (White et al. 2006 and White and Hodges 2005).

FILTERING TOOLS

Use of a median filter allows for identification and removal of undesirable data irregularities, i.e. "spikes," that satisfy particular size requirements. Since the data is recorded sequentially in time along the boat track, the relationship between adjacent points can be utilized to aid in filtering. White and Hodges (2005) identify a filter half-length, *N*, based upon distance between adjacent points and upon the width, *L*, of objects to be filtered (see equation below). For each data point, a point subset is developed using *N* records preceding and *N* records following the data point; the depth of the original data point is replaced with the median depth from the subset (White and Hodges 2005).

$$N_{median} \geq \frac{L}{\overline{\Delta x} - \sigma}$$

Where, N_{median} = filter half-length
L = width of objects to filter
$\overline{\Delta x}$ = average distance between raw data points
σ = standard deviation of distance between raw data points

To filter objects with a width, *L*, of 1 meter, the filter half-length is determined from the average and standard deviation of the distance between raw data points. For a data set where the distance between points is normally distributed, a constant value of *N* may be suitable across the entire data set; however, a typical data set is more variable and σ is typically on the order of $\overline{\Delta x}$. Composed of many thousands (perhaps hundreds of thousands) of points measured under a range of conditions, the variability in distance between points arises from changing boat speed to avoid obstacles or during changes in heading.

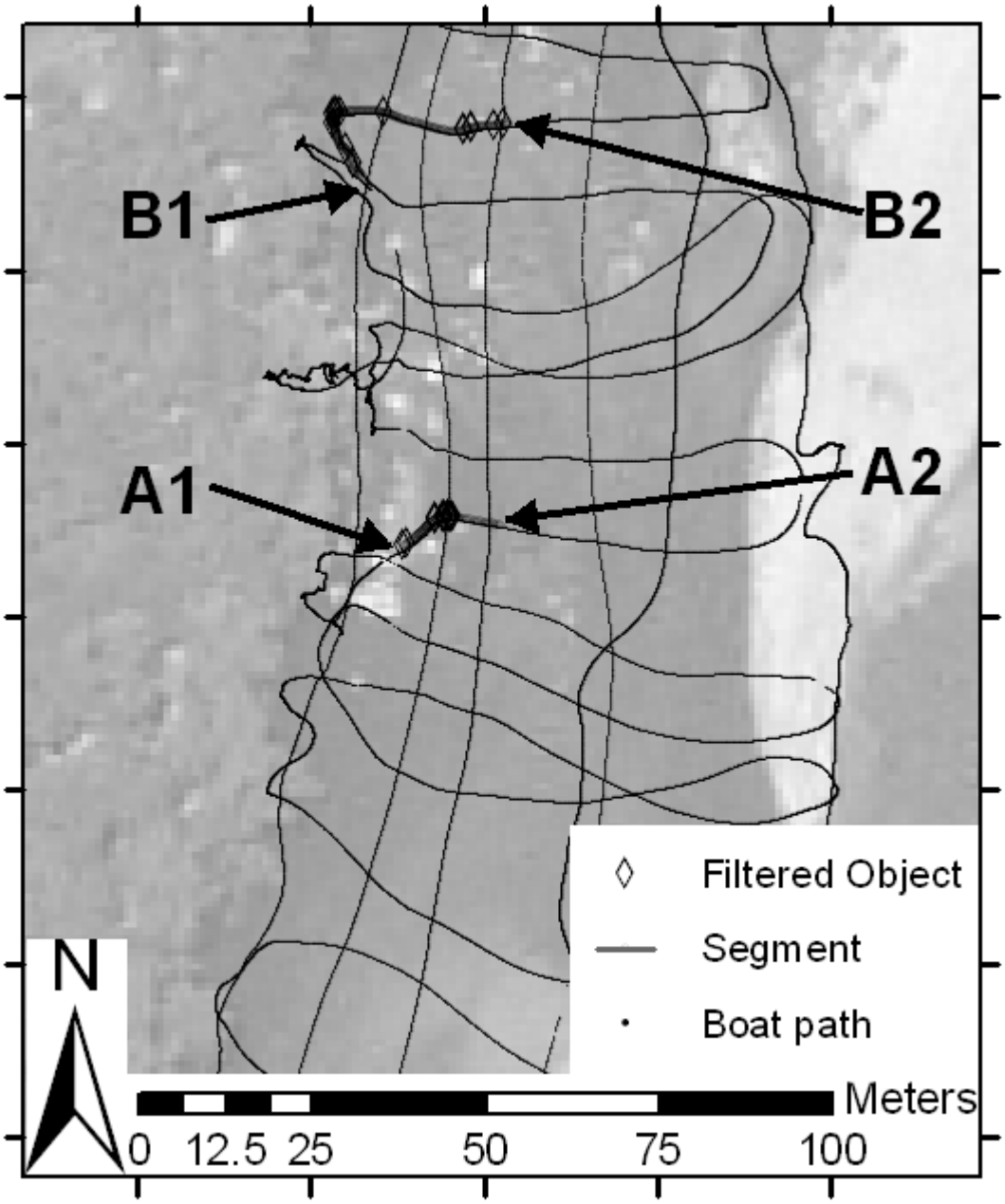

Figure 1 – Site map showing boat track, Segments A and B, and filtered objects.

APPLICATION

This paper presents application of the median filter to a large data set. Calculated across an entire raw data set of approximately 250,000 data points, the average distance between points, $\overline{\Delta x}$, is 0.105 meters and σ is 0.074. To filter objects having width, *L*, of 1 meter, the filter half-width, *N*, is 32.

For segments A1-A2 and B1-B2 (Figure 1), application of the data filtering is shown in Figure 2 (segment A1-A2) and Figure 3 (segment B1-B2). The small dots in Figures 2 and 3 represent the original raw data set. The filtered set developed using the constant half-width of 31 is shown as a light dotted line labeled "Filter 1." Near the distance stations of 29,042 and 29,049 meters, the Filter 1 line successfully filters spikes spanning less than 1 meter (Figure 3). However, the Filter 1 line is not representative of the raw data between stations 28,407 and 28,414 (Figure 2) and between stations 29,073 and 29,078 (Figure 3).

To expand the White and Hodges (2005) median filter method to account for varying distance between points, a varying half-length filter is applied. For the "Filter 2" set, the half-length is determined locally according to point spacing in the vicinity of each raw data point. Across the data set, the value of N ranges from 2 (where spacing between points is large because the boat is moving fast) to 1,141 (where spacing between points is extremely small); the mean value of N is 47.

The heavy solid lines labeled "Filter 2" on Figures 2 and 3 represent the filtered set developed from the locally-varying half-length. As with the Filter 1 set, the Filter 2 set successfully filters spikes spanning less than 1 meter (e.g., stations 29,042 and 29,049 on Figure 3). In addition, the Filter 2 line is representative of the raw data between stations 28,407 and 28,414 (Figure 2) and between stations 29,073 and 29,708 (Figure 3).

Objects filtered from the Filter 2 set that exceed 0.15 meter in height are identified as diamonds within each segment on Figure 1. The objects identified near the beginning and middle of Segment A1-A2 are consistent with raw data higher than the Filter 2 set (Figure 2). Similarly, the location of objects throughout segment B1-B2 (Figure 1) is consistent with the relationship of raw data to the Filter 2 set (Figure 3). Additionally, the location of filtered objects is consistent with location of instream boulders and near-bank debris depicted in the aerial photo (Figure 1).

CONCLUSION

Processing raw bathymetric data using a median filter is an effective means of smoothing spikes out of a raw data series of echosounder data. Analysis of the filtered data is also useful for evaluating roughness coefficients since locations where data is filtered represents locations with submerged objects (Osting et al. 2004).

Compared to the ordinary median filter method (Filter 1), the expanded method (Filter 2) results in a smooth processed data set more representative of the raw data. Consistent with the expanded method presented in this paper, the use of a median half-length calculated locally is recommended when the distance between raw data points varies.

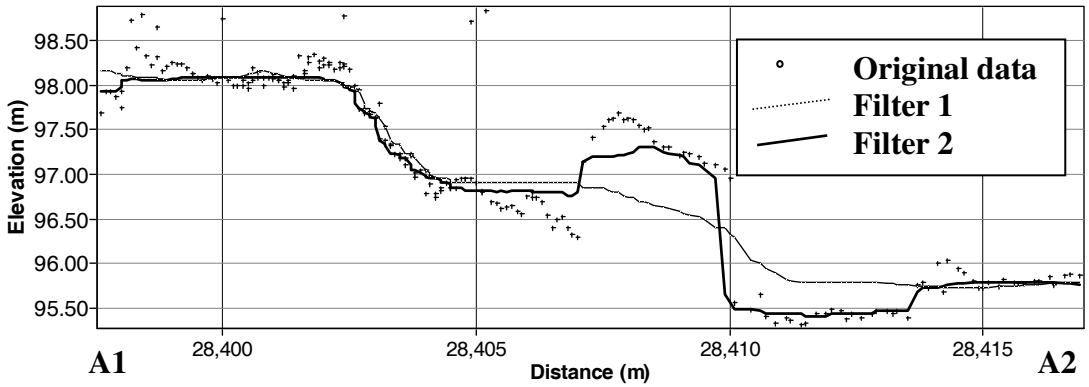

Figure 2 – Data filtering for Segment A.

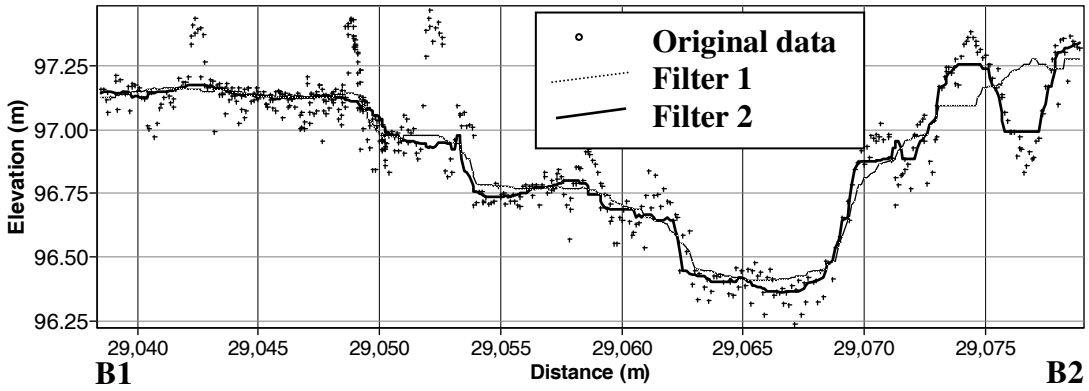

Figure 3 – Data filtering for Segment B.

REFERENCES

BIO-WEST. (2008). "Lower Colorado River, Texas, Instream Flow Guidelines; Colorado River Flow Relationships to Aquatic Habitat and State Threatened Species: Blue Sucker." Prepared for Lower Colorado River Authority and San Antonio Water System. http://www.lcra.org/library/media/public/docs/lswp/findings/BIO_LSWP_IFguidelines_FINAL.pdf >(Accessed January 1, 2009).

Bowen, Z.H., Bovee, K.D., and Waddle, T.J. (2003). "Effects of channel modification on fish habitat in the Upper Yellowstone River." USGS Open File Report 03-476.

Hardy, T.B., Addley, R.C., Saraeva, E. (2006). "Evaluation of instream flow needs in the Lower Klamath River – Phase II final report." Institute for Natural Systems Engineering, Utah Water Research Laboratory, Utah State University. http://www.engineering.usu.edu/uwrl/inse/klamath/report.html

Osting, T. Mathews, R. and Austin. B. (2004). "Analysis of instream flows for the Sulphur River – Hydrology, Hydraulics and Fish Habitat Utilization." Texas Water Development Board report to US Army Corps of Engineers. http://hyper20.twdb.state.tx.us/data/Inflow/Sulphur04/Sulphur2004.html >(Accessed January 1, 2009).

Osting, T. and Hodges, B. (2007). "Estimating uncertainty in 2D hydraulic models for instream flow studies." University of Texas at Austin, Center for Research in Water Resources http://www.crwr.utexas.edu/reports/pdf/2007/rpt07-03.pdf >(Accessed January 1, 2009).

White, L. and Hodges, B. (2005). "Filtering the signature of submerged large woody debris from bathymetry data." *Journal of Hydrology,* 309, 53-65.

White, L., Hodges, B.R, Austin, B., and Osting, T. (2006). "Identification of submerged large woody debris from single-beam echo soundings." *Journal of Hydroinformatics,* 8(1), 1-12.

Numerical Simulation of Chemical Spills Using CCHE2D Model and Chemical Property Database

Xiaobo Chao[1], Tingting Zhu[2], Munther Hammouri[3] and Yafei Jia[4]

[1]Research Scientist, National Center for Computational Hydroscience and Engineering, The University of Mississippi, University, MS 38677, USA, e-mail: chao@ncche.olemiss.edu
[2]Research Scientist, National Center for Computational Hydroscience and Engineering, The University of Mississippi, University, MS 38677, USA, e-mail: tzhu@ncche.olemiss.edu
[3]Research Assistant, Department of Electronic Engineering, The University of Mississippi, University, MS 38677, USA, e-mail: muntherhammouri@gmail.com
[4]Research Professor, National Center for Computational Hydroscience and Engineering, The University of Mississippi, University, MS 38677, USA, e-mail: jia@ncche.olemiss.edu

ABSTRACT

Chemical spills in surface waters often occur in modern societies, which cause significant impact on water quality, eco-environment and drinking water safety. In this paper, chemical spill contamination in water resources is studied by using a depth-integrated computational model, CCHE2D, modified for predicting fate and transport processes of chemical contaminants in surface waters. The processes of volatilization, photolysis, hydrolysis, adsorption, desorption, degradation, etc. were included, and the interaction between sediment bed and water column were also considered. To simulate the fates and transport processes of chemicals using the developed chemical spill module, many parameters of the chemical materials are needed. A database was developed to provide information for involved chemical processes. Hypothetical chemical spill cases were simulated using the CCHE2D model and the developed chemical property database.

Keywords: Chemical spills, CCHE2D Model, Database, Chemical property,

INTRODUCTION

A large number and wide variety of chemicals are used in manufacturing facilities and transported near water bodies, raising potential dangers of chemical spill incidents. In recent years, the number of accidents by which large quantities of toxic chemicals are discharged into water bodies has increased. In March 1993, About 65,000 gallons of toluene spilled from a ruptured line into the Ohio River while being pumped from a barge into a factory (New York Times, 1993). This incident caused a

lot of potential environmental impacts on the Ohio River. In November 2005, an explosion at a chemical factory in China's Jilin Province released about 100 tons of highly toxic benzene into the Songhua River, a tributary of the Amur (Kim and Murphy, 2006). The blasts created a 80 km long toxic slick in the Songhua River. As the slick travelled downstream, dead fish washed up on the banks and many water supply facilities had to be shut down for a couple of days.

When a chemical accident occurs, it is imperative to know where the released chemical may go and what the chemical concentration in water is. Numerical model provides a useful tool for predicting the trajectory and fate of chemical spill in water body.

A two dimensional numerical model, CCHE2D, has been developed by the National Center for Computational Hydroscience and Engineering (NCCHE) to simulate the flow, sediment, pollutant transport, water quality, as well as chemical spills in natural water bodies. This model has been verified and validated rigorously using analytical methods, many sets of physical model data, and applied to many nature water cases (Jia and Wang 1999, Jia et al. 2002, Zhu 2006). In order to simulate the fate and trajectory of chemical spill in water body, the chemical properties are important parameters. In CCHE2D chemical module, the following parameters are required: Degradation rate in water, Degradation rate in soil, Organic-carbon partition coefficient, Molecular weight, and Henry's constant.

To provide those chemical properties, a database CHEMBASE was established using Microsoft ACCESS 2007, with objects such as table, query, report, form, macro, and module, etc. The CHEMBASE database can be used to provide the chemical property information for numerical simulation of chemical contamination. It also provides additional information for users to review so that the selected parameters can fit better to the conditions of the environment under investigation. For example, the ranges of the parameters Koc (organic-carbon partition coefficient), Degradation rate in water, and Degradation rate in soil, vary depending on the conditions, such as PH, temperature, etc. Measured values and the corresponding experimental conditions were provided by this database for users to review and select the reasonable values. The output parameters of the chemical database can be directly taken by the Graphical Users Interface of CCHE2D model as inputs (Zhang, 2008). Due to the fact that no field datasets with sufficient information has been found, two hypothetical chemical spill incidents in the Ross Barnett Reservoir, Mississippi, were simulated to demonstrate the capabilities of the developed CCHE2D model and CHEMBASE database

CCHE2D CHEMICAL MODULE DESCRIPTION

Governing Equations

CCHE2D chemical module has been developed and integrated into CCHE2D model to simulate the distributions of chemical concentrations in the water column as well as sediment layers (Zhu 2006). The processes of transportation, volatilization, sedimentation, adsorption, degradation, etc. were considered.

In the water column, the chemical concentrations can be described by the following mass transport equation:

$$\frac{\partial C}{\partial t} + u\frac{\partial C}{\partial x} + v\frac{\partial C}{\partial y} = \frac{\partial}{\partial x}(D_x \frac{\partial C}{\partial x}) + \frac{\partial}{\partial y}(D_y \frac{\partial C}{\partial y}) + \sum S_i \quad (1)$$

in which u and v = depth-averaged velocity components in x and y directions, respectively; C = depth-averaged chemical concentration in water column; D_x and D_y = dispersion coefficients; $\sum S_i$ = effective source terms, which include source terms due to external loading, volatilization, adsorption, desorption, degradation, and vertical diffusion at water-sediment interface.

In sediment layers, it is assumed that pore water may infiltrate in and out of those layers and thus induce additional chemical transfer. In the present module, a multiple-layer approach proposed by DiToro (2001) was used to simulate the chemical transport in sediment layers. The governing equations can be expressed as:

$$\frac{\partial h_j C_j}{\partial t} = \sum S_j \quad (2)$$

where C_j =concentration of chemical in sediment layers; h_j =depth of sediment layers; $\sum S_j$ is the effective source term. In the first sediment layer, $\sum S_j$ includes source terms due to external loading, vertical diffusion at water-sediment interface, degradation, and vertical diffusion between the first and second sediment layers. In other sediment layers, $\sum S_j$ includes source terms due to external loading, vertical diffusion between neighboring sediment layers, and degradation in sediment layers.

Chemical Fate Processes in the Chemical Module

In CCHE2D chemical module, some major chemical fate processes, including volatilization, adsorption, desorption, degradation, etc. were considered.

Volatilization is the movement of chemical across the air-water interface as the dissolved neutral concentration attempts to equilibrate with the gas phase concentration. The rate of exchange is proportional to the gradient between the dissolved concentration and the concentration in the overlying atmosphere and the conductivity across the interface of the two fluids. The conductivity is influenced by molecular weight, Henry's Law constant and environmental conditions at the air-water interface. In this model, a formula obtained from the "two-film" theory was used to calculate the volatilization rate (Wool et al. 2001).

The adsorption process occurs in the water column between dissolved chemical and particulate matter. Adsorption reactions are usually fast relative to other environmental processes, and equilibrium may be assumed. In the present model the processes of adsorption-desorption were assumed to reach equilibrium at each time step and a linear adsorption isotherm was applied to describe the kinetics of adsorption and desorption. The ratio between the concentrations of particulate and dissolved chemical was taken as a constant and defined as partition coefficient. Its value could be obtained from the experimental measurement or calculated based on the organic carbon partition coefficient (Karickhoff et al 1979).

Degradation encompasses the broad and complex processes of enzymatic attack by organisms on organic chemicals. In this model, a first order decay algorithm was used to simulate the degradation process of chemical, and constant decay rates were specified for chemical degradation in water and sediment systems. The degradation rate of a chemical in water or soil could be obtained based on the experimental measurements.

In this study, a chemical property database, CHEMBASE, was developed to provide the necessary parameters regarding chemical fate processes, such as Degradation rate in water, Degradation rate in soil, Koc (organic-carbon partition coefficient, Molecular weight, Henry's constant, etc.

Numerical Solution and Model Verification

Numerical Method

CCHE2D is a two dimensional depth-averaged computational model for simulating flow, sediment, pollutant transport, water quality, as well as chemical spills in natural water bodies. It was developed using the finite element method, and the structured conformal mesh was adopted in the model. The chemical spill module was decoupled with the CCHE2D free surface hydrodynamic model (Jia et al 2002). The unsteady flow equations were solved using the time marching scheme. A velocity correction method was applied to solve the dynamic pressure and enforce mass conservation. Provisional velocities were solved first without the pressure term, and the final solution of the velocity was obtained by correcting the provisional velocities with the pressure solution (Jia et al 2002). The system of the algebraic equations was solved using the Strongly Implicit Procedure method (SIP). Flow fields, including water elevation, horizontal and vertical velocity components, and eddy viscosity parameters were computed by CCHE2D hydrodynamic model and set as inputs for chemical simulations. The concentration distributions of chemical in the water column and sediment layers were simulated by solving mass transport Eq. (1) and (2) numerically.

Model Verification

To verify the chemical spill module, the numerical model was tested against an analytical solution for predicting concentrations of a non-conservative substance in a one-dimensional river flow with constant depth and velocity. At the middle of the river, there is a point source with constant concentration (Fig 1).

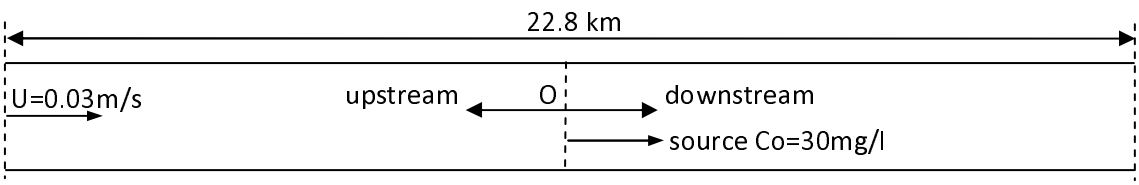

Fig. 1. Test river for model verification

Under this condition, the concentration of the substance throughout the river can be expressed as:

$$U\frac{\partial C}{\partial x} = D_x\frac{\partial^2 C}{\partial x^2} - KC \tag{3}$$

where U is the velocity; C is the substance concentration; D_x is the dispersion coefficient; x is the displacement from O point; and K is the decay rate. An analytical solution given by Thomann and Mueller (1988) is:

$$C(x) = C_0 \exp\left[\left(\frac{u+\sqrt{u^2+4KD_x}}{2D_x}\right)x\right] \quad \text{(upstream, } x \le 0\text{)} \tag{4}$$

$$C(x) = C_0 \exp\left[\left(\frac{u-\sqrt{u^2+4KD_x}}{2D_x}\right)x\right] \quad \text{(downstream, } x > 0\text{)} \tag{5}$$

where C_0 is the concentration at O point. In this test case, it was assumed, the water depth = 10 m and D_x=30 m^2/s, the values of K = 0, 1.0/day and 2.0/day, respectively, Fig. 2 shows the concentration distributions obtained by the numerical model and analytical solution. The maximum error between the numerical result and analytical solution is less than 2%.

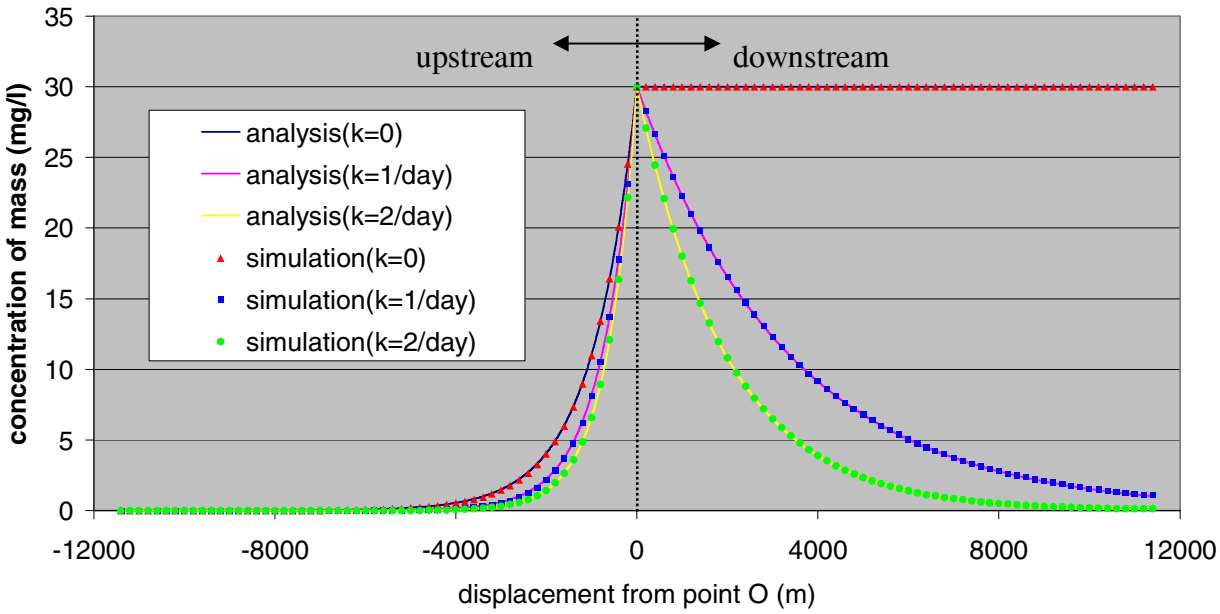

Fig. 2 The concentration distribution along the river

DEVELOPMENT OF CHEMICAL PROPERTY DATABASE

To provide necessary parameters for CCHE2D chemical module, a chemical property database, CHEMBASE, was developed using Microsoft Access 2007. The major objects in this database include table, query, report, form and macro.

Table

A table is used to store data in MS Access 2007. In the CHEMBASE database, all the parameters of physical-chemical properties were included in a table. For each chemical, the table contained more than 20 parameters for computing the processes of volatilization, photolysis, hydrolysis, adsorption, desorption, degradation, as well as the interaction between sediment bed and water column.

The parameters of physical-chemical properties in this table were collected from a few sources, including ChemFate (SRC 2008), and some other references (Mackay et al., 2006, Texas Register 2007). The database system allowed users to add new chemicals in the table and modify some parameters of physical-chemical properties for their specific needs.

Some parameters, such as Koc (organic-carbon partition coefficient), Degradation rate in water, and Degradation rate in soil, range widely. The minimum, maximum, and mean values were provided, and the mean values were set as defaults.

Query

A query is used to filter and retrieve data from the table. In order to provide required parameters of a chemical for numerical simulation, the database should allow the user to have the following operations:

(1) Identify a chemical based on the chemical name, CAS number, or chemical formula;
(2) Search the needed chemical parameters contained in the table.

Those operations can be accomplished using a parameter query. In order to select a chemical based on the Chemical name, CAS number or Chemical formula, the “Query by Form” technology was used to build a few criteria of the parameter query. The criteria of the parameter query were set as the name of combo boxes displayed on a form shown in Fig.3. For the current chemical spill module, the following physical-chemical property parameters are required:

(1) Degradation rate in water (mean)
(2) Degradation rate in soil (mean)
(3) Koc, organic-carbon partition coefficient (mean)
(4) Molecular weight
(5) Henry's constant

Report

A report is an object designed for summarizing the selected data. The recorded source of the report was the query. After choosing a chemical, the physical-chemical property parameters were displayed in the report.

Form (User Interface)

Form is an object designed primarily for data input or display or for a control of application execution. In this database, a form was built as a user interface, and it can be used to select a chemical. It can also be used to activate a few command buttons to show the report of physical-chemical properties, export data for CCHE2D model, and exit the database system. In this form, a button "Edit Parameters" was provided to active processes for reviewing and adjusting some parameters based on different experimental conditions (Fig.3).

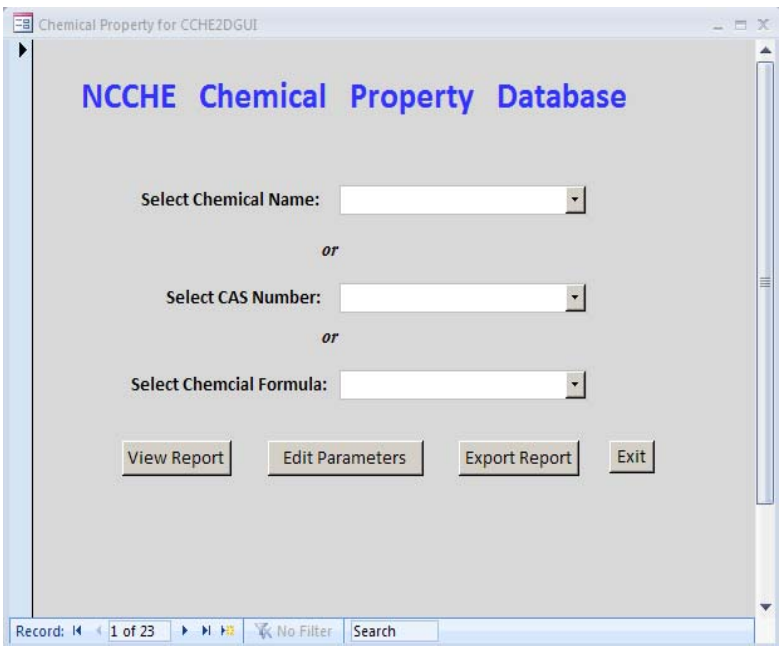

Fig.3 The form of CHEMBASE database

Adjust Chemical Parameters for more Reliable Results

Some parameters, such as Koc (organic-carbon partition coefficient), Degradation rates in water and soil range widely due to different conditions. In this database, the measured values and the corresponding experimental conditions were provided for users to review. Then the user may select a reasonable value based on the particular experimental conditions. In this developed database, the experimental information and related parameters were obtained from a public source: ChemFate (SRC 2008).

After load the data from ChemFate web (SRC 2008) based on CAS number, Formula or Chemical Name, a software "ChemFate Analyzer.exe", developed by NCCHE was applied to process those data. Two Microsoft access tables were generated to save the parameters and related experimental conditions for Koc and Degradation rates in soil and water.

In this database, a program was developed using the C# language to operate the "Edit Parameters" button for reviewing the measured values as well as experimental conditions and updating the output parameters in the report. This program provides a useful tool for the user to select reasonable values for his application based on experimental conditions.

LINK CHEMBASE DATABASE TO CCHE2D MODEL

After the values of chemical properties are finalized, the report can be exported as a ".txt" file by clicking "Export Report" button (Fig. 4). The CCHE2D model can load this text file automatically for model simulation (Fig. 5).

The chemical partition coefficient K_p in the model is calculated by

$$K_p = K_{oc} f_{oc} \tag{6}$$

in which K_p = partition coefficient; K_{oc} = organic/carbon partition coefficient, which can be obtained from the developed database; f_{oc}= organic carbon fraction of the solid and it is given by the CCHE2D model.

After loading all the data, the CCHE2D model can be applied to simulate the trajectory and fate of chemical spill in a water body.

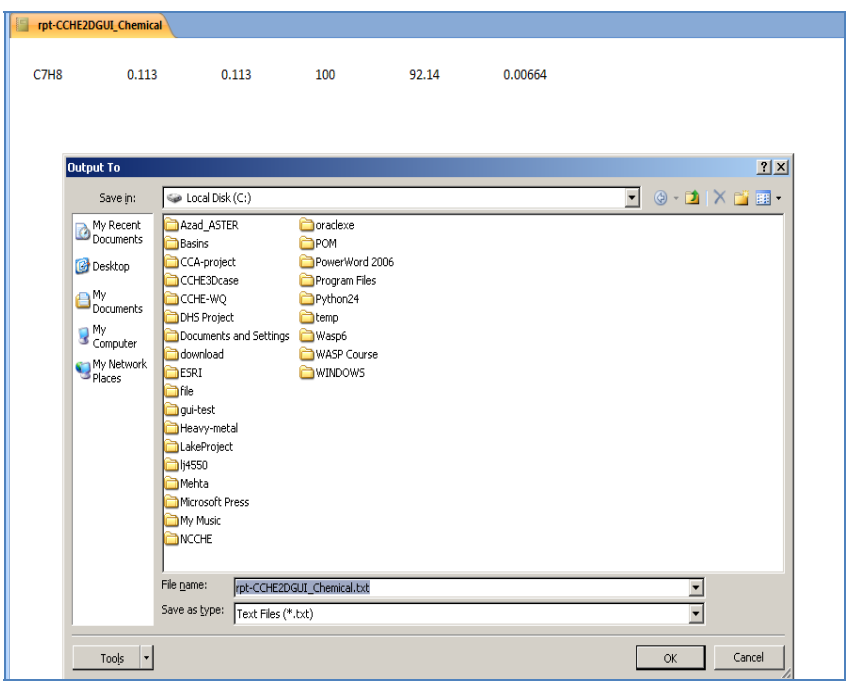

Fig.4 Export of chemical property parameters as a text file

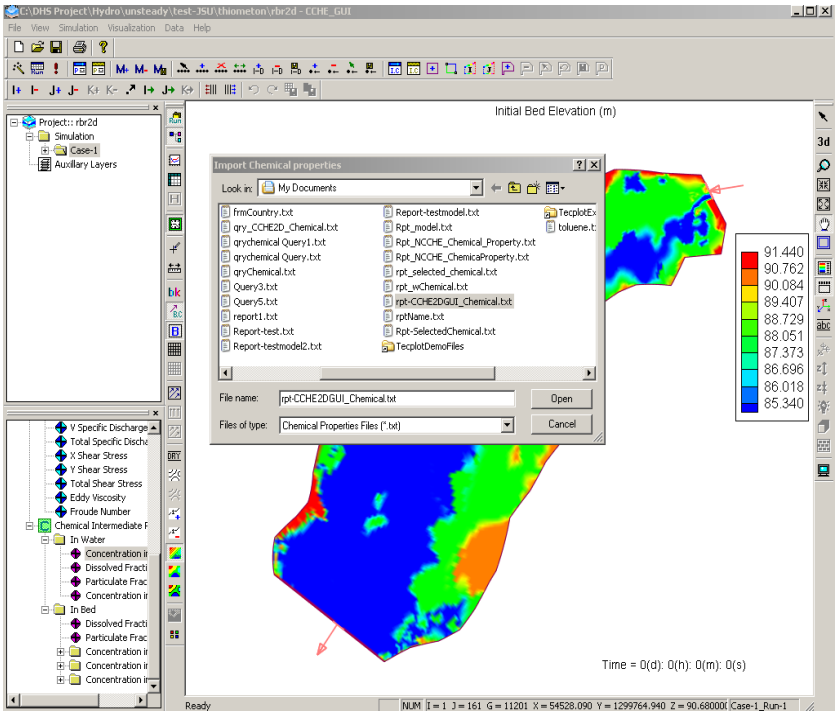

Fig.5 Import of the chemical property .txt file to CCHE2D Model

APPLICATION OF CHEMBASE DATABASE AND CCHE2D MODEL TO HYPOTHETICAL CHEMICAL SPILL CASES

In order to test the capabilities of developed CHEMBASE database and CCHE2D model for simulating chemical spills in natural waters, two hypothetical chemical spill case occurred at Ross Barnett Reservoir in Mississippi were studied. This reservoir serves as the primary drinking water supply for the city of Jackson, and it also provides recreational opportunities in the forms of campgrounds, parks, boat launches, multi-purpose trails, etc.

It was assumed that 30 tons of toluene, one of toxic chemicals, was accidentally discharged into a river from a plant located 65 miles upstream of the reservoir, the chemical then flowed through a stream into the reservoir. When transporting in the river, about 1/3 of the toluene was lost due to evaporation, dissolution, decay, etc. It took 12 hours for the remaining 20 tons of toluene to completely discharge into the reservoir. In another case, it was assumed that 2000 kg of the toxic pesticide, thiometon, was dumped into the reservoir due to a traffic accident on a highway near the west shoreline. It took 12 hours for all the thiometon to release into water. Fig.6 shows the location of the two hypothetical incidents.

Flow Simulation

Wind stress and upstream discharge are the most important driving forces for flow currents in the reservoir. The period from Jan 1 to 31, 2005, was chosen for

model simulation. After obtained flow discharges at inlet, water surface levels at outlet, as well as wind speeds and directions during this period, CCHE2D model can be applied to simulate the flow fields in the reservoir. Fig. 7a and Fig. 7b show the velocity vectors at the first day and second day, respectively. The flow results were used for simulating the concentration of chemicals in the two hypothetical cases.

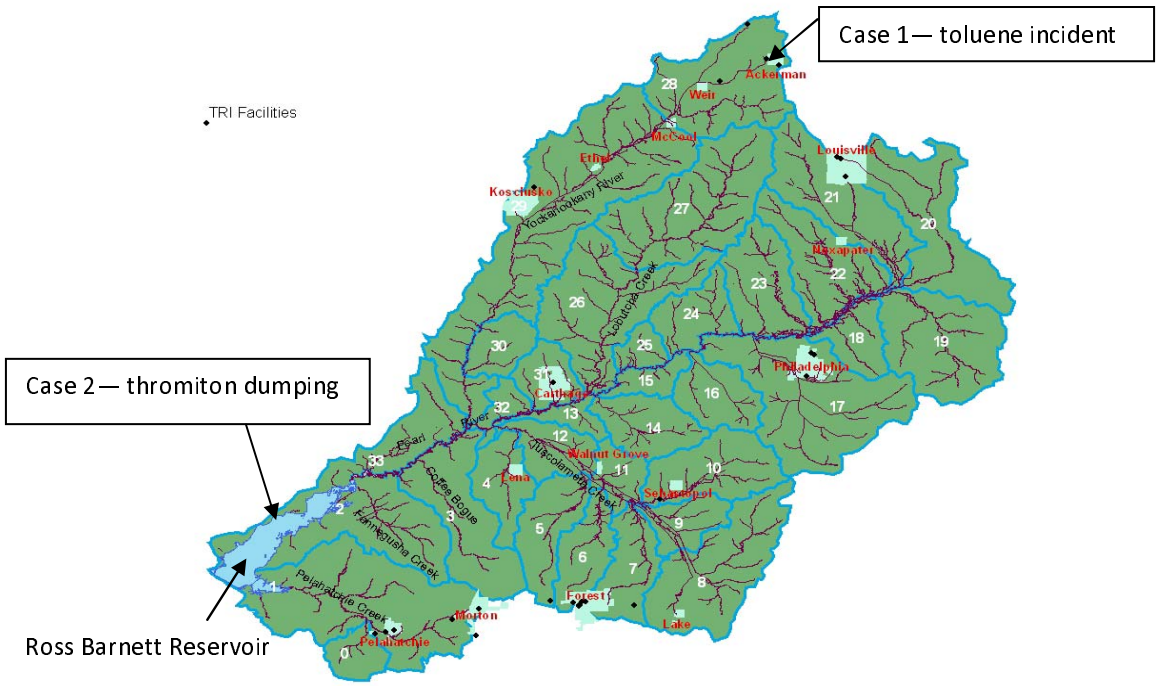

Fig.6 Two hypothetical chemical incident cases

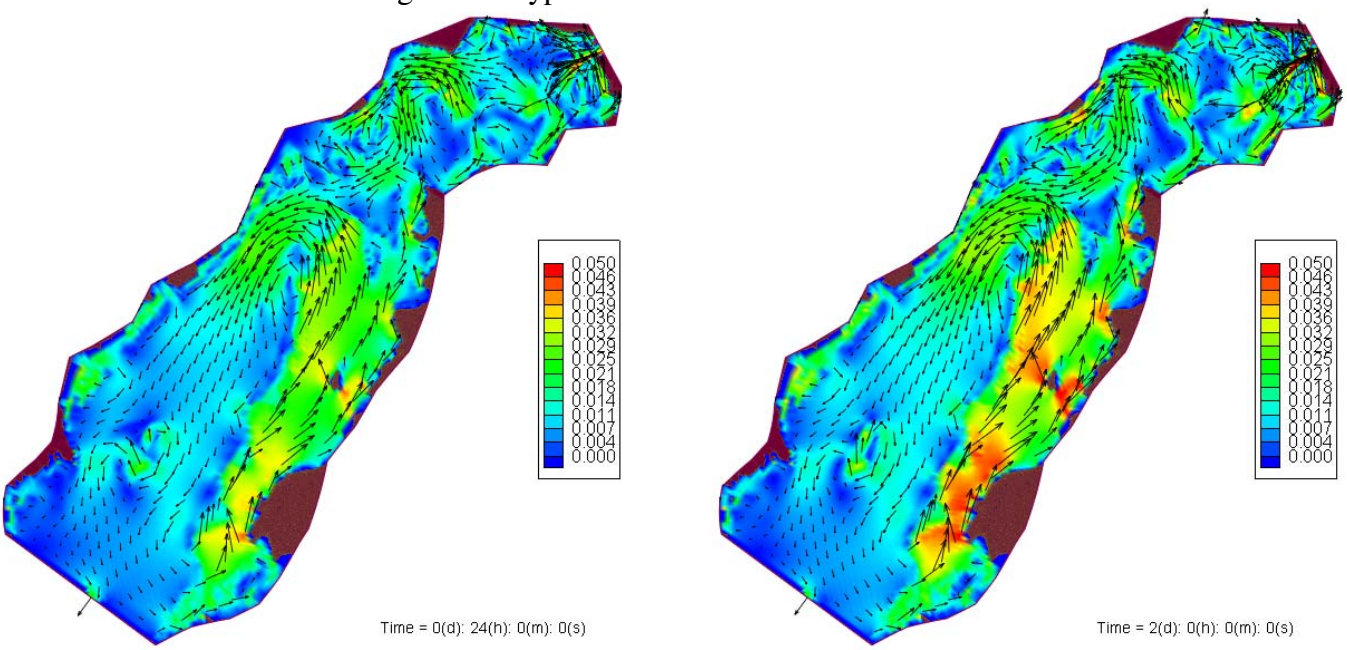

a. At the first day b. At the second day

Fig.7 Numerical results of velocity vectors

Numerical Modeling of Two Hypothetical Chemical Spills Cases

Using CHEMBASE database, the physical-chemical parameters of toxic chemicals toluene and thiometon required by the model can be obtained (Fig. 4). These parameters can be loaded to CCHE2D model automatically, and used for model simulation (Figs. 5).

After all the parameters were set up correctly, CCHE2D model was used to simulate the fate and trajectory of chemical spills. Fig.8 shows the simulated concentration distributions of toluene at first day, third day and fourth day after toluene discharged into reservoir, respectively. It can be observed that during the first four days, the upstream of the reservoir is the major polluted area, and the concentration is greater than the 1ppm of the Maximum Contaminant Level (MCL) suggested by EPA. After four days, the concentration in the whole reservoir is less than the MCL. Fig. 9 shows the concentration distribution of thiometon at the 1st day, 10th day and 25th day after thiometon releasing into the reservoir. Without operating any decontamination processes, the concentration of thiometon would be greater than the 3 ppb of MCL for about 25 days. This chemical incident may cause huge impacts on the aquatic environment in the reservoir.

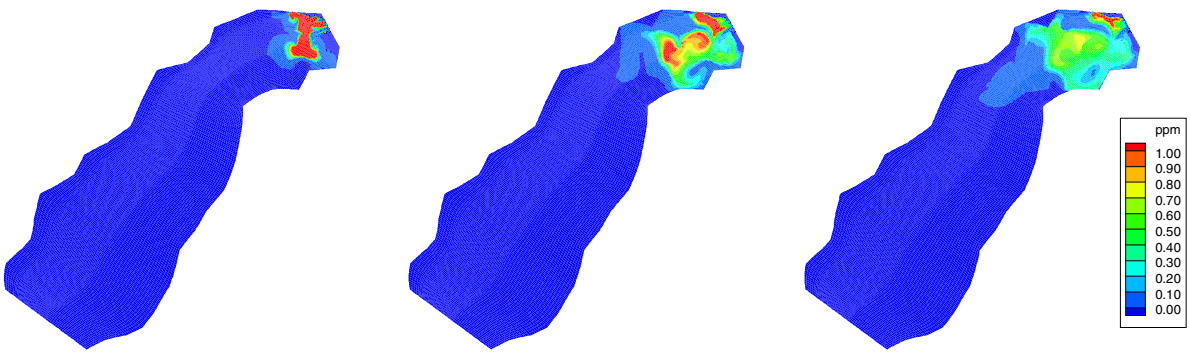

Fig. 8 Concentration distributions of toluene in the reservoir (ppm)

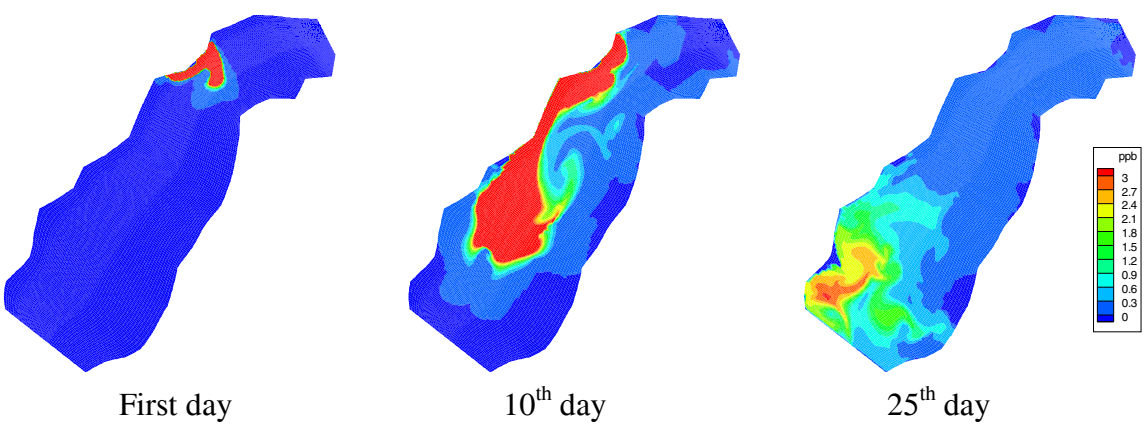

Fig. 9 Concentration distributions of thiometon in the reservoir (ppb)

These simulation results provide useful information to estimate the polluted area after a chemical incident occurs.

CONCLUSIONS

A depth-integrated computational model, CCHE2D, has been developed for predicting fate and transport processes of chemical contaminants in surface waters. A case with non-conservative substance in a one-dimensional river flow was used for model verification. To simulate the fates and transport processes of chemicals, some parameters of the chemical property are needed. A database, CHEMBASE, was developed using Microsoft Access 2007 for providing those parameters. In this database, the main table contained a number of physical-chemical properties for chemicals. This table can be expanded by simply adding more chemicals and their physical-chemical properties. The search of the chemical could be performed based on its name, CAS number, or chemical formula. A report was built to display the physical-chemical properties of the selected chemical. The user could review and adjust the parameters based on different experimental conditions. The parameters contained in the final report can be exported as a text file, and easily loaded by CCHE2D model for simulating the fate and trajectory of chemical spills. Two hypothetical chemical spill cases were simulated to demonstrate the capabilities of CCHE2D model and CHEMBASE database. This system provides useful tool for developing and implementing an emergency response plan, and it is also valuable for environmental impact assessment.

ACKNOWLEDGMENTS

This research was funded by US Department of Homeland Security. The suggestions and advices provided by Dr. Yaoxin Zhang of the University of Mississippi are highly appreciated.

REFERENCES

DiToro (2001). Sediment Flux Modeling, Wiley-Interscience.

Jia, Y., Wang, S.S.Y.(1999). "Numerical model for channel flow and morphological change studies." *Journal of Hydraulic Engineering*, Vol. 124, No. 9, 924-933.

Jia, Y., Wang, S.S.Y., and Xu, Y. (2002). "Validation and Application of a 2D Model to Channels with Complex Geometry." *International Journal of Computational Engineering Science*, Vol. 3, No. 1, 57-71.

Karickhoff, W.S. , Brown, D. S., and Scott, T.A. (1979). "Sorption of hydrophobic pollutants on natural sediments." Water Research, 13, 241–248.

Mackay, D., Shiu, W.Y., Ma, K.C. and Lee, S.C. (2006). *Physical-Chemical Properties and Environmental Fate for Organic Chemicals*, Taylor & Francis.

Kim, J. S. and Murphy, M. (2006). "Trans-boundary river tensions — opportunities for collaboration." China Environment Series, Issue 8, p. 209, The Woodrow Wilson Center, Washington, DC.

New York Times (1993). "Chemical Spills in Ohio River". On March 12, Website: http://query.nytimes.com/gst/fullpage.html?res=9F0CE4DA1630F931A25750C0A965958260 (accessed in June 2008).

State of Texas (2007). "Texas commission on environmental quality." *Texas Register*, Vol. 32, No. 11, 1604-1620.

Syracuse Research Corporation's (SRC) (2008), *CHEMFATE Chemical Search*, http://www.syrres.com/esc/chemfate.htm (accessed in May 2008).

Wool, T.M. et al (2001). Water Quality Analysis Simulation Program (WASP) version 6 User's Manual, US Environmental Protection Agency, Atlanda, GA.

Zhu, T., (2006). *A depth-averaged two-dimensional water quality model as a research and management tool*, Ph.D dissertation, The Univ. of Mississippi.

Zhang, Y. (2008). *CCHE-GUI – Graphical Users Interface for NCCHE Model User's Manual – Version 3.20*, Technical Report No. NCCHE-TR-2008-01, The Univ. of Mississippi.

One-Dimensional Modeling of Water Quality and Aquatic Ecosystems in Streams

Podjanee Inthasaro[1], Weiming Wu[2], and Sam S.Y. Wang[3]

[1]Ph.D. Student, National Center for Computational Hydroscience and Engineering (NCCHE), The University of Mississippi, 102 Carrier Hall, University, MS 38677, USA; email: podjanee@ncche.olemiss.edu
[2]Research Associate Professor, NCCHE, The University of Mississippi; email: wuwm@ncche.olemiss.edu
[3]F.A.P. Barnard Distinguished Professor and Director, NCCHE, The University of Mississippi; email: wang@ncche.olemiss.edu

ABSTRACT

CCHE1D is a one-dimensional channel network model developed at the National Center for Computational Hydroscience and Engineering, the University of Mississippi. Recently, the CCHE1D has been enhanced to simulate water quality and aquatic ecosystems in streams. The numerical model computes stream water temperature by considering heat fluxes across the water surface. The aquatic ecosystem model considers a simple food-chain model of phytoplankton, zooplankton and fish. It simulates the changing concentrations of biotic organisms and couples with water quality parameters by considering processes of photosynthesis, respiration, mortality, decomposition and nutrient cycling. The integrated CCHE1D water quality and ecosystem model has been tested in the Tualatin River, Oregon. It well predicts the water temperature, phytoplankton biomass, zooplankton biomass and other water quality parameters along the simulation domain.

INTRODUCTION

During the past decades, many streams and rivers faced pollution problems that were directly relevant to human and environmental health. When a waterway is contaminated by chemical substances, aquatic organisms such as vertebrates and invertebrates are directly affected. Moreover, these aquatic organisms can be a source of human exposure to contaminants via food chain. Due to advanced computer technology and increased public health and environmental awareness, mathematical models have currently become an important tool in the study of complex systems. A variety of water quality and aquatic ecosystem software, such as WASP7 (Di Toro et al., 1983) and AQUATOX (Park and Clough, 2004), have been developed by various organizations with specific objectives. The newly integrated water quality and aquatic ecosystem model in the CCHE1D is focused on the simulation of water quality parameters and biotic and abiotic components in freshwater riverine ecosystems.

Because of the one-dimensional simulation, the model has a great advantage in computational speed and is suitable for long-term simulation.

CCHE1D WATER QUALITY AND AQUATIC ECOSYSTEM MODEL

The current CCHE1D version released in 2002 simulates unsteady open-channel flow by solving the St. Venant shallow water equations using the Preissmann implicit scheme, and computes non-uniform sediment transport using a non-equilibrium approach (Wu and Vieira, 2002). Recently, CCHE1D has been enhanced to simulate water quality and aquatic ecosystems in streams. The water temperature model describes heat transfer in the water column based on the first law of thermodynamics. The model computes the stream water temperature taking into account the combination of heat fluxes— short-wave solar radiation, long-wave radiation, latent heat flux and sensible heat flux (Wu, 2008). The aquatic ecosystem model considers a simple food-chain model of phytoplankton, zooplankton and fish; it simulates the changing concentrations of biotic organisms and water quality parameters including dissolved oxygen (DO), carbonaceous biological oxygen demand (CBOD), nitrogen (ammonia, nitrate, and organic nitrogen) and phosphorus (phosphate and organic phosphorus) by considering processes of photosynthesis, respiration, mortality, decomposition and nutrient cycling. The conceptual framework of the CCHE1D aquatic ecosystem model is illustrated in Figure 1.

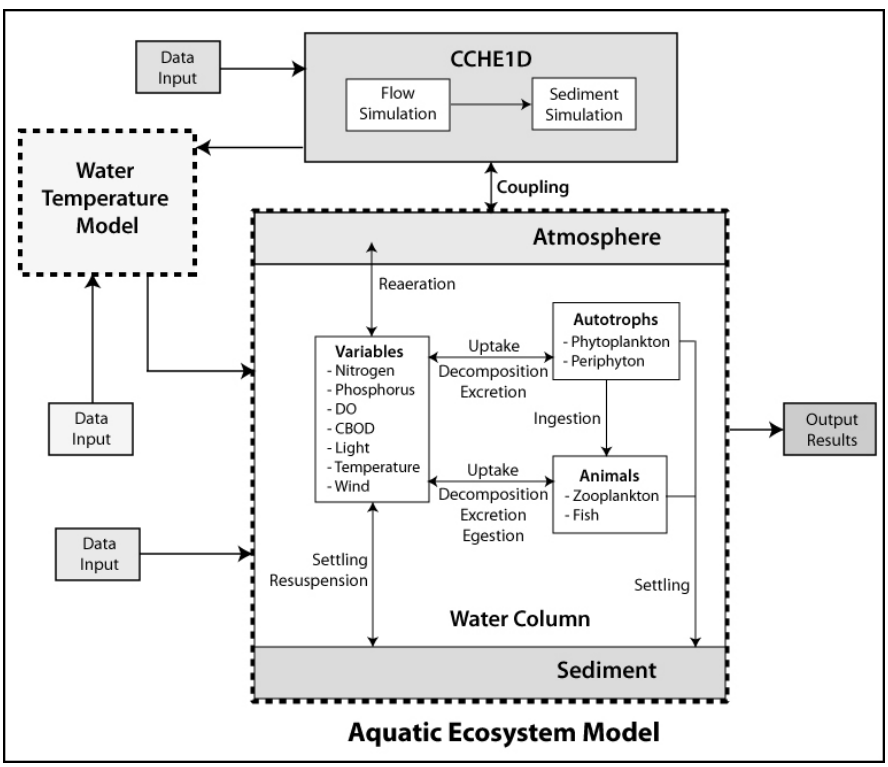

Figure 1. Conceptual framework of the aquatic ecosystem model.

The model simulates fate and transport of chemicals through drainage networks under steady or unsteady flow conditions. The transport equation is

described by the advection-dispersion equation based on the principle of conservation of mass and Fick's law:

$$\frac{\partial(AC)}{\partial t}+\frac{\partial(QC)}{\partial x}=\frac{\partial}{\partial x}\left(E_L A\frac{\partial C}{\partial x}\right)+S_c A \tag{1}$$

where x and t are the spatial and temporal axes; A is the cross-sectional flow area; Q is the flow discharge; C is the concentration of a constituent; E_L is the longitudinal effective diffusivity; and S_c is a net source term for each constituent due to biochemical and physical changes and/or due to lateral input to the channel by runoff. The rate of change for each source term is described as follows.

Phytoplankton. Source term for phytoplankton rate (S_a) is calculated by

$$S_a=\left(k_{ag}-k_{ar}-k_{ae}-k_{am}\right)C_a-k_{zg}\frac{C_a-\mu_z}{h_{zg}+C_a}C_z-\frac{\omega_a}{h}C_a \tag{2}$$

where C_a and C_z are biomass concentrations of phytoplankton and zooplankton, respectively; k_{ag} is the photosynthetic rate given in Eq. (3); k_{ar}, k_{ae}, k_{am} and k_{zg} are the maximum rates of phytoplankton respiration, excretion, non-predatory mortality and zooplankton grazing, respectively; μ_z and h_{zg} are the threshold and half-saturation phytoplankton concentrations for zooplankton grazing, respectively; h is the water depth; and ω_a is the settling velocity of phytoplankton.

The photosynthetic rate is calculated by

$$k_{ag}=k_{ag,\max}\frac{1}{\gamma h}\ln\left(\frac{h_L+I_0}{h_L+I_0e^{-\gamma h}}\right)\min\left(\frac{C_{PO4}}{h_P+C_{PO4}},\frac{C_{NH3}+C_{NO3}}{h_N+C_{NH3}+C_{NO3}}\right) \tag{3}$$

where $k_{ag,\max}$ is the maximum photosynthetic rate; γ is the total light extinction; I_0 is the average light intensity; h_L is the half-saturation light intensity for photosynthesis; C_{PO4}, C_{NH3} and C_{NO3} are phosphate, ammonia and nitrate nitrogen concentrations, respectively; and h_P and h_N are the half-saturation phosphorus and nitrogen concentrations for photosynthesis, respectively.

Zooplankton. The net source term for zooplankton rate (S_z) is described by

$$S_z=\left(e_{zg}k_{zg}\frac{C_a-\mu_z}{h_{zg}+C_a}-k_{zr}-k_{ze}-k_{zm}\right)C_z \tag{4}$$

where k_{zr}, k_{ze} and k_{zm} are the maximum rates of zooplankton respiration, excretion and mortality, respectively; and e_{zg} is the assimilation efficiency.

Dissolved Oxygen (DO). DO is affected by several factors such as atmospheric reaeration, photosynthesis, respiration, decomposition and nitrification. The DO source term (S_{DO}) is described by

$$S_{DO} = k_{re}\left(C'_{DO} - C_{DO}\right) + \left(\frac{32}{12} + \frac{48}{14}\alpha_{NC}\left(1 - p_{NH3}\right)\right)k_{ag}C_a - \frac{32}{12}\left(k_{ar}C_a + k_{zr}C_z\right) - k_{CBOD}\left(\frac{C_{DO}}{h_{CBOD} + C_{DO}}\right)C_{CBOD} - \frac{64}{14}k_{NH3}\left(\frac{C_{DO}}{h_{NH3} + C_{DO}}\right)C_{NH3} - \frac{s_{SOD}}{h} \quad (5)$$

where C_{DO} is the DO concentration; C'_{DO} is the saturation DO concentration; k_{re} is the reaeration rate; k_{CBOD} is the rate of deoxygenation; h_{CBOD} is the half-saturation DO concentration for deoxygenation; and s_{SOD} is the sediment oxygen demand.

Carbonaceous biological oxygen demand (CBOD). CBOD represents the oxygen demand by bacteria in the oxidation of organic material. The change rate in CBOD concentration (S_{CBOD}) can be determined by

$$S_{CBOD} = \frac{32}{12}\left(k_{am} + k_{ae}\right)C_a + \frac{32}{12}\left(k_{zm} + k_{ze}\right)C_z - \frac{5}{4}\frac{32}{14}k_{NO3}\left(\frac{h_{NO3}}{h_{NO3} + C_{DO}}\right)C_{NO3} + \frac{32}{12}\left(1 - e_{zg}\right)k_{zg}\frac{C_a - \mu_z}{h_{zg} + C_a}C_z - k_{CBOD}\left(\frac{C_{DO}}{h_{CBOD} + C_{DO}}\right)C_{CBOD} - \frac{\omega_{CBOD}}{h}f_{PCBOD}C_{CBOD} \quad (6)$$

where C_{CBOD} is the CBOD concentration; f_{PCBOD} is the fraction of particulate CBOD in the total CBOD; and ω_{CBOD} is the setting velocity of CBOD.

Nitrogen cycle. Three nitrogen compartments— ammonia (NH_3), nitrate (NO_3) and organic nitrogen (ON), are modeled in this study. The source terms for organic nitrogen (S_{ON}), ammonia (S_{NH3}) and nitrate (S_{NO3}) are expressed as

$$S_{ON} = f_{ON}\alpha_{NC}\left(k_{am}C_a + k_{zm}C_z\right) - k_{ON}\left(\frac{C_a}{h_{ON} + C_a}\right)C_{ON} - \frac{\omega_{ON}}{h}f_{PON}C_{ON} - \frac{s_{ON}}{h} \quad (7)$$

$$S_{NH3} = \left(1 - f_{ON}\right)\alpha_{NC}\left(k_{am}C_a + k_{zm}C_z\right) - k_{ag}p_{NH3}\alpha_{NC}C_a + \alpha_{NC}k_{ze}C_z + k_{ON}\left(\frac{C_a}{h_{ON} + C_a}\right)C_{ON} - k_{NH3}\left(\frac{C_{DO}}{h_{NH3} + C_{DO}}\right)C_{NH3} - \frac{s_{NH3}}{h} \quad (8)$$

$$S_{NO3} = k_{NH3}\left(\frac{C_{DO}}{h_{NH3} + C_{DO}}\right)C_{NH3} - k_{NO3}\left(\frac{C_{DO}}{h_{NO3} + C_{DO}}\right)C_{NO3} - k_{ag}\alpha_{NC}\left(1 - p_{NH3}\right)C_a - \frac{s_{NO3}}{h} \quad (9)$$

where C_{ON}, C_{NH3} and C_{NO3} are the concentrations of ON, ammonia and nitrate, respectively; α_{NC} is the nitrogen to carbon ratio; k_{ON}, k_{NH3} and k_{NO3} are the rates of mineralization, nitrification and denitrification, respectively; f_{ON} is the fraction of dead organic material to ON pool; f_{PON} is the fraction of particulate ON in total ON; h_{ON}, h_{NH3} and h_{NO3} are the half-saturation for mineralization, nitrification and denitrification, respectively; ω_{ON} is the settling velocity of ON; s_{ON}, s_{NH3} and s_{NO3}

are ON, ammonia and nitrate fluxes to the sediment bed, respectively; and p_{NH3} is the ammonia preference factor and can be estimated by

$$p_{NH3} = \frac{C_{NH3}C_{NO3}}{(h_N + C_{NH3})(h_N + C_{NO3})} + \frac{C_{NH3}h_N}{(C_{NH3} + C_{NO3})(h_N + C_{NO3})} \quad (10)$$

where h_N is the half-saturation constant for nitrogen uptake.

Phosphorus cycle. Phosphorus is divided into two groups: organic phosphorus (OP) and inorganic phosphorus (orthophosphate, PO_4). The source terms for organic phosphorus (S_{OP}) and phosphate (S_{PO4}) are expressed as

$$S_{OP} = f_{OP}\alpha_{PC}(k_{am}C_a + k_{zm}C_z) - k_{OP}\left(\frac{C_a}{h_{OP} + C_a}\right)C_{OP} - \frac{\omega_{OP}}{h}f_{POP}C_{OP} - \frac{s_{OP}}{h} \quad (11)$$

$$S_{PO4} = (1 - f_{OP})\alpha_{PC}(k_{am}C_a + k_{zm}C_z) - \alpha_{PC}k_{ag}C_a + \alpha_{PC}k_{ze}C_z + k_{OP}\left(\frac{C_a}{h_{OP} + C_a}\right)C_{OP} - \frac{s_{PO4}}{h} \quad (12)$$

where C_{OP} and C_{PO4} are the concentrations of OP and phosphate, respectively; α_{PC} is the phosphorus to carbon ratio; k_{OP} is the mineralization rate; h_{OP} is the half-saturation for mineralization; f_{OP} is the fraction of dead organic matters recycled to OP pool; f_{POP} is the fraction of particulate OP in total OP; ω_{OP} is the setting velocity of OP; and s_{OP} and s_{PO4} are the OP and phosphate fluxes to the sediment bed, respectively.

CASE STUDY

The Tualatin River is located on the west side of the Portland metropolitan area in northwestern Oregon. The river originates in the Coast Range and flows generally eastward before joining the Willamette River near West Linn. During summer, the river encountered water quality problems such as low dissolved oxygen level, high pH level and high phytoplankton concentrations.

The study domain for the main Tualatin River is approximately 50 km, from River Mile (RM)38.4 (Rood Bridge at Hillsboro) to RM5.5 (Stafford Road near Lake Oswego), shown as the CCHE1D interface (see Figure 2). The average bed slope is approximately 0.025%, and the average river width is 15 m. Flow discharge results mainly from precipitation. Within the study reach, the Tualatin River has two major tributaries (Rock Creek and Fanno Creek) and several minor creeks. The Rock Creek has both agricultural and urban influences while the Fanno Creek flows almost exclusively through an urban area. In addition to tributaries, two wastewater treatment plants (WWTPs–Rock Creek WWTP at RM38.1 and Durham WWTP at RM9.3) discharge treated effluent into the river. At several locations in the study domain, water is withdrawn for public water supply, irrigation, and power generation.

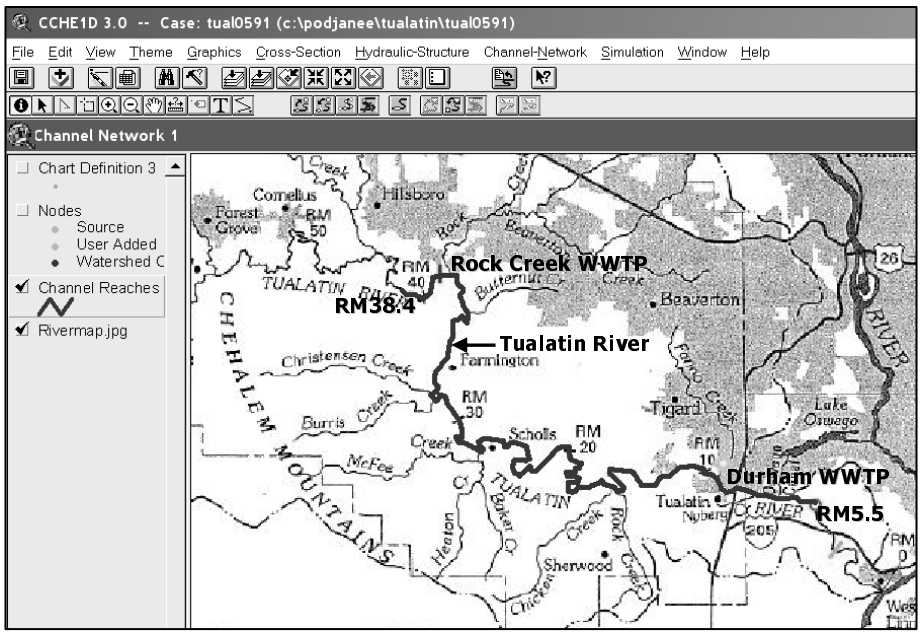

Figure 2. Simulation domain for the Tualatin River study.

The simulation period starts from May 01, 1991 to October 31, 1991. The simulation domain is represented by 132 cross-sections. Each cross-section is divided into 11 panels. Discharge hydrographs for the upstream boundary and the two major tributaries are obtained from the U.S. Geological Survey (USGS) site (http://waterdata.usgs.gov/or/nwis/). Irrigation withdrawal is documented by Rounds et al. (1999).

The unsteady flow from May 01 through Oct. 31 is simulated and compared to the field measurement (see Figure 3). The simulation result is in a good agreement in phase with the measurement, but the magnitude is slightly over-estimated. The differences between the simulated (RM5.5) and measured (RM1.8) rates are due to water's travel time and possible point and nonpoint discharges between two locations.

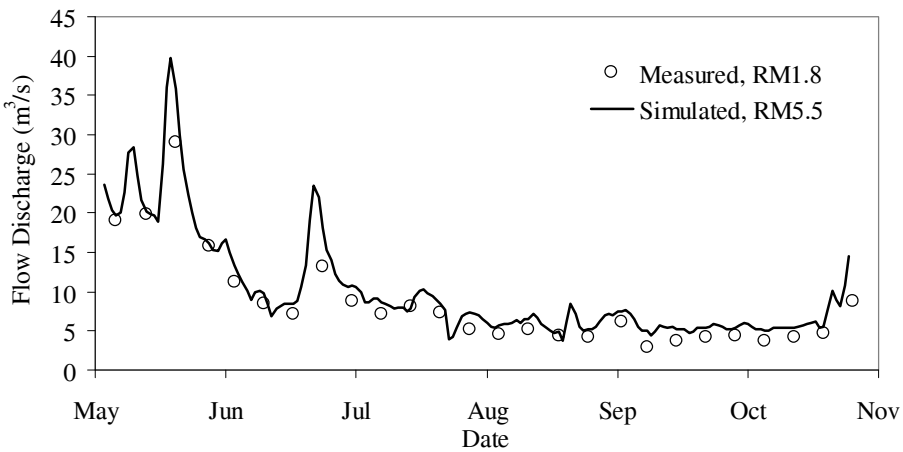

Figure 3. Comparison of measured and simulated flow discharges at the downstream of the Tualatin River.

Meteorological data at the Portland Airport weather station is used as input in the water temperature model. The transfer of intraregional data may contribute to some prediction errors, which, however, are assumed to be negligible in this study. Due to 1-D heat transport equation, the simulated water temperature is cross-sectionally averaged. The field data obtained from Doyle and Caldwell (1996) was mostly collected at the depth of 3 ft (approximately 0.9 m) below the water surface. Although both locations are possibly not at the exact depth, the phase and magnitude of both data is comparable (see Figure 4).

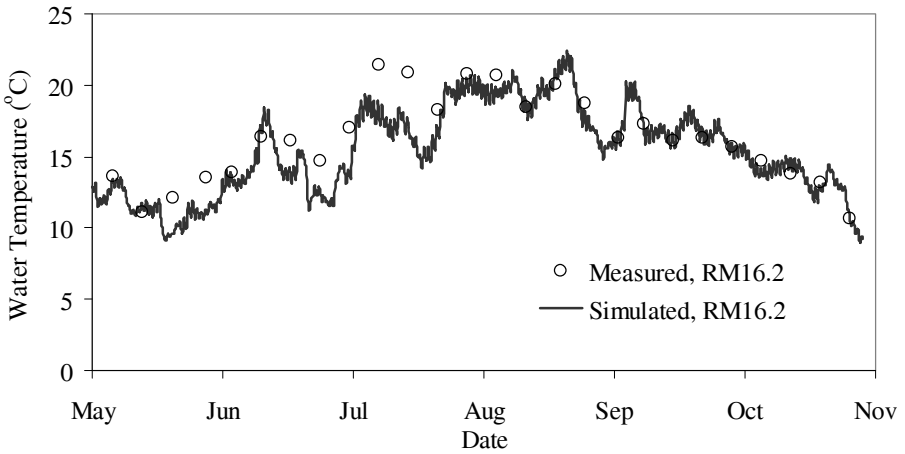

Figure 4. Comparison of measured and simulated water temperatures.

The phytoplankton and zooplankton concentrations and some water quality parameters are obtained from field study which was surveyed and documented by Doyle and Caldwell (1999). Most chemical and biological reaction rates used in this study are obtained from Rounds et al. (1999) and other literatures. The simulated phytoplankton biomass and the measurement data for a selected cross-section (see Figure 5) and the averaged phytoplankton concentrations over the simulation period (see Figure 6) are compared. The simulation results and the field data are in a good agreement in the upstream locations.

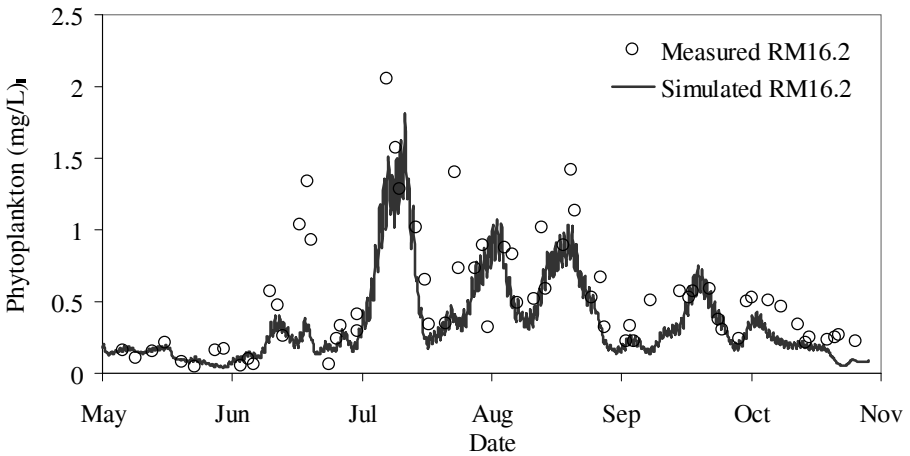

Figure 5. Simulated and measured phytoplankton biomasses at RM16.2.

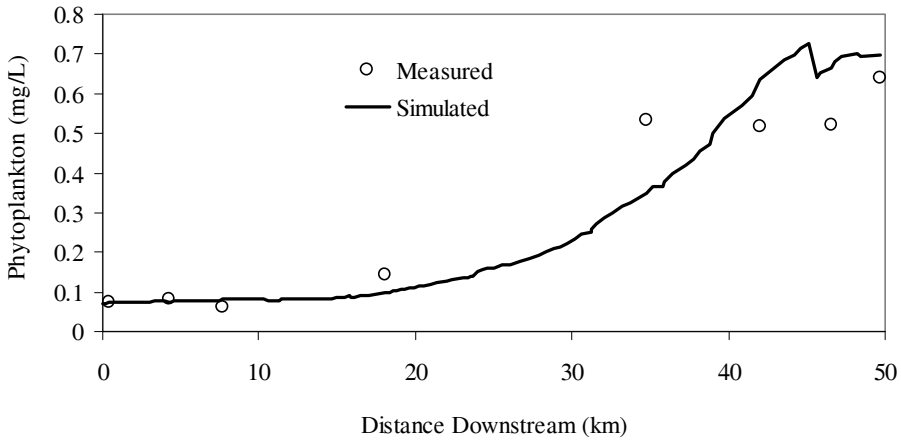

Figure 6. Comparison of the mean measured and simulated phytoplankton biomasses during May-October, 1991.

The comparison of simulated zooplankton concentration and measured data surveyed by Doyle and Caldwell (1996) is presented in Figure 7. The zooplankton abundances from the field data have been converted to the biomass concentrations by length-weight regression relations. These relationships have been taken from various literatures for calculating biomass of each zooplankton species at the specific life stage. Due to the limited zooplankton biomass at the upstream cross-section and the initial concentration of zooplankton biomass for some locations, the performance of the zooplankton dynamics model is rather undesirable. The simulated data is in the acceptable ranges for several times during the 5-month simulation period. The model will be further tested by studying its sensitivity.

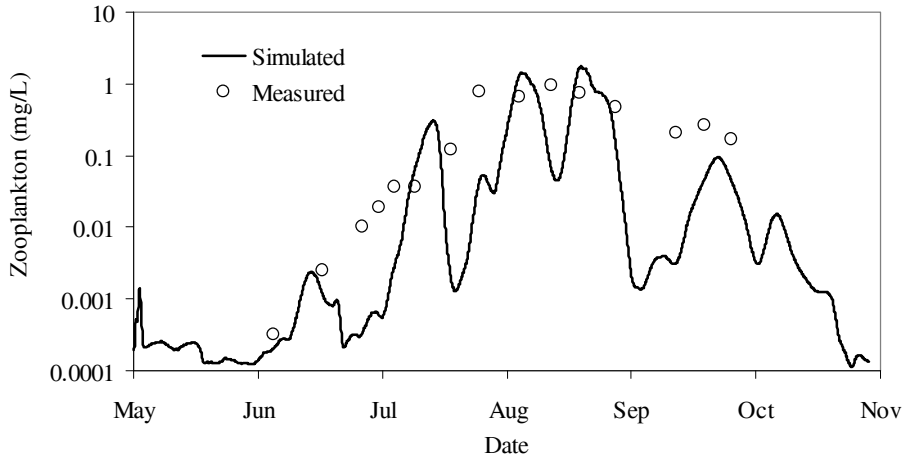

Figure 7. Simulated and measured zooplankton biomasses at RM5.5.

The simulated and measured ammonia and nitrate at the downstream cross-section (RM5.5) are compared in Figure 8. The model can well capture seasonal variations of nitrogen concentrations during the simulation period.

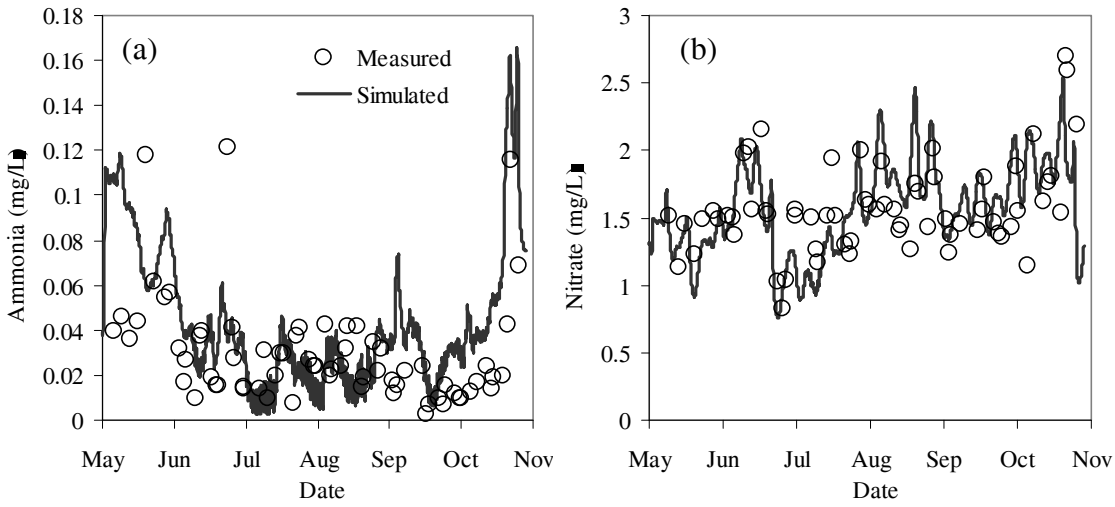

Figure 8. Comparison of the measured and simulated (a) ammonia and (b) nitrate concentrations at downstream cross-section.

Simulated DO and phosphate concentrations compared to the mean measurement data averaged over the simulation period are shown in Figure 9. Among various sources of DO, the photosynthesis process seems to be the most significant influence on DO in the Tualatin River. The overall profile of DO simulation and the field data are in a good agreement (see Figure 9a). Figure 9b presents a sudden change of phosphate concentration due to the effluents from the Durham WWTP. The overall trend of simulated phosphate concentration in the Tualatin River is comparable to the measured concentration; however the simulated concentration is slightly higher than the field data in some reaches.

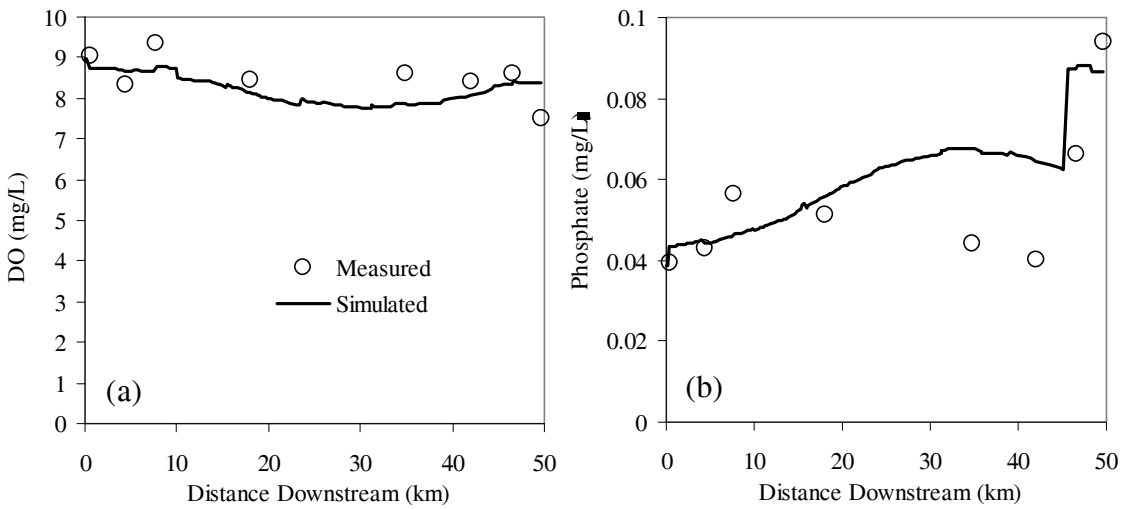

Figure 9. Comparison of the mean measured and simulated (a) DO and (b) phosphate concentrations along the Tualatin River during May-October, 1991.

CONCLUSION

The water temperature model and aquatic ecosystem model have been implemented in the CCHE1D package. The developed model is capable of simulating the heat transfer, transport and fate of chemicals, and concentrations of living organisms in channel networks under unsteady flow conditions. The model has been tested in computation of water temperature, water quality, and ecosystem components in the Tualatin River from May 01 until Oct. 31, 1991. Although the water temperatures simulated by the model are cross-sectionally averaged values and the field data are integrated samples measured at approximately 0.9 m below the water surface, both simulated and measured data are in a good agreement in both phase and magnitude. The model well predicts the time-series concentrations of the water quality parameters along the simulation domain. It has a good potential to simulate the concentration changes due to the lateral inputs from the wastewater treatment plants and the river's tributaries. The overall simulated biomass of phytoplankton is comparable to the measured data even though they are slightly different in some cross-sections. The model can roughly capture the trend of the zooplankton dynamics. The performance of the aquatic ecosystem model will be further validated in more cases.

ACKNOWLEDGEMENTS

This study is a part of the research project sponsored by the USDA ARS Specific Research Agreement No.58-6408-7-236 and the University of Mississippi.

REFERENCES

Di Toro, D. M., Fitzpatrick, J. J. and Thomann, R. V. (1983). *Documentation for Water Quality Analysis Simulation Program (WASP) and Model Verification Program (MVP)*. EPA-600/3-81-044, U.S. Environmental Protection Agency (USEPA), Office of Research and Development, Minnesota.

Doyle, M. C. and Caldwell, J. M. (1996). *Water-Quality, Streamflow, and Meteorological Data for the Tualatin River Basin, Oregon, 1991-1993*. U.S. Geological Survey (USGS) Open-File Report 96-173. Portland, Oregon.

Park, R. A. and Clough, J. S. (2004). *AQUATOX (RELEASE 2): Modeling Environmental Fate and Ecological Effects in Aquatic Ecosystem – Volume2: Technical Documentation*. EPA-823-R-04-002. USEPA, Office of Water, Washington, D.C.

Rounds, S. A., Wood, T. M. and Lynch, D. D. (1999). *Modeling Discharge, Temperature, and Water Quality in the Tualatin River, Oregon*. USGS Water Supply Paper 2465-B, Oregon.

Wu, W. (2008). *Computational River Dynamics*. Taylor and Francis, London.

Wu, W. and Vieira, D. A. (2002). *One-Dimensional Channel Network Model CCHE1D Version 3.0 – Technical Manual*. Technical Report No. NCCHE-TR-2002-1. National Center for Computational Hydroscience and Engineering, The University of Mississippi.

Use of Artificial Neural Networks for Habitat Unit Composition Modeling

Jian-Ping Suen[1]

[1] Department of Hydraulic and Ocean Engineering, National Cheng Kung University, No.1 University Road, Tainan 701, TAIWAN; Phone 886-6-2757575-63243; Fax 886-6-2741463; Emails: jpsuen@mail.ncku.edu.tw

ABSTRACT

Understanding the fish assemblage composition and assessing habitat preferences is an important requirement for ecological engineering practices for river restoration. This study collects fish and habitat data in the Tsengwen River Basin and Kaoping River Basin to provide criteria for fish habitat restoration projects. Fish samples were collected used prepositioned areal electrofishing devices designed for repeated grid sampling. The electrofishing data were used to identify habitat preferences and develop fish community-habitat models. A fuzzy rule-based model was used to characterize habitat units as deep pool, deep riffle, shallow riffle, and shallow pool based on measured depth and current velocity. The artificial neural networks then is used to model the connection between the autecology matrix analysis values and surveyed habitat unit compositions. The utility of the model was furthered using historical fisheries data in addition to the data collected as part of the study. The fish community-habitat model results provide a reference condition that can be used to guide stream restoration and ecological engineering decisions aimed at maintaining the natural ecological integrity and diversity of Taiwanese rivers.

INTRODUCTION

Management of water resources is highly developed in Taiwan due to the high density of people living on the island and the uneven spatial distribution of seasonal precipitation. Traditionally, water resources projects emphasized utility; flood defense projects including bank protection, erosion control, and dike construction have traditionally used concrete structures and designs with high safety factors to protect public safety and prevent economic losses from flooding. But recent projects have begun to incorporate additional principles of ecological engineering (Mitsch and Jorgensen, 2003). The Public Construction Commission began to promote ecological engineering approaches for river restoration in late 1990's. At present, environmentally-friendly and ecologically-appropriate engineering projects are being designed that shift the focus from river bank stabilization to instream structures such as riffles and pools (Kuo, 2006; Wu et al., 2006).

The physical habitat of rivers plays an important role in sustaining fish populations and maintaining biodiversity. The relationships between fish community and

physical habitat reveal repeatable ecological processes and are useful for river restoration and ecological engineering activities in rivers (Lamouroux and Cattaneo, 2006). But while it is known that many environmental factors are important to the presence and abundance of each fish species (Bovee, 1982; Jowett, 2002), the strong interrelation between factors makes it difficult to determine which of these factors play a dominant role in the maintenance of fish community structure (Lamouroux et al., 1999). The combinations of depth, velocity, and substrate have been used regularly as surrogates for an overall physical complexity and to describe the physical habitat for fish in rivers (Clifford et al., 2006). Physical habitat simulation models have been used for fish in river restoration projects worldwide (Bockelmann et al., 2004; Mouton et al., 2007). Physical habitat variables such as flow velocity, depth, and substrates can be related to the presence and abundance of a species to describe the species' preferred habitat. Habitat suitability curves based on these relationships can be used to determine the potential effects of hydraulic variation on fish species (Bovee, 1982). However, this type of analysis is limited in its application to multiple species; most physical habitat models are developed only for target or dominate species (Tomsic et al., 2007), and just a few of them are for fish communities rather than an individual species (Lamouroux and Souchon, 2002).

This paper aims to develop reference conditions based on historical fish community data for designing the instream structures in river restoration and ecological engineering projects. Fish data is collected using prepositioned areal electrofishing devices that allow identification of preferred habitat in an undisturbed environment; the physical variables of each habitat location are subsequently surveyed. Fish data then is analyzed using the fish autecology matrix to determine the environmental habitat requirements. Finally, an artificial neural network model is developed to connect the field work measurements to the fish autecology matrix analysis. This process provides a way that engineers can use the artificial neural networks models to analyze historical fish data and develop reference conditions for the design of ecologically-relevant instream structures.

Method

Sampling Design

This study focuses on an ecological analysis of fish habitat units mainly in mid- to upper-order streams. Fish were sampled using 1 meter-by-1 meter prepositioned areal electrofishing devices (PAEDs). Using this approach minimizes sampling method disturbance of fish position and provides a consistent method of sampling the same habitat over time (Schwartz and Herricks, 2004). The goal is to ensure all individuals are caught their most natural environment, and the physical environmental conditions of each location can be effectively measured and connected to habitat unit simulation models.

Artificial Neural Networks (ANNs)

Natural neural networks (the brains of animals) learn from experience and can perform difficult operations and recognize complex patterns, even if those patterns are noisy. The artificial neural networks research of recent years has attempted to mimic these networks to attain the advantages of their flexible and powerful calculating abilities. Although the concept of artificial neurons was first introduced by McCulloch and Pitts (1943), the major applications of ANNs have arisen only since the development of the back-propagation method of training by Rumelhart et al. (1986). ANN research following this development has resulted in successful solution of some complicated problems not easily solved by traditional modeling methods. The details of ANNs model operation are provided by Zurada (1992) and are not reported here.

Fish Autecology Matrix

The autecology matrix assembles information from scientific literature, reports, and field work observations into a database of habitats and life history requirements of fish species. The database provides easy access to ecological information in a form that can be readily and consistently used to support fish habitat and autecological analysis. In its present form, the autecology matrix divides factors into five sub-matrices: physical habitat, spawning requirements, ecological issues, water quality tolerance, and human values. Together, these five sub-matrixes include approximately 230 habitat and life history factors for each fish species. The matrix can be used in two primary ways: (1) to identify environmental requirements or ecological characteristics for a species by providing a summary of the expected habitat requirements or ecology and life history characteristics of the species, and (2) to identify a fish community that has specific environmental requirements or ecological characteristics by providing a list of species that share common habitat requirements (Suen and Herricks, 2006).

The autecology matrix can also be useful when emphasizing a limited set of factors that are important in providing both species and community information. In an analysis of the matrix for a community of organisms, it is possible to determine the proportion of species within the community with similar habitat preferences or life history requirements. Since these proportions are determined from a listing of species known to occur in a stream reach, it is possible to identify community habitat preferences or ecological characteristics based on a weight-of-evidence presented in matrix summaries (Suen and Herricks, 2006).

We have reviewed the literature and developed a Taiwan-specific freshwater fish autecology matrix that includes approximately 65 freshwater fish species and 230 environmental factors and ecological characteristics. Table 1 shows part of the matrix used in this study. In the matrix, a value of one (1) indicates that the environmental factor can be applied to the particular species, while a value of zero (0) indicates that the factor cannot be applied. These data for individual species can be used to analyze the environmental requirements of the fish community. For example, if the first five species of Table 1 are recorded in a sampling site, those five species

are considered the resident community. Because two of these species prefer deep pool locations, 40 % of this fish community's preferred location is deep pool. Similarly, three of the five species prefer gravel, so 60 % of this fish community's preferred substrate is gravel. The percentages of all of the 230 environmental factors can be easily calculated within the matrix.

The environmental preference percentages calculated in this way are used as input variables in the habitat ANNs models. In this research, the twelve environmental factors of deep pool, shallow pool, deep riffle, shallow riffle, no current, slow current, medium current, fast current, silt/sand substrate, gravel substrate, cobble substrate, and boulder substrate are used as independent variables in the habitat simulation ANNs models. These factors are generally physical habitat factors and are reasonable for habitat simulation models.

Table 1 A demonstrative excerpt of the fish autecology matrix

Fish	Preferred locations				Current				Substrate			
	Deep pool	Shallow pool	Deep raffle	Shallow raffle	None	Slow	Medium	Fast	Silt/ Sand	Gravel	Cobble	Boulder
Microphysogobio brevirostris	0	1	1	0	1	1	0	0	1	0	0	0
Zacco pachycephalus	0	1	0	1	1	1	1	0	1	1	1	0
Channa maculata	1	1	0	0	1	1	0	0	1	1	0	0
Rhinogobius giurinus	1	1	1	0	1	1	1	0	1	1	1	0
Rhinogobius candidianus	0	0	0	1	0	0	0	1	0	0	1	1
Acrossocheilus formosanus	0	1	1	1	1	1	1	1	1	1	1	1
Candidia barbatus	1	1	0	0	1	1	0	0	1	1	1	0
Sinogastromyzon puliensis	0	1	1	1	0	0	1	1	0	1	1	1
Varicorhinus barbatulus	1	1	1	1	0	1	1	1	1	1	1	1

RESULTS AND DISCUSSION

Habitat-Specific Fish Collection

The study areas are the Tsengwen River and Kaoping River, located in southwestern Taiwan. Electrofishing sample sites were selected such that stream depth, velocity, and substrate could be related to the samples to develop an

understanding of fish habitat preference under existing environmental conditions. The sampling locations were identified as providing a wide variation of depth and velocity with relatively stable substrate conditions.

Fish were sampled at about one hundred habitat units within the four major sampling locations from 2007 to 2009 using the PAED technique. Ninety-eight units produced fish communities, while six of the units had no fish. A total of 1,035 individuals were obtained, including six genera and seventeen species. The dominant species were Pulin river loach (Sinogastromyzon puliensis), Freshwater minnow (Zacco pachycephalus), and two species of Goby (Rhinogobius giurinus and Rhinogobius rubromaculatus). The velocity at these habitat units varied from 0.01 to 1.58 m/s, and the depth varied from 3 to 160 cm.

The surveyed depth and velocity data of the same electric grid units were analyzed by the fuzzy rule-based model to identify habitat types (Suen and Su, 2009). Deep riffle (DR) is the most abundant habitat type, and the number of riffles is greater than the number of pools. This is likely because the study locations are within mid- to upper-order streams where riffle habitats and deeper water are more abundant than in low-order reaches. The habitat type results of the fuzzy rule-based model echo those of the field observations, but the fuzzy model classification procedure provides a quantitative way to define fish habitat types. It provides a clear, measurable procedure that is easier for engineers to apply.

Model Development

Historical fish sampling results usually show fish abundance or presence data in reach-scale sampling sites. Because this study uses PAEDs to sample fish in 1-by-1-meter habitat unit, the habitat scales between historical and recent data are different. To allow comparison between the datasets, 20 units were selected randomly from the habitat units. The habitat conditions of these units were used to mimic the habitat conditions at the historical reach-scale sampling sites. The combined fish data for the 20 units represented the fish abundance data for a reach-scale sampling site, and the compositions of the four types of habitat unit conditions of the 20 units represented the actual habitat condition at a sampling site. The fish data was then analyzed using the fish autecology matrix to determine the proportion of the communities that prefer each the of the twelve environmental factors (deep pool, shallow pool, deep riffle, shallow riffle, none current, slow current, medium current, fast current, silt/sand substrate, gravel substrate, cobble substrate, and boulder substrate). These percentages are used as input variables in the ANNs model. The percentages of each habitat type within the twenty units are used as output variables in the ANNs model. This process of randomly selecting twenty habitat units and calculating percentages is repeated twenty times, resulting in twenty sets of data to be used in developing the habitat ANNs model.

Table 2 shows the summary of habitat composition simulation models developed by the ANNs. The percentages of the 4 simulated habitat types may not sum to one, but

the percentages can still represent a relative comparison for engineering consideration. Most species sampled in riffle areas (e.g. Sinogastromyzon puliensis) only prefer riffle type habitats, but some species sampled in pool areas (e.g. Zacco pachycephalus and Rhinogobius giurinus) are habitat generalists which can also be caught in riffle type areas (Yu and Lee, 2005). This may cause the validation's r^2 value of the deep pool habitat unit model to be relatively low (0.508) and the validation's r^2 values of the two riffle habitat unit models to be relatively high (0.947 and 0.653). Improved sampling efficiency in deep pool areas and increased collection of guild species that use deep pool habitats (e.g. Hemiculter leucisculus) may increase the r^2 value of the deep pool habitat unit model.

Table 2 ANNs model results

	Training events			Validation events		
	RMSE	RMSE_P	r^2	RMSE	RMSE_P	r^2
Deep pool	0.0273	17.433	0.807	0.0370	24.657	0.508
Deep riffle	0.0208	4.599	0.944	0.0540	11.999	0.947
Shallow pool	0.0279	16.107	0.920	0.0748	39.382	0.543
Shallow riffle	0.0317	14.850	0.866	0.0598	27.172	0.653

While developing the regression models, autecology matrix analysis uses fish presence and absence data instead of abundance data. Although fish abundance data may provide more information, it is a snapshot-type result that reflects the antecedent environmental conditions. Besides that, the goal of the habitat simulation models is to reconstruct habitat unit compositions based on historical fish data; commonly, presence and absence data are all that can be found in the literature.

SUMMARY

This research develops a physical habitat simulation model by using historical fish data for river restoration and ecological engineering in mid- to upper-order streams in Taiwan. The simulated composition of four types of habitat units (deep pool, shallow pool, deep riffle, and shallow riffle) of a designed streamflow condition could guide the design of instream structures in creating pool-riffle systems with ecological reference. Although the compositions of habitat types in rivers may vary with streamflow variation, and the maintenance of instream structures for habitat composition is difficult, the habitat simulation model demonstrates how the design of an instream engineering structure can be guided by fish community information.

ACKNOWLEDGEMENTS

The authors gratefully acknowledge the research support of the National Science Council, Taiwan under grant number NSC 96-2221-E-006-264-MY3 and National

Cheng Kung University under grant number R046. Wei-Che Su, Shih-Kai Chou, Tsung-Chi Chang, Ying-Sheng Lyu, Ruei-Hong Wang, and Chin-Yuan Lin provided field assistance. The authors also acknowledge the assistance of Dr. Edwin Herricks and Dr. Cathy Marcinkevage in the various aspects of this work.

REFERENCES

Bockelmann, B.N., Fenrich, E.K., Lin, B., Falconer, R.A., 2004. Development of an ecohydraulics model for stream and river restoration. Ecological Engineering 22(4-5), 227–235.

Bovee, K.D., 1982. A guide to stream habitat analysis using the instream flow incremental methodology. Instream Flow Information Paper 12, US Fish and Wildlife Service, Fort Collins, Colorado, 248 pp.

Clifford, N.J., Harmar, O.P., Harvey, G., Petts G.E., 2006. Physical habitat, eco-hydraulics and river design: a review and re-evaluation of some popular concepts and methods. Aquatic Conservation: Marine and Freshwater Ecosystems 16(4), 389-408.

Jowett, I.G., 2002. In-stream habitat suitability criteria for feeding inanga (Galaxias maculatus). New Zealand Journal of Marine and Freshwater Research 36(2), 399–407.

Kuo, C.C., 2006. Using ecotechnology to redirect Taiwan's construction work away from conventional method. Ecological Engineering 28(4), 325-332.

Lamouroux, N., Olivier, J.M., Persat, H., Pouilly, M., Souchon, Y., Statzner, B., 1999. Predicting community characteristics from habitat conditions: fluvial fish and hydraulics. Freshwater Biology 42(2), 275-299.

Lamouroux, N., Souchon, Y., 2002. Simple predictions of instream habitat model outputs for fish habitat guilds in large streams. Freshwater Biology 47(8), 1531-1542.

McCulloch, W.S., Pitts, W., 1943. A logical calculus of the ideas imminent in nervous activity. Bulletin and Mathematical Biophysics 5, 115-133.

Mitsch, W.J., Jorgensen, S.E., 2003. Ecological engineering: A field whose time has come. Ecological engineering 20(5), 363-377.

Mouton, A.M., Schneider, M., Depestele, J., Goethals, P.L.M., de Pauw, N., 2007. Fish habitat modelling as a tool for river management. Ecological Engineering 29(3), 305-315.

Rumelhart, D.E., Hinton, G.E., Williams, R.J., 1986. Learning internal representations by error propagation. Parallel Distributed Processing, vol. 1, chap. 8, Rumelhart D.E., McClelland, J.L. eds., MIT Press, Cambridge, Mass. 318-362.

Schwartz, J.S., Herricks, E.E., 2004. Use of prepositioned areal electrofishing devices with rod electrodes in small streams. North American Journal of Fisheries Management 24(4), 1320–1330.

Suen, J.P., Herricks, E.E., 2006. Investigating the causes of fish community change in the Dahan River (Taiwan) using an autecology matrix. Hydrobiologia 568, 317-330.

Tomsic, C.A., Granata, T.C., Murphy, R.P., Livchak, C.J., 2007. Using a coupled eco-hydrodynamic model to predict habitat for target species following dam removal. Ecological Engineering 30(3), 215-230.

Wu, H.L., Feng, Z.Y., 2006. Ecological engineering methods for soil and water conservation in Taiwan. Ecological Engineering 28(4), 333-344.

Yu, S.L., Lee, T.W., 2005. Habitat segregation by fishes in western Taiwan rivers. Journal of Applied Ichthyology 21(6), 531-534.

Zurada, J. M. Introduction to Artificial Neural Systems. West Info Access. Singapore.

Considering River-Scale Ecological Improvements within Flood Management Planning: The Lower Menomonee River Watercourse Status Report

Michael Schwar[1] and Tom Chapman[2]

[1]HNTB Corporation, 11414 W. Park Place Suite 300, Milwaukee WI 53224; PH (414) 359-2300; email: mschwar@hntb.com
[2]Milwaukee Metropolitan Sewerage District, 260 West Seeboth Street, Milwaukee WI 53204-1446; PH (414) 272-5100; email: tchapman@mmsd.com

ABSTRACT

Between 2000 and 2012, nearly $180M in flood management and ecological improvements will be made in the lower seven miles of the Menomonee River and Underwood Creek in Milwaukee and Wauwatosa Wisconsin. When complete, these improvements will alter areas along at least one bank over nearly 70 percent of the river, resulting in more than 130 acres of riparian land conversion in that highly urban reach. These improvements were and will be undertaken by multiple parties for a variety of land development, flood management, and ecological restoration purposes.

To identify opportunities for providing multiple benefits from planned projects, the Milwaukee Metropolitan Sewerage District (MMSD) developed the Lower Menomonee River Watercourse Status Report. This report characterized the existing hydrologic, physical and ecological conditions of the river and its riparian area as it passes through a highly urbanized corridor. It summarized improvements made in the last seven years and identified remaining ecological and flood management concerns to be addressed by future projects. Additional projects are currently in various states of planning, and there is interest among various stakeholders to develop these projects in ways that provide additional environmental benefits beyond their primary flood management objectives.

Like many urban rivers, the Menomonee River is highly channelized. The status report identified four distinct reaches with varying degrees of channelization, natural substrate and riparian function. Prime opportunities for improvement include removing concrete sections that serve as fish barriers and providing additional riparian functionality in the mid-reach areas, both of which would help connect relatively high quality habitat upstream with Lake Michigan downstream. Several opportunities to enhance ecological function were identified associated with ongoing flood management projects and the report will serve as a basis for guiding additional efforts along the lower Menomonee River.

BACKGROUND

The Menomonee River is the second largest of three rivers that flow into Lake Michigan through the Milwaukee Harbor. Industrial development in the Menomonee River watershed began to occur rapidly following completion of the railroad connecting Chicago and Milwaukee in 1855 and the rate of urban growth along the lower Menomonee River peaked in the 1900s through 1920s. Industrial land use occurred

along the river, where water was used for both a resource and means of disposing of waste products. During this time, filling and dredging operations along the lower Menomonee River to satisfy industrial development interests resulted in a channelized river and filled floodplains.

Historically the Menomonee River, Milwaukee River Estuary and Lake Michigan supported a diverse and abundant fish and aquatic life community. The fishery included commercially and recreationally important cold, cool and warm water resident and potadromous species from Lake Michigan. The life requisites of many fish species were dependent, in whole or in part, on access to unique and seasonal habitats present in the lake, estuary and riverine environs.

Beginning with European settlement in the early 1800s, habitat for fish and aquatic life along the river and estuary was extensively modified or destroyed. The previously mentioned river channelization and filling of the floodplain resulted in the loss of over 10,000 acres of wetland habitat in the estuary and along the lower Menomonee River. A low-head dam, grade controls and concrete channel lining constructed in the lower Menomonee River acted as barriers to resident and potadromous fish movement. These structures also caused increases in water temperature, sedimentation and other impacts to water quality

Since the mid-1990's, a number of flood improvement and redevelopment projects in the area have resulted in significant changes to riparian land use (Table 1). Most of these projects have been implemented to improve flood flow conveyance for flood management. Some of these have had secondary benefits to improving the character of the river channel and riparian margins. A few have been implemented entirely for the purpose of improving the environmental characteristics of the river and the immediate riparian corridor.

While the loss of historical fish habitat is not fully reversible, some of the barriers to fish movement have been removed or abated. For example, the Falk Dam, formerly located at the Menomonee River estuary boundary, was removed in 2001. More significantly, in 2000 MMSD removed the six-foot high concrete grade control structure at N. 45th St. and 1,200 feet of concrete lining and replaced them with natural stone as the channel bed. The remaining 3,300-feet of concrete-lined channel remains a barrier to fish movement and an impediment to water quality goals. This section of the Menomonee River has not attained the State of Wisconsin’s assigned biological use for this reach.

Within this context the MMSD undertook the Lower Menomonee River Status Report. This report characterized the existing hydrologic, physical and ecological conditions of the river. With this information existing limitations to ecological function within the river corridor were evaluated, and the potential for planned or proposed projects to contribute to improved ecological function was explored.

Table 1. Completed Projects along the Lower Menomonee River.

Project	Status	River Mile	Date Built	Owner	Impact on River Corridor
Menomonee Valley Shops Redevelopment: Redeveloped 100-acre Shops site along 1,000 feet of north bank of the river	Complete	2.45 to 2.86	2006	City of Milwaukee	Increased floodplain area and improved riparian margin
Miller Park Riverbank Widening and Stabilization: Widened and stabilized 2,000 feet of riverbank; created trail and enhanced river access	Complete	3.06 to 3.56	2002	SWPBPD	Increased floodplain area and improved riparian margin
Valley Park Floodwall: Installed about 2,000 feet of floodwall to protect Valley Park	Complete	3.70 to 4.05	2001	MMSD	No impact on river channel
Wisconsin Avenue Viaduct Wetland: Created half acre wetland adjacent to the river	Complete	4.08 to 4.23	2000	City of Milwaukee	No impact on river channel
Drop Structure Removal: Removed impassible drop structure and 1,000 ft concrete and restored more natural gradient and bed	Complete	4.28 to 4.52	2000	MMSD	Provided fish passage
Hawley Road Bridge Removal: Removed Hawley Road Bridge and improved conveyance	Complete	5.13 to 5.14	2006	MMSD	No impact on river channel
Hart Park Project: Lowered 48 acres of floodplain, increased riparian corridor, expanded and stabilized riverbank, created trail	Complete	5.51 to 6.40	2006	MMSD	Increased floodplain area and improved riparian margin
Milwaukee County Grounds, Phases I and II: Creates a 960 acre-foot detention facility that will decrease flood flows in Hart Park by 3,000 cfs in a 100-yr event	Partially Complete	7.42 to 8.30	2008	MMSD	No impact on river channel
Hoyt Park Bank Stabilization: Stabilized 600 feet of riverbank and a headcut in the channel	Complete	7.51 to 7.62	2001	MMSD	Improved riparian margin

RIVER HYDROLOGY

While extreme peak flows are used to design flood management projects, base flows and frequent but minor flows tend to have a larger influence on ecological conditions in the river. Base flows occur in the periods between storm events and determine conditions experienced by aquatic biota during a large portion of the year. The typical daily flow in the lower Menomonee River is 44 cubic feet per second (cfs), and 70 percent of the time flow in the river is between 10 and 100 cfs. River flows show a clear seasonal pattern. The river exhibits a pronounced rise due to snowmelt in the spring, and then flows recede during the late summer and fall (Figure 1). During the spring melt, which generally occurs between February and April, the river experiences sustained 10-day or longer

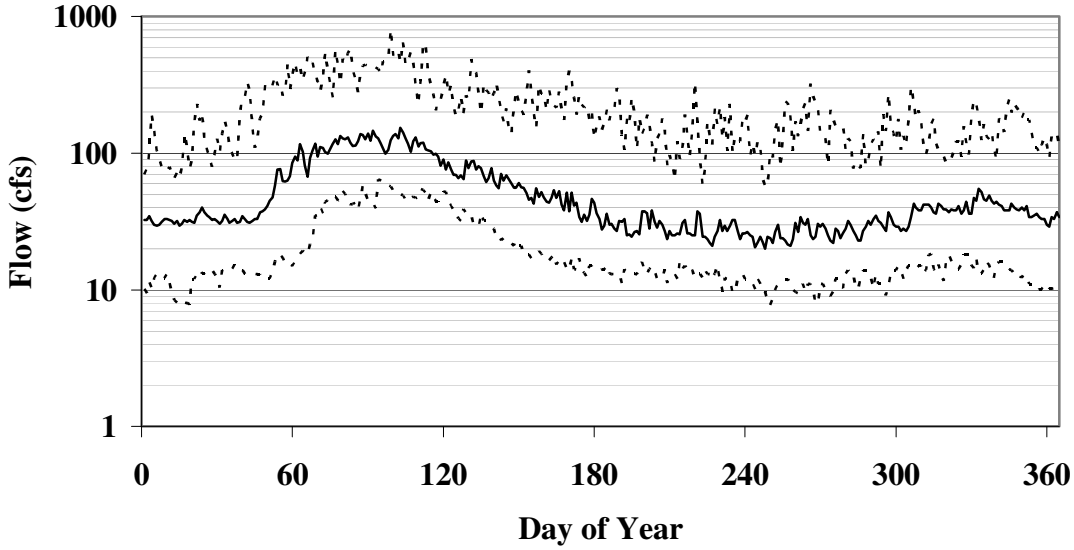

Figure 1. Median daily flow (solid line) and 10- and 90-percent limits (dashed lines) for Menomonee River at Wauwatosa (USGS Gage 04087120) based on Water Years 1962-1985 and 1987-2004.

periods of flow in the 150 to 400 cfs range, and often during that period there are one or two days with average flows of 1200-1500 cfs. Low flows during average years are around 20-30 cfs. High flow events can occur at any point throughout the year, and on almost any day there is at least a ten percent probability that flows in the river will exceed 100 cfs.

Character of high flows. On the lower Menomonee River larger flows (larger than the 50 percent annual probability, also known as the 2-year flow, equal to approximately 4,000 cfs) tend to occur quickly and last for a brief period. The peaks tend to be driven by a combination of two tributary inflows, Underwood Creek and Honey Creek, with contributions from upstream areas arriving after the highest flows have passed. Analysis of the 15-minute instantaneous flow records for the largest flows between 1986 and 2006 indicate two types of typical events. The first type is a "flashy" event, during which flows quickly rise and then steeply fall back. The second type is an "extended" event, during which flows fall back, but remain at an elevated level. The extended events occur at about the same frequency as flashy events, but the extended events tend to be larger and appear to reflect storms that fall over most of the watershed.

Ecological significance. Based on the preceding evaluation of the character of base flows and frequent higher flows, several flow thresholds of ecological significance were developed based on duration and frequency of occurrence. These include flows within the channel (300 cfs and less) and flows that inundate the stream banks and the immediate riparian margin (1,200 to 4,000 cfs). These flows, their duration and frequency are presented in Table 2.

Table 2. Qualitative threshold flows of ecological significance for the lower Menomonee River.

Flow (cfs)	Average Duration	Incidence	Seasonality
30	Months	Every year	Average daily flow during summer and fall
160	Weeks	Every year	Average sustained spring melt flow
300	Days	Nearly every year	Common peak daily flow during snow melt
1,200	8-24 Hours	Nearly every year, average daily flow that occurs twice a year on average	Can happen in any season
2,100	Few Hours	Nearly every year, average daily flow that occurs every other year on average	Generally in March through September
4,000	Minutes	Peak flow occurs approximately every other year	Usually in June through August

PHYSICAL AND ECOLOGICAL CONDITIONS

During the 1950s to 1980s, MMSD constructed concrete-lined channel waterways in an effort to improve conveyance and reduce the risk of flooding of structures and property within these floodplains. Nearly all of the approximately 26 miles of these concrete-lined channels are in need of repair or replacement. In some areas, the concrete-lined riverbed and banks are failing, and in many others, the concrete is nearing the end of its functional lifespan. These concrete-lined stream segments fragment and limit linear and lateral connectivity within the stream and their corridor habitat and ecosystems; limit or prevent fish and wildlife movement; increase water temperature; destroy fish, aquatic life and wildlife habitat; limit recreational use including those attendant to navigation, fishing and aesthetics; and may actually increase flooding and decrease public safety.

The conditions of the 6.3-mile long reach of the lower Menomonee River under study reflect these historic river and floodplain modifications. This section of the document presents a description of the physical and ecological condition of the streambed, banks and riparian margin within the study area.

Existing streambed and stream bank condition. The materials that comprise the streambed and stream banks of the Menomonee River were documented in 2000 as part of a geomorphic inventory of the entire watershed (Inter-Fluve 2001). The bed and banks of the lower Menomonee River consist of alluvial materials (gravels and cobbles), bedrock, riprap, concrete and WPA Walls.

WPA walls were constructed in the 1920s and 1930s as part of the Works Progress Administration to serve as flood management and river controlling structures. These walls consist of mortared limestone blocks and are up to 12 feet high. The WPA walls in the Menomonee River watershed range in condition from stable and functional to flanked, crumbling and non-functional. Throughout the study area, the WPA walls are functioning, although two segments exhibit degradation of the stone and mortar and are at risk for potential failure (Inter-Fluve 2000). Also, throughout the study area

approximately 17 percent of the bed and 50 percent of the banks consist of man-placed materials, indicating the extent of human-induced impacts along this section of river.

Inundation of riparian margins. The interaction of land and water at the riparian margin is one of the critical factors that influences riparian and channel quality and function. For this study, a HEC-RAS hydraulic model was used to characterize the aerial extent of inundation within the riparian margin along the lower Menomonee River study area. First, the modeled water surface elevations associated with the flows of ecological significance were determined. Then, using the bank line location and elevations, the floodplain topography, and the modeled water surface elevations, the areas of inundation for three different flows (600; 1,200; and 4,000 cfs) were determined. These inundation areas, as well as an average inundation width, were compiled for each reach. The inundation area and width are negligible in certain reaches because of the constrained channel geometry. The most upstream reach has the most functional floodplain, as this reach exhibits the largest inundation area and width at 4,000 cfs, but other reaches also provide important habitat because they contain pockets of habitat that inundate at the lower flows.

Fisheries. While many fish species are resident to the middle and headwater reaches of the Menomonee River, many others use—or could use—the lower river as a transitory corridor from the lake and estuary to access the habitat available in the river and tributaries. As one of its more integral fish habitat functions, the lower Menomonee River provides an important biological connection to the entire Menomonee River watershed. Additionally, the lower river also provides spawning, rearing and adult habitat to a variety of game and non-game fish, other aquatic life and wildlife.

Fish populations in the lower Menomonee River are less than optimal due to the impacted habitat conditions of the river. Factors responsible for the limited habitat include land use and resulting stormwater and pollutant loads; extreme flow conditions; and modifications to the original physical habitat along the river and its corridor. Habitat modifications include the 3,300-foot long reach of semi-impassible concrete channel lining, a lack of channel margin refuge caused by extended segments of smooth, vertical limestone block walls and reduced in-stream habitat diversity resulting from several causes, such as floodplain encroachment and a lack of woody material recruitment. Benefits from enhancements to river habitat could include fish access to historical upstream and newly created local habitats necessary for reproduction, development and other life requisites; enhanced genetic diversity; access to over wintering habitat; access to and increased production of food supplies; and enhanced water quality.

ECOLOGICAL LIMITATIONS

Local-scale ecological function is limited by the interrelated factors of channel bed condition, channel bank condition and the potential for fish passage, as well as the nature of the wetland or floodplain vegetative community. At the reach scale, the primary ecological limitation within the lower Menomonee River is a 3,300 length of concrete river bed which limits the connectivity of fisheries between the estuary and the rest of the river over all ranges of flow experienced by the river. The downstream areas of the river have very limited margin habitat, meaning that natural flow variations do not

inundate additional riparian land. Since the river banks are nearly all concrete wall, rip rap, other steep (3:1 and greater) slopes to the river, there are very limited floodplain wetlands and inundation of land during normal seasonal flow variations. The inundation of riparian margins during seasonal variations in flow is one of the key requirements for ecological function. Finally, the downstream portions of the river also have limited wooded riparian corridors, which provide shade and woody debris for the river.

POTENTIAL FOR IMPROVEMENT

This report evaluated the projects that may be constructed in the next several years from both a flood risk reduction perspective and from an ecosystem function benefit. Some projects such as the Western Milwaukee project and Phase 2 of Milwaukee County Grounds will be built primarily for flood management. Other projects such as the Airline Yards project will be more specifically focused on ecological restoration. Table 3 summarizes the improvements that will result from each of these projects. It was determined that, with proper design these projects could contribute to improvements in each of the areas of ecological limitation noted above.

CONCLUSIONS

- A key project for the entire system is completing Phase 2 of Milwaukee County Grounds. An undesired consequence of removing concrete in the Underwood Creek and Valley Park would be raising 100-year water surface elevations. The Milwaukee County Grounds project will lower the downstream100-year water surface elevation sufficiently to compensate for the increases caused by concrete removal. Without County Grounds, these projects would not be feasible due to unacceptable increases in the water surface elevation beyond existing elevations.

- The Western Milwaukee Floodwater Management Project will significantly improve conditions within Reaches 2 and 3 through creation of 1.5 acres of new floodplain wetlands, a day-lighted Schoonmacher Creek, and 31 acres of primarily wooded riparian corridor.

- Creation of a pilot channel in the Valley Park area is feasible without increasing the 100-year flood water surface elevations above existing elevations assuming that the County Grounds project is functional. The pilot channel would greatly improve the ecological connectivity throughout the entire watershed and allow fish to migrate from the estuary to the rest of the river.

- The feasibility for concrete side slope removal in the Valley Park area requires more study. Preliminary modeling suggests that in order to due this, additional land would need to be purchased to widen the channel so that 100-year water surface elevations would not be increased above the current conditions.

- Overall, the floodplain projects proposed by the MMSD will lower the 100-year water surface elevations and provide key ecological improvements in the lower river.

Table 3. Summary of Potential Ecological Improvements Along the Lower Menomonee River.

Project	Reach	Improved Condition				
		Channel Bed	Channel Bank	Fish Passage	Floodplain Wetland	Woody Riparian Vegetation
Phase 1 Western Milwaukee Flood Management	3	N/C	Converts 800 feet of WPA wall to riparian margin	N/C	Creates 0.5 acres	Creates 7 acres of tall grass prairie
Phase 2 Milwaukee County Grounds	4	Provides reduced flow conditions which allow channel bed improvement	Provides reduced flow conditions which allow bank improvement	N/C	N/C	N/C
Menomonee Valley – Airline Yards	1	N/C	Creates 2,500 feet of stabilized bank	N/C	Creates 1 acre	Creates 10 acres
Falk Corporation Floodwall	1	N/C	N/C	N/C	N/C	N/C
Phase 2 Western Milwaukee Flood Management	3	N/C	Converts 400 feet of WPA wall to riparian margin. Opens 500-feet of enclosed tributary creek	N/C	Creates about 1 acre	Creates 31 acres
Valley Park Concrete Removal –Pilot Channel Alternative	2	Replaces 3,900 feet of concrete bed with stone for fish passage	N/C	Provides fish passage	N/C	N/C
Valley Park Concrete Removal – Improve Bottom and One Side Alternative	2	Replaces 3,900 feet of concrete bed with stone for fish passage	Converts 400 feet of concrete bank to riparian margin	Provides fish passage	N/C	N/C

N/C = No Change

Developing Linkages between Biological Impairment and Stream Siltation: A Case Study in the Northern Great Plains Ecoregion

John S. Schwartz, PhD, PE[1], Andrew Simon, PhD[2]; and Lauren Klimetz[2]

[1]University of Tennessee, Department of Civil and Environmental Engineering; 63 Perkins Hall, Knoxville, Tennessee 37996-2010; PH (865) 974-7721; jschwart@utk.edu

[2]USDA ARS National Sedimentation Laboratory; P.O. Box 1157, Oxford, Mississippi 38655; PH (662) 232-2918; Andrew.Simon@ars.usda.gov, Lauren.Klimetz@ars.usda.gov

Abstract

Loss of biological integrity in streams due to excessive suspended sediment is a major cause of water quality impairment in the United States today. States monitor and assess streams for biotic integrity, and list streams as "impaired" according to §303(d) of the Clean Water Act for those that do not meet biological criteria. Biological criteria are set by states based on benthic macroinvertebrates or fish community metrics, developed as indices of biotic integrity (IBI) per Level IV ecoregions. In many cases, causes for biological impairment are not clear, and commonly states list causes as "siltation" and/or habitat alteration without strong evidence. A critical need exists to improve analytical tools to link loss of biological integrity with "siltation", and to estimate total maximum daily loads (TMDLs) for these impaired streams. This study tested an idea using autecological fish data and USGS suspended sediment concentration (SSC) data to better link causes of biological impairment to SSC metrics. The study was located in Northern Great Plains Level III Ecoregion, in which 77 USGS gauging stations with flow and suspended sediment data were co-located with fish data from federal and state agencies. Autecological data was summarized by fish species found in this ecoregion, including attributes on mesohabitat preferences, water quality tolerance, trophic structure, and feeding, diet, and spawning behaviors. An autecological data matrix was created using the species autecological information and site fish presence/ absence data, forming a matrix that included, per site, the number of occurrences an autecological attribute occurred for fish species present. Ecological analysis found significant differences for several autecological attributes between stable and unstable channels. Fish located at unstable sites tended to: 1) prefer open-water mesohabitat, 2) be dominated by herbivores with algae diet, and 3) exhibit non-guarding spawning behavior. Use of fish autecological data and the protocols applied in this study were found useful to improve "strength of evidence" approaches to link biological impairment to excessive SSC.

Introduction

Loss of biological integrity due to excessive erosion, transport, and deposition in rivers and streams is a major water quality (WQ) problem in the United States. The 2000 National WQ Inventory found that siltation was a leading cause of impairment, second to pathogens, representing 31% of the assessed and designated impaired rivers and streams. Siltation is generally defined as an impaired condition resulting from excessive fine sediments suspended in the water column, embedded in course bed sediments, and/or deposited in the active channel degrading habitat (USEPA, 2006). Siltation-impaired

streams on state §303(d) lists require states to development and implement sediment total maximum daily loads (TMDLs) (USEPA, 1999a). A TMDL represents a pollutant load allocation that meets a pollutant WQ standard (USEPA, 1999b). However for suspended sediment, no state to date has adopted a WQ standard although Minnesota has adopted a 25 NTU turbidity standard as a surrogate for suspended sediment. Most state WQ assessments rely on indices of biotic integrity (IBI) to designate biologically-impaired streams, and if no identifiable chemical degradation causes are identified, siltation is generally inferred in human-dominated watersheds. A critical need exists for a TMDL linkage analysis that can relate excessive fine sediments with loss of ecological function, so that sediment load reduction targets can be set in impaired watersheds.

In order to implement sediment TMDL targets that can potentially achieve a positive ecological response in degraded watersheds, targets must be ecologically-based. Stream ecosystems can be impacted by increased levels of suspended sediment in various ways including a reduction of primary production and macroinvertbrate abundance, which in turn can limit food availability for fish (Waters, 1995; Henley *et al*., 2000). Particularly with clear-water fishes, excessive suspended sediment over prolonged periods of time can cause mortality, depress growth, reproduction and recruitment, and elicit avoidance behavior inducing out migration from impacted reaches (Newcombe and MacDonald, 1991; Servizi and Martens, 1992; Newcombe, 2003). Although ecological responses can be complex, loss of ecological function can be observed by changes in fish community structure (Lamouroux *et al.*, 2002; Walters *et al.*, 2003).

Quantifying impacts on fish community structure from excessive suspended sediment has been problematic because of the episodic nature of elevated suspended sediment levels, and species-specific responses to sediment dose, and their regional differences (Newcombe, 2003; Schwartz *et al*., 2008). Simon *et al*. (2004) found significant differences of suspended sediment concentrations at the 1.5-year recurrence frequency ($Q_{1.5}$) among ecoregions in the United States, in which the $Q_{1.5}$ represents the effective sediment discharge. Effective discharge is defined as a discharge or range of discharges that over the long term transports the largest proportion of annual suspended sediment load (Wolman and Miller, 1960). Utilizing the $Q_{1.5}$ and a field-based geomorphic assessment technique to distinguish stable and unstable conditions, annual sediment yields ($T/yr/km^2$) was computed for watersheds and condition, providing a means to set a sediment TMDL allocation (Simon *et al*., 2004). This methodology reasonably assumes sediment loads estimated for unstable conditions were at levels that can induce biological impairment. However no linkage analysis has been attempted to test this hypothesis.

It is important as one of the outcomes of a TMDL linkage analysis is identifying what ecological functions have been lost due to elevated suspended-sediment levels (USEPA, 2006). Reliance on species data can introduce undue variance into the linkage analysis, and fails to identify what ecological functions have been lost. Ecological function can be expressed by species traits or autecological attributes, e.g. for fish, feeding and spawning behavior, mesohabitat preferences, microhabitat availability for predation avoidance and flood refugia (Schwartz, 2002). Use of autecological data in a linkage analysis may provide a means to identify specific losses of these ecological functions, which then sediment TMDLs can specifically target corrections through best management practices.

The objective of the study was to explore whether fish autecological data can be used in a linkage analysis relating biological impairment to suspended sediment metrics. A change in fish community structure, parameterized by autecological data based on species traits information, and related to channel stability may provide a useful methodology to link biological impairment to stream siltation.

Methods

Study Design: The study area was the Northwestern Great Plains Ecoregion (ER43), which includes western North and South Dakota, eastern Montana, and northeastern Wyoming (Fig. 1). Study sites included watersheds having United States Geological Survey (USGS) gauging stations with instantaneous discharge data and 15 or more suspended sediment collections. Suspended sediment collections contained wash load clays and silts, and suspended load sands. Basin drainage areas and elevations above MSL were also obtained from the USGS database for each site. Overall, a "strength of evidence" interpretive approach was to test an idea whether fish autecological data could be used to identify biologically impaired streams due to "siltation" by correlating autecological data to suspended sediment metrics. Fish data were obtained from federal and state agencies co-located at the USGS gauging station sites with flow and suspended sediment data, in which 77 sites were found. This "strength of evidence" is recommended for watershed-scale ecological analysis by USEPA (2000) guidance document on stressor identification.

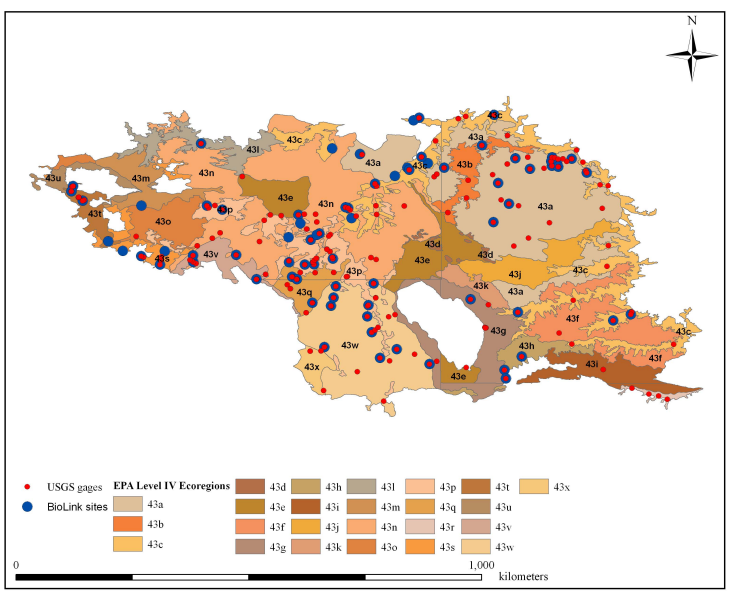

Figure 1. Location map of study sites in the NW Great Plains Ecoregion (43), showing USGS gauging stations and fish data sites.

Suspended Sediment Loads at the $Q_{1.5}$ for Stable and Unstable Channels: The $Q_{1.5}$ was computed by a log-Pearson Type III distribution using the annual-maximum peak-flow series for each of the sites with available data (Simon *et al*., 2004; 2008). Suspended-sediment yield at the $Q_{1.5}$ was obtained by using the sediment-transport relation developed for the site, substituting the $Q_{1.5}$ into the relation and solving for suspended sediment load. As part of the analytic procedure, the maximum sampled discharge is compared at the $Q_{1.5}$ to make sure that it falls within the flow range sampled. If the $Q_{1.5}$

exceeds the maximum sampled discharge by 50%, the site is not used in further analysis. This is because considerable error can occur in calculating loads high flows, particularly if the sediment-transport relation is extended beyond the measured bounds of the data. To normalize data for watersheds of different size, sediment load was divided by drainage area, providing calculations of sediment yield ($T/d/km^2$) and presented by quartile measures to describe data ranges and central tendencies.

Channel stability at each site was determined by a rapid geomorphic assessment (RGA), a field-based technique using nine metrics to infer dominant processes and magnitude of instabilities (Simon *et al*., 2004, 2008). The RGA was created based on geomorphic concepts from the channel evolution model, in which disturbance to an alluvial channel initiates a systematic response of downcutting followed by channel widening (Simon and Hupp, 1989; Simon, 1989; Simon and Darby, 1999). The RGA provides a quick assessment of channel stability providing an index score based on nine metrics consisting of: 1) primary bed material; 2) bed/bank protection; 3) degree of incision; 4) degree of constriction; 5) stream bank erosion; 6) stream bank instability; 7) established riparian woody-vegetative cover on banks; 8) occurrence of bank accretion; and 9) stage of channel evolution. ER43 field assessments were conducted in 2007 (Simon *et al*., 2008). Unfortunately, it is not uncommon suspended-sediment sampling was carried out over decades earlier, and measured suspended sediment loads do not represent current channel stability conditions. This issue was addressed by establishing stability condition during the sampling periods for suspended sediment using available USGS data and the following techniques: 1) examination of stage-discharge relationships and cross-sectional data noting whether bed elevation changed over time; and 2) analysis of long-term suspended-sediment data computing rating curve relationships by decade, and observing for changes in rating curve power function coefficients and exponents. Changes in rating relations imply channel adjustments with time, and possible unstable conditions. Study sites were designated as stable or unstable for current conditions based on the field RGA, and measured suspended sediment loads were used for matched conditions (Simon *et al*., 2008).

Autecological Data: Fish data were obtained from federal and state agencies, in which fish were sampled between the 1997 and 2006, with the majority of samples occurring between 2000 and 2003. Data sources included: 1) USEPA Region VIII EMAP and REMAP datasets; 2) North Dakota Division of Health (NDDH); 3) USGS Coop Unit at South Dakota State University, Dr. Charles Berry; and 4) Montana Department of Fish, Wildlife and Parks, online Fisheries Information System database (http://maps2.nris.state.mt.us/scripts/esrimap.dll?name =MFISH&Cmd=Main&Pc) accessed March 2, 2008. Fish data sites were co-located with USGS gauging station locations by latitude and longitude coordinates, in which a total of 77 sites were found. Per site, species presence and absence data were compiled from these four key data sources. Presence and absence data were used because: 1) analysis of this data type alleviates issues associated with differences in sampling gear and effort, important when abundance data are used, and 2) this study's focus on attributes of ecological function based on species traits, and essentially grouped as guilds. A summary list of fish species found within the final fish presence/absence dataset, and the number of occurrences per stable and unstable sites can be found in Table 1.

Table 1. Fish species with ordination codes, and the number of each species found within the dataset, at stable and unstable sites.

Ordination Name Code	Common Name	Number of sites fish species was present	Percent of 77 sites fish species was present	Number of stable sites fish species present	Number of unstable sites fish species present
BGMSHR	BIGMOUTH SHINER	4	5.2	2	2
BKBULL	BLACK BULLHEAD	22	28.6	10	11
BKSTKB	BROOK STICKLEBACK	6	7.8	6	0
BLCRAP	BLACK CRAPPIE	7	9.1	3	3
BLNSDC	BLACKNOSE DACE	8	10.4	6	2
BLSDDR	BLACKSIDE DARTER	0	0.0	0	0
BLUEGL	BLUEGILL	2	2.6	2	0
BROWNT	BROWN TROUT	5	6.5	2	3
BRSSMW	BRASSY MINNOW	11	14.3	7	4
BURBOT	BURBOT	2	2.6	1	1
CHCATF	CHANNEL CATFISH	32	41.6	11	18
CKCHUB	CREEK CHUB	16	20.8	9	6
CMCARP	COMMON CARP	46	59.7	22	20
CMSHIN	COMMON SHINER	0	0.0	0	0
CUTTHR	CUTTHROAT TROUT	1	1.3	1	0
EMRSHR	EMERALD SHINER	12	15.6	5	6
FATHMW	FATHEAD MINNOW	42	54.5	19	22
FLCHUB	FLATHEAD CHUB	38	49.4	14	19
FRDRUM	FRESHWATER DRUM	3	3.9	0	2
GLDSHR	GOLDEN SHINER	5	6.5	2	2
GOLDEY	GOLDEYE	16	20.8	6	8
GRSUNF	GREEN SUNFISH	33	42.9	16	16
IOWADR	IOWA DARTER	10	13.0	5	5
JOHNDR	JOHNNY DARTER	6	7.8	3	3
LGNSDC	LONGNOSE DACE	31	40.3	12	14
LKCHUB	LAKE CHUB	12	15.6	9	2
LMBASS	LARGEMOUTH BASS	10	13.0	6	4
LNNSKR	LONGNOSE SUCKER	11	14.3	4	5
MSCULP	MOTTLED SCULPIN	1	1.3	1	0
MTNSKR	MOUNTAIN SUCKER	10	13.0	3	5
MTNWTF	MOUNTAIN WHITEFISH	4	5.2	2	2
NOPIKE	NORTHERN PIKE	21	27.3	8	12
NPKILL	NORTHERN PLAINS KILLIFISH	3	3.9	2	1
NDBDC	NORTHERN REDBELLY DACE	3	3.9	2	1
OSSUNF	ORANGESPOTTED SUNFISH	2	2.6	2	0
PKSEED	PUMPKINSEED	7	9.1	3	3
PLKILL	PLAINS KILLIFISH	11	14.3	8	2
PLNSMW	PLAINS MINNOW	17	22.1	5	10
PLTOPM	PLAINS TOPMINNOW	1	1.3	0	1
PRLSHR	PEARL DACE	0	0.0	0	0
QUILLB	QUILLBACK	3	3.9	1	2
RAINBW	RAINBOW TROUT	3	3.9	2	1
RBSUNF	REDBREAST SUNFISH	1	1.3	0	1
RCARPS	RIVER CARPSUCKER	25	32.5	10	13
REDSHR	RED SHINER	5	6.5	1	4
ROCKBS	ROCK BASS	5	6.5	2	2
SATINF	SATINFIN SHINER	0	0.0	0	0

Ordination Name Code	Common Name	Number of sites fish species was present	Percent of 77 sites fish species was present	Number of stable sites fish species present	Number of unstable sites fish species present
SAUGER	SAUGER	5	6.5	3	1
SFCHUB	SICKLEFIN CHUB	1	1.3	1	0
SMBASS	SMALLMOUTH BASS	11	14.3	4	4
SMBUFF	SMALLMOUTH BUFFALO	1	1.3	0	0
SNDSHR	SAND SHINER	39	50.6	18	18
SPTSHR	SPOTTAIL SHINER	2	2.6	1	0
SREDHR	SHORTHEAD REDHORSE	29	37.7	10	16
STCHUB	STURGEON CHUB	4	5.2	1	3
STNCAT	STONECAT	27	35.1	10	14
TDMADT	TADPOLE MADTOM	1	1.3	1	0
WALLEY	WALLEYE	7	9.1	2	5
WHBASS	WHITE BASS	1	1.3	1	0
WHCRAP	WHITE CRAPPIE	2	2.6	1	1
WHTSKR	WHITE SUCKER	56	72.7	25	27
WSILVY	WESTERN SILVERY MINNOW	21	27.3	9	10
YLBULL	YELLOW BULLHEAD	7	9.1	4	2
YLPERC	YELLOW PERCH	2	2.6	2	0

Autecological data are species trait information for this study included: rearing mesohabitat preference (open water, pool, riffle), water quality tolerance, trophic structure, feeding location (bottom, pelagic, surface), feeding behavior (grazing, sorting, stalking, pursuit), diet (algae, crustaceans, insects, fish, etc.), and spawning behavior (guarding, nest builder type, egg dispersion/laying type) (Table not shown due to space limitations). Data were compiled for each species from the following references: Smith (1979); Etnier and Starnes (1993); Barbour *et al*. (1999); Coker *et al*. (2001); and on-line Search FishBase (www.fishbase.org) accessed February 18, 2008. Compiled data consisted of a spreadsheet matrix with fish species by rows and autecological attribute by columns, and when the attribute applied it was given a value of "1", and when it did not apply it was given a "0" value (Table not shown due to space limitations). A second spreadsheet matrix was generated that consisted of study site by autecological attribute, in which the number of occurrences an autecological attribute occurred for that site based on fish species presence were enumerated (Table not shown due to space limitations).

The approach to this ecological analysis was to first use ordination statistics to: 1) examine whether patterns of fish presence and absence correlated in ordination space with channel stability, accounting for the potential effects of basin attributes drainage area and elevation, and 2) through ordination statistics, examine what autecological attributes correlate with channel stability, which can be interpreted as to the potential losses of various ecological functions. Parametric statistics were then used to examine whether autecological attributes, summed by the number of occurrences by fish species per site, differed between stable and unstable sites. These statistics were used to support the qualitative findings observed by the ordination statistics.

Statistical Analysis: Ordination techniques included principal components analysis (PCA) and canonical correspondence analysis (CCA). PC-ORD (version 5.0) was used to perform these analyses (McCune and Mefford, 1999; McCune and Grace, 2002).

Typically for the CCA, site x fish species +/- data was used as the main data matrix, and site x physical variables was used as the secondary matrix. For the autecological analysis, "site x autoecological attributes" was used as the secondary data matrix. A t-test for unequal variances was used to test the statistical hypothesis that the means for an autecological attribute was significantly different between stable and unstable sites (Excel™ Data Analysis Tool). Each autecological attribute was tested separately and significance levels reported.

Results and Discussion

Fish distribution has been shown to be strongly influenced by site drainage area and elevation (Schwartz, 1991; Newall and Magnuson, 1999), particularly in this ecoregion (Rahel and Hubert, 1991; Kral and Berry, 2005; Hoagstrom *et al*., 2006). Therefore, a preliminary analysis tested whether channel stability was equal or greater in importance as drainage area and elevation influencing fish distribution. This analysis was necessary to provide evidence that the stability attribute could be effectively used in the analysis of fish autecological attributes. Site drainage area, elevation, and channel stability were found to be equally important as influencing basin-scale fish distribution for some species as observed by the CCA ordination (Fig. 2). In Figure 2, the channel stability eigenvector appeared to be slightly less dominant compared to drainage area and elevation plotted by axes 1 and 2, however, a better orientation of three basin attributes was observed by axes 2 and 3. A fish assemblage that clustered dominantly with stable sites included: brook stickleback, johnny darter, walleye, black crappie, pumpkinseed, yellow bullhead, brown trout, lake chub, mountain whitefish, and plains killifish (Fig. 2b). In this CCA ordination, the Pearson's correlation coefficients (*r*) for drainage area were -0.59, -0.59, and -0.26, elevation were -0.76, 0.77, and 0.22, and channel stability were -0.28, 0.41, and 0.86 (axes 1, 2, and 3, respectively).

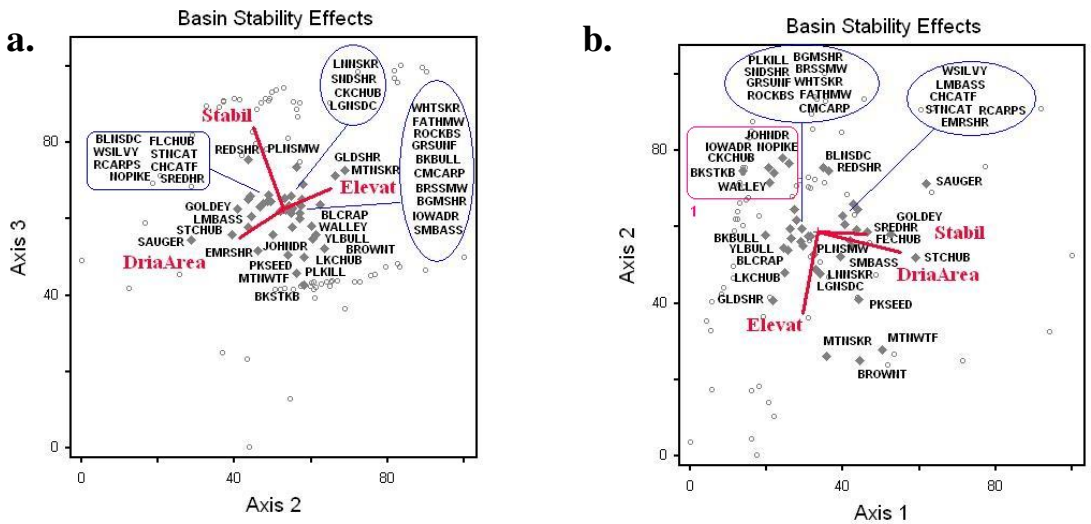

Fig. 2. CCA ordination of fish species by site, with secondary environmental attributes accounting for effects of site drainage area (DraiArea), elevation (Elevat), and channel stability (Stabil). Ordination plot shows a) axis 1 and 2; and b) axes 2 and 3. Ordination codes for fish species can be found in Table 1.

PCA ordination was used to examine the orientation of eigenvectors relative to site channel stability and various sets of autecological attributes. Fish with pool and riffle mesohabitat preferences strongly orientated with stable sites, whereas fish with open channel habitat preference and water-quality tolerant fish oriented more with unstable sites (axes 1 and 2 accounted for 72.8% of the variance). Ordination figures are not shown due to proceedings space limitations. By definition, unstable sites generally lack bed substrate suggesting channels for these sites would characteristically have more open channel, glide-type mesohabitat. The PCA examining site relationships of fish trophic structure and channel stability found unstable sites aligning strongly with herbivores (axes 1 and 2 accounted for 56.6% of the variance). Other trophic levels, e.g., insectivores and piscivores, did not orientate near clusters of stable or unstable sites. This relationship between unstable sites and herbivores is interesting considering that fish with open channel mesohabitat preference orientated with unstable site too. Herbivores tend to occupy shallow-water, glide habitat (Schwartz and Herricks, 2008).

The PCA examining site relationships of fish feeding behavior and channel stability was weak, but showed a slight tendency for stalking and pursuit behaviors to align with the stability eigenvector and unstable sites. In general, stable and unstable sites did not cluster in ordination space. Axes 1 and 2 in this PCA ordination with feeding behavior accounted for 64.2% of the variance. The PCA examining site relationships of fish diet and channel stability found unstable conditions aligning strongly with algae (axes 1 and 2 accounted for 73.1% of the variance). This result was consistent with findings where the herbivore eigenvector aligned with the stability eigenvector. It is possible watersheds with unstable channels tended to have nutrient rich waters from human and agricultural waste promoting algae growth, however this is only speculative without further analysis. Also, fish diets consisting of annelids, crustaceans and molluscs tended to orientate towards stable sites. The fact these secondary trophic prey oriented with stable sites is interesting from an ecosystem perspective, possibly inferring a broader food web structure in stable sites in contrast with unstable sites.

The PCA examining site relationships of fish spawning behavior and channel stability found unstable sites aligning strongly with egg non-guarders, egg deposition submerged open water and substrate, and egg adhered to substrate (axes 1 and 2 accounted for 51.1% of the variance). In contrast, stable sites aligned to some degree with egg guarders and nest builders. This result suggests that non-guarders that disperse eggs into the water column or on substrate do not require stable channel morphology, but guarders need adequate substrate to build nests, therefore their annual recruitment is dependent of stable bed morphology.

Statistical comparisons of site occurrences of autecological attributes, using a t-test to compare the attribute means between stable and unstable channels, resulted in 14 significant differences. Of the mesohabitat preference attributes, open water preference occurred more in unstable channels than stable channels ($p = 0.04$). Of the trophic level attributes, herbivores and piscivores species occurred more in unstable channels than stable channels ($p = 0.0021$, 0.09, respectively). Pelagic feeders and pursuit behavior occurred more often in unstable channels than stable channels ($p = 0.01$, 0.03, respectively). Grazing feeders and fish that prefer an algae diet were found more often in unstable channel than stable channels ($p = 0.10$, < 0.01, respectively). Of the spawning

behavior attributes, non-guarders, and egg dispersion into open water/substrate and on substrate occurred more often in unstable channels than stable channels ($p = 0.028$, 0.001, 0.068, respectively). Spawners that build nests were found more often in stable channels than unstable channels ($p = 0.01$). Also, fish that that prefer an annelid diet were found more often in stable channel than unstable channels ($p = 0.07$). Findings from this statistical analysis follow similarly the ordination statistics, in which the significant autecological attributes included: open water mesohabitat preference, herbivores, pursuit feeding behavior, algae diet, egg non-guarders, egg dispersion into open water/substrate and on substrate, and egg nest builders.

Conclusion

Sufficient evidence was found in the ecological analysis to support the utility of RGA determinations of stable-unstable reaches, and subsequent sediment transport differences summarized by suspended-sediment yield and dose (Simon *et al*., 2008). Whether the ecological consequences are from direct or indirect stressors, fish species that preferred open water channels occurred more often at unstable sites. In addition, herbivores with algae diet, pelagic piscivores with stalking and pursuit feeding behaviors, and fish with non-guarding spawning behavior that disperse eggs into the water column or adhere to loose substrate tended to occur more often in unstable channels. Fish that preferred pool-riffle habitat structure and had guarding spawning behavior occurred more often at stable sites. Ecologically, a "strength of evidence" interpretation suggests mesohabitat structure is degraded at some sites by sedimentation forming channels with open water, glide-pool habitat that appears to promote algae growth, and creates bed material dominated by sands which appears to promote fish recruitment by non-guarding spawners. In addition, non-guarding spawners that disperse eggs would benefit from more frequency events with high suspended sediment, increasing more days with higher turbidity. Findings from this study suggest the general approach to assess channel stability, and analyze for autecological differences between stable-unstable determinations hold promise as a linkage analysis protocol for sediment TMDLs. Autecological results, as described above, provide a means to guide development of additional studies focusing monitoring parameters. In addition, outcomes can support watershed corrective actions plans to meet required TMDL targets for sediment load reductions.

Acknowledgements

The study was funded by the USEPA Region VIII, Ecosystems Protection and Monitoring Program through a cooperative agreement with the USDA National Sedimentation Laboratory (Project # 6408-13000-017-31). We would like to thank Kris Jensen, USEPA Team Leader, and Tom Johnson and Tina Laidlaw for EMAP data support. Additional assistance with compiling fish data included: Mike Ell and Joe Gross with the North Dakota Department of Health, Division of Water Quality; Dr. Charles Berry with the South Dakota USGS Cooperative Unit at South Dakota State University, and Ann Harrie with the Montana Department of Environmental Quality. USDA NSL staff assisting in field work included Brian Bell, Danny Klimetz, and Mark Griffith**.** Danny Klimetz and Wendy Disckerson provided GIS and database support.

References

Barbour MT, Gerritsen J, Synder BD, Stribling JB. 1999. *Rapid Bioassessment Protocols for Use in Wadable Streams and Rivers: Periphyton, Benthic Macroinvertebrates, and Fish*. EPA 841-B-99-002. US Environmental Protection Agency, Washington DC.

Coker GA, Portt CB, Minns CK. 2001. *Morphological and Ecological Characteristics of Canadian Freshwater Fishes*. Can. MS Report Fish. Aquat. Sci. 2554: iv+89p.

Etnier DA, Starnes WC. 1993. *The Fishes of Tennessee*. University of Tennessee Press, Knoxville. 688p.

Henley WE, Patterson MA, Neves RJ, Lemly AD. 2000. Effects of Sedimentation and Turbidity on Lotic Food Webs: A Concise Review for Natural Resources Managers. *Reviews in Fisheries Science* **8**(2): 125-139.

Hoagstrom CW, Wall SS, Duehr JP, Berry CR. 2006. River size and fish assemblages in southwestern South Dakota. *Great Plains Research* **16**: 117-126.

Kral JG, Berry CR. 2005. Fishes at randomly selected sites on wadable streams in South Dakota. *Proceedings of the South Dakota Academy of Science* **84**: 305-313.

Lamouroux N, Poff NL, Angermeier PL. 2002. Intercontinental convergence of fish community traits along geomorphic and hydraulic gradients. *Ecology* **83**(7): 1792-1807.

McCune B, Mefford MJ. 1999. PC-ORD. *Multivariate Analysis of Ecological Data, Version 4*. MjM Software Design, Gleneden Beach Oregon, USA.

McCune B, Grace JB. 2002. A*nalysis of Ecological Communities*. MjM Software Design, Gleneden Beach Oregon, USA.

Newcombe CP. 2003. Impact Assessment Model for Clear Water Fishes Exposed to Excessively Cloudy Water. *J. American Water Resources Association* **39**(3): 529-544.

Newcombe CP, MacDonald DD. 1991. Effects of Suspended Sediment on Aquatic Ecosystems. *North American Journal of Fisheries Management* **11**: 72-82.

Newall PR, Magnuson JJ. 1999. The importance of ecoregion versus drainage area on fish distributions in the St. Croix River and its Wisconsin tributaries. *Environmental Biology of Fishes* **55**: 245-254.

Rahel FJ, Hubert WA. 1991. Fish assemblages and habitat gradient in a Rocky Mountain-Great Plains stream: biotic zonation and additive patterns of community change. *Transactions of the American Fisheries Society* **120**: 319-332.

Schwartz JS. 1991. *Influence of Geomorphology and Land Use on Distribution and Abundance of Salmonids in a Coastal Oregon Basin*. MS Thesis. Oregon State University, Corvallis.

Schwartz JS. 2002. *Stream Habitat Characterized by Stage-specific Flows and Three-dimensional Geomorphological Complexity: Development of Ecological Criteria for Stream Restoration Design*. PhD Dissertation. University of Illinois, Urbana.

Schwartz JS, Dahle M, Robinson RB. 2008. Concentration-frequency-duration curves for stream turbidity: possibilities for use assessing biological impairment. *J. American Water Resources Association* **44**(4): 879-886. DOI 10.1111/j.1752-1688.2008.00186.x.

Schwartz JS, Herricks EE. 2008. Fish use of ecohydraulic-based mesohabitat units in a low-gradient Illinois stream: implications for stream restoration. *Aquatic Conservation: Marine & Freshwater Ecosystems* **18**: 852-866. DOI 10.1002/aqc.905.

Servizi JA, Martens DW. 1992. Sublethal Responses of Coho Salmon (*Oncorhynchus kisutch*) to Suspended Sediments. *Can. J. Fish. Aquat. Sc*. **49**: 1389-1395.

Simon, A. 1989. A model of channel response in disturbed alluvial channels. E*arth Surface Processes and Landforms* 14(1): 11-26.

Simon A., Darby SE. 1999. The nature and significance of incised river channels. Pages 3-18 I*n Incised Rivers Channels: Processes, Forms, Engineering, and Management*. SE Darby, A. Simon editors. John Wiley and Sons, UK.

Simon A, Heins A, Dickerson W. 2004. Suspended-sediment transport rates at the 1.5-year recurrence interval for ecoregions of the United States: transport conditions at the bankfull and effective discharge? *Geomorphology* **58**: 243-262.

Simon A., Klimetz L, Schwartz JS. 2008. Characterization of "Reference" Suspended-Sediment Transport and Bed Material Conditions for Selected Ecoregions in EPA Region VIII: The Mountains and Plains. USDA, Agricultural Research Service, National Sedimentation Laboratory Technical Report 61, Watershed Physical Processes Research Unit, April 2008.

Smith PW. 1979. *The Fishes of Illinois*. University of Illinois Press, Urbana. 314p.

USEPA. 1999a. Protocols for Developing Sediment TMDLs. EPA-841-B-99-004. U.S. Environmental Protection Agency, Office of Water, Washington DC.

USEPA. 1999b. Draft Guidance for Water Quality-based Decisions: The TMDL Process. EPA-841-D-99-001. U.S. Environmental Protection Agency, Washington DC.

USEPA. 2000. Stressor Identification Guidance Document. EPA/822/B-00/025. U.S. Environmental Protection Agency, Office of Research & Develop., Washington DC.

USEPA, 2000. Water Quality Report, Appendix A. Available online at: http://www.epa.gov/305b/2000report/appendixa.pdf Accessed 4/2/08

USEPA. 2006. Framework for Developing Suspended and Bedded Sediments (SABS) Water Quality Criteria. EPA-822-R-06-001. U.S. Environmental Protection Agency, Office of Water, Office of Research and Development, Washington DC.

Walters DM, Leigh DS, Bearden AB. 2003. Urbanization, sedimentation, and the homogenization of fish assemblages in the Etowah River Basin, USA. *Hydrobiologia* **494**: 5-10.

Waters TF. 1995. *Sediment in Streams, Sources, Biological Effects and Control*. American Fisheries Society Monograph 7, Bethesda, Maryland. 251 p.

Wolman MG, Miller JP. 1960. Magnitude and frequency of forces in geomorphic processes. *Journal of Geology* **68**: 54-74.

The Effect of Natural Hydrological Disturbances (Defined From HSPF Simulated Hydrographs) on Trout Populations in Ungaged Streams of the Great Smoky Mountain National Park

Keil J Neff[1] Joseph Parker[1] John Schwartz[2] Matt Kulp[3] Steve Moore[3] Meijun Cai[1]

[1]Graduate Research Assistant, University of Tennessee, Department of Civil and Environmental Engineering, 223 Perkins Hall, Knoxville, TN 37996 kneff1@utk.edu; jparke33@utk.edu; mcai@utk.edu
[2]Assistant Professor, University of Tennessee, Department of Civil and Environmental Engineering, 63 Perkins Hall, Knoxville, TN 37996 jschwart@utk.edu
[3]Fisheries Biologist, National Park Service, Great Smoky Mountains National Park, 107 Park Headquarters Road, Gatlinburg, Tennessee 37738, USA; (865) 436-1250; Matt_Kulp@nps.gov; Steve_E_Moore@nps.gov

Abstract

Hydrological processes impact the functioning of ecosystems and influence fish population dynamics. In the Great Smoky Mountains National Park (GRSM), native brook trout (*Salvelinus fontinalis*) and rainbow trout (*Oncorhynchus mykiss*) populations have declined in some watersheds over the past two decades. Since 1986, 69 streams (369 sites) are routinely sampled by GRSM fisheries biologists, in which detailed data have been collected on fish condition (length, weight), abundance, year class strength, and biomass. To evaluate the impact of floods and droughts on trout, indicators of hydrologic alteration (IHA) were computed for 127 fish sampling sites between 1990 and 2007. The Hydrological Simulation Program - FORTRAN was used to model flows at each ungaged fish-sampling stream site. Outlets were defined for each site, and flow was calculated for the period of record. The model was calibrated by adjusting parameters including storage, infiltration, runoff, and ground water for three elevation classes (low < 800 m ≤ medium < 1200 m ≤ high) to fit flow output from model with two USGS gaging stations and one NPS gaging station. The ecohydrologic regimes, characterized using the IHA method, were compared with trout abundance and biomass at each site. Results indicated the abundance of young-of-the-year brook and rainbow trout significantly declined after extreme floods and droughts. In particular, low-flows during droughts significantly reduced recruitment for both brook and rainbow trout, which is likely due to decreased spawning habitat. Brook trout populations in larger low-elevation streams showed more stability compared to smaller headwater streams.

Key Words: drought, Great Smoky Mountains, flood, HSPF, IHA, trout

Introduction

The flow regime of a stream affects the structure, composition, and productivity of fish communities by regulating abiotic habitat conditions and biotic processes (Poff et al. 1997; Richter et al. 1996). In the Great Smoky Mountains National Park (GRSM), native brook trout (*Salvelinus fontinalis*) and rainbow trout (*Oncorhynchus mykiss*) populations have declined in some watersheds over the past two decades. Although it is believed that trout have primarily been impacted by episodic acidification, the effect of natural hydrological extremes or disturbances on brook trout populations in GRSM streams is examined in this research.

Floods and droughts are the major forms of natural hydrologic disturbances that regulate riverine biological communities (Cattaneo et al. 2002). The natural flow regime of a river plays a critical role in determining the distribution, diversity, and abundance of riverine species. A river's flow regime can affect abiotic characteristics such as flow depth and velocity, temperature, oxygen content, turbidity, streambed substrate, and morphology (Richter et al. 1997), and biotic processes in the riverine community (Poff et al. 1997). The timing, frequency, duration, and magnitude of a disturbance may dictate the success or failure of populations in stream ecosystems (Lake 2000). The severity of the hydrologic event to biota is dependent on the timing of the event relative to the fish developmental stage. Mountain headwater streams, such as those in the GRSM, are more sensitive to variations in streamflow which affects the availability of habitat for communities to grow, forage, and reproduce (Elwood and Waters 1969).

High-elevation stream communities are especially prone to large disturbances caused by floods (Roghair et al. 2002; Swanson et al. 1998). Floods may cause rapid effects on fish populations primarily from high in-stream velocities and debris flow, which may cause death, displacement, or reduce effective habitat (Elwood and Waters 1969). Harvey (1987) concluded that the ability of fish to maintain their position in-stream under high flows increased rapidly with size because larger fish are stronger and have better swimming abilities. Extreme high flows can destroy or damage fish eggs or larvae in redds (Carline and McCullough 2003) or increase sedimentation of fine material on spawning gravel decreasing oxygen availability to developing embryos and physically trapping emerging alevins (Jensen and Johnsen 1999). Additionally, fish can be stranded in isolated pools from the main channel once a flood flow has receded. Severe flooding in salmonid streams commonly destroys the year class of fish that are still incubating or have recently emerged and can take two to three years to recolonize (Carline and McCullough 2003). Timing is important as winter flooding can destroy redds of fall-spawning brook trout and spring floods can destroy redds of spring-spawning rainbow trout.

Droughts can affect the fish communities by physically decreasing the surface area and volume of the water body, and by altering the water quality, particularly temperature and oxygen (Closs and Lake 1996; Cowx et al. 1984; Matthews and Marsh-Matthews 2003). Drought reduces habitat leading to increased fish density, causing increased biotic interactions including predation and competition for diminishing food. Low water levels may prevent aquatic species access to spawning grounds leading to possible loss of a year class (Lake 2003; Richter et al. 1996).

Severe drought may reduce groundwater flow into streams thereby negatively affecting spawning grounds for fish species that utilize discharging groundwater to regulate temperature, chemistry, and hydrology within redds (Curry et al., 1995). Low flow can cause brook trout eggs to become infected with the fungus *Saprolegnia* reducing the recruitment class (Hakala and Hartman 2004). Lack of food abundance has been attributed to a loss of benthic macroinvertebrate populations, reduction in surface area available to catch falling terrestrial insects, and diminished invertebrate drift, the principal food source for salmonids (Canton et al. 1984; Hakala and Hartman 2004).

The objective of the current study was to evaluate the impact of floods and droughts on trout populations for 127 fish sampling sites in the GRSM between 1990 and 2007. The Hydrological Simulation Program - FORTRAN (HSPF) was used to model flows at each ungaged fish-sampling stream site. The ecohydrologic regimes, characterized using the indicators of hydrologic alteration (IHA) method, were statistically correlated with trout population data to evaluate the influence of hydrological disturbances to trout populations in the GRSM.

Methods

Study Area

The GRSM lies in the Blue Ridge physiographic region, located in the Southern Appalachians in eastern Tennessee and western North Carolina. The physiographic region is characterized by rugged topography, heavily forested slopes, and steep mountain streams. Streambeds are dominated by boulder and cobble, and gradients of the stream channels increase with elevation (Larson and Moore 1985). The climate of the GRSM can be described perhumid mesothermal with seasonal temperature variation and precipitation distributed throughout the year.

The average annual rainfall varies significantly throughout the park with lower elevations generally receiving near 127 cm and some higher elevation sites more than 215 cm (NCDC 2008). Most summer rainfall occurs during thunderstorms and an occasional tropical storm. Winter precipitation is associated with large-scale frontal systems. Summer and early spring generally have the most abundant precipitation, with rainfall averages of 12.7 cm and 20.3 cm per month in lower and upper elevations, respectively. Autumn is the driest season due to slow-moving high pressure systems, with rainfall averages around 7.6 cm and 12.7 cm per month in lower and upper elevations, respectively.

Brook trout is the only salmonid species indigenous to the southern Appalachian Mountains. Rainbow trout were introduced into GRSM streams in the early 1900's and often live sympatrically with the native brook trout (Larson and Moore 1985). Rainbow trout usually dominate lower elevation streams, whereas brook trout are predominantly found in headwater streams.

GRSM fishery biologists have surveyed brook and rainbow trout populations at 369 sites in 69 different streams since 1990 (Moore and Kulp 2007). Trout samples are collected in the summer and early fall (May to October) using backpack electroshocking units. Most sites are surveyed every 3-5 years; approximately 25 sites are surveyed annually. Trout are collected from a 100 m representative section of stream by a standard three-pass removal technique (Reynolds 1996). Trout are

separated into two age groups, young of year (YOY) and adults, and are measured for total length (mm) and weight (g). Trout less than 100 mm in length are classified as YOY. Using a maximum likelihood estimator, population estimates are generated based on the number of trout sampled from a section of stream. Trout densities are calculated as population per unit area of stream (number of trout/100 m^2). Trout biomass is reported as kilograms of trout per hectare (kg/ha).

The current study evaluates trout survey data for the period 1990-2007. We assumed trout sites within a 700 m reach did not have significantly different hydrology, and combined sites within this distance when confluences and physical barriers did not separate them. Trout data was averaged for combined sites.

Hydrology Model

HSPF, developed through the U.S. Environmental Protection Agency (USEPA), was used to model flows at the 127 ungaged fish-sampling stream sites. Watersheds for each of the study sites were delineated using a Digital Elevation Model (DEM; cell size = 9.13 m^2) in ArcMap 9.2 and brought into Better Assessment Science Integrating Point and Nonpoint Sources (BASINS). Watersheds were characterized using manual delineation to represent the topography (DEM), streams (National Hydrologic Dataset), and ArcMap created subbasin boundaries. BASINS used these three layers to create the map layers required for setting up the HSPF model, including defining and physically characterizing the stream network, calculating subbasin slopes and areas, and defining outlets. Additionally, a landuse layer was created, characterized as forest or field, and incorporated into the model.

Three gaged watersheds were used to define and calibrate hydrologic parameters in HSPF. This included two USGS gages (Stations 03497300 and 03460000) and a high-elevation H-flume at Noland Divide (Cai and Schwartz 2008). A three-tier hydrologic parameter band was used assuming the major change in the hydrologic parameters was primarily due to elevation differences. Subwatersheds were associated with outlets a) above 1200 m with the Noland Divide high-elevation parameters, b) between 800 m and 1200 m with Station 03460000 middle-elevation parameters, and c) below 800 m with Station 03497300 low-elevation parameters.

Time series data including hourly potential evapotranspiration (calculated from daily high and low temperatures and latitude) and hourly precipitation were required to simulate hydrology in HSPF. Hourly rainfall and daily temperature data were acquired for 16 stations from sources including the Tennessee Valley Authority, the National Oceanic and Atmospheric Administration through the National Climatic Data Center (NCDC), and the National Park Service (NPS). Seven different climate layers containing a unique combination of the weather stations were used to simulate the study watersheds throughout the GRSM. Weather data was segregated into high- and low-elevation classes, defined at 1000 m.

The model was calibrated by adjusting hydrologic parameters including storage, infiltration, runoff, and groundwater for three elevation classes (low<800 m $\leq$ middle $\leq$ 1,200 m < high) to observed flows from the aforementioned gaging stations. The calibration period for both USGS stations (03497300 and 03460000) was approximately 10 years. First, the annual water volume balance and parameters controlling groundwater and evapotranspiration losses were adjusted. Monthly

volumes and baseflows were examined by adjusting parameters including infiltration, monthly evapotranspiration rates, and storage capacities. To fine-tune the peak of the hydrograph and the recession rate, the hydrograph shape, and interflow and upper zone storage parameters were adjusted. Yearly and monthly volumes were examined during calibration. During model calibration, annual volume differences less than 15% were deemed acceptable (Donigian et al. 1983). Models with a coefficient above 0.6 were considered to perform satisfactorily (BASINS 2007). Additionally, the Nash and Sutcliffe (1970) coefficient of efficiency (NSE) was used to evaluate model performance, with NSE values greater than 0.36 considered acceptable (Kim et al. 2007). After the model was calibrated and met the visual and goodness-of-fit criteria, Station 03460000 was modeled for a five-year validation period. Finally, the hydrology of each of the 127 trout sites were simulated for the period between January 1, 1990 and December 31, 2007 corresponding to the years the GRSM has surveyed trout populations.

Indicators of Hydrologic Alteration

Hydrologic regimes were assessed using a method proposed by Richter et al. (1996) referred to as the IHA method. Once hydrology simulations of the trout sites were completed, daily flows for each site were characterized into ecologically relevant parameters using IHA software developed by the Nature Conservancy. The IHA program calculated 32 parameters organized into five hydrological groups to statistically characterize hydrologic variation in the flow regime, including ecologically-significant flow parameters of magnitude, timing, frequency, duration, and rate of change. Additionally, environmental flow components (EFCs) were calculated to include five components important to river ecosystem health; including extreme low flows, low flows, high-flow pulses, small floods, and large floods. The IHA and EFC parameters were calculated using non-parametric (median and percentile) statistics because of the non-normal nature of the hydrology data.

Statistical Analyses

The relationship between trout populations and hydrology patterns over the entire study period was examined. The 67 IHA hydrology parameters were statistically compared to brook and rainbow trout metrics including density (YOY and adult), total biomass, and ratio of brook adult density to rainbow adult density for each site. The means of IHA variables were normalized among sites by taking IHA variables with units of flow and dividing them by the mean flow (average of the monthly medians). Nonparametric multivariate analyses were performed to define significant correlations between the trout metrics and normalized IHA variables. Relationships between each IHA hydrology variable and trout metric were examined using the Spearman's Rho. A relationship among trout and predictor variables was considered significant if the p-value was less than 0.05.

The relationship between trends in trout populations and hydrology were also evaluated. We defined a trend as a discernable decrease or increase in a trout metric for three or more consecutive years with a correlation coefficient above 0.70. YOY trout were excluded from this analysis because of high variability in the data. Once trends were identified, a linear regression was performed; the slope of the regression

was used to characterize the trend. The IHA hydrology variables during the periods of the identified trout population trends were characterized. Nonparametric multivariate analysis of trends of trout metrics and corresponding IHA parameters were used to identify significant correlations between trout population trends and hydrology. An additional variable, trout watershed area (in thousandths of hectares – same order of magnitude), was incorporated in this analysis as well. The criteria set for examining significant results was $p < 0.01$ for brook trout and $p < 0.05$ for rainbow trout.

To evaluate the relationship between hydrological extremes and trout abundance, three IHA variables were chosen to represent hydrological extremes including the 10-year flood, the two most extreme 90-day minimum flows, and the two largest 2-year floods. The 90-day minimum was used because it characterized an extended dry period which has been shown to significantly affect aquatic communities (Lake 2003). Trout populations were examined for a four-year period during these extreme hydrologic events. Adult brook and rainbow densities, and total biomass were examined before, during, after, and two years following the floods and droughts. The affects of the floods and droughts on the YOY brook and rainbow trout population densities were evaluated by comparing the mean YOY population and the post-drought population. Over 50 data points were used for each year in both the flood and drought analyses. Means were compared using Student's t pairwise comparison test and considered significant at the $\alpha = 0.05$ level. Outliers, determined by standardized residuals by finding the residual and sample standard deviation, were omitted. A least squares difference matrix and ordered difference report were used to examine the results of the means comparison.

Results

The visualization plots and goodness of fit measures for calibration and validation indicated the HSPF hydrology model was able to adequately represent the hydrological processes in GRSM and were aligned with USEPA recommendations (USEPA 2000). Output from the calibrated models of the two USGS gaging sites indicated better than satisfactory model performance and met simulation objectives. The hydrologic modeling results from Station 03460000 during the validation period verified the performance of the model and also met stipulated criteria. Calibration and validation results by month showed the model generally met the 15% volume difference, but consistently overestimated fall flow rates, although the majority of R^2 values and Sutcliffe values were within the acceptable range.

Brook trout were more abundant in streams with larger fall flows as evidenced by positive correlations with mean stream flows in September, October, and November. Additionally, brook trout were also positively correlated with high and low pulse lengths. Brook trout were less abundant when streams had larger spring flows as indicated by the negative relationships with mean stream flows in February, March, April, and May. Brook trout were also negatively correlated with the fall rate and reversals. A higher ratio of brook trout adult densities were found in streams with higher mean monthly flows in the fall; alternatively, lower density ratios corresponded to higher mean monthly flows in the spring. Rainbow trout were more abundant in streams with larger mean spring flows indicated by positive correlations

with stream flows in March, April, and May. Rainbow trout were also positively correlated with reversals. Rainbow trout were less abundant in streams with longer high and low pulse lengths.

Brook trout in smaller watersheds have greater increases and decreases in population such that larger streams have less steep trends than headwater streams. Brook trout increases in abundance positively correlated with increases in high and low pulse lengths. A decrease in the ratio of brook trout adult density to rainbow trout adult density was correlated with decreases in February and March mean flows.

YOY brook and rainbow trout populations decreased in following droughts and floods. Adult brook trout densities and total brook trout biomass significantly increased two years following droughts. Adult rainbow trout densities and rainbow trout total biomass significantly decreased following droughts and recovered the following year. Adult brook densities were not significantly affected by larger floods. Adult rainbow densities did not significantly decline a year following floods, but significantly decreased two years following the extreme hydrologic event.

Discussion

Brook trout were found to be more abundant in streams with larger mean flows in autumn which corresponds to spawning (Etnier and Starnes 1993; Moore and Kulp 2008). Lower mean flows during these critical months were found to harm recruitment especially after severe droughts occurring in late summer and early fall. Low flows associated with a severe drought may have influenced brook recruitment in several ways: 1) adult brook trout surviving the drought months likely had diminished body fat reserves leading to reduced egg deposition (Canton et al. 1984); 2) low water levels during autumn months would expose more streambed and decrease available spawning habitat (Hakala and Hartman 2004); and 3) lower flows may have enabled sediment to deposit on redds, possibly reducing oxygen for the embryos (Reice et al. 1990). Hydrograph fall rates were also seen to be negatively correlated with brook trout abundance and may have impacted recruitment by exposing eggs and thereby causing desiccation of redds. Adult brook trout were found to be more resistant to severe drought than YOY trout. YOY trout may be less tolerant than older trout of increased temperatures and decreased oxygen content associated with lower flows (Closs and Lake 1996). Decreased riffle habitat may have also led to the increased mortality of YOY trout (Cowx et al. 1984). Similar to brook trout, rainbow trout were found more abundant in streams with a larger mean flows when spawning occurs. Rainbow trout spawn from late winter to early summer, and would similarly have better recruitment with better habitat conditions influenced by hydrology.

The strong influence severe droughts have on rainbow trout abundance was apparent from the results. Similar to brook trout YOY, rainbow YOY densities declined significantly after major droughts. Unlike adult brook trout, adult rainbow densities and total rainbow biomass significantly declined after severe droughts. These declines could possibly be attributed to: 1) adult rainbow trout being significantly larger than brook trout and having a harder time finding refugia (Moore and Kulp 2008); 2) diminishing habitat and food both of which would cause increased competition during drought conditions (Canton et al. 1984); and 3) rainbow trout are

not native and would not have evolved survival traits specific to streams of the Southern Appalachians (Moore and Kulp 2008). Adult rainbow abundance did show a strong recovery the second year after the drought to near pre-drought levels, which indicated the resilience of the species.

Brook trout were found less abundant in streams with larger mean spring flows and this may be due to smaller yearly recruitments associated with loss of redds, or displacement of recently hatched YOY by stronger currents (Harvey 1987). Large flood events also usually occurred in late winter or early spring, corresponding to incubation and emergence of the brook trout year class. There were significantly fewer YOY brook trout after large flood events. This may be attributed to incubating eggs and YOY trout not being able to maintain their position under strong currents and being swept downstream against debris and substrate. Seegrist and Gard (1972) and Carline (2003) both found similar results and concluded winter floods destroyed incubating or recently emerged year classes. Adult brook densities, however, did not change significantly after large flood events. This is likely due to their strong swimming ability and ability to find refugia in complex habitat morphology. Like brook trout, rainbow YOY densities sharply declined after larger floods, where as adult densities did not.

The reason smaller streams have steeper shifts in brook trout populations may be attributed to increased frequency of extreme hydrological events and less habitat and refugia to take shelter in during large disturbances (Elwood and Waters 1969). Larger streams may be more diverse and would be able to provide more refugia such as deep pools which would be utilized under extreme hydrological events (Pearsons et al. 1992). Smaller streams would also have smaller numbers of trout and be limited in their total production, and thereby would be more vulnerable to larger shifts in abundance caused by extreme hydrological events.

Characterizing stream ecosystems and evaluating the ecohydrology relationships was better utilized when the species traits were examined. Mathews and Richter (2007) suggested looking at ecohydrology relationships utilizing IHA metrics in stages corresponding to important life cycles of the aquatic species of interest. Their proposed IHA methodology was successfully demonstrated in this study. By identifying the important life cycles of both brook and rainbow trout, such as spawning and emergence, and splitting the trout populations into two separate age-groups, the ecohydrology relationships were identified and useful conclusions were made on how hydrological patterns influence the population dynamics of brook and rainbow trout in the GRSM.

Stream hydrological patterns do play an important role in determining the abundance of brook and rainbow trout in the GRSM. The magnitude and timing of extreme hydrological events, such as droughts and floods, was shown to be a major regulator of trout assemblages. The mean magnitude of monthly water conditions demonstrated dominant controls in the distribution and abundance of rainbow and brook trout. Trout spawning success was also strongly dependent on hydrology with the strength of yearly recruitments shown to correspond to certain hydrological patterns. In addition, the IHA software was shown to adequately characterize the flow regime into manageable ecohydrology parameters that could be statistically compared to brook and rainbow trout abundance. The conclusions of this study helps

GRSM fisheries biologist understand how certain hydrology patterns and extremes influence the brook and rainbow trout populations, allowing them to more effectively manage valuable GRSM resources.

References

Cai, M., and Schwartz, J. S. (2008). WinHSPF Model Simulations of Nitrogen and pH for a Low-Alkalinity Stream Impacted from Atmospheric Acid Deposition. ASCE/EWRI World Environmental & Resources Congress: Honolulu, HI, May 12-16, 2008.

Canton, S. P., Cline, L. D., Short, R. A., and Ward, J. V. (1984). "The Macroinvertebrates and fish of a Colorado stream during a period of fluctuating discharge." *Freshwater Biology*, 14(3), 311-316.

Carline, R. E., and McCullough, B. J. (2003). "Effects of floods on brook trout populations in the Monongahela National Forest, West Virginia." *Transactions of the American Fisheries Society*, 132(5), 1014-1020.

Cattaneo, F., Lamouroux, N., Breil, P., and Capra, H. (2002). "The influence of hydrological and biotic processes on brown trout (Salmo trutta) population dynamics." *Canadian Journal of Fisheries and Aquatic Sciences*, 59(1), 12-22.

Closs, G. P., and Lake, P. (1996). "Drought, differential mortality and the coexistence of a native and an introduced fish species in a south east Australian intermittent stream." *Environmental Biology of Fishes*, 47(1), 17-26.

Cowx, I. G., Young, W. O., and Hellawell, J. M. (1984). "The influence of drought on the fish and invertebrate populations of an upland stream in Wales." *Freshwater Biology*, 14(2), 165-177.

Donigian, A. S., Jr., Imhoff, J. C., and Bicknell, B. R. (1983). "Predicting water quality resulting from agricultural nonpoint source pollution via simulation - HSPF." *Agricultural management and water quality*, 200-249.

Elwood, J. W., and Waters, T. F. (1969). "Effects of floods on food consumption and production rates of a stream brook trout population." *Transactions of the American Fisheries Society*, 98(2), 253-&.

Etnier, D. A., and Starnes, W. C. (1993). The Fishes of Tennessee. Knoxville: The University of Tennessee Press.

Hakala, J. P., and Hartman, K. J. (2004). "Drought effect on stream morphology and brook trout (Salvelinus fontinalis) populations in forested headwater streams." *Hydrobiologia*, 515(1-3), 203-213.

Harvey, B. C. (1987). "Susceptibility of young-of-the-year fishes to downstream displacement by flooding." *Trans. Am. Fish. Soc.*, 116, 851-855.

Jensen, A. J., and Johnsen, B. O. (1999). "The functional relationship between peak spring floods and survival and growth of juvenile Atlantic Salmon (Salmo salar) and Brown Trout (Salmo trutta)." *Functional Ecology*, 13(6), 778-785.

Kim, S. M., Benham, B. L., Brannan, K. M., Zeckoski, R. W., and Doherty, J. (2007). "Comparison of hydrologic calibration of HSPF using automatic and manual methods." *Water Resources Research*, 43(1).

Lake, P. S. (2000). "Disturbance, patchiness, and diversity in streams." *Journal of the North American Benthological Society*, 19(4), 573-592.

Lake, P. S. (2003). "Ecological effects of perturbation by drought in flowing waters." *Freshwater Biology*, 48(7), 1161-1172.

Larson, G. L., and Moore, S. E. (1985). "Encroachment of exotic rainbow trout into stream populations of native brook trout in the southern Appalachian mountains." *Trans. Am. Fish. Soc.*, 114, 195-203.

Mathews, R., and Richter, B. D. (2007). "Application of the indicators of hydrologic alteration software in environmental flow setting." *Journal of the American Water Resources Association*, 43(6), 1400-1413.

Matthews, W. J., and Marsh-Matthews, E. (2003). "Effects of drought on fish across axes of space, time and ecological complexity." *Freshwater Biology*, 48(7), 1232-1253.

Moore, S. E., and Kulp, M. A. (2007) Great Smoky Mountains National Park Trout Data Base, Data Base Prepared by the U.S. NPS, Gatlinburg, TN.

Moore, S. E., and Kulp, M. A. (2008). Personal Communication with Great Smoky Mountains National Park Fisheries Biologists, J. Parker, ed., Gatlinburg, TN.

NCDC. (2008). Climate Norms: Climate of Tennessee. Retrieved September 1, 2008, from the National Oceanic and Atmospheric Administration, http://www5.ncdc.noaa.gov/climatenormals/clim60/states/Clim_TN_01.pdf.

Pearsons, T. N., Li, H. W., and Lamberti, G. A. (1992). "Influence of habitat complexity on resistance to flooding and resilience of stream fish assemblages." *Trans. Am. Fish. Soc.*, 121, 427-436.

Poff, N. L., Allan, J. D., Bain, M. B., Karr, J. R., Prestegaard, K. L., Richter, B. D., Sparks, R. E., and Stromberg, J. C. (1997). "The natural flow regime." *BioScience*, 47(11), 769-784.

Reice, S. R., Wissmar, R. C., and Naiman, R. J. (1990). "Disturbance regimes, resilience, and recovery of animal communities and habitats in lotic ecosystems." *Environmental Management*, 14(5), 647-659.

Reynolds, J. B. (1996). "Chapter 8: Electrofishing." Fisheries Techniques, B. R. Murphy and D. W. Willis, eds., American Fisheries Society, Bethesda, Maryland, 221-253.

Richter, B. D., Baumgartner, J. V., Powell, J., and Braun, D. P. (1996). "A method for assessing hydrologic alteration within ecosystems." *Conservation Biology*, 10(4), 1163-1174.

Richter, B. D., Baumgartner, J. V., Wigington, R., and Braun, D. P. (1997). "How much water does a river need?" *Freshwater Biology*, 37(1), 231-249.

Roghair, C. N., Dolloff, C. A., and Underwood, M. K. (2002). "Response of a brook trout population and instream habitat to a catastrophic flood and debris flow." *Transactions of the American Fisheries Society*, 131(4), 718-730.

Seegrist, D. W., and Gard, R. (1972). "Effects of floods on trout in Sagehen Creek, California." *Trans. Amer. Fish. Soc.*, 101, 478-482.

Swanson, F. J., Johnson, S. L., Gregory, S. V., and Acker, S. A. (1998). "Flood disturbance in a forested mountain landscape - Interactions of land use and floods." *Bioscience*, 48(9), 681-689.

USEPA. (2000). BASINS Technical Note 6: Estimating Hydrology and Hydraulic Parameters for HSPF. Office of Water, EPA-823-R00-012.

Upper Mississippi River Basin Envirohydrologic Observatory

Jeremy Bril[1], J.V. Loperfido[1], Craig Just[2], and Nathan Young[2]

[1]Graduate Research Assistant, IIHR – Hydroscience & Engineering, Dept. of Civil and Environmental Engineering, The University of Iowa, Iowa City, IA 52245; email: jeremy-bril@uiowa.edu; jloperfi@engineering.iuowa.edu
[2]Associate Research Engineer, IIHR – Hydroscience & Engineering, Adjunct Assistant Professor, Dept. of Civil and Environmental Engineering, The University of Iowa, Iowa City, IA 52245; email: craig-just@uiowa.edu; nathan-young@uiowa.edu

Abstract

The University of Iowa's IIHR - Hydroscience & Engineering is creating an *envirohydrologic* observatory on Pool 16 of the Upper Mississippi River. Centered at the Lucille A. Carver Mississippi Riverside Environmental Research Station (LACMRERS), the observatory's sensor network will collect highly time resolved data to support modeling efforts for water quality and watershed process studies. Coupling sensor data with models will enable testing of existing hypotheses and will generate new hypotheses focused on water quality, nutrient, and sediment fluxes as they relate to food webs containing freshwater mussels and microbes. One hypothesis currently under investigation is that intense deposition of particulate organic matter from extreme flooding alters these food webs through physical and chemical means.

1. Introduction

Society's current water use practices have caused much concern for diversity and health of water-cycle systems at local and regional scales. Natural processes within watersheds can often be significantly altered by human activity. Studying these human-water dynamics has proven to be quite difficult due to complexity of the processes involved. However, the environmental engineering and hydroscience communities have developed a new investigative approach which considers all water cycle components and their interactions with the ecological, biogeochemical, and human systems at the watershed-scale (Muste et al. 2009). The new approach responds to the challenges of the human-water dynamics by creating *envirohydrologic* observatories, utilizing digitally-based remote and in-situ observation and communication technologies integrated with relational geospatial databases and high-performance computing.

The creation of these observatories is being led by two relatively new National Science Foundation (NSF) communities: the Consortium of Universities for the Advancement of Hydrologic Science, Inc. (CUAHSI) and the Water and Environmental Research Systems Network (WATERS Network). These two organizations have been promoting the development and implementation of the cyberinfrastructure (CI)-based environmental observatories for the investigation of watershed processes. The observatories facilitate full-scale hypothesis testing and verification of pilot-study findings through the observations made at large scales in comparable settings (Muste et al. 2009). The observatories enable the cross-disciplinary process discovery and understanding through observation, simulation, analysis, and knowledge synthesis using components and connections similar to those illustrated in Figure 1.

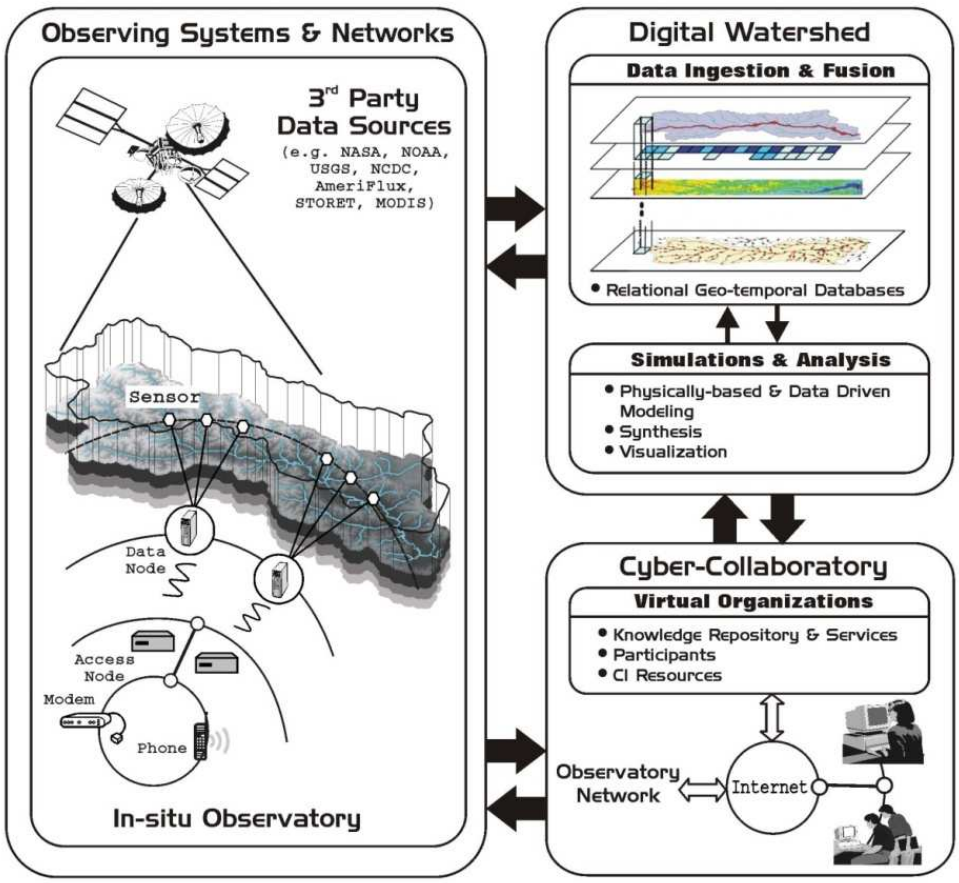

Figure 1: Conceptual configuration of the CI-based environmental observatory (Muste et al. 2009).

Figure 1 illustrates integration of the in-situ observatory, compiled digital watershed, and collaboration of virtual organizations for the Clear Creek watershed, located near Iowa City, Iowa. With the successful creation of an observatory at this small local scale, the investigators seek to implement an observatory along a segment of the Mississippi River near Muscatine, Iowa.

2. Observatory Location

The University of Iowa's IIHR - Hydroscience & Engineering (IIHR) is in the process of creating an Environmental - Hydrologic Observatory on Pool 16 of the Upper Mississippi River Basin (UMRB). Pool 16 of the UMRB extends 41 kilometers from Mississippi Lock and Dam 15 near Rock Island, Illinois to Lock and Dam 16 near Muscatine, Iowa (see Figure 2a). The only major tributary to Pool 16, the Rock River, enters just south of Rock Island. The Andalusia Island Complex dominates a significant stretch of the pool (see Figure 2b). IIHR's Lucille A. Carver Mississippi Riverside Environmental Research Station (LACMRERS) is located adjacent to Pool 16 in Fairport, Iowa. This project will provide proof of concept in acquisition and application of highly time resolved data to accurately predict the movement of water, nutrients, or sediments over broad geospatial and temporal scales.

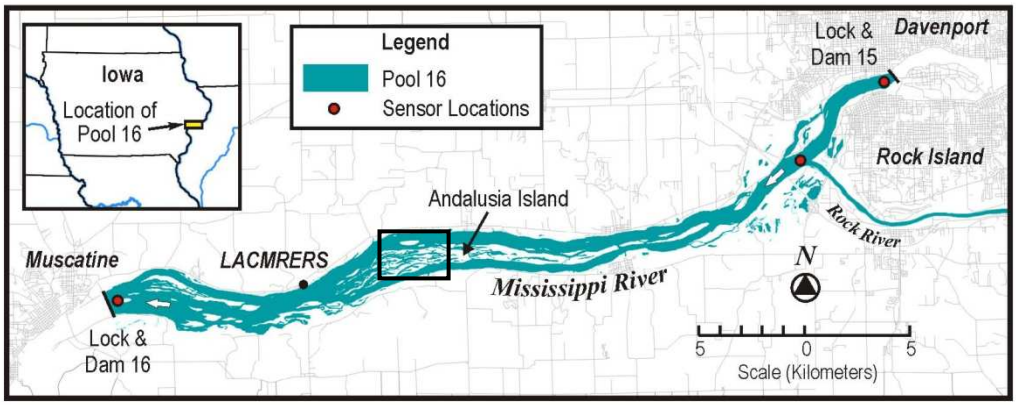

(a)

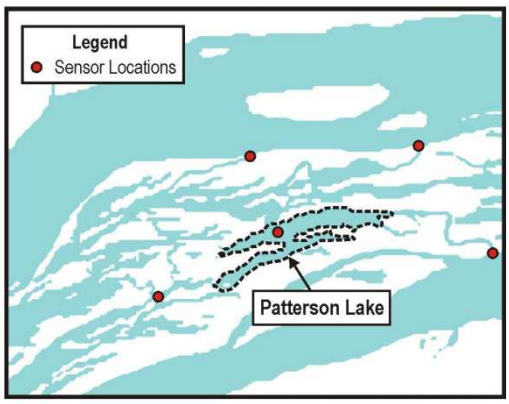

(b)

Figure 2: (a) Navigation Pool 16 on the UMRB with locations for primary monitoring stations. (b) Five stations will be used to monitor primary inlets and outlets to Patterson Lake and within the lake in the Andalusia Island Complex.

High-frequency observations at different scales will allow conservation and transport equations for water, nutrients, and sediment to be parameterized, optimized, and solved. This will enable accurate analyses of water quantity and quality subject

to changing climate, nonpoint sources of nutrients causing coastal hypoxia, and total dissolved and suspended solids. Sensors deployed within Clear Creek watershed have proved dependable for measuring water constituents.

Past studies of nutrient levels in the Mississippi River generally focused on data from single locations, which was then used to upscale nutrient loads for entire pools. Concurrent data from multiple locations will enable more accurate modeling of nutrients along a defined stretch of the river due to major events (from major floods, to isolated events along a tributary, to agricultural trends), seasonal fluctuations, and role of nutrient processing within the pool.

State-of-the-art sensors featuring the latest remote communication technologies are placed at the entrance and exit of Pool 16 at the mouth of the Rock River and within the Andalusia Island Complex for long-term study of:

1) Water Balance: Continuous information on the volume of water entering Pool 16 via the main Mississippi channel, tributaries, and precipitation, and the volume of water exiting Pool 16 over several years will enable more accurate modeling of river response to climatic events and very accurate modeling of the mass of transported sediment and nutrients.

2) Nutrient Load: Continuous monitoring of nutrient transport at the inlet and outlet of Pool 16, the Rock River, and other locations within the Pool will allow the researchers to track changes over time and space. Results from this study may create a more complete understanding of nutrient transport in the Mississippi River from its upper reaches to the Gulf, and have significant implications on our understanding of hypoxia.

3) Sediment Load: Like nutrient load, sediments entering and exiting Pool 16 will be closely monitored to quantify sediment load in the Pool and to establish temporal and geospatial trends. Sediment transport within the river channel, erosion/deposition trends along the banks, sediment composition, sediment provenance, and other parameters will be examined.

3. Sensor Network

Each sensor cluster in Pool 16 (currently at various levels of completion) is data logging and telemetry-enabled via a Campbell Scientific CR1000 datalogger, an AirLink Communications Raven CDMA cellular modem, two NP12 rechargeable batteries and charge controllers, and two BP SX20U solar panels (see Figure 3).

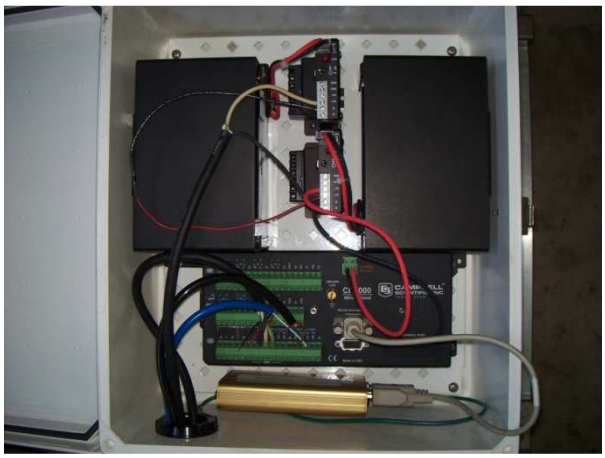

Figure 3: Components of sensor cluster including datalogger, cellular modem, batteries and charge controllers.

The networking equipment has been coupled with a Hach DS5X water quality sonde, a Forestry Technology Systems DTS-12 turbidity probe, and a Hach Nitratax UV sc plus nitrate sensor (see Figure 4). Real-time parameters measured at these sites include: dissolved oxygen, pH, conductivity, temperature, turbidity, and nitrate-N.

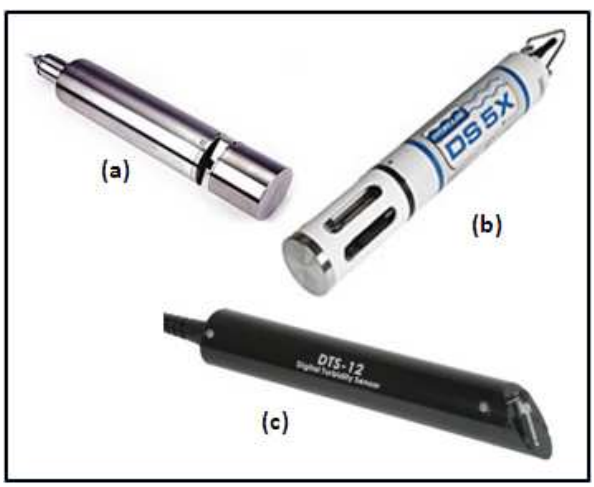

Figure 4: Sensors used to measure water quality include (a) a Hach Nitratax UV sc plus nitrate sensor, (b) a Hach DS5X water quality sonde, and (c) a Forestry Technology Systems DTS-12 turbidity probe.

For field deployment, each of the three sensors is individually housed in constructed PVC pipe units and placed in the selected location. The housing units provide protection for the sensors. Holes drilled in the PVC pipes allow water parameters to be measured (see Figure 5a). Sensor cables are attached to a log chain and submerged. The cable ends are attached to the networking equipment located at the top of a 14-foot ladder (see Figure 5b).



(a) **(b)**

Figure 5: (a) Sensor housing unit placed in water connected to (b) the networking and logging equipment placed on top of ladder.

Ladders (secured to nearby trees) were utilized to maximize the modem's antenna signal, as well as to insure the networking equipment would not be inundated during floods. Locating the network equipment well above the normal pool level will prevent damage caused by devastating floods such as those which occurred in Eastern Iowa and nearly the entire UMRB during May-July 2008. In Pool 16, waters abruptly rose from a highly managed stage of approximately 10 feet to 20 feet and then to nearly 24 feet from May-June 2008 (see Figure 6).

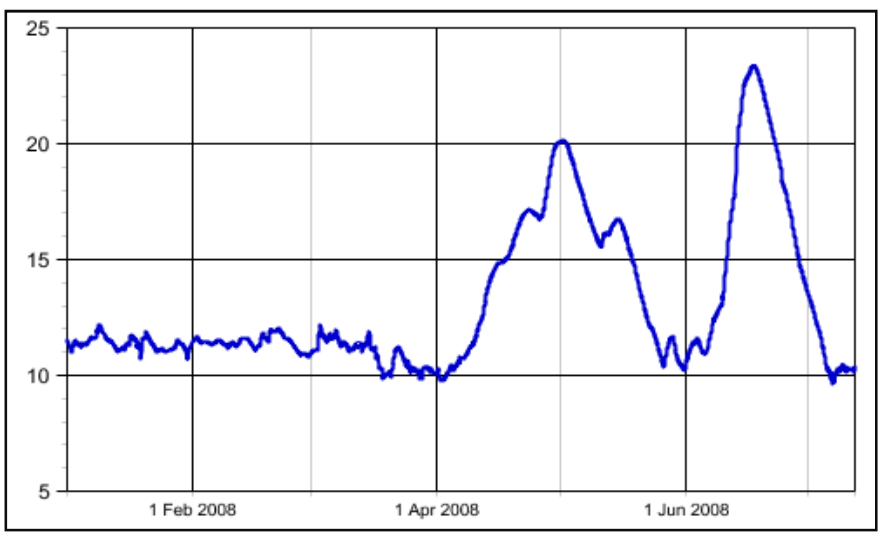

Figure 6: A hydrograph showing Pool 16 stage (in feet) versus time during 2008 (derived from USGS data).

Sensors in the envirohydrologic observatory have collected concurrent data at 15-minute intervals (e.g. dissolved oxygen, turbidity, nitrate, pH, temperature) from multiple locations to enable the modeling of diurnal phenomena and processes

associated with extreme events. As more data are collected over time, measurements will enable the study of seasonal fluctuations and will help to better determine Pool 16's nutrient processing dynamics.

4. Impact of Extreme Events on Mussels and Nutrient Processing

Data collected using the Pool 16 envirohydrologic observatory is currently being used to investigate the influence of extreme flood events on freshwater mussels and nutrient processing. Freshwater mussels and bacteria play a major role in nutrient processing in large river ecosystems by further cycling nutrients taken up by phytoplankton and zooplankton. Under typical ecosystem conditions, mussels appear to process nitrogen more rapidly than denitrifying bacteria (Gardner et al. 1995). Substantial deposition of carbon-rich sediment resulting from extreme flooding may increase nitrogen cycling rates by bacteria and thus alter overall denitrification rates.

It is also known that mussels and bacteria play a major role in nutrient cycling in the broad food web containing phytoplankton, zooplankton, micro-zooplankton, dissolved and particulate organic matter, and benthos (see Figure 7).

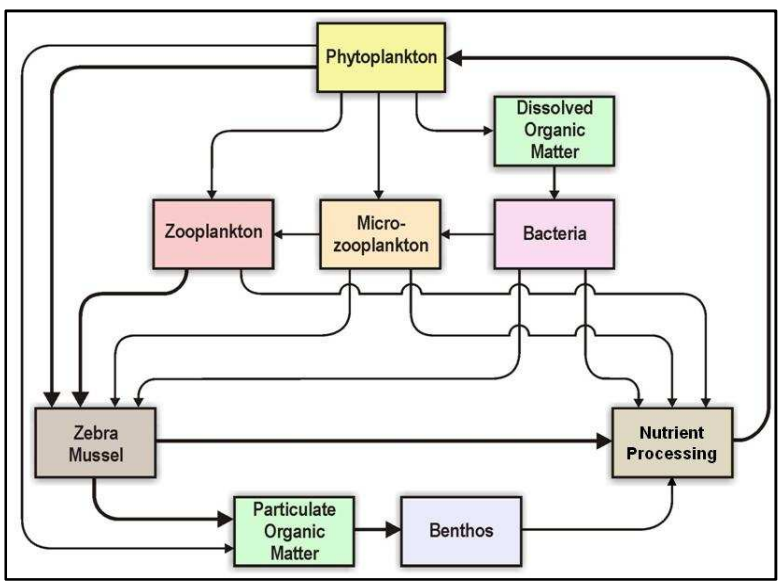

Figure 7: Nutrient cycling during quiescent conditions. Bold lines indicate more significant processing pathways.

Currently, researchers have been focusing on a well characterized Pool 16 mussel bed near Buffalo, Iowa. A substantial number of adult and juvenile mussels, including the federally endangered Higgins Eye mussels, were observed at the site in October 2003 (Helms 2003) and again by the investigators in October 2008. Physical features of the mussel habitat will be characterized using multibeam sonar, and will be compared with bathymetric data collected in 2005 to quantify sediment deposition (Young 2006). Sediment cores will be obtained throughout the bed to determine particulate deposition characteristics from the 2008 flood.

In addition, flow data from USGS and US Army Corps of Engineers gauging stations in Pool 16 will be used in conjunction with nutrient data collected from

municipal drinking water treatment plants and the USGS National Water-Quality Assessment Program (NAWQA) to estimate nutrient mass fluxes before, during, and after the flood. Data from these existing sources will complement data compiled from several post-flood installed sensors located in Pool 16. Data analysis will determine how the mussels' ability to process nutrients may have been affected by the flood event.

Lab experiments are being conducted to explore the effect of intense organic matter deposition on mussels. Using intact sediment cores from the mussel bed in Pool 16, the researchers will use two sets of pseudo-sterilized habitats, one with microbes only and one with a microbial-mussel co-habitated system (Lavrentyev, Gardner and Yang 2000). Mussels to be introduced to the microbial-mussel systems have been collected from the Pool 16 habitat.

One set of the microbes only and microbial-mussel lab systems will contain sediment cores of carbon-rich, flood deposited sediment while another set will contain cores containing older sediments. River water will be continuously pumped through each of the systems at a flow rate of 1 mL min^{-1}. To measure nitrogen processing rates for the bacteria and mussels, the stable isotope ^{15}N-ammonium will be fed into the systems. Microbial denitrification rates will be measured through acetylene blockage techniques. Initial studies on nitrate transformation capacity revealed that bacteria in the organic rich sediments from the mussel bed were capable of completely removing nitrate within 72 hours, compared to no removal in the mildly organic sediments (see Figure 8).

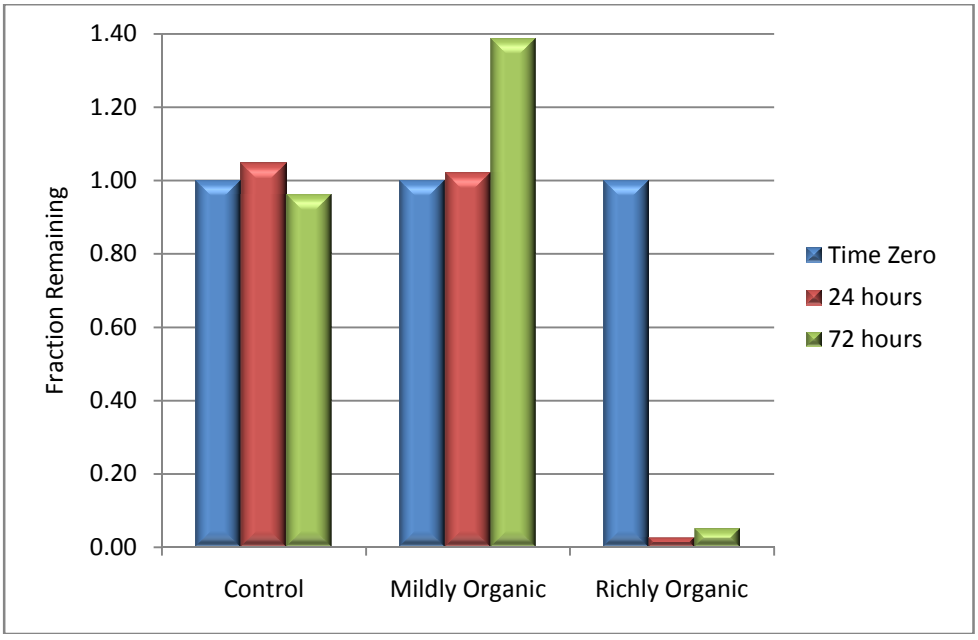

Figure 8: Initial studies on nitrate transformation capacities in mussel bed sediments.

Also, most probable number techniques will be used to quantify total heterotroph and total denitrifying populations. Finally, the researchers will use molecular methods to measure reductase enzyme activities in the microcosms.

5. Scaling Research

Scientific understanding of water related processes is currently limited by an inability to describe how heterogeneous processes interact at different scales to produce the variability witnessed in the water environment (Butcher and Covington 1995). For example, Figure 9 displays dissolved oxygen (D.O.) measurements for the Clear Creek headwaters, mid-point, and tailwaters.

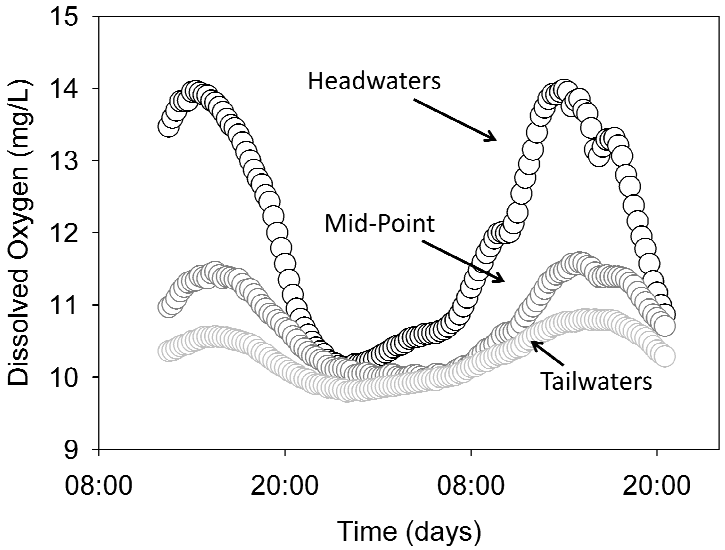

Figure 9: Dissolved oxygen (DO) data collected at three sensing stations located in the Clear Creek Watershed. The largest changes in concentration occurred at the headwaters, and the smallest changes occurred at the tailwaters.

The magnitude of the diurnal cycle for D.O. (in Figure 9) is greatest at the headwaters of Clear Creek then decreases with distance downstream. This provides evidence to support the concept of scaling phenomena in water chemistry processes from small to larger watershed drainage areas. The investigators hypothesize evidence of these scaling phenomena will continue to be observed as research is expanded to the Iowa River and the Upper Mississippi River Basins.

6. Conclusions

Recent historic floods in the Midwest present unique, and short-lived, opportunities to test scientific hypotheses related to a highly perturbed, large river ecosystem. The Pool 16 ecosystem of braided channels and natural backwaters is just one of many Mississippi River subsystems that inadequately process nutrients that contribute to Gulf of Mexico hypoxia. Extreme, flood-related sediment deposition almost certainly impacts the nutrient processing cycle in the short and long term.

This research will expand our limited scientific knowledge of how aquatic environments are affected by increasing human and climate induced changes by using freshwater mussels as a sentinel species. Freshwater mussels have been likened to the "canary in a coal mine" in that their presence in a waterbody is generally indicative of

good sediment and water quality. In addition, mussels provide an integrated record of water quality and current day nutrient dynamics. Understanding how mussels process nutrients in this large river ecosystem is important for engineering, managing, and setting policy to improve and sustain the health of this valuable societal resource. Additionally, the creation of the envirohydrologic observatories will assist in the comprehension of the processes that govern watershed environmental systems, which will in turn aid in watershed management, restoration, and resource optimization.

Acknowledgements

The authors would like to acknowledge the support provided by the National Science Foundation, the Carver Charitable Trust, LACMRERS, and the following individuals: Travis Anderson, Brandon Barquist, Andy Craig, Jon Durst, Paul Eastling, John Foster, Pete Haug, Mike Kundert, Teresa Newton, Gene Parkin, Jesse Piotrowski, Maclaine Putney, Doug Schnoebelen, and Mike Schubert.

References

Butcher, J. B. & S. Covington (1995) DISSOLVED-OXYGEN ANALYSIS WITH TEMPERATURE-DEPENDENCE. *Journal of Environmental Engineering-Asce,* 121**,** 756-759.

Gardner, W. S., J. F. Cavaletto, T. H. Johengen, J. R. Johnson, R. T. Heath & J. B. Cotner (1995) Effects of the zebra mussel, Dreissena polymorpha, on community nitrogen dynamics in Saginaw Bay, Lake Huron. *Journal of Great Lakes Research,* 21**,** 529-544.

Helms, D. (2003) Mussel Survey for the Blackhawk Barge Fleet PCS Site in Mississippi River Pool 16 River Mile 470 Scott Co., Iowa. Helms and Associates, Bellevue, Iowa.

Lavrentyev, P. J., W. S. Gardner & L. Y. Yang (2000) Effects of the zebra mussel on nitrogen dynamics and the microbial community at the sediment-water interface. *Aquatic Microbial Ecology,* 21**,** 187-194.

Muste, M., Kim, D., Arnold, N., Whiteaker, Just, C., and Kruger, A. (2009) Digital Watershed Inception Using Community Project Components. Special Issue on Cyberinfrastructure for Hydrology and Environmental Engineering, *Proceedings of Institution of Civil Engineers Water Management,* Thomas Telford Journal, London, UK.

Young, N.C. (2006) Physical Characterization of Freshwater Mussel Habitats in Upper Mississippi River Pool 16. Doctoral Dissertation, The University of Iowa.

A COMPARISON OF FORMED SUCTION INLETS FOR FLOOD CONTROL APPLICATIONS

By

David Werth[1], Mark Allen[2] and Brent W. Nicholas[3]

Formed suction inlets (FSI) are commonly used with large vertical pumps in flood control applications. The US Army Corps of Engineers Type 10 FSI is used extensively throughout the southeastern United States. However, variations of this inlet have been utilized with increasing frequency for a variety of reasons including cost, flexibility of use in existing intakes and smaller foot prints.

Type 10 formed suction inlets have a proven record of success in a wide variety of approach flow conditions including high cross flow applications and with less than ideal vertical or horizontal transitions. Published guidelines and extensive field experience provide reliable design guidance for this type of inlet. While design guidance has been published on alternative inlets there is very little information or data available providing a direct comparison of effectiveness between a Type 10 with an alternative FSI.

This paper presents the results of a physical model study which was conducted with the specific goal of comparing the Army Corps of Engineer Type 10 FSI with an alternative "shoe box" version. The model was used to identify surface vortex activity for both types of inlets as well as a comparison of flow straightening and vortex suppression abilities. A side by side comparison of the two different formed suction inlet designs is presented which is useful when evaluating various station and equipment alternatives in flood control applications.

Background

Formed suction inlets (FSI) are very common in flood control applications and have often been used to replace the typical pump bell for a variety of reasons. A discussion by Werth and Zheng (2008) outlined a number of advantages including insensitivity to high cross flow conditions, an ability to eliminate sub-surface vortex activity, and the potential to reduce the required minimum pump submergence to minimize surface

[1] David Werth, Ph.D., P.E. Principal, Clemson Engineering Hydraulics, Inc. Anderson, SC 29625, e-mail: dwerth@ceh-lab.com, Ph. 864-231-9585

[2] Mark Allen, P.E., M. ASCE, Camp Dresser & McKee Inc., Denver, CO. e-mail: AllenME@cdm.com, Ph. 303-383-2300

[3] Brent W. Nicholas, P.E., Camp Dresser & McKee Inc., Houston, TX. e-mail: NicholasBW@cdm.com, Ph. 713-423-7300

vortex activity. Numerous configurations of formed inlets exist with the most familiar of these designs developed by the U.S. Army Corps of Engineers and referred to as the Type 10 FSI. Design guidelines for the minimum size of the inlet were published by the Corps (Fletcher and Oswald, 1992) and distributed widely in the 1998 Hydraulic Institute Standards (ANSI, 1998). Photo 1 shows a typical Type 10 FSI.



Photo 1 Typical Type 10 Formed Suction Inlets (attaches to pump column)

While the Type 10 FSI is relatively well known there are several other variations of formed inlets, scoops or elbows. Werth and Cheek (2004) presented guidelines for an Alternative FSI which was intended for use under existing pumps with suction bells already installed. The internal geometry of the Alternative FSI varies from the Type 10 FSI in that most surfaces are flat rather than curved but both inlet functions in much the same way. The most significant variation between the two is that the Type 10 FSI attaches directly to the pump column and replaces the pump bell and the Alternative FSI attaches to the floor directly below the pump bell. Photo 2 shows the Alternative FSI.

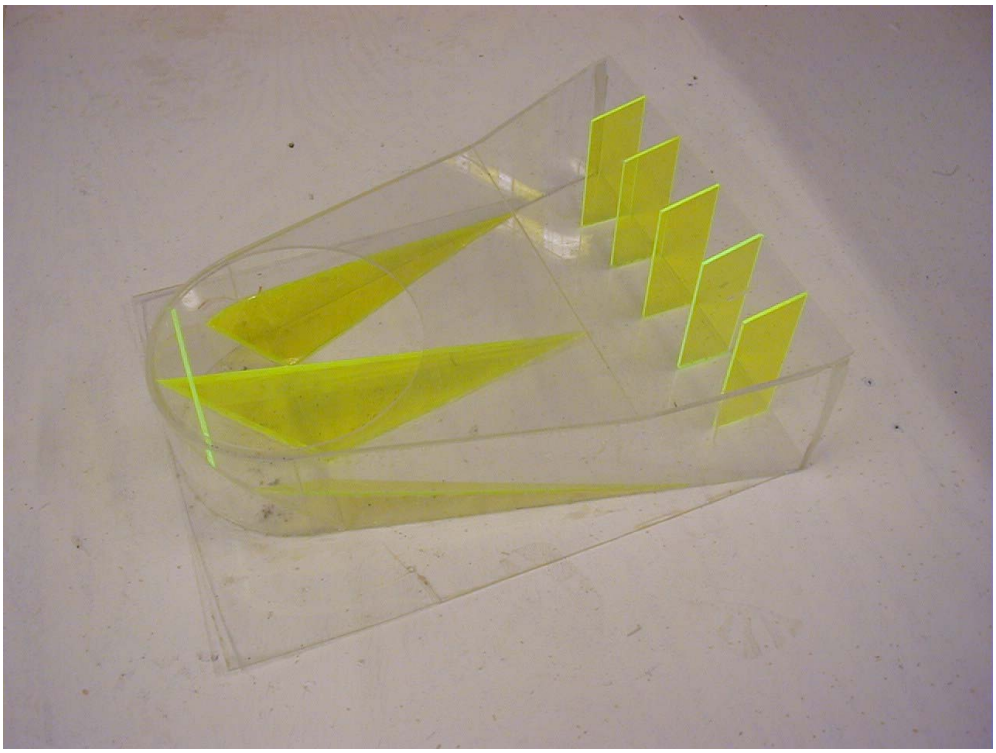

Photo 2 Alternative Formed Suction Inlet (sits under pump bell)

Project Background

Clemson Engineering Hydraulics, Inc. conducted a physical hydraulic model study of the Henderson Bayou Levee, Floodgate and Storm Water Pumping Station for Camp, Dresser, & McKee Inc. (CDM). The intake structure, designed by CDM, will be located in Ascension Parish on the Henderson Bayou and will serve as a flood control pump station. The intake will house a total of three (3) lift pumps, each with a rated capacity of 500-cfs. The pumps will serve as lift pumps by passing flow from the bayou protected side of the pump station to a higher discharge elevation on the opposite side. The primary purpose of the pump station is to protect the Henderson Bayou Watershed from a combined storm event coupled with a high backwater elevation from the Amite River.

The model was used to evaluate the hydraulic conditions within the intake structure and directly compare the Type 10 and "Alternative FSIs. The model was also use to develop recommended modifications as needed to remediate any adverse hydraulic phenomena which could impact pump performance as well as to evaluate the potential for debris accumulation.

Model Configuration

The Henderson Bayou intake will be located within an existing channel that will also house run-of-river sluice gates and a navigation channel. During a coincident storm event and high Amite River backwater event, the sluice gates and navigation channel

gate will be closed and the pump station will operate. Flow transitions from the invert of the channel and station entrance to the invert of the sump via a sloped ramp. The full width of the channel, including the floor topography of the channel entering into the lift station and the floor topography of the navigation channel were included in the model. The entire geometry of the pump station, including the individual bays housing the trash screens, as well as the sloped transition was simulated in detail in the model. Photo 3 shows a model overview.



Photo 3 Model Overview

The Henderson Bayou model was constructed at a 1:12 scale and operated according to Froude scaled flow rates. At this scale the model Reynolds number at the entrance to each inlet (based on an equivalent diameter) was on the order of 1.5×10^5, which is well above the value of 1.0×10^5 recommended by the Hydraulic Institute (1998) for modeling closed conduit pump approach flows.

The individual model pump flow rates, as well as the total model flow rate were determined with an ASME standard orifice meter with an accuracy of +/- 2 percent or better. The water levels in the pump sump were recorded with a staff gauge referenced to the sump floor with an accuracy of 3-mm (0.01-ft) or better Dye was used to visually evaluate hydraulic phenomena including vortex formations. Velocity fluctuations and turbulence levels were measured just upstream of the pump impeller location using a miniature rotor velocity meter. A swirl meter was installed in each pump at the prototype impeller location to measure the level of pre-swirl of flow

entering the pump. Each swirl meter consists of 4 straight vanes mounted on a shaft with low friction bearings. Photo 4 shows the model Type 10 (left and center) and Alternative Inlets (right side) in place in the model.

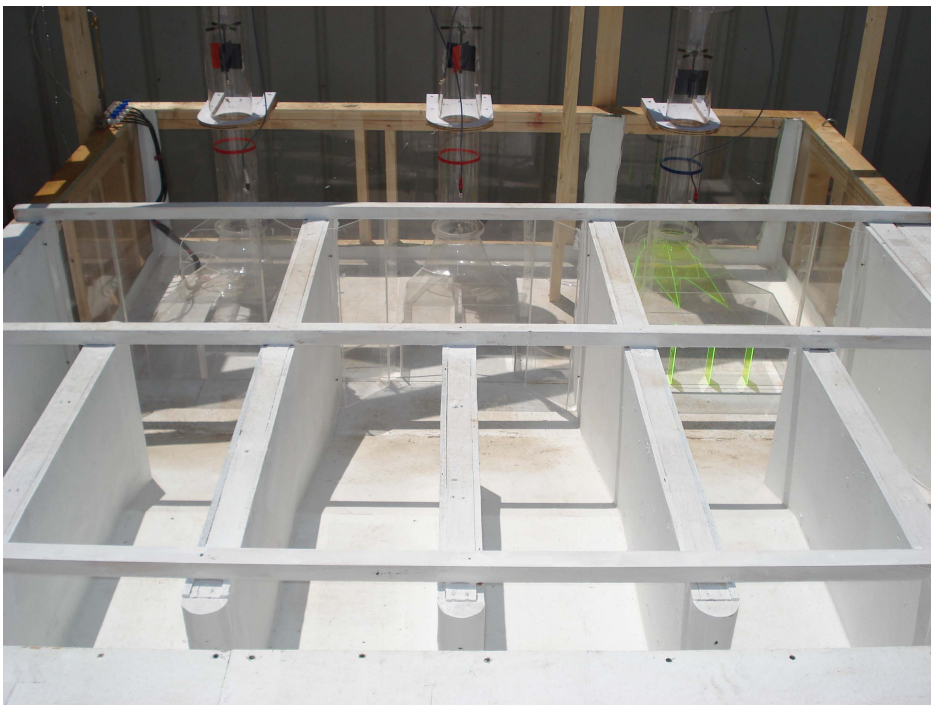

Photo 4 Type 10 FSI (left side) and Alternative FSI (right side)

The Type 10 FSIs were fabricated per the US Army Corps of Engineer Guidelines. The Alternative FSI was fabricated according to Werth and Cheek (2004) as shown below in Figures 1 and 2.

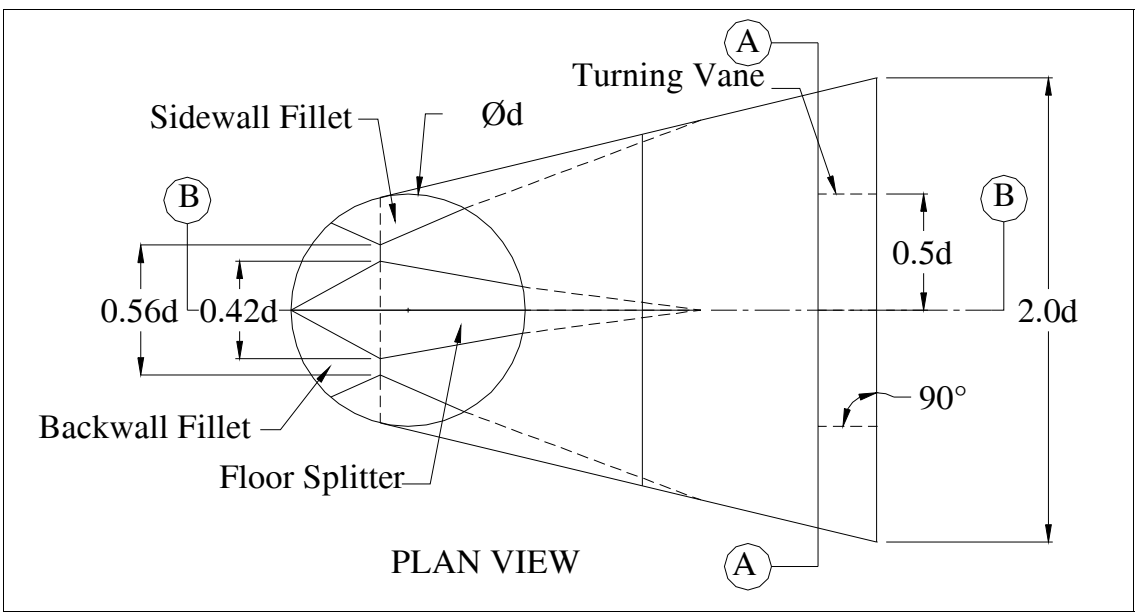

Figure 1 Alternative FSI – Plan View

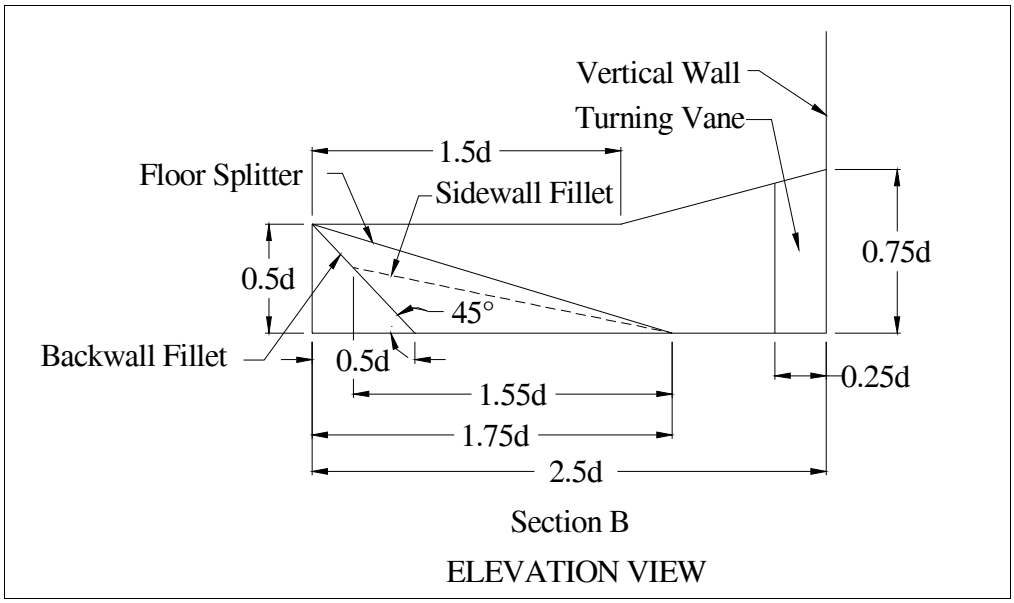

Figure 2 Alternative FSI – Elevation View

Test Results

The intention of the original study was to evaluate the overall performance of the intake structure, including the run-of-river gates and overall approach flow conditions. The intention of this paper is to provide a direct comparison between the Type 10 and Alternative FSI designs in the same intake with nearly identical approach flow conditions. While the project report contains considerable detail this paper presents only conditions observed within the inlets. Flow rates and water levels were the same for both types of inlets allowing for a direct comparison of the results.

The data collected in each type of inlet included velocity measurements around the pump throat location, flow pre-swirl entering the pumps, and vortex activity and overall flow conditions within the intake. Because the intake housed a total of three pumps a Type 10 FSI and an Alternative FSI were installed in the outside pump bays. A slightly modified Type 10 was installed in the center bay but is not part of this comparison. Acceptance criteria was established per the 1998 HI guidelines and included velocity data presented as the maximum individual point deviation from the overall average and should be less than +/- 10%. Turbulence is defined as the standard deviation of the approximately 15,000 velocity samples taken at a single point over a 30-second period divided by the average of those velocity readings. Turbulence should be less than 10%. Pre-swirl should be less than 5-degrees for a traditional pump bell but experience has shown that most FSIs have pre-swirl values less than 2.5-degrees. No organized vortex activity should reach the pump throat.

Ten different pump combinations and water levels were investigated during the baseline portion of the study. While several issues were identified for improvement with the overall structure related to the run-of-river gates and screen chambers the conditions were generally uniform and stable within the inlets.

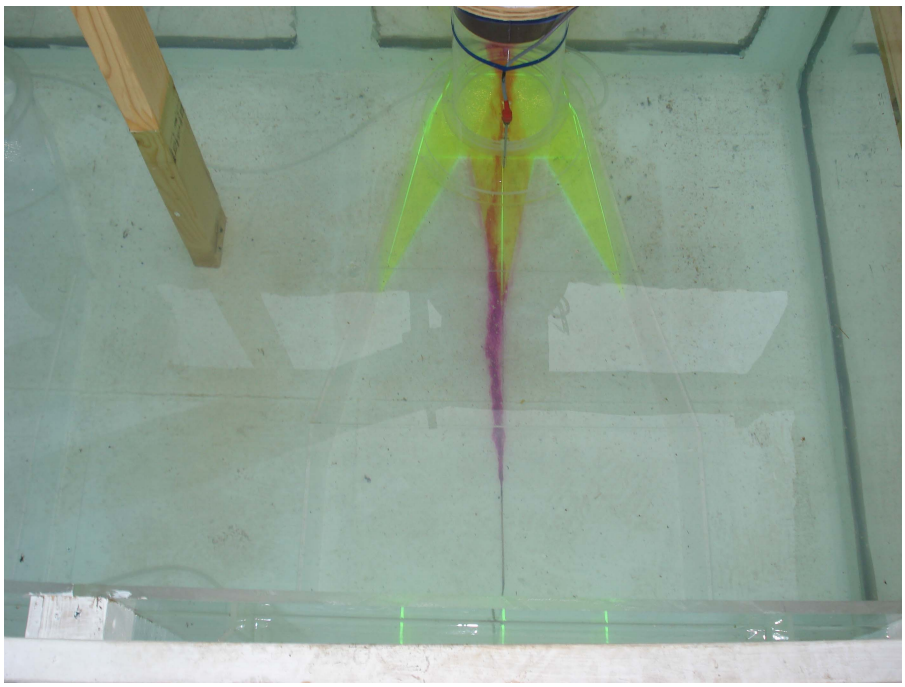

Photo 5 Uniform Flow Inside Alternative FSI

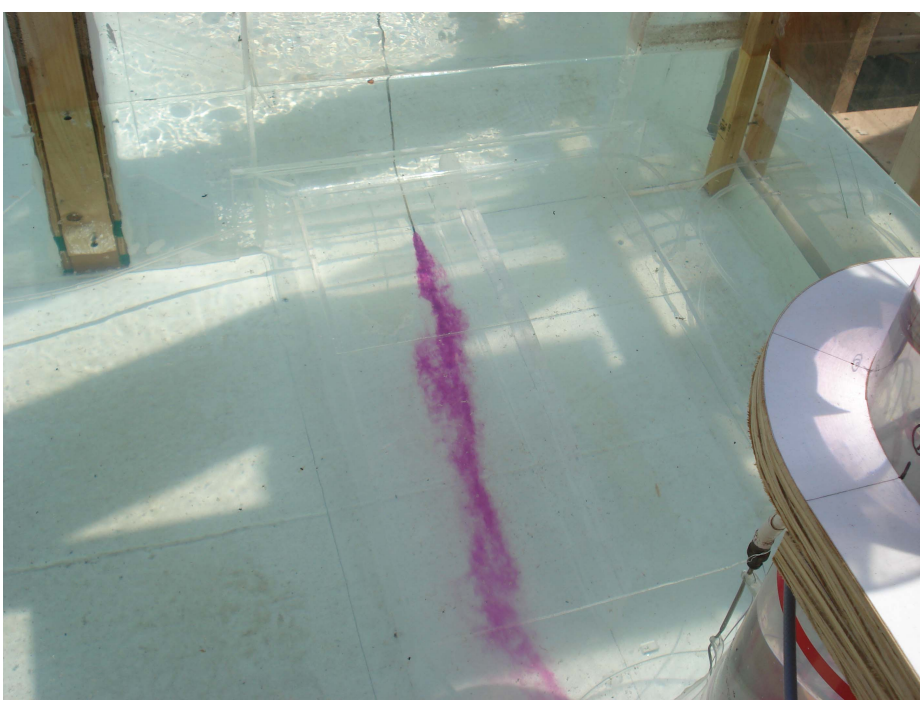

Photo 6 Uniform Flow Inside Type 10 FSI

During all baseline tests the pre-swirl values were less than 1.0-degree in both the Type 10 and Alternative FSI configurations. Velocity and turbulence readings were also within criteria.

Surface vortex activity was present and entered both the Type 10 and Alternative FSIs. Surface vortex suppression beams were installed upstream of each inlet and dissipated this vortex activity. A previous paper by Werth and Zheng (2007) investigated submergence requirements of formed suction inlets and the reader is encouraged to refer to this for additional details regarding submergence requirements.

Conclusions

In any discussion regarding a comparison of different types of pump intakes it is important to note that very few intake structures have identical approach flow conditions, site constraints and operational characteristics. This makes a direct comparison of different types of modifications or inlet alternatives from different studies difficult.

The purpose of this paper was not to determine whether one FSI was better than the other. The purpose was determine whether the two types of formed suction inlets were equally effective in providing pump approach flows within acceptable criteria. Each of the two inlets investigated have advantages and disadvantages and specific project requirements or constraints may dictate a preferred configuration.

The results of this study indicate that both the Type 10 FSI and the Alternative FSI are equally effective at providing acceptable flow conditions at the entrance to the pump impeller. Previous experience has shown both FSI designs to be effective over a wide range of intake configurations but little information existed to determine if they were equally effective under similar approach flow conditions. Both FSI configurations resulted in a similar reduction of pre-swirl, an equal ability to suppress sub-surface vortex activity, an equal tendency for surface vortex formation and both resulted in pre-swirl and turbulence readings that were within established guidelines.

This suggests that design engineers have an additional alternative when evaluating formed suction inlets. In cases where the pump can be readily attached to the inlet a Type 10 FSI may be feasible. In other cases, such as an existing sump, where a pump bell already exists or where a narrower pump bay is desired then the Alternative FSI may be more practical.

Again, the intent of this paper is not to suggest one type of formed inlet is more effective than the other but rather to provide the results of a relatively rare study involving the direct comparison of the two under nearly identical approach flow conditions. These results suggest that both are equally effective at improving the approach flow and resulting in conditions which are well within the established HI

Guidelines. The actual model study is ongoing and no final selections had been made at the time of publication.

References

Zheng, Yifan., and Werth, David. (2008). "Optimize Pump Intake Design With Formed Suction Inlets." Proceeding of the 2008 EWRI Conference, Honolulu, HI

Fletcher, B. P., and Oswalt, R. (1992). "Geometry Limitations for the Formed Suction Intake." Engineering Technical Letter No. 1110-2-327, US Army Corps of Engineers, Washington, D.C.

American National Standard for Pump Intake Design. *Hydraulic Institute*. 1998. ANSI/HI 9.8-1998

Werth, D.E., and Cheek, D.E. (2004). "Design Guidelines for Alternative Formed Suction Inlets". Journal of Water Management, *Proceedings of the Institution of Civil Engineers*, London, 157(WM3), 151-158.

Werth, David., and Zheng, Yifan. (2007). "Reducing Pump Submergence With Formed Suction Inlets." Proceedings of the 2007 EWRI Conference, Tampa, FL.

CASE STUDY: IMPACT OF VARYING MITERED SUCTION ELBOWS ON LARGE WASTEWATER PUMPS

By

David Werth[1] and Ted Stolinski[2]

Mitered elbows are commonly used for suction inlets on large vertical raw waste water pumps. While information exists regarding the appropriate number of miters or maximum angles to prevent flow separation, little information is available in regards to the impacts on the approach flow conditions into the impeller when used in pump suction piping.

Pump manufacturers commonly use mitered elbows in dry-pit and occasionally in wet pit pump applications. Each manufacturer has a "typical" design with a specific number of miters that is used across a wide range of elbow sizes and turning radii. Experience has shown that in some applications, an insufficient miter design can lead to severe instability of the approach flow into the impeller. Limited design guidance is available to evaluate the impact of mitered elbow design for varying flow rates and suction sizes. The Hydraulic Institute Standard does not address mitered suction elbows mounted directly on a pump suction.

This paper presents the results of a physical model study which was conducted to evaluate an existing raw wastewater pumps station housing five large (40,000 gpm) pumps. The existing station has exhibited a number of issues over the years and when a sixth pump was added, a model study was conducted to evaluate the approach flow conditions. Testing indicated that the mitered suction inlets were causing excessive flow separation and significant velocity variations at the pump inlet. Test results are presented which outline the impact of varying the miter design on pump inlet conditions.

Background

Black & Veatch Corp. is currently overseeing an upgrade to the existing MSD Lemay waste water treatment plant pump station. Currently the station houses five (5) 40,000 gallon per minute (gpm) raw sewage pumps but has an existing suction pipe already in place for a sixth pump. Black & Veatch Corp. is planning to install the sixth pump, also rated at 40,000 gpm in the available pump location. Given a history of

[1] David Werth, Ph.D., P.E. Principal, Clemson Engineering Hydraulics, Inc. Anderson, SC 29625, e-mail: dwerth@ceh-lab.com, Ph. 864-231-9585

[2] Ted Stolinski P.E., Black & Veatch Corp., Kansas City, MO, e-mail: stolinskit@bv.com, Ph. 913-458-3448

accelerated impeller and wearing ring wear Clemson Engineering Hydraulics was commissioned to conduct a physical hydraulic model study of the intake to evaluate the existing and future conditions within the wet-well and suction piping.

Existing Intake

Flow is introduced into the circular structure which is divided into two symmetrical halves, via a common influent channel. After entering the intake flow splits into one of the two halves, each housing up to three pumps. Currently three pumps are installed in one half and two in the other. A series of three (3) 60-inch diameter suction lines withdraw flow from each side of the intake for a total of six (6) pumps. The existing five pumps utilize mitered elbows which transition from the 60-inch suction lines to a 42-inch elbow discharge and then a 36-inch pump suction. The new pump was proposed to utilize a nearly identical mitered elbow but transitions from the 60-inch pipe directly to a 36-inch elbow discharge.

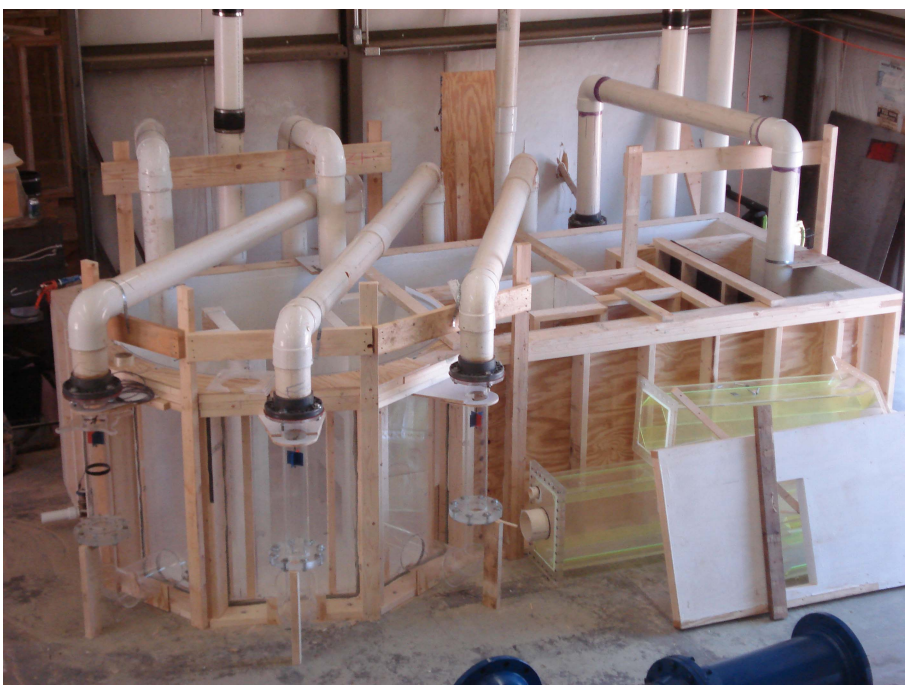

Photo 1 Overview of Pump Station Model

The station currently has the 60-inch suction line for the new pump installed but does not have the mitered elbow in place. The only constraints on the new elbow design was that it be attached to the existing 60-inch suction line and maintained the same pump centerline and discharge location as the existing pumps. The pump manufacturer was responsible for the suction elbow design and utilized a design very similar to the existing elbows. Photo 2 shows a close-up view of the original mitered elbow.

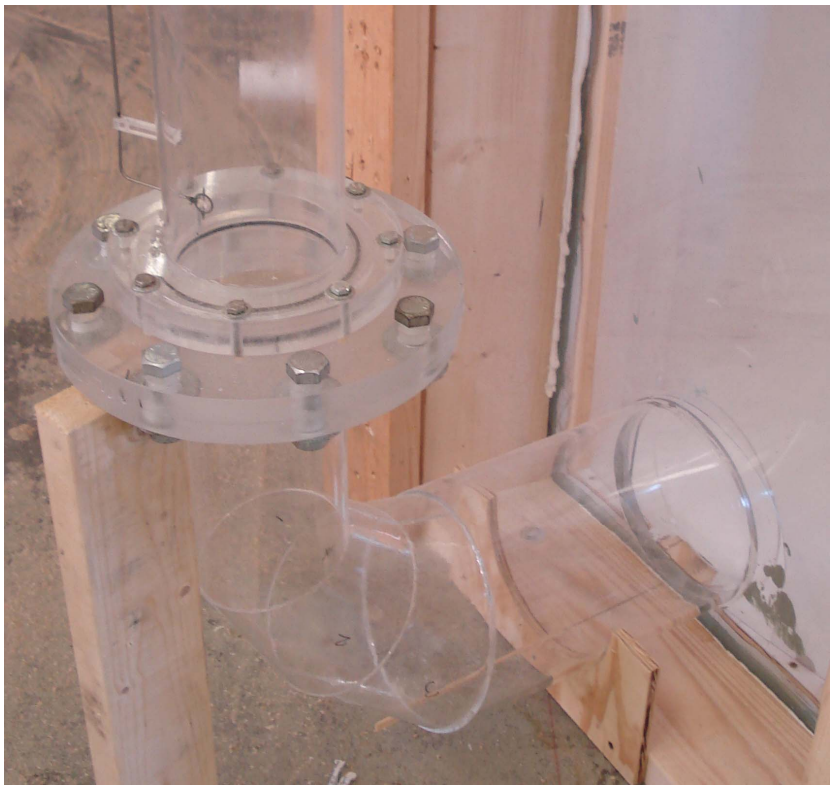

Photo 2 Original Three-Miter Model Elbow

Model Configuration

The Lemay model was constructed at a 1:8.0 scale. The resulting Reynolds number will be on the order of 1.0×10^5 at the 60-inch suction piping and 1.7×10^5 in the suction piping at the pump. The resulting Weber number was approximately 620.

The individual model pump flow rates, as well as the total model flow rate were determined with an ASME standard orifice meter with an accuracy of +/- 2 percent or better. The water levels in the pump sump were recorded with a staff gauge referenced to the sump floor with an accuracy of 3-mm (0.01-ft) or better). Vortex formation was visually observed. Dye was used to aid in the visualization of vortex formation.

Velocity fluctuations and turbulence levels were measured in just upstream of the pump impeller location. A free spinning miniature propeller was used to measure the velocities. A swirl meter was installed in each pump at the prototype impeller location to measure the level of pre-swirl of flow entering the pump. Each swirl meter consists of 4 straight vanes mounted on a shaft with low friction bearings. A lab pump was used to re-circulate flow from the wet well, through the model elbows and back to the model head box.

The original miter elbow proposed for the new pump application was very similar to the existing elbows with the exception of the elbow discharge diameter. The existing

elbows terminate at 42-inches and then utilized a reducer to transition to 36-inches. The new elbow transitioned from 60-inches directly to 36-inches. Figure 1 shows the initial elbow design.

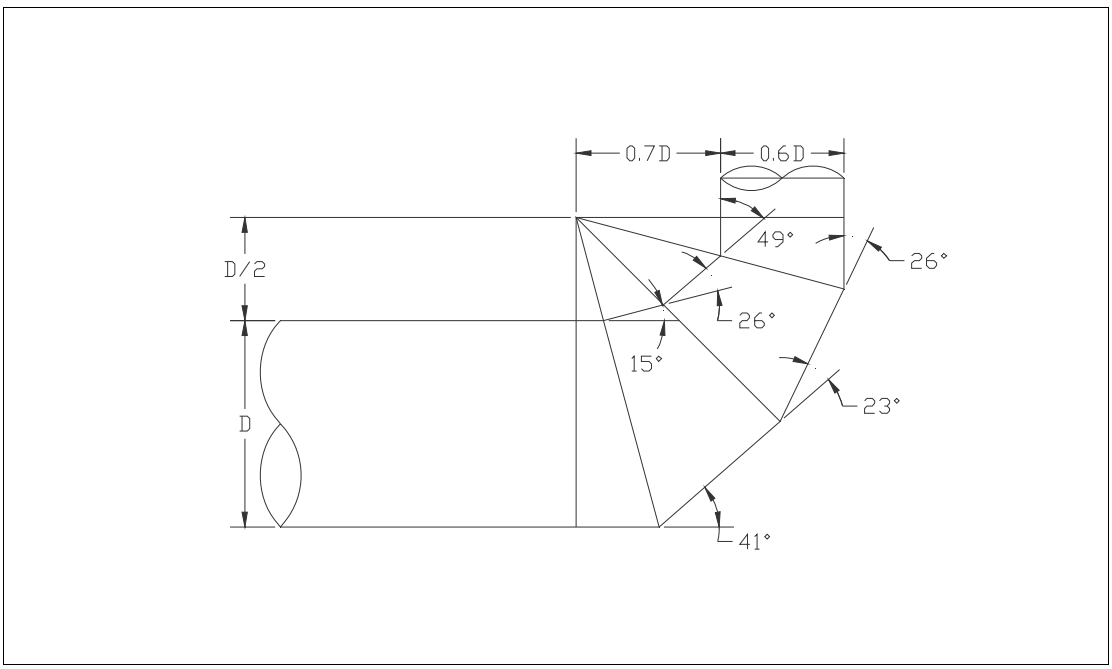

Figure 1 Original Miter Elbow Design

As shown on Figure 2, the drawing the initial design included diverging angles which varied from 15-degrees to 49-degrees. Most design guidelines suggest keeping diverging angles to 10-degrees or less.

Test Results

The intention of the original study was to evaluate the overall performance of the intake structure, including the overall approach flow conditions. The intention of this paper is to provide a comparison between varying mitered elbow designs as part of the overall design. While the project report contains considerable detail this paper presents only conditions observed within the actual mitered elbows. Flow rates and water levels are the same for both types of elbows allowing for a direct comparison.

The data collected in each type of inlet included velocity measurements around the pump throat location, pre-swirl, vortex activity and overall flow conditions. Velocity data is presented as the maximum individual point deviation from the overall average and should be less than +/- 10%. Turbulence is defined as the standard deviation of the velocity samples taken at a single point over a 30-second period divided by the average of those velocity readings. Turbulence should be less than 10%. Pre-swirl

should be less than 5-degrees for a traditional pump bell but pre-swirl values less than 2.5-degrees is preferred. No organized vortex activity should reach the pump throat.

Numerous different pump combinations and water levels were investigated during the baseline portion of the study. During all tests there were significant variations in the velocity profile around the pump throats. Testing revealed a significant region of low velocity on the upstream (short radius) side of the mitered elbow. Velocity readings indicated that velocities on the upstream side were in excess of 30-percent lower than the sides and back of the elbow. The flow rates were adjusted to simulate the velocities going through the existing 40-inch discharge elbows and testing revealed very similar results even with the lower elbow velocities. Photo 3 shows a large region of dye which indicates the low velocity separation zone.

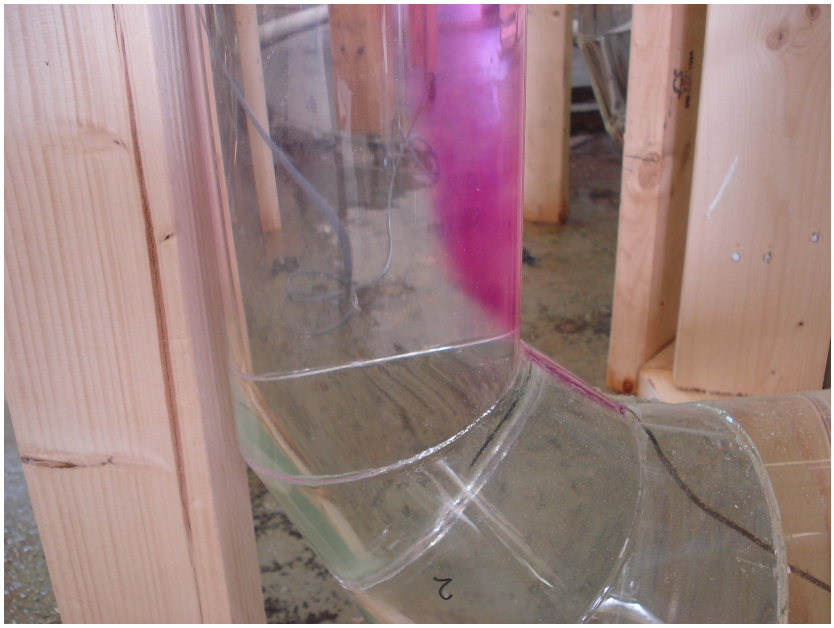

Photo 3 Separation on Upstream Side of Elbow

Numerous turning vane arrangements were investigated but because this is a raw sewage station the design needed to be “open vane” to minimize the potential for debris accumulation. As a result they had limited effectiveness.

Given that the elbow was not yet fabricated for the new pump it was decided to vary the miter design. The elbow was changed from a 3-miter to a 5-miter design. This decreased the maximum diverging angle from 49-degrees to 33-degrees as shown in Figure 2.

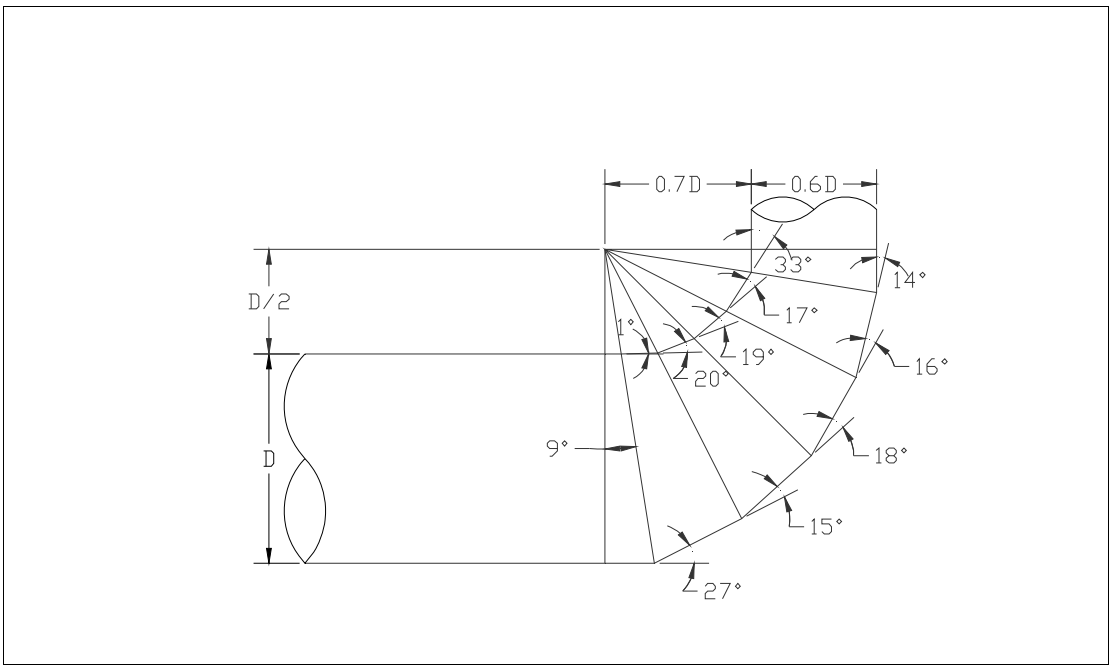

Figure 2 Revised Miter Elbow Design

Photo 4 shows the revised model elbow.



Photo 4 Uniform Flow Inside Type 10 FSI

The model was operated with the revised elbow in place and observations indicated that the separation zone was significantly reduced. Velocity variations decreased from

in excess of 30-percent with the original design to less than 8-percent with the revised elbow design. Virtually no separation was observed on the upstream (short radius) side of the elbow.

Conclusions

The results of the model study show that relatively small variations in mitered elbow design can have a significant impact on conditions within the elbow. In this application a maximum divergence angle of 49-degrees resulted in significant flow separation and a large region of low velocities at the pump impeller location. Revising the elbow to reduce the maximum divergence angle to 33-degrees significantly improved impeller entrance flow conditions and virtually eliminated the separation on the short radius side of the elbow.

However, it should be noted that flow separation in elbows is also related to the flow velocity. Additional studies would prove useful in attempting to quantify a maximum angle versus elbow velocity. A sufficient amount of test data is not yet available to determine a maximum miter angle as a function of velocity.

In this application the maximum elbow velocity was just over 12-ft/sec and testing indicated that a miter angle of 33-degrees was acceptable. Based on this data it is likely that future design could utilize miter angles up to 30-degrees on inlets with velocities of 12-ft/sec or less. Additional work could determine if this angle, or another, would be acceptable at higher and lower velocities.

References

American National Standard for Pump Intake Design. *Hydraulic Institute*. 1998. ANSI/HI 9.8-1998

Culvert Retrofit and Fish Passage: An Update

Joseph R. Webb[1], Rollin H. Hotchkiss[2]

1. Graduate Research Assistant, Dept. of Civil and Environmental Engineering. 368 Clyde Bldg, Brigham Young University, Provo, UT 84602. Email: joseph.r.webb@gmail.com.
2. Professor, Dept. of Civil and Environmental Engineering. 368 Clyde Bldg, Brigham Young University, Provo, UT 84602. Email: rhh@et.byu.edu.

Abstract

Culverts throughout the country are approaching or are past their original design lives. These 'baby boomer' culverts will need to be repaired, rehabilitated, or replaced. Because entire culvert replacement is so expensive and intrusive, alternate measures to extend the culvert project life are growing increasingly popular. One such method is slip lining, where a 'sleeve' is installed within an existing culvert barrel and stabilized. Plastic pipe sleeves are very popular for slip lining primarily because the plastic material's lower Manning's roughness values allow for the culvert capacity to be maintained despite a reduction in culvert size.

Unfortunately, the reduced friction within the barrel can create a barrier to fish passage due to increased water velocities. The increased velocities also cause greater outlet scour which can result in further obstacles to fish passage. These new fish barriers can greatly affect aquatic ecosystems by limiting the access that fish have to smaller tributaries used for spawning and rearing—access that is critical to the life-cycles of many fish, including stream salmonid populations.

It is suggested that mitigation of the increased velocities should go hand-in-hand with slip lined culvert design projects where fish passage (present or future) is to be considered. Can the demand for hydraulic capacity as well as the demand for fish passage be satisfied?

A literature review and survey of all U.S. state Departments of Transportation as well as state Fish and Wildlife Departments has shown that there has been very limited experience in providing for fish passage through slip lined culverts. Site visits have been made to the few states with this experience to assess developing technologies and record successful and unsuccessful installations. Additional hydraulic analysis using current software is also underway to determine ranges of flows and sizes of culverts where slip lined retrofits can adequately serve as fish corridors.

Introduction

The vast majority of pipe culverts in the United States were built over 40 years ago, during a massive transportation infrastructure upgrade; our culverts are reaching a kind of middle age. A Transportation Research Board Research Needs Statement explains that the highway infrastructure is characterized by a huge inventory of damaged and decaying culverts. Because entire culvert replacement is so expensive and intrusive, alternate measures to extend 'baby boomer' culvert life are growing increasingly popular. One such method is slip lining, where a 'sleeve'—usually plastic—is installed, or slipped, within the existing culvert barrel and stabilized. The sleeve's lower roughness value allows for the smaller pipe to convey the same capacity. This slip lining method is attractive because it does not require any excavation of the existing pipe and roadway fill, providing an opportunity for culvert replacement without the undesired disruption to highway traffic, not to mention the advantage of rehabilitating the culvert without less right of way concerns. Culvert and pipe fabricators have begun to design and manufacture product conducive to this new technology (TRB 2007).

The huge inventory of aging culverts was designed solely on the basis of peak design flows, and likely did not take into account fish passage. Many of these culverts have turned out to be significant barriers for fish. In 1973 the United States Government signed into law the Endangered Species Act (ESA). Once a species is listed as threatened or endangered, the ESA requires that 'critical habitat' be designated for that species, including areas necessary to recover the species. Federal agencies are forbidden from authorizing, funding, or carrying out any action which "destroys or adversely modifies" critical habitat (USC 1973). Unfortunately, the increased velocities due to slip lined culvert retrofit can result in further obstacles to fish passage. These new fish barriers can greatly affect aquatic ecosystems by limiting the access that fish have to smaller tributaries used for spawning and rearing—access that is critical to the life-cycles of many fish, including stream salmonid populations.

It is suggested that mitigation of the increased velocities should go hand-in-hand with slip lined culvert design projects where fish passage (present or future) is to be considered. Can the demand for hydraulic capacity as well as the demand for fish passage be satisfied? To this point, there has been very limited experience in providing for fish passage through slip lined culverts. The objective of this paper is to introduce slip lining as an option for culvert retrofit and discuss fish passage implications associated with this method. Additionally, this paper contains a review of the currently available literature on mitigation techniques, a survey of transportation and fisheries agencies who have utilized mitigation techniques, and reports on visits to various project locations to identify successful implementation of slip lined culvert retrofits. The scope and objectives of an ongoing Utah Department of Transportation research project relating to mitigation techniques to allow fish passage in slip lined culvert retrofits is also included.

Slip Lining and Fish Passage

Slip lining involves three major steps. First, the existing culvert must be inspected and prepared for lining. This process includes flushing or cleaning the existing culvert to eliminate obstructions. Second, a smooth plastic (generally) pipe end is placed into the culvert and pushed through the culvert. Finally, the culvert ends are capped and the annular spaces between the existing culvert and the new liner are grouted to fix the liner in place and provide additional structural support (Campbell 1995). These culvert lining techniques often reduce construction costs by 50-75% (DeMarco 1993, Campbell 1995). Additionally, slip lined retrofits often take half the time as regular culvert replacement, often with only very minor to no traffic impedance (DeMarco 1993).

The 1973 ESA requires that critical habitat be designated for all listed species and that federal agencies are forbidden from authorizing, funding, or carrying out any action which "destroys or adversely modifies" this critical habitat. All listed aquatic organisms are therefore a concern when considering both culvert design and culvert retrofit. While all aquatic organisms are of concern, this report focuses solely on fish passage. There are at least seven reasons that a culvert is considered a barrier to fish passage. These barriers and possible effects were summarized in the following table, found in the recent Federal Highway Administration document "Design for Fish Passage at Roadway-Stream Crossings: Synthesis Report" (FHWA 2007).

Table 2. Description of Barriers to Fish Passage and Possible Effects (from FHWA 2007)

Barrier Type	*Description*	*Impact*
Drop	Drop at outlet exceeds fish jumping ability, or jump pool is insufficient to generate sufficient thrust.	Fish cannot enter structure, can be injured, or will expend too much energy entering the structure to traverse other obstacles.
Velocity	High velocity exceeds fish swimming	Fish tire before passing the crossing.
Turbulence	Turbulence within culvert prevents fish from entering, or confuses sense of	Fish do not enter culvert, or are unable to successfully navigate the waterway.
Length		Fish may not enter structure due to darkness. Fish may fatigue before traversing the structure.
Depth	Low flow depth causes fish not to be fully submerged.	Fish will be unable to swim efficiently or unable pass the structure.
Debris	Caught within a culvert, debris can block flow, or portions of flow.	Fish may not be able to pass by debris, or constricted flow may create a velocity or turbulence barrier within the culvert.
Cumulative	Series of culverts, each of which stresses fish during passage.	Group of culverts, each marginally passable, may be a combined barrier.

Although slip lined culvert retrofits may be extremely appealing when considering cost, time, and culvert discharge capacity, this method is fraught with fish passage issues, and therefore, basic slip lined retrofits are not terribly conducive to the ESA. The same hydraulic characteristic that makes slip line retrofit possible—increased velocities due to low roughness—can be a barrier to fish passage, not to mention the cause of several other barriers. The decreased roughness can cause increased

scouring at the outlet of the culvert, causing it to be perched. This increase in velocity can also create a steep velocity gradient between channel and culvert velocities. Many of the baby boomer culverts are already significant barriers to fish. A simple hypothetical example shows how culvert outlet velocities can be increased by 20% after slip lined retrofit (Webb 2008). This example of a change in velocity is used to highlight the fact that slip-lining methods can make a bad fish passage issue even worse without proper consideration of mitigation techniques.

Survey of Current Practices

There are several mitigation techniques available for application when culverts represent velocity barriers. The majority of the literature on this topic centers on baffles and weirs both inside and outside of a barrier culvert. The concept and function of the baffled culvert is similar to most fishways in that the baffles create a series of short high velocity runs between the baffles and a series of low velocity backwater areas behind the baffles. These areas allow the fish to swim in short bursts and then rest (Bryant 1981). A second prevalent idea is to place tailwater control weirs near the outlet of retrofitted culverts. This causes water to slow down and back up into the culvert itself, providing favorable depth and reduced velocities within the culvert.

A nation-wide survey of all U.S. state Departments of Transportation as well as state Fish and Wildlife Departments has shown that there has been very limited experience in providing for fish passage through slip lined culverts. The Oregon Department of Fish and Wildlife requires that a structure is completely backwatered throughout the entire migration period at all discharges. In order to provide this condition, baffles, weirs, bedload retention grids, tailwater control weirs, and over-steepened channel reconstruction are utilized. The California Department of Transportation has little experience with liners where fish passage is a concern, and warns that attaching baffles to HDPE liners can be difficult and may be prone to getting torn out during heavy storms. Another study suggests that baffled culverts may create a barrier to the downstream passage of juvenile Chinook salmon smolt, as the smolt avoided the structural complexity provided by baffles and selected a control channel over a baffled channel (Kemp 2008). The Ohio Department of Transportation often buries the invert of slip lined culverts to decrease culvert velocity. The Connecticut Department of Transportation has completed several slip lined retrofits on culverts 1.8-m (6-ft) in diameter or larger. The Maine Department of Transportation discourages considering slip lined culvert retrofits which will result in a culvert less than 1.2-m (4-ft) in diameter. Smaller retrofits can cause too great of a velocity change, as well as create maintenance issues due to the increased possibility debris impaction. Maine also suggests that careful attention be paid to the increased elevation of culvert inverts due to slip lined retrofitting, which can cause outlet pool degradation.

The Vermont Agency of Transportation rarely slip lines culverts, but also mentions that they “have had success only in those instances where backwater through the full

length of the barrel could be achieved." Vermont has been very creative in their mitigation techniques.

> "In large multi plate systems where the problem is confined to the invert area of the structure, where deformation has not progressed, where the danger appears to be loss of fines from around the pipe, we have installed up to a foot of concrete in the invert. Rebar is placed on a 12 x 12in grid and tack welded where possible. This type of repair can be used with a roughened surface, baffles, or random placement of embedded stone. In these cases, the goal is to simulate velocity and depth in the adjacent stream reach. Well placed stone clusters may recruit sediment and debris that could facilitate passage. Bottom characteristics will change yearly based on timing and distribution of large storm events that may scour the concrete surface."

The following photos from a visit to Vermont show many of these mitigation techniques used in non-lined culvert retrofits.



Figure 1, 2, 3. Various techniques for velocity mitigation in stream crossings.

Unfortunately, as is true with much advancement in engineering practice, the survey has also shown that many of the treatments for velocity mitigation remain unproven. Several respondents suggested that finding funding for post-construction monitoring is often difficult to obtain. This leaves the hydraulic engineer or biologist with untested conduits and without feedback necessary for design development and adaptive management in culvert rehabilitation. In order to further the science and continue creative developments in culvert treatments, both pre- and post-construction monitoring must be a priority. Following are four case studies which have undergone some type of pre-construction assessment, and post-construction monitoring.

Site Visits

As a result of information provided by survey respondents, site visits have been made a few states with this experience to assess developing technologies and record successful and unsuccessful installations. Visits were made to slip lined culvert retrofits in northern California, Maine, Vermont and Connecticut. These culvert tours included discussions on design considerations, post-construction observations, and general recommendations from those familiar with the installations. Brief case studies of four of these improved crossings follow.

Mendocino County Retrofit

The California Fish and Game approved a slip lined retrofit of a culvert in Mendocino County. In this case, a 0.91-m (3-ft) corrugated metal pipe culvert was lined with a 2.5-ft steel pipe with corner baffles, and was enhanced with three tailwater controls with removable notches, as shown in Figure 4



Figure 4. Outlet of slip lined culvert retrofit in Mendocino County, CA, showing corner baffles and one of three tailwater control barriers.

This culvert is on an intermittent, flashy and highly degrading stream. The stream bottom is at least 6-m (20-ft) below the road level and is adjacent to upstream private property. Because the stream is intermittent and because of a fish barrier upstream, this retrofit was installed as a case study, to learn more about the effects of corner baffles and tailwater controls. Study has shown that the baffles don't change the water surface profile or the overall culvert capacity significantly. However, the baffles have significantly increased sediment loading, which is flushed out only in high flows.

Cape Elizabeth Retrofit

The first stream crossing in Maine to be discussed is located near Cape Elizabeth, Maine. The 2.13-m (7-ft) CMP culvert at the Cape Elizabeth site is replaced by a 1.8-m (6-ft) Weholite pipe. The aquatic organisms of interest in this case are the American Eel and Alewife, which come inland in the spring as adults to spawn, and whose elvers return in the following spring. These animals are strong swimmers, but exhibit no leaping ability; therefore, it was expedient that water be backed up into and through the culvert during spring flows. A HDPE weir, costing approximately $3000 was placed downstream of the culvert and creates a subcritical condition to within roughly 1.5 to 2-m (5 to 6.5-ft) of the culvert inlet. Figure 5 shows the retrofitted culvert with the tailwater weir submerged.

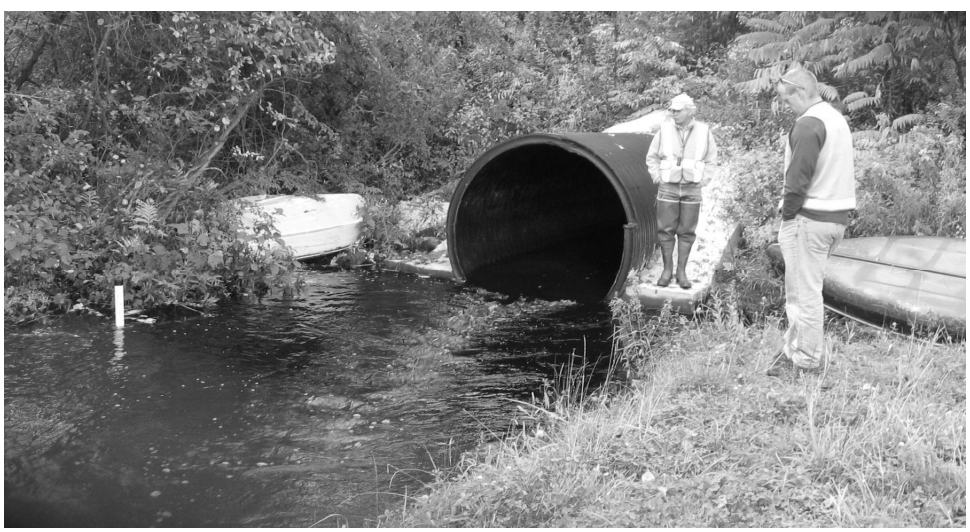

Figure 5. Culvert retrofit near Cape Elizabeth, ME. Tailwater weir is submerged.

Since construction, alewives have been found upstream and within the retrofitted culvert. It is suggested that observational, as well as formal post-construction monitoring is essential to determining the viability of such retrofits under similar conditions.

Belfast Retrofit

State Highway 1 runs along the Atlantic coast of Maine. This highway is the only road which connects the quaint coastal villages on the east coast of Maine which are so important to the tourism industry of the state. Given that the seasonal construction window coincides with the peak of the tourist season, full replacement of this culvert

would create a dramatic disruption. This culvert is only about 60-m (200-ft) from the ocean, and is a thermal refuge for juvenile brook trout. As a conduit for juvenile brook trout, the retrofit was designed for low flows. Roughly 16-18 baffles are inside the 1.8-m (6-ft) culvert. These weirs are 7.7-cm (3-in) tall with 5-cm (2-in) notches. Readily available jersey barriers were used for tailwater control weirs, and are designed to back the water into the culvert at a depth of 7.7-cm (3-in) over each baffle at the design flow. Figures 6 and 7 show the culvert outlet, as well as an image of the baffles within the HDPE pipe.



Figure 6. Culvert retrofit outside Belfast, ME, showing tailwater control weir.



Figure 7. Baffles within Belfast culvert retrofit.

Prior to the retrofit of this culvert, the roughly 60-m (200-ft) of stream above the culvert had no juvenile brook trout. A study after the retrofit found 80 juvenile brook trout in the same reach. Further observation has revealed that rocks tend to pile up below the downstream weirs, and between larger flows, rocks and sediment build up

next to the baffles. In all, the Department of Transportation was able to retrofit this culvert for fish passage without closing the road for long periods of time and saved more than $100,000 dollars.

Falmouth Retrofit

An interesting case study is the retrofit of a stream crossing near Falmouth, Maine. The Town of Falmouth applied to the Maine Department of Environmental Protection to lengthen a culvert using slip lined techniques, which were favored due to steep ravines which would cause entire culvert replacement to be extremely costly. The Maine Department of Inland Fisheries and Wildlife (MDIFW) reviewed the application and were concerned that this improvement might prevent or limit the passage of juvenile wild brook trout which persist in the stream system. Calculations performed by MDIFW resulted in the suggestion that corrugated metal pipe be used for the retrofit, in conjunction with a tailwater control at the outlet pool in order to back water into the pipe. "The Town really wanted to try plastic pipe . . . (and because of) an existing manmade barrier to passage was located a short distance downstream, it was decided to proceed with (the) project on an experimental basis" with the Town agreeing to provide a grade control structure downstream and that further modifications would take place if fish were unable to pass the retrofitted pipe. The outlet of the pipe is shown in Figure 8.

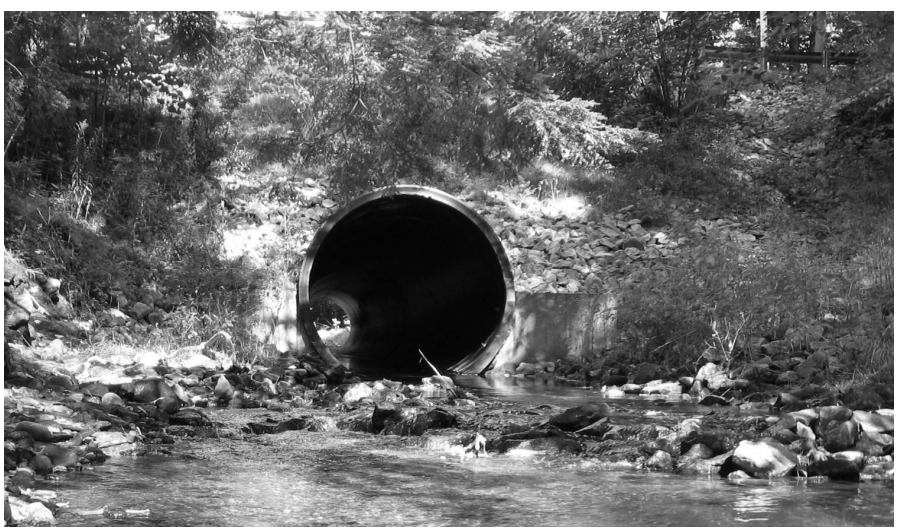

Figure 8. Outlet of Falmouth slip lined culvert retrofit. Rock tailwater grade control also shown.

In order to verify the success of the project, 60 marked hatchery farmed brook trout were introduced just downstream from the culvert, with nets downstream from the outlet pool and 112 m upstream from the inlet. After 24 hours, the site was revisited and fish were caught using an electrofishing unit. The study found 62% of the fish within the pipe, 28% of the fish upstream of the culvert and 10% unaccounted for. The retrofit was deemed a success, and no further construction was done on the site.

It has been shown that many states have begun utilizing slip lined culvert retrofit technology. Some agencies refuse to use slip lining when fish passage is an issue,

while others have chosen to modify retrofit designs to provide for passability. These have been done using varying techniques and have been met with varying degrees of success. This paper has shown four such cases. It is almost certain that there are more slip lined culvert retrofit success stories throughout the country, as well as more failures. Unfortunately, many of these retrofits have not been documented, and have not included pre-construction assessment and post-construction monitoring. It is suggested that increased documentation of design methods and monitoring results is essential to identifying conditions where slip lined retrofits are favorable, as well as evaluating the plethora of structural improvement methods that can be applied to the retrofitting process.

Current Work

The Utah Department of Transportation, in cooperation with Brigham Young University (BYU) and Utah State University (USU), intends to identify measures that can be used to mitigate the increased velocities associated with lined culverts. This is a two-Phase project. The project will provide broad guidelines, as well as some specific alternatives, for potential implementation of slip lined culvert retrofits that are passable to fish. Phase I includes the following objectives:

1. Determine what fish passage measures are currently being used to provide for fish passage in slip lined culverts.

2. Visit a limited number of sites to inspect and measure flow characteristics in slip lined culverts retrofitted for fish passage.

3. Perform analyses (no lab work) to establish ranges of hydraulic characteristics of flow that may be expected in slip lined culverts retrofitted for fish passage.

4. Determine the range of fish species for which passage may be feasible when retrofitting slip lined culverts for fish passage.

5. Prepare for Phase II of the study.

A survey of current design methods, along with culvert site visits, is complete. Hydraulic analysis currently being performed on this culvert data to determine ranges of flow characteristics possible in slip lined culverts retrofitted for fish passage. Much of this analysis has employed HY-8, a culvert hydraulics software package developed by the Federal Highway Administration. This analysis will provide information for task 4, which is to determine the ranges of fish species in Utah for which retrofitting slip lined culverts may be feasible. The final steps to Phase I of the research is to address constructability, durability, sedimentation retention and maintenance issues. After Phase I, several potential design alternatives will have been identified and examined using general hydraulic principles.

Phase II will be completed by Utah State University. Phase II will involve installing several of the potential alternatives in the field and testing them in detail in the laboratory. The lab tests will provide information on the propensity for retrofit designs to retain or evacuate sediments. The field tests will be tested for actual fish passage. At the end of Phase II, specific design procedures for retrofit and installation will be available based upon both field and lab tests.

Summary

The highway infrastructure of America includes a huge inventory of damaged and decaying culverts. Entire culvert replacement is so expensive and intrusive that alternate measures to extend culvert life are growing in popularity. One method of culvert retrofit that doesn't require any excavation or disruption to traffic is slip lining, where a 'sleeve' is installed within an existing culvert barrel and stabilized. Sleeves are typically made of plastic because the plastic material's lower roughness value allows for culvert capacity to be maintained despite a reduction in culvert size.

Unfortunately, the same hydraulic characteristic that makes slip line retrofit possible—increased velocities due to low roughness—can create barriers to fish passage. Since the ESA of 1973 requires that federal agencies are forbidden from authorizing, funding, or carrying out any action which "destroys or adversely modifies" this critical habitat, it is imperative that mitigation of the increased velocities accompany the inevitable culvert inventory upgrade where fish passage is to be considered.

There has been very limited experience in providing for fish passage through slip lined culverts. The relatively sparse amount of literature on this subject centers on baffles and weirs both inside and outside of a barrier culvert, which create a series of short high velocity runs between the baffles and a series of low velocity backwater areas behind the baffles. These areas allow the fish to swim in short bursts and then rest. A key concept put forth in the literature is that a very wide range of baffle sizes can be effective.

A survey of various transportation and fish and game agencies has shown that many forms and combinations of these ideas have been creatively put into practice with varying degrees of success. Visits to several sites have shown a range of solutions which have had positive results. Post-construction monitoring has proven essential in these cases to make determinations toward the viability of various approaches. A Utah Department of Transportation (with BYU and USU) project involving research and a review of current methods, as well as development of new design methods is currently in progress.

References

Anon. (1994). "Highway Drainage Restored Without Impending Traffic." *Public Works*. v.125, n.9, p.46.

Behlke, C. E., Kane, D. L., McClean, R. F., and Travis, M. D., (1991). "Fundamentals of Culvert Design for Passage of Weak-Swimming Fish." *Rep. No. FHWA-AK-RD-90-10*, U.S. Department of Transportation Federal Highway Administration.

Bryant, M. D. (1981). "Evaluation of a Small Diameter Baffled Culvert for Passing Juvenile Salmonids." *Res. Note PNW-384*. Portland, OR: U.S. Department of Agriculture, Forest Service, Pacific Northwest Forest and Range Experiment Station.

Campbell, S. (1995). "Culvert Rehabilitation at the Kennedy Space Center." *Public Works*. v.126, n.3, p.52.

DeMarco, J., Muenchmeyer, G. (1993). "Trenchless Technology Keeps Traffic Flowing." Water Engineering & Management. v. 140, n.9, p.36-38.

FHWA (Federal Highway Administration). (2007). "Design for Fish Passage at Roadway-Stream Crossings: Synthesis Report." *Rep. No. FHWA-HIF-07-033*. U.S. Department of Transportation Federal Highway Administration. p. 60-67.

Kemp, P. S., and Williams, J. G. (2008). "Response of migrating Chinook salmon (Oncorhynchus Tshawytscha) smolts to in-stream structure associated with culverts." *River Research and Applications,* 24(5), 571-579.

MacDonald, and J.I., Davies, P. E. 2007. "Improving the Upstream Passage of Two Galaxiid Fish Species Through a Pipe Culvert." *Fisheries Management and Ecology*. v.14, iss.3, p.221-230.

MDOT (Maine Department of Transportation), (2004). "Fish Passage Policy and Design Guide: 2nd Edition." Maine Department of Transportation.

Rajaratnam, N., Katopodis, C., and Lodewyk, S., (1991). "Hydraulics of Culvert Fishways IV: Spoiler Baffle Culvert Fishways." *Canadian Journal of Civil Engineering*, v.18, iss.1, p.76-82.

Robison, E. G., Mirati, A., and Allen, M., (1999). Oregon Road/Stream Crossing Restoration Guide: Spring 1999.".

TRB (Transportation Research Board). (2007). "Culvert Rehabilitation to Maximize Service Life While Minimizing Direct Costs and Traffic Disruption." *Transportation Research Board Research Needs Statement*. http://rns.trb.org/dproject.asp?n=12691, 12-28-2007.

USC (United States Congress) (1973). "Endangered Species Act". *16 U.S.C 1531-1544, 87 Stat. 884*, as amended. Washington GPO.

Webb, J., Hotchkiss, R. (2008). "Culvert retrofit and fish passage: At odds?" *Proceedings of the World Environmental and Water Resources Congress 2008*, American Society of Civil Engineers.

Field evaluation of engineered large woody debris for structure performance and habitat value

Kendra Russell[1] and Elaina Holburn[1]

[1]Technical Service Center, Bureau of Reclamation, Denver Federal Center Bldg 67 (86-68240), Denver CO 80225-007; PH (303) 445-2552; FAX (303) 445-6351; email: krussell@do.usbr.gov

ABSTRACT

Engineered large woody debris (LWD) structures are frequently used for habitat restoration and enhancement, bank protection and stabilization, and to alter flow within a channel. This paper discusses current LWD guidelines as well as ongoing field investigations on constructed LWD structures in the Middle Fork John Day River near John Day, OR. Low altitude balloon photogrammetry was completed for seventeen structures on the Middle Fork John Day to complete a stability and effectiveness assessment of the LWD structures. A habitat evaluation of the structures was also completed. The structures have experienced just over a 2-year peak discharge since constructed and are still in place. Preliminary findings show that the structures are generally acting as intended by altering channel morphology through locally narrowing the channel, adding pools, forming bars, and providing cover for fish habitat. The next step for the field analysis is to look at the stability of each LWD structure and perform quantitative comparisons.

INTRODUCTION

Many forested river ecosystems with minimal anthropogenic impacts commonly have the presence of large woody debris (LWD). Much of the natural LWD in channels was removed during the 20th century. However, replacement efforts are becoming widespread due to increased understanding of the many varied benefits of LWD. Engineered LWD structures are frequently used for habitat restoration and enhancement, bank protection and stabilization, and to alter flow within a channel. One major ecological benefit of LWD within rivers is the improvement to floodplain connectivity and creation of habitat through hydraulic complexity and cover (holding and rearing refuge habitats) for important fish species.

The Bureau of Reclamation (Reclamation) is using engineered LWD structures in habitat restoration efforts to provide short-term benefits to supplement long-term riparian vegetation recovery. To maximize the success of these structures, as measured through stability and habitat value, an increased understanding of the linkages between design parameters, structural stability, and resultant habitat is needed. To achieve this, Reclamation is involved in an ongoing research effort to evaluate LWD designs through field investigations and physical modeling in a laboratory setting. This paper discusses a few important habitat benefits and design guidelines identified through a literature review and presents an example of a field investigation of constructed LWD structures in the Middle Fork John Day River. This information will be used as the foundation for determining structure configurations in future physical modeling of LWD structures.

Short-term habitat benefits related to the presence of LWD within channels has been well documented. Previous studies have shown that more wood in rivers causes greater numbers and complexity of textural grain size patches (Buffington and Montgomery 1999). The addition of wood has led to increased habitat heterogeneity and overall macroinvertebrate richness and density (Lester et al. 2007). Based on these studies' findings, when used appropriately, LWD can enhance habitat for certain important fish species. Benefits of these structures have been monitored and evaluated. Among those monitored and published, Cederholm et al. (1997) and Shields et al. (2003) recorded marked biological responses. Cederholm et al. (1997) measured a 20-fold increase in the population of coho salmon during winter months at engineered LWD sites in a tributary to the Chehalis River, Washington. Within a 2 kilometer stretch of the Little Topashaw Creek in Mississippi, Shields et al. (2003) identified an increase in the average number of species, the number of fish, and the size of the fish following installation of 72 structures. However, the long-term ecological recovery in the latter study was doubtful due in part to the instability of most of the structures.

Important analysis steps and design considerations were identified through a literature review. An understanding of river processes within the system proposed for LWD installations is imperative so as to understand the historical presence of LWD, how recruitment and input of LWD has changed over time, and how well the current river processes coalesce with the installations of LWD. This type of assessment is needed to determine if a LWD structure is appropriate and if so, the type of structure that would be successful based on the geomorphology, hydrology, hydraulics, and human features (Abbe et al. 2005). Another important step is to identify the physical and biological objectives of the structure(s), such as additional cover and slow water rearing habitat for juveniles, scour pool development for adult holding, spawning gravel depositional zones, or hiding or resting locations from predators.

Following completion of analyses to determine that LWD structures can effectively be used as part of a habitat restoration effort and identification of structure objectives, several design parameters need consideration. Objectives should be consistent with the proposed stability of the structure, design life, and potential downstream risks. Parameters such as drag, scour, spacing, angle, burial, wood characteristics, and backwater effects all require examination and quantification. Key design variables that can be directly linked to increased success in meeting habitat goals include structure orientation with respect to flow and structure spacing. Results of research performed by Cherry and Besctha (1989) provided evidence that the vertical and horizontal orientation of wood affects channel scour and stability. In their flume study, pieces of wood lying on the bottom of the bed produced the greatest scour surface area. This information can be expanded to LWD complexes and points to having an understanding of what range of angles from the bank produces the greatest stability and scour pool volume.

Multiple LWD structures in series may increase the success of meeting structural objectives. Structures should be spaced closely enough that fish can rest between consecutive structures. However, structures spaced too closely may limit the maximum development of scour holes and area of spawning gravel deposition between the structures. Montgomery et al. 1995 developed a relationship between pool formation and natural LWD loading across multiple channel types. This relationship can be used to compare naturally effective LWD loading with constructed LWD loading. Alternatively, a relationship may be developed specifically within a river of interest based on the availability of historical data documenting the presence of LWD (e.g. pre-disturbance aerial photography).

Many other studies have been conducted documenting useful guidance and important considerations for the design of engineered LWD. By combining documented relationships in published literature with findings in the field, we can begin to compare how closely engineered structures fit published data, evaluate the performance of the structures in achieving their intended habitat goals, identify successful designs as well as those that could be improved, and ultimately recognize where data gaps exist that can be further examined in a physical laboratory setting.

EXAMPLE FIELD INVESTIGATION

The field investigation in the Middle Fork John Day River is part of a comprehensive program to use field investigations and physical modeling to determine stable LWD configurations, placement, and sizing to create habitat through depositional and scouring mechanisms. Information from the field investigations will assist designers, resource managers, and stakeholders understand how habitat characteristics and structure stability vary based on the location of the LWD structure within the channel and design the most stable structures with the highest habitat value. Upon completion of data processing from the field investigations, key design parameters from the literature review will be compared with the structures along the Middle Fork to determine if the designs fit with previously conducted studies.

LWD structures were installed on the Middle Fork John Day River near John Day, OR in July–August, 2007 and July-August, 2008 (MWH 2006). Seventeen total structures were installed; seven were designed as collector v-logs, four were designed as scouring v-logs, and six were designed as deflector v-logs. The structures are split into two groups separated by approximately one mile: the upstream section has ten structures and the downstream section has seven structures. Figures 1 and 2 show the locations of the LWD structures. Scouring v-logs were intended to provide salmonid resting habitat and depth cover as well as physical cover and shade. Deflector v-logs were meant to create friction within the structure and cause the river flow to go around the structure, resulting in narrowing and deepening of the channel. Instream cover and habitat diversity was anticipated to be created by these structures. Collector v-logs were designed to collect woody debris in the channel and create cover, resting, and hiding refuge for adult and juvenile fish. The scouring v-logs have a pre-excavated pool unlike the deflector or collector v-logs. Based on design drawings, the collector v-log and scouring v-log have 4 key log members; the deflector v-log has 5

key log members. All log members of the structures are bolted together. The collector v-log was designed with a root wad at the structure apex that extends into the river; the deflector v-log did not incorporate this feature. All structures are similar in size spanning approximately 35 feet along the river bank and extending roughly 20 feet into the river.

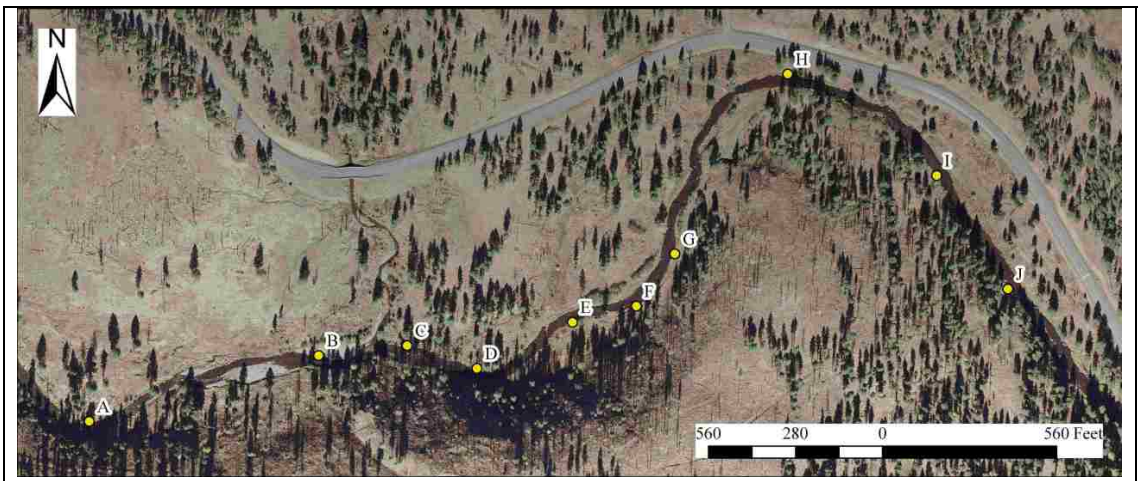

Figure 1. Overview of upstream portion of LWD structures on the Middle Fork John Day River. Structures are labeled A through J. Flow is from right to left.

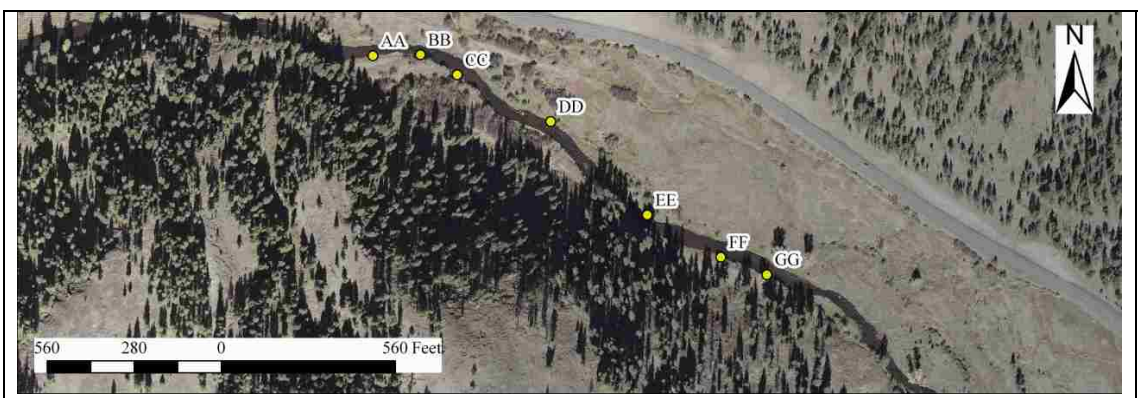

Figure 2. Overview of the downstream portion of LWD structures on the Middle Fork John Day River. Structures are labeled AA through GG. Flow is from right to left.

A site visit to these structures was conducted in November, 2008. The largest peak flow the 2007 structures have experienced to date was approximately 1,200 to 1,500 cubic feet per second (cfs) based on 2,300 cfs measured 30 miles downstream from the structures (recorded at USGS 14044000 Middle Fork John Day River at Ritter, OR). This flow is between a 2-year and 5-year event for the Middle Fork John Day based on a recent hydrologic analysis (Reclamation, 2008). The 2008 structures had only experienced base flow conditions (less than 100 cfs) between the time of their installation and the site visit.

Since the goal of the field investigation is to compare the structural stability and habitat value of the LWD structures to determine the most efficient configuration for future designs, detailed surveys are needed to measure previously identified key parameters. This information will help determine which parameters have the most influence on stability and habitat. The quantity of structures, time allotted for the field investigation, and poor satellite coverage made a detailed topographic survey with a total station or GPS equipment at each structure not feasible. Therefore, low altitude balloon photogrammetry was used.

Low altitude balloon photogrammetry is an emerging technology. Originally photogrammetry was limited to professionals with the required training, equipment, and software. However, with the development of high quality digital cameras, Adam technology developed a "system that retains all of the rigor of a state-of-the art photogrammetric system but with a degree of performance and automation that make it accessible to anybody who can capture a photographic image (Birch 2006)." The Adam technology has been used by Reclamation to map vertical rock faces and seemed appropriate to test in collecting topographic information within rivers.

Reclamation has been working to expand the areas in which small scale photogrammetry is applicable. To acquire photographs for mapping ground surfaces and in-channel features, the digital camera was attached to an 8-foot diameter helium balloon. The balloon was tethered to the ground and manually moved to the location of concern. Pan and tilt camera movements were remotely controlled using a control unit designed for flying small airplanes and helicopters. The live image from the camera was transmitted to a receiver on the ground, enabling the operator to see directly through the camera lens and remotely trigger the camera at specific overlapping intervals for development of accurate terrain models. In the field investigation of the Middle Fork John Day River, the balloon was approximately 100 to 150 feet above the ground for the photographs. Figure 3a and 3b show the balloon and camera used to take photographs of the LWD structures.

The low altitude balloon digital photogrammetry provides high resolution spatial information in a fraction of the time it would take to survey the same number of points using traditional methods. Ground survey control was established by placing small targets along the channel corridor and using GPS equipment to obtain spatial information for each target. In addition to the target survey points, GPS survey was completed on top of and adjacent to the log structures to compare with the photogrammetry results. Qualitative information about the structures and the river were also collected including: planform location, bed material size, vegetation on the banks, bank material, and structure burial.



Figure 3a. Helium balloon used to carry digital camera. The balloon can carry approximately 12 pounds.

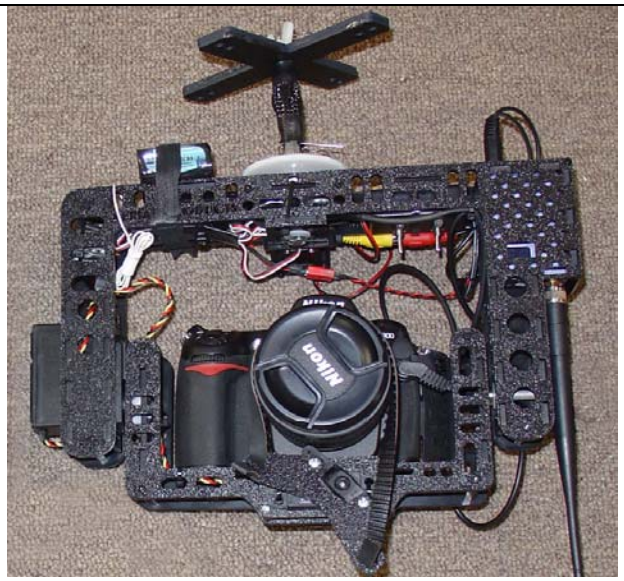

Figure 3b. D300 Nikon camera mounted to frame with pan (360° rotation) and tilt (from horizontal to straight down) servo motors to control orientation.

Qualitative habitat evaluations of the structures were completed by a local biologist (Wilson personal communication, 2008), who examined each structure trying to determine whether structures were providing micro or macro habitat, how they differed from one another, and potential ideas for improvement. For this habitat evaluation, micro habitat features generally provided areas for cover and hiding. Macro habitat generally referred to structures with scour pools or larger channel morphology changes occurring. Snorkel surveys were completed on the Middle Fork John Day River prior to construction. However, to date not enough post-construction data has been collected to quantitatively evaluate the structures.

PHOTOGRAMMETRIC PROCESSING

Photographs acquired from the helium balloon were imported into Adam Technology's 3DM Analyst Mine Mapping Suite. An example photograph is shown in Figure 4. Using the software, images were paired, and common points were generated between the images. The software experienced difficulty finding common points within the river channel, and therefore, multiple points were added manually to accurately match the images. Control points and associated GPS information were added to the targets in the images to orient the photos spatially.



Figure 4. View of an engineered LWD structure in the Middle Fork John Day River as seen from a helium balloon about 120 feet above the ground (flow is from left to right).

The software needs a least three control points with known locations to form an absolute orientation (Birch 2006). Four targets were placed at each structure, and overlapping images were taken from one structure to the next to orient the entire project in the State Plane coordinate system. Figure 5 shows a pair of images in the Adam Technology software with labeled common and control points.

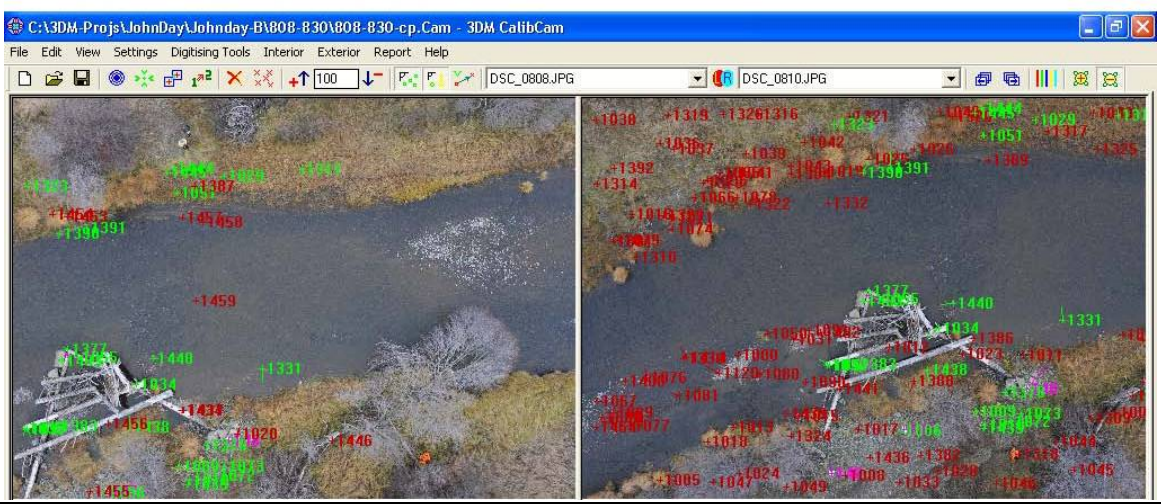

Figure 5. Common points are either automatically generated by the Adam Technology software or entered manually. Control points from the surveyed targets are also input into the program to create a digital terrain model (DTM) from the photographs.

The digital terrain model (DTM) generator within the Adam Technology software was used to create spatial points with elevation and orthophotographs. The accuracy of the DTM points varied within each photo-image pair; the total residual ranged

from 0.04 to 0.19 feet for 36 of the control points. Figure 6a shows the orthophotograph for LWD structure CC. Figure 6b shows the same structure with the DTM points overlaid. There are over 50,000 points generated for the one photograph. As seen from the DTM points, the software had difficulty in generating elevation points across the water surface and also in locations with trees.

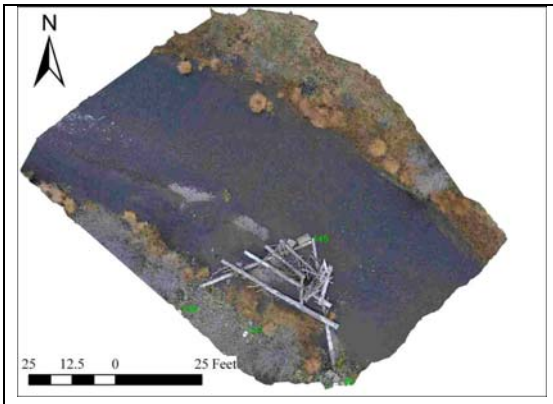

Figure 6a. Orthophotograph generated by Adam Technology software for LWD structure CC on the Middle Fork John Day River.

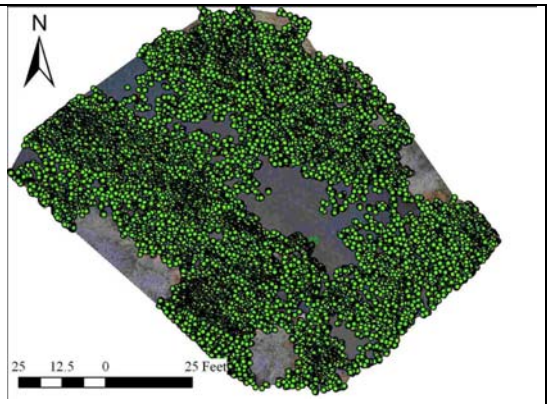

Figure 6b. Orthophotograph of LWD structure CC with elevation points from Adam Technology software processing overlaid.

Since there were multiple structures in series the orthophotographs were merged to create a continuous image. Three of the downstream site structures (AA, BB, and CC) are shown in Figure 7. Continuous images can be used to evaluate changes in morphology upstream and downstream of the structure as well as the interaction between the structures. For example, bars are beginning to form between the structures illustrated in Figure 7,



Figure 7. Ten merged orthophotographs generated from Adam Technology software that cover a portion of the downstream site from LWD structure AA to CC. Flow is from right to left.

HABITAT EVALUATION

Fourteen of the seventeen LWD structures were visited in November, 2008 with a local biologist. Key limiting factors for salmonid species on this section of the Middle Fork John Day River include high summer temperatures, a lack of large wood debris structure for shade and hiding, and a lack of mature trees in the riparian for shade and food production (Wilson 2008). Many species use the LWD structures including bull trout, spring Chinook, summer steelhead, and long nose dais. Table 1 lists each of the structures, their type, and the habitat they provide based on the qualitative evaluation performed by the local biologist.

Table 1. Summary of habitat evaluation completed in November, 2008.

Structure ID	Type	Pre-dug scour	Macro-habitat	Habitat Functionality	Physical Changes
B	Scouring	X	X	Spawning, Rearing, Thermal refuge, Cover, Hiding	Pool
C	Deflector			Hiding	
D	Deflector			Cover, Hiding	
E	Deflector			Cover, Hiding	Scour on opposite bank
F	Collector			Cover, Hiding	Deeper channel
G	Collector			Cover, Hiding	Deeper channel
H	Scouring	X	X	Adult Holding	Pool, divided run in channel
AA	Collector			Cover, Hiding	Channel narrowing, scour
BB	Deflector		X	Spawning, Cover, Hiding	Bar formation, gravel deposition, scour
CC	Deflector			Cover, Hiding	Bar formation
DD	Collector			Little cover, Hiding	Channel narrowing, scour
EE	Scouring	X	X	Thermal refuge, Spawning, Adult holding, Juveniles	Pool, channel narrowing, gravel deposition
FF	Deflector				Bar formation, scour, channel narrowing
GG	Collector			Juvenile rearing	Bar formation, deeper channel, gravel deposition, channel narrowing

Based on the field evaluation by the biologist, all structures did provide habitat value to the system. However, the downstream portion (Structures AA-GG) seems to be outperforming the upstream section in creating habitat complexity, locally narrowing the channel, and changing the river morphology. In particular, structure EE is working to narrow the channel and add complexity through an approximately 50 foot river segment. Also, structure B is providing thermal refugia and was one of two places fish lived during the 2007 fish kill due to high water temperatures (Wilson 2008). Some of the recognized benefits may relate to localized morphologic conditions, such as bed rock outcrops, in addition to variations in structure configurations.

PRELIMINARY RESULTS AND DISCUSSION

At the time of this report, field data from the Middle Fork John Day are being processed. A qualitative examination of the habitat evaluation results suggests that

structures are generally performing as intended. All scouring structures have maintained some scour pool, although comparisons with the pre-excavated scour pool volume have not been examined. Deflector structures, such as E or FF, are deflecting flows against the opposite bank creating a scouring mechanism and narrowing localized flow conveyance. Finally, collector structures appear to be providing cover and hiding for fish (Wilson, personal communication, 2008). In addition, several structures are providing habitat benefits that were not considered in the design. For example, although structure GG was designed as a collector, it is creating greater channel complexity by causing bar formation and channel narrowing. Next steps for the field component of the research include finishing data processing and measuring structure attributes, such as flow constriction, spacing, and key member lengths. Quantitative information from the field investigation will then be compared to the habitat evaluation and the existing design guidelines and coupled with results from the physical modeling to best understand the relationships between geometric variables of the structure, structure stability, and habitat benefits.

REFERENCES

Abbe, T. B., D. R. Montgomery, et al. (2005). DRAFT Bank Protection and Habitat Enhancement using Engineered Log Jams: An Experimental Approach Developed in the Pacific Northwest, *Natural Resources Conservation Service*.

Bureau of Reclamation (2008). *Middle Fork and Upper John Day River Tributary Assessments, Grant County, Oregon*, Denver, CO.

Birch, J. S. (2006) "Using 3DM Analyst Mine Mapping Suite for Rock Face Characterization." *Laser and Photogrammetric Methods for Rock Face Characterization Workshop*, 13-32.

Buffington, J. M. and Montgomery, D. R. (1999). "Effects of hydraulic roughness on surface textures of gravel-bed rivers." *Water Resources Research*, 35(11), 3507-3521.

Cederholm, C. J., R. E. Bilby, et al. (1997). "Response of juvenile coho salmon and steelhead to placement of large woody debris in a coastal Washington stream." *North American Journal of Fisheries Management*, 17, 947-963.

Cherry, J. and Beschta, R. L. (1989). "Coarse woody debris and channel morphology: a flume study." *Water Resources Bulletin*, 25(5), 1031-1036.

Lester, R. E., W. Wright, et al. (2007). "Does adding wood to agricultural streams enhance biodiversity? An experimental approach." *Marine and Freshwater Research*, 58(8), 687-698.

Montgomery, D. R., J. M. Buffington, et al. (1995). "Pool spacing in forest channels." *Water Resources Research*, 31(4), 1097-1105.

MWH (2006). *Middle Fork John Day Habitat Improvement Conceptual Design Report.*

Shields, F. D., S. S. Knight, et al. (2003). "Response of fishes and aquatic habitats to sand-bed stream restoration using large woody debris." *Hydrobiologia*, 494, 251-257.

Wilson, W. (2008). Habitat Value of Engineered Log Jam Structures for Nature Conservancy Property Middle Fork John Day River Data Sheet. (November 4, 2008)

NUMERICAL ANALYSIS OF THE PERFORMANCE OF ROCK WEIRS: EFFECTS OF STRUCTURE CONFIGURATION ON LOCAL HYDRAULICS

Christopher L. Holmquist-Johnson[1,2]

1 Ph.D. Candidate, Colorado State University, Fort Collins, CO 80523
2 (current address) U.S. Geological Survey, 2150 Centre Ave., Fort Collins, CO 80526; PH (970) 226-9382, email: h-johnsonc@usgs.gov

ABSTRACT

River spanning rock structures are being constructed for water delivery as well as to enable fish passage at barriers and provide or improve the aquatic habitat for endangered fish species. Current design methods are based upon anecdotal information applicable to a narrow range of channel conditions. The complex flow patterns and performance of rock weirs is not well understood. Without accurate understanding of their hydraulics, designers cannot address the failure mechanisms of these structures. Flow characteristics such as jets, near bed velocities, recirculation, eddies, and plunging flow govern scour pool development. These detailed flow patterns can be replicated using a 3D numerical model. Numerical studies inexpensively simulate a large number of cases resulting in an increased range of applicability in order to develop design tools and predictive capability for analysis and design.

The numerical model U^2RANS is used to investigate how variations in structure geometry affect local hydraulics, scour hole development, and overall structure performance. An automatic mesh generator was developed to expedite the process of generating 30 structure geometries in a simulated straight trapezoidal channel. Variations in structure geometry include: arm angle, arm slope, drop height, and throat width. Various combinations of each of these parameters are modeled at 3 flow rates: 1/3 bankfull discharge, 2/3 bankfull discharge and bankfull discharge. The numerical modeling focuses on how variations in structure geometry affect local flow patterns and scour development. Numerical modeling results duplicated both field observations and lab results by quantifying high shear zones near field and lab scour areas and low shear zones near field and lab depositional areas.

The analysis and results of the numerical modeling, laboratory modeling, and field data provide a process-based method for understanding how structure geometry affects flow characteristics, scour development, fish passage, water delivery, and overall structure stability. Results of the numerical modeling allow designers to utilize results of the analysis to determine the appropriate geometry for generating desirable flow parameters. The end product of this research will develop tools and guidelines for more robust structure design or retrofits based upon predictable engineering and hydraulic performance criteria.

1 INTRODUCTION

River spanning rock structures provide sufficient head for irrigation diversion, permit fish passage over barriers, protect banks, stabilize degrading channels, activate side channels, reconnect floodplains, and create in-channel habitat. Vertical drop height, lateral constriction, size of rock material, and construction methods are common design considerations for these structures. The use of in-stream structures for habitat and stream restoration dates back to the early 1900s; however, the design, effectiveness, and performance of these types of structures have not been well documented. A review of international literature on grade control structure design by Nagato (1998) found that no official standard guidelines for designing

low-head drop structures exist. The review found that design guidelines were relatively tentative or provisional and site specific in nature. While recently there have been a large number of laboratory experiments and empirical relationships developed from field data, efforts to link these relationships with field engineering practices are lacking.

Monitoring of in-stream restoration projects has focused primarily on whether structures produce the desired physical response rather than understanding the physical processes that cause the physical response and how that response might change with differing structure configurations. While general monitoring of in-stream restoration projects provides some information pertaining to success and failure rates, it usually does not provide enough detailed quantitative information to determine the physical processes associated with the success or failure of a given structure geometry. As a result, current design methods are based upon anecdotal information applicable to narrow ranges of channel conditions. Complex flow patterns and performance of rock weirs are not understood, and methods and standards based upon predictable engineering and hydraulic performance criteria currently do not exist. Without accurate hydraulics, designers cannot address the failure mechanisms of structures.

In 2005, the Bureau of Reclamation (Reclamation) initiated a program to evaluate the performance of these structures and develop design guidelines using a multi-faceted approach that consists of field reconnaissance, physical modeling, and numerical modeling. Integration of field, lab, and numerical data sets provides a scientific basis for predicting structure performance under various river conditions and for developing the most-effective design criteria. This paper focuses on the numerical modeling of rock weirs and the effects that variations in the structure geometry have on local hydraulics. A design matrix consisting of approximately 30 different structure configurations along with a field validation case are presented. The following section takes a closer look as to why lower order (1D and 2D) models are not suitable for simulating the complex flow patterns associated with rock weirs.

2 PRELIMINARY COMPARISON OF NUMERICAL MODELING OF ROCK WEIR FLOW PATTERNS

Numerical modeling provides an opportunity to test design parameters over large ranges. A numerical model must capture significant flow patterns and replicate the important dominant physical processes. One-dimensional (1D) numerical simulations model downstream changes in hydraulics while neglecting vertical and lateral variation. Two-dimensional (2D) models incorporate lateral differences in velocity and water surface elevation, but neglect flow patterns that are not parallel to the stream bed. Three-dimensional (3D) modeling simulates the motion of water in all directions and most accurately captures flow patterns. Estimating structure performance with lower dimensional methods requires understanding the impact of representing a feature with methods farther divorced from real world processes. The limited understanding of the complex flow patterns around rock weirs require 3D simulations.

Flow characteristics such as jets, near bed velocities, recirculation, and plunging flow govern scour pool development. 3D numerical models capture these patterns without requiring prior and possibly incorrect assumptions typically required when using lower order models. Figure 1 shows a U-Weir in the field and the corresponding water surface and velocity output from the 3D numerical model U^2RANS (Lai et al, 2003). In the photograph, entrained air reveals areas of high velocity and turbulence. The 3D model captured flow features including the draw down curve, hydraulic jump, and variations in velocity. Dry areas in the photograph, such as the protruding rocks in the upper left corner match the 3D model water surface. Figure 1 demonstrates the capability of three-dimensional numerical modeling to match field conditions.

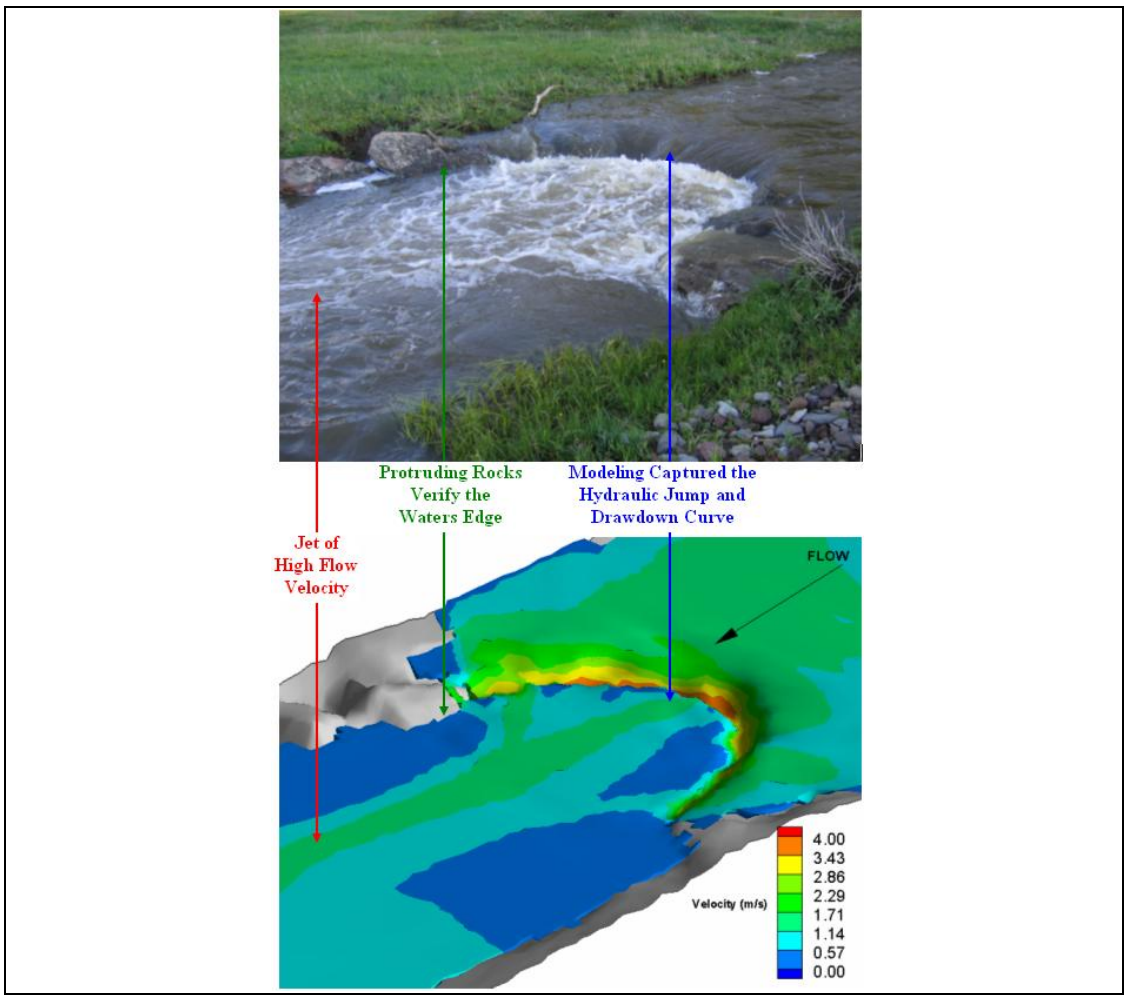

Figure 1. Field Photo and Corresponding Numerical Modeling Results

Figure 2 shows a plan view with water surface elevation contours. The areas upstream and downstream of the structure show little lateral variation. The water surface drops rapidly over the structure and follows the weir crest topology. 1D modeling assumes gradually varied flow and constant water surface elevation across a transect. Methods to meet 1D water surface requirements include constructing cross sections tracing water surface elevation contours or coding multiple cross section perpendicular to the thalweg.

Figure 3 shows surface velocity vectors. In the channel upstream and downstream of the structure water generally flows parallel to the banks. Over the weir, the flow paths rapidly converge and then slowly expand. A jet through the center of the channel creates abrupt lateral changes in velocity. 1D modeling requires cross section lines perpendicular to the velocity vectors and therefore must accommodate lateral variability through bending the cross section.

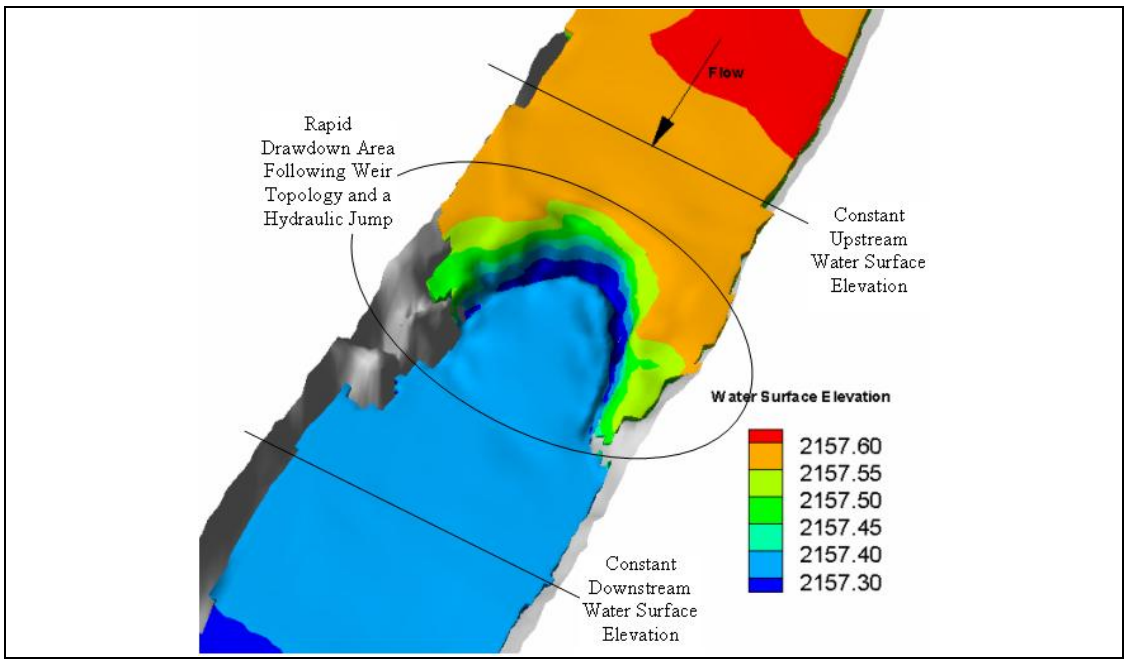

Figure 2. Modeled Water Surface Elevation (Z-Axis Scaled Factor of 5)

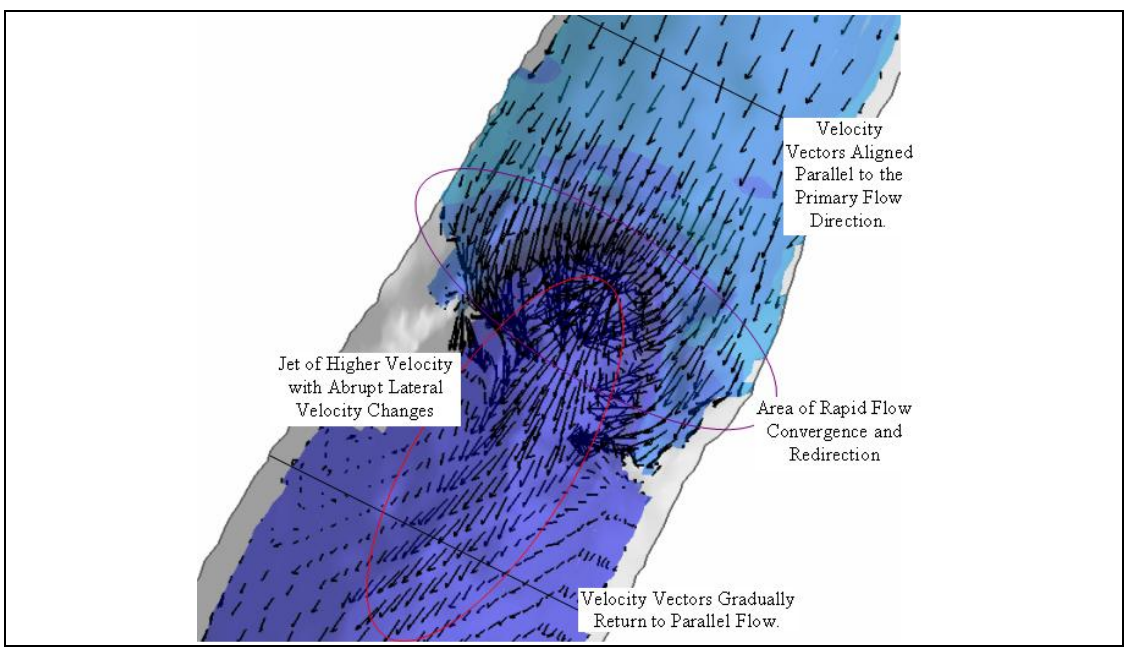

Figure 3. Plan View Velocity Vectors and Wetted Area

Figure 4 shows a vertical profile view for velocities along a longitudinal section of the thalweg. Water flows parallel to the bed upstream and downstream of the structure. The stream lines rapidly converge and diverge vertically through the structure. The velocity profile contains a jet midway through the water column rather than the logarithmic profile of a typical river section. Vertical velocity components in the scour pool show plunging flow. 2D modeling requires velocity vectors perpendicular to a vertical plane while 1D modeling requires perpendicular velocity vectors in both vertical and lateral planes. As a result, these lower order models are not able to properly represent the flow patterns associated with these types of structures.

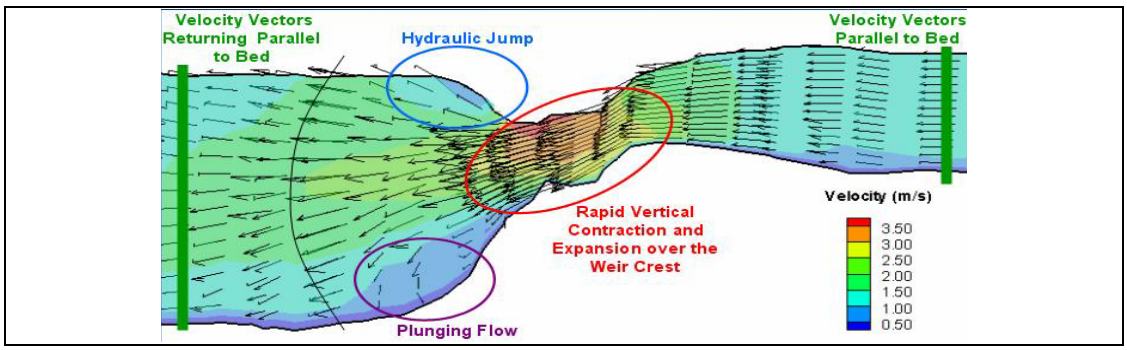

Figure 4. Thalweg Profile View and Velocity Magnitude

Figure 5 illustrates attempts to reconcile the cross sectional 1D requirement with observed field conditions. A cross section model can meet either water surface requirements or velocity requirements, but not both. Figure 5 demonstrates why 1D models require adjustments for multi-dimensional effects. HEC-RAS contains placeholders, but the magnitude of the adjustment is unknown for rock weirs. The adjustment will depend on the throat width, profile and plan arm angle, drop height, and more. After understanding the 3D processes, developing 1D and 2D adjustment parameters may be possible.

In addition to the field data comparison, with the recent completion of the rock weir laboratory testing, measured water surface elevations, velocities, and bed topography are currently being analyzed and compared to results from the 3D numerical model in order to develop rating curves and scour prediction equations for various rock weir configurations.

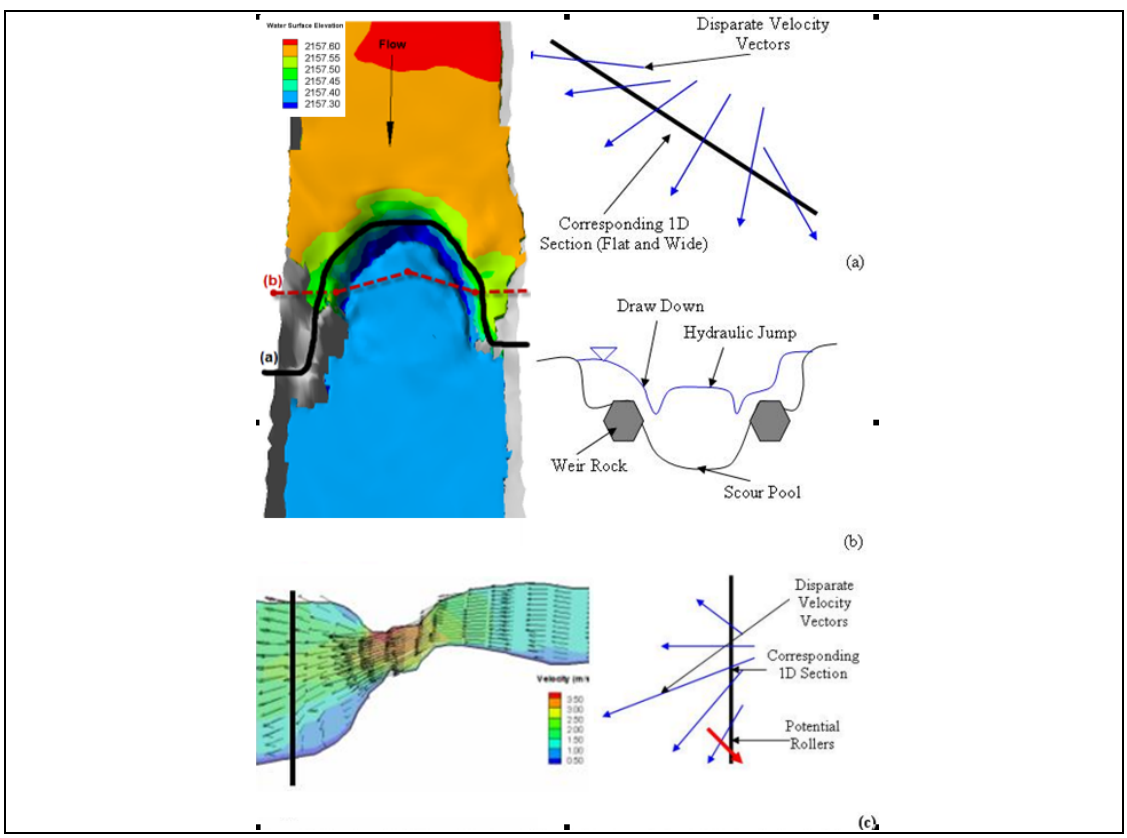

Figure 5. Meeting 1D Water Surface Criteria Fails to Meet Velocity Criteria (a) and vice versa (b). No Method captures jumps or plunging flow (c).

3 3D MODEL SETUP AND DESIGN

The numerical model U^2RANS (Lai et al, 2003) is used to investigate how variations in structure geometry affect local hydraulics, scour hole development, and overall structure performance. An automatic mesh generator was developed to expedite the process of generating 30 different structure geometries in a simulated straight trapezoidal channel. Variations in structure geometry include: arm angle, arm slope, drop height, and throat width. The following sections describe how the design matrix was generated.

3.1 Included Variables

The following variables were included in compiling the final design matrix:

- Bed Material
- Channel Slope
- Throat Width
- Drop Height (fish passage criteria per WDFW 2003)
- Arm Length (Planform Angle and Profile Angle)

3.2 Excluded Variables

The following variables were considered but not included in the final design matrix:

- Bank Height: Water depths will not exceed weir depth. All model runs are at bank full or less, no superbank discharge.
- Bank Angle (Side Slope): 0.75:1 (H:V) Assuming wide-rectangular is adequate.
- Top Width: set by hydraulic geometry equations.
- Bankfull Design Discharge: set by hydraulic geometry equations.
- Asymmetric Geometries: This is a limitation of the study scope.
- Radius of Curvature: This is a limitation of the study scope.

3.3 Matrix Configuration

3.3.1 Bed material

Grain sizes were selected to match field conditions in which river spanning rock structures are most commonly used (ie. gravel bed rivers). The distributions for the D84 and D16 were set to plus and minus one phi class. Three D50 grain diameters were selected using the geometric mean of the AGU classification system, a log base 2 scale:

- Coarse Gravel: D50 = 22.63 mm, D84 = 45.25 mm, D16 = 11.31 mm
- Small Cobble: D50 = 90.51 mm, D84 = 181.0 mm, D16 = 45.25 mm
- Large Cobble: D50 = 181 mm, D84 = 256 mm, D16 = 90.51 mm

3.3.2 Bankfull Channel Geomerty

Previous research has shown that it is possible to define a ‘‘bankfull channel geometry’’ [Leopold and Maddock, 1953; Leopold et al., 1964] in terms of a bankfull width B_{bf}, bankfull depth H_{bf} and down-channel bed slope S. More recently, Parker et al. (2007) used a baseline data set consisting of four differing stream reaches from Canada, USA, and Britain to determine bankfull hydraulic relations for alluvial, single-thread gravel bed streams with definable channels and floodplains. Their results (eqns, 1-3 below) show a considerable degree of universality and the exponents of Q_{bf} in these equations are similar to those found by other authors (e.g., Millar, 2005).

$$S \cong 0.101 \cdot \left(\frac{Q_{bf}}{\sqrt{gD_{s50}} D_{s50}^2} \right)^{-0.344} \quad \text{Equation 1}$$

$$W_{bf} \cong \frac{4.63}{g^{1/5}} Q_{bf}^{0.4} \left(\frac{Q_{bf}}{\sqrt{gD_{s50}} D_{s50}^2} \right)^{0.0667} \quad \text{Equation 2}$$

$$H_{bf} \cong \frac{0.382}{g^{1/5}} Q^{2/5} \quad \text{Equation 3}$$

Where,

S = bed slope;

Q_{bf} = bankfull discharge (m^3/s);

D_{s50} = median particle diameter, (m);

W_{bf} = bankfull width (m);

H_{bf} = bankfull depth (m).

Because of the degree of universality and ease of use of the hydraulic geometry equations presented by Parker et al., they were selected for determining the bankfull hydraulic geometry used in this study. Given the bed material grain sizes listed above and a range of representative channel slopes (0.001, 0.004, and 0.01), Equations 1, 2, and 3 were used to compute central width, depth, and discharge tendency in the design matrix. In order to analyze each structure configuration and its effects on the local flow patterns, the discharge for each structure configuration was varied to include 1/3, 2/3, and bankfull discharges.

3.3.3 Throat width

Initial structure throat width was set to 1/3 the bankfull width as specified in Rosgen (2001) and following observed field applications. To study how flow patterns are affected by changes in structure throat width, the throat width was varied from 1/4, 1/3, and 1/2 the calculated bankfull width for each of the three grain sizes and corresponding channel geometry.

3.3.4 Drop height

Drop height was set to 0.8ft as prescribed by the WDFW (2003) for the maximum drop height allowed for fish passage. In order to study how the drop height over the structure effects flow patterns, this parameter was varied by 0.5 and 1.5 times the value prescribed by WDFW (2003). This results in a range of drops heights of 0.4, 0.8, and 1.2ft.

3.3.5 Arm length

Initial structure arm lengths were designed to approach as close as possible the midpoint of the design ranges specified in Rosgen (2001). Rosgen's recommended plan angles were between 20 to 30 degrees and profile angles range from 2 to 7 percent. Target angles were 25 degrees for plan angles and 4.5 percent for profile angles. The solver function in Microsoft Excel® was then used to calculate the weir arm length that minimized the relative distances on the planform and profile angles of the weir arms. This minimized solution was then used to calculate the arm length ranges that would be used in the numerical modeling in two ways;

multiplying the minimized values by ½ and 2. This provided a wide range of planform (10.31 to 48.35 degrees) and profile angles (1.47 to 10.11 percent) to be tested (Figure 6).

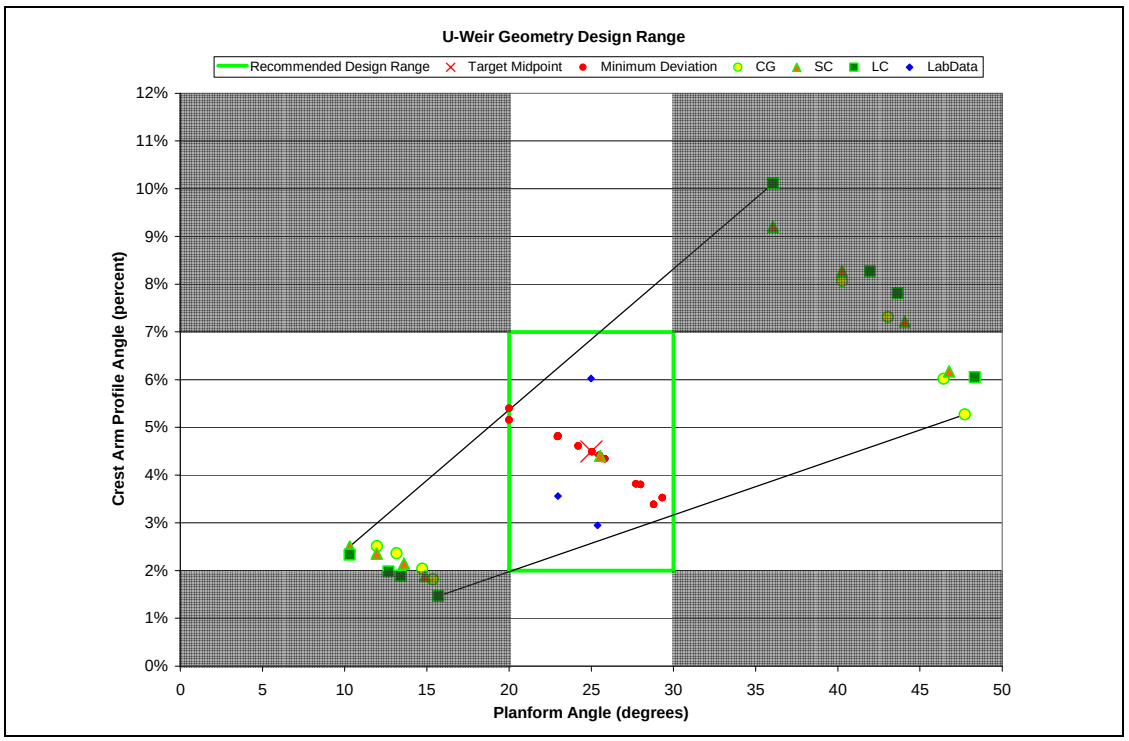

Figure 6. Plot of variation in structure parameters used in design matrix.

3.4 Mesh Generator

The automesh generator simplifies the process of 3D numerical modeling by allowing the generation of multiple structure geometries in a quick and cost effective manner. Five lateral definition lines describe a structure in the 3D mesh generator: upstream bed, upstream header, downstream header, downstream footer, and downstream bed. Overbank, top of bank, and toe lines describe the channel. Each line consists of eight definition points. Combinations of river left or river right, toe, top of bank or overbank, upstream or downstream, bed, header or footer, and pool uniquely identify each definition point. Dashed lines show the intersection of the structure with the channel bank. Each point can be uniquely identified through selecting one from each column in Table 1. Figure 7 shows the conceptualized structure with definition lines and definition points.

Table 1. Structure Definition Point Identification

Flow-Wise	Bank-Wise	Structure-Wise	Laterally
Upstream	Left	Bed	Throat
Downstream	Right	Header	Toe
		Footer	Top bank
		Pool	Overbank

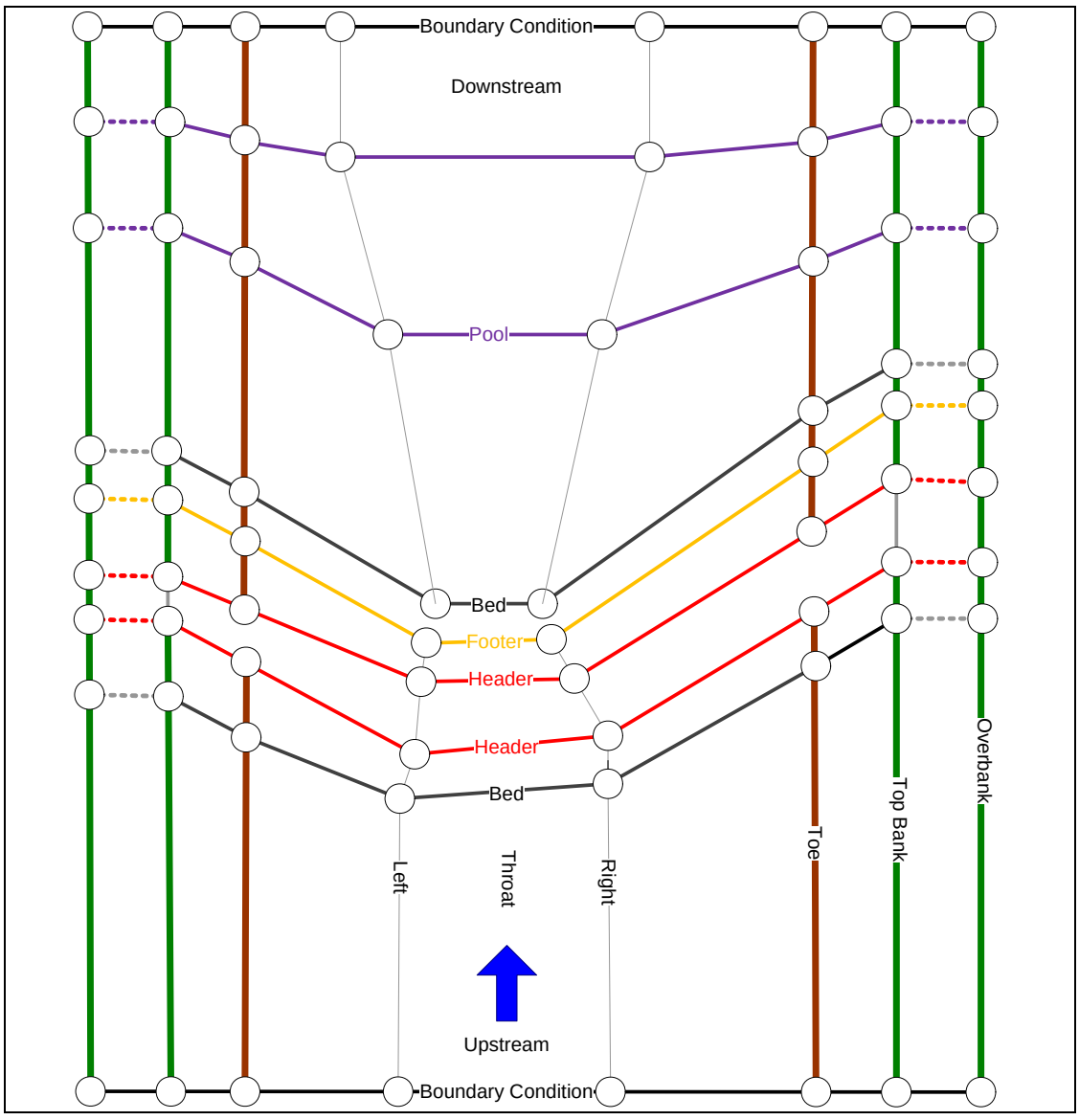

Figure 7. Profile of 3D Structure Line and Point Definition

The definition lines can be identified by the endpoints. For example, the line from the downstream right footer toe to the downstream right footer top of bank identifies where the downstream face of the structure intersects the bank on river right (looking downstream). Definition lines create structure faces that can be identified as left arm, throat, and right arm.

4 PRELIMINARY ANALYSIS OF STRUCTURE CONFIGURATION AND RESULTING HYDRAULICS

Analysis of the effects that variations in rock weir arm length (arm angle and slope), throat width, and drop height have on local hydraulics is currently underway. The following are being analyzed to determine how variations in structure geometry affect local hydraulics: velocity field, bed shear stress, conveyance or flow constriction, energy dissipation, eddies and flow re-direction, and near bank velocities and shear stresses. Figure 8 and Figure 9 show how the velocity field and bed shear stresses are altered for various structure configurations.

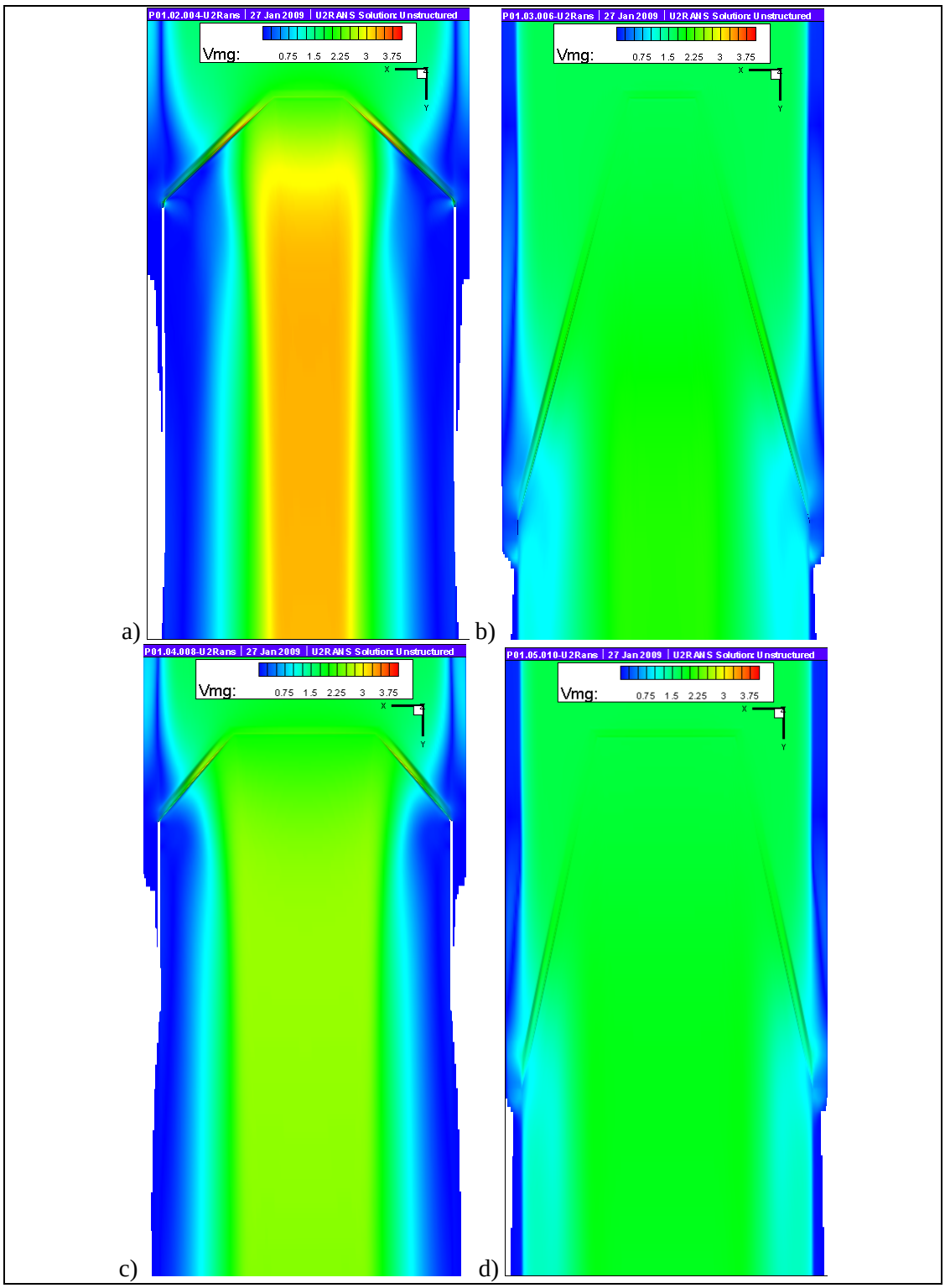

Figure 8. Change in surface velocity for various structure configurations: a) .25Width-.5Arm Length, b) .25Width-2Arm Length, c) .5Width-.5Arm Length, d) .5Width-2Arm Length.

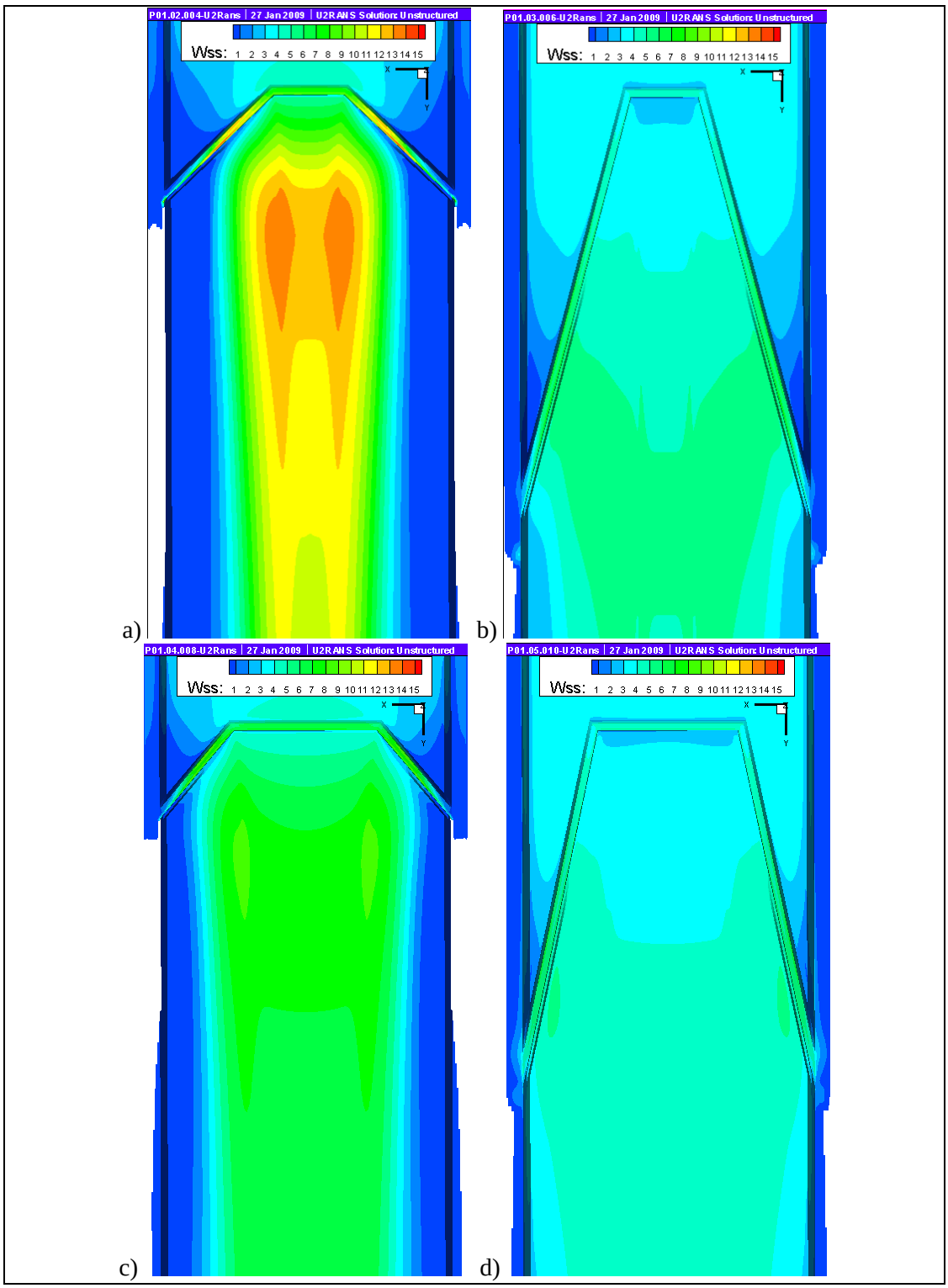

Figure 9. Change in bed shear stress for various structure configurations: a) .25Width-.5Arm Length, b) .25Width-2Arm Length, c) .5Width-.5Arm Length, d) .5Width-2Arm Length.

5 CONCLUSIONS

The numerical modeling focuses on how variations in structure geometry influence local flow patterns and scour development. Current numerical modeling results have duplicated both field observations and laboratory results by quantifying high shear zones near field and lab scour areas and low shear zones near field and lab depositional areas. Results of the numerical modeling allow designers to determine the appropriate geometry for generating desirable flow parameters. The results may also be coupled with the results of the physical model to develop a method to predict critical variables, such as bed shear stress and scour depths, using a 1D model.

The analysis and results of the numerical modeling, laboratory modeling, and field data provide a process-based method for understanding how structure geometry affects flow characteristics, scour development, fish passage, water delivery, and overall structure stability. The end product will develop tools and guidelines for more robust structure design or retrofits based upon predictable engineering and hydraulic performance criteria.

6 REFERENCES

Lai, Y.G., Weber, L.J., Patel, V.C., "Non-Hydrostatic Three-Dimensional Method for Hydraulic Flow Simulation - Part I: Formulation and Verification," ASCE J. Hydraulic Engineering, Vol.129, No.3, pp.196-205, 2003.

Lai, Y.G., Weber, L.J., Patel, V.C., "Non-Hydrostatic Three-Dimensional Method for Hydraulic Flow Simulation - Part II: Application," ASCE J. Hydraulic Engineering, Vol.129, No.3, pp.206-211, 2003.

Millar, R. G. (2005), Theoretical regime equations for mobile gravel-bed rivers with stable banks, Geomorphology, 67, 204– 220.

Nakato, T. (1989). A Review of International Literature of Design Practice and Experience with Low-Head Alluvial-Channel Grade-Control Structures, Prepared by the Iowa Institute of Hydraulics.

Parker, G., P. R. Wilcock, C. Paola, W. E. Dietrich, and J. Pitlick (2007), Physical basis for quasi-universal relations describing bankfull hydraulic geometry of single-thread gravel bed rivers, J. Geophys. Res., 112, F04005

Rosgen, D. L. 2001. The cross-vane, W-weir, and J-hook vane structures...Their description, design, and application for stream stabilization and river restoration, ASCE conference Reno, Nevada 2001.

Quantitative Evaluation of Rock Weir Field Performance

David Varyu, Kendra Russell, Elaina Holburn,

Hydraulic Engineers, Sedimentation and River Hydraulics Group, Technical Service Center, Bureau of Reclamation, Denver, CO (dvaryu@do.usbr.gov)

Abstract

River spanning loose-rock structures are used in channels for a variety of purposes ranging from grade control to habitat complexity. Despite the use of in-channel rock weirs for a myriad of purposes, there is a lack of widely applicable guidelines for the design of the structures. Integration of field, laboratory, and numerical data sets will provide a scientific basis for predicting structure performance under various river conditions and for developing the most-effective design criteria. Investigation of surveyed structures in the field identified several important relationships between structure parameters and the degree of failure. The most notable include the relationships with throat width, open angle of the structure, profile arm angle, and distance to next upstream or downstream rock structure. In general, structures with wider throats relative to the channel width failed less frequently than those with smaller throats. Structures characterized by wider open angles and greater arm slopes tended to fail more frequently than those with narrower open angles and milder slopes. Structures placed in close sequence tended to fail less frequently than those with wide distances between structures. Additional field data continues to be collected and their inclusion in the field data set will further refine observable trends between structure parameters and degree of failure. The quantitative analysis performed in this study must be coupled with the results from the laboratory and numerical modeling components to best understand the relationships between geometric variables of the structure and structure stability.

1. Introduction

River spanning loose-rock structures are used in channels for a variety of purposes ranging from grade control to habitat complexity. The most common objectives in implementing these structures in rivers are to provide sufficient head for diversion without creating migration barriers for fish, to increase channel and bank stability, and to improve habitat features for endangered fish species. Due to the wide range in their application, designs of the structures and determinations of structure functionality are highly variable. However, common performance objectives of most river spanning rock structures include the ability to withstand high flow events and preserve their intended functions over a range of flow conditions.

Despite the use of in-channel rock weirs for a myriad of purposes over the last 50 to 100 years, a literature review of available information on river spanning rock structures identified a lack of widely applicable guidelines for the design of the structures (Mooney et al, 2007). The review found that methods and standards for designing rock weirs based upon predictable engineering and hydraulic performance criteria currently do not exist. As such, Reclamation initiated a multi-faceted research effort to improve design criteria for river spanning rock structures. Ongoing research consists of three primary components:

1. Field investigations of river spanning rock structure performance,
2. Physical modeling in a laboratory setting, and
3. Numerical modeling of hydraulics resulting from the presence of river spanning rock structures.

Integration of field, laboratory, and numerical data sets will provide a scientific basis for predicting structure performance under various river conditions and for developing the most-effective design criteria. This paper focuses on the results of field investigations and the correlation between failure mechanisms and physical design parameters.

Field investigations identified structure performance and hypothesized failure mechanisms at each structure (Mooney et al., 2007). Of the 127 structures evaluated, over 70% were determined to have at least partially failed based on the definition used to define failure, which was predominantly related to structural stability of constituent rocks. The most common failure mechanism was the growth of the scour pool and subsequent slumping of the footer rocks. Field observations suggest that most structures were comprised of rocks adequately sized to prevent failure by sliding and rolling through incipient motion. Qualitative investigations also identified a need for a greater understanding of system processes (e.g. sediment loads and channel migration rates) and recognized structure tie-in to the bank and depth of foundations as critical components of structure designs.

The purpose of this report is to utilize field measurements and topographic surveys collected during field investigations to correlate specific design parameters and to identify possible failure mechanisms. River spanning rock structures evaluated for this report include rock weirs comprised of loose rocks that extend across the width of the channel. Results from the quantitative evaluation of field performance will inform other aspects of the research effort and assist engineers, planners, and manager in improving rock weir designs through increased focus on critical design parameters.

2. Methods

2.1. Data Collection and Processing

Of the 127 structures evaluated, topographic surveys were performed on 76 river-spanning loose rock structures between June, 2005 and November, 2007. Fifty-four of these structures are included in the quantitative analysis. The remainder of the original 127 structures either were non-river spanning, not rock structures, too newly constructed (minimal flows experienced), or were not surveyed sufficiently to quantify structure dimensions. Structures surveyed include A-weirs, U-weirs, Asymmetrical U-weirs, W-weirs, and VW-weirs (Figure 1). To maintain consistency for comparing parameters (i.e. arms and angles) across multiple structures, a consistent method of identifying arms and angles was developed. The most commonly surveyed structures were U-weirs and A-weirs. Examples of both are included in this section.

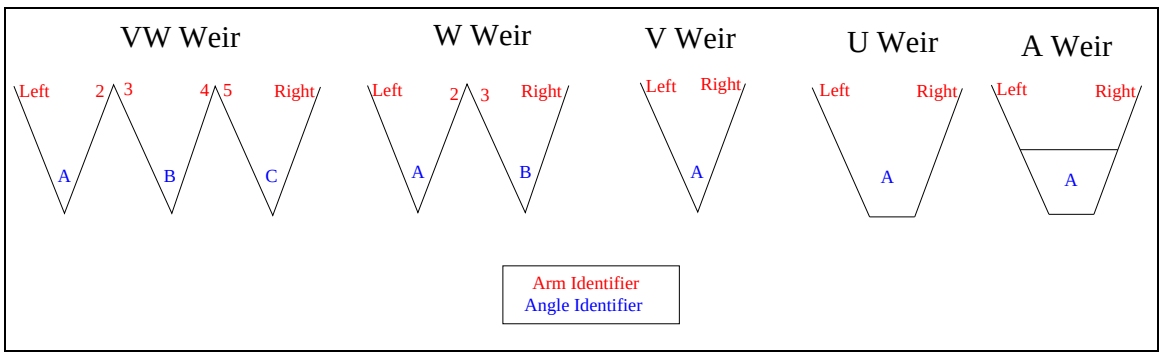

Figure 1. Arm and Angle Identifiers for surveyed structure types.

Following collection of river and structure topography, data were imported into ArcMap (ESRI Version 9.2). Structure planforms were digitized within ArcMap, along with other site characteristics such as bank line locations, structure opening, location of maximum scour depth, etc. Digitized lines were used to calculate parameters such as arm lengths, throat widths, cross arm lengths, bankline and structure angles, and distance from the location of maximum scour to specified points on the structure crest. Figure 2 displays some of the common structure parameters considered during analysis.

All structure parameters were gathered into a single database to determine ranges of different elements of constructed rock structures and to develop any statistical correlations that could be used to direct the design of future structures to prevent or minimize the observed failure mechanisms.

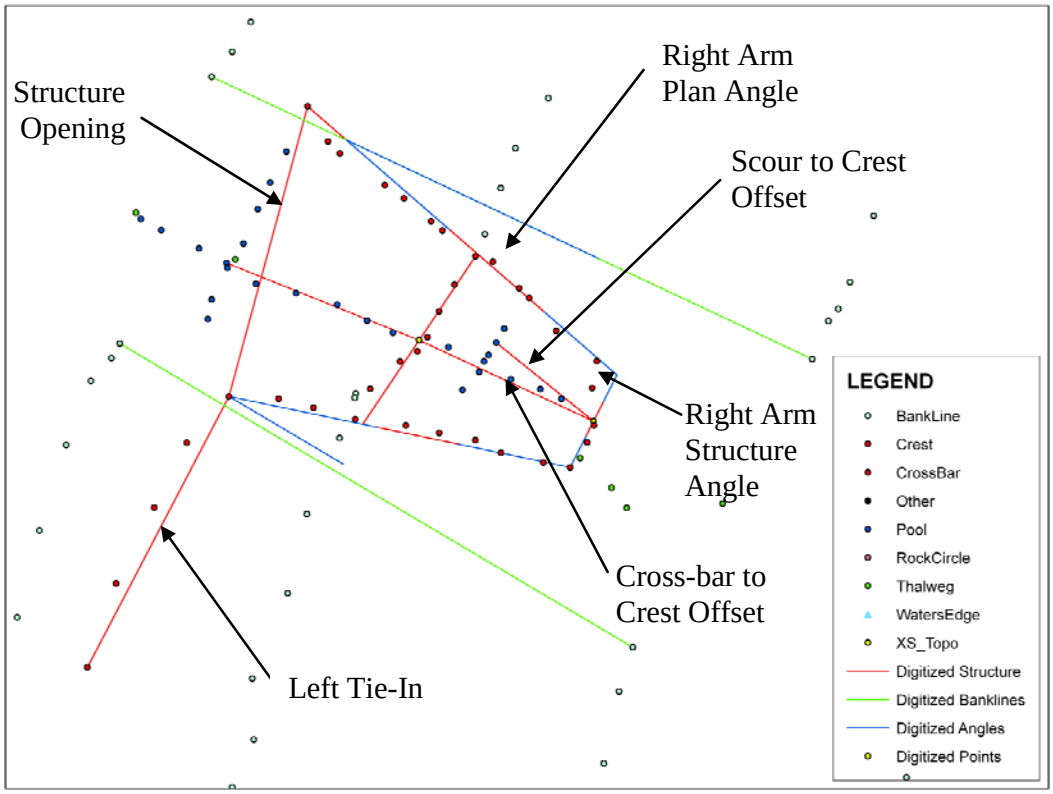

Figure 2. A-weir structure K at Rio Blanco site with some parameters identified.

3. Results

3.1. Distribution of each structure by type and whether failure, partial failure, or success.

In the qualitative investigation of in-channel structures (Mooney et al., 2007), a total of 127 structures were evaluated to evaluate structure performance and identify potential failure mechanisms. This quantitative report focuses on river spanning rock structures. Because the type and amount of data collected at each structure varied greatly, a total of 54 structures were suitable for quantitative analysis (river spanning and with sufficient survey data). Table 1 presents the river spanning rock structures that are considered in the results section, broken down by degree of failure.

One W weir and one VW weir were surveyed during the qualitative evaluation. Due to the small number of each of these structures, no quantitative comparison could be conducted across the individual structure types to determine which parameters are important to structure success. Note that both the W-weir and the VW-weir failed. In addition to these 52 structures (54 less one W-weir and one VW-weir), eight structures on Red Hill Creek in Canada were surveyed. These eight Red Hill Creek structures were surveyed shortly after there installation and had not experienced any substantial flows; therefore, identifying a degree of failure and failure mechanisms for these structures was not possible.

Table 1. Usable structures considered by degree of failure

Structure Type	Count	Usable	NoFail	PartialFail	Fail	Unknown
V-weir	13	5	0	0	5	0
U-weir	37	22	7	8	6	1
A-weir	11	8	0	6	2	0
Asymmetric U-weir	22	17	3	8	5	1
VW-weir	1	1	0	0	1	0
W-weir	3	1	0	0	1	0
Total	**87**	**54**	**10**	**22**	**20**	**2**

Some structures are installed in series along a river, sometimes with structure types varying from structure to structure. Distances to upstream and to downstream structures were identified for those structures that were not stand-alone structures. Also, if the next structure (upstream or downstream) was not a river spanning rock structure, then the distance to the next river spanning rock structure was measured. Table 2 presents the number of structures that did have upstream and downstream structures, whether river spanning or not.

Table 2. Structures with upstream and downstream structures.

Structure Type	Usable	US structure	US RSRS	DS structure	DS RSRS
V-weir	5	3	3	2	2
U-weir	22	21	20	21	21
A-weir	8	5	5	7	7
Asymmetric U-weir	17	17	16	16	16
VW-weir	1	0	0	1	1
W-weir	1	1	1	1	0

Some parameter values common to U-weirs, V-weirs, A-weirs, and asymmetrical U-weirs are presented in Table 3, along with maximum, minimum, and mean values, delineated by degree of failure. Table 4 presents additional data relevant to A-weirs in terms of cross bars. Note that one A-weir consisted of dual cross bars (a double drop). Also note that all of the A-weirs considered were categorized as partial failures or full failures. Due to a lack of A-weirs that did not fail, and because only two A-weirs were full failures, trends between degree of failure and various parameters can not be substantiated by the structures surveyed in this analysis alone.

Table 3. Value ranges for select parameters common to all structures by degree of failure

	Open angle A (deg)	Scour A to Crest offset (ft)	River Widths to Upstream Structure (ft)	River Widths to Upstream RSRS (ft)	River Widths to Downstream Structure (ft)	River Widths to Downstream RSRS (ft)	Scour Depth A (ft)	Min Structure Arm Profile Slope (ft/ft)	Max Structure Arm Profile Slope (ft/ft)	Min Structure arm angle (deg)	Max Structure arm angle (deg)	Throat Width / Structure Width	Min arm Length / Structure Width	Max arm Length / Structure Width	Min Plan Angle	Max Plan Angle
max	99.1	67.9	22.5	22.5	83.6	83.6	4.6	0.13	0.22	47.6	60.1	0.9	1.6	2.6	50.4	61.9
min	20.7	3.0	0.5	0.5	0.5	0.5	1.3	-0.03	0.02	-2.9	0.0	0.0	0.1	0.2	6.8	8.7
mean	55.1	14.3	4.9	6.3	6.7	7.9	2.7	0.04	0.08	20.9	32.4	0.3	0.6	0.9	22.7	34.3
max	65.8	31.6	11.4	11.4	11.7	16.2	3.9	0.08	0.15	31.7	41.8	0.9	0.9	1.2	29.5	36.4
min	20.7	5.0	0.7	0.7	0.7	0.7	1.4	-0.03	0.03	2.6	14.6	0.1	0.2	0.3	7.1	13.8
mean	44.5	15.4	3.9	5.5	3.4	5.3	2.6	0.04	0.08	16.9	27.6	0.4	0.6	0.9	19.7	27.2
max	99.1	19.7	11.8	19.3	21.4	21.4	4.6	0.08	0.17	45.9	53.2	0.6	1.6	2.6	41.7	60.3
min	29.2	3.0	1.3	1.3	0.5	0.5	1.3	0.00	0.02	5.2	15.2	0.1	0.2	0.3	6.9	14.2
mean	50.9	11.4	4.6	6.9	5.1	5.8	2.9	0.04	0.07	20.2	30.6	0.3	0.7	1.1	18.1	32.4
max	94.1	67.9	22.5	22.5	83.6	83.6	4.3	0.13	0.22	47.0	60.1	0.6	1.1	1.6	50.4	61.9
min	32.7	3.4	0.7	0.7	0.8	0.8	1.3	-0.02	0.03	-2.9	0.0	0.0	0.1	0.2	6.8	8.7
mean	62.4	16.5	6.1	6.5	10.8	12.3	2.7	0.04	0.09	22.3	35.1	0.2	0.5	0.8	28.1	38.5

Black = All Structures, Blue = No Failure, Green = Partial Failure, Red = Failure

Table 4. Value ranges for select parameters relevant to A-weirs by degree of failure

	CrossBar width (ft)	CrossBar 2 width (ft)	CrossBar offset from throat (ft)	CrossBar 2 offset from throat (ft)	CrossBar Scour to Crest offset (ft)	CrossBar 2 Scour to Crest offset (ft)	Cross bar scour depth (ft)	CrossBar 2 scour depth (ft)	CrossBar Drop Height (ft)	CrossBar 2 Drop Height (ft)
max	39.9	43.6	24.4	69.5	49.3	9.7	5.5	4.5	1.9	1.8
min	14.6	43.6	8.0	69.5	2.9	9.7	1.7	4.5	0.5	1.8
mean	24.5	43.6	17.8	69.5	23.0	9.7	2.9	4.5	1.0	1.8
max	30.4	43.6	24.4	69.5	27.8	9.7	3.5	4.5	1.9	1.8
min	14.6	43.6	8.0	69.5	2.9	9.7	1.7	4.5	0.8	1.8
mean	20.6	43.6	16.9	69.5	15.5	9.7	2.4	4.5	1.2	1.8
max	39.9	N/A	21.4	N/A	49.3	N/A	5.5	N/A	0.5	N/A
min	33.1	N/A	19.4	N/A	34.1	N/A	3.1	N/A	0.5	N/A
mean	36.5	N/A	20.4	N/A	41.7	N/A	4.3	N/A	0.5	N/A

Black = All Structures, Green = Partial Failure, Red = Failure

3.2. Observable Trends of Degree of Failure with Structure Parameters

A comparison of parameters across all structures was presented in Table 3. A further comparison of parameters by degree of failure for each structure type was performed. U-weirs and V-weirs were combined, with V-weirs being described as U-weirs with throats of zero-width. For analysis of trends, U-weirs and V-weirs are combined into the category U,V weirs. Ranges of selected structure parameters were compared across the degree of structure failure to determine the presence of trends and identify where strong relationships exist between specific design parameters and degrees of failure.

Scour depth relative to foundation depth was expected to be an important factor in the success of a structure's stability due to the fact that the most prevalent mode of failure observed was the growth of scour pool and subsequent slumping of the header and footer rocks (Mooney et al. 2007). The data indicate no trend relating the scour depth to the degree of failure. However, the lack of a trend may be due to the fact that scour depth was not evaluated as a ratio to foundation depth. Evaluating scour depth as a ratio to footer depth is expected to be the most useful way to non-dimensionalize this parameter. Foundation depths were not surveyed in the original data collection plan. Therefore, attempts were made to non-dimensionalize scour depth to parameters that showed significant correlations to scour depth, including arm length, throat width, and structure opening. However, these ratios involving scour depth did not show improved trends with degree of failure. Attempts were also made to non-dimensionalize scour depth to the relative size of the channel, such as structure/channel width. Again, no improved trends with degree of failure were realized. Future analyses that incorporate footer depths as a surrogate for foundation depths may display improved trends with the degree of failure.

Certain trends were observed in considering degree of failure relative to various parameters. These trends were not necessarily observed in all structure types, however. For instance, Figure 3 presents structure open angle for U,V-weirs and Figure 4 shows the same parameter for asymmetrical U-weirs. U,V-weirs tended to fail when the open angle exceeded 45 degrees, and asymmetrical U weirs experienced a full failure when the open angle exceeded 60 degrees.

Proximity of structures to the next upstream or downstream structure showed a trend with the degree of failure for U,V-weirs. No trends were present for structure spacing of asymmetrical U-weirs. U,V-weirs with structures (regardless of type) of closer proximity to other structures, either the upstream or downstream direction, were less likely to fail than widely spaced structures.

Another parameter that suggested some correlation with the degree of failure included throat width. To compare throat width across varying river conditions, throat width was non-dimensionalized through the use of the ratio of throat width to channel width. Throat width relative to channel width shows trends with degree of failure for U,V-weirs, asymmetrical U-weirs, and even A-weirs. Data suggest that the more of the channel width that is blocked by the throat (as opposed to arms), the likelihood for failure decreases.

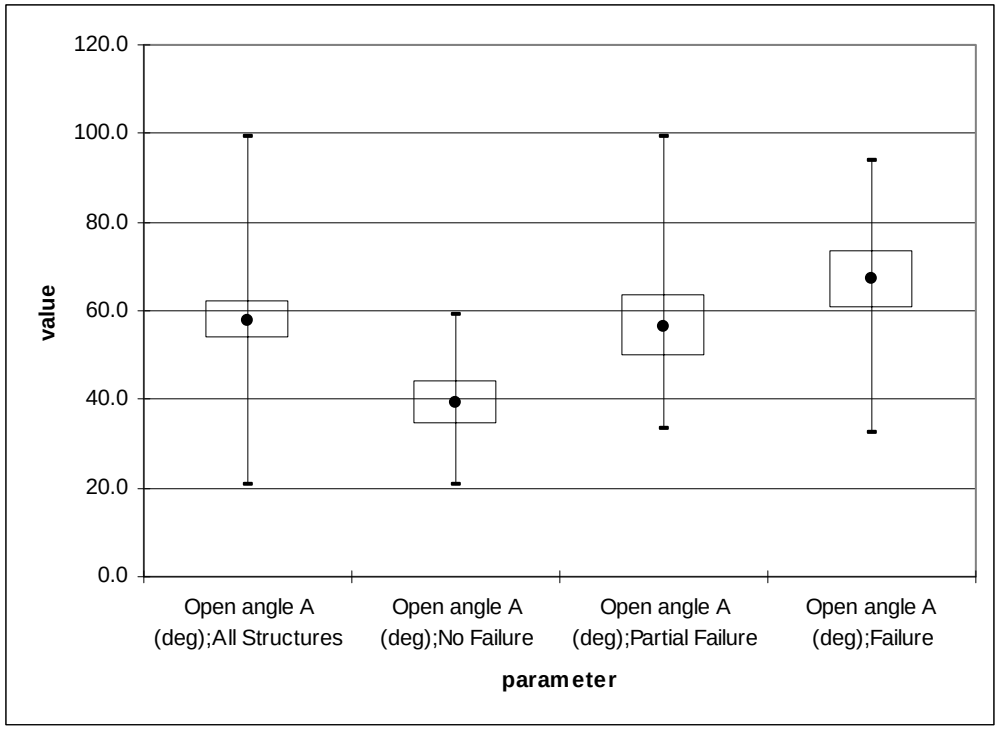

Figure 3. Degree of failure compared to open angle; U,V-weirs

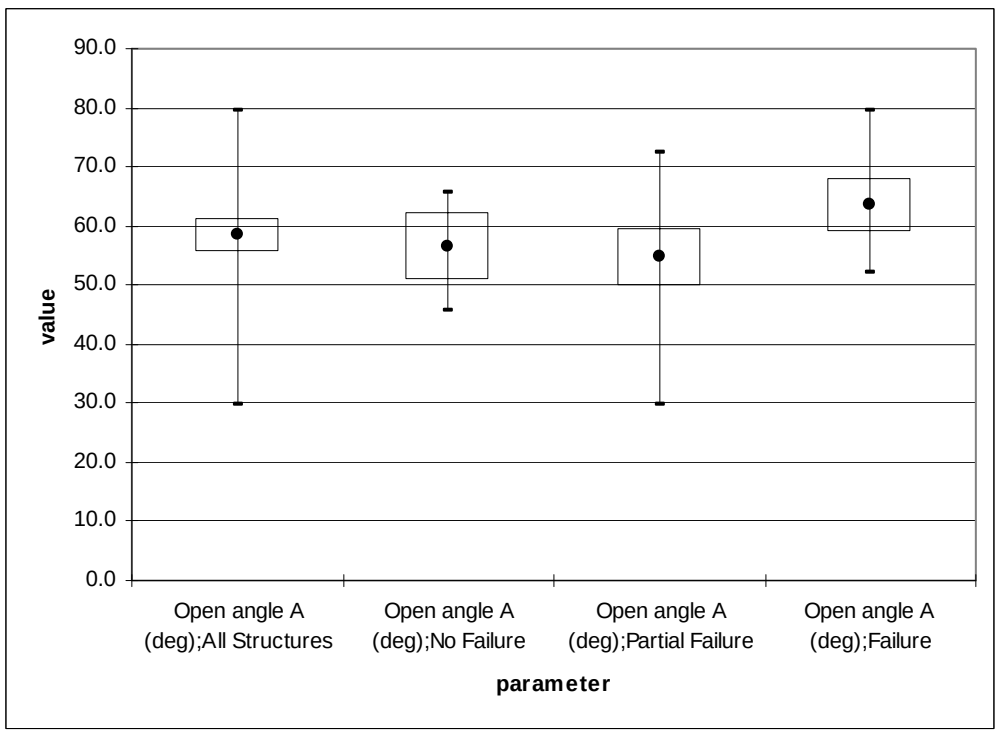

Figure 4. Degree of failure compared to open angle; asymmetrical U weirs

.

Observable trends were categorized as increasing or decreasing, depending on if the likelihood of failure was observed to increase with an increase or decrease of the parameter value. For instance, open angle was determined to have an increasing relationship with the degree of failure since the greater the value, the more likely the structure was to have experienced some degree of failure. Throat width divided by structure width was determined to have a decreasing relationship with the degree of failure since the lower the value, the more likely the structure was to have experienced some degree of failure. Scour depth can be described as not showing a trend. Table 5 presents whether select parameters show an increasing or decreasing trend. These trends are strictly observations and are not described based on their statistical significance. Since all A-weir structures were observed to have partially or fully failed, the relationships presented only indicate whether there is a tendency for the structure parameter to have experienced a greater degree of failure with a variation in the parameter value. Incorporating fully functioning A-weirs that have never required maintenance could change the presented relationships.

Table 5. Observations of trends by structure type for select parameters.

Parameter	U,V weir	Asymmetrical U weir	A weir
Open angle A (deg)	Increase	Increase	Increase
Scour A to Crest offset (ft)	None	None	Increase
River Widths to Upstream Structure (ft)	Increase	Decrease	None
River Widths to Upstream RSRS (ft)	None	None	None
River Widths to Downstream Structure (ft)	Increase	Decrease	None
River Widths to Downstream RSRS (ft)	None	None	None
Scour Depth A (ft)	None	None	None
Min Structure Arm Profile Slope (ft/ft)	Increase	Decrease	Increase
Max Structure Arm Profile Slope (ft/ft)	Increase	Decrease	Decrease
Min Arm Length (ft)	None	None	Increase
Max Arm Length (ft)	None	None	Increase
Min Structure arm angle (deg)	Increase	None	Decrease
Max Structure arm angle (deg)	Increase	Increase	Increase
Throat Width / Structure Width	Decrease	Decrease	Decrease
Min arm Length / Structure Width	None	None	None
Max arm Length / Structure Width	None	None	None
Min Plan Angle	Increase	None	None
Max Plan Angle	Increase	Increase	None

4. Discussion and Conclusions

Within the context of this report, quantitative analyses were performed on 54 structures that contained adequate survey information for development of a consistent data base of information. Surveys collected were processed and digitized in ArcGIS and Microsft Excel to quantify up to 80 geometric parameters at each site. Each site, however, varied in the number of quantifiable parameters based on the topographic surveys. The parameters were used as predictor variables to understand the relationships between the individual variables and the degree of failure associated with each structure type. While hydraulic processes can partially explain the relationships between the parameters and failure, some limitations are recognized by the sample size of each of the parameters. Each parameter was evaluated based on its individual relationship with structural

integrity. However, multiple parameters are interacting to produce a specific outcome of structural stability. By separating out relationships between the structure and individual parameters, the analysis is lacking the ability to incorporate all potential interactions between the predictor variables. Using the current data that were collected in the field across a relatively small sample size, these relationships represent a first attempt to correlate specific parameters with degrees of failure. A more robust analysis could be performed if the response variables were described with discrete quantitative values as opposed to categories of degree of failure or failure mechanisms. Based on field findings, quantification of each of the response variables requires additional data. Therefore, multiple regression analyses were not conducted on this initial set of data, but may be evaluated in the future.

The investigation identified several important relationships between structure parameters and the degree of failure. The most notable include the relationships with throat width, open angle of the structure, profile arm angle, and distance to next upstream or downstream rock structure. In general, structures with wider throats relative to the channel width failed less frequently than those with smaller or no throats (V-weirs). Structures characterized by wider open angles and greater arm slopes tended to fail more frequently than those with narrower open angles and milder slopes. Structures placed in close sequence tended to fail less frequently than those with wide distances between structures. However, the installation of multiple structures should consider the project objectives and the hydraulics to determine adequate spacing so as not to limit pool development or impact structure submergence at lower than design flows.

Two parameters that were evaluated as part of this analysis but did not illustrate notable trends included scour depth and the structure location relative to lateral channel morphology. The scour depths surveyed did not represent the maximum scour experienced by the structure prior to failure, as scour pools may fill at lower flows and on receding limbs of hydrographs while maximum scour depths will be experienced during significant storms. The location of the structure with respect to meander pattern did not illustrate a trend with the degree of failure. This may be in part related to the small sample size evaluated, system interactions such as lateral channel migration, or to flow path realignments associated with the structure geometry.

The parameters included in this analysis did not address system wide processes that would need to be evaluated on a larger scale to evaluate potential impacts to structure stability. Lateral channel migration, sediment transport throughout the system, changes in slope through the system, and root strength present along the channel banks, among many other system-wide processes, may all play a role in how well a structure performs in a given location. One substantial finding of this analysis is that an understanding of the fluvial geomorphic processes must be gained prior to installing these structures to best recognize their potential for success in reaching a specific project objective and to realize the level of maintenance required at each site.

The quantitative analysis performed in this study must be coupled with the results from the laboratory and numerical modeling components to best understand the relationships between geometric variables of the structure and structure stability. The variability across structure performance as identified in this field investigation portion of the research was based on a small sample size of structures surveyed with large ranges in geometric

parameters. Numerous landowners perform undocumented “maintenance” on the structures, which convolutes the ability of the field data alone to quantify structure performance. Modification to one variable while maintaining the values of all other parameters would be necessary to isolate how changes to the parameter impact the structure performance. Interactions between the variables add further complexity to the ability to evaluate an individual variable. An evaluation of the interactions of multiple variables is more suitable to numerical and physical modeling than to the field investigations. However, the relationships identified through the field investigation help inform inputs to the numerical and physical modeling and can be used to assess ranges of specific parameters that drive structure stability. Furthermore, the information from the field investigations can be used to determine how well relationships developed from the physical and numerical modeling translate to the field.

5. Planned Additional Tasks

A large amount of topographic information was collected during the site evaluations. During the analysis, several parameters were identified that were not collected but could be used to further the statistical analysis and might be strongly correlated to the degree of structure failure and possibly the mechanism for failure. The parameters include: sediment size upstream of the structure, sediment size in structure scour pools, sediment size downstream of the structure, size of rock material used in structure, elevations of structure foundation rocks, distance of the spacing or voids between the rocks used in the structure, and throat and cross-bar drop heights from the original bed elevation.

In addition, during the analysis, two parameters were identified that were not consistently collected throughout the first stage of site evaluations. These were the dimensions of the scour pool and delineation of the river banks near the structures. Some parameters still need to be calculated, including channel slope and bank lines for some sites. The channel slope based on the thalweg needs to be calculated at all sites.

Multiple sites are missing a few key topographic survey measurements needed to include them in our dataset. During the completion of this quantitative analysis, several sites were revisited during October, 2008, including the East Fork Salmon River, Bear Creek, Catherine Creek, and the Entiat River. Data from these sites need to be digitized and added to the quantitative analysis to increase the population size for statistical analysis and to perform more detailed evaluations on several parameters that were not previously collected.

6. References

Meyer, J. (2007) Restoration Structure Inventory and Survey Results from the Little Snake River and Tributaries, Northern Colorado. Masters Thesis, Colorado State University, Fort Collins.

Mooney, D., Holmquist-Johnson, C., and E. Holburn (2007) Qualitative Evaluation of Rock Weir Field Performance. Bureau of Reclamation, Technical Service Center, Sedimentation and River Hydraulics Group, Denver, CO

A Digital Floc Camera for Nonintrusive Measurement of Floc Parameters

Remya G. Kumar[1], Ariel Ruiz[2] and Kyle B. Strom[3]

[1] Graduate Research Assistant, Department of Civil and Environmental Engineering, University of Houston, Houston, TX, rgkumar@uh.edu
[2] Postdoctoral Fellow, Department of Electrical Engineering, University of Houston, Houston, TX, ariel.ruiz@mail.uh.edu
[3] Assistant Professor, Department of Civil and Environmental Engineering, University of Houston, Houston, TX, kbstrom@uh.edu

ABSTRACT

This paper discusses the use of a digital camera setup developed for the in-situ measurement of floc size distributions as a function of time in a turbulent field. The camera assembly consists of a CCD camera fitted with a 2X objective lens coupled with an LED spotlight and a strobe controller. The setup allows for the measurement of a wide spectrum of particle sizes, ranging in size from 5 micron to a few millimeters, in a single image. The system was tested for accuracy using suspensions of known particle sizes (Coulter Counter standard particles) and compared to. The camera system is then used to measure floc particle size distributions of kaolin clay in fresh and salt water suspensions.

1. INTRODUCTION

The evolution of flocculated particle size distributions is a fundamental component in the transport and deposition processes of fine muddy sediments in estuaries, lakes, and oceans. Floc particle size distributions can change as a function of the local turbulent stress field and the biological/chemical properties of the sediment-water mixture. Important for the development and testing of analytic floc population dynamic models is the accurate measurement of floc grain size distribution as a function of the driving turbulent fluid motion. This type of data can be quite difficult to obtain since flocs are both fragile and dynamic, meaning that an accurate measurement requires nonintrusive in-situ measurements of the size distribution as a function of time. Digital cameras have proven to be one of the best technologies for accomplishing this (Ridd and Alessandra (2006); Mikkelson et al. (2005); Esima and Kalf (1996)).

The camera setup is a nonintrusive, automated assembly which provides a direct mechanism to measure the floc size distribution without disturbing the original floc structure. The camera assembly consists of a data acquisition system which is controlled by a current source controller (regulating the current pulses for illumination and trigger signals), a data logger (recording data) and the storage unit (storage of the data). The major focus of this paper is on the validation of the camera setup developed at the University of Houston for the in-situ measurement of floc size distributions. Section 2 describes the camera assembly. Section 3 elaborates the camera method and the steps involved in the validation process of the camera technique. Section 4 presents the application of the camera setup. Section 5 presents the concluding thoughts on the camera technique to measure floc size distribution.

2. CAMERA ASSEMBLY

The camera assembly consists of a 1392 X 1040 AVT Firewire progressive scan, monochrome CCD camera fitted with a 2X primary magnification objective lens coupled with an LED spotlight. The spotlight is attached to a strobe controller which can be triggered or run in continuous mode. The camera can capture single images using an external trigger or can capture images at a speed of up to 17 fps. The camera shutter speed, gain, brightness, gamma, resolution (camera settings) are set to particular values in order to achieve a desirable image as per the test sample conditions. The camera captures images of flocs which are then processed using an image analysis tool (Image J).

The lens system consists of the front objective and a rear assembly, the Modular Magnification System kit R200 plus Objective 9 from Edmunds Optics. The lens has a magnification of 2X with a field of view of 3.2 mm X 3.2 mm and has a working distance of 91 mm. The in-line system of the objective lens is equipped with a C-Mount. The C-Mount is inserted between the rear assembly and the front objective and then threaded to a tripod. The adjustable screw on the side of the front objective is used to regulate the amount of light to pass through the aperture of lens assembly. The LED spotlight acts as a source of illumination for the camera and is connected to the strobe source which allows to vary the light intensity on the LED spotlight as per requirement.

The S4000 Advanced Illumination Strobe source runs on three different modes - continuous, test and trigger. The continuous mode is used for very slow moving or static fluid flow conditions. However for rapidly moving turbulent flow fields, it becomes difficult to capture clear floc images with the continuous mode. This problem is resolved by strobing the light, which makes it possible to freeze the motion of fast moving flocs. The strobing of the light is achieved by simultaneously triggering the camera and the strobe source to achieve minimum blurred and clear images. Trigger lines from the camera and the strobe controller are connected to the Data Acquisition device (NI-DAQ) which is controlled through LabView (8.7.1) National Instruments. Figure 1 is a pictorial representation of the test setup. Figure 2 shows an example of fast moving microspheres in water. Microspheres are polystyrene particles (Large Polymers BB03N –Bangs Lab) with particle size less than 90 µm.

3. VALIDATION OF THE CAMERA METHOD

In order to validate the camera technique, tests were performed on suspensions of standardized particle sizes, used in calibrating Coulter Counter. The goal was to validate the results given by the imaging system. The camera and lens specifications yield a pixel size of 2.2 µm/pixel and allow for the measurement of a wide spectrum of particle sizes ranging from approximately 5-10 µm to a few millimeters in size, in a single image. The Coulter Counter solution consists of standard Polystyrene Latex particles (L10, L20, L30) with nominal size of 10 µm, 20 µm and 30 µm. Images of Coulter Counter particles (10 µm, 20 µm and 30 µm) were captured using the camera system (Figures 3, 4 and 5). The back lit images were then processed to obtain the imaged particle size distribution. The

imaged samples of Coulter Counter particles were tested in a Coulter Counter particle size analyzer to compare the results with the camera method.

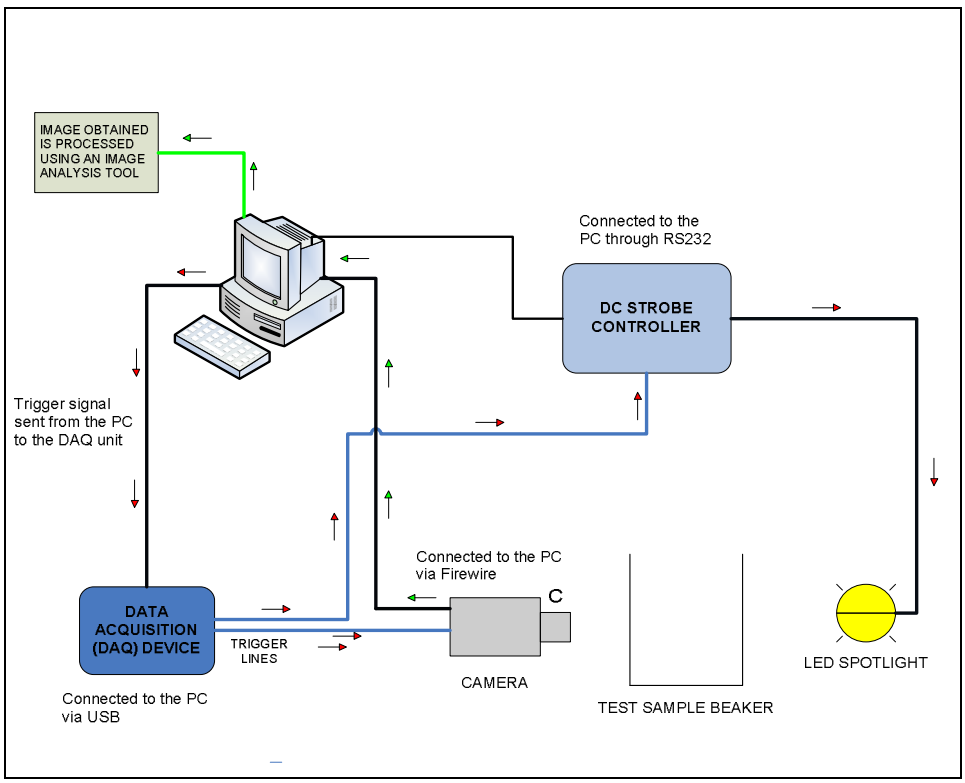

Figure 1 - Camera Assembly Network

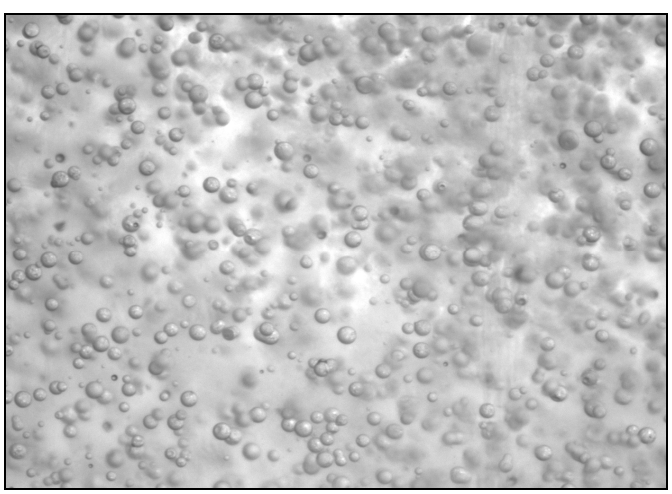

Figure 2 - Image of Microspheres with size < 90 µm taken in the camera setup

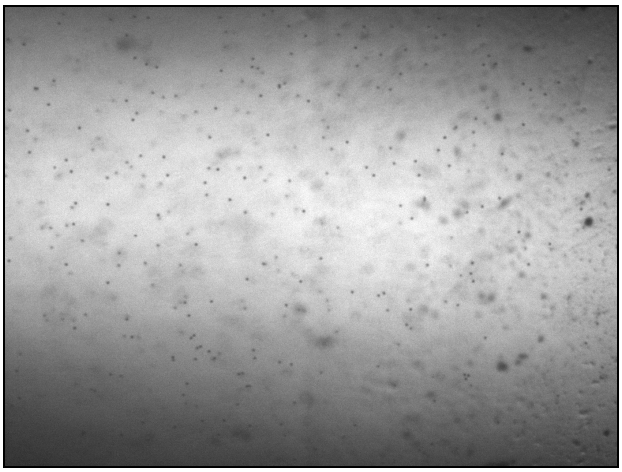

Figure 3 - L10 Coulter Counter standard solution 10 µm particles taken in the camera setup



Figure 4 - L20 Coulter Counter Standard Solution 20 µm particles taken in the camera setup

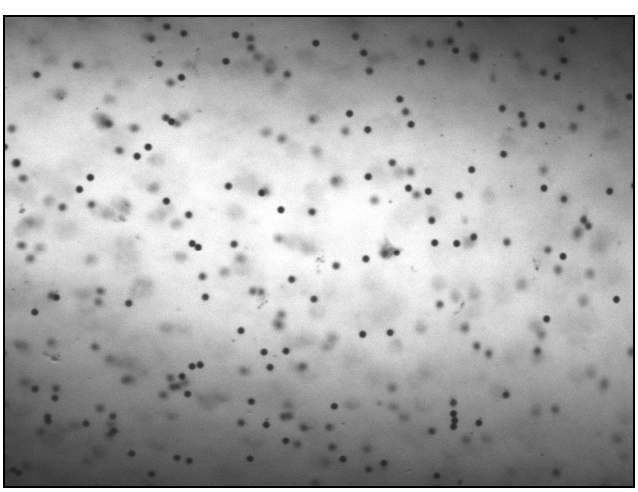

Figure 5 - L30 Coulter Counter Standard Solution 30 µm particles taken in the camera setup

The images of the Coulter Counter particles were processed using the image analysis tool (ImageJ). The results were then compared with that obtained from the Coulter Counter (Tables 1 and 2). The average particle size measured by the camera setup varied from the values obtained from the Coulter Counter in the order of 3 - 4 µm.

Table 1- Mean and Standard Deviation for L20

L20	COULTER COUNTER	CAMERA SETUP
Mean	20.32µm	17.51µm
Standard Deviation	1.76µm	2.79µm

Table 2- Mean and Standard Deviation for L30

L30	COULTER COUNTER	CAMERA SETUP
Mean	32.19µm	27.49µm
Standard Deviation	0.99µm	3.36µm

The results showed that the camera under estimated the particle sizes. This could be due to over exposure of light, which could have made the flocs look smaller in size. There is this possibility of an error in the calibration of the camera, which could have lead to the underestimation of the particle sizes.

4. APPLICATION OF THE CAMERA METHOD

The camera method is used to measure the floc size distribution of kaolin clay. Figure 6a shows an image of kaolin flocs. The image is then processed using an image analysis procedure for automated grain size measurement (Strom et al. 2007) (Figure 6). The camera method can also be applied to measure the fall velocity of flocs and to study the time evolution of flocs.

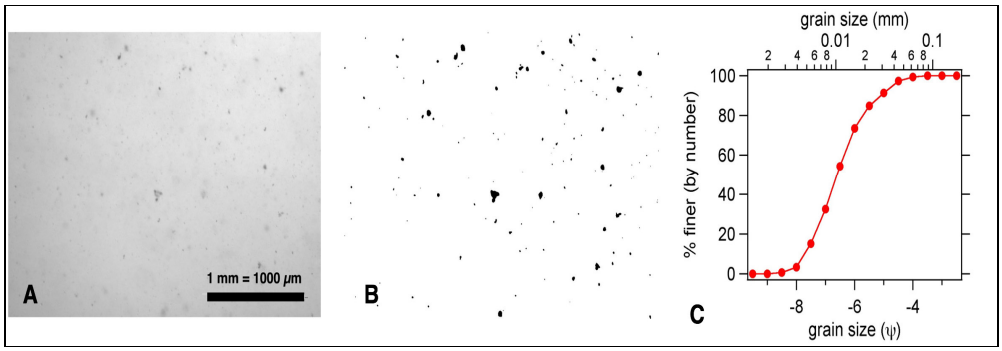

Figure 6 - Application of camera setup for floc measurement. (A) imaged flocs, (B) threshold image for automated grain sizing, and (C) resulting grain size distribution.

5. CONCLUSIONS

The floc camera assembly is capable of providing comprehensive information on the floc size, structure, floc formation, and the temporal evolution of flocs. This enables the study and characterization of flocs and their various parameters such as settling velocity, fractal dimension, and excess density. Collecting quality images for analysis are, however, non-trivial; since the camera setup is dependent on several parameters such as the sediment concentration, the amount of lighting, the speed at which the particle moves, and the camera specifications. The validation process results suggest that the particle sizes estimated for the standard size particles (L20 and L30) by the camera and Coulter Counter are reasonably close. An offset of 2-3 microns in the average particle size is observed between the camera measured distributions and the standardized sizes. The camera method did yield greater spread in the measured particles comparatively to the Coulter Counter results. This may be due in part to over exposure of the particles, having particles at varying depths of field, or other measurement errors.

6. REFERENCES

Esima, D., Kalf, J (1996). "In situ particle (floc) size measurements with the NIOZ in situ camera system." Journal of Sea Research, (36), 49-53.

Mikkelson, O. A, Hill, P. S., Milligan, T. G., Chant, R. J. (2005). "In situ particle size distributions and volume concentrations from a LISST-100 laser particle sizer and a digital floc camera." Continental Shelf Research, (25), 1959-1978.

Ridd, P.V, Alessandra, M (2006). "Devices to measure settling velocity of cohesive sediment aggregates: A review of the in situ technology." Journal of Sea Research, (56), 199-226.

Strom, K. B., Hilldale, R. C., and Kuhns, R. D. (2007). "Comparison of grain size distributions derived from digital images to sieve and pebble count derived distributions". In Hydraulic Measurements and Experimental Methods, pages 415–420, Lake Placid, NY. ASCE/EWRI and IAHR.

Multi-Criteria Assessment of Pallid Sturgeon Habitat Restoration for the Missouri River

John Stansbury[1], PhD, PE, M.ASCE; Jennifer Gitt[2], EI, S.M.ASCE; and Istvan Bogardi[3], PhD

The U.S. Army Corps of Engineers (USACE) in cooperation with other agencies such as the U.S. Fish and Wildlife Service is currently planning, designing, and constructing projects designed to restore habitat for the endangered pallid sturgeon (Scaphirhynchus Albus) and associated species in and along the Missouri River. Management and restoration of habitat is a complex process with many and often conflicting priorities, and habitat restoration success is difficult to measure, in part because there is often a significant lag time between the restoration activity and the biological response by the target species. This project develops a multi-criteria assessment tool to help the USACE and cooperators assess the status and the progress of the habitat restoration efforts on the Missouri River. The multi-criteria assessment method uses composite programming which assesses the overall condition of the habitat based on multiple indicators (e.g., water velocity, depth, substrate). Indicator values were determined at different locations and times, and weights were assigned to the indicators to represent their relative importance. The result obtained from the assessment is a river bend-scale value that characterizes the overall quality and quantity of habitat at different points in time for that bend. Conversely, the method can be used to characterize conditions before and after a habitat restoration project or to compare the effectiveness of different habitat restoration methods on different bends within the river reach. The assessment method will also be used to identify data gaps and deficient habitat components that require further restoration.

[1]Assoc. Prof. and Assoc. Chair Dept. of Civil Engineering, Univ. of Nebraska-Lincoln
[2]Grad. Res. Asst., Dept. of Civil Engineering, Univ. of Nebraska, PKI 225, Omaha, NE 68182; PH (402) 880-6268; FAX (402) 554-3288; email: jgitt@mail.unomaha.edu
[3]Prof. Dept. of Civil Engineering, Univ. of Nebraska-Lincoln

INTRODUCTION

The U.S. Army Corps of Engineers (USACE) in cooperation with other agencies including the U.S. Fish and Wildlife Service (FWS) is currently planning, designing, and constructing projects designed to restore habitat for the endangered pallid sturgeon (Scaphirhynchus Albus) and associated species in and along the Missouri River. Management and restoration of habitat is a complex process with many and often conflicting criteria, and habitat restoration success is difficult to measure, in part because there is often a significant lag time between the restoration activity and the biological response by the target species. This need for habitat assessment using a diverse set of components may be fulfilled by the multi-criteria habitat assessment (MCHA) tool presented in this paper. The multi-criteria assessment method uses composite programming which assesses the overall condition of the habitat based on multiple indicators (e.g., water velocity, depth, substrate). The focus of the assessment is for the habitat required by pallid sturgeon fry and juveniles, age 0 to 1 year.

Missouri River History and Problems

The Missouri River flows 3734 km (2321 mi) from the Rocky Mountains near Three Forks, Montana to its confluence with the Mississippi River near St. Louis, MO. The river's basin drains all of Nebraska, and parts of Colorado, Iowa, Kansas, Minnesota, Missouri, Montana, North Dakota, South Dakota and Wyoming. Figure 1 shows the Missouri River drainage basin.



Figure 1: Missouri River, source USACE

As recently as 1923, the Missouri River was a predominantly meandering stream with channel widths ranging from 457 to 1893 m (1500 to 6500 ft) (USFWS, 2000). Six Missouri River main stem dams, built between 1933 and 1964, have inundated approximately 36 percent of the river length and associated riverine habitat creating a lacustrine environment behind each dam and altering the natural downstream temperature, hydrograph, and sediment loads, as well as creating fish migration barriers. In addition, 40 percent of the Missouri River has been channelized (from Sioux City, IA to its confluence with the Mississippi River near St. Louis, MO) as part of the Bank Stabilization and Navigation Project. This reach of the river has been narrowed into a stable, self-scouring channel maintained at widths of 180 to 270 m (600 to 900 ft) containing a 90 m (300 ft) navigation channel maintained at a minimum depth of 2.7 m (9 ft). The channelization greatly reduced the meander belt habitat, including riparian timber,

sandbars, and shallow water habitat. Additionally, the dams and channelization have reduced substrate diversity and bottom structure (USFWS, 2000).

Habitat and Ecological Issues for the Pallid Sturgeon

Pallid sturgeons are native to the Mississippi and Missouri Rivers and their major tributaries including the Yellowstone and Platte Rivers. The pallid sturgeon was listed as an endangered species on October 9, 1990. The reasons for listing are habitat modification, apparent lack of reproduction, commercial harvest, and hybridization (USFWS, 2000). In 2000, the FWS issued a jeopardy opinion for the pallid sturgeon (Korschgen, 2007). Habitat modification is listed as the most significant cause for the species decline. Pallid sturgeon can travel long distances to find suitable habitat with an average home range of 78.6 km (48.8 mi). The maximum recorded migration distance is 319.7 km (198.6 mi), and they have been reported to travel 20.9 km per day (13 mi/day) (USFWS, 2000). However, dams restrict movement in the upper Missouri River, possibly preventing sturgeon from reaching spawning habitat and preventing fry from reaching recruiting grounds. In addition, habitat homogenization by channelization in the middle and lower reaches has reduced available habitat by decreasing channel variability with the loss of islands, sand bars, and scour holes.

In the upper reaches of the Missouri River, pallid sturgeon have been found to reach lengths of 1.8 m (6 ft), weigh up to 36 kg (80 lbs), and live in excess of 60 years. They are benthic fish having a streamlined body with a flat rostrum and large pectoral fins allowing them to exploit river bottoms as current refugia (USFWS, 2000). Gut analyses indicate pallid sturgeon diet consists of benthic macro-invertebrates, and as the sturgeon grows, the diet includes an increasing proportion of fish (USFWS, 2000).

Spawning cues are thought to be the combination of rising stream flow and temperature, which historically occurred between late April and July (USFWS, 2000). There have been reports of recent spawning activity by the pallid sturgeon; however, a lack of young-of-the-year pallid sturgeons found in the River indicates a problem with recruiting the young fish to adulthood. The population is currently being sustained by efforts to breed and stock the fish throughout its historical range. This study is focused on the early life-stage, age zero to one, to address the needs of the juvenile pallid sturgeon at the recruitment bottle-neck that is suspected to be hindering the survival of the species.

Current Habitat Restoration Efforts

Historically, the Missouri River was a wide meandering stream with 98 percent of the main channel less than 3 m (10 ft) deep and with velocities generally between 0.3 to 0.75 m/s (1 and 2.5 fps) during the late summer and fall (USFWS, 2000). Shallow water habitat (SWH) was found to be lacking in the modified Missouri River and was defined to fill the gap between historically available habitats and those which are found in the river today. SWH is defined as area having water velocities less than 0.6 m/s (2.0 ft/s) at depths less than 1.5 m (5.0 ft) at the effective discharge (50 percent exceedance discharge from August flow duration curves) (USACE, 2007). The habitat restoration goal, as set forth by the FWS in the 2000

Biological Opinion is to create 12.4 to 18.6 ac/km (20 to 30 ac/mi) of shallow water habitat (SWH). According to the USACE SWH program interoffice management plan, dated August 2003, the long-term goal is to convert an average of 61 m (200 ft) of the top width, about 24 acres per river mile, to SWH while maintaining all authorized project purposes. Habitat restoration efforts on the channelized portion of the Missouri River include notching dikes and building in-stream chevrons, which create scour holes, sand bars, promote bank erosion, and catch passing woody debris. In addition, historic side chutes are being reopened to create backwaters and channels with low velocities.

Multi-Criteria Habitat Assessment Process

The multi-criteria habitat assessment (MCHA) tool is similar to other habitat assessment methods, for example the US Environmental Protection Agency's Rapid Bioassessment Protocols. The MCHA is designed to help evaluate the status and progress of the habitat restoration efforts on the Missouri River using composite programming. The overall condition of the habitat in a river bend is assessed using multiple indicators resulting in a value that characterizes the overall habitat quality and quantity at a single point in time. The resulting value may be used to evaluate changes through time or to compare habitats in multiple locations. The assessments will be used to assess restoration progress and effectiveness.

The indicators are the habitat components in the river system that significantly affect the pallid sturgeon. Each indicator is given a weight, w, that reflects the importance of the indicator. Each indicator has a normalized value, c, that places the measured condition (e.g., velocity magnitude) within the range of the best and worst case values. Normalization scales the indicator condition values between zero and one using Equation 1. A normalization value of one represents the best case and zero is the worst case.

$$c_i = (\text{Measured Value} - \text{Worst}) / (\text{Best} - \text{Worst}) \quad (1)$$

The normalized indicators are then compiled into groups of increasingly less specific categories as shown in Figure 2. The indicators in each group are traded off using Equation 2:

$$c_T = [(w_1 * c_1)^p + (w_2 * c_2)^p + (w_3 * c_3)^p + \ldots]^{(1/p)} \quad (2)$$

where

c_i = normalized condition for criterion i,

c_T = composite condition value for a criteria group,

p = balancing factor, usually 1-3, which removes bias and emphasizes outstanding criteria,

w_i = weight for criterion i, (sum of weights in criteria group must equal one).

This equation is iterated through all the indicator groups until a single value for the overall habitat condition is reached (see Figure 2). The result obtained from the assessment is a river bend-scale value that characterizes the overall quality and quantity of habitat for that bend.

Habitat management and restoration is a complex process with many and often conflicting criteria making MCHA a fitting tool for monitoring the progress and effectiveness of the restoration efforts. The process of data collection to support the assessment can help managers evaluate their data collection priorities and to fill data gaps. The structure may also be used to evaluate impaired bends to identify conditions that need improvement by finding the categories and indicators with the lowest values.

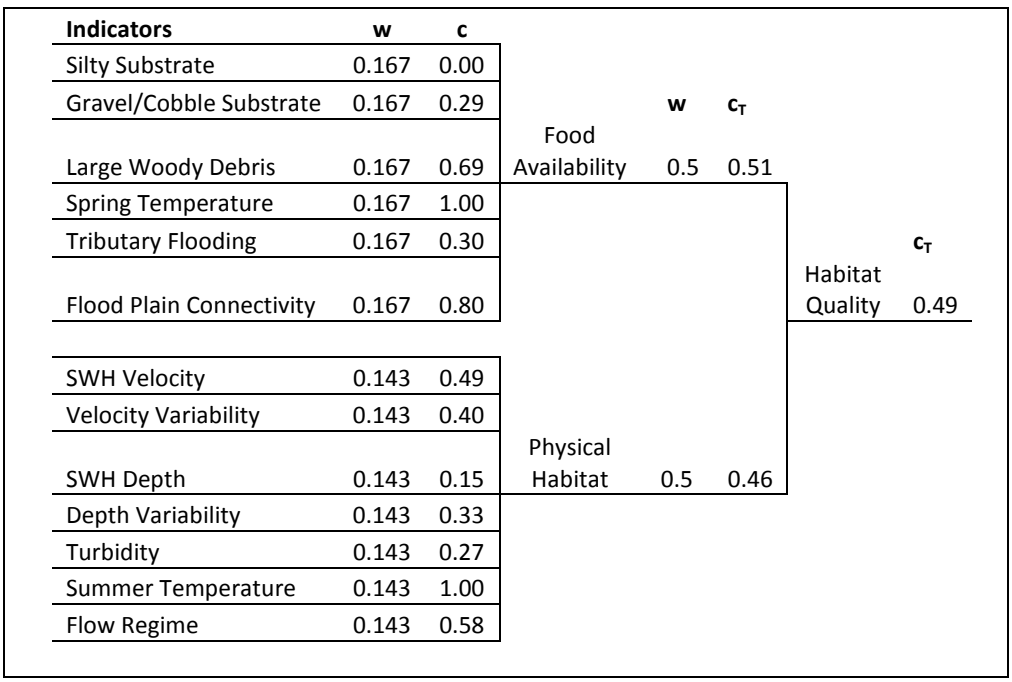

Figure 2: The MCHA Structure for Age 0-1 Pallid Sturgeon in the Missouri River. Note that this figure shows a balanced weighting scheme; other weighting schemes can be used as discussed below. A balancing factor (p) of 1 is used for this figure. Criterion values (c) are for Lower Little Sioux Bend 2006.

MCHA Challenges

The primary difficulty of using the MCHA for pallid sturgeon habitat is gathering sufficient data for each indicator and linking the indicators to specific ecological functions. For example, studies have been implemented to locate pallid sturgeon and track their movements, and those studies can be overlaid by physical data, such as substrate. However, it is unknown whether the fish are in that particular location because they prefer that type of substrate, the substrate supports a food source, or that the substrate is all that is available. The lack of clear links between habitat conditions and ecological function limits the ability to definitively assess habitat conditions.

The data required to use the MCHA tool for pallid sturgeon on the Missouri River are extensive, and data collection can require a great deal of time and money. Because of limited available data, estimates have been required for some of the indicator values for this analysis. This will be a problem for applying the MCHA

method until data collection is done specifically to meet the needs of the MCHA process.

METHODS

Develop Goals and Uses of the MCHA Tool

The MCHA method can be used to characterize conditions through time (e.g., before and after a habitat restoration project) or to compare the effectiveness of different habitat restoration methods on different bends within the river reach. The assessment method could also be used to identify data gaps and deficient habitat components that require further restoration. Habitat restoration success is difficult to measure, in part because there is often a significant lag time between the restoration activity and the biological response by the target species. The MCHA tool can assist resource managers by helping them identify the best locations and methods for restoration, the types of habitat monitoring and data collection to focus on, as well as to assess the status and the progress of the habitat restoration efforts.

Selection of Composite Programming

Composite programming was selected for use in the MCHA tool because it allows for the comparison of multiple indicators within common groupings as shown in Figure 2 (e.g., Food Availability), and these broader categories are then traded off for the overall condition. Dividing criteria into smaller groups decreases the number of criteria in each group and helps maintain the relative importance of each criterion within a group. Conversely, multi-criteria assessment tools such as compromise programming multiattribute utility theory allows all criteria to be traded off together, the larger number of criteria traded off together may allow a fatally flawed criterion to pass through undetected in an otherwise outstanding habitat and mislead improvement efforts.

Selection of Habitat Assessment Sites

The Habitat Assessment and Monitoring Program (HAMP) collects data from 20 river bends from Ponca, NE to Rulo, NE in the USACE's Omaha District, providing a wealth of physical and biological data. Three habitat assessment sites were selected from the HAMP bends in the channelized portion of the Missouri River based on data availability. The three bends including Lower Little Sioux bend, downstream of Decatur, NE at river mile (RM) 672.8 to RM 670.5, Upper Civil bend at RM 574.8 to RM 572.8, and Nebraska bend at RM 562.9 to RM 560.4, the latter two are near Nebraska City, NE. The results presented in this paper are from the Lower Little Sioux Bend, data for the other two bends are still being developed.

Identify Criteria

The value of the overall Habitat Quality, the final indicator, is defined by two second-level indicator categories, Food Availability and Physical Habitat, which are each composites of first-level indicators. The composite structure is made up of 13 first-level indicators, described in detail below. Each indicator was selected because it represents an important component in the habitat of the juvenile pallid sturgeon.

Identify Best and Worst Values for Each Criterion

The best and worst values define the potential range of values of each criterion. For this study, these values are developed from literature sources and from expert

opinion (e.g., from fisheries biologists studying the pallid sturgeon). There have been numerous studies of pallid sturgeon habitat and behavior; however, little data were collected before construction of the main stem dams, limiting the availability of historical data such as unrestricted population size and habitat preferences. As noted above, the modern habitat studies can only identify preferences for what is available under current conditions which, in many cases, are strikingly different from the historic river. The values for the worst case condition are based on conditions that would likely not support pallid sturgeon survival. The best values could be defined by one of two sets of conditions, these include: the "reasonable and prudent" conditions detailed by the 2000 Biological Opinion, or the untouched natural conditions of the river Lewis and Clark experienced in 1804 to which the pallid sturgeon are adapted. The "reasonable and prudent" version of the best values is the choice for the MCHA structure for two reasons: first it is the selected goal of the managing agencies overseeing the restoration of the sturgeon habitat, and second it is likely impossible to return to predevelopment conditions.

The choice of the values of the best and worst conditions affects the trade-off results. For example, as the best condition increases (i.e., moves farther away from the actual condition), the value of the trade-off result will be lower (i.e., farther from the best). For some applications of multi-criteria analysis, this phenomenon must be carefully evaluated. However, for this study, the trade-off results will be used as relative values for comparing the condition of a site through time or comparing the conditions of different sites. Since all of the analyses will use the same "best" and "worst" values, the selection of these values will not materially affect the comparisons.

Determine Values of the Criteria under Each Treatment

1. Silty Substrate

Juvenile pallid sturgeon diets consist mainly of invertebrates. Silty substrates provide a higher density of invertebrates than sand substrates due to the instability and tight packing of sand grains which reduces the ability of the substrate to trap detritus and may limit available oxygen (Allen, 2007). However, high silt levels can reduce heterogeneity by filling interstitial spaces and coat consumers and food resources, so a mix of sand in the silty substrate is desired (Allen, 2007). Substrate data are collected at the end of each HAMP fish collection trawl as a grab sample and with the USACE's physical survey around a small selection of channel structures in each HAMP bend. These data do not provide a good representation of the entire width of the channel, but are reflective of what is likely occurring in the shallow fringe. Ideally, this indicator would be represented by the area, in acres/mile, of silty substrate, defined by the Unified Soil Classification System as grain sizes less than 0.075mm in a sieve analysis (Das, 2006). However, due to the current lack of substrate data points to compile realistic areas, a preliminary data model was developed using the fraction of samples out of the total number collected that fall into this substrate classification. The best indicator value is up to 20 percent of the total number of samples collected, and the worst is zero.

2. Gravel/Cobble Substrate

Gravel and cobble substrates are important for the incubation of the pallid sturgeon eggs because they require an adequate supply of oxygenated water circulating through the coarse substrate; the embryos will suffocate in an overly silty substrate. The gravel also protects the eggs from predators and sweeping currents (Allen, 2007). This indicator is also represented by a preliminary model using the fraction of samples out of the total number collected that fall into the gravel/cobble substrate classification for the same reasons noted above. With a more complete dataset, this indicator would be represented by the area, in acres/mile, of gravel or cobble substrate defined by the Unified Soil Classification System as grain sizes 76.2 to 4.75mm in a sieve analysis (Das, 2006). The best indicator value is up to 20 percent of the total number of samples collected, and the worst is zero. Substrate data for this indicator is the same data used in the Silty Substrate indicator.

3. Large Woody Debris and Rocky Substrate

Large woody debris (LWD) is a minor energy source itself because few invertebrates feed on it directly; however, it does provide food and habitat for a number of species serving as an important substrate for biofilm development. LWD traps organic material and leaves and creates a depositional area, where sediments and organic matter settle and decompose, providing nourishment through primary production for the inhabitants of the microhabitat (Allen, 2007). Large wood and rock structures or boulders in a river are thought to be mostly interchangeable as suitable substrates for biofilms and as flow obstructions for organic material retention. This indicator is represented by the area, in acres per mile, of LWD and rock structures. The best indicator value is one acre per mile of LWD and rock structures, and the worst value is zero.

4. Spring Temperature

Temperature has a strong influence on secondary production in a river system by limiting the availability of food at several levels of the food chain. Temperature affects the organic matter decomposition rate, the accrual and loss rate of benthic algae, and determines metabolic rates of organisms (Allan, 2007). The main stem dams release cold water from the bottom of the reservoirs keeping the downstream river water colder than the natural system. Certain insect species have lifecycles requiring exposure to near freezing followed by rapidly warming temperatures to break egg diapauses. This temperature cue cannot occur in the cold waters below dams until late in the season if at all (Allen, 2007). If insects do not hatch, there could be a shortage of food in these river reaches for insectivores, which include juvenile pallid sturgeon.

This indicator is represented by the number of degrees below 17°C (62°F) for the average May temperature as recorded by the USGS stream gage nearest to the given river bend. The best indicator value is zero, signifying that the average May temperature has warmed to at least 17°C, and the worst value is ≥5, meaning the temperature did not exceed 11°C (51°F).

5. Tributary Flooding

Tributary flooding is an important ecological function because it brings organic matter into the river. This organic matter in turn provides the base of the food chain for the pallid sturgeon. Since much of the natural flooding for the river has been eliminated through dams and levees, tributary flooding is now likely a major source of organic matter for the system. This indicator is represented by the number of tributary floods within 50 miles upstream of the bend within the last 10 years as found on USGS stream gage data for the major tributaries. Flooding is defined as out of bank events. The best value is 10, an average of one flood per year, and the worst value is zero.

6. Flood Plain Connectivity

The importance of a flood plain to a river ecosystem is substantial, as production by aquatic and terrestrial macrophytes in the flood plain along with inputs from flooded forest make up approximately 90 percent of carbon production (Allen, 2007). A connectivity model was developed for the Missouri River Master Water Control Manual Revised Draft Environmental Impact Statement (RDEIS) in 2001 to measure inundation of low-lying lands along the channelized portion of the river. The model outputs the number of acres inundated vs. the percent of years flooded for a minimum of two days. The best value is 4000 acres inundated at a 33 percent frequency, meaning 4000 acres will be flooded approximately every three years, the same frequency as the FWS's requirement in their Biological Opinion (2000) for Gavin's Point Dam to release an artificial spring rise. The worst value is zero.

7. Shallow Water Habitat Velocity

Shallow water habitat for the pallid sturgeon recovery is defined as areas in the river with velocities less than or equal to 0.6 m/s (2.0 ft/s) and depths less than or equal to 1.5 m (5.0 ft). Low velocity is important to provide refugia for fish (especially juveniles) and to provide other ecological functions (e.g., macro-invertebrate production) associated with low velocity. Since much of this type of habitat has been eliminated due to dams and channelization, the presence of this habitat attribute is important to the recovery of the sturgeon. The indicator SWH Velocity accounts for the presence of the shallow water habitat velocity component in the river bend. The total area, in acres per mile, with velocity magnitude less than or equal to 0.6 m/s (2.0 ft/s) is the indicator value. The best indicator value is the upper limit of the USACE goal of 18.6 ac/km (30 ac/mi), and the worst value is zero.

The USACE collected in-channel velocity data in the selected HAMP bends using an Acoustic Doppler Current Profiler (ADCP) concurrently with hydrographic data and recorded the data as depth averaged velocity magnitude and direction (USACE, 2007). The ADCP data were recorded at low flows; therefore, the depth averaged velocities are not representative of effective discharge (USACE, 2007). The ADCP data were fit to run a 2D model to delineate SWH at various flow exceedances, including the effective discharge. The 2D model output is the data used in this study which allows for a detailed set of data around all structures at the effective discharge. The data used for this research is true to the 2D model but is not a perfect representation of what is occurring in the river. The GIS environment

ArcMap was used to calculate areas of given velocity classes, such as the SWH component 0 to 0.6 m/s (0 to 2 ft/s), by generating a triangulated irregular network (TIN) surface for each bend representative of the velocity magnitudes using the velocity data.

8. Velocity Variability

Velocity variability is a measure of the complexity of the habitat conditions which can be considered an indication of the ecological complexity and stability. A frequency distribution of the areas in the river with various measured classes of velocity represents the in-channel variability for the indicator, Velocity Variability. The velocity variability model normalizes the number of acres in each velocity class to the total number of submerged acres in the bend to get the frequency, f, at the effective discharge. The sum of all frequencies should equal one. The data were compiled into six velocity classes in feet per second, see Table 1. The number of frequencies equal to or greater than 0.10, representing 10 percent of the total bend area, is the indicator value. The greater the number of classes where $f \geq 0.10$, the higher the variability in the bend and better the indicator value. The best indicator value is six, which is the total number of defined velocity classes; and the worst value is one, representing no variability in the bend. The data used for this indicator is the same as for the SWH Velocity indicator.

Table 1: Frequency Distribution Model for Velocity Variability

Velocity Range, fps	Acres in Velocity Range	Frequency, f	$f \geq 0.1$
0 - 1	17.66	0.080	0
1 - 2	18.93	0.086	0
2 - 3	27.08	0.123	1
3 - 4	78.85	0.358	1
4 - 5	77.75	0.353	1
5 - 12	0.01	0.000	0
Total	220.27	1.000	3
# Velocity Classes $f \geq 0.1$ =			**3**

9. Shallow Water Habitat Depth

The indicator SWH Depth accounts for the presence of the shallow water habitat depth component in the river bend. The total area, in acres per mile, with depth less than or equal to 1.5 m (5.0 ft) is the indicator value. The best indicator value is the upper limit of the USACE goal of 30 acres per mile, and the worst value is zero. The USACE measured and recorded the in-channel depths in the selected HAMP bends, with cross sections every 15.2 m (50 ft), concurrently with the velocity data previously described. Backwaters and chutes were not included (USACE, 2007).

10. Depth Variability

A frequency distribution of the areas within measured depth classes characterizes the indicator, Depth Variability. The depth variability model is the same as the method used for Velocity Variability. The data were compiled by the

USACE into four depth classes in feet; see Table 2 and Figure 3. The classes are divided into uneven increments about the desired SWH criteria including a two foot fringe class above and below the SWH criteria; however, only the inundated areas during effective discharge are considered for this model. The best indicator value is four classes with a frequency of at least 0.1, indicating good depth variability, and the worst value is one.

Table 2: Frequency Distribution Model for Depth Variability

Depth Range, feet	Acres in Depth Range	Frequency, f	f ≥ 0.10
12+	135.53	0.678	1
7 to 12	45.53	0.228	1
5 to 7	7.45	0.037	0
0 to 5	11.3	0.057	0
Total	199.81	1.000	2
# Depth Classes f ≥ 0.10 =			**2**

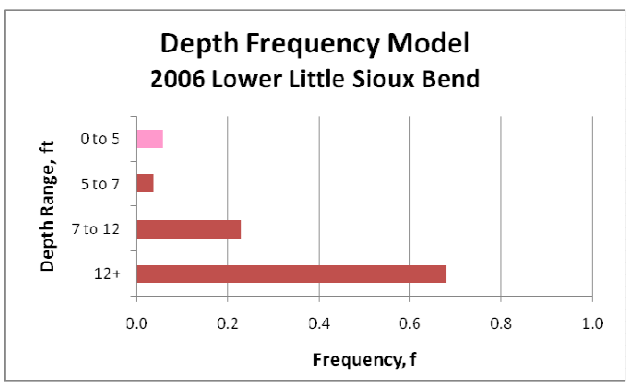

Figure 3: Depth Variability Frequency Chart

11. Turbidity

Turbidity is caused by suspended sediments, including algae and colloidal matter, restricting light transmission through the water providing the sturgeon with cover for protection from predators as well as for feeding on unsuspecting invertebrates and fish (Allen, 2007). The suspended sediment load has decreased by 69 to 99 percent from historic conditions, depending on downstream distance from the nearest dam, due to sediment trapping behind dams (USFWS, 2000). A decrease in turbidity allows sight-feeding species to increase in abundance which in turn could increase predation, competition, and reduce food availability (Allen, 2007).The Turbidity indicator is represented by the average Nephelometric Turbidity Units (NTU) as sampled by the HAMP data collection teams during the summer months. The best value is 100 NTUs, and the worst value is zero. The pallid sturgeons avoid areas without turbidity and current and are even suspected to be photophobic (USFWS, 2000).

12. Summer Temperature

Temperatures on the Missouri and Mississippi Rivers typically range from 0°C to 30°C (32°F to 86°F), and pallid sturgeons are found within the entire range (USFWS, 2000). There are point sources of heat pollution along the length of the Missouri River, for example the discharge of industrial cooling water, that have the potential to increase the nearby water temperature to the point that it is uninhabitable by most aquatic species. This indicator is represented by the number of degrees above 30°C for the average July temperature as recorded by the USGS stream gage nearest to the given river bend. The best indicator value is zero, signifying the average July temperature did not exceed 30°C, and the worst is ≥5, meaning the temperature exceed 35°C (95°F).

13. Flow Regime

A seasonally varied discharge is important to a river ecosystem because high flows entrain organic matter from stream banks, side channels, and other depositional areas unavailable during base flow (Allen, 2007). Many individual species have specific adaptations associated with particular flow regimes that cue various life history stages, for example high flows in spring cue spawning in some species including the pallid sturgeon, these adaptations may also allow them to exploit historical cycles of floods and drought (Allen, 2007). The indicator, Flow Regime, is a qualitative analysis of how closely the hydrograph follows historical seasonal variations, for example spring rise and summer low flows. The indicator value is determined by the number of months with 10-year average flows that fit within ±142 cubic meters per second (± 5000 cfs) of the proposed GP2021 hydrograph, defined in the RDEIS, using the USGS stream gage data monthly mean discharge. The best value is 12, representing a strongly correlated hydrograph where each month's 10-year mean discharge is within the hydrograph envelope, and the worst value is zero.

Determine the Weighting for the Criteria

The weight given to each indicator is based on the perceived importance of the criterion to the pallid sturgeon. There are a number of weighting techniques commonly used in multi-criteria assessment and decision modeling, these include: fixed point, which splits a total value among all indicators; rating, where each indicator is placed on a scale 1-10 and then the values are normalized; and paired comparisons, where each indicator is compared to all the others in pairs most popularly done using Saaty's analytic hierarchy process calculating eigenvalues to represent weights (Hajkowicz et al., 2000). The fixed point method was used for this study to demonstrate the effect of weights on the final outcome. This will be discussed in the results section. Saaty's method of paired comparisons is planned for use in further research when a select group of pallid sturgeon and habitat experts aid in the ranking of the indicators presented in this paper.

Application of CP Method

Once the indicators have been determined, weighted, and measured they may be placed into the structure for calculation. The final composite value is telling of the conditions in the assessed bend, and comparison of the value to other

temporally, spatially, or structurally varied assessment values will show improvement or deterioration over time, or reveal the most effective habitat types.

Uncertainty

There is considerable uncertainty in this assessment. Two primary sources of uncertainty are: lack of knowledge of the links between habitat conditions and ecological function related to juvenile sturgeon, and lack of measurement data regarding conditions in the river (e.g., extents of substrate types). Assessment of these uncertainties is critical to the proper use of the MCHA. For some of the data (e.g., flow frequencies) statistical analyses can be done to assess uncertainty. In cases where statistical analysis is not possible (i.e., where distributions are not known), fuzzy set theory may be used. In the cases where uncertainty is associated with lack of knowledge (e.g., ecological links), a more qualitative analysis based on expert opinion may be needed. Unfortunately, at this time, these analyses have not been completed. A proposed approach will be to conduct the trade-off analysis while directly incorporating uncertainties using fuzzy set methods.

RESULTS

Trade-off values

The trade-off of the criteria including the normalized values of the first-level indicators, the trade-off values for the second-level indicators, and the overall habitat quality value for the Lower Little Sioux study bend is shown in Figure 2.

The trade-off values provide relative estimates of the overall habitat quality of the bend at a particular point in time. It is important to note that the trade-off values are relative values indicating the quality of the overall habitat relative to worst-case and best-case conditions. While each trade-off value can be use to gain improved understanding of how a site compares to “best” and “worst”, the most reliable use of the tool is to compare how a site changes with time or how different sites compare. This is because consistent analyses will provide consistent comparisons.

From Figure 2, it can be seen that the condition of the Silty Substrate criterion is the worst possible, while the Spring and Summer Temperature criteria are the best possible. The overall Food Availability criterion trade-off value is 0.51, indicating that the condition is about half way between the best and worst. The overall trade-off value, Habitat Quality, is also half way to the best mark. Note that several of the data, as mentioned above, are preliminary and the results should only be considered for method demonstration purposes. However, once the complete data sets are available, these results will be useful for habitat managers because with this information, they can see where more effort is needed and where efforts have provided the most improvement. They can also see which types of remediation efforts have led to the greatest overall habitat improvements, or how a site has changed with time. Note that at this time, data are available for only one year, so the year-to-year comparison is not yet available.

In addition to the overall habitat quality (final trade-off value), important information can be found from the lower-level trade-offs and from the values of the indicators themselves. While managers may be more interested in the overall

habitat quality comparisons, scientists may be more interested in the more specific information found in the lower-level trade-offs. For example, to gain a better understanding of how food production/availability might compare between two bends (or two remedial treatments), a comparison of the trade-off values from the upper bracket in Figure 2 could be made.

Analysis of Criteria Weighting

The weighting of the criteria is developed by the habitat experts. Either the experts can develop a consensus of the weighting system, or each expert can assign weights according to his beliefs. The first case will provide a single final trade-off result that reflects the consensus weighting. The second case will result in a different final trade-off value for each expert. The second case method can be instructive as it will show the range of results reflected by the range in expert judgments. In both cases it is important to conduct sensitivity analyses of the weighting systems to understand how the weights affect the final trade-off values. For the study to-date, the expert judgments on the weights have not been solicited. Therefore, several possible weighting schemes (which are likely similar to schemes that will be proposed by the experts) have been assumed by the authors. These weighting schemes are shown in Table 3. The final trade-off values for each given weighting scheme are also shown in Table 3. Weighting scheme 1 makes all weights within a trade-off group equal; weighting scheme 2 emphasizes the importance of substrates over flow regime, shallow water habitat over turbidity/temperature/flow, and food production over physical habitat; weighting scheme 3 is the opposite of scheme 2.

Table 3: Weighting Schemes and the overall Habitat Values

Indicators/Criteria	Weight 1	Weight 2	Weight 3	Ideal	Worst	Value
Food Availability	**0.500**	**0.700**	**0.300**			
Silty Substrate	0.167	0.250	0.080	20	0	0
Gravel/Cobble Substrate	0.167	0.250	0.080	20	0	20
Large Woody Debris	0.167	0.250	0.090	1	0	0.69
Spring Temperature	0.167	0.090	0.250	0	5	0
Tributary Flooding	0.167	0.080	0.250	10	0	3
Flood Plain Connectivity	0.167	0.080	0.250	4000	0	3200
Physical Habitat	**0.500**	**0.300**	**0.700**			
SWH Velocity	0.143	0.250	0.063	30	0	14.6
Velocity Variability	0.143	0.250	0.063	6	1	3
SWH Depth	0.143	0.250	0.063	30	0	4.6
Depth Variability	0.143	0.063	0.063	4	1	2
Turbidity	0.143	0.063	0.250	100	0	27.3
Summer Temperature	0.143	0.063	0.250	0	5	0
Flow Regime	0.143	0.063	0.250	12	0	7
Habitat Quality Value	**0.49**	**0.41**	**0.57**			

CONCLUSIONS

Several conclusions can be drawn from this preliminary study of multi-criteria habitat assessment that may help guide further study, they include:

- A multi-criteria habitat assessment tool was successfully developed to assess habitat quality for pallid sturgeon on the Missouri River
- A great deal more research is needed to develop a scientific understanding of the links between habitat attributes and ecological functions related to pallid sturgeon
- The MCHA can be used to compare changes in habitat quality for a site over time or to compare habitat quality at different sites and across remedial treatments
- More data collection (e.g., mapping substrates and flood plain) is needed to fully support the MCHA
- The MCHA tool can help managers identify data gaps and direct data collection efforts
- The MCHA tool can be useful in forcing managers to consider the entire range of pertinent habitat attributes
- The MCHA tool and data collection efforts need to be coordinated so data collection supports tool and the tool supports decision-making

Need for further research

Considerable research is needed to support the efforts to restore the pallid sturgeon habitat in the Missouri River. Much research is needed in the basic sciences to better establish the links between habitat conditions and ecological functions related to the sturgeon. For example, it is generally assumed that pallid sturgeon eat macro-invertebrates. However, the actual invertebrate species that are preferred and needed by the sturgeon at various life stages are not known. As a consequence, it is not known what types of substrates are needed to support these macro-invertebrates.

Further research directly related to the MCHA tool includes developing species diversity indices both for macro-invertebrates and for fish species. These indices would be good indicators of not only the physical habitat attributes but also of the ecological functions working in the habitat. Another area of further research for the MCHA tool is to develop the method to directly assess uncertainties using fuzzy set theory methods. Understanding uncertainties is critical for decision-makers, and it is easy to overlook or misinterpret the effects of uncertainty if they are not directly incorporated into the assessment, so the incorporation of fuzzy set methods into the MCHA tool would be a very useful improvement.

ACKNOWLEDGEMENTS

The authors would like to thank the US Army Corps of Engineers – Omaha District for providing funding, technical support and data for this research. We would also like to gratefully acknowledge the biologists and engineers from the Habitat Assessment and Monitoring Program, the Nebraska Game and Parks Commission, the Shallow Water Adaptive Management Team, the US Fish and Wildlife Service, the US Geological Survey, and the US Army Corps of Engineers for providing their time and knowledge.

REFERENCES

Allan, J. D., and Castillo, M. M. (2007). *Stream Ecology Structure and Function of Running Waters*, Second Edition. Springer, Dordrecht, The Netherlands.

Das, B. M. (2006). "Origin of Soil and Grain Size." *Principles of Geotechnical Engineering, Sixth Edition*, Thompson Canada Limited, Toronto, Ontario, Canada, 2.2 - 2.6.

Hajkowicz, S. A., G. T. McDonald, P. N. Smith, 2000. An Evaluation of Multiple Objective Decision Support Weight Techniques in Natural Resource Management. Journal of Environmental Planning and Management, 43(4), 505-518.

Korschgen, C. E., ed., (2007). *Factors Affecting the Reproduction, Recruitment, Habitat, and Population Dynamics of Pallid Sturgeon and Shovelnose Sturgeon in the Missouri River,* U.S. Geological Survey Open-File Report 2007–1262, 280 p.

U.S. Army Corps of Engineers (USACE) (2001). *Missouri River Master Water Control Manual Review and Update Revised Draft Environmental Impact Statement Summary*, U.S. Army Corps of Engineers Northwestern Division, 29p.

USACE (2003). *Program Management Plan: Shallow Water Habitat, Missouri River, Ponca to the Mouth*, USACE Omaha District, Office Report, August 2003.

USACE (2007). *Missouri River 2006 Shallow Water Habitat Data Collection and Analysis*, USACE Omaha District, Office Report, January 2007.

U.S. Fish and Wildlife Service (USFWS) (2000). *Biological opinion on the operation of the Missouri River main stem reservoir system, operation and maintenance of the Missouri River bank stabilization and navigation project, and operation of the Kansas River reservoir system*, Bismarck, ND, 286 p.

U.S. Geological Survey (USGS) (2008). *USGS Surface-Water Data for the Nation*, <http://waterdata.usgs.gov/nwis/sw> (Jan. 27, 2008).

River Bed Sediment Classification Using ADCP

F. Douglas Shields, Jr.[1]

[1]National Sedimentation Laboratory, USDA Agricultural Research Service, PO Box 1157, Oxford, MS 38655-1157; PH (662) 232-2919; FAX (662) 232-2988;email: doug.shields@ars.usda.gov, Member, ASCE

ABSTRACT

Description of physical aquatic habitat often includes data describing distributions of water depth, velocity and bed material type. Water depth and velocity in streams deeper than about 1 m may be continuously mapped using an acoustic Doppler current profiler from a moving boat. Herein we examine the potential of using the echo signal strength from the bed as an indicator of bed material type. Mean signal strength from soft, muddy beds was consistently 10 to 20 dB lower than mean signal strength from noncohesive (gravel or sand) beds. Sand beds tended to have complex signatures with large variances.

INTRODUCTION

Restoration or rehabilitation of degraded stream and river habitats requires definition of a target condition and preferably post-implementation monitoring to measure progress toward the target. A physical habitat condition, rather than some state of biotic populations, is often selected as a target because biotic conditions are more difficult to sample and describe and often exhibit great variation driven by variables outside the stream ecosystem (e.g., climate or ocean events). Stream physical aquatic habitat has been described as the joint distribution of water depth, water velocity, bed type and sometimes cover (e.g., Gorman and Karr 1978, Shields et al. 1994). Practically, stream habitat has been characterized by computing statistics based on measurements of water depth and velocity at each point of a horizontal grid. In many cases stream bed type and cover, both qualitatively assessed, were included as additional grid variables. Resultant statistics describing the central tendency, variability and spatial distribution of these three or four variables and their combinations have been used to explain key differences between more- and less-degraded streams and to infer biotic responses. Usually the required data are collected by wading observers.

Collection of water depth and velocity information may be automated across a wide range of stream sizes using an acoustic Doppler profiler (ADCP). Here we suggest that ADCP data may also be used to infer bed hardness and thus bed sediment type. Acoustic seabed classification for mapping habitats and other marine features is a rapidly expanding field (Anderson et al. 2008). Many workers have advanced methods for using specialized equipment and software to acoustically explore or classify underwater sediments (Chivers et al. 1990, MacDougall and Black 1999, Preston et al. 2000, Cholwek et al. 2000 and 2005, Wienberg and Bartholoma 2005); here we propose use of off-the-shelf technology to simply map the distribution of bottom types based on sediment at the bed surface. Bottom types (hardness and surface roughness) may be determined by extracting the return signal strength from

the bottom track echo and using this information to compute the echo intensity at the bed. Bed echo intensity is a function of the sediment bulk density, the amount of gas in voids near the bed surface, the amount and type of submersed vegetation (if any), and the geometric uniformity (flatness) of the bed. All of these qualities are related directly or indirectly to sediment grain size and bed shear stress. The discussion below is based on use of a Teledyne RDI 1200 kHz Workhorse Rio Grande ADCP in streams, rivers and lakes with depths ranging from 1 to 7 m and velocities ranging from 0 to 2.5 m s^{-1}.

COMPUTATIONS

The echo intensity detected by the instrument is given by (Gordon 1996):

$$EI = SL + SV + K - 20\log(R) - 2\alpha R \tag{1}$$

where

EI = echo intensity recorded by the instrument (dB),

SL = source level or transmitted power (dB),

SV = bottom backscattering strength (dB),

K = transducer-specific constant based on the relationship between pressure at the transducer face and the measured signal strength

R = distance from the transducer to the bottom measured along the beam (m) = $r/\cos\theta$, where r = vertical distance from the transducer to the bottom (m) and θ = beam angle (20°), and.

α = sound absorption coefficient (dB/m).

The last two terms account for signal strength decay due to beam spreading and absorption of acoustic energy, respectively. Solving for *SV*,

$$SV - K = EI - SL + 20\log(R) + 2\alpha R \tag{2}$$

Below we compute *SV- K* for various river and lake bottom types and compare results. We use *dB** as a symbol for *SV – K*.

EI, the echo intensity was determined by converting the RSSI (return signal strength indicator) recorded by the ADCP in "counts" to units of dB by multiplying RSSI by the echo intensity scale factor supplied by the manufacturer (RD Instruments 1999)

$$scale\_factor = \frac{127.3}{(273 + T_e)} \tag{3}$$

where T_e is the temperature of the instrument in degrees C, assumed equal to the water temperature .

Source level, *SL*, is given by the equation

$$SL = 10\log\left(\frac{P}{P_0}\right) \tag{4}$$

where

P_0 = reference pressure (1 μPa) and

P = pressure of the signal propagated by the ADCP, given by

$$P = \sqrt{\rho c I} \tag{5}$$

where

ρ = density of the medium (kg m^{-3}),

c = speed of sound (assumed to be constant = 1450 m s^{-1}), and

I = power density (W m^{-2}).

Power density, I, was computed by assuming the transmitted power is spread out over a surface area equal to the area of a circle with a diameter equal to one beamwidth 1 m from the transducer.

$$I = \frac{4 A_{rms} V_{rms} P_F E}{\pi d^2} \tag{6}$$

where

A_{rms} = rms current for transmitted signal(amp),

V_{rms} = rms voltage for transmitted signal (volts),

P_F = power factor (assumed = 0.5),

E = efficiency (assumed = 0.5), and

d = beam diameter (m).

The transmit voltage and current were obtained from the binary output file (RDI 2001, p. 122) and converted from counts to amps and volts as follows:

A_{rms} = 0.011451 * ADC_Counts, and

V_{rms} = 0.253765* ADC_Counts

For the 1200 kHz Workhorse Rio Grande, the far field beam is conical with a side angle of 1.4° (RDI Instruments 1996). Therefore, the beam diameter, d, at a distance of 1 m from the transducer would be

d = 2 tan 0.7 = 0.0244 m (RD Instruments 1999, personal communication, Kent Deines).

Transducer constants, *K,* were unknown, but it was assumed that each of the four transducers on a given ADCP would have different constant values. We adjusted dB* values from transducers 2, 3 and 4 to a common reference based on regression against dB* values measured simultaneously by transducer 1.

Because the sound beam is approximately cylindrical in the near field and then spreads as a cone in the far field, the expression for beam spreading, $20\log(R)$, is valid only for R in excess of a near-zone distance. The near-zone distance is specified by the ADCP manufacturer as R = 2.1 m (RD Instruments 1999). For computation, the value of R in the term $20\log(R)$ was replaced by an expression proposed by Libicki et al. (1989) and used by Thorne et al. (1991) whenever $0.4 < R \leq 2.1$ m. Values with $R < 0.4$ m were discarded.

$$R \times \left[\frac{2 + \frac{\varepsilon r_n}{R}}{3} \right] \tag{7}$$

where $\varepsilon = 1$ and $r_n = 2.1$ m.

The sound absorption coefficient, α, is dependent on water temperature, salinity, and suspended sediment concentration. However, variation over the range of water temperatures observed in this study is slight, and no information was available regarding suspended sediment concentrations. Therefore a constant value of 0.35dB m^{-1} was assumed based on the work of Francois and Garrison (1982a and b) for the (http://resource.npl.co.uk/acoustics/techguides/seaabsorption/) given an assumed temperature of 19 C^o, 1228.28 kHz frequency in freshwater. The assumption of a constant α likely introduced error for sites with sand in suspension.

DATA COLLECTION

Bottom track data were collected using a 1228.28 Teledyne RDI Rio Grande Workhorse ADCP from an aluminum boat anchored in a range of fluvial environments as shown in Table 1. Stations were selected to represent a range of bed types, and samples of bed material were collected at each station with either a BM60 bed material sampler or a petite Ponar dredge. Qualitative, visual descriptions were recorded for each bed sample, and sediments were returned to the lab and subjected to standard analysis for grain size distributions. Additional ADCP data were collected from river reaches encompassing the points where bed samples had been collected.

ANALYSIS

Values for $SV - K$ (also referred to here as dB^*) were computed using the procedure outlined above. Initial analysis focused on ensembles with good data for all four beams. Beams 1 and 3 (which point port and forward, respectively) produced dB^* site means within 1-5% of each other while beams 2 and 4 (pointing starboard

and aft, respectively) produced site means within 2-22% of each other. Beams 2, 3, and 4 were corrected to the same relative magnitude as Beam 1 using regression formulas based on data ensembles with good values for all four beams (Figure 1). After correction, correlation coefficients and coefficients of determination were computed between *dB** and each term in equation 1. Mean *dB** values were computed for the four beams in each ensemble, and frequency distributions were computed for each site and for each major sediment type and hydraulic environment.

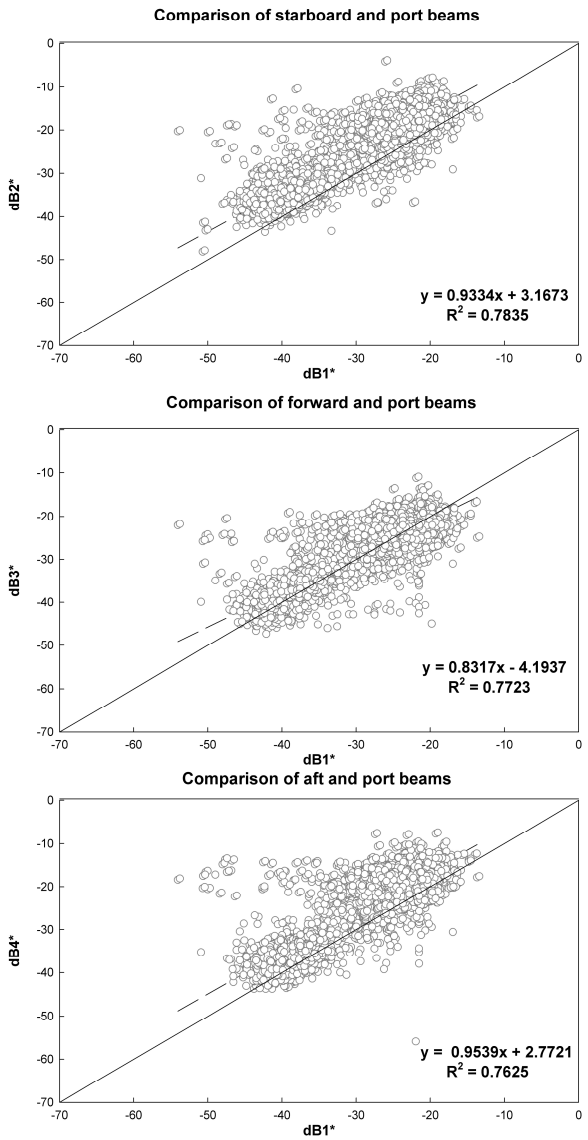

Figure 1. Comparison of simultaneous measurements of bottom backscattering strength using different transducers on the same ADCP.

An entire meander bend of the Little Tallahatchie River in Mississippi was acoustically scanned on the same day that point samples of sediment and bottom

backscatter strength were obtained. Resulting data were used to generate contour maps of bottom backscatter strength, water depth, and current velocity in order to create a synoptic view of physical aquatic habitat.

RESULTS

From 59% to 68% of the variation in *dB** was due to variation in *EI*, the bottom echo intensity for a database comprised of more than 7500 measurements. Power level varied little within our data set, and r^2 values between *dB** values for each beam and *SL* ranged from 1 to 3%. The variation in terms in equation 2 representing losses due to beam spreading and sound absorption in the water column accounted for 3% to 8% and 7% to 13% of the variation in *dB**, respectively.

Table 1. General characteristics of sites sampled for bottom signal strength

Water body	Environment	Bed type	Water Depth, m	Mean current velocity, m/s
Big Sunflower River	Channelized river	Silt and clay	1 to 5	0.02 – 0.03
Deep Hollow Lake	Natural oxbow	Silt and clay	1.0	nil
Little Tallahatchie River	Meandering river	Sand and gravel	1 to 4	0.3 – 0.7
Luxapalila Creek	Channelized river	Fine gravel and sand	1 to 4	.06 – 0.14
Sylamore Creek	Meandering river	Gravel	2.9	0.02
White River	Meandering river	Sand	2.6	11.14
		Gravel	2.5 – 2.8	0.6 – 0.7

Initial exploration of data focused on well-sorted (narrowly graded) sediments from quiescent environments (lakes or low-velocity rivers). Frequency distributions associated with each major sediment type are provided in Figure 2a and summary statistics are shown in Table 2. Cohesive and noncohesive bed material had distinct signatures. Gravel beds produced backscatter strengths about 10 to 20 dB greater than for soft muddy, bottoms. Sandy bottoms had backscatter strengths intermediate to mud and gravel, and sand produced a much wider range of *dB** than other bed types (Figure 2a), likely due to the range of sediment transport and bedform regimes at the sand bed sites. Addition of data from similar well-sorted beds located in higher energy environments indicated that sands and gravels produce similar average backscatter strengths, but that sand again had much higher variance (Figure 2b), perhaps due to sand transport or bedforms. The higher mean *dB** for sand from the White River sand bottom site relative to the Little Tallahatchie sites (Table 3) may be related to bed roughness. Bathymetric data from the ADCP indicated that the White River sand site had a plane bed while the Little Tallahatchie sites (Table 3) exhibited dunes.

Table 2. Mean bottom backscattering strength, *dB, for low-energy sites.**

Water Body	Bed Type	% by weight				No. of values	Mean *dB**	Std dev
		Gravel	Sand	Silt	Clay			
Deep Hollow Lake	Soft mud	D_{50} = 0.012 mm, Mean = 0.043 mm, Std dev = 0.063 mm				388	-43	1.3
Big Sunflower River	Soft mud	0	3	40	56	319	-38	1.5
		0	8	38	55	435	-42	1.0
Luxapalila Creek	Sand	8	91	1	0	150	-30	3.4
		4	96	1	0	152	-23	1.3
	Gravel	86	14	0	0	151	-22	1.0
Sylamore Creek	Gravel	96	4	0	0	1523	-23	1.2

Table 3. Mean bottom backscattering strength, *dB, for high-energy sites.**

Water Body	Bed Type	% by weight			No. of values	Mean *dB**	Std dev
		Gravel	Sand	Fines			
Little Tallahatchie River	Sand	0	98	1	210	-27	1.4
		0	100	0	95	-24	0.9
		1	99	0	44	-23	0.7
		0	100	0	39	-26	0.9
		1	99	0	57	-24	0.9
		0	100	0	61	-27	0.8
White River	Sand	0	89	11	165	-19	1.0
	Gravel	99	1	0	344	-20	1.1
		93	6	1	346	-22	3.1

Contour maps of *dB**, water depth and current velocity for a large, complex bend of the Little Tallahatchie River are presented in Figure 3. "Ground truth" for the *dB** measurements was obtained by sampling bed sediments and bottom

backscatter strength simultaneously as described above at the points shown as red crosses in Figure 3b. The three numbers adjacent to the crosses indicate the composition of bed samples as gravel, sand and fines in percent by weight Bottom habitats were complex, exhibiting the influence of bend flow hydraulics and inflows of coarse sediments from a tributary mouth on the downstream left descending bank. A large area of finer sediments on the upstream left descending bank was associated with a slackwater overflow channel.

CONCLUSION

Synoptic maps of three of the major components of riverine physical aquatic habitat, current velocity, water depth, and bottom type can be made using commercially available boat-mounted ADCP. However, conversion of signal strength values recorded by the instrument to bottom hardness requires use of instrument-specific coeffiecients that must be obtained by ground-truthing each ADCP using bed sediment samples and ADCP data collected simultaneously. Furthermore, the return signal strength for sandy bottoms varies widely based on bedforms and sediment bulk density.

ACKNOWLEDGEMENTS

Kent Deines and Doug Shields, Sr. provided helpful suggestions and insights. Sam Testa and John Massey assisted with field data collection. Daniel Wren and David Mueller read an earlier version of this paper and made many helpful suggestions.

REFERENCES

Anderson, J. T., Holliday, D. Van, Kloser, R., Redid, D. G., and Simard, Y. (2008). "Acoustic seabed classification: current practice and future directions." *ICES Journal of Marine Science: Journal du Conseil,* 2008 65(6),1004-1011.

Chivers, R., Emerson, N., and Burns, D. (1990). "New acoustic processing for underway surveying." *Hydrographic Journal*, 56, 9-17.

Cholwek, G., Bonde, J., Li, X., Richards, C., and Yin, K. (2000). "Processing RoxAnn sonar data to improve its categorization of lake bed superficial substrates." *Journal of Marine Geophysical Researches*, 21, 409-421.

Cholwek, G., Yule, D., Eitrem, M., Quinlan, H., and Doolittle, T. (2005). *Mapping potential lake sturgeon habitat in the Lower Bad River Complex*, USGS, Washington, D.C.

Gorman, O. T., and Karr, J. R. (1978). "Habitat structure and stream fish communities." *Ecology,* 59(3), 507-515.

Francois, R. E., and Garrison, G. R. (1982a). "Sound absorption based on ocean measurements: Part I:Pure water and magnesium sulfate contributions." *Journal of the Acoustical Society of America*, 72(3), 896-907.

Francois, R. E., and Garrison, G. R. (1982b). "Sound absorption based on ocean measurements: Part II:Boric acid contribution and equation for total absorption." *Journal of the Acoustical Society of America*, 72(6), 1879-1890.

Gordon, R. L. (1996). *Acoustic Doppler current profiler: Principles of operation, a practical primer*, RD Instruments, San Diego.

Libicki, C., Bedford, K. W., and Lynch, J. F. (1989). " The interpretation and evaluation of a 3MHz acoustic backscatter device for measuring benthic boundary layer sediment dynamics." *Journal of the Acoustical Society of America*, 85,1501-1511.

Mac Dougall, N., and Black, K.D. (1999). "Determining sediment properties around a marine cage farm using acoustic ground discrimination: RoxAnn." *Aquaculture Research,* 30, 451-458.

Preston, J.M., Rosenberger, A., and Collins, W.T. (2000). "Bottom classification in very shallow water." *In: OCEANS 2000 MTS/IEEE Conference and Exhibition,* 3, 1563-1567, September 9-11, 2000.

RD Instruments. (1999-2003). *WinRiver Application 1.06. Help screens*, RD Instruments, San Diego.

RDI. 2001. "Workhorse commands and output data format." *P/N 957-6156-00*, RD Instruments, San Diego.

Shields, F. D., Jr., Knight, S. S., and Cooper, C. M. (1994). "Effects of channel incision on base flow stream habitats and fishes." *Environmental Management*, 18(1),43-57.

Thorne, P.D., Vincent, C. E., Hardcastle, P. J., Rehman, S., and Pearson, N. (1991). "Measuring Suspended Sediment Concentrations Using Acoustic Backscatter Devices." *Marine Geology*, 98, 7-16.

Wienberg, C., and Bartholoma, A. (2005). "Acoustic seabed classification in a coastal environment (outer Weser Estuary, German Bight)- a new approach to monitor dredging and dredge spoil disposal." *Continental Shelf Research,* 25, 1143-1156.

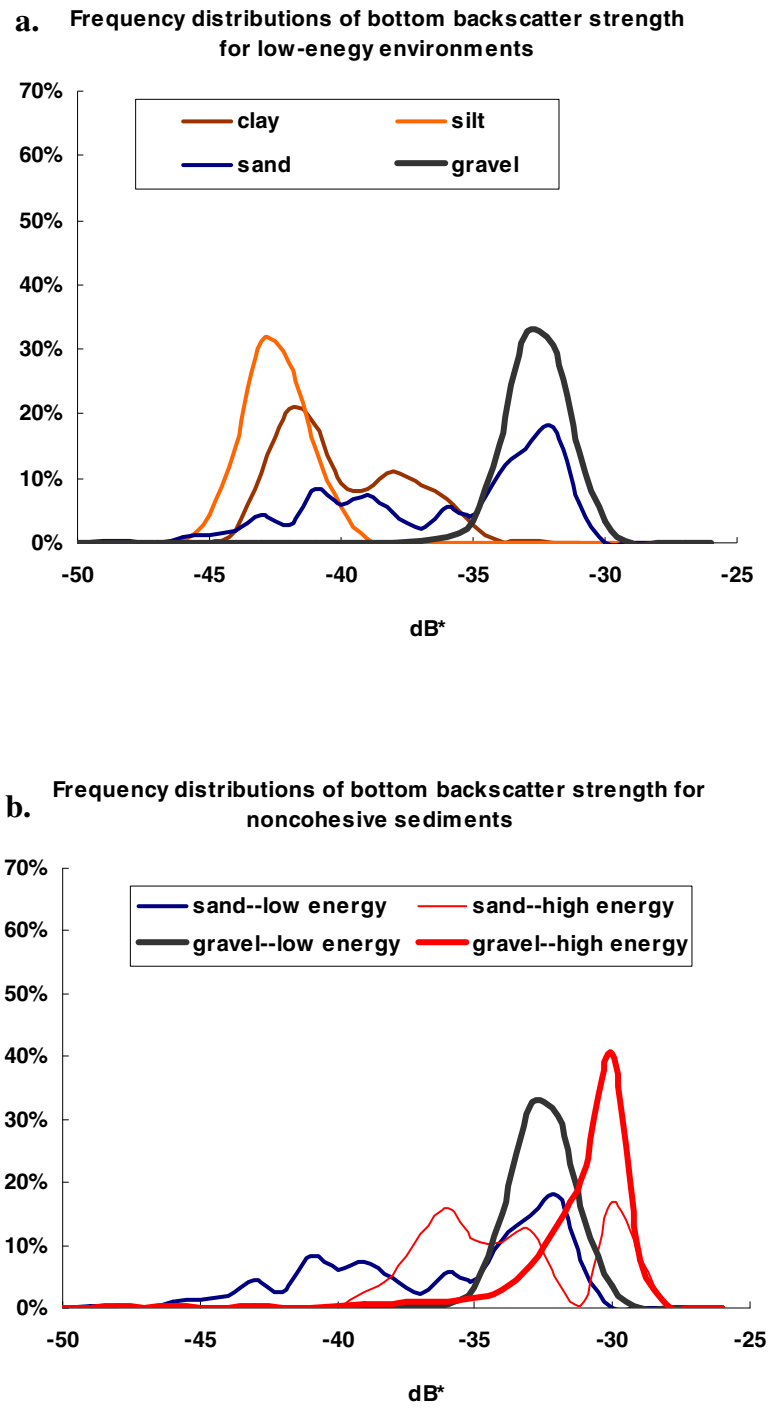

Figure 2. Frequency distributions for dB* measured over various types of river bed sediments. (a) Low-energy environments. (b) Sands and gravels in low- and high-energy environments.

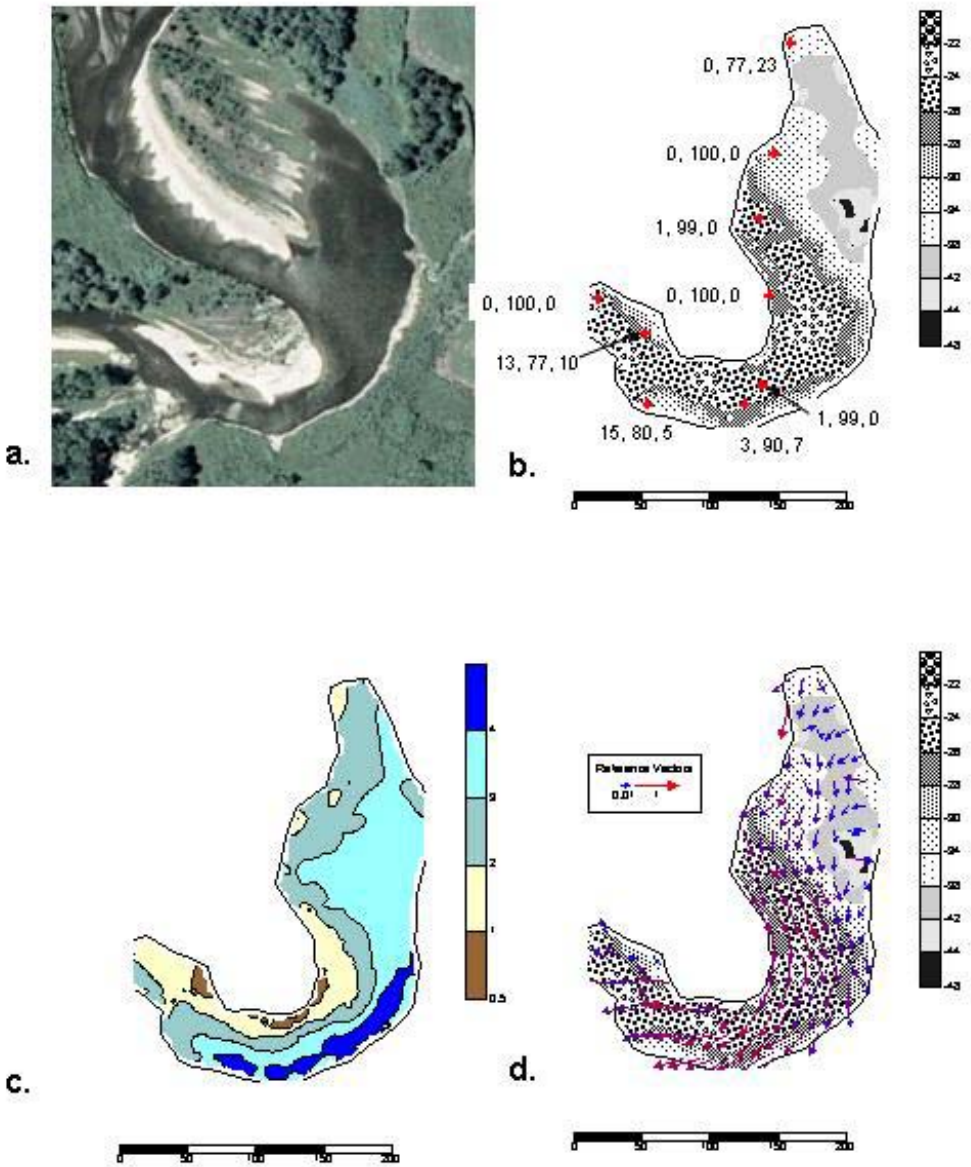

Figure 3. Habitat maps for Jones Creek, bend, Little Tallahatchie River, Mississippi based on ADCP data collected 11 September 2008. A) Air photograph taken 11 August 2007 with water level about 1.58 m lower than for ADCP collection one year later. However, note tributary mouth at lower left of photo and backwater area at upper right. B) Average bottom return signal strength *dB in dB. Red crosses show sites where bed samples and simultaneous 5 min ADCP runs were collected. Numbers represent percent gravel, sand and fines for bed samples. C) Water depth in m with vertically-averaged water velocity in m/s shown by superimposed vectors. D) Bottom track signal strength contour map shown in B with velocity vectors superimposed.**

Environmental Aspects of Dredging: What About Air Quality?

Mark J. Anderson[1] and Brian D. Barkdoll[2], F.ASCE

[1]USACE, Rock Island District, IL, 61204, PH (309) 794-5735 ext.6108, FAX: (309) 794-5712, email: mark.j.anderson@usace.army.mil
[2]Civil & Environmental Engineering Dept., Michigan Tech University, Houghton, MI 49931, PH: (906) 487-1981, FAX: (906) 487-2943, email: barkdoll@mtu.edu

ABSTRACT

Dredging has historically been important for keeping the nation's waterways navigable, mining, and more recently for the removal of contaminants and restoring natural habitat. The placement of dredged material, re-suspension of sediments, and contaminated dredged material could all result in adverse environmental impacts. These impacts have all been, and are being, studied extensively. What has not been investigated, however, are the air emissions resulting from dredging operations. The incorporation of air emissions into management decisions such as the selection of dredging technology is needed and would allow decisions based on environmental impacts and not solely on cost. This analysis lends itself to a limited life cycle and ecoefficiency analysis.

IMPORTANCE OF DREDGING

Dredging is the underwater excavation of accumulated sediments. The removal of sediment from a water body can be done for several reasons. The primary purposes are: navigation, mining, ecosystem restoration, and the removal of contaminants. Once sediment has been removed from the channel it is referred to as dredged material. In fiscal year (FY) 2006 the U. S. Army Corps of Engineers (USACE) dredged a total of 204.2 million cubic yards (CY) of sediment (NDC 2007). Navigation maintenance dredging accounted for 137.8 million CY or 67.5% of this total. Two types of dredging equipment performed 66.6% of the total dredging completed in FY 2006. Cutterhead pipeline dredges removed 118.6 million CY of material or 58.1% and mechanical dredges removed 17.4 million CY or 8.5% of the total material dredged in 2006.

Navigation maintenance dredging is an integral and necessary operational component of our waterborne transportation system. Waterborne commerce in the United States totaled 2,588 million short tons in 2006 (IWR 2006). Of that total 702.1 million short tons were transported within the Mississippi River System with 490.6 million short tons being classified as internal traffic. Internal traffic is defined as "vessel movements (origin and destination) which take place solely on inland waterways. An inland waterway is one geographically located within the boundaries of the contiguous 48 states or within the boundaries of the State of Alaska" (IWR 2006). Nearly 25% or 120.4 million short tons of the Mississippi River System internal traffic were transported on the Illinois Waterway. The waterborne transportation system would be crippled if navigation maintenance dredging was not performed in a regular and timely manor.

TYPES OF DREDGES

There are numerous types of dredges used for the various purposes including: cutterhead pipeline (CPD), mechanical bucket or clamshell (MBD), hopper, sidecaster,

and dustpan dredges. Each type of dredge is well suited for different site conditions (both dredge cut and placement site), sediment characteristics, quantities of sediment to be dredged, production rates, and distance that the material must be transported to a placement site (USACE 1983).

COMPARISON OF DREDGING METHODS

The type of equipment included in this analysis will be limited to that which is commonly used for navigation channel maintenance dredging on the Illinois Waterway (IWW) and Upper Mississippi River (UMR) within the U. S. Army Corps of Engineers, Rock Island District. The equipment selected was used by Rock Island District for navigation channel maintenance dredging on the IWW during the 2005 dredging season. It included a 16-inch cutterhead pipeline dredge owned and operated by an independent contractor and a mechanical bucket dredge owned and operated by Rock Island District (Graham 2007/08).

Cutterhead pipeline dredges are capable of pumping dredged material approximately 5,000 to 12,000 feet with just the pump on the dredge itself, depending on the size dredge, elevation change to the placement site, and sediment characteristics. In order to transport dredged material over longer distances, additional inline booster pumps must be added. Typically, only two booster pumps can be efficiently added to the dredging process, increasing the transport distance by 1,000 to 3,000 feet per booster pump. If the distance between the dredge cut and placement site exceeds the total distance with booster pumps then an intermediate placement site within the water body must be identified and approved. The sediment would be dredged to this intermediate placement site then the dredge would be moved from the original dredge cut to the intermediate placement site and the material would be dredged a second time and transported to the final placement site, commonly referred to as re-handling or double handling the dredged material. This process significantly increases the environmental impacts and the cost per CY which usually makes a cutterhead pipeline dredge unsuitable for dredging and transporting dredged material distances greater than that reachable with two booster pumps. The transport distances for the 16-inch contractor-owned dredge used by Rock Island District for the 2005 dredging season are 8,000 feet for the dredge alone, with each booster pump capable of increasing the transport distance by 2,000 feet. Once a cutterhead pipeline dredge has been mobilized and set up at a dredge cut it is capable of nearly continuous dredging with few interruptions except for routine maintenance for the equipment, movement of the discharge pipeline to minimize delays to navigation, and relocation of the pipeline within one or to another placement site. This results in relatively high production rates. Cutterhead pipeline dredges generate a considerable quantity of water that must be managed at the placement site to meet water quality standards.

Mechanical bucket dredges are well suited when the dredge material must be transported distances greater than 12,000 feet. Once the material has been dredged and loaded onto a barge it can be transported long distances without requiring re-handling. Another situation where mechanical bucket dredges are well suited is for small quantities of material to be dredged from one location, because they are relatively quick and inexpensive, compared to cutterhead pipeline dredges, to mobilize and demobilize. Another consideration for dredging equipment is the distance from the river channel to

the placement site. Either an excavator or a dozer would be used to transfer the dredged material from the barge to the placement site as long as the site is adjacent to the river channel. If the placement site is not immediately adjacent to the channel, material dredged by a mechanical bucket dredge would need to be transferred from the barge to a truck for transport overland to the placement site. This would add expense, negative environmental impacts, and reduce production rates over a cutterhead pipeline dredge. A cutterhead pipeline dredge could extend the discharge pipeline over land to the placement site as long as the total transport distance doesn't exceed the maximum distance for that dredge.

Each type of dredge has distinct advantages and disadvantages that contribute to the decision-making process (USACE 1983). Mechanical bucket dredges are quicker and more economical to mobilize, are capable of transporting dredged material over long distances, require less supporting equipment, and have relatively low production rates. Cutterhead pipeline dredges are more difficult and costly to mobilize, are limited in the distance they can transport dredged material, require more support equipment, and have relatively high production rates. In general terms this means that mechanical bucket dredges are better suited to small quantities of material to be dredged at a given location and/or long (greater than 12,000 feet) transport distances while cutterhead pipeline dredges are better suited to large quantities and shorter transport distances (less than 12,000 feet).

Typically, dredging decision makers utilize multiple criteria for selection of dredging equipment and placement site for each dredge cut(s) (USACE 2003-A). These criteria are used to identify and implement the most suitable combination of equipment and placement site(s) for navigation channel maintenance dredging over a 20 to 40 year planning horizon.

DREDGED MATERIAL PLACEMENT SITES

Dredged material placement sites used in Rock Island District fall into five broad categories including: thalweg, bankline, near shore, upland, and confined. The thalweg is the deepest part of a river channel cross section which usually has the highest flow rates. A bankline placement site would be within the flood plane and immediately adjacent to the river channel. Beach nourishment would be one example of a bankline placement site. Near shore placement sites would also be located within the flood plane but further away from the river channel than a bankline placement site. Upland placement sites are located outside of the flood plane, frequently behind a levee. Confined disposal placement sites are engineered facilities that contain dredged material within a specified footprint.

Thalweg Dredged Material Placement Sites

Thalweg placement of dredged material could be done using either a cutterhead pipeline or mechanical bucket dredge. The site would be located in a reach of river that is particularly deep, usually 20 to 30 feet in depth or more, this compares to the navigation channel mandated minimum depth of nine feet. Not all reaches of the UMR or IWW have thalweg conditions that are suitable for dredged material placement. This is not a particularly desirable option since it does not remove the sediment from the river channel and could result in additional environmental impacts. There are some

advantages to thalweg placement that must be taken into account before eliminating this type of placement site from consideration. Thalweg placement is economical as long as the distance between the dredge cut and placement site are within the dredges transport distance capabilities. Also, there is no return water to manage when using a cutterhead pipeline dredge.

Bankline Dredged Material Placement Sites

Bankline placement could be done using either a cutterhead pipeline or mechanical bucket dredge. The dredged material is placed on the river shore or bankline for habitat restoration, beach replenishment or nourishment, or erosion protection. A bankline placement site for habitat restoration could be to stabilize tree root systems that have been exposed due to erosion, increase the land surface elevation in areas to provide safe havens for wildlife to use during flood events, and create or enhance islands. Recreational facilities along the river are highly desirable to state and local governments along with the public. Dredged material can be used to nourish beaches and enhance the recreational experiences for boaters and swimmers. On occasion dredged material can be placed on banklines for erosion protection of cultural and historic sites that are not easily accessible for more traditional erosion protection systems such as riprap. In addition, dredged material can be used as short-term erosion protection or as fill to restore a bankline in preparation for riprap or some other erosion protection system.

Near Shore Dredged Material Placement Sites

Near shore placement sites would include those sites that are within the floodplain but beyond the bankline. These placement sites can be used for habitat restoration similar to bankline sites or as long-term placement sites. The preferential option for long-term placement sites is typically to locate them outside of the floodplain to avoid adverse impacts to flood water surface elevations and the risk of re-suspension of the sediment and transport back into the river channel during high water events. However there are locations where the floodplain extends beyond practical and economical limits of transporting dredged material so near shore sites must be considered.

Upland Dredged Material Placement Sites

Upland sites are located outside the floodplain and are typically the preference of resource and regulatory agencies since they will have no impact on flood water surface elevations and they eliminate the potential for transport back into the river channel during floods. Upland sites could include: placement on the landside of levees (as long as the level of flood protection is not increased); placement on existing agricultural fields; beneficial use stockpiles; and for habitat restoration.

Confined Dredged Material Placement Sites

Confined dredged material placement facilities (CDF) are engineered and constructed sites that will retain the dredged material within a specified footprint. CDFs can be used for island creation, long-term dredged material placement sites, commercial and recreational site development, and for contaminated dredged material to ensure contaminates do not migrate off-site.

DREDGING EQUIPMENT EMISSIONS TO THE ATMOSPHERE

Navigation channel maintenance dredging equipment used on the IWW and UMR, as with most locations, needs to be mobile and capable of operation without an external power source, making diesel fuel the predominate choice. All of the equipment included in this study is diesel powered. The combustion of diesel fuel releases pollutants into the atmosphere that can be quantified and compared between dredging crews to determine the lowest adverse environmental impacts for each type of equipment and scenario. These contaminants impact air quality and may add to global climate change considerations.

CURRENT KNOWLEDGE

The U.S. Army Corps of Engineers (USACE) was first tasked with maintaining and improving a waterborne navigations system in 1824. Deepening and clearing out rivers and harbors was added to the USACE responsibilities in 1826 (USACE 2007) and remains an integral part of the USACE mission. Typical types of equipment and placement sites utilized for navigation channel maintenance dredging are outlined in the "Types of Dredges" and "Dredged Material Placement Sites" sections respectively. USACE, both independently and in collaboration with the U. S. Environmental Protection Agency (USEPA), have developed several manuals for dredging operations, including dredged material placement sites, and environmental impacts from dredging.

Even though navigation maintenance dredging has been done for hundreds of years the environmental effects are fairly recent considerations. Environmental impacts of dredging have been studied and documented with most of the information having been developed over the past 10 to 15 years (Bridges 2008). The areas of primary focus have been the identification and implementation of beneficial uses for dredged material, environmental dredging, emissions to air from the placement and/or re-suspension of contaminated dredged material, and the regulation of emissions to the air from marine engines. Though environmental impacts of dredging have been studied, no efforts have been applied to the evaluation of air emissions from comparable types of dredging equipment, as in this study.

Beneficial Use of Dredged Material

Beneficial use of dredged material is it's productive use as a resource material. Some possible uses include construction materials, aquaculture, topsoil, beach nourishment, berm creation, capping, land creation, land improvement, fill, shore erosion protection, habitat enhancement, and wetland restoration.

The Great Lakes Commission, responding to the findings of the Great Lakes Beneficial Use Task Force, has identified the beneficial use of dredged material as a "priority management option" and has adopted a resolution for increasing federal funding, research, and USACE authority for beneficial use (Pebbles 2002). The emphasis on identifying and implementing beneficial uses for Great Lakes dredged material will help to minimize environmental impacts from dredging but does not address the air emissions from dredging equipment.

The loss of Louisiana coastal wetlands is being addressed through the beneficial use of dredged material. USACE, New Orleans District has utilized approximately 27 million CY of the 90 million CY of sediment dredged from federal navigation channels

for coastal wetlands restoration projects. This has resulted in the restoration of approximately 10,000 acres of wetlands (Creef and Mathies 2002).

The Illinois River, a major segment of the Illinois Waterway, is part of a large flyway for North American migratory birds. Extensive sedimentation in the backwaters has severely degraded this habitat. The restoration of this migratory flyway will require the removal and placement of a considerable volume of sediment (Marlin and Darmody 2002). Beneficial use applications for this dredged material are being investigated including: island creation and enhancement, topsoil, fill, and urban renewal (Marlin and Darmody 2002).

USACE, Rock Island District has been actively involved in identifying and implementing beneficial uses for navigation channel maintenance dredged material. Examples of beneficial uses for dredged material from the IWW and UMR are levee repair, island creation, fill/construction materials, beach nourishment, and habitat enhancement.

Environmental Dredging

Environmental dredging can be defined as "dredging performed specifically for the removal of contaminated sediments for the purpose of remediating environmental risks" (Bridges 2008). An environmental dredging workshop sponsored by the U.S. Army Corps of Engineers (USACE) and U.S. Environmental Protection Agency (USEPA) focused on re-suspension of sediments, release of contaminants from in-situ and suspended sediments, residual contaminated sediments, and environmental risks (Bridges 2008). None of these focus areas included the air emissions from dredging operations.

According to W. D. Rokosch and N. J. Berg, selection of the best dredging technique for a particular project should be based on several criteria including: dredging location conditions such as water depth, extent of dredge cut, navigation, structural obstructions, sediment characteristics, potential for debris, and underwater structures; environmental regulations; cost considerations; and the positive and negative effects of the dredging operations (Rokosch and Berg 2002). None of the considerations for selection of dredging techniques are air emissions from the dredging equipment.

Several stakeholders from four European countries, France, the United Kingdom, Belgium, and the Netherlands, developed New!Delta, a project to promote the sustainable development of ports and port related activities. One of New!Delta's strategies is sustainable dredging defined as "a strategy in which management of dredging operations is a part of an integrated estuary management that strikes a balance between environmental, economic, social and technical aspects while respecting the legal requirements" (NEW!Delta 2007). The focus of their sustainable dredging strategy is on the potential changes to the physical and sedimentary processes, ecology and habitats, and the existing and future use of the estuary. The primary effects of dredging and dredged material disposal, as outlined in their report, include changes to the hydromorphology, loss of habitat, sedimentation, suspended sediment and turbidity, dispersion of contaminated sediment, reduction in oxygen levels, and disturbances such as noise, light, and movement (New!Delta 2007). Again, there is no consideration for the air emissions from the dredging equipment included in their sustainable dredging strategy.

A rating system similar to that used with Leadership in Energy and Environmental Design (LEED) could be utilized to promote sustainable port development and operation (Abood 2007). The LEED system includes the following six categories: "1.) sustainable sites, 2.) water efficiency, 3.) energy and atmosphere, 4.) materials and resources, 5.) indoor environmental quality, and 6.) innovation and design process". A total of 69 points can be awarded within these categories. According to Abood LEED Categories 4, Materials and Resources, and 6, Innovation, would be the primary sources for dredging and dredged material placement to achieve points (Abood 2007). These points could be received for beneficial use of dredged material, enhancement of aquatic life, and minimizing the loss of habitat. In addition, LEED Categories 2, Water Efficiency, and 5, Indoor Environmental Quality could achieve points for dredged material treatment and reductions in dredging equipment air emissions (Abood 2007). Specifically, Abood identifies the reduction in emissions from ships through the use of alternative fuels, retrofitting engines, addition of emission reduction devices such as catalysts, and reductions in light loading and tidal delays by deepening channels. Interestingly, the deepening of channels would require additional dredging that could increase rather than reduce air emissions. This study addresses reductions in air emissions but does not look at selecting the dredging equipment that would reduce emissions while maintaining navigation channel dredging.

The U.S. Environmental Protection Agency (USEPA) and USACE have collaborated in the development of a document titled "Evaluating the Environmental Effects of Dredged Material Management Alternatives – A Technical Framework" (USEPA, 2004). This framework provides overall guidance for the application of detailed testing manuals developed by USACE and USEPA. These technical testing and design manuals address aquatic and terrestrial impacts from the dredging and placement operations, including the potential for volatization of contaminants into the atmosphere. None, however, consider the air emissions from the dredging equipment in the design and equipment selection process.

Dredged Material Emissions to the Atmosphere

Emissions to the atmosphere from dredging operations include the volatization of chemicals from contaminated dredged material within both the placement site and re-suspended in the water column and emissions from marine engines used to power dredging equipment. The rate at which specific chemicals volatize from dredged material has been studied using various models. Volatization rates for hydrophobic organic compounds from four different locations were modeled to tentatively rank the magnitude of emission rates. The four locations were the dredging location or cut, the exposed placement site location, the ponded placement site location, and the placement site location with vegetated cover (Valsaraj 1995). The results indicated that the greatest emissions resulted from the exposed placement site followed by the dredge cut location with high levels of suspended solids (Valsaraj 1995). Air quality impacts from odorous or toxic compounds in dredged material and effects on inhabitants near dredging operations can be costly to control (Zimmer 2004). Multiple models were tested with differing operational and remediation alternatives. The results were evaluated against acute air quality standards and odor threshold (Zimmer 2004). Neither of these studies considered the air emissions from dredging equipment.

Regulation of Air Emissions From Marine Engines

Air emissions such as Nitrogen Oxides (NOx) from marine engines are being regulated under both the USEPA's "Control of Emissions of Air pollution from New Marine Compression Ignition Engines at or Above 37 kW" and Individual State Implementation Plans (SIP) (Gore 2002). Actions taken to comply with these standards include using shore power instead of marine power when tied up to pier, voluntarily reducing speed when in port to below normal, and potentially limiting industrial equipment operations to a specified number of hours each day (Gore 2002). These standards address air emissions but do not examine the dredging equipment selection process as a source for reducing emissions to the atmosphere.

The significance of United States port air quality concerns are increasing. In response, the USEPA generated the transportation and general conformity rules (Rhoads 2004). These rules require project sponsors to include air quality analysis in their planning process. An approach has been developed based on emission reduction plans that allow projects to maintain general conformity status. Cost estimates are developed that include the type and size of equipment to be used, production rates, hours of operation, and labor requirements that meet existing standards without supplementary air emission control considerations (Rhoads 2004). This approach utilizes a similar approach to that done in this study for quantifying air emissions from diesel equipment but does not use the results for selection of equipment. Nor does it focus on navigation maintenance dredging but considers all equipment required for unspecified projects.

SUMMARY

Considerable effort has been put forth to identify and reduce environmental impacts from dredging operations. Reductions in adverse impacts have been achieved through the identification and implementation of beneficial uses for dredged material, development of environmental dredging techniques, minimization of the volatization of compounds from contaminated dredged material, and striving toward compliance with air quality standards. The reuse of dredged material for construction materials, aquaculture, topsoil, beach nourishment, berm creation, capping, land creation, land improvement, fill, shore erosion protection, habitat enhancement, and wetland restoration has minimized the need for long-term placement sites and the resulting impacts to both aquatic and terrestrial environments. Removal of contaminated sediments minimizes the risk of contaminants migrating into the water column or biota. Identifying solutions that minimize volatization of contaminates from dredged material either from a placement site or when re-suspended in the water column help to reduce environmental impacts. In addition, the adaptation of air quality standards for marine engines reduces adverse impacts to the environment. All of these efforts significantly improve the sustainability of dredging operations and reduce environmental impacts. One potential area for reducing adverse environmental impacts that is conspicuously missing from this list is the quantification and selection of comparable dredging equipment based on the air emissions. By identifying the type of dredging equipment with the lowest air emissions, when cost, site conditions, and equipment availability are comparable, environmental impacts can be minimized without compromising the dredging project.

REFERENCES

Abood, K. A., (2007). "Sustainable and Green Ports; Application of Sustainability Principles to Port Development and Operation", *Proc. Ports 2007 30 years of Sharing Ideas, 1997 – 2007,* ASCE, San Diego, CA.

Bridges, T. S., Ells, S., Hayes, D., Mount, D., Nadeau, S.C., Palermo, M.R., Patmont, C., and Schroeder, P. (2008). The Four Rs of Environmental Dredging: Resuspension, Release, Residual, and Risk. United States Army Corps of Engineers Dredging Operations and Environmental Research Program, Washington D.C., GPO.

Creef, E. D, and Mathies, L. G., (2002). "Investigation of the Excavation, Transport and beneficial use of Illinois River Dredged Material", *Proc. Third Specialty Conference on Dredging and Dredged Material Disposal*, ASCE, Orlando, FL.

Gore, D. J., (2002). "Maritime Administration's Formulation of a Maritime Energy and Clean Emissions Program", *Proc. 2002 Spring Technical Conference of the American Society of Mechanical Engineers International Combustion Engine Division,* International Combustion Engine Division, ASME. Rockford, IL

Graham, Willis. "Dredge Information." Personal communication. 28 Nov. 2007 to 19 June 2008

IWR (2006) "Waterborne Commerce of the United States Calendar year 2006, Part 5 National Summaries", U.S. Army Corps of Engineers, Alexandria, VA.

Marlin, J. C. and Darmody, R. G., (2002). "Beneficial Use of Great Lakes Dredged Material", *Proc. Third Specialty Conference on Dredging and Dredged Material Disposal*, ASCE, Orlando, FL.

Navigation Data Center, U.S. Army Corps of Engineers (NDC) (2007). ''The United States Waterway System Transportation Facts'', http://www.iwr.usace.army.mil/ndc/factcard/fc07/factcard.pdf (9 June 2008)

New!Delta (2007). "Framework for a Sustainable Dredging Strategy", www.newdelta.org (11 November 2007)

Pebbles, V., (2002). "Beneficial Use of Great Lakes Dredged Material", *Proc. Third Specialty Conference on Dredging and Dredged Material Disposal*, ASCE, Orlando, FL.

Rhoads, R., (2004) "A Breath of Fresh Air?". *Dredging and Port Construction,* 31(Nov), 16-19

Rokosch, W. D. and Berg, N. J., (2002). "Dredging Efficiently – dredging techniques and its effects to the environment." *Proc., Third Specialty Conference on Dredging and Dredged Material Disposal*, ASCE, Orlando, FL.

United States Army Corps of Engineers (USACE) (1983). Dredging and Dredged Material Disposal. EM 1110-2-5025, Washington D.C., GPO

USACE (2003-A). Dredged Material Management Plan for Dredged Material Placement, Upper Mississippi River Miles 300.2 – 303.4, Pools 22 and 24, Site Plan for the Lock and Dam 22 Reach, Lock and Dam 22 Upper and Lower Approach Dredge Cuts. Rock Island IL, U.S. Army Corps of Engineers, Rock Island District

USACE (2007), "A Brief History", http://www.hq.usace.army.mil/History/brief.htm (2 July 2008)

USEPA (2004). Evaluating Environmental Effects of Dredged Material Management Alternatives – A Technical Framework. EPA842-8-92-008, Washington D.C., GPO

Valsaraj, K. T., Thibodeaux, L. J., and Reible, D. D., (1995). "Modeling Air Emissions from Contaminated Sediment Dredged Materials", *Proc. 1995 Symposium on Dredging, Remediation and Containment of Contaminated Sediments,* ASTM, Montreal, CAN

Zimmer, M. P., Schewe, G. J., and Wagner, J., (2004). "Comparison of Air Concentrations and Odors From ISCST3 and AERMOD Modeling: Implications for Remediation", *Proc. Air and Waste Management Association's 97th Annual Conference and Exhibition,* A and WMA; Cinergy Corp., Indianapolis, IN

Integrating fluvial geomorphology and two-dimensional hydraulic and sediment transport modeling to support sustainable design of large river and floodplain improvements: The Trinity River Corridor Project, Dallas, Texas, USA.

Mark R. Tompkins, P.E., Ph.D.[1], Greg Ajemian, P.E.[2], Gregory Welch, P.E.[3], Anthony Falzone[4], Kyle Winslow, P.E., Ph.D.[5], Paul Frank, P.E.[1], Beatriz Dongell[3], Denny Mengel[6]

[1] CH2M HILL, 155 West Grand Avenue, Suite 1000, Oakland, CA 94612; PH (510) 587-7793: e-mail: mark.tompkins@ch2m.com
[2] Senior Program Manager, Trinity River Corridor Project Office, City of Dallas; 1500 Marilla, Room 6B South, Dallas, TX 75201 PH (214) 671-9504: e-mail: gregory.ajemian@dallascityhall.com
[3] CH2M HILL, 12377 Merit Drive, Suite 1000, Dallas, TX 75251; PH (972) 980-2188: e-mail: greg.welch@ch2m.com
[4] CH2M HILL, 33 New Montgomery Street, Suite 2000, San Francisco, CA 94105; PH (415) 541-7220: e-mail: afalzone@ch2m.com
[5] CH2M HILL, 402 W. Broadway Ste. 1450, San Diego, CA 92101; PH (619) 687-0120; email kyle.winslow@ch2m.com
[6] CH2M HILL, 322 East Front Street, Suite 200, Boise, ID 83702; PH (208) 345-5314; email Denny.Mengel@ch2m.com

ABSTRACT

The Trinity River Corridor Project in Dallas, Texas will realign and naturalize eight miles of the Trinity River channel and create a wide variety of recreational and habitat features on the floodplain within the boundaries of the Dallas floodway. Major flood control projects in the 1920s and 1950s relocated, straightened, and channelized the river, and regular mowing on the floodplain has maintained homogenous conditions with limited habitat value. Primary river naturalization elements of the project include restoration of channel meanders, creation of more natural channel geometry, integration of natural geologic controls into the channel profile, and creation of an oxbow lake. Floodplain improvements include creation of wetlands, lakes, recreational features such as trails and playing fields, and establishment of more natural vegetation assemblages. This suite of channel and floodplain improvements will create more complex hydraulics and sediment transport characteristics that will strongly influence the operation and maintenance of the Project area, and therefore the overall sustainability of the Project. Therefore, the design of channel and floodplain features has been guided by detailed analysis of historical geomorphology of the Project site and the region, and two-dimensional hydraulic and sediment transport modeling of the proposed channel and floodplain design. We present results from the integrated fluvial geomorphology and two-dimensional hydraulic and sediment transport modeling based design process introduced in Tompkins et al (2008) and describe how these results, which included velocity and shear stress distribution and sediment deposition patterns, were used to develop and refine channel alignment, geometry, and bank treatment designs as well as configuration and design of floodplain features.

INTRODUCTION

The Balanced Vision Plan (BVP) for the Trinity River (City of Dallas 2003) struck a balance between the following diverse and potentially conflicting goals for the Trinity River Corridor:

1) Provide undiminished flood protection for the full length of the corridor in a way that supports the achievement of environmental, recreational, mobility, and economic goals;
2) Complete bold initiatives of environmental responsibility, restoration, and proper management in the midst of an intensely urban setting;
3) Create a magnificent recreation and urban open space amenity while co-existing successfully with flows of vehicular traffic as well as periodic floodwaters;
4) Meet stated regional transportation goals in a way that supports economic development, air quality improvement, and appreciation for the park; and
5) Create critically important community and economic opportunities for the neighborhoods bordering the Trinity River, for downtown, and as the centerpiece of a major urban region.

One of the primary motivations for the development of the BVP is the current degraded condition of the largely single-purpose Trinity River floodway in the City of Dallas. The Trinity River in Dallas has experienced dramatic change over the past century, with the most rapid and extensive changes occurring during the construction of the original Dallas Floodway project in the late-1920s and the US Army Corps of Engineers (USACE) reconstruction of the floodway in the mid-1950s. These projects relocated, straightened, and channelized the Trinity River in the vicinity of Dallas (Figure 1), creating a homogenous river corridor with limited habitat and aesthetic value.

Furlong et al (2003) describe in detail the changes that have occurred to the Trinity River in Dallas since the mid-1800s. While some change has continued to occur since the USACE project was completed (e.g. the Dallas Floodway improvements in 1990), the channel realignment portion conceptualized in the BVP and designed as part of the ongoing Trinity River Corridor Project (Project) will result in perhaps the most significant change to the Trinity River since the 1920s-era Dallas Floodway project.

The Trinity River channel is a central feature of the BVP, as it influences the design and sustainability of nearly all of the other proposed features for the floodway. The BVP describes significant physical changes to the channel and floodway including restoration of channel meanders, creation of a mid-channel island, alterations to channel geometry, and construction of two lakes in the floodway adjacent to the channel. This paper summarizes hydrologic and geomorphic assessments conducted to document and quantify historical and ongoing channel and floodway change, and presents a design process that combines these historical analyses with approaches from landscape architecture and state-of-the art hydraulic and sediment transport modeling to translate the Balanced Vision for the Trinity Lakes project into the most sustainable detailed design possible for the site.



Figure 1: Oblique aerial photograph of the Trinity River near Dallas in 1929. Note the straightened channel under construction in the center of the photo and the vegetated, meandering natural channel to the right of the new channel. Downtown Dallas is on the right side of the photograph. Flow direction is from top to bottom.

HYDROLOGY ASSESSMENTS

The hydrology of the Trinity River watershed (Figure 2) has been a critical consideration in the channel realignment design process as it will govern not only flow magnitude, frequency, duration, and timing that Project features will be exposed to, but construction scheduling and post-project operation and maintenance requirements as well. We assessed all available hydrology data and reports to characterize river stage-discharge relationships, daily streamflow characteristics, flood frequency, influence of reservoir regulation, and seasonality and inter-annual variability. The Project reach of the Trinity River has a drainage area of 6,100 square miles and includes approximately 8 miles between the confluence of the Elm and West Forks and the Dallas Area Rapid Transit (DART) Bridge downstream. The climate in this part of the watershed is humid subtropical with hot summers and mild winters. Average annual rainfall in the watershed is between 30 and 40 inches. Most of the annual precipitation occurs during thunderstorms, with occasional very heavy rainfall occurring over short time periods. Thunderstorms can occur throughout the year, but are more frequent in the late spring and early summer.

River Stage – Discharge Relationships

The relationship between river stage (i.e. depth of flow above a datum) and discharge is an important consideration in channel design as rapid changes in stage can lead to bank failure due to increased pore water pressure that develops as high flows recede from the floodplain back into the river channel. Flow and stage in the Trinity River near Dallas change rapidly in response to rainfall in the watershed. This is due in large part to urbanization that has increased impervious watershed area and decreased travel time of runoff entering the Trinity River and tributaries. The estimated stage-

discharge rating curve (Figure 3) illustrates that river stage increases approximately 40 feet between 200 cfs and 80,000 cfs. Flow and stage increases of this magnitude frequently occur over short periods of time, often less than twenty four hours.



Figure 2: Trinity River watershed. Project reach is in the Dallas Metro Area.

Daily Streamflow

Daily streamflow characteristics are important to consider in channel design as they largely dictate the day-to-day flow conditions that will be experienced by people accessing and recreating in the Project area and by the river corridor ecosystem. The United States Geological Survey (USGS) maintains a streamflow gauge (#0805700) in the Project reach that began recording in 1903. Mean daily flows in the Trinity River during the period of record range from a low of approximately 10 cfs (which has occurred less than 0.3% of the time) to a high of 152,000 cfs on June 26, 1908. The average daily flow is approximately 1,700 cfs, and "base" flow is between 500 and 600 cfs.

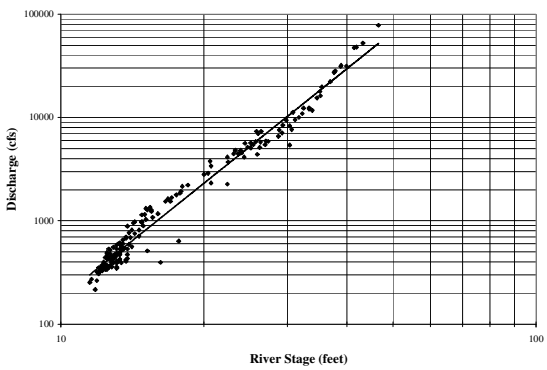

Figure 3: Estimated stage-discharge rating curve from observed data (1982-2007) at USGS Gage #08057000 (Trinity River at Dallas)

Flood Frequency

The frequency and magnitude of peak floods at the Project site will influence many facets of the final channel realignment design, including erosion control measures, riparian vegetation planting schemes, recreational features, and operation and maintenance. While high magnitude, low frequency floods are not the primary focus of the channel realignment design, an understanding of extreme event hydrology is crucial as it will inform assessments of sustainability of Project elements and development of long-term operation and maintenance procedures. Annual peak floods in the Trinity River range from 4,540 cfs (05/28/1978) to 184,000 cfs (flood of record on 05/26/1908). The Flood of Record occurred after 10 to 15 inches of precipitation in the watershed over a three day period, when the stage and discharge at the Dallas gage were 52.6 feet and 184,000 cfs, respectively, and the river was over two miles wide between West Dallas and downtown Dallas (Furlong et al. 2003). The average annual flood is approximately 30,000 cfs and the median flood is 21,400 cfs.

Influence of Reservoir Regulation

Reservoir regulation at the Project site is an important consideration for channel design because the reservoirs in the watershed have altered the historical frequency and magnitude of floods that will be experienced by Project design elements. Further, because the large storage reservoirs were constructed around the middle of the period of record for the USGS Dallas gage, the changes they have caused influenced selection of hydrology to consider for design (i.e. pre- vs. post-reservoir hydrology). Upstream of Dallas, the Trinity River watershed is regulated by 15 reservoirs and lakes with total storage capacity of over 5.5 million acre feet (Bureau of Economic Geology 1997). By 1960 seven large reservoirs had been constructed with a combined maximum observed storage volume of almost 2.4 million acre-feet. Two additional reservoirs were constructed in the 1980's with a combined maximum observed storage volume of almost 1.5 million acre-feet. Peak flows have been reduced significantly post-1960, except relatively frequent floods (i.e. up to the 1.10 year flood) which have increased slightly since 1960. It is unclear whether this increase is a result of reservoir regulation, changes in the watershed, or some combination of the two.

Hydrologic Seasonality and Interannual Variability

The timing of flows in the Project area is important because it will influence construction scheduling as well as operation and maintenance of the Project. The temporal distribution of flows in the Trinity River near Dallas is relatively constant throughout the year. Median monthly streamflow (calculated using the entire period of record) ranges from 300 to 500 cfs for all months except April, May, and June, when median monthly streamflow increases to between 700 and 1,100 cfs. Large precipitation events typically occur during the months of April, May, and June, which explains the rise in median flow values as well as the increase in peak flows during these months. Reservoir regulation has not changed these patterns significantly;

however it has altered the magnitude of difference between streamflows during different seasons. Prior to dam construction, median monthly streamflow varied over a wider range throughout the year and maximum monthly streamflows were higher. In addition to seasonal variability, flows in the Trinity River vary from year to year as hydrologic conditions change. Interannual differences in flow are important to consider in the design of the Trinity River channel because conditions in the channel and floodway will vary from year to year and will influence potential uses of the channel as well as maintenance requirements. While low flows are similar across water year types, the duration of periods with high flows (and the magnitude of those high flows) varies significantly. For example, in 1978 (an extremely dry year) daily average discharge was approximately 200 cfs for most of the year, with brief peaks of 4,000 cfs or less, while in 1989 (an extremely wet year), peaks between February and June kept daily average discharges above 5000 cfs for much of the year and as high as 43,000 cfs during large storms. The final channel design will consider differences between water year types of this scale.

TRANSLATING HYDROLOGY AND CHANNEL GEOMORPHOLOGY INTO DESIGN

A variety of fluvial geomorphic assessments were conducted in the Trinity River Corridor Project area (Tompkins et al 2008) to develop a template for the preliminary alignment, geometry, and profile design for the realigned channel that would satisfy the project's multiple objectives. Table 1 summarizes the process by which the hydrologic, hydraulic, and geomorphic characteristics described above were translated into the initial channel design. The initial design alignment, geometry, and profile was evaluated and refined in an iterative application of two-dimensional hydraulic (RMA) and sediment transport (SED-2D) models to identify and minimize potential problem areas, thereby producing a final schematic design that incorporated a thorough understanding of hydrology and fluvial geomorphology and maximizes sustainability through natural processes.

TABLE 1: CHANNEL CONDITIONS AND RELATED DESIGN GUIDANCE

River Corridor Characteristic	Conditions in Trinity River at Dallas Floodway	Related Channel Realignment Design Guidance
Stage – Discharge Relationship	Rapid changes in stage with changes in flow	To minimize the erosive effects of these rapid changes and maintain better recreational access and aquatic and riparian habitat, channel geometry should be designed with flatter slopes than the 1:1 slope used in the 1955 USACE channel design
Flood Frequency	Frequent (every 1.4 years on average) bankfull flows of approximately 13,000 cfs, and flows above 13,000 inundate the floodway	Consider expanding cross-sectional area to increase conveyance and protect future floodway developments; Design geometry that is relatively stable during flows of at least 13,000 cfs
Hydrologic Seasonality and Interannual Variability	Periods of extended low and high flow conditions that vary seasonally and with water year type	Create features (e.g. terraces, floodplain benches, etc.) that are appropriately situated in relation to low, high, and intermediate flow stage
Riparian Vegetation	Narrow band of riparian vegetation along channel margins reduces extent of bank erosion and imparts roughness to in-channel flow.	Create channel geometry that facilitates growth of desired riparian vegetation and achieves aesthetic and recreational objectives

TABLE 1: CHANNEL CONDITIONS AND RELATED DESIGN GUIDANCE

River Corridor Characteristic	Conditions in Trinity River at Dallas Floodway	Related Channel Realignment Design Guidance
Channel Geometry	Relatively stable since initial adjustment to USACE channel improvements (8 – 20 feet of widening); Extensive local bank erosion "repaired" by sediment deposition and revegetation	Maintain at least 50 foot bottom width from USACE improvement design and sideslopes flatter than 1:1 to reduce extent of bank erosion; Increase top-of-bank width to minimize channel widening immediately after implementation; Armor banks in close proximity to sensitive floodway developments
Channel Profile	Stable reach slope with undulations in channel invert profile that vary in location and magnitude	Minimize alterations to existing profile slope; Incorporate gradient control or plan for channel dredging where slope must be changed significantly
Channel Alignment	Stable channel centerline alignment, even in large meanders with strong eddy currents; channel width varies between 120 and 200 feet within Project area	Incorporate a 120 to 200 foot-wide buffer area between channel margins and no-encroachment area boundaries so that channel adjustments will not threaten critical areas; Where corridor is not wide enough to accommodate buffer, armor channel banks (or install sub-surface "cut-off wall") to protect sensitive floodway developments

Figure 4 shows the model grid developed to represent the proposed conditions for both the channel and floodway elements of the project. Note the varied channel geometry shown in different colors in the oblique view in Figure 4. Given the complex nature of both in-channel and overbank hydraulics expected with the proposed conditions, this two-dimensional representation was critical in adequately describing and gaming both channel and floodplain design features.

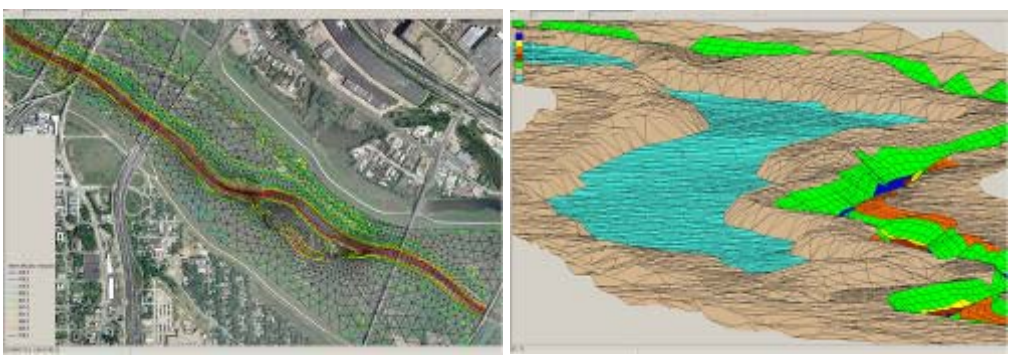

Figure 4: Plan view (left) and oblique 3-D view of the RMA-2 two dimensional model grid developed to represent the proposed Trinity river channel and floodplain conditions.

Figure 5 shows the RMA-2 model output for an overbank model run of approximately 38,000 cfs. The velocity and shear stress magnitudes and locations were used to develop design criteria for bank treatments and in-channel habitat features, and to design complex park features on the floodplain such as the weirs that control flow into and out of the floodplain lakes and the outfall channel that connects the lakes to the channel.

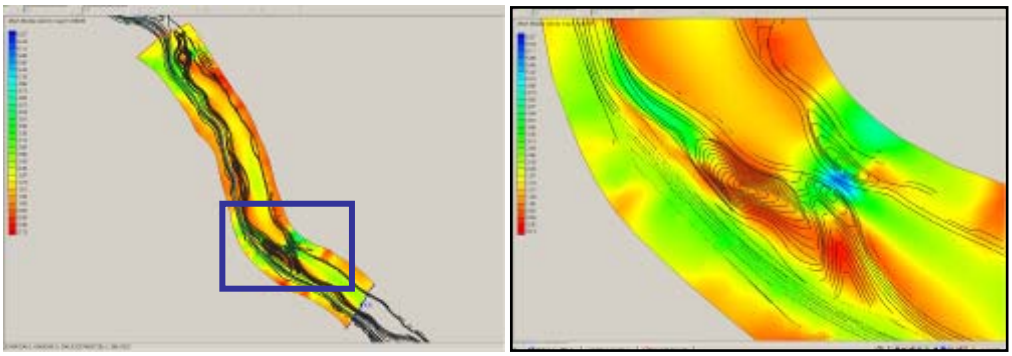

Figure 5: 2-D velocity contours showing channel and floodplain hydraulics for a flow of approximately 38,000 cfs. Blue areas are high velocity and red areas are low velocity.

Figure 6 shows the SED-2D model output that was used to further refine channel and floodplain designs, and to guide development of operation and maintenance requirements and costs. Because the floodplain will become a heavily used park in the City of Dallas, a detailed understanding of likely sedimentation patterns was essential throughout the design process.

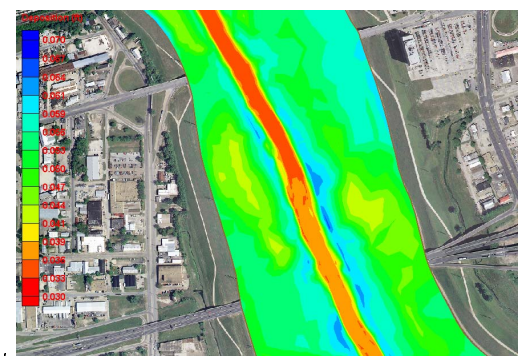

Figure 6: 2-D elevation contours showing depths and locations of expected erosion and deposition in the channel and on the floodplain.

While two-dimensional hydraulic and sediment transport modeling tools are not necessary on every channel realignment or restoration project, they have proved to be an extremely useful on the highly complex Trinity River Corridor Program where major changes are proposed to both the channel and floodplain. They provided meaningful design feedback with respect to hydraulics and sediment transport and helped identify areas where small-scale design modifications could significantly improve conditions in ways that would not have been possible using traditional one-dimensional tools.

REFERENCES CITED

Bureau of Economic Geology, 1997. Existing reservoirs from the 2001 State Water Plan. Digital data provided by, Texas Water Development Board.

City of Dallas. 2003. A Balanced Vision Plan for the Trinity River Corridor. Dallas. 2003.

Furlong, J.N., G. Ajemian, and T. McPherson. 2003. History of the Dallas Floodway. Fall 2003 ASCE Meeting.

Tompkins et al 2008. The Dallas Trinity Lakes Project: challenges and approaches to designing a channel realignment scheme to satisfy multiple objectives. EWRI World Environmental and Water Resources Congress. Honolulu, HI.

REHABILITATION OF THE MIDDLE RIO GRANDE NEAR BERNALILLO, NEW MEXICO

Drew C. Baird[1] and Carolyn Donnelly[2]

[1]Hydraulic Engineer, U.S. Bureau of Reclamation, Technical Service Center, Denver Technical Service Center, Denver, Colorado 80225 PH (303) 445-2564, FAX (303) 445-6351: email:dbaird@do.usbr.gov
[2]Hydraulic Engineer, U.S. Bureau of Reclamation, Albuquerque Area Office, 555 Broadway Blvd, NE, Albuquerque, NM, 87102 PH (505) 462-3632; FAX (505) 462-3794: email: cdonnelly@uc.usbr.gov

Abstract

Along the Middle Rio Grande near Bernalillo, New Mexico, sediment loads and flood peaks have been reduced, and the river channel is incising and has converted from a low flow braided sand-bedded channel to a single thread gravel-controlled bed channel (often bi-modal sediment transport conditions), with a slightly sinuous planform. As a result, the river has migrated laterally, and before the project, was closer to the levee that provides flood protection for the adjacent developed areas. A project has been implemented to prevent levee failure, safely pass peak flows, re-establish some measure of floodplain connectivity, and improve habitat conditions for two endangered species. Project features include a new channel relocated away from the levee, bendway weirs, a low floodplain surface along the outside of the new river bend, a secondary channel, rootwads, and native vegetation plantings. The new low floodplain surface is intended to provide a new riparian zone near the existing riparian zone that has become decadent as a result of channel incision and reduced flood peaks. Data include post project cross sections showing the re-connected floodplain and the initial riparian zone re-establishment, and main channel and near bank vertical velocity profiles. Initial channel response is qualitatively evaluated.

Background

During most of the 20th century the Middle Rio Grande in the vicinity of Bernalillo, New Mexico, has been a low-flow braided, relatively straight or slightly sinuous aggrading channel with a shifting sand substrate and low banks, with high floodplain connectivity. Since the 1950's, upstream reservoirs and channelization works have been constructed to reduce sediment supply and flood peaks, increase sediment transport capacity, and protect riverside facilities and infrastructure. During this period there have been extended periods of drought and high flows affecting the channel. The altered flow and sediment regimes, largely from upstream dam and channelization construction, have affected channel conditions. The post-Cochiti Dam and channelized river in this area is a gravel-controlled bed which is mostly single thread with a slightly sinuous planform. Sediment transport is bi-modal during gravel mobilizing events. The channel changes (Reclamation, 2007) include

- Channel bed incision began after dam construction and continued through the 1990's. Historical floodplains have been abandoned and are now terraces with bank heights larger than 6 ft (Massong et. al., 2006).
- The reduced supply of sand size sediment material since dam construction, together with the availability of coarser sediments, has resulted in the bed material size changing to gravel and cobble size material.
- Planform conversion occurred in the 1990's. The channel is now predominantly a single thread, deep thalweg, with side channels becoming inundated only during high flow events (the 2-year flow or greater).
- Medial bars or islands were transient prior to planform conversion and are now relatively stable channel features with partial vegetation. These medial bars or islands now act as high-flow floodplain surfaces narrowing the active channel and in many cases have become attached to the banks.
- A series of migrating bends is developing as a result of planform conversion, narrowing, incision, and bed coarsening.
- The channel bank height, at present, is mostly tall enough that the thalweg elevation intersects the bankline beneath the root zone of the riparian vegetation on the abandoned terraces.
- Small patches of riparian vegetation are growing on the new smaller floodplain surfaces being created by the migrating incised channel, while the historical floodplain is becoming increasingly isolated from the main channel and 2-year return period peak flows.

The channel incision and narrowing have degraded native aquatic and terrestrial habitats, including that of two endangered species, the Rio Grande silvery minnow (*Hybognathus amarus*) (RGSM) and the Southwestern willow flycatcher (*Empidonax traillii extimus*) (SWFL). Habitat needs for the RGSM include low velocity, low depth, silt/sand substrate habitats, inundated floodplains and inlets to side channels (Dudley and Platania, 1997; SWCA, 2007; Reclamation, 2007). The SWFL habitat needs are dense growth of trees and shrubs, about 13 to 15 feet tall, located in riparian ecosystems associated with wetlands, and other areas near rivers and lakes (Reclamation, 2007). An incised channel with coarse substrate, tall banks, and small patches of floodplain connectivity does not generally provide suitable habitat for these two endangered species.

The river rehabilitation project near Bernalillo, New Mexico, was initiated to address bed and bank erosion threatening river side facilities and the degradation and loss of native habitat in this reach. The protection of river side facilities, rehabilitation of riverine habitat to one more favorable to the RGSM, and the development of a riparian zone connected to the river's hydrology are the primary objectives of the project.

Project Description

Near the town of Bernalillo, New Mexico, the river channel has moved close to the levee on the east side, and the angle of the upstream bend directed flows at this bank. Based upon a time sequence of visual observation, there was concern that, at moderately high flows of 3,000 to 5,000 cfs, the bank could erode, causing the levee to fail and the river to

flow into the Bernalillo Riverside Drain and flood an extensive area east of the river, with both residential and agricultural uses (Sixta and Nemeth, 2005). The site is located on the east side of the Rio Grande, approximately 3,300 feet south of the U.S. Highway 550 Bridge in Bernalillo, New Mexico (Figure 1).

To protect the levee from future damage, the main channel of the Rio Grande was realigned slightly to the west, bendway weirs were installed, a low floodplain surface along the outside of the bend was created, and a secondary channel was constructed (Figure 1). The low floodplain surface and secondary channel are intended to reduce erosion potential on the east bank and create more favorable habitat. The project was designed by Bio-West, Inc. (Bio-West, 2005), under contract with the Bureau of Reclamation, and construction was performed by a Reclamation crew from August 2006 to March 2007.

To reduce the energy directed at the east bank, the main channel was realigned as shown in Figure 1. This realignment decreases the bend angle and also increases the distance from the river channel to the levee. A low floodplain surface was established by placing alluvial fill in the old main channel with a sloping and multi elevation surface. The alluvial fill volume was about 42,000 cubic yards, and was taken from the new channel alignment and the secondary channel. The secondary channel was excavated to the west of the existing main channel (Sixta and Nemeth, 2005).

Re-establishing the terrestrial-aquatic connectivity in river rehabilitation and inundation of the floodplain is essential for ecosystem health (Brookes, 1996). The new riparian zone is about 120 ft wide (Figure 2) and varies in width throughout the project area (Figure 1) with a total land area of 2.4 acres. Various levels of floodplain surfaces were established with some being inundated with about 1 to 1.5 feet of water depth at about 5,000 cfs (Sixta and Nemeth, 2005). These varied flow depths are intended to encourage natural recruitment of native riparian forest species at different flow rates on the multiple levels of the low floodplain surfaces (Figure 2). Planting of native willow and cottonwood on the new low floodplain surfaces also encourages establishment of a riparian forest. Finally, numerous rootwads and woody debris piles were included to provide short term habitat enhancement (Figure 1).

The 13 bendway weirs were constructed on the outside of the bend along the east bank of the river to prevent bank erosion. Bendway weirs are upstream angled stone sills, submerged at high flows, and placed along the outer banks that are designed to control and redirect currents through the bend (Derrick, 1997). A new thalweg location develops at the tips of the bendway weirs. Bendway weirs are typically constructed with a top width of two to three times the maximum diameter of the rock used to construct the weir, and typical heights range from one half to one times the bendway weir top width (McCullah and Gray, 2005). The bendway weirs at the Bernalillo site were constructed of 12 inch nominal diameter riprap, with an approximate width of four feet, and a length projecting 25 feet into the flow. To prevent flanking by possible future lateral migration, an additional length of riprap extends into the bank, and is typically about 75 feet. The weirs are approximately four feet high at the bank and taper to three feet high at the tip.

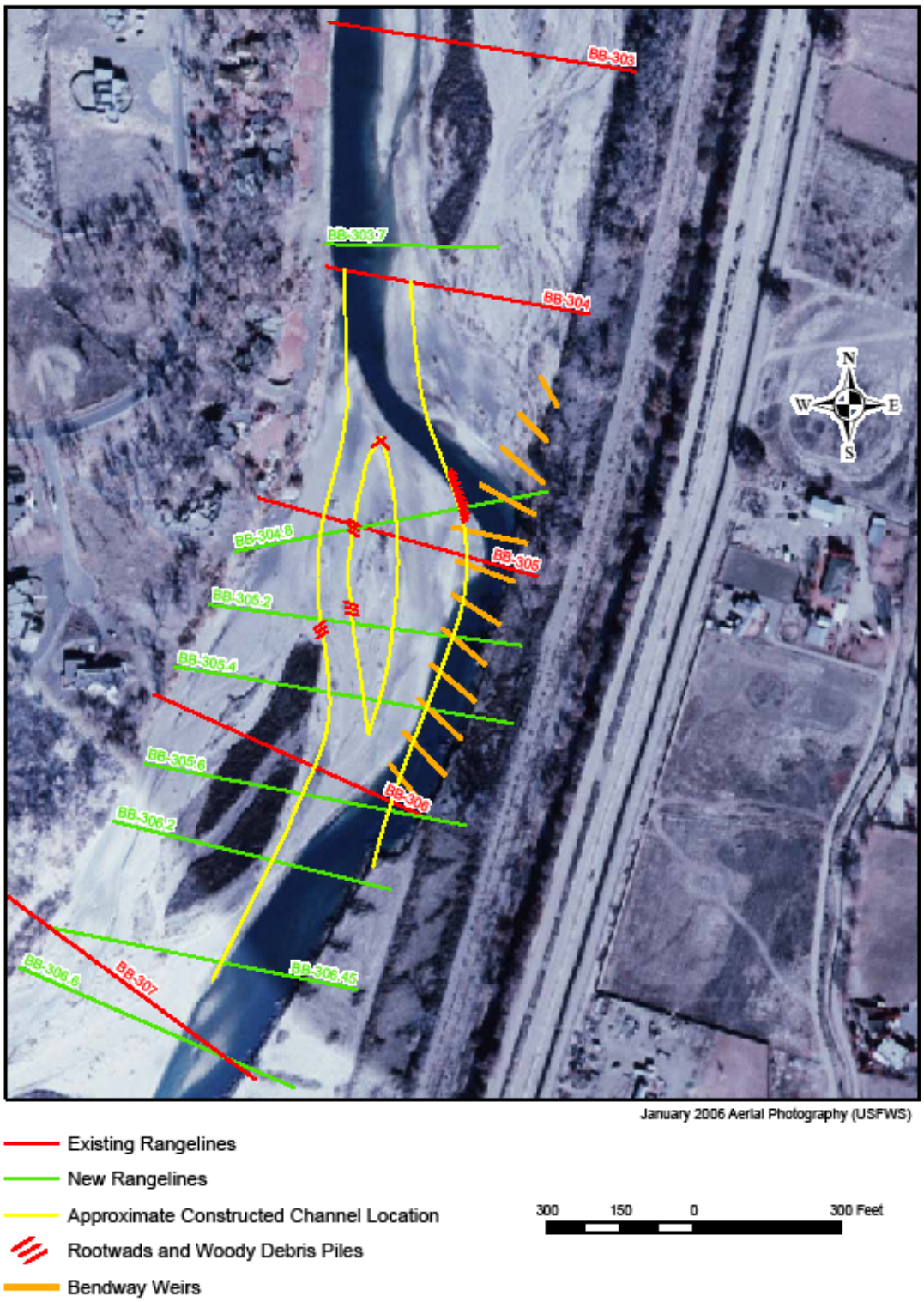

Figure 1. Bernalillo Project plan view showing relocated channel, secondary channel, bendway weirs, and range line locations.

The four foot height corresponds to the 500 cfs water surface elevation at the bank, and to slightly less than half of the modeled 5,000 cfs water surface elevation. These flows correspond to a typical low and high flow, respectively. The weirs were constructed at a spacing of 75 feet and oriented 20 degrees upstream of a perpendicular line extending from the bank (Sixta and Nemeth, 2005).

Since it is difficult to precisely estimate potential project outcomes for river rehabilitation, adaptive management is included in the project. Adaptive management consists of post project data collection and observation, evaluation, and modifications to the project to meet project goals. Adaptive management for the project (Sixta and Nemeth, 2005) includes 1) replanting vegetation if initial survival rate is low, 2) additional earthwork to maintain the new channel alignment until the new bankline is stabilized by vegetation and the bendway weirs, 3) earthwork to adjust the elevation of the constructed low surface floodplain to improve establishment of a new riparian zone, 4) additional rock to replace rock which may erode from the bendway weir tips or for field weir modifications, and 5) replacing dislodged rootwads and debris piles.

Post Project Assessment

The objective of the post project assessment plan is to determine the overall effectiveness of the project features and channel response to provide for improved future project function. Specifically, the post project assessment includes the following: 1) determine initial and longer term channel response to project construction in terms of channel plan view, hydraulic geometry, and channel profile; 2) measure the velocity and estimate shear stress in the main channel and along the bankline between weirs; 3) determine the actual frequency of overbank flows in the excavated floodplain, 4) estimate sediment transport rates through the project area, 5) observe and document the stability of the bendway weirs and the constructed bank line.

The initial channel cross section changes, velocity, and shear stress (in both the main channel and along the bankline between weirs), and discharge measurements are reported in this paper.

Data Collection, Analysis, and Results

Cross sections were collected in May 2007 and May 2008. A discharge measurement was made during May 2008 to determine the flow split between the main channel and the secondary channel. A series of point velocity and vertical velocity profiles were measured to estimate velocity and bed shear stress in the main channel and along the bankline between the bendway weirs during May 2008. Comparative cross sections, for section 304.8 are shown in Figures 2 and 3. The pre project (August 2004) cross section is 305 (Figure 2). The location was slightly changed after the project was constructed so the cross section would be oriented perpendicular to the new channel alignment. The thalweg elevation is higher and the main channel flow depth is reduced post construction (Figure 2). This is attributed to increasing the local centerline bend radius, and the new secondary channel (Figure 2) which, at high flows, conveys a significant portion of the

flow. In the pre-construction cross section, there was an abandoned channel from about station 340 to about station 575, which was not a secondary channel. The secondary channel (measured in May 2007) is much wider and conveys more flow than originally designed. During construction a small secondary channel was excavated. The new main channel was blocked and all river flows were directed down the secondary channel. A larger than anticipated flow event occurred during construction, enlarging the secondary channel beyond the design dimensions (May 2007 in Figure 2).

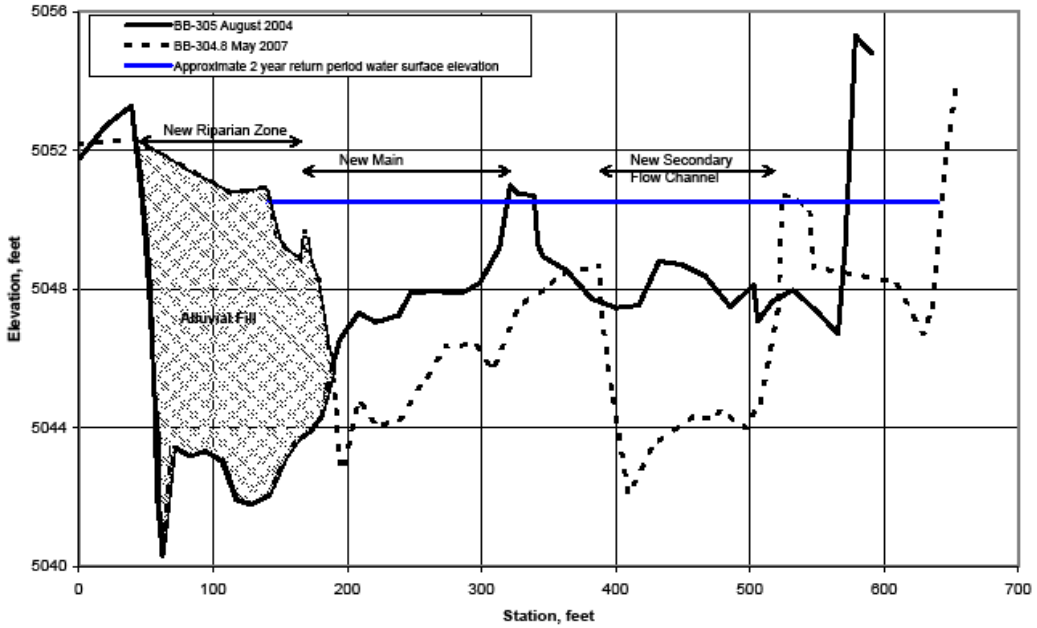

Figure 2. Rangeline comparison before and after construction, showing the alluvial fill for the new riparian zone, and the new main and secondary channel locations.

Between May 2007 and May 2008, there was scour in the main channel between station 200 and about 300 (Figure 3). There was scour in the secondary channel between stations 310 and 400, and fill between stations 395 to about 510. During the May 2008 discharge measurement there was 1970 cfs flowing between stations 180 to 310 in the main channel, and about 1660 cfs flowing in the secondary channels between stations 310 to 520. During May 2008, a series of velocity measurements were made near the bendway weirs. Velocity measurements consisted of instantaneous measurements made using an ADV manufactured by SonTek/Ysi in San Diego, California. A sampling rate of 25 Hz for 60 seconds was made with the ADV mounted to a standard 50 lb USGS

weight. The effectiveness and limitations of the weight mounted ADV are described by Baird (2004).

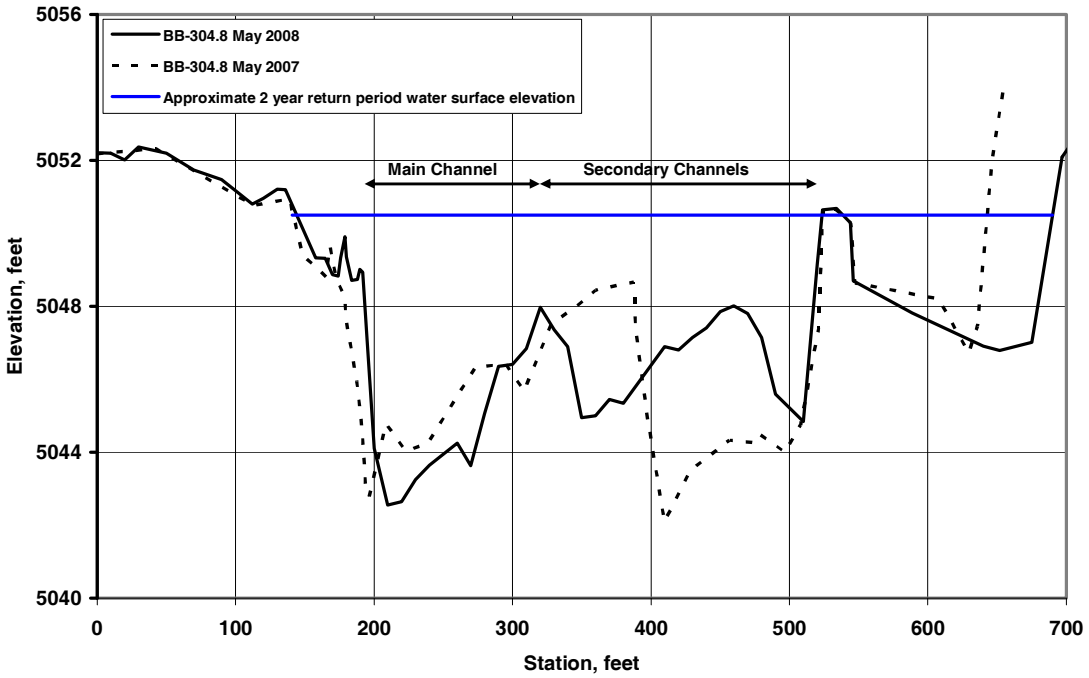

Figure 3. Same rangeline as Figure 2, comparing May 2007 and May 2008 data and showing some main channel scour, and secondary channel scour and filling.

At some locations, 3-point velocity measurements were made in the vertical at 0.2, 0.6, and 0.8 *y*/*d*. At other locations, a series of 19 point velocities were made to develop a vertical velocity profile. The purpose of the vertical velocity profile is to estimate bed shear velocity (u_*) and bed shear stress (τ_o) in the main channel and along the bankline between bendway weirs. The velocity profile also was collected for the purpose of gaining an understanding of this part of the flow field and thus erosion patterns around the bendway weirs. The main channel velocity, velocity profile, and shear stress were collected and estimated to compare with same variables along the bankline between bendway weirs. The difference between the main channel and bank line velocity and shear stress is the reduction as a result of the bend way weirs. The bank line vertically averaged bank line velocity and shear stress will be compared with published bank stability criteria based upon bank material soil types and sizes. Estimating u_* from the velocity profile relies upon the logarithmic velocity profile law being valid. Whether a logarithmic zone existed near the bank between the bendway weirs was an unknown at the time of data collection. Assuming a logarithmic zone exists its thickness was also an unknown. To aid in these purposes the measured vertical velocity profile was also compared to the log wake flow law given by Nikora and Goring (2000) using estimated values of shear velocity zero velocity roughness height, and the Coles (1956) wake flow parameter:

$$\frac{\bar{u}}{u_*} = \frac{1}{\kappa}\ln\left(\frac{y}{y_o}\right) + \frac{2\Pi}{\kappa}\sin^2\left(\frac{\pi y}{2d}\right) \quad (1)$$

where u_* is the shear velocity in ft/s, κ is the von Karman constant equal to 0.4, y_o is the zero velocity roughness height in ft, and Π is the dimensionless Coles wake flow parameter. For the flow region from the bed to about 0.2 y/d (inner region), a logarithmic profile exists (Figures 4 and 5). This is sufficient thickness to estimate u_*. For the flow region about y/d > 0.2 (outer region) the flow deviates from the logarithmic law. Secondary currents have also been shown to cause this departure (Baird, 2004).

The main channel shear velocity was 0.585 ft/s, compared to 0.159 ft/s twelve feet downstream of the sixth bendway weir from the upstream end (bendway weir 6). Using the relationship $\tau_o = \rho u_*^2$ bed shear stress was estimated (Table 1). The value of the Coles wake flow parameter was -0.16 for the main channel, and -0.05 for the bankline downstream of bendway weir 6. A negative Cole's wake flow parameter is caused by flow retardation from secondary currents. The main channel flow velocity profile (Figure 4) is in good agreement with the profile of the log-wake law with a logarithmic zone in the inner region, and some deviation near the top of the water column. The bankline line velocity profile (Figure 5) has a logarithmic zone in the inner region, and deviates significantly from the log-wake law in the outer region, attributed to bank line (side wall) effects. Main channel vertical mean velocity (average of 0.2, and 0.8 y/d values) was 4.00 ft/s, the bankline 12 feet upstream of each weir measured was 2.85 ft/s, the bankline 12 feet downstream of each weir measure was 2.96 ft/s, and the bankline halfway (35 feet) between each weir was 3.21 ft/s. The bank line would remain stable under these shear stress and velocity conditions for particle sizes larger than 0.3 to 0.6 inches in diameter (Table 1). During data collection the banks were not actively eroding and are comprised of sand and gravel sizes.

Initial Post Project River Response

Post project visual observations show few naturally-seeded cottonwoods that have grown beyond several inches, even though the newly established floodplain was inundated after spring runoff of 2006. Willows and cottonwoods planted as part of the project have experienced some mortality, and some continued growth. Those closest to the water surface have experienced mortality attributed to extended periods of inundation. Further up the bankline plantings are generally more successful. The bendway weirs have remained stable and variable depth and velocity flow conditions have been established as a result of scour at their tips and downstream eddies. However, the downstream eddies were only observed during low flow conditions. Data from May 2008 showed that no eddies existed downstream of the weirs along the bankline. Between the time the project was constructed and the May 2008 data collection period, no bank erosion had occurred between the bendway weirs. Post runoff observations indicate that there is some bank erosion along the outside of the realigned meander bend between the bendway weirs.

Measurements made at 3,900 cfs, in May 2008, show that the near bank shear velocity and depth averaged velocity were reduced (Table 1).

Table 1 Material Sizes Which are Stable for the Measured Velocity and Shear Stress. Sizes are from Fischenich (2001).

Location	Vertically Averaged Velocity (ft/s)	Stable Boundary Type for the Measured Velocity	Local Shear Stress (lb/sq ft)	Stable Boundary Type for the Measured Velocity
Main Channel	4.0	Graded Loam to cobbles and 6 inch gravel	0.661	Graded silts to cobbles and 1-2 inch gravel
Near the Bank Line between Bendway weirs	2.85 to 3.21	1-2 inch gravel	0.159	Fine loam 0.6 to 1.3 inch gravels

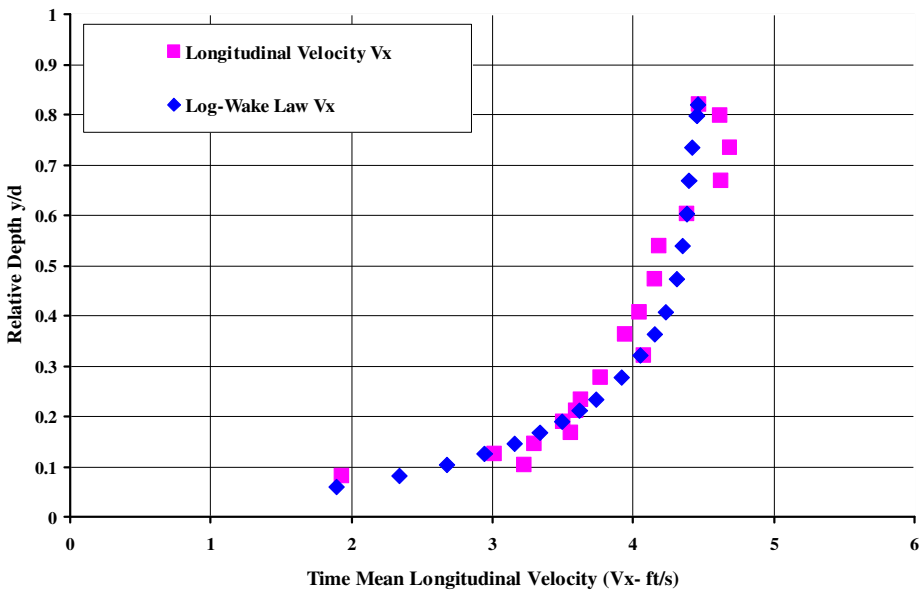

Figure 4. Main channel vertical velocity profile 12 ft. from the tip of weir 6.

For the flow rate in May 2008 (3,900 cfs), the near bank shear velocity 12 feet downstream of bendway weir 6 was 27.2% of the main channel shear velocity, the near bank depth averaged velocity either 12 feet or upstream or downstream of the bendway weirs was 72.6% of the main channel depth averaged velocity, and the near bank depth averaged velocity at the midpoint between two bendway weirs was 80.3% of the main channel depth averaged velocity. The large secondary channel conveyed a significant

portion of the flow. Post-runoff observations indicate that it is filling with sediment, while the main channel appears to be scouring. Additional data collection is planned to confirm these post runoff observations. The low floodplain surface area between about

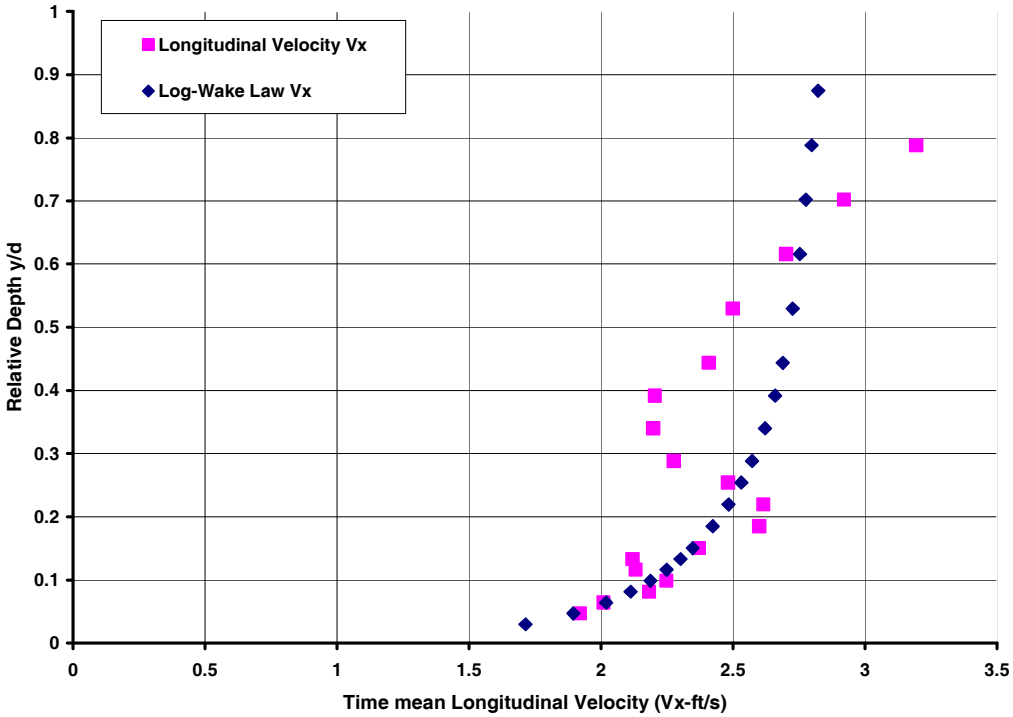

Figure 5. Main Channel vertical velocity profile along the bankline 12 ft. downstream of weir 5.

station 40 and station 120 was constructed with a slope for habitat and revegetation purposes. The bankline velocity and shear stress have also been reduced. For the time period up to the May 2008 data set, the bankline remained intact without scalloping or bank erosion between groins, indicating sufficient near bank velocity reduction to maintain bank stability. The peak of the 2008 runoff occurred later in May and was 5,150 cfs. After the recession of the hydrograph it was observed that the large secondary channel had filled significantly with sediment, and that bank scalloping between bendway weirs occurred. .

Conclusions and Recommendations

Successful rehabilitation of incised, narrowed river channels can include re-establishing connectivity between the main channel and floodplain by either raising the riverbed or lowering the banks or terraces. In some cases, smaller inset floodplains will establish within the abandoned terraces as the channel migrates laterally. Floodplains may need to be re-established by excavation when incision prevents floodplain connectivity, and raising the river bed is not possible. In other cases where channel incision is mild or doesn't exist, removal of barriers can create floodplain connectivity. These could be spoil berms from channel excavation, or longitudinal dikes which are no longer needed.

For this project, a new low floodplain surface was created by relocating the river and placing alluvial fill material in the previous main channel. At the Bernalillo project site, the initial response shows that a riparian zone is not developing naturally and additional plantings may be needed to ensure long term establishment of a riparian zone. At present the riverside infrastructure is adequately protected, and the bendway weirs are stable, although scallops have developed between weirs. If scour in the main channel and sediment deposition in the secondary channel continue, the weirs may erode away and the main channel could migrate laterally.

Large river rehabilitation and floodplain connectivity may require a great deal of earth work, depending upon the local topography and geomorphology. This project illustrates the challenge of achieving multiple, diverse goals in a highly managed natural system. Goals such as maintaining flood conveyance and protecting riverside infrastructure may require a different approach than creating or improving habitat for endangered species. Habitat restoration projects generally attempt to mimic conditions that evolved before the system was managed. The initial response at this site indicates that the project may require adaptive management and additional post project maintenance. This is a work in progress, and, with additional data, findings and conclusions may be added or altered based on future observations.

It is recommended that additional data be collected and evaluated to understand and document post project channel processes affecting the flood conveyance, protection of riverside facilities, floodplain connectivity, bank stability near the bendway weirs, and the variable depth and velocity conditions found near the bendway weirs. Additionally, longer reach river response assessment would be useful to determine any channel changes as a result of the project.

Acknowledgements

The authors gratefully acknowledge the contributions made by others which benefited this paper. Mark Nemeth reviewed the manuscript, and Paula Maker reviewed the background section. Discussions with Darren Olsen from Bio-West added greatly to the general understanding of the project concepts and design. Suzanne Devergie and Vincent Benoit joined in to collect the 2007 and 2008 cross section data sets and the discharge measurements with Carolyn Donnelly. Connie DeMoyer collected the ADV velocity profile data sets with Drew Baird and estimated turbulence flow statistics using WINADV. Conclusions in this paper are the findings of the authors and do not represent the official policy of the U.S. Bureau of Reclamation.

References

Baird (2004), “Turbulent Flow and Suspended Sediment Transport in a Mobile, Sand Bed Channel with Riprap Side Slopes,” Dissertation submitted in partial Fulfillment of the requirements for the Degree of Doctor of Philosophy, University of New Mexico, May 2004.

Bio-West Inc., (2005), "Middle Rio Grande Project, Bernalillo Priority Site, Final Design Report," Bio-West, Inc. Logan, UT.

Brookes, A., (1996), "Floodplain Restoration and Rehabilitation," In "Floodplain Processes," edited by Anderson, M.G., Walling, Des, E., and Bates, P.D., John Wiley and Sons, NY.

Bureau of Reclamation, (2007), "Middle Rio Grande River Maintenance Plan Part 1 Report," Middle Rio Grande Project, NM, Upper Colorado Region, Albuquerque Area Office, NM.

Coles, D.E. (1956) "The Law of the Wake in Turbulent Boundary Layer," J. Fluid Mechanics, 1, Pg. 191-226.

Derrick, D.L., (1997). "Harland Creek Bendway Weir/Willow Post Bank Stabilization Demonstration Project," In the "Proceedings of the Conference on the Management of the Landscapes Disturbed by Channel Incision," Oxford, MS.

Dudley, R.K. and Platania, S.P., (1997), "Habitat Use of Rio Grande Silvery Minnow," Report to the NM Department of Game and Fish, Santa Fe, NM, and U.S. Bureau of Reclamation, Albuquerque, NM.

Fischenich, C (2001), "Stability Thresholds for Stream Restoration materials," EMRRP Technical notes Collection (ERDC TN-EMRRP-SR-29), U.S. Army Engineer Research and Development Center, Vicksburg, MS.

Julien, P.Y., (1995), "Erosion and Sedimentation," Cambridge University Press., Cambridge England.

Massong, T., Tashjian, P., and Maker, P., (2006), "Recent Channel Incision and Floodplain Evolution within the Middle Rio Grande, NM," Proceedings of the 8th Federal Interagency Sedimentation Conference, Reno, NV.

McCullah, J., and Gray, D. (2005), " Environmentally Sensitive Channel and Bank Protection Measures," National Cooperative Highway Research Program NCHRP report 544, and Project 24-19, Transportation Research Board, Washington DC.

Nikora, V., and Goring, D., (2000) "Flow Turbulence over Fixed and Weakly Mobile Gravel Beds" J. Hydr. Engrg., ASCE Vol. 126 (9), Pg. 679-690.

Sixta, M., and Nemeth, M., (2005), "Bernalillo Project Site Description," U.S. Bureau of Reclamation, Albuquerque Area Office, Albuquerque, NM.

SWCA, (2007), "Characterization of Rio Grande Silvery Minnow Egg and Larval Drift and Retention in the Middle Rio Grande," Prepared by SWCA Environmental Consultants, Broomfield CO, and Albuquerque, NM.

USACE River Ecosystem Restoration Planning: Lessons Learned From the Illinois River Study

Michael Schwar

HNTB Corporation, 11414 W. Park Place Suite 300, Milwaukee WI 53224;
PH (414) 359-2300; email: mschwar@hntb.com

ABSTRACT

Planning undertaken by the U.S. Army Corps of Engineers for the Illinois River (IL) Basin Restoration Study utilized formulation techniques that could be adapted for other river ecosystem restoration planning efforts. The USACE planning process requires quantification of benefits in order to evaluate the relative merit of alternative approaches. Historically, these benefits have often been quantified in terms of "acres of habitat created or improved". However, when altered abiotic processes or biotic interactions limit ecosystem function to a larger degree than habitat limitation it is necessary to incorporate both spatial and functional considerations to develop meaningful measures of restoration benefit.

In the Illinois River system, ecosystem function is generally considered to be limited by a combination of abiotic processes (including sediment transport, water level and water quality), biotic interactions (including lost connectivity and exotic species), and habitat limitation (including deep waters, connected backwaters and floodplains). For the Illinois River Basin Restoration study, developed by the USACE in partnership with the State of Illinois seven overall restoration goals were developed, each addressing one of the identified limiting factors. Each objective was quantified using individually specific criteria, such as tons of sediment delivered to the river, degree of water level fluctuation, miles of connected tributary mainstem and acres of connected backwater multiplied by a depth distribution function. Alternatives were then developed based on differential attainment of the various criteria relative to the level necessary to reach full functionality.

Sophisticated hydrologic and hydraulic modeling, supplemented with GIS analyses, were used to quantify tributary-, basin- and reach-level effects of alternative implementation. HSPF was used to evaluate hydrologic and sediment transport benefits within tributaries from implementation of different levels of infiltration and storage practices. UNET hydraulic modeling was used to estimate the reduction of water level fluctuation due to tributary improvements and reconnection of floodplain areas. The relationships between level of implementation and modeled effect were used to determine the level of effort (or number of individual projects) required along the river or throughout the watershed to reach the desired criterion levels for each particular alternative.

The ecological function of impacted rivers, wetlands and their watersheds tends to be degraded by factors above and beyond habitat loss. Identifying the relevant factors and formulating plans that adequately address each is crucial to developing successful

restoration projects. Combining sophisticated models of physical processes with the input of ecologists with extensive local knowledge allows the development of ecologically meaningful planning and design criteria for these projects.

INTRODUCTION

The Illinois River Basin Restoration Program is a joint Federal-State effort to restore ecosystem function to the Illinois River. In the Illinois River system, ecosystem function is generally considered to be limited by a combination of abiotic processes (including sediment transport, water level and water quality), biotic interactions (including lost connectivity and exotic species), and habitat limitation (including deep waters, connected backwaters and floodplains). The project team, led by the USACE and the Illinois DNR established an overarching goal: "Restore and maintain ecological integrity, including habitats, communities and populations of native species, and the processes that sustain them.". To reach the overarching goal, the team developed seven overall restoration goals, each addressing one of the identified limiting factors and associated with specific measurable criteria. Projects will be developed to address one or more goals and the level of effort and focus of the restoration determines the number and types of projects implemented.

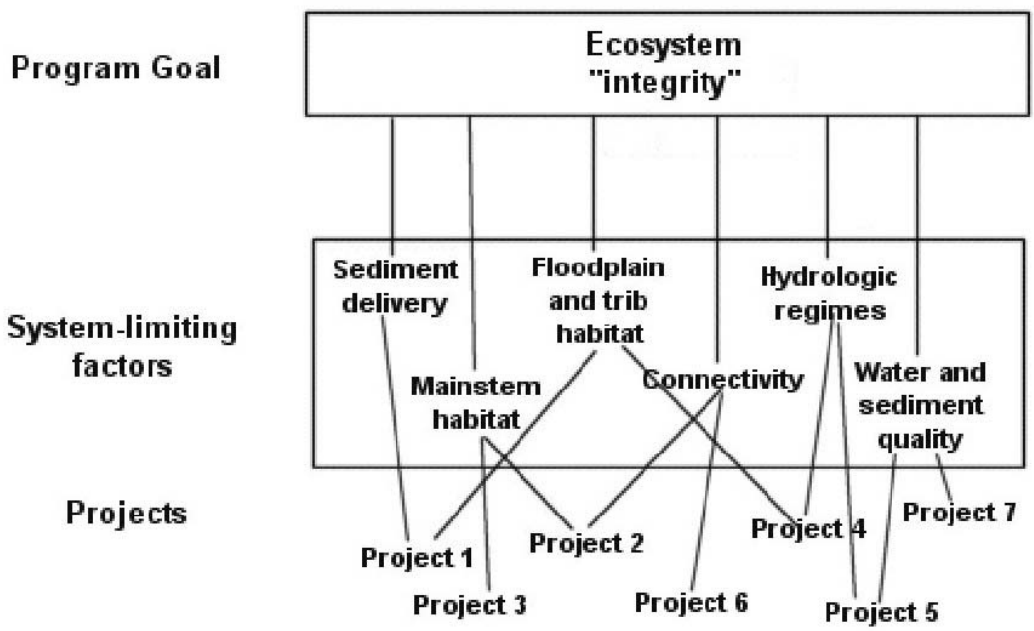

Illinois River Basin Overall Restoration Goals

Goal	Measures of Success
Reduce sediment delivery to the Illinois River from upland areas and tributary channels with the aim of eliminating excessive sediment load	– Reduced tons of sediment delivered to the River – Reduced tons of sediment delivered to high-value habitat areas
Restore aquatic habitat diversity of side channels and backwaters, including Peoria Lakes, to provide adequate volume and depth for sustaining native fish and wildlife communities	– Acres of diverse backwaters – Acres of side channel and island habitats – Maintained connections between backwaters and main channel – Improved substrate conditions for plants and animals (compaction)
Improve floodplain, riparian and aquatic habitats and functions	– Acres of mainstem floodplains – Acres of tributary floodplains – Miles of riparian habitat
Restore aquatic connectivity (fish passage) on the Illinois River and its tributaries, where appropriate, to restore or maintain healthy populations of native species	– Passage at dams
Naturalize Illinois River and tributary hydrologic regimes and conditions to restore aquatic and riparian habitat	– Reduced low water fluctuations along mainstem – Reduced tributary peak flows – Increased tributary base flow – Pool drawdowns for 30 days at least once every 5 years
Improve water and sediment quality in the Illinois River and its watershed	– Achieving full use support (first for aquatic life, later for all uses) – Encouraging remediation – Achieving nutrient standards – Maintaining existing full use waters

HYDROLOGIC RESTORATION ANALYSIS

A number of modifications within the basin, notably extensive land use change, has led to flashier hydrologic regimes in tributaries and increased water level stability in the mainstem Illinois River. Since tributary hydrology and mainstem water levels are often linked, the effects of restoration had to be evaluated holistically. Watershed restoration effects were modeled using HSPF using long-term (30-year) rainfall inputs and river water levels were modeled using a UNET model of the river, also using long-term inputs and run at two hour timesteps. For example, the effects of adding various quantities of floodplain storage along the river was hydraulically modeled; it was determined that such storage could smooth water level regime locally and for a short distance downstream but would have little effect upstream.

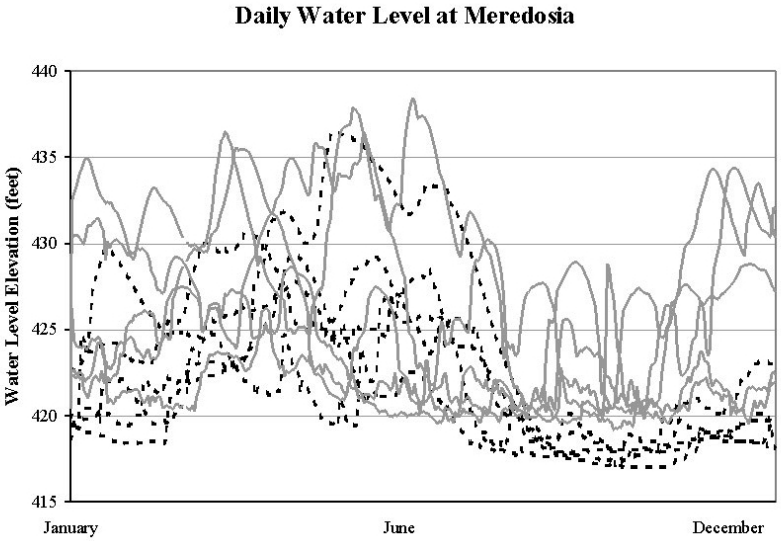

(Dashed lines are pre-1900 river levels, solid lines are from 1990-2000)

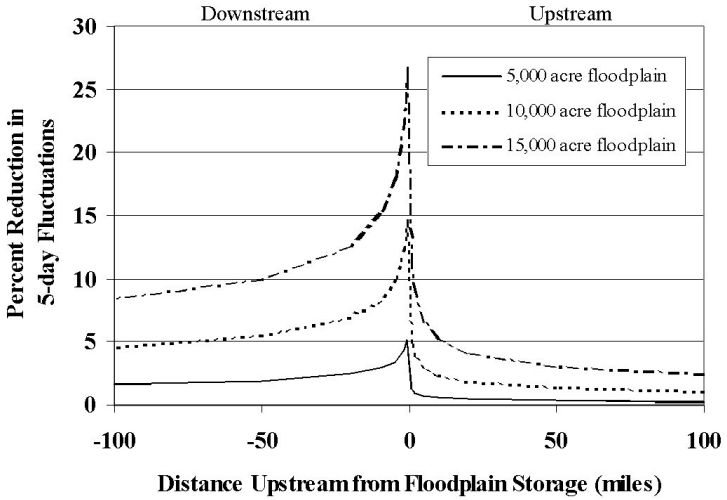

The UNET model was also used to evaluate potential drawdown opportunities. The model was run using long term flows to probability of maintaining extended exposure upstream of the Peoria and La Grange dams if drawdowns were attempted at different times of the year. The figure below shows the assumed ecological benefits from drawdowns at various times of the year, and by combining the relative benefit with the probability of success the expected benefit of different strategies can be determined. Although summer drawdowns have the highest potential benefits, they were found to have a low likelihood of success due to the incidence of storms that would flood exposed areas. Later drawdowns are more likely to succeed and despite the lower benefits during that time of year, the average expected benefit per attempt is highest for drawdowns beginning in August.

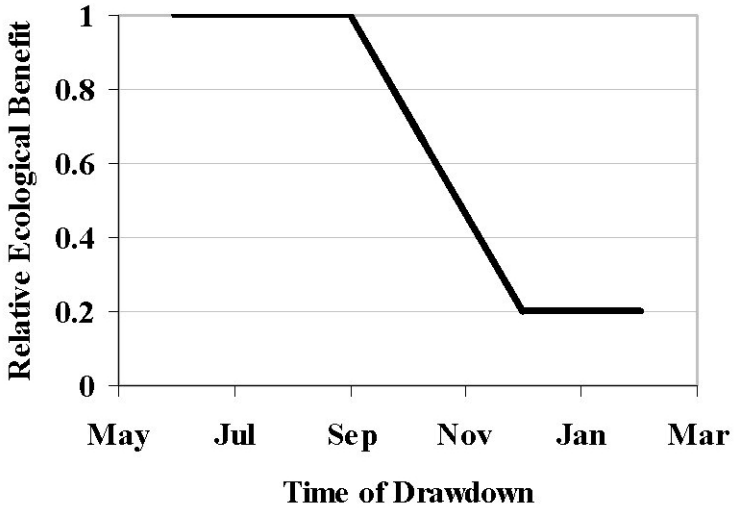

Starting Date		Jun 1	Jul 1	Aug 1	Sep 1	Oct 1	Nov 1	Dec 1
Suitability (30-day)		1.0	1.0	1.0	0.8	0.6	0.4	0.2
Suitability (70-day)		1.0	0.97	0.86	0.66	0.46	0.29	0.2
30-day attempt	Full success rate	0.15	0.3	0.6	0.65	0.65	0.55	0.4
	Expected benefit (per	**4.5**	**9**	**18**	**15.6**	**11.7**	**6.6**	**2.4**
70-day attempt	Full success rate	0.1	0.2	0.45	0.45	0.4	0.3	0.2
	Expected benefit (per	**7**	**13.6**	**27.1**	**20.8**	**12.9**	**6.1**	**2.8**
	30-day but not 70-day rate	0.4	0.6	0.4	0.4	0.4	0.4	0.55
	Expected benefit (per	**12**	**18**	**12**	**9.6**	**7.2**	**4.8**	**3.3**

Watershed and tributary benefits were quantified using HSPF simulations of four tributaries that are considered to represent the range of conditions present in the basin. Various implementation levels of restoration techniques were modeled and the benefit curves for the four tributaries were used to generate a mean curve that was used to represent basinwide implementation. The output from these simulations was also used as input to the river UNET model to evaluate the effects on mainstem water level fluctuations and other downstream benefits.

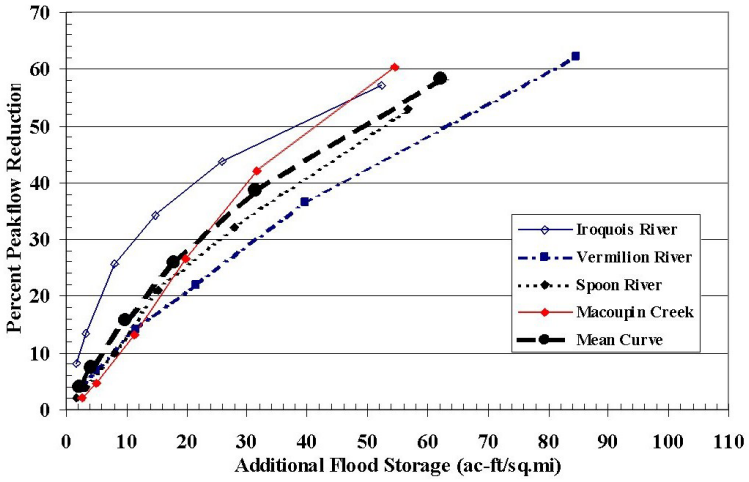

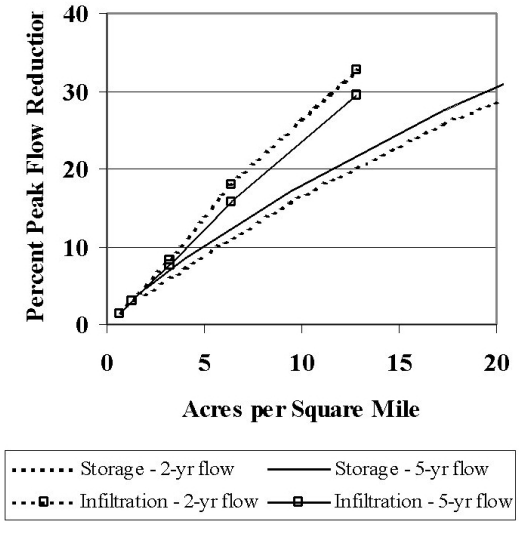

PLAN FORMULATION

After determining the benefits of individual restoration measures, plans to address the hydrologic restoration goal were developed by combining various levels of implementation of these measures. Costs were then estimated for each of these plans. Selected plans for each individual goal were assembled to create alternatives with different ecological integrity endpoints.

	Initial Cost ($M)			Tributaries		Reduced Main Stem Fluctuations	
Alternative	**Construction**	**Real Estate**	**Total**	**Reduced Peak Flow**	**Increased Baseflow**	**Growing Season**	**Winter**
R0, I0, M0, WP0, WL0	0	0	0	0	0	0%	0%
M1	6.6	0	6.6	0	0	65%	73%
M2	7.6	0	7.6	0	0	65%	73%
R1	**108**	**62**	**170**	**1.50%**	**0.1%**	**0%**	**0%**
R2	180	104	284	2.50%	0.1%	0%	0%
M1, R2	187	104	291	2.50%	0.1%	65%	73%
M1, R3	367	207	574	5%	0.3%	65%	73%
M1, R4	647	368	1015	8%	0.6%	66%	73%
M1, R5	1508	863	2371	16%	1.6%	67%	78%
I1	100	33	133	0.80%	5%	0%	0%
M1, I2	207	65	272	1.50%	10%	67%	73%
M1, I3	407	131	538	3%	20%	65%	73%
M1, I4	1008	326	1334	7.60%	50%	65%	73%
M1, I5	2009	653	2662	16%	80%	65%	73%
R1, I1	**208**	**95**	**303**	**2.30%**	**5%**	**0%**	**0%**
M1, R1, I1	**215**	**95**	**310**	**2.30%**	**5%**	**65%**	**73%**
M1, R3, I3	**767**	**338**	**1105**	**8%**	**20%**	**65%**	**73%**
M1, R4, I3, P4, L6	**1047**	**499**	**1546**	**11%**	**20%**	**66%**	**73%**
M1, R5, I4	2509	1189	3698	23%	50%	67%	78%
M1, R5, I4, WP2	2809	1189	3998	23%	50%	70%	79%
M1, R5, I4, WL2	2809	1189	3998	23%	50%	70%	79%
M1, R5, I4, WP2, WL2, P4, L6	**3109**	**1189**	**4298**	**23%**	**50%**	**72%**	**80%**

Key:
(R) - storage in tributary areas
(I) - infiltration in tributary areas
(M) - dam management
(WP) - modification of Peoria wicket dams
(WL) – modification of La Grange wicket dams
Bold type - alternative combinations that were used as system plans

	Overarching Goal	Goal 1	Goal 2	Goal 3	Goal 4	Goal 5	Goal 6
Alternative	Ecological Integrity	Sediment Delivery	Backwaters and Side Channels	Floodplain, Riparian, and Aquatic	Connectivity	Water Level Management	Water Quality
No Action	decline	some increase delivery	decline 1%/ yr	No Change	potential improvement	more fluctuations	minor improvement
1	regional improvements	0% upper Tribs 20% Peoria Tribs 0% lower Tribs	3,600 BW acres 10 side channel 10 island protect	5,000 acres MS 5,000 acres Trib 25 stream miles		-1.5% TPF 0% TBF 0% MSF	minor regional improvements
2	maintain current habitat at system level	0% upper Tribs 40% Peoria Tribs 0.5% lower Tribs	6,100 BW acres 20 side channel 15 island protect	5,000 acres MS 10,000 acres Trib 50 stream miles		-2.3% TPF +5% TBF 0% MSF	regional improvement
3	begin system improvements - sediment focus	11% upper Tribs 40% Peoria Tribs 4% lower Tribs	8,600 BW acres 30 side channel 15 island protect	20,000 acres MS 20,000 acres Trib 100 stream miles	Fox, DuPage, Des Plaines	-2.3% TPF +5% TBF 66% MSF	some system improvement
4	begin system improvements - tributary focus	11% upper Tribs 40% Peoria Tribs 4% lower Tribs	6,100 BW acres 20 side channel 15 island protect	5,000 acres MS 20,000 acres Trib 100 stream miles	Fox, DuPage, Des Plaines, Kankakee, Spoon, Aux Sable	-8% TPF +20% TBF 66% MSF	some system improvement
5	ecosystem integrity stable	11% upper Tribs 40% Peoria Tribs 4% lower Tribs	8,600 BW acres 30 side channel 15 island protect	40,000 acres MS 40,000 acres Trib 250 stream miles	Fox, DuPage, Des Plaines, Kankakee, Spoon, Aux Sable	-8% TPF +20% TBF -66% MSF	some system improvement
6	measurable increase at system level	11% upper Tribs 40% Peoria Tribs 20% lower Tribs	12,000 BW acres 35 side channel 15 island protect	75,000 acres MS 75,000 acres Trib 500 stream miles	Fox, DuPage, Des Plaines, Kankakee, Spoon, Aux Sable	-11% TPF +20% TBF -66% MSF	some system improvement
7	reasonable upper bound to system improvements	11% upper Tribs 40% Peoria Tribs 20% lower Tribs	18,000 BW acres 40 side channel 15 island protect	150,000 acres MS 150,000 acres Trib 1000 stream miles	Fox, DuPage, Des Plaines, Kankakee, Spoon, Aux Sable, 3 Main Stem Dams	-23% TPF +50% TBF -73% MSF	some system improvement

Overarching Goal – Ecological Integrity will be addressed by the other goals through prioritization and specifications on restoration measures.
Goal 1 - Sediment delivery benefits are expressed in percentage reductions in tributary delivery resulting from in-channel stabilization and upland practices.
Goal 2 - Backwater (BW) Benefits are expressed in acres dredged, but will benefit larger reaches. Side Channel benefits associated with increased structure and some dredging.
Goal 3 - Main stem (MS) floodplain and riparian (trib) areas are expressed as acreages. Aquatic areas are expressed in stream miles.
Goal 4 - Connectivity (Fish Passage) lists reaches to be addressed. Main stem passage is at Starved Rock, Marseilles, and Dresden Island.
Goal 5 - TPF and TBF are tributary peak flow and base flow, respectively. MSF is the change in the main stem fluctuation regime, representing an average of 5-day windows in the lower river fluctuations over the course of the average growing season. Auto gates allow increased management to smooth flow releases and are included in Alternatives 6 and 7. Wicket dam replacements are considered for the Peoria and La Grange pools in Alternative 7.
Goal 6 - Water quality issues will be addressed through other goals. Greatest benefits likely associated with Goals 1 and 3.
Only rough benefits estimations are included in table; see writeup for additional details.

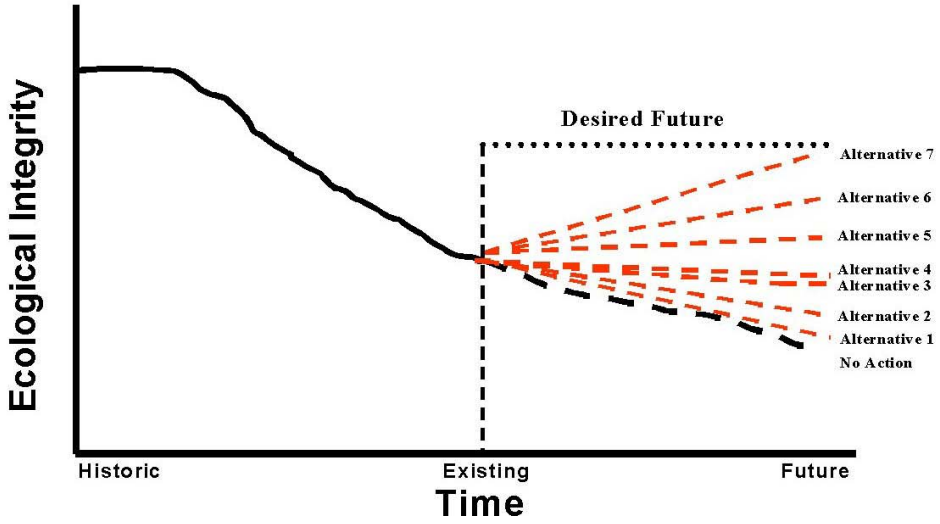

CONCLUSIONS

At this point, the field of large-scale river restoration necessarily includes many non-quantitative elements. Overall goals of ecosystem integrity can rarely be assigned specific measurable values, the restoration measures necessary to reach such goals are not usually understood with precision and available large-scale monitoring data is often inadequate to evaluate trends over relatively short time scales. But there are certain aspects that are sufficiently understood that processes can be simulated and restoration alternatives can be quantitatively compared. By incorporating such information into the planning process, more meaningful evaluations of project benefits can be developed where "acres of habitat" is not a sufficient indicator.

ACKNOWLEDGEMENTS

Chris Trefry and Renjie Xia from the Hydrology and Hydraulics Branch, Rock Island District, U.S. Army Corps of Engineers conducted much of the modeling that forms the basis of the hydrologic benefits analysis. Planners from the Rock Island District were responsible for the plan formulation briefly described here, most notably Brad Thompson, Jodi Staebell, Marshall Plumley and Steve Russell.

A Depth-Averaged 2-D Model of Non-cohesive Dam/Levee Breach Processes

Weiming Wu[1] , Zhiguo He[2], and Sam S.Y. Wang[3]

[1]Research Associate Professor, National Center for Computational Hydroscience and Engineering, University of Mississippi, 102 Carrier Hall, University, MS 38677, USA; PH (662) 915 6561; Email: wuwm@ncche.olemiss.edu
[2]Postdoctoral Research Associate, National Center for Computational Hydroscience and Engineering, University of Mississippi, 102 Carrier Hall, University, MS 38677, USA; PH (662) 915 6561; Email: hzg@ncche.olemiss.edu
[3]F.A.P. Barnard Distinguished Professor and Director, NCCHE, University of Mississippi, 102 Carrier Hall, University, MS 38677, USA; PH (662) 915 7788; Email: wang@ncche.olemiss.edu

ABSTRACT

A depth-averaged 2-D model has been developed to simulate the breach processes of non-cohesive dams and levees caused by overtopping flows. It solves the 2-D flow and sediment transport equations using an explicit finite volume method on a rectangular grid, with the HLL approximate Riemann solver to handle the mixed-regime flows near the breach. It considers interactions among transient flow, strong sediment transport and rapid bed change by including bed change and variable flow density in the continuity and momentum equations of flow. The model adopts the non-equilibrium approach for total-load sediment transport, and specifies different repose angles for the sediments below and above the water surface when handling the non-cohesive embankment slope avalanching. It uses a varying time step length that satisfies both the CFL condition and the limitation that the bed change is less than about ten percent of the local flow depth at each time step. The test using laboratory experiments shows the developed model predicts well the breach dimensions and flow characteristics.

INTRODUCTION

Thousands of dams and levees have been built around the world for flood defense, water supply, navigation, power generation, etc. Failure of any dam or levee poses significant risks to people and property nearby and the services provided by the structure. Examples of such incidents include the failure of the Tenton dam in 1976 and the levee failures in the Mississippi River in 1993 and in the Yangtze River in 1998. Therefore, understanding and prediction of dam/levee failure processes is crucial for decision making for safety and maintenance of dams and levees. The most common reasons for dam failures are surface erosion due to overtopping flow and internal erosion due to downstream seepage and piping. In the last decades, many embankment breach models have been developed. Singh (1996) introduced and

evaluated several analytical and empirical earthen dam breach models available in that time, whereas Mohamed et al. (2005) reviewed many existing dam/levee breach models. In most of these models, the breach section is simplified as a rectangle, trapezoid or triangle, the flow at the breach is estimated using the broad-crested weir relation, and the erosion is estimated using different simplified models. Uncertainties in predicted breach parameters and flood hydrograph exist due to significant model simplifications (Mohamed et al. 2005).

Unlike the above simplified breach models, 1-D and 2-D numerical models can simulate the flow and morphodynamic processes due to dam/levee breach more realistically (Wu and Wang, 2008; Faeh, 2007). Because dam breach flows are usually in mixed flow regimes and with discontinuities, the often used numerical schemes are the shock-capture schemes, such as approximate Riemann solvers and TVD (Total Variation Diminishing) schemes. Many of these methods have been verified and successfully applied in the simulation of dam-breach flow over fixed beds (Toro, 2001). However, the simulation over movable beds is much more challenging and encounters additional difficulties due to high sediment concentration and rapid bed change that might significantly affect the flow. The depth-averaged 2-D model of Faeh (2007) decouples the governing equations of flow and sediment transport and thus ignores the effect between them. Wu and Wang's (2008) model considers the effect of sediment concentration and bed change on the flow, so that it is extended herein to the depth-averaged 2-D case. The governing equations, numerical methods and validation of the developed 2-D model are presented in this paper.

GOVERNING EQUATIONS

For dam breach due to overtopping flows, the interaction of flow, sediment transport and channel bed becomes significant. The generalized 2-D shallow water equations considering this interaction are (Wu, 2007)

$$\frac{\partial(\rho h)}{\partial t}+\frac{\partial(\rho uh)}{\partial x}+\frac{\partial(\rho vh)}{\partial y}+\rho_b\frac{\partial z_b}{\partial t}=0 \tag{1}$$

$$\frac{\partial}{\partial t}(\rho uh)+\frac{\partial}{\partial x}\left(\rho u^2h\right)+\frac{\partial}{\partial y}(\rho uvh)+\rho gh\frac{\partial z_s}{\partial x}+\frac{1}{2}gh^2\frac{\partial \rho}{\partial x}+\rho g\frac{n^2m_buU}{h^{1/3}}=0 \tag{2}$$

$$\frac{\partial}{\partial t}(\rho vh)+\frac{\partial}{\partial x}(\rho uvh)+\frac{\partial}{\partial y}\left(\rho v^2h\right)+\rho gh\frac{\partial z_s}{\partial y}+\frac{1}{2}gh^2\frac{\partial \rho}{\partial y}+\rho g\frac{n^2m_bvU}{h^{1/3}}=0 \tag{3}$$

where t is the time, x and y are the longitudinal and lateral coordinates, h is the flow depth, u and v are the flow velocities in x and y directions, $U=\sqrt{u^2+v^2}$, $\partial z_b/\partial t$ denotes the rate of change in bed surface elevation, z_b is the bed surface elevation above a reference datum, z_s is the water level, n is the Manning roughness coefficient, g is the gravitational acceleration, ρ is the density of the water and

sediment mixture in the water column determined by $\rho = \rho_w(1-C_t)+\rho_s C_t$ with C_t being the volumetric concentration of total-load sediment, ρ_b is the density of the water and sediment mixture in the bed surface layer determined by $\rho_b = \rho_w p'_m + \rho_s(1-p'_m)$ with p'_m being the porosity of the surface-layer bed material, ρ_w and ρ_s are the water and sediment densities, and $m_b = \sqrt{1+(\partial z_b/\partial x)^2+(\partial z_b/\partial y)^2}$ considering the bed slope.

Simulation of the fluvial processes under dam breach flow can be achieved by computing bed load and suspended load separately or the total load directly in the case of non-cohesive sediments. Here, the latter approach is used, so that the sediment transport equation is (Wu, 2007)

$$\frac{\partial(hC_t)}{\partial t}+\frac{\partial(huC_t)}{\partial x}+\frac{\partial(hvC_t)}{\partial y}=-\frac{1}{L}(UhC_t-m_b q_{t*}) \tag{4}$$

where C_t is the actual total-load sediment concentration, q_{t*} is the total-load sediment transport capacity or the so-called equilibrium transport rate per unit channel width, and L is the non-equilibrium adaptation length of sediment transport. Note that the coefficient m_b introduced in Eq. (4) considers the lateral erosion along the side slope.

The bed deformation is determined with

$$(1-p'_m)\frac{\partial z_b}{\partial t}=\frac{1}{L}(UhC_t-m_b q_{t*}) \tag{5}$$

The sediment transport capacity is determined using the formula of Wu et al. (2000), with the modification suggested by Wu (2004) to consider the effect of gravity on sediment transport over steep slope. In addition, to consider the effect of sediment concentration, the settling velocity ω_s used in Wu et al. (2000) formula is determined by Richardson and Zaki's (1954) method: $\omega_s = \omega_{s0}(1-C_t)^m$, with m≈4.0 and ω_{s0} being the settling velocity of single sediment particles in quiescent, distilled water.

NUMERICAL METHODS

To establish an explicit algorithm, Eqs. (1)–(3) are reformulated by eliminating the flow density on their left-hand sides using the relation of $\rho = \rho_w(1-C_t)+\rho_s C_t$ and Eq. (4). The new continuity and momentum equations are

$$\frac{\partial h}{\partial t}+\frac{\partial(uh)}{\partial x}+\frac{\partial(vh)}{\partial y}=-\frac{1}{1-p'_m}\frac{UhC_t-m_b q_{t*}}{L} \tag{6}$$

$$\frac{\partial(uh)}{\partial t}+\frac{\partial(u^2h)}{\partial x}+\frac{\partial(uvh)}{\partial y}=-gh\frac{\partial z_s}{\partial x}-\frac{1}{2}gh^2\frac{1}{\rho}\frac{\partial\rho}{\partial x}-g\frac{n^2m_buU}{h^{1/3}} + u\frac{\rho_s-\rho_w}{\rho}\left(1-\frac{C_t}{1-p'_m}\right)\frac{UhC_t-m_bq_{t*}}{L} \tag{7}$$

$$\frac{\partial(vh)}{\partial t}+\frac{\partial(uvh)}{\partial x}+\frac{\partial(v^2h)}{\partial y}=-gh\frac{\partial z_s}{\partial y}-\frac{1}{2}gh^2\frac{1}{\rho}\frac{\partial\rho}{\partial y}-g\frac{n^2m_bvU}{h^{1/3}} + v\frac{\rho_s-\rho_w}{\rho}\left(1-\frac{C_t}{1-p'_m}\right)\frac{UhC_t-m_bq_{t*}}{L} \tag{8}$$

Eqs. (6)–(8) and (4) are written in the following compact form:

$$\frac{\partial\mathbf{\Phi}}{\partial t}+\frac{\partial\mathbf{F}(\mathbf{\Phi})}{\partial x}+\frac{\partial\mathbf{G}(\mathbf{\Phi})}{\partial y}=\mathbf{S}(\mathbf{\Phi}) \tag{9}$$

where $\mathbf{\Phi}$, $\mathbf{F}(\mathbf{\Phi})$, and $\mathbf{G}(\mathbf{\Phi})$ represent the vectors of unknown variables and fluxes

$$\mathbf{\Phi}=\begin{bmatrix}h\\uh\\vh\\hC_t\end{bmatrix},\quad \mathbf{F}(\mathbf{\Phi})=\begin{bmatrix}uh\\u^2h\\uvh\\huC_t\end{bmatrix},\quad \mathbf{G}(\mathbf{\Phi})=\begin{bmatrix}vh\\uvh\\v^2h\\hvC_t\end{bmatrix} \tag{10}$$

and $\mathbf{S}(\mathbf{\Phi})$ includes the remaining terms in each equation.

Consider the finite-volume mesh shown in Figure 1. Each control volume (cell) is embraced by four faces. Non-staggered (collocated) grid system is used here. The primary variables h, u, v and C_t are defined at cell centers and represent the average values over each cell, while the fluxes are calculated at cell faces.

Integrating Eq. (9) over the (i, j) control volume, applying the Green theorem, and using the Euler scheme for the time derivative, one can derive the following discretized equation:

$$\mathbf{\Phi}_{i,j}^{n+1}=\mathbf{\Phi}_{i,j}^{n}-\frac{\Delta t}{\Delta x_{i,j}}\left(\mathbf{F}_{i+1/2,j}^{n}-\mathbf{F}_{i-1/2,j}^{n}\right)-\frac{\Delta t}{\Delta y_{i,j}}\left(\mathbf{G}_{i,j+1/2}^{n}-\mathbf{G}_{i,j-1/2}^{n}\right)+\Delta t\,\mathbf{S}_{i,j} \tag{11}$$

where Δt is the time step length, $\Delta x_{i,j}$ and $\Delta y_{i,j}$ are the cell lengths in x and y directions, $\mathbf{F}_{i+1/2,j}^{n}$ is the flux at face $(i+1/2, j)$, and $\mathbf{G}_{i,j+1/2}^{n}$ is the flux at face $(i, j+1/2)$.

The HLL approximate Riemann solver (Harten et al., 1983) is used to determine the fluxes at cell faces. The terms on the right-hand side of Eq. (6) and the last three terms on the right-hand side of Eqs. (7) and (8) are evaluated using the values at cell centers and the central difference scheme at time level n. The water

surface gradient term is discretized using the backward difference when the velocity is positive and the forward difference scheme when the velocity is negative. The numerical method has the first-order accuracy in both time and space.

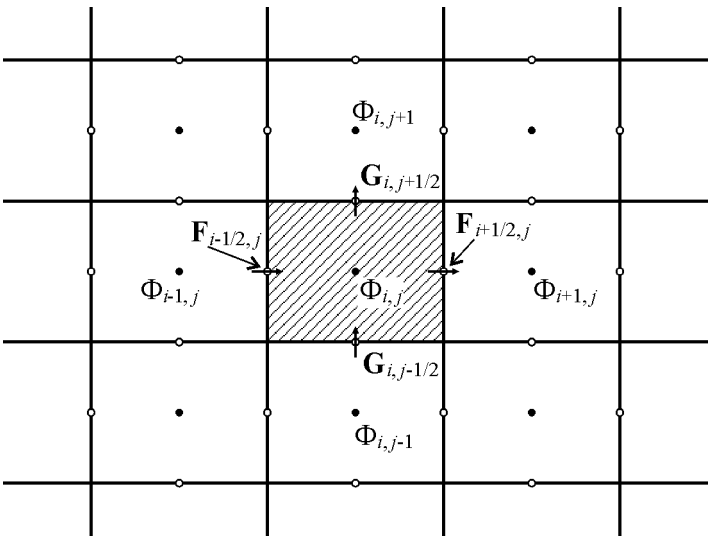

Figure 1. 2-D finite-volume mesh

The bed deformation equation (5) is discretized as

$$\Delta z_b = \frac{\Delta t}{1-p'_m}\frac{UhC_t - q_{t*}}{L} \tag{12}$$

Because the above solution procedure is explicit, the computational time step should be limited by numerical stability conditions, such as the Courant-Friedrichs-Lewy (CFL) condition for flow computation and additional conditions for sediment transport and bed change computations. By trial and error, it has been found that to obtain a stable solution, the bed change at each time step should be less than about 10% of the local flow depth. This, in addition to the CFL condition, limits the time step length.

Considering nearly vertical side walls of the breach observed in laboratory and field experiment even for non-cohesive dam/levee materials, a specially designed avalanching algorithm is adopted here. The non-cohesive slope avalanching algorithm presented by Wu (2007, pp. 278-279) is modified by specifying two different repose angles for the submerged materials and the dry materials above the water surface. The submerged repose angle is about 33 degrees as normally used, while the dry repose angle is about 79 degree for the test case present in the following case.

MODEL TEST

The present model has been validated quantitatively using the laboratory experiments carried out by HR Wallingford, UK (Morris et al., 2005). The experimental flume was about 50 m long and about 10 m wide, schematically shown in Figure 2. A series

of experimental runs were conducted under different flow and sediment conditions. The experimental test case #2 is selected here to validate the present numerical model. The model dam was located at about 36 m downstream of the flume entrance. It was 0.5 m high and had a crest of 0.2 m in width. Its upstream and downstream slopes were 1V:1.7H. The dam materials were non-cohesive. A wide grading and a narrow grading sediment mixture were tested; however, both had the same median diameter of 0.25 mm.

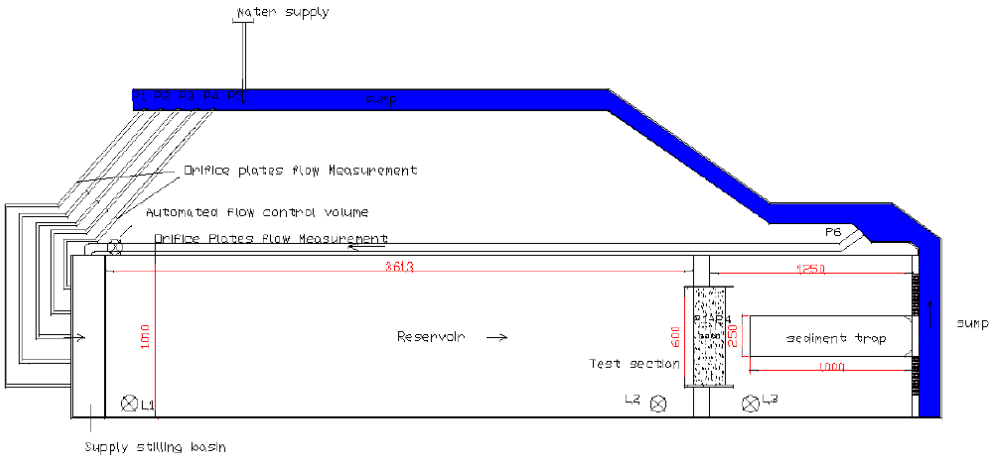

Figure 2. Schematic plan of the experimental flume at HR Wallingford (Morris et al., 2005)

The experiment started from pumping water into the reservoir. When the reservoir water level rose to the bottom of the pilot channel, the flow overtopped the dam. Water eroded the downstream slope first, so the downstream slope became milder and the dam crest retreated and eroded downward. No headcutting was observed in this test case because the non-cohesive sediment was used. Once the material was nearly eroded to the base, the material below the water level is eroded. This undermined the slopes and leaded to block failure. These processes continued until there was not enough water to erode more material. In the meantime, the upstream slope was also eroded leading to a curved "bell mouth" entrance to the breach. This "bell mouth" weir controlled the flow through the breach. Slumping was also observed on the upstream face due to this erosion (Morris et al., 2005).

A uniform mesh consisting of 1000×200 nodes in longitudinal and lateral directions is used in the simulation. The dam material porosity is estimated as 0.36, and the Manning roughness coefficient n is estimated as 0.018. The sediment adaptation length is set as 0.05 m, which is close to the longitudinal grid spacing as suggested by Wu (2007) and Wu and Wang (2008) to avoid the appearance of anti-dunes in the simulation. The time step length is determined by setting a Courant number of 0.5 but limiting the ratio of bed change to flow depth to be less than 0.1. This means that the time step length varies in different time steps. The initial pilot channel is 0.02 m deep and 0.2 m wide. The bed material repose angle is set to be 33° in the submerged condition and about 79° in the emergent condition. The inflow

discharge of 0.07 m^3/s is specified at the flume entrance, while a free overfall flow condition (Froude number =1) is applied at the end of the flume.

Figure 3 shows the simulated bed topography and Figure 4 shows the simulated water surface profile and flow pattern at the peak breach flow. A breach of 2.83 m in width forms at the time of peak flow. The water surface exhibits a shape of "bell mouth" weir flow, which agrees with the observation in the experiment. At the downstream of the breach the flow spreads laterally and a hydraulic jump exists.

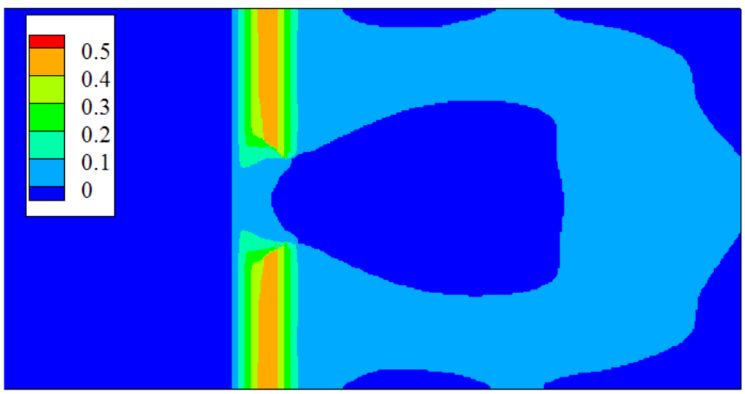

Figure 3. Simulated bed topography at the peak breach flow (contour levels in meter)

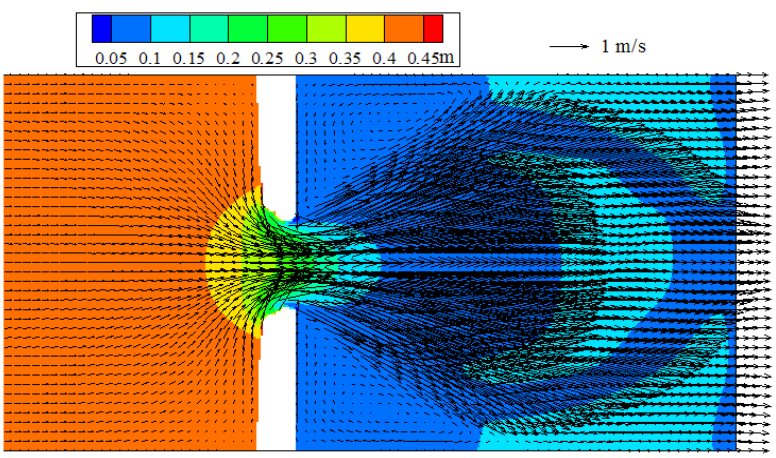

Figure 4. Simulated flow pattern and water surface at the peak breach flow

Figure 5 compares the measured and simulated breach flow discharges varying with time, and Figure 6 compares the measured and simulated breach widths. The measured data were obtained using both wide and narrow grading materials. Because the numerical simulation uses only a uniform sediment size and does not consider the gradation of sediment mixture, only one set of simulation results is obtained. The simulated breach flow hydrograph has a steeper rising limb than the

measured ones, as shown in Figure 5, while Figure 6 also shows a faster widening process in the simulation than in the experiments. However, the simulation results agree generally well with the measured data; in particular, the peak breach flow discharge and the final breach width are well predicted by the model.

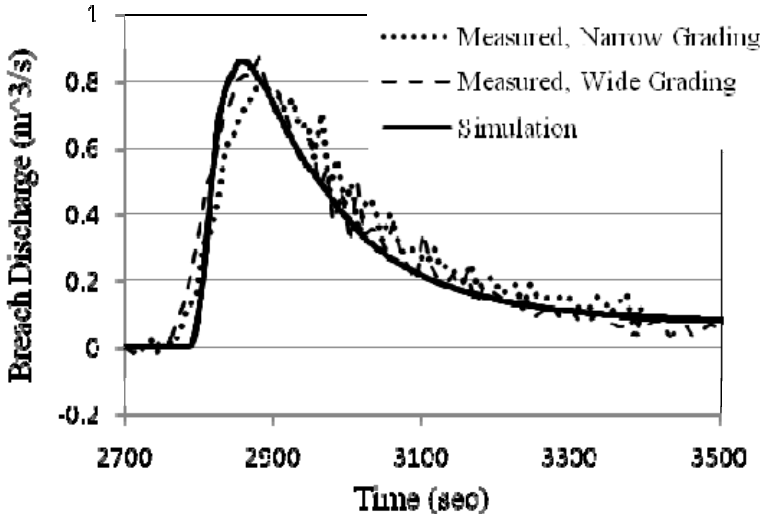

Figure 5. Measured and simulated breach flow discharges

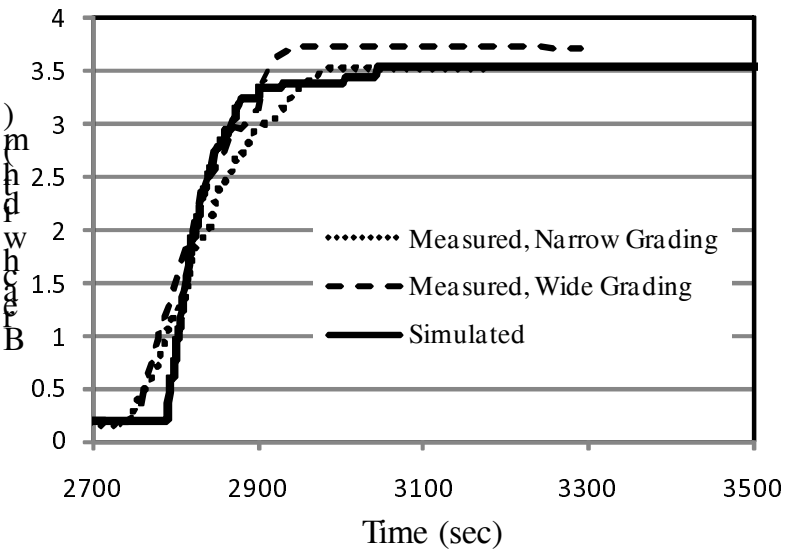

Figure 6. Measured and simulated breach widths

CONCLUSIONS

A depth-averaged 2-D finite-volume model has been established to simulate the earthen dam/levee breach processes due to overtopping flows. The effects of sediment concentration and bed change on the flow are considered in the continuity and

momentum equations. The sediment transport model simulates the non-equilibrium transport of total load. An explicit algorithm based on the finite volume method is adopted to solve flow, sediment transport and bed change equations. The model adopts the HLL approximate Riemann solver to handle the mixed-regime flows near the breach and the wetting-drying problem efficiently. A specially designed avalanching algorithm is adopted in this model, to consider different repose angles for the submerged materials and the dry materials above the water surface. To enhance the performance of the model, a varying time step is used that satisfies the CFL condition and ensures the bed change at each time step is less than ten percent of the local flow depth.

The developed model has been tested using the laboratory experiments conducted at HR Wallingford. The model predicts generally well the breach width, the flow pattern near the breach, and the breach flow hydrograph.

ACKNOWLEDGEMENT

This study is part of the research project sponsored by the USDA-ARS Specific Research Agreement No. 58-6408-7-236 (monitored by the USDA-ARS National Sedimentation Laboratory) and the University of Mississippi.

REFERENCES

Faeh, R. (2007). "Numerical modeling of breach erosion of river embankments." *J. Hydraulic Eng.*, ASCE, 133(9), 1000–1009.

Harten, A., Lax, P.D. and van Leer, B. (1983). "On upstream differencing and Godunov-type schemes for hyperbolic conservation laws." *SIAM Review*, 25(1), 35–61.

Mohamed, M. A. A., Samuels, P. G., Morris, M. W., and Ghataora, G. S. (2005), "Improving the accuracy of prediction of breach formation through embankment dams and flood embankments." HR Wallingford, UK. http://www.samui.co.uk/impact-project/publications/wp2_pub1.pdf.

Morris, M., Hassan, M., and Vaskinn, K. (2005). "Conclusions and recommendations from the IMPACT project WP2: Breach formation." HR Wallingford, UK. http://www.samui.co.uk/impact-project/cd4/Presentations/THUR/17-1_WP2_10Summary_v2_0.pdf.

Richardson, J. F. and Zaki, W. N. (1954). "Sedimentation and fluidisation, part I." *Trans., Inst. Chem. Engrs.*, 32(1), 35–53.

Singh, V. P. (1996). *Dam Breach Modeling Technology*, Kluwer Academic Publishers.

Toro, E. F. (2001). *Shock-Capturing Methods for Free-Surface Shallow Flows*, Wiley.

Wu, W. (2004). "Depth-averaged 2-D numerical modeling of unsteady flow and nonuniform sediment transport in open channels." *J. Hydraulic Eng.*, ASCE, 130(10), 1013–1024.

Wu, W. (2007). *Computational River Dynamics*, Taylor & Francis, UK.

Wu, W. and Wang, S. S. Y. (2008). "One-dimensional explicit finite-volume model for sediment transport with transient flows over movable beds." *J. Hydraulic Research*, IAHR, 46(1), 87–98.

Wu, W., Wang, S. S. Y. and Jia, Y. (2000). "Nonuniform sediment transport in alluvial rivers." *J. Hydraulic Res.*, IAHR, 38(6), 427–434.

A Lattice Boltzmann Model for Dam Break Flows

H. Liu, J. G. Zhou, R. Burrows and Y. Peng

Department of Engineering, University of Liverpool, Liverpool L69 3GQ, UK
Haifei.Liu@Liverpool.ac.uk

Abstract

A two-dimensional lattice Boltzmann model (LBM) for dam break flows is developed. Shallow water equations coupled with the large eddy simulation model is numerically simulated by the lattice Boltzmann method, so that the turbulence can be taken into account and modeled efficiently. The model is verified and applied to two cases: (a) partial dam break flow; (b) circular dam break flow. The objectives of this study are to validate the two-dimensional LBM in transient flow simulation and analyze the detailed transient processes in open channel flows.

Key words: dam break flow, lattice Boltzmann method, large eddy simulation, shallow water equations, LABSWE

1 Introduction

Catastrophic flash flooding occurs when a dam fails and the impounded water escapes through the breach into the downstream valley. The suddenness and disastrousness of the shock wave make the dam break flow attract many interests from both engineers and academicians. The dam break flow has two-dimensional characteristics and is usually turbulent. This phenomenon is mathematically described by the set of two-dimensional nonlinear shallow water equations, the solutions of which can be obtained only by numerical integration, except some simplified cases. There are many numerical schemes that can be used to solve the SWE, such as finite difference and finite volume methods. However, a good solution to the SWE for the transient flows depends on the accuracy, the efficiency and sometimes the shock-capturing ability. During recent decades, the lattice Boltzmann method has developed into an alternative method for simulating surface water flow (Chen and Doolen, 1998). It is derived firstly to avoid the drawbacks of lattice-gas cellular automata in late 1980s. In the early 1990s, the

Navier-Stokes equations were recovered by the LBM with the Bhatnagar- Gross-Krook (BGK) model (Chen et al., 1992; Qian et al., 1992; Sukop and Thorne, 2006). Later, Zhou (2001, 2002a) proposed improved theories on the lattice Boltzmann methods for nonlinear shallow water equations (LABSWE), which introduced the LBM into river and coastal engineering. Compared with traditional methods, the LABSWE is a simple and efficient model with easy treatment of boundary conditions (Zhou, 2007), and so is adopted in this study. In order to accelerate the computing speed with-out loss of the accuracy, the multi-block algorithm with acceleration technique proposed by Dupuis and Chopard (2003) is incorporated in the LABSWE.

The present study aims to develop an efficient two-dimensional numerical model using the lattice Boltzmann method for dam break flows. Providing the depth-averaged features, the nonlinear shallow water equations with the large eddy model embedded in are selected as the governing equations. The model is verified and applied to two cases: (a) partial dam break flow; (b) circular dam break flow.

2 Theoretical Backgrounds

2.1 Governing Equations

The shallow water equations describe the evolution of a hydrostatic, incompressible flow with comparatively large ratio of the horizontal scale to vertical scale. The general two-dimensional governing equations for shallow water flows can be derived from the Navier-Stokes equations. The nonlinear shallow water equations can be written in a tensor form as (Zhou, 2004):

$$\frac{\partial h}{\partial t}+\frac{\partial (hu_j)}{\partial x_j}=0 \tag{1}$$

$$\frac{\partial (hu_i)}{\partial t}+\frac{\partial (hu_iu_j)}{\partial x_j}=-\frac{g}{2}\frac{\partial h^2}{\partial x_i}+\nu_k\frac{\partial^2 (hu_i)}{\partial x_j\partial x_j}+F_i \tag{2}$$

where the Cartesian coordinate system and the Einstein summation convention over Latin indices are used; h is water depth; x_j and u_j are the distance and instantaneous velocity components in the j direction respectively, i.e. for $j = 1$, $x_j = x$ and $u_j = u$; for $j = 2$, $x_j = y$ and $u_j = v$. x and y are defined as longitudinal and lateral directions of the channel; v_k is the kinematic viscosity; $g = 9.81 m/s^2$ is gravitational acceleration; t is time. In addition, F_i is the force term and is defined as:

$$F_i=-\frac{\tau_{bi}}{\rho}-gh\frac{\partial z_b}{\partial x_i} \tag{3}$$

Where z_b is bed elevation above datum. The bed shear stress τ_{bi} in the i direction is given by the depth-averaged velocities,

$$\tau_{bi} = \rho C_b u_i \sqrt{u_j u_j} \tag{4}$$

In which C_b is the bed friction coeffcient.

In natural water, turbulence is a quite common phenomenon. Generally, introducing the Reynolds equations and turbulent stress as in the $k-\varepsilon$ model is the usual way to model the turbulence, giving the time-averaged properties. However, this type of method cannot provide the detailed structure of the turbulence. Large eddy simulation, using space-filtered governing equations with subgird-scale stress model for the unresolved scale stress, can efficiently simulate vorticity larger than a prescribed scale, but needs only moderate computational effort (Tutar and Hold, 2001), so is used in this paper.

If u_j is regarded as the velocity component after being space-filtered, it can be defined by

$$u_j(x, y, z, t) = \int_{\Delta V} u_j^b G(x, y, z, x', y', z') dV \tag{5}$$

With a spatial filter function G and u_j^b is the velocity component before being space-filtered; $\Delta V = \Delta x' \Delta y' \Delta z'$; x', y' and z' are the coordinates of the space chosen for velocity filter; v_t is the total viscosity ($=v_k + v_e$), replacing v_k in Eq. (2); v_e is the eddy viscosity, defined by

$$v_e = (C_s l_s)^2 \sqrt{S_{ij} S_{ij}} \tag{6}$$

Where C_s is the Smagorinsky constant, l_s is the characteristic length scale ($l_s = \Delta x$ in the present study) and S_{ij} is the magnitude of the large scale strain-rate tensor,

$$S_{ij} = \frac{1}{2h}\left[\frac{\partial(hu_i)}{\partial x_j} + \frac{\partial(hu_j)}{\partial x_i}\right] \tag{7}$$

The depth-averaged subgrid-scale stress τ_{ij} with eddy viscosity is calculated by

$$\tau_{ij} = 2hS_{ij} \tag{8}$$

2.2 Lattice Boltzmann Model

The lattice Boltzmann model for nonlinear shallow water equations with turbulence (LABSWE^{TM}) has been presented by Zhou (2002b). After incorporating the subgrid-scale model, for motion in the i direction within a collision step, the lattice Boltzmann equation with 9-speed square lattice and force term is

$$f_a(x+e_a\Delta t,t+\Delta t)=f_a(x,t)-\frac{1}{\tau_t}\left[f_a(x,t)-f_a^{eq}(x,t)\right]+\frac{\Delta t}{N_a e^2}e_{ai}F_i \tag{9}$$

Where f_a is the particle distribution function; e=Δx /Δt; Δx is the lattice size; F_i is the force term calculated by Eq. (3); Δt is the time step; N_a is a constant, decided by the lattice pattern.

$$N_a=\frac{1}{e^2}\sum_a e_{ax}e_{ax}=\frac{1}{e^2}\sum_a e_{ay}e_{ay} \tag{10}$$

$\tau_t=\tau+\tau_e$ is the total relaxation time, wherein τ is the single relaxation time and τ_e is the eddy relaxation time with respect to the eddy viscosity which can be calculated (Hou et al., 1996)

$$\tau_e=\frac{-\tau+\sqrt{\tau^2+18C_s^2/(e^2h)\sqrt{\prod ij\prod ij}}}{2} \tag{11}$$

Where

$$\prod ij=\sum_a e_{ai}e_{aj}(f_a-f_a^{eq}) \tag{12}$$

e_{ai} is the particle velocity vector in the i spatial coordinate. For the two-dimensional 9-speed square lattice the velocity vector of particles is defined by

$$e_a=\begin{cases}(0,0), & a=0\\ e\left[\cos\dfrac{(a-1)\pi}{4},\sin\dfrac{(a-1)\pi}{4}\right], & a=1,3,5,7\\ \sqrt{2}e\left[\cos\dfrac{(a-1)\pi}{4},\sin\dfrac{(a-1)\pi}{4}\right], & a=2,4,6,8\end{cases} \tag{13}$$

One can obtain N_a = 6, if substitute Eq. (13) into Eq. (10). The local equilibrium distribution function is expressed as

$$f_a^{eq}=\begin{cases}h-\dfrac{5gh^2}{6e^2}-\dfrac{2h}{3e^2}u_iu_i, & a=0\\ \dfrac{gh^2}{6e^2}+\dfrac{h}{3e^2}e_{ai}u_i+\dfrac{h}{2e^4}e_{ai}e_{aj}u_iu_j-\dfrac{h}{6e^2}u_iu_i, & a=1,3,5,7\\ \dfrac{gh^2}{24e^2}+\dfrac{h}{12e^2}e_{ai}u_i+\dfrac{h}{8e^4}e_{ai}e_{aj}u_iu_j-\dfrac{h}{24e^2}u_iu_i, & a=2,4,6,8\end{cases} \tag{14}$$

From the distribution function, the water depth h and flow velocity u_i can be calculated through:

$$h = \sum_a f_a , \qquad u_i = \frac{1}{h} \sum_a e_{ai} f_a \tag{15}$$

2.3 Boundary Conditions

The discrete particle distribution must satisfy imposed constraints for water depth and momentum along the boundaries of the lattice. Several schemes that can be used for solid boundaries, such as bounce-back scheme of no-slip boundary conditions and elastic-collision scheme of slip boundary conditions; periodic and zero-gradient conditions for inflow and outflow boundaries, etc.

3 Numerical Tests

3.1 Partial Dam Break Flow

A benchmark test of partial dam break, initially used by Fennema and Chaudhry (1990), is investigated using the multi-block LABSWE. A dam is located in the central line of a 200m × 200m square reservoir with still upstream and downstream water depths being 10m and 5m, respectively. The dam fails at time t = 0s with a 75m break, as depicted in Fig. 1. The generated bore wave propagates downstream and in the mean time, a depression wave moves upstream. A uniform coarse grid of 100 × 100 is applied to the computational domain, and a fine block of Δx_f = $0.5\Delta x_c$
(I.e. m = 2) covers the adjacent area of the dam (x = 25 ~175m shown in Fig.1). The time step is 0.01s and the single relaxation time τ is 0.52. The Smagorinsky constant C_s is 0.3.

The contours of the water depth based on simulation results of the partial dam break flow at t = 2s, t = 4s and t = 7.2s have been plotted at the left column in Fig. 2. They agree well with previous results from the adaptive Q-tree Godunov scheme by Rogers et al. (2001). Additionally, the corresponding plots obtained from the simulation with only coarse grid have been presented at the right column in Fig. 2. As shown in the figure, the coarse gird models provide rough and inaccurate results.
Compared with the simulation results of the multi-block model and the previous researches (Rogers et al., 2001; Anastasiou and Chan, 1997), the dam break wave obtained by coarse grid model influences farther distances, indicating that the model may suffer from numerical dispersion when only coarse grid is used.

3.2 Circular Dam Break Flow

Another popular test examines the wave propagation of a circular dam break (Mingham and Causon, 1998). A uniform 200 × 200 grid is used to cover a 2000m × 2000m square frictionless domain, where the bed slope is zero. The time step is 0.1s and the single relaxation time τ is 0.506. The Smagorinsky constant C_s is 0. The initial condition in Eq. (16) is discontinuous and flow velocity is zero, when the circular dam is suddenly removed.

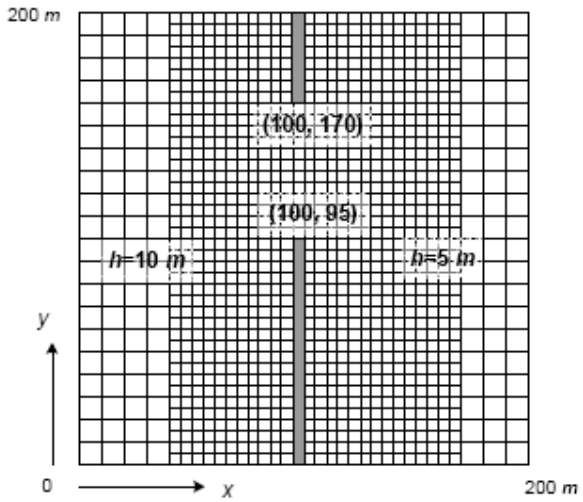

Fig. 1. Indicative Grid Layout and Channel Size for Two-dimensional Dam Break

The water depth evolutionary process along a radial up to 50 seconds has been presented in Fig. 3. Figure 4 shows the three-dimensional plots of the water depth at t = 20s and t = 50s. A uniform finer grid with lattice ratio m = 2 is also used to test the grid convergence, based on which the fractional error is only 0.82%. It illustrates that the model with the prior grid has produced the solution of acceptable accuracy. These results can be compared with those from other high resolution schemes (Murillo et al., 2006), giving the excellent agreements.

$$h(r) = \begin{cases} 10, & r < 800m \\ 5, & r \geq 800m \end{cases} \tag{16}$$

4 Conclusions

In this study, a two-dimensional lattice Boltzmann model for dam break flows has been developed and validated, in which the large eddy simulation model is coupled with nonlinear shallow water equations (LABSWE^{TM}) for turbulence modeling.

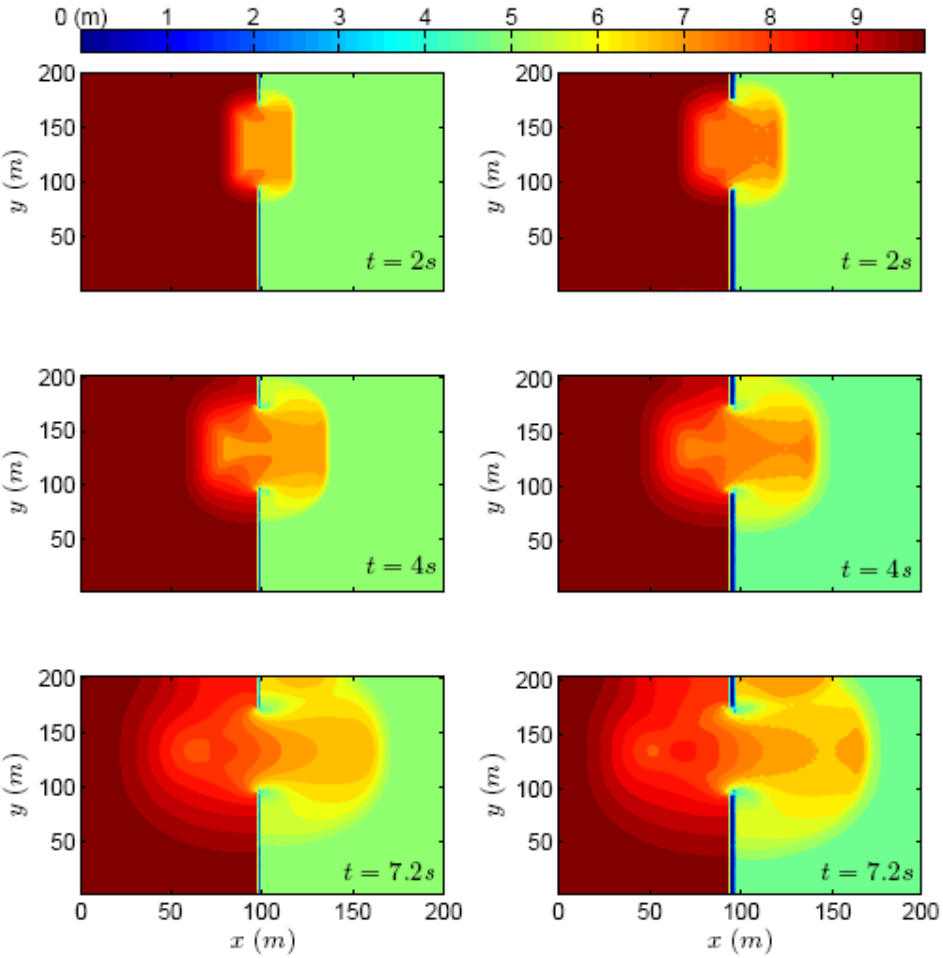

Fig.2.Contours of Water Depth at Different Time Using Multi-block (Left Column) and Coarse Grid (Right Column)

Numerical simulations have been verified by two tests and the detailed flow processes in unsteady state have been presented. Overall, it is found that the two-dimensional multi-block model is efficient and capable of producing depth-averaged hydrodynamic characteristics of dam break flows.

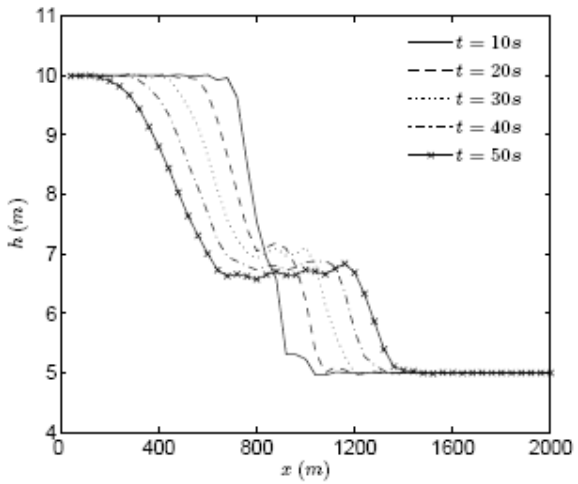

Fig. 3. Water Depth Evolution after Dam Break along a Radial

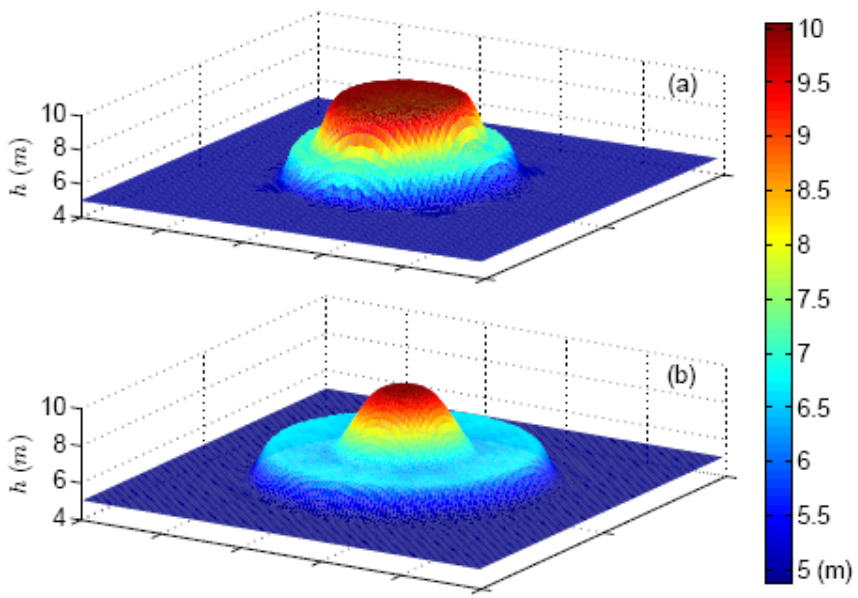

Fig. 4. Three-dimensional Plots of Water Depth for $t = 20s$ (a) and $t = 50s$ (b)

References

Anastasiou, K., Chan, C. T., 1997. Solution of the 2D shallow water equations using the finite volume method on unstructured triangular meshes. International Journal for Numerical Methods in Fluids 24, 1225-1245.

Chen, H., Chen, S., Matthaeus, W. H., 1992. Recovery of the navier-stokes equations using a lattice-gas boltzmann method. Phys. Rev. A. 45, R5539-5542

Chen, S., Doolen, G. D., 1998. Lattice boltzmann method for fluid flows. Annu.Rev. Fluids Mech. 30, 329-364.

Dupuis, A., Chopard, B., 2003. Theory and applications of an alternative lattice Boltzmann grid refinement algorithm. Physical Review E 67 (066707).

Fennema,R.J.,Chaudhry, M. H., 1990. Explicit methods for two-dimensional unsteady free-surface flow. Journal of Hydraulic Engineering, ASCE 116, 1013-1034.

Hou, S., Sterling, J., Chen, S., Doolen, G. D., 1996. A lattice Boltzmann subgrid model for high Reynolds number flows. Fidlds Institute Communications 6, 151-166.

Mingham, C. G., Causon, D. M., 1998. High-resolution finite-volume method for shallow water flows. Journal of Hydraulic Engineering, ASCE 124(6), 605-614.

Murillo, J., Garcia-Navarro, P., Burguete, J., Brufau, P., 2006. A conservative 2D model of inundation flow with solute transport over dry bed. International Journal for Numerical Methods in Fluids 52, 1059-1092.

Qian, Y. H., D'Humieres, D., Lallemand, P., 1992. Lattice BGK models for navier-stokes equation. Europhys. Lett 17, 479-484.

Rogers, B., Fujihara, M., Borthwick, A. G. L., 2001. Adaptive Q-tree Godunov type scheme for shallow water equations. International Journal for Numerical Methods in Fluids 35, 247-280.

Sukop, M. C., Thorne, D. T., 2006. Lattice Boltzmann Modeling-An Introduction for Geoscientists and Engineers. Spinger. NewYork.

Tutar, M., Hold, A. E., 2001. Computational modelling of flow around a circular cylinder in sub-critical flow regime with various turbulence models. Int. J. Num. Meth. Fluids, 35, 763-784.

Zhou, J. G., 2001. An elastic-collision scheme for lattice Boltzmann methods. International Journal of Modern Physics C 12:387-401.

Zhou, J. G., 2002a. A lattice Boltzmann model for the shallow water equations. Comput. Methods Appl. Mech. Engrg. 191, 3527-3539.

Zhou, J. G., 2002b. A lattice Boltzmann model for the shallow water equations with turbulence modeling. International Journal of Modern PhysicsC, Vol.13, No.8, 1135-1150.

Zhou, J. G., 2004. Lattice Boltzmann Methods for Shallow Water Flows. Springer, Berlin, Germany.

Zhou, J. G., 2007. Comparison study of lattice Boltzmann method and Godunov method for shallow water flows. Proceedings of 32nd Congress of IAHR, Venice, Italy.

Comparison of Dam Breach Parameter Estimators

D. Michael Gee[1]

[1] Senior Hydraulic Engineer, Corps of Engineers Hydrologic Engineering Center, 609 2nd St., Davis, CA 95616; email: michael.gee@usace.army.mil.

ABSTRACT

Analytical techniques for the estimation of dam breach parameters were evaluated and compared. The development of potential flooding from a dam failure requires several elements; the hydrologic scenario, the possible dam failure modes, breach parameters that are associated with the failure modes, and the routing and mapping of the consequent discharge hydrograph. This paper presents recent research into the use and application of several dam breach parameter estimators to describe the physical characteristics of a dam breach, use of those parameters within the unsteady flow routing model HEC-RAS, and the computation and display of the resulting downstream impacts. The breach parameter estimators that were used include both empirical and embankment erosion process models.

INTRODUCTION

Many agencies are reviewing and updating dam safety and risk studies. The Corps of Engineers is performing a portfolio risk analysis of their projects. Included in that study is the updating of probable maximum flood inflow hydrographs and routing of potential dam break floods to ascertain downstream consequences. The estimation of possible breach dimensions and development times is necessary in any assessment of dam safety. The breach parameters will directly and substantially affect the estimate of the flows, inundated areas and warning times at downstream locations. The breach location, size, and formation time are often the most uncertain pieces of information in a dam failure analysis. Application of several commonly used analysis techniques to several projects is described in this paper.

The geometric description of a dam breach must be estimated to simulate the resultant flood wave and downstream consequences. Some readily available models that can be used for performing dam breach outflow hydrograph computation and downstream routing are HEC-RAS (HEC, 2006a), HEC-HMS (HEC, 2006b), NWS-DAMBRK (Fread, 1988b), NWS-FLDWAV (Fread, 2000), and a few others. These models require that the potential breach characteristics be estimated outside of the model. Several "process" models are also available, or being developed, that attempt to simulate the progression of a dam breach using sediment transport equations to estimate erosion rates and soil mechanics relations to predict mass slope failures. One process model that is discussed herein is the NWS-BREACH model (Fread, 1988a).

Breach dimensions and time of development must be estimated for various failure scenarios. This requirement includes different failure modes as well as different hydrologic events. The breach parameters associated with a hydrologic event of the scale of the probable maximum flood may differ from those for a sunny day failure triggered, perhaps, by a seismic event. Therefore, a set of breach parameters needs to be developed for each combination of antecedent pool elevation (hydrologic event) and failure scenario.

The breach characteristics can be estimated in several ways; including: comparative analysis (comparing the study project to historical failures of dams of similar size, materials, and water volume); regression equations (equations developed from historical dam failures in order to predict peak outflow or breach size and development time); and physically based computer models (computer programs that attempt to model the physical breaching process by using sediment transport/erosion equations, soil mechanics, and principles of hydraulics). All of these methods are viable techniques for estimating breach characteristics.

Reasonable values for the breach size and development time are needed to make a reliable estimate of the outflow hydrographs and resulting downstream inundation, flood travel times, water velocities, etc. These parameters describing the breach have large uncertainty. The HEC-RAS and HEC-HMS software require the following information to describe a dam breach:

Failure Location

The breach failure location depends on many factors, such as; type and shape of dam, failure mode, and structural elements of the dam. All factors concerning the dam, particularly any historical records of seepage and foundation problems, should be considered in order to place the breach in the most probable location for each failure mode. If a most probable location cannot be identified, then the centerline of the breach should be set to the centerline of the downstream main channel

Failure Mode

The hydraulic algorithms in HEC-RAS and HEC-HMS are designed to simulate the hydraulics of overtopping and piping failures. The failure mode is the mechanism for starting and growing the breach. Overtopping failures start at the top of the dam and grow to maximum extents, while a piping failure can start at any elevation/location and grow to the maximum extents. The ultimate breach size and breach development time are much more critical in the estimation of the outflow hydrograph than the actual failure mode.

Breach Development Time

Both HEC-RAS and HEC-HMS require as input data a breach development time. That time is described as follows:

Overtopping Failure: The time, from when the breach has eroded back to the upstream side of the top of the dam, to when the breach is fully formed (ie., significant erosion has stopped, not the time until the reservoir pool is emptied).

Piping Failure: The time from when a significant amount of flow and material are moving through the piping failure to when the breach is fully formed

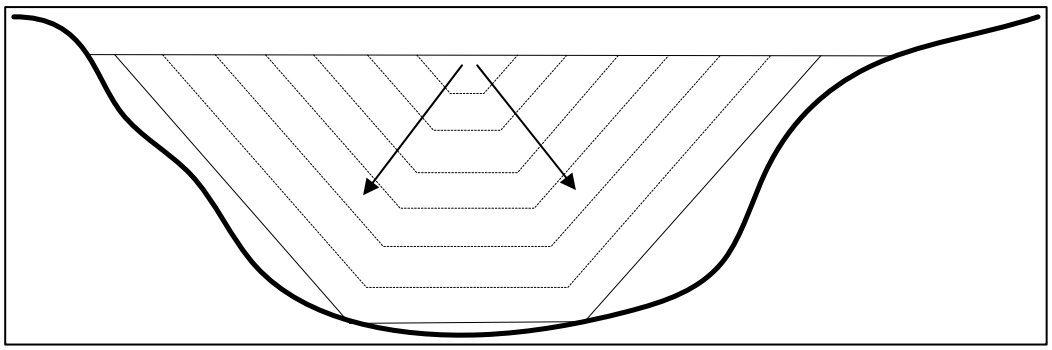

Figure 1. Generalized Trapezoidal Breach Progression

(significant erosion has stopped, not the time until the reservoir pool is emptied).This paper focuses on the description and hydraulics of overtopping breaches. The ultimate size of the breach must be described. This is the size expected when breach has stopped growing. The breach may stop growing because the entire dam has eroded or because the reservoir has drained and there is no more water available to erode the dam. The ultimate bottom elevation is the point at which erosion stops; usually either bedrock or the bottom of the reservoir pool. The breach size is described by a bottom width and side slopes. The conceptual development of a generalized trapezoidal overtopping breach is shown on Fig. 1.

It is necessary to define the circumstances of breach initiation (trigger mechanism) and how long it takes for the breach to progress to the ultimate size. The development time is the elapsed time from significant flow through the breach to the time at which ultimate size is reached. For overtopping failures the breach parameters should describe the initiation and progress of the hydraulic control (weir) that governs the release of water from storage.

Several options are available for identifying the breach initiation time. One option is to specify the duration that the pool elevation exceeds some threshold. This information may be the result of a geotechnical investigation. A second option is to specify a pool elevation; the breach begins to form as soon as that elevation is reached. The final option is a specific time during the simulation regardless of the pool elevation. This is useful for "sunny day" type failures that are not associated with a hydrologic event.

The breach shape develops in time from initiation to its ultimate configuration. The simplest development rate is linear; that is, the breach dimensions grow at a uniform rate. Options are available to simulate a breach that initially grows very quickly then slows down towards the end of the development time. Information for defining these growth rate parameters could be obtained from geotechnical information or from use of a process model such as NWS-BREACH (Fread, 1988a).

REVIEW OF GUIDANCE FOR BREACH PARAMETERS

Federal Agency Guidelines

Many federal agencies have published guidelines in the form of possible ranges of values for breach width, side slopes, and development time. Shown in Table 1 is a summary of guidance to date (USACE, 1980: USACE, 2007).

Table 1. Ranges of Possible Values for Breach Characteristics

Dam Type	Average Breach Width B_{ave}	Horizontal Component of Breach Side Slope (H) H:1V	Failure Time t_f (hrs)	Agency
Earthen/ Rockfill	(0.5 to 3.0) x HD (0.5 to 5.0) x HD (1.0 to 5.0) x HD (2.0 to 5.0) x HD	0 to 1.0 0 to 1.0 0 to 1.0 0 to 1.0 (slightly larger)	0.5 to 4.0 0.1 to 4.0* 0.1 to 1.0 0.1 to 1.0	USACE (1980) USACE (2007) FERC (1988) NWS (Fread, 2006)
Concrete Gravity	Multiple Monoliths Usually ≤ 0.5 L Usually ≤ 0.5 L	Vertical Vertical Vertical	0.1 to 0.5 0.1 to 0.3 0.1 to 0.2	USACE (2007) FERC NWS
Concrete Arch	Entire Dam (0.8 x L) to L Entire Dam (0.8 x L) to L	Valley wall slope 0 to valley walls 0 to valley walls 0 to valley walls	≤ 0.1 ≤0.1 ≤ 0.1 ≤ 0.1	USACE (1980) USACE (2007) FERC NWS
Slag/ Refuse	(0.8 x L) to L (0.8 x L) to L	1.0 to 2.0	0.1 to 0.3 ≤ 0.1	FERC NWS

Where: HD = Height of the dam.
L = Length of the dam crest.

* Note: Dams that have very large volumes of water, and have long dam crest lengths, will continue to erode for long durations (i.e. as long as a significant amount of water is flowing through the breach), and may therefore have wider breach widths and longer times than what is shown.

Determining the size and growth rate for breaches is not a precise exercise. Therefore, simulation models such as HEC-RAS allow for the user to quickly evaluate the impacts of a range of parameters on the results. The Bureau of Reclamation (Wahl, 1988) offers an excellent literature review of this subject.

Regression Equations

The following regression equations have been used for several dam safety studies found in the literature and are being considered for inclusion in guidance for the Corps of Engineers Portfolio Risk Assessment study:

- Froehlich (1987,1995a,1995b)
- MacDonald and Langridge-Monopolis (MacDonald, 1984)
- Von Thun and Gillette (1990)

Froehlich utilized 63 earthen, zoned earthen, earthen with a core wall (i.e. clay), and rockfill data sets to develop a set of equations to estimate average breach width, side slopes, and failure time. In the application of these equations reported herein, the height of the breach is calculated by assuming that the breach goes from the top of the dam to the natural ground elevation at the centerline of the breach location.

MacDonald and Langridge-Monopolis (MacDonald, 1984):

MacDonald and Langridge-Monopolis utilized 42 data sets (predominantly earthfill, earthfill with a clay core, and rockfill) to develop a relationship for the "Breach Formation Factor." The Breach Formation Factor is a product of the volume of water released from the dam (V_{out}) and the height of water above the dam. They then related the breach formation factor to the volume of material eroded from the dam's embankment. The V_{out} parameter is not exactly known before performing the

breach analysis as it is the volume of water that passes through the breach (not including flow from gates, spillways, and overtopping of the dam away from the breach area). A good first estimate, however, is the volume of water in the reservoir at the time that the breach initiates. Once a set of parameters are estimated and a breach analysis is performed, a better estimate of the actual volume of water that passes through the breach can be made. Then the parameters can be recalculated using that volume. The recalculation of the volume makes the method iterative in these situations. The resulting ultimate breach dimensions are a function of the volume eroded and the embankment geometry. The MacDonald and Langridge-Monopolis paper states that the breach should be trapezoidal with side slopes of 0.5H:1V. The breach size is computed by assuming that the breach erodes vertically to the bottom of the dam and then erodes horizontally until the maximum amount of material has been eroded or the abutments of the dam have been reached. The base width of the breach can be computed from the dam geometry with the an equation given in (Washington, 1992). Note that the MacDonald and Langridge-Monopolis paper states that the equation for the breach formation time is an envelope of the data from earthfill dams. An envelope equation implies that the equation will tend to give high estimates of the actual breach time (for homogenous earthfill dams).

Von Thun and Gillette (Von Thun, 1990):

Von Thun and Gillette used 57 dams from both the Froehlich (1987) and MacDonald and Langridge-Monopolis (1984) papers to develop their methodology. The method suggests the use of breach side slopes of 1.0H:1.0V; except for dams with cohesive soils, where side slopes should be on the order of 0.5H:1V to 0.33H:1V. Von Thun and Gillette developed two different sets of equations for the breach development time depending upon the embankment material.

NWS-BREACH (Fread, 1988a):

The NWS-BREACH model is a "process" model in that it uses sediment mechanics and transport relationships to simulate the breach development. The model uses sediment transport equations to compute the rate of erosion and size of a breach given information regarding the soil characteristics of the dam material, the inflow hydrograph, etc. Enlargement of the breach over time is computed by sediment transport equations, sudden collapse due to excess hydrostatic pressure and width expansion by slope stability. Sediment transport equations are available for either cohesive or noncohesive materials.

Other process models such as SIMBA (Hanson, et al., 2005; Temple, et al., 2005) and HR-BREACH (Mohamed, 2002) are currently under development. At this time these models are undergoing testing with various field data and are not yet available for general use.

DAM BREACH FLOW SIMULATION USING HEC-RAS

The implementation of these breach parameters in the HEC-RAS modeling system is depicted on Fig. 2.

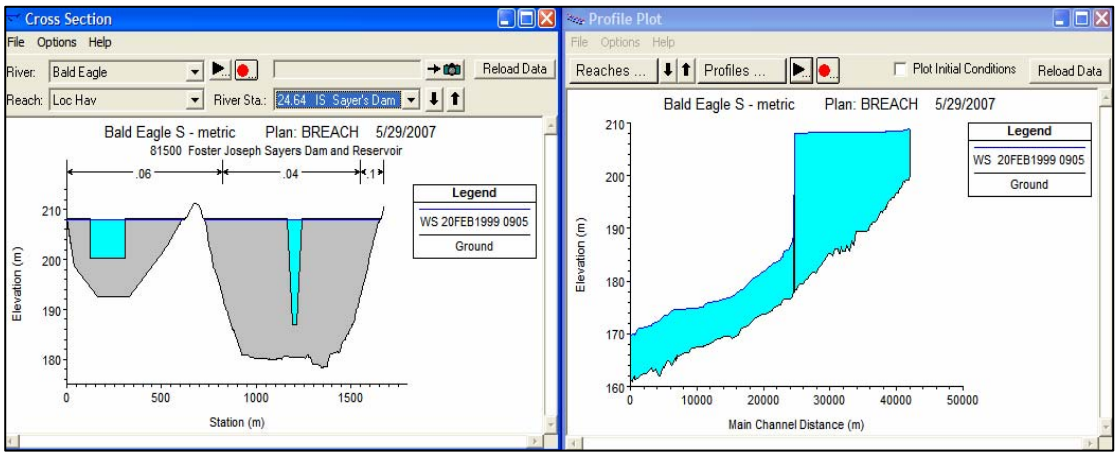

Figure 2. HEC-RAS Dam Breach Model

The graphical depiction of the breach size, location and progression associated with the computed upstream and downstream water surface profiles provides useful information for the analyst as well as the clients of the study. HEC-RAS uses dam breach parameters developed externally (using the techniques outlined above or any others deemed appropriate) to compute the temporal progression of a breach in an inline structure (dam). The flows through that structure are computed considering breach flow, overtopping flow, spillway discharges, gated flow, and submergence effects due to downstream backwater. Those several flow components are used as an internal boundary condition for unsteady flow modeling of the pool and the downstream reach. The pool may be analyzed using either simple level pool routing or as an unsteady flow reach using cross sections. Differences in breach outflow hydrographs due to different breach parameters will decrease as the floodwave is routed through the downstream reach.

SOME COMPARISONS

At this time, the breach parameter estimation methods described above have been applied to five situations. Two are hypothetical failures at actual projects. One of these has measured cross sections in the pool and the downstream reach so that the effects of in-pool and downstream routing can be examined. Three actual historic failures are also reproduced; one of which was a planned experiment. All of the cases discussed here are overtopping failures. In all cases the breach development was assumed to be linear in time. The hypothetical cases were assumed to start breaching when the overtopping was about 0.3 m; the reported beginning time of failure was used for the historic cases. Only the applications to the two historic failures are presented here due to space limitations; complete results can be found in (Gee and Brunner, 2007).

APPLICATIONS TO SOME HISTORIC OVERTOPPING FAILURES

Oros Dam

Oros dam (Brazil) was under construction when it failed by overtopping in

March of 1960 (CEATI). The dam height was about 35.5m. It was composed of a clay core with sand and rock shoulders. The empirical methods of MacDonald, Froehlich and VonThun were applied to this structure along with the BREACH process model. The volume of water released was estimated to be $660*10^6$ m^3 (1). Table 2 summarizes the resulting breach parameters computed by these methods.

Table 2. Breach Parameters for Oros Dam

Oros	Parameter			
Method	W_b (m)	Side Slopes (h:v)	t_f (hrs)	Vol eroded (m^3)
MacDonald	900	0.5	3.7	$2.38*10^6$
Froehlich	305	1.4	4.8	
VonThun	132	0.33	1	
BREACH	284	0.6	7.3	
Reported	200	0	6.5 to 12	$0.87*10^6$

The breach outflow hydrographs computed using these parameters are shown on Fig. 3 with the estimated outflow hydrograph. The outflow hydrograph was deduced from the record of water level during the event (CEATI).

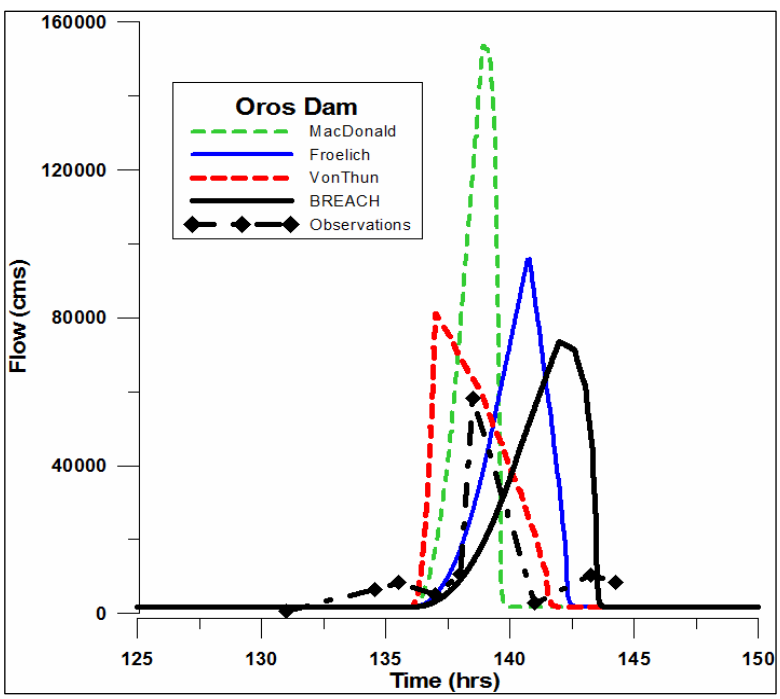

Figure 3. Breach Hydrographs for Oros Dam

Banqiao Dam (China)

Banqiao Dam failed by overtopping from a large storm in 1975 (CEATI). The dam was constructed of a clay core containing shale. The upstream and downstream fill was homogeneous earth. It can be assumed that, due to construction methods (primarily non-mechanized), that the core was poorly compacted. The dam

was about 24.5 meters high with a crest elevation at 116.34m. Crest width was 6m and length 2020m. The upstream slope was 3H:1V and downstream 2.5H:1V. The design capacity for the spillway and outlet works was 1742 m^3/sec; the estimated peak inflow was about 13,000 m^3/sec when breaching occurred. The estimated breach parameters are shown in Table 3.

The breach outflow hydrographs computed using these parameters are shown on Fig. 4. Field observations for this event consist of the pool elevation time history. These observations can be compared with the pool drawdown computed using HEC-RAS with the estimated breach parameters as shown on Fig. 5.

Table 3. Breach Parameters for Banqiao Dam

Banqiao	Parameter			
Method	W_b (m)	Side Slopes (h:v)	t_f (hrs)	Vol eroded (m^3)
MacDonald	1037	0.5	3.4	$1.85*10^6$
Froehlich	281	1.4	7	
VonThun	108	0.33	0.7	
BREACH	641	0.6	3.6	
Reported	210	0	1.5	$0.6*10^6$

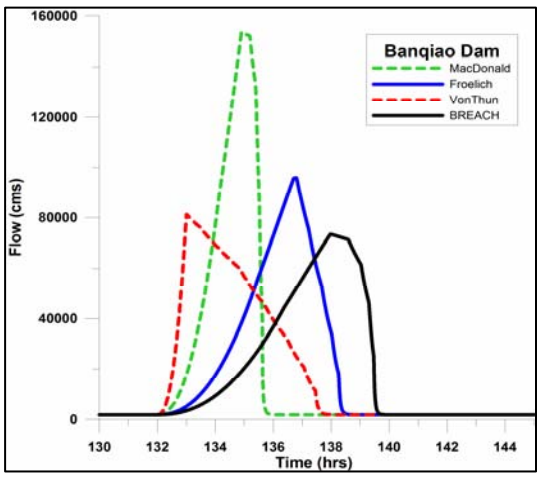

Figure 4. Breach Hydrographs for Banqiao Dam

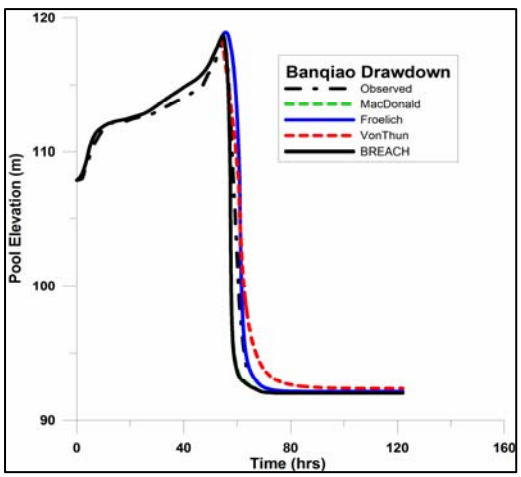

Figure 5. Pool Drawdown for Banqiao Dam

CONCLUSIONS AND OBSERVATIONS

Several techniques are available for estimating the breach parameters resulting from dam overtopping and subsequent failure. These techniques are predominately empirical, based on fitting relationships between key parameters such as water depth behind the dam and historic observations. One process model, NWS-BREACH, was also applied for comparison.

Estimation of dam breach parameters is a necessary first step in performing the analysis of the downstream consequences of possible dam failures. These parameters are used to compute breach outflow hydrographs using estimated inflow hydrographs, reservoir elevation-capacity data, and spillway and gate hydraulic capacities. Techniques are being developed to interpret and utilize the breach parameters estimated by application of these methods in an unsteady flow model; HEC-RAS. The methods predict a wide range of breach parameters and therefore, a large difference in outflow hydrographs. The MacDonald method routinely produced the largest peak outflows. The only comparison to an estimated historic outflow hydrograph (Oros) showed that all of the methods produced flows larger than those observed. For the case in which the pool drawdown data were available, all of the methods, when used in the HEC-RAS simulation model, produced comparable results.

The methods tested suggest use of flatter breach side slopes than are typically observed. The bases for development of the empirical techniques must be kept in mind. The breach configuration used in developing the regression equations was typically the ultimate shape that was observed at the after the event. What is needed for computing outflow hydrographs is the progression of the hydraulic control; be it a weir flow in the case of overtopping or an orifice flow in the case of piping. The hydraulic computations done in HEC-RAS assume that the hydraulic control progresses based on a failure time estimated from the method applied. Downstream submergence of the control is possible and is included in the outflow computation.

Process models are currently being developed and tested (Wahl, et al., 2008). The expected advantage of this type of model will be the ability to relate breach parameters to the materials and construction of the structure of interest. Tracking of the progression of the hydraulic control during breaching should be improved as well.

REFERENCES

CEATI Dam Safety Interest Group R&D Project "Erosion of Embankment Dams," Dam Breaching Database, https:\\database.dam-breaching.org

FERC (1988), USA Federal Regulatory Commission – Notice of Revised Emergency Action Plan Guidelines, February 22, 1988.

Fread, D. L. (1988a), BREACH: An Erosion Model for Earthen Dam Failures, National Weather Service, Office of Hydrology, Silver Spring, MD (revised 1991)

Fread, D.L. (1988b), "The NWS DAMBRK Model: Quick Users Guide," Hydrologic Research Laboratory, Office of Hydrology, National Weather Service, NOAA, June 20, 1988 (Revision 4, August 1991)

Fread, D.L. (2000), "NWS FLDWAV Model: Theoretical Description," Hydrologic Research Laboratory, Office of Hydrology, National Weather Service, NOAA, March 6 2000.

Fread, D.L. (2006), ASDSO Advanced Technical Seminar, "Dam Failure Analysis"

Froehlich, D. C. (1987), "Embankment Dam Breach Parameters," Hydraulic Engineering, Proc. 1987 ASCE National Conference on Hydraulic Engineering, New York, 570-575.

Froehlich, D. C. (1995a), "Embankment Dam Breach Parameters Revisited," Water Resources Engineering, Proc. 1995 ASCE Conf. on Water Resources Engineering, New York, 887-891.

Froehlich, D. C. (1995b), "Peak Outflow from Breached Embankment Dam," J. Water Resour. Plan. Management Div. , ASCE 121(1), 90-97.

Gee, D. Michael and Brunner, Gary W., (2007), "Comparison of Breach Predictors," Association of State Dam Safety Officials (ASDSO), Dam Safety 2007, Austin, TX, 9-13 September 2007.

Hanson, G. J., Temple, D. M., Morris, M., Hassan, M., Cook, K. (2005), Simplified breach analysis model for homogeneous embankments: Part II, Parameter inputs and variable scale model comparisons, Proceedings of 2005 the U.S. Society on Dams Annual Meeting and Conference, Salt Lake City, Utah. p. 163-174, 2005.

Hydrologic Engineering Center (HEC, 2006a), *HEC-RAS River Analysis System*, User's Manual, U.S. Army Corps of Engineers, Davis, CA. http://www.hec.usace.army.mil/software/hec-ras/

Hydrologic Engineering Center (HEC, 2006b), *HEC-HMS Hydrologic Modeling System*, User's Manual, U.S. Army Corps of Engineers, Davis, CA. http://www.hec.usace.army.mil/software/hec-hms/

MacDonald, T. C., and Langridge-Monopolis, J. (1984), "Breaching Characteristics of Dam Failures," ASCE J. Hydraulic Engineering, 110(5), 567-586,

Mohamed, M. (2002), "Embankment Breach Formation and Modelling Methods". Ph.D. Thesis. The Open University.

Temple, D. M., Hanson, G. J., Neilsen, M. L., Cook, K. R. (2005), Simplified breach analysis model for homogeneous embankments: Part I, Background and model components, Proceedings of the 2005 U.S. Society on Dams Annual Meeting and Conference, Salt Lake City, Utah. p. 151-161, 2005.

U.S. Army Corps of Engineers (USACE, 1980), Hydrologic Engineering Center, "Flood Emergency Plans – Guidelines for Corps Dams," RD-13, June 1980.

U.S. Army Corps of Engineers (USACE, 2007), Risk Assessment for Dam Safety, Dam Failure Analysis Toolbox, September 2007.

Von Thun, J. L., and Gillette, D. R. (1990), "Guidance on Breach Parameters," Internal Memorandum, U.S. Dept. of the Interior, Bureau of Reclamation, Denver, CO.

Wahl, Tony L. (1988), "Prediction of Embankment Dam Breach Parameters – A Literature Review and Needs Assessment," DSO-98-004, Dam Safety Research Report, U.S. Department of the Interior, Bureau of Reclamation, Dam Safety Office, July 1998. http://www.usbr.gov/pmts/hydraulics_lab/twahl/breach/breach_links.html

Wahl, Tony L., et al. (2008), "Development of Next-Generation Embankment Dam Breach Models," United States Society on Dams, 28th Annual USSD Conference, Portland, OR, April 28-May 2, 2008, pp. 767-779.

Washington State Dept. of Ecology (1992), Dam Safety Guidelines, Tech. Note 1 Dam Break Inundation Analysis and Downstream Hazard Classification, Water Resources Program, Dam Safety Office, P.O. Box 47600, Olympia, WA 98504-7600, July 1992, http://www.ecy.wa.gov/programs/wr/dams/Images/pdfs/technote_1.pdf

Representation of Linear Terrain Features in a 2D Flood Model with Regular Cartesian Mesh

Mustafa Altinakar[1], Marcus McGrath[2], Yavuz Ozeren[3], and Edie Miglio[4]

[1]NCCHE, The University of Mississippi. Carrier Hall, Room 102, P.O. Box 1848, University, MS, 38677-1848; PH (662) 915-3783; FAX (662) 915-7796; email: altinakar@ncche.olemiss.edu
[2]NCCHE, The University of Mississippi. Carrier Hall, Room 102, P.O. Box 1848, University, MS, 38677-1848; PH (662) 915-3960; FAX (662) 915-7796; email: mzmcgrat@ncche.olemiss.edu
[3]NCCHE, The University of Mississippi. Carrier Hall, Room 102, P.O. Box 1848, University, MS, 38677-1848; PH (662) 915-6559; FAX (662) 915-7796; email: yozeren@ncche.olemiss.edu
[4]MOX, Dept. of Mathematics "F. Brioschi", Politecnico di Milano. Piazza Leonardo da Vinci, 32, 20133 Milano, Italy; PH +39-02-239 94 600; FAX +39-02-239 94 606, email: edie.miglio@polimi.it (visiting scientist at NCCHE during 2007)

ABSTRACT

Highly transient floods resulting from the failure of dams and levees can lead to loss of life and property damage. Two-dimensional (2D) numerical simulations that use modern shock-capturing schemes are particularly suited to simulate these mixed-regime floods for flood mapping, consequence analysis and emergency management planning. The Digital Elevation Models (DEM) are often used as a regular computational mesh. Unfortunately, linear terrain features, such as road and railroad embankments and dikes, which may influence flood patterns, are not adequately captured in DEMs. This study describes a two-sided cut-cell boundary method for representing linear terrain features on a regular Cartesian mesh. The proposed method is briefly described and some test simulations are presented.

INTRODUCTION

Dams and levees are one of the eighteen critical infrastructures/key- resource sectors that require protective actions to prepare for, or to mitigate against, a terrorist attack or other hazards. Their failure leads to highly transient flows that can cause loss-of-life, property damage and cascading failures in other critical sectors.

US National Inventory of Dams (NID, 2008) currently lists about 79,000 dams in the USA, including those in Guam and Puerto Rico. Only about 5% of these dams are owned by the federal government. The majority of the remaining dams are privately owned and they are under the responsibility of the states. Out of the 79,000 existing dams, 11,243 are classified as high hazard and 12,656 as significant hazard dams. All high hazard dams are required to have an Emergency Action Plan (EAP) identifying potential emergency conditions at a dam and specifying preplanned actions to be followed to minimize property damage and loss of life. The EAP also contains inundation maps and the procedures and information to assist the dam owner/operator in issuing early warning and notification messages to responsible downstream emergency management authorities. Unfortunately, 5,035 high hazard dams and 6,013 significant hazard dams do not yet have an EAP. Among these, 1,858 high-hazard dams and 2,533 significant hazard dams were built before 1940.

Two-dimensional (2D) numerical models based on modern conservative shock-capturing schemes can provide a cost effective way to prepare EAPs for all high-hazard and significant-hazard dams. The 2D numerical models can directly use Digital Elevation Maps (DEM), which are readily available from federal and state owned geospatial data clearinghouses. This greatly facilitates input data preparation. The 2D simulation captures the highly dynamic nature of these floods and provides reliable results even in flat areas without channelized flow. Moreover, simulation results can be readily imported into a GIS platform, as raster or shape files, to be used for map creation, risk and vulnerability analyses, and flood emergency management and decision support.

Using a DEM directly as computational mesh, however, presents certain drawbacks. For typical DEM resolutions of 30m to 100m used in dam-break studies, the DEMs do not adequately capture linear terrain features, such as road and railroad embankments, which may constitute obstacles and influence the flood propagation and inundation limits. Increasing the resolution or using a locally refined unstructured triangular mesh is not always desirable as it may lead to longer computational times due to CFL (Courant-Friedrichs-Lewy) condition.

The present paper discusses the implementation of a two-sided cut-cell boundary method (or immersed boundary method) in a 2D numerical model in order to represent linear terrain features on a regular Cartesian mesh without penalizing the time step. A few test cases are also presented.

DESCRIPTION OF THE NUMERICAL MODEL CCHE2D-FLOOD

Consider the two-dimensional shallow water flow depicted in Figure 1. Two-dimensional unsteady shallow water equations governing the flood flow can be written in the following vector form:

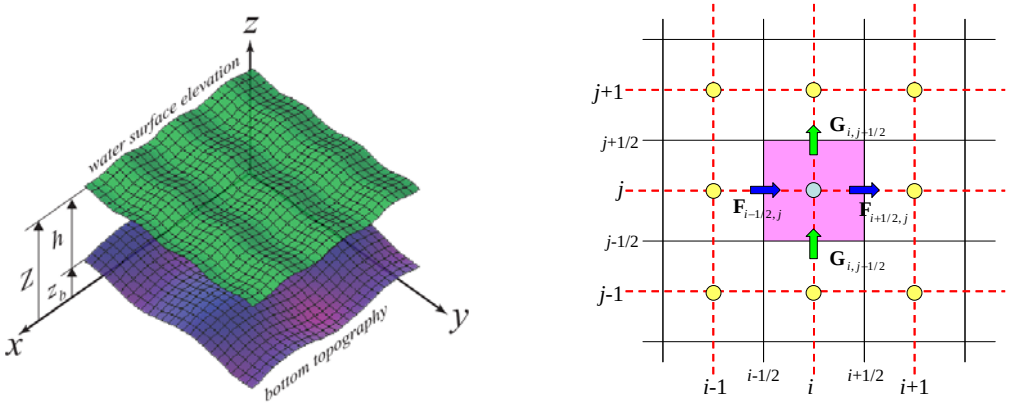

Figure 1. Left: Definition sketch for a two-dimensional shallow water flow; Right: Regular Cartesian computational grid.

$$\frac{\partial \mathbf{U}}{\partial t}+\frac{\partial \mathbf{F}(\mathbf{U})}{\partial x}+\frac{\partial \mathbf{G}(\mathbf{U})}{\partial y}=\mathbf{S}(\mathbf{U}) \tag{1}$$

where $\mathbf{U}$ is the vector of conserved variables; $\mathbf{F}(\mathbf{U})$ and $\mathbf{G}(\mathbf{U})$ are the flux vectors in horizontal x and y directions:

$$\mathbf{U}=\begin{bmatrix} h \\ hu \\ hv \end{bmatrix}=\begin{bmatrix} h \\ Q_x \\ Q_y \end{bmatrix} \quad ; \quad \mathbf{F}=\begin{bmatrix} Q_x \\ Q_x^2/h \\ Q_xQ_y/h \end{bmatrix} \quad ; \quad \mathbf{G}=\begin{bmatrix} Q_y \\ Q_yQ_x/h \\ Q_y^2/h \end{bmatrix} \tag{2}$$

In the above equations, h is the water depth, u and v are the components of horizontal velocity vector in x and y directions. The components of volume flux (discharge) in x and y directions are represented by Q_x and Q_y. The vector of source terms $\mathbf{S}(\mathbf{U})$ is given by:

$$\mathbf{S}=\begin{bmatrix} q_v \\ -gh(\partial Z/\partial x)-g\left(u\sqrt{u^2+v^2}/C^2\right) \\ -gh(\partial Z/\partial y)-g\left(v\sqrt{u^2+v^2}/C^2\right) \end{bmatrix} \tag{3}$$

where q_v is a volume source or sink located in the cell, Z is the water surface elevation with respect to the reference plane and C the Chezy friction coefficient.

Referring to the computational grid represented in Figure 1, cell-centered finite-volume discretization of Eq. 1 over a rectangular control volume leads to the following explicit scheme:

$$U_{ij}^{n+1}=U_{ij}^{n}-\frac{\Delta t}{\Delta x_i}\left(F_{i+1/2,j}-F_{i-1/2,j}\right)-\frac{\Delta t}{\Delta y_j}\left(G_{i,j+1/2}-G_{i,j-1/2}\right)+\Delta t\, S_{ij} \tag{4}$$

where Δx and Δy represent the cell dimensions in x and y directions, and Δt is the time step. The terms $F_{i+1/2,j}$, $F_{i-1/2,j}$, $G_{i,j+1/2}$ and $G_{i,j-1/2}$ represent the *intercell*

fluxes along the four cell edges. The two-dimensional (2D) numerical model CCHE2D-FLOOD, which was developed at the National Center for Computational Hydroscience and Engineering of the University of Mississippi, uses the first order upwinding method to compute the intercell fluxes:

$$\mathbf{F}_{i+1/2\,j} = \begin{bmatrix} Q_x \\ Q_x^2 / h \\ Q_x Q_y / h \end{bmatrix}_{i+k} \quad k = \begin{cases} 0 & Q_x \geq 0 \\ 1 & Q_x \leq 0 \end{cases}; \quad \mathbf{G}_{ij+1/2} = \begin{bmatrix} Q_y \\ Q_y Q_x / h \\ Q_y^2 / h \end{bmatrix}_{j+m} \quad m = \begin{cases} 0 & Q_y \geq 0 \\ 1 & Q_y \leq 0 \end{cases} \tag{5}$$

The above upwinding relationships for intercell fluxes are supplemented by additional relationships to take into account special conditions, such as wet and dry cell interactions, converging flows, very steep ground elevations, etc. The source terms are discretized in the following manner:

$$\mathbf{S} = \begin{bmatrix} q_v \\ -gh_{ij}^{n+1}\left[\left(\partial Z / \partial x\right)\right] - g\left(u_{ij}\sqrt{u_{ij}^{\,2} + v_{ij}^{\,2}} \Big/ \left(h_{ij}^{1/6}/n\right)^2\right) \\ -gh_{ij}^{n+1}\left[\left(\partial Z / \partial y\right)\right] - g\left(v_{ij}\sqrt{u_{ij}^{\,2} + v_{ij}^{\,2}} \Big/ \left(h_{ij}^{1/6}/n\right)^2\right) \end{bmatrix} \quad \text{with} \quad C = \frac{h_{ij}^{1/6}}{n} \tag{6}$$

where n represents the Manning's roughness coefficient.

The CCHE2D-FLOOD model handles dry-bed condition by maintaining a very small water depth, which is chosen sufficiently small not to cause any noticeable change in the propagation speed of the wet/dry front. When a wet cell and dry cell share a common edge, only the mass flux is allowed into the dry cell (momentum flux is set to zero) during that particular time step.

The numerical code resulting from this discretization is stable, robust and oscillation-free near discontinuities. It has been shown to rigorously conserve mass and momentum. No special entropy fixes are needed to ensure physically plausible solutions. CCHE2D-FLOOD has been verified and validated using analytical solutions as well as data from laboratory experiments, model tests, and past dam break events (see Ying et al., 2003a and b; Ying and Wang, 2004; and Ying et al., 2004).

Different types of boundary conditions are implemented in CCHE2D-FLOOD: 1) fully reflecting impervious solid boundary; 2) open boundary (which allows the flow to exit the computational domain freely); 3) stage-time boundary (which allows to specify the water surface elevation at the boundary as a function of time); 4) inlet boundary (which allows definition of a discharge hydrograph entering or leaving through the boundary).

CCHE2D-FLOOD uses an explicit scheme to solve the shallow water equations. It is, therefore, subjected to the Courant-Friedrichs-Lewy (CFL) condition for stability and convergence. Given a mesh size, $\Delta x \times \Delta y$, the CFL condition places an upper bound on the time step as follows:

$$N_{CFL} = \text{Max}\left[\frac{\Delta t}{\Delta x}(|u| + \sqrt{gh}), \frac{\Delta t}{\Delta y}(|v| + \sqrt{gh})\right] \le 1 \quad (7)$$

The time step can be either automatically selected by the program based on the consideration of the CFL condition or directly specified by the user.

CUT-CELL BOUNDARY METHOD AND LINEAR TERRAIN FEATURES

A two-sided cut-cell boundary (or immersed boundary) method was implemented in CCHE2D-FLOOD to represent linear terrain features on a regular rectangular Cartesian mesh. Referring to Figure 2, the linear terrain feature to be represented in the 2D model is projected onto the DEM from a GIS shape layer by imposing the following rules: 1) a cell can only be cut by a single straight line; 2) The line joining the centers of two adjacent cells can only be cut by a single straight cut-line, 3) When two adjacent cells are both cut by a line, the cut lines should meet at the same point on the common edge. The projected line cuts through computational cells and divides them into two irregular-shaped parts. Some of the irregular-shaped cells can be very small. The main challenge resides in developing a scheme that does not require smaller time steps to meet the CFL condition for stability. The oscillation-free shock-capturing property of the scheme must also be preserved.

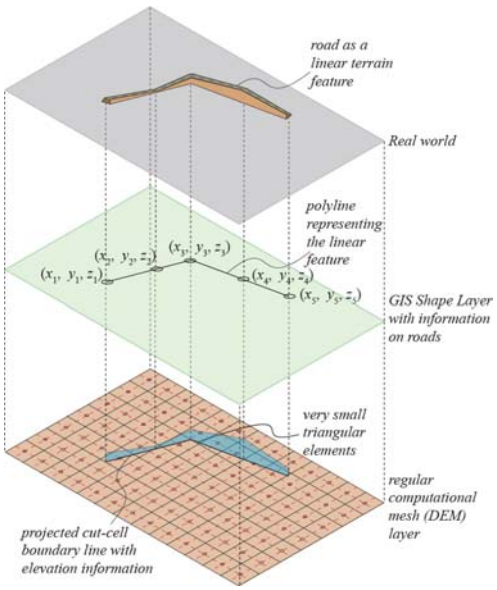

Figure 2. Projection of a linear terrain feature on the regular Cartesian Mesh.

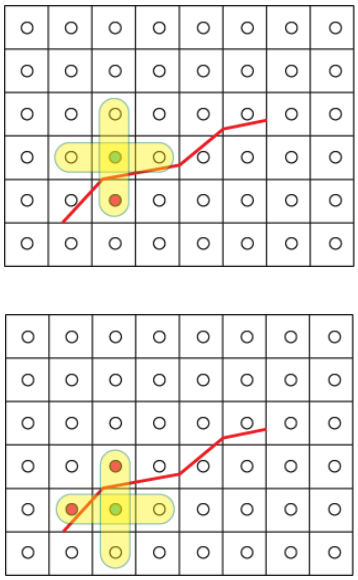

Figure 3. Computational stencils in the presence of a cut-cell boundary.

Several methods have been proposed to deal with cut-cells in two and three-dimensional meshes. Causon et al. (2000) combines cut-cells with adjoining regular cells to avoid small time steps. The h-box method (Helzel et al., 2005) use a rotated control volume for calculating the flux through the cut-cell boundary. The present study has adopted the Ghost Fluid Method (GFM) (Ghias et al., 2007), which is a special form of a class of techniques called Immersed Boundary Method (IBM) (Mittal and Iaccarino, 2005). The two-sided version of GFM implemented in CCHE2D-FLOOD is described in Miglio et al. (2008). Here only a brief presentation of the method will be given and some test cases will be presented.

Figure 3 shows the computational stencil in the presence of a cut-cell boundary. In the upper figure, the computed point (shaded green) is located in the upper side of the cut line representing the linear terrain feature. The cell below (shaded red) lies on the other side of the boundary; thus, the variables at the cell center are not available for applying the stencil. When calculating the cell below the cut line, the values of variables for cells above and on the left are not available for applying the stencil. The missing cells of the computational stencil are said to be *ghost cells* (GP) with respect to the cell being computed. The idea behind the GFM method is to use specially computed values for the variables in ghost cells in such a way that the following boundary conditions are enforced along the cut-line:

$$Q_n = q, \qquad \frac{dQ_t}{dn} = 0, \qquad \frac{dZ}{dn} = 0, \tag{8}$$

where Q_n and Q_t are the normal and the tangential components of the discharge, Z the water surface elevation, $\mathbf{n} = \lfloor n_x, n_y \rfloor$ the vector normal to the immersed boundary and q represents the overtopping discharge, if any, which can be calculated using an appropriate weir equation, for example.

The computational procedure to determine the values of the variables in ghost cells will be explained referring to Figure 4. In both left and right cases, the cell (i, j) is being computed. In the left hand side configuration, the cell $(i, j-1)$ is a ghost point (GP) with respect to the computed cell (i, j). To compute the flux across the lower edge, the values of the unknown must be defined at GP in such a way that the boundary conditions along the immersed boundary are correctly represented. To find the unknown values at GP, the point GP is first reflected onto the other side of the immersed boundary to find the *reflected point* RP. Note that the line segments $GP - B_{34}$ and $B_{34} - RP$ have the same length. The value at RP can be calculated by bilinear interpolation using the known values of the variables at the surrounding cells.

The values at GP are then linearly extrapolated from RP using the boundary conditions at B (Eq. 8). Once the values to be used at GP are determined, the computational stencil can be directly applied to compute the next step values for the cell (i, j). This was the simplest situation where all the four corner nodes of the

interpolation cell are on the same side of the cut-cell boundary as the computed cell. A different situation arises when all the corners of the interpolation cell are not on the same side as the computed cell. Such a case is depicted on the right hand side of Figure 4. The corner 1 of the interpolation cell is on the opposite side of the cut-cell boundary and, thus, its value is not defined. The fix in such cases is to replace the missing corner by the boundary condition; in this case condition at B_{34}. The rest of the procedure basically remains the same. Details of the method and derivation of the equations for different situations are presented in detail in Miglio et al. (2000).

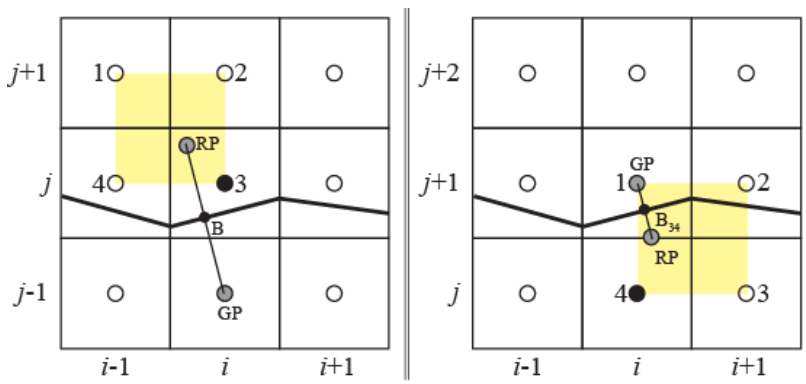

Figure 4. Procedure for determining the values of the variables in a ghost cell.

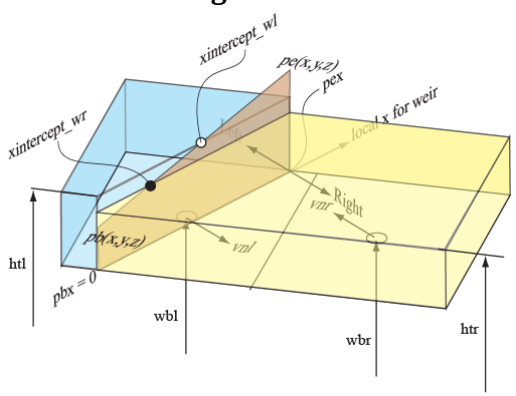

Figure 5. Definition sketch of a cut-cell boundary reach with overtopping.

Depending on the height of the cut-cell boundary and the water surface elevation on both sides, an overtopping discharge of q may be flowing from one side to the other. Figure 5 shows a cut-cell boundary reach with regions of unsubmerged flow, submerged flow and no flow. In order to be able to take into account all possible flow situations, the reach is divided into a number of equal-length sub-reaches. Using the ogee weir equation, the incremental overtopping discharge, Δq_j is separately calculated for each sub reach based on the elevation of the weir at the sub-reach center and the water depths on both sides. These incremental discharges are then summed up to determine the total discharge passing over the reach, q.

VALIDATION OF CUT-CELL BOUNDARY METHOD AND TEST CASES

Circular dam break in a closed square domain

The case of a 4m-diameter circular dam in a 15×15m close rectangular domain filled with 1m-deep still water is used to validate the cut-cell boundary method. Referring to Figure 6, the square domain for the reference case is defined along the grid lines by imposing a fully reflecting wall boundary condition. In the test case, the 15×15m square domain is defined inside a 25×25m domain by using cut-cell boundaries making an angle of 45° with the gridlines of the computational mesh. In both cases the computations are carried out with $\Delta x = \Delta y = 0.5m$ and $\Delta t = 0.1s$.

Computed water surface contours for both solutions are shown in Figure 7 for the first 5 seconds. The test-case solution is rotated 45° counter clockwise to facilitate comparison with the reference solution. The color-bar range is varied with time for better readability. However at each time, the test solution and the reference solution use the same color-bar range. As it can be seen, the water depth patterns obtained with cut-cell boundary method are almost identical to those of the reference solution.

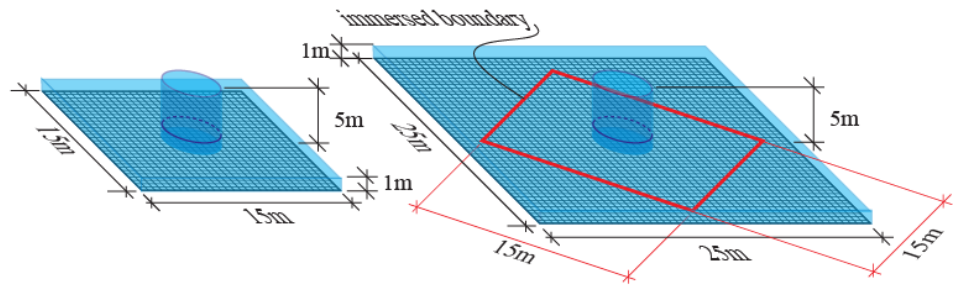

Figure 6. Set-up for circular dam break case with and without cut-cell boundary capability.

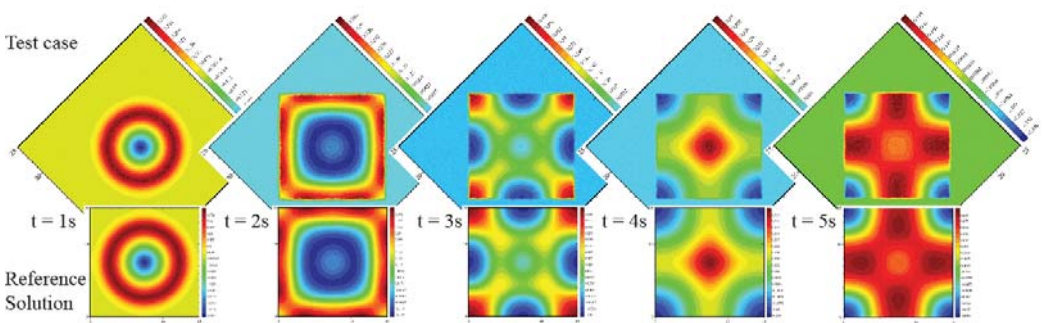

Figure 7. Circular dam break simulation with and without cut-cell boundary.

Dam-break flood over a variable height cut-cell boundary

Figure 8 shows the experimental set-up for this test case. The wedge shaped cut-cell boundary has a very low height near the apex. The height of the cut-cell

boundary increases towards both extremities. The dam located along the upper boundary of the computational domain breaks at the beginning of the simulation. Everywhere else there is still water with a depth of 0.5m.

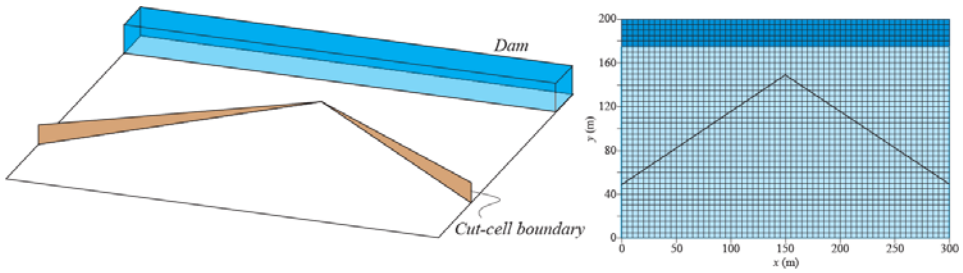

Figure 8. Set-up for dam-break flood over a variable-height cut-cell boundary.

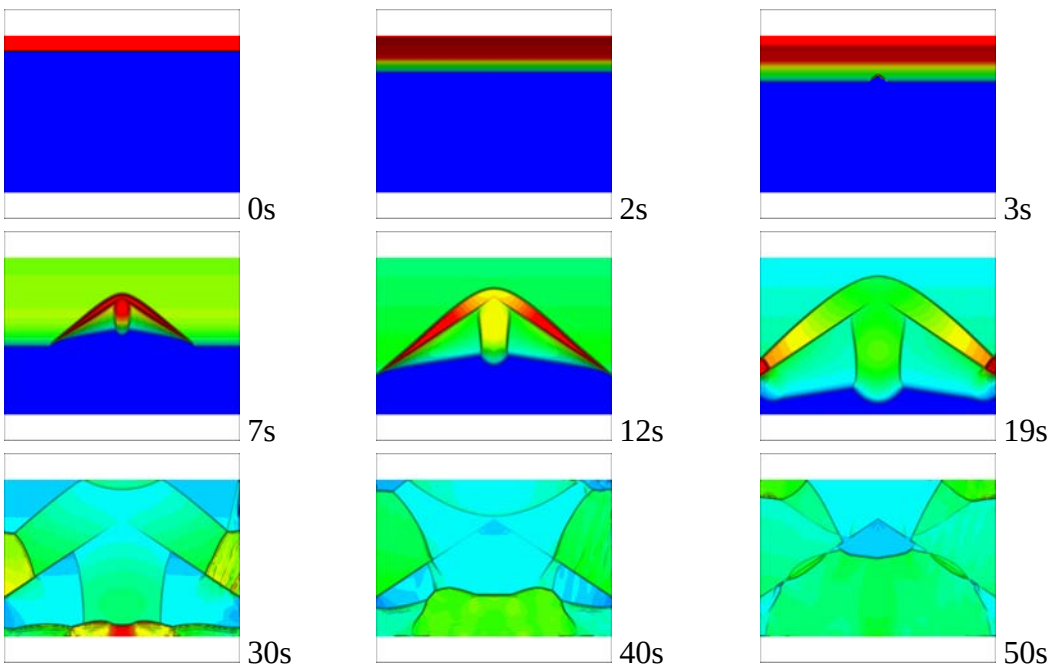

Figure 9. Water surface contours for dam-break flood over a variable-height cut-cell boundary. Numbers below the frames represent time in seconds.

Computed water-surface elevations are plotted in Figure 9 at different times after the dam break. When the dam-break flood reaches the cut-cell boundary, the flow partly overtops boundary (in the middle part); partly it is reflected, leading to the formation of a moving hydraulic jump. As more water arrives toward the cut-cell boundary, eventually the overtopping takes place over its entire length. The following images show the interaction of various wave fronts resulting from this complex configuration. Since four sides of the computational domain are declared as a fully reflecting wall boundary, mass conservation can be easily verified. Loss of mass at the end of several hundred seconds of simulation is found to be less than 1%.

CONCLUSIONS

The paper described the implementation of a two-sided cut-cell boundary method in the numerical model CCHE2D-FLOOD, which uses a first order upwinding finite-volume scheme to solve 2D shallow water equations on complex topography defined by a DEM. This two-sided cut-cell boundary method allows representing the linear terrain features on a Cartesian regular mesh, which cannot be adequately captured in a DEM. The implemented method allows overtopping of the cut-cell boundary. The results of two selected test cases demonstrate the effectiveness of the method.

REFERENCES

Causon, D.M., Ingram, D.M., Mingham, C.G., Yang, G. and Pearson, R.V. (2000). "Calculation of Shallow Water Flows Using a Cartesian Cut Cell Approach." Advances in Water Resources, 23:545-562.

Ghias, R., Mittal, R. and Dong, H. (2007). "A sharp interface immersed boundary method for compressible viscous flows." J. Comput. Phys., 225, pp.528-553

Helzel C., Berger M.J. and Leveque R.J. (2005). "A high-resolution rotated grid method for conservation laws with embedded geometries." SIAM Journal on Scientific Computing, vol. 26, no. 3, pp. 785-809.

Miglio, E., Altinakar, M.S., and Tayfur, G. (2008). "Representation of Linear Terrain Features in 2D Free Surface Model using Cut-Cell Boundary Method." Proc. Int. Conf. on Fluvial Hydraulics River Flow 2008, 3-5 September 2008, Cesme, Turkey.

Mittal, R. and Iaccarino, L. (2005). "Immersed Boundary Methods, Annual Review of Fluid Mechanics." Vol. 37: 239-261.

Ying, X., Khan, A.A. and Wang, S.S.Y. (2003a). "An Upwind Method for One-Dimensional Dam Break Flows." Proc. of 30th IAHR Congress, pp. 245-252, Thessaloniki, Greece, August, 2003.

Ying, X., Khan, A. A. and Wang, S.S.Y. (2004). "An Upwind Conservative Scheme for Saint-Venant Equations." Journal of Hydraulic Engineering. Vol.130, No.10, pp. 977-987, 2004.

Ying, X. and Wang, S.S.Y. (2004). "Two-Dimensional Numerical Simulations of Malpasset Dam-Break Wave Propagation." Proc. of 6th International Conference on Hydroscience and Engineering, Brisbane, Australia, Book of Abstracts, pp.137-138, Manuscript on CDROM, May, 2004.

Ying, X., Wang, S.Y. and Khan, A.A. (2003b). "Numerical Simulation of Flood Inundation Due to Dam and Levee Breach." Proceedings of ASCE World Water & Environmental Resources Congress 2003 (CD-ROM), Philadelphia, USA, June 2003.

Flood Risk Assessment of Complex Riverine Systems

By Christopher N. Dunn P.E.[1] and Michael K. Deering P.E.[2]

[1] Director, U.S. Army Corps of Engineers, Institute for Water Resources, Hydrologic Engineering Center, 609 Second Street, Davis, CA 95616; PH (530) 756-1104; FAX (530) 756-8250; email: christopher.n.dunn@usace.army.mil

[2] Chief, Water Resources Systems, U.S. Army Corps of Engineers, Institute for Water Resources, Hydrologic Engineering Center, 609 Second Street, Davis, CA 95616; PH (530) 756-1104; FAX (530) 756-8250; email: michael.k.deering@usace.army.mil

ABSTRACT

For over two decades, the U.S. Army Corps of Engineers (USACE) has required that all of their planning processes address the Nation's water resources needs in a systems context. Corps policy also requires that all flood damage reduction studies adopt risk analysis. While the USACE has these requirements, there is little guidance and few tools to support them. For this reason, the USACE Institute for Water Resources (IWR) sponsored investigations into the development of a new tool to analyze complex riverine systems while implementing the current flood risk analysis and systems requirements. This new tool, currently called HEC-FRM or Flood Risk Management, is the next generation of the Hydrologic Engineering Center's Flood Damage Analysis (HEC-FDA) model. This paper will present the model development for this tool which will be used for levee certification and assessment, planning and design studies, and advance the Corps modeling approach for risk analysis.

Introduction

A primary mission of the U.S. Army Corps of Engineers is to provide flood protection for communities and rural areas throughout the United States. During flood episodes the Corps operates flood control projects and conducts emergency management activities. At the direction of Congress, the Corps studies and implements flood risk management measures and over the years the Corps Flood Risk Management programs have significantly reduced flood risks by implementing many structural and non-structural flood damage reduction measures such as dams, levees and floodplain management initiatives. The Corps Hydrologic Engineering Center continues to develop new procedures and programs to meet the changing needs of the country and utilize new science & technology. These new programs need to be aligned with current Federal policies. One such policy that has regained significant interest is performing systems studies with risk analysis.

For this reason, the U.S. Army Corps of Engineers (USACE) Institute for Water Resources (IWR) sponsored investigations into the development of a new tool to analyze complex riverine systems while implementing current flood risk analysis and systems requirements. This new tool, currently called HEC-FRM or Flood Risk Management, is the next generation of the Hydrologic Engineering Center's Flood Damage Analysis (HEC-FDA) model. It will include a systems approach, event-based sampling, the ability to do scenario analysis, and structure-by-structure, cost, non-structural, loss-of-life, and agricultural damage analysis. The tool will accommodate many, if not all, of the recommendations that the Corps agreed with from the National Research Council report on the Corps' implementation of risk analysis for flood damage reduction (NRC, 2000). It will also aide in implementing the Chief of Engineers' Actions for Change.

This paper will present the HEC-FRM model development including sampling and solution techniques, uncertainty definitions, and system-wide component fragility and performance interactions/relationships for these complex riverine systems. The paper will describe the capabilities as detailed in the recently written software design document, "Flood Damage & Risk Analysis of Complex Riverine Systems" which proposes significant advancements to the USACE modeling approach for risk analysis. The new tool would be used nationwide for levee certification, levee assessment and planning and design studies.

Need for Systems Approaches and Risk Analysis

The U.S. Army Corps of Engineers Engineer Regulation ER 1105-2-100, Planning Guidance Notebook has required that the Corps planning processes address the Nation's water resources needs in a systems context. However, Corps policy does not provide guidance on how to perform system-wide analyzes. Also, Corps policy, ER 1105-2-101, Risk Analysis for Flood Damage Reduction Studies requires "All flood damage reduction studies will adopt risk analysis…" While EM 1110-2-1619, Risk Analysis for Flood Damage Reduction Studies, provides procedures on how to conduct risk analysis for local projects, it provides little support for risk analysis in a systems context. Therefore, while the Corps has requirements for systems approaches using risk analysis, there is little guidance and few tools to support these requirements.

Problem with Current Approaches

In spite of the fact that few tools are available for using risk analysis with system studies, risk analyses have occurred. These studies are being performed using the tool HEC-FDA or Flood Damage Reduction Analysis. HEC-FDA is a plan evaluation and plan formulation tool that helps to answer the question, "Which proposed flood damage reduction plan is the best from an economic standpoint?" It provides the capabilities to evaluate the with and without project plans and compares the plans using expected damage and damage reduction benefits. It also develops project performance metrics for comparison of alternatives and levee certification and since 1996 has included the capabilities to perform risk analyses.

However, even with these advanced capabilities, HEC-FDA still looks at a system of projects as a number of independent projects. This issue and others raised by the National Research Council, current users of HEC-FDA and HEC have clearly shown that HEC-FDA needs to include explicit systems analysis capabilities. Other needs identified to improve HEC-FDA include: re-plumbing FDA's Monte Carlo sampling to address a combination of damage reaches; include providing risk and uncertainty capabilities about non-structural measures, adding agricultural damage and project costs; providing correlated sampling of dependent relationships (e.g. rating curve versus the reservoir inflow/outflow curve); adding additional failure modes and features; analyzing impacts of project failure for residual risk requirements (e.g. loss-of-life); and addressing additional H&H support of risk analysis (e.g. realistic physical limits on frequency analysis and update the equivalent record length procedures).

Another problem the Corps faces when trying to conduct comprehensive watershed studies is the requirement to identify a local sponsor. Since the1986 Water Resources Development Act became law, water resources development and research to support it has been accomplished project-by-project because of the need for a local sponsor. Therefore, we are in a catch 22. Current policy requires a systems context but current legislation still requires the identification and support of a local sponsor. Is the sponsor willing to participate in a comprehensive study or only their local project?

Corps' Actions for Change

Nowhere has the need for a systems approach been more apparent than in New Orleans. The city is protected from flooding by a series of levees. During Hurricane Katrina some of the levees failed demonstrating that no matter how strong some of the levees were, if all of the levees are not robust, catastrophic flooding can still occur.

Because of the unacceptable systems performance of the New Orleans hurricane protection system, the Corps developed the Corps' Actions for Change (AFC). The goal of these actions is to improve public safety and the Nation's water resources infrastructure. Several actions were identified such as shifting decision making from individual, isolated projects to that of an interdependent system and communicating risk in simple and clear terms. In addition, a complete Theme was created to focus on employing risk analysis concepts with the goal to address many of the needs identified in the section above.

One of the first products addressing the systems approach is Engineer Circular (EC) 1110-2-6067. This circular requires that the Corps use risk analysis and a systems approach when performing levee certifications. This process evaluates components as an interconnected system necessary to insure protection of the associated floodplain. These items can include the levee, floodwall, closure structures, pumping stations, culverts and interior drainage works.

White Paper for the Development of HEC-FRM

Another product addressing the AFC was the development of a White Paper titled "Risk-Based Flood Damage Analysis: Software Design Document, Model Design for Flood Damage and Risk Analysis of Complex Riverine Systems." Written by Dr. David W. Watkins, Ph.D. while on a temporary assignment at HEC as the Roy Beard Visiting Scholar, the paper proposed an initial design for the new tool that will perform risk analyses for complex river systems. The goal of the proposed new tool, HEC-FRM, is to perform systems approaches for assessing risks in complex, interdependent systems. It will incorporate social and environmental consequences and include capabilities to perform levee assessments and certifications. It will also assist in effectively communicating risk. To accomplish these tasks, HEC-FRM will have to incorporate new computational methodologies. He conducted a thorough literature review where he uncovered previous efforts including the Sacramento and San Joaquin River Basins Comprehensive Study, the recommendations of the Interagency Performance Evaluation Team, the software used for estimating coastal storm damage (Beach-fx), the Corps dam and levee safety programs and several European projects. Each provided valuable lessons and insights on how to conduct a systems approach including risk analysis.

The White Paper became the basis for HEC-FRM's Project Management Plan and defined the domain of the new tool as that dealing with riverine systems with floodplain consequence areas. The tool would include a linear system representation of the components including levees, floodwalls, closure gates and loading and resistance assumed uniform for a specific reach. Both structural and non-structural measures were to be addressed.

A suggested computational flow starts with each project alternative, a single scenario of the project life cycle (e.g. 50 years), being simulated by sampling the annual maximum flood events over the duration of the life cycle. Of course, if agricultural damage is to be considered, seasons within a year will have to be sampled as well. The system performance and flood characteristics will determine when and if breaches occur to the various projects. If breaches do occur, the impacts will be calculated based on flood inundation and related consequences. The consequences shall include economic, social, environmental and loss-of-life. Life cycle modeling will include rehabilitation, repair and flood recovery when necessary. So, if the damage is substantial the characteristics of the consequence area may be altered prior to the next flood event. This process would then be repeated for the next scenario.

Several key issues were identified. A primary issue is how to generate the flood events themselves, i.e., should HEC-FRM use frequency curves like HEC-FDA or use synthetic events. Other problems include how to automate thousands of hydrodynamic simulations, model multiple failure modes, evaluate consequences and; reduce the computational burden necessitated by the comprehensive systems approach. One way to reduce the computational burden is to examine the trade off between detailed modeling and important sources of uncertainty. If only a few sources of uncertainty

are examined, then the burden could be significantly reduced. Regardless of how these issues are addressed, it is clear that flexibility or varying levels of fidelity will be key to the success of the software.

Software Design Concepts

In a parallel effort, HEC is developing the Watershed Analysis Tool (HEC-WAT) to help the Corps and its study partners conduct watershed and water resources management studies with risk analysis. Funding for the development of HEC-WAT (WAT) is being provided through the System-wide Water Resources Program and the Flood and Coastal Storm Damage Reduction Research and Development program. The R&D program is also contributing toward the development of HEC-FRM.

WAT modeling teams benefit because they develop their models in a closely coordinated manner, track progress of other models, and automatically retrieve results from previous model runs thus assuring more efficient and coordinated results. The team benefits by using a common interface to track project status through each modeling component and displaying results during public and project status meetings.

The WAT streamlines and integrates the analytical process using software commonly applied by multi-disciplinary teams (HEC-HMS, HEC-RAS, HEC-ResSim, and HEC-FIA, etc.). The integration of the software is accomplished through the use of a concept called a "plug-in" as shown in Figure 1. The "plug-in" concept allows the WAT to know little about individual software, but provides an analysis framework for the software. A "plug-in" can provide the ability to access and edit software parameters, and view results available from the software through the WAT framework.

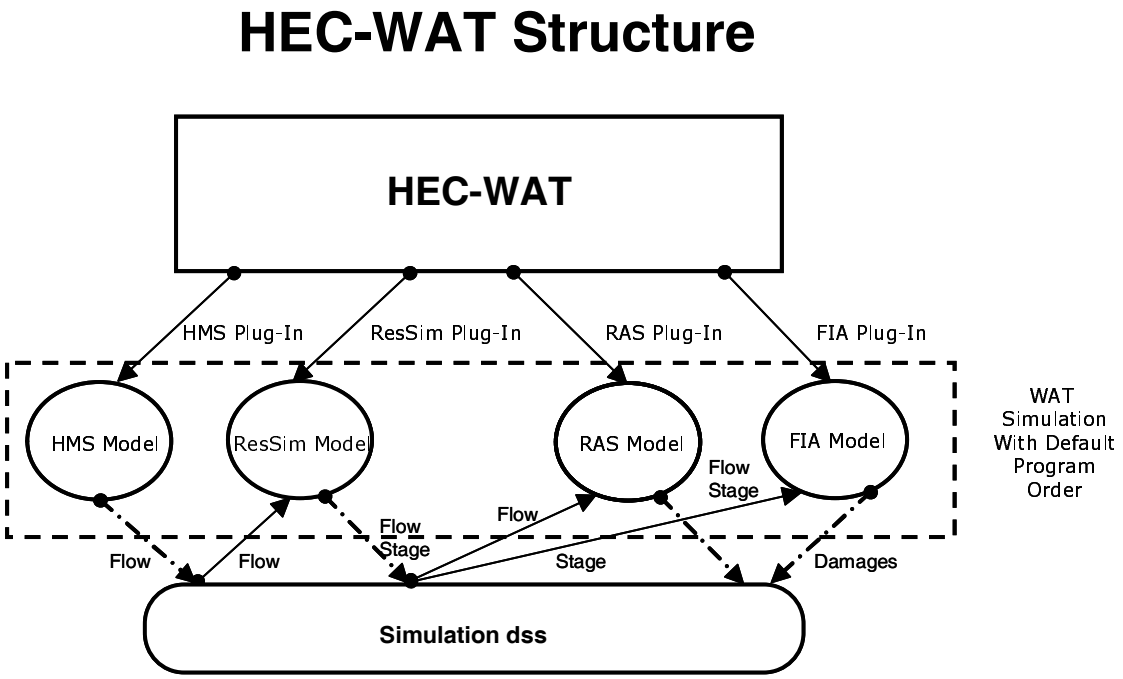

Figure 1. HEC-WAT Structure

HEC-FRM Framework

The HEC-FRM framework starts from the organization and structure of the WAT. FRM will operate within the WAT as a computational option if the user chooses to perform plan formulation or system performance analyses. The basic FRM organizational structure is shown in Figure 2. FRM will have the capability to sample from a pre-defined flow-frequency with associated inflow hydrographs as shown in Figure 2, or utilize the HEC-HMS (Hydrologic Modeling System) and HEC-ResSim (Reservoir Simulation) models in the WAT to generate inflows to the system (not depicted in Figure 2). A fragility sampler plug-in will set failure elevations to be used in HEC-RAS (River Analysis System) which would then route the inflow hydrographs down the system. Where failures occur breach hydrographs will be made available to a spreading model to delineate inundation areas and compute depths, velocities and duration in the consequence area of interest. Once the inundation and gridded hydraulics data is determined, that data is made available for HEC-FIA (Flood Impact Analysis) to compute consequences. The FRM process will apply the Monte Carlo simulation, a numerical-analysis procedure that computes the expected value of consequences ($ damage, loss-of-life, etc) while explicitly accounting for the uncertainty in the parameters used to determine those flood inundation consequences. FRM will be configured to allow for a life-cycle type computation of consequences and associated performance indices.

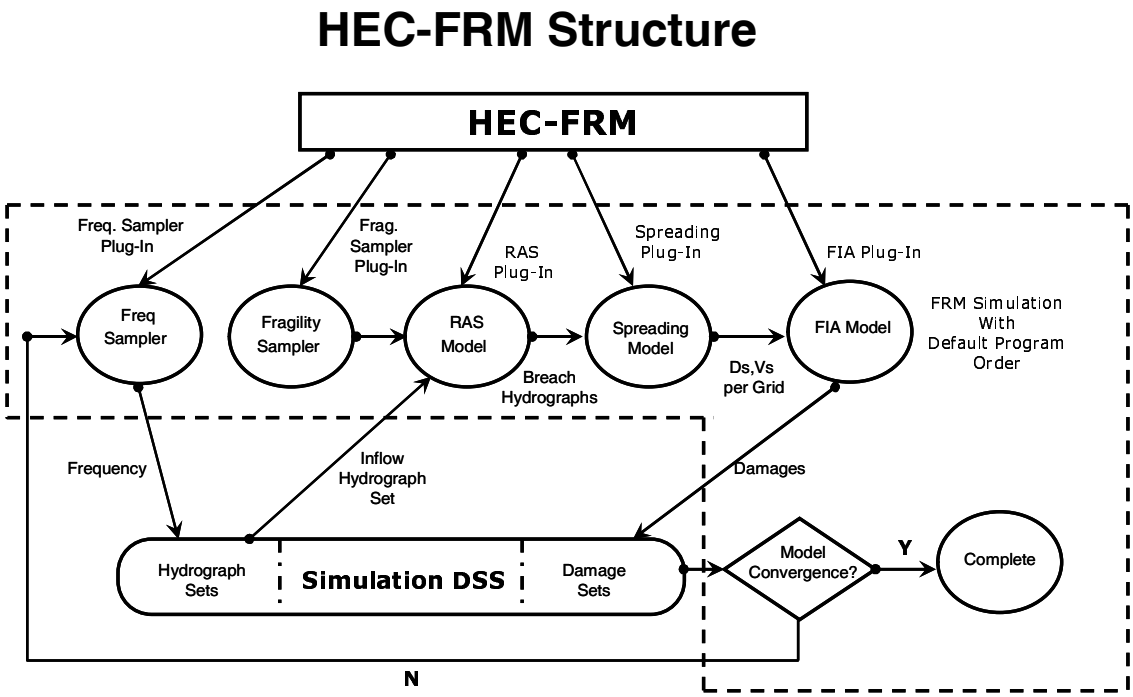

Figure 2. HEC-FRM Structure

Hydrologic Definition and Sampling

The hydrologic inputs to develop system loadings can be defined in FRM in two ways. Two distinct methods were discussed. First, FRM could use HMS and ResSim with sampling of key parameters for each simulation to capture uncertainties and to

generate loading hydrographs. This method would use all models in the WAT and allows for explicit evaluation of alternatives having upstream storage features as shown in Figure 3. The second method uses pre-defined flow-frequency functions with uncertainties and associated hydrographs defined for each frequency. This is the method depicted in Figure 2. From either of these methods, sets of 50 year sequences would be developed; each set representing one realization of a project life-cycle. The 50 year sequences would allow for inclusion of asset management activities, system degradation, etc.

System Load Distribution

System loadings would involve the application of HEC-RAS routing of the inflow hydrographs, $Q_{i,}$ to be tested against fragility functions at pre-defined locations in the system (see Figure 3). These pre-defined locations, or index locations, are representative of a levee reach (shown as segments around a consequence area in Figure 3) or of other system components such as gates, floodwalls, etc. As the system components fail, reduced flows are subsequently delivered to the downstream extents of the system, Q_o. Flows leaving the system via a failed system component produce a breach inflow hydrograph, depicted by $Q_{b.}$

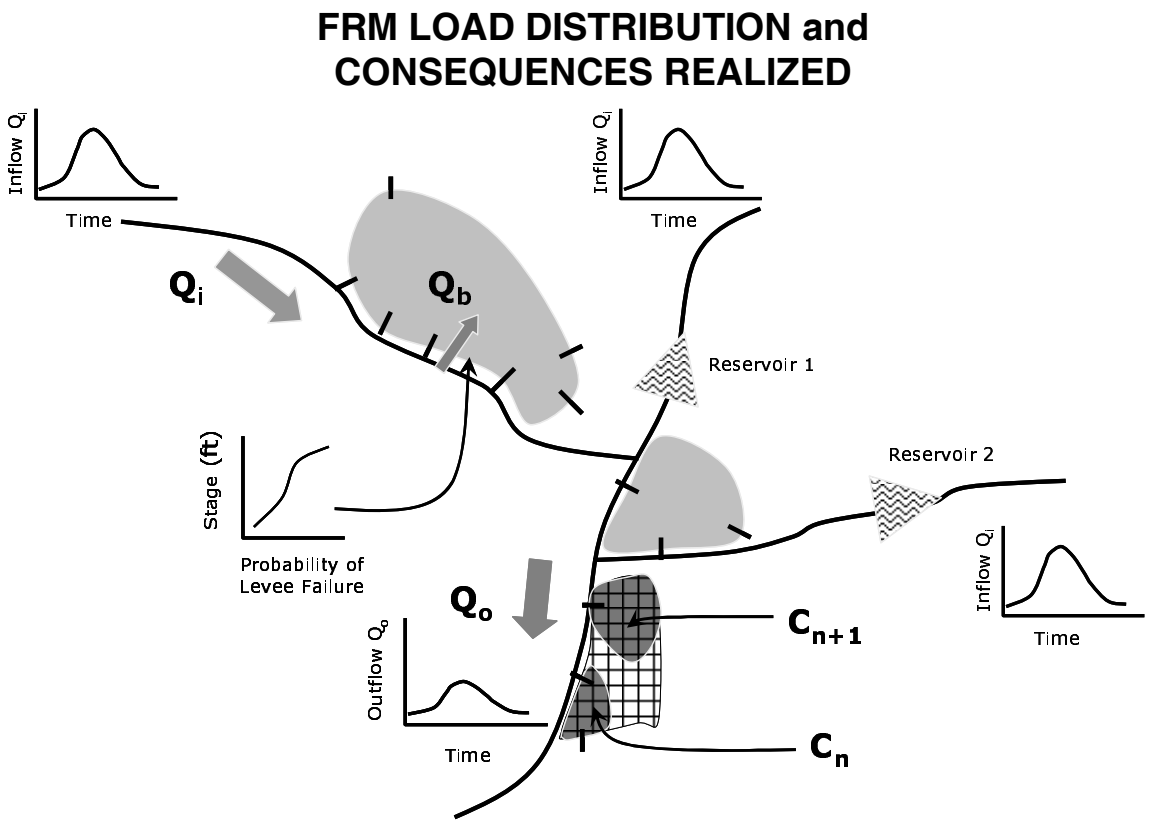

Figure 3. HEC-FRM Load Distribution and Consequence Realized

Sampling of Fragility Curves

As described above, the fragility curves will be sampled at each location for each routing/loading simulation. A random sampling between 0.0 and 1.0 will set the elevation of failure which in turn is set in HEC-RAS for testing against hydrologic loadings. The traditional way of interpreting a levee fragility curve (stage vs. probability of failure) is that when water reaches a given stage on the levee, there is a certain chance of the levee failing. For example, at a stage of 7 feet, the fragility curve shown below in Figure 4 shows a 29% change of failing, and a 71% chance of not failing. At 8 feet, the same curve shows an 88% chance of failing, and so a 12% chance of not failing. From a simulation standpoint, if water level reaches 7 feet, we actualize the chance of failure by drawing a uniform random number between 0 and 1 and choose failure if it is less than 0.29.

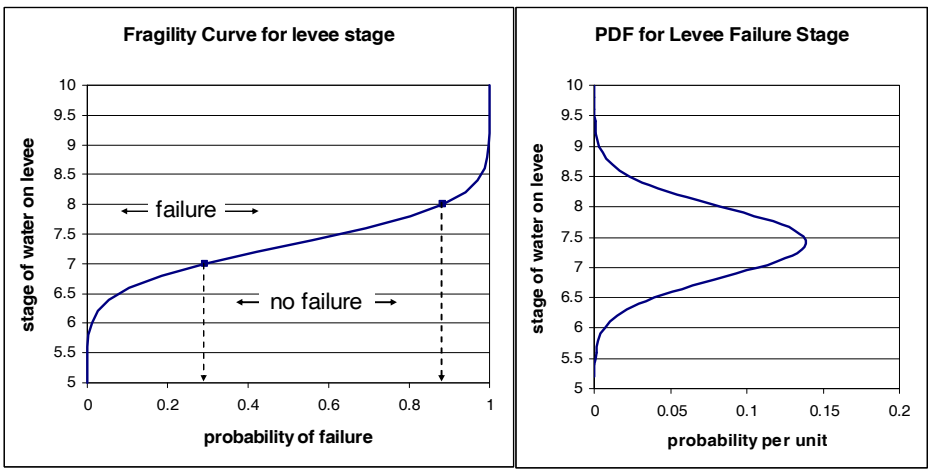

Figure 4. Fragility Curve

Another way to look at the fragility curve is to recognize that it is a non-decreasing function that spans probability from 0 to 1. The curve can be considered a cumulative distribution function (CDF) of the stage at which failure occurs. This also allows us to infer a PDF (probability density function) or bell curve of the failure distribution, in the figure above right. With this interpretation, with the CDF we'd say that there is a 29% chance that the failure stage is less than or equal to 7 feet, and there is an 88% chance that the failure stage is less than or equal to 8 feet. We're using the same information, but instead of a yes or no outcome at a given stage, we have linked failure stage to a "non-exceedance" probability. Using the second method of interpreting the fragility curve allows us to actualize the random element with a single random number (choosing levee failure stage for that realization) rather than needing to query a random number at every time step to say "at this stage, does it fail or not?" Once the levee failure stage is chosen, randomness is gone, and it remains only to route the hydrograph to determine if and when stage reaches the failure stage.

In a systems context with multiple failure modes/locations, sampling of those fragility curves, including uncertainty, is required for each realization of a FRM simulation. The fragility sampling plug-in would generate for each realization a set of random numbers between 0 and 1 for each index location and then determine failure stages from each fragility curve. These stages are then exported to RAS for use in that simulation. After a large number of simulations, this would result in the evaluation of the full range of failure possibilities over the entire system. This sampling and failure routine would define the system load distributions as well as inundation delineations in the consequence areas of interest.

Inflow Spreading

As failures occur in the consequence area, RAS computes the inflow/failure hydrograph shown as Q_b in Figure 3 and is then distributed with a "spreading" or inundation model. FRM will have options for the spreading model plug-in and could be accomplished with a simple or complexly linked ponding area option in RAS, ERDC's SMS or other 2D models depending on topography and inundation hydraulic characteristics. Whichever technique is used to generate inundation parameters, the information will be cast into a gridded format using the same grid definition as FIA. This gridded data will then be made available for computation of consequences in FIA.

Consequence Modelling

Consequences will be computed using FIA including economic damages and Loss-of-Life estimates. Depth, duration and velocity gridded data would be passed from the spreading model to FIA for those computations. FIA is also used to determine flood damage reduction benefits attributed to individual flood control projects (reservoirs, levees and diversions) and for real-time response activities as part of the Corps Water Management System. For a specified event or for each of 50 yr life cycle sequences, HEC-FIA can compute urban and agricultural flood damage, area inundated, number of structures inundated, and population at risk. Damage analysis of crops involves a complex series of factors and considerations. Among these are the type of crop, season of the year, cropping patterns, duration and magnitude of flooding, and much more. Monetary damage values are determined from investment losses, mature-crop price values, harvest costs, and may include secondary business losses. The new version the software, FIA will include a graphical user interface with GIS capabilities from either FIA itself or through the WAT structure.

Computational Challenges

The major issue that confronts this effort is the computational demand inherent in this type of methodology. Areas of focus will be on sequencing and "stacking" of multiple RAS simulations using multi-processors, hot-start techniques and various forms of "importance" or "intelligence" sampling for minimizing simulations. Of all of the technical aspects of this proposed modelling approach for computation of risk assessment parameters, reduction of the computational burden is the largest challenge.

Conclusion

The USACE will conduct risk assessments in a system context with recognition of system uncertainties about the key variables in an explicit manner and assesses them holistically. FRM model development will include sampling and solution techniques, uncertainty definitions, and system-wide component fragility and performance interactions/relationships for these complex riverine systems. It will include a systems approach, event-based sampling, the ability to do scenario analysis, and structure-by-structure, cost, non-structural, loss-of-life, and agricultural damage analysis. The new tool will accommodate many, if not all, of the recommendations that the Corps concurred with from the National Research Council report on the Corps' implementation of risk analysis for flood damage reduction (NRC, 2000), and it will also aide in implementing the Chief of Engineers' Actions for Change. FRM would be used nationwide for levee certification, levee assessment and planning and design studies.

References

Hydrologic Engineering Center, (2008) "HEC-FDA, Flood Damage Reduction Analysis" User's Manual, Version 1.2.4, CPD-72, U.S. Army Corps of Engineers, Institute for Water Resources, 609 Second Street, Davis, CA 95616

National Research Council, (2000) "Risk Analysis and Uncertainty in Flood Damage Reduction Studies," National Academy of Sciences, 2101 Constitution Ave., N.W. Washington D.C. 20418

ER 1105-2-100, (2000) "Planning Guidance Notebook," U.S. Army Corps of Engineers, Washington D.C.

ER 1105-2-101, (2006) "Risk Analysis for Flood Damage Reduction Studies," U.S. Army Corps of Engineers, Washington D.C.

EM 1110-2-1619, (1996) "Risk-Based Analysis for Flood Damage Reduction Studies," U.S. Army Corps of Engineers, Washington D.C.

Hydrologic Engineering Center, (2008) "HEC-WAT, Watershed Analysis Tool," User's Manual, Beta Version 1.0, CPD-88, U.S. Army Corps of Engineers, Institute for Water Resources, 609 Second Street, Davis, CA 95616.

Hydrologic Engineering Center, (2008) "HEC-HMS, Hydrologic Modeling Systems," User's Manual, Version 3.3, CPD-74A, U.S. Army Corps of Engineers, Institute for Water Resources, 609 Second Street, Davis, CA 95616.

Hydrologic Engineering Center, (2007) "HEC-ResSim, Reservoir System Simulation," User's Manual, Version 3.0, CPD-82, U.S. Army Corps of Engineers, Institute for Water Resources, 609 Second Street, Davis, CA 95616.

Optimal Design of Water Diversion System: A Case Study

Mohammad Karamouz[1], Siyamak Doroudi[2], Azadeh Ahmadi[3], Ali Moridi[4]

[1] Professor, School of Civil Engineering, University of Tehran, Tehran, Iran. karamouz@ut.ac.ir
[2] M.Sc. Student, Engineering Department, Islamic Azad University- Science & Research Branch of Tehran, Iran. siyamak.doroudi@yahoo.com
[3] Ph.D. Candidate, School of Civil Engineering, University of Tehran, Tehran, Iran. azadehahmadi@ut.ac.ir
[4] Ph.D, School of Civil Engineering, Amirkabir University (Tehran Polytechnic), Tehran, Iran. moridi@cic.aut.ac.ir

ABSTRACT

Study of uncertainties in the design of dam diversion is of great importance due to its high economic impact on the construction cost. It is important to study the carrying capacity of the diversion systems, considering the hydrologic uncertainties due to climate change phenomenon and its impacts in decision making. In order to consider these uncertainties, the historical rainfall data of the nearest gauge stations have been analyzed, then the rainfall variations in the future have been predicted using down-scaling of the GCM (general circulation model) data. The runoff of the basin is simulated using rainfall runoff modeling. The results of uncertainties evaluation have been incorporated in an optimization model.

In this paper, a GA-based optimization model for determining the optimal sizing of a dam diversion system is developed. The proposed model minimizes the flood damages and costs based on the optimal size of the dam diversion system in a probabilistic framework. The proposed algorithm considers risk in the decision making about diversion dam height and diversion tunnel characteristics. In this model, the hydrological uncertainties and the climate change impacts in design of dam diversion system are considered in the objective function of the optimization model. The proposed methodology is applied to the Karoun-4 Dam in the south-western part of Iran. The results show the significance value of considering flood risk and climate change impact on the design of dam diversion systems.

Keywords*:* Genetic Algorithm, Optimization, Dam Diversion System, Climate Change, Hydrological Uncertainties, General Circulation Model

INTRODUCTION

In order to construct a structure on a river, it would be inevitable to use a diversion system in order to have dry construction site. As there are different types of diversion systems, the diversion system type depends on topographic conditions, site characteristics (geologically and geo-technically), river's hydrologic features, expected cost, etc. A common diversion system is using an upstream cofferdam accompanied with one or more tunnels. The dimensions of a diversion system should be constructed in a way that can safely pass the possible flood with regular return periods, and if it fails to do so, the flood damages should be minimized. Therefore there is a tradeoff between construction costs and flood damages.

The cost of diversion works depends, among other factors, on: the tunnel dimensions

and the intended tunneling support measures during and after excavation; quality and specifications of the rock through which the tunnel should be excavated. The dimensions of the upstream (and downstream) cofferdams; the characteristics of the required spillway, should be designed to divert the floods.

Yen (1985) attempted to introduce a predictable error made by project designer through definition of a risk-based design methodology. Pate-Cornell and Tagaras (1986) designed dam hydrological components considering risks and hydrological uncertainties. Following a similar approach, Afshar and Marino (1994) optimized the dam overflow capacity based on the risk concept. Tang (1975) optimized discharge of a drainage system based on risk-based design, considering hydrological uncertainties for the first time. Saeedi (2007) optimized the construction costs through selecting the dimensions of a diversion system considering tunnel covering material, type of drilling, supporters, and type of upstream cofferdam soil through mathematical solving of assumed equations.

In this paper, an uncertainty based optimization model is developed for determining the optimal characteristic of a diversion system to the proposed model which analyzes the influence of hydrologic uncertainties. SDSM (Statistical Downscaling model) is used to forecast different floods during dam construction, then a rainfall-runoff model is used to simulate the rainfall flowing to the diversion dam. The probable floods are routed to calculate the flood damages. An optimization model is developed to minimize the construction costs and the expected damages for determining the optimal diversion dam characteristics. The decision variables in the GA-based optimization model are the tunnel diameter, covering material, length, the height of upstream cofferdam and down stream cofferdam, due to floods with different return periods. The proposed model is applied for optimizing the Karoon 4 diversion system in the south-western part of Iran as a case study.

METHODOLOGY

In this case study, an optimization model is proposed to minimize costs and damages. The objective function of the optimization model includes construction costs, and the damages cost due to floods with different return periods. This model determines the best tunnel diameter and support and lining types of the tunnel according to the Manning coefficient and it also specifies level and length of the tunnel, heights of the upstream cofferdam and downstream cofferdam. It shows whether or not a Spillway for upstream cofferdam is needed. The proposed model has the three following steps:

Step 1: The recorded data as the inputs of the model is gathered and analyzed. The data consists of observed rainfall series, cross section, slope, Manning coefficient of the river and the climatic conditions of the case study.

Step2: A rainfall forecasting model is used to predict the rainfall and flood events in real time operation. In this study, SDSM (Statistical Downscaling model) which downscales General Circulation Model (GCM) output data according to climate change scenarios is used as a forecast model. Based on the obtained results of the SDSM model, the rainfall- runoff model is used to estimate the flood volumes during the construction dams. Then the flood hydrograph of different return periods are

estimated leading to calculate the probabilities of flood events.

Step 3: The objective function of the optimization model is estimated based on the construction dams for different decision variables (such as tunnel diameters, heights of cofferdams) and damages due to different floods. In order to calculate the damages, according to the decision variables, the floods are routed in the diversion system. It is a tradeoff between construction costs of spillway, tunnel with different characteristics and cofferdams. Using iterative procedure in the optimization model, the best values of decision variables to minimize the costs and damages are determined

CASE STUDY

The Karoon 4 dam is located on Karoon River in the southwestern part of Iran. The characteristics of the Karoon watershed and the Karoon 4 dam are presented in Table 1. The potential runoff inflow to the reservoir is about 4549 MCM.

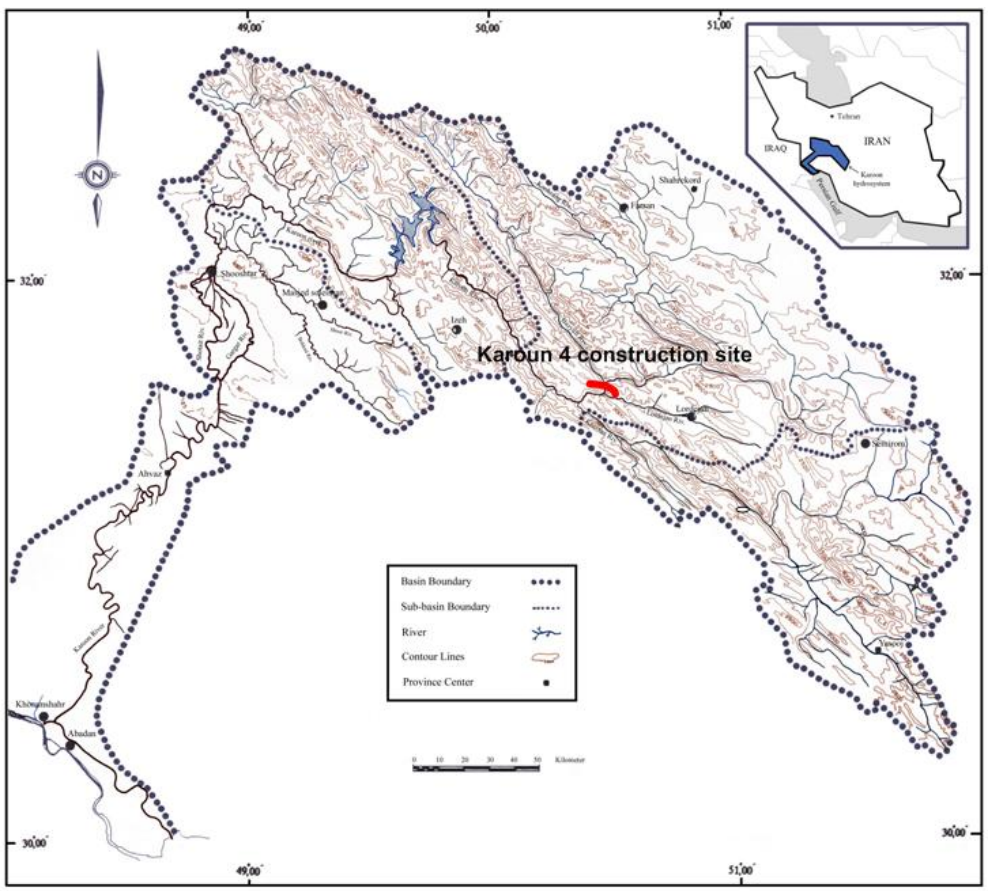

Figure 1: Karoon watershed and location of Karoon 4 construction site

During construction of dams, the river water has to be diverted away from the dam

site so that the construction of the dam can be undertaken in the dry. The usual method of river flow diversion involves construction of tunnels and cofferdams. The tunnel is excavated in either of the abutments to divert the entire river flow and both its normal and flooding condition, around the dam site. The cofferdams are watertight structures, usually earth embankments, constructed upstream and downstream of the site to isolate the construction area that is to be kept dry. The tunnel entrance is upstream of the upstream cofferdam and discharges into the river downstream of the downstream cofferdam (Saedi, 2007). Figure 1 shows the location of the Karoon 4 construction site.

Table 1: The characteristics of the Karoon watershed and the Karoon 4 dam

Area (km^2)	Average rainfall (mm)	Dam capacity (MCM)0	Length of diversion tunnels	Number of outlets	Hydropower energy (Mw)
12813	680	2192	655 , 664	3	1000

The diversion system of Karoon 4 reservoir has two tunnels, an upstream cofferdam and a downstream cofferdam. The average upstream and downstream side slopes of the cofferdams are considered 1 vertical over 2.5 horizontal. Manning roughness coefficient is about 0.014, 0.022 and 0.03 for different tunnel lining 1) rockbolts and shotecrete and reinforced concrete 2) rock bolts and shotcrete 3) little rock bolts and shotcrete. The tunnel dimensions, tunnel support types, heights cofferdams, construction of upstream cofferdams spillway, the upstream and downstream tunnel elevations (slope of the tunnel) are determined. There are some limitations on the tunnel diameter ($7.0m < D < 13.0m$) and height of the upstream cofferdam ($15m < H < 75.0m$).

METHODS AND MATERIALS

In this study SDSM is used as a forecasting rainfall model, HEC-HMS is used to estimate the runoff due to forecasted rainfall and Genetic Algorithm (GA) is used to solve the optimization model. In the following sections, brief descriptions of the models used are given.

SDSM Model

Even though global climate models in the future are run at a high resolution, the need will remain to "downscale" the results from such models to individual sites or localities for impact studies (Department of the Environment, 1996).

Downscaling techniques are divided into two main groups: Statistical and dynamical. In situations where low–cost, rapid assessments of localized climate change impacts are required, statistical downscaling (currently) are more effective. In this study, SDSM has been used for long-lead rainfall prediction for an individual site at daily time–scales, by using grid resolution GCM output.

During downscaling with SDSM, a multiple linear regression model is developed between a few selected large-scale predictors and local scale predictands such as temperature and precipitation. Figure 2 shows a schematic illustrating the general approach to downscaling.

The parameters of the regression equation are estimated using the efficient dual simplex algorithm. Large-scale relevant predictors are selected using correlation analysis, partial correlation analysis and scatter plots, and also considering physical sensitivity between selected predictors and predictand for the region. Ideally, predictor variable candidates should be physically and conceptually sensible with respect to the predictand (precipitation) and accurately modeled by GCMs. For precipitation downscaling, it is also recommended that the selected predictor should contain variables describing atmospheric circulation such as thickness, stability and moisture content. In practice, the choice of predictor variables is constrained by data availability from GCM archives.

Structure and operation of SDSM includes five distinct tasks: (1) preliminary screening of potential downscaling predictor variables; (2) assembly and calibration of SDSM(s); (3) synthesis of ensembles of current weather data using observed predictor variables; (4) generation of ensembles of future weather data using GCM-derived predictor variables; (5) diagnostic testing/analysis of observed data and climate change scenarios.

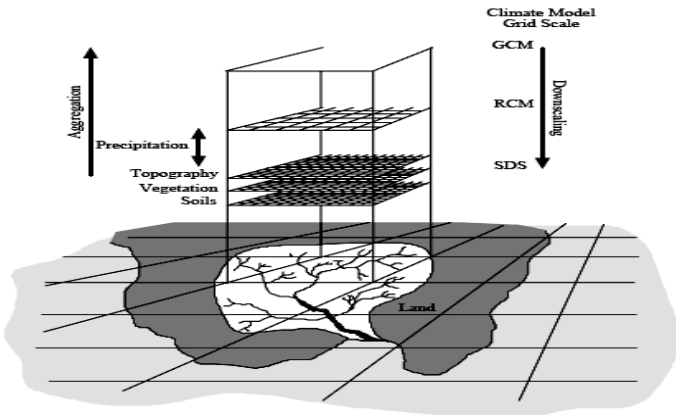

Figure 2: A schematic illustrating the general approach to downscaling. (Wilby &Dawson, 2004)

Model Formulation

The objective function of the optimization model is the total construction costs and expected damages that might occur during the project. The probabilities of flood events with different return periods are considered by the expected value of flood damages and the construction expenses of the diversion system. The objective function and the constraints of the proposed optimization model are as follows:

$$Minimize\ Z = E(damage) + Cost_C = \sum_{i=1}^{6} P(i)(D_{T_i}) + Cost_C \quad (1)$$

$$D_{T_i} = Damege_{i,UC} + Damege_{i,DC} + Damege_{i,Tunnel} + Damege_{i,Site} \quad (2)$$

$$Cost_C = (Cost_{Tunnel} + Cost_{Upstreamcofferdam} + Cost_{Downstreamcofferdam}) \quad (3)$$

$$Cost_{Tunnel} = C_e + C_l + C_S \quad (4)$$

$$C_e = V_e \times U_e = \frac{\Pi}{4} L\left[D + 2(T + 0.1)^2\right] \times U_e \tag{5}$$

$$C_l = V_l \times U_l = \Pi LT[D + T] \times U_l \tag{6}$$

$$C_S = V_S \times U_S = \Pi LT[D + 2T] \times U_S \tag{7}$$

$$Cost_{Upstreamcofferdam} = U_{UC} * V_{UC} + XU_{SP}V_{SP} \tag{8}$$

$$V_{UC} = W[(B + 0.5(z_u + z_d)(H + F)](H + F) \tag{9}$$

$$V_{SP} = W_{SP}(b + z_d k)k + 0.5W(B \times k) \tag{10}$$

$$Cost_{Downstreamcofferdam} = U_{DC} * V_{DC} \tag{11}$$

$$V_{DC} = W_{DC}[(B_{DC} + 0.5(z_{du} + z_{dd})(H_{DC} + F_{DC})](H_{DC} + F_{DC}) \tag{12}$$

$$IF(0 < h/D < 0.5) \Rightarrow Q = (\frac{D}{4}\left[\frac{\sqrt{1-a^2}a}{(Arc\cos a)}\right])^{2/3} \frac{AS^{1/2}}{n}, a = (\frac{D/2 - h}{D/2}) \tag{13}$$

$$IF(0.5 < h/D < 1.0) \Rightarrow Q = (\frac{D}{4}\left[\frac{\sqrt{1-a^2}a}{(\Pi - \arccos a)}\right])^{2/3} \frac{AS^{1/2}}{n}, a = (\frac{h - D/2}{D/2}) \tag{14}$$

$$1.0 < h/D < 1.5 \Rightarrow Q = 0.62 \sqrt{\frac{1}{1 - \left[\frac{D}{h + D/2}\right]^4}} A\sqrt{2gh} \tag{15}$$

$$1.5 < h/D \Rightarrow Q = A\sqrt{2g}\left[\frac{h + L.S_T - \xi D}{1 + Ke + \frac{2gn^2 L}{R^{4/3}}}\right]^{1/2} \tag{16}$$

$$Q_{SP} = C_0 W_{SP} h_{SP}^{1.5} \tag{17}$$

where :

i : the index of flood occurrence with given return period, $P(i)$: probability of flood occurrence with different return periods, D_{T_i} : the flood , $Cost_C$: construction, $Cost_{Tunnel}$: cost of tunnel construction, C_e : cost of tunnel excavation, U_e : unit cost of tunnel excavation, V_e : volume of tunnel excavation, C_l : cost of tunnel lining, U_l : unit cost of lining of tunnel, V_l : volume of tunnel lining, : C_S cost of tunnel support, U_S unit cost of tunnel support, V_S : volume of support, T: lining thickness, L: tunnel length, D: tunnel diameter, $Cost_{Upstreamcofferdam}$: construction cost of upstream cofferdam, W: the crest length of upstream cofferdam, B: is the cofferdam top width, z_u : the upstream side slope of upstream cofferdam section, z_d : the downstream side slope of upstream cofferdam section, H: height of upstream cofferdam , F : upstream cofferdam free board , U_{UC} : unit cost of upstream cofferdam, X : variable of spillway $(\{1,0\})$, V_{SP} : concrete volume of spillway, U_{SP} : unit cost of spillway, parameters, b: cofferdam downstream length, k: spillway

lining thickness, Wsp: width spillway $Cost_{Downstream cofferdam}$: cost of building downstream cofferdam length, V_{DC} : volume of downstream cofferdam W_{DC} : length of downstream cofferdam, B_{DC} : the downstream cofferdam top width z_{du} : the upstream side slope of downstream cofferdam section, z_{dd} : the downstream side slope downstream cofferdam, H_{DC} : height of downstream cofferdam, F_{DC} : down stream cofferdam free board, U_{DC} :: unit price of. downstream cofferdam, : C_0 variable discharge coefficient, Q : Discharge outlet of tunnel, S : The longitudinal slope of tunnel, R : Hydraulic radius, n : Manning roughness coefficient, h : the water head above tunnel intake, A : tunnel cross section, g : gravitational acceleration, Ke : the tunnel entrance loss coefficient , ξ : variable of tunnel outlet $(\{1,0.5\})$ Q_{SP} : spillway Discharge , W_{SP} : width spillway.

Equations 2-4 show the construction costs including tunnel, downstream and upstream cofferdams costs and the damages due to flood damages of tunnel, cofferdams and the working site. The construction costs are estimated using Equations 5-12, considering the volume of the materials. Equations 13-16 are used to calculate the discharge of the tunnel. Since the capacity of water transfer from diversion tunnels is limited, in large floods the spillway is constructed for increasing the passing capacity Therefore, the upstream cofferdam with a spillway is usually built. Equation 17 shows the passing discharge over the spillway.

In this study in order to find the optimal characteristic of the diversion system, the Genetic Algorithm (GA) optimization method is utilized. Genetic algorithm is an adaptive method trying to imitate the biological and genetic process and can successfully be applied to optimization problems

GA is a population of individuals, named chromosomes. Each chromosome represents a potential solution to a problem. This solution is evaluated by its fitness function. As each chromosome represents a potential solution, the fitness of each chromosome as a candidate solution, must be evaluated by a random search process to form the decision space. Additionally, fitness is a function of the problem constraints, and must be satisfied. Through successive generation, fitness should progressively be improved towards an optimum solution. The new population is generated using the genetic operators including Selection, Crossover, and Mutation.

More details of genetic algorithms can be obtained in the works of Michalewicz (1992a, b) and Gen and Cheng (2000). Genetic algorithms usually consist of the following steps:

1. Encoding of the decision variables and placing them in a chromosome.
2. Creating an initial population (first generation).
3. Determination of fitness for every chromosome in the current population (fitness
4. Setting the probability for mutation and crossover.
5. The selection of better chromosomes for matching and running a cross over operator for shuffling the selected chromosomes.
6. Performing mutation for selected chromosomes.

7. Repeat steps 3–6 to obtain the optimal or near optimal solutions.

In general, GAs start with a population of chromosomes and later modifies them through genetic operators to produce better fitting chromosomes. The main fields of application of GAs include problems with high complexity and non-linear behavior.

RESULTS

The SDSM model was calibrated for 1961-1995 with correlation factor (R^2) of 0.81 and 0.79 for HadA2 and HadB2 scenarios respectively. The validation results for 1995-2005 give a correlation factor (R^2) of 0.64 and 0.58 for HadA2 and HadB2 respectively.

The predicted monthly average precipitation of two selected scenarios (HadA2 and HadB2) and observed data are shown in Figure 3. The 10 year predicted average monthly data are from 2006- 2016 and the observed data is based on the monthly average from 1961- 2005.

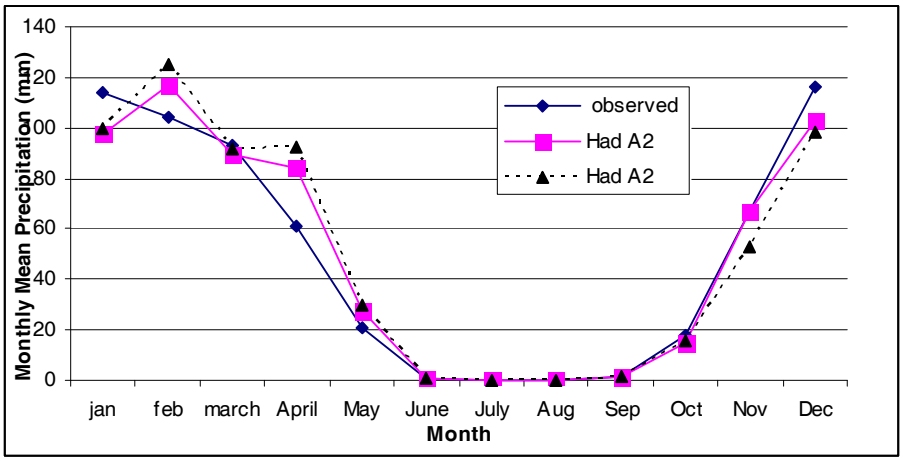

Figure 3: Comparison between precipitation Output of Had A and Had B scenarios from SDSM, and Observed Monthly precipitation.

A rainfall-runoff model has been developed using HEC-HMS software. Sub-basins of the study area have been characterized and modeled in HEC- HMS software using the SCS method. The hydrograph of March 9-12, 2004 flood has been used for model calibration. The hyetograph of rainfall has been estimated using central patterns of SCS hyetographs because of monotonous and steady intensity during the rain time in the region. The SCS curve method has been used for runoff estimation and an average curve number (CN) of 42 has been estimated for the watershed. The observed and simulated Hydrograph after rainfall-runoff model calibration for March 9-12, 2004 are shown in Figure 4. The forecasted flood hyetograph has been entered into the HEC- HMS model and the amount of flood at the construction site is estimated.

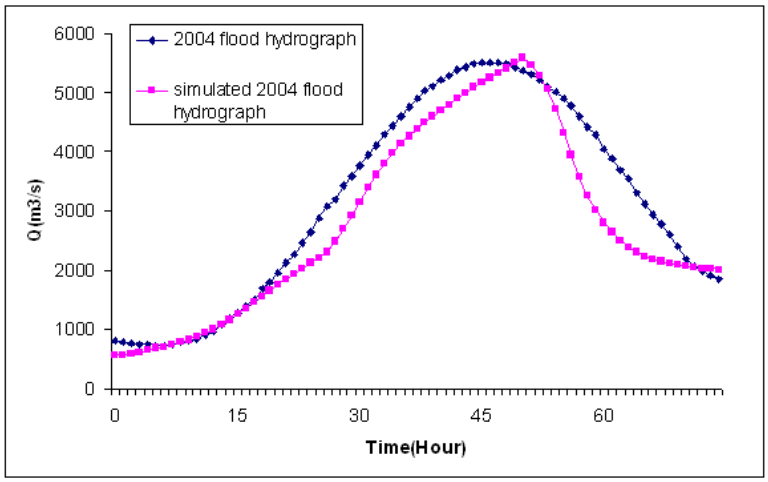

Figure 4: Comparison between simulated and observed flood hydrograph

The developed optimization model considers different alternatives for construction of the diversion system with a minimum cost that could yield low damages. According to the results, by investing about 2.4 million Dollars for the construction of a diversion system, the expected value of damages is reduced to 1.18 million Dollars. This considerable gain shows the significant value of utilizing the proposed approach.

Table 2 shows the optimal characteristics of the diversion system. The result of the optimization model maintains the construction of a cofferdam with a height of 40 meters with a spillway with the capacity of 3500 cms. The model has also proposed construction of a tunnel, 9.5 meter diameter and 655 meter length and a second tunnel with a 9.5 meter diameter and 644 meter length.

Table 2: Optimal characteristic of diversion system

Tunnel diameter(1)	Tunnel diameter(1)	Tunnel support(1)	Tunnel support(2)	Upstream tunnel elevation(1)	Upstream tunnel elevation(2)
9.5m	9.5m	Type1	Type2	850.5m	860m
Downstream Tunnel elevation(1)	Downstream Tunnel elevation(2)	Upstream cofferdam height	Downstream cofferdam height	Spillway construction	Spillway capacity
842.55m	853m	40m	20m	Yes	$3500\,m^3/s$

SUMMARY AND CONCLUSION

In this paper, an optimization model is used to design a diversion system for Karoon 4 dam site in the southern part of Iran. The proposed optimization model utilizes a Genetic algorithm model in order to select the best diversion system. The proposed optimization model minimizes the cost construction and expected value of damages. The expected values of damages are obtained based on the return period of

forecasted floods in the study area. In the proposed model, the HEC-HMS model is used for the hydrologic simulation of different precipitation events forecasted based on down scaling of GCM model results. A hydrological model is used for routing of flood in the cofferdam reservoir with and without a spillway. The innovative aspect of this study is the application of the Genetic Algorithm optimization model utilizing engineering, economic and flood probability in optimal design of a diversion system. The results include an explicit economic valuation of the cost and damages and an economical-based plan for the diversion system.

REFRENCES

Afshar,A., Barkhordary,A., Marino, M.A. (1994), "Optimizing river diversion under hydraulic and hydrologic uncertainties." J. Water Resour. Plng. and Mgmt., ASCE.,120(1),36-47.

Gen M.R., Cheng L. (2000), Genetic algorithms and engineering optimization Wiley, Europe.

Michalewicz Z. (1992a), Genetic algorithms data structure evolutionary programs, Springer , New York.

Michalewicz Z. (1992b), Genetic algorithms + data structure evolutionary programs, Springer New York.

Pate-Cornell, M.E., Tagaras, G. (1986), Risk costs for new dams: Economic analysis and effects of monitoring , Water Resour. Res., 22(1), 5-14.

Saiedi S. (2007), "Optimum diameter of diversion tunnels in dam construction" J. Dam Engineering , XVIII (1), 51-70.

Tung ,Y.K. (1987), "Effects of uncertainties on optimal risk-based design of hydraulic Structures" J. Water Resours .Plng. Mgmt., ASCE.113(5), 709-722.

YEN, B.C. (1985), Reliability of Hydraulic Structure Possessing Random Loading and Resistance,.University of Illinois at Urbana Champaign Press.

Wilby, R.L., Dawson, C. (2004) “Using SDSM Version 3.1- A decision support tool for the assessment of regional climate change impacts”, A Consortium for the Application of Climate Impact Assessments (ACACIA) Canadian Climate Impacts Scenarios (CCIS) Project Environment Agency of England and Wales.

KANSAS RIVER BANK STABILIZATION AND POST-PROJECT CONDITIONS

John Blancett[1], PE, M.ASCE and Pete Jarchow[2], PE, M.ASCE

[1]HNTB Corporation, Water Resources Group - Project Engineer / Assistant Department Leader, 715 Kirk Drive, Kansas City, MO 64105; PH (816) 527-2539; FAX (816) 221-9016; email: jblancett@hntb.com
[2]HNTB Corporation, Water Resources Group - Project Manager / Department Leader, 715 Kirk Drive, Kansas City, MO 64105; PH (816) 527-2248; FAX (816) 221-9016; email: pjarchow@hntb.com

Abstract

In addition to the original design and construction information from the 2003 EWRI publication, this paper also includes follow-up regarding the Kansas River bank stabilization project condition.

The Kansas River is a major Missouri River tributary. The project site is 43 miles (70 kilometers) upstream from their confluence, with a drainage area of 58,610 square miles (151,800 square kilometers). The channel ranges from 590 to 1180 feet (180 to 360 meters) wide in an 8860-foot (2,700-meter) floodplain. The project area was a channel bulge along the left bank of the river, at an inflection point where the channel meanders from the north (left) side of the floodplain to the south side of the floodplain. A bridge is located downstream, in the middle of an east-west reach; downstream of the bridge, another meander returns the channel to the north. The sandy channel banks ranged from 20 to 30 feet (6 to 9 meters) tall, stood at slopes from 1.0 horizontal to 1.0 vertical, to nearly vertical, and tended to collapse into the channel thalweg and washed away whenever water levels receded.

During the wet decade of the 1940s the channel moved 670 feet (200 meters) eastward. The great 1951 flood resulted in an eastward shift of over 980 feet (300 meters), plus a significant channel shift southward, upstream of the bridge. At the channel bend between the project site and the bridge, three long right bank rock dike structures were built by Douglas and Leavenworth Counties in the mid 1950s; three short left bank structures were added in the late 1950s. These structures have been effective in stabilizing the reach upstream of the bridge. In the late 1970s, a Corps of Engineers demonstration project stabilized the bend upstream of the project site, mainly using windrow revetment that eventually launched and formed relatively uniform and stable bank armor. The 1993 flood initiated a left bank channel bulge between these two stabilized bends. The bulge steadily pushed eastward, progressing about 820 feet (250 meters) by 1999 and threatened existing stabilization.

Many different stabilization methods were considered, including Bendway Weirs, Bank Revetments, Rock Dikes, Longitudinal Peak Stone Toe Protection, and L-Head Dikes. The L-Head dikes were selected as a combination of the most cost effective and environmentally friendly alternative. The first four dikes were constructed in early 2002, and the fifth and sixth were installed in early 2003.

The protective works have been performing as expected, and ongoing monitoring and possible maintenance is recommended. The structures successfully moved the channel thalweg away from the bank, allowed the channel slopes to vegetate, and accretion / re-vegetation between the L-Heads and the banks.

Introduction

The site is located on the left bank of the Kansas River, 43 miles (70 kilometers) upstream of its confluence with the Missouri River. The project reach is in Douglas and Leavenworth Counties, north of Eudora, Kansas, 7 miles (11 kilometers) east of Lawrence and 20 miles (32 kilometers) west of Kansas City, Missouri. The Kansas River floodplain is 8860-feet (2,700-meters) wide at the site, and widens upstream of the site, reaching 15,100-feet (4,600 meters) in about 3 miles (5 kilometers). The Wakarusa River channel joins the Kansas River channel over 3,200 feet (one kilometer) downstream of FAS 209 Bridge (roadway: Highway 1 / extension of Main Street north of Eudora, KS).

The river channel location transitions from the extreme northern portion of the floodplain to the extreme southern portion as it flows past the site. The floodplain is heavily agricultural in the general vicinity of the site. Areas of trees and thick natural vegetation exist, mostly near the channel and generally in areas of recent accretion.

Unchecked, the left bank erosion and channel meander migration would eventually impact FAS Route 209 and its existing bridge over the Kansas River. This bridge is jointly maintained by Douglas and Leavenworth Counties, and serves as a major north-south Kansas River crossing. The nearest alternative crossing requires approximately a 20-mile (32-kilometer) detour. The eroding left bank was roughly 3,600 feet (1,100 meters) long and was migrating toward the FAS Route and the north bridge abutment. Earlier localized stabilization measures had not stabilized the entire reach.

The Soil Survey Reports indicate that the topsoil material in the erosion area consists of Sarpy-Haynie Complex and Eudora Complex. The former is described as a loamy fine sand and fine sand; the latter is defined as a silt loam and fine sand loam. Both readily erode. The bridge substructure (piers) is founded on concrete-filled sheet piling rings driven approximately 40 feet (12 meters) below the channel thalweg at the bridge.

Channel Movement and Previous Stabilization Efforts

The site history and movement of the Kansas River were investigated back to the early 1940s. The bank shifts were defined from aerials and mapping, and are superimposed on a 2001 aerial (Exhibit 1). The USGS map base contours (based on 1948 aerial photography) show the location of the channel prior to the 484,000 cubic feet per second (cfs) (13,700 cubic meters per second (cms)) 1951 flood, and its movement relative to a 1941 aerial photograph. In that period, the bank moved over 660 feet (200 meters), an average of 100 feet (30 meters) per year. USGS peak flow data at the Lecompton gage show annual peaks in 1941 through 1945 exceeded 100,000 cubic feet per second (2,830 cubic meters per second) every year. By comparison, subsequent to the 1951 flood, annual peak discharges have exceeded 100,000 cfs (2,830 cms) only five times. The 1951 flood caused a 1000 foot (300 meter) bank shift eastward, and nearly as much migration southward in the reach upstream of the FAS 209 bridge. In reaction to the 1951 channel movements, in 1953 three major dike structures were constructed from the right bank of the river into the channel upstream of the bridge to stabilize the reach, and a 600 foot (183 meter) wide channel was excavated. The dike structures from upstream to downstream, were 1500, 1260 and 1250 feet (457, 384, and 381 meters) long, respectively. The rock portions of these structures generally had a 6-foot (2-meter) top width and side slopes of 1.25

horizontal to 1.00 vertical. The structures ranged from a minimum of 4 feet (1.3 meters) tall, up to 20 feet (6 meters) in height. The channelization included a 30-foot (9-meter) base width pilot channel.

In 1959, three shorter rock dikes were constructed on the left bank, just upstream of the westernmost 1953 rock structure. These dikes, likely intended to stabilize the flow direction to the 1953 dikes, were keyed about 100 feet (30 meters) into the bank, had 12-foot (4-meter) top widths, side slopes of 1.25 horizontal to 1.00 vertical, and ranged from 170 to 330 feet (52 to 101 meters) in length. The dikes were angled downstream at about 60 degrees to the bank line. The area between the 1953 and 1959 structures and the Eudora Bridge has since been relatively stable. Some right bank erosion occurred in the 1990s, and as a result, the counties recently restored the river ends of the two right bank structures closest to the Eudora Bridge.

The left to right channel bend upstream of the 1950s protection measures and the project site moved significantly eastward in the early 1970s. A peak discharge of 140,000 cfs (4,000 cms) occurred in an October 1973 flood. A COE demonstration project was then implemented using windrow revetments at the bend upstream of the current project site, in 1979. The bank protected by the COE project appears to have been stable until the 1993 flood, which at 190,000 cfs (5,380 cms) was the second largest event since 1908.

The genesis of the current bulge at the project site may have been during a 1967 flood with a peak discharge in excess of 106,000 cfs (3,000 cms). The downstream end of the bulge was at the farthest upstream of the three left bank rock dikes constructed in 1959. The entire left bank, from the COE stabilization project to the Eudora Bend bridge, appears to have been stable from 1974 through 1990. There had been no discharges in excess of 100,000 cfs (2,830 cms) during this period. By 1992, a channel constriction had developed at the upstream end of the bulge, located between the downstream end of the left bank COE protection and heavy vegetation of a sandbar on the right. The 1993 flood resulted in floodplain flows moving eastward across the inside of the river channel loop north of the FAS 209 bridge. Significant damage occurred to the county road resulting from the flood flows. The eastward bulge between the two prior protection projects expanded significantly. Floodwater crossed the inside of the channel meander, along the north side of the floodplain, north of the current channel bulge.

The site was visited many times by the co-authors, from October 1998 through early 2003, before final construction of the protection. During that time the bank had moved approximately 160 feet (50 meters). Most of the recent bank movement occurred in late 1998 and in 1999, a period of extended above average flows with several higher peaks as well.

Site Hydrology and Hydraulics

The Kansas River has a drainage area of 58,460 square miles (151,400 square kilometers) at the USGS streamflow gage at Lecompton. That gage is at River Mile 63.8, which is 20 miles (32 kilometers) upstream of the left bank bulge site. The study site is at River Mile 43.5, with a drainage area of 58,610 square miles (151,800 square kilometers). The next USGS gage downstream is at Desoto, at River Mile 31.0, with a drainage area of 59,770 square miles (154,800 square kilometers). Approximately 60% of the drainage area lies within the State of Kansas. The hydrology at the project location is influenced by many reservoirs, located on most major tributaries to the Kansas River. The

oldest major reservoir went into service in 1948; the newest reservoirs began operating in the 1960s. Subsequent to the construction of the reservoirs, both average and peak discharges on the Kansas River have been reduced in comparison with the natural, pre-reservoir conditions. The average velocity of bank-full flows varies from 11 feet per second (3.3 meters per second) at the most constricted width to 4 feet per second (1.2 meters per second) in the widest areas, assuming that the channel is of uniform depth. It is likely that a significant scour area exists in conjunction with the constriction, reducing the actual maximum velocities somewhat.

Project Process

The justification of project need was necessary to proceed into project design. This required the project be designed in steps, each performed to determine the necessity, cost and direction of the next step. Therefore, Kansas City District Corps of Engineers retained HNTB Corporation of Kansas City, Missouri to assess, develop and design a stabilization project under the Section 14 Emergency Bank Stabilization Program. The steps of the project were as follows:

Site Assessment. The Site Assessment consisted of a site visit, acquisition of historical mapping, soils information and previous project plans. During the site visit, observations of active erosion were noted and measured against known landmark features.

The Kansas River is an active river that experiences significant and frequent movement over most of its length, and has an erodible silt and sandy floodplain which frequently lacks armoring vegetation on the banks. Previous bank stabilization measures have had mixed results; the 1953, 1959, and 1979 projects have all performed well but likely created hard points, perhaps causing the bulge at the project site. Historically, most of the major channel movements in the project area appear to be related to the occurrence of significant river flows. These high flows recede quickly, causing the saturated steep sandy banks to collapse. This material typically falls into or next to the channel thalweg adjacent to the bank, and is washed away.

The bulge erosion site at Eudora Bend changed the flow direction in a relatively short distance. The Site Assessment considered that the likely continuation of this pattern would accelerate the progression, until the bulge pushed all the way through the left bank to a short distance upstream of the FAS 209 bridge. This would adversely affect the flow alignment into the bridge opening and isolate the left bank 1959 dikes. Therefore, the Site Assessment recommended proceeding to the next step, and identified three possible stabilization measures for consideration.

Concept Design and Alternatives Analysis. The Concept Design and Alternatives Analysis involved the conceptual design of three (3) bank protection arrangements. The alternatives were selected based on the site conditions and the potential funds available for implementation. All alternatives were based on an efficient use of rock and a reasonable compromise between an ideal design and a limited construction budget. They were:

- **Rock Dikes.** A series of rock dikes projecting out from the bulge area, and a flow guiding dike at the upstream end of the bulge, would relocate the channel and cause sediment accretion downstream of the each dike. It would be used to direct flows towards the former main channel location, away from the bulge, similar to the success observed in the existing downstream right

bank dikes just upstream of the FAS 209 bridge. Due to severity of the bulge and the flow entry angle, flow would still impinge the bulge bank, and flow anomalies could result at the dike ends.

- **LPSTP**. Nearly bank aligned Longitudinal Peak Stone Toe Protection (LPSTP) would protect the toe and stabilize the bank within the bulge area. Minimal flow pattern improvements would result, versus the pre-constructed condition, allowing continual stress on the right bank from reflected flow off of the revetment.

- **L-Head Dikes.** A series of bankline re-establishing rock L-Head Dikes within the bulge, and a flow guiding dike at its upstream end, would relocate the channel, and cause sediment accretion downstream and behind the dikes. The bank paralleling portions of the L-heads would direct flows along or towards the former main channel location, away from the bulge. This was suggested by David Derrick of the U.S. Army Corps of Engineers, in lieu of a Bendway Weir alternative originally considered by the Site Assessment. David Derrick visited the site to assess the potential of Bendway Weirs, and recommended they be replaced with the L-Head Dike alternative. Bendway Weirs were dropped from consideration because of the flow entry angle into the upstream bend, the length of that bend and the relatively straight channel reach upstream, and because the various older stabilization measures were not considered compatible with Bendways.

All alternatives included rock protection / re-establishment of the upstream and downstream protection measures immediately outside of the erosion area, to inhibit erosive progression or a flanking of the proposed protective works. A comparison matrix was developed for evaluating the alternatives. The matrix assessed stability issues, potential hydraulic and environmental effects, and maintenance issues. The results of Step 2 were a report and a recommended alternative for design.

Design. The L-Head Dikes alternative was selected for design. A topographic and contour map of the river channel and the left bank throughout the bulge was necessary to obtain accurate quantities and an optimum design. To develop the map, the site was surveyed in October of 2000, but due to the rapid progression of the erosion it was necessary to resurvey the bank edge in September of 2001 and the entire southern portion in November of 2002. It was necessary to design for staged construction over two years, because of funding limitations. The locations of the proposed structures are shown on Exhibit 2, in addition to the 1953 Dikes and 1959 Dikes. The following describes the design elements:

- **Rock Blanket.** The stable upstream left bank, at the northwest extent of the erosion, is protected with a proposed 75 foot (23 meter) long full height Graded Stone blanket. The blanket has a minimum thickness of 3 feet (1 meter) and a bed surface placed rock toe, 10 feet (3 meters) wide by 5 feet (1.5 meters) thick. The revetment requires smoothly tapering 50 foot (15 meter) upstream and 80 foot (24 meter) downstream transitions.

- **Upstream Dike 1.** Downstream of the Rock Blanket, a 200 foot (60 meter) long rock dike is aligned along the pre-existing bank. Like the other project dikes, the side slopes are 1.5 horizontal to 1.0 vertical with a top crown width of 6 foot (2 meters).

- **L-Head Dikes 1 through 4.** The remaining downstream length of the erosion site is protected by four L-Head Dikes, two which were planned for construction in the first phase. The L-Head Dikes each consist of three segments: transverse (from the bank out into the river), curved (radial

direction change for construction equipment turning), and longitudinal (from the curve, downstream parallel with the river flow direction). The alignments were determined by aligning a curve from the stable bank upstream to the downstream end of the second 1959 left bank dike end, to create the desired future bank line (see Exhibit 3). The transverse portions of these dikes are perpendicular to the arc and are roughly perpendicular to the eroding bank, approximately 30, 105, 215 and 230 feet (9, 32, 66 and 70 meters) long respectively for L-Head Dikes 1 through 4. The curved portions have a 55-foot (17-meter) radius, and are approximately 80, 80, 80 and 66 feet (24, 24, 24 and 20 meters) in length along the baseline of the alignment, respectively for L-Head Dikes 1 through 4. The longitudinal portions are aligned from chords on the arc, aligned from the transverse riverward end, toward the riverward end of the next dike downstream. The longitudinal segments are roughly 40 percent of the gap distance between the transverse dikes, approximately 350, 190, 190 and 150 feet (107, 58, 58 and 46 meters) long respectively for L-Head Dikes 1 through 4.

Phase 1 Design and Construction. The L-Head Dikes were placed in two construction steps. First, the root (buried tie-back) was constructed and a full length platform was installed outward to approximately elevation 788.0 feet (240.2 meters), to relocate the thalweg and provide a work surface to nearly the elevation of the 1-year return period event 789.0 feet (240.4 meters). The platform included a riverward quantity of rock that could launch during thalweg adjustment. The deepest part of the channel was on the outside of the bend, along the eroding bank. The transverse portion of the dike blocked and redirected the existing thalweg outward. The flow was then directed along the face of the longitudinal portion of the dike, relocating the thalweg. It was presumed that this would cause the riverward stone to launch, protecting the dike toe from undercutting at the increased depth. In actuality, due to favorable flow conditions, minimal amounts of stone launched during construction. The contractor then completed (capped-off) the L-Head Dikes to the full design height of 794.0 feet (242.0 meters), starting from the river end and working back towards the bank, where the dike top slopes upward toward the bank. Additional Rock Blankets were installed along the bank adjacent to the tie-in of each L-Head Dike. Construction of Phase 1 was completed in March, 2002.

Phase 2 Design and Construction. Additional surveys were taken in November 2002 of the topography and contours at the location of proposed L-Head Dike 4, and at a possible tie-in location to the remnants of the 1959 Dike 1. The co-authors, with the assistance of Warren Mellema, a private consultant formerly with the Corps of Engineers, revisited the site, re-evaluated the un-constructed portion of the original design, and developed the Phase 2 design and construction plans.

- **L-Head Dike and Rock Blanket.** The L-Head Dike 4 was slightly relocated and re-aligned from the original design, as a result from observations of the constructed L-Head Dikes and in coordination with the newly proposed Crowned Revetment. A Rock Blanket at the bank was included at the tie-in of L-Head Dike 4.

- **Crowned Revetment.** At the time of Phase 1 design and construction, it was determined that the ground adjacent to 1959 Dike 1 was eroding too rapidly for that dike to be saved. However, drought conditions and the subsequent lack of high flows following the Phase 1 construction minimized additional erosion in that area during 2002. Therefore, it was decided to save 1959 Dike 1 and incorporate it into the project. As a result, the exposed and partially flanked east end of the existing 1959 Dike 1 was connected to the eroded bank by constructing a Crowned Revetment,

essentially converting the old dike into the streamline paralleling portion of an L-Head Dike. The new portion of the revetment has a similar section as the completed L-Head Dike 4, not including the launchable rock. It has a 6-foot (2-meter) top crown width and 1.5 horizontal to 1.0 vertical side slopes. The alignment was set parallel to the transverse portion of L-Head Dike 4.

It was determined necessary to minimize the disturbance to the existing 1959 Dike 1. Originally, lowering the top elevation of the existing dike was considered. However, it was decided to leave the dike unchanged, due to concerns regarding environmental disturbance to potential eagle perch trees, lack of construction safety for those working atop a potentially unstable steep rock structure, and the loss of hydraulic protective rock as compared to the current height.

Current Conditions

The majority of the 1970's Corps of Engineers windrow revetment upstream of Dike 1 has launched and protected the bank as expected. The transition into the project area will need regular monitoring to prevent flanking.

Accretion of material has been creating a depositional area suitable for natural re-vegetation behind the protective works (see Exhibit 4). The accretion was immediate and has decelerated through time. The depth of the accretion appears to be related to the dike height and frequency of inundation. The apparent vegetation is dictated by its survivability from inundation. As this area's deposition slowly increases in depth, it is expected to become populated with hardy maturing species.

Banks behind the protected works have slumped some, reaching stable equilibrium as evidenced by grasses and other vegetation on the banks.

The thalweg has paralleled the riverward face of the longitudinal portion of the L-Heads. The sacrificial riverward stone has only partially launched in some locations, leaving the remaining stone available for undercutting scour protection. The thalweg has also maintained an acceptable entry angle to the reach stabilized in the 1950s. The right bank upstream of the 1953 dikes was actively eroding due to flow impingement and has recently subsided. High flows that overtop the crowned revetment have been vaned between the upstream 1959 Dike (# 1) and the middle 1959 Dike (#2), causing slight erosion, debris accumulation and re-entry erosion. The channel and these structures will require monitoring and possible maintenance in the future.

The project plantings along the top of the bank, did not survive, due to dry weather, lack of sponsor maintenance, and the adjacent land owner's desire to re-cultivate the land for agricultural purposes.

The southern farm field runoff drains down the river bank into the accretion area immediately downstream of the L-Head Dike 3 tie-back, which is the best location for this slowly developing head-cut. The post-project attempts to arrest this have only been marginally successful.

The stabilization measures utilized rock blanket, dike and revetment designs in a cost effective manner, but are localized in nature, and as such are vulnerable to possible long term changes in the river that cannot be economically prevented, or to atypical flow conditions and extreme flooding that might occur.

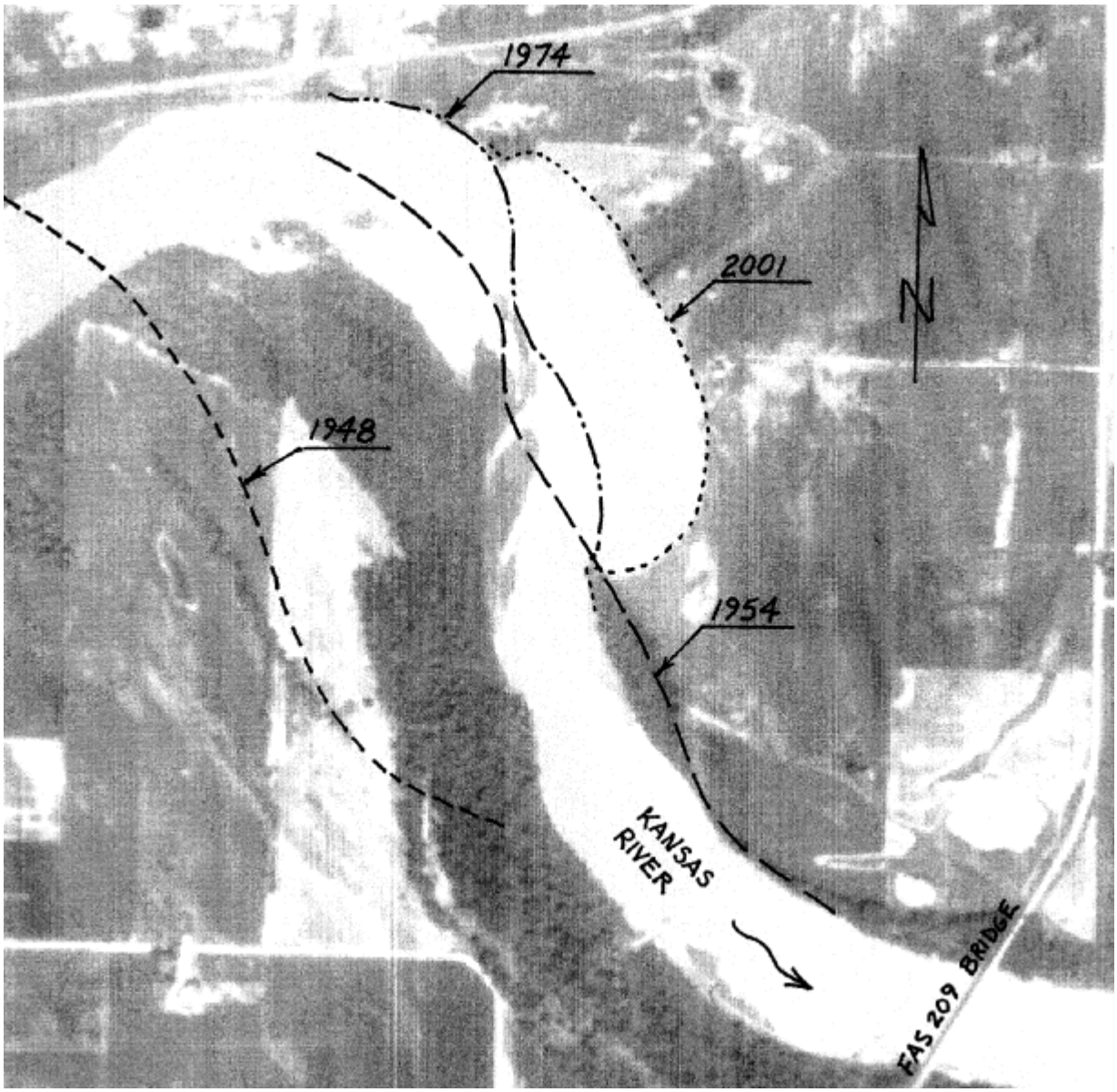

EXHIBIT 1 - Left Bank Progression, Kansas River near Eudora, Kansas

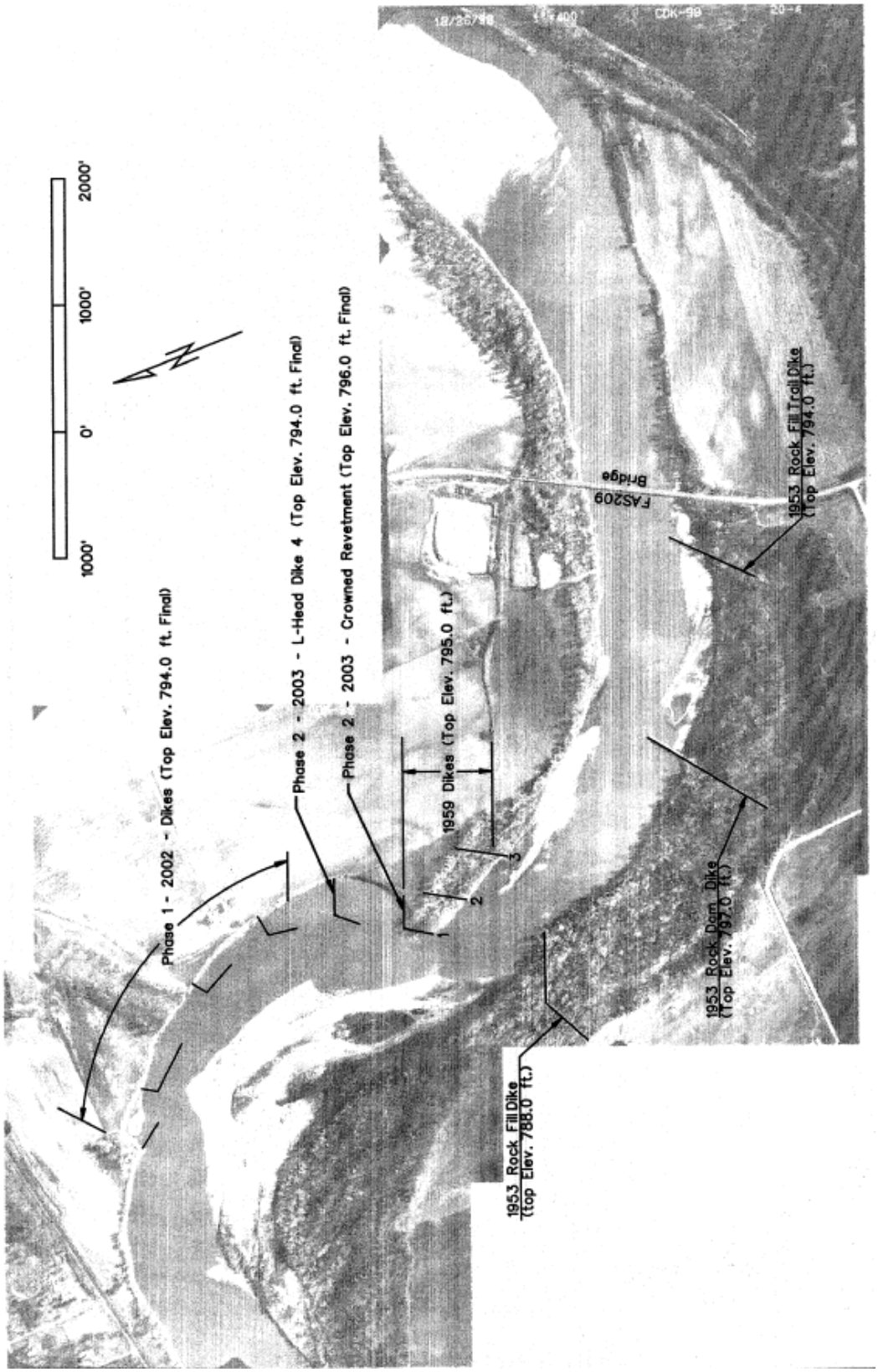

EXHIBIT 2 - 1953, 1959, 2002 and 2003 Bank Stabilization Structures, Kansas River

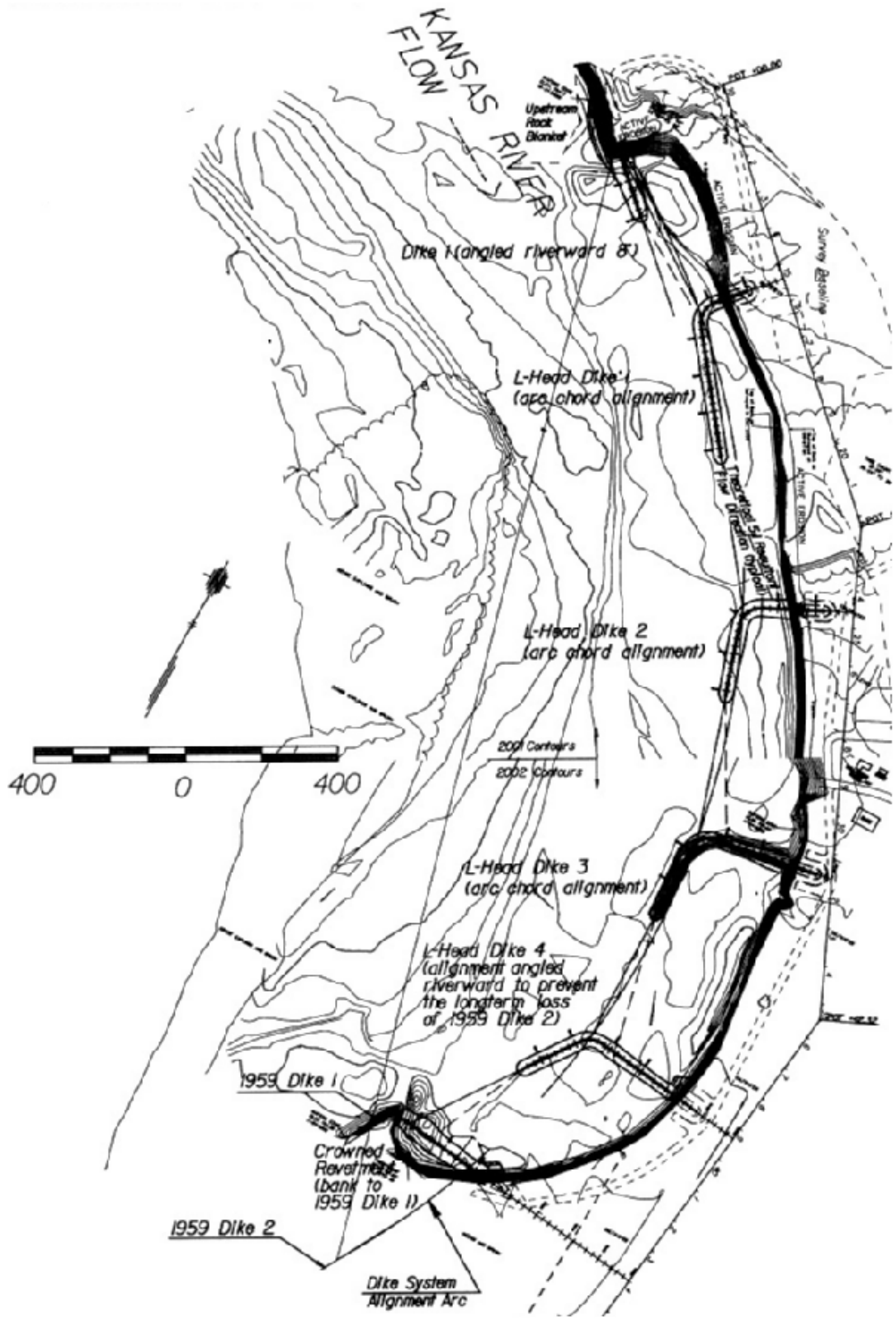

EXHIBIT 3 – Dike Layout on the Kansas River



Year 2000 – facing south (downstream) at L-Head Dike 3



Year 2006 – facing south (downstream) at L-Head Dike 3

EXHIBT 4 – same locations views - pre-project and post-project conditions

Adverse Affects of Flood Flow at Skewed Railroad Crossings

William Yord A.M.[1], Jerry R. Richardson M., D.WRE [2], Vincent J. Zink S.M.[3]

This poster presents a case study documenting the hydraulic issues relating to skewed bridge crossings. Although Hydraulic Engineering Circular Number 20 (HEC-20) discusses these adverse affects, the illustrations and discussions of the issues relating to skewed bridges are brief. This is not a failing of HEC-20 but an acknowledgement that, given the extensive scope of the subject matter contained in HEC-20, this document can only provide a very broad treatment of the methods and process for evaluating and designing bridges in a variable morphological environment.

This study presents the hydrologic investigation of a flood event from historic, eye witness, and post flood investigation. Analysis of this data clearly indicates that due to embankment skew, the water levels on the approach embankment were as much as 1.5 m (5 ft) higher than at the bridge opening. The consequences of this are graphically illustrated by photos taken during the flood, and analysis of post-flood hydrographic survey data.

Heavy rains from June 27 through July 1, 2007, over east-central Kansas (Southern Miami and northern Linn counties) resulted in widespread flooding in the Marais des Cygnes River basin. In less than five days, this region of Kansas received approximately 44% of the mean annual precipitation for Eastern Kansas (USDA 1942). This rainfall resulted in widespread flooding on the Marais des Cygnes River and its tributaries near the towns of La Cygnes and Pleasanton, Kansas. In some areas, the resulting flood waters overtopped the embankment and rails owned and operated by the Burlington Northern Santa Fe Railway Company (BNSF), eroded embankment material and mobilized the ballast for the rails. Specifically, significant flooding occurred at various locations between Milepost (MP) 47 and 63 of the Fort Scott subdivision, and one train was derailed due to the erosion of the embankment.

The following information was obtained from the National Oceanic and Atmospheric Administration's (NOAA) website (NOAA 2007):

> "Numerous rounds of heavy rainfall affected much the lower Missouri River Valley between Wednesday June 27 and Saturday July 1, resulting in widespread flooding across the region. Some of the harder hit areas include locations along the Marais des Cygnes river including Osawatomie and La Cygne Kansas and into Bates county of Missouri...locations along the South Grand river in Missouri...including the town of Urich...and Big Creek in Missouri...including the Blairstown area."

---

1 Project Manager, H&H Rail Wilson & Co, 903 E. 104th street, Suite 210, Kansas City Missouri 64110

2 Associate Professor, School of Computing and Engineering, University of Missouri Kansas City, 5100 Rockhill Road, Kansas City, MO, 64110

3 Intern Engineer, Wilson & Co, 903 E. 104th street, Suite 210, Kansas City Missouri 64110

Table 1 and Figure 1, also obtained from the NOAA website; provide a more detailed description of the rainfall totals and aerial extent of this event.

Table 1 Rainfall Totals Documented by NOAA (NOAA 2007)

City	County	Rainfall Total between June 27 and July 1, 2007, inches
Pleasanton	Linn, KS	15.80
Mound City	Linn, KS	15.01
La Cygnes	Linn, KS	14.90
Trading Post	Linn, KS	13.28

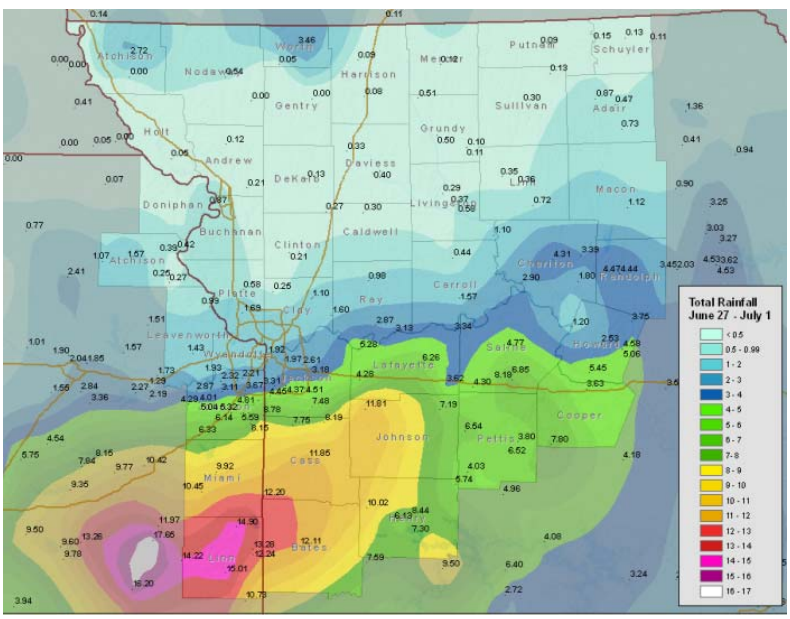

Figure 1 Isohyetal rainfall map June 27-July 1, 2007 (after NOAA 2007)

The flood that affected the Marais des Cygnes River basin in the summer of 2007 was between a 75 year and 100 year event (Table 2) based on review of the rainfall records, and flood frequency analysis of USGS stream gage data from two gages in the area during the time of the flood.

Table 2 Summary of Flood Frequency Analysis

Summary of Flood Frequency Analysis					
Trading Post Gage	**Gage # 6916000**				
	10-Year	**25-Year**	**50-Year**	**100-Year**	**200-Year**
Log Pearson III , cfs	59,036	92,026	123,900	163,123	211,141
Gumbel, cfs	74,764	100,236	119,133	137,890	156,579
PeakFq Bulletin 17 B	57,220	85,000	110,100	139,300	173,000
La Cygne Gage	**Gage # 6915800**				
Log Pearson III , cfs	60,792	91,544	121,658	160,227	181,125
Gumbel, cfs	74,270	97,420	114,593	131,640	148,625
PeakFq Bulletin 17 B	59,670	83,520	104,400	128,100	155,100

In addition to stream gage data and NOAA resources, there were other very valuable sources of information used in this study, which include reports dated September 25, 2007, Helicopter photos taken July 2, 2007, eyewitness accounts, FEMA Flood Insurance Rate Maps (FIRMs) and Flood Insurance Studies (FISs), and data collected during our 2008 field investigation.

The first data source that was reviewed was the Hanson-Wilson report dated September 25, 2007. This report addressed some of the bridge capacity issues along MP 47 to MP 70 on the Fort Scott Subdivision. The 2007 report did not go into detail regarding actual flood elevations with respect to the elevation of the rail facilities in those areas that received damage during the June 2007 event.

Hanson-Wilson was also provided pictures taken from a helicopter on July 2, 2007 showing the areas of flooding along the Fort Scott Subdivision. The photos were invaluable in locating landmarks and water surface elevations that could be field surveyed along the route, and sections of track that were showing signs of conveyance (water moving from one side of the track to the other).

The purpose for attempting to acquire FEMA FIRMs or FISs was to compare actual water surface elevations on the July 2, 2007 event with elevations shown within the FIRMs or FISs. This could only take place if there were previous detailed studies in the area to set base flood elevations (100 year flood elevations) along the Marais Des Cygnes River or its tributaries.

Unfortunately, there have been no previous detailed studies in either Miami or Linn County. The only FIRMs that are available are the Linn County FIRMs, which show the entire Marais Des Cygnes flood plain area in FEMA Zone A.

A field investigation was conducted on June 23, 2008. The team obtained data to better map the actual extents and water surface elevations associated with the flood. This effort was greatly assisted by the photographs taken from the air on July 2, 2007, and from the recollection of BNSF lookout Mr. Rex Hall, who was an eye witness to the flood event. His recollection was invaluable in locating points on the ground which could be surveyed to establish high water mark elevations.

The flooding caused by this storm system had severe consequences to the communities in the region (most notably La Cygne, and Pleasanton, Kansas). Significant stretches of BNSF's Fort Scott Subdivision was submerged between Milepost 47 and 63.

An important and significant source of information that was critical to this study was a series of photographs taken from the air at the peak of the flood (July 2, 2007 - Figure 2). These photos allowed us to survey flood elevations along the BNSF facilities with GPS and allowed us to identify areas of low-velocity ponded water and regions along the railroad where overtopping velocities were elevated.

7-2-07 Ft. Scott Subdivision Washout between Ft. Scott and Paola
Looking South from MP 49.3



Coal Train Parked on Main Line at LaCygne, Kansas Fort Scott Sub
Looking North from South LaCygne



Coal Train Parked on Main Line at LaCygne, Kansas Fort Scott Sub
Looking North from South LaCygne

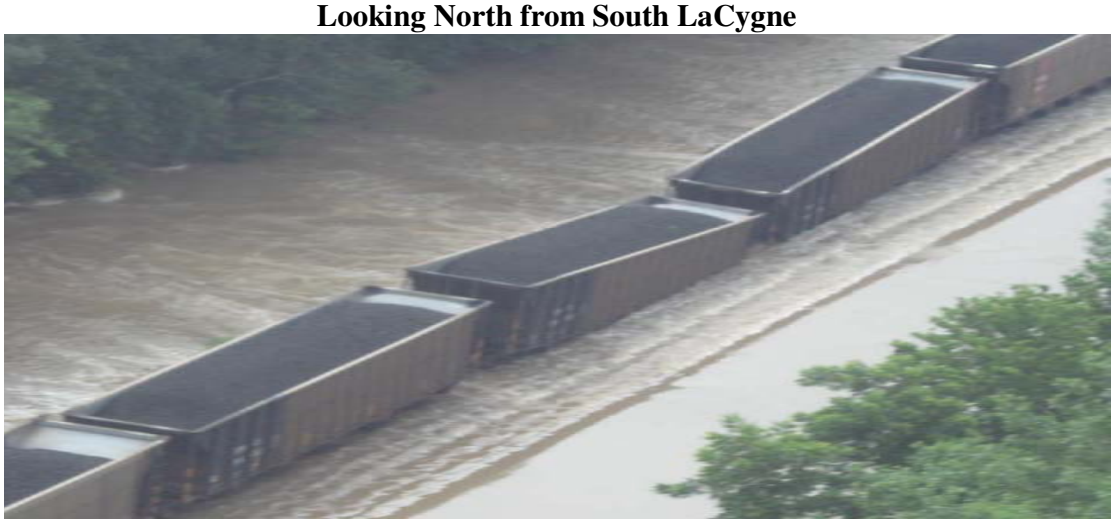

Figure 2 Air Photos of Overtopping Flow of Railroad Embankment

Although most of the railroad embankment and rail was inundated from MP 47 to 70, not all of the inundated embankments were damaged due to washout of the subgrade or ballast. Washouts were limited to locations where there was a significant cross-flow over and through the embankment.

Areas where there is a strong potential for washout is best determined from the air photos taken during the peak of the flood in early July 2007. Areas where the water surface elevations on each side of the railroad were nearly identical have minimal potential for washout. These can be easily identified because of the lack of waves or other disturbance of the water surface.

Inundated embankments without cross-flow are also subject to failure due to the potential loss of strength of the embankment material because the saturation of these soils; however, if the embankment is not loaded during saturation, and allowed to drain after the flood, the potential for embankment failure of these inundated areas is reduced.

Where the embankments were overtopped (cross-flow), the water is nearly at critical depth, and the wave action downstream is due to a weak hydraulic jump. Due to the uniqueness of the flow depth at critical depth, the overtopping flow velocity was estimated to be between 5 and 8 feet per second.

Differential water surface elevations from each side of the railroad embankments caused potential hydraulic energy and cross-flow that is available to move water through the embankment and ballast as sub-surface flow. Large differential heads result in hydrodynamic forces that can easily mobilize embankment and ballast materials. Because of this, damaged areas where the embankment has been washed out should be carefully rebuilt using standard geotechnical methods and compaction requirements.

The hydraulics and flood potential for MP 66.7-67.0 required special consideration. In this area the embankment of the railroad runs between the Marais des Cygnes River and Middle Creek (Figure 3). Since these two rivers share the same floodplain, the presence of the railroad embankment serves as a left overbank and right overbank levee for the Marais des Cygnes and Middle Creek, respectively.

If Middle Creek is flooding without the Marais des Cygnes flooding, water will flow through the relief bridges under the railroad from east to west. For very large floods on Middle Creek, water can overtop the railroad with a potential for washout of the west side of the railroad embankment. If (as in the case of the July 2007 flood) the Marais des Cygnes is flooding more than Middle Creek, the flow will be from west to east and the eastern embankments would be prone to washout. Finally if the flood on the Middle and Marais des Cygnes were nearly equal, the embankment could be inundated without washout potential.

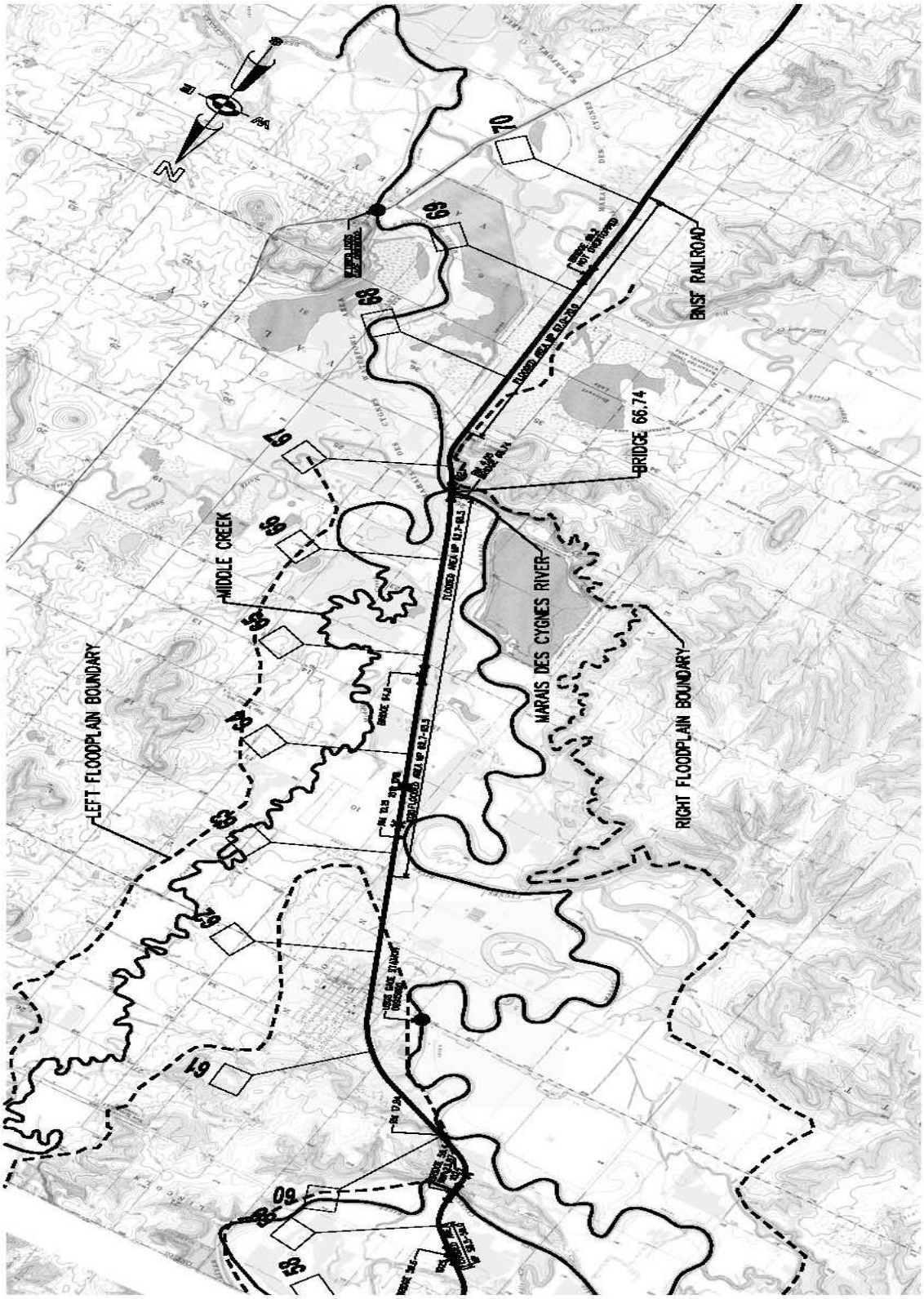
BNSF RAILROAD
BRIDGE 66.74
MIDDLE CREEK
MARAIS DES CYGNES RIVER
LEFT FLOODPLAIN BOUNDARY
RIGHT FLOODPLAIN BOUNDARY
70
69
68
67
66
65
64
63
62
61
60
59

Figure 3

As discussed previously, the flood that inundated and damaged the BNSF railroad from MP 47 to 70 had an exceedence probability of approximately 0.01 (100-year flood). However, due to the inundation and damage that occurred during this flood, the Ft. Scott Subdivision does not meet current design guidelines for hydraulic design.

We offered BNSF several options for dealing with this problem which are listed below:

1. Upgrade the line segment to meet current hydraulic design standards. This would require a comprehensive hydrologic and hydraulic study of the Marais des Cygnes River and tributaries. The design would require that most of the railroad would have to be raised between MP 47 and 70 and most of the relief structures would need to be modified or upgraded. The major river bridges would not need to be modified since they were not overtopped during the flood.
2. Stabilize the railroad embankment to mitigate/minimize washout potential. This option would accept having this line segment go out of service during a flood of similar magnitude but minimize damage and repair requirements. Service could resume soon after the flood waters recede. In this option the team of hydraulic and geotechnical engineers would assess the potential washout locations, prioritize them, and implement a plan to stabilize the embankment slopes so that the potential for washout is minimized. It is likely that areas of embankment would be required to be rebuilt and stabilized using a variety of techniques.
3. It may also be advantageous to accept that the flood was a rare event and repair only as needed. If another significant flood occurred it should be accepted that the railroad will go out of service and that washed out embankments will need to be repaired again. It should be noted that since the embankment repairs that were conducted after the 2007 event were not engineered, the extent of embankment damage may be larger the next time an event of this magnitude occurs.
4. Finally, it may be desirable to pursue a phased approach to upgrade the railroad to current design standards over a period of time. This option is a hybrid of option 1 and 3. In considering this approach it is noted that the main river bridges are sufficient to pass the 100-year flood. Furthermore, the areas that were overtopped and washed out are on sag vertical curves which would allow the rail to be raised relatively easily.

The most appropriate course of action depends on many factors such as the importance of this line segment to BNSF overall operations and the available alternative routes around this location when this line segment is flooded again.

Bridge river crossings that are skewed to a river or floodplain may require careful consideration regarding the effects to approach embankment, and abutment degradation caused by overtopping flood flows such as those that were experienced on the Fort Scott Subdivision. The data that was gathered during the flood by pictures helped provide a better understanding of what takes place and why during these events.

References

Flooding-June 2007." National Oceanic and Atmospheric Administration. 7 Jul. 2007. Jun. 2008. <http://www.crh.noaa.gov/eax/?n=flooding-june2007>.

Physical Modeling of River Spanning Rock Structures: Evaluating Interstitial Flow, Local Hydraulics, Downstream Scour Development, and Structure Stability

Kent L. Collins[1], Christopher I. Thornton[2], Brent Mefford[3], and Christopher L. Holmquist-Johnson[4]

[1]Sedimentation and River Hydraulics, Technical Service Center, U.S. Bureau of Reclamation, Denver, CO 80225; PH (303) 445-2563; FAX (303) 445-6351; email: kcollins@do.usbr.gov
[2]Hydraulics Laboratory, Engineering Research Center, Colorado State University, Fort Collins, CO 80253; PH (970) 491-8394; email: thornton@engr.colostate.edu
[3]Water Resources Research Laboratory, Technical Service Center, U.S. Bureau of Reclamation, Denver, CO 80225; PH (303) 445-2149 FAX (303) 445-6324; email: bmefford@do.usbr.gov
[4]Fort Collins Science Center, U.S. Geological Survey, Fort Collins, CO 80525; PH (970) 226-9382; email: h-johnsonc@usgs.gov

ABSTRACT

Rock weir and ramp structures uniquely serve a necessary role in river management: to meet water deliveries in an ecologically sound manner. Uses include functioning as low head diversion dams, permitting fish passage, creating habitat diversity, and stabilizing stream banks and profiles. Existing information on design and performance of in-stream rock structures does not provide the guidance necessary to implement repeatable and sustainable construction and retrofit techniques. As widespread use of rock structures increases, the need for reliable design methods with a broad range of applicability at individual sites grows as well.

Rigorous laboratory testing programs were implemented at the U.S. Bureau of Reclamation (Reclamation) and at Colorado State University (CSU) as part of a multifaceted research project focused on expanding the current knowledge base and developing design methods to improve the success rate of river spanning rock structures in meeting project goals. Physical modeling at Reclamation is being used to measure, predict, and reduce interstitial flow through rock ramps. CSU is using physical testing to quantify and predict scour development downstream of rock weirs and its impact on the stability of rock structures.

INTRODUCTION

River spanning rock structures can provide energy dissipation, create and enhance aquatic habitat, allow fish passage, relieve pressure on failing banks, establish grade control, and function as water diversion. Information on the design and performance of these structures is largely anecdotal based on empirical professional experience without the engineering rigor required for duplicability. Site specific design requires a

substantial design effort that in some cases can consume more resources than construction. Over the course of the past several years, the use of rock ramp and weir structures has spread from use as habitat restoration and fish passage as part of salmon recovery projects in the Pacific Northwest, to examination of alternatives to bank stabilization as part of the Middle Rio Grande River Maintenance Project in New Mexico. There is little systematic information on how well these structures meet project goals. Realizing the need for more qualitative assessment of the function of various structures, laboratory test program was designed and implemented.

Current in-stream rock structures research seeks to streamline the design process, increase understanding of the performance of river spanning rock structures, and improve the chances for successfully meeting management objectives. The laboratory physical modeling forms part of a multifaceted approach incorporating a quantitative evaluation of field data to provide empirical validation, laboratory physical modeling for controlled testing of complicated processes, and numerical simulations to expand the range of applicability and analytic capability. Field measurements, physical testing, and numerical modeling will combine to relate structure performance to interstitial flow, local hydraulics, and scour quantification processes. Laboratory tests will assist in developing tools and guidelines for more robust design or retrofits of river spanning rock structures based upon predictable engineering and hydraulic performance criteria.

Physical testing facilities in the hydraulic laboratories at the U.S. Bureau of Reclamation (Reclamation) and at Colorado State University were selected to investigate the impacts of interstitial flow and downstream scour development on the design, installation, function, and maintenance of river spanning rock structures. Current physical testing being conducted at Reclamation's Water Resources Research Laboratory at the Technical Service Center in Denver is focused on methods for quantifying and limiting interstitial flow through rock ramps. The Hydraulics Laboratory at the Colorado State University's Engineering Research Center in Fort Collins is being used to examine the downstream bed scour and structural stability in various rock weir structures. The physical modeling component will provide information for the development of sustainable construction and retrofit techniques, minimizing the structure lifecycle costs and maximizing their ability to reliably meet management objectives.

ROCK RAMP PHYSICAL MODELING

During periods of low stream flow, it is vital that rock ramps convey sufficient surface flow to meet fish passage requirements. Physical modeling facilities at the U.S. Bureau of Reclamation's Water Resources Research Laboratory at the Technical Service Center were used to determine design guidelines that identify the ratio of interstitial flow to surface flow passing down rock ramps and identify the effectiveness of adding "choke material" to the riprap to reduce permeability.

Project Need. Rock ramps are riffle like structures constructed in a stream to provide passage of aquatic species over low barriers. Ramps are typically constructed using loose riprap placed on a gravel or synthetic filter overlying a foundation of native

material. The size and gradation of the rock is based on achieving stability of the material under maximum design flow conditions. Ramp slope is generally selected based on achieving flow criteria required for aquatic specie passage. Ramps are typically constructed at slopes less than about three percent, however slopes up to five percent are used, and slopes up to ten percent have been considered.

The current state of the art does not provide the designer with sufficient guidelines to establish a low flow limit of operation for rock ramps. In many previous designs, uncertainty of interstitial flow capacity has lead to grouting to ensure sufficient water flows above the surface to support fish passage during periods of low river flow. Grouting is costly and often not favored by resource agencies. Surface grouting can also create structural problems over time by reducing the ability of the structure to adjust to foundation settlement or river degradation.

Project Objectives. This study was designed to provide the basis for selecting a rock gradation that includes estimation of the interstitial flow of the new structure. The study further investigated reducing ramp porosity by post construction choking of the ramp with selected fines and, to a limited degree, by natural sediment passage. The major objectives of the study were to:

- Conduct a literature review of flow through rock structures to develop a current basis of technology for predicting interstitial flow. The literature review also included other technologies incorporating flow through rock components. Some of these technologies are earth dam riprap overtopping protection, rock-fill dams, rock jetties, rock storm water detention levees, and water filtration.
- Develop a correlation between riprap gradation, slope, porosity and interstitial flow velocity that can be used for design of rock ramps.
- For steep rock ramps, determine the viability of post construction choking of riprap with a gradation of finer material to reduce interstitial flow.

Study Design. The framework for this study was developed as a series of tasks building on each other:

Task 1. The first task was to initiate the literature review with the goal of consolidating applicable design methods and prior research findings identified from published and gray literature sources. Current algorithms published for predicting and parameters that influence interstitial flow velocity interstitial flow velocity were documented.

Task 2. The next task was the modification of an existing physical model to obtain data on flow over and through rock ramps. The sketch in Figure 1 represents the basic conceptual design of the rock ramp test facility. The facility incorporated a 4-foot-wide by 22-foot-long by 6-foot-high Plexiglas flume in which sectional models of rock ramps were constructed. Water was supplied to the model from the laboratory sump using a 40 horsepower pump capable of discharging a maximum of about 8 ft^3/s flow. At the downstream terminus of the model, a 25 hp sediment pump provided up to an additional 8 ft^3/s flow and recirculation of sediment when required. The flume was instrumented with a vertical array of pressure piezometers and

temperature sensors located mid-channel at 5 ft stationing. Temperature probes were used to measure interstitial velocity. Hot water from a hot water heater was injected through a vertical ported pipe embedded in the rock ramp 1 ft downstream of the upstream cutoff wall. The time between injection and a rise in water temperature measured at the downstream probes equated to average interstitial flow velocity between stations. Interstitial flow was be measured at the terminus of the ramp by routing water passing through the rock to a separate channel and measuring weir. End effects in the model were avoided by adjusting a porosity plate located at the downstream end of the ramp.

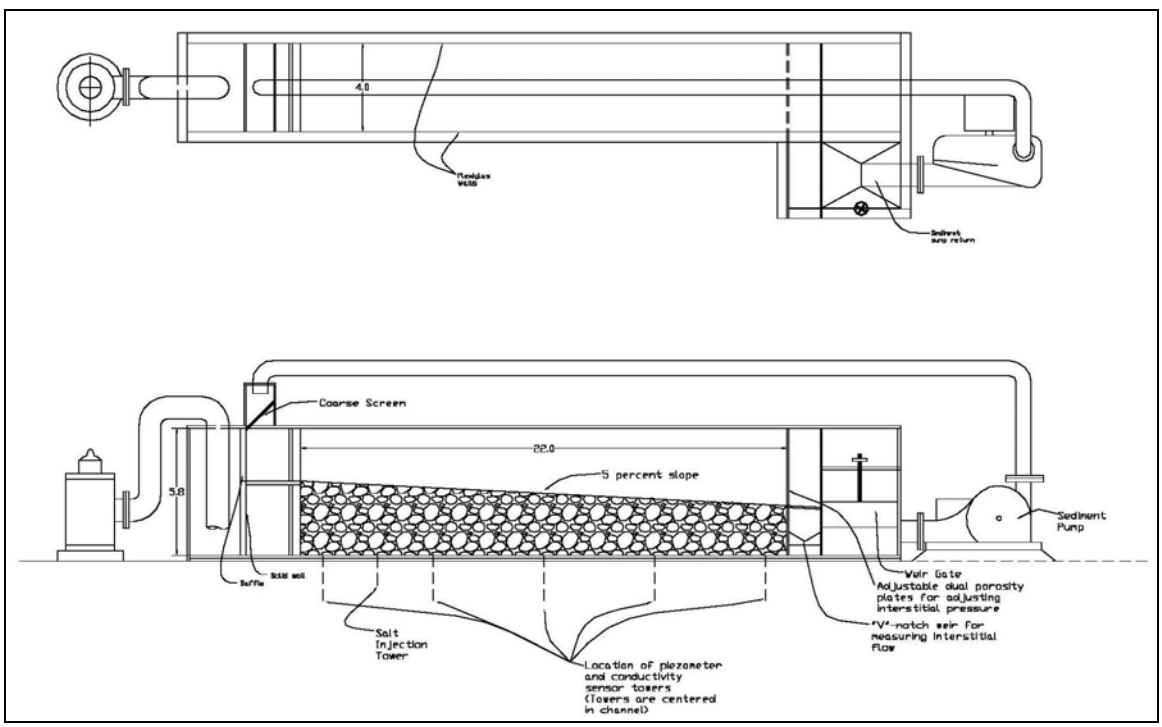

Figure 1. Plan and profile view schematics of rock ramp physical model

Originally, a saline water injection system with conductivity probes was planned for measurement of interstitial velocity. In the end, hot water injection with temperature probes was chosen instead. Figure 1 represents the proposed design before the final interstitial velocity measurement decision was made, but the basic design concept and flume configuration did not change.

Task 3. Prior studies of flow through rock for embankment overtopping protection suggest interstitial flow velocity is dependent on slope, median material size and material gradation. Frizell et al. (1998) conducted prototype studies of flow through rock on 2:1 embankment slopes using rock with medium diameters of 2.1 ft and 0.9 ft. They found interstitial velocity could be represented by the following relationship

$$\frac{V_i}{\sqrt{gd_{50}}} = 2.48 S^{0.58} C_u^{-2.22}$$

where V_i is the interstitial flow velocity, d_{50} is the median stone size, g is the acceleration of gravity, S is the embankment slope, and C_u is coefficient of uniformity, (d_{60} /d_{10}).

In similar studies with smaller material (d_{50}<0.8 ft) Abt et al. (1991) found V_i could be expressed by the empirical relation

$$V_i = 19.29\left(C_u^{-0.074} S^{0.46} n_p^{4.14}\right)^{1.064} \left(g d_{50}\right)^{0.5}$$

where n_p represents rock layer porosity.

As rock layer porosity, n_p, is often unknown for field conditions, Abt dropped n_p as a dependent variable and reanalyzed the data based on material size fractions d_{50}, d_{40}, d_{30}, d_{20}, d_{15}, and d_{10}. The correlation of the data increased with decreasing size fraction. Abt found a reasonably good relationship (correlation coefficient = 0.92) for V_i given by

$$V_i = 0.232\left(g d_{10} S\right)^{0.5}.$$

In Abt's tests the d_{10} material size ranged from about 1.5 inches to 2.0 inches.

The Frizell et al. (1998) and Abt et al. (1991) studies focused solely on defining stability of riprap exposed to flow on steep slopes. The current study expanded prior work to the design of rock ramps placing greater emphasis on control and prediction of interstitial flow.

Ongoing physical testing proposes to accomplish project objectives by constructing sectional models of rock ramps in the test facility described in Task 2. The six proposed test configurations based on two ramp slopes and three uniformity coefficients are given in the Table 1.

Table 1. Proposed rock ramp physical test matrix

Test No.			1	2	3
	Proposed Test Matrix		**Coefficient of Uniformity, C_u**		
A	**Ramp**	5 percent	1.5	2.2	3.0
B	**Slope**	10 percent	1.5	2.2	3.0

Physical testing of the rock ramps at 5 percent slope is complete for all three uniformity coefficients listed in Table 1. Based on completed tests and engineering experience with design, installation, and monitoring, physical testing at 10 percent ramp slopes has been abandoned. Data and experience indicate that 10 percent ramps may be too steep, producing turbulent, high velocity surface flows that could prevent fish passage and would present significant challenges in the design of a stable structure. Configurations for remaining rock ramp physical tests will be determined primarily based on feedback from clients currently designing and implementing these types of structures.

Task 4. Choking the voids within riprap with a material of finer gradation has been used during rock ramp construction as a method to achieve a lower porosity of the ramp. Although not well defined for rock ramps steeper than 3 percent, choke

material is typically a sandy-gravel material and standard road base material can be used. This choke material has been successfully used on ramps of slope less than about 2 percent. No data or case studies have been found on the validity of this approach for steeper slopes. For this series of tests, post construction choking was evaluated by spreading choke material on the surface after testing of the ramp stability and interstitial flow measurement without finer material was completed. The choke material was selected to meet filter criteria for the riprap. The choked ramps were tested for extended periods with clear water to evaluate the potential for loss of choke material effectiveness where a surface treatment approach is used.

Task 5. The final study task is to evaluate ramp sealing due to bed load transport for the 5 percent slope ramps. Approximately 1mm-diameter-minus sand would be introduced and allowed to re-circulate for an extended period. Sand would be added at a rate of 1.5 ft^3/day until an equilibrium transport rate is reached.

ROCK WEIR PHYSICAL MODELING

Previous testing and field investigations identified development of a downstream scour pool as the dominant failure mechanism for rock weir structures. Existing methods do not accurately predict scour or capture the hydraulic processes controlling growth of scour holes and undermining of rock weirs. Physical modeling facilities at Colorado State University's Engineering Research Center Hydraulics Laboratory were used to test a near prototype range of weir configurations and bed material sizes to determine scour magnitudes and trends, measure hydraulic conditions associated with structure type, and assess the stability of each weir configuration.

Project Need. Reclamation's Pacific Northwest Region designs and constructs numerous in-stream rock weir structures every year for fish passage and habitat restoration as part of various salmon recovery projects. In addition, the Middle Rio Grande, River Maintenance Project in New Mexico is exploring alternate means to stabilize banks by reducing flow velocity along eroding banks. Current design methods have had mixed success, primarily relying on individualized professional experience and anecdotal information. Development of design recommendations through systematic data collection, testing, and analysis is required for new structures and retro-fits to reliably meet management objectives. A scientific and mechanistic based understanding of structure behavior leads to supportable planning and management decisions and improves adaptability to new circumstances.

The rock weir physical modeling component of the river spanning rock structures research project is being conducted at the Hydraulics Laboratory located at the Engineering Research Center of Colorado State University (CSU). Physical modeling was conducted on three types of in-stream rock structures: U-weir (similar to V-weir but with a throat), W-weir, and A- weir (also called a double drop). The physical testing program was developed by CSU, in conjunction with Reclamation, to investigate the hydraulics specific to the three weir types and the associated bed scour development. For all three rock weir types, physical tests were performed using consistent methodology to document and improve understanding of how the

structures function up to a state of instability and to add to the existing data set and expand the range of applicability of rock weirs.

Project Objectives. The rock weir physical modeling component of this research will help to develop design packages to simplify the engineering of in-stream structures. There were three primary research objectives designated for the rock weirs physical testing:

- Quantify the dimensions of the bed scour downstream of rock weirs.
- Measure water surface elevations to develop water surface profiles and head-discharge relationships. Provide an empirical water surface profile for developing modeling techniques in one-dimensional numerical hydraulic model (HEC-RAS).
- Collect three-dimensional velocity measurements to analyze velocity and shear stress distributions in the physical model. Obtain calibration points for three-dimensional hydraulic modeling.
- Describe the scour failure mechanism of rock weirs.

Study Design. Physical modeling involved the construction of a scale model of each weir with a unique length scale for each selected bed material. A flume 16-ft-wide by 50-ft-long and 4-ft-deep, with a pump and head-box system capable of discharges up to 40 ft^3/s was selected for this study. A data-collection platform spanning the width of the flume was added to facilitate data collection. Conceptual design sketches of the rock weir testing facility are shown in Figure 2. Each configuration had a unique combination of weir shape, bed material, and bed slope.

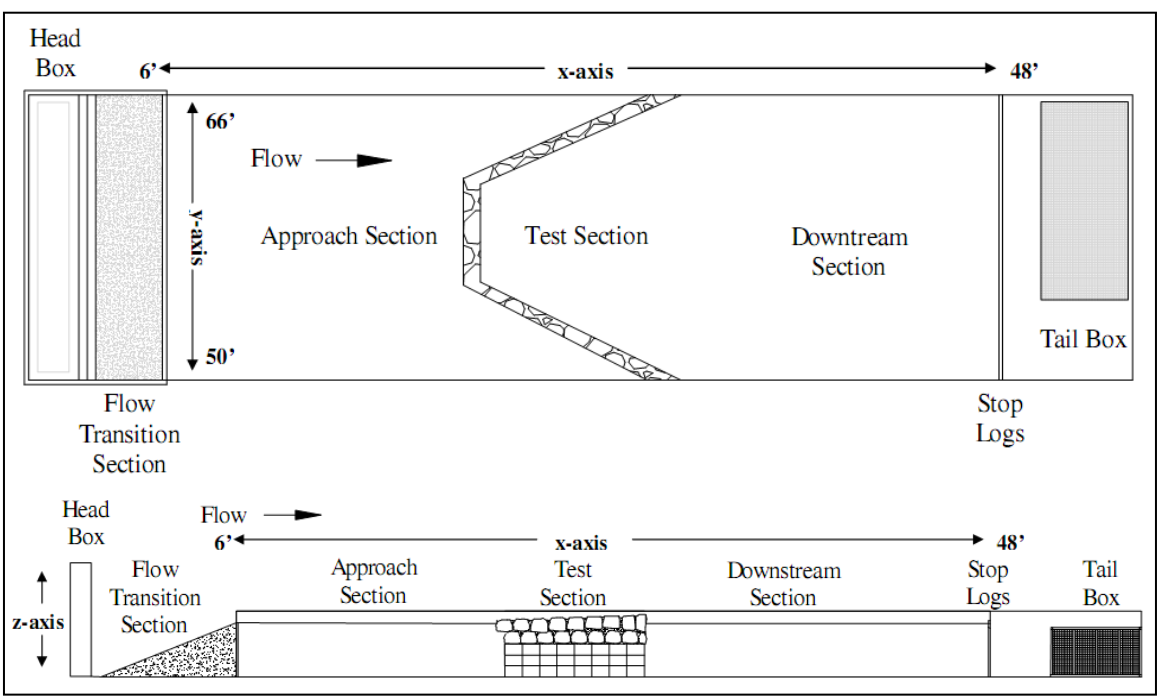

Figure 2. Plan and profile schematics of rock weir physical model

The test matrix for the rock weir physical modeling is listed in Table 2.

Table 2. Rock weir physical test matrix

Configuration	Weir Type	Weir Rock Size (in)	Drop (ft)	Bed Grain Size (mm)	Bed Slope (ft/ft)	Arm Length (ft)	Arm Slope (degrees)
1	W	6.87	None	15.0	0.0047	11.00	5.37
2	U	6.87	None	15.0	0.0047	11.44	4.08
3	U	6.87	0.14	15.0	0.0047	11.44	4.08
4	U	10.00	0.18	5.0	0.0021	11.24	1.70
5	A	10.00	0.36	5.0	0.0020	9.24	1.02
6	W	10.00	0.18	5.0	0.0020	7.97	2.38
7	U	8.80	0.17	9.8	0.0030	12.58	2.05
8	A	8.80	0.34	9.8	0.0030	9.41	1.69
9	W	8.80	0.17	9.8	0.0030	9.35	2.76
10	A	6.87	0.28	15.0	0.0050	10.69	2.40
11	W	6.87	0.14	15.0	0.0050	11.00	3.13

Three distinct of rock weirs types and three different bed gradations were tested at three separate discharges. W- and U-weirs were initially tested with the bed elevation equal to the crest elevation at the weir throat (no drop) resulting in a total of 11 unique configurations of weir shape, bed material, and bed slope that were constructed and tested.

Hydraulic Geometry. Independent variables were reduced to discharge and grain size using hydraulic geometry from Julien (2002). Three grain sizes were determined that corresponded to field conditions in areas where natural stone weirs were proposed to be built or were already in use. Using these pre-selected grain sizes and an estimated prototype discharge, regime equations from Julien (2002) were used, in an iterative process, to determine width and slope for the prototype. The design of the model was constrained by the available dimensions of the flume. Using the 16 foot width, 4 foot depth, and a maximum discharge capacity of 40 ft^3/s, scaling ratios could be adjusted to enable proper sizing of the prototype and the scale model. Prototype slope and width were calculated from the following two equations

$$S \cong 0.0124 Q^{-0.4} d_s{}^{1} \tau_*{}^{1.2}$$

$$W \cong 5.0035 Q^{0.53} d_s{}^{-0.33} \tau_*{}^{-0.27}$$

where S is the bed slope, Q is the bankfull discharge in m^3/s, d_s is the median particle diameter in mm, τ_* represents the Shields number and was assumed equal to 0.047 (Reclamation, 2006), and W is the bankfull width in meters.

Normal Depth. Normal depth, y_n, was calculated using Manning's equation

$$Q = \frac{\Phi}{n}(by_n)(S_o)^{1/2}\left(\frac{by_n}{b+2y_n}\right)^{2/3}$$

where y_n is normal depth, n is Manning's roughness coefficient, Q is discharge, b is bottom width, S_o is bed slope, and Φ is a conversion coefficient (equal to 1.486).

Manning's roughness, *n*, was calculated using Strickler's relationship (Richardson et al., 1990)

$$n = k_u \, d_s^{1/6}$$

where, k_u Strickler's constant (equal to 0.0421).

Scaling. The hydraulic testing of the model was designed to use an undistorted scale to best represent flow patterns and sediment transport. The available width of the flume in relation to the prototype width was used to determine the length scaling parameters. Length scaling ratios were prescribed as 1:4.36, 1:4.61, and 1:5.75 corresponding to the 5-mm, 9.8-mm, and 15-mm median grain diameter bed materials used in the physical testing, respectively. Since the model was considered undistorted, the slope did not require scaling. Froude similitude governs the hydraulic characteristics

$$Fr = \frac{U}{\sqrt{g \cdot Y}}$$

where *Fr* is the Froude number, *U* is the mean channel velocity, *g* is the acceleration due to gravity, and, *Y* is the characteristic depth of flow.

Froude similitude scaling requires the velocity ratio to equal the square root of the vertical scaling ratio

$$U_r = \sqrt{Y_r}$$

where U_r is the ratio of velocity in the prototype to velocity in the model and Y_r is the ratio of characteristic depth in the prototype to characteristic depth in the model.

Froude scaling results in the following relationship between flow scale and length scale:

$$Q_r = L_r^{5/2}$$

where Q_r is the ratio of discharge in the prototype to discharge in the model and L_r is the ratio of length in the prototype to length in the model.

Flow resistance was not considered to be a significant effect in this model, since local hydraulics and local scour conditions were the primary focus.

The Rouse number defines the vertical distribution of sediment in suspension. For scour testing, this parameter represents the interaction of the bed material with the water column due to turbulent hydraulic processes. The Shields parameter represents bed mobility through shear stress processes such as rolling and sliding. The Rouse numbers for the prototype conditions were expected to be relatively high suggesting bed motion processes governed and therefore the Shields parameter was the most applicable scaling condition (Reclamation, 2006). Julien (2002) reports that Shields' similitude governs the scour under clear water conditions. Therefore, Shields' scaling was used to size the model grain diameter according to the length ratio (Reclamation, 2006).

The "drop" is the distance from the crest of the weir to the surface of the bed. A prototype drop height of 0.8 feet was used in accordance with Reclamation Pacific Northwest Regional Office criteria. Model drop heights were determined by dividing the prototype drop height by the length scaling ratios. Drop heights, prescribed by Reclamation, were 0.14 ft., 0.17 ft., 0.18 ft. corresponding to the 6.87-inch, 8.8-inch, and 10-inch weir rocks, respectively. For the A-weirs, a "double-drop" design was used. The cross arm was set at the calculated drop height and the crest of the weir was set at twice the calculated drop height.

Weir-rock sizes were prescribed by Reclamation and were based on recommendations by Rosgen (2001) to use weir rocks that are three times the drop height of the weir. Rock sizes were 10 in, 8.8 in, and 6.87 in measured along the intermediate axis and corresponded to the 5-mm, 9.8-mm, and 15-mm bed material, respectively. Larger weir rocks were used with a smaller bed material to simulate field conditions.

Bed Material. Three d_{50} grain diameters for the prototype were selected to match field conditions over a range of areas where rock weir structures have been built or are proposed to be constructed. The small cobble is representative of streams in the Pacific Northwest, while course gravel is representative of Rio Grande headwater streams. The need to minimize scaling required for model testing was also a factor in grain size selection (Reclamation, 2006).

Model bed material sizes were determined using Shields scaling. The median diameters (d_{50}) of the prescribed bed materials were 5 mm, 9.8 mm, and 15 mm. The actual median diameters achieved were approximately 4.2 mm, 9.81 mm, and 12.3 mm for the U-weir tests. For the A-weir and W-weir tests, the actual median diameters achieved were approximately 4.2 mm, 9.81 mm, and 15.38 mm.

Weir Dimensions. Structures were designed to approach as close as possible the midpoint of the design ranges specified in Rosgen (2001). Recommended plan angles were between 20 to 30 degrees and profile angles between 2 to 7 percent. Target angles were 25 degrees for plan angles and 4.5 percent for profile angles. Reclamation used the solver function in Microsoft Excel® to calculate the weir arm length that minimized the relative distances on the planform and profile angles of the weir arms. No information on the importance of one angle over another could be found so the relative errors were kept equal (Reclamation, 2006). Figure 3, Figure 4, and Figure 5 show the design layout and basic dimensions for the U-, A-, and W-weirs tested.

Prototype grain size and discharge were used in an iterative process utilizing the solver function in Microsoft Excel® to determine prototype dimensions and model length scaling. The dimensional constraints of the flume influenced the design process. Froude and Shields scaling were used to determine model sizing ratios.

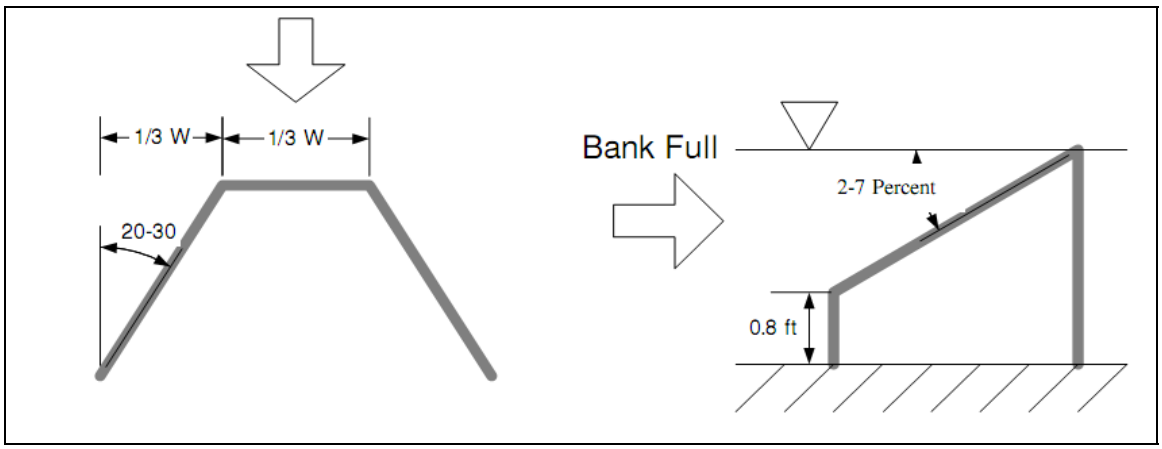

Figure 3. U-Weir conceptual design sketch (Reclamation, 2005)

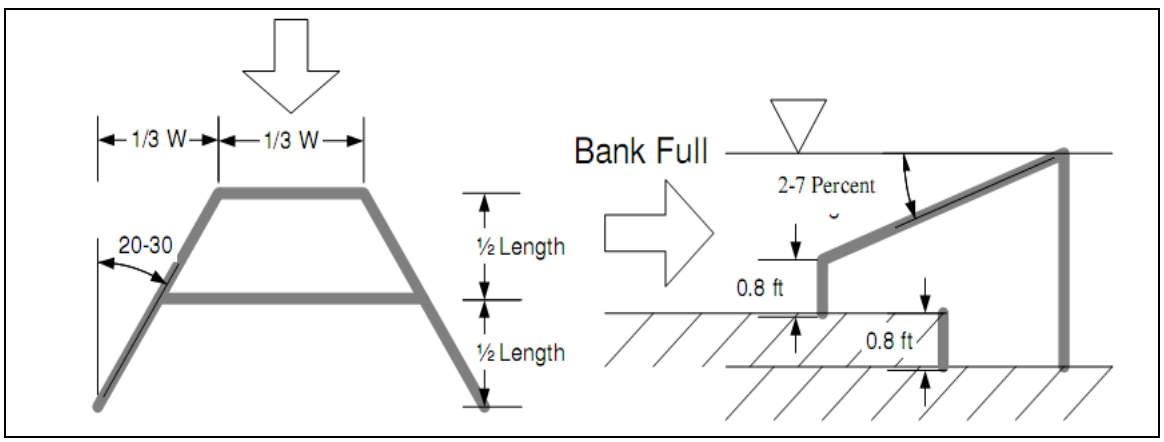

Figure 4. A-Weir conceptual design sketch (Reclamation, 2005)

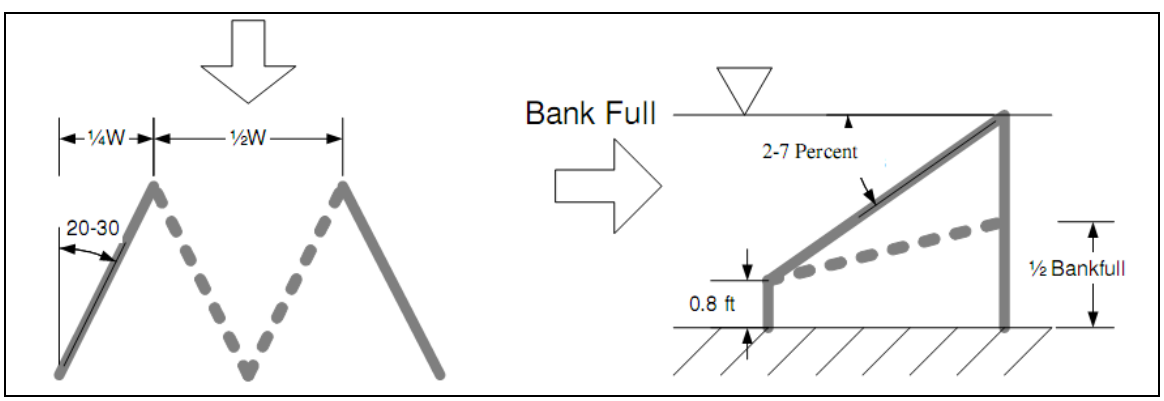

Figure 5. W-weir conceptual design sketch (Reclamation, 2005)

CONCLUDING REMARKS

In-stream rock structures are increasingly being used to serve a wide variety of aquatic habitat, fish passage, stream stabilization, and water diversion purposes. The current state of the art does not provide sufficient design and performance information for new structures and retrofits to reliably meet management objectives. Current design methods are largely based on individualized professional experience and anecdotal information with a narrow range of applicability. A clear need exists to

expand the current knowledge base and develop design procedures that would allow site specific application and improve the sustainability of rock ramps and weirs.

Physical modeling currently in progress at the U.S. Bureau of Reclamation (Reclamation) and at Colorado State University (CSU) is focused on the development of recommendations for improving the design of river spanning rock structures. Computation, measurement, and reduction of interstitial flow through steep rock ramps is being studied at Reclamation's Water Resources Research Laboratory. The Hydraulic Laboratory at CSU's Engineering Research Center is conducting physical tests to quantify and predict the development of scour downstream of rock weirs and the effects of downstream scour on structure stability. As an integral part of a multifaceted approach including collection and analysis of field data, numerical modeling, and laboratory testing, the physical modeling component will provide information for the development of improved river spanning rock structures design methods and guidelines.

REFERENCES

Abt, S.R., Khattak, M.S., Nelson, J.D., Ruff, J.F., Shaikh, R.J., Wittler, R.J., Lee, D.W., and Hinkle, N.E. (1987) May. "Development of Riprap Design Criteria by Riprap Testing in Flumes: Phase I," NUREG/CR-4651, ORNL/TM-10100/V1, prepared for the U.S. Nuclear Regulatory Commission, Washington D.C.

Abt, S.R., Wittler, R.J., Ruff, J.F., LaGrone, D.L., Khattak, M.S., Nelson, J.D., Hinkle, N.E., and Lee, D.W. (1988) Sept. "Development of Riprap Design Criteria by Riprap Testing in Flumes: Phase II; Followup Investigation," Vol 2, NUREG/CR-4651, ORNL/TM-10100/V2, prepared for the U.S. Nuclear Regulatory Commission, Washington D.C.

Frizell, K.H., Ruff, J.F., and Mishra, S. (1998). Oct. "Simplified Design Guidelines for Riprap Subjected to Overtopping Flow," Proceedings of the Annual Association of State Dam Safety Officials (ASDSO) Conference, Las Vegas, NV, October 1998.

Holmquist-Johnson, C.L. and Mooney, D.M. (2005). Alphabet Weir Physical Model Statement of Work. U.S. Bureau of Reclamation, Technical Service Center, Denver, CO. Sedimentation and River Hydraulics Group. Correspondence, July 2005.

Holmquist-Johnson, C.L. and Mooney, D.M. (2006). Alphabet Weir Physical Model Design Write-Up. U.S. Bureau of Reclamation, Technical Service Center, Denver, CO. Sedimentation and River Hydraulics Group. Correspondence, July 2006.

Julien, P.Y. (2002). *River Mechanics*. Cambridge University Press, Cambridge, United Kingdom. pp 408.

Mefford, B., Collins, K.L., and Baird, D. (2006). Hydraulic Model Study Proposal: Design and Evaluation of Interstitial Flow through Rock Ramps Constructed on Steep Slopes. U.S. Bureau of Reclamation, Technical Service Center, Denver, CO.

Meneghetti, A.M., Thornton, C.I., and Cox, A.L. (2008). Alphabet Weir Physical Modeling – Interim Report. Colorado State University, Department of Civil Engineering, Engineering Research Center, Fort Collins, CO, prepared for U.S. Bureau of Reclamation, Denver, CO.

Mercure, J.J., Robeson, M.D., Thornton, C.I. (2006). Alphabet Weir Physical Modeling. M.S. Plan B Paper. Colorado State University, Department of Civil Engineering, Fort Collins, CO.

Richardson, E.V., Simons, D.B., and Julien, P.Y. (1990). *Highways in the River Environment.* Federal Highway Administration.

Rosgen, D.L. (2001). *Applied River Morphology.* Wildland Hydrology, Pagosa Springs, CO.

Redesign and Rehabilitation of Railroad Bridges with Advanced Adverse Lateral Migration

William Yord A.M.[1], Jerry R. Richardson M., D.WRE [2], Vincent J. Zink S.M.[3]

Much of the railroad infrastructure in the United States was initially built over a century ago, whereas the highway infrastructure is roughly half as old. Consequently, the existing railroad infrastructure presents more cases with advanced stream stability issues. These include advanced lateral and vertical migration which must be addressed when assessing, mitigating, or redesigning railroad bridges for stream stability and scour. Bridge 433.3 on the Union Pacific Railroad near Chickasha, Oklahoma is used as a case study to illustrate the problems with redesigning a railroad bridge crossing which has experienced advanced long-term lateral stability issues, and to demonstrate how mitigating for stream stability and scour at railroads differs from similar work within the National Highway System.

In this case the Washita River has had extensive lateral migration over approximately the last eighty years. Two railroad bridges exist on the Washita River at this location, which are the main river bridge (Bridge 433.5) and the left bank overflow bridge (Bridge 433.3). Upstream of this location, a tortuous meander bend exists which is migrating down-valley at a rate of approximately 6 m/yr (20 ft/yr) (Figure 1). Downstream of Bridge 433.3 the west bank of the Washita River is showing signs of degradation and severe head cutting toward the bridge opening. The most likely location for this cutoff is through this relief bridge (Bridge 433.3) located 0.3 km (0.2 mi.) north of the main bridge crossing (Bridge 433.5).

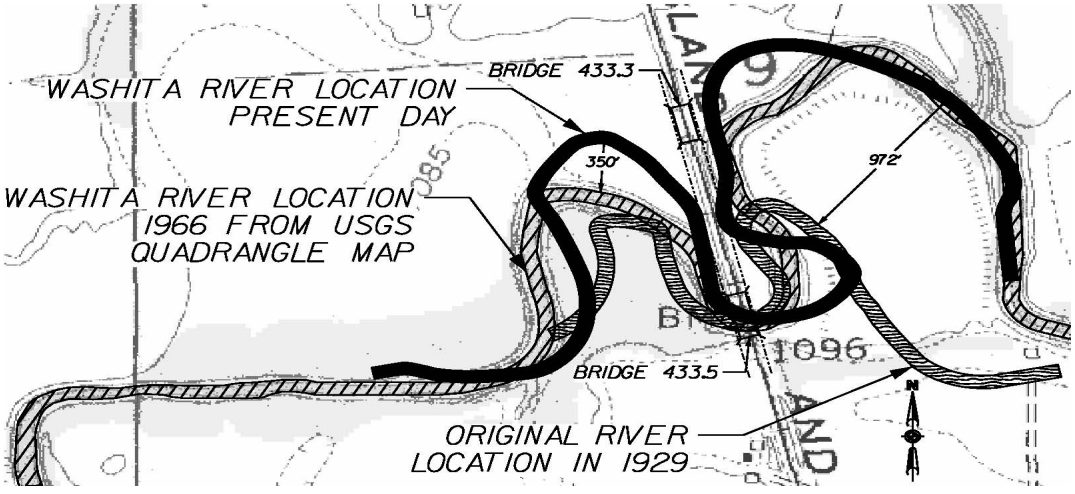

Figure 1: Stream Migration Snapshots in Time

1 Project Manager, H&H Rail Wilson & Co, 903 E. 104th street, Suite 210, Kansas City Missouri 64110

2 Associate Professor, School of Computing and Engineering, University of Missouri Kansas City, 5100 Rockhill Road, Kansas City, MO, 64110

3 Intern Engineer, Wilson & Co, 903 E. 104th street, Suite 210, Kansas City Missouri 64110

The channel length around the meander loop is nearly 5 times longer than the down valley length near Bridge 433.3, and given the rate of movement it is likely that a cutoff through the overflow bridge will occur within the next few years unless river training measures are taken.

In order to design the replacement for the relief structure (Bridge 433.3), the potential for meander cutoff had to be carefully considered. Multiple options were considered including retaining the existing channel using countermeasures, designing the replacement bridge to account for the potential cutoff, and physically cutting off the river and abandoning the main channel bridge as part of the new design. Each presented technical, geomorphic, flood control, and permitting issues.



Figure 2: Washita River Upstream of Bridge 433.3. Note Bridge 433.3 in Background and Scour on Left Bank

OPTIONS

The first option considered was to make the overflow bridge (Bridge 433.3) the main river bridge and leave the existing main river bridge in place. Do not encourage the cut-off of the Washita River through Bridge 433.3. Let the cut-off occur naturally and make adjustments to Bridge 433.3 after this cut-off occurs. This would mean that the overflow bridge would need to be sized and configured as a main river bridge (approximately 3-steel spans).

Uncertainty and extra risk to UPRR infrastructure exists regarding this option in that the Washita River may cut-off at unexpected locations (most likely between Bridge 433.3 and 433.5) and adversely affect bridge abutments or railroad fill embankments. The existing railroad embankments between Bridge 433.3 and 433.5 would need to be monitored during and after major flood events to ensure the stability of the railroad embankment, abutments of the main river bridge and the abutments and piers of the

proposed Bridge 433.5. After the Washita River cut-off through Bridge 433.3, remediation would need to take place to stabilize any areas where scour has occurred. The flow in the meander loop after this is complete would be much less problematic as most of the flow would be through Bridge 433.3 instead of the main river bridge. The existing meander bend of the Washita River through Bridge 433.5 would likely fill with sediment after a period of time.



Figure 3: Washita River Channel Showing Lateral Migration on the Left Bank

Another option was to make the overflow bridge (Bridge 433.3) the main river bridge and leave the existing main river bridge in place. Encourage the cut-off of the Washita River through Bridge 433.3 by excavating a channel from upstream of the Bridge through the structure and connect it to the main Washita River Channel downstream of Bridge 433.3. This would mean that the overflow bridge would need to be sized and configured as a main river bridge. A grade control structure could be installed upstream of Bridge 433.3 to maintain the slope of the river, help control head cutting and help maintain flow in the existing meander bend through Bridge 433.5

The Washita River cut-off would be much more predictable and controllable under this option. The flow in the meander loop after this is complete would be much less problematic as most of the flow would be through Bridge 433.3 instead of the main river bridge. The existing meander bend of the Washita River through Bridge 433.5 would likely fill with sediment after a period of time.



Figure 4: Washita River Channel Downstream of Bridge 433.5. Note Lateral Stream Migration on Outside Embankment

The final option we considered was to maintain the existing configuration of Bridge 433.3 as an overflow structure and Bridge 433.5 as the main river bridge and armor Bridge 433.3 with deep buried rip-rap and guide banks to enhance stability if the Washita River tries to cut-off through the overflow bridge. In effect, this would be a deep buried heavy rock weir (Type III Rock). The volume of the heavy rock for the weir structure beneath Bridge 433.3 is approximately 8570 cubic yards. Extra rock would be recommended for protection of bridge abutments. This rock weir is shown conceptually on the Plan & Profile Exhibit Bridge 433.3 on the following page.

CONCLUSIONS

In order to design the replacement for the UPRR Bridge 433.3, the potential for a meander cutoff had to be carefully considered. These options included retaining the existing channel using countermeasures, designing the replacement bridge to account for potential cutoff, and physically cutting off the river and abandoning the Bridge 433.5 as part of the new design. Each presented technical, economic, geomorphic, flood control and permitting issues for the crossing. Bridge 433.3 and 433.5 offer a glimpse into the future for the National Highway System as lateral migration and stream stability issues present themselves such as that experienced by infrastructure that has been in service twice as long. Scour analysis for bridges in the National Highway System should also include stream stability and geomorphologic studies upstream and downstream of the bridge crossing to properly locate bridges to account for lateral and vertical migration of existing rivers as well as general and local scour analysis.

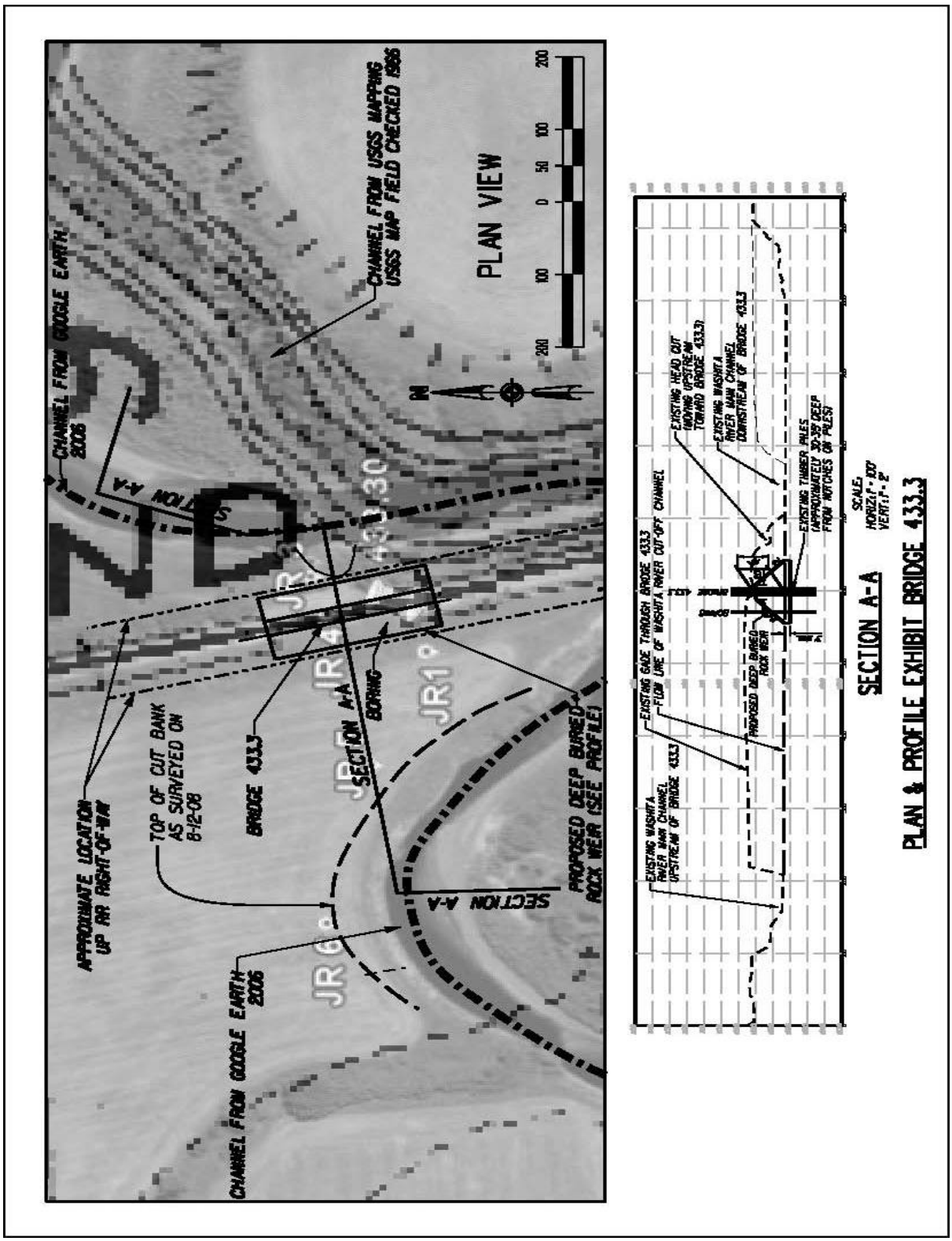

Figure 5 Plan and Profile Exhibit Bridge 433.3

A Direct Method for Determining Riprap Size for Erosion Protection in Rivers

Yongliang Jin[1] and Brian D. Barkdoll, F. ASCE[2]

[1]Graduate Research Assistant, Civil & Environmental Engineering Dept., Michigan Tech Univ., Houghton, MI 49931, PH: (906) 487-1981, FAX: (906) 487-2943, email: yjin@mtu.edu
[2]Associate Professor, Civil & Environmental Engineering Dept., Michigan Tech Univ., Houghton, MI 49931, PH: (906) 487-1981, FAX: (906) 487-2943, email: barkdoll@mtu.edu

Abstract: In cases where an open channel needs bed and bank protection riprap is a common lining material, of which riprap size is the main design parameter needing determination. The current solution procedure is a cumbersome iterative one. A direct solution (one not needing iteration) is proposed here that improves computation time by 98% and adds less than 8% error.

Introduction

One of the current methods for calculating riprap size is from Anderson et al. (1970) and is an extension of the tractive force concept outlined in Chow (1959). The method is summarized as follows (Sturm 2001):

1. Choose a riprap diameter and obtain φ and θ from figures of which the values are approximated by the following
$$\varphi = 1.3445\text{-}ln(d_{50}) + 34.197$$
$$\theta = 1.9366 + 0.518\,\varphi$$
in which φ is the angle of repose in degrees, θ is the side slope angle in degrees, and d_{50} is the median particle size in feet;
2. Calculate the critical bed and wall shear stresses from
$$\tau_{Oc} = 4d_{50}$$
$$K_r = \frac{\tau_{Oc}^{w}}{\tau_{Oc}} = \left[1 - \frac{\sin^2\theta}{\sin^2\varphi}\right]^{1/2}$$
in which τ_{Oc} is the critical shear stress required for initiation of motion in lbs/ft^2 and K_r is the tractive force ratio;
3. Determine Manning's n from
$$n = 0.04 d_{50}^{1/6}$$
4. For a given channel bottom width, b, discharge, Q, and slope, S, find the normal depth from Manning's equation;
5. Calculate the maximum bed ,$(\tau_O)_{max}$, and wall ,$(\tau_O{}^w)_{max}$, shear stresses from :
$$(\tau_O)_{max} = 1.5\gamma RS$$
$$(\tau_O{}^w)_{max} = 1.2\gamma RS$$

---

[1] Graduate Research Assistant, Civil & Environmental Engineering Dept., Michigan Tech University, Houghton, MI 49931
[2] Associate Professor, Civil & Environmental Engineering Dept., Michigan Tech University, Houghton, MI 49931, barkdoll@mtu.edu

where γ is the specific weight of water, R is the hydraulic radius, and S is the longitudinal bed slope; and

6. Repeat with another riprap diameter and/or bottom width until the maximum shear stresses are just smaller than the critical values.

This process is effective but time consuming with iterations not only in Steps 1 through 6 outlined above, but also within Step 4 in which iterations must be performed to obtain the normal depth from Manning's equation for a trapezoidal channel.

Procedure

To find a direct method for obtaining the minimum riprap size, one without iteration, the method outlined above was solved for over 1000 different values of the input variables Q, S, and b. A direct equation was then obtained that gave predictions of riprap size that closely matched the "true" values from the method outlined in Steps 1 through 6 above. Values of Q, S, and b were chosen to be inclusive of values found in natural channels so that the direct method acquired herein would not require extrapolation outside the range of values employed in its development (Table 1).

Table 1. Input data range

Parameter	Minimum value	Maximum value	Unit
Q	100	1,072,600	cfs
S	0.00001	0.01057	ft/ft
b	1	5,281	ft

See Jin (2006) for all of the various forms of equations tried.

Results

Of all the equations attempted, it was found that the following equation yields the most accurate results:

$$d_{50} = \frac{2.41 Q^{0.60355} S^{0.79358} b^{-0.51341}}{1 + 1.65 e^{-0.5 b/y}} \qquad 1 < \text{b/y} < 50$$

Fig. 1 shows the predictions and true values as a function of b/y. Note that for values of b/y less than 1, the error can be unacceptably high, but that otherwise the error is less than 8%.

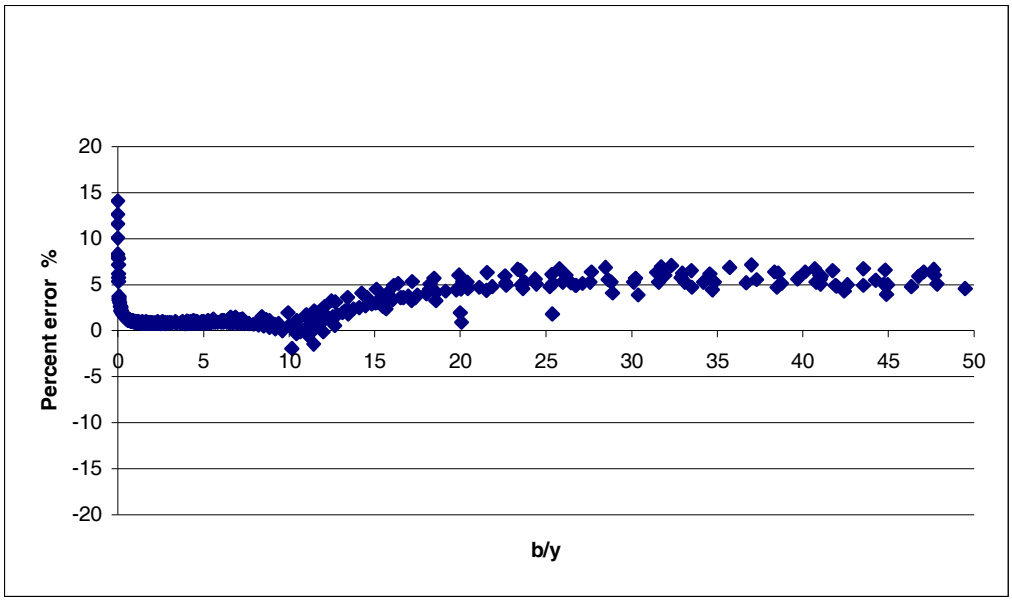

Fig. 1. Error between predicted and true values of minimum riprap size as a function of b/y.

Both the iterative and direct methods were run on the same computer for over 1000 times and it was found that there was a time savings of 98% by the direct solution.

Conclusions

The direct method found here of calculating the minimum riprap size to avoid erosion in channels improves computation time by 98% while adding an error of less than 8% and, therefore, can be used in computations of this sort. Even though the computation time of the existing iterative method may not be considered excessive, the present method does constitute a substantial time savings with not much additional error. In addition, the present solution is simpler and more pedagogically attractive.

Acknowledgements

Katrina Finn and Rebecca Spicer worked on earlier versions of this project.

Notation

The following symbols are used in this paper:

b	=	bottom width in ft;
d_{50}	=	median riprap diameter in ft;
K_r	=	tractive force ratio;
n	=	Mannings roughness coefficient;
Q	=	discharge in ft^3/s;
R	=	hydraulic radius in ft;
S	=	longitudinal channel bed slope;
y	=	normal flow depth in ft;
φ	=	angle of repose in degrees;
θ	=	side slope angle in degrees;
τ_{Oc}	=	critical shear stress required for initiation of motion in lbs/ft^2;

$(\tau_O)_{max}$ = maximum bed shear stress in lbs/ft^2;
$(\tau_O^w)_{max}$ = maximum wall shear stress in lbs/ft^2;
φ = angle of repose in degrees; and
γ = specific weight of water.

References

Anderson, A.G., Paintal, A.S., and Davenport, J.T. (1970) *Tentative Design Procedure for Riprap-Lined Channels*, NCHRP Report 108. National Cooperative Highway Research Program, Highway Research Board, National Research Council, Washington, DC.

Chow, V.T. (1959) *Open Channel Hydraulics*, McGraw Hill, New York, N.Y.

Jin, Y. (2006) *Direct Method to Determine the Optimal Riprap Size for Erosion Protection in Rivers*," MS Thesis, Michigan Tech University, Houghton, MI 49931.

Sturm, T.W. (2001) *Open Channel Hydraulics*, McGraw-Hill, Boston, MA.

Modeling of Sediment Particle Deposition and Resuspension Processes Using a Stochastic Jump Diffusion Particle Tracking Model

Jungsun Oh[1] and Christina W. Tsai[2]

[1] Research Assistant, Civil, Structural and Environmental Engineering, State University of New York at Buffalo, 207 Jarvis Hall, Buffalo, NY 14260; email:joh8@buffalo.edu

[2] Associate Professor, Civil, Structural and Environmental Engineering, State University of New York at Buffalo, 233 Jarvis Hall, Buffalo, NY 14260; email:ctsai4@eng.buffalo.edu

ABSTRACT

Although river beds generally tend to reach an asymptotic equilibrium, it may be abruptly altered by occurrences of natural extreme flow events or establishment of man-made structures. These causes lead to significant morphological changes in the bed profile through erosion and deposition processes. The change of river bed can be quantified for predicting the stability of a river channel. The status of a geomorphological equilibrium can be determined by two transport phases, i.e., water and sediment transport. In particular, the bed profile in sediment transport models can be employed as the initial condition, and the calculated movement of sediment can set a new bed profile. Herein, we propose to use the stochastic jump diffusion particle tracking model (SJD-PTM) to simulate the movement of sediment and particle deposition and resuspension processes. The stochastic diffusion jump particle tracking model is a Lagrangian particle tracking model governed by stochastic equations. When simulating the particle trajectories from the mean drift, settling velocity, diffusivity and extreme events, we can calculate the probabilities of deposition/scouring of a sediment particle by comparing the particle shear stress with the critical shear stress. As the result, we can trace particles and obtain particle trajectories and their statistical characteristics such as the ensemble mean and variance. Furthermore, we will be able to simulate particle deposition and resuspension processes.

INTRODUCTION

One of the major environmental concerns about sediment transport is the geomorphological change due to scouring and deposition. Estimating the change of river bed is beneficial to predicting the stability of a river channel. Souring / deposition processes become more significant during extreme flow events. It is of practical significance to determine whether sediment particles settle down on the bed or resuspend from the bed when simulating movement of sediment particles.

River beds generally tend to reach an asymptotic equilibrium. However, river bed may be altered by natural extreme flow events or man-made structures. These causes lead to significant morphological changes in the bed profile through erosion and deposition processes. Many of earlier models assumed equilibrium conditions in which the actual sediment transport rate is equal to the capacity of flow carrying sediment at equilibrium conditions at each computational point. In reality, alluvial river systems change continuously with respect to time and space so that absolute equilibrium states rarely exist in natural conditions. The local equilibrium assumption may not be realistic, particularly in cases of erosion and deposition during extreme events, because sediment cannot instantaneously reach a new equilibrium condition. Since extreme flow events are likely to cause strong net erosion and deposition, it is more realistic to consider non-equilibrium erosion and deposition processes when estimating the effect of extreme flow events on sediment transport. Bed shear stress is a basic shear parameter governing deposition / erosion processes. Employing the criteria of deposition / resuspension can determine if sediment particles are depositing or resuspending when the sediment particles reach the bed. The deposition / erosion processes of sediment particles also inherit the stochastic property from the stochastic instantaneous flow velocity. In other words, the stochastic flow velocity results in the randomness of bed shear stress, and such bed shear stress due to turbulence and occurrences of extreme events play a significant role in the deposition / erosion processes. Therefore, considering the stochastic bed shear stress can model more comprehensively deposition / erosion of sediment particles and then quantify the impact of extreme flow events on deposition / erosion processes.

To simulate flow and morphodynamic processes, many numerical models have been developed from theoretical equations or a combination of theoretical equations and empirical relations (Jia and Wang 1999; Molinas and Yang 1986; Lee et al. 1997). Lei et al. (1998) developed a finite-element model for rill erosion by controlling flow hydraulics and erosion processes according to altered morphology. Herein, the

proposed SJD-PTM adopts a Lagrangian particle tracking approach that traces sediment particles. Thus, it is more suitable to describe movement of particles in a probabilistic manner. Krone (1962) and Ariathurai et al. (1977) suggested the probability of cohesive sediment particles sticking to the bed based on their laboratory studies. Nagaraja (2008) attempted to simulate sediment transport with a particle tracking model using the probability of deposition / resuspension suggested by Krone (1962). However, the probability of deposition in the above studies (Nagaraja, 2008) is mainly targeting cohesive sediment particles. In the proposed study, we propose to derive the bed shear stress based on the essential stochastic characteristics of flow velocity and then use the critical shear stress to determine whether the particle would deposit or resuspend. The main objective of this study is to simulate movement of sediment particles and the particle deposition and resuspension processes.

STOCHASTIC JUMP DIFFUSION MODEL

The stochastic jump diffusion processes have been used for describing random abrupt changes of variables in time in various fields (Hanson, 2007). Movement of sediment particles in an open channel can also be controlled by an abrupt change of flow due to the passing of extreme flow events. Therefore, the stochastic jump diffusion process is pertinent to modeling movement of sediment particles in open channel flows (Oh and Tsai, 2008). The governing equations can be written as following stochastic differential equations.

$$d\mathbf{X}_t = \underbrace{\bar{\mathbf{u}}(t, \mathbf{X}_t)dt}_{\text{drift term}} + \underbrace{\boldsymbol{\sigma}(t, \mathbf{X}_t)d\mathbf{B}_t}_{\substack{\text{random term} \\ \text{due to turbulence}}} + \underbrace{\mathbf{h}(t, \mathbf{X}_t)d\mathbf{P}_t}_{\text{jump term}} \quad \text{or} \tag{1a}$$

$$\mathbf{V}_p = \frac{d\mathbf{X}_t}{dt} = \underbrace{\bar{\mathbf{u}}(t, \mathbf{X}_t)}_{\text{drift term}} + \underbrace{\boldsymbol{\sigma}(t, \mathbf{X}_t)\frac{d\mathbf{B}_t}{dt}}_{\substack{\text{random term} \\ \text{due to turbulence}}} + \underbrace{\mathbf{h}(t, \mathbf{X}_t)\frac{d\mathbf{P}_t}{dt}}_{\text{jump term}} \tag{1b}$$

where $\mathbf{X}_t$ is the position or trajectory of a particle, $\bar{\mathbf{u}}(t, X_t)$ is the drift velocity vector, $\boldsymbol{\sigma}(t, X_t)$ is the diffusion coefficient tensor (3×3 diagonal matrix in flow), $\mathbf{B}_t$ is the three-dimensional vector of the Wiener process. $\mathbf{h}(t, X_t)$ is the jump amplification factor and $\mathbf{P}_t$ denotes a Poisson process so that the inter-arrival time between extreme events is exponentially distributed. The mean drift motion of particles is represented by

$$\bar{\mathbf{u}}(t,\ X_t) = \bar{\mathbf{U}} + \nabla \mathbf{D} = \begin{cases} \bar{U}(t,x,y,z) + \partial D_x / \partial x \\ \bar{V}(t,x,y,z) + \partial D_y / \partial y \\ \bar{W}(t,x,y,z) - w_s + \partial D_z / \partial z \end{cases} \quad (2)$$

which is a deterministic component. The random turbulent motion term and jump term are stochastic components including random processes. The magnitude of extreme flow events is characterized by the jump amplification factor. The jump amplification over the extreme event duration T can then be expressed as

$$\mathbf{h}(t, \mathbf{X}_t) = \int_t^{t+T} \left(\int_0^T \frac{\mathbf{u}_f(t) - \mathbf{V}_p(t_0)}{\tau_p} d\tau \right) dt \quad (3)$$

where $\mathbf{u}_f(t)$ is the increased mean flow velocity due to an extreme event, $\mathbf{V}_p(t_0)$ is particle velocity before the extreme event and τ_p is the particle relaxation time. It is assumed that only one extreme event occurs within a time interval [t, t+dt].

DEPOSITION / EROSION PROCESSES

We set channel bottom boundaries associated with the stochastic jump diffusion particle tracking model (SJD-PTM) and simulate the movement of sediment under non-equilibrium conditions. Deposition / resuspension of a sediment particle can be determined by comparing the bed shear stress with the critical shear stress.

The bed effect in an open channel flow produces a logarithmic mean velocity profile in the longitudinal direction. The logarithmic velocity profile in the longitudinal direction is

$$\frac{\bar{u}}{u_*} = \frac{1}{\kappa} \ln\left(\frac{z_{sh}}{z_0} \right) \quad (4)$$

where $\bar{u}$ is the time-averaged streamwise velocity, u_* is the friction velocity, κ is the von Karman universal turbulence constant, z_{sh} is the elevation at which u is measured and z_o is the "virtual origin" of the profile (i.e., roughness length). Equation (4) can be used for the mean drift velocity in the longitudinal direction.

Bed shear stress is a basic shear parameter governing erosion processes. The bed shear stress can be usually calculated from the measured velocity profile. The bed shear stress, τ_o, can be estimated from the shear velocity:

$$\tau_0 = \rho u_*^2 \qquad (\rho : \text{water density}) \quad (5)$$

The shear velocity, u_*, can be estimated by the logarithmic velocity formula as

$$u_* = u\kappa \frac{1}{\ln(z_{sh} / z_0)} \tag{6}$$

where u is stochastic instantaneous flow velocity. Similar to stochastic particle velocity, the stochastic flow velocity can be estimated as

$$u = \bar{\mathbf{u}}(t, \mathbf{X}_t) + \boldsymbol{\sigma}(t, \mathbf{X}_t) \frac{d\mathbf{B}_t}{dt} + \mathbf{h}(t, \mathbf{X}_t) \frac{d\mathbf{P}_t}{dt}$$

where the jump amplification factor is expressed with the Dirac-delta function to explain abrupt change of flow velocity due to extreme flow events during a very short time period.

$$\mathbf{h}(t, \mathbf{X}_t) = \int_t^{t+T} \int_0^T (\boldsymbol{u} - \boldsymbol{V}_p) \delta(T/2) d\tau dt = \int_t^{t+T} (\boldsymbol{u} - \boldsymbol{V}_p) dt$$

Substituting equation (6) into equation (5), the bed shear stress is rewritten as equation (7).

$$\tau_0 = \rho \left[u\kappa \frac{1}{\ln(z_{sh} / z_0)} \right]^2 \tag{7}$$

Herein, the bed shear stress calculated from equation (7) can then be compared to the critical shear stress, i.e., criteria of deposition / resuspension of sediment particles. The estimated bed shear stress is inherently stochastic because of the stochastic particle velocity. The randomness originates from both flow turbulence and occurrences of extreme events.

APPLICATION AND SIMULATION RESULTS

The proposed SJD-PTM can be applied to particle movement in an enclosed domain subject to boundary deposition and erosion processes. As the result of the proposed model, we can trace particles and obtain stochastic particle trajectories, including their ensemble mean and variance.

The mean drift velocity of a regular flow in the following examples are $\bar{u} = 0.4$ m/s in the longitudinal direction and $\bar{w} = 0.0$ m/s in the vertical direction. The longitudinal diffusivity is $\sigma_x = 0.1$ m^2/s, and the vertical diffusivity is $\sigma_z = 0.008$ m^2/s. The longitudinal diffusivity is normally an order of magnitude larger than the vertical diffusivity in open channel flow. The occurrence of the extreme events can be represented by a Poisson process with a mean rate of 0.05/s, i.e., the mean frequency of occurrences with λ=180. The overall flow velocity during the extreme events is increased to 2.5 m/s in the longitudinal direction, and 1.5 m/s in the vertical direction. The total simulation time is 3600 s. The normalized total

simulation time is 1, and the normalized time step is 1/3600.

Case 1: Not considering bed shear stress

Figures 1 and 2 present sediment particle trajectories during a part of the total simulation time. Figure 1 displays the movement of sediment particles released at the center of depth. The solid line (blue) is the particle trajectory by the stochastic diffusion model. The dashed dotted line (black) is particle trajectory by the stochastic jump diffusion model. As shown in Figure 1, a sediment particle moves randomly due to flow turbulence gaining the velocity from extreme flow events occurring randomly and eventually settles down in the course of movement. The particle may be entrained or resuspended under the influence of turbulence and occurrences of extreme flow events. In other words, when the bed shear stress criteria are not being enforced, we mainly consider particle movement in response to ambient flow (both flow turbulence and extreme flows). Therefore, compared to Case 2 (where the bed shear stress criteria are established), the particle is more prone to resuspension. Figure 2 shows an ensemble mean trajectory of the 500 scenarios. The ensemble mean trajectories indicate that sediment particles move farther longitudinally and may have a higher probability for resuspension in the occurrences of extreme flow events.

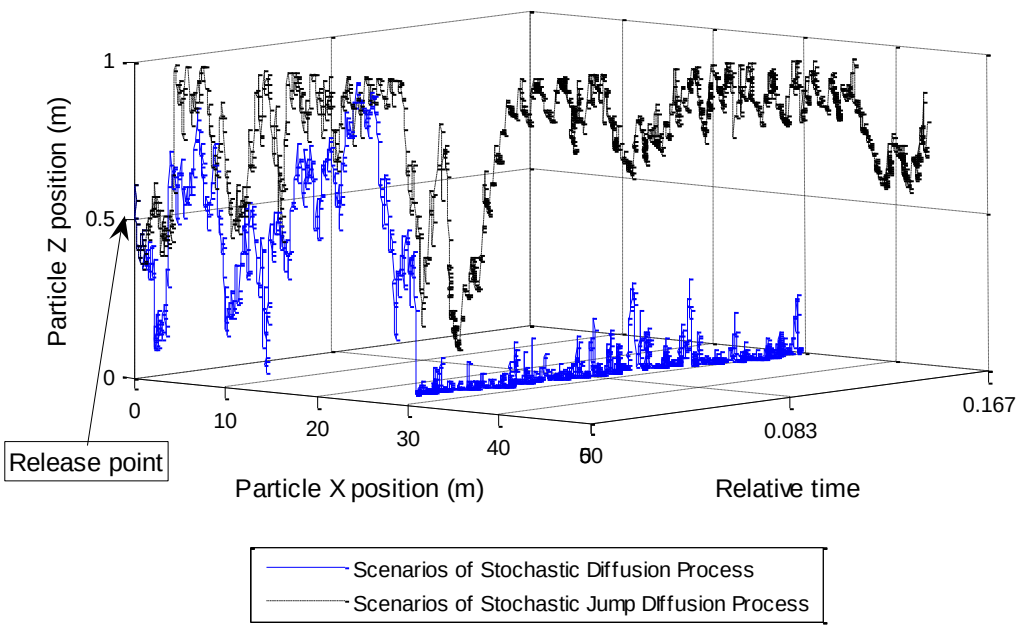

Figure 1. Sediment particle trajectories in a 2-D flow

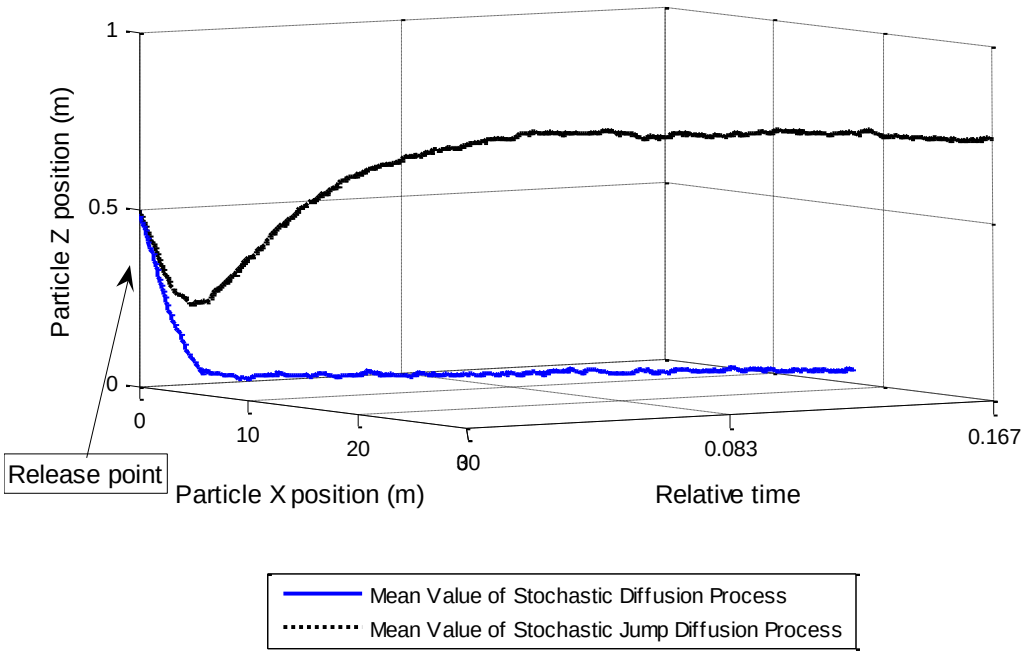

Figure 2. Ensemble mean of sediment particle trajectories in a 2-D flow

Case 2: Considering bed shear stress

Movement of sediment particles in open channel flows can be simulated including deposition / resuspension in the following examples. Herein, deposition / resuspension of sediment particles can be determined by comparing the bed shear stress with the critical shear stress. Since the bed shear stress is probabilistic attributed to stochastic particle velocity, we can obtain various realizations of particle trajectory. Figure 3 demonstrates the deposition / resuspension of sediment particles in an open channel flow. In this example, a sediment particle is also released at the center of the channel depth. Compared to Figure 1, because of the critical shear stress criterion, a particle is subject to less frequent resuspensions. The flow velocity needs to exceed the critical shear stress for particle incipient motion. The critical shear stress is 0.1 Pa for particle size 0.1 mm. Figure 4 illustrates the ensemble means of 500 simulations of the scenarios in Figure 3. From the comparison of Figures 2 and 4, it is demonstrated that the ensemble mean particle trajectory, when considering the bed shear stress criterion, travels farther longitudinally and is subject to less frequent resuspensions on the average. Also, particles in the presence of extreme events are prone to resuspensions, as can be seen in Figures 2 and 4. Overall, as shown in Figures 3 and 4, in the occurrence of extreme flow events, particles are prone to entrainment and resuspension.

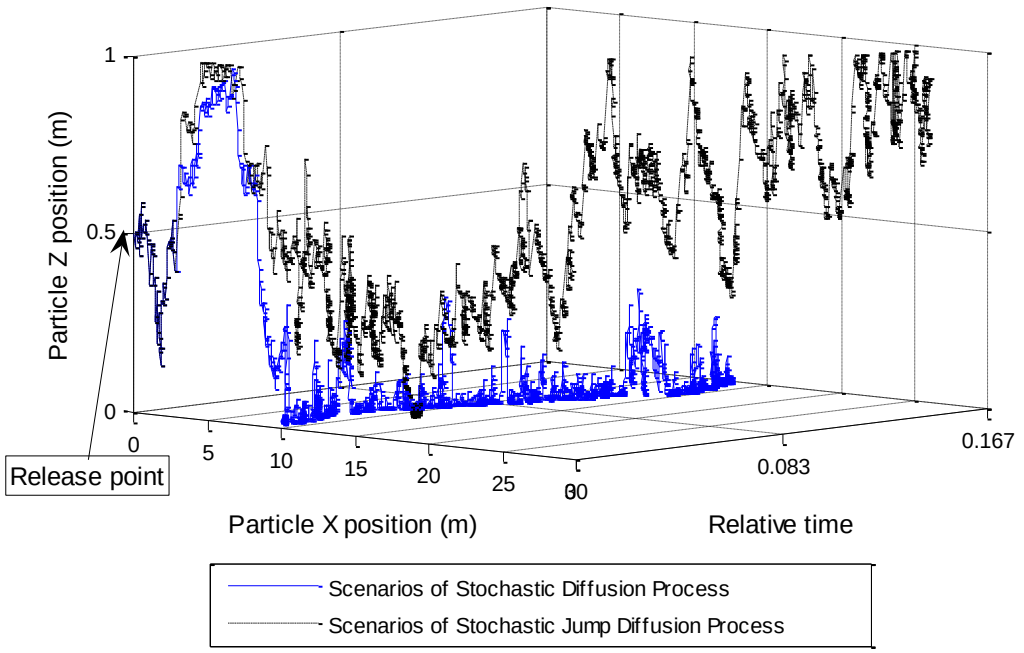

Figure 3. Sediment particle trajectories (depositing) in a 2-D flow

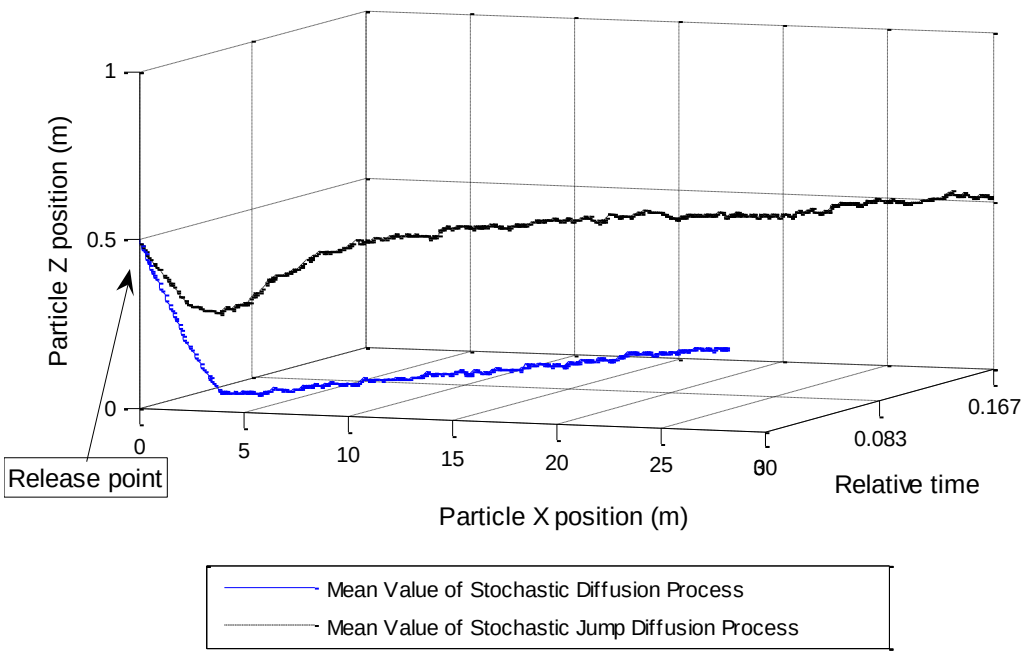

Figure 4. Ensemble mean of sediment particle trajectories in a 2-D flow

Particle Deposition and Resuspension

Figure 5 shows the position of 200 particles with respect to time after being released at the center of the channel depth. Figure 5 demonstrates diffusion, deposition and resuspension of particles. Figures 5 presents particle deposition and resuspension without any extreme flow events during total simulation time, i.e., particles move under the influence of subcritical flow (Fr = 0.13). The critical shear stress is 0.1 Pa for particle size 0.1 mm.

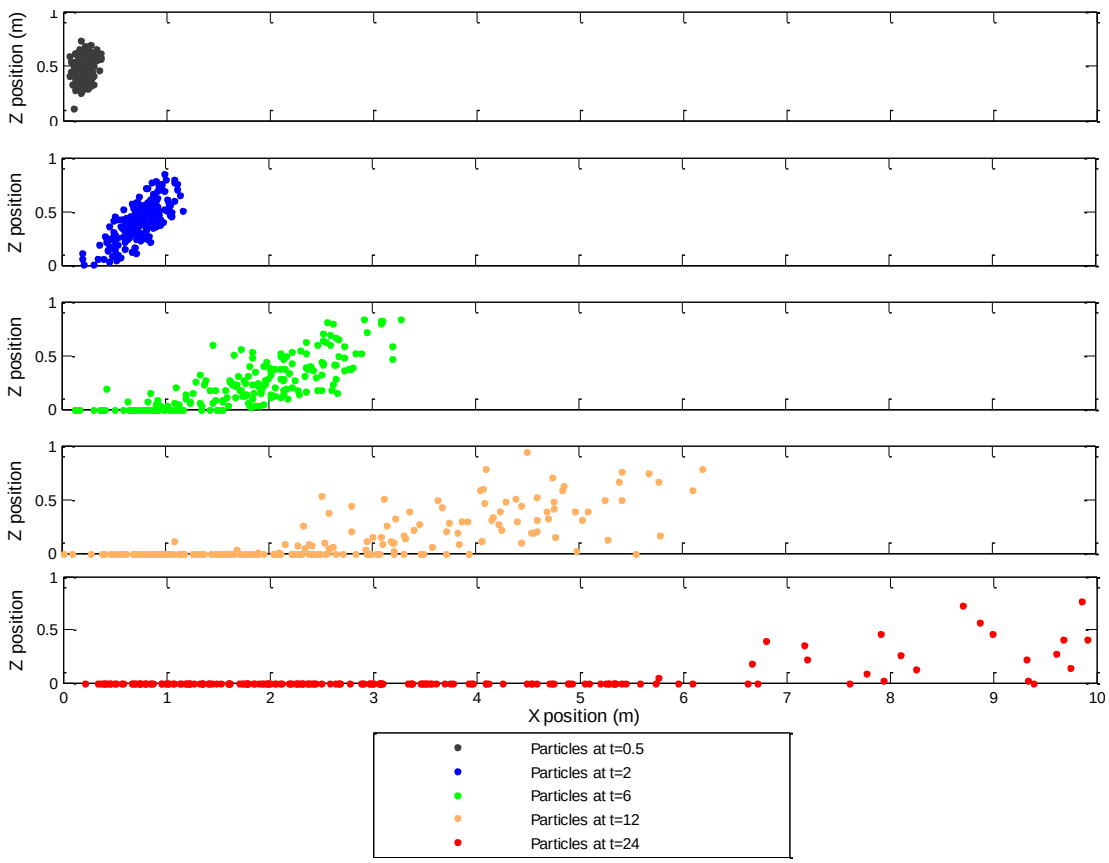

Figure 5. Snapshots of particle mass movement for each time

CONCLUSIONS

The proposed stochastic jump diffusion particle tracking model (SJD-PTM) can be developed to simulate deposition and resuspension of sediment particles in open channel flows. Movement of sediment particles in open channel flows is under the influence of the bed boundary effect. In this study, we attempt to use a logarithmic velocity profile to discuss the bed boundary effect such as deposition / resuspension processes of the particles. The channel surface and bottom are bounded and then whether sediment particles settle down on the bed or resuspend from the bed can be determined. Simulation of particle deposition and resuspension

is achieved by employing the logarithmic velocity profile formulae and the stochastic bed shear stress. As a result, the stochastic property inherently included in deposition / erosion processes is realized by the randomeness of bed shear stress from the stochastic instantaneous flow velocity. The particle trajectory in a regular flow in the previous examples presents the deposition and resuspension patterns of particles in a regular flow (Figure 5). The occurrences of extreme flow events result in net particle entrainment due to larger flow capacity carrying sediment particles (Figure 3). The proposed model is expected to predict the geomorphological changes due to scouring and deposition, which is important to channel bed and bank stability. Besides, since extreme flow events tend to result in non-equilibrium conditions, a non-equilibrium model is more realistic when estimating the effect of extreme flow events on sediment transport.

ACKNOWLEDGEMENT

The authors gratefully acknowledge the financial support from National Science Foundation under grant contract number EAR-0748787.

REFERENCES

Ariathurai, R., MacArthur, R.C., and Krone, R.B. (l977). "Mathematical model of estuarial sediment transport." Technical report D-77-12, US Army Corps of Engineers (USACE) Waterways Experiment Station, Vicksburg, MS.

Hanson, F. B. (2005). "Applied stochastic processes and control for jump-diffusions: modelling, analysis and computation." Society for Industrial and Applied Mathematics.

Krone, R.B. (1962). "Flume studyies of the transport of sediment in estuarial shoaling processes." Final report, Hydraulic Engineering Laboratory and Sanitary Engineering Research Laboratory, University of California, Berkeley, CA.

Jia, Y. and Wang, S.S.-Y. (1999). "Numerical model for channel flow and morphological change studies." *Journal of Hydraulic Engineering*, ASCE, 125(9), 924-933.

Lee, H.Y., Hsieh, H.M., Yang, J.C. and Yang, C.T. (1997). "Quasi-two-dimensional simulation of scour and deposition in alluvial channels." *Journal of Hydraulic Engineering*. ASCE, 123(7), 600-609.

Nagaraja, P. (2008). "Particle tracking sediment transport model for the buffalo river." MS thesis, State University of New York at Buffalo, Buffalo, N.Y.

Numerical Model of Channel Meandering in the Middle Sacramento River

Jianchun Huang, Ph.D., P.E., David R. Varyu, M.S., and Blair P. Greimann, Ph.D., P.E.

Sedimentation and River Hydraulics Group, Technical Service Center, Bureau of Reclamation, Denver, CO 80225 USA (vhuang@do.usbr.gov)

Abstract

SRH-Meander was used to predict the channel migration in the Middle Sacramento River. SRH-Meander is a model developed in the Technical Service Center, Bureau of Reclamation to simulate the bed topography, flow field, and bank erosion rate in a curved channel with an erodible bed. The study area extends 101 miles from Red Bluff (RM 243) to Colusa (RM 142).

The model was first calibrated by comparing the simulated channel alignment to the actual channel alignments for the period from 1976 to 1999. The erosion coefficients and the cutoff ratio were adjusted during the calibration. The calibrated model was used to predict the channel alignment in 2019 starting from the channel alignment in 1999. The terrain elevation was updated by tracking the erosion or deposition in the channel and by exchanging information between the 1D channel and 2D terrain.

1. Introduction

Because most hydraulic and sediment transport models assume the channel position stays fixed in the horizontal plane, a channel migration model (SRH-Meander) must be used to predict future channel alignments in response to variable hydrology, upstream sediment supply, and bank material conditions. Channel migration is helpful to the colonization of cottonwoods because channel migration creates bare soil on which seedlings can establish. A channel migration model can be used to evaluate whether the channel can migrate outward and downstream in areas targeted for cottonwood establishment, or whether the channel is constrained by natural geomorphic features or human placed bank protection. If the channel cannot migrate outward and create a new bar surface, cottonwoods can have a difficult time establishing because the area of a point bar where they germinate is repeatedly reworked causing desiccation of any seedlings that do establish.

The model was first calibrated with the channel alignments in 1976 to 1999. The calibration process adjusted the erosion coefficients and the cutoff ration. After calibration the model was validated by comparison between the simulated and filed 2004 alignments. The model was used to predict the channel alignment in 1999 starting from the channel alignment in 2019. The averaged channel character values, such as mean radius of curvature, half wave length, entrance angle, sinuosity, and migration rate, were calculated for different restoration strategies. The terrain elevation was updated by tracking the erosion or deposition in the channel and by exchanging information between the 1D channel and 2D terrain.

2. Model description

SRH-Meander is a computer model that simulates the bed topography, flow field, and bank erosion rate in curved channel with an erodible bed. In each time step, SRH-Meander first calculates the flow field based on the standard step method, normal depth method, or a predefined table. It then computes the channel bank erosion rate. Finally, the channel alignment is updated with the erosion rate, followed by the channel cutoff if needed. The model can be used to predict the channel migration in meandering rivers

SRH-Meander uses the meander method proposed by Johannesson and Parker (1989). It is a re-derivation of the analysis by Engelund (1974). The basic idea behind these analyses is to write the flow variables as a sum of two parts. The first part is the solution to the case of flow in a straight channel. The second part is equal to the deviation from the straight channel solution for the case of a slightly curved channel. The deviation is assumed to be linearly related to the maximum curvature of the channel. These perturbed flow variables are substituted into the 3D flow equations. The equations are then simplified and grouped into the terms responsible for the straight channel solution and those due to the channel curvature. The equations become ordinary differential equations and can be solve analytically or through relatively simple numerical methods. The sediment transport is assumed to be a function of the local velocity and shear stress.

Sun at al. (2001a, b) improved Johannesson and Parker's (1989) linearization theory to calculate bank erosion in river meanders by incorporating multiple-size sediment transport equation. Johannesson and Parker (1989) assume the bank erosion rates are related to the near-bank depth-averaged flow velocity, which is calculated by a small perturbation approach. The near bank depth-averaged flow velocity is decomposed into two parts: the component characterized by local curvature forcing (e.g. point bars) and the component characterized by the free system (e.g. alternate bars).

SRH-Meander extends the linearization analyses of Johannesson and Parker (1989) and Sun et al. (2001a, b) to include the sediment mass balance. The incoming and exiting sediment in a reach are calculated by a non-equilibrium sediment transport model. The sediment erosion or deposition is calculated using a sediment mass balance between the incoming and outgoing sediments and sediment erosion due to bank migration. The channel width is assumed to be constant. The terrain elevation is updated by tracking the erosion or deposition in the channel and by exchanging information regarding bed elevation and bed material fractions between the 1D channel and 2D terrain.

3. Model Calibration

A calibration to historic meander rates was completed because "it is not possible to determine the erodibility coefficients a priori, based on bank properties, presence of vegetation, etc." for real rivers without "calibrating the erodibility coefficients on field observations" (Crosato, 2007). The period of record used for model calibration was from 1976 to 1999. This interval was chosen based on the availability of data and the quality of that data. Selected sub-reaches of the study reach (river mile 243 to river mile 142) were isolated to simplify the calibration process. Due to the space limit of this paper, only one sub-reach from RM 224.5 to RM 218 is presented here. The data collected and used for the calibration of the middle Sacramento River is described below, but in general, the source and quality of data will vary for each project and vary the results.

Flow data from gages operated by the State of California Department of Water Resources (CDWR) were utilized for model calibration. Mean daily flows for the period of record from 10/01/76 to 09/30/99 for CDWR gage 'VIN' were used for the selected reach.

Profile and cross-sectional geometry information was taken from a United States Corps of Engineers publication, "Sacramento and San Joaquin River Basins, Comprehensive Study" (U.S. Army Corps of Engineers, 2002). This study produced a HEC-RAS geometry model of the river that was used in this study. River planform geometry was made available by CDWR in the form of aerial photographs and GIS maps consisting of traces of the active channels.

From the 2002 USACOE publication, information on channel roughness, namely Manning's roughness coefficient values, was obtained. Also from the study, information on bed material size was gathered and used as input to the model.

No modifications were made to the flow data acquired from CDWR. However, a filter is present in SRH-Meander so that flow data that may not effect river meandering can be excluded. For instance, it is generally accepted that base flows do not cause changes in channel morphology. However, due to the linear nature of the computer model, these base flows yield a calculated meander length, however minor. Conversely, when flows of a river exceed the carrying capacity of a channel, the excess flow spills out on to the floodplain, and the excess flood waters have little affect on channel-forming processes. Without an imposed upper bound on the flow rates, the rate of bank erosion would increase as the flow rate increases even above the bank full discharge. Thus, an upper limit above which the flow is capped and lower limit below which the flows are ignored was applied to the input flow data set. Based on the flow hydrograph and the results of the RAS model, lower and upper limits of 35,000 and 90,000 cfs, respectively, were used for the Sacramento River.

The HEC-RAS model associated with the 2002 USACOE study was used to derive cross-sectional and profile geometry parameter values. Rather than assume a cross-sectional shape and associated descriptive parameters (e.g., sideslope and bottom width for a trapezoidal cross-section) to represent the river, a more generic approach was taken. The HEC-RAS model was run with a series of steady flow rates. Cross-sections were sorted by sub-reach, and average hydraulic parameters were calculated. The geometry parameters were tabulated into a format that SRH-Meander can interpret. Thus, for each sub-reach, a table was created with flow rates from 30,000 to 90,000 cfs along with associated sub-reach averaged values for velocity, friction slope, hydraulic depth, top width, and hydraulic radius. SRH-Meander linearly interpolates hydraulic parameters for flow rates between the tabulated values.

The GIS maps made available by the DWR were used for planform geometry data. The SRH-Meander meander model uses a GIS point file (which represents the centerline of the river) to compute radii of curvature and other parameters which are necessary to estimate the rate of river meander. The GIS maps provided by the DWR contained polygons which depicted the 'active' channel alignments for various years. It was necessary to digitize a polyline (representing the centerline) based on the polygons provided by CDWR, and further transform the line into a point file. A polyline was digitized in ArcGIS to represent the centerline of the 1976 channel and the 1999 channel, which are the 'starting' and 'ending' conditions to which the model was to be calibrated.

In addition, a valley axis for the 1976 channel was digitized, which is used in the computation of channel cutoffs. The cutoff ratio is a calibration parameter. When the length of the channel divided by the length of the valley exceeds the cutoff ratio, the model allows a cutoff to occur. The cutoff ratio for the sub-reach was adjusted during the calibration process.

To calibrate the model, the simulated channel alignment was compared against the actual channel alignment at the end of the time interval being modeled. An iterative approach was taken in calibrating the model to the sub-reach. Erosion coefficients were adjusted after an observed model run as necessary until the model output alignment represented the actual channel alignment sufficiently well.

Table 3-1 presents a summary of the parameters – both calibration parameters as well as those determined before calibration – used during calibration of the SRH-Meander model to the Sacramento River. All of the erosion coefficients are not listed, but rather the minimum, average, and maximum values for each sub-reach are presented.

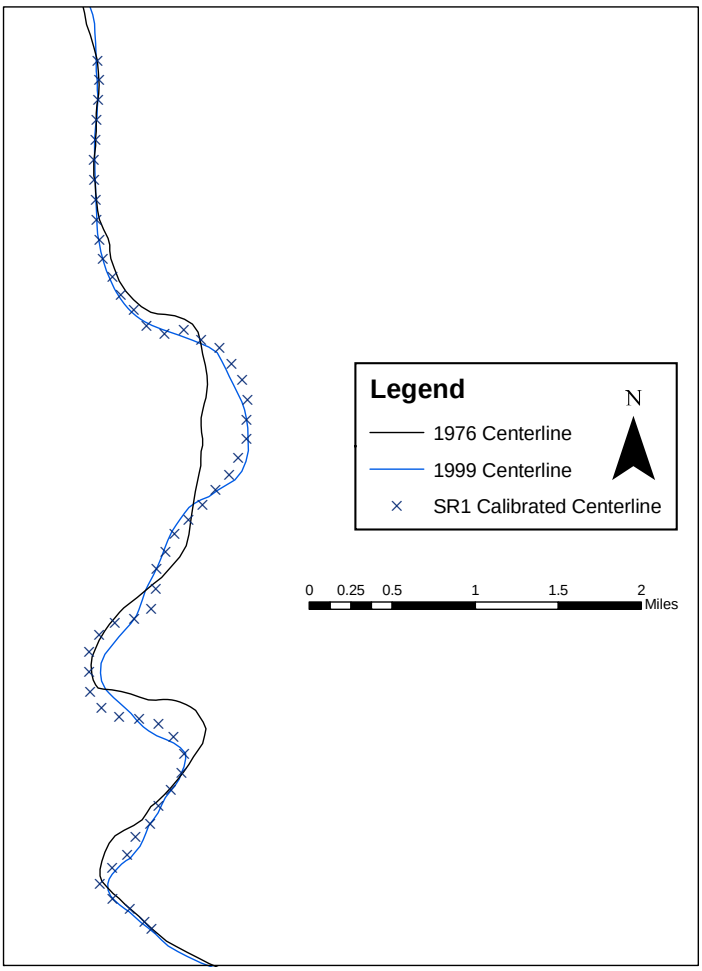

Figure 3-1. displays the centerline for the 1976 channel, the centerline for the 1999 channel, and the SRH-Meander output nodes representing the model output channel centerline.

Table 3-1. Summary of parameters used during SRH-Meander model calibration

Pre-determined parameters	**Ave. Channel Width (ft)**	1058
	Manning n (-)	0.032
	Ave. Energy Slope (ft/ft)	0.00056
	Bed Material Size (mm)	14
	Number of Polygons	18.00
Calibration parameters	**Grid Spacing (-)**	0.6
	Cutoff Ratio (-)	2.0
	Min. Erosion Coefficient (-)	9.80E-08
	Ave. Erosion Coefficient (-)	7.23E-05
	Max. Erosion Coefficient (-)	3.80E-04

The average absolute distance of the model output coordinates to the actual channel centerline was 46 feet. This value is small relative to the average channel top widths of 1,058 feet. Adjusting the grid spacing for each sub-reach yielded slightly better results, but for the sake of consistency one grid spacing value was determined for all sub-reaches. The value of 0.60 for the grid spacing agrees with the finding of Crosato for numerical meander models that the "optimal distance between successive grid points had the order of half the channel width" (Crosato, 2007).

In general, the SRH-Meander was better at modeling changes in bend amplitude than at modeling bend translation. Whether the model predicts translation versus amplification is primarily a function of the channel roughness input parameter combined with the calculated curvature of the centerline. Calibrating one bend with a given curvature may cause poor model performance in a subsequent bend of similar curvature. Another limitation of SRH-Meander lies in modeling portions of a river that migrate 'inward'; that is, when the bend amplitude decreases rather than increases and the river slightly straightens. This process is usually due to local chute cutoffs as opposed to larger scale neck cutoffs. Meander cutoffs within SRH-Meander depend on the input valley axis, and it effectively only allows for neck cutoffs. The model does not have the capability to account for straightening phenomenon, especially for two continuous bends. The only successful inward migration caused with SRH-Meander involves an over-amplification of the immediate upstream or downstream bend.

Correlating the erosion coefficients resulting from the model calibration to the existing bank properties as provided by CDWR was attempted. A meaningful correlation between existing bank properties and the calibrated erosion coefficients was not identified. It is hypothesized that the bank properties being considered reflect only at most the last couple years of a twenty-four year modeled time interval (1976-1999). In SRH-Meander, one polygon, representing one erosion coefficient, reflects the outer-bank of a bend for the entire time interval simulated. As a river meanders across its floodplain, different materials are encountered, the bank height and angle will change, geological controls may be reached, and unknown riprap may have been placed at any time during the modeled interval. Thus, the next step of the correlation process is to gather and apply more historical data to the problem to represent the conditions spanning the entire time interval and not just the last few years of the time interval. Ideal data to collect includes the time and location of riprap placement, aerial photographs for many years within the modeled time interval, and a geospatial mapping of soil types across the floodplain, which includes soil data for regions below the surface soils. When more time-dependant information becomes available, the SRH-Meander model may be re-calibrated with additional erosion coefficient polygons to reflect changes in bank properties through time.

The above limitations do not allow for future river meander prediction that would occur if bank properties were changed (e.g., riprap removed or added) due to the inability to predict an erosion coefficient based on bank properties. The model is currently capable of determining the most likely areas of future channel migration as a function of in-flow hydrographs, which would be based on release management actions occurring at Shasta and Keswick Dams. A correlation is anticipated with the collection of more historical data representing the modeled time interval.

4. Model Prediction

The calibrated model was used to predict the channel alignment in 2019 with initial channel alignment taken from 1999 photography, the CALSIM simulated hydrology at Red Bluff Diversion Dam, and lateral flows. The erosion coefficients, the channel roughness, the grid spacing, the cutoff ratios, and all other parameters were kept unchanged from the calibration model. The 2004 photography was used to verify that the predicted channel alignment was reasonable.

The future flows were taken from a water operations model (CALSIM II) that used a monthly time step. The monthly flows were downscaled to daily flows. The operations model using historical hydrologic conditions and the period from 10/1/1983 to 9/30/2003 was used to predict channel meander from 1999 to 2019. Flow data from the gage at Red Bluff Diversion Dam (RM 243.0) was used as upstream incoming flow. Three different alternative flow scenarios were simulated, corresponding to various water operations strategies. For the purposes of this paper they are designated as FNA, WQ1B, and AF1B.

The predicted channel alignment in 2019 is shown in Figure 4-1. The Sacramento River continues to meander at the same rate. Results show that a channel cutoff might happen at the largest bend in this subreach unless the channel bank is stabilized at this location.

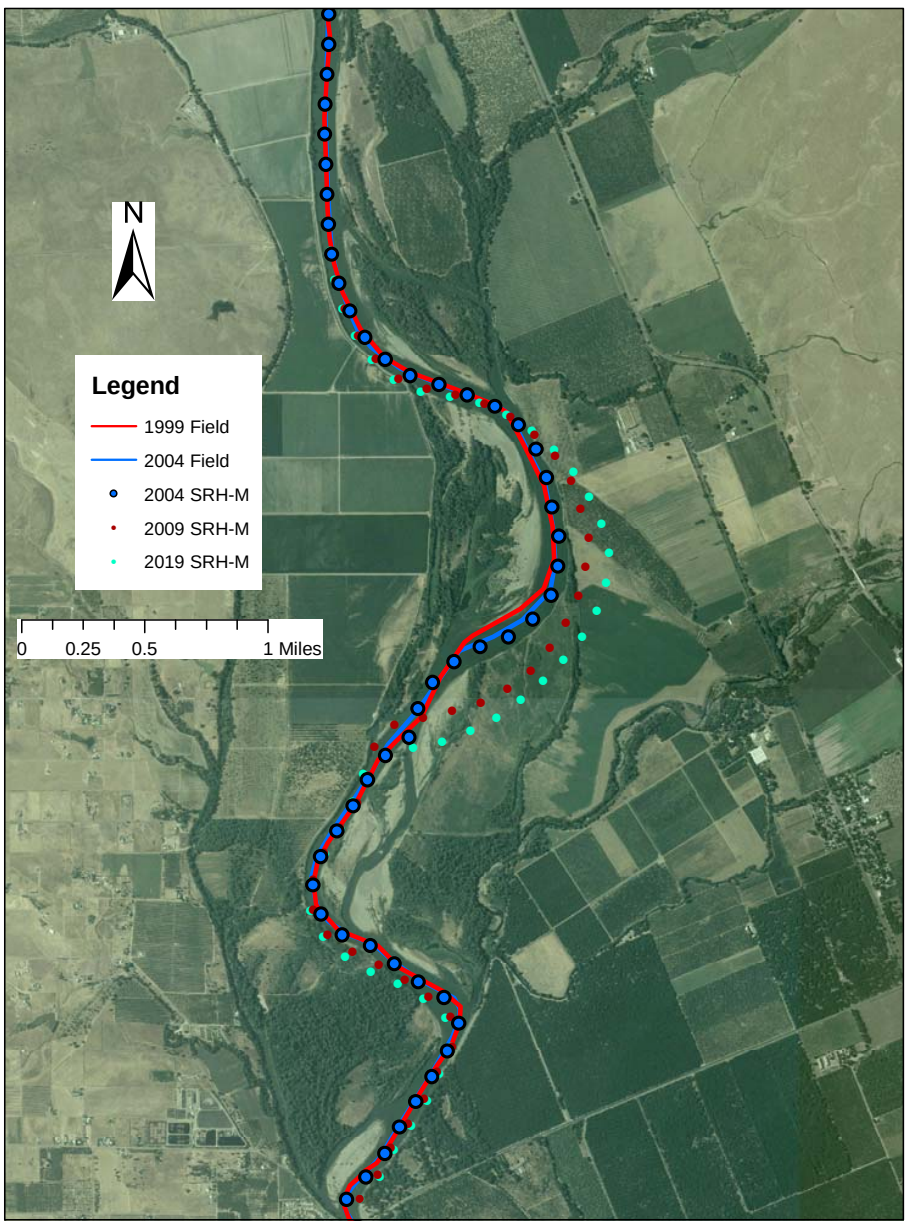

Figure 4-1. SubReach 1 prediction results

Figure 4-2 compares the channel migration rates with historical data (Larsen, 2007). Larsen mapped the channel centerlines in the middle Sacramento River from Red Bluff to Colusa from historic topographic maps (1904) and aerial photographs (in 6 time periods between 1937 and 1997). The channel migration rates are calculated for progressive migration, partial cutoff, and partial chute cutoff. Progressive migration is lateral channel adjustment that occurs via a continual and gradual process of bank erosion. Chute cutoffs occurs when overbank flows are sufficient to concentrate shear stresses to a degree capable of carving a new channel across the floodplain. "The partial cutoff category describes episodes of channel avulsion that affect only a portion of a meander bend" (Larsen, 2007). Since SRH-Meander cannot distinguish chute and partial cutoffs, the results are given for progressive migration and cutoff. Results show similar trends of migration rates with historical data. The progressive migration rate is about 4.1 m/year for FNA and AF1B, and 4.0 m/year for WQ1B. The cutoff migration rate is about 15.5 m/year for FNA and AF1B, and 15.4 m/year for WQ1B.

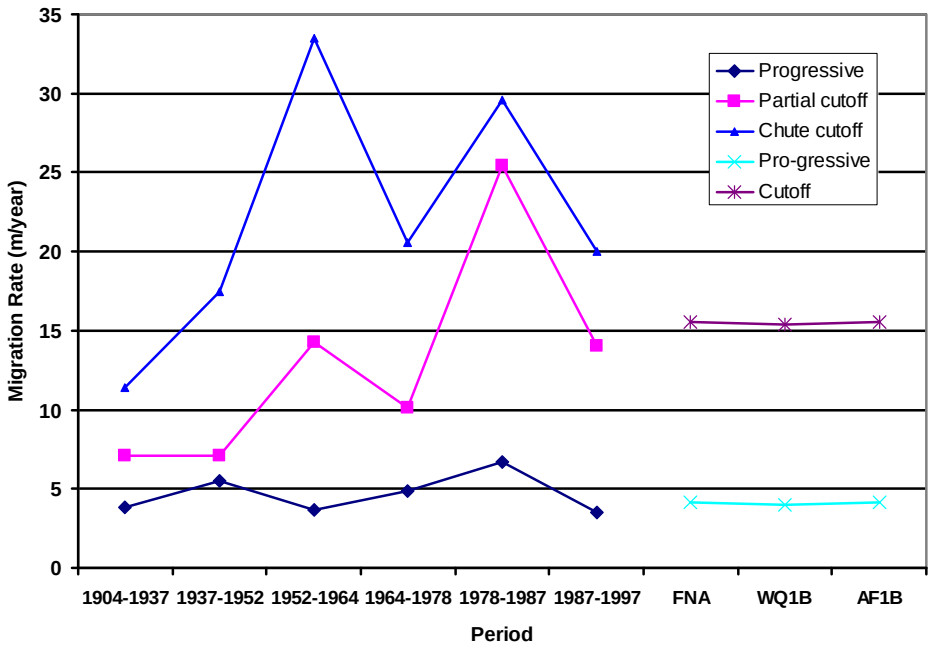

Figure 4-2. Predicted Dimensionless Migration Rates compared with historical data (Larsen, 2007)

SRH-Meander also can calculate terrain elevation changes during channel migration. The model calculates the terrain elevation by tracking the erosion or deposition in the channel and by exchanging information regarding channel elevation and bed material between the 1D channel and 2D terrain. During the simulation, the channel width was assumed constant. 2D terrain elevation was stored in a raster format generated with ARC-GIS. Since the 2D data required huge memory and the study reach covers about 100 miles, the study reach was divided into 7 sub-reaches to obtain high resolution in representing terrain elevation. Figure 4-3 shows the terrain elevation for the initial year 1999 when the field data is available. Figure 4-4 shows the predicted terrain elevation in 2019. Elevation data are only available in 1999 and no other data is available to determine the accuracy of SRH-Meander in predicting terrain elevation revision due to channel migration. Figure 4-5 shows the predicted terrain change from 1999 to 2019, which displays the erosion (red) near the outside of the bend and deposition (green) near the inside of the bend. The black polygon shows the total area that the channel would have swept in the 20-year period. Accurate prediction of terrain elevation change is helpful to determine the area targeted for cottonwood establishment.

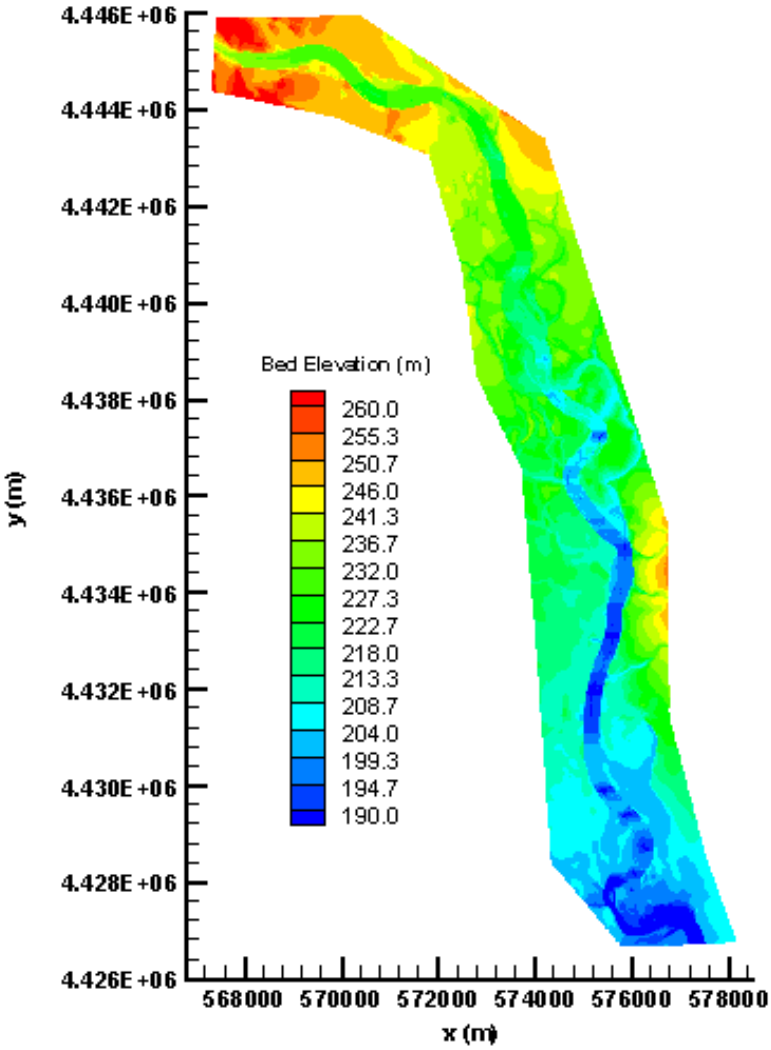

Figure 4-3. Initial terrain elevation in 1999

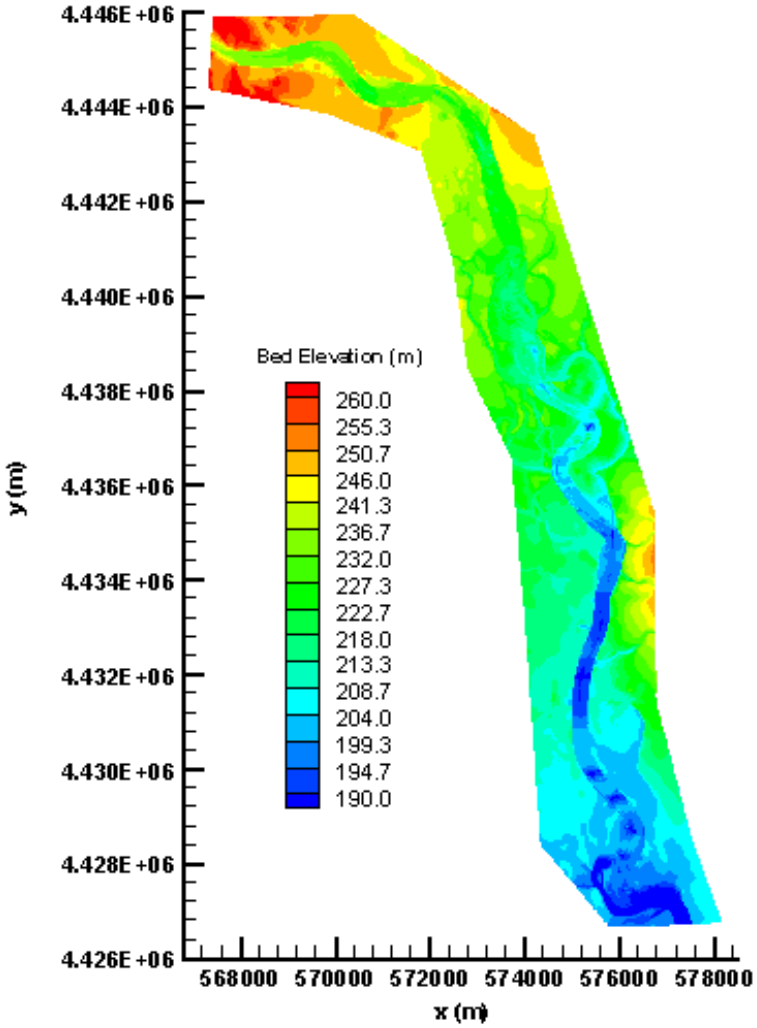

Figure 4-4. Final terrain elevation in 2019

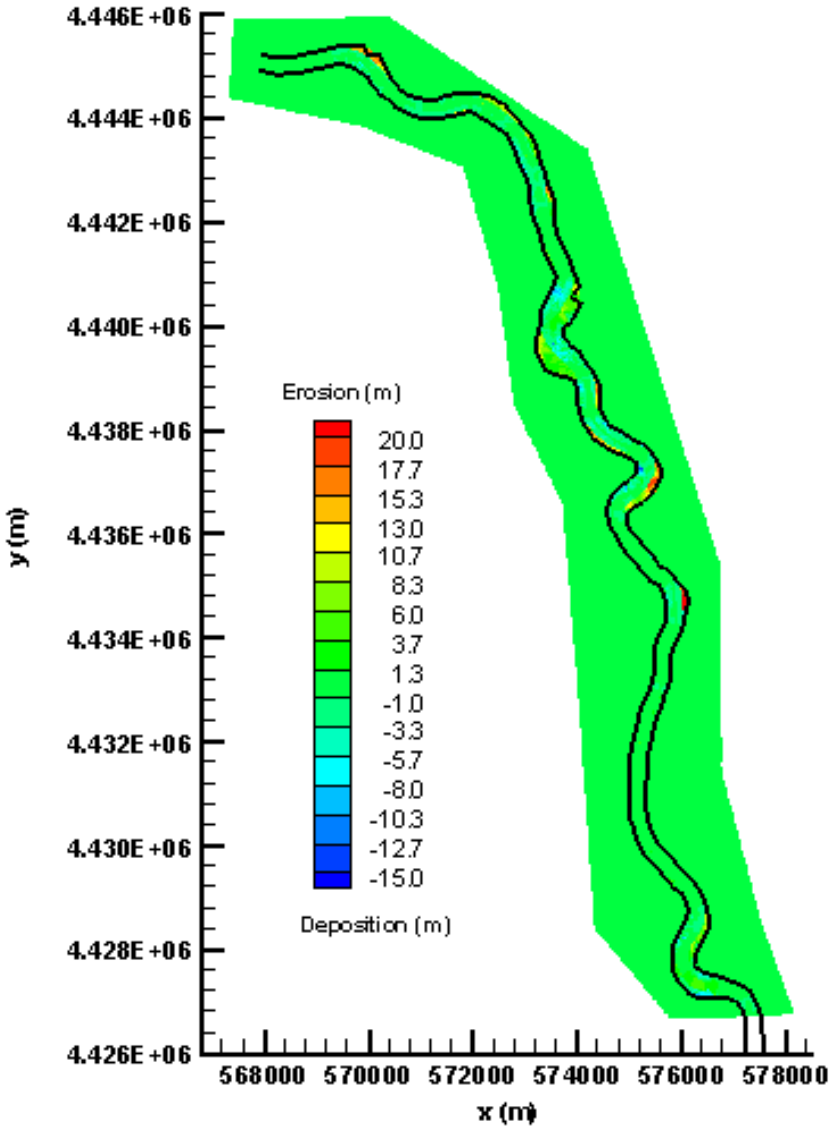

Figure 4-5. Terrain elevation change from 1999 to 2019

5. Summary

The SRH-Meander model was used in the Middle Sacramento River extending 101 miles from Red Bluff (RM243) to Colusa (RM142) to predict the channel migration. The model was first calibrated with the channel alignment from 1976 to 1999. The model reproduced the general movement of most large bends in the river. The average absolute distance of the model output coordinates to the actual channel centerline was 46 feet. This value is small relative to the average channel top widths of 1100 feet. The calibrated model was used to predict the channel alignment in 2019. The terrain elevation was also calculated and the results could be used to evaluate whether the channel can migrate outward and downstream in areas targeted for cottonwood establishment.

Acknowledgements

The Mid-Pacific Reclamation Regional Office and the Reclamation Science and Technology Program have supported the development of SRH-Meander.

References

Crosato, A., (2007). "Effects of smoothing and regridding in numerical meander migration models", Water Resources Research, VOL. 43, W01401.

Engelund, F. (1974). "Flow and Bed Topography in Channel Bends," *ASCE Journal Hydraulics Division*, Vol. 100(11), 1631-1648.

Johannesson, H., and Parker, G. (1989). "Linear Theory of River Meanders," in *Water Resources Monograph No. 12: River Meandering*, edited by S. Ikeda and G. Parker, American Geophysical Union, Washington DC, 181-213.

Larsen, E., (2007). *Predicting Modes and Magnitude of River Channel Migration and Chute Cutoff Based on Bend Geometry, Sacramento River, California, USA*, Report prepared for the Bureau of Reclamation.

Sun, T., Meakin, P., and Jøssang, (2001a). "A computer model for meandering rivers with multiple bed load sediment sizes, I. Theory," *Water Resources Research*, Vol.37(8), 2227-2241.

Sun, T., Meakin, P., and Jøssang, (2001b). "A computer model for meandering rivers with multiple bed load sediment sizes, II. Computer simulations," *Water Resources Research*, Vol.37(8), 2243-2258.

One- and Two-dimensional Modeling of Deep Gravel Mining in the Rio Salado

Dong Chen[1], Mingfa Liu[2]

[1] Ph.D., P.E., M. ASCE, Division of Hydrologic Sciences, Desert Research Institute, 755 E. Flamingo Road, Las Vegas, NV 89119; PH (702) 862-5541; FAX (702) 862-5427; Email: dchen@dri.edu

[2] Department of Finance, University of Nevada, Las Vegas, 4505 S. Maryland Parkway, Box 456008, Las Vegas, Nevada 89154-6008. Phone: 702-338-9004; Fax: (702) 895-4650; Email: lium4@unlv.nevada.edu

ABSTRACT

Impact of deep sand and gravel mining pits (with a depth of 10 meters) on flood zone coverage and riverbed change of the Rio Salado, Salt River, Phoenix, Arizona were simulated using one- and two-dimensional numerical models. Two commonly used models are applied in the study, i.e., HEC-RAS and CCHE2D. HEC-RAS is a one-dimensional hydrodynamic and sediment transport model developed by the U.S. Army Corps of Engineers, while CCHE2D is a depth-averaged two-dimensional hydrodynamic and sediment transport model developed at the University of Mississippi. The bed material was treated as three layers on the channel bed with multiple grain-sized sediment mixtures. Changes in bed elevation were calculated by solving the sediment mass conservation equation. The modeling results of CCHE2D were compared with the HEC-RAS modeling results and field observations, which showed that the 2D model was more robust in simulating flood zone coverage, non-uniform sediment sorting, and channel geomorphologic changes.

INTRODUCTION

The Salt River (Rio Salado in Spanish) drains 14,500 square miles of mountainous desert terrain in central and eastern Arizona and is the largest tributary to the Gila River in Arizona. The river originates in eastern Arizona and flows westward to its confluence with the Gila River west of downtown Phoenix (Figure 1). Prior to agricultural development and urbanization of the Phoenix metropolitan area, the Rio Salado was a perennial stream fed by snowmelt from mountains in eastern Arizona. Flow in the river had a distinct seasonal pattern, with highest flows occurring in December and January and lowest flows in October. The yearly-averaged discharge was about 570 cfs before 1938. However, perennial flows on the Salt River have ceased due to dam and diversion construction in the early 1900s. In the early part of the 20th century, major modifications to the river system occurred as part of the Salt River Project, which placed several dams along the Salt River to allow diversions of water for agricultural and urban uses. Sand and gravel

mining operations and development along the river induced additional changes to the river channel and hydrology. The materials extracted from the river have been used extensively throughout the development of the Phoenix Metropolitan area. Since 1965, the channel has carried a yearly-averaged discharge of only 400 cfs, with less than 14 cfs in almost three-fifths of the years (USACE, 2005). Now the water in the channel is dominated by the releases from upstream dams. The highest recent discharge occurred on February 13, 2005, of approximately 35,000 cfs as recorded by the USGS gauge at 51st Avenue (http://waterdata.usgs.gov/az/nwis/rt).

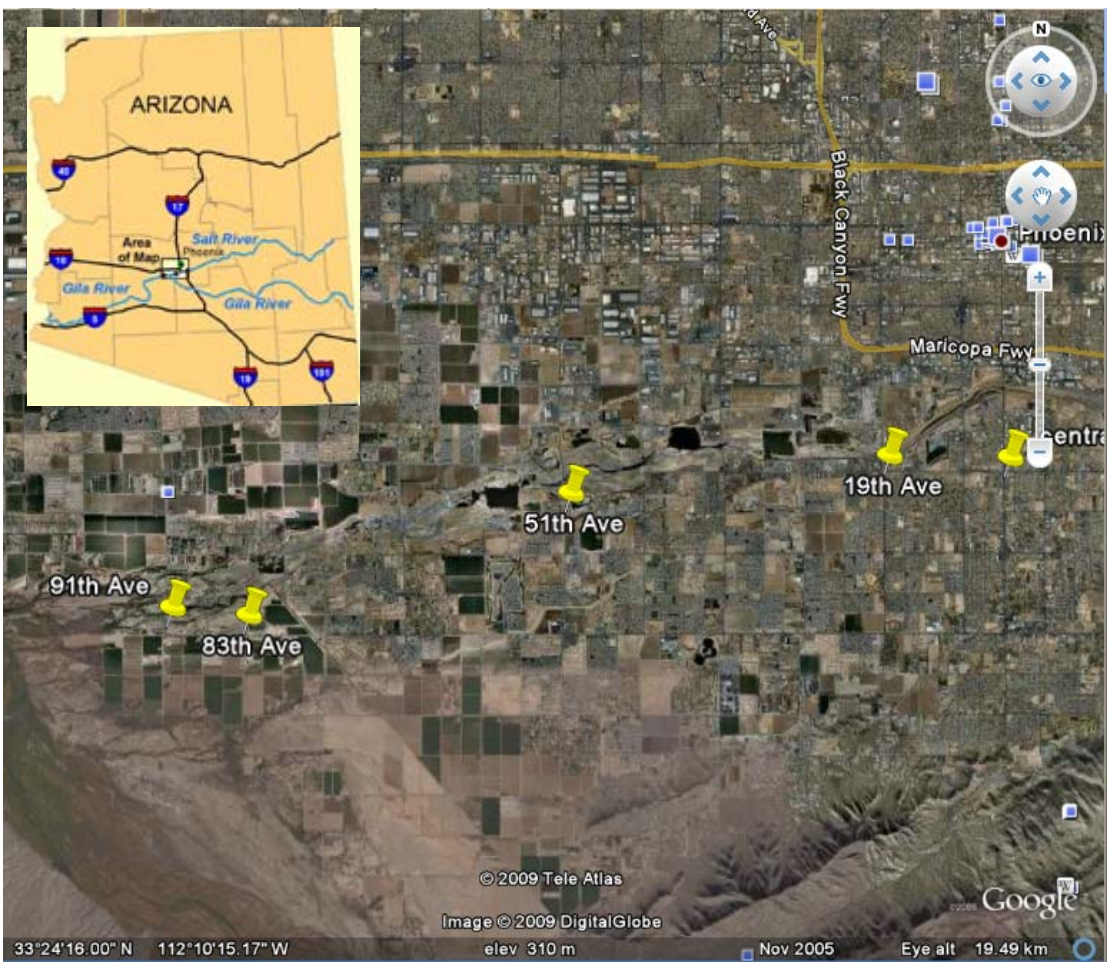

Fig. 1 Map of the Rio Salado, Salt River, Phoenix, Arizona

Sediment transport is an issue of importance in the Salt River special in the vicinity of city of Phoenix where recently unprecedented amount of growth has occurred. Previous sediment transport analyses have showed that sediment dynamics was more significant in the proximity of mining operations (USACE, 2005). Sand gravel mining has been going on in the Salt River for generations. There are numerous large mining pits in the Salt River around the city of Phoenix and the

demands of more mining pits are growing day by day (shown in Fig. 1). Sand and gravel mining operations can cause changes in channel geomorphology as well as hydrology. Therefore, it is very important to understand the sediment transport dynamics in the Salt River along with the impact of gravel mining pits along the river bed. This study was designed to understand the sediment transport dynamics due to various flood events and the impact of gravel mining operations in the Oeste reach of the Salt River. The Oeste reach (study reach) is approximately 9.5 miles of the Salt River extending from 19th Avenue on the east to 91rd Avenue on the west. The study area is within the boundaries of the City of Phoenix, Arizona.

Bed Material Gradation along the River

Bed material gradations along the channel were obtained through a combination of Pebble Count Method and Sampling Materials at five accessible locations (Chen et al, 2007). Less than 0.6% surface material consists of wash load (clay and silt) whose size is less than 0.0625 mm. About 2% bed material belonged to fine sand at 19th and 91st Avenues. Bed surface material mean size D_{50} ranges from 20mm to 40mm. More than 90% of the bed surface material consists of very coarse sand and gravels. Materials at the 51st Avenue are coarser than the bed material at other locations.

Introduction to HEC-RAS and CCHE2D

The U.S. Army Corps of Engineers' River Analysis System (HEC-RAS) is software that allows you to perform one-dimensional steady and unsteady flow river hydraulics calculations and sediment transport calculations. Both one-dimensional energy equation and momentum equation are considered in various situations including mixed flow regime calculations, i.e., hydraulic jumps, hydraulics of bridges, and evaluating profiles at river confluences. The effects of various obstructions such as bridges, culverts, weirs, spillways in the flood plain may also be considered in the computations. The sediment transport potential is computed by grain size fraction, thereby allowing the simulation of hydraulic sorting and armoring. HEC-RAS is widely used in engineering firms in U.S (USACE, 2002).

CCHE2D is an integrated package for two-dimensional simulation and analysis of river flows, non-uniform sediment transport, morphologic processes, coastal processes, pollutant transport and water quality. These processes are solved with the depth integrated Reynolds equations, transport equations, sediment sorting equation, bed load and bed deformation equations. This model is based on Efficient Element Method, a collocation approach of the Weighted Residual Method. Internal hydraulic structures, such as dams, gates and weirs, can be formulated and simulated synchronously with the flow. Dry and wet capability enables one to simulate flows with complex topography with ease. Three turbulence closure schemes, depth-averaged parabolic, mixing length eddy viscosity models and k- e model, are

available. The numerical scheme can handle subcritical, supercritical flows and their transition (NCCHE, 2005).

HYDRODYNAMIC SIMULATION

The effect of mining pits on inundated areas during different discharges was simulated in this study. Fig.2 provides an example of the calculated inundated areas with and without the mining pits at 500-year event. Based on Fig. 2, HEC-RAS and CCHE2D have similar calculated results which indicate that the inundated area has been reduced around the pits. However, this modification is minor comparing to the whole inundated area because the mining area only occupied a small part in the whole domain. Similar conclusions were drawn under other discharges which are not included in the report. However, our results suggested that mining pits altered the local flow direction and magnitude. Prior studies elsewhere have shown that over the years the Salt River around city of Phoenix has experienced severe bank erosion (USACE, 2005). The maximum riverbank shift has been as much as one-half mile in some locations through the area between 19th and 91st Avenues, Phoenix. The meander belt varies from approximately 2 miles in width at some places (19th Avenue) to approximately 4 miles in width at other places (91st Avenue; USACE, 2005). Previous sediment transport analyses have showed that sediment dynamics were more significant in the proximity of mining operations (USACE, 2005). However, the quantitative relation between bank erosion and gravel mining activities has not been formulated yet.

SIMULATION OF BED ELEVATION CHANGE

The effect of mining pits on bed elevation change was also simulated in this study. Fig. 3 and 4 show the bed topography change induced by gravel mining operation at 500-year flood event with HEC-RAS and CCHE2D models, respectively. Based on the simulation results, there was substantial erosion occurring upstream and downstream of the pits, however, the modeling results of HEC-RAS and CCHE2D model differed with each other. HEC-RAS results indicated serious head-cutting occurred upstream the pits, while CCHE2D results suggested “downstream erosion” was more noticeable. Modeling results of HEC-RAS showed the maximum bed degradation were 3.6 meters and 2.9 meters upstream of the Pit #1 and Pit #3, respectively. However, modeling results of CCHE2D exhibited the maximum bed degradation was 3.3 meters which occurred downstream the Pit #1. Besides, modeling results of CCHE2D indicated most sediment deposition was occurred in the upstream end of the mining pits. The maximum bed aggradations were 1.7 meters and 1.9 meters in the Pit #1 and Pit #2, respectively. Based on laboratorial/field observations and previous modeling study (Chen et al., 2008), the 2D model was more robust in simulating flood zone coverage, non-uniform sediment sorting, and channel geomorphologic changes.

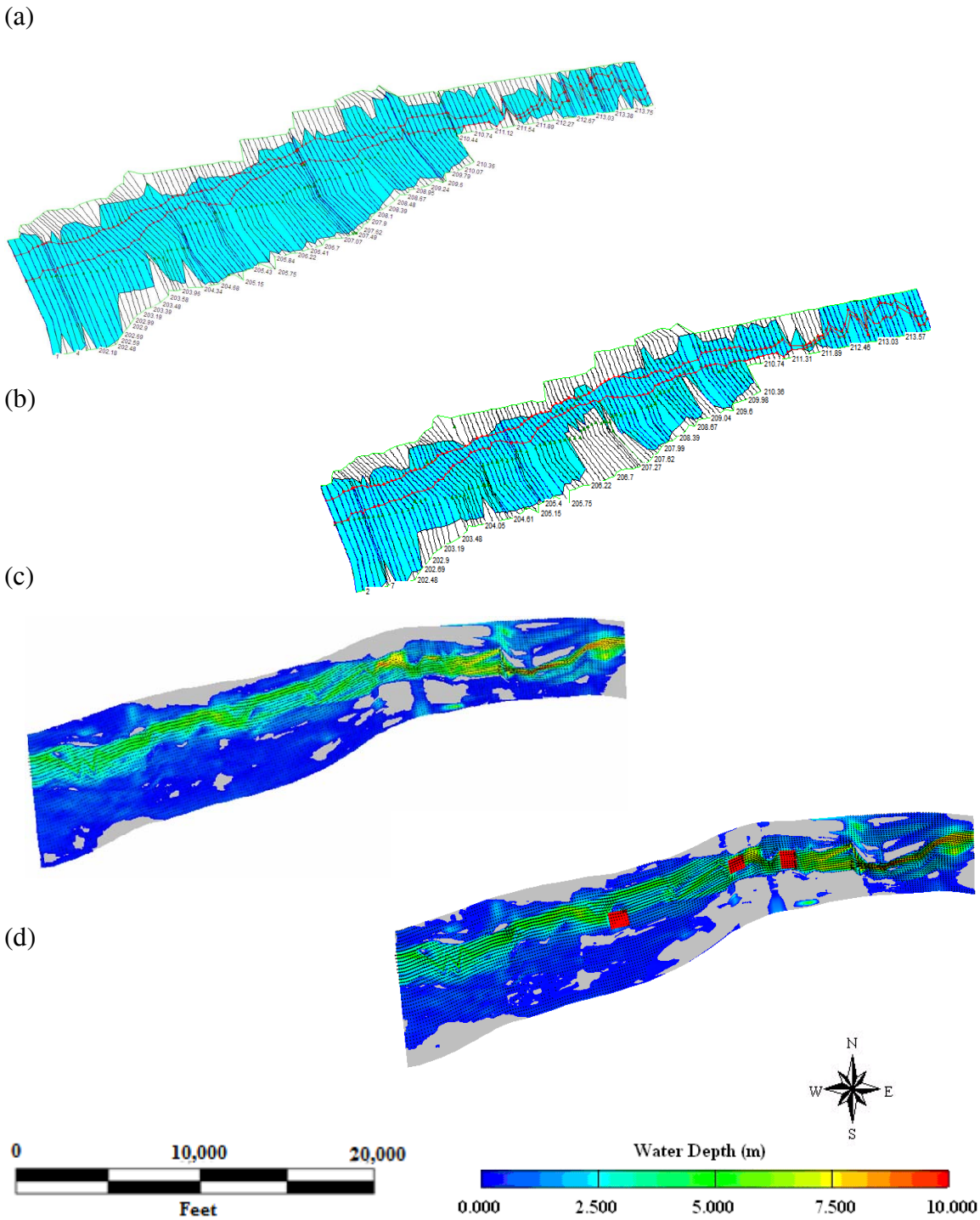

Fig.2. Calculated inundated areas at 500-year event (a) HEC-RAS without mining pits; (b) HEC-RAS with three 10m pits; (c) CCHE2D without mining pits; (d) CCHE2D with three 10m pits

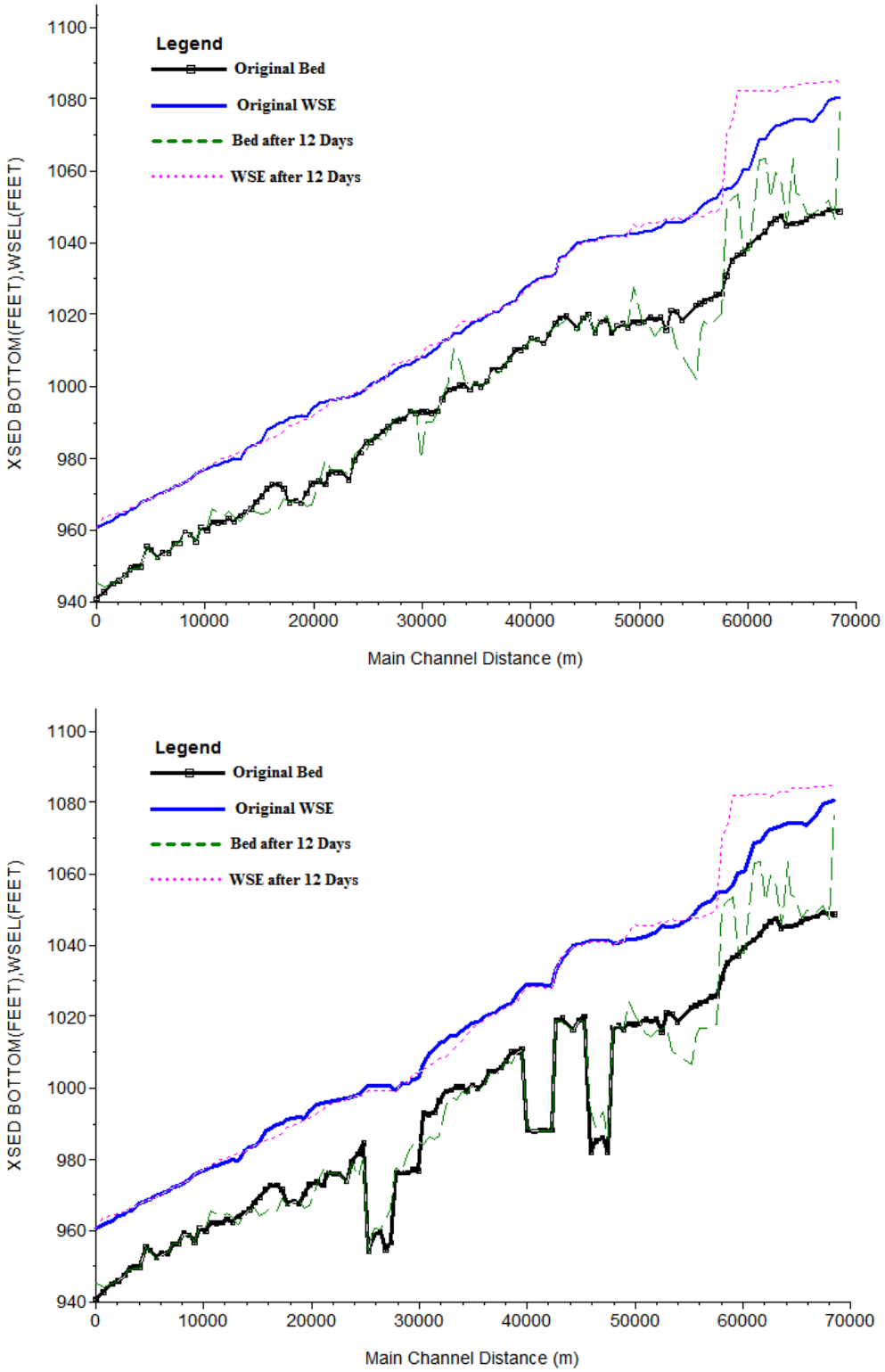

Fig. 3. Calculated bed topography change with HEC-RAS (a) without mining pits; (b) with two 10m mining pits (500-year event).

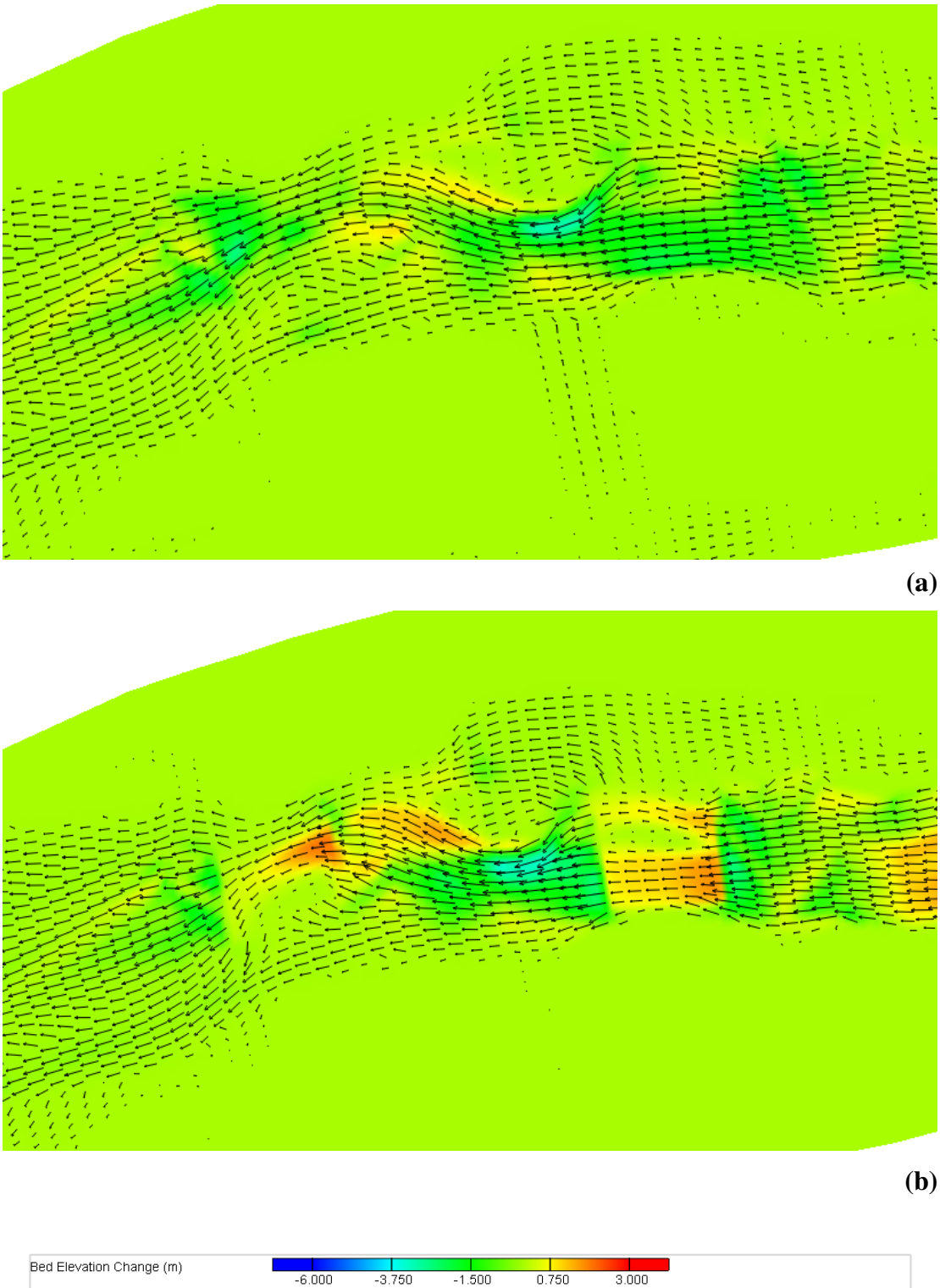

Fig. 4. Calculated bed topography change with CCHE2D (a) without mining pits; (b) with two 10m mining pits (500-year event).

CONCLUSIONS

Impact of sand and gravel mining on flood zone coverage and riverbed change of the Rio Salado, Salt River, Phoenix, Arizona were simulated using HEC-RAS and CCHE2D under 500-year frequency floods in the present study.

a) Hydrodynamic results of HEC-RAS are similar to the calculated results of CCHE2D. Presence of mining pits insignificantly reduced the inundate area, however, those pits changed the local flow directions and magnitudes which may accelerate stream bank erosion.

b) Bed Elevation calculated results of the two models differ with each other. There was substantial erosion occurring upstream and downstream of the pits, however, HEC-RAS results indicated serious head-cutting occurred upstream the pits, while CCHE2D results showed "downstream erosion" was more noticeable.

c) CCHE2D results indicated most sediment was deposited in the upstream end of the pits.

d) The 2D model was more robust in simulating flood zone coverage, non-uniform sediment sorting, and channel geomorphologic changes.

FUTURE STUDY

Flow structure around a deep mining pit (deeper than flow depth) has strong three-dimensional characteristics. The feasibility and accuracy of one- or two-dimensional models under those situations are unknown. We will look into the possibility of simulating deep mining pits in laboratories by using three-dimensional models and verified by measurements in our future studies.

ACKNOWLEDGEMENT

This study was funded by US Corps of Army Engineers (USACE), Department of Defense under Urban Flood Demonstration Program of Arid and Semi-Arid Regions (UFDP). We thank the personnel of Flood Control District of Maricopa County and Phoenix district office of the USACE for their assistance in data collection and providing over view of the sites. We would also like to acknowledge the National Center for Computational Hydro-science and Engineering at the University of Mississippi for CCHE2D model.

REFERENCES

Chen, D., Acharya, K., and Stone, M. (2008). "Modeling of Gravel Mining in the Rio Salado, Arizona". *World Water & Environmental Resources Congress, ASCE 2008*. Honolulu, Hawaii.

Chen, D., Zhang, Y., Duan, J., Stone, M., and Acharya, K. (2007). "2D Simulation of hydrodynamic and sediment transport in a gravel bed channel: the Salt River."

World Water & Environmental Resources Congress, ASCE 2007. Temple, Florida.

NCCHE (2005) website - http://www.ncche.olemiss.edu/

US Army Corps of Engineers (2005). *Rio Salado Oeste Interim Feasibility Report (Alternative Formulation Briefing)*. pp63

US Army Corps of Engineers (2002). HEC-RAS River Analysis System, Hydraulic Reference Manual

Effects of Gas Ebullition on Cohesive Sediment Resuspension and Cap Stability

Pinar Cakir Kavcar[1] and Steven J. Wright[2]
[1] Bechtel Corporation – Geotechnical and Hydraulic Engineering Services, Houston, TX, USA; email: pkavcar@bechtel.com
[2] Civil and Environmental Engineering, University of Michigan, Ann Arbor, MI, USA; email: sjwright@umich.edu

ABSTRACT

Sediment resuspension can significantly contribute to the mass transport of sediment-bound contaminants into the overlying water column. This study considers the influence of gas ebullition (due to microbial activity) on resuspension rates as observations indicate that fine-grained sediments may be lifted into the water column in the bubble wakes. Capping aims to minimize contaminant migration to the water column by reducing sediment resuspension rates. In addition to the influence of gas fluxes on resuspension rates for uncapped cohesive sediment beds, this experimental investigation considers the effectiveness of two types of caps, sand and AquaBlok®. The investigation involved experiments conducted on sediments (d_{50}=10 μm) collected from the Anacostia River in Washington DC. Gas ebullition fluxes were selected based on values reported in the literature. The experimental results for the zero gas flux case indicated that the resuspension increases as the square of the bed shear stress level above a threshold or critical shear stress required to initiate resuspension. With regards to the ebullition experiments, it was observed that air migration occurs as a series of discrete bubbling events through semi-permanent channels in the sediment bed associated with a cyclical buildup and release of gas pressure within the sediment. A significant amount of sediment was carried in the wakes of released bubbles. When the same conditions were studied with sediment caps applied over the bed surface, no sediment resuspension was observed over the duration of the experiments with the sand cap. AquaBlok® cap heaved up and ruptured if the pressure head differential across the cap reached a level on the order of 20-25 cm.

INTRODUCTION

Resuspension process may result in increased contaminant concentrations within the water column due to the increased exposed surface area. Many factors have been demonstrated to contribute to the resuspension rates for fine-grained cohesive sediments. Hydraulic shear stress has been assumed to be the major factor leading to erosion. The theories established for the determination of the rate of erosion of cohesive sediment beds considering the bed shear stress involve different approaches to the phenomenon. More importantly, inclusion of any other mechanism such as gas

ebullition that could result in additional resuspension needs to be incorporated into the proposed framework.

Both laboratory and in-situ measurements of cohesive sediment erosion generally involve a series of stepwise increasing bed shear stress levels over fixed duration-time steps (e.g., Ravens and Gschwend, 1999; Aberle et al., 2006). The erosion rate is typically calculated using measured fluxes of suspended sediment concentration. The conclusions of these investigations vary and the most appropriate mathematical formulation to compute erosion rate from measurements is still under discussion. Interpretation of time dependent erosion rates which are typically high at the beginning of an experimental shear stress step and then decrease with time (e.g., see Parchure and Mehta, 1985; Amos et al., 2003) requires a somewhat arbitrary definition of the erosion rate. Variation in the outcomes of these investigations depend also on the types of beds considered with some experiments performed with remolded sediments with uniform properties over the bed thickness or in a form that the sediments were allowed to consolidate while suspended sediment deposits on the bed over time. The effect of consolidation on the erosion rates has been related to the bulk density by several researchers such as Jepsen et al. (1997).

A power relationship defining erosion rates has been widely used in the interpretation of experimental results in the general form of

$$E = K(z_0)(\tau - \tau_c(z_0))^m \tag{1}$$

where E is the erosion rate per unit area of bed surface [$ML^{-2}T^{-1}$], $K(z_0)$ is an empirical erosion coefficient with its dimensions depending on the exponent m, τ is the applied bed shear stress [FL^{-2}], $\tau_c(z_0)$ is the critical bed shear stress for erosion, and z_0 is the depth of erosion [L] (e.g., Maa et al., 1998; Ravens and Gschwend, 1999).

An expression expressing the time-dependency of the erosion rate over a shear stress step was given by Sanford and Maa (2001) as

$$E = \rho_d(z_0)\beta(\tau - \tau_{c0})e^{-\varphi\beta(t-t_0)} \tag{2}$$

where $\rho_d(z_0)$ is the dry bulk density at sediment depth z_0, β is a local parameter, τ_{c0} is critical bed shear stress when τ is first applied at $t = t_0$, t is time, t_0 is time at which a new shear stress is applied, and $\varphi = d\tau_c / dz_0$. For a uniform bed ($\varphi = 0$), Equation 2 reduces to $E = K(\tau - \tau_c)$ with $K = \rho_d\beta$. For a non-uniform bed ($\varphi \neq 0$), Equation 2 describes an exponential decay of erosion rate with time.

No comprehensive studies have been reported in the literature related to the effect of ebullition on bed stability or on resuspension rates. Ebullition is the result of a series of processes in which excess gases are generated by micro-organisms from organic matter. In cohesive sediment beds under organic rich conditions, ebullition leads to accumulation of gas dissolved in pore water and in bubbles. Gas bubbles are produced when the sum of the partial pressures of dissolved gases exceeds the ambient pressure (Fendinger et al., 1992). Bubbles grow until a pressure threshold is

reached as they build up sufficient buoyancy to overcome the cohesive strength of the sediment and migrate upward. Ebullition generally occurs episodically due to changes in shear stress or pressure (especially in tidal systems) that affect the gas bubble release potential (Joyce and Jewell, 2003). In fine-grained sediments, bubbles fracture the sediment and these fractures combine and form channels reaching to the water-sediment interface (Huls et al., 2003a-b). One effect of the gas bubbles is to increase sediment porosity and reduce bulk density, thus potentially decreasing the critical shear stress for resuspension (Joyce and Jewell, 2003; Jepsen et al., 2000). Bubbles rising through the sediment matrix exert an erosive force along their path, and as a result have the potential to move the sediments to the surface.

Ebullition fluxes reported in the literature vary considerably. A wide range of ebullition fluxes ranging from 0.01 cm/d to 48 cm/d was reported by Chanton and Martens (1988). These measurements were obtained from several sites under different temperature, pressure, salinity levels, water depths and sediments having variable organic contents.

Limiting the resuspension hence contaminant migration due to advective flow induced shear stresses and/or gas ebullition flux is possible using caps. However, there have been no systematic investigations on the use of sediment caps in controlling resuspension. Assessment of the effectiveness of caps as a remedial technology requires an understanding of contaminant fluxes from sediments both in the presence and absence of caps in order to understand the potential for contaminant transfer to the water column.

EXPERIMENTAL SETUP AND METHODS

Fine-grained Anacostia River cohesive sediment with d_{50} on the order of 10 μm was used in the laboratory experiments. An exploratory investigation was performed to observe various aspects of the sediment behavior when a gas ebullition flux was applied to the sediment bed with or without cap. The flume experiments were different as they involved application of an erosive force to the surface of the sediment or the cap material by creating a flow over the relevant test surface in the laboratory flume. The exploratory experiments were performed with no such flow but were conducted in glass aquaria that had a horizontal cross-section of approximately 45 cm by 90 cm. It was developed through observations that side wall effects can be avoided by using a distribution system under the sediment bed that releases gas away from the container walls. In the case of the exploratory experiments this was achieved through bubble bars and in the case of the flume experiments, perforated soaker hoses were used.

The flume experiments were conducted in a 7.5 m long, 0.6 m wide flume. The test section was approximately 2.00 m long located about 3.5 m downstream from the flume inlet. A 0.3 m wide depressed cavity was installed in a false floor in the flume bottom to be filled with the sediment and capping material. The depth of the sediment cavity in the flume was adjusted according to the specific experiment. The bed thickness was fixed to 10 cm for the Anacostia River sediment beds. For the experiments where the Anacostia River sediment together with the cap material was used, each layer was 10 cm.

The injection system consisted of a set of parallel soaker hoses connected to a common source and ran the length of the test bed. During the experiments with gas injection if an injection rate was set with a flow meter, initially the gas would flow into the sediment, increasing the internal sediment pressure which decreases gas flow rate through the meter. Increasing the control valve setting to increase the flow would only build the pressure until eventually the gas erupted from the sediment. At this point, the resistance to gas flow would suddenly decrease and the gas flow rate would dramatically increase. This inconsistent flow rate was resolved by adopting a methodology to ensure a relatively constant long term average gas flux through the sediment. It was presumed that gas release will actually occur through a series of discrete release events and a procedure was developed that would mimic this behavior. The apparatus consisted of two bottles connected in series to each other and then to the bubble bars or perforated soaker hoses. When water was supplied to the first bottle at the desired rate of the gas flux in a series of discrete additions, the air pressure in this bottle and hence in the second bottle was gradually increased to initiate bubbling through the sediment. The bubbling event then relieved pressure in the bottles and the bubbling subsided until the addition of more water increased the pressure again to a level required to initiate a new event. By this procedure, a constant long term average air injection rate was achieved. Considering the range of ebullition fluxes reported in the literature, 1.2, 12 and 48 cm/d were the initial selected rates for the resuspension experiments. A flux of 2.4 cm/d was added to the experimental schedule as 12 and 48 cm/d were observed to create continuous air bubbling which is considered to be incompatible with what would be observed in natural systems.

The flume experiments were conducted by increasing the bed shear stress in five, discrete hour long steps in the re-circulating flume starting from a low bed shear stress and increasing the shear stress each time step. The depth in the flume was approximately 0.25 m. Discharge rates were measured by an orifice meter installed in the return pipeline. Sediment concentrations in the re-circulating water were inferred by monitoring the flow with a turbidimeter connected to the return pipeline in the flume system downstream from the recirculation pump. In order to compute resuspension rates, a flow-through cell enabling continuous turbidity measurements was attached to the turbidimeter. The approach to estimate bed shear stress was to obtain local turbulence measurements close to the bed surface and to develop a procedure for converting these results to bed shear stress and to directly relate bed shear stress to flow velocity. Several sets of Acoustic Doppler Velocimeter (ADV) data were collected for this purpose (Cakir Kavcar, 2008).

All the experiments were conducted with unconsolidated sediment beds and homogenized constant bulk density. Letting each sediment bed sample to consolidate for an extended period of time (weeks) would have caused some scheduling problems in conducting the number of planned experiments. In addition, there were issues of how to treat the gas ebullition aspect of the experiments during this consolidation period. In the end, it was decided to perform the experiments by placing the sediment as a slurry and allowing it to settle for approximately 12-15 hours before each experiment.

Additional experiments were also conducted in the presence of the sand cap and the AquaBlok® cap. Other experiments were performed in glass aquaria with an AquaBlok® cap. AquaBlok® is a system prepared by placing bentonite-coated gravel as the cap; the hydration of the bentonite produces an effectively impermeable cap material.

OBSERVATIONS AND RESULTS

Similar behavior was observed in both the aquaria and flume experiments. As air was applied at the bottom of the sediments, gas pressure built up and at some point a bulge would develop on the sediment surface. Initially larger bubbles (up to 5 cm) would erupt from the bulge carrying significant amount of sediment into the water column in the bubble wake, and then followed by several smaller diameter bubbles (0.5-1 cm) with less sediment entrained (Figure 1). Typically if the air pressure applied was not excessive, bubble release would stop after a short period of time and the process would repeat itself, gas pressure build-up, bubble release, pressure drop, and cessation of bubble production. Channels at fixed locations in the sediment bed were formed by the bubbles. As the bubble diameters became smaller over time, less sediment was carried up into the flow and it is thought that some sort of armoring process on the channel walls occurs.

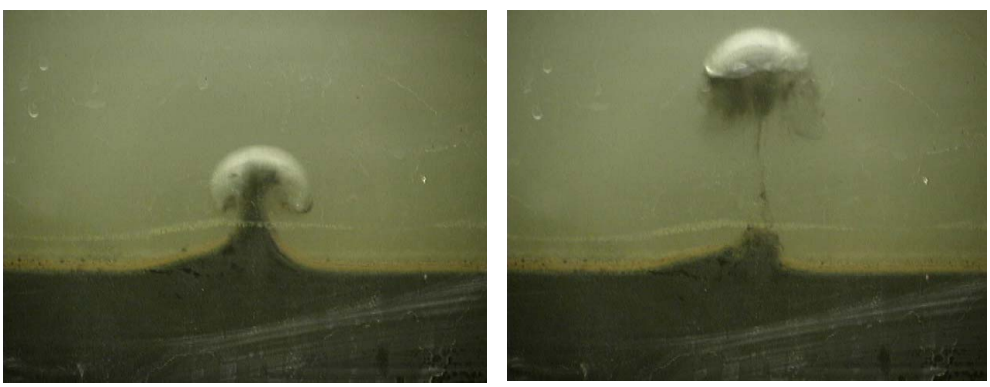

Figure 1: Air bubble is released and some sediment is entrained into the water column in its wake.

Additional exploratory experiments were performed to bubble air through sediment covered with a sand cap. The bubbles tended to be more constant diameter (0.5-1.0 cm) throughout the duration of the experiment. Again the air is observed to flow through distinct channels. Although no Anacostia River sediment was observed in the water column during the course of the experiments, the excavation after the experiment in the sand cap showed some degree of cohesive sediment migration into the cap layer indicating a potential of sediment resuspension in a longer duration experiment.

Samples of AquaBlok® aggregate obtained from the manufacturer were allowed to hydrate for at least a day in glass aquaria sub-divided to produce horizontal sections of 45 cm by 45 cm. Gas pressure was applied beneath different thicknesses of AquaBlok® layers. Sand was placed under the AquaBlok® cap as a medium to

ensure uniform pressure distribution beneath. Observations of the rupture of the AquaBlok® in the various experiments as a result of pressure built-up indicated a potential practical issue. These failures were observed at a pressure differential of 20-25 cm across the cap material. Two major rupture patterns were identified as either lifting along one wall or mounding near the center of the tank. This mound would grow until eventually the layer ruptured. Initial set of flume experiments involved shear stress applied to the bed without air injection flux (advective flow experiments). Experimental protocol dictated a five-step bed shear stress increase from 0.153-0.309 N/m^2 on average. Each flume experiment was repeated multiple times until consistent results were achieved. Suspended sediment concentration measurements collected by the turbidimeter show that there is no significant bed erosion during the first two hours of the experiment and then resuspension is apparent with increasing rates as the shear stress level is increased. The trend within each one hour interval shows that resuspension rates are usually higher initially which indicates a time dependence at a given shear stress level (see Figure 2).

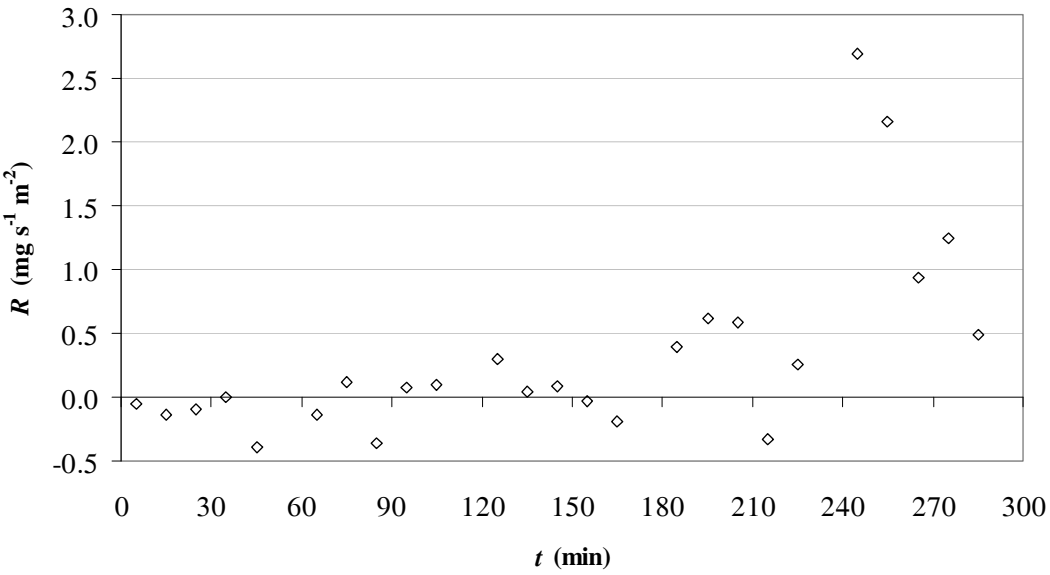

Figure 2: A resuspension rate (*R*) versus time (*t*) graph presenting time dependency of the resuspension rates during each hour of the five hour long experiment (no air injection).

Time dependency of the resuspension rates required averaging of the rates over an hour for each shear stress level for comparison purposes. This yielded relatively consistent results when the results of the repetitions of the same experiment were compared. The erosion threshold or critical shear stress was determined to be approximately 0.19 N/m^2 at which resuspension rates approach zero. An empirical relationship for the resuspension rate, R was derived as:

$$R = M(\tau - \tau_c)^2 \tag{3}$$

where M is the resuspension rate coefficient, τ is the applied bed shear stress and τ_c is the critical shear stress. For the experiments without air flux, M can be approximated to be 96.7 mg s^{-1} m^{-2} Pa^{-2} where τ_c is 0.19 N/m^2 as shown in Figure 3.

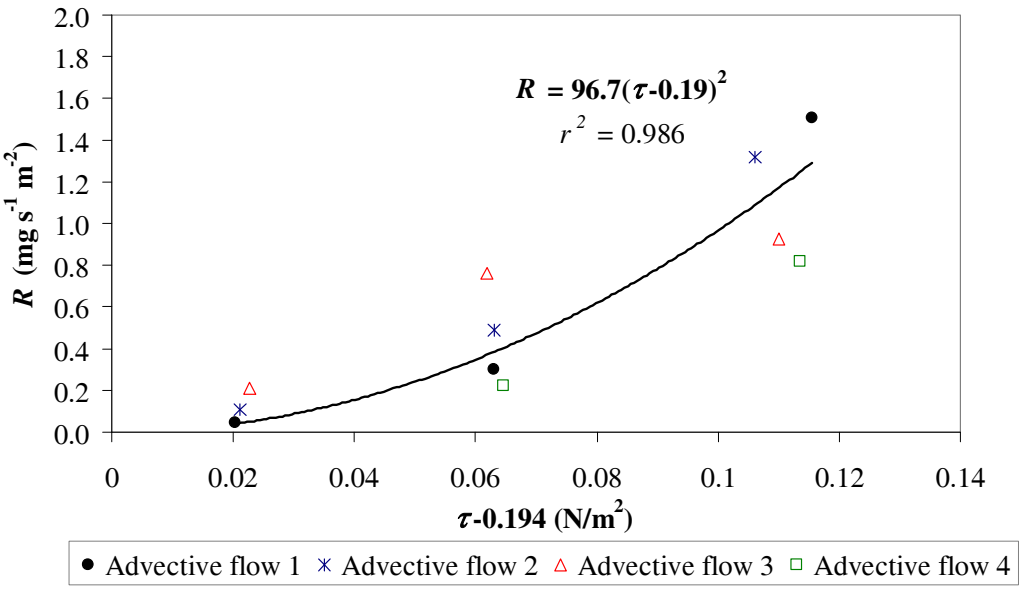

Figure 3: Quadratic relationship fit according to the "Advective flow 1" experiment and the results of all the advective flow experiments with respect to the curve fit.

When flume ebullition experiments were conducted, air migration occurred with a cyclical buildup and release of gas pressure with discrete bubbling events. This is likely to be observed in Anacostia River as the tidal fluctuations in water level will create a cyclical variation in overlying pressure that should have a strong influence on the release of gas from the sediments. The observations showed that the amount of sediment resuspended depends on several factors such as bubble size, bubbling frequency and duration of bubbling. Once a channel is well-established in the sediment bed, there appears to be a reduction in the resuspension rate. This observation is based on both visual observations as well as turbidity measurements. The size of the bubbles coming from the same channel tends to reduce over time if the bubbling is continuous. If a bubbling event from a channel stops at some point in time and restarts at a later time, the channel may heal itself to some extent. Consequently, the resuspension rates due to ebullition appear to be correlated to two time dependent processes, how long a bubbling event lasts and the time interval between successive events. It appears to be random where the channels form and at how many discrete points bubbling occurs at a given air flux rate. Therefore, considerable variation was observed among repeated experiments involving gas ebullition.

The initially selected ebullition fluxes were 1.2,12, and 48 cm/d. These rates were considered in the experiments together with the step-wise increased advective flow induced shear stress. Several experiments were conducted to investigate the effect of

each ebullition rate. The investigations showed that 12 cm/d was a very high rate creating continuous air bubbling and this is felt to not be representative of occurrences in natural systems. 48 cm/d ebullition experiments were eliminated from further consideration because of this observation. On the other hand, 1.2 cm/d ebullition fluxes usually ended up with a situation where no air bubbling events occurred during some one hour measurement periods. One or two bubbling events lasting 20 minutes during the whole 5 hours of a single experiment was not definitive for the purpose of determining the added effect of ebullition on resuspension rate. An additional ebullition flux of 2.4 cm/d was investigated in an effort to observe more ebullition events throughout the duration of an experiment.

As can be seen from a synthesis of all the data (Figure 3), ebullition results in greater sediment resuspension compared to advective flow only experiments. This effect increases with the ebullition rate. However, the data also suggest that once bubbling channels are formed in the sediment bed, the contribution of ebullition to the resuspension rates becomes minimal. It is generally observed in ebullition experiments that during the last hour of the experiment (highest shear stress level) resuspension rates closely correspond to those observed in an advective flow experiment with no ebullition. There are two possible explanations for that observation; one is that no ebullition occurs during that period of time such as often occurred for the ebullition rate of 1.2 cm/d and a second possibility is that the channels are formed in a well-defined configuration and the contribution of ebullition to the resuspension rates is minimal such as for the 2.4 and 12 cm/d ebullition rates which created sustained bubbling in most of the repetitions.

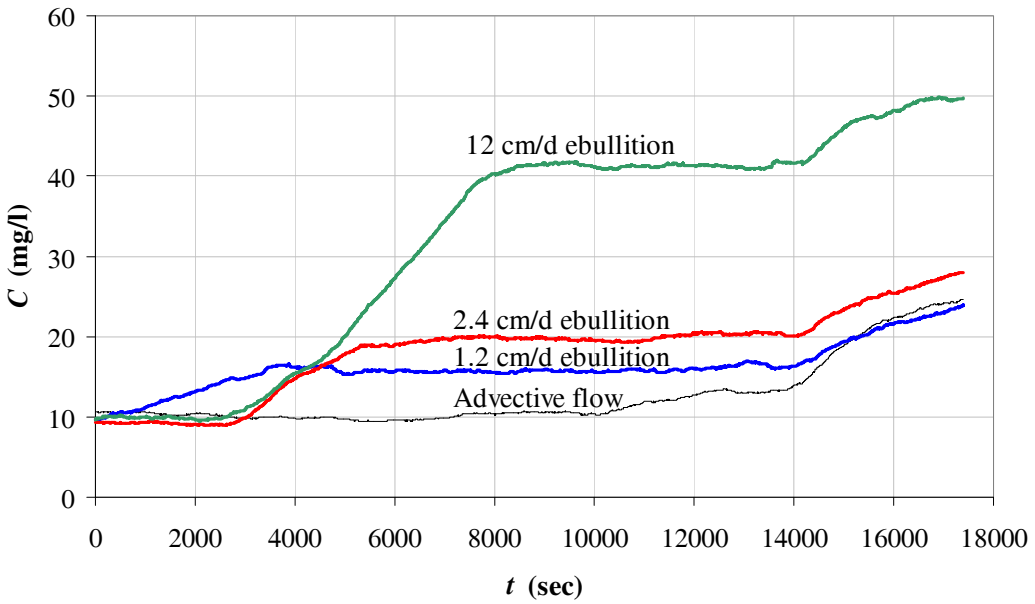

Figure 3: Comparison of suspended sediment concentration measurements (*C*) among ebullition experiments with different ebullition fluxes and an advective flow experiment.

It was noted that the computation of resuspension rates was not straightforward. The issue arises from the apparent random nature of ebullition events. As opposed to the hourly resuspension rates computed for advective flow experiments, it is not possible to compute rates in a time-averaged manner for the ebullition experiments. Each ebullition event seems to have its own resuspension potential and this potential basically depends on several parameters as explained previously. The data suggest that the amount of pressure build-up between the events affects the resuspension rates significantly. If somehow bubbling does not occur for an extended period of time, pressure builds up significantly creating very high resuspension rates when the pressure is released. However, the relationship between the pressure build-up and the resuspension rates does not seem to follow a well-defined trend.

In order to identify the contribution of ebullition to resuspension rates, the amount of sediments in suspension was calculated for three repetitions of the 2.4 cm/d ebullition experiments. The amount of sediment suspended due to bed shear stresses was approximated using Equation 3 as 40 g on average. The contribution of the ebullition to the total was calculated as 50 g on average. However, two of the ebullition experiments involving discrete ebullition events throughout the duration of the experiments resulted in 140 g on average. The one with the continuous bubbling resulted in approximately 80 g of sediment resuspension. It is apparent that resuspension rates are highly depended on on the specific nature of the ebullition process

When the sand cap (d_{50}=340 μm) was examined for its effectiveness in minimizing the resuspension rates, none of the air injection fluxes (1.2 cm/d, 2.4 cm/d, and 12 cm/d) caused any detectable suspended sediment concentration in the flume within the duration of the experiments. This result indicates that the cap material filtered all the cohesive sediment transported by bubbles from the sediment layer beneath it. However, it is not known if any resuspension would occur over extended periods of time.

As the issues related to AquaBlok® caps subjected to gas ebullition flux were identified in small scale experiments, no further experiment in the flume setup was performed on this type of cap for gas ebullition. However, advective flow induced shear stress flume experiments showed that AquaBlok® is very stable under even very high bed shear stresses. The stress values were increased up to a value of approximately 2.6 N/m^2 to indetify the limitation to the stability of the AquaBlok® bed. By looking at the surface of the bed after the experiment, it was seen that some bentonite material was eroded from the surface and some small aggregate particles were carried downstream by bed load transport. Nevertheless, the majority of the aggregate adhered to the bentonite layer underneath creating an armoring layer.

ACKNOWLEDGMENTS

This investigation was conducted as part of a comprehensive research project sponsored by the Strategic Environmental Research and Development Program. Further support was provided by the Department of Civil and Environmental Engineering and the Program of Environmental and Water Resources Engineering at the University of Michigan.

REFERENCES

Aberle, J., Nikora, V., and Walters, R. (2006). "Data Interpretation for In Situ Measurements of Cohesive Sediment Erosion." *Journal of Hydraulic Engineering*, ASCE, 132(6), 581-588.

Amos, C. L., Droppo, I. G., Gomez, E. A., and Murphy, T. P. (2003). "The Stability of a Remediated Bend in Hamilton Harbour, Lake Ontario, Canada." *Sedimentology*, International Association of Sedimentologists, 50, 149-168.

Cakir Kavcar, P. (2008). "Stability of Cohesive Sediments Subject to Pore Water and Gas Ebullition Fluxes and Effectiveness of Sand and AquaBlok® Caps in Reducing the Resuspension Rates." Ph.D. Thesis, 89-94.

Chanton, J. P., and Martens, C. S. (1988). "Seasonal Variations in Ebullitive Flux and Carbon Isotropic Composition of Methane in a Tidal Freshwater Estuary." *Global Biogeochemical Cycling*, 2(3), 289-298.

Fendinger, N.J., Adams, D.D., and Glotfelty, D.E. (1992) "The Role of Gas Ebullition in the Transport of Organic Contaminants from Sediments." *The Science of the Total Environment*, 112, 189-201.

Huls, H., Costello, M. (Service Engineering Group), and Sheets, R. (Soil Technology, Inc.) (2003a). "Gas, NAPL, and PAH Flux Assesment in Sediments." *Proceedings of the Second International Conference on Remediation of Contaminated Sediments*, Venice, Italy.

Huls, H., Costello, M. (Service Engineering Group), and Sheets, R. (Soil Technology, Inc.) (2003b). "Bench Test Design Evaluation of a Remedial Wetland Cap (with Regard to Ebullition and Its Control)." Presented at: In-Situ Contaminated Sediment Capping Workshop, Cincinnati, OH.

Jepsen, R., Roberts, J., and Lick, W., (1997). "Effects of Bulk Density on Sediment Erosion Rates." Water, Air and Soil Pollution, 99, 21-31.

Jepsen, R., McNeil, J., and Lick, W. (2000). "Effects of gas generation on the density and erosion of sediments from the Grand River." Journal of Great Lakes Research, 26(2), 209-219.

Joyce, J., and Jewell, P.W. (2003). "Physical Controls on Methane Ebullition from Reservoirs and Lake." Environmental and Engineering Geoscience, IX(2), 167-178.

Maa, J. P.-Y, Sanford, L., and Halka, J. P. (1998). "Sediment Resuspension Characteristics in Baltimore Harbor, Maryland." International Journal of Marine Geology, Geochemistry and Geophysics, 146, 137-145.

Parchure, T. M., and Mehta, A. J. (1985). "Erosion of Soft Cohesive Sediment Deposits." *Journal of Hydraulic Engineering*, ASCE, 111(10), 1308-1326.

Ravens, T. M., and Gschwend, P. M. (1999). "Flume Measurements of Sediment Erodibility in Boston Harbor." *Journal of Hydraulic Engineering*, ASCE, 125(10), 998-1005.

Sanford, L. P., and Maa, J. P.-Y. (2001). "A Unified Formulation for Fine Sediments." *International Journal of Marine Geology, Geochemistry and Geophysics*, 179, 9-23.

Empirical Equation for Abrasion of Stilling Basin Caused by Impact of Sediment

M.E Banihabib [1*] and M. Elahi[2]
[1] Assistant professor, Department of Irrigation and Drainage Engineering, University of Tehran, Iran; Email:Banihabib@ut.ac.ir
[2] M.Sc. Irrigation and Drainage Engineering, University of Tehran, Iran

Abstract
This research studies empirical equation for abrasion of stilling basin caused by impact of the sediment. Review of previous papers shows that in previous researches, the mixture effects of erosion and impact are studied without determination of the share of impact in the mixture effect. Also in those researches, the sediment grain size is not as large as debris size in debris flow or experiments are done without tail water depth. Therefore, in this research, the impact of large grain size is determined on concrete stilling basin with tail water. One dimensional analysis is carried out. The experiment includes concrete samples with three different cement contents, five depth of tail water, three grain sizes. Abrasion of each grain impact is measured and recorded. Uni-variable and multivariable regression analysis was employed to possible relation between abrasion ratio and the dimensionless parameter of the experiment. The empirical equations are judged using mean relative error of the equations. Later a multivariable power equation is proposed for abrasion determination of the sediment impacts. The equation shows the abrasion is a function of dimensionless energy of sediment grain and the ratio of the grain velocity on stilling basin to the grain velocity on water surface. The results of the present research are used in estimating the longevity of Diversion Dams and concrete check dams in contact with debris flood.

Key words: Diversion Dams, debris flow, abrasion of stilling, Impact of Sediments

[*]Corresponding author: Department of Irrigation and Drainage Engineering, University college of Aburaihan, University of Tehran, Pakdasht, Islamic Republic of Iran, e-mail: banihabib@ut.ac.ir

1.Introduction

Debris flow is defined as the flows with high concentrations of sediments which more than 50 % of their weight include sand stone and rock. Some reports of damaging caused by passing debris flood from different dams including Iran (Ruzbahan Diversion Dams), china, India, (Ichari and Manri dams in the mountainous areas of Himalaya), Swiss and France [3, 4, 7]. In those dams, abrasions and holes on spillway and stilling basin were seen. They have noticed the reason of all these abrasions, passing sand, stone and rocks. For solving this problem they have some methods like using metal plates, angle for the sharp edges of flip bucket and its teeth in Ichari dam, metal cover with metal halter on concrete spillway and stilling basin in Manri dam, high strength concrete and epoxy resins in china, installing granite blocks and covers for Baril stilling basin of railway in Swiss, acorn and pine woods as a protective cover in France. Eighteen dams in Swiss had the same abrasion and Reyn national company tested the resistance against impact and abrasion for various materials [1, 4, 7, 8]. Bargua and Muris has reported the damages imposed to spillways and stilling basin of reservoir and hydropower dams due to passing large grained sediment in different part of the world [4, 7, 8]. The reports and articles clarify the necessity of research in basis of the damaging effect of transitory debris flood along stilling basin and spillway. Liu et al. (2006) represented that abrasion and sediment impact on the surface are two factors for abrasion of stilling basin and spillway in dams [6]. The standards compiled for examining concrete by sediment, mainly discussed the effect of abrasion not sediment impacts' distraction. In the latest standard offered by the American Society of Testing and Materials, it is emphasized on the quality of the experimental results [9, 10]. In the research carried out by liu, jet flow containing sand is sprinkled on a concrete piece and the effect of the mentioned jet on different type of concrete with different percentages of water to cement was discussed(6). In the mentioned research the effect of abrasion and impact of fine sand sediment are combined. So a necessary knowledge of the impact effect was not detected clearly and the method and type of discussion is concentrated on comparing the effect of suggested method for concrete with different percentage of water to cement. This research shows that the percentage of abrasion on concrete samples is related to the work done per unit mass. According to the tests we can know damaging mechanism on stilling basin caused by large sized sediment of debris flood in two points. In above tests damaging mechanism is gained by modeling abrasion and impact that the share of abrasion is a lot but not distinguished. Also the grain size used as sediment (8-32 mm) compared to large sediments of debris flood mentioned in reference 5 and 2 (300, 500mm) is small. In this case a research was done by Banihabib, which in, the damaging effect of sediment impact on stilling basin of diversion dams was studied and a relation between percentage of abrasion and the potential energy of the sediments of debris flood was derived [2]. But in that research the effect of water and tail water in stilling

basin is not studied and no equation is given. Therefore the purpose of this research is to study the damaging effect of sediment impact on stilling basin and to give an equation for estimating the damages of concrete stilling basin with different depths of tail water. Also the effect of sediment impact on concrete slab of stilling basin in different water depths is studied. Then different empirical equations are evaluated.

2. Methodology

2-1- Physical Methods

Experiments are included 135 tests. The mixing plan of concrete samples are according to ACI 12 11 /1 are presented. As it is specified in these tables the ratio of water to cement was 0.5. Sand and gravel derived from river are used to make concrete.

Construction and caring of concrete samples has been in a way that after mixing materials in a mixer in a laboratory, 135 cylindrical samples with the height of 40mm and the diameter of 141mm was prepared. After 24 hours the samples were taken out from the block and till the end of the twenty eighth days was put in water. For the experiment of the impact they used 3 types of spherical object. Their weight and diameter are present in table 4. Other instruments which were used for the experiment include

- Digital scale with the accuracy of 0.01 grams for weighting
-Ruler and metal meters
-Laboratory system include water basin attended with guide pipe for hitting of bullet to the center of concrete samples.

2-2- Experiments

The main question of the research is the possibility of having an empirical relation between the percentage of damaging and the potential energy of debris sediment hitting on a concrete sample with considering the depth of tail water. Therefore the test system include water basin attended with guide pipe as in figure 1, is in dimensions 1.6 * 0.8 * 0.6. The process of the experiment begins with putting the concrete sample under and center of the guide pipe. In fact the basin was use as a model stilling basin and the impacting sediment was modeled by a metal bullet. The reason of using metal bullet instead of stone is the unchangeable weight and shape of the bullet during the test. In every test the metal bullet was dropped with the initial velocity of zero toward the concrete. Samples were placed in five depths of tail water, zero, 8, 20, 32, 40 centimeter. When the depth of water on the sample was zero, the weight of concrete sample was measured before and after impact with numerical scale but when the sample was in water the scaling of weight carried out after 3 times of impaction. Impaction and measuring weight was continued until the failure of concrete sample and dividing into some parts (figure 2).
For extracting relation and its validation three sets for each test were done. Therefore with considering 5 water depths and three concrete content the number of tests had been 45 that a number of impaction test was done till the failure of the concrete sample.



Figure 2 : concrete sample failure

3-2 - Analysis

Due to discuss on result and to study the empirical relation between damaging of the concrete and potential energy of impacting stone, the abrasion ratio is defined as follows:

$$A* = \frac{concrete weight \ \ after\ nth\ impact - superior\ concrete\ weight}{superior\ concrete\ weight} \quad (1)$$

Where $A*$ is the ratio of concrete abrasion after n time impacting to the concrete sample. Because this abrasion ratio is caused by the first impact to the impact number n. Accumulative potential energy that is spend to impact and production of this abrasion is defined as follow:

$$E = \sum_{i=1}^{n} W_{si} H \quad (2)$$

Where H_i is the height of bullet drop and W_{si} weight of bullet in the impact number i. In addition to accumulative potential E, the water depth in basin and the height of bullet drop has effect on $A*$ therefore with dimension analysis the dimensionless parameter was achieved:

$$E_* = \frac{E}{W_0 \times D} = \frac{\sum W_{si} H}{W_0 \times D} \quad (3)$$

$$P_* = \frac{P}{D} \quad (4)$$

$$Y_* - \frac{y}{D} \quad (5)$$

Where p is drop height, D is sediment diameter, W_0 is the weight of the first sample, Y is the water depth. For analysis data in each cement content, data were divided in to three individual sets that the first set was used to analysis and study of relations and the second and third sets for validation of relations gained from the first set. One-variable relation include linear, power, logarithmic and multi-variable relations include linear and power.

3-Result and discussion

According to dimension analysis we can consider cement content, dimensionless energy imposed to sample as the effective parameters on concrete abrasion ratio. Since the impaction of stones to the stilling basin is generally in a depth that is equals to that of a jumping, its essential to analysis the effect of existing water on the base of available theories and accuracy limitations should be clarify. For achieving to this goal we use the model describe in figure 3 for analyzing.

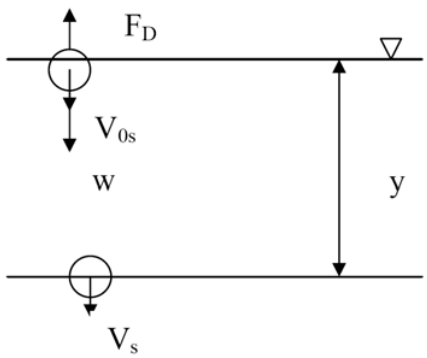

Figure 3: scheme model used for analysis

The averaged velocity of stone can be determined as follow:

$$V = \frac{V_{0s} + V_0}{2} \tag{6}$$

Sediment with the above velocity will produce a resisting force which can be determined as follow:

$$F_D = \frac{1}{2} C_D A \rho V^2 \tag{7}$$

Where in this equation FD is resisting force, CD is the shape factor, A is the stone area and p is the special mass. From dynamic balance of weight, resisting and second law of Newton forces, we can have the following relation (2):

$$C = \frac{V}{V_{0s}} = \frac{-0.056\frac{y}{D} \pm \sqrt{(0.056\frac{y}{D})^2 - [(1+0.056\frac{y}{D})(0.056\frac{y}{D} - 1 - \frac{(y/D)/(p/D)}{(1-(y/D)/(p/D))})]}}{1+0.056\frac{y}{D}} \quad (8)$$

Where Y is the water depth in stilling stone diameter, v_{0s} and v_s are respectively stone velocity when entering the water and impact to bed. This relation has been shown in a group of curves in figure 4. In this figure P_1 is the height of spillway. This figure shows that if the dimensionless depth is less than one means the flow depth is less than the sediment diameter the effect of reduction in water depth on the velocity of impaction on the bed is less than 10%.

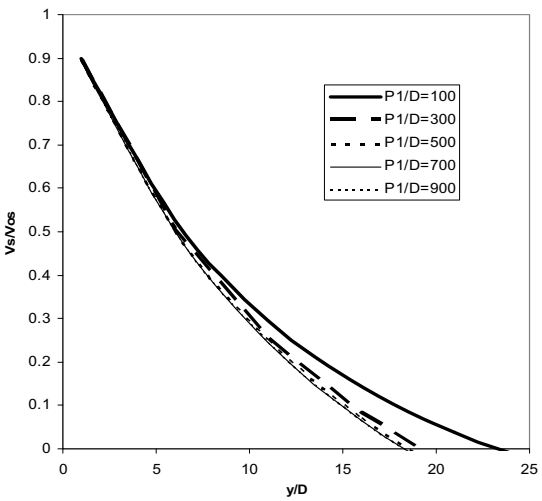

Figure 4. The ratio of velocity of sediment before entering water to after it

Water depth in stilling of dams reaches to many times as much the sediment diameter so it is necessary to consider the flow water analysis. In this research different depth water is considered on concrete samples while hitting bullet. The regression between dimensionless factors is studied. To study these relations, SPPS software was used so that the best formula which could clarify the effect of debris sediment impaction on stilling basin was derived. As mentioned before the effective parameters can be known as the value of energy imposed to the sample, P_0 and Y_*. So the value of factors of each formulas change according to the value of cement content and for different cement content individual relations was gained. Due to reduction of the number of dimensionless parameters ratio of the grain velocity on stilling basin to the grain velocity on water surface (c) was used as a dimensionless parameter. This dimensionless parameter is a function of Y_0, P_0. There for c is used instead of dimensionless parameter Y_0, P_0. Therefore, the dimensionless energy of impact will be modified and the new parameter $E_{*,m}$ named modified dimensionless energy is defined as follow:

$$E_{*m} = E_* C \quad (9)$$

By having dimensionless value of energy, 3 data groupes of empirical relations was studied.

-One variable linear, logarithmic quadratic between abrasion ratio and dimensionless parameter.

-Multi variable linear relation between abrasion ratio and dimensionless parameter.

For studying the error of above relation, averaged relative error with the following definition was used.

$$MARE = \frac{\sum_{i=1}^{n} |A_0 - A_c|}{A_0} \quad (10)$$

Where in this relative A_0 and A_c are respectively observed and calculated values. And n is the number of data in each Data group.

The data of the first data group is used for extracting relations and the data of the second and third data groups were used for comparing the results of determining A* with derived relation with this data group of data so that it was possible to validate the extracted relations

3.1. One variable Equations

The one variable relation below was derived based on the first set data and the results of determining A* was compared with relations Extracted by the use of the data of first, second and third data groups based on MARE:

$$A_* = a\,E_{*m} + b \quad (11)$$

$$A_* = a\,E_{*m}{}^{b} \quad (12)$$

$$A_* = a\,\ln(E_{*m}) + b \quad (13)$$

$$A_* = a\,E_{*,m}{}^{2} + bE_{*m} + c \quad (14)$$

$$A_* = a\,E_{*,m}{}^{3} + bE_{*,m}^{2} + cE_{*,m} + d \quad (15)$$

The parameters of 11 to 15 relations and MARE base data and validated data are present in table . This table shows that the error of one variable power relation with base data and validated data was less than the error of one variation linear, logarithmic and 8888888888.

3.3 Multi-variable linear relation based on dimensionless parameter E*, P*, Y*

Multi-variable relation between concrete abrasion ratio caused by impact and dimensionless parameters of energy, depth and the drop height are extracted for the first set of data using SPSS and averaged relative error of extracted relation was estimated with the second and third sets of data. Extracted relation is as following and the regression factor and MARE for the relation is present in the table 5.

$$A_* = a\left(\frac{y}{D}\right) + b\left(\frac{y}{D}\right) + c\left(\frac{y}{D}\right) + dE_{*,m} \quad (16)$$

Comparing MAREs of the mentioned table shows that multi variable linear relation has larger error comparing to relation 13 and using the multi variable relation can not improve the estimation of mentioned formula.

3.3. Multi-variable linear and power relation and parameter E*, C

Multi-variable relation between concrete abrasion ratio caused by impact of sediment and dimensionless parameter E*, C was derived for the first using SPSS, second and third sets are compared in tables 11 and 12.the mentioned multi variable relation are

$$A_* = a + bC + dE_* \tag{17}$$

$$A_* = a\, C^b E_*^{\,d} \tag{18}$$

Comparing the value of averaged relative error for these relations with relations 11 to 16 shows that relation number 18 has minimum error with first data set and validation data(second and third) and can be the best relation among all studied relations to determine the concrete abrasion ratio caused by impact of sediment. The parameters of this relation are different for different cement content. The result shows the effect of cement content to resist the abrasion by impact of sediment. Therefore the relation between parameters a, b, and d and cement content cc was studied and the following relation was derived as follows:

$$a = -0.0017 \times c - 4.848 \tag{19}$$

$$b = 0.0004 \times c - 1.495 \tag{20}$$

$$d = 0.0005 \times c + 1.086 \tag{21}$$

By these relations and the relation number 18, the following relation is derived.

$$A_* = (-0.0017 \times c - 4.848) \times c^{(0.0004 \times c - 1.495)} \times E_*^{(0.0005 \times c + 1.086)} \tag{22}$$

4. Conclusion

In the present research which is based on doing experiments of impacting debris sediments on submerged concrete samples and to analysis the available empirical relations between experimental results, the following results has been achieved:

-The value of abrasion caused by the impact of sediments is a function of dimensionless energy and the ratio of the grain velocity on water surface to the grain velocity on concrete stilling basin, and the cement content.

-From studied relations the multi-parameter power relation between concrete abrasion and dimensionless energy and the ratio of the grain velocity on water surface to the grain velocity on concrete stilling basin had the minimum averaged relative error and the parameters of multi-parameter power relation was a function of cement content.

Table 1. MARE parameters and regression ratio of equations

Formula	Cement content	a	b	C	d	R	Mare(1)	Mare(2)	Mare(3)
	350	3×10^{-5}	-0.001	-	-	0.7854	1.1045	1.2324	1.0494
	400	3×10^{-5}	0	-	-	0.78	1.7868	1.7074	1.4301
11	450	6×10^{-5}	-0.001	-	-	0.832	2.2126	2.0815	1.9268
	350	9×10^{-6}	1.1521	-	-	0.7696	0.61511	0.914	0.4836
	400	4×10^{-6}	1.321	-	-	0.663	0.7461	0.7434	0.6947
12	450	3×10^{-6}	1.3592	-	-	0.8936	0.3702	0.3275	0.3826
	350	0.0026	-0.0085	-	-	2.0781	2.0781	2.4249	2.323
	400	0.002	-0.008	-	-	4.0162	4.0162	3.7242	3.5684
13	450	0.002	-0.006	-	-	1.5949	1.5949	1.5396	1.0962
	350	9×10^{-8}	3×10^{-8}	0.0005	-	0.8576	0.9117	1.0347	0.783
	400	7×10^{-8}	2×10^{-5}	-5×10^{-5}	-	0.791	1.116	1.1094	0.9564
14	450	6×10^{-8}	-4×10^{-5}	0	-	0.976	3.9208	3.7604	3.5211
	350	5×10^{-10}	6×10^{-8}	2×10^{-5}	0.0004	0.8578	0.8807	1.0367	0.7472
	400	-1×10^{-10}	1×10^{-7}	2×10^{-5}	0	0.8578	0.783	0.7912	0.718
15	450	5×10^{-1}	6×10^{-7}	2×10^{-5}	0	0.882	4.9242	4.3425	4.4124
	350	-0.001	9×10^{-5}	-	2.5×10^{-5}	-	1.4186	1.2493	1.3699
	400	-0.001	-5×10^{-5}	-	2.5×10^{-5}	-	1.4062	1.9309	1.257
16	450	0	0	-	2.5×10^{-5}	-	1.0914	0.9227	1.0353
	350	-3.465	2.935	-	0.005	-	1267.312	974.4984	1186.956
	400	-3.429	3.429	-	0.005	-	1593.545	1541.864	1518.011
17	450	-4.101	3.425	-	0.006	-	1618.68	620.68	757.88
	350	-5.4437	-1.355	-	1.261	-	0.416205	0.533451	0.3428453
	400	-5.5287	-1.335	-	1.286	-	0.539277	0.545723	0.3376697
18	450	-5.6137	-1.315	-	1.311	-	0.346155	0.561944	0.3536187

5.Reference

[1] Banihabib, M " Factor of flow insurgence with high density" 4th River Engineering conference. Ahvaz 1997.
[2] Banihabib, M and Iranpoor, "Evaluation of impact sediment practical stilling basin of dams", Civil Engineering International Conference, Iran, Tabriz, 2007.
[3] Banihabib, M.E. ,H. Shantia & Sh. Ghotbi.2002. Measures for problems of hydraulic Structures in rivers transporting Deloris flow. Procc. of International Conference on Fluvial Hydraulics. Sept. 4-6 . 2002 .Louvain- La – Neuve, Belgium.
[4] Bhargava, D.N., Narair ,L. Tiagai , S.S. and Gupta ,P P.1987. sedimentation problems at low dams in the Himalayas. Water power & Dam Construction.
[5] Horszczaruk, E. 2004. The model of abrasive wear of concrete in hydraulic structures. Wear 256 (2004) ELSEVIER , pp 787-796.
[6] Liu , y.w., T, yen & T.Hsu,2006. Abrasion erosion of concrete by water-borne sand. Cementand Concrete Research ELSEVIER No 36 pp 1814-1820.
[7] Morris, G. and Fan. J. 1997. Reservoir sedimentation handbook Mc Graw –Hill.
[8] Schnable Engineering Associate , Inc, 2001. Laboratory Tests and Field studies on Erosion and Abrasion Resistance of soil cement and Roller-Compacted concrete – Results of Riterature Review PCAR & D No2436.
[9] The American Society for testing and Materials , Standard Test Method for Abrasion Resistance of concrete or Mortar surface by the Rotating-cutter Method, ASTM Designation C944 , Philadephia, 1999.
[10] The American Society for Testing and Materials, standard Test Method for Abrasion Resistance of concrete (under water Method) , ASTM Designation C1138, Philadephia, 1999.

INVESTIGATION OF LAND-USE CHANGE AND HYDROLOGIC FORCING UPON STREAMBANK EROSION AND IN-STREAM SEDIMENT PROCESSES USING A WATERSHED MODEL AND SEDIMENT TRACERS

J. P. Russo,[1] J. F. Fox[2], and D. Martin[3].

[1,3]S.M.ASCE, Graduate Assistant, Department of Civil Engineering, University of Kentucky, 161 O.H. Raymond Bldg., Lexington, KY 40506-0281; PH (859) 257-4093; FAX (859) 257-4404; email: joseph.paul.russo@gmail.com.

[2]M.ASCE, Assistant Professor, Department of Civil Engineering, University of Kentucky, 161 O.H. Raymond Bldg., Lexington, KY 40506-0281; PH (859) 257-8668; FAX (859) 257-4404; email: jffox@engr.uky.edu.

ABSTRACT:

In stream erosion represents a significant portion of the watershed sediment budget for lowland watersheds, but current modeling strategies do not often include accurate methods for estimating the yield from stream bank sources or accurate representation of the stream bank erosion process at the watershed scale. This research presents a method for estimating the yield from stream bank sources using sediment carbon and nitrogen isotopic tracer results coupled with a watershed scale erosion and sediment transport model. The coupled fingerprinting-watershed modeling framework is presented in the following steps: 1) measure the sediment yield from the study watershed; 2) estimate fraction of sediment yield eroding from stream banks using sediment fingerprinting data and use this and other collected data for the watershed model calibration and verification; 3) create a conceptually simple, yet representative, model of bank erosion processes and integrate the subroutine into the watershed erosion and sediment transport model, calibrate, and verify. Land use and climate change sceneries will then be used with the calibrated model to predict the effect on the sediment transport budget.

KEYWORDS: streambank erosion, sediment transport, watershed modeling, sediment yield, isotopes, tracers.

INTRODUCTION

Sediment loss, transport, and fate are a significant environmental problem. Sediment is a pollutant that can kill fish and other aquatic life, and other potentially hazardous substances, such as fertilizers or pesticides, attach themselves onto the soil particles and eventually end up in the stream (US EPA, 1999). Turbid waters reduce

the available dissolved oxygen for aquatic life and inhibit respiration and photosynthesis (Wood and Armitage, 1997) Excess sediment deposits can smother fish eggs, reduce the storage capacity of reservoirs, and in stream sediment decomposition can contribute significant CO_2 to the atmosphere (Richardson and Jowett, 2002). Understanding sediment erosion, transport, and fate processes is a vital step toward controlling sediment pollution and creating a complete environmental model (Walling 2005).

Stream bank and stream bed erosion are watershed processes that are very difficult to model at the watershed scale due to the variability of their sediment make-up across a watershed and fluid turbulence complexity throughout a stream segment. Even small watersheds contain several miles of stream banks which can be heterogeneous and estimating erosion rates for these banks is compounded due to the varying degrees of vegetation coverage, exposure to sidewall shear stresses, mass failure, and root density which can make quantifying an erosion rate/yield very difficult. Seasonal variations in the watershed such as flow variations, microbial decomposition, pore pressure, and interflow also effect erosion rates.

Sediment yield measured at the outlet of the watershed is the sum of all watershed erosion processes, including stream banks, stream beds, and upland sediment sources (Simons and Senturuk 1992). Differentiating between these different sources is a difficult task, but much headway has been made with sediment fingerprinting toward estimating the yield from different sediment sources in the watershed (Collins and Walling, 1998). Sediment fingerprinting using natural tracers has become a feasible, acceptable method for estimating sediment yield from different sources of erosion in a watershed (Collins and Walling, 1998; Motha et al. 2004; Walling 2005; Davis 2008). The method involves collecting samples of suspended sediment using sediment traps and analyzing the collected sediment for naturally occurring tracers, e.g., inorganic elemental composition, carbon and nitrogen stable isotopic composition. Sediment samples from potential sources of suspended sediment are then collected and analyzed for the same tracers, and, using an un-mixing model, the fraction of sediment eroding from each source can be estimated (Collins and Walling, 1998; Fox and Papanicolaou, 2008).

While sediment fingerprinting provides a useful data-based tool for quantifying sediment sources in a watershed and their respective sediment loads, there is a need for performing watershed erosion and sediment transport modeling across an entire watershed in order that future land-use scenarios and climate changes can be modeled and investigated. Previous studies indicate that sediment from channel banks can be a dominant sediment source in some watersheds (Trimble, 1997; Smith and Dragovich, 2008) however, a review of recent literature suggests that hydrologically driven watershed prediction models typically do not accurately represent bank erosion processes. The modeling limitation is partially due to the fact that while empirical equations of bank erosion are available accurate process-based bank erosion models are less developed, particularly for composite watershed modeling applications where simple, computationally inexpensive subroutines with low data requirements are desirable (Borah and Bera, 2003; Merritt et al., 2003; Kalin

et al., 2003). There is a need to build erosion models that are conceptually simple, but capture all the necessary sediment processes with simple data requirements while providing some physically based structure.

The present research works towards the coupling of sediment fingerprinting with watershed erosion and sediment transport modeling in order that stream bank erosion can be more accurately modeled at the watershed scale. The long-term objective of this research works towards development and the watershed modeling tool and application for land-use change and climate change scenarios. In this paper, the goal is to present the data collection, fingerprinting, and model development components of this work. The coupled fingerprinting-watershed modeling framework is presented in the following steps: 1) traditional sediment transport data collection methods are used to measure the sediment yield from the study watershed; 2) the fraction of the sediment yield derived from the stream banks is estimated using the sediment fingerprinting approach, and the data is thereafter used for the watershed sediment transport model calibration and verification; 3) a conceptually simple yet representative model of bank erosion processes is constructed, calibrated, and integrated into a watershed erosion and sediment transport model.

STUDY AREA

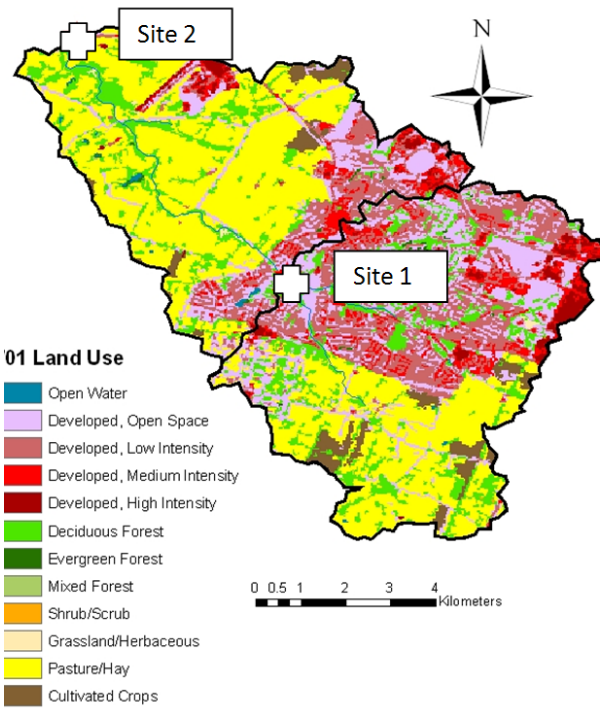

Figure (1) Map of the South Elkhorn Watershed, Lexington Ky.

The study area for this research is the South Elkhorn watershed located near the University of Kentucky in Lexington, Kentucky (see Figure 1). The South Elkhorn is approximately 61 km^2. The South Elkhorn was chosen for the coupled model development due to the fallowing reasons. (1) The South Elkhorn experiences stream bank erosion as its dominant source of transported sediments. (2) Overland erosion processes such as rill and inter-rill erosion are only a small contribution to sediment loads in the South Elkhorn watershed, thus model development can be achieved under fairly controlled conditions. (3) The South Elkhorn has been an experimental watershed where tracer development and sediment fingerprinting methodologies have been improved over the past four years. Tracer data has been previously collected for the watershed (Davis 2008) thus making it ideal for development of coupled modeling strategy. (4) Stream flow and precipitation data is available for the watershed. Weather data is readily available from NOAA. The Lexington Airport is located inside the study watershed and hourly precipitation, temperature, and wind speed data are easily accessible. Flow and water depth data is also easily accessible from USGS gage 03289000 located at the outlet of the watershed. (5) The South Elkhorn is very close to the University of Kentucky and is easily accessible to the researchers on a daily basis. (6) The South Elkhorn is a multi land use lowland watershed with urban and non-urban land cover, and is representative of other small scale basins in the bluegrass region of Kentucky. At this time, the region has pronounced sedimentation problems in its streams primarily as the result of bank erosion processes, thus making the model development a regional environmental need.

In general, the banks of the South Elkhorn have low erodibility and are stable in the watershed upstream of Site 1 in Figure 1. . From Site 1 to the outlet of the watershed at site 2 the banks become progressively more incised with less vegetation. Stream bank, stream bed erosion and deposition are the dominant sediment processes within this reach of the watershed.

In development of the coupled modeling tool for the South Elkhorn, emphasis was placed upon data collection and performing sediment fingerprinting using data from sites 1 and 2 in Figure 1. Thereafter, the watershed model was further developed for the problem reach.

(1) Measure Sediment Yield

In order to provide data for calculation of suspended sediment yield in the watershed, suspended sediment was collect and thereafter the Einstein approach was used to estimate sediment yield.

Suspended sediment was collected from the South Elkhorn watershed using a Teledyne ISCO water sampler. 500ml samples were collected on a storm by storm basis on either a one hour or two hour time step. The samplers were then transported to the University of Kentucky Hydrosystems Laboratory where they were individually run through a pre-weighed dry filter, and then dried for an additional twenty four hours, and the sediment was measured. A total of 5 storm events were used for estimation of sediment yield. The yield for the storm events were evaluated

using Einsteins approach (1950) which is described in (Chang, 1988). The suspended sediment discharge was obtained by integrating

$$q_{ss} = \int_a^D Cudz \qquad \text{Eq(1)}$$

where q_{ss} is the discharge of suspended sediment per unit channel width, a is the lower limit where suspension begins, C is the sediment concentration, and D is the depth. The Einstein integration yields the equation

$$q_{ss} = 11.6 C_a U_*^{'} \left[2.303 \log\left(\frac{30.2D}{\Delta} \right) I_1 + I_2 \right] \qquad \text{Eq(2)}$$

where

$$I_1 = 0.216 \frac{A^{z_*-1}}{(1-A)^{z_*}} \int_A^1 \left(\frac{1-\eta}{\eta} \right)^{z_*} d\eta \qquad \text{Eq(3)}$$

$$I_1 = 0.216 \frac{A^{z_*-1}}{(1-A)^{z_*}} \int_A^1 \left(\frac{1-\eta}{\eta} \right)^{z_*} \ln(\eta) d\eta \qquad \text{Eq(4)}$$

I_1 and I_2 are function of A and z^* and were integrated numerically using (Nakato, 1984). The sediment concentration, C, can be calculated at any time instant with the equation

$$C(y) = C_a \left[\left(\frac{D-y}{y} \right) \left(\frac{a}{D-a} \right) \right]^{z^*} \qquad \text{Eq(5)}$$

where C_a is a reference concentration and a is a reference level. z^* is the Rouse number defined as

$$z_* = \frac{\omega_s}{\kappa U_*} \qquad \text{Eq(6)}$$

where w_s is sediment fall velocity in m/s, κ is the dimensionless von Karman constant equal to approximately 0.40, and U^* is the shear velocity in m/s. U^* is defined as

$$U_* = (gHS)^{1/2} \qquad \text{Eq(7)}$$

The reference level a is treated as the transition from bed load to suspended load and occurs on the order of 5% of the flow depth (Chang 1988). C_a typically corresponds to this reference level, however, here C_a will be calculated using concentration at the ISCO sampler inlet depth, C_Y, which can be used in Equation (5) and rearranged as

$$C_a = \frac{C_Y}{\left[\left(\frac{H-Y}{Y}\right)\left(\frac{a}{H-a}\right)\right]^{z^*}} \qquad \text{Eq(8)}$$

where Y is the depth of the depth at the inlet as defined before.

The yields for an individual storm event were determined by integrating the sediment rate function Equation (2) over the entire storm hydrograph.

$$S_y = \int_0^T Q_s dt \qquad \text{Eq (9)}$$

Where 0 is the onset of the storm event, T is the end of the event, and Q_s is the sediment flow rate (q_{ss}) integrated over the width of the channel.

A storm hydrograph is defined as the flow period between the onset of the hydrograph until the point in time when significant flow acceleration ceases and the flow regime returns to base flow conditions. This base flow separation method was taken from (Chow, 1988). The onset of acceleration of the flow over time was defined as the point when flow acceleration begins, and the end of the flow acceleration was determined as a function of the peak flow (Q_p)

$$N = 4.094e^{0.004Q_p} \qquad \text{Eq(10)}$$

where N is the length of time from the time of peak flow to the time when storm acceleration ends and the flow regime returns to base flow conditions.

Using the Einstein method, the sediment yields were calculated. Thereafter, a power law was used to fit the relationship of sediment yield to peak flow rate. Figure (2) show the yields and peak flow rates for the sediment transporting storm events in the South Elkhorn.

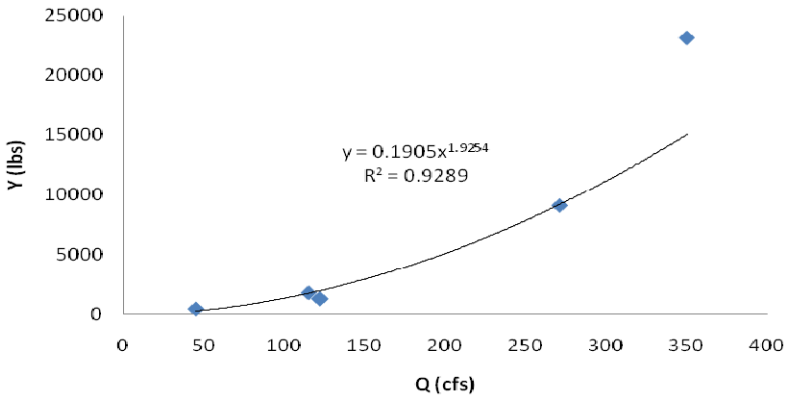

Figure (2) Sediment Yield and Peak Flow Rate for the Sampling Period

(2) Sediment Yield Estimation Using Tracer Data and Sediment Fingerprinting

The contribution of the sediment yield derived from bank erosion was estimated using sediment fingerprinting with carbon and nitrogen isotope (δ^{13}C and δ^{15}N) natural tracers.

The isotopic tracers are a signature of the sediment and a result of carbon and nitrogen cycling. δ^{13}C and δ^{15}N are dependent upon environmental variabiles including the spatial properties of the land cover (e.g.,. vegetation type) and land management (e.g., tillage, biostabilzation methods) making the tracers ideal for comparison of different spatial sources of erosion in a watershed. In other words, two different tracks of land will have two different isotopic signatures, and sediment can be traced back to its source by analyzing its isotopic signature. This method can be applied to the watershed by collecting and analyzing suspended sediment captures at an outlet. The sediment at the outlet is a mixture of all sediment sources in the watershed, and by comparing the signature of the sediment at the outlet with the signature of the sediment sources a fraction of total sediment yield can be derived for each sediment source.

Sediment tracer samples were collected using *in situ* sediment trapping devices (Walling and Amos 1999; Phillips et al. 2000; Russell et al. 2000; Gruszowski et al. 2003; Fox 2005; Walling et al. 2006; Fox and Papanicolaou 2007). The sediment traps were collected and replaced weekly. The traps were emptied and the contents centrifuged to remove as much water as possible without losing sediment. The samples were then freeze dried, weighed, and wet sieved to separated the d<53 μm, where d is particle size diameter, fine fraction. The fine fraction was then freeze dried and weighed again to determine the mass of suspended sediment captured inside the trap for the sampling time.

A characteristic of the South Elkhorn is the predominance of bank erosion in the lower reach of the watershed between sites 1 and 2 (see Figure 1) and the lack of overland (rill and inter rill) erosion in the uplands. The majority of sediment collected at the outlet is either from the stream banks or streambed of the ephemeral and perennial streams throughout the basin and the bed of the main channel. Past research has shown that the δ^{15}N signature of the stream banks is statistically unique in comparison with the in-stream sediments of the streambeds (Davis 2008). The differences are due to the in-stream biochemical processes that the sediments undergo, e.g., microbial processesing, once deposited in the stream of the channel. The fingerprinting study collected samples at two locations, site one near the uplands before the incised stream banks and site two at the outlet of the watershed. The sediment collected at each sampling site was analyzed for their N^{15} isotopic signature.

Because of the small contribution from sediment sources other than the stream banks and streambed, the isotopic signature of the sampling site before the bank erosion reach (site 1) was assumed to be the signature of the stream banks and all other sediment sources except the stream banks, and the signature of the sediment at the outlet (site 2) was assumed to be the signature of the all sediment sources plus the stream banks in the lower reach where bank erosion was a severe problem.

$$\delta_{outlet}^{15} = X_{banks}\delta_{banks}^{15} + X_{other}\delta_{other}^{15} \quad \text{(Eq 11)}$$

where X_{Banks} is fraction of material coming from the banks, X_{Other} is the fraction of material coming from all sources except the banks, and δ^{15} is the isotopic signature from its respective source. By definition

$$X_{banks} + X_{other} = 1 \quad \text{(Eq 12)}$$

and by substitution.

$$X_{banks} = \frac{\delta_{outlet}^{15} - \delta_{other}^{15}}{\delta_{bank}^{15} - \delta_{other}^{15}} \quad \text{(Eq 13)}$$

Using this method a fraction of sediment yield from stream bank erosion is determined. Figure 3 shows the yield of sediment for each source for weekly samples collected during the sampling period. The stream banks show higher sediment yield with discharge but also show variability. The streambed erosion shows a consistent trend with increasing peak flow that erodes a greater load of streambed sediments.

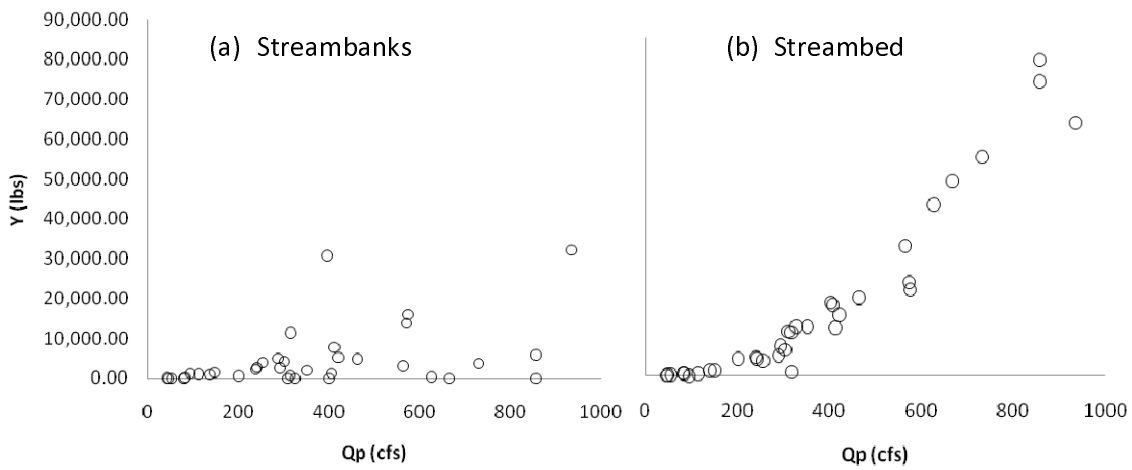

Figure (3) Yield from streambank and streambed sediments

(3) Watershed Bank Erosion Model

The sediment fingerprinting results were used in a coupled modeling framework to calibrate bank erosion at the watershed scale. The watershed model Hydrological Simulation Program – FORTRAN (HSPF) (Bicknell et al., 1997) was chosen to be used as the watershed model for the South Elkhorn. HSPF was chosen for the hydrological model for the South Elkhorn because 1) HSPF has the ability to model on a variety of time steps including hourly and daily, 2) HSPF is a very comprehensive watershed model that includes a multitude of overland and in-stream processes, 3) HSPF is easily available via download from the EPA.

HSPF is a deterministic lumped parameter model that has been used successfully on large (Bergman et al., 2002; Ackerman et al., 2005; Ribarava et al,

2008) and small (Mishra et al., 2006) watersheds. HSPF can also be used as a semi-distributed parameter model as it divides the watershed into different hydrological homogeneous land segments (i.e. forest cover, urban cover, est.), and calculates runoff and pollutant values for these land segments independently. HSPF considers three types of modeling segments, permeable land, impermeable land, and reaches. These modeling segments have several components that calculate runoff and pollutant values for each land segment. The flow and pollutants are routed through the reaches, and the resulting hydrograph and pollutant graphs can be exported for any reach/land segment desired. HSPF requires time series data of precipitation and potential evapotranspiration as a minimum data requirements, although certain pollutants require additional time series including daily temperature, percent cloud cover, dew point temperature, wind speed, and solar radiation.

HSPF simulates sediment detachment and transport for upland sources as a function of runoff shear stress and of raindrop detachment. Sediment detachment, transport, and entrainment are modeled in the bed of the channel as a function of reach mean velocity, particle settling velocity, and entrainment/transport/scour velocity thresholds. HSPF models three sizes of sediment (sand, silt, and gravel). HSPF does not include a bank erosion component and therefore a bank erosion component was developed as a separate subroutine that was input to the model.

Flow calibration and verification was performed by first performing a simple sensitivity analysis to determine which parameters the model is most sensitive too by adjusting routing, permeable land, and impermeable land parameters from their maximum to their minimum value and analyzing the resulting hydrograph. Once sensitive parameters were determined, the sensitive parameters were adjusted until the outflow from the model matched the observed values for the calibration period (2006 to 2008). The was calibrated as a two step process: 1) Routing parameters were adjusted until yearly volumes of water and were matched with observed data as well as possible, 2) cross sectional geometry parameters were adjusted using cross sectional data to match average stream velocities with observed values as well as possible 3) permeable land and impermeable land parameters such as interflow and soil storage capacities were adjusted until the base flow and hydrograph shape were as closely matching observed data as possible. Figure 4 shows the observed and simulated flows for a six month period, and figure 5 shows the verification period.

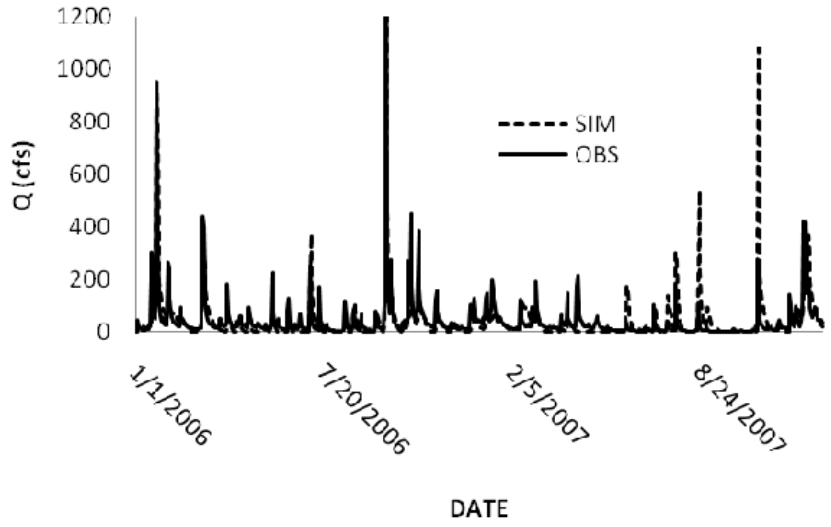

Figure (4) Observed and Simulated flow for the Calibration Period

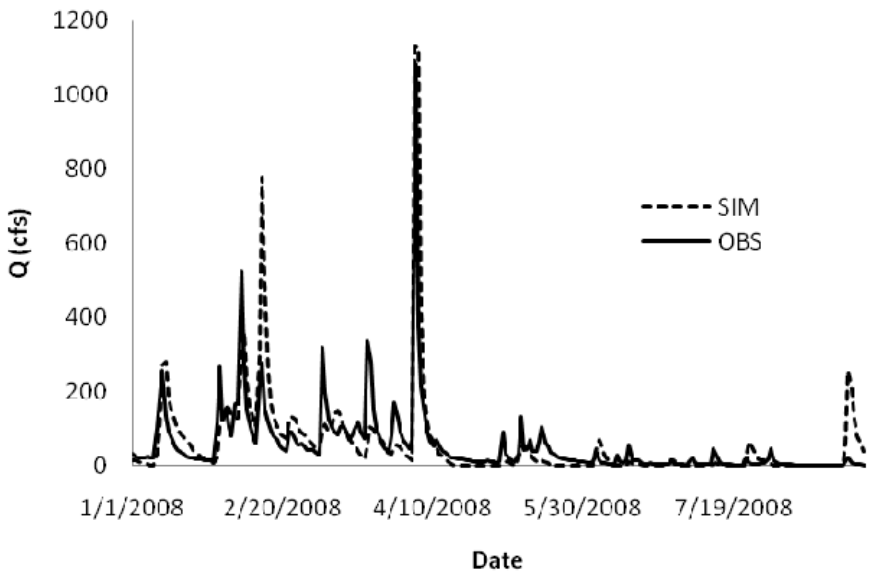

Figure (5) Observed and Simulated flow for the Validation Period

After calibrating for flow, the sediment component, including the bank erosion component, were added to HSPF. For the time being, the bank erosion model used was a conceptually simple model that relates sediment yield from the banks in the reach as a function of the excess shear stress as

$$S_y = m\left(\frac{\tau}{\tau_c} - 1\right)^n \qquad \text{Eq (14)}$$

where τ is the shear stress at the banks and τ_c is the critical shear stress for the reach, and m and n are calibration coefficients. The sediment fingerprinting results were used to calibrate the bank erosion model. Common values for the critical shear stress were used based on the published literature and were varied from 2 to 5 Pa. Values

were iterated through the bank erosion model until reasonable values of sediment yield were calculated. The coefficients m and n were also calibrated and equaled 2211 and 1.44, respectively.

Using the calibrated flow data from the model, the daily sediment yield was predicted using Equation 14 and a time series was built. Bank erosion was modeled as a point source in the affected reach, and this time series was used as the daily load of sediment delivered from the banks into the reach. The sediment was then routed to the outlet of the watershed and the final fine sediment time series was compared with the observed sediment yield. The calibration procedure was as follows: 1) Predict sediment yield from the banks using the simulated flow data and Equation 14 and create a time series of sediment load delivered into the reach from the banks, 2) Use the bank sediment load time series as the loading data for a point source in the affected reach, 3) compare the sediment yield at the outlet with the observed values of sediment yield, and 4) adjust model parameters and repeat steps one through four until simulated values match observed values.

Figure 6 shows the comparison between simulated and obverted sediment yield at the outlet that is derived from the stream banks and the total sediment yield.

The model shows reasonable results for the stream bank estimates with the exception of the last event, however the total sediment yield comparisons need additional refinement, which is on-going. While flow is modeled reasonable well, velocity and total yield estimates have considerable error. Table (1) contains the correlation and error of observed velocity, flow, and yield measurements with the simulated values.

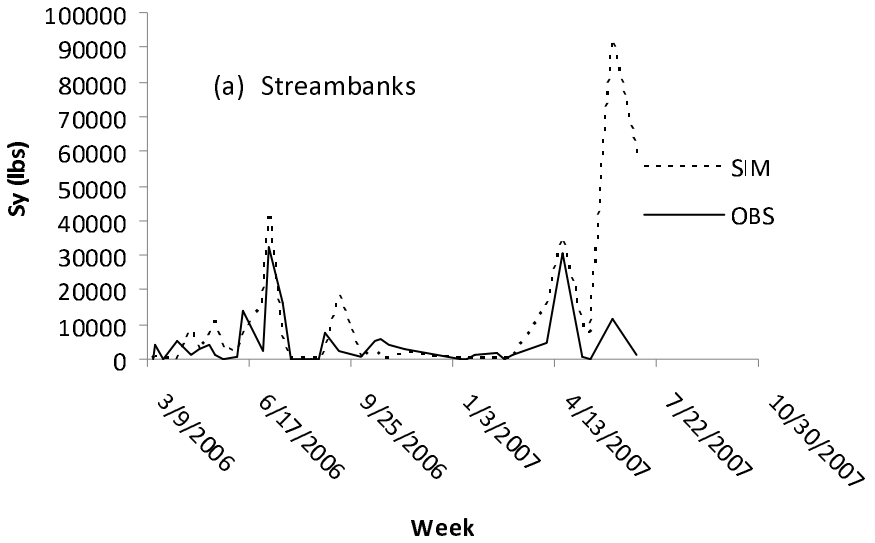

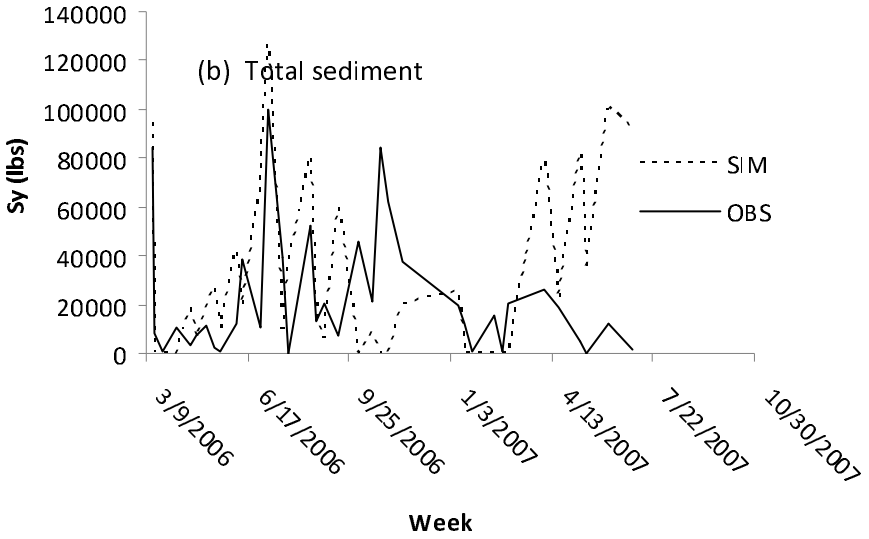

Figure (6) Bank and total Sediment Yield SIM and OBS VS Date

Table (1) Table Statistical Observations

	Correlation With Observed Data	Percent Error
Flow Calibration Period (06-07)	0.80	-1.10
Flow Verification Period (08)	0.77	-6.79
Velocity Calibration Period (06-07)	0.68	-28.48
Velocity Verification Period (08)	0.81	-34.16
Bank Sediment Yield (06-07)	0.46	57.25
Total Sediment Yield (06-07)	0.47	36.73

The percent error is the difference between the simulated and the observed values while the correlation coefficient is a measure of how well the trends of the simulated data match the trends of the observed data.

DISCUSSION

This paper presents a new coupled methodology for estimating and modeling stream bank erosion yields using sediment fingerprinting and watershed erosion and sediment transport modeling. This research is ongoing and areas of ongoing improvement include the following:

- Further refine the stream bank model component to account for spatial distribution laterally and vertically in the reach. The sediment yield estimation for the bank estimation shows a low correlation with the peak flow for the sampling period (0.43). Other processes are occurring that are affecting stream bank erosion besides the peak flow rate, and these processes must be investigated.
- Refine the sediment yield and the tube mass relationship. The sediment yield data represents the mass of sediment transported out of the reach for the entire sampling period, which is about one week. The current relationship between flow and yield is based on the peak flow for that sampling period. This data needs to be refined so that we can draw a relationship between a single storm event, and the peak flow for that event.
- Increase the resolution of the model. Stream banks are currently modeled as a point source in one reach of the model. The next step needs to be to differentiate the different sections of stream bank erosion, estimate erosion yield for each of these sections, and increase the resolution of the model by simulating stream bank erosion in each of these sections.
- Further calibration of the flow, velocity, and sediment models. The most important parameter for the HSPF stream bed erosion model is the velocity of the flow in the reach. Velocity and sediment yield all show a low correlation with observed values and large percent errors. Further calibration is needed to enhance the models predictive capacities.

After refining the coupled model, the model will be used for performing watershed erosion and sediment transport modeling across the watershed in order that future land-use scenarios and climate changes can be modeled and investigated for the Bluegrass.

REFERENCES

Ackerman, Drew. Kenneth C. Schiff, and Stephen B. Weisberg. (2005). "Evaluating HSPF in an Arid urbanized watershed." JAWRA. 477-486.

Bera, M., Borah, D.K.. 2003. "Watershed-Scale Hydrological and Nonpoint-Source Pollution Models: Review of Mathematical Bases. American Society of Agricultural Engineers." 46(6): 1553-1566.

Bergman, M.J. W. Green, and L. J. Donnangelo. (2002). "Calibration of storm loads in the South Prong Watershed, Florida, Using BASINS/HSPF." Journal of American Water Resources Association. Vol 38. No 5. 1423-1436

Bicknell, B. R., John C. Imhoff, John L. Kittle, Jr., Thomas H. Jobes, Anthony S. Donigian, Jr.. (1997). "Hydrologic simulation program-Fortran, user's manual for version 11 (EPA/600/R-97/080)." Athens, GA: US EPA, Ecosystems Research Division, Environmental Research Laboratory.

Chang, Howard. Fluvial Processes in River Engineering. (Florida: Krieger Publishing Company, 1988), 131-185.

Chow, Ven Te. Applied Hydrology. (New York: McGraw-Hill, 1988), 132-135.

Collins, A.L., D.E. Walling. (1998). "Use of composite Fingerprinting to determine the provenance of the contemporary suspended sediment load transported by Rivers." Earth Surfae Processes and Landforms. Vol 23 31-52.

Davis, C. M. (2008). "Sediment fingerprinting using organic matter tracers to study streambank erosion and streambed sediment storage processes in the South Elkhorn Watershed." M.S. Dissertation, University of Kentucky, Lexington, Kentucky.

Fox, J. F. (2005). "Fingerprinting using biogeochemical tracers to investigate watershed processes." Ph.D. Thesis, University of Iowa, Iowa City, Iowa.

Fox, J.F., and Papanicolaou, A.N. (2007). "The use of carbon and nitrogen isotopes to study watershed erosion processes." J. Am. Wat. Resour. Assoc., 43(4), 1047-1064.

Fox, J.F. and Papanicolaou, A.N. (2008). "An un-mixing model to study watershed erosion processes." Advances in Water Resources, 31(1), 96-108.

Fox, J.F., and Papanicolaou, A.N. (2008b). "Application of the spatial distribution of nitrogen stable isotopes for sediment tracing at the watershed scale." J. Hydrol., 358, 46-55.

Gruszowski, K.E., Foster, I.D.L., Lees, J.A., and Charlesworth, S.M. (2003). "Sediment sources and transport pathways in a rural catchment, Herefordshire, UK." Hydrol. Proc., 17, 2665-2681.

Mishra, Ashok. S. Kar and V. P. Singh . (2006) "Determination of runoff and sediment yield from a small watershed in sub-humid subtropics using the HSPF model." Hydrological Processes. 3035-3045.

Kalin, Latif. Rao S. Govindaraju[a], Mohamed M. Hantush . (2003). "Effects of geomorphological resolution on modeling of runoff hydrograph and sedimentograph over small watersheds." Journal of Hydrology. (276) 89-111.

Merritt, W.S., R.A. Letcher, and A.J. Jakeman. 2003. „A review of erosion and sediment transport models." Environmental Modeling and Software. 18, 761-799.

Motha, J.A., Wallbrink, P.J., Hairsine, P.B., and Grayson, R.B. (2004). "Unsealed roads as suspended sediment sources in an agricultural catchment in south-eastern Australia." J. Hydrol., 286, 1-18.

Nakato, T., "Numerical Integration of Einstein's Integrals," Journal of Hydraulic Engineering. ASCE, 110(12), 1863-1868, December 1984.

Phillips, J.M., Russell, M.A., and Walling, D.E. (2000). "Time-integrated sampling of fluvial suspended sediment: a simple methodolgy for small watersheds." Hydrol. Proc., 14, 2589-2602.

Ribarava, Irina. Plamen Ninov, and David Cooper. (2008). "Modeling nutrient pollution during a first flood event using HSPF software: Iskar River case study, Bulgaria. Ecological Modelling." (211) 241-246.

Russell, M.A., Walling, D.E., Hodgkinson, R.A., 2000. "Appraisal of a simple sampling device for collecting time-integrated fluvial suspended sediment samples." In: Stone, M. (Ed.), The Role of Erosion and Sediment Transport in Nutrient and Contaminant Transport, IAHS Publ. No. 263. IAHS Press, Wallingford, pp. 119–127.

Richardson, J., I.G. Jowett. (2002). "Effects of sediment on fish communities in East Cape streams, North Island, New England." New Zealand Journal of Marine and Freshwater Research. Vol 36. 431-442.

Simons and Senturk. Sediment Transport Technology. Water Resources Publications, LLC, 1992.

Smith, Hugh G., Deirdre Dragovich. (2008). "Sediment budget analysis of slope-channel coupling and in-channel sediment storage in an upland catchment, southeastern Australia." Geomorphology. 101, 643-654.

Trimble, Stanley W. Contribution of Stream Channel Erosion to Sediment Yield from an urbanizing watershed. Science 278. 1442.

Walling, D.E., and Amos, C.M. (1999). "Source, storage, and mobilisation of fine sediment in a chalk stream system." Hydrol. Proc., 13, 323-340.

Walling, D.E. (2005). "Tracing suspended sediment sources in catchments and river systems." Sci. of the Tot. Environ., 344, 159-184.

Walling, D.E., Collins, A.L., Jones, P.A., Leeks, G.J.L., and Old, G. (2006). "Establishing fine-grained sediment budgets for the Pang and Lambourn LOCAR catchments, UK." Journal of Hydrology, 330, 126– 141.

Wood, Paul J., Patrick D. Armitage. (1997). "Biological Effects of fine sediment in the lotic environment." Environmental Management. Vol. 21, No.2. 203-217.

This page intentionally left blank

Retrofitting Stormwater BMPs in a Supercritical Flow Regime
A Hydraulic Perspective

I. J. Tye – CH2M HILL
MIE Aust, PE,
Level 7, 9 Help Street, Chatswood NSW, 2067, Australia
Email: ivan.tye@ch2m.com.au

ABSTRACT

A computational hydraulic model toolkit was required to facilitate designs that would permit retrofitting stormwater Best Management Practices (BMPs) and flow diversion structures on covered and open channels flowing under supercritical flow conditions:

- Without exacerbating flooding, and
- Maximizing the capture of suspended solids.

This paper outlines the development of the computational hydraulic model toolkit.

The paper addresses:

- The computational hydraulic modeling of the base case – pre installation of the BMP,
- The use of a Diversion Channel to divert the treatable flow from the Main Channel to the BMP via a weir or gate,
- The transitioning of the flow regime from supercritical to subcritical immediately upstream of the BMP and wholly within the Inlet Diversion Channel to optimize the settlement of sediments in the BMP and limit sediment drop out in the Inlet Diversion Channel,
- The transitioning of the flow regime from subcritical to supercritical immediately downstream of the BMP and wholly within the Outlet Diversion Channel to minimize flow depths,
- The strategic positioning of the hydraulic jump outside of the Main Channel to prevent overtopping and the likely flooding of adjacent residences,
- The design of flood mitigation works and the mitigation of sediment drop out upstream of the weir in the Main Channel, and
- Retaining Main Channel capacity.

A physical model was constructed of a proposed BMP retrofit and tested for a range of flows. The physical model was used to check and refine the computational model as well as for determining the optimum angle for flow diversion and the total force on weirs. The latter was used in the design of collapsible weirs.

The computational hydraulic model has been successfully used to design the diversion channel bed slopes and the lengths and dimensions of inlet and outlet Diversion Channels to optimize pollutant capture and to manage potential flooding.

1. INTRODUCTION

Many of the stormwater channels that were constructed in our cities and towns pre-1980 were typically constructed from concrete or brickwork (Refer to Photographs 1, 2 and 3). Hydraulic analyses indicate that the majority of these channels flow under supercritical flow conditions, thus the ability to settle out suspended sediments within a stormwater best management practice (BMP) is made more difficult by the fast moving water. Attempts to slow the water down to enhance settlement generally lead to a raising of the flood level and in some instances the flooding of private property and the deposit of sediment in the Main Channel instead of in the BMP (Refer to Photograph 4). This paper sets out the techniques that were developed to overcome these issues.



Photo 1 - Typical concrete lined stormwater channel



Photo 2 - Typical brick lined stormwater channel

Photograph 4 illustrates an example of a BMP and weir retrofitted in the 1990's. This method is still commonly used and creates the following hydraulic issues:

- Establishment of a hydraulic jump at the diversion weir which results in floodwaters overtopping the channel wall, and
- Establishment of a slow moving body of water immediately upstream of the weir resulting in sediment dropping out from the water column in the Main Channel. The drawback is that during the next flood event the sediment can become re-suspended and then carried over the weir instead of to the BMP. Other negative issues; include unsightliness, provision of a habitat for mosquitoes and vermin and public complaints.



Photo 3 - Typical covered concrete channel.



Photo 4 – A weir retrofitted to divert stormwater towards a BMP for treatment.

2. HYDROLOGY

In hydrologic terms the channels generally had capacities of the order of a 1 in 10 year to a 1 in 20 year storm event. In most instances the flow rate that was adopted for diversion to the BMP for treatment was the 1 in 3 month peak flow. The 1 in 3 month storm event was selected as it represents in excess of 90% of the total yearly volume of runoff.

3. HYDRAULICS

The computational hydraulic modeling toolkit developed for this project was to be later used by a number of sub-consultants to carry out the detailed hydraulic modeling and design work and it was thus necessary to find a program that was readily available, within target budget and reasonable straight forward to use. Computational Fluid Dynamic Models and other complex hydraulic models were not considered due to cost and the need for experienced hydraulic modelers.

The public domain hydraulic program HEC-RAS was selected as it was readily available and there were reasonable number of modelers who were familiar or experienced users of that particular model.

3.1 Current Practice

Prior to this project, the practice was to retrofit the BMP as economically as possible and often in locations with limited space. Thus a Diversion Weir was placed across the Main Channel and the Inlet Diversion and Outlet Diversion Channels were kept as short as possible (refer to Figure 1) and their hydraulic impacts were not fully appreciated. Often a hydraulic jump would occur in the Inlet Diversion Channel and it would extend into the Main Channel resulting in a slow moving body of water at the weir and subsequent settling out of sediments and debris immediately upstream of the weir (Photo 4). Additionally, early overtopping of the weir would occur, resulting in a lesser quantity of suspended sediment being diverted to the BMP.

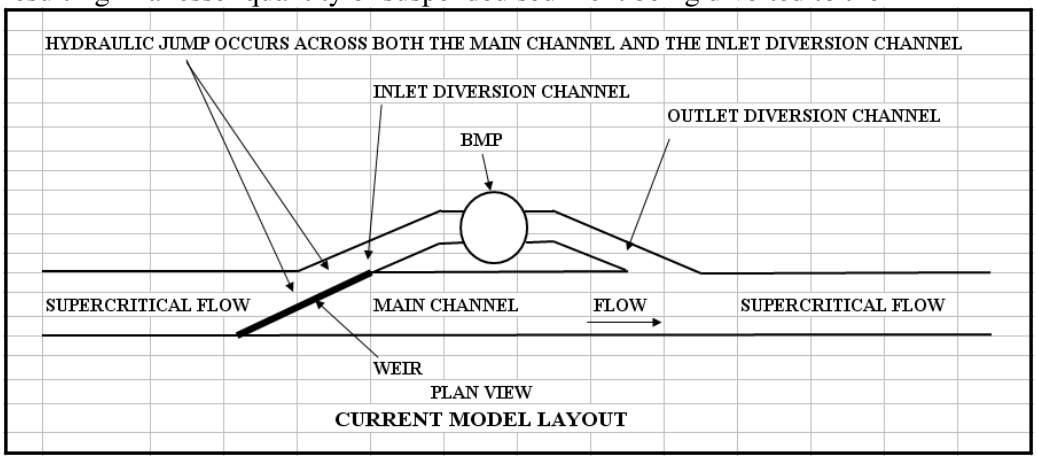

Figure 1 – Current Practice BMP Retrofit Layout

3.2 Conceptual Model

A conceptual model (Figure 2) was developed which laid out all the requirements of the hypothesis and which if achieved would significantly enhance the capture of pollutants, in particularly sediments and also manage flooding which is typically associated with placing obstructions within channels flowing under supercritical conditions.

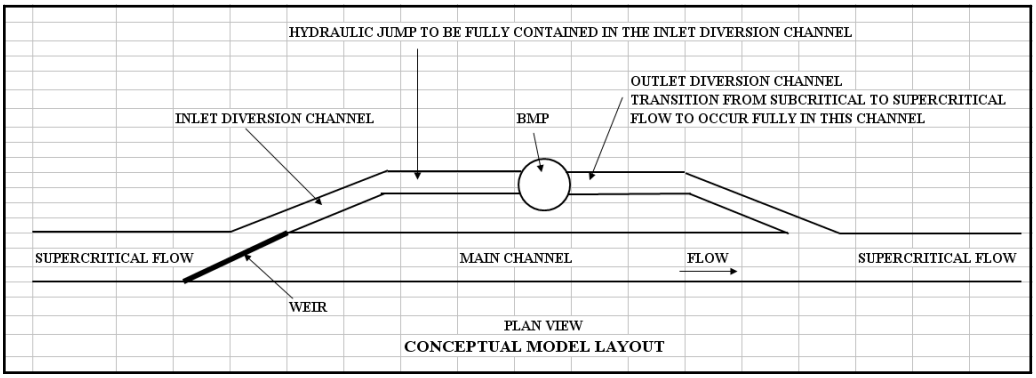

Figure 2 – Conceptual Model Layout

3.3 Computational Model Components

To simplify the modeling and to provide ease of review the computational hydraulic model was broken up into three (3) separate models.

Model 1 (Figure 3) was developed to determine the base case. That is, to determine the capacity (Q_c) of the existing channel just before overtopping occurred and to determine the flow depth for the treatable flow rate. In HEC-RAS, the channel is constructed from a number of channel cross sections (also known as River Stations). For our project, cross sections were surveyed at typically 20 meter intervals and at least 200 meters upstream and downstream of the selected BMP location. Where other hydraulic control structures, such as culverts, existed within the 200 meter limit then the survey and the model was extended a further 200m beyond the hydraulic control structure.

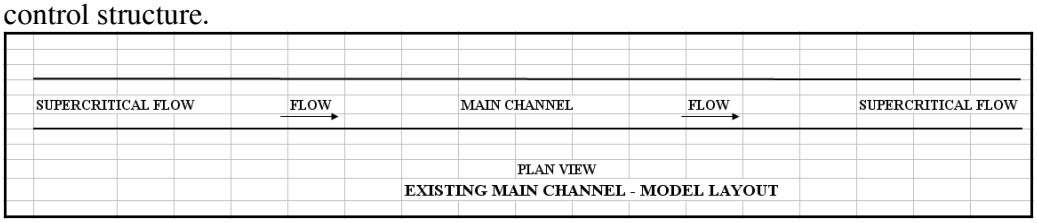

Figure 3 – Existing Main Channel Layout – Model 1

Model 2 (Figure 4) was developed to model the treatable flow rate only and to determine the lengths, grades and dimensions of the Inlet Diversion Channel and the Outlet Diversion Channel such that:

- The flow immediately upstream of the BMP was subcritical in order to optimize settlement of sediments in the BMP,

- The hydraulic jump is fully contained within the Inlet Diversion Channel in order to provide the minimum allowable weir height (preferable equal to the supercritical depth of the treatable flow in the Main Channel for the base case plus the estimated super-elevation),
- The hydraulic jump does not overtop the walls of the Inlet Diversion Channel,
- The flow when it departs the BMP is subcritical, and
- The flow transitions from subcritical back to supercritical within the Outlet Diversion Channel and before it reaches the Main Channel.

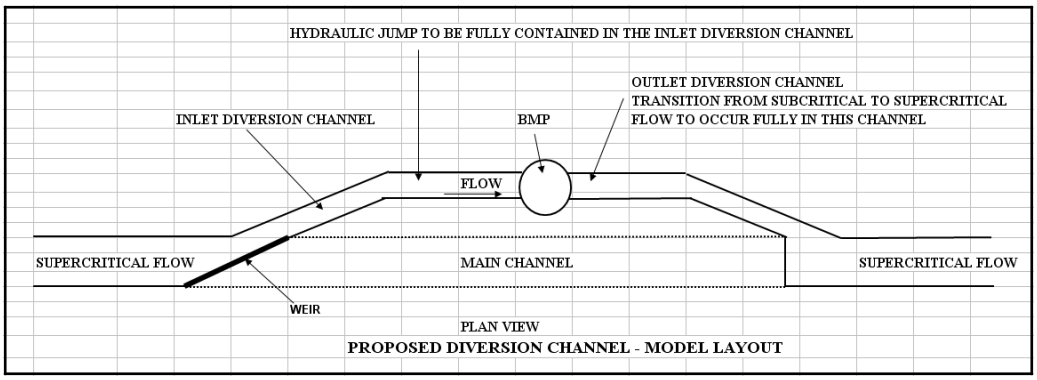

Figure 4 – Proposed Diversion Channel Layout – Model 2

Model 3 (Figure 5) was developed after the location of the start of the Inlet Diversion Channel and the end of the Outlet Diversion Channel had been determined in Model 2 above. This model was necessary to determine the impact of including a fixed weir and sudden expansion and contraction sections in the Main Channel and assuming that the BMP is fully blocked. The model was then amended to include flood mitigation works to prevent over topping of the channel for the previously determined full capacity flow (Q_c).

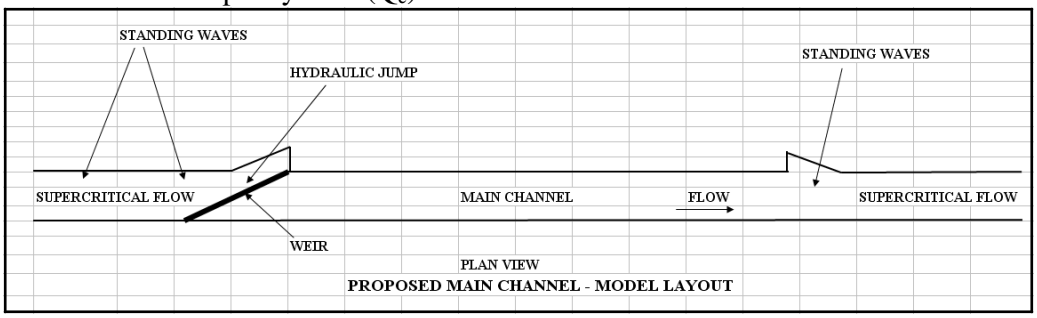

Figure 5 – Proposed Main Channel Layout – Model 3

3.4 Physical Model

A physical model of an actual design was constructed at the University of Technology - Sydney, hydraulics laboratory. The physical model was used to check the conceptual model, the hydraulic behavior predicted by the computational model,

determine where the computational model required refining and what assumed computational model parameters required adjustment.

Photograph 5 illustrates the 1 in 20 scale model which was constructed from Perspex. The BMP was represented by a section with a dropped invert and removable vertical plates with different sized holes. The different size holes represented the percentage blockage of the BMP.

The model shown in Photograph 5 included a collapsible weir (and not a skewed weir as shown in Figure 4). A strain gauge was used to measure the force on the weir at the design flow. This was later used to design the counter-weight for the collapsible and self righting weir.

Fourteen Piezometers (Photograph 7) were used to record the hydraulic head at various locations within the Main Channel and the Diversion Channel. This data was used to compare the computational model results against the physical model results. Key areas of difference between the physical model and the computer model were the predicted behavior at weirs that were located at right angles to the Main Channel and the magnitude of the disturbances at the confluence of the Diversion Channel with the Main Channel. The physical model showed the water profile super-elevating at bends but also banking up at the downstream end of the weir (Photograph 8).



Photo 5 - 1 in 20 scale model of actual design to determine overall system behavior. (Flow direction is from top to bottom of photo.)



Photo 6 - 1 in 10 scale model to obtain better details at the confluences and at the weir. (Flow direction is from top to bottom of photo.)

Photograph 6 illustrates a 1 in 10 scale model but with geometrically simplified Main and Diversion Channels. The larger model was used to obtain better definition of the behavior of the water surface at the weir and the confluence of the Diversion Channel and the Main Channel as well at the hydraulic forces on the collapsible weir.

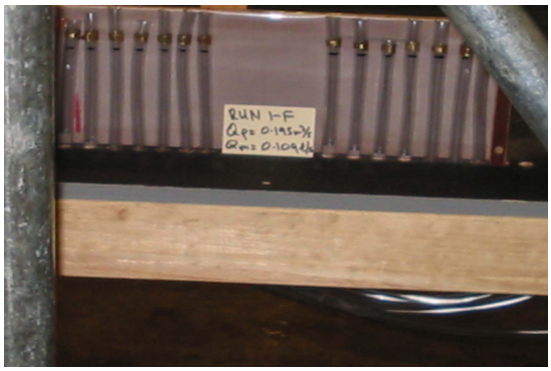

Photo 7 - Piezometers indicating the hydraulic head at various locations in the Main Channel and in the Diversion Channels.

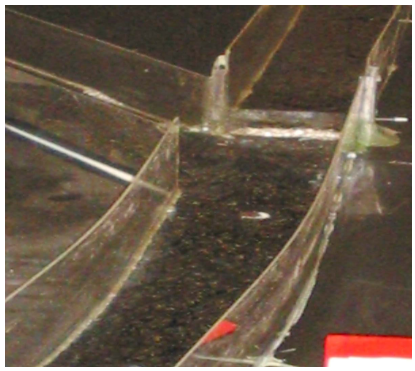

Photo 8 - Close up of the weir, positioned at right angles to the main Channel. (Flow direction is from bottom left to top of photo.)

The physical model was invaluable in identifying hydraulic behavior that was not evident in the computer model results and in providing the computational modelers with the:

- Data to permit model calibration, and
- The confidence that the computer model was providing realistic results.

3.5 Computer Model Calibration

The computer model that was initially developed for the concept design, and which was later used in the construction of the physical model, was revisited and some model parameters amended to reproduce flow profiles that more closely matched the physical model profiles.

Typically Manning's n value is adjusted in computer models to produce profiles to match recorded levels, however in this instance, the flow profiles between the physical and computer models were a good match except at the confluence of the Diversion Channel and the Main Channel and at the weir. Thus the Manning's n value of 0.013 for both concrete and brick channels was retained. The default contraction and expansion values at the River Stations that represented the confluences were increased, from 0.1 to 0.3 and 0.3 to 0.5 respectively. The "ineffective flow area" facility in the HEC-RAS Model was also used to exclude non active flow areas.

3.6 Computer Model

The HEC-RAS Model was developed with three separate geometry files. The geometry files represented:

- Main Channel (Refer to Figure 3),
- Diversion Channel with Diversion Weir and BMP (Refer to Figure 4), and
- Main Channel with Diversion Weir and confluences of Diversion Channels (Refer to Figure 5).

The geometric data file and model and the hydraulic profile in the Diversion Channel with BMP for the treatable flow are shown in Figure 6. Note, in the example in Figure 6, the hydraulic jump commences at River Station 25.8, thus the section of channel between RS 25.8 and RS 46.5 was not necessary from a hydraulic perspective. That section of channel was provided to allow the channel to be located around a large tree that was of significant value to the local community.

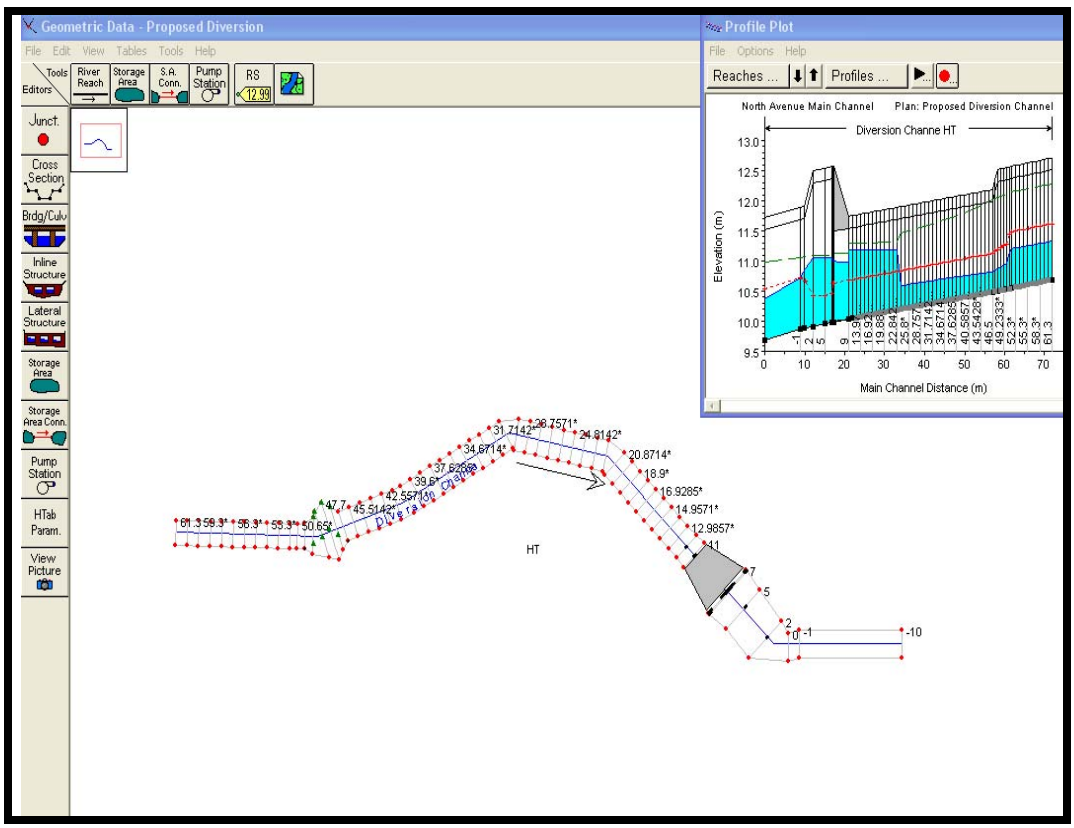

Figure 6 – Plan showing HEC – RAS Geometric Layout and inset the Hydraulic Profile for the treatable flow rate

4. LESSONS LEARNT

During the design of the computational model, the main lesson learnt when working with super critical flow, was the need to avoid abrupt changes to the channel geometry. Abrupt changes to the channel geometry, whether to the invert or the side walls resulted in short sharp spikes in the hydraulic profile.

The effect of placing fixed weirs in the Main Channel resulted in the development of a hydraulic jump and overtopping of the channel walls. Thus flood mitigation works included raising of the channel walls. To reduce the height of hydraulic jumps, the employment of hydraulically efficient ogee and half-circle weirs was determined to be an effective strategy.

5. EARLIER EXAMPLE

Initial designs were trialled on smaller channels with small treatable flow rates and an example is illustrated by Photographs 9, 10 and 11.



Photo 9 – Shows the Main Channel (looking downstream) with a broad curved weir and with the Inlet Diversion Channel on the left.



Photo 10 – Shows the Inlet Diversion Channel and the entrance to the BMP.



Photo 11 – Shows the outlet from the BMP and the Outlet Diversion Channel

Note that the walls of the Diversion Channel are much higher than the walls of the Main Channel. The flow in the Main Channel is supercritical whereas the flow in the Diversion Channels is both supercritical and subcritical.

Also of interest is that the Main Channel can be observed to be free of settled sediment.

For the earlier designs, a separate physical model was developed to investigate the optimum angle for the Diversion Channel (and the diversion weir). The physical model was trialled with diversion channels set at angles of 45^0, 30^0 and 15^0 to the main channel. An angle of 30 degrees was adopted for the designs as:

- The disturbance to the hydraulic profile in the Main Channel remained manageable, and
- It was shown to be optimal in matching the length required for the Inlet and Outlet Diversion Channels and the space for the BMP. (The flatter the angle, the greater the length of the diversion channels to provide sufficient separation from the Main Channel to fit the BMP.)

6. CONCLUSIONS

The decision to invest in a physical model to verify the computational model was invaluable.

The conceptual hydraulic model toolkit developed for the purpose of analyzing the retro-fitting of BMPs on channels that flowed under supercritical conditions was successful. The HEC-RAS computer model performed very well when run under mixed flow (sub-critical and super-critical) conditions and it proved to be a robust and reliable hydraulic modeling tool.

The computational hydraulic model toolkit was used at 15 sites that flowed under supercritical flow conditions and all 15 designs have been successfully constructed, withstood the rigors of a number of actual storm events and have to date not received adverse feedback from adjoining residents.

7. ACKNOWLEDGEMENTS

The author wishes to thank all those who assisted on the project, but in particular: Thilaka Mampitiyarachchi, Sydney Water's Senior Hydraulic Modeler, for her invaluable contribution and the many hours spent reviewing computer model runs and providing guidance in the development of the toolkit, Neil Davis, Azzurra Consulting, for his many useful tips in computational hydraulic modeling, and to Rudi van Drie, Balance R&D Consulting, for constructing and running the physical models.

8. REFERENCES

Brater, E.F. and King, H.W. (1976). *Handbook of Hydraulics for the Solution of Hydraulic Engineering Problems*, 6th ed., Publisher, McGraw-Hill Book Company.

EPA - NSW Australia (October 2007). *Managing Urban Stormwater: Treatment Techniques.* Consultation Draft.

Henderson, F.M. (1966). *Open Channel Flow*, Publisher, Macmillan Publishing Co., Inc.

Sydney Water (2002). *Guildford Regional GPT (SEIP#34), Duck Creek – Options Report.*

Tye, I. J. (January 2009). *Pollutant Capture Optimisation Technique in a Supercritical Flow Regime*, Environmental and Water Resources Institute (EWRI) of the American Society of Civil Engineers (ASCE), Bangkok, Thailand,

US Army Corps of Engineers (2002). *HEC RAS River Analysis System, User's Manual*.

Numerical Simulation of Sediment Transport and Morphological Change of JiJi Weir Reservoir

Yaoxin Zhang[1], Yafei Jia[1], Keh-Chia Yeh[2], Chung-Ta Liao[2] and Sam S.Y. Wang[1]

[1]National Center for Computational Hydroscience and Engineering
102 Carrier Hall, The University of Mississippi, University, MS 38677; Email: yzhang@ncche.olemiss.edu

[2]Natural Hazard Mitigation Research Center
1001 Ta-Hsueh Road, National Chiao Tung University, Taiwan, Hsin Chu, 30010; Email: kcyeh@mail.nctu.edu.tw

ABSTRACT

JiJi Weir was built across a mountain river, Chuoshui Creek, Taiwan. Because of deep slope, abundant sediment supply and tropical Typhoon climate, channel changes are very fast and occur in Typhoon seasons. Since its normal operation in 2002, the shallow reservoir of the JiJi Weir had a serious sediment problem: it could be filled up in just one strong typhoon event. Sediment will be completely carried through the reservoir and the spillway of the Weir. In this paper, a computational model, CCHE2D, was used to simulate the sediment transport of the JiJi Weir Reservoir. Transport of both suspended load and bedload sediments with multiple grain-sizes was simulated, and the geomorphology changes were studied within the reservoir during nine typhoon events. Simulation results were compared with the measurements of morphological change, and it shows that the CCHE2D model is capable of producing reasonable and realistic morphological changes.

INTRODUCTION

The JiJi Weir was built in the Chuoshui Creek, a mountain river with a large amount of sediment and affected strongly by floods due to Typhoon. Since the reservoir is shallow and the sediment transport rate is high, the sediment could fill up the reservoir quickly; then once the reservoir is full, the sediment will be completely carried through the reservoir to the downstream. Since its operation in 2002, the JiJi Weir reservoir had serious sediment depositions. Sediments are mainly carried by large flood events in typhoon seasons.

Figure 1. shows the study area from JiJi Weir to JiLu Bridge; the reservoir is about 2 km long. The delta of sedimentation is separated by the main channel into two large areas A and B. According to the measurements in 2003, the total amount of sediment from upstream is about 14.77 million m^3, but only about 13% was transported downstream of the spillway, so the reservoir lost about 1.92 million m^3 in

that year.

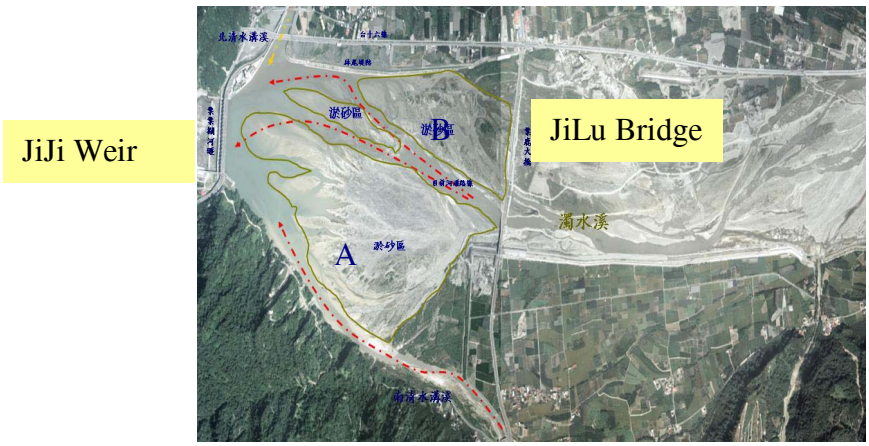

Figure 1. Study Area

In this study, the CCHE2D model was used to simulate the sediment transport and bed morphological changes in this reservoir during nine typhoon events in three years from 2004 to 2007. Simulation results were compared to the measurements of morphological changes.

*C*CHE2D Hydrodynamic and Sediment Transport Model

The CCHE2D model is a state-of-the-art numerical modeling system for two-dimensional, unsteady, turbulent river flow, sediment transport, and water quality prediction. The model is also designed for applications to multiple-process simulations in surface waters with complex geometry such as river bed and bank erosion with both uniform and non-uniform sediment and meander river migration. The model can be used for designing and evaluating the effects of the hydraulic structures, such as grade control structures, dikes, etc. The CCHE2D model uses a hybrid numerical method, the Efficient Element Method (EEM), which takes the advantages of both the Finite Element Method (FEM) and the Finite Volume Method (FVM). Depth-integrated two-dimensional equations (the continuity equation, the momentum equations, the k-ε turbulent equations, the sediment transport equations, etc) are solved with multiple capabilities such as turbulent flow, wind-driven flow, tidal flow, and flow with vegetation effects (Jia and Wang, 1999, 2001a, and 2001b).

The CCHE2D model can simulate the transport of non-uniform sediment mixtures of multiple size classes with bed slope effects, secondary flow effect in curved channels, and avalanche effects. The capability of simulating the non-equilibrium sediment transport process is achieved by solving the following equations (Wu et al., 2000):

Suspended Load:

$$\frac{\partial(hC_k)}{\partial t}+\frac{\partial(UhC_k)}{\partial x}+\frac{\partial(VhC_k)}{\partial y}=\frac{\partial}{\partial x}\left(\varepsilon_s h\frac{\partial C_k}{\partial x}\right)+\frac{\partial}{\partial y}\left(\varepsilon_s h\frac{\partial C_k}{\partial y}\right)+\alpha\omega_{sk}\left(C_{*k}-C_k\right) \quad (1)$$

Bed Load:

$$\frac{\partial(\delta_b\bar{c}_{bk})}{\partial t}+\frac{\partial(\alpha_{bx}q_{bkx})}{\partial x}+\frac{\partial(\alpha_{by}q_{bky})}{\partial y}+\frac{1}{L_t}\left(q_{bk}-q_{b*k}\right)=0 \quad (2)$$

Bed Change:

$$(1-p')\frac{\partial z_{bk}}{\partial t}=\alpha\omega_{sk}\left(C_k-C_{*k}\right)+\left(q_{bk}-q_{b*k}\right)/L_t \quad (3)$$

where h is the local water depth, U and V are the depth-integrated velocity components in the x and y directions, respectively; ε_s is the eddy diffusivity of sediment; C_k is the concentration of the k-th size class, and C_{*k} is the corresponding transport capacity; α is the adaptation coefficient for suspended load; ω_{sk} is the sediment settling velocity; q_{b*k}, q_{bk}, q_{bkx} and q_{bky} are the bed load transport capacity, the bed load transport rate, and transport rate components in x and y directions, respectively; L_t is the adaptation length for bed load; p' is the porosity of bed material, and z_{bk} is the bed change.

The non-equilibrium adaptation length L_t characterizes the distance for a sediment process adjusting from a non-equilibrium state to an equilibrium state, which is related to the scales of sediment transport processes, bed forms and channel geometry.

CURRENT STUDY

Mesh Generation

The study area in the JiJi reservoir is about 2km long. Mesh generation is based on the topographic data measured along cross sections in the reservoir in October, 2004 and January, 2007. A computational mesh (40 x 161) was generated by the 2D structured mesh generator---CCHE-MESH (Zhang, 2006), as shown in Figure 2.

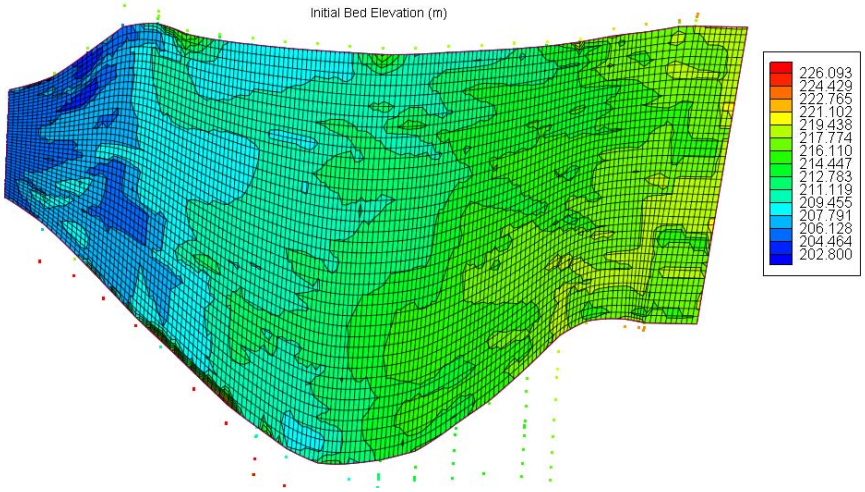

Figure 2. Computational Mesh

Bed Material and Grain Size

Bed material samples obtained in July 2004 were used as initial bed composition within the reservoir. Figures 3. and 4. show the locations of the bed material samples and the representative grain sizes of these samples, respectively. As one can see, within the area about 1000m to the weir, the bed material is very fine, while beyond this area the bed material becomes coarser.

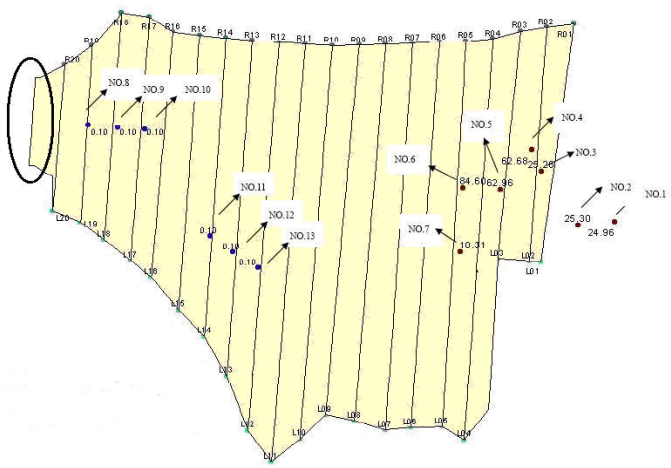

Figure 3. Bed Samples

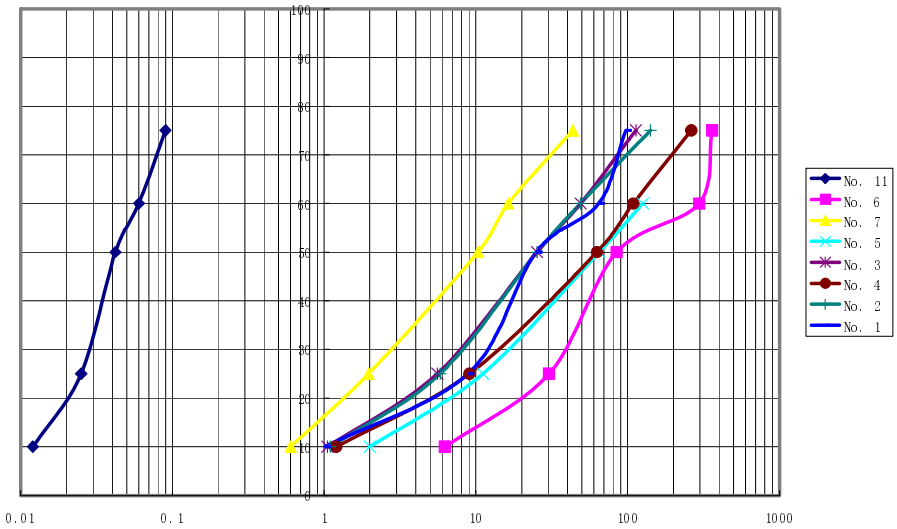

Figure 4. Grain Sizes in JiJi Reservoir

In this study, 6 size classes were defined to simulate the sediment transport in the JiJi reservoir (Table 1).

Table 1 Sediment Size Classes

Classes (mm)	Lower Limit (mm)	Upper Limit (mm)
0.0272	0.001	0.074
0.297	0.074	0.59
2.38	0.59	4.76
9.52	4.76	19.1
152	19.1	305
457	305	610

Boundary Conditions

Table 2 indicates the typhoon events from July 2004 to June 2006 used to calibrate the model, and those events June 2007 to October 2007 were used to validate the model. The sediment hydrograph data was obtained according to the observed relationship between the flow discharge and the sediment concentration. The flow hydrograph and the sediment hydrograph at JiLu bridge, and the stage hydrograph at JiJi weir are plotted in Figs. 5 and 6, respectively.

Table 2 Typhoon Events

Time	Peak Flow at JiLu Bridge (cms)	Time	Peak Flow at JiLu Bridge (cms)
2004/07/01	8,343	2005/08/12	1,201
2004/08/24	4,841	2005/09/01	1,333
2004/12/04	1,050	2005/09/29	1,122
2005/07/18	2,486	2006/06/03	4,567
2005/08/05	2,486		

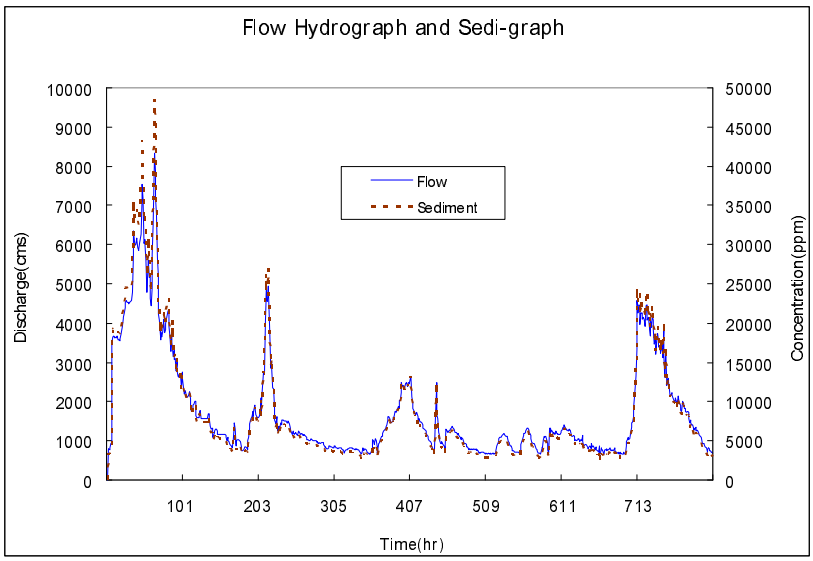

Figure 5. Flow Hydrograph and Sedi-graph at JiLu Bridge

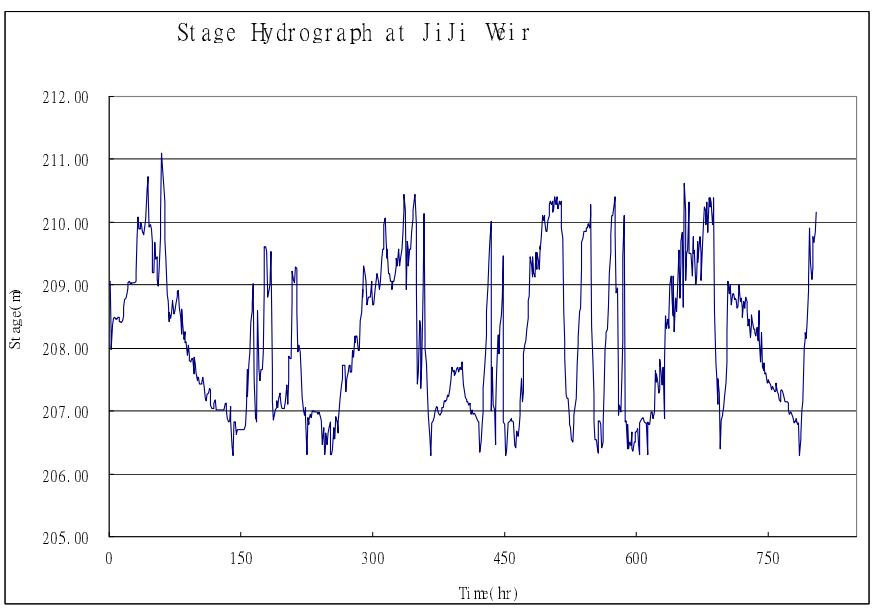

Figure 6. Stage Hydrograph at JiJi Weir

Simulation Results

The bed elevation was interpolated onto the computational mesh using the topographic data of October 2004 and January 2007, respectively. Figure 7. shows the comparisons of the bed elevation change in this period (from 2004 to 2007). A big erosion area (A) was observed on the delta where deposition usually occurs, which was caused by extensive dredging in the simulation period. The delta with fine sediment extended further downstream toward the Weir Site and formed two big depositions (B and C) which stopped a few hundred meters from the weir. A scour hole (D) appeared immediately behind the weir, which could be caused by three dimensionality of the flow and associated sediment transport.

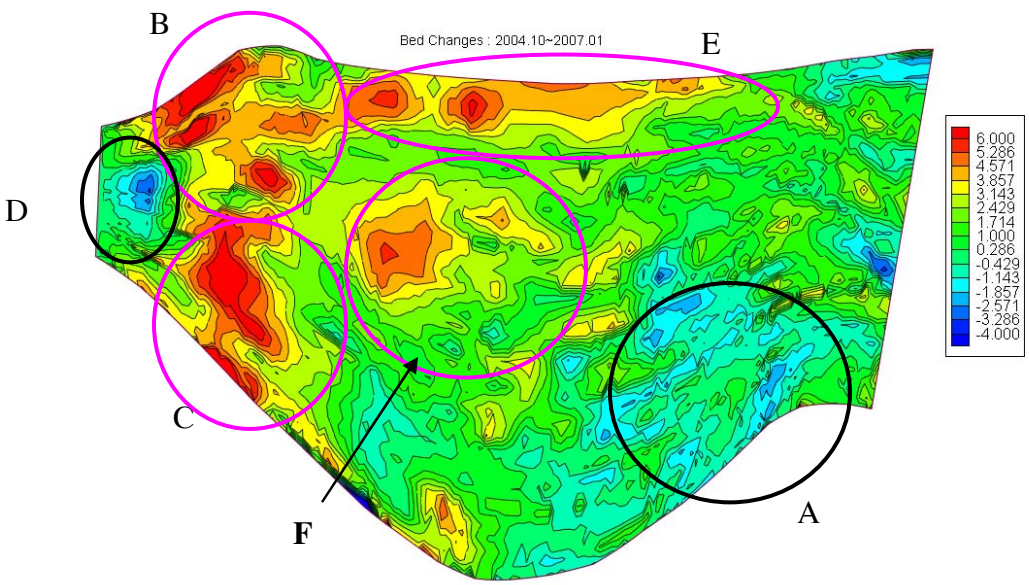

Figure 7. Measured Bed Changes

The model was calibrated using the bed topography of October of 2004, the flow and sediment hydrograph from July 2004 to June 2006. Sensitivity studies were performed on the following main model parameters: (1) Ratio of bed load and suspended load (90% suspended sediment, 10% bed load; 95% suspended sediment, 5% bed load; and, 99% suspended sediment, 1% bed load); (2) Bed load adaptation length $\boldsymbol{L_t}$ (= 1000m, 1500m, 2000m, and 3000m); (3) Suspended load adaptation coefficient $\boldsymbol{\alpha}$(= 0.01, 0.015, and 0.02); and, (4) Bed roughness $\boldsymbol{n}$ (= 0.04, 0.032, and 0.025). According to the simulation tests, 95% suspended load and 5% bed load produced more reasonable results, and the combination of bed roughness, bed load adaptation length and suspended load adaptation coefficient ($\boldsymbol{L_t}$ = 3000m, $\boldsymbol{\alpha}$=0.010, and n = 0.025) produced the best results.

Figure 8. shows the simulated bed changes, Figure 9 (a) and (b) show the final

flow field and the water surface level, and Figure 10 (a) and (b) show the peak flow field and water surface level. When the flow discharge was low, large dry areas over the Delta appeared. In the erosion zone A, the simulated results show slight depositions; in the deposition zones B and C, the model under-estimated the depositions; in the deposition zone E, under-estimated results were observed as well; the model predicted two scour holes instead of one in zone D; and, in deposition zone F, the simulation agrees well with the measurements.

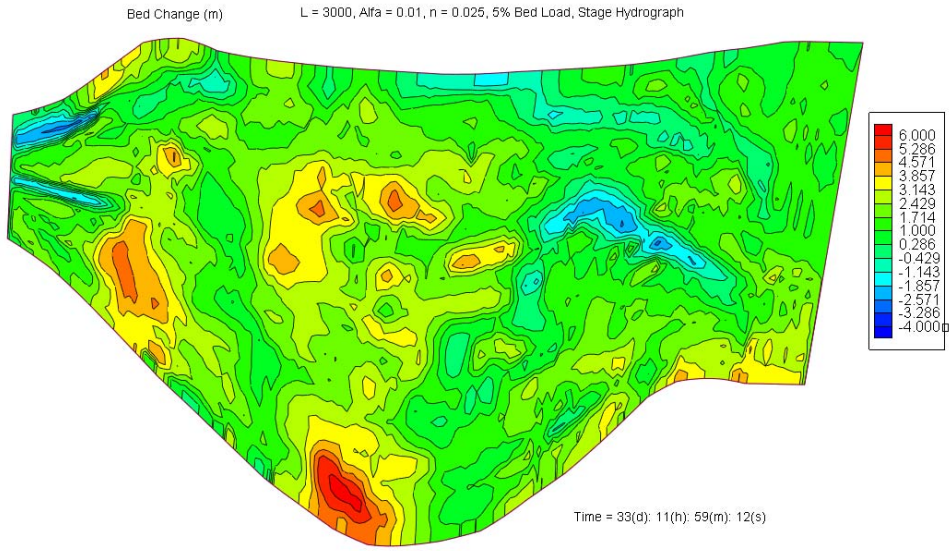

Figure 8. Simulated Bed Changes

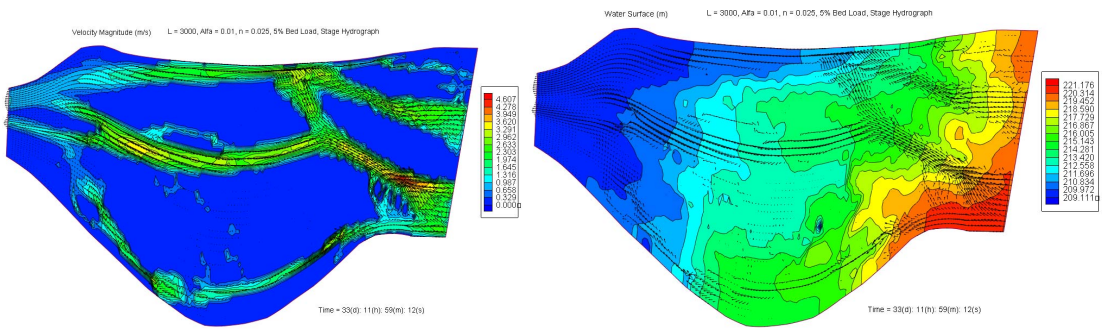

(a) (b)

Figure 9. Simulated Flow Field and Water Surface Level

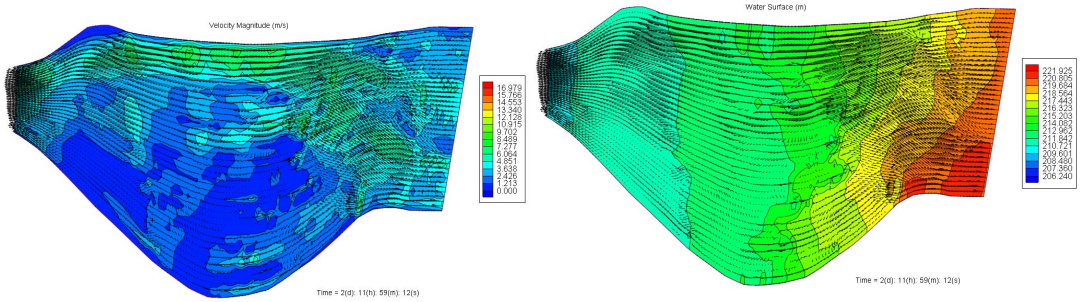

(a) (b)

Figure 10. Peak Flow Field and Water Surface Level

Figure 11. shows the cross sections where the simulated bed elevations are compared with those measured in October 2004 and January 2007. For CS 1~4, the simulated results basically showed good agreements with the measurements except some small scour holes; for CS 5~10, the simulated results under predicted the big erosions over the delta dredging area (zone A, Figure 7.); for CS 11~15, the simulation correctly predicted depositions, but underestimated near the right bank and over-estimated near the left bank; for CS 16~19, the simulated results under-estimated the depositions; and, for CS 20, the big scour hole in front of the Weir was not predicted well.

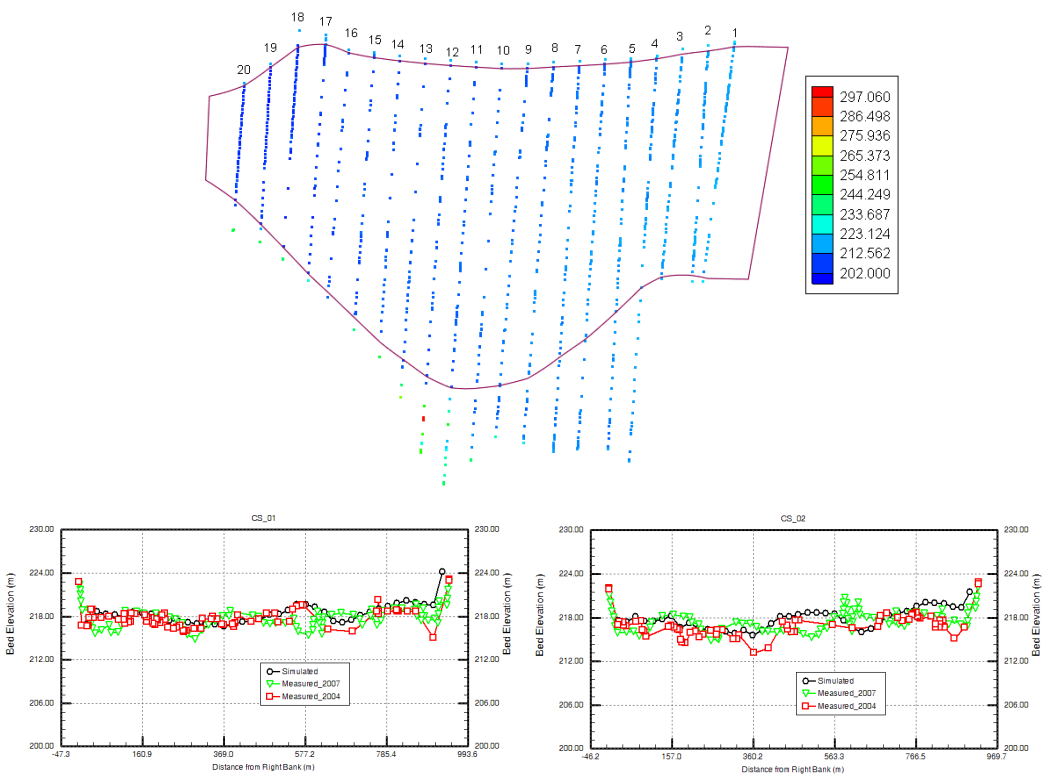

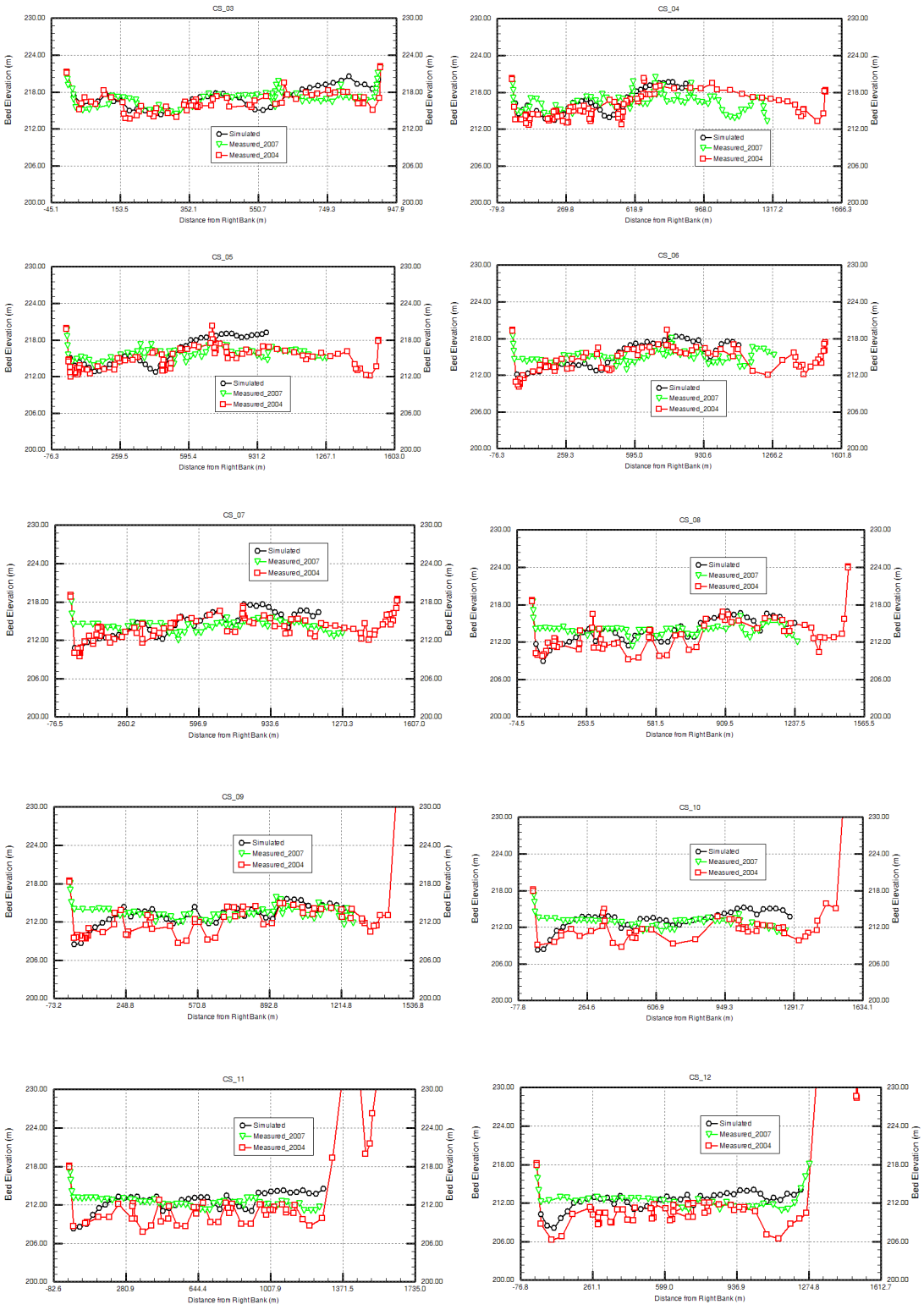
CS_03
CS_04
CS_05
CS_06
CS_07
CS_08
CS_09
CS_10
CS_11
CS_12
Bed Elevation (m)
Distance from Right Bank (m)
Simulated
Measured_2007
Measured_2004

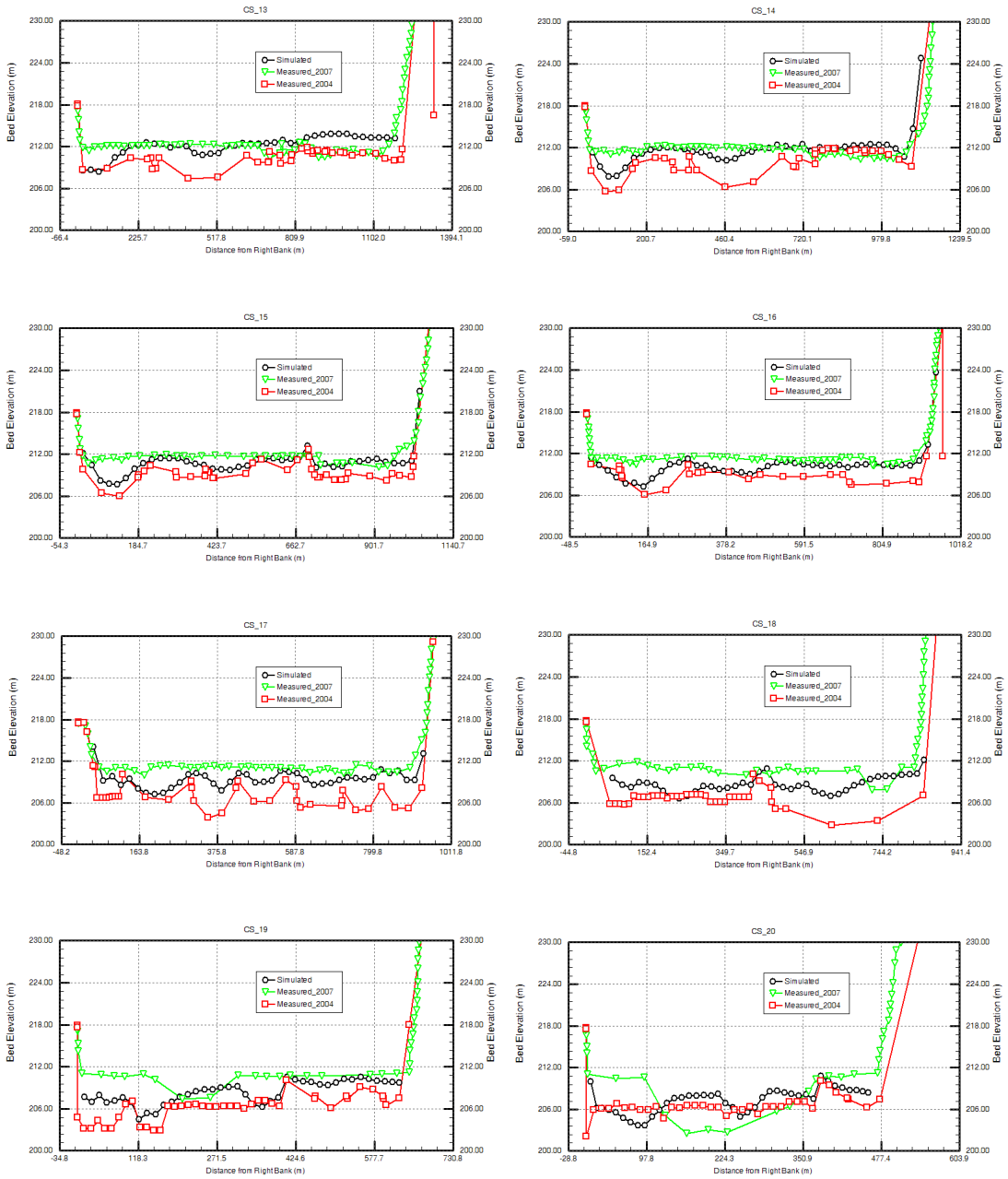

Figure 11. Comparisons of Cross Sections

CONCLUSIONS

The CCHE2D model was used to simulate the sediment transport and the bed morphological changes in the JiJi Reservoir. The followings conclusions are made according to the analysis of simulated results and measurements:

(1) Morphological changes occurred mainly during big flood events. Erosions are near the inlet and in the Weir front. More depositions are distributed in

the lower part of the reservoir, and near the right (North) bank.

(2) The suspended sediment is dominant, which contributes most of the depositions. 95% of suspended load and 5% of bed load are found to be an appropriate sediment combination. The adaptation length of bed load L = 3000 and the adaptation coefficient of the suspended load Alfa = 0.01 produced the best results.

(3) Generally, the trend of the simulated bed change agreed with the observed pattern, but differences remain obvious. The model under-predicted a big scour hole close to the weir and large erosions over the delta which are partially affected by the unknown amount of dredging. The scour hole in front of the weir could be due to the three dimensionality of the flow and sediment transport, which could be resolved better with a 3D model.

(4) The CCHE2D model is capable of simulating sediment transport and morphological changes within the JiJi Weir reservoir with unsteady boundary conditions for the flow and sediment. The dry-wet capability makes simulations with complex morphology very efficient.

(5) The uncertainty of the data such as sediment load, its composition and bed material composition may affect the accuracy of the numerical model prediction.

AKNOWLEDGEMENT

This work is a result of research sponsored by National Chiao Tung University of Taiwan under Research Agreement No. 300212267A and The University of Mississippi.

REFERENCES

Jia, Y., and Wang, S. S-Y.(1999), "Numerical Model for channel flow and morphological changes studies", *ASCE J. Hydraulic Engrg*, 125(9): 924-933.

Jia, Y., and Wang, Sam S.Y. (2001a), "CCHE2D: Two-dimensional Hydrodynamic and Sediment Transport Model for Unsteady Open Channel Flows Over Loose Bed", Technical Report, NCCHE-TR-2001-1, Aug. 2001.

Jia, Y., and Wang, Sam S.Y. (2001b), "CCHE2D Verification and Validation Tests Documentation", Technical Report, NCCHE-TR-2001-2, Aug. 2001.

Wu, W., Wang, S. S. Y. and Jia, Y. (2000) "Nonuniform sediment transport in alluvial rivers", *J. Hydraul. Res.*, Vol. 38, 2000, No. 6, pp. 427-434.

Zhang, Yaoxin (2006). "CCHE-MESH 2D Structured Mesh Generator Users' Manual—Version 3.0." NCCHE Technical Report. NCCHE-TR-2007-01, March 2007.

One-Dimensional Modeling of Sedimentation Processes on the Puyallup River

Brian G. Wardman[1], P.E.; Brad R. Hall[1], P.E.; and Casey M. Kramer[2], P.E.

[1]Northwest Hydraulic Consultants, 3950 Industrial Blvd. #100c, West Sacramento, CA 95691; PH (916) 371-7400; FAX (916) 371-7475; email: bwardman@nhc-sac.com

[2] Washington State Department of Transportation, 310 Maple Park SE, PO Box 47329, Olympia, WA 98504-7329; PH (360) 705-7262, FAX (360) 705-6832 email: kramerc@wsdot.wa.gov

Abstract

This paper presents the results of a sedimentation study using the one-dimensional sediment transport capabilities of HEC-RAS 4.0 to quantify sedimentation processes in the lower Puyallup River, WA. The HEC-RAS 4.0 model used in this study was calibrated using USGS measured sediment transport rates and verified by reproducing the observed deposition of the reach between 2001 and 2007. Historical USGS flow data observed on the lower Puyallup River was used to create average annual flow-duration curves used as hydraulic input into the model, while averaged NOAA observed tidal elevations for the mean high tide, mean sea level, and mean low tide within Commencement Bay were used as downstream hydraulic boundary conditions. Depositional trends in the model results were compared with existing trends noted in historical cross-section comparison and gage adjustments to a nearby USGS streamflow gage. Results of the model show the bed elevations are expected to increase by as much as 5 feet over the next 50 years. The overall trap efficiency of the reach is expected to decrease as tidal influences begin to control the sedimentation processes over time.

Introduction

Located in Western Washington, the Puyallup River along with its major tributaries, the White and Carbon Rivers, convey the majority of flood flows from the slopes of Mount Rainier into Commencement Bay. Recent hydrological and hydraulic analyses associated with updating Federal Emergency Management Agency (FEMA) floodplain maps on the Puyallup River have shown that predicted flood elevations are higher than estimated in previous flood hazard mapping efforts (**nhc** 2007). This increase in flood profile elevations is hypothesized to be caused by ongoing sediment deposition within the river channel as the Puyallup River carries a significant sediment load. To quantify the changes in the hydraulic characteristics of the river channel, a sedimentation study was completed to characterize the sediment conditions of the lower Puyallup River. As part of this study, the numerical sediment transport model provided in HEC-RAS 4.0 (Hydrologic Engineering Center, 2006) was utilized to predict the sediment movement through the study reach; specifically the location, volume, and depth of sediment deposition or erosion.

The HEC-RAS 4.0 sediment transport module incorporates much of the HEC-6 "Scour and Deposition in Rivers and Reservoirs" code (Hydrologic Engineering Center, 1993) into the graphical HEC-RAS interface. This one-dimensional, movable boundary, open channel flow model simulates streambed profile changes resulting from varying river flow and tailwater conditions. The model was developed to assess spatial and temporal variations in non-equilibrium sediment transport conditions due to an imbalance of sediment inflow, existing bed material characteristics and sediment transport capacity on alluvial channels. The model is based on one-dimensional, gradually varied flow hydraulics and sediment transport theory and is capable of calculating sedimentation in dendritic, closed loop and distributary networks of river systems.

Such one-dimensional sediment transport models are dependant upon both hydraulic and sediment transport computations. Hydraulic inflows into the sediment module are inputted as a flow hydrograph segmented into a series of steady flow events of variable duration. For each flow sequence, the one-dimensional conservation of energy equation is solved to determine the water surface profile and pertinent hydraulic parameters such as energy slope, velocity, depth, hydraulic roughness, and width at each cross-section. Sedimentation process (i.e. erosion, entrainment, transportation, deposition, and compaction of sediment particles) are then computed at each cross-section by solving the sediment continuity equation (i.e. the Exner equation) and a user defined sediment transport function.

The proper application of the HEC-RAS 4.0 sediment transport model requires the calibration of both hydraulic and sediment transport parameters. Hydraulic calibration includes the adjustment of effective conveyance limits, Manning's n values, and expansion and contraction energy loss coefficients. Calibration to the sediment transport computations includes the selection of the proper transport relationship (i.e. Ackers-White, Laursen-Copeland, etc.), as well as the adjustment of sediment inflows to obtain reasonable agreement between measured and modeled sediment deposition and erosion. This paper provides the methods and results of the calibration of the HEC-RAS 4.0 model for simulating sedimentation processes on the lower Puyallup River.

Study Site

The modeled study reach includes the lower 37,800 feet (7.15 miles) of the Puyallup River from Commencement Bay to a few miles upstream of the Puyallup River USGS Stream Gage (Station 12101500). Streambed elevations in the study reach range from -10 feet (NAVD88) near the mouth of the Puyallup River at Commencement Bay to about 25 feet (NAVD88) near the confluence with the White River (River Mile 10.1). Slopes range from approximately 0.00035 ft/ft near the mouth of the Puyallup River to approximately 0.0006 ft/ft near the confluence with the White River (River Mile 10.1) with a break in gradient near River Mile 3.75. Sediment samples indicate that bed materials are primarily medium and fine sand, with gravel. Field observations show that the median particle size decreases in the downstream direction.

Objective

The primary objective of this sediment modeling investigation is to provide a 50-year forecast of bed adjustments as it pertains to the locations and characteristics of sediment deposits that may affect channel flood carrying capacities. To meet this objective, information from surveyed channel cross sections, site specific measurements of sediment transport rates, measurements of existing bed material characteristics, and analysis of hydrologic conditions were used to calibrate the sedimentation model. The model was then used to estimate future channel aggradation occurring throughout the model reach. The results provide estimates of future channel geometry, which when input into the HEC-RAS hydraulic model will reveal how flood profiles are likely to be affected by sediment deposition 50-years in the future.

Methodology

The following major steps were incorporated into the methodological design to achieve the study objectives:

1. Calibration of hydraulic parameters to match existing hydraulic conditions in the lower Puyallup River.
2. Choice of proper sediment transport function to best simulate the flow and sediment capacity relationship of the lower Puyallup River.
3. Calibration of sediment inflow rating curves to match sediment loading characteristics in the lower Puyallup River.
4. Model Verification.
5. Model Application.

Hydraulic Calibration

Sediment transport capacities calculated in the HEC-RAS 4.0 sediment module are based on locally computed hydraulics (i.e. depth, velocity, hydraulic radius, friction slope). (Hydrologic Engineering Center,2008). Based on this dependence, inaccuracies in the hydraulic computations can be reflected in the results of the sedimentation computations. To ensure the most accurate representation of overall sedimentation processes, user-defined parameters in the hydraulic computations must be adjusted to best match the computed and measured hydraulic results. In the HEC-RAS 4.0 model, these user-defined parameters primarily consists of adjusting effective conveyance limits, Manning's n values, and expansion and contraction energy loss coefficients to obtain reasonable agreement between measured and computed hydraulic characteristics.

A previously calibrated unsteady HEC-RAS model from the **nhc** (2007) floodplain study was used as a basis for this sedimentation modeling study. The calibrated unsteady HEC-RAS model included 67 cross-sections over the lower 8.2 miles of the Puyallup River cut from recent topographic and bathymetric surveys. Levees along the Puyallup River were modeled as lateral weirs connecting the river to large floodplain storage areas. Hydraulic roughness and energy loss coefficients were

calibrated to match computed water surface elevations to observed water surface elevations observed in a February 1996 flood (**nhc,** 2007).

For this study, the geometry was adjusted to incorporate only the lower 7.15 miles, from the mouth of the Puyallup River at Commencement Bay to a point approximately 4 miles upstream of upstream of the Puyallup River USGS Gage (Station 12101500) near the confluence of the White and Puyallup Rivers. Floodplain storage areas and lateral weirs utilized for defining floodplain inundation limits in HEC-RAS can not be utilized in the sediment transport algorithms within HEC-RAS, and were removed from the geometric representation of the reach. Bridge sections were modified as needed to properly simulate hydraulic losses and sediment transport through the bridge sub-sections for sedimentation modeling. To account for the hydraulic affects of bridges, blocked obstructions replaced bridge piers and the Manning's n coefficient was adjusted to obtain similar hydraulic characteristics as the original model. The last adjustment was the addition of a simplified "inflow" reach from River Mile 7.15 (STA 377+50) to River Mile 10.18 (STA 537+50), which was adjusted to maintain a constant cross-sectional shape and bed slope, typical of the uppermost sections in the vicinity of STA 377+50. This inflow reach provides sufficient distance for developing a sediment inflow in equilibrium with the bed material and hydraulic conditions at the upstream boundary of the study area.

Choice of Transport Equation

HEC-RAS 4.0 provides the user with a choice of the following seven published sediment transport functions to be used to compute potential sediment transport capacity:

1. Ackers-White (1973)
2. England and Hansen (1967)
3. Laursen-Copeland (1968/1989)
4. Meyer-Peter and Muller (1948)
5. Toffaleti (1968)
6. Yang (1973/1984)
7. Wilcock (2001)

Although each of these functions is well-founded and widely accepted, the assumptions and empirical data used to create each do vary. This variance may result in the results of equations varying by orders of magnitude for equivalent flow conditions. Appendix E of the HEC-RAS reference manual provides insight on selecting the most applicable function for the project conditions.

For this study, the Laursen-Copeland transport function was used to compute bed material sediment transport capacity on the Puyallup River. The Laursen-Copeland transport function is a total load formula developed for computing sediment transport of coarse silt to gravel sized sediments. This particular transport function was chosen based on our experience in sedimentation modeling studies and on the formula's

ability to most accurately replicate the sediment load rating curve derived from USGS measured data from the Puyallup River gage (Station 12101500) shown in Figure 1.

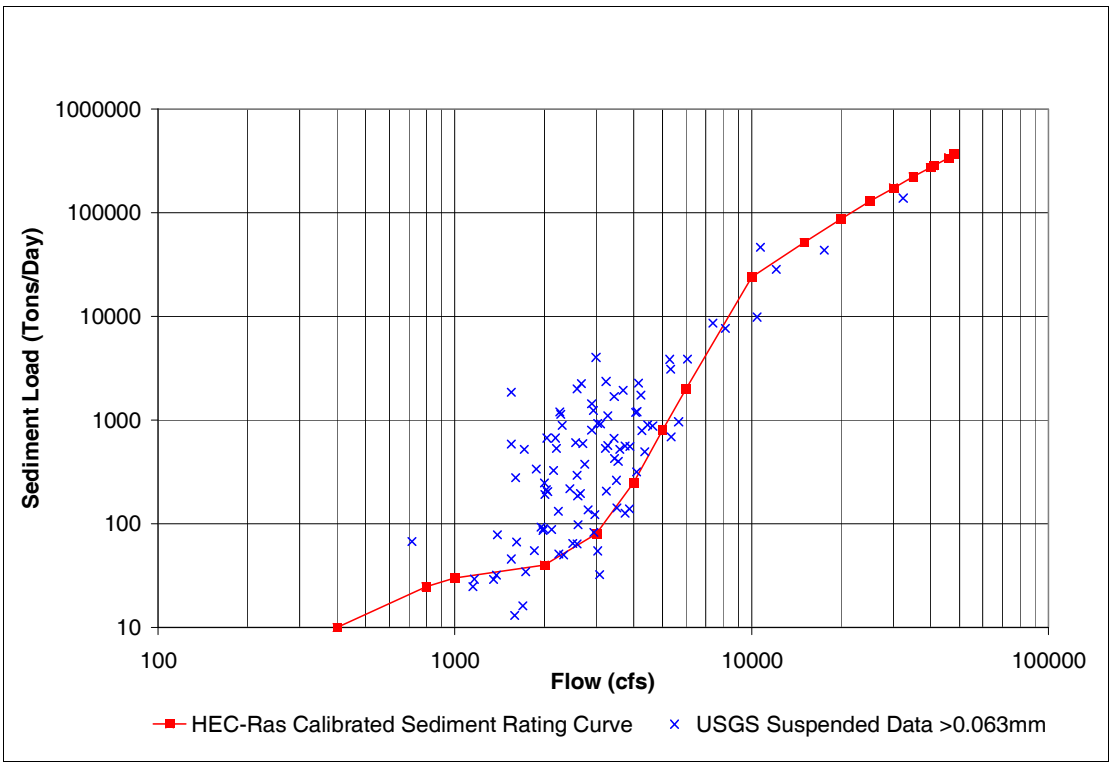

Figure 1: Sediment Inflow Rating Curve With USGS Suspended Sediment Data

Sediment Inflows

The HEC-RAS 4.0 model requires the user to specify a sediment inflow as an upstream boundary condition. This boundary condition can be set as an equilibrium load based on model calculations, a sediment load series defined by the user, or based on a user-defined rating curve. For this study, historical measured suspended sediment loads measured by the USGS at the Puyallup River Gage near Puyallup, WA (Station 12101500) were used as an initial assumption to create a rating curve for the sediment inflow boundary condition.

Figure 1 shows a sediment rating plot created from suspended sediment discharges (tons/day) and stream flow (cfs) both recorded by the USGS in the Puyallup River at USGS Gage 12101500 from January 1978 through July 1994. Only the fraction coarser than 0.063mm (very fine sand) is plotted, because this closely matches the minimum size of the sampled bed material. It is assumed that the finer silts and clays do not deposit but are carried downstream to Commencement Bay. The final HEC-RAS calibrated rating curve shown in Figure 1 was originally developed from the USGS suspended data and adjusted to match historic depositional patterns in the modeled reach as discussed below in the *Model Verification* section.

Model Verification

To determine the locations and quantities of sediment deposition and erosion for model adjustment and verification, an analysis of historic cross-sectional survey data and a field reconnaissance was performed. In all, twenty-nine cross-sections ranging from River Mile 0.20 (STA 10+75) to River Mile 9.63 (STA 508+25) were compared using data from a 2002 **nhc** survey and a 2007 Minister and Glaeser survey. Changes in average bed elevation from erosion and deposition were calculated for each cross-section. Depositional volumes were computed using the end area approach, and bed level surveys were extrapolated to channel banklines if bed coverage was incomplete

The HEC-RAS 4.0 model was then run using historical flow rates reported at the Puyallup River USGS Gage (Station 12101500) for the same time period as the surveyed cross sections (i.e. April 2002 to March 2007). By slightly adjusting the sediment rating curve developed from the USGS field measurements, a close agreement between the measured and modeled changes in bed elevation caused by sediment deposition were obtained. The final sediment rating curve is shown in Figure 1. Figure 2 shows the comparison of measured deposition to modeled deposition for each modeled cross section. Figure 2 shows reasonable agreement between measured and computed sediment deposition locations and magnitudes over the entire study reach.

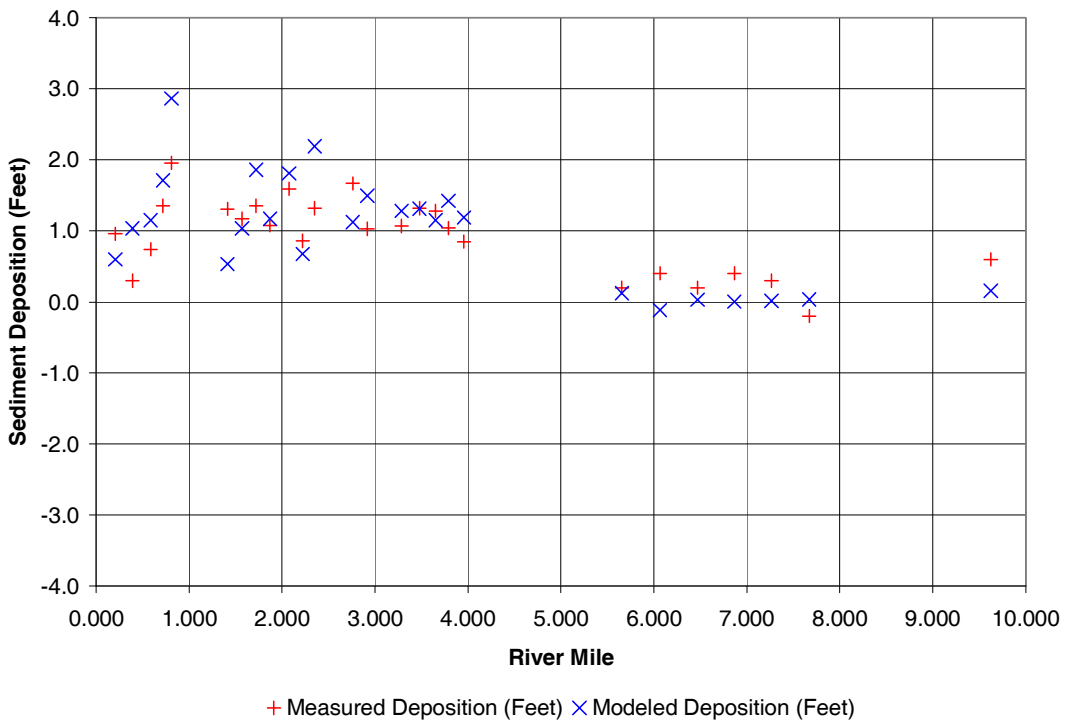

Figure 2: Comparison of Measured Deposition to Modeled Deposition

Model Application

Once the HEC-RAS 4.0 sediment model was calibrated, it was applied to forecast future sedimentation processes on the lower Puyallup River. A cumulative frequency curve, also known as a flow duration curve was developed based on historic flow-duration statistics of the lower Puyallup River. The Puyallup River USGS Stream Gage (Station 12101500) mean daily flow record from WY 1945 through WY 2006 was used for this analysis. The mean daily flows were sorted by magnitude and the number of days or fractions of days that the flow exceeded a given range of flows was determined. Dividing the number of days a given flow rate is exceeded by the total number of days in the streamflow record provides the expected value of the percent time that a given flow is exceeded. This relationship can be scaled to any time period of interest for assessing net water and sediment discharge for numerical modeling purposes.

The downstream water surface elevations in the Puyallup River are controlled by the tidal elevation at the river's mouth in Commencement Bay. Time variant water surface elevations can be specified as a function of time in the HEC-RAS 4.0. Tidal stage elevations for the sedimentation assessment were based on tidal records at the National Oceanic and Atmospheric Administration gage in Tacoma, WA (Station 9446484). The tidal elevations recorded at this gage yield the approximate tidal stage elevations (NAVD 88) for the mouth of the Puyallup River:

- Mean High Water 8.27 ft
- Mean Sea Level 4.22 ft
- Mean Low Water 0.17 ft

These mean tidal elevations were specified to occur within each flow increment in the sedimentation model simulations. To simulate the effects of the varying tidal elevations in the quasi-unsteady hydraulic simulations of the HEC-RAS 4.0 model, the Mean High Water and Mean Low Water elevations were specified for 25% of the duration for a given flow as determined in the flow duration analysis described above. The Mean Sea Level was specified for the remaining 50 % of the flow duration

Results

A useful way to assess the sedimentation dynamics of a stream is to plot the "total accumulated load" of sediment as a function of stream distance. The total accumulated load is the total mass (or weight) of sediment that passes a given section of the river for the total time period of the analysis. A reduction in total accumulated load in the downstream direction can be interpreted as sediment deposition in the reach, as the total load has decreased, and the decreased sediment load manifests itself as channel aggradation in the intervening reach. Conversely, an increase in total accumulated load in the downstream direction can be interpreted as sediment erosion in the reach, as the total load has increased, and the increased sediment load manifests itself as channel incision in the intervening reach.

The total accumulated load on the modeled reach of the Puyallup River for 10- and 50-year simulation periods is shown in Figures 3 and 4, respectively. The computed total load is fairly horizontal for entire upper reach to approximately River Mile 5, indicating sediment passes through this reach without significant erosion or

deposition of sands in the bed material. This is consistent with the small amounts of sediment deposition observed from the field measurements upstream of River Mile 5. The computed accumulated load then decreases as the river approaches Commencement Bay, consistent with observations of significant deposition on these lowermost reaches of the Puyallup River. The modeled reach trap efficiency, or the percentage of sediment inflow which deposits in the reach, decreased over time. Over the initial ten years of simulation, the reach traps around 13% of all inputted bed material sediment whereas over the last ten years of simulation time the reach traps less than 5% of bed material sediment transported into the reach. This trend suggests that without any major changes to the bed configuration (i.e. dredging) the channel will progress towards higher bed elevation, steeper profile, and quasi-equilibrium state where the long-term deposition in the reach will be nearly equivalent to the long-term erosion of the reach.

Figures 3 and 4 also include the load composition throughout the reach. The transported sediment is primarily sands with trace amounts of gravel. This is consistent with field observations, where bed material sampling in the lower reach found no appreciable amounts of gravel. During the first two decades of simulation, the deposition in the downstream portion of the modeled reach is primarily composed of coarse sands. During the final three decades of the simulation, the composition of the load remains fairly constant throughout all of the cross-sections suggesting that equal amounts of each inflowing grain size are being deposited.

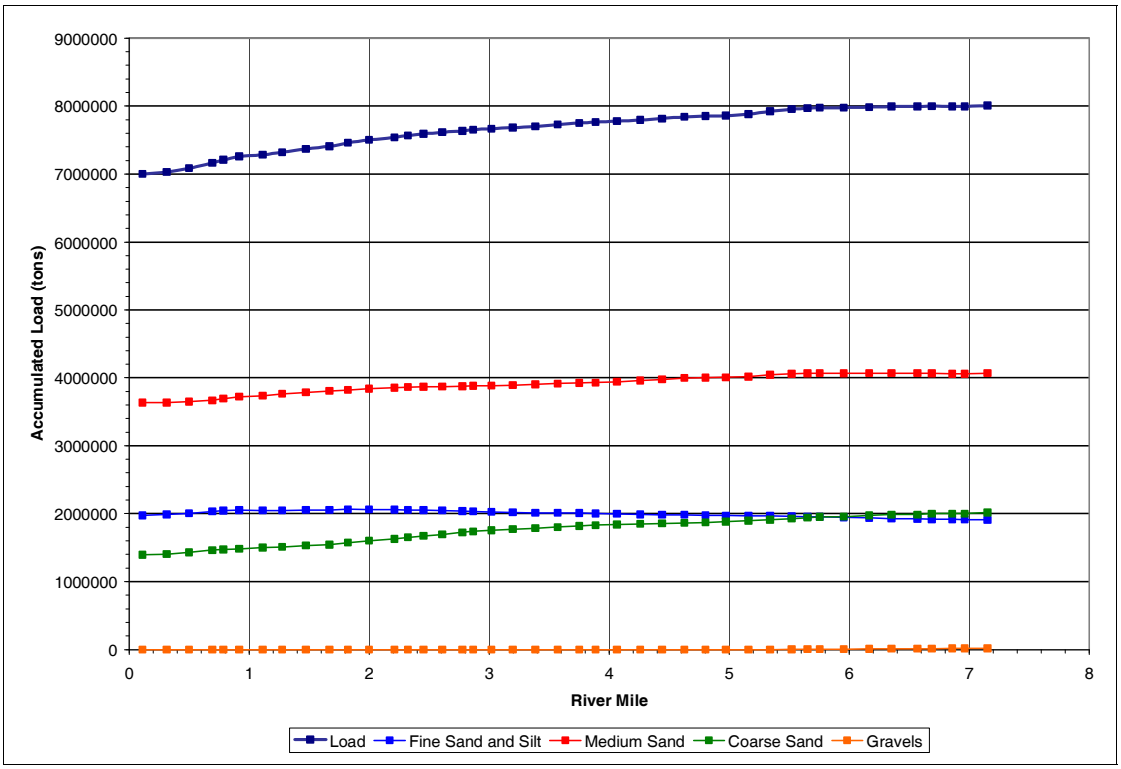

Figure 3: Total Accumulated Load Over Ten Years of Simulation

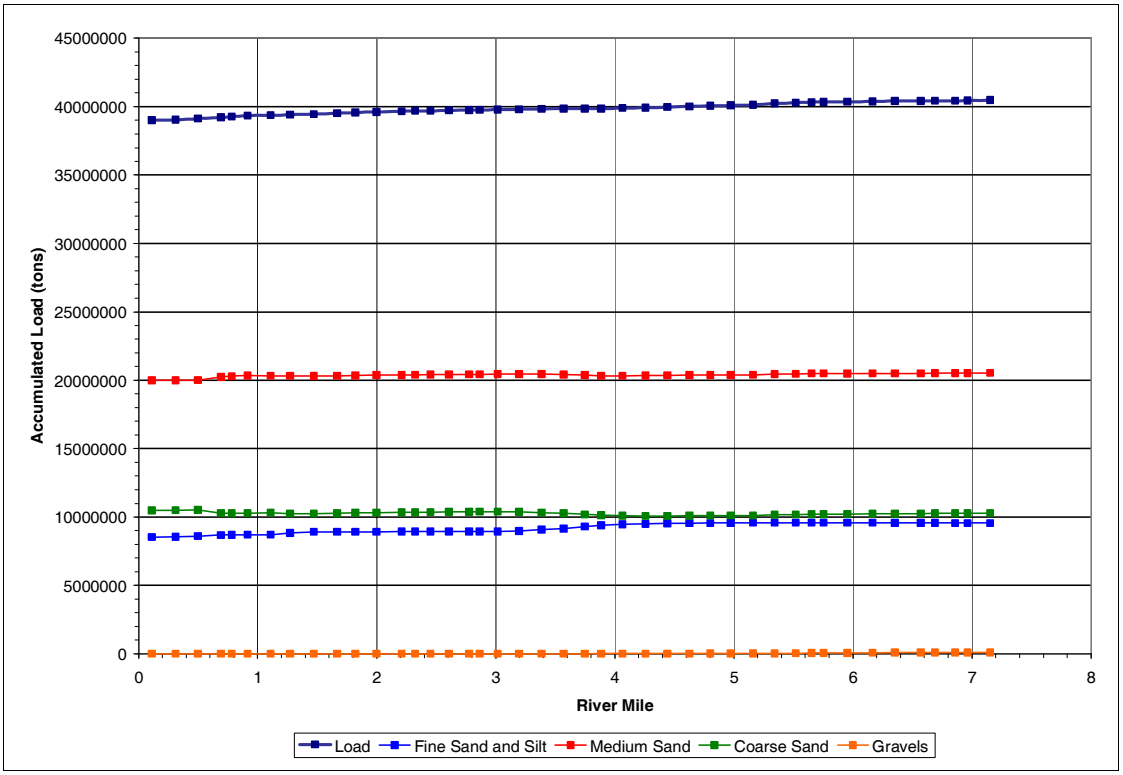

Figure 4: Total Accumulated Load Over Fifty Years of Simulation

Conclusions

As discussed in the previous sections, significant increases in bed elevation are expected to occur in the Lower Puyallup River. These estimates of sediment deposition over a 50 year time period into the future are developed from application of the calibrated sediment transport model using observed values for flow duration characteristics, tidal elevations, and sediment loads. A detailed analysis of the stationarity (i.e. invariance of statistical properties over time) of hydrologic and sediment data has not been completed, however obvious trends in peak discharge magnitude or flow duration are not evident in the review and incorporation of this data into the sedimentation model. Rates and locations of aggradation and subsequent increases in flood elevation profile over the next 50 years are reasonably presented by this analysis.

Examination of both the accumulated load curves and specific gage analysis (**nhc,** 2008) suggest that the Puyallup River is tending towards a state of quasi-equilibrium. The accumulated load curves show a trend of decreasing trap efficiency in the study reach. As the trap efficiency approaches zero, the downstream reach would achieve a steady state condition with nearly equivalent amounts of sediment leaving and entering the system over a period of time. The specific gage analysis shows an overall increase in peak flood water surface elevations during the first ten years of simulation and a much smaller increase throughout the remainder of the 50 year simulation. The actual time needed for the system to reach a quasi-equilibrium state is dependant upon the flow events and sediment loading. Variability of the

hydrologic conditions may affect the time required to reach the quasi-equilibrium state, but should not affect the final bed changes.

The primary control on the reduction over time in the rate in sediment deposition and trap efficiency on the lower Puyallup River is a result of the control of the bed and water surface elevation on the Puyallup River Delta from Commencement Bay. Although the size of the Delta appears to be significant from aerial photos, this tidal sand flat is worked by currents resulting from diurnal tides of approximately a 10 foot tide range, and additionally worked from wind waves during periods of inundation and high winds, a not uncommon occurrence in the Puget Sound. Commencement Bay beyond the limits of the delta is a significant sink for additional sediment deposition, given adjacent depths of the bay are on the order of 100 or more feet and worked by the relatively strong tidal currents of the region. Transects were surveyed over the sand flat delta surface in 1997, and a bathymetric survey of the same area completed by the Corps of Engineers in 2001. These transects indicate that both erosion and deposition have occurred over this time period, but the average elevation of the delta is approximately equivalent between the two surveys.

Acknowledgements
The authors gratefully acknowledge the insight and feedback of Harold Smelt of Pierce County, Tony Melone of Tetra Tech, and Jeff Johnson of **nhc**.

References

FEMA/**nhc** (2007). *Flood Insurance Mapping Study for Puyallup River*. Prepared by Northwest Hydraulic Consultants on behalf of the Federal Emergency Management Agency (FEMA). Hydraulic modeling for the FIS initiated in 2002; the report was submitted in July 2004 and the report was revised in May 2007.

Hydrologic Engineering Center (1993). HEC-6 Scour and Deposition in Rivers and Reservoirs, Users Manual

Hydrologic Engineering Center (2006). *HEC-RAS, Version 4.0 Beta* [Computer Program]. Davis, CA

Hydrologic Engineering Center (2008). HEC-RAS Hydraulic Reference Manual. Davis, CA

nhc (2008). *Puyallup River Flood Investigation Report.* Prepared by Northwest Hydraulic Consultants.

Physical Experimentation and CFD Modeling to Evaluate Sediment Scour in Catchbasin Sumps

Humberto Avila[1] and Robert Pitt[2]

[1]Professor of Water Resources Engineering, Department of Civil and Environmental Engineering, Universidad del Norte, Km 5 Via Puerto Colombia, Barranquilla, Colombia. PH: (575) 3509236, e-mail: havila@uninorte.edu.co
[2]Cudworth Professor of Urban Water Systems, Department of Civil, Construction, and Environmental Engineering, The University of Alabama, P.O. Box 870205, Tuscaloosa, AL 35487.PH:(205)348-2684, Fax:(205)348-0783, e-mail: rpitt@eng.ua.edu

ABSTRACT

The sediment removal capacity in catchbasin sumps and other hydrodynamic separators does not necessarily imply the ability to prevent the sediment from being scoured, especially when the remaining sediment capacity volume of the device is small and the flow rates are high. The sediment removal ability of catchbasin sumps and hydrodynamic separators must be balanced with their ability to retain the captured material by preventing scour. Therefore, understanding and quantifying scour processes in catchbasin devices is an important need when considering these devices as part of a stormwater management plan. This study investigated the sediment scour from a conventional catchbasin sump for different particle sizes, sediment depths, and flow rates. Full-scale physical experimentation and Computational Fluid Dynamics (CFD) modeling were conducted to determine a wide range of conditions at which different particles sizes are scoured.

METHODOLOGY

The methodology includes two main parts: full-scale physical modeling and computational fluid dynamic (CFD) modeling.

Physical modeling. The geometry of the catchbasin sump used for the experiments was based on the optimal geometry recommended by Lager et al. (1977) and tested by Pitt et al. (1979, 1985, 1998). For this geometry, if the outlet diameter is d, the total height of the catchbasin sump is $6.5d$, and the inside diameter is $4d$; the outlet has to be located $4d$ above the bottom and $1.5d$ below the top of the catchbasin. The outlet diameter (d) was selected as 300 mm (approximately 12 inches) (see Figure 1).

The scour tests consisted of the measurement of the suspended sediment concentration (SSC) at the effluent of the catchbasin sump to determine the sediment mass loss. Turbidity and particle size distribution (PSD) were also measured. A 50-cm wide rectangular inlet was used as the inlet.

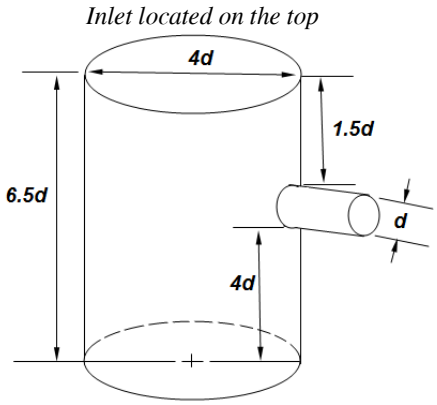

Figure 1. Optimal catchbasin geometry (Larger et al. 1977) used to build the full-scale physical model.

Two types of scour tests were performed. The first series of scour tests were performed with a sediment mixture at Lake Lureen State Park, Northport, AL, as once-through tests using the lake water. The second scour tests were performed with sediment with a homogeneous particle size at the facilities of the University of Alabama. The first PSD mixture was a prepared sediment mixture having a PSD similar to the measured values from deposited sediment sampled from catchbasin sumps observed by Valiron and Tabuchi (1992) and Pitt and Khambhammettu (2006). The characteristic diameters of this sediment mixture are D_{10} = 90 μm, D_{50} = 500 μm, and D_{90} = 2000 μm. Figure 2 shows the PSD of the sediment mixtures and also the particle size distributions for the separate components used to make the mixture. Four overlaying water depths were evaluated: 10, 25, 46, and 106 cm. Each overlaying water depth was tested with five consecutive flow rates, each lasting 25 min; the flow rates were: 0.3, 1.3, 3.0, 6.3, and 10 L/s. Composite samples (1.0 L) were collected for the first 5 min and for the last 20 min of test.

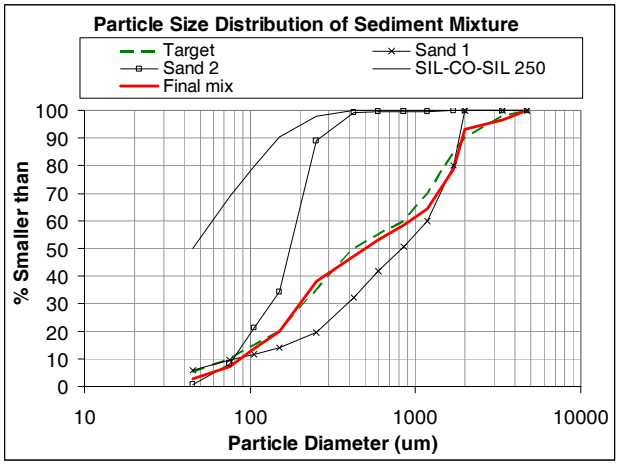

Figure 2. Particle Size Distribution (PSD) of sediment mixture prepared for scour test.

The wide range of this PSD in the sump contributes to the formation of bed armoring, which is the development of an erosion-resistant layer of relatively large particles created by the preferential washing of fine particles from the surface layers due to the velocity field acting on the sediment surface.

The second PSD mixture corresponded to a sediment material with a fairly homogeneous PSD, with D_{10} = 80 μm, D_{50} = 180 μm, and D_{90} = 250 μm (the PSD corresponds to Sand 2 in Figure 2). The sediment scour results obtained with this homogeneous PSD were used for calibration and validation of the CFD model.

CFD modeling. Sediment scour evaluation was conducted for homogeneous sediment materials by using a scour model customized for a 2D-CFD model implemented in *Flow-3D v.9.2*. The simulations were performed assuming a 50-cm wide rectangular inlet. A new scour model code was written and implemented that considered the specific conditions of the phenomenon as well as the limitations of the CFD software package. A total of 40 scenarios, including the calibration and validation cases, were simulated. The scenarios included combinations of three flow rates, five overlaying water depths, and four sediment particle sizes. Figure 3 shows a CFD output from a series of scour simulations.

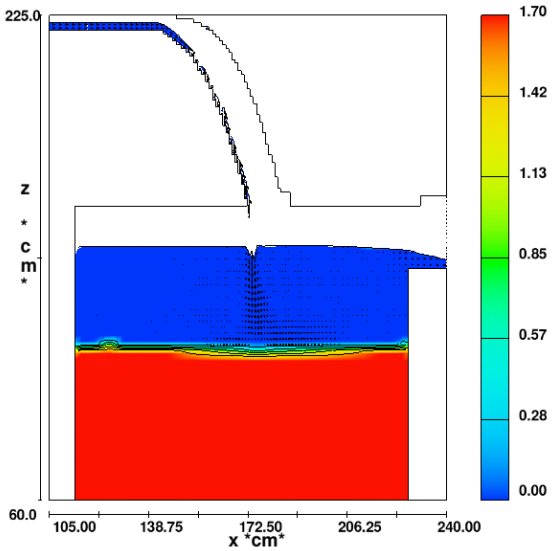

Figure 3. Total sediment concentration (g/cm^3) at 20 min of continuous flow. Flow rate: 10 L/s, overlaying water depth: 24 cm, particle size: 180 μm.

The sediment scour simulations were performed assuming clear water as the influent. The use of clear water is conservative when determining the scour rate. Clear water has a larger sediment-carrying capacity and therefore a larger scour potential compared to heavily silt-laden water. However, this assumption does not greatly differ from typical conditions of stormwater runoff in urban areas. The scour tests with the full-scale physical model were performed with lake water having a maximum SSC of 6 mg/L. The National Stormwater Quality Database reported median suspended solid concentrations of 50 to 100 mg/L for different land uses for data collected throughout the U.S. (Pitt and Maestre 2008); however, concentrations

as high as several thousand mg/L were also reported. Stormwater runoff with high suspended sediment concentrations has a somewhat lower carrying capacity and therefore less scour potential than clear water. The list of case scenarios simulated is presented in Table 1.

Table 1. List of Case Scenarios Simulated with the 2D-CFD Model

		Flow rate (L/s)											
		50			180			500			1000		
		Particle size (μm)											
		5	10	20	5	10	20	5	10	20	5	10	20
Overlaying water depth (cm)	15	■	■	■	■	■	■	■	■	■		■	■
	24	■	■	■	■	■	■	■	■	■		■	■
	35	■	■	■	■	■	■		■	■			■
	40		■	■		■	■			■			
	45			■			■			■			

RESULTS OBTAINED WITH A SEDIMENT MIXTURE

The turbidity time series showed that with this specific PSD, the scour had an exponential decay pattern under steady flow conditions, having a maximum turbidity value at the beginning of the flow when the plunging impact of the incoming water had its greatest effect and decreasing exponentially over time. This pattern was more evident when the sediment was located relatively close to the outlet (with shallow water layers over the sediment), where it is more exposed to scour (Figure 4).

The turbidity time series tests showed that an armoring layer of large sediment particles is formed on the sediment surface during steady flow conditions. This finding reveals that if relatively large particles (D_{75}=1500 μm, D_{90}=3350 μm, and D_{max}=4750 μm for this experiment) are present in the pre-deposited sediment in a catchbasin sump, the scour potential of underlying smaller particles is rapidly decreased as an armoring of the larger particles rapidly form on the sediment surface. Therefore, only a few centimeters of the surface sediment will be exposed to scour. However, the effectiveness of the armoring is relative to the fraction or proportion of large particles in the pre-deposited sediment and their proximity to the sediment surface.

The SSC for different flow rates and overlaying water depths for the 0-5 min composite samples is shown in Table 2. SSC increases as a fractional power function of the flow rate. A maximum SSC of 1139 mg/L was measured when the overlaying water depth was 10 cm during the 10 L/s flow rate. The difference between the flux rate at 6.5 L/s (1045 mg/L) and at 10 L/s (1139 mg/L) is not large, considering that an armoring layer had already been formed after 100 min of continuous flow at the lower rate before the 10 L/s flow rate was applied. The pattern for SSC for the 5-25-min composite samples is similar to the pattern seen for the 0-5-min composite samples; however, the SSC values were between 40 and 80% lower (see Table 2).

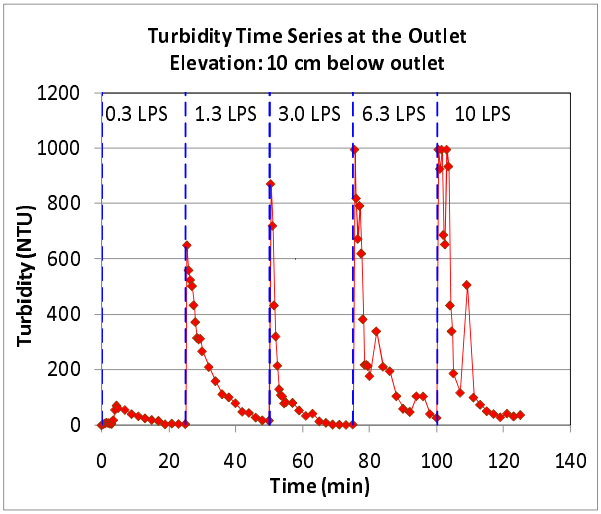

Figure 4. Turbidity time series at the outlet for scour tests: 10 cm (left) and 46 cm (right).

Table 2. Total SSC (mg/L) of Scoured Sediment for the Composite Samples

Depth below the outlet (cm)	Flow rate (L/s)									
	0.3	1.3	3.0	6.3	10.0	0.3	1.3	3.0	6.3	10.0
	SSC (mg/L) 0-5 min composite sample					SSC (mg/L) 5-25 min composite sample				
10	55.6	392	427	1045	1139	13	55	102	244	684
25	7.0	8.0	42	108	46.4	1.6	5.5	20	22	44
46	4.9	4.1	6.5	12.0	10.6	2.0	1.5	4.8	10.8	11.2
106	1.7	2.6	3.3	2.9	1.7	0.6	1.1	2.0	2.1	4.0

The total scour-mass time series presented in Figure 4 shows that with an overlaying water depth of 10 cm, the maximum scoured mass, after 125 min, was about 16 Kg. The scoured particles were all smaller than 4750 μm. This scoured mass is equivalent to a scour depth of about 0.9 cm in the catchbasin. In contrast, with an overlying water depth of 25 cm, the total scoured mass, after 125 min, was reduced to less than 1 kg (930 g), which is about 17 times less than that observed with the 10 cm water depth. With an overlaying water depth of 46 cm, the total scoured mass was further reduced to only 360 g in the 120 min period of flow. With a 106 cm water depth, the total scoured mass was reduced even further to only 90 g during the 125 min test. At 106 cm below the outlet, only particles smaller than 45 μm were detected in the effluent water.

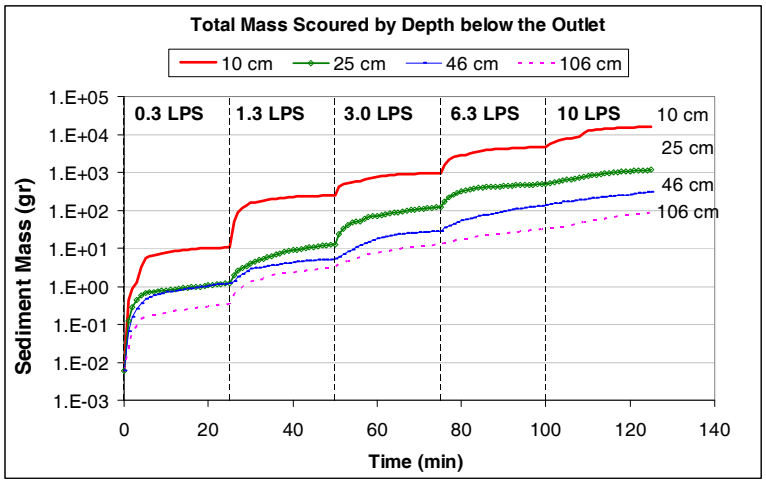

Figure 5. Total sediment mass scoured by water depth over the sediment for all scour tests.

Regression analyses were conducted to examine the effects of overlaying water depth and the scoured sediment mass. The depth of the water was found to be a significant factor, with a highly significant p-value of 0.006. A similar conclusion was also found by Avila et al. (2007) with CFD modeling. These results show that the overlaying water depth over the sediment significantly contributes to a reduction in scour potential. As the overlaying water depth increases, the armoring formation decreases, because the sediment is less exposed to scour. However, at shallow overlaying water depths, the armoring layer plays an important role in reducing the scour potential. If no armoring mechanism is present at shallow overlaying water depths, the sediment scour will be considerably higher. Figures 6 and 7 show the experimental response surfaces of suspended sediment concentrations obtained with the sediment mixture for the 0 -5 and 5 – 25 min composite samples, respectively.

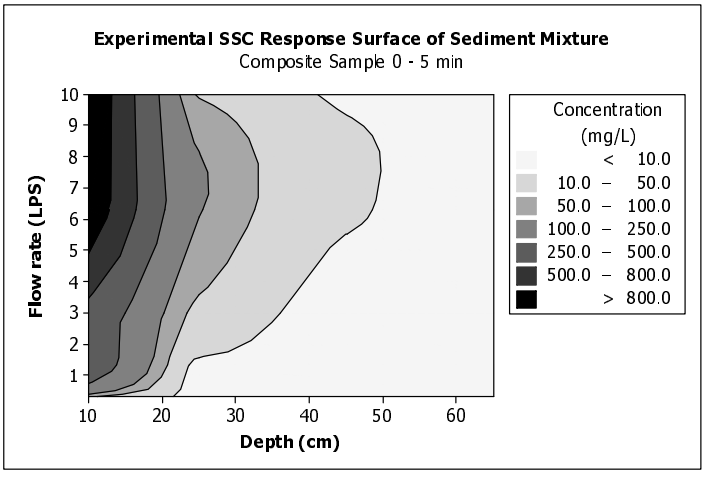

Figure 6. Response surface plots of experimental suspended sediment concentration (SSC), mg/L as a function of flow rate (L/s) and overlaying water depth (cm). 0 – 5 min composite sample.

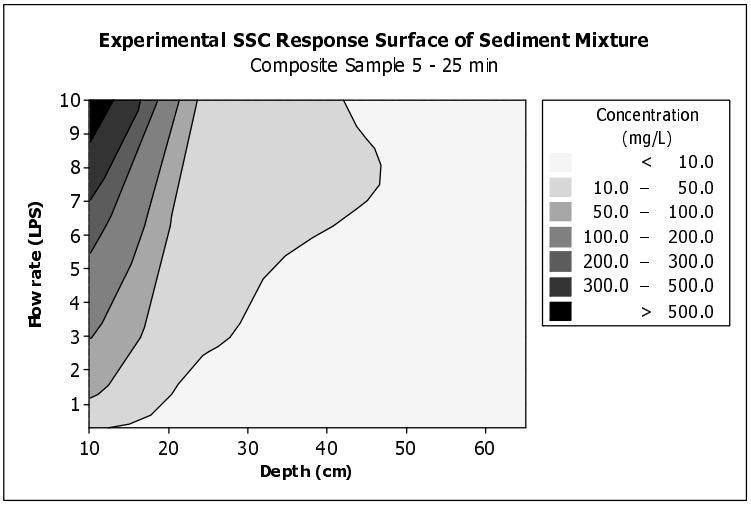

Figure 7. Response surface plots of experimental suspended sediment concentration (SSC), mg/L as a function of flow rate (L/s) and overlaying water depth (cm). 5 – 25 min composite sample.

The regression model for SSC (mg/L) of the 0-5 min composite samples with a R^2 = 0.92 is given as:

$$SSC = (670)^2 \cdot H^{-3.32} \cdot Q^{(0.92H^{-0.15})}.$$

The regression model for the 5-25 min composite samples with a R^2 = 0.93 is given as:

$$SSC = (115)^2 \cdot H^{3} \cdot [\ln(H)]^{-15} Q^{(1.6H^{-0.19})},$$

where *SSC* is the Suspended Sediment Concentration (mg/L), *H* is the overlaying water depth, or depth below the outlet (cm), and *Q* is the flow rate (L/s or L/s).

Both regression models fitted the experimental data very well and the residuals achieved the assumptions of normality.

RESULTS OBTAINED WITH A HOMOGENEOUS SEDIMENT MATERIAL

Initially, it was expected that the SSC values in the effluent with homogeneous sediment material would have an exponential pattern similar to the one obtained with the sediment mixture. However, the results showed that the SSC was approximately constant during the 30 min of continuous flow. This finding is attributed to the absence of an armoring layer formed by large particles which protect smaller particles from scour within minutes after the water jet impact. In the case of sediment with a homogeneous particle size, all particles on the sediment surface were exposed continuously to scour during 30 min of continuous flow. However, the scoured mass was not large enough to increase the overlaying water depth to the point where sediment scour would decrease. Nevertheless, it is expected that after longer periods of time with continuous flow, the scour rate would decrease as the overlaying water

depth increased, especially below the plunging water jet, where a hole is created in the sediment surface. Table 3 shows the experimental SSC values obtained for tests with sediment at 24 and 35 cm below the outlet, 10 L/s flow rates, and with a 50-cm wide rectangular inlet.

Table 3. Experimental SSC of 3-min Composite Samples (Scour Tests with Sediment Material with Homogeneous Particle Size, Flow rate: 10 L/s, Overlaying Water Depth: 24 and 35 cm)

Composite Samples - Time Interval (min)	SSC (mg/L) at 24 cm below the outlet	SSC (mg/L) at 35 cm below the outlet
0 – 3	600	170
3 – 6	479	161
6 – 9	491	203
9 – 12	556	182
12 – 15	521	153
15 – 18	425	179
18 – 21	574	172
21 – 24	562	206
24 – 27	569	182
27 – 30	557	178

Table 4 shows the computed SSC obtained with the CFD model. These results show that in the absence of armoring, SSC decreases exponentially as a function of the homogeneous sediment particle size (Figure 8) and approximately linearly as a function of the overlaying water depth above the sediment (Figure 9).

Table 4. Mean SSC obtained with a calibrated CFD modeling for different flow rates, overlaying water depth and sediment particle size. Homogeneous sediment particle size.

Flow rate (L/s)		SSC (mg/L)											
		50			180			500			1000		
		Particle size (mm)											
		5	10	20	5	10	20	5	10	20	5	10	20
Overlaying water depth (cm)	15	1554	1296	1051	1107	1086	838	381	571	565		110	198
	24	348	800	766	225	579	636	17	163	264		14	65
	35	5	527	567	1	189	428		37	111			13
	40		185	428		40	274			55			
	45			218			112			15			

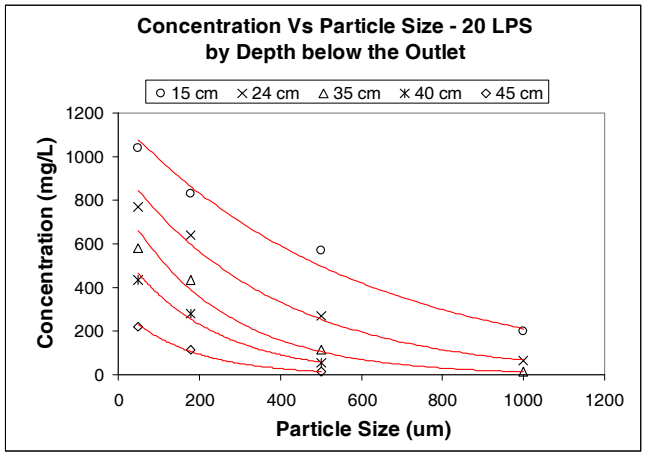

Figure 8. Suspended sediment concentration (mg/L) versus sediment particle size (μm) plotted by overlaying water depth (cm) (20 L/s flow rate).

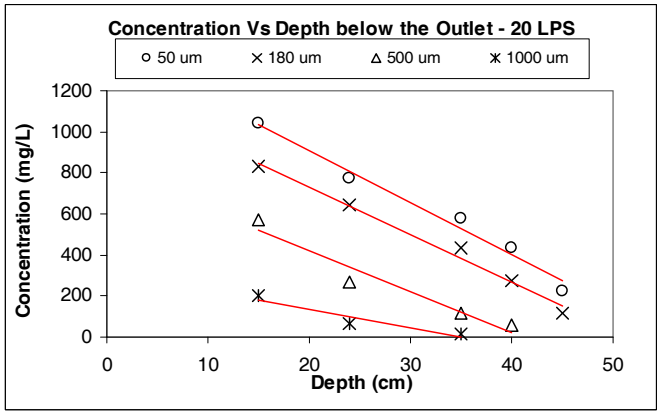

Figure 9. Suspended sediment concentration (mg/L) versus overlaying water depth (cm) plotted by sediment particle size (μm) (20 L/s flow rate.)

CONCLUSIONS

Two protection mechanisms occurred when conducting the tests with the sediment mixture: the overlaying water depth and an armoring layer. In this case, the overlaying water depth protected the sediment surface from the first impact of the plunging water jet. However, the plunging water jet still had enough energy to scour the sediment material directly below it. Then, due to the high shear stresses generated by the first water impact, all particle sizes (large and small) are suspended. Consequently, a *"washing machine effect"* occurs with the suspended sediment while the plunging water jet retreats upward because of the air buoyancy. The washing machine effect consists of the preferential removal of fine material from the suspension of the whole mixture, leaving a layer of large particles on the sediment surface which forms the armoring layer. Only the overlaying water will serve as a protection mechanism against scour if armoring is not present.

In contrast, the variation of SSC over time using sediment having a homogeneous particle size showed that SSC has a magnitude that was statistically constant during the 30 min period of evaluation. Initially, it was expected that the SSC magnitudes with homogeneous sediment material would have an exponential decay pattern similar to the one obtained with the sediment mixture, with high concentrations within the first minutes of flow and then undergoing a substantial decrease for the remaining flow duration. However, the results showed that the SSC maintained an approximate constant magnitude. This phenomenon is attributed to the absence of an armoring layer that protects the sediment from being scoured. SSC will decrease only when the overlaying water depth is high enough to dissipate the eroding energy of the velocity field and therefore reduces the acting shear stress on the sediment surface.

REFERENCES

Avila, H., R. Pitt, and S.R. Durrans. "Factors affecting scour of previously captured sediment from stormwater catchbasin sumps." In: *Stormwater and Urban Water Systems Modeling*, Monograph 16. (edited by W. James, E.A. McBean, R.E. Pitt and S.J. Wright). CHI. Guelph, Ontario, pp. 197 – 218. 2008.

Flow Science, Inc., *Flow-3D User's Manual, V-9*. Santa Fe, NM: Flow Science, 2007.

Lager, J.A., W.G. Smith, W.G. Lynard, R.M. Finn, and E.J. Finnemore. "Urban Stormwater Management and Technology: Update and Users' Guide." U.S. EPA-600/8-77-014. Cincinnati, OH, September 1977.

Pitt, R. "Characterizing and Controlling Urban Runoff through Street and Sewerage Cleaning." U.S. EPA. Contract No. R-805929012. EPA/2-85/038. PB 85-186500/AS. Cincinnati, OH, June 1985.

Pitt, R. "Demonstration of Nonpoint Pollution Abatement Through Improved Street Cleaning Practices." U.S. EPA. Grant no. S-804432. EPA-600/2-79-161. Cincinnati, OH, August 1979.

Pitt, R. and R. Field. "An Evaluation of Storm Drainage Inlet Devices for Stormawter Quality Treatment." Procedures WEFTEC (Water Environmental Federation Technical Exposition). Orlando, FL, 1998.

Pitt, R. and U. Khambhammettu. (2006), "Field Verification Tests of the UpFlow™ Filter. Small Business Innovative Research, Phase 2 (SBIR2)" U.S. EPA, Edison, NJ. 275 pages. March 2006.

Pitt, R. and A. Maestre. *The National Stormwater Quality Database - A Compilation and Analysis of NPDES Stormwater Monitoring Information*. U.S. EPA Office of Water. Washington, D.C., September 4, 2005, Updated: February 3, 2008.

Valiron F. and J. P. Tabuchi. *Maitrise de la pollution urbaine par temps de pluie, étatde l_art. Lavoisier*. Paris, France, 1992.

Sedimentation Characteristics of the Lower Nakdong River Upstream of the Nakdong River Estuary Barrage

Sang-Kil Park M.ASCE[1], Un Ji[2], Byungdal Kim[3], Dohoon Kim[4]

[1]Professor, Dept. of Civil Engineering, Pusan National Univ., Busan, South Korea. E-mail: sakpark@pusan.ac.kr
[2]Research Professor, Dept. of Civil and Environmental Engineering, Myoungji University, Yongin, South Korea. E-mail: jiuncivil@gmail.com
[3]Department of Project Design, Korea Water Resources Corporation, Daejeon, Korea
[4]Ph.D Student, Dept. of Civil Engineering, Pusan National Univ., Busan, South Korea.

Abstract

The Nakdong River Estuary Barrage (NREB) was constructed in 1987 to prevent saltwater intrusion and to provide the sustainable water supply in the upstream channel of the NREB. The upstream channel of the NREB has experienced sedimentation problems requiring annual dredging operation after the construction. The main purpose of sediment dredging is to prevent flooding during late summer. According to the past records, the annual average dredging volume is about 524,170 m^3 in the upstream channel of the NREB. Fluvial changes and sedimentation problems have been continued due to urbanization and development in the watershed as well as construction and management (sediment dredging) of the NREB. However, the sufficient field monitoring and researches for sedimentation characteristics and bed changes have not been performed after construction of the NREB. Therefore, bed elevation changes for 14 years (1990-2003) after construction of the NREB were analyzed using the Hec-6 model and relatively short term changes of bed elevation were simulated using RMA2 and SED2D programs with field data to review the superficial changes. Field survey before and after sediment dredging was conducted at various points of time to examine the natural flushing effect of sediment by moderate and high discharge before flood season (late July to early September) during low tide.

Introduction

The Nakdong River flows 510 km through the southeastern region of South Korea from the Taebaek Mountains to the East Sea (Park et al, 2008). The Nakdong River is the second largest river in Korea and flows through the major cities such as Daegu and Busan. The Nakdong River has a drainage area of about 23,384 km^2 with frequent typhoons and floods from June to September. Among the annual typhoons, Typhoon Maemi of September 12, 2003 was the worst typhoon to hit South Korea for more than a decade and the old Gupo Bridge partially collapsed with the loss of a pier due to high velocities by the large flood and bridge pier scour by Typhoon Maemi (Ji and Julien, 2005).

Near the Nakdong Estuary, there are wetlands, sand islands and deltas, which provide an ideal habitat for migratory birds and waterfowls. The Nakdong River Estuary Barrage (NREB) was built in 1983-87 near the Eulsuk Island to prevent salt-water intrusion in the estuary. The 2.3-km-long barrage includes 510 m of 10 gates section and 1,720 m of a closed dam section with a navigation lock, fish ladder, and other related structures. The NREB provides the control of the upstream water level and the local road for auto-traffic, and prevents salt-water intrusion into the Lower Nakdong River.

Since the construction of the barrage, the Lower Nakdong River has experienced sedimentation problems requiring dredging. The main purpose of dredging sediments is to maintain the flood conveyance capacity of the upstream channel on the Lower Nakdong River during typhoons and floods, which are coupled with high water levels. Historical records (1990 to 2007) indicate an average of 524,170 m^3 per year of dredging with an annual cost estimated at $2 million. The material dredged is primarily non-cohesive fine sand. Most of the sedimentation occurs after floods and during low flows. The gates cause a backwater effects upstream of the barrage, which results in sediment deposition.

The objectives of this study are to perform historical data collection, numerical simulation, and field surveying for the Lower Nakdong River and to analyze sedimentation characteristics. Therefore, outcomes in this study should be used to improve the present method to control sediment deposition and to propose a new approach to solve sedimentation problem upstream of the Nakdong River Estuary Barrage.

Site Description of the Lower Nakdong River

The Lower Nakdong River has a drainage area of about 23,384 km^2 and spans 510 km from the north across South Korea. The average width of the Nakdong River is approximately 45 m and reaches 250 m in the Lower Nakdong River. Based on the Mulgeum station, the average water depth is 2 – 3 m on the Lower Nakdong River (from the NREB to Samryangjin). The Lower Nakdong River has a very mild bed slope of approximately 0.0001 to 0.0002 m/m and has one tributary, the Yangsan River. The mean annual precipitation of the Nakdong River basin is 1,186 mm and the mean annual temperature ranges from 12 to 16 $°C$. The median grain size of bed material at the Gupo Bridge is 0.25 mm and the bed is mainly fine sand.

The Nakdong River Maintenance General Planning Report (KMOCT, 1991) presented the roughness factor of 0.023 for Manning's n which was determined for the Lower Nakdong River using the field data of historic floods, bed materials, and bedforms. Also, a Darcy-Weisbach friction factor (f) of 0.03 was used to compute the backwater profile of the Lower Nakdong River in the NREB maintenance manual (ISWACO-NEDECO, 1987). If the averaged depth 3m of the Lower Nakdong River is applied to their relations between different friction factors, Manning's n of 0.023 produced the Darcy-Weisbach friction factor of 0.03.

Because resistance to flow depends largely on bedform configurations, three methods (Simons and Richardson (1963, 1966), Bogardi (1974), and van Rijn (1984)) to predict bedform configurations are selected to verify the feasibility of given roughness factors. The backwater profile was calculated based on the mean daily flow of the Lower Nakdong River, and then the bedform configurations were determined by three methods. The calculation results show that the bedform configurations of the Lower Nakdong River consist of ripples and dunes and the results are described in Figure 1 and Figure 2 is the field observations in 2006 using the sound navigation ranging, which is in good agreement with the bedform calculation results. For the roughness factor, the Darcy-Weisbach friction factor of 0.03 was used for numerical modeling.

Korea Water Resources Corporation (KOWACO) collected sediment field data in 1995 at the Jindong Station, which is located in 80 km upstream of the NREB, and presented calculated total sediment load of Jindong Station. Measured sediment field data and the Modified Einstein Procedure (Colby and Hembree, 1995) were used to estimate the total sediment load at Jindong Station (KOWACO, 1995).

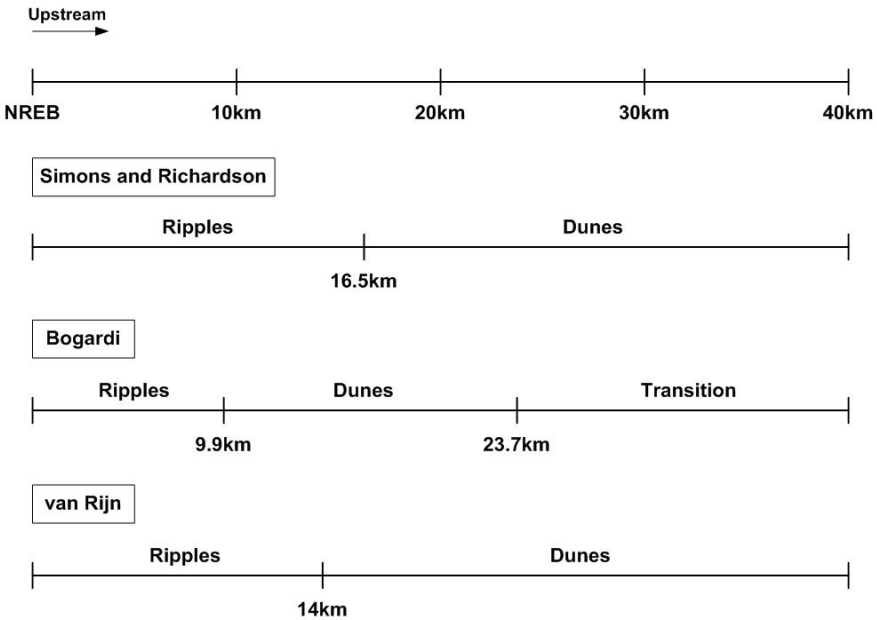

Figure 1. Bedform calculation results on the Lower Nakdong River

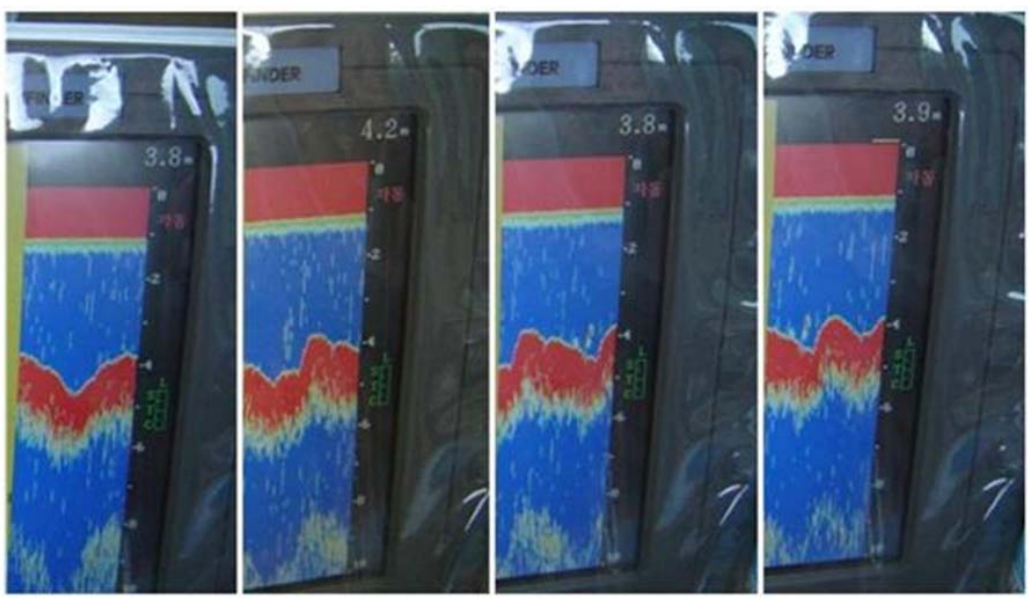

Figure 2. Field observation of bedform configuration in 2006

Because presently used suspended sediment sampler such as point and depth integrated samplers cannot collect the sediments for the entire water column, the unmeasured load must be estimated and added to the measured load to estimate the

total load using the Modified Einstein Procedure. Sediment field data include suspended sediment concentrations, and particle size distributions of suspended sediment and bed material. Calculated sediment discharge data of Jindong Station by KOWACO were compared with several total sediment load equations in Figure 3. The total sediment load calculated by the Modified Einstein Procedure is referred to as field data in this study. The Engelund and Hansen (1967) method overestimated the total load at Jindong Station. Shen and Hung (1972), Ackers and White (1973), Yang (1979), and Brownlie (1981) equations show relatively good agreement with the field data.

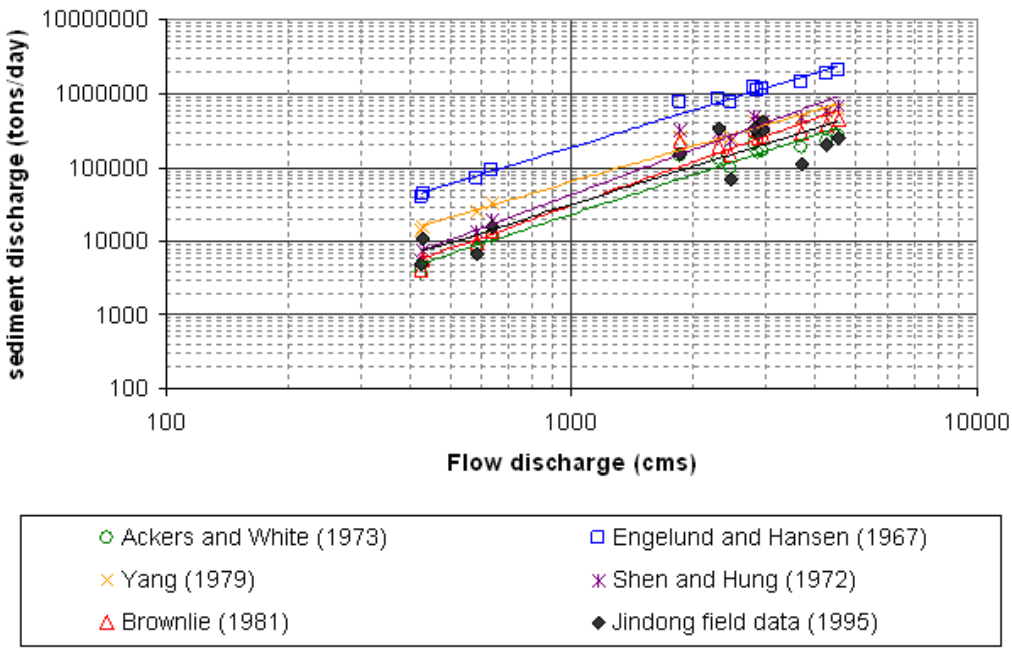

Figure 3. Sediment transport equations comparison of Jindong Station

Numerical Simulation

1D Simulation of Bed Elevation Changes Using the Hec-6 model

Bed elevation changes from the NREB and 50 km upstream of the NREB were simulated using the Hec-6 model for one month with Typhoon Maemi in 2003. Yang's method for sediment transport equation, which was relatively consistent with field measurement of Jindong Station as shown in Figure 3, was adopted in the

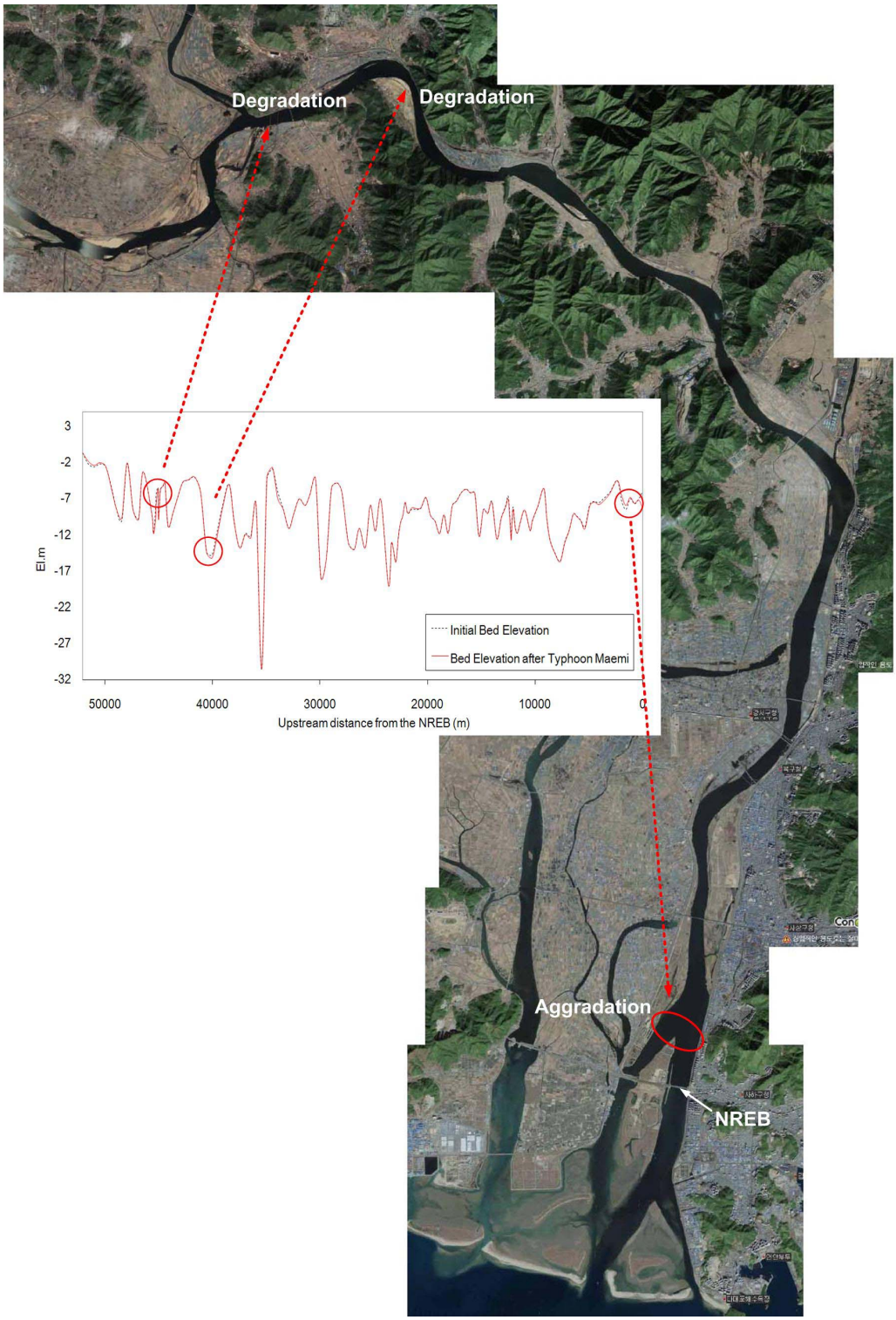

Figure 4. Hec-6 result for bed elevation changes for 30 days in Sept. 2003



Figure 5. Hec-6 result for bed elevation changes for 14 years (1990-2003)

model. Typhoon Maemi hit the Lower Nakdong River on September 12, 2003 and simulation time in the model was one month of September 2003. The simulation result is shown in Figure 4. The maximum degradation of 1.59 m occurred near the 4.5 km upstream of the NREB and bed elevation at the 4 km upstream of the NREB was decreased 70 cm. Also, the downstream area near the NREB had sediment deposition of 80 cm because the expanded channel width resulted in the velocity decrease.

To analyze the long-term changes of bed elevation in the upstream approached channel (3 km upstream form the NREB) after construction of the NREB, the gauging data for flow discharge and water stage form 1990 to 2003 was used. Bed changes from NREB to Jindong Station (80 km upstream of the NREB) were calculated for 14 years after construction of the NREB and the result is plotted in Figure 4. Bed elevation from Samrangjin (40 km upstream of NREB) to Jindong was degraded after the placement of NREB. Also, it was represented in the simulation results that bed elevations near the NREB, 20 km, and 35 km were increased. The results of the Hec-6 model to analyze the characteristics of bed changes in the Lower Nakdong River show typical features of sediment deposition near the estuary barrage or dam due to the decreased velocity.

2D Simulation of Flow and Bed Elevation Changes

RMA2 and SED2D models were used for 2-dimensional numerical simulations of flow and bed changes for 3 km area in the approached channel of NREB in this study. Field data surveyed by KOWACO in April 3rd 2008 were

utilized to construct topographical data for numerical modeling. Finite element and node numbers of constructed geometry were corresponding to 2,831 and 8,830. Daily mean discharge in Sanrangjin and water surface elevation in NREB from April 1st to July 15th 2008 were collected as shown in Figure 6 and used for boundary conditions. Discharge and water surface elevation data were classified to three groups and representative values of each groups are summarized in Table 1.

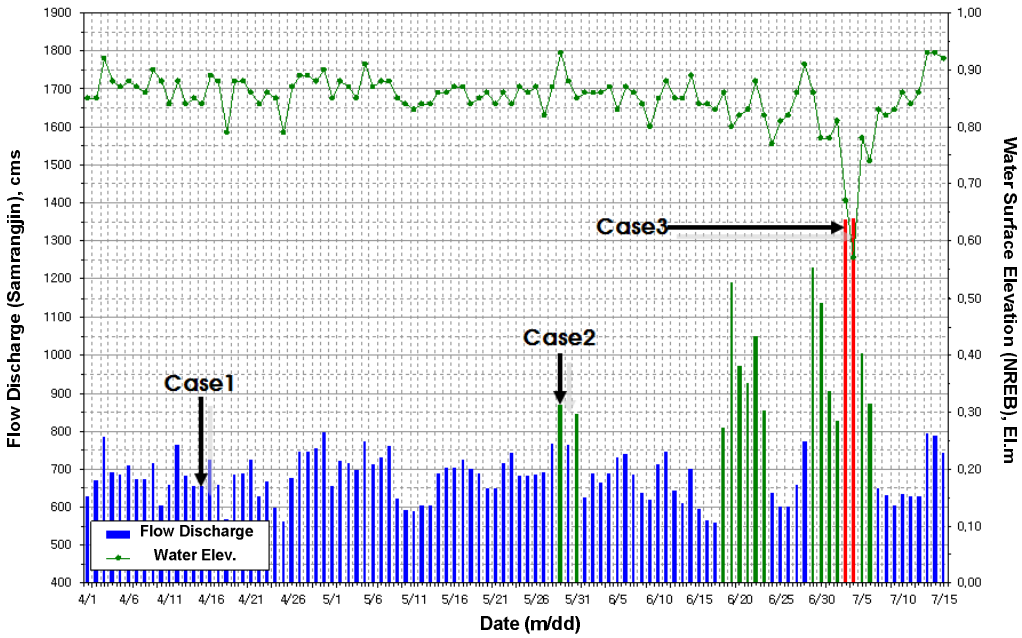

Figure 6. Discharge and water surface elevation from April 1st to July 15th 2008

Table 1. Boundary conditions of simulation cases

Groups	Discharge range [m³/s]	Averaged discharge [m³/s]	Averaged water elevation [m]	Corresponding time [day]	Sediment discharge [tons/day]	Initial sed. [kg/m³]
Case1	0 ~ 800	678.30	0.86	90	16204.20	0.27650
Case2	800 ~ 1250	963.75	0.82	14	29602.58	0.35551
Case3	1250 ~ 1400	1359.28	0.62	2	53399.13	0.45469

RMA2 and SED2D models were used for 2-dimensional numerical

simulations of flow and bed changes for 3 km area in the approached channel of NREB in this study. Field data surveyed by KOWACO in April 3rd 2008 were utilized to construct topographical data for numerical modeling. Finite element and node numbers of constructed geometry were corresponding to 2,831 and 8,830. Daily mean discharge in Samrangjin and water surface elevation in NREB from April 1st to July 15th 2008 were collected as shown in Figure 6 and used for boundary conditions. Discharge and water surface elevation data were classified to three groups and representative values of each groups are summarized in Table 1.

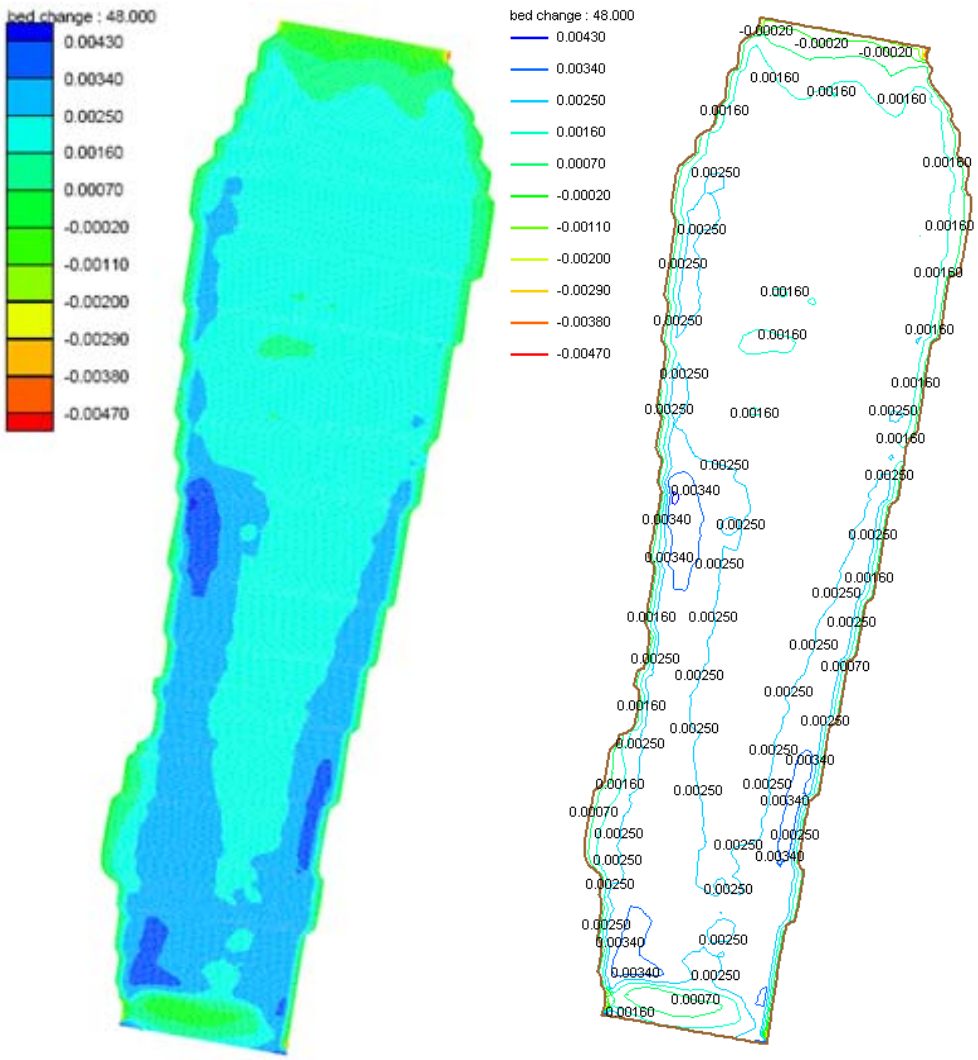

Figure 7. Bed change results of Case 3 (Flow direction from upside to downside)

According to the results of RMA2, maximum velocities for Cases 1 and 2 wer 0.2 m/s and 0.3 m/s in the vicinity (100 m) of the NREB. The water depth was ranged from 4 m to 10 m and the deepest point was 1.5 km upstream of the NREB. The calculation results of the SED2D model represented that most of the simulated area had sediment deposition and the aggradation was increased in the direction of the NREB for Cases 1 and 2. The velocity distribution of Case 3 was 0.02 m/s to 0.47 m/s and maximum velocity occurred in the similar location of Cases 1 and 2. Superficial bed changes for Case 3 are shown in Figure 7. Sediments were deposited in the main channel and bed was scoured in the edge of the river bank and upstream and downstream boundaries. There was no sediment deposition near the NREB because of the lower water stage by gate opening.

Field Surveying Results for Bed Changes before and after Floods

Volumetric analysis of bed changes was performed using field surveying data of 3km in the upstream direction from the NREB. Addition field surveying for volumetric analysis of bed changes was executed three times except two regular annual surveying in April and September (Figure 8). Sediment dredging was

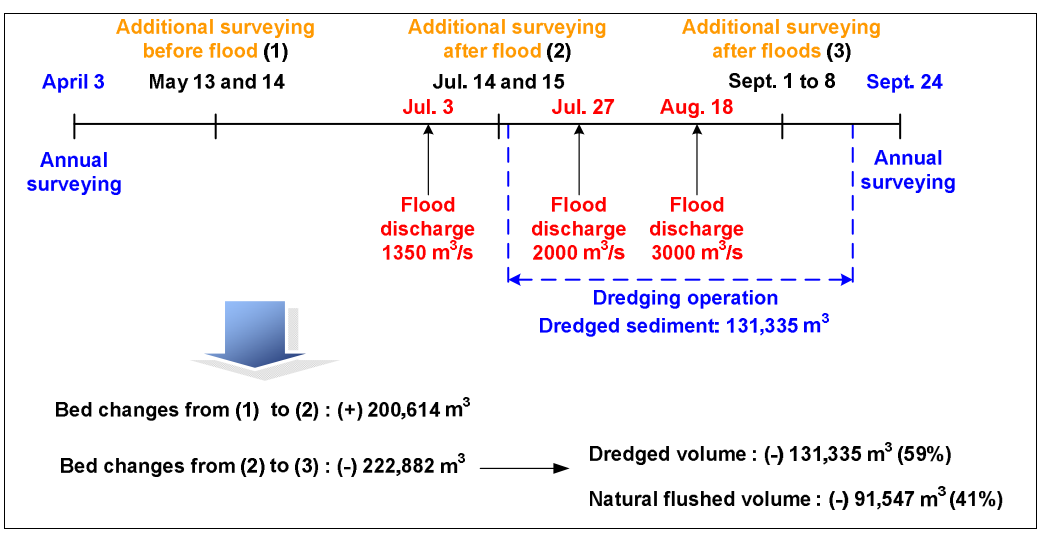

Figure 8. Volumetric analysis of bed changes using field surveying data (2008)

operated from July 16th to September 19th 2008 and dredged sediment volume was corresponding to 131,335 m^3. The sediment volume of bed change between

additional surveying before and after first flood is (+) 200,614 m^3 as shown in Figure 8 and the sign of (+) represents deposition. It is similar results of 2D numerical simulation from April 1st to July 15th 2008. Also, the volumetric bed change between additional surveying (2) and (3) was (-) 200,614 m^3. The sediment volume of (-) 91,547 m^3 was flushed by natural flow because sediment dredging of (-) 131,335 m^3 was operated in this period

Conclusion

Historical data collection, numerical simulation, and field surveying for the Lower Nakdong River were conducted to analyze sedimentation characteristics near the NREB. The bedform calculation results show that the bedform of the Lower Nakdong River consist of ripples and dunes and the field observations in 2006 using the sound navigation ranging shows good agreement with this results. The results of Hec-6 modeling to analyze the characteristics of bed changes in the Lower Nakdong River show typical features of sediment deposition near the estuary barrage or dam due to the decreased velocity. As a result of 2D numerical modeling, sediments were deposited in the main channel and bed was scoured in the edge of the river bank and upstream and downstream boundaries. There was no sediment deposition near the NREB because of the lower water stage by gate opening. Lastly, volumetric analysis of bed changes was performed using field surveying data of 3km in the upstream direction from the NREB and analysis results were similar to the 2D numerical simulation conducted in this study.

References

Ackers, P., and White, W.R., 1973. Sediment transport: New approach and analysis. J. Hyd. Div. ASCE, 99, no. HY11:2041-60.

Bogardi, J., 1974. Sediment Transport in Alluvial Streams. Budapest: Akademiai Kiado.

Brownlie, W.R., 1981. Prediction of flow depth and sediment discharge in open-channels. Report no. KH-R-43A. Pasadena, California Institute of Technology, W. M. Keck Laboratory.

Colby, B.R., and Hembree C.H., 1955. Computation of Total Sediment Discharge, Niobrara River near Cody, Nebraska. U.S. Geological Survey, Water-Supply Paper 1357.

Engelund, F., and Hansen, E., 1967. A Monograph on Sediment Transport to Alluvial Streams. Copenhagen, Teknik Vorlag.

Ji, U. and Julien, P.Y., 2005. The Impact of Typhoon Maemi on the Nakdong River, South Korea. Hydrology Days, Colorado State University, March 7, 2005, pp. 103-110.

KOWACO, 1995. A Study on Sedimentation Characteristics in Nakdong Estuary Barrage. Korea Water Resources Corporation (KOWACO), Korea.

Park, S.K, Julien, P.Y., Ji, U., and Ruff, J.F, 2008. Retrofitting Large Bridge Piers on the Nakdong River, South Korea. J. Hyd. Eng. ASCE, 134, no 11: 1639-50.

Shen, H.W., and Hung, C.S., 1972. An engineering approach to total bed-material load by regression analysis. Proc. sedimentation Symposium, ed. H.W. Shen. Berkeley, Calif.: Water Resources Pub., chap 14.
Remodified Einstein procedure for sediment load. J. Hyd. Div. ASCE, 109, no. 4 (1983): 565-78.

Simons, D.B. and Richardson, E.V., 1963. Form of bed roughness in alluvial channels.
Trans. ASCE, 128(1963): 284-323

Simons, D.B. and Richardson, E.V., 1966. Resistance to flow in alluvial channels.
Professional Paper 422-J. Washington, D.C., U.S. Geological Survey.

van Rijn, L.C., 1984. Sediment transport, Part III: Bedforms and alluvial roughness. J. Hyd. Div. ASCE, 110, no 12: 1733-54.

Yang, C.T., 1979. Unit Stream Power Equation for Total Load. J. Hyd. Div. ASCE,

vol. 40: 123-138.

Experimental Results on the Stability of Non-Cohesive Sediment Beds Subject to Vertical Pore Water Flux

Pinar Cakir Kavcar[1] and Steven J. Wright[2]

[1] Hydraulic Engineer, Bechtel OG&C, Inc., 3000 Post Oak Blvd., Houston, TX 77056. E-mail: pkavcar@bechtel.com

[2] Member ASCE, Professor, Civil and Environmental Engineering, 113 EWRE, University of Michigan, Ann Arbor, MI 48109-2125; PH (734) 764-7148; FAX (734) 763-2275, email: sjwright@umich.edu

ABSTRACT

Due to conflicting conclusions in the literature, this study considers the influence of vertical pore water flux on the initiation of motion criterion for noncohesive bed sediments subject to an applied shear stress. A key issue with respect to interpretation of experimental results may be associated with the determination of bed shear stress, a quantity that cannot be measured directly and thus relies on indirect methods to estimate. Another issue is the determination of the key variable characterizing the bed seepage as many studies characterize seepage in terms of the velocity while others account for the piezometric head gradient.

A modification of the traditional Shields' parameters to account for the effects of bed seepage was developed suggesting that the bed hydraulic gradient is the key parameter in characterizing initiation of sediment motion. Experiments were performed for three different sand sizes subject to both vertically upward and downward bed flow to test the validity of the formulation over a wide range on the Shields curve. Experimental results interpreted using the modified dimensionless shear stress are shown to be consistent with the conventional Shields curve.

INTRODUCTION

Lu, et al (2008) present an excellent review of the existing literature related to the effects of bed seepage on turbulence intensity, bed shear stress, and sediment transport rates. In their Table 1 which is a summary of existing studies, they indicate that each of these variables have been reported to decrease, increase, or remain unchanged. The current study is concerned with the effect of bed seepage on initiation of sediment motion which is clearly related to these same variables. Both conditions of injection (vertically upward pore water flow) and suction (downward flux) are considered. Simons and Richardson (1966) suggested that seepage of water into the bed would increase the effective weight of the bed particles and, therefore, increase the stability of the bed. Cheng and Chiew (1999)

reported a tendency for lowered critical shear stress as injection velocities were increased for median grain sizes ranging from 0.63 mm to 1.95 mm. On the other hand, Martin (1970) reported that inflow seepage does not enhance incipient motion of the sediment particles even up to a quick bed condition. However, Rao and Sitaram (1999) investigated bed stability using seven different sizes of sand (0.32-3.0 mm) under the effect of either injection or suction. They concluded that suction reduces the stability of the bed particles and increases mobility whereas injection does the opposite.

A review of the specifics of previous experimental studies indicates a number of potential explanations for these conflicting conclusions. One critical issue is that the initiation of motion is generally characterized by the bed shear stress such as through the Shields' curve which relates sediment stability to two dimensionless parameters:

$$\tau_* = \frac{\tau}{(\gamma_s - \gamma)d} \text{ and } \mathrm{Re}_* = \frac{u_* d}{\upsilon} \quad (1)$$

in which τ is the bed shear stress, γ_s and γ are the unit weight of sediment and water, respectively, d is the effective sediment diameter, u_* is the shear velocity defined by $\tau = \rho u_*^2$ and υ is the kinematic viscosity of the fluid. bed shear stress cannot generally be measured directly and must be inferred from the measurement of other flow variables. Another issue is the definition of the key variable characterizing the bed seepage. Most previous studies have used the seepage velocity to establish a relationship to bed stability. The development by Cakir and Wright (2006) of a modified Shields' parameters to account for the effect of bed seepage suggests that the piezometric head gradient is the more relevant parameter. Since seepage velocity and gradient are related related to grain size, the possibility exists that previous studies did not choose a relevant range of flow variables in order to observe an effect. In order to address these issues, an experimental study was performed using sands with different diameters selected to span a wide range on the Shields' curve. Experiments with both injection and suction were performed. The results of these experiments are presented in this study.

MODIFIED SHIELDS PARAMETERS

The conventional Shields parameters in Equation 1 may be derived by several different approaches, all of which involve a consideration of forces acting on the bed material; Cakir and Wright (2006) chose an approach using a moment balance considering three principal forces acting on an idealized (spherical) non-cohesive sand particle: a drag force F_D, the submerged weight of the particle F_W and a lift force F_L. Flow through the bed may be included as a seepage force F_J in this balance. The seepage force is assumed to be produced by a linear vertical pressure gradient deviation from hydrostatic conditions and this gradient i produces a force similar to the buoyant force (included in the submerged weight term in Equation 2) and in the same direction in the case of injection. Suction conditions are described

with a negative value of i. Since these forces are both due to linear pressure variations acting through the center of volume of the sediment particle, regardless of actual shape, the effect of the seepage force can be directly incorporated into a modified definition of τ_* although possibly with a correction factor to account for the local variation of the head gradient at the sediment/water interface as suggested by Martin and Aral (1971). Their approach assumes that a constant correction of the piezometric head gradient within the sand bed can be used to estimate the local gradient at the sediment/water interface. The moment balance yields the scaling that $\rho u_*^2 \propto (\gamma_s - (1+Si)\gamma)d$ at incipient instability and there suggests that the dimensionless shear stress in the conventional Shields; parameters can be replace with

$$\tau_{*m} = \frac{\tau}{(\gamma_s - \gamma(1 + Si))\, d} \qquad (2)$$

where S represents an adjustment to the internal hydraulic gradient within the sediment bed representing the effect of the altered flow pattern at the sediment/water interface as proposed by Martin (1970), and Martin and Aral (1971). The value of S value was estimated as 0.85 from an arithmetic average of the individual experimental values reported in Martin and Aral (1971). It is noted that minor changes of this coefficient does not have a significant effect on the current results as demonstrated by Kavcar (2008). From Equation 2, it can be seen that i must be fairly large, at least greater than about 0.1, in order to have at least a five percent effect on τ_{*m}. Many previous studies were conducted with hydraulic gradients considerably less than this value.

EXPERIMENTAL INVESTIGATION

Experiments were conducted in a 7.5 m long, 0.6 m wide flume with the front of the test section located 3.5 m downstream from the flume inlet. The test section was approximately 2.00 m long, with a 0.3 m wide sediment filled cavity installed in a false floor in the bottom of the flume. A platform covered with geotextile was installed within the cavity to support approximately 10 cm of sediment while allowing free migration of pore water into or out of the sediment depending on the applied pressure beneath. The hydraulic head at the bottom in the cavity beneath the sand bed was measured with a piezometer and the head difference between the cavity and the water flowing above the sand bed was measured. The injection or suction discharge was also metered.

There are various definitions for initiation of motion criterion in the literature (Buffington, 1999). Initiation of motion was observed visually in this study. Specifically, it was observed that if each flow rate was run for an extended period of time (20-30 minutes), bed ripples would be initiated at a given flow and then spread over the entire bed. This approach provided a more repeatable methodology for defining initiation of motion than other approaches investigated. All the sands were commercially produced and referred to as *beach/lake sand* and have a fairly rounded shape. Three sizes of sands, d_{50}=160 μm, 500 μm and 1200 μm were used.

As mentioned previously, there is no direct way to measure bed shear stress in experiments with injection or suction. It was considered unacceptable to achieve a fully developed boundary layer by performing experiments at depths of only a few cm since the resulting bulk flow Reynolds Numbers would only nominally be above the transition from laminar to turbulent flow and therefore not representative of typical field conditions. Flow depths were held in the range of 25-30 cm for all experiments and a typical value for the local boundary layer thickness over the sediment bed was on the order of 5 cm. The bed shear stress was estimated by measuring local turbulence measurements close to the bed surface and developing a procedure for converting these to bed shear stress. An Acoustic Doppler Velocimeter (Sontek MicroADV, down-looking probe) is capable of measuring the instantaneous velocity components of the flow in all three dimensions. Vertical velocity profiles were measured at the center of the flume width over the sediment bed as well as on a rigid boundary that temporarily covered the test bed. The ADV measurements also provided statistics on the velocity fluctuations, and consequently the Reynolds Stress term which is proportional to the local turbulent shear stress. The details of the procedure for determination of bed shear stress are provided in Kavcar (2008). Although this approach has its own limitations, it was considered to be preferable to experiments with water depth of a few cm (Rao and Sitaram, 1999) in order to ensure a fully developed boundary layer that changes considerably with distance along the test bed due to the requirements for a significant inflow or outflow.

For each sand size, a baseline experiment without pore water flux was conducted to define a critical bed shear stress at which incipient motion was observed. After a critical bed shear stress induced by the no bed seepage case was determined for each sand size, positive (injection) or negative (suction) hydraulic gradients were applied to the bed to investigate the effect of pore water gradients on the bed stability. In theory, the range for the applied injection hydraulic gradients would have an upper limit of 1 which implies a quick sand condition. The applied hydraulic gradients were selected to be sufficiently large that an effect on sediment stability could be observed and they would cover as wide a range of values as possible. Overall, three injection and two suction cases with different pressure gradients were investigated. The flow rate through the bed was metered in both injection and suction experiments while the piezometric gradient was determined by measuring the head difference across the bed. An injection or suction experiment was conducted by first setting the hydraulic gradient to a predetermined value and increasing the flume discharge until incipient motion was observed.

RESULTS

It is useful to explore the effect of suction and injection on velocity and Reynolds stress profiles. ADV measurements were made for flows with and without vertical flux through the sand bed. The results of typical experiments are provided in Figures 1 and 2. The measured velocity profiles demonstrate the intuitive result

that when the pore water flow is upwards into the free stream flow, the lower velocities near the bed are displaced further away from the boundary. Similarly,

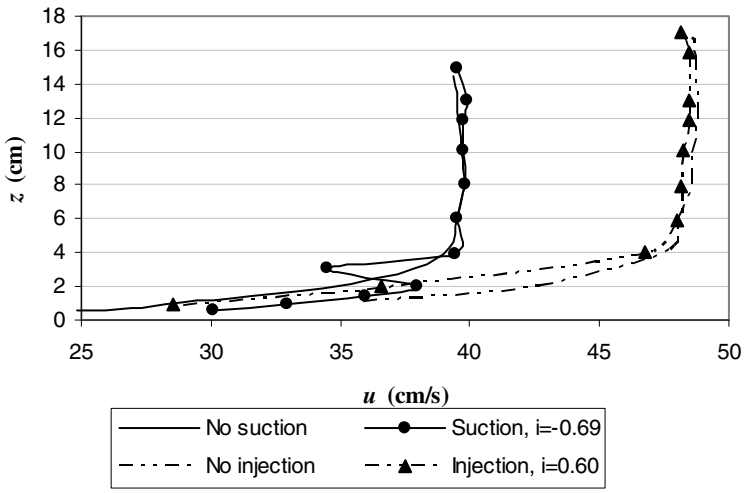

Figure 1. Comparison of mean velocity profiles of experiments with strong injection (hydraulic gradient=0.60)and strong suction (hydraulic gradient=-0.69) with experiments at same free stream velocities and no suction or injection (d_{50}=1200 μm).

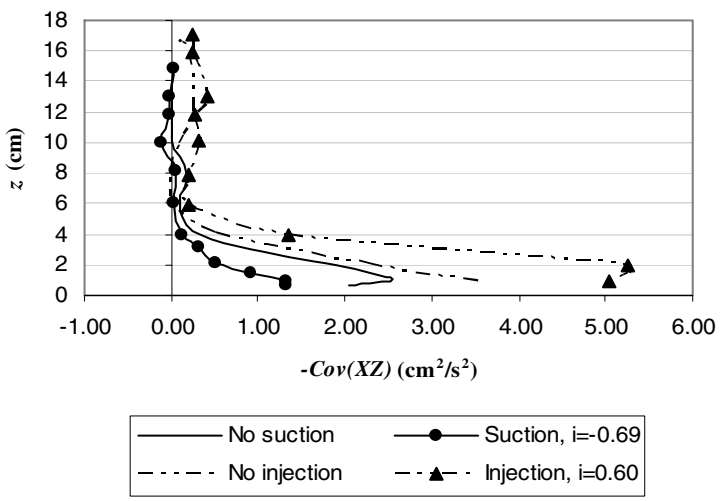

Figure 2. Comparison of covariance profiles of experiments with strong injection (hydraulic gradient=0.60) and strong suction (hydraulic gradient=-0.69) with experiments at same free stream velocities and no suction or injection (d_{50}=1200 μm).

when there is suction into the bed, higher velocities persist closer to the bed surface as the lower momentum flow near the boundary is removed from the main flow.

The two sets of measurements contain velocity profiles where the free stream velocity is similar in a case without suction or injection and in experiments with high injection or suction rates. These results imply that if one used the surface velocity or the cross-sectional averaged velocity to characterize the flow (e.g., to estimate the bed shear stress from the Manning equation), each set of measurements would experience the same bed shear stress. It is believed that this situation has led to confusion to some previous discussions on the influence of bed injection or suction on sediment stability. Since most accepted bed stability criteria are shear-stress based, it is irrelevant how the velocity or discharge required to initiate sediment transport varies with injection or suction; the only thing that is important is how the shear stress varies. Thus it was observed during this experimental investigation that sometimes a greater discharge was required to initiate sediment motion but at the same time, a lower estimated bed shear stress was experienced and therefore by shear stress-based criteria, the bed is less stable

Considering the covariance profiles, the results indicate that at the same free stream velocity, injection increases the local turbulent shear stress while suction decreases it. The effects are more pronounced the larger the hydraulic gradient. Prinos (1995) studied numerically the effects of bed suction on the structure of turbulent flow by solving the Reynolds-averaged Navier-Stokes equations for the experimental data by Maclean (1991) and reported the same behavior of decreased turbulent shear stress in case of bed suction.

These results are counter to some of the qualitative behavior discussed in the literature (e.g, Cheng and Chiew, 1998a) on the role of suction or injection on bed shear stress and this may have led to some of the contradictions in the literature on bed stability in experiments with pore water seepage. One could argue that in the case of injection the smaller local velocity gradient due to the displacement of a given velocity further out into the flow would indicate a smaller bed shear stress; nevertheless this would only be valid for a laminar flow where the shear stress is directly proportional to the local velocity gradient. In this study, the flow was turbulent over the test section, implying that the bed shear stress was dominated by the turbulent characteristics of the flow.

The bed shear stresses corresponding to the conditions when incipient motion was observed were computed employing the procedure explained above in cases of suction, injection and in the absence of injection or suction; results are given in Table 1. The suction experiments for 500 μm are not included here since no ADV measurements were available for determination of bed shear stress. The results are consistent with a greater bed shear stress required to initiate sediment motion when bed suction is applied and a reduced shear stress with injection. Figure 3 shows the Shields curve defined by the van Rijn (1984) functional relationships. When the data measured in this study are plotted but without the modified shear stress defined in Equation 2 the results indicate scatter that is somewhat greater than traditionally observed in experiments without suction or injection. However the trends for individual grain sizes, especially the 160 and 1200 μm sizes don't follow the general trends of the Shields' curve. When the dimensionless shear stress is

modified to account for the effects of suction and injection, Figure 4 demonstrates the results using a value of 0.85 for the S coefficient suggested by Martin and Aral (1971). The data for d_{50}=1200 μm lie below the Shields curve but basically parallel to it. This may be due to the fact that the grain size distribution is fairly broad for that particular sand and smaller grain sizes in the distribution are responsible for the observed initiation of motion, but it is also noted that many researchers suggest that the limiting value of τ_* for large R_* should be around 0.03 (e.g. Garcia, 2008, Chapter 3) and thus consistent with the current results. The main issue is that Figure 4 presents a more consistent presentation than Figure 3.

Table 2. Hydraulic gradient, seepage velocity, free stream velocity and estimated bed shear stresses.

d_{50}=160μm			
i	I (m/s)	u_s (m/s)	τ_i (N/m^2)
0.000	0.000000	0.2978	0.1741
0.320	0.000033	0.2890	0.1696
0.480	0.000065	0.2796	0.1548
0.700	0.000090	0.2763	0.1602
-0.441	-0.000057	0.3279	0.2849
-0.844	-0.000108	0.3363	0.2492
d_{50}=500μm			
i	I (m/s)	u_s (m/s)	τ_i (N/m^2)
0.000	0.000000	0.3229	0.2344
0.248	0.000059	0.3229	0.1994
0.481	0.000117	0.3117	0.1951
0.706	0.000173	0.3047	0.1915
d_{50}=1200μm			
i	I (m/s)	u_s (m/s)	τ_i (N/m^2)
0.000	0.000000	0.4515	0.4918
0.300	0.001150	0.4684	0.3461
0.450	0.001760	0.4737	0.3341
0.600	0.002236	0.4815	0.3526
-0.383	-0.001455	0.4233	0.6996
-0.689	-0.002619	0.3952	0.9087

There are a number of assumptions that were employed in the determination of the bed shear stress used in the computation of the modified dimensionless shear stress and the grain Reynolds number. It is likely that a more rigorous procedure to determine the bed shear stress would result in better agreement with the traditional Shields curve, but there is a fair disagreement in the literature regarding even what the Shields curve is supposed to be. The presented results are considered

satisfactory in verifying the methodology for incorporating the effects of suction or injection on bed stability with a straightforward and simple modification of the dimensionless shear stress used in the conventional Shields curve.

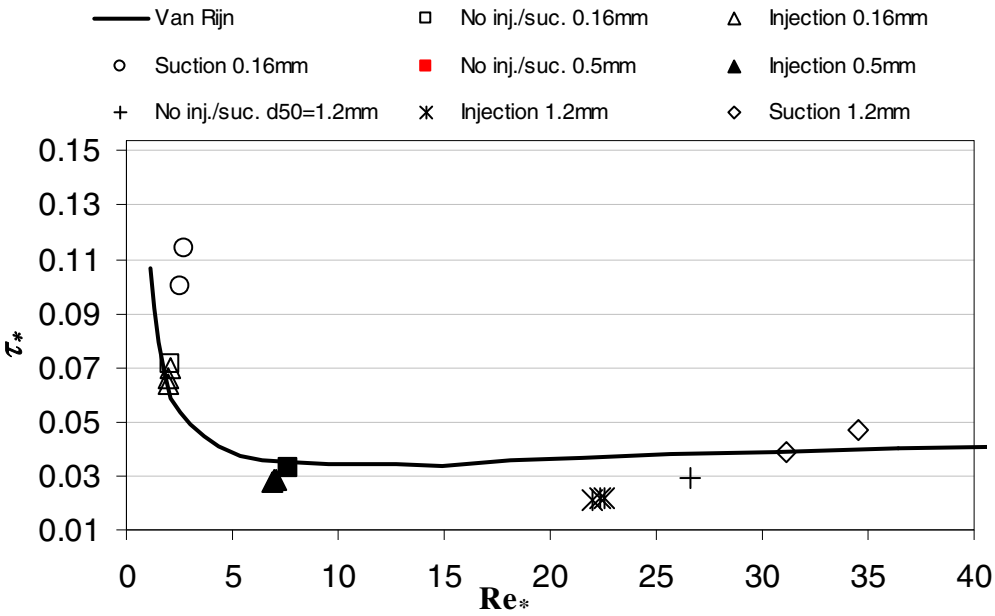

Figure 3. Experimental data on conventional Shields curve.

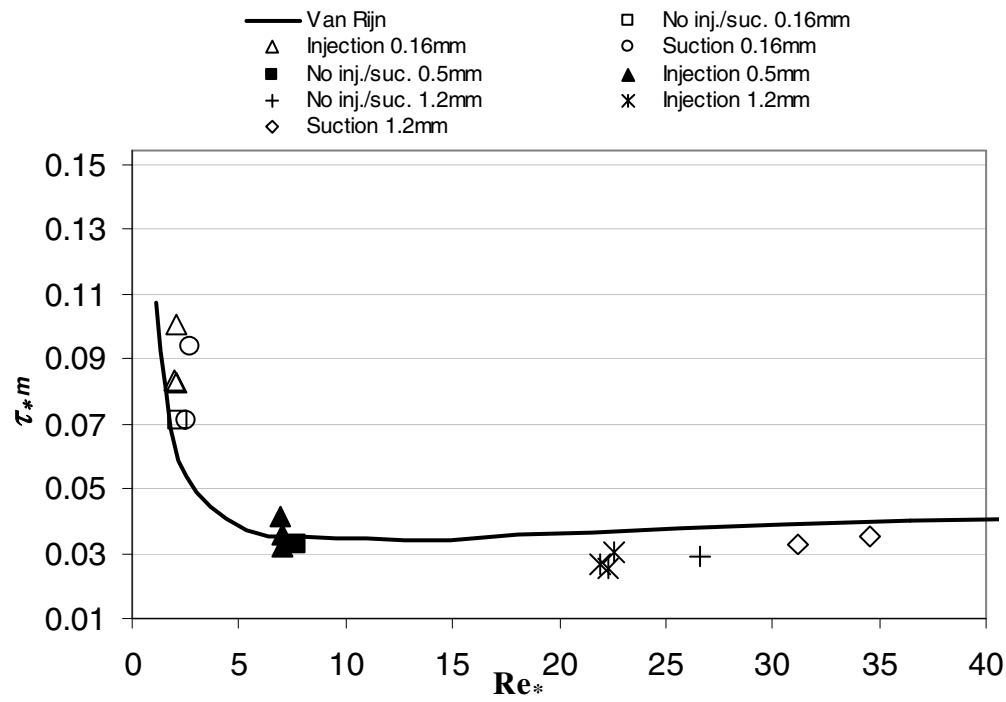

Figure 4. Experimental data on modified Shields curve.

SUMMARY AND CONCLUSIONS

This study was undertaken in part to resolve contradictory findings in the literature regarding the effect of bed seepage on the initiation of motion of non-cohesive sediments. Although several studies report that positive upwards bed flow (injection) reduces the stability of bed sediments and downwards seepage (suction) reduces it, other studies report the opposite conclusion. A review of previous studies suggests that one issue may simply be the inability to accurately estimate bed shear stress especially in the spatially non-uniform flow conditions presented by significant bed seepage. An alternative method for estimating bed shear stress was developed, relying on the measurement of turbulence close to the bed. When the methodology was applied for measurements without suction or injection, the results are consistent with the conventional Shields curve. The same methodology was applied to analyze measurements with relatively high suction and injection rates and the results compared to a modified Shields curve formulation that was developed to describe the influence of suction or injection. Different sand sizes were selected for testing to cover relevant ranges of the Shields curve to avoid the possibility of the results being only valid for certain ranges of noncohesive sediment. The following conclusions are generated from this study:

- Injection or positive upwards bed seepage tends to reduce the bed shear stress required for incipient motion of bed sediments while downwards seepage into the bed increases the required bed shear stress;
- The experimental results can be made consistent with the conventional Shields curve when the modified dimensionless shear stress is used in the Shields curve;
- Hydraulic gradient through the bed is the most relevant parameter related to bed seepage influencing non-cohesive sediment stability. Gradients greater than 0.1 are required to have a noticeable effect on bed stability

ACKNOWLEDGMENT

This research was conducted under a project sponsored by the Strategic Environmental Research and Development Program. Support for this research is gratefully acknowledged.

REFERENCES

Buffington, J. M. (1999). "The Legend of A. F. Shields." *Journal of Hydraulic Engineering*, 125(4), 376-387.

Cakir, P. and Wright, S.J. (2006) "Stability of Non-cohesive sediments under conditions of pore water flux," Proceedings of World Water and Environmental Resources Congress, ASCE, paper 40856-13842.

Cheng, N.-S., and Chiew, Y.-M. (1998). "Turbulent Open-channel flow with upward seepage." *Journal of Hydraulic Research*, 36(3), 415-430.

Cheng, N.-S. and Chiew, Y.-M. (1999). "Incipient sediment motion with upward seepage." *Journal of Hydraulic Research*, 37(5), 665-681.

Garcia, M. (2008) "Sedimentation engineering: Processes, measurements, modeling and practice," ASCE Manual 110, New York.

Kavcar, P.C. (2008), "Stability of cohesive sediments subject to pore water and gas ebullition fluxes and effectiveness of sand and Aquablok caps in reducing the resuspension rates," Ph.D. dissertation, Civil Engineering, The University of Michigan, Ann Arbor, MI.

Lu, Y., Chiew, Y.-M. and Cheng, N.-S. (2008) "Review of seepage effects on turbulent open-channel flow and sediment entrainment," Journal of Hydraulic Research, 46(4), 476-488.

Maclean, A. G. (1991). "Open channel velocity profiles over a zone of rapid infiltration." *Journal of Hydraulic Research*, 29(1), 15-27.

Martin, C.S. (1970). "The effect of a porous sand bed on incipient sediment motion." *Water Resources Research*, 6(4), 1162-1173.

Martin, C. S., and Aral, M. M. (1971). "Seepage Force on Interfacial Bed Particles." *Journal of the Hydraulics Division*, ASCE, 101(7), 1081-1100.

Prinos, P. (1995). "Bed-Suction Effects on Structure of Turbulent Open-Channel Flow." *Journal of Hydraulic Engineering,* ASCE, 121(5), 404-412.

Rao, A.R., and Sitaram, N. (1999). "Stability and mobility of sand-bed channels affected by seepage." *Journal of Irrigation and Drainage Engineering*, ASCE, (125)6, 370-379.

Simons, D.B. and Richardson, E.V. (1966). "Resistance to flow in Alluvial Channels." *U.S. Geological Survey Professional Paper 422-J.*

van Rijn, L. C. van (1984). "Sediment Transport, Part I: Bed Load Transport." *Journal of Hydraulic Engineering,* ASCE, 110(10), 1431-1455.

Suspended Sediment Concentration Measurements of Muddy Sediments with an ADV

M. Salehi[1] and K. B. Strom[2]

[1]Graduate Research Assistant, Dept. Civil and Environmental Engineering, University of Houston, Houston, TX, USA, e-mail: msalehi@mail.uh.edu
[2]Assistant Professor, Dept. Civil and Environmental Engineering, University of Houston, Houston, TX, USA, e-mail: kbstrom@uh.edu

1 ABSTRACT

This paper presents a laboratory study which examines the relationship between suspended sediment concentration and the signal to noise ratio recorded by a Nortek Vectrino Doppler velocimeter for two velocimeter acoustic output power levels. Tests are conduced in a tank with tap water and Kaolin clay for the concentration range of $0.0008 - 2.8$ g/L. Results indicated that the velocimeter signal to noise ratio saturates at approximately 10 mg/L for a High power level setting and at 100 mg/L for a Low+ level power setting. For concentrations less than the saturation condition, the signal to noise ratio was found to be proportional to the logarithm of concentration, indicating that the velocimeter is a useful tool for measuring synchronized velocity and suspended sediment concentration time series.

2 INTRODUCTION

Acoustic Doppler velocimeters are designed to measure time varying turbulent velocity signatures of fluids flows, and are common tools for doing so in both field and laboratory settings (Voulgaris and Trowbridge, 1998; Nikora and Goring, 2000; Maddux et al., 2003; Strom and Papanicolaou, 2007). However, since the Doper system measure velocity using an acoustic reflection from small particulate matter in the water, they also are capable of recording information concerning the suspended particulate matter in the water column (Lohrmann et al., 1994; Lohrmann, 2001; Nikora and Goring, 2002; Hosseini et al., 2006). Studies have shown that data mining of the strength of the acoustic return signal recorded by Doppler velocimeters can yield very reliable suspended sediment concentration measurements of fine sediment (Fugate and Friedrichs, 2002; Voulgaris and Meyers, 2004; Hosseini et al., 2006). If the strength of the acoustic return recorded by the Vector signal is properly calibrated, it has been shown that in some cases, the Doppler systems can give estimates of suspended sediment concentration (SSC) that are as good as Optical Backscatter Sensors (OBSs) and Sequoia instrument's

LISST-100x, both of which are designed to measure suspended sediment concentration (Fugate and Friedrichs, 2002; Voulgaris and Meyers, 2004).

If the strength of the acoustic return signal can be adequately calibrated to the suspended sediment concentration, then Doppler systems provide a single platform for simultaneous velocity-SSC measurements at turbulent frequencies. A unique feature of this is that the turbulent sediment flux term in the advection-diffusion equation for suspended sediment can be evaluated directly. Term 3 in the following equation represents the spreading of sediment concentration due to random turbulent motion:

$$\frac{\partial C}{\partial t} + \frac{\partial}{\partial x_i}\left(U_i C\right) + \frac{\partial}{\partial x_i}\left(\overline{u_i' c'}\right) = S_e - S_D \tag{1}$$

where the molecular diffusion term has been dropped and $u_i(\mathbf{x},t) = U_i(\mathbf{x}) + u_i'(\mathbf{x},t)$ is the velocity vector (note: $u_3 = w = W - w_s + w'$, where w_s is the fall velocity), $c(\mathbf{x},t) = C(\mathbf{x}) + c'(\mathbf{x},t)$ is the suspended sediment concentration, and S_e and S_D represent sediment deposition and erosion rates. The turbulent spreading terms, $\partial_i(\overline{u_i' c'})$, is typically modeled as a diffusive process,

$$\overline{u_i' c'} = -D_{Ti}\frac{\partial C}{\partial x_i} \tag{2}$$

where D_{Ti} is the turbulent diffusion coefficient in the x, y, z directions and needs to be determined via other relations or calibrated experimentally. However, with the coupled velocity-SCC measurements, the turbulent flux can be directly measured with the Doppler system. Furthermore, if the assumptions of 2D, steady, uniform flow are made, Eq. 1 reduces to,

$$w_s\frac{\partial C}{\partial z} + \frac{\partial}{\partial z}\left(-\overline{w'c'}\right) = 0 \tag{3}$$

and a direct estimation of the fall velocity can be made from the measured vertical turbulent flux; since integration of Eq. 3 in the z and application of the boundary condition gives,

$$w_s = \frac{\overline{w'c'}}{C} \tag{4}$$

Therefore, the bulk fall velocity w_s can be estimated either through a single point measurement of the average concentration and turbulent flux, or through linear regression of measured profiles along z.

This paper examines the use of a Nortek Vectrino velocimeter for quantifying the suspended sediment concentration and turbulent sediment flux of muddy sediments in a laboratory setting. The impetus for this, in addition to measurement of turbulent flux, is the quantification of site-specific critical erosional and depositional conditions of estuarine muds.

3 BACKSCATTER AND SSC

The Acoustic Doppler velocimeter used in the study was a 10 MHz Nortek Vectrino with a side-looking 3D/2D probe. The system is a dual-pulse Doppler system

which calculates velocity using the phase shift between an emitted and reflected signal. The Vectrino has a single acoustic emitter ($f = 10$ MHz) and four receivers located a fixed distance from the emitter and angled to receive reflected sound from the sampling volume which is located 5 cm from the emitter. The sample volume is 6 mm diameter and has a variable length of $3 - 15$ mm. The Vectrino has an internal sampling frequency of $426 - 2564$ Hz, a data output range of $1 - 200$ Hz, and a dynamic echo intensity range of 25 dB. The Vectrino represents a second generation acoustic velocimeter and has shown excellent performance for turbulent measurements, especially in low SNR conditions (Rusello et al., 2006)

As mentioned, the strength of the return echo from sediment in the the sampling volume is a function of the SSC. Rayleigh scatter theory shows that the volume backscatter strength, S_v is,

$$S_v = 10 \log \left(\frac{3\phi k^4 r^3}{\rho_s} C \right) \tag{5}$$

where ϕ is a material property, k is the acoustic wave number ($k = 2\pi/\lambda$, where λ is the wavelength), ρ_s is the density of the sediment, r is the particle radius, and C is the concentration (mass/volume). For a given emitted frequency and sediment type/size, Eq. 5 shows that,

$$S_v \propto 10 \log(C), \quad \text{or} \quad C \propto 10^{S_v/10} \tag{6}$$

when $kr < 1$ (Urick, 1983). For the acoustic Doppler system, we can model the strength of the backscatter using the following version of the sonar equation in dB units (Lohrmann, 2001; Gartner, 2004; Hoitink and Hoekstra, 2005),

$$S_v = K_c(E - E_r) + 20 \log(R) + 2\alpha R \tag{7}$$

Here E is echo strength (counts), E_r is the reference receiver noise (counts), K_c is a conversion factor (counts/dB), α is a water and sediment adsorption factor, and the R is the range to the sampling volume. The last two terms in Eq. 7 are known as the major contributors to the two-way transmission loss, $2TL$, in acoustic energy as a wave travels from the emitter to the control volume and back,

$$2TL = 20 \log(R) + 2\alpha R \tag{8}$$

The first term in Eq. 8 accounts for loss due to spreading, and the second term accounts for adsorption. The adsorption coefficient, α, can be decomposed to reflect adsorption from the water and that due to sediment, $\alpha = \alpha_w + \alpha_s$. α_w is a function of pressure, salinity, and frequency; however, for $f = 10$ MHz, α_w can be taken as $\alpha_w = 26.9$ and does not vary with salinity (Lohrmann, 2001). Estimates for α_s can be made assuming uniform size particle (Urick, 1983) as,

$$\alpha_s = \left[\frac{k^4 r^3}{96\rho_s} + \frac{ks(SG-1)^2}{2\rho_s(s^2 + [SG + \delta]^2)} \right] \frac{20}{\ln(10)} C \tag{9}$$

where, k is the wave number (m^{-1}), r is particle radius (m), $s = [9/(2\beta r)]\,[1 + 2/(\beta r)]$, $\beta = \sqrt{\pi f/\nu}$, f is frequency, ν is the kinematic viscosity of water (m^2/s), SG is the specific gravity of the sediment, $\delta = [1 + 9/(\beta r)]\,/2$, and C is the concentration (kg/m^3).

For the Vectrino, R and α_w are constants ($R \approx 0.05$), and combining Eq. 6 and 7 gives,

$$\log(C) = K_c(E - E_r)/10 + c_1 + c_2\alpha_s \tag{10}$$

where $\alpha_s = \alpha_s(C)$. For reasonably low concentrations ($C \leq 1000$ mg/L), $\alpha_s 2R$ is relatively small compared to the other terms and can be neglected. Taking $K_c(E - E_r) \cong SNR$, results in linear relationship between the Signal to Noise Ratio, SNR (dB), and the logarithm of C,

$$\log(C) = c_1 SNR + c_2, \quad \text{or} \quad C = 10^{(c_1 SNR + c_2)} \tag{11}$$

The coefficients c_1 and c_2 are sediment and velocimeter dependent parameters that can be found through linear regression applied to experimental measurements of C and the corresponding average SNR value. It should be stressed that such calibrations are intrinsically dependent on the sediment properties of the suspension.

4 METHODS

This relation between S_v and C was examined for the Vectrino over the concentration ranges from $0.0008 - 2.8$ g/L using tap water and Kaolin clay. For the tests, the Vectrino "power" and "velocity range" parameter settings were varied at each concentration level to explore the effect of the user set parameters on the $C = C(SNR)$ relationship for a range of typical values, i.e. Power = (High, Low+) and Nominal Velocity Range = (± 0.3, ± 1.0 m/s). The test were conducted in a tank of known volume of water, and Kaolin clay ($d_{50} \approx 10$ μm) was systematically added to create the desired concentrations. All suspensions were continuously mixed at a constant rate during data acquisition. 3000 data points were collected at 25 Hz (2 minute samples) for each of the 148 different experimental combinations.

5 RESULTS

At each concentration level, the average SNR (dB) values for the time series were averaged per receiver and then averaged over the four receivers to give an overall average SNR for each experimental condition. The data was grouped first by transmitter power level and then by velocity range setting and plotted to examine the linearity expected by Eq. 11 (Fig. 1). Fig. 1a shows that the Vectrino quickly reached a saturation level around $SNR \approx 23$ (dB) where increases in concentration result in no further increase in SNR value. As expected, the concentration at which this happens, C_{sat}, is a function of the power setting since a reduction in the emitted intensity will result in a reduction in the echo. For Low+ power,

C_{sat} = 100 mg/L, whereas for the High power setting, C_{sat} = 10 mg/L (Fig. 1b,c). Overall, user set nominal velocity range had no significant effect on the measured *SNR* values.

Below the saturation condition, $C < C_{sat}$, both power levels yield the linear response of $C \propto 10^{(c_1 SNR + c_2)}$ anticipated by Eq. 11 (Fig. 1c). Increasing the power from Low+ to High results in a constant shift of the linear portion of the response towards higher *SNR* values for a given concentration (Table 1). Since the slope remains constant, the linear portion of the curve for which $C_i < (C_{sat})_i$ can be modeled with the coefficients obtained for the Low+ power settings and a modified signal to noise ratio, $SNR^* = SNR - \Delta$, where Δ is the difference in dB between the two power settings (Fig. 1d). For the Vectrino, $\Delta = 7.5$ dB between Low+ and High power settings.

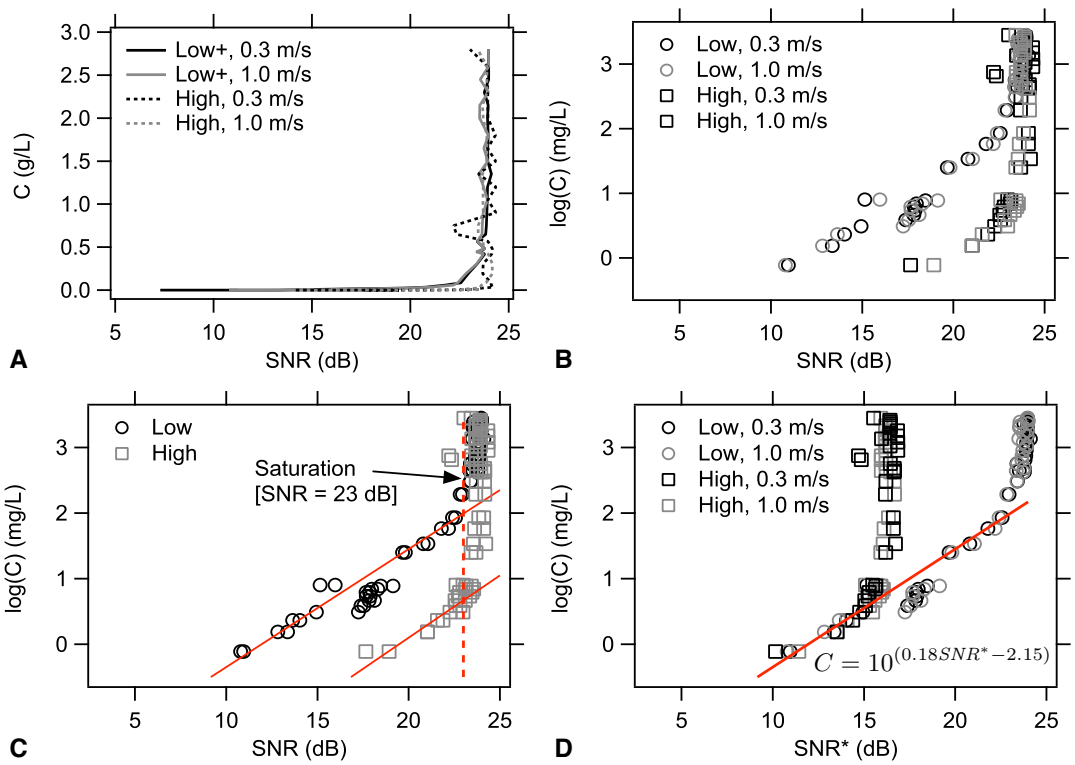

Figure. 1: Summary of results for the four conditions. (A) Suspended sediment concentration C in g/L as a function of *SNR*; (B-C) log(C) versus *SNR* (C in mg/L); and (D) C versus SNR^* along with the fit regression equation.

Table 1: Regression results for C in mg/L

Power	C_{sat} (mg/L)	c_1	c_2
Low+	100	0.18	-2.15
High	10	0.19	-3.7

6 CONCLUSIONS

This study has examined the relationship between the suspended sediment concentration of Kaolin clay and the Vectrino measured *SNR* value in a laboratory. Results show that the Vectrino reaches a saturation condition in *SNR* response at $C = 10$ mg/L for a power setting of High and $C = 100$ mg/L for a power setting of Low+. The user setting for the nominal velocity range had little effect on the relationship between concentration and *SNR* . For concentrations less than saturation, a proportionality between the logarithm of concentration and the *SNR* was found. This suggests that within this range, the Vectrino is a useful tool for recording simultaneous velocity and SSC time series data for sediment flux and fall velocity analysis.

A practical limitation in the methodology outlined in the study is the limit set on particle size by the acoustic frequency. The relationships discussed are based on the Rayleigh scattering model which is restricted to the particle size range $d < k^{-1}$, which translates to $d < 50$ μm for the 10 MHz system(Lohrmann, 2001; Hoitink and Hoekstra, 2005). The Kaolin primary particles do fit the criteria of $d < 50$ μm; however, it is unknown as to how flocculation might have affected the results.

REFERENCES

Fugate, D. C. and Friedrichs, C. T. (2002). Determining concentration and fall velocity of estuarine particle populations using ADV, OBS, and LISST. *Continental Shelf Research*, 22(11-13):1867–1886.

Gartner, J. W. (2004). Estimating suspended solids concentrations from backscatter intensity measured by acoustic Doppler current profiler in San Francisco Bay, California. *Marine Geology*, 211:167–187.

Hoitink, A. and Hoekstra, P. (2005). Observations of suspended sediment from adcp and obs measurements in a mud-dominated environment. *Coastal Engineering*, 52(2):103–118.

Hosseini, S. A., Shamsai, A., and Ataie-Ashtiani, B. (2006). Synchronous measurements of the velocity and concentration in low density turbidity currents using an Acoustic Doppler Velocimeter. *Flow Measurement and Instrumentation*, 17(1):59–68.

Lohrmann, A. (2001). Monitoring sediment concentration with acoustic backscattering instruments. Nortek Technical Note 003, Nortek AS.

Lohrmann, A., Cabrera, R., and Kraus, N. (1994). Acoustic-doppler velocimeter (ADV) for laboratory use. In *Proceedings of Conference on Fundamentals and Advancements in Hydraulic Measurements and Experimentation*, pages 351–365, Buffalo, NY. American Society of Civil Engineers.

Maddux, T. B., Nelson, J. M., and McLean, S. R. (2003). Turbulent flow over three-dimensional dunes: 1. free surface and flow response. *Journal of Geophysical Research*, 108(F1):6009.

Nikora, V. and Goring, D. (2000). Flow turbulence over fixed and weakly mobile gravel beds. *Journal of Hydraulic Engineering*, 126(6):679–690.

Nikora, V. I. and Goring, D. G. (2002). Fluctuations of suspended sediment concentration and turbulent sediment fluxes in an open-channel flow. *Journal of Hydraulic Engineering*, 128(2):214–224.

Rusello, P. J., Lohrmann, A., Siegel, E., and Maddux, T. (2006). Improvements in acoustic doppler velocimetery. In *The 7th International Conference on Hydroscience and Engineering*, Philadelphia, USA. IAHR and Drexel University.

Strom, K. B. and Papanicolaou, A. N. (2007). ADV measurements around a cluster microform in a shallow mountain stream. *Journal of Hydraulic Engineering*, 133(12):1379–1389.

Urick, R. J. (1983). *Principles of underwater sound*. McGraw-Hill.

Voulgaris, B. and Trowbridge, J. H. (1998). Evaluation of the acoustic Doppler velocimeter (ADV) for turbulence measurements. *Journal of Atmospheric and Oceanic Technology*, 15:272–289.

Voulgaris, G. and Meyers, S. T. (2004). Temporal variability of hydrodynamics, sediment concentration and settling velocity in a tidal creek. *Continental Shelf Research*, 24:1659–1683.

The Connectivity of Upland and Instream Processes

Athanasios (Thanos) N. Papanicolaou[(1)] and Philip Ellis[(2)]

[(1)]Associate Professor, Robert and Virginia Wheeler Faculty Fellow in Engineering, Dept. of Civil and Environmental Engineering, IIHR-Hydroscience and Engineering, University of Iowa, Iowa City, IA 52242, U.S.A., phone: +1 319 335 6448; fax: +1 319 335 5238 ; e-mail: apapanic@engineering.uiowa.edu

[(2)]Graduate Research Assistant, Dept. of Civil and Environmental Engineering, IIHR-Hydroscience and Engineering, University of Iowa, Iowa City, IA 52242, U.S.A., phone: +1 319 335-5638; e-mail: philip-ellis@uiowa.edu

ABSTRACT

The transport dynamic and fate of sediments in rivers is closely interrelated to upland activities within a watershed. Commonly, much of the degradation of surface waters in rivers is linked to excessive fine sediment and sediment-bound pollutants coming from the uplands. Phosphorus, some pesticides, most metals, and many organic compounds are transported to the stream primarily adsorbed to fine sediment. Different land use activities in a watershed contribute to the increased influx of fine sediments and pollutants into streams. This research seeks to provide a methodology to qualitatively describe the inputs from the uplands into a stream segment, i.e., to account for the connectivity of upland and instream processes.

In order to link fate of sediment within the river with upland activities, this research aims to integrate two models, namely, WEPP an upland non-point source pollution model with 3ST1D, an instream model that can handle inputs of silts and clays. The analysis is performed in the Clear Creek Watershed of Eastern Iowa using existing data for model calibration and verification.

INTRODUCTION

The components of a watershed may be simplified into three parts: hill-slopes, floodplains, and streams (Figure 1). Each element has its own complexities and interactions with the others. First, the hill-slopes shall be considered to be made up of two different mechanisms: rill and inter-rill areas. The rill areas are considered to be ditch-like in nature and carry concentrated flow directed towards the nearest link to lesser elevations. The inter-rill areas are sections of land that are in-between and above the rills carrying overland flow. These two components are considered the most temporally complex because of the intricacies of sediment movement. Second, the flood plains are directly adjacent to the streams and allow for inundation during large events. Though a large part of the floodplain's functionality is for inundation, it too has many different components that can affect the morphology of the system. The floodplain's mechanisms include wetlands, gullies, stream-bank (collapse and erosion), an assortment of head-cuts, and other nuances making up the various

sinks/sources involved with sediment entrainment and availability. Lastly, the streams, which are the connectors for the vast watershed systems and have been the heaviest studied, seem to maintain a certain level of ambiguity. Researchers have been able to model and predict some of the hydraulic and transport mechanisms of in-stream processes, but predictions are mostly reserved for some finite control volumes and specific characteristics. Even under these circumstances, the models must then be verified by some amount of ground truth. Therefore, whatever amount of knowledge we have concerning a watershed system's components, we know much less about the connectivity and interactions of each.

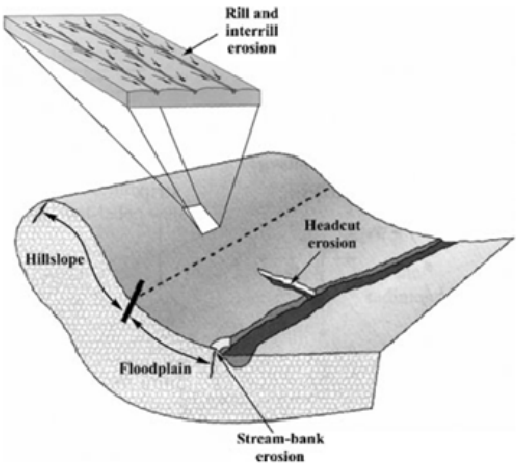

Figure 1. Sketch of the hillslope, floodplain and instream components

OBJECTIVE

The overarching objective of this research is to show the plausibility of numerical models simulating upland erosion and transport throughout a watershed. Specifically, this research will provide, for the first time, the interconnectivity between upland erosion and instream sediment transport processes using a didactic blend of field data and numerical models.

METHODOLOGY

Study Area

The study area is located within the Clear Creek Experimental Watershed (CCEW). The CCEW is a HUC-10 (Hydrological Unit Code) watershed located in east-central Iowa within Iowa and Johnson Counties (Figure 2). The CCEW drains approximately 270 km^2 into the Clear Creek River which discharges into the Iowa River slightly North of Iowa City, IA. This research is focused in the headwaters of the system, more specifically within the South Amana Catchment (SAC). The SAC is in the northwest corner of the CCEW and encompasses 26 km^2. Some of the highest erosion rates in the CCEW are in this catchment and result from a combination of swelling and highly erodible soils with steep gradients and intensive

agriculture. It is predominantly rural with only single farmsteads in the catchment borders. The SAC is mostly row-crop agriculture generally consisting of maize and soybean production. The dominant soil layer in the SAC is silty clay loam. As can be seen in Figure 4, the southern sub basin of the uplands is comprised mostly of Tama, and in the northern region Downs is the most prominent, while the floodplain soils are predominantly Colo (Papanicolaou and Abaci 2008). When simulating overland flow, topography of the watershed is vitally important, specifically for determining the shape of hillslopes (concave vs. convex). Through GIS analysis techniques it has been determined that the SAC consist mainly of concave hillslope structure. In addition, the elevation ranges from 235 to 274 m above mean sea level, and the average gradient is 4%, with a range of 1 to 10% (Papanicolaou and Abaci 2008). The outlet for the Clear Creek South Amana Catchment is a typical stream of the Midwest. Being a fairly small, 2nd order stream, it is un-gauged with no historical record concerning the flow regime.

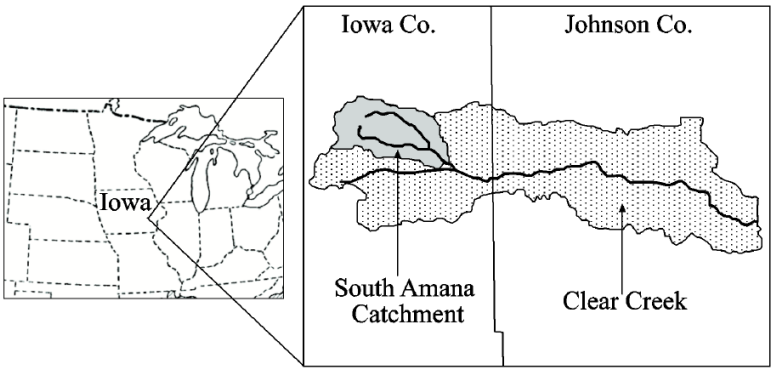

Figure 2. The South Amana Catchment in the Clear Creek Watershed, IA

Field data and instrumentation

Various instruments were deployed at the SAC outlet to record the topography of the region of interest, determine the bed composition, perform flow measurements, and gauge the suspended load. Surveying was carried out by using a Leica-TC 605 Total Station in order to determine the exact geometry of the SAC outlet. Extensive bed sampling was undergone to determine the grain size distribution of the bed. Flow measurements were conducted by using a 3-D Side Looking Flow Tracker ADV manufactured by SonTek. The Flow Tracker ADV had a velocity range of 0.001 – 4 m/s and an accuracy of ±1% of the measured velocity. Mean flow measurements of the velocity in a cross-section were used to determine the flow discharge.

Turbulent measurements were conducted by using a field ADV with a higher sampling frequency than the Flow Tracker ADV. Although turbulence strongly influences the velocity distribution, shear stress, energy transfer, sediment transport, and spread of pollutants in river channels (Sukhodolov, 1998), results from ADV measurements are outside the scope of this paper. It is important to note, though, that accurate measurements of depth-averaged velocity were derived from these measurements and are vital for validation purposes. Stage measurements were taken using Pressure Transducers manufactured by Global Water Instrumentation Inc. One pressure transducer was fixed at the exit of the reach at a known location, and another

was installed for redundancy at the entrance of the reach. In order to verify the pressure transducers, rulers were fixed at two locations along the stream and relative stages were recorded during site visits. The pressure transducers recorded the depth and time at an interval of 15 minutes, giving us data to create continuous stage hydrographs for any given precipitation event. From this stage information, once coupled with flow data, a stage discharge curve was created and is useful for any storm event. Suspended sediment loads were measured by way of a volumetric sediment sampler, namely Sigma 900 Max Portable Samplers. Volumetric samples were taken regularly on a 24hr schedule, and select precipitation events were captured at a 1 hour sampling rate.

Uplands Erosion Model

To numerically simulate upland erosion the Water Erosion Prediction Project (WEPP) model was utilized. WEPP is a process-based erosion simulation model developed by the United States Department of Agriculture (USDA). based on physical parameters. A physically based distributed watershed model (such as WEPP) ventures to account for an exhaustive amount of parameters while allowing the user to specify a forcing. A comprehensive review of the model formulation is available in Flanagan and Nearing (1995). Papanicolaou and Abaci (2008) have shown that WEPP, as a physical-based distributed model, can adequately simulate runoff and erosion processes for larger watersheds (e.g., 26 km^2) when the flow/sediment pathways are well understood. The key data needed for WEPP simulations are the following: rainfall patterns for specific events (depth, distribution, and intensity), topography, soil characteristics (hydraulic conductivity, erodibility criteria, etc.), and land management regimes.

One of WEPP's most defining and appealing assets is the model's ability to predict rill and interrill erosion. WEPP solves the sediment continuity equation for rill erosion and provides results of rill width and depth within a hillslope profile. The driving sediment transport equation for rill erosion in the model includes the steady-state sediment continuity equation for a hillslope given as

$$\frac{dG}{dx} = D_f + D_i$$

where G is sediment load (kg/s/m), D_i is the interrill erosion rate (kg/s/m^2) or interrill source term, and D_f can be rill detachment or deposition rate (kg/s/m^2). D_f is detachment in rills when the applied hydraulic shear stress exceeds the critical shear stress of the soil and when the sediment load is less than the sediment carrying capacity. Rill detachment is

$$D_f = K_r(\tau_f - \tau_c)\left(1 - \frac{G}{T_c}\right)$$

where K_r is a rill erodibility parameter (s/m), τ_f is bed shear stress exerted by the fluid (Pa), τ_c is the critical shear stress (Pa), and T_c is sediment transport capacity (Kg/s/m). Net deposition in the rill is computed when sediment lad, G, is greater than sediment transport capacity, T_c. The equation for deposition follows:

$$D_f = \frac{\beta V_f}{q}(T_c - G)$$

where V_f is the effective fall velocity for the sediment (m/s), q is unit discharge in the rills (m^2/s), and β is a raindrop induced turbulence coefficient.

Instream Model

To simulate flow and sediment transport within the SAC outlet the Steep Stream Sediment Transport 1-Dimensional (3ST1D) model was utilized (Papanicolaou et al. 2004). 3ST1D was chosen based on the following considerations: First, the section of interest (the SAC outlet) is comprised of a heterogeneous bed material (Figure 3), classified as silty-sand (ASTM D2488), and 3ST1D can handle bed mixtures consisting of cohesive and sand materials. Second, the stream reach being modeled, is predominantly unidirectional and free from any sinuosity. Therefore, secondary currents are minimal and computationally expensive programs, such as 2-Dimensional and 3-Dimensional models are unnecessary.

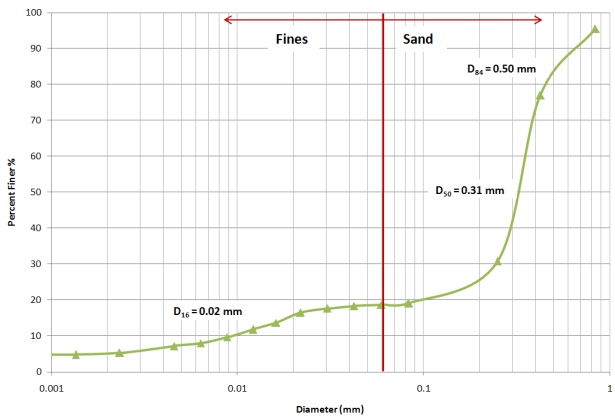

Figure 3. Grain size distribution for the outlet of the SAC. D_{16}, D_{50} and D_{84} represent the characteristic grain sizes for the 16th, 50th and 84th percentiles, respectively (i.e. 84% of the bed material is less than 0.50 mm in diameter)

Instream numerical modeling is explicitly intertwined with the uplands from which it is fed, but, from the modeling perspective, streams operate under an entirely different set of parameters. Descriptions of the stream reach such as geometry and bed composition are imperative parameters. Also, specific flow characteristics, such as depth, discharge, and velocity, are vital for attaining accurate simulations.

Flow is calculated by means of the 1-D Saint-Venant equations. The Saint-Venant equations are derived from the Navier-Stokes equations which express the law of conservation of mass and momentum along the flow direction (Papanicolaou et al. 2004). Sediment calculations require the user to apply sound engineering judgment. There are a plethora of empirical equations in the literature that may be utilized, but only for specific physical and climatic conditions. Understanding the sediment composition, flow regime, channel form and other such properties of the SAC outlet are vital when determining appropriate transport equations.

The sediment calculations follow a step by step process. First, the channel's resistance to flow is determined (Manning's n and friction factor). Next, incipient motion criterion for the commencement of sediment motion is determined based on the critical erosional strength. Critical erosional strength is defined as the strength

provided by interparticle forces that resist erosion and the value is set by the user during the calibration process. Next, the flow's transport capacity for a given section is calculated via an equation formulated by Yalin (1963). Next, an erosion and deposition algorithm is employed (Papanicolaou et al 2004), followed by a suspended concentration model, and finally the bed is updated for each successive time-step.

Calibration and Verification

The simulations for this study are meant to replicate the natural environment, but the user must exploit some ground truth measurements to anchor them in the real world. Therefore a calibration and verification process is used to improve the accuracy of our models.

For a watershed model a successful calibration will minimize the difference between observed and predicted values of sediment yield while maintaining validity over a range of events. Calibration starts with flow and then moves to sediment (Santhi et al., 2001), and this is the philosophy we will consider with our design. Since the input parameters in a watershed model are cumbersome in number, it is important to know the meaningful ranges for each of the parameters. The dominant factors governing the sediment yield from a watershed are precipitation, rill/interrill erodibility, rill and interrill residue cover, critical erosional strength, and hydraulic conductivity (Nearing 1990).

For the calibration of instream models, the process should prove accurate prediction of flow velocities and depths in the channel, while predicting closely the deposition and detachment rates within the reach. Similar to the watershed model, predictions should be based on input parameters and boundary conditions that are reasonable and reflect the natural processes that occur within the stream reach.

RESULTS

Below are some of the results that will aid describing the interactions between uplands erosion and instream processes via field data and numerical modeling. First we shall present some of the input data for the uplands erosion model WEPP; this will include historical rainfall data for the SAC, soil characteristics, land management practices, and topography. Second we shall present some of the input data for the instream numerical model 3ST1D; this will include bed composition, stage hydrograph, stage discharge relationship and velocity measurements. Also, to compliment both models, a sediment rating curve and ADV measurements are presented.

WEPP inputs include the following: Topography, which was previously discussed, soil characteristics (Figure 4), and land management regimes (Figure 4), and rainfall patterns for specific events (Figure 5). With these inputs WEPP will estimate the water discharge and sediment yield resulting from specific precipitation events. In order to validate the upland erosion model we shall utilize the following tools: continuous stage hydrograph (Figure 5) coupled with the stage discharge relationship (Figure 6), and the sediment rating curve (Figure 7) created from numerous suspended sediment samples.

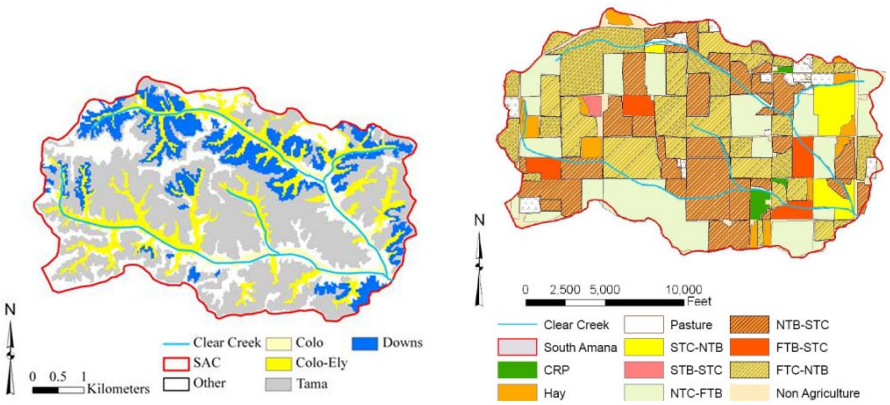

Figure 4. Soil characteristics and crop rotations for the SAC (Papanicolaou and Abaci 2008)

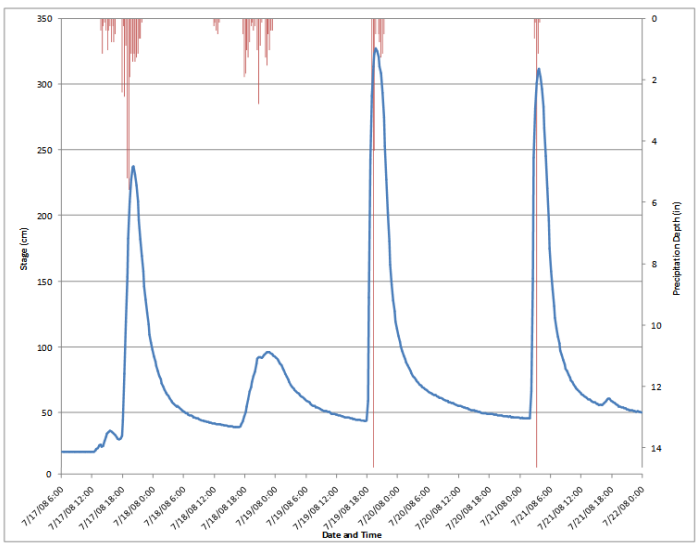

Figure 5. Time series showing rainfall in the SAC and stream hydrograph for the SAC outlet

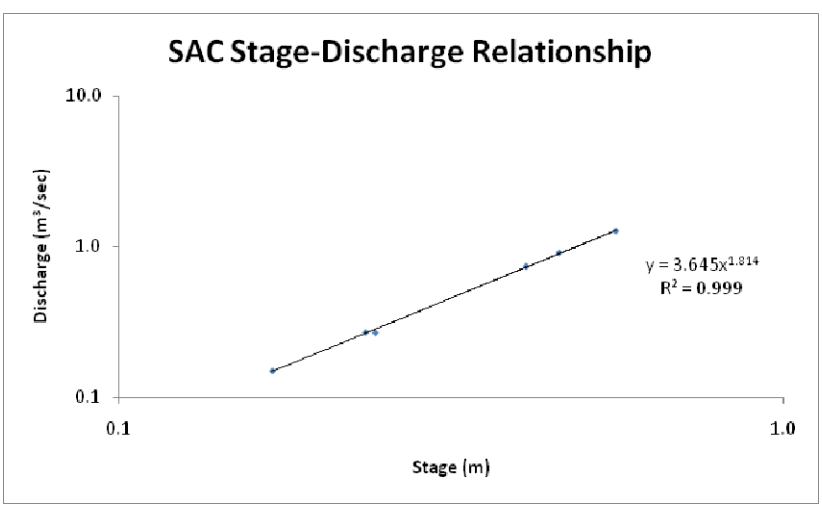

Figure 6. Stage discharge relationship for the SAC outlet

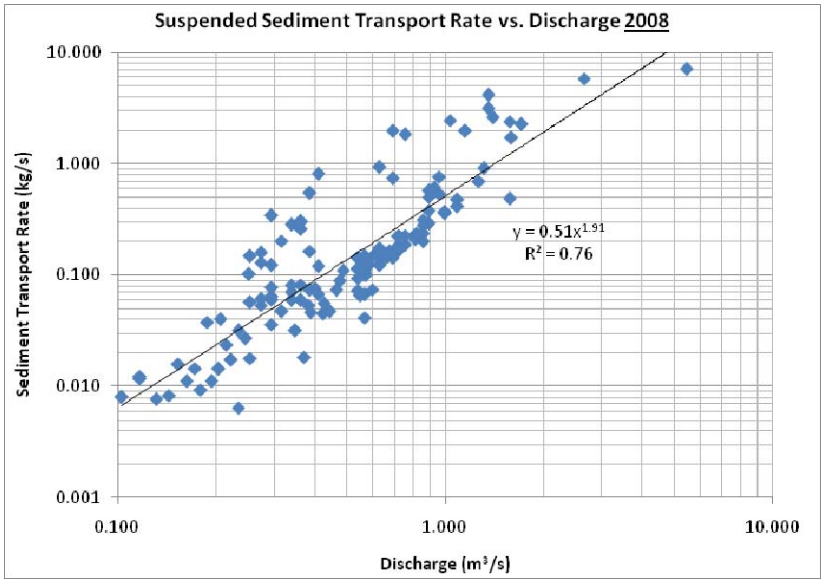

Figure 7. Sediment rating curve for the SAC

3ST1D model inputs are summarized in Table 1. With these inputs 3ST1D will estimate the flow velocity and depth, bed evolution, and sediment transport rate resulting from specific precipitation events (WEPP inputs). In order to validate the in-stream model we shall utilize the ADV velocity measurements (Figure 8) and the stream hydrograph (Figure 5) for the hydrodynamic component, whereas for the sediment transport component we shall use the sediment rating curve (Figure 7).

Table 1. Input variables for the 3ST1D model and their respective sources of origin

Input	Source
Geometry and bed elevation	Survey
Discharge	WEPP
Depth	Stage-discharge relationship
Sediment Inflow	WEPP
Bed Composition	Grain Size Distribution
Sediment Transport Equation	Yalin (1963)
Erosion deposition algorithm	Papanicolaou et al. (2004)
Incipient motion criterion	Set during calibration process
Manning's n	Set during calibration process
Active layer thickness	Papanicolaou et al. (2004)

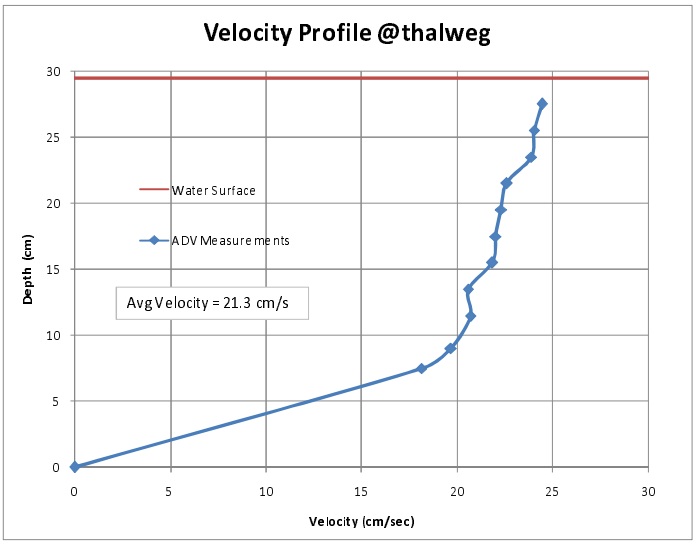

Figure 8. ADV velocity measurements at the SAC outlet

CONCLUSION

Through the various instrument measurements and constant observations, we hope to have developed a concise representation of the in-stream processes of the South Amana Catchment outlet, along with a quantitative assessment of erosion occurring in the uplands of the watershed. By coupling the already established models (WEPP and 3ST1D) a digital watershed may be developed for the South Amana Catchment. Though the technology is not fully developed this research will further the knowledge of interactions of the fluvial system at a catchment level, and can lay the framework for watershed management on larger scales.

REFERENCES

Chang (1988), Fluvial Processes in River Engineering, John Wiley and sons, Inc.

Flanagan, D. C., and Nearing, M. A. _1995_. "Water erosion prediction project hillslope profile and watershed model documentation." NSERL Rep. No. 10, National Soil Erosion Research Laboratory West Lafayette, Ind.

Nearing (2005), "Modeling responses in soil erosion and runoff to changes in precipitation and cover," Catena 61 (2005) 131-154.

Papanicolaou (2004), "One-dimensional hydrodynamic/sediment transport model applicable to steep mountain streams," Journal of Hydraulic Research, VOL. 00, No. 0 (2004), pp. 1-19.

Papanicolaou and Obaci (2008), "Upland Erosion Modeling in a Semihumid Environment via the Watershed Erosion Prediction Project Model," Journal of Irrigation and Drainage Engineering, ASCE, VOL. 134, No. 6.

Santhi et al. (2001), "Validation of the SWAT model on a large river basin with point and non point sources," Journal of the American Water Resources Association, Volume 37, No 5.

Sukhodolov (1998), "Turbulence structure in a river reach with sand bed," Water Resources Research, Volume 34, No 5 pages 1317-1334.

Yalin (1963), "An expression for bed-load transportation," Journal of Hydraulic Division, VOL. 89, No. HY3, pp. 221-250.

Upstream Intrusion Effect of CSO Event in Bubbly Creek, IL

XIAOFENG LIU [1], SUMIT SINHA[2], DAVIDE MOTTA[3], and MARCELO H. GARCIA[4]

[1] Post-doctoral Research Associate, Dept. of Civil and Environmental Engineering, University of Illinois, Urbana, Illinois 61801, USA. E-mail: liu19@illinois.edu
[2] Research Assistant, Dept. of Civil and Environmental Engineering, University of Illinois, Urbana, IL 61801, USA. E-mail: sinha6@illinois.edu
[3] Research Assistant, Dept. of Civil and Environmental Engineering, University of Illinois, Urbana, IL 61801, USA. E-mail: dmotta2@illinois.edu
[4] Professor and Director of the Ven Te Chow Hydrosystems Lab., Dept. of Civil and Environmental Engineering, University of Illinois, Urbana, IL 61801, USA. E-mail: mhgarcia@illinois.edu

ABSTRACT

Bubbly Creek is a tributary of the Chicago River, IL. It is used mainly as a Combined Sewer Overflow (CSO) route to the Chicago River. The CSO events from the Bubbly Creek carry sewers into the main channel and have a great impact on the overall water quality downstream. The sewer water mixed with particles usually has a higher density than the ambient water in the main channel. Upstream intrusion of sewer water is possible during the CSO event. In this paper, the three-dimensional environmental fluid dynamics code (EFDC) is used to simulate the CSO event in Bubbly Creek. The main purpose is to investigate the extent of the upstream intrusion and its implications for the water quality effects on the Chicago River. The results show that the front location is a function of the relative CSO flow and the CSO particle concentration.

INTRODUCTION

The Chicago River is a vital part of Chicago, Illinois, which is the third largest city in the United States with a population of more than 3 million. Bubbly Creek is a tributary, which is also known as South fork of the Chicago River's South branch. The location of the river system is shown in Figure 1. Bubbly Creek is notorious for its heavy pollution because the meatpacking industry used it as an open sewer and massive quantities of animal remains were dumped into it in the 1900s (Hill, 2000).

Under wet weather condition, the discharge of Combined Sewer Overflow (CSO) from Bubbly Creek into the Chicago River induces high flow velocities and high shear stresses on the stream bed which has poor sediment quality. Therefore, Bubbly Creek, which is a frequent source of contaminant into the Chicago River, plays an important role for the water quality of the whole river system.

To fully understand the transport and fate of the pollutants, it is important to know the flow structures associated to the CSO events. Because of its high content of particulate matters and the resuspension/deposition process, the sewer flow in the Bubbly Creek could be heavier than the ambient water in the Chicago River and density current could happen at the junction. Polluted heavy water might flow upstream in the Chicago River as an intruding underflow. In this research, the specific questions which need to be answered are how long the impaired water can travel upstream, what the control factors

are, and what are their environmental implications. Besides this density current study, water quality modeling has also been done using a two-dimensional BOD and DO model to study both short term and long term changes (Motta *et al*, 2009) .

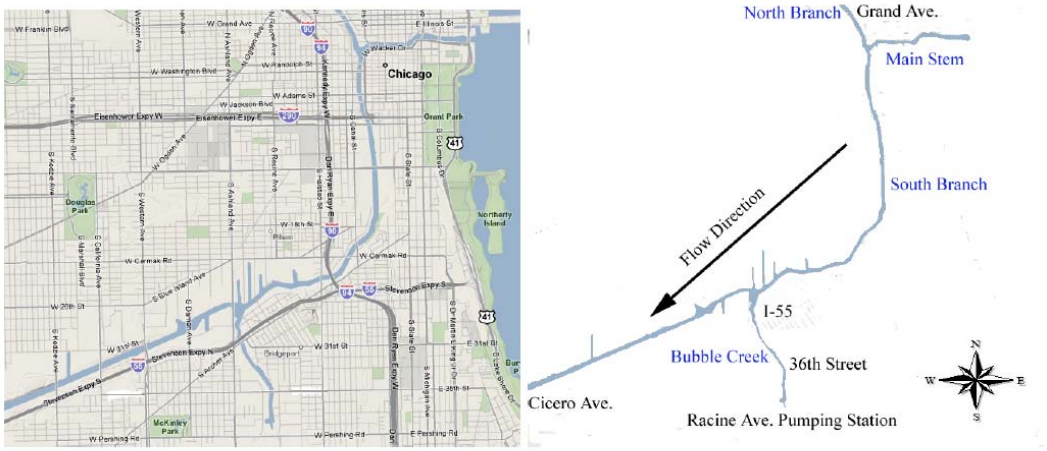

Figure 1. Aerial view of the Chicago River, Illinois: (a) Whole River Domain (b) River Segmentation and Boundaries.

The three-dimensional Environmental Fluid Dynamics Code, EFDC, is used to simulate the CSO dynamics (Hamrick 1992). EFDC is a public domain code which is supported by the US Environmental Protection Agency (EPA) and has been widely used for many rivers and estuaries. EFDC uses stretched or sigma vertical coordinate and Cartesian or curvilinear, orthogonal horizontal coordinate. It solves the three-dimensional vertically hydrostatic, free surface, turbulent-averaged equations of motions for fluid. Water quality models are also implemented. For this paper, only the hydrodynamics and the sediment transport part of the EFDC code are used. For calibration purpose, the domain includes the North branch up to Grand Avenue, the Chicago River main stem, the South branch down to Cicero Avenue, and the Bubbly Creek. The total length of the waterway in this domain is 20.3 kilometers (about 12.6 miles). For simulations of density currents due to CSO events, only the portion of the Bubbly Creek and its junction with the main channel is included (Figure 2(b)). The bathymetry data are provided by the United States Geological Survey (USGS) and are shown in Figure 2.

CALIBRATION

Before the model can be used for the density current study, the hydrodynamic part needs to be calibrated. The bottom resistance is one of the important factors which affect the behavior of the river system. In EFDC, the only parameter which needs to be specified for the resistance of river bottom is the roughness height. Equivalent to Manning's roughness coefficient n, it is used in the log law formula when computing the bottom shear stress. Even with the information on the sediment, vegetation, and river geometry, the determination of the roughness height is still a challenge. In this paper, the roughness height is selected as a calibration parameter.

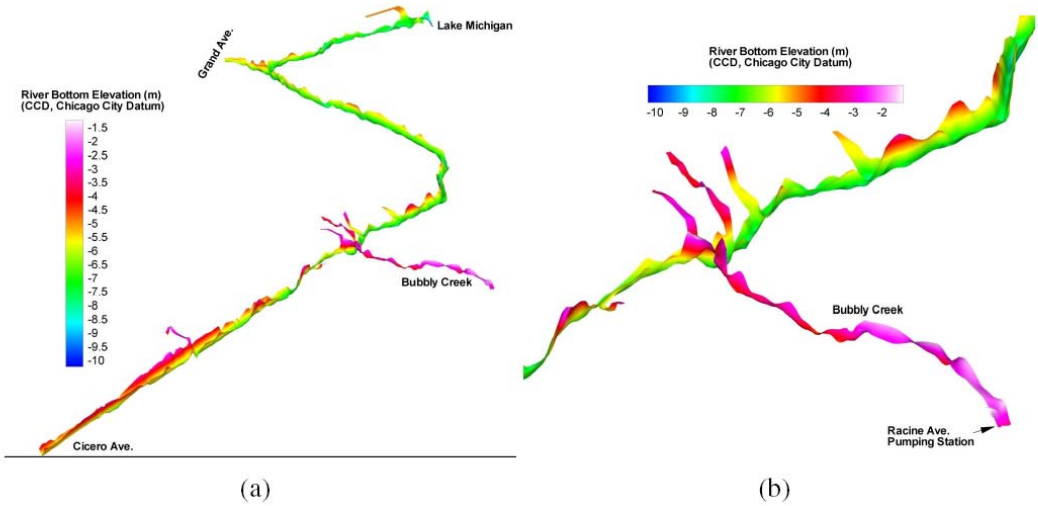

Figure 2. Bathymetry of the Chicago River, IL: (a) Bathymetry of the Whole River (b) Bathymetry near Bubbly Creek.

The boundary conditions and the calibration data are provided by the USGS gauge stations along the river. They include station 05536118 at Grand Avenue, station 05536123 at Columbus Drive, and a new gauge station which is installed at Cicero Avenue. At these gauge stations, water-stage recorders, acoustic velocity meters, and water-temperature sensors are installed. The discharge at the Grand Avenue gauge station and the stage at the Cicero Avenue gauge station form the boundary conditions for the calibration simulation. The measurement from the USGS gauge stations are plotted in Figure 3. The goal of the calibration is that the water surface elevations at the Grand Avenue and Columbus Drive gauge stations are matched. The calibration period is from 01/01/2008 to 03/01/2008. During this period, the Chicago Lock at Lake Michigan is closed and the leakage from the lock is neglected. So the boundary condition for main stem at the Chicago Lock is set as a rigid wall.

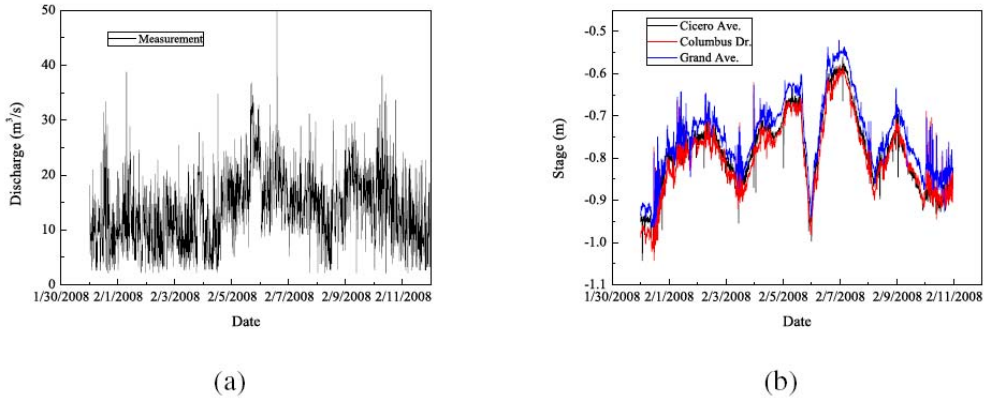

Figure 3. Measurement Data for the Calibration of the Hydrodynamic Model: (a) Flow Discharge at Grand Avenue Gauge Station (b) Stages at Grand Avenue, Columbus Drive, and Cicero Avenue Gauge Stations.

The river system is divided into four segments: North branch, South branch, main stem, and Bubbly Creek. This segmentation is similar to Barkau (1991) and Shrestha and Melching (2003). In each segment, the roughness height (i.e., Manning's *n* coefficient) is uniform. The calibration results for the roughness height are shown in Table 1. The Bubbly Creek has a roughness height of 0.2 m (Manning's *n* value of 0.026) which is higher than the rest of the river system. The calibrated stages at Grand Avenue, Columbus Drive, and Bubbly Creek Junction are plotted in Figure 4.

TABLE 1. Calibrated Values for Roughness Height and Equivalent

Name	Roughness Height	Manning's n from Strickler's formula $n = 0.034 k_s^{1/6}$
North Branch (NB)	0.1	0.023
South Branch (SB)	0.1	0.023
Main Stem (MS)	0.15	0.025
Bubbly Creek (BC)	0.2	0.026

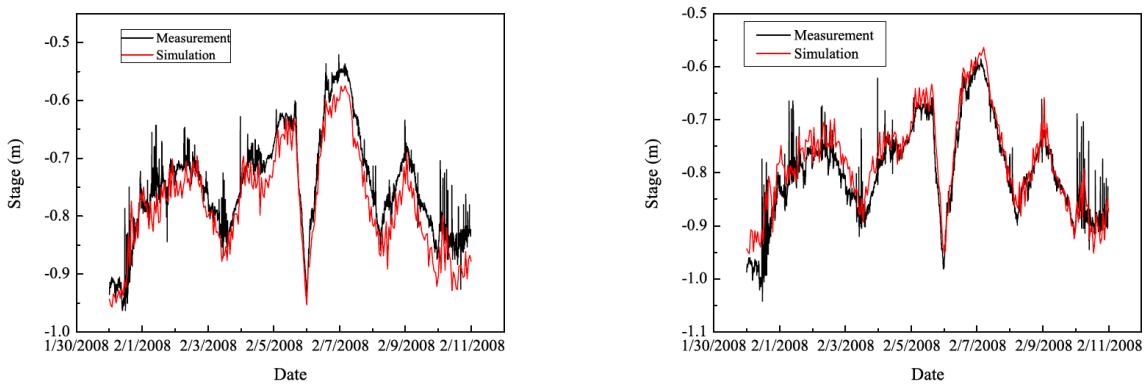

Figure 4. Calibrated Results from the Hydrodynamic Model: (a) Stages at the Grand Avenue Gauge Station (b) Stages at Columbus Drive Gauge Station.

APPLICATION

Since the model is calibrated, the next step is to investigate the transport of the particles and use the results to infer how the CSO event effects on the water quality in Chicago River. The parameters of the CSO particles and river bottom sediments are from measurement. The particle density in the bed cores and the bed surface grabs at the Bubbly Creek junction are 2392 kg/m^3 and 2423 kg/m^3, respectively (Yin *et al.*, 2007). According to USACE (2005), the particle density along the whole length of the Bubbly Creek ranges from 1370 kg/m^3 to 2570 kg/m^3. In this paper, an average value of 2000 kg/m^3 is selected for the particle density. The porosity for the Bubbly Creek is set to a

value of 0.7 from the analysis in Yin *et al.* (2007). For the main channel, a typical value of 0.4 is used. The sediments in Bubbly Creek (both the cores and the grab samples) are fine sand, which have an average diameter of 82 μm, with maximum and minimum diameters of 258 μm and 20 μm (USACE 2005). Particle size distribution measurements were also done for the main channel in 2004 at Archer Avenue, which locates upstream of the junction. The mean diameter in the main channel ranges from 57 μm to 191 μm. Since only one typical particle is used in current research, the mean diameter D_{50} is set to 100 μm.

Following, three major variables are studied, i.e., the main channel (the Chicago River) flow, the CSO flow, and the CSO particle concentration.

Effects of the main channel flow

In order to investigate the effects of the main channel flow, seven cases are simulated (see Table 2). The main channel flow ranges from 1 m^3/s to 30 m^3/s at the Grand Avenue gauge station, according to the USGS measurement. The CSO flow from Bubbly Creek is fixed at 35 m^3/s, which is a typical value when half of the CSO pumps at the Racine Avenue Pumping Station are turned on. The CSO particle concentration is fixed at a typical value which is 1000 mg/l.

TABLE 2. Test Cases for the Effects of the Main Channel Flow

Case #	Main Channel Flow (m^3/s)	CSO Flow (m^3/s)
1	1	35
2	5	35
3	10	35
4	15	35
5	20	35
6	25	35
7	30	35

The typical flow features can be observed in Figure 5. It shows the flow streamlines and particle concentration field around the Bubbly Creek junction at T = 4 hours. The CSO flow from Bubbly Creek is split into three parts due to the effect of density difference, i.e., flow upstream, flow downstream, and flow going up the step into the first slip. Due to the effect of high concentration of particles, the water from the CSO event is denser than the ambient water in the main channel and therefore the density current is formed. Instead of uniquely flowing downstream, part of the CSO flow from Bubbly Creek plunges under the water surface and flows upstream. The distance of this upstream-traveling current is one of the main features which will be investigated. This distance depends on the relative strength of the CSO flow and the particle concentration. Another apparent flow feature is the big recirculation at the junction when the CSO event happens. The big open water space is called the turning basin and is used for the commercial ship transportation. From the water quality perspective, the big recirculation

will stir the bottom of the turning basin and resuspend the polluted sediment and the upstream traveling underflow will bring the pollutant upstream.

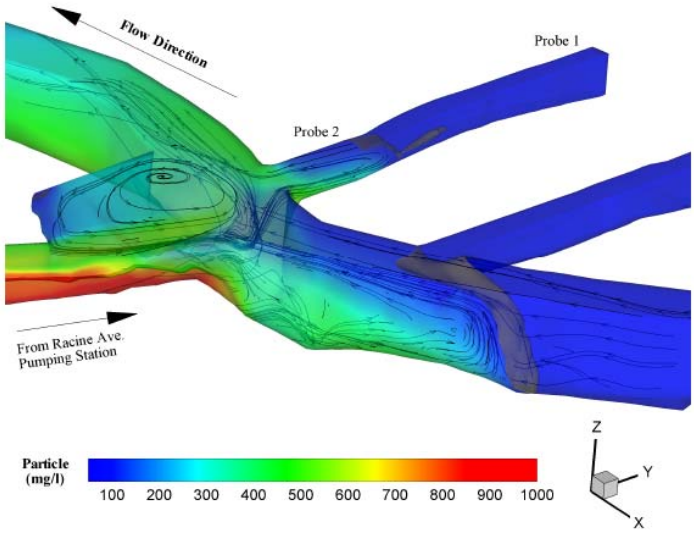

Figure 5. Flow Features at T = 4 Hours for Case 1 (Main Channel Flow = 1 m^3/s, CSO Flow = 35 m^3/s, CSO Particle Concentration = 1000 mg/l).

Figure 6 shows the flow streamlines in the turning basin at different stages of the CSO event. This figure allows for visualizing the flow field around the junction. From the beginning to the end, there is always a big vortex in the turning basin. This is due to the effect of the main channel or the CSO flow, or both. At the initial stage (T = 2 hours), there is another vortex around the first slip. This might be caused by the initial momentum of the CSO flow. With the flow developing, the second vortex around the first slip disappears (T = 4 hours). The flow structure around the turning basin does not significantly vary during the CSO event (compare time = 4 hours and 6 hours). Again, due to the effect of the density current, the CSO flow travels both upstream in the main channel and into slips, as it is evident from the streamlines. When the CSO event ends, the vortex in the turning basin becomes smaller.

In order to evaluate the effects of the main channel flow (when the CSO flow is fixed at 35 m^3/s), the front location and the plunging point are measured. The front point is measured at the point where the front meets the ambient sediment concentration (100 mg/l). The plunging point is defined as the location where the sediment concentration is 150mg/l at the water surface. The coordinate L along the river starts from the downstream origin (Cicero Avenue). The Bubbly Creek junction is located at about L = 700 m. Figure 7 shows the quantitative relation between the front location, plunging point, front slope, and the main channel flow. It is observed that with the increase of the main channel flow, the front location and the plunging point are pushed downstream. The front becomes sharper as the main channel flow increases.

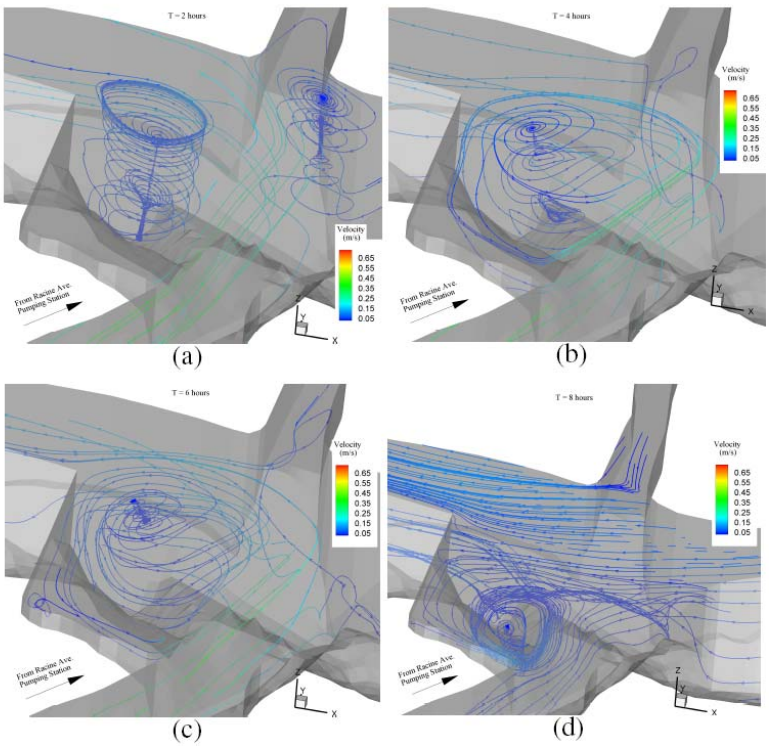

Figure 6. Details of the Flow Feature in the Turning Basin at Different Time: (a) T = 2 Hours (b) T = 4 Hours (c) T = 6 Hours (d) T = 8 Hours

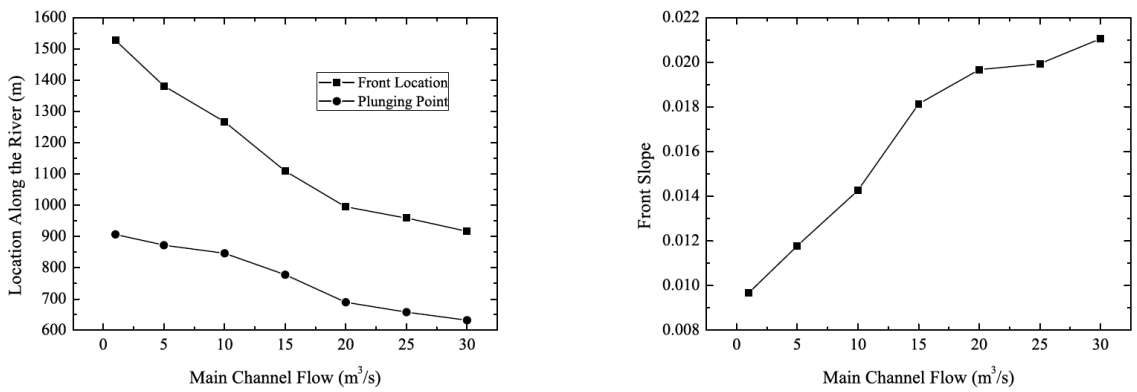

Figure 7. Effects of the Main Channel Flow on the Front Location, Plunging Point, and Front Slope: (a) Front Location and Plunging Point (b) Front Slope.

Effects of the CSO flow

For the effects of the CSO flow, seven cases are simulated (see Table 3). The main channel flow is fixed at 10 m^3/s, which is the average flow in the river according to the USGS measurements. The CSO flow ranges from 20 m^3/s to 120 m^3/s, which corresponds to the cases where only one pump to all six pumps are turned on at the Racine Avenue Pumping Station. The main channel ambient particle concentration is set

to 100 mg/l and the CSO flow particle concentration is set to 1000 mg/l. Case 9 in Table 3 is the same as Case 3 in Table 2.

TABLE 3. Test Cases for the Effects of the CSO Flow

Case #	Main Channel Flow (m^3/s)	CSO Flow (m^3/s)
8	10	20
9	10	35
10	10	50
11	10	75
12	10	90
13	10	105
14	10	120

Figure 8 shows the simulation results for front location, plunging point, and the front slope. The effects of the CSO flow are not as significant as the effects of the main channel flow. With the increase of the CSO flow, the front point and the plunging point quickly increase to their asymptotic values. For CSO flow greater than 50 m^3/s, the front location and the plunging point almost keep constant. This is because the momentum of the CSO flow is restricted in the area of the junction. The upstream intrusion of the pollution is dominated by the buoyancy effect. The slope of the front decreases slightly as the CSO flow increases. However, it reaches an asymptotic value very quickly. The small increase of the slope when the CSO flow is 90 m^3/s may be due to the uneven bottom of the river.

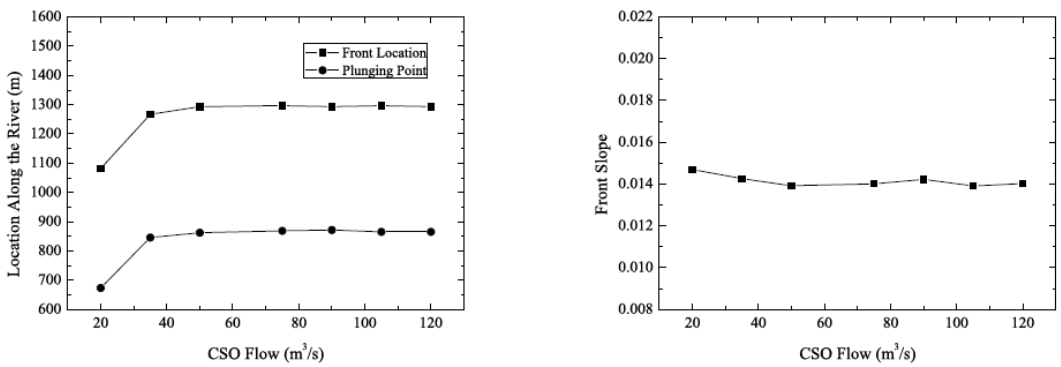

Figure 8. Effects of the CSO Flow on the Front Location, Plunging Point, and Front Slope: (a) Front Location and Plunging Point (b) Front Slope.

Effects of the CSO particle concentration

In this section, the effects of the CSO particle concentration are studied. The main channel flow is fixed at 10 m^3/s and the CSO flow is set at 35 m^3/s, which are both typical values for the river. The main channel ambient particle concentration is set as 100 mg/l. The CSO flow particle concentration ranges from 300 mg/l to 2200 mg/l. This

range was defined according to the CSO water sampling at the Bubbly Creek pumping station.

TABLE 4. Test Cases for the Effects of CSO Particle Concentration

Case #	Main Channel Particle Concentration (mg/l)	CSO Particle Concentration (mg/l)
15	100	300
16	100	600
17	100	1000
18	100	1300
19	100	1600
20	100	1900
21	100	2200

With the increase of the CSO particle concentration, the front travels further upstream. But the momentum of the front getting from the CSO event is not as significant as those cases by varying the CSO discharge. For cases from 17 to 21, since there is a small step just upstream the junction, the front is stopped there for all the cases simulated. That is the reason the front location did not change even the CSO particle concentration is increased to a very high value. The only difference between cases 17 to 21 is that the front concentration is higher when the CSO particle concentration is higher. The slope of the front is a function of the CSO particle concentration. With the increase of the CSO particle concentration, the front slope becomes smaller, i.e. the front becomes less steep. Figure 9 shows the quantitative relationship between the front location, plunging point, front slope and the CSO particle concentration.

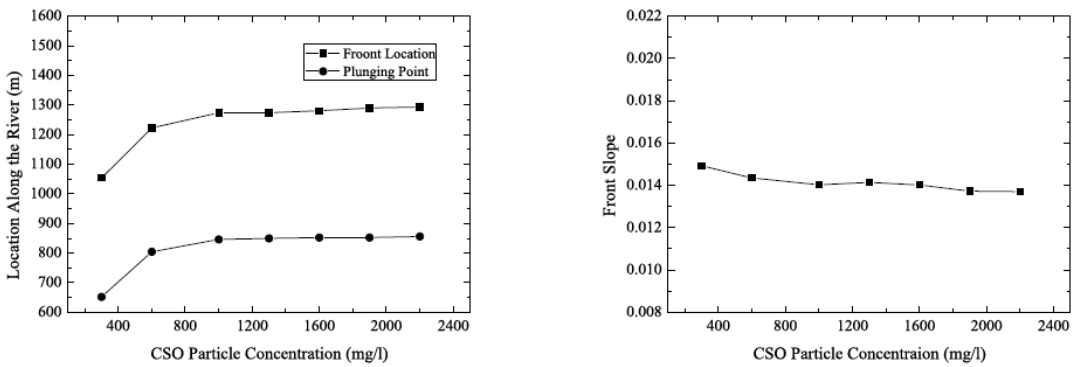

Figure 9. Effects of the CSO Particle Concentration on the Front Location, Plunging Point, and Front Slope: (a) Front Location and Plunging Point (b) Front Slope.

DISCUSSION

From the simulations, the CSO flow and the main channel flow are two competing factors which drive the current when the CSO particle concentration is fixed. Figure 10 shows the dimensionless front location as a function of the relative CSO flow. The dimensionless front location is defined as L_f/H_r, where L_f is the front location and H_r is

the river depth. The relative CSO flow is defined as Q_{cso}/Q_{main}, where Q_{cso} is the CSO flow and Q_{main} is the main channel flow. Regression relations are developed to quantify the dependence of the front location and shape on the relative CSO flow (Figure 10).

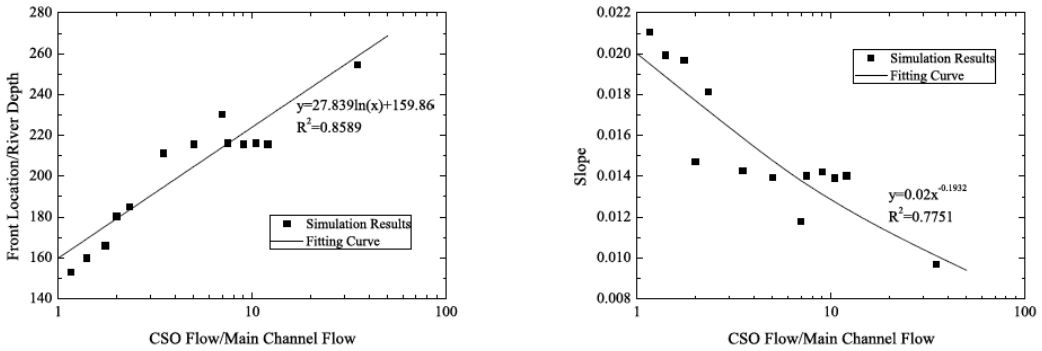

(a) (b)

Figure 10. Effects of the Dimensionless CSO Flow on the Front Location and Front Slope: (a) Dimensionless Front Location (b) Front Slope.

CONCLUSION

Using the CSO particles as an indicator for water quality, it was shown that the pollutant discharged into Bubbly Creek travels upstream in the main channel and also intrudes into the slips. Three most important variables, main channel flow, CSO flow, and CSO particle concentration, were investigated. With the increase of the main channel flow, the front location and the plunging point are shifted downstream. This is due to the flushing effect of the main channel flow. Increasing both the CSO flow and the CSO particle concentration moves the front location further upstream. However the effect of increasing the CSO particle concentration is not as significant as that of increasing the CSO flow.

ACKNOWLEDGEMENTS

This research is supported by the Metropolitan Water Reclamation District of Greater Chicago (MWRDGC). The authors gratefully thank Dr. John M. Hamrick for his helpful discussion and suggestions.

REFERENCES

Barkau, R. (1991). "Modeling of Chicago tunnel and canal system, Appendix 13." *Data Collection and Model Revisions*, Christopher B. Burke Engineering Ltd. to the U.S. Army Corps of Engineers, Chicago District.

Motta, D, Abad, J.D., Liu, X, and García, M.H. (2009).Two-dimensional BOD and DO Water Quality Model for Engineering Applications: The Case of Bubbly Creek in Chicago, Illinois. In Proceedings of ASCE EWRI World Environmental & Water Resource Congress, Kansas City, Missouri

Hamrick, J. (1992). "A three-dimensional environmental fluid dynamics computer code: Theoretical and computational aspects", Virginia Institute of Marine Science, School of Marine Science, The College of William and Mary, Gloucester Point, VA 23062.

Hill, L., (2000), "The Chicago River: A Natural and Unnatural History", Lake Claremont Press.

Shrestha, R. and Melching, C. (2003). "Hydraulic calibration of an unsteady flow model for the Chicago waterway system", submitted to the Metropolitan Water Reclamation District of Greater Chicago, Institute for Urbana Environmental Risk Management, Marquette University, Milwaukee, WI 53201-1881.

USACE (2005). "Collection and analysis of sediment samples from the south fork of south branch, Chicago river", United States Army Corps of Engineers Chicago District.

Yin, K., Viana, P., Zhao, X., and Rockne, K. (2007). "Active capping remediation project: Bubbly Creek turning basin bore log", Applied Environmental Biotechnology Laboratory, Department of Cicil and Material Engineering, UIC.

A Simple Analytical Design Method for Small Alluvial Channels

Bruce M. McEnroe[1], John E. Shelley[2] and C. Bryan Young[3]

[1]Dept. of Civil, Environ. and Arch. Engrg., Univ. of Kansas, 1530 W. 15th St., Lawrence, KS 66045; PH (785) 864-2925; e-mail: mcenroe@ku.edu
[2]Dept. of Civil, Environ. and Arch. Engrg., Univ. of Kansas, 1530 W. 15th St., Lawrence, KS 66045; PH (785) 864-2924; e-mail: johnnyjazzman@ku.edu
[3]Dept. of Civil, Environ. and Arch. Engrg., Univ. of Kansas, 1530 W. 15th St., Lawrence, KS 66045; PH (785) 864-2999; e-mail: cbyoung@ku.edu

ABSTRACT

This paper presents an analytical design method for realignment of small alluvial channels with non-cohesive bed material. This method follows the general approach recommended by the U.S. Army Corps of Engineers and the Natural Resources Conservation Service. The realigned reach is designed to convey the same bankfull discharge and sediment load as a stable reach directly upstream. The length, slope, sinuosity and cross-sectional dimensions of the realigned reach are obtained from an analytical solution to Manning's equation for flow resistance and a simplified version of the Meyer-Peter and Muller equation for bed-load transport. The bankfull width and meander wavelength are obtained from geomorphic relationships for stable natural streams. Consequently, the realigned reach should have stable geomorphic characteristics that are typical of a natural stream in a similar setting.

INTRODUCTION

Highway departments occasionally find it necessary to realign short reaches of small streams in connection with highway improvements or to protect the highway embankment against stream encroachment. Several key goals guide the design of the realigned reach. First, the new reach should have geomorphic characteristics that are typical of a natural stream in a similar setting. These characteristics include the channel's bankfull capacity, cross-sectional dimensions, planform, bottom profile, and bed and bank materials. Second, the realigned reach should be stable, with little change in the bottom profile, planform or cross-sectional dimensions once the channel is established. Third, the realigned reach should eventually provide similar in-stream and riparian habitat as a natural stream in a similar setting. If the stream that must be realigned has been degraded by prior channelization, then a realignment project that meets these objectives will help to restore the natural stream functions.

Analytical methods for natural channel design use hydraulic equations for flow resistance and sediment transport, as well as geomorphic relationships, to determine the channel's cross-sectional dimensions, slope and sinuosity. The objective is a stable configuration with natural geomorphic characteristics that will convey the natural bankfull discharge and the associated sediment load. The Army Corps of Engineers' *Hydraulic Design of Meandering Channels* (Copeland, et al., 2001) and

the Natural Resources Conservation Service's *National Engineering Handbook, Part 654* (NRCS, 2007) present a general framework for the analytical approach to natural channel design.

This paper presents the main elements of a simple analytical design method, termed the Kansas Analytical Method, for small alluvial channels with non-cohesive bed materials. In the Kansas Analytical Method, the realigned channel is designed to convey the same bankfull discharge and sediment load as the nearest stable reach upstream of the design reach. A hydraulic geometry equation relates the bankfull width to the bankfull discharge.

PRELIMINARIES AND FIELDWORK

The design process necessarily starts with the establishment of some boundary conditions and the selection and characterization of the "upstream supply reach." The endpoints of the project reach should be located at riffles wherever possible. The thalweg elevations at the endpoints must be surveyed. The designer must lay out the general alignment of the new reach, exclusive of meanders. The length of this non-meandering alignment is termed the valley length.

A stable reach on the same stream, preferably directly upstream of the project reach, is selected as the upstream supply reach. The selected reach should start and end at riffles and should contain at least one intermediate riffle. The thalweg profile and the channel cross-section at the most representative intermediate riffle are surveyed. The bankfull stage at the representative riffle is identified from field indicators. A bed-material sample from the representative riffle is analyzed to determine the d_{50} particle size (the sieve-opening size through which 50% of the material, by weight, would pass). The Manning resistance coefficient for bankfull flow through the reach is estimated by the best available method, considering the bed and bank roughness and other relevant factors. The bankfull flow condition is approximated as uniform flow, and the bankfull discharge is calculated with the Manning equation using the average bottom slope for the reach and the bankfull cross-section at the representative riffle.

CHANNEL SLOPE AND CROSS-SECTIONAL DIMENSIONS

Three main considerations determine the slope and cross-sectional dimensions of the realigned reach. The new reach should convey the same bankfull discharge and sediment load as the upstream supply reach, and its bankfull width should be typical of natural streams with the same type of bed material and the same bankfull flow. Discharge continuity is achieved by setting the bankfull discharge for the design reach equal to the previously estimated bankfull discharge in the upstream supply reach.

Bankfull flow through the design reach is approximated as uniform flow governed by the Manning resistance equation, which can be stated in terms of the wetted perimeter and hydraulic radius as

$$Q_b = \frac{c}{n_d} P_d R_d^{5/3} \sqrt{S_d} \quad (1)$$

in which Q_b is the bankfull discharge, n_d is the Manning resistance coefficient, P_d is the wetted perimeter, R_d is the hydraulic radius, S_d is the channel slope (the "d" subscripts designate the design reach), and c is a units-related constant (1.49 for U.S. units; 1 for SI units) .

Bed-load transport is modeled with the following simplified form of the Meyer-Peter and Muller (MPM) equation:

$$Q_s = \frac{8P}{\sqrt{\rho}} \left[\gamma R S - 0.047 (\gamma_s - \gamma) d_{50} \right]^{3/2} \quad (2)$$

in which Q_s is the bed-load transport rate (submerged weight per unit time), ρ is the density of water, γ is the specific weight of water, γ_s is the specific weight of the sediment, and d_{50} is the median sediment size by weight. This form of the MPM equation, applicable to channels with plane beds and large width-to-depth ratios, is a satisfactory approximation for design applications. The first term inside the brackets is the average shear stress over the wetted perimeter, and the second term is the critical shear stress required to initiate motion of the d_{50}-size sediment. Therefore, the sediment transport rate varies with the 3/2 power of the excess shear stress (the amount by which the average shear stress exceeds the critical value).

Equating the sediment-transport rates in the upstream supply reach and the design reach yields the sediment-transport continuity equation:

$$P_u \left[R_u S_u - 0.047 (G_s - 1) d_{50} \right]^{3/2} = P_d \left[R_d S_d - 0.047 (G_s - 1) d_{50} \right]^{3/2} \quad (3)$$

in which the "u" subscripts designate the upstream supply reach and G_s is specific weight of the sediment.

A preliminary bankfull width, W_b, for the design reach is obtained from a hydraulic geometry equation. The recommended equation for sand-bed streams in the U.S. is

$$W_b = 2.34 \sqrt{Q_b} \quad (4)$$

and the recommended equation for gravel-bed streams in the U.S. is

$$W_b = 2.03 \sqrt{Q_b} \quad (5)$$

for W_b in feet and Q_b in cfs (NRCS, 2007).

The three unknowns in the discharge and sediment-transport continuity equations are the wetted perimeter, hydraulic radius and slope of the design reach. In the Kansas Analytical Method, the wetted perimeter is assigned a value equal to 110% of the bankfull width obtained from the hydraulic geometry equation:

$$P_d = 1.1\, W_b \tag{6}$$

Solving Eqs. 1 and 3 simultaneously for S_d by eliminating R_d yields the following equation for the slope of the design reach:

$$S_d = \left(\frac{c\, P_d}{Q_b\, n_d} \right)^{\frac{6}{7}} \left\{ \left(\frac{P_u}{P_d} \right)^{\frac{2}{3}} R_u\, S_u + \left[1 - \left(\frac{P_u}{P_d} \right)^{\frac{2}{3}} \right] \left[0.047 \left(G_s - 1 \right) d_{50} \right] \right\}^{\frac{10}{7}} \tag{7}$$

The corresponding length of the design reach, L_d, is computed from the slope and the thalweg elevations at the end-points. The hydraulic radius of the design reach is then obtained from the discharge equation, rearranged as follows:

$$R_d = \left(\frac{Q_b\, n_d}{c\, P_d} \right)^{\frac{3}{5}} S_d^{\,-\frac{3}{10}} \tag{8}$$

The cross-sectional area of the design reach is the product of the wetted perimeter and the hydraulic radius:

$$A_d = P_d\, R_d \tag{9}$$

The design reach would normally have a trapezoidal cross-section for constructability. The area and wetted perimeter of a trapezoidal channel can be expressed in terms of the bottom width, B_d, the depth, y_d, and the side slope, m, as follows:

$$A_d = B_d\, y_d + m\, y_d^{\,2} \tag{10}$$

$$P_d = B_d + 2\sqrt{1 + m^2}\, y_d \tag{11}$$

Solving Eqs. 10 and 11 simultaneously for y_d by eliminating B_d yields the following explicit equation for depth:

$$y_d = \frac{P_d - \sqrt{P_d^2 - 4A_d\left(2\sqrt{1+m^2} - m\right)}}{2\left(2\sqrt{1+m^2} - m\right)} \tag{12}$$

The bottom width is then obtained from either Eq. 10 or Eq. 11. The bottom width, depth, and side slope determine the actual top-width of the design reach, W_d:

$$W_d = B_d + m\,y_d \tag{13}$$

This top width might differ slightly from the preliminary bankfull width used to establish P_d.

The computed channel slope and cross-sectional dimensions must be checked for reasonableness and practicality. The realigned reach should be no steeper than the existing reach (i.e., no loss of stream length). The channel length is also checked by examining the associated sinuosity. Sinuosity is defined as the ratio of the channel length to the valley length (the length of the desired alignment exclusive of meanders). Most natural streams have sinuosities between 1.2 and 2.0. If the preliminary design calculations yield a reach length that is too short or a sinuosity that falls outside the normal range, then the design should be revised. A different bankfull width is selected, a new slope is computed, and the slope and sinuosity are re-checked.

The practicality of the computed channel depth should also be checked by comparing the bankfull level with the level of the natural floodplain at various points along the desired alignment. The bankfull level should not exceed the natural floodplain level, but also should not be far below the natural floodplain level, so that the desired connection between the channel and the natural floodplain is maintained. If the channel depth lies outside the desired range, then a different bankfull width is selected and the analytical design calculations and the design checks are repeated.

PLANFORM

The meanders of a natural stream, although irregular and varied, can be characterized by dimensions such as the average meander wavelength and the average radius of curvature of meander bends. In channel realignment design, the objective is a planform with the desired sinuosity and meander characteristics that are typical of a natural stream.

A stream's meander wavelength, λ, tends to be proportional to its bankfull width. Soar and Thorne (2001) examined the ratio of meander wavelength to bankfull width for 438 sites from nine independent datasets, and found that this ratio has a mean value of approximately 12. Therefore, in the Kansas Analytical Method, the meander wavelength is initially set to 12 times the bankfull width:

$$\lambda = 12\ W_d \tag{14}$$

Typical meander patterns of natural streams are often idealized by mathematical functions such as Leopold's "sine-generated curve" (NRCS, 2007). The sine-generated curve has some theoretical justification, but it is difficult to apply in practice. Numerical integration is required to calculate the coordinates of points along the curve. Sine-generated meander bends are complicated to describe on a plan sheet and difficult to lay out and construct in the field.

The form of the sine-generated curve can be approximated satisfactorily by a series of circular arcs and straight lines, which are easier to describe, lay out, and construct. Figure 1 shows the relevant variables for this meander geometry, in which

ω = angle at which stream intersects longitudinal axis of symmetry
L_s = length of each line segment
L_c = length of each circular arc
R_c = radius of curvature of each circular arc

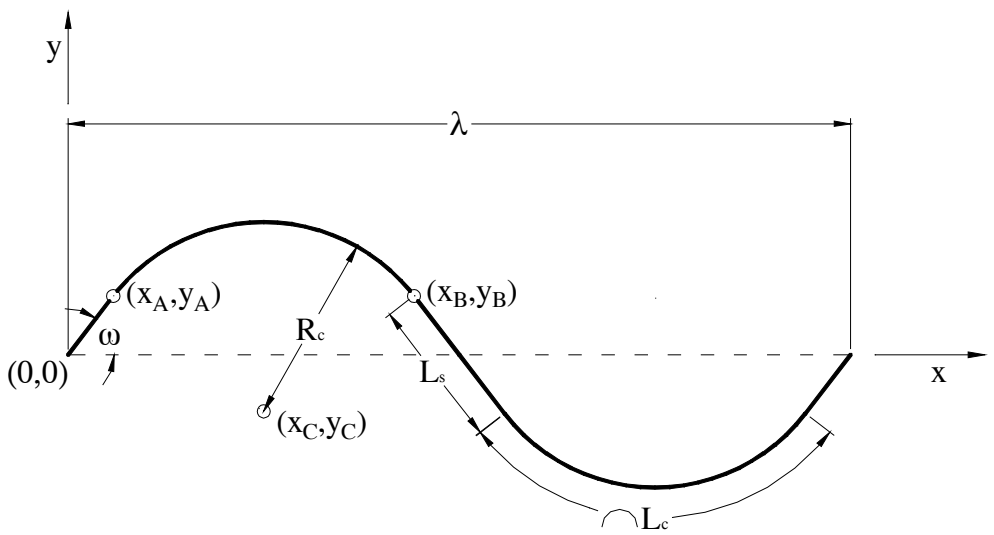

Figure 1. Representation of meander geometry by circular arcs and line segments

The sinuosity, p, is related to the characteristic angle, ω, and the ratio $L_s/(L_s+L_c)$, the fraction of the channel length composed of line segments. Setting the ratio $L_s/(L_s+L_c)$ equal to 0.3 yields meanders that closely resemble sine-generated meanders. With $L_s/(L_s+L_c)$ set to 0.3, the sinuosity and the characteristic angle in radians are related as follows:

$$p = \frac{1}{0.3\cos\omega + 0.7\frac{\sin\omega}{\omega}} \tag{15}$$

In the meander design problem, the desired sinuosity is known and the characteristic angle must be calculated. Eq. 4-26 cannot be solved closed-form for ω. However, over the range $1 \le p \le 3$, Eq. 4-26 is fitted very well by the following explicit equation for ω in radians:

$$\omega = -0.0032 + 1.9947\,z - 0.2438\,z^2 + 0.5457\,z^3 \tag{16}$$

in which

$$z = \sqrt{\frac{p-1}{p}} \tag{17}$$

The lengths L_s and L_c, the radius of curvature R_c, and the coordinates of points A, B and C are given by the formulas:

$$L_s = 0.15\,\lambda\,p \tag{18}$$

$$L_c = 0.35\,\lambda\,p \tag{19}$$

$$R_c = \frac{L_c}{2\omega} \tag{20}$$

$$x_A = \frac{L_s}{2}\cos\omega \tag{21}$$

$$x_B = \frac{\lambda}{2} - \frac{L_s}{2}\cos\omega \tag{22}$$

$$y_A = y_B = \frac{L_s}{2}\sin\omega \tag{23}$$

$$x_c = \frac{\lambda}{4} \tag{24}$$

$$y_c = \frac{L_s}{2}\sin\omega - R_c\cos\omega \tag{25}$$

These relationships provide a starting point for laying out a planform for the realigned reach. The meander characteristics can be varied and adjusted to fit the project constraints, provided that the realigned reach has the desired length and slope.

BOTTOM PROFILE

The bottom profiles of most alluvial streams exhibit a somewhat regular sequence of riffles and pools. The riffles tend to occur near the inflection points of meander bends, and the pools tend to be deepest about two-thirds of the way through the meander bends. The pools retain water and provide valuable aquatic habitat during periods of little or no flow.

If the design for the realigned reach incorporates riffles and pools, the cross-sectional dimensions computed with the analytical relationships should be applied at the riffles. The bankfull depth at the deepest point in the pools should be approximately 150% of the bankfull depth at the riffles. Riffles should be located at the inflection points, or at the midpoints of the line segments connecting the circular arcs. The deepest point in a pool should be located downstream of the bend apex approximately one-third of the distance from the bend apex to the downstream riffle. The bankfull depth can be varied linearly between the upstream riffle and the deepest point, and between the deepest point and the downstream riffle, which results in a saw-tooth bottom profile.

CONCLUSIONS

The analytical design method presented in this paper is appropriate for realignment of small alluvial channels with non-cohesive bed material. This method follows the general approach recommended by the USACE and the NRCS. The realigned reach is designed to convey the same bankfull discharge and sediment load as a stable reach directly upstream. The bankfull width and meander wavelength are obtained from geomorphic relationships for stable natural streams. Consequently, the realigned reach should have stable geomorphic characteristics that are typical of a natural stream in a similar setting.

ACKNOWLEDGMENT

This work was supported by the Kansas Department of Transportation (KDOT) through the Kansas Transportation Research and New Developments (K-TRAN) Program. James Richardson, P.E., Brad Rognlie, P.E., and Michael Orth, P.E., of KDOT all provided valuable guidance.

REFERENCES

Copeland, R. R., D. N. McComas, C. R. Thorne, P. J. Soar, M. M. Jonas, and J. B. Fripp (2001). *Hydraulic Design of Stream Restoration Projects*, Technical Report ERDC/CHL TR 01–28, U. S. Army Corps of Engineers, Engineer Research and Development Center, Vicksburg, MS.

McEnroe, B. M., C. B. Young and J. E. Shelley (2009). *Guidelines for Stream Realignment Design,* Report No. K-TRAN:KU-08-2, Kansas Department of Transportation.

NRCS (2007). *Stream Restoration Design*, National Engineering Handbook, Part 654, Natural Resources Conservation Service.

Soar, P. J., and C. R. Thorne (2001). *Channel Restoration Design for Meandering Rivers*, Technical Report ERDC/CHL CR-01-1, U. S. Army Corps of Engineers, Engineer Research and Development Center, Vicksburg, MS.

Bankfull Discharge for Kansas Natural Alluvial Channel Design

J. Shelley[1], C. B. Young[2], B. McEnroe[3]

Dept. of Civil, Environmental, and Architectural Engineering, University of Kansas, 1530 W. 15th St. Rm. 2150, Lawrence, KS 66045.

[1]PH (785) 864-2924; FAX (785) 864-5631; E-mail: johnnyjazzman@gmail.com
[2]PH (785) 864-2999; FAX (785) 864-5631; E-mail: cbyoung@ku.edu
[3]PH (785) 864-2925; FAX (785) 864-5631; E-mail: mcenroe@ku.edu

Abstract

In this study we present an equation that predicts bankfull discharge for Kansas streams based on watershed characteristics. This equation can be used for natural channel design projects such as stream realignments and restorations. To develop this equation, we first determined that the recurrence intervals of bankfull flow on 46 natural streams in Kansas range between <1.0 and 1.7 years. The median and mean recurrence interval are both 1.2 years. We then derived a multivariate regression equation for the 1.2-year discharge from a database of 72 small rural streams in Kansas, using ten different watershed characteristics as possible predictors. The regression analysis led to an equation that predicts the 1.2-year discharge as a function of the drainage area, the mean annual precipitation, and the length of the longest flow path. This equation can be used for natural channel design in Kansas.

Introduction

Engineers design river modification projects for a number of reasons, including flood protection, highway safety and capacity improvements, drinking water supply, navigation, hydropower, and recreation. In the past, river designers sought to maximize these human benefits while minimizing costs. Today, engineers also see the importance of maximizing environmental benefits such as habitat enhancement, bed and bank stability, decreased sediment transport rates, and water quality. Often, the best way to maximize these environmental benefits is for the designed channel to simulate the form and function of a self-formed channel. A stream design that simulates important features of self-formed streams is termed a natural channel design.

One of the most important aspects of a natural channel design is the design discharge. This discharge should be similar to the capacity that a stable, self-formed stream in the same location would have. The capacity of a self-formed channel that is well connected to its floodplain is termed the bankfull flow (FISRWG, 2001). Equations that predict the bankfull flow in self-formed streams can be used to determine the design discharge for a natural channel design. Equations for bankfull flow must be based on region-specific data because of the high variability in the driving hydrologic and geomorphic factors.

In this paper we present a multivariate regression analysis for bankfull flow in Kansas streams, based on local hydrologic records and geomorphic surveys. We derived this equation during the development of the Kansas Analytical Method, a natural channel design method for small rural streams in Kansas. In the sections that follow, we first describe the datasets used in the analysis. Then, we present the results of a recurrence interval analysis of bankfull flow in Kansas streams. Next, we discuss the development of the regression equation. Finally, we discuss the uses and limitations of the equation.

Datasets

The equation developed for this study is based on two datasets. Both datasets consist of stream and watershed data for rural basins in Kansas. The first dataset contains bankfull stage, bankfull discharge, and other geomorphic data for 46 stable, gaged streams. We selected these 46 streams from a larger geomorphic dataset that was developed with funding from the Kansas Water Office and US Environmental Protection Agency (Emmert and Hase, 2001). We selected the 46 streams by removing streams for which: (1) The surveyors could not identify the bankfull stage with certainty, (2) The stream was degraded, (3) The survey was incomplete or of poor quality, (4) The stream bottom was predominantly bedrock, or (5) The streamflow record was too short to determine a return period.

The majority of the streams in this dataset are far larger than streams that are typically candidates for realignment or restoration. Only four of the streams in this first dataset have drainage areas less than 30 square miles, whereas 34 of the 46 streams have drainage areas of over 500 square miles. We used this dataset to determine the average recurrence interval (annual maximum series) of bankfull flow in Kansas rivers and streams, but we needed additional stream data to produce a design equation.

The second dataset used in this study contains extensive hydrologic and watershed data for 72 gaged Kansas streams with drainage areas under 30 square miles. This dataset has been used in previous research to derive flood frequency estimates for Kansas rural, ungaged streams (McEnroe, et al., 2007). These streams are similar in size to streams that might be considered for realignment and restoration. However, geomorphic surveys were not available for these locations. We used this dataset in the regression analysis to create a design equation for discharge capacity.

Recurrence Interval of Bankfull Flow

Figure 1 displays the distribution of the recurrence intervals (annual maximum series) for bankfull flow for streams in the first dataset. These recurrence intervals ranged from < 1.01 years to 1.7 years, with both a median and a mean recurrence interval of 1.2 years. This range of recurrence intervals is consistent with numerous studies in other regions, including the pioneering work of Wolman and Leopold (1957). The recurrence interval of bankfull flow appears to be independent of geographic location and of channel material, as shown in Figure 2. In addition, the recurrence interval of bankfull flow is independent of drainage area (see Figure 3). We conclude that the

1.2-year discharge is an appropriate approximation for bankfull flow for design purposes in Kansas.

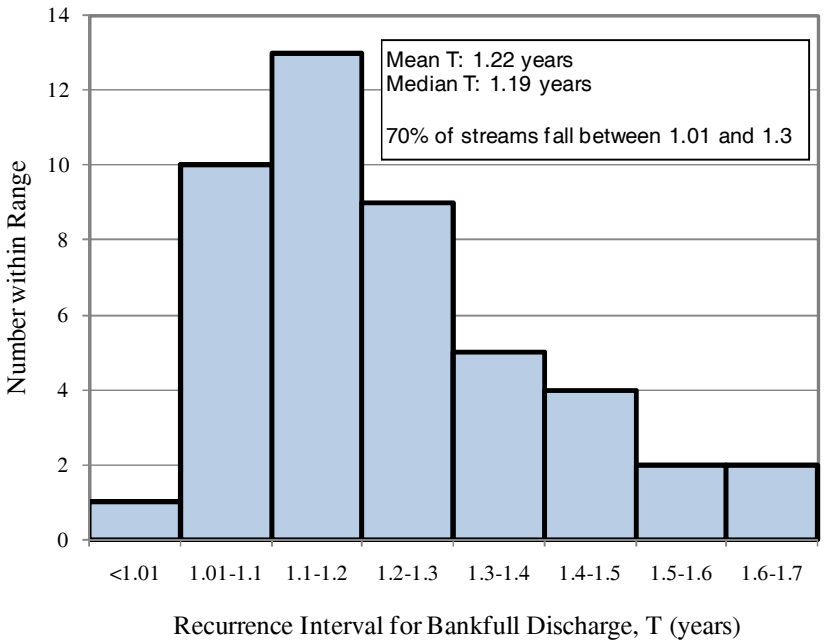

Figure 1. Recurrence Intervals for Bankfull Flow in Kansas Streams

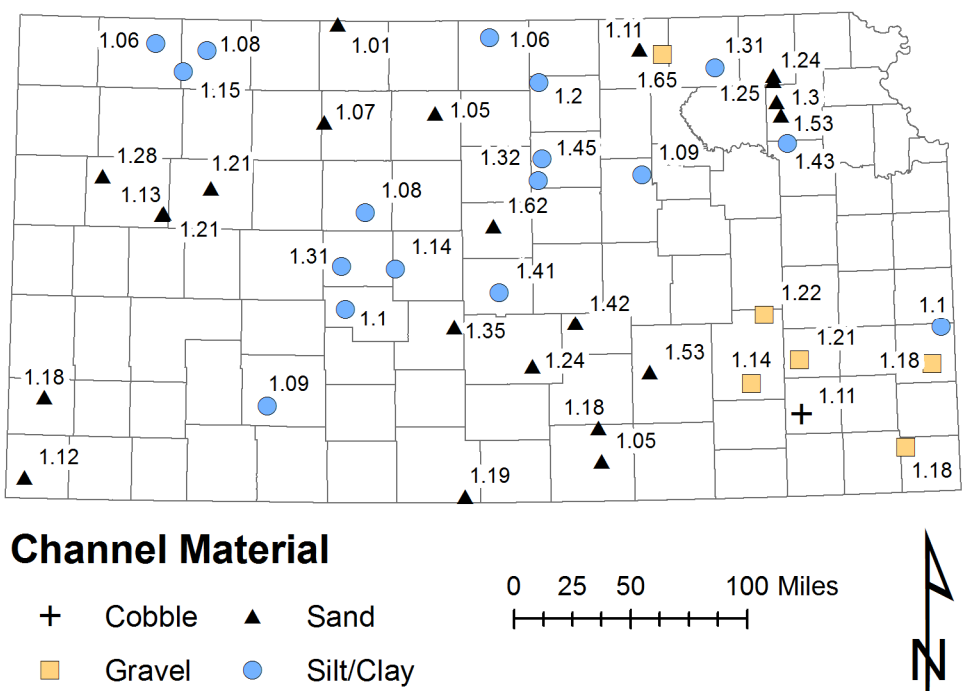

Figure 2. Recurrence Intervals for Bankfull Flow in Kansas Streams, Sorted by Channel-Bed Material

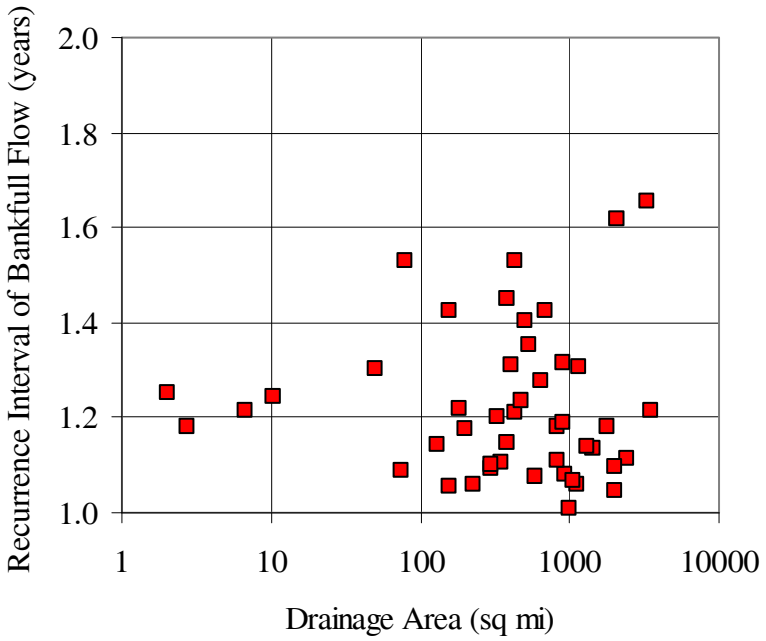

Figure 3. Independence of Recurrence Interval from Drainage Area

Regression Analysis

We used forward stepwise linear regression to develop a predictive equation for the 1.2-year discharge for small Kansas streams, following the methodology used by McEnroe, et al. (2007). We removed five stations from the dataset because they had $Q_{1.2}$ values equal to zero. Table 1 lists the five stations excluded from the regression analysis. Four of these stations are located in western Kansas, where zero-flow years are not uncommon. The fifth station excluded from the analysis is a small watershed (1.62 mi^2) located in Washington County, Kansas.

Table 1. Stations with $Q_{1.2}$ Equal to Zero

Site #	Station name	County	CDA (mi^2)	MAP (in)
6884100	Mulberry Creek tributary near Haddam	Washington	1.62	30.1
6846200	Beaver Creek tributary near Ludell	Rawlins	10.55	20.5
6873300	Ash Creek tributary near Stockton	Rooks	0.88	23.0
7141600	Long Branch Creek near Ness City	Ness	29.58	21.4
7141800	Otter Creek near Rush Center	Rush	17.20	22.9

Table 2 lists the predictors that were considered in the regression analysis. The 2-year rainfall intensity (for duration equal to the watershed time of concentration) was used in lieu of the 1.2-year rainfall, as tables of 1.2-year rainfall intensities are not available in Kansas. Details on the determination of these watershed characteristics can be found in McEnroe et al. (2007).

Table 2. Watershed Characteristics used in the Regression for $Q_{1.2}$

Symbol	Watershed Characteristic	Units
CDA	Contributing Drainage Area	mi^2
Sh	Basin Shape Factor	--
Sl	Average Slope of Main Channel	ft/mi
SP	Generalized Soil Permeability	in/hr
CN	NRCS Runoff Curve Number	--
i_2	2-year Rainfall Intensity for Duration t_c	in/hr
MAP	Mean Annual Precipitation	in
MAE	Mean Annual Lake Evaporation	in
MAD	Mean Annual Precipitation Deficit	in
L	Length of the Longest Flow Path	mi

The regression analysis led to the following equation for $Q_{1.2}$:

$$Q_{1.2} = 0.00258\,CDA^{1.26}\,MAP^{3.17}\,L^{-1.10} \qquad (1)$$

where $Q_{1.2}$ is in cfs. The mean annual precipitation, MAP, is determined from Figure 3. The longest flow path, L, is measured along the channel from the watershed outlet to the drainage divide. Eq. 1 has a standard error of estimate of 0.217 log units (-39%, + 65%) and a coefficient of determination, R^2, of 0.827. This standard error and coefficient of determination are similar to previously published equations for 2, 5, 10, 20, 50, and 100-year discharges (McEnroe et al., 2007).

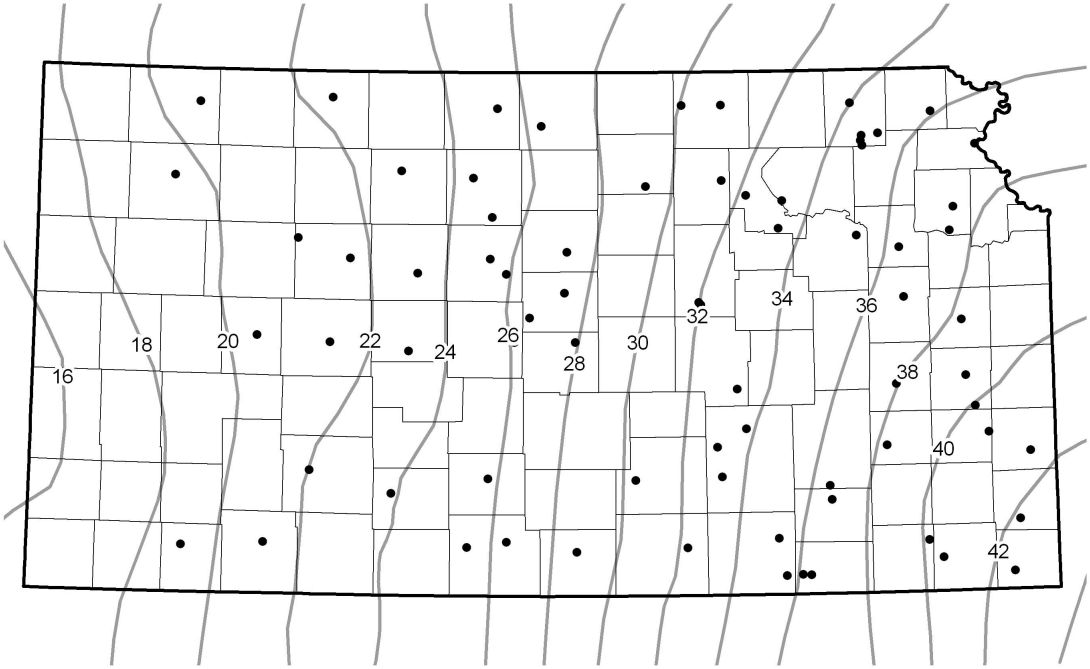

Figure 3. Mean Annual Precipitation (inches) in Kansas along with Gages used in Regression Analysis

Equation Uses and Limitations

The bankfull discharge for small rural streams in Kansas can be approximated by the 1.2-year discharge, estimated from Eq. 1. This equation can be used to determine the discharge capacity in a natural channel design, such as a stream realignment or restoration. However, the following limitations should be kept in mind: First, the use of local data to derive Eq. 1 makes it applicable to Kansas streams only. Second, Eq. 1 only applies to non-degraded channels with a mobile bed. Third, this equation may not be applicable in stream systems that regularly experience zero-flow years, as is the case for many streams in western Kansas. Finally, Eq. 1 should not be applied to urban stream design, because urban streams were not included in the recurrence interval analysis or the regression analysis. Future research that derives a bankfull flow equation using urban watershed parameters, such as percent impervious, is warranted.

References

Emmert, Brock and Hase, Kristen (2001). "Geomorphic Assessment and Classification of Kansas Riparian Systems." Kansas Water Office.

FISRWG (2001). *Stream Corridor Restoration: Principles, Processes, and Practices.* Chapter 7. "Analysis of Corridor Condition." Federal Interagency Stream Restoration Working Group (15 Federal agencies of the US gov't). GPO Item No. 0120-A; SuDocs No. A 57.6/2:EN 3/PT.653. ISBN-0-934213-59-3.

McEnroe, B.M. and C. B. Young (2007). *Flood Frequency Relationships for Small Watersheds in Kansas*, Report No. K-TRAN: KU-06-4, Kansas Department of Transportation.

Wolman, M. Gordon and Leopold, Luna B. (1957). "River Floodplains: Some Observations On Their Formation." *Geological Survey Professional Paper 282 – C.*

Sediment Load Based Single Thread Alluvial Channel Classification

Gregory Wilkerson[1] and Gary Parker[2]

[1]Department of Civil and Environmental Engineering; Southern Illinois University Carbondale; 1230 Lincoln Dr. (MC 6603); Carbondale, Illinois, U.S.A. 62901; Ph.: 618-453-7810; Fax: 618-453-3044; Email: gwilkers@siu.edu.
[2]Department of Civil and Environmental Engineering and Department of Geology| University of Illinois at Urbana-Champaign; Hydrosystems Laboratory, MC-250; 205 N. Matthews Ave.; Urbana, Illinois, U.S.A. 61801; Ph.: 217-244-5159; Fax: 217-333-0687;Email: parkerg@uiuc.edu.

ABSTRACT

Past studies have demonstrated the relation between channel-perimeter sediment type (i.e., the weighted mean percent silt-clay in the channel and banks, M) and channel shape (i.e., the width-depth ratio). Moreover, M was found to be an indicator of the predominant sediment transport mode. Motivated by the reasoning and results of this earlier work we propose a classification scheme for single thread rivers that relies on the median bed material grain size (D_{50}) to classify streams as predominantly transporting either a fine suspended load (D_{50} <= 0.062 mm), coarse suspended load (0.062 mm < D_{50} <= 0.50 mm), mixed load (0.50 mm < D_{50} <= 25.0 mm), or bedload (D_{50} > 25.0 mm). For classifying channels, we use Shields curve to define conditions of incipient sediment motion and the criterion $u_* = w_s$ (u_* = shear velocity and w_s = sediment fall velocity) to define the onset of significant suspended load transport. This work is warranted because in most studies of rivers and canals the D_{50}, rather than M, is the only measure recorded for describing channel-perimeter sediment type. Distinctive relationships between B_{bf} and Q_{bf}, and H_{bf} and Q_{bf} are noted for each of the stream classes we propose, that is, trendlines for these variable differ systematically between stream classes. In contrast, width-to-depth ratios for the stream classes are not distinctive; the width-to-depth ratios range from 3 to 100 across all stream types and values as large as 1,000 are common for coarse suspended-load streams.

INTRODUCTION

Classification schemes are generally proposed with the intention of imposing some sort of rational order on the wide variety of channels formed by fluids flowing in erodible channels (Knighton, 1998) and a variety of criteria have been proposed for classifying channels (e.g., Davis 1899; Harvey 1969; Rosgen 1996, Schumm 1960, 1963; and others). Herein we present a basis for classifying stable, single-thread alluvial rivers with a median bed-material size, D_{50}, between 0.062 mm and 25 mm. Rivers meeting this criteria are both common in the natural environment and studied extensively.

The analyses which are presented herein are in part motivated by earlier work reported by Schumm (1960, 1963). That work, therefore, is briefly reviewed. Schumm (1960) showed that the weighted mean percent silt-clay in the channel and banks (M) could be used as a sediment parameter for predicting channel shape expressed as a width-to-depth ratio (F or B/H). Specifically, stream shape was shown to vary according to:

$$F = \frac{B}{H} = 255M^{-1.08} \tag{1}$$

Figure 1 shows a plot of this relationship and the data used to derive it. Neither the percentage of silt and clay in the banks nor in the channel alone showed a correlation with the width-to-depth ratio. Also, neither mean annual discharge nor the mean annual flow significantly affects this relationship in spite of the importance of discharge to the absolute width and depth of a channel. Equation (1) indicates the importance of channel-perimeter sediment type to channel shape.

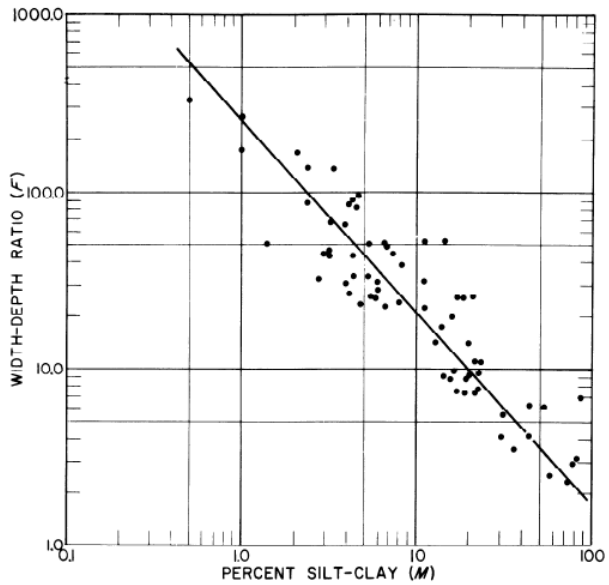

Figure 1 – Relation between width-to-depth ratio and weighted mean percent silt-clay at different cross sections. The regression line was determined graphically. Standard error is 0.202 log units and correlation coefficient is 0.81. (Source: Schumm 1960).

Schumm (1963) proposed tentative classification criteria for alluvial channels that are similar to the criteria described herein. The criteria are similar because in both cases the delineative criteria are based on channel perimeter sediment and the proposed channel classes are differentiated by their predominant sediment transport mode. In his analyses Schumm used M as a sediment parameter. Also, three channel types were identified: bed-load ($M < 8$), mixed-load ($8 \leq M \leq 30$), and suspended-load ($M > 30$). As used by Schumm, the term suspended load is synonymous with wash-load and is

generally comprised of sand and clay particles. The term bed-load is synonymous with bed-sediment load and is generally comprised of sand and coarser sediment. Schumm also provided a range of width-to-depth ratio's for stable channels of each type. For bedload, mixed load, and suspended load channels, the respective ranges were >25, between 7 and 25, and less than 7.

Schumm (1968) provides additional data that supports the tentative alluvial river classification proposed by Schumm (1963). As a result of the additional data, the limits for the three classes of channels were revised as follows: bed-load ($M < 5$; $F > 40$), mixed-load ($5 \leq M \leq 20$; $10 \leq F \leq 40$), and suspended-load ($M > 20$; $F < 10$). Also noted by Schumm (1968) were the following limitations to the proposed classification:

(1) application must be restricted to alluvial rivers which contain less than about 20 percent gravel in their channel and which are not influenced by bedrock outcrops in their channels, and

(2) compared to river channels in sub-humid, semiarid, and arid regions, major perennial streams of humid regions seem to show much less variability and may be more difficult to relate to the proposed classification.

The results presented by Schumm (1960, 1963, 1968) indicate that channel-perimeter sediment composition significantly influences channel shape and the mode by which sediment load is transported in a channel. Schumm (2003) further outlines the basis for the classification system outlined above by noting that discharge is an independent variable that largely determines the size of stream channels and the amplitude of wavelength of meanders but is not a valid basis for stream channel classification. The other independent variable noted by Schumm (2003) is sediment load. Schumm proposes that either the type of material transported or the predominant mode of sediment transport should be used as the basis for classification rather than the median grain size of the bed material. The given reason being that great changes in the morphology of a stream can occur when the median grain size of bed material is essentially constant. Ultimately, Schumm's tentative classification scheme is founded on data from a restricted range of sand-bed streams, which may limit its overall applicability, and rests on the assumption the M adequately reflects transport mode (Knighton, 1998; Schumm 2003).

Schumm (1960, 1963, 1968, 2003) uses M to characterize channel-perimeter sediment type, the predominant mode of sediment transport, and ultimately to classify channels. In contrast, Rosgen (1996) uses D_{50} to represent channel material in his stream classification scheme (where bimodal particle distributions are observed the particle size observed most frequently is take as the dominant particle size). In addition to D_{50}, Rosgen's classification scheme uses an entrenchment ratio (width of flood prone area at an elevation twice the maximum bankfull depth/bankfull width), and the width-to-depth (ratio of bankfull width/mean bankfull depth), water surface slope, and sinuosity as principle measures for "Level II" classification of channels. Rosgen recommends Level II classification as for addressing questions pertaining to

sediment supply, stream sensitivity to disturbance, potential for natural recovery, channel response to changes in flow regime, and fish habitat potential.

Herein we discern classes of single thread alluvial channels using the particle size Reynold's number, the Shields number at bankfull discharge, and criteria for specifying the onset of (1) bed sediment motion and (2) significant bed sediment suspension. We compare the findings of this study with those reported by Schumm (1960, 1963, 1968, 2003) and attempt to identify similarities and reconcile differences in the findings.

METHODS/DATA

An extensive review of published literature in which bankfull discharge and bankfull channel morphology data were reported was conducted by the writers. It is concluded from that effort that in the overwhelming majority of cases where bankfull data are reported, the D_{50} is the only reported information regarding channel perimeter sediment. The only notable exception to this observation pertains to stream reaches identified as having riffle-pool geometry. Reaches of channel with riffle-pool geometry characteristically have heterogeneous bed material; for such reaches separate D_{50} values for pools and riffles were commonly reported. None of the stream reaches represented in this study is known to contain pool-rifle sequences. Given that D_{50} is the only generally available information about channel sediment, we are motivated to identify a means for using D_{50} to characterize channels. Given the results reported by Schumm (1960, 1963, 1968), we have reason to expect that a channel's dominant sediment transport mode can be predicted from a characteristic channel perimeter particle size such as the D_{50}.

We obtained stream reach data (data points) for this study from numerous published sources and then assigned each data point to one of four stream classes: fine suspended load ($D_{50} \leq 0.062$ mm), coarse suspended load ($0.062 \text{ mm} < D_{50} \leq 0.50$ mm), mixed load ($0.50 \text{ mm} < D_{50} \leq 25.0$ mm), bedload ($D_{50} > 25.0$ mm). The number of points obtained for each stream class is summarized in Table 1. As will be discussed later, the stream classes indicate the predominant sediment transport mode during bankfull discharge. Parameters for the coarse suspended-load stream data span the following ranges: $12.0 \text{ cfs} \leq Q_{bf} \leq 21{,}600$ cfs, $9.75 \text{ m} \leq B_{bf} \leq 9{,}450$ m, $0.57 \text{ m} \leq H_{bf} \leq 48.0$ m, $8.75E\text{-}6 \leq S \leq 6.40E\text{-}3$, $0.094 \text{ mm} \leq D_{50} \leq 0.50$ mm.

Table 1. Number of streams sites in each stream class.

Stream Class	No of Points
Fine suspended-load ($D_{50} \leq 0.062$ mm)	7
Coarse suspended-load ($0.062 \text{ mm} < D_{50} \leq 0.50$ mm)	60
Mixed-load ($0.50 \text{ mm} < D_{50} \leq 25.0$ mm)	86
Bedload ($D_{50} > 25.0$ mm)	72

In selecting streams for this study, we have attempted to choose only stable single-thread alluvial streams that could be considered stable. In addition, streams were included only if the reported value of Q_{bf} was measured. Excluded were streams for which Q_{bf} was presumed equal to $Q_{1.5}$, Q_2, or $Q_{2.33}$ (i.e., discharges having return periods of 1.5, 2, and 2.33 years, respectively); assumed equal to the mean annual flood; or derived from the Manning-Strickler equation or some other flow resistance equation.

Basis for Stream Channel Classification

Presented in the following paragraphs is the basis for the stream classification we propose. We note that the approach was originally developed and presented by Parker (2004).

Bed sediment motion occurs when flow conditions are such that the bankfull Shield's parameter (τ^*_{bf}) exceeds the critical value of the Shield's parameter (τ^*_c). Shields parameter is given by:

$$\tau^*_{bf} = \frac{\tau_{bf}}{\rho R g D_{50}} = \frac{H_{bf} S}{R D_{50}} \tag{2}$$

where

$$\tau_{bf} = \rho g H_{bf} S \tag{3}$$

is the bed shear stress corresponding to bankfull discharge, ρ = fluid density, g = gravitational constant, H_{bf} = bankfull depth, S = bed slope, and R = submerged specific gravity for sediment. The submerged specific gravity is given by:

$$R = \frac{\rho_s}{\rho} - 1 \tag{4}$$

where ρ_s = sediment density. For natural quartz sediments, R is usually close to 1.65 and therefore we assume this value, with one exception, for the streams represented herein. The exception is for the 23 bedload streams reported in Parker et al. (2007) and originally described by Charlton et al. (1978). Charlton et al. reported measured values of R ranging from 1.49 to 1.76.

For estimating values of τ^*_c we use Parker (2003):

$$\tau^*_c = \frac{1}{2}\left[0.22\ Re_p^{-0.6} + 0.06 \cdot 10^{\left(-7.7\, Re_p^{-0.6}\right)}\right] \tag{5}$$

where Re_p is the Reynold's particle number and is given by:

$$Re_p = \sqrt{R g D_{50}}\, D_{50} / \nu \tag{6}$$

and ν = kinematic viscosity of water.

Significant suspended sediment motion occurs when the bed shear velocity at bankfull discharge ($u_{*,bf}$) exceeds the bed sediment fall velocity (w_s), that is, when $u_{*,bf} / w_s > 1.0$, where:

$$u_{*,bf} = \sqrt{\frac{\tau_{bf}}{\rho}} = \sqrt{\rho g H_{bf} S} \tag{7}$$

For discussing w_s, we use the dimensionless parameter W_*, given by:

$$W_* = \frac{w_s^3}{Rg\nu} \tag{8}$$

Dietrich (1982) developed the following relation for estimating values for W_*:

$$\begin{aligned} \log W_* = &-3.76715 + 1.92944(\log D_*) - 0.09815(\log D_*)^{2.0} \\ &- 0.00575(\log D_*)^{3.0} + 0.00056(\log D_*)^{4.0} \end{aligned} \tag{9}$$

in which D_* is a dimensionless particle size defined by:

$$D_* = \frac{RgD_n^3}{\nu^2} = Re_p^2 \tag{10}$$

In applying (10) we replace D_n with D_{50}. Equation (9) is valid for $0.05 \le D_* \le 5E9$ which corresponds to $0.20 \le Re_p \le 7.0E4$. Given (7) to (10), the ratio $u_{*,bf} / w_s$ can be expressed as follows:

$$\frac{u_{*,bf}}{w_s} = \frac{\sqrt{\tau_{bf} / \rho} \Big/ \sqrt{RgD_{50}}}{w_s \Big/ \sqrt{RgD_{50}}} = \frac{\sqrt{\tau_{bf}^*}}{\left(W_* / Re_p\right)^{1/3}} \tag{11}$$

When $u_{*,bf} / w_s$ = 1.0, the corresponding value of Shield's parameter is the critical shear stress for the onset of significant suspended sediment transport, $\tau_{c,sus}^*$, that is:

$$\tau_{c,sus}^* = \frac{W_*^{2/3}}{D_*^{1/3}} \tag{12}$$

Equations (5) and (12) can be used, respectfully, to plot curves representing the onset of significant bed and suspended sediment motion as a function of D_* or D_{50} as shown in Figure 2. Also plotted in Figure 2 are data for the streams represented in Table 1.

Figure 2 illustrates is that streams having $D_{50} \leq 0.50$ mm tend to plot above Dietrich's curve and therefore significant suspended sediment motion is expected in such streams. Streams for which 0.50 mm $\leq D_{50} \leq$ 25.0 mm plot in the region between Dietrich's and Shield's curve, and therefore sediment transport in suspension and as bedload is expected in these streams. Streams where $D_{50} >$ 25.0 mm plot in a narrow region near Shield's curve and therefore sediment transport as bedload sediment is expected. Respectfully, we designate these streams as being suspended-load, mixed-load, and bedload streams to reflect their prevailing sediment transport mode. Further, we sub-classify suspended-load streams as being fine ($D_{50} \leq 0.062$ mm) or coarse (0.062 mm $< D_{50} \leq$ 0.50 mm) since cohesive forces are generally significant for particles smaller than about 0.062 mm.

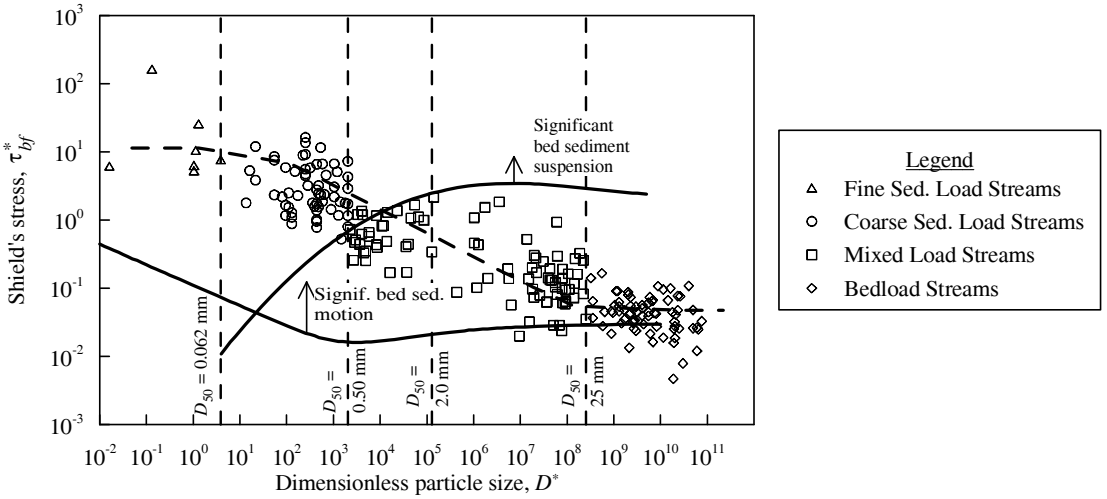

Figure 2. Shields regime diagram with (1) Shields curve (as modified by Parker et al. 2003) indicating the onset of bed sediment motion, (2) Dietrich's (1982) relation for particle settling velocities to indicate the onset of significant suspension of bed sediment.

RESULTS AND CONCLUSIONS

A physical basis for stream classification is developed using Shields curve to define conditions of incipient sediment motion and the criterion $u_* = w_s$ (u_* = shear velocity and w_s = sediment fall velocity) to define the onset of significant bed sediment suspension. Considering bankfull discharge, Figure 2 indicates that the predominant sediment transport mode in a channel can be predicted from D_{50}. We propose the use of D_{50} for classifying channels rather than M (the weighted mean percent silt-clay in the channel and banks), as proposed by Schumm (1960, 1963, 1968) because for most studies of rivers and canals the D_{50}, is the only channel-perimeter sediment parameter recorded.

Also, based on Figure 2, we classify streams as predominately transporting sediment as either fine suspended-load ($D_{50} \leq 0.062$ mm), coarse suspended-load (0.062 mm < $D_{50} \leq 0.50$ mm), mixed load (0.50 mm < $D_{50} \leq 25.0$ mm), or bedload ($D_{50} > 25.0$ mm). It is commonplace for channels with 0.062 mm $\leq D_{50} \leq 2.0$ mm to be classified as sand bed-rivers. Noting that the particle size that separates coarse suspended-load and mixed-load streams is 0.50 mm, we recommend reconsidering the practice of using 2.0 mm as the particle size separating sand and gravel.

Based on the reasoning and results presented by Schumm (1960, 1963, 1968) we expect the shape of single thread alluvial channels is significantly influenced by the predominant sediment transport mode in a stream channel. To demonstrate, width-to-depth ratios (F) are plotted against D_{50} values in Figure 3 but there are no noticeable trends. As noted earlier, Schumm (1960, 1963) made the same observation so this result is not a completely surprising.

What is noteworthy in Figure 3 is the wide range of F values. Earlier we mentioned that Schumm (1968) identified three stream classes and provided corresponding M and F value ranges. Since M is not known for the channels in this study they cannot be grouped into the stream classes identified by Schumm to directly compare F value ranges. However, the F values in Figure 3 range from 3 to 100 across all stream types and F values as large as 1,000 are common for coarse suspended-load streams. We believe, therefore that the narrow range of F values observed by Schumm (i.e., from 0.5 to about 100; Figure 1) is not truly representative of sand bed alluvial channels in the natural environment.

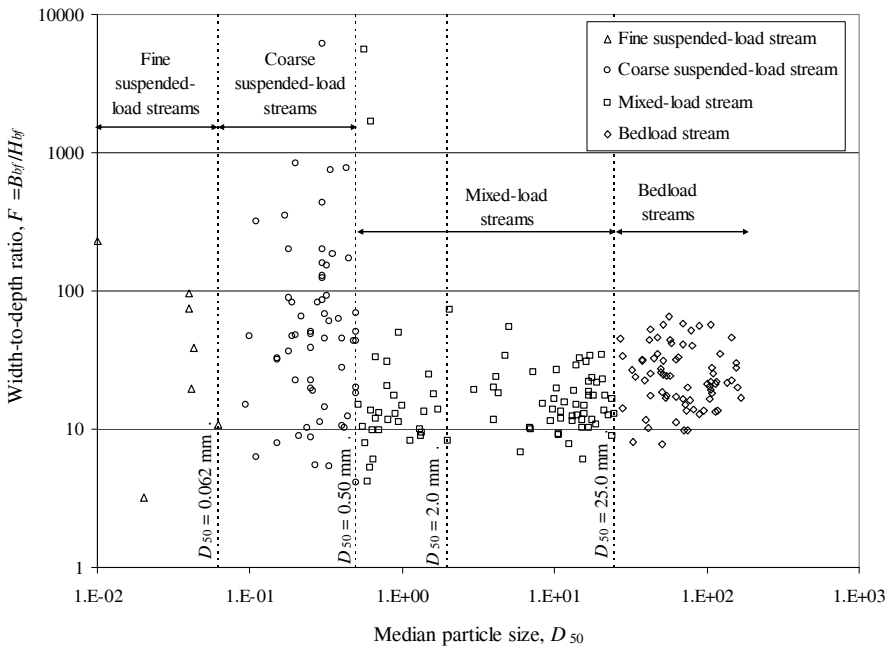

Figure 3. Width-to-depth ratio's for streams included in study.

Evidence that the proposed stream classes have distinct shapes is still needed and thus we plotted B_{bf} and H_{bf} against Q_{bf} in Figure 4. In Figures 4a and 4b different symbols are shown and separate trend lines are plotted for each stream class. To facilitate discussing the trend lines they are plotted alone in Figures 4c and 4d. Figure 4c shows trendlines for the relationship between B_{bf} and Q_{bf}. Ordering the stream classes by the D_{50} sizes represented, that is, from fine suspended-load to the bedload rivers, we find that as the stream class (or D_{50}) increases, the trendline slopes decrease. Trendlines for the relationship between H_{bf} and Q_{bf} are shown in Figure 4d. Again ordering the stream types by D_{50}, what Figure 4d shows is that as D_{50} increases, the trendline slopes increase.

In spite of not finding distinctive width-to-depth ratios for the proposed stream classes, Figure 4 indicates that for each stream class there are distinctive relationships between B_{bf} and Q_{bf}, and H_{bf} and Q_{bf} for the four stream classes we propose. Ultimately this result supports the notion that the shape of single thread alluvial channels is significantly influenced by the predominant mode by which sediment is transport in the channel. Nonetheless, additional work is needed to improve understanding of the interrelationship between sediment transport, channel perimeter sediment, and channel shape.

ACKNOWLEDGEMENTS

This work was supported by the STC program of the National Science Foundation via the National Center for Earth-surface Dynamics under the agreement Number EAR-0120914.

REFERENCES

Charlton, F.G., Brown, P. M., and Benson, R. W. (1978). *The hydraulic geometry of some gravel rivers in Britain* (Report No. IT 180), Hydraulics Research Station, Wallingford, England.

Davis, W. M. (1899). "The geographical cycle." *Geographical Journal*, 14, 481-504.

Dietrich, W. E. (1982). "Settling velocity of natural particles." *Water Resources Research*, 18(6), 1615-1626.

Harvey, A. M. (1969). "Channel capacity and the adjustment of streams to hydrologic regime." *Journal of Hydrology*, 8, 82-98.

Knighton, D. (1998). *Fluvial forms and processes*, Arnold, London.

Parker, G. (2004) *1D Sediment Transport Morphodynamics with Applications to Rivers and Turbidity Currents*, edited, copyrighted e-book, http://www.cee.uiuc.edu/people/parkerg/morphodynamics_e-book.htm (Jan. 27, 2009).

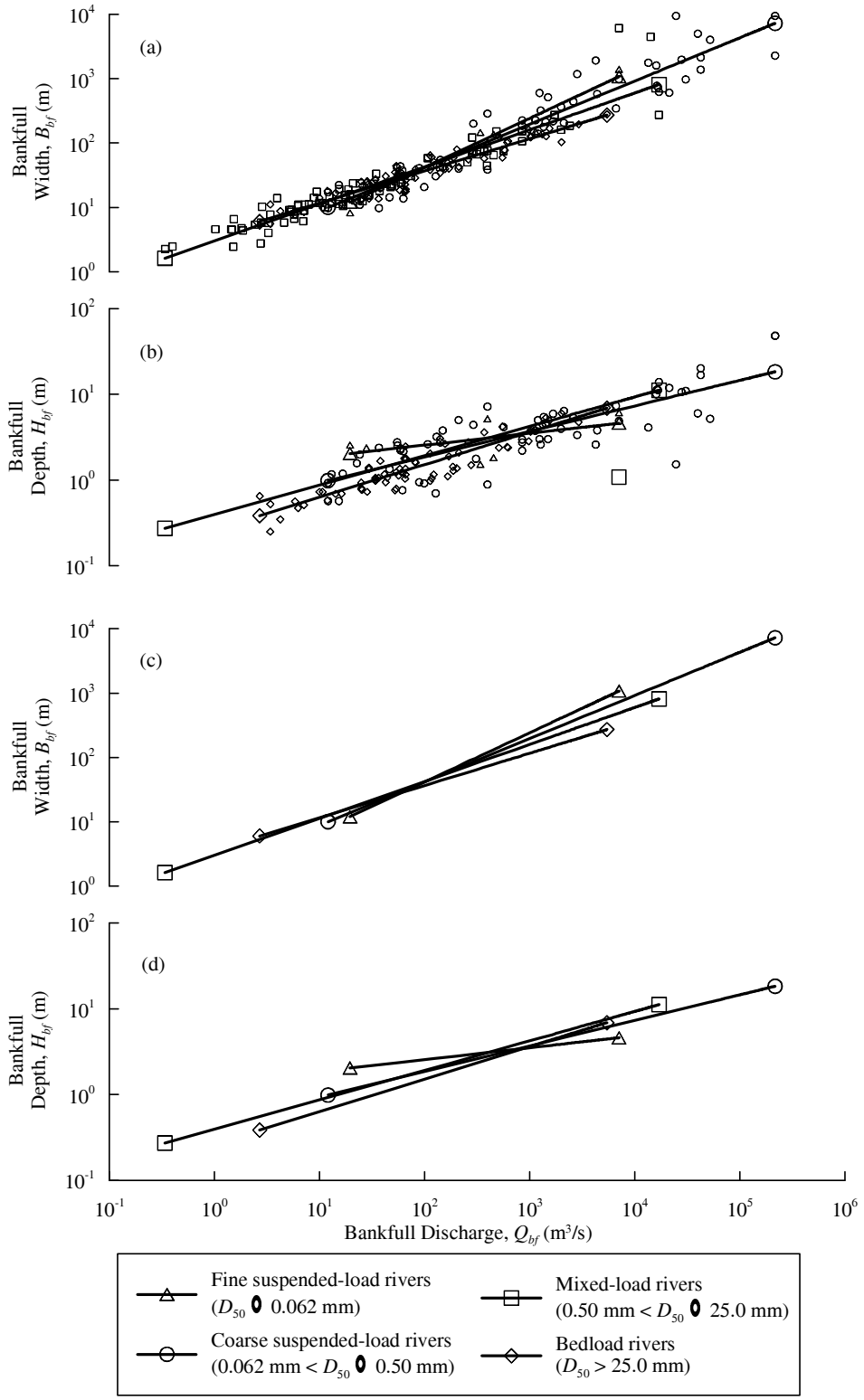

Figure 4. Plots showing bankfull width and depth against bankfull discharge. Parts (a) and (b) show trendlines and data. Trendlines alone are shown in parts (c) and (d).

Parker, G., Toro-Escobar, C. M., Ramey, M. and S. Beck (2003). "The effect of floodwater extraction on the morphology of mountain streams." *Journal of Hydraulic Engineering*, 129(11), 885-895.

Parker, G., Wilcock, P. R., Paola, C., Dietrich, W. E., and Pitlick, J. (2007). "Physical basis for quasi-universal relations describing bankfull hydraulic geometry of single-thread gravel bed rivers." *Journal of Geophysical Research*, 112, F04005, doi:10.1029/2006JF000549.

Rosgen, D. L. (1996). *Applied river morphology*, Wildland Hydrology, Pagosa Springs, Colorado.

Schumm, S. A. (1960). *The shape of alluvial channels in relation to sediment type*. U.S. Geological Survey Professional Paper 352-B, U.S. Government Printing Office, Washington, DC.

Schumm, S. A. (1963). *A tentative classification of alluvial river channels.* U.S.G.S Circular 477, U.S. Government Printing Office, Washington, DC.

Schumm, S. A. (1968). River adjustment to altered hydrologic regimen, Murrumbidgee River and paleochannels, Australia: U.S. Geological Survey Professional Paper 598, 65 pp. http://pubs.er.usgs.gov/usgspubs/pp/pp598.

Schumm, S. A. (2003). *The Fluvial System*, Blackburn, Caldwell, New Jersey.

USING WATERSHED SCALE GEOMORPHIC ASSESSMENT TO IMPROVE URBAN STREAM RESTORATION DESIGN

Sue L. Niezgoda, Ph.D., P.E., Affiliate Member, ASCE[1]

[1]Assistant Professor, Department of Civil Engineering, Rose-Hulman Institute of Technology, 5500 Wabash Avenue, Terre Haute, IN 47803, PH (812)877-8814; FAX (812)877-8440; email: niezgoda@rose-hulman.edu

Abstract

The initial phases of a stream restoration project typically include a watershed geomorphic assessment to classify, identify, and assess a variety of environmental problems that can occur over a fairly large geographic area. There are three phases of geomorphic assessment at the watershed-scale, including the desktop phase, the qualitative field study phase, and the quantitative field study phase. Each phase successively offers more detailed information on system-wide instability; however, each phase also successively requires more resources to implement. An evaluation of the methods involved with each phase of assessment is needed to offer the restoration community guidance on selecting a method or combination of methods that can be used to assess system-wide stability based on time and funding constraints. This paper examines existing quantitative and qualitative assessment techniques, the strengths and weaknesses of those techniques, and their applicability to urban stream restoration design. In particular, those methods that are most beneficial to urban stream restoration are examined and how they can potentially be used to improve the stream restoration design effort by focusing on the watershed scale. An example of the selection and application of qualitative and quantitative assessment techniques to an urban stream restoration design in Bloomington, Indiana is also presented.

Introduction

The initial phases of a stream restoration project typically include a watershed assessment to identify and assess a variety of environmental problems that can occur over a fairly large geographic area. A watershed scale assessment of channel stability in the urban setting requires four main tasks: 1) delineate the watershed, 2) divide the stream network into reaches with similar characteristics, 3) categorize those reaches, and 4) characterize each reach according to level of stability and the protection of critical infrastructure (Chin and Gregory 2005). Watershed delineation is typically completed with topographic maps or GIS data. However, in the urban setting, delineation becomes more complicated due to the existence of ephemeral stormwater drainage channels and roadways that can act as stormwater drainage channels.

Topographic maps, field surveys, remote sensing data, planning documents, and aerial surveys should all be used in conjunction with stormwater drainage plans to identify the total channel network.

Once the watershed has been delineated, it is necessary to subdivide the urban stream network into segments of similar characteristics for geomorphic analysis. In an urban setting, it is difficult to segment a stream based on a standard length or homogeneous geomorphic characteristics due to the fact that infrastructure and other urban constraints act to fragment the drainage network. Therefore, it is suggested that streams be segmented based on hydraulic controls, including road crossings, bridge or utility crossings, or stormwater outfall locations (Chin and Gregory 2005). By segmenting the channel in this manner, management units are delineated because crossings and outfalls are often points at which channel runoff is augmented by stormwater flow and hazard potential is high (Chin and Gregory 2004).

Following network segmentation, each reach can be characterized through geomorphic assessment. Jokay and Watson (2005) suggest that there are three phases of geomorphic assessment, including the desktop phase, qualitative field study phase, and quantitative field study phase. The desktop phase typically includes gathering data and information on land use, soils, and geology from maps and aerial photographs. During this phase, conclusions with respect to channel planform, gradient, valley width, riparian zone width, watershed development, and soil erodibility are inferred from map and soils data (Jokay and Watson 2005). The qualitative field study phase includes conducting a Rapid Geomorphic Assessment (RGA) that field truths data collected during the desktop phase. Qualitative site specific data are gathered on indicators of stream instability (e.g., bank cutting, mass wasting). The quantitative phase involves characterizing reach-level, site specific measurements on geometry and bed material to quantify stream form and processes.

Evaluation of Available Assessment Methods

Chin and Gregory (2005) and Johnson (2005) provide excellent summaries of many existing qualitative and quantitative channel assessment methods. In addition, a collaborative work effort between George Mason University and the National Park Service has resulted in the development of an Ecological Assessment Methods Database (http://assessmentmethods.nbii.gov/). This searchable database focuses on methods and includes selected guidance documents. Based on a review of this material, existing assessment methods can be grouped into four general categorizations (Chin and Gregory 2005): (1) quantitative methods that involve a comprehensive inventory describing characteristics; (2) quantitative methods that emphasizes channel change using thresholds, degree of disturbance, and stability analyses; (3) qualitative methods that focus on management and include the rapid assessment of channel stability using rating systems; and (4) qualitative methods that focus on management of critical infrastructure and include the rapid assessment of channel stability using rating systems. The selection of an appropriate category and method for the characterization of urban stream condition requires consideration of the following specific qualities (Parsons et al. 2002):

- Level of resources required to implement;

- Incorporation of parameters that are relevant to determining channel stability based on biotic, chemical, energy, habitat, and flow regime factors;
- Conformity with a rapid philosophy of data collection and analysis;
- Scientific outputs presented in a form that is easily interpreted by managers;
- Adaptability and applicability to a wide range of river types;
- Ability to predict physical stream characteristics;
- Ability to account for high-hazard urban constraints (e.g., bridges) and;
- Ability to identify environmental problems within an urban drainage network (e.g., exposed utility pipes, fish migration blockages, etc.).

The representation of each of these qualities within the four categories of assessment methods is summarized in Table 1.

Application of Assessment Methods to an Urban Stream Restoration Project

The City of Bloomington, Indiana plans to renovate Cascades Park which is located within the city limits. In order for the city to continue with their renovation plans, Cascades Creek, which runs through the park, needed to be stabilized. A thorough environmental engineering investigation was completed as part of a senior design project conducted by students at Rose-Hulman Institute of Technology. In order to meet project requirements, the student team needed to apply methods that examine stability parameters (chemical and biotic factors, energy source, habitat structure, and flow regime), that were rapid in data collection and analysis, that could potentially predict physical stream characteristics, that account for high-hazard urban constraints (retaining walls, concrete ford, bridges, etc.), and that identify environmental problems within an urban setting. According to Table 1, to meet all these needs, the students needed to apply a combination of quantitative and qualitative approaches presented in Categories 1 and 3.

Prioritization of Reaches

The student team used the Natural Resource Conservation Service's (NRCS) Stream Visual Assessment Protocol (SVAP) to evaluate various reaches of Cascades Creek and prioritize which have the greatest need for restoration. First, the team divided the section of Cascades Creek under investigation into separate smaller reaches (12 total). In this case, the student team found the presence of bank retaining walls to be the major factor in reach delineation. Next, the student team scored each reach in ten different SVAP categories on a scale of one to ten (ten being the best). The categories presented in the SVAP that were rated included 1) channel condition, 2) hydrologic alteration, 3) riparian zone, 4) bank stability, 5) water appearance, 6) nutrient enrichment, 7) barriers to fish movement, 8) in-stream fish cover, 9) pools, and 10) insect/invertebrate habitat. Rankings for each category within each reach were based on the NRCS criteria (NRCS 1998). An example of an individual reach result from the application of the SVAP is displayed in Figure 1. Figure 2 provides photographs of the example reach to provide an illustration of reach conditions at the time the SVAP was applied. The SVAP results for the entire 12 reaches of Cascades Creek are summarized in Table 2. The reach ratings given in Table 2 provide a general indication of the relative health of the reach, especially when compared to the ratings of surrounding reaches.

Table 1 - Evaluation of four categories of assessment against desired qualities of an assessment protocol for urban streams. Representation of qualities is designated as yes (Y), no (N) or potentially (P). (Adapted from Parsons et al. 2002)

Qualities of an Urban Stream Assessment Protocol	Category 1 Methods that Provide a Comprehensive Inventory of Stream Characteristics	Category 2 Methods that Emphasize Channel Change using Thresholds, Degree of Disturbance, and Stability Analysis	Category 3 Methods that Focus on Management and Include Rapid Stability Assessment using Rating Systems	Category 4 Methods that Focus on the Management of Infrastructure and Include Rapid Stability Assessment using Rating Systems
Example References	Rosgen (1994), Rosgen (1996), Downs (1995), Newson et al. (1998), , Thorne (1998)	Simon (1989, 1994), Simon and Downs (1995), Montgomery and Buffington (1997)	Pfankuch (1978), NRCS (1998), Barbour et al. (1999), Yetman (2001), VANR (2007)	Shen and Schumm (1981), Annandale (1994, 1999), Lagassee et al. (2001), Johnson (2005)
Type of Assessment	Quantitative	Qualitative/Quantitative	Qualitative	Qualitative
Level of Resources Required	High	Moderate to High	Moderate	Moderate
Incorporate parameters relevant to:				
Chemical Factors	N	N	Y	N
Biotic Factors	N	N	Y	N
Energy Source	N	N	Y	N
Habitat Structure	Y	Y	Y	N
Flow Regime	Y	Y	Y	Y
Rapid data collection and analysis	N	N	Y	Y
Output form easily interpreted	P	P	Y	Y
Adaptability and applicability to a wide range of river types	Y	Y	Y	Y
Predict physical characteristics	Y	Y	N	N
Account for high-hazard urban constraints (e.g., bridges)	P	P	P	Y
Identify environmental problems	P	P	Y	Y

Reach Number 1

Channel condition	9
Hydrologic alteration	9
Riparian zone	5
Bank stability	4
Water appearance	9
Nutrient enrichment	9
Barriers to fish movement	8
In-stream fish cover	5
Pools	3
Invertebrate habitat	5



Overall Score *(Total divided by number scored)* 66/10	**6.6**	<6.0	**Poor**
		6.1-7.4	**Fair**
		7.5-8.9	**Good**
		>9.0	**Excellent**

Figure 1 - Example of SVAP applied to Reach 1 in Cascades Creek.

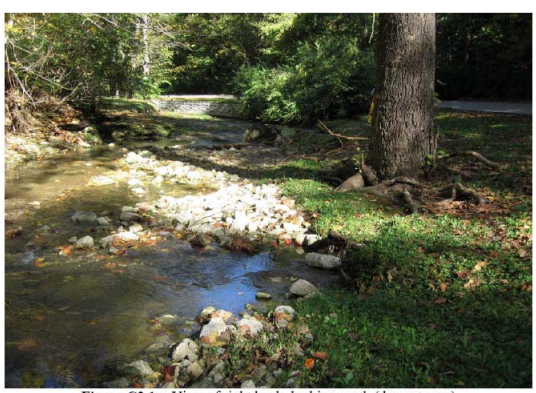

Figure C2.1a: View of right bank, looking north (downstream).



Figure C2.1b: View of right bank, looking northwest (downstream).

Figure 2 - Photos of Cascades Creek Reach 1

Table 2 - USDA SVAP Summary for Reaches in Cascades Creek

Reach Number	Overall Score	Rating
1	6.6	Fair
2	6.1	Fair
3	5.5	Poor
4	6.1	Fair
5	5.7	Poor
6	4.2	Poor
7	5.0	Poor
8	5.2	Poor
9	5.2	Poor
10	5.5	Poor
11	6.1	Fair
12	5.4	Poor

As part of the environmental engineering study, the student team also collected stream survey data for use in stream classification and hydraulic model studies. The survey results were applied to the Rosgen (1994) classification system to classify each reach and provide insight into stream type (Category 1). The determination of bankfull stage in urban streams for use in the Rosgen (1994) classification was difficult as there was typically no clear indicator of bankfull elevation (breaks in slope, tops of point bars, vegetation lines, changes in sediment size, etc.). To better represent the main channel in Cascades Creek the team looked beyond the use of bankfull indicators and examined other key stream features that were determined to be more appropriate in the urban setting: 1) changes in channel roughness (Manning's n) – point where channel boundary characteristics change such that it indicates a change in roughness characteristics; 2) channel top of banks – where there is a clear break in slope from the channel banks to the floodplain (i.e., top of retaining walls); 3) elevation of flooding impact - elevation at which flooding would significantly impact adjacent infrastructure or property. For most reaches in Cascades Creek the main channel top of bank indicator ("bankfull indicator") was identified as a break in slope or top of a retaining wall. The results of the Rosgen (1994) classification are summarized in Table 3.

Stream bank erodibility was characterized through the application of Rosgen's (1996) Bank Erodibility Hazard Index (BEHI). At each reach cross section location, stream bank erosion potential variables were determined including (1) bank height, (2) bankfull height (if possible to determine in the urban stream) (3) riparian root depth (4) riparian root density (5) bank angle (6) surface protection (7) bank materials, and (8) bank stratification. Rosgen (1996) organized these streambank erosion variables into a hazard rating procedure that includes indices that are used to estimate streambank erodibility. The BEHI results for Cascades Creek are summarized in Table 4. Based on these results, the team determined that the natural banks range from very low to extreme erodibility and used this information to prioritize the banks for erosion protection.

Table 3 – Rosgen (1994) Classification Results for Cascades Creek

Reach	Stream Type	Sensitivity to Disturbance	Recovery Potential	Sediment Supply	Stream Bank Erosion Potential	Vegetation Controlling Influence
1	C5	very high	fair	very high	very high	very high
2	B1c	very low	excellent	very low	very low	negligible
3	F1	low	fair	low	moderate	very high
4	B1c	very low	excellent	very low	very low	negligible
5	F1	low	fair	low	moderate	very high
6	F1	low	fair	low	moderate	very high
7	F1	low	fair	low	moderate	very high
8	C1	low	very good	very low	low	moderate
9	NA	NA	NA	NA	NA	NA
10	F1	low	fair	low	moderate	very high
11	B3	low	excellent	low	low	moderate
12	F1	low	fair	low	moderate	very high

Note: Reach 9 was not classified because the reach consisted mostly of the man made ford.

Table 4 – BEHI (Rosgen 1996) Results for Cascades Creek

BEHI ID Number	Left Bank Erodibility Classification	Right Bank Erodibility Classification
1	Moderate	Low
2	Very Low	Very High
3	Low	Moderate
4	Low	n/a
5	n/a	Moderate
6	n/a	Moderate
7	n/a	Extreme
8	n/a	Extreme
9	Low	High
10	n/a	High
11	n/a	Low
12	n/a	Moderate
13	n/a	High
14	High	Very High

Reach 1 Summary and Preliminary Recommendation Based on Assessment Results

Reach 1 is located at the southernmost, upstream end of the project area (Figure 1). The reach is approximately 79 meters long and is characterized by a gently sloping bank to the right side of the stream. The bank extends at a gentle slope until it reaches the road. Most of the right bank does not appear to be eroding and is almost entirely covered by grass with one large tree and a patch of shrubbery at its northern edge (Figure 2). However, severe erosion was observed at the most downstream portion of the reach along the right bank. The eroded area is about 3.7 meters wide and extends the entire height of the bank. The erosion is coming dangerously close to an adjacent road. The left bank is steeply sloped and extends upward in elevation for more than 15 meters, forming the left edge of the valley. The slope of the left bank is covered in moderate to dense vegetation consisting of trees, brush, and some grasses. The left bank is also eroding, characterized by exposed roots (Figure 2) The stream bed is made up of a range of sediment from bedrock in places, to small pebbles, and small boulders.

Based on the results of the Category 1 and 3 assessments, the student team recommended that a rehabilitation structure be placed along the right bank at the downstream end of the reach to stop the erosion that is threatening the road. They further suggested the placement of boulder revetments or rock vanes to correct the deficiency. Also, with a moderate to high bank erosion potential, the team recommends planting more vegetation on the right and left banks to better hold the soil in place during large storm events. Although grass provides good soil cover, vegetation with larger root structures can provide more stability and protection.

Summary

There are a number of advantages and disadvantages of assessment techniques that need to be considered. The desktop assessment requires the least amount of resources but also provides the least amount of information regarding reach level stability. Conversely, the quantitative field study offers the most site-specific data for analyzing fluvial forms and processes, but it also requires the most resources to implement. Most restoration resources are devoted to the actual restoration design, leaving little available for initial watershed-scale assessments or post-construction monitoring (Bernhardt et al 2005). As a consequence, most projects begin with only a desktop assessment which produces a report that contains little information based on recent observations and may not be very useful for decision making (Jokay and Watson 2005). Qualitative assessment using RGA techniques (Categories 3 and 4) can provide a better understanding of the natural processes and stream reach condition throughout the watershed while only requiring a moderate amount of resources (Chin and Gregory 2005, Jokay and Watson 2005, Johnson 2005). Quantitative field studies (Categories 1 or 2) may only be necessary when focusing on a given high priority reach, in which specific information on fluvial forms and processes are necessary for design (Chin and Gregory 2005). In general, qualitative assessments (or RGA's) appear to be the most suitable to the urban environment, because they validate desktop assessments by assessing various parameters

qualitatively in a short amount of time (Chin and Gregory 2005). Ultimately, conducting a qualitative assessment using methods presented in Categories 3 and 4 in Table 1 can help prioritize impacted stream reaches and better direct future stream restoration and stabilization efforts within an urban watershed. This prioritization can ensure long-term effectiveness of future restoration projects and serve as a foundation for a coordinated and effective watershed management plan.

References

Annandale, G. W. (1994). "Guidelines for the hydraulic design and maintenance of river crossings, Volume VI: Risk analysis of river crossing failure." *Rep. No. TRH 25:1994*, Department of Transport, Pretoria, South Africa.

Annandale, G. W. (1999). "Risk analysis of river bridge failure." *Proc., Stream Stability and Scour at Highway Bridges*, E. V. Richardson and P. F. Lagasse, eds., ASCE, Reston, Va., 1003–1012.

Barbour, M.T., Gerritsen, J., Snyder, B.D., and Stribling, J. B. (1999). "Rapid bioassessment protocols for use in streams and wadeable rivers: periphyton, benthic macroinvertebrates, and fish." Second Edition, *EPA 841-B-99-002*, Office of Water, U.S. Environmental Protection Agency, Washington, D.C.

Bernhardt E.S., Palmer M.A., Allan J.D., Alexander G., Barnas K., Brooks S., Carr J., Clayton S., Dahm C., Follstad-Shah J., Galat D., Gloss S., Goodwin P., Hart D., Hassett D., Jenkinson R., Katz S., Kondolf G.M., Lake P.S., Lave R., Meyer J.L., and O'Don T.K. (2005). "Synthesizing U.S. river restoration efforts." *Science* 308: 636-637.

Chin, A., and Gregory, K.J. (2005). "Managing urban river channel adjustments." *Geomorphology*, 69, 28-45.

Downs P.W. (1995). "River channel classification for channel management purposes." *Changing River Channels*, Gurnell, A., and Petts G. (eds.). John Wiley & Sons, Ltd., Chichester, UK: 347-365.

Johnson, P.A. (2005). "Preliminary assessment and rating of stream channel stability near bridges." *ASCE, Journal of Hydraulic Engineering*, 131(10), 845-852.

Jokay, N., and Watson, B. (2005). "Conducting rapid fluvial geomorphic assessment based on the channel evolution model: A case study in Griffin, Georgia." *Proceedings of the 2005 Georgia Water Resources Conference*, held April 25-27, 2005, at the University of Georgia, Hatcher, K.J. (ed.), Athens, Georgia.

Lagasse, P. F., Schall, J.D., Johnson, F., Richardson, E.V., Richardson, J.R., and Chang, F. (2001). "Stream stability at highway structures, third edition." *Rep. No. FHWA-IP-90-014, HEC-20-ED-2*, Federal Highway Administration, Washington, D.C.

Montgomery, D.R., and Buffington, J.M. (1997). "Channel-reach morphology in mountain drainage basins." *Geological Society of America Bulletin*, 109, 596-611.

Newson M.D., Clark, M.J., Sear, D.A., and Brookes A. (1998). "The geomorphological basis for classifying rivers." *Aquatic Conservation: Marine Freshwater Ecosystems,* 8, 415-430.

Parsons, M., Thomas, M., and Norris, R. (2002). "Australian river assessment

system: Review of physical river assessment methods — A biological perspective." Cooperative Research Centre for Freshwater Ecology, Monitoring River Health Initiative, *Technical Report Number 21*, Environment Australia, <http://ausrivas.canberra.edu.au/Geoassessment/Physchem/Man/Review/chapter3.html.> (November 28, 2008). *ISSN* 1447-1280, *ISBN* 0-642-54887-0

Pfankuch, K.J. (1978). "Stream reach inventory and channel stability evaluation." U.S. Department of Agriculture Forest Service, *Northern Region Report*, Missoula, MT.

Rosgen, D.L. (1994). "A classification of natural rivers." *Catena,* 22, 169-199.

Rosgen, D.L. (1996). *Applied River Morphology*. Wildlife Hydrology, Pagosa Springs, CO.

Shen, H.W. and Schumm, S.A. (1981). "Methods for assessment of stream-related hazards to highways and bridges." Office of Research and Development Report *FHWA/RD-80/160*. Federal Highway Administration, Washington, DC.

Simon, A. (1989). "A model of channel response in disturbed alluvial channels." *Earth Surface Processes and Landforms,* 14, 11 –26.

Simon, A. (1994). "Gradation processes and channel evolution in modified west Tennessee streams: process, response, and form." *U.S. Geological Survey Professional Paper 1470*, Reston, Virginia.

Simon, A. and Downs, P.W. (1995). "An interdisciplinary approach to evaluation of potential instability in alluvial channels." *Geomorphology,* 12, 215– 232.

Thorne C.R. (1998). *Stream Reconnaissance Handbook*. John Wiley & Sons, Ltd., Chichester, UK.

USDA-NRCS (1998). "Stream visual assessment protocol." *National Water and Climate Center Technical Note 99-1*, Washington DC.

Vermont Agency of Natural Resources (VANR). (2007). "Vermont stream geomorphic assessment." *Phase 2 Handbook, Rapid Stream Assessment Field Protocols*. Vermont Department of Environmental Conservation, Water Quality Division, River Management Section, <http://www.vtwaterquality.org/rivers/htm/rv_geoassesspro.htm.> (November 28, 2008.)

Yetman, K.T. (2001). "Stream corridor assessment survey, survey protocols." Watershed Restoration Division, Chesapeake & Coastal Watershed Services, Maryland Dept. of Natural Resources Annapolis, MD

Habitat Restoration on the Middle Fork John Day River

E.R. Holburn[1], T. Turner[2], L. Piety[3], R.E. Klinger[3]

[1] Hydraulic Engineer, Bureau of Reclamation, Denver, CO, eholburn@usbr.gov;
[2] Hydraulic Engineer, Bureau of Reclamation, Boise, ID, tturner@usbr.gov;
[3] Geomorphologist, Bureau of Reclamation, Denver, CO, lpiety@usbr.gov and rklinger@usbr.gov.

ABSTRACT

Multi-disciplinary stream assessments are currently being conducted on tributaries to the Columbia River, including the Methow, Wenatchee, Entiat, and John Day River Basins. The primary objective of these studies is to develop an improved understanding of the physical processes acting on the watershed to identify river restoration opportunities that address limiting factors of ESA-listed species. This objective is met through interpretation of the biological conditions, including the fisheries and vegetation ecosystems, the geologic setting, anthropogenic constraints, geomorphic processes, basin hydrology, and hydraulic and sediment transport processes. Local knowledge, compiled data and modeling results are synthesized to evaluate potential physical and biological response to restoration actions. In particular, hydraulic modeling, sediment transport analyses, and geomorphic studies help define the spatial and temporal scale of river processes and offer a predictive tool to assess proposed actions. This paper presents an example of how this objective is being accomplished along a 23-mile reach of the Middle Fork John Day River located in northeastern Oregon.

Results of these investigations assist other technical staff, resource managers, planners, and stakeholders in determining how and where to focus resources for implementation of identified restoration projects. In this paper, we also illustrate a scientific methodology for evaluating the linkages between fluvial processes and biological response to proposed habitat improvements and present results from a two-dimensional hydraulic model to quantify potential increases in floodplain connectivity and channel complexity.

INTRODUCTION

In compliance with the Federal Columbia River Power System Biological Opinion (NOAA, 2008), the Bureau of Reclamation (Reclamation), U.S. Army Corps of Engineers, and Bonneville Power Administration are working to implement habitat restoration projects in the Upper and Lower Columbia River basin. Recovery efforts are focused on limiting factors for the survival of Endangered Species Act (ESA)-listed and other culturally important species within the four general sectors of harvest, hatcheries, hydropower, and habitat. Implementation of a combination of actions in all four sectors is expected to be necessary for recovery of ESA-listed species. Within the habitat sector, Reclamation provides technical assistance for project identification, design, and construction in partnership with States, Tribes, Federal agencies, and other local workgroups. Initially, technical assistance was provided to address critical path projects such as stream flow improvement, removal of in-stream barriers, and fish screen enhancement projects. More recently, Reclamation has been incorporating

habitat complexity projects, which have been a challenging endeavor for both scientists and resource managers.

Reclamation initiated assessments in multiple tributaries to the Columbia River, including the Methow, Wenatchee, Entiat, and John Day Rivers, to develop planning tools that can be used collectively by partners within a subbasin to focus resources to identify and prioritize floodplain connectivity and channel complexity restoration/ protection projects. Within this paper, we present how scientific assessments are being developed and applied in the Middle Fork John Day River (MFJDR).

The John Day River is a tributary to the Columbia River and drains nearly 8,000 square miles. The Middle Fork subbasin originates in the Blue Mountains of the Malheur National Forest and flows 75 miles to its confluence with the North Fork John Day River north of Monument, Oregon. The assessment area of the MFJDR is a 23-mile stretch of river located in Grant County, Oregon, from the confluence of Camp Creek to just downstream of the confluence of Crawford Creek. This area has a range of private and federal ownership, including some national forest lands. Multiple properties are owned by the Confederated Tribes of the Warm Springs Reservation of Oregon (CTWSRO) and by The Nature Conservancy.

Within the MFJDR, substantial changes to channel processes and resulting habitat have occurred over the last century. Populations of several important fish species, including spring Chinook (*Oncorhynchus tshawytscha*), summer steelhead (*Oncorhynchus mykiss*), and bull trout (*Salvelinus confluentus*), have markedly decreased. Spring Chinook and summer steelhead are of particular importance to the region because the John Day River is managed exclusively for wild fish production (NPCC, 2005).

METHODS

To develop habitat restoration strategies, a multi-disciplinary team worked to provide a cross-discipline understanding of important river processes that help create and sustain habitat conditions important to ESA-listed and other culturally important species. Habitat restoration projects implemented with a clear understanding of the existing physical processes are more likely to provide both short- and long-term benefits to important fish species. A sound understanding also helps reduce the likelihood for unanticipated, potentially adverse impacts to landowners and even the species itself.

Stream evaluation efforts aim for a high degree of certainty by using state of the art tools and more quantitative than qualitative data. While quantitative methods provide more certainty to results than qualitative methods, they are not always necessary and are more costly and time consuming to employ, particularly for large study areas. Therefore, a multi-tiered spatial approach was used in the MFJDR that began with a coarse-scale analysis of physical processes, and then focused in more detail in areas identified to have more complex river processes. The initial coarse-scale analysis, referred to as a stream assessment, provided the technical basis for proposed restoration concepts. Upon completion of the stream assessment, resource managers worked with the technical team to determine where impacts are localized and design work can begin, or alternatively, where a refined analysis within a specific reach of

river was needed. The reach-scale evaluation addresses questions specifically tailored to processes operating within that reach that are important to further understand prior to implementing a restoration action. Reach assessments typically occur in areas with a high degree of impacts and a high potential for improving habitat complexity.

Stream Assessment. To determine the degree of impact to altered habitat availability and quality, a conceptual model was developed for the MFJDR to outline typical channel processes and expected river functions that may have existed prior to widespread anthropogenic impacts. Not all river reaches can support the same level of floodplain complexity due to variations in geologic control, floodplain width, sediment size, channel slope, and local hydrology. Comparison of the present river setting to a conceptual model of the MFJDR prior to anthropogenic impacts helps determine which processes may have been altered and to what degree. It is recognized that processes cannot be fully returned to pre-development conditions due to changes in vegetation, the physical setting, or current land use. Documented historical changes in morphological river features (e.g., channel form, floodplain character, presence and type of riparian vegetation) can help define the rate of change from pre-development conditions, how the changes relate to historical floods and anthropogenic activities, and whether the changes are continuing or have stabilized. Following the compilation of previously existing data, components of the ecosystem were further explored to improve understanding of system processes influencing the generation and maintenance of salmonid habitat, including:

Fisheries- An investigation of historical trends of ESA-listed and other culturally important species was conducted based on past work to understand changes in abundance, spatial distributions, and potential habitat factors limiting their populations. An understanding of current species presence and habitat use relative to historical presence and habitat use laid the framework for how anthropogenic impacts or processes that influence the availability and quality of habitat important to their continued survival may have been altered over time.

Geomorphic/Geologic setting- Existing geologic information was collected at a regional level to understand the geologic history of the basin and identify the presence of major geologic structures (i.e., faults, folds, rock types, and their spatial relationships) that may be important to the present-day morphology of the MFJDR. Within the stream assessment area, aerial photography, Light Detection and Ranging (LiDAR) data, regional geology maps, and field reconnaissance were used to define surficial geologic units (floodplain, stream terraces, landslides, and alluvial fans) and identify specific geologic controls that may restrict the lateral and vertical position of the river (e.g., resistant bedrock, large boulders, talus). Historical trends of channel position, slope, and width were evaluated to document rates of change and relate changes to anthropogenic impacts or natural river processes.

Reaches within the stream assessment area were defined on the basis of their physical characteristics and dominant processes affecting channel form and function needed to maintain habitat features. Initially, geologic controls such as alluvial fans and bedrock outcrops were identified through field evaluation of the assessment area. Other physical characteristics used in identifying the reaches included valley width, tributary inputs of flow and sediment, and present riparian vegetation. Other more

subtle geomorphic processes that influence the physical characteristics of the river, such as changes in channel form and position, channel slope, sediment transport capacity, and notable areas of erosion or deposition, were also evaluated to further define reach characteristics

Hydrology- A hydrologic analysis was conducted to identify historical flood events that may have impacted channel morphology, to characterize significant impacts to the flow regime within the basin, and to provide an estimate of the recurrence interval of specific peak discharges for input to hydraulic and sediment transport models. The analysis relied primarily on literature documenting diversion magnitude and timing, long-term stream gage data, and documented accounts of historical floods. A geographical information system (GIS) layer was then created to provide easy access to flood frequency estimates anywhere in the basin based on regional regression equations for northeastern Oregon.

Hydraulics and sediment transport- Hydraulic and sediment transport analyses were performed to evaluate floodplain connectivity, identify potential areas of bed degradation, and examine the influence of anthropogenic activities on hydraulics and sediment transport. The hydraulic analysis consisted of the development of a one-dimensional, steady flow hydraulic model using Hydrologic Engineering Center-River Analysis System (HEC-RAS). For evaluation of channel processes in the stream assessment, cross-sectional averaged hydraulic parameters were sufficient to approximate water surface elevations, extent of inundation, and in-channel velocities for selected peak discharges. Various surrogates, which included incipient motion, unit stream power, total stream power, and sediment transport capacity, were used to evaluate how sediment moves through the MFJDR under various peak discharges. These surrogates provide an improved understanding of the relative degree to which channel forming processes vary throughout the system and of the relative capacity of reaches to transport sediment.

Riparian Vegetation- Large areas of riparian vegetation clearing have occurred along the MFJDR over the last century. To locate and quantify the impacts, aerial photography from 1939, 1956, 1976, and 2006 were used in combination with LiDAR data to visually interpret canopy vegetation community classes such as conifer, hardwoods, shrub, or meadows. Vegetation communities in the floodplain were mapped in GIS, and changes in vegetation over time were quantified. Based on the mapping of present day conditions, the potential for recruitment of large woody debris (LWD) and shading by trees along the river channel was characterized. These data could be further refined and validated using a field assessment of species present.

Anthropogenic constraints and impacts- Anthropogenic activities including logging, grazing, and mining of placer deposits immediately adjacent to or in the river have occurred for over a century in the Middle John Day basin. A literature review was conducted to capture major changes in land use since the late 1800s. Mapping of constructed features on and adjacent to the floodplain, including levees, roads, bridges, and water diversions, was conducted using aerial photography and LiDAR data and verified with field observations (Reclamation, 2008). Impacts of the constructed features on floodplain connection and channel position were also quantified and mapped.

Findings from each of the components described above were integrated to identify reaches that displayed the greatest impacts to the physical river setting relative to the conceptual model of typical channel processes. Inferred changes to river processes were then interpreted to determine how the impacts may have potentially influenced habitat conditions. From this information, a technical ranking of reaches was developed to provide other technical staff, resource managers, planners, and stakeholders with a way to identify, sequence, and prioritize opportunities for protecting or restoring channel and floodplain connectivity and channel complexity at the reach-scale. Proposed rankings consider potential for protection of existing habitat, restoration opportunities, degree of departure from fully-functioning conditions, and present fish use.

Reach-scale Evaluation. Results from the stream assessment of physical processes on the MFJDR combined with landowner willingness led to a refined investigation of restoration opportunities within one segment of the stream assessment area. The reach selected lies within the Oxbow Conservation Area (OCA), an area that was drastically altered by dredge mining operations in the 1940s. The key objective of the reach assessment was to further investigate hypotheses on river process identified in the stream assessment and by a working group of stakeholders that would lead to implementation of restoration projects with the greatest opportunity for success. These hypotheses included (1) mining activities have severely impacted floodplain connection and lateral channel migration, (2) returning all flow to the historical South Channel would benefit habitat without adversely impacting channel morphology, and (3) geomorphic conditions within the reach influence potential restoration options. To accomplish the objective, these steps were followed:

Data gap analysis- An interdisciplinary team comprised of geomorphologists, biologists, ecologists, hydraulic engineers, design engineers, and stakeholders was convened to help identify missing information needed to better understand reach processes relative to implementation of restoration actions. Specific items identified were longitudinal and seasonal variations in stream temperature, composition of native vegetation within the riparian corridor, and a refined interpretation of the channel morphology including the hydraulic properties of the river associated with multiple channels, substantial flow splits, a meandering channel, and a channel with extensive point bar and pool-riffle formation.

Geomorphic investigations- Coarse-scale geologic mapping completed for the stream assessment was refined to gain a better understanding of geomorphic processes controlling the channel morphology, the history of development, and evolution of the channel over the last several thousand years. In addition, specific information regarding the character of the floodplain, terraces, and deposits from the tributaries was needed. A single mapped unit of surficial deposits associated with the river was subdivided into four alluvial units based primarily on surface morphology, relative age, and elevation above the active channel. Shallow pits were excavated on each of the alluvial units to describe the character of the sediment comprising the deposits, document the extent of soil formation (an indicator of relative age and landscape stability) and collect detrital charcoal and sediment samples in an attempt to evaluate the type of vegetation growing adjacent to the river pre-historically.

2D hydraulic model- The OCA is comprised of a complex network of multiple channels and tributaries. Therefore, a 2D hydraulic model was developed using Reclamation's Sedimentation and River Hydraulics 2D hydraulic model (SRH-2D; Lai, 2006) to gain insight and predictions of floodplain processes, side channel connectivity, and split flow dynamics through the selected reach. Simulations were conducted for the 2- through 100-year peak discharges with inlet flows ranging from 881 cubic feet per second (cfs) to nearly 2700 cfs. In addition, the model was applied to evaluate a "proposed conditions" scenario to examine how hydraulic parameters and habitat features may change following a specified restoration action. Proposed conditions included blocking off the North Channel, an artifact of dredge mining, downstream from the bifurcation of the historical South Channel, and just upstream of the confluence with a major tributary, Granite Boulder Creek (Figure 1).

Following completion of these individual tasks, results from the geomorphic investigations were linked with results from the hydraulic modeling to better understand pre-disturbance physical processes in the reach, identify potential restoration opportunities, and identify limitations to habitat restoration.

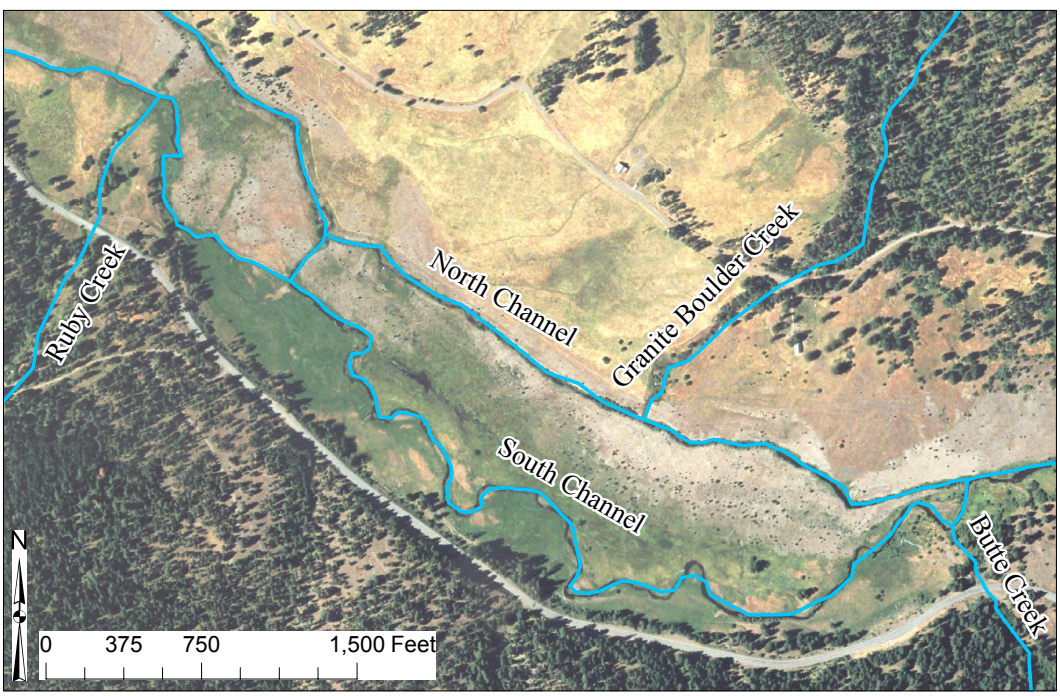

Figure 1. Aerial image of key features examined in the Reach Evaluation.

RESULTS AND DISCUSSION

Summary of stream assessment findings. The form of the river and channel processes can be affected by changes in flow regime, sediment regime, and topographic elements, such as constructed features and vegetation. The flow regime in the MFJDR is relatively unaffected by historical development with the exception of minor flow diversions. The sediment regime is mainly affected by short-term increases in fine sediments from anthropogenic activities, localized changes in channel slopes resulting from channelization, and possibly localized degradation or bed coarsening. The greatest apparent impacts to river form and habitat result from

historical changes to the topography and riparian vegetation due to anthropogenic activities. Notable changes to topography, vegetation, and the river form that impact the availability and quality of habitat for spring Chinook and steelhead include: (1) reduced side channel access and floodplain connectivity due to bridges, roads, levees, and bank protection measures that disconnect the channel from the historical channel migration zone and floodplain area; (2) reduced access to the historical channel migration zone through increased channel slope and decreased sinuosity due to confinement of high flows, manual channel straightening, and bank protection measures; (3) reduced quantity of large trees available for recruitment to the river and altered rates of regeneration of riparian vegetation due to timber harvest, conversion of riparian forests to agricultural fields, and minimal lateral reworking of the channel and floodplain; (4) reduced habitat complexity within the channel, along channel margins, and within the floodplain due to alterations in cover, LWD inputs, and hydraulic and sediment diversity (e.g. wet meadows, beaver ponds) and due to the conversion of banks to rock protection; (5) reduced competency of the channel to rework floodplain materials due to dredge mining activities; and (6) increased water temperatures resulting from alterations in channel complexity, increased width-to-depth ratios, disconnected floodplains, and reduced shade.

Development of restoration concepts. Results of the stream assessment were used to evaluate the potential for restoring channel processes that create and maintain desired habitat. It was determined that actions with the greatest potential to create habitat are those that restore natural river processes and generate habitat complexity, particularly in reaches that experience frequent channel migration and floodplain inundation. Short-term actions, such as the placement of LWD, may be needed to supplement long-term riparian vegetation recovery. Protection and monitoring opportunities were also identified as part of a restoration strategy to maximize beneficial effects of restoration projects in adjacent areas.

Several restoration concepts were recommended for long-term recovery of habitat complexity. First, a major revegetation effort is needed to restore healthy riparian processes, provide shade and cover to the channel, provide a source for the future recruitment of LWD, and moderate lateral channel migration and bank erosion. A second important restoration concept in areas with a wide floodplain is the setback or removal of topographic (anthropogenic) features that negatively impact river processes, including floodplain connectivity, lateral channel migration, and the availability and formation of off-channel and main channel complexity features. In areas with narrow floodplains, the largest impacts to habitat function result from the loss of riparian vegetation and the presence of bank armoring (rock spurs, riprap). Modification or removal of these features in conjunction with riparian planting offers the best opportunity for improving habitat.

Technical ranking of reaches. Within the MFJDR, three of the twenty defined reaches were ranked considerably higher than all other reaches based on their potential for restoration of floodplain connectivity and channel complexity. These three reaches included properties at the Dunstan Ranch managed by The Nature Conservancy and the Oxbow and Forrest Conservation Area managed by the CTWSRO. All of the high-ranking reaches are characterized by wide floodplains with

high potential for frequent floodplain inundation, lateral migration and formation of side channels, which encourages continual regeneration of a healthy riparian corridor that would add shade, organic material, and additional complexity to the channel. The final prioritization for further analyses on the OCA was made on the basis of stakeholder preference, availability of funding opportunities and prior dedication of resources to site-specific restoration efforts

Substantial findings of the reach-level evaluation of the OCA. The 3.5 mile stretch of the OCA selected for reach-level evaluation has been substantially modified, primarily due to ranching, grazing, timber harvest, road and levee construction, channel stabilization, and dredge mining. The first three activities mentioned led to the removal of vegetation from the floodplain and adjacent valley floor. Road and levee construction resulted in disconnection of floodplain, while bank stabilization structures, consisting principally of rock spurs and riprap, have constrained lateral channel migration. The most substantial impact, however, was the dredge mining activities that occurred on the property in the early 1940s. This activity altered the channel and floodplain characteristics dramatically by changing the location, geometry, and planform of the channel, as well as the number of channels. Dredging operations turned over floodplain deposits, winnowed out available fines, and altered the size of the channel bed and floodplain sediment. After mining ceased, stream flow was split between two channels, the North and South Channels (Figure 1). The South Channel is the remnant of the natural channel to the south of the dredge tailings; the North Channel was constructed through the dredge tailings and across the toe of the Granite Boulder Creek alluvial fan. During high flows, most of the stream flow is routed through the South Channel, but during low flows, the hydraulic conditions are reversed due to the conveyance conditions at the bifurcation of the North Channel.

Two significant contributors of stream flow and sediment to this reach are Granite Boulder Creek, located downstream from the bifurcation of the North and South Channels, and Ruby Creek, just downstream from the confluence of the North and South Channels (Figure 1). Both tributaries would have provided substantial physical constraints on the river geomorphology, particularly on lateral channel migration. However, parts of each fan were dredged, and the creeks have been at least partially diverted into artificial channels. Channelization resulting from the dredge activities now severely impacts channel position and river function.

Geomorphology. Several important aspects of the geology, how it influences the river geomorphology, and the processes controlling it were observed in the OCA. In general the three larger tributaries, Ruby, Butte, and Granite Boulder Creeks, shed alluvial fans into or across the valley. The formation of these alluvial fans directly influences the channel gradient and channel form immediately upstream of each tributary. Material shed onto the valley floor by Ruby Creek is in general very coarse grained, and primarily of volcanic composition. As a consequence, the Ruby Creek alluvial fan has a strong influence on the position of the MFJDR in the valley pushing it northeast (Figure 1). In combination with a landslide at this location, the Ruby Creek alluvial fan provides a constraint on the valley width, and as a result, controls the channel gradient locally and channel form immediately upstream.

The valley is significantly wider downstream of Ruby Creek, and as a consequence, the areal extent of the floodplain historically was much greater as the MFJDR migrated laterally across this area. Despite impacts of the mining locally, evidence for this is provided by channel scars on the valley floor visible in the 1939 aerial photographs. Older stream terraces preserved along the margins of the valley are indicative of an overall trend of incision by the MFJDR into older alluvial valley fill during the last 7600 years. However, the wide floodplain and numerous abandoned channels on the valley floor visible in the 1939 photographs suggest that the recent history of the river (for at least the last 1200 years) has been predominately of lateral migration (Bandow, 2003).

The Granite Boulder Creek alluvial fan also has a strong influence on the position and character of the MFJDR in the valley pushing it south (Figure 1). Unlike the Ruby Creek fan, its areal extent is significantly larger. Historically, the distal portion of the alluvial fan (toe) was modified by the MFJDR. Evidence for this is provided by abandoned channel scars and other lineations that are subparallel to the course of the MFJDR and by patterns in the vegetation visible on the 1939 aerial photography. As implied by its name, material shed onto the valley floor from Granite Boulder Creek is very coarse and primarily of granitic composition. Based on the areal extent of its alluvial fan, it is apparent that the Granite Boulder Creek drainage is the major contributor of coarse-grained gravelly sediment to the MFJDR. The Granite Boulder Creek alluvial fan constrains the channel position of the MFJDR where it pushes the river against the Butte Creek alluvial fan (at the present day split between the North and South Channels). The result once again is that the alluvial fan is a control on the channel gradient locally and channel form immediately upstream.

The Butte Creek alluvial fan is small in terms of its areal extent relative to Granite Boulder Creek. However, its steep gradient, which is similar to that of the Ruby Creek alluvial fan, allows very coarse-grained material to be delivered from its basin directly to the margin of the MFJDR valley. And as with Ruby Creek, the sediment comprising the fan is primarily of volcanic composition. The coarse-grained nature and steep form allows the Butte Creek alluvial fan to exert some influence on the position of the MFJDR pushing it north against the upstream margin of the Granite Boulder Creek alluvial fan (Figure 1).

Because vegetation on the valley floor was removed as a result of logging and agricultural activities and later by mining, little is known about the type and extent of historical riparian vegetation on the OCA. Thirty-four charcoal samples were collected from each of the stream terraces and alluvial fan deposits, either in soil pits or natural exposures. Each sample was identified to genus level in an attempt to document the type of large woody vegetation present prehistorically. Several trends were recognized in the type and distribution of paleobotanical material recovered. First, samples recovered from terrace deposits along the MFJDR are dominated by conifer charcoal. A single fragment of Alder (*Alnus*) charcoal was recovered from the youngest stream terrace deposit. Typically, samples recovered from the floodplain and youngest terrace deposits include material representing riparian species, for example willow (*Salicaceae*) and cottonwood (*Populus*). Also, the youngest deposits (in this case the youngest terrace and floodplain deposits) generally contained

charcoal indicative of the diverse riparian ecosystem. While there was diversity in the type of charcoal recovered along the MFJDR, more commonly represented riparian species were missing. An interesting finding was the presence of Hemlock (*Tsuga*) charcoal in the older terrace deposits (>1200 years). Apparently hemlock is not found in the area today. Sediment samples were also collected to examine pollen content; results of these analyses are pending.

2D hydraulics. Using the results of the 2D model, split flow dynamics were evaluated and several habitat indicators, including side channel access, floodplain connectivity, and high quality high flow habitat, were investigated. Comparisons were made between existing and proposed conditions (blocking off the North Channel) based on predicted changes to water surface elevation, depth-averaged velocity, and bed shear stress. These hydraulic parameters were compared along the channel thalweg and across the floodplain.

Flow split patterns were evaluated to better understand complicated hydraulics between the North and South Channels and through several smaller alternative channels (e.g. abandoned ditches). Model results indicate that the North Channel has a reduced influence on flood conveyance as the peak discharge increases in magnitude. The capacity of the North Channel is estimated to be approximately 450 cfs (17 percent of the total) at a 100-year peak discharge, with the remaining flow being conveyed through the South Channel and across the adjacent floodplain. The model also improved the ability to predict the influence of other constructed flow paths and abandoned side channels on floodplain inundation.

Present floodplain connectivity was determined by quantifying the area of the floodplain outside of the low flow channel that experienced depths exceeding 0.5 feet. Model results predicted substantial floodplain connectivity at the 2-year peak discharge throughout a substantial portion of the study area. Locations not experiencing floodplain connectivity under the peak flows evaluated were channelized portions of the river, which were artifacts of mining activities. The model also predicted that almost all of the side channels present were connected at flows equivalent to the 2-year peak discharge and greater. Side channels that may have been present historically through the dredged areas were drastically altered during the dredging operations of the 1940s. One channel that appears to have been the main low flow channel in the 1939 aerial photographs begins to convey flow at the 10-year peak discharge and is well connected at the 100-year peak discharge. High-quality high-flow habitat, which was defined as areas experiencing greater than 0.5 feet of flow depth with velocities less than 2 feet per second, accounted for 10% to 17% of the floodplain, depending on peak discharge.

Comparisons of the channel hydraulics under existing and proposed conditions suggest slight improvements to the habitat indicators. Notable changes only occurred in a 1.5 mile section downstream of the North and South Channel bifurcation. Models of the proposed conditions predicted increased floodplain connectivity along the South Channel, which decreased in magnitude as the peak discharge increased. At discharges exceeding a 10-year annual exceedance probability, areas of floodplain connectivity lost along the channel margins of the North Channel were greater than those gained along the floodplain of the South Channel. Although most of the flow

across the South Channel floodplain was not conveyed through well-defined side channels, the proposed conditions did result in increased overbank flow. The proposed condition resulted in more high flow habitat at 2-year peak discharges, but was slightly less for all other peak discharges evaluated. This change was primarily due to a loss of habitat along the margin of the North Channel. Comparisons of hydraulic parameters between the two conditions indicated minimal changes in channel depths, velocities, and bed shear stresses along the South Channel. However, the model predicted increased inundation and flow velocities along the South Channel floodplain.

Linking results of the assessments to restoration options. Currently, several restoration options are being considered on the OCA. The first, discussed above, is focused on blocking the North Channel and returning all of the stream flow into the South Channel. Due to conditions resulting from dredge mining in the area of the bifurcation, concerns have been raised as to potential impacts of increased depths, velocities, and shear stresses in the South Channel and along the channel bed, banks, and floodplain. Hydraulic modeling results suggest that these parameters will not substantially change from current conditions. Based on geomorphic characteristics of the river that are visible in the 1939 aerial photography, it is evident that the proposal to block the North Channel would essentially return the river to a position in the valley that it occupied historically. While the current channel form appears to be quite similar to that of the river in 1939, data does not exist to allow comparison of the current channel geometry relative to the geometry of the river in 1939. However, a dramatic change in the channel morphology of the South Channel is not expected as a result of blocking the North Channel given the character of the Granite Boulder Creek alluvium and current processes, which further alleviates recognized concerns.

An additional option under consideration is the reconnection of Granite Boulder Creek to the South Channel as a result of a channel reconfiguration. If reconnected, Granite Boulder Creek would serve as an important source of colder water inflow to the MFJDR, which could help mitigate high water temperatures not conducive to salmonids. As a result of dredging operations, much of the fine-grained sediment may have been winnowed out of the alluvium in the area between the confluence of Granite Boulder Creek with the North Channel and the South Channel floodplain. Concerns with this reconnection are the potential loss of a surface flow connection due to the disruptions by mining activity in the grain size of the Granite Boulder Creek alluvium. However, geomorphic evidence suggests that loss of this surface connection would not be expected given three factors: (1) evidence of such a connection in 1939, (2) similarities in the character of the sediment between the confluence of Granite Boulder Creek and the South Channel and the character of the sediment across which the North Channel currently flows downstream to Ruby Creek confluence, and (3) the general nature of alluvial fan deposition.

In additional to restoration alternatives discussed previously, several more restoration actions have been proposed for consideration based on the results of the hydraulic modeling and geomorphic conditions. Results from the geomorphic analysis will continue to be evaluated in conjunction with the 2D model and used as tools to investigate additional restoration actions and subsequent results on habitat.

CONCLUSIONS

This report presents the results of an assessment approach designed to address restoration of floodplain connectivity and habitat complexity based on integration of information from multiple disciplines including biology, geomorphology, hydraulic engineering, and other natural sciences. A coarse-scale analysis of the river system processes (a stream assessment) provides essential technical information to help guide resource managers and decision makers with potential restoration actions and the locations where such actions may have the most benefit to habitat. The multi-tiered approach allows for the addition of information as needed to address reach-specific restoration questions and concerns in a reach-level evaluation. Specific questions regarding the effects of restoration actions or additional information needs can be further investigated and developed through refined analyses of a given reach.

Findings from the stream assessment for the MFJDR resulted in a focused reach-level evaluation on the OCA, a property managed by CTWSRO. Due to mining activity, installation of bank protection, water diversions, and vegetation changes related to agriculture and logging, the majority of the study area on the OCA has experienced dramatic changes in river processes resulting in disconnection of floodplain, constrained lateral channel migration, and a lack of floodplain and channel complexity. A refined understanding of the geomorphic and hydraulic conditions was applied to investigate existing habitat and how blocking the artificial North Channel may influence processes and resultant habitat. Comparisons of the channel hydraulics suggest slight improvements to habitat indicators when the North Channel is blocked. Results of the effort also indicate minimal changes in channel depths, velocities, and bed shear stresses along the South Channel and alleviate concerns regarding potential changes to the morphology of the South Channel and the potential loss of a surface flow connection between Granite Boulder Creek and the South Channel. The 2D model and refined understanding of geomorphic processes will be applied in the future to understand the viability of additional proposed restoration actions within the reach and determine the most suitable actions for habitat improvement.

REFERENCES

Bandow, J.R., 2003. Holocene alluvial history of the Middle Fork John Day River, Oregon: M.S. thesis, University of Oregon, Eugene, OR.

Bureau of Reclamation, 2008. Middle Fork and Upper John Day River Tributary Assessments, Grant County, Oregon: Bureau of Reclamation, Denver, CO.

Lai, Y.G. 2006. Theory and User's Manual for SRH-W, Version 1.1: Bureau of Reclamation, Denver, CO.

Northwest Power and Conservation Council (NPCC), 2005. John Day Subbasin Revised Draft Plan, Prepared by Columbia-Blue Mountain Resource Conservation & Development Area.

NOAA-Fisheries, 2008. Consultation on Remand for Operation of the Federal Columbia River Power System, 11 Bureau of Reclamation Projects in the Columbia Basin and ESA Section 10(a)(I)(A) Permit for Juvenile Fish Transportation Program (Revised and reissued pursuant to court order, NWF v. NMFS, Civ. No. CV 01-640-RE (D. Oregon))

Hungry Canyons Alliance: Streambed Stabilization in Western Iowa

J. T. Thomas[1]

[1]Hungry Canyons Alliance, Golden Hills RC&D Office, P.O. Box 189, Oakland, IA 51560-0189; PH (712) 482-3029; email: john.thomas@rcdnet.net

ABSTRACT

The Hungry Canyons Alliance (HCA) was formed locally to provide financial and technical assistance for streambed stabilization projects in the 19 counties of the deep loess region in western Iowa. Stream straightening and land-use changes, coupled with the erosive nature of loess, caused streams to downcut and widen, undermining bridges, farmland, and utility lines. The most efficient and affordable way to stop channel degradation has proven to be the construction of grade control structures (GCS). GCS allow a drop in stream elevation in a controlled setting, prevent further degradation, decrease sediment loads and turbidity, and increase water quality. With over 750 GCS of all types in western Iowa, western Iowa has been referred to as a "laboratory" for GCS design. The HCA has conducted research on GCS design and fish passage, the use of directional drilling to control gully erosion, the use of scrap tires in GCS, knickpoint migration, and aerial stream classification.

THE PROBLEM

In western Iowa, 19 counties contain deposits of loess ranging from 4 m to over 61 m deep. Loess is highly erodible and very susceptible to stream channel erosion and degradation. Beginning with settlement of the area around the late 1840's and early 1850's, land use changed dramatically from prairie to farmland, likely causing rapid erosion in upland areas and deposition in stream networks. Stream channel dredging and straightening from the early 1900's to the 1950's was done to reduce flooding, increase the amount of farmland in production, and to clean out the sediment clogged channels.

After straightening, streambed bed slopes were steeper because streams still had the same fall per mile, yet there was a shorter distance over which that fall occurred. The steeper bed slopes increased water velocities, increasing stream erosion. Streams could either re-meander or downcut. Due to the high erodibility of loess soils, streams downcut, causing accelerated soil erosion in western Iowa (Fig. 1). Knickpoints, which are naturally occurring overfalls (Fig. 2), would form and rapidly advance upstream, eventually affecting the entire watershed. Unstable, vertical stream banks would slump to a more stable slope; if high flow events flushed the slumped bank debris, vertical banks would again be unstable and slump, widening the channel. Tributaries of degraded streams would also erode and adjust to the lowered base level, often initiating gully formation where no channel had previously existed.

These erosional processes recurred until the streambed stabilized. As streams downcut bridge pilings were destabilized, and as streams widened bridges would collapse. Many bridges were forced to be closed (Fig. 3), or replaced with taller, longer, more expensive bridges.

What might have been a 1.5 m high stream bank 50 years ago may now be a 9.1 m deep canyon with bare vertical banks. Erosion of streams into "hungry canyons" has undermined bridges, farmland, and utility lines, and already caused an estimated $1.1 billion in damage to public and private infrastructure in western Iowa in the 19 county area of the deep loess soils region of western Iowa (Baumel, 1994). Stream degradation has also eroded away thousands of acres of valuable farmland, increased stream sediment loads, and decreased water quality. A survey of western Iowa bridges in 2000 revealed that 404 were endangered due to stream channel degradation.

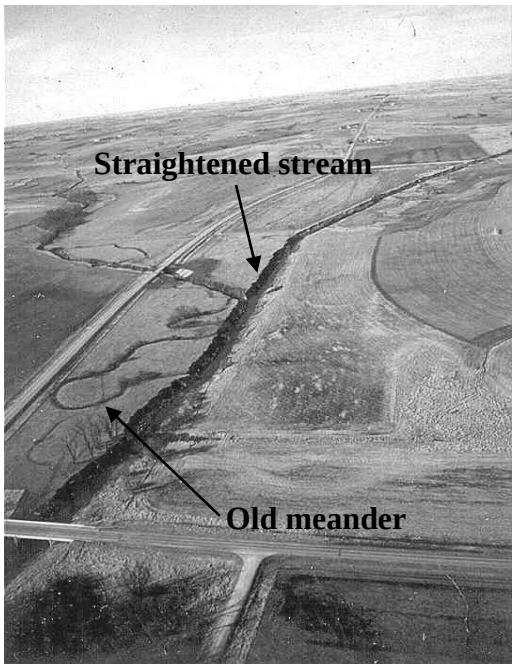

Figure 1. Straightened versus meandering stream. (Walnut Creek, Pottawattamie County).



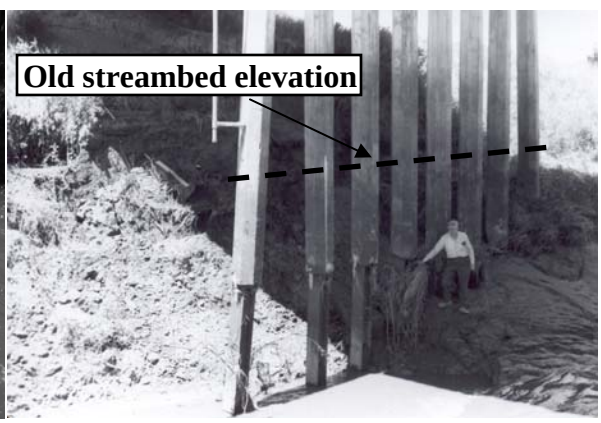

Left: Figure 2. Knickpoint eroding headward upstream. Scour hole is up to 3.1 m deep. Right: Figure 3. Bridge endangered by exhumation of pilings.

THE SOLUTION – GCS AND HCA

A proven, affordable solution to this problem is to build grade control structures in streams. Grade control structures (GCS) at regular intervals help streams stabilize by changing their longitudinal profile from an erosive steep incline to a stable stair-step pattern. Streambed stabilization is the key to preventing further erosion and protecting infrastructure (Fig. 4).

GCS design is largely dependent on drainage area. Small drainage areas < 7.8 km^2 can often be controlled with reinforced concrete box (RCB) or corrugated metal pipe (CMP) culverts with drop inlets and/or flume outlets (Fig. 5). Large drainage areas > 7.8 km^2 are often controlled with weirs constructed with steel sheet pile, driven into the streambed 6.1 m, with a riprap and concrete grout slope immediately downstream, a riprap stilling basin downstream of the weir slope, and riprap covered banks (Fig. 6). Only limestone bedrock is available in western Iowa, and it is found in relatively thin ledges (< 2.4-3.1 m), but due to bedding planes and stratification boulders greater than a 0.77 m^3 are very rare. Riprap also tends to fracture due to freeze/thaw processes and then move under higher flow conditions, so concrete grout is used to lock the riprap in place. Both RCB/CMP and weir designs allow the stream elevation to drop in a controlled setting, restore lost stream grade, prevent further degradation, and reduce streambed slope upstream creating a calm backwater condition where silt can settle out, decreasing sediment loads and turbidity and increasing water quality. Sediment re-deposited upstream also helps support exposed bridge pilings.

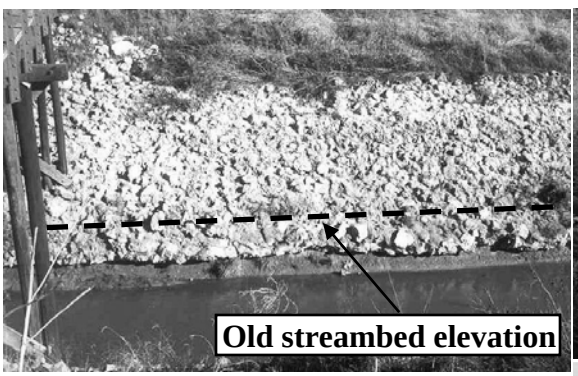





Above: Figure 4. An NRCS-EWP bank stabilization site that did not include streambed stabilization in Page County. After the stream downcut 1.8 m in 7 years, the bank stabilization was left high and dry.
Upper right: Figure 5. RCB flume in Fremont County with 7.6 m of fall.
Lower right: Figure 6. Crawford County sheet pile weir with grouted riprap slope.

The Hungry Canyons Alliance (HCA) provides financial and technical assistance to the 19 counties affected by streambed degradation in western Iowa with deep loess soils. State and federal money appropriated to the HCA is made available to the counties through a GCS cost share program; county governments provide a minimum of 20% match for each GCS. Approximately 20 GCS are constructed every year. From 1992-2008, the HCA provided $16 million in state and federal cost share, enough to complete 297, and approve another 22, GCS in 17 counties in western Iowa. These structures will protect an estimated $77.75 million in property value. It is estimated that 231 hectares of land, equivalent to 18.1 million metric tons of

sediment, will be protected from erosion by construction of the 319 GCS. HCA GCS, with an average cost of $64,737, protect approximately $243,742 in property per structure. For every $1 invested in HCA GCS, more than $4.24 of property value and an average of 889 kg of sediment are protected from streambed degradation. A second HCA program, funded with the interest earned from state appropriations, provides funding to landowners where grade control is necessary to stabilize active gully erosion. With the help of the NRCS, this program has built 84, and approved another 9, structures for a total cost share of $619,406. The HCA has quarterly meetings at which issues concerning stream erosion and streambed stabilization are discussed. Regular attendees include county engineers, county supervisors, NRCS employees, Soil and Water Conservation District commissioners, Iowa Department of Natural Resources fisheries biologists, engineer consultants, contractors, and landowners.

Severe rains in May 2007 and June 2008 caused widespread flooding and stream channel damage; this was the worst flooding to hit western Iowa since 1993. However, Federal Emergency Management Agency (FEMA), Natural Resources Conservation Service (NRCS), the Hungry Canyons Alliance (HCA), and counties have all seen evidence that GCS have directly reduced flood damage costs and FEMA/NRCS Emergency Watershed Protection (EWP) Program claims in numerous instances. The vast majority of GCS were undamaged, and infrastructure protected by GCS had no damage. A small proportion of these GCS also suffered damages during the flooding; however, the damages to these structures are minimal compared to the total loss of our bridges that may have resulted without these GCS. The HCA is providing technical assistance to the counties by documenting which erosion control measures have worked, which have not, and what new techniques can be used to enhance performance of the original erosion control design if it has not adequately solved the erosion problem.

Over 750 GCS of all types have been constructed in western Iowa by county governments, HCA, NRCS, NRCS-EWP, Iowa Department of Transportation, cities, utility (water, gas, telephone, electric, etc.) companies, railroad companies, Army Corps of Engineers, Iowa Department of Natural Resources, landowners, and Soil and Water Conservation Districts. With so many GCS located in one area, western Iowa has been referred to as a "laboratory" for GCS design. Because western Iowa has, and still is experiencing such dramatic streambed degradation, the Hungry Canyons Alliance is one of the unheralded leaders in innovative GCS research, design, and construction (Thomas, 2007).

A CASE STUDY

A 1.5 m concrete grade control structure (Fig. 7A), built and maintained by Northern Natural Gas (NNG) since the early 1970's, had been destabilized and nearly destroyed by advancing, in-stream, knickpoint migration (Fig. 7B). Streambed downcutting had caused the structure to vertically control approximately 4.9 m (Fig. 7C), when it was only designed to vertically control 1.5 m. The spillpad itself was starting to crumble (Fig. 7D), was almost completely undermined, and was separating from the sheet pile, causing the sheet pile to begin to bow. The structure had a

projected life of 0.5 to 1 year. NNG had spent millions of dollars since building the original structure, trying to protect the structure from knickpoint migration. NNG had given up on the structure and was planning on re-drilling their pipelines under the stream to a greater depth, at a cost of $2.4 million, and allowing their structure to fail.

In 2002, the HCA became aware of the problem and knew that allowing the structure to fail would destabilize Walnut Creek upstream from the structure, endangering 23 bridges and hundreds of hectares of farmland. The HCA and NNG began discussing how the site could be stabilized. An agreement was reached in which the HCA provided technical assistance and coordinated repair of the existing NNG grade control structure and construction of three new GCS downstream. Repair work was completed in spring of 2004 (Fig. 7E), at a total cost of about $68,000, and construction of the three new GCS (Fig. 7F-H) were completed in spring of 2005 at a total cost of about $372,000. NNG and HCA paid for $358,000 and $82,000, respectively. The project saved NNG and its customers over $2 million. NNG has repeatedly expressed their appreciation for the HCA's assistance and has begun modifying more of their GCS throughout the Midwest in accordance with what they learned in western Iowa.

HCA RESEARCH PROJECTS

Controlling Erosion While Allowing Fish Migration

The HCA has been working with the Iowa Department of Natural Resources (DNR) to design and construct weirs that will allow fish to migrate upstream yet be cost effective to construct. Streams were prioritized for importance of fish, such as catfish, to be able to migrate up and down. A proposed GCS design for fish passage, consisting of a 1:20 or 1:15 (rise/run), grouted rock slope downstream from a V-notch sheet pile weir was agreed upon and several existing weir structures were modified to this design. Before and after the modifications, the DNR and the Natural Resource Ecology and Management Department at Iowa State University caught, tagged, and released fish from above and below the weirs (Larson et al., 2004; Litvan, 2006; Litvan, et al., 2008a-c). The major results of these studies were: 1) catfish were documented moving over the 1:15 weirs, 2) fish communities were slightly better (5%) near the weirs compared with reaches without weirs, and 3) macroinvertebrate abundance and diversity was 60% greater near the weirs compared to reaches without weirs. A second study, performed by the University of Iowa's IIHR–Hydroscience and Engineering Department, measured velocities on different weir backslopes and performed modeling of different weir slopes to optimize for channel catfish migration while reducing flow velocities, slope lengths, and costs (Papanicolaou and Dermisis, 2006; Papanicolaou and Dermisis, in press). The variable controlling fish passage was either the flow depth or maximum velocity, dependent on the drainage area. Both 1:20 and 1:15 weirs allowed fish passage, however, 1:15 was recommended because it was less expensive. This subject is discussed in much greater detail in an accompanying paper in these proceedings entitled "Fish Passage and Abundance around Grade Control Structures on Incised Streams" by Thomas, et al.



Figure 7. NNG structure A) originally before any erosion in fall of 2000, B) with knickpoint moving upstream toward structure in fall of 2000, C) after knickpoint erosion in fall of 2001, D) spillpad starting to crumble in summer of 2003, E) after completion of repair work in spring of 2004, F) after completion of three 1.2 m weirs downstream in spring of 2005, G) close-up of lowest weir in spring of 2005, H) water backed up to base of original structure in spring of 2005.





Top: Figure 8. Scrap tire project designed like a weir.
Bottom: Figure 9. Scrap tire project designed like a toewall.

Using Scrap Tires in GCS

The HCA has built two experimental GCS with scrap tires (Fig. 8-9). Scrap tires are difficult to recycle and often reduce landfill capacity. Theoretical and experimental research was done by Iowa State University followed by construction of the prototype weirs with the help of the NRCS and landowners. Scrap tires were arranged in layers, bolted together with lag screws, and filled with flowable concrete grout. A design manual which described construction technique and evaluated its cost, effectiveness, and structural stability compared to traditional grade control structure designs and materials was disseminated to county engineers and NRCS offices in western Iowa so similar structures may be built.

Aerial Stream Classification

The HCA has conducted an aerial assessment and classification of streams in the deep loess region of western Iowa (Fig. 10) to determine areas of active stream erosion and the impact GCS have on controlling stream degradation (Thomas and Cutler, 2003). Upon encountering locations of extremely erosive streams and threatened bridges, responsible county/agencies were notified. The stream assessment consisted of flying along streams in a small helicopter while videotaping the stream channel and recording positions with a global positioning system receiver. Streams were classified based on a six-stage channel evolution model to describe the dominant channel processes occurring along stream reaches. Streams across the region in 1993 and 1994, and in a smaller area in 2000, were similarly classified. Comparison of the recent classification to those of the past allows us to describe how GCS have impacted the streams and make predictions as to

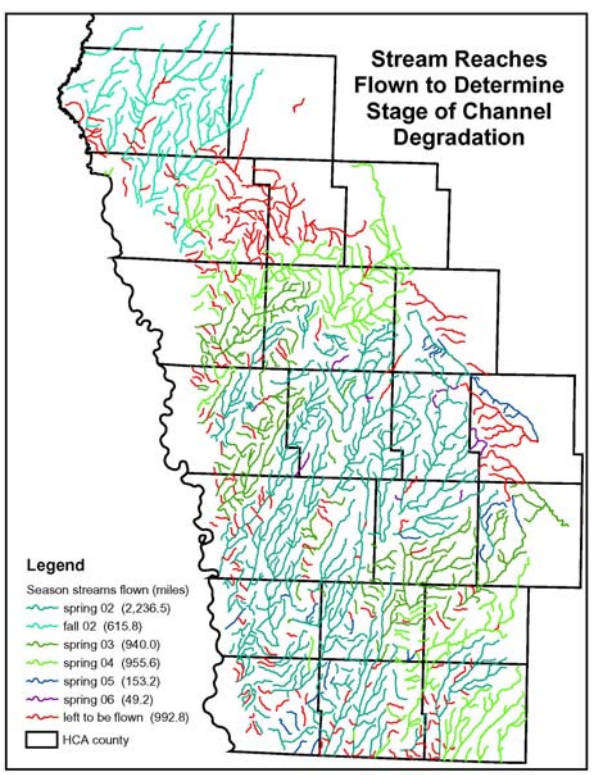

Figure 10. Stream reaches flown to determine the stage of channel evolution.

where future stream erosion will occur. Approximately 9,560 km of stream in 22 western Iowa counties will be classified during the 2002-2010 project. Videos and maps are made available to county engineers and NRCS offices for stream stabilization project planning.

Experimental Bored Headcut Basin Projects

Some gullies in the deep loess soils of western Iowa, especially in the loess hills region, can be very deep, reaching depths of approximately 21.3 m, with near-vertical headcuts and side walls (Fig. 11). Primary deposits of loess soil are highly erodible and unstable when wet, but unlike other types of sediment deposits, they are very stable when vertical and dry. Gullies expand and erode upstream during rain events due to surface runoff, entering the gully via the headcut, and due to groundwater flow, entering the gully at the base of near-vertical walls, both of which de-stabilize the gully walls causing bank collapse. Runoff then carries away the collapsed bank debris, preparing the walls again for collapse.

Stabilization or control techniques are limited to pipe-drop structures, but associated fill of the gully and excavation of a core trench in an area of such high relief makes these types of structures often cost-prohibitive, and definitely not cost-effective. The HCA is experimenting with the use of directional drilling techniques to bore at an angle through the primary loess soil from upstream of the headcut to the base of the gully wall. A plastic PVC pipe is inserted into the borehole and the bentonite slurry, used to drill the hole, acts as the sealant that makes the borehole watertight as it dries. A vertical PVC riser is added to the angled pipe to serve as an inlet. A water-retention basin is excavated upstream of the inlet, and a terrace is built downstream of the inlet, between the inlet and the headcut (Fig. 12). The basin allows a larger storm event to be controlled by a smaller pipe. No work is done in the gully and there is no filling of the gully, dramatically reducing earthwork costs. The near-vertical gully headcut will gradually slump to a stable slope over time because collapsed debris will not be carried away by runoff.



Top: Figure 11. The headcut was located at the second fence (behind one in foreground) only five years ago. Bottom: Figure 12. Basin (in which the directional drilling machine sits) built upstream of the terrace (at right) which is built upstream of the gully headcut (out of picture to the right).

The HCA has built three of these experimental Bored Headcut Basin (BHB) structures to control three 9.1-12.2 m deep gully headcuts with small drainage areas (< 6.9 hectares) in the deeply incised small watersheds of the Loess Hills. Non-

terraced sites were chosen to limit the amount of infiltration occurring upstream of the BHB's. Survey and design assistance was provided by the USDA-NRCS. The three BHB's have averaged only $10,560 and have weathered > 76.2 mm rain events without problem. Considering a typical pipe drop structure may have cost as much as $60,000, the BHBT has proven to be very cost-effective. We are continuing to monitor their progress, while planning for future more BHB projects.

Knickpoint Migration Study

An actively eroding stream knickpoint is being monitored closely to: (1) measure knickpoint propagation rates in the field, (2) examine the morphodynamics of actively migrating knickpoints for different flow conditions, and (3) to develop a knickpoint erosion model that is applicable to the deep loess area of western Iowa. An accurate knickpoint erosion model for loess will aid in the placement of future GCS. The study is being conducted by the University of Iowa's IIHR–Hydroscience and Engineering Department and the HCA.

Stage-Discharge Project

There are no gaged (measures water discharge) medium to small sized (≤ 259 km^2 drainage area) streams in western Iowa, which limits our ability to predict erosion. To remedy this, a semi-automatic, permanent, sensor network is being installed on 11 representative, ungaged streams in the deep loess area of Western Iowa. Stage-discharge relationships for these streams will be developed. The project is being implemented by the University of Iowa's IIHR–Hydroscience and Engineering Department, the HCA, and possibly the U.S. Geological Survey.

REFERENCES

Baumel, C. (1994). "Impact of degrading western Iowa streams on private and public infrastructure costs." *Stream Stabilization in Western Iowa*, Iowa DOT HR-352, Golden Hills Resource Conservation and Development, Oakland, Iowa, 4.1-4.39.

Larson, C. J., Atchison, G. J., and Menzel, B. W. (2004). *Annual Progress Report to the Iowa Department of Natural Resources Fisheries Bureau for an Evaluation of Effects of Weirs in Walnut Creek on Fish Abundance and Movement*, Cold Springs Southwest Regional Office, Iowa Department of Natural Resources.

Litvan, M. E. (2006). *An Evaluation of Effects of Grade Control Structures on Fish Movement and Fish Communities in Turkey Creek, Cass County, IA and Macroinvertebrate Communities in Walnut Creek, Montgomery County, IA*. M.S. Thesis, Iowa State University, Ames, Iowa.

Litvan, M. E., Pierce, C. L., Stewart, T. W., and Larson, C. J. (2008a). "Fish Passage in a Western Iowa Stream Modified by Grade Control Structures." *North American Journal of Fisheries Management*, 28:1384–1397.

Litvan, M. E., Pierce, C. L., Stewart, T. W., and Larson, C. J. (2008b). "Fish Assemblages in a Western Iowa Stream Modified by Grade Control

Structures." *North American Journal of Fisheries Management*, 28:1398–1413.

Litvan, M. E., Stewart, T. W., Pierce, C. L., and Larson, C. J. (2008c). "Effects of Grade Control Structures on the Macroinvertebrate Assemblage of an Agriculturally Impacted Stream." *River Research and Applications*, 24: 218–233.

Papanicolaou, A. N., and Dermisis, D. C. (2006). *Field Investigation of Hydraulic Structures Facilitating Fish Abundance and Passage through Bridges in Western Iowa Streams*, Iowa DOT TR-521, IIHR-Hydroscience & Engineering, University of Iowa, Iowa City, Iowa.

Papanicolaou, A. N., and Dermisis, D. C. (In press). "Fish passage over hydraulic structures in Midwestern Rivers of the USA." *J. River Basin Management*.

Thomas, J. T., and Cutler, B. A. (2003). "Using Aerial Videography and GIS for Stream Channel Stabilization in the Deep Loess Region of Western Iowa." *Proceedings of the 8th National Watershed Conference, June 9-11, Council Bluffs, IA*. National Watershed Coalition: Chandler, OK.

Thomas, J. T. (2007). "Grade control in western Iowa streams." *Stream Restoration Design Part 654 National Engineering Handbook*. United States Department of Agriculture Natural Resources Conservation Service, CS12.1-CS12.20.

Thomas, J. T., Papanicolaou, A. N., Pierce, C. L., Dermisis, D. C., Litvan, M. E., and Larson, C. J. (this volume). "Fish Passage and Abundance around Grade Control Structures on Incised Streams."

Rehabilitation of Mine Impaired Creek in Idaho

Brian Murphy, PE, PH, CFM[1], Moosub Eom, PhD, PE[2], Bill Adams[3], and Jeff Johnson[4]

[1]Camp Dresser & McKee (CDM), 555 17th Street, Suite 1100, Denver, CO 80202; PH (303) 383-2429; email: murphybm@cdm.com
[2]CDM, 555 17th Street, Suite 1100, Denver, CO 80202; PH (303) 383-2449; email: eomm@cdm.com
[3]U.S. Environmental Protection Agency, Mail Stop ECL-113, 1200 Sixth Avenue, Suite 900, Seattle, WA 98101; PH (206) 553-2806; email: adams.bill@epa.gov
[4] U.S. Forest Service, 3815 Schreiber Way, Coeur d'Alene, ID 83815; PH (208) 765-7442; email: jkjohnson@fs.fed.us

ABSTRACT

The stream rehabilitation design for Tributary Creek in the Coeur d'Alene National Forest, Shoshone County, Idaho, was performed using the following general design concepts: reference reach selection, stream geometry and slope modifications, evaluation of stream habitat features, and channel stability. The stream rehabilitation used undisturbed reference reaches and the Rosgen method to aid in stream rehabilitation design. An overview of the hydraulic modeling and U.S. Fish and Wildlife Service Habitat Suitability Index (HSI) models for the target species will be presented in addition to design plans.

INTRODUCTION

Tributary Creek is a highly degraded stream located within the Jack Waite Mine and Mill site in the Coeur d'Alene National Forest, Shoshone County, Idaho (see Figure 1). Historic mining activities have disturbed the entire Tributary Creek drainage impacting water quality, geomorphology, and aquatic habitat. The mine operated from 1909 until the early-1960s primarily mining silver, lead, and zinc ore. Four tailings piles (TP-1, TP-2, TP-3, and TP-4) were constructed along Tributary Creek by placing tailings along and over the stream channel (see Figure 2).

The U.S. Environmental Protection Agency (EPA) and the U.S. Forest Service (USFS) are currently implementing mine reclamation activities at the Jack Waite Mine and Mill site under an Action Memorandum. One of the goals of the reclamation activity is long-term aquatic restoration of Tributary Creek. As part of these activities,

the USFS would like to rehabilitate the impaired channel to a "natural" stream channel because the stream is an important Westslope Cutthroat Trout habitat and potential Bull Trout recovery habitat area.

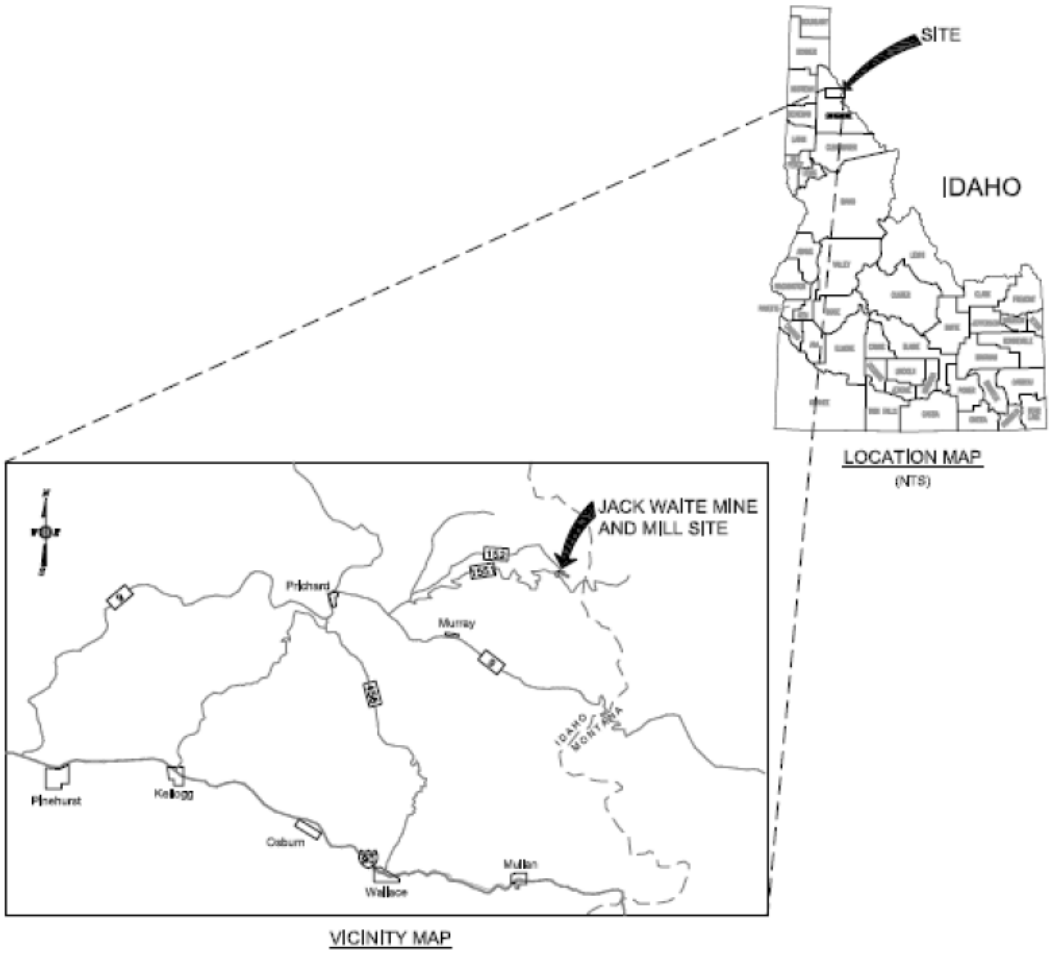

Figure 1. Site Location Map of Jack Waite Mine and Mill Site

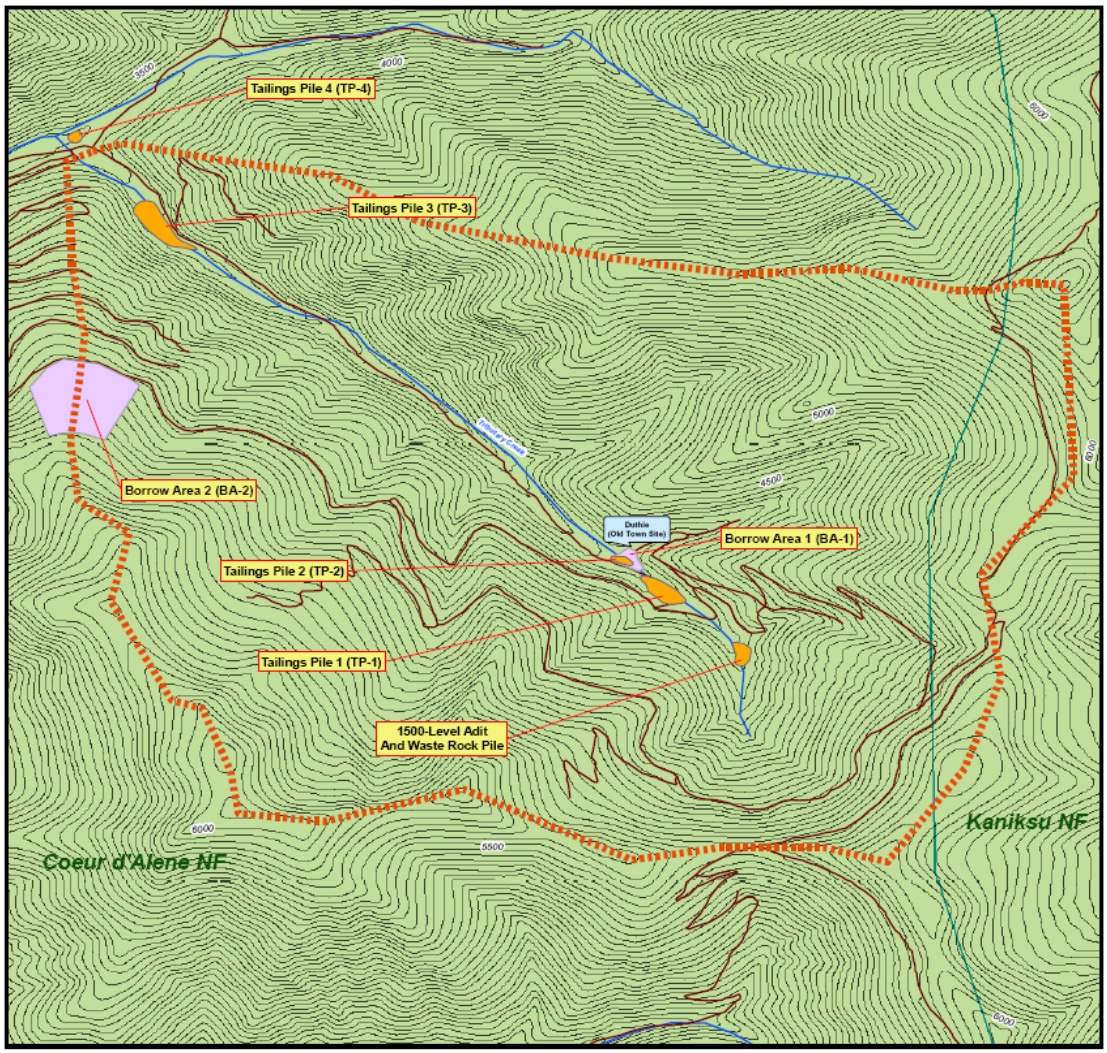

Figure 2. Site Feature Map of Jack Waite Mine and Mill Site

DESIGN APPROACH

The new stream alignment, slope, channel geometry, and in-stream structures of the design reach were determined based on a reference reach downstream of TP-2 (see Figure 2), the Rosgen stream classification method, 1937 aerial photographs, 2007 field photographs and the 2007 aerial photogrammetric and light detection and ranging (LIDAR) survey data.

The major elements of the design approach used for the rehabilitation design included:

1. Reference channel morphological analysis
2. Stream rehabilitation structures
3. Fish habitat design
4. Hydraulic analysis
5. Rock sizing

REFERENCE CHANNEL MORPHOLOGICAL ANALYSIS

The limited spatial extent of the aerial and LIDAR survey data required the selection of a reference reach within the Upper Tributary Creek basin. Therefore, a 1,000-foot reach located downstream of TP-2 was selected as the reference reach. This reference reach was classified according to the Rosgen classification scheme (Rosgen, 1996).

The reference reach was classified as Rosgen A3-type due to the steep slope (~8%), channel geometry (deeply entrenched and confined channel) and channel material (coarse depositional soil). A3-type channel slopes range from 4 to 10 percent and streamflows at bankfull state are typically described as a step-pool, cascading channel, which often stores large amounts of sediment in the pools. The width to depth ratios and entrenchment ratios are low (< 12 and < 1.4, respectively), with low sinuosity (< 1.2). These A3-type channel features were used as stream rehabilitation design criteria (Rosgen 1996).

A new alignment was developed for Upper Tributary Creek because historical information indicated the stream channel was initially located to the east of its current alignment (beneath the current TP-1 location) and curved up at tributary junctions prior to mining activities (see Figure 3). The proposed alignment was determined by inspection of the aerial photos and LIDAR data. Also, the existing stream channel alignment did not follow the natural channel meandering pattern shown in the reference reach and typical of Rosgen A3-type channels.

Following selection of a stream alignment, geometric properties were determined. The proposed stream channel has a width to depth ratio and entrenchment ratio of approximately 9 and 1.2, respectively. The sinuosity for the proposed stream channel is approximately 1.1, which are consistent with Rosgen A3-Type channels.

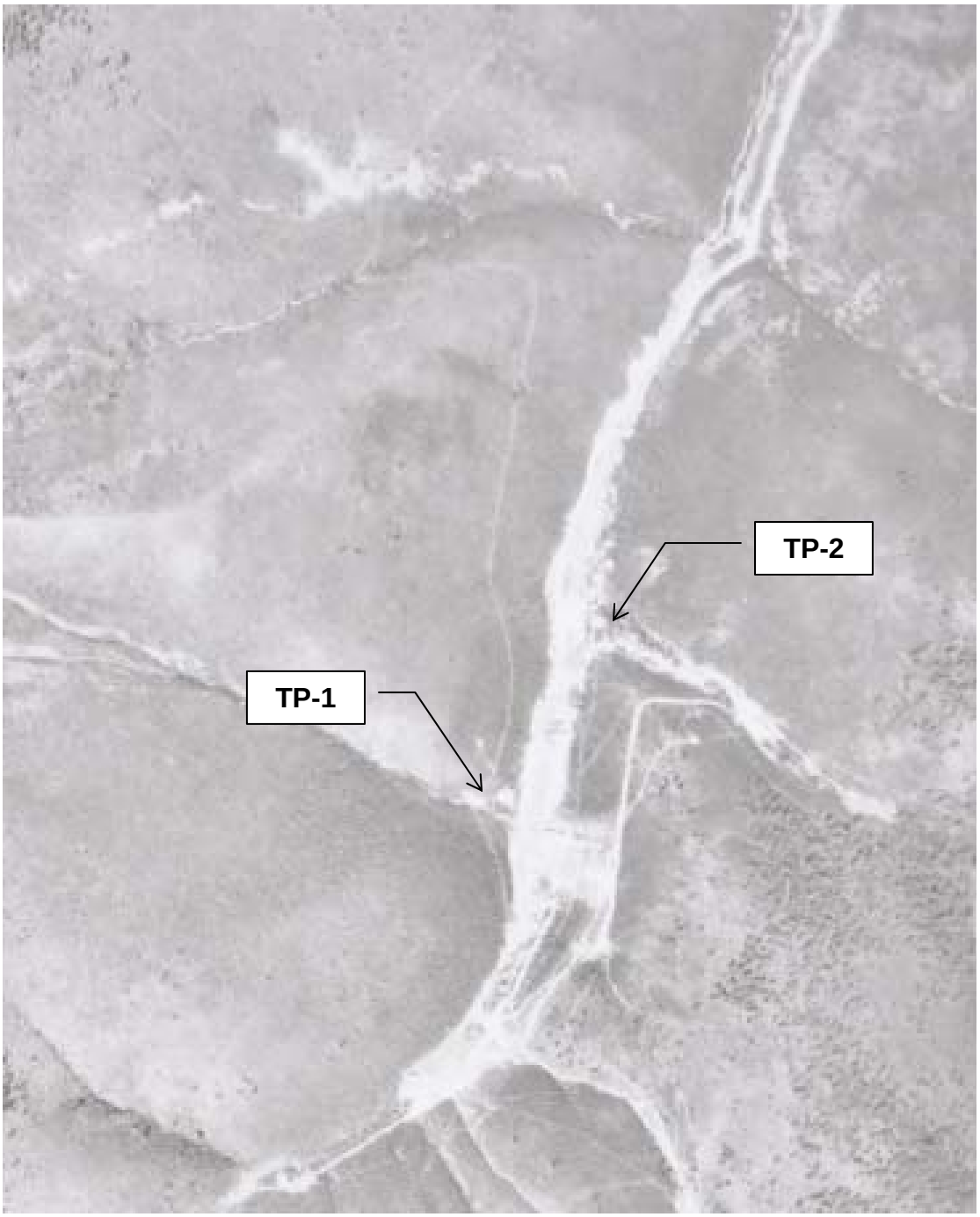

Figure 3. Historical Aerial Photograph – Upper Tributary Creek

STREAM REHABILITATION STRUCTURES

River restoration design guidelines, including Rosgen, recommend the following in-stream structures to create step-pool/riffle-pool sequences. The bed profile of the existing stream channel does not show step-pool sequences; however, the step-pool sequences are shown in the reference reach and are typical of Rosgen A3-type channels. These in-stream structures will recreate critical habitat for native fish species and maintain a desired stream bed elevation. The structures will also stabilize the channel banks.

Rock Vortex Weirs with Downstream Pools

Rock vortex weirs will be installed to create aquatic habitat in the form of scour pools and for grade control, while still maintaining the bed load sediment transport regime of the stream. In addition, the downstream side of the vortex weirs will be excavated by 2- to 3-feet to increase the depth of scour pools required for fish habitat. By shifting the apex of the structure toward one bank or the other, vortex weirs will be used to control the thalweg location through meander bends and prevent bank erosion.

Weirs should point upstream with the arms angling downstream. The angle the arms make with the upstream banks should be approximately 20 to 50 degrees so that flows are directed away from the banks and deeper pool areas are created directly downstream of weirs. The arms are carried up the streambank to just above the bankfull elevation. Rock vortex weirs are constructed first by placing a foundation of boulders (footer rocks) two to three feet in size in a trench excavated along the stream bottom. Large rocks (vortex rocks) are then placed in the trench behind and against the footer rocks so that they extend up to the desired elevation. The key component of rock vortex weirs is that the vortex rocks do not touch each other with the exception of the end rocks. Most design details call for spacing the vortex rocks 1/3 and 1/2 a rock diameter apart. The overall drop controlled by the weir should be less than 2 feet for stability reason (Maryland 2000).

Root Wad Revetments

Root wad revetments will be installed at outer bends of the stream to prevent stream bank erosion by directing the flow away from the outer bank. The root wads will also trap sediment between revetments and create in-stream habitat structure for fish spawning and rearing.

Footer logs should be positioned in the trench below the stream invert such that each upstream log is shingled over its downstream neighbor. The root mass should be oriented perpendicularly to the direction of flow. An angle of 30 to 60 degrees to the channel center line is usually adequate. The root wad revetment should be backfilled, and fill material should be tightly packed in the joints, connections, and gaps to firmly secure all components. Stone may be necessary on flashy stream (Maryland 2000).

Toe Protection

Two tributaries join Upper Tributary Creek within the rehabilitation reach. At junctions with the tributaries, flexible and/or rigid protection will be installed to reinforce bank

toes and protect against bank erosion. Types of protection include vegetation, bioengineered materials, and riprap.

Step-Pool Sequences

Step-pool sequences will be constructed in steep reaches for grade control and the creation of aquatic habitat through flow diversification. Step-pool sequences are characterized by a succession of channel-spanning steps formed by large grouped boulders that separate pools containing finer bed sediments. As higher velocity flow tumbles over the step, energy is dissipated in roller eddies causing lower velocity flow within the downstream plunge pool. Typical spacing for pools is 1 to 4 times of channel width.

Step rocks shall be placed on footer rocks so that they rest on two halves of each footer rock below, and so that the step rock is offset in the upstream direction. Footer rocks should extend below the scour hole elevation (Maryland 2000).

Stream Crossings (Modified Newbury Riffles)

USFS Road #152 crosses the existing alignment of Upper Tributary Creek at six culvert locations. The rehabilitation design removes all six culverts. Under the rehabilitation design, USFS Road #152 crosses the proposed stream alignment at only two locations. In place of culverts, modified Newbury Riffles will be constructed to provide stream crossings for vehicles while facilitating the natural passage of fish. According to the typical Newbury Riffle design (see Figure 4: Newbury and Gaboury 1993), the downstream slope is very gradual at 20H:1V while the upstream slope is steeper at 4H:1V. However, due to the steep slopes of the design reach, the downstream slope of 10H:1V was used. Also, the typical Newbury Riffle does not include a top crest width; however in this channel design, a top crest width of 20 feet was used to provide stream crossings for vehicles.

Newbury Riffle substrate is composed of gravels, cobbles and boulders. Riffle height generally runs 1 to 3 feet. On the crest and downstream face of the riffle, large boulders are placed to create a range of chutes between them, which are observed in the natural riffles. These boulders create locally-varied flow conditions. Hydraulic jumps and aeration zones occur in different areas on the riffle surface as the water stage rises and falls. At the lowest stages, the flow dwindles into two or three smaller channels crossing the riffle surface between the large boulders. Therefore, to create this kind of natural varied flow conditions, large boulders should be placed randomly or close to natural riffle conditions.

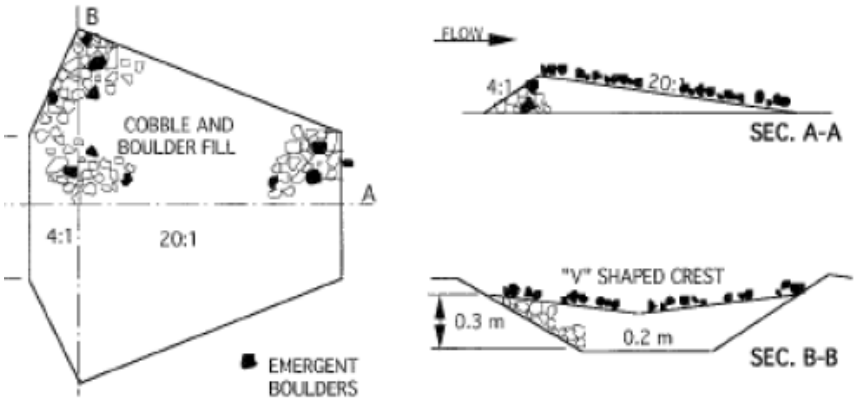

Figure 4. Newbury Riffle typical plan view (Newbury and Gaboury, 1993)

FISH HABITAT DESIGN

The rehabilitation design includes design of fish habitat to improve available fish habitat for target fish species in Tributary Creek. The USFS Idaho Panhandle National Forests identified the West Slope Cutthroat Trout as the target species with long term restorative goals of targeting Bull Trout.

To find the relationship between in-stream habitat area and channel hydraulic parameters, U.S. Fish and Wildlife Service (USFWS) Habitat Suitability Index (HSI) models were reviewed. HSI models were available for three trout species; Cutthroat, Brook and Rainbow Trout (USFWS 1982a;1982b;1984). A Bull Trout HSI was not available. Suitability index graphs of these three species were compared to determine the most appropriate habitat conditions. The comparison found that these three species have the same optimum suitability conditions for the following variables:

1. Average thalweg depth during the late growing season low water period > 30 cm (1.0 ft) for stream width ≤ 5 m (16.4 ft)
2. Average thalweg depth during the late growing season low water period > 45 cm (1.5 ft) for stream width > 5 m (16.4 ft)
3. 30 cm/sec (1 ft/sec) < Average velocity over spawning areas during embryo development < 60 cm/sec (2 ft/sec)
4. Pool class rating during the late growing season low flow period (Aug-Oct): ≥ 30% of the area is comprised of first-class pools (First-class pool: the greatest pool depth ≥ 1.5 m (4.9 ft) in streams ≤ 5 m (16.4 ft) wide or ≥ 2 m (6.6 ft) in streams > 5 m (16.4 ft) wide)

The rehabilitation design incorporates these variables through the in-stream structures mentioned above.

HYDRAULIC ANALYSIS

To evaluate the designed fish habitat, a HEC-RAS model (USACE 2005) was constructed for the existing and proposed stream. The model was run for 2-, 5-, 10-, 25-, 50-, and 100-year peak discharges. Due to the absence of measured flow data, these peak discharges were estimated using U.S. Geologic Survey (USGS) regionalized flood-frequency equations for Idaho (USGS 2002). The standard errors of these USGS equations range from 60 percent to 69 percent. Therefore, to consider these errors associated with these equations, the calculated discharges were increased by the standard errors. Table 1 presents estimated peak discharges.

Table 1. Estimated Peak Discharges

	For Tributary Creek above TP1		For Tributary to Tributary Creek above Duthie	
Frequency	Calculated (cfs)	Increased by SE (cfs)	Calculated (cfs)	Increased by SE (cfs)
2-year	27.5	44.0	17.5	28.1
5-year	40.7	65.2	26.1	41.8
10-year	50.8	81.9	32.6	52.6
25-year	63.9	104.8	41.2	67.5
50-year	73.5	122.1	47.4	78.7
100-year	83.7	141.0	54.0	91.0

The maximum flow depths and velocities were calculated by the HEC-RAS model for each of peak discharges. Figures 5 and 6 present 100-year discharge water surface profiles of the existing and proposed conditions, respectively. The output from the HEC-RAS model is summarized in Attachment B. The calculated values were used to evaluate the change in HSI habitat variables between the existing and proposed stream. The discharge of the late growing season low flow period was estimated as the 2-year discharge (44 cfs) since flow data was not available.

A comparison of the existing and proposed stream flow depths illustrates the reach length where the maximum flow depth is greater than 2 feet increases from 50 feet to 265 feet (see Table 2). The increase shows the creation of more pool habitat area. Also, the reach length having maximum flow depth greater than 2.5 feet and 3 feet increases from 0 feet to 85 feet and from 0 feet to 30 feet, respectively. The reach length having flow velocity between 1 and 1.5 ft/sec, which is the optimum velocity range for the trout spawning area during embryo development, increases from 0 feet to 90 feet.

Table 2. Comparison of Predicted Habitat Parameters

	Reach length that the maximum flow depth is greater than			Reach length that the flow velocity is between 1 and 1.5 ft/sec
	3 ft	2.5 ft	2 ft	
Existing	0 ft	0 ft	50 ft	0 ft
Proposed	30 ft	85 ft	265 ft	90 ft

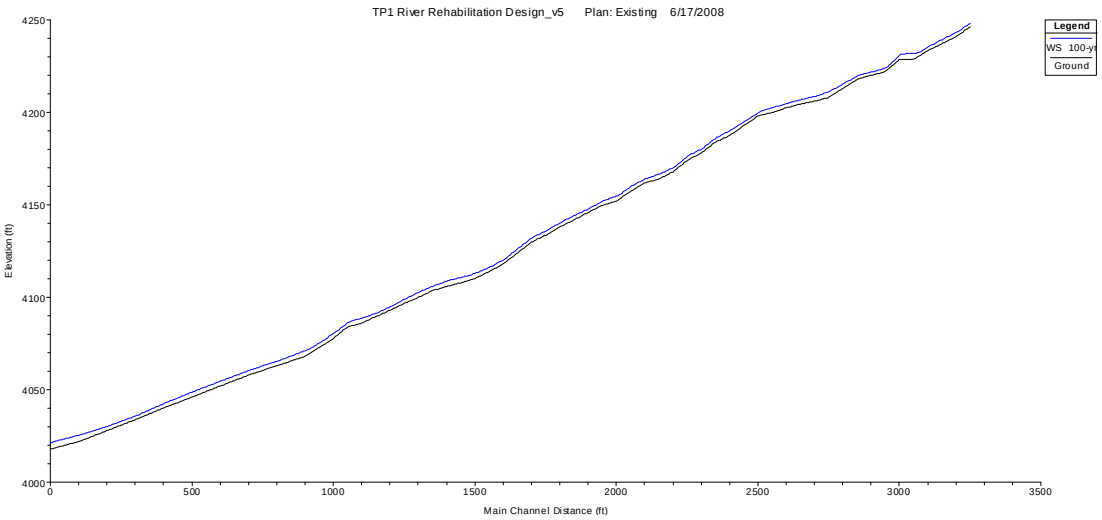

Figure 5. Water surface profile of existing conditions model (100-year discharge)

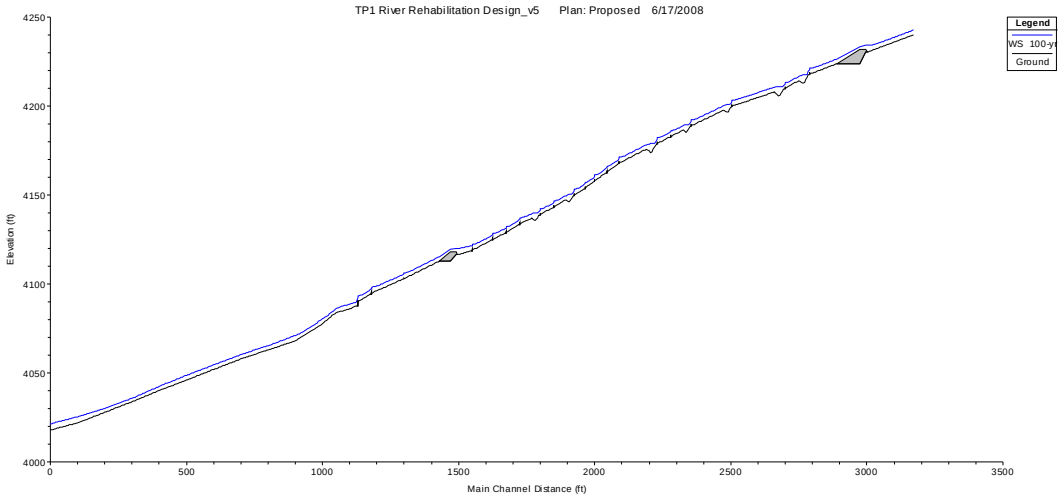

Figure 6. Water surface profile of proposed conditions model (100-year discharge)

ROCK SIZING

Rock for vortex weirs and stream crossings was sized to be stable at the 100-year peak discharge, which was estimated at 141 cfs. The USFS recommends 24 inch diameter boulders for construction of the vortex weirs. The stream crossings generally requires cobble-sized rock. The USACE riprap design program, CHANLPRO was used to determined the rock size required for the vortex weirs and stream crossings (USACE 1999).

The maximum flow velocity and depth overtopping the weirs and stream crossings were calculated from the HEC-RAS model, and CHANLPRO was run for these values. As shown in Attachment C, D_{100}(max) = 9 inches was suggested for both the vortex weirs and stream crossings. However, USACE riprap gradation D_{100}(max) = 18 inches (D_{50}(max) = 12 inches), which is specified in Specification 02380 RIPRAP (Table 3), was selected for the stream crossings. 24-inch boulders was selected as the appropriate size for the vortex weirs based on the USFS designs.

Table 3. Gradation for Riprap Placement (USACE 1994)

Limits of Stone Weight in Pounds for Percent Lighter by Weight								
D_{max} in inches	D_{100}		D_{50}		D_{15}		$D_{30(min)}$ in inches	$D_{90(min)}$ in inches
	Max	Min	Max	Min	Max	Min		
9	36	15	11	7	5	2	5	7
18	292	117	86	58	43	18	9	13
24	691	276	205	138	102	43	12	17

Specific weight of stone = 165 lbs/cu ft

REFERENCES

Maryland Department of the Environment. (2000). *Waterway Construction Guidelines*.

Newbury, R. W. and Gaboury, M. N. (1993). *Stream analysis and fish habitat design, a field manual*. Newbury Hydraulics, Ltd, Gibsons, B. B., Canada.

Rosgen, D. L. (1996). *Applied river morphology*. Wildland Hydrology, Pagosa Springs, Colorado.

USACE. (1999). Program CHANPRO Version 2.0. November.

USACE. (2005). HEC-RAS Version 3.1.3. May.

USFWS. (1982a). *Habitat Suitability Index Models: Cutthroat Trout*. February.

USFWS. (1982b). *Habitat Suitability Index Models: Brook Trout*. September.

USFWS. (1984). *Habitat Suitability Index Models: Rainbow Trout*. January.

USGS. (2002). *Estimating the Magnitude of Peak Flows at Selected Recurrence Intervals for Streams in Idaho*. Water-Resources Investigations Report 02-4170.

The Value of Protecting Ozark Streams: An Economic Evaluation of Stream Bank Stability for Phosphorus Reduction

E. Dove[1], K. Rodgers[2], and M. Keener[3]

[1]Water Resources, Olsson Associates, 1525 E. Republic Rd B100, Springfield, MO 65804; PH (417) 890-8802; email: edove@oaconsulting.com
[2]Water Resources, Olsson Associates, 1525 E. Republic Rd B100, Springfield, MO 65804; PH (417) 890-8802; email: krodgers@oaconsulting.com
[3]Watershed Committee of the Ozarks, 320 N. Main Ave, Springfield, MO 65806; PH (417) 866-1127; email matt@watershedcommittee.org

ABSTRACT

Keywords: stream restoration, phosphorus, removal cost, TMDL

One of the many appealing features of the Ozarks is the quality and beauty of our lakes and streams. Frequent algae blooms in the James River arm of Table Rock Lake however threatened not only valuable tourism dollars but also the quality of Ozark life. A nutrient based TMDL focusing on phosphorus and nitrogen was adopted for the James River in 2002. As we move into implementation, the question of the most cost effective method to reduce phosphorus loads is paramount. This paper compares the local cost of phosphorus removal from point sources as well as non-point sources. Specific Ozarks examples investigated included phosphorus reduction from a waste water treatment plant, stormwater BMP's, stream buffers and stream stabilization. The paper findings indicate Stream restoration is an excellent solution to preventing this phosphorus from being transferred to Ozark lakes and is cost efficient when compared to other non-point source reduction strategies. This paper briefly introduces the audience to many other economic benefits to stream restoration such as flood attenuation, greenways trails, and home price increase.

1.0 Introduction

As the Ozark's see increased development, area streams are beginning to show the telltale signs of urbanization. One common impact from urbanization is accelerated stream bank erosion.



Picture 1. Bank erosion threatening an Ozark condominium building (2008 photograph by Olsson)

Stream and bank erosion liberates a tremendous amount of sediment and causes the loss of property. The City of Springfield and Greene County are making progress toward restoring degraded streams. As part of Springfield's stormwater management plan, the city began daylighting Jordan Creek. This project removes drainage tunnels and reconstructs the stream corridor. The daylighted area also features a greenway trail connecting two parks.



Picture 2. Jordan Creek Daylighting Project (Springfield MS4 Report, 2007). This entire portion was previously in an undersized box culvert. Small fish are now prevalent in the base flow stream, and the trail system is heavily used.

Greene County completed a stream restoration project in 2007, stabilizing Ward Branch using geomorphic and bioengineering approaches instead of concrete. This project was 1,289 feet long, made extensive use of native plantings, and, in the future,

will incorporate a greenway trail. The cost for restoring Ward Branch was $347,000 or $269 per linear foot.

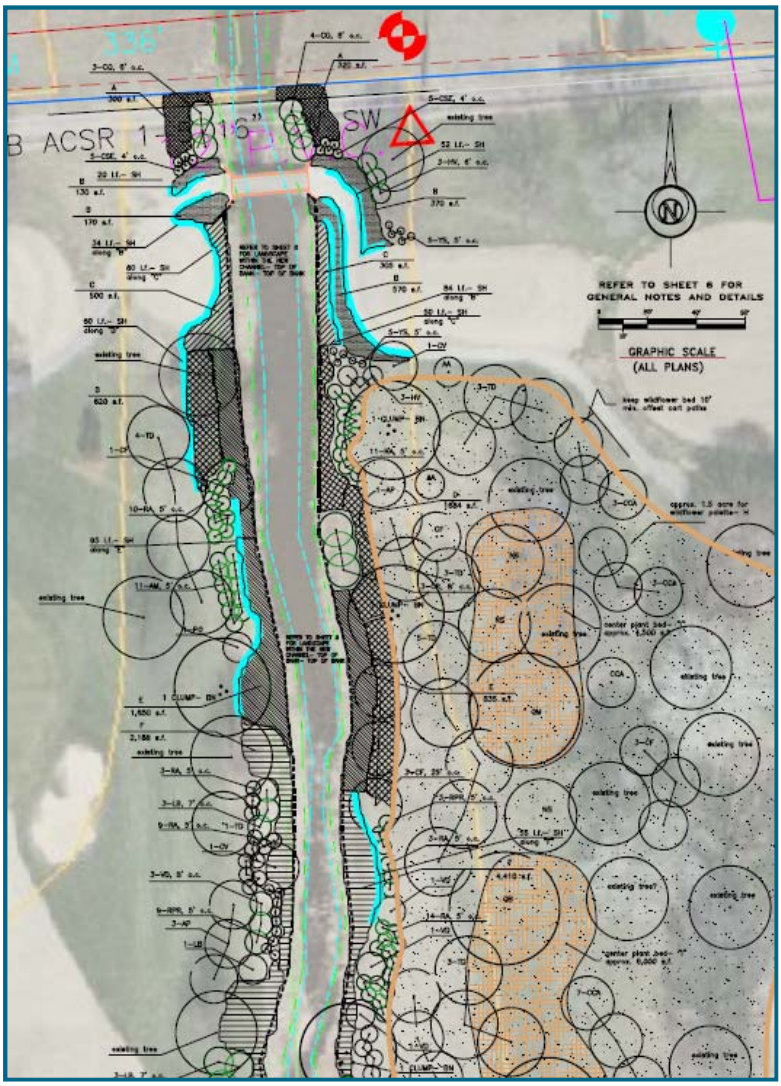

Picture 3. Map of Ward Branch restoration project. Located adjacent to Twin Oaks Country Club Golf Course in southern Springfield, the stream bank was heavily eroded and contributed to phosphorus pollution in James River.

Using Ward Branch as an example, at a cost of $269 per linear foot, is it worth stabilizing the Ozark streams? This paper presents some of the economic impacts from not stabilizing the Ozark streams. The discussion focuses mainly on phosphorus (P) impacts and costs, but some of the benefits associated with a stable greenway are also considered. Local studies and local examples are used when possible and are compared to national data.

2.0 Background

2.1 Impact of Phosphorus (P) on Water Quality

P is a particular concern because many of the Ozark's waterways and lakes are P limited (DNR 2001 TMDL). Nutrient loading analysis typically focuses on either P or nitrogen, depending on which is the limiting factor in a water body. A nitrogen to P ratio of greater than 10:1 indicates that the water body is P limited and vice versa. Stating that the nutrient is "limited" does not mean that there isn't much of it; it means that it will limit the total productivity of the water body. The following table shows published Nitrogen Limiting Thresholds taken from the DNR Total Maximum Daily Load (TMDL) for James River:

Table 1. Nitrogen:Phosphorus limiting thresholds

Information Source	N Limiting Threshold	Transition	P Limiting Threshold
Schanz and Juon (1983)	<10:1	10:1-20:1	>20:1
Petersen et al. (1993)			>20:1
Stockner and Shortreed (1978)			>20;1
Pringle (1987)	<10:1		
Grimm and Fisher (1986)	<10:1		
Dodds et al. (1998)	<12.6:1		
Borchardt (1996)			>17:1
Lohman (1988)	<12:1		

The high sediment trap efficiencies of lakes cause them to become sinks for pollutants. In addition, through sedimentation and anaerobic digestion, P can be recycled through the water column. Dissolved P is quickly utilized by algae, macrophyte, and epyphite communities for increased cellular growth. The resulting biomass shades out larger plants and benthic micro-algae or macrophytes. Picture 4 shows the relation between P and algal chlorophyll a. The implication of this relationship is that every pound of P can sustain approximately 200 lbs of biomass when all other nutrients are abundant. In comparison, one pound of nitrogen can only support 12.5 lbs of biomass (CE-QUAL, 1995).

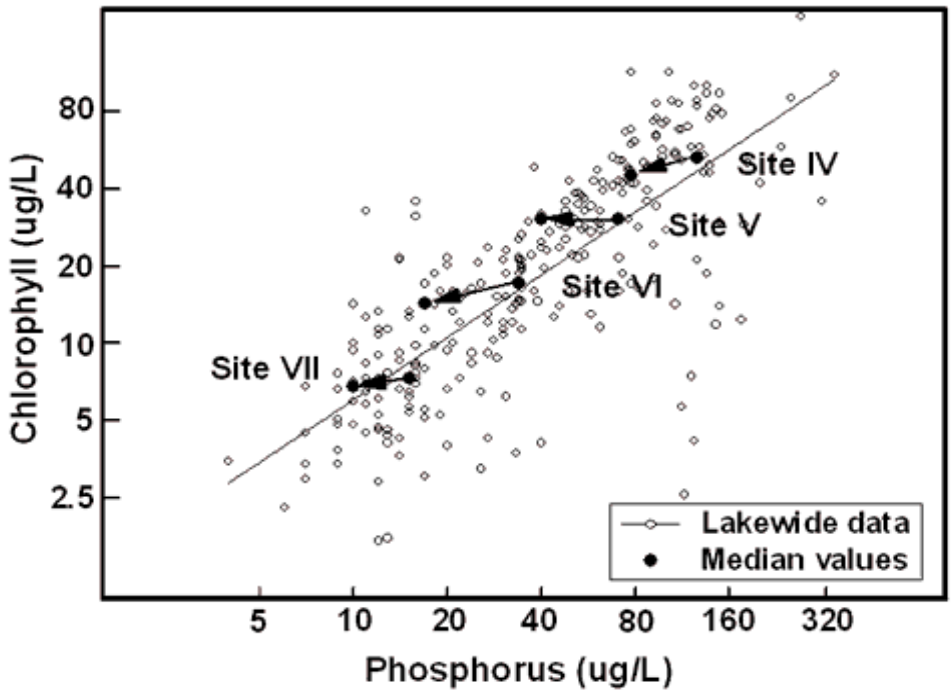

Picture 4. Graph showing relation between chlorophyll and total phosphorus concentrations in Table Rock Lake.

2.2 Table Rock Lake Eutrophication

In the 1990s, the James River Arm of Table Rock Lake, located near Branson, Missouri, started experiencing frequent algae blooms. This high dollar tourism location was well known for its crystal clear water, and the algae blooms became a stark reminder that a lake's water quality is a reflection of its watershed and streams. In the James River Basin, tourism brings over $900 million per year to the local economies (DNR TMDL 2001). Local officials and businesses understood the potential impact of poor water quality on the local economy. This led the Table Rock Lake/Kimberling City Area Chamber of Commerce to form the corporation Table Rock Lake Water Quality, Inc. in 1998. The Chamber's board of directors recognized that improving and preserving Table Rock Lake's water quality was vitally important. They concluded that the corporation would be an action group dedicated to projects that would stop pollution resulting from non-point sources such as nutrient enrichment, bacterial contamination, and contamination from point sources. This group was instrumental in formalizing and implementing the James River TMDL.



Picture 5. Table Rock Lake (algae bloom of 1999 in the James River Arm of Table Rock Lake – Missouri DNR photo).

Water quality studies performed as far back as 1969 have indicated that high nutrient loads existed in the James River. In May of 2001, the James River TMDL of 0.075 mg/L of P and 1.5 mg/L of in-stream total nitrogen was approved. The first phase of the TMDL implementation plan focuses on point sources. A P limit of 0.5 mg/L was imposed on all point sources discharging greater than or equal to 22,500 gallons per day. A major result of this first phase was the 2001 improvement to the City of Springfield Southwest Treatment Plant to reduce average P discharge to 0.5 mg/L.

The second phase of the TMDL (Total Maximum Daily Load) focuses on non-point sources and relies on riparian corridor restoration, Best Management Practices (BMPs), septic tank cleanouts, and soil testing. The City of Springfield's Stormwater Management Plan has been put into place and has helped by upgrading/creating stormwater treatment in addition to performing full spectrum detention, acquiring floodplain areas, cleaning streets, and improving the de-icing procedures. The James River Basin Partnership and the Watershed Committee of the Ozarks have also helped by contributing volunteer time, organizing cleanups, educating the public, and managing grant funds. The following chart from the DNR's TMDL Data Sheet shows the difference in P loads before the TMDL and after the combined point and non-point source controls have been partially implemented:

Table 2. James River TMDL

Mean Nutrient Levels for Two Locations on James River Comparing Data from 1999 to 2003 (in mg/L)				
Nutrient	**James R. near Boaz**		**James R. at Galena**	
	1999	**2003**	**1999**	**2003**
Total P	0.62	0.15	0.51	0.21

The dramatic reduction in P is notable but is largely a result of improvements at the wastewater treatment plant. Non-point sources of P, however, are much more elusive to treat. According to the TMDL for the James River Basin, 0.033 to 0.06 tons/acre/year of sediment is released from stream bank erosion. The amounts of sediment that can be liberated from modest reaches of streams are extensive. The rate of erosion found at Ward Branch produced 77 tons of soil liberated in eight months from only a 1,000-foot long stretch (OEWRI, 2007).

2.3 Phosphorus (P) Loaded Stream Banks

Fine-grain sediment in alluvial deposited stream banks is laden with nutrients such as P. This is not a surprise; the agricultural community has long valued the highly productive floodplain bottoms. Research performed by Iowa State University (Moeller, Kovar, Russell, and Haan, 2006) has found that total P concentrations of 200-to-500 mg/kg were common in grazing land in Colorado. Soil testing performed by Missouri State University on Ward Branch Stream in Green County, Missouri, has found a similar range of total P. The average P found in the stream banks was 400 mg/kg (0.035 lbs of P per cubic foot of bank material). This implies that even minor amounts of stream bank erosion have a large potential to release P into the stream and ultimately into sensitive water bodies such as Table Rock Lake.

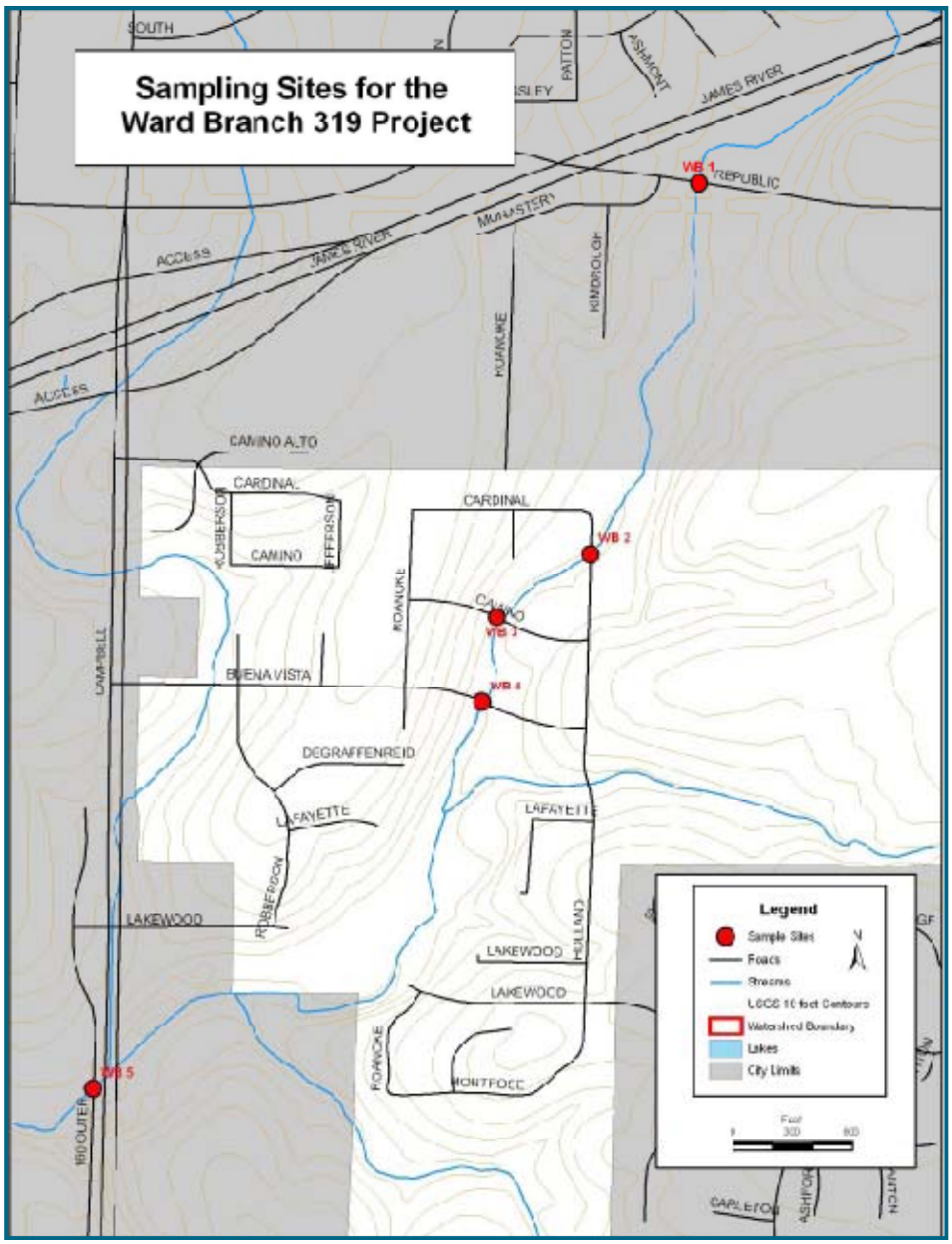

Picture 6. Sampling sites for Ward Branch (OEWRI, 2007)

Using the averages mentioned above for the Ward Branch Study, it was estimated that erosion would liberate 93 lbs of P per 1,000 feet of channel per year. Testing found that the total P load in the stream was 175 lbs/year, so this bank alone contributed 53 percent of the P load in the stream.

The Ward Branch findings on the volume of sediment generated from stream banks are not the only such findings. Based on reservoir water quality studies performed by Olsson Associates in Nebraska, 20-to30 percent of sediment and nutrients are from stream bank erosion (Cunningham, 2003). Studies on San Diego Creek in suburban Los Angeles found that over 60 percent of the

sediment resulted from channel erosion (Trimble, 1997). Likewise, a study on Goodwin Creek in northern Mississippi found that better than 80 percent of the total sediment yield originated as channel and gully erosion (Grissinger, 1990). A study of a channelized stream in Illinois found that one storm eroded as much as 1,150 tons of soil from a single bank in 1982 (Roseboom and Russell, 1985). The amounts of sediment liberated from stream banks can be greatly increased as a result of channelization, urbanization, and widespread stream instabilities such as incision (head cuts).

A link exists between the riparian buffers and stream bank stabilization. A study of 748 stream bends found that 67 percent of bends without vegetation suffered erosion during a storm, while only 14 percent of bends with vegetation were eroded (Beeson and Doyle 1995). Keep in mind, the bank erosion potentially could have removed the vegetation rather than the de-nuded banks causing the erosion. Nevertheless, this 1995 study makes it clear that bends void of vegetation are 30 times more likely to erode.

Studies have shown that P removal has been measured along a healthy stream segment (Watson, 2001). Unhealthy or deforested riparian areas cause channel narrowing, which reduces the total amount of stream habitat and ecosystem per-unit channel length and compromises in-stream processing of pollutants (Sweeny, et al., 2004). Sweeny has suggested, "Forested stream channels have a wider and more natural configuration, which significantly affects the total in-stream amount and activity of the ecosystem, including the processing of pollutants. Riparian corridors and grass filter strips work together to cause sedimentation of clay particles containing phosphorus and to slow the water as it enters the stream. The woody vegetation further assists in stream bank stabilization. These results reinforce current policies used in the U.S. to incentivize riparian buffers as BMPs resulting in re-forestation for stream restoration and water-quality." A forest and grass buffer combination not only reduces non-point source pollutants from entering streams; they also enhance the in-stream processing of both non-point and point source pollutants, thereby reducing their impact on downstream rivers and impoundments (Welsch, 1991, Lowrance, 1997). This in-stream P processing further improves the cost efficiency for stream restoration.

2.4 Other Non-Point Sources of Phosphorus (P)

The point source wastewater treatment plants are only one of the many sources of P to our streams. Urban runoff contains a considerable amount of non-point P. Table 3 breaks down sources of P pollution from an area in Marquette, Michigan (Steuer, Selbig, Hornewer, and Prey, 1997). The table also summarizes event mean concentrations in runoff from residential and commercial areas completed by the Watershed Committee of the Ozarks on Pierson Creek. Pierson Creek is located along the eastern edge of Springfield, Missouri. The 1994 Pierson Creek study sampled runoff downstream from a

general residential or commercial area, so the land use was not itemized as discreetly as the Michigan study.

Table 3. Sources of phosphorus in urban areas from various data sources.

Source Area Sampled	Michigan Study Total P (mg/l)	Pierson Creek Study Total P (mg/l)	NURP Data (mg/l)
Commercial Parking Lot	0.2	0.281	0.201
High Traffic Street	0.31	-	
Medium Traffic Street	0.23	-	
Low Traffic Street	0.14	-	
Commercial Rooftop	0.09	-	
Residential Rooftop	0.06	0.40	0.383
Residential Driveway	0.35		
Residential Lawns	2.33		
Basin Outfall	0.29		

Based on the MS4 monitoring being performed by the City of Springfield in areas of the community that do not have water quality stormwater treatment, total P concentrations range from 0.05 mg/L to 0.8 mg/L, with an average of 0.26 mg/L, which compares favorably to the Michigan study. The Michigan study and the Nationwide Urban Runoff Program (NURP) data have focused on these urban sources, but many of these studies neglect stream bank erosion sources of P.

The City of Springfield has begun a notable stormwater treatment program for all new developments over one acre in size. The water quality storm of one inch must be treated using systems such as rain gardens, bioswales, extended detention, filter strips, porous concrete, and several other mechanisms to decrease the water quality impairments to our streams. Watershed groups in the area are working hard to reduce the amount of P and other stormwater pollutants from entering streams. The James River Basin Partnership sponsored the 2006 James River Watershed 319 Project. This $3.1 million project created a variety of BMPs, including riparian corridor restoration, septic tank cleanout, urban and agricultural soil testing, and educational/outreach programs. The Watershed Committee of the Ozarks is currently working with the City of Springfield to install storm water education signage at key locations around the city. In addition, the Watershed Center at Valley Water Mill is being developed as an educational showpiece for a variety of water quality BMPs.

3.0 Phosphorus (P) Removal Costs

The impacts of hyper utrophic conditions caused by excess P are well documented, but what about the costs to remove P from Ozark waterways? P enters our water from both point and non-point sources. This section will discuss an Ozark's example on the costs of P removal from a point source and will also discuss the costs of non-point source P removal using stormwater BMPs.

3.1 Point Source Phosphorus (P) Removal Costs

Point source pollution can contribute a high percentage of P to our water, but our research indicates it is much cheaper to reduce the amount of P being discharged from point sources than non-point sources. In response to the imposed TMDL on James River and the algae blooms on Table Rock Lake, the Springfield Southwest Treatment Plant performed treatment upgrades to decrease P discharges into the James River. The upgrade began in 1997 and was completed March of 2001. The project cost was $2.2 million and involved installing an alum treatment system. The most recent project followed a 1993 project, which also reduced the discharge concentrations of P.

Table 4. Wastewater treatment plant upgrades and the associated pre and post total phosphorus discharges to Wilson Creek.

Southwest Treatment Plant Upgrade	Completion Date	Cost	Post-Upgrade Avg. Lbs of P to Creek	Prior Avg. Lbs of P to Creek
Plant Expansion	1993	$30 million	850 lbs/day	1,650 lbs/day
Alum Treatment	2001	$2.2 million	110 lbs/day	850 lbs/day

Including the operation and maintenance cost of the alum system, the cost for P removal at the treatment plant, due to the 2001 upgrade, resulted in approximately $4.60 per pound of P removed per year, assuming a 50-year life cycle and including an estimated O&M cost of 54 percent of construction.

3.2 Non-Point Source Stormwater BMP Phosphorus (P) Removal Costs

Olsson Associates and Wright Water Engineers recently completed a stormwater BMP retrofit cost analysis study for Overland Park, Kansas. We specifically evaluated the costs associated with constructing and maintaining various non-point source pollution treatment methods. The cost for these systems varied but is generally summarized in Picture 7.

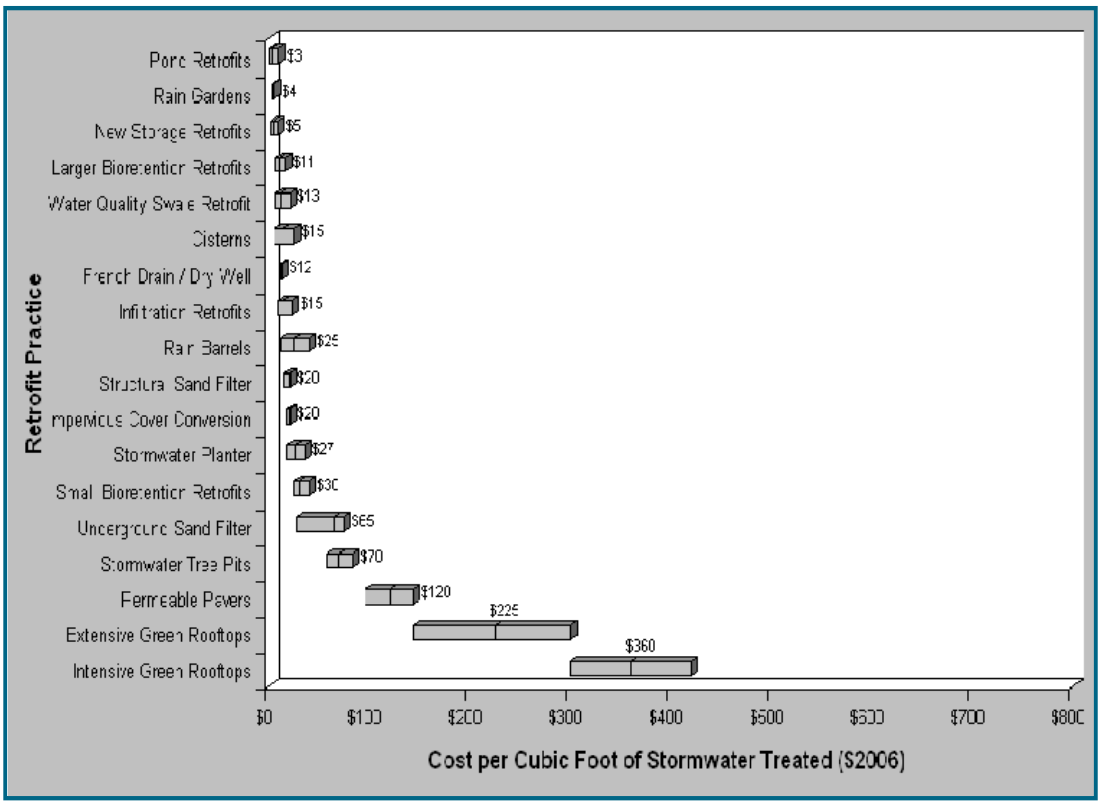

Picture 7. Graph of BMP Cost (Olsson, 2007)

Based on the monitoring being performed by the City of Springfield in areas of the community that do not have water quality stormwater treatment, total P concentrations range from 0.05 mg/L to 0.8 mg/L, with an average of 0.26 mg/L (City of Springfield, 2007). Mean average cost was used from the graph above for a BMP of $10 per cubic foot for a 50-acre development site, which gives a total BMP cost of $1.12 million (including 4.5 percent operation and maintenance costs). BMPs all have varying percent removal rates for P, which range from zero percent for green roofs, 15 percent for grass channels, and up to 75 percent removal for wetlands (EPA, 1999). We should note that an increasing amount of data has been suggesting the removal efficiency of BMPs that may not be the most appropriate measure used in designing these systems due to the variability of inflow concentrations and a practical lower limit of removal. For simplicity, we are using a 40 percent removal rate for an average inflow concentration of 0.26 mg/L P. Using these inflow and removal rates, the BMPs would cost $466 per pound of P removed per year (EPA, 1999). Some agricultural BMPs are cheaper, such as terracing. These BMPs result in average costs of $185 per pound of P removed per year (Tippett, 1995).

3.3 Cost of Stream Stabilization Using Geomorphic and Bioengineering Approaches

National data indicates a wide range in costs for stream stabilization, from $42 per linear foot to as much as $1,000 per linear foot (especially for daylighting culverts). Projects performed by Olsson Associates in Nebraska, Kansas, and Missouri have found a range of costs from $260 per linear foot to $350 per linear foot. The Ward Branch stabilization in Greene County resulted in a cost of $269 per linear foot. Assuming a 4.5 percent operation and maintenance cost, the total cost for 1,000 feet of stream would be $874,250. In 1,000 feet of stream channel on Ward Branch, MSU measured 93 lbs of total P being exported per year from bank erosion. For Ward Branch, the cost in terms of the amount of total P prevented was $188 per pound annually for a 50-year life cycle.

It should be pointed out that these approaches do not completely eliminate stream bank erosion. Natural systems in dynamic equilibrium will migrate over time, and sediment will be liberated and subsequently deposited so that the net transport out of the system balances with the net sediment inflow rate.



Picture 8. Before and after stream restoration done by Newbury Hydraulics – Waukegan Brook – Washington Park, Michigan: 1991 before restoration (left), and three years post-construction in 1995 (right).

One approach historically taken to reduce stream bank erosion is to concrete line or enclose the stream. This approach is quite expensive and also reduces environmental benefits. Using lower Ward Branch as an example, the upstream culvert is a 10-by-12-foot concrete box culvert. Assuming this culvert was extended with the same size structure, it would result in a construction cost of nearly $1.6 million ($1,580 per linear foot) for the culvert and fill necessary to the cover 1,000 feet of conduit. This cost does not include permitting costs and downstream erosion protection. This cost is over five times more costly than the natural stream design.

3.4 Stream Buffers

To arrive at a unit cost basis, several design parameters were applied. Using a 100-foot wide buffer with woody vegetation for the first 50 feet next to the

stream and a 50 grass filter outside the woody area yielded a 50 percent removal efficiency using a relatively flat slope of 1-to-5 percent (Wenger 1999). A flow through velocity of 0.5 fps with a design depth of 1-inch deep during the two year storm was used to establish the number of acres a unit width of buffer could treat (Harner et al 2000). Combined with an assumed predominantly residential land use, the buffer could treat 0.0148 drainage area acres per foot of width. Installation bid tabulations from the Jordan Creek daylighting project in Springfield and projects in Christian County, Missouri, were reviewed, and, based on these local Ozark projects, an average installation cost of $15,000 was estimated. The installation cost includes three-to-five gallon trees, shrubs, native grass seeding, erosion control, and grading to ensure sheet flow through the buffer. Maintenance costs are estimated to be similar to stormwater BMPs at 4.5 percent of construction. The sediment accumulated in buffers must be removed to maintain the buffer treatment efficiency (Daniel and Moore, 1997). An assumed 10 year cleanout of the accumulated sediment in the grass area, followed by reseeding, was assumed at a 10 year interval over the 50 year design life. These calculations indicate that a 100-foot wide grass and tree buffer would cost approximately $20 per linear foot to install and an additional $140 per linear foot to maintain for a 50 year period. The amount of phosphorus removed during the 50 year design life was estimated at 0.58 lbs per foot of buffer. The cost efficiency is calculated at $278 per pound of phosphorous removed.

4.0 Cost Efficiency Comparison

We have presented some of the costs associated with removing P from the water column once it has been liberated and also the costs associated with stabilization measures taken to prevent the P from being eroded from the stream banks. Is an ounce of prevention worth a pound of cure? The following table summarizes the results:

Table 5. Phosphorus removal cost comparisons

P Removal Method	Data Source	Cost per Pound Removed Annually
Wastewater Treatment Plant	Springfield WWTP Upgrades, EPA Guidance Documents	$4.60
Stormwater BMPs	EPA 1999 Study	$698 to $1,535
	Olsson 2006 Study	$466
Stream Restoration	Ward Branch and Other Restoration Plans in Nebraska, Kansas, and Missouri	$188
Stream Buffers	Jordan Creek, Springfield Christian County, Missouri	$278

Point source reductions stood out as the most effective method to reduce P entering the James River. Of the three non-point source methods reviewed, the data indicates that performing stream stabilization projects is a cost-efficient method to reduce the amount of P in our streams and lakes. Stream bank stabilization projects should be an integral portion of a watershed plan and a TMDL implementation strategy. However, if full-spectrum detention and adequate stream buffers are in place, the stabilization projects may not be needed, and the phosphorus processing of the healthy corridor is, in essence, "free" treatment. The associated prevention of stream instabilities offers an even more attractive economic proposal, as do the added benefits of healthy streams and the ensuing recreational opportunities.

5.0 Other Economic Benefits of Stream Restoration and Greenways Trails

The prior discussion was limited to quantifiable dollars spent to prevent P from reaching critical areas. As the Ozarks continue to see urban development, increasing pressures will encourage us to encroach on our streams. Riparian areas are dynamic and provide many functional benefits to the stream ecosystem. Effective riparian management could ameliorate many ecological issues related to land use and environmental quality. Riparian corridors should play an essential role in conducting water and landscape planning, in the restoration of aquatic systems, and in catalyzing institutional and societal cooperation for these efforts (Nainmen et al 1993). Riparian zones need to be viewed as an active river area framework, which includes a spatially explicit, holistic view of rivers that comprises both the channels and the riparian lands necessary to accommodate the physical and ecological processes associated with the river system. The framework informs river conservation by providing an approach to account for the areas and processes that form, change, and maintain a wide array of habitat types and conditions in and along rivers and streams.

By leaving a buffer around streams during construction, developers realize not only immediate cost savings, but also the possibility of gaining long-term value to the property. The developer realizes an economic advantage for keeping the stream open and employing an adequate stream buffer, full-spectrum detention, and erosion control during construction and stormwater quality treatment.

The National Park Service has well-documented studies on the economic value of greenways (NPS, 1995). Greenways that border streams offer many benefits, one of which is a marked increase in home values. In a subdivision in Springfield, the assessed valuations of the homes that back to the South Creek greenway is 15 percent higher than comparable homes in the remainder of the subdivision. In Boulder, Colorado, a study of property values found that homes next to a greenway had 32 percent higher property values than homes 3,200 feet away. In Apex, North Carolina, developers of the Shepherd's Vineyard subdivision found that they could charge $5,000 more for a home adjacent to a greenway. In Brown County, Wisconsin, homes along the Mountain Bay Trail sold for nine percent more than similar property not adjacent to a trail. Assuming an average lot width of 120 feet, an average lot value of $35,000, and residential houses backing to both sides of the stream, the benefit is

approximately $87 per linear foot of stream. In a 2002 survey of recent homebuyers sponsored by the National Association of Realtors, trails ranked as the second most important community amenity out of a list of 18 choices. The increase in home values also leads to increased property tax revenue. In Boulder, Colorado, a study of one subdivision revealed that the greenway increased the aggregate property value by $5.4 million. This resulted in $500,000 more in potential property tax revenue, which could pay for the $1.5 million greenway in three years.

Greenway trails also decrease the amount of pollution reaching our streams by serving as alternative modes of transportation. Studies have shown that two-thirds of the trips that people living in urban areas make are less than five miles in distance. Using the trails for walking and biking has also been shown to decrease public health costs $3 for every $1 spent on trail development (Wang, Macera, Scudder-Soucie, Schmid, Pratt, and Buchner, 2005).

Greenway trails can be incorporated as floodplain acquisitions. FEMA estimates that flooding causes over $1 billion in damages every year, and approximately 10 million homes are currently located in floodplains. After flooding in Tulsa, Oklahoma, the city designed a greenway along Mingo Creek that included woods, wetlands, and parks to enhance the floodplain. As a result, flood insurance rates in Tulsa dropped 25 percent. The Minnesota DNR found that the average value of one acre-foot of flood storage is $300. Therefore, if one acre-foot of floodplain or wetland is developed, it would cost the public $300 to replace the water storage. Preserving and maintaining an "active river area" provides for future economic return while at the same time preventing future costly restoration or remediation projects.

Streams, trails, and lakes also bring tourism dollars to communities. In the James River Basin, tourism brings over $900 million per year to the local economies (DNR TMDL 2001). The recreational benefits of trails, healthy streams, and lakes can be quantified using the "willingness-to-pay" system (National Parks Service, 1995). These values (converted to 2008 dollars) show what the average person would be willing to pay to have certain activities available to them per person, per day.

Table 6. Willingness to Pay

Average Willingness to Pay by Activity	
Activity	**Average Value per Activity Day**
Picnicking	$25
Hiking	$40
Non-motorized Boating	$68
Warm Water Fishing	$41
Non-consumptive Wildlife	$28

6.0 Conclusion

This study has shown that stream restoration can be one of the most cost-effective methods of preventing phosphorus from entering lakes. BMPs are more expensive,

though necessary, because not only do they treat a myriad of pollutants, including phosphorus, they also decrease the rate of runoff, thereby preventing some erosion. The calculations in this study show that phosphorus emissions from point sources such as treatment plants are the least-costly to reduce. However, as the James River TMDL states, non-point source pollution needs to be addressed in conjunction with point source pollution to decrease the amount of nutrient loading in our lakes.

Our streams and lakes are very valuable resources. What would happen today if the entire Table Rock Lake was affected the way the James River arm was affected by the algae blooms of 1998? As recent as the spring and summer seasons of 2008, visitation to Table Rock Lake decreased dramatically due to two factors: 1) lake levels remaining at or near record flood stages for several weeks due to large amounts of rainfall, and 2) public perception and fear that the lake was contaminated and unsafe to swim or boat in (Table Rock Lake Water Quality). As a result, local business owners realized decreased revenues. This recent event emphasizes the impacts impaired water quality has to local economies. Considering alone the amount of P that is released by eroding stream banks, compared to the cost of removing P by other non-point source removal methods, it is obvious that our streams need to be protected. The economic benefits of having healthy streams and lakes equate to millions of dollars per year in tourism, health care benefits, and home values. Protecting streams in urban settings generates approximately $250 worth of increased land value per linear foot and results in one of the least costly methods of reducing non-point source P. Protecting Ozark Streams is a necessary investment into the sustainability of the environment and the future economic viability of the region.

REFERENCES

Sweeney, B. W., Bott, T. L., Jackson, J. K.,* Kaplan, L. A., Newbold, J. D., Standley, L. J., Hession, W. C., and Horwitz, R. J, (2004). "Riparian deforestation, stream narrowing, and loss of stream ecosystem services." *Proceedings of the National Academy of Sciences of the United States of America*. September 28, 101(39): 14132–14137.

Bullard, L., (1994) *Pierson Creek Watershed Studies*. Watershed Committee of the Ozarks. Springfield, MO.

Center for Watershed Protection (CWP) (2004). *Stormwater Pond and Wetland Maintenance Guidebook* (draft).

Center for Watershed Protection (1997). *The Economics of Stormwater BMPs in the Mid-Atlantic Region.*

City of Springfield Storm Water Services Division, Department of Public Works. (2007). *NPDES Storm Water Permit Annual Report July 2006 – June 2007*

Cole, T. and Buchak, E. (1995). *CE-QUAL-W2: A Two-Dimensional, Laterally Averaged, Hydrodynamic, and Water Quality Model, Version 2.0*

Daniel, T.C. and Moore, P.A. (1997). Managing Phosphorus in Manure: Causes, Concerns, and BMPs. In: *Proceedings of the Southeastern Sustainable Animal Waste Workshop*. University of Georgia. Athens, GA.

Daniels, R. B. and Gilliam, J.W. (1996). Sediment and chemical load reduction by grass and riparian filters. *Soil Science Society of American Journal* 60:246-251.

Dinnes, D. (2004). *Assessment of Practices to Reduce Nitrogen and Phosphorus Nonpoint Source Pollution of Iowa's Surface Waters.* USDA-ARS National Soil Tilth Laboratory, Ames, Iowa.

Wang, G., Ph.D., Macera, C. A., Ph.D., Scudder-Soucie, B., Med., Schmid, T., Ph.D., Pratt, M., MD, MPH, Buchner, D., MD. (2005). *Cost-Benefit Analysis of Physical Activity Using Bike/Pedestrian Trails.* Health Promotion Practice Vol. 6, No. 2, p174-179.

Heaney, J. and J. Lee (2004). *Methods for Optimizing Urban Wet-weather Control Systems*, Prepared for EPA.

Lampe. L., Andrews, H., Martin, P., Barrett, M., Jefferies, C., Woods-Ballard, B., Kellagher, R., and M. Hollon (2005). *Post-project Monitoring of BMPs/SUDs to Determine Performance and Whole-Life Costs: Phase 2*. Prepared for WERF, AwwaRF, and UKWIR. Report No. 01-CTS-21T.

Moeller, S. L., Kovary, J. L., Russell, J. R., and Haan, M. M. (2006) *Grazing Management Effects on Potential Sediment and Phosphorus Loss from Streambanks*

Missouri Department of Natural Resources (2001). *Total Maximum Daily Load (TMDL) for James River, Webster, Greene, Christian, and Stone Counties, Missouri; Jefferson City, Missouri.*

Northern Virginia Planning District Commission, Engineers & Surveyors Institute (1992). *Northern Virginia BMP Handbook.*

National Parks Service (1995) *Economic Impacts of Protecting Rivers, Trails, and Greenway Corridors.*

The Ozarks Environmental and Water Resources Institute (2007). *Preconstruction Report for the Ward Branch Stream Restoration Project.*

Smith, M.P., Schiff, R., Olivero, A. and MacBroom, J.G. (2008). *The Active River Area: A Conservation Framework for Protecting Rivers and Streams*. The Nature Conservancy, Boston, MA.

Tippett, J. (1995). *Cost Effectiveness of Agricultural BMPs for Nutrient Reduction in the Tar-Pamlico River Basin (NC).*

U.S. Environmental Protection Agency, Office of Water (2007). *Biological Nutrient Removal Processes and Costs, EPA-823-R07-002.*

U.S. Environmental Protection Agency (2002). *Costs of Urban Stormwater Control.*

U.S. Environmental Protection Agency, Office of Water (1999). *Preliminary Data Summary of Urban Storm Water Best Management Practices. EPA-821-R99-012.*

Sample, D., Heaney, P., Wright, L., Fan, C., and R. Field (2003). Costs of Best Management Practices and Associated Land for Urban Stormwater Control, *Journal of Water Resources Planning and Management*, Volume 129, Issue 1, February.

Steuer, J., W. Selbig, N. Hornewer and J. Prey (1997). *Sources of Contamination in an Urban Basin in Marquette, Michigan, and an Analysis of Concentrations, Loads, and Data Quality*. U.S.G.S. Water Resources Investigations Report 97-4242. Wisconsin DNR and EPA. 25pp.

Strecker, E., Huber, W., Heaney, J., Bodine, D., Sansalone, J., Quigley, M., Leisenring, M. Pankani, D., and A. Thayumanavan (2005). *Critical Assessment of Stormwater Treatment and Control Selection Issues*, Prepared for WERF." See Section 6.3, Cost Considerations.

Watershed Management Institute (1997). *Operation, Maintenance, and Management of Stormwater Management.* Prepared in cooperation with the U.S. Environmental Protection Agency.

Watson, C. (2001). *Development and Evaluation of Reactive Near-Stream-Structures for Reducing Agrichemical Contamination.*

Weiss, P.T., Gulliver, J.S. and A.J. Erickson (2007). Cost and Pollutant Removal of Stormwater Treatment Practices, *Journal of Water Resources Planning and Management*, May/June.

Wenger, S. (1999). *A Review of The Scientific Literature on Riparian Buffer Width, Extent and Vegetation,* Office of Public Service & Outreach, Institute of Ecology, University of Georgia.

Wossink, A. and W. Hunt (2003). *The Economics of Structural Stormwater BMPs in North Carolina,* WRRI Research Report No. 344.

ASCE-EWRI 2009 – World Environmental & Water Resources Congress

Developing Probability of Failure Estimates for Stream Restoration Design Components

Timothy M. Sliwinski S.M.ASCE, [1] Sue L. Niezgoda Ph.D., P.E., Aff.M.ASCE, [2] Michael DeVasher Ph.D. [3]

[1]Rose-Hulman Institute of Technology, 5500 Wabash Avenue, Campus Mail 1319, Terre Haute, IN 47803; email: sliwintm@rose-hulman.edu

[2]Department of Civil Engineering, Rose-Hulman Institute of Technology, 5500 Wabash Avenue, Campus Mail 4047, Terre Haute, IN 47803; PH (812) 877-8814; email: niezgoda@rose-hulman.edu

[3]Department of Mathematics, Rose-Hulman Institute of Technology, 5500 Wabash Avenue, Campus Mail 4009, Terre Haute, IN 47803; email: devashe1@rose-hulman.edu

Abstract:
Stream restoration projects are proliferating in all regions of the country to provide improvements to streams disturbed by highway construction, urbanization, and channel modifications. The morphologically-based natural channel design method is commonly used to design stream restoration projects; however, the design approach is often vague, qualitative, and lacking in guidance. This can lead to an increase in project uncertainty and costs. A two-step method of incorporating uncertainty and risk in stream restoration design has been developed as a combination of Design Failure Modes and Effects Analysis (DFMEA) and risk quantification. The purpose of DFMEA is to prioritize failures in accordance with their risk. The definition of risk contains two components: (1) probability of failure and (2) consequence of failure. Probability of failure of stream restoration design components is often difficult to determine due to lack of published failure data. In the existing risk assessment method, the likelihood of occurrence ratings from the DFMEA are used to estimate the probability of failure. A set of tasks were carried out to improve the application of the two-step risk assessment method by developing better estimates of probability of failure for stream restoration design components. A literature review was performed to compile potential failure modes, causes of failure, associated predictor variables, and uncertainty in the predictor variables for stream restoration design components. Following this, advanced probabilistic techniques, namely Logistic Regression Analysis (LRA) and Monte Carlo

Simulation (MCS), were applied to develop improved failure probabilities for stream restoration design. MCS was used to incorporate the results of the literature review and to select values for the predictor variables for use in the LRA. The LRA provided a model that was used for prediction of the probability of occurrence of an event. The results were incorporated into the existing risk assessment method to create a better decision making tool for stream restoration design. The incorporation of the resulting risk assessment method in the design phase of stream restoration projects can be important to decision making and will improve the likelihood of success.

Introduction:

Stream restoration projects are proliferating in all regions of the country to provide improvements to streams disturbed by highway construction, urbanization, and channel modifications. The morphologically-based natural channel design method (Rosgen 1996) is commonly used to design stream restoration projects; however, the design approach is often vague, qualitative, and lacking in guidance. This can lead to an increase in project uncertainty and costs (Kondolf 1998, Johnson and Brown 2001). A two-step method of incorporating uncertainty and risk in stream restoration design has been developed as a combination of Design Failure Modes and Effects Analysis (DFMEA) and risk quantification (Niezgoda and Johnson 2007).

Design Failure Modes and Effects Analysis:

DFMEA is a qualitative procedure for systematically identifying potential component failure modes and the effects associated with those failures on the operation status of the system (Dushnisky and Vick 1996). Previously, the DFMEA method has been used to evaluate and rank potential problems in the manufacturing processes. It has also been applied to advance the understanding of complex electrical and mechanical systems including numerous applications in nuclear safety (McCormick 1981, American Nuclear Society 1983, Fullwood and Hall 1988, Henley and Kumamoto 1992, Shimizu et al. 1993).

In the case of stream restoration design, the components consist of elements such as cross sectional geometry, cross rock vanes, rootwads, and meander pattern that are utilized by practitioners to design a stable, functional stream. The failure modes for each component typically consist of dislocation, unintended scour or unintended deposition. The consequence of a specific failure mode for a specific component is an estimate of the cost of restoration or damage to the stream as a whole, induced by said component failure. Additionally, there are a set of detection methods used by the designer to determine if a given failure will occur prior to implementation. These detection methods can be indirect, such as an incipient motion analysis, or direct, such as checking state mandated installation guidelines to ensure that each component is designed according to existing standards.

The DFMEA method is performed in the design stages prior to implementation allowing time to assess the risk/cost of component or system failure and so that changes to the implemented design can be made early and at low cost. The purpose

of DFMEA is to prioritize failures in accordance with their risk (Kmenta and Ishii 2000). The definition of risk contains two components: (1) probability of failure and (2) consequence of failure. Based on this definition, the following mathematical expression is used to calculate risk:

$$Risk = C_o + \sum_{i=1}^{n} (p_i C_i) \quad (1)$$

where, C_o = initial cost of the project, including assessment, design, and construction costs; p_i = probability of failure of component *i;* C_i = consequence of failure of component *i* in terms of costs of repair, replacement, and damage; and n = the total number of components in the system. Probability of failure of stream restoration design components is often difficult to determine due to lack of published failure data. In the existing risk assessment method, the likelihood of occurrence ratings from the DFMEA are used to estimate the probability of failure (Niezgoda and Johnson 2007).

The results of this project will improve upon this risk assessment method by creating a method of empirically calculating the probability of failure. Failure, for this project, is determined by the following definitions:

- *Overall Design Failure:* When a stream no longer operates as intended due to instability. This can happen if the incoming sediment is greater than the outgoing or vice versa.
- *Component Failure:* When an element no longer operates as intended and either induces stream instability or causes any unintended change downstream. A design component can fail both structurally and/or functionally.
- *Structural Failure:* This refers to a collapse of the physical system or components of the system sufficient to prevent fulfillment of the design objectives (Brown and Johnson, 2001).
- *Functional Failure:* This implies that the project objectives cannot be realized due to the ineffectiveness of the design, although the structure or form may be intact and in place (Brown and Johnson, 2001).

The requirements to execute the DFMEA method include the following (McCollin 1999):

- A hierarchical structure for the system illustrating all system components
- Failure modes of all components of the system
- An objective criterion for implementing corrective action (typically a risk priority number)

The goal of this project is to develop a more accurate way of determining stream failure and component failure when performing the DFMEA. This is accomplished by

performing advanced probabilistic techniques on data that is collected for real streams.

Current Study:

The following set of tasks were carried out to improve the application of the two-step risk assessment method by developing better estimates of probability of failure for stream restoration design components:

- A literature review was performed to compile potential failure modes, causes of failure, associated predictor variables, and uncertainty in the predictor variables for stream restoration design components.
- A survey was developed and sent out to various agencies to collect failure information for actual stream restoration projects.
- This data was used to run advanced probabilistic techniques, namely Logistic Regression Analysis (LRA) and Monte Carlo Simulation (MCS). These techniques were applied to develop improved failure probabilities for stream restoration design.
- Results were incorporated into the existing risk assessment method to create a better decision making tool for stream restoration design.

The incorporation of these results into the risk assessment method in the design phase of stream restoration projects can be important to decision making and will improve the likelihood of success with a stream restoration project.

Literature Review:

In the risk assessment method presented above, failure probabilities of design components are highly uncertain. To improve the risk assessment method for wide-spread use, it is proposed here that LRA and MCS techniques be used to develop improved estimates of failure probability and risk. Currently, the probability of failure for design components and the expected failure costs are estimated based on engineering judgment, experience with similar projects, and the review of literature (Brown 2000).

To supplement this data, a literature search of more current material was completed to compile component information used to develop a data survey. The component information gathered includes commonly used components within stream restoration (e.g., cross sectional geometry), typical failure modes of these components (e.g., excessive degradation) as well as all traditional design methods (i.e., detection methods) for each component (e.g., incipient motion analysis). The survey results were used to run the LRA and MCS techniques to better understand failure probabilities.

Stream Failure Data Survey:

The survey created was in an excel spreadsheet that was sent out to numerous agencies to obtain stream failure data, as seen in Figure 1.

	#	Component	Component Failure	Failure Mode	Design Method (Direct/Indirect)	Design Detection Method
9						
10	1	Boulder Placement	Yes	Unintended movement/dislocation	Direct	Boulder diameter 2'-5' (no more than 1/8 of stream width)
		Boulder Placement Brush Layering Brush Mattresses Cross Sectional Geometry Construction Cross Vanes Culvert Baffles Gabions Imbricated Riprap			Indirect	Shear Stress
12	1				Direct	Boulder volume 35-70 cubic feet
13	2	Brush Mattresses	Yes	Other	Direct	Live branches are cut from fresh, green, healthy, dormant parent plants that are adapted to site conditions
14	2				Direct	Wood branches 5'-10' length
15	3	OTHER	Yes	Describe in Other Values	Indirect	Judgement/Experience

Design Detection Method	Predictor Variables List	Known Predictor Variables Values	Other Values
Boulder diameter 2'-5' (no more than 1/8 of stream width)	*Boulder diameter*	Diameter = 6'	
Shear Stress	*Shear Stress, Critical Shear Stress, Hydraulic Radius, Channel Slope, Particle Size, Reynolds Number, Dimensionless Stress, Shields Parameter*	Shear Stress = …, Critical Shear Stress = …, etc.	Particle Size is unknown, etc.
Boulder volume 35-70 cubic feet	*Boulder volume*	Boulder Volume = …	
Live branches are cut from fresh, green, healthy, dormant parent plants that are adapted to site conditions	*Live branch material*	Branch Material = …	Failure Mode = …
Wood branches 5'-10' length	*Branch length*	Branch Length = …	
Judgement/Experience	*Please describe methodology and known data*		Component = …, Failure Mode = …, Methodology = …, etc

Figure 1. Example Survey Results

First, the user would fill out general stream information, such as if the stream failed to meet its design objectives and if so then how. This general stream information is above the cells depicted in Figure 1. Then the user would select the stream component from a list of common components utilized within stream restoration projects, such as "Boulder Placement" as seen in the first component row of Figure 1. Next, the user would select "Yes" if the component failed and "No" if it did not. This forces the user to decide upon component failure and prevents the grey area associated with varying engineers' opinions. The user would then select the failure mode associated with the selected component, such as "Unintended movement/dislocation." Following this it would be necessary to select the first design method, either "Direct" or "Indirect." Here "Direct" refers to design of a stream component by state guidelines for materials and installation and "Indirect" refers to design of a stream component by calculating its affect on the stream as a whole. The final selection by the user is the first design detection method from a list associated with the component and design method already chosen. From this selected information the spreadsheet fills the following cell with a list of predictor variables associated with the chosen design detection method. If the user selected the same information as that in the first component row in Figure 1, the predictor variable list would output "Boulder Diameter." The user would then fill in the following cell with the known predictor variable values, in this case the actual boulder's diameter. There is also an Other Values column for any additional data the user may have.

The survey was a simple to use tool that allowed the user to select component information from a series of drop boxes and fill out unique information in allocated cells. This survey provided the component and predictor variable information necessary to run the numerical methods.

Logistic Regression Analysis (LRA):

LRA is a model used to predict the probability of occurrence of an event by fitting data to a logistic curve. In this model the input data is a set of independent variables, often called covariates, that are continuous, discrete, and/or dichotomous (1 or 0) and the result is categorical and dichotomous (Hosmer and Lemeshow 2004).

LRA is used extensively in the medical sciences, social sciences and in marketing applications. For example, LRA could be used to predict a customer's inclination to purchase a product or if an adult will have a heart attack within a specified time period. To develop the predicting function a set of covariates are required. In the examples given the covariates could consist of the customer's purchase habits or the adult's body mass index. In the case of stream restoration the covariates would consist of the predictor variables associated with each component.

Monte Carlo Simulation (MCS):

MCS is a method for iteratively evaluating a deterministic model using sets of random numbers as inputs. This method is often used when the model is complex, nonlinear, or involves uncertain parameters (Ayyub and McCuen 2003).

MCS has been useful for modeling phenomena having significant uncertainty associated with their inputs and for studying systems with a large number of coupled degrees of freedom. Specifically, MCS has been used in the physical sciences, visual design, finance, mathematics, and for solving "What If" scenarios.

Results:

The results of the literature review and survey will consist of a list of stream failure data. Most importantly stream restoration component details, whether or not the component failed, and if the stream as whole did not meet the design objectives. This data is necessary to perform the LRA and MCS.

One additional goal of the survey is to collect data for later use. Such data includes the failure mode of each component. This can be used to judge whether or not a component's failure caused the stream as whole to not meet its design objectives. Similarly the detection method (Direct or Indirect) can be later used to judge if a component's failure could have been prevented. This is valuable information that can lead to a better understanding of stream restoration design.

Future Work:

For this project, LRA will incorporate the results of the literature review and survey to develop a function that models the probability of failure of each component. The covariates for each component's function are a set of predictor variables. The result will be a binary definition of component success or failure.

From the component function generated by the LRA we can develop distributions for each predictor variable. The distributions will give insight into how sensitive component success is to each predictor variable. Furthermore, once the functions are generated for all common components the functions can be combined into a tool that calculates risk in Equation (1), where p_i is determined by the function for component i and the predictor variable values are input by the user.

For this project, MCS will incorporate the results of the literature review and survey to perform uncertainty propagation for each component's predictor variables. The final MCS results will be evaluated using a histogram to visualize the uncertainty in the calculated risk. The mean, median, and standard deviation will also be evaluated to best describe the distribution and results. This provides improved quantitative estimates of risk for a given design configuration.

Previously MCS has been incorporated within stream restoration as a method to perform sensitivity analyses for the Goulburn River in Australia (Grayson et al. 2005). The sensitivity analyses were conducted to identify key variables for predicting bank

erosion rates using a particular bank erosion model. Similarly, MCS can be conducted to determine the predictor variables for stream restoration.

Summary:

The ultimate goal of this project is to develop a tool that incorporates the results of the LRA and MCS analysis in the determination of the risk using Equation (1). This tool will improve upon the current DFMEA method which utilizes engineering experience to determine the probability of component failure. Here the probability of component failure will be determined through the function developed in the LRA and inputs given by the user. The desired inputs will be chosen based on the results of the LRA and MCS.

This tool will reduce the uncertainty that is inherent to the stream restoration design process. It will provide practitioners with a straight forward way to predict the failure of stream restoration design components and through this whether or not the stream itself will meet the design objectives. Furthermore, the data collected in this project will advance the stream restoration community's understanding of stream failure. Additionally, this data can prove useful beyond the scope of this project. The data can later be used to better understand the consequence of failure associated with each component failure.

References:

American Nuclear Society, 1983. *Probabilistic Risk Assessment Guide: A Guide to the Performance of Probabilistic Risk Assessments for Nuclear Power Plants*. NUREG/CR 2300, Vol. 1, Office of Nuclear Regulatory Research, U.S. Nuclear Regulatory Commission, Washington, D.C.

Ayyub, B.M., and McCuen, R.H. (2003). *Probability, statistics, and reliability for engineers and scientists, 2nd edition.* Chapman and Hall/CRC, New York.

Brown, K. (2000). "Urban stream restoration practices: an initial assessment." The Center for Watershed Protection, Elliot City, Maryland, <http://www.cwp.org.> (accessed Feb. 4, 2005).

Dushinisky, K. and S. G. Vick, 1996. "Evaluating Risk to the Environment From Mining Using Failure Modes and Effects Analysis." *In:* Uncertainty in the Geologic Environment: From Theory to Practice. *Proceeding of Uncertainty* 1996, July 31-August 3, pp. 848-865

Fullwood, R. and R. Hall, 1988. *Probabilistic Risk Assessment in the Nuclear Power Industry*. Pergamon Press, Oxford, United Kingdom.

Grayson, R. B., I. D. Rutherford, S. Jha, A. W. Western, 2005. *Testing Uncertainty in a Model of Stream Bank Erosion,* in Zerger, A. and R.M. Argent (EDs) MODSIM 2005 International Congress on Modelling and Simulation Society of Australia and New Zealand, 2714-2720

Henley, E. and H. Kumamoto, 1992. *Probabilistic Risk Assessment – Reliability Engineering, Design, and Analysis*. Institute of Electrical and Electronics Engineers, IEEE Press, New York, New York.

Hosmer, D. and S. Lemeshow, 2004. *Applied Logistic Regression: Textbook and Solutions Manual*. Wiley-IEEE.

Johnson, P.A., and Brown, E. (2001). "Incorporating uncertainty in the design of stream channel modifications." *Journal of the American Water Resources Association*, 37(5), 1225-1236.

Kmenta, S., and Ishii, K. (2000). "Scenario-based FMEA: a life cycle cost perspective." *Proceedings*, American Society of Mechanical Engineers, 2000 Design Engineering Technical Conference, Baltimore, Maryland.

Kondolf, G.M. (1998). "Lessons learned from river restoration projects in California." *Aquatic Conservation: Marine and Freshwater Ecosystems* 8, 39-52.

McCollin, C., 1999. "Working Around Failure". *Manufacturing Engineering* 78(1), 37-40.

McCormick, C., 1981. *Reliability and Risk Analysis.* Academic Press, Orlando, Florida.

Niezgoda, S.L., and Johnson, P.A. (2007). "Case study in cost-based risk assessment for selecting a stream restoration design method for a channel relocation project." *ASCE, Journal of Hydraulic Engineering*, 133(5), 468-481.

Rosgen, D.L. (1996). *Applied river morphology.* Wildland Hydrology, Fort Collins, Colorado.

Shimizu, S., M. Sugawara, S. Sakurai, T. Mori, and K. Saikawa 1993. "Decision-Making Support Systems for Reliability-Centered Maintenance." *Journal of Nuclear Science and Technology*, 30(6), 505-515

Bedload Composition and Development of 2D Stream Sediment Model for Stream Restoration Design Applications in Urbanizing Watersheds

William R. Cantrell, E.I.[1]; John S. Schwartz Ph.D, P.E[2], and William K. Barry, P.E., D. WRE[3]

[1,2] Graduate Student, Assistant Professor; University of Tennessee, Department of Civil and Environmental Engineering, Knoxville, TN 37996-2010; PH (865) 974-7721; wcantrell@utk.edu, jschwart@utk.edu.

[3] Senior Engineer; S&ME, Inc., 1413 Topside Road, Louisville, TN 37777; PH (865) 970-0003; kbarry@smeinc.com

Abstract:

A central problem in the field of stream restoration is that of designing a stable channel that supports a healthy benthic population. Many stream restoration projects take place in urban or urbanizing watersheds. The relationship between changing watershed characteristics and local channel conditions within that watershed is poorly understood. This study is made up of two major components that address aspects of this problem: first, a physical study of bedload flux in watersheds representing rural, urban, and developing conditions and second, verification of results from the Computational Hydraulic Engineering Two-Dimensional Sediment Model (CCHE2D) on the reach scale and correlation of CCHE2D results with Rapid Bioassessment Protocol III (RBP III) scores. Study sites were selected in Knox County, Tennessee including twelve sites for the bedload study and a single site for the CCHE2D model verification. The bedload flux portion of the study combines field collection of bedload via portable bedload traps and an estimate of energy slope from peak stage recorders. Information derived from the field collection will be combined with watershed data via geographic information system (GIS) analysis. Watershed metrics including percent impervious area, roadways adjacent to streams, and average watershed slope determined via GIS will be correlated with the measured bedload composition for each research site. The CCHE2D model verification will combine the study of bedload flux with a previous study correlating the surficial bed material composition with macroinvertebrate biotic integrity scores (RPB III) for 76 reaches in East Tennessee. The combination of this information will provide a valuable tool in stream restoration design in allowing practitioners to have an empirical metric with which to design/predict channel substrate composition as an indicator of physical habitat quality.

Introduction:

Urbanization and Hydrology:
Urbanization in a watershed begins a chain reaction of effects in the water resources of that watershed (Bledsoe and Watson, 2001; Booth and Jackson, 1997; Walsh et al., 2005). Hydrologic changes lead to changes in sediment flux which lead to changes in form and function of the streams from both a biological and structural perspective. As infiltration and storage capacities are altered due to construction activities including clearing and grubbing, paving, and building construction; hydrograph values and shapes change, with peaks and durations increasing. Delivery paths to the streams are concurrently altered by use of stormwater collection and distribution infrastructure which delivers high volumes to the stream with a low time of concentration. USGS Flood Regression Equations suggest that the Q2 of Tennessee watersheds increase by a factor of

1.9 at 10% impervious surface in the watershed and by a factor of 2.5 at 20% impervious over values from watersheds with no impervious surface. Percentage of impervious surface is commonly used to quantify urbanization due to the availability of USGS raster files produced by spectral analysis techniques (Arnold and Gibbons, 1993).

Stream Restoration in Urban Environments:
Goals of stream restoration in urban areas include geomorphic stabilization and reestablishment of biotic integrity while leaving established infrastructure intact. Input from stakeholders in the community along with engineering and scientific perspectives must be balanced in a way that is acceptable to all parties in order to be fully and successfully implemented (Rhoads et al., 1999). As new information on the effects of urbanization is compiled, a more complete understanding of natural versus anthropogenic influence is developed. A better understanding of the interaction between these two classes of influence on streams allows for incorporation of natural processes in stream restoration practice.

Urbanization's Effects on Channel Stability:
Hydrologic and sediment changes both in turn affect channel stability. Higher flow rates with lower upstream sediment loads tend to lead to channel widening, incision, or a combination of the two. Incision can increase transport of fine sediment downstream through both erosion and by isolating the channel from its floodplain. Separate from hydrologic changes, other effects on the channel are felt. Riparian areas are often removed during urbanization activities, removing a valuable habitat resource as well as a sediment filtering feature (Hook, 2003). Bank armoring due to close proximity construction or stormwater collection features can cause down-cutting or widening of the channel as new hydraulic forces are developed in a reach. Simon (1995) identified six stages of channel evolution in a disturbed watershed; the primary features of the post-disturbance channel being downcutting and widening. As channel area has been sufficiently increased, aggradation takes place, leading to restabilization.

Urbanization's Effects on Sediment Supply:
Three significant stages of sediment availability are noted in the typical shift from non-urban to an urbanized watershed: the undisturbed condition, for which the stream is assumed to be in regime; the construction phase, which can lead to sediment loads up to 100,000 tons/sq.mi/year; and finally the urbanized phase, where many previous sediment sources have been altered or removed completely (Wolman, 1967). Efforts to mitigate the effects of the construction phase have improved over the years with the development of Best Management Practices (BMPs) for construction work. New sources of sediment are also introduced including slope instability and roadway erosion. Coarse substrate can be stripped due to higher flows but may not be replenished due to sealing of upland sediment sources (Nelson and Booth, 2004). Fining of bed sediment toward sand due to changes in sediment sources has been noted in urbanized portions of watersheds (Simon et al., 2004). Sampling of bedload in non-urban, urbanizing, and urban watersheds to determine effects on bedload composition is not extensive at this point.

Project Objectives:
This study intends to address a central problem in the discipline of stream restoration: that of designing a stable channel that adequately supports biological activity. Bedload composition of various watersheds will be analyzed to determine the effects of urbanization on bedload supply, combining this information with previous regional research linking fine sediment substrate with Rapid Bioassessment Protocol III (RBP III) scores. This will provide a powerful design tool that relates the primary concern of regulators (improving biological conditions in the stream) with a critical design component that is currently addressed only by semi-quantitative or qualitative methods.

Study Design:
This study is made up of two major components: First, an analysis of bedload composition in rural, urbanizing, and urban watersheds in the Knox County, TN area to determine if significant bedload is present in these systems and if so to determine if impervious surfaces have an effect on the composition. Geographic Information System (GIS) analysis of the watersheds is used to quantify these characteristics of the research watersheds. Watersheds were chosen to represent various percentages of impervious area, which is a surrogate for urbanization in this study. Figure 1 is an overview map of the research watersheds.

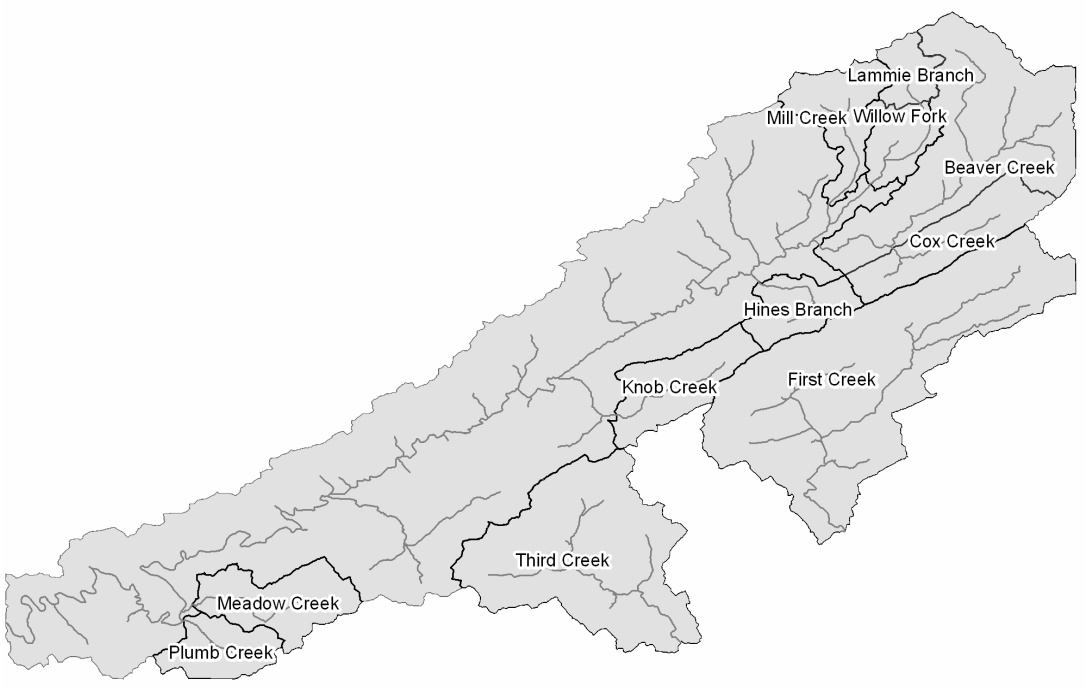

Figure 1. Map of Research Sites

Secondly, verification of results of the CCHE2D sediment model on a short, hydraulically simple reach that is typical of potential stream restoration sites in the area. The model output will be combined with previous research in the area by Williams (2005) which analyzed the relationship between channel stability/bed material and Rapid Bioassessment Protocol III (RBPIII) scores. Boundary conditions developed from one storm event will be used to generate the simulation. Previous attempts to use this model

to predict bed composition (Johnson, 2008) were hampered by insufficiently dense sediment rating curve information, so monitoring will continue throughout the runoff event.

Methods:

Selection of Research Sites:
Bedload sampling sites were selected in a limited geographic/geologic area in an effort to limit extensive differences in sediment yield due to variation in geologic processes. Nine of the research watersheds are subwatersheds of Beaver Creek in Knox County, Tennessee. The other two watersheds are adjacent to the Beaver Creek watershed. Beaver Creek is a high priority watershed in the area and is the focus of hydrologic remediation activities by the Knox County government and has an active watershed association. Watershed size was not a consideration due to the prevalence of moderate urbanization at any appreciable downstream distance in any area with basin sizes ranging from just over 1 mi^2 to almost 12 mi^2. GIS analysis of watersheds above sampling sites provided the primary variable of percent impervious surface, along with two additional secondary variables: average watershed slope and length of roadways within 50 ft of the stream. Table 1 shows the watersheds chosen, total area, and percent impervious surface.

Table 1. Percent Impervious in Research Watersheds

	Total Area (ac)	Percent Impervious
Third Creek	7541.2	27.3
Hines Branch	1408.9	20.9
Plumb Creek	1481.8	18.4
First Creek	11950.8	17.7
Knob Fork	2163.5	14.9
Meadow Branch	2278.4	12.1
Cox Creek	2363.8	5.5
Beaver Creek	9597.0	5.4
Mill Branch	1985.3	3.0
Willow Fork	2098.1	1.3
Lammie Branch	842.0	1.2

Bedload Sampling Method:
Temporary bedload sampling devices with capacity to sample during the duration of the flow event were modeled after a combination of Bunte's (2004) bedload traps and the Helley-Smith (1971) bedload sampler. The final design consisted of 5/16" x 3 ½" aluminum bar stock frame with an opening measuring 3" x 12"; an interior sampling net with openings sized .05"; and an exterior reinforcing net. Figure 3 shows the assembled sampling device. Before a predicted storm event, the samplers were secured to the bed in a riffle area of each sampled research reach using #8 rebar driven into the bed. After the peak stage has decreased by at least half, the samplers are removed and returned to the laboratory. Organic material is removed from the collected sample and the remaining soil particles are initially dried. Smaller organic debris is then burned in an ignition oven and

a dry sieve is performed, providing the information to develop a particle size distribution (p.s.d.).



Figure 2. Assembled Bedload Sampler

Data Processing:
In order to determine possible correlations with indicator variables, a matrix of watershed properties will be produced. GIS produced watershed metrics, stream order values, d_{85}, d_{50}, and d_{35} particle size values will be included. Multiple linear regression techniques will be applied to this data in order to assess any trends present. Peak stage recorders were placed upstream and downstream at each site. These will be used to generate an approximate energy slope at peak flow for the reaches. As a sanity check, bed shear will be checked against pebble count sizes to determine the presence of any non-mobile bed material. Peak stage will also be used to classify flow events as a percent of bankfull stage.

Modeling:
The Willow Fork site was chosen as the one to be modeled in CCHE2D. A topographic survey of the channel and immediate flood plain was performed using a total station and prism. Mesh generation, hydraulic simulation, and sediment simulation will be performed in the National Center for Computational Hydroscience and Engineering's CCHE2D two dimensional sediment model. Sediment rating curve and current bed composition information will be gathered in the field. Hydrograph information will be recorded at the upstream and downstream boundaries with Global Water stage recorders. If sufficient data is not recorded for a successful modeling run, a sensitivity analysis will be performed on the reach to determine threshold conditions for degradation and aggradation, particularly of fine sediment. These threshold values of bed composition will be determined through the work of Williams (2005), in which channel stability and bed composition were correlated with EPA RBPIII scores. In this way, the biological connection will be made.

Preliminary Results:

Eleven bedload samples have been collected from six sites as of January 2009. A map of the research watersheds is included as Figure 1. The particle size distribution summary and percent impervious in the watershed are included in Table 2. Figure 3 shows a flooded research site with the peak stage recorder near the lower left corner. Consistent values have been obtained in the 3rd Creek and Beaver Creek watersheds only. Figure 3 shows this research site at flood stage with the peak stage recorder near the lower left corner. Other sites have either had p.s.d. values that are not stable over the first two measurements or have only one or no samples. It is expected that d_{85} values will drop with an increase in impervious area, with d_{50} and d_{35} values remaining consistent or decreasing. Large amounts of organic debris and small samples of present biota have been noted in the samples that have been processed. Insufficient data has been collected for statistical analysis at this time.

Table 2. Particle Size Summary

Site Location	Storm Date	d_{85} (mm)	d_{50} (mm)	d_{35} (mm)
3rd Creek	11/14/2008	2.32	0.81	0.66
3rd Creek	12/10/2008	2.24	0.59	0.40
3rd Creek	1/7/2009	2.60	0.53	0.41
Beaver Creek	12/10/2008	1.14	0.58	0.38
Beaver Creek	1/7/2009	1.10	0.70	0.51
Willow Fork	12/10/2008	1.70	0.42	0.30
Willow Fork	1/7/2009	0.91	0.43	0.35
Lammie Branch	1/7/2009	>9.75	0.65	0.29
Cox Creek	12/10/2008		9.36	3.55
Cox Creek	1/7/2009	1.52	0.51	0.28
Hines Branch	1/7/2009	1.55	0.31	0.18



Figure 3. Third Creek Research Site at Flood Stage

Sediment sampling is ongoing and with sufficient storm events will reach 2-3 values for each site. Any anomalies noted in nested watersheds will be followed up by field investigation with a goal of identifying impoundments, active construction, and other disturbances such as cattle crossings. As the research draws to a close, a relationship between impervious area and bedload composition will be developed as well as a valuable modeling tool for stream restoration practitioners. Developments such as this are hoped to develop stream restoration as an activity integrating both geomorphological and biological perspectives.

Acknowledgements:

I would like to thank both the University of Tennessee, Knoxville and S&ME, Inc. for their continued financial support for this research. Dr. John Schwartz and Ken Barry have been instrumental in defining the research priorities and providing insight into the problems at hand. Construction of the bedload traps would not have been possible without the help of Larry Roberts and Ken Thomas in the Civil and Environmental Engineering Department Shop. Laura DeVilbiss, Andy Dodson, Michael Hamrick, and Daniel Johnson have provided indispensable help with field work, technical advice, or both.

References:

Arnold Jr., Chester L. and James C. Gibbons. (1996) Impervious Surface Coverage. Journal of the American Planning Association. 62:2,

Bledsoe, Brian P. and Chester C. Watson. (2001) Effects of Urbanization on Channel Instability. Journal of the American Water Resources Association. 37:2, 255-270.

Booth, DB and Jackson, CR. (2007) Urbanization of Aquatic Systems – Degradation Thresholds, Stormwater Detection, and the Limits of Mitigation. Journal of the American Water Resources Association, 33. 1077-1090

Bunte, Kristen; Steven R. Abt; John P. Potyondy; and Sandra E. Ryan. (2004) Measurement of Coarse Gravel and Cobble Transport Using Portable Bedload Traps. Journal of Hydraulic Engineering. 130:9, 879-893.

Hook, P.B. (2003) Sediment Retention in Rangeland Riparian Buffers. Journal of Environmental Quality. 32:2, 1130-1137.

Johnson, Daniel. (2008) The Application of a Two-Dimensional Sediment Transport Model in a Cumberland Plateau Mountainous Stream Reach with Complex Morphology and Coarse Substrate.

Nelson, Erin J., Booth, Derek B. (2002) Sediment Sources in an Urbanizing, Mixed Land-Use Watershed. Journal of Hydrology. 264, 52-68.

Rhoads, B.L., D. Wilson, M. Urban, and E.E. Herricks. (1999) Ineraction Between Scientists and Nonscientists in Community-Based Watershed Mangagement: Emergence of the Concept of Stream Naturalization. Environmental Management. 24:3, 297-308.

Simon, A. (1995) Adjustment and Recovery of Unstable Alluvial Cahnnels: Identification and Approaches for Engineering Management. Earth Surface Processes and Landforms. 20. 611-628.

Simon, A., Langendoen, E.J., Bingner, R.L., Wells, R., Yuan, Y. and Alonso, C.V. (2004) Suspended-Sediment Transport and Bed-Material Characteristics of Shades Creek, Alabama and Ecoregion 67: Developing Water-Quality Criteria for Suspended and Bed-Material Sediment. *National Sedimentation Laboratory Report No. 43*, 150 p.

Walsh, C.J.; Roy, A.H.; Feminella, J.W.; Cottingham, P.D.; Groffman, P.M.; Morgan, R.P. (2005) The Urban Stream Syndrome: Current Knowledge and the Search for a Cure. Journal of the North American Benthological Society. 24:3. 706-723.

Williams, Kelly. (2005) Linking Channel Stability and Bed Sediment Characteristics to Biological Integrity in Tennessee Ridge and Valley Streams.

Wolman, M. Gordon. (1967) A Cycle of Sedimentation and Erosion in Urban River Channels. Geografiska Annaler. Series A, Physical Geography. 49:2/4. 385-395.

Two-dimensional BOD and DO water quality model for engineering applications: the case of Bubbly Creek in Chicago, Illinois

Davide Motta[1], Jorge D. Abad[1], Xiaofeng Liu[1], Marcelo H. García[1]

[1] Research Assistant, Dept. of Civil and Environmental Engineering, University of Illinois, Urbana, IL 61801, USA. E-mail: dmotta2@illinois.edu
[2] Post-doctoral Research Associate, Dept. of Civil and Environmental Engineering, University of Illinois, Urbana, Illinois 61801, USA. E-mail: abad@illinois.edu
[3] Post-doctoral Research Associate, Dept. of Civil and Environmental Engineering, University of Illinois, Urbana, Illinois 61801, USA. E-mail: liu19@illinois.edu
[4] Professor and Director of the Ven Te Chow Hydrosystems Lab., Dept. of Civil and Environmental Engineering, University of Illinois, Urbana, IL 61801, USA. E-mail: mhgarcia@illinois.edu

ABSTRACT

Bubbly Creek was historically used as a drainage channel for the waste resulting from Chicago's stockyards. Nowadays there is flow in the creek only during rainfall events resulting in Combined Sewer Overflows (CSO) and water quality is a very important issue, particularly during the summer months, when the dissolved oxygen levels are extremely low and sediment oxygen demand is expected to be large.

Due to the particular flow regimes of the creek and the conditions of the benthic sediments in the bed, a special BOD-DO (Biochemical Oxygen Demand - Dissolved Oxygen) water quality module was developed and implemented into the two-dimensional depth-averaged numerical model STREMR-HySedWq. The approach illustrated represents a substantial improvement to the state-of-the-art of water quality modeling methodologies.

The model was able to capture the key processes and provide useful preliminary results for the two following scenarios: [1] CSO events, for which the model was coupled to a one-dimensional cross-section-averaged BOD-DO water quality model, and [2] potential "purification" solutions, such as flow augmentation and supplemental aeration, with the goal of increasing the DO levels in the creek during dry weather periods.

DESCRIPTION OF BUBBLY CREEK

Bubbly Creek, located South-West of Chicago (Figure 1), is the South Fork of the South Branch of the Chicago River and has a length of approximately 2000 meters, a mean width of about 44 meters (varying between 23 and 61 m) and a mean water depth of 2.2 m (ranging from 1.2 to 3.6 m). The mean channel bottom slope is about 0.0013. From 1865 to 1939, Bubbly Creek was used as a drainage channel for the waste resulting from Chicago's stockyards (Hill, 2000). Today, this historically industrial area is being transformed into a residential development, with strip malls and residences, and therefore there is a revived interest in Bubbly Creek.

Four different regimes characterize Bubbly Creek: [1] during dry periods, the water in the creek is essentially stagnant; [2] with light rainfall events, there are no noticeable changes, since the combined sewage conveyed from the 36 square miles service area to the Racine Avenue Pumping Station (RAPS, Figure 1) is pumped to the Stickney Water Reclamation Plant of the Metropolitan Water Reclamation District of Greater Chicago (MWRDGC) and not discharged into the creek; [3] during heavy storms, the RAPS discharges Combined Sewer Overflow (CSO) into the creek, so that there is a northward flow in Bubbly Creek which finally discharges into the South Branch of the Chicago River; [4] for excessively heavy storms, several CSO outfalls located along the channel (Figure 1) may discharge into the creek depending on the intensity of the rainfall event.

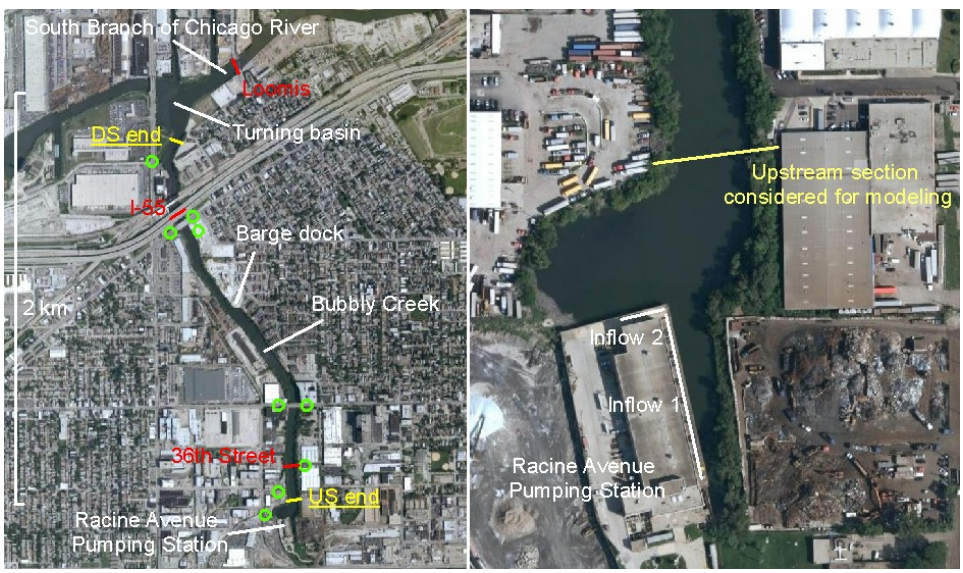

Figure 1. Aerial view of Bubbly Creek (left) and detail of the Racine Avenue Pumping Station (right). Circles denote outfalls along the banks.

MODELING SCENARIOS

As part of a larger study of Chicago's waterways, the water quality dynamics in Bubbly Creek was modeled for two scenarios: CSO events (indicated above as regime [3]) and potential "purification" solutions, such as flow augmentation and supplemental aeration, to increase the Dissolved Oxygen (DO) levels in the creek during dry weather periods, which are particularly low during the summer months due to the presence of oxygen demanding sediments along the bottom of the creek.

Density currents in Bubbly Creek caused by CSO events and the upstream intrusion of denser flow both upstream and downstream of the South Branch of the Chicago River have been observed and modeled by Liu *et al.* (2009).

CSO SCENARIO

Characteristics. During a CSO event, resuspension of the organic sediments can occur, with a consequent additional oxygen demand in the water column, which

cannot be modeled as benthic oxygen demand from the bed (Briskin *et al.*, 2002). A theoretical and quantitative approach for the evaluation of the transport of organic matter across the bed/water interface was therefore derived and implemented numerically, by coupling hydrodynamics, sediment transport and water quality.

Notice that a CSO event is an intermittent discharge scenario. As mentioned, when water is flowing in the creek ("Phase 1"), sediment resuspension can occur. For the following phase, characterized by quiescent flow ("Phase 2"), the situation reduces to a dispersion-reaction problem. This is evident from the observation of the biggest CSO event in the period 2005-2007, which occurred on September 13, 2006, and was characterized by a measured CSO volume of 505.84 MG, overflow lasting 7.66 hours and producing a mean flow rate of 69.4 m^3/s (Figure 2).

From Figure 2 it can be observed that: [1] once the CSO event starts the DO concentration increases at both monitoring stations at 36th Street and Interstate Highway I-55 (whose location is indicated in Figure 1). As shown by the numerical modeling presented below, this increase is mainly due to high DO content of the CSO input, while reaeration of the flow plays a minor role; [2] once the CSO discharge ends, an increased oxygen demand, due to the Biochemical Oxygen Demand (BOD) input and/or BOD resuspension from the bed associated to the CSO flow, causes DO depletion; [3] this depletion is recovered relatively quickly at the I-55 Station, which is closer to the South Branch of the Chicago River, whereas it is observed to persist for days in the case of the 36th Street Station, far from the South Branch.

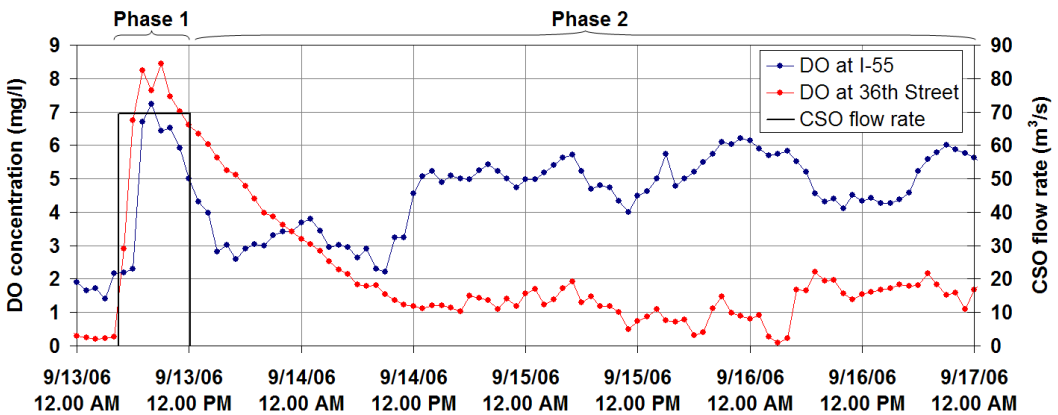

Figure 2. Dissolved Oxygen (DO) concentration measured at the 36th Street and I-55 monitoring stations and input hydrograph at the Racine Avenue Pumping Station (RAPS) for the CSO event on September 13, 2006.

Modeling. "Phase 1", with the RAPS discharge flowing into the creek was modeled with the code STREMR-HySedWq, which is able to handle the bed/water exchange of organic matter and whose two-dimensional nature allows for accounting of the cross-sectional variation of the shear stress and BOD resuspension and settling. "Phase 2", when water in Bubbly Creek is quiescent again, was modeled with a one-dimensional, area-averaged, dispersion-reaction model.

Two-dimensional depth-averaged STREMR-HySedWq model for "Phase 1". Bernard (1993) developed a two-dimensional depth-averaged hydrodynamic model called

STREMR. It includes a k-ε turbulence model and a correction due to secondary flow, and it imposes a rigid lid approximation for the free surface which requires the specification of the water surface elevation. For the case of flows in Bubbly Creek, the rigid-lid assumption was verified to be adequate (Motta *et al.*, 2007). Abad *et al.* (2008) incorporated a sediment transport module (bedload and suspended sediment for multiple size classes) and the model was renamed STREMR-HySed. The original assumption of fixed bottom elevation was relaxed according to the Exner formulation, while maintaining the water surface elevation constant.

The water quality module implemented in the new version STREMR-HySedWq considers the oxygen balance. It solves the depth-averaged mass balance equations for the concentration of Biochemical Oxygen Demand (C_{BOD} in mg/l) and Dissolved Oxygen (C_{DO} in mg/l), which consider the net rate of production S, in terms of concentration/time, properly defined for BOD and DO. The kinetic processes involving the BOD are oxidation and bed/water exchange

$$S_{BOD} = -K_D \Theta_D^{(T-20)} \left(\frac{C_{DO}}{K_{BOD} + C_{DO}} \right) C_{BOD} + Bed\ /\ water\ exchange \qquad (1)$$

where K_D is the oxidation coefficient at 20 °C, Θ_D is the temperature coefficient for oxidation, T is the water temperature in °C and K_{BOD} is the half saturation constant for the BOD oxidation.

The source/sink terms involving the DO are reaeration, oxidation, bed sediment oxygen demand and any localized DO input (e.g. supplemental aeration)

$$S_{DO} = K_a \Theta_a^{(T-20)} \left(C_s - C_{DO} \right) - K_D \Theta_D^{(T-20)} \left(\frac{C_{DO}}{K_{BOD} + C_{DO}} \right) C_{BOD} - \frac{SOD}{H} \Theta_s^{(T-20)} + W_{DO} \qquad (2)$$

where K_a is the reaeration coefficient, Θ_a is the temperature coefficient for reaeration, C_s is the dissolved oxygen concentration at saturation, SOD is the bed sediment oxygen demand per unit area and time, H is the water depth and Θ_s is the temperature coefficient for the bed sediment oxygen demand.

As regards the bed/water exchange in equation (1), extensively illustrated by Motta (2008), the bed is divided into top and lower layers (Figure 3). The thickness of the top layer is considered to be constant in time at each location. BOD can be present, both in the water column and in the bed top layer, as dissolved constituent or attached to sediments (Figure 3). The dissolved (subscript "d") BOD concentrations in the water column $C_{BOD,w,d}$ (subscript "w") and in the top layer pore water $C_{BOD,b,d}$ (subscript "b") are expressed as

$$C_{BOD,w,d} = f_{w,d} C_{BOD,w} \quad , \quad C_{BOD,b,d} = f_{b,d} \frac{C_{BOD,b}}{n} \qquad (3a,b)$$

where $C_{BOD,w}$ is the BOD total concentration in the water column (indicated so far as C_{BOD}), $C_{BOD,b}$ is the BOD total concentration in the sediment top layer, $f_{w,d}$ and $f_{b,d}$ are the dissolved fractions (between 0 and 1) in the water column and sediment

bed top layer respectively (assumed as constant) and n is the bed porosity. The BOD concentrations attached to the particles (subscript "p") in the water column, $C_{BOD,w,p}$, and in the bed top layer, $C_{BOD,b,p}$, are expressed as

$$C_{BOD,w,p} = (1 - f_{w,d}) C_{BOD,w} \quad , \quad C_{BOD,b,p} = (1 - f_{b,d}) C_{BOD,b} \tag{4a,b}$$

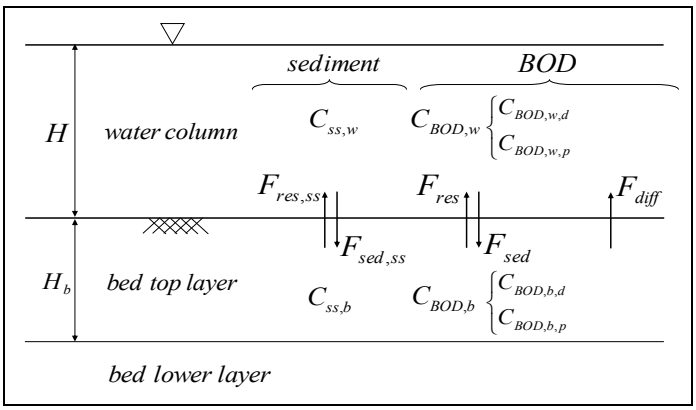

Figure 3. Sediment (SS) and Biochemical Oxygen Demand (BOD) concentrations in the water column and in the bed top layer with fluxes across them.

The total exchange of BOD between the bed and the water column in the equation (1) is given by the algebraic sum of three fluxes in the vertical direction (Figure 3): sedimentation flux F_{sed}, resuspension flux F_{res} and diffusive exchange flux F_{diff}. The sedimentation flux F_{sed} is given by the sum of the settling of BOD attached to the sediments and the inclusion of pore water due to the bed aggradation caused by sedimentation of suspended sediments:

$$F_{sed} = v_s (1 - n) \frac{C_{BOD,w,p}}{C_{ss,w}} + v_s n C_{BOD,w,d} \tag{5}$$

$C_{ss,w}$ is the suspended sediment concentration in the water column (Figure 3) and v_s is the sedimentation rate. The resuspension flux F_{res} is given by the sum of the resuspension of BOD attached to the sediments in the bed and the release of pore water due to the bed erosion caused by sediment resuspension:

$$F_{res} = v_r (1 - n) \frac{C_{BOD,b,p}}{C_{ss,b}} + v_r n C_{BOD,b,d} \tag{6}$$

v_r is the erosion rate. The diffusive exchange flux F_{diff} is proportional to the difference between the concentration in the bed interstitial water, $C_{BOD,b,d}$, and in the water column, $C_{BOD,w,d}$, with E_{diff} indicating the BOD diffusion coefficient and H_b the thickness of the bed top layer:

$$F_{diff} = \frac{E_{diff}}{H_b}\left(C_{BOD,b,d} - C_{BOD,w,d}\right) \tag{7}$$

The sedimentation and erosion rates v_s and v_r refer respectively to the sedimentation (deposition) of sediments $F_{sed,ss}$, which depends on the sediment concentration in the water column, and the resuspension (entrainment) of sediments $F_{res,ss}$, which is related to the bottom shear stress exerted by the flow (Figure 3):

$$v_s = \frac{F_{sed,ss}}{(1-n)} = \frac{F_{sed,ss}}{C_{ss,b}} \quad , \quad v_r = \frac{F_{res,ss}}{(1-n)} = \frac{F_{res,ss}}{C_{ss,b}} \tag{8a,b}$$

$C_{ss,b}$ is the sediment volume concentration in the bed (m_{ss}^3/m^3). The deposition rate v_s is proportional to the sediment settling velocity and the sediment volume concentration at the bed/water interface (Abad *et al.*, 2008). The erosion rate v_r can be calculated, in absence of an *in situ* relation, with one of the formulations presented in literature for non cohesive sediments, once sediment size and density are known. For this study, the formula by Smith and McLean (1977) was used, the details of which are reported by Motta (2008).

From equations (1) for BOD and (2) for DO it can be seen how the BOD bed/water exchange affects the DO levels in the water column: the bed/water interaction terms in (1) have an impact on the BOD concentration in the water column C_{BOD}, and, as a consequence, on the DO concentration C_{DO}, since the BOD-DO system is coupled through the oxidation term.

One-dimensional area-averaged model for "Phase 2". The one-dimensional area-averaged conservation equation is written, for both the concentrations of BOD and DO, as

$$\frac{\partial C}{\partial t} + u\frac{\partial C}{\partial x} = \frac{1}{A}\left(\frac{\partial}{\partial x}EA\frac{\partial C}{\partial x}\right) + S \tag{9}$$

where C is the concentration of BOD or DO, t is time, u is the flow velocity in the x direction, x is the longitudinal distance, A is the flow area, E is the dispersion coefficient and S is the source/sink term. In this case, after the CSO discharge, there is no advection (i.e., $u = 0$). The sink term S_{BOD} is similar to (1) and considers only oxidation and settling (obviously no resuspension occurs), while the source/sink term S_{DO} is similar to (2) and considers oxidation and bed sediment oxygen demand. Equation (9) is solved numerically for a reach by setting appropriate initial and boundary conditions.

Results. For most of the data needed for modeling purposes, measurements are available for Bubbly Creek. However, some information was taken from literature and some other parameters were calibrated.

The bathymetry of Bubbly Creek was provided by the Illinois Water Science Center of the U.S Geological Service (USGS) and it is displayed in Figure 4a, in terms of water depths for a constant horizontal typical water stage of 175.9 m a.s.l.

For the CSO event of September 13, 2006, a suspended sediment and BOD input concentration of $C_{ss,w,input}$ = 604.8 mg/l and $C_{BOD,w,input}$ = 68.1 mg/l, respectively, were calculated with the regression formulations proposed by Alp and Melching (2006) for a CSO volume of 505.84 MG. It was assumed that all BOD in the water column, as well as in the bed, is attached to the particles. The input of DO was calibrated to match the DO concentration measurements in the creek (Figure 2) and was set equal to 9 mg/l, which is slightly less than the value at saturation (9.4 mg/l for a measured temperature of 18.9 °C) given that the combined sewage comes from a system of shafts and pipes which promotes the aeration of the turbulent flow.

A spatially constant bed sediment oxygen demand of 2.32 g/m^2/day (MWRDGC, 2007) was used. The porosity of the bed is on average 0.82 (Yin *et al.*, 2007). The density of the sediment at the upstream boundary as well as at the bottom was set to 2100 kg/m^3 (USACE, 2005). The particle size, expressed as median size D_{50}, is on average 82 μm, corresponding to fine sand - coarse silt (USACE, 2005).

As regards the BOD concentration in the bed sediments, relevant discrepancies were found in the literature in terms of its quantification; therefore, it was calibrated, resulting in a value of 5000 mg/l, assumed spatially and temporally constant and corresponding to a concentration over the mass of sediments of 13.2 mg/g. Currently, there are plans to measure SDO in-situ along Bubbly Creek.

The settling velocity of the CSO suspended sediments is also a parameter very difficult to estimate, because it is characterized by a strong *in situ* variability. In absence of measured data, its value was calibrated and set equal to 4.5 m/day.

Figure 4b shows the flow velocity field in the creek for the September 13, 2006 event. Observe that the upstream portion of Bubbly Creek is characterized by water depths of around 1.5-2.5 m, while the downstream portion, because of navigation, is characterized by higher depth values of about 2.5-3.5 m (Figure 4a). This difference has a direct impact on the erosion pattern during a CSO event, since lower depths are associated with higher velocity and friction coefficient values and therefore higher bed shear stresses, erosion rates and sediment resuspension. From Figure 4b, velocities are higher in the upstream portion (around 0.8-1.0 m/s), while downstream the values are lower (around 0.5-0.7 m/s).

The CSO event dynamics is dominated by advection, bed/water interaction and kinetics, while diffusion plays a minor role. The flow regime is net erosional. Erosion is especially high in the upstream portion of the creek, varying from 80-90 cm at the upstream end of the creek to about 20-30 cm at the downstream end.

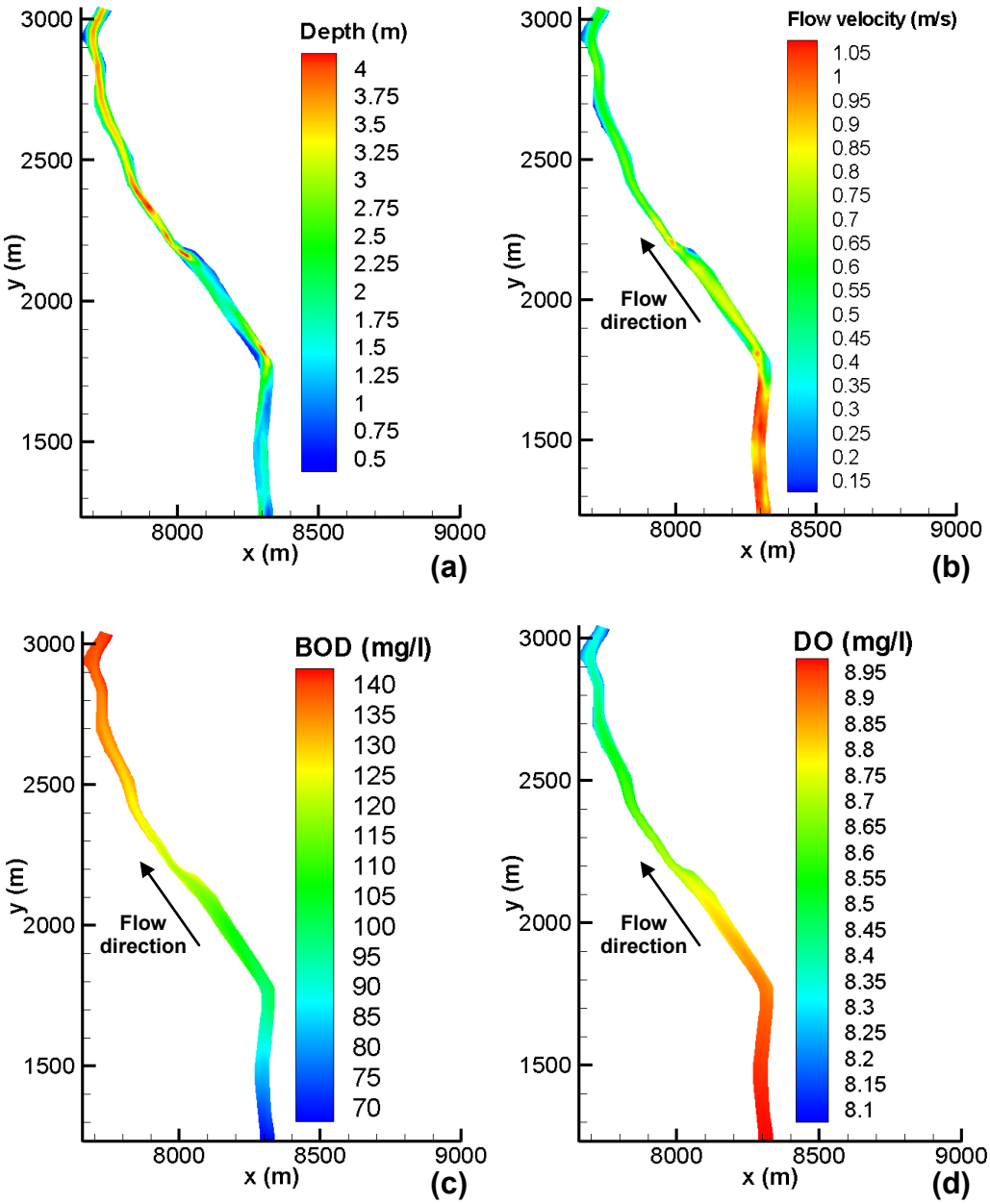

Figure 4. (a) Bathymetry of Bubbly Creek for a constant horizontal water stage of 175.9 m a.s.l. (b) Flow velocity field for a discharge of 69.4 m^3/s; (c) BOD and (d) DO concentration in the water column after 7.66 hours.

Since the regime is net erosional, both the suspended sediments and BOD concentrations in the water column increase in the downstream direction. In particular, the BOD concentration, from the input value of 68.1 mg/l at the Racine Avenue Pumping Station, reaches a value of about 140 mg/l at the downstream end (Figure 4c). Its concentration after 7.66 hours is essentially determined by the input concentration in the upstream portion of the creek and mainly by the resuspension of BOD from the bed in the rest of the channel. The DO field (Figure 4d) is dominated by the upstream input, while the oxidation and bed sediment oxygen demand

processes cannot cause a significant depletion in the downstream direction during the relatively limited discharge period. Therefore, the effect of a CSO event, as observed in Figure 2 for "Phase 1", is to temporarily increase the DO levels in the creek.

The post CSO discharge stage ("Phase 2") was modeled using the averaged measured DO level at the Loomis Street station in the South Branch (Figure 1), equal to 6.86 mg/l, as downstream boundary condition for DO, while a BOD concentration of 5 mg/l (Alp and Melching, 2006) was used. The dispersion coefficient for BOD and DO, which "lumps" the effect of the continuous water stage variation in the South Branch on the scalars transport in Bubbly Creek (estuarine effect), was calibrated and set equal to 4 m^2/s in the downstream portion of the creek (last 1000 m of the creek) while upstream the BOD and DO concentrations are exclusively governed by kinetics, since the constriction of the creek and the abrupt decrease in water depth at mid-channel (Figure 4a) damp down the estuarine effect.

Three days after the end of the CSO discharge, conditions in Bubbly Creek were simulated, assuming, from measurements, a constant water temperature of 21.9 °C, and starting from the modeled conditions in the creek at the end of "Phase 1". Figures 5a and 5b show the temporal evolution of the concentration of BOD (modeled) and DO (modeled vs. measured) at the monitoring stations at 36th Street and I-55 (Figure 1) after the end of the CSO discharge.

Several observations can be made: [1] the model predicts a monotonic temporal decrease of the BOD concentration in the water column for both stations, because of BOD settling and oxidation. The decrease rate is higher at the I-55 Station, characterized by a higher BOD content in the water right after the CSO discharge (effect of the BOD resuspension from the bed); [2] the model is also able to capture, qualitatively and quantitatively, the evolution of the DO level at both the stations: at I-55, that is close to Bubbly Creek's mouth, the DO decreases very rapidly for the first hours, due to the oxygen demand exerted by the BOD in the water column, entering from the pumping station but especially resuspended from the bed. At the 36th Street Station, which is about 1800 m far from the South Branch of the Chicago River, the DO concentration decreases without recovering in the days following the CSO discharge, because the effect of higher DO concentration in the South Branch is not felt; [3] the predicted DO levels at the 36th Street Station after about 30 hours are lower than the measured ones: this was expected, since the model presented does not adjust the bed sediment oxygen demand, which is important for the DO depletion once most of the BOD in the water column has been oxidized or has settled down on the bottom, for anaerobic conditions, which do occur in the upstream portion of the river after about 30 hours. In anaerobic conditions the bed sediment oxygen demand decreases, explaining why the DO concentration in reality does not go to zero.

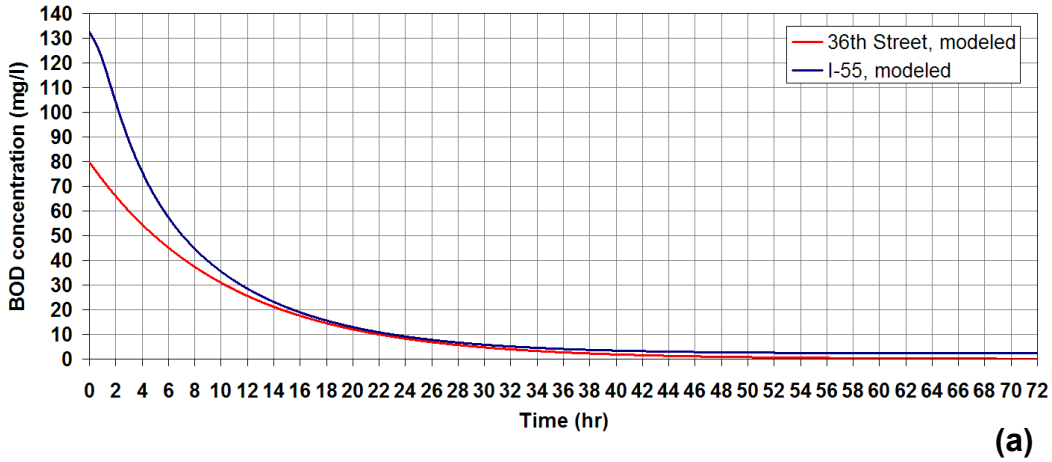

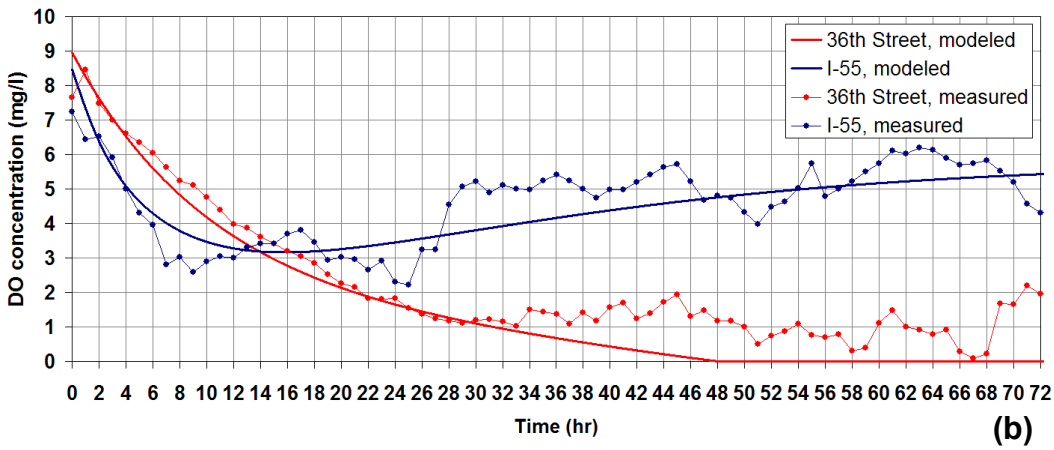

Figure 5. Temporal evolution of the concentration of (a) BOD (modeled) and (b) DO (modeled vs. measured) at the monitoring stations in Bubbly Creek at 36th Street and I-55, after the CSO discharge of September 13, 2006.

"PURIFICATION" SCENARIOS

Characteristics. Recently, two possible flow augmentation scenarios, with or without coupling with supplemental aeration, were proposed with the goal of improving the dissolved oxygen levels in Bubbly Creek, which are very low especially after CSO discharge events and in general during the summer months. The two main solutions proposed were opening a gate at the Racine Avenue Pumping Station and drawing flow backward from the South Branch of the Chicago River, inducing reaeration (MWRDGC, 2003; 2004), or drawing flow with a pipe from the South Branch towards Bubbly Creek headwaters, inducing flow in the creek and discharging back into the South Branch (Alp and Melching, 2006). Both scenarios plan to take water from the South Branch: this means that the water quality in Bubbly Creek would essentially depend on the water quality of the South Branch. To avoid this situation and, in general, any interaction with the South Branch, three alternative solutions were preliminarily analyzed using STREMR-HySedWq: [1] flow recirculation (northward flow in the creek). Flow is withdrawn by a pipe at the

downstream (North) end of the creek, and it is discharged back into the creek at its upstream (South) end; [2] flow recirculation plus supplemental aeration at one location in the creek; [3] flow recirculation plus supplemental aeration in the recirculation pipe.

Modeling. The analyses were performed for a "worst case" scenario: the initial conditions for BOD and DO, as well as the water temperature, were selected with reference to a typical summer period after CSO is discharged from RAPS. BOD in the water column was assumed to be oxidized and to settle down; DO is used for oxidation of the BOD in the water column and by the sediment oxygen demand from the bed, while reaeration from the atmosphere, once flow is forced in the creek, is a positive contribution to the DO levels.

The scenario modeled is indeed idealized; on the other hand, its analysis allowed for a first evaluation of the potential effectiveness of some "purification" technologies. The "purification" goal was set, in terms of DO concentration, to 4 mg/l suggested by the Illinois Pollution Control Board (IPCB).

Results. The results obtained for the three "purification" solutions listed above are herein briefly illustrated, considering a recirculation discharge of 50 MGD (2.19 m^3/s), for which sediment resuspension from the bed is avoided. Figure 6a shows the corresponding flow velocity field, which is on average 0.02 m/s, with a maximum value of 0.04 m/s.

The O'Connor and Dobbins formula (1958) was used to compute the reaeration coefficient K_a ($K_a[day^{-1}] = 3.93(U[m/s])^{1/2}/(H[m])^{3/2}$, where H is the water depth and U is the flow velocity) and Mortimer formula (1956) for the DO concentration at saturation C_s ($C_s[mg/l] = \exp[7.71 - 1.31\ln(T[°C] + 45.93)]$,where T is the water temperature). The BOD settling velocity was conservatively assumed equal to 1 m/day (Alp and Melching, 2006).

Scenario 1: flow recirculation. Figures 6c and 6d show respectively the spatial field of the reaeration coefficient K_a in day^{-1} and the difference between the reaeration (DO source term) and bed sediment oxygen demand (DO sink term) in mg/l/day for a flow rate of 50 MGD and a typical summer temperature of 25 °C (the diurnal variation of temperature, which is in general in the order of 1-2 °C, was neglected). Rearation is relevant especially in the upstream portion of the creek, where the flow is faster and shallower. The overall effect of flow recirculation is to increase the DO levels. Figure 6b shows the DO field at equilibrium starting from an initial concentration of 1 mg/l, typical value after a CSO event. The equilibrium condition for DO, ultimately determined by the balance between reaeration and bed sediment oxygen demand, is reached after about three weeks, when considering an initial post-CSO BOD concentration of 60 mg/l in the water column, which gradually goes to zero because of settling and oxidation.

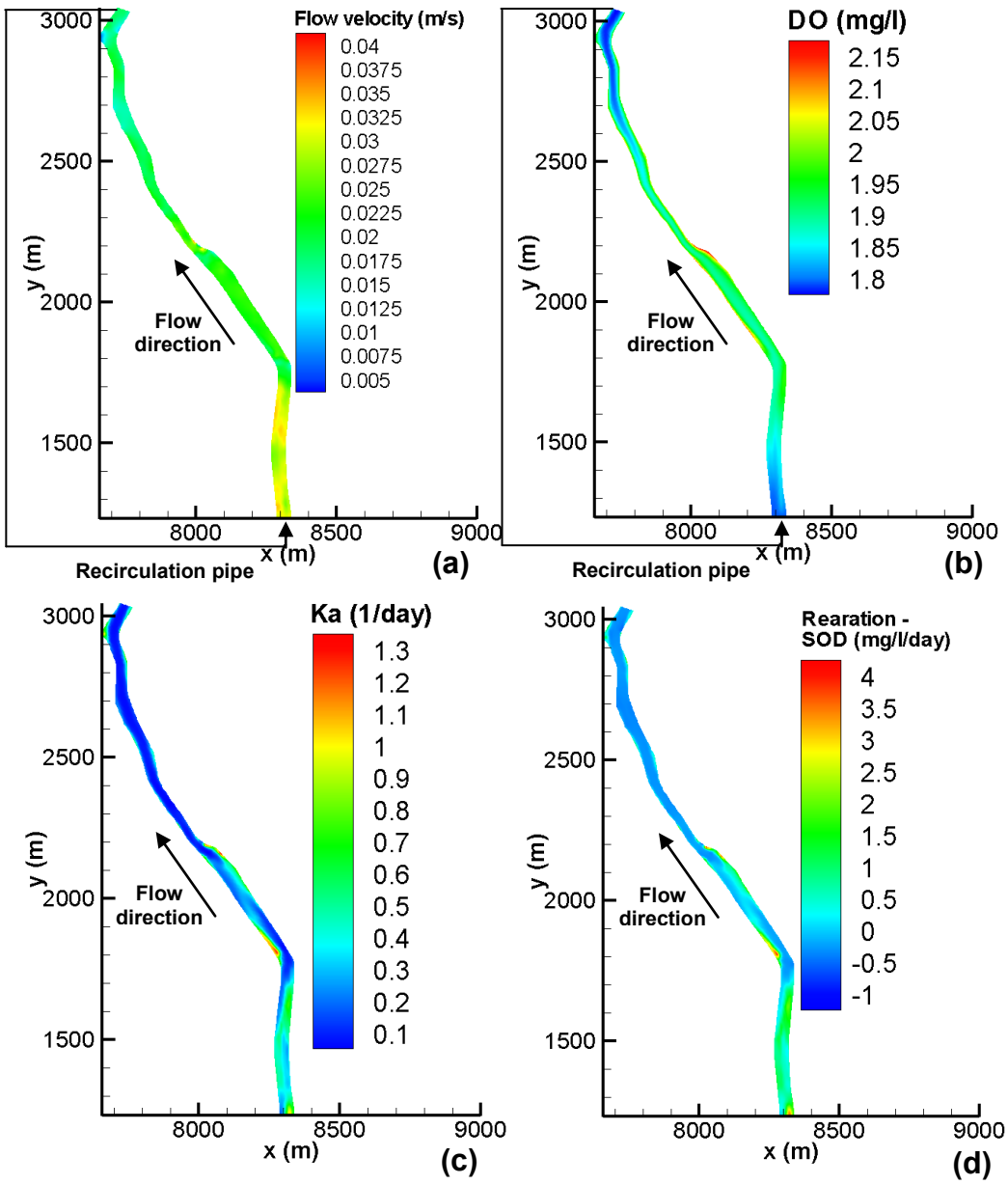

Figure 6. (a) Flow velocity field for a flow rate of 50 MGD. (b) DO concentration field at equilibrium. (c) Reaeration coefficient. (d) Difference between the reaeration (source) and bed sediment oxygen demand (sink) terms.

Scenario 2: flow recirculation plus supplemental aeration in the creek. From Scenario 1 it appears that a flow recirculation of 50 MDG is not enough to meet the IPCB standard of 4 mg/l for DO (Figure 6b). Supplemental aeration can therefore be coupled with flow recirculation. Figure 7a shows the DO field at equilibrium, when a continuous DO supplemental input of 1.31 g/s, minimum required to meet the IPCB standard of 4 mg/l everywhere in the creek, is introduced at about mid-channel.

Scenario 3: flow recirculation plus supplemental aeration in the recirculation pipe. The location of the DO supplemental aeration input can be alternatively set in the

recirculation pipe, rather than in the creek. This solution allows for complete mixing of the oxygen in the water before it flows into the upstream (South) end of the creek. Obviously, the minimum DO input rate that is necessary for meeting the IPCB standard everywhere in the creek is the same as calculated for Scenario 2. However, if the additional oxygen is introduced in the pipe, the time to reach equilibrium of the DO field in the creek is noticeably reduced, since mixing occurs in the pipe and not in the creek itself: only a bit more than one day is enough to reach, in the summer, the equilibrium field in Figure 7b.

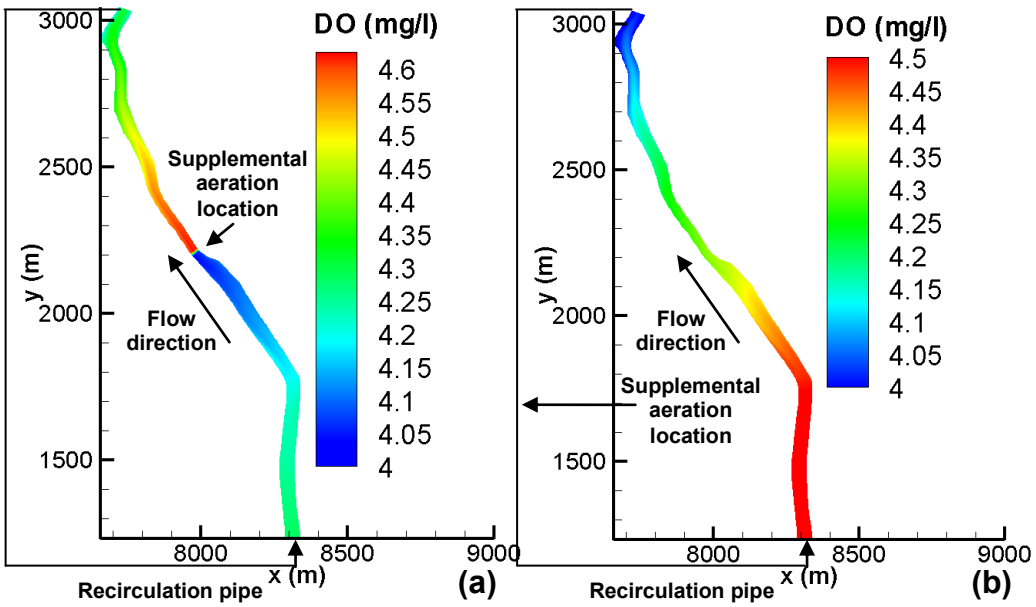

Figure 7. (a) DO concentration field at equilibrium for Scenario 2. (b) DO concentration field at equilibrium for Scenario 3.

The analysis presented shows that flow recirculation, when coupled with supplemental aeration, represents a potential solution for the creek restoration in terms of DO levels. The disconnection from the South Branch appears to be convenient, since the water quality in Bubbly Creek would not depend on the water quality of the Chicago River. Moreover, recirculation allows for significantly reducing the supplemental aeration rates.

CONCLUSION

A new two-dimensional depth-averaged water quality BOD-DO model was implemented in the numerical code STREMR-HySedWq. The model allowed for evaluating two different scenarios for Bubbly Creek in Chicago, i.e. Combined Sewer Overflow events and potential "purification" technologies such as flow augmentation, flow recirculation and supplemental aeration.

In particular, a quantitative framework for the evaluation of the BOD transport across the bed/water interface in rivers was derived, in order to capture the additional oxygen demand in the water associated with the resuspension of organic sediments

from the bottom. The process was described in terms of its dependency on the properties of the flow, the sediments and the bed.

The application of the model to Bubbly Creek showed its potential use in the evaluation of the DO depletion associated to high BOD content in the water column, both in the short and long term period after a CSO event. The results showed that the described conceptual framework is able to capture, both qualitatively and quantitatively, the DO dynamics during and after a CSO discharge, through calibration against measurements of DO levels. It also provides physical insight into the processes which govern the water quality in the creek and guidance for implementing water quality remediation and sediment management solutions in the future.

ACKNOWLEDGEMENTS

The financial support of the Metropolitan Water Reclamation District of Greater Chicago (MWRDGC) through a research grant to the Ven Te Chow Hydrosystems Laboratory of the Department of Civil and Environmental Engineering at the University of Illinois at Urbana-Champaign is gratefully acknowledged.

REFERENCES

Abad, J.D., Buscaglia, G.C., and Garcia, M.H. (2008). "2D stream hydrodynamic, sediment transport and bed morphology model for engineering applications." *Hydrological Processes*, 22, 1443–1459.

Alp, E. and Melching, C.S. (2006). "Calibration of a model for simulation of water quality during unsteady flow in the Chicago Waterway System and application to evaluate use attainability analysis remedial actions." *Marquette University,* Milwaukee WI, TR 18 for MWRDGC.

Bernard, R.S. (1993). "STREMR: numerical model for depth-averaged incompressible flow." *Tech. Report REMR-HY-11, USACE.*

Briskin, B.J., Cantero, M.I., and Garcia, M.H. (2002). "In-situ measurements of suspended oxygen demand by suspended biosolids." *IAHR Hydraulic measurements and experimental methods*.

Hill, L., (2000), "The Chicago River: A Natural and Unnatural History", Lake Claremont Press.

Liu, X., Sinha, S., Motta, D., and Garcia, M.H. (2009). "Upstream Intrusion Effect of CSO Event in Bubbly Creek, IL". In *Proc. of ASCE EWRI World Environmental & Water Resource Congress,* Kansas City, Missouri, 2009.

Metropolitan Water Reclamation District of Greater Chicago (MWRDGC), (2003). "Bubbly Creek water quality improvement, a demonstration project in 2002." Report No. 03-1.

Metropolitan Water Reclamation District of Greater Chicago (MWRDGC), (2004). "2003 Bubbly Creek water quality improvement, demonstration project." Rep. No. 04-8.

Metropolitan Water Reclamation District of Greater Chicago (MWRDGC), (2007). "Water quality within the Waterways System of the Metropolitan Water Reclamation District of Greater Chicago." Report No. 07-38, 2006.

Motta, D., Soares Frazao, S., and Garcia, M.H. (2007). "Hydrodynamic modeling of Bubbly Creek, Chicago, Illinois: flow patterns during combined-sewer-overflow events." *Proceedings ISEH V*, Phoenix, AZ.

Motta, D. (2008). "Two-dimensional hydrodynamic, sediment transport and water quality model for Bubbly Creek, Chicago, Illinois." M.S. Thesis, University of Illinois at Urbana-Champaign, IL.

Mortimer, C.H. (1956). "The oxygen content of air-saturated fresh waters, and aids in calculating percentage saturation." *Intern. Ass. Theoret. Appl. Commun.*, No. 6.

O'Connor, D.J., and Dobbins, W.E. (1958). "Mechanisms of reaeration in natural streams." *Trans. Amer. Soc. Civil Engrs.*, 123, p. 655.

Smith, J., and McLean S. (1977). "Spatially averaged flow over a wavy surface." *Journal of Geophysical Research*, 83, 1735-1746.

U.S. Army Corps of Engineers Chicago District (USACE), (2005). "Collection and analysis of sediment samples from the South Fork South Branch, Chicago River."

Yin, K., Viana, P., Zhao, X., and Rockne, K.J. (2007). "Active capping remediation project: Bubbly Creek Turning Basin bore LOG." *UIC Report*.

Using HEC-RAS Hydraulic Design Functions for Geomorphic Channel Design and Analysis

By John Shelley[1] and A. David Parr[2]

Dept. of Civil, Environmental, and Architectural Engineering, University of Kansas, 1530 W. 15th St. Rm. 2150, Lawrence, KS 66045.

[1]PH (785) 864-2924; FAX (785) 864-5631; E-mail: johnnyjazzman@gmail.com
[2]PH (785) 864-2925; FAX (785) 864-3808; E-mail: parr@ku.edu

Abstract

The Copeland method for designing geomorphologically stable channels has been included in the Army Corps of Engineers' Hydraulic Engineering Circular River Analysis System (HEC-RAS). This method requires the bottom width, depth, and side slopes of a representative cross-section from a stable, upstream reach as input. This assumes the upstream cross-section can be approximated by a trapezoidal channel, but no instruction on how to derive this trapezoidal approximation is given in available literature. Additionally, the method requires a side-slope Manning 'n' value, for which the available documentation provides only qualitative guidance. This paper presents a step-by-step design example for using the Copeland method, including approximating the upstream channel as a trapezoid and calculating the sidewall Manning 'n'.

Introduction

The Army Corps of Engineers' Hydraulic Engineering Circular River Analysis System (HEC-RAS) includes capabilities for calculating bankfull discharge and for designing geomorphologically stable channels. One of these tools is the Copeland method for stable channel design.

The Copeland method is an analytical stable channel design method. The goal of this method is to design the bottom width, depth, and slope (side slopes are a required input) of a trapezoidal channel so that the sediment transport capacity in the designed channel equals the sediment transport capacity of a stable, upstream supply reach. The method uses Brownlie's resistance and sediment transport functions, which apply only to sand bed channels (Brownlie, 1981). Additional limitations on the method's applicability are presented in the HEC-RAS Hydraulic Reference Manual (USACE, 2008) and should be consulted prior to using the method. The basic steps for performing a Copeland stable channel design are provided in the HEC-RAS Users Manual (USACE, 2006). Unfortunately, currently available scientific literature, users manuals, and case studies do not provide sufficient guidance in selecting several crucial input parameters. The bottom width, depth, and side slopes of a representative

cross-section from a stable, upstream reach are required as input. These inputs assume the upstream channel is a trapezoid. Since the upstream channel will typically be a natural cross-section, question arises as to how the trapezoidal measurements are to be supplied. Also, the Copeland method requires a Manning 'n' value for the sidewalls of the main channel. While engineers are familiar with choosing Manning 'n' values for the entire main channel, they seldom need to choose sidewall 'n' values. Only qualitative guidance exists in the literature.

This paper provides a complete step-by-step example of how to use the Copeland method for stable channel design in HEC-RAS. It demonstrates how to calculate an equivalent trapezoid for the upstream cross-section and how to calculate the side-wall Manning 'n' values. Required inputs include a surveyed cross-section and slope for an upstream supply reach, and channel average Manning 'n' values for the upstream cross-section and the project reach.

Stable Channel Design (Copeland Method)

Given:

$n_{upstream}$ = .0388
n_{des} = .0345

I. Field Reconnaissance

A. Perform a cross sectional survey at a stable upstream riffle or inflection point. Record the station/elevation of the left and right edges of the moveable bed and the elevation of the bankfull stage. This is shown in Table 1 below.

Table 1. Cross-sectional Survey

Sta	Elev	Notes	Sta	Elev	Notes	Sta	Elev	Notes	Sta	Elev	Notes
0	1298.54		30	1293.55		50	1292.37		66	1293.6	
2	1298.41		32	1293.05		51	1292.5		68	1293.87	
4	1298.03		34	1293.24		52	1292.74		70	1294.44	
6	1297.81		36	1293.22		53	1292.76		72	1294.81	RB
8	1297.12		38	1293.32	LEOMB	54	1292.78		74	1294.93	
10	1296.5		40	1293.27		55	1292.87		76	1295	
12	1295.84		41	1292.95		56	1292.77		78	1294.86	
14	1295.22		42	1292.82		57	1292.74		80	1294.96	
16	1294.81		43	1292.73		58	1292.81		82	1294.99	
18	1294.72		44	1292.56		59	1293.11		84	1295	
20	1294.58		45	1292.58		60	1292.89		86	1295.1	
22	1294.36		46	1292.44		61	1292.87		88	1296.16	
24	1294.35	LB	47	1292.53		62	1292.84		90	1296.98	
26	1293.66		48	1292.45		63	1293.09				
28	1293.74		49	1292.41		64	1293.14	REOMB			

LB = Left bank
LEOMB = Left edge of moveable bed
RB = Right bank
REOMB = Right edge of moveable bed

B. Determine the slope of the upstream section from riffle to riffle or inflection point to inflection point.

Slp = 0.00473

C. Estimate the bankfull stage by geomorphologically observation or some other method.

Bankfull stage (h_{bnk})= 1294.81 ft

D. Take a bed-sediment sample to determine the sediment gradation of the upstream cross section, consisting of the d_{16}, d_{50}, and d_{84} (sieve size for which, 16%, 50%, and 84% of the material is finer by weight.) Note that a by-weight sediment characterization is not the same as a "pebble count," (a by-number characterization).

d_{16} = 0.8 mm
d_{50} = 1 mm
d_{84} = 1.5 mm

II. HEC-RAS

A. Calculate the design bankfull flow

1. Create a new HEC-RAS project.
2. Create a new river and reach in the geometry editor window.
   River name: Schaffer Creel North
   Reach name: Reach1
3. Create a new cross section. *[Cross Section, Options, Add a new Cross Section]*
4. Paste the surveyed station/elevation points into the new Cross section then add the location of the left and right bank stations (14 and 72 feet, respectively). *[Using Ctrl C and Ctrl V for the copy and paste commands, respectively, is often need in building HEC-RAS models.]*

5. Choose the *Run/Hydraulic Design Functions…* menu item from the main menu.
6. Choose the *Type/ Uniform Flow* menu item.
7. If it is not already selected, choose the correct river and reach from the drop down combo boxes.
8. Enter the elevation of the field-selected bankfull stage and the channel slope into the appropriate fields. (1294.81 ft and 0.00473, respectively.)

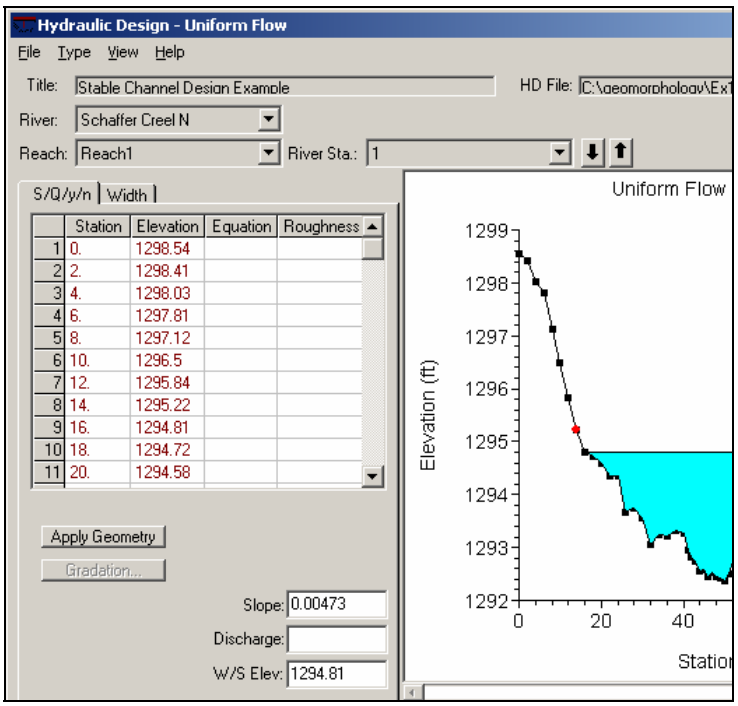

9. Click on the field next to the elevation on left most station/elevation point, under the heading "Equation" and choose Manning as the resistance equation.
10. Enter the Manning 'n' value for the upstream reach of 0.0388.
11. Click inside of the "Discharge" field then click the "Compute" button to calculate the discharge.

$Q_{bnkfull}$ = 266 cfs

B. Choose a Manning's n-value for the channel side walls and bed

1. Click on the field next to the elevation on the station/elevation point for the start of the movable bed under the heading "Equation" and choose the Brownlie resistance equation. The station/elevation values for this point are (38, 1293.32).
2. Choose the Manning's resistance equation for the left-most station/elevation point in the cross section and for the point at the end of the moveable bed. Enter the same Manning's n-value at these points. Here those station/elevation points are (0, 1298.54) and (64, 1293.14). Note that a resistance equation will apply from the station/elevation point where it is entered across the channel from left to right (down the table) until a different equation is specified. The table below shows the location of the Manning and Brownlie resistance equations and the n-values for this example. The initial n-value used was 0.039.

Station	Elevation	Equation	Roughness
0	1298.54	Manning	0.039
2	1298.41		
4	1298.03		
Hidden Cells			
36	1293.22		
38	1293.32	Brownlie	
40	1293.27		
41	1292.95		
Hidden Cells			
62	1292.84		
63	1293.09		
64	1293.14	Manning	0.039
66	1293.6		
68	1293.87		
Hidden Cells			
88	1296.16		
90	1296.98		

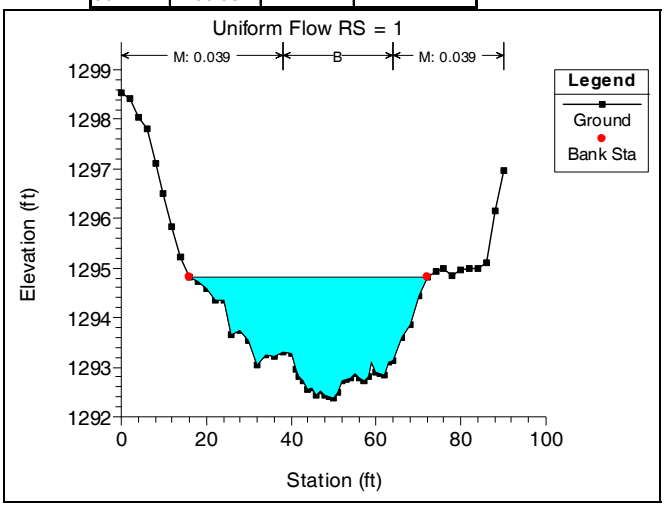

3. Click the compute button to calculate the discharge. Compare the discharge to the calculated bankfull discharge, $Q_{bnkfull}$. Adjust the two Manning's n-values and click Compute again. Readjust the Manning's n-values until the discharge equals the expected discharge. The Brownlie resistance equation applied for the movable bed portion of the channel throughout the calculations.

Sta	Equation	n	Q	$Q_{bnkfull}$
0 and 64	Manning	0.039	292	266
0 and 64	Manning	0.04	288	266
0 and 64	Manning	0.043	275	266
0 and 64	Manning	0.045	268	266
0 and 64	Manning	0.0454	264	266

$n_{sides} = 0.0454$

This Manning's n-value is the sidewall Manning's n-value for use in the Copeland method stable channel design.

4. Change the resistance formula for the moveable bed region from "Brownlie" to "Manning." Enter an intial n-value for the movable bed region (station 38) and click compute. Readjust this Manning's n-value until the discharge equals the expected discharge without altering the two sidewall Manning's n-values. Here the sidewall n-value is 0.0454.

Station	Equation	n	Q	$Q_{bnkfull}$	
38	Manning	0.03	271	266	
38	Manning	0.032	263	266	
38	Manning	0.0310	266	266	OK

$n_{bed} = 0.0310$

The Manning's n-value found is the Manning's n for the movable bed at bankfull flow. In summary the Manning's n-values are 0.0454 for the overbanks and 0.0310 for the main channel.

C. Create a Prismatic Hydraulic Model for the Upstream Reference Cross Section.

Use the river, reach and cross section created earlier.

1. Set the bank stations to the edges of the moveable bed (not the bankfull level) and set the overbank and main channel n-values to 0.0454 and 0.0310, respectively.

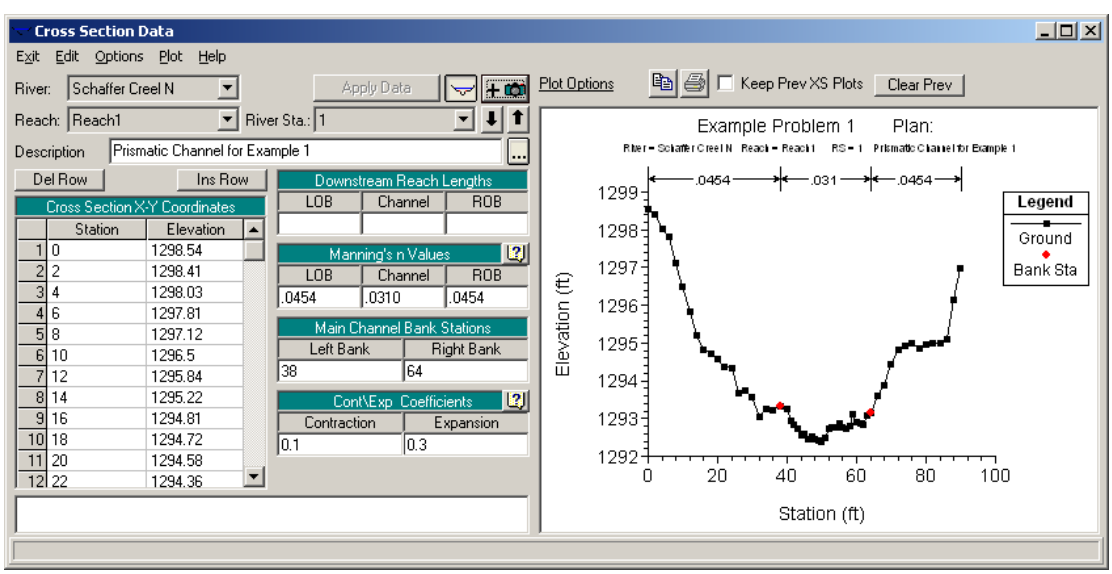

2. Copy Cross Section 1 to Cross Section 100. [*Options, Copy Current Cross Section*]
3. Adjust the elevations of Cross Section 100 by 100*slope. [*Options, Adjust Elevations*]
    1. +100 * Slp = +100 * 0.00473 = +0.473

4. Set the downstream reach lengths for Cross Section 100 to 100.
5. Copy the Cross Section 100 to Cross Section 200. [*Options, Copy Current Cross Section*]
6. Adjust up the elevations of Cross Section 200 upward by 0.473 ft. [*Options, Adjust Elevations*]
7. Exit the cross section editor then in the Geometric Data editor, save the geometric data as Prismatic. *[File, Save Geometry Data As….., Prismatic]*
8. From the main menu open the Steady Flow Editor and input the design bankfull discharge of 266 cfs determined above. [*Edit, Steady Flow Data*]
9. In the Steady Flow Editor, input the "normal depth" downstream boundary condition. Enter the slope. [*Reach Boundary Conditions, Downstream, Normal Depth, 0.00473*].
10. From the main menu, run the steady flow analysis of the prismatic upstream reach. [*Run, Steady Flow Analysis, Subcritical, Compute*]
11. Use the HEC-RAS Profile Summary Tables to determine the following parameters from the upstream prismatic reach:

Table 2. Parameters

Parameter	Symbol	HEC-RAS Designation
Hydraulic radius of the channel above the moveable bed	R_{mov}	Hydr Radius C
Wetted perimeter of the moveable bed	P_{mov}	W.P. Channel
Cross sectional flow area of the entire bankfull channel	A_{bank}	Flow Area
Wetted perimeter of the entire bankfull channel	P_{bank}	W.P. Total

12. To find these values, perform the following steps from the main menu *View/Profile Summary Table, Options, Define Table, Clear All Table Headings.* You can then double click on the variables until the following table is created. Then hit *OK, Options, Save Table.., Example 1 Prismatic*.

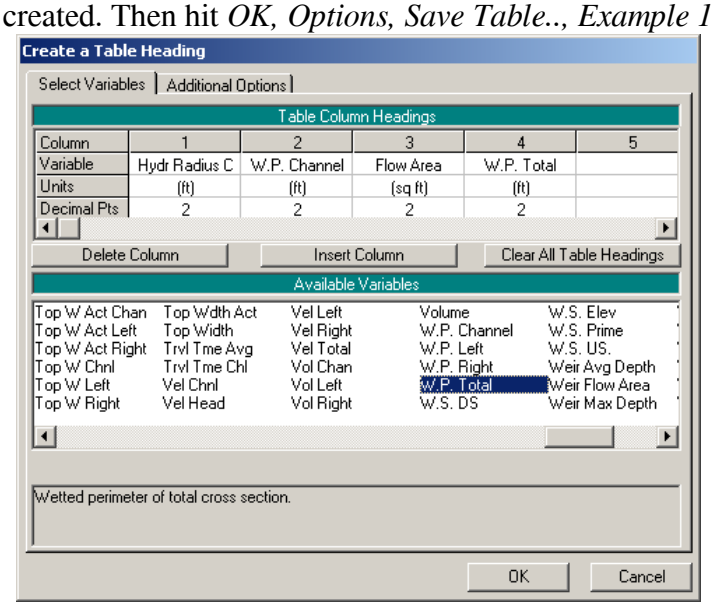

Profile Output Table - Example 1 Prismatic

File Options Std. Tables User Tables Locations Help

HEC-RAS Plan: Plan 01 River: Schaffer Creel N Reach: Rea

Reach	River Sta	Profile	Hydr Radius C	W.P. Channel	Flow Area	W.P. Total
			(ft)	(ft)	(sq ft)	(ft)
Reach1	200	Bankfull Flow	1.77	26.25	67.55	51.28
Reach1	100	Bankfull Flow	1.77	26.25	67.54	51.28
Reach1	1	Bankfull Flow	1.77	26.25	67.38	51.23

13. Determine the bottom width and height of the equivalent upstream trapezoid. Use the values from Cross Section 200.

$b = P_{mov} = 26.25$ ft
$y = R_{mov} = 1.77$

14. Calculate the side slopes of the equivalent trapezoidal channel for the upstream cross section, using the following equation, where m is defined in the drawing below.

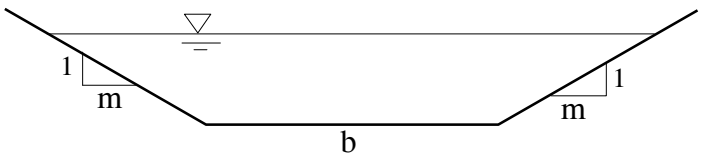

$$\frac{(A_{bank})^5}{(P_{bank})^2} = \frac{(by + my^2)^5}{\left(b + 2y\sqrt{m^2+1}\right)^2} \rightarrow \frac{(67.55)^5}{(51.28)^2} = \frac{(26.25(1.77) + my^2)^5}{\left(26.25 + 2(1.77)\sqrt{m^2+1}\right)^2}$$

By trial and error or by using the Solver in EXCEL one can solve for m = 6.33.

A_{bnk} =	67.55 ft^2
P_{bnk} =	51.28 ft
b =	26.25 ft
y =	1.77 ft
m =	**6.33**

-8E-07 ← $\frac{(A_{bank})^5}{(P_{bank})^2} - \frac{(by+my^2)^5}{\left(b+2y\sqrt{m^2+1}\right)^2}$

C. Calculate a Copeland Stable Channel Design

1. Choose the *Run/Hydraulic Design Functions…* menu item from the main menu.
2. Choose the *Type/Stable Channel Design…* menu item and the *Copeland* tab.
3. Enter the design discharge. Keep the defaults for the specific gravity and temperature. The Optional Input boxes can be left blank.
4. Click the *Gradation* button and enter the values of d_{16}, d_{50}, and d_{84}.

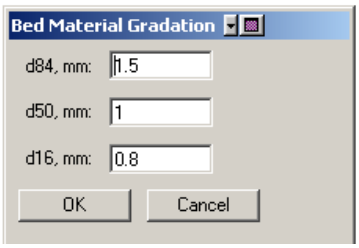

5. Enter the side slopes and the side slope Manning's n-values for the design channel. The side slopes should be chosen for stability and constructability. 2 to 3H:1V (m=2 to 3) may be appropriate. Here we will use a side slope n-value of 0.0454 for the design channel. Probably an n-value with two significant digits would be preferable. For instance, 0.045 rather than 0.0454. Here we have kept the extra significant digit to maintain the equivalent conveyances using different methods.

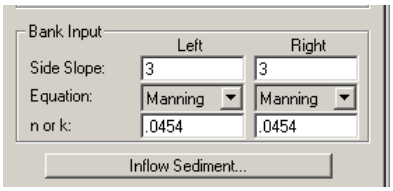

6. Click the *Inflow Sediment…* button and a window will appear. Choose the option to let HEC-RAS calculate the inflow sediment concentration. Enter the bottom width (b), bank height (y), Energy Slope (channel slope) and side slopes (m), calculated earlier for the upstream representative channel. If the upstream section is a meandering channel and the channel design will be a meandering channel, the same n-value for the side slopes should be used in both the upstream and the design section. When the upstream section is stable, but non-meandering, and a meandering channel will be designed downstream, or when a straight channel will be designed downstream from a meandering channel, then the n-values should be different.

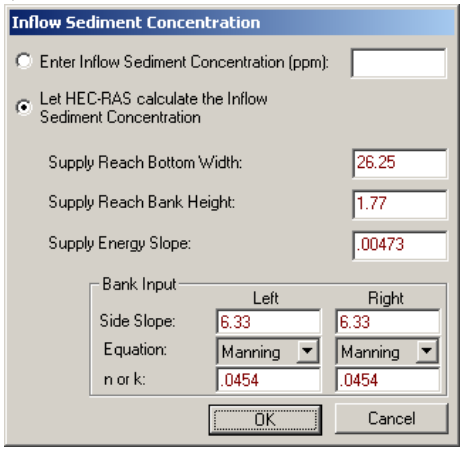

7. Click the *Compute* button. The values that go into this table are for the upstream reference cross section. The program computes the sediment inflow

from the upstream reference reach and provides many design options for the design channel.

8. Choose the desired design from the table of solutions. HEC-RAS plots the chosen solution. The channel has been designed to carry incoming bankfull flow at the bankfull stage and to have the same sediment transport capacity at bankfull flow as the upstream cross section.

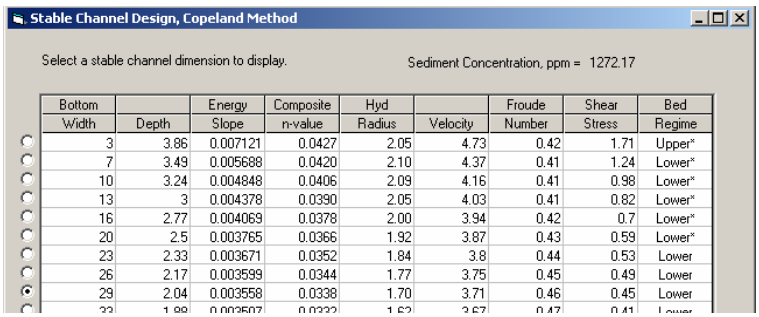

Bottom Width	Depth	Energy Slope	Composite n-value	Hyd Radius	Velocity	Froude Number	Shear Stress	Bed Regime
3	3.86	0.007121	0.0427	2.05	4.73	0.42	1.71	Upper*
7	3.49	0.005688	0.0420	2.10	4.37	0.41	1.24	Lower*
10	3.24	0.004848	0.0406	2.09	4.16	0.41	0.98	Lower*
13	3	0.004378	0.0390	2.05	4.03	0.41	0.82	Lower*
16	2.77	0.004069	0.0378	2.00	3.94	0.42	0.7	Lower*
20	2.5	0.003765	0.0366	1.92	3.87	0.43	0.59	Lower*
23	2.33	0.003671	0.0352	1.84	3.8	0.44	0.53	Lower
26	2.17	0.003599	0.0344	1.77	3.75	0.45	0.49	Lower
29	2.04	0.003558	0.0338	1.70	3.71	0.46	0.45	Lower

Conclusion

A procedure was developed for designing a geomorphologically stable channel using the Copeland method of stable channel design within HEC-RAS. An example was presented that applied the procedure to a natural channel reach.

Acknowledgments

This project was sponsored by the Kansas Department of Transportation through KTRAN project KU-08-5. Special thanks are due to Mr. Jim Richardson, the project administrator, and to Mr. Brad Rognlie for their support in this endeavor.

References

Brownlie, William R. (1981). "Prediction of Flow Depth and Sediment Discharge in Open Channels," Report No. KH-R-43A, California Institute of Technology, W.M. Keck Laboratory of Hydraulics and Water Resources.

USACE (2008). Hydraulic Reference Manual. United State Army Corps of Engineers. Available at http://www.hec.usace.army.mil/software/hec-ras/hecras-document.html .

USACE (2006). HEC-RAS Users Manual. United States Army Corps of Engineers. Available at http://www.hec.usace.army.mil/software/hec-ras/hecras-document.html .

A Monitoring and Assessment Framework to Evaluate Stream Restoration Needs in Urbanizing Watersheds

John S. Schwartz[1], Sue L. Niezgoda[2], Louise O. Slate[3], Donald D. Carpenter[4], William K. Annable[5], Tess M. Wynn[6], Christine Pomeroy[7], and Munsell McPhillips[8],

[1]University of Tennessee, Dept. of Civil and Environmental Engineering, 63 Perkins Hall, Knoxville, Tennessee 37996; PH (865) 974-7721; jschwart@utk.edu.

[2]Rose-Hulman Institute of Technology, Department of Civil Engineering; 5500 Wabash Avenue, Terre Haute, Indiana 47803; PH (812) 877-8814; niezgoda@rose-hulman.edu.

[3]MACTEC Engineering & Consulting, Inc., Raleigh, North Carolina 27612; PH (919) 876-0416; loslate@mactec.com.

[4]Lawrence Technological University, Civil Engineering Department, 21000 W. Ten Mile Road; Southfield, Michigan 48075; PH (248) 204-2549; carpenter@ltu.edu.

[5]University of Waterloo, Dept. of Civil Engineering, 200 University Avenue West, Waterloo, Ontario, Canada N2L 3G1. PH (519) 888-4567 ext 2955; wkannabl@uwaterloo.ca.

[6]Virginia Tech, Biological Systems Engineering Dept., 302 Seitz Hall, Blacksburg, Virginia 24061; PH (540) 231-2454; tesswynn@vt.edu.

[7]University of Utah, Dept. of Civil and Environ. Engineering, 122 S. Central Campus Dr., 212 CME, Salt lake City, Utah 84112; PH (801) 585-7300; Christine.Pomeroy@utah.edu.

[8]Intuition & Logic, GP, 1306 Autumn Trace, Amelia Island, Florida 32034; PH (904) 261-5555, munsell@ilincworld.com.

Abstract:

Urbanization has a significant impact on rivers and streams, modifying flows, sediment loads, channel morphology, water quality and nutrient processing, and aquatic biota. Because of these impacts, a majority of the streams in urban and urbanizing watersheds are reported on §303(d) state lists as impaired from siltation, habitat alteration, nutrients, bacteria, and other stressors. States are required to develop total maximum daily loads (TMDLs) under 40 CFR 130, and watershed-scale implementation plans are produced to rehabilitate impaired streams by achieving target TMDL allocations. Stream restoration practices are commonly used as corrective measures to meet TMDLs, particularly for siltation and habitat alteration. However, urban stream restoration typically consists of reach-scale projects that may not be well integrated into a watershed corrective plan. Rather, project scope and location are commonly determined by local perceptions of need and accessibility. Watershed planning is needed in urbanizing watersheds for various reasons. Most importantly, planning is needed because hydrology and sediment loads change as developments occur over time until ultimate build-out, and future infrastructure constraints affect channel planform stability. These reasons underscore the critical need for restoration projects to be implemented based on a watershed plan, and a plan that integrates implementation of stormwater management best management practices (BMPs). The objective of this paper is to present a framework for monitoring and assessment protocols for urban and urbanizing watersheds, with the aim to better support planning of stream restoration projects and improve restoration outcomes. This is the

product of a joint task committee by the Urban Stream Committee of the Urban Water Resources Research Council and the River Restoration Committee of the Hydraulics and Waterways Council.

Introduction:

Watersheds impacted by urbanization have altered chemical, physical and biological processes, impacting how water, sediment, organic matter, nutrients, and pollutants are transported from a more impervious land cover to the stream (Paul and Meyer 2001; Chin and Gregory 2005; Palmer et al. 2005; Bernhardt and Palmer 2007). Meyer et al. (2005) terms this degradation of watershed processes as the "urban stream syndrome". Impacted streams range in size from 1st to approximately 5th order, which is of a scale where land cover in entire watersheds can be converted to urban. Impacts to urban streams include degradation of water quality by increased nutrients, suspended sediments, toxins and water temperatures (Carle et al. 2005; Walsh et al. 2005). Altered hydrological patterns can include increased stormflow peaks, decreased lag time to peaks, greater frequencies and duration of erosive flows, and altered summer baseflow (Booth and Jackson 1997; Walsh et al. 2005). Channel morphologies in early stages of watershed urbanization adjust by deepening and widening, typically referred to as channel incision (Hammer 1972, Booth 1990; Bledsoe and Watson 2001). Less systematic responses occur in channel adjustments such as excessive local scour, altered pool-riffle spacing, and reach-scale bed aggradation or degradation (MacRae 1996; Chin and Gregory 2005; Kang and Marston 2006). Ecologically, organic matter retention is lowered and algae biomass frequently increases, simplifying benthic macroinvertebrate communities (Moerke et al. 2004; Meyer et al. 2005). Fish assemblages are less diverse in urban streams, typically consisting of tolerant, pool-dominant species (Moerke and Lamberti 2003; Schwartz and Herricks 2007). Based on clear needs, the numbers of restoration projects in these impacted watersheds have greatly increased to contend with the urban stream syndrome (Bernhardt et al. 2005).

In the United States, increased use of stream restoration practices in urban watersheds has been driven, in part, by Clean Water Act (CWA) regulations. Many urban streams are identified as impaired on CWA §303(d) state lists because they do not meet state water quality and/or biocriteria standards due to siltation, habitat alteration, nutrients, bacteria, and various toxic pollutants. Once listed as impaired, states are required to develop total maximum daily loads (TMDLs) under 40 CFR 130 for these reaches (EPA 1997, 1999). TMDLs are issued at the hydrologic unit code (HUC) 8 scale, in which annual load reductions are prescribed along with suggested corrective action plans. Because impairment in urban watersheds is a function of multiple stressors on aquatic biota, corrective action plans require an array of best management practices (BMPs) that are integrated spatially at the watershed or subwatershed scales (Schueler 2005). Also, it must be recognized that different regulatory rules guide BMP implementation. For example under CWA §402 National Pollutant Discharge Elimination System (NPDES), stormwater permits require municipalities and urban counties to complete stormwater management plans. Plans include watershed maps of stormwater outfalls and predict future hydrology through models that account for runoff changes from proposed urban land developments (Schueler and Kitchell 2005). BMPs commonly used include

detention ponds, grass swales, solids removal devices, and community retrofits using low impact development (LID) and integrated management practices (IMP). Stream mitigation banks and BMPs are promoted by federal and state regulators when urban developments require CWA §404 permitting.

In fact, the stream restoration practice has grown into a major business with over one billon dollars spent on projects annually (Bernhardt et al. 2005). Support for restoration projects by state and local governments are endorsed, in part or combined, by CWA regulations §130, §303(d), §402, §404, and others (Deason et al. 2009). However, recent concerns as to what constitutes project success have arisen within the restoration practice community, largely due to vague project objectives and a lack of post-construction monitoring (Brown 2000; Bernhardt et al. 2007). Slate et al. (2007) also noted engineering liability issues have arisen due to conflicts between design methodologies, regulatory guidelines, and project failures related to instream structures and channel stability. The concern over project success is driven by the legal requirement to return streams to a "fully supporting" status with respect to designated uses such as aquatic life, and community-level accountability for project expenditures. It is difficult to predict or assess success for watershed-scale objectives when stream restoration projects are implemented at the local reach scale, and impairment occurs from modified land uses and multiple stressors throughout a watershed.

It is imperative that stream restoration projects in urban watersheds be implemented within a broader watershed-scale context, in which project objectives are clearly linked to stressors. In addition, project designs must take into account constraints imposed by urban infrastructure, and the changing hydrology, sediment yield, and channel morphology over time from urbanization. Project objectives and designs differ in urban and urbanizing watersheds than those in rural watersheds; therefore, urban-specific monitoring and assessment information must guide the pre-design decisions to optimally target projects. In general, urban stream restoration objectives include: flood mitigation; channel stability; mitigation credit to offset CWA §404 permitted impacts; infrastructure protection; stream channel relocation; aesthetics, water quality improvement; and, stream riparian habitat enhancement. Because of the difficulty in setting specific objectives linked to measurable stressors, it has been noted that objectives for restoration projects are often vague (Johnson and Brown 2001; Bernhardt et al. 2007). This is particularly true when restoration projects are implemented without adequate watershed monitoring and assessment.

Because most stream reaches in urbanizing watersheds are not in a geomorphic equilibrium state, this precludes monitoring and assessment guided by an analog, or reference reach approach (Fischenich 2001). It is commonly recognized that urbanization permanently alters watershed processes, and that restoring a stream back to a preexisting morphology is highly unlikely. Monitoring and assessment in urban and urbanizing watersheds needs to comprehensively identify stressors on aquatic biota and describe current environmental conditions. Future conditions must be predicted by use of watershed modeling guided by municipal land use planning documents (Schueler 2005). Many monitoring and assessment tools are freely available that can be used in urban streams and support restoration practices. For example, HEC-HMS and HEC-RAS can be used predict future stream flows based on the composition of land use types at

ultimate build-out (USACE 2002, 2008). Engineering regime equations can then be applied to assess channel stability once channel morphology and future flows have been established (Copeland et al. 2001; Shields et al. 2003). Indirectly, placement of stormwater detention affects predicted flows and sediment yield; thus, it must be part of the watershed restoration planning so that hydrological modeling can more accurately estimate future flows. Within the current restoration practice, a greater recognization and integration of available monitoring and assessment tools is needed to address the "urban stream syndrome" and to better aid in the recovery of degraded urban streams.

The objective of this paper is to propose a framework for monitoring and assessment protocols that integrates currently available, public domain tools specific to urban and urbanizing watersheds. The framework recognizes the need to assess present and future urban conditions, and to integrate stormwater management into watershed-scale stream restoration plans. It is suggested that this integration can be cost effective because many municipalities already fund watershed hydrological studies, and for larger cities studies are funded through stormwater utility fees. In this proposed framework, monitoring tools are those that quantify baseline conditions and support modeling efforts to predict future channel morphology and water quality. Assessment outcomes from the framework prioritize restoration project needs within watersheds, and support restoration planning and design. Project implementation will always be one reach at a time as currently practiced, however a scheduled program of projects through a watershed planning process would better guarantee watershed recovery.

Framework for Monitoring and Assessment Protocols

The framework for monitoring and assessment protocols has four main components and many supporting protocols within each main component (Figure 1). The four main components are: 1) delineate watershed boundaries to define hydrological management units; 2) conduct watershed-scale analysis using various monitoring and assessment tools; 3) delineate reach boundaries based location of instream hydraulic controls to define reach-scale management units; and, 4) develop a watershed plan for restoration projects. Monitoring and assessment protocols are described below.

The framework is based on an engineering modeling perspective that is essential to predict future streams flows and sediment loads over time accounting for urbanization of the watershed. Coordinated with municipal land use plans, hydrological models (e.g., HEC-HMS, SWMM, WinHSPF) and sediment yield models (e.g., AnnAGNPS, SWAT) can be used to predict future watershed conditions. Watershed-scale assessments rely on many different monitoring tools that are multidisciplinary in origin. These tools quantify necessary data for hydrological/sediment yield model development, and identify spatial problems including channel stability, pollutant sources for poor water quality, and degraded physical habitat. The framework, hierarchical in structure, allows watershed assessments to guide selection of reaches for more detailed modeling and assessment at the reach scale. Reach boundaries are defined at hydraulic controls in the channel, tributary confluences, and major stormwater outfalls to run hydraulic models for channel stability and ecohydraulic habitat investigations (e.g., HEC-RAS, ConCEPTS, PHABSIM, River2D). This hierarchical approach links observed impairments between

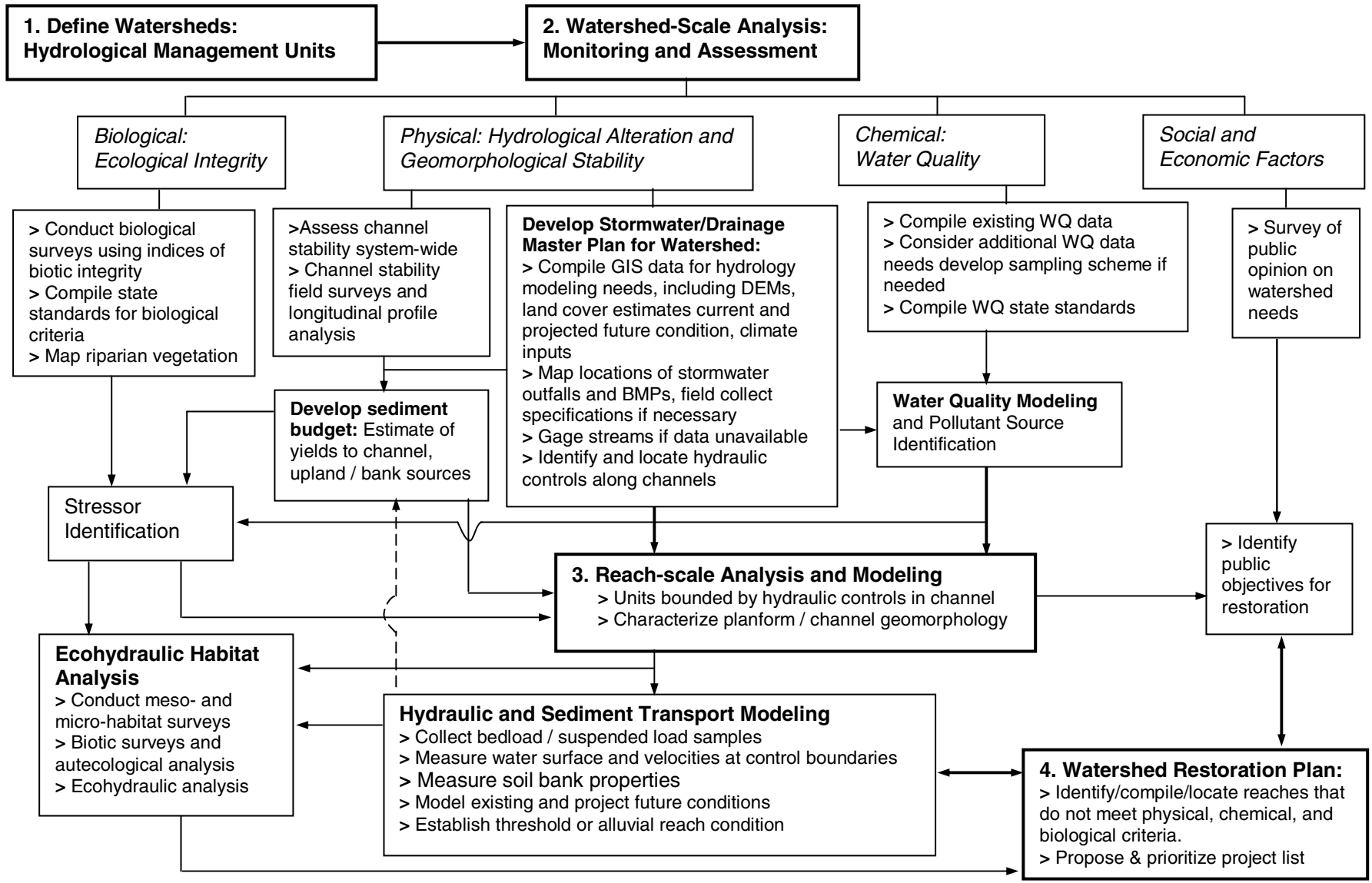

Figure 1. A monitoring and assessment framework for watershed planning to support urban stream restoration practices.

watershed and reach scales, and provides the critical information for appropriate use of stream restoration practices.

Descriptions of the monitoring and assessment protocols within the framework are illustrated below:

1. Define Watersheds: Hydrological Management Units

The first step in any watershed assessment is to define boundaries of the hydrological management unit. Watershed size can vary depending on state, but management units will likely be either HUC-12 or -14 designations. GIS tools are available to delineate watershed boundaries from DEMs, such as ArcHydro and BASINS (EPA 2001). USGS seamless spatial databases can provide the DEMs. The Center for Watershed Protection also provides a general procedural description for delineating watershed boundaries (Schueler 2005).

2. Watershed-scale Analysis: Monitoring and Assessment Protocols

In this framework the focus of the watershed-scale analysis is two-fold: one is to quantify existing conditions of water quality, hydrology, channel morphology and stability, habitat quality, biotic integrity, and mapping urban infrastructure and land uses; and two, is to develop a stormwater/drainage master plan to predict future hydrology and sediment yields. Thorne (1998) and FISRWG (1998) are good resources for basic watershed reconnaissance protocols. Developing a stormwater/drainage master plan requires use of municipal land use plans to model runoff changes from urbanization. In addition, social and economic factors need to be identified, and public opinion must be considered as part of the decision-making process for watershed corrective action plans (Wade et al. 2002). Many urban centers have watershed associations that provide a means of communication between citizens and technical professionals.

Accomplishment of the watershed-scale analysis includes seven tasks, which will be described in detail in a future joint task committee product. The tasks are:

a. Develop stormwater/drainage master plan;
b. Assess channel stability system-wide;
c. Develop watershed sediment budget;
d. Conduct biotic integrity and physical habitat surveys;
e. Conduct riparian vegetation surveys;
f. Conduct water quality analysis and modeling; and
g. Conduct a stressor identification (CADDIS) analysis.

Outcomes from the watershed-scale analysis provide a fundamental understanding of the causes of the impaired condition, identifying reaches that fail to meet water quality standards, levels of biotic integrity, and/or channel stability. At the watershed scale, qualitative field studies are beneficial to field truth the data collected during desktop analysis efforts (Schueler and Kitchell 2005). Qualitative site-specific data are gathered on geomorphic indicators of stream instability, such as bank cutting and mass wasting, local bed erosion, and debris jams that are contributing to local erosion. Rosgen (2006) has developed protocols for watershed-scale reconnaissance and assessment to identify geomorphically unstable reaches that may attribute excessive sediment to channels; the protocols are known as WARSSS (Watershed Assessment of

River Stability and Sediment Supply). The CADDIS analysis can be used to systematically link multiple stressors to sources of biological impairment (USEPA 2000). To accomplish the hydrological and water quality modeling, an essential task requires the drainage network to be delineated into nodes and links, a standard practice for hydraulic modeling in watersheds (Morris 1996).

Key to the effort is to delineate nodes at existing hydraulic controls, i.e., road crossings, bridge or utility crossings, stormwater outfall locations, major channel slope changes, lateral constrictions, or bedrock outcrops. Although seemingly simplistic, identifying hydraulic controls is critical because geomorphic characteristics and reach stability are typically bounded by these controls. From a holistic view of the watershed, an integrated strategy of using both stream restoration practices and stormwater BMPs can be planned. Locations of problem reaches are mapped for interpretation and prioritization of potential project needs. Identified problem reaches may need further monitoring and assessment utilizing tools appropriate at the reach, or local scale.

3. Reach-scale Analysis and Modeling

Once a watershed has been analyzed and reaches identified with potential restoration needs, monitoring and assessment specific to the reach-scale can be implemented at these locations only. Potential restoration needs are based on identified locations of stressors, including geomorphic, water quality, and biological conditions. Geomorphic data collected at this reach scale can be used to quantify stream channel form and processes, and supplement sediment transport modeling activities (Niezgoda and Johnson 2005; Smith and Prestegaard 2005). Reach-scale geomorphic analyses can be accomplished with spreadsheet-type aids, e.g., STREAMS (Ward and Mecklenburg 2005), and GeoTools (Bledsoe et al 2007). Important elements of this analysis include the determination of threshold or alluvial reach conditions. Bank stability models based on fluvial and geotechnical processes include the USDA Bank Stability and Toe Erosion Model (Simon et al. 2008). Sediment transport models to estimate whether aggradation/degradation processes dominate include: SAM, ConCEPTS, CCHE2D, and other models. In addition, stream habitat and biological data can be collected (Barbour et al. 1999; Kaufmann et al. 1999), and ecohydraulic models applied for detailed ecological assessments (Schwartz 2003; Bockelmann et al. 2004; Pasternack et al. 2004).

Accomplishment of the reach-scale analysis includes three tasks, which will be described in detail in a future joint task committee product. The tasks are:

a. Geomorphic and bed sediment characterization;
b. Hydraulic and sediment transport modeling;.and,
c. Ecohydraulic habitat analysis.

Outcomes from the reach-scale analyses include a prioritization of restoration needs, and compilation of monitoring data that can support the design process. Geomorphic, hydraulic, and ecological data are integrated in this analysis to recommend ecohydaulic habitat-based restoration projects (Rabeni and Jacobson 1993; Schwartz et al. 2001; Jannsson et al. 2005). If additional monitoring data are needed for project design, a monitoring plan can be developed.

4. Watershed Restoration Plans

Watershed restoration plans are developed based on urban-specific monitoring and assessment efforts at both the watershed- and reach-scales. A system-wide interpretation of the data is completed and reaches with restoration needs are prioritized. Stormwater BMPs must also be identified and prioritized because future stream flows are dependent on implementation of these practices. The final watershed restoration plan must be achieved through community acceptance, where technical professionals and community leaders discuss the technical outcomes from the monitoring and assessment findings.

Summary Conclusions

Because urbanizing streams are impaired by multiple stressors, and these stream systems are continually evolving to a new geomorphic state while infrastructure development persists, approaches to stream restoration will differ from those applied to rural watersheds. Specific monitoring and assessment protocols are needed for urban watersheds, relying on engineering-based hydrological models to predict future stream flows as impervious surfaces increase. This does not preclude the use of other geomorphological- and ecological-based tools; they are needed as well. Watershed restoration plans must incorporate thorough hydrological modeling of existing and future conditions, including the use of stormwater management BMPs. Restoration objectives need to be clearly linked with quantified stressors, to systematically rehabilitate impaired watersheds. Because municipalities with stormwater management programs typically have completed hydrological-based modeling for existing and future conditions, it would be cost effective to develop watershed restoration plans that integrate stormwater management BMPs and instream restoration practices.

Acknowledgements

Many thanks to members on the ASCE/EWRI Urban Stream Committee of the Urban Water Resources Research Council and the River Restoration Committee of the Hydraulics and Waterways Council that provided input on this group effort.

References

Barbour MT, Gerritsen J, Synder BD, Stribling JB. 1999. *Rapid Bioassessment Protocols forUse in Wadable Streams and Rivers: Periphyton, Benthic Macroinvertebrates, and Fish*. EPA 841-B-99-002. US Environmental Protection Agency, Office of Water, Washington DC.

Bernhardt ES, Palmer MA. 2007. Restoring streams in an urbanizing world. *Freshwater Biology* **52**: 738-751.

Bernhardt ES, Sudduth EB, Palmer MA, Allan JD, Meyer JL, *and 7 others*. 2007. Restoring rivers one reach at a time: results from a survey of U.S. river restoration practitioners. *Restoration Ecology* **15**(3): 482-493.

Bernhardt ES, Palmer MA, Allan JD, Alexander G, Barnas K, Brooks S, Carr J, *and 15 others*. 2005. Synthesizing U.S. River Restoration Efforts. *Science* **308**: 636-637.

Bledsoe BP, Watson CC. 2001. Effects of urbanization on channel stability. *Journal of the American Water Resources Association* **37**: 255-270.

Bledsoe BP, Brown MC, et al. 2007. Geotools: a toolkit for fluvial systems analysis. *Journal of the American Water Resources Association* **43**(3): 757-772.

Bockelmann BN, Fenrich EK, Lin B, Falconer RA. 2004. Development of ecohydraulics model for stream restoration and river restoration. *Ecological Engineering* **22**: 227-235.

Booth DB. 1990. Stream channel incision following drainage basin urbanization. *Water Resources Bulletin* **26**: 407-417.

Booth DB, Jackson CR. 1997. Urbanization of aquatic systems - degradation thresholds, stormwater detection, and the limits of mitigation. *Journal of the American Water Resources Association* **33**: 1077-1090.

Brown K. 2000. *Urban Stream Restoration Practices: An Initial Assessment*. Center for Watershed Protection, Ellicott City, MD. www.cwp.org.

Carle MV, Halpin PN, Stow CA. 2005. Patterns of watershed urbanization and impacts on water quality. *Journal of the American Water Resources Association* **41**(3): 693-708.

Chin A, Gregory KJ. 2005. Managing urban river channel adjustments. *Geomorphology*, **69**: 28-45.

Copeland RR, McComas DN, Thorne CR, Soar PJ, Jonas, MM, Fripp JB. 2001. Hydraulic Design of Stream Restoration Projects. *Technical Report ERDC/CHL TR-01-28*, U.S. ACOE: Engineer Research & Development Center; Vicksburg, MS.

Deason JP, Dickey GE, Kinnell JC, Shabman LA. 2009. An integrated planning framework for urban river restoration. *Journal of Water Resources Planning and Management* (in review).

Federal Interagency Stream Restoration Working Group (FISRWG). 1998. *Stream corridor restoration: principles, processes and practices.* National Technical Information Service, U.S. Dept. of Commerce, Springfield, Virginia. http://www.nrcs.usda.gov/ technical/ stream_restoration.

Fischenich, JC 2001. Technologies for urban stream restoration and watershed management. U.S. Army Corps of Engineers *Technology News: Ecosystem Management and Restoration Program.* EMRRP Bulletin No. 01-1.

Hammer TR. 1972. Stream channel enlargement due to urbanization. *Water Resources Research* **8**: 1530-1540.

Jannsson R, Backx H, Buolton J, Dixon M, Dudgeon D, Hughes FMR, Nakamura K, Stanley EH, Tockner K. 2005. Stating mechanisms and refining criteria for ecologically successful river restoration: a comment on Palmer *et al*., 2005. *Journal of Applied Ecology* **42**: 218-222.

Johnson PA, Brown ER. 2001. Incorporating uncertainty in the design of stream channel modifications. *Journal of the American Water Resources Association* **37**(5): 1225-1236.

Kang RS, Marston RA. 2006. Geomorphic effects of rural-to-urban land use conversion on three streams in the Central Redbed Plains of Oklahoma. *Geomorphology* **79**: 488-506.

Kaufmann PR, Levine P, Robinson EG, Seeliger C, Peck DV. 1999. *Quantifying Physical Habitat in Wadable Streams*. EPA/620/R-99/003. US Environmental Protection Agency, Office of Research and Development, Washington DC.

MacRae, CR. 1996. Experience from morphological research on Canadian streams: is control of the two-year frequency runoff event the best basis for stream channel protection? In *Effects of Watershed Development and Management on Aquatic Ecosystems*. Roesner LA (ed). American Society of Civil Engineers, Reston, VA; 141-162.

Meyer JL, Paul MJ, Taulbee WK. 2005. Stream ecosystem function in urbanizing landscapes. *Journal of the North American Benthological Society* **24**(3): 602-612.

Moerke AH, Lamberti GA. 2003. Responses in fish community structure to restoration of two Indiana streams. *North American Journal of Fisheries Management* **23**: 748-759.

Moerke AH, Gerard KJ, Latimore JA, Hellenthal RA, Lamberti GA 2004. Restoration of an Indiana, USA stream: Bridging the gap between basic and applied lotic ecology. *Journal of the North American Benthological Society* **23**(3): 647-660.

Morris S. 1996. Evaluation of urban stream corridor restoration design alternatives using HEC-2. *Journal of the American Water Resources Association* **32**(5): 891-899.

Niezgoda SL, Johnson PA. 2005. Improving the urban stream restoration effort: Identifying critical form and processes relationships. *Environmental Management* **35**: 579-592.

Paul MJ, Meyer JL. 2001. Streams in the urban landscape. *Annual Review of Ecological Systems* **32**: 333-365.

Palmer MA, Bernhardt ES, Allan JD *and 19 others*. 2005. Standards for ecologically successful river restoration. *Journal of Applied Ecology* **42**: 208-217.

Pasternack GB, Wang CL, Merz JE. 2004. Application of a 2D hydrodynamic model to design of reach-scale spawning gravel replenishment on the Mokelumme River, California. *River Research and Applications* **20**: 205-225.

Rabeni CF, Jacobson RB. 1993. The importance of fluvial hydraulics to fish-habitat restoration in low-gradient alluvial streams. *Freshwater Biology* **29**: 211-220.

Rosgen D. 2006. *Watershed Assessment of River Stability and Sediment Supply (WARSSS).* Wildland Hydrology, Ft. Collins, Colorado.

Schueler T. 2005. *An Integrated Framework to Restore Small Urban Watersheds.* Version 2.0. Center for Watershed Protection, Ellicott City, MD. www.cwp.org.

Schueler T, Kitchell A. 2005. *Methods to Develop Restoration Plans in Small Urban Watersheds.* Version 2.0. Center for Watershed Protection, Ellicott City, MD. www.cwp.org.

Schwartz JS. 2003. Use of a 2D hydrodynamic model for stream restoration design of high-flow habitat in low-gradient Midwest streams. Pages 242-251 In *Proceedings of the Symposium on Protection and Restoration of Urban and Rural Streams* June 23-25, 2005, Philadelphia, PA. M. Clar, D. Carpenter, J. Gracie, and L. Slate (eds). American Society of Civil Engineers, Reston, VA.

Schwartz JS, Herricks EE. 2007. Evaluation of pool-riffle naturalization structures on habitat complexity and the fish community in an urban Illinois stream. *River Research and Applications* **23**: 451-466.

Schwartz JS, Herricks EE, Rhoads BL. 2001. Integrating geomorphology, hydraulics, and ecological criteria to support stream naturalization in East-Central Illinois. In *Proceedings from the World Water and Environmental Resources Congress*. Orlando, Florida, May 2001. American Society of Civil Engineers, Reston, VA.

Shields FD, Copeland RR, Klingeman PC, Doyle MW, Simon A. 2003. Design for stream restoration. *ASCE Journal of Hydraulic Engineering* **129**(8): 575-584.

Simon A, Thomas R, Curini A, Bankhead N. 2008. *Bank Stability and Toe Erosion Model User's Manual version 5.0*. USDA National Sedimentation Laboratory, Oxford, MS.

Slate LO, Shields FD, Schwartz JS, Carpenter DD, Freeman G. 2007. Engineering design standards and liability for stream channel restoration. *ASCE Journal of Hydraulic Engineering* **133**: 1099-1102.

Smith SM, Prestegaard KL. 2005. Hydraulic performance of a morphology-based stream channel design. *Water Resources Research* **41** (W11413): doi:10.1029/ 2004WR003926.

Thorne CR. 1998. *Stream Reconnaissance Handbook*. John Wiley & Sons, Ltd., Chichester, UK.

USACE. 2008. *HEC-HMS Hydrologic Modeling System, User's Manual Version 3.3*. US Army Corps of Engineers, Hydrologic Engineering Center, Davis CA.

USACE. 2002. *HEC-RAS River Analysis System, User's Manual Version 3.1*. US Army Corps of Engineers, Hydrologic Engineering Center, Davis CA.

USEPA 1997. *Compendium of Tools for Watershed Assessment and TMDL Development*. EPA 841-B-97-006. US Environmental Protection Agency, Office of Water, Washington D.C.

USEPA. 1999. *Protocols for Developing Sediment TMDLs.* EPA 841-B-99-004, US Environmental Protection Agency, Office of Water, Washington D.C.

USEPA. 2000. *Stressor Identification Guidance Document*. EPA/822/B-001/025. US Environmental Protection Agency, Office of Water, Washington DC.

USEPA. 2003. *Better Assessment Science Integrating Point and Nonpoint Sources, BASINS version 3.0*. EPA 823-B-01-001. U.S. Environmental Protection Agency, Office of Water, Washington DC.

Wade RJ, Rhoads BL, Rodriguez J, Newell M, Wilson D, Herricks EE, Bombardelli F, Garcia, M, Schwartz JS. 2002. Integrating science and technology to support stream naturalization near Chicago, Illinois. *Journal of the America Water Resources Association* **38**: 931-944.

Walsh CJ, Roy AH, Feminella JW, Cottingham PD, Groffman PM, Morgan RP. 2005. The urban stream syndrome: current knowledge and the search for a cure. *Journal of the North American Benthological Society* **24**(3): 706-723.

Ward AD, Mecklenburg DE. 2005. Design discharge procedures in the STREAMS spreadsheet tools. In *Proceedings from the World Water and Environmental Resources Congress*. Anckorage, AK; May 2005. American Society of Civil Engineers, Reston, VA.

Post Project Appraisal of Riparian, Wetland, and Aquatic Habitat Restoration at Best Slough, Beale Air Force Base, Marysville, CA

M.R. Tompkins[1], D. Mengel[2], and T. Hamaker[3]

[1] CH2M HILL, 155 Grand Avenue, Suite 1000, Oakland, CA 94612; PH (510) 587-7793; email Mark.Tompkins@ch2m.com
[2] CH2M HILL, 322 East Front Street, Suite 200, Boise, ID 83702; PH (208) 345-5314; email Denny.Mengel@ch2m.com
[3] CH2M HILL, 2525 Airpark Drive, Redding, CA 96001-2443; PH (530) 243-5831; email Tim.Hamaker@ch2m.com

ABSTRACT

Best Slough flows through Beale Air Force Base and used to come into contact with groundwater contaminated by trichloroethene (TCE) at Site 17 during low flow periods when it was a gaining stream. An interim remedial action was developed for Site 17 to halt further migration of the contaminated groundwater plume by surrounding it with a slurry wall and establishing a phytoremediation system on top of the site within the slurry wall. The portion of Best Slough in contact with the contaminated groundwater plume was realigned upgradient of the plume with more natural channel morphology and riparian vegetation as well as sufficient hydraulic capacity and channel stability to protect the remedial features on the site. Channel banks were designed with terraced slopes to provide additional acreage for riparian vegetation habitat. Side-channel islands were included in the channel design to provide isolated riparian habitat for waterfowl as well as for aquatic reptiles and amphibians. A complex of deep-water channels was incorporated into the design to provide rearing habitat and thermal refuge for warmwater fish. And all channel features were incorporated, where possible, into the overall erosion control and bank stability design for the channel. Project construction was completed in 2000, and periodic site visits have documented development of aquatic and riparian habitat features and performance of the channel realignment and restoration elements of the project with respect to their design objectives. We summarize observations of channel, riparian, and vegetation performance over the past eight years and present lessons learned from this complex, multi-objective river restoration project.

INTRODUCTION

Past land-use practices on Air Force Bases throughout the United States altered channel form in many Base streams. In addition, past waste disposal practices contaminated soil adjacent to Base streams and degraded water quality in Base streams connected to groundwater (Mengel et al 2000). In the mid 1900's, a 500 meter reach of Best Slough on Beale Air Force Base in an area known as Site 17 (Figure 1) was channelized. Riparian vegetation was also removed in the reach flowing through Site 17. The intent of both of these modifications was to enhance agricultural use of the area (Bruce Reinhardt, Beale Air Force Base, personal communication). Also in the mid 1900's, several years after the channel modifications occurred, several thousand liters of trichloroethylene (TCE), a known carcinogen, were disposed of by draining large drums of the material into shallow pits adjacent to Best Slough (Bruce Reinhardt, Beale Air Force Base,

personal communication). The TCE infiltrated the soil surface and collected on the underlying bedrock about 12 meters deep. TCE also entered the groundwater and flowed into Best Slough during the summer months. Though the TCE in Best Slough volatilized quickly, potentially harmful concentrations were regularly detected. The uniform geometry and degraded water quality (from TCE and increased temperatures) in this 500 meter reach of Best Slough impaired local habitat conditions and created a discontinuity in the aquatic and riparian habitat present upstream and downstream of Site 17.

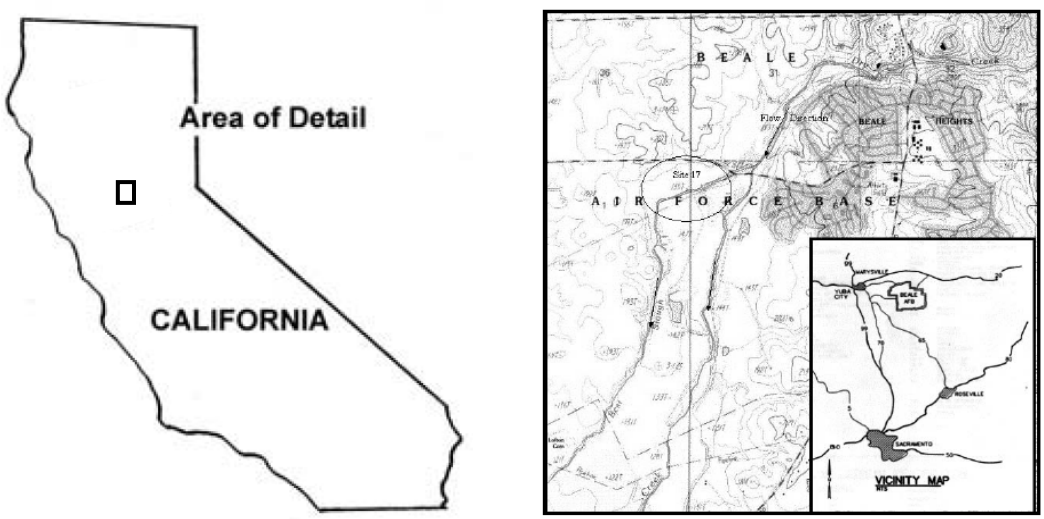

Figure 1: Location maps for Beale Air Force Base and Best Slough

In the 1990's, the Air Force Center for Environmental Excellence (AFCEE) initiated a process to remediate the contaminated soil and groundwater on Air Force bases throughout the country and, when possible, restore or enhance stream corridors adjacent to the contamination sites. As part of this process, Beale Air Force Base designed a solution to the groundwater contamination and stream corridor habitat degradation problems at Site 17. The design (Figure 2) consisted of the following components:

- Impervious slurry wall enclosing the TCE-contaminated area
- Native tree phytoremediation system within the area enclosed by the slurry wall
- Realignment of the reach of Best Slough flowing through the contaminated area
- Temporary and permanent erosion control on the banks of the realigned reach
- Aquatic and riparian habitat creation in and along the realigned reach

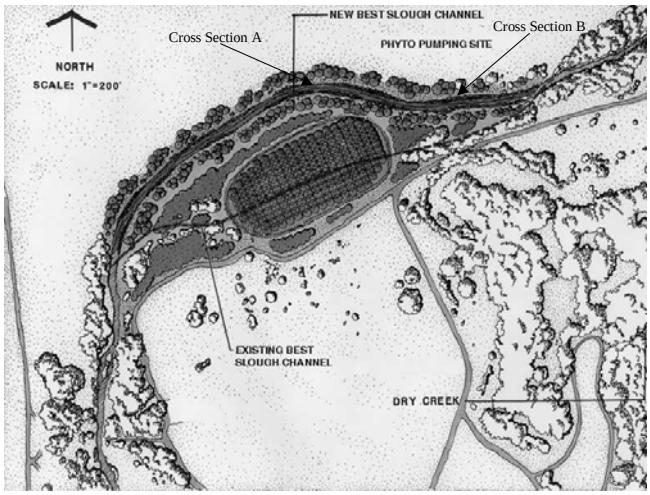

Figure 2: Conceptual design drawing of the Best Slough realignment and restoration project. The locations of the cross sections surveyed for this study are also shown.

The project design team selected a realignment route that removed Best Slough from contact with the contaminated area and designed channel planform and geometry that resembled the planform and geometry of the system upstream and downstream of the project site. The design team selected a variety of erosion control and habitat creation techniques for this project. Erosion control techniques included bioengineering (willow pole plantings, brush bundles, and root-wad boulder clusters), biodegradable fabrics, riprap, and various combinations of each of these treatments. Habitat creation techniques included protection of a backwater wetland area, varied channel geometry, revegetation with native plants, and placement of woody debris. When possible, the design team selected techniques that provided both erosion control and habitat creation benefits.

The design was completed in 1999 and construction was completed in August of 2000. The design team developed a plan and budget for post-project monitoring of chemical, physical, and biological conditions, however funds were only available for chemical monitoring. Therefore, no formal monitoring of channel form, vegetation success, or habitat colonization was performed in the first year after construction was completed. Because of the complexity of fluvial systems and the length of time required to observe change in restored streams, the true success of stream restoration projects can be difficult to adequately assess (Kondolf and Micheli 1995) without such monitoring. We conducted a quantitative post project appraisal approximately one year after construction and a qualitative post project appraisal approximately nine years after construction to assess how the realigned and restored stream corridor performed with respect to the objectives of the project. This simple study highlighted the importance of post-project monitoring to the evaluation of the project and to the planning and design of future stream restoration projects.

STUDY APPROACH

We reviewed the design documents for the geomorphic channel realignment, riparian revegetation, and aquatic habitat enhancement elements of this project (CH2M HILL 1999). We also reviewed the “as-built” drawings (Versar 2000) produced by the contractor at the

completion of the project. The design documents and as-built drawings provided information about the objectives and design criteria of the project, and the physical conditions at the project site immediately after construction was completed. Our post-project appraisal protocol was designed to provide useful information about the performance of the realignment and restoration project on Best Slough and was divided into two general categories:

- Geomorphology
- Biology

Geomorphology

In 2001 (approximately one year after construction) we collected information on the topography of the realigned channel and banks by surveying longitudinal profiles and channel cross sections. We measured longitudinal profiles along the channel thalweg and along the tops of both banks of the realigned reach and compared them to the "as-built" profiles surveyed immediately after the project was completed. We also surveyed two channel cross sections in locations that we suspected would be most prone to change given their location and configuration in the realigned reach, and compared them with the "as-built" geometry generated at the completion of the project. We also identified the location of the base-flow water surface elevation relative to the elevation of specific channel design features described in the design documents. In 2009 (approximately eight years after construction), we observed and documented reach-scale geomorphic conditions and compared them with conditions observed in 2001 and in 2003.

Biology

In 2001, we estimated percent cover in each of the five revegetation zones (tule and emergent wetland, scrub riparian, mixed riparian, valley oak, and valley oak and cottonwood) identified in the riparian revegetation document by randomly sampling three different square meter plots in each zone. We visually estimated percent cover in each sample plot and then averaged the three values for each zone. We also collected kicknet samples in each of the aquatic habitat enhancement treatments to assess aquatic insect colonization. We performed three kicknet samples at each site and recorded the families present at each site. In 2009, we observed and documented reach-scale biological conditions (primarily riparian vegetation condition) and compared them with conditions observed in 2001 and in 2003.

RESULTS AND DISCUSSION

Geomorphology

The slope of the thalweg through the project reach immediately after construction ("as-built") and in 2001 ("post-project") was essentially flat. However, the project team designed a long, relatively deep run-pool (Figure 3) in the middle third of the realigned reach to provide cool water habitat and refugia for resident fish. As described in the aquatic habitat enhancement design document, the run-pool design depth was based on the depths of naturally formed pools upstream and downstream of the project area. However, the length of the run-pool was not based on natural channel forms observed elsewhere in Best Slough. The 2001 post-project profile shows that sediment had accumulated at the upstream end of the run-pool. We also surveyed longitudinal profiles along the top-of-bank on both sides of Best Slough in 2001. Because the

winter of 2000 was relatively dry, and no overbank flows occurred in the realigned reach, only insignificant changes (due to vegetation) were apparent in the top-of-bank longitudinal profiles. The extensive development of microtopography on the channel banks and on the floodplain adjacent to the top of bank observed in 2009 suggests that overbank flow events have occurred between 2001 and 2009.

We surveyed two cross sections in the realigned reach of Best Slough (A and B in Figure 2) in 2001. Cross section A (Figure 4), located in the deep run-pool, shows the cross-sectional component of the sediment accumulation observed in the longitudinal profile of the thalweg in 2001. It appeared that additional sedimentation had occurred between 2001 and 2009, however some deeper areas were still present in 2009. These smaller deep pools may have persisted in this portion of the realigned reach due to complex local hydraulics. Therefore, it appears that the extensive excavation required to create the large run-pool was probably not necessary or sustainable with respect to habitat creation goals. The resources used to excavate this large area could have been used to determine the geomorphic processes responsible for creating the deep pools upstream and downstream of the project reach and to restore those processes to create sustainable pool habitat under the existing hydrologic conditions. Cross section B (Figure 5) was located near the upstream end of the realigned reach of Best Slough. In this section of the realigned and restored reach, the design team created a terraced cross section (Figure 5) to support emergent wetland species. This cross section also shows sediment accumulation in 2001. This accumulation could be attributed to the absence of flows large enough to scour sediment from the pool in the winter of 2001. In 2009, this cross section had developed extensive aquatic and riparian vegetation that has likely accelerated deposition. In general, this reach appears have become more geomorphically stable over the past eight years.

We also surveyed the water surface elevation in 2001 as an assessment of the geomorphic design, the revegetation effort, and the aquatic habitat enhancements in the context of the base flow water surface elevation. The design documents supporting each of these project elements stressed the importance of the base flow water surface elevation to the performance of each element of the realigned stream reach. The measured water surface elevation is shown on the thalweg longitudinal profile plot and the cross section plots (Figures 3, 4, and 5, respectively). No significant rainfall had occurred in the Best Slough watershed immediately prior to the 2001 survey, so the measured water surface elevation was a good approximation of the base flow water surface elevation at the project site. The revegetation design document and the geomorphic design document indicated that the terrace on this cross section should have been approximately 0.15 to 0.30 meters below the base flow water surface elevation. At the time of the 2001 survey, the base flow water surface elevation was approximately 0.63 meters above the terrace elevation (Figure 5). Several beaver dams downstream of the project reach appeared to be controlling water surface elevations. It appears that ongoing beaver activity between 2001 and 2009 has controlled base flow water surface elevations and therefore the establishment and succession of aquatic and riparian vegetation.

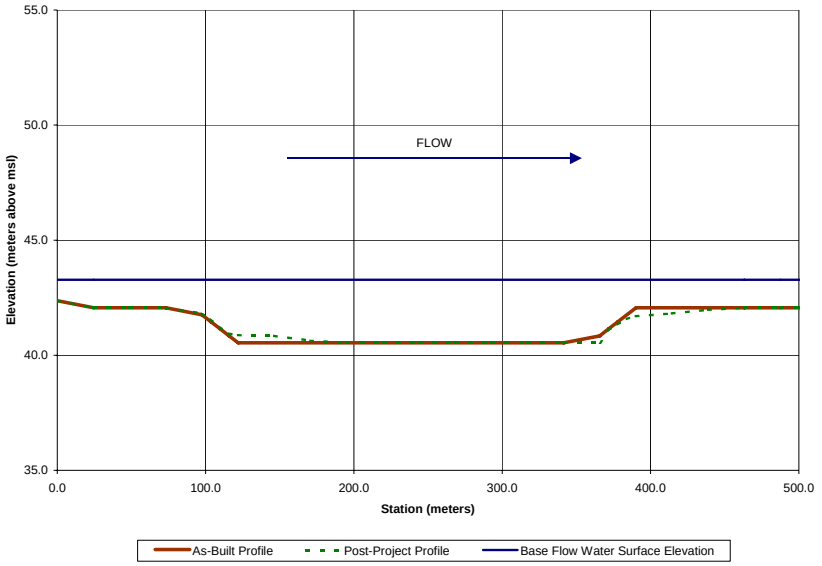

Figure 3: Thalweg longitudinal profile showing as-built elevations and elevations one year after construction. The location of the large run-pool is indicated in the middle third of the profile.

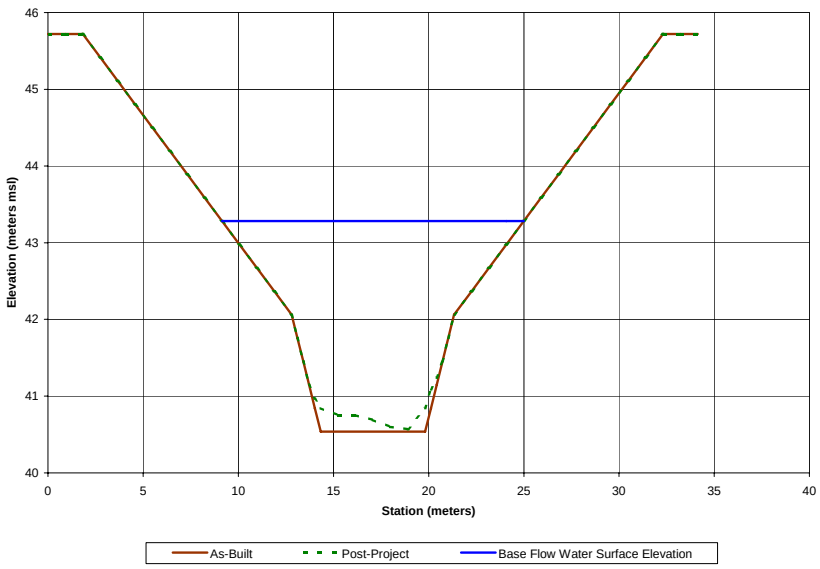

Figure 4: Channel cross section showing as-built elevations and elevations one year after construction. The location of this cross section is shown in Figure 2. Note the sediment accumulation at the head of the run-pool.

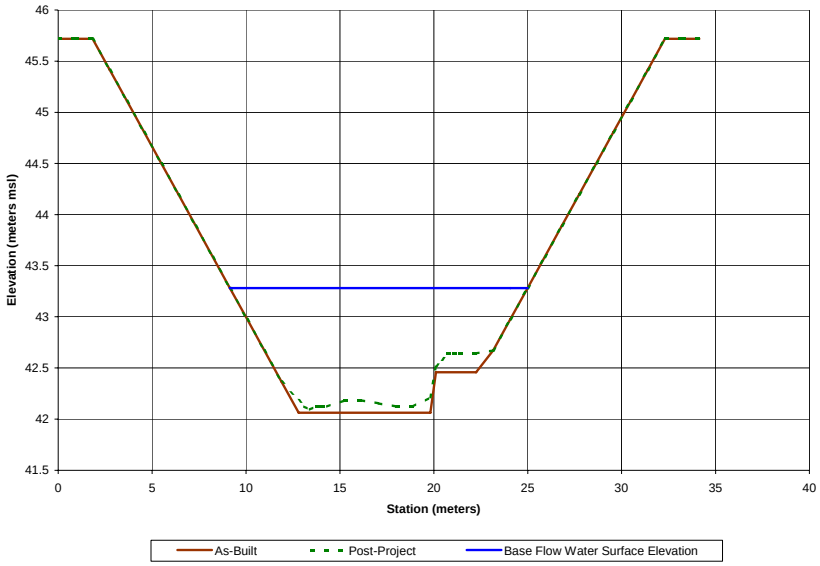

Figure 5: Channel cross section showing as-built elevations and elevations one year after construction. The location of this cross section is shown in Figure 2. Note the sediment accumulation on the terraced portion of the cross section.

Biology

Figures 6 and 7 show the same location just after construction of the realigned and restored reach was completed and in 2001. To the casual observer, the rapid and lush establishment of riparian vegetation could be seen as an indication of project success. However, a structured examination of the vegetation indicated potential performance issues in 2001. Table 1 shows the estimated percent cover of each of the five planting zones specified in the revegetation design document. The percent cover of the scrub riparian, mixed riparian, valley oak, and valley oak and cottonwood plant assemblages were all at or above the desired levels listed in the revegetation design document. However, the tule and emergent wetland plantings covered only 24% of the area in the zones where they were planted. This is approximately 50% less than the desired area listed in the revegetation design document. The high base-flow water surface elevation described in the section above is the most likely reason that the tule and emergent wetland species planted on the channel terraces had not become successfully established by 2001. However, by 2009 coverage of emergent and wetland vegetation appeared to meet and in many locations exceed design objectives.

Table 1: Percent cover in the design revegetation zones

Revegetation Zone	*Percent Cover*
Tule and Emergent Wetland	24%
Scrub Riparian	81%
Mixed Riparian	90%
Valley Oak	75%
Valley Oak and Cottonwood	73%

Revegetation zones were shown on the design drawings and the native species to be planted in each zone were listed in the revegetation design document.



Figure 6: Realigned channel before revegetation. The new channel banks were completely bare before vegetation and erosion control fabrics were installed.



Figure 7: Realigned channel 1 year after construction. The flowering plants are native lupines and the grasses include a range of native riparian species.

We also sampled for the presence and absence of aquatic insect families in the three primary aquatic habitat restoration types included in this project to assess the early colonization in each area in 2001. Table 2 lists the aquatic insect families collected from the aquatic habitat restoration areas. The backwater wetland was a portion of the old Best Slough channel that the design team connected to the new channel alignment as an off-channel slackwater area. The insect families collected in this area were indicative of lentic habitats (Thorp and Covitch 1991), and were dominated by predatory damselfly nymphs (Coenagrionidae). This could indicate the local presence of high concentrations of prey species, as damselflies are commonly voracious feeders. We collected very few aquatic insects (4 individuals) from the rootwad / boulder clusters in 2001. We also collected crayfish and small fish fry from these structures. This could indicate that the root-wad / boulder clusters were an inappropriate choice for aquatic habitat in Best Slough. However, we also observed several bass and sunfish in and around the root-wad / boulder clusters in 2001, so the lack of aquatic insects could also have been due to fish predation. We collected high numbers (113 individuals) of mayfly larvae (baetidae) from the shallow water habitat areas in 2001. The shallow water habitat areas of the realigned reach generally included banks with willow pole plantings interspersed with native riparian vegetation, a toe-of-slope constructed with 0.15 – 0.30 meter diameter riprap, and invert elevations similar to the invert elevations upstream and downstream of the realigned reach. Mayflies are commonly sensitive to poor water quality conditions (Thorp and Covitch 1991) and their presence indicates that water quality in this section of the realigned reach of Best Slough is at least good enough for organisms with pollution tolerance levels similar to Baetid mayflies. We also collected high numbers (54 individuals) of caddis fly larvae (hydropsychidae) in 2001. These organisms feed on fine particulate organic matter (Merritt and Cummins 1996) and their abundance indicates an adequate nutrient supply in this section of the realigned reach. The aquatic insect colonization in the shallow water habitat areas and the backwater wetland area in 2001 indicates that these areas were appropriately designed and created habitat for aquatic species. The appropriateness of the root-wad / boulder cluster design was uncertain in terms of aquatic insects, however it appears to have been beneficial to fish. No sampling was conducted in 2009, however aquatic insect observations indicated that aquatic insect abundance and diversity has likely increased over the past eight years.

Table 2: Aquatic insect families collected in aquatic habitat restoration areas

Habitat Type	*Aquatic Insect Families Present*
Backwater Wetland	Coenagrionidae, Libellulidae, Carabidae, Caenidae, Ameletidae
Root-wad / Boulder Clusters	Corixidae, Chironomidae, Caenidae
Shallow Water Habitat	Hydropsychidae, Baetidae, Simuliidae, Corduliidae, Coenagrionidae, Haliplidae, Philopotamidae, Chironomidae

CONCLUSION

We observed specific successes and failures of the Best Slough realignment and restoration project through a simple post-project appraisal one year and eight years after construction. Elements of the geomorphic design, the revegetation design, and the aquatic habitat design have been successful to date. However, the resources expended to design and build this project could probably have been used more efficiently. Additional pre-design surveys could have provided more appropriate pool lengths and aquatic habitat types, and indicated the importance of beaver activity on water surface elevations. The observations from this simple post-project appraisal highlight the importance of post-project monitoring programs and showed that even a relatively unsophisticated monitoring program can detect problems that could easily be remedied by adaptive management actions.

REFERNCES

California Department of Water Resources – Division of Flood Management. California Data Exchange Center. http://cdec.water.ca.gov/cgi-progs/reports/PRECIPOUT.1998.html.

CH2M HILL. 1999. Site 17 Interim Remedial Action Best Slough Realignment and Restoration Design. Prepared for Beale Air Force Base – Air Force Center for Environmental Excellence.

Downs, P.W. and G.M. Kondolf. In press. Post-project appraisals in adaptive management of river channel restoration.

Kondolf, G.M. and E.R. Micheli. 1995. Evaluating stream restoration projects. Environmental Management 19:1 pp. 1-15.

Mengel, D., Baisal, M., Lawson, P., and M.R. Tompkins. Riparian habitat restoration and in-situ trichloroethylene remediation at Best Slough, Beale Air Force Base, California. Proceedings from the American Water Resources Association 2000 Annual Meeting.

Merritt, R.W. and K.W. Cummins. 1996. An Introduction to the Aquatic Insects of North America. Chapter 17. Kendall/Hunt Publishing Company. Dubuque.

Thorp, J.H. and A.P. Covitch. 1991. Ecology and Classification of North American Freshwater Macroinvertebrates. Chapter 17. Academic Press. San Diego.

Versar Construction Company. 2000. As-built drawing set for the Site 17 Interim Remedial Action Project. Prepared for Beale Air Force Base – Air Force Center for Environmental Excellence.

Predicting Streambank Seepage Flows: Sensitivity to Soil Properties and Layering

D.M. Heeren[1], G.A. Fox[2], M.L. Chu-Agor[3], and G.V. Wilson[4]

[1]Research Engineer, Department of Biosystems and Agricultural Engineering, Oklahoma State University, 114 Agricultural Hall, Stillwater, Oklahoma 74078; PH (405) 744-8459; FAX (405) 744-6059; email: derek.heeren@okstate.edu

[2]Assistant Professor, BAE, OSU, 120 Agricultural Hall, Stillwater, OK 74078-6016; PH (405) 744-8423; FAX (405) 744-6059; email: garey.fox@okstate.edu

[3]Ph.D. Candidate, BAE, OSU, 120 Agricultural Hall, Stillwater, OK 74078-6016; PH (405) 744-5431; FAX (405) 744-6059; email: magor@okstate.edu

[4]Research Hydrologist, Watershed Physical Processes Research Unit, USDA-ARS National Sedimentation Laboratory, 598 McElroy Drive, Oxford, MS 38655; PH (662) 232-2927; FAX (662) 281-5706; email: gvwilson@ars.usda.gov

2009 ASCE EWRI World and Environmental Resources Congress

Abstract. Streambank failures result in loss of land and increased stream sediment loads. Variably saturated flow models integrated with bank stability models are being used to predict bank failure; however, understanding of the level of soil characterization necessary to predict when seepage contributes to bank failure is needed. ROSETTA, a pedotransfer function, was used to estimate hydraulic parameters for various levels of soil data (from texture class to saturated hydraulic conductivity, K_s). A two-dimensional groundwater flow code, SEEP/W, was used to model a hypothetical streambank and estimate seepage velocity. Results suggested that K_s and/or percent clay measurements are necessary to adequately predict seepage. A layered bank was also simulated with several combinations of soil types. Results indicated that only one order of magnitude difference in K_s (equivalent to a resistance ratio of 10) may be necessary to induce perching and seepage from the top layer. This research suggested that, if a field reconnaissance is performed to locate streambanks susceptible to perching, K_s and/or bulk density measurements are necessary to indicate the presence of a restrictive layer.

Introduction

Streambank failures result in loss of land, increased stream sediment loads, and increased nutrient loads if soil nutrient levels are high. At least three groundwater mechanisms of streambank failure have been observed. An increase in soil moisture can reduce cohesion and soil frictional strength. The importance of this instability mechanism has led to work by Darby et al. (2007) and Rinaldi et al. (2008) in linking groundwater flow, fluvial hydraulics, and streambank stability models. Second, seepage gradient forces exert body forces on streambank sediment proportional to the hydraulic gradient (Lobkovsky et al. 2004), which has been incorporated into slope stability analyses for noncohesive banks. Finally, undercutting due to fluvial or seepage erosion can contribute significantly to bank collapse (Fox et al. 2006; Wilson et al. 2007).

Hagerty (1991) discussed the difficulty of identifying sites with seepage in the field, especially since seepage is often intermittent. Could sites with the potential for seepage erosion be predicted during a field reconnaissance based on easily defined soil properties (e.g. textural class)? Seepage often results from a perched water table above a restrictive layer. It is uncertain what difference in saturated hydraulic conductivity (K_s) is required to induce seepage. Field observations of seepage include 1.0-2.5 order of magnitude difference in K_s (Fox et al. 2007; Wilson et al. 2007).

Variably saturated flow models integrated with bank stability models are used to predict bank failure (Chu-Agor et al. 2008a,b); however, an improved understanding of the soil conditions under which seepage mechanisms become prevalent is needed. Groundwater seepage is driven by several soil hydraulic properties. However, data on water retention and hydraulic conductivity functions often are not available and are uneconomical and/or laborious to acquire. Pedotransfer functions (PTFs) are a convenient option for estimating missing parameters based on readily available soil data. ROSETTA is a neural network model that predicts hydraulic parameters (residual water content (θ_r), saturated water content (θ_s), van Genuchten parameters (α and n), and K_s) for various levels of soil data (Schaap et al. 2001).

It is unknown what degree of site characterization is necessary, and what soil properties should be targeted in the characterization, in order to predict bank failure from seepage erosion. The objective of this study was to determine the necessary level of soil data needed to adequately model streambank seepage velocity and to predict the occurrence of perched seepage.

Materials and Methods

Flow Modeling: SEEP/W & ROSETTA

Following Chu-Agor et al. (2008a), a hypothetical streambank was modeled with SEEP/W (Geo-Slope International Ltd.) to simulate the variations in the soil-water pressure and cumulative discharge. SEEP/W is a finite element model of Richards' equation for two-dimensional variably saturated flow (Krahn 2004). Specifying and assigning material properties in SEEP/W involves defining the water retention function, $\theta(h)$, and the hydraulic conductivity function, $K(h)$, where h is the soil-water pressure (Krahn 2004). The van Genuchten (1980) model, which requires hydraulic parameters (θ_r, θ_s, α, n, and K_s), was used to represent $\theta(h)$and $K(h)$.

Hydraulic parameters were estimated with the ROSETTA program (Schaap et al. 2001), which is composed of five hierarchical PTFs for five levels of input data: soil textural class only, textural distribution (percent sand, %S; silt, %Si; and clay, %C), textural distribution and bulk density (BD), the previous parameters and water pressure at field capacity, or the previous parameters and water pressure at wilting point. This research utilized the second and third PTFs.

Soil Properties

First, SEEP/W was used to estimate the average seepage velocity (v_s) for a homogenous, single-layer bank. Soil types (sand, S; loamy sand, LS; sandy loam, SL; sandy clay loam, SCL; and loam, L) were selected that could serve as conductive layers within a more complex bank profile. Boundary conditions included a zero flux boundary for the top and bottom boundaries and a fixed water table (WT) on the side opposite the bank face. The bank height (BH) was 1 m and the width was 1 m. The WT ranged from 0.25 to 1.00 m, resulting in WT/BH ratios of 25, 50, 75, and 100%. SEEP/W continued until dynamic equilibrium was reached.

Eight levels of soil data were simulated, resulting from combinations of the following: known or unknown %S (representing a sieve analysis), K_s, and BD. Researchers have used the centroid of a polygon on the soil texture triangle to estimate %S, %Si, and %C when only the textural class was known (Shirazi et al. 2001a,b). These values (Shirazi et al. 2001a) were used as the baseline %S, %Si, and %C for each soil type (Table 1). Similarly, the K_s that ROSETTA estimated for the centroid %S, %Si, and %C was used as the baseline K_s. These values were used to find the baseline v_s. Finally, the BD for which ROSETTA estimated the baseline K_s (an iterative process) was considered to be the baseline BD.

When only the textural class was known, each of the points on the exterior of its polygon on the soil texture triangle (gray circles in Figure 1) was simulated. For each point, a SEEP/W simulation was performed, using the ROSETTA estimated hydraulic parameters for that point. In this way, v_s was estimated for the potential worst case scenarios (i.e. largest deviations in v_s from the baseline v_s).

When a hypothetical sieve analysis was performed, the %S was assumed equal to the %S at the centroid, making a line of possible clay and silt contents through the centroid. For this situation, the two endpoints on this line of constant %S (white circles in Figure 1) were simulated. If BD was known, the third PTF in ROSETTA was used to estimate hydraulic parameters. For simulations where K_s was known, the baseline K_s was used instead of the K_s estimated by ROSETTA.

Table 1: Baseline soil parameters used for calculating baseline seepage velocity. The %S, %Si, and %C are the centroid of the polygon for the soil textural class. The K_s and BD were determined with ROSETTA.

Soil Texture	Sand (%)	Silt (%)	Clay (%)	K_s (cm d^{-1})	BD (g cm^{-3})
S	92	5	3	469	1.54
LS	82	13	5	117	1.57
SL	65	26	9	43	1.50
L	41	41	18	11	1.48
SCL	60	14	26	13	1.59

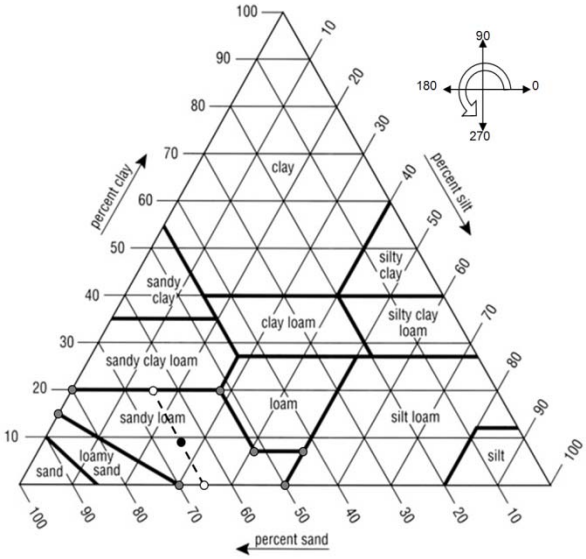

Figure 1: USDA Soil texture triangle. Data points selected for sandy loam are illustrated. The black dot is the centroid (65% S, 26% Si, and 9% C). Gray dots represent the worst case scenarios if only textural class is known. White dots represent the worst case scenarios if a sieve analysis was performed.

Output v_s was compared with the baseline v_s for each run, and the percent difference was calculated. Within each level of soil data, the maximum and minimum (e.g. most negative) errors were used to illustrate the range of possible error. The data analysis also utilized a relative sensitivity coefficient:

$$S_r(y/x) = \frac{\frac{y - y_b}{y_b} \times 100}{\frac{x - x_b}{x_b} \times 100} \quad (1)$$

where $S_r(y/x)$ = relative sensitivity coefficient for output y relative to input parameter x, y = output under consideration, y_b = baseline value for output y, x = parameter under consideration, x_b = baseline value for parameter x. $S_r(y/x)$ is essentially the percent change in output divided by the percent change in input.

Bank Layering

In order to determine the conditions necessary to induce a perched water table, a hypothetical streambank with two layers of equal thickness was modeled with SEEP/W. The finite element grid for the numerical simulation and a flow example is shown in Figure 2. The simulated BH was 1 m and the width was 5 m. Boundary conditions included a zero flux boundary for the bottom and the side opposite the bank face, and a constant infiltration rate for the top surface. The infiltration rate was set to either 10 or 15% of K_s in the top layer (in order to ensure no ponding and therefore an equivalent infiltration volume in each case), and continued until a 5.1 cm rainfall had been applied. All possible combinations of soil types in the soil texture triangle (using the centroid %S, %Si, and %C for each) were considered. Subsoils with higher K_s values were also included in order to simulate dense restrictive layers.

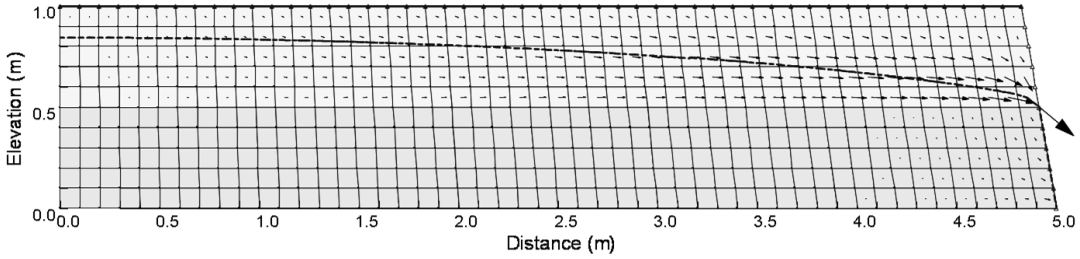

Figure 2: SEEP/W flow data at the end of the simulation for an S layer (light gray) over an L layer (dark gray) resulting in perched seepage. The bank face is on the right. The dotted line is the water table. Arrows are flow vectors. In this case, 74% of the total discharge emerged from the top layer.

For each combination of soil layers, perched seepage was determined as the ratio of seepage in the top layer to the seepage from both layers (based on cumulative discharge). Perched seepage was compared to the bank layer resistance ratio:

$$R_r = \frac{\frac{L_b}{K_{s,b}}}{\frac{L_t}{K_{s,t}}} \qquad (2)$$

where R_r = resistance ratio, L_b = thickness of the bottom soil layer, $K_{s,b}$ = saturated hydraulic conductivity of the bottom soil layer, L_t = thickness of the top soil layer, and $K_{s,t}$ = saturated hydraulic conductivity of the top soil layer. Soil layer resistance accounts for the impact of the thickness of a restrictive layer on its ability to induce lateral flow. It is noted that R_r (bottom/top) is equal to the K_s ratio (top/bottom) for these simulations since the bank layers have the same thickness.

Results and Discussion

Soil Properties

The range of seepage velocity errors across the five different textures indicated the range of possible error for a given level of soil data (Figure 3). Results were the average of the results for the four water table heights (different WT/BH ratios had little impact on the results). Knowing textural class only resulted in considerable errors in predicted v_s across all simulated soil textures. Potential errors ranged from -65% to 272%.

Sieve analysis beyond knowledge of the texture (using the baseline %S) reduced the potential error in estimating v_s for sand-dominated textures (i.e., S and LS), but only minimally reduced the potential error for SL and L textures. Sieve analysis was beneficial for the coarse grained materials, where seepage process often occur; however, as the percent fines increased, the determination of %S by sieving became of little value.

Knowledge of the K_s consistently reduced potential errors in predicted v_s across all simulated soil textures. Percent error in predicted v_s when measuring K_s only (-7% to 16%) were comparable to the errors when having a detailed knowledge of the %S (sieve analysis) and K_s (-4% to 13%).

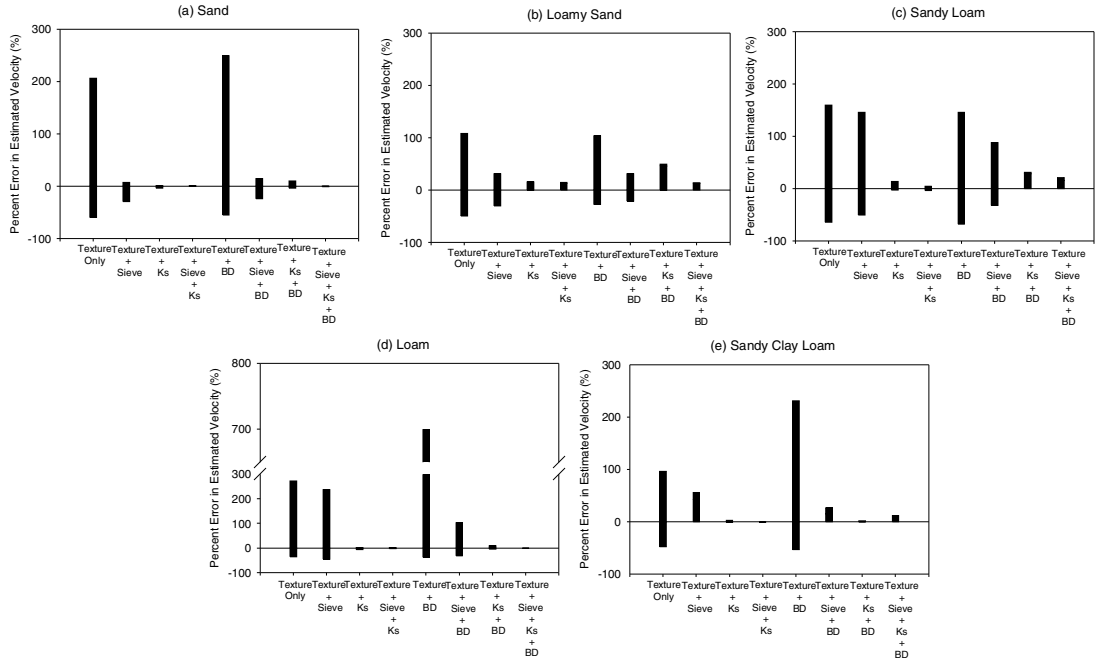

Figure 3: Range of seepage velocity error for varying levels of soil data. Data reported are for average of all WT/BH ratios.

Distance and Direction of Divergence across the Soil Texture Triangle

The $S_r(y/x)$ was calculated for the seepage velocities relative to change in soil texture input, based on results from runs when neither K_s nor BD was known. Due to the difficulty of measuring change in texture (e.g. %S can not be changed while holding %Si and %C constant), an innovative approach was needed. The $S_r(v_s/d)$ was calculated as the percent change in v_s divided by the distance (d) moved across the soil texture triangle, a surrogate for change in texture from the centroid.

The $S_r(v_s/d)$ did not correlate well to location on the soil texture triangle, when represented by %S, %Si, or %C. The $S_r(v_s/d)$ did, however, correlate well with the direction of divergence on the soil texture triangle (Figure 4a). The angle from the centroid to each point was measured counter-clockwise from the horizontal, as indicated in Figure 1.

Also, the correlation was more apparent when the logarithmic nature of the seepage velocity was accounted for by using $\log(v_s)$ instead of v_s (Figure 4b). The $S_r(\log(v_s)/d)$ relationship resembles a negative sine wave. The peak occurred near 270° (straight down on Figure 1), which was when %C decreased and %Si and %S increased. In other words, this was the direction of divergence that resulted in the greatest increase in v_s for a given distance. Likewise, 90° was the direction that resulted in the greatest decrease in v_s.

When a sieve test was performed, error was reduced partly because the direction of divergence was limited to 120° or 300° (as well as the limit on the possible distance of divergence when %S was known). If %C would have been known, the direction of divergence would have been limited to 0° and 180°, where $S_r(\log(v_s)/d)$ was near zero. Data points with angles near 0° and 180° have $S_r(\log(v_s)/d)$ values between -0.25 and 0.25. The implication is that testing for %C (which is easier than measuring

K_s) and using a PTF for other soil parameters may reduce error in v_s sufficiently. While the relationship in Figure 4 did not hold for the entire soil texture triangle (the data set included S, LS, SL, SCL, and L), it was applicable to soils where seepage problems are most likely.

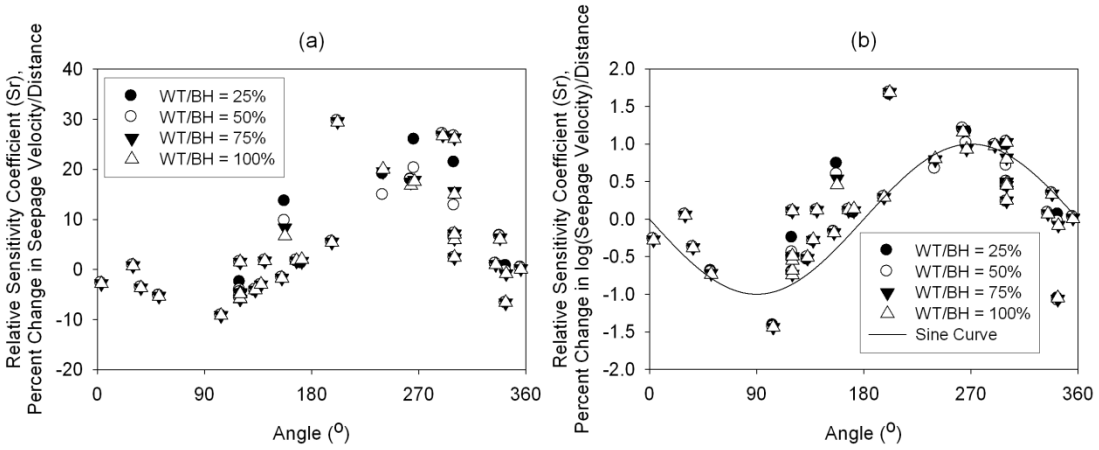

Figure 4: Correlation of the sensitivity coefficient, based on v_s (a) or log(v_s) (b), with the angle of divergence. Moving 0° or 180° (horizontally) across the soil texture triangle results in minimal change in seepage velocity.

Impact of BD on K_s and Seepage Velocity

Although a higher level of soil data would be expected to improve seepage estimates, knowledge of BD provided little if any reduction in error (Figure 3). Since K_s is the primary driving parameter (compared to other hydraulic parameters) for impacting v_s in the SEEP/W model, the relationship between K_s and BD was analyzed. Laboratory data from Chu-Agor et al. (2008b) were compared to ROSETTA estimated K_s values for two soil samples and three BDs (Table 2). The $S_r(K_s/BD)$ indicated the high sensitivity of K_s to changes in BD. Also, SEEP/W was used to estimate v_s for both laboratory and ROSETTA K_s values. BD had a disproportionate impact on v_s, with $S_r(v_s/BD)$ based on lab data ranging from -29.5 to -5.4; however, $S_r(v_s/BD)$ based on ROSETTA estimates ranged from -5.6 to 0.4.

Table 2: Comparison of saturated hydraulic conductivity (K_s) and seepage velocity (v_s) sensitivity to bulk density (BD) for both laboratory and ROSETTA (PTF) K_s.

Soil	S	Si	C	BD	K_s (cm d^{-1})		$S_r(K_s/BD)$		v_s (μm s^{-1})		$S_r(v_s/BD)$	
Text	(%)	(%)	(%)	(g/cm^{-3})	Lab	PTF	Lab	PTF	Lab	PTF	Lab	PTF
S	99	1	0	1.6	665	1248	-5.4	-1.7	104	194	-5.4	-1.7
				1.45	1521	1512	n/a	n/a	237	235	n/a	n/a
				1.3	2454	1467	-5.9	0.3	377	226	-5.8	0.4
LS	85	13	2	1.7	52	113	-8.0	-4.7	8	17	-8.1	-4.8
				1.6	104	160	n/a	n/a	15	24	n/a	n/a
				1.5	294	215	-29.3	-5.5	43	32	-29.5	-5.6

It is uncertain why an increased level of input data resulted in an increase in error. Based on Table 2, it appeared that ROSETTA may not be sensitive enough to BD. It should also be noted that ROSETTA is a neural network model. That is, it does not use physically based equations to account for the impact of parameters, including BD. Rather, it is highly dependent on the amount, extent, and quality of data used in developing the model. For example, the unexpected positive $S_r(v_s/BD)$ and $S_r(K_s/BD)$ in Table 2 may indicate that ROSETTA has little available data on both K_s and BD for sand samples. Also, the use of two separate PTFs within Rosetta (one for known BD and one for unknown BD) may be a confounding factor for the results in Figure 3. Another observation is that some PTFs which account for BD include both texture and organic matter content (Kaur et al. 2002; Nemes et al. 2005).

Bank Layering

A perched water table was predicted based on soil textural class only. All possible combinations of soil textures were considered, using baseline data (hydraulic parameters) for each textural class. The presence of a perched water table was indicated by seepage from the top layer (Table 3). According to these data, either an S or LS top layer was necessary for perching to be possible, but this was not consistent with field observations (Fox et al. 2007; Wilson et al. 2007). A primary limitation of this approach was neglecting variation in BD. It is quite possible that subsoils may have a higher BD than topsoils. Due to the large impact of BD on v_s (Table 2), soil texture alone was not sufficient to predict perching during a field reconnaissance. Data such as BD or K_s was necessary to indicate the presence of a restrictive layer.

Dense subsoils with a lower K_s than ROSETTA predicted (without inputting BD) were simulated in SEEP/W, together with the four topsoils that had the highest K_s values (S; LS; silt, Si; and silt loam, SiL). The correlation between perched seepage and R_r is shown in Figure 5. According to these SEEP/W simulations, an R_r of approximately 10, equivalent to only a one order of magnitude difference in K_s, was required to induce a perched water table. This was consistent with field observations of Fox et al. (2007) who also noted small differences in K_s resulting in perched seepage, not the two or three order of magnitude contrast in K_s as was previously expected.

Table 3: Percent of the total seepage that emerged from the top layer due to a perched water table, without accounting for variation in BD.

		Bottom Layer											
Soil Texture		S	LS	Si	SL	SiL	C	SC	SiC	SCL	SiCL	L	CL
K_s (cm d^{-1})		469	117	44	43	29	17	16	15	13	12	11	7
Top Layer	S	0	0	18	20	41	63	65	67	71	73	74	84
	LS		0	0	0	0	0	0	0	0	0	0	40
	Si			0	0	0	0	0	0	0	0	0	0
	SL				0	0	0	0	0	0	0	0	0

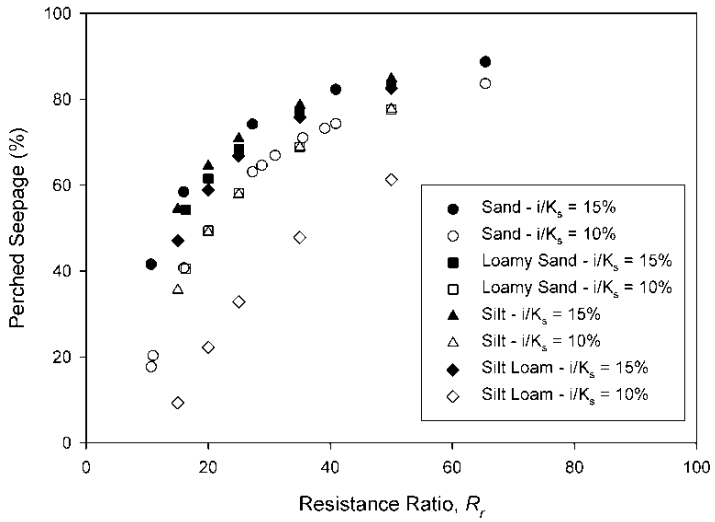

Figure 5: Perched seepage for S, LS, Si, and SiL soils (top layer) and infiltration (*i*) rates at 10 or 15% of K_s.

Conclusions

A two-dimensional groundwater flow code, SEEP/W, was used to model a hypothetical streambank. The sensitivity of groundwater seepage relative to various levels of soil data was determined. Sole use of the soil texture's centroid %S, %Si, and %C as a surrogate for soil texture (i.e., only textural class was known) resulted in considerable errors in predicted v_s across all simulated soil textures. Sieve analysis in addition to knowledge of the texture reduced the potential error for sand-dominated textures (i.e., S and LS), but only minimally reduced the potential error for SL and L textures. Knowledge of K_s consistently reduced potential errors in predicted v_s across all simulated soil textures to levels comparable to the error when knowing both K_s and %S. Measuring %C may be an economical alternative to K_s for minimizing error for conductive layers.

A dense, restrictive layer (high BD) was the necessary condition for perching, not the more commonly assumed difference in soil types. Subsoils may have a lower K_s than ROSETTA predicted for a particular soil textural class due to a high BD. For a field reconissaince, either BD or K_s may be needed to identify sites with potential for perched seepage. Only one order of magnitude difference in K_s may be necessary to induce perching.

Acknowledgments

This material is based upon work supported by the Cooperative State Research, Education, and Extension Service (CSREES), U.S. Department of Agriculture (USDA), under Award No. 2005-35102-17209.

References

Chu-Agor, M.L., Wilson, G.V., and Fox, G.A. (2008a). "Numerical modeling of bank instability by seepage erosion undercutting of layered streambanks." *Journal of Hydrologic Engineering,* 13(12), 1133-1145.

Chu-Agor, M.L., Fox, G.A., Cancienne, R., and Wilson, G.V. (2008b). "Seepage caused tension failures and erosion undercutting of hillslopes". *Journal of Hydrology,* 359(3-4), 247-259. doi:10.1016/j.jhydrol.2008.07.005.

Darby, S.E., Rinaldi, M., and Dapporto, S. (2007). "Coupled simulations of fluvial erosion and mass wasting for cohesive river banks." *Journal of Geophysical Research,* 112, F03022. doi:10.1029/2006JF000722.

Fox, G.A., Wilson, G.V., Periketi, R.K., and Cullum, R.F. (2006). "Sediment transport model for seepage erosion of streambank sediment." *Journal of Hydrologic Engineering,* 11(6), 603-611.

Fox, G.A., Wilson, G.V., Simon, A., Langendoen, E.J., Akay, O., and Fuchs, J.W. (2007). "Measuring streambank erosion due to ground water seepage: correlation to bank pore water pressure, precipitation and stream stage." *Earth Surface Processes and Landforms,* 32(10), 1558-1573.

Hagerty, D.J. (1991). "Piping/sapping erosion. 2: Identification-diagnosis." *Journal of Hydraulic Engineering-ASCE,* 117(8), 1009–1025.

Kaur, R., Kumar, S., and Gurung, H. P. (2002). "A pedo-transfer function for estimating soil bulk density from basic soil data and its comparison with existing PTFs." *Australian Journal of Soil Research,* 40(5), 847-857.

Krahn, J. (2004). *Seepage modeling with SEEP/W: An engineering methodology*. GEO-SLOPE International Ltd., Calgary, Alberta., Canada.

Lobkovsky, A.E., Jensen, B., Kudrolli, A., and Rothman, D.H. (2004). "Threshold phenomena in erosion driven by subsurface flow." *Journal of Geophysical Research-Earth,* 109(F4), F04010.

Nemes, A., Rawls, W.J., and Pachepsky, Y.A. (2005). "Influence of organic matter on the estimation of saturated hydraulic conductivity." *Soil Science Society of America Journal,* 69, 1330-1337.

Rinaldi, M., Mengoni, B., Luppi, L., Darby, S.E., and Mosselman, E. (2008). "Numerical simulation of hydrodynamics and bank erosion in a river bend." *Water Resources Research,* 44, W09428. doi:10.1029/2008WR007008.

Schaap, M.G., Leij, F.J., and van Genuchten, M.Th. (2001). "ROSETTA: A computer program for estimating soil hydraulic parameters with hierarchical pedotransfer functions." *Journal of Hydrology,* 251(3), 163-176.

Shirazi, M.A., Boersma, L., and Johnson, C.B. (2001a). "Particle-size distributions: Comparing texture systems, adding rock, and predicting soil properties." *Soil Science Society of America Journal,* 65(2), 300-310.

Shirazi, M.A., Boersma, L., Haggerty, P.K., and Johnson, C.B. (2001b). "Spatial extrapolation of soil characteristics using whole-soil particle size distributions." *Journal of Environmental Quality,* 30, 101-111.

van Genuchten, M.Th. (1980). "A closed-form equation for predicting the hydraulic conductivity of unsaturated soils." *Soil Science Society of America Journal,* 44(5), 892-898.

Wilson, G.V., Periketi, R.K., Fox, G.A., Dabney, S.M., Shields, F.D., and Cullum, R.F. (2007). "Soil properties controlling seepage erosion contributions to streambank failure." *Earth Surface Processes and Landforms,* 32(3), 447-459.

A Seepage Erosion Sediment Transport Function and Geometric Headcut Relationships for Predicting Seepage Erosion Undercutting

M.L. Chu-Agor[1], G.A. Fox[2], and G.V. Wilson[3]

[1] Ph.D. Student and Graduate Research Assistant, Oklahoma State University, Department of Biosystems and Agricultural Engineering, 209 Agricultural Hall, Stillwater, OK 74078

[2] Assistant Professor, Oklahoma State University, Department of Biosystems and Agricultural Engineering, 209 Agricultural Hall, Stillwater, OK 74078

[3] Hydrologist/Soil Physicist, USDA-ARS National Sedimentation Laboratory, Oxford, MS 38655

Abstract

Seepage erosion is an important factor in hillslope instability and failure. However, predicting erosion by subsurface flow or seepage and incorporating its effects into stability models remain a challenge. Limitations exist with all existing seepage erosion sediment transport functions, including neglecting the three-dimensional geometry of the seepage undercut. The objective was to develop a sediment transport model that can predict sediment mobilization (i.e., seepage erosion and undercutting) with time based on previously reported three-dimensional soil block experiments covering a wide range of hydraulic, soil type, and packing (i.e., slope and bulk density) combinations. The transport function was represented by an excess velocity equation wherein the rate of erosion was related to the difference between the steady state velocity and the critical velocity (R^2 = 0.62). The critical velocity was derived from a critical head measured in the laboratory using the three-dimensional soil block. The relationship between the eroded volume per bank face area and the amplitude of the headcut was also derived. Using a three-dimensional Gaussian function, the geometric relationships between the lateral and vertical dimensions of the headcut were then estimated. Linear regression analysis between the predicted and observed time at which a given amount of headcut developed resulted in an R^2 of 0.86. The ground water velocity exfiltrating a hillslope can be used with the derived sediment transport function to predict the dimensions of the headcut and the geometry of the undercut which enables the prediction of the impact of seepage erosion undercutting on hillslope stability.

Introduction

Seepage erosion is an important factor in hillslope instability and failure. However, predicting erosion by subsurface flow or seepage and incorporating its

effects into stability models remain a challenge. The complexity results from the difficulty in quantifying the soil, hydrologic, and geotechnical mechanisms affecting this phenomenon as well as understanding the interaction between them. To start with, measuring subsurface flow and seepage erosion in the field is difficult (Hagerty, 1991; Fox et al., 2007; Wilson et al., 2007). Furthermore, the variability and heterogeneity of the porous media add another level of uncertainty to seepage flow and erosion estimation (Hagerty, 1991). According to Sidorchuk (2005), the nature of soil erosion is determined by the interaction between water flow and structured soil. This interaction is stochastic in nature due to the complexity and microscopic scale of the geo-mechanical and electro-chemical forces between particles in the soil and of the velocity oscillations in water flow.

Another aspect adding to the complexity of seepage erosion analysis is its three-dimensional nature (Crosta and di Prisco, 1999; Chu-Agor et al., 2008a). Since seepage erosion is not uniformly distributed throughout the bank, but is isolated to the preferential flow path of the seep, the dimensions of the seepage undercut is important in quantifying the amount of sediment eroded. According to Crosta and di Prisco (1999), bank failure due to seepage erosion is the final result of a complex chain of events taking place during a certain time period. Because of these factors, seepage erosion is not extensively studied compared to fluvial erosion other than the seepage influence on the soil pore-water pressure (Darby and Thorne, 1996; Crosta and di Prisco, 1999; Rinaldi and Casagli, 1999; Simon et al., 1999), although it has been demonstrated to be an important instability mechanism (Cancienne et al., 2008; Chu-Agor et al., 2008b).

Several studies to date have developed relationships that predict sediment transport due to seepage. Seepage erosion has been analyzed by different researchers as either due to: (1) individual particle mobilization (Howard and McLane, 1988; Dunne, 1990; Lobskovsky et al., 2004), or (2) small mass failure employing Coulomb's failure mechanism (Dunne, 1990; Chu-Agor et al., 2008a,b). Sediment transport models (i.e., Howard and McLane, 1988; Fox et al., 2006) have also been developed based on laboratory experiments on specific, usually noncohesive, soils. Equations for initiation of particle motion attempt to predict the limiting conditions when the seepage force across the grain exceeds the shear strength of the particle resulting in that particle detaching out of its intergranular "pocket" (Dunne, 1990). Mass failure analysis evaluates the balance of forces acting on a soil element of an infinite slope. It attempts to predict the conditions when the resultant of the driving forces exceeds the resultant of the stabilizing forces causing small or large masses of soil to fall.

Most studies on seepage erosion have focused their analysis on one failure mechanism, specific soil types, and/or specifically for noncohesive soils, limiting their application to the conditions under which they were derived. Furthermore, seepage undercutting in the field has a three-dimensional geometry not addressed in previous studies. In this study, a sediment transport model which can predict sediment mobilization (i.e., seepage erosion and undercutting) over time will be derived and evaluated based on previously reported three-dimensional soil block experiments (Chu-Agor et al., 2008a) covering a wide range of hydraulic, soil type, and packing (i.e., slope and bulk density) combinations.

Materials and Methods

Three-dimensional Soil Block Experiments

Data gathered from the three-dimensional block experiments of Chu-Agor et al. (2008a) were used in this research. The three-dimensional soil block was constructed of Plexiglas with dimensions 50 cm by 50 cm by 50 cm. It had two compartments: a water reservoir at one end where a constant water head was maintained and a soil compartment that simulated a single-layered streambank (Figure 1). Water flowed from the water reservoir to the soil compartment through a 10 cm by 10 cm inlet centered at the bottom of the wall dividing the two compartments. Two soil textures were used in the experiments: sand and loamy sand. Each soil type was packed in the box at various bulk densities (ρ_b): 1.30, 1.45, and 1.60 Mg m^{-3} for the sand and 1.30, 1.45, 1.50, 1.60, and 1.70 Mg m^{-3} for the loamy sand. All experiments consisted of soil blocks with heights of 25 cm, widths of 50 cm, and lengths of 25 cm. The bottom of the soil block was lined with a 2.5 cm densely packed clay layer to serve as a restrictive layer. The rest of the block was packed with soil to the desired ρ_b in 2.5 cm lifts. The soil was then cut to simulate various bank angles, α' (90, 75, and 60 degrees), such that the horizontal centerline for each bank remained 20 cm away from the water inlet. For the experiments, heads (H) of 15, 25, or 35 cm were maintained in the inflow reservoir.

During the experiment, a three-dimensional, medium-range laser scanner (3D Digital Corporation, Sandy Hook, CT) was used to monitor seepage erosion at the bankface of the soil block. Scanned images were taken at regular intervals to capture the change in the bank due to seepage erosion (Figure 2). The scanned images were then exported to ASCII files in terms of the xyz coordinates and used to create 2.0 mm square grids. A program was developed to compute the eroded volume by subtracting the scanned surface at a given time from the scanned surface of the initial bank. A five-parameter Gaussian function (Weisstein, 1999) was fit to the volume of the eroded surface in order to determine the typical undercut shape and dimensions (Chu-Agor et al., 2008a), where the function is given as the following:

$$z(x,y) = A\exp\left[-\left\{\left(\frac{x-x_o}{\sigma_x}\right)^2 + \left(\frac{y-y_o}{\sigma_y}\right)^2\right\}\right] \quad (1)$$

where $z(x,y)$ is the measured seepage headcut from the original bank face, A is the amplitude or maximum distance of seepage erosion, x_o and y_o is the center of the amplitude, and σ_x and σ_y are spreads of the seepage headcut (Figure 2). The variables σ_x and σ_y are related to the full width at half-maximum ($FWHM_j$) of the Gaussian function:

$$FWHM_j = 2\sqrt{2\ln(2)}\sigma_j \quad (2)$$

where j is either x or y (Weisstein, 1999).

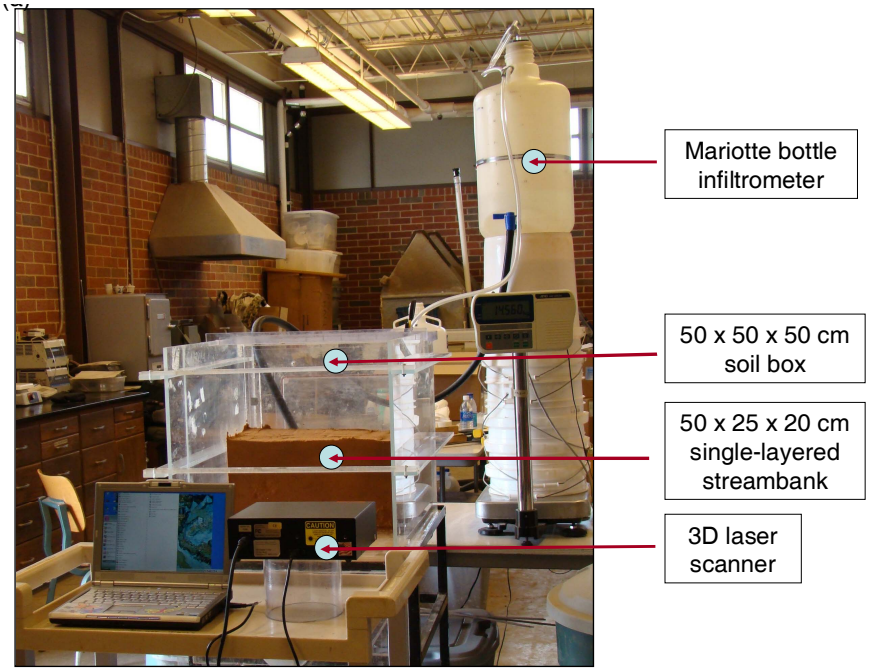

Figure 1. Three-dimensional soil block set-up used to simulate seepage erosion of single-layer, repacked soil banks.

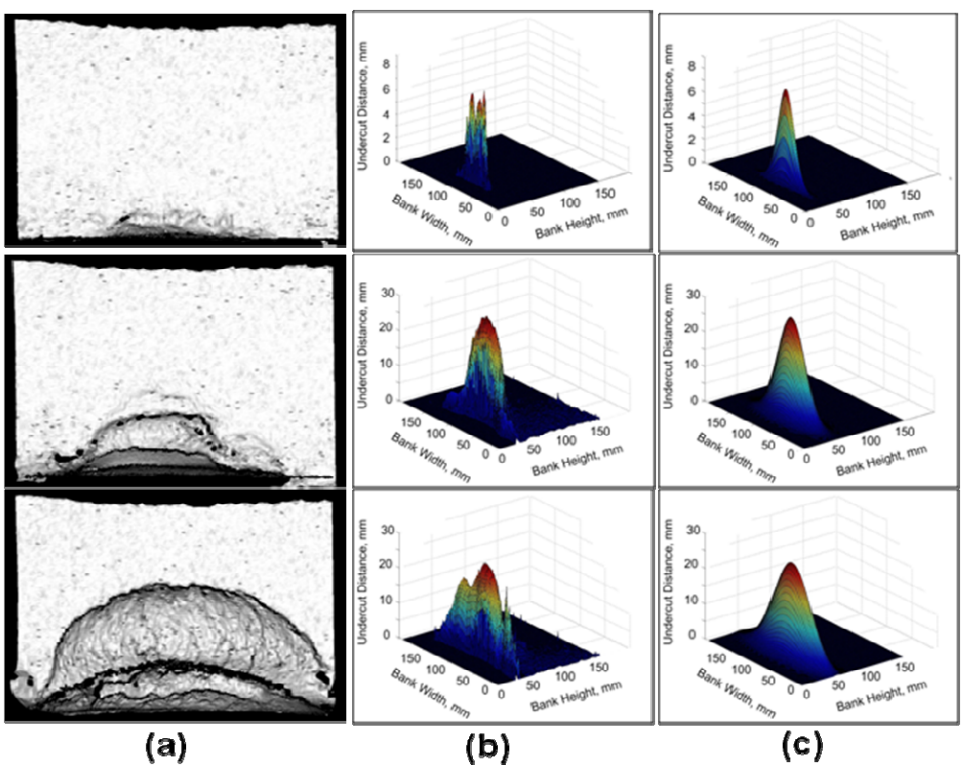

Figure 2. (a) Time sequence of seepage particle mobilization and undercutting. (b) Distance of seepage undercutting (vertical axis). The bank face is the x-y plane. (c) A Gaussian function fit to the seepage particle mobilization data.

Derivation of a Sediment Transport Model

The sediment transport function was represented by an excess velocity equation, where velocity, v, was the steady-state ground water velocity:

$$E_{rs} = K_{ds}\left(v - v_c\right)^a \tag{3}$$

where E_{rs} is the seepage erosion rate (i.e., volume of sediment per bank face area per time, m^3 of sediment per m^2 of bank face per s), K_{ds} is the seepage erodibility coefficient, v_c is the critical velocity, and a is an exponent. The steady-state ground water velocity was estimated from Darcy's Law with Dupuit-Forcheimmer assumptions:

$$v = \frac{q}{n} = \frac{KH\sin(\alpha')}{nL_{sc}} \tag{4}$$

where q is the flow per area of the seepage undercut per time, L_{sc} is the length of the soil block, K is the saturated hydraulic conductivity, and H is the hydraulic head. Thus, v is equivalent to the pore water velocity.

For cases with undercutting by seepage erosion, the imposed ground water velocity, v, was estimated from the steady-state flow based on the imposed hydraulic gradient (i.e., a function of the head, H) and corrected for the measured depth of undercutting (A) from the laser scanner during each experiment, such that the path length is $(L_{sc}\text{-}A)$ (i.e., increases in A increases v by reducing the flow path length):

$$v = \frac{q}{n} = \frac{KH\sin(\alpha')}{n(L_{sc} - A)} \tag{5}$$

Critical Velocity

The critical groundwater velocity necessary for seepage erosion initiation, v_c, was a function of the critical gradient, i_{cr} (i.e., the gradient that must be imposed on the sediment before seepage erosion initiates). The critical gradient was determined by dividing the critical head, H_{cr}, which was measured using the three-dimensional soil block set-up of Chu-Agor et al. (2008a), by the length of the soil block. The soil block was packed with sand and loamy sand at various ρ_b. The bank face was maintained at a 90-degree angle. At the start of the experiment, the head in the water reservoir was set at 4 cm (i.e., 1.5 cm above the clay layer). Once steady state flow was reached, the head was increased by 1 cm and the system was allowed to reach equilibrium. If no undercutting was observed, this process was repeated until a sufficient head was reached that was capable of propagating an undercut. Each experiment with a given set of soil and hydraulic controls was carried out in duplicate. Since the head was increased in 1 cm increments, a minimum and a maximum were used to define the critical head. The minimum value being the head before undercutting occurred and the maximum value when undercutting propagated.

Model Development

Experiments conducted by Chu-Agor et al. (2008a) that experienced seepage undercutting were divided into two groups. Two-thirds of the experiments (34

experiments) were used for model development and the remaining one-third (18 experiments) for model evaluation. The groups were chosen randomly based on a random number generator. Each experiment consisted of one or more scanned images representing the evolution of the undercut before mass wasting occurred. Thus, each experiment contained measurements of A at different times during the experiment (i.e., 93 observations for model development and 40 observations for model evaluation).

From the laboratory experiments, the observed erosion rate, E_{rs}, was computed by dividing the ratio of the eroded volume to the bank face area of the undercut, V/A, by the observed time. The average value of i_{cr} was used with the soil properties for the specific type and packing to calculate the critical velocity, v_c (equation 4). A nonlinear regression of E_{rs} versus v-v_c was fit to all 34 experiments with varying soil type, bulk density, H, and bank angles. A limitation of the proposed sediment transport function is that it assumes laminar flow conditions. Therefore, the equation is only valid for i_{cr} less than a maximum gradient at which turbulent flow occurs. Laminar flow conditions should be prevalent in the field except under cases of macropore or pipe flow (Wilson, 2007). Also, for model development, relationships were derived between V/A and A. Geometric relationships between A and σ_x and σ_y for the experiments in the model development data set were also defined.

Model Evaluation

The model was evaluated by comparing the predicted time using the relationships discussed previously to the observed time for a given A. First, a value of A as measured during the model evaluation experiment was selected. The ratio V/A was then computed using the relationship between V/A and A obtained during model development. The steady-state velocity, v, was computed as a function of the selected A using equation (5). The critical velocity, v_c was determined based on the measured critical head, H_{cr}, using equation (4). Next, the erosion rate, E_{rs}, was calculated using the empirical equation derived from the model development dataset; i.e., equation (3). The time required for a given amount of A to develop was then calculated as:

$$t_{pred} = \frac{V / A}{E_{rs}} \tag{6}$$

Finally, a linear regression analysis was performed between the observed time to reach the specific, A, to the predicted time, t_{pred}, calculated using the seepage erosion sediment transport function and the geometrical headcut relationships.

Estimating the Headcut Dimensions

From knowledge of A, σ_x and σ_y, the five-parameter Gaussian function can be simplified to approximate the height (h) or width (w) of the undercut at different distances along A. For example, at the bank face, one can solve for h_{bf} and w_{bf} (i.e., height and width of the undercut at the bank face, respectively) when z is reasonably close to zero (i.e., $z = \varepsilon$). To solve for the h_{bf}, simply substitute $x = 0$ with $x_o = 0$ and $y_o = 0$ into equation (1) and solve for $y = h_{bf}/2$; to solve for w_{bf}, substitute $y = 0$ with

$x_o = 0$ and $y_o = 0$ into equation (1) and solve for $x = w_{bf}/2$. The following equations are derived:

$$h_{bf} = 2\sigma_y \sqrt{-\ln\left(\frac{\varepsilon}{A}\right)} \quad , \; w_{bf} = 2\sigma_x \sqrt{-\ln\left(\frac{\varepsilon}{A}\right)} \tag{7}$$

Similarly, solving for the h and w at any z, where $z < A$, results in the following equations that allow prediction of the entire undercut shape:

$$h(z) = 2\sigma_y \sqrt{-\ln\left(\frac{z}{A}\right)}, \; w(z) = 2\sigma_x \sqrt{-\ln\left(\frac{z}{A}\right)} \tag{8}$$

In order to compute h_{bf} and w_{bf} using equation (7), it was assumed that ε was equal to the average particle diameter or the median particle size, d_{50}, of the particle size distribution since an undercut cannot be formed until at least one particle is dislodged from the bank. The values of σ_y and σ_x were computed using the Gaussian function for a given A. The scanned images of experiments with 60-degree banks did not show the full extent of the width of the undercut and were excluded from the analysis.

Results and Discussion

Model Development and Evaluation

Results of the non-linear regression between experimental data on E_{rs} versus v-v_c for all the 34 experiments with varying soil type, bulk density, H, and bank angles resulted in regression constants of a and b equal to 0.001 and 0.5, respectively, with a coefficient of regression, R^2, of 0.62 (Figure 3). This function covered a wide range of variability (i.e., different hydraulic controls, different packing conditions, and two soil types) as well as the three-dimensional nature of the seepage erosion. The function also related the erosion rate to the seepage velocity. Unlike that of Howard and McLane (1988), the derived sediment transport model does not use empirical coefficients which are difficult, if not impossible, to estimate. The function however, requires an estimate of i_{cr}.

Prior to deriving the sediment transport model, the critical gradient, i_{cr}, was determined. Using H_{cr}, the relationship between i_{cr} and effective cohesion, c', was established. Cohesion in soil added an extra force that has to be exceeded in addition to gravity and water forces before mobilization could occur. According to Dunne (1990), for soil with some amount of cohesion, an extra force is acting on the soil mass resisting the separation of the mass. He added that i_{cr} depended on the thickness of the volume that eventually separated. Cohesion therefore is a parameter which can also be used to estimate i_{cr}. Regardless of soil type and packing condition, i_{cr} and c' followed a logarithmic relationship ($R^2 = 0.99$) as follows:

$$i_{cr} = 0.19\ln(c') + 0.09 \tag{9}$$

Since the model considers the three-dimensional nature of seepage erosion, the geometry of the headcut has to be defined. For the model development data sets consisting of data from both soil types (coarse sand and loamy sand) and across a range of several different bulk densities (1.3 to 1.7 Mg m^{-3}), heads (15 to 35 cm), and bank angles (60 to 90 degrees), a linear relationship was observed between V/A and A,

with $A = 2.8\ V/A$. The ratio V/A represents the average depth of the undercut. Using this relationship, the average depth of undercut, V/A, was related to the maximum depth, A, which can be predicted from E_{rs} at a given time.

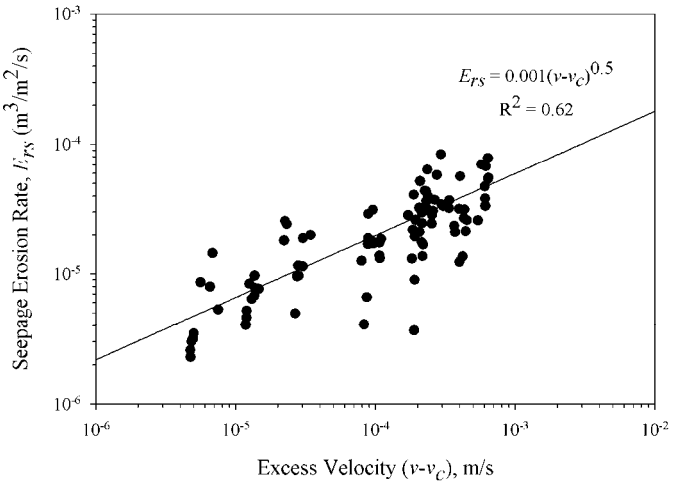

Figure 3. Relationship between seepage erosion rate (E_{rs}) and excess velocity (v) above the critical velocity (v_c) from model development studies.

The model was evaluated using the remaining 18 experiments by comparing the observed time with the predicted time for which a chosen headcut amplitude, A, developed. The linear regression analysis between the predicted time and the observed time resulted in an R^2 of 0.86 (Figure 4). The model was found to slightly over predict the time to develop a given A at large time. Larger observed times corresponded to experiments performed on stable banks (i.e., lower α' and H, and higher ρ_b). This means that for more stable banks, the model under estimated E_{rs}.

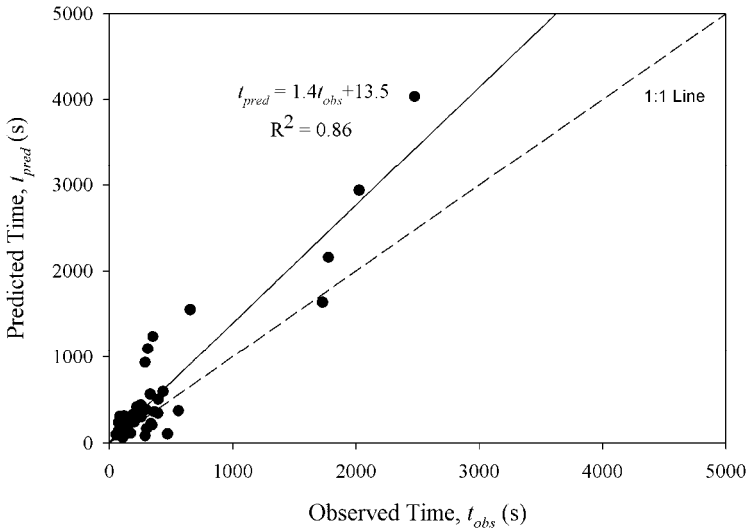

Figure 4. Linear regression between predicted time (t_{pred}) and observed time (t_{obs}) calculated using the seepage erosion sediment transport function and geometrical headcut relationships to obtain the observed headcut amplitude (A) for the model evaluation studies.

From a prediction of A, Chu-Agor et al. (2008a) and this research documented the appropriateness of a Gaussian distribution, from which predictions of σ_x and σ_y of the undercut could be made. Relationships between A and σ_x and σ_y included:

$$\sigma_x = 2.4A \qquad \sigma_y = 0.2A^{0.7} \tag{10}$$

Once σ_x and σ_y are known, w_{bf} and h_{bf} were computed using equation (7). When assuming ε equal to d_{50}, linear regression analysis between the measured and computed w_{bf} and h_{bf} for the model evaluation data set yielded slopes of 1.4 and 1.6, intercepts of -0.1 and 0.0, and R^2 of 0.85 and 0.84 for w_{bf} and h_{bf}, respectively.

Summary and Conclusions

A sediment transport function was developed and evaluated based on the three-dimensional soil block experiments conducted by Chu-Agor et al. (2008a). Two-thirds of the 54 experiments were used for model development and the remaining for model evaluation. The transport function was represented by an excess velocity function wherein the rate of erosion was related to the difference between the steady-state velocity and the critical velocity. The former was estimated from Darcy's Law with an adjusted hydraulic gradient to take into account the depth of seepage undercut measured by the laser scanner. The latter was determined as a function of the critical gradient which was measured in the laboratory using a three-dimensional soil block. The critical gradient was related to the effective cohesion through a logarithmic relationship. A power relationship (R^2 = 0.62) was established between erosion rate and excess velocity. The relationship between the eroded volume per bank face area and the amplitude of the headcut was also derived. Using a three-dimensional Gaussian function, the geometric relationships between the dimensions of the headcut were established. The model was evaluated by comparing the predicted time to the observed time at which a given amount of headcut developed. The linear analysis between the predicted time and measured time resulted in an R^2 of 0.86. The sediment transport model together with the derived relationships between the dimensions of the headcut and its geometry can be used to incorporate the effects of seepage erosion undercutting into bank stability analysis with integrated groundwater flow and stability models.

Acknowledgments

This material is based upon work supported by the Cooperative State Research, Education, and Extension Service (CSREES), U.S. Department of Agriculture (USDA), under Award No. 2005-35102-17209.

References

Cancienne, R., G.A. Fox, and A. Simon (2008), Influence of seepage undercutting on the root reinforcement of streambanks, *Earth Surf. Proc. Land.,* 33(11), 1769-1787, DOI: 10.1002/esp.1657.

Chu-Agor, M.L., G.A. Fox, R. Cancienne, and G.V. Wilson (2008a), Seepage caused tension failures and erosion undercutting of hillslopes, *J. Hydrol.*, 359, 247-259.

Chu-Agor, M.L., G.V. Wilson, and G.A. Fox (2008b), Numerical modeling of bank stability by seepage erosion. *J. Hydrol. Eng.*, 13(12): 1133-1145.

Crosta, G., and C. di Prisco (1999), On slope instability induced by seepage erosion, *Can. J. Geotech.*, 36, 1056-1073.

Darby, S.E., and C.R. Thorne (1996), Numerical simulation of widening and bed deformation of straight sand-bed rivers. I. Model development, *J. Hydraul. Eng.-ASCE*, 122, 184-193.

Dunne, T. (1990), Hydrology, mechanics, and geomorphic implications of erosion by subsurface flow, *Geological Society of America,* Special Paper 252.

Fox, G.A., G.V. Wilson, R.K. Periketi, and R.F. Cullum (2006), Sediment transport model for seepage erosion of streambank sediment, *J. Hydrol. Eng.*, 11(6), 603-611.

Fox, G.A., G.V. Wilson, A. Simon, E. Langendoen, O. Akay, and J.W. Fuchs (2007), Measuring streambank erosion due to ground water seepage: Correlation to bank pore water pressure, precipitation, and stream stage, *Earth Surf. Proc. Land.*, 32(10), 1558-1573.

Hagerty, D.J. (1991), Piping/sapping erosion. 1. Basic considerations, *J. Hydraul. Eng.-ASCE*, 117(8), 991-1008.

Howard, A.D., and C.F. McLane, III (1988), Erosion of cohesionless sediment by ground water seepage, *Water Resour. Res.*, 24(10), 1659-1674.

Lobkovsky, A.E., B. Jensen, A. Kudrolli, and D.H. Rothman (2004), Threshold phenomena in erosion driven by subsurface flow, *J. Geophys. Res.-Earth*, 109(F4), Art. No. F04010.

Rinaldi M., and N. Casagli (1999), Stability of streambanks formed in partially saturated soils and effects of negative pore water pressures: The Siene River (Italy), *Geomorphology*, 26, 253-277.

Sidorchuk, A. (2005), Stochastic modeling of erosion and deposition in cohesive soils, *Hydrol. Process.*, 19, 1399-1417.

Simon A., A. Curini, S.E. Darby, and E.J. Langendoen (1999), Streambank mechanics and the role of bank and near-bank processes in incised channels, In *Incised River Channels*, S.E. Darby and A. Simon (eds), John Wiley and Sons, Chichester, UK, pp. 193-217.

Weisstein, E.W. (1999), Gaussian function, in *CRC Concise Encyclopedia of Mathematics*, CRC Press, New York, pp. 716-717.

Wilson, G.V. (2007), Ephemeral gully erosion by preferential flow through continuous soil-pipes, *Earth Surf. Proc. Land.*, in review.

Wilson, G.V., R. Periketi, G.A. Fox, S. Dabney, D. Shields, and R.F. Cullum (2007), Soil properties controlling seepage erosion contributions to streambank failure, *Earth Surf. Proc. Land.*, 32(3), 447-459.

A Blueprint for Advancing Hydrologic Predictability in Developing Countries: A Case Study for the Nile River Basin

M. Gebremichael

Civil & Environmental Engineering, University of Connecticut, Storrs, CT 06269; PH (860) 486-2771; FAX (860) 486-2298; email: mekonnen@engr.uconn.edu

ABSTRACT

Lack of reliable hydrologic monitoring and prediction tool in the Nile River basin is hindering the planning and management of water resources in the region. This paper presents the broad outlines of an emerging approach for improving hydrologic monitoring and predictability in the Nile basin. The new approach embraces the space-time heterogeneities of hydrologic processes, and the integrative observations-modeling uncertainty in characterizing those processes. Instead of relying solely on sparse ground-based measurements, it will take advantage of recent developments in satellite remote sensing technology to observe space-time patterns of hydrologic variables. It will acknowledge the various observational and modeling error sources, and quantify the residual errors. Instead of using hydrologic models that have not been proven to work in the Nile basin, it will seek to identify the level of complexity needed maximize the performance of models driven by satellite datasets for the Nile basin. The defining feature of the new approach will be a sharp focus on the use of satellite data, hydro-meteorological models of appropriate complexity, establishment of a ground validation site and implementation of field campaigns for error characterization. This new focus will advance hydrologic monitoring and predictability in the Nile basin, and improve the accuracy of water balance components that would feed directly into the making of more-efficient, more-equitable and better-informed water management and planning decisions.

1. Introduction

The Nile River Basin (NRB) covers an area of over 3 million km^2, and a length of about 6700 km, the longest in the world. Water is a scarce resource in the NRB countries, and 'water resource management' is often a top priority in these countries. Proper utilization of the Nile water requires a good scientific understanding of (1) the space-time variability of Nile hydrology, and (2) assessment of the impacts of land use and climate changes on Nile hydrology. However, due to the sparse network of ground-based observation systems in the NRB, the space-time variability of Nile hydrology remains largely unknown. This problem could potentially be addressed by the use of satellite remote sensing (SRS) systems. SRS systems involve the detection and recording of electromagnetic radiation reflected/emitted by the Earth's surface/atmosphere, and the use of inverse techniques to convert those energy measurements to magnitudes of hydro-meteorological variables (e.g., precipitation, soil moisture, clouds, etc.). Retrieval equations are typically empirical algorithms, and this situation has led to the development of a plethora of such retrieval techniques. For example, one can apply different retrieval equations to a remotely sensed measurement to obtain quite different estimates of the same physical variable. For this reason, existing SRS products exhibit significant variations that limit our ability to improve the scientific understanding of the space-time variability of hydrological variables in the NRB.

Although satellites can observe key hydrological variables (mainly rainfall and evapotranspiration), there are still other important hydrological variables, particularly basin responses to rainfall forcing, such as, streamflow and groundwater flow, which cannot be observed by current SRS technology. To estimate the latter at ungauged locations, hydrologic models are typically used. Hydrologic models also play a crucial role in decision making for water management by simulating the basin responses under possible future scenarios (e.g., land use change, climate change, drought and flood forecasts, etc.). There are a number of hydrologic models developed in different regions of the world with different levels of complexity. Similar as with the SRS retrieval techniques, different models could give different simulation results, and there is no consensus on the hydrologic model most appropriate for the NRB as such consensus would need to be supported by exhaustive ground validation.

As a summary, we note that addressing the following two questions is the key to improve hydrologic monitoring and predictability in the NRB:

1. How can existing SRS systems lead to enhanced understanding of the space-time variability of rainfall and evapotranspiration at the NRB basin scale?

2. How can hydrologic models lead to enhanced understanding of the space-time variability of hydrological responses, particularly streamflow and groundwater flow?

In this paper, we present an approach that can be used to address these questions. Although we use the NRB to demonstrate our point, our approach can be applied to any major transnational river basin particularly in developing countries with inadequate ground-based observation systems.

2. How can existing SRS systems lead to enhanced understanding of the space-time variability of rainfall and evapotranspiration?

Rainfall

Background

Rainfall is the major driving force of the hydrologic cycle, and its estimation accuracy affects significantly the prediction accuracy of basin responses. Furthermore, rainfall is the most significant source of uncertainty in river basin hydrology. Data from rain gauges are commonly used in hydrological applications; however, the existing network of rain gauges in the NRB is by far inadequate for any hydrological application. Maintaining an adequate rain gauge network is difficult in this region, due to the vastness of the basin as well as the insurmountable operational issues to run such a large network in developing countries that do not have the resources to do so. As an alternative, spatial rainfall information over large basins could also be obtained from weather radar or SRS. Although weather radars are commonly used in most developed countries, there is no radar coverage in the NRB due the expensive capital and operational cost to run a radar network. This leaves us with SRS as the only currently viable means of obtaining spatially distributed rainfall data over the NRB.

Uncertainty in SR products

SR products are contaminated by several sources of error, which can be broadly grouped into temporal (sampling) and retrieval (algorithm) error. Temporal sampling errors arise from infrequent satellite visits and the variability of rainfall fields in space and time (e.g., Bell and Kundu 2000; Gebremichael and Krajewski 2004). Algorithm errors are associated with the algorithm approximation to the physical process (e.g., Wilheit et al. 1991). Information on rainfall estimation error is as critical as the rainfall estimate itself. In addition to providing objective measures to ensure progress in the satellite rainfall algorithm, estimation errors also help the user by providing information necessary for making rational decisions, enabling the user to take risk explicitly into account. To quantify the errors in the SR estimates, comparison of the SR estimates with independent, high-quality, ground-based rainfall observations are needed at selected locations. Sites that provide such high-quality ground-based rainfall observations are typically referred to as validation sites. Validation sites have been established or are underway in several developed countries. Such sites are now available in the US, UK, Spain, Italy, Japan, Kwajalein, and Australia, among others (Smith et al. 2007).

To assess the errors in the SRS estimates in the NRB region, recently we carried out the first validation field campaign in the Beressa watershed (BW) of the NRB in the summer of 2008. The BW is a mountainous, 220 km^2 watershed, located in the headwater of the NRB in Ethiopia (Figure 1). The watershed fairly represents most of the highlands of the NRB. During this field campaign, we installed 22 non-recording rain gauges within an area of 5 km × 5 km inside the BW, and collected daily measurements of rainfall at each of these locations for 40 days, from July 1 to August 9, 2008. Superimposed in Fig. 1 is the location of the rain gauges. We used these data to evaluate the accuracy of CMORPH (NOAA's Climate Prediction Center MORPHing technique; Joyce et al. 2004) rainfall product. CMORPH is the global rainfall product with the finest resolution (30 min, and ~ 8km × ~8km). CMORPH products rely exclusively on passive microwave and geostationary infrared measurements, with no ground-based measurement information.

Figure 1 shows that one of the CMORPH pixels contains about 19 rain gauges. This dense rain gauge network provides a very good reference dataset to evaluate the accuracy of CMORPH. We obtained area-averaged daily rainfall values from the rain gauge network by averaging the daily rainfall data from all 19 rain gauges. We aggregated the half-hourly CMORPH products to daily time scales, and compared them to the area-average values derived from the rain gauge network. As can be seen from Fig. 2, CMORPH performance varied by day. Overall, CMORPH tends to underestimate daily rainfall by 27%.

In a separate study, we had evaluated the accuracy of CMORPH in the central United States (see Zeweldi and Gebremichael 2008), and found that CMORPH overestimates rainfall in this region by a factor of 2 in July. The differences in the CMORPH accuracy over Little Washita and BW could be explained by the regional differences in climate and topography. Compared to BW, Little Washita is hotter in July and therefore has more evaporation below the cloud base that typically leads to overestimation by the SR product. Compared to Little Washita, BW is also characterized by more complex terrain rainfall.

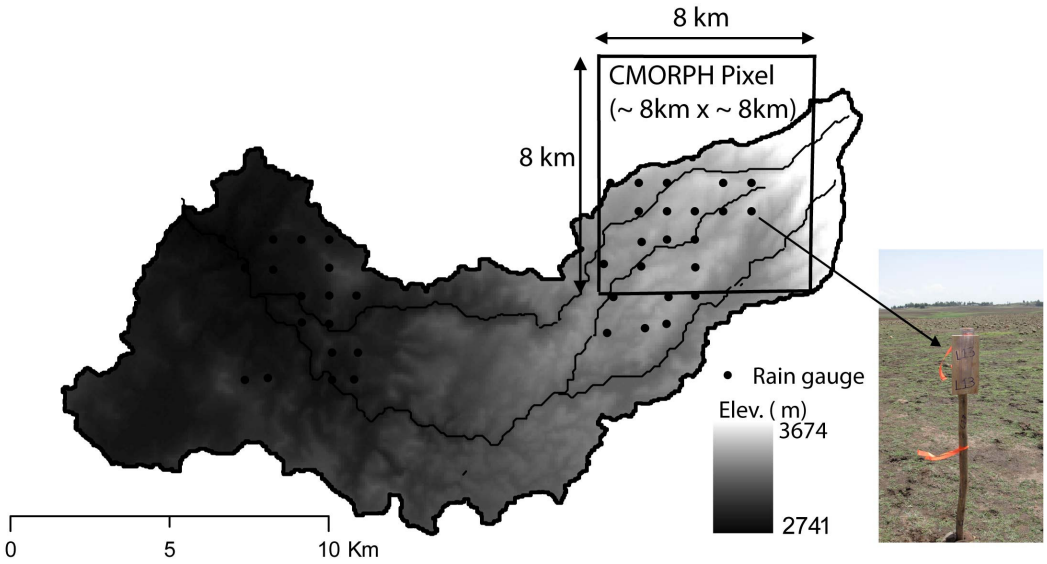

Figure 1. The 220-km^2 Beressa Watershed within the Nile River Basin, and its topographic characteristics derived from a 90-m digital elevation model. The inset shows the CMORPH rainfall product pixel (~8 km by ~ 8km), and a network of 19 rain gauges within this pixel. The rain gauges are graduated cylinders as shown in the picture, and manual readings were taken every morning.

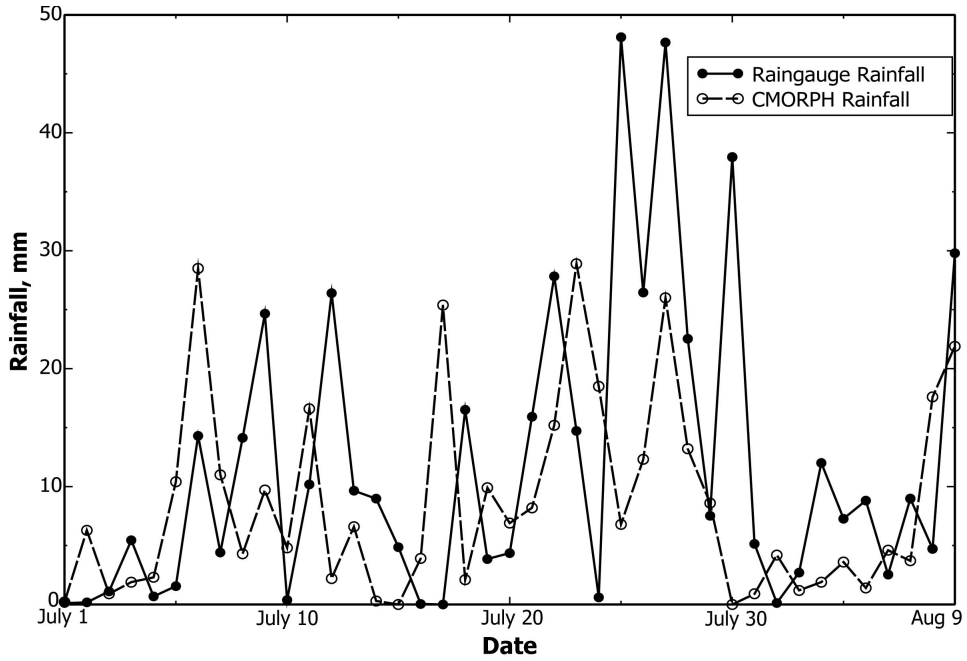

Figure 2. Comparison of time series of daily CMORPH and gauge-averaged rainfall values over one CMORPH pixel (see Fig. 1) within BW. The gauge-averaged rainfall is obtained by averaging daily rainfall data from 19 rain gauges within the CMORPH pixel.

Proposed Solution

It follows from the above discussion that information on the SR error is critically important to use the SR products as well as to improve the accuracy of the SR products. The NRB does not yet have a permanent validation site that can be used to quantify the errors in the SR estimates. We propose the establishment of a validation site in the NRB. The validation site should be equipped with a dense, permanently deployed, tipping bucket rain gauge network. SRS systems coupled with a validation site could make a breakthrough in characterizing the space-time variability of rainfall in the NRB.

Evapotranspiration

Background

Actual Evapotranspiration (ET) in the NRB is a major component of the hydrologic cycle, and so there is a strong interest in its accurate estimation. The traditional techniques for determining ET are either direct measurements in lysimeters (point scale) or from dedicated installations measuring gradients of temperature and water vapor (plot scale), or indirect estimation approaches based on the partitioning of the energy balance at the land surface (plot scale) (Brutsaert 1982; Monteith and Unsworth 1990). ET rates vary with soil moisture content, surface roughness and vegetation type, and so, it is often difficult to estimate ET using only ground-based measurements. For example, in the heterogeneous landscape in the central plateau of Spain, as many as 13 ground ET measurements in a relatively small area of 5000 km^2 were not sufficient to predict the area-averaged ET rate (Pelgrum and Bastiaanssen 1990). Thus, SRS remain the only viable alternative.

Uncertainty in SET products

Errors in Satellite ET (SET) estimates mainly result from uncertainties in the retrieval algorithms. SET retrieval algorithms contain a series of empirical equations, and so these equations might need some adjustments when they are applied to different regions. Most of the SET algorithms solve for ET as a residue of the energy balance equation. In these schemes, estimation of the sensible heat flux is the most significant source of error in SET estimates. Quantifying the uncertainty in the SET or sensible heat flux estimates over the NRB will help to (1) select the best SET algorithm, (2) modify the empirical equations involved in the SET algorithm, and (3) quantify the uncertainty of the resulting ET estimates. Information on the SET uncertainty is currently missing for the NRB.

Proposed Solution

We propose that well-organized field experiments designed to assess, improve, or develop new, SET algorithms be carried out in the NRB. This requires deploying ground-based sensors that provide accurate ET estimates at scales that are comparable to satellite pixels. This could be done by combining scintillometers and weather stations. Scintillometer can provide reliable measurement of sensible heat flux from the propagation statistics of an electromagnetic wave emitted over a certain distance along the surface (DeBruin 2002). The scintillometer has a

unique advantage over other ground-based sensors (e.g., eddy covariance sensors) in that it provides (1) measurements at scales comparable to remote sensing methods, (2) high temporal resolution, (3) access to remote areas, and (4) high accuracy.

3. How can hydrologic models lead to enhanced understanding of the space-time variability of hydrological responses, particularly streamflow and groundwater flow?

Reliable quantification of the temporal and spatial variability of basin responses (e.g., streamflow, groundwater flow) in a basin requires the use of a hydrologic model. A very important step in applying hydrologic models is selecting the optimal model complexity level. The model complexity level refers to the numerical method used for representing a basin: lumped, semi-distributed or fully-distributed. The premise that the explicit representation of spatially varying fields should lead to significant advances in the skill to simulate and forecast hydrologic response is the central hypothesis in the development of distributed hydrologic models (e.g., Beven 1989; Goodrich et al. 1995). The ability for detailed representation of spatial information (e.g., topography, soils, vegetation, and meteorological forcing) and hydrological dynamics comes at the expense of computational burden. Many studies also point out the possible overparameterization of the process description (e.g., Refsgaard 1994, 1997) and the general inability to validate the distributed dynamics with currently available spatial data (Grayson et al. 2002). Jakeman and Hornberger (1993) and Woolhiser (1996) have questioned the need for complex, physically-based models. This leads to the question: how much complexity is optimally needed in a hydrologic model for the NRB? Grayson and Bloschl (2001) argue that the performance of hydrologic models depends on the relationship between data availability/uncertainty and model complexity (Fig. 3). The level of model complexity required, and the relationship between this complexity level and sub-basin area and data uncertainty is yet to be assessed for the NRB.

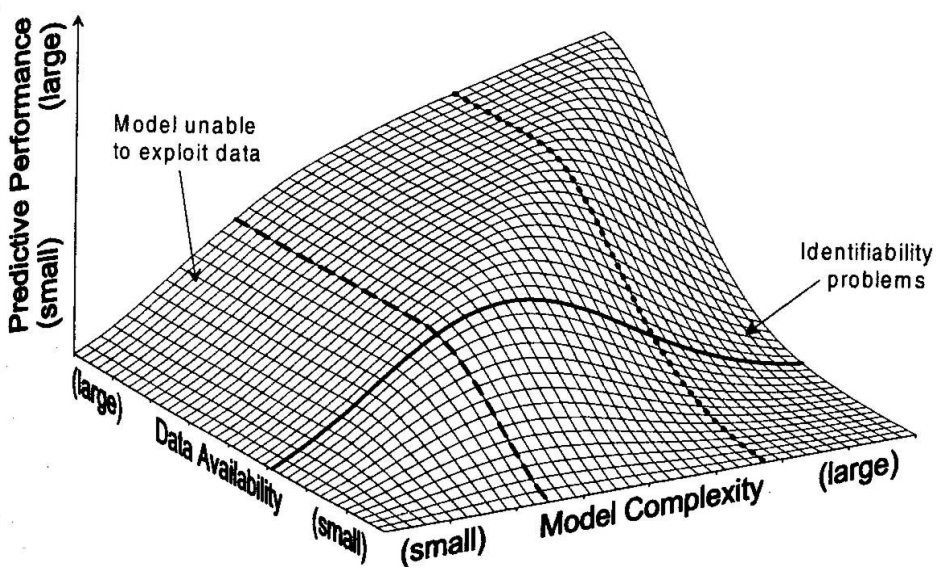

Figure 3 – Predictive performance of hydrologic models as a function of model complexity and data availability (Grayson and Bloschl 2001).

Proposed Solution

Research is needed to quantify the appropriate model complexity level for the NRB, given the availability of spatially distributed inputs from satellites and their uncertainty. This may depend on the space-time scale of interest, and season. To perform this research, it is important to maintain high-quality streamflow gauges at different spatial scales. The existing streamflow gauges network within the NRB can provide a good starting point for this research.

4. A blueprint for Advancing Hydrologic Monitoring and Predictability in the Nile River Basin

The NRB does not yet have a reliable hydrologic monitoring and assessment/prediction tool. This places serious limitations for the planning and management of the water resources in the Nile basin. Based on the discussion in the foregoing sections, we propose a new approach for advancing hydrologic monitoring and predictability in the NRB. As depicted in Figure 4, the approach stands on four pillars: establishement of a validation site, deployment of field campaigns, and integration of satellite data with hydrologic models. The validation site is important to provide ground reference for satellite rainfall estimates and hydrologic model streamflow simulations. The field campaign will provide ground reference data for satellite ET estimates. Major progress on the subject of Nile water management can be achieved by integrating the above research aspects to improve our understanding of Nile hydrology and lead to advanced data-modeling tools. To realize the transition to the new approach, we provide a brief assessment of the current strengths and existing barriers.

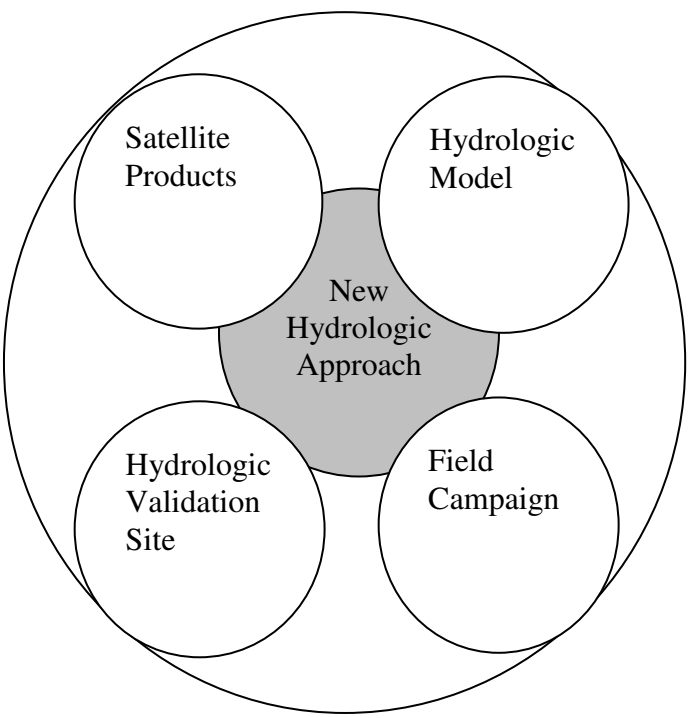

Figure 4 – The key components of the proposed hydrologic approach to advance hydrologic monitoring and predictability in the Nile River Basin.

References

Bell, T. L., and P. K. Kundu, 2000: Dependence of satellite sampling error on monthly averaged rain rates: Comparison of simple models and recent studies. J. Climate, 13, 449-462.

Beven, K.J. 1989: Changing ideas in hydrology — The case of physically based models. J. Hydrol., 105, 157–172.

Brutsaert, W., 1982: Evaporation into the atmosphere: theory, history, and applications. Kluwer Academic, Dordrecht, The Netherlands.

DeBruin, H.A.R., 2002: Renaissance of scintillometry, Boundary-Layer Meteor., 105, 1-4.

Gebremichael, M., and W. F. Krajewski, 2004: Characterization of the temporal sampling error in space-time averaged rainfall estimates from satellites. J. Geophys. Res., 109, D11110, doi:10.1029/2004JD004509.

Goodrich, D. C., J. -M. Faures, D. A.Woolhiser, L. J. Lane, and S. Sorooshian, 1995: Measurement and analysis of small-scale convective storm rainfall variability. J. Hydrol., 173, 283–308.

Grayson, R. B., G. Bloschl, A. W. Western, and T. A. McMahon, 2002: Advances in the use of observed spatial patterns of catchment hydrological response. Adv. Water Resour., 25, 1313–1334.

Grayson, R., and G. Bloschl, 2001: Spatial Modelling of Catchment Dynamics. In: Spatial Patterns in Catchment Hydrology. Grayson, R., and G. Bloschl, Ed., 51-81.

Jakeman, A.J., and G.M. Hornberger, 1993: How much complexity is warranted in a rainfall-runoff model? Water Resour. Res., 29(8): 2637-2649.

Joyce, R. J., J. E. Janowiak, P.A. Arkin, and P. Xie, 2004: CMORPH: A method that produces global precipitation estimates from passive microwave and infrared data at high spatial and temporal resolution. J. Hydromet., 5, 487-503.

Monteith, J., and M. Unsworth, 1990: Principles of Environmental Physics. London: Edward Arnold.

Pelgrum, H., and W. G. M. Bastiaanssen, 1996: An intercomparison of techniques to determine the area-averaged latent heat flux from individual in-situ observations: A remote sensing approach using the European Field Experiment in a Desertification-Threatened Area data, Water Resour. Res., 32(9): 2775-2786

Smith, E. A., and coauthors, 2007: International Global Precipitation Measurement (GPM) Program and Mission: An Overview. In: Measuring Precipitation From Space, (Eds.) Lizanni, V., P. Bauer, and J. Turk, Springer, Vol. 28, 611-653.

Wilheit, T. T., A. T-C Chang, and L. S. Chiu, 1991: Retrieval of monthly rainfall indices from microwave radiometric measurements using probability distribution functions. J. Appl. Meteorol., 16, 551-56

Woolhiser, D. A., 1996: Search for Physically-based Runoff Model – A hydrologic El Dorado. J. Hydrol. Eng., 122(3): 122-129.

Zeweldi, D., and M. Gebremichael, 2008: Evaluation of CMORPH Rainfall Products at Fine Space-Time Scales, J. Hydromet., (in press).

Distributed Hydrologic Model for Flood Prevention in the Yuna River Watershed, Dominican Republic

H. J. Robinson[1], Z. Fang[2], and P. B. Bedient[3]

[1]Department of Civil and Environmental Engineering, Rice University, M.S. 317, Houston, TX 77005-1827; PH (713) 348-3798; FAX (713) 348-5239; email: hilaryr@rice.edu
[2]Department of Civil and Environmental Engineering, Rice University, M.S. 317, Houston, TX 77005-1827; PH (713) 348-2398; FAX (713) 348-5239; email: nickfang@rice.edu
[3]Department of Civil and Environmental Engineering, Rice University, M.S. 317, Houston, TX 77005-1827; PH (713) 348-4953; FAX (713) 348-5239; email: bedient@rice.edu

ABSTRACT

The Yuna River basin, a watershed of about 5500 km^2 in the Dominican Republic (DR), is affected by both broad floods in the valley and flash flooding in the upper mountainous reaches. A better understanding of flood behavior and an assessment of flood control options is necessary in this watershed to protect human life and property, as highlighted by the particularly active 2008 hurricane season. Distributed hydrologic models using *Vflo*™ of both 250m and 500m cell resolution have been developed to provide flood prediction and flood control assessment in the basin. The Upper Yuna subwatershed is topographically diverse, with steep tributaries falling from 3,000m mountains into a main channel through a relatively flat valley. The *Vflo* software has great applicability for this watershed compared with more standard hydrologic models because it can model the challenging topography, provide flow outputs for any portion of the watershed, and handle variable-detail GIS inputs of elevation data, soil, and land-use maps. An analysis has been performed that compares influence of cell size and hydrologic detail on tributaries of varying steepness and flow output, which proves important for location selection of flood control options. A main goal of this work is to aid this flood-prone community by getting a first model running that can provide inputs to flood timing prediction, basic floodplain mapping, and flood control assessment, but that can be quickly refined as more data of greater detail becomes available.

INTRODUCTION

Flooding along the Yuna River, which is the second largest river in the Dominican Republic, is deadly and frequently damaging to the economy and agriculture of the region. Between 2000 and 2008, approximately 8 tropical storms and hurricanes hit or affected the Dominican Republic, and multiple storms took the

lives of citizens. The basin of the Yuna River covers approximately 5500 km^2 of land, and drains along two major tributaries into the larger Lower Yuna River and eventually into the Caribbean Sea (see Figure 1 below).

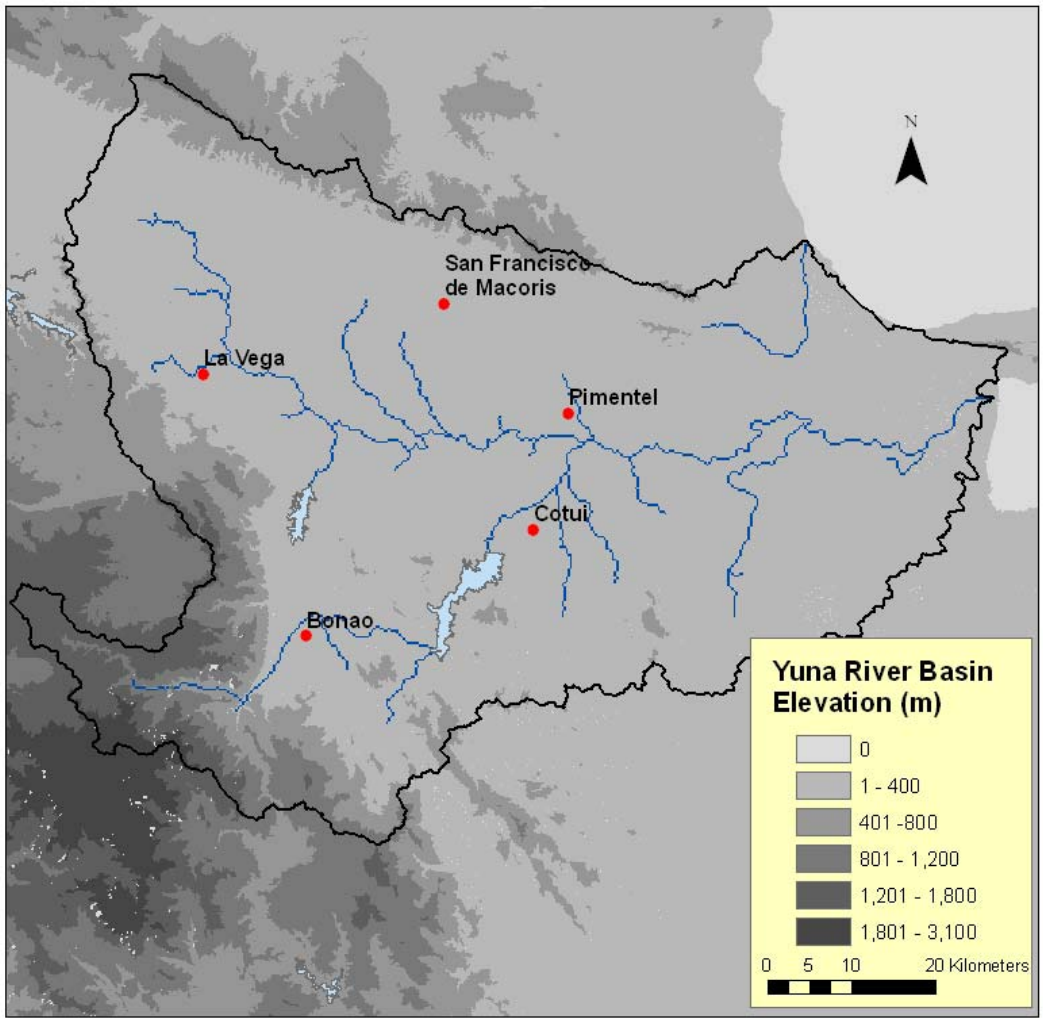

Figure 1: Yuna River Basin and Elevation Map

The Yuna River basin is characterized by steep tributaries that flow into the Lower Yuna River through a relatively flat valley. The runoff through the steep regions creates dangerous flash-flooding behavior in the Upper Yuna River through the city of Bonao. In the valley, wide floods occur that maintain high water for multiple days. The floodplain is estimated to be nearly 15 km wide in some places. There are fewer people living in the valley but many homes are clustered next to rivers for resources and access.

Agriculture is a vital component of the Yuna River Basin economy. The lower valley is very productive in rice, and the upper valley is used for mixed crops. A better understanding of flood behavior is necessary in this watershed to protect agricultural property. Currently, no comprehensive study of flood risk or flood control potential exists for the Yuna River basin. The model created in this study

provides a foundation for understanding flood risk in the basin and for making plans to mitigate it.

BACKGROUND

Hydrologic models can run calculations in a lumped, distributed, or semi-distributed format, which is a hybrid version between the former two. Each has more appropriate applications, as established in Das et al (2008). In this study, semi-distributed models outperformed, though comparison was based on only discharge at the outlet, for which the semi-distributed and lumped models were created (Das et al 2008). Distributed models, specifically, are designed to simulate flows along an entire channel. Zimmerman et al (2007) confirmed that a distributed model can successfully predict peak flows when results are needed at all points along a channel. They showed that the cumulative effects of detention ponds can be determined using a distributed model for which hydrographs can be extracted at every point along a tributary.

Various distributed hydrologic models are available, requiring different sets of parameter inputs. These models also address topography in different ways, which is an important focus in variable watersheds. Yang et al (2000) compared topography simulations within three distributed models: MIKESHE, TOPMODEL, and GB (geomorphology-based). MIKE SHE is thorough but slow in computation time; TOPMODEL requires greater calibration yet utilizes variable data better; GB is flexible and was determined by Yang et al (2000) to be the best for hydrologic modeling of large watersheds. The methodology in MIKE SHE parallels the gridded system that is run by the distributed model, *Vflo*™, which is provided by Vieux and Associates out of the University of Oklahoma (Vieux 2004). *Vflo*™ is a fully distributed model that provides outputs at both the local- and broad-scale without modification of the model setup. The platform of its flow computations is physically-based and requires the finite element method, which is used to solve the following kinematic equations:

Overland flow $$\frac{\partial h}{\partial t} + \frac{S^{1/2}}{n}\frac{\partial h^{5/3}}{\partial x} = R - I$$

Channel flow $$\frac{\partial A}{\partial t} + \frac{\partial Q}{\partial x} = q$$

where h = flow depth, S = slope, R = rainfall rate, I = infiltration rate, n = hydraulic roughness, Q = discharge or flow rate, q = rate of lateral inflow per unit length, and A = cross-sectional area (Vieux 2004). *Vflo*™ is an established model that can hot-start to minimize computation time and can handle very large basins (Vieux 2004). *Vflo*™ has been able to successfully replicate historical flood events, as seen in Vieux (2004) and Tachikawa et al (2003) and has been used in large, tropical watersheds, such as in Puerto Rico in Rojas and Harmsen (2007).

MODEL SETUP

The development of the Yuna River basin model involved a compilation of remotely sensed data into a detailed *Vflo*™ model of interconnected cells. One model was created with cells of 250m on a side, the other with cells of 500m. The flow direction grid that establishes the basis of the model was derived from NASA SRTM 90x90m data, which is comparable with SRTM 30mx30m data provided for the mainland United States. LiDAR data is expected to become available in Summer 2009 from the University of Texas Center for Space Research, which will provide important detail to the hydraulic model. However, the hydrologic model, running with 250m cells, should be adequately formed by the SRTM data.

Parameterization

Major inputs to a *Vflo*™ model are imperviousness, Green and Ampt infiltration parameters, overland and channel roughness, slope, and channel width. For the Yuna River basin, slopes were derived from the same elevation data that was used for determining flow direction. Channel width and roughness were estimated from the satellite imagery of GoogleEarth, in the absence of higher-detail images. Supplementary photos were taken during a helicopter flight over the watershed to obtain detail of bank erosion and stream vegetation.

Overland roughness Manning's coefficients are derived from a land use map created by the National Institute for Hydraulic Resources (INDRHI) of the Dominican Republic. The map's texture indicates the land use parcels were pulled from satellite images in an automated process. Manning's coefficients have been defined for each of the land use categories, ranging from 0.015 to 0.4. Over 30 categories are displayed, specifying a number of crops that are grown in the region.

Infiltration parameters for the local soil types were created using average values of the Soil Conservation Service's (SCS) four main soil groups. Descriptions of local soils obtained from INDRHI aided in determining which soil group was most appropriate, and Green-Ampt parameters were assigned based on these groups.

Precipitation

Full parameterization of the watershed allows for simulation of rainfall frequency storms. A Log-Pearson III frequency analysis was performed for three gages. The area represented by each gage slightly surpasses common limits seen with areal reduction coefficients, but no other gage operated for long enough to perform a statistically significant analysis. Annual 24-hr 100-yr storm maximums ranged from 160 to 320 mm for these gages, which is a high level of variation and is probably accounted for by coastal and topographical effects.

Typical rainfall distribution must be estimated to input a frequency storm at a given gage. Telemetered rainfall gage data is available on an hourly basis in certain Yuna locations starting in 2006. Cumulative plots of significant Yuna River basin storms have been compared to the four common distributions that have been developed by the Soil Conservation Service to approximate storms seen in the United States: Types I, II, III, and IV. This method provides dimensionless coefficients that can be multiplied by storm depth to depict hyetograph shape and placement of peak

intensity (McCuen 2005). The Yuna River basin is best approximated by the Type III curve.

RESULTS

The goal of these hydrologic simulations is to better our understanding of flood behavior along the Yuna River. The influence of a tributary is a telling indicator of its flood control potential. A comparison has been performed to assess this potential for the main tributaries of the Yuna River, even without sufficient data to represent historical storms. Figure 2 shows the tributary assignment in the watershed, with channel cells created for any cell draining more than 400 other cells for the 500m model.

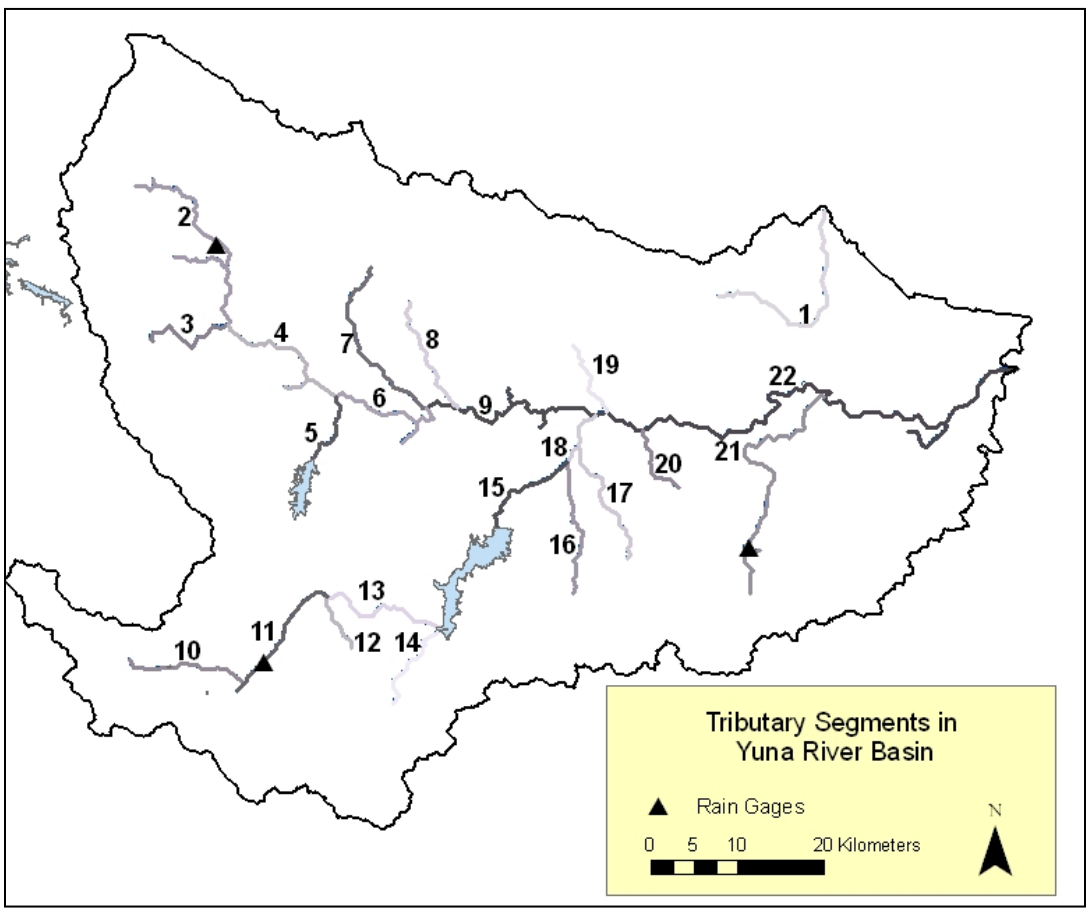

Figure 2: Labeled tributaries and segments of river for Tributary Comparison Analysis in Table 1

A 24-hr synthetic uniform storm of 200 mm was used for this analysis. Tributary influence is shown as a relative percentage of volume and peak flow, as compared with the river outlet. Where volume can be controlled, the potential to mitigate wide downstream floods may be present; where peak flow can be controlled, there may be the potential to mitigate flash flooding. The full tributary comparison is

shown in Table 1. While a local flood assessment or calibration might be best performed with the 250m cell model, the 500m cell model was used for this broad analysis, limiting computation time significantly.

Table 1: Comparison of tributary contributions using 500m preliminary model

Tributary Segment	% Volume of Outlet	% Peak Flow of Outlet		Tributary Segment	% Volume of Outlet	% Peak Flow of Outlet
1	5	5		12	5	5
2	14	19		13	21	33
3	6	10		14	5	8
4	27	31		15	29	36
5	5	6		16	6	8
6	36	40		17	5	6
7	5	4		18	39	44
8	5	4		19	5	4
9	50	50		20	1	3
10	5	14		21	10	11
11	13	26		22	100	100

DISCUSSION

A tributary analysis has been performed that denotes each tributary's contribution (at its outlet) as a proportion of the total flow. This process normalizes the results to eliminate calibration issues and still provides valuable information for selecting flood control locations. Because of the steep slopes and varied infiltration in the watershed, comparisons are possible that would otherwise not be obvious.

Table 1 highlights differences in tributary influence, such as the relative importance of tributaries 2, 3, 10 and 21 over tributaries 7, 8, 17, and 19. These tributaries have larger runoff volume or peak flow than would be expected from their relative length and size. Tributary 21 may be particularly influential, or for some storms, insignificant, because its timing is far off from other tributaries of similar size. Further investigation of historic storm movement is needed to determine timing specifics, but this analysis quickly narrows the list of potential flood control locations.

An interesting optimization of flood control location can be made for tributaries 10, 11, and 13, which drain into each other successively toward Bonao. The change in peak flow from tributary 10 to 11 is from 14% to 26%, or almost double. The change in peak flow from tributary 11 to 13, as more area is drained and slopes flatten, is from 26% to 33%, or just over a quarter larger. The volume comparison shows similar results, with volume increasing 160% between tributaries 10 and 11, yet increasing less then two thirds between tributaries 11 and 13. The relative increases do not match up linearly between peak flow and volume, showing the importance of the model in understanding behavior. Perhaps a flood control would be better located in tributary 11 than in tributary 13 if geography or expense made it more difficult to construct downstream. There would still be sufficient influence to affect the local runoff.

Tributary 15 results are particularly significant, as they indicate flood control effectiveness in the Hatillo Reservoir. About a quarter of the watershed's full volume enters the reservoir, while the peak flow through the reservoir is about a third of the greatest expected flow. These comparisons show useful conclusions can be reached using the tributary analysis, even without full calibration to historical events.

CONCLUSION

The preliminary hydrologic model has great potential for use in hydraulic modeling and floodplain delineation. As greater elevation and hydraulic detail becomes available, HEC-RAS modeling will be able to produce floodplains using the results of the Yuna River model. As it is, the tributary comparison is particularly useful for selecting flood control locations. Certain tributaries have been shown to have greater influence than is first discernible, especially when drainage area does not linearly match peak flow rates. A preliminary list of significant tributaries can be easily compiled. For future work, one of the benefits of using the distributed model, *Vflo*™, is that hydrographs can be pulled from the existing basin model at any location desired. An engineer selecting specific sites for flood controls can focus in on a cell within one of the more influential tributaries. Storage can be added at that specific site to determine extent of possible volume and peak flow mitigation. The distributed model is an ideal template for this work, as it remains calibrated at the scale of the watershed, and yet permits comparison of flood controls for very small shifts in location down to 250m .

REFERENCES

Das, T., Bardossy, A., Zehe, E., and He, Y. (2008). "Comparison of conceptual model performance using different representations of spatial variability." *J. of Hydrology*, 356(1-2), 106-118.

McCuen, R. (2005). *Hydrologic Analysis and Design*, Pearson Prentice Hall, New Jersey.

Rojas, A., and Harmsen, E. (2007). "Hydrologic Studies Using Vflo in Western Puerto Rico." *Seventh Carib. Islands Water Res. Congress*, 81-85.

Tachikawa, Y., Nawarathna, B., Vieux, B., and Takara, K. (2003). "Hydrologic Prediction Using Weather Radar Information and Distributed Hydrological Modeling." *The XXIII Gen. Assembly of the Intnl. Union of Geodesy and Geophys.,* Sapporo, Japan.

Vieux, B. (2004). *Distributed Hydrologic Modeling Using GIS*, Kluwer Academic, The Netherlands.

Yang, D., Herath, S., and Musiake, K. (2000). "Comparison of different distributed hydrological models for characterization of catchment spatial variability." *J. of Hydrological Proc.*, 14(3), 403-416.

Zimmerman, A. (2007). *The Use of a Distributed Hydrologic Model to Evaluate the Location of Development and Flood Control Reservoirs*. Rice University, Houston, TX.

Evaluation of Land Use Land Cover Changes in Palleru (K-11) Sub Basin of River Krishna using GIS and NDVI

M.V.S.S.Giridhar[1] and Dr.G.K.Viswanadh[2]
[1] Asst. Prof., Centre for Water Resources, Institute of Science & Technology, JNTU, Hyderabad, [2] Professor, Dept. of Civil Engg., J.N.T.U. C.E., JNTU, Hyderabad

Abstract

In the present study, Palleru sub basin (K-11) has been considered for the evaluation of land use land cover changes. Ten rain gauge stations were identified in and around the study area and accordingly the sub basin was divided into ten sub areas namely Palakurthy, Kodagandla, Torrur, Tungaturthy, Aravapally, Maripeda, Noothankal, Atmakur, Kushmanchi and Mothey based on Thiessen polygon network. The land use/land cover classification was made based on Normalized Difference Vegetation Index (NDVI) with two scenes in a year. The areal extent of bare soil was computed as 26.16 sq km and 372.03 sq km for the years 2000 and 2002 respectively in the Rabi season and 87.73 and 182.82 sq km for the years 2000 and 2002 respectively in the summer season. Bare soil increased by 345.87 sq km and 95.09 sq km in Rabi and summer seasons respectively. The areal extent of fallow lands with bushes decreased from the year 2000 to 2002 with respect to Rabi and summer seasons due to limited rainfall in the year 2002. However, the cropped area did not register much difference. The areal extent of water bodies in Rabi season was estimated as 198.83 sq km and 92.57 sq km for the years 2000 and 2002 respectively. The decrease in water spread area from the year 2000 to 2002 was due to corresponding decrease in rainfall in the study area from 920mm to 556 mm. Similarly, the areal extent of water bodies in summer season was estimated as 22.74 sq km and 18.27 sq km for the years 2000 and 2002 respectively.

Introduction

Land use/land cover inventories are essential for the optimal utilization and management of resources in a given sub basin. Land cover refers to different features covering the earth's surface including vegetation cover, water bodies, open scrub etc. It integrates the sum of human activities having an influence on the environment. The USGS has devised a land use/land cover classification system for use with remote sensor data (Anderson et al., 1976). Land use and land cover information should be presented on separate maps and should not be

intermixed (Lillesand et al., 1979). With the latest advancements and the wide range of applications in the field of remote sensing, Geographic Information System (GIS) facilitates the adoption of new methodologies which prove to be highly efficient. (Sahai et al., 1985) used multidate, multispectral Landsat imagery of pre and post monsoon studies. The overlay of the toposheet on the satellite image with appropriate ground truth provides the features of the land use/land cover of the selected area. The same study if implemented periodically enables to understand the variations in resources. ERDAS 8.7 has been used to study land use/ land cover features of the sub basin. The objective of the present study is to study and evaluate the land use and land cover changes in the sub basin of River Krishna, Andhra Pradesh, India. Nayak and Jaiswal (2003) observed that the conventional hydrologic data are inadequate for the purpose of design and operation of water resources systems. In such cases, remote sensing data are of great use for the estimation of relevant hydrological data. RS data can serve as a model input for the determination of river catchment characteristics such as land use /land cover, geomorphology, slope, drainage etc. GIS offers the potential to increase the degree of definition of spatial sub units, both in number and descriptive detail.

Holben (1986) studied that Normalized Difference Vegetation Indices (NDVI) increased as one proceeds from water through ice, snow, opaque clouds, bare soil, to green vegetation. (Wiegand et al., 1991) have argued that, at a specific site, the cumulative evapotranspiration and cumulative vegetation index should be highly correlated because the same green plant tissue measured by NDVI is due to absorbed active photo synthetic radiation. Reddy (1997) described that satellite data provides integrated information on rock types, land forms, geological structures, weathering, soil types, erosion, land use/land cover, surface water bodies, distribution of ground water, slope details, soil type, rainfall, irrigated areas and their acreage etc., All these data, incorporated into the GIS package, it will form an excellent data base and becomes useful for judicious planning, proper development and effective management of water resources.

Study area

The Krishna basin is situated between longitudes $73^0$21' to $81^0$09'E and $13^0$07' to $19^0$25' N in the Deccan plateau covering large areas in the States of Maharashtra, Karnataka and Andhra Pradesh. The Krishna basin extends over an area of 2,58,948 km^2, which is nearly 8% of the total geographical area of the country. Krishna catchment was divided in to 12 sub basins. In the present study, K-11 sub basin i.e Palleru basin of River Krishna has been considered to analyze land use/land cover at each rain gauge sub area. The Palleru sub basin lies between

latitudes 16^0 $39^{'}$ and 17^0 $50^{'}$ North and longitudes 79^0 $17^{'}$ and 80^0 $09^{'}$ East. The Palleru sub basin has a catchment area of 3,263km^2, which constitutes 1.3% of the total basin area. The catchment area of the Palleru sub basin entirely lies in the State of Andhra Pradesh. In the present study, sub basin has been considered up to Palleru reservoir only (2068km^2) as shown in Fig.1.

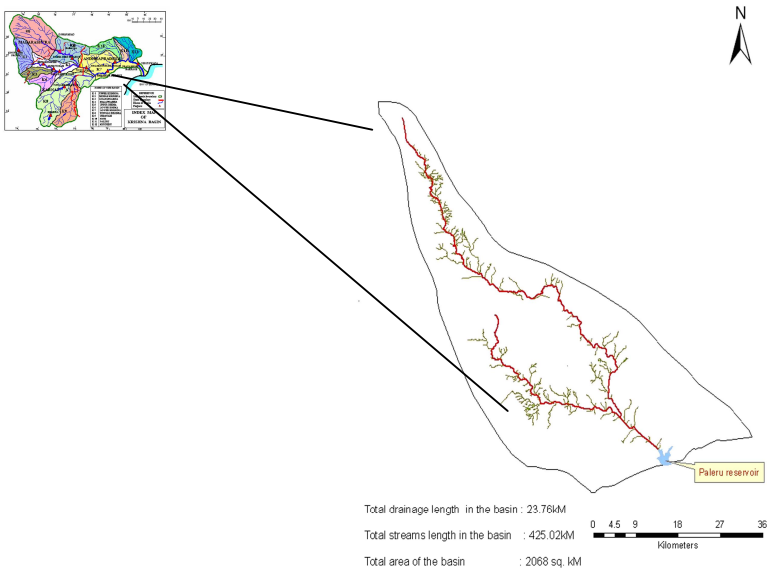

Fig 1 : Location plan of Palleru sub basin (K-11).

Data Used

Spatial data in the form of satellite imageries for the preparation of Land use/Land cover details at sub basin level were procured from National Remote Sensing Agency (NRSA), the details being listed in Table 1. These satellite imageries for both Kharif and Rabi seasons for two years pertain to Indian Remote Sensing Satellite (IRS) 1C & 1D, Linear Imaging and Self Scanning Sensor (LISS –III) with a resolution of 23.5m. The topographic maps used namely 56 O7, O10, O11, O12, O15, O16, 56P13, 65C4 and 65D1 on a scale of 1:50,000 were collected from Survey of India (SOI), Uppal, Hyderabad on 1:50,000 scale for the delineation of watershed boundary.

Table 1 Details of Satellite Imageries

Sl. No	Date of pass	Path, Row, Shift and Scanner	IRS	Season
1	09-04-2000	101, 60, 50% SHIFT, LISS-III	IC	Rabi
2	29-12-2000	101, 60, 50% SHIFT, LISS-III	IC	Kharif
3	11-05-2002	101, 60, 50% SHIFT, LISS-III	ID	Rabi
4	22-12-2002	101, 60, 50% SHIFT, LISS-III	ID	Kharif

Methodology

Identification and delineation of Land use/Land cover, location, extent and their spatial distribution patterns are possible because of the synoptic view provided by the Satellites and their ability to resolve both macro and micro details on a single imagery. It provides periodic coverage of the same area thus enabling to obtain Multi-temporal data useful for monitoring the dynamic aspects of Land use/Land cover. It provides data both in analog and digital form. Such data is amenable for both visual interpretation and digital analysis for extracting thematic information. It is relatively fast, cost effective and economical for inventorying several details of LU/LC than the most of the other methods of surveying. The different Multi-spectral and Spatial data can be merged with other satellite data for optimizing the LU/LC identification and discrimination.

Image classification: The overall objective of image classification procedures is to automatically categorize all pixels in an image into land cover classes or themes. Different feature types manifest different combinations of Digital Numbers (DN) based on their inherent spectral reflectance and emittance properties. The elements of image interpretation are shape, size, pattern, tone (or hue), texture, shadow, site, association and resolution.

Spectral Response of Vegetation: The visible and near infrared bands on the satellite multi spectral sensors allow monitoring of the greenness or vigor of vegetation. Green vegetation is highly absorptive in the visible part of the spectrum, mostly owing to the presence of chlorophyll. Beyond a wavelength of about 700nanometers, the absence of absorbing pigments and leaf structure results in high reflectivity for green vegetation. In contrast, other features such as bare ground, water, snow and clouds have similar reflectance in visible channel compared to near infrared channel. Stressed vegetation is less reflective in the near infrared channel than non-stressed vegetation and also absorbs less energy in the

visible band. Stratification of the Normalized Difference Vegetation Index (NDVI) response to broad scene components was shown in Table 2. Vegetation indices were found to increase as one proceeds from water through ice, snow, opaque clouds, bare soil, to green vegetation Holben (1986). Out of the various vegetation indices available, NDVI is very widely used as it minimizes the effect of change in illumination condition and surface topography (Holben, 1986). The NDVI is defined as the ratio of difference between the near infrared and red reflectance to their sum.

$$NDVI = \frac{CH2 - CH1}{CH2 + CH1} \quad (1)$$

where,

CH1 = Spectral reflectance from red band / channel

CH2 = Spectral reflectance from near infrared band / channel

Table 2 Albedo Values for Different Cover Types.

Sl. No	Cover Type	Planetary Albedo		
		CH1	CH2	NDVI
1	Dense green leaf vegetation	0.050	0.150	0.500
2	Medium green leaf vegetation	0.080	0.110	0.140
3	Light green leaf vegetation	0.100	0.120	0.090
4	Bare soil	0.269	0.283	0.025
5	Clouds	0.227	0.228	0.002
6	Snow and Ice	0.375	0.342	-0.046
7	Water	0.022	0.013	-0.257

The thematic map of Land Use / Land Cover has been prepared using ERDAS 8.7. The classification of land Use / Land Cover classes were evaluated using NDVI. Of all the available methods of image classification with regard to vegetation and its sub classification, NDVI forms the basis for a better classification and hence

adopted for the present study. And also, as the study area is considerably large comprising predominantly of vegetation, NDVI classification is better suited and hence employed for the classification of Land Use / Land Cover. This data is used as an input for direct runoff estimation.

Preparation of Land Use / Land Cover Thematic Map

Spatial data in the form of satellite imageries for the preparation of Land Use/Land Cover details at sub basin level were procured from National Remote Sensing Agency (NRSA) the details are listed in Table 1. These satellite imageries for both Kharif and Rabi seasons for two years pertain to Indian Remote Sensing Satellite (IRS) -1C & 1D, Linear Imaging and Self Scanning Sensor (LISS –III) with a resolution of 23.5m. The collected satellite images were georeferenced in ERDAS 8.7 then rectified and finally projected. The delineated watershed in vector form was overlaid on projected satellite imagery to get sub set of the study area. Thiessen polygon coverage which was prepared in GIS in vector form was overlaid on sub set image of the study area in ERDAS 8.7 to get delineation for all ten sub areas namely Palakurthy, Kodagandla, Torrur, Maripeda, Tungaturthy, Noothankal, Aravapally, Atmakur, Mothey and Kushmanchi. Normalized Difference Vegetation Index (NDVI) was employed as the basis for Land Use / Land Cover classification. This method of classification has been found to be suitable for the study area i.e., Palleru sub basin as the data used was pertaining to the past period i.e., years 2000 and 2002 and also the study area is considerably large comprising predominantly of vegetation. Study area has been classified for Land Use / Land Cover into four classes viz., Water bodies, Crop land, Bare soil and Fallow land with bushes in each sub area based on NDVI values generated in ERDAS 8.7. Area under each class has been calculated from the attribute table in Arc.GIS9.1. The flow chart used in this analysis has shown in Fig. 2. The classified thematic map was converted from raster to vector format for further analysis. The Land Use / Land Cover thematic map and soil map were intersected in command tools of ARC/INFO.

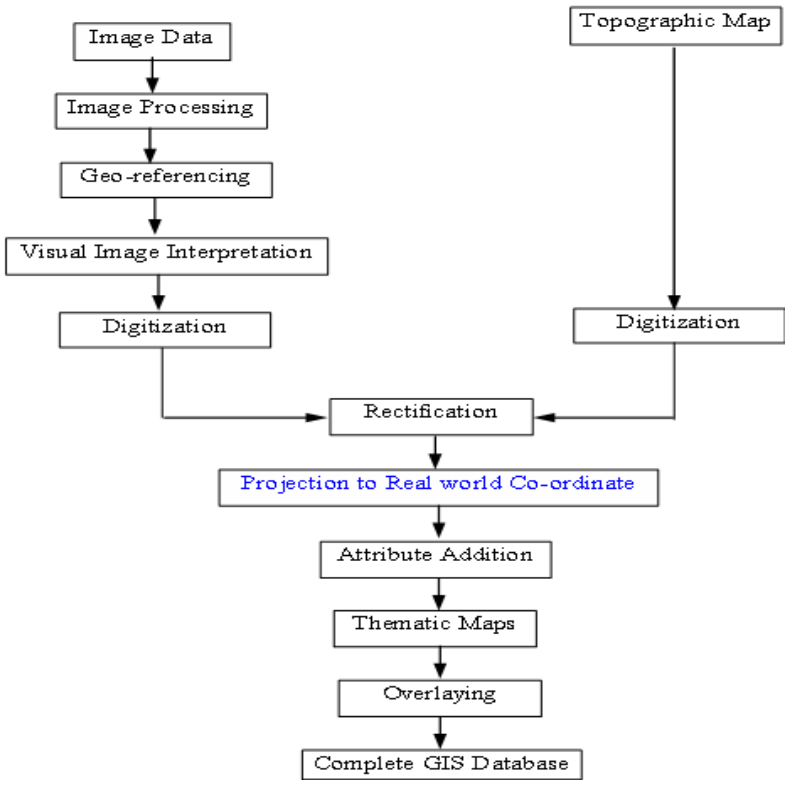

Fig 2. Flow chart for the preparation of land use and land cover thematic map.

Results and discussion

Four satellite imageries were analyzed using ERDAS 8.7, two of them pertaining to Rabi season and another two related to summer season in the years 2000 and 2002 respectively. The thematic map of Land Use / Land Cover has been prepared using ERDAS 8.7 for all imageries. The land Use / Land Cover classes were evaluated using Normalized Difference Vegetation Index (NDVI). Study area has been classified into four classes viz., Water bodies, Crop land, Bare soil and Fallow land with bushes in each sub area based on NDVI values for Land Use / Land Cover classification. Areal extent under each class has been calculated from the attribute table of ERDAS 8.7. The areal extent of Water bodies, Crop land, Bare soil and Fallow land classes has been listed in Table 3 for each sub area.

Table 3 Land Use Land Cover Details in the Study Area

Date of pass: 09-12-2000

	Pala Kurthy	Kodagandla	Torrur	Maripeda	Tungaturthy	Noothankal	Aravapally	Atmakur	Mothey	Kushmanchi	Total
Water Bodies	8.18	27.64	17.88	24.31	27.81	34.90	8.43	13.13	10.19	26.36	198.83
Crop land	118.78	126.95	71.30	219.18	123.03	176.27	39.84	97.17	70.14	143.26	1185.92
Bare soil	4.95	4.85	1.53	1.68	4.12	2.58	2.41	1.85	1.61	0.58	26.16
Fallow land	107.80	90.40	37.05	59.18	92.34	66.77	66.64	66.54	50.05	28.44	665.22

Date of pass: 29-12-2002

	Pala Kurthy	Kodagandla	Torrur	Maripeda	Tungaturthy	Noothankal	Aravapally	Atmakur	Mothey	Kushmanchi	Total
Water Bodies	6.21	8.65	2.56	11.08	10.81	17.95	6.45	8.88	4.94	15.03	92.57
Crop land	90.30	86.45	56.12	195.75	117.51	174.44	33.12	86.74	60.09	123.51	1024.02
Bare soil	56.03	65.47	24.15	33.73	49.66	31.08	32.32	31.70	25.29	22.60	372.03
Fallow land	86.89	89.30	44.85	63.70	69.02	56.84	45.40	51.38	41.84	37.48	586.73

Date of pass: 09-04-2000

	Pala Kurthy	Kodagandla	Torrur	Maripeda	Tungaturthy	Noothankal	Aravapally	Atmakur	Mothey	Kushmanchi	Total
Water Bodies	1.20	1.24	1.09	1.09	1.92	1.08	0.34	1.12	0.73	12.93	22.74
Crop land	29.39	30.34	19.61	37.79	35.85	44.48	7.67	28.82	15.63	85.61	335.18

Bare soil	7.54	14.43	8.41	6.15	15.70	12.04	10.96	7.35	4.42	0.72	87.73
Fallow land	201.39	203.80	98.68	259.31	193.37	223.05	98.40	141.34	111.53	99.35	1630.23

Date of pass: 11-05-2002

	Pala Kurthy	**Kodagandla**	**Torrur**	**Maripeda**	**Tungaturthy**	**Noothankal**	**Aravapally**	**Atmakur**	**Mothey**	**Kushmanchi**	**Total**
Water Bodies	0.67	0.57	0.69	0.96	0.64	0.77	0.23	0.42	1.28	12.21	18.27
Crop land	25.57	26.67	21.09	75.43	34.56	72.14	6.39	35.43	19.87	83.43	400.58
Bare soil	28.12	29.73	14.18	7.06	27.04	18.67	23.92	17.63	10.61	5.86	182.82
Fallow land	185.16	192.84	91.83	220.90	184.78	189.06	86.82	125.14	100.54	97.12	1474.21

The areal extent of water bodies in Rabi season was estimated as 198.83 sq km and 92.57 sq km for the years 2000 and 2002 respectively. The decrease in water spread area from the year 2000 to 2002 was due to corresponding decrease in rainfall in the study area from 920mm to 556 mm. Similarly, the areal extent of water bodies in summer season was estimated as 22.74 sq km and 18.27 sq km for the years 2000 and 2002 respectively.

The areal extent of bare soil was computed as 26.16 sq km and 372.03 sq km for the years 2000 and 2002 respectively in the Rabi season and 87.73 and 182.82 sq km for the years 2000 and 2002 respectively in the summer season. Bare soil increased by 345.87 sq km and 95.09 sq km in Rabi and summer seasons respectively. The areal extent of fallow lands with bushes decreased from the year 2000 to 2002 with respect to Rabi and summer seasons due to limited rainfall in the year 2002. However, the cropped area did not register much difference. The variation of areal extent of water bodies, Crop land, Bare soil and Fallow land classes of land use and land cover in each sub area has shown in Figs. 3 to 5.

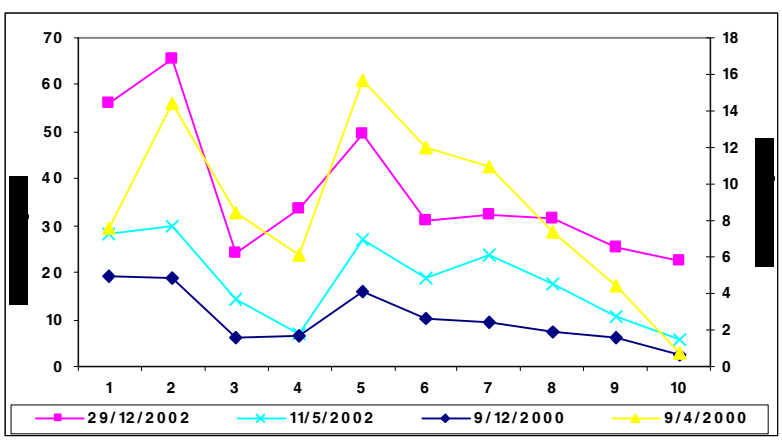

Fig. 3 Variation of areal extent of bare soil in different sub areas.

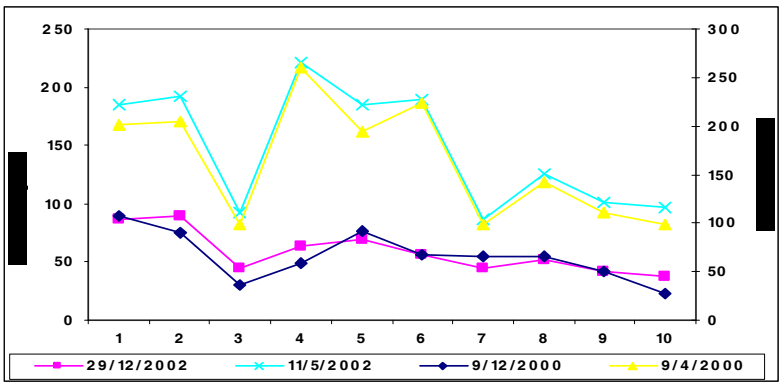

Fig. 4 Variation of areal extent of fallow land in different sub areas

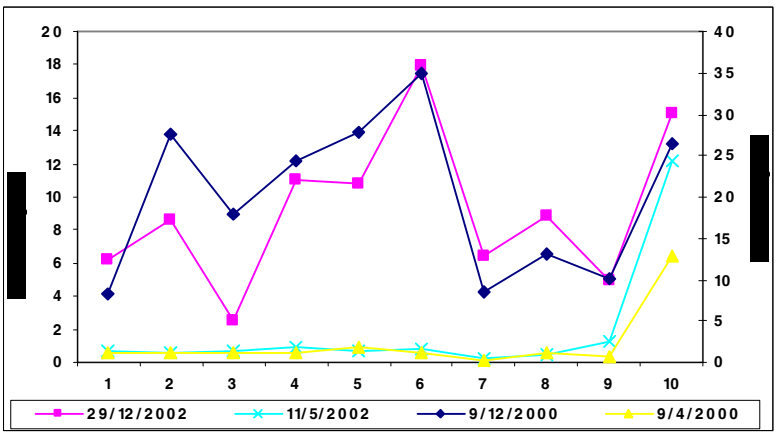

Fig. 5 Variation of areal extent of water bodies in different sub areas.

Conclusions

The classification of land Use / Land Cover classes were evaluated using NDVI. Of all the available methods of image classification with regard to vegetation and its sub classification, NDVI formed the basis for a better classification. It can also be safely concluded that for the considerably large areas comprising predominantly of vegetation, NDVI classification is better suited. NDVI classification is found to be especially suitable in such cases where the analysis was carried out using either past imageries or present imageries with no ground truth data.

References

Anderson, J.R., et al, "A Land use and land cover classification system for use with Remote Sensing Data", USGS professional paper 964, U.S.Gov. Printing Office, Washington, D.C., 1976.

Holben, B.N. 1986, "Characteristics of Maximum -Value Composite Images from Temporal AVHRR Data". Int. J. Rem. Sen. 26: 651-656.

Lillesand, T.M. and Kieffer, R.W. 1979, "Remote Sensing and Image Interpretation", John Wiley and Sons, New York, U.S.A, 721p.

Nayak. T.R., and Jaiswal. R.K., 2003, "Rainfall-runoff modeling using satellite data and GIS for Bedas river in Madya Pradesh", Indian Institute of Engineers (India) Journal, Vol 84, May, pp:47-50.

Reddy, P.R 1997, "Use of Satellite Data in Development and Management of Ground Water Resource", Proceedings Ground Water Development in Hard Rock Hydro systems, Central Ground Water Board, Hyderabad.

Sahai, Baldev, Kalubarme, M.H. and Jadav. K.L. 1985, "Ecological studies in Vkai Command area", Int.J.Remote Sensing, 6(3&4): 401-409.

Wiegand, C.1., Richardson, A.J., Escobar, D.E., and Gerbermann, A.h. 1991, "Vegetation Indices in Crop Assessments", Rem. Sen. Env., 35:105-119.

On the Local-scale Spatial Variability of Daily Rainfall in the Highlands of the Blue Nile: Observational Evidence

MENBERU M. BITEW[1], M. GEBREMICHAEL[1], F. A. HIRPA[1] , Y. MICHAEL[2], Y. SELESHI[2] , AND Y. GIRMA[3]

[1] University of Connecticut Civil and Environmental Engineering Department Storrs, CT 06269-2037. PH (860) 486 2771 FAX (860) 486 2298 email: mekonnen@engr.uconn.edu, menberu@engr.uconn.edu, feyera@engr.uconn.edu
[2] Addis Ababa University, Civil Engineering Department.
Addis Ababa, Ethiopia email: yonasm@ceng.aau.edu.et, base_et@ethionet.et
[3]Amhara Agricultural Organization. Debrebrehan Research Center.
Addis Ababa, Ethiopia. yonas@yahoo.com

Abstract

The HEXB (Hydrological EXperiment in Blue nile) experiment provided an opportunity, via dense network of rain gauges, to study the spatial variability of daily rainfall at a 5 km × 5 km scale in a tropical and mountainous part of the Blue Nile river basin, for the period of July 1 – August 9, 2008. The results of daily rainfall spatial analyses are shown in this paper. High intensity rainfall events have more absolute spatial variability (e.g., standard deviation) and less relative spatial variability (as measured by coefficient of variation), compared to lower intensity events. The coefficient of variation varies from 12% to 320%, with a median of 50%, indicating that there is a significantly large variability from one gauge observation to the other, and one gauge does not represent 5 km × 5 km grid-average daily values. A careful rain gauge layout design is critical to get accurate estimates at smaller number of rain gauges.

1. Introduction

It is known that rainfall events in the tropics can have large spatial variability over short distances. This variability has implications in the establishment of rain gauge networks and assessment of spatial sampling uncertainty. However, quantitative information on this variability is missing in tropical mountainous regions due to the lack of adequate ground observations.

The HEXB (Hydrological EXperiment in Blue nile) experiment has provided the opportunity, via a dense network of rain gauges, to explore a range of issues related to spatial rainfall characteristics. In this study, we consider the variability within a 5 km × 5 km area, here called "local" scale, which is commensurate with the resolution of high-resolution satellite rainfall products, such as PERSIANN-CCS (Precipitation Estimation from Remotely Sensed Information using Artifical Neural Networks – Cloud Classification System; Hong et al. 2004) and CMORPH (NOAA's Climate Prediction Center MORPHing technique; Joyce et al. 2004), and therefore, is important to validate these satellite products.

Firstly, we characterize the spatial statistics of daily rainfall using marginal statistics (probability distribution, standard deviation, and coefficient of variation) as

well as bivariate statistics (correlation coefficient as a function of separation distance). The effect of temporal aggregation on the spatial statistics is also considered. Secondly, we assess the sampling uncertainty introduced by the use of smaller number of rain gauges to estimate local-scale-averaged rainfall estimates.

2. The Watershed

The Beressa Watershed is located in the central highlands of Ethiopia, within 9°33′43″N to 9°42′27″N and 39°28′34″E to 39°44′23″E (Fig. 1). It covers an area of 283 km^2. Geologically, it is part of the highlands that largely owe their altitude to the uplift during the rifting process. The Beressa watershed is on the western plateau edge of the rift system. It is characterized by diverse topographic conditions; elevation ranges from 1850 m to 3700 m. Climate is considered humid, with 1100 mm of annual precipitation. Most of the annual rainfall comes from summer monsoon.

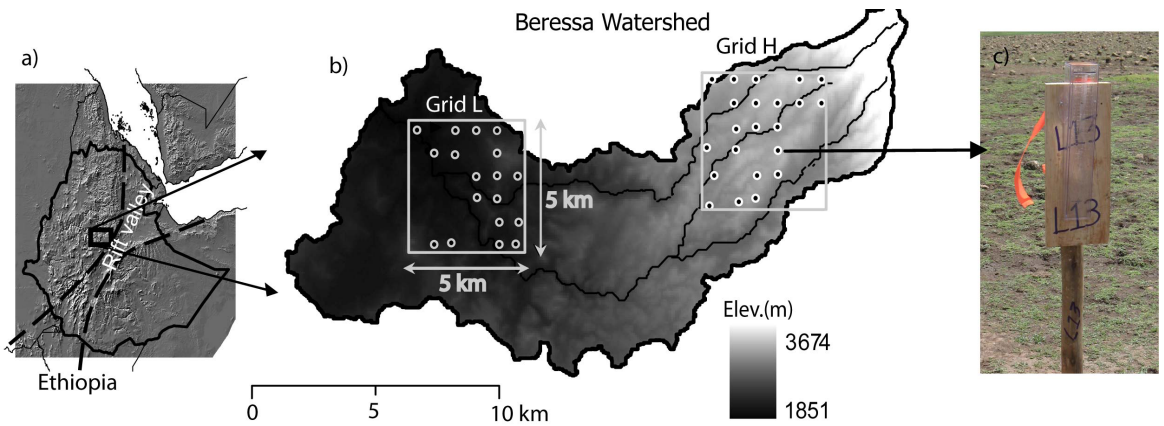

FIG. 1. (a) Map of Ethiopia showing the location of the Beressa watershed with respect to the rift valley. (b) The Beressa Watershed (283 km^2) delineated using a 90-m DEM. The inset contains two grids (5 km × 5km) located in the high-elevation and low-elevations areas of the watershed; and the rain gauges within them. (c) A picture showing an example of one of the installed non-recording rain gauges.

3. The Experiment

The HEXB project started in June 2008, with the aim of advancing hydrological science in a tropical and mountainous region through gaining a better understanding of the space-time variability of rainfall, as sensed by rain gauges network and remote sensors, and how this variability influences hydrologic simulation at the catchment scale. The project has been administered by the University of Connecticut, in collaboration with Addis Ababa University and the Amhara Regional Agricultural Research Institute-Debreberhan Research Center. It has been funded by the National Science Foundation.

An important focus of the project was a set of experimental facilities within the Beressa Watershed. This comprised two new networks of non-recording rain gauges (Fig. 1). The first network consisted of 21 non-recording rain gauges over a 5 km × 5

km area, in the upstream mountainous region of the watershed, we call "Grid H". The second network consisted of 18 non-recording rain gauges over a 5 km × 5 km area, in the downstream hilly region of the watershed, we call "Grid L". The separation distance between two neighboring rain gauges was about 1 km, within each grid. Initially, we put rain gauges every kilometer within each grid, but we lost some of them during the experimental period. We believe that the remaining density of 18 or 21 rain gauges is adequate to capture the spatial pattern of rainfall, and to estimate accurately the mean rainfall over each grid.

We selected the two grids to look at the effect of elevation on rainfall's spatial variability. Figure 2 presents the elevation of each rain gauge. Grid H's rain gauges have elevations ranging from 3100 to 3270 m, while Grid L's have elevations ranging from 2730 m to 2900 m. Grid H has higher elevation than Grid L. However, both grids have similar sub-grid variability in elevation; for example, the range of elevations within each grid is about 170 m.

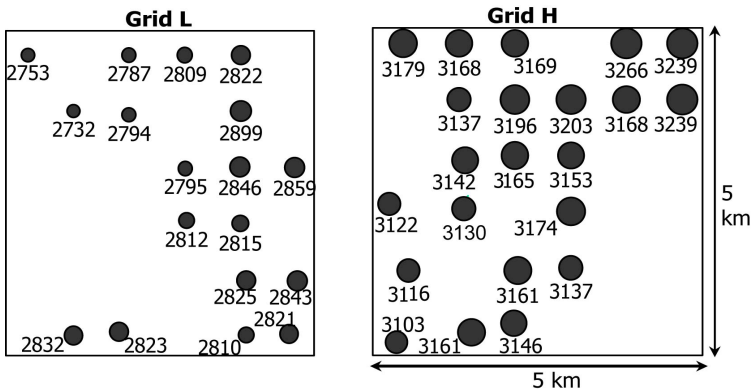

FIG. 2. Elevation (m) of each rain gauge location over (left panel) Grid L, and (right panel) Grid H.

The non-recording rain gauges used were the "Tru-Chek®" plastic rain gauges manufactured by the Forestry Suppliers. The gauges have scales permanently marked on the front side. We mounted each gauge vertically on a wooden pole at a height of 2 m above the ground. A typical rain gauge installation is shown in Fig. 1c. Our research group and trained local research assistants took readings off each rain gauge, every morning from 7 to 8 am, for the period of July 1 to August 9, 2008. This is the major rainy period in the region; there were 38 rainy days during the 40-day experimental period.

4. Results and Discussions

a. Spatial Variability of Rainfall: Marginal Statistics

In Figs. 3a and 3b, we show the distributions of spatial variability of daily rainfall within an area of 5 km × 5 km, for Grids L and H. The spatial variability of rainfall varies from day to day. Higher spatial means tend to have more sub-grid variability than lower ones. We found a sample correlation coefficient of 0.74 for Grid L (and 0.84 for Grid H) between the interquantile range (i.e. the difference between the 75% and 25% quantiles of spatial rainfall) and spatial mean, indicating that the spatial mean explains about 55% for Grid L (and 71% for Grid H) of the day-to-day

variation in the spatial variability of daily rainfall, for 50% of the cases. For 80% of the cases, the spatial mean explains about 65% for Grid L (and 74% for Grid H) of the day-to-day variation in the spatial variability of daily rainfall.

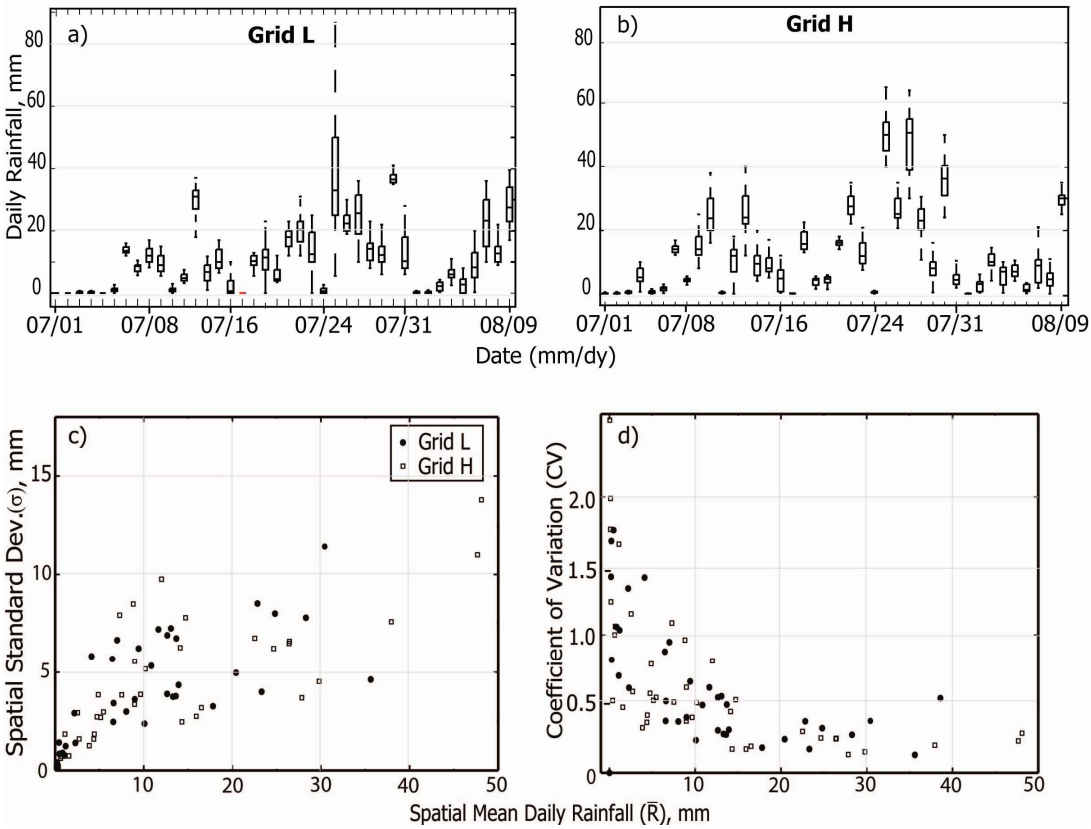

FIG. 3. Spatial variability of daily rainfall over each grid. (a) Box plots for the distribution of spatial rainfall on each day over Grid L. (b) Same as in Fig. (a), but for Grid H. (c) Spatial standard deviation versus the spatial mean rainfall. (d) Spatial coefficient of variation versus spatial mean rainfall. The statistics are obtained using all 18 gauges within Grid L and 21 gauges within Grid L, for each day within the observation period. The box plots represent 10%, 25%, 50%, 75%, and 90% quantiles, from the bottom up.

In Fig. 3c, we present the spatial standard deviation (σ) as a function of the spatial mean daily rainfall ($\overline{R}$). Overall, σ increases with increasing $\overline{R}$, indicating that higher spatial means tend to have more absolute sub-grid spatial variability. However, the relationship between σ and $\overline{R}$ is non-linear: the slope is steeper and the scatter is narrower for low $\overline{R}$ values, than for high values.

The increase in σ with increasing $\overline{R}$ is consistent with the fact that absolute variability tends to be greater for higher values of measured positively defined random variables than for small values. To filter out the effect of this fact, we normalized σ against $\overline{R}$, and looked at how this relative variability (expressed as coefficient of variation, CV=$\sigma / \overline{R}$) behaves with respect to the spatial mean. Figure 3d shows that, overall, high spatial means have less sub-grid relative variability than

lower spatial means. The relative variability decreases exponentially with increasing $\overline{R}$, for $\overline{R}$ smaller than 15 mm/day, and then remains fairly constant for $\overline{R}$ exceeding 15 mm/day. The CV varies from 12% to 320%, with a median of 50%, indicating that there is a significantly large variability from one gauge observation to the other. For the days with CV above 100%, the rainfall intensities were of low to medium intensity.

Let us look at the effect of temporal aggregation on spatial variability. We calculated σ, CV, and $\overline{R}$ for 5-day accumulations, and show the results in Fig. 4. The absolute variability (σ) exhibits a strong linear dependence on $\overline{R}$: it increases linearly with increasing $\overline{R}$. However, the relative variability does not show a clear dependence on $\overline{R}$. This indicates that aggregating the data to longer time scales filters out the effects of other factors (e.g., rain type, storm direction, etc.) that could cause spatial variability. From the comparisons of 1-day and 5-day accumulations, it becomes clear that (1) at the daily time scale, the absolute spatial variability depends on $\overline{R}$ in a non-linear way; and the relative variability shows a strong dependence (exponential decay) on $\overline{R}$, particularly for small to medium events; (2) aggregating the daily data to longer time scales (for example, 5-day) will lead to spatial variability, where the absolute spatial variability depends on $\overline{R}$ strongly in a linear way, and the relative variability does not depend on $\overline{R}$.

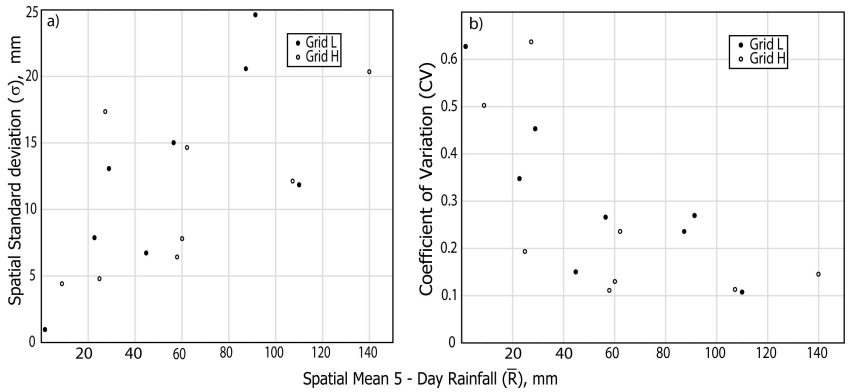

FIG. 4. Spatial variability of 5-day rainfall accumulation over each grid. (a) Spatial standard deviation and (b) coefficient of variation versus the spatial mean rainfall.

b. Spatial Variability of Rainfall: Joint Statistics

To quantify the spatial correlation structure, a plot of correlation coefficients between time series data of pairs of rain gauge observations, with respective separation distances, is often examined (e.g., Morrissey et al. 1995; Ciach and Krajewski 1999; Gebremichael et al. 2003). Using a similar approach, the results are shown in Fig. 5 for each grid. The results show that correlation does not depend on distance, suggesting that the large variability (CV) observed from one rain gauge to the other has a random characteristic.

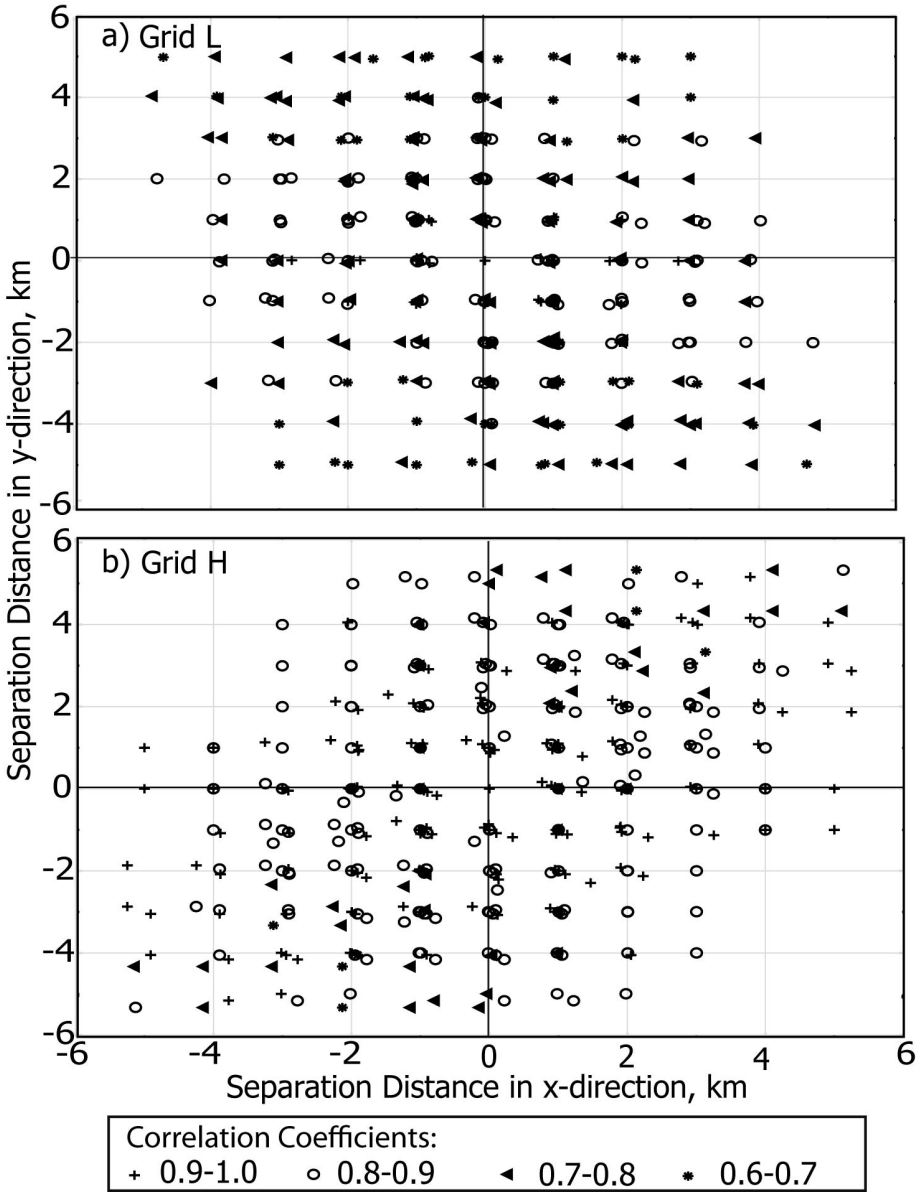

FIG. 5. Correlation coefficient between daily time series data of pairs of rain gauges with separation distances in both directions, for (a) Grid L, and (b) Grid H.

c. Rain Gauge Spatial Sampling Uncertainty

One of the impacts of the spatial variability of rainfall is the number of rain gauges required to accurately estimate grid-averages, and the uncertainty level resulting from the use of smaller number of rain gauges. Let us assume that the spatial mean of rainfall from all rain gauges within each grid, hereafter referred to as "Reference rainfall $\overline{R}$) represents the "true" rainfall. The expression for $\overline{R}$ is:

$$\overline{R} = \frac{1}{n}\sum_{i=1}^{n} R_i,$$

where, $i = 1, 2, \ldots, n$ (number of all rain gauges within Grid L or H).

By sampling smaller number of rain gauges, we can simulate the "Estimated rainfall $\overline{R}_e$" resulting from these gauges::

$$\overline{R}_e = \frac{1}{n}\sum_{i=1}^{n} R_i \delta_i,$$

where, the Kronecker delta function, δ_i, is one if the rain gauge is selected and zero otherwise. The estimation error is, therefore, the difference between $\overline{R}$ and $\overline{R}_e$, and it obviously depends on the number of rain gauges as well as the network configuration.

Consider two daily events over Grid H: the July 15 and July 30 events. The July 15 event had a spatial mean of 9 mm/day, which is equivalent to the 50% quantile of the spatial mean time series data. The July 30 event had a spatial mean of 38 mm/day, equivalent to the 90% quantile of the spatial mean time series data. So the July 15 event represents typical event, while the July 30 event represents an extreme event. Our interest is to quantify $\overline{R}_e$ and estimation error resulting from the use of smaller number of rain gauges (1, 2, 4, 8, 16) in estimating area-averaged values for these typical and extreme events. For each gauge density, we simulated 16 realizations of rain gauge networks by randomly generating each network from a uniform distribution, and show the results in Figs. 6a and 6b.

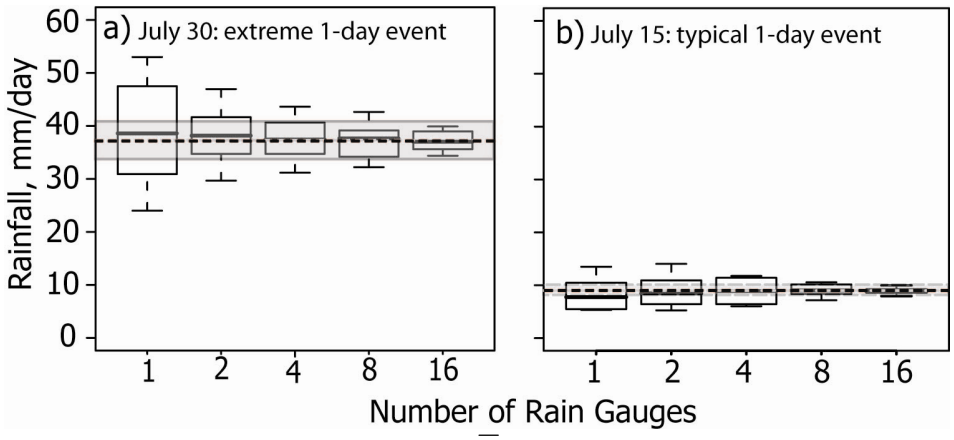

FIG. 6. Distribution of rainfall estimates ($\overline{R}_e$) as a function of rain gauge network density, for (a) the July 30 extreme event, and (b) the July 15 typical event. The bold dashed line shows the reference $\overline{R}$. The shaded region indicates the ±10% deviation from $\overline{R}$.

Consider the event of July 30 ($\overline{R} = 30$ mm/day), which is the 90% quantile extreme value. When only one rain gauge is used to estimate this grid-average rainfall, the estimate could be anywhere from 24 to 53 mm/day (equivalent to estimation error of -14 to 15 mm/day, or –37% to 39% of $\overline{R}$) for 80% of the configurations, and from 31 to 48 mm/day (estimation error of -7 to 10 mm/day, or –18% to 26% of $\overline{R}$) for 50% of the configurations. When four rain gauges are used, the rainfall estimate ranges from 31 to 44 mm/day (estimation error of -7 to 6

mm/day, or –18% to 16% of $\overline{R}$) for 80% of the configurations, and from 35 to 41 mm/day (estimation error within ± 3 mm/day, or ± 8% of $\overline{R}$) for 50% of the configurations.

Let us look at the corresponding values for the typical event of July 15 ($\overline{R} = 30$ mm/day). When one rain gauge is used, the rainfall estimate ranges from 5.3 to 13.5 mm/day (estimation error of -3.7 to 4.5 mm/day, or –40% to 50% of $\overline{R}$) for 80% of the configurations, and from 5.5 to 10.5 mm/day (estimation error of -3.7 to 4.5 mm/day, or –39% to 16% of $\overline{R}$) for 50% of the configurations. With four rain gauges, the rainfall estimate ranges from 6.4 to 11.8 mm/day (estimation error within ± 2.8 mm/day, or ± 30% of $\overline{R}$) for 80% of the configurations, and from 6.4 to 11.4 (estimation error within ± 2.6 mm/day, or ± 30% of $\overline{R}$) for 50% of the configurations.

Let us compare and contrast the estimation errors for the two rainy events. The first feature is that the magnitude of the estimation error is larger for the extreme event than for the typical event. This can be explained by the fact that strong events have more absolute spatial variability than those of weaker events (see Fig. 3c). The second feature is that the proportion of the estimation error to $\overline{R}$ is smaller for the extreme event than for the typical event. This can be explained by the fact that strong events have less relative variability than those of weaker events (see Fig. 3d).

How many rain gauges do we need to obtain a reliable estimate of the grid-average daily rainfall estimate? It depends on the level of uncertainty we accept. Let us say, we accept 10% level of uncertainty. For the extreme event, this can be achieved by having (i) 16 rain gauges of pretty much any configuration used in this study, or (ii) 2, 4, or 8 rain gauges with any of the 50% of the configurations used in this study. This indicates that a careful rain gauge layout design is critical to get accurate estimates at smaller number of rain gauges. There are studies that looked at optimal network configuration (e.g., Moore et al. 2000). For the typical event, the 10% uncertainty level can be achieved by having (i) 16 rain gauges of pretty much any configuration used in this study, or (ii) 8 rain gauges having any of the 50% of the configurations used in this study. Apparently smaller numbers of rain gauges, that were deemed adequate for the extreme event, were found inadequate for the typical event. This is due to the fact that our objective measure (i.e. 10% level of uncertainty) is relative to the actual rainfall value, and strong events have lower percentage of estimation errors with respect to their rainfall value.

5. Conclusions and Recommendations

HEXB provided an opportunity, via dense network of rain gauges, to study the spatial variability of daily rainfall at a 5 km × 5 km scale in a tropical and mountainous part of the Blue Nile river basin. High intensity rainfall events have more absolute spatial variability (e.g., standard deviation) and less relative spatial variability (as measured by coefficient of variation), compared to lower intensity events. The coefficient of variation varies from 12% to 320%, with a median of 50%, indicating that there is a significantly large variability from one gauge observation to

the other, and one gauge does not represent 5 km × 5 km grid-average daily values. The correlation does not depend on distance, suggesting that the large variability observed from one gauge to the other has a random characteristic. The smallest number of rain gauges required to estimate grid-average rainfall depends on the rainfall magnitude. It is generally smaller for high intensity events than for low intensity events. A careful rain gauge layout design is critical to get accurate estimates at smaller number of rain gauges. Four rain gauges with the right configurations can have better performance than ill-placed 16 gauges.

Acknowledgment. This research was supported by the National Science Foundation (NSF Grant OISE-0651783).

REFERENCES

Ciach, G. J., and W. F. Krajewski, 1999: On the estimation of radar rainfall error variance. *Adv. Water Resour.,* **22,** 585–595.

Gebremichael, M., and W. F. Krajewski, 2003: M. Morrissey, D. Langerud, G. J. Huffman, and R. Adler, 2003: Error uncertainty analysis of GPCP monthly rainfall products: A data-based simulation study. *J. Appl. Meteor.,* **42,** 1837–1848.

Hong, Y., K. L. Hsu, S. Sorooshian, and X. Gao, 2004: Precipitation Estimation from Remotely Sensed Imagery Using an Artificial Neural Network Cloud Classification System. *J. Appl. Meteor.*, **43**, 1834–1852.

Joyce, R. J., J. E. Janowiak, P. A. Arkin, and P. Xie, 2004: CMORPH: A method that produces global precipitation estimates from passive microwave and infrared data at high spatial and temporal resolution. *J. Hydromet*., **5**, 487-503.

Moore, R. J., D. A. Jones, D. R. Cox, and V. S. Isham, 2000: Design of the HYREX raingauge network. *Hydrol. Earth Sys. Sci*., **4**(4), 525-530.

Morrissey, M. L., J. A. Maliekal, J. S. Greene, and J. Wang, 1995: The uncertainty in simple spatial averages using raingage networks. *Water Resour. Res.,* **31,** 2011–201

Characteristics of Integrated Water Resource Management in the Zambezi River and Great Lakes Basins: A Comparison of Two Approaches

Jonathan W. Bulkley[1], Imasiku Nyambe[2], and Christine J. Kirchhoff[3]

[1]Professor of Natural Resources, School of Natural Resources and Environment and Professor of Civil and Environmental Engineering 440 Church Street, Ann Arbor, MI 48109-1041; PH (734) 764-3198; FAX (734) 647-5841; e-mail:jbulkley@umich.edu
[2]Professor and Coordinator, Integrated Water Resource Management Center, C/o School of Mines, University of Zambia, Great East Road, Lusaka 10101 Zambia; PH 260-211-294086 / 290165; FAX 260-211-294086 / 290165; e-mail:inyambe@gmail.com
[3]Ph.D Candidate, School of Natural Resources and Environment, 440 Church Street, Ann Arbor, MI 48109-1041; PH (734) 764-1412; FAX (734) 647-5841; e-mail:orange@umich.edu

ABSTRACT

"The Provision of adequate fresh-water resources for people and ecosystems will be one of *the most critical and potentially contentious issues facing society and governments at all levels during the 21st century*" (American Meteorological Society, 2008).

Integrated Water Resources Management (IWRM) is evolving as a contemporary means to address complex and critical issues associated with making the most effective and efficient use of water resources. Water resource challenges in the Zambezi River Basin include both quality and quantity issues including potential diversions from the basin to localities outside the basin and lack of an agreed upon institutional framework for the management of the Zambezi River system. In 1972, the United States and Canada signed the first Great Lakes Water Quality Agreement. This agreement committed the two countries who share the trans-boundary waters of the Great Lakes to restore and enhance water quality in the Great Lakes System. Amendments in 1987 resulted in establishing the goal to virtually eliminate persistent toxic substances into the Great Lakes resulting from human activities. In 2008, the Great Lakes Compact was approved by all of the eight Great Lakes States plus the Provinces of Ontario and Quebec. This compact was subsequently approved by the Congress of the United States and signed by President Bush on October 3, 2008. Both the Zambezi River Basin and the Great Lakes Basin offer valuable insights into the application of IWRM to critical water resource planning and management challenges in their respective geographical locations.

INTRODUCTION

Integrated Water Resource Management (IWRM) has evolved during the last two decades of the 20th Century. IWRM has developed in response to population growth placing greater demands upon water resources that are showing reduced quality and

increasing shortages in certain geographic regions. The IWRM approach is one that is evolving from a supply-oriented, engineering-based approach towards a demand-oriented, multi-sector approach (Loucks and van Beek, 2005). Loucks and van Beek (2005) develop the relationship between the importance of providing sustainable water resource systems and IWRM by citing the importance of the Dublin Principles developed in early1992 prior to the Rio Sustainability Conference. The Dublin Principles are as follows:

1. Water is a finite, vulnerable and essential resource, essential to sustain life, development and the environment.
2. Water resources development and management should be based on a participatory approach, involving users, planners and policy makers at all levels.
3. Women play a central role in the provision, management and safeguarding of water.
4. Water has an economic value in all its competing uses and should be recognized as an economic good.

In 2000, the Global Water Partnership made a clear connection between Integrated Water Resource Management (IWRM) and sustainability as follows: "IWRM is a process which promotes the coordinated development and management of water, land and related resources, in order to maximize the resultant economic and social welfare in an equitable manner without compromising the sustainability of vital ecosystems" (Global Water Partnership, 2000). IWRM clearly moves away from "top down" master water planning towards a more comprehensive approach that includes the inter-relationships between different water sectors as well as the institutional requirements and capacity building needed to implement the priority water programs (Loucks and van Beek, 2005).

ZAMBEZI RIVER BASIN: CHARACTERISTICS AND CHALLENGES

The Zambezi River Basin (ZRB) is located between 9-20° South and 18-36° East in Southern Africa (Figure 1). The basin, with total area of 137 million hectares (1.37 million km^2) is the fourth largest in Africa after the Congo, Nile, and Niger River basins. It extends through Angola (18.2%), Botswana (2.8%), Malawi (7.7%), Mozambique (11.4%), Namibia (1.2%), Tanzania (2.0%), Zambia (40.7%) and Zimbabwe (16.0%)

The basin receives a mean annual rainfall of about 950 mm, with a rainfall pattern characterized by a distinct wet and hot summer and a dry period in the remainder of the year. The north and east of the basin receive significantly more precipitation than the south and west. Climate change may have an effect on evaporation from reservoirs, on crop production and fish stocks. Less than 10% of the mean annual rainfall in the basin contributes to the flow of the Zambezi River into the Indian Ocean whereas more than 90% evaporates and returns to the earth's atmosphere. Given the relatively high rainfall in summer, it is a safe assumption that a significant part of the resulting water resource is temporarily stored in sub-soil aquifers. However, detailed information about the availability and use of these

groundwater resources is, as yet, not available. Even so, groundwater may become a more prominent source of water over time.

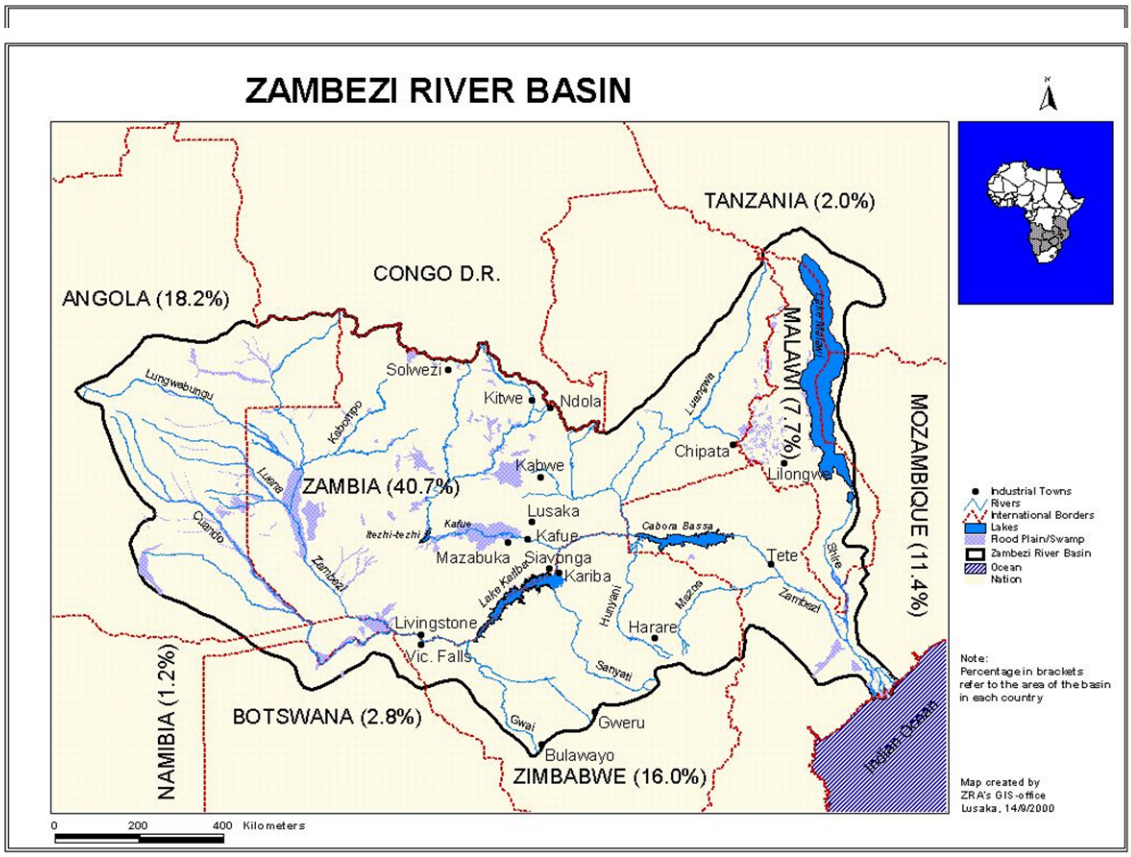

Figure 1: The Zambezi River Basin [adapted from Zambezi River Authority (ZRA), 2000]. Note the area occupied by the Basin in each riparian state).

Most of the Zambezi River Basin is high plateau land varying between 800 and 1,450m above mean sea level with most of the basin above 1,000m. This high elevation contributes to the significant hydropower potential of the Basin.

The population in the Zambezi River Basin (ZRB) is estimated to be 40 million people, of which about 7.5 million live in the urban centers. This is expected to increase to 47 million by 2025 with urbanization steadily increasing. Two economies exist in the basin: a fast high income generating and growing economy centered on exploitation of mineral resources, and a rural economy with high levels of poverty and low coverage of basic services. In recent years, most riparian countries have witnessed encouraging economic growth and therefore a need to consolidate and sustain this through the sustainable development of the water resources of the Zambezi Basin. However, there are a number of major water resources challenges that must be overcome to satisfy the fast growing population and economic development. These challenges are summarized in Table 1.

Table 1: Challenges of water resources in the Zambezi River Basin

Physiography	Climate Change & Variability	• Increased frequency of droughts and floods • Small change in rainfall ► Large change in river flow
	Ecosystems	• Biodiversity e.g. effects of deforestation for agriculture & woodfuel • Desertification • Wetland degradation e.g. the Kafue flats in Zambia
	Surface Water	• Limited resources, unevenly distributed and over-exploited and poorly known in terms of quantity and quality • Assessment and monitoring of the resource are lacking • Industrial and municipal effluent loading in Kafue River Basin – Copperbelt Zambia (pollution) • Pollution from industrial and urban centre activities e.g. Lusaka, Harare
	Groundwater	
Socio-Economy	Demography	• High population growth rate in urban areas • Poor water and sanitation coverage and service delivery e.g. the karstic aquifer in Lusaka is a non-renewable water resource that is highly affected by poor sanitation coverage. • Water-related diseases (Cholera) & HIV/AIDS. Region has a higher incidence of HIV/AIDS and Cholera outbreaks due to inadequate access to clean water and sanitation in peri-urban and rural areas • Agriculture is the most important economic activity and the biggest water consumer (~80%) resulting in competition for water e.g. there is high competition between irrigation and hydropower in the Kafue River Basin…
	Economy	
Management	Legislation	• Water legislation is varied across the riparian countries • Inadequate institutional strength and capacity • Establishment of cooperative frameworks for managing shared waters in the context of IWRM is still in its infancy. • ZAMCOM not yet operational
	Institutional	
	Knowledge	• Data access, sharing, reliability and standardization is not available • Monitoring is scattered, except for example the reservoirs such as Lake Kariba by Zambezi River Authority. • Gaps o Insufficient insight into climate change and variability o Water pollution inadequately addressed o Groundwater recharge largely unknown o Environmental flow requirements largely unknown

A principle challenge for the Basin concerns water quantity. The Zambezi River has an average run-off of 103,224 Mm^3. Approximately 20% of this stream flow is used currently. However, use is expected to increase to 41% if the various ambitious plans by riparian states for irrigation and hydropower development are implemented by 2025. Given the high degree of seasonal and spatial variability in available water resources, and the possible effects of climate change, increasing demands on the Zambezi River are likely to push the river to its limits. In addition to issues of water quantity, there are a number of water quality issues that demand attention. These challenges include: point pollution around manufacturing and mining centers, municipal effluents, and the spread of aquatic weeds, wetland degradation among others. These challenges are highlighted in Table 1.

Two examples of challenges are given here to illustrate some of the issues in ZRB:

(a) Hydropower: This sector is by far the largest water user because of the evaporation from hydropower reservoirs estimated at approximately 17 km^3 (17 billion m^3). Only three existing reservoirs in the ZRB have a regulating

capacity of significance: Kariba, Cahora Bassa and Itezhi-Tezhi. A total capacity of 4,684 MW has been developed in the Zambezi River basin, of which 75% is on the Zambezi River itself, producing an average of almost 33,000 GWh per year. Of the total developed capacity 5% is in Malawi, 45% in Mozambique, 36% in Zambia and 14% in Zimbabwe. Zambia, for example is planning to further develop another 2,870 MW through expansion and new ones.

(b) Water and Sanitation Coverage: In Zambezi River Basin, water and sanitation coverage of the member states is at its lowest level (Table 2) such that even the better economy of Botswana is below 50% for rural.

Table 2. Water (W) and Sanitation (S) Coverage for selected 4 riparian states of ZRB

	Angola		Malawi		Mozambique		Zambia	
	W(%)	S(%)	W(%)	S(%)	W(%)	S(%)	W(%)	S(%)
Urban	70	56	96	66	76	51	86	41
Rural	40	16	62	42	24	14	37	13
Total	50	30	67	46	42	27	53	23

ZAMBEZI RIVER BASIN: OVERCOMING CHALLENGES

In trying to overcome some of these challenges, the Southern Africa Development Community (SADC) Water Division adopted IWRM as an intervention strategy to manage transboundary water resources within the SADC region. The Zambezi River Basin sits within the SADC region wherein which IWRM is being applied.

SADC Water Division established an enabling environment for IWRM through the ratification of the SADC Protocol for Shared Water Courses (Protocol) in 1997. The Protocol was revised in 2000 by SADC member states. This is the main instrument for guiding reform processes at transboundary basin levels. However, additional instruments are now in place that compliments the Protocol:

- Regional Strategic Action Program (RSAP I) for IWRM and development, 1999 to 2004, with 7 priority areas and more than 33 IWRM projects at Regional and National Level
- In 2000, SADC vision on Water, Life and Environment was developed and sets out the overall SADC Water vision
- RSAP II was developed in 2005 and is being implemented & provides a regional IWRM implementation framework
- 2005 Regional Water Policy Developed
- 2005 Regional Water Strategy Developed

In addition to these instruments and the Protocol, several commissions have been established. One such commission is the Zambezi Watercourse Commission (ZAMCOM). ZAMCOM will provide a governance structure for the ZRB once ratified by all the riparian countries. Until then, the only joint management of the ZRB is through the Zambezi River Authority (ZRA) (1980), a bilateral institution

between Zambia and Zimbabwe. The ZRA provides a success case story of basin level cooperation and management for Lake Kariba on the Zambezi River and perhaps hints at the cooperation possible in the ZRB.

At present Zambia is the only country that has not signed the ZAMCOM Agreement entitled: "Agreement on the Establishment of the Zambezi Watercourse Commission" despite being a signatory to SADC Protocol on Shared Water Courses. The ZAMCOM Agreement has a broad and challenging agenda for regional cooperation including: synchronizing water resources development plans; revising reservoir operation so as to serve a wide variety of functions (e.g., such as flood control, support to flood plain agriculture, river and estuarine fishery and navigation); cooperation in the control of aquatic weeds; and the development of climate change adaptation strategies appropriate to the Basin (e.g., the use and recharge of groundwater). To further enable the sharing of the benefits of cooperation the ZAMCOM Agreement also focuses on joint planning of electricity grids, road networks and navigation opportunities.

Implementation of the ZAMCOM Agreement at the national level will be equally challenging particularly because except for Zimbabwe and Namibia, who have incorporated the main elements of an IWRM approach in their institutional frameworks, the others are still in progress. Malawi and Zambia have their IWRM plans completed but the institutional and legal frameworks are yet to be adopted or enacted into law.

GREAT LAKES BASIN: CHARACTERISTICS AND CHALLENGES

The combined U.S. and Canadian population within the Great Lakes Basin is about 40 million people. The political jurisdictions include the two countries, eight states (U.S.), two provinces (Canada) plus a very large number of sub-state and sub-province units of government. Four of the Great Lakes plus a portion of the St. Lawrence River comprise the boundary waters between the United States and Canada in the Great Lakes Region of North America. The most direct route from the western shore of Lake Superior to the exit from Lake Ontario into the St. Lawrence River is 1,249 miles (2,011 kilometers).

.

GREAT LAKES BASIN: OVERCOMING CHALLENGES THROUGH IMPLEMENTATION OF "IWRM LIKE" APPROACHES

Three examples of actions with the Great Lakes Basin are presented that illustrate aspects of IWRM in the context of the Great Lakes Water System. The first example is the 1909 Boundary Waters Treaty between the U.S. and Canada which includes the waters of the Great Lakes. As the population grew and industrial development took place in these boundary water regions of the U.S. and Canada including the Great Lakes, the two countries recognized that means needed to be provided to ensure the long-term productive use of the shared waters. The Treaty established processes to enable disputes regarding the use of the boundary waters

between the two countries to be settled. The Treaty established the International Joint Commission (IJC) to address issues identified by the governments of Canada and the United States impacting the Boundary waters and to make recommendations for issue resolution. The IJC's Mission Statement is as follows:

> "The International Joint Commission prevents and resolves disputes between the United States of America and Canada under the Boundary Waters Treaty and pursues the common good of both countries as an independent and objective advisor to the two governments. In particular the Commission rules upon applications for approval of projects affecting boundary or transboundary waters and may regulate the operation of these projects; it assists the two countries in the protection of the transboundary environment, including the implementation of the Great Lakes Water Quality Agreement and the improvement of transboundary air quality; and it alerts the governments to emerging issues along the boundary that may give rise to bilateral disputes" (IJC, 1998).

On April 15, 1972, Prime Minister Pierre Trudeau and President Richard Nixon met to sign the Great Lakes Water Quality Agreement. This milestone event committed Canada and the United States to control pollution in the Great Lakes and to clean up waste waters from industries and communities. The major issue at that time was phosphorus over-enrichment (Environment Canada: Great Lakes Water Quality Agreement, 2009). This agreement committed the two countries who share the trans-boundary waters of the Great Lakes to restore and enhance water quality in the Great Lakes System. This first Great Lakes Water Quality Agreement was replaced in 1978. Subsequent amendments in 1987 resulted in establishing the goal to virtually eliminate persistent toxic substances into the Great Lakes resulting from human activities. The IJC monitors and assesses progress towards achieving the eventual goal of eliminating persistent toxic pollutants from the Great Lakes (IJC, 1998). This action requires addressing the atmospheric deposition of toxic pollutants as well as contaminated sediments, ground water sources, and non-point source pollution into the Great Lakes. The long-term goal is one example of the value and importance of IWRM and its necessity in viable planning and management of trans-boundary water resources. The eventual achievement of this long-term goal requires not only the coordination of leadership and activities of government at international, national and sub-national levels but also the additional critical participation of civil, public and private sector interests.

A second example is the control of untreated discharge of ballast water into the waters of the Great Lakes. Ocean vessels navigate into and out of the Great Lakes through the St. Lawrence Seaway and the Welland Ship Canal. The discharge of ballast water from these ships into Great Lakes waters has enabled the introduction of aquatic invasive species into the Great Lakes. Previous introductions of invasive species, such as the zebra mussels via vessels' untreated ballast have cost states and provinces millions of dollars in damage to municipal, industrial, and recreational infrastructure, loss of fisheries, and loss of recreational water uses (Ballast Water Final Determination, 2005). On April 13, 2005, the Michigan

Department of Environmental Quality (MDEQ) issued a rule that effective January 1, 2007, all ocean going vessels shall obtain a permit from the MDEQ to operate in state waters. This permit will only be issued if the applicant can demonstrate that the ocean going vessel will not discharge aquatic nuisance species or if the ocean going vessel discharges ballast water, it will use one of the several technologies approved for use by the MDEQ.

It should be noted that the U.S. EPA had exempted ballast water discharges from the provisions of the Clean Water Act in 1973. The failure of the Federal government to effectively regulate ballast water discharges has shifted the responsibility to individual states. The Rule issued by the MDEQ was challenged by a consortium of shipping interests in March 2007 in federal court in the Eastern District of Michigan. The Federal court upheld the state's new law requiring shipping vessels to obtain a ballast water discharge permit to operate in state waters. The shipping consortium appealed this decision to the U. S. Court of Appeals for the Sixth Circuit. In November 2008, the Federal appeals court issued a decision upholding Michigan's ballast water statue. In this specific situation, a legal remedy developed by the MDEQ to address issues not effectively regulated by the federal government is being implemented to protect the Michigan waters of the Great Lakes. Other states within the Great Lakes are actively considering similar legislation since they too have a legal obligation to protect their waters from invasive species (Hall, 2008). This example demonstrates that IWRM must include the broad legal and policy framework necessary to protect critical water resources.

A third example illustrating the importance of IWRM in the Great Lakes Basin is the Great Lakes Compact. This Compact agreement was signed by President Bush on October 3, 2008. It is a working example of trans-boundary IWRM activities. The driving force that motivated the creation of the Great Lakes Compact dates from 1997 when a Canadian entrepreneur developed the concept of sending Lake Superior water to the Far East via tanker ships. Basically, the idea was to bring an empty tanker ship with a liner in its cargo hold that would fill its cargo space with Lake Superior water and then transport this liquid cargo (158 million gallons per year by tankers) to the Far East to be sold (Annin2006). In March 1998, a permit to export the Lake Superior water was issued to this entrepreneur by the Ontario government. The news of this potential diversion spurred action in both the United States and Canada. The individual who was issued the permit was convinced by Canadian officials to withdraw the permit with the assurance that if diversions from Lake Superior were permitted in the future, he would be the first inline to receive such permission (Annin, 2006). These events began a nearly decade long period of intense discussion and negotiation between the eight Great Lake states and the provinces of Ontario and Quebec to craft a legally binding agreement between all of the parties that would provide a reasoned approach to evaluate any and all applications for diversion of waters from the Great Lakes. It was paramount that all applicants be treated fairly. The resulting legally binding approach was to craft a Great Lakes Compact that would be approved by all of the Great Lakes states plus the two Canadian provinces. All have to pass equivalent binding legislation for their jurisdictions. In addition, the U.S. Congress would approve the Compact and the Compact would then be signed by the President of the United States.

The key provisions of the legally binding Great Lakes Compact include the following:

1. Economic development will be fostered through sustainable use and responsible management of Basin waters.
2. A ban on new diversions of water from the Basin but limited exceptions could be allowed for communities near the basin when rigorous standards are met.
3. Communities that apply for an exception will have a clear and predictable decision making process: standards to be met and opportunities to appeal decisions. These processes do not exist under current law.
4. The States and Provinces will use a consistent standard to review proposed uses of Basin waters. The States and Provinces will have flexibility regarding their water management programs and how to apply this standard.
5. Regional goals and objectives for water conservation and efficiency will be developed, and they will be reviewed every five years. Each State and Province will develop and implement a water conservation and efficiency program that may be voluntary or mandatory.
6. There is a strong commitment to continued public involvement in the implementation of the Compact.

These key elements of the Great Lakes Charter incorporate the IWRM process as articulated by the Global Water Partnership in 2000.

OBSERVATIONS

IWRM interventions are new concepts to the riparian states of ZRB. The adoption of IWRM and the creation of relevant enabling environments (policies), institutional, legal and management instruments are indeed at their infancy. Except for Zimbabwe (fully adopted with IWRM focused policies, law and institutions), Namibia (partially), Zambia (policy and implementation plan), Malawi (plan), the remaining four basin states are still in the very early stages. Interestingly, IWRM has been adopted as a way through which water should be managed in the broader SADC region of which the ZRB is a part. This high level of embracing IWRM in the region coupled with the many challenges in ZRB (Table 1) requires first, a human resource capacity development of individuals that have an understanding of IWRM and second, data and information for decision making.

The lack of data, information, and human capacity for decision making has important implications. For example, Zambia has not signed the ZAMCOM Agreement. There may be many answers to the question "Why has Zambia not yet signed the Agreement?" One clear constraint is lack of data or information for decision making. Another example is that most economies in ZRB would like to diversify and improve the productivity and value-added of the sectors that provide the bulk of the employment, services and agriculture, and hence achieve sustainable development. To achieve this goal of sustainable development ZRB countries must also achieve sustainable use of ZRB water resources. Data, information and data exchange, expanding on the Zambezi Water Information System (ZAMWIS) that set

up ZACPRO II will ultimately provide for an effective Zambezi Watercourse Commission and contribute to effective governance of the ZRB.

UNZA IWRM Centre in collaboration with U.S. universities such as the University of Michigan therefore finds itself at an opportune moment to contribute in education & training, research and consultancy in ZRB providing the much needed manpower first to implement IWRM interventions in ZRB and second, to assist in the development of data, information and data exchange for the well-being of ZRB citizens.

REFERENCES

American Meteorological Society (2008). Policy Statement, May 12, 2008

Annin (2006). *The Great Lakes Water Wars.* Peter Annin, Island Press, Washington, D.C. 2006

Chenje M (editor), 2000. State of the Environment – Zambezi Basin 2000. SADC/IUCN/ZRA/SARDC, Maseru/Lusaka/Harare.

Environment Canada: Great Lakes Water Quality Agreement, 2009. http://www.on.ec.gc.ca/greatlakes/default.asp?lang=En&n=EE1B7E6A-1

Euroconsult Mott MacDonald (2007). Integrated Water Resources Management Strategy for the Zambezi River Basin. SADC-WD/Zambezi River Authority, SIDA, DANIDA, Norwegian Embassy, Lusaka

Global Water Partnership (2000). "Effective water governance." Stockholm, Sweden, Tac Background Papers No. 7, 2000

Hall, (2008) http://www.glelc.org/blog/2008/11/federal-appeals-court-upholds-michigan-ballast-water-law-allows-states-to-take-action-to-stop-the-sp.html Noah Hall, Wayne State University Law School; Executive Director, Great Lakes Environmental Law Center. November 23, 2008

Hirji R., Johnson P., Maro P., and Chiuta T. M (editors), 2002. Defining and Mainstreaming Environmental Sustainability in Water Resources Management in Southern Africa. SADC/IUCN ROSA/SARDC/ World Bank: Maseru/Harare/Washington DC.

Hollingworth B. and Chiramba T (editors), 2005. Implementing the SADC Regional Strategic Action Plan for Integrated Water Resource Management (1999-2004): Lessons and Best Practice. Hot Dot Print. 135p.

IJC (1998) The International Joint Commission and The Boundary Waters Treaty of 1909. IJC, Ottawa and Washington, D.C.

Loucks and van Beek (2005). *Water Resource Systems, Planning and Management.* United Nations Educational, Scientific and Cultural Organization. UNESCO 2005 and WL Delft Hydraulics 2005. The Netherlands.

Determining the Causes of Declining Upper Great Lakes Levels – Phase I of the International Upper Great Lakes Study by the St. Clair River Task Team

Anthony J. Eberhardt[1] and Syed M. A. Moin[2]

[1]U.S. Army Corps of Engineers, Institute for Water Resources, 7701 Telegraph Road, Alexandria, VA 22315-3868; PH (703) 428-6291; FAX (703) 428-6686; e-mail: anthony.j.eberhardt@usace.army.mil.
[2]International Joint Commission, Canadian Section, 234 Laurier Avenue West, 22nd Floor, Ottawa, ON K1P 6K6; PH (905) 220-6742; FAX (613) 993-5583; e-mail: moins@ottawa.ijc.org.

ABSTRACT

The purpose of the International Upper Great Lakes Study (IUGLS) is to investigate improvements to the regulation of the outflow of Lake Superior given the impacts regulation may have on water levels, flows, and consequently affected resources throughout the upper Great Lakes system. It also is closely examining the physical processes driving current Great Lakes water level conditions, and possible ongoing changes in the St. Clair River and their impacts on river flow and Lakes Michigan and Huron levels (Phase I). The issues are being investigated by two Task Teams (TTs): the Lake Huron Outflow/ St. Clair River Task Team (SCR TT) and the Lake Superior Regulation Task Team (LSR TT). This paper describes the investigations being conducted by the SCR TT for Phase I of the Study which is scheduled for completion in October 2009. The entire Study will be completed in April 2012.

INTERNATIONAL UPPER GREAT LAKES STUDY

The International Upper Great Lakes Study was initiated in March 2006 by the International Joint Commission (IJC), a U.S.-Canadian Commission formed by the International Boundary Waters Treaty of 1909, to oversee issues and settle disputes related to boundary waters between the two countries. The purpose of the Study was to develop alternative outflow management plans to Plan 1977-A, the plan which has been used to specify outflows from Lake Superior since June 1990, that better serve the interests upon which that plan was developed (hydropower, commercial navigation and water uses) and emerging interests (recreational boating, riparian issues and the ecosystem) under various hydrologic conditions including climate change. However, due to recently declining levels on the upper lakes, the scope of the work was modified to examine the St. Clair River and its possible conveyance changes that may be responsible for the decline.

The geographic scope of the Study is shown in Figure 1 and a detail of the St. Clair River investigative area is shown in Figure 2.



Figure 1. Upper Great Lakes

The Lake Huron Outflow/ St. Clair River Task Team

The Lake Huron Outflow/ St. Clair River Task Team has focused on that part of the Study which addresses the issues related to historic changes in the hydraulic conveyance capacity of the St. Clair River due to man-made changes (dredging, gravel mining, ship wrecks, hardening of the shoreline, conveyance constrictions due to bridges and other infrastructure, etc), natural conveyance changes, physical changes associated with glacial isostatic rebound, overall reduction in net basin supplies due to climate change and variability effecting the Lake Huron outflow, or a combination of all of the aforementioned causes. There is a concern that physical changes in the St. Clair River, which is part of the connecting channel between Lake Huron and Lake Erie, may have increased the flow conveyance, thereby significantly contributing to the lowering of the levels of the Upper Lakes.

The SCR TT is organized into three Technical Work Groups (TWG): Data Verification and Reconciliation/ Surveys and Monitoring, Hydraulic Modelling, and Sediment Studies. The TT has also worked closely with the Study's Hydroclimatic Group which is investigating hydrologic factors which may be responsible for the decline.

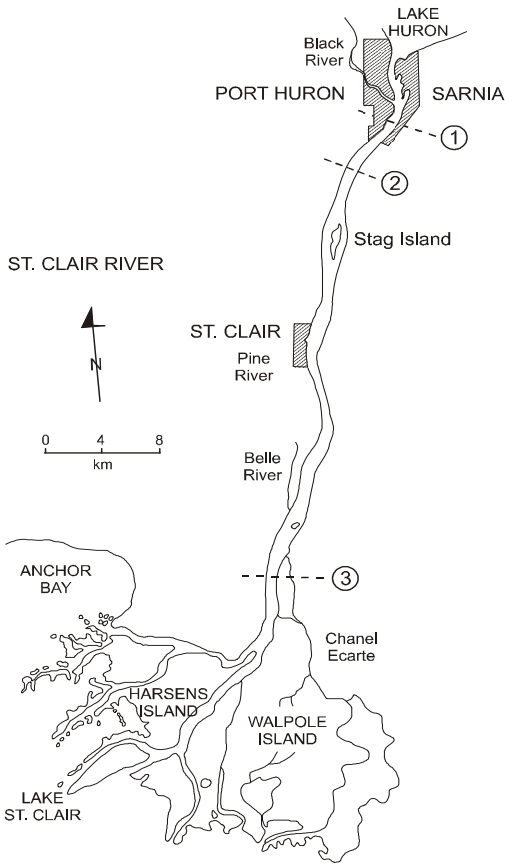

Figure 2. The St. Clair River

Data Verification and Reconciliation/ Surveys and Monitoring TWG

The Data Verification and Reconciliation/ Surveys and Monitoring TWG is responsible for investigations related to defining the bathymetry of the river, how it may have changed due to natural and man-made factors, level and flow verification and issues related to glacial isostatic adjustments. The following activities were initiated for the group by various agencies and universities:

- U.S. Army Corps of Engineers, Detroit District gathered archived data on cross-sections and dredging from 1954, 1962, 1971 and also collected new bathymetric data in 2007;
- U.S. Geological Survey, Woods Hole Science Center conducted side-scan sonar mapping of the upper reach (Fort Gratiot to mouth of the Black River) of the river;
- U.S. Geological Survey, Great Lakes Science Center performed GIS analysis of fluvial mapping;
- U.S. Geological Survey, Woods Hole Science Center in conjunction with the University of Illinois-Urbana-Champaign conducted multi-beam echo sounding and acoustic Doppler profiler mapping.

At issue through all these investigations has been the extent of coverage throughout the period of investigation. Single beam bathymetric data are available for 1971 and 2000, but not in years between these dates. The latest survey was taken in 2007 using multi-beam technology. Coverage has varied from 11,000 points in 1971 to 13 million points in 2007. The differences in coverage at transects has created a level of uncertainty regarding how river cross-sections may have changed. Figure 3 demonstrates this issue showing a possible ("actual") bed surface and what a survey may show.

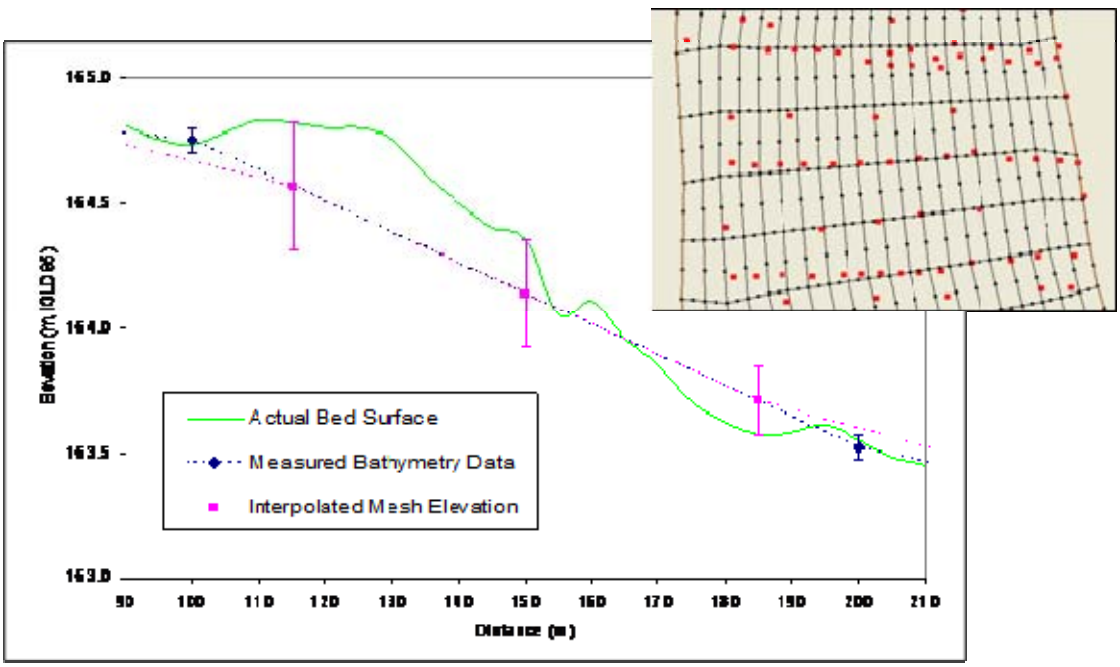

Figure 3. Cross-sectional Uncertainty

Studies are underway to verify river rating curves, by the University of Illinois- Urbana-Champaign, since precise calibration of lake levels and river flows is critical for both phases of the Study. Determination of flows is also being substantiated by new international side-looking acoustic Doppler current profilers, installed by the USGS in four locations on the St. Marys, St. Clair and Detroit Rivers.

Hydraulic Modelling TWG

The Hydraulic Modelling TWG is conducting various studies, some of which are complementary, while others provide a level of redundancy, through various techniques. The following agencies and universities are performing studies to determine how conveyance may have changed:

- U.S. Army Corps of Engineers, Detroit District developing 1-D models;
- U.S. Geological Survey, Michigan Water Science Center developing 1 -D models;

- U.S. Army Corps of Engineers, Hydrologic Engineering Center developing 1 - D modelling and performing sensitivity analyses;
- U.S. Army Corps of Engineers, Cold Regions Research and Engineering Lab modelling of ice-restricted flow events;
- Environment Canada developing 1 and 2-D models;
- In collaboration with the Sediment Studies TWG University of Illinois-Urbana-Champaign developing limited reach 3-D sediment and full reach 1.5 and 2-D mobile bed models.

Sensitivity has been examined through the modelling with various cross-sectional and Manning's "n" assumptions. These models have resulted in various results and are being refined in an attempt to reduce uncertainty.

Sediment Studies TWG

The Sediment Studies TWG has investigated the nature of the river bed to determine the sediment transport capabilities. Environment Canada performed video-mapping of bed features to determine the nature and estimation of sediment transport. These investigations are continuing. The work of the USGS, Woods Hole Science Center and the University of Illinois-Urbana-Champaign are also evaluating the fluvial nature of the river in critical reaches.

Hydroclimatic Group

To determine the hydrology impacting changing water levels and flows, the Hydroclimatic Group is performing the following investigations:

- NOAA- Great Lakes Environmental Research Lab (GLERL)/ Case Western University are determining which net basin supply and climate change and variability scenarios to consider;
- Environment Canada is developing atmospheric and land coupled numeric models to generate regional climate and hydrology;
- The net basin supply sensitivity for both component and residual techniques is being evaluated.

The University of Colorado and Environment Canada have installed an eddy co-variance evaporation measurement device at Stannard Rock in Lake Superior. A second device will be installed at a location on Lake Michigan.

Table 1 shows the studies and investigations that are underway or completed. The investigations are grouped under two headings intended to answer questions relative to 1962 dredging which was the last significant man-made activity that may have altered the river's conveyance.

Result Integration - St. Clair River Tasks

		Science Questions Framework					
		Has the "Conveyance" of the St. Clair River Changed since the 1962 dredging?			Has the "Morphology" of the St. Clair River altered since the 1962 dredging?		
		SQ1	SQ2	SQ3	SQ4	SQ5	SQ6
No.	Project	What is causing the declining head difference between Lakes Michigan/Huron - Erie?	Has the St. Clair River flow regime (i.e. water level-discharge relationship) changed with time and if so, why?	Has the velocity patterns in the St Clair River been modified and if so, what are the implications?	Is the St. Clair River bed stable or eroding?	If the bed of the St Clair river is eroding, what initiated it, and when?	Has the sediment budget for the St. Clair River changed and if so, what are the implications?
P21	Net Basin Supplies Comparison and Water Balance Closure	❑	❖				
P22	Glacial Isostatic Adjustment	❑	❖				
P2	Review of St. Clair & Detroit River Rating Curves and Develop Hydraulic Performance Graphs	❑	❑		❖	❖	
P7	Discharge Computation of the River Using the Standardized HEC-RAS Model	❑	❑		❖	❖	
P3	Development of a Basic 1-D Modelling of St. Clair River Using HEC-RAS	❖	❑	❖	❖		
P4	1-D Conveyance Analysis of the St. Clair River Using the Standardized HEC- RAS Model	❖	❑	❖	❖		
P8	Ice Effects of Flows and Levels Using Standardized Geometry Model of HEC-RAS	❖	❑	❖	❖		
P10	1-D Conveyance Analysis of the St. Clair River using the Mobile Bed MOBED Model	❖	❑	❖	❑	❖	❖
P23	2-D Conveyance / Morphological Analysis of the St. Clair River using SED2D or equivalent	❖	❑	❖	❑	❖	❖
P5	Application of 2-D Modelling Using Existing RMA2 Model of the St. Clair River with Different Bathymetric Data Sets	❖	❑	❑	❑	❑	
P6	Application of 2-D Model of the St. Clair River Using Telemac Modules with Different Bathymetric Data Sets	❖	❑	❑	❑	❑	
P24	Quantification of Uncertainties in 1-D and 2-D Modeling	❖	❑	❑	❑	❑	❖
P1	Bathymetry of St. Clair River 1971 - 2007		❑		❑	❑	❖
P13	Analysis of Bathymetric and Planform Changes in the Past 130 years and Registration into Common GIS		❑		❑	❑	❖
P15	Obtain and Analyze the Bottom Velocity Data from ADCP		❖	❑	❑	❖	
P16	New Coincident ADCP and Multi-beam Data for Hydraulic/sediment Model Verification		❖	❑	❑	❖	
P18	Extract Bed Movement Velocity from Existing or New ADCP Data		❖	❑	❑	❖	
P11	Side-scan Sonar and Video of Substrate in Upper St Clair River		❖		❑	❖	
P12	Sediment Coring and Physical Testing of Substrate in the ST. Clair River		❖		❑	❖	
P9	Video Transects of River Bed, Monthly Sediment Load Measurements, Cross-section Surveys, Grab samples of Bed Material - Sarnia-Pt Lambton		❖		❑	❑	❑
P17	Analysis of Ship Effects, Both Movement and Sinking on Sediment and Erosion Regimes				❖	❑	❖
P19	Reports and Data on Surficial Geology, Littoral Transport, St Clair River and Delta				❖	❖	❑
P20	Conduct Sedimentation Studies of the St Clair River Delta		❖		❖		❑
P14	History of St. Clair River and Detroit River Dredging and Compensation Works				❖	❖	❖

Legend:

Primary focus	❑
Secondary focus	❖

Table 1. Investigations linked to Science Questions Framework

The strategies being proposed for the various investigations are being reviewed by an independent peer group (IPG) composed of experts in respective fields of study. The IPG review, managed by and reporting to the International Joint Commission, is being conducted through ASCE-EWRI and the Canadian Water Resources Association.

PRELIMINARY FINDINGS

Studies of conveyance appear to indicate that there may have been a decrease in the modeled level of Lake Huron of about 0.12 m (+/- 0.03 m) between 1971 and 2007. Since 2000, the modeled level of Lake Huron may have increased by 0.03 m (+/- 0.02 m) between 2000 and 2007.

Contributing factors are:

- Conveyance changes due to natural and man-made impacts;
- Net basin supply changes and spatial changes over the upper and lower lakes; and
- Glacial isostatic rebound.

The exact contribution of each factor is uncertain, which complicates the justification for remedial actions.

FURTHER INFORMATION

Further information about the investigations of the IUGLS, its findings under Phase I and the continuing study work under Phase II, studies to develop alternates for Lake Superior outflow management plans, can be found at the Study web site: www.iugls.org. The International Joint Commission web site, www.ijc.org, also provides information about the Study and its other Study and Control Boards.

REFERENCES

Upper Lakes Plan of Study Revision Team (2005). “Upper Lakes Plan of Study for Review of the Regulation of Outflows from Lake Superior” prepared for the International Joint Commission.

Economic Sustainability Evaluation of an Inter-basin Water Transfer Project Using GWP* Statement

Mohammad Karamouz[1], S. Ali Mojahedi[2], Asghar Elyasi[3], Vahid Askarinejad[4]

[1]Professor, School of Civil Engineering, University of Tehran, Tehran, Iran, Phone No +98 21 88 555 884, Fax No. +98 21 88 701 507 (Primary contact), Karamouz@ut.ac.ir
[2]M.S. in Water Resources Engineering, Ministry of Energy, Iran, Email: ali.mojahedi@gmail.com
[3]MS Student, School of Civil Engineering, University of Tehran, Tehran, Iran, aaelyasi@gmail.com
[4]M.S Student, School of Civil Engineering, University of Tehran, Tehran, Iran, vahid_asn@yahoo.com

Abstract

One of the strategic components of progress in societies is Water Resources Development Projects that have a key role for expanding regional infrastructures in safe and affordable water. These plans have direct and indirect economic impacts. In order to measure them, one needs to consider different parameters affected by regional conditions and project characteristics.

Among the newest approaches to utilize water is to evaluate it as a "socio-economic good". Global Water Partnership (GWP) guideline has been developed using this point of view. It follows economic sustainability evaluation in water projects and considers two main terms of full cost and full value. The former consists of: Full Supply Cost, Opportunity Cost, Economic and Environmental Externalities, and the later includes: Economic Value and Intrinsic Value. This statement explains that economic sustainability will be attained when the full value is equal or greater than the full cost of the project.

In this paper, evaluation of economic sustainability based on GWP guidelines has been applied for an Inter-basin Water Transfer Project (IWTP) in Iran. The goal of this project is to supply water from the Karoon River in the South-Western part to the central region in Iran for agricultural activities.

For this purpose, different components of the project are identified, and then its full cost (such as capital investment, loss of revenue from hydropower generation and crop production and the cost of improving water quality in the basin of origin) and full value (such as benefit from agricultural production, aquifer restoration) are calculated by using a simulation model and an accounting method. The results show the value and cost of each component of the project as a basis for identifying the stable economic elements of the project. Finally, certain recommendations for improving the sustainability of the system are presented.

Keywords: Full Value, Full Cost, GWP, Inter-basin Water Transfer

* Global Water Partnership

1. Introduction

Water Resources Development Projects play a key role in society's progress. In regions with non-uniform temporal and spatial distribution of water resources an alternative to balance the water resources and demands is the Inter-basin water transfer project. Diversions of water from one river basin to another are multi-disciplinary problems (yevjevich, 2001), which involve complex issues and may cause a variety of negative social and environmental impacts. They require careful consideration of the costs and benefits, environmental issues, along planning period, and painstaking negotiations between numerous stakeholders before decisions can be made (Ghassemi and White, 2007).

These are geomorphologic, hydrological, water quality, water resources planning, and hydraulic engineering components, which are intimately connected with political, administrative, economic, environmental, cultural and legal components. Controversies that have surrounded water diversion scheme in the past have many issues in common. However, each case also has its own specific problems (Committee on Western Water Management, 1992).

Economic appraisal assists the decision-making process among projects competing for limited government funds. Since the beginning of rapid urbanization and industrialization that have caused water quantity and quality impacts, some other economic aspects of the projects are considered in addition with the capital and operational costs (Ghassemi and White, 2007).

In 1992, the statement at Rio de Janeiro during the WCED claimed that water should be regarded as an integral part of the ecosystem, as a natural resource and as a social and economic good. The charging mechanisms should reflect as far as possible both the true cost of water when used as an economic good and the ability of consumers to pay (Agenda 21, 1992). The 1992 Dublin Statement on Water and Sustainable Development further affirmed that water has an economic value in all its competing uses and that it should be recognized as an economic good (Zhong and Mol, 2007). In 2003, the Asian Development Bank [ADB] said that: it will support the evolution of water allocation through markets of transferable water rights once the necessary policy, legal, and institutional frameworks for Integrated Water Resources Management in a river basin context have been put in place (ADB, 2003,pp.18–19). After that a lot of effort has been put into introducing water as a valuable good and developing effective water pricing policies for the main water consumers e.g. urban, agriculture and industry (Schuck and Green,2001; Gomez and Riesgo, 2004; Arpke and Strong, 2005; Shiferaw *et al.*, 2008; Webber *et al.*, 2008). Global Water Partnership (GWP), formally established in 1996, formulated the concept of water as an economic good and explained, in practical terms, the economic tools that can be used to effect the environmentally, socially, and economically efficient use of water (GWP, 1998). In this paper, an Inter-basin Water Transfer Project (IWTP) in Iran is evaluated based on GWP guideline. For this purpose different components of the project are identified and evaluated. Then to evaluate the amount of these components, some indicators and a simulation model (WEAP) have been used. After calculation of full cost and full value, the degree of sustainability of the project is assessed. Finally some recommendations are given followed by a summary and conclusion.

2. Methodology

After AGENDA 21 and THE DUBLIN PRINCIPLES put the concept of water as an economic good, Global Water Partnership (GWP) in 1998 developed a guideline for evaluation of the sustainability of vital environmental systems. This guideline can be used to consider the environmental, social, and economical aspects of water usage, by formulating the concept and explaining in practical terms. It follows economic sustainability evaluation in water projects and considers two main terms of Full Cost and Full Value. The former consists of: Full Supply Cost, Opportunity Cost, Economic and Environmental Externalities Cost, and the later includes: Economic Value and Intrinsic Value. This statement explains that economic sustainability will be attained when the Full Value is equal or greater than the Full Cost of the project.

The full cost was calculated for the IWTP project includes capital investment, Operation and Maintenance (O&M) costs, loss of revenue from hydropower generation and crop production (as the opportunity cost), the cost of river dredging and improving water quality in the river (as the economic externalities). Moreover Full value involved benefit from agricultural production (as the Value of the users of water) and aquifer restoration (as net benefit from return flows) was calculated for estimating the degree of suitability of the project.

3. Case Study

Rafsanjan plain is located in the central part of Iran between 55° and 57° longitude and 29°, 53' and 31°, 15' latitude with a 16096 km^2 area. In this plain, 97 percent of 73607 ha cultivated area is pistachio arbor. Groundwater is a common property resource in Daranjir watershed and the approximate total demand (agricultural, industrial and domestic demands) in the case study is supplied by groundwater resources (See Table 1). Frequent droughts and groundwater depletion are critical constraints to improving agricultural productivity in this plain.

Table1. Rafsanjan water resources, consumption and irrigation efficiency

Plain	Surface Resources		Underground Resources		Total Consumption	Average Consumption	Irrigation Efficiency
	MCM	%	MCM	%	MCM	m^3/ha	%
Rafsanjan	8.00	1.14	695.00	98.86	703.00	10848	36.5

In the Rafsanjan plain each year, 212 MCM in excess of the aquifer safe yield is discharged. Furthermore; the water salinity has been increased to three times the standard upper limit EC for pistachio production in recent years. The average of annual water drawdown has been 0.75 m in the last 10 years. For improvement of this problem the inter-basin water transfer has been suggested.

Transferring 250 MCM water from Solegan (origin of water transfer in the headwaters of the Karoon River) which is located 450 Km away from the Rafsanjan plain (as destination), is an alternative for supplying water demand in this plain (see Figure 1). The goal of this project is supplying water demands for 110000 ha agricultural area and accordingly economic improvement, social satisfaction and aquifer restoration will be achieved.

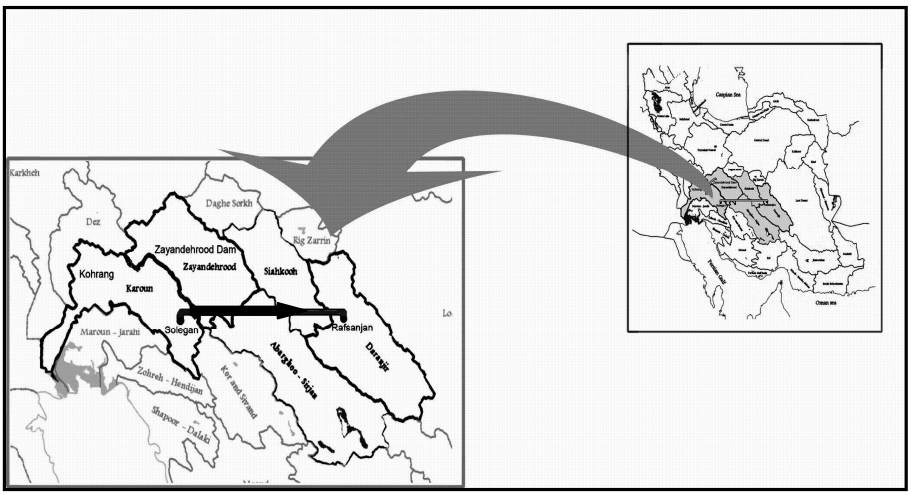

Figure1. Divided main watersheds in Iran and the transfer project

In the origin basin, Karoon River flows from Zagros range into the Persian Gulf. A part of the river that is located downstream of the Gotvand Dam, plus the Dez River as a middle section of river, supply the water demands for more than 660,000 hectares of agricultural networks, eight cities and several industries.
On this river there are 5 reservoirs out of which three reservoirs are operational with the objective of supplying water, hydropower generation and flood control and the rest are under construction (For more details see Table 2). Increasing water demands and waste-loads of domestic and agricultural sectors have severely decreased the water quality of the Karoon River. Due to these circumstances, local resistances against inter basin water transfer projects from this basin (including the project mentioned above) are increased.

Table2. Specifications of dams on Karoon System

Dam	Operation status	Capacity (MCM)	Height (m)	Lake Expansion (ha)	Target of Operation
Karoon 1	operational	3139	177	5500	Water supply & Hydropower generation
Karoon 3	operational	2970	205	4600	Water supply Hydropower generation Flood control
Gotvand	under construction	4500	178	7500	
Godarlandar	operational	230	177	600	
Karoon 4	under construction	2192	230	2700	Water supply & Hydropower generation

4. Results & Discussion

In this section all of the elements of full cost and full value are evaluated based on GWP Guideline, 1998. The terms are set at a 30-year horizon begins by 2008, with an

interest rate of 10% (i=0.1).

4.1. Full cost

a. *Capital Charge:* this term includes the cost of setting up a diversion dam, excavating a transferring tunnel and establishing a pipeline set. (951 million dollars)

b. *O&M cost:* this term is calculated for operating and maintaining the infrastructures mentioned above. (95 million dollars)

c. *Opportunity cost:* In this project, the losses of agricultural development (calculated by Eq.1) and revenue from hydropower generation (used WEAP model) caused of water transfer have been evaluated as the opportunity cost in origin basin.

$$\mathrm{Cost_C} = V \times \overline{\mathrm{CPD}}_{\mathrm{origin}} \times \alpha \times \overline{\mathrm{P}}_{origin} \qquad (1)$$

$\overline{P}_{origin}$ = Price of crop in origin basin

V = Volume of water transfer

$\overline{\mathrm{CPD}}_{\mathrm{origin}}$ = Crop per Drop coefficient in origin basin

α = Net benefit coefficient

$\mathrm{Cost_C}$ = Annual cost of agriculture's losses (37.54 million dollars)

Assessing the impact of the IWTP on the hydropower generation of Karoon Reservoirs, WEAP model (a water Evaluation and planning software) is developed (Figure 2). The model consists of all urban, agricultural and industrial users, Reservoirs and the IWTP. The results show that the average difference in cost between scenarios with and without performing the project is 562.1 GWh/yr. (10.2 million dollars)

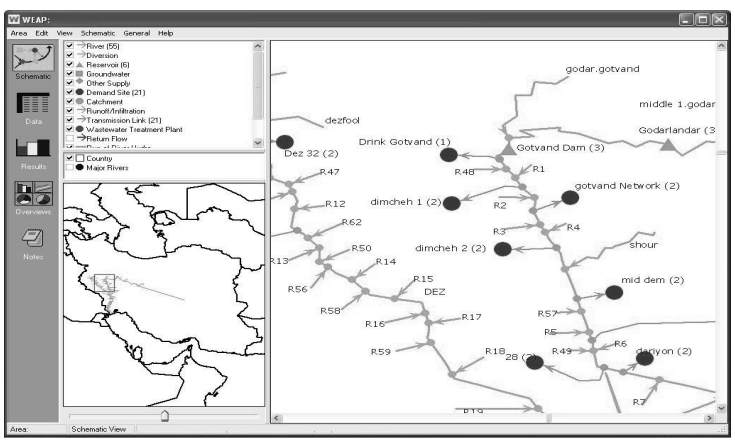

Figure2.Karoon-Daranjir WEAP model interface

d. Economic Externalities

As the lower discharge of the river causes more sedimentation, therefore diversion of water from upstream of Karoon River increases the dredging costs (8 million dollars/year). For calculating this term a diagram was developed by Zahiri and Kordestani (2004) was used to estimate the dredging cost with and without the water transfer plan.
The cost of improving water quality up to its threshold has been defined as another element of Economic Externalities. Agricultural wastewater inflow to the Karoon River is about 1.6 BCM with an average concentration of EC equal to 2600 µmhos/cm. The power of declining the salinity depends on the volume of freshwater in the river and the volume of the wastewater drainages into the river. By diminishing the volume of the freshwater in the river because of the IWTP implementation, the volume of the wastewater needs to be decreased. For achieving this, a ratio of the wastewater could be diverted to large wastelands. The cost of buying these lands for maintaining the water quality is considered as economic externalities (224 million dollars).

e. Environmental Externalities
Although an important factor, it is not yet explored in this study.

4.2. Full Value

f. Value To Users of Water
The marginal value of products in the Rafsanjan plain is calculated as follows:

$$VWA = \frac{NVOI - NVOWI}{VWDI} \tag{2}$$

Where *VWA* is the value of water in agriculture, *NVOI* is the net value of output with irrigation, *NVOWI* is the net value of output without irrigation and *VWDI* is the volume of water of diverted for irrigation.
Because of the complete dependence of agricultural products on irrigation in the destination basin, the *NVOWI* is equal to zero. Therefore *VWA* is the ratio of *NVOI* to *VWDI* (107.25 million dollars).

g. Net Benefits From Return Flows
Although the return flows from agriculture activities could not met the aquifer because of its significant depth (more than 150m), the IWTP allows aquifer to restore itself by reducing the groundwater pumping (0.53 million dollars /year).

h. Net Benefits From Indirect Use
There are no Indirect Users in this project and so the "Net Benefit from Indirect Users" estimated to be zero.

i. Adjustment For Societal Objectives & Intrinsic Value (not considered in this paper)

In order to analyze economic sustainability of this project, all of the estimated values are changed to Cent (1 Cent = 0.01 dollar) per cubic meter per year (Figure 3). Results show in the full value term, the "value to users of water" has the major character (42.9 Cents/m^3) and almost the "net benefit from return flows" is negligible (0.2 Cents/m^3). In the full cost term, the "full supply cost" (14 Cents/m^3) and the "opportunity cost" (19.1 Cents/m^3) have the main role, also the amount of "economic externality" (6.2 Cents/m^3) is considerable.

4.3. Analysis of Economic Stability of Water Use

Economic stability is achieved by differing full value and full cost. Therefore, in this project it is equal to 3.8 Cents/m^3 (=43.1(full value) – 39.3 (full cost)). It shows a stability situation, because of the enormous difference between the price of pistachio in Rafsanjan (destination region) and wheat in the origin basin.

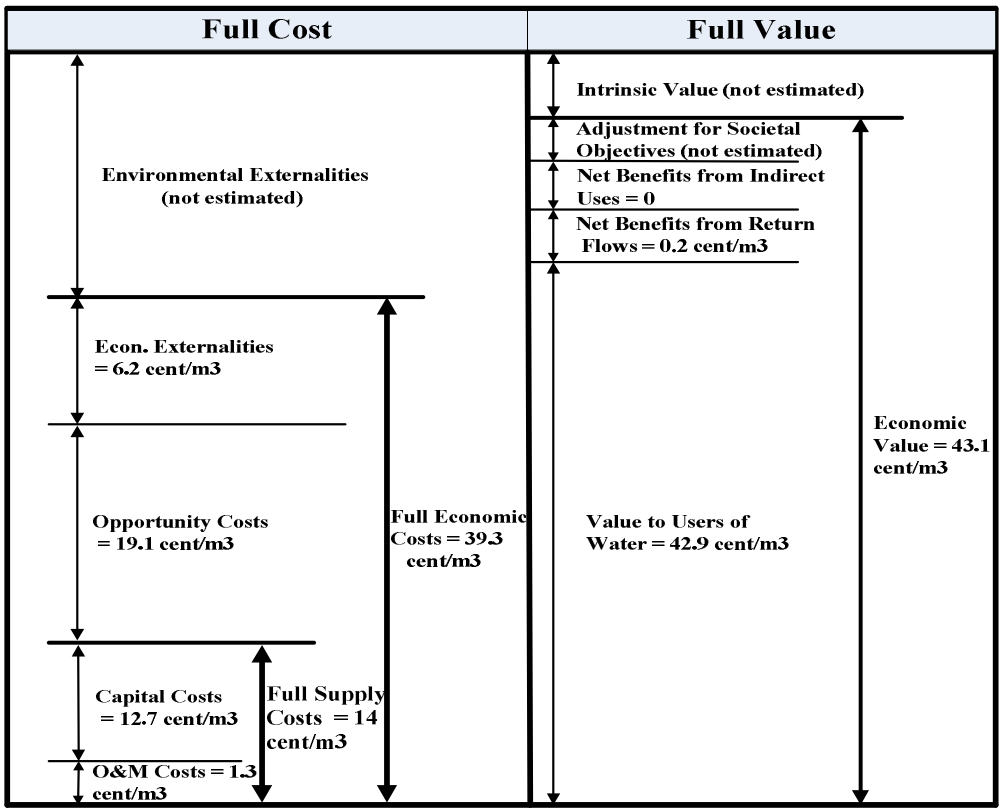

Figure3. Comparison of Estimation of costs and values for the IWTP (Not to scale)

5. Summary & Conclusion

GWP has formulated the concept of water as a socio-economic good to be applied in practice. In this paper, an IWTP in the central part of Iran is evaluated based on GWP guidelines. For this purpose the components of full cost and full value which could be estimated using the available data, are employed. The analysis of the full cost and the

full value of the project show the economic stability of the project. However the difference of these values is too low. This might be because of neglecting some effective terms such as intrinsic value and environmental externalities. Therefore, in order to increase the suitability of the region, some considerations should be involved in the project assessment process. The main recommended issues could be summarized as follows:

- Considering indirect users such as hydropower generators to make a more accurate estimation of "Net Benefit from Indirect Users" (which has been considered equal to zero in this study).
- Developing a method for computing the "Intrinsic Value" for aquifer restoration.
- Utilizing the methods of the efficient water use to decrease the aquifer depletion.

6. References

Agenda 21, (1992), "United Nations Conference on Environment and Development", p174.

Arpke, A., Kelly Strong, (2006), "A comparison of life cycle cost analyses for a typical college dormitory using subsidized versus full-cost pricing of water" journal of Ecological Economics (58) 66– 78.

Committee on Western Water management, National Research Council, Water Transfer in the West: Efficiency, Equity and the Environment. National Academy Press, Washington, D.C.

Ghassemi, F., and White, L. (2007) "Inter-Basin Water Transfer: Case Studies from Australia, United States, Canada, China and India" Cambridge University Press (2007) - ISBN 0521869692.

Rogers, P., Bhatia, R., and Huber, A., (1998), "Water as a Social and Economic Good: How to Put the Principle into Practice", Global Water Partnership Technical Advisory Committee (TAC).

Schuck, E., Green, G., (2002), "Supply-based water pricing in a conjunctive use system: implications for resource and energy use Resource and Energy Economics 24 175–192.

Shiferaw, B., Reddy, R., and Wani, S., (2008) "Watershed externalities, shifting cropping patterns and groundwater depletion in Indian semi-arid villages: The effect of alternative water pricing policies", journal of ecological economics, (67):327 –340.

Webber, M., Barnett, J., Finlayson, B., and Wang, M., (2008) "Pricing China's irrigation water", journal of.gloenvcha. doi: 10.1016.

Yevjevich, V. (2001) "Water Diversions and Inter-basin Transfers." Water Int., 26(3): 342–348.

Zahiri, A., and Korestani, S. (2004) "The effects of Inter-basin Water Transfer on the Dredge Activities in the Karoon River." *Proceeding of Water Transfer Seminar*, Tehran, Iran, Feb, 2004. (In Farsi).

Zhong, L., Mol, A., (2008), "Participatory environmental governance in China: Public hearings on urban water tariff setting" Journal of Environmental Management 88 899–913.

Recent Developments in Water Policy in the Americas

Mark W. Killgore, P.E., D. WRE, M. ASCE

Mark W. Killgore, P.E, D. WRE, M. ASCE, Puget Sound Energy PO Box 97034 PSE-09S, Bellevue, WA 98009, (PH) 425-462-3293, mark.killgore@pse.com

Abstract

This paper reviews recent work by EWRI, AWRA, ANEAS, FECIC and other entities actively developing water policy statements in preparation for the Fifth World Water Forum, scheduled for Istanbul, Turkey, March 16 through 22, 2009. EWRI participated in many of the preparatory events including:

- International Symposium on the 5th World Water Forum held in conjunction with the EWRI World Environmental & Water Resources Congress 2008 in Honolulu Hawaii in May 2008.
- Fourth National Water Resources Policy Dialogue, September, 2008, Washington, DC (sponsors included AWRA, EWRI and NWF).
- 22nd Annual Convention of ANEAS and the North American Regional Water Forum, Guadalajara, Mexico, November, 2008.
- Mexican Federation of Colegios (Sections) of Civil Engineers' (FECIC) 2nd World Congress on Water and Climate Change, Merida, Yucatán, Mexico, November 2008.
- Water Forum of the Americas, Iguazu Falls, Paraná, Brazil, November 2008.

Introduction

As of January 2009, preparations are well underway for the Fifth World Water Forum scheduled for March 16 through 22, 2009 in Istanbul, Turkey. Since the America's Regional Process plays a prominent role in identifying current water policy issues in the Western Hemisphere, and EWRI is participating in this process, this paper attempts to summarize many of the key concerns in this arena and policy related initiatives such as the recent FECIC Congress in Mexico.

For the Fifth World Water Forum, six principal themes have been identified including:

1. Global Change & Risk Management
2. Advancing the Human Development and the Millennial Development Goals

3. Managing and Protecting Water Resources and their Supply Systems to Meet Human and Environmental Needs
4. Governance and Management
5. Finance
6. Education, Knowledge and Capacity Building

Efforts for the Americas Region are sub-divided into 4 different sub-regions: Central America, Caribbean, North America and South America. Each sub-region is working in order to identify its main subjects of interest and to give answers to the different usual problems inside their own region. Each subregion developed its own Subregional document. In preparing for the Regional Process, for the Fourth World Water Forum, the Committee for the Americas identified the following challenges in water management in the Americas region:

1. Coastal zone management
2. Dam safety
3. Decentralization, Municipal role and local community
4. Energy options: hydropower
5. Financing water infrastructure
6. Flood, droughts, and risk management
7. Governance, institutional quality, and public participation
8. Groundwater management
9. Health implications of sanitation
10. Legal and regulatory framework for IWRM: advances and reforms
11. New frontiers in irrigation approaches
12. Payment for environmental services
13. Privatization: options for financing
14. Public versus private irrigation
15. Reaching the Millennial Development Goals
16. River basin organizations and institutions-appropriate level
17. Rural sanitation
18. Transboundary river basins
19. Urban water management
20. Water and Trade
21. Water as a human right
22. Water as an end versus water as a means
23. Water management of indigenous population
24. Water quality management-adequate water quality standards.

A key issue identified in the new North American Subregional Document (Herrera, 2008) is the need for mitigating flood risks in vulnerable areas and improved forecasting systems. Clarifying hydrometeorological risk and better forecasting systems combined with disaster prevention will improve the status

quo. An area of special relevance is transboundary watersheds, particularly the U.S. Mexico border in the case of drought and flood risk along the US Canada border. Herrera also characterizes the hydrology of the North American subregion and identifies key stakeholders in the region.

Climate change is another factor adding stress to water scarce regions. Developing Methods to address water scarcity under increasing populations in an ecologically sustainable way is identified as key.

The document identified the US and Canada as using an ecosystem approach to solve water problems. This approach includes land, air and water media. Considerable focus deals with water quality impacts from atmospheric contaminants along with land use.

The case of Mexico illustrates the need to provide clean drinking water and sewerage services, particularly in the southeast and in rural communities, where the problems is more serious. The document also states that "in the case of the United States and Canada, it is necessary to address new demands of quality standards for drinking water and the eradication of some contaminants, like the presence of lead in some places. In these countries, it is also necessary to make investments to renew the drinking water supply and sewerage infrastructure, which is reaching the end of its useful life." The latter item has been a key focus of ASCE's Infrastructure Report Card Program.

The Message of Iguazu Falls

The participants in the Water Forum of the Americas in Iguazu Falls, Brazil developed a message for the Fifth World Water Forum. The Water Forum of the Americas served as the conclusion of the Americas Regional Process in preparation for the 5th Forum. More than 250 people from different sectors of water management throughout the Americas participated. Participants included Ministers of State, Governors, Mayors, Parliamentarians, international organizations, academics, the private and public sectors, non-governmental organizations and river basin committees. Key participants in Brazil were the Ministers of Environment from Brazil and Turkey.

Over the course of several interactive sessions, the following recommendations were made by the participants:

- Promote social inclusion and the eradication of poverty through universal access to water supply and sanitation as well as through the productive use of water, by means of the usage of hydroelectric power, irrigation for food production, transportation, tourism and recreation, within a sustainable development context.

- Institutional strengthening of management bodies and promotion of internal and external integration of water resources policies with other sect oral policies.
- Incorporate the principle of common but differentiated responsibilities in water resources management, and the need for technology transfer and additional financial resources, in particular in strategies to face climate change.
- Because of the transversality principle, water management must be at the core of public policy in all three phases; planning, implementation, and control.
- Within specificities of each region, one should consider the multiple use of water on an efficient and rational basis, incorporating environmental conservation, protection and reclamation as necessary actions toward the improvement of water availability.
- Water sustainability requires good regulation and economic incentives.
- Promote agreements on the management of transboundary aquifers and basins.
- Decentralized, participative and integrated management of water resources with local stakeholders and indigenous and traditional communities, taking into account a gender perspective.
- We need to promote cleaner production by making investments in applied research, technological development and capacity development.
- The challenge of water management in small islands (SIDS) and the wider Caribbean region must be recognized and receive special attention due to their vulnerability to global climate changes.
- Support capacity development to help cope with the impacts of climate change.
- Need to raise awareness about water with training and education for everybody at different socio-economic levels connecting people with the basins where they interact.

Fourth Water Policy Dialogue

On September 22, 2008 EWRI (Kyle Schilling, Mark Killgore and Daene McKinney) along with EWRI Director, Brian Parsons and ASCE's Senior Manager, Government Relations, Michael Charles participated in the American Water Resources Association's (AWRA) Fourth National Water Resources Policy Dialogue. The Dialogue was cosponsored by EWRI and the National Wildlife Federation and included over 70 water leaders and others from around the nation including several congressional staff members with active interests in water resources' policies. This event built on the International Symposium on the 5th World Water Forum held in conjunction with the EWRI Congress in Honolulu in May, 2008.

The theme of the Fourth Dialogue was "Moving from Concepts to Action." The purpose of the Dialogue was to discuss how the outcomes of the first three Dialogues might best be moved from concepts to legislative and executive action. The outcomes of the Fourth Dialogue may provide input to the presidential

campaigns. Richard Engberg, AWRA's Technical Director and Jerry Della Priscolli from the Corps facilitated the discussions.

Three major issues were discussed including "Reconciling Contradictory Water Policies"; "Improving Collaboration"; and "Broadening the Role of Science"; as they relate to the overarching concerns of drought, flooding, infrastructure, population demographics, and climate change among many others. At the conclusion of the Dialogue, AWRA Past President (and active EWRI member) Gerald Galloway, EWRI President Kyle Schilling and David Conrad, Senior Water Resources Specialist for the National Wildlife Federation provided their insights gained from the dialogue. Conclusions from the Policy Dialogue were presented at the Water Forum of the Americas at Iguazu Falls in Brazil in November. Schilling stressed the importance of lessons learned from a historical perspective about implementing integrated water resources planning in North America, particularly the importance of both water quality and quantity. Other major conclusions included needs for a fresh assessment of the nation's water resources, better coordination, updated principles on water and development and planning for water resources in both a political and watershed context.

The offices of the co-chairs of the Congressional Water Caucus (Rep. John Linder, R-Ga.; Rep. Jim Costa, D-Calif.; Rep. Bart Stupak, D-Mich.; Rep. Grace Napolitano, D-Calif., and Rep. George Radanovich, R-Calif) welcomed the participants. The Caucus was formed to promote a dialogue about water issues and provide timely, scientific information about water resources and water use. The box below lists the Twelve Principles of Water Policy developed by the Caucus.

Twelve Principles of Water Policy
Congressional Water Caucus

1. Ensure an adequate supply of fresh water for U.S. citizens, securing a sufficient water supply for both urban and rural areas;
2. Consider all available technologies for increasing water supply efficiently, while safeguarding the environment, including the use of best management practices;
3. Recommend a means of capturing and storing excess water for future droughts;
4. Implement strategies to improve water use efficiencies and reduce water waste;
5. Support adequate funding to implement water re-use strategies wherever appropriate;
6. Advocate the coordination of efforts by Congress, the President, and state and local government to solve water issues;
7. Consolidate and streamline efforts between local, state, and Federal government agencies to reduce the bureaucratic red tape many local communities face when trying to build water reservoirs and other infrastructure needs;
8. Protect the rights of state and local governments;
9. Suggest financing options for new public works water projects;

10. Encourage Federal assistance to state and local governments to identify potential groundwater banking as part of sustainable water supplies;
11. Recognize international implications for water resources shared with other nations; and;
12. Collect and share data related to water use and water quality to determine effectiveness of policy.



Kyle Schilling, Mark Killgore and Brian Parsons along with others participate in breakout session at the Fourth National Water Resources Policy Dialogue at the Nation's Capitol.

Following the Dialogue, the sponsors consolidated many of the remarks and published a four page summary entitled "National Water Policy Dialogue". The summary was submitted to the President Obama Transition Team and ultimately published on the Obama Transition Website (AWRA, 2008).

The primary conclusions of the Dialogue included:

- There is an immediate need for an assessment of the Nation's water resources to include the current status of the resource, the future needs for water and identification of gaps that exist in fulfilling these needs.

- The federal government, in cooperation with state and local agencies, needs to develop a national vision and overarching principles to guide water resources development activities supported by the federal government.

- There is increasing need for mechanisms that will better coordinate the water related activities of federal agencies and among congressional committees. The absence of effective coordination is apparent in the conflicts and overlaps that exist in legislation, programs, and agency activities.
- The relationship among the federal government, states and local communities is changing and must be addressed. The federal government's role in water resources, long seen to be a driving force, must be reevaluated in light of growing state attention and direction of water resource activities.

- Federal actions with regard to water resources must be taken in a watershed context where the underlying planning is conducted in partnership with the states and local entities.

The conclusions of the policy dialogue echo many of the twelve principles above.

Conclusions

Many challenges face water planners and government officials as we gather in Istanbul to share experiences and ideas. EWRI will be participating in a session on Hydrosolidarity (Falkenmark, 2005). Hydrosolidarity is described as an increasingly integrated approach to managing water resources that relies heavily on participation and coordination among community stakeholders, water-related management agencies, and local, state, and national governments. A fundamental goal of hydrosolidarity is the cooperative, unified management of transboundary water resources, whether at the national or the international level.

Another session to be possibly included in the sessions is "Utility of IWRM Lessons Learned by Developed Countries for Developing Countries". Additionally EWRI has proposed a short course "How to Develop a Tool Box to Facilitate Transboundary Water Resources with an Emphasis on Water Quality".

Under Theme 6 "Education, Knowledge and Capacity Building", EWRI will share lessons learned in effective outreach via institute international programs and

participation. Specifically EWRI is participating in Topic: 6.1 Education and Capacity Development Strategies."

The Water Forum promises to be a stimulating discussion on where our field is headed and may directly contribute to EWRI's strategic planning initiatives.

Acknowledgements

The author acknowledges the support of ASCE, the EWRI Governing Board and the 5th World Water Forum Task Committee for participating in the meetings and helping contributing to the material in this paper.

References

1. ANEAS, XXII Conference description accessed online at http://www.aneas.com.mx/XXII%20Convencion_en.html
2. Herrera Toledo, Cesar, 2008. Water Forum of the Americas, Report of the North American Sub-Region Prepared for the Interamerican Development Bank.
3. World Water Forum, 2008. Session Summary for 3.1.1 From the December 15, 2008 summary template. Accessed online at http://portal.worldwaterforum5.org/wwf5/en-us/themes/Theme3/Topic3.1/Pages/default.aspx
4. AWRA, 2008 and coauthors EWRI and National Wildlife Federation. Water Policy Dialogue. http://change.gov/open_government/entry/national_water_policy_dialogue/
5. Falkenmark, Malin in co-operation with the Symposium Scientific Programme Committee, 2005. Towards Hydrosolidarity, Ample Opportunity for Human Ingenuity.

The Memorandum of Understanding (MOU) Between The University of Zambia and the University of Michigan Conception and Subsequent Implementation Goals

Jonathan W. Bulkley[1], Imasiku Nyambe[2], and Christine J. Kirchhoff[3]

[1]Professor of Natural Resources, School of Natural Resources and Environment and Professor of Civil and Environmental Engineering 440 Church Street, Ann Arbor, MI 48109-1041; PH (734) 764-3198; FAX (734) 647-5841; e-mail:jbulkley@umich.edu
[2]Professor and Coordinator, Integrated Water Resource Management Center, C/o School of Mines, University of Zambia, Great East Road, Lusaka 10101 Zambia; PH 260-211-294086 / 290165; FAX 260-211-294086 / 290165; e-mail:inyambe@gmail.com
[3]Ph.D Candidate, School of Natural Resources and Environment, 440 Church Street, Ann Arbor, MI 48109-1041; PH (734) 764-1412; FAX (734) 647-5841; e-mail:orange@umich.edu

ABSTRACT

In April 2008 the University of Michigan and the University of Zambia signed a Memorandum of Understanding (MOU) that approved a cooperative agreement to foster the development of a collaborative research and exchange program focused on concepts of integrated water resources management (IWRM) to be applied in the Zambezi River Basin in Southern Africa and the Great Lakes Basin in the U.S. The Zambezi River Basin, home to nearly 40 million people, is the largest river basin in Southern Africa covering 1.37 million square kilometers in eight countries. The Great Lakes Basin watershed is home to about 40 million people living in eight U.S. States and two Canadian Provinces and covers over 1/2 million square kilometers.

The MOU marks the culmination of a sixteen month effort which began in January 2007 and included two trips to Southern Africa, one in August 2007 and a second in November 2007. Individuals from The Nature Conservancy's Great Rivers Program, which includes the Zambezi River, facilitated the first trip to the basin through their contacts at the African Wildlife Foundation Zambezi Heartland team based in Kariba, Zimbabwe. The first trip provided an introduction to the range of problems and issues confronting application of IWRM in the Zambezi River and served to establish contact with a number of key organizations and people working to enhance and improve the management of the Zambezi's water resources. Following the first visit, we were invited to participate in the "Championing Effective IWRM in the Zambezi Basin" Conference held in Victoria Falls, Zimbabwe in November of 2007. The second trip and Conference provided an opportunity to reconnect with colleagues met during the first visit to the basin and, in addition, to meet new colleagues including Professor Imasiku Nyambe.

INTRODUCTION

In the summer of 1960, one of the authors of this paper, Jonathan Bulkley (age 22), traveled to Ghana as a member of an Operations Crossroads Africa two-month work camp project. One purpose of this work camp experience was for a racially mixed group of young Americans and Canadians to join with a counterpart group of young Ghanaian students in order to build a water supply system for a rural training camp located in the rainforest of the Ashanti Region. An equally important objective of the experience was to expose the Crossroads team to the 1960 realities of living and working in a tropical rainforest region in West Africa. For me, this overall experience had a profound impact on my life. First, as a consequence of the direct observation of the critical need for a safe and secure water supply system, I changed my civil engineering major from transportation engineering to water resources. Second, I became highly motivated to seek graduate education since I believed the most effective way I could assist these types of situations was to acquire as much education as possible. Finally, I had never before lived as a minority in a society where I was different from the population as a whole. All of these factors combined and guided me to graduate school in the field of water resources and to seek an academic position for my professional career.

As my forty year career in teaching and research at the University of Michigan is coming to a close, I want to explore the possibility of providing a similar 21st Century experience for Michigan. These students working to resolve water related problems here in the U.S. would meet and interact with a counterpart group of students from an African University working to resolve water related problems and issues in their country and region.

In January, 2007, we became aware of the recently established Great Rivers Program of The Nature Conservancy (TNC). One of the Great Rivers identified by TNC is the Zambezi River in Southern Africa. Contacts were made with TNC and they subsequently provided an important introduction to the African Wildlife Foundation. These two organizations (TNC and the African Wildlife Foundation) provided outstanding assistance that greatly facilitated our first trip to Southern Africa.

INITIAL TRIP

The initial trip to Southern Africa by Jonathan Bulkley and Christine Kirchhoff occurred in late August and early September, 2007. As noted earlier, both the itinerary and logistics of the visit were greatly facilitated by the staff of the African Wildlife Foundation based in Kariba, Zimbabwe. This working visit to Zambia, Zimbabwe and Botswana resulted in a series of nineteen meetings in fourteen days in the three countries with key water related agencies, non-governmental organizations and members of the faculty at the University of Zambia

and the University of Zimbabwe. All of these meetings were greatly aided through the good offices of the Great Rivers Program of The Nature Conservancy (TNC).

TNC provided us with an introduction and subsequent close association with Mr. Jimmiel Mandima, Director of the Zambezi Heartland, an African Wildlife Foundation (AWF) designated protected area. The Zambezi Heartland encompasses 18,000 square miles including a significant length of the Zambezi River from Lake Kariba in Zimbabwe to Lake Cahora Basso in Mozambique. Jimmiel and his staff are based in Kariba, Zimbabwe, not far from the Zambia border. This close association with AWF enabled us to have a very productive and valuable visit to the Zambezi River Basin by facilitating numerous meetings and contacts and by providing extensive logistical support. The latter included arranging for all of our transportation needs, facilitating border crossings and making reservations for all of our overnight accommodations in Kariba and Harare, Zimbabwe as well as in Kasane, Botswana and Lusaka, Zambia.

SECOND TRIP

As a consequence of the meetings held during the initial visit, we were invited to attend the annual Zambezi River Basin Stakeholders Forum (Forum) in Victoria Falls, Zimbabwe on November 25-27, 2007. The Victoria Falls meeting marked the third Stakeholder Forum. As a consequence of teaching responsibilities at Michigan, Jonathan Bulkley was not able to accept this invitation. However, Christine Kirchhoff and a second Ph.D student from the University of Michigan whose African research focuses upon fisheries, Mr. Ted Lawrence, did attend and both made presentations at the Forum. The overall Forum objective was to develop a shared vision for the Zambezi Basin including the following specific objectives: (1) Share knowledge and experiences regarding sustainable management of the Zambezi River Basin; (2) Identify key issues and challenges that need to be addressed to guarantee sustainability; (3) Collect ideas for an Integrated Water Resource Management (IWRM) strategy for the Zambezi River; and (4) Network with Zambezi River Basin Stakeholders.

Integrated Water Resource Management (IWRM) is an ongoing process in the Zambezi River Basin with the objective of creating and subsequently implementing the Zambezi Action Plan. The Southern Africa Development Community (SADC) is the custodian of the Zambezi Action Plan. SADC encompasses 15 different countries and brings more than 200 million people together in Southern Africa. Furthermore, the SADC region is notable because 70% of the water resources and 15 major river basins in the region are shared by two or more countries. Progress has been made in developing the IWRM strategy. Effective participation and stakeholder involvement has advanced through efforts such as the annual Forums. In addition, a platform has been established for each basin country to address local and national concerns. However, a number of challenges must be overcome in order to fully realize IWRM in the Zambezi River Basin. In his

Keynote Address at the Stakeholder Forum, Mr. Khupe, a retired government hydrologist, identified the following challenges in the Zambezi River Basin:

(a) Ecosystems transcend national boundaries and as such need to be jointly managed;

(b) Water management doesn't abide by boundaries;

(c) Upstream activities affect downstream;

(d) Decisions (mostly made by politicians) impact everyone but not everyone is included in the deliberation (e.g., Communities are not adequately represented at the Stakeholder Forum); and,

(e) Multiple stakeholders.

Mr. Khupe offered the following observations to overcome the above challenges:

(a) Information sharing builds trust. Need to exchange information and be open.

(b) Stakeholders need to be included. Communities, civil society – haven't been involved.

(c) Approach the media**.**

One of the challenges to implement the IWRM is the full realization of the Zambezi Action Plan which includes the establishment of a joint governance and implementation mechanism through the creation of the Zambezi Watercourse Commission (ZAMCOM). Further insights regarding progress of establishment of this joint governance/implementation structure was presented by Dr. Z. Phiri during the first day of the Stakeholder Forum. Dr. Z. Phiri, Professor at the University of Zambia School of Engineering, noted that ZAMCOM was signed in 2004 and is now undergoing ratification by the eight riparian countries. The objectives of the agreement are to efficiently develop and utilize the water resources of the Zambezi River. Dr. Phiri noted a number of challenges that had emerged during the ratification process including:

(a) Water governance constraints;

(b) Weak stakeholder participation; and,

(c) Inadequate infrastructure.

Dr. Phiri suggested two responses to facilitate the ratification process:

(a) National agendas must move to cooperative agendas; and,

(b) Perception of benefits for ratification is of key importance.

A number of other speakers at the Forum weighed in on the IWRM strategy itself. One speaker, Ms. Tabeth Chiuta, an International Union for the Conservation of Nature (IUCN) wetlands policy expert, provided a number of key recommendations IUCN hoped to see in the final IWRM strategy. These recommendations included:

(a) Mainstream wetlands functions into IWRM;

(b) Improve understanding and appreciation of wetlands functions;

(c) Invest in wetlands ecosystem functions;

(d) Manage water infrastructure and development to maintain environmental Functions; and,

(e) Facilitate partnerships to facilitate mainstreaming wetland functions.

Other speakers discussed the need to include environmental flows in the IWRM strategy, to provide incentives to local people who would implement the strategy, the promotion of co-management strategies, and the importance of funding.

This second trip focused upon the Zambezi River Basin Stakeholders Forum (Forum) plus subsequent follow-up visits at the University of Zambia in Lusaka, Zambia. It should be noted that Ms. Kirchhoff and Professor Nyambe from the University of Zambia made presentations at the same Water Quality session at the Forum. Their meeting at Victoria Falls together with the subsequent discussions at the University in Lusaka laid the foundation for the drafting and approval of the Memorandum of Understanding between the University of Michigan and the University of Zambia.

THE MEMORANDUM OF UNDERSTANDING (MOU)

The overall objective of the Memorandum of Understanding signed on April 17, 2008 is to provide an opportunity for students and faculty members from the two universities to meet and learn from one another in the context of undertaking important and relevant water resources research. This joint experience will strengthen the overall capacity for these young men and women to be come leaders in their professions and to function more effectively in the global world of the 21st Century.

Four major activities will be undertaken to further the achievement of this overall objective. These four major activities are as follows:

(a) Joint Research: Undertake joint research of mutual benefit and interest focused upon identifying effective water policies and practices, and related

institutions and institutional frameworks to provide more efficient and sustainable management of trans-boundary water resources.

(b) Workshops: Conduct at least two workshops each year one in Southern Africa and one in the United States where the research teams would meet together at the host institutions to share results and identify further research initiatives.

(c) Report Research Results: Seek opportunities to report research results at annual water meetings held in the United States and in Southern Africa.

(d) Capacity Building: Participate in scholarly exchange and learning through the joint research efforts, workshops and research presentations. Also, jointly explore and identify appropriate short courses designed to assist in capacity building among students, staff and the wider community.

Activities to be carried out during the implementation of the MOU include the following:

(a) External Funding: Each of the parties shall seek external funding to support the implementation of this MOU. The parties may, through joint proposals, also jointly seek funding.

(b) Time Period: The MOU should be for an initial time period from the date it is approved by the parties through September 2011.

(c) Annual Review: There will be an annual review conducted to evaluate the yearly accomplishments and identify any changes needed to further the future effective implementation of this MOU.

(d) Comprehensive Review: During the last six months of this MOU, a comprehensive assessment of the accomplishments achieved will be undertaken and any modifications required for the continuance of the MOU will be identified.

UNIVERSITY OF ZAMBIA: REASONS TO UNDERTAKE THE MEMORANDUM OF UNDERSTANDING (MOU)

In 2006, the University of Zambia (UNZA) established the UNZA IWRM Centre (IWRMC) a centre of "excellence" in line with the UNZA's motto of "service and excellence" guided by University's development **Mission** of "meeting the needs of individuals and society through excellence in teaching and learning, research and service in order to foster sustainable human development and a culture of peace, human rights and justice".

The Centre was established as a response to the Water Sector Support program through the Ministry of Energy and Water Development (MEWD) in collaboration with Royal Danish Embassy (RDE) (MEWD-Danida, 2005). It is based on the concepts and policies that are underlying the draft Water Resources Management Bill and the Human Resources Capacity study in the Water Sector in Zambia, which pointed out critical shortages of human resources to champion IWRM interventions in Zambia (Nyambe, 2005). In addition, the Government of Zambia also realized the pivotal role water plays in the socio-economic development of Zambia through the Fifth National Development Plan (2006-2010) and Vision 2030 (Ministry of Finance and Planning, 2006), where agriculture and tourism are priority areas aimed at creating wealth and reduction in poverty and community levels.

The Center's **Vision** is therefore that of "advancing and implementation of IWRM interventions in Zambia and the region through education and training, advanced research and consulting services for a sustainable water sector performance" with the main objective of "to build capacity in IWRM in Zambia focusing on water resources covering surface and groundwater employing techniques for assessments, quantifications, quality analysis and modeling (e.g. use of remote sensing and GIS). Also to improve water sector performance and ensure that there is sustainable management of the water resources through human resource development and capacity building" with the following specific objectives:

- To contribute to capacity building (human resource development, institutional strengthening and policy reform) in the water sector.
- To promote and undertake the training of water sector personnel and trainers in technical, managerial, economic and social issues to increase performance and productivity.
- To develop an independent advisory service to government, local authorities, private sector and international organizations in management of water and environment.
- To develop an information support service for information pertaining to Integrated Water Resource Management.
- To promote and undertake applied research in the work place and at graduate and postgraduate levels in the area of Integrated Water Resource Management and Environment.

The IWRMC is a hub currently with seven schools represented on its technical committee (Agricultural Sciences, Engineering, Education, Humanities and Social Sciences, Law, Mines and Natural Sciences). These seven schools bring together geology (hydrogeology), civil and environmental engineering – hydrology

of surface water focused), agriculture, mining, physical sciences (biology, chemistry, physics), life sciences (human and veterinary medicine), socio-economic, law and education. The IWRMC is also a hub for collaboration with stakeholders in Zambia and universities and NGOs outside of Zambia. The Zambia Water Partnership sits within the premises of the centre.

To advance its objectives, with support from Danida, IWRMC put in place a twinning arrangement with Danish universities in which Zambians are trained, followed by a Swiss program. However, despite the two arrangements, the academic quality and breadth, and teaching and research enhancement at the departments contributing to the center is at its lowest infancy. Accordingly, exchanges and collaboration with other universities is still a must. As a result a Memorandum of Understanding (MOU) was signed with the University of Michigan in order to pursue the Center's objectives.

THE UNIVERSITY OF MICHIGAN AND THE SCHOOL OF NATURAL RESOURCES AND ENVIRONMENT: REASONS TO UNDERTAKE THE MEMORANDUM OF UNDERSTANDING (MOU)

In late February and early March 2008, University of Michigan President Mary Sue Coleman led a delegation to South Africa and Ghana to extend existing collaborations with several African universities, forge new relationships between the University of Michigan and African counterparts, and develop new initiatives. President Coleman's trip occurred during the very time that the drafting of the MOU between the University of Zambia and the University of Michigan took place. This joint effort between our universities reflects the ongoing activities of both universities to join in partnerships across the globe to bring together faculty and students to engage and learn from and with each other in order to address the problems facing our societies individually and globally.

The School of Natural Resources and Environment (SNRE) at the University of Michigan is the active party to our MOU. A prime reason for SNRE to become a partner with the University of Zambia through this MOU is articulated in the MOU provision that addresses joint research. Through the MOU, the SNRE and the University of Zambia will undertake joint research of mutual benefit and interest focused upon identifying effective water policies and practices, and related institutions and institutional frameworks to provide more efficient and sustainable management of trans-boundary water resources. It is the achievement of "more efficient and sustainable management of trans-boundary water resources" that ties the MOU directly to the roles and mission of the SNRE at the University of Michigan.

"Achieving a sustainable society is the core focus of the University of Michigan's SNRE. Its overarching objective is the protection of the earth's resources for the benefit of present and future humanity as well as that of all other life on the globe. The only way that protection can be achieved is through creation

of knowledge and strategies that result in current needs being met in a way that creates a foundation for future generations to thrive. Hence SNRE's mission is to foster wise stewardship of environmental resources through effective and just strategies for achieving sustainable societies over the long term. This need for SNRE's work is seen in rising U.S. and worldwide demands on water, land, food and energy resources along with unsustainable land use and consumption patterns and ineffective decision making processes. Climate change, globalization, demographic change and economic insecurity all exacerbate these fundamental problems, and result in the loss of biodiversity in terrestrial and aquatic systems and diminished health and quality of human life" (SNRE Executive Committee, January 10, 2009). We enter into this MOU with hope and optimism that this small, joint undertaking will inform and ultimately lead to more sustainable management of water resources in the U.S. and Southern African and beyond.

OBSERVATIONS

The signing of the MOU between the two universities indicates commitments by the university administrators for this collaboration. Continuous exchange of ideas between the Principle Investigator of the Joint UM/UNZA Collaboration (Professor Jonathan W. Bulkley and the Coordinator, The University of Zambia IWRM Center (Professor Imasiku A. Nyambe) has resulted in two papers to be presented at EWRI/ASCE conference in Kansas City, Missouri in May 2009. These papers ultimately demonstrate the resolve of the two universities to collaborate in one area of River Basin management where UNZA is lacking experience. Current programs at IWRMC are designed for national water resources covered by Zambezi River Basin, and yet the Zambezi River itself is shared by eight countries in Southern Africa.

The coming in of the University of Michigan, to foster a partnership on the study of the Zambezi River Basin with a comparative approach to the Great Lakes Region of the U.S., which has been studied and researched for many years will provide a rich experience to the basin management of the Zambezi that is still at its infancy. The emphasis in the MOU by the two universities on staff and student exchange is to ensure the transfer of knowledge and skills that will enhance capacities for programs at UNZA's IWRMC and associated Department levels to deliver high-quality science, social science, and engineering programs (education and research related to resource assessment, modeling, monitoring and its application to developmental sectors of Zambia particularly natural resource management with a focus on stakeholder participation). Above all, our understanding of basin level management focusing
on the intersection of natural resources, socio-economic development, and environmental sustainability will be enhanced.

It is IWRMC's hope that relationships with stakeholders (e.g., "consumers" of students and research products such as agriculture, industry, government agencies, and public interest entities) and partners in the region and abroad will be

strengthened through provision of relevant accessible information for decision making. This in turn may open the doors for IWRMC to access relevant and appropriate development assistance, student and program support, collaboration and resource sharing, and endowment and foundation gifts.

These collaborative relationships will build and strengthen the UNZA IWRMC's capacity to assist the Zambian Government in attainment of the water resources goals articulated in Zambia's Vision 2030. The opportunity for students and faculty from the University of Zambia and the University of Michigan to work together on key water resources research is of critical importance. These students, young men and women, will represent a new level of achievement in global water resource collaboration. These students in both countries are among the water resource professionals who will provide the leadership in the integrated planning, implementation and management of water resources for the 21st Century.

REFERENCES

MEWD-Danida, 2005: Water Sector Programme Support Zambia, Component Description Final, Component 3, Support to Integrated Water Resources Management, November 2005

Ministry of Finance and National Planning (MFNP), 2006. Fifth National Development Plan 2006-2010. Lusaka, Zambia. 384p.

MOU between University of Zambia and University of Michigan, April 17, 2008.

Nyambe, I. A., 2005: Water Sector Identification and Preparation Study Part 5: Options for collaboration between Zambian and Danish institutions on water sector research –Assessment of human resources in the sector, April 2005

SNRE Executive Committee (January 10, 2009), SNRE and Sustainability, 01.10.09 Document

Title: Environmental & Water Resources in Developing Countries

Sub Title: Development of Micro Irrigation Facility at Parsoda Village

Agale P.K[1], Wankhede N.N[2]., Bhave P. B.[3] and Mhaske S. Y.[4]

1 Faculty of Civil and Environment Engineering Department, V.J.T.I. Matunga, Mumbai - 400 019, India, Ph(+91 022) 24198325; Fax (+91 022) 24198425; email-priyanandagale@gmail.com

2 Faculty of Chemistry Department, V.J.T.I. Matunga, Mumbai - 400 019, India, Ph(+91 022) 24198127; Fax (+91 022) 24198425; Mumbai, email-nil_w@rediffmail.com

3 Faculty of Civil and Environment Engineering Department, V.J.T.I. Matunga, Mumbai - 400 019, India, Ph(+91 022) 24198325; Fax (+91 022) 24198425; email-pbbhave@vjti.org.in

1 Faculty of Civil and Environment Engineering Department, V.J.T.I. Matunga, Mumbai - 400 019, India, Ph(+91 022) 24198325; Fax (+91 022) 24198425; email-symhaske@vjti.org.in

Abstract

India is developing country among the world. Most of the people in India depend on agricultural industry. Near about 70% population depends on agriculture. Hence, India's development mostly depends on development of agricultural sector. But it is very difficult to construct big dams across the rivers due to environmental damage and protest of farmers against acquisition of land. Also major or medium irrigation project cannot provide the irrigation benefit to every farmer. Due to scarcity of water for irrigation, one lac farmers did suicide in last ten years in India. If the micro irrigation facilities are provided then there will be considerable recharge of ground water aquifer take place. It will create agricultural reform without causing natural hazard.

The present paper deals with development of micro irrigation facility at Parsoda village, district Aurangabad, Maharashtra State in India. In this project micro irrigation techniques like farm pond, earthen bunds are used for development of irrigation facility, near about 3500 acres of agricultural land is benefited due to micro irrigation technique with minimum expenditure.

INTRODUCTION

India is one of the developing countries in the world. Near about 75 percentages Indian population is dependent on the agricultural sector and they are living in rural areas, so it is very clear that development of the country like India is totally dependent on development of its agricultural sector. Indian Agriculture accounts for almost 25 percentage of the total GDP.

Agricultural sector is interlinked with natural resources such as land, water, vegetation and humans. Moreover Agricultural sector does not have any negative effects on the environment. If agricultural industry is developed by considering the environmental factors then we come to know that it is the only industry which becomes a part of environmental and water conservation. All the crop plants form the engines of the Oxygen regeneration cycle of the earth. Crop vegetation also acts as an infiltrator of rain water into ground by leading the stagnated rain water into the soil up to the full depth of the roots thereby recharging the water table. This increased water table is very helpful for the irrigation purpose. Hence the economy of the nation depends on the natural resources and its management.

In recent past suicide of farmers is a big issue in India. The rate of farmer suicides in India is increased and it will affect the economy of country nearly 150000 farmers committed suicide in nine years from 1997 to 2005,while farmer suicides have occurred in many states, nearly two third of these deaths are concentrated in five states. The five worst-hit states are Maharashtra, Andhra Pradesh, Karnataka, Madhya Pradesh, and Kerala. Maharashtra is the worst affected state in the country. Farmer suicide rate is from 1083 in 1995 to 3925 in 2005 (TISS, 2005).

There are many causes for this tragic situation one of the major causes being lack of irrigation facilities. Day by day the ground water table is getting depleted, hence the farmer are not getting water for irrigation. Construction of large reservoir creates many socio –environmental problems also it cannot provide benefit to each and every farmer. Hence development of country and agricultural sector is dependent on Micro watershed development. This is the only solution to overcome the above problems.

LAND AND WATER MANAGEMENT

Land and water resources are limited and their wide utilization is imperative especially for countries like India where the population increase day by day and it creates the pressure on land and water resources. Thus proper planning and management of natural resources is essential for the development of country. The economical development of an India depends to a significant extent on the natural Resources and its management. The average annual rainfall in India is around 114 cm and in terms of volume, it is in the order of 370 million mm (M) ha-m of Which 123 M ha-m is lost in evaporation, 167 M ha-m are runoff and the rest of The 80 M ha-m goes into the subsoil annually. While about 43 M ha-m gets absorbed in the top layer of the soil, thereby contributing to soil moisture, the remaining 37 M ha-m accounts for the ground water from rainfall. According to Raghunath (1987), the average annual ground water recharge from rainfall and seepage from canals and irrigation systems is in the order of 67 M ha-m of which 40% is extractable economically. The present utilization of ground water is approximately 13 M ha-m and about 14 M ha-m is available for further exploitation and utilization. Agriculture in India is heavily

dependent on Rainfed Farming Systems. Out of about 328 M ha of geographical area in the country, the net cultivated area is around 142.2 m ha of which about around 33.3% (47.4 M ha) is under irrigation. About 56% of the total food grain is produced from the irrigated area while the remaining 44% is contributed by 95.8 M ha. rainfed areas (Sarkar, 1997). This data reveals that the rain water inflow is good but its utilization is poor. On the other hand, the dependency on rainfed agriculture is very high. Hence the strategy to meet the increasing demand of agricultural produce is to initiate micro level watershed planning. Watershed development provides an Opportunity for optimum utilization of land and water resources and increasing the crop yield by over two folds. Apart from the area under agricultural lands, there are vast stretches of denuded forests, overgrazed pastures and barren lands. It is estimated that about 100 M. ha wastelands are presently lying underutilized or idle, and posing a threat to agriculture and environment.

Watershed development program creates employment through development of wasteland and for countries like India where population growth rate is high it is very essential to create the employment. It will more helpful for increasing economy of country.

MICRO-WATERSHED DEVELOPMENT

The watershed management concept recognizes the inter-relationships among the linkage between uplands and low lands, land use, geomorphology, slope and soil (Tideman, 1996).Considering watershed conservation work it is not feasible to take the whole are at once. Thus the whole basin is divided into several smaller units, each unit is called micro –watershed.

Micro- Watershed is more beneficial rather than construction of big reservoir from socio - environmental point of view. For the construction of big reservoir land acquisition and rehabilitation of people is the major problem in highly populated country like India, also large reservoir creates environmental problems. So that micro watershed development is the only way for the developing country like India.

Micro-watershed development consisting of following methods

A) Structural methods
B) Vegetative measures

A) Vegetative Measures: It consist of watershed measures in the following forms so that soil erosion in the watershed is controlled,

- Cover crops
- Horticulture
- Afforestation along bunds
- Block plantations

B) Structural Methods: It consisting of following engineering structures for the rain water harvesting, these structures are economical also required less maintains cost. Such type of structures does not cause any harm to socio - environmental. Table no. 1 shows salient features of watershed structures

- Gully checks
- Staggered trenches
- Continuous contour trenches
- Mini percolation tanks
- Sunken gully pits
- Rock fill dams
- Bunding
  Contour Bunding
  Boundary Bunding
- Farm ponds
- Percolation tanks
- Check dams

ECONOMIC ANALYSIS

Economic Analysis can be done for the following Structures taken up under water - shed Development.

- Bunding
- Percolation tanks
- Check dams
- Farm ponds

Benefits of Micro Watershed Structures

- Soil erosion due to runoff can be controlled
- Crop damage due to runoff can be controlled
- It provides facility for easy ground water recharge
- Less land required for its construction. Hence there is no possibility of land acquisition
- Irrigated areas stabilized and yields increased in the crops raised in these stabilized areas
- The additional areas come under irrigation from fallow (before) to single crop (after) and their yields
- The additional areas come under irrigation during second crop and their yields
- The additional areas brought under irrigation from fallow (before) to double crop and their yields

Case Study of Parsoda Village:

The Parsoda village is the one village of Maharashtra State situated at Aurangabad district having population 6000 and nearly 3500 acres of land is used for agriculture. The permeable soil is available .It is one of the drought prone village of Aurangabad. It is on going project in Parsoda village we are awareing the people about development and construction of Micro watershed through ECO NEEDS FOUNDATION (NGO)

In this village micro watershed development carried out through Farm ponds, Percolation tanks, and bunding .These structures are very economical as it required only soil and stones and it is locally available.

Farm pond Details

Farm pond is the excavated trench into ground for harvesting the rain water .It controls the soil or agricultural loss due to runoff. It also very help full for ground water recharge. Hence at Parsoda village close network of form pond is proposed, for avoiding silt deposition in farm pond depth of farm pond is divided in to different part so that it provides the soil stability to farm pond and facility for cleaning. One of the advantages of such pond after rainy season is over it can be used for manufacturing of compost fertilizer Following are the some details of farm pond considering ground water recharge.

Size:-
For top part = 9m x 9 m x 2.5 m
For bottom part = 6m x 6m x 2.5 m
Total storage available for water or volume of pond =292.5 cubic meters
As per local survey it is found that there are five maximum rainfalls during which maximum runoff taken place. It means that farm pond store the water and recharge the ground water in five times during rainy season.

Total ground water storage due to each farm pond = 5x 292.5
= 1462.5 cubic meters
= 1462000 liters

Proposed 25 Number of farm pond at Parsoda village

Total ground water storage possible due to farm pond = 25 x 1462000
= 36550000 liters
= 36.55 M liters

Conclusion

Micro watershed promotes socio cultural, socio economical and socio ecological development .the present paper deals with different micro watershed structures and its utilization according to the topographical situation. These structures are economical and are very help full for raising the farm income, enhancing agricultural productivity, soil and water conservation and also for, generating rural employment.

References

Raghunath H.M., 1987. Ground Water. Willey Eastern Ltd. p. 1-2.
Sarkar A.N., 1997. Status of Organizing Training for Watershed Development And Management in India
Tideman, E. M., *Watershed Management, Guidelines for Indian Conditions*, Omega Scientific Publishers, New Delhi, 1996, p. 372.
Tata Institute of Social Science (TISS), Tuljapur, Dist. Osmanabad, 2005, Enquiry Report, “Causes of farmers suicides in Maharashtra”, Submitted to Bombay High Court.

Table 1: Salient features of watershed structures

Name of the structures	Objectives	Visualization
Gully Checks	Arresting of soil –erosion promoting infiltration of rain-water Improving the soil-moisture.	Over a period of time Gully checks heal up the small gullies, prevention of further deepening and widening of gullies. Help in increasing vegetation leading to stabilization of gullies.
Rock fill dams	Increasing soil moisture Recharges of ground-water arresting of soil erosion	Improved vegetation in the vicinity of structures
Staggered Trenches	Increasing soil moisture Reducing soil erosion	Improved vegetation
Continuous contour Trenches	Increasing soil moisture Reducing soil erosion Recharge of Ground-Water	Improved vegetative growth, increase in the well population, and increased crop yields in the influence area.
Percolation Tanks	Recharge of ground-water through percolation by impounding water.	Increased crop yields, Increase in the cropped area, Increase in the well population
Sunken gully pits	Controlling the erosion Recharging of ground-water	Improved vegetative growth on the banks of stream.
Bunding	Soil-moisture conservation	Increase in crop yields. Increase in the cropped area.
Farm ponds	Storage of surface water	Utilization of stored water for pesticide spraying, drinking water for cattle and life saving irrigation to the crops.
Check dams	Basically Recharge of ground-water through percolation by impounding water.	Increased crop yields-Increase in the cropped area. Increase in the well population

Feasibility Study for Implementing Renewable Energy to Power a Groundwater Pump in Rural Guatemala

Will Granich[1] and Andrew Curtis Elmore[2]

[1]Department of Geological Engineering, Missouri S&T, 125 McNutt Hall, Rolla, MO 65409;
PH (573) 690-0276; e-mail: wagr38@mst.edu
[2] Associate Professor of Geological Engineering, Missouri S&T, 125 McNutt Hall, Rolla, MO 65409;
PH (573) 341-6784; e-mail: elmoreac@mst.edu

Abstract:

Communities in rural Guatemala often struggle with obtaining adequate, clean drinking water. A deep groundwater well can provide a clean and sustainable water source for near-by communities. To obtain the groundwater, an electric submersible pump must be installed in the well. Utility power in rural Guatemala can be unreliable and expensive, thus a study has been conducted to establish if using alternative energy is sustainable and economically viable for a groundwater pump for a rural Guatemalan community. The study focused on effectiveness, reliability and cost. A weather station was erected in Sacala las Lomas to collect baseline data for the feasibility study. Wind velocity, wind direction, solar radiation, temperature, precipitation and barometric pressure data were collected. The data were analyzed to determine the potential power generated with solar and wind power. Although the location was in a particularly superior location for sun and wind exposure, installing solar panels and/or a wind turbine would not be feasible for supplying the amount of energy required for a submersible groundwater pump that would meet the needs of the community.

Introduction:

Throughout Guatemala a lack of sanitation infrastructure and poor solid waste management has left most of the country with drinking water infected with pathogens. Coliform bacteria are often used as indicator organisms of pathogens. This is because coliforms consist mainly of the species Escherichia coli (E. coli) which thrive in the intestines of warm-blooded animals (Reynolds and Richards 1996). Since E. coli bacteria occur in the intestines, the presence of E. coli suggests that the water is being contaminated from fecal matter. Some strains of E. coli bacteria can lead to sickness and possibly death. This problem has led to Guatemala producing one of the highest infant mortality rates in Central America (WHO 2000).

Guatemala is topographically separated into the lowlands and highlands. The lowlands, located in northern Guatemala and along the coastlines, consist of a flat terrain with a tropical climate. The highlands of Guatemala are mountainous with a

very rugged terrain. The highlands have a temperate climate with a wet season (May-October) and a dry season. Water sources for most villages in the highlands usually are spring water systems distributed by gravity for several kilometers. The spring water is often contaminated with E. coli at the source, and often becomes more contaminated from bacterial growth in the pipeline (Elmore et al. 2005).

A proven, safe and sufficient water source in Guatemala is deep aquifers (Elmore et al. 2005). A submersible pump is used to bring the groundwater to the surface where it can be distributed. In many rural villages in the highlands of Guatemala, electricity is costly and there can be long power outages (EIA 1997). Therefore, if a groundwater pump is being used and there is a power outage, the community only has the volume of water in a storage tank until the electricity is restored. Typically a storage tank contains three days volume of water. Possible resolutions to avoid this problem are the implementation of alternative energy sources, such as solar and wind power, to run the pump without relying on grid-power.

Project Background:

Sacala las Lomas (Sacala) is a rural village in the highlands of Guatemala. Sacala is located approximately 1,910 meters (m) above mean sea level (amsl) in the Sierra Madre mountain range, in the Department of Chimaltenango. Sacala is approximately 4 kilometers southwest of the city of San Martin Jilotepeque as shown on Figure 1.

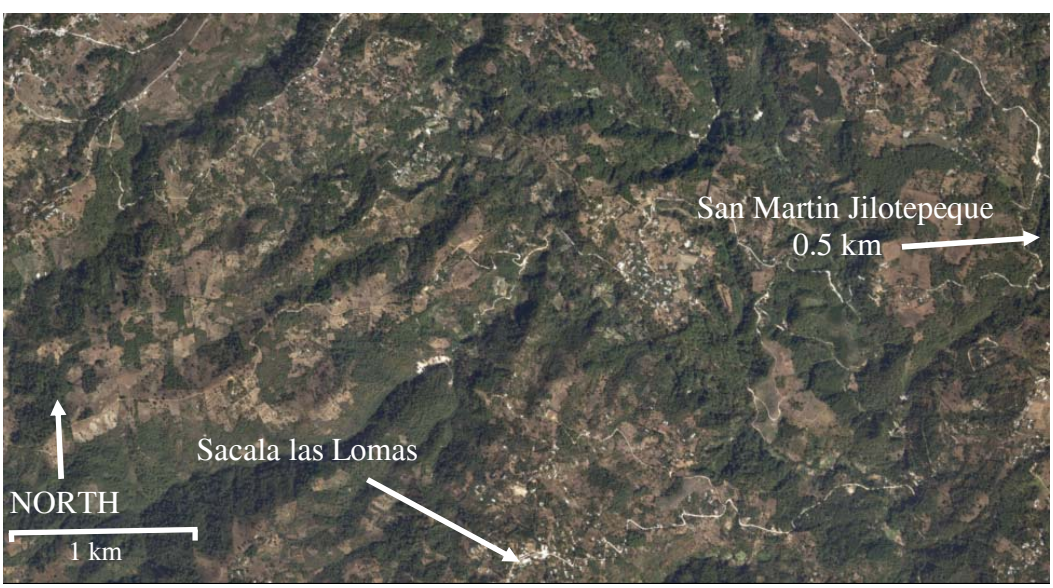

Figure 1. Location Map of Sacala

As of 2001, Sacala's population is 662, and there are 223 homes dispersed throughout the mountain side (Martin 2001). Sacala has been trying to attain funding, with assistance from a non-profit group from Canada, to drill and develop a deep groundwater well. The community is asking for a groundwater well because the current drinking water supply, a spring-based system, runs dry during the dry season. Lepper and Elmore (2005) found that a groundwater well in rural Guatemala is beneficial to both water quantity and quality if installed properly.

Although deep groundwater wells are costly and rare in rural Guatemala, a few deep groundwater wells have been installed in the highlands of Guatemala. According to a Guatemalan drilling company, Daho Pozos, a typical groundwater well in the area has a dynamic water level around 150 meters below ground surface and will cost around US $60,000. Although the solution is very costly, it may be the most effective solution to the water problems in Guatemala.

A feasibility study has been conducted to determine if an alternative source of energy can replace the utility power grid. The study compared solar power, wind power, and utility power to determine the best method to providing reliable energy to the submersible pump. Weather data was collected using a weather station set up in Sacala. Upon concluding the study, a recommendation was given to the community of Sacala and the non-profit group searching for finances for the groundwater well.

Weather Station:

There are a limited number of weather stations collecting solar and/or wind data in Guatemala. The closest known functioning weather station to Sacala is located 35 kilometers away near Guatemala City, at an elevation of 1,490 m amsl. Due to the horizontal distance, elevation change and topographical features (mountains and valleys) between Guatemala City and Sacala, it was decided that on-site data would be required to determine the feasibility of using solar and/or wind power to run a groundwater pump. In March of 2008, a three-meter weather station with a Campbell Scientific Datalogger was installed on a piece of property in Sacala. The Datalogger was powered by a 12V battery which was charged using a 10W solar panel. The Datalogger was programmed to collect data averages every minute from a pyranometer and anemometer located three meters above ground surface, and 30 minute averages from a temperature probe, barometric pressure meter and precipitation tipping bucket. Table 1 shows the manufacturer and model numbers of each piece of equipment of the weather station.

Table 1. Equipment List

Item:	Manufacturer:	Model Number:
Datalogger	Campbell Scientific, Inc.	CR800-ST-SW-NC
Tipping Bucket	Texas Electronics	TE525
Barometric Pressure	Setra	CS100
Temperature Probe	Campbell Scientific, Inc.	107
Anemometer	R.M. Young	05103-L15
Pyranometer	Apogee Instruments	CS300-L15
Tripod Stand (10ft)	Campbell Scientific, Inc.	CM110
Tripod Crossarm(4ft)	Campbell Scientific, Inc.	CM204
10W Solar Panel	Campbell Scientific, Inc.	SP10
12V Power Supply	Campbell Scientific, Inc.	PS100-SW
Datalogger Enclosure	Campbell Scientific, Inc.	ENC10/12-ES-MM

The location for the weather station was selected based on: land ownership, land elevation, adjacent suitable sites for a groundwater well, wind potential, solar radiation potential, and security. The selected site was near a suitable site for a

groundwater well, on a steep saddle with good wind potential (few trees and buildings), on land with little shade and not easily seen by passer-bys.

For a renewable energy feasibility study, the longer the data is collected, the more reliable the values (Derrick 1992). However, since Sacala wants a groundwater well as soon as possible, a long-term collection of data is not possible. Derrick (1992) states that study periods can be reduced to 12 months or less if there are sufficient long-term data elsewhere in the vicinity. Therefore, a short-term collection plan was implemented, and, if needed, more data could be attained from other Guatemalan weather stations to correlate the sites

Photovoltaic Performance Prediction Methodology:

The performance of a photovoltaic (PV) array was predicted using the pyranometer data from the datalogger. The sunlight potential is called the solar radiation and is measured in kilowatts per meter squared (kW/m^2). The pyranometer is located in a horizontal position, thus the horizontal radiation is measured. To maximize the amount of power generated from a fixed solar array, the solar panels are tilted to match the latitude of the site (Ewing 2007). Since the solar radiation is measured from a horizontal position while solar panels are installed at a tilted position, the tilted solar radiation is calculated. Also, since the energy used by pumps is generally measured in kilowatt-hours (kW-hrs), the average daily horizontal radiation measured at the site is converted to $kW\text{-}hrs/m^2/day$ by multiplying the horizontal radiation by 24. The tilted radiation is calculated using Equation 1 (Honsberg and Bowden 2002):

$$S_{module} \approx \frac{S_{horizontal} * \sin(\alpha + \beta)}{\sin(\alpha)} \qquad (1)$$

Where: S_{module} is the tilted radiation ($kW\text{-}hrs/m^2/day$),
$S_{horizontal}$ is the horizontal radiation ($kW\text{-}hrs/m^2/day$),
α is the elevation angle of the sun (degrees), and
β is the tilt angle of the solar panel measured from horizontal (degrees)

The elevation angle of the sun (α) differs with each day, and can be calculated using Equations 2 and 3 from Honsberg and Bowden (2002):

$$\alpha \approx 90 - \phi + \delta \qquad (2)$$

Where: ϕ is the latitude (degrees) and
δ is the declination angle:

$$\delta \approx 23.45 * \left(\sin\left(\frac{360}{365}\right) * (284 + d) \right) \qquad (3)$$

Where: d is the day number of the year (i.e. January 1st is 1, January 2nd is 2, etc.)

The daily kilowatt-hours required for the groundwater pump was calculated by multiplying the pump power, in kilowatts, by the efficiency of the pump and the daily pumping time in hours. To size the pump, the water demand was calculated. The system was designed for a life of ten years. The design population was used assuming the current population growth of 3% for the next ten years with a safety

factor of 10% (Martin 2001). A typical rural Guatemalan community uses about 84 liter/day/capita of water (Trigg 2000). That means, for the design population of 920 people, the pump is required to pump 77,280 liters per day. A storage tank, installed on the ground surface, was assumed to hold three days worth of water which will act as a buffer if there is an increase in water demand or lack of power. Using a total dynamic head of 188 m (150 m to the dynamic groundwater level and a 25% safety factor) and a flowrate of 235 liters per minute (lpm), an 11.19 kW pump, similar to the Grundfos Model 85S150-13, was selected for the design. At the flowrate of 235 lpm the pump operates at an efficiency of about 70%, and would require 7.84 hours per day to pump the average daily demand. Using these numbers, the daily power draw from the pump is 87.7 kW-hrs.

From the power required and the tilted solar radiation values, the number of solar panels required can be calculated using Equation 4 from Ewing (2007):

$$S \approx \frac{P_{req}}{(P_{\max} * \eta * S_{\mathrm{mod}})} \qquad (4)$$

Where: S is the solar panels required,

P_{req} is the power draw from the equipment used (kW-hrs/day)

P_{max} is the maximum power generated from the solar panel (kW/panel)

η is the system efficiency

S_{mod} is the calculated tilted solar radiation (kW-hrs/m^2*day)

The study assumed the parameters of Sharp ND-216U2 solar panels. The maximum power generated from one solar panel is 216 W and the system efficiency, assuming a Fronius IG 2000 inverter, is about 90%. Using the maximum number of solar panels over any three day span and the average cost for solar panels, the cost of solar power for a submersible pump was calculated. A three day span was used because this is the size of the proposed storage tank.

Wind Power Methodology:

Wind velocity is measured using an anemometer. Placement of the anemometer is crucial in wind energy studies. As height from the ground surface is increased, wind velocity also increases and can be approximated using a power law equation, typically the one-seventh power-law (Johnson 2001). The increase in velocity is due to the reduced friction from the ground, vegetation and buildings. Wind velocities are generally higher on ridges with steep slopes on either side of the ridge. This phenomenon occurs when the wind is compressed on the prevailing wind side of the hill. The wind blows up the side of the hill and upon reaching the ridge the air expands and quickens its velocity to the low pressure zone on the other side of the hill (Johnson 2001). So by placing the wind turbine in a well chosen location, the output can be increased significantly.

Wind velocities were collected on one minute averages for the study period. The anemometer was placed three meters above ground surface. For a high wind resource area, a typical wind turbine for the power that is required for the Sacala project (87.7 kW-hrs/day) is similar to the Bergey Excel S 10 kW wind turbine. Bergey Windpower has developed a spreadsheet using a Weibull distribution to predict the wind energy generated at different heights. The spreadsheet takes into

consideration the elevation, predicted Weibull K value, the estimated wind shear exponent, the anemometer height, the hub height of the wind turbine, and the turbulence factor. The elevation is known as 1,910 m amsl, the Weibull K is estimated as 2, the wind shear exponent is assumed 0.22 for rough terrain, the anemometer height is 3 m, the wind turbine height is assumed to be 36.5 meters and the turbulence factor is assumed to be 0%. Upon plotting the equation's results, the wind turbine power produced each day was calculated for the study period.

Solar Power Results:

Upon collecting eight months of data (April through November of 2008), the solar power for Sacala was analyzed. The Datalogger was non-functional from July 1-July 4 for unknown reasons; however, all other days in the study produced consistent data. The average tilted radiation value for the eight month period was 4.41 kW-hrs/m^2/day. The month with the highest solar radiation value was April with a value of 5.96 kW-hrs/m^2/day.

For each day during the study period, the number of sunlight hours each day was more than the hours of pumping time required. Knowing that there was sufficient day light to power the pump, the number of solar panels required was calculated. Figure 1 shows the number of solar panels required for each day of the study period.

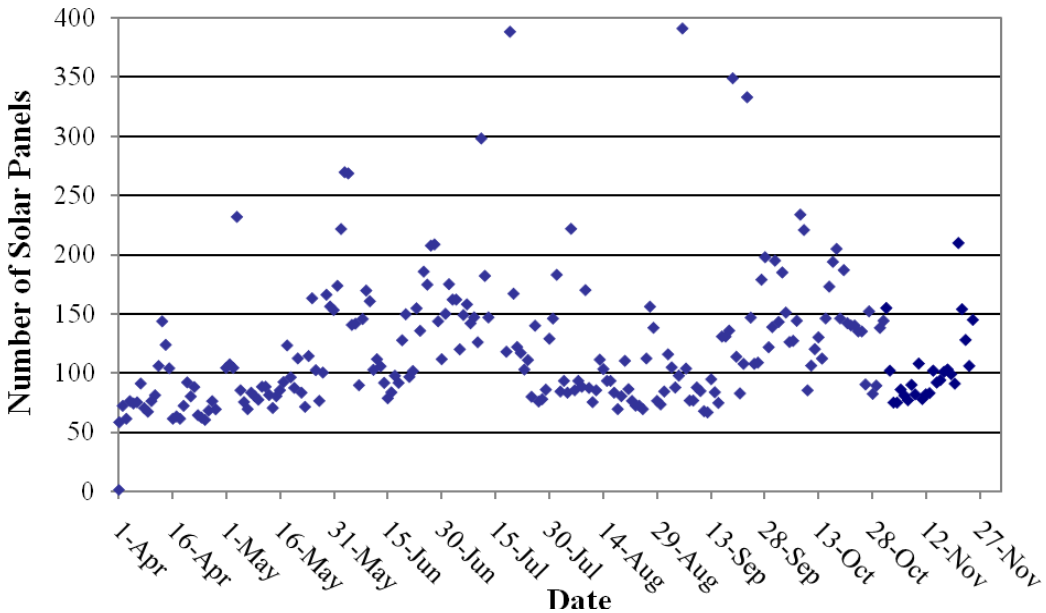

Figure 1. Solar Panels Required to Produce 87.7 kW-hrs/day

Wind Power Results:

The Bergey Windpower worksheet was used to determine how much potential power was produced from April through November using a 36.5 m tower. The Datalogger was non-functional from July 1-July 4 for unknown reasons; however, all other days in the study produced consistent data. The average wind velocity for the study period was 1.15 m/s at 3 m, which corresponds to about 1.99 m/s at 36.5 meters. The month with the highest average wind velocity was April with an average

velocity of 1.5 m/s at 3 m, or 2.60 m/s at 36.5 meters. Using the Bergey Windpower worksheet, the daily average power produced with one wind turbine was 1.94 kW-hrs. The month with the highest daily average was April with an average of 2.49 kW-hrs per day.

Figure 2 shows the estimated number of wind turbines required to produce the 87.7 kW-hrs needed per day.

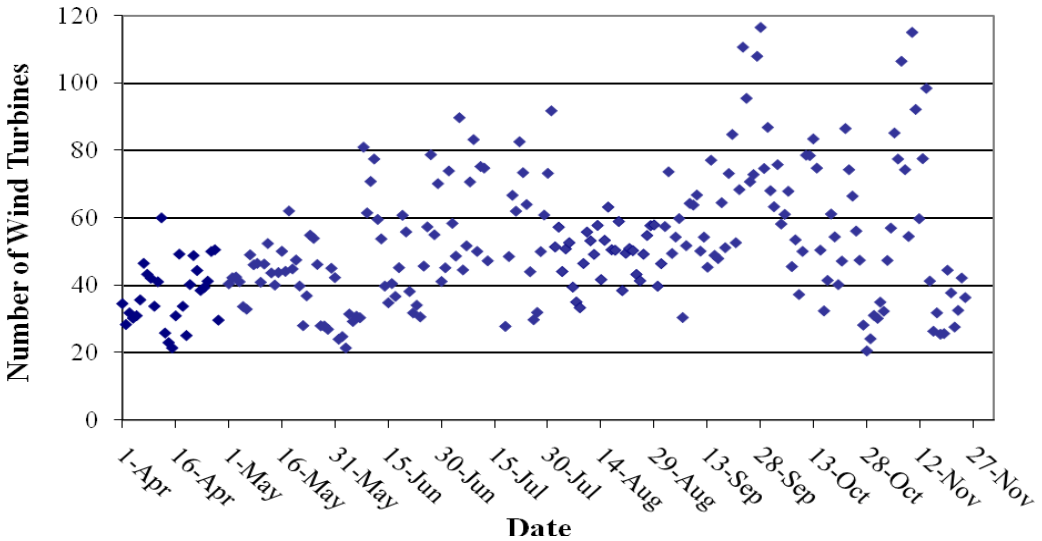

Figure 2. Wind Turbines Required to Produce 87.7 kW-hrs/day

Hybrid Results:

Since a large number of both solar panels and wind turbines would be required to power the pump, a hybrid analysis was considered. Using the average daily power generated by one wind turbine over the study period, the difference in energy produced and energy required was recovered by solar panels. Figure 3 shows the total number of solar panels needed to produce sufficient energy with the assistance of a 36.5 meter tall wind turbine.

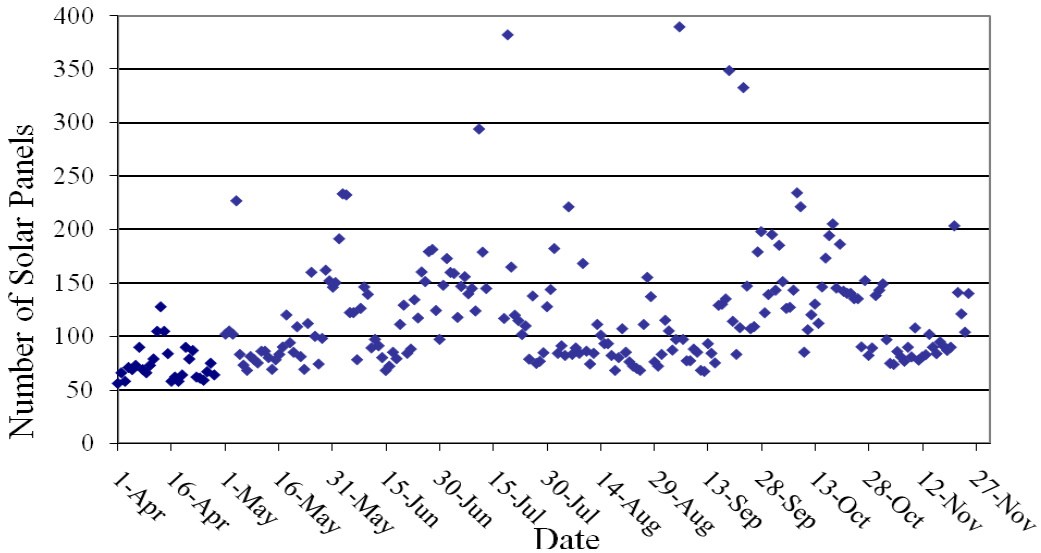

Figure 3. Solar Panels Required for 87.7 kW-hrs/day Using One Wind Turbine

Table 2 shows the cost estimates of the PV array, grid power, wind turbine, and hybrid system. Equipment and installation costs for the solar array and wind turbine were based on costs from the manufacturer in 2008.

Table 2. Cost Estimation of the Alternative Energy Generation Methods

PV Array Cost

Item:	Unit Price:	Quantity:	Est. Cost After 10 Years
Sharp ND-216 U2	$1,100	222	$244,200
Fronius IG 2000 Inverter	$1,800	4	$7,200
Ground Mount Racks	$800	23	$18,400
		Total:	**$269,800**

Grid-Power Cost

Item:	Unit Price:	Quantity:	Est. Cost After 10 Years
Electricity	$0.20/kW-hr	87.7/day	$64,021
		Total:	**$64,021**

Wind Turbine Cost

Item:	Unit Price:	Quantity:	Est. Cost After 10 Years
Bergey Excel S Turbine	$27,900	78	$2,176,200
Guyed Lattice Tower	$11,920	78	$929,760
Installation	$14,000	78	$1,092,000
		Total:	**$3,105,960**

Hybrid Cost

Item:	Unit Price:	Quantity:	Est. Cost After 10 Years
Sharp ND-216 U2	$1,100	191	$210,100
Fronius IG 2000 Inverter	$1,800	4	$7,200
Ground Mount Racks	$800	20	$16,000
Bergey Excel S Turbine	$27,900	1	$27,900
Guyed Lattice Tower	$11,920	1	$11,920
Installation	$14,000	1	$14,000
		Total:	**$287,120**

Discussion:

The solar and wind power potential for Sacala was calculated using measurements collected for eight consecutive months. Although Sacala has a relatively high solar power potential, the power required from a 11.19 kW submersible groundwater pump is significant and would require approximately 222 216W solar panels, which would require 23 ground mounts and 4 inverters (maximum of 60 panels per inverter).

The current price for electricity is $0.20 per kW-hr for Sacala. Although this is relatively expensive, there are no maintenance costs incurred over the design life of the pump. There are also no installation costs since the well can be situated near power lines.

The wind resource of Sacala is considerably lower than needed for the groundwater pump. To power the pump, 78 10 kW wind turbines, 36.5 m tall would have to be installed. Clearly, this would require a lot of space and a huge installation cost for one groundwater pump.

If a hybrid system would be installed, using one wind turbine would be most economically feasible. However, 191 solar panels would still have to be used to power the pump. This would require 20 ground mounts and 4 inverters.

Conclusions and Recommendations:

Even though grid-power in rural Guatemala is often unreliable, the community of Sacala has expressed that they have experienced no significant loss of electricity, and they feel grid-power is reliable in Sacala. With the current electricity cost for Sacala at $0.20 per kW-hr, and the community of Sacala having high faith and little complaints about the utility company's reliability, there is no reason to abandon grid-power.

When financing is possible, alternative energy has become a popular alternative to traditional power plants. The highlands of Guatemala offer good solar power potential; however, to power energy demanding products, such as a deep groundwater pump, solar power is not feasible. Also, Sacala has a low wind potential, and the installation of a wind turbine would not be economically favorable. Even when environmental interests are a higher priority than economic interests, the area of land needed to install the required solar panels or wind turbines for this project is more than what is feasible.

Acknowledgments

The feasibility study was funded by a grant from the National Science Foundation award number 0623091. Additional support was provided by the Sisters of Saint Joseph, the community of Sacala las Lomas and Missouri University of Science and Technology.

References:

Bowden, S. and Honsberg, C.B. (2002). Photovoltaics CDROM. Retrieved December 18, 2008, from http://pvcdrom.pveducation.org/index.html

Derrick, A. (1992). "Development of the measure-correlate-predict strategy for site assessment" Proc. *Wind Energy Converstion*, BWEA, Britain, 259-265.

EIA (1997). "Guatemala: Electricity" Energy Information Administration, U.S. Government. Retrieved December 12, 2008 from http://www.converger.com/eiacab/guatemal.htm#ELEC

Elliott, D.L., Holladay, C.G., Barchet, W.R., Foote, H.P., & Sandusky, W.F. (1986). Wind energy resource atlas of the United States. DOE/CH 10093-4. Golden, CO: U.S. Department of Energy Pacific Northwest Laboratory.

Elmore A.C., Miller G.R. and Parker P. (2005). "Water Quality in Lemoa, Guatemala" Environmental Geology, 48(1), 901-907.

Ewing, R.A. (2007). "Calculating Your Daily Solar Energy Harvest" Countryside and Small Stock Journal, May/June 2007. Retrieved December 2, 2008 from http://www.countrysidemag.com/issues/91/91-3/Rex_A_Ewing.html

Johnson, G.L. (2006). Wind Energy Systems. Electronic Edition from http://eece.ksu.edu/~gjohnson/Windbook.pdf , Manhattan, Kansas.

Martin, E. (2001). Solicitud de Financiamiento por el ejercicio 2004. Unidad Ejecutora del Programa de Acueductos Rurales.

Reynolds Tom, D. and Richards Paul, A , (1996). Unit Operations and Processes in Environmental Engineering. PWS Publishing Company. Boston, Massachusetts.

Trigg, M. (2000). "Domestic water consumption and its determination in rural Guatemala." Water and Environmental Management; Journal of the Institution of Water and Environmental Management, 14(1), 45-50.

World Health Organization (WHO) (2000). Global Water Supply and Sanitation Assessment Report 2000, UNICEF, New York.

Drinking Water Field Analyses for the Detection and Enumeration of Coliform Bacteria in Rural Guatemalan Highlands

Jenna Tune[1] , and Andrew Curtis Elmore, Ph.D., P.E., M.ASCE[2]

[1]Graduate Student Geological Engineering; 127 McNutt Hall, University of Missouri-Rolla, Rolla, MO 65409; PH (573) 578-1055; email: jstpkd@mst.edu

[2]Assistant Professor of Geological Engineering; 127 McNutt Hall, University of Missouri-Rolla, Rolla, MO 65409; PH (573) 341-6784; FAX (573) 341-6935; email: elmoreac@mst.edu

ABSTRACT

An analysis of drinking water contaminant concentrations in the highlands of rural Guatemala evaluated the Coliscan EasyGel as a field method for the detection and enumeration of coliform bacteria in drinking water and found it adequate. In developing countries like Guatemala, many deaths among infants and young children may be due to dehydration, malnutrition, or other complications of waterborne bacterial infections. Students and engineers are challenged to find sustainable means to provide safe drinking water. A field applicable method of quantifying microbiological contamination is needed to improve the evaluation of engineering solutions. A pour plate method using the patented Coliscan EasyGel medium is commercially available and marketed for field use by Micrology Labs Incorporated. However, the validity of the field data is called into question when the results are compared qualitatively and quantitatively to duplicate Membrane Filtration (MF) analysis using M-Endo medium, an ASTM accredited method. To evaluate comparability, this work splits subsets of the samples for duplicate MF analysis and non-parametric statistical evaluation due to the non-normal nature of data distribution.

INTRODUCTION

In developing countries like Guatemala, the costs of disease and productivity losses linked to inadequate clean water and sanitation are equivalent to 2% of gross domestic product (Swedish Water House 2007). Many deaths among infants and young children are due to dehydration, malnutrition, and other complications of waterborne bacterial infections. More than 2 billion people living in poverty in the developing world are considered at high risk. Students and engineers are challenged to find sustainable means to provide safe drinking water supplies in the rural highlands of Guatemala and other locations in similar stages of development. In an effort to improve evaluation of engineering solutions, this work measured the density of coliform bacteria, an indicator organism, to determine the presence and/or degree of fecal pollution rather than presence of pathogens.

Few naturally occurring bodies of water are free of indicator organisms; however, the presence of coliform bacteria in treated water is cause for concern because standard treatment processes are expected to remove naturally occurring nonfecal coliform bacteria. It is customary, therefore, to test for the total coliform group rather than for fecal coliforms, specifically *Escherichia coli* (*E. coli*). This distinction is useful when characterizing a pollution source

because nonfecal members of the coliform group are known to survive longer in a stressed environment. Both the Membrane Filtration (MF) procedure and the Coliscan EasyGel method have been modified to determine *E. coli* density.

As a result of the U.S. EPA Total Coliform Rule (TCR), the presence or absence of microbiological contaminants in drinking water is typically analyzed using a qualitative binary method. Yet such methods do not quantify or provide data on the magnitude of contamination needed to evaluate the effectiveness of an engineering solution. Prior to adoption of the TCR, an MF procedure was used to analyze samples transported to certified laboratories. Because this method was developed for a laboratory setting, it is impractical and costly when applied to field work in remote locations. A simplified method designed for field interpretation and requiring little equipment and training, therefore, would be valuable.

MATERIALS AND METHODS

In 2003, Micrology Labs Inc. developed Coliscan Easygel, a medium targeted specifically for field use with the pour plate method. This method appears designed for typical field conditions; however, the validity of field data is questionable when compared qualitatively to a well documented technique such as MF. The MF technique uses a typical vacuum filtration apparatus to target bacterial cells on a cellulose membrane. After the water is filtered, the membrane filter is incubated on a 5 mL plate of appropriate medium at a set temperature for a specific period of time. Several types of medium are marketed for detection of total coliforms using the MF technique. The United States Environmental Protection Agency (USEPA) approves the use of MF with M-endo LES medium, and this has become the method of choice for routine analysis of drinking water (Grabow 1979). The MF technique is considered useful for analysis of a wide range of sample volumes or dilutions because it detects a wide range of contamination levels. Whether using m-Endo agar on pre-poured plates or m-Endo liquid broth and nutrient pads, total coliform forming units appear as colonies with a metallic green sheen. The MF technique should be avoided when sampling highly turbid water or water expected to have large amounts of non-target organisms that could clog the filter and generate data. Rarely, non-coliform organisms may produce the characteristic total coliform sheen, creating a potential source of errors, such as false positives. Because MF uses the same non-disposable equipment (vacuum filtration setup) for each sample, data is reliable when samples are analyzed in a sterile laboratory setting and isolated to control cross contamination. With the use of disposable equipment MF may be easily adapted to field testing. Considering the cost of the incubator and glassware, however, this technique may not be feasible for students or professionals interested in analyzing water samples in remote field locations. Despite these limitations, however, the effectiveness of MF using m-Endo is well documented; and the method requires less space and time than other equally established methods.

The pour plate technique using Coliscan EasyGel is sold in a kit of 10 for $20.00. Each kit includes all required equipment. A user friendly method promising reliable results with little equipment and low cost, Coliscan Easygel lends itself to field work. The medium is formulated to distinguish between total coliforms (represented by pink/magenta colonies) and *E. coli* (represented by blue/purple colonies). A sample of 1-5 mL, depending on sample source and expected contamination level, is mixed with Coliscan EasyGel broth and poured onto a

pretreated Petri dish. The Coliscan EasyGel medium contains pectin-gel that solidifies approximately 40 minutes after pouring. At the discretion of the technician, the sample is then incubated either at 35°C for 24 hours or at room temperature for 48 hours. Occasionally, colonies display a range of color, thus complicating identification of colony types. Despite these limitations and the novelty of the technology, the Coliscan EasyGel is an innovative method assumed to be superior in terms of cost feasibility and amount of equipment required.

A public health study in Guatemala analyzed water samples using the Coliscan EasyGel technique to measure the concentration of total coliforms and *E. coli* in drinking water. To evaluate the validity of the data, a subset of the samples was split for testing with MF using m-Endo. Because data involving micro-organisms is likely to assume a non-normal distribution, the Mann-Whitney hypothesis test was used to perform a non-parametric analysis of results and thus to compare the data generated by the Coliscan EasyGel with that from MF with m-Endo. The results of this initial comparison were evaluated against those of a parallel analysis using the same procedure performed in the laboratory with water samples of known concentration. During both laboratory and field analyses, samples were read after varying periods of incubation. To evaluate the effect of unforeseen field conditions, duplicate samples were incubated at temperatures outside those recommended for each method.

RESULTS

Table 1 is the result of a trial and error analysis evaluating the feasibility for field application of several MF medium options approved by the USEPA and available commercially in various forms. Because the field site was extremely remote, the samples analyzed there could not be transported for duplicate laboratory analysis. Therefore, comparison of the field results generated by the Coliscan Easygel method with those produced by MF may not permit conclusive evaluation of the accuracy of the Coliscan Easygel method. Each water sample collected was assumed to have a uniform contaminate distribution; however, all samples (including dilutions) were analyzed in triplicate to accommodate the possibility of significant variance.

The comparative analysis was performed in both the laboratory and the field to ensure appropriate characterization of discrepancies independent of field conditions. The results are shown in Fig. 1. Using standard methods, a batch of E. coli was cultured to provide a sample of contaminated drinking water for laboratory analysis by both Coliscan Easygel and MF techniques. To quantify the contamination in the sample, a duplicate serial dilution was analyzed by turbidimetry and plated on nutrient broth.

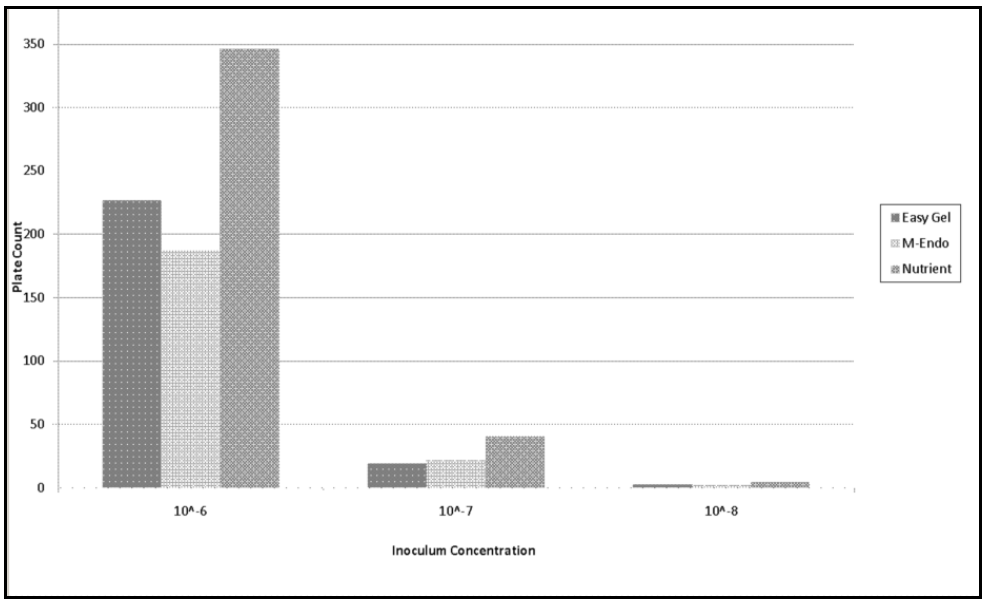

Fig. 1: Laboratory Comparative Analysis

Medium	Positive Reaction	Preparation		Transportation		Cost (per 50ml)
		Advantages	Disadvantages	Advantages	Disadvantages	
m-endo LES (2 mL ampules)	TC metallic green sheen	Pre-measured, pre-mixed, & pre-sterilized	none	Small, easy to pack	Must be kept cold	$10*
MI agar (50 mL glass bottle)	TC blue	Pre-mixed	Must be measured & sterilized between testing	none	Breakable & must be kept cold	$21.75
MI broth (50 mL bottle)	TC blue	none	Must be measured, mixed, & sterilized between testing	none	Breakable & must be kept cold	$22.35

All medium must be incubated at 35°C +/- 0.5°C. Table does not include shipping costs.
*Sold only in sets of 50.
TC = Total coliforms

Table 1: MF medium selection analysis

The Coliscan Easygel method is capable of detecting a contamination level as low as 1 coliform forming unit (CFU) per 100 mL; however this level is too dense to generate linearity among absorbency data. Therefore, samples were diluted to absorbency in the linear range and multiplied by the dilution factor to obtain a more representative value. During incubation, the Coliscan Easygel plates were counted every hour from hour 18 through hour 22, as illustrated in Figure 2. To evaluate further the usefulness of incubation temperature flexibility offered by in the Coliscan Easygel method, samples were analyzed in duplicate using incubation temperatures of approximately 37°C, 30°C, and 25°C for 24 hours (see Table 2). Plated samples were counted every hour from hour 18 through hour 22, as shown in Figures 2 and 3.

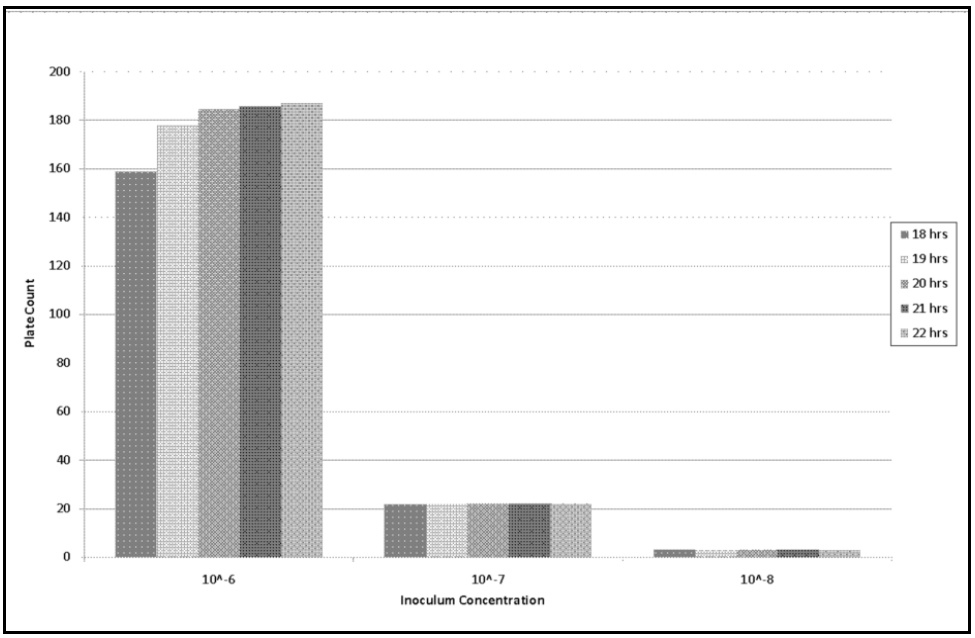

Fig. 2: Coliscan Easygel Laboratory Analysis

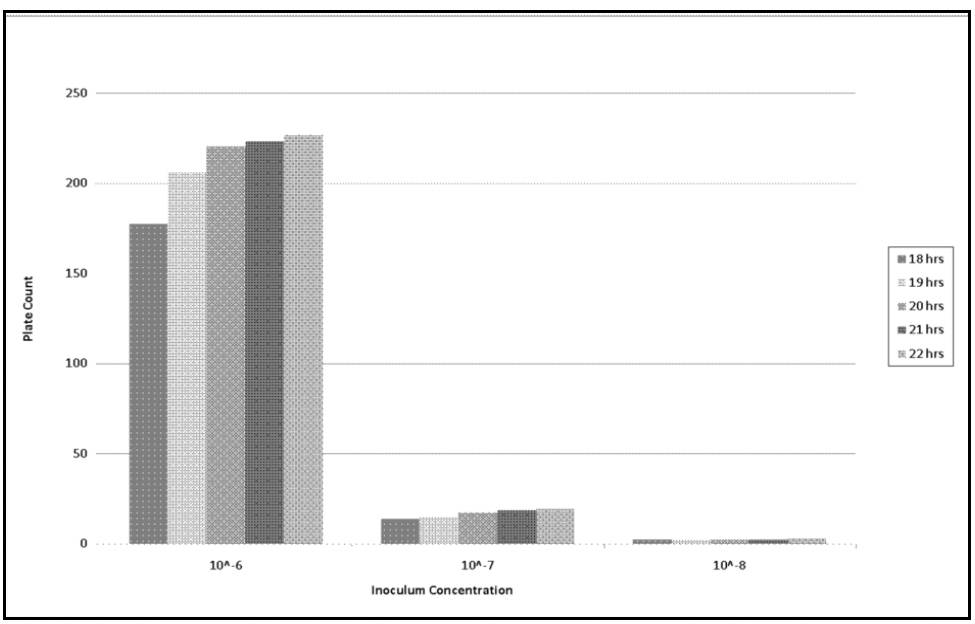

Fig. 3: Membrane Filtration Laboratory Analysis

Table 3 summarizes the costs associated with field analysis of 10 samples using Coliscan Easygel and MF with m-endo. Comparing advantages and disadvantages of Coliscan Easygel, Table 4 more clearly evaluates the comprehensive cost of this method. The Mann-Whitney hypothesis test was used as a nonparametric analog of the two-sample hypothesis tests, comparing the medians of the Easygel and MF data sets rather than the means, thus adjusting for the non-normal distribution. Table 5 presents the results of the statistical evaluation for the comparative analyses performed both in the field and in the laboratory.

Time (hrs)		Temperature		
		37 °C	30 °C	25 °C
12	EG	34	0	0
	m-endo	30	0	0
23	EG	29	8	0
	m-endo	37	21	0
46	EG	28	20	15
	m-endo	38	30	29
58	EG	28	18	18
	m-endo	38	27	31
*Each value represents the average of 3 plate counts				

Table 2: Laboratory comparative analysis results

Required Materials		Price ($) per 10 tests
Easygel	All inclusive kit	19.65
	Incubator	40
	Sterile dilution H_2O	0-50
	TOTAL	**59.65-109.65**
m-endo method	m-endo ampules	10*
	Glassware	0-500
	Portable vacuum pump	0-500
	Buffer rinse solution	0-50
	Plates	5*
	Nutrient pads	20*
	Filters	10*
	Sterilizing solution	0-50
	Incubator (hova-bator)	40
	Pipets	5-10*
	TOTAL	**90-1195**
*Value adjusted for test quantity of 10; actually sold in greater quantities.		

Table 3: Coliscan EasyGel versus MF using m-endo cost comparison

Table 3 summarizes the costs associated with field analysis of 10 samples using Coliscan Easygel and MF with m-endo. Comparing advantages and disadvantages of Coliscan Easygel, Table 4 more clearly evaluates the comprehensive cost of this method. The Mann-Whitney hypothesis test was used as a nonparametric analog of the two-sample hypothesis tests, comparing the medians of the Easygel and MF data sets rather than the means, thus adjusting for the non-normal distribution. Table 5 presents the results of the statistical evaluation for the comparative analyses performed both in the field and in the laboratory.

LAB RESULTS				
Dilution Series		**10^{-6}**	**10^{-7}**	**10^{-8}**
1	**P**	0.0122	0.6015	-
	H_o	Reject	Fail to reject	Fail to reject
FIELD RESULTS				
Dilution Series		**3ml**	**4ml**	**5ml**
1	**P**	-	0.0809	0.0809
	H_o	-	Fail to reject	Fail to reject
2	**P**	-	0.1904	0.1489
	H_o	-	Fail to reject	Fail to reject
3	**P**	0.0809	0.1489	0.1489
	H_o	Fail to reject	Fail to reject	Fail to reject
H_o (null hypothesis) – The two population medians are equal. H_a (alternative hypothesis) – The two population medians are not equal. Alpha – 0.05				

Table 4: Mann-Whitney hypothesis test results

Advantages	Disadvantages
Easier to differentiate colonies with larger plates	Plate lids fit loosely – plates must be stationary 40 minutes prior to traveling to ensure no spilling
Incubation temperature is flexible	Unable to detect less than 1 CFU/100mL
Decreased cost in terms of time spent testing and training	Larger plates require more space in incubator, limiting number of tests that can be performed simultaneously
Decreased monetary cost (less equipment required)	Positive reaction capable of producing various shades of color causing uncertainty in results

Table 5: Qualitative Coliscan EasyGel

DISCUSSION

Although its use of minimal equipment makes Easygel relatively inexpensive in monetary terms, time spent training and testing depends largely on the medium. Not only must the composition of the medium be considered, but the physical state in which the medium is available also affects the ease with which this method can be used in the field and the validity of its results. This work found that medium sold in pre-measured, pre-sterilized ampoules decreased the number of sample results discarded due to spills, fractures, and possible contamination. The MI medium results showed a better recovery rate for EasyGel than for m-endo medium (USEPA 1992); however, the MI medium is commercially available as both powered broth and bottled agar. Further, additional equipment and care are required to prepare and protect pre-pour plates prior to and during travel.

Small discrepancies found between duplicate samples analyzed using both techniques appear to reflect the nature of the medium used or the technician's ability to distinguish colonies representing a positive reaction. This ability may be affected by incubation temperature, size of Petri dish relative to magnitude of contamination, or amount of training and experience in identifying and counting colonies.

Table 2 indicates that although dependant on contamination level and dilution, both techniques offer valid results an incubation time of less than 24 hours. Reliance this conclusion is ill-advised when conducting field work due to uncertain levels of contamination in field samples. As expected, samples analyzed using the Coliscan Easygel technique showed similar results at varying temperatures. In some cases, the number of colonies representing a positive reaction decreased over time, perhaps because colonies grew together or because the technician was unable to quantify colonies representing a positive reaction. For example, non-coliform colonies may have been identified as a positive reaction before color uptake was absolute. A similar analysis was performed in the field using duplicate Coliscan Easygel results after incubation at 95°F (32°C) for 24 hours, then at room temperature for 48 hours; as suggested by Micrology Labs Inc. These results are unavailable for quantitative analysis, however, because due contamination levels were misjudged resulting in an unproductive dilution series. Nonetheless, the colonies identified as total coliforms were better differentiated after incubation at a higher temperature for a short period of time.

In general, the MF technique using m-Endo LES broth ampoules produced a slightly better recovery of total coliforms in both laboratory and field settings. This method, however, was significantly more expensive and required more time for both training and testing. In both field and laboratory comparative analyses using the Mann-Whitney hypothesis test, the duplicate samples analyzed using Coliscan Easygel and MF techniques were shown to come from the same population within a 95% confidence level. The Coliscan Easygel data meet the data quality objectives for characterizing the magnitude of contamination found in natural field samples, permitting more accurate calculation of the effectiveness of engineering solutions. Samples, however, should be analyzed in duplicate or triplicate to account for inherent variance. Further, due to limitations specified by the manufacturer on sample volume, the Coliscan Easygel technique is practicle only for a specific range of expected contamination.

ACKNOWLEDGEMENTS

The data collection described here was supported by Grant 0623091 from the National Science Foundation– International Research Experiences for Students program.

REFERENCES

Brenner KP, Rankin CC, Roybal YR, Stelma GN, Scarpino PV, and Dufour AP (1993) New medium for the simultaneous detection of total coliforms and *Escherichia coli* in water. Applied and Environmental Microbiology 59:3534-3544.

Helsel DR and Hirsch RM (1992) Statistical methods in water resources. In: Studies in environmental science. Elsevier Science Publishing Company Inc. 49: 522-530.

Myers DN and Sylvester MA (1997) National field manual for the collection of water-quality data, biological indicators. In: U.S. Geological Survey techniques of water-resources investigations A7:49-54

Norstrom, A. Planning for drinking water and sanitation in peri-urban areas. Swedish Water House Report 21. SIWI, 2007.

Toranzos GA, McFeters GA, and Borrego JJ (2004) Detection of microorganisms in environmental freshwaters and drinking waters. In: Manual of environmental microbiology. Am Society for Microbiology, ASM Press 18:205-219.

U. S. Environmental Protection Agency. 1992. Manual for the certification of laboratories analyzing drinking water. EPA-814B-92-002. Office of Ground Water and Technical Support Division, USEPA, Cincinnati, Ohio.

Sustainability of Rural Water Supply Projects in Nicaragua

Jairo Hernandez Alvarado

Fondo de Inversion Social de Emergencia (FISE), Direccion de Operaciones y Desarrollo Local (DODL), Managua, Nicaragua. FAX (505) 278-1673; PH (505) 412-9135; email: jairoihernandez@hotmail.com

Abstract

Access to safe and freshwater service without sustainability is a critical issue for many developing countries. From the past decade, Nicaragua has been working on increasing access to water and sanitation services with sustainability in rural areas through the Emergency Social Investment Fund (Fondo de Inversion Social de Emergencia, FISE) which is the governmental agency in charge of investments in rural water and sanitation solutions. The experience with rural water and sanitation rural systems began in 1977 with the Rural Basic Sanitation National Plan (PLANSAR). PLANSAR was designed to increase coverage of water and sanitation services, using technical solutions of the urban sector. During the period 1977 through 2000 there was no community participation at all. In 2000, The World Bank conducted an evaluation of the social fund and found that half of the sampled systems supplied water on a regular basis, and half supplied water on average only three days per week. The low supply systems experienced operations and maintenance difficulties. In these sampled systems, the operations and maintenance was under the responsibility of the central and municipal agencies and community participation and training was virtually non-existent.

Currently, FISE efforts are focused on providing adequate access to safe water for human consumption and on improving sustainability of water supply and sanitation projects. The enhancement of sustainability is based on the application of a current rural model that has incorporated lessons learned from previous experiences. The key to this improvement is the community participation in the entire project cycle. In addition to technical aspects, the rural model strengthens the local community's capacity to manage services by supporting an effective community participation process during the project cycle, by introducing sound financial and economic principles to value water and sanitation services, by training community-based water committees and by clarifying the roles and responsibilities of the various stakeholders including the municipalities. Since 2004, FISE has been applying the rural model and has funded 117 water supply and sanitation projects and trained the same number of Water and Sanitation Committees with the main task of operating and managing their water supply and sanitation systems in coordination with their municipalities.

Introduction

The purpose of this paper is to present the experience of the Emergency Social Investment Fund (FISE) at the rural water sector in Nicaragua. In this paper are summarized the processes implemented by FISE and the lessons learned in the field under the perspective of a participatory approach at local level as a central element in the sustainability of rural water supply projects in Nicaragua.
The paper starts by describing the background and the evaluation process practiced for the 2002-2004 period. Afterwards, it explains the rural model, the decentralization process and the institutional mechanisms currently implemented by FISE. Further it outlines the project cycle highlighting the community participation in every stage. Finally, the paper concludes by stating the community participation as a decisive component in the project cycle with emphases in the reinforcement of other components from the last stage of such cycle.

Background

FISE is a governmental agency created in 1990 as a decentralized institution and a temporary body to alleviate the poverty caused by the lack of investment in basic social infrastructure in the countryside of Nicaragua. Some years later, FISE became a permanent entity and innovative institution concerned about the impact and sustainability of its investments in sensitive issues such as education, health, road infrastructure and potable rural water and basic sanitation.
Nicaragua's rural water and sanitation sector is characterized by a low coverage level. In this context, FISE has increased the allocation of national and international funding for projects on the rural water sector as part of the National Development Program (NDP) to provide adequate access to safe water for human consumption. Currently, FISE is committed not only to increase coverage of water and sanitation services but also to improve sustainability of projects developed under the rural water sector program. From lessons learned in the field, sustainability has become a major concern of water supply projects once the infrastructure has been completed. The problem is mainly characterized by a short-term disuse or premature deterioration of part or sometimes the entire water systems.
As part of a an institutional initiative of summarizing the experiences and impacts in the rural water sector, FISE conducted a survey for the 2002 – 2004 term in which collected water supply project information was connected with construction, management, operation, maintenance, community participation and environmental protection. That survey showed serious problems threatening the long-term sustainability for water supply projects (Martinez, A., 2005). More than one third (36%) of the sampled systems were not working properly since they were supplying water only three or four days per week. Some of the main weaknesses identified in this evaluation can be summarized as follows:

Low Cost Recovery. In small piped systems using electric pumps often the tariffs are modified by reducing them to rates generally lower than the pre-established tariff

rates established in the formulation stage of the project. Many times, this situation pushes municipalities towards subsiding operation and maintenance costs in order to keep the systems working properly to supply water on a regular basis. Eventually, these subsidies are withdrawn leading to a total collapse of the system.

Poor Communication. Lack of communication at the local level weakens project the sustainability. In the evaluation, community members mentioned that they do not understand how the tariffs were calculated or even worse how much money was needed for the system operations and maintenance in any given month. Such lack of communication creates problems of distrust among the project beneficiaries.

Poor Planning Work at Local Level. At the feasibility stage, technical consultants in charge of the planning were not interested in getting feedback from community members and then integrating the public comments into the final plan. Typically the consultants developed their studies by focusing only on technical aspects without including interaction at local level.

Community Participation

Typically, in Nicaragua the rural water supply systems can be gathered into five groups: (1) small piped systems using electric pumps (Miniacueducto por Bombeo Eléctrico, MABE), (2) small gravity-fed piped systems (Miniacueducto por Gravedad, MAG), (3) boreholes with hand pumps (Pozos Perforados Equipados con Bombas de Mano, PPBM), (4) hand-dug wells with hand pumps (Pozos Excavados Manualmente Equipados con Bomba de Mano, PEBM) and (5) Rehabilitation and Extension of Existing Systems (Mejoramiento y Ampliación de Sistemas Existentes, MASE). While these types of water systems do not represent complex technologies, when governmental agencies or international donor organizations practice their periodical evaluations, a high number of those systems are non-functional or poorly maintained, being consequently classified as non-sustainable in the long-term.

A lesson learned over the past few years is that community participation in rural water supply and sanitation projects is vital. The higher the level of community participation in establishing a service, in implementing it and in operating it and maintaining it, the better sustained the service (Olatunji, 2003). Therefore, communities should be properly involved throughout the entire project cycle process, from identification, investment, selection of technologies, financial contribution, construction and the operation and maintenance stage.

There is no a precise definition for community participation, but it can be understood in terms of activities performed by the communities in development projects including elements such as assessment of the local situation, definition of the problems, setting of priorities, making decisions, planning of action programs to solve the problems, sharing responsibilities in project implementation and evaluating and modifying the project (Whyte, 1986). This kind of definition involves all the role players regardless of age, gender, educational level or socio-economic standing. Historically in Nicaragua, the ‘idea’ of community participation was limited to the

concept that plans and decisions were made by major leaders and consultants and then communities were informed of the decisions taken on their behalf.

Although community participation is nowadays an essential foundation-stone of water and sanitation projects in developing countries, this alone is no automatic guarantee of success. The only way of approaching such a guarantee is to build in all stages, in as many aspects as possible, and for all stakeholders, a clear understanding that participation is more worthwhile than non-participation (Carter, Tyrrel and Howsam, 1999). In order to encourage greater participation from community, municipalities, civic groups and all stakeholders, FISE implemented a project development model in which municipalities and communities play a paramount role in all stages of the project cycle. This model is implemented under the decentralization process where all the responsibilities in the project cycle including long-term support to the community organizations are transferred to municipalities.

From evidence in the field, it is known that both municipalities and communities are not capable of developing, at least in the short-term, all stages of a water supply or sanitation project without institutional support. The need of institutional support at local levels is a concern addressed by National Decentralization Policy "defining" FISE as the institution in charge of implementing actions or mechanisms aimed at developing local capacities focused on improving the investment management and strengthening organizations at the local tier (Reglamento Operativo, 2006). The implemented mechanisms are accompanied by integral approaches such as gender, environmental management and social inclusion. The application of these approaches takes into consideration the fact that Nicaragua presents a diversity of cultural, ethnical and lingual aspects and considers poor's needs for the selection of technical service options and training needs.

Institutional Support

The institutional support to strengthen municipality and community capacities is provided through three modalities: (1) Direct Technical Assistance (from FISE), (2) From External Technical Assistance (Service Providers) and (3) Training.

Direct Technical Assistance. It is provided by Municipal Advisors directly from FISE and is aimed at Municipal Technical Unit (Unidad Técnica Municpal, UTM) personnel to be supported in the process of formulation, assessment, tender procedures, hiring, supervision, training and community organization. Direct Technical Assistance is also in charge of verifying the accomplishment of the all procedures established for the water supply project cycle.

External Technical Assistance. Outside consultants are hired by municipalities in order to deal with a specific stage in the project cycle. Usually, this kind of assistance is hired for cases in which municipalities need to carry out a task that requires a multidisciplinary staff. Municipalities have to guarantee that the assistance developed by the contractor (service provider) takes into account the application of the integral

approaches (genre, environmental management and social inclusion) and the training for community members on the aforementioned topics.

Training. Training has as its main objective the improvement of capacity building for local government, local stakeholders and community organizations. In this context, training has been conceived to update and extend the knowledge of investment management in a decentralized environment, cycle project administration, supervision, operation and maintenance of water systems and their legal aspects.

Integral Approaches

Gender. The gender policy implemented by FISE has the purpose of contributing to the equality of rights and opportunities among men and women to take part in the decision making process of a water supply project, assuming responsibilities and benefits from the human, social and economic development as an instrument to struggle against poverty (Reglamento Operativo, 2006). In rural regions of Nicaragua historically women and children spend a good part of the day fetching water from rivers or wells (World Bank, 2008). As part of the decentralization process undertaken by FISE, gender policy highlights the principles of equality of opportunities to have access to services through the empowerment of men and women in all stages of the project implementation.
The application of gender approach in water supply projects not only requires a positive attitude towards gender issues, but also the acquisition of relevant skills. Thus training modules for all categories of staff should have a gender component tailored towards their specific job performance with the aim of sensitizing all on the need to ensure women's participation in projects (Yankson, Dotse and Laryea, 1997). To ensure the application of gender approach, the following actions have been implemented as part of the decentralization process undertaken by FISE:

- Incorporation of gender approach into regulatory documents, operating manuals, educational materials, institutional programs, terms of references and contracts to be applied at any stage of the project.
- Incorporation of gender workshops into the institutional budget.
- Involvement of municipalities in the creation and implementation of their own gender policy promoting a wider women's participation as members of UTM staff. In the case of communities, women's participation in local committees should be encouraged to at least a level of 30% to include senior positions such as president or treasurer.
- Support the materialization of socio-economic infrastructure projects aimed to raise women's incomes and strengthen their self-esteem and leadership skills.
- Monitoring of the gender approach indicators for evaluating impacts of gender policy on projects (Reglamento Operativo, 2006).

Environmental Management. In Nicaragua, the regulatory framework that organizes the environmental evaluation system is contained in Decree No. 76-2006.

This framework is part of the strategy that Ministry of Environment and Natural Resources (Ministerio del Ambiente y Recursos Naturales, MARENA) is implementing to decentralize the national environmental administration. The purpose of this initiative is to see that the environmental assessment and permits requested by the General Law of the Environment (Law 217) can be obtained in more efficient and effective way.

According to Decree No. 76-2006, projects not included in its classification are those that can cause low potential environmental impacts and therefore, are not subject to an Environmental Impact Assessment (EIA) for a further environmental permission. In this Decree, rural water supply systems (MABE, MAG, PPBM, PEBM and MASE) are classified as projects that cause low environmental impacts and therefore are excluded from the Decree Classification. For this type of projects, municipal authorities can establish their own environmental procedures in the conferral of environmental permission. To support the municipalities and as part of the decentralization process, FISE developed the Environmental Management System (Sistema de Gestión Ambiental, SISGA) to incorporate all the environmental aspects and risk management in the respective stages of project cycle. SISGA allows municipalities apply preventive actions to mitigate possible adverse effects caused to the environment by the construction of water supply infrastructures.

Basically, SISGA is constituted by a set of instruments that establishes the procedures to be incorporated in the different project cycle stages in order to prevent or mitigate possible negative effects caused by the construction of water supply infrastructure. The major instruments used in the SISGA are the following: (1) Environmental Community Diagnosis, (2) Environmental Classification According to Decree No.76-2006, (3) Emplacement Evaluation, (4) Environmental Basic Requirements, (5) Environmental Analysis and (6) Environmental Assessment Report.

Social Inclusion. Social inclusion means state of being included in a community and society as a whole; a condition in which individuals and groups can access the range of available opportunities, services and resources and contribute to their planning and decision making. It also refers to the actions and processes needed to transform situation of those who are socially excluded, by influencing institutions and changing the perceptions that create and sustain exclusion (Beall, 2002).

The main objectives of the FISE social inclusion policy are: (1) promote social, economic and cultural development of vulnerable groups living in severe poverty, (2) guarantee facilities aimed at easing access to handicapped people and (3) sensitize local governments for inclusion of indigenous people in municipal programs (Reglamento Operativo, 2006).

Community Organization: Drinking Water and Sanitation Committee

Drinking Water and Sanitation Committee (Comité de Agua Potable y Saneamiento, CAPS) is the local organization in charge of leading community participation in all project cycle stages. CAPS is constituted by six members regardless of the type of water system (MABE, MAG, PPBM, PEBM and MASE). The positions in

hierarchical order are: President, Vice-President, Treasurer, Secretary, Hygiene and Environment Officer and Propaganda Officer. It is expected that women take at least 30% of the leading positions such as President, Vice-President and/or Treasurer (Manual de Administración del Ciclo de Proyectos Municipal, MACPM, 2007).
The CAPS constitution is carried out in a general assembly which is conducted by a municipal representative. The election process is valid with the attendance of at least 80% of head of the household. In the case of attendance less than 80%, another assembly should be carried out; if the next assembly attendance is still below 80% of head of the households, permanent project suspension from Multiyear Municipal Investment Plan (Plan de Inversión Municipal Multianual, PIMM) should be considered.

Project Cycle and Community Participation

The activities established for the rural water project cycle developed by FISE, emphasizes on the application of gender approach, environmental protection, community participation and community strengthening in management, operation and maintenance of water systems. The rural water and sanitation project cycle comprises the following stages (see Figure1): (1) Identification, (2) Pre-investment, (3) Construction and (4) Monitoring.

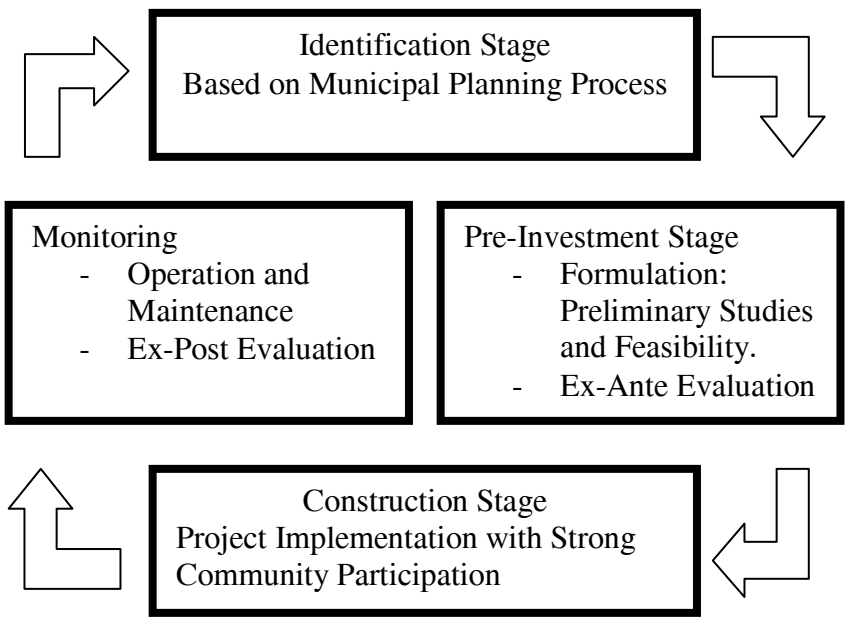

Figure 1. Project Cycle

Identification. This stage is based on a Municipal Planning Process (MPP) managed by the governmental agency Nicaraguan Institute of Municipal Development (Instituto Nicaragüense de Fomento Municipal, INIFOM). MPP is a participative

process at municipal level with the main purpose of establishing priorities in municipal investments (World Bank, 2008). This process involves consultations with all communities through participatory micro-planning workshops to review local problems, identify projects and analyze how the community, through its participation, can implement those projects. MPP leads to a Multi-year Municipal Investment Plan (PIMM) which is a tool for programming the use of municipal resources for every four- year period. Currently, FISE allocates funds only for projects included in the PIMM.

Pre-investment. In this stage all the activities related to formulation and project evaluation are developed. Formulation is divided in two phases: (i) Preliminary studies and (ii) Feasibility. Preliminary studies are conducted by municipal staff or a project formulator and comprise all the actions aimed at guiding community participation and establishing technical proposals. Preliminary studies are initiated when municipal representative or formulator meets local leaders and confirms the project request. Hence, it is set the date for the community assembly. In this case, local leaders assume the responsibility of guaranteeing the minimum attendance of household representatives.

Community assembly is the mechanism to confirm project demand and the occasion to organize local residents in the form of CAPS taking into consideration women's participation in leading positions. After the community has been organized, project formulator with CAPS support collects socio-economic and technical information, prepares and presents a preliminary report in a general assembly. The preliminary report should present the different alternatives proposed by formulator with pros and cons in each, so that local residents have the opportunity to select the most convenient and affordable alternative to fulfill their needs.

Once a community has selected what it considers its best alternative the formulator initiates the feasibility studies. In these studies the consultants are required to clearly demonstrate to the community and the municipality that the proposed project is technically, socially, legally, environmentally and economically viable through analyses, designs and all subsequent activities necessary for project completion. In addition to technical aspects, the formulator must include the two following community oriented training components: (1) Community Organization, Health, Environment and Gender (OSAG) and (2) Management, Operation and Maintenance in Water and Sanitation Projects (AOM). The OSAG training is aimed at water supply and sanitation project beneficiaries while AOM training is aimed at CAPS members.

As part of pre-investment stage, the Ex-ante Evaluation process basically will act as a quality control mechanism to ensure municipalities meet the necessary requirements to undertake a water and sanitation project. Currently, this process is still under FISE responsibility and is a mandatory step to obtain the project approval by donors or funding agencies. The Ex-ante Evaluation Stage implies verification of the appropriate technical regulations, community participation in the formulation process as stated in the MACPM and accomplishment of sustainability criteria.

Construction. At the beginning of this stage, the contractor along with the municipal representative present to local residents in a general assembly a detailed schedule of the different activities to be performed in the construction process, including the necessary community and CAPS training workshops. If the community undertakes to provide labor the community should be organized in task groups updating schedules monthly. Special attention should be paid to training workshops to guarantee full beneficiary participation. CAPS will be in charge of coordinating all the actions involving community participation and reporting to community about the project development.

Monitoring. Upon project completion, municipalities are in charge of monitoring the operation and maintenance of the project over a six-month period. During this time, municipal technicians are in charge of verifying the project sustainability through the effectiveness of operation and maintenance stage of the water system. In addition, the municipal technicians are responsible for assessing the CAPS performance and corroborating the implementation of the preventive maintenance annual plan designed in the pre-investment stage (project formulation).

Ex-Post Evaluation. Part of the author's duties as FISE Municipal Advisor is to monitor and evaluate the project sustainability once construction has been completed. In 2008 the author conducted an evaluation on small scale water supply projects finished in 2007 in the northern region of Nicaragua. The monitored projects had at least one year operating after their completion. In the inspection process, the author sampled 18 projects from which 4 were MABE, 1 MAG and 13 PPBM. From the sampled projects 6 (33%) were not supplying water to community mainly due to the following problems: (1) mishandling of electrical equipment, (2) vandalism (electrical equipment was destroyed), (3) reluctance to pay the pre-establish tariff, usually beneficiaries pay a lower tariff than that defined in the formulation stage to cover operation and maintenance costs and (4) lack of implementation of the preventive maintenance annual plan by CAPS. This was mainly observed in the PPBM equipped with hand pump whose major component is a rope that has to be replaced when wasted. The replacement of rope is not a complex activity since it does not represent a high cost for the maintenance stage and it does not require an expert labor for its installation. These systems were not operational due to the lack of rope which was not considered in the preventive maintenance annual plan.

Conclusion

The success about sustainability is determined by the understanding of this is a long-term process that requires full community participation in every stage of the project cycle. Comparing the lessons learned from the communities visited in 2007 to those learned from the 2002-2004 survey, there is a slight improvement in the proportion of operational projects after their completion. This small improvement is due to the remarkable local involvement in the entire project cycle in which community developed the sense of ownership and user's responsibilities. On the other hand, the

projects that did not produce the expected results after their completion, presented problems associated to the lack of community participation in the operation and maintenance stage. Hence, the encouragement of local participation in this stage is also crucial to avoid the waning of both the community enthusiasm and the CAPS motivation for keeping functioning.

References

Martinez, A. (2005). *Informe Final Sistematización de Experiencias del Programa de Agua y Saneamiento Rural (PASR), Durante el Periodo 2002-2004*. Fondo de Inversion Social de Emergencia (FISE).

Olatunji, T. (2003). *Towards Making Rural Water Supply Work and Sustainable*. 29th WEDC International Conference Towards the Millennium Development Goals. Nigeria 2003.http://wedc.lboro.ac.uk/conferences/pdfs/29/Olatunji.pdf.

Whyte, A. (1986). *Guidelines for Planning Community Participation Activities in Water Supply and Sanitation Projects*. World Health Organization (WHO).

Carter, R.C., Tyrrel, S. F., and Howsam, P. (1999). *Impact and Sustainability of Community Water Supply and Sanitation Programmes in Developing Countries*. Journal of the Chartered Institution of Water and Environmental Management, Vol.13, pp 292-296.

Fondo de Inversión Social de Emergencia, FISE. *Reglamento Operativo 2006-2010*. Julio 2008.

World Bank, (2008). *Rural Water Supply and Sanitation Project*. Project Appraisal. Document. Report No. 42908-NI..

Yankson, B., Mawuena Dotse, F., and Odai Laryea, N. (1997). *Integrating Gender Issues into Water Programmes*. 23rd WEDC Conference. Water and Sanitation For All: Partnerships and Innovations. Durban, South Africa.

Beall, J., (2002). *Globalisation and Social Exclusion in Cities: Framing the Debate with Lessons from Africa and Asia*. Working Paper Series 02-27, Development Studies Institute, London School of Economics and Political Science.

Fondo de Inversion Social de Emergencia, FISE. *Manual de Administración del Ciclo de Proyectos Municipal*, MACPM, 2007.

Framework for Improving Water Security in the Middle East

John A. Kliem, PE

Commander, Civil Engineer Corps, U.S. Navy, Graduate, Industrial College of the Armed Forces, National Defense University, Fort McNair, Washington D.C. 20340. PH (703) 571-9780; email john.kliem@js.pentagon.mil. The information contained in this paper is solely the opinion of the author and in no way reflect the policy of the United States Department of Defense or any other agency of the U.S. Government.

Abstract

Middle Eastern water demands are going to exceed the supply by 2040 potentially exacerbating an already tense situation. Any lasting peace plan needs to address scarce water resource commodities. All stake holders need to play a role in determining the allocation of water to ensure water security needed for further economic development. The United States as part of an international coalition needs to guide the Jordan River riparian states in the development of a regional water governance body to provide the required transparency to fairly allocate water resources and to ensure that water does not become the flash point for future Middle Eastern conflicts.

Statement of the Problem

The water demands of the Israelis, Palestinians, and Jordanians by the year 2040 will exceed supply by 3,500 million cubic meters per year (mcm)(Shlomo, 2007). Any peace plan for this region will have to address many elements to include security for Israel, return of the Golan Heights for Syria, and an Independent Palestine. However, under this scenario each country would be free to manage the natural resources in the best interest of their country. The Palestinians and Jordanians have made valid claims that Israel is using more than their fair share of water from Lake Tiberias and the Mountain Aquifer that is partially located under the occupied portion of the West Bank. Additionally, Syria is demanding access to Lake Tiberias and the water that runs off the Golan Heights to support their settlements and recreation. These forces are aligned to reduce Israel's water supply. Consequently, it is difficult to imagine a stable peace in the Middle East without addressing the region's scarcest resource – water.

Background of the Issue Including U.S. Objectives

Water is an essential element of any civilization. Countries cannot thrive or begin to develop without water since it is required to support agricultural and industrial growth not to mention sustain and grow populations. The Syrians, Lebanese, Jordanians, Israelis and Palestinians all require water in order to develop their societies. All of these groups share principally the same water sources, the Jordan River watershed with associated springs and the Mountain Aquifer located beneath the West Bank and Israel, *figure 1*. Syria and Lebanon have several other better options for water than the Jordan River Watershed. Increases in population and agriculture are driving higher demand for this limited resource (Dillman, 1989).

Pollution from industry, sewage, and mineral deposits also threatens to diminish portions of the water supply in the region (Starr, 1989).

The water flows into the Jordan River in three ways surface water, ground water, and rainfall runoff. Four main tributaries the Hasbani, Dan, Banias and the Yarmuk Rivers feed the Jordan River (El Nasar, 2008). Prior to 1964 the flow of the Jordan River was 1,300-1,500 mcm (Amery and Wolf, 2000) today the flow is about 125 mcm (El Nasar, 2008). This reduction is due to the Israeli National Water Carrier and other water diversion projects by Syria and Jordan (El Nasar, 2008). The remaining 125 mcm has a high salinity and mineral content (El Nasar, 2008). Also during low flow periods a greater proportion of the flow consists of agricultural and sanitary sewer discharges. These discharges are most likely high in nitrates and biochemical oxygen demand making the water of little value and a potential pollutant to the Dead Sea that receives the flow from the Jordan River ("Jordan Water Resources", 2008).

During the 1967 War Israel took the Golan Heights from Syria and the West Bank from Jordan. The outcome of the conflict improved the hydro strategic situation for Israel. As a result of the 1967 War, Syria lost access to Lake Tiberias and its watershed including the Golan Heights but also lost access to the Banias Springs and River (Amory and Wolf, 2000). Not only did Israel gain access to more of the Jordan River Watershed but also exercised control over the aquifers in the occupied portions of the West Bank. Jordan and the Palestinians lost the most from this war from a hydro strategic stand point.

Israel's water requirements have grown to meet increased supplies as a result of the 1967 War. The country is known for its aggressive water development strategies that have made the "desert bloom" (Kay, 2003). However, with a finite supply of water and with many regional demands for this single resource some accommodations must be arrived at. Israel gets one third of its water from Lake Tiberias with the rest coming from the West and North Eastern Mountain Aquifer (Dillman, 1989). A large portion of the Mountain Aquifer is under the occupied portion of the West Bank, *figure 2*. Israel uses about 60 percent of its water for agricultural and only about a third of that water is made up of reclaimed wastewater (Amory and Wolf, 2000).

Jordan is truly a water limited country that shares most of its rivers with other countries ("Jordan Water Resources", 2008). The Yarmuk River, supplies Jordan with about 40 percent of its water distributed via the King Abdullah Canal with the rest of the required water comes from ground water supplies exceeding the safe yield for the aquifer by 120 mcm per year (Amory and Wolf, 2000). About 75 percent of Jordan's water goes to support agriculture of which only seven percent is from reclaimed wastewater ("Jordan Water Resources", 2008).

Palestinians living on the West Bank have very limited options for water supply (Amory and Wolf, 2000). As stated earlier, removing water from the Jordan River is not a good option due to upstream diversion projects and the remaining water being of very poor quality. The Israeli Government limits the number of wells and how much water the Palestinians can withdraw from the Mountain Aquifer (Dillman, 1989). Due to this practice Palestinians have access to about 18 percent of the ground water that is available in their territory (Amory and Wolf, 2000).

Syria wants access to Lake Tiberias as a source of national pride. It is doubtful that Syria would pump water out of Lake Tiberias simply due to the expense of pumping the water up and over the Golan Heights *(All Things Considered,* 2000 and Omestad; et al, 2000). Syria's primary water sources are from the Euphartes and other sources to the north which could be more economically developed. Once Syria gained access to the Golan Heights and Lake Tiberias they could begin to collect water run-off from the Golan for their settlements. One legitimate concern that Israel may have is that Syria since it is un-interested in water from Lake Tiberias may not be as rigorous in controlling the quality of water run-off from the Golan Heights. Settlements could substantially degrade the quality of water from point source and non-point source pollution (Omestad; et al, 2000).

It will be difficult for Israel's economy to relinquish control over the water resources of the Golan Heights and the Mountain Aquifer. However, this appears to be the course required for peace and peace is more important to Israel that any water source (Author Interview, 2008). The Palestinians and Jordanians are anxious to have more water resources and claim that Israel is taking more than their fair share of water. In addition to Israel's water quantity requirements equally important is Israel determination to maintain the quality of its water sources.

The 2006 National Strategic Strategy, Section IV states that the United States will "work with others to defuse regional conflicts" (Bush, 2006). This is not a new objective similar wording was used in the 2002 National Security Strategy. In 2002 we were concerned that even if the U.S. does not have a stake in the conflict we should work to defuse the conflict because our enemies may capitalize on the situation to achieve their own objectives (Bush, 2006). There is the potential of withdrawal of Israeli forces from portions of the Northern West Bank and the establishment of a Palestinian government. One possible next step could be the establishment of an independent Palestine and the return of the Golan Heights to Syria. Simultaneously we must create an environment to ensure security for Israel in order to realize lasting peace in the region.

It is in our country's interest to establish conditions that will lead to prolonged stability and economic growth for the Jordan River States Region. The issue of water supply for Jordan, Palestine and Israel is essential to lasting peace in the region and must be approached in a regional systemic manner as described in the 2006 National Strategic Strategy which has proved successful in dealing with past Israeli-Palestinian Issues (Bush, 2006).

Economic growth is certainly a requirement for stability in the Jordan River watershed area. Clean water is essential to economic growth and would be an essential ingredient in the creation of the Middle East Free Trade Area by 2013 as described in the 2006 National Security Strategy (Bush, 2006).

The creation of a stable Middle East is in the best interest of the United States. In order for our country to continue to serve as a viable World Leader we have an obligation to work for a fair and equitable solution to this issue. However, we have a credibility issue in the eyes of the Middle East. We have been seen as willing to go it alone and attack an Arab country as in the case of Iraq. Our country has been a very close ally of Israel since its inception. We have branded Syria as a state supporting terrorism and have recalled our ambassador. The Palestinian leadership is being run

by a state that we consider to be terrorists supported by Syria. In light of our credibility issue we must play a role of encouraging a resolution to this problem through a neutral party that has credibility in this region.

The water right issues that exist in the Jordan River watershed are very controversial and are closely linked to future economic if not survival of the countries involved. The solution must be brokered and monitored by a neutral party. It will take the United States to bring the interested parties to the table and establish the frame work that will lead to resolution of this issue. Fair water allocation is critical to regional stabilization and economic growth.

Analysis of Policy Options

As part of any peace agreement between Israel, Jordan, and the Palestinian Authority water rights need to be addressed for the Jordan River Watershed and the Mountain Aquifer. This paper presents several policy options to resolve the Jordan River and Mountain Aquifer rights. One possible option is the United States could adopt a policy that the water that is contained within a country's borders or on the boundary at the time of the Peace agreement would be retained by that country. The U.S. could promulgate a policy to transport water from "water rich" countries like Turkey and Egypt to meet the growing demands of the region. An alternative policy would involve the water resources of the riparian states and the Mountain Aquifer to be leased to a multinational water management company by the stakeholder countries. Finally, the Jordan River and the Mountain Aquifer could be declared a part of an International Water Management District led by a coalition of stakeholder countries and members of a United Nations Water management group.

One option would be for each stakeholder to control the water that is within its borders. Consequently, Israel, Jordan, Lebanon, Palestine, and Syria would have some claim to the Jordan River watershed and Israel and Palestine would have rights to the water in the Mountain Aquifer. The chief benefit to this option would be the U.S. could take a "hands-off" approach and not get bogged down in resolving regional water issues. Each country would be free to develop their water resources as they see fit. Most likely all countries to some extent would be in a race to exploit the existing water resources for their own benefit. We would see the existing supplies begin to become depleted or polluted through irresponsible drilling and uncontrolled agricultural and sanitary sewer run-offs (Dillman, 1989). Wealthier nations in the region would then invest in desalinization plants to sustain their countries leaving the poorer nations to fend for themselves. As the water becomes increasingly scarce tensions in the region would rise with a potential for environmental terrorism or attacks on other country's water resources out of frustration at the inequality of the water supplies. There would be a possibility that the region would continue to be unstable.

Another possibility is to transport water from water rich countries such as Turkey and Egypt or construct a large desalinization plant financed by the European Union or the US (Shuval, 1991). One author suggested that the price for a desalinization plant option is 3-5 Billion dollars (Shuval, 1991). This price tag appears low and most likely does not include the cost of distributing the water from the plant to the region. The price for desalinated water has decreased recently due to technological advances from two dollars a cubic meter to fifty cents a cubic meter

(Fry, 2006). However, the cost of moving water from a desalinization plant to the region's inland inhabitants would drive this cost much higher. The construction of a large desalinization plant is certainly possible with outside financing for the construction of the plant and possibly the distribution system. The simple construction of a plant and infrastructure is possible but this option lacks the overarching structure that would ensure continuity of service. Care would have to be taken to assure the region that the shipment of water from the desalinization plant would be stopped during times of political crisis as was recently done to the inhabitants of the Gaza Strip.

The idea of transporting water from Egypt or Turkey to the region is amazingly short-sighted and does not address the issues at hand leading to the water scarcity such as population control, predominance on an economy driven by a water intensive industry of agriculture. If water is piped into the region in the so called "Peace Pipeline" from Turkey, it would cost about 20 billion dollars to bring water from the Seyhan and Ceyhan Rivers to Israel, Jordan and Palestine (Cowell, 1991). Not to mention once these countries became dependent on Turkish or Egyptian water what would happen when a drought hit those countries. It is very doubtful that Turkey would support such an initiative as they are looking to ensure their own water supplies for the future (Author Interview, 2008).

The once international boundaries are agreed upon for the countries of Israel, Palestine, Syria, and Jordan. The countries of Jordan, Palestine, Israel, and Syria could jointly award a lease to an international water resource management firm consisting of principles from each stakeholder country. This water management firm would allocate the regions water supplies and develop water management projects that would enhance the economic development of the region. Each country would be charged for the water that they used. The poorer countries of the region would benefit from the capital of the multinational firm to use as leverage for water development packages that the might not have been able to afford normally. The Water Management firm would be responsible for getting water to all of the stakeholders' citizens in the region. They would have to work with each stakeholder country to ensure pollution control and that no one drills illegal wells into the aquifer.

This option has its benefits in that the entire region's water would be controlled by a single entity ensuring responsible management of the region's resources. If the company failed to manage the water resources appropriately, then the company would face economic penalties and possible the revocations of the lease. Poorer countries would have access to water development projects that may not have otherwise occurred. Each country would pay the same price for the water that is used. No longer would the strongest country get all the water.

There are some significant drawbacks for privatizing the region's water supply. It would be difficult to find an interested international company that would have the capital and other resources to take on this responsibility. An undertaking of this size in a region with such a troubled past possibly would pose too significant of a risk to be practical. A cost analysis is required determine the operational and maintenance costs of the existing distribution system with the capital expenditures required to bring the plants up to standards as well as future projects. These costs would have to be allocated across the regional water users to determine if such a

venture would be profitable. The economics and risk involved with this solution make this option unattractive.

The UN would declare the Jordan River Watershed and the Mountain Aquifer to be an International Water Management District. Declare the regional water sources to be an international resource to be managed by all stakeholders jointly under the leadership of a United Nations appointed Water Management Director. Each of the region's countries would appoint officials to be apart of the Water Management District. The district would set water rates for public and private consumption and establish water management policies concerning run-off and usage allocation. Rates would be developed to ensure operation and Maintenance of Plants, distribution systems and to ensure future capital development projects.

One attribute for this option is that the region's water resources are managed by a consistent entity in an attempt to fairly distribute the water resources. However, once again a major issue with this policy would involve if the stakeholders could trust the UN to manage their water resources. This is why it is important to ensure that each stakeholder appoints representatives to be involved in leadership of the Water Management District. In this way water management issues could become a source of cooperation vice conflict (Interview with Author, 2008). This Watershed Management entity would have to work closely with the stakeholder countries to oversee water quality to ensure that urbanization and pollution does not affect water quality. Each country would be required to enforce jointly agreed surface run-off water quality.

Another draw back for this option is the significant international financing required to get the water management district has established with the required infrastructure and initial water development projects. Eventually the International Water Management District could become self sustaining through water usage rates but this will take a substantial amount of time. The international community must decide if this region worth investing in to ensure peace and prosperity in the Middle East.

Policy Recommendation

The United States needs to work with the international community and the UN to establish an International Water Management District for the Jordan River Countries and the Mountain Aquifer. The U.S. should play a role in developing an international coalition to support this initiative to convince Jordan, Israel, Syria, Lebanon and Palestine to support the existence of an International Water Management District. It is critical that all stake holders fill leadership roles in the Water Management District under the leadership of a UN appointed director. This body has the greatest possibility of success since the stakeholders will be directly and jointly involved in solutions to their problems. This solution also removes the United States from the role of mediator or peace broker as previous administrations have done. The Arab world cannot view the United States has playing too heavy a role in the development of this solution as we are seen as an ally of Israel and not an honest broker.

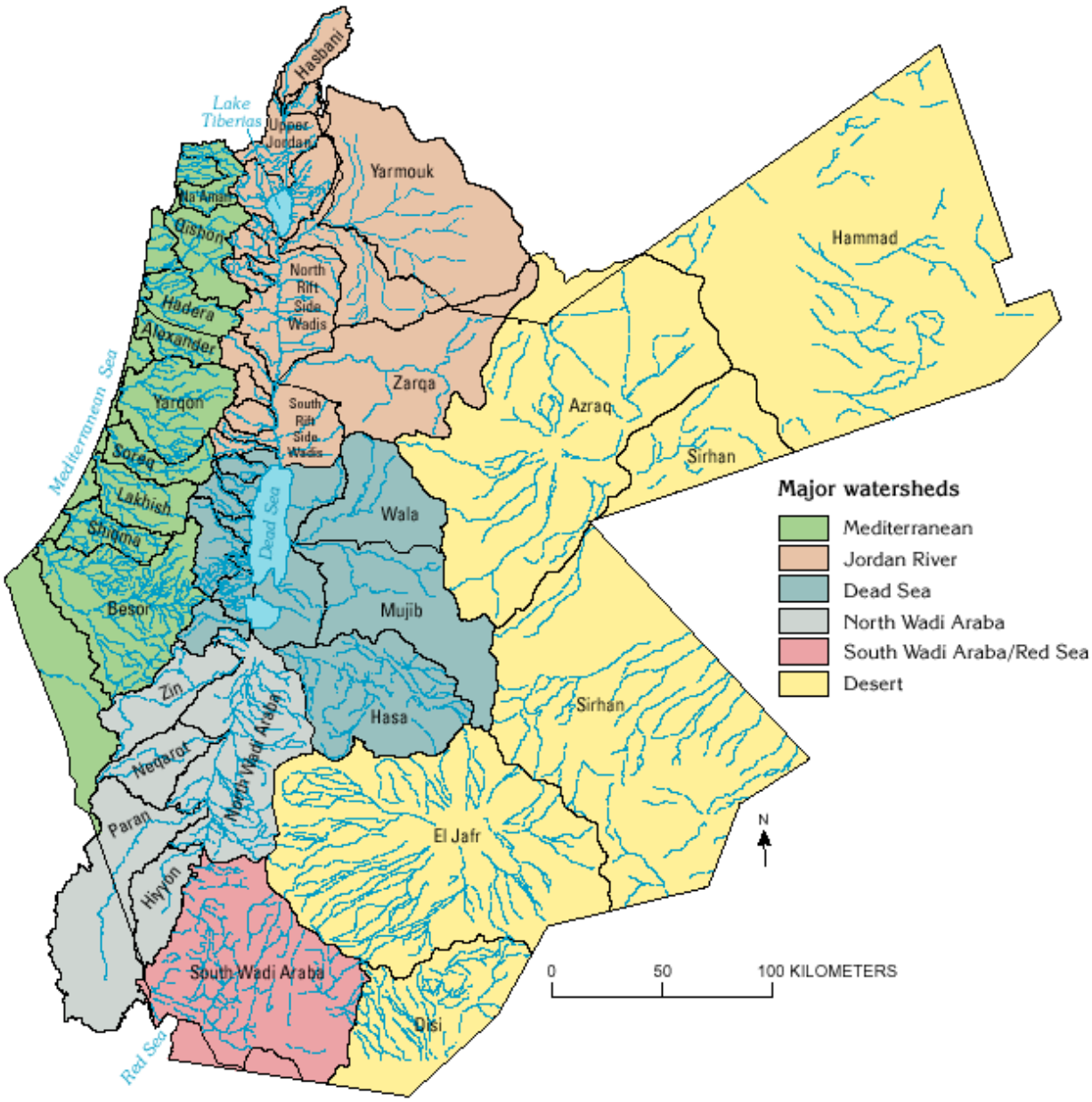

Figure1. The Jordan River Watershed (El-Naser, 1998)

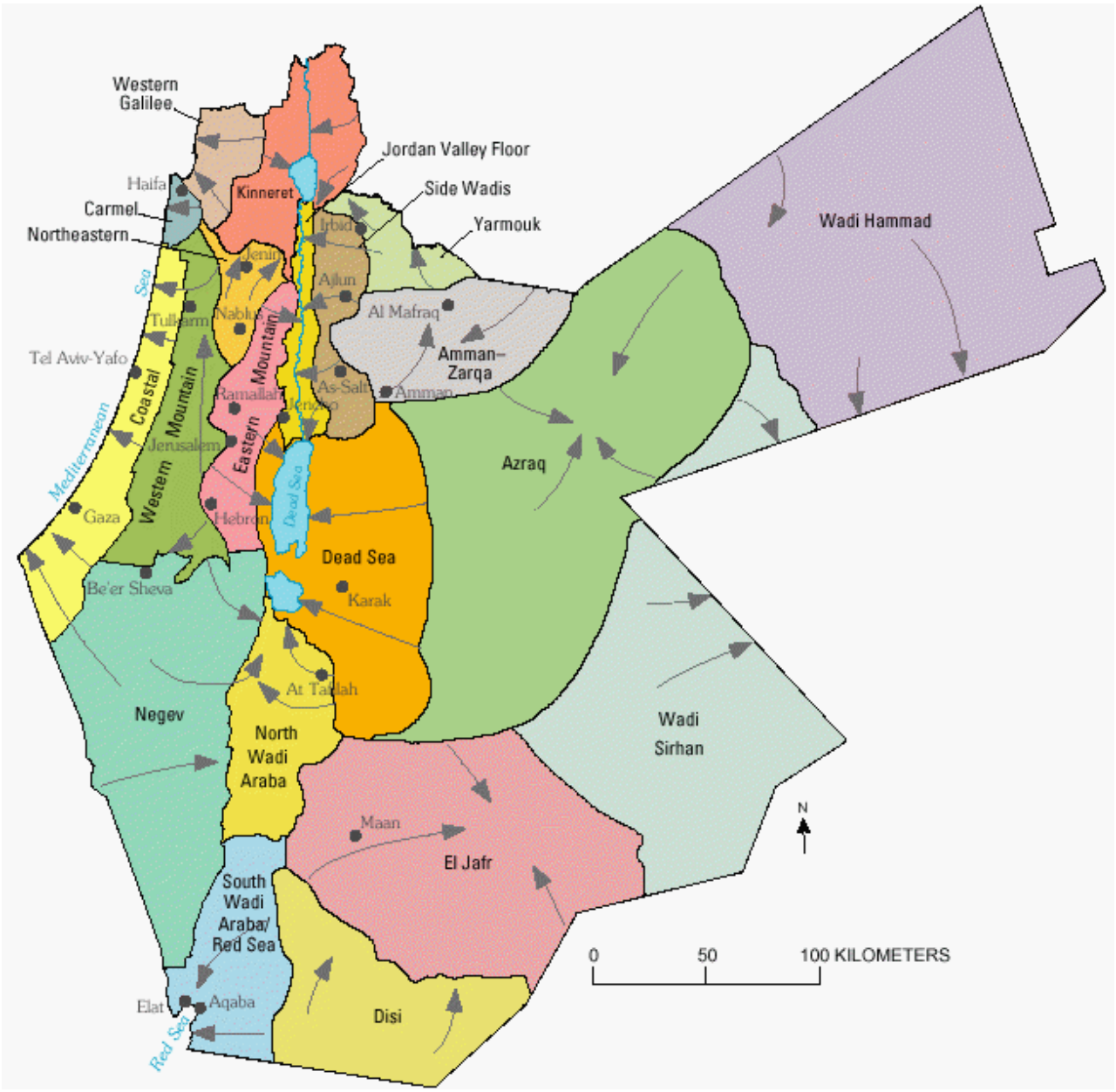

Figure 2. Groundwater resources (El-Naser, 1998)

Bibliography

"Good Water Neighbors Newsletter." 1, no. 42 (January 7, 2007, 2007): January 17, 2008, http://www.foeme.org/docs/newsletter42.htm.

"Syria and Jordan Launch Al-Wahda Dam." *The Syria Report* no. 16 (Mar, 2004): 12.

"International: Peace Walks on Water." *The Economist* 356, no. 8190 (Sep 30, 2000): 45.

"Profile: Water Rights Fight between Israel and Syria in the Golan Heights." *All Things Considered* (Jan 6, 2000): 1.

"Jordan Water Resources." Food and Agricultural Organization of the United Nations. http://www.fao.org/nr/water/aquastat/countries/jordan/index.stm (accessed 25 January, 2008, 2008).

Author Interview, This portion of the paper was derived from interviews with senior members of the Diplomatic Community from the affected countries. Their names are not listed in keeping with the "Non-Attribution" Policy of the National Defense University. The interview occurred on 4 February 2008.

Amery, Hussein A. and AaronT Wolf, eds. *Water in the Middle East: A Geography of Peace*. First ed. Vol. 1. Austin, Texas: University of Texas Press, 2000.

Bush, George W. *The National Security Strategy of the United States of America*National Security Council, 2006.

Cowell, Alan. "The World; More Precious than Oil, and Maybe as Volatile." *New York Times,* Mar 17, 1991.

Dillman, Jeffrey D. "Water Rights in the Occupied Territories." *Journal of Palestine Studies* Volume 19, no. Autumn (1989, 1989): 46-71, http://www.jstor.org/view/0377919x/di009632/00p0151f/0 (accessed January 11, 2008).

El-Naser, Hazim, Mustafa F. Nuseibeh, Karen K. Assaf, Shmuel Kessler, and Meir and Ben-Zvi. *Overview of Middle East Water Resources*Executive Action Team, Middle East Water Data Banks Project, 1998, http://www.exact-me.org/overview/toc.htm (accessed January 10, 2008).

Fry, Al. *Facts and Trends: Water,* World Business Council for Sustainable Development, 2006.

Kay, Paul A. "Making the Desert Bloom." *Alternatives Journal* 29, no. 2 (Spring, 2003): 44.

Maital, Shlomo. "Six Myths." *The Jerusalem Report* (Jun 25, 2007): 22.

Omestad, Thomas, David Makovsky, and Rachel Stroumsa. "The Struggle Over Water A Failed Summit Highlights Rival Claims to Water Sources in the Thirsty Mideast; Jerusalem; the Golan Heights." *U.S.News & World Report* 128, no. 14 (Apr 10, 2000): 32.

Plushnick-Masti, Ramit. "A Torrent of Problems for the Hallowed Jordan; Evangelical Christians Who Value the Mideast River for Baptism have Joined Environmental Activists in Seeking to Stem its Degradation." *Los Angeles Times,* Sep 24, 2006.

Shuval, Hanan I. "Water for Peace." *The Jerusalem Report* (Nov 21, 1991): 39.

Starr, Joyce Shira. *Covenant Over Middle Eastern Water Key to World Survival*. First ed. Vol. One. New York: Henry Holt and Company Inc., 1995.

Swain, Ashok. "A New Challenge: Water Scarcity in the Arab World." *Arab Studies Quarterly* 20, no. 1 (Winter, 1998): 1.

"A War for Water"

by
Jonah-Jong M Lee

HDR Engineering, Inc. Water Business Group, 3230 El Camino Real Suite 200, Irvine, CA 92602-1377; Phone (714) 730-7300; Fax (714) 730-2301; email: Jonah.Lee@HDRinc.com

ABSTRACT

It is the most precious commodity on earth, and billions of people do not have adequate means of obtaining it. Water both for drinking and sanitation use is essential to human life. Yet in a world where we have come so far in technological advancement, we still live amongst 2 billion people who do not have access to modern sanitation facilities and 1 billion people without safe and drinkable supplies of water. We have failed to address a problem that should have spurred world interest long ago. There are countries with millions of people, including children, dying each year due to a lack of clean drinking water and poor sanitation services. With a continuous rise in population throughout the world and an ineffective distribution of water resources, there can be as many as 140 million water-related deaths by 2025.

INTRODUCTION

"When the well is dry, we learn the worth of water." –Benjamin Franklin

For those of us who live in parts of this world where we are fortunate enough to have the luxury of clean sources of water, we may never fully comprehend the meaning of this phrase. Unfortunately, those living in underdeveloped countries may not understand it either. How can they appreciate the value of something as precious as water if the well was dry long before they even tried to pump? Sufficient and clean water is essential for the wellbeing of all living creatures. In an era where we have advanced in civilization, it is an unfortunate state of affairs that we are amongst a population where one in every six people lives without an adequate source of water.

Around the world today, poor developing countries are struggling with the lack sufficient and clean sources of water. A single person needs 4-5 gallons of water per day in order to survive. On average, a family in Africa uses about five gallons of water each day compared to that of the average American who uses 140 gallons of water at home each day. Water-related deaths are in the millions each year, and roughly 840,000 of these deaths are children under the age of 14. These deaths are not due to the lack of drinking water alone; the lack of proper sanitation systems brings a large risk of infection. There are more deaths caused by poor water sanitation and a lack of safe drinking water than by war, terrorism, and weapons of mass destruction combined.

WATER SOURCES

Water resources are classified in the form of surface water, sub-surface water, or frozen water. Surface water comes in the form of rivers, lakes, or fresh water wetlands. As they are constantly pumped out for human consumption, they are naturally replenished by precipitation. The volume of water also depends upon the rate it is lost through discharge into the oceans, evaporation rate, artificial reservoirs, permeability of the soil, and runoff characteristics of the land in the watershed. The sub-surface water known as groundwater is the fresh water located in the pore space of soil and rock or the water flowing within aquifers below the water table (Figure 1). The natural input to sub-surface water is seepage from surface water. The natural outputs from sub-surface water are springs, which are where the groundwater flows out of the ground and the aquifer surface meets the ground surface. The other form of output for sub-surface water is through seepage that leads into the ocean. Of all the Earth's water only 2.5 percent is found to be fresh water, with two thirds of that frozen in glaciers and polar ice caps. Several schemes have been proposed to make use of these glaciers but nothing has been done to date.

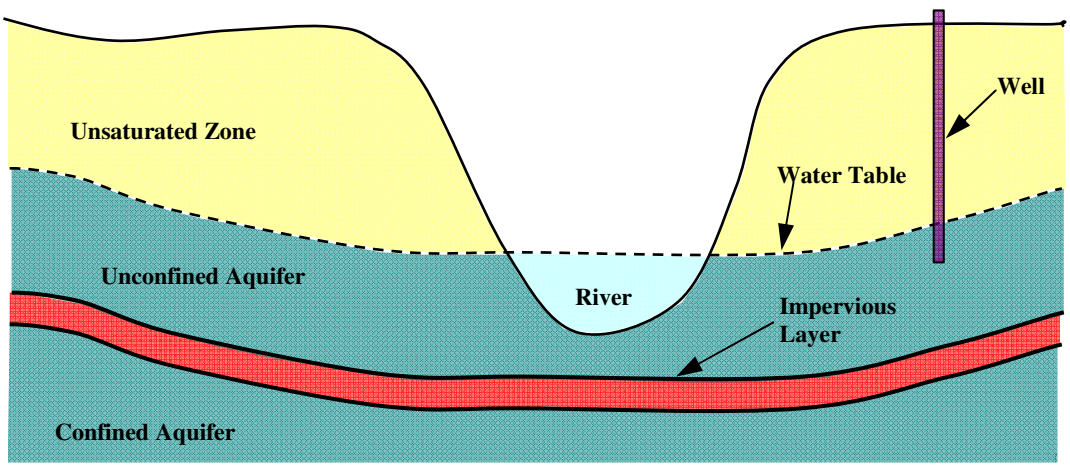

Figure 1. Water Table Varying With the Surface Topography

A new technology that has been widely used in arid areas such as the Persian Gulf is desalination. Currently there are over 7,500 desalination plants in operation worldwide with three out of five plants located in the Middle East. Desalination is an artificial process that takes sea water and converts it into fresh water. The more common practices of desalination are distillation and reverse osmosis. This technology has yet to make a major impact due to its high costs of operation. Most believe that as technology continues to advance, the costs will be significantly less. The cost to produce water from a desalination plant can range anywhere from $1,000 to $4,000 per acre-foot, compared to a cost of $20 to $150 per acre-foot for water pumped from rivers and lakes and $50 to $300 per acre-foot for reclaimed/recycled water depending on location. Groundwater pumping costs range typically from $600 to $700 per acre-foot. Small desalinations are slowly becoming more prominent but

until the cost is reduced to what communities can reasonably afford, this may not be an option.

With ongoing trends, many nations have fallen into a state of water stress or even worse, from water scarcity. Water stress is defined as occurring in an area where there is not enough water for all uses whether agricultural, industrial, or domestic. Water stress occurs when less than 1,500 cubic meters (or 52,972 cubic feet) of water is available per person within a year, while water scarcity occurs when less than 1,000 cubic meters (or 35,315 cubic feet) of water is available per person within a year. It is estimated that by 2025, more than 2.8 million people living in 48 countries may face either water stress or water scarcity.

POPULATION & GROWTH

The world's population has been growing steadily especially in the last century. Compared to the 1.6 billion inhabitants in the early 1900s, the population has grown exponentially to more than four times that over the past hundred years, now exceeding 6.7 billion people. The population is expected to grow to 7.8 billion by 2025 and 9 billion by 2050. Ninety percent of that growth is expected to take place in less developed nations. It has already been noted that over a billion people do not have safe and adequate sources of drinking water and that two and a half billion people are without adequate sanitation systems. What is even worse is that in 2025, it is expected that two out of every three people could possibly be without safe drinking water and basic sanitation services.

In 2000, the per capita average water usage in the United States was 1,430 gallons per day, which was down from 1,620 gallons per day in the previous decade. The U.S. is also the third largest population with very little or no threat of water scarcity. With a population of 305 million, Americans use up to 408 billion gallons per day. This includes water for drinking, bathing, cooking, washing, and maintaining lawns and gardens. In addition, water is in constant demand for the industrial and manufacturing sector to create products; the agriculture industry to provide food; and the energy industry to provide illumination, heat, and air conditioning. These are all critical needs to the consumer, who has long depended on such luxuries.

WATER-SCARCE NATIONS

The two largest countries, China and India, contain respectively 20 percent and 17 percent of the world's total population. That is a combined 37 percent of the world's population, and these two nations are also headed towards a scarcity of water, which should peak in the not too-distant future. Countries such as China and India may face severe water crises unless changes are made in their water management practices. China has already been regarded by the United Nations as one of the 13 water-deficient countries in the world. Though China has been diligently implementing seawater desalination plants along the coast of the southeast and near northern parts of China, there is still a shortage throughout the country. Currently there are an

estimated 400 cities throughout the country that are running short. With an expected 1.6 billion population by 2030, the water resources will likely plunge by more than 25 percent. In the past, India had greatly benefited from investing in the development of large water infrastructures, which resulted in enormous gains in food security and in the reduction of poverty. Unfortunately, India does not have the funds to develop new or upgrade existing facilities. In addition to that, India does not have the sources of water to provide for its growing economy and rising population. Due to its poor water supply services, farmers and urban dwellers have resorted to pumping out groundwater, which in turn has rapidly reduced water tables and depleted aquifers. In addition, 90 percent of India's territory is drained by inter-state rivers, and it is estimated that within the next decade, India's demand for water will exceed all sources of supply.

To some it may sound like a joke when one hears that the leaders in innovation of water technologies may be going through a water shortage crisis. Israel, the captain of the water industry who developed the technology of desalination and drip irrigation, has been fast approaching a water crisis. They currently have only three desalination plants with a fourth being built, which may not be completed until 2013. One of the factors that Israel is facing is poor management. Israel is in great need of a highly informed government that will address the problems that need the most focus and attention. After years of drought that have been plaguing their nation, and with increasing demand caused by a growth in population and the need to supply water pursuant to international undertakings, their resources have dwindled to a great extent.

In a country that's also a continent on its own, Australia anticipated that within the next decade, nearly every city will have to find and develop a new water supply. Next to Antarctica, Australia is the driest continent in the world. Due to a combination of a growth in population and recent prevailing climate changes, the already at-risk water resources have slipped into further jeopardy. Many of Australia's citizens have already experienced several water restrictions such as bans on washing cars, using sprinklers, and watering gardens. Australia will have to find new ways to provide water within the next 5 to 10 years. Building new infrastructure could very well cost up to $25 billion and would need to be paid for by higher charges to the consumers.

The hardest reality to accept is that there are potential water wars between countries that share rivers and lakes. Nearly 80 of Africa's river and lake basins are shared between two or more countries. Many countries also depend upon the inflow of water from outside their nation's boundaries. War and disputes over water may very well be the case within the next 25 years throughout Africa. Currently about half the population suffers from one of the major water-related diseases. More alarmingly, experts have estimated that one in every two people will face water scarcity. By 2025 it is predicted that 12 more African countries will join the 14 that are already suffering from water stress or water scarcity (Figure 2). Africa's water shortage woes result primarily from uneven distribution. One such example lies in the Congo basin,

an area where 30 percent of the continent's water drains but only 10 percent of the continent's population lives.

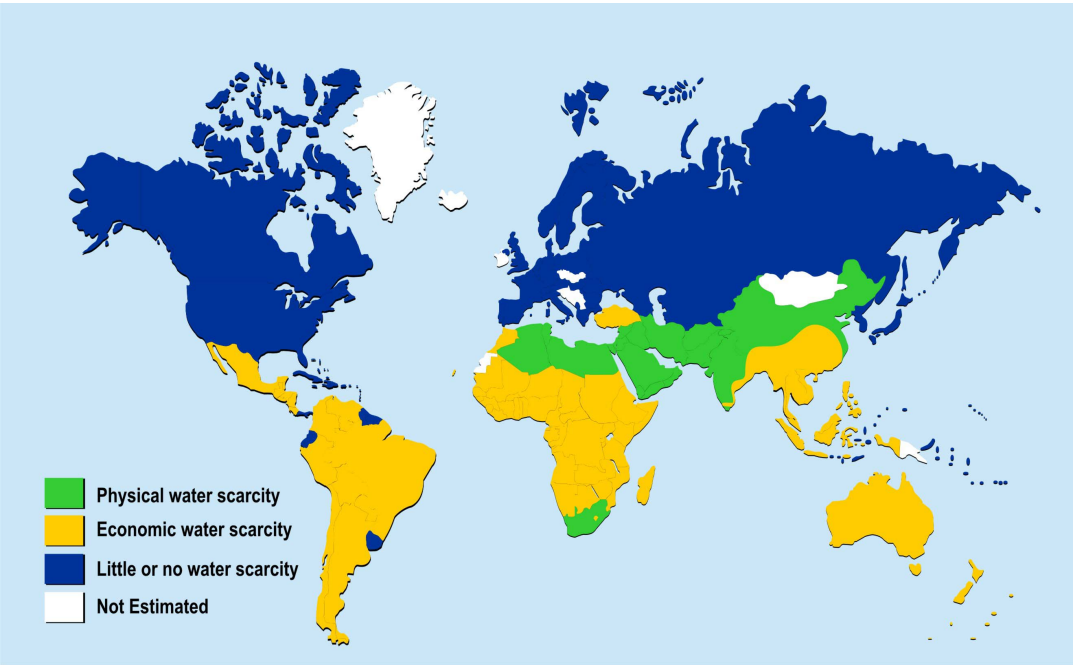

Figure 2. 2002 Trend of Worldwide Water Scarcity

WATER-BORNE DISEASES

It is a frightening thought that at any given moment, half the population of the developing world is suffering from a water-borne disease. A water-borne disease is any disease that is transmitted or spread through contaminated water. A disease can be spread by microorganisms such as protozoa, viruses, bacteria, and intestinal parasites. Contracting a disease can be easier than possibly imagined. It is as simple as eating food that was prepared by an individual who has already contracted a disease and did not wash their hands. It can also be contracted by touching something that was handled by an infected person and then transferring microorganisms to the mouth. The diseases just to list a few include:

- Diarrhea – Has been the leading cause of childhood death. Due to infection, may last from a few days to several weeks. Constant diarrhea may result in severe dehydration and shock. It can become life threatening due to fluid loss in water diarrhea especially in small infants or malnourished individuals.
- Cholera – Is one of the most rapidly fatal illnesses and a perfectly healthy person can become hypertensive with in an hour of the onset of symptoms. If proper medical treatment is not given immediately, an infected patient may die within three hours.
- Amoebiasis – Can be transmitted through the fecal-oral route in which water had come into contact with feces, poor sewage treatment, or

from the absence of cleaning after handling feces. It is estimated to have caused 70,000 deaths on an annual basis.

- Crytosporidiosis – A parasitic disease, whose symptoms include stomach pains, cramps, and a low fever. This disease is transferred by material such as earth water or uncooked or cross contaminated food that has come into contact with feces of an infected individual.
- Giardiasis – Caused by eating food contaminated by the unwashed hands of an infected person or drinking groundwater polluted by an infected animal. Symptoms include loss of appetite, fever, blood in urine, watery stools, upset stomach, and projectile vomiting. When present, symptoms may last one to three days.
- Schistosomiasis – Is transmitted when the larvae of the parasite are sheltered by snails and infect humans who come into contact with the infected water. The larva enters through the skin and travels through the bloods vessels and nests in the lungs. It is second following malaria as the most socioeconomically distressing disease. Schistosomiasis can damage internal organs and impair growth and cognitive development in children if it becomes chronic.
- Typhoid – Has been a continuous problem in less-industrialized countries mainly due to problems of unsafe drinking water, poor sewage disposal, and problem flooding. Transmission can be from contaminated water or milk. Symptoms include high fever, rose colored spots on the chest, and/or enlargement of the spleen and liver.

This is just a small list of over dozens of water-related diseases that have been a constant threat to the well-being of millions of people worldwide. An alarming 80 percent of illnesses in developing countries are water-related. The spread of these diseases is caused primarily by drinking water tainted with urine or feces of infected human beings or animals.

RECOMMENDATIONS

The first step to reducing this problem is to keep clean water clean and to dispose and treat sanitary waste in a safe manner. A common misconception is that the cost to repair the infrastructure of multiple countries would be too much for wealthier donor nations. Opportunities to help less developed countries do not lie in high-cost centralized water treatment and distribution systems alone. Practical innovative solutions such as point-of-use disinfection and safe water storage vessels can relieve short-term problems of water storage. The water supply, both clean and sanitary, is disinfected to kill any pathogens and to further prevent them from prevailing again in the distribution system. Without the disinfection process, the risk of water-borne disease is increased, and the problems will persist.

A fundamental answer to managing a water crisis begins with negotiating a standard of which nations are entitled to their share of water in a river or lake. Water crises are closely related to regional tensions, but history has shown that there has been far less

conflict over water than there has been conflict over cooperation. Formation of strong international institutions has been characterized as the way forward; they prevent costly disputes over a resolution and result in early intervention and management. Organization and collaboration are the keys to developing treaty agreements that promotes co-operative opportunities.

Another affordable method would be using electrolytic generators that produce sodium hypochlorite from salt water, then appropriately storing the treated water to prevent recontamination. This method has been proven to be effective in numerous households in Central America, Africa, and the Middle East. Much speculation has been developed that there is a short-term and a long-term measure to solving this large array of water-related issues. The short-term assessment should be for people to wash their hands as much as possible, boil water, and store it. Fifty percent of the places with unsafe water once had a system that functioned, but fell apart due to a lack of maintenance.

One of the major benefits that most are not seeing is that there can be a major return; for every dollar spent, there can be an economic return of $3 to $34 depending on the country. However, what can be far more precious is eliminating disease and death due to unclean water and poor sanitation, while supporting health and productivity gains. The United Nations has been diligently working to diminish by half the number of people without access to safe drinking water and basic sanitation by the year 2015. The United Nations created the Millennium Development Goals which is to reduce the number of people without access to safe drinking water by half and to stop unsustainable utilization of water resources. In 2002, two other goals were adopted which are to aim to develop integrated water resource management and water efficiency plans. By 2015 the goal is to halve the total number of people who do not have access to basic sanitation.

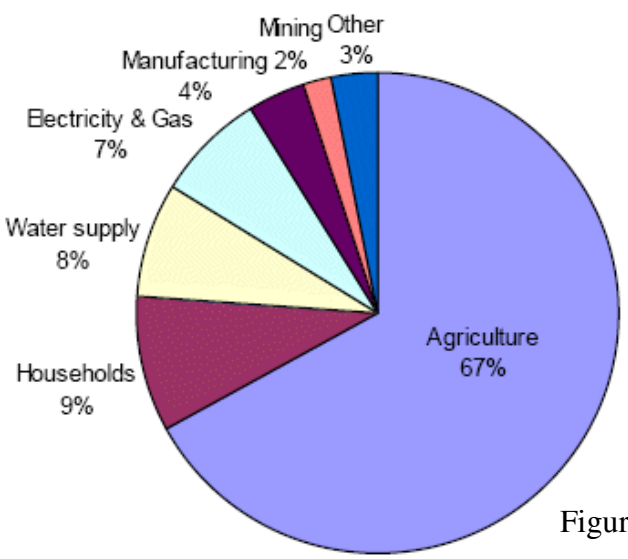

Figure 3. Breakdown of Water Usage

A long-term measure that can further impact the conservation of water would be the agricultural business. Worldwide agriculture plays a vital role in every economy and

therefore should be attended to. Most of our world's water supply is heavily focused on the agricultural business (Figure 3). But much of that water is being wasted from over-watering of crops. Developing countries especially would have to begin to produce more crop per liter of water, promote equitable access to water, and conserve their water resources. In order to avoid a future food shortage, there must be more investment to achieve productivity gains using existing and new technologies. For instance, if one farmer were to reduce water usage by a mere 1 percent, that would save over 7,000 cubic feet of water per year, which is enough to provide drinking water for 150 people. Irrigation technologies need to be upgraded, such as drip irrigation, which puts water where it is needed and is far more efficient than the use of sprinklers and flooding fields. Inexpensive technologies such as treadle (pump designed to lift water) or mechanical pump irrigation equipment on a smaller scale have also proven to be successful in increasing crop production and income. Further investment is not only cheap, but will ultimately save money on a much broader scope.

CONCLUSION

Water is the essence of life. Without water there is no life on earth and there is no more existence. We must treat water not as a commodity to be sold to the highest bidder or treat it as a right to only the privileged and wealthy, but as an indispensable component of human life. We, the nations of all mankind, must learn not only the system and practice of sharing equitably, but we must also embrace the furthering technologies and principles of protecting the environment and the sources of fresh water that belongs to us all.

It is not the obligation of the wealthy to establish an infrastructure of water conservation and sanitation facilities. However, for the sake of humanity and moral fiber, it would be a wise investment to help those less fortunate in the global mainstream. Repairing the damage that has already been done must take place immediately, eliminating water-borne diseases before they spread to the larger population. The more fortunate nations have an opportunity to do what is ethical and can reorganize the approach to providing water and sanitation services while at the same time protecting their existing establishments and preventing a similar fate. Unless these degrading conditions in poor, developing nations can be managed properly, even wealthier prominent countries will ultimately feel the impact of diminishing supplies of drinkable, useable clean water. Perhaps nations will one day be going to war not for oil, land, or other treasures, but the most important resource, water!

REFERENCE

http://www.greenbiz.com/news/2006/08/22/water-crisis-hits-rich-countries-says-report

Lenntech Water Treatment & Air Purification, http://www.lenntech.com/Waterborne-diseases/waterborne-diseases.htm

Johannesburg Summit 2002. Johannesburg Summit Secretary-General Calls for Global Action on Water Issues. http://www.johannesburgsummit.org/html/media_info/pressrelease_prep2/global_action_water_2103.pdf (downloaded August 2002).

Kirby, Alex, BBC news Online: Why world's taps are running dry. http://news.bbc.co.uk/2/hi/science/nature/2943946.stm

Lecturer. Professor Emeritus Dan Zaslavsky, Definition of Israel's Water Problems or Water as a Metaphor, June 2000.

Shah, Anup, Water and Development: Global Issues. http://www.globalissues.org/article/601/water-and-development

Smith, Russell, BBC News Online: Africa's potential water wars. http://news.bbc.co.uk/1/hi/world/Africa/454926.htm

Water Encyclopedia, Population and Water Resources. http://www.waterencyclopedia.com/Po-Re/Population-and-Water-Resources.html

WHO. 1995. Community Water Supply and Sanitation: Needs, Challenges and Health Objectives. 48th World Health Assembly, A48/INEDOC./2, April 28, Geneva, Switzerland.

WHO. 2000. Global Water Supply and Sanitation Assessment 2000 Report. Available in full at http://www.who.int/water_sanitation_health/Globassessment/GlobalTOC.htm. (downloaded August 2002).

Water Resources in Jordan: Challenges and Accomplishments

S. Merayyan[1], S. Mrayyan[2], and M. Mihyar[3]
[1]Assistant Professor, Department of Civil Engineering, California State University, Sacramento, 6000 J. St., Sacramento, CA 95819-6029; PH (916)278-5349; FAX (916)278-7957; email:merayyan@csus.edu
[2]Vice Dean, AL-Balqa Applied University, Al-Huson, Jordan; email:salwa_mrayyan@yahoo.com
[3]Water Resources Engineer, California Dept of Water Resources, Sacramento, CA 95819; email:mmihyar@water.ca.gov

Abstract

The Hashemite Kingdom of Jordan, or simply Jordan, is a small county located in the Middle East. Jordan has borders with Saudi Arabia, Syria, Iraq, and Israel (see Figure 1). Jordan was established in 1921 and has very limited natural resources. Jordan's current (2008) population is estimated to be 6.5 million. The country has a total area of 750,000 km2, about one third (92,300 km2) of which is dry land while the other two thirds (329,000 km2) is irrigated land.

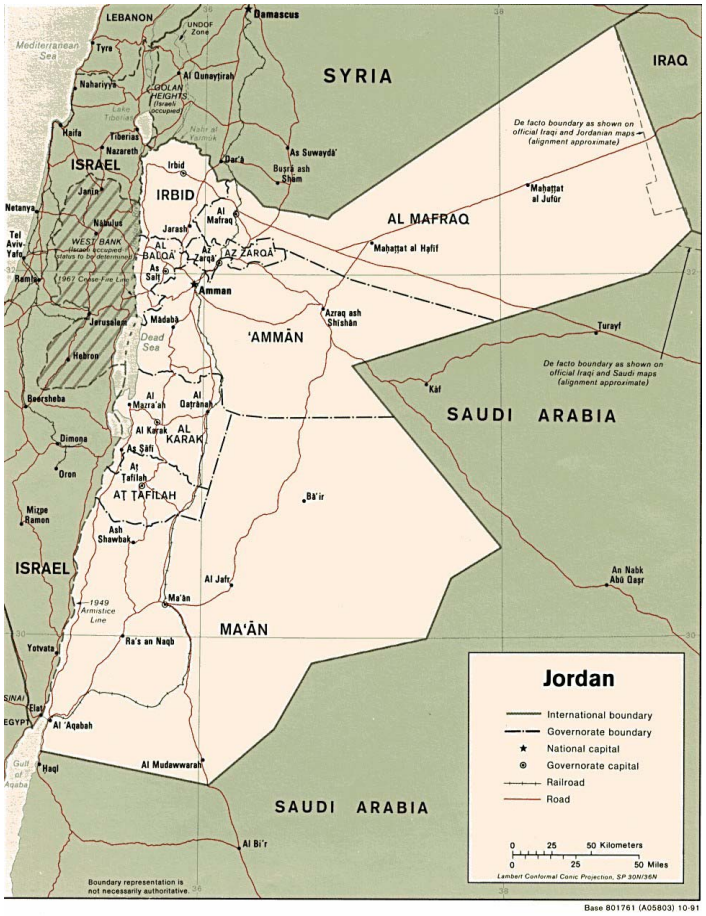

Figure 1. Map of Jordan (M. Mohsen, 2007)

Jordan's limited water resources fluctuated around a stationary. The normal population growth, in addition to the massive influx of refugees from neighboring countries, made the limited water resources in the country even worse. The majority of water resources experts classify countries with less than 1000 m^3 per (year-capita) as water poor countries. In 1997, Jordanians consumed only 883 million cubic meters (MCM), which translates to about 200 m^3 per (year-capita). The 1997 water consumption rate - when compared to the rates of neighboring countries - was 65% less than that consumed in Syria and Israel, and 85% less than that of Egypt.

The gap between water supply and demand is expected to increase due to the steady increase in population. If the current population growth trends follow what is projected, in 2025 the annual water consumption per capita will decrease from its 1997 level of 200 m^3 per (year-capita) to 91 m^3 per (year-capita).

In 2000, Jordan needed 1258 MCM to meet its domestic, industrial and agriculture demands. Faced with these challenges, the Jordanian government devised a plan aimed at reducing the demand and increases the supply of water. The increase of the water supply was partly achieved as an outcome of the peace treaty that was signed between Jordan and Israel in 1994, which ensures an additional estimated 215 MCM of water via the building of additional dams, as well as pipelines on the Yarmouk and Jordan rivers. Other projects that the Jordanian government proposed to improve water supply are purchasing water from other countries (i.e. Turkey) and/or constructing a canal "The Two Seas Canal or the Peace Conduit" to bring water form the Red Sea to the Dead Sea. The proposed Two Seas Canal will be constructed with the participation of Israel and the financial support of the United States and the European Union. The Canal will bring 1.8 billion m^3/yea of sea water which will then be treated using desalination to provide about 850 MCM of portable water to Jordan, Israel and Palestine.

The water issue in the Middle East is not only a limited resource, it's also a source of conflict that might require world intervention. Participation in and funding of such projects will, on the long run, provide the people of Jordan with the necessary supply of water , hence improving the overall status of the population as well as reducing any potential for conflict.

Climate

Jordan's weather is classified as semi-arid to arid with hot and dry summers, and cold and wet winters. Jordan's precipitation (see Figure 2) varies in magnitude, intensity, and distribution. Most of the precipitation in Jordan occurs between the months of October and May of each year. The average annual precipitation in Jordan is 50-200 mm, 100-300 mm, and 200-600 mm in Jordan's Desert, Jordan's Valley, and Highlands, respectively. In a typical wet year, the total precipitation is about 1200 MCM and is half of that in a typical dry year. The evaporation rates in Jordan vary form 63% from the highlands to 99% from the desert. The typical long-term evaporation average is 93%.

Surface Water Resources

The majority water re-charge comes from precipitation, which dramatically varies from year to year. The surface water, base flow, and runoff long-term averages are 713 MCM, 451 MCM, and 256 MCM, respectively. There are three major surfaces water systems in Jordan; theses systems are: Jordan River that has a catchment area of 18,194

km^2. The Yarmouk River which has a catchment area of 6,7890 km^2. About 1,160 km^2 of the Yarmouk River catchment area is located in Syria. The third major river in Jordan is the Zarqa River. The Zarqa River has a catchment area of 4025 km^2 and its water is not shared with any of Jordan's neighboring countries. The Zarqa River catchment area is densely populated; where about 65% of Jordan's population resides and about 80% of Jordan's industry located. The effluent form several wastewater treatment facilities (e.g. As-Samra, Jeresh, and Ba'qa WWTP) discharge to the Zarqa River. The Zarqa River is controlled by the King Talal Reservoir and its water is mainly used for agriculture and live stock demands. The percentage of treated sewerage that is discharged into the Zarqa River is 50% in the winter months and about 60% in the summer months. There are two surface water bodies in Jordan: The Dead Sea and the Gulf of Aqaba. Figure 3 shows the fifteen surface water basins while Table 1 provides a summary of the annual flow from each basin.

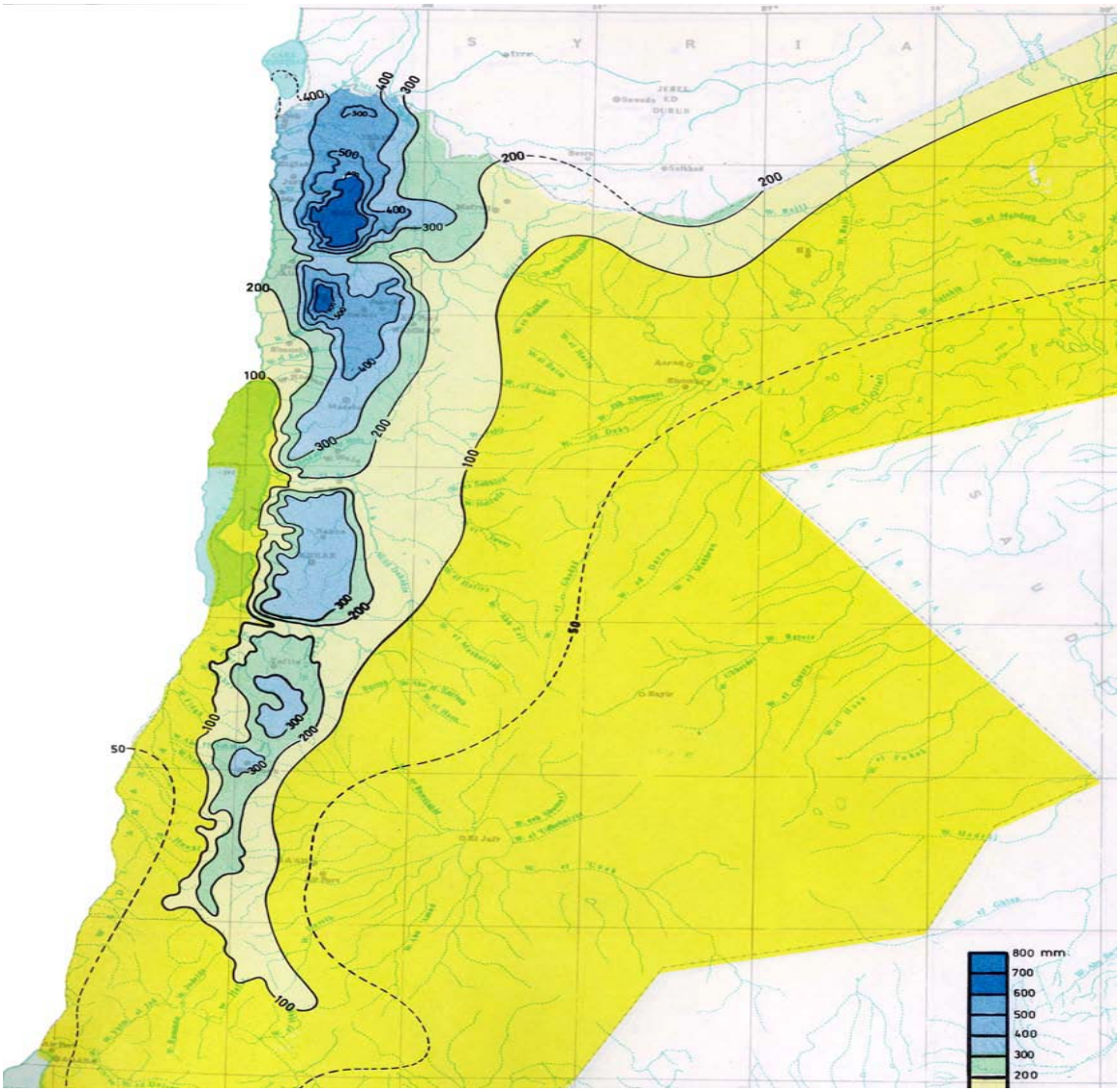

Figure 2. Annual Precipitation (M. Mohsen, 2007)

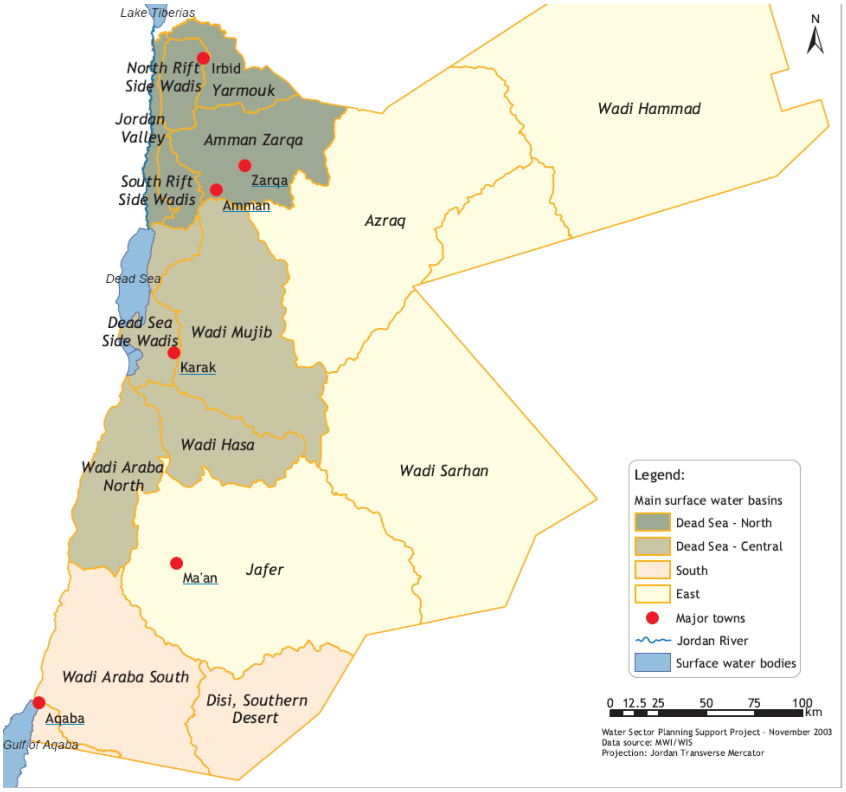

Figure 3. Surface Water Basins

Table 1. Catch Basin Flow

Basin	Annual flow (MCM)
Yarmouk	166
Zarqa	84
N. Side Wadi	58
S. Side Wadi	58
Jordan Valley	8
Wadi Mujib	102
Dead Sea Side Wadi	43
Wadi Hasa	43
Azraq	41
Wadi Hammad	24
Wadi Sarhan	18
Jafer	13
Disi, Southern Desert	1
N. Wadi Araba	46
S. Wadi Araba	8
Total	713

Groundwater Resources

Groundwater is considered to be the main source of water supply in many regions of Jordan and is the only water supply in other regions. More than half of the water supply in Jordan comes from groundwater basins. There are twelve groundwater basins in Jordan (see Figure 4). The Disi and Jafer basins are considered to be "fossil" aquifers. The annual safe yield from these two aquifers is 12 MCM. Recent studies showed that the Disi aquifer can support annual abstraction of 125 MCM for about 50 years. The two largest aquifers that are rechargeable aquifers are the Amman-Zarqa basin and the Dead Sea basin. The maximum annual safe yield from these two basins is 144 MCM. Table 2 provides a summary of the annual safe yield supply from various aquifers in Jordan.

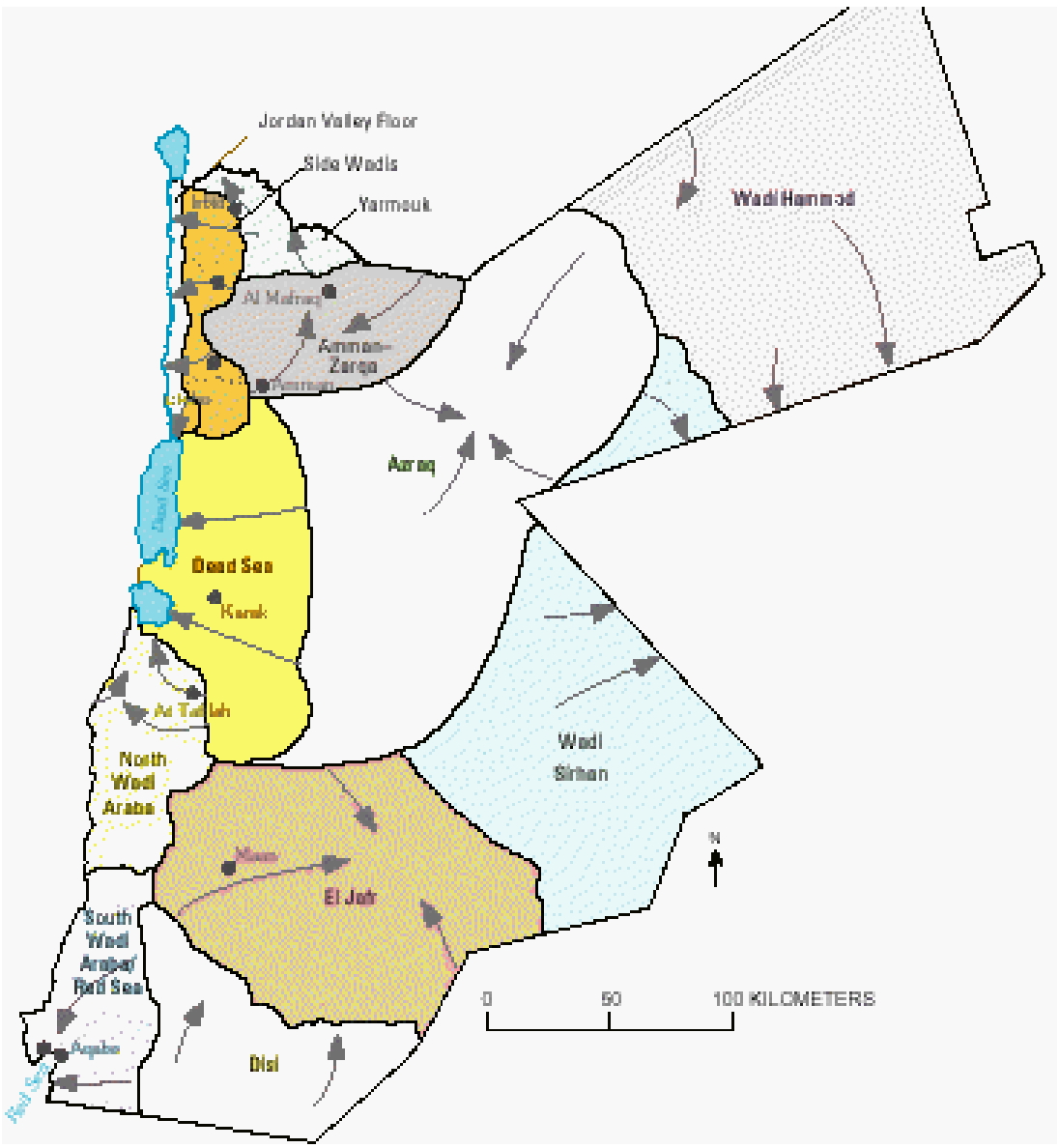

Figure 4. Groundwater Basins

Table 2. Annual Aquifers' Yield

Basin	Safe Yield (MCM)
Amman-Zarqa	87
Dead Sea	57
Yarmouk	40
Azraq	24
Jordan River	21
Jordan River Side Wadis	15
Jafer (Fossil)	9
Wadi Hammad	8
S. Wadi Araba	6
Wadi Sarhan	5
N. Wadi Araba	4
Disi (Fossil)	3
Total	279

Wastewater Resources

Twenty-six of Jordan's cities are served by nineteen wastewater treatment plants (WWTP). The Majority of these treatment plants are stressed. The treated wastewater is considered an integral part of Jordan's sustainable water resources system. About 70% of the population living in urban areas is serviced with sewer collection system. The annual treated wastewater effluent form theses serviced areas is about 80 MCM. The treated effluent is typically used to meet agriculture and live stock demands and as a groundwater recharge source. The agriculture demands are mainly directed towards the Jordan Valley, where the majorly of Jordan's agricultural is located.

The two largest wastewater treatment plants in Jordan are the As-samra and Irbid (Wadi AL-Arab) WWTP. The design capacity of the As-samra WWTP is 68,000 m^3/day and Irbid (Wadi Al-Arab) WWTP design capacity is 21,000 m^3/day.

Additional sustainable source of water in Jordan is obtained from desalination plants. There are two operating desalination plants in Jordan. They are the Abu Zeghan and Zara plants with a total combined treatment capacity of About 31 MCM (10 MCM from Abu Zeghan and 21 MCM form Zara). The desalinated water from these two plants is added to the overall water supply in Jordan. Desalination treatment plants are typically expensive to build and operate in a country with limited resources like Jordan.

Challenges

There are several challenges facing the water sector in Jordan. These challenges include elevated levels of normal population growth rates (including population migrations due to regional conflict), degrading surface and groundwater qualities, and changes in precipitation patterns due to climate change.

The annual average population growth rate is about 2.5%, which is relatively high when compared to other countries of Jordan's size and resources. The massive fluxes of

thousands of refugees (in the span of few months at a time) from neighboring countries as a result of several regional conflicts (e.g. the first Gulf War, the continuous Arab-Israeli conflict, and the second Gulf War) caused an alarming and sudden increase on the water demands in Jordan. In addition to the population increase, the living standards in Jordan are steadily improving and as a result the industrial and agricultural demands are increasing.

To make things worse, Jordan's population projections for the year 2020 is about 9.9 millions with 65% of the populations will be served with sewer service. The projected sewerage generation is about 237 MCM, which is a bout three times the sewerage generation form the current population estimates.

In 1999, the domestic water consumption was 231.5 MCM (29% of the total consumed water in the country). About 79% of the water supply for domestic uses comes from groundwater sources with the exception of the water that is pumped form the Yarmouk River to meet Amman's water demand. The portable water infrastructure in Jordan is not very efficient. Only 45% of the daily domestic consumption accounted for and about 55% of the daily domestic consumption is lost. Table 3 provides a summary of Jordan's water demands and their sources.

Table 3. Water Demand in MCM by Sector in 1999 (S. Tutundjian)

Use	Groundwater Sources (GWS)	% of Total GWS	Surface Water Sources (SWS)	% of Total SWS	Total Supply Sources TSS	% of Total TSS
Domestic	183	79	49	21	231	29
Industrial	35.5	94.4	2.1	5.6	37.6	5
Agriculture	256	49.1	265	50.9	521	65
other	7.3	64.6	4	35.4	11.3	1
Total	481		320		801	

The effluent's salinity from WWTP in Jordan is typically higher than normal due to low domestic use levels (due water conservation efforts, and intermittent service) and the use of standard treatment technologies like stabilization ponds in the current WWTP. In addition, to the reasons mentioned above, the high evaporation rate in Jordan results in loss of liquid sewerage water from the stabilization ponds to the atmosphere, which in turn increases the sewerage water salinity. The use of the brackish water to recharge groundwater sources result in additional degradation of the groundwater supply

The regulation on industrial discharge to the public sewer collection lines is loosely enforced in Jordan. Therefore, industrial effluent from various types of industries with varying industrial wastewater strengths are currently being discharged into public sewers collection lines and eventually treated by municipal WWTP using standard technologies that is used to treat domestic sewerage. As result, when released, the treated effluent from the municipal WWTP is less desirable for agricultural purposes.

Industrial demands accounts for about 5% (see Table 3) of Jordan's total water supply. About 94% of the industrial demand comes from groundwater resources. This is projected to increase due to improvements in the industrial sector in the country, Jordan's

inclusion in the World Trade Organization (WTO) and the signed free trade agreements between Jordan and the United States and the establishments of the free zones in different regions of Jordan. These agreements make Jordan a desirable destination for regional investors and manufacturers.

The agriculture sector in Jordan is the largest water consumer. This sector uses about 65% (see Table 3) of the total water demand in Jordan. About 49% of the agricultural demand comes from groundwater resources. The majority of the irrigated land in Jordan is located in the highland and the desert (about 52,700 hectars), and in the Jordan Valley (about 31,600 hectars).

It's clear the importance of groundwater in Jordan's overall water resources plan to meet its current water demand. Yet there is a shortage of about 40% in the groundwater supply to reach the current total water demand. The 2005 estimates of available water supplies in Jordan from various sources is 816 MCM (275 MCM from Groundwater, 56 MCM groundwater recharge, 395 MCM surface water, 80 MCM from WWTP effluent, and 10 MCM from desalinated water). The projected increase in the water demand form the three major sectors (99% of the total water demand) in Jordan are presented in Table 4.

Table 4. Previous, Current and Projected Water Demands in MCM (M. Mohsen)

Use	Year			
	1999	2005	2010	2020
Domestic	231	382	434	611
Industrial	37.6	81	99	146
Agriculture	521	858	904	890
Total	789.6	1321	1436	1647

A quick comparison of the water supply in 2005 (used as a reference for the comparison) with water demand in 1999, 2005, 2010 1 and 2020 (see Table 5) reveals major water deficit in all years analyzed expect in 1999. It's clearly demonstrated that the problem of water shortages in Jordan is a chronic problem for years to come. If the current domestic, agricultural and industrial practices are not addressed, the water supply in Jordan will deplete in quantity and quality with time. This will also make the problem of water shortages even worse than actually shown in Table 5. Overdraft of groundwater and surface water is creating a tremendous stress on the water supply in Jordan. Large losses from surface waters (i.e. the Dead Sea) are also a problem that the Jordan has to address in order to at least to reduce these losses.

Table 5. Water Management and Projections in MCM

Year	Available Water Supply	Demand	Deficit
199	801	789.6	+11.4
2005	816	1321	505
2010		1436	620
2020		1647	831

Accomplishment

In order for Jordan to balance its water budget, support the growth plans envisioned in the country, and provide the basic element of life to Jordanians, the government needs to take certain steps to increase the water supply and reduce demands.

Increasing supply should be the most important objective of Jordan's water planners. In order to achieve this objective, the government is forging ahead with major joint projects with neighboring countries (Egypt, Syria, Israel, and Palestine) and applying water conservation practices. The steps the government is proposing to meet and exceed the water demand is listed below.

1. Building Al-Wehda dam will add 100 MCM to the water supply in Jordan. The project is on hold until a peace treaty is forged between Syria and Israel.
2. The main source of additional water supply in Jordan will come from the Dead Sea-Red Sea channel project (or the Peace Conduit). This project is in its early phases. The environmental assessment study and feasibility study were just awarded to French and British companies. When completed, this project will provide Jordan with 570 MCM in 2022. The project is in co-operation between Jordan, Egypt, Israel, and Palestine with the financial support form the world community (the United States of America, the European Union, the World Back and other financial agencies). This is a major piece in the water supply puzzle for Jordan to meet its future water supply.
3. The Disi Project will increase the water supply from the Disi basin (fossil basin) by 100 MCM by the year 2011, which is projected to be depleted in 50 years. This is a temporary fix but it's necessary.
4. More surface water can be harvested by employing better water management practices and building small earthen dams. The exploitation of additional surface water will add 139 MCM to the current 395 MCM.
5. Employing non-traditional water management practices will increase water supply. Some of these practices include but not limited to: improvement of the effluent quality form WWTP by employing new technologies and improve water retention in the WWTP stabilization ponds. These practices will add about 89 MCM in 2020 to the current level of 80 MCM.
6. Invest in desalination technology utilizing sustainable energy sources like solar and wind energies. Jordan implemented two projects that will add 65.5 MCM of available water in 2020 to the current levels of desalinated water of 31 MCM.
7. Utilizing surface runoff to recharge groundwater will add about 26 MCM above the current recharge amount of 56 MCM.

Evaluation of the completed and proposed projects and the implementation of the strategies suggested by Jordan's government one can see that Jordan will be able to or close to meet its water demands by 2020. Until then, Jordan needs to apply short-term fixes like:

1. Improve the portable water infrastructure which will save about 30-40% of the water that is being lost.
2. Enforce existing and propose stricter laws on sewerage and industrial effluent to municipal WWTPs.
3. Increase outreach efforts to citizens and provide incentives to water conservation efforts especially from the agricultural sector.

References

Tutundjian S. Water Resources in Jordan, Online Resource, 2001.

Mohsen, M. Water Needs in the Middle East Region, From Red Sea to Dead Sea-Water and Energy, Geneva Conference, 2007.

Raddad, K." Water Resources and Use Workshop on Environment Statistics", Dakar, Senegal, 2005.

Halasah, N. and Ammary, B. "Groundwater Resources in Jordan" Online resources, 2007

Impacts of Mining in the Upper Zambezi River Basin: an overview of the Zambian Copperbelt

Imasiku A. Nyambe
Professor and Coordinator, Integrated Water Resource Management Center, C/o School of Mines, University of Zambia, Great East Road, Lusaka 10101 Zambia;
PH 260-955-793600; FAX 260-211-294086 / 290165;
e-mail:inyambe@unza.zm

ABSTRACT: The Zambezi River Basin (ZRB) is the largest river basin in Southern Africa, covering some 1.37 million square kilometers across eight countries: Angola, Botswana, Malawi, Mozambique, Namibia, Tanzania, Zambia, and Zimbabwe. It is home to approximately 30 million people who rely on the river for drinking water, fisheries, irrigation, hydropower production, mining and industry, ecosystem maintenance, and other uses such as tourism at Victoria Falls and wildlife viewing along the river banks. Water management in the basin is especially difficult because there are multiple countries with multiple and competing interests; competing issues other than water that demand time, attention, and money; inadequate basin-level institutional structures; institutional, legal, economic, and human resource constraints within each country; and poor data collection, poor communication, and inadequate training. However, Zambia has a lion's share of the basin with 105.2km^3/ac of water resources covering 75% of the country of a total area of 752,614 sq. km.

Zambia's life line is depended on the Zambezi River Basin's waters, for example, the Kafue River sub-basin is home to the Zambian Copperbelt where huge copper mining have been practiced for almost a century. Further to the west, more new mines have come on line or are about to do so. The middle of the sub-basin occur Lusaka – the capital with a very fast growing population and further down are the large scale sugar-cane farms and industries such as Nitrogen Chemicals of Zambia at Kafue Town. In addition, energy needs, in form of electricity, are drawn from the same Kafue River resulting in competing needs between agriculture (both small & large) and energy. These land uses in addition to growing population have threatened the water resource of the Zambezi River Basin particularly the Kafue River sub-basin both in quantity and quality. Mining in particular has been blamed for water pollution in the Zambezi River Basin. Indeed, recent studies indicate that mining activities have contributed to contaminated soils, stream sediments and water, and agricultural plants such as cassava and sweet-potatoes leaves. These studies have recommended to the Zambian Government as a way of mitigating mining contamination as follows:

- Monitoring and evaluation of long-term trends of contaminated mapped parts of the Copperbelt is highly desirable for the high-quality environmental management.
- A new progressive technology including dust limiting electro-static filters is necessary to reduce the impact of dust fall from smelters and processing plants.
- Reducing the amount of airborne particles that originate from impoundment beaches, capping of beaches by a mixture of clayey laterite and ground limestone is suggested together with overlaping of remedied surfaces with plant residues (i. e. trash conservation or mulching).
- The use of treated municipal seawage to improve the fertility of reclaimed surfaces of tailing impoudments.
- Thickening of tailings should be preferred over wet deposition, combined with high quality seepage barriers and return systems.

1.0 Introduction

The Zambezi River Basin is the largest river basin in Southern Africa, covering some 1.37 million square kilometers across eight countries extending through Angola (18.2%), Botswana (2.8%), Malawi (7.7%), Mozambique (11.4%), Namibia (1.2%), Tanzania (2.0%), Zambia (40.7%) and Zimbabwe (16.0%) (Figure 1).

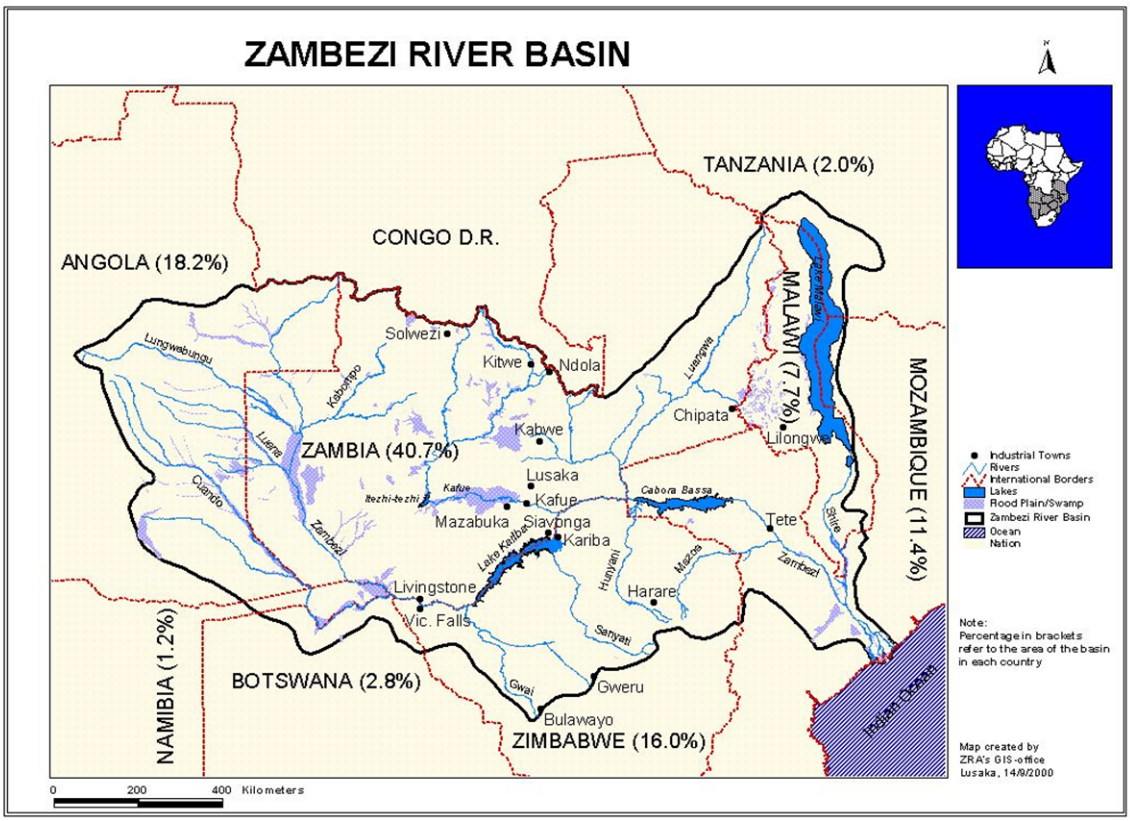

Figure 1: The Zambezi River Basin [adapted from Zambezi River Authority (ZRA), 2000]. Note the area occupied by the Basin in each riparian state)

Renewable water resources in the ZRB as contributed by each riparian country are given in Table 1 (Scholes and Biggs, 2004).

Table 1: Renewable Water Resources by ZR basin country (*after Scholes and Biggs 2004*)

Basin Countries	**Renewable Water Resources**			
	Total (km^3/ac)	**Withdrawals (km^3/ac)**	**Withdrawals % of Total**	**Water 2001 (m^3/person)**
Angola	184.0	0.4	0.19%	13,620
Botswana	14.4	0.1	0.97%	8,471
Malawi	17.3	0.6	3.65%	1,641 [a]
Mozambique	216.1	0.6	0.29%	11,960
Namibia	17.9	0.3	1.51%	10,022
Tanzania	91.0	2.0	2.20%	2,642
Zambia	105.2	1.7	1.65%	10,233
Zimbabwe	20.0	2.6	13.05%	1,560 [a]
[a] Indicates water stress (<1,700 m^3/person)				

From Figure 1, it is clear that Zambia has a lion's share of the basin's surface area covering 75% of the country's total area of' 752,614 sq. km whereas Table 1 indicates that Zambia takes 3rd place in the total water resource of 105.2km^3/ac after Angola (184.0km^3/ac) and Mozambique (216.1km^3/ac).

Zambia's life line is depended on the Zambezi River Basin's waters, for example, the Kafue River sub-basin is home to the Zambian Copperbelt where huge copper mining have been practiced for almost a century. Further to the west, more new mines have come on line or are about to do so. The middle of the sub-basin occur Lusaka – the capital with a very fast growing population and further down are the large scale sugar-cane farms and industries such as Nitrogen Chemicals of Zambia at Kafue Town. These land uses in addition to growing population have threatened the water resource of the Zambezi River Basin particularly the Kafue River sub-basin both in quantity and quality. Mining in particular has been blamed for water pollution in the Upper Zambezi River Basin of the Kafue River sub-basin (Figure 2).

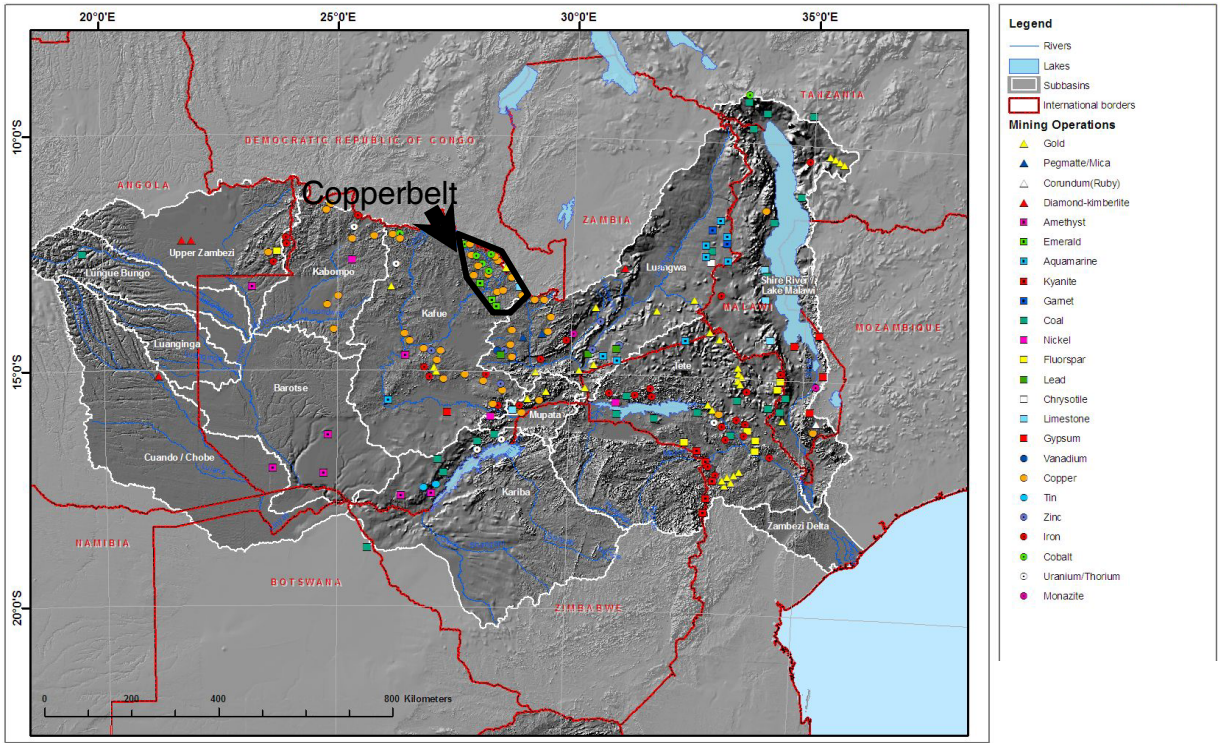

Figure 2: Zambezi River Basin showing location of Zambian Copperbelt (modified from Euroconsult Mott MacDonald, 2007)

This paper therefore looks at the water and stream sediment of the Zambian Copperbelt as impacted by mining and whether it is practical to have standard water quality for the entire Zambezi River Basin.

2.0 Mining on the Zambian Copperbelt

Zambia is an irregularly shaped, land-locked country which contains vast mineral resources. The most important of these are the copper and cobalt metals mined on the Zambian Copperbelt (Figure 3).

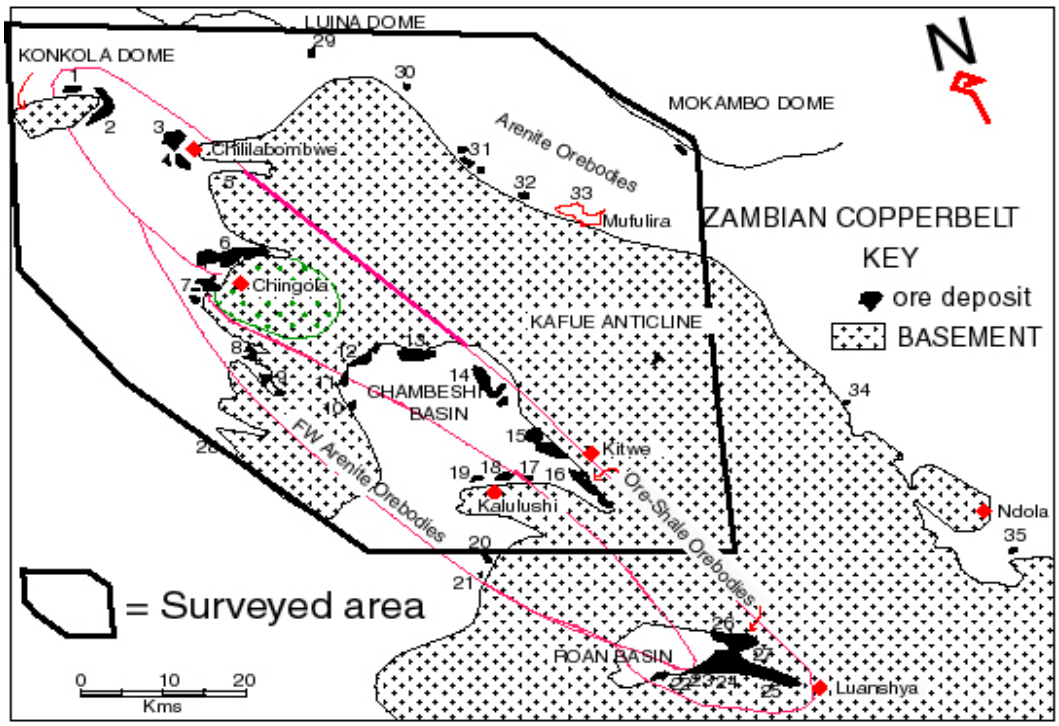

Figure 3: Map of Zambian Copperbelt showing the mining copper ore districts of Chililabombwe (Konkola Mine), Chingola (Nchanga Mine), Mufulira (Mufulira Mine), Chambeshi (Chambeshi Mine), Kalulushi (Chibuluma Mine) Kitwe (Nkana Mine) in the studied area.

For many years, copper mining has supported the social and economic development of the country accounting for about 93% of all Zambia's foreign exchange earnings in 1991, but declined to 72% in 1995. Minerals of all types accounted for 9.8% of export earnings in 1992. On the overall, the Mining Industry was the main contributor to the country's Gross Domestic Product (GDP), contributing an average of 35% (1965-1970), which significantly reduced to an average of 8% during the period 2000 to 2005 rising up to 11.8% in 2006 (Figure 4). For example, in 2004, mining contributed K 2,550 Billion to the total GDP of K32, 141 Billion i.e. 8% of GDP.

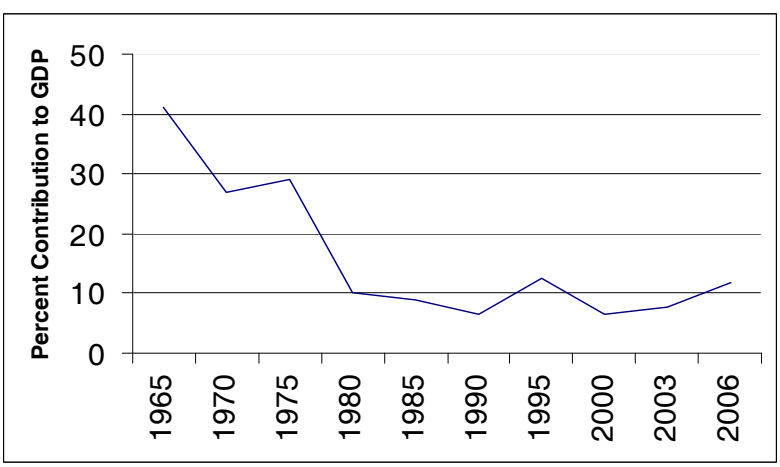

Figure 4: Percent Contribution of Mining to GDP (Source: Central Statistics Office)

Since 1914 to 2002, Zambia has produced enormous tonnages of copper (Figure 5).

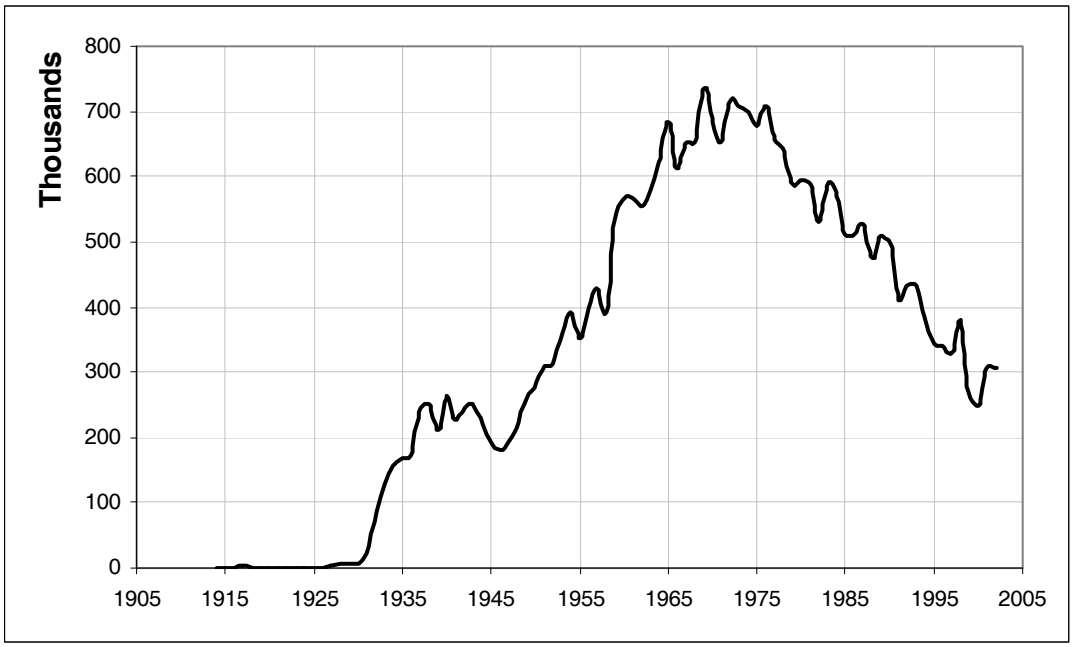

Figure 5: Copper production in Zambia (1914-2002) (Nyambe and Kawamya, 2005)

With these huge copper tonnages, over 600,000 tones between 1964 and 1980 for example, meant that the mining companies had to have licenses to discharge waste into the environment. For example, former Zambia Consolidated Copper Mines Limited, held 9 licenses, to discharge tailings effluent into public streams. It further held 25 licenses to operate tailings dams, 7 licenses to operate domestic waste disposal sites, 7 licenses to operate slag dumps and 8 licenses to transport tailings to tailings dams. The mining activities have led to some pollution of surface and ground waters, degradation of arable land and siltation.

3. Environmental Impacts

Increased levels of mining activities coupled with many years of mining particularly copper has impacted negatively on the surface cover, especially the large-scale mining operations on the Copperbelt (e.g. Nchanga Open Pit and Nkana Smelter (Figure 6a & b).

Open-cast operations have a huge tonnage of overburden consisting of waste rocks and overburden disposed of in waste dumps, overburden dumps and waste rock dumps (Figure 6a). There are 32 overburden dumps in Zambia's mining industry containing 1.899 million tones of overburden and covering an area of about 206,465ha.Waste rock is generated in underground shaft mining. There are 21 waste rock dumps with approximately 77 million tones of waste rock. They cover an area of 388 ha. Slag is waste material produced from smelting of concentrates. It is delivered for disposal in molten or granulated state. There are 9 slag dumps containing 40 million tones of slag. They cover an area of 279 ha. There 45 dumps/dams containing 791 million tones of tailings covering an area of approximately 9,562ha. As at 2005, a total of 216,257 ha were covered by overburden, slag, tailings and waste rock dumps occupying land that could otherwise be used for other purposes.



(a)



(b)

Figure 6: (a) Nchanga Open Pit on the Copperbelt and (b) Overview of Nkana Smelter on the Copperbelt.

Underground mining operations have also impacted negatively on the environment affecting an area of 4,000 ha that is prone to subsidence and thus protected. De-watering from underground workings adds about 500,000m ^{3}/day of water into the Kafue River, a major Zambian river that flows through this mining zone. The river is the source of water for household (including drinking water) and industrial use.

These mining activities have a broad range of effects on the environment and the ecosystem (terrestrial systems, river drainage patterns & human health) that result, for example, from tailings (slimes), slag and minor amounts of toxic hazardous chemical wastes as sources of chemical pollution to water resource due mainly from oxidation of the sulfides.

Processing facilities consisting mainly of crushers, concentrators, smelters and refineries produce among others tailings that feed into tailing impoundments (Figure 7a) providing dust fallout (Figure 7b) on dry sections ("beaches") affecting plant leaves to a distance of a few kilometers from the source of pollution, whereas their dams leak, discharging a pulp rich in iron. The contents of Cu in these precipitates vary between 800 and 2 500 ppm, Co between 780 and 1 900 ppm As 2.7 up to 350 ppm, and Pb 14 and 270 ppm (Kříbek and Nyambe, 2004).



(a)



(b)

Figure 7: (a) Tailing impoundment – wet part; (b) dry part providing dust fallout affecting plant leaves

Effluents from the mines have already been blamed for loss of aquatic life down-stream along the Kafue River locally. For example, cattle losses have been reported due to consuming copper-rich sediment (and possibly vegetation) stirred up at the time of drinking near the Mwambashi River (ZCCM, 1982).

Recent studies undertaken by Kribek et. al, (2002, 2004, and 2006) indicate that main sources of strong anthropogenic contamination with heavy metals (As, Hg, Co, Cu, Pb and Zn) are:

- industrial water released from processing plants and smelters,
- solid and gaseous emissions from smelters,
- seepage through the tailings impoundment dams,
- wash-out of fine-grained material from spoil banks,
- airborne particles from beaches of tailings pond and, airborne particles from crushers.

Contamination of surface waters is ascribed to (i) siltation that results from washout of fine particles from dumps and ore-processing plants, (ii) overflow of water from tailing facilities, (iii) leakage of water through the tailing facilities dams and (iv) the drainage of technological waters from smelters and acid plants.

The contamination of the Copperbelt region by cobalt (Co), copper (Cu), manganese (Mn), selenium (Se), sulphates (SO_4), calcium (Ca) and magnesium (Mg) markedly exceeds the permissible values for surface waters in the European Union. The pH of waste waters from ore dressing plants employing chemical technologies fluctuates between 2.04 and 3.62 when insufficiently limed. The contents of metals in these acid waters exceed the permissible values for surface waters in the European Union by ten times. Limits for cadmium (Cd), nickel (Ni), selenium (Se) and zinc (Zn) also exceed the standards. The contents of toxic elements in stream sediments reach 1,296 ppm As, 3,660 ppm Co, 1257 ppm chromium (Cr), 65 460 ppm Cu (Figure 8), 6.47 ppm Hg, 48 ppm molybdenum (Mo), 360 ppm Ni, 1 370 ppm Pb, 3 590 ppm Zn and 2.1 % sulphur total ($S_{tot.}$). Fortunately, the acid neutralising capacity of river sediments and riverbed rocks is high and the contamination of water significantly decreases downstream of the contaminated sources.

These studies have also shown that on the Copperbelt, soils are general elevated in copper because of the high natural background levels. In contaminated areas contents of copper in fresh agricultural products of cassava and sweet potato leaves reach as much as 253.8 ppm, cobalt 18.9 ppm, arsenic 7ppm, nickel 3.4 ppm, lead 5.04 ppm and zinc 161 ppm.

The elevated natural background levels of copper on the Copperbelt, for example, cannot be substituted with a standard from Mongu in the Barotse flood plains of western Zambia that is entirely made up of Kalahari quartz-rich sands. This will definitely condemn the entire Copperbelt as inhabitable. For the Zambezi River Basin, regional standards are thus recommended.

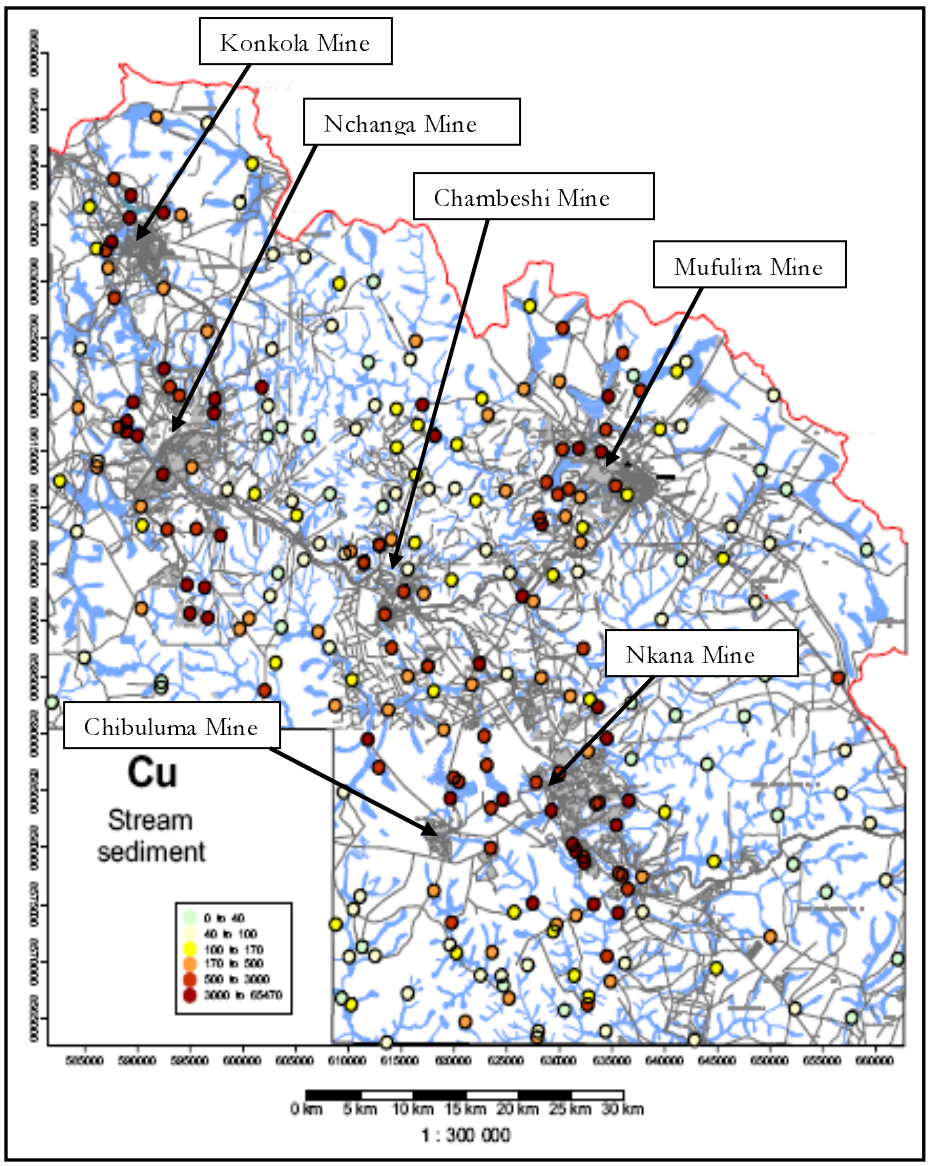

Figure 8: Copper (Cu) in stream sediments. Note high values are related to an operating mine with a maximum up to 65 460 ppm Cu.

4. Observations and Recommendation

Mining activities have indeed contaminated water and stream sediments and in some cases agricultural plants such as cassava and sweet-potatoes leaves have been affected. The significant decrease in contamination levels and the high background levels for a given metal e.g. copper in this case is an indication that a blanket figure for water quality cannot be used for the entire Zambezi River Basin. For example a value of a metal from a district where such a metal does not occur cannot be applied in a district where it occurs despite that they occur in the same basin. Use of local standards per region or district is recommended.

It is therefore useful as recommendations to the Zambian Government to mitigate mining contamination as follows:

- Monitoring and evaluation of long-term trends of contaminated mapped parts of the Copperbelt is highly desirable for the high-quality environmental management.
- A new progressive technology including dust limiting electro-static filters is necessary to reduce the impact of dust fall from smelters and processing plants.
- Reducing the amount of airborne particles that originate from impoundment beaches, capping of beaches by a mixture of clayey laterite and ground limestone is suggested together with overlaping of remedied surfaces with plant residues (i. e., trash conservation or mulching).
- The use of treated municipal seawage to improve the fertility of reclaimed surfaces of tailing impoudments.
- Thickening of tailings should be preferred over wet deposition, combined with high quality seepage barriers and return systems.

References

Kříbek, B. – Nyambe, I. (eds.) (2002): Evaluation of the environmental impacts of copper and cobalt mining in the Zambian part of the Copperbelt and a heavy metals and sulfur contamination and monitoring system proposal. Kitwe area. – Project of the Technical Aid of the Czech Republic to the Republic of Zambia in the year 2002. – MS Czech Geological Survey, Praha, 140 p.

Kříbek, B. – Nyambe, I. (eds.) (2004): Impact assessment of mining and processing of copper and cobalt ores on the environment in the Copperbelt, Zambia. Project of the Technical Aid of the Czech Republic to the Republic of Zambia in the year 2004. – MS Czech Geological Survey, Praha, 160 p.

Kříbek, B. – Nyambe, I. (eds.) (2005): Impact assessment of mining and processing of copper and cobalt ores on the environment in the Copperbelt, Zambia. Kitwe and Mufulira areas. – Project of the development assistance program of the Czech Republic for the years 2004-2006. Final report for year 2004. – MS Czech Geological Survey, Praha, 196 p.

Kříbek, B. – Nyambe, I. (eds.) (2006): Impact assessment of mining and processing of copper and cobalt ores on the environment in the Copperbelt, Zambia. Eastern part of the Kitwe and Mufulira areas. – Project of the Technical Aid of the Czech Republic to the Republic of Zambia in the year 2005. – MS. Czech Geological Survey, Praha, 135 p (in Czech).

Nyambe I. A., and Kawamya M. V., 2005. Approaches to sustainable minerals development in Zambia in Marker B. R., Petterson, M.G., McEvoy, F., and Stephenson, M. H., (Eds). Sustainable Minerals Operations in the Developing World. Journal of the Geological Society of London Special Publications, 250, pp.73-86.

Scholes, Robert J. and R. Biggs (2004). *Ecosystem services in Southern Africa: A Regional assessment.* Pretoria: Council for Scientific and Industrial Research.

ZCCM – Zambia Copper and Cobalt Mining Investment Holdings Plc. (1982): Environmental assessment of the Copperbelt and Kabwe areas. MS E 539. – MS ZCCM Investment Holding Plc. Nkana, Zambia, 268 p.

Improving the Water Quality of One of the World's Great Lakes: Tai Lake Case Study of Environmental Responsibility in the Developing World

D. P. Albers, PE[1]

[1]Ecology and Environment, Inc., 368 Pleasant View Drive, Lancaster, New York, 14086; PH (716) 684-8060; email: dalbers@ene.com

ABSTRACT

China's Tai Lake is one of the world's great lakes. Located in eastern China near the city of Shanghai, over 30 million people live within the lake's watershed. In 2007 Tai Lake experienced a major algal bloom, which resulted in the suspension of water supplies to Wuxi City. In response, the Chinese central government tasked the China Development Bank (CDB) with creating an environmental loan program to assist in improving the lake's water quality.

Ecology and Environment, Inc. (E & E) was hired by the CDB to assist in identifying loan opportunities that could be used to improved Tai Lake's water quality. A principle finding was the willingness of local authorities to fund large-scale environmental projects. Another significant finding was the recognition within the watershed of the need to shift funding away from wastewater treatment plants and toward measures to intercept polluted runoff from non-point sources.

The approach presented in this paper provides a model for developing countries to create effective and comprehensive environmental loan programs and the supporting strategies needed to help ensure their success.

INTRODUCTION AND APPROACH

This case study provides an example of how a proposed large-scale environmental loan program was developed for China, a rapidly developing nation facing severe environmental challenges. Tai Lake, which is located in eastern Chine near the city of Shanghai, is one of the world's great lakes: the lake has a surface area of greater than 2,300 square kilometers (900 square miles), and over 30 million people live within its watershed (see Figure 1). The lake basin is a resource of national significance, and it is afflicted with serious water quality problems. For several years the water quality of Tai Lake has been below the goals set by China's Ministry of Environment. The most significant issues affecting water quality are algal blooms, high levels of nutrients in the lake's waters, and high levels of oxygen demand. These issues are the direct result of the region's recent industrial, agricultural, and



Figure 1. Tai Lake Basin Map

residential development and represent significant challenges to improving the water quality of Tai Lake.

In 2007 Tai Lake experienced a major algal bloom, which resulted in the suspension of water supplies to Wuxi City. In response, the Chinese central government (in coordination with other efforts) tasked the China Development Bank (CDB) with creating an environmental loan program to assist in improving the lake's water quality. Major international development banks have been making environmental loans to China for decades. This effort reflects China's desire to create a similar environmental loan program for a major Chinese bank.

Comprehensive planning and secure sources of project funding are needed if the problems affecting Tai Lake are to be effectively addressed. Significant planning efforts have been made. Additional coordination will focus efforts on addressing the causes of the lake's water quality problems to achieve lasting improvements.

Ecology and Environment, Inc. (E & E) was hired by the CDB to assist in the development an environmental loan program to address the water quality problems faced by Tai Lake. Our understanding of these problems was developed through a combination of site visits, literature and data reviews, and interviews with government officials and scientists. We then reviewed remedies that had been applied in developed nations to lakes with similar problems.

Based on our findings, a summary of the general causes of the lake's poor water quality was developed and presented to the CDB staff so that they could understand the types of problems that environmental projects should focus on to improve Tai Lake's water quality. Next, projects proposed by municipal and provincial governments to address the water quality problems in Tai Lake were summarized and evaluated for their likely impact on water quality. This was done using an evaluation procedure developed to rank the proposed projects. E & E then developed a work plan for the next phase, which involved developing a coordinated water quality management strategy for Tai Lake that includes all of the major stakeholders. Finally, we developed a detailed approach for an environmental loan program and presented the approach to the CDB.

WATER QUALITY UNDERSTANDING

Although the region depends on Tai Lake for most of its water supply, the water quality in much of Tai Lake is so poor that the water is, in places, not even fit for use as irrigation water. The most prominent water quality problem in Tai Lake—large blooms of blue-green algae—is caused by high levels of phosphorus. The high phosphorus levels are resulting in eutrophication of the lake, which has been accelerating in recent years.

The data relating to sources and quantities of nutrients entering the lake are incomplete and contradictory. No single agency is collecting or coordinating this information, and existing data collection arrangements do not adequately cover the agricultural areas from which the largest nutrient flows likely come.

It is clear from the available data, however, that rapid economic development, urbanization, and population growth in the Tai Lake basin have caused a large increase in water demand for residential, agricultural, and industrial purposes, and has resulted in the discharge of significant amounts of untreated and partially treated wastewater into the lake basin. Industrialization of the region began in the 1970s, and by the year 2000, 460 million cubic meters of domestic wastewater, 1 billion cubic meters of industrial wastewater, and an unknown but large volume of non-point source wastewater (e.g., agricultural runoff) was being discharged into the lake annually. Treatment capacity has increased significantly, but it has not kept up with the need.

CURRENT PROJECTS

The governments in the Tai Lake basin have been working diligently to develop water quality improvement projects for several years. An extensive list of projects that could have a positive impact on the water quality of Tai Lake was developed based on trips to the Tai Lake basin, projects proposed by the local governments and projects identified in the 11th Five-Year Plan (MEPA, 2007). This list contained over 300 projects in various stages of development and was organized into the following project types:

- Effective stop-gap measures that could reduce the steep decline in the lake's water quality and safeguard drinking water supplies;
- More and better wastewater treatment plants;
- More effective treatment of potable water;
- Control of runoff from agricultural lands;
- Focused interventions on industrial discharges based on contaminants of concern; and
- Alternate sources for drinking water.

The criteria we used to evaluate and rank projects for funding and implementation are summarized below. We ranked each criterion for each project based on the presumed likelihood the proposed project would meet the criteria and computed an overall score for each project.

- Magnitude of Impact
- Cost-Effectiveness
- Long-term Effectiveness

- No Environmental Harm
- Induced Impacts
- Location/Proximity Benefits
- Amenity Enhancements
- Proven/Reliable
- Implementable
- Status of Project Planning/Design

COORDINATED WATER QUALITY MANAGEMENT STRATEGY

We developed a coordinated water quality management strategy to meet the goals established in the 11th Five Year Plan to clean up Tai Lake. These goals include the following:

- Improve Tai Lake water quality to protect drinking water
- Control industrial pollution sources to meet discharge standards
- Effectively control all water pollution discharges to the lake
- Strengthen the water quality monitoring and water pollution alarm system

The following short-term objectives are based on meetings and with local and national environmental agencies:

- Improve lake water quality from below Class V to Class V
- Improve the water quality of the eastern portion of the Lake from Class V to Class IV
- Halt the trend in increasing eutrophic levels in Tai Lake
- Improve the quality of the major drinking water sources and transport canals to Class III
- Improve the percent compliance with water quality standards in rivers and canals from 18.6% to 40%

The following long-term objectives were also based on meetings and with local and national environmental agencies:

- Improve lake water quality to Class IV
- Improve the eutrophic level of the lake
- Improve the percent compliance with water quality standards in rivers and canals to 80%

To achieve these objectives, we developed a strategy based on a review of several large international water quality programs, incorporating the best parts and most applicable approaches to the situation at Tai Lake, while paying close attention to lessons learned from those programs.

Based on our review, we recommended the creation of a management structure to properly plan and coordinate the efforts needed to achieve the short- and long-term water quality objectives set for Tai Lake. To help ensure success, this body should include representatives from the major stakeholders that would be involved in the overall program.

Some of the functions of this management body include:

- Coordinating the efforts of cities, provinces, and various government agencies involved in the effort to improve the water quality of Tai Lake;
- Reducing or eliminating duplications of efforts; and
- Reducing the difficulties in sharing information about successes and failures associated with the various projects.

We suggested calling this group the "Tai Basin Water Quality Steering Committee." Working under the Steering Committee, a newly created "Tai Basin Program Management Office" comprising the Technical Resource, Research, and Finance Groups would manage day-to-day concerns such as administration and strategy implementation. The Technical Resource Group would oversee the Design and Construction sub-groups, while the Research Group would house the Modeling and Monitoring sub-groups. This proposed management structure is presented in Figure 2.

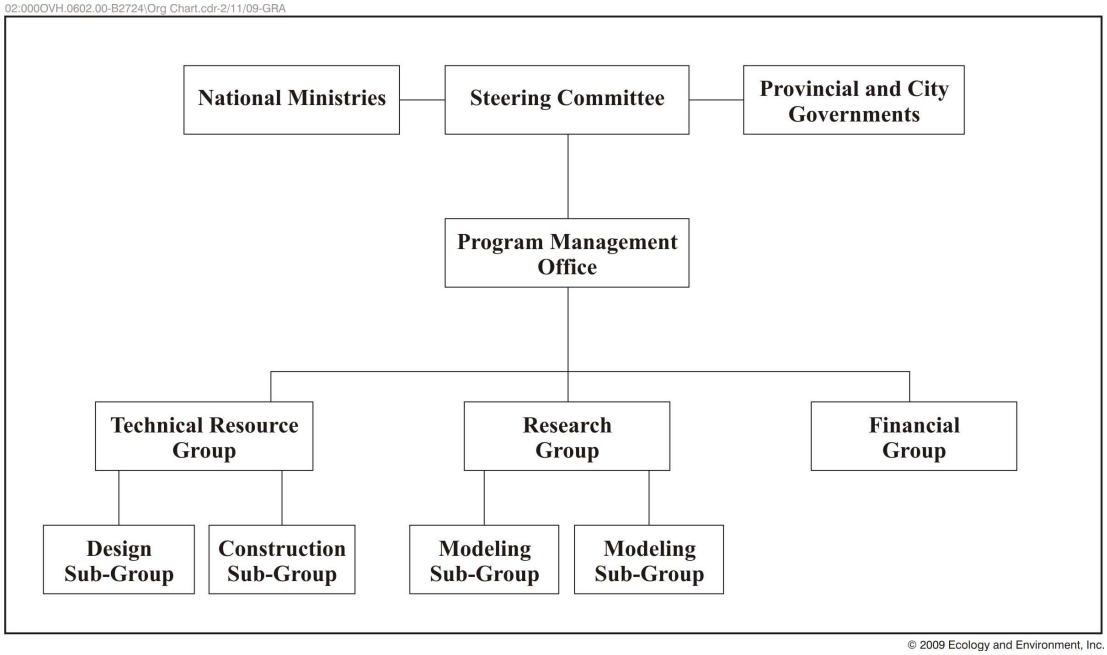

Figure 2. Proposed Tai Lake Water Quality Management Program Structure

The Steering Committee. The Tai Basin Water Quality Steering Committee would provide executive-level management for the Water Quality Management Program and

act as a high-level consultation and coordination body. A principal function of the Steering Committee would be to coordinate the numerous water quality improvement efforts that are now dispersed among many national ministries and agencies, several provinces, numerous large cities, and many smaller cities, and it would work to resolve intergovernmental conflicts on water quality issues. The Steering Committee should have sufficient power to enforce its decisions. It would also ensure the close coordination of the water quality management program with regional economic, environmental, and social development programs.

The Program Management Office. The main role of the Tai Basin Program Management Office (PMO) would be to develop and undertake the Water Quality Implementation Plan. In undertaking the implementation plan, the PMO would deal with day-to-day management affairs, including human resources, administration, public notification and press releases, resource administration (buildings, equipment, laboratories, etc.), day-to-day problems, and crisis management. It would also gather the data necessary to gauge the success of the program and make suggestions to the Steering Committee about how the program might be altered to be more successful.

The Technical Resource Group. The main role of the Technical Resource Group would be to review project designs and monitor construction of water quality management projects. This group would report to the PMO and would be comprised of two major sub-groups: the Design Sub-Group and the Construction Sub-Group.

The main role of the Design Sub-Group would be to review the technical designs of projects with regards to their technical adequacy. The goals of the Design Sub-Group would be to ensure that proposed project designs are technically sound, that they would address the water quality problem they are intended to address, and that lessons learned from previous projects can be incorporated into the designs of newly proposed projects.

The main role of the Construction Sub-Group would be to provide oversight and monitoring during project construction. The goals of this sub-group would be to ensure the proper utilization of resources and the completion of the construction work as presented in earlier planning and design stages.

The Research Group. The main role of the Research Group would be to provide a scientific understanding of the root causes of Tai Lake's water quality problems and a scientific method for predicting the relative effectiveness of various management strategies. The Research Group would be a consortium of government research organizations, universities, and industrial research organizations. This group would report to the PMO and would be comprised of two major sub-groups: the Monitoring Sub-Group and the Modeling Sub-Group.

Monitoring provides accountability for management actions. A coordinated and comprehensive monitoring network would provide the information required by the managers to make informed decisions, adapt their actions as needed, and provide effective stewardship of Tai Lake's water resources. It is anticipated that the bulk of the Tai Lake monitoring effort would be conducted by various organizations already involved to some extent in monitoring Tai Lake's water quality. The goal of the Monitoring Sub-Group would be to coordinate and standardize these various efforts and to centralize the collected data.

The goal of the Modeling Sub-Group would be to develop descriptive tools relating pollutant sources to water quality impacts and to use these tools to predict the effectiveness of alternative pollution control strategies.

The Financial Group. The main role of the Financial Group would be to identify funding sources and to match available funding to proposed projects. The Financial Group would also assess whether proposed projects are financially viable and sustainable. The Financial Group would ensure that entities proposing to implement water quality projects are financially capable and, where necessary, would provide guidance and recommendations to improve their financial management systems.

ENVIRONMENTAL LOAN PROGRAM APPROACH

Having determined, in principle, which projects the CDB and the local governments wish to pursue as part of the comprehensive program to improve water quality in Tai Lake, the next tasks would be to prepare the projects for funding, obtain the necessary funding, and then implement the projects. The project preparation phase begins with an initial concept for a project backed by feasibility studies. To determine whether a proposed project is feasible, sustainable, and suitable for CDB funding requires considerable effort on the part of the Implementing Entity (i.e., the entity that would construct and operate the project), consultants, local government officials, and CDB staff.

This effort is divided into two parts. The first part of the project preparation process is to undertake a detailed review and assessment of each potential project to determine its initial suitability for CDB financing. This assessment would consist of the following types of activities:

- Technical analysis
- Environmental impact assessment
- Social and health impact analysis
- Resettlement assessment
- Public consultation
- Financial analysis
- Economic analysis

- Creating a management information system
- A managerial and organizational review
- Creating a Project Performance Monitoring System
- Recommending loan covenants and loan review procedures

Based on the results of the review and analysis work described above, the CDB would make a determination as to whether the proposed project is potentially suitable for funding. If suitable, a detailed loan report would be written for the consideration of the CDB Board of Directors. The loan report would include a description of the project and a discussion of the need for the project, its objectives and goals, the necessary inputs and outputs, associated activities and milestones, and a summary of the reviews listed above.

After the loan report for a specific project has been approved and funding has been put in place, project-specific implementation activities begin (e.g., final design, tendering, and construction). The purpose of these activities is to provide assurances to CDB (and the Tai Lake Water Quality Steering Committee) that each project approved for funding is designed appropriately, constructed according to the design, constructed to a high standard of quality, and constructed safety. The successful completion of these activities would ensure that the constructed project functions as intended and results in the expected improvement in water quality in Tai Lake.

SUMMARY

To select appropriate project types and projects to improve water quality in the Tai Lake basin, it was necessary to identify and understand the various factors affecting water quality in the lake. Therefore, E & E undertook a high-level qualitative investigation of the causes of the poor water quality in the lake. The investigation included a review of numerous studies, examination of environmental data, and meetings with various local experts in water management, pollution control, and civil engineering. In addition, since many cities in the Tai Lake basin are actively working to develop projects to correct the water quality problems, we examined many of the recent restoration plans and actions taken to restore the lake.

The water quality problems in the Tai Lake basin are serious but not unique: over the years, many developed countries have tackled similar problems. An assessment of the restoration programs undertaken by these countries, as well as the effectiveness of the measures included in those programs, provided another basis for understanding appropriate projects and management structures to improve water quality in Tai Lake basin.

Based on our understanding of the causes of poor water quality in the Tai Lake basin and the successful restoration measures used in developed countries, we have developed a framework that the CDB can use to evaluate loan applications for Tai

Lake water quality project. This framework involves applying the evaluation criteria developed to rank the projects in terms of their likely achievements.

Once restoration projects have been selected for CDB financing, the proposed environmental loan program would need to be implemented. As part of the loan program, the projects would be monitored to ensure they are properly designed, constructed, and implemented. This would ensure that the individual projects provide their anticipated results and that the ultimate goal of enhancing water quality in the Tai Lake basin is achieved.

This case study presents an approach to improve the water quality of a large lake in a heavily populated part of one of the world's leading developing nation. It also presents the first attempt by a Chinese state bank to create a large-scale environmental loan program, which is a major milestone in the development of environmental policy in China. The approach presented here provides a model for developing countries to create effective and comprehensive environmental loan programs and the supporting strategies needed to ensure their success.

REFERENCES

MEPA, 2007. *National Master Plan of Water Pollution Control for the Key Water Basins (2006-2010)* – Appendix IV (Draft).

Investigating aquatic ecosystems of small lakes in Khorezm, Uzbekistan

Laurel Saito,[1] M. ASCE, Julian Scott,[2] Michael Rosen,[3] Bakhriddin Nishonov,[4] Sudeep Chandra,[5] John P.A. Lamers,[6] Dilorom Fayzieva,[7] and Margaret Shanafield[8]

[1] Graduate Program of Hydrologic Sciences, University of Nevada Reno, Mail Stop 186, 1664 N. Virginia Street, Reno, NV 89557; PH (775) 784-1921; Fax (775) 784-4583; email: lsaito@cabnr.unr.edu
[2] Graduate Program of Hydrologic Sciences, University of Nevada Reno, Mail Stop 186, 1664 N. Virginia Street, Reno, NV 89557; PH (775) 784-1061; Fax (775) 784-4583; e-mail: scottj01ster@gmail.com
[3] Nevada Basin and Range Study Unit, United States Geological Survey, 2730 N. Deer Run Road, Carson City, NV 89701; PH (775) 887-7683; Fax (775) 887-7629; e-mail: mrosen@usgs.gov
[4] Laboratory of Surface Water Quality Investigation, Hydrometeorological Research Institute, 72 K. Makhsumov Str., Tashkent 700052 Uzbekistan; PH (011) 998-71-1331150; e-mail: bnishonov@mail.ru
[5] Department of Natural Resources and Environmental Science, University of Nevada Reno, Mail Stop 186, 1664 N. Virginia Street, Reno, NV 89557; PH (775) 784-6221; Fax (775) 784-4583; e-mail: sudeep@cabnr.unr.edu
[6] UNESCO-ZEF German-Uzbek Khorezm Project, 14, Khamid Almjan Street, Khorezm 220100 Uzbekistan; PH (011) 998-62-226-2119; e-mail: j.lamers@zef.uzpak.uz
[7] Institute of Water Problems, Academy of Sciences of the Republic of Uzbekistan, N. Khadjibayev Str. 49, Tashkent 100041, Uzbekistan; PH (011) 998-71-169-1270; e-mail: dfayzieva@gmail.com
[8] Division of Hydrologic Sciences, Desert Research Institute, 2215 Raggio Parkway, Reno, NV 89512; PH (775) 673-7391; e-mail: mshanafield@yahoo.com

ABSTRACT

The Khorezm province of Uzbekistan, located in the Aral Sea Basin, suffers from severe environmental and human health problems due to decades of unsustainable land and water management. Agriculture is the dominant land use in Khorezm, and agricultural runoff water has impacted many small lakes. In this water-scarce region, these lakes may provide a water source for irrigation or fish production. Samples have been collected from 13 of these lakes since 2006 to assess water quality, the aquatic food web, and possible limits to aquatic production. Lake salinity varied from 1 to >10 g/L both between and within lakes. Although hydrophobic contaminants concentrations were low (82-241 pg toxic equivalents/mL in June 2006, October 2006, and June 2007), aquatic species diversity and relative density were low in most lakes. Ongoing work is focused on 4 lakes with pelagic food webs to estimate fish production and assess anthropogenic impacts on the food web. Lake sediment cores are also being examined for organic contaminants, and hydrology is being assessed with stable isotopes.

INTRODUCTION

The Khorezm province of Uzbekistan is located in the Aral Sea Basin, where decades of unsustainable land and water management have led to severe environmental and human health problems and concerns (Allouche 2007). Agriculture is the dominant land use in Khorezm (Wehrheim and Martius 2008), and agricultural runoff water has impacted many small lakes in the province. In this water-scarce region, these lakes may provide a suitable source of water for irrigation or fish production. This study involves collecting and assessing information on the hydrology, water quality, and ecology of these lakes to evaluate their potential for such uses. The project is a collaboration between scientists and students in Uzbekistan, the United States, and Germany.

APPROACH

Since May 2006, we have collected and measured monthly data from as many as 13 lakes. These data include pH, nutrient and major ion concentrations, and depth profiles of water temperature, dissolved oxygen, and specific conductivity. We also collected zooplankton, aquatic macroinvertebrate, and fish samples twice per year in 2006 and 2007 for stable isotope analysis and characterization of the food webs of the lakes. Beginning in August 2007, sampling was modified to focus on 4 lakes with pelagic food webs and nutrient bioassays were added to the monthly sampling regime to examine nutrient limitation over time in the lakes. In summer 2008, shallow piezometers were installed to monitor the exchange of water between shallow groundwater and the lakes. Pressure transducers monitored water level in the piezometers and the lakes, and water samples were collected from wells, piezometers, nearby water bodies, and the lakes on a weekly basis. In addition to the nutrient and ion analyses, these samples were analyzed for stable isotopes of water (hydrogen and oxygen). To measure the toxicity of hydrophobic organic contaminants to aquatic organisms, passive organic samplers (Huckins et al. 1990, 1993) were deployed three times in the lakes and the Amu Darya, and in summer 2008 they were also deployed in piezometers at three of the lakes. We have also taken some preliminary lake sediment cores to examine the history of the lakes in terms of sedimentation and anthropogenic chemical inputs associated with agriculture to the lakes. Training of Uzbek and American students on field and laboratory work has been an important component of the project.

PRELIMINARY RESULTS

The lakes varied in salinity from 1 to over 10 g/L both between and within lakes depending on the lake and season. Concentrations of hydrophobic contaminants in the lakes were low (120-210 pg toxic equivalents (TEQ; Rosen et al., 2006)/mL in June 2006; 82-160 pg TEQ/mL in October 2006; and 83-241 pg TEQ/mL in June 2007). However, results from one of the piezometers in Summer 2008 showed moderate levels of toxicity (approximately 400 pg TEQ/mL is considered moderate). A 100 cm sediment core taken near the edge of one of the lakes showed relatively

constant concentrations of DDT (average 0.007 mg/kg), γ-HCH (0.0012 mg/kg), and their degradates with depth below a depth of about 15 cm depth, with lower concentrations above 15 cm depth (DDT average of 0.004 mg/kg; γ-HCH average of 0.0007 mg/kg). Age dating of this core using ^{137}Cs and ^{210}Pb indicates that the total sediment package represented over 100 years of sedimentation, but interpretation of the age dating profile is ongoing. New cores have also been taken near the center of the lakes.

Despite low concentrations of hydrophobic organic contaminants in lake water columns, aquatic species diversity and relative density were low in most lakes examined. Ammonium and nitrate concentrations in the lakes were higher in the spring in 2007 and 2008 when agricultural fields in the vicinity of the lakes were being leached with excess water. Phosphorus concentrations were highest in 2006 and much lower in 2007 and 2008. Water isotope and major ion analyses have been completed, and preliminary results indicate that groundwater was a major source to one of the lakes during much of the summer of 2008. Food web samples are currently being analyzed to assess food web structure and composition.

Since the project began, seven Uzbek and two American students have been part of the project. Many have participated in training by the senior Uzbek and American personnel related to sampling and analysis procedures. All of the students have also interacted with German and Uzbek students working on related projects through our German collaborator.

FUTURE WORK

Ultimately, the combined datasets will be used for assessing the hydrology of the lakes, examination of possible land management options, and estimation of the economic, ecologic, and water quality impacts of such changes on the lakes. In addition, the project team recently received funding to take additional lake sediment cores and perform microbial experiments to examine processes which might be reducing pesticide concentrations in lake waters and sediments. This information will be useful not only for understanding current and future conditions in the lakes, but also the historical usage and development of these lakes.

REFERENCES

Allouche, J. (2007). “The governance of Central Asian waters: national interests versus regional cooperation.” In Vingard, K. (ed.). *Disarmament Forum: Central Asia at the Crossroads*, no. 4. Geneva: United Nations Institute for Disarmament Research. Pp. 45-56.

Huckins, J.N., Tubergen, M.W., and Manuweera, G.K. (1990). “Semipermeable membrane devices containing model lipid: a new approach to monitoring the bioavailability of lipophilic contaminants and estimating their bioconcentration potential.” *Chemosphere*, 20, 533-522.

Huckins, J.N., Manuweera, G.K., Petty, J.D., MacKay, D., and Lebo, J.A. (1993). "Lipid-containing semipermeable membrane devices for monitoring organic contaminants in water." *Environmental Science and Technology*, 27, 2489-2496.

Rosen, M.R., Rowe, T.G., Goodbred, S.L., Shipley, D.O., and Arufe, J.A. (2006) "Importance of land use, streamflow, and water quality on toxicity of SPMD extracts deployed in streams from the Lake Tahoe and Truckee River watersheds." In Hughes, R.M., Wang, L., and Seelbach, P.W. (eds.). *Influences of landscapes on stream habitats and biological assemblages.* American Fisheries Society Symposium, 48, 125-149.

Wehrheim, P., and Martius, C. (2008) "Farmers, cotton, water and models – introduction and overview." In Wehrheim, P., Schoeller-Schletter, A., and Martius, C. (eds.). *Continuity and change: land and water use reforms in rural Uzbeksitan*. Halle(Saale): IAMO. Pp. 1-15.

Prediction of Thermal Stratification in Proposed Bakhtyari Reservoir with CE-QUAL-W2

Mehrdad Nazariha[1],Erfan Danaei[2],Seyyed hosein hashemi[3],Amir Hosein Izad Doustdar[4]

1.Assistant Professor, Faculty of Environment, University of Tehran,No.25, Qods St. , Enqelab Ave., Faculty of Environment, University of Tehran.
Phone:+982161113165,
E-mail:mnazariha@ur.ac.ir
2.Post Graduate Student of Environmental Engineering, Faculty of Environment, University of Tehran.Phone:+982122420658,E-mail: erfandanaei@gmail,com
3.Assistant Professor, Environmental Sciences Research Institute, Shahid Beheshti University, Environmental Sciences Research Institute, Shahid Beheshti University, Evin Ave, Shahid Chamran highway, Tehran, Phone:+982122431971
E-mail:H_hashemi@sbu.ac.ir
4.Manager of Base,Environmental and cultural heritage studies of Iran Water and Power Resources Development.No.40, Bidar Ave, Africa cross, Modarres highway, Tehran
Phone: +982123151932,E-mail: amirensi@yahoo.com

ABSTRACT

Construction and operation of dams have two main effects on streams. At first it increases detention time and then leads to thermal stratification. Changing of water quality is the result of these effects and the outflow has different physical, chemical and biological characteristics from inflow.

In this study thermal regime in proposed Bakhtyari reservoir was simulated with CE-QUAL-W2 model. The inputs are reservoir topography, hydrological and meteorological data. As there is no chance to calibrate or verify the model, they will be done in monitoring and operation period. Three different inflow scenarios were simulated based on dry, normal and wet year .Simulation results represent that in dry year stratification starts at April and remains up to September, but the results of normal year indicates that Stratification is between May and November. In wet year because of short detention time, thermal gradient variation is different from dry and normal year and temperature of middle layers imitate inflow water temperature. In all scenarios a stagnant layer could be seen in downward of outlet structure(700mASL).It is concluded that in dry years which dam has a major effect in inflow regime, turnover is mostly conform thermal stratification theories in reservoirs.

Key words: Bakhtyari dam , thermal stratification, modeling , CE-QUAL-W2

INTRODUCTION

In recent decades and by beginning of new century, one of earth planet's inhabitant population's worries and particularly countries located in dry lands such as our country is water problem in a way that availability to water with appropriate quality and quantity has been converted to a challenge(Soltani 1384).As it was customary from the past, reserving water by construction of dam for provision of water for agricultural consumption, industry, potable water, controlling flood, production of aquatic electric energy, quality control and … seems necessary (karamuz 1382).Flowing water under affection of phenomena such as deaeration, cellular breathing , mixing etc. has uniform quality. But surface water flow reservation could cause of unfavorable effects on water quality of the river (Soltani 1384).The most important changes which may occur on reservoirs is thermal stratification. Anyhow other changes such as eutrophication, evaporation, reservoir basin effects , dissolved solids , dissolved gas , smell problem, etc.are such issues which affect on water quality of reservoir (Soltani 1384).

The preliminary step in study of bio-physical processes within reservoir, is understanding thermal stratification and the consequence of formation, as temperature affects decomposition of organic materials and increasing rate of chemical reactions and on the other hand affects the time varying concentration of these materials(Tajrishi 1385).Temperature related features and stability of reservoirs could be predicted by use of mathematical modeling and in case of environmental problem, can be taken remedial way for decreasing problems by various ways.

Use of multilevel outlet structures, destroying of reservoir's stratum or mixture, aeration of outflow water by use of hydraulic jumping creation and so on are recommendable examples of remedial ways in various ages of a dam from study to utilization (Tajrishi 1385).

Before dam construction, a few studies have been done by researchers on thermal stratification, because it needs calibration by future sampling in reservoir. Gunduz et al by use of two dimensional model(CE-QUAL-W2) simulated quality related behavior of proposed Isikli reservoir for provision of potable water. This model used for determination of potential water quality deterioration by entering of various contaminants charges and its resultants compared with potable water quality standards in order to determining of reservoirs water control managements strategies and watershed area (Gunduz et. Al., 1998).Encon consultant company by use of one dimensional model "DYRESM" studied effects of Yusufeli dam -which was under construction in Turkey- on thermal stratification of reservoir (ENCON,2006).

With regarding to Bakhtiari dam reservoirs shape which its length to width is high (approximately 1:60) and has dendrite like shape, the CE-QUAL-W2 model has been used which has the capability of two dimensional simulation of reservoir in depth and lengh.In this article effect of various programming scenarios of inflow water resources to reservoir in formation of thermal stratification has been surveyed by use of this model.

Study Region

Bakhtyari dam is located in west south of Zagros chain mountains' skirt over a river under the same name in border of Lorestan province (right wing) and Khuzestan

province (Left wing).Surface of basin area is 6503 Sq Km and maximum altitude of the area is 4080 m from the free sea level. At normal level reservoir's altitude is 830 m in ratio to sea level, lake total volume is 4845 cubic million meters and live storage of that is 2647 cubic meters, area at full supply level is 55 Sq Km,length of that about 60 Km and maximum depth at dam wall is 300 meters. Six unit of turbine each of them in capacity of 250 megawatts and in total 1500 megawatts will be installed in power generation section of dam.

MATERIALS AND METHODS

For simulation of reservoirs water quality CE_QUAL-W2 model has used.CE-QUAL-W2 is a two dimensional (longitudinal-depth) hydrodynamic and quality related model. Due to lateral homogeneity assumption, it is appropriate for long water bodies. Development and completing of this model has been begun from three decades ago and has been used for reservoirs, lakes and estuaries in all over the world. This two dimensional model based on finite difference, has ability of simulation of vertical and longitudinal distribution of thermal energy and chemical and biological parameters which has been selected in water bodies. also in water bodies, it simulates appropriately volume, density, vertical and longitudinal concentration of quality parameters. Hydrodynamic simulation engine, impose effects of density changes on flow. Quality modules have the ability of simulation of about 30 quality parameters along with temperature and cyclic pattern of temperature. It also has the below ability: A) simulation for long time period B) Several branches modeling in water body with geometrical complexity C)Multiple joints of water bodies D)variable Longitudinal and height related distances in segmentation. Model along with multi assumption and approximate which is applied for simulation of hydrodynamic processes, transformable and quality based issues has limitations. The model is get used to solve equations in vertical and longitudinal directions, but ignore lateral changes. There is no algorithm for momentum in vertical direction and results for bodies with high vertical acceleration may not be accurate. Water quality parameters which is represented by models has complex interactions. Several processes such as transfer and accumulation of sediments, poisonous materials and dynamic sediment oxygen demand would not be simulated. (William2007)

Four series of data related to reservoir's geometry, simulation period, boundry condition and meteorological parameters have been used for modeling.

Reservoir's Geometry

Topographic and Geometrical information and of Bakhtyari reservoir has been excerpted from topological maps in scale of 1:20000.

For define of reservoir's geometry in model, water body has been divided to 51 pieces with a length of 1.5 Km and 2 and 3 meters depth layers. (Fig.1)

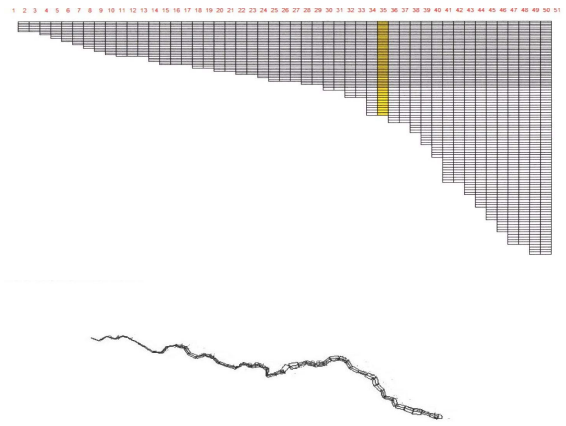

Fig.1 lateral and up view of reservoir's geometry

Simulation Time Period

With regard to that various aquatic years, dry, wet and normal are registered in statistical periods, for each aquatic year, a two year simulation period is included of first year belonging to loading and the second year belonging to water taking from reservoir has been assumed. Information regarding to inflow flow rate to reservoir and outflow flows from the reservoir excerpted from" environmental Impact Assessment" report which has extracted from" water resources programming and optimum energy production". For surveying of yearly varying, three aquatic year of very dry, normal and very wet have been entered separately in model input for comparing of thermal profiles.

Model Boundry Condition

Upward boundry conditions are defined in the model by inflow rate to reservoir and inflow water temperature and downward boundry condition is defined by outflow rate from outlet structure. Hydrological information extracted from water measurement station of TangPanj, which is located in proximity of Bakhtyari river and Cesar river incidence (Fig.2).

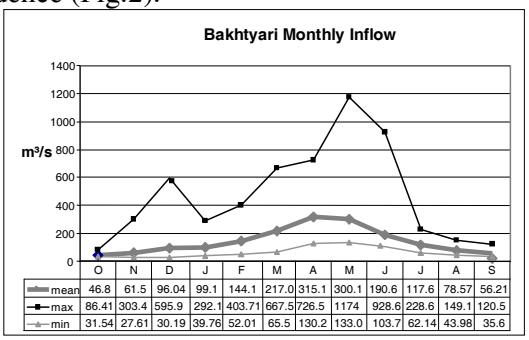

	O	N	D	J	F	M	A	M	J	J	A	S
mean	46.8	61.5	96.04	99.1	144.1	217.0	315.1	300.1	190.6	117.6	78.57	56.21
max	86.41	303.4	595.9	292.1	403.71	667.5	726.5	1174	928.6	228.6	149.1	120.5
min	31.54	27.61	30.19	39.76	52.01	65.5	130.2	133.0	103.7	62.14	43.98	35.6

Fig.2-Mean, maximum and minimum of bakhtyari river monthly flow

Meteorological Data

Meteorological data included of air temperature degree, dew point temperature, wind speed and direction and cloud coverage. Required meteorological data has been extracted from Tangpanj and Aligoodarz stations. In this simulation, Meteorological information in a monthly period has been entered into model and has been used from 2004-2005 aquatic year information. With regard meteorological report of the project which indicates the similarity of various year air temperature, monthly mean values for two continuous years has been entered into the model.

Due to the lack of the reservoir and lack of availability of information about reservoir water temperature and level, model calibration is made at the time of reservoir shaping. Based on previously made studies (Mohammadi Khalf Badam 2004, Williams2007), two factors of wind direction to reservoir' and shades resulted from plants coverage from the surroundings are the most affecting factors on layering phenomenon which both factors with regard to collected data are determined.

Management Scenarios:

In order to simulate Bakhtaran thermal behavior based on mean probable changes in inflow flow rate into reservoir, three scenarios has been defined. In first scenario reservoir thermal behavior due to inflow water decreasing based on one of a very dry year had been simulated. The given year has been 1970-1971.In the second scenario thermal gradients in mean inflow rate into reservoir has been surveyed. For this purpose normal aquatic year of 1988-1989 has been selected. In third scenario thermal regiment of reservoir for the year of 1993-1994 which was very wet year has simulated. Outlet structure level in all scenarios was selected 700 meters above sea level.

RESULTS

Figure 3,4,5 depicting vertical water temperature profile for 12 months of the year near the dam wall. for dry, normal and wet year, respectively.

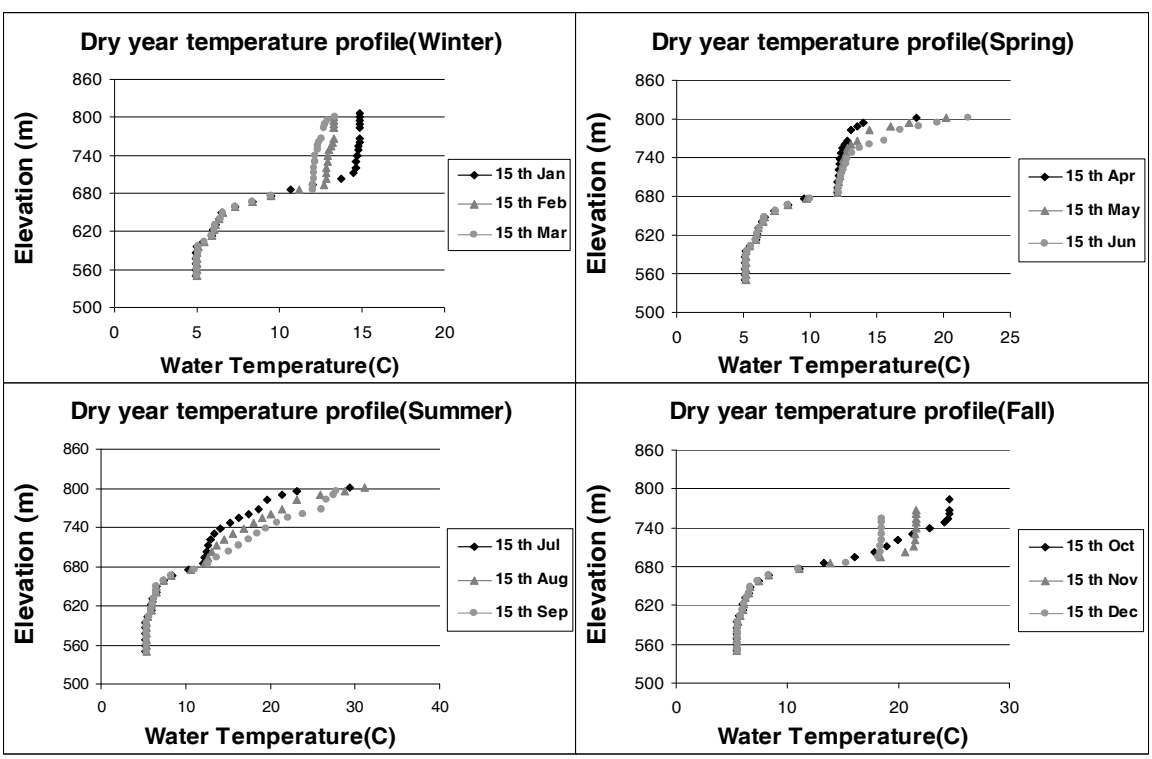

Fig.3-Dry year vertical temperature profile

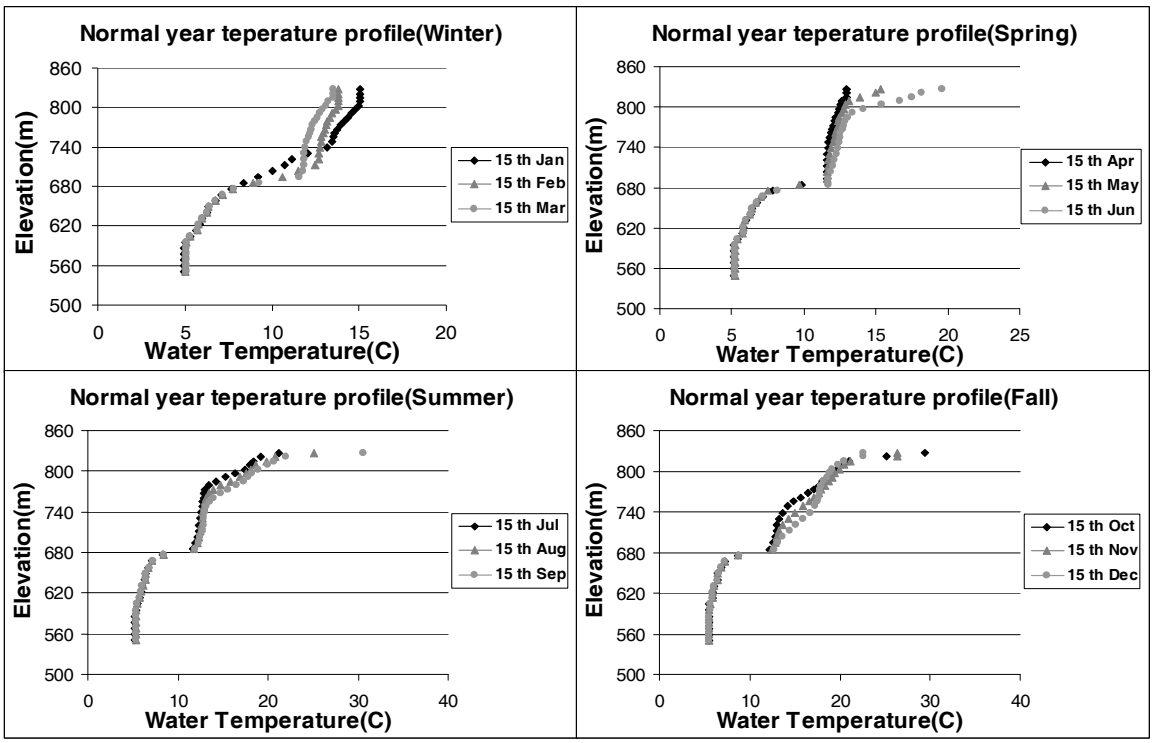

Fig.4-Normal year vertical temperature profile

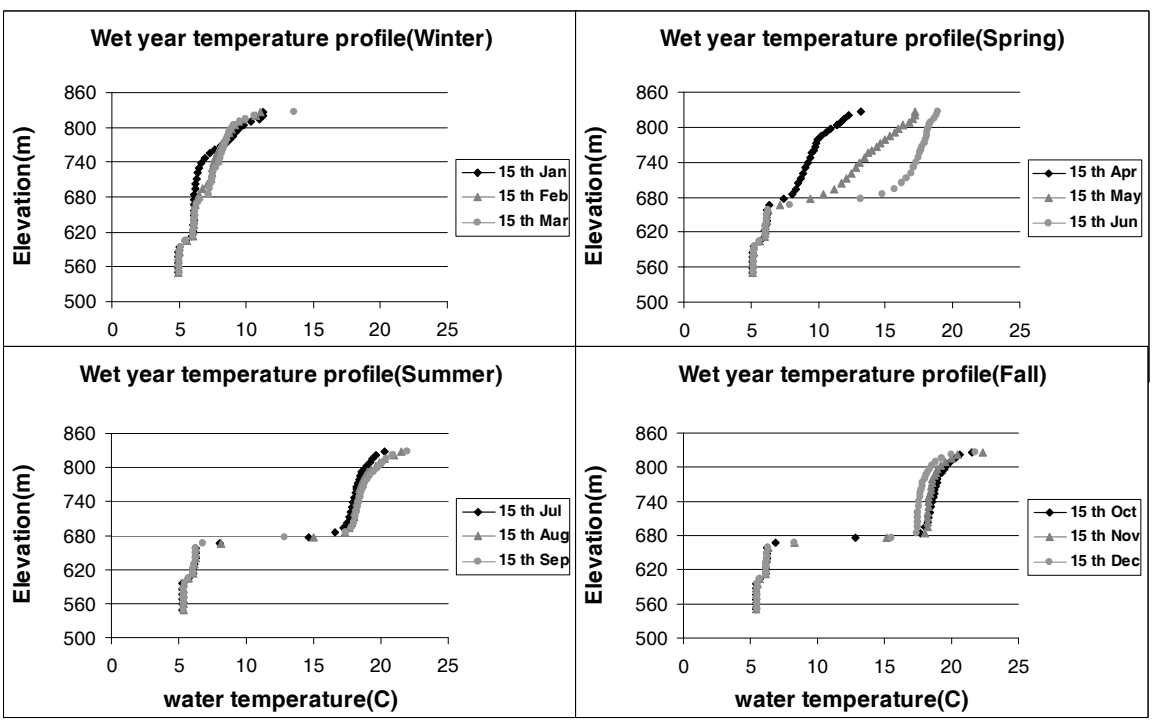

Fig.5-Wet year vertical temperature profile

Discussion and conclusion

It is observed that under 700 meters level which is selected as outlet structure level, temperature profile have stagnant behavior and seasonal changes could not be observed on that and water temperature would be uniform and about 5 degree centigrade. At preliminary test it has determined that depth of this stagnant area is a function of changes in outlet structure level.

Fig.3 show that in dry year from the beginning days of April, layer forming has been begun from high altitudinal level and would maximize up to mid of September, in a way that 16 degree changes of temperature in depth of 100 meters is observable and surface water could reach to 30 degree centigrade. From the mid of September up to January depreciation of stratification would be commenced and again an isothermal layer would begun to form and during temperature decreasing, depth of the layer increase from 35 to 60 meters and January, February and March isothermal conditions are observed about 13 to 15 degree centigrade up to 100 meters depth.Resevoir is warm monomictic and the turnover at the beginning of fall would be happened and stratification is observed about 5 month.

But based on Fig.4 changes are begun from the mid of May and maximize to its magnitude up to November. In a way that 13 degree changes of temperature in depth of 140 meters is observed and surface water temperature is near 27 degree centigrade and depreciation of formed layers would be commenced from last days of March and repeatedly an isothermal layer would begun to form and during decreasing of temperature, depth of the layer would increase from 10 meter to 115 meter and in March and April conditions of thermal uniformity is about 11 to 13 degree and is observed up to depth of 130.Reservoir is warm monomictic and turnover is happened at the beginning of winter and stratification is observed in a 7 month period of the year.

What is perceived from Fig.5 is indicating a layer along with variable thermal gradient which has temperature about 9 to 13 degrees centigrade in April up to 15 to 22 degree centigrade in beginning of winter. It seems like that, except from surface water which is a function of monthly variation of temperature, middle layers are mostly depends on inflow water and reservoir. Due to difference in operation with dry and normal years, expectable stratification would not be come true.

In comparison between two scenarios of normal and dry year it could be concluded that, with regard to long detention time in dry year, thermal gradient is high, but the period of that is shorter. The reason of shortness of stratification could be referred to reaching of a low flow rate of water period and taking of water from middle layers which give absorption opportunity of sun light to upper layers. As well as it can be concluded that , more effects of dam on aquatic regiment (dry year), more is the expectation of circumstances closeness to lake like situation and yearly circulations more would be under affection of geometrical conditions, winding and as a whole effective processes on layer formation. But by decreasing dam effect in flow regiment (wet year), outflow water quality more would be under effect of inflow regiment and reservoir's effects whether on hydrodynamic parameters such as temperature or quality parameters such as dissolved oxygen , nitrogen and phosphorus changes in depth and etc. would decrease.

References

Gunduz, O, Soyupak, S. and Yurteri, C. 1998."Development of water quality management strategies for the proposed Isikli Reservoir". Wat. Sci. Tech Vol. 37,No2: 369-376.

Karamouz, M.Karachian, R, (2003).Water resources systems quality management and programming.Amirkabir University of Technology Publications (Polytechnics Tehran).

Mahab Qods consultant Engineering company.(2005).Bakhtiari power plant and dam project Environmental Impact Assessment report.

Soltani.J, Alavi Moghddan.S.M.(2005)" experience resulted from the effects of thermal stratification on water quality of some reservoirs in country"

Tajrishi.M, Abrishamchi.A, Afshar.A, Sarangh.A, (2006)"surveying and analysis of thermal stratification in reservoirs" set of workshop specialized articles in eutrophication and management in reservoirs.

Mohammadi Khalf Badam, H."Reservoirs eutrophication -two dimensional modeling (Karkheh dam casual study). Dissertation, Science and Techmology University of Iran, 2005

Williams N T,(2007)." Modeling Dissolved Oxygen In Lake Powell Using CE-QUAL-W2" Dissertation, Department of Civil and Environmental Engineering, Brigham Young University

ENCON. 2006. Hydro modeling report (reservoir water quality and downstream flow modeling)

U S Army (1987),"Reservoir Water Quality Analysis", Engineering and design,1110-2-1201

Physiological and Yield Response of Green Bell Pepper to Soil Moisture Sensor Controlled Drip Irrigation

Lincoln Zotarelli, Michael D. Dukes. Agricultural and Biological Eng. Department, University of Florida. PO Box 110570, Gainesville, FL, 32611, ph: (352) 392-1864. lzota@ufl.edu; mddukes@ufl.edu.

The objectives of this study were to evaluate the physiological and yield response of pepper to different soil moisture thresholds using soil-moisture-sensor (SMS) irrigation control. Irrigation treatments were set at specific threshold of volumetric-water-content (VWC) which was allotted five irrigation windows/day and bypassed events if the VWC exceeded the established threshold. Treatments were: threshold of 4, 8, 12%VWC single irrigation-drip at center of the bed (SS); threshold of 8, 12%VWC with double drip-irrigation (SD); $TIME_{2h}$ with fixed 2hr irrigation/day and $TIME_{4x24}$ with 4 fixed events of 30min/day. The use of SMS reduced irrigation water applied (81; 118; 138; 112; 201; 341 and 260mm for SS_4; SS_8; SS_{12}; SD_8; SD_{10}; $TIME_{2h}$ and $TIME_{4x24}$, respectively). For the same order, the pepper yield was 26; 31; 35; 30; 42; 33; 41 Mg/ha. Water and NO_3-N captured in lysimeters were lower on SMS irrigation controlled compared to TIME based irrigation commonly used by producers.

Keywords: *nitrogen leaching, vadoze zone, fertigation, drainage lysimeters, best management practices*

Introduction

Vegetables are a major component of Florida agriculture encompassing about 72,000 ha for production with a crop value of 1.5 billion dollars. Bell pepper is the second most important vegetable produced in Florida in terms of value. With a crop value of 209 million dollars, the average acreage annually planted with bell peppers in Florida is 7,500 ha. Vegetable crops in Florida are irrigated due to the coarse-textured soils with low water holding capacity and soil organic matter content(Carlisle et al. 1988). Since irrigation and fertilization are intrinsically linked, appropriate irrigation management is required for these soils in order to avoid nitrate leaching. Despite the N-fertilizer rate recommendation for mineral soils with drip irrigation in Florida of 224 kg N ha^{-1}, growers may opt to apply excessively high N rates to minimize risk of yield reduction due to nitrogen limitations. In addition, on sandy soils, proper irrigation management is decisive to maximize yield, fertilizer and water use efficiency for vegetable crop production. On the other hand, significant reductions in water availability for irrigation use in southeast U.S. have increased the importance of implementation of water conservation practices in agriculture. Agricultural practices such as the use of plastic mulch, drip irrigation and quantitative irrigation scheduling are common in Florida, and they provide growers with a viable option to reduce crop water requirements and thus conserve water resources. Even with these advances, there remains a need for advancement in irrigation management by using real-time monitoring techniques combined with high frequency irrigation application methods based on actual plant water requirements. The use of frequent but low volume irrigation applications via drip irrigation is superior to the more traditional scheduling of few large applications (Locascio 2005). In the past few years, sensor technology that permits continuous on-farm monitoring of soil water status has become increasingly accessible to commercial producers. Soil moisture

sensors (SMS) measure volumetric soil water content (SWC), which can be used to more accurately balance specific crop water requirements. The use of SMS–based irrigation systems can maintain soil water status within upper and lower limits determined by type of soil and crop preventing over irrigation and saving water (Dukes and Scholberg 2005; Zotarelli et al. 2008; Zotarelli et al. 2009) . The objective of this study was therefore to identify suitable irrigation scheduling methods, drip irrigation system design to reduce crop water use and to evaluate their effect on pepper development and yield. We hypothesized that alternative irrigation designs and improved irrigation management will reduce irrigation water requirements of intensively managed pepper production systems.

Materials and Methods

A field experiment was carried out at the University of Florida, Plant Science Research and Education Unit, near Citra, FL, during the spring of 2008. The soil has been classified as Candler sand (Buster 1979). These soils contain 97% sand-sized particles in the upper 1 m of the profile (Carlisle et al. 1988) with a field capacity in the range of 0.10-0.12 ($v\ v^{-1}$) in the 0-30 cm depth (Icerman 2007). The area was rototilled and raised beds were constructed with 1.8 m between bed centers. Granulated fertilizer was incorporated into the beds at a rate of 112 kg ha^{-1} of P_2O_5. Beds were fumigated (80% methyl bromide, 20% chloropicrin by weight) 13 days before transplanting at a rate of 604 kg ha^{-1} after placement of drip tape and plastic mulch in a single pass. Irrigation was applied via drip tape (Turbulent Twin Wall, 0.20 m emitter spacing, 0.25 mm thickness, 0.7 L hr^{-1} at 69 kPa, Chaplin Watermatics, NY). Water applied by irrigation and/or fertigation was recorded by positive displacement flowmeters (V100 16 mm diameter bore with pulse output, AMCO Water Metering Systems, Inc., Ocala, FL, USA). Weekly manual meter measurements were manually recorded while data from transducers that signaled a switch closure every 18.9 L were collected continuously by data loggers (HOBO event logger, Onset Computer Corp., Inc., Bourne, MA, USA) connected to each flow meter. Pressure was regulated by inline pressure regulators designed to maintain an average pressure in the field of 69 kPa during irrigation events. The plots were 15 m long, and a tractor mounted hole puncher was used to make 50 mm wide openings at 30 cm intervals in twin staggered rows with each approximately 7 cm from the bed center. A weather station located within 500 m of the experimental site provided precipitation, temperature, relative humidity, solar radiation and wind speed data and this information was used to calculate daily reference evapotranspiration (ET_0) according to FAO-56(Allen et al. 1998). Crop evapotranspiration (ET_c) was based on the product of ET_0 and the crop coefficient (K_c) for a given growth stage (Simonne et al. 2007) and values were reduced by 30% to account for the effect of plastic mulch on crop ET (Amayreh and Al-Abed 2005) until the plant canopy was 80% full cover of raised bed area. Pepper transplants (*Capsicum annuum* var. "Brigadier") were set on 9 April 2008. Weekly fertigation consisted of injecting dissolved fertilizer salts into fertigation lines. All plots received 247 kg ha^{-1} of K_2O as potassium chloride and 12 kg ha^{-1} of Mg as magnesium sulphate. The experimental design had seven irrigation treatments randomized within four blocks. The N-rate corresponded to 220 kg ha^{-1} of N applied as calcium nitrate (Olson et al. 2005).

The irrigation treatments were identified as single drip irrigation (SS) in the center of the bed and double drip (SD) beside plant rows. The irrigation treatments were regulated by the commercial RS500 soil moisture sensor (SMS) controller manufactured by Acclima, Inc. (Meridian, ID). The RS500 unit controls irrigation application by bypassing time clock initiated irrigation events if soil moisture was at or above a preset threshold of volumetric water content

(VWC) depending on irrigation treatment (Table 1). The soil moisture sensor probes were installed at a 45 degree angle between two plants that measured the soil moisture in the top 0.15 m of the bed. Timed irrigation windows were specified as five possible events per day, starting at 8:00 am, 10:00 am, 12:00 pm, 2:00 pm, and 4:00 pm for 24 minutes each (2 hr/day total). Two reference treatments were established, a time-based irrigation treatment with one fixed 2 hr ($TIME_{2h}$, approx. 6 mm/day) irrigation event per day and fixed 4 irrigation events per day of 24 min ($TIME_{4x24}$, approx. 4.8 mm/day), both with a single drip line. An overview of irrigation treatments are outlined in Table 1.

Table 1. Outline and description of irrigation treatments along with threshold volumetric water content (VWC), total cumulative and daily irrigation application depth.

Treat. codes	Irrigation description	Threshold VWC	Max. irrigation	Max. daily	Number of irrigation events		
		$m^3\ m^{-3}$	frequency (events/d)	irrigation (mm)	Sched.	Irrigated	Skipped
SS_4	Acclima Digital TDT RS-500	0.04	5	6.0	266	77	189
SS_8	Acclima Digital TDT RS-500	0.08	5	6.0	266	106	160
SS_{12}	Acclima Digital TDT RS-500	0.12	5	6.0	266	117	149
SD_8	Acclima Digital TDT RS-500	0.08	5	6.0	266	172	94
SD_{12}	Acclima Digital TDT RS-500	0.12	5	6.0	266	171	95
$TIME_{2h}$	No soil moisture sensor, daily fixed time irrigation	-	1	6.0	54	54	0
$TIME_{4X24}$	No soil moisture sensor, reduced daily fixed time irrigation	-	4	5.0	216	216	0

Plots were harvested on 62 and 76 days after transplanting (DAT). The harvested area consisted of a central 10.5 m long region within each plot. Pepper fruits were size graded into culls, medium, large, and extra-large. Marketable weight was calculated as total harvested weight minus the weight of culls. Irrigation water use efficiency (IWUE) expressed in kg of fruit per m^{-3} of irrigation applied was calculated. Plant biomass accumulation was evaluated by harvesting two representative plants per treatment replicate at transplanting, 23, 34, 49 and 68 DAT. Vegetative and reproductive plant parts were separated. Leaf area was determined for each sample using a LI-300 (Li-cor, Lincoln, Nebraska). Shoot and fruit tissues were dried at 65 ^{o}C for subsequent dry weight determination. Leaf stomatal conductance (g) was measured with a diffusion porometer (Model AP4, Delta-T Devices, Burwell, Cambridge, UK). Measurements were performed at middle of vegetative stage and at begging of the flowering stage. Four leaves (two sunlit, two shaded) were sampled from the upper part of pepper plants, giving twelve measurements per treatment (Verhoef 1997). The results of stomatal conductance were multiplied by the corresponding plant leaf area for each treatment and the results presented in mmol s^{-1} $plant^{-1}$.

The volumetric water content of the top soil of the production beds was monitored by coupling time domain reflectometry (TDR) probes (CS-615, Campbell Scientific, Inc. Logan, UT, USA) with a datalogger (CR-10X, Campbell Scientific, Inc., Logan, UT, USA). Soil

moisture probes were placed in the beds at two subsequent soil layers which recorded soil moisture values. The upper probe was inserted at an angle in order to capture soil moisture in the top 0.15 m of the profile and the lower probe was inserted vertically below the upper probe recording soil moisture between 0.15 m and 0.30 m. Drainage lysimeters were installed 0.75 m below the surface of the bed three years prior to the bed formation. Leachate extraction via a vacuum pumping system occurred weekly, one day before each fertigation event. Total leachate volume was determined gravimetrically, and subsamples collected from each bottle were analyzed for NO_3-N so that total N loading rates could be calculated. Soil solution and soil core extracts were stored at –18 ºC (0 ºF) until nitrate and nitrite analysis. Samples were analyzed using an air-segmented automated spectrophotometer (Flow Solution IV, OI Analytical, College Station, TX) coupled with a Cd reduction approach (modified US EPA Method 353.2).

Statistical analyses were performed using PROC GLM procedure of (SAS 2002)to determine treatment effects for yield, IWUE and stomatal conductance. Means separation testing was performed as needed using Duncan's Multiple Range Test at a confidence level of 95%. For repeated measurements such as plant biomass accumulation volume leachate nitrate leaching, the PROC MIXED procedure of SAS with residual maximum likelihood estimation approach and least squares means of fixed effects were pair-wise compared.

Results and Discussion

The cumulative rainfall at the final harvest was 174 mm. Overall temperatures increased over time, during establishment period average temperature was 19 ºC and the minimum temperature dropped below 10 ºC on several occasions. During the plant vegetative and reproductive stages the average daily temperature was 25 ºC, with maximum temperatures ranging between 27 and 35 ºC and minimum temperature ranging between 11 and 23 ºC.

In the first 23 days after transplanting, a plant establishment phase was characterized by the application of approximately 5.5 mm day^{-1} divided in 4 irrigation events, totaling 123 mm applied to each treatment. After the pepper plants were well established, the irrigation treatments were initiated. Each soil moisture sensor controller was programmed to bypass irrigation if the probe read soil moisture at or above the set threshold at the beginning of an irrigation window. During the crop season, programmed irrigation events were skipped which significantly reduced the amount of water applied to soil moisture sensor (SMS) based treatments (Fig. 1). The volume of irrigation increased in order $SS_4 < SD_8 < SS_8 < SS_{12} < SD_{12} < TIME_{4x24} < TIME_{2h}$ (Fig. 1). For the same order, the water savings compared to $TIME_{2h}$ treatments corresponded to 76%; 67%, 65%, 60%; 41% and 24%, respectively. The daily application rates can be translated to 1.5, 2.1, 2.2, 2.6, 3.8 and 4.9 mm d^{-1}, respectively. The cumulative ETc for the period after the plant establishment was 170 mm (Fig. 1), which indicates that only treatments SD_{12}, $TIME_{4x24}$ and $TIME_{2h}$ received amount of irrigation water above the cumulative ETc at end of the season.

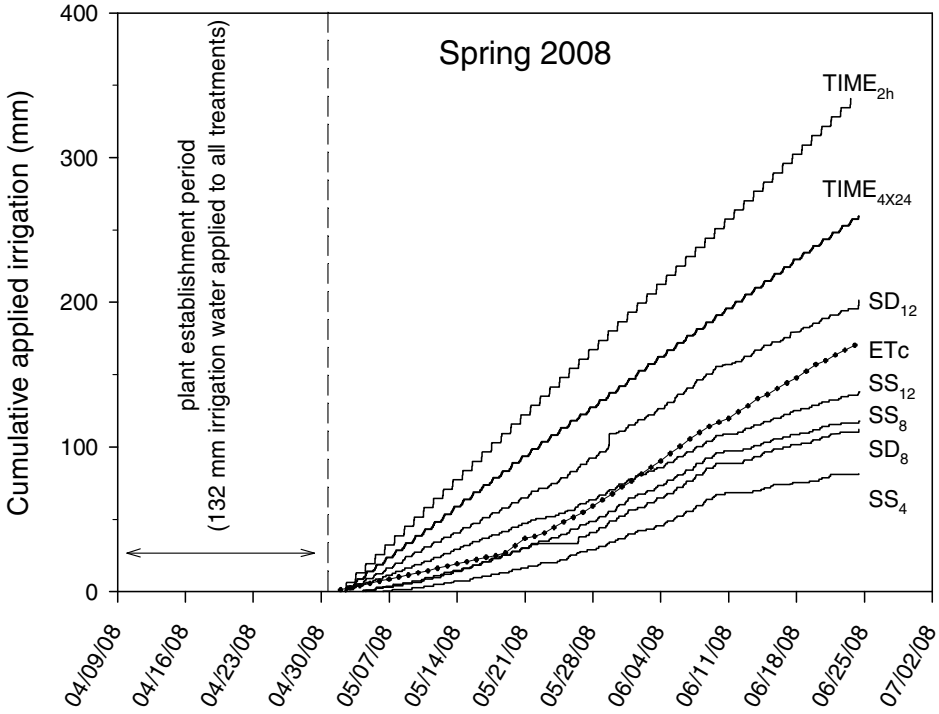

Fig.1. Cumulative irrigation and estimated evapotranspiration (ET_c) after initial plant establishment as affected by different irrigation scheduling and soil moisture sensor irrigation treatments during spring 2008.

The soil moisture content as measured by TDR probes had a noticeable increase in soil moisture after each irrigation event throughout the growing season (Fig. 2). Soil moisture sensor based irrigation treatments irrigated for short periods of time which resulted in a relatively small increase in soil moisture, consequently decreasing the volume of percolate. On the other hand, the $TIME_{2h}$ treatment was irrigated for a longer time period which resulted in very pronounced soil moisture fluctuations (Fig. 2 bottom row). These spikes in soil moisture were only temporary, as excess soil moisture that rapidly drained in this sandy soil (Fig. 3). Soil moisture content returned to field capacity within 12 h. The spikes also indicate that the soil water content as measured by the TDR probes rapidly reaches a point above the soil water holding capacity in the soil upper layer, inducing percolation to deeper soil layers, and explaining the higher percolate values for the $TIME_{2h}$ treatment compared to the other treatments (Fig. 3 left). In fact, similar spikes in soil water content were observed at below15 cm showing appreciable soil water percolation though the soil profile throughout the entire production. In terms of soil water availability to plants, the $TIME_{2h}$ treatment initially may provide more favorable growth conditions since the soil remains wetter, thus reducing potential water stress. However, excessive water percolation also may reduce N retention and crop N supply and thereby reduce yield for pepper (Fig. 4).

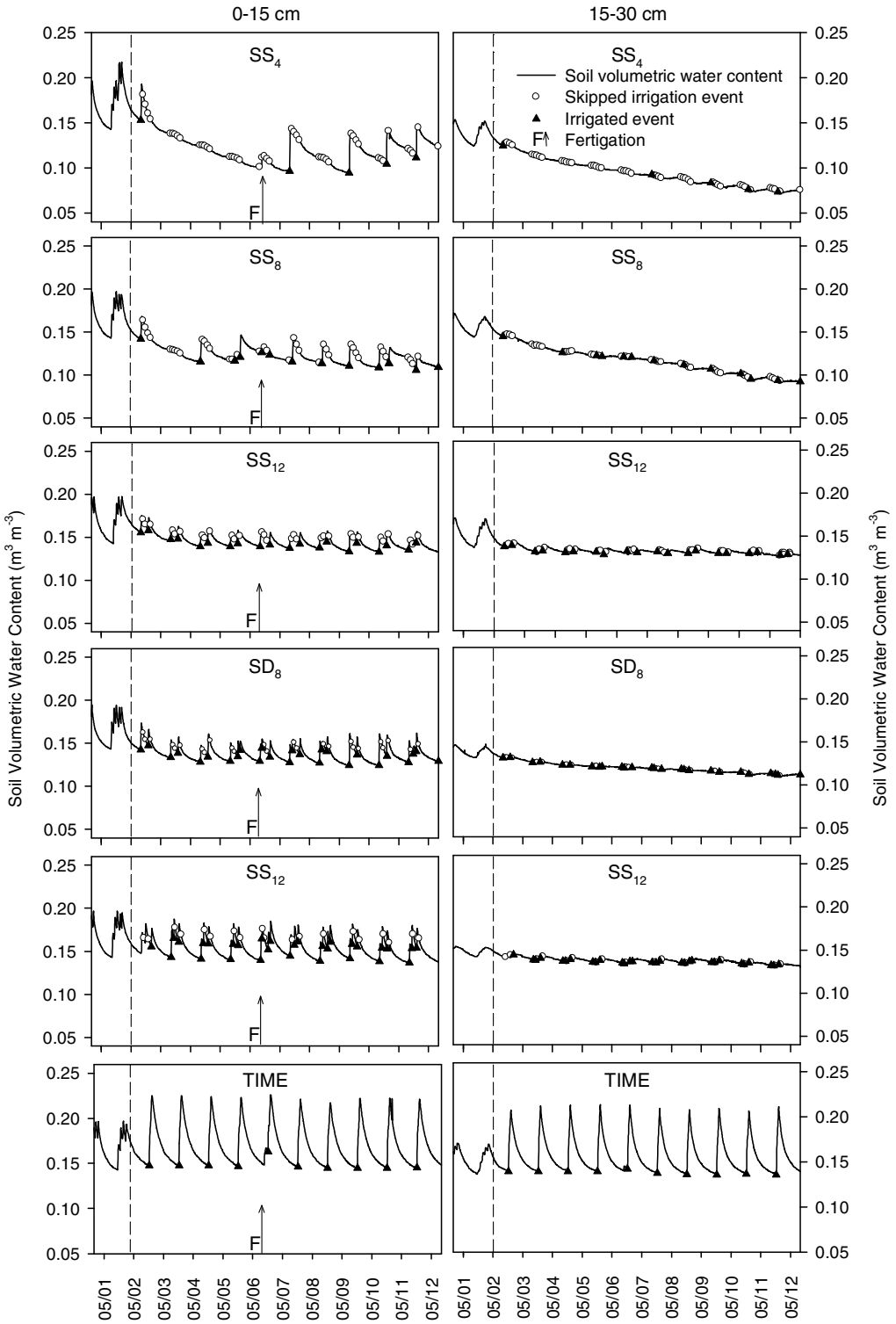

Fig. 2. Soil volumetric water content measured at 0-15 cm (left graphs) and 15-30 cm depth (right graphs) with schedule irrigation events during pepper vegetative development in spring of 2008. The dotted line represents the initiation of soil moisture sensor treatments.

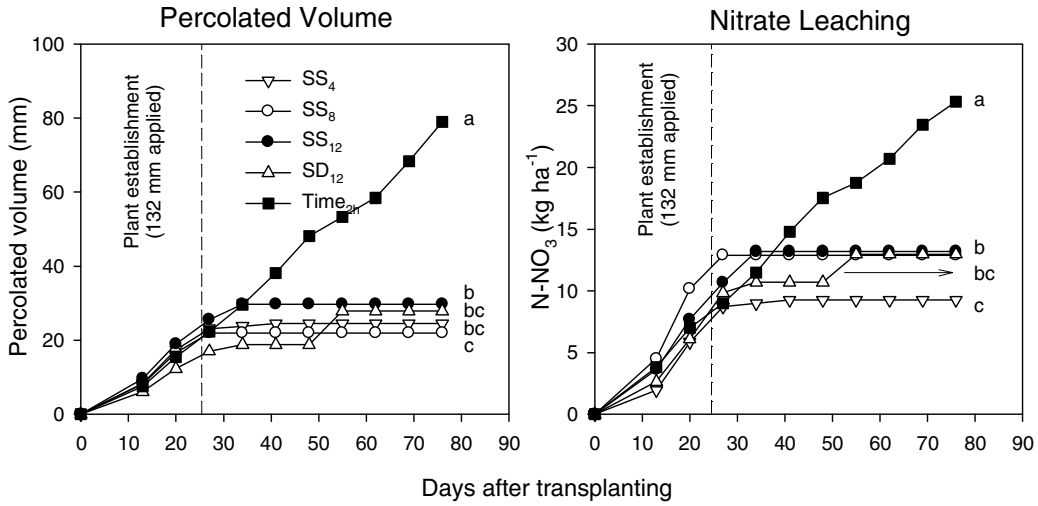

Fig.3. Cumulative leachate volume (left) and cumulative NO_3-N mass leached for different irrigation scheduling and soil moisture sensor irrigation treatments during spring 2008. Treatment means followed by same letter are not different according to Duncan's Multiple Range Test at $P \leq 0.05$.

The overall leachate amounts since the transplanting date were 24, 22, 30, 27 and 80 mm, for SS_4, SS_8, SS_{12}, SD_{12} and $TIME_{2h}$, respectively. However, most of the water percolation occurred during the establishment period, except for $TIME_{2h}$, which percolated about 7-8 mm wk^{-1} (Fig. 3 left). Cumulative nitrate leaching at the end of the crop season was significantly higher for $TIME_{2h}$ with 25 kg NO_3 ha^{-1} leached. The measured values for SS_4, SS_8, SS_{12} and SD_{12} ranged from 9 to 13 kg NO_3 ha^{-1} following the same patterns observed for percolated volume (Fig. 3 right).

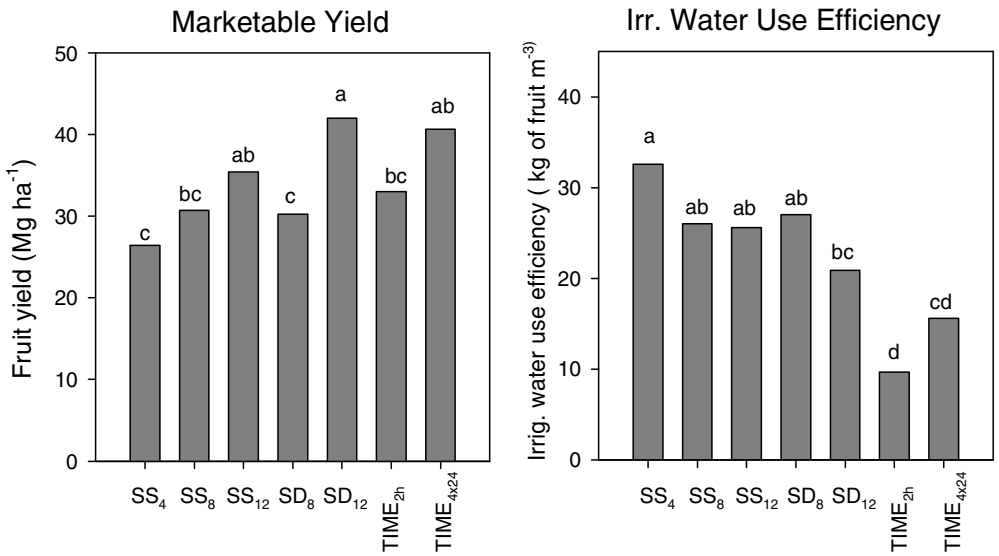

Fig. 4. Pepper total and marketable yield (culls minus total yield) and irrigation water use efficiency as affected by different irrigation scheduling and soil moisture sensor irrigation treatments during spring 2008. Treatment means followed by same letter are not different according to Duncan's test at $P \leq 0.05$.

Irrigation treatments had an important impact on IWUE and pepper yield (Fig. 4). The use of SMS with 12% VWC threshold and $TIME_{4x24}$ significantly increased marketable pepper yield when compared to the other treatments (Fig.4). Pepper yield obtained in these experiments were in the range of those reported in the literature for sandy soils in Florida.

The use of SMS control at 12% VWC threshold increased the water use efficiency of peppers without reducing yield compared to $TIME_{2h}$. Overall shoot (leaves and stem) dry weight ranged between 1.4 and 1.9 Mg ha^{-1} with no differences between treatments (Fig. 5 bottom). A reduced leaf area was observed for SS_4 and SS_8 treatments, while other treatments showed a leaf area above 3400 cm^2 $plant^{-1}$. Interestingly, the leaf area for $TIME_{2h}$ treatment reached a plateau around 50 DAT, indicating earlier plant maturity, which may be associated to the excessive leaching and lack of nitrogen, compared to the other treatments (Fig. 5 top). On the other hand, the reduction in leaf area for treatments SS_4 and SS_8 was related to the soil water availability and irrigation water distribution. Besides the reduced number of irrigation events for SS_4 and SS_8 compared to the other SMS treatments, the amount of water applied to these two treatments was not enough to wet soil between 15-30 cm and VWC decreased below 10% several days after the treatments started (Fig. 2 right column).

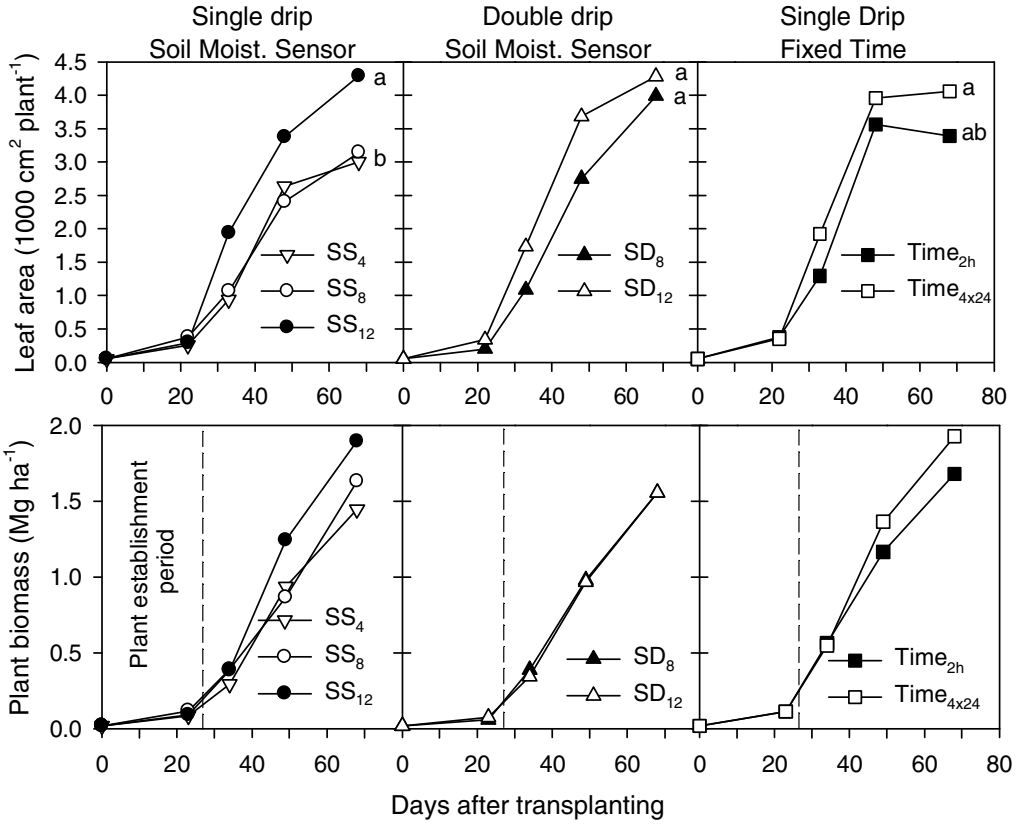

Fig.5. Leaf area (top row) and cumulative plant biomass (bottom row) of pepper as affected by different irrigation scheduling and soil moisture sensor irrigation treatments during spring 2008.

The irrigation frequency reported for treatments SS_{12}, SD_8 and SD_{12} resulted in higher levels of VWC (15-18%) at 0-15 cm and 15-30 cm soil layer (11-14%) without excessive drainage (Fig. 3). The soil moisture patterns influenced directly leaf stomatal conductance. Initially at 33 DAT, leaf stomatal conductance ranged between 7 to 15 mmol s^{-1} $plant^{-1}$, but no

patterns leaf stomatal conductance was correlated to the irrigation treatments (Fig. 6 left). During the flowering at 48 DAT, leaf conductance was again measured (Fig. 5 right, notice different scale for axis), and the $TIME_{4x24}$, SD_{12} and SS_{12} showed the higher leaf stomatal conductance and these results followed the similar patterns of yield results. Furthermore, more frequent measurements within a day and in season are required to reduce the large uncertainty of approximately 20% (Bragg et al. 1991) in conductance data estimated using porometry.

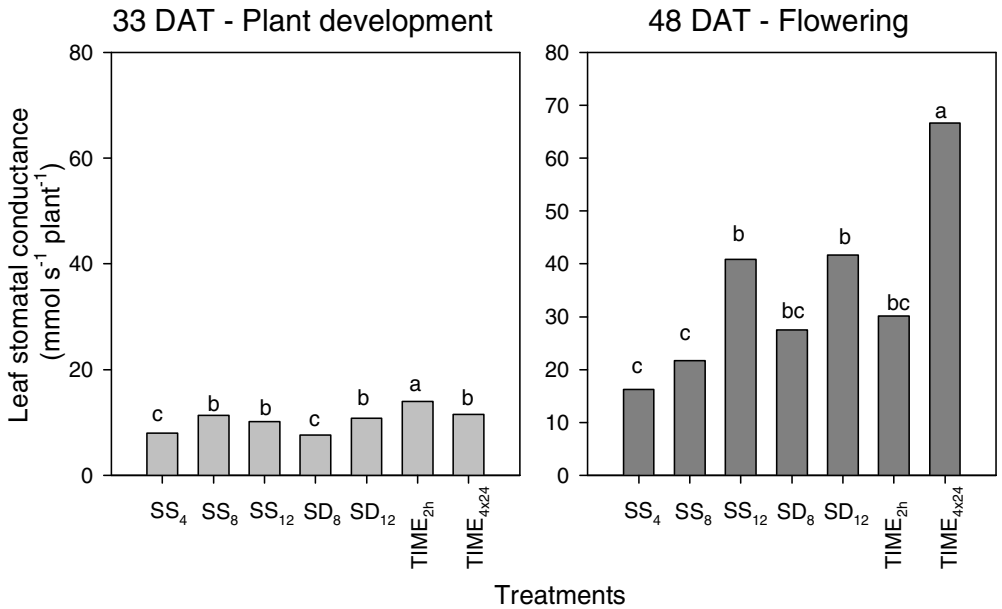

Fig.6. Pepper leaf stomatal conductance as affected by different irrigation scheduling and soil moisture sensor irrigation treatments during spring 2008. Treatment means followed by same letter are not different according to Duncan's test at $P \leq 0.05$.

Conclusion

Soil-moisture sensor (SMS) based irrigation systems in pepper significantly reduced the applied irrigation resulting in 41%-60% less irrigation water applied compared to fixed time irrigation ($TIME_{2h}$) without reducing yield. Soil moisture sensor controller thresholds below 8% of volumetric water content significantly reduced the amount of water applied, but also resulted in a significant decrease of marketable yields. The treatment ($TIME_{4x24}$) with four fixed irrigation events a day resulted in similar marketable yields as SD_{12}, SS_{12}, but with lower irrigation water use efficiency. The use of double drip improved water distribution across bed, which resulted in an increase of leaf area for SD_8 compared to SS_8 treatment, however, no additional yield benefit was measured due to the use of double drip comparing SS_{12} and SD_{12} to SS_8 and SD_8.

References

Allen, R. G., L.S.Pereira, Raes, D., and Smith, M. (1998). *Crop evapotranspiration: guidelines for computing crop water requirements*, Food and Agriculture Organization of the United Nations, Rome.

Amayreh, J., and Al-Abed, N. (2005). "Developing crop coefficients for field-grown tomato (*Lycopersicon esculentum* Mill.) under drip irrigation with black plastic mulch." *Agricultural Water Management*, 73(3), 247-254.

Bragg, T., Webb, N., Spencer, R., Wood, J., Nicholl, C., and Potter, E. (1991). *AP4 Porometer User Manual. Version 2. Delta T Devices Ltd. Cambridge, UK.*

Buster, T. P. (1979). *Soil survey of Marion County, Florida*, Washington, D.C.

Carlisle, V. W., Sodek III, F., Collins, M. E., L.C., H., and Harris, W. G. (1988). "Characterization data for selected Florida soils. University of Florida-Institute of Food and Agricultural Sciences." *Soil Sci. Res. Report . Gainesville, FL.*, 88-1.

Dukes, M. D., and Scholberg, J. M. (2005). "Soil moisture controlled subsurface drip irrigation on sandy soils." *Applied Engineering in Agriculture*, 21(1), 89-101.

Icerman, J. (2007). "Approaches for two-dimensional monitoring and numerical modeling of drip systems," University of Florida, M.Sc. Thesis, Gainesville.

Locascio, S. J. (2005). "Management of irrigation for vegetables: Past, present, and future." *HortTechnology*, 15.

Olson, S. M., Simonne, E., Maynard, D. N., Hochmuth, G., Vavrina, C. S., Stall, W. M., Pernezny, K. L., Webb, S. E., Taylor, T. G., and Smith, S. A. (2005). "Pepper production in Florida." Vegetable Production Handbook for Florida 2005-2006, S. M. Olson and E. Simonne, eds., IFAS, Gainesville, 291-303.

SAS. (2002). *The SAS system for Windows. Release 9.0.*, SAS Inst. Inc., Cary, NC.

Simonne, E. H., Dukes, M. D., and Haman, D. Z. (2007). "Principles and Practices of Irrigation Management for Vegetables." In Vegetable Production Guide for Florida, U. of Fla., Gainesville, Fla., O. a. Simonne, ed., Univ. of Fla., Gainesville, FL, 33-39.

Verhoef, A. (1997). "The effect of temperature differences between porometer head and leaf surface on stomatal conductance measurements." *Plant Cell and Environment*, 20(5), 641-646.

Zotarelli, L., Dukes, M. D., Scholberg, J. M., Hanselman, T., Le Femminella, K., and Munoz-Carpena, R. (2008). "Nitrogen and water use efficiency of zucchini squash for a plastic mulch bed system on a sandy soil." *Scientia Horticulturae*, 116, 8-16.

Zotarelli, L., Scholberg, J. M., Dukes, M. D., Muñoz-Carpena, R., and Icerman, J. (2009). "Tomato yield, biomass accumulation, root distribution and irrigation water use efficiency on a sandy soil, as affected by nitrogen rate and irrigation scheduling." *Agricultural Water Management*, 96(1), 23-34.

Water Production Functions for High Plains Crops

Thomas Trout, Gerald Buchleiter and Walter Bausch

USDA-Agricultural Research Service, 2150 Centre Ave., Bldg D, Fort Collins, CO. 80526; PH 970-492-7419; email: Thomas.trout@ars.usda.gov.

ABSTRACT

Declining water supplies is the critical resource issue for irrigated agriculture in the High Plains and much of the western U.S. Farmers need to maximize production per unit water consumed to remain economically viable and sustain irrigated agriculture. The Agricultural Research Service (ARS) Water Management Research Unit is developing water production functions for High Plains crops that can help farmers make decisions for allocating limited water supplies among crops. The Unit has developed an irrigated research farm to measure total water balance for a 4 crop rotation (wheat, corn, sunflower, dry beans). The goal is to develop water production functions based on consumptive use, relate yields to soil water deficits and plant stress indicators, and improve existing plant growth models to more accurately reflect water stress effects. Results for the first year corn crop show both grain and total biomass yields nearly proportional to water consumptive use with water use efficiencies of 2.4 and 3.9 kg/m^3, respectively.

INTRODUCTION

Population growth, environmental needs, water table declines, and reduced precipitation, possibly due to climate change effects, are resulting in reduced water supplies for irrigated agriculture in the High Plains and much of the western U.S. These trends will likely continue. As our understanding of the hydrology of the region has improved, it has become apparent that increases in irrigation system efficiency alone will not create sufficient water supplies to meet future water needs. Irrigated area will likely decline, jeopardizing the viability of rural agricultural economies throughout the High Plains.

Sustaining irrigated agriculture will require maximizing economic output per unit of the most limiting resource – water. This will require both conversion to higher value crops, which has been occurring for several years in California and the southwestern U.S., and maximizing productivity per unit of water consumed.

Many studies have shown that the marginal productivity per unit of irrigation water applied tends to increase as water application declines. This may be due either to increased efficiency of water use (less deep percolation and evaporation losses from irrigation and better utilization of precipitation), or to a physiological responses in plants that increases productivity per unit water consumed. The first effect is likely, but, as stated above, may not produce the needed additional water supplies. Past studies that show a linear relationship between yield and water consumption

(Doorenbos and Kassam 1986) indicate that there may not be water productivity efficiency gains from decreasing water use.

The objective of this project is to measure water productivity (production per unit water use) of four crops common in the high plains under a range of water application and consumption amounts. Precision water application and measurement systems are used to separate out irrigation efficiency and crop water productivity. Plant responses to water stress are monitored to better understand physiological responses and to provide indicators of levels of stress. Plant growth models will be compared with the results and modified to better model stress effects, so that the results can be extended to other environments and conditions.

METHODS

A 16 ha field research facility northeast of Greeley, CO was developed to enable the precision field measurements required to accomplish the above objectives. Four blocks (one per crop) were laid out near the center of the facility with 4 replications and 6 water treatments. Each block has 6 outside buffer rows. Each plot includes twelve 40 m long rows (76 cm spacing), of which the center four are used for measurements. The predominately sandy loam soils in the plot area were mapped according to apparent electromagnetic measurements and with visual surveys of open irrigation pipe trenches. Soil cores were sampled to 2 m to determine soil types and water holding characteristics.

Four crops – winter wheat, field corn, sunflower (oil), and dry beans (pinto) are rotated through the four blocks. Crops are planted, fertilized, and managed for maximum production under fully irrigated conditions. All blocks are managed with no or minimum tillage except for one 7.6 m end of each replication across all plots which is conventionally tilled to allow comparison of the water balance under the two tillage systems.

Six water treatments are applied to each crop:

- #1 – 100%: fully meet predicted water requirements
- #2 - 85%: 85% of treatment #1
- #3 - 70%: 70% of treatment #1
- #4 - 70%: 70% of treatment #1
- #5 - 55%: 55% of treatment #1
- #6 - 40%: 40% of treatment #1

Treatment 3 is applied proportional to treatment #1 at each irrigation. Treatments #2, 4, 5, and 6 are targeted to be seasonally proportional to treatment #1 but the water applications are distributed in response to critical growth periods (Stewart et al. 1975, Stegman 1982). This results in applications below the treatment amount between establishment and reproductive stages and during plant maturation stages, and application above the treatment amount during the critical reproductive stage. This water management scenario is designed to maximize production per unit of water applied. Comparison of treatments 3 and 4 will indicate the advantages of this

scenario. All treatments are irrigated equally during the germination and plant establishment period.

Irrigation water is delivered to the corner of each plot and applied through polyethylene header pipes to drip irrigation tubing (Point Source Irrigation 41T163-12 [16 mm thick walled tubing with 1.1 L/h conventional inline emitters on 30 cm spacing])[1] laid on the soil surface near each plant row. Flow rates and volumes to each treatment are measured with turbine flow meters (BadgerMeter Recordall 1 ½" Turbo 160 meters with RTR transmitters). Irrigation applications to each treatment are controlled and recorded with Campbell Scientific CR 1000 data loggers. A portable sprinkler system (Nelson Poly 2000 with R10 Turbo heads on 9 m spacing) is used as needed to germinate crops and incorporate herbicides. Water is supplied from groundwater (1.9 dS/m), stored in a 22,000 L storage tank, and pressurized with a pressure-controlled variable frequency drive booster pump.

An automated weather station is located at the edge of the plots near the center of a 0.5 ha grass plot. Hourly data from the station is used to calculate ASCE Standardized Penman-Monteith alfalfa reference evapotranspiration (ETr). Soil water content (SWC) in each plot between 15 and 200 cm depth is measured by neutron attenuation (503 Hydroprobe, Campbell Pacific Nuclear) from an access tube in the center of each plot. Soil water content in the surface 15 cm is measured with a MiniTrase portable TDR system (SoilMoisture). Irrigations are scheduled using measured soil water depletion and predicted soil water depletions based on ETr measurements.

Plant measurements are taken periodically to indicate responses to the water treatments. Plant growth stage is assessed visually. Canopy cover is measured both with a photosynthetically active radiation sensor (AccuPAR LP-80, Decagon Devices), and a NIR,R,G digital camera (ADC, TetraCam Inc.). Spectral radiometers and an infrared thermometer mounted on a mobile platform (along with the TetraCam camera) measure canopy reflectance and temperature, respectively (Fig 1). Stomatal conductance is measured with a porometer (Model SC-1, Decagon Devices), and leaf water potential with a plant water status console (Model 3000, SoilMoisture, Inc.). At the end of the season, seed yield and quality and total biomass is measured from an approximately 70 m^2 area in the center of each plot.

Two adjacent 2 ha fields are each planted to one of the four crops so that each crop is grown in alternate years. Bowen Ratio energy balance instrumentation is installed in the center of each field to estimate actual crop ET. The crop in the field is irrigated to meet full water requirements, and the measured ET is compared to calculated water use in the 100% treatment. The measured ETc is also used to calculate a crop coefficient for the crop under well watered conditions. The fields adjacent to these fields and the plot areas are used as buffer areas and for variety trials under water stress conditions.

[1] Mention of product and trade names are for the benefit of the reader and do not imply endorsement of the product by USDA.



Figure 1. Mobile radiometer platform used to measure reflectance and canopy temperature from 7.2 m above the ground.

Results will be compared with three types of models. A simple water balance spreadsheet is used to track ET and SWC and to schedule irrigations. This model estimates ETc (FAO 56 methodology), surface evaporation, and deep percolation losses and compares measured and predicted SWC. The FAO AquaCrop model (Steduto et al. 2007, Raes, et al. 2007) is a semi-empirical model designed to predict crop water production functions. We will calibrate the model with initial results and verify its accuracy against future year data. The RZWQM2 model (Ma et al. 2000, Ahuja et al. 2000) is a process-based soil and plant model. It will be coupled with the DSSAT (Jones et al. 2003) suite of plant models and compared with measured results. Once the various components of the model are verified (soil water balance, ETc, plant growth, yield), it will be used to project the field results to other conditions and environments and generate data for economic comparisons of alternative water management options. The RZWQM2 model produces a single stress parameter to describe water stress. We will attempt to relate this stress parameter to our measurements of plant stress and add measurable stress indicators that could be used as triggers for deficit irrigation scheduling.

RESULTS

This project began in 2008 so we have completed one crop year. We will present 2008 results for corn in this paper. Due to land preparation requirements (deep ripping and land planing), the first year crop was not planted "no-till". Nitrogen fertilizer applications, based on soil samples and agronomic practices, were split between preplant broadcast (50 kg/ha), sidedress at planting (33 kg/ha), and water-applied nitrogen (34 kg/ha). DeKalb 52-59 AF2 (VT3) corn seed was planted May 12 at 80,000 seeds per ha. Germination was nearly 100%.

The corn, which was sprinkle irrigated May 21 (20 mm), emerged about June 1 and received 30 mm of precipitation on June 6. This was the last measureable rainfall until Aug 6, allowing fully controlled water treatments throughout the vegetative stage. Ten irrigations (287 mm) were applied to the 100% treatment and 7 irrigations (110 mm) to the lowest water treatment in this interval. On Aug 4, soil water deficits to 90 cm depth varied from about 40 mm in the 100% treatment to 90 mm in the driest two treatments. Figure 2 shows the dramatic effects of the water stress treatments on corn vegetative growth.



Figure 2. Comparison of corn growth condition on July 31 just before entering the reproductive growth stage. Rows at the left and background are treatment 1; rows at right (short with curled leaves) are treatment 6.

Table 1. Water application and consumptive use for the six irrigation treatments for the 2008 corn crop. Applications are divided between vegetative (Veg) and reproductive (Repro) growth stage (before/after Aug 3). Percents are relative to treatment #1. Soil water content (SWC) change is to 0.9 m depth from June 10 to Oct 9.

Tmnt	Target	Irrigation Application			Irrig. + Precipitation			Evapotranspiration			Transpiration			Deep Perc.	Surface Evap.	SWC Change
		Veg	Repro	Total	Veg	Repro	Total	Veg	Repro	Total	Veg	Repro	Total	Total	Total	Total
		mm	*mm*	*mm*	*mm*	*mm*	*mm*	*mm*	*mm*	*mm*	*mm*	*mm*	*mm*	*mm*	*mm*	*mm*
1	100%	287	150	437	326	340	667	299	265	564	263	250	513	117	50	-14
		100%	*100%*	*100%*	*100%*	*100%*	*100%*	*100%*	*100%*	*100%*	*100%*	*100%*	*100%*			
2	85%	225	111	336	264	302	566	272	252	523	235	237	471	55	50	-2
		79%	*74%*	*77%*	*81%*	*89%*	*85%*	*91%*	*95%*	*93%*	*89%*	*95%*	*92%*			
3	70%	199	80	279	238	271	509	252	247	499	219	232	451	32	47	-7
		69%	*53%*	*64%*	*73%*	*80%*	*76%*	*84%*	*93%*	*88%*	*83%*	*93%*	*88%*			
4	70%	184	85	269	223	276	499	236	245	481	203	229	433	40	47	-15
		64%	*57%*	*62%*	*68%*	*81%*	*75%*	*79%*	*92%*	*85%*	*77%*	*92%*	*84%*			
5	55%	134	45	178	173	235	408	191	194	385	158	174	332	42	52	-20
		46%	*30%*	*41%*	*53%*	*69%*	*61%*	*64%*	*73%*	*68%*	*60%*	*69%*	*65%*			
6	40%	110	25	135	149	216	365	172	184	356	137	160	298	32	56	-23
		38%	*17%*	*31%*	*46%*	*63%*	*55%*	*57%*	*69%*	*63%*	*52%*	*64%*	*58%*			

The corn tasseled and entered the reproductive stage about Aug 3. A 42 mm rainfall on Aug 6 replenished the soil water in all treatments to start the reproductive stage, and 95 mm rainfall on Aug 14/15 filled the 0.9 m root zone profile in all treatments. Irrigation treatments were re-started on Aug 26 and continued until a rainfall on Sept 12. First frost occurred Oct 12 and the crop was harvested Nov 6.

Table 1 lists water applications and consumption for the 6 treatments. The 100% treatment received 437 mm of irrigation and 230 mm of rainfall, of which about 117 mm was lost below the root zone; and evapotranspired about 564 mm, of which about 50 mm was estimated to be surface evaporation. Although the range of irrigation applications exceeded the range of treatment targets, the range of ETc and transpiration (T) was reduced due to the August rainfall. The soil water storage change from the beginning to end of the season was relatively small in all treatments due to late season rainfall.

Although the low water treatments were severely stressed in July and early August and successful pollination seemed questionable, the well-timed rainfalls allowed even the driest treatment to produce viable yields. Seed yields varied from 12.9 Mg/ha (205 bu/ac) for tmnt #1, an above average yield for the area, down to 8.6 Mg/ha (137 bu/ac) for treatment #6. The harvest index increased only slightly with increasing deficits (from 0.58 to 0.62). Figure 3 shows the water production relationship for the crop. The relationships for both total biomass and seed yield are fairly linear over the range tested. The intercepts of both the biomass and grain yield vs. ETc and T are small meaning that the responses are nearly proportional and the water productivity (yield per unit water) is nearly constant over the range. The grain yield averaged 2.7 and 2.4 kg per m^3 of water and biomass yield averaged 4.4 and 3.9 kg/m^3 of water transpired and evapotranspired, respectively. For the 2008 year, the grain yield per unit irrigation water applied increased from 3.0 kg/ m^3 for treatment #1 up to 6.4 kg/ m^3 for treatment #6. These values will vary widely with precipitation amount and timing.

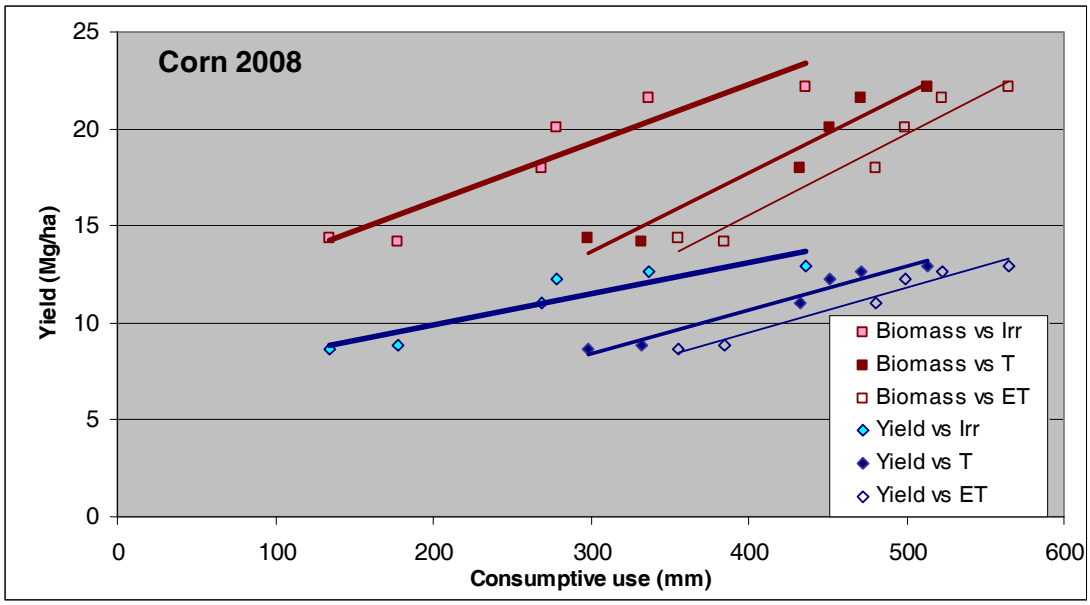

Figure 2. Water production functions for 2008 corn. Red lines are total biomass (dry wt.). Blue lines are grain yield (15.5% moisture content). Yields are plotted relative to irrigation amount (Irr), crop transpiration (T), and crop ET (ET). Lines are linear least squares regression fits to the 6 data points.

DISCUSSION

Many water production function studies in the High Plains have related production to irrigation water applied, and they show increasing productivity with decreasing irrigation applications, as we measured in this study. This is because deficit irrigation increases the effective use of precipitation, may increase irrigation efficiency by reducing deep percolation and soil evaporation losses, and may result in soil water mining. However, since the impact of irrigation on the regional hydrology is often more closely related to water consumed than irrigation water applied (assuming unconsumed water returns to useable supply sources such as groundwater or return flows to streams), consumptive use should be the more relevant parameter. By relating production to consumptive use, the results can be transferred to other environments and irrigation methods.

These results which show that water productivity does not change with consumptive use indicate little opportunity to increase water productivity through deficit irrigation. Even though stress during the vegetative stage resulted in dramatically reduced vegetation (Fig. 2), the reduction in stress during reproduction resulted in relatively good yields from deficit irrigated plots and relatively constant water productivity for both biomass and grain. Whether these results are borne out over a range of environmental conditions will be determined by future results.

REFERENCES

Ahuja, L.R., K.W. Rojas, J.D. Hanson, M.J. Shaffer, and L. Ma (eds). 2000. The Root Zone Water Quality Model. Water Resources Publications LLC. Highlands Ranch, CO. 372pp

Doorenbos, J., and A.H. Kassam. 1986. Yield response to water. FAO Irrigation and Drainage paper #33. FAO, Rome.

Jones, J.W., G. Hoogenboom, C.H. Porter, K.J. Boote, W.D. Batchelor, L.A. Hunt, P.W. Wilkens, U. Singh, A.J. Gijsman, and J.T. Ritchie. 2003. The DSSAT cropping system model. Eur. J. Agron. (18):235-265.

Ma, L., L.R. Ahuja, J.C. Ascough, II, M.J. Shaffer, K.W. Rojas, R.W. Malone, and M.R. Cameira. 2000. Integrating system modeling with field research in agriculture: Applications of Root Zone Water Quality Model (RZWQM). Adv. Agron. 71:233-292.

Raes, D., P. Steduto, T.C. Hsiao, E. Fereres and L. Heng. 2007. AquaCrop crop water productivity model – calculation procedures. FAO LWDD, Rome, Italy.

Steduto, P., D. Raes, T.C. Hsiao, E. Fereres, L. Heng, G. Issi, and J. Hoogeveen. 2007. AquaCrop: A new model for crop prediction under water deficit conditions. Options Mediterraneenees, Series A, No 80: 285-292.

Stegman, E.C. 1982. Corn grain yields as influenced by timing of evapotranspiration deficits. Irrig. Sci. (3):75-87.

Stewart, J.I., R.D. Misra, W.O. Pruitt, and R.M. Hagan. 1975. Irrigating corn and grain sorghum with deficient water supply. Trans. ASAE. (18):270-280.

Water Retention and Hydraulic Conductivity of Different Media Used for Containerized Agriculture Systems

Vivek Kumar[1], M. Reza Savabi[2], Felipe M. Guerrero[1], Berrin Tansel[1]

1 Florida International University, Civil and Environmental Engineering Department, 10555 West Flagler Street, Engineering Center Miami, FL, 33174
2 United States Department of Agriculture, ARS, Miami, FL

Abstract

Containerized plant production represents an extremely intensive agricultural practice and a large amount of water and chemical fertilizer is applied. Hydo-physical characteristics such as water infiltration, texture and structure, particle size distribution affect the quality of the media used in containerized agricultural systems and the water availability to plants. Water retention characteristics depend on particle size distribution as well as the composition of the media used. Materials with coarser particles allow faster percolation of water and also retain relatively higher amounts moisture per unit weight due to higher porosity But drain faster due to less surface area.. Faster drainage can result into air flow through coarser materials causing the media to dry. As the media desaturates, hydraulic conductivity is reduced. The objective of this study was to analyze the different media used by nurseries to characterize the physical properties which would explain the soil-water interactions. In this study we measured soil's hydraulic conductivity in the laboratory using three methods, constant head permeability test, falling head permeability test and tension Infiltrometer. The results were compared in relation to particle size distribution characteristics of samples. The results of the study indicate that the four common media being used in nurseries in South Florida have distinct hydro-physical properties. The result of this should assist the land managers while selecting the Best Management Practices.

Keywords: Nurseries, Water Infiltration, Best Agricultural Practices, Water Retention, Particle Size Distribution, Containerized Agriculture Systems, Soil-Water Interactions

Introduction

Florida is the second-leading horticulture state in the nation. Florida greenhouse/nursery sales are more than $1.6 billion annually. Containerized plant production represents an extremely intensive agricultural practice and a large amount of water and chemical fertilizer is applied. Considering that three national parks (Everglades, Biscayne and Big Cypress) in south Florida surround agriculture, a major challenge in agricultural production is the development of appropriate technology that combines optimum crop production with environmental protection. Non-point source water pollutants (nutrients, pesticides, and other chemicals) resulting from agricultural areas have been implicated as a source of water quality degradation in southern Biscayne Bay. In 1996, the United States Environmental Protection Agency published an interim report on South Florida Ecosystem Assessment. The report stated that the nutrient loading from agricultural and urban areas had significantly increased nutrient concentrations,

particularly phosphorus. The report also indicated that discharging phosphorus at the current control target of 50 μg/L would continue to allow eutrophication of over 95% of the Everglades marshes.

Farming methods can alter soil mechanisms such as soil structure, porosity, as well as the hydraulic conductivity and water retention. Transition to container production is driven by market demands and numerous production advantages including greater production per acre, faster plant growth, higher plant quality, and lack of dependence on arable land (Colangelo and Brand, 2001). In agriculture systems, environmental conditions affect the longevity of fertilizer availability and release. Because environmental conditions fluctuate, regular monitoring of the medium's nutrient status is essential. Lack of essential elements will result in slow and aesthetically unacceptable growth. Conversely, excessive nutrient concentrations result in root injury, hindering the plant's ability to absorb water and nutrients; which increases the potential for environmental contamination (Water Quality Handbook for Nurseries). Leaching of nutrients is a major field of study and a major concern in agricultural practices, and the ability of a soil to hold nutrient depends on the mechanics and dynamics of its interaction with water which in turn acts a major source of nutrient transport. Extent of leaching depends directly with the hydraulic conductivity. The mass leaching is substantially reduced when the hydraulic conductivity lowers for a stabilized soil and substantially increases when the hydraulic conductivity is increased.

The objective of this study was to analyze the different media used by nurseries to characterize the physical properties which would explain the soil-water interactions. The study involved measuring soil's hydraulic properties in the laboratory by three methods (i.e., constant head permeability test, falling head permeability test and tension Infiltrometer. The results were compared in relation to the particle size distribution of each sample.

Materials and Methods

The samples analyzed where from four different nurseries across South Miami-Dade county Florida, Pine Island Mix, Nursery Mix, Greenhouse mix and Costa farms mix. The characteristics of the study samples are illustrated in Table1. The samples have high organic content. This is in contrast to soil in the region which have a high percentage of clay, sand, loam and silt. The high organic content of the four nursery samples is due to the efforts of the nursery operators who add certain media in the soil sample to increase the moisture retention capacity.

Pine Island	**Nursery Mix**	**Greenhouse Mix**	**Costa Farms**
Hardwood Fines	Pine Bark (50%)	Pine Bark (37.5%)	Pine Bark
Pine Bark Fines	Sand (10%)	Sand (7.5%)	Sand
Eco-Soil	Coir Pith (40%)	Coir Pith (30%)	Coir Pith
Dolomite	Dolomite	Perlite (25%)	Dolomite
Talstar	Micro Mix	Dolomite	Styrofoam
Minors		Micro Mix	
Total Organic Content (65.17 %)	Total Organic Content (39.13 %)	Total Organic Content (62.29 %)	Total Organic Content (48.8 %)

Table 1. Materials in nursery mixtures under study.

The study involves the following experimental procedures to develop characterize selected physical properties of nursery mixtures:

1. Sieve Analysis: Fisher Scientific (US Standard Sieve Series).
2. Constant Falling Head Permeability Test: ELE International Permeameter.
3. Falling Head Permeability Test: ELE International Permeameter.
4. Infiltration: Tension Infiltrometer Soil Measurement System Tension Infiltrometer.

It has long been recognized that hydraulic conductivity is related to the grain-size distribution of granular porous media (Freeze and Cherry, 1979). Knowledge of saturated hydraulic conductivity of soil is necessary for modeling the water flow in the soil, both in the saturated and unsaturated zone, and transportation of water-soluble pollutants in the soil. Permeability is the ease with which the water flows through a soil medium. Tension Infiltrometer measures the unsaturated hydraulic properties of a given soil sample. Water is allowed to infiltrate soil at a rate which is lower that free fall rate of water through a column, which is accomplished by maintaining a negative pressure on the water.

Methodology

- Sieve Analysis:

A defined amount of oven dry soil sample was subjected to a stack of 13 sieves ranging from 38.1mm to 0.075mm. The duration of the sieve shaking process was kept at a constant value of 15 minutes for all the four samples. After the allotted time of 15 minutes for the shaker, the individual sieves were analyzed for their respective weights and the several parameters were calculated, Cumulative percent of soil retained on the nth sieve, Cumulative percent of soil passing through the nth and the Weight gain of soil during sieve analysis.
Unlike the usual soils mixtures which tend to lose some mass during the course of the experiment, the nursery mixtures gained some weight during the course of the experiments which was about 20 minutes from the time of coming out of the oven to the final step of measuring the individual sieve weight.

Sr. No	Sample	Initial mass of soil	final mass of soil	coefficient of uniformity (Cu)	coefficient of gradation (Cc)	Weight Gain during the sieve analysis
		gm	gm			%
1	Pine Island	350	359.5	7.257	0.626	2.71
2	Nursery mix	300	302.2	2.738	0.721	0.73
3	Green house Mix	225	227.7	3.385	0.816	1.20
4	Costa Farms	200	201.6	8.276	0.920	0.80

Table 2: Sieve analysis coefficients.

- Constant Head Permeability Test:

Constant Head Permeability Test were conducted with ELE International Permeameter model EI25-0623 (Loveland, Colorado). This Instrument consists of a transparent acrylic cylinder that holds the soil sample which is to be tested. The permeameter has two different opening one at the top and the other at the bottom for the continuous movement of fluid. To distribute the flow over the entire cross-sectional area of the permeameter two Porous stones are used at either ends of the cylinder. Since the flow of water through the media may cause actual movement of the soil particle or even the soil fragments, a spring is placed on the top porous stone to pack/contain the soil media movement .the constant head permeability test requires a constant flow of water through the medium, hence to fulfill the requirement a Constant-head supply device which is just a large funnel, with an overflow held up over the permeameter. Once the assembly is in place oven dry soil specimen is filled upto about two-thirds the length of the tube. The spring packing of the oven dry sample enable the calculation of the dry density:

$$\rho_d = \frac{W}{AL}$$

Where, W is the Weight of the Specimen in the Permeameter: L is the Length of specimen *(*cm) and A is the Area of specimen ($A = (\pi/4)\, D^2$, cm^2).
Upon the measurement of time and the constant head the hydraulic conductivity of the particular sample can be calculated as:

$$K = \frac{QL}{Aht}$$

Where, Q is the Volume (cm^3), t is the Time of collection (s) and h being the Head difference (cm)

- Falling Head Permeability Test:

Falling Head Permeability Test were conducted with ELE International Permeameter model EI25-0623 (Loveland, Colorado)The equipment and assembly is similar to the Constant Head permeability test but unlike the Constant-head supply device, the head is allowed to fall with the help of a burette instead of the funnel assembly. The hydraulic conductivity is calculated as:

$$K = \frac{aL \ln \frac{h_1}{h_2}}{At}$$

Where, a = area of falling head tube (cm^2); L=final length of specimen (cm); A=area of specimen (cm^2); t = falling time (sec); h_1= initial drop height (cm) and h_2= final drop height (cm).

- Infiltration Test

Infiltration tests were conducted with tension infiltrometers by Soil Measurement Systems model SW-080B which has a 20 cm base plat that was separated from the water tower. Tension Infiltrometer measures the unsaturated hydraulic properties of a given soil sample. Water is allowed to infiltrate soil at a rate which is lower than the free fall rate of water through a column, which is accomplished by maintaining a negative pressure on the water. This is done to prevent the infiltration through cracks and wormholes, which would otherwise give high hydraulic conductivity values, which are not representative of the soil matrix (SMS Infiltrometer manual). Tension Infiltrometer measures the unsaturated hydraulic properties and the infiltration rate decreases as the soil becomes saturated till it attains a stabilized rate. The range of tensions attainable in the Infiltrometer is between 0 and –30 cm H2O, and each cm corresponds to 1 mbar pressure. Therefore at tensions close to zero, the infiltration rate should be approximately equal to saturated hydraulic conductivity of the soil.

When similar infiltration experiments involving two different negative pressures are performed the saturated hydraulic properties of the soil can be computed. The experiments when performed with a slight negative pressure difference (negative pressure of 5 vs. 40) yield nearly identical infiltration results, but the distinct behavior was eminent when the negative pressure difference was increased (negative pressure of 5 vs. 40). The volume of water entering the soil per unit time (cm^3/hr) can be computed as:

$$Q(h_X) = \pi r^2 K_{sat} \exp(\alpha h_X)\left[1 + \frac{4}{\pi r \alpha}\right]$$

Where, Q is the volume of water entering the soil per unit time (cm^3/hr); K is the hydraulic conductivity (cm/hr); α is coefficient (cm^{-1}) and h is the tension (cm). Also

$$K(h) = K_{sat} \exp(\alpha h)$$

Different negative pressures (h_x) provide different Q values, upon comparing two different Q values for the same medium hence

$$\alpha = \frac{\ln\left[\frac{Q(h_2)}{Q(h_1)}\right]}{h_2 - h_1}$$

The above equations can be used to generate a variety of values for the varying negative pressure. The saturated hydraulic conductivity value calculated and the saturated hydraulic conductivity value measured directly with the Infiltrometer might not be the same (SMS Infiltrometer manual).

Table 3. Tension Infiltrometer parameters and observation

Sr. No	Sample	Negative pressure -h1 (cm)	Negative pressure -h2 (cm)	Infiltration Rate at h_1 cm/hr	Infiltration Rate at h_2 cm/hr	Tension Infiltrometer (cm/hr)
1	Pine Island	154	40	6.12	32.04	7.2
2	Nursery mix	181	50	24.4	33.6	57.6
3	Green house Mix	153	40	23.6	36.4	25.2
4	Costa Farms	135	40	22.8	28.8	21.6

*Average of experiment done twice.

- Moisture retention capacity Evaluation

The moisture retention capacity and moisture absorption rate of the Nursery mixture is alarmingly high compared to usual soil media as evident form the sieve analysis, where the oven dry soil sample absorbs moisture from the surroundings which increases the total weight of a sample by a mean of 1.5% in a span of 20 minutes.

Table 4. Moisture gain during sieve analysis of the nursery mixtures

Sr. No	Sample	Weight Gain during the sieve analysis (In 20 minutes) %
1	Pine Island	2.71
2	Nursery mix	0.73
3	Green house Mix	1.20
4	Costa Farms	0.80

The saturated water retention capacities of the media were estimated using two different procedures, the first consists of adding water to the soil till it saturates and the second is to submerge the soil sample in water till it absorbs moisture to reach saturation. The amount of oven dry soil sample for each experiment was 50 grams. To prevent the intermixing and loss of the soil media Cheese cloth was used. The error related to the cheese cloth‘s ability to absorb water were duly noted and evaluated to get the best possible Moisture retention measurement of the Nursery mixture. The Moisture retention capacity of the media was computed as

$$\text{Saturation Water Content (\%)} = \frac{W - S - E}{S} \times 100$$

Where, W is the total weight of the saturated specimen (g); S is the soil sample weight (g); E is the error due to the cheese cloth. The high water retention capacity may be attributed to the high organic content of the Nursery mixtures.

Results

The media samples under study have been enriched by the nurseries to satisfy their respective needs and the major requirement was to retain as much moisture as the sample can. Hence a lot of organic contents where added like pine barks, manure with only fraction of sand. And a simple water saturation experiment illustrates the following results in Table 5. Figure 1 presents the particle -size distribution of the nursery mixtures. All four mixtures had similar particle size distribution, in general.

Table 5. Water saturation characteristics of the nursery mixtures.

Sr. No	Sample	Saturation Water Content (%)
1	Nursery mix	138.3 ± 13.2
2	Green house Mix	155.3 ± 3.3
3	Pine Island	213.2 ± 16.6
4	Costa Farms	201.2 ± 5.8

*Average of 3 tests

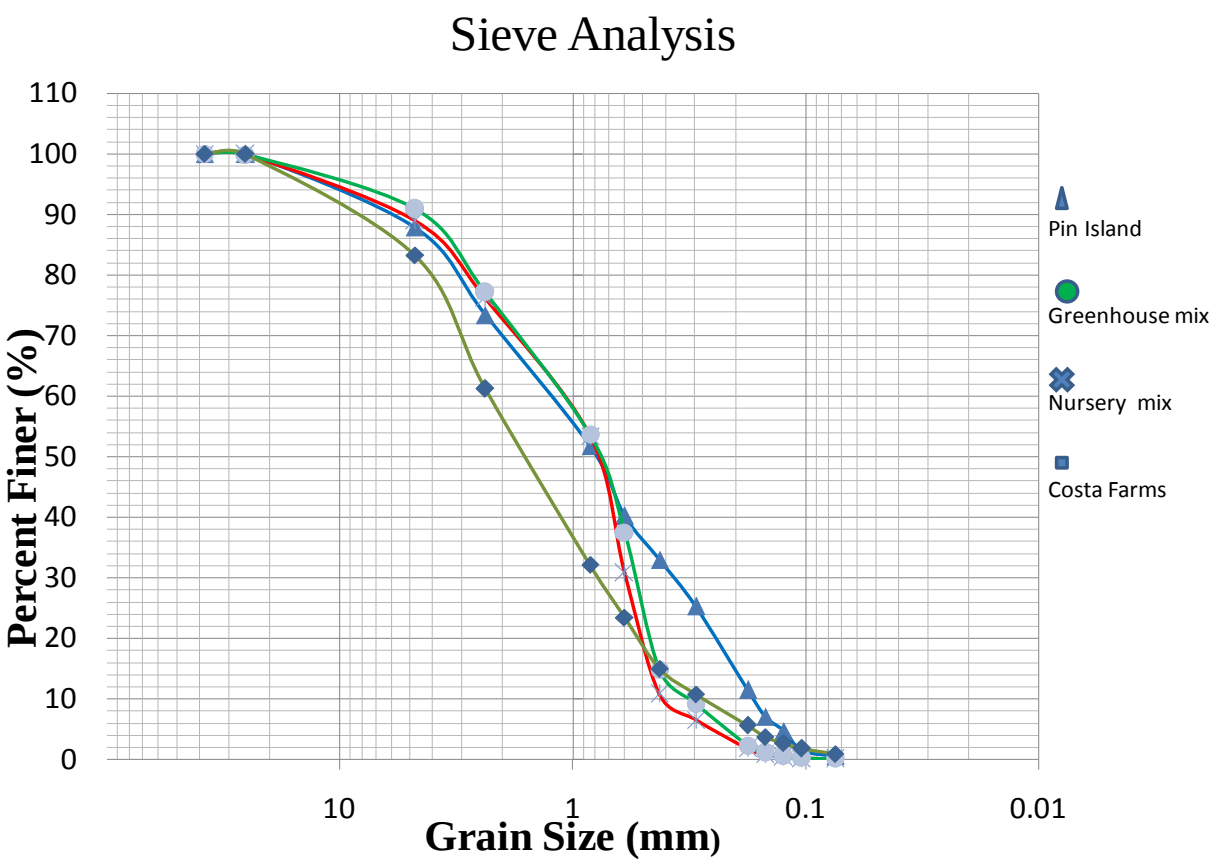

Figure 1. Particle -size distribution of the nursery mixtures.

To characterize the hydraulic conductivity of different size particles within the nursery mixtures, each sample was divided into 3 different particle size ranges by sieving. The sieving process consisted of a small sieve (0.425mm - Pan), medium sieve (2mm - 0.6mm) and large sieve (38.1mm- 4.75mm). The constant head permeability experiments provided the dry density and the hydraulic conductivity of each particle size mixture as presented in Figures 2 and 3. The decrease in particle size results in the increase of dry density and in the decrease of hydraulic conductivity. The hydraulic conductivity of the sample medium as whole follows the particle size analysis behavior, for example the Pine Island sample has larger particle size distribution hence the hydraulic conductivity is similar to the hydraulic conductivity of the lager sieve range of Pine Island sample. Tension infiltrometer was used to measure the unsaturated hydraulic properties of the nursery soil samples. Since saturated hydraulic was required, the experiments were performed with two different negative pressure. The experiments were performed in containers simulating the conditions in containerized agriculture systems. Figure 4 presents the plots of cumulative infiltration versus time. The hydraulic conductivities of the three different methods yield the results which are presented in Table 7.

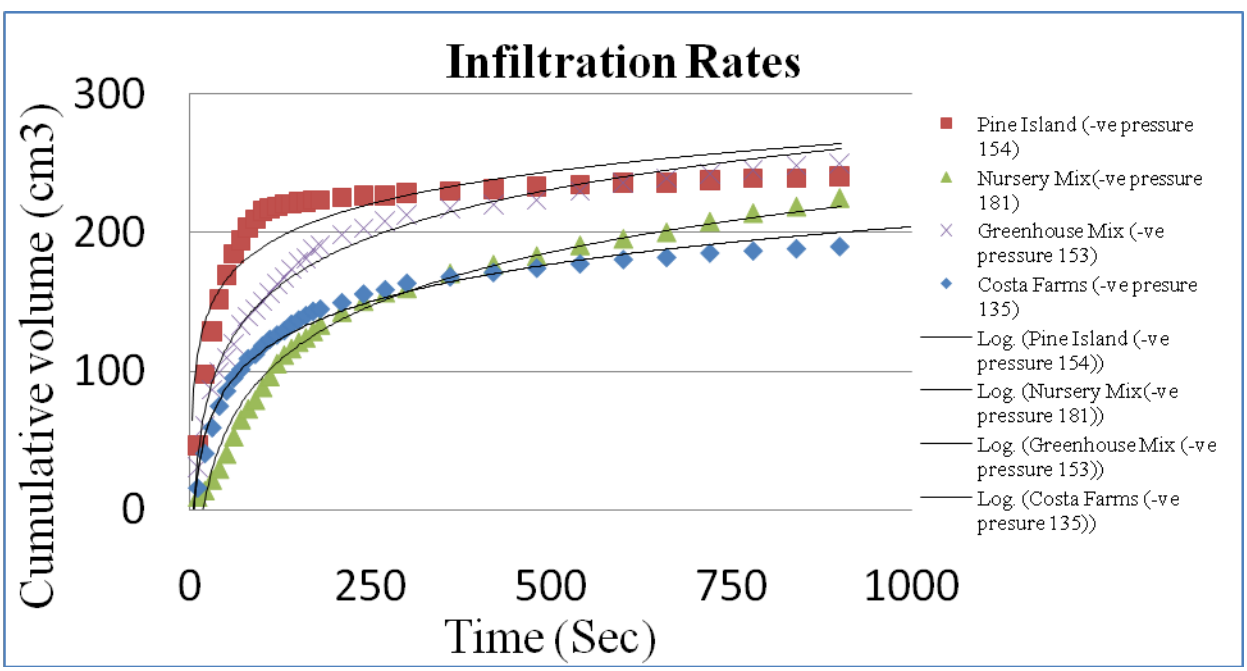

Figure 4. Results from tension Infiltrometer tests

Table 6. Equation of the Infiltrometer fit curves.

Sample	Curve Fit Equation	
Nursery mix	y = 39.01ln(x) - 65.14	R^2 = 0.981
Green house Mix	y = 49.81ln(x) - 78.45	R^2 = 0.986
Pine Island	y = 55.90ln(x) - 161.2	R^2 = 0.974
Costa Farms	y = 33.92ln(x) + 33.76	R^2 = 0.767

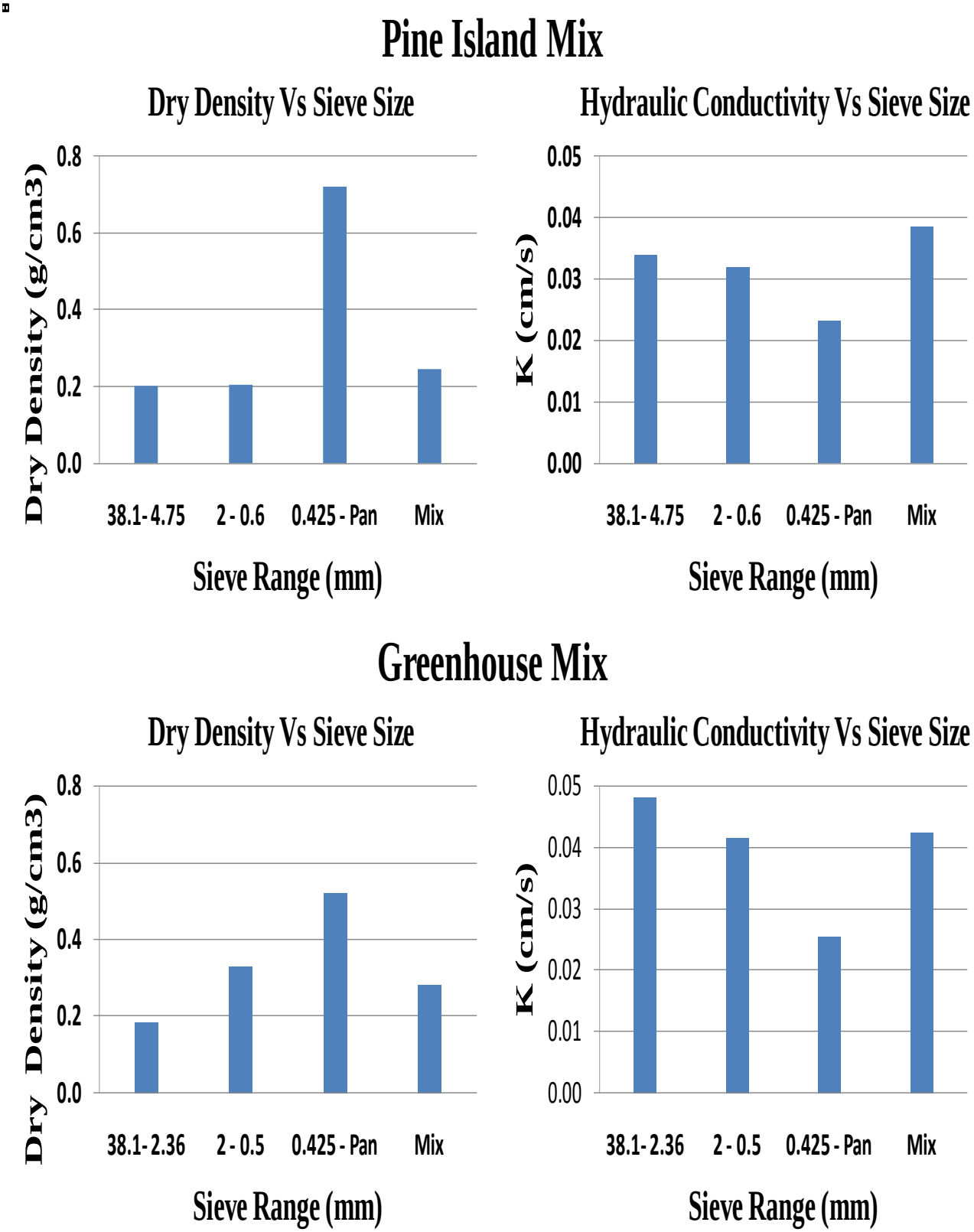

Figure 2. Variation of dry density and the hydraulic conductivity in relation to particle size in Pine island Mix and Greenhouse Mix samples.

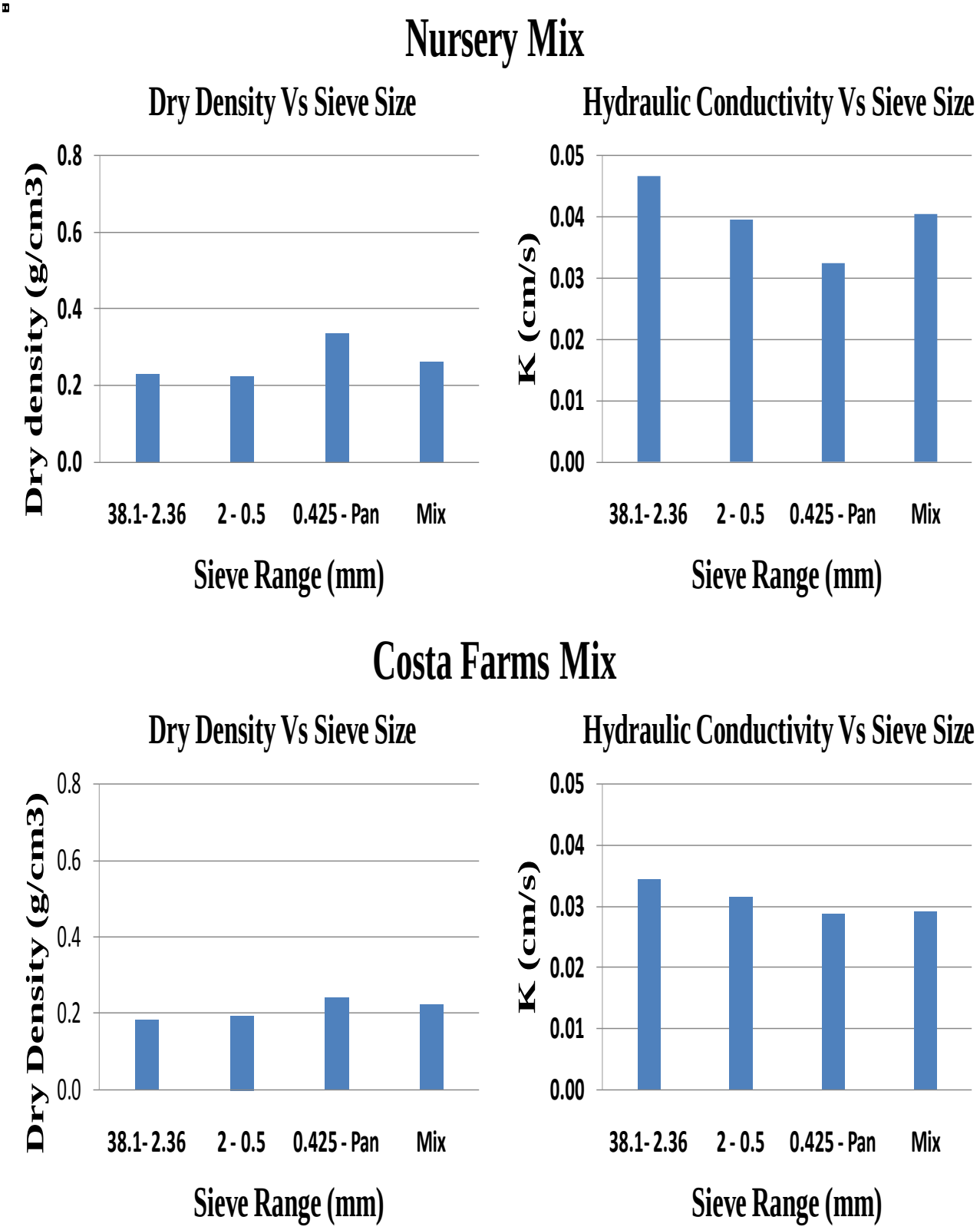

Figure 3. Variation of dry density and the hydraulic conductivity in relation to particle size in Nursery Mix and Costa Farms samples.

Table 7. Saturated hydraulic conductivity of nursery mixtures measured by three different test methods.

Saturated Hydraulic Conductivity	Pine Island	Nursery Mix	Greenhouse Mix	Costa Farms
Constant Head Permeability Test (cm/hr)	136.8 ± 21.6	151.2 ± 18	144 ± 5.76	104.4 ± 7.2
Falling Head Permeability Test (cm/hr)	381.6 ± 41.7	334.8 ± 23.2	280.8 ± 36.6	403.2 ± 17.8
Tension Infiltrometer (cm/hr)	7.2	57.6	25.2	21.6

* Constant Head Permeability Test was performed 6 times, Falling Head Permeability Test 4 time and Tension Infiltrometer 2 times.

Conclusions

Hydro-physical characteristics such as water retention and hydraulic conductivity of four different nursery mixtures were characterized by laboratory experiments. Effect of particle size on hydraulic conductivity was analyzed after separating each sample by using three 3 different size sieve sizes. The hydraulic conductivity measurements varied significantly between different test methods. The results of these types of characterization can provide a scientific basis for understanding of the non-point source water pollution from containerized horticultural and floricultural production systems and assist in the development of the Best Management Practices (BMP) for operation of environmentally sustainable agricultural enterprises in South Florida.

References

1. D.J. Colangelo and M.H. Brand “Nitrate Leaching Beneath a Containerized Nursery Crop Receiving Trickle or Overhead Irrigation,”. J Environ. Qual. 30:1564–1574 (2001).
2. N. Babacar, M. Jérome, H. Vincent, G. Chantal, H. Yannick “Effects of Agricultural Practices on Hydraulic Properties and Water Movement in Soils in Brittany (France),” Soil & Tillage Research, 93: 251-263(2007).
3. Jean Caron and David Elrick “Measuring the Unsaturated Hydraulic Conductivity of Growing Media with a Tension Disc,” Soil Science Soc. America, 69:783-793 (2005).
4. Water Quality Handbook for Nurseries, Oklahoma Cooperative Extension Service Division of Agricultural Sciences and Natural Resources Oklahoma State University.

Water Use and Evapotranspiration Coefficients for Camelina Sativa

D.J. Hunsaker[1], A.N French[1], T.R. Clarke[1] and D.M. El-Sheikha[2]

[1]USDA-ARS, Arid Land Agricultural research Center, Maricopa, Arizona 85238; PH (520) 316-6372; FAX (520) 316-6330; email: doug.hunsaker@ars.usda.gov

[2]University of Arizona, Maricopa Agricultural Center, Maricopa, Arizona 85238; PH (520) 316-6348; FAX (520) 568-2556; email: elsheikd@yahoo.com

ABSTRACT

The water use characteristics of *Camelina sativa*, an oilseed crop, were evaluated in an irrigation experiment in Maricopa, Arizona. Camelina (cv. Robinson) was grown between November 2006 and April 2007 in plots, each 10 by 17 m. Thirty-two of the field plots were replicated in a randomized block design consisting of irrigation treatments of four levels of soil water depletion: 40, 50, 65, and 75%. Six supplemental plots evaluated water stress at 85% soil water depletion. Weekly soil water content measurements were obtained over a soil profile of 1.9 m for all plots using neutron probes. In January 2007, following initial irrigations uniformly applied to all treatments, treatments received one to four additional surface irrigations. The camelina extracted soil water to a depth of 1.5 m. The seasonal evapotranspiration, calculated from soil water balance data, varied from 285 mm for the water stress plots to 371 mm for the 40% treatment. Excluding the water stress plots, seed yields for treatments varied from 950 to 1130 kg ha^{-1}, though differences were not significant. Mid-season camelina crop coefficients were on the order of 1.13 to 1.20. A camelina crop coefficient curve is presented as a function of days after planting.

INTRODUCTION

Camelina sativa (L.) Crantz is an oilseed crop that is currently being investigated by U.S. industry as a source for biodiesel, but has a number of other potential industrial and food applications as well (Vollmann et al., 2007). Camelina has a relatively short growing season when sown as a summer annual in northern Midwestern U.S. areas, e.g., 80 to 100 days (Putnam et al., 1993), but in Northern and Central Europe the season length is reportedly longer ≈120 days (Zubr, 1997). Camelina has also been shown to perform well as a biannual winter crop in certain areas (Putnam et al., 1993). Prior research has listed several attractive agronomic attributes of camelina (see, e.g., Putnam et al., 1993; Vollmann et al., 2007). These include the ability to grow well at low-fertility inputs (e.g., seasonal application of 60 kg N ha^{-1}) and under saline soils. It can survive frost and freeze cycles after emergence, is competitive with annual weeds, needs little insect control, and has drought-avoidance characteristics.

Researchers at the USDA-ARS research center in Maricopa, AZ, are working with industry to develop several alternative crops, including camelina, for production in the arid southwestern U.S. Successful commercialization efforts of camelina could ultimately create opportunities for growers in the area with limited cropping alternatives. Camelina commercialization may also create new areas of production with limited competition from major commodity crops. However, little is known about the crop's water use characteristics and yield response to irrigation. Consequently, we currently lack the information that will lead to appropriate irrigation management for its production in the desert Southwest (French et al., 2009). Thus, a field experiment was conducted to evaluate camelina water use and yield under irrigated conditions in the desert southwestern U.S. The main objectives were to determine: (1) the crop's soil water use characteristics, (2) crop evapotranspiration (ETc), and (3) yield response to variable irrigation levels. Experimental objectives also included development of camelina crop coefficients compatible with the FAO-56/ETc guidelines (Allen et al., 1998) and applicable to southwestern U.S. growing conditions.

METHODS AND MATERIALS

A camelina irrigation experiment, the first of a two-year field investigation, was conducted from November 2006 to April 2007, on a laser-leveled, 1.25 ha field site (fig. 1) located at the University of Arizona, Maricopa Agricultural Center, in central Arizona (33˚04'N, 111˚58'W, 361 m above M.S.L.). The field soil is a Casa Grande series (Typic Natrargids, fine-loamy, mixed, hyperthermic) with predominantly sandy clay loam texture. Crops grown at the site in the years prior to the experiment were wheat, oats, barley, and jojoba. On 06 November 2006, camelina seed was broadcast-planted to dry soil over the entire field at a rate of 8.2 kg ha^{-1}. The seed, a 'Robinson' variety, was supplied by Technology Crops International (TCI, www.techcrops.com). Immediately after planting, measurements were made to mark 40 plots, each 10 m x 17 m in area, within the site (fig. 1).

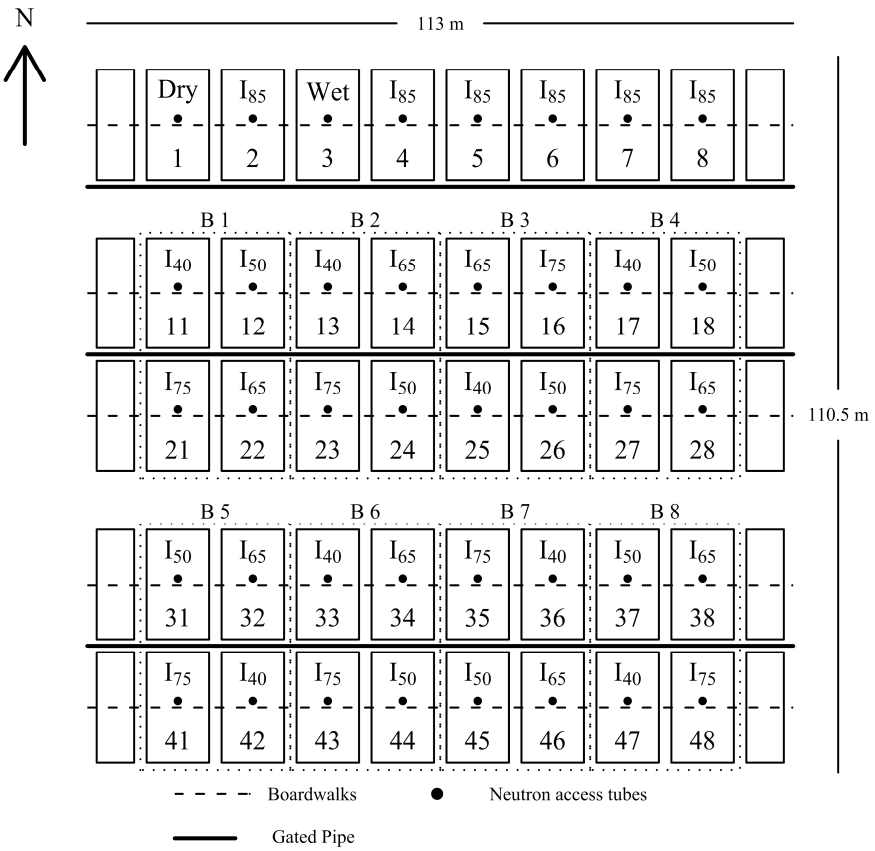

Figure 1. Camelina experiment field site at Maricopa, Arizona, showing 40 plots, each 10 m x 17 m. Treatment identifiers at the top of each plot correspond to irrigation soil water depletion levels: I_{40} at 40%, I_{50} at 50%, I_{65} at 65%, I_{75} at 75%, and I_{85} at 85%. Block design is indicated by dotted-lines with identifiers B1-B8. The top row that includes six of I_{85} plots was not blocked.

A tractor-mounted Giddings[3] soil sampler (Model 25-TS, Giddings Machine Company, Windsor, CO) was then used to install neutron access tubes to a depth of 2.0 m in 38 of the plots (fig. 1). During the installation of the access tubes, soil samples in each plot were extracted in 0.3-m increments to a depth of 1.8 m. The soil samples were then taken to the laboratory and analyzed for -33 kPa (field capacity) and -1500 kPa (wilting point) soil water retention using pressure membrane extractors (Model 1000, Soilmoisture Equip. Corp., Santa Barbara, CA) and soil particle size fraction using the hydrometer method (Gee and Bauder, 1986). Following access tube installation, border dikes were formed to separate plots and to control surface irrigation water applications to plots. Three gated pipe irrigation systems, 152-mm diameter, were installed in the east-west direction extending the length of the field (indicated by heavy east-west lines in fig. 1). Irrigation water was controlled by valves located on the west end of each system, and gated-ports spaced

[3] Mention of products and trade names does not imply endorsement by USDA

1.0 m apart were used to control water application to individual plots. In-line propeller water flow meters were used to measure the amount of water applied to plots during the season. Raised mid-plot boardwalks (dashed lines in fig. 1) were also installed to provide non-destructive access to plots.

Starting on 14 November 2006, prior to the first irrigation of the dry-planted camelina, frequent monitoring of volumetric soil water contents were begun for all plots. Soil water contents (θ_v) were measured from 0.1 to 1.9 m in 0.2 m increments using field-calibrated neutron moisture gauges (Model 503, Campbell Pacific Nuclear, CPN, Martinez, CA). Since neutron gauge accuracies can be unreliable at the 0.1 m depth, the neutron data were supplemented by measuring soil water contents for the 0 to 0.3 m soil surface using a time domain reflectometry (TDR) system (Trase1, Soilmoisture Equip. Corp., Santa Barbara, CA), where the TDR rods were placed 0.5 m away from the access tube in each plot. For each plot, the θ_v measurements made during the season were combined with field capacity (θ_{fc}) and wilting point (θ_{wp}) soil water content data determined in the laboratory to estimate soil water depletion percentage (SWD_p). The SWD_p, expressed as a percentage of total available water, was calculated as:

$$SWD_p = [(\theta_{fc} - \theta_v)/(\theta_{fc} - \theta_{wp})] \times 100$$

A randomized block experimental design was employed to investigate four irrigation treatments each replicated eight times. The 32 plots used in the blocked irrigation study were 11-18, 21-28, 31-38, and 41-48 (fig. 1). Eight other plots (1-8) not included in the blocked irrigation treatment design were used for other experimental purposes, i.e., unplanted dry and wet soil plots (1 and 3) and planted plots, imposed with severe water stress (2, 4, 5, 6, 7, and 8). Thus, data from these water stress plots, though omitted from analysis of variance procedures, will be presented for reference purposes. Plants in the two soil plots were removed by herbicide applications, whereas planted buffer areas on the east-west sides of the field and alleyways between plots north to south (fig. 1) provided cropped surfaces outside of plot areas. To obtain uniform crop emergence and establishment, all plots were irrigated three times (15 and 21 November 2006, and 5 December 2006) early in the season before irrigation treatments were begun. Layout size and field logistics did not allow testing effects due to fertilization. Consequently, on 5 December 2006, all plots were fertilized with 50 kg N ha^{-1} by injecting 32% solution urea-ammonium-nitrate (32%) through the irrigation system.

After crop establishment, irrigation for treatments were governed by measured SWD_p where the four levels selected, 40, 50, 65, and 75%, corresponded to treatments defined as I_{40}, I_{50}, I_{65}, and I_{75}, respectively (fig.1). The depletion level used for the six stress plots in the northern portion of the field was 85% (where stress treatment is denoted as I_{85}). For irrigation scheduling purposes, soil water depletion levels were based on a conservative crop rooting depth of 0.7 m. When the median measured SWD_p at the 0.7-m depth for replicates within a treatment reached the specified level, irrigations were then applied to all treatment plots with water depths approximately

1.1 times the depth needed to restore an individual plot to field capacity. Consequently, plots within a given treatment, though irrigated on the same day, often received different irrigation application depths due to differences in soil water depletion prior to irrigation and water holding capacities among plots.

Weekly photographic data were collected on 13 occasions to document camelina canopy cover fractions. A digital camera was mounted at the end of a 2.6-m hand-carried aluminum pole, allowing nadir-views for all plots with a field of view of about 1.6 m x 1.2 m. Pixel resolution was better than 1 mm at mid-season canopy heights of about 0.5 m. Image data were originally collected in raw mode, then converted to 3-band (red, green, blue) TIFF format. Weekly fractional crop cover estimates for each plot were generated using a green index classification method developed and presented by French et al. (2009).

Camelina evapotranspiration (ETc) rates for plots were estimated throughout the growing season using soil water balance procedures described in Hunsaker et al. (2005). For each plot, ≈ weekly estimates of ETc were calculated by the change in soil water content from one measurement date to the next over an estimated effective root extraction depth, accounting for water gains in the soil profile from irrigation and rainfall, and water losses below the root zone. The ETc data, combined with estimated fractional cover and plant height for a given plot, and the FAO-56 grass reference evapotranspiration (ETo) provided by a nearby MAC farm AZMET weather station (Brown, 1989), were used to back–calculate basal crop coefficients (Kcb, Allen et al., 1998) following procedures developed by Hunsaker et al. (2005):

$$Kcb = ETc/ETo + Ke$$

where Ke is the soil evaporation coefficient and all other parameters are as defined above.

On 19 April 2007, seed yield samples were harvested from each plot using a Hege plot combine (Wintersteiger AG, Austria) equipped with a 1.5-m cutter bar. The samples were harvested within designated areas measuring approximately 24 m^2 in the south half of each plot (south of the boardwalk in fig. 1). Unfortunately, seed was lost while harvesting plot 28 (treatment I_{65}), and this particular plot will be omitted from data analyses. Each harvest area was individually marked and measured for total area and all seed yields were subsequently adjusted to 0% moisture. Total oil content was measured with a TD-NMR mini-spectrometer (Model mq20, Bruker Optics Inc., Billerica, MA).

RESULTS AND DISCUSSION

The November-planted camelina crop was 156 days old when harvested on 19 April 2007. However, it was initially anticipated that a winter-planted camelina crop in Arizona would about 120 days or less from planting to harvest and that this would then allow field preparation for our rotation to cotton by mid-March, 2007. Even

though irrigations to the treatments were terminated by early March, subsequent air temperatures were not high enough to fully dry the seed until mid-April. The early March cut-off of irrigation water to the crop likely affected final yields, which averaged about 1300 kg ha^{-1} for the 50% top-yielding plots. Thus, our yields were considerably lower than those reported elsewhere, e.g., 1574 to 2248 kg ha^{-1} as reported by Vollmann et al. (2007) in eastern Austria. Limitations to camelina yield for the longer than expected growing season in Arizona may also have been induced to some extent by insufficient nitrogen application. However, the average total oil content, 41%, for the Arizona crop was comparable to other total oil contents reported (Zubr, 2003; Vollmann et al., 2007).

Water application schedules for the five irrigation treatments are summarized in table 1. All treatment plots were irrigated three times (15 and 21 Nov. 2006, and 5 Dec. 2006) early in the season before irrigation treatments were begun. More irrigation water was needed during the initial irrigation for the I_{85} treatment plots to achieve uniform coverage for germination in those plots. After the irrigations of 5 December, in which all plots were also fertilized with 50 kg N ha^{-1}, the I_{40}, I_{50}, I_{65}, and I_{75} received another 4, 3, 2, and 2 irrigations respectively, whereas the I_{85} received only one more irrigation. Between planting and harvest, the field site received a total of 38 mm of rain.

Mean soil water content profiles presented for the I_{40} treatment show that crop soil water extraction was confined to the upper 0.7 m soil profile through about mid Jan. 2007 (fig. 2a). During this early season period, water from irrigations gradually moved downward in the soil profile to about 1.3 m. After mid Jan., camelina extracted stored soil water at deeper depths (fig. 2b). By 5 March 2007, soil water extraction had occurred to about 0.9 m. Following the final irrigation to I_{40} (6 March), the camelina depleted soil water as deep as 1.5 m by early April.

Based on the above evaluation of camelina soil water profiles, ETc was calculated by the soil water balance using a 1.5-m root zone. As there was no observed movement of water below 1.5 m for any treatment, deep drainage was assumed to be negligible.

A statistical difference occurred between irrigation treatments for seasonal ETc, calculated from 15 Nov. 2006 through 1 April 2007. The I_{40} (371 mm) and I_{50} (354 mm) treatments both had greater seasonal ETc than for the I_{65} treatment (table 2), whereas the ETc for the I_{50} was not significantly different from that for I_{75}. Unlike seasonal ETc, neither final yield nor water use efficiency (final yield per unit of evapotranspiration) was significantly different between treatments (table 2). However, within-treatment yield was highly variable compared to that for seasonal ETc. Consequently, these results indicated that seed yield was independent of irrigation schedule and crop water use. Results for the I_{85} treatment, though outside of the experimental design, suggested a substantial decrease in both ETc and yield ($\approx$ 20 % reduced compared to other treatments) may occur when only a single irrigation is given after emergence.

Table 1. Irrigation event dates and mean irrigation depths for camelina treatments during the 2006-07 growing season at Maricopa, Arizona.

Treatments	I_{40}	I_{50}	I_{65}	I_{75}	I_{85}
Date	Treatment mean irrigation depth (mm)				
15 Nov. 2006	48.4	48.8	49.4	48.8	59.3
21 Nov. 2006	37.0	38.4	37.4	39.3	38.8
5 Dec. 2006[a]	66.3	67.1	67.1	67.0	83.0[b]
17 Jan. 2007	47.6				
6 Feb. 2007		60.0			
9 Feb. 2007			62.9	68.6	
13 Feb. 2007	48.9				
22 Feb. 2007		48.6			
26 Feb. 2007	41.8				
1 Mar. 2007			64.6		
2 Mar. 2007					78.5
6 Mar. 2007	39.5	50.5		71.4	
Totals	329	313	281	295	260

[a] All treatment plots were fertilized with 50 kg N/ha during irrigation on 5 Dec. 2006.
[b] One plot in this treatment was inadvertently irrigated twice on 5 Dec. 2006.

Table 2. Camelina irrigation treatment means for seasonal crop evapotranspiration (ETc), seed yield (Y), and water use efficiency (WUE_{ETc}) for the 2006-07 season.

	Treatments[a]				
Variable	I_{40}	I_{50}	I_{65}	I_{75}	I_{85}[b]
Crop evapotranspiration, ETc (mm)	371a (0.06)	354ab (0.09)	325c (0.09)	333bc (0.04)	285 (0.09)
Seed yield, Y (kg ha^{-1})	1058a (0.21)	1077a (0.32)	950a (0.27)	1130a (0.29)	857 (0.48)
Evapotranspiration water use efficiency, WUE_{ETc} (kg m^{-3})	0.28a (0.18)	0.30a (0.32)	0.28a (0.23)	0.34a (0.28)	0.30 (0.48)

[a] Treatment coefficients of variation for variables are shown in parenthesis below means.
[b] Note I_{85} is excluded from the analysis of variance since it was not part of the block design.
a, b, c Treatment means followed by different letters in a row are significantly different at the 0.05 level according to the Tukey (HSD) test.

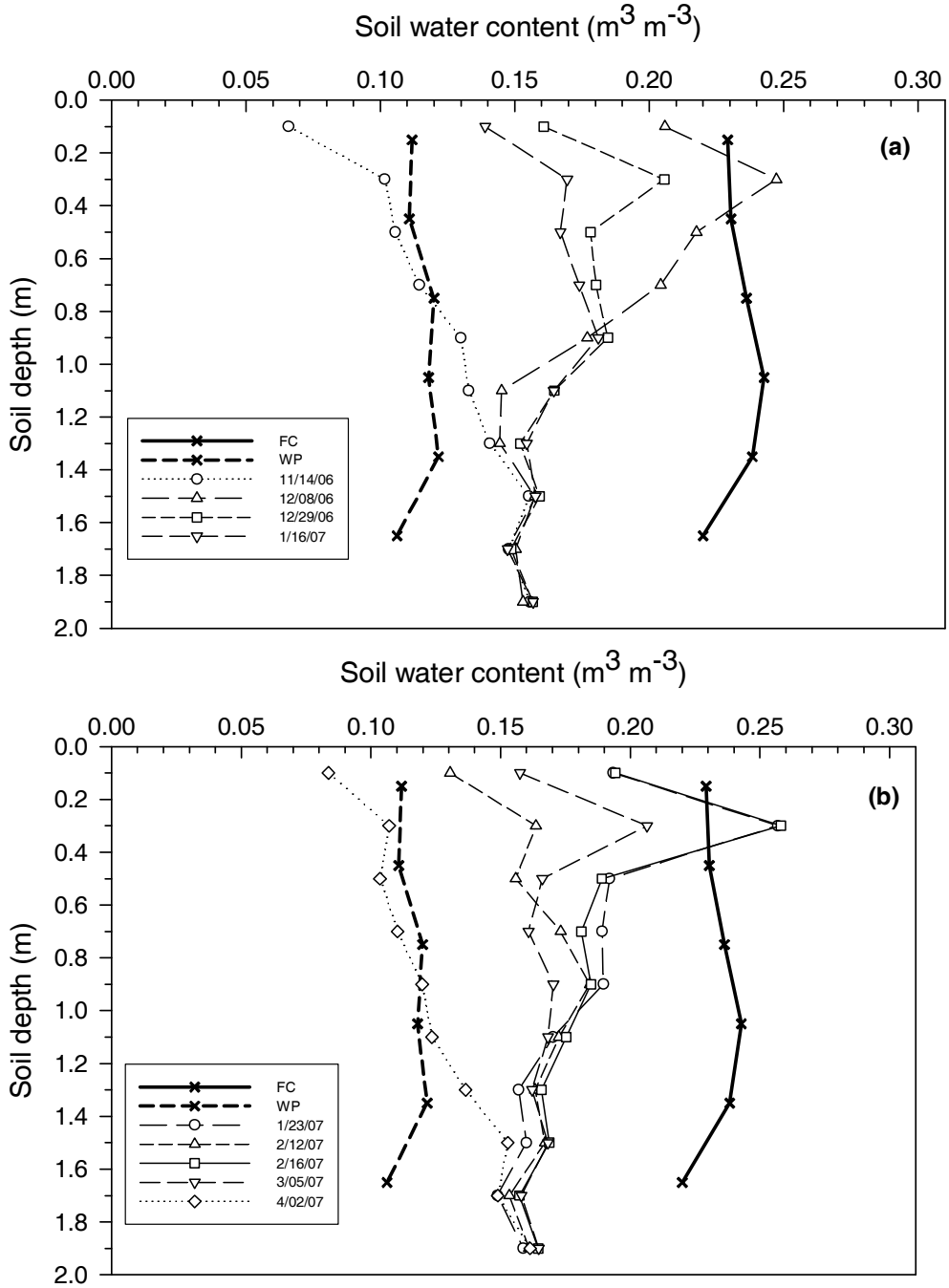

Figure 2. Mean soil water content profiles and mean field capacity (FC) and wilting point (WP) for the I_{40} treatment during the (a) early and (b) late camelina season.

Data for the 50% top-yielding plots (16 plots) were used to back-calculate basal crop coefficients (Kcb) and then derive a camelina Kcb curve as a function of days after planting (DAP). The Kcb increased slowly for the first 50 DAP (fig. 3). This trend is likely explained by retarded growth during the cold temperatures in December and January. The Kcb increased more rapidly after 50 DAP to maximum Kcb values at about 100 to 120 DAP. The effects of different treatment irrigation scheduling regimes beginning 63 DAP (17 Jan. 2007) induced higher Kcb variability than during the early season. In general, the Kcb for the I_{65} and I_{75} were lower than those of the more frequently irrigated treatments, I_{40} and I_{50}, once irrigation treatments were initiated. While different models could be employed to describe Kcb as a function of DAP, a 4th order polynomial regression model appeared to provide a reasonable representation (fig. 3). The 4th order model agreed well with data during the early season and estimated negligible Kcb after 140 DAP. The model also predicts maximum Kcb values from 1.13 to 1.20 from 100 to 120 DAP.

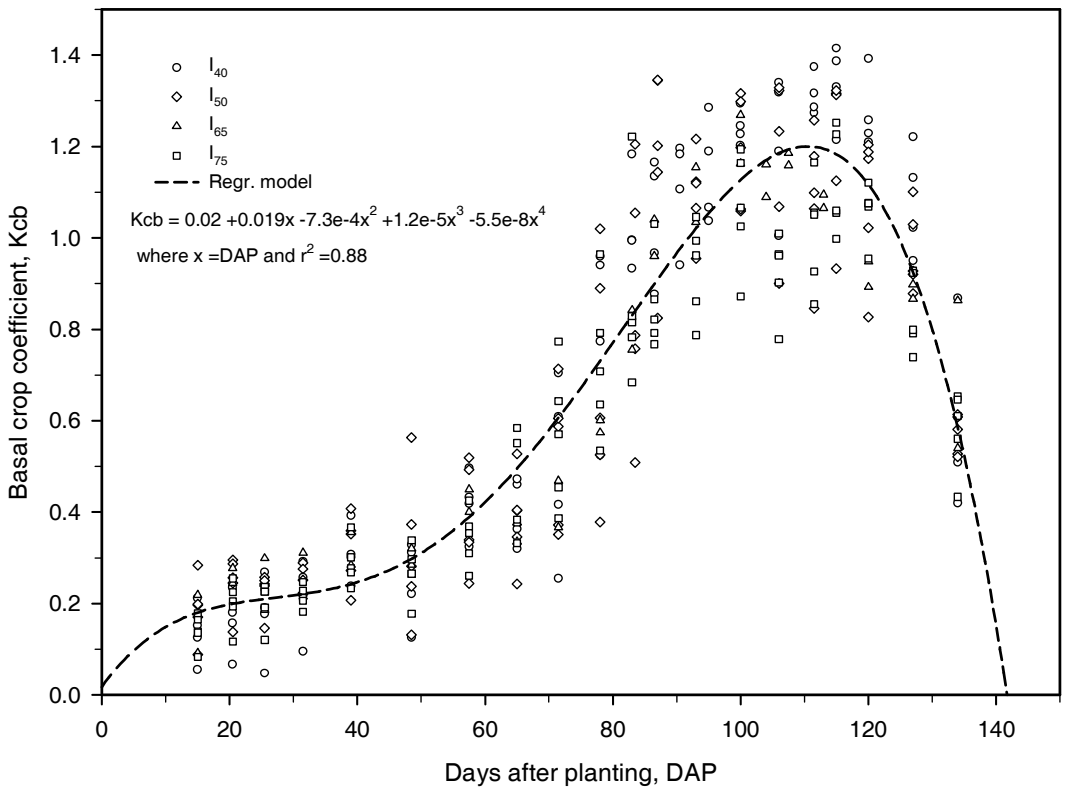

Figure 3. Camelina basal crop coefficients (Kcb) for 16 treatment plots with days after planting (DAP) and Kcb regression model as a function of DAP.

CONCLUSIONS

An irrigation field experiment with camelina sativa was conducted in Maricopa, Arizona during 2006-07 to evaluate the crop's water use and ETc crop coefficients. Results from this initial camelina experiment indicated that differing levels of irrigation affected total evapotranspiration. However, the different amounts of water applications and ETc achieved did not significantly affect final seed yields, which varied from 950 to 1130 kg ha^{-1}, for blocked treatments. A preliminary Kcb curve for camelina as a function of days after planting was derived from the experimental data. Subsequent camelina investigations underway in Arizona utilized fertilization levels and planting dates markedly different from those of this experiment and will be used to extend these results to a wider range of conditions.

REFERENCES

Allen, R.G., Pereira, L.S., Raes, D., and Smith, M. (1998). *Crop Evapotranspiration*. FAO Irrigation and Drainage Paper 56, FAO, Rome, Italy.

Brown, P.W. (1989). Accessing the Arizona Meteorological Network (AZMET) by computer. Ext. Rep. No. 8733, University of Arizona, Tucson, Arizona.

French, A.N., Hunsaker, D., Thorp, K. and Clarke, T. (2009). Evapotranspiration over a camelina crop at Maricopa, Arizona, Ind. Crops Prod. (in press)

Gee, G.W., and Bauder, J.W. (1986). Particle-size analysis, In: Klute, A. (ed.), *Methods of soil analysis, Part I*, Amer. Soc. Agron., Madison, WI, pp. 383-411.

Hunsaker, D.J., Pinter, P.J., Jr., and Kimball, B.A. (2005). Wheat basal crop coefficients determined by normalized difference vegetation index, *Irrig. Sci.* 24(1): 1-14.

Putnam, D., Budin, J., Field, L. and Breene, W. (1993). Camelina: a promising low-input oilseed, In: Janick, J., Simon, J. (eds.), *New Crops, Exploration, Research, and Commercialization,* Proc. 2nd Nat. Symp., Indianapolis, IN, Oct. 6-9, 1991, John Wiley & Sons, Inc., New York, pp. 313-322.

Vollmann, J., Moritz, T., Kargl, C., Baumgartner, S., and Wagentristl, H. (2007). Agronomic evaluation of camelina genotypes selected for seed quality characteristics, Ind. Crops Prod. 26(x):270-277.

Zubr, J. (1997). Oil-seed crop: Camelina sativa, Ind. Crops Prod. 6(2):113-119.

Zubr, J. (2003). Qualitative variation of Camelina sativa seed from different locations, Ind. Crops Prod. 17(3):161-169.

[1] Irrigation Scheduling for Deficit Irrigation

Norman L. Klocke, P.E.[2], Loyd R. Stone[3], Dale A. Bolton[4]

ABSTRACT

Many irrigators face the prospect that they will not be able to fully irrigate their crops. In these cases, they still need to schedule their water applications to make the best economic use of available water. Major scheduling questions for deficit irrigation include: (1) will pre-season irrigation be beneficial; and (2) when should irrigation be started and stopped during the growing season. Traditional irrigation scheduling has been developed for irrigation systems that can supply the full irrigation requirements of the crop and produce maximum crop yields. Irrigation schedules are based on current crop water requirements and predict irrigation needs in the immediate future. Irrigators practicing deficit irrigation need to predict irrigation schedules in advance of the growing season and make appropriate adjustments based on potential crop yields and economic returns. A computerized decision tool, the Crop Yield Predictor (CYP) has been developed to predict yields from alternative irrigation schedules. The user determines soil water status before or during the cropping season and formulates a potential schedule of irrigation dates and amounts. Soil water holding capacity and irrigation system water delivery capacity are constraints on the ability to supply water to the crop. CYP uses a daily soil water balance coupled with computations of effective evapotranspiration (ETe) to predict crop yields from regional yield-ET relationships. Multiple executions of CYP with alternative irrigation schedules lead to the schedules that project optimum net economic returns from the management scenarios.

INTRODUCTION

Maximum net economic returns for irrigators with adequate water supplies usually have corresponded to irrigation management to obtain maximum crop yields. Irrigation in excess of crop water needs reduces net economic return, but the marginal increases in crop yields usually covered marginal production costs. When water supplies cannot match crop needs and deficit irrigation management is anticipated, optimum net economic return from irrigation is the appropriate measure of best management (English et al. 2002). Crop selection for optimum net return may involve multiple crops in rotation, a single crop with reduced irrigation, or irrigation on a smaller area (Martin et al. 1989). In addition to crop selections, irrigation needs to be allocated among crops, using crop production functions and production costs for optimum economic return (English, 1981, Martin et al. 1989, Klocke et al. 2006).

Scheduling irrigation events during the growing season for crops that have a non-limited water supply has involved the estimation of non-stressed crop ET (ETc) from current weather parameters, producing a reference ET (ETr) that is modified with a crop coefficient (Kc) to account for changing crop growth stages. A soil water balance of ETc, effective precipitation, net irrigation, drainage, runoff, and run-on produces daily values for available

[1]Partially funded by the Ogallala Aquifer Project, USDA, Agricultural Research Service
[2] Professor, Water Resources Engineering, Kansas State University, 4500 East Mary St., Garden City, KS 67846. E-mail: nklocke@ksu.edu.
[3]Professor, Soil Science, Kansas State University, Manhattan, KS
[4]Data Processing Specialist, Kansas State University, Garden City, KS

soil water (ASW). For irrigation schedules with the goal of crops with no water stress, irrigation needs are calculated to keep ASW between field capacity and an ASW content that does not cause stress, usually 50-60% of the ASW remaining in the active root zone. The starting dates for irrigation events are established by calculating the days until the crop will experience stress at the point of the end of the irrigation cycle (no later than starting date) and when there is room to store the irrigation event amount at the point of the beginning of the irrigation cycle (no sooner than date) (Kansas State University, 2007)

When the water supply for irrigation is less than the water required for non-stressed conditions, water deficits can be anticipated. Irrigation schedules for deficit irrigation need to anticipate the potential for crop yields and net economic returns prior to and during the growing season. The major irrigation scheduling decisions for deficit irrigation are: (1) whether or not pre-season irrigation is needed (Stone et al. 2008), and (2) when irrigation growing season irrigation should start and stop. Between the start date and stop date, irrigation systems often operate on a fixed frequency depending on the capacity of the well to supply water.

The objective for this study was to develop an interactive decision model that would help users to predict optimum irrigation schedules for crops that are expected to experience water stress. The model predicted ASW during the growing season, crop yields, and the net economic return for the crop with the proposed irrigation schedule. Model users could simulate alternative irrigation schedules for years with less than average, average, and more than average precipitation.

MODEL DESCRIPTION

The CYP was an adaptation of the Kansas Water Budget (KSWB) model (Khan et al., 1996 Stone et al., and Stone et al., 2006). The KSWB was a coupled model of a daily soil water balance and an estimation of daily evapotranspiration (ET) (figure 1). The ET side of the model started with a reference ET (ETr) using the equation of Jensen and Haise (1963) with inputs of average daily maximum and minimum air temperature, average daily solar radiation, and an expression for latent heat of vaporization (Wright, 1982). Maximum ET (ETm) was derived from ETr with a bare-soil water coefficient during the non-growing season and a crop coefficient (Kc) during the growing season (Doorenbos and Pruitt, 1977). ETm values assumed that the crop was not stressed by soil water content, atmospheric conditions, disease, or lack of nutrients. ETm was modified with a soil water stress coefficient (Ks) during the growing season to produce actual ET (ETa). The soil Ks values were developed according to the function reported by Jensen et al. (1970):

$$Ks = \ln(ASW + 1)/\ln(101) \quad [1]$$

where ASW is available soil water (%).

ETa transferred to the soil water balance side of the model:

$$SW_E = SW_B + P_E + I_N - ETa - D_P \quad [2]$$

where SW_E was total SW at the end of each day; SW_B was total SW at the beginning of each day; P_E was the daily average effective precipitation from 30 years of weather records minus

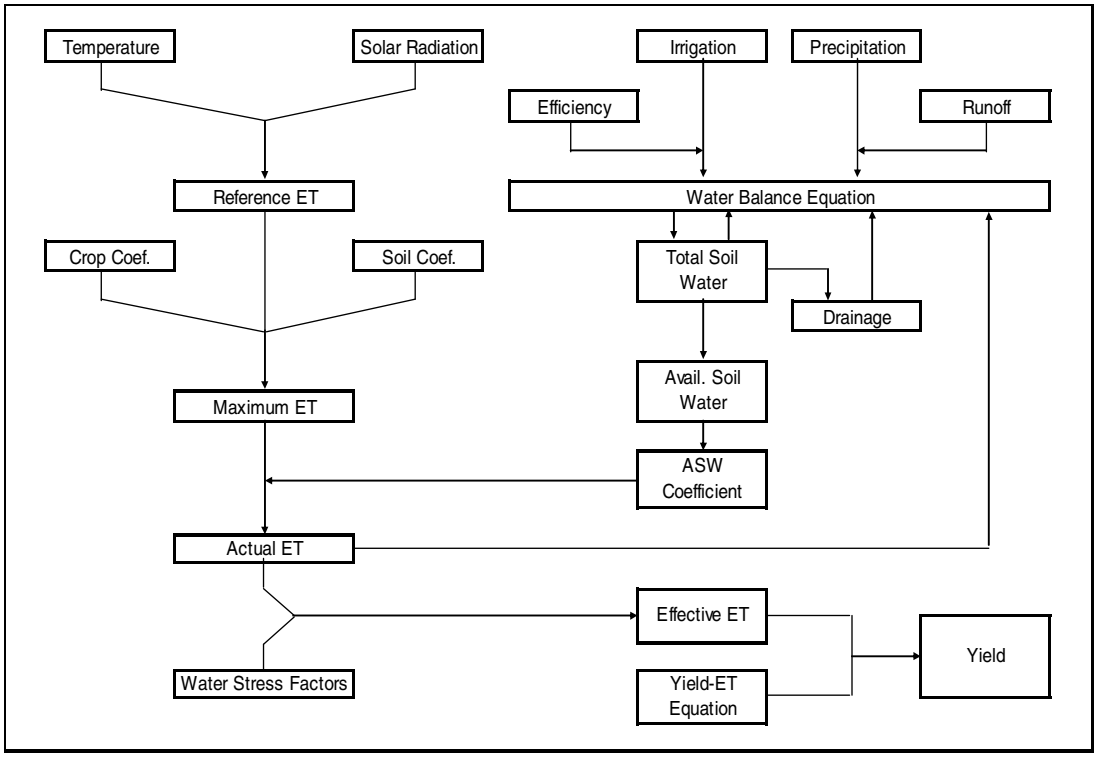

Figure 1. Flow chart for Kansas Water Budget adapted to Crop Yield Predictor

runoff, I_N was net irrigation that infiltrated into the soil and D_P was drainage from the 1.83 m soil profile. Daily drainage was calculated by using the Wilcox method as described by Miller and Aarstad (1972). Daily drainage for a Ulysses silt loam soil (Stone et al., 1987) was:

$$D_P = 42.7(TSW/729)^{18.06} \quad [3]$$

where TSW is total soil water of the 1.83 m profile (mm).

Effective ET (ETe) was derived from ETa using the ratio of ETa and ETm along with the crop's sensitivity to water stress during the stages of growth, including vegetative, flowering, seed formation, and ripening. ETe for corn that actually contributed to crop yield (Ye), was calculated with:

$$Ye\ [Mg\ ha\text{-}1] = -11.5\ [Mg\ ha\text{-}1] + 39.8\ [Mg\ ha\text{-}1\ mm\text{-}1]\ X\ ETe\ [mm] \quad [4]$$

USER INPUTS FOR CYP

Reference evapotranspiration was calculated daily by CYP for the geographic location selected by the user. Average daily maximum air temperature, minimum air temperature, and solar radiation for each default location were calculated from thirty years of weather data for each location. The average daily weather factors for each location were used to calculate daily reference evapotranspiration (ETr) from Jensen and Haise (1963). ETr was for a well watered crop with full canopy cover in semiarid and arid regions. ETr was

increased to account for advective energy when the average maximum air temperature was more than 33°C.

Annual precipitation was determined by the model user. Precipitation probability values were also available for each default location. Precipitation amounts for occurrence 2 out of 10 years, 5 out of 10 years, and 8 out of 10 years were suggested so the user could simulate wet, normal, or dry years.

Soil texture was selected by the user from a listing of silt loam and loamy sand soils. The ASW storage capacity and volumetric soil water contents at field capacity and permanent wilting were displayed for each soil texture.

Irrigation system efficiency was defined as the ratio of water infiltrated (net irrigation) and the water pumped or supplied to the field (gross irrigation). The user entered irrigation efficiency and the program supplied suggested efficiencies for types of irrigation systems.

Crop selection was for corn, grain sorghum, sunflower, soybean, winter wheat or alfalfa. CYP furnished default dates for growing season milestones, but the user could change the defaults for to match other crop cultivars. Kc values and water stress factors were adjusted for the days in each growth stage.

Irrigation schedule was a series of dates for irrigation events and the corresponding gross irrigation amounts. Irrigation dates and amounts could be entered into the program directly or imported from an Excel file. Multiple irrigation schedules could be developed in Excel for input into the program. The program also could generate uniform frequency schedules from user entries of (1) starting dates and ending dates for the growing season irrigation events, (2) irrigation season gross irrigation, (3) gross irrigation for each irrigation event, where the gross irrigation was the same for all irrigation events, (4) area irrigated, and (5) irrigation system pumping capacity.

Runoff was the percentage of daily precipitation that did not infiltrate. The user could enter the runoff percentage or CYP calculated a runoff factor using crop type, total annual precipitation, and soil texture.

Initial available soil water could be entered for any date by the user and CYP used it for water balance calculations from that date forward. Default ASW on January 1 was determined by CYP from annual precipitation and total irrigation for the growing season.

Crop prices and production operating costs could be entered to predict net economic return without considering fixed costs from the projected crop yield:

$$\text{Net Return} = \text{Price X Yield} - \text{Operating Costs.} \qquad [5]$$

CYP OUTPUTS

Effective crop evapotranspiration (ETe) was the crop's evapotranspiration that contributed to crop yield. ETe was calculated with coefficients that modified ETr to account for crop growth stage (Kc), crop water stress from less than optimum soil water content (Ks), and the crop's susceptibility to stress during different growth stages. ETm was the crop's ET with no water stress and only dependent on crop growth stage; ETa was the crop's ET when soil

water stress reduced ETm; and ETe was the crop's ET that also included the influence of growth stages on stress susceptibility.

During the non-growing season a bare soil evaporation coefficient modified ETr to generate daily evapotranspiration values.

Crop yield (Ye) was calculated from linear relationships of yield as a function of ETe, which were developed form long-term field studies in west-central Kansas.

Maximum Potential Yield (Ym) was calculated with the yield-ET relationships using ETm for the non-stressed condition.

Relative Yield (Yr) was the ratio of Ye and Ym. The predicted relative yields may be more important to the model user than field yields. The user could use expected maximum field yields and simulated relative yields to calculate deficit irrigated yields.

Daily drainage was calculated using a Wilcox-type drainage equation (Miller and Aarstad, 1972) that was field calibrated for each soil texture.

Daily available soil water was charted by CYP from a soil water balance of:

$$ASW_t = ASW_{t-1} + \text{effective precipitation} + \text{net irrigation} - \text{drainage} - ETe$$

The model user can visually inspect the daily ASW charts to find its relationship to field capacity and permanent wilting.

MODEL TESTING

Field data. Crop yields, daily ASW, and ETa for continuous corn were predicted with CYP and compared with field results from a cropping system study conducted at the West Central Research and Extension Center of the University of Nebraska at North Platte, Nebraska (41.1°N, 100.8°W, 860 m above sea level) (Schneekloth et al. 1991 and Hergert et al. 1993, and Klocke et al., 2007). The average annual precipitation is approximately 508 mm, which is 36% of annual reference ET (ETr). Approximately 80% of the annual precipitation occurs during the summer growing season, which extends from late-April until mid-October. Predominant soil texture was Cozad silt loam (Fluventic Haplustoll) with pH of 7.5. Plant available soil water holding capacity was 0.17 m^3 m^{-3} for volumetric soil water contents from 32% for field capacity to 15% for permanent wilting over 0 to 3 m of soil depth. The land slope was less than 1%.

There were three water treatments: full irrigation, limited irrigation, and non-irrigated. The full irrigation treatment was scheduled to meet full crop ET by replacing soil water extractions. The limited irrigation treatment received an annual irrigation allocation of unless there was sufficient soil water to achieve full water needs. Limited irrigation was scheduled to favor applications during critical growth stages for crop development. Irrigation was reduced or withheld during the vegetative period and concentrated on reproduction and grain fill.

Soil water was measured weekly to a depth of 1.8 m in 0.3 m increments with the neutron attenuation method (Evett and Steiner, 1995). Precipitation, net irrigation, and changes in soil water from one measurement to the next were used to calculate weekly ETa. Drainage

was assumed to be minimal within the one week sampling interval of soil water and was not included in the soil water balance. Water runoff and run-on to the plots were observed to be zero.

CYP testing. Continuous corn data from the North Platte location for 1994 and 1995 were compared with simulations by the CYP. Daily irrigation events, precipitation events, and ETr from the field study were used as inputs to the CYP. ASW storage capacity, field capacity and permanent wilting soil water characteristics for a Ulysses silt loam soil were used for the simulations with CYP.

Annual precipitation amounts for 1994 and 1995 were nearly the same but the monthly values were quite different (table 1). January through May, 1994 had less precipitation than 1995, but July and August 1995, months with more crop water needs, had very little precipitation.

Table 1. Precipitation (mm) for North Platte, NE.

Year	Jan-Mar	Apr	May	Jun	Jul	Aug	Sep	Oct-Dec	Annual	May-Sep[+]
1994	11	45	26	89	126	25	19	86	428	285
1995	23	76	128	74	43	0	62	10	416	307
Avg.	41	43	74	80	75	54	45	57	468	328

[+]Growing season precipitation

With more than normal precipitation during July and August, 1994 less irrigation was required in 1994 than 1995. Simulated corn yields were less than field measure yields in 1994, but simulated yields for limited and full irrigation treatments in 1995 were more than in 1994. The simulation of these yield better approximated field yields (table 2). The relative yields may be more important than the actual yields because the model user can use their expected fully irrigated yields and the relative yields to estimate deficit yields. Simulated maximum yields can be calculated from ETm.

Table 2. CYP simulated and North Platte field corn yields.

Year	Irrigation Treatment	Irrigation	Simulated Yield	Field Yield	Yield Deviation Field-Sim.	Simulated Relative Yield	Field Relative Yield
		mm	Mg ha^{-1}	Mg ha^{-1}	%	%	%
1994	Dryland	0	5.8	7.4	22	80	76
1994	Limited	76	7.0	10.0	30	95	103
1994	Full	152	7.3	9.6	24	100	100
1995	Dryland	0	2.3	3.2	28	20	32
1995	Limited	152	8.8	8.2	-7	77	81
1995	Full	381	11.5	10.2	-13	100	100

Soil water contents from the field study, the discrete data points, were compared with CYP simulations, which were daily estimations (figures 2 and 3). Field and simulated soil water contents were similar in 1994 over the dryland, limited, and full water treatments. Limited irrigation field data were less than the simulated estimations during the middle of the growing season. The dryland and limited irrigation treatments compared well in 1995

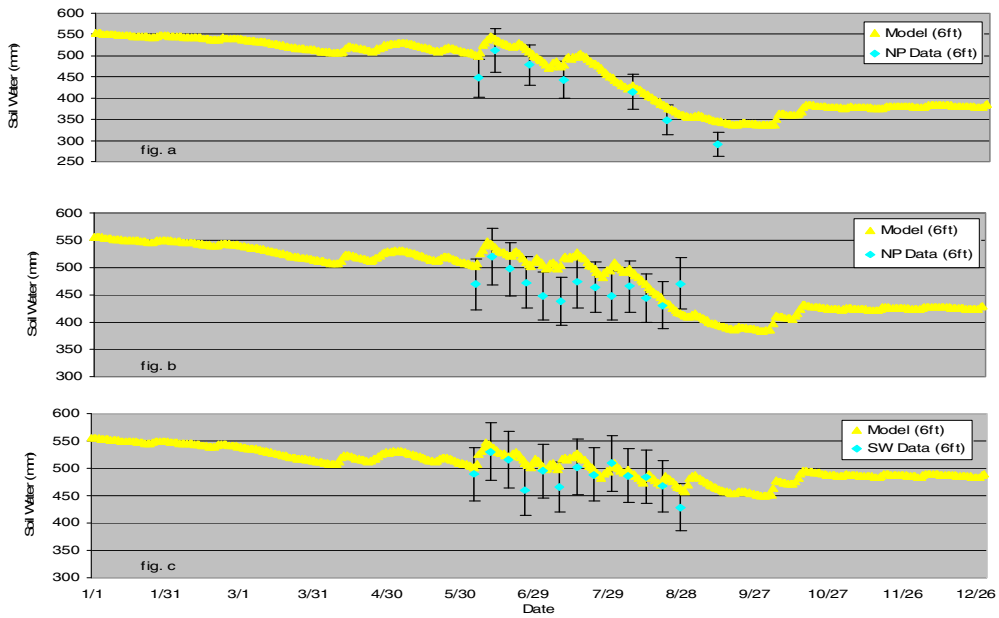

Figure 2. Total soil water simulated from CYP and measured in the plots for dryland (a), limited (b), and full (c) water treatments with ±10% deviation for each field SW measurement for 1994.

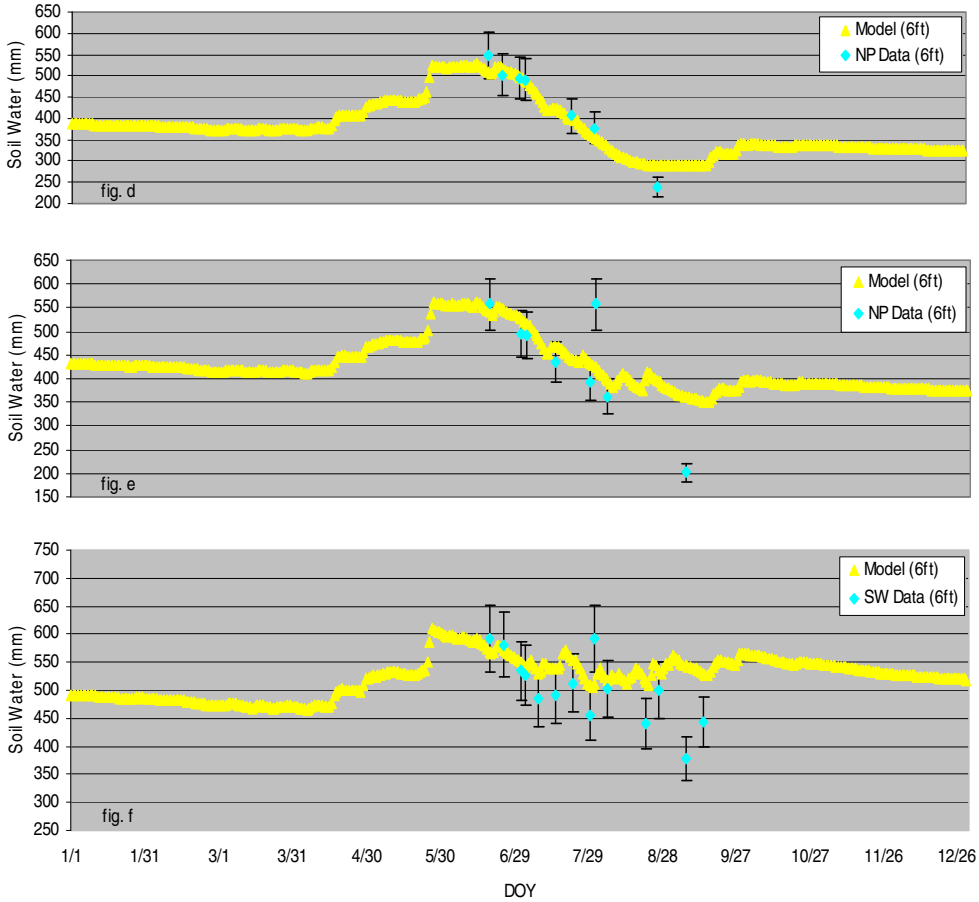

Figure 3. Total soil water simulated from CYP and measured in the plots for dryland (d), limited (e), and full (f) water treatments with ±10% deviation for each field SW measurement for 1995.

except for two outlying field data points in the limited irrigation treatment. Field data for the full irrigation treatment tended to be more than simulated during the early growing season and lower during the end of the growing season. These comparisons are encouraging for the application of CYP for simulations.

CONCLUSIONS

The Crop Yield Predictor (CYP) has been adapted from the Kansas Water Budget (KSWB) to become and interactive model where the user can enter a western Kansas location, annual precipitation, soil texture, crop type, a potential irrigation schedule, runoff, initial soil water (SW) content, crop production costs, and commodity prices to predict grain yield, relative grain yield, daily SW content, daily drainage, daily crop ET and net economic returns. Alternative irrigation schedules and annual precipitation can be entered into CYP to predict changes in results. The alternative schedules can guide CYP users in choosing irrigation starting dates ending dates and irrigation frequencies.

Simulated and measured grain yields relative to fully irrigated yields for each year compared better than actual yields. CYP simulated and measured soil water contents showed similar trends through the growing season with better agreement with the dryland water treatment than the fully irrigated treatment.

Literature Cited

Buller, O., H.L. Manges, L.R. Stone, and J.R. Williams. 1991. Modeled crop water use and soil water drainage. Agricultural Water Management 19:117-134.

Doorenbos, J., and W.O. Pruitt. 1977. Guidelines for predicting crop water requirements. Rev. ed. Irrig. and Drainage Paper 24. FAO, Rome.

English, M.J. 1981. The uncertainty of crop models in irrigation optimization. Trans. of the ASAE. 24(4):917-921, 928.

English, M.J. 2002. A paradigm shift in irrigation management. J. Irrig.of Drain. and Div. of ASCE. 128(5):267-277.

Evett, S.R., and J.L. Steiner. 1995. Precision of neutron scattering and capacitance type water content gauges from field calibration. SSSA J. 59:(4)961-968.

Hergert, G.W., N.L. Klocke, J.L. Peterson, P.T. Nordquist, R.T. Clark, and G.A. Wicks. 1993. Cropping systems for stretching limited water supplies in the central Great Plains. J. Prod. Agric. 6(4)520-529

Jensen, M.E., and H.R. Haise. 1963. Estimating evapotranspiration from solar radiation. J. Irrig. and Drain. Div. of ASCE 89:15-41.

Jensen, M.E., J.L. Wright, and B.J Pratt. 1971 Estimating soil moisture depletion from climate, crop and soil data. Trans of the ASAE. 14:954-959.

Kansas State University. 2007. KanSched2: KSU Mobile Irrigation Lab. Available at www.oznet.ksu.edu/mil.

Khan, A.H., L.R. Stone, O.H. Buller, A.J. Schlegel, M.C. Knapp, J.-I. Perng, H.L. Manges, and D.H. Rogers. 1996. Educational software for illustration of drainage, evapotranspiration, and crop yield. J. Nat. Resour. Life Sci. Educ. 25:170-174.

Klocke, N.L., L.R. Stone, G.A. Clark, T.J. Dumler, and S. Briggeman. Water allocation model for limited irrigation. J. App. Eng. In Agric. 22(3):381-389.

Klocke, N.L., J.O. Payero, and J. P. Schneekloth. 2007. Long-term response of corn to limited irrigation and crop rotations. Trans. of the ASABE. 50(6):2117-2124.

Martin, D.L., J.R. Gilley, and R.J. Supalla. 1989. Evaluation of irrigation planning decisions. J. Irrig. Drain and Div. of ASCE. 115(1):58-77.

Miller, D.E., and J.S. Aarstad. 1972 Estimating deep drainage between irrigations. Soil Sci. Soc. Am. Proc. 36:124-127.

Schneekloth, J.P., N.L. Klocke, G.W. Hergert, D.L. Martin, R.T. Clark. 1991. Crop rotations with full and limited irrigation and dryland management. Trans. of the ASAE. 34(6)2372-2380.

Stone, L.R., R.E. Gwin, Jr., P.J. Gallagher, and M.J. Gattendorf. 1987 Dormant-season irrigation: grain yield, water use, and later loss. Agron. J. 79:632-636.

Stone, L.R., O.H. Buller, A.J. Schlegel, M.C. Knapp, J.-I. Perng, A.H. Khan, H.L. Manges, and D.H. Rogers. 1995. Description and use of KS Water Budget v. T1 software. Resource Manual, Dep. of Agron., Kansas State Univ., Manhattan, KS.

Stone, L.R., and A.J. Schlegel. 2006. Yield-water supply relationships of grain sorghum and winter wheat. Agron. J. 98:1359-1366.

Stone, L.R., F.R. Lamm, A.J. Schlegel, and N.L. Klocke. 2008. Storage efficiency of off-season irrigation. Agron. J. 100(4):1185-1192.

Wright, J.L. 1982 New evapotranspiration crop coefficients. J. Irrig. Drain. Div. of ASCE. 108:57-84.

The Arkansas Irrigation Scheduler

Earl Vories[1], Phil Tacker[2], and Steve Hall[3]

[1]Cropping Systems and Water Quality Research Unit, USDA-ARS, Delta Center, P.O. Box 160, Portageville, MO 63873; PH (573) 379-5431; FAX (573) 379-5875; email: Earl.Vories@ars.usda.gov
[2]Cooperative Extension Service, University of Arkansas, P.O. Box 391, Little Rock, AR 72203; PH (501) 671-2245; FAX (501) 671-2303; email: ptacker@uaex.edu
[3]Cooperative Extension Service, University of Arkansas, P.O. Box 391, Little Rock, AR 72203; PH (501) 671-2199; FAX (501) 671-2163; email: shall@uaex.edu

ABSTRACT

In the US Mid-South, annual rainfall is generally sufficient for limited crop production, but periods of drought during the growing season make irrigation essential for optimum yields. However, factors such as cloudy weather, rainfall, and temperature swings caused by the movement of weather fronts all complicate irrigation scheduling. The Arkansas Irrigation Scheduler has been in use for over twenty years in Arkansas and surrounding states, with the current version released in 2008. The current version retains most of the objectives of the earlier versions, with the exception of being field-, rather than system-based, allowing users to view the soil water status of more of their fields at one time and group the fields as they feel most appropriate. Other changes made the program easier to learn, allowed the user to take advantage of more extensive weather data if it is available, and made the program applicable to more areas than before. Crop coefficient functions developed in the region are needed, but are not currently available. Future versions of the program may be limited to the internet, but no internet version is currently available for public use. In addition to improving yields, using the program to properly schedule irrigation can save energy and therefore money by reducing unnecessary pumping, and help to alleviate water shortages being experienced in many agricultural areas.

INTRODUCTION

The US Department of Agriculture's National Agricultural Statistics Service (NASS) divides the US into 20 Water Resource Areas, with the Lower Mississippi (WRA 08), also called the Mid-South, containing portions of Missouri, Kentucky, Arkansas, Tennessee, Mississippi, and Louisiana. The region has a humid subtropical climate and irrigation has been a fairly recent addition to many farmers' production systems. For example, the 2002 Census of Agriculture showed that Arkansas was the fourth leading state in terms of irrigated land (USDA-NASS, 2004), but as recently as 1975

approximately 95 % of the soybean and cotton harvested in the state were produced without irrigation (USDA-NASS, undated).

In the Mid-South, annual rainfall is generally sufficient for limited crop production, but periods of drought during the growing season make irrigation essential for optimum yields. Timely irrigation has been shown to increase yields of corn (Vories et al., 1993) and cotton (Vories et al., 2007), and irrigation has also been shown to reduce corn earworm damage and aflatoxin production (Smith and Riley, 1992). However, irrigation scheduling, the correct timing of irrigation during the growing season, is more difficult in humid regions like the Mid-South than in arid locations. Factors such as cloudy weather, rainfall, and temperature swings caused by the movement of weather fronts all complicate irrigation scheduling. Weather conditions in humid regions vary greatly from year to year, and even within a year, and the variability must be accounted for.

Too often, people in the Mid-South decide when to irrigate by the appearance of the crop; however, by the time stress is visible on the plants, the yields have probably already been reduced from the lack of water. Someone with quite a bit of experience can do a good job with the "feel method," or examining the soil in the root zone. In fact, one study reported that after "calibrating" with a tensiometer, better results were obtained by feel than with other scheduling methods (Phipps, 2003). However, more objective methods are usually needed for effective irrigation management.

Most commonly used methods either measure or estimate the soil water content. Evett (2007) provided an in-depth discussion of soil water and many of the methods for available for measuring soil water content. Although many types of instruments have been developed to measure soil water content, using many different kinds of technology, all have drawbacks. In addition, the highly variable soils in the region have limited the use of soil water measurements for irrigation scheduling.

The complexity of scheduling irrigation can be greatly reduced by the use of publicly available computer programs. Henggeler (2002) summarized eight programs developed in locations ranging from Arizona to North Dakota and varying greatly in complexity and input requirements. One of the programs discussed by Henggeler (2002) was the Arkansas Irrigation Scheduler (AIS), which was developed in the 1970s and early 1980s under the leadership of Dr. James Ferguson to aid Arkansas farmers in managing irrigation. Arkansas producers were just beginning to irrigate their crops, rather than depending solely on rainfall to meet the crop's water needs. In fact, during the years 1972 through 1981, the first ten years with separate records collected for irrigated and nonirrigated crops in Arkansas, an average of only 8% of the soybean and 14% of the cotton crops were irrigated (USDA-NASS, undated).

The program has gone through many changes as both knowledge and personal computing power have advanced. The earliest versions were mainframe-computer based (Yar, 1984), since personal computers (PCs) were fairly rare and not very powerful at that time. An early PC version of the program was written in BASIC for

the Radio Shack TRS-80[1] computers (Radio Shack Corporation, Fort Worth, Tex.) in many University of Arkansas Cooperative Extension Service (CES) and some farm offices. Several updated versions were released by CES for the MSDOS operating system, and the most recent versions were written in FoxPro for Microsoft Windows (Microsoft Corp., Redmond Washington). The initial program was only for use with stationary center pivot systems, but later versions included support for towable center pivot systems (Edwards, 1986). Support for furrow, flood, and graded border irrigation were included in subsequent revisions. Cahoon et al. (1990) reported five objectives for the AIS: 1) to be user friendly and easily operated; 2) to require minimal input data; 3) to be applicable to Mid-South climatological conditions and crops; 4) to be system-based as opposed to field-based; and 5) to be useful as a prediction tool, as opposed to a monitoring tool. While increases in computing power have reduced the need to be system based, the other four objectives still apply.

ARKANSAS IRRIGATION SCHEDULER PROGRAM DESCRIPTION

Like many scheduling programs, the AIS uses a water-balance approach to scheduling irrigation, similar to managing a checkbook. The system balance represents the soil water deficit (SWD), the difference between the soil's existing moisture content, summed over the rooting depth, and the moisture content of the soil at its well drained upper limit (~24 hours after surface water was removed). Deposits to the system include rainfall and irrigation. Withdrawals from the system include crop evapotranspiration (ET_c), runoff, and deep percolation below the root zone. Deep percolation is considered negligible when the SWD > 0 and is therefore not considered in the program. Rooting depth is not used explicitly in the program, but is implicit in the choice of a maximum allowable SWD. Cahoon et al. (1990) provided a detailed description of the program and that information will not be repeated. Instead, this report will deal primarily with changes made to the program since their article was written.

User friendly and easily operated. Each winter from 2005 through 2008 a group of program users met to discuss ways to improve the program for the next release. One of the most commonly heard comments was that the program should operate similarly to other Windows-based programs, making it easier for new users to learn to operate the program. Therefore, many of the changes were intended to make the program more user friendly as stated in objective 1. An updated version was released in 2008 (version 2.2.166) that included improvements to incorporate knowledge gained since the 2000 release of version 1.1w, to feature more intuitive operation similar to other Windows-based programs, and to be more universally applicable, rather than just aimed at users in Arkansas and surrounding states.

Require minimal input data. The program was developed for Arkansas producers, and much of the funding for developing and supporting the program was provided by Arkansas soybean producers through their checkoff funds. One of the problems

[1] Mention of trade names or commercial products in this publication is solely for the purpose of providing specific information and does not imply recommendation or endorsement by the U.S. Department of Agriculture or University of Arkansas.

facing Arkansas farmers when the AIS was developed was a lack of detailed weather information, which was one reason for objective 2 (to require minimal input data). Even though many states have networks of electronic weather stations with data available to the public, no such system was employed in Arkansas. However, producers in the states surrounding Arkansas also used the program and many researchers use the program as well. Therefore, the program needed to be flexible enough to meet the needs of producers with little weather information available and researchers or producers in other states with access to more weather data.

Rainfall. Several changes have dealt with rainfall and how it is considered in the daily water balance. As before, the program doesn't attempt to estimate runoff; instead the user is asked to input the effective rainfall, or the amount in excess of runoff. Knowing net rainfall would be advantageous, since considerable runoff can result from the thunderstorms common in the Mid-South. However, much more detailed information concerning topography and soil would be necessary than is currently required of the user. Furthermore, the resulting estimate would probably not be highly accurate. The relatively flat topography in most of the region increases the likelihood that rainfall will be effective at reducing the SWD before running off of the field.

In addition, the limit reported by Cahoon et al. (1990) that rainfall could replace no more than 90% of the estimated SWD was removed from the program. The numerical value of the limit seemed somewhat arbitrary given the wide range of rainfall amounts and intensities common in the region. In addition, the fact that rainfall could never eliminate the SWD seemed to be a point of confusion for program users.

Another change had to do with the lower limit for rainfall amount effective in reducing the SWD. Cahoon et al. (1990) ignored daily rainfall amounts < 5 mm. Their modified crop coefficient used to calculate ET_c included a soil surface wetness coefficient that served to raise the modified crop coefficient to 1 on the day of irrigation or a rainfall > 5 mm, to account for evaporation of water from the wet surfaces of the soil and/or leaves. They also included a lesser surface wetness coefficient on the following day. Rainfall < 5 mm was felt to be offset by the increased evaporation. However, an 8 mm rainfall could be reported as two 4 mm rainfalls and be ignored by the program, or it could be reported as one 8 mm rainfall and be accounted for in the program depending on the timing of the rain relative to the measurement. Later program revisions eliminated both the 5 mm limit and effect of the surface wetness coefficient on the second day. For small rainfalls, the impact of the wetness coefficient was limited by the rainfall amount (i.e., a 2 mm rainfall could not increase ET_c by more than 2 mm).

Reference evapotranspiration. Since one of the problems facing Arkansas farmers was a lack of detailed weather information, the program developers needed to estimate reference evapotranspiration from minimal data. Cahoon et al. (1988) used regression analyses to investigate relationships for estimating pan evaporation, which was measured at several sites in the region. Pan evaporation was related to a short grass reference evapotranspiration (ET_o) using a pan coefficient of 0.86. They developed quadratic equations for six locations in or near Arkansas (Fig. 1) of the form:

$$Pan = C_1 + C_2(T_{max}^2) + C_3(T_{max}) + C_4(DL) \quad (1)$$

where:
Pan = daily pan evaporation;
T_{max} = maximum daily temperature;
DL = day length;
C_1, C_2, C_3, C_4 = regression coefficients.

Day length was calculated from the latitude of the site and the day of the year, so that only rainfall and T_{max} were entered daily by the user. Other relationships were investigated, but Equation 1 appeared to provide the best combination of acceptable accuracy and minimal input data. Furthermore, it was believed that small day-to-day errors would be reduced somewhat during the days between irrigations (i.e., a small negative error one day would be partially offset by a small positive error the following day).

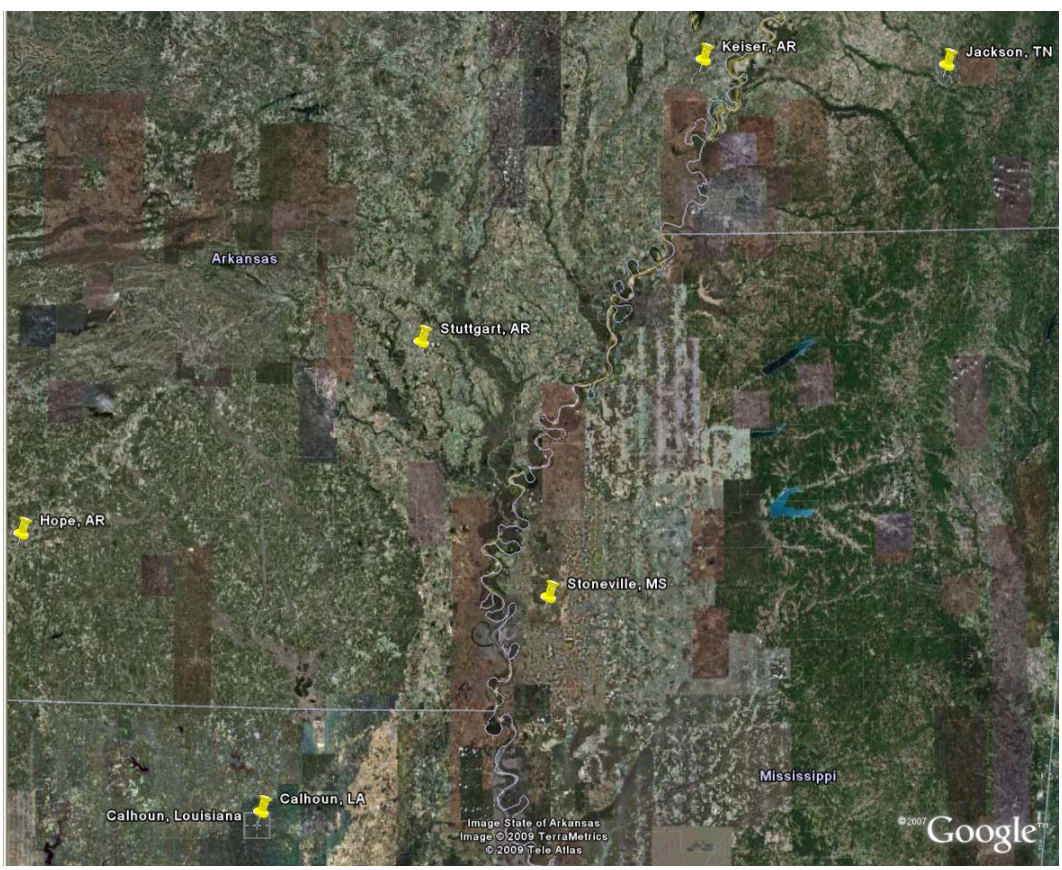

Figure 1. Locations of climatological data analyses for pan evaporation estimates.

Before 2008, producers or researchers with extensive weather data were only able to use T_{max} and rainfall data and required to select one of the six locations (Stuttgart, Keiser, and Hope, Ark.; Jackson, Tenn.; Stoneville, Miss.; and Calhoun, La.) most similar to their own location for estimating ET_o. Many researchers and some farmers from nearby states, including Louisiana and Missouri, had access to data from electronic weather stations that provided more extensive weather data than was

available to most Arkansas producers. Therefore, the latest version of the program allows users to input a value for ET_o directly using estimates derived from some other method believed to be more accurate, rather than having the program estimate one. Those with limited data can still allow the program to estimate ET_o in the same way as before. Therefore, while only minimal input data are still required to use the program, the change allows the user to take advantage of additional data when it exceeds the minimum required.

Long-time program users must exercise care if they change to another method of ET_o estimation, even if it provides more accurate estimates. Vories and Tacker (2006) reported that ET_o values calculated with the AIS for Keiser, Ark., were consistently higher than values calculated with the Standardized Penman-Monteith equation (ASCE-EWRI, 2004). Hypothetical irrigation schedules developed from the ET_o values resulted in consistently earlier first irrigations and two additional irrigations were scheduled each year with the AIS values. Vories et al. (2009) reported agreement between ET_o values from the AIS and from observed pan evaporation from the National Climatic Data Center (NOAA, undated) using the pan coefficient used in the AIS (0.86). However, both were higher than the values calculated using the standardized Penman-Monteith equation (ASCE-EWRI, 2004). Some of the differences could be accounted for by varying the maximum allowable SWD for different ET_o estimation methods. Farmers are currently advised to adjust the maximum allowable SWD to best fit individual fields as they become more familiar with using the AIS, and similar adjustments could be especially important if a different ET_o estimation method is used. However, for most producers in Arkansas and many other areas, using more data-intensive methods is not an option until more detailed weather data become widely available.

Applicable to Mid-South climatological conditions and crops. While the program will be applicable to more areas than before, it is still intended primarily for use in the Mid-South or areas with similar humid climates as suggested in objective 3. Wet soil conditions typical of winter and early spring simplify the choice of a starting SWD. In addition, small errors that accumulate over time from the use of limited weather data will usually be erased by rainfall or in some cases by surface irrigation. However, better crop coefficient functions are needed for the Mid-South. Lysimeter-based functions have not been developed in the region, so some of the functions were adapted from different climates. Weighing lysimeters have been installed by the US Department of Agriculture's Agricultural Research Service (ARS) in Stoneville, Miss., (Fisher, 2004) and by Louisiana State University in Saint Joseph, La. (Clawson and Hendrix, 2007). Both systems have been used to study cotton ET_c, but will likely be available for other crops in the future. Similarly, photographic techniques being developed (Purcell, 2000; Trout and Johnson, 2007) may result in simpler methods for developing crop coefficients than using weighing lysimeters. Until better functions are developed, irrigators in the Mid-South must rely on published values and experimental data from other regions.

System-based as opposed to field-based. Recent versions of the program have changed from system-based (obj. 4) to field based. In the early versions, computer memory and storage restricted the program to only consider a small number of fields.

A representative situation was selected as a four-field system, representing quadrants of a stationary center pivot field, halves of two towable center pivot fields, or four fields sharing one well for surface irrigation. Recommendations were made for when to irrigate each of the fields in the system. More powerful PCs allow many more fields to be considered simultaneously. Being able to view the soil moisture status of most or all of the fields on a farm at the same time was believed to be more advantageous than retaining the system base. The user could then choose to group the fields in whatever way best fit the situation.

Useful as a prediction tool, as opposed to a monitoring tool. The program has kept its utility as a prediction tool, rather than just a monitoring tool (obj. 5). The predictive capability of the program is one of its most important assets under Mid-South conditions, where multiple crops are often irrigated from the same water supply. In addition, irrigation decisions are often coordinated with pesticide applications or other field operations. User's can project irrigation needs for the next ten days, assuming no rainfall and the expected T_{max}.

Other factors. Even with improvements to the AIS, users must remember that many things can still affect the accuracy of the program output. In addition to excessive rainfall, runoff can result from application rates on the outer portions of a center pivot that are too high for the soil. An application efficiency of 90% is assumed for sprinkler irrigation and cannot be changed by the user. However, since runoff-inducing application rates waste water and energy, they should be avoided. With furrow irrigation, soil crusting, irrigating every other middle, or irrigating a field with appreciable slope may result in less than saturated conditions following irrigation, even though the assumption in the program is SWD = 0 (Cahoon et al., 1990).

Another assumption in the program is no standing water (i.e., all rainfall or irrigation applied in excess of the SWD will run off the field). Standing water can cause the soil to remain saturated for several days, stressing the crop and continuing to affect water use after the standing water is removed. Estimates for water use in the program are based on a healthy, well watered crop. A crop that has been drought stressed or experienced oxygen stress from standing water may never recover to the expected water use rate. However, between the humid climate and the relatively flat topography, standing water is often unavoidable, particularly in lower portions of the fields.

Internet version. CES has decided to move most of their supported software to the internet. While the internet has been used for program distribution for several years, most of the programs were downloaded from the website and operated on the user's computer. However, future plans are for programs to run on the server without residing on the user's computer. Advantages to such a system include: "bugs" can be repaired without having to contact users and provide "patches" or updated versions; the user is always assured of using the latest version of the program; and the user doesn't have to bother with installation and setup of the software on their computer. However, the main disadvantage is that the program cannot be used without internet service. Users without internet service would not be able to use the program, and users with relatively slow dial-up service might not be willing to wait the time

necessary to run the program for many fields. Although the internet version is in beta testing, no internet version is currently available for public use.

Finally, the current version of the program is applicable to more areas than before, and offers improvements for users already familiar with the program. Using the program will aid producers in determining the optimum irrigation schedule for their situation. In addition to improving yields, properly scheduling irrigation can save energy and therefore money by reducing unnecessary pumping. Reducing unnecessary pumping can also help to alleviate water shortages being experienced in many agricultural areas.

SUMMARY

The AIS has been in use for over twenty years in Arkansas and surrounding states, with the current version released in 2008. The current version retains most of the objectives of the earlier versions (user friendly and easily operated, requires minimal input data, applicable to Mid-South climatological conditions and crops, and useful as a prediction tool, as opposed to a monitoring tool). The one changed objective was to be field-, rather than system-based, allowing users to view the soil water status of more of their fields at one time and group the fields however they feel most appropriate. Other changes made the program easier to learn, allowed the user to take advantage of more extensive weather data if it is available, and made the program applicable to more areas than before. Changing only the ET_o calculation method was shown to suggest fewer irrigations per year in one study. Therefore, previous users that take advantage of more extensive weather data will need to exercise care to see if other changes such as maximum allowable SWD are also needed. Crop coefficient functions developed in the region are needed, but are not currently available. Future versions of the program may be limited to the internet, if service becomes extensive enough to reach all of the users. However, no internet version is currently available for public use. In addition to improving yields, using the program to properly schedule irrigation can save energy and therefore money by reducing unnecessary pumping, and help to alleviate water shortages being experienced in many agricultural areas.

REFERENCES

ASCE-EWRI, 2004. The ASCE standardized reference evapotranspiration equation. Technical Committee report to the Environmental and Water Resources Institute of the American Society of Civil Engineers from the Task Committee on Standardization of Reference Evapotranspiration. 173 p.

Cahoon, J., Ferguson, J., Edwards, D., and Tacker, P. (1990). A microcomputer-based irrigation scheduler for the humid mid-South region. Applied Engineering in Agriculture 6(3), 289-295.

Cahoon, J., Ferguson, J., and Costello, T. (1988). Empirical pan evaporation equations for the Mid-South region. ASAE Paper No. SWR 88-100. ASABE, St. Joseph, MI.

Clawson, E. L., and Hendrix J. A. (2007). Weighing lysimeters in northeast Louisiana: First year's experience. Proc. Beltwide Cotton Conf., National Cotton Council, Memphis, Tenn., p. 1754.

Edwards, D. R. (1986). Development and evaluation of a microcomputer program to schedule center pivot irrigation in sub-humid climates. Unpublished M.S. thesis. University of Arkansas, Fayetteville.

Evett, S. R. (2007). Soil water and monitoring technology. In: Lascano, R. J., and Sojka, R. E. (Eds). Irrigation of agricultural crops. American Society of Agronomy, Madison, Wis., pp. 25-84. Available at: http://hdl.handle.net/10113/1098. Accessed 26 January, 2009.

Fisher, D.K. (2004). Simple and inexpensive lysimeters for monitoring reference- and crop-ET. Proc. Irrig. Assoc. Tech. Conf. Irrig. Assoc., Falls Church, VA (unpaginated CDROM).

Henggeler, J. (2002). Software programs currently available for irrigation scheduling. Proc. Irrig. Assoc. Tech. Conf. Irrig. Assoc., Falls Church, VA (unpaginated CDROM).

Phipps, B. (2003). Specialists Speaking. In "Cotton Farming" June 2003. Available at: http://www.cottonfarming.com/home/2003_JuneCF-SS.html#Missouri. Accessed 25 July, 2009.

NOAA. (undated). National Climatic Data Center. Washington, DC, US Dept. of Commerce. Available at: http://www.ncdc.noaa.gov/oa/ncdc.html. Accessed 3 May 2007.

Purcell, L. C. (2000). Soybean canopy coverage and light interception measurements using digital imagery. Crop Sci. 40, 834-837.

Smith, M. S., and Riley, T. J. (1992). Direct and interactive effects of planting date, irrigation, and corn earworm (Lepidoptera : Noctuidae) damage on aflatoxin production in preharvest field corn. J. Econ. Entomol. 85, 998-1006.

Trout, T. J., and Johnson, L. F. (2007). Estimating crop water use from remotely sensed NDVI, crop models, and reference ET. Proc. Fourth Int. Conf. on Irrig. and Drain. USCID, Denver, Colo., pp. 275-285 [CDROM].

USDA-NASS. (2004). Farm and ranch irrigation survey (2003). AC-02-SS-1. Washington, DC, USDA.

USDA-NASS. (undated). Quick Stats: Agricultural Statistics Data Base. Available at: http://www.nass.usda.gov/QuickStats/. Accessed 21 July, 2009.

Vories, E. D., and Tacker, P. L. (2006). Effect of ET calculation method on irrigation scheduling in Midsouth. ASABE Paper No. 062205. ASABE, St. Joseph, MI.

Vories, E. D., Tacker, P. L., Lancaster, S. W. and Glover, R. E. (2009). Subsurface drip irrigation of corn in the United States Mid-South. Agric. Water Management (in press).

Vories, E. D., Hogan, R., Tacker, P., Glover, R. and Lancaster, S. (2007). Estimating the impact of delaying irrigation for Midsouth cotton on clay soil. Trans. ASABE 50(3):929-937.

Vories, E. D., Pitts, D. J., and Ferguson, J. A. (1993). Sprinkler irrigation response of corn on clay. Ark. Farm Res. 42, 6-7.

Yar, A. (1984). On-farm irrigation scheduling by computer simulation in Arkansas. Unpublished Ph.D. diss. University of Arkansas, Fayetteville.

The Next Generation of Irrigation Management Programs

Robinson, P.M.[1]

[1] Water Management Engineer, P.E., West National Technology Support Center, USDA, Natural Resources Conservation Service, 1201 NE Lloyd Blvd, Portland, OR, 97232 (Ph.) 503.273.2417. e-mail:peter.robinson@por.usda.gov

ABSTRACT

A number of states have developed advisory software to assist farm managers with irrigation scheduling. The fundamental procedures for irrigation scheduling are relatively straightforward and simple, but the diversity of the programs that have recently been developed is remarkable and significant. The range of analytical options offered by these programs is increasing; some have evolved from simple irrigation scheduling programs into comprehensive and sophisticated irrigation planning and management programs, driven in part by the accelerating competition for water. The next generation of irrigation management software will need to address the challenge of optimizing irrigation management; i.e. maximizing net economic returns rather than maximizing yields. But the software to do that is inherently very complex, and development of such software is beyond the resources of most individual states or agencies.

This paper provides an overview of existing and developing irrigation management programs in the U.S. and suggests some potential components of the next generation of irrigation management software.

INTRODUCTION

The Natural Resources Conservation Service (NRCS) is the lead agency of the United States Department of Agriculture charged with carrying out the Department's conservation mission on private lands. The agency addresses the resource concerns of landowners with an individually designed conservation plan composed of conservation practices. One of the natural resource concerns that the conservation plans can address is inefficient use of water on irrigated lands.

Among the 160 plus NRCS conservation practices is the "irrigation water management" practice. Irrigation scheduling and irrigation water management are among the preferred tools NRCS has for assisting a landowner in mitigating the inefficient use of irrigation water.

In 2008, NRCS applied the Irrigation Water Management Conservation Practice on 1,307,457 acres nationwide (NRCS, 2008). The NRCS has encouraged the use of irrigation scheduling software through both technical and financial assistance to landowners. In addition, some developers of irrigation schedulers have received financial assistance from the agency. Other developers have received indirect assistance through the encouragement or requirement of using a specific irrigation scheduler.

IRRIGATION GOALS

Determining when and how much to irrigate is fundamental to the operation of any irrigated farm. Optimizing an irrigation schedule can have a variety of goals, including (Martin, 1990):

- maximizing net return,
- minimizing irrigation costs,
- maximizing yield,
- optimally distributing a limited water supply,
- minimizing groundwater pollution or
- optimizing the production from a limited irrigation system capacity.

Current irrigation schedulers often assume that the sole goal of the irrigator is to maximize yield. In this case, the scheduler looks at the immediate situation, i.e. when is the next recommended irrigation. This assumes that the water is available on that date. The irrigator usually is not given guidance of how best to manage several fields in a water limited environment. Going forward, we can expect US irrigators to be in a water limited situation more frequently, and effective schedulers will need to be able to recommend an irrigation schedule based on the irrigator's selected goal and the amount of water the farmer has available.

SCHEDULING STRATEGIES

Every irrigated farm uses some type of decision making process to schedule irrigations, though that process may be as basic as "water is delivered every seventh day". Table 1 indicates that the current preference of deciding when to irrigate is based on the "crop condition" or "feel of soil". All other methods have a relatively low level of use.

Table 1. Methods Used in Deciding When to Irrigate (USDA, 2004)

Respondents could choose more than one method.	1998	2003	% of 2003 value	% Change 1998-2003
Number of irrigated farms	223,932	220,163		-1.7%
Any method	220,770	220,163	100.0%	-0.3%
Condition of crop	163,303	175,560	79.7%	7.5%
Feel of soil	90,434	76,731	34.9%	-15.2%
Soil moisture sensing device	17,869	14,452	6.6%	-19.1%
Plant moisture sensing device	(NA)	3,193	1.5%	
Commercial or government scheduling service	7,238	14,190	6.4%	96.0%
Reports on daily crop-water evapotranspiration (ET)	10,841	15,323	7.0%	41.3%
Scheduled by water delivery organization	22,567	26,537	12.1%	17.6%
Personal calendar schedule	40,338	42,551	19.3%	5.5%
Computer simulation models	2,237	1,285	0.6%	-42.6%
When neighbors begin to irrigate	(NA)	14,080	6.4%	
Other	15,601	19,298	8.8%	23.7%

Scientific irrigation scheduling follows one of three strategies (Jones, 2004):

- Soil water measurement
- Soil water balance calculations
- Plant 'stress" sensing.

Irrigation schedulers typically use the checkbook method to calculate the daily soil water balance and recommend irrigations dates and amounts. The checkbook method of irrigation scheduling is one variation of the soil water balance strategy, and can be represented mathematically as (Howell, 2007):

$$\Theta z_{i+1} = \Theta z_i + (P_i - Q_{roi}) + I_{ni} - ET_i - Dz_i$$

where Θz_i is the soil water content on day i integrated over the root zone depth z, P is rainfall, Q_{ro} is runoff, I_n is net applied irrigation, ET is the crop water use from the root zone, and D_z is the deep percolation beneath the root zone at depth z.

The checkbook method requires inputs of crop ET, effective rainfall, and irrigation depth. The development of state and regional weather and evapo-transpiration networks has allowed irrigators to have access to daily evapo-transpiration values. However, the checkbook method, even when integrated with a weather/ET network, typically relies on the irrigator to record and enter the effective rainfall and irrigation events. Even if the crop ET data is completely accurate, the irrigator may have difficulty in determining the effective precipitation or the net irrigation depth. Errors can be introduced into the checkbook method early and often.

Consequently, it is universally recommended to field truth the results of irrigation schedulers. Errors are cumulative in the checkbook method, and unless an effective rainfall or irrigation fills the root zone to field capacity, measuring the soil moisture is critical to ensure that the scheduling calendar reflects what is happening in the field.

IRRIGATION SCHEDULING SOFTWARE

To facilitate the calculations required for the checkbook method, a variety of organizations have developed irrigation scheduling software. This section highlights selected schedulers. All of these schedulers discussed use some form of the soil water balance calculation to predict the next date and amount of irrigation. Table 2 summarizes the schedulers.

AZSCHED

AZSCHED (Martin, 2003, 2005) was developed by the University of Arizona; it has most of the features common to schedulers. The software is standalone; the user downloads the program and runs it off of a personal computer. The program connects to the AZMET weather network to access real time ET data. There are 28 crops in the AZSCHED database. The program uses growing degree days rather than days after planting to determine the crop stage.

Arkansas Scheduler

The Arkansas Scheduler (Tacker, 2006) is designed for the irrigated crops in the mid-south, and can be used to schedule irrigations of cotton, soybeans, grain sorghum or corn. Arkansas Scheduler allows the user to import ET data, but does not access any weather network. In the absence of ET data, it will calculate a daily ET value based

on the day's maximum temperature. It also has a predictive function; the user can enter in the forecasted weather and Arkansas Scheduler will develop an irrigation calendar.

Wateright

Wateright (C.I.T., 2009) is a web application created by the Center for Irrigation Technology in Fresno, CA. It has a wide area of application because of its ability to access the ET networks of California (CIMIS), and Oregon, Washington and Idaho (Agrimet). The user is able to schedule a total of 15 fields, and the results are shown in tabular form. The soils data is limited to seven soil types e.g. "fine sandy loam". If the weather station selected is in California, the user can choose from among 63 crops. For fields in the Pacific Northwest, Wateright has access to the crop database of Agrimet. Wateright also provides the option of specifying a cover crop with its own crop coefficient; the cover crops also can have their own start and stop dates. The user can also select the criterion for the irrigation schedule, e.g a schedule based on the management allowable depletion, a preferred length of irrigation set, or a preferred irrigation rotation.

KanSched

KanSched2 (Clark, 2002) (Rogers, 2006) was developed by Kansas State University. This is a standalone program. It has been used successfully as a research tool in at least one instance (Dogan, 2006) and has been adopted for use by NRCS as the preferred scheduling tool in Kansas. It does not access an online ET network, though this does have one advantage because it can be used easily outside of its "design' area. The program has 19 internal crops, and the crop coefficients can be edited so that virtually any crop can be modeled. It uses generic soil names and data, e.g. clay loam, for its available water capacity, but, again, this data can be easily edited. Notable features include its graphing output and its irrigation pumping cost tool.

NDAWN (North Dakota Agricultural Weather Network) Irrigation Scheduler

The NDAWN Irrigation Scheduler (Scherer, 2008) is a web-based application for use in North Dakota. It uses a soil water balance algorithm to determine the soil water deficit in the effective root zone on a daily time step. The application has a GIS interface that allows the user to delineate the field of interest based on aerial photographs; the soil information is then immediately imported. The user is able to make a selection from three nearby weather stations for ET data. The soil data includes available water capacity from the NRCS Soil Data Mart, and this information is automatically added to a table so the user doesn't have to enter it.

A tabular irrigation schedule is then produced, with historical ET data for dates in the future. The user must enter the precipitation and irrigation events, and has the option of adjusting the soil moisture content as needed. The soil water balance is calculated for the three major soils of the delineated field.

IMO (Irrigation Management Online)

IMO (Irrigation Management Online) (Hillyer, 2007) is a web application that is currently in field testing. While the original development was centered in Oregon, the developers are now working cooperatively with the University of California,

Washington State University and the University of Idaho to utilize IMO in those states. IMO incorporates sophisticated analytical and decision support capabilities not found in conventional irrigation decision support software, including:

- modeling of application efficiencies and crop yields, both of which are normally assumed *a priori* in conventional irrigation management but must be explicitly analyzed for partial irrigation,
- conjunctive management of all fields that share a single source of water (as opposed to the conventional approach of managing each field independently) in order to facilitate optimal allocation of limited water among multiple fields,
- explicit modeling of uncertainties coupled with a Bayesian decision model for irrigation management under uncertainty,
- linking of simulation models to enterprise budget spreadsheets tailored to the economic circumstances of individual farms to facilitate rapid economic assessment of alternative water use strategies and associated crop yields.

Additionally the developers anticipate moving to 'controlled' open source code options that would permit local users to adapt the system to accommodate local circumstances, science and preferred practices while still insuring the integrity of the system.

Citrus MicroSprinkler Irrigation Scheduler

The Citrus MicroSprinkler Irrigation Scheduler (FAWN, 2009) was developed by the University of Florida and is hosted on the Florida Automated Weather Network site. It is an easy to use web application for citrus. It accesses the Florida Automated Weather Network's 35 weather stations. The user enters some basic data about the tree spacing of a mature citrus orchard, the irrigation system, and selects one of nine available soils. The web application then returns a statement on the recommended timing of the irrigation events for the next two weeks. For example, the result may be: "Irrigate every 5 days for 11 hours and 2 minutes."

TrueISM

Often left out of the discussion of irrigation schedulers are the efforts of private software firms. One such effort is sponsored by the El Dorado Irrigation District (EID) in northern California. EID uses the TrueISM software (Taylor, 2009) that was specifically developed for the irrigation district by TruePoint Solutions. This software is a web application and resides on one of the EID servers. There are two main sub-components to the current software package. The first is the day-to-day operations where a majority of the tasks are automated including weather data downloads and grower report delivery by e-mail. The second component is the field application where all of the data logger information and neutron probe readings are recorded on a tablet computer. At the end of the day this tablet is connected to the network and the prediction database updated. The software then re-calculates all of the irrigation predictions automatically based on the most recent data. The district has developed accurate irrigation system efficiencies for each farm based on the dense network of soil moisture sensors and irrigation flow measurement devices. The farmer has the option of waiting for the weekly e-mail, or accessing the most current information online.

THE NEXT GENERATION (NG) OF IRRIGATION SCHEDULERS

Irrigation scheduling software development will continue. As a starting point for discussion on where the development should lead, several suggestions are listed here.

1. The NG irrigation schedulers will be online applications. Although there will continue to be a need for legacy software, the ability to access real time online data requires that the user have an internet connection. Fortunately, the number of farmers without broadband internet will continue to decline. One attractive aspect of online applications will be the ability to evaluate the real time use of the software.
2. The NG irrigation schedulers will be able to access relevant on-line databases that expand the functionality of the software. Among the relevant databases are:
   - weather networks that report daily ET and real time rainfall and weather forecasts,
   - soil databases,
   - aerial photography,
   - water rights databases, and other information that is important for individual watersheds and irrigation districts.

   Many of the current schedulers are capable of accessing several existing ET networks. The NDAWN irrigation scheduler accesses the NRCS soils database and aerial photography. Leveraging the work of other agencies, particularly federal and state databases, will create added value, and generate support from those agencies.
3. The NG irrigation schedulers will allow for the quality weighting of various inputs. Currently, most schedulers replace calculated soil moisture data with measured soil moisture data, assuming the measured soil data is flawless. In fact, all data points have some inherent error. Determining the relative uncertainty of all data will be an important function.
4. The NG irrigation schedulers will have integrated crop yield models. In addition, they will allow the user to make decisions based on the current economic situation, i.e. commodity and water prices.
5. The NG irrigation schedulers will allow for deficit irrigation, and in fact, allow the farmer to choose among several goals in order to optimize irrigation.
6. The NG irrigation schedulers will schedule whole farms, and their multiple fields and water sources.
7. The NG irrigation schedulers will allow irrigation districts and watershed organizations to access water use information to improve planning.
8. The NG irrigation schedulers will be integrated with irrigation hardware. For example, the scheduler will be linked to the flow meters, rain gauges and soil moisture monitoring devices of the farm, so that this data does not have to be entered manually. This will provide a feedback loop so that the scheduler can be a data management tool that mitigates the uncertainties inherent in data collection. For example, although not fully integrated, TrueISM inputs soil moisture data gathered on a tablet computer in the field and automatically updates its irrigation schedule.

Table 2. Irrigation Scheduler Summary

Program Name and Version	Standalone or WebApp	Weather Network	Area of Use	Crops & Coeffficients	Soil Information Available	Other interesting information
KanSched2 2.1.8	Standalone	ET data entered manually	Anywhere, but crop coefficients are for Kansas	19 internal crops, plus ability to add/edit custom crop coefficients	11 generic soil textures e.g. clay loam. Can be edited.	Good Soil Moisture Charts. Pumping Cost tool.
NDAWN Irrigation Scheduler	WebApp	NDAWN: 70 stations, mostly in ND.	North Dakota	9 crops	Soil information seamlessly imported when field is delineated	User delineates field from aerial photography
AZSCHED 1.17	Standalone	AZMET: 28 active stations in January 2009, all in AZ.	Arizona	24 crops	User enters the available water capacity for the soil.	Uses growing degree days to monitor crop status
Wateright	WebApp	CIMIS and Agrimet	California, Oregon, Washington, Idaho	63 crops in CA. In the Pacific Northwest the number varies based on the Agrimet station	7 generic soil textures	Wide variety of crops and locations
IMO (Irrigation Management Online)	WebApp	Agrimet	Oregon, Washington, Idaho	It uses the ET crop data provided by Agrimet, which varies by station	11 generic soil textures, plus can create new soil type	Good graphing capabilities.
Arkansas Scheduler 2008	Standalone	ET data entered manually	Arkansas	cotton, corn, soybeans, grain sorghum	5 generic soil texture class	Projection aspect: user enters expected weather
Citrus MicroSprinkler Irrigation Scheduler	WebApp	FAWN: 35 stations in Florida	Florida	Citrus only	9 soils	One page entry, one click and the user gets the result.
TrueISM (as configured for the El Dorado Irrigation District)	WebApp	1 CIMIS station	El Dorado Irrigation District (EID), Placerville, CA	41 crops	All 42 soils of the EID	Interactive Soil Triangle, accurate system efficiency database

REFERENCES

Allen, R. G., L. S. Pereira, D. Raes, and M. Smith. (1998) *Crop evapotranspiration. Guidelines for computing crop water requirements. FAO Irrigation and drainage paper 56,* Rome, Italy: FAO.

Center for Irrigation Technology (2009) "Welcome to Wateright". http://www.wateright.org>(January 26, 2009).

Clark, G.A., Rogers, D.H., and Briggeman, S. (2002) "KanSched: An ET-Based Irrigation Scheduling Tool for Kansas Summer Annual Crops"

Dogan, E. Clark, G.A., Rogers, D.H., and Vanderlip, R.L. (2006) "On-Farm Scheduling Studies and CERES-Maize Simulation Of Irrigated Corn." *Applied Engineering in Agriculture*, ASABE, 22(4), 509-516.

Florida Automated Weather Network: FAWN. (2009) http://fawn.ifas.ufl.edu/tools/irrigation/citrus/scheduler>January 23, 2009

Henggeler, J. (2002a) "Software programs currently available for irrigation scheduling." 2002 Conference Proceedings, Irrigation Association International Irrigation Technical Conference. Falls Church, Va.: Irrigation Assn.

Henggeler, J. (2002b) "Programs Available for Irrigation Scheduling." 2002 Conference Proceedings, Improving Irrigation Efficiency in Agriculture, Las Cruces, NM.

Hillyer, C., Abou Rached, C., English, M.J. (2007) "A Web-based Advisory Service for Optimum Irrigation." 2007 Conference Proceedings, Irrigation Association International Irrigation Technical Conference. Falls Church, Va.: Irrigation Assn.

Howell T.A. and Meron, M. (2007) "Irrigation Scheduling." In: *Microirrigation for Crop Production*. (F.R. Lamm, J.E. Ayars, F.S. Nakayama, eds.) Elsevier.

Jones, H.G. (2004) "Irrigation scheduling: advantages and pitfalls of plant-based methods." *Journal of Experimental Botany*, Water-Saving Agriculture Special Issue 55(407), 2427–2436.

Martin, D. L, Stegman, E.C. and Ferres, E. (1990) "Chapter 7: Irrigation Scheduling Principles." In: *Management of Farm Irrigation Systems*. (Hoffman, G.J., Howell, T.A., Soloman, K.H. eds.) ASAE.

Martin, E.C., Slack, D.C., Detwiler, H. and Jones, J (2003) "Arizona Irrigation Scheduling System (AZSCHED) Users Handbook", http://ag.arizona.edu/crops/irrigation/azsched/azsched.html>(Jan. 23, 2009)

Martin, E.C., Slack, D.C. (2005) "AZSCHED V2.0: Climate-Based Irrigation Scheduling In Arizona." 2005 Conference Proceedings, Irrigation Association International Irrigation Technical Conference. Falls Church, Va.: Irrigation Assn.

NRCS (2008) "2008 PRS Reports." http://ias.sc.egov.usda.gov/prsreport2008 >(January 26, 2009).

NRCS (2005) "Natural Resources Conservation Service, Conservation Practice Standard: Irrigation Water Management." http://www.nrcs.usda.gov/technical/Standards/nhcp.html> (Jan 23, 2009)

Rogers, D.H., Clark, G.A., Alam, M., and Shaw, L.K. (2006) "Kansas progress in ET based scheduling: Improvements in KanSched." 2006 Conference Proceedings, Irrigation Association International Irrigation Technical Conference. Falls Church, Va.: Irrigation Assn.

Scherer, T.F., Morlock, D.J. (2008) "A Site Specific Web-based Irrigation Scheduling Program." 2008 ASABE Annual International Meeting. Providence, RI.

Tacker, P.L., (2006) "Computer Programs Used for Improved Water Management in Arkansas." 2006 ASABE Annual International Meeting. Portland, OR.

Taylor, K. (2009). *Final Report of the "Scheduling irrigation for commercial agricultural growers within the El Dorado Irrigation District using permanently placed soil moisture sensors" Project.* Unpublished.

USDA (2004) *Farm and Ranch Irrigation Survey (2003)*, National Agricultural Statistics Service, Washington, D.C.

Woodruff Irrigation Charts

J.C. Henggeler [1]

[1] Department of Biological Engineering, University of Missouri, PO Box 160, Portageville, MO 63873; PH (573) 379-5431; FAX (573) 379-5875; email: henggelerj@missouri.edu

ABSTRACT

The Woodruff Irrigation chart method of irrigation scheduling began as a graphical chart solution of when to irrigate for a specific crop, location, planting date, and soil in Missouri. It has been expanded to a web-based chart maker that can be used for corn, cotton, and soybeans in Missouri and adjacent states. Survey data indicates that irrigators who use the Woodruff charts increase their yields over non-schedulers by 14.0 bu/ac more corn, 104 lbs/ac more cotton, and 10.7 more bu/ac soybeans. In southeast Missouri approximately 16%, 6%, and 5% of corn, cotton, and soybean irrigators use the Woody method, while 12%, 17%, and 7% use the ***Arkansas Scheduler***. Total impact since 2001 is estimated to be $54 M.

INTRODUCTION

Dr. "Woody" C.M. Woodruff was born in1910 in Kansas City and passed away in 2003 still maintaining an active presence in agronomic research. He had worked for the University of Missouri's Agronomy Department since 1929. He graduated from the University of Missouri College of Agriculture in 1932. He received has master's degree in agronomy from the University of Missouri-Columbia in 1939 and after civilian wartime service completed his doctorate in 1953.

He was a many-talented man. Because of his keen mind, he served with the United States Army Signal Corps doing research during World War II on radar systems and airborne magnetic submarine detectors. He was primary a soil chemist, and developed the Woodruff buffer equation commonly used in soil analysis. He was the first person to break the 100-bushel per acre yield level on corn. He did this by reverse analysis determining the number of kernels per acre needed and the amounts of N, P and K required to provide kernel mass to attain 100 bu/ac. He later said that he was lucky because the first season right after Word War II when he did this had well-timed rains.

He was keenly aware of weather patterns and their effect on yield. He determined that yield suppression in corn can occur if the previous season has received too much rain. He showed that this was due to micro-nutrients becoming tied up in chelates that caused the micro-nutrients not to be readily available to corn next season. This awareness of the problem of too much late-season moisture led to a tool he developed to help irrigators so that they would not over-irrigate crops. This became know as the Woodruff Chart, or as what we in Missouri call the Woody chart.

BACKGROUND

The Woodruff chart consists of a graph containing two parallel lines that serve as a graphical means to schedule irrigation. The top one represents the accumulative crop water use of the crop. The bottom line indicates when drought would occur and is offset a vertical distance equal to the available water holding capacity of the soil. Thus, the X axis (horizontal axis) of the graph represents time, while the Y axis (vertical axis) represents inches of water.

Original Woodruff chart. Woodruff had determined that the average daily water use of corn was 0.15 inches per day (ipd), but since he knew that it was important to end the season with some amount of available storage, he used the value of 0.14 ipd to develop the curve of accumulation. Also, his study of weather patterns in central Missouri indicated that in 95% of all years soil moisture was adequate through May, so the irrigation chart starts in June. Figure 1 shows the original double-line graphic that was used in Missouri guidesheet from the 1970s (Woodruff, 1975).

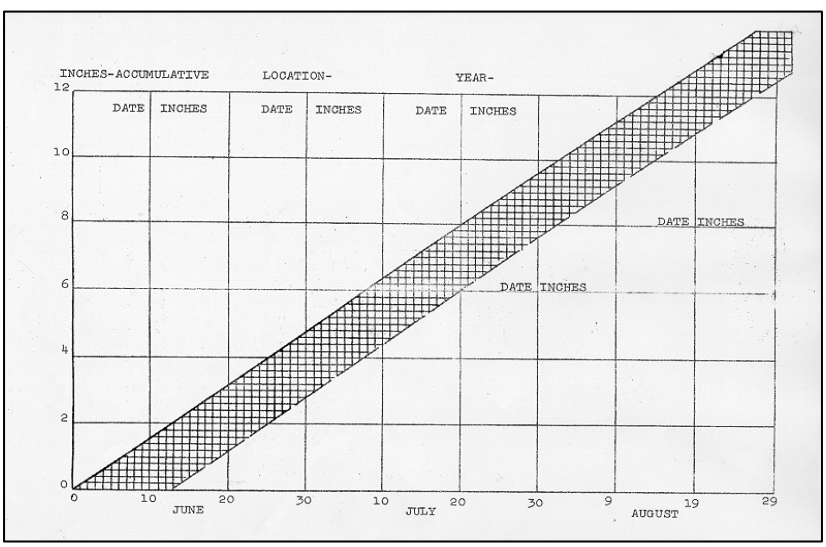

Figure 1. A Woodruff graph as it appeared in a Missouri guidesheet from the 1970s.

To schedule irrigations, the user merely pencils in the rainfall amounts in an up-and-down fashion on the day they occur, using the same vertical units that the crop water use curve is plotted with. The second and subsequent rainfall events are penciled in on the graph on their appropriate date and start at a level equal in elevation to the top of the last penciled in rainfall event, creating a stair step pattern. Irrigation occurs before the stair step crosses the bottom (drought) line. Irrigation amounts are penciled in the same manner as rainfall events. If a rainfall or irrigation amount takes the stair step across the top line (accumulative water use), any portion above the accumulative curve is considered deep percolation, and is discounted. In this case, the irrigator

begins the stair step, not at the top of the rainfall line, but at a level equal to where the rainfall line and the accumulative water use line cross.

Woodruff charts had great popularity with Missouri irrigators, most of whom had little irrigation experience.

Updating the Woodruff chart method. As mentioned, the original chart was developed specifically for corn planted about May 1 and grown on claypan soils in central Missouri making it site-, crop-, and date-sensitive. In the 1980s agricultural engineers at the University of Missouri expanded the concept with a BASIC computer program that allowed weather data to be an input variable. Also, additional crops, emergence dates and soils could be utilized. A value of 80% of Blaney-Criddle evapotranspiration (ET_{BC}) was used as the reference value (Gregory and Schottman, 1982). This method did not construct a chart, but instead used a generated table.

Existing Woodruff chart method. The current Internet Woodruff site was opened up to growers in June, 2001. The system was designed to require minimal data from the irrigator, who on one of the opening screens (Figure 2), chose crop, soil type, irrigation method, and county in Missouri.

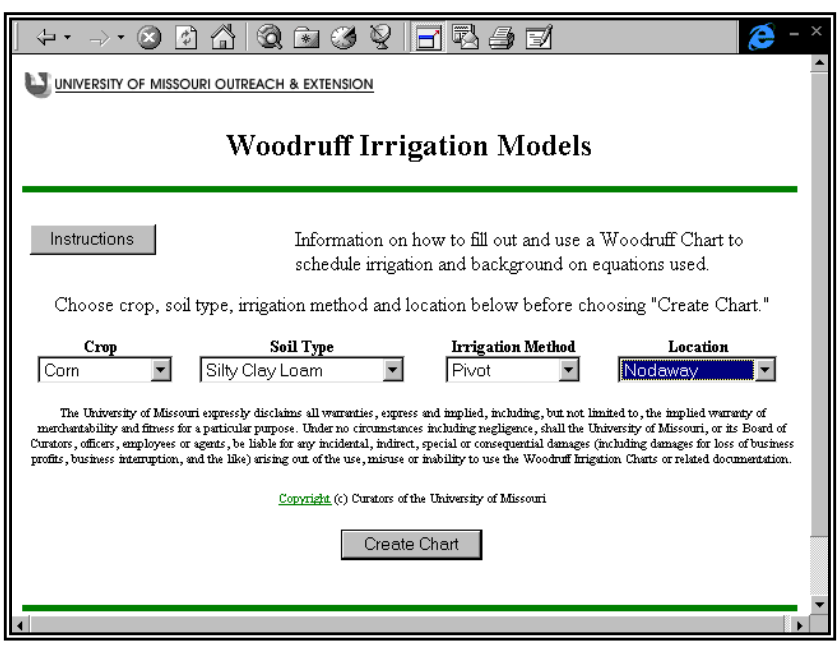

Figure 2. Opening query screen of the Woodruff Irrigation Chart Internet site.

The ET_{BC} equation is used in the Internet version. Daily values of evapotranspiration are calculated using a splining function on published 30-year monthly mean values of daily maximum and minimum temperatures. Latitudinal values are used to calculate daylight hours, part of the Blaney-Criddle equation. A database was established that

contains, for each Missouri county, latitude, daily maximum temperature, daily minimum temperature, and daily ET_{BC}.

The next screen that a viewer sees (Figure 3) asks for additional information including emergence date, field name, acreage and Relative Maturity or Maturity Group, depending on whether corn or soybeans had been chosen. It was found that "field name" was important as some growers had a number of various fields that Woodruff charts were printed up for. Acreage data was asked for so that developers could measure total impact.

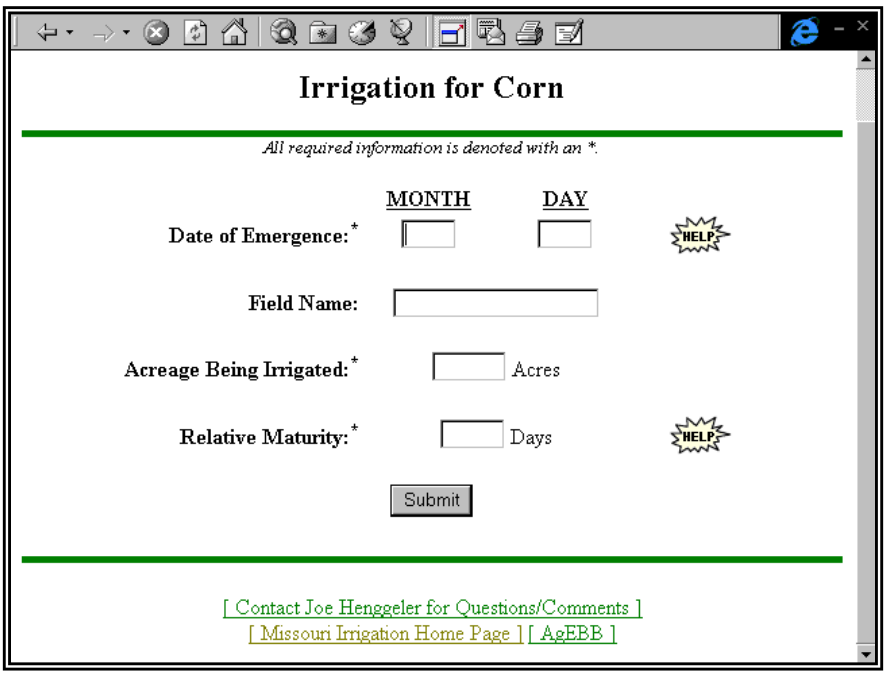

Figure 3. The second query screen that collects data for developing the Woodruff chart.

The final screen (Figure 4) before the graph is created, presents computer-suggested data including date crop will cease up-taking water, estimated water holding capacity of the soil, the ideal soil moisture status at the end of the season, and the deficit at which to trigger irrigations. These values are derived from data already supplied by the user, and can be adjusted if needed to be.

Cessation of crop water use. The final maturity of the crop is based on empirical relationships. Corn maturity is based on an estimate of corn Heat Units (HUs) (base 50° with 86° degrees as upper limit on maximum) to reach "black layer" that uses the Relative Maturity of the hybrid in use. Once the required HU value is calculated, the associated historical weather file is used to determine the date this will occur. A grower can change this date if he feels that it is not correct. The crop coefficient curve is based on % of HUs.

For soybeans, final maturity (R8) is based on a derived empirical relationship using Maturity Group, latitude and date of emergence. Again, once emergence and date of R8 are determined, a coefficient curve is developed based on standard Hus (60-degrre base).

Cotton is by nature a perennial, so cessation of its water use is dependent on either the occurrence of sufficiently cold enough weather or the application of crop desiccants. For Missouri conditions, the occurrence of 55°F-weather in the fall is close in time to normal applications of crop termination chemicals. Once the emergence date and the date of the first 55° fall weather (determined by interrogating the county data file) are known, the seasonal Heat Units (base 60 with no upper limit on maximum) can be calculated. Daily crop coefficient values are based on % of seasonal Heat Units experienced up to that date.

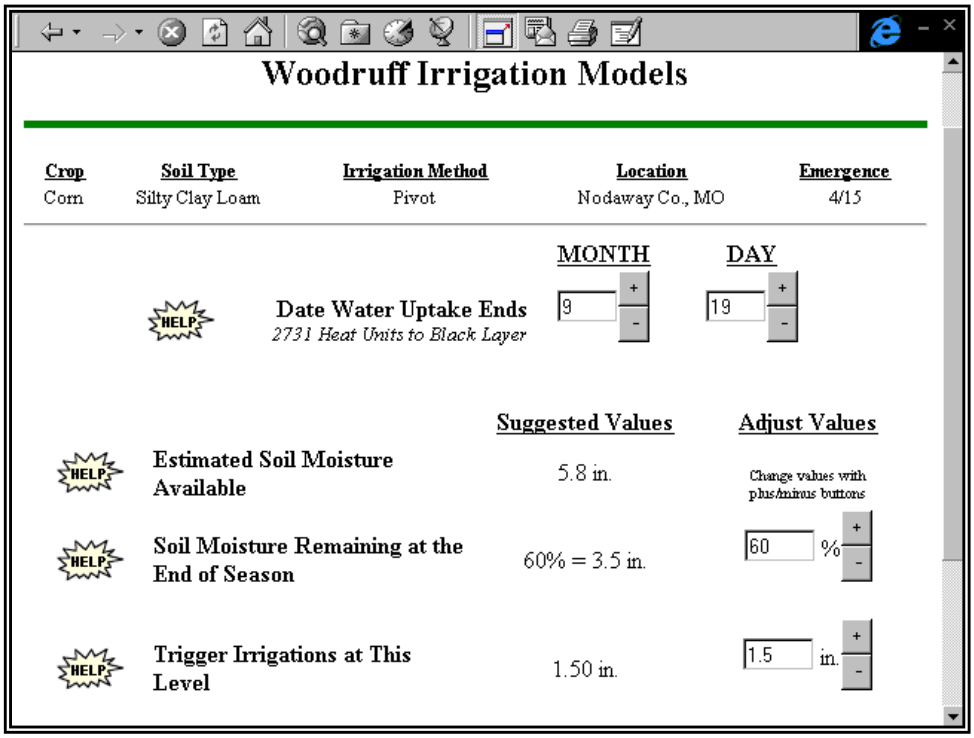

Figure 4. The last query screen that collects data for developing the Woodruff chart and allows for default estimates to be modified.

Irrigation trigger points. The soil type, crop, and method of irrigation determine the irrigation trigger (a.k.a., deficit) to default to (Table 1). This value represents the off-set between the bands in the chart. These suggested values are based on empirical research done by the University of Arkansas and are employed in their computer program, ***Arkansas Scheduler*** (Ferguson, 2000).

A sample Woodruff chart for 119-RM corn, emerging on May 1 in Clay County, MO is seen in Figure 5. Full information on crop coefficient values used and other items are found in the documentation section of the web-based program. The site of the program is:

http://agebb.missouri.edu/irrigate/woodruff/

Table 1.Default irrigation deficits for various crops, soil types and irrigation methods.

Soil Type	CORN		SOYBEAN		COTTON	
	Pivot	Flood	Pivot	Flood	Pivot	Flood
	-------- inches per irrigation application ----------					
Coarse Sand	0.75	1.00	1.00	1.50	1.00	1.50
Fine Sand	1.00	1.50	1.50	2.00	1.50	2.00
Loamy Sand	1.00	1.50	1.05	2.00	1.05	2.00
Sandy Loam	1.25	1.75	1.75	2.25	1.75	2.25
Fine Sandy Loam	1.25	1.75	1.75	2.25	1.75	2.25
Very Fine Sandy Loam	1.25	1.75	1.75	2.25	1.75	2.25
Clay	1.25	1.75	1.50	2.00	1.50	2.00
Clay Loam	1.25	1.75	1.50	2.00	1.50	2.00
Silty Clay	1.50	2.00	2.00	2.50	2.00	2.50
Silty Clay Loam	1.50	2.00	2.00	2.50	2.00	2.50
Silt Loam	1.50	2.00	2.00	2.50	2.00	2.50

IMPACT

The two prime scheduling methods in Missouri are the computer program ***Arkansas Scheduler*** developed by the University of Arkansas (Ferguson et al., 2000) and the Woodruff chart.

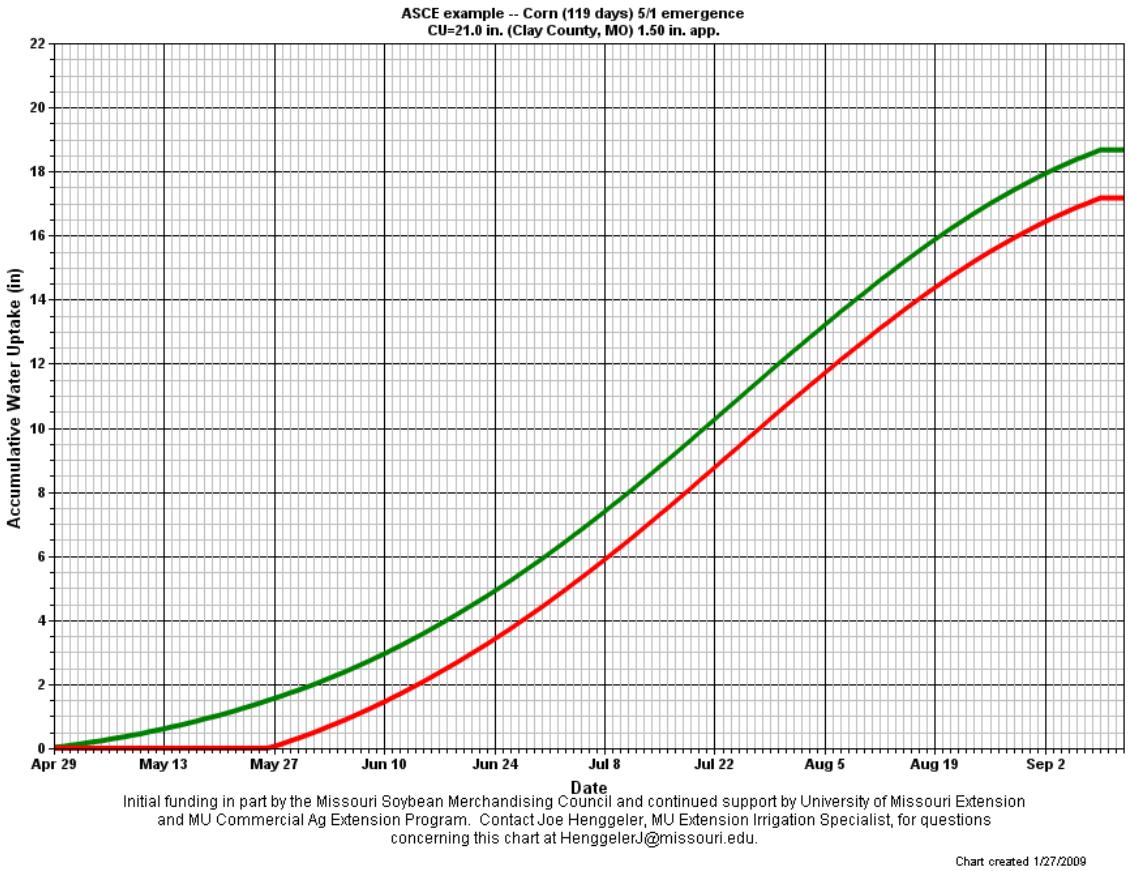

Figure 5. A sample Woodruff chart for 119-RM corn, emerging on May 1 in Clay County, MO.

The **Bootheel Irrigation Survey** (**BIS**) was initiated in 1987 and collects data from irrigators in southeast Missouri. Since 2000 the **BIS** has collected data on the method of irrigation scheduling the farmer used. Survey data indicates that irrigators who use the Woodruff charts increase their yields over non-schedulers by 14.0 bu/ac more corn, 104 lbs/ac more cotton, and 10.7 more bu/ac soybeans. In southeast Missouri approximately 16%, 6%, and 5% of corn, cotton, and soybean irrigators use the Woody. Figures 6 a through c show the yields of non-schedulers, users of the ***Arkansas Scheduler***, and users of the Woodruff irrigation charts.

Using the information on yield increase, % of users, and amount of irrigated acres it is estimated that the Woodruff irrigation website has increase the gross profits of Missouri irrigators by $54M since its inception in 2001. This is based on increased gross profits of $30M, $7M, and $17M for corn, cotton, and soybean, respectively.

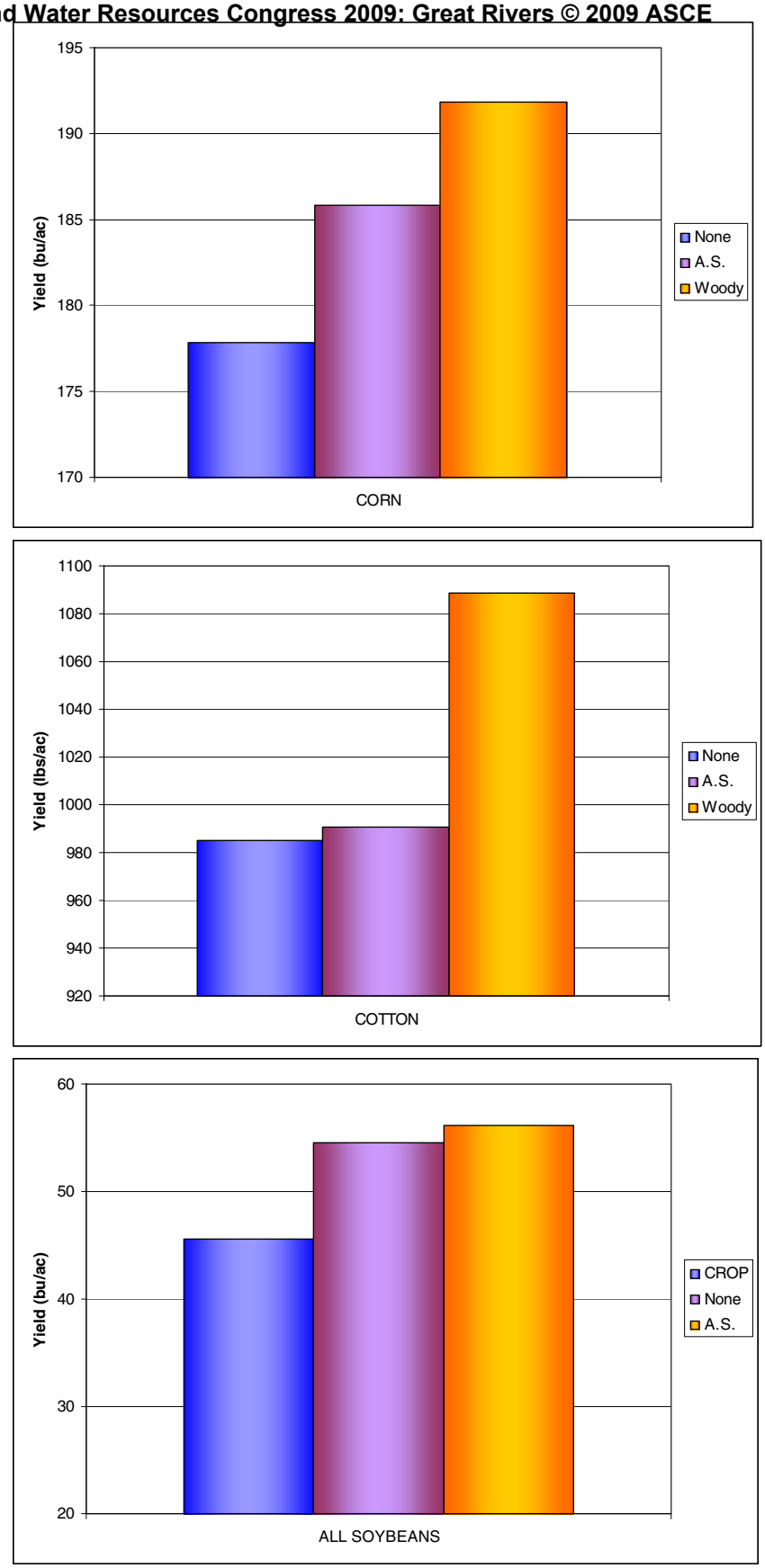

Figures 6a,b,c. Irrigated yields of corn (6a), cotton (6b), and soybean (6c) for non-schedulers (None), users of Arkansas Scheduler (A.S.), users of Woodruff charts (Woody) for period 2001-2008.

REFERENCES

Ferguson, J., D. Edwards, J. Cahoon, E. Vories, and P. Tacker. 2000. UACES Irrigation: Microcomputer Based Irrigation Scheduler, Ver. 1.1w. University of Arkansas.

Gregory, J.M. and R.W. Schottman. 1982. Irrigation scheduling procedure for subhumid areas. Transactions of ASAE. Vol (25) 4: 1290-1294.

Henggeler, J. 2009. 2000 - 2008 Bootheel Irrigation Surveys. http://agebb.missouri.edu/irrigate/survey/index.htm. > (Jan 26, 2009)

Henggeler, J and J. Travlos. 2009. Woodruff Irrigation Charts. http://agebb.missouri.edu/irrigate/woodruff > (Jan 26, 2009)

Woodruff, C.M. 1975. Irrigating corn on claypan soils in Missouri. UMC Guide No. 4137. Published by University of Missouri, Columbia.

A Web-Based Advisory Service For Optimum Irrigation Management

Charles Hillyer[1], Marshall English[1], Carole Abourached[1], Chadi Sayde[1], Kent Hutchinson[1] and John Busch[2]

1 Biological and Ecological Engineering Dept., Oregon State Univ., 116 Gilmore Hall, Corvallis OR 97331-3906; emails: hillyer@engr.orst.edu, englishm@engr.orst.edu, abouracc@onid.orst.edu, hillyer@engr.orst.edu, khutchinson1@verizon.net

2 USDA-Natural Resource Conservation Service, Baker City Service Center 3990 Midway Dr Baker City, OR 97814-1453; email: John.Busch@or.usda.gov

Abstract

The optimum (profit maximizing) level of irrigation water use is usually less than the yield maximizing level, particularly when water has an associated opportunity cost. However, the amount of analysis required to implement a profit maximizing strategy is usually too time consuming to be practical for most farmers. Furthermore the practical operational constraints imposed on typical irrigation practices are usually too complicated to be fully encapsulated in software.

Oregon State University and the NRCS have cooperatively developed a web-based, user-directed application for optimum irrigation management. This system has already completed two years of field trails and has a demonstrated capacity for delivering conventional irrigation schedules. The system is now entering a second phase of development where we are adding new analytical tools that enable easy generation of optimum irrigation schedules. This system, known as Irrigation Management Online (IMO), explicitly analyzes irrigation efficiency and yield reductions for deficit irrigation, performs simultaneous, conjunctive scheduling for all fields in the farm that share a limited water supply, and employs both ET and soil moisture measurements in a Bayesian decision analysis to enhance the accuracy of the irrigation schedules. To mitigate the complexities of irrigation constraints the system has been designed so that the user is an integral part of the irrigation optimization procedure.

Relevant theoretical background on irrigation optimization has have been articulated in papers by (English et al., 2002) and (English and Orlob, 1978). The system described herein is comprised of two key elements: (i) a general model of irrigation system performance that analyzes the ultimate disposition of applied water, the spatial distribution of water, and corresponding yield responses to applied water; (ii) a web based advisory program for optimal irrigation scheduling that analyzes farm water demands in individual fields and aggregate farm water demand, allocates farm water supply according to the management rules stipulated by the user, and facilitates the development of optimum irrigation schedules. These two elements are described in greater detail below.

The Irrigation Efficiency Model (IEM)

The Irrigation Efficiency Model was initially designed to model the relationship between sprinkler irrigation intensity, water losses and crop water use. IEM was originally developed by Oregon State University and the New Zealand Ministry of Agriculture and Fisheries (English, 1992), then further developed and refined with funding from a USDA National Research Initiative grant (Isbell, 2005). The model is implemented in C# and uses a variant of the MODCOM simulation framework (Hillyer, 2003). The implementation is modular and has been designed with the anticipation of future extensions and modifications. Complete details of IEM's functions are described by (Isbell, 2005) and are also available online at http://oiso.bioe.orst.edu. What follows is a brief description of the four key features of IEM.

Calculated Efficiency. IEM functions as a soil water balance model, tracking irrigation and precipitation inputs, estimating potential crop ET, adjusting the potential ET to account for low soil moisture or wet surface conditions, and partitioning ET into its component parts of evaporation and transpiration using the algorithms outlined in FAO 56 (Allen et al., 1998). A system diagram of the water balance is shown in Figure 1. When soil moisture is depleted to a user-specified level of allowable depletion, the model calculates the gross irrigation requirement, expressed as the amount of irrigation required to replenish soil moisture to a user specified refill level. Calculations of gross irrigation requirements are based on net irrigation requirement and an assumed application efficiency provided by the user. Subsequently, when an irrigation event occurs, IEM simulates *actual* application efficiencies by modeling the principal determinants of irrigation losses, spatial

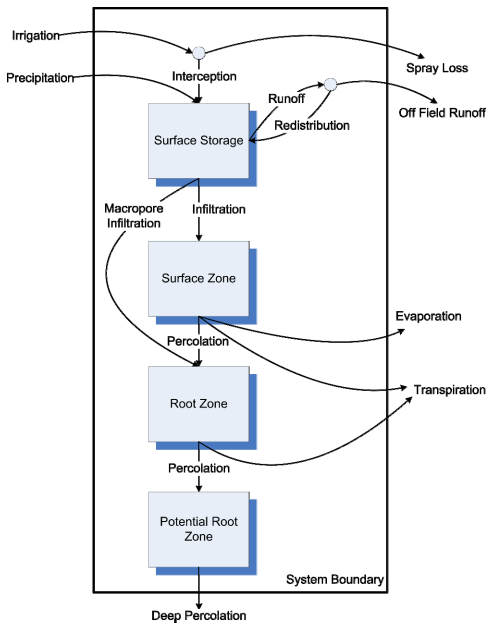

Figure 1. IEM System Diagram

variability of soil characteristics, irrigation timing and adequacy, patterns of applied water, wind effects on spray losses, wind distortions of sprinkler patterns, variability of surface infiltration rates, and surface water accumulations and associated redistribution. By simulating these factors the model analyzes the disposition of applied water in terms of evaporative losses, deep percolation, and runoff in addition to water stored in the crop root zone.

Spatial Variability. All irrigation systems are, to some degree, non uniform in their application of water. Furthermore, soil physical properties vary throughout a field. These two sources of non-uniformity combine to produce varying levels of available water in the field. It has also been demonstrated (Isbell, 2005) that the statistical distribution of cumulative crop ET will change shape with varying levels of irrigation intensity. Given such progressive distortions of ET patterns (and therefore yield) simulation of spatial variability will be of central importance in estimating the statistical characteristics of yield predictions. IEM attempts to quantify this variability through a Monte Carlo approach. The water balance model described above is replicated with varying soil physical properties. During any irrigation event each replicated water balance receives a different depth of applied water based on the uniformity characteristics of the irrigation system. Figure 2 shows the simulated distributions of crop ET from a field irrigated at 60%, 80%, and 100% of potential ET. By using this method IEM is able to simulate the distribution of crop ET without assuming *a priori* the distribution of available water. This method does, however, require that we be able to quantify the magnitude of spatial variable physical properties. At present this issue is left to the user's judgment, although default values are provided.

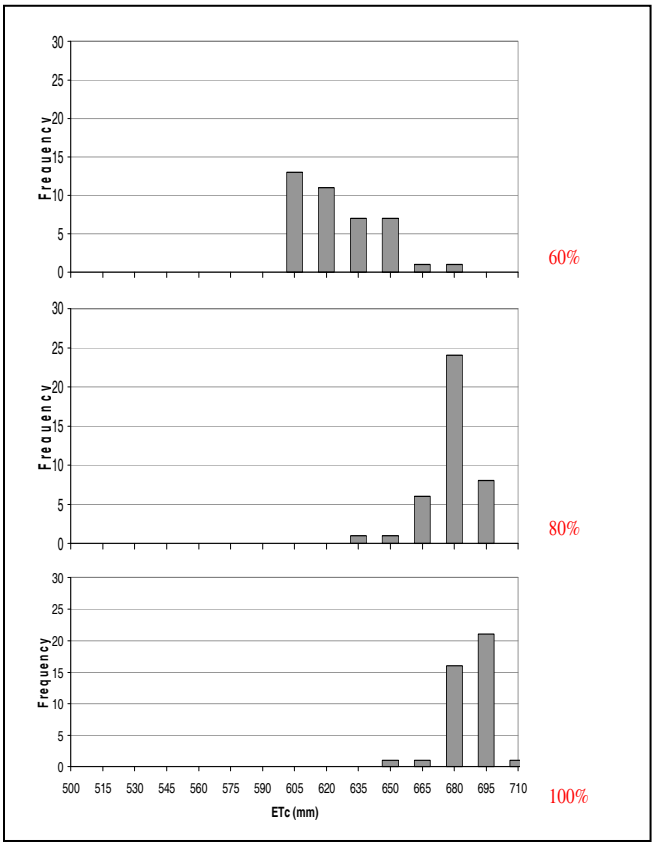

Figure 2. Histograms of Cumulative Crop ET at varying levels of Irrigation Intensity

Yield Modeling. Currently IEM uses the procedure described in FAO Irrigation and Drainage Paper No. 33 to estimate yield reduction from under irrigation. Also, a model described by (Solomon, 1985) is used to estimate yield reductions associated with over irrigation. Though FAO 33 is a widely used model, the authors experience and the experience of many others with the use of this model under ordinary field

conditions has been unsatisfactory. During the last few years, a team of climate, crop, soil, irrigation, and water scientists from various countries have been working under the auspices of FAO to develop a new crop-water production model to replace the FAO 33 model. The new FAO model, known as "AquaCrop, is a simple, accurate, robust, menu-driven and user-friendly program that is designed for a wide range of users. The model is being calibrated for a variety of crops based on experiments conducted in a number of countries (Raes et al., 2006). We intend to integrate the AquaCrop model into IEM once it has been calibrated for a sufficient number of crops.

Combining Soil Moisture Estimates. Figure 3 shows a histogram of measured 'field capacities' in a small area (one acre) of a silt loam soil that illustrates the innate variability of soil water holding characteristics (Isbell, 2005). This variability has two important implications. First, since net irrigation requirements are commonly based in part on field capacity, the variability indicated by Figure 3 implies that net irrigation requirements depend upon which part of a heterogeneous field is considered the 'control' sector for scheduling purposes. Secondly, since it is common practice to rely on soil moisture measurements to determine 'true' soil moisture, the variability shown in Figure 3 implies that such soil moisture measurements must be treated as highly uncertain. These two conclusions are known to experienced irrigation managers, and they illustrate the rationale for simulating spatial variability.

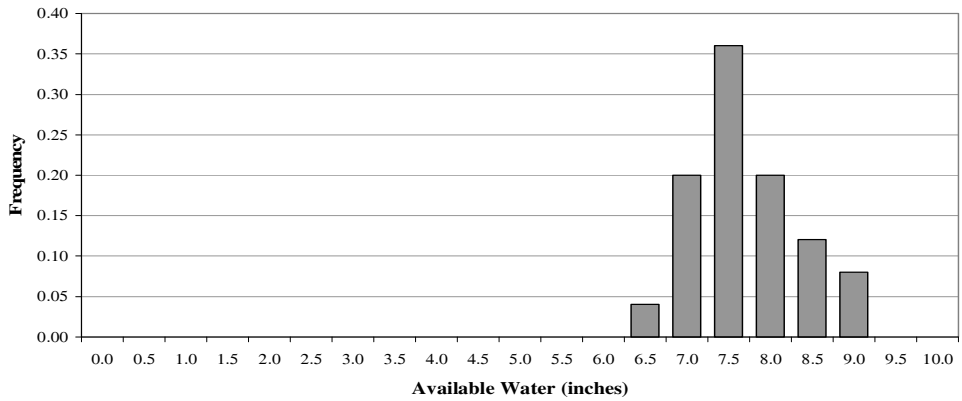

Figure 3. Measured 'field capacities' in a relatively homogeneous silt loam soil

Reference ET, even under the best conditions, is still an estimate and will have some associated error. It is clear that both estimated ET and measured soil moisture are subject to error, but at the same time both embody valuable information. Rather than arbitrarily dismissing one in favor of the other, a more rational approach is to estimate the uncertainty of each, and then derive a hybrid estimate that weights each source of data according to its estimated uncertainty. Bayes Rule provides a way of integrating the information about each estimator to derive an a-posteriori estimator of depletion that is both more precise (reduced variance) and more accurate. The analysis involves using the statistical distribution of one estimator (or source of information; e.g., cumulative ET) as a prior probability distribution for depletion, and then using the other estimator (e.g., as obtained from soil moisture measurements) to update that distribution, creating an a-posteriori distribution of the estimated depletion. Space

does not permit duplicating the complete details of this analysis, the reader is referred to (English et al, 2008) for more complete details of the procedure.

Irrigation Management Online

A web based irrigation advisory service known as Irrigation Management Online (IMO)[1] has been cooperatively developed by Oregon State University and the National Resource Conservation Service. IMO is currently undergoing its third year of field trails and has been successfully used in Oregon, Washington, and Idaho. The service has a demonstrated ability to provide conventional scientific irrigation scheduling advice. Development of IMO has proceeded in two phases. The first phase, now largely complete, involved development of a tool that enables farm managers to actively search for irrigation strategies that minimize water use and allow management of irrigation when water supplies are limited. The second phase, now underway, involves development of user interface tools that allow farm managers to actively search for optimal irrigation strategies and analyze their potential impact on yields and net economic returns. A complete description of all of IMO's features is not possible with the space restrictions here. Instead we will describe some of the features relevant to optimum irrigation scheduling and some of the features that make IMO different from other irrigation scheduling applications.

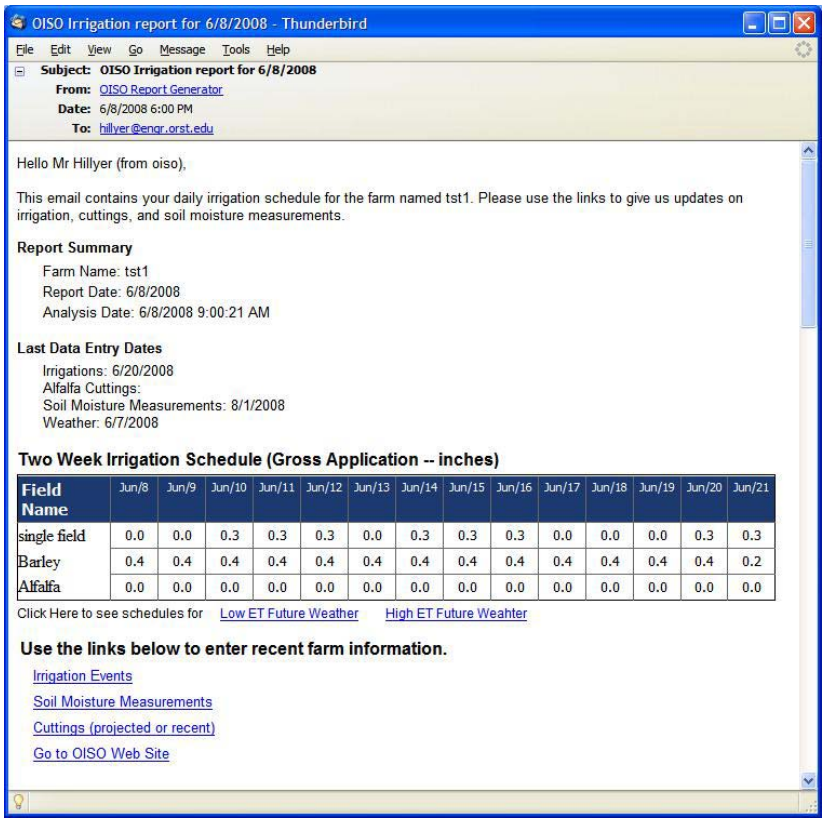

Figure 4. Sample Email

[1] IMO was formerly known as Oregon Irrigation Scheduling Online (OISO) and some of the figures in this document retain references to that name.

IMO was designed with the KISS principle in mind. Collecting information from the user is usually one of the more complicated and/or frustrating steps in using any application. To address this problem all setup information is collected through a series of wizards. These wizards provide explanations for each piece of information collected and, wherever possible, reduce the amount of information required for setup. The wizards both reduce the effort required to setup a farm and inform the user about the terminology and concepts used by IMO.

A second simplifying feature of IMO is automatic weather downloads. Part of the setup process involves choosing a site and source of weather data. Once this choice has been made IMO will automatically download updated weather information and use it to generate new irrigation schedules. The system is currently configured to use weather data from either the USBR AGRIMET weather network or IFPNet (Dalles, OR). We are actively working to extend the system to connect to the CIMIS network in California for a pilot program there.

Once a farm has been setup the user is kept informed via daily emails from the website. A sample of one such email is shown in Figure 4. These emails include inquiries about recent irrigation operations and links that bring the user back to the data input pages of the website. These emails serve as a recurring reminder to the farm manager to evaluate their water use and plan for short term supply limitations.

One feature that distinguishes IMO from other systems is forecasting of crop water demand that extends from the current date to the projected end of season. An example forecast for a single field is shown in Figure 5. This graph shows the projected soil moisture, soil moisture measurements (black squares), precipitation, past irrigations, and proposed future irrigations that are recommended by IEM.

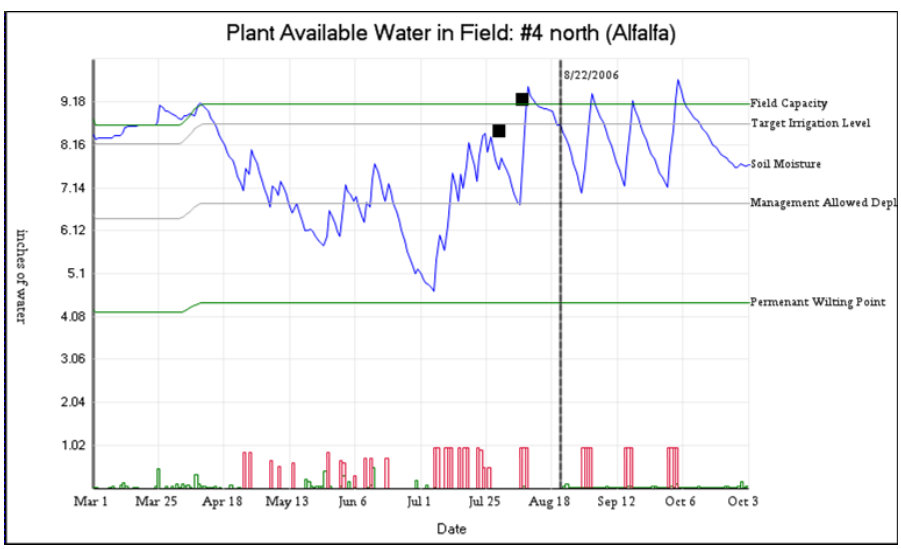

Figure 5. Sample Soil Moisture plot produced by IMO

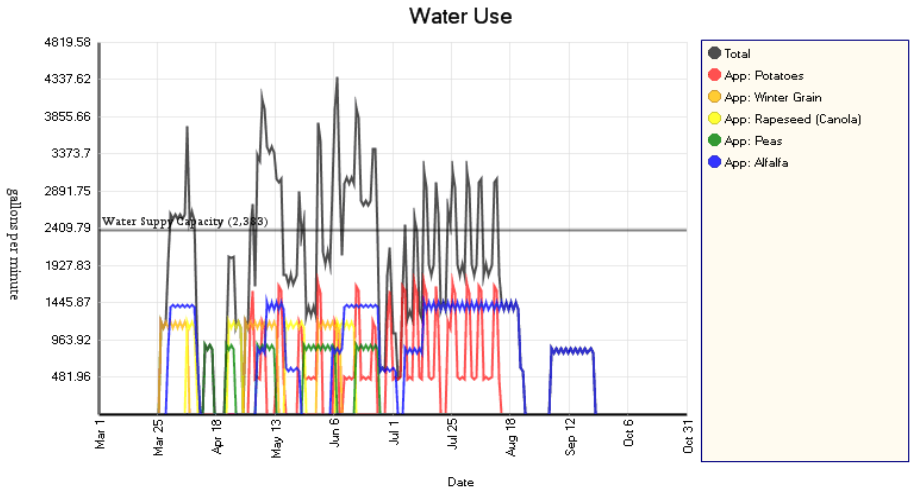

Figure 6. Full Season water use plot produced by IMO

Managing Long Term Constraints. An example seasonal water use plan from a cooperating farm is shown in Figure 6. The different coded lines show projected irrigation dates and delivery rates (gallons per minute) for irrigation of five crops on seven fields of various sizes with a variety of irrigation systems. The resulting aggregate farm water demand, summed for all fields, is also shown (upper line). Total farm water delivery capacity, about 2400 gpm, is shown as a horizontal line. As the graph indicates, the water demand would exceed supply for much of the season, particularly in May and June, so the initial water use plan shown here is not feasible. Several changes might then be proposed to deal with this water shortage; (i) a small field of alfalfa in its last year of production could be fallowed, (ii) a second field of alfalfa could be deficit irrigated, (iii) alfalfa cutting dates could be shifted slightly, and (iv) a field of winter wheat could be deficit irrigated.

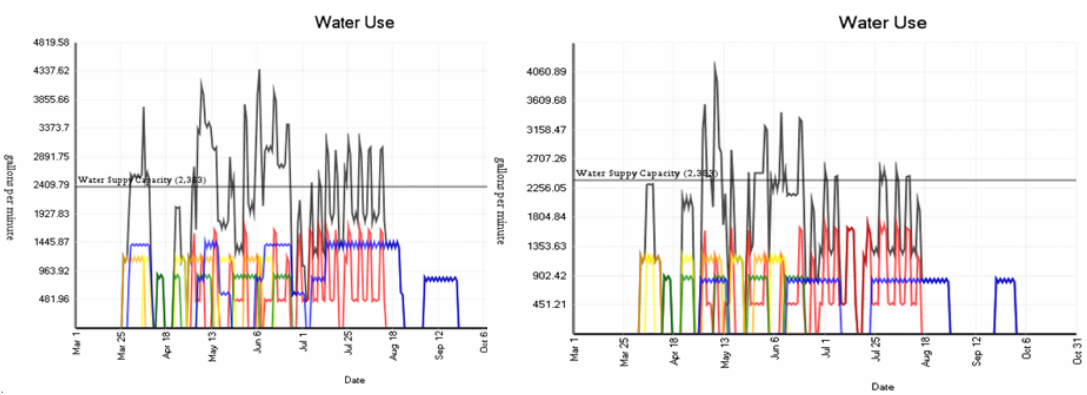

Figure 7. Original (left) and revised (right) water use plots

Figure 7 is a comparison of the initial water demand graph (left) with the resulting revised graph (right) produced after inputting the proposed changes into IMO. The proposed changes would substantially reduce overall demand, and shorten most periods of excess demand, making the water shortages more manageable. The irrigation schedule might then be adjusted on a day-by-day basis, shifting irrigations

from high demand days to days when capacity is under-utilized. These day-by-day adjustments are performed using an interactive two week schedule described in the next section.

Another long term management feature is the ability to use multiple weather profiles for estimating water use. When a farm is set up IMO uses the selected weather station to generate a historical weather data set that represents high, average, and low ET years. Then, whenever forecasts are produced, IMO uses IEM to generate three different forecasts corresponding to the high, average, and low ET weather profiles. This feature allows farm managers to see a range of water use scenarios and plan accordingly. Figure 8 shows three soil moisture graphs that show the irrigation forecast for a field of Alfalfa based on the historical weather downloaded from the AGRIMET station in Powel Butte, OR.

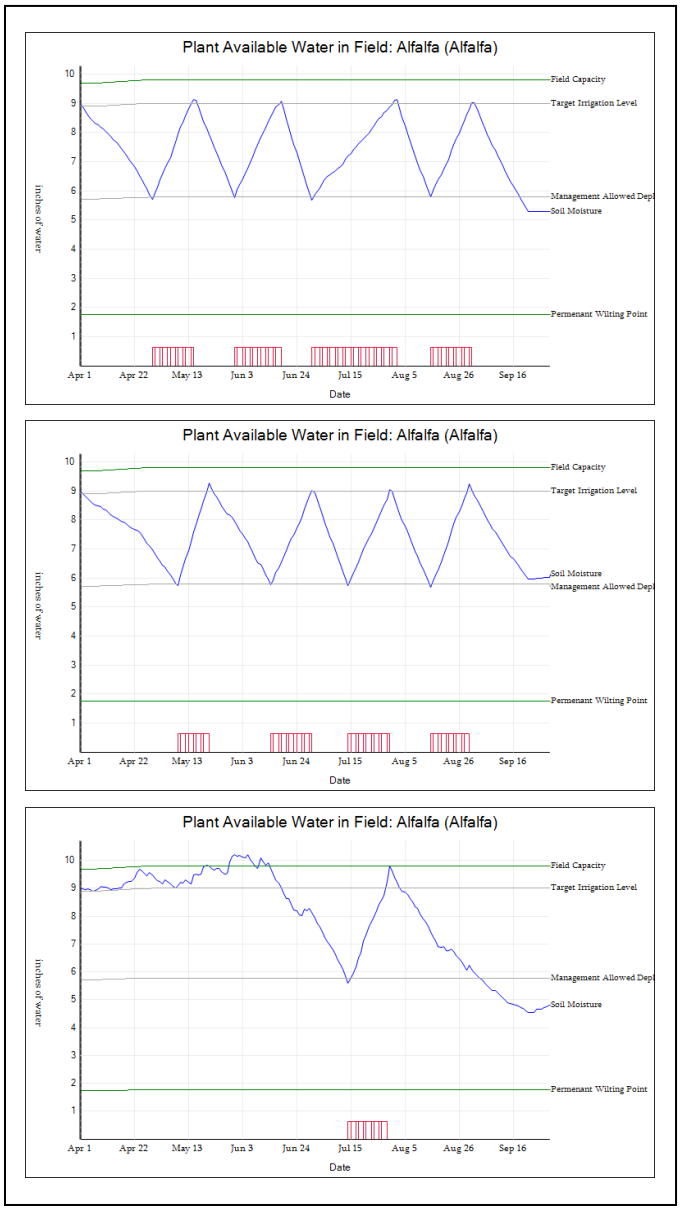

Figure 8. Forcast Irrigation schedules for high (top), average (middle), and low (bottom) ET estimates.

Managing Short Term Constraints. Figure 9 shows a sample two week irrigation schedule generated by IMO. The bottom row of the table indicates that the irrigation demand is exceeding the supply capacity of the water management unit[2]. The user can edit this schedule by moving some events around, deleting some of them, or adding new ones. All of this data entry is performed via drag-and-drop style interaction with the two week schedule. After sufficient manipulation the schedule will appear as shown in Figure 10. Note that now the bottom row indicates (via a change in color) that the supply constraints are not being

[2] Color is used on the website to emphasize the excess condition.

exceeded. After performing these manipulations IMO will re-evaluate the soil moisture calculations for each field and present the user with revised estimates of soil moisture conditions, water use, and predicted yields.

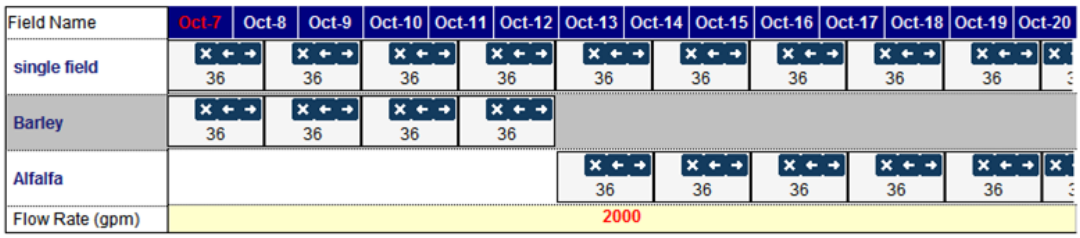

Figure 9. Editable Calendar Schedule screenshot

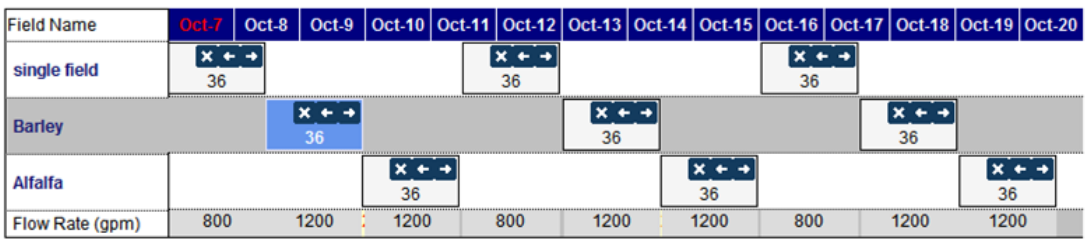

Figure 10. Editable Calendar Schedule screenshot (after editing)

Economic Analysis. We have recently added an economic analysis component to IMO. Each farm manager has different preferences regarding how they track costs relating to irrigation. The IMO website cannot possibly accommodate every person's preferences in this regard. The economics package is implemented as an Excel spreadsheet that downloads information from the IMO website. Excel allows the user the flexibility to setup and enumerate their costs in a way that is convenient to them and it eliminates the security concerns associated with storing sensitive financial information on a web server. Once the initial setup is complete (performed via VBA macros) a Web Service is used by the spreadsheet to download updated information on number of irrigations, total water use, and yield estimates projected to the end of the season. This update procedure can be performed by the user each time they want to re-evaluate their irrigation operations. The spreadsheet and Web Service are currently in a beta form and will be field tested during the coming year.

Conclusion

IEM is a robust numerical model that estimates efficiency of irrigation by modeling the disposition of applied water. This model uses well established algorithms and procedures for estimating consumptive use of water, stress related reduction in consumptive use, and for yield estimation. Furthermore, the model explicitly accounts for spatial variability of non-uniform irrigation and soil physical properties. The model is also able to combine ET based estimates and measurement based estimates of soil moisture to provide more accurate results.

IMO is a web-based advisory service for irrigation management. The website provides farm managers with a set of tools that enables them to actively search for optimum irrigation strategies. The system is being used in a pilot program for implementation of conventional irrigation scheduling and optimum irrigation strategies when water supplies are limited or expensive. Originally developed for use in Oregon, IMO is now being field tested inWashington, Idaho, and California.

References

Allen, R.G. Pereira, L.S. Raes, D. Smith, M.1998. Crop evapotranspiration: Guidelines for computing crop water requirements. Food and Agriculture Organization of the United Nations irrigation and drainage paper No. 56.

Doorenbos, J. and Kassam, A.H. 1979. Yield response to water, Food and Agriculture Organization of the United Nations irrigation and drainage paper No. 33.

English, M.J. and G.T. Orlob. 1978. Decision Theory and Irrigation Optimization, California Water Resources Center Contribution No. 174.

English, M.J. Taylor, A.R. and Abdelli, S.1992. A Sprinkler Efficiency Model. ICID Bulletin, 41(2):153-162.

English, M.J., Solomon, K. H., and Hoffman, G.J. 2002. "A paradigm shift in irrigation management." Invited paper, Jubilee Year Edition, J. Irrigation and Drainage Engineering, ASCE. Vol. 28, No 5.

English, M., Chadi Sayde, Alix Gitelman and Louraine Khoury, 2008. A Feedback System to Optimize Crop Water Use Estimates in Irrigation Scheduling. IN: World Environmental & Water Resources Congress 2008 , May 13-16, 2008, Honolulu, Hawaii

Hillyer, C.H. Bolte, J., van Evert, F. Lamaker, A. 2003. The ModCom modular simulation system. European Journal of Agronomy 18: 333 – 343.

Isbell, B. M. 2005. An Irrigation Efficiency Model for Optimum Irrigation Management. MS Thesis. Corvallis, Oregon. Oregon State University, Department of Bioengineering.

Raes, D. Steduto, P. Hsiao, T.C. Fereres, E. 2006. Structure, algorithms and functionalities of the crop-water productivity model AquaCrop. Available at: http://symp2006.cu.edu.tr/Osman%20Tekinel/pdf/Raes_AquaCrop_Turkey_2006.pdf. Accessed 15 February 2007.

Solomon, K.H. 1985. Typical crop water production functions. Presented at the 1985 winter meeting of the American Society of Agricultural Engineers. December 15-17, Chicago, IL, USA.

Estimating Crop Coefficients from Fraction of Ground Cover and Height

Richard G. Allen[1] and Luis S. Pereira[2]

[1] Professor of Water Resources Engineering, University of Idaho, 3793 N. 3600 E., Kimberly, Idaho 83341. 1 208 423 6601, rallen@kimberly.uidaho.edu
[2] Professor, Superior Institute of Agronomy, University of Lisbon, Portugal

ABSTRACT

The crop coefficient is the ratio of actual ET to reference ET and is heavily controlled by the amount of vegetation present to transpire water. This relationship can be used to estimate values for the crop coefficient as functions of the amount of ground covered by vegetation. A method established in the FAO-56 publication is expanded in this paper to estimate the crop coefficient from the fraction of ground cover and height of vegetation. In addition, when estimates of average background soil evaporation are made, then the 'mean' or single crop coefficient can be estimated. Estimates from the method are compared with measured crop coefficients reported for a number of vegetable crops during the crop development periods. Results are promising.

INTRODUCTION

The two-step crop coefficient (K_c) x reference evapotranspiration (ET_{ref}) method has been a successful and dependable means to estimate evapotranspiration (*ET*) and crop water requirements. The method utilizes weather data to estimate *ET* for a reference condition and multiplies that estimate by a crop coefficient that represents the relative rate of *ET* from a specific crop and condition to that of the reference. The reference condition is generally *ET* from a clipped, cool season, well-watered grass (ET_o) or from a taller full-cover alfalfa crop (ET_r). The calculation of *ET* from these surfaces has been standardized by FAO (Allen et al., 1998, 2006) and the American Society of Civil Engineers (ASCE-EWRI 2005).

The K_c ET_{ref} approach provides a simple, convenient and reproduceable way to estimate *ET* from a variety of crops and climatic conditions (Doorenbos and Pruitt, 1977, Wright 1982, Snyder et al., 1989a,b, Allen et al., 1998). Crop coefficient 'curves' have been developed and reported for a wide range of agricultural crops (Allen et al., 1998, 2007). The K_c is regarded as generally transferable among regions and climates under the assumption that the ET_{ref} accounts for nearly all variation

caused by weather and climate and the K_c represents the relative fraction of ET_{ref} that is governed by amount, type and condition of vegetation. These characteristics are more consistent for agricultural vegetation than, for example, natural vegetation, and thus the K_c values are more consistent and accuracy of the K_c ET_{ref} approach is usually highest for agricultural applications. Therefore, tabular values for K_c are often successfully used over a wide range of agricultural applications. The developed K_c curves or values represent the ratios of ET_c to ET_{ref} during various growth stages.

Conversely, the vegetation amount, height and density of many systems including natural vegetation, orchards, and residential and rural landscapes is highly variable, even during the middle part of the growing season, so that substantial uncertainties exist with tabularized values for these systems. Under these conditions, K_c values can be more accurately estimated by basing the estimates on the fraction of ground covered or shaded by vegetation, the height of the vegetation and the amount of stomatal regulation under moist soil conditions. The value for K_c for conditions of low soil water availability is generally determined by reducing the K_c estimate via a stress coefficient K_s using a daily soil water balance model.

This paper describes a relatively simple approach for estimating the K_c value based on a physical description of the vegetation. The method traces to the FAO-56 publication (Allen et al., 1998) with extensions made to account for background evaporation from soil and better seamlessness of the procedure. The procedure is intended for estimating both basal and average K_c for natural vegetation, orchards and landscape systems for different portions of the growing season based on amount of vegetation present and background evaporation from soil.

BACKGROUND

Basal Crop Coefficient. Basal crop coefficients, K_{cb}, represent primarily the transpiration component of *ET* and a small evaporation component from soil that is visibly dry at the surface. The use of K_{cb} over long periods requires adjustment for evaporation from wet soil during periods following rain or irrigation. The total crop coefficient, K_c is computed from K_{cb} as:

$$K_c = K_s K_{cb} + K_e \quad (1)$$

where K_s is a dimensionless 'stress' coefficient whose value is dependent on available soil water and K_e is a coefficient that adjusts for increased evaporation from wet soil following rain or irrigation. The procedure in eq. 1 has been referred to as the 'dual' K_c approach (Allen et al., 1998, 2005). The value for K_s is 1 unless available soil water limits transpiration, in which case it has a value less than 1. The values for K_e create "spikes" in the K_c curve as shown in fig. 1. Estimation of K_e for bare soil conditions is described in Wright (1982) and Allen et al., (1998, 2005).

Single Crop Coefficients. In basin-wide water balance studies or irrigation systems planning, use of 'single' crop coefficients that imbed averaged effects of evaporation from wet soil are more useful and convenient than computing a daily K_c based on K_{cb}, K_s and K_e. The single crop curve, K_{cm}, shown in fig. 1 lies above the basal curve by an amount that depends on the frequency of soil wetting. The K_{cm} is in essence a 'time-averaged' K_c as opposed to the 'dual K_c'. When a single crop coefficient is used, usually no additional adjustment is made for the effects of surface soil wetness. Adjustments are made for the effects of limited soil water as:

$$K_c = K_s K_{cm} \tag{2}$$

where K_s is calculated from Allen et al., (1998, 2005). Values for K_{cm} during partial crop cover depend not only on the amount and type of vegetation cover, but on frequency of precipitation and irrigation and whether irrigation wets all or part of the soil surface. K_{cm} curves can be generated from K_{cb} curves for known or simulated precipitation or irrigation frequencies following the dual K_{cb} approach and daily timestep.

Segmented Crop Coefficient Cuves. Figure 1 shows realistic K_c curves that have smooth, continuous transitions during the growing season. K_c curves have often been constructed, for simplicity in construction and estimation, using the FAO segmented approach shown in fig. 2 where the continuous seasonal curve is broken into four linear segments representing the initial, development, midseason and late season periods (Doorenbos and Pruitt, 1977, Allen et al., 1998, 2005). The appeal of the FAO style curve is that only three key values for K_c need to be determined: $K_{c\ ini}$ during the initial period, $K_{c\ mid}$ during the midseason period, and $K_{c\ end}$ at the end if the late season period. Values for $K_{c\ ini}$, $K_{c\ mid}$ and $K_{c\ end}$ are listed in FAO-56 (Allen et al. 1998) and Allen et al., (2007). The FAO style curve can be applied equally well to basal and single K_c applications in both dual and single mode. Examples of successful application of the FAO style K_{cb} curves in dual model include Hunsaker (1999), Tolk and Howell (2001), de Medeiros (2001), Hunsaker et al. (2002, 2003, 2005), Howell et al. (2004), Mutziger et al. (2005) and Allen et al. (2005a, 2007).

The procedures for constructing K_c curves presented in the following apply to both grass and alfalfa reference bases. Therefore, distinction is made between those K_c that apply to grass reference and those that apply to the alfalfa reference by denoting the former as K_{co} and the latter as K_{cr}. The two types of K_c's should not be interchanged, since those for the grass reference basis tend to be 20 to 30% larger than those for the alfalfa reference basis because ET_r tends to be 20 to 30% stronger than ET_r.

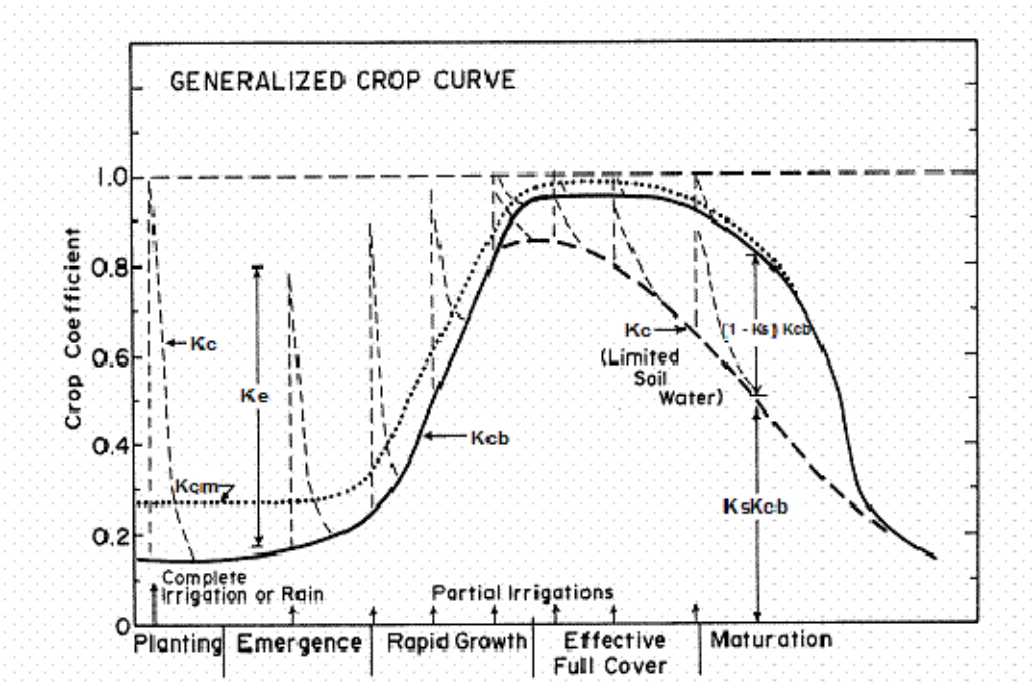

Fig. 1. Generalized crop coefficient curves over a growing season showing the effects of increasing K_c during midseason caused by plant development, wet soil surface and (long-dashed curve) limited available soil water (after Wright 1982; Jensen et al. 1990).

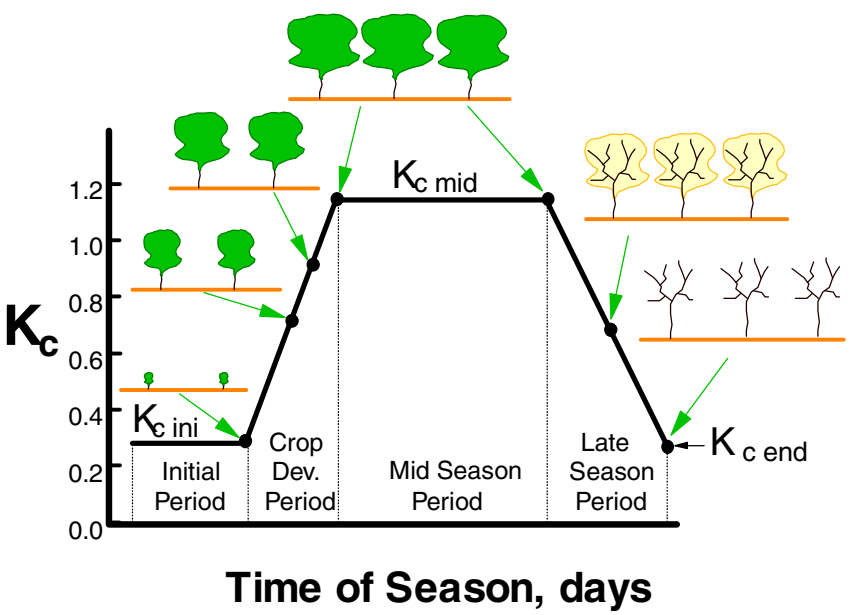

Fig. 2. FAO segmented crop coefficient curve and four growing stages (after Allen et al. 1998).

Adjusting K_{co} for Climate. The ratio of ET_c to grass ET_o for many crops increases as wind speed increases and as minimum daily relative humidity decreases (Doorenbos and Pruitt, 1977). This is due primarily to differences in roughness between taller agricultural crops and the clipped grass reference. The result is a higher K_{co} value caused by increased roughness and perhaps leaf area making the aerodynamic aspects of vapor transport more important and significant. The adjustment to K_{co} is generally required only for coefficients based on the grass ET_o reference. No adjustment for climate is necessary for coefficients based on the alfalfa ET_r reference because of the greater roughness of alfalfa that is more similar to most crops (Wright, 1982, Pereira et al. 1999). The FAO procedure for adjusting K_{co} values uses mean daily minimum relative humidity and wind speed. For climates with RH_{min} greater than or less than 45% or with mean wind speeds at 2 m over grass (u_2) that are more than or less than 2.0 m s^{-1}, the standardized values for all $K_{co\ mid}$ and $K_{cbo\ mid}$ from FAO-56 and for $K_{co\ end}$ and $K_{cbo\ end} > 0.4$ are adjusted as:

$$K_{co\ mid/end} = K_{co\ mid/end\ (table)} + \left[0.04\left(u_2 - 2\right) - 0.004\left(RH_{\min} - 45\right)\right]\left(\frac{h}{3}\right)^{0.3} \qquad (3)$$

where $K_{co\ mid/end(table)}$ is the value for $K_{co\ mid}$, $K_{cbo\ mid}$, $K_{co\ end}$ or $K_{cbo\ end}$ for the standardized climate and h is the mean maximum plant height, m, during the midseason period, or full cover period. Eq. 3 is valid for h to 20 m (Allen et al., 1998, 2005). The values for RH_{min} and u_2 need only be approximate values averaged over the midseason and late season periods.

ESTIMATING K_C CURVES FROM FRACTION OF GROUND COVER

Natural vegetation systems tend to have extensive variability in vegetation density, plant height, and water availability, both within a single expanse and between expanses of the same vegetation. Therefore, the distribution of K_c and thus ET populations can be broad, as shown in fig. 3, where a frequency distribution of ET for the month of June and calendar year for cottonwood and salt cedar populations along a 100 km stretch of the Middle Rio Grande valley is shown as derived from satellite-based energy balance (Allen et al. 2007b). ET from salt cedar showed larger variance due to its tendency to grow across a broad range of water availability (water table depth), soil types and salinity conditions, whereas cottonwoods, which exhibited a smaller variance in the population of ET, are typically found close to stream channels and consistent water supply. Wide variation was also noted for tree population density, which added to variance in the populations of ET.

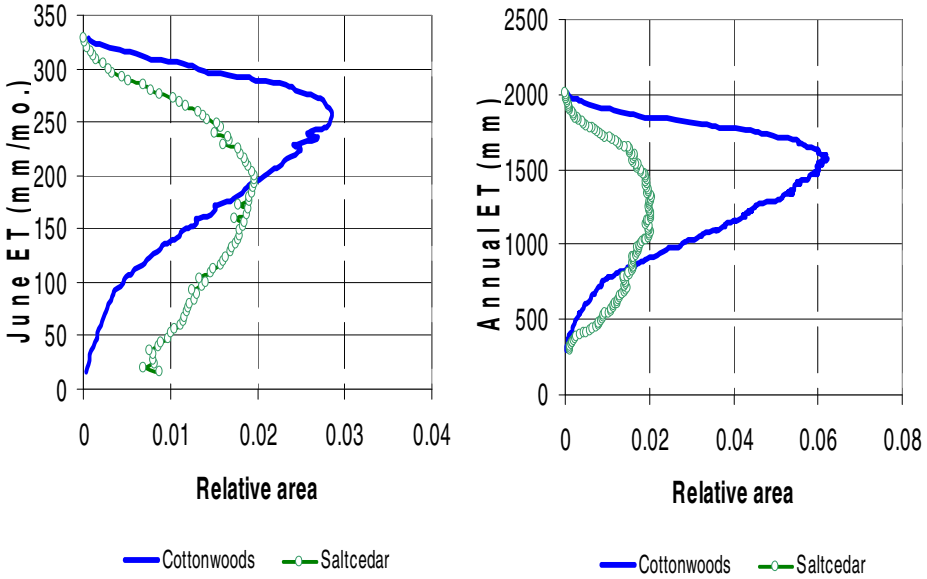

Fig. 3. Frequency distributions of ET from 6,000 ha of cottonwood and salt cedar along the Middle Rio Grande in New Mexico during June and all of 2002.

For expanses of vegetation large enough that an equilibrium boundary is established so that general one-dimensional equations such as the Penman-Monteith apply, a maximum upper limit on *ET* is established due to the law of conservation of energy. Therefore, for large expanses of vegetation (larger than about 500 to 2000 m^2) , the K_c development process has upper limits for K_{cr} of about 1.1 for the alfalfa reference and upper limits for K_{co} of about 1.3 for the grass reference. K_c's for smaller expanses (< 500 m^2) should also adhere to these limits when the vegetation height and leaf area is less than or equal to that of surrounding vegetation and soil water availability is similar. Only under conditions of "clothesline effects" (where vegetation height exceeds that of the surroundings) or "oasis effects" (where vegetation has higher soil water availability than the surroundings) will peak K_c's exceed the limits stated. The user should exercise caution when extrapolating ET measurements from small vegetation stands or plots to large stands or regions, as overestimation of ET may occur.

The upper, energy-constrained limit on K_c can be used to advantage in estimating K_c for vegetation for which the K_c is unknown, by using it to set the upper limit for vegetation having full or nearly full ground cover. The value for K_c reduces when plant density or leaf area fall below full ground cover which, in some cases has been defined as when leaf area index, *LAI,* < 3. Because the K_c tends to decrease in proportion to the amount of vegetation, the basal K_{cb}, which correlates with amount of vegetation because it represents mostly transpiration, can be expressed in terms of a density coefficient, K_d, where:

$$K_{cb} = K_{c\min} + K_d \left(K_{cb\,full} - K_{c\min}\right) \quad (4)$$

where K_{cb} is the approximation for K_{cb} for conditions represented by the density coefficient, K_d, $K_{cb\ full}$ is the estimated basal K_c during peak plant growth for conditions having nearly full ground cover (or $LAI > 3$), and $K_{c\ min}$ is the minimum basal K_c for bare soil ($K_{cb\,min} \sim 0.15$ under typical agricultural conditions and $K_{cb\,min} \sim 0.0$ to 0.15 for native vegetation, depending on rainfall frequency). The density coefficient K_d can be estimated as a function of measured or estimated leaf area index LAI or as a function of fraction of ground covered by vegetation. The density coefficient is defined in eq. 7.

For tree crops having grass or other ground cover, eq. 4 can take the form:

$$K_{cb} = K_{cb\,cover} + K_d \left(\max\left[K_{cb\,full} - K_{cb\,cover}, \frac{K_{cb\,full} - K_{cb\,cover}}{2} \right] \right) \quad (5)$$

where $K_{cb\ cover}$ is the K_{cb} of the ground cover in the absence of tree foliage. The second term of the *max* function reduces the estimate for $K_{cb\,mid}$ by half the difference between $K_{cb\ full}$ and $K_{cb\ cover}$ when this difference is negative. This accounts for impacts of shading by vegetation having K_{cb} that is lower than that of the surface cover due to differences in stomatal conductance. Eq. 4 and 5 can be applied to estimate K_{cb} during any period, including the midseason period. The value for K_{cb} from Eq. 4 and 5 should be applied as a basal coefficient using the dual $K_{cb} + K_e$ method, since the actual K_c may increase to 1.0 for ET_r or 1.2 for ET_o following precipitation even if the estimated K_{cb} is small, due to surface evaporation from among sparse vegetation. In addition, K_c should be reduced via K_s when soil water is low.

The approach of Eq. 4 and 5 can be similarly applied to estimate a single K_{cm} coefficieint for any period having less than full vegetative cover by accounting for the effect of evaporation from predominately exposed areas of soil among the vegetation, much the same as is done in the dual $K_{cb} + K_e$ approach:

$$K_{cm} = K_{soil} + K_d \left(\max\left[K_{c\,full} - K_{soil}, \frac{K_{c\,full} - K_{soil}}{2} \right] \right) \quad (6)$$

where K_{soil} represents the average K_c from the non-vegetated (exposed) portion of the surface and reflects the impact of wetting frequency, soil type and relative ET rate (i.e., ET_o) during the same period as K_d and $K_{c\ full}$. The K_{cm} represents an average K_c value that considers the mean impact of evaporation from soil, as does $K_{c\ full}$, representing K_c.from a fully covered soil with some background evaporation. K_{cm} can be used to represent the midseason or other period as defined by K_d, K_{cm} and $K_{c\ full}$.

For large stand size (greater than about 500 m^2), $K_{cb\ full}$ for use with ET_o can be approximated as a function of mean plant height and adjusted for climate following Allen et al. (1998):

$$(for\ ET_o)\ .....\ K_{\text{cb full}} = F_r \left(\min\left(1.0 + 0.1h,\ 1.20\right) + \left[0.04(u_2 - 2) - 0.004(\text{RH}_{\min} - 45)\right]\left(\frac{h}{3}\right)^{0.3} \right) \quad (7a)$$

For use with alfalfa reference ET_r, $K_{cb\ full}$ can be estimated as:

$$(for\ ET_r)\ .....\ K_{\text{cb full}} = F_r\ \left(\min\left(0.8 + 0.1h,\ 1.0\right)\right) \quad (7b)$$

where h is mean maximum plant height in m, u_2 is the mean value for wind speed at 2 m height during the mid-season in m s^{-1}, and RH_{min} is the mean value for minimum daily relative humidity during the mid-season in %. The climatic correction is not required for $K_{\text{cb full}}$ when used to derive the K_{cb} for ET_r because of the aerodynamic and canopy characteristics of the alfalfa reference crop. $K_{c\ full}$ can generally be estimated as equivalent to $K_{cb\ full}$ or equal to $K_{cb\ full}$ + 0.05 following Wright (1982) and Allen et al., (1998).

The value for $K_{c\ full}$ represents a general upper limit on $K_{cb\ mid}$ for tall vegetation having full ground cover and LAI > 3 under full water supply. Eq. 7a and 7b produce general approximations for the increase in $K_{cb\ full}$ with plant height and climate. The estimate from eq. 7 may need adjustment downward if the vegetation exhibits more stomatal control on transpiration than is typical for agricultural crops, for example, for types of trees or natural vegetation.

Density Coefficient. The density coefficient describes the increase in K_c with increase in amount of vegetation. The shape of the K_d curve is curvilinear with LAI or fraction of ground cover because of effects of microadvection of convective and radiative energy from exposed soil and height of vegetation. Where *LAI* can be measured or approximated, K_d can be approximated under normal conditions using an exponential function by Allen et al. (1998):

$$K_d = \left(1 - e^{[-0.7\,LAI]}\right) \quad (8)$$

where *LAI* is defined as the area of leaves per area of ground surface averaged over a large area with units of $m^2\ m^{-2}$. Only one side of 'green,' healthy leaves that are active in vapor transfer is counted. The relationship in eq. 8 is similar to one used by Ritchie (1974).

Where estimates of the fraction of ground surface covered by vegetation, f_c, are available, the K_d is estimated similar to Allen et al. (1998) as:

$$K_{\mathrm{d}} = min\left(1, M_L\, f_{c\,eff}, f_{c\,eff}^{\left(\frac{1}{1+h}\right)}\right) \tag{9}$$

where $f_{c\,eff}$ is the effective fraction of ground covered or shaded by vegetation [0.01 - 1] near solar noon, M_L is a multiplier on $f_{c\,eff}$ describing the effect of canopy density on shading and on maximum relative ET per fraction of ground shaded [1.5 – 2.0], and h is the mean height of the vegetation in m. Estimation of $f_{c\,eff}$ was described in Allen et al. (1998). For canopies such as trees or randomly (nonrow) planted vegetation, $f_{c\,eff}$ can be estimated as:

$$f_{c\,eff} = \frac{f_c}{\sin(\beta)} \qquad \leq 1 \tag{10}$$

where β is the mean angle of the sun above the horizon during the period of maximum ET (generally between 11.00 and 15.00) and f_c is the fraction of surface covered by vegetation as observed from directly overhead. f_c is often determined from visual inspection. However, digital image analysis or other measurement means can be employed. Generally, $f_{c\,eff}$ can be calculated at solar noon (12.00), so that β can be calculated as:

$$\beta = \arcsin\left[\sin(\varphi)\sin(\delta) + \cos(\varphi)\cos(\delta)\right] \tag{11}$$

where parameters φ and δ are latitude ($-\pi/2 \leq \varphi \leq \pi/2$) and solar declination in radians. Allen et al. (1998) provided equations for estimating β for row crops as a function of row orientation. A schematic showing f_c, $f_{c\,eff}$ and β is shown in fig. 4.



Fig. 4. Schematic showing extent of f_c, $f_{c\,eff}$ and β for tree vegetation where f_c is the fraction of surface covered by vegetation as measured from directly overhead.

The M_L multiplier on $f_{c\,eff}$ in eq. 9 imposes an upper limit on the relative magnitude of transpiration per unit of ground area as represented by $f_{c\,eff}$ (Allen et al. 1998) and is expected to range from 1.5 to 2.0, depending on the canopy density and thickness. Parameter M_L is an attempt to simulate the physical limits imposed on water flux through the plant root, stem and leaf systems. The value for M_L can be modified to fit the specific vegetation.

Fig. 5 shows values for K_d over a range of $f_{c\,eff}$ and a range of h for M_L = 1.5 and for M_L = 2 when h = 5 m, showing the effect of h and M_L on the estimate. Only K_d for h greater than about 1 m is impacted by varying the value for M_L from 1.5 to 2.0. The estimates by eq. 9 closely reproduce individual functions previously suggested by Fereres (1981) for orchards (using M_L = 2.0) and Hernandez and Suarez (1988) for vegetables. The function by Fereres (1981) is the same as one recommended by Snyder and Eching (2005).

Eq. 9 suggests that as h increases, total leaf area and resulting net radiation capture will increase, thereby increasing K_c. In addition, as h increases, more opportunity for microadvection and radiation of heat from soil to canopy occurs and turbulent exchange within the canopy increases for the same amount of ground coverage. Both of these increases increase the relative magnitude of K_{cb} or K_c. Values for K_{cb} or K_c can be scaled from estimates by Eq. 6 or 7 in proportion to the health and leaf condition of the vegetation at termination and the length of the late season period (i.e., whether leaves senesce slowly or are killed by frost). The f_c parameter and h are probably the simplest indices to estimate in the field.

When the mean stomatal control by the vegetation is greater than that characteristic of agricultural vegetation, Allen et al. (1998) suggested that the estimate by Eq. 6 or 7 be reduced by about 10 or 20 percent for each doubling of leaf resistance above 100 s m^{-1}. A more specific reducer for effects of stomatal control was introduced by Allen et al. (1998) where a stomatal resistance factor F_r was developed based on the FAO Penman-Monteith equation assuming full cover conditions:

$$F_r \approx \frac{\Delta + \gamma(1 + 0.34u_2)}{\Delta + \gamma\left(1 + 0.34u_2 \frac{r_l}{100}\right)} \qquad (12)$$

where r_l is mean leaf resistance for the vegetation in question [s m^{-1}], Δ is the slope of the saturation vapor pressure vs. air temperature curve, kPa C^{-1}, and γ is the psychrometric constant, kPa C^{-1}. Factor F_r is multiplied against the estimate for $K_{cb\,full}$ in Eq. 7 to reduce its value. The standard value for F_r is 1.0, which is applicable to most agricultural crops, where r_l is approximately 100 s m^{-1}. Values for r_l for many agricultural and non-agricultural plants can be found in Körner *et al*. (1978) and Allen *et al*. (1996).

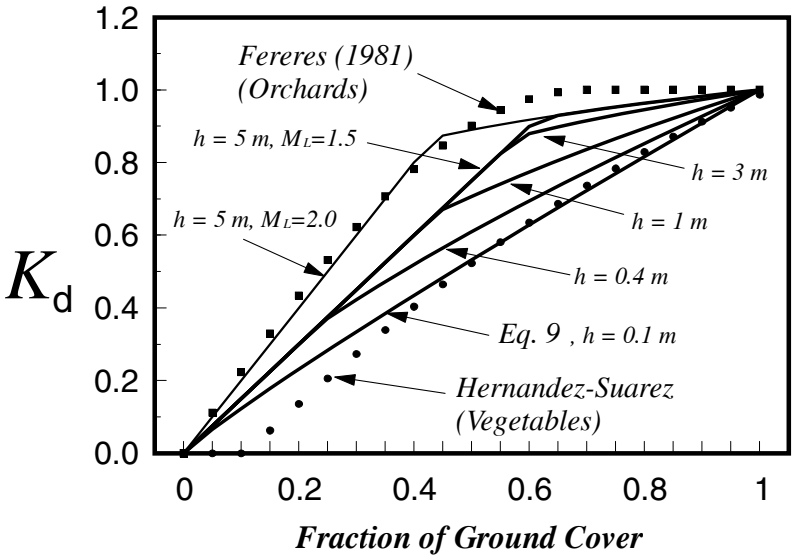

Fig. 5. Density coefficient, K_d, estimated from eq. 9 with M_L = 1.5 over a range of fraction of ground cover and various plant heights, and compared with estimates by Fereres (1981) for orchards and Hernandez-Suarez (1988) for vegetables.

COMPARISON OF K_C FROM EQ. 6 BASED ON K_D FROM EQ. 9 WITH DATA

The close agreement with Fereres (1981), Snyder and Eching (2005) and Hernandez and Suarez (1988) suggests that the general form of Eq. 9 is appropriate for a range of vegetation types and heights. The estimation of K_c from Eq. 6 using $K_{c\ full}$ from Eq. 7a and K_d from Eq. 9 was further compared with K_c data and regression equations reported by Grattan et al., (1998) and Hanson and May (2006). Grattan et al., (1998) reported the progression of K_c during plant development for seven vegetable crops in California as measured using Bowen ratio systems. They expressed K_c as a function of percent of ground cover, which is equivalent to f_c so that their data can be compared directly to that from Eq. 6 and 9. Hanson and May (2006) additionally reported a polynomial equation for K_c vs. f_c for tomatoes in California.

Eq. 6 for K_c was applied rather than Eq. 5 for K_{cb} since some background soil evaporation appeared to be present for some of the crops. $K_{c\ full}$ was estimated as equivalent to $K_{cb\ full}$. In addition, f_c was used in Eq. 9 rather than $f_{c\ eff}$ because specific dates of vegetation development were not reported. Because the sun angle during late spring is high, differences between f_c and $f_{c\ eff}$ will be small. The parameters used in Eq 6, 7a and 9 for the vegetable crops are summarized in Table 1 as are root mean square error (RMSE) for the Eq. 6/9 combination and for the original regression equations of Grattan et al. (1998). Comparisons of Eq. 6/9, the regression

equations by Grattan et al., and the Grattan et al. data are shown in Figure 6 for the seven crops. Vegetation height was varied over time in Eq. 9 in proportion to the maximum estimated height times the ratio of specific f_c to f_c at full cover reported by Grattan et al., (1998), with the exception of cantaloupe, which was assumed to have nearly constant height due to its vine nature. Maximum values for h were taken from tables in Allen et al., (1998). A standard climate was assumed due to lack of reported data by Grattan et al. (1998). Due to the relatively short height of the crops, the adjustment for climate in Eq. 7a would be small.

Table 1. Parameters used in Equations 6, 7 and 9 to simulate the crop coefficients measured by Grattan et al. (1998) and Hanson and May (2006).

Crop	**Arti-choke**	**Beans**	**Brocolli**	**Lettuce**	**Canta-loupe/ Honey -dew**	**Onion**	**Straw - berry**	**Tomato**
K_{soil}	0.15	0.50	0.15	0.15	0.15	0.40	0.05	0.15
M_L	2.0	2.0	2.0	2.0	2.0	2.0	2.0	2.0
Max h, m	0.6	0.4	0.3	0.3	0.3	0.4	0.2	1.2
h vs. t	in prop. to *fc*	in prop. to *fc*	in prop. to *fc*	in prop. to *fc*	Constant	in prop. to *fc*	in prop. to *fc*	in prop. to *fc*
u_2, ms^{-1}	2	2	2	2	2	2	2	2
RH_{min}, %	45	45	45	45	45	45	45	45
no. obs.	11	27	34	39	35	14	10	--
$RMSE_{Grattan}$	0.09	0.09	0.13	0.16	0.09	0.10	0.05	--
$RMSE_{Eq.\ 6/9}$	0.15	0.10	0.14	0.17	0.10	0.11	0.10	--

The agreement between K_c from Eq. 6, 7a and 9 and the data of Grattan et al. (1998) was nearly as good as the fitted regression equations reported by Grattan et al. (1998), with the exception of artichokes where the Grattan regression fit the data better with its stronger curve (Fig. 6a). The accuracy of K_c from Eq. 6, 7a and 9 appears to be within the measurement error of the reported K_c data. When K_{soil} = 0.15, Eq. 6 reverts to Eq. 4 that was developed for the basal K_c. The larger values required for K_{soil} in Eq. 6 for beans and onion suggest that the soil surface was relatively moist for these two crops, as evidenced by values for measured K_c at low f_c. The publication of Hanson and May (2006) did not report the measurement data so that only their regression equation was compared against the product of Eq. 6, 7a and 9. The two estimates compared closely, suggesting that Eq. 6, 7a and 9, using readily estimated physical parameters can be used to estimate K_c if visually assessed or other estimates of f_c are available.

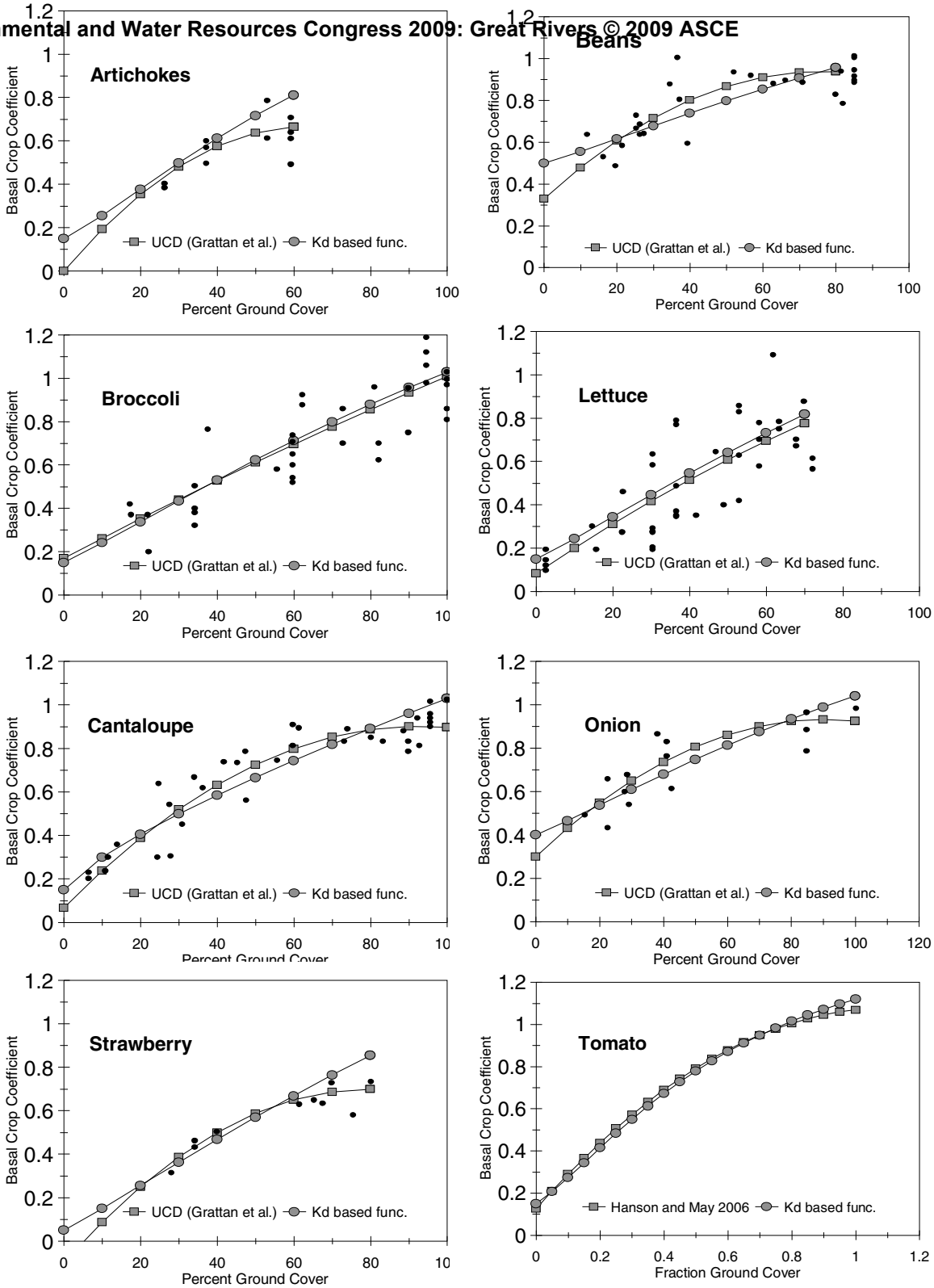

Fig. 6. K_c vs. f_c for seven vegetable crops in California reported by Grattan et al. (1998) (a-g) and tomatoes in California by Hanson and May (2006) (i), showing data and regression equations by Grattan et al. and Hanson and May (2006) with K_c estimated using Eq. 6, 7a and 9.

CONCLUSIONS

The crop coefficient is the ratio of actual ET to reference ET and is heavily controlled by the amount of vegetation present to transpire water. This relationship can be used to estimate values for the crop coefficient as functions of the amount of ground covered by vegetation. A method established in the FAO-56 publication is expanded in this paper to estimate the crop coefficient from the fraction of ground cover and height of vegetation. In addition, when estimates of average background soil evaporation are made, then the 'mean' or single crop coefficient can be estimated. Estimates from the method are compared with measured crop coefficients reported for a number of vegetable crops during the crop development periods. Results are promising.

REFERENCES

Allen, R.G., Pereira, L.S., Raes, D. and Smith M., (1998). "Crop Evapotranspiration: Guidelines for Computing Crop Water Requirements." *Irrig. and Drain. Paper No. 56*, United Nations Food and Agriculture Organization, Rome, Italy, 300 pp.

Allen, R.G., Pereira, L.S., Smith , M., Raes, D. and Wright, J.L. (2005a). FAO-56 dual crop coefficient method for estimating evaporation from soil and application extensions. *J. Irrig. and Drain. Engrg.,* ASCE 131(1):2-13.

Allen, R.G., Pruitt, W.O., Businger, J.A., Fritschen, L.J., Jensen, M.E., and Quinn, F.H. (1996). "Evaporation and Transpiration." Chap. 4, pp. 125-252 *In*: Wootton et al. (Task Com.), *ASCE Handbook of Hydrology, 2nd ed*" Am. Soc. Civ. Engrs., New York, NY., 784 pp.

Allen, R.G., Pruitt, W.O., Raes, D., Smith, M. and Pereira, L.S. (2005b). "Estimating evaporation from bare soil and the crop coefficient for the initial period using common soils information." *J. Irrig. and Drain. Engrg.,* ASCE 131(1):14-23.

Allen, R.G., Pruitt, W.O., Wright, J.L., Howell, T.A., Ventura, F., Snyder, R., Itenfisu, D., Steduto, P., Berengena, J., Yrisarry, J.B., Smith, M., Pereira, L.S., Raes, D., Perrier, A., Alves, I., Walter, I., Elliott, R. (2006c). "A recommendation on standardized surface resistance for hourly calculation of reference ET_o by FAO56 Penman-Monteith method." *Agric. Water Manage.*, 81:1-22.

Allen, R.G., Wright, J.L., Pruitt, W.O., Pereira, L.S. and Jensen, M.E. (2007). "Water requirements." pp. 208-288, *In*: Hoffman, G.J., Evans, Evans, R.G., and Jensen, M.E. (eds), *Design and Operation of Farm Irrigation Systems*, Am. Soc. Agr. and Biol. Eng., St Joseph, MI.

ASCE-EWRI. (2005). *The ASCE Standardized Reference Evapotranspiration Equation*. Allen, R.G., I.A. Walter, R.L. Elliott, T.A. Howell, D. Itenfisu, M.E. Jensen, and R.L. Snyder.(eds), Am. Soc. Civ. Engrs., 69 pp. +App. A-F and Index.

deMedeiros, G.A de, Arruda, F.B., Sakai, E. and Fujiwara, M. (2001). The influence of crop canopy on evapotranspiration and crop coefficient of beans (*phaseolus vulgaris* L.). *Ag. Water. Man*. 49:211-224.

Doorenbos, J., and Pruitt, W.O. (1977). "Guidelines for predicting crop water requirements." *FAO Irrig. and Drain. Paper No. 24, 2nd ed*, Food and Agriculture Organization, United Nations, Rome, Italy. 156 pp.

Fereres, E., TM Aldrich, H Schulbach, DA Martinich. 1981. Responses of Young Almond Trees to Late-Season Drought. California Agriculture 35:77, 11-12, 1981

Grattan et al. . 1998. New crop coefficients estimate water use of vegetables, row crops. California Agriculture, Jan-Feb p16-17.

Hanson, B. and D. May. 2006. Crop coefficients for drip-irrigated processing tomato. Agricultural Water Management. 81(3):381-399.

Hernandez-Suarez, M., 1988. Modeling irrigation scheduling and its components, and optimization of water delivery schedules with dynamic programming and stochastic ETa data. Ph.D. dissertation. University of California, Davis, CA.

Howell, T.A., Evett, S.R., Tolk, J.A. and Schneider, A.D. (2004). Evapotranspiration of Full-, Deficit-Irrigated, and Dryland Cotton on the Northern Texas High Plains. *J. Irrig. and Drain. Engrg.*, ASCE 130(4):277-285.

Hunsaker, D.J. (1999). Basal crop coefficients and water use for early maturity cotton. *Trans. ASAE* 42(4):927-936.

Hunsaker, D.J., Pinter, Jr., P.J. and Cai, H. (2002) Alfalfa basal crop coefficients for FAO–56 procedures in the desert regions of the southwestern U.S. *Trans ASAE*. 45(6):1799–1815.

Hunsaker, D.J. Pinter, P.J. Jr., Barnes, E.M. and Kimball, B.A. (2003). Estimating cotton evapotranspiration crop coefficients with a multispectral vegetation index. *Irrig Sci* 22:95–104.

Hunsaker, D.J., Barnes, E.M., Clarke, T.R., Fitzgerald, G.J., Pinter Jr, P.J. (2005). Cotton Irrigation Scheduling Using Remotely-Sensed and Fao-56 Basal Crop Coefficients. *Trans ASAE*. 48(4):1395-1407.

Jensen, M.E., Burman, R.D. and Allen, R.G. (1990). *Evapotranspiration and Irrigation Water Requirements*. ASCE Manuals and Reports on Engineering Practice No 70, 350 pp.

Körner, C., Scheel, J.A., and Bauer, H. (1979). "Maximum leaf conductance in vascular plants." *Photosynthetica*, 13(1):45-82.

Mutziger, A.J., Burt, C.M., Howes, D.J. and Allen, R.G. 2005. Comparison of measured and FAO-56 modeled evaporation from bare soil. *J. Irrig. and Drain. Engrg.*, 131(1):59-72.

Pereira, L.S., Perrier, A., Allen, R.G., and Alves, I. (1999). "Evapotranspiration: Concepts and Future Trends." *J. Irrig. and Drain. Engrg.*, 125(2):45-51.

Pereira, L.S., Smith, M., and Allen, R.G. (1999). "Crop water requirements." pp. 213-262, *In*: CIGR (*International Association of Agricultural Engineers) Handbook of agricultural engineering*. Vol. I, Sec. 1.5.1, Am. Soc. Agr. Engrs., St. Joseph, MI.

Ritchie, J. T. (1974). "Evaluating irrigation needs for southeastern U.S.A." pp. 262-273. *Proc., Irrig. and Drain. Spec. Conf.*, Am. Soc. Civ. Engrs.,

Snyder, R.L., Lanini, B.J., Shaw, D.A., and Pruitt, W.O. (1989a). "Using reference evapotranspiration (ETo) and crop coefficients to estimate crop evapotranspiration (ETc) for agronomic crops, grasses, and vegetable crops." Coop. Ext., Univ. of Calif., Berkeley, CA, Leaflet No. 21427, 12 p.

Snyder, R.L., Lanini, B.J., Shaw, D.A., and Pruitt, W.O. (1989b). "Using reference evapotranspiration (ETo) and crop coefficients to estimate crop evapotranspiration (ETc) for trees and vines." Coop. Ext., Univ. Calif., Berkeley, CA, Leaflet No. 21428, 8 p.

Snyder, R.L. and S. Eching. 2005. Urban Landscape Evapotranspiration. California State Water Plan, vol. 4, 691-693

Manure Application to Soybeans in the Chesapeake Bay Watershed

William F. Ritter[1]

[1]Professor of Bioresources and Civil and Environmental Engineering, Bioresources Engineering Department, University of Delaware, Newark, DE 19716. email: writter@udel.edu.

ABSTRACT

Corn and soybeans are major crops grown in the Chesapeake Bay watershed. The watershed has significant numbers of poultry, dairy and swine in certain areas. Land application of manure is a standard practice in the watershed. Over the years phosphorus concentrations have built up in manure applied soils because application rates have been based upon crop nitrogen requirements. In some cases research has shown manure application will increase soybean yields. One of the environmental concerns of applying manure to soybeans is the risk of increasing nitrate concentrations in the groundwater or tile drainage. Another concern is the buildup of phosphorus in the soil, which may cause phosphorus leaching on sandy soils or increase phosphorus loads in surface runoff.

INTRODUCTION

Today the livestock and poultry industry has become much more concentrated than in the 1960s. The broiler industry is concentrated in the southeastern and south-central states. Georgia, Arkansas, Alabama, Mississippi and North Carolina account for more than 60% of all broiler production in the U.S (Paudel and McIntosh, 2005). Several counties on the Delmarva Peninsula account for 18% of the product. Iowa, North Carolina and Minnesota account for 54% of the hog production in the U.S. (USDA, 2008).

As livestock and poultry operations have become larger and more concentrated, manure management has become more intensive and challenging. In many cases producers cannot use all the manure produced on their own farms and transportation costs for manure are a concern. Ideally corn and cotton are ideal crops for the application of swine and poultry manure. In many areas where swine and poultry are produced, corn and soybeans are the major crops grown. With excess manure produced in some areas, this has led to the application of manure applied to soybeans. Soybeans are a legume crop which fix nitrogen, so the nitrogen in the manure may not be efficiently used. Also if manure is applied to soybeans based upon nitrogen needs of the crop, phosphorus application rates will exceed crop uptake needs. This paper will discuss the potential environmental effects and summarize research on the utilization of manure on soybean production as it relates to water quality.

IOWA BAN ON LEGUINE MANURE APPLICATION

In 2003 a number of environmental organizations in Iowa proposed banning the application of liquid swine manure to soybeans. For several years the Iowa Environmental Protection Commission (EPC) considered banning the practice of applying liquid manure to soybeans. After several years of public comment and a number of hearings the EPC voted in April 2008 by a 5-2 vote to establish the rate of liquid manure application on land to be planted to soybeans in a manure or nutrient management plan at 112 kg/ha of available nitrogen. The rule took effect May 14, 2008. The 112 kg/ha does not apply on or after June 1 of each year, but the rate of 0.063 kg of N per kg of soybean yield applies. Many farmers in Iowa apply liquid manure or nitrogen fertilizer in the fall or early spring in Iowa.

IMPACT ON YEILD

The average soybean yield in Iowa in 2006 was 3089 kg/ha and is estimated to have a nitrogen removal of 194 kg N/ha (Helmers et al., 2008). Varel et al (1992) found soybeans can remove up to 200 kg N/ha. The amount of nitrogen that can be fixed by soybeans over a growing season has been reported to range from 70 to 120 kg N/ha (Tisdale and Nelson, 1975). Soybeans may be unable to fix the total quantity of nitrogen needed for yields obtained under optimal growing conditions today. These comparisons should be made with care, however, because soybean yields today are higher than in 1975.

There have been a number of studies reported in the literature where manure applications have increased soybean yields. Rakshit (2002) applied liquid swine manure to multiple plots at nitrogen target rates of 112 and 224 kg N/ha. Soybean yields increased at all sites receiving manure but only three of the five sites had a statistically significant yield increase. Schmitt et al. (2001) applied swine manure at sever field locations in Minnesota to multiple soybean cultivars at zero, low and high rates of nitrogen. Low rates ranged from 43 to 230 kg N/ha and high rates ranged from 72 to 460 kg N/ha. Soybean yields increased at three of the seven field locations with increasing manure nitrogen application rates. Yields increased on sites having low available soil nitrogen during mid-June.

Adeli et al. (2005) applied broiler litter and commercial fertilizer to soybeans on a Leeper silty clay loam soil in Mississippi. Treatments were broiler litter application at the rates of 0, 40, 80 and 160 kg N/ha of plant available nitrogen and commercial fertilizer applications at broiler litter equivalent nitrogen rates. Soybean grain yield and nitrogen uptake rate increased with increasing broiler litter and fertilizer application rates. Soybean grain yields and nitrogen uptake rates were significantly greater from broiler litter application than from commercial fertilizer applications. Soybean yields for broiler litter application ranged from 2770 kg/ha for the 40 kg N/ha application rate to 3180 kg/ha for the higher broiler application rate.

RESIDUAL SOIL NITRATE AND GROUNDWATER QUALITY

Rakshit (2002) found when the swine manure application rate was less than 200 kg N/ha, post harvest nitrate profiles at all the sites revealed only one instance where concentrations were above the non-manure soil nitrate levels. Schmidt et al. (2000) in a study evaluating the impact of swine manure application nodulating and non-nodulating soybeans found post harvest soil nitrate concentrations followed a quadratic relationship. The results indicate increases of 4, 17 and 35% increases in post-harvest soil nitrate levels from 0 to 120 cm with application rates of 56, 112 and 168 kg N/ha, respectively when compared to 0 kg N/ha.

Kanwar et al. (2006) reported on a six year study at the Iowa State University Northeast Iowa Research Farm in Floyd County where liquid swine manure was applied to plots in a corn-soybean rotation. Swine manure was applied at the rate of 168 kg N/ha before soybeans. The manure was applied in the fall. Tile drainage samples were analyzed for nitrates. The fall applied manure resulted in the highest average nitrate concentration in tile water compared to other fertilizer and manure treatments. The average six-year nitrate concentration for the corn-soybean rotation was 39.8 mg N/l and for the soybean-corn rotation 36.6 mg N/L. Average yearly concentrations ranged from 20.7 to 70.4 mg N/L. Spring application of manure in no-till corn only resulted in the lowest average nitrate concentration of 16.2 mg N/L.

In a four year study in Pocahontas County, Iowa, liquid swine manure was applied at a rate of 168 kg N/ha before both corn and soybeans and compared to a rate of 224 kg N/ha applied every other year before corn. The total of 336 kg N/ha application rate every two years versus the 224 kg N/ha application rate every two years resulted in average nitrate concentrations increasing in the tile drainage on an average from 17 to 23 mg N/L, a 35% increase that was statistically significant (Helmers et al., 2008).

Adeli et al. (2005) found no significant differences in residual soil nitrate concentrations following two years of soybean production where broiler litter and fertilizer were applied at 0, 40 and 80 kg/ha of available nitrogen. At an application rate of 160 kg N/ha of available nitrogen, residual nitrate concentrations increased in the top 30 cm of the soil profile. At the high application rate soil residual nitrate concentrations were significantly greater with commercial fertilizer than broiler litter. Nitrates did not leach below the 90 cm depth.

Vasilas (1997) conducted a two-year study to evaluate the effect of timing of broiler litter application to soybeans. The study was conducted at the University of Delaware Research and Education Center in Sussex County on Ingleside sandy loam soil. Broiler litter was applied in November, January, March and two weeks prior to planting in May. Broiler litter was applied at a rate of 9 Mg/ha. The experimental design was a randomized complete block with three replications. Two groundwater sampling wells 3.6 m deep were installed in each plot. Monthly groundwater samples were taken from June 1994 to May 1996.

When groundwater sampling started, nitrate concentrations were below 10 mg N/l Nitrate levels in the November and January applications increased to above 10 mg N/l in November 1994. The May and March applications caused nitrate levels to increase to above 10 mg N/l in January 1995 and April 1995, respectively. For each sampling date the November and January applications generally had the highest groundwater nitrate concentrations. In February 1996, the nitrate concentration for the November application was almost 30 mg N/l. Post harvest soil nitrate concentrations in 1995 were 60 mg/kg at the 60 to 90 cm depth and 101 mg/kg at the 90 to 120 cm depth for the November application.

Vasilas (1997) concluded from the study that timing of the broiler litter application was unlikely to affect soybean yields and that the recovery of broiler litter nitrogen by soybeans is low. This means the potential for groundwater contamination is high. In order to maximize the recovery of broiler litter nitrogen by soybeans, application of the broiler litter should be close to the planting date and double cropping winter wheat or planting a cover crop after harvesting the soybean to recover the soil residual nitrogen.

DELAWARE STUDY

Methods And Materials: Broiler litter was applied to four large plots 0.25 ha in size in 194 and 1995 at the University of Delaware Research and Education Center in Sussex County. Manokin soybeans were planted in 75 cm rows at a rate of approximately 350,000 seeds/ha in late May each year. One plot was used as a control where no broiler litter was applied. The other three plots received 2.24, 4.48 and 9.6 Mg/ha of broiler litter each year. The nutrient content of the broiler litter varied somewhat from year to year. In 1994, nitrogen application rates for the three treatments with broiler litter were 73, 146 and 292 kg N/ha. In 1995, nitrogen application rates were 115, 230 and 460 kg N/ha. Phosphorus application rates were 66, 132 and 264 kg P_2O_5 /ha in 1994 and 12, 24 and 48 kg P_2O_5/ ha in 1995. No commercial fertilizer was applied to the control plot. The plots were located on a Klej loamy sand soil. From 1989 to 1991 the plots were used for a winter cover crop non-irrigated corn study. For that experiment three monitoring wells were installed in each plot at a depth of 4.5 m. All monitoring wells were constructed from 3.25 cm PVC pipe with the bottom 0.75 m screened with 2.5 mm slot size PVC screen. The monitoring wells were installed by the auger drilling method. The annulus around all wells was sealed with bentonite. Two background monitoring wells were also installed.

In 1992 and 1993 soybeans were planted on the four plots but no experiments were conducted. In 1996 soybeans were also planted, but no broiler litter or fertilizer was applied.

Groundwater samples were collected every two or three months from November 1993 to October 1996 and analyzed for nitrates by the Bioresources Engineering Water Quality Laboratory. All monitoring wells were sampled with a battery operated

peristaltic pump. The wells were pumped dry and allowed to recharge before a sample was taken. Water table depth measurements were taken each time groundwater samples were taken. Nitrates were analyzed by the ion chromatograph method.

Groundwater Quality: Average nitrate concentrations for the different treatments are presented in Table 1. Nitrate concentrations where 9.6 Mg/ha of broiler litter was applied for two years increased somewhat. There was no trend in nitrate concentrations for the other broiler litter treatments or the control. Average nitrate concentrations for the control ranged from 7.25 to 11.1 mg N/l. Nitrate concentrations for 2.24 and 4.48 Mg/ha broiler litter application rates decreased in 1995 and 1996 when compared to concentrations in 1993 and 1994 before the broiler was applied. In February, 1994 the average nitrate concentration for the 4.48 Mg/ha treatment was 11.1 mg N/l. In September of 1994 the nitrate concentration decreased to 7.20 mg N/l for the remainder of the sampling period. For the 9.6 Mg/ha treatment nitrate concentrations reached a high of 15.9 mg N/l in November of 1995. Nitrate concentrations in the two background wells were below 10 mg N/l.

Table 1. Average Groundwater Nitrate Concentrations (mg N/l) for Broiler Litter Application

	Broiler Litter Rate (Mg/ha)			
Sampling Date	2.24	4.48	9.6	Control
11-12-93	6.42	12.2	9.42	8.27
2-28-94	7.13	11.1	10.7	9.69
4-26-94	9.50	10.2	9.05	10.3
5-31-94	7.64	10.6	9.55	10.1
7-1-94	8.26	10.2	10.8	9.23
9-11-94	9.32	7.88	9.80	9.30
11-4-94	9.51	8.07	11.8	8.37
1-31-95	9.68	8.20	12.9	9.46
3-16-95	7.60	6.82	13.7	10.4
5-23-95	4.81	4.91	12.1	10.0
7-25-95	5.65	5.51	10.5	10.1
9-29-95	7.39	5.86	12.9	9.61
11-20-95	5.73	6.65	15.9	10.4
1-3-96	7.31	7.12	15.0	11.1
3-26-96	4.84	4.67	13.5	10.0
5-31-96	4.42	4.94	12.7	10.0
7-25-96	3.74	7.09	10.7	7.53
10-2-96	3.49	4.69	10.8	7.25

Rainfall varied considerably during the growing season from 1994 to 1995. In 1994 a total of 553 mm of rainfall occurred during the growing season while in 1995 the

rainfall was 276 m. In 1994 soybean yields for the different treatments ranged from 1781 to 2059 kg/ha and in 1995 they ranged from 510 to 886 kg/ha. Both years the control had the lowest yield.

In 1994, the total rainfall was 758 mm after the manure was applied. The high rainfall probably caused the nitrates on the high rate broiler litter applications to leach to the groundwater as indicated by the higher groundwater nitrate concentrations in January, 1995. For the lower application rate treatments, probably most of the mineralized nitrogen was taken up by the soybean plants since yields were normal for dry land soybeans grown on sandy soils in Delaware. Although during the growing season rainfall was low in 1995, 277 mm of rainfall occurred in October and November. It is surprising nitrate concentrations did not increase in the groundwater for all three broiler litter treatments in January 1996 because of the low soybean yields in 1995.

PHOSPHORUS

A 5925 kg/ha soybean crop will remove 35kg/ha of phosphorus (P_2O_5) 170 kg/ha of nitrogen and 62 kg/ha of potassium (K_2O). Soybeans will use the phosphorus in the manure, but if either broiler litter, liquid swine manure or dairy manure is applied to soybeans at a rate of 112 kg/ha of nitrogen, phosphorus will build up in the soil. If liquid swine manure from a grower-finishing operation was applied at a rate of kg N/ha, the phosphorus application rate may be 77 kg/ha (P_2O_5). With broiler litter, a 112 kg N/ha nitrogen application rate could result in a phosphorus application rate of 70 kg/ha (P_2O_5). For semi-solid earthen basin dairy manure, a 112 kg N/ha nitrogen application rate may result in a 54 kg/ha phosphorus (P_2O_5) application rate (MWPS, 2000). Adding phytase to the broiler or swine ration may decrease the phosphorus in the manure by up to 25 to 30% (Sutton and Humenik, 2003) Long term buildup of phosphorus in the soil would be of a concern with surface runoff and also on sandy soils phosphorus leaching may occur. Maryland, Pennsylvania, Delaware and Virginia all have nutrient management regulations based upon phosphorus. If the soil tests high or very high in phosphorus no more phosphorus can be applied than what is removed by the crop based upon a three year average.

CONCLUSION

There are some benefits to applying manure to soybeans and some negative aspects. On the positive side, manure can supply nitrogen phosphorus, potassium and other nutrients for the crop and reduce commercial fertilizer cots. In some cases manure application may increase soybean yields. With a corn-soybean rotation incorporating manure into cornstalks instead of soybean stubble will reduce the erosion potential because of the greater residue cover with corn stalks.

Manure application to soybeans will increase the risk of nitrate losses to groundwater or tile drainage. Applying manure in a corn-soybean rotation to both crops to meet

nitrogen needs or even applying manure at a rate of 112 kg/ha to soybeans will result in a buildup of phosphorus in the soil.

If manure is applied to soybeans it should be applied as close to planting as possible. Manure should not be applied in the fall of the year to soybeans. A winter cover crop such a rye or winter wheat should be used to remove the residual nitrogen since nitrate leaching will occur during the winter months and early spring.

REFERENCES

Adeli, A., Sistani, K.R., Rowe, D.E. and Tewolde, H. (2005). "Effects of broiler litter on soybean production and soil nitrogen and phosphorus concentrations." *Agronomy Journal*, 97: 314-321.

Helmers, J.J., Moody, L.B. and Burns, R. (2008). "Utilization of manure nutrients for crop production." National Pork Board, Des Moines, IA., *Technical Report*.

Kanwar, R. Pederson, C., Helmer, M. Sawyer, J. and Mallarino, A. (2006). "Impact of swine manure application on water quality." Northeast Research and Demonstration Farm. ISRF 06-13, Iowa State University, Ames, IA.

Midwest Plan Service. (2000)."Manure characteristics." MWPS 18, *Manure Management System Series,* Iowa State University, Ames, IA.

Paudel, J. and McIntosh, C.S. (2005) "Country report: broiler industry and broiler litter-related problems in the southeastern United States." Waste Management, 25 (60) 1083-1088.

Rakshit, S. (2002). "Liquid swine manure as a nitrogen source for corn and soybean production." *MS Thesis*, Iowa State University, Ames, IA.

Schmidt, J.P., Schmitt, M.A., Randall, G.W., Lamb, J.A., Orf, J.H. and Gollany,J.T. (2000). " Swine manure application to nodulating and nonnodulating soybeans." *Agronomy Journal*, 92, 987-992.

Schmitt, M.A., Schmidt, J. P., Randall, G.W., Lamb, J.A. Orf, J.H. and Gollany, J.T. (2001). "Effect of manure on accumulation of dry matter, nitrogen and phosphorus by soybeans." *Communications in Soil Science and Plant Analysis,* 32(11-12), 1931-1941.

Sutton, A. and Humenik, F, (2003). "Technology options to comply with land application rules." CAFO Fact Sheet #24, Environmental and Land Stewardship Curriculum, Midwest Plan Service, Iowa State University, Ames, IA.

Tisdale, S.L. and Nelson, W. L. (1975). "*Soil fertility and fertilizers*." 3rd edition, MacMillian, New York, NY.

U.S. Department of Agriculture. (2008). "*Kentucky agricultural statistics and annual report*." National Agricultural Statistics Service, Field Office, Louisville, NY.

Varel, G.E. and Peterson, T.A. (1992). "Nitrogen recovery by soybeans in monoculture and rotation systems." *Agronomy Journal*, 84, 215-218.

Vasilas, L.M. (1997). "Agronomic and environmental implications of broiler litter amendments to soybeans." *MS Thesis*, University of Delaware, Newark, DE.

ON-LINE IRRIGATION SCHEDULING WITHIN THE BELLE FOURCHE IRRIGATION DISTRICT

Jared K. Oswald[1] and Hal D. Werner[2]

[1] Staff Engineer, RESPEC Water & Natural Resources, P.O. Box 725, Rapid City, SD 57709; PH 605.394.6400; FAX 605.394.6456; email: *Jared.Oswald@respec.com*

[2] Professor Emeritus, South Dakota State University, P.O. Box 2120, Brookings, SD 57007; PH 605.688.5673; FAX 605.688.6764; email: *Hal.Werner@sdstate.com*

ABSTRACT

On-line irrigation scheduling consultant software is being developed for producers within the Belle Fourche Irrigation District (BFID). This project, which is funded for 3 years by a Conservation Innovation Grant (CIG) through the Natural Resources Conservation Service (NRCS), is entering its second irrigation season.

The BFID is a gravity-fed, canal-based system located in western South Dakota. Recurring droughts often limit the amount of water available for irrigation in the BFID. The purpose of this project is to provide producers with a reliable, easy-to-use means to monitor and schedule irrigations that will conserve water and reduce the amount of sediment-laden irrigation return flows that are discharged into the adjacent Belle Fourche River, historically listed as impaired for total suspended solids (TSS) by the South Dakota Department of Environment and Natural Resources (SD DENR).

The on-line irrigation scheduling consultant software allows producers with internet access to create a secure, personalized Web page that provides irrigation scheduling advice for a particular field. The software collects daily weather data and uses it to estimate rainfall and calculate crop evapotranspiration (ET) utilizing the American Society of Civil Engineers (ASCE) Penman method and locally adapted crop coefficients. Irrigation delivery amounts entered online by the producer are added to the rainfall estimates for that location. The irrigation scheduling software then calculates a soil water balance and irrigation schedule for soil types in the field. Soil moisture sensors installed at two depths are recorded to provide on-line tracking of relative soil water changes throughout the irrigation season. The producer has the option to adjust the calculated soil water balances or measured rainfall amounts based on his observations at the field.

The results of the first year of irrigation scheduling were used to evaluate the on-line software and methods. User feedback is also being collected to fine tune the on-line user interface. The second season of irrigation will expand the user base and be used to further evaluate the software.

KEYWORDS: Irrigation, Evapotranspiration, Soil Moisture, Computer Software, NRCS

INTRODUCTION

The Belle Fourche Project is located immediately north of the Black Hills in western South Dakota (Figure 1). The Belle Fourche Irrigation District (BFID) serves over 480 individual producers who irrigate 57,183 acres. Typical irrigated farms in the BFID are small to medium in size (100–300 acres) and are family owned. Alfalfa and hay production accounts for about 65 percent of crop production, with small grains and corn accounting for most of the remainder of crops produced. Irrigation methods are almost entirely surface irrigation.

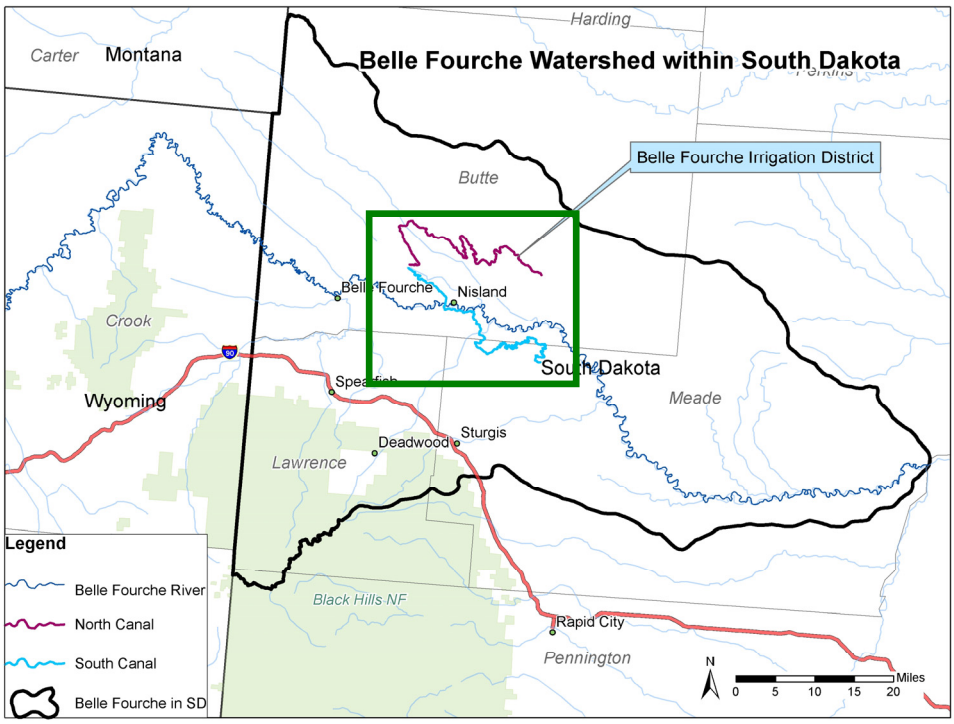

Figure 1. Location of the Belle Fourche Irrigation District within the Belle Fourche River Watershed.

The Belle Fourche River has been historically listed as impaired for total suspended solids (TSS) by the South Dakota Department of Environment and Natural Resources (SD DENR). The project began when the BFID participated in the Belle Fourche River TSS Total Maximum Daily Load (TMDL) study. The study determined that a significant portion of the TSS entering the river could be eliminated by reducing the amount of unused irrigation waters flowing into the river and its tributaries (Figure 1). Horse Creek, also impaired because of excessive TSS, receives much of the irrigation return flows originating in the BFID. The TMDL recommended that reductions in return flow be accomplished through canal automation, updating their water order and billing system, and implementing on-farm improvements such as scientific irrigation scheduling and converting surface irrigated fields to sprinkler irrigation.

Recurring droughts often limit the amount of water available for irrigation in the BFID. Research has documented how scientific irrigation water management (IWM) can improve water conservation and productivity. In the Steele et al. [2000] study, savings of 30 percent of the seasonal irrigation depths were achieved using IWM versus grower practices. Scientific IWM considers factors such as soil water-holding capacity, crop water use, and allowable depletions necessary to apply the optimum amount of water needed for crop production.

When water is limited, IWM allows the best use of irrigation water by applying water during the most critical crop growth periods. Studies on corn in North Dakota, Kansas, and Nebraska have shown deficit irrigation can save water with minimal yield reduction. Melvin and Payero [2003] stated, however, that "the deficit irrigation strategy is the most challenging to manage." Heeren et al. [2008] modeled 30 irrigation strategies with a simulated center pivot at Nisland, South Dakota (located within the BFID). They found that it is critical to use specific scheduling strategies to achieve the greatest water and production efficiency. Thus it is critical to use scientific irrigation scheduling to achieve the greatest productivity with the available water.

Shearer and Vomocil [1981] found that adoption of scientific irrigation scheduling was well accepted by growers but the practice was not sustained once technical support was reduced. Leib et al. [2002] determined that the number of irrigators using scientific irrigation scheduling, even with the availability of consultants for technical support, may have been as low as 18 percent as of 1998. Technical service providers in many parts of the country provide IWM assistance but serve a relatively small number of growers. Dr. Hal Werner, consultant available to the project, conducted extension educational efforts on IWM for over 30 years. His experience indicates that use of scientific irrigation scheduling will be limited unless user-friendly methods are available to the producer.

Presently, irrigation scheduling for most farmers relies largely on past practice. Even though it is generally accepted that scientific scheduling can increase water efficiency, scientific input is minimal because of constraints of training, experience, time, and other resources. This is in spite of the fact that tools are now widely available for scientific irrigation scheduling, including evapotranspiration (ET) information and stand-alone scheduling software. Many locations publish ET and crop water use information on the Web; however, an interactive Web-based irrigation scheduler that requires minimal input and effort from the producer is not available at this time for producers in the BFID.

Consultants to the project developed the software logic and framework that would be implemented by this project. The software includes the ASCE Penman and locally adapted crop coefficients. The software model considers on-site ET, rainfall, irrigation amount, soil water capacity, soil water balances, and forecasted ET to plan irrigation amounts and timing.

METHODS

The goal of this 3-year project is to implement a Web-based, interactive irrigation scheduling calculator that is customized to each producer's crop, planting date, soil type, rainfall and irrigation amounts, and method of irrigation. The calculator will allow any producer with internet access to create a personalized Web page with irrigation information for a particular field. To accomplish this, an extensive real-time weather network was implemented that ties into an existing radio network the BFID uses to monitor structure settings and flow throughout the BFID. The weather network includes four full-weather stations that provide the necessary inputs to calculate daily evapotranspiration (ET) using the American Society of Civil Engineers (ASCE) Penman method and also nine rainfall monitoring sites (Figure 2).

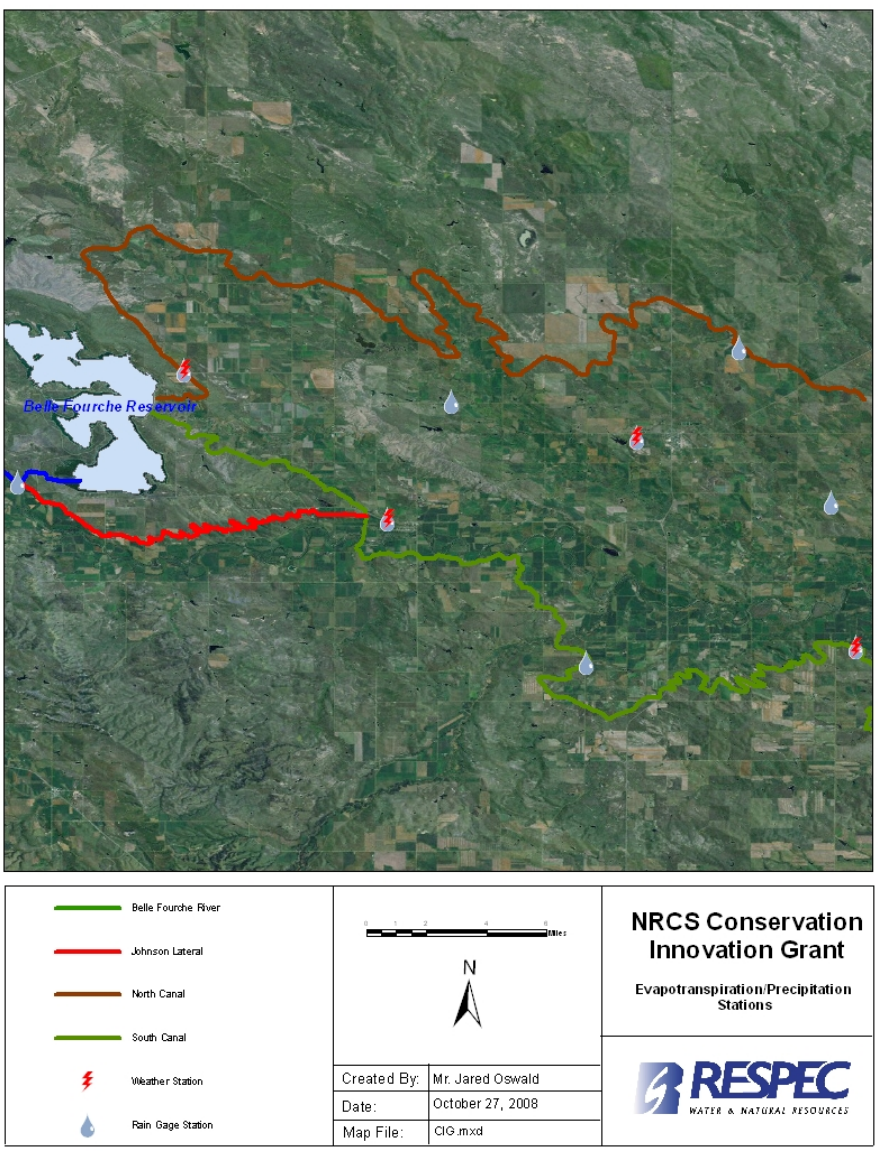

Figure 2. Location of the weather stations and rain gages throughout the Belle Fourche Irrigation District.

Producers are able to establish site-specific irrigation scheduling for each crop and irrigated field on their farm using the on-line scheduling application. Currently, scheduling routines have been developed for alfalfa (both new crop and established), corn, barley, and wheat.

At the beginning of the growing season, the producer must log on to their personalized Web page and then, using a custom Web mapping application, draw a polygon around the field that they plan to use with the on-line scheduler. Once the producer selects the location of their field and inputs the current crop and planting date, the database system retrieves the water-holding capacity of the soil and calculates the total area to be irrigated. It also assigns the appropriate rain gage and weather station along with BFID lateral that supplies water to the field. From that day forward throughout the irrigation season, the on-line irrigation consultant software will calculate and track crop water use and soil water balances for each soil type in the field.

The on-line irrigation consultant software provides projections of future crop water use that allows the producer to plan irrigations and water deliveries. This is accomplished by averaging the crop water use from the previous 3 days and projecting that amount on the next 4 days. This prediction is essential because there can be up to a 3-day lag from when the producer orders water from the BFID to when it actually arrives at the field.

The producer is required to enter the amount and timing of irrigation deliveries. Ten-minute readings from soil moisture instruments installed at ¼ and ¾ of the crop rooting depth are collected weekly and are provided online as a means to track relative soil water changes throughout the irrigation season. The on-line scheduling application provides the producer with the ability to input actual rainfall amounts when those are measured on site. They can also adjust the calculated soil water balance based on soil moisture measurements or field inspection.

ANALYSIS

Development and testing of the irrigation scheduling consultant software during the first year of this project precluded use by producers during the first irrigation season. Instead, the irrigation scheduling routine was developed using Microsoft Excel. The tracking of the calculated field soil water balance along with the soil water tension, measured with Watermark® blocks, was provided via email on a weekly basis.

During the first irrigation season, the producers based their irrigation decisions more on the information being provided to them from the soil moisture sensors rather than the soil water balance being calculated using weather, rainfall, and the irrigation model. This was partially because the information was provided on two separate graphs using two different scales—tension in centibars for the measured balance and soil water balance in inches for the calculated balance. Producers also stated that they

were more comfortable with something that was concrete and visible rather than the equations in the model. Because of the expense of not only buying the soil moisture data loggers and sensors but also the expense of collecting the data, the success of the on-line irrigation scheduling consultant application as an economical, systemwide application depends on the producers trusting the calculated balance while using the measured balance from soil moisture sensors as occasional ground truth.

After the irrigation season was completed, project staff attempted to devise a method of in-season indexing these two datasets. This was done to identify any discrepancies between the calculated and measured soil water balance and also for a visual aid that would allow the producers to correlate the two forms of information. It was hypothesized that the calculated values should lie somewhere in between those measured at the two rooting depths since the calculated value is essentially an average of the entire soil profile.

An initial analysis was completed on a relatively small 23-acre field with established alfalfa (Figure 3). The field contains a soil with a water-holding capacity of 2.12 inches per foot, which is assumed to be homogeneous throughout its 4-foot rooting depth. The soil moisture sensors are located in the northeast corner of the field. Irrigation is delivered via gated pipe from the west end of the field and travels from southwest to northeast.



Figure 3. Aerial imagery of a 23-acre field used for initial analysis.

The 2008 irrigation season was wetter than normal, with 14.89 inches of rainfall occurring between April 15 and September 1 in a region that normally receives approximately 13 inches of annual precipitation. The producer irrigated the field twice during the growing season, July 12–15 and August 25–28. For the purpose of the calculated water balance, the irrigation volume was distributed uniformly across the entire field while assuming a 50 percent application loss.

To index the two datasets, the measured values of soil moisture tension and the calculated values of soil water deficit were divided by their full scale range, or range of available water from 0 to 100 centibars, to determine the percentage of soil water deficit (Figure 4). The full scale value was assumed to be 75 percent of field capacity (6.4 inches) for the calculated water deficit in this soil type, based on literature. The percentage of soil water deficit measured and calculated tracked similarly until irrigation was delivered from July 12–15. At this point, the soil moisture sensors recorded zero centibars of tension (soil was saturated) and the calculated deficit dropped to approximately 20 percent and then immediately began to rise again. This caused the calculated percent deficit after this point to be much greater than the measured percent deficit. Assuming the Watermark® sensors were correct in measuring saturated soil, a reindexing algorithm was applied that reset the calculated percent deficit to 0 percent when the average reading of the two soil moisture sensors was below 10 centibars of tension (Figure 5). With this correction, the calculated value stayed within the range of the 1-foot and 2-foot sensors for nearly the entire irrigation season. The anomaly that coincides with the final irrigation is because an implement tire track was created inadvertently upstream of the soil moisture station, causing water to be diverted around the sensors. The 3-foot sensor responded to the irrigation amount, but at a later date than was predicted.

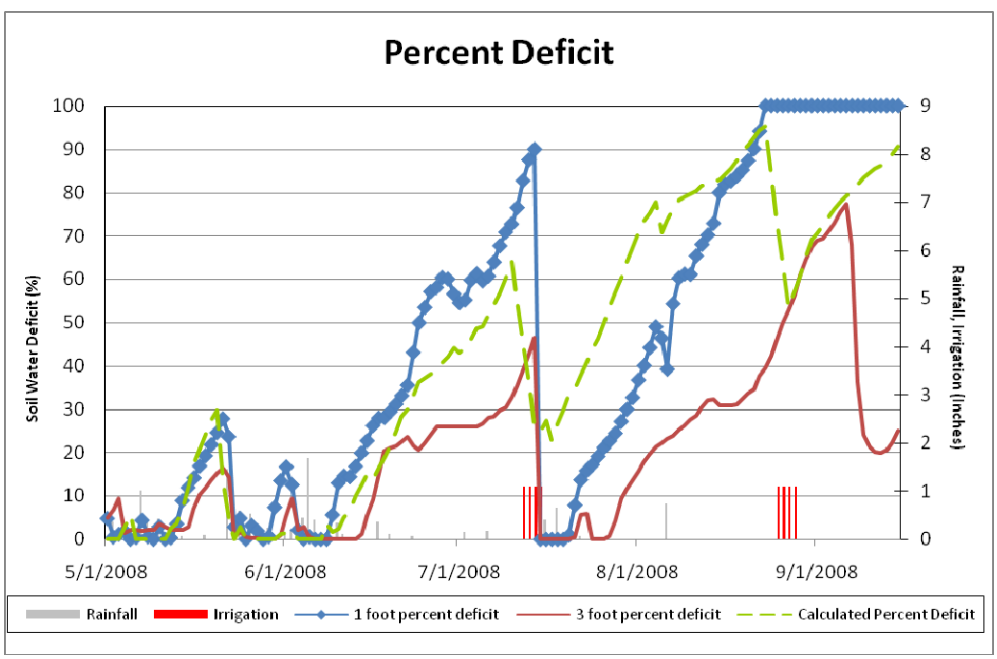

Figure 4. Measured and calculated values of soil water deficit.

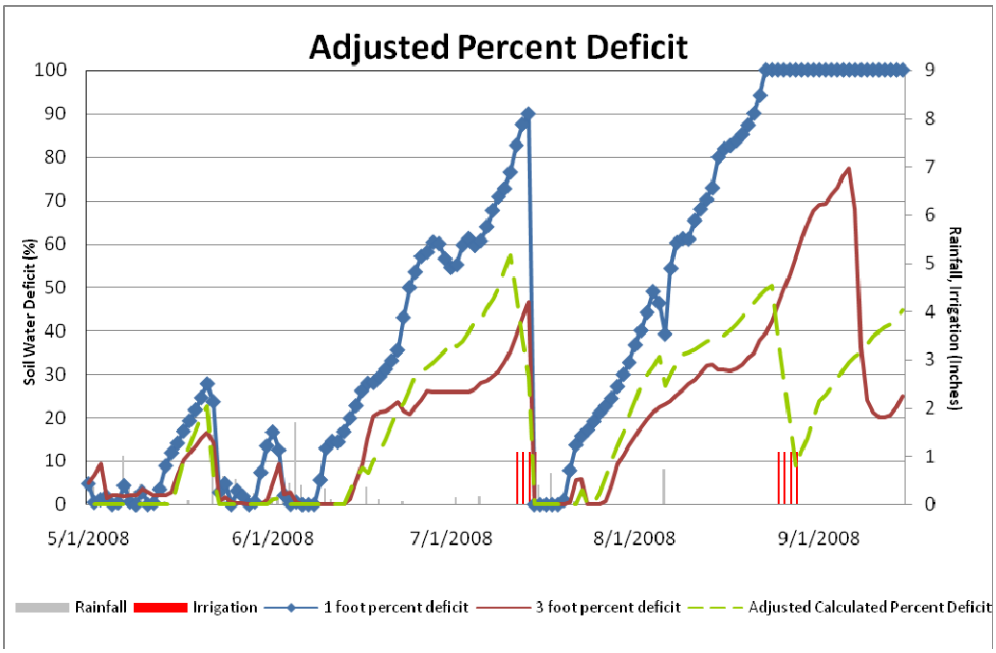

Figure 5. Percentage of measured and calculated soil water deficit with calculated being adjusted to 0 percent when the average of the two sensor readings is below 10 centibars of tension.

The effectiveness of using this indexing method is directly correlated to the reliability of the soil moisture information. There were several soil moisture stations that reported erroneous information that could not be used to compare to the water balance that is being calculated, as in the values reported in Figure 6.

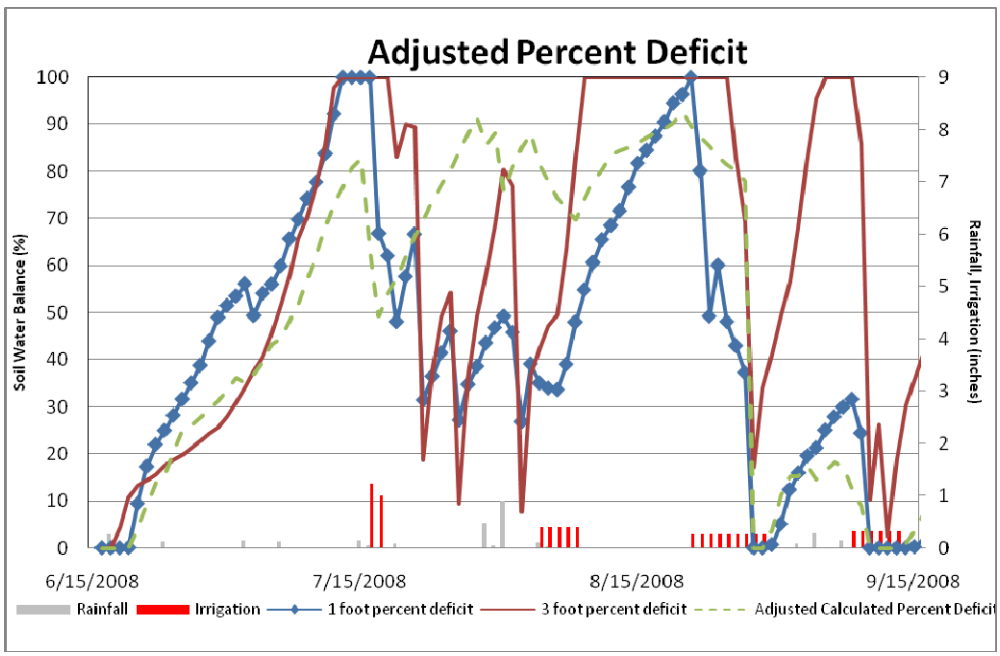

Figure 6. Adjusted percent deficit for a soil moisture station with erroneous readings.

SUMMARY

The goal of this 3-year project, funded by a Conservation Innovation Grant (CIG) through the Natural Resources Conservation Service (NRCS), is to develop a reliable, Web-based irrigation scheduling tool that is easy for producers in the Belle Fourche Irrigation District to set up, understand, and maintain. The Web-based application was being developed and tested during the first irrigation season, so cooperating producers were provided with calculated soil water balances that were developed using the model logic from the Web-based application input into a Microsoft Excel spreadsheet. Producers were also provided with readings from Watermark® soil moisture sensors placed at ¼ and ¾ of the crop's effective rooting depth.

After the irrigation season was completed, project staff devised a method of comparing the measured and calculated soil moisture balances that would identify any discrepancies between the two datasets and also provide a visual aid that would allow the producers to correlate the two forms of information. The two sets of data were normalized by dividing the calculated values of soil water deficit in inches and measured values of soil moisture tension in centibars by their full range (range of plant available water from field capacity to 100 centibars) and were represented as a percentage of the soil water deficit. The calculated soil water deficit was then set to zero when the soil moisture sensors had an average tension of less than 10 centibars.

In the first year, producers had a tendency to rely more heavily on the measured soil moisture information than what was being calculated using weather data collected from a network of weather stations and rain gages. This was justified in the fact that the calculated balance before indexing was often much higher than what would be expected, especially following irrigation applications. Because of the expense to the producer of not only buying the soil moisture data loggers and sensors but also the expense of collecting the data, the success of the on-line irrigation scheduling consultant application as an economical, broad-reaching application depends on the producer trusting the calculated balance and using the measured balance as an occasional ground truth.

The goal for the next 2 years of the project will be to deploy the Web-based application and continues to monitor if the indexing method developed after the first year continues to apply. Gravimetric tests will be run on all soil types so the inches of available water from 0 to 100 centibars is represented more precisely rather than relying solely on literature values.

REFERENCES

Heeren, D. M., Werner, H., and Trooien, T. (2008). "Evaluation of deficit irrigation strategies for corn," *Proceedings of the Irrigation Association International Irrigation Conference*, June 18–20, Falls Church, VA.

Lieb, B. G., Hattendor, M., Elliot, T., and Matthews, G. (2002). "Adoption and adaptation of scientific irrigation scheduling: trends from Washington, USA as of 1998," *Agricultural Water Management*, 55:105–120.

Melvin, S., and Payero, J. (2003). "Future equipment and research needs gleaned from farmer reactions to an irrigation water conservation education program in southwest Nebraska," *Proceedings of the Irrigation Association International Irrigation Conference*, June 18–20, Falls Church, VA.

Shearer, M. D., and Vomocil, J. (1981). "Twenty-five years of modern irrigation scheduling support efforts," *Proceedings of the ASAE Irrigation Scheduling Conference*, ASAE, St. Joseph, MI. pp. 208–212.

Steele, D. D., Stegman E. C., and Knighton, R. E. (2000). "Irrigation management for corn in the northern great plains," *Irrigation Science*, 19:107–114.

Agricultural Drainage Management Systems Task Force (ADMSTF)

A Partnership Group that Promotes and Implements Drainage Management Systems on Cropland in the Mississippi River Basin to Improve Water Quality of Drainage Flows.

James L. Fouss[1] and Michael Sullivan[2]

ABSTRACT

The Agricultural Drainage Management Systems (ADMS) Task Force was initiated during a charter meeting in the fall of 2002 by dedicated professional employees of Federal, State, and Local Government Agencies and Universities. The Agricultural Drainage Management (ADM) Coalition was established in 2003 by drainage industry officials, trade associations and non-government organizations. These two groups formed a working partnership to promote and implement drainage water management systems that can significantly improve the quality of drainage water flows from agricultural cropland. Earlier research had shown that a large percentage of the nitrate-nitrogen that migrates down the Ohio and Mississippi Rivers comes from surface and subsurface drainage discharge from agricultural cropland in the Midwest region. An initial primary goal of the partnership groups was to reduce the loss and transport of fertilizer nutrients, particularly nitrate-nitrogen, from drained agricultural croplands in the Midwestern States on a farm-by-farm basis. They installed and conducted field demonstrations for farmers to promote and encourage them to install and implement drainage water management practices (controlled-drainage) for both new drainage installations and by retrofitting their existing drainage systems with drainage outlet controls. Previous research that had been conducted at multiple locations to evaluate controlled-drainage systems documented that the decrease in nitrate-nitrogen loss in drainage discharge was almost directly proportion to the reduction in drainage outflow volume accomplished by installing control structures on the drainage outlets. A 50% reduction in drainage outflow and nitrate loss was a common research finding at most of these locations. The desired ultimate goal of the ADMSTF and ADMC partnership efforts was to implement drainage water management on a large enough scale (watershed-by-watershed) in the Midwest to decrease transport of excess nutrients through the Mississippi River drainage basin to the Gulf of Mexico. EPA and USGS had reported this source of nitrate-nitrogen as one of the major sources contributing to the persistent formation of the large hypoxic zone ("dead zone") in the Gulf of Mexico.

[1] Chair of ADMS Task Force, and Research Leader (Supervisory Agricultural Engineer), Soil & Water Research Unit, Agricultural Research Service (ARS), USDA, Baton Rouge, LA 70808; PH (225) 578-0743; FAX (225) 757-7728; email: james.fouss@ars.usda.gov

[2] Co-Chair of ADMS Task Force, and Mississippi River Basin Coordinator for the Natural Resources Conservation Service (NRCS), USDA, North Little Rock, AR 72116; PH: (501) 758-2544 (Ext. 115); email: Michael.Sullivan@wdc.usda.gov

Background and Need for Change in Agricultural Drainage Management Practices

In agricultural cropland areas where soil profiles have seasonal shallow water tables, a centuries old management practice has been to install subsurface (tile) drainage systems to reduce the duration of excess soil-water occurrences in the root-zone that damage crop growth and yield. The subsurface drainage practice provides other beneficial benefits as well, including improved filtration, reduced surface runoff and thus less soil erosion, and improved crop growth and yield when compared to the same or similar soil without a subsurface drainage system (Skaggs and van Schilfgaarde, 1999). It has been known for many years that subsurface drains reduce the losses of phosphorus and sediment from agricultural cropland, however, the loss of nitrate-Nitrogen was found to increase in sub-drainage outflows because of leaching from the soil profile by the subsurface drainage system (Gilliam et al., 1999). The nitrate leaching into subsurface drains has been studied, but during the last two decades concerns have been raised about the increasing size of hypoxic zone formed each year in the northern Gulf of Mexico (and elsewhere around the world). This concern has focused a renewed interest and need for additional subsurface drainage studies. The new studies provided a focus on drainage management because drainage of the soil profile was needed for optimum agricultural production, but a way needed to be found to avoid or greatly reduce the losses of fertilizer nutrients (especially nitrate-Nitrogen) with the drain outflows to surface receiving waters and streams. The original focus of the ADMS Task Force activities was the 8-State Midwest area including MN, IA, MO, IL, IN, OH, MI, and WI, because earlier EPA and USGS reports indicated that this region was the major source of the nitrate-Nitrogen lost from agricultural cropland that was carried down the Mississippi River System to the northern Gulf of Mexico and contributed to formation of the hypoxic zone.

The Concept of Nutrient Reduction by Drainage Water Management

There are two components involved to explain the nutrient reduction in the drainage outflow with drainage water management (controlled drainage); see example implementation in Fig. 1. First, the outflow drainage volume reduction by DWM results in a decreased discharge of nutrients (mostly nitrates) in almost direct proportion to the percent that the drain volume outflow is reduced (Gilliam et al., 1979; Evans et al 1989; Skaggs et al., 1994; Thomas et al., 1995). Second, by elevating the drainage outlet, any resulting decrease in the depth to the water table will cause the soil to become anaerobic and thus increase denitrification (Gilliam et a., 1979; Evans et al., 1989b; Kliewer and Gilliam, 1995; Thomas et al., 1995; Drury et al., 1997; Power et al., 2000). These effects of these two outcomes work together rather than separately, thus enhancing the reduction in nutrients discharged from the drain outlet.

Drainage water management research has shown reductions in nitrate outflow from subsurface drainage system by about 50% (Meek et al., 1970; Gilliam et al., 1979; Gilliam and Skaggs, 1986; Evans et al., 1989b; Skaggs and Chescheir, 1999; USDA-ARS, 2002; Fausey, 2004). In Sweden, Westrom et al. (2001) reported that during a dryer than normal or average year, nitrate loads in drainage outflow were reduced by 78% to 94% from drainage water management plots when compared to conventional drainage. Skaggs and Cheschier (1999) predicted with the DRAINMOD-N model that drainage water management reduced nitrate losses most effectively in closely spaced, deeper drains.

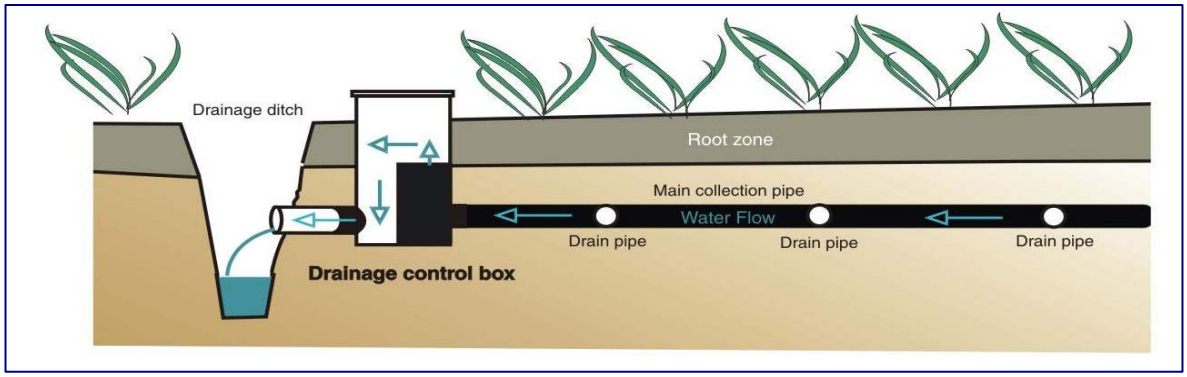

Fig. 1. Conceptual Drainage Outlet Control Structure in Subsurface Drain Main

As drainage water management (controlled-drainage) holds more water is in the soil profile, denitrification occurs, reducing nitrate concentrations in the saturated portion of the soil (Meek et al., 1970; Jacinthe, et al., 1999; Power et al., 2000). Jacinthe, et al. (1999) reported that during a 130 day study, 24% to 43% of the nitrogen present was denitrified when the water table was controlled at 10 cm below the soil surface.

The majority of nitrate load decrease observed from drainage water management is due to the volume of water and the nitrates in that water being held back within the soil profile (Gilliam et al., 1979, Evans et al., 1989b; Gilliam et al., 1999; Evans and Skaggs, 2004).

Drainage water management has the advantage that it does not require land to be removed from production because the soil profile is utilized for both water storage and creates the conditions for denitrification. A disadvantage is that drainage water management can only be used on relatively flat fields (i.e., 1% slope or less is preferred), but some recent technological flow-control developments may make it applicable to lands of greater slopes.

The ADMS Task Force and its Organizational Membership and Meetings

The Task Force was formally established in early 2003 as a technical work group (TWG) of USDA's Partnership Management Team (PMT) to assist in addressing and resolving water quality issues on agriculturally drained lands. The PMT was a collaborative effort among the USDA Agricultural Research Service (ARS); Natural Resources Conservation Service (NRCS); and the Cooperative State, Research, Education, and Extension Service (CSREES). Agricultural drainage management was one of 14 priority national research and technology development needs that were already identified by NRCS under the PMT Need-Request System, before it became a TWG.

Besides the principal Federal Government Agencies, ARS, NRCS, and CSREES that made up the PMT, other Federal Agencies that took an active part were the Environmental Protection Agency (EPA) and the U.S. Geological Survey (USGS). The main cooperative state agencies were the Minnesota Department of Agriculture and some Midwest State Departments of Environmental Quality (DEQ).

The Land Grant Universities in the Midwest had several members of their faculty, researchers, extension specialists, and instructors who initially took a very active role in the formation and activities of the Task Force, such as Iowa State University, University of Minnesota, University of Illinois, Purdue University, The Ohio State University, North Carolina State University, and Louisiana State University. By the second year of the ADMSTF, the University of Missouri, Michigan State University, and University of Wisconsin.

The Technical Committee and leadership of the ADMSTF was provided by a Chair – responsible for Technology, co-Chair – responsible for Implementation (these may be two co-Chairs), and an Executive Secretary – responsible for Education and Extension. In the first few years the Technology was handled by ARS, Implementation by NRCS, and Education and Extension by one of the Land Grant University professors in association with CSREES.

Although the ADM Coalition members were not official members of the ADMS Task Force (to avoid any legal conflicts of interest when voting on action items) they were invited to attend and participate in the discussions at Task Force meetings. Many of the ADMC members were representatives of drainage materials manufacturers and most were also members of the Corrugated Polyethylene Plastic Pipe Assoc. (CPPA) of the Plastic Pipe Institute, Inc. (PPI). At some of the Task Force meetings local drainage contractors were invited to attend and some made formal presentations or put on field demonstrations for the Task Force. Some drainage and water management consultants, who were members of the ADMC, often attended Task Force meetings to keep up to date with the technology. In addition, representatives from several non-Government Organizations have attended TF meetings, such as the National Corn Grower's Association; Sand County Foundation; IN Drainage District Association; IA Drainage District Association; Gulf of Mexico Program; Lower Mississippi River Basin Sub-Committee on Hypoxia; National Association of Conservation Districts (NACD); The Fertilizer Institute; The Nature Conservancy (TNC); and Ducks Unlimited. From 2002-2009, Task Force meetings have been held in IA (3), OH (4), IL (2), IN (2), FL, MN (3), LA, and NC, for a total of 17 meetings.

ADMS Research Findings

On behalf of the Task Force, Dr. Wayne Skaggs (c/o NCSU) completed a summary of past research findings. This summary report emphasizes that "Drainage Water Management" includes conventional drainage, controlled drainage, and subirrigation. While the emphasis has been on subsurface drainage, drainage water management includes surface drainage as well. Over the years the terms "water table management", "water table control", "reversible drainage", and "controlled and reversible drainage" have been coined to describe drainage systems that have facilities for some level of management, as opposed to passive, conventional drainage systems. Recently the term "drainage water management" has been proposed as a descriptive and politically acceptable term that can be used to describe any and all combinations of the above practices.

The report supports the conclusion -- based largely on the research in Ohio, Illinois, North Carolina, Michigan, and Louisiana -- that drainage water management can effectively reduce water flow and nitrate-Nitrogen loading during the non-growing season by an annual average of 30 to 60 percent. Producers can also receive an economical benefit from reduced losses of

inputs. Moreover, by using additional drainage management during the growing season, producers can mitigate dry spells or drought by capturing more water within the soil profile, mitigating yield reductions by 10-15 bushels of corn per acre. For example, research results from a 4.5-year field study, comparing controlled drainage to other drainage treatments in Northwest Ohio, showed that controlled drainage treatment reduced drainage outflows to about 60 percent of conventional drainage flows and nitrate-nitrogen loadings by more than 45 percent compared to conventional drainage; see Fig. 2.

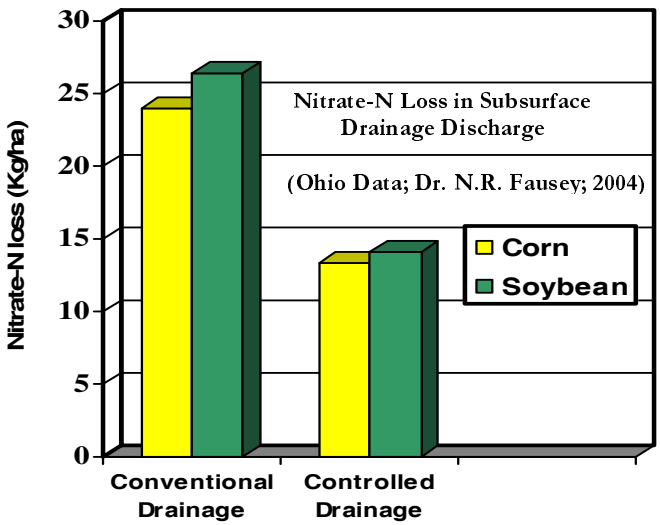

Fig. 2. Research Findings from Northwest Ohio

Field Implementation of Agricultural Drainage Management

Based on research findings documenting the water quality benefits of drainage water management, NRCS has provided funding for demonstrating the practice and further documenting benefits through the NRCS Conservation Innovation Grants Program (CIG) over the past several years. Six National CIG projects with almost $3 million in federal funds have been approved since 2004.

Technical and financial assistance has been made available to producers for implementing drainage water management through the Environmental Quality Incentives Program (EQIP) and the Conservation Security Program (CSP). Since 2004, approximately 56,000 acres have been planned and 23,000 acres implemented for drainage water management nationwide. Drainage water management practices have been planned on approximately 14,600 acres and applied on 6,700 acres within the 8-state focus area of the Task Force.

Challenges exist, however, in achieving widespread acceptance and adoption on the cropland potentially suitable for drainage water management. Producers have shown interest in drainage water management but mainly for the potential to increase yields that is not well documented. Technical capacity is limited for developing sound drainage water management plans – to help address this, Illinois NRCS offered an EQIP Ground and Surface Water Conservation Project in 2007 targeting development of drainage water management plans.

Recent ADMS Accomplishments

The Task Force worked with NRCS to develop a Fact Sheet for products and revised the Practice Standard 554, "Drainage Water Management," which highlights, in particular, the use of "control structures" that are placed in the main lines of subsurface drainage systems. The Fact Sheet points out that users need to consider drainage water management as part of conservation management system (CMS). Conservation practices such as drainage water management are normally implemented as part of a CMS that includes other practices such as nutrient management, riparian buffers, cover crops, filter strips, wetlands, etc. as needed to address identified natural resource concerns. Standards for the practices are available in the NRCS electronic Field Office Technical Guide (eFOTG; 2004): http://www.nrcs.usda.gov/Technical/Standards/nhcp.html

The Task Force has also developed a website on The Ohio State University computer system that contains the Charter, Action Plan, Goals and Objectives, Fact Sheet, and Flyer: http://www.ag.ohio-state.edu/~usdasdru/ADMS/ADMSindex.htm Other information such as an education and extension bulletins, recent summary of research findings, and linkages to other drainage water management conferences, activities, and meetings will be added to the website.

The Task Force organized its first technical session in 2004 entitled "*Drainage Water Management for the Midwest"* with a series of papers presented at the American Society of Agricultural Engineers (ASAE) **8th International Drainage Symposium**. The Task Force continues to plan, organize and participate in other conferences and symposiums that provide detailed engineering and scientific information on drainage water management practices and systems along with the latest status on Task Force projects and activities.

A recent research modeling/simulation accomplishment by Task Force members involved a preliminary evaluation of the potential water quality impact of applying drainage water management in an 8-state region of the Midwestern U.S. (Jaynes and Thorp, 2008; Thorp, et al. 2008). Their simulations were made with the hybrid model RZWQM-DSSAT,[3] to predict both conventional subsurface drainage and drainage water management performance in terms of hydrologic and nitrogen cycles over a 25-year period of historical weather at 48 locations across the 8-state region (MO, IA, MN, MI, WI, IL, IN, OH). They showed the DWM was suitable for about 7.2 million ha of cropland in the corn belt region. Their simulated average reduction in drain flow with DWM for the region was 151 mm/yr, and the regional reduction over the long term was predicted at 53%. This predicted reduction in nitrogen load down the Mississippi River System to the Gulf of Mexico was about 7% of the proposed 45% reduction by the year 2015 as recommended by the EPA National Research Council (NRC).[4] They estimated costs and indicated that the DWM practice was cost effective for reducing N-load at $1.53/kg-N/yr, and this was less than for other practices or methods compared (Jaynes and Thorp, 2008). The predicted regional reduction in nitrate-nitrogen losses through the drains was 18.9 kg-N/ha/yr, and the regional percent reduction over the long term was 51% (Thorp et al., 2008).

[3] The RZWQM-DDSAT hybrid model combines the Root Zone Water Quality Model with components of the Decision Support Systems for Agrotechnology Transfer model (Ma et al., 2005; Ma et al., 2006).
[4] Recent EPA reports indicate the year 2015 may no longer be realistic to reach the 45% reduction target goal.

Joint ADMC and ADMSTF Projects and Future Activities

NRCS developed a Drainage Water Management (DWM) Practice Standard 544 and conservation practice standards for the Midwestern States to provide cost-sharing assistance through NRCS to farmer's who implement DWM on their farms. When farmers began to ask more questions about how well DWM would work on their farms and in their soils, the ADMC and partnering members of the ADMSTF in the 5 States of IA, MN, IL, IN, and OH applied for and was granted a $1 million NRCS Conservation Innovation (CIG) Grant to install and conduct DWM demonstration projects on paired field-size demonstration sites in each of the 5 States. This CIG project is now in its third year of the 3-year grant period, and data collected will demonstrate the effectiveness of the DWM Systems for reducing nitrate loss is drainage outflows, reducing drainage volumes, and effects on crop yields. Rainfall is measured (monitored) at all demonstration sites and water table depth monitored at each DWM site. All sites have a satellite link that allows downloading of site data to remote PC equipment. Field Days and Workshops on DWM are conducted at each of these demonstration sites for farmers, contractors, consultants, State and Federal government agencies, and the General Public. Future endeavors to be undertaken by the Task Force will include promoting complementary conservation practices that can be combined with DWM, such as winter cover crops to further reduce the potential of nitrate loss from the cropland sites following annual crop harvest, and improvements in fertilizer application methods or fertility management practices. Other projects have evaluated the reduction in nitrate in subsurface drainage discharge by biofilters, saturated buffers, recycling of drainage water, and diversion of the drainage waters through wetland resource areas to reduce nitrate-load.

The Task Force is concentrating first on transferring drainage management technologies in demonstration projects in areas with suitable tile drainage systems. As these areas are identified, the Task Force will work with local sponsors and producers to develop and implement economically feasible research and demonstration projects. These will include the use of other management practices in combination with multiple drainages management practices. To further refine the existing technology, data will be gathered from these areas by conducting research and monitoring at the sub-watershed scale. A part of the project design would be to create the monitoring strategy for each project to assess water quality, such as reducing nonpoint source pollution; agronomic affects, such as yield changes and other crop growth attributes; water conservation effects for varying management strategies; soil quality affects for varying management strategies; and economic attributes, such as economic return on investment from drainage water management practices and systems. The researchers will collaborate with the landowner and local drainage district personnel to ensure the best-designed project and that no off-site problems with water drainage would develop.

The Task Force also is working to increase technical assistance, education, and extension activities. For example, ARS technical specialists are being asked to identify the best locations in the states on which to focus drainage water management projects identify pollutants to address, identify opportunities for wildlife habitat enhancement, and provide information to landowners. The Task Force plans to work with NRCS to draft practice standards at the state level for the projects. The Task Force is also interested in opportunities to cooperate with education and extension programs to educate landowners, conservation groups, and local and

state farm groups on drainage water management options that could be deployed in certain areas across a particular state. This will be instrumental in building support for the effort as well as in identifying potential landowning participants.

References

Drury, C.F., C.S. Tann, J.D. Gaynor, T.O. Oloya, I. J. van Wesenbeeck, and D.J. McKenney. 1997. Optimizing corn production and reducing nitrate losses with water table control-subirrigation. Soil Sci.Soc. Am. J. 61: 889-895.

EFOTG. 2004. National Resource and Conservation Service Field Office Technical Guide. Document can be found at the NRCS website: http://efotg.nrcs.usda.gov/technical/efotg/.

Evans, R.O., J.R. Cummings, and J.W. Gilliam. 1989a. Controlled drainage: A best management practice in North Carolina. ASAE Paper 892695. ASAE. St Joseph, MI.

Evans, R.O., J.W. Gilliam, and R.W. Skaggs. 1989b. Effects of agriculture water table management on drainage water quality. Tech. Rep. 237. Water Res. Inst., University of North Carolina, Raleigh.

Evans, R.O., J.W. Gilliam, R.W. Skaggs. 1991. Controlled drainage management guidelines for improving water quality. Publication NO. AG-443. N.C. Coop. Extension Service.

Evans, R.O., R.W. Skaggs, and J.W. Gilliam. 1995. Controlled drainage versus conventional drainage effects on water quality. J. of Irrig. Drain. Eng. 121(4): 271-276.

Evans, R.O. and R.W. Skaggs. 2004. Development of controlled drainage as a BMP in North Carolina. In: Drainage VIII Proceedings of the Eighth International Symposium, 21-24 (Sacramento, California USA). Ed. R. Cooke. Publication Date March 21, 2004. ASAE Publication Number 701P0304. ASAE, St Joseph, MI. Pp 1-15.

Gilliam, J.W., J.L. Baker, and K.R. Reddy. 1999. Chapter 24: Water Quality Effects of Drainage in Humid Regions. In: R.W. Skaggs and J. van Schilfgaarde eds. Agricultural Drainage. Agron. Monogr. 38. American Society of Agronomy, Inc., Crop Science Society of America, Inc., Soil Science Society of America, Inc., Madison, Wisconsin, USA. Pp. 801-830.

Gilliam, J.W. and R.W. Skaggs. 1986 Controlled agricultural drainage to maintain water quality. J. Irrig Drain. Eng. 112: 254-263.

Gilliam, J.W., R.W. Skaggs, S.B. Weed. 1979. Drainage control to diminish nitrate loss from agricultural fields. J. Environ. Qual. 8(1): 137-142.

Jacinthe, P.A., W.A. Dick, and L.C. Brown. 1999. Bioremediation of nitrate-contaminated shallow soils using water table management techniques: Nitrate removal efficiency. Transactions of the ASAE. 42(5): 1251-1259.

Jaynes, D.B. and K.R. Thorp. 2008. Potential water quality impact of drainage watere management in the Midwest Cornbelt. ASABE Paper 084767. ASABE. St Joseph, MI.

Ma, L., G. Hoogenboom, L. R. Ahuja, D. C. Nielsen, and J. C. Ascough II. 2005. Development and evaluation of the RZWQM-CROPGRO hybrid model for soybean production. *Agronomy J.* 97(4): 1172-1182.

Ma, L., G. Hoogenboom, L. R. Ahuja, J. C. Ascough II, and S. A. Saseendran. 2006. Evaluation of the RZWQM-CERES-Maize hybrid model for maize production. *Agric. Systems* 87(3): 274-295.

Meek, B.B., L.B. Grass, L.S. Willardson, and A.J. MacKenzie. 1970. Nitrate transformation in a column with controlled water table. Soil Sci. Soc. Am. Proc. 34(2): 235-239.

NRCS Performance Results System 2004 – 2008 data.

NRCS Conservation Innovation Grant Program information. (http://www.nrcs.usda.gov/programs/cig/)

Pitts, Donald J. 2008. Drainage Water Management: The Illinois Experience, Prepared for presentation at University of Minnesota, Southwest Research and Outreach Center at Lamberton, MN on August 13-14, 2008.

Power, J.F., R. Wiese, and D. Flowerday. 2000. Managing nitrogen for water quality –Lessons from management systems evaluation area. J. Environ. Qual. 29: 355-366.

Skaggs, R.W., M.A. Breve, and J.W. Gilliam. 1994. Hydrology and water quality impacts of agricultural drainage. Critical Reviews in Environmental Science and Technology. 24: 1-32.

Skaggs, R.W. and G.M. Chescheir. 1999. Chapter 15: Application of drainage simulation models. In: R.W. Skaggs and J. van Schilfgaarde eds. Agricultural Drainage. Agron. Monogr. 38. American Society of Agronomy, Inc., Crop Science Society of America, Inc., Soil Science Society of America, Inc., Madison, Wisconsin, USA. Pp. 537-564.

Skaggs, R.W. and J. van Schilfgaarde (Eds.). 1999. Agricultural Drainage, Agronomy Monograph 38, 1328 pp. American Society of Agronomy, Madison, Wisconsin.

Thomas, D.L., C.D. Perry, R.O. Evans, F.T. Izuno, K.C. Stone, and J.W. Gilliam. 1995. Agricultural drainage effects on water quality in Southeastern U.S. J. of Irrig. Drain. Eng. 121(4): 277-282.

Thorp, K.R., R.W. Malone, and D.B. Jaynes. 2007. Simulating long-term effects of nitrogen application rates on corn yield and nitrogen dynamics. Transactions of the ASABE 50(4): 1287-1303.

Thorp, K.R., D.B. Jaynes, and R.W. Malone. 2008. Simulating the long-term performance of drainage water management across the Midwestern United States. Transactions of the ASABE. 51(3): 961-976.

USDA, ARS. 2002. Draining the land without polluting the waters. Agricultural Research. Vol. 50, No. 10, October 2002. p. 4-8.

Wesstrom, I., I. Messing, H. Linner, and J. Lindstrom. 2001. Controlled drainage – effects on drain outflow and water quality. Agricultural Water Management. 47:85-100.

DENITRIFYING BIOREACTORS FOR TREATMENT OF TILE DRAINAGE

Laura E. Christianson[1], Alok Bhandari[1], Matthew H. Helmers[1] and Martin St. Clair[2]
[1]Department of Agricultural & Biosystems Engineering, Iowa State University, Ames, IA
[2]Department of Chemistry, Coe College, Cedar Rapids, IA

Abstract

Much of the hypoxia in the Gulf of Mexico has been attributed to agricultural nonpoint pollution sources in the Midwestern states. There is, therefore, a critical need to develop practical and cost effective methods to reduce nitrate loadings from these areas. As the hypoxic zone is thought to be larger this year than ever before, the time is ripe for new technologies to reduce nutrient loads in the Mississippi River. Denitrifying drainage bioreactors can provide cost-effective treatment of tile water at the field scale while requiring minimal system maintenance. These bioreactors consist of a trench filled with an available carbon source (usually woodchips) that is readily colonized by bacteria and fungi capable of utilizing nitrate as an electron acceptor. A handful of such bioreactors have been installed in the US Midwest and have shown good nitrate removal. This poster describes the design, field installation, and cost estimates of full-scale denitrifying bioreactors.

Background

The history of artificial agricultural drainage in the US middle west began in the 1800's and has grown to include more than 20.8 x 10^6 ha in Midwestern states (Dinnes et al. 2002). Increased use of fertilizers over the past 60 years has resulted in elevated concentrations of nitrate in agricultural drainage, often above the drinking water limit (Baker et al. 1975; Kalita et al. ; Mirek 1999) with annual nitrate loadings to surface waters of tens of kg per ha (Jaynes et al. 2008). Nitrate from agricultural sources has been identified as a major source of non-point source pollution, and nitrate loadings in the Mississippi River are key causes of water quality impairment in the Gulf of Mexico (Rabalais et al. 1996) with the hypoxic zone in the Gulf expected to be the second largest this year (NOAA 2008).

The magnitude and intensity of agricultural nitrate losses depends upon many management factors such as tillage (Kanwar 2006), cropping (Kanwar 2006; Mirek 1999), fertilizer type (Kanwar 2006), and tile drain spacing (Kladivko et al. 2004). Several options have been proposed to reduce nitrate loadings to surface waters including more soil testing, abandoning drainage systems, increased use of wetlands, better crop rotations, increased use of cover crops, and better fertilizer application rate, placement and timing (Dinnes et al. 2002; Jaynes et al. 2004). However, regardless of better management strategies, nitrate concentrations in drainage waters can still exceed the drinking water standard (Baker et al., 1975), because in addition to management factors, precipitation timing and organic matter mineralization can affect nitrate loss (Randall and Goss 2001; Kanwar 2006; Kladivko et al. 2004).

In watersheds where agriculture is a major land use, high nitrate mass loadings to surface waters often result. For example, in the Embarrass River watershed in Illinois where 70-85% of the land is cropped, annual total nitrogen losses were 39 kg N/ha (Kovacic et al. 2000). Jaynes et al. (1999) documented that nitrate losses in an Iowan agricultural watershed ranged from 4-66 kg N per ha annually. Similarly, Kalita et al. (2006) found that Illinois drainage water nitrate losses ranged from 23-33 kg NO_3-N/ha/yr with average concentrations (range of 15-20 mg/L) above the drinking water limit. Such nitrate losses have been documented for several decades, with early work by Baker et al. (1975) showing that the nitrate nitrogen concentrations in drainage water ranged from 2.3-44.2 mg/L with an average of 21 mg/L. While nitrate concentrations from individual drains are relatively consistent on a day-to-day basis (Baker et al. 1975), nitrate concentrations can vary by season as Mirek (1999) found that drainage nitrate-nitrogen concentrations were highest in the spring and lowest in the summer (spring: 14.7 mg/L, summer: 9.8 mg/L, fall: 11.5 mg/L, winter: 11.7 mg/L). Note that drainage volumes also vary by season which has implications for mass loadings. Mirek (1999) documented the greatest drain flow volumes during the spring and the least drain flow during the summer.

Denitrifying Bioreactor Technology.

Although denitrification, or nitrate-removal, occurs naturally in soil, the rapid transport of drainage water in tile drains decreases the available time for the nitrate to be depleted before the water is discharged into a receiving stream (Kellman 2005). Edge-of-field treatment systems can be designed to intercept tile drainage and remove nitrate biologically by the action of soil microorganisms. Biological denitrification requires the presence of suitable bacteria, nitrate, a carbon or energy source, and the absence of oxygen (Korom 1992). In the simplest terms, denitrifiers "breathe" the nitrate and "feed on" the carbon source.

Denitrifying bioreactors such as those filled with woodchips ('woodchip bioreactors'), provide a new option for nitrate removal from agricultural drainage. This can be accomplished by directing tile flow into an underground trench containing woodchips as a carbon source for denitrification activity. Denitrifying bioreactors for agricultural drainage are based loosely on the concept of flow-through denitrification systems proposed for treatment of septic effluent (Robertson and Cherry 1995) and for groundwater remediation (Schipper and Vojvodic-Vukovic 2000; Schipper et al. 2005). Jaynes et al. (2004) compared various nitrate reduction strategies including deep tiles, denitrification walls, phytoremediation, and usage of a cover crop and observed that the denitrification wall had the highest nitrate removal with no yield losses or land taken out of production. Bioreactors occupy a land area that is typically $1/10^{th}$ that of wetlands (Kovacic et al. 2000). Van Driel et al. (2006) recently showed that bioreactor nitrate removal rates could be an order of magnitude higher than those associated with wetlands.

The first bioreactor for agricultural drainage was installed in Ontario, Canada and consisted of three 200 L barrel reactors that were partially buried in a stream bank 100 m from a tile outlet. Influent nitrate-nitrogen concentrations (2-6 mg/L) were reduced to nearly zero inside the organic matter and sand filled barrels (Blowes et al. 1994). Early research on denitrifying bioreactors has also been conducted at the University of Illinois (Appleford et al. 2008; Cooke et al. 2001; Wildman 2001) and the USDA-ARS National Soil Tilth Lab in Ames, Iowa (Jaynes et al. 2008; Moorman 2008, personal communication).

The USDA National Soil Tilth Lab bioreactors have been modeled most closely after denitrification wall research with their design consisting of flow-through woodchip walls

adjacent to tile lines. Their wall treatment resulted in a nitrate reduction of 55% (results averaged over five years) with no detrimental effect on crop yields (Jaynes et al. 2008). The placement of these walls on each side of the tile line, however, limits the practicality of this design for widespread field implementation. The Soil Tilth Lab has also conducted laboratory scale bioreactor studies involving carbon source for the bioreactor (Greenan et al. 2006) and production of nitrous oxide (Moorman 2008, personal communication).

The University of Illinois has done substantial work on bioreactors. Rodrigue (2004), documented that a bioreactor (0.9 m wide and 1 m deep below 0.97 m soil; drainage area: 13 acres) experienced variations in effluent nitrate most likely due to fluctuations in microbial activity. Effluent nitrate concentrations exceeded 10 mg/L nitrate-N, but only after large storm events (Rodrigue 2004). Wildman (2001) reported that a field reactor was only $1/8^{th}$ of the required size but still achieved 100% nitrate reduction. Other bioreactors deployed in Illinois have been successful in removing 50-60% of nitrate concentration in drainage waters (Appleford et al. 2008).

Bioreactor Design

It is thought that designing a denitrification bioreactor for eight to ten hours of retention time (RT) is sufficient for denitrification of most agricultural drainage waters in Iowa (Van Driel et al. 2006). Retention periods that are too long will encourage sulfate reduction and RTs which are too short will result in insufficient denitrification. Another major consideration is that it is impractical to design a bioreactor to treat 100% of agricultural drainage flow throughout the entire drainage season. To do so would require a bioreactor of uneconomical proportions. Van Driel et al. (2006) has argued that designing a reactor to handle peak flows is not cost-effective while designing for base flows that occur during the growing season is most appropriate. Therefore, it is thought that designing these systems to treat approximately 20% of the peak flow will result in the treatment of the majority (approximately 70%) of total annual flow. In this case, the peak volume is estimated to be the drainage design coefficient for which many drainage systems in Iowa have been designed, usually about 1.3 cm/day (0.5 inches/day).

Based on these considerations, designers must find a balance between the RT, percentage of peak flow to be treated and design volume. Ideally, an RT of eight hours with treatment of 20% of peak flow will result in a volume that is not to big so as to be impractical. The porosity, hydraulic conductivity, and head gradient across the bioreactor all affect these values.

A special note must be made for the distinction between the volume of the bioreactor versus the volume of carbon needed for denitrification to be sustained for a significant length of time (years to decades). The amount of carbon needed is determined by the stoichiometry of denitrification; it is well established that about 1 kg of carbon is needed to denitrify about 1 kg of nitrate (Blowes et al. 1994; Robertson and Cherry 1995). The total volume of the bioreactor based on the retention time and percent of peak flow is usually far more than the amount of carbon needed for actual denitrification. Because the carbon source in denitrifiers, usually woodchips, may be difficult to obtain and expensive in large quantities, the idea naturally follows that inert materials (gravel, etc.) may be mixed in with the carbon source to make up the required volume in the bioreactor excavation while still allowing the sufficient carbon (Wildman 2001).

Recent Bioreactor Installations

Within Iowa, a handful of such bioreactors have been installed to treat a variety of drainage areas under differing *in situ* conditions (table 1). The oldest, a bioreactor near Pekin, Iowa, was installed by Iowa State University and the Iowa Department of Agriculture and Land Stewardship in 2004. This bioreactor is 0.5m x 30.5m (1.5ft x100 ft) and treats drainage from 1.2 ha (3 ac). Another bioreactor that has been operating for several years is the bioreactor installed in the Lime Creek watershed in Buchanan County, Iowa by a local watershed group for approximately $2,050. This bioreactor is 1.5m x 12.2m (5ft x 40ft) with a drainage treatment area of approximately 40.5 ha (100 ac). The first year of data indicated nitrate reduction increased within the bioreactor over the course of the summer months (May through September) (figure 1). In figures 1 and 2, “near bioreactor outlet” refers to a sampling well within the bioreactor approximately 5 m from the outlet. Outlet concentrations in this case

were elevated, most likely due to backflow into the outlet control structure from bypass flow. Sulfate reduction follows this same temporal pattern within the bioreactor meaning that sulfate reducing bacteria are utilizing the carbon source in addition to the denitrifiers especially in late summer (figure 2). This additional process may possibly decrease the longevity of this bioreactor.

Table 1: Denitrification bioreactors in Iowa

Location	Funding Organization	Length	Width	Depth	Drainage Treatment Area
Pekin, Iowa	Iowa State University and Iowa Department of Ag and Land Stewardship	30.5 m	0.5 m	1.2 m	1.2 ha
Buchanan County, Iowa	Local watershed group	12.2 m	1.5 m	1.2 m	40.5 ha
Central Iowa	Iowa Soybean Association	15.2 m	7.6 m	Approx. 1.8 m	16.2 ha

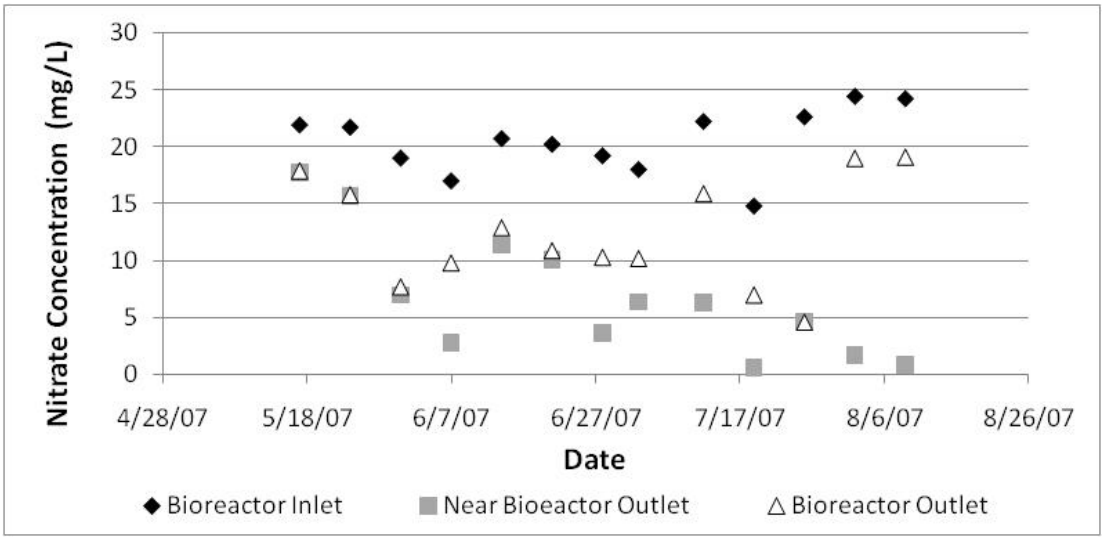

Figure 1: Lime Creek nitrate concentrations throughout bioreactor for summer 2007

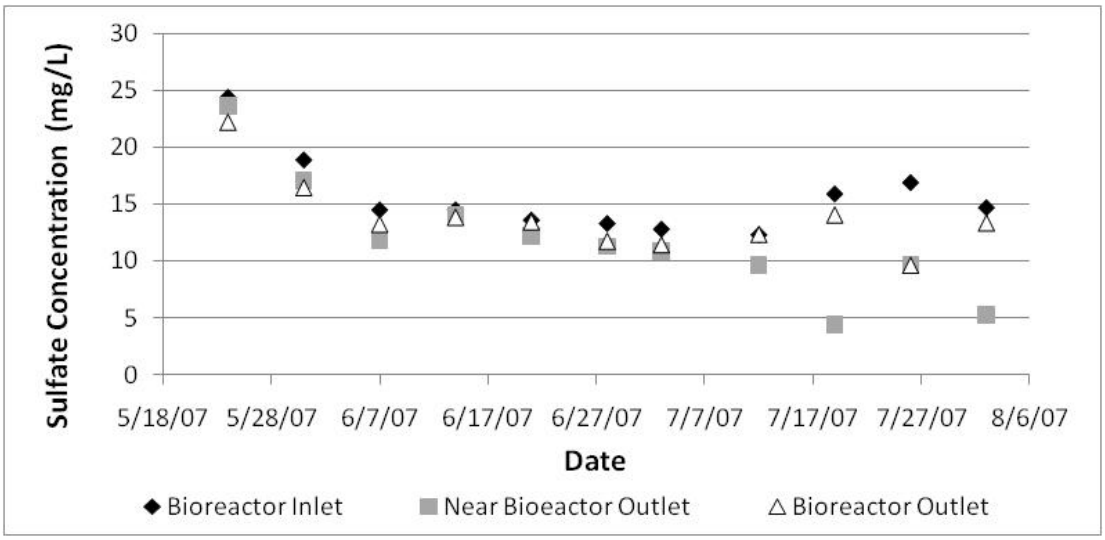

Figure 2: Lime Creek sulfate concentrations throughout bioreactor for summer 2007

The Iowa Soybean Association organized and funded the most recent bioreactor installation of a 7.6m x 15.2m (25ft x 50ft) rectangular bioreactor in central Iowa. Preliminary data has shown initial losses of organics in the effluent. Many researchers have documented these flushing losses especially during start-up (Diaz et al. 2003; Robertson and Cherry 1995; Vogan 1993; Volokita et al. 1996). The cost of this bioreactor was estimated at approximately $8000 (Iowa Soybean Association 2008, personal communication). Capital cost per unit drainage area for this bioreactor was $495/ha ($200/ac). Approximately half of the woody material obtained for this bioreactor was free and consisted of shredded woody debris provided by a local city government. The other half of woody material included conventional woodchips (approximately 76.5 m^3 or 100yd^3) bought for $975 including transportation costs.

One of the obstacles for bioreactor installation has been the ability to locate and hire a contractor who has an opening in his schedule during a window when soil conditions allow for excavation. Another hurdle has been encountered in locating enough woodchips. It is important to have access to a woodchip supplier who is both close in proximity and can provide reasonably priced woodchips. Moreover, the quality of woodchips should be consistent between batches so as to allow for some consistency between loads. Lastly, regarding implementation, the location of the bioreactor at the chosen site is important. An additional

denitrification bioreactor not mentioned above was located in a very sandy soil. Because of this, while there is significant inflow, there is very little outflow. It is thought that it would have been better to install a plastic liner in this bioreactor to attempt to reduce the leaching out of this system.

Conclusions

Denitrification bioreactors in Iowa and the Midwest have shown good potential to be an additional technology to add to the existing slate of nitrate reduction options such as wetlands and in-field management. With further research into the hydraulic and biological processes that occur within bioreactors, it is believed their performance can be enhanced. Though challenges remain for design and installation, increased understanding of the basic science of these systems combined with increased experience of *in situ* applications will help make this a viable option for many landowners.

References

Appleford, J. M., Rodriguez, L. F., Cooke, R. A. C., Zhang, Y., Kent, A. D., and Zilles, J. (2008). "Characterization of Microorganisms Contributing to Denitrification in Tile Drain Biofilters in Illinois." *2008 ASABE Annual International Meeting*, Providence, RI.

Baker, J. L., Campbell, K. L., Johnson, H. P., and Hanway, J. J. (1975). "Nitrate, phosphorus, and sulfate in subsurface drainage water." *Journal of environmental quality*, 4(3).

Blowes, D. W., Robertson, W. D., Ptacek, C. J., and Merkley, C. (1994). "Removal of agricultural nitrate from tile-drainage effluent water using in-line bioreactors." *Journal of Contaminant Hydrology*, 15(3), 207-221.

Cooke, R. A., Doheny, A. M., and Hirschi, M. C. (2001). "Bio-reactors for edge of field treatment of tile outflow." *2001 ASAE Annual International Meeting*, Sacramento, CA.

Diaz, R., Garcia, J., Mujeriego, R., and Lucas, M. (2003). "A Quick, Low-Cost Treatment Method for Secondary Effluent Nitrate Removal through Denitrification." *Environmental Engineering Science*, 20(6), 693-702.

Dinnes, D. L., Karlen, D. L., Jaynes, D. B., Kaspar, T. C., Hatfield, J. L., Colvin, T. S., and Cambardella, C. A. (2002). "Nitrogen management strategies to reduce nitrate leaching in tile-drained midwestern soils." *Agronomy Journal*, 94(1), 153-171.

Greenan, C. M., Moorman, T. B., Kaspar, T. C., Parkin, T. B., and Jaynes, D. B. (2006). "Comparing carbon substrates for denitrification of subsurface drainage water." *Journal of Environmental Quality*, 35(3), 824-829.

Iowa Soybean Association. (2008). Personal Communication. Ankeny, Iowa.

Jaynes, D. B., Hatfield, J. L., and Meek, D. W. (1999). "Water quality in Walnut Creek Watershed: Herbicides and nitrate in surfce waters." *Journal of Environmental Quality*, 28.

Jaynes, D. B., Kaspar, T. C., Moorman, T. B., and Parkin, T. B. (2004). "Potential methods for reducing nitrate losses in artificially drained fields." American Society of Agricultural Engineers, St. Joseph, MI 49085-9659, United States, Sacramento, CA, United States, 59-69.

Jaynes, D. B., Kaspar, T. C., Moorman, T. B., and Parkin, T. B. (2008). "In situ bioreactors and deep drain-pipe installation to reduce nitrate losses in artificially drained fields." *Journal of Environmental Quality*, 37(2), 429-436.

Kalita, P. K., Algoazany, A. S., Mitchell, J. K., Cooke, R. A. C., and Hirschi, M. C. (2006). "Subsurface water quality from a flat tile-drained watershed in Illinois, USA." *Agriculture, Ecosystems and Environment*, 115.

Kanwar, R. S. (2006). "Effects of cropping systems on NO3-N losses to tile drain." *Journal of the American Water Resources Association*, 42(6), 1493-1501.

Kellman, L. M. (2005). "A study of tile drain nitrate -15N values as a tool for assessing nitrate sources in an agricultural region." *Nutrient Cycling in Agroecosystems*, 71.

Kladivko, E. J., Frankenberger, J. R., Jaynes, D. B., Meek, D. W., Jenkinson, B. J., and Fausey, N. R. (2004). "Nitrate leaching to subsurface drains as affected by drain spacing and changes in crop production system." *Journal of Environmental Quality*, 33(5), 1803-1813.

Korom, S. F. (1992). "Natural Denitrification in the Saturated Zone: A Review." *Water Resources Research*, 28(6), 1657-1668.

Kovacic, D. A., David, M. B., Gentry, L. E., Starks, K. M., and Cooke, R. A. (2000). "Effectiveness of constructed wetlands in reducing nitrogen and phosphorus export from agricultural tile drainage." *Journal of Environmental Quality*, 29(4), 1262-1274.

Mirek, S. T. (1999). "Effect of nitrogen fertilizer management and seasonality of tile flow on nitrate leaching through tile drains," University of Illinois at Urbana-Champaign, Urbana-Champaign.

Moorman, T. (2008). Personal Communication. USDA National Soil Tilth Lab, Ames, Iowa.

NOAA. (2008). "Survey Cruise Records Second-Largest 'Dead Zone' in Gulf of Mexico Since Measurements Began in 1985." <http://www.noaanews.noaa.gov/stories2008/20080728_deadzone.html>.

Rabalais, N. N., Wiseman, W. J., Turner, R. E., Sen Gupta, B. K., and Dortch, Q. (1996). "Nutrient changes in the Mississippi River and system responses on the adjacent continental shelf." *Estuaries*, 19.

Randall, G. W., and Goss, M. J. (2001). "Chapter 5: Nitrate Losses to Surface Water through Subsurface, Tile Drainage." In: *Nitrogen in the Environment: Sources, Problems, and Management*, R. F. F. a. J. L. Hatfield, ed., Elsevier Science.

Robertson, W. D., and Cherry, J. A. (1995). "In situ denitrification of septic-system nitrate using reactive porous media barriers: field trials." *Ground Water*, 33(1), 99-111.

Rodrigue, A. L. (2004). "Effects of sampling frequencies in the evaluation of nitrate-N transport from drainage –related BMPs," University of Illinois at Urbana-Champaign, Urbana-Champaign.

Schipper, L. A., Barkle, G. F., and Vojvodic-Vukovic, M. (2005). "Maximum rates of nitrate removal in a denitrification wall." *Journal of Environmental Quality*, 34(4), 1270-1276.

Schipper, L. A., and Vojvodic-Vukovic, M. (2000). "Nitrate removal from groundwater and denitrification rates in a porous treatment wall amended with sawdust." *Ecological Engineering*, 14(3), 269-278.

Van Driel, P. W., Robertson, W. D., and Merkley, L. C. (2006). "Denitrification of agricultural drainage using wood-based reactors." *Transactions of the ASABE*, 49(2), 565-573.

Vogan, J. L. (1993). "The use of emplaced denitrifying layers to promote nitrate removal from septic effluent," University of Waterloo, Waterloo, Ontario, Canada.

Volokita, M., Belkin, S., Abeliovich, A., and Soares, M. I. M. (1996). "Biological denitrification of drinking water using newspaper." *Water Research*, 30(4), 965-971.

Wildman, T. A. (2001). "Design of field-scale bioreactors for bioremediation of nitrate in tile drainage effluent," University of Illinois at Urbana-Champaign, Urbana-Champaign.

Drainage Main Rehabilitation in Iowa

M. J. Helmers[1], S. Melvin[2], and D. Lemke[3]

[1]Assistant Professor, Department of Agricultural and Biosystems Engineering, Iowa State University, Ames, IA 50011; Ph: 515-294-6717; Email: mhelmers@iastate.edu
[2]Professor Emeritus, Department of Agricultural and Biosystems Engineering, Iowa State University
[3]Chief, Water Resources Bureau Iowa Department of Agriculture and Land Stewardship

Abstract

Subsurface drainage systems installed throughout much of north central region of Iowa have provided substantial crop production benefits. However, most of these systems were installed in the early 1900's and as such they are reaching their design life. With the aging infrastructure of these systems, better economic conditions, and the potential for more financial gains for better drainage; there will need to be significant rehabilitation that occurs in the future. This paper will discuss some of what is known about the existing infrastructure in this area, some potential opportunities for future redesign, and potential economic returns of drainage district redesign. The future redesign would need to include environmental as well as economic considerations and might include the integration of drainage and wetland systems. While this paper focuses on a specific location, the concepts should have relevance to many areas where existing drainage infrastructure is aging.

Keywords. Subsurface drainage; drainage design

Introduction

Subsurface drainage is a common water management strategy for agricultural productivity in areas with poorly drained soils and seasonal high water tables. This is especially the case in the north central region of Iowa. This is an area where local drainage districts were formed in the early 1900's to provide outlets to landowners in flat poorly drained areas with no natural outlet on their property. In many areas the existing drainage outlet or main may be significantly undersized such that the water cannot be removed quickly enough to minimize crop damage even if there is adequate field drainage installed. Also, these systems are nearing or exceeding their design life, so there will likely be significant maintenance, rehabilitation, or redesign of these systems in the future. This comes at a time when there is the potential for financial gains with better drainage. This paper discusses some of what is known about the existing infrastructure in this area, some potential opportunities for future redesign, and potential economic returns of drainage district redesign.

Background

Within Iowa there are approximately 3.6 million ha that have been artificially drained (Baker et al., 2004). About two-thirds of this drainage area is within organized drainage districts. Based on the soil conditions (mineral) and field crops grown in this area along with the need for surface inlets in most cases, the modern design standards would call for a drainage coefficient of between 1.27 to 2.54 cm/day (1/2 to 1 inch/day). A 1980's study (Schult et al., 1981) investigated drainage conditions in parts or all of 10 counties studied in north central Iowa. Of an estimated 395,098 ha (975,551 acres) in the study area, 76,031 ha (187,732 acres) were considered to be naturally well drained soils needing no artificial drainage. On the remaining 319,067 ha, 273,542 ha (675,414 acres) were estimated to have a high level of field drainage (drainage coefficient of at least 1.27 cm/day), 31,353 ha (77,415 acres) were estimated to be at an intermediate level of field drainage (drainage coefficient of at least 0.95 cm/day), and 14,171 ha (34,990 acres) were estimated to have no tile drainage. While the majority of the area was estimated to have adequate field drainage, nearly all the area was estimated to have inadequate outlet capacity through the drainage main. Of the 319,067 ha (787,819 acres) that were potentially drainable in the study area, approximately 95% of the area (302,952 ha) was estimated to have a drainage district outlet capacity that was less than 0.95 cm/day. So, while in most cases adequate field drainage existed, the actual drainage of most fields was estimated to be constrained by the drainage district system.

Based on this 1980's study, they estimated based on surveys of farmers that within the study area 68% of the maximum yield was being realized but if all drainage district outlets were sized to at least a 0.95 cm/day drainage coefficient 90% of the maximum yield could be realized (Kanwar et al., 1983). While it has been estimated that significant yield improvement could result from improved outlet capacity of these drainage district systems there have been few upgrades to the design capacity. Drain outlet improvements have been hampered by poor economic conditions as well as a requirement for the majority of landowners to approve additional drainage taxes to pay for improved systems. Improvements in grain commodity prices may increase the interest in drainage main improvement and it is important to understand potential impacts of drainage main rehabilitation on crop yields and water flow.

While the 1980's study provides a basis for evaluating the impacts of drainage main improvement, we used a drainage model, DRAINMOD, to evaluate the potential impacts of drainage main design. The field scale deterministic hydrologic model, DRAINMOD (Skaggs, 1978) simulates a soil-water regime of surface and subsurface drainage systems, and predicts surface runoff, infiltration, evapotranspiration, subsurface drainage and seepage (vertical and lateral) from subsurface drained landscapes. The daily precipitation, maximum and minimum temperature for a period from 1945 to 2004 (Fig. 1) were used from the Humboldt weather station, located in Humboldt County, IA. The average monthly temperature varied from -9°C in January to 23°C in July. The average monthly precipitation varied from 20 mm in January to 120 mm in June with an average annual precipitation of 785 mm. The rest of the input parameters such as soil, crop, and trafficability parameters were the same as

summarized by Singh et al. (2006). For drainage system design, a drain spacing of 24 m was used which is consistent with recommendations for many soils in north central Iowa (Anonymous, 1987) and the drainage coefficient was varied to evaluate the impact of drainage outlet design on water flow and crop production on a field-scale. Using the crop production estimates, an example county in north central Iowa was used to evaluate the potential impacts of drainage redesign on crop production. This example county had approximately 101,250 ha (250,000 acres) in drainage districts with an average drainage capacity of 0.46 cm/day.

Results and Discussion

Based on the DRAINMOD simulations, as expected, average annual subsurface drainage over the 60 year simulation period is predicted to increase as drainage coefficient increases and, conversely, as drainage coefficient increases surface water runoff is predicted to decrease (Figure 1). Potential increases in subsurface drainage would have water quality implications since increased subsurface drainage would be expected to increase the export of water soluble contaminants with nitrate-nitrogen of particular concern. However, decreased surface water runoff would be expected to decrease export of those contaminants most closely associated with sediment export (e.g., phosphorus, pesticides, and bacteria).

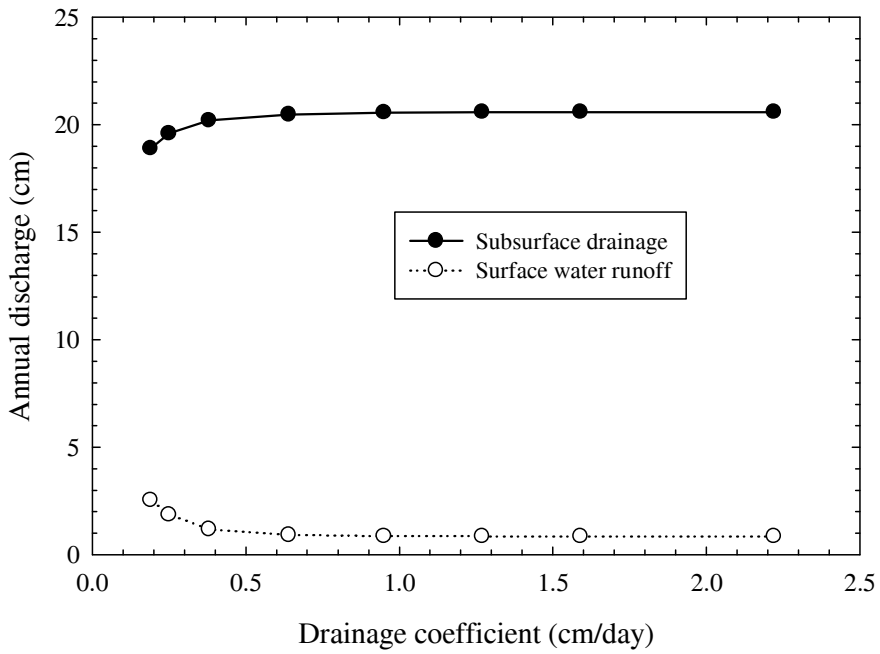

Figure 1. Predicted impact of drainage outlet coefficient on surface runoff and subsurface drainage.

Also, as expected, increases in drainage coefficient is expected to have a positive impact on crop production with average predicted relative yield increasing from about 87% at a drainage coefficient of 0.46 cm/day to a relative yield of about 97% at a drainage coefficient of 0.95 cm/day (Figure 2). Using the predicted relative yield values shown in Figure 2 along with the drainage capacity estimations for the

example county, the overall yield increase of improving the drainage from existing conditions to a drainage coefficient of 1.27 cm/day was estimated to be 7.7%. This value assumes that well-drained soils would not benefit from improved outlet capacity and that drainage districts with a very low drainage coefficient would have disproportionate benefits. Considering a potential 7.7% increase in yield for both corn and soybeans, a base corn yield of 11,915 kg/ha (190 bushels/acre) and a base soybean yield of 3,695 kg/ha (55 bushels/acre), and 65% corn area with 35% soybean area; drainage redesign in this example county (101,250 ha) would be predicted to provide an annual increase of 63.6 million kg (2.5 million bushels of corn) and 10.6 million kg (0.39 million bushels) of soybeans.

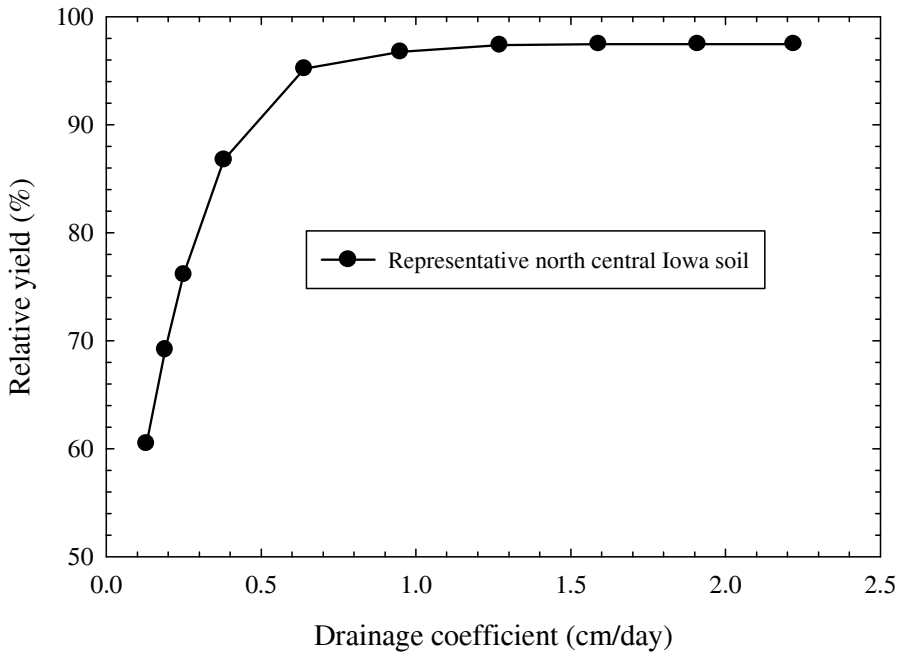

Figure 2. Predicted impact of drainage outlet coefficient on relative crop yield.

An additional factor to consider in upgrading the outlet capacity is the possibility for improved drainage in farmed wetland areas where farmed wetlands are partially drained wetlands that may contain some tile and can often be farmed. However, the degree of drainage in continuously cropped farmed wetlands cannot be improved beyond what it was in 1985, when Swampbuster took effect in the United States. So, while improving the outlet capacity may provide increased crop production for the majority of the drainage area and potentially reduce surface runoff there could be potential concern with improved drainage of continuously cropped farmed wetlands in addition to nitrate loss. Overall, the current situation results in poor drainage conditions for the prior converted cropland, and relatively unproductive farmed wetlands that are continuously farmed with little value as cropland or as wetland.

A potential strategy to mitigate concerns regarding drainage and wetland protection would be to integrate nitrate-removal wetlands into the redesigned drainage systems. In this type of integrated system, the water from the drainage district would be routed

through a wetland prior to release to a downstream waterbody. Using this type of integrated strategy, wetlands would be specifically sited to capture and treat drainage water and these wetlands would also provide important ecological functions on the landscape while providing a better outlet condition for prior converted cropland.

Conclusions

Subsurface drainage is essential for crop production in north central Iowa but currently many of the systems are not optimally designed relative to crop production. Many of the systems have a drainage coefficient that is well below the recommended design standards and the systems are likely reaching the end of their design life. So, with recent increased commodity prices there may be renewed interest in drainage outlet improvements. As discussed, a redesign of the drainage systems could have significant positive impacts on crop production and there is the potential to reduce surface water runoff. However, the potential increase in nitrate-nitrogen export from improved drainage would need to be considered in this redesign and nitrate-removal wetlands could provide an opportunity for treating the drainage water before discharging to downstream waters. In addition, these nitrate-removal wetlands may provide improved ecological functioning compared to continuously cropped farmed wetlands that are likely present in many of these drainage areas of north central Iowa.

References

Anonymous, 1987. Iowa Drainage Guide. Special Report (Revised), Cooperative Extension Service, Iowa State University, Ames, IA 50011.

Baker, J.L., S.W. Melvin, D.W. Lemke, P.A. Lawlor, W.G. Crumpton, and M.J. Helmers. 2004. Subsurface drainage in Iowa and the water quality benefits and problem. Drainage VIII Proceedings of the Eighth International Symposium. ASAE Meeting Paper No. 701P0304. St. Joseph, MI.

Kanwar, R.S., H.P. Johnson, D. Schult, T.E. Fenton, and R.D. Hickman. 1983. Drainage needs and returns in north-central Iowa. Trans. of the ASAE 26(2): 457-464.

Schult, D.L., T.E. Fenton, R.D. Hickman, H.P Johnson, R.S. Kanwar, and J.F. Timmons. 1981. Present and potential agricultural drainage situations in the ipper Des Moines River basin – Ten County Area. Special Report, Departments of Agricultural Engineering, Agronomy, and Economics, Iowa State University, Ames, IA.

Singh, R., M. J. Helmers, and Z. Qi. 2006. Calibration and validation of DRAINMOD to design subsurface drainage systems for Iowa's tile landscapes. Agricultural Water Management. 85: 221-232.

Alfalfa reference ET from a weighing lysimeter and estimates from the ASCE Standardized Reference ET Equation in the Arkansas Valley of Colorado

Allan Andales[1], Dale Straw[2], Thomas Ley[2], Abdel Berrada[1]
[1] Department of Soil and Crop Sciences, Colorado State University, Fort Collins, CO 80523-1170; email: Allan.Andales@colostate.edu
[2]Colorado Division of Water Resources

ABSTRACT

The American Society of Civil Engineers (ASCE) standardized reference ET equation has been prescribed for use in the Arkansas Valley of Colorado for estimation of reference evapotranspiration (ET) and subsequent estimation of crop consumptive use. In 2006, a precision weighing lysimeter (mechanical lever scale – load cell combination) was installed at Rocky Ford, Colorado to verify the performance and predictive accuracy of the ASCE standardized ET equation for calculating alfalfa reference (tall reference) ET values. The undisturbed soil monolith is contained in a tank that is 3 m x 3 m in area and 2.4 m deep. The standard deviation of the weight measurements was less than 0.02%, based on calibration of the load cell with known weights. Alfalfa was established on the lysimeter and surrounding field (4 ha) in 2007. Instrumentation for micrometeorological measurements as well as soil temperature, soil heat flux, and soil moisture measurements were installed. Calculated ET from the ASCE standardized equation (ET_{rs}) and ET measured from the lysimeter (ET_r) were compared during periods in the 2008 season when the alfalfa crop on the lysimeter and surrounding field were considered to be in reference conditions. Calculated ET_{rs} agreed well with ET_r from the lysimeter when wind conditions were relatively calm and vapor pressure was relatively stable. However, ET_{rs} tended to be greater than ET_r under advective conditions. Also, calculated ET_{rs} was notably less than ET_r from the lysimeter on a number of days late in the growing season. The underlying causes of these differences need further investigation.

INTRODUCTION

Accurate estimates of crop consumptive use (evapotranspiration) are needed to effectively manage irrigation in the Arkansas River Basin of Colorado and to maintain compliance with the Arkansas River compact with Kansas. The American Society of Civil Engineers (ASCE) standardized Penman-Monteith equation (PME) (Allen et al., 2005) has been approved by the U.S. Supreme Court as the method of determining evapotranspiration (ET) for compact compliance, but has not been tested in the Arkansas Basin. A validated ASCE-PME can be a widely-applicable tool for irrigation management in the Arkansas River Basin of Colorado.

An accurate way to quantify actual ET rates from a crop is to use a precision weighing lysimeter that directly measures ET based on changes in weight of an intact soil monolith containing an actively growing crop. In 2006, construction of a precision weighing lysimeter was completed at Rocky Ford in the Arkansas River Basin of Colorado. One purpose of the lysimeter is to provide accurate measurements of crop ET for the evaluation of the ASCE-PME for conditions in the Arkansas River Basin. The objective of this paper is to present a preliminary evaluation of the performance of the ASCE-PME compared to hourly alfalfa ET measurements from the weighing lysimeter in 2008.

DESCRIPTION OF THE LYSIMETER

The lysimeter is located at the Arkansas Valley Research Center (38° 2´ 17.30´´ latitude and 103° 41´ 17.60´´ longitude), approximately 3.2 kilometers east of Rocky Ford in Otero County, Colorado (NW1/4 Sec 21, T23S, R 56W). The elevation at the site is approximately 1,274 m above mean sea level. The soil type is Rocky Ford; coarse-loamy, mixed, superactive, mesic Ardic Argiustoll.

The long-term average annual precipitation at the site is 300 mm, with May through August having the highest rainfall. The total average annual snowfall is 589 mm. The annual average minimum temperature is 2.4 °C and the annual average maximum temperature is 21 °C. The last spring frost (0.3 °C) occurs on or before May 1 and the first fall frost on or before October 5 in 50% of the years; thus the average length of the growing season for warm-season crops like corn is 158 days.

The crop lysimeter was patterned after the lysimeters at Bushland, Texas operated by USDA-Agricultural Research Service. Marek et al. (1988) provide details of the lysimeter design. The lysimeter consists of an inner tank with dimensions of 3.0 m x 3.0 m surface area x 2.4 m depth and an outer containment tank. Installation and calibration of the crop lysimeter was completed in 2006. The inner tank was filled with undisturbed soil (soil monolith) from the same field where the lysimeter is located (Fig. 1). The soil tank moves freely within the outer tank and the top edges of the two are separated by a few millimeters. The chamber between the two tanks houses the weighing mechanism, the drainage tanks, data loggers and has standing room for half-a-dozen people. The weighing mechanism consists of a mechanical lever scale-load cell combination (mV V^{-1} output; 0.02% accuracy). Based on calibration of the load cell to measure the weight of the inner tank containing the soil monolith, a unit change in load output (1 mV V^{-1}) is equivalent to 76 mm of water. Thus, changes in load cell output are simply multiplied by 76 to obtain the amount of water lost through ET or amounts of water gained through precipitation or irrigation. Water that percolates through the soil monolith is collected in two drainage tanks suspended from the scale frame that supports the soil tank, so that there is no overall weight change registered by the scale as water drains into the tanks. One tank collects water from the internal portion of the monolith and the other tank collects water from the perimeter of the monolith. Berrada et al. (2008) provide details on the installation, calibration, and management of the crop lysimeter.



Figure 1. The inner tank plus soil being lowered inside the containment tank of the crop lysimeter. Photo taken by Michael Bartolo.

The crop lysimeter and surrounding field were seeded with alfalfa (Genoa variety) on 9 August 2007. The dimensions of the surrounding field are 158.5 m x 256.1 m (4.06 ha). Instrumentation for measuring rainfall, wind speed and direction, air temperature, humidity, incoming and reflected radiation, photosynthetically active radiation, and canopy temperature were installed above the lysimeter (Fig. 2). Soil temperature sensors were installed at 0.01 m, 0.04 m, 0.5 m, 1.0 m, and 2.0 m below the soil surface of the monolith. Heat flux plates were also installed 0.1 m below the soil surface. Two 3.8-cm diameter electromechanical steel tubes (EMT) were installed in the monolith to monitor soil water content with a neutron probe. Also, soil temperature sensors and neutron probe access tubes were installed adjacent to the lysimeter. The lysimeter load cell and sensor outputs are logged by a Campbell Scientific CR-7 data logger mounted in the underground chamber. Detailed descriptions of the sensors and their placement were given by Berrada et al. (2008).



Figure 2. View of the crop lysimeter looking to the east. The manhole for accessing the data logger, weighing mechanism, and drainage tanks is on the left; and micrometeorological sensors are mounted above the lysimeter.

METHODS

The lysimeter load cell output was recorded every 10 seconds throughout the 2008 growing season. Fifteen-minute averages of the load cell output were used in the calculation of ET. The difference between beginning and ending load cell outputs (mV V^{-1}) on each hour were multiplied by 76 mm mV^{-1} V to obtain hourly rates of ET (mm h^{-1}).

The alfalfa crop on the lysimeter and the surrounding field were managed similarly. Both the lysimeter and surrounding field were furrow-irrigated at the same times (Table 1). Furrow irrigation of the lysimeter was done manually with the use of a metered hose to approximate water application rates on the surrounding field. Furrow spacing was 0.76 m, with 4 furrows on the lysimeter.

Table 1. Irrigation dates and amounts for the lysimeter (4/1/2008 – 9/1/08).

Date	Net irrigation amount (mm)
April 2	114
May 12	119
June 20	121
July 1	165
July 25	164
August 4	146
Total	829

Alfalfa on the lysimeter and surrounding field was harvested three times: 6/11/2008; 7/21/2008; 9/1/2008. After each cutting, alfalfa canopy height was about 0.08 m, which was significantly below the standard reference height of 0.50 cm specified by the ASCE-PME. For purposes of comparing ET_r from the lysimeter and ET_{rs} from the ASCE-PME, we assumed that the alfalfa crop was approximately at reference conditions when the observed height was greater than 0.30 m. The alfalfa height remained below 0.30 m for about 2 to 3 weeks after each harvest. We assumed that ET_r from the lysimeter was comparable to the ASCE-PME ET_{rs} values during the following periods, when alfalfa crop height was at least 0.30 m: 4/30/2008 – 6/10/2008; 6/30/2008 – 7/20/2008; and 8/3/2008 – 8/31/2008.

The hourly version of the ASCE-PME (Allen et al., 2005) was used to calculate alfalfa reference ET_{rs} using hourly averaged micrometeorological data recorded directly above the lysimeter. The hourly ASCE-PME is given below.

$$ET_{rs} = \frac{0.408\Delta(R_n - G) + \gamma \frac{C_n}{T + 273} u_2 (e_s - e_s)}{\Delta + \gamma(1 + C_d u_2)}$$

where:

ET_{rs} = standardized reference crop evapotranspiration for tall surfaces (mm h^{-1}),

R_n = calculated net radiation at the crop surface (MJ m^{-2} h^{-1}),

G = soil heat flux density at the soil surface (MJ m^{-2} h^{-1}),

T = mean hourly air temperature at 1.5 to 2.5-m height (°C),

u_2 = mean hourly wind speed at 2-m height (m s^{-1}),

e_s = saturation vapor pressure at 1.5 to 2.5-m height (kPa),
e_a = mean actual vapor pressure at 1.5 to 2.5-m height (kPa),
Δ = slope of the saturation vapor pressure-temperature curve (kPa $°C^{-1}$),
γ = psychrometric constant (kPa $°C^{-1}$),
C_n = 66; numerator constant for tall reference and hourly time step (K mm s^3 Mg^{-1} h^{-1}) and C_d = 0.25 (daytime), 1.7 (nighttime); denominator constants for tall reference and hourly time step (s m^{-1}).
Units for the 0.408 coefficient are m^2 mm MJ^{-1}.

Hourly ET_{rs} values calculated from the ASCE-PME were compared to hourly ET_r values measured from the lysimeter on days when alfalfa crop height was at least 0.30 m. Agreement between ET_{rs} and ET_r values were evaluated with the following statistics:

- RE = relative error of mean (%); zero is best
- RMSE = root mean square error (mm); average error of hourly ET_{rs}
- d = index of agreement (0 – 1; see Willmott, 1981); 1 means perfect agreement between ET_{rs} and ET_r
- p-value = probability of ($T \leq t$) from a 2-tailed t-test comparing means; p-value > 0.05 indicates mean ET_{rs} is not significantly different from mean ET_r (from lysimeter) at 0.05 significance level.

RESULTS AND DISCUSSION

The cumulative alfalfa ET measured from the lysimeter (4/1/2008 – 9/1/2008) was 1042 mm (Fig. 3). In contrast, precipitation during the same period was only 196 mm. The irrigations applied during the season (Table 1) typically penetrated down to 50 cm below the monolith surface (Fig. 4) but could not refill the deeper soil layers in mid-season. However, the irrigation on August 4 plus several rainfall events later in August penetrated down to 190 cm.

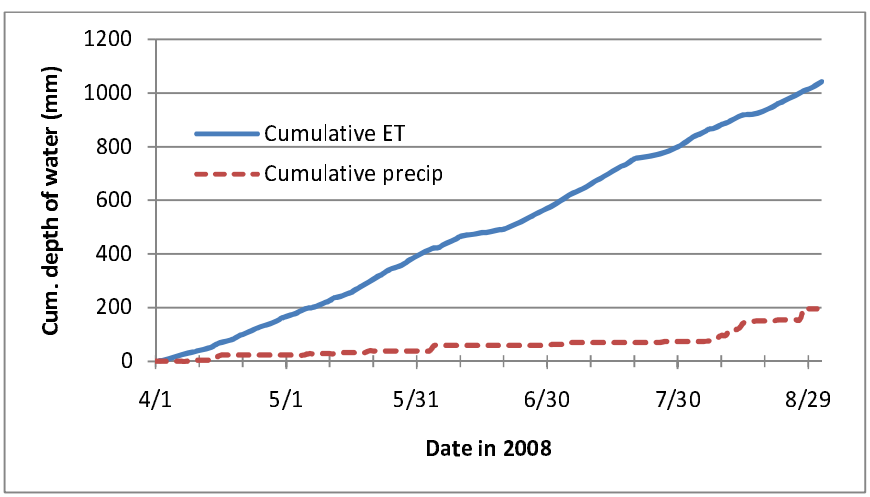

Figure 3. Cumulative alfalfa ET and precipitation on the lysimeter in 2008.

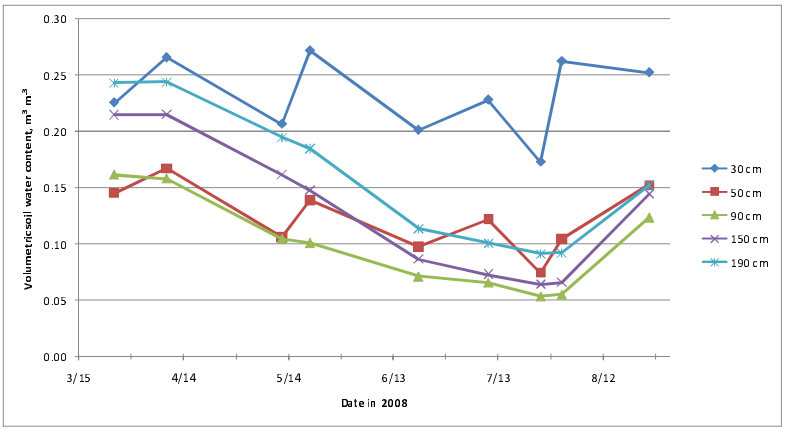

Figure 4. Volumetric soil water content at selected depths in the lysimeter for 2008.

Figures 5 to 8 show representative comparisons of hourly ET computed from the ASCE-PME (ET_{rs}) versus ET measured from the lysimeter (ET_r) for three different days during the 2008 season, when the alfalfa crop on the lysimeter and surrounding field was considered to be in reference condition. June 7 (Fig. 5) is an example of a day (early season) when ET_{rs} and ET_r matched well throughout the day. Wind conditions were relatively calm and vapor pressure was relatively stable (Fig. 8). Consequently, relative error and RMSE were low and the index of agreement (d) was close to 1.

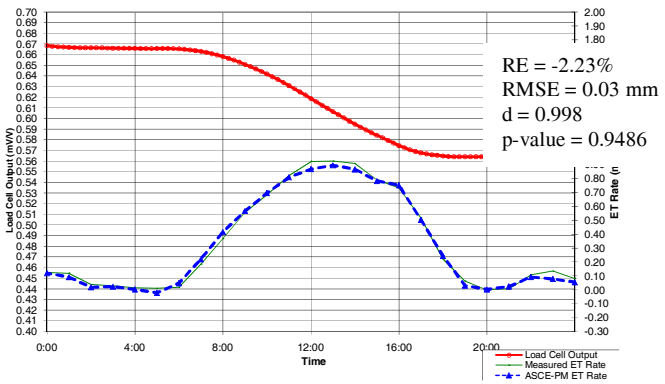

Figure 5. ET rate and lysimeter load cell output on 7 June 2008 (before 1st alfalfa cutting).

June 2 (Fig. 6) was also early in the season but had elevated afternoon temperatures, higher afternoon wind speeds, and a drop in vapor pressure (Fig. 8). The drop in solar radiation after 1200 h (Fig. 8) indicated increased cloud cover, which was reflected in the drop in both the lysimeter and ASCE-PME ET rates. However, the ASCE-PME seemed to be overly sensitive to higher wind speed and decreased vapor pressure that occurred after 1400 h. The equation over-predicted ET under these conditions (Fig. 6). Relative error and RMSE were considerably higher

and d was lower compared to those on June 7. The late afternoon to early evening (1600-2000 h) ET rates from the lysimeter ranged from 0.25 to 0.72 mm h^{-1} on June 2 compared to a range of 0.00 to 0.70 mm h^{-1} for the same period on June 7 (Fig. 5). On June 2, the strong winds that came after 1400 h came from the WSW (235-250 azimuth from true N). The source of this advected hot dry air was a large expanse of dry prairie in the aforementioned direction from the lysimeter.

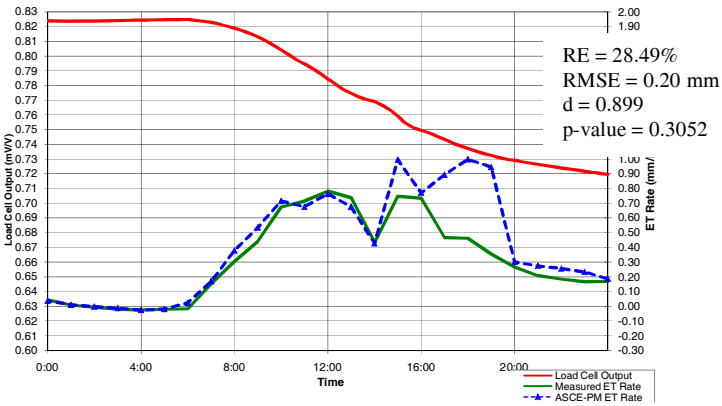

Figure 6. ET rate and lysimeter load cell output on 2 June 2008, showing overestimation of afternoon ET_r by ASCE-PM equation.

Figure 7 shows a comparison late in the season (August 28) where the computed ET_{rs} from the ASCE-PME was notably less than the measured ET_r from the lysimeter during midday. This under-prediction was noted on a number of days late in the season. No unusual weather conditions were evident (Fig. 8). However, the increased soil water content of the monolith profile (Fig. 4) and the 0.6 m alfalfa canopy height that was slightly higher than ASCE-PME standard height (0.5 m) may have contributed to the underestimation. The underlying causes of these differences need further investigation.

In all the comparisons between ET_r from the lysimeter and ET_{rs} calculated from the ASCE-PME, the p-values were greater than 0.05. This indicated that the calculated alfalfa ET rates from the ASCE-PME were not statistically different from the ET rates measured from the lysimeter (at 0.05 significance level).

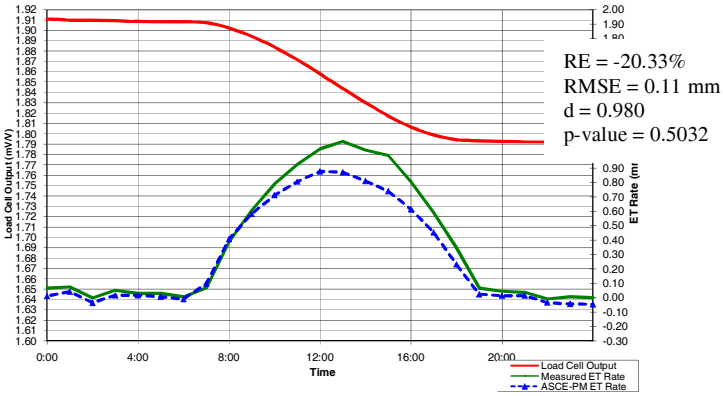

Figure 7. ET rate and lysimeter load cell output on 28 August 2008, showing mid-day under-estimation of ET_r by the ASCE-PM equation. Alfalfa crop height was about 0.6 m.

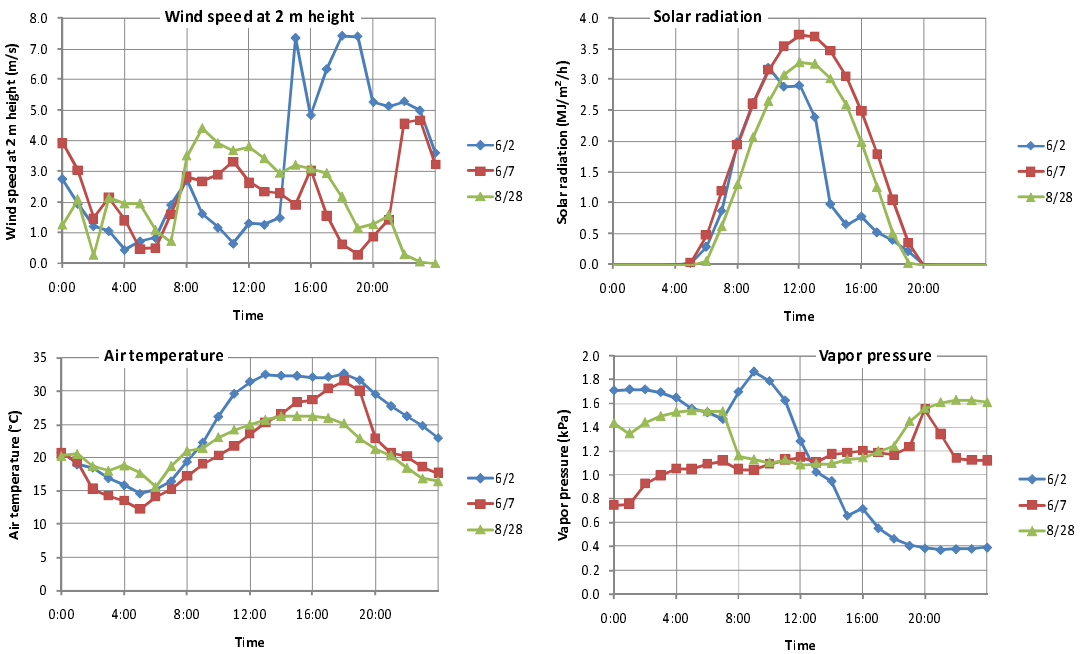

Figure 8. Comparisons of primary weather variables among the three sample dates.

CONCLUSION

This paper presented preliminary comparisons between hourly alfalfa reference ET calculated from the ASCE-PME and measured values in 2008 from a newly installed precision weighing lysimeter at Rocky Ford, Colorado. The ASCE-PME gave alfalfa ET estimates that agreed well with lysimeter measurements when sensible heat advection was not significant. The equation tended to over-estimate hourly ET rates when high wind speeds (> 5 m s^{-1}) occurred with elevated air

temperature and decreased vapor pressure. On the other hand, the equation under-estimated mid-day alfalfa ET rates on some days late in the season, possibly because of the assumed canopy height (0.5 m) being less than the actual canopy height and/or soil water and root water uptake dynamics that are not accounted for. Further studies are needed to evaluate the accuracy of the ASCE-PME in estimating alfalfa reference ET for different conditions in the Arkansas River Basin.

REFERENCES

Allen, R.G., Walter, I.A., Elliott, R., Howell, T., Itenfisu, D., and Jensen, M. (Eds.) (2005). *The ASCE standardized reference evapotranspiration equation*. Environmental and Water Resources Institute of the American Society of Civil Engineers, Reston, Virginia.

Berrada, A., Simmons, L., Straw, D., Bartolo, M., and Ley, T. (2008). "The large lysimeter at the Arkansas Valley Research Center: Ojectives and accomplishments" *Technical Bulletin TB08-02*, http://www.colostate.edu/Depts/AES/Pubs/pdf/tb08-2.pdf, Agricultural Experiment Station, Colorado State University, Fort Collins, Colorado.

Marek, T.H., Schneider, A.D., Howell, T.A., and Ebeling, L.L. (1988). "Design and construction of large weighing monolithic lysimeters." *Trans. ASAE* 31(2), 477-484.

Willmott, C. J. 1981. "On the validation of models." *Physical Geography* 2, 184-194.

ACKNOWLEDGEMENTS

The lysimeter project is a joint effort between the Colorado Water Conservation Board, Colorado Division of Water Resources, Colorado Water Institute, and CSU. Technical support has also been provided by USDA-Agricultural Research Service engineers and scientists in Fort Collins, CO and Bushland, TX.

ASCE Standardized Penman-Monteith Alfalfa Reference ET and Crop ET Estimates for Arkansas River Compact Compliance in Colorado

Thomas W. Ley PE, M. ASCE, Dale E. Straw PE[2], and Robert W. Hill PE, M.ASCE[3]

[1] Colorado Division of Water Resources, Pueblo, CO 81004; PH (719) 542-3368; FAX (719) 544-0800; email: thomas.ley@state.co.us
[2] Colorado Division of Water Resources, Denver, CO 80203; PH (303) 866-3581; FAX (303) 866-3589; email: dale.straw@state.co.us
[3] Professor, Dept of Biological and Irrigation Engineering, Utah State University, Logan, UT 84322; PH (435) 797-2791; FAX (435) 797-1248; email: robert.hill@usu.edu

Abstract

In the fourth report in the case of Kansas v. Colorado (No. 105, Original, U.S. Supreme Court), regarding compliance with the Arkansas River Compact, the Special Master hearing the case recommended specific changes by which Arkansas River streamflow depletions at the Colorado-Kansas Stateline are determined. One of the major changes was the recommendation to move away from the modified Blaney-Criddle method and adopt a reference crop evapotranspiration-mean crop coefficient approach to determine crop consumptive use estimates for input to the computer model used to determine compact compliance. This paper discusses some of the steps the State of Colorado has taken to comply with this recommendation.

Introduction

The lower Arkansas River Valley of southeastern Colorado is characterized as a long, relatively narrow and shallow valley, extending approximately 260 km (160 mi) from below Pueblo Reservoir near Pueblo, Colorado on the western end, to the Colorado-Kansas Stateline on the eastern end, east of the town of Holly, Colorado (Figure 1). Within the lower Arkansas River Valley east of Pueblo there are approximately 260,000 acres of irrigated cropland. Forage crops, specifically alfalfa, are predominant, followed by grains (corn, wheat, sorghum) and vegetables (onions, peppers, melons).

Historically, the modified Blaney-Criddle method has been used to determine crop consumptive use, or potential crop evapotranspiration (PET) estimates for input to the Hydrologic-Institutional (HI) Model. The HI Model was developed to determine depletions to usable Arkansas River streamflows at the Colorado-Kansas Stateline

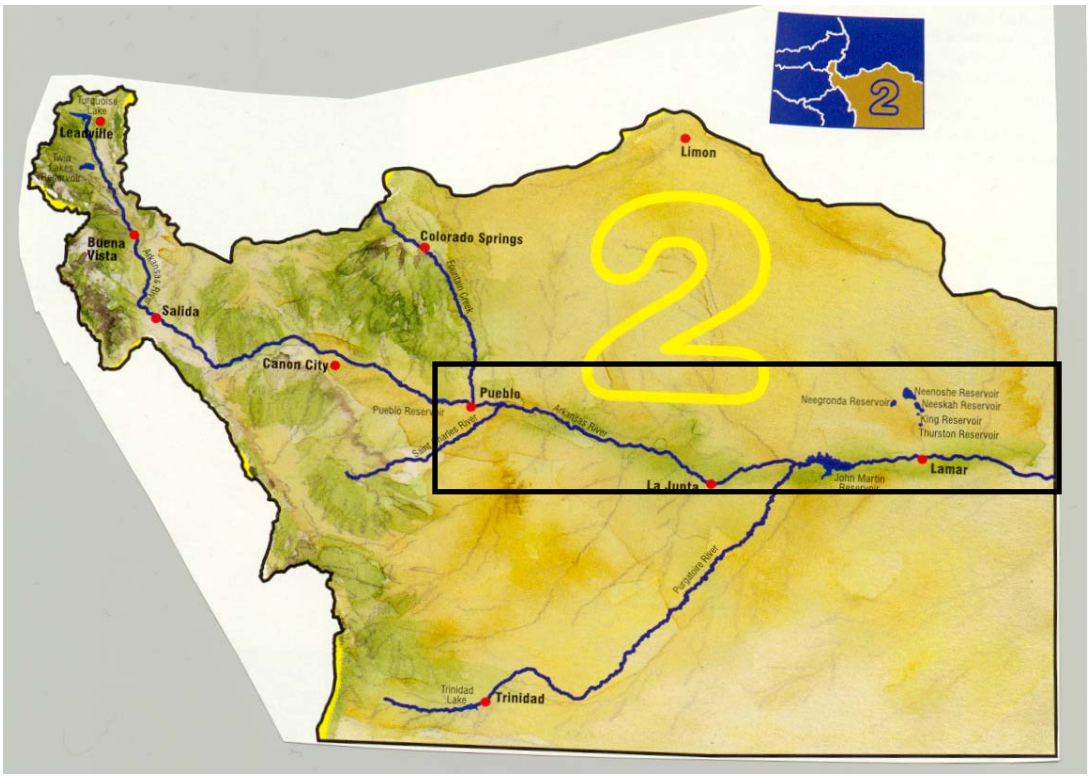

Figure 1. Lower Arkansas River Valley in Southeastern Colorado.

caused by post-Compact well pumping in Colorado, and evaluate whether the State of Colorado is in compliance with the Arkansas River Compact between the two States. The HI Model uses estimates of potential crop water use to predict diversions for irrigation by ditches in Colorado and to calculate actual crop water use. Modified Blaney-Criddle crop consumptive use estimates were developed using monthly maximum and minimum air temperature data from six NOAA Cooperative Observer weather station network sites located near Pueblo, Rocky Ford, La Junta, Las Animas, Lamar, and Holly, Colorado. These long term NOAA Coop stations are relatively evenly distributed down the Arkansas River Valley from Pueblo to the Colorado-Kansas Stateline.

In his fourth report (Littleworth, 2003) in the case of Kansas v. Colorado (No. 105, Original, U.S. Supreme Court), regarding compliance with the Arkansas River Compact, the Special Master hearing the case recommended specific changes by which PET was to be determined, for both the historical period, and for annual updates. Based on expert testimony regarding the inaccuracy of the Blaney-Criddle method, and the increasing availability of electronic weather station data in the area, the Special Master recommended that crop consumptive use estimates for input to the HI Model should be based on a reference crop ET-mean crop coefficient approach. Specifically, the ASCE standardized reference evapotranspiration equation (ASCE-EWRI, 2005) and available electronic weather station data should be used to estimate tall (alfalfa) reference crop ET_{rs}, and alfalfa-reference based mean crop coefficients adapted for the major crops grown in the area used to compute crop ET.

This paper will discuss:

1) evaluation of existing automated electronic weather station sites at the time of the Special Master's recommendation, various weather station siting issues, and steps taken to improve the network of electronic weather stations within irrigated agricultural areas of the Arkansas Valley of southeastern Colorado;
2) cooperation and collaboration with the State of Kansas to evolve and improve processes in the review and quality assurance of the weather data used in the ASCE standardized equation to compute tall crop (alfalfa) reference evapotranspiration, $ET_{rs;}$
3) brief review of the development of mean crop coefficients used to estimate crop ET for the major crops produced in the area.

Further discussion and background of steps taken by the States of Colorado and Kansas to implement this recommendation are discussed in companion papers in these proceedings (Andales et al., 2009, Book and Brengosz, 2009; Brengosz, 2009; Ley et al., 2009).

Weather Data Requirements

All versions of the Penman combination equation, including the ASCE standardized reference ET equation (ASCE-EWRI, 2005), require detailed weather data. Ideally, these weather data (intended for reference ET estimation) should be collected at weather stations sited over well-watered, clipped grass surfaces in open, irrigated settings. For daily estimates, required daily weather data are total daily solar radiation, daily maximum and minimum air temperature, mean daily dewpoint temperature or actual air vapor pressure as determined from measurements of relative humidity, and mean daily wind speed at 2 m above the surface. Beginning in the early to mid-1980's, automated electronic weather station networks were installed in agricultural areas of Nebraska and California. Since then, additional States have installed similar networks, including, for example, Washington State PAWS, Oklahoma Mesonet, and the Texas North Plains PET network. In Colorado, the Colorado Agricultural Meteorological Network (CoAgMet) began in the early 90's (Duke, 1996). Many of these weather station networks collect data for the purpose of, among others, computing reference ET and crop ET for crops of interest in their respective areas. These data should not be taken at face value, but carefully assessed using recommended data integrity and quality control procedures. Such procedures must also evaluate the weather collection site and local and regional environment to determine if the weather data were collected in the prescribed reference environment. These issues are discussed further below.

Weather Station Site Assessment

It is recommended that weather data intended for reference ET estimation be collected at weather stations sited over well-watered, clipped grass surfaces in open,

irrigated settings (Allen et al, 1998; ASABE, 2004; Allen, 1996). Reference ET (and therefore crop ET) estimates will be artificially high when weather data are collected in environments that are drier than these reference conditions (Brown and Ley, 1993; Ley, et al., 1996). Specifically, when located in environments that are drier than the reference condition, weather stations will measure increased air temperatures, reduced water vapor in the air, and potentially greater wind speeds, resulting in increased reference ET estimates compared to the reference environment. In such cases, a greater portion of the energy available is used in sensible heating of the air and soil and less in evaporation (which results in cooling and humidification of the air) because of the reduced amount of environmental moisture available for evaporation. This effect has generally been termed an aridity effect.

Each weather station proposed for use in calculation of reference ET estimates should be visited and assessed as to potential aridity effects. Siting information to note include whether the station is located in a generally irrigated agricultural environment, what the local siting conditions are out to a radius of several hundred feet, what the ground cover is immediately under and around the station and how is it maintained, and what the condition is of the fetch (surface and moisture characteristics of the land) in the primary upwind direction. Deviations from prescribed reference conditions described above indicate that the weather data collected at the site need to be carefully evaluated for aridity effects. This includes a very careful evaluation of the relative humidity data and the relationship between daily minimum air temperature and dewpoint temperature (ASCE-EWRI, 2005). Suggested procedures for correcting weather data for potential aridity effects are given in Allen (1996) and ASCE-EWRI (2005). Any corrections to the weather data should be noted and maintained as part of the record.

At the time of trial testimony, and the Special Master's subsequent formulation of recommendations regarding crop ET methodology, circa 2002, only 4 CoAgMet stations were in existence in the lower Arkansas River Valley (Vineland, Avondale, Rocky Ford, and Lamar01). Of these, the Vineland, Avondale, and Rocky Ford sites were found to be located in irrigated environments, while the Lamar01 station was found to be located in a dry, rangeland environment about 5 miles south of irrigated land near Lamar CO. As a result, the Lamar01 data have generally been considered unusable for reference ET computation. This left essentially two CoAgMet weather stations: Avondale and Rocky Ford to represent the lower Arkansas Valley, from Pueblo CO to the Colorado-Kansas Stateline. The Avondale and Vineland CoAgMet stations are only about 6 miles apart, and for reasons discussed later, the Vineland station data are only used to fill in for missing data at Avondale. Figure 2 is a satellite image of the lower Arkansas River Valley of Colorado showing the current locations of CoAgMet weathers stations. In 2002, the Special Master's recommendation was to determine crop ET for the entire valley using only the Avondale and Rocky Ford stations located in the western half of the lower valley.

Mean monthly ratios of crop ET (computed using ASCE standardized alfalfa reference ET and mean crop coefficients) to modified Blaney-Criddle crop

consumptive use, for the 7-year period: 1994-2000 and for 10 different crops, were developed to calibrate the modified Blaney-Criddle method to the ASCE standardized reference ET-mean crop coefficient method. The Avondale CoAgMet site was used to calibrate the Pueblo NOAA site, while the Rocky Ford CoAgMet site was generally used to calibrate the Rocky Ford, La Junta and Las Animas NOAA sites for the historic period. The trend in calibration factor change between Pueblo and Rocky Ford was used to develop extrapolated calibration factors for use at Lamar and Holly. Calibration factors were applied to modified Blaney-Criddle crop consumptive use estimates for the historic compact period, 1950-1993, to adapt them to standardized reference ET-mean crop coefficient-based crop ET estimates. For the period 1994-2004, Avondale and Rocky Ford CoAgMet data were directly used to compute alfalfa reference ET and subsequently, crop ET at those sites. However, again, the extrapolated calibration factor trend was used to calibrate the NOAA sites from Rocky Ford east to the Stateline for this period.

Weather Station Density

A question of the "representativeness" of the Avondale and Rocky Ford CoAgMet weather stations of conditions in Lamar and Holly, much less La Junta and Las Animas immediately arose. Hubbard (1994) investigated the spatial variability of daily weather variables measured at 24 locations of the High Plains Automated Weather Data Network of the central US during the period 1988-92. The coefficient of determination, r^2, the ratio of the explained variation to the total variation between parameter values at pairs of locations, was computed through regression techniques and then plotted as a function of time of year for given separation distances between stations. To explain 90% of the variation in daily weather variables between sites, Hubbard found that a 60-km (37 mi) station spacing was needed for maximum temperature; 30-km (19 mi) spacing for minimum temperature, relative humidity, solar radiation, and reference ET; 20-km spacing (12.5 mi) for soil temperature, and 10-km (6.2 mi) spacing for wind speed. Seasonal weather differences were observed to strongly affect spatial variability.

Spatial dependence structure of multivariate time series at several locations in space (i.e., electronic weather station data collected at several locations) can be analyzed through an evaluation of the cross-correlations between the multiple series. For example, a multivariate autoregressive model of order one, AR(1), of a state variable (weather parameter or reference ET) describes a state-space process with lag-zero and lag-one correlation in space and lag-one temporal correlation (Bras and Rodriguez-Iturbe, 1985). Lag-zero spatial correlation describes the spatial coherence of a given variable measured on the same day at a number of sites. Lag-one spatial correlation describes the spatial coherence of a given variable measured at one site with the same measured variable at a number of other sites on the previous day. Lag-one temporal correlation describes the temporal dependence structure of a given variable measured at one site with the same measured variable at the same site on the previous day. Ley (1995) developed multivariate AR(1) models of daily weather variables (max, min and dewpoint temperatures, solar radiation, and wind run) and daily alfalfa reference

ET for a 33-station agricultural weather network in Eastern Washington for the period 1989-91. Spatial variability was analyzed by plotting lag zero cross-correlation coefficient matrixes of the standardized zero-mean detrended residuals of each variable versus a matrix of interstation distances. These plots revealed that for spatial cross-correlation of no less than 0.95 (which for comparison to results of Hubbard (1994) is equivalent to a coefficient of determination of $r^2 = 0.90$); maximum interstation distances for the weather variables and reference ET were: maximum temperature approximately 50 km (31 mi); minimum temperature approximately 10 km (6 mi); dewpoint temperature approximately 10 km (6 mi); solar radiation approximately 30 km (19 mi); wind run approximately 6 km (3.7 mi); and reference ET approximately 20 km (12.5 mi). The narrower station distances are attributed to the more complex topography and influence of prevailing weather patterns in eastern Washington as compared to the High Plains area of Hubbard's study.

Hill and Ley (Appendix C, 2002) used these same procedures to evaluate spatial variability of electronic weather station data collected over the 7-year period 1994-2000 at the Avondale, Vineland, and Rocky Ford CoAgMet weather station sites and the Kansas State University site at Garden City KS. Assuming a minimum acceptable lag zero cross-correlation coefficient equal to 0.90 (somewhat more relaxed than the two studies previously described), Hill and Ley showed the Rocky Ford CoAgMet station could be considered an appropriate predictor as follows: maximum temperature for all NOAA locations east to the state line; minimum temperature, dewpoint temperature, solar radiation and alfalfa reference ET for La Junta and Las Animas NOAA locations, but not Lamar and Holly; daily wind run for the La Junta NOAA location, but not Las Animas, Lamar and Holly. The La Junta and Las Animas sites are within 26 miles east of Rocky Ford, however, Lamar is 60 miles east and Holly is about 86 miles east of Rocky Ford. These results indicated the Rocky Ford CoAgMet station does not provide representative reference ET estimates for computing crop ET for all locations of the Arkansas Valley from Rocky Ford east to the Colorado-Kansas Stateline.

Two new CoAgMet stations had just been established at about the time of the Special Master's recommendation in 2002: Lamar02 and Holly01. The Special Master recommended the data collected at these stations be evaluated and used as well. These sites and the data collected during 2002-2004 were evaluated. In each case, the weather stations were established in large un-irrigated fields on the fringe of irrigated areas. The Lamar02 data were considered usable for reference ET, but it was felt there was some aridity impact due to the local dry environment surrounding the station. The Holly01 site was considered to be too heavily impacted by dry, advected air and it was agreed to not use the data from this site for reference ET estimation.

Weather Station Network Development

Beginning in the spring of 2005, the CoAgMet weather station network in the lower Arkansas River Valley of Colorado was the focus of considerable enhancement.

Based on the analyses of spatial variability of weather variables by Hill and Ley (2002) and problems with the Lamar02 and Holly01 sites described above, a network of weather stations usable for reference ET purposes was developed (Figure 2). The established stations at Avondale, Vineland, and Rocky Ford remained in place. New electronic weather stations were established at Fowler, in the irrigated area between La Junta and Las Animas, and in the irrigated area east of Las Animas, between Las Animas and Lamar. The Fowler station was located on a golf course. The La Junta and Las Animas stations were located in large irrigated alfalfa fields. The Lamar02 site was moved, and is now known as Lamar04. It is located in a large irrigated alfalfa field. The Holly01 site was also moved and is called Holly02. It is also located in a large irrigated alfalfa field. Due to cooperator interest in the weather data, the Holly01 site was eventually re-established with another weather station. Supplies of spare sensors and parts (anemometer bearings) were procured to support maintenance. Routine weather station site visits were initiated for the purpose of maintaining vegetation growth in the immediate vicinity of the stations and to check/clean sensors. Since 2005, minor modifications have been implemented: the Avondale station was moved approximately 175 m north of its old location in June 2007 due to two new center pivots installed to the SW and NW that were irrigating the station. The Lamar04 station was moved approximately 30 m south of its old location in June 2007 to obtain separation distance from the corn crop that had been planted on the immediate north side of the old location.

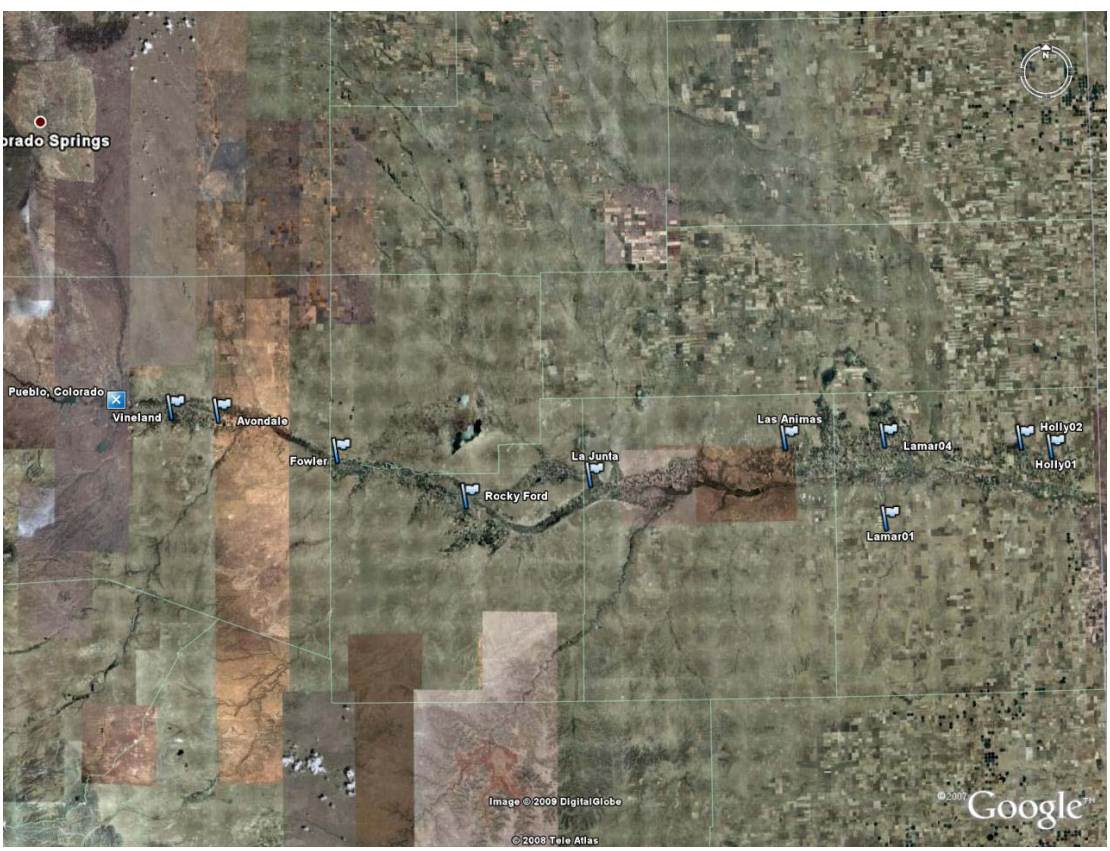

Figure 2. Current (2009) CoAgMet electronic weather station network in the lower Arkansas River Valley of Colorado.

When enough good quality weather data have been collected at Lamar04 and Holly02 (i.e., 5 years minimum), the two States have agreed to develop new calibration factors to re-calibrate the modified Blaney-Criddle method at each of the Lamar and Holly NOAA sites. New crop ET estimates for the period 1950-2004 will be used in the HI Model to determine if significant differences between the two calibration methods result.

Locating weather stations in irrigated alfalfa fields, as opposed to the recommended irrigated clipped grass, was considered necessary due to a lack of large irrigated grass fields or pastures in the lower Valley. The effects of the growing, and harvested, alfalfa on wind speeds measured at 2 m above the ground surface have been identified as a concern. A study of these effects was initiated in 2008 and results are reported in Ley et al. (2009).

Weather Data Integrity Assessment

Faulty weather measurement sensors (poor calibrations, poor or inadequate maintenance practice, sensor failure etc.) and inadequate weather data quality control/quality assurance procedures can result in inaccurate reference ET estimates. Procedures and guidelines for assessing the integrity of weather data for reference ET estimation have been developed (Allen, 1996; ASCE-EWRI, 2005; Allen et al., 1998). Methods for "correcting" data collected by poorly calibrated sensors, for adjusting temperature data collected at non-reference sites to reflect reference conditions, and for filling in missing weather data are also described in these same references. Officials for both the States of Colorado and Kansas have independently performed weather data integrity assessments using some combination of the methods referred to above and summarized below. In most cases, very similar "corrected" data sets have been developed. Where differences are found, further interaction between the two States occurs until a final data set agreeable to both sides is developed. Any corrections to the weather data are noted and maintained as part of the record.

Generally, the following steps are taken to assess weather data integrity at a single station. Trends among neighboring stations are similarly assessed. Missing data are often filled in using checked weather data from a neighbor station or regression analyses of a given weather parameter during identified good periods of data from neighboring weather stations.

1) Graph daily maximum and minimum air temperatures to check for obvious outliers (data values which do not follow the trends of the preceding or following periods) and/or inconsistent trends.
2) Graph daily minimum air temperature and daily dewpoint temperature together over time. Check for outliers and inconsistent trends in dewpoint temperature. In an irrigated reference environment, dewpoint temperature should generally be within 2-5 °C below minimum air temperature, although during periods of annual crop development, when the crops in the area are

providing less than 70% ground cover, some local aridity impact due to sensible heating is often evident and acceptable. Figure 3 shows a comparison of measured daily minimum air temperature and dewpoint temperature at the Las Animas CoAgMet station during 2007. The small differences between the two data sets, particularly during the growing season, indicates this is a well-watered reference type environment.

3) Graph daily maximum and minimum relative humidity (RH) to assess the performance of the RH sensor and potential calibration problems. If the daily maximum RH values consistently exceed 100% by 3-5% then a sensor or sensor calibration problem should be suspected. The same would be true of extended periods of maximum daily RH less than 80-85% if the station is located in an irrigated reference environment. Figure 4 is an example of an obvious RH sensor problem during the first part of the year, and replacement of the sensor during 1995 at the Rocky Ford CoAgMet site.
4) Graph daily solar radiation data and compare with expected clear sky short wave solar radiation for the site. Both States have adopted methodology for clear sky short wave solar radiation given in Appendix D of ASCE-EWRI (2005), which considers effects of sun angle and water vapor on absorption of short wave radiation, and separates the components of beam and diffuse radiation. Measured solar radiation should be expected to be nearly equal to clear sky solar radiation values on clear days. If there are obvious periods when the maximum measured solar radiation does not approach or is in excess (by more than ±3-5%) of the clear sky values a sensor calibration problem should be suspected and the data "re-calibrated". Figure 5a shows measured daily total solar radiation at the Rocky Ford CoAgMet station during 2008 versus the clear sky envelope. Due to relatively low values during most of January-September as compared to the clear sky curve, a calibration factor of 1.04 was determined and applied to the measured data. The resulting "re-calibrated" total daily solar radiation data are shown in Figure 5b.
5) Graph daily mean wind speed and check for periods of consistently low readings that might indicate bearing fatigue, or for periods in mid to late summer when crops in nearby fields have begun to mature and may be sheltering the weather station and wind sensor. Figure 6 is a comparison of mean daily wind speeds during 2003 at Avondale and Vineland. These sites are only about 5 miles apart and should experience relatively the same wind. The Vineland site is perennially surrounded by corn crops within a few meters on two or three sides. The wind speed differences seen in Figure 6 from about day 170 to day 255 are due to sheltering of the anemometer as the corn grows to full height (mid June) and up until harvest (mid September).

Crop Coefficients

ASCE-EWRI (2005) suggests that published sets of crop coefficients may be used with the ASCE standardized equation, as long as the basis for the crop coefficient and the reference crop, i.e., alfalfa or grass, is consistent. Mean crop coefficients

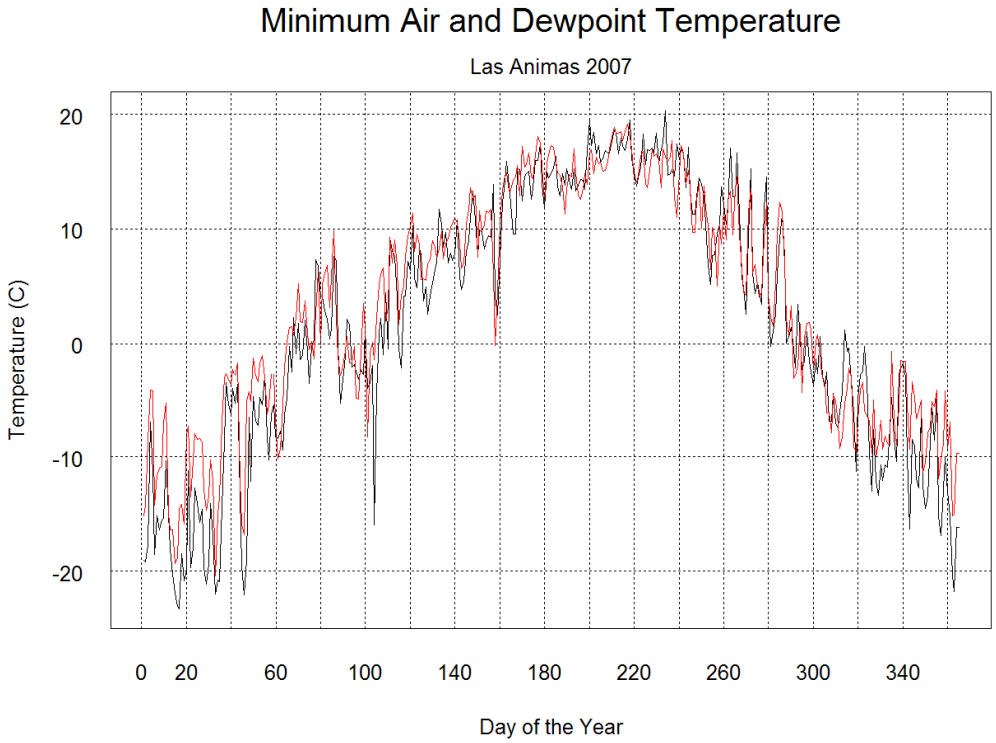

Figure 3. Comparison of measured minimum air temperature (black) and dewpoint temperature at Las Animas CoAgMet station during 2007.

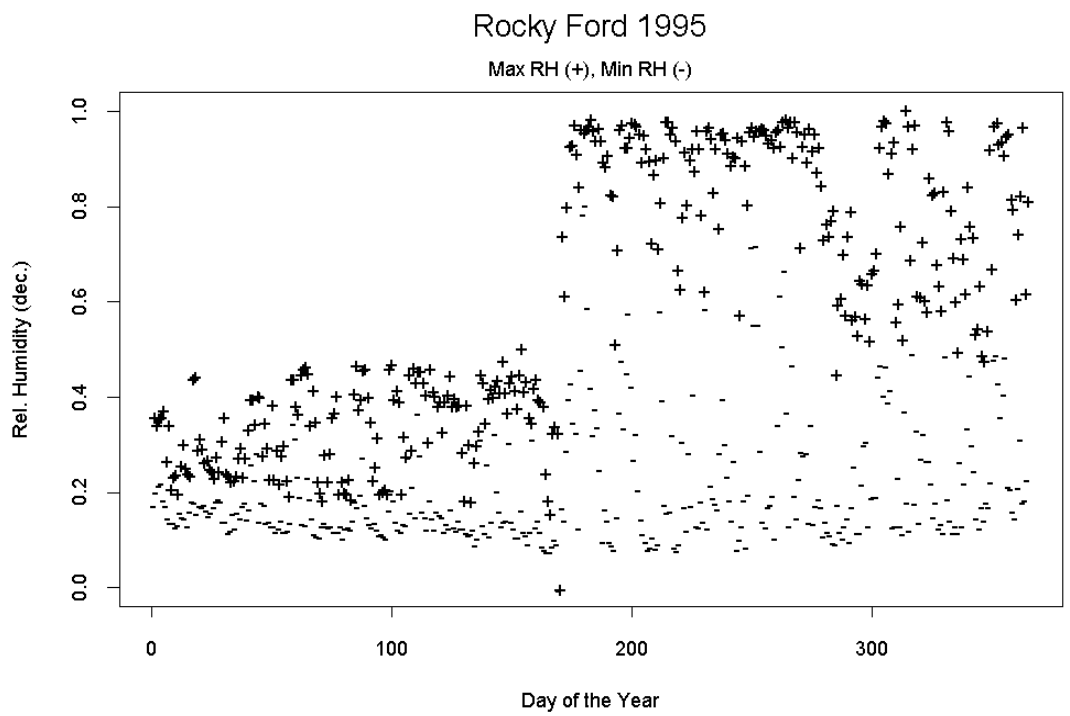

Figure 4. RH sensor problem and replacement with a good sensor at Rocky Ford CoAgMet site in 1995.

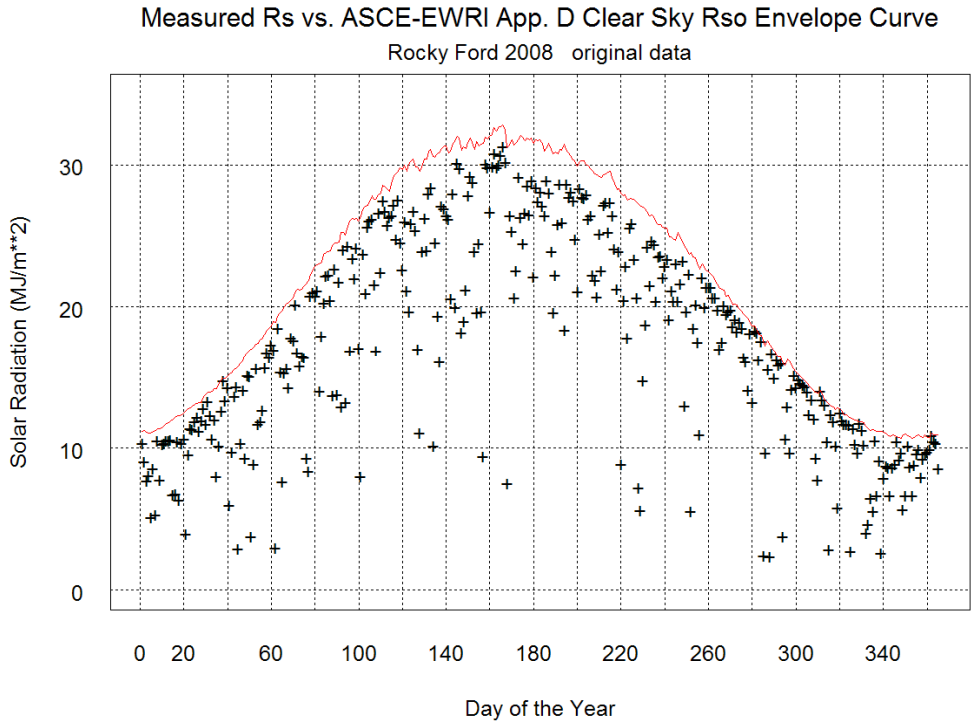

Figure 5a. Measured daily total solar radiation during 2008 at Rocky Ford CoAgMet station and ASCE_EWRI App. D clear sky solar radiation.

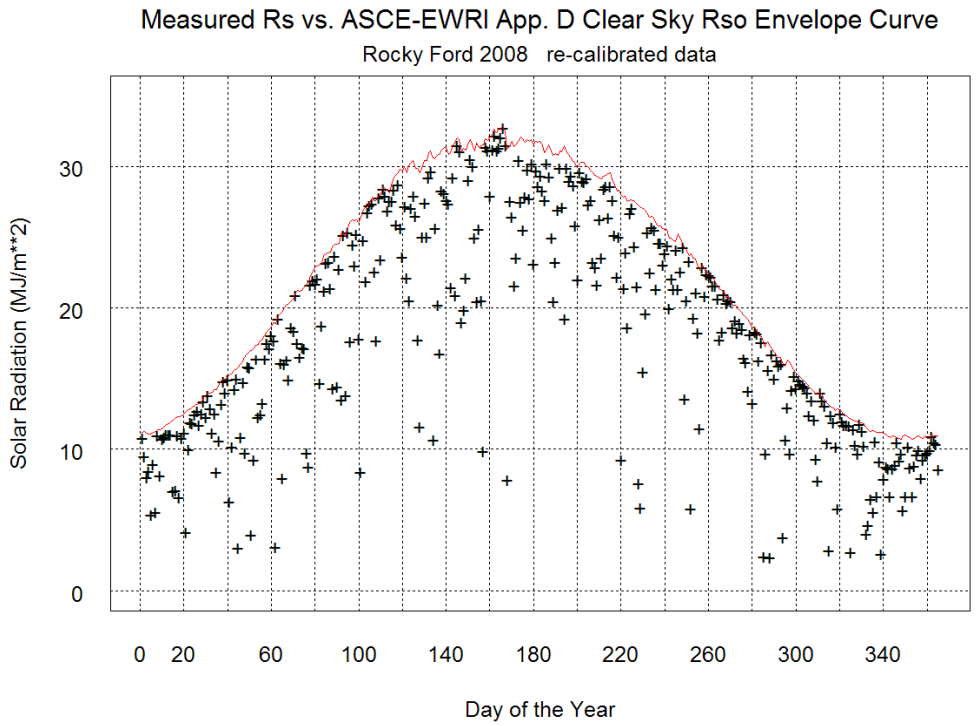

Figure 5b. "Re-calibrated" daily total solar radiation during 2008 at Rocky Ford CoAgMet station and ASCE_EWRI App. D clear sky solar radiation.

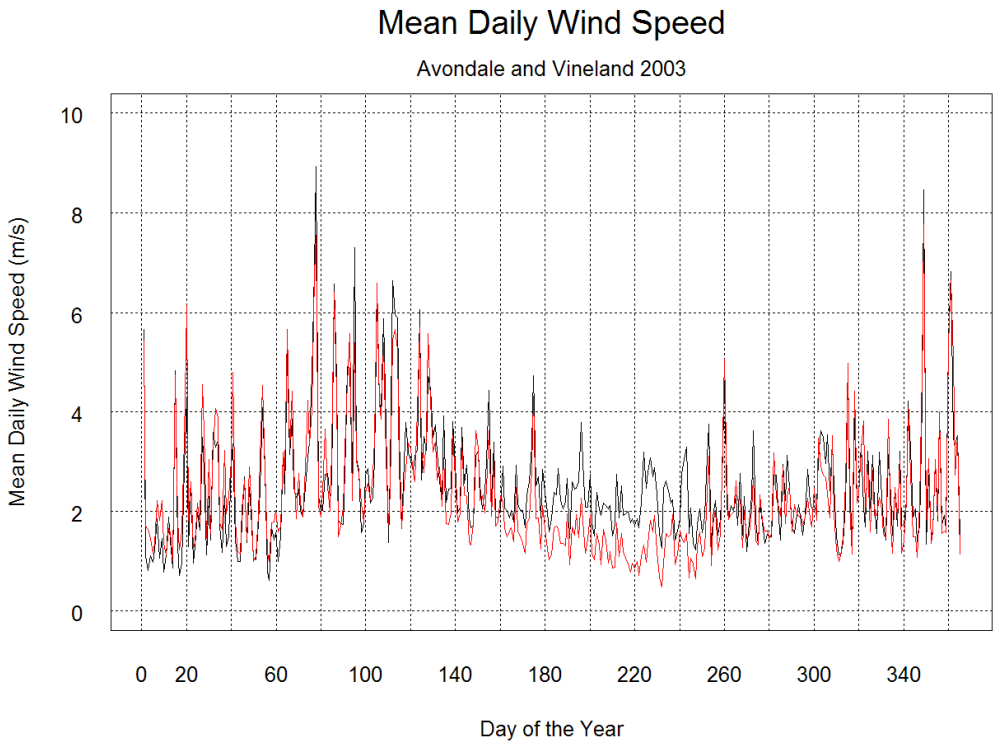

Figure 6. Mean daily wind speeds measured at the Avondale (black) and Vineland (red) CoAgMet stations in 2003.

ultimately adopted are based on Table 6.9 of ASCE Manual 70 (Jensen et al. 1990), adjusted for the differences in crop planting, development and harvest dates between southeastern Colorado and Kimberly, Idaho. The Manual 70 crop coefficients were developed specifically for 1982 Kimberly Penman equation which gives alfalfa reference ET estimates. The ASCE standardized equation for the tall (alfalfa) reference crop differs from the 1982 Kimberly Penman in that ASCE standardized equation assumes a constant 0.50 m tall hypothetical reference (alfalfa) while the 1982 Kimberly Penman does not. As a result, the ASCE standardized tall reference equation tends to predict higher than the 1982 Kimberly Penman equation during the spring and fall months (Mar-May, Sept-Oct) and predicts equal to or slightly lower during the peak summer months (Jun-Aug). Thus, the adopted mean crop coefficients were adjusted to account for the differences between the two methods.

The Special Master did understand and recognize that improvements in the computation of crop consumptive use can be made. Specifically,

> "This is not to say that the Kansas' values, as calculated with the Penman-Monteith equation and crop coefficients, can never be changed. As more information is developed on conditions in the Arkansas River Valley, adjustments made in accordance with recognized professional procedures may be appropriate." (Littleworth, 2003).

The State of Colorado in cooperation with Colorado State University has undertaken the design, construction, and operation of precision weighing lysimeters located at the Colorado State University Arkansas Valley Research Center near Rocky Ford, Colorado. The purpose of the lysimeter project is to research and develop crop coefficients for use with the ASCE standardized reference ET equation for climate conditions and crops produced in southeastern Colorado. A companion paper in these proceedings (Andales et al., 2009) describes lysimeter research work accomplished to date.

References

Allen, R.G. 1996. "Assessing Integrity of Weather Data for Use in Reference Evapotranspiration Estimation". *Journal of Irrigation and Drainage Engineering*, ASCE, Volume 122, No. 2:97-106.

Allen, R.G., L.S. Pereira, D. Raes, and M. Smith. 1998. "Crop Evapotranspiration: Guidelines for Computing Crop Water Requirements". *FAO Irrigation and Drainage Paper 56.* Rome, Italy.

ASABE. 2004. "EP505: Measurement and Reporting Practices for Automatic Agricultural Weather Stations". American Society of Agricultural and Biological Engineers, St. Joseph, MI.

ASCE-EWRI. 2005. "The ASCE Standardized Reference Evapotranspiration Equation". Edited by R.G. Allen, I.A. Walter, R.E. Elliott, T.A. Howell, D. Intenfisu, M.E. Jensen, and R. L. Snyder. Task Committee on Standardization of Reference Evapotranspiration of EWRI. Amer. Society of Civil Engineers, Reston, VA.

Andales A., D. E. Straw, T. W. Ley, and A. Berrada. 2009. "Alfalfa Reference ET from a Weighing Lysimeter and Estimates from the ASCE Standardized Reference ET Equation in the Arkansas Valley of Colorado". Proceedings of the ASCE World Environmental and Water Resources Congress, May 17-21, 2009. Kansas City, MO.

Book, D.E. and M. K. Brengosz. 2009. "Overview of Development and Use of Crop ET estimates with Hydrological Models for Interstate Compacts". Proceedings of the ASCE World Environmental and Water Resources Congress, May 17-21, 2009. Kansas City, MO.

Bras, R.L. and Rodriguez-Iturbe, I. 1985. *Random Functions and Hydrology*, Addison-Wesley, Reading, MA.

Brengosz, M.K. 2009. " Interstate Collaboration in the Arkansas River Compact Compliance Process: The "Nuts and Bolts" of Developing PET for Canal Service Areas for Input to the H-I Model". Proceedings of the ASCE World Environmental and Water Resources Congress, May 17-21, 2009. Kansas City, MO.

Brown, P.W. and T.W. Ley, 1993. "Siting Agricultural Weather Stations". In: *Management of Irrigation and Drainage Systems: Integrated Perspectives, Proc. of the ASCE Irrigation and Drainage Division Specialty Conference*, Park City, UT, July 21-23. pp. 985-992.

Duke, H. R. 1996. "COAGMET - Colorado Agricultural Meteorological Network". In: *Evapotranspiration and Irrigation Scheduling. Proc. of the ASAE International Conference*, San Antonio, Texas, Nov. 3-6. pp. 704-709.

Hill, R.W. and T.W. Ley. 2002. "Crop Water Use Estimates For The Arkansas River Basin in Southeastern Colorado". Expert Report Prepared for Colorado State Engineer, Kansas v. Colorado, No. 105, US Supreme Court.

Hubbard, K.G. 1994. "Spatial variability of daily weather variables in the High Plains of the USA". *Agric. and Forest Meteorology* 68:29-41.

Jensen, M.E., R.D. Burman and R.G. Allen, Eds. 1990. *Evapotranspiration and Irrigation Water Requirements.* ASCE Manual No. 70. New York, N.Y.

Ley, T. W. 1995. "Spatial Variability and Error Limits of Reference Evapotranspiration Estimates", dissertation presented in partial fulfillment of the requirements for the degree of Doctor of Philosophy, Utah State Univ., Logan UT.

Ley, T.W., R.G. Allen, and R.W. Hill. 1996. "Weather Station Siting Effects on Reference Evapotranspiration". *Evapotranspiration and Irrigation Scheduling. Proc. of the ASAE Int'l Conference*, San Antonio, Texas, Nov. 3-6. pp. 727-734.

Ley, T. W., R. G. Allen, and M. E. Jensen. 2009**. "**Adjusting Wind Speed Measured over Variable Height Alfalfa for Use in the ASCE Standardized Penman-Monteith Equation". Proceedings of the ASCE World Environmental and Water Resources Congress, May 17-21, 2009. Kansas City, MO.

Littleworth, A. L. 2003. "Fourth Report of the Special Master". State of Kansas vs. State of Colorado and the United States of America. No. 105, Original. Supreme Court of the United States. October.

Interstate Collaboration in the Arkansas River Compact Compliance Process:
The "Nuts and Bolts" of Developing PET for Canal Service Areas
for Input to the H-I Model

Mary Kay Brengosz[1]

[1]Senior Water Resources Engineer, Spronk Water Engineers, 1000 Logan Street, Denver, CO 80203; PH (303) 861-9700; Fax (303) 861-9799; email: mkb@spronkwater.com

ABSTRACT

The Hydrological-Institutional (H-I) Model is a computer model used to determine compliance with the Arkansas River Compact. The States of Kansas and Colorado complete an annual update of the model to compute the effects of well pumping on Stateline river flows. The annual update process requires the two States to agree on the crop mix, weather data and potential evaporation (PET) estimates for the canal service areas (among other things). The H-I Model is highly sensitive to the crop evapotranspiration input, so the update of this input data set is given particular attention by both States. This paper describes the evolution of the PET estimates over time, and the steps involved in the annual update process, emphasizing the collaboration and cooperation that occur in order to reach a final PET data set.

INTRODUCTION

The Arkansas River Compact (Compact), ratified in 1949, allocates the water supply of the river between the States of Colorado and Kansas. In 1985, Kansas sought enforcement of its compact rights in the United States Supreme Court. The case is now awaiting approval of the Proposed Decree by the Court. The history of Kansas v. Colorado (No. 105, Original, U.S. Supreme Court) is discussed in more detail in another paper in these proceedings (Book and Brengosz, 2009). The end of the case signaled a shift in the interactions between the two States, from "litigation mode" which is necessarily adversarial, to "update and monitoring mode", which requires cooperation and collaboration. One of the areas in which cooperation is essential is the annual update of the H-I Model.

THE H-I MODEL IN KANSAS V. COLORADO

In this case, the H-I Model, in the FORTRAN language, was developed in the late 1980s and submitted to court by Kansas at the trial in 1990. It was intended to calculate the depletions to useable flow in the Arkansas River at the Colorado-Kansas Stateline, caused by well pumping after the Compact was signed. Both States adopted it for modeling in the case, and it is now being used to determine if Colorado

is in compliance with the Compact. The model is updated annually, but compliance is determined on the basis of a rolling ten-year accounting period.

The model contains twenty-three water users under canals diverting from the Arkansas River, located from near the city of Pueblo to near the Stateline. Fourteen users are upstream of John Martin Reservoir and nine are downstream. John Martin Reservoir represents a break-point in the valley, physically and operationally. Canal service areas range from about 600 acres to more than 90,000 acres. Input data and parameters, such as streamflow, canal diversions, precipitation, and irrigation pumping, are read in from a file containing 34 data sets. The file PET.DAT, which is, inexplicably, data set 50, contains the monthly crop PET for each user. Surface water delivered to farms from the canals for irrigation use is subject to on-farm lateral losses, surface runoff and deep percolation losses. The remaining surface supply, as well as effective precipitation and pumped groundwater (a separate input data set), is available for consumptive use by the crops. The H-I Model then simulates consumptive use by crops, soil moisture storage and on-farm losses as part of the overall calculation of Stateline flows.

In the model's original incarnation, crop PET for the years 1950-1985 was calculated with the Modified Blaney-Criddle formula (USDA, SCS 1970), and was later updated through 1999 during the continuing litigation. The Modified Blaney-Criddle formula was well-accepted in water rights matters in Colorado at the time the trial began. The Blaney-Criddle method requires only average monthly temperature data, which is readily available from numerous weather stations in the cooperative observer network of the National Oceanic and Atmospheric Administration/National Weather Service (NOAA/NWS) for long periods of record. The PET estimates for the model were based on six NOAA/NWS weather stations distributed across the valley, near the Colorado towns of Pueblo, Rocky Ford, La Junta, Las Animas, Lamar, and Holly. Figure 1 is a map of the model area showing the river, irrigated areas and weather stations.

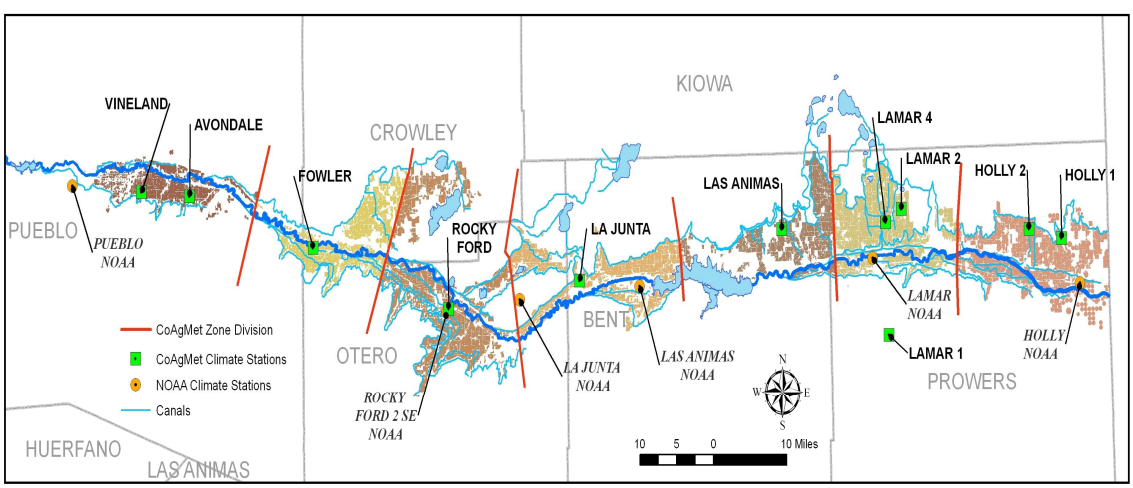

Figure 1. Location Map of Irrigated Areas and Weather Stations
(Irrigated parcels and zone divisions are from Colorado Division of Water Resources)

During the decades of litigation, the science of computing crop evapotranspiration (ET) was advancing. The Penman-Monteith and the 1982 Kimberly Penman methods gained favor in the engineering community, but few weather stations collected the more extensive data need for these newer methods. In 1992, the first weather stations collecting the necessary data in the Arkansas Valley were installed at Avondale and Rocky Ford. By 2002, there were four such stations (at Vineland, Avondale, Rocky Ford and Lamar01) that were part of the Colorado Agricultural Meteorological Network (CoAgMet). At trial in 2002, the engineers for Kansas recommended that the Penman-Monteith Method be used for calculation of PET for model input. The form of the Penman-Monteith equation used by the Kansas engineers was the standardized form that had been recommended in 2000 by the ASCE Task Committee on Standardized Evapotranspiration Calculations. This later became the ASCE Standardized Reference Evapotranspiration Equation (ASCE-EWRI, 2005). During this trial phase, the CoAgMet stations were evaluated for their suitability for use in the Penman-Monteith equation in the Arkansas Valley. As more fully described in another paper in these proceedings (Ley et al., 2009a), Vineland and Lamar01 were determined to be unusable for calculating reference ET. The two States agreed to use the two remaining CoAgMet weather stations, Avondale and Rocky Ford. Some Vineland data were used to fill in missing data at Avondale. In his fourth report in 2003 (Littleworth, 2003), the Special Master recommended the use of the ASCE standardized Penman-Monteith (ASCE std. Penman-Monteith) for development of crop consumptive use estimates that are input to the H-I Model for both historical and future years, using the Avondale and Rocky Ford stations.

ADJUSTMENT OF HISTORICAL BLANEY-CRIDDLE INPUT

The H-I Model had been calibrated to the PET input based on the Blaney-Criddle Method. Because there are significant differences in the PET results from the Blaney-Criddle Method and the Penman-Monteith Method, the model was recalibrated to the new input (Spronk & Papadopulos, 2002). In addition, adjustment was needed for the 1950-1994 PET input, years for which the data needed to calculate Penman-Monteith were not available. To achieve a consistent data set, the Blaney-Criddle PET values were "calibrated", or adjusted, to more closely resemble the Penman-Monteith values by applying monthly adjustment factors for each crop and weather station.

The adjustment factors, which are the ratio of the monthly Penman-Monteith Crop PET to the Blaney-Criddle Crop PET, were derived from the period of overlapping record at the time of the derivation, approximately 1993-1999, at the NOAA and CoAgMet stations. The Penman-Monteith at the Avondale/Vineland CoAgMet station was used to adjust the Pueblo NOAA station Blaney-Criddle. The CoAgMet station at Lamar was not used to calculate adjustment ratios. The Rocky Ford CoAgMet Penman-Monteith was used to adjust the Blaney-Criddle at all the remaining NOAA stations at Rocky Ford, La Junta, Las Animas, Lamar, and Holly, a distance of about 90 miles.

The Penman-Monteith/Blaney-Criddle monthly adjustment factors ranged from 0.28 for Winter Wheat in November at Rocky Ford, to 8.13 for Hay/Pasture in March at Pueblo. The adjustment factors were close to 1.0 for the peak growing months of each crop, but differed by a greater amount at the start and end of the growing seasons (Franzoy, 2001). The adjustment ratios for each station were presented at trial in 2002, and were agreed to by both States after several exchanges of expert reports in the case. An example of the ratios for alfalfa and winter wheat are shown in Table 1.

Table 1. Example of Blaney-Criddle to Penman-Monteith Adjustment Ratios

Crop	Month	Pueblo	Rocky Ford, La Junta & Las Animas	Lamar & Holly
Alfalfa	Apr	3.04	2.27	2.16
	May	1.45	1.34	1.28
	Jun	1.23	1.17	1.11
	Jul	1.01	1	0.95
	Aug	0.95	0.95	0.9
	Sep	1.1	1.02	0.97
	Oct	1.12	1.23	1.17
Winter Wheat	Mar	5.59	2.72	2.46
	Apr	1.85	1.56	1.41
	May	1.43	1.34	1.21
	Jun	2.62	2.67	2.41
	Jul			
	Aug			
	Sep	0.91	0.85	0.77
	Oct	0.65	0.56	0.5
	Nov	0.41	0.31	0.28

There was a question about whether data from Rocky Ford was appropriate for adjusting the Blaney-Criddle values all the way to the Stateline, and general agreement by the parties that more stations were needed because of the long distance. Colorado actively worked to encourage the expansion of the CoAgMet network, and was successful in establishing new stations. However, as discussed by Ley et al. in their paper in these proceedings, there were issues relating to the siting of the CoAgMet stations, particularly those downstream of John Martin Reservoir, and how they would be used in calculation of future PET input data and adjustment of the Blaney-Criddle estimates. There were several more years of discussion, and location and relocation of weather stations, needed to resolve these issues, culminating in the PET Agreement in 2005.

2005 PET AGREEMENT

In 2005, the State Engineer for Colorado, Hal Simpson, and the Chief Engineer for Kansas, David Pope, entered an agreement (the PET Agreement) regarding the computational procedures for PET used in the H-I Model, and a method for adjusting SCS Blaney-Criddle values in the future when more weather stations were

operational. The PET Agreement, Appendix B.2 of the Decree (Littleworth, 2008) confirms the use of the adjustment ratios proposed at trial for the 1950-1993 PET estimates for canal areas upstream of John Martin Reservoir (Pueblo NOAA with Avondale/Vineland CoAgMet and Rocky Ford NOAA with Rocky Ford CoAgMet). For 1994-2004, PET would be calculated directly by the ASCE std. Penman-Monteith method at the Avondale/Vineland and Rocky Ford CoAgMet stations. For calculations in 2004 and into the future, it was anticipated that three new CoAgMet stations would be installed at Fowler, La Junta and Las Animas, and the PET would be calculated directly. The States agreed to jointly develop a new distribution of canal service areas to the weather stations when acceptable data became available from the new stations. In 2008, the new stations were incorporated into the distribution as shown on Figure 1.

For canal areas located downstream of John Martin Reservoir, the1950-2002 Blaney-Criddle PET estimates at the Lamar and Holly NOAA stations were adjusted with the Rocky Ford CoAgMet station. For 2003-2004, PET would be calculated directly by the ASCE std. Penman-Monteith method at the Lamar02 CoAgMet station, and this would be used for the entire area downstream of John Martin Reservoir. For 2005 and 2006, PET would be calculated directly by the ASCE std. Penman-Monteith method at the Lamar02, Lamar04 and Holly02 CoAgMet stations. It was thought by the parties that at the end of 2009, there would be at least five years of overlapping data at the Lamar and Holly NOAA and CoAgMet stations, and new Blaney-Criddle to Penman-Monteith ratios could be calculated for the 1950-2002 data. However, as Tom Ley indicated in another paper in these proceedings (Ley et al., 2009a), the stations were moved during the time frame specified in the Agreement, and some of the data are not of sufficient quality for this purpose. The Holly station in particular had persistent data problems through 2007. This has been an area of ongoing discussion, and will be another area of opportunity for cooperation as the 2008 data are reviewed for the update in 2009.

ANNUAL UPDATES

The States of Kansas and Colorado complete an annual update of the model to compute the effects of well pumping on Stateline river flows. Although all input data sets are updated, the Stateline flows calculated by the H-I Model are highly sensitive to the crop PET input. Because of this sensitivity, the update of the PET input data set is given particular attention by both States. Every step of this process includes collaboration between the States. The update process requires the two States to agree on the crop mix, weather data and final PET estimates for the canal service areas.

The Decree and the PET Agreement form the framework within which the annual updates are done. The PET Agreement specifies which weather stations will be used. Because several weather stations have been relocated more than once, this has not been as straightforward as it appears, and the States have cooperatively agreed to defer some parts of the schedule in the PET Agreement in order to accomplish the objectives of the Agreement. The Decree in Appendix B.1 addresses the

methodology for calculating the county crop distribution, evaluating and correcting data from the weather stations, and calculating the PET, and sets out the schedule of the annual updates.

Colorado's engineers collect and compile the data and create the updated data sets, and provide them to the Kansas engineers by March 31. The Kansas engineers review the material from Colorado and proceed with their own analysis, and provide the model results and any proposed modifications to the data sets to Colorado by May 15. In acknowledgement of the give-and-take nature of this process, the Decree specifies that if the States have not reached agreement on H-I Model results by June 1, they shall be submitted to the "Dispute Resolution Procedure" prescribed in Appendix H of the Decree. In the updates that have been performed so far, the States have agreed on the PET input in sufficient time to avoid this situation.

THE PET UPDATE PROCESS

Overview

Although the Decree states that Colorado is responsible for the data compilation and creation of the update data set, Kansas engineers collaborate in the update of all the data sets in order to check the information provided by Colorado on March 31 each year. The calculations are done by engineers for the two States with different tools, adding to the confidence in the final results. The "two States" are in reality several persons who review the data, "crunch the numbers", and exchange results in order to ultimately agree on an input data set. For Colorado, they are Thomas Ley and Dale Straw of the Colorado Division of Water Resources, and Robert Hill of Utah State University. For Kansas, three employees of Spronk Water Engineers perform this work: Dale Book (President), Mary Kay Brengosz (Senior Water Resources Engineer), and Angela Schenk (Assistant Hydrogeologist). Both States have also had the benefit of input from Dr. Richard Allen of the University of Idaho.

The steps involved in the annual update process for the PET data set are:

1. Weather data assessment and correction.
2. Calculation of Reference ET.
3. Calculation of crop PET at the weather stations.
4. Determination of the county-wide crop distribution.
5. Determination of irrigated acreage under each canal.
6. Distribution of the crop ET to the canal service areas.

At each step, there can be differences of opinion and interpretation. The canal/user PET results are input to the Model to compute the actual crop ET, based on available water supply.

The Kansas engineers use the Ref-ET program developed at the University of Idaho (University of Idaho, 2000) to calculate the reference ET, and a series of spreadsheets to process the results and produce the input data set. The Colorado engineers use the S-Plus program for the weather data integrity assessment and for calculation of the ASCE std. Penman-Monteith equation (coded by Tom Ley). The S-Plus output is daily weather and reference ETr, which are input to a spreadsheet where the monthly mean crop coefficients are applied to produce the monthly crop PET. A series of "C" language programs developed by Dale Straw are used to produce the input data set. (Ley, 2009b) The two methods give almost identical results when using the same input data. The results are shared with and reviewed by each State's engineers. Comparison of the results helps to pinpoint areas of differences in the data integrity assessment. The cooperative review and calculation by the two States has become an important component of the process.

Weather Station Data Assessment and Correction

Daily weather data are used with the ASCE std. Penman Monteith equation to compute daily alfalfa reference ETr at each weather station. Before use in the equation, the data are reviewed and corrected. "Data Correction" is a concept unfamiliar to engineers in many areas of practice. There is a well-deserved attitude of suspicion towards, and a taboo against, altering data to better fit the desired outcome. However, correcting the data is precisely what is required to ensure that use of the ASCE std. Penman-Monteith equation will result in a good, representative reference ETr for the weather station. Faulty or missing data, whether from sensor error, battery failure, operator error, or other causes, should be corrected or replaced with values that are reasonable for a given weather station. Even before any data are collected, the location of a weather station is important. The PET Agreement specifies that the States will cooperate in the siting of weather stations. In practice, Colorado has sited the weather stations and Kansas has not objected. However, the multiple locations of the Holly station (Holly01 and Holly02) and the Lamar station (Lamar02, Lamar02 and Lamar04) since the locations were first evaluated could be interpreted as an extreme example of the concept of data correction, in that the stations have been moved to provide data that is more representative of reference conditions.

The Decree provides that data corrections to faulty or missing data identified by the Colorado engineers during the data integrity assessment or by the Kansas engineers during their review of the data shall be corrected or estimated using standard engineering principles. The report of the ASCE Task Committee (ASCE-EWRI, 2005), in Appendices D and E, provides procedures for siting a weather station, and for assessing and correcting the various weather parameters. Both States follow these procedures in general, but the results can be different depending on the actual

procedure used for data replacement or adjustment. Data adjustment can include using an average of surrounding days, replacing with data from a nearby station, or using a regression based on one or more nearby stations. The process of selecting a proper location for the weather stations and assessing the daily data is described more fully in another paper in these proceedings, (Ley et al., 2009a).

Data integrity assessment and correction is the most time-consuming part of the annual PET update. This was especially true in the first rounds of the update process, where multiple years were processed. Review of daily data for each parameter is tedious, and evaluation of the weather parameters, especially the solar radiation data, is subject to some interpretation, and therefore some disagreement between the States. The areas most subject to interpretation have been wind speed and solar radiation. For example, is a period of low solar radiation readings just an extended cloudy period, or is something wrong with the sensor? Is the wind speed regionally low during a certain period of time, or is there tall vegetation, a pile of hay bales, or a structure obstructing the anemometer? Are there other conditions at the site that do not meet reference conditions? Even if the States agree that adjustments to a certain parameter are needed, they must then agree on when to apply the adjustments and how much should they be.

Calculation of Reference ET

After the data assessment and corrections, the calculation of alfalfa reference ET is fairly straightforward since the Decree specifies the ASCE std. Penman-Monteith will be used. However, through each State's detailed review of the other's work, some issues have been identified. Although the ASCE std. Penman-Monteith equation was developed for wind measurements at a height of 2 m over a smooth grass surface, some of the CoAgMet stations are located over and near tall alfalfa. Tom Ley, Rick Allen and Marvin Jensen investigated this issue in 2008 at two CoAgMet sites and a lysimeter operated by Colorado State University, and they will report on their investigation in another paper in these proceedings (Ley et al., 2009c). Another issue that has arisen in this case is the impact of soil and irrigation water salinity and irrigation management practices and their relation to reference crop conditions. The Special Master considered this issue and decided that an adjustment for salinity should not be made to the PET, but should instead be accounted for in the irrigation efficiency of individual canals, if needed.

The daily values of reference ETr are summarized to monthly totals for further use in development of the input data set. The engineers on both sides of this case are indebted to the ASCE Committee for developing and publishing the ASCE std. Penman-Monteith Equation, and to the researchers through the preceding decades who contributed to the development of the equation. They have provided a tool that is capable of hourly estimates of evapotranspiration when used with accurate data. However, field conditions are not as controlled as research conditions, and the developers may be appalled that we have taken their elegant and carefully tuned hourly equation and are using it as the equivalent of a year-at-a-glance calendar.

Calculation of Crop ET

The summarized monthly reference ETr is used to calculate crop ET for nine different crops plus a winter (or non-growing season) ET in the months November through March, and the results are summarized to a monthly PET for each crop at each weather station.

Crop Coefficients

The crop coefficients for the Penman-Monteith Method that were ultimately adopted at trial in 2002, and are still being used, are based on Table 6.9 of ASCE Manual 70 (Jensen et al, 1990) adjusted for the differences in climate and crop planting/harvest dates in Colorado compared to Kimberly, Idaho, and further refined for differences between the Kimberly Penman and ASCE std. Penman-Monteith equations. The crop coefficients are shown in Table 2. Gene Franzoy, a consultant for Kansas, developed the crop coefficients in consultation with Dr. James Wright who had developed the Manual 70 coefficients, Dr. Robert Hill who was a consultant for Colorado, and several other locally-based researchers who supplied invaluable information on local harvest and planting dates (Franzoy, 2001).

Table 2. Mean Monthly Crop Coefficients for Use with Alfalfa Reference ETr as Calculated with the ASCE std P-M Equation (Table 2 from Franzoy, 2001)

Month	Wheat Kcm	Dry Beans Kcm	Corn Grain Kcm	Corn Silage Kcm	Spring Grain Kcm	Sorghum Kcm	Vegetables Kcm	Alfalfa Kcm	Hay Kcm
Jan									
Feb									
Mar	0.33				0.15			0.45	0.38
Apr	0.82				0.39		0.17	0.71	0.58
May	0.93	0.19	0.19	0.19	0.88	0.19	0.29	0.79	0.63
Jun	0.67	0.38	0.40	0.40	0.90	0.42	0.64	0.85	0.68
Jul	0.15	0.91	0.89	0.89	0.34	0.93	0.68	0.88	0.70
Aug		0.64	0.95	0.95		0.85	0.35	0.86	0.69
Sep	0.30		0.76	0.82		0.48		0.75	0.60
Oct	0.29							0.55	0.44
Nov	0.25								
Dec									

County-wide Crop Mix

The Decree requires that the crop distribution for each user be derived from county agricultural statistics, unless more detailed records are available for individual canal systems. In practice, more detailed information has not been available. The two States use the county crop statistics from the National Agricultural Statistics Service's Colorado Field Office each year to develop a crop mix for each canal/user.

Differences in interpretation of the county statistics are resolved before proceeding. The crop statistics for the year being updated may not be available by the deadlines specified in the Decree, so a place-holder value, usually the same value as the previous year, is used until the revised data are available. The Decree requires that when final crop statistics become available, the States shall make a revised H-I Model run based on the final crop statistics, if the States are in agreement on the other aspects of the data sets.

Irrigated Acreage

Appendix B.4 of the Decree documents another agreement between the States to resolve issues relating to the periodic updates of irrigated acreage. In order to analyze and document changes in irrigated areas that would affect the model results, Colorado acquires Landsat satellite imagery every five years (the last year was 2008) and annual aerial photographs from the United States Department of Agriculture (USDA) Farm Service. In addition, Colorado's farm verification program investigates twenty percent of the wells and their associated acreage each year, so that all are reviewed every five years. The engineers for Kansas review the information provided by Colorado and provide feedback on any changes in parcels that have been proposed by Colorado.

Canal/User PET

Allocation of canal service areas to weather stations is done by assigning area-weighted irrigated areas under each canal to the nearby weather stations and to each county (Tables 3 and 4). When the model was developed, GIS was not a readily available tool. The area-weighting factors were developed using paper maps and visual inspection. The early county-to-canal weighting factors, used in the crop distribution allocation, have not changed since they were developed, but a change could be needed if there is a significant change in irrigated parcels over time. The early canal-to-weather station weighting factors were used until 2008, when the Fowler station was added to the process, and the latest locations of the remaining weather stations were included. The current method of determining the canal-to-weather station is based on a GIS map analysis by Colorado in 2008, and the then-current weather station locations. Another change in weather station locations is not anticipated, but could be possible.

The canal/user PET is calculated with the annual crop distribution (weighting factors by county) and the crop PET (weighting factors by weather station) for nine crops, plus a winter (or non-growing season) ET in the months November through March. Calculation of canal/user PET is done collaboratively by the two States. Different tools are used and the States compare and agree to each other's estimates of user PET for input to the H-I Model. The Kansas team imports the crop PET at each station into a spreadsheet that distributes the PET to canal areas based on the weightings. The method used by the Colorado team runs the PET through a series of "C" programs that give almost identical results when used with the same data.

Table 3: Weather Station Weighting Factors by H-I Model User

User Name	Pueblo	Fowler	Rocky Ford	La Junta	Las Animas	Lamar	Holly
Bessemer	100%						
Booth Orchard	100%						
Excelsior	100%						
Collier	100%						
Colorado	4%	53%	43%				
Rocky Ford Highline		42%	58%				
Oxford		100%					
Otero		4%	96%				
Catlin		5%	95%				
Fort Lyon			1%	23%	36%	40%	
Rocky Ford			100%				
Holbrook			44%	56%			
Las Animas Consolidated				100%			
Baldwin-Stubbs		100%					
Fort Bent					15%	85%	
Keesee					100%		
Amity						19%	81%
Lamar / Manvel						50%	50%
Hyde						100%	
XY Graham							100%
Buffalo							100%
Sisson							100%
Stateline Pumpers							100%

Table 4: County Weighting Factors by H-I Model User

User Name	Pueblo	Crowley	Otero	Bent	Prowers
Bessemer	100%				
Booth Orchard	100%				
Excelsior	100%				
Collier	100%				
Colorado		100%			
Rocky Ford Highline	12%		88%		
Oxford	33%		67%		
Otero			100%		
Catlin			100%		
Fort Lyon			6%	56%	38%
Rocky Ford			100%		
Holbrook			95%	5%	
Las Animas Consolidated				100%	
Baldwin-Stubbs		100%			
Fort Bent				6%	94%
Keesee				100%	
Amity					100%
Lamar / Manvel					100%
Hyde					100%
XY Graham					100%
Buffalo					100%
Sisson					100%
Stateline Pumpers					100%

The winter ET is still calculated by the Blaney-Criddle method with a crop coefficient of 0.2. Winter ET is applied to all the user acreage in the months December through February. The growing season for several crops extends into March and November, so the winter ET cannot be applied to 100% of the acreage in these months. In November, the winter ET is applied to the total acreage less the percentage of winter wheat in the user's crop distribution. In March, winter wheat, pasture grass, alfalfa and spring grain have begun growth, so the winter ET is applied to the total acreage less the percentage of these crops. The total PET for March and November is thus the sum of the crop ET on the cropped acreage and the winter ET on the uncropped acreage.

The engineers for Kansas proposed in 2008 that the winter ET be calculated with the Penman-Monteith method instead of Blaney-Criddle. The Kansas engineers also suggested further investigation into adjustment of wind speeds measured over alfalfa. The Colorado engineers had already begun planning such an investigation, and it was performed in 2008. The results of that study are the subject of another paper in these proceedings (Ley et al., 2009c). These will be areas for discussion between the States in 2009 or future years.

ONGOING OPPORTUNITIES FOR COOPERATION

Because of the process defined in the Decree and the PET Agreement, many areas of disagreement have already become areas of cooperation and collaboration. The annual update process, at least regarding the issues already resolved, becomes smoother every year. The people on both sides have become familiar with each other's approaches and personalities, as well as each State's viewpoints. This makes it easier to anticipate areas of agreement which may require less review, and focus on potential areas of disagreement, which will require a closer look. In general, disagreements in the annual PET update process have been resolved in an amicable and timely manner. However, because of the ongoing evolution and improvement in the science of ET, potential advancements in the equipment at the weather stations, changes in cropping patterns and land and water use, it is almost certain that new issues will arise in the future. Although past agreement is not a certain predictor of future solutions, all of us who are involved in the annual updates hope that future legal action can be avoided on the issue of PET if we continue the collaboration that has served us well in past years.

REFERENCES

ASCE-EWRI. 2005. "The ASCE Standardized Reference Evapotranspiration Equation". Edited by R.G. Allen, I.A. Walter, R.E. Elliott, T.A. Howell, D. Intenfisu, M.E. Jensen, and R. L. Snyder. Task Committee on Standardization of Reference Evapotranspiration of EWRI. Amer. Society of Civil Engineers, Reston, VA.

Book, D.A. and M. K. Brengosz. 2009. "Overview of Development and Use of Crop ET estimates with Hydrological Models for Interstate Compacts". Proceedings of the ASCE World Environmental and Water Resources Congress, May 17-21, 2009. Kansas City, MO.

Franzoy, C.E. 2001. "Comparison of Crop Evapotranspiration Calculated using ASCE Standardized Penman-Monteith and TR-21 Blaney-Criddle". Expert Report Prepared for Colorado State Engineer, Kansas v. Colorado, No. 105, US Supreme Court.

Jensen, M.E., R.G. Allen, and R.D. Burman (ed.). 1990. "ASCE Manual and Report on Engineering Practice No. 70, Evapotranspiration and Irrigation Water Requirements". New York, NY.

Ley, T.W., D.E. Straw and R.W. Hill. 2009a. "ASCE Standardized Penman-Monteith Alfalfa Reference ET and Crop ET Estimates for Arkansas River Compact Compliance in Colorado". Proceedings of the ASCE World Environmental and Water Resources Congress, May 17-21, 2009. Kansas City, MO.

Ley, T.W. 2009b. Personal communication.

Ley, T.W., R.G. Allen and M.E. Jensen. 2009c. "Adjusting Wind Speed Measured over Variable Height Alfalfa for Use in the ASCE Standardized Penman-Monteith Equation." Proceedings of the ASCE World Environmental and Water Resources Congress, May 17-21, 2009. Kansas City, MO.

Littleworth, A. L. 2003. "Fourth Report of the Special Master". State of Kansas vs. State of Colorado and the United States of America. No. 105, Original. Supreme Court of the United States. October.

Littleworth, A. L. 2008. "Fifth and Final Report of the Special Master, Volume II, Proposed Judgment and Decree". State of Kansas vs. State of Colorado and the United States of America. No. 105, Original. Supreme Court of the United States.

Spronk Water Engineers, Inc. and S.S. Papadopulos & Associates, Inc. 2002. "Kansas Analysis of Compact Compliance with the Arkansas River Compact 1997-1999 and Prospective Compact Compliance". Expert Report Prepared for Colorado State Engineer, Kansas v. Colorado, No. 105, US Supreme Court.

USDA, Soil Conservation Service. 1970. "Irrigation Water Requirements", Technical Release 21.

University of Idaho and R.G. Allen, 2000. User Manual, "Ref-ET: Reference Evapotranspiration Calculation Software for FAO and ASCE Standardized Equations".

Overview of Development and Use of Crop ET Estimates with Hydrological Models for Interstate Compacts

Dale E. Book[1] and Mary Kay Brengosz[2]

[1]President, Spronk Water Engineers, 1000 Logan Street, Denver, CO 80203; PH (303) 861-9700; Fax (303) 861-9799; email: debook@spronkwater.com
[2]Senior Water Resources Engineer, Spronk Water Engineers, 1000 Logan Street, Denver, CO 80203; PH (303) 861-9700; Fax (303) 861-9799; email: mkb@spronkwater.com

ABSTRACT

Crop Evapotranspiration (ET) is an important element in hydrological modeling in river basins with significant irrigation. The State of Kansas currently participates in ongoing modeling in two river basins for the purpose of monitoring compliance with interstate compacts: the Arkansas River in Colorado and Kansas and the Republican River in Kansas, Nebraska and Colorado.

The decree in *Kansas v. Colorado* (No. 105, Original, U.S. Supreme Court) provides for annual updates of the Arkansas River Hydrological-Institutional Model (H-I Model) to compute the effects of well pumping and offsets on Usable Stateline flows. The model was originally developed for the litigation, and has been modified for use in monitoring compact compliance. The Republican River Groundwater Model was developed through negotiation as part of a settlement in the case of *Kansas v. Nebraska & Colorado (*No. 126 Original, U. S. Supreme Court*)*. The Republican River model is used each year to determine the Calculated Beneficial Consumptive Use attributed to groundwater pumping in the Republican River Basin in the States of Nebraska, Colorado and Kansas. The settlement stipulation requires that each state calculate the crop irrigation requirement by county and compare those estimates to the pumping. This paper discusses the development and function of crop ET in each setting.

INTRODUCTION

Enhancement of crop evapotranspiration (ET) is the goal of irrigation and an important hydrologic parameter to quantify when assessing impacts of water use on streamflows and basin water supply in the western United States. The estimation of crop ET has been used for design and operation of irrigation systems and planning water resource projects for many years. The science of ET is well established, and collection of climatologic data for purpose of crop management is widespread. Formulas to determine crop water use have evolved into sophisticated methods, as water scarcity leads to more careful use of water for crops.

Hydrologic modeling involves complex relationships of the movement, distribution and consumption of water supply. Water supply projects often involve reservoir storage and conjunctive use of ground and surface water. The use of water for irrigation results in partial consumption of the water supply, with a residual returning to the drainage and stream system. Water is stored in the root zone and aquifers as it flows through the irrigation process, to be "reused" again downstream in the system. It is these processes of application, soil moisture storage, crop consumption, percolation through the aquifer to the stream as return flow and diversion or storage downstream that make up essential elements of the hydrologic model of a stream system used for irrigation supply.

Crop ET determination has been applied for many years to quantify the consumptive use of irrigation water, for the purpose of facilitating water rights transfers. The basic principal of limiting future consumption of water to historical crop consumption has been a staple of water rights engineering as water supplies are shifted from irrigation to municipal and industrial uses in stream systems of limited supplies. Methods of analysis range from deterministic methods to compute crop ET and return flows to more sophisticated stream system models, with calibrated parameters to match streamflow or water level measurements. This paper discusses the application of two such calibrated models, one in the Arkansas River basin and one in the Republican River basin, and the role of crop ET in each. Both models are being applied in the context of administration of interstate compacts, where methods have been established to assess compact compliance.

ARKANSAS RIVER COMPACT

The Arkansas River Compact (Compact) allocates the water supply of the river between the States of Colorado and Kansas. Ratified in 1949, the Compact required protection of water uses existing at the time of the Compact in the two States as additional development occurred. Since 1949, additional water development consisted of groundwater development in each state and construction of two federal reservoirs in Colorado. Although some municipal and industrial use of water occurs in the basin in both states, the primary use of water, as in most western states, is for irrigation. The Compact did not provide a fixed allocation to either of the states, but instead provided for maintenance of conditions enjoyed by the water uses existing at the time of the Compact. The Compact was reached after a long history of litigation between the two States dating back to 1907. The Compact was centered on the allocation of benefits of John Martin Reservoir, constructed during the 1940's to provide supplemental water supply in Colorado and Kansas, and prescribed the operations of the reservoir.

The Arkansas River in Colorado and Kansas is fully allocated and was extensively developed for irrigation by the time of the Compact. The basin is characterized by water shortages after the snowmelt runoff season in most years and throughout dry years. Construction of reservoir storage provided supplemental supplies, but water available for storage was still less than demand, as John Martin Reservoir was

emptied in most years before the irrigation season ended. Groundwater pumping was developed to supplement the surface water supplies in both states after the Compact.

Kansas v. Colorado (No. 105, Original) was initiated in the United States Supreme Court in 1985 for enforcement of Kansas' compact rights. The case has been brought to a close, pending the Court's issuance of a final decree, which has been prepared and submitted to the Court by the Special Master, Arthur L. Littleworth. (Littleworth, 2008). Because of the provisions in the Compact requiring protection of water uses in place as of 1949 from effects of post-compact water uses, it was necessary to develop analyses of such effects over the variable hydrologic conditions that have occurred since the time of the Compact. This ultimately led to the development and use of a hydrologic basin model to assess impacts of water use in Colorado at the Stateline.

Physical Setting

The Arkansas River begins in the headwaters of the eastern slope of the Rocky Mountains in Colorado and flows generally west to east across the eastern high plains into Kansas, across most of that state and into Oklahoma. However, it is the western reach that was most extensively developed for irrigation beginning in the late 1800's, and continuing into the 1970's with construction of federal reservoirs and development of groundwater by wells. The Arkansas River Compact between the states of Kansas and Colorado requires that development and use of water in Colorado not diminish the flow allocated to Kansas under the Compact. The water crossing the Stateline to Kansas is normally used within the western reach down to Garden City or a short distance downstream, where the river alluvium overlies and recharges the Ogallala Aquifer. The river has normally been dry at Dodge City, approximately 120 river miles east of the Stateline, since the early 1970's, except during periods of very high streamflow. The river begins to flow again in the vicinity of Great Bend, Kansas.

At issue in Kansas v. Colorado was the effect of post-compact use by groundwater pumping in Colorado on Stateline flows. Most of the groundwater development occurred in the 150-mile reach of the river extending from Pueblo to the Stateline and was limited to the alluvial aquifer along the mainstem of the Arkansas River (Figure 1). Major tributaries in this reach are sparse. Fountain Creek drains the Pikes Peak area and enters the river at Pueblo. The Purgatoire River drains the southern Front Range, extending to New Mexico, and flows in the Arkansas River at Las Animas, just upstream of John Martin Reservoir. The basin water supply is largely derived from snowmelt in the headwaters. Streamflow from rainfall is relatively limited and of short duration most years. A shallow aquifer of sands and gravels along the river extends about three miles wide with depths of less than 100 feet.

The reach between Pueblo to the Stateline was extensively developed for irrigation prior to the turn of the 20th century. Canals and reservoirs in Colorado are allocated water from the river on the basis of dates of appropriation, with the "senior" rights

entitled to appropriations before more "junior" water rights are entitled to divert. By 1900, the dependable flow in the western reach had been appropriated in Colorado and a number of off-channel reservoirs had been constructed. Downstream diversions depended on runoff and return flows for water supply. Between Pueblo and the Stateline, about 300,000 acres have been irrigated from a number of canals. Due to the limited and variable water supply, wells were developed for supplemental supply wherever the aquifer would produce usable well capacities. Twenty three canals diverted flows from the river. All of the canals had water rights with dates of appropriation that were integrated into Colorado's administrative system to allocate water along the entire length of the river in the State.



Figure 1: Arkansas River Basin Location Map (Littleworth, 2008)

The primary crops irrigated are alfalfa, corn, sorghum and small grains. The region is also famous for the melons and vegetables grown in parts of the valley, where dependable water rights were secured and favorable soils exist. The climate is considered arid, noted for high winds, clear days and high temperatures during the peak of the summer. Elevation ranges from approximately 4,700 feet at Pueblo to approximately 3,300 feet at the Stateline.

When John Martin Reservoir was constructed and placed into operation, supplemental water supply was provided for eight canals downstream in Colorado and eight canals in Kansas. Some of the smaller canals were subsequently taken out of operation and their water supply was obtained from wells. With a conservation capacity of approximately 350,000 acre-feet, the reservoir does not fill most years and was typically drained by late summer.

The Arkansas River Compact specified how the supply stored in the reservoir would be divided between Colorado and Kansas. The outlet gates are closed in the winter and all inflows are stored. The Compact divided the water supply in John Martin Reservoir 60% to Colorado and 40% to Kansas, measured at the Stateline, 60 miles downstream of the reservoir. When the reservoir was empty, administration of the river reverted back to the pre-compact condition and water was allocated to canals in Colorado by appropriation date, and return flows and stream gains flowed into Kansas. An agreement entered in 1980 between the states established separate accounts in the reservoir which encouraged more carryover storage from year to year since then.

Hydrologic Model

The technical issues involved in Kansas v. Colorado were complex. It was necessary to define the standard of compliance and the "compact condition" against which new water uses could be quantified. The addition of John Martin Reservoir into the system at the time of the Compact rendered the pre-compact stream conditions obsolete for purposes of measuring allocations. This meant it was not possible to use the pre-compact water supply, diversions and stateline flow to develop index flows. The complex operation of the priority system in Colorado meant that water supplies were variable from canal system to system, depending on the seniority of the water rights and available flow. The yield of the Arkansas River is also quite variable from year to year. Since the canals on the lower end of the system divert mostly return flows, their supplies are dependent on upstream operations in addition to intermediate runoff conditions. Finally, the Compact provision protecting Kansas uses existing at the time of the Compact was conditioned on flows being usable in Kansas, such that upstream depletion of streamflow deemed unusable in Kansas was allowed under the Compact.

All of this complexity in the system of canals and reservoir, administration of water rights, the operations of John Martin Reservoir and consideration of conditions in Kansas resulted in the need for a hydrologic model of the river from Pueblo to the Stateline. The purpose of the model was to determine the effect of post-compact groundwater pumping in Colorado on Stateline flows into Kansas. The model has been referred to as the H-I Model, in reference to the hydrologic and institutional processes simulated by it. The model simulates the surface water system and processes groundwater interaction with the river through response functions derived from a separate groundwater flow model.

The H-I Model was developed initially to quantify the effects of the groundwater pumping in Colorado since the time of the Compact through the date of the filing with the court (1985), and subsequently extended to the present in several phases. After it was determined that the groundwater development had resulted in compact violations, controls were necessary in Colorado to obtain compact compliance. The model has evolved into a tool for measuring compliance. The model and its use going forward for assessing the adequacy of replacement operations in Colorado is

documented in the proposed decree pending before the Supreme Court (Littleworth, 2008).

Colorado promulgated Rules in 1996 to require that any continued pumping would be subject to providing offsets so that depletions of Stateline flows prohibited by the Compact would be mitigated. Sources of offsets could include irrigated acreage retirement, reservoir water, net of historical return flows, or transmountain water from the western slope not native to the Arkansas River, usually return flows from the first use.

The model is to be used each year to measure the combined effect of post-compact pumping and operation of replacement plans in Colorado on Stateline flows. Data for actual water supply, climate data, reservoir operations and groundwater pumping are compiled each year and input to the model. The model operates by using measured streamflow supplies, and predicts diversions and storage for pre-compact canals and reservoirs in Colorado. The model contains calibration parameters that were used to calibrate the model to historical streamflows and canal diversions.

Crop ET in the H-I Model

A major module of the model is the simulation of crop water demand and use. The model computes crop water consumptive use and return flows, based on the water supply predicted to be available to the irrigated land. The difference between stream diversions and return flows is commonly referred to as stream depletion, which is a measure of consumptive use by irrigated crops and the delay of return flows reaching the stream.

The crop water demand, or potential ET, is an important model parameter for computing the actual crop ET, limited by the available water supply. Other important model parameters for determining the actual crop ET are irrigated area and water supply. Potential crop ET is calculated outside of the model and used as a model input. The process to calculate crop water demand is a comprehensive combination of climatological data, reference crop ET, application of crop coefficients and derivation of a composite demand for each canal based on cropping patterns across the model domain (Brengosz, 2009). The model uses the crop water demand to compute a demand for water from the river for the canals. The water supply in the river is allocated to the canals and reservoirs based on their demands, locations and relative priorities. Groundwater pumping is added to the supply available for lands served by wells. The total available water supply is applied to meet the crop water demand to determine actual crop ET. The structure of the model, to determine crop water use based on the crop water demand and water supply, reflects the generally water-short condition of the study area.

Potential crop ET was originally computed for the model using the Modified Blaney-Criddle formula, which was developed by the U.S. Department of Agriculture (USDA), Soil Conservation Service (SCS) (USDA-SCS, 1970). This method has had

wide acceptance for calculating historical crop water demand in settings where weather data were limited. The only data requirements were mean monthly temperature at several locations within the study area. Monthly precipitation is also an input to the model and effective precipitation is computed by a routine in the model.

As it became apparent that the H-I Model would be used going forward in time to assess compact compliance, the State of Kansas recommended that the methodology being used to compute the potential crop ET be improved to incorporate available weather data sufficient for application of the Penman-Monteith formula. This proposal was submitted to the Special Master in a trial phase dealing with future remedies, in 2002.

Since the time of the first submittal of the H-I Model to the Special Master in 1990, a weather station network had been installed in the Arkansas River Valley in Colorado, maintained by the Colorado Agricultural Meteorological Network (CoAgMet). The use of Penman-Monteith for reference crop ET had become more streamlined, with progress being made on the development of the ASCE Standardized Reference ET equation, by the ASCE Task Committee on Standardization of Reference Evapotranspiration (ASCE-EWRI, 2005). ASCE Manual 70, Evapotranspiration and Irrigation Water Requirements, had been published in 1990, which described various methods of ET estimation and evaluated and compared the accuracy of various methods under various climatic conditions (Jensen et al., 1990).

The conversion of the method used to estimate potential crop ET from Modified Blaney-Criddle to Penman-Monteith for the H-I Model involved a number of considerations. Because the potential crop ET was a model input, the change did not require any modifications to the structure of the H-I Model. The primary issues that needed to be addressed included the source, sufficiency and reliability of weather data, adaptation of crop coefficients that would be applicable for the study area and any recalibration issues for the H-I Model.

1. The sufficiency and reliability of weather data are discussed in papers presented in these proceedings by Brengosz and by Ley, et al. (Brengosz, 2009 and Ley et al., 2009). Data from four weather stations were available in the study area in 2000. Three of the sites had data for seven years of record available at the time of conversion. Additional weather stations subsequently have been added to the network since 2000 and are now utilized in preparing annual updates.

2. Crop coefficients for application to the Arkansas River Valley were derived from ASCE Manual 70 for use with alfalfa reference crop ET. Adjustments were made for the local growing season conditions in the Arkansas River valley (Franzoy, 2001).

3. The potential effect of the implementation of the Penman-Monteith method on calibration of the H-I Model was addressed by comparing the results from

Penman-Monteith with those obtained with Modified Blaney-Criddle for the overlapping period of record, seven years for most of the weather stations. ASCE Manual 70 had documented differences in the ability of each method to predict crop ET, which indicated an overall difference between the two methods for arid climates. This difference was substantiated by the comparison made for the Arkansas River valley.

The H-I Model was calibrated over the period of 1950 – 1994, using the prior estimates as input. To provide a set of potential crop ET input to the model for the calibration period that would be consistent with the extensions of the model past 1994 using Penman-Monteith, the potential crop ET estimates for 1950 – 1994, obtained with the Modified Blaney-Criddle formula, were transformed to values consistent with Penman-Monteith results. This was accomplished by deriving monthly adjustment factors for each crop and weather station. The H-I Model was then recalibrated with the transformed potential crop ET data.

The evidence submitted by Kansas and Colorado at trial is described in the Special Master's fourth report (Kansas v. Colorado, No. 105 Original, 2003) (Littleworth, 2003). The Special Master considered extensive evidence and decided a number of issues involving the adoption of Penman-Monteith for use in the H-I Model. He concluded that Blaney-Criddle tended to underestimate potential ET in arid locations. He also concluded that Penman-Monteith was generally the method recommended by the scientific community when adequate data were available. He noted data issues were reasonably addressed with integrity assessments and appropriate adjustments which could be relied on into the future, with the expectation that data collection methods would also improve with time.

Issues raised at trial for consideration of the change were related to the applicability of results computed with Penman-Monteith formula to real-world conditions in the field when computing actual crop ET. This is an issue that continues to be important for modeling applications, here and elsewhere: to what extent can results obtained from direct application of the Penman-Monteith and commonly used crop coefficients be accepted without adjustment, or if adjustments are needed, what information or data are necessary to substantiate any adjustments? The H-I Model of course accounted for the availability, or shortage, of water supply because that was the underlying structure of the model. The issues of effects of irrigation management and water quality on crop water use were addressed with evidence and testimony. The Special Master decided that the results of the equation could be used in the model in this case without downward adjustment for real world conditions and management.

The Arkansas River in eastern Colorado is somewhat remarkable for high concentrations of salinity. However, the water supply continues to be a valuable resource for irrigated agriculture in the region, implying that water users have adapted management to the water quality. The issue of the effect of water quality on crop yield and ET was considered by the Special Master. He concluded that the interrelationships of water quality, soil salinity, irrigation management and crop yield

were complex and a relatively simplified adjustment to potential crop ET rates was not appropriate for this modeling application, suggesting that reduced irrigation efficiency to account for leaching practice would be sufficient for this model.

The technical issues considered in this case are examples of details that may need to be considered for direct use of reference or crop specific ET results in other hydrologic models. As the Special Master noted, "While experts speak in terms of 'equations', the mathematical certainty that one might be led to expect from this terminology is not real. Clearly, under some conditions, adjustments are made to reflect local conditions, and these adjustments are not without subjective input." (pg 73, Fourth report) (Littleworth, 2003).

Current Status of Arkansas River Model

The Special Master's findings that the Penman-Monteith equation should be used to compute crop potential ET for input to the H-I Model laid the groundwork for the ongoing updates to the modeling done by the two states each year. The Draft Decree and Appendices provide specifications for annual updates, including schedules, data requirements and procedures for making future changes to the methods (Littleworth, 2008). The decree contains specifications for climate data to be used, crop coefficients, and weather data integrity assessment and correction procedures. Model results are currently updated through year 2007.

REPUBLICAN RIVER COMPACT

The Republican River Compact allocates the water supply of the Republican River Basin between the States of Nebraska, Kansas and Colorado by percentages and tributary basin. The basin is located in the high plains, from eastern Colorado, through southwestern Nebraska and northwestern Kansas (Figure 2). The river flows into Kansas near Hardy, Nebraska, continuing to its confluence with the Smoky Hill River near Junction City, Kansas. Streamflow is derived principally from baseflow and precipitation runoff. The Republican River Compact was adopted in 1943. Water development for irrigation has included early surface water diversions, construction of several federal reservoirs and canal systems, and groundwater development throughout the basin. Much of the basin is underlain by the Ogallala Aquifer. The largest reservoir, Harlan County Reservoir, located about 65 miles upstream of the final crossing of the Kansas-Nebraska Stateline, is a joint project between the Corps of Engineers and Bureau of Reclamation, supplying water to lands in both Nebraska and Kansas.

The State of Kansas brought an action for enforcement of the Republican River Compact in 1999 to the U. S. Supreme Court (Kansas v. Nebraska and Colorado, No. 126 Original). The Republican River Compact allocated beneficial consumptive use to each of the States. Compact compliance is assessed by tabulating the consumptive uses in each state, computing the allocable water supply by adding the stream gage

flows to the computed consumptive uses and comparing each states use to its allocation.

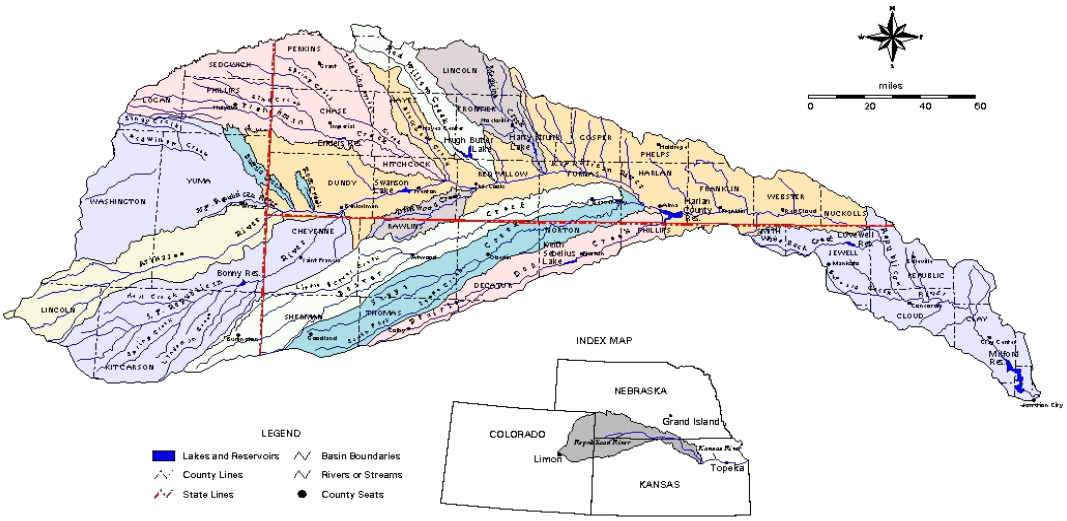

Figure 2: Republican River Location Map based on Appendix C.1 of McKusick, 2003.

In this case, the Special Master issued a ruling requiring that effects of groundwater pumping on streamflows be included and accounted for within each State's allocations. The three states then entered negotiations to resolve issues related to measuring compact compliance. An important element of the settlement was the development and acceptance of a groundwater model used to compute the effects of pumping in each state on streamflows. The Final Settlement Stipulation was submitted to the court in December, 2002 and the Groundwater Model was finally adopted in September, 2003 (McKusick, 2003).

ET Calculations for Republican River Compact

The Groundwater Model is used each year to compute the streamflow effects of pumping in each state. The updates and accounting are accomplished through the Republican River Compact Administration. The methods and data requirements are specified in the Accounting Procedures and Reporting Requirements, Appendix C to the Final Settlement Stipulation. Model documentation is contained in Appendix J to the Final Settlement Stipulation and the Final report of the Special Master. The model determines the effects of pumping for irrigation supply by using the concept of net pumping. Total pumping and recharge of applied water are input to the model.

Crop ET is not an explicit input or result from the model. The Accounting Procedures contain a requirement for each state to annually tabulate and provide estimates of crop irrigation requirement, on a county format. This information has

been and continues to be developed by each State using the Hargreaves method for reference ET, calibrated to the Penman-Monteith equation. The reference crop ET derived with Hargreaves is used with locally derived crop coefficients to obtain the crop specific ET values. Composite values are then obtained by county, using county-wide crop statistic data. Effective precipitation is computed from the monthly totals of potential crop ET and precipitation, using the methods set out in Technical Release No. 21 (USDA, 1970).

REFERENCES

ASCE-EWRI. 2005. "The ASCE Standardized Reference Evapotranspiration Equation". Edited by R.G. Allen, I.A. Walter, R.E. Elliott, T.A. Howell, D. Intenfisu, M.E. Jensen, and R. L. Snyder. Task Committee on Standardization of Reference Evapotranspiration of EWRI. Amer. Society of Civil Engineers, Reston, VA.

Brengosz, M.K. 2009. "Interstate Collaboration in the Arkansas River Compact Compliance Process: The "Nuts and Bolts" of Developing PET for Canal Service Areas for Input to the H-I Model". Proceedings of the ASCE World Environmental and Water Resources Congress, May 17-21, 2009. Kansas City, MO.

Final Settlement Stipulation dated December 15, 2002, approved by the states of Colorado, Nebraska and Kansas and filed in the case of *Kansas v. Nebraska and Colorado*, No. 126, Original, in the Supreme Court of the United States

Franzoy, C.E. 2001. "Comparison of Crop Evapotranspiration Calculated using ASCE Standardized Penman-Monteith and TR-21 Blaney-Criddle". Expert Report Prepared for Colorado State Engineer, Kansas v. Colorado, No. 105, US Supreme Court.

Jensen, M.E., R.G. Allen, and R.D. Burman (ed.). 1990. "ASCE Manual and Report on Engineering Practice No. 70, Evapotranspiration and Irrigation Water Requirements". New York, NY.

Ley, T.W., D.E. Straw and R.W. Hill. 2009a. "ASCE Standardized Penman-Monteith Alfalfa Reference ET and Crop ET Estimates for Arkansas River Compact Compliance in Colorado". Proceedings of the ASCE World Environmental and Water Resources Congress, May 17-21, 2009. Kansas City, MO.

Littleworth, A. L. 2003. "Fourth Report of the Special Master". State of Kansas vs. State of Colorado and the United States of America. No. 105, Original. Supreme Court of the United States.

Littleworth, A. L. 2008. "Fifth and Final Report of the Special Master, Volume II, Proposed Judgment and Decree". State of Kansas vs. State of Colorado and the United States of America. No. 105, Original. Supreme Court of the United States.

McKusick, V.L. 2003. “Final Report of the Special Master”. State of Kansas v. State of Nebraska and State of Colorado, No. 126, Original. Supreme Court of the United States.

McKusick, V.L. 2003. “Second Report of the Special Master (Subject: Final Settlement Stipulation”. State of Kansas v. State of Nebraska and State of Colorado, No. 126, Original. Supreme Court of the United States.

USDA, Soil Conservation Service. 1970. “Irrigation Water Requirements”, Technical Release 21.

Adjusting Wind Speed Measured over Variable Height Alfalfa for Use in the ASCE Standardized Penman-Monteith Equation

Thomas W. Ley PE, M. ASCE[1], Richard G. Allen M. ASCE[2], and Marvin E. Jensen M. ASCE[3]

[1] Colorado Division of Water Resources, Pueblo, CO 81004; PH (719) 542-3368; FAX (719) 544-0800; email: thomas.ley@state.co.us
[2] Professor, Research and Extension Center, University of Idaho, 3793 N. 3600 E., Kimberly, Idaho 83341; PH (208) 423-6601; email: rallen@kimberly.uidaho.edu
[3] (retired) USDA-ARS and Colorado State University, Ft. Collins, CO; email: MJensen419@aol.com

Abstract

The ASCE Standardized Reference Evapotranspiration Equation expects the weather station wind speed data to represent that occurring at a height of 2 m over and downwind of a smooth measurement surface such as clipped grass. The Task Committee on the Standardized Equation provided guidance for adjusting wind speed measured at height other than 2 m, or, for situations when the wind speed is measured over and downwind of 0.5 m alfalfa. The latter adjustment attempts to account for the effects of both grass and alfalfa crop characteristics (height, roughness) on the wind profile. A more physically representative approach to adjust wind speeds at various heights and various weather measurement surface conditions to equivalent wind speed at 2 m height over clipped grass is tested. Wind speeds were simultaneously measured during the 2008 growing season at 2-m and 3-m heights above ground surface over variable height alfalfa at two Colorado Agricultural Meteorological Network (CoAgMet) electronic weather stations and at the research alfalfa lysimeter installation at the Colorado State University Arkansas Valley Research Center. These wind speed measurements were adjusted to estimated wind speed at 2 m over grass, and compared.

Introduction

In his fourth report (Littleworth, 2003) in the case of Kansas v. Colorado (No. 105, Original, U.S. Supreme Court), regarding compliance with the Arkansas River Compact, the Special Master hearing the case recommended specific changes by which Arkansas River streamflow depletions at the Colorado-Kansas Stateline are determined. One of the major changes was the recommendation to use the ASCE Standardized Reference Evapotranspiration Equation (ASCE-EWRI, 2005) as the

method to determine reference crop evapotranspiration and the basis for determining crop consumptive use. Steps taken by the States of Colorado and Kansas to implement this recommendation are discussed fully elsewhere in these proceedings (Book and Brengosz, 2009; Brengosz, 2009; Ley et al., 2009). One activity undertaken by the State of Colorado, in cooperation with the Colorado Climate Center, was to expand and improve the collection of weather data suitable for use in the Standardized Equation. To this end, new Colorado Agricultural Meteorological Network (CoAgMet) electronic weather stations were installed, or existing stations moved, into large, private, commercial irrigated alfalfa fields in the lower Arkansas Valley of Colorado. Locating stations in irrigated alfalfa fields was done because of the need to collect weather data for the Standardized Equation in an irrigated environment with adequate fetch (ASCE-EWRI, 2005), and because of a lack of large irrigated grass or pasture fields that could be used for this purpose.

American Society of Agricultural and Biological Engineers Engineering Practice EP505: Measurement and Reporting Practices for Automatic Agricultural Weather Stations recommends that wind speed be measured at 2 m or 3 m height over uniform, low cover vegetation such as grass (ASABE, 2004). The standard wind speed measurement height on CoAgMet weather stations is 2 m above the surface. Some weather station networks measure wind speed at 3 m to avoid or minimize effects of measurement surface vegetation height.

The parameterization of the ASCE Standardized Reference Evapotranspiration Equation (ASCE-EWRI, 2005) expects the wind speed measurement, if not measured at 2-m height over and downwind of a smooth measurement surface such as clipped grass, to be translated to an equivalent value. Specifically, the zero plane displacement, 0.08 m, used in the Standardized Equation for the tall reference crop, is for a weather measurement surface similar to clipped grass, with vegetation height of 0.12 m. The purpose of this was to accommodate a majority of weather stations collecting data over a smooth surface like grass. The Task Committee on the Standardized Equation provided guidance in Appendix B of EWRI-ASCE (2005) for adjusting wind speed measured at height other than 2 m, or, for situations when the wind speed is measured over and downwind of 0.5 m tall alfalfa using standard logarithmic wind speed profile theory. Equation B.14c (ASCE-EWRI, 2005) was developed to adjust wind speed measured over and downwind of 0.5 m alfalfa to an equivalent wind speed over clipped grass for use in the Standardized Equation.

$$u_2 = u_z \frac{\ln\left(\frac{2-d}{z_{om}}\right)}{\ln\left(\frac{z_w-d}{z_{om}}\right)} = u_z \frac{\ln\left(\frac{2-0.08}{0.062}\right)}{\ln\left(\frac{z_w-0.335}{0.062}\right)} = u_z \frac{3.44}{\ln(16.3z_w-5.42)} \quad \text{(B.14c)}$$

where u_2 is wind speed at 2 m above ground surface (m s^{-1}), u_z is wind speed at height z_w over 0.5 m alfalfa (m s^{-1}), d is zero plane displacement height (m) taken as 0.67 h, and z_{om} is aerodynamic roughness length (m) taken as 0.123 h, where h is crop height

(m). The d and z_{om} values in the denominator are for the 0.5 m alfalfa weather measurement surface, while the d and z_{om} in the numerator are a combination of the zero plane displacement for clipped grass (0.08) and roughness length for 0.5 m alfalfa (0.062). This combination is an attempt to account for the effects of both grass and alfalfa crop characteristics (height, roughness) on the wind profile. However, there is some question on whether Eq. B.14c functions correctly in translating wind speed measured over a rough surface such as full cover alfalfa to an equivalent for a smooth grassed standard weather surface.

The States of Colorado and Kansas have agreed to temporarily use Eq. B.14c with a seasonal average alfalfa crop height of 0.3 m to adjust the 2-m wind speed data collected at the CoAgMet weather stations located in commercial alfalfa fields. This results in a nominal 1.7% upwards adjustment to measured wind speeds. It is felt that the true ratio of 2-m wind speed measured over clipped grass to 2-m wind speed over alfalfa will exceed this value on a seasonal average basis, and potentially significantly exceed it, during periods when alfalfa is growing at reference conditions. This paper presents the results of initial studies to better define the adjustment of wind speed data measured at 2-m above ground surface over variable height alfalfa.

Background

The second and third authors have performed a considerable amount of research along with Dr. James L. Wright, USDA-ARS (retired), in the development of Penman and Penman-Monteith type evapotranspiration equations, including the ASCE Standardized Reference ET Equation. Much of this work was done at the USDA-ARS research facility in Kimberly Idaho using alfalfa as the reference crop and with wind measurement over a standard grassed weather station surface. This ultimately influenced the final values for surface resistance used in the Standardized Equation, and thus, the wind data input to the equation should be collected over grass (or adjusted to a grass condition) (Allen et al., 1989; Allen and Wright, 1997; ASCE-EWRI 2005). In that case, the wind profile adjusted to grass should be constructed using zero plane displacement and roughness for grass, which, as discussed above, may not be properly done in Eq. B.14c.

A suggested better approach (than Eq. B.14c) to adjust wind data collected over non-standard measurement surface conditions to an equivalent wind at 2 m over clipped grass is to use the full wind speed translation algorithms presented in Allen and Wright (1997) that correctly account for impacts of height and roughness of vegetation of each surface. These algorithms apply the concept of 'blending height' where the wind profiles over the measurement surface and the surface to which wind is being translated are both extended upward to the top of the internal (or inertial) boundary layer, IBL, over each respective surface. At this elevation, the wind speeds (or at least friction velocity) can be assumed to be equal for both surface conditions. The wind speed at the top of the IBL is then extrapolated downward from this height to the surface to which the wind speed is being translated. Equation 13 of Allen and Wright (1997), repeated here as Eq. 1, illustrates this translation algorithm:

$$u_{z,v} = u_{z,w} \frac{\ln\left(\frac{z_{IBL,w} - d_w}{z_{om,w}}\right)\ln\left(\frac{z_{IBL,v} - d_R}{z_{om,R}}\right)\ln\left(\frac{z_v - d_v}{z_{om,v}}\right)}{\ln\left(\frac{z_w - d_w}{z_{om,w}}\right)\ln\left(\frac{z_{IBL,w} - d_R}{z_{om,R}}\right)\ln\left(\frac{z_{IBL,v} - d_v}{z_{om,v}}\right)} \quad (1)$$

where $u_{z,w}$ is the measured wind speed (m s^{-1}) at a weather station at height z_w (m) having vegetation type W, and $u_{z,v}$ is the equivalent wind speed (m s^{-1}) estimated to have occurred at height z_v (m) above a surface of vegetation type V. $z_{IBL,w}$ and $z_{IBL,v}$ are the heights (m) of the IBL over the weather measurement surface (W) and over the surface (V) to which wind is being translated. d_w, d_R, and d_v are the zero plane displacement heights (m), taken as 0.67 h, for the weather measurement vegetation, the regional vegetation, and, the vegetation of surface V. $z_{om,w}$, $z_{om,R}$, and $z_{om,v}$, are aerodynamic roughness lengths (m) taken as 0.123 h, for the weather measurement vegetation, the regional vegetation, and, the vegetation of surface V. The variable h is vegetation height (m) for each surface condition (W, R, and V).

Eq. 1 is a multiplicative combination of the basic logarithmic wind speed profile relationship and extrapolates wind measured at z_w upward to $z_{IBL,w}$, then from $z_{IBL,w}$ upward to $z_{IBL,R}$, then from $z_{IBL,R}$ downward to $z_{IBL,v}$, and finally from $z_{IBL,v}$ downward to z_v. The intermediate steps to extrapolate up from the weather measurement surface IBL to the regional internal boundary layer and back down to the IBL for surface V is necessary when the heights of the IBL's for the weather measurement surface and for surface V are expected to be different from each other due to different vegetation roughness and fetch lengths for each condition. The regional IBL is assumed to occur directly above the IBL's of the two underlying surfaces and integrates the effects of surface conditions for a large area on the regional wind speed profile. One limitation of the approach of Eq. 1 is that it assumes that neutral boundary layer buoyancy conditions hold. This is generally the case for reference and agricultural conditions when vegetation is near full-ground cover (Allen and Wright, 1997) and the same assumption is used in the derivation and application of the standardized reference ET equation (ASCE-EWRI 2005).

Use of Eq. 1 requires estimating the thickness or height the IBL for each surface condition and the region. The thickness of the IBL depends on the size of the area having similar surface properties, including roughness, vegetation characteristics, and moisture conditions. Allen and Wright (1997) present an approach developed by Brutsaert (1982) to approximate the growth of the IBL over an individual field downwind of a surface discontinuity. Their Eq. 14 is repeated here as Eq. 2:

$$z_{IBL} = d + 0.33 z_{om}^{0.125} x_f^{0.875} \quad (2)$$

where z_{IBL} is the height of the IBL over a surface having roughness, z_{om}, and zero plane displacement, d, at a horizontal distance downwind, x_f, of a substantial change

in surface or vegetation characteristics, all in (m). Surface roughness, z_{om}, and zero plane displacement, d, are approximated as 0.123 h, and 0.67 h, respectively, where h is vegetation height (m).

It should be noted that when the weather station measurement surface (W) and the surface to which wind speed is being translated (V) are both alfalfa with the same fetch conditions, then Eq. 1 reduces to the standard wind speed profile adjustment equation, which is simply an adjustment for wind speed measurement height. The leftmost part of Eq. B14c (as presented above) shows this adjustment, where the d and z_{om} values in both the numerator and denominator are for variable height alfalfa. For example, the adjustment could be from wind speed measured at 3 m above ground surface over alfalfa to 2 m above ground surface over alfalfa.

Methods and Materials

Concerns on the effects of full canopy alfalfa on wind speed measured at 2 m above the ground surface prompted the outfitting of three weather stations along the Arkansas River valley of southeastern Colorado that were in the interiors of alfalfa fields with additional wind speed measurement instrumentation at 3-m height. The three stations comprised two CoAgMet stations located in large alfalfa fields, Las Animas and Holly 02, and the meteorological station at the research alfalfa lysimeter site at the Colorado State University Arkansas Valley Research Center (CSU-AVRC) near Rocky Ford. The outfitting was completed in early June 2008 (see Table 1). In all instances, RM Young Wind Sentry cup anemometers were used at both 2-m and 3-m heights above the ground surface. The existing 2-m height cup anemometers were serviced with new upper and lower shaft bearings and were cleaned at the time of the installation of the 3-m height anemometers, which were all brand new. The CSU-AVRC lysimeter installation is also equipped with a RM Young Wind Monitor (propeller anemometer with integrated vane). The CoAgMet stations are equipped with CR-10X data loggers programmed to measure attached sensors every 10 seconds. Final wind speed data values stored in the CoAgMet database are the mean hourly wind speed (m s^{-1}) and the daily wind run (km d^{-1}). The CSU-AVRC lysimeter meteorological instrumentation is measured by a CR-7X data logger programmed to measure on a 6-sec interval. Final output data includes 5-minute, 15-minute, and daily average wind speed (m s^{-1}).

The typical growth pattern of alfalfa (green chopped or harvested for hay) in the lower Arkansas Valley of Colorado is for spring greenup to begin in late March/early April. Four harvests are usual, occurring approximately the first week of June, the middle of July, the end of August and mid to late October. Fall dormancy and or killing frosts occur by late October. Alfalfa crop growth and harvest data were documented at the CSU-AVRC site, and monitored and documented with photos at the two CoAgMet sites. Cutting dates were obtained from the cooperators at the CoAgMet sites. See Table 1. Crop height curves through the season were approximated at each site using these data, and a simple linear-segmented crop height model similar in structure to the simple single crop coefficient model described in

Table 1. 3-m anemometer installations and crop growth dates during 2008 at the three study sites.

Site	Lat	Long	Elev (m)	3-m anem. installation date	Spring Greenup	First harvest	Second harvest	Third harvest	Fourth harvest
CSU-AVRC	38.04	103.70	1274	Jun 12	Apr 1	Jun 11	Jul 19	Aug 29	Nov 3
Las Animas	38.15	102.86	1187	Jun 4	Apr 1	Jun 14	Jul 22	Aug 28	Nov 11
Holly 02	38.14	102.24	1088	Jun 4	Mar 20	May 30	Jul 8	Aug 21	Oct 18

FAO-56 (Allen et al., 1998). Crop height during the initial growth stage was taken as 0.12 m, and during full canopy stage as 0.50 m, except during the last growth cycle of the season, when maximum alfalfa height attained was only about 0.35 m at all sites. Crop growth between harvests was broken into 3 or 4 intervals, the initial period, rapid development, full canopy, and late. The initial period is normally 5-7 days, except during the first cycle when growth is slower due to cooler temperatures. Rapid development occurs over about 20 days, and full canopy and late stages are from 10-15 days during the mid-season. The impact of alfalfa vegetation height on reducing the ratio of wind speed measured at 2-m height above ground surface to that made at 3-m height above ground surface became more pronounced as the alfalfa grew.

Eqs. 1 and 2 were used to translate both the 2-m and 3-m measured mean daily wind speeds (m s^{-1}) at each site to an equivalent 2-m mean daily wind speed (m s^{-1}) over clipped grass, termed adjusted 2-m and adjusted 3-m mean daily wind speeds in the discussion of results. The alfalfa weather station measurement surface (crop height) at each site varied with time as described above. The fetch of similar surface conditions in each case, i.e., x_f, in Eq. 2, was taken as 200 m for all three deployments, although in the case of CSU-AVRC, there were corn fields or plots 83 m to the north and 100 m to the south of the meteorological instrumentation on the lysimeter field. East and west fetch distance was well over 200m.

An additional measure of wind speed was made at the Rocky Ford CoAgMet station during 2008, over a surface that approximates a standard clipped grass surface. However, these wind data were not reliable for 2008 because corn research plots were located in the near vicinity of the anemometer (5-60 m to the south and west/NW). During June – mid October, when the corn on the plots was taller than about 1 m, sheltering effects on wind speed measurements from the CoAgMet station were evident. Therefore, and unfortunately, the wind speed measurements from the grassed Rocky Ford CoAgMet station could not be used for comparison and as a reality check for the alfalfa wind speed data that were translated to an equivalent wind speed at 2 m over grass.

Eq. 1 was applied to translate measured wind speeds to values representing equivalent wind speeds expected to have occurred over 0.12-m grass having 200 m of

fetch and at the 2-m height (i.e., conditions for a standard weather station). The regional condition in each case was taken as having 1000 m of irrigated fetch with an average vegetation height of 0.5 m. The 0.5 m height represents a mixture of agricultural crops including alfalfa, field corn, grains and vegetables.

Eq. 1 was also applied in reduced form (as discussed above) to translate the 3-m measured wind speeds over alfalfa to estimated 2-m wind speeds over alfalfa at each site. The estimated 2-m wind speeds were then compared to the measured 2-m wind speeds. This translation allows a check on the whether the logarithmic adjustment holds over the alfalfa fields and that the assumption of neutrality is generally valid.

Results

The measured 3-m mean daily wind speed is plotted against measured 2-m mean daily wind speed (upper graph), and the adjusted 3-m mean daily wind speed is plotted versus the adjusted 2-m mean daily wind speed (lower graph), for each of the three sites, respectively, in Figures 1, 2, and 3. Wind speeds typically increase as one moves west to east in the Lower Arkansas Valley of Colorado. For the period June 15 to Oct 31, 2008, the cumulative daily wind run measured at 2-m and 3-m height, respectively, was 23,143 km and 26,577 km at CSU-AVRC; 33,511 km and 37,379 km at Las Animas; and, 33,900 km and 39,180 km at Holly02. The average ratio of measured 3-m to 2-m mean daily wind speeds for this period was 1.148 at CSU-AVRC; 1.116 at Las Animas; and, 1.156 at Holly02. During this period, CSU-AVRC had 62 days, Holly02 had 63 days, but Las Animas had only 41 days when the alfalfa height was 0.35 m and taller. This partially explains the smaller 3-m to 2-m wind speed ratio at Las Animas for the period.

The factor, computed using Eqs. 1 and 2, to adjust the measured 2-m wind speed to the standard weather station condition ranged from 1.00 to 1.18 for alfalfa crop heights of 0.12 m and 0.50 m, respectively, at all 3 sites. The average adjustment factor for April 1 to October 31 across all three sites was 1.09. Conversely, the factor to adjust the measured 3-m wind speed ranged from 0.92 to 1.03 for crop heights of 0.12 m and 0.50 m, respectively, with an April 1-October 31 average adjustment factor of 0.98 across all three sites. The 3-m adjustment factor ranged from 0.98 to 1.03 during periods when the alfalfa crop could be considered at full canopy, 0.30 to 0.50 m in height.

An objective of this study was to adjust measured 2-m and 3-m wind speeds so that the adjusted wind speeds from both heights, representing equivalent wind speeds measured at 2 m over 0.12 m grass, was the same and reflected wind speeds expected over a grassed surface. In Figures 1-3, the measurements made at 2 m over the ground surface for alfalfa were increased following adjustment, and acquired values similar to those derived when adjusting the 3-m measurements over alfalfa to 2 m over a standardized grass surface. Table 2, part (A) is a summary of the measured and adjusted 2-m and 3-m wind speed data for all three sites for the study intervals

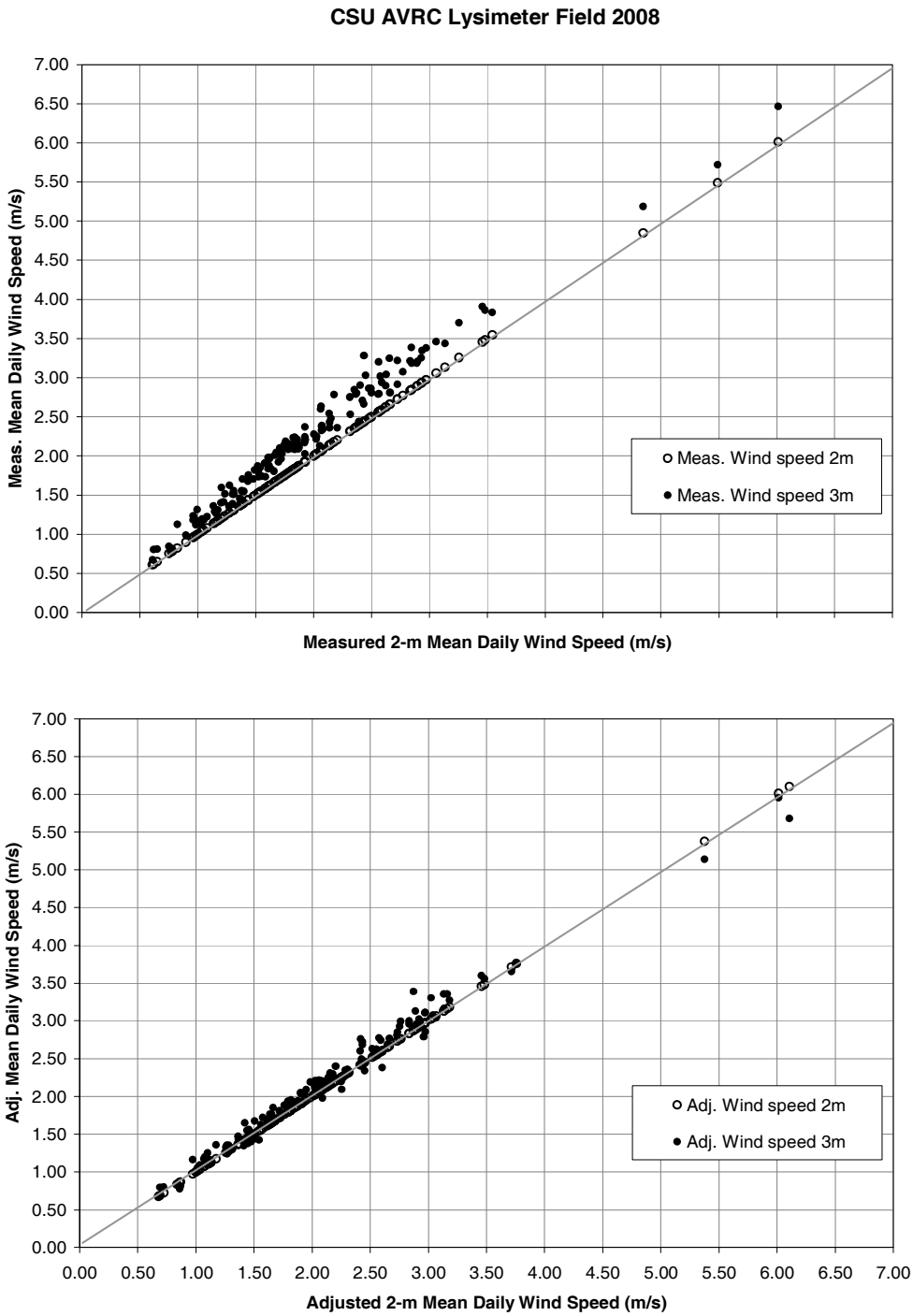

Figure 1. Comparison of measured 2-m and 3-m mean daily wind speeds (upper graph) and adjusted 2-m and 3-m mean daily wind speeds (lower graph) at CSU AVRC.

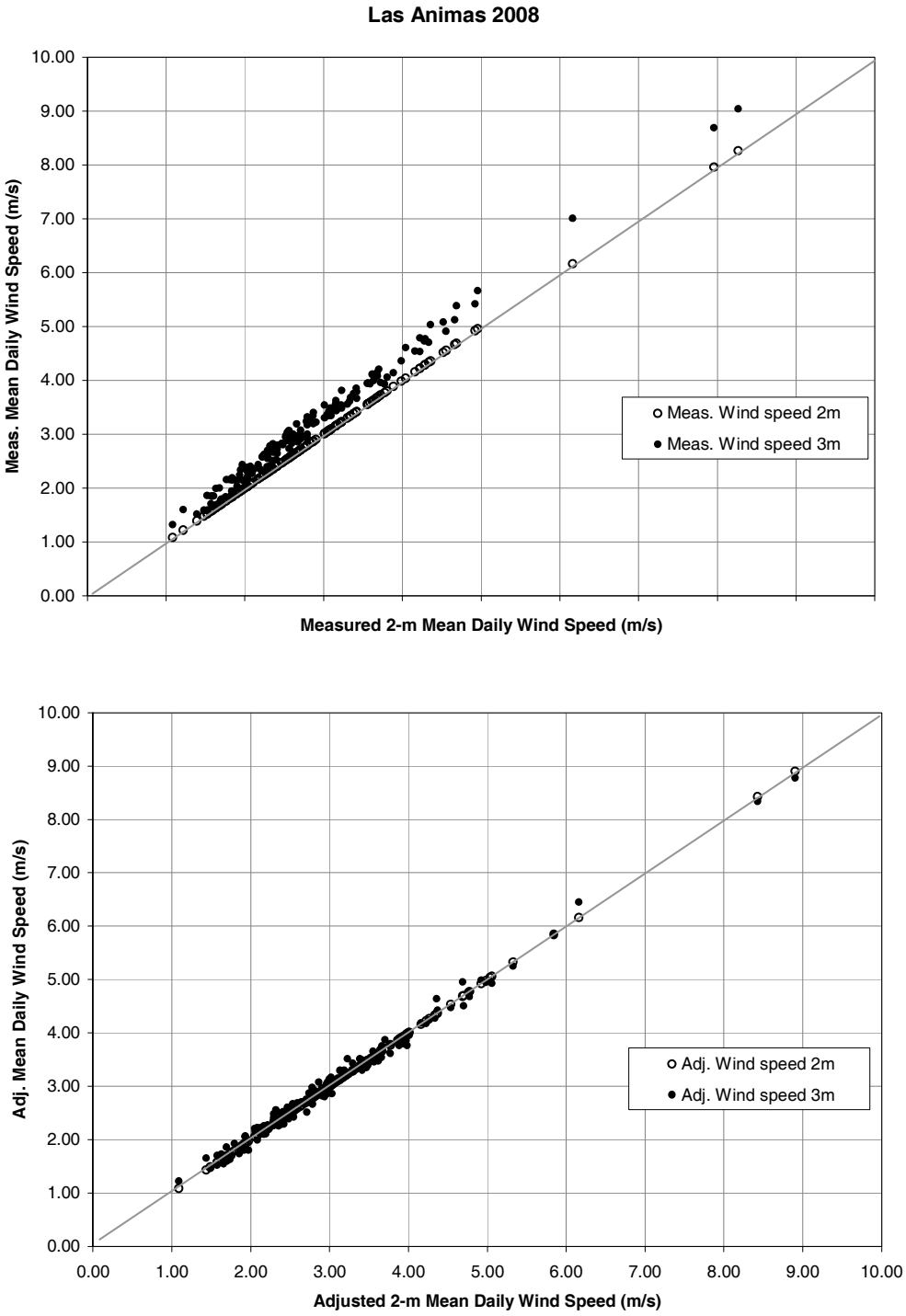

Figure 2. Comparison of measured 2-m and 3-m mean daily wind speeds (upper graph) and adjusted 2-m and 3-m mean daily wind speeds (lower graph) at Las Animas CoAgMet station.

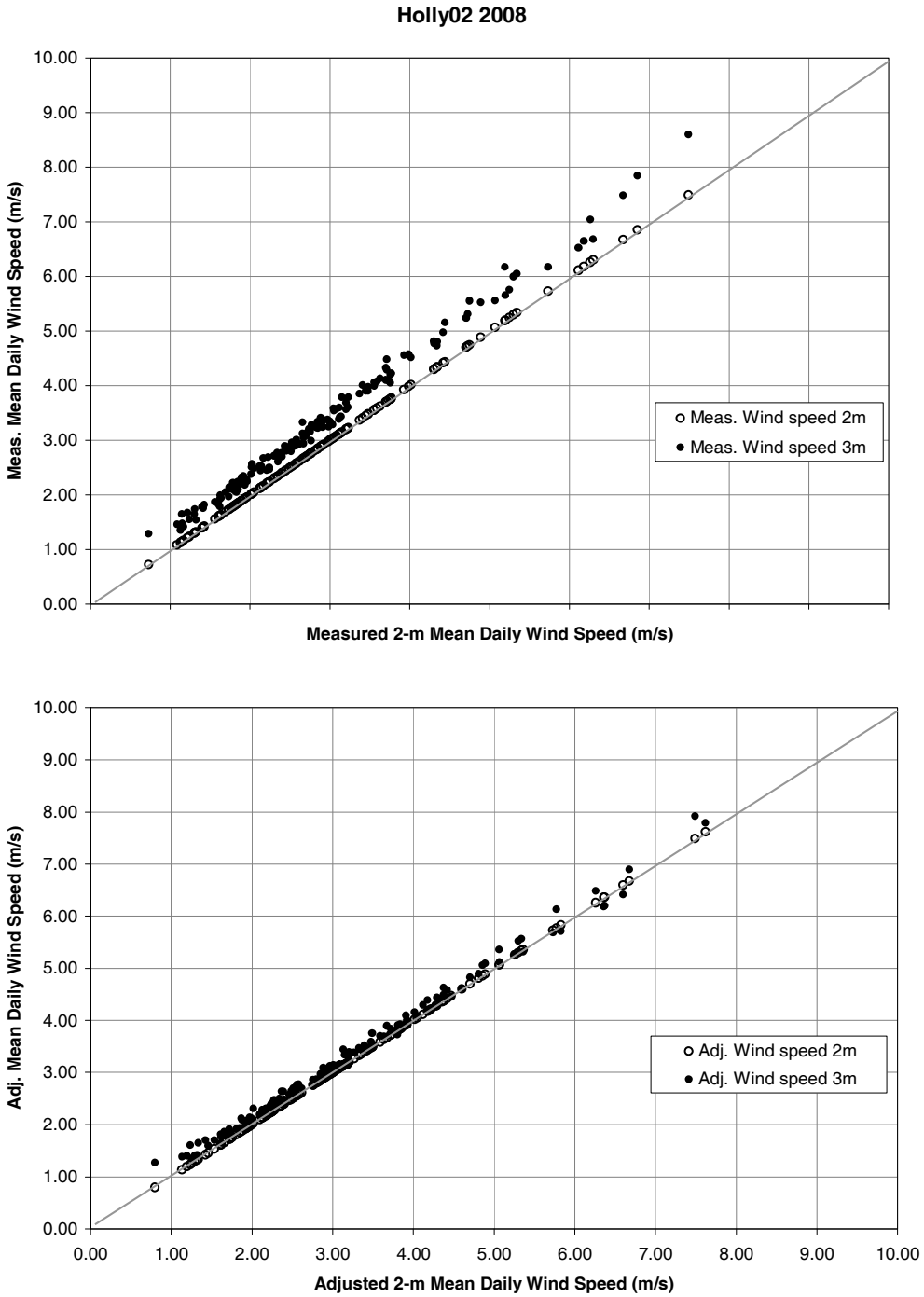

Figure 3. Comparison of measured 2-m and 3-m mean daily wind speeds (upper graph) and adjusted 2-m and 3-m mean daily wind speeds (lower graph) at Holly02 CoAgMet station.

indicated. These results and lower graph in each of Figures 1-3 show the adjustment method is relatively effective and internally consistent, in that the adjusted wind speeds are similar. For example, the results in Table 2 show the mean difference between the measured 2-m and 3-m daily wind speeds was 0.28 m s^{-1} at CSU-AVRC, 0.33 m s^{-1} at Las Animas, and 0.43 m s^{-1} at Holly02. After adjustment using Eq. 1, the mean difference between the adjusted 2-m and 3-m daily wind speeds was 0.07 m s^{-1} at CSU-AVRC, 0.02 m s^{-1} at Las Animas, and 0.12 m s^{-1} at Holly02. The adjustment procedure reduced the difference by 75% at CSU-AVRC, by 94% at Las Animas, and by 72% at Holly02. The variability of the performance of the adjustment algorithm suggests additional investigation is needed on the sensitivity of the error closure to the values used for regional fetch length, regional vegetation height, the estimation method for the height of the IBL's, etc.

The last column of Table 2 indicates the standard deviation of the average difference between the adjusted daily 2-m and 3-m wind speeds to be within 3-5% of the mean adjusted 2-m wind speeds.

At CSU-AVRC, adjustment statistics were also computed for a subset of days, designated as CSU-AVRC (subset) in Table 2, when mean daily wind direction was from either of two 90-degree sectors: NE to SE or SW to NW. This was done to determine if the corn crops to the north and south of the lysimeter field affected the measured and adjusted wind speeds. The measured and adjusted mean daily 2-m and 3-m wind speeds were slightly less for the subset of days at CSU-AVRC. The standard deviation of the daily difference between adjusted 2-m and 3-m wind speeds was also slightly less. Filtering days from the data set when the mean wind direction was from the areas of the corn fields does not appear to have much impact on the results.

Least squares linear regression relationships were computed for each of the adjusted 2-m and 3-m wind speeds versus the measured 2-m wind speed at all three sites. As well, least squares linear regression relationships were computed for adjusted 3-m wind speed versus the adjusted 2-m wind speed at all three sites. At CSU- AVRC, these linear regressions were computed for both the full data set and the wind direction-filtered subset of days. Results are summarized in Table 3. The values for r^2 were high, as expected, due to the large covariance between wind speed measurements at the two heights. In general, no improvement in r^2 was found for the CSU-AVRC subset, when the data were filtered for wind direction. The individual site regression equations, or the overall mean regression equations for adjusting 2-m wind speed measured over alfalfa and presented at the bottom of Table 3, part (A) may provide a simple means for adjusting wind speeds collected over variable height alfalfa to equivalent wind speeds for the standard weather station conditions when nothing is known about alfalfa growth periods and harvest dates, especially in the case where wind speed measurement height is to be standardized at 2 m, as in the case of CoAgMet. Adjustments to measured 2-m wind speeds over alfalfa using the overall mean regression equation developed using the CSU-AVRC subset compared to those made using the full logarithmic wind speed profile translation algorithm, Eq.

Table 2. Comparison of measured mean daily wind speeds, adjusted mean daily wind speeds, average difference between adjusted wind speeds, standard deviation of the difference, and standard deviation of the difference as percent of mean adjusted 2-m mean daily wind speed at the three study sites: (a) comparison for Eq. 1-adjusted 2-m and 3-m mean daily wind speeds, (b) comparison for Eq. 1-adjusted 2-m mean daily wind speed and regression equation adjusted 2-m mean daily wind speed, and (c) comparison for 2.7 m mean daily wind speeds over alfalfa with Eq.1 adjusted 2-m mean daily wind speeds (grass equivalent).

Site	Interval	Measured mean daily wind speed (m/s)		Adjusted mean daily wind speed (m/s)		Ave. Difference (m/s)	Std. Dev. of Diff. (m/s)	Std. Dev. of Diff. as Percent of Adj. 2-m Mean Daily Wind Speed
(A)		**2-m**	**3-m**	**2-m**	**3-m**			
CSU-AVRC	6/13-10/31	1.95	2.23	2.11	2.18	0.07	0.11	5.27
CSU-AVRC (subset)	6/13-10/31	1.91	2.20	2.09	2.16	0.07	0.10	4.90
Las Animas	6/5-10/31	2.83	3.16	3.06	3.08	0.02	0.11	3.53
Holly 02	6/5-10/31	2.94	3.37	3.16	3.28	0.11	0.11	3.36
(B)					**Regression**			
		2-m	**3-m**	**2-m**	**Eq.[1/]**			
CSU-AVRC	6/13-10/31	1.95	2.23	2.11	2.12	0.01	0.14	6.41
CSU-AVRC (subset)	6/13-10/31	1.91	2.20	2.09	2.09	-0.01	0.13	6.32
Las Animas	6/5-10/31	2.83	3.16	3.06	3.03	-0.03	0.20	6.65
Holly 02	6/5-10/31	2.94	3.37	3.16	3.14	-0.02	0.19	6.13
(C)				**grass**	**alfalfa**			
		2-m	**3-m**	**2-m**	**2.7-m**			
CSU-AVRC	6/13-10/31	1.95	2.23	2.11	2.11	0.00	0.11	5.08
Las Animas	6/5-10/31	2.83	3.16	3.06	3.06	0.00	0.16	5.07
Holly 02	6/5-10/31	2.94	3.37	3.16	3.17	0.01	0.16	5.20

[1/] Adjusted mean daily wind speed computed using overall mean regression of adjusted 2-m wind speed versus the measured 2-m wind speed for all sites and the CSU-AVRC subset of days (see Table 3).

Table 3. Results of linear regression analyses of: a) adjusted 2-m and 3-m mean daily wind speed (m s^{-1}) to a standardized wind speed at 2 m over clipped grass versus measured 2-m mean daily wind speed (m s^{-1}) over alfalfa, b) adjusted 3-m mean daily wind speed (m s^{-1}) versus adjusted 2-m mean daily wind speed (m s^{-1}) where both are adjusted to a standardized wind speed at 2 m over clipped grass, and c)) adjusted 3-m mean daily wind speed (m s^{-1}) versus measured 2-m mean daily wind speed (m s^{-1}) where both are over alfalfa.

Regression Parameter	CSU-AVRC (all days)	CSU-AVRC (subset of days)	Las Animas	Holly02
(A)				
regression of adjusted 2-m wind speed versus the measured 2-m wind speed				
slope	1.04	1.07	1.06	1.01
intercept	0.09	0.05	0.07	0.19
r^2	0.98	0.97	0.97	0.98
regression of adjusted 3-m wind speed versus the measured 2-m wind speed				
slope	1.01	1.05	1.05	0.99
intercept	0.21	0.14	0.13	0.35
r^2	0.95	0.95	0.97	0.98
overall mean regression of adjusted 2-m wind speed versus the measured 2-m wind speed				
	All sites (all days)	All sites (CSU-AVRC subset of days)		
slope	1.04	1.03		
intercept	0.11	0.12		
r^2	0.98	0.98		
(B)				
regression of adjusted 3-m wind speed versus the adjusted 2-m wind speed				
slope	0.98	0.99	0.98	0.98
intercept	0.11	0.09	0.07	0.16
r^2	0.98	0.98	0.99	0.99
(C)				
regression of adjusted 3-m wind speed versus the measured 2-m wind speed (both over alfalfa)				
slope	0.98	0.99	0.99	0.99
intercept	0.10	0.09	0.05	0.14
r^2	0.99	0.98	0.99	0.99

1, with time variable crop height data, resulted in less than ±1% difference in the adjusted seasonal mean daily wind speed. See Table 2, part (B).

The results shown in Table 3, part (B) are best fit equations for the data plotted in the lower graph of each of Figures 1-3 (with the exception that the CSU-AVRC subset data have not been plotted). The r^2 values are generally higher in this case compared with those in Table 3, part (A), because the time-variable impacts of alfalfa vegetation height are factored out, i.e., both data sets have been adjusted to the same datum (grass roughness). These regression results (with slopes near 1.00 and small intercepts) indicate the wind speed translation algorithm (Eq. 1) is internally consistent, i.e., the adjusted 3-m wind speeds are nearly the same as the adjusted 2-m wind speeds.

Table 3, part (C) shows the results of regressions of the measured 3-m wind speed adjusted to a 2-m height above ground over alfalfa versus the measured 2-m wind speeds above ground over alfalfa at each site. These results indicate the logarithmic wind profile adjustment holds over the alfalfa fields and that the assumption of neutrality is generally valid.

Estimate of neutral wind speed measurement height over alfalfa. The range of the adjustment factors to adjust the 2-m and 3-m mean daily wind speeds measured over alfalfa (as computed using Eq. 1) to equivalent mean daily wind speed at 2 m over grass suggests there is an intermediate height for wind speed measurement above ground surface over variable height alfalfa that is neutral and approximates wind speed at 2 m over grass without need for adjustment. By setting $u_{z,w}$ equal to $u_{z,v}$ in Eq. 1, one can solve directly for z_w, the alfalfa wind speed measurement height as a function of the alfalfa crop height. The result is a z_w time series reflecting the alfalfa growth and harvest periods. Neutral, seasonal mean wind speed measurement height over alfalfa that is equivalent to mean wind speed measured at 2 m over grass was computed in this fashion for the periods of data collection at all three locations in 2008. The mean neutral alfalfa weather station wind speed measurement heights were 2.73 m for CSU-AVRC, 2.67 m for Las Animas, and 2.70 m for Holly02; or, across all three sites, the average is 2.70 m. Anemometers deployed at this height in actively growing and harvested alfalfa fields (having similar growth and harvest patterns as the study area, Table 1) would be expected to measure wind speeds over alfalfa that do not need adjustment prior to computing alfalfa reference ET_{rs}. This was evaluated by adjusting the measured 2-m wind speeds at each location to a height of 2.70 m using logarithmic wind profile adjustment for height (discussed previously), and comparing the resultant values with the Eq.1 adjusted 2-m wind speeds (that represent equivalent wind speed at 2 m over grass). Results are shown in Table 2, part (C), in the format similar to previously discussed results. The results show there is very good agreement between the two sets of wind speed estimates at all three sites (average differences near 0.00), but with more scatter/dispersion in the differences, (similar or larger values for the std. deviation of the differences).

Impacts on computed reference ET. ASCE standardized equation alfalfa reference ET_{rs} was computed for the period of data collection during 2008 at all three sites using the following wind speed data sets: a) measured 2-m mean daily wind speed, b)

measured 3-m mean daily wind speed, c) Eq. 1 adjusted 2-m mean daily wind speed, d) Eq. 1 adjusted 3-m mean daily wind speed, and e) mean daily wind speed adjusted using the overall mean regression equation for all sites with the CSU-AVRC wind direction-filtered subset of days (i.e., Equiv. 2-m wind speed over grass (m s^{-1}) = 1.04 * measured 2-m wind speed over alfalfa (m s^{-1}) + 0.12). Results are presented in Table 4. The period of data collection at each site essentially covers three alfalfa growth cycles. Computed ET_{rs} using measured 3-m mean daily wind speed is from 4.3-5.6% greater, using adjusted 2-m mean daily wind speed is from 1.4-3.2% greater, and using adjusted 3-m mean daily wind speed is from 3.1-4.5% greater than when computed using the measured (over alfalfa) 2-m mean daily wind speed. Using the regression-equation adjusted mean daily wind speed (based on the general equation listed earlier in this paragraph) results in an increase of computed alfalfa reference ET by 2-3% compared to using measured (over alfalfa) 2-m mean daily wind speed. The 'true' ET_{rs} values, (i.e., as computed using measured wind speed at 2 m above ground surface over clipped grass), would likely have been in the range of 2 to 4% greater than the ET_{rs} calculated using the wind speeds collected at 2-m height above ground surface over the alfalfa crops. On average, ratios of the 3-m to 2-m unadjusted wind speeds averaged about 1.15, as noted earlier, and ratios of ET_{rs} using these two wind data sets averaged about 1.05. This suggests that, in the context of weather data along the Arkansas River, the 15% increase in measured wind speed from 2-m to 3-m height causes the seasonal ET_{rs} estimate to increase by 5%, or a ratio of about 1 to 3.

Table 4. Comparison of computed Standardized Alfalfa Reference ET for measured and Eq. 1 adjusted 2-m and 3-m mean daily wind speed data sets, and regression equation adjusted mean daily wind speed data. Values in parentheses are the ratio of the ET_{rs} value to the ET_{rs} computed using the measured 2-m mean daily wind speeds.

Standardized Alfalfa Reference ETrs (mm)						
Site	Period (DOY)	Meas. 2-m mean daily wind speed	Meas. 3-m mean daily wind speed	Adj. 2-m mean daily wind speed	Adj. 3-m mean daily wind speed	Regression equation adj. mean daily wind speed
CSU-AVRC	165-305	999	1042 (1.043)	1013 (1.014)	1030 (1.031)	1019 (1.020)
Las Animas	157-305	1058	1110 (1.049)	1092 (1.032)	1098 (1.038)	1090 (1.030)
Holly02	157-305	975	1030 (1.056)	1003 (1.029)	1019 (1.045)	1001 (1.027)

Summary and Conclusions

Wind speed data measured at 2-m and 3-m height above ground surface over variable height (growing) alfalfa during 2008 at three sites in the lower Arkansas Valley of Colorado were adjusted to represent wind speeds expected at 2 m over 0.12-m grass having 200 m or more fetch. Wind speed translation algorithms were applied where the wind profiles over the measurement surface and the surface to which wind is

being translated are both extended upward to the top of the internal boundary layer over each respective surface. At this elevation, the wind speeds (or at least friction velocity) are assumed to be equal for both surface conditions. The adjustment method was found to be internally consistent—i.e., the adjusted 2-m and 3-m wind speeds at each site were nearly equal in value. This requires, however, careful documentation of alfalfa growth and harvests at the alfalfa weather station. The sensitivity of the method to weather measurement surface fetch, and the vegetation height of the general region, which affects the height of the internal boundary layer over the measurement surface and the translation surface, needs further study.

Measured 3-m wind speed over alfalfa was adjusted to 2-m height above ground over alfalfa and compared to the measured 2-m wind speeds above ground over alfalfa at each site. Results indicate the logarithmic wind profile adjustment holds over the alfalfa fields and that the assumption of neutrality is generally valid.

Ideally, adjusted wind run should be compared to measured 2-m wind run over 0.12-m grass at a standard weather station with 200 m or more fetch. The Rocky Ford CoAgMet site, which is near the CSU-AVRC lysimeter site, approaches these conditions, however, measured wind speed data at this site during 2008 were affected by nearby corn crops.

Adjustments made to wind speed measured at 2-m height above ground over alfalfa to translate the measurements to that expected at 2-m height above ground over clipped grass ranged from 1.00 to 1.18, when the alfalfa height ranged from 0.12 m to 0.50 m. The seasonal (Apr 1-Oct 31) average adjustment factor was 1.09. The maximum, 1.18, and average, 1.09, upward adjustment factors are substantially greater than the 1.7% upward adjustment calculated using Eq. B.14c (ASCE-EWRI, 2005) with seasonal average alfalfa height of 0.30 m. Eq. B.14c appears to underestimate the required adjustment, and we recommend that it not be used to adjust wind speed measured over a rough surface such as alfalfa to the standardized smoother surface of clipped grass that is expected by the standardized reference ET equation.

A single mean regression relation developed using data collected in 2008 may be a suitable method to adjust wind speeds collected over variable height alfalfa to represent wind speeds at 2 m over 0.12-m grass with 200 m of fetch, especially in cases where nothing is known about alfalfa growth periods and harvests at the weather station, and when standard wind speed measurement height is 2 m. Such regression equation-based adjustments when compared to those made using the full logarithmic wind speed profile translation algorithm, Eq. 1, with time variable crop height data, resulted in less than ±1% difference in seasonal mean daily wind speed. This approach needs further study and would benefit from an additional year or two of data to assess variability.

A mean neutral wind speed measurement height over alfalfa (for the alfalfa growth conditions of this study), i.e., which produces equivalent wind speeds at 2-m over grass, of 2.70 m was determined through manipulation of the full wind speed adjustment algorithm expressed here as Eq. 1. Measured 2-m wind speeds over

alfalfa adjusted for height to 2.70 m compared well with Eq. 1 adjusted 2-m wind speeds (grass equivalent).

References

Allen, R. G. and J. L. Wright. 1997. Translating Wind Measurements from Weather Stations to Agricultural Crops. *Journal of Hydrologic Engineering*, 2(1): 26-35. Amer. Society of Civil Engineers, Reston, VA.

Allen, R. G., M. E. Jensen, J. L. Wright, and R. D. Burman. 1989. "Operational Estimates of Reference Evapotranspiration". *Agron. Jour.* 81:650-662.

Allen, R. G., L. S. Pereira, D. Raes, and M. Smith. 1998. "Crop Evapotranspiration: Guidelines for computing crop water requirements." *Irrigation and Drainage Paper No. 56,* FAO, Rome.

ASABE. 2004. EP505: Measurement and Reporting Practices for Automatic Agricultural Weather Stations. American Society of Agricultural and Biological Engineers, St. Joseph, MI.

ASCE-EWRI. 2005. The ASCE Standardized Reference Evapotranspiration Equation. Edited by R.G. Allen, I.A. Walter, R.E. Elliott, T.A. Howell, D. Itenfisu, M.E. Jensen, and R. L. Snyder. Task Committee on Standardization of Reference Evapotranspiration of EWRI. Amer. Society of Civil Engineers, Reston, VA.

Book, D.E. and M. K. Brengosz. 2009. Overview of Development and Use of Crop ET estimates with Hydrological Models for Interstate Compacts. Proceedings of the ASCE World Environmental and Water Resources Congress, May 17-21, 2009. Kansas City, MO.

Brengosz, M.K. 2009. Interstate Collaboration in the Arkansas River Compact Compliance Process: The "Nuts and Bolts" of Developing PET for Canal Service Areas for Input to the H-I Model. Proceedings of the ASCE World Environmental and Water Resources Congress, May 17-21, 2009. Kansas City, MO.

Brutsaert, W. 1982. *Evaporation into the Atmosphere.* Reidel Publishing Co. Dordrecht. The Netherlands.

Ley, T. W., D. E. Straw, and R. W. Hill. 2009**.** ASCE Standardized Penman-Monteith Alfalfa Reference ET and Crop ET Estimates for Arkansas River Compact Compliance in Colorado. Proceedings of the ASCE World Environmental and Water Resources Congress, May 17-21, 2009. Kansas City, MO.

Littleworth, A. L. 2003. Fourth Report of the Special Master. State of Kansas vs. State of Colorado and the United States of America. No. 105, Original. Supreme Court of the United States. October.

Estimation of evaporation and evapotranspiration during nongrowing seasons using a dual crop coefficient

Richard G. Allen[1] and James L. Wright[2]

[1] Professor of Water Resources Engineering, University of Idaho, 3793 N. 3600 E., Kimberly, ID 83341, (208) 423 6601. rallen@kimberly.uidaho.edu
[2] Soil Scientist (ret), USDA-ARS, 3793 N. 3600 E., Kimberly, ID 83341, (208) 423 6601.

ABSTRACT

Evapotranspiration and net irrigation water requirement estimates were updated in 2007 by Allen and Robison (2007; Allen et al., 2007) for agricultural areas in Idaho. ET calculation procedures were employed that use an updated procedure to calculate crop coefficients that considers the impact of surface wetting by irrigation and precipitation on total evapotranspiration. ET was calculated for daily, monthly and annual timesteps for 123 weather station locations across Idaho for complete, available periods of record. ET estimates were made for all times during the calendar year including winter to provide design and operation information for managing land application of agriculture, food processing and other waste streams and to provide full-calendar year estimates of E and ET for hydrologic studies and to estimate beginning of growing season soil water content.

Crop evapotranspiration, abbreviated ET_c, was calculated on a daily timestep basis for improved accuracy. Daily calculation timesteps allowed for the calculation of evaporation of water from wet soil surfaces following precipitation or irrigation events. ET_c for monthly, growing season and annual periods were summed from the daily calculations. The FAO-56 method for estimating evaporation from bare, wet soil, was utilized where a daily water balance was computed for the top 10 cm of soil as a means for reducing evaporation losses as the soil surface dries. Precipitation runoff was estimated using the NRCS Curve Number method where antecedent moisture was computed from the daily surface soil water balance.

Snow cover data as observed at many of the NWS stations were used to modify winter time estimates of evaporation caused by high albedo of snow and energy required for heat of fusion and was also used during adjustment of cumulative growing degree days for winter wheat during winter.

INTRODUCTION

Evaporation during nongrowing (wintertime) periods varies widely, based on availability of moisture, freezing of soils, snow cover, impacts of surface organic mulches (dead vegetation) and availability of energy for evaporation. Quantification of winter time evaporation is important when performing hydrologic water balances and when estimating effectiveness of wintertime precipitation in recharging the soil profile to supply water to vegetation during the subsequent growing season. Evaporation losses during winter, following soil wetting events, reduces the effectiveness of precipitation in recharging soil profiles.

Few studies have measured and documented wintertime evaporation. Wright (1991, 1993) conducted a series of wintertime measurements of evaporation using the dual precision weighing lysimeter systems at Kimberly. The following figures 1 and 2 show mean K_c values derived by Wright (1991) that correspond to evaporation during nongrowing (winter) seasons at Kimberly over a six year period from 1985 – 1991. The lysimeter surface conditions included clipped fescue grass on one lysimeter that was dormant during the winter period and various 'bare soil' conditions on the other lysimeter that represented soil conditions in between annual agricultural crops. The bare soil conditions included disked wheat stubble, disked alfalfa, disked soil, alfalfa and winter wheat. The basis for the mean K_c values in the figures is the ASCE standardized Penman-Monteith method (original K_c's by Wright were transformed to the ASCE PM basis). The ASCE PM alfalfa reference ET_r standard represents 0.5 m tall green alfalfa, even during winter (the crop is a hypothetical potential reference). The K_c at Kimberly during winter time rarely reached 1.0. However, mean K_c (K_{cm}) did typicalloy approach or exceed 0.8 during Dec. 1988 - Mar. 1989 for the disked soil, a period having a nearly continuous distribution of precipitation.

THE CROP COEFFICIENT APPROACH

A common approach for ET is the crop coefficient – reference ET method, where a reference ET_r is multiplied by a crop coefficient. The reference ET_r represents ET from a defined, fully vegetated surface such as full-cover alfalfa or clipped cool season grass and incorporates the influence of weather on the ET quantity. The K_c is defined as the ratio of actual or potential ET by a specific crop or land-cover condition to ET_r. The K_c therefore incorporates plant and cultural factors that cause ET to vary from ET_r. These factors are typically related to stage of vegetation development and wetting by irrigation or precipitation. The K_c ET_r method is widely used due to its simplicity, reproducibility, relatively good accuracy, and transportability among locations and climates. The method, when applied carefully, can produce estimates of ET that are sufficiently accurate for irrigation systems design and operation.

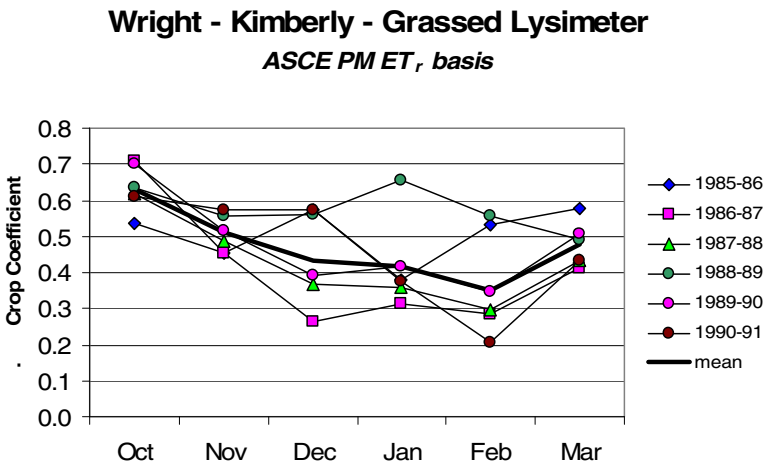

Figure 1. Mean monthly K_c measured by Wright (1993) from a grassed (dormant) lysimeter during nongrowing periods at Kimberly, Idaho converted for use with the ASCE Penman-Monteith alfalfa reference ET_r equation.

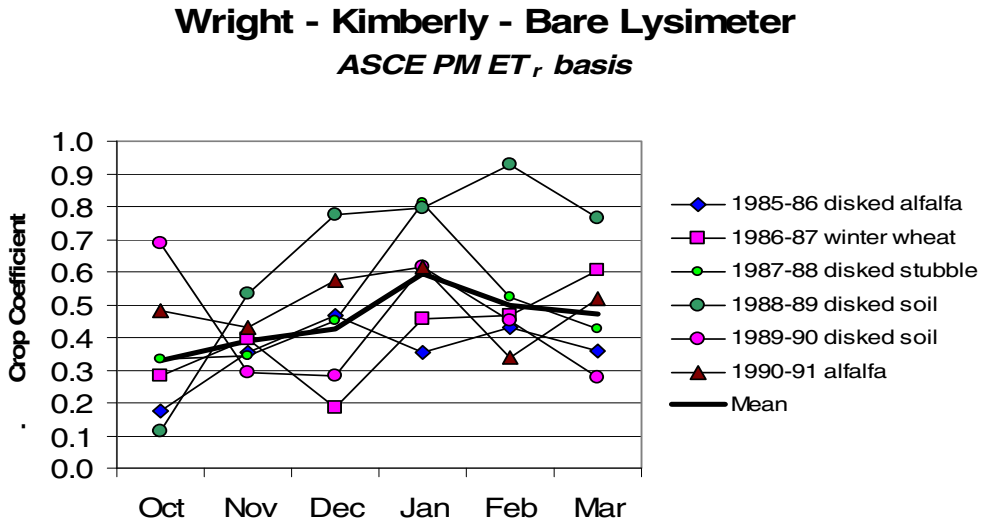

Figure 2. Mean monthly K_c measured by Wright (1993) during nongrowing periods at Kimberly, Idaho for various types of surface cover, converted for use with the ASCE Penman-Monteith alfalfa reference ET_r equation.

Two approaches to K_c have historically been applied. The first approach uses a 'mean' K_c where all time-averaged effects of evaporation from the soil surface are averaged into the K_c value. The mean K_c represents, on any particular day, average evaporation fluxes expected from the soil and plant surfaces under some 'average' wetting interval (by rain or irrigation). The second K_c approach is the 'dual' K_c method, where the K_c value is divided into a 'basal' crop coefficient, K_{cb}, and a separate component, K_e, representing evaporation from the soil surface. The basal crop coefficient represents ET conditions when the soil surface is dry, but with sufficient root zone moisture present to support full transpiration. The K_e component

is calculated separately, according to actual or simulated wetting events and is then added to the K_{cb} to produce the total K_c. Generally, a daily calculation time-step is required to apply the dual K_c method. The form of the equation for actual $ET_{c\ act}$ in the dual K_c approach is:

$$ET_{c\ act} = \left(K_s\, K_{cb} + K_e\right) ET_r \tag{1}$$

where K_{cb} is the basal crop coefficient [0 - ~1.0 when used with ET_r], and K_e is a soil water evaporation coefficient [0 - ~1.0 when used with ET_r]. All K terms are dimensionless. K_{cb} is defined as the ratio of ET_c to ET_r when the soil surface layer is dry, but where the average soil water content of the root zone is adequate to sustain full plant transpiration. K_e quantifies the evaporation component from wet soil in addition to the evapotranspiration represented in K_{cb}. K_s is a reduction coefficient for when there is stress caused by low soil moisture [0 - 1] (dimensionless). K_s reduces the value of K_{cb} when the average soil water content of the root zone is not adequate to sustain full plant transpiration. K_s = 1.0 when there is no water stress.

The dual K_{cb} approach is considered to be a superior approach for estimating wintertime evaporation than the mean K_c approach because the evaporation process is dominated by frequency of wetting events and relative wetness of the surface soil layer. A daily soil water balance is required to calculate K_s, since its value can change daily as soil water contents decline. This soil water balance incorporates the full effective root zone as simulated on a particular date during the growing season and an evaporation layer during the nongrowing season. A separate soil water balance estimates K_e where only the water content of the upper 0.1 m of soil is simulated, since it is this upper soil layer that supplies water for direct evaporation from the soil surface. The calculation of the crop coefficient curve during the growing season followed general practice of FAO-56 and Allen et al., (2005).

The daily water balance calculations and the calculation of K_s and K_e follow directly the procedure established in the FAO-56 publication (Allen et al., 1998) and extended by Allen et al., (2005). Departures from the Allen et al., (2005) FAO-56 procedure were made for the Idaho application to account for use of alfalfa reference ET_r rather than grass reference ET_o that is generally applied with the FAO-56 procedure. The general model for K_e (Allen et al. 1998) for use with the basal crop coefficient is:

$$\begin{aligned} &K_e = K_r\,(\,K_{c\,max} - K_s K_{cb}\,) \\ &\textit{such that} \\ &K_e \le f_{ew}\ K_{c\,max} \end{aligned} \tag{2}$$

where $K_{c\ max}$ is the maximum value of K_c following rain or irrigation, K_r is a dimensionless evaporation reduction coefficient [0-1] that in the FAO-56 dual K_c approach, is expressed as a function of the cumulative depth of water depleted by evaporation from the soil. Parameter f_{ew} is the fraction of soil surface from which

most of the evaporation occurs and is generally taken as the fraction of soil surface that is both exposed to drying and is 'wetted' during the wetting event. The use of cumulative depth of evaporation to estimate K_r tends to stretch out drying periods when ET_{ref} is low and shorten them when ET_{ref} is high.

The FAO-56 K_c approach represents a compromise between complexity and general application by conducting a daily water balance of the upper soil layer where upward flux of water or vapor to the layer from below is considered to be negligible or is ignored, and the effective depth of the evaporating layer is specified as the depth of soil that dries, on average, to a threshold dryness point. In the case of the FAO procedure, the threshold point is taken as the mean soil water content half-way between air dry and wilting point. This is an arbitrary dry point, but one that is relatively straight forward for field application and one that is reproducible. The maximum depletion depth for the layer provides a consistent stopping point for the evaporation cycle to ensure conservation of mass and can be customized for each application to fit observations.

The FAO procedure assumes that evaporation takes place in two stages following Ritchie (1971): the energy limiting stage 1, and the falling rate stage 2. When the soil is wet (in stage 1), the evaporation reduction coefficient in eq. 2, K_r = 1.0. When the water content in the effective evaporation layer begins to limit evaporation (in stage 2), K_r decreases. The value for K_r is set to zero when the total amount of water in the effective evaporation layer is depleted during the drying cycle. Assuming the soil is at field capacity (θ_{fc}) shortly after rainfall or irrigation and that it can dry to halfway between 0 and the wilting point (θ_{wp}), the total amount of water that can be depleted by evaporation (*TEW*) from the effective evaporation layer during a drying cycle is estimated as:

$$TEW = 1000\,(\theta_{fc} - 0.5\,\theta_{wp})\,z_e \tag{3}$$

where *TEW* is the 'total evaporable water' in mm, θ_{fc} and θ_{wp} are $m^3\ m^{-3}$ and z_e is the effective depth of the surface layer that is dried by evaporation in m. The cumulative depth of evaporation, D_e, at the end of stage 1 is defined as readily evaporable water (*REW*) and normally ranges from 5 to 12 mm depending on soil texture (Ritchie 1972).

Downward adjustment of *TEW* was recommended by Allen et al. (1998, 2005b) during extended periods of low ET_{ref} (i.e., ET_o < 5 mm d^{-1}) commonly experienced during nongrowing periods. During cool conditions, for example during winter or other cool periods, less radiation energy is available for heating the soil surface layer and evaporate water, and total effective *TEW* representing a drying event will typically be smaller than during a warm period. Allen et al. (1998) suggested using ET_o as a surrogate for temperature and radiation conditions to reduce the value for *TEW*. When ET_o < 5 mm d^{-1}, *TEW* is estimated as:

$$TEW = 1000(\theta_{fc} - 0.5\theta_{wp})z_e\sqrt{\frac{ET_o}{5}} \quad (4)$$

where ET_o is an average representing the general estimation period. A monthly average for ET_o was used. Varying ET_o on a daily basis is not recommended since it will cause *TEW* to vary daily, which can cause numerical inconsistencies. The value for REW was limited to less than or equal to 0.7 ($TEW_{applied}$).

During the falling rate stage when $D_e > REW$, evaporation is estimated to be proportional to the amount of water remaining in the surface soil layer, and K_r becomes:

$$K_r = \frac{TEW - D_{e(i-1)}}{TEW - REW} \quad (5)$$

where $D_{e(i-1)}$ is the cumulative depth of evaporation at the end of day $(i - 1)$, or the previous day.

Estimation of K_e requires a daily water balance for the f_{ew} fraction of the surface soil layer:

$$D_{e,j} = D_{e,j-1} - (P_j - RO_j) - \frac{I_j}{f_w} + \frac{E_j}{f_{ew}} + T_{ei,j} + DP_{ei,j} \quad (6)$$

where $D_{e,j-1}$ and $D_{e,j}$ are cumulative depletion depth at the ends of days j-1 and j [mm], P_j and RO_j are precipitation and precipitation runoff from the soil surface on day j [mm], I_j is the irrigation depth on day j that infiltrates the soil [mm], E_j is evaporation on day j (i.e., $E_j = K_e\ ET_{ref}$) [mm], $T_{ei,j}$ is the depth of transpiration from the exposed and wetted fraction of the soil surface layer on day j [mm], and $DP_{ei,j}$ is the deep percolation from the f_{ew} fraction of the soil surface layer on day j if soil water content exceeds field capacity [mm]. Assuming that the surface layer is at field capacity following heavy rain or irrigation, the minimum value for $D_{e,j}$ is zero. The limits imposed on $D_{e,j}$ are consequently $0 \le D_{e,j} \le TEW$. The irrigation depth I_j is divided by f_w to approximate the infiltration depth to the f_w portion of the soil surface. Similarly, E_j is divided by f_{ew} because it is assumed that all E_j (other than residual evaporation implicit to the K_{cb} coefficient) is taken from the f_{ew} fraction of the surface layer. It is recognized that soil water content can exceed field capacity for a few days following a large wetting event and that some drainage in soil occurs at very small rates at water contents below field capacity. To some extent, impacts of these simple assumptions can be compensated for in setting the value for z_e or *TEW*.

CALCULATING WINTERTIME EVAPORATION

In estimating K_c for nongrowing season periods, a basal $K_{cb} = 0.1$ was used for bare soil conditions, for surfaces covered with some amount of mulch, and for dormant turf/sod systems. The K_{cb} represented conditions when these surfaces had a

dry soil surface, but with sufficient moisture at depth to supply some diffusive evaporation. The evaporation (K_e) component was estimated separately in the daily soil water balance, where $K_{c\ max}$ during the nongrowing period was set at 0.9 for bare soil, 0.85 for mulched surfaces and to 0.8 for dormant grass cover. The lower value for grass is to account for insulative effects of the grass and higher albedo. The *third surface cover class* of 'mulch', was used to represent surfaces that are part way between bare and grassed conditions. The assumed effective fraction of 'cover' f_{ew} used during estimation of K_e was 0.7 for dormant grass, 0.4 for mulch and 0 for bare soil. The use of a low value for K_{cb} permitted the K_e function in the daily calculations to increase the value for total K_c according to wetting frequency by rain and snow.

An effective 'rooting zone' of 0.10 m was used for the fraction of surface under the cover. For all surfaces, a daily soil water balance was conducted and a stress coefficient is applied when soil water content drops below a critical value for the upper 0.10 to 0.15 m. Thus, actual K_c reduced below K_{cb} when both the ground surface and subsurface soil were dry.

The nongrowing season (winter) period was defined as the period beginning at the end of a K_{cb} curve representing the growing cycle for a specific crop or the occurrence of a killing frost, and ending at greenup or planting of the same crop the following year (or Oct. 1 in the case of winter wheat). All land use types, including agricultural, landscape, horticultural and natural vegetation, were assigned one of the three winter cover conditions (dormant grass, bare soil or mulch classes) for estimating evaporation losses during winter.

Adjustment for snow cover. Snow cover depth and new snowfall are reported for a number of National Weather Service cooperature stations. Snow cover information was used to adjust the K_c ($K_{c\ max}$) value to account for higher albedo of snow and absorption of heat by melt. The following algorithms were applied:

$$K_{c\_multiplier} = 1 - K_{radiation\_term\_winter} + \frac{(1 - albedo_{snow})}{(1 - albedo_{surface})} K_{radiation\_term\_winter} \quad (7)$$

where $K_{RadiationTermWinter}$ represents the weighting of (or contribution to) winter time reference ET estimates by the radiation term of the Penman-Monteith method, $albedo_{snow}$ is the mean albedo of snow cover and $albedo_{surface}$ is the mean albedo of the bare surface. $K_{RadiationTermWinter}$ is equivalent to:

$$K_{radiation\_term\_winter} = \frac{\Delta}{\Delta + \gamma\left(1 + \frac{r_s}{r_a}\right)} \quad (8)$$

where Δ is slope of the saturation vapor pressure-temperature curve, γ is the psychrometric constant, r_s is surface resistance to vapor flow and r_a is aerodynamic resistance to heat and vapor flow above the surface. The intent of Eq. (7) is to adjust the ET_r estimates by the Penman-Monteith method, which is parameterized to estimate ET for a vegetated surface to those that would have occurred from snow cover. The primary adjustment is for albedo of the surface, which is higher for snow cover. For ease of calculation, $K_{RadiationTermWinter}$ was calculated as a function of day of year based on a relation derived using full years of Kimberly weather data and the ASCE standardized Penman-Monteith equation:

$$K_{RadiationTerm} = 2.2E-08\ J^3 - 2.42E-05\ J^2 + 0.006J + 0.011 \quad (9)$$

An additional reduction in evaporation of 30% was made to account for absorbed latent heat of fusion of any melting snow prior to evaporation. Albedo of snow was set at 0.8 in calculations and albedo of the surface was set to 0.25.

Occaisionally, some stations reported snow fall (daily), but did not report observations of accumulated snow cover. In these cases, estimated depth of snow on the ground was made by accumulating snow fall and applying a simple melt rate function:

$$Snow\_accumulation_i = Snow\_accumulation_{i-1} + \frac{Snowfall}{2} - Melt_i \quad (10)$$

$$Melt = 4\ T_{max} \quad (11)$$

where *snow_accumulation* is snow depth accumulation in mm, *Snowfall* is reported snowfall depth for the day in mm, *Melt* is melt rate in mm/day and T_{max} is daily maximum air temperature in ^oC. The *snow_accumulation* parameter was calculated for all stations and periods and was used if it exceeded reported snow depth, as a precaution. The reported depth of snowfall was halved to reflect consolidation of the snow cover. The snow melt rate function was based on about 50 years of snowcover observations for Ashton, Idaho.

INFILTRATED PRECIPITATION

Runoff during precipitation events is strongly influenced by soil texture, soil structure, sealing and crusting of the soil surface, land slope, local land forming (tillage and furrowing), antecedent moisture, precipitation intensity and duration. Generally, estimation of runoff during precipitation is fraught with uncertainty. For general purposes, runoff can be estimated using the USDA-NRCS Curve Number approach. The NRCS curve number is simple to apply and is widely used within the hydrologic, soils and water resources communities. Required data are daily precipitation depth and computation of a daily soil water balance by which to select the antecedent soil water condition.

Once the surface runoff depth is estimated using the curve number procedure, the depth of rainfall infiltrated is calculated as:

$$P_{inf} = P - RO \tag{12}$$

where P_{inf} is the depth of infiltrated precipitation [mm], P is the measured precipitation depth [mm], and RO is the depth of surface runoff [mm]. If the soil will not hold the amount infiltrated, the remainder goes to deep percolation.

EXAMPLES OF WINTERTIME ESTIMATES

Examples of calculated K_{cb} and $K_{c\ actual}$ curves ($K_{c\ actual} = ET_{c\ actual} / ET_r$), including wintertime evaporation are shown in Figure 3 for a crop of spring wheat and potatoes during the 2004 calendar year near Ashton. The $K_{c\ actual}$ traces include the evaporation (K_e component) that appear as 'spikes' above the K_{cb} curves following precipitation and irrigation events. The $K_{c\ actual}$ during winter time peaked at about 0.6 for the spring wheat crop that was assumed to have a mulched soil surface during the nongrowing season and at 0.8 or less for the potato crop that was assumed to have a bare soil surface during the nongrowing season. $K_{c\ actual}$ peaks during winter were reduced when snow cover was noted to account for higher reflectance of the snow (January – March for 2004). $K_{c\ actual}$ was below K_{cb} when soil stress was estimated to occur during the nongrowing season or prior to initiation of irrigation (generally begun when $K_{cb} > 0.22$). The duration of K_e spikes (time-wise) tends to increase during spring and fall as weather cools and more days are required to dry the soil surface. Even though the value estimated for $K_{c\ actual}$ was relatively high during the nongrowing season, the actual ET rate was relatively low (bottom figure in Figure 3) due to the low value for reference ET_r, which represents the drying power of the atmosphere and energy available for evaporation.

An example of a time series of daily K_c over a multiyear period is shown in Figure 4 for six crop categories at Parma, Idaho for the 1988-1990 period. The K_c values shown are the basal K_{cb} curve (solid line) and actual K_c curve (symbols). During processing, these K_c values were converted to crop ET_c by multiplying by reference ET_r. The difference between actual K_c and basal K_{cb} when K_c exceeds K_{cb} represents evaporation from the bare or partially covered soil surface. K_c is occasionally below K_{cb} when there is insufficient soil moisture to support the evaporation process. Even though values for total K_c are 'high' during winter following wetting events, the resulting ET_c is relatively low, since ET_r averages less than 1 mm d^{-1} during much of winter. This was demonstrated in Figure 3. The values for K_c during winter varied with crop type due to assumptions made regarding the type and nature of cover during winter (mulch, bare soil or dormant sod-like surface).

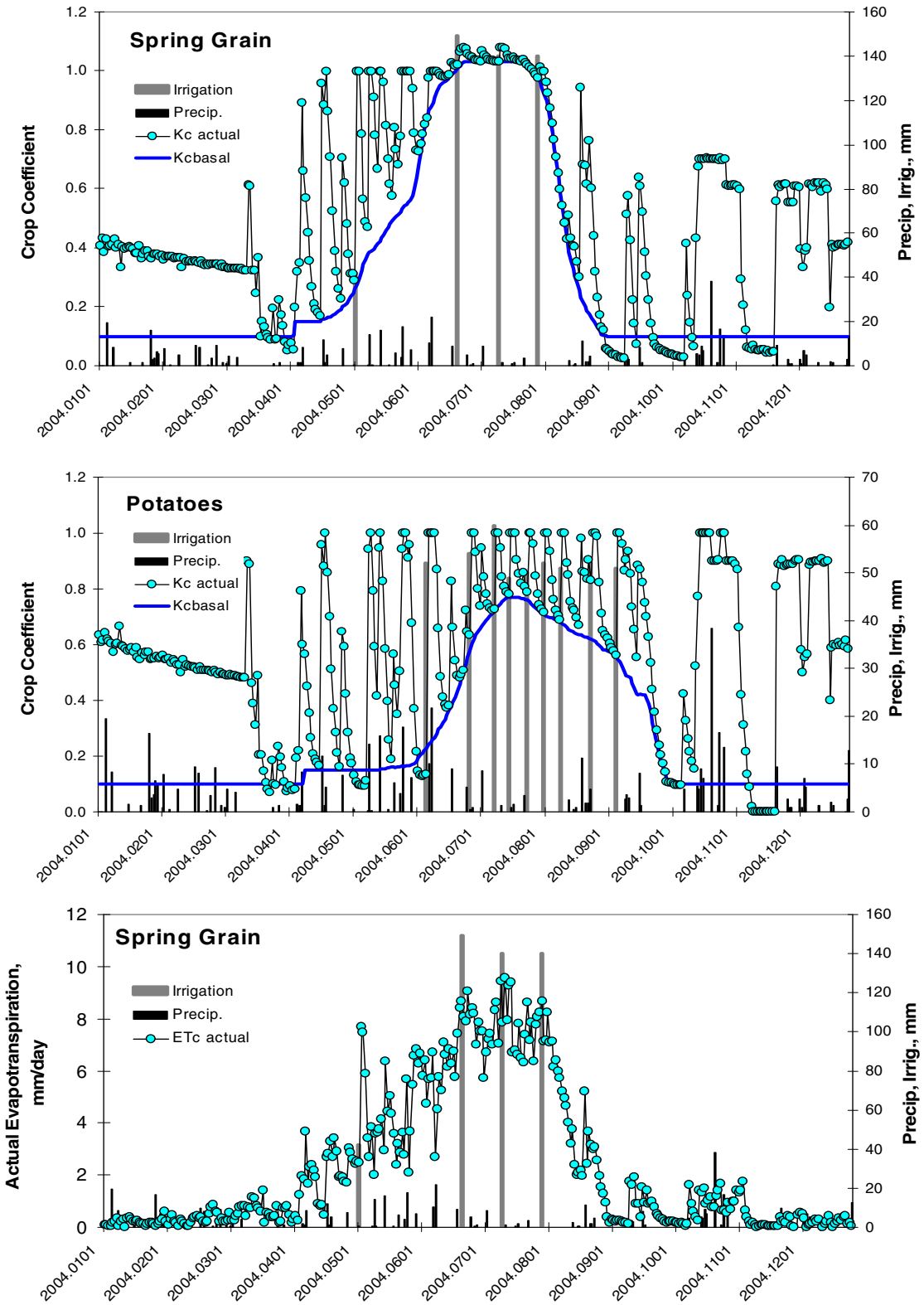

Figure 3. Example K_{cb} ('Kcbasal') and $K_{c\ actual}$ curves for spring wheat and potato crops near Ashton during 2004. Simulated irrigation events are shown as vertical bars. The $K_{c\ actual}$ traces include the evaporation (K_e component) that appear as 'spikes' above the K_{cb} curves following precipitation and irrigation events. Also shown in the bottom figure is daily actual ET_c for the spring grain.

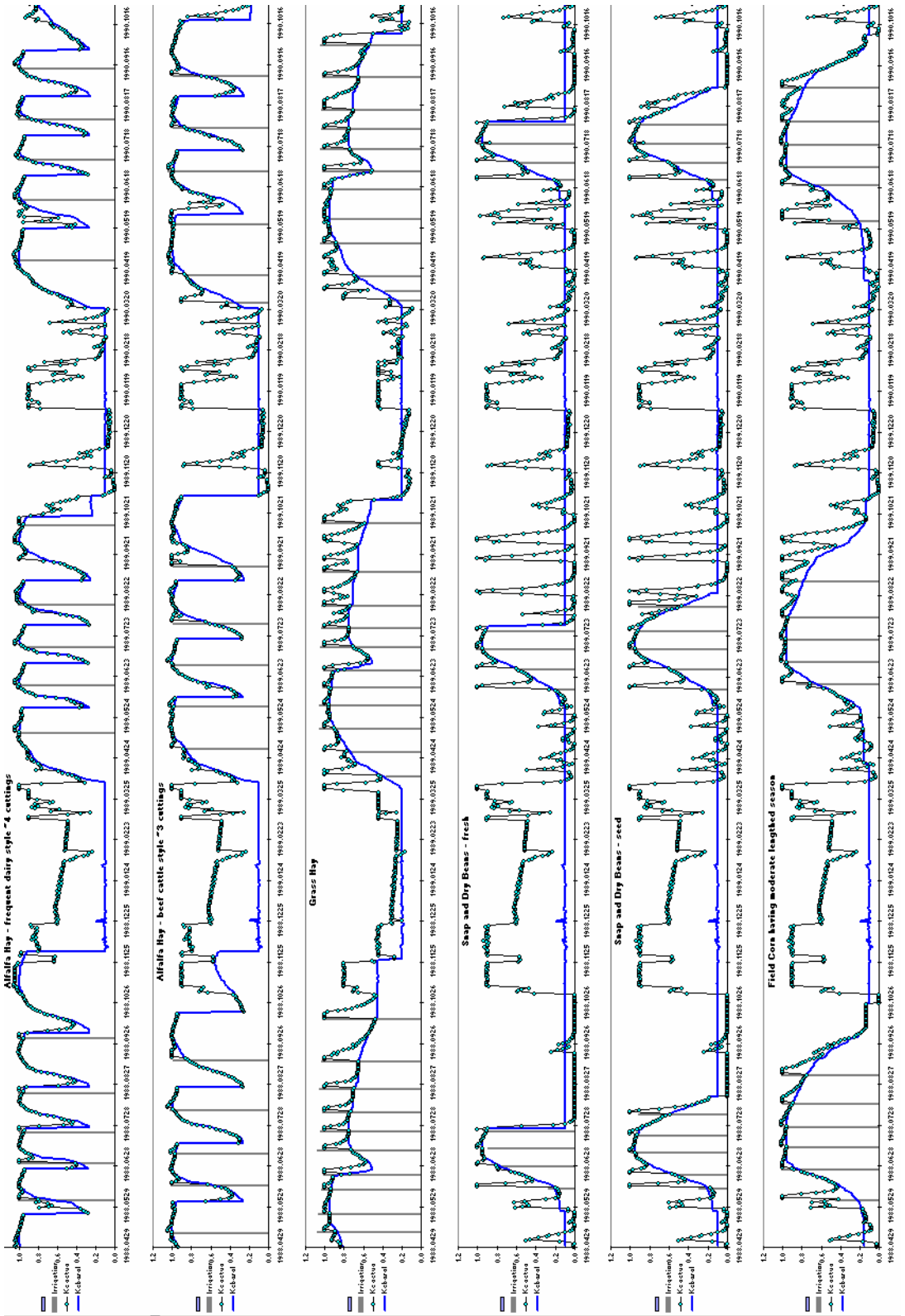

Figure 4. A time series of daily crop coefficients for alfalfa hay (top two crops for frequent and less frequent cutting), grass hay (third crop), dry beans harvested fresh (fourth), dry beans harvested dry (fifth) and field corn (bottom) over a three year period (1988-90) including wintertime at Parma.

COMPARISON OF ESTIMATES AGAINST THE WRIGHT LYSIMETER DATA

Figures 5 and 6 below show simulations from the "ETIdaho" calculations of Allen and Robison (2007) for Kimberly, Idaho for the same years as shown in Figures 1 and 2, estimated using a daily time step and the dual K_{cb} approach described above and using reference ET calculated using the ASCE PM for alfalfa reference based on National Weather Service data (maximum and minimum air temperature only, with dewpoint, solar radiation and wind speed estimated).

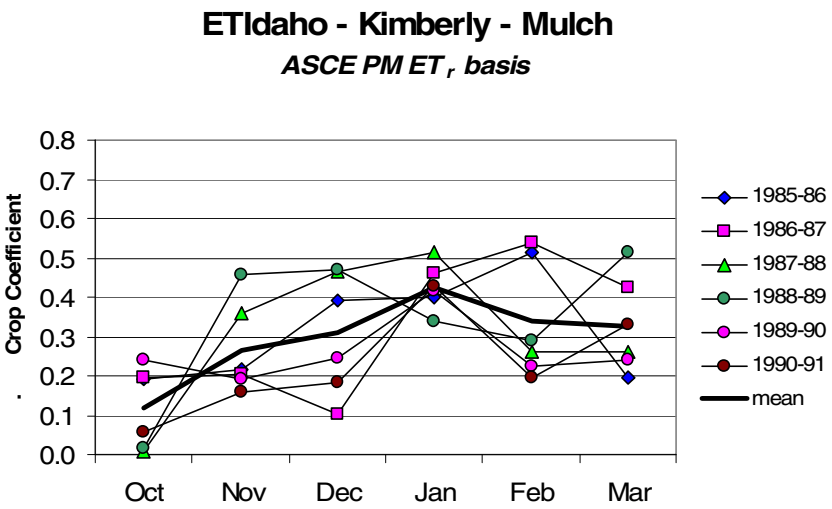

Figure 5. Monthly K_c for mulched soil cover condition during winter at Kimberly, Idaho for the same years as shown in Figure 1, estimated using a daily time step and the dual K_{cb} approach.

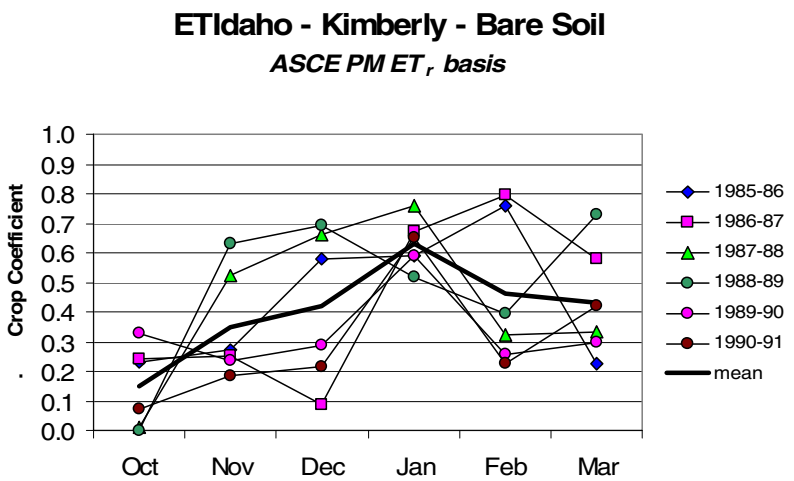

Figure 6. Monthly K_c for bare soil during winter at Kimberly, Idaho for the same years as shown in Figure 2, estimated using a daily time step and the dual K_{cb} approach.

The estimates for the mulched cover (Figure 5) are similar to those measured by Wright (1993) for the dormant turfgrass (Figure 1), although somewhat lower, especially during October, when the ETIdaho routine estimated lower ET due to the assumption of no irrigation. The lysimeters at Kimberly were irrigated. The estimates for bare soil (Figure 6) follow the measurements shown in Figure 2 relatively closely, with similar year to year variation in K_c caused by variation in precipitation amounts and frequencies as well as snow cover. Estimates by ETIdaho for dormant turf were lower than measurements shown in Figure 1 due to lack of irrigation assumed in ETIdaho for the cover.

SUMMARY AND CONCLUSIONS

The FAO-56 method for estimating evaporation from bare, wet soil, was utilized at 123 locations in Idaho over a more than 100 year period of record at some sites. A daily water balance was computed for the top 10 cm of soil as a means for reducing evaporation losses as the soil surface dries. Available water holding capacity and texture of soil for each station was determined using information from the National StatsGo soils information data base using a GIS analysis of the national soil data base for the area assigned to each station. Precipitation runoff was estimated using the NRCS Curve Number method where antecedent moisture was computed from the daily surface soil water balance. The curve number was determined from soil texture based on the StatsGo soils data base. Snow cover data as observed at many of the NWS stations were used to modify winter time estimates of evaporation caused by high albedo of snow and energy required for heat of fusion and was also used during adjustment of cumulative growing degree days for winter wheat during winter. Monthly winter evaporation estimated for Kimberly over a six year period compared relatively well with lysimeter measurements reported by Wright (1993).

REFERENCES

Allen, R.G. and C.W. Robison. (2007). "Evapotranspiration and consumptive irrigation water requirements for Idaho." *Univ. of Idaho Rep.*, submitted to the Idaho Dept. Water Resources. 149 pp. (revised)

Allen, R.G., L.S. Pereira, D. Raes, and M. Smith. 1998. *"Crop Evapotranspiration: Guidelines for computing crop water requirements."* Irrig. and Drain. Paper 56, Food and Agriculture Organization of the United Nations, Rome, 300 pp.

Allen, R.G., L.S. Pereira, M. Smith , D.Raes , and J.L. Wright. 2005. FAO-56 Dual Crop Coefficient Method for Estimating Evaporation from Soil and Application Extensions. *J. Irrig. and Drain. Engrg.,* ASCE 131(1):2-13.

Allen, R.G., Pruitt, W.O., Raes, D., Smith, M. and Pereira, L.S. (2005b). "Estimating evaporation from bare soil and the crop coefficient for the initial period using common soils information." *J. Irrig. and Drain. Engrg.,* ASCE 131(1):14-23.

Allen, R.G., C.W. Robison and J.L. Wright. 2007. Updated procedures for calculating state-wide consumptive use in Idaho. in the Role of Irrigation in a

Sustainable Future. USCID Conference on Irrigation, Sacramento, CA proceedings: 189-212.

ASCE – EWRI. (2005). The ASCE Standardized reference evapotranspiration equation. ASCE-EWRI Standardization of Reference Evapotranspiration Task Comm. Report, available at http://www.kimberly.uidaho.edu/water/asceewri/

Ritchie, J.T. (1971). "Dryland evaporative flux in a subhumid climate: I. Micrometeorological influences." *Agron. J.*, 63:51-55.

Ritchie, J.T., (1972). "Model for predicting evaporation from a row crop with incomplete cover." *Water Resour. Res.,* 8:1204-1213.

State Soil Geographic (STATSG0) Data Base Data use information. United States Department of Agriculture Natural Resources Conservation Service, National Soil Survey Center. Miscellaneous Publication Number 1492. Issued August 1991, Slightly revised May 1993, Revised December 1994. Converted to .PDF September 1995

USDA-SCS. 1972. National Engineering Handbook, Section 4, Table 10.1.

Wright, James L. 1991. Using weighing lysimeters to develop evapotranspiration crop coefficients. pp. 191-199. In: R.G. Allen, T.A. Howell, W.O. Pruitt, I.A. Walter & M.E. Jensen (eds.). Proc. of the International Symposium on Lysimetry, July 23-25, Honolulu, Hawaii. ASCE, 345 E. 47th St., New York, NY 10017-2398.

Wright, James L. 1993. Nongrowing season ET from irrigated fields. p. 1005-1014. In: R.G. Allen and C.M.U. Neale (eds.) Management of Irrigation and Drainage Systems: Integrated perspectives. Proc. Workshop ASCE Irrigation and Drainage Division, Park City, UT, 21-23 July, 1993

Evapotranspiration and Net Irrigation Water Requirements for Nevada

J. L. Huntington[1] and R. G. Allen[2]

[1] Hydrologist, Nevada Division of Water Resources, 901 S. Stewart Street, Carson City, NV, 89701; PH (775) 684-2867; FAX (775) 684-2811; email: jhuntington@water.nv.gov

[2] Professor of Water Resources Engineering, University of Idaho, Research and Extension Center, 3793 N. 3600 E., Kimberly, Idaho, 83301; PH (208) 423-6601; FAX (208) 423-6699; email: rallen@kimberly.uidaho.edu

ABSTRACT

Evapotranspiration (ET) of water is a primary component of the hydrologic cycle and is becoming more significant as increasing demands are placed on finite water supplies in Nevada and across the western U.S. Local, state, and federal water resource agencies have a great need for accurate estimates of net irrigation water requirements for evaluating irrigation development, transfers of irrigation water for municipal use, and litigation of water rights applications and protests. The major objective of this study is to update estimates of crop ET and net irrigation water requirements for Nevada. Estimates of ET and net irrigation water requirements are made for all major crops grown in Nevada at over 200 locations using National Weather Service weather stations located throughout the state. The methods for estimating ET follow the new ASCE-EWRI Standardized Penman-Monteith approach, while the net irrigation water requirement for crops is estimated using a dual crop coefficient and daily soil water balance approach. Results show that in central and northern parts of Nevada, the net irrigation water requirement for alfalfa, the primary crop grow in Nevada, is less than the typical permitted amount of irrigation water rights of 4 ac-ft/ac, indicating that if irrigators wish to change or sell their water rights to more consumptive uses, they would not be able to transfer the entire water right. These revised estimates of ET and net irrigation water requirements for various crops will be used for updating basins water budgets and establish the amount of irrigation water that is available for water transfers in the future.

INTRODUCTION

Irrigation water requirements are primarily controlled by the evapotranspiration (ET) of agricultural crops. Quantifying the amount of ET for a particular type of vegetation and region is necessary for proper design of irrigation systems, basin water balance estimates, and irrigation water management, review and litigation of water right applications and disputes, all of which continue to receive high priority attention. In the past, the State of Nevada has based ET and net irrigation water requirement estimates on a combination of reports, mainly from the USDA Nevada Irrigation Guide (USDA-SCS, 1992), State of Nevada Report No. 3 (Pennington, 1980), and studies used in hearings associated with the Alpine Decree (Mahannah, 1979; Hill, 1979; Guitjens and Mahannah, 1977). These publications primarily utilized temperature based Blaney-Criddle, modified Blaney-Criddle, Jensen-Haise, and Penman equations for computing reference ET, as well as correlation of estimated consumptive use with crop yields, and soil moisture balance (depletion) estimates of ET, resulting in a wide range of estimates. While these reports have been extremely useful, their dated methods and limited spatial coverage have created a need to update ET and net irrigation water requirement estimates with large spatial coverage using newly available standardized methods.

The major objective of this report is to update crop ET and net irrigation water requirement estimates for Nevada. Estimates are made for major crops grown in Nevada using more than 200 National Weather Service stations located throughout the state, providing sufficient spatial coverage for estimating the spatial distribution of crop ET and net irrigation water requirements, however, in this paper only alfalfa ET and net irrigation water requirements will be discussed.

EVAPOTRANSPIRATION CALCULATION APPROACH

The approach applied in this study for computing crop ET is the common crop coefficient – reference ET approach, where the reference ET is multiplied by a crop coefficient for estimating the actual ET of a vegetative surface. There are many methods available for estimating the reference ET, ET_o, while many are simple temperature-based techniques, others are data intensive as required for more physically based models. Estimates of ET_o vary widely among the methods, and there is considerable debate as to which is the more correct method. Generally, the lack of weather variables such as incoming solar radiation, dew point temperature, and wind speed needed for more physically based models of ET_o has led to the use of simple temperature based methods, even though investigators are often aware that more physically based methods result in more accurate and representative estimates of ET_o. Given that the number of weather stations that collect incoming solar

radiation, relative humidity, and wind speed are extremely limited, there is a great need to utilize basic National Weather Service (NWS) data of maximum and minimum temperature and precipitation and apply an ET_o method that is robust and currently accepted in the literature and scientific community to estimate state-wide crop ET and net irrigation water requirements.

The Penman-Monteith method for calculating ET_o is currently accepted as a standard method (ASCE-EWRI, 2005) for calculating a standardized and consistent value for ET_o, referred to here as ET_{sz}. The Penman-Monteith method, however, requires weather variables that are not routinely measured at NWS stations. Recent advancements in estimating weather variables such as incoming solar radiation (Thornton and Running, 1999; ASCE-EWRI, 2005), generalization of dew point temperatures representative of irrigated areas (ASCE-EWRI, 2005; Allen et al., 1998; Allen and Robison, 2007) and regionalizing of wind speed (Allen and Robison, 2007) have proven useful for estimating ET_{sz} using the Penman-Monteith equation while maintaining sufficient accuracy and spatial coverage for state-wide application. The grass reference Penman-Monteith equation has been widely applied by Arizona and California State agencies for computing consumptive use (i.e. AZMET and CIMIS), as well as the U.S. Bureau of Reclamation for their Lower Colorado River Accounting System (LCRAS) model, therefore the State of Nevada has adopted the daily time step grass reference evapotranspiration equation (ET_{os}) as the basis for computing crop ET and net irrigation water requirements, which is used in this study.

Given that ET_{sz} refers to ET from a reference crop that is actively growing, not limited by soil moisture, and is at full cover and peak height, the ratio of actual ET to the ET_{sz}, otherwise known as a crop coefficient (K_c) representing specific crop types, must be applied to adjust the ET_{sz} to simulate the actual ET of a particular crop or surface (ET_{act}). The majority of crop coefficients in the literature were derived from research weighing lysimeter measurements of actual ET from stress-free crops and calculated ET_{sz} at the lysimeter sites, mainly from Davis, CA, and Kimberly, ID (Doorenbos and Pruitt, 1977; Wright, 1981, 1982). This study utilizes a dual crop coefficient and daily soil water approach to compute the ET_{act}, where the K_c value is separated into a 'basal' crop coefficient, K_{cb}, and a soil evaporation coefficient, K_e (Allen et al., 2005). The heritage of many of the K_{cb} values used in this study can be traced to Wright (1982).

METHODS

Standardized Penman-Monteith Equation

As a part of a standardization effort, the ASCE Penman-Monteith (ASCE-PM) equation and associated equations for calculating aerodynamic and bulk surface

resistance have been combined and condensed into a single equation that is applicable to both grass and alfalfa surfaces by changing standardized constants (ASCE-EWRI, 2005). The ASCE-PM equation is intended to simplify and clarify the presentation and application of the method. As used in this analysis, the term ET_{os} refers to the standardized grass reference ET. Calculation of parameters required in the ASCE-PM equation was accomplished using guidelines from ASCE-EWRI (2005). Methods for estimating variables of daily incoming solar radiation, dew point temperature, and wind speed required are discussed below.

NCDC Weather Data Assembly

Weather station data from the NWS used in the computation of ET_{os} and net irrigation water requirements include daily maximum and minimum air temperature and precipitation, and observations of snowfall and snow cover depth for some stations. These data are officially collected and housed by the National Climatic Data center (NCDC) of the National Oceanic and Atmospheric Administration (NOAA). Data are generally available from the NCDC from about 1930 onwards, however lengths of records vary widely from station to station, ranging from less than 1 month to 120 years. Limiting weather station datasets to those stations having at least 4 years of complete annual records resulted in over 200 usable weather stations in Nevada.

Incoming Solar Radiation Estimation

Time series estimates of solar radiation (R_s) for each NWS station were calculated following an empirical method described by Thornton and Running (1999), which is based on the difference between daily maximum and minimum air temperature. The general premise of the method is based from the principle that during cloud cover maximum air temperatures generally decrease, and the minimum temperature is increased due to increased downward emission and reflection of long wave radiation by clouds at night (Allen, 1997). Application of the Thornton-Running equation to NWS station temperature data has produced satisfactory results when compared to measured R_s at 14 nearby weather stations. The average ratio of daily estimated to measured R_s for all 14 stations is 1.02 with a standard deviation of 0.05, while the average RMSE for daily estimated R_s is 3.75 $MJ/m^2/d$. In general, the Thornton-Running equation provides reasonable estimates over the ranges of R_s experienced and during all months of the year. The Thornton-Running equation was applied in similar applications for Idaho by Allen and Robison (2007).

Dewpoint Temperature Estimation

Dew point temperature (T_{dew}) is defined as the temperature at which a parcel of air must be cooled to become saturated with water vapor. The dewpoint temperature can be used to represent the humidity of the lower air mass, for example the relative humidity (RH) is at 100% when the air temperature is at the dewpoint. Because NWS stations do not record relative humidity, the estimated T_{dew} is used to represent the humidity of the lower air mass. In an irrigated setting T_{min} will usually approach T_{dew}, especially in the early morning when winds are calm and soil moisture is high. Weather stations located in non-irrigated settings typically record higher maximum air temperatures and lower daily RH than those located in irrigated areas due to the lack of available water, causing the net radiation to be partitioned into sensible heat instead of latent heat or ET. The use of humidity data collected from non-irrigated settings can cause overestimation of ET_{sz} to as much as 20-26% (Brown, 2001; ASCE-EWRI, 2005).

The daily T_{dew} at each NWS weather station is estimated in this study as $T_{dew} = T_{min}-K_o$, where T_{min} is the daily minimum air temperature (^oC) and K_o is an offset coefficient (^oC) and is synonymous with the dew point depression. It is common in arid and semiarid regions to have a T_{dew} of 2 to 5 ^oC below T_{min} under well watered conditions (Allen, 1996). Rather than assign NWS stations spatially constant mean monthly K_o values, spatially distributed mean monthly K_o values were derived and assigned to NWS stations. There are very few weather stations in Nevada that measure RH in irrigated areas, therefore mean monthly K_o values were computed from weather stations located in irrigated areas from the AZMET (Arizona Meteorological Network), CIMIS (California Irrigation Management Information System), AGRIMET, and Utah Agriculture Weather Network, as well as U.S. Geological Survey (USGS) micrometeorological stations located in irrigated areas in Nevada from studies by Maurer et al., (2006) and Allander et al., (2009) (Figure 1a). Calculated mean monthly K_o values for the different weather stations are shown in Figures 1b, where it is apparent that mean monthly K_o values vary depending on the location. For instance, in southern locations the K_o value for a given month is greater than in northern locations, primarily due to the temperature, length of growing season, amount and seasonality of precipitation, and magnitude of regional advection of dry air. Mean monthly K_o values were ultimately assigned to NWS stations by spatial interpolation using inverse distance weighting, averaging spatially interpolated K_o surfaces to individual hydrographic areas, and then assigning NWS stations respective mean monthly spatially averaged hydrographic area K_o values. Measured mean monthly K_o values were assigned to NWS stations in basins where measurements occurred. For illustration purposes the spatial distribution of mean annual K_o is shown in Figure 1c.

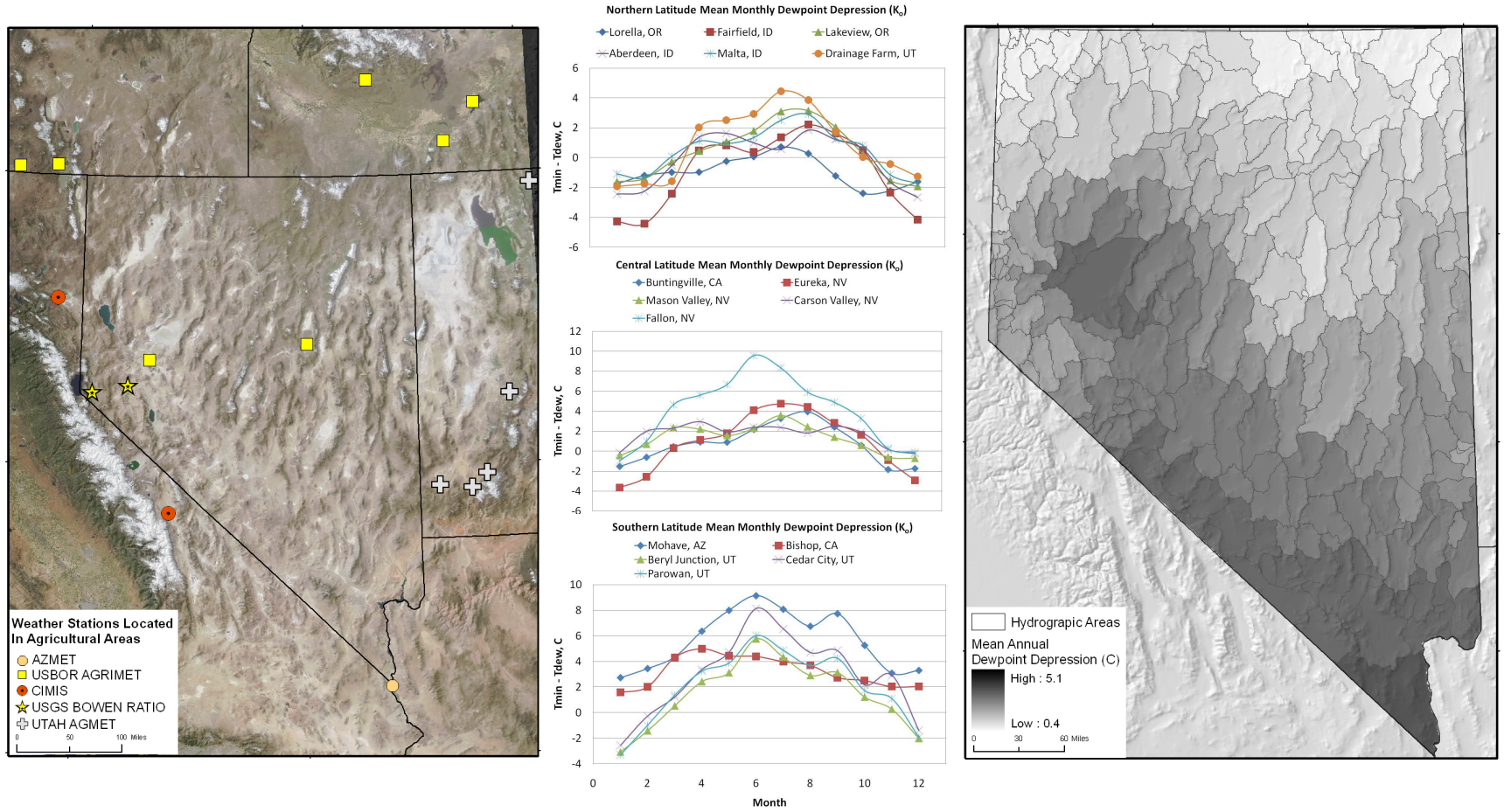

Figure 1a-c. (a)Weather stations measuring RH located in irrigated areas used for calculation of and spatial interpolation of dew point depression (K_o). (b) Mean monthly K_o for southern, central, and northern weather station locations shown in figure 1(a). (c) Spatially averaged mean annual K_o illustrating the extreme spatial variability of K_o (i.e. T_{min}-T_{dew}).

As expected, southern locations have a larger dew point depression (i.e. larger K_o value) while northern areas have a smaller dew point depression. This spatial trend is likely due to regional scale advection of dry air, and more specifically the climatology that governs regional scale advection such as the amount of valley floor precipitation, energy balance from the natural vegetation on valley floor areas, and typical air mass origins or jet stream patterns. Using weather stations located in irrigated areas as the basis for computing mean monthly K_o values likely minimizes local advection effects while preserving regional advection effects that most irrigated areas in Nevada are likely experiencing due to the arid climate and smaller scale irrigation projects. For example, the mean monthly K_o for Fallon, central Nevada, is significantly higher than surrounding stations shown in Figure 1b. After a detailed analysis of K_o from surrounding stations in the Fallon area that are located in non-irrigated settings, the mean annual K_o at these stations is above 8°C, while the Fallon AGRIMET site is reporting a mean annual K_o of 4°C. This finding suggests that the Fallon AGRIMET K_o can be interpreted as being 'representative' of the K_o occurring in the irrigated project area. The irrigated areas surrounding the AGRIMET site in Fallon are highly discontinuous, as there are many fallowed fields. However, this is a common occurrence in the Fallon project area, therefore the Fallon AGRIMET site is likely 'seeing' the effect of regional advection more than other areas in central Nevada that have more continuous irrigated areas and receive more annual precipitation.

Wind Speed Estimation

Wind speed (U) is not measured at NWS stations except at airport stations, therefore wind speed from NWS airport stations and weather stations from a variety of networks located on valley floor areas with sufficient period of record, totaling 60 stations, were used to compute the mean monthly wind speed. The mean monthly wind speed at each NWS station was estimated as

$$U_2 = U_{2mean \cdot monthly_i}$$

where U_2 is the estimated daily 2 meter height wind speed for each NWS station, and $U_{2\ \text{mean monthly i}}$ is the measured mean monthly 2 meter height equivalent wind speed or hydrographic area spatially averaged 2 meter wind speed. Similar to the assigning of K_o values to NWS stations with no measurements within the hydrographic basin, spatially interpolated mean monthly wind speed surfaces were generated using inverse distance weighting and were then spatially averaged to hydrographic areas,

where NWS stations were assigned respective spatially averaged mean monthly wind speed values.

Crop Evapotranspiration

Actual crop ET, ET_{act}, in this study is calculated as

$$ET_{act}=(K_sK_{cb} + K_e)ET_{os}$$

where ET_{os} is the grass reference ET, K_{cb} is the basal crop coefficient, and K_e is the soil water evaporation coefficient. K_{cb} and K_e are dimensionless and range from 0 to 1.4 when used with ET_{os}. When the soil water content is less than that needed to sustain full rates of transpiration a stress coefficient, K_s, is applied ranging from 0 to 1. K_s is equal to 1 when there is no water stress, as is the case for fully-irrigated crops during the irrigation season as opposed to rain fed crops or native vegetation. A daily soil water balance is required to calculate K_s, which incorporates the available soil moisture for the simulated effective root zone. An additional soil water balance is maintained for the estimation of K_e, and is limited to the upper 0.1m of the soil since this zone is assumed to be the only layer that supplies water for direct evaporation from the soil surface. Further details of the daily water balance used in this study can be found in Allen et al.,(2005) and Allen and Robison (2007).

The K_{cb} curve represents impacts on ET stemming from changes in vegetation phenology, which can vary from year to year depending on the start, duration, and termination of the growing season, all of which are dependent on temperature conditions during spring, summer, and fall periods. Depending on the crop, the start, duration, and termination of the growing season are estimated each year according to a 30-day moving average temperature or a cumulative growing degree method prior to the start date, with specified temperatures defining the killing frost. For alfalfa, spring green up was estimated when cumulative growing degree day (CGDD) since January 1 reached 300 ^oC-days using a temperature base of 0^oC. The cumulative growing degree day was normalized following Wright (2001) by the quantity of CGDD required to advance the K_{cb} curve from green up to effective full cover and harvest.

Three different alfalfa K_{cb} curves were constructed according to the cycle of growth, that being a initial cycle curve, a intermediate or mid cycle curve, and a late cycle curve according to Wright (1981, 1982) and lysimeter records in Kimberly, ID (Figure 2). Implementation of three different K_{cb} curves for alfalfa is consistent with the fact that the first cycle or cutting of alfalfa has the largest yield and hence water consumption, with subsequent cuttings having less yield, and the final cutting having the least amount of yield. The CGDD values for the first growth cycle are accumulated beginning at green up of the crop in spring, and from the time of cutting

for all subsequent growth cycles. The killing frost temperature of -7°C defines termination of the growing season for alfalfa.

Calibration of CGDD values controlling the simulation of the green up and cutting dates was accomplished by minimizing the error in simulated vs actual green up and cutting dates documented from previous studies in Nevada, and 'typical' green up and cutting dates obtained from farmers located in southern, central, and northern Nevada (Table 1). The best fit CGDD value from January 1 until green up was 300 °C-days, while the best fit CGDD value for time from green up until the first cutting was 880 °C-days, and CGDD value of 740 °C-days since the first cutting until the next cutting. These CGDD values gave promising results across the state considering the extreme spatial variation of air temperature. Details on the development of the curves shown in Figure 2 and CGDD calculations are given in Allen and Robison (2007) and Allen et al., (2007). The alfalfa reference-based curves of Allen and Robison were converted to grass reference-based curves in this Nevada application by dividing by 1.20, which is the standardized ratio for alfalfa to grass reference for the standard climate condition proposed by FAO (Allen et al., 1998) where mean wind speed at 2 m is 2 m/s and mean daily minimum relative humidity is 45%. Departures from the standard climate condition are however accounted for by adjusting the daily K_{cb} value upward based on the estimated daily RH and wind speed following procedures outlined in FAO-56 (Allen et al., 1998).

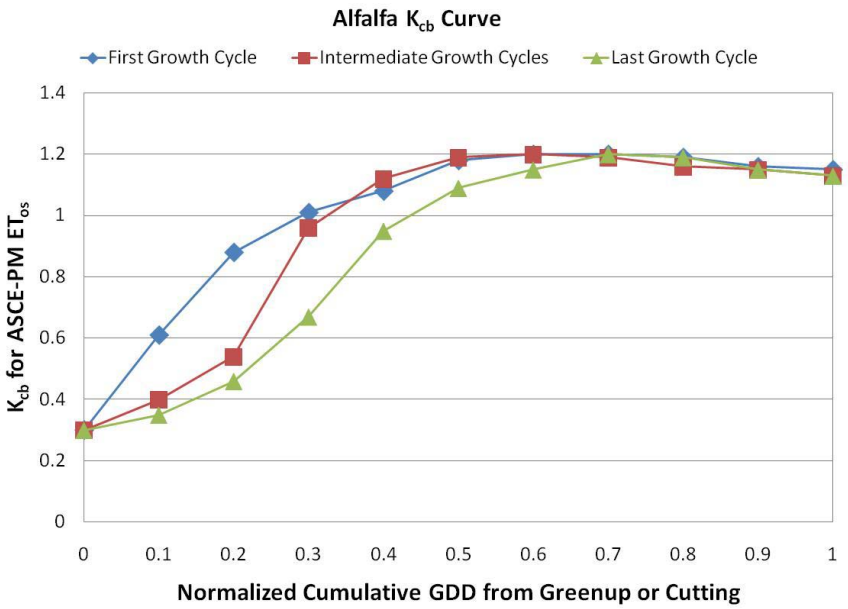

Figure 2. Basal crop coefficient curves for alfalfa representing different stages of growth.

Table 1. Documented/typical green up and cutting dates vs simulated green up and cutting dates for alfalfa using calibrated CGDD parameter values.

Crop	Hydrographic Area	NWS Weather Station Used for Analysis	Documented/ Typical Green Up Dates	Simulated Mean Green Up Dates	Documented/Typical Cutting and Harvest Dates	Simulated Mean Cutting/Harvest Dates	Source
Alfalfa	Carson Desert	Fallon EXP	3/20	3/23	6/15, 7/19, 9/1, 10/21	6/12, 7/22, 9/1, 10/21	Rashedi (1983)
Alfalfa	Carson Desert	Fallon EXP	3/20-4/1	3/21	6/1, every 30-40 days after, 3-4 cuttings	6/8, every 40 days after, 3-4 cuttings	Latin Farms (2008), Verbal Communication
Alfalfa	Carson Valley	Minden	3/20-4/5	4/2	6/15, 8/1, 9/15	6/19, 7/29, 9/10, sometimes a 4th cutting at 10/29	Aldax (2008), Verbal Communication
Alfalfa	Carson Valley	Minden	3/20-4/5	3/27	6/8, 7/28, 9/20, no 4th cutting	6/15, 7/26, 9/4, no 4th cutting	Aldax (2006), Written Communication via USGS
Alfalfa	Carson Valley	Minden	3/20-4/5	3/27	6/8, 7/21, 9/5, no 4th cutting	6/14, 7/24, 9/3, no 4th cutting	Godecke (2006), Written Communication via USGS
Alfalfa	Mason Valley	Yerington	3/15-4/1	3/20	5/25-6/5, every 35-45 days after, typically 4 cuttings	6/3, every 39 days after, 9 out of 10 years have 4 cuttings (6/3, 7/12, 8/17, 9/28)	Snyder Livestock (2009), Verbal Communication
Alfalfa	Moapa Valley	Overton	2/1-2/20	2/9	4/5-4/15, every 30 days after, typically 7 cuttings	4/18, every 32 days after, 7-8 cuttings	Hardy (2008), Verbal Communication
Alfalfa	Antelope Valley	Antelope Valley Farr	4/1-4/15	4/6	6/15, 8/5, 10/15, no 4th cutting	6/24, 8/3, 10/17, no 4th cutting	Farr Farms (2008), Verbal Communication

RESULTS

Estimated ET_{os} vs Calculated ET_{os}

Assessing the error in estimated ET_{os} using estimates of R_s, T_{dew}, and U_2, verses using measured data is of significant concern because estimation of these weather variables provides the ability to use NWS stations for sufficient spatial coverage and statewide application. To address this issue a comparison was made between estimated ET_{os} at NWS stations and calculated ET_{os} at nearby stations located in irrigated areas that measure the full suite of weather variables. Results of the comparison indicate that the ratios of annual estimated ET_{os} to calculated ET_{os} range from 1.01 to 1.06, with an average of 1.04, and an average RMSE for daily estimated ET_{os} of 0.95 mm/d (Table 2). These results are acceptable considering the overall error and that estimated ET_{os} is entirely dependent on spatially interpolated dew point depression, wind speed, and estimated R_s using T_{max} and T_{min}. The bias in slightly overestimating ET_{os} is attributed to a small bias of NWS station reported local temperatures.

Table 2. Estimated ET_{os} vs calculated ET_{os} at NWS and nearby irrigated area weather stations that measure the full suite of weather variables.

Name of NWS Station for ET_{os} Estimation	Basin of NWS Station Location	Name of ET_{os} Measurement Station	Basin of ET_{os} Measurment Station Location	Type of ET_{os} Measurement Station	Period of Record Used for Comparison	Ratio of Estimated Annual ET_{os} for NWS stations to Measured Annual ET_{os}	RMSE for Daily Estimated ET_{os} (mm d^{-1})	Estimated Mean Annual ET_{os} (mm)	Measured Mean Annual ET_{os} (mm)
Diamond Valley USDA	Diamond Valley	Eureka Agrimet	Diamond Valley	AGRIMET	8/01 - 6/06	1.06	0.82	1280	1209
Fallon EXP STN	Carson Desert	Fallon Agrimet	Carson Desert	AGRIMET	3/01 - 12/05	1.01	0.74	1295	1273
Laughlin	Colorado Valley	Mohave	Mohave Valley, AZ	AZMET	1/03 - 5/07	1.01	1.50	1958	1938
Yerington	Mason Valley	B11	Mason Valley	USGS Bowen Ratio	3/05 - 3/07	1.04	0.79	1245	1196
Minden	Carson Valley	ET-2	Carson Valley	USGS Bowen Ratio	4/03 - 11/04	1.06	0.92	1276	1353
					Average of Ratios and RMSE	1.04	0.95		
					Std. Dev. of Ratios and RMSE	0.03	0.42		

Actual Crop ET and Net Irrigation Water Requirements

Actual crop ET (ET_{act}) was calculated at a daily time step for the period of record for all NWS stations using the ASCE-PM equation and dual crop coefficient and soil water balance approach following Allen et al., (2005), Allen and Robison (2007), and Allen et al., (2007). An example of the daily ET_{act} for Fallon, NV, during 2002 is illustrated in Figure 3, which also illustrates cutting effects and the response of the K_c curve (K_{cb}*K_s+K_e) to precipitation and simulated irrigations due to the evaporative component of the K_c curve. The mean annual net irrigation water requirement of alfalfa for all NWS stations analyzed were computed for the last 30

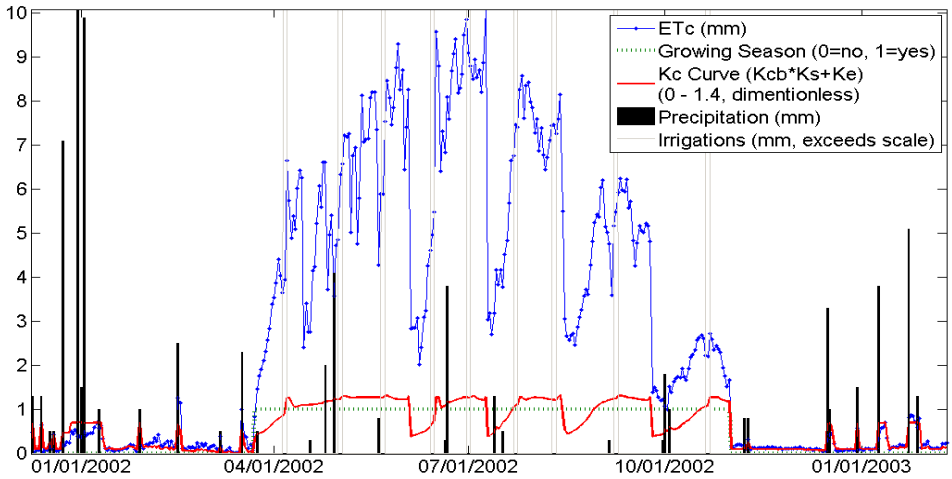

Figure 3. Simulated alfalfa ETc using the NWS Fallon, NV weather station. The computed Kc curve, simulated irrigations, and measured precipitation are also shown to illustrate the response of the K_c curve due to wetting events and cuttings.

years of record available. Results were then spatially distributed and averaged to hydrographic area boundaries for illustration purposes only (Figure 4). The net irrigation water requirement is defined as the ET_{act} – precipitation residing in the root zone, and represents the amount of additional water that the crop would evapotranspire beyond precipitation residing in the root zone if water were made available at the right time during the growing or non growing season. The net irrigation water requirement is synonymous with the net consumptive use. Figure 4 illustrates the large spatial variation in the net irrigation water requirement of alfalfa, primarily due to the extreme spatial variability in air temperature affecting the ET_{os} and growing season length. In southern parts of Nevada, the net irrigation water requirement is larger than the typical permitted irrigation water right of 5ft/yr (1,524mm/yr), and in central and northern areas of Nevada the net irrigation water requirement is less than the typical permitted irrigation water right of 4ft/yr (1,219mm/yr).

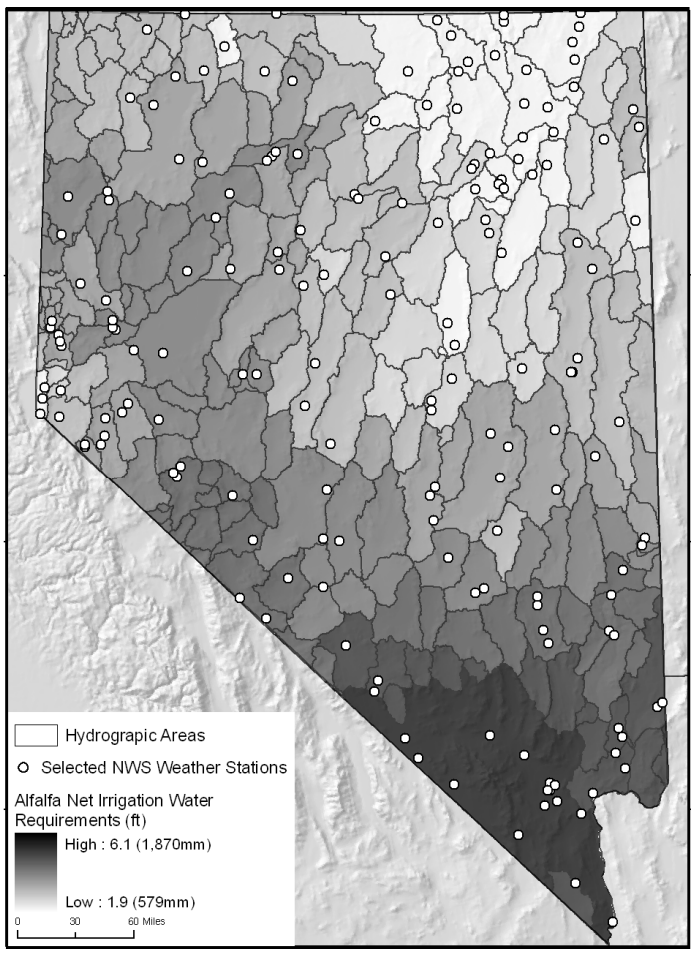

Figure 4. Mean annual alfalfa net irrigation water requirements (net consumptive use) and NWS stations used for computations. Results are spatially averaged to hydrographic area for illustration purposes only.

CONCLUSIONS

The objective of this study was to update crop ET and net irrigation water requirements for assessing water transfers from agriculture to new uses. In order to provide adequate spatial coverage, NWS stations were used; however NWS stations do not measure all weather variables needed for application of the widely accepted standardized ASCE-PM equation. Therefore, solar radiation was estimated at NWS stations with acceptable levels of error, and mean monthly measurements of dew point depression and wind speed from weather stations located in irrigated areas and valley floor areas, respectively, were assigned to NWS stations by spatially distributing mean monthly measurements. Estimates of ET_{os} vs computed ET_{os} using weather stations that measure the full suite of weather variables are in good agreement and provide confidence in weather variable estimation methods and net irrigation water requirement estimates. Results indicate that in central and northern parts of Nevada, if irrigators decide to change their irrigation water right to a new use by fallowing their fields, Nevada water law allows for the irrigation water right available for transfer to be reduced to the net irrigation water requirement (i.e. net consumptive use). These revised estimates of ET and net irrigation water requirements for various crops will be used for determining the amount of irrigation water that is available for water transfers in the future, as well as assist in basin water budget studies.

REFERENCES

Allen, R.G. (1996). "Assessing Integrity of Weather Data for use in Reference Evapotranspiration estimation." *Journal of Irrigation and Drainage Engineering*, ASCE. 122(2):97-106.

Allen, R.G. (1997). "A Self-Calibrating Method For Estimating Solar Radiation From Air Temperature." *Journal of Hydrologic Engineering*, 2(2), 56-67.

Allen, R.G., L.S. Pereira, D. Raes, and M. Smith. (1998). "Crop Evapotranspiration: Guidelines for Computing Crop Water Requirements." *Irrigation and Drainage Paper 56,* Food and Agriculture Organization of the United Nations, Rome, 300 pp.

Allen, R.G., L.S. Pereira, M. Smith, D.Raes, and J.L. Wright. (2005). "FAO-56 Dual Crop Coefficient Method for Estimating Evaporation from Soil and Application Extensions." *Journal of Irrigation and Drainage Engineering*, ASCE, 131(1):2-13.

Allen, R.G. and C.W. Robison. (2007). "Evapotranspiration and Consumptive Irrigation Water Requirements for Idaho." *University of Idaho Report,* 222 pp.

Allen, R.G., C.W. Robison and J.L. Wright. (2007). "Updated procedures for calculating state-wide consumptive use in Idaho." *Role of Irrigation in a Sustainable Future*. USCID Conference on Irrigation, Sacramento, CA proceedings: 189-212.

Allander, K.K., Smith, J.L., and Johnson, M.J. (2009). "Evapotranspiration in the Lower Walker River Basin, West-Central Nevada, Water Years 2005-07." *U.S. Geological Survey Scientific Investigations Report,* In preparation*,* xx-2009, xx p.

ASCE-EWRI. (2005). "The ASCE Standardized Reference Evapotranspiration Equation." *Report of the Task Committee on the Standardization of Reference Evapotranspiration*, Environmental and Water Resources Institute of the American Society of Civil Engineers. 171 p.

Brown P.W. (2001). "Siting and Maintenance of Weather Stations." *University of Arizona Cooperative Extension. Turf Irrigation Management Series*, No 3.

Doorenbos, J., and Pruitt, W.O. (1977). "Crop Water Requirements." *Irrigation and Drainage Paper No. 24,* Food and Agriculture Organization of the United Nations, Rome.

Guitjens, J. C. and C. N. Mahannah. (1977). "Upper Carson River Water Study, Water Year 1976." *Cooperative Extension, Agriculture Experimental Station*, Max C. Fleischmann College of Agriculture, University of Nevada, Reno, Nevada. R120. 32p.

Hill, R.W. (1979). "Water Requirements, Carson River Valley, California/Nevada." *United States vs. Alpine Land and Reservoir Company*, Civil No. D-BRT, USDC, Nevada. Keller Engineering. 19 p.

Mahannah, C.N. (1979). "Report on Irrigation Requirements for the Carson Valley Above Lahontan." *Report Prepared in Accordance with Pretrial Order for U.S.A. v. Alpine*, et al. in Equity No. D-183 BRT. 40 p.

Maurer, D.K., Berger, D.L., Tumbusch, M.L., and Johnson, M.J. (2006). "Rates of evapotranspiration, recharge from precipitation beneath selected areas of native vegetation, and streamflow gain and loss in Carson Valley, Douglas County, Nevada and Alpine County, California." *U.S. Geological Survey Scientific Investigations Report,* 2005-5288, 70 p.

Pennington, R.W. (1980). "Evaluation of empirical methods for estimating crop water consumptive use for selected areas in Nevada." *Nevada Division of Water Planning Report 3*, 206 p.

Thornton, P.E. and S.W. Running. (1999). "An improved algorithm for estimating incident daily solar radiation from measurements of temperature, humidity, and precipitation." *Agricultural and Forest Meteorology*, 93:211-228.

USDA-SCS. (1992). "Nevada Irrigation Guide." Subpart F, part 683, *Water Requirements*, July 1992, pp. 683-19 – 683-71.

Wright, J. L. (1981). "Crop Coefficients for Estimates of Daily Crop Evapotranspiration." *Irrigation Scheduling for Water and Energy Conservation in the 80's*, ASAE, St. Joseph, Michigan, 18-26.

Wright, J. L. (1982). "New Evapotranspiration Crop Coefficients." *Journal of Irrigation and Drainage Division*, 108(1), 57-74.

Integrated Water Management in an Ancestral Water Scheme in a Mountainous Area of Southern Spain

G. Vivas[1], E. Gómez-Landesa[2], L. Mateos[3], J.V. Giráldez[4]

[1]BEFESA, Avda. de la Buhaira, 2, 41018, Sevilla, Spain; formely Instituto de Agricultura Sostenible, CSIC; PH +34 608 796075; email: gonzalo.vivas@befesa.abengoa.com
[2]Instituto de Agricultura Sostenible, CSIC, Alameda del Obispo s/n, 14071 Córdoba, Spain; PH +34 957 499228; FAX +34 957 499252; email: ag1mainl@uco.es
[3]Formely, New Mexico State University, Las Cruces, NM
[4]Universidad de Córdoba and Instituto de Agricultura Sostenible, CSIC, Alameda del Obispo s/n, 14071 Córdoba, Spain; PH +34 957 499208; FAX +34 957 499252; email: ag1gicej@uco.es

ABSTRACT

The snow pack of Sierra Nevada, Southern Spain, melts during spring and early summer feeding ancestral irrigation canals in the region called Alpujarra. This study compared the traditional supply, based on proportional division, with the actual supply, based on up-downstream priority, in a representative watershed in the Alpujarra. A combination of three models was used for the analysis. Snow melt and runoff were simulated using the Snow Runoff Model and satellite images to determine snow cover. A second model (based on a water balance with capacity constraints) simulated the distribution of water either following proportional supply or up-downstream priority. Crop irrigation requirements were simulated using the FAO approach. The equity inherent to the proportional supply did not diminish adequacy overall. Because of the reuse of return flows in the watershed, irrigation efficiency at the watershed scale was significantly greater than irrigation efficiency at the irrigation canal scale.

INTRODUCTION

Irrigation in Spain flourished in the Middle Age. The Muslims introduced in Southern and South-eastern Spain not only new irrigation techniques, but also the concept of collective management in the governance of the water resources. The actual organization of the water users' associations in Spain is based on the principles that were developed at that time. Moreover, some irrigation systems and their organization have remained almost unchanged in mountainous areas of Southern Spain. Alpujarra is one of those areas. Traditionally, water was divided based on proportional supply among canals and then rotated within the canals. These water distribution rules (reported in historical documents dated in the XVI century) have been in use until today, but the whole system is declining rapidly.

Another feature of these systems was integrated water management. In fact, the new paradigms of water and irrigation management (Mateos et al., 1998; Mateos, 2008; Clemmens et al., 2008) were implicit in the ancestral systems of the Alpujarra. First, the excess of water in sectors of the system were reused downstream. Second, when supply

was greater than demand, natural springs were recharged to extend the availability of water into the dry season.

The performance of these systems may be quantified using indicators defined by several authors (Molden and Gates, 1990; Malano and Burton, 1998; Mateos et al., 2002).

This study analyses using simulation models and performance indicators the integrated water management of a representative watershed (the Poqueira River) in the Alpujarra. The traditional proportional supply is compared with the actual supply, which is based on up-downstream priority.

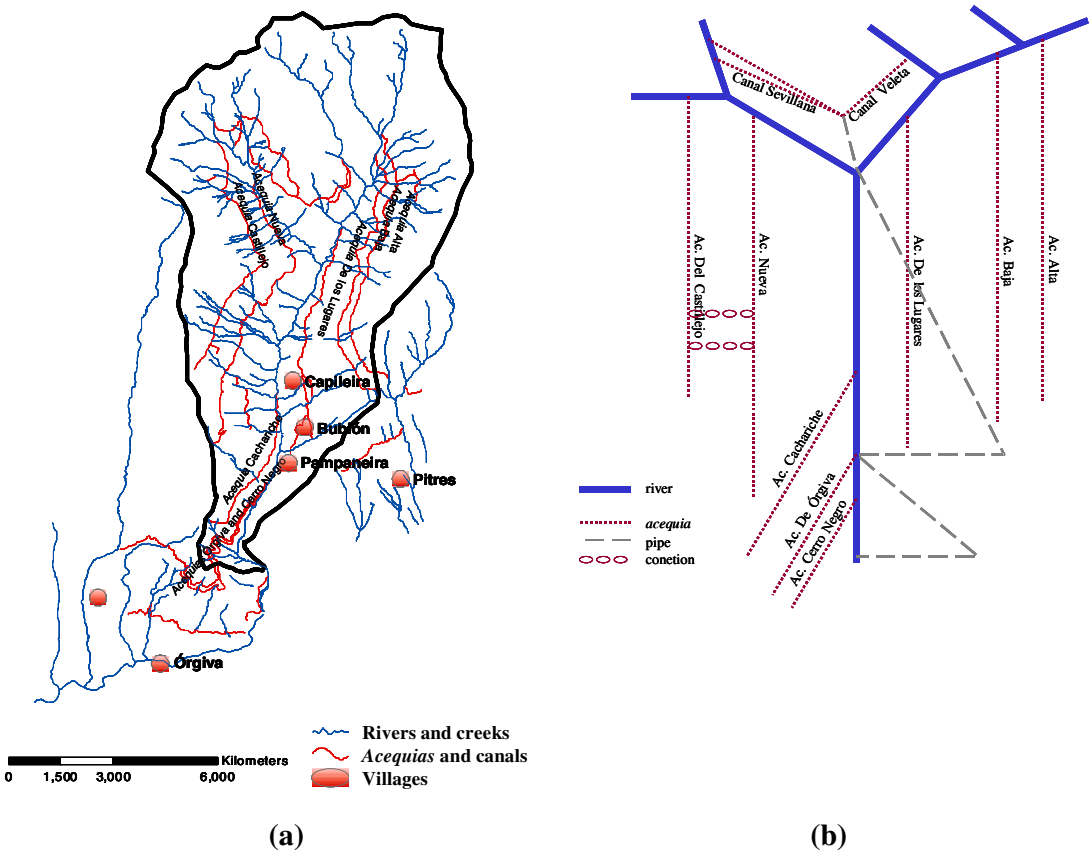

Figure 1. Map of the study watershed (a) and sketch of the fluvial and *acequias* networks (b)

THE STUDY WATERSHED

The study was carried out in the Poqueira River watershed (Fig. 1a). This watershed covers 90 km^2 of mountainous land in the southern face of Sierra Nevada, Southern Spain. Its altitude varies from 400 m a.s.l where the Poqueira River joins the Guadalfeo River to 3479 m a.s.l. at the summit of the Mulhacén peak. Mean annual rainfall in the Poqueira watershed varies from 450 mm in its lowest part to about 1000 mm in the mountain

summits. The rainfall distribution along the year is typical of a Mediterranean climate; the summer is dry and maximum precipitation occurs between November and February. Above 2000 m, 75% of the precipitation is as snow.

Table 1. Characteristics of the *acequias* and canals in the study watershed, including number of *pagos* and number of turns

Acequia	Length (m)	Area (ha)	Lining	Capacity ($L\ s^{-1}$)	*Pagos*	Turns
del Castillejo	8332	803	Unlined	200	6	11
Amoladeras	3502		Unlined			
Nueva	10045	827	Concrete/Earth	459	5	15
de los Lugares	8952	266	Concrete/Earth	246	6	8
Cachariche	4960	107	Concrete/Earth	243	7	9
Cerro Negro	6354	489	Concrete/Earth	191	5	9
Baja	9239		Unlined			
Alta	9003		Unlined			
Órgiva	8589		Concrete/Earth			
Canal Sevillana	2837		Concrete			
Canal Veleta	1906		Concrete			

The Poqueira watershed has a complex water conduit network consisting of *acequias*, canals that transport water to hydropower plants, and pipes (Fig. 1b). The total length of open canals (*acequias* plus hydropower canals) is 73.7 km. Table 1 gathers the main characteristics of the *acequias* and canals. There are five *acequias* for irrigation within the watershed: Castillejo, Nueva, De los Lugares, Cachariche and Cerro Negro (Fig. 1). Other two *acequias* run along the eastern slope of the watershed, *acequias* Baja and Alta, transferring water to the watershed of the Trevélez River, where they divert water to the neighbour watershed (Fig. 1). The *acequia* Órgiva also transfers water by crossing the western slope of the watershed and transposing to the watershed of the Chico River, where it flows to irrigate the lowland of the nearby village, Órgiva (Fig. 1).

The irrigated crops are mainly vegetables (abundant in *acequia* Cerro Negro, the most active in the watershed) and pasture for animal grazing (abundant in *acequia* Castillejo). Nevertheless, an increasing proportion of the irrigable land is being abandoned, mainly in *acequia* Cachariche. *Acequia* de los Lugares was built for irrigation purposes too, but it supplies water for domestic use to the villages Capileira, Bubión and Pampaneira.

The water supplied by an *acequia* is divided into irrigation sectors locally called *pagos*. The number of *pagos* in the *acequias* of the Poqueira watershed is 5 or 6 (Table 1). Each *pago* has the right to a number of hours or days during the rotation, (which duration varies) with a variable time period between 8 and 15 days (Table 1). Within a *pago*, water is rotated among farms from upstream to downstream. The canal master controls the water turns. The rules governing water distribution are precise and they have long tradition, so they are observed tacitly by all farmers.

The flow rate at the head of the *acequias* is determined by the water availability at the river where they derive from, and by the agreements that regulate the water use in the watershed. Nowadays, these agreements are not always equitable: in the dry year 2005, when the water was insufficient to satisfy all the demand, only the downstream *acequias* farmers suffered the scarcity. More just rules governed water distribution in the past.

An activity related to the *acequias* is dedicated to hydropower production. Three power plants are connected in cascade by means of pipes starting at a basin at 2100 m of altitude (Fig. 1b). There is an agreement between the electricity company and the farmers of *acequia* Nueva, according to which as the discharge in the creek decreases the diversion for hydropower production must be reduced, giving priority to the *acequia* Nueva.

MATERIALS AND METHODS

Three models were combined for the simulation study: the Snow Runoff Model, the crop irrigation requirements model, and the water distribution model.

The Snowmelt-Runoff Model (SRM) was designed to simulate and forecast daily stream flow in mountain basins where snowmelt is a major runoff contributor. SRM was developed by Martinec (1975) in small European basins. Each day, the water produced from snowmelt (calculated on a degree-days base) and from rainfall is computed, superimposed on the calculated recession flow and transformed into daily discharge from the basin (Martinec et al., 2005). Model variables are derived from actual observations of temperature, precipitation, and snow covered area. Model parameters can either be derived from measurements or estimated by hydrological judgement taking into account the basin characteristics, physical laws, and theoretical or empirical relationships. The application of SRM involved the determination of snow cover using images collected with the sensor MODIS on board of the satellite Terra. Temperature and precipitation data were obtained from a weather station located in the village of Lanjarón.

The crop irrigation requirements were calculated using a soil water balance equation. Two water contents were used to characterize each soil class: the drained upper limit or field capacity and the lower limit of plant extractable water or wilting point. Drainage below the root zone was computed as the excess of water over field capacity. Crop evapotranspiration was calculated from reference evapotranspiration and crop coefficients (Doorembos and Pruitt, 1977; Allen et al., 1998). Reference evapotranspiration was estimated by the Hargreaves equation (Hargreaves and Sammani, 1985). The balance equation was used to calculate net irrigation as the depth of water needed to refill the soil profile when the water content reached the allowable depletion. Net irrigation was divided by an application efficiency accounting for percolation and runoff losses.

For the purpose of formulating the water distribution model, the watershed was divided in three subsystems, each consisting of the water source (the point were snow melt runoff is assumed to concentrate), natural channels, *acequias*, canals and *pagos*. The water distribution model was based on the principle of the water balance at the nodes of the distribution network accounting for capacity constraints. The capacity of each *acequia* and

canal (Table 1) was calculated based on Manning's equation. Filtrations along the *acequias* and canals were estimated as a function of their construction material and length (Table 1). The simulation step was daily. The turns within each *pago* were simulated according to the traditional organizational rules (Table 1).

The division of water among *acequias* and canals was simulated according to two distribution modes: proportional supply (the traditional mode) and supply according to up-downstream priority (the current mode). Under proportional supply the available water at one node was divided proportionally to the irrigable area downstream each of the two branches starting at that node. Under the division by priority, the available water was diverted to the *acequias* or canals until filling their capacity, thus the water rights had an up-downstream priority. Then, the volume simulated for each *pago* was compared with the irrigation requirements calculated previously. The excess of water at the *pagos* or *acequias* was circulated according to the diagram in Fig. 1b. From here on, proportional supply will be denoted by PRO and supply according to up-downstream priority, by PRI.

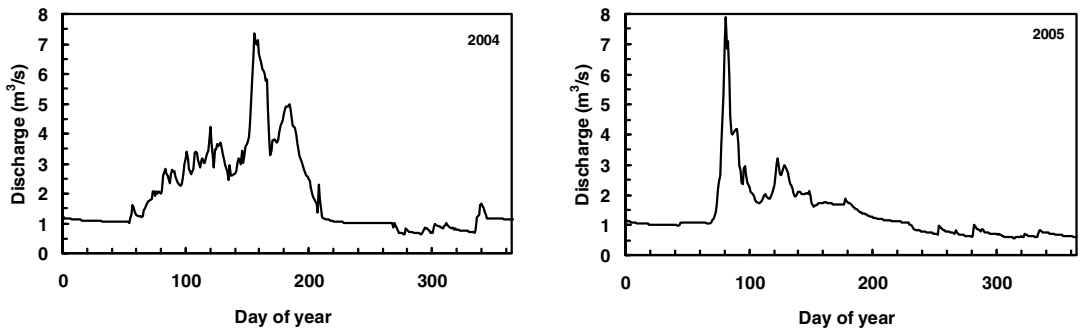

Figure 2. Simulated runoff hydrographs for the study watershed in 2004 and 2005

RESULTS AND DISCUSSION

The snow melting period varied in the years of study (2001 to 2005) notably. Typically it started during March and it ended during June or July, resulting in periods between two and four months. The runoff hydrographs reflected the occurrence of intense rain events and of snow meeting peaks consequence of temperature increases (Fig. 2). 2001, 2003 and 2004 were wet years, with annual runoff volumes between 45.99 and 60.19 hm^3, whereas 2002 and 2005 were dry years, with runoff volumes 30.86 and 34.39 hm^3, respectively.

Simulated volumes that were diverted to the canals system were greater the wet years, for both distribution modalities: 14.04 hm^3 in 2001 or 2004 and 14.33 hm^3 in 2003, for PRO, and between 11.31 hm^3 in 2001 and 11.80 hm^3 in 2003, for PRI; whereas the smaller volumes corresponded to the dry years: 10.71 hm^3 in 2005 and 11.83 hm^3 in 2002 for PRI and 7.38 hm^3 in 2005 and 10.11 hm^3 in 2002 for PRO (Table 2).

The mean, simulated volume flowing in the watershed was 45.67 hm^3. Under PRI, the mean volume diverted to the canals system was 12.99 hm^3, representing 28.4 % of the available volume. Whereas under PRO, this averaged volume was 10.39 hm^3 only, or 22.7

% of the volume available in the watershed. This difference was expected because under PRO a fraction of the available water was allowed to flow at the outlet of the watershed. While the runoff volume simulated in 2005 at the outlet of the watershed was 1.19 hm^3 under PRI it was 3.48 hm^3 under PRO. In a wet year as 2001, the runoff volume at the outlet of the watershed reached 25% of the available volume, with little difference between both distribution modalities.

Table 2. Simulated volume of water, hm^3, diverted to the canals system and to some specific *acequias* of the study watershed in the period March to August, years 2001 to 2005, for the two water distribution modalities considered (PRO: Proportional supply and PRI: supply according to an up-downstream priority)

Year		Total	Castillejo	Nueva	Lugares	Cachariche	Cerro N.
2001	PRI	14.04	1.88	2.13	2.15	2.60	1.99
	PRO	11.31	1.65	1.68	1.37	1.83	2.05
2002	PRI	11.83	2.14	2.09	2.64	1.96	0.18
	PRO	10.11	1.87	1.52	2.24	0.61	1.93
2003	PRI	14.34	1.89	2.19	2.26	2.60	1.90
	PRO	11.80	1.63	1.98	1.69	1.50	2.05
2004	PRI	14.04	2.14	2.63	2.64	1.97	1.07
	PRO	11.34	1.97	2.09	2.32	0.75	1.78
2005	PRI	10.71	1.56	1.05	1.58	2.59	1.42
	PRO	7.38	1.20	0.81	0.78	0.77	2.05

The total volume of water diverted to the canals system depended on the water availability and the distribution modality. However, the share of water for each canal depended on its location within the watershed as well. The *acequias* located in the upper part of the watershed diverted under PRI a greater share of water than under PRO (Table 2), and vice versa. Compare for instance the volumes diverted to the *acequias* Castillejo (the highest) and Cerro Negro (the lowest) (Table 2).

The return flows of the irrigated land plus the intentioned diversions for recharging natural springs varied from year to year and depended on the distribution modality as well. In the wet years, the volume of return flows that were re-circulated were 0.04 hm^3 and 0.02 hm^3 for PRI and PRO, respectively, while in the dry years these volumes were halved.

These differences among years and between distribution modalities had differential effects on the irrigation performance of the different canals. For instance, the relative irrigation supply for *acequia* Castillejo (the highest) and *acequia* Cerro Negro (the lowest) in 2003 (wet year) and 2005 (dry year) showed a contrasting evolution along the irrigation campaign. In *acequia* Castillejo, the relative irrigation supply (RIS, defined as the ratio between the diverted water and the irrigation water required for maximum yield) under PRO decreased with respect to the RIS under PRI as the season progressed. This decrease corresponded with the RIS increase under PRO with respect to the RIS under PRI observed in *acequia* Cerro Negro. Moreover, note that the contrast was in the dry year more marked than in the wet year. This contrasting performance indicated that PRO, contrary to PRI, approached the water distribution that avoids water excess and crop water deficit.

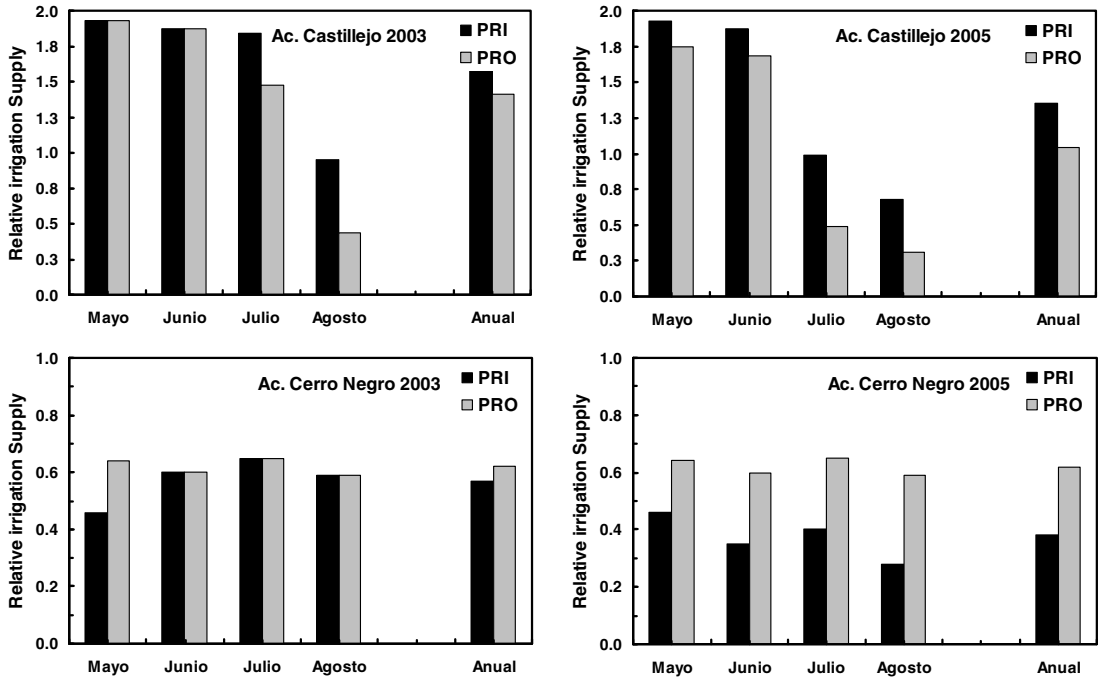

Figure 3. Relative irrigation supply in *acequias* Castillejo and Cerro Negro, years 2003 and 2004, for the water distribution modalities PRO (proportional supply) and PRI (supply according to an up-downstream priority)

Table 3. Equity among the *acequias* of the three subsystems and the whole system of the study watershed, years 2001 to 2005, for the water distribution modalities PRO (proportional supply) and PRI (supply according to an up-downstream priority)

Year	Subsys. Toril		Subsys. Mulhacén		Sunsys. Poqueira		Whole system	
	PRI	PRO	PRI	PRO	PRI	PRO	PRI	PRO
2001	0.50	0.55	0.89	0.94	0.26	0.43	0.54	0.53
2002	0.56	0.64	0.74	0.98	0.00	0.78	0.39	0.67
2003	0.49	0.48	0.88	0.96	0.25	0.52	0.58	0.67
2004	0.47	0.52	0.73	0.92	0.18	0.70	0.53	0.69
2005	0.72	0.72	0.65	0.90	0.18	0.75	0.25	0.42

As it should be expected, PRI resulted in equity significantly greater than PRI (Table 3). Equity (EQ) is defined herein as one minus the quotient between the average of the absolute differences between the irrigation water depths and their average (numerator), and the average of the irrigation water depths (denominator). Globally, the difference between EQ under PRI and PRO widened in the years of less precipitation, exactly when equity is more important.

Note that, although distribution capacity is not discussed herein, both RIS and EQ were conditioned by it. The same occurred with efficiency (E, defined as the quotient between the diverted volume minus the return flow and the diverted volume), which resulted under PRO higher than under PRI (Table 4). Again, the difference of this indicator applied to

both distribution modalities was under dry years greater than under wet years. This interaction is affected by the distribution capacity of the *acequias*, which it not discussed herein.

But perhaps the most interesting point regarding E is the difference between the efficiency of the subsystems and that of the whole system. The later is always greater than the former, reflecting the water reuse within the watershed.

Table 4. Efficiency in the *acequias* of the three subsystems and the whole system of the study watershed, years 2001 to 2005, for the water distribution modalities PRO (proportional supply) and PRI (supply according to an up-downstream priority)

Year	Subsys. Toril		Subsys. Mulhacén		Sunsys. Poqueira		Whole system	
	PRI	PRO	PRI	PRO	PRI	PRO	PRI	PRO
2001	0.74	0.80	0.83	0.85	0.73	0.91	0.90	0.96
2002	0.74	0.83	0.82	0.86	0.61	0.97	0.92	0.99
2003	0.75	0.85	0.83	0.88	0.72	0.94	0.90	0.98
2004	0.75	0.89	0.82	0.88	0.71	0.97	0.93	0.99
2005	0.75	0.82	0.84	0.89	0.71	0.96	0.87	0.98

CONCLUSIONS

The results showed that the equity inherent to the traditional proportional supply overall did not diminished the relative irrigation supply of the land irrigated from each of the irrigation canals. Moreover, the relative irrigation supply of the downstream irrigation canals improved in the dry years with little effect on the relative irrigation supply of the upstream canals. It was concluded that the abandonment of the agricultural activity in the Poqueira watershed and the relaxation of the ancestral irrigation organisational rules is degrading the irrigation performance. On the other hand, thanks to the integrated use of water and to the reuse of return flows, irrigation efficiency at the watershed scale was significantly greater than at the scale of irrigation canal. The study case illustrated a paradigm of water governance and integrated management that should enlighten scientists, engineers and professionals dealing with the world water crises.

REFERENCES

Allen, R.G., Pereira, L.S., Raes, D., and Smith. M. (1998). *Crop evapotranspiration – Guidelines for computing crop water requirements.* Irrigation and Drainage Paper 56. FAO, Rome, Italy.

Clemmens A. J., Allen, R.G., and Burt, C.M. (2008). "Technical concepts related to conservation of irrigation and rainwater in agricultural systems." *Water Resour. Res.*, 44, W00E03, doi:10.1029/2007WR006095

Doorembos, J., and Pruitt, W.O. (1977). *Crop Water Requirements.* Irrigation and Drainage Paper 24. FAO, Rome, Italy.

Hargreaves, G.H., and Samani Z.A. (1985). "Reference crop evapotranspiration from temperature." *Trans. ASAE,* 1(2), 96-99.

Malano, H, and Burton, M. (2001). *Guidelines for benchmarking performance in the irrigation and drainage sector.* International Programme for Technology and Research in Irrigation and Drainage (IPTRID). FAO, Rome, Italy.

Mateos, L. (2008). "Identifying a new paradigm for irrigation system performance." *Irrig. Sci.*, 27, 25-34.

Mateos, L., López-Cortijo, I., and Sagardoy, J.A. (2002). "SIMIS: The FAO decision support system for irrigation scheme management." *Agric. Water Manage.*, 56, 193-206

Mateos, L., Young, C.A., Wallender, W.W. and Carlson, H.L. (2000). "Simulating spatially distributed water and salt balances." *J. Irrig. Drain. Engrg.*, 126, 288-295.

Molden, D.J., and Gates, T.K. (1990). "Performance measures for evaluation of irrigation-water-delivery systems." *J. Irrig. Drain Engrg*., 116(6), 804-823.

Comparison of Sensible Heat Flux Measurements by a Large Aperture Scintillometer and Eddy Correlation Methods

Xinhua Jia[1], Xiaodong Zhang[2], and Dean D. Steele[3]

[1]Xinhua Jia, Assistant Professor, Department of Agricultural and Biosystems Engineering, North Dakota State University, P.O. Box 6050, Fargo, ND 58108-6050; PH (701) 231-6453; FAX (701) 231-1008; email: xinhua.jia@ndsu.edu

[2]Xiaodong Zhang, Associate Professor, Department of Earth Systems Science and Policy, University of North Dakota, P.O. Box 9011, Grand Forks, ND 58202-9011; PH (701) 777-6087; FAX (701) 777-2940; email: zhang@aero.und.edu

3Dean D. Steele, Associate Professor, Department of Agricultural and Biosystems Engineering, North Dakota State University, P.O. Box 6050, Fargo, ND 58108-6050; PH (701) 231-7268; FAX (701) 231-1008; email: dean.steele@ndsu.edu

ABSTRACT

The eddy correlation (EC) method has been recommended as one of the standard methods for measuring actual evapotranspiration. One of the challenges in interpreting eddy correlation measurements is that the balance between various energy components measured and the total energy received can sometimes be off by up to 30%. An independent measurement of sensible heat flux by scintillometry is often used to resolve this energy balance closure problem.

An EC system was set up at a 47 ha commercial corn field in southeastern North Dakota in 2008. Net radiation, latent heat flux, sensible heat flux, soil heat flux and other weather parameters were measured continuously at a 30-min interval during the growing season. A Scintec Boundary Layer Scintillometer 900 (BLS900) was temporarily deployed for seven days when clear sky conditions were satisfied. During the synchronous experiment, both systems were adjusted to at least 1 m above the canopy and collected data at an increased frequency of every minute. The EC system was placed at approximately the midpoint of the scintillometer path. The comparison of sensible heat fluxes measured by the two methods showed good agreement. The results will be used to validate the eddy correlation system in an attempt to reconcile the closure of energy balance.

INTRODUCTION

Sensible heat (H) is the transfer of heat energy driven by temperature difference between the surface and the air. Latent heat (LE) is released when water condenses and is required for evaporation. Thus we have the latent heat of vaporization, i.e., the heat required to evaporate water. In a vegetated area, LE is determined by the evapotranspiration rate, and the direct measurement of evapotranspiration by eddy correlation (EC) method has been widely used and accepted as one of the standard methods for LE determination (Farahani et al., 2007). The EC

station can be deployed over a large area above the crop or tree canopy, which overcomes the actual surface conditions. However, one of the challenges with EC is to reconcile the measurements of various energy components. The unbalanced energy amount can be off by up to 30% of the total measured energy (Wilson, et al., 2002). It is normally assumed that the unbalanced energy is evenly distributed between sensible and latent heat fluxes, according to the Bowen Ratio (H/LE) (Twine et al., 2000, Jia et al., 2007). Therefore an independent estimate of sensible heat flux can help to determine the unbalanced energy and reduce the error.

Scintillometry measures atmospheric scintillation caused by refractive index fluctuations and applies the Monin-Obukhov Similarity principle to derive the sensible heat flux from the structure parameter of the temperature (Hemakumara et al., 2003; Lagouarde et al., 2006). This is the only micrometeorological method, though indirect, that can be used to provide an estimate of sensible heat flux averaged over a distance and over a continuous time period (DeBruin et al., 1995; DeBruin, 2002; Meijninger and DeBruin, 2000). It can operate over a variety of landscape scales. Kleissl et al. (2008) measured sensible heat flux over a homogenous area with natural vegetation using six large aperture scintillometers deployed at different heights and locations and found only 10% differences in the results. Asanuma and Iemoto (2007) compared sensible heat flux measured by eddy correlation and a large aperture scintillometer, but indicated that an accurate measurement of sensible heat flux depends on additional temperature and wind speed measurements as well as an estimate of the roughness length.

During the growing season of 2008, an eddy correlation system was used to measure actual ET in a maize field over a subsurface drainage. A large aperture scintillometer (LAS) was set up with the eddy correlation station for a comparison. This paper describes the experimental setup and presents preliminary comparison of the sensible heat flux measured by the two methods.

MATERIALS AND METHODS

Experimental Site

The experiment was conducted in 2008 over a 47 ha maize field at Fairmount, Richland County, ND. An eddy correlation system was set up (46.00895^{o} N, 96.60368^{o} W, 296 m above the sea level) at the southwest quarter of the field, at which a subsurface drainage system was installed in the fall of 2002. A scintillometer (BLS900, Sentic, German) was setup with the EC station in the middle of transect between the transmitter and the receiver. The path length was 584 m. Figure 1 shows the schematic layout of the instrumentation setup.

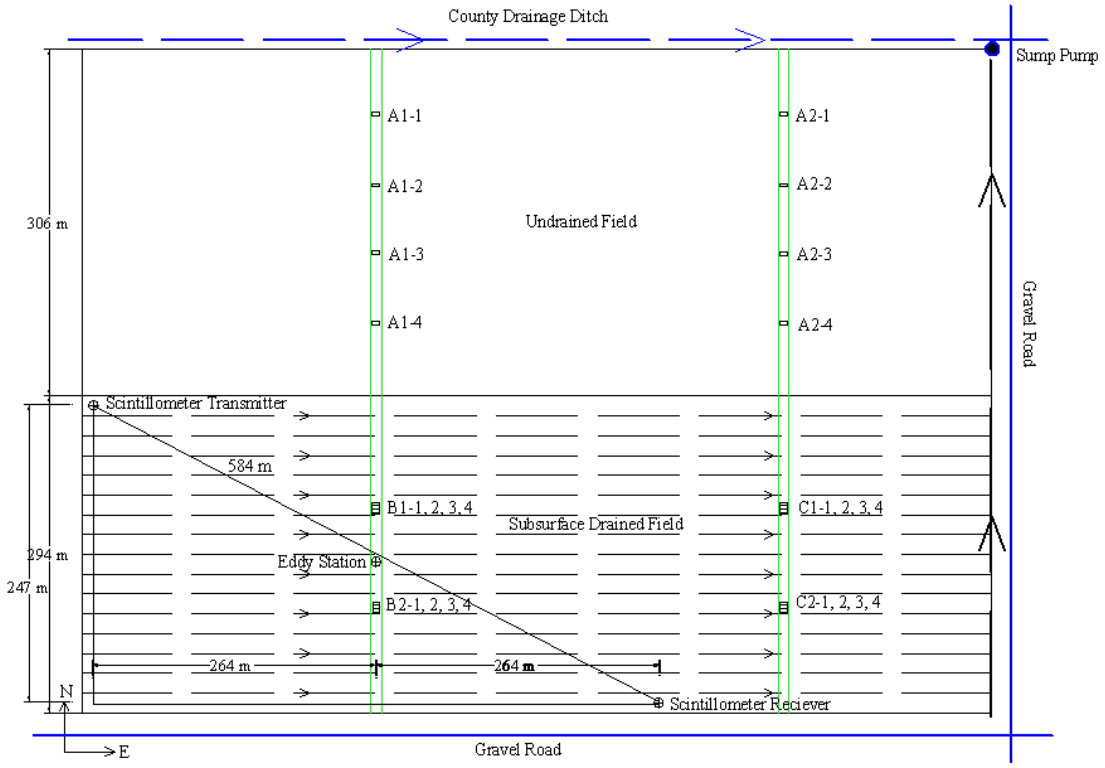

Figure 1. Schematic diagram of the experimental setup.

The EC station consists of a CSI (Campbell Scientific Inc., Logan, UT) CSAT3 3-D Sonic Anemometer and a CSI KH20 Krypton Hygrometer. The sampling frequency was 10 Hz and 1 to 2 min moving averages were used during the comparison with the scintillometer. The same average was applied to the meteorological measurements, such as net radiation, temperature, soil temperature, soil moisture, etc.

The scintillometer used in this study is a Large Aperture Scintillometer, model BLS900, manufactured by Scintec Inc., Germany. The BLS900 transmitter emits radiation through 924 light emitting diodes (LED) on two disks. The LEDs can operate in 4 different pulse repetition rates from 1Hz to 125 Hz; in this study, the rate was set at 5 Hz. The BLS900 is insensitive to transmitter vibrations because of its large emitting surface area and relatively large disperse angle.

During the experiment, the path length of scintillometer was fixed at 584 m, but its height along with that of EC was adjusted according to the maize height (Figure 2). The EC and LAS comparison was conducted on July 5, 8, 9, 13, 14 and August 5 and 6, 2008.

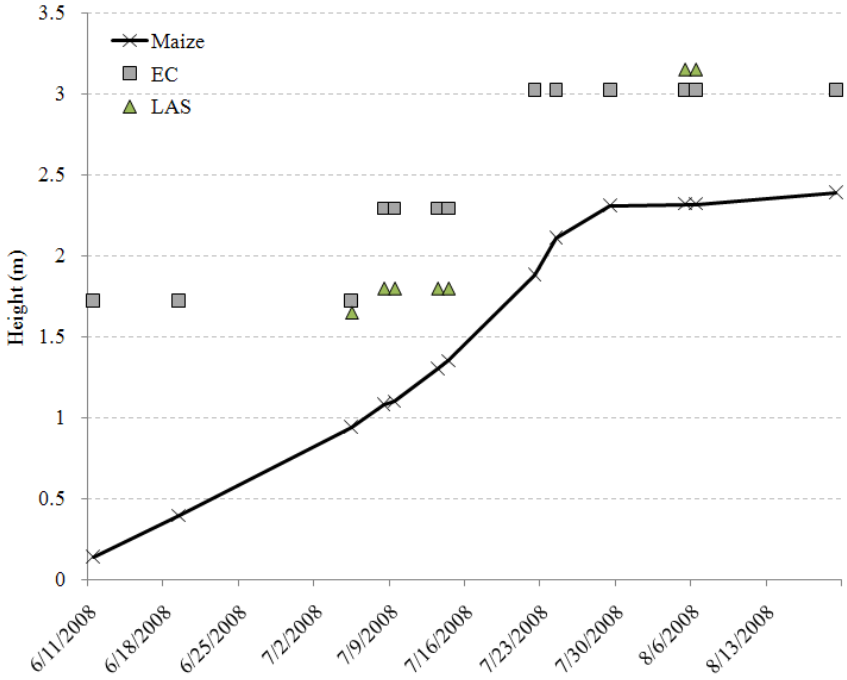

Figure 2. Arrangement of crop and instrumentation heights during the 2008 growing season at Fairmount, ND.

Sensible heat flux calculation

The description of EC method used in this research has been detailed by others (Sumner, 2001, Jia et al., 2006, 2007) and will not be repeated in this paper. Sensible heat flux estimation from scintillometer measurements have been addressed by Clifford et al. (1974), Hill et al. (1992), Hill (1997), and Lagouarde et al. (2006). In this paper, we only review the equations used for H estimation by the BLS900 large aperture scintillometer.

The refractive index (C_n^2, $m^{-2/3}$) integrated along the optical path was directly provided by the BLS900 processing unit. The structure function constant of temperature (C_T^2, $K^2\ m^{-2/3}$) can be calculated using

$$C_n^2 = \alpha_1^2 \frac{p^2}{T^4} C_T^2 \qquad (1)$$

where α_1 is wavelength dependant proportionality factor. At wavelength 880 nm, α_1 is 0.005759 $K\ Pa^{-1}$; p is the air pressure in Pa; and T is air temperature in K. This equation was listed in the manufacturer manual (Scintec, 2007).

The Bowen ration (β) correction listed by others (Wesely, 1976; DeBruin et al., 1995; Lagouarde et al., 2006) was not applied. The use of scintillometer is intended to compare the H

by LAS (H_{LAS}) with H by EC (H_{EC}). The use of β from EC will not allow the independent estimation of H_{LAS}. As stated by Savage (2009), when β is small, the correction for H is large, but the absolute value of H is small. When the β is large, the correction for H is small with possible little impact on the estimated energy balance.

Once C_T^2 is known, the temperature scale T_* can be calculated from a universal function $f_1[(z\text{-}d)/L_m]$ based on Monin-Obukhov similarity theory (MOST):

$$C_T^2 = T_*^2 (z-d)^{-2/3} f_1[(z-d)/L_m] \qquad (2)$$

where z is the height of the optical beam above ground in m. The d term is the zero displacement height in meters and can be determined from 0.67h, where h is the mean maximum height of the plant canopy in meters (ASCE, 1996).

The temperature scale T_* is used to calculate the H_{LAS}:

$$H = \rho C_p u_* T_* \qquad (3)$$

where ρ is air density in kg m^{-3} and C_p is specific heat of air in J kg^{-1} K^{-1} (1.225 J kg^{-1} K^{-1}).

The friction velocity, μ_*, can be obtained from surface to air application based on measured wind speed at height z, and an integrated stability correction function for momentum transfer:

$$\mu_* = k u_z \left[\ln \frac{z-d}{z_{om}} - f_2\left(\frac{z-d}{L_m} \right) \right]^{-1} \qquad (4)$$

where k is the von Karman constant, 0.41, u_z is wind speed at height z in m s^{-1}, and z_{om} is momentum roughness height of the surface and is estimated from 0.123 h.

The L_m term is the Obukhov length. When neglecting the latent heat flux correction, it is a function of friction velocity μ_*, and temperature scale T_*.

$$L_m = -\frac{T\mu_*^2}{kgT_*} \qquad (5)$$

Where T is air temperature in K, k is the von Karman constant, and g is gravitational acceleration, 9.81 m s^{-2}.

The two functional equations in eq. (2) and (4) are based on the status of $(z\text{-}d)/L_m$.

When $(z\text{-}d)/L_m \leq 0$, the boundary layer is under unstable condition:

$$f_1\left(\frac{z-d}{L_m}\right) = a_u\left(1+b_u\left|\frac{z-d}{L_m}\right|^{-2/3}\right) \quad (6)$$

When $(z-d)/L_m > 0$, the boundary layer is under stable condition:

$$f_1\left(\frac{z-d}{L_m}\right) = a_s\left(1+b_s\left|\frac{z-d}{L_m}\right|^{2/3}\right) \quad (7)$$

From De Bruin et al. (1993), constants $a_u = 4.9$, $b_u = 9.0$, $a_s = 4.9$, and $b_s = 0$ will be used in this study.

For the unstable condition with $(z-d)/L_m \leq 0$ (Paulson, 1970),

$$f_2\left(\frac{z-d}{L_m}\right) = 2\ln\left(\frac{1+x}{2}\right) + \ln\left(\frac{1+x^2}{2}\right) - 2\arctan(x) + \frac{\pi}{2} \quad (8)$$

For the stable condition, $(z-d)/L_m > 0$ (Webb, 1970),

$$f_2\left(\frac{z-d}{L_m}\right) = -5.2\left(\frac{z-d}{L_m}\right) \quad (9)$$

where x is calculated from

$$x = \left(1-\frac{16(z-d)}{L_m}\right)^{1/4} \quad (10)$$

In summary, input parameters are refractive index, air temperature, height of the optical beam of the LAS, mean maximal height of the plant canopy, and wind speed through the calculations. The H_{LAS} value is calculated from iteration by assuming an initial value of μ_*. Once the $(z-d)/L_m$ stabilizes after 3-4 iterations, the H_{LAS} value is calculated.

ACKNOWLEDGEMENTS

This project is supported by the North Dakota Agricultural Experiment Station, the North Dakota State Water Commission, and the North Dakota Department of Health. The authors wish to thank Mr. James Moos and Mr. Kevin Horsager for their technical support. Mention of trade names is for information purposes only and does not imply endorsement by the authors or NDSU.

REFERENCES

ASCE. 1996. Hydrology Handbook. ASCE, Reston, VA P125-252.

Asanuma, J., and Iemoto, K. (2007). "Measurements of regional sensible heat flux over Mongolian grassland using large aperture scintillometer." *J. of Hydrol.* 333:58-67.

Clifford, S., Ochs, G., and Lawrence, R. (1974). "Saturation of optical scintillation by strong turbulence." *J. Opt. Soc. Amer.,* 64:148-154.

De Bruin, H.A.R., Kohsiek, W., and van den Hurk, B.J.J.M. (1993). "A verification of some methods to determine the fluxes of momentum, sensible heat, and water vapour using standard deviation and structure parameter of scalar meteorological quantities." *Boundary-Layer Meteorol.* 63, 231-257.

DeBruin, H.A.R., van den Hurk, B.J.J.M., and Kohsiek, W. (1995). "The scintillation method tested over a dry vineyard area." *Boundary- Layer Meteorol.,* 76:25-40.

De Bruin, H.A.R. (2002). "Introduction, renaissance of scintillometry." *Boundary- Layer Meteorol,.*105:1-4.

Farahani, H.J., Howell, T.A., Shuttleworth, W.J., and Bausch, W.C. (2007). "Evapotranspiration: progress in measurement and modeling in agriculture." *Trans. of ASABE.* 50(5):1627-1638.

Hemakumara, H., Chandrapala, L., and Moene, A. (2003). "Evapotranspiration fluxes over mixed vegetation areas measured from a large aperture scintillometer." *Agric. Water Manag.,* 58:109-122.

Hill, R. J. (1992). "Review of optical scintillation methods of measuring the refractive-index spectrum, inner scale and surface fluxes." Waves Random Media, 2:179-201.

Hill, R.J. (1997). "Algorithms for obtaining atmospheric surface-layer fluxes from scintillation measurements." *J. Atmos. Oceanic Tech.,* 14:456-467.

Jia, X., Dukes, M.D., Jacobs, J.M., and Irmak, S. (2006). "Weighing lysimeters for evapotranspiration research in a humid environment." *Trans. of ASAE* 49(2):401-412.

Jia, X., Swancar, A., Jacobs, J.M., Dukes, M.D., and Morgan, K. (2007). "Comparison of evapotranspiration rates for flatwoods and ridge citrus." *Trans. of the ASABE,* 50(1):83-94.

Kleissl, J., Gomez, J., Hong, S.H., Hendrickx, J.M.H., Rahn, T., and Defoor, W.L. (2008). "Large aperture scintillometer intercomparison study." *Boundary- Layer Meteorol,.*128:133-150.

Lagouarde, J.P., Irvine, M., Bonnefond, J.M., Grimmond, C.S.B., Long, N., Oke, T.R., Salmond, J.A., and Offerle, B. (2006). "Monitoring the sensible heat flux over urban areas using large aperture scintillometry: case study of Marseille city during the Escompte experiment." *Boundary- Layer Meteorol,.* 118:449-476.

Meijninger, W., and DeBruin, H. (2000). "The sensible heat flux over irrigated areas in western turkey determined with a large aperture scintillometer." *J. Hydrol.,* 229:42-49.

Paulson, C.A. (1970). "The mathematical representation of wind speed and temperature profiles in the unstable atmospheric surface layer." *J. Appl. Meteorol.,* 9:857-861.

Savage, M.J. (2009). "Estimation of evaporation using a dual-beam surface layer scintillometer and component energy balance measurements." *Agricultural and Forest Meteorology,* doi:10.10016/j.agrformet.2008.09.012.

Scintec (2007). "Scintec boundary layer scintillometer, User Manual for BLS450, BLS900, BLS2000." Scintec, German.

Sumner, D.M. (2001). "Evapotranspiration from a cypress and pine forest subjected to natural fires in Volusia County, Florida, 1998-99." USGS Water Resources Investigations report 01-4245.

Twine, T.E., Kustas, W.P., Norman, J.M., Cook, D.R., Houser, P.R., Meyers, T.P., Prueger, J.H., Starks, P.J., and Wesely, M.L. (2000). "Correcting eddy-covariance flux underestimates over a grassland." *Agricultural and Forest Meteorology,* 103:279-300.

Webb, E. K. (1970). "Profile relationships: the lon-linear range, and extension of strong stability." *Quart. J. Roy. Meteorol. Soc.* 96:67-90.

Wesely, M.L. (1976). "The combined effect of temperature and humidity on the refractive index." *J. Appl. Meteorol.* 15:1177-1188.

Wilson, K.B., Goldstein, A.H., and Falge, F. (2002). "Energy balance closure at FLUXNET sites." *Agricultural and Forest Meteorology,* 113:223-243.

Mid-summer Deficit irrigation of Alfalfa as a Strategy for saving Water

B.R. Hanson[1], K.M. Bali[2], S.B. Orloff[3], B.L. Sanden[4], and D. Putnam[5]

[1]Department of Land, Air and Water Resources, One Shields Ave., University of California, Davis, CA 95616; PH (530) 752-4639; FAX (530) 752-5262; email: brhanson@ucdavis.edu
[2]University of California Cooperative Extension, Imperial County, 1050 East Holton Road, Holtville, CA 92250; PH (760) 352-9474; email: kmbali@ucdavis.edu
[3]University of California Cooperative Extension, Siskiyou County, 1655 South Main Street, Yreka, CA 96097; PH (530) 842-2711; email: sborloff@ucdavis.edu
[4]University of California Cooperative Extension, Kern County, 1031 South Mount Vernon Avenue, Bakersfield, CA 93307; PH (661) 868-6218; email: blsanden@ucdavis.edu
[5]Department of Plant Sciences, One Shields Ave., University of California, Davis, CA 95616; PH (530) 752-8982; email: dhputnam@ucdavis.edu

ABSTRACT

Evapotranspiration (ET) of fully-irrigated and deficit-irrigated (no irrigation in July, August, and September) was measured in five alfalfa fields at various locations throughout California. Seasonal ET ranged from 838 to 1,651 mm, which differed from historical seasonal ET. Deficit irrigation reduced ET, but the ET difference between fully-irrigated and deficit-irrigated alfalfa was site specific. Yields were reduced by deficit irrigation.

INTRODUCTION

Alfalfa is California's single largest agricultural water user due to the amount grown, typically about 405,000 ha, and its long growing season. Seasonal alfalfa water applications generally range from 494,000 to 679,000 ha-m. Because of the high water usage, interest exists in better defining the seasonal water use of fully irrigated alfalfa for different climatic areas of California and in midsummer deficit irrigation (no irrigation in July, August, and September) of alfalfa as a strategy for coping with limited water supplies and also as a strategy for providing water for transfer from water-rich areas such as the Sacramento Valley to water-short areas such as the San Joaquin Valley and southern California. In theory, the amount of water available for transfer is the difference between the ET of fully-and deficit-irrigated alfalfa. This midsummer deficit irrigation strategy maintains the relatively high yields of the first part of the year and eliminates irrigations during the summer when yields are small and quality usually is poor.

Previous studies on mid-summer deficit irrigation of alfalfa showed that no irrigation during the midsummer reduced the alfalfa yield, but did not stop all plant growth (Frate et al., 1991, Guitjens, 1993, Ottman et al., 1996, Putnam et al., 2000, Robinson et al., 1994). As a result, some evapotranspiration occurred during the period of deficit irrigation. No information exists on differences in midsummer evapotranspiration amounts between fully-and deficit-irrigated alfalfa.

This study investigated the seasonal ET requirements of fully-irrigated alfalfa and the effect of midsummer deficit irrigation on yield and evapotranspiration in commercial alfalfa fields at various locations in California.

METHODS AND MATERIALS

Alfalfa evapotranspiration (ET) was determined at Tulelake (Klamath Basin), Scott Valley (near Yreka in the intermountain area of northern California), Sacramento Valley (near Davis), Kern County (near Buttonwillow), and the Imperial Valley (near Holtville). All sites were commercial fields except for the Tulelake site, which was located at the University of California Intermountain Research and Extension Center, Measurements were made at the Davis site from 2005 to 2008, and at the other sites in 2007 and 2008.

These sites reflect mid-summer climate conditions ranging from warm summer temperatures in the Intermountain areas (Scott Valley, Tulelake) to very hot summer temperatures (Imperial Valley). Border (flood) irrigation was used at the Sacramento Valley, Kern County, and Imperial Valley sites, while sprinkle irrigation was used at the Scott Valley and Tulelake sites, reflecting the irrigation practices of each area. Most of each field was fully irrigated; a section of each field was deficit irrigated during the mid-summer. The fully-irrigated alfalfa was irrigated according to the irrigators' normal practices.

The ET was determined using the eddy covariance (Tanner et al., 1985) and surface renewal meteorological methods (Paw U and Brunet, 1991; Paw U et al., 1995; Snyder et al., 1996; Spano et al., 1997). The eddy covariance system consisted of a CSAT3 sonic anemometer (Campbell Scientific, Inc.), four Hukseflux self-calibrating soil heat flux plates installed at 8 cm deep, two sets of spatially averaging soil temperature probes (Campbell Scientific, Inc.) installed at 2 and 6 cm deep, two CS616 soil water sensors (Campbell Scientific, Inc.) installed 2.5 cm deep, and a Q7.1 net radiometer (Radiation and Energy Balance Systems, Inc.). The sensors were connected to a CR5000 data logger (Campbell Scientific, Inc.). Logger software from Campbell Scientific, Inc. was used to process the data and to calculate covariances and average flux densities of net radiation (R_n), latent heat (LE), sensible heat (H), and soil heat (G) every 30 minutes. The CSAT3 anemometer also measured horizontal wind speed, wind direction, and air temperature. Relative humidity was measured with a HMP45C temperature and relative humidity probe (Campbell Scientific, Inc.).

The surface renewal system consisted of a Q7.1 net radiometer, two soil heat flux plates (Radiation and Energy Balance Systems, Inc.), one set of spatially averaging soil temperature probes, and two fine wire thermocouples (0.076 mm diameter) (Campbell Scientific, Inc.) mounted about 1.5 m above the ground surface to measure air temperature. The sensors were connected to either a CR23X, a

CR10X, or a CR1000 data logger (Campbell Scientific, Inc.), depending on the site, which recorded high frequency temperature data and low frequency data of other variables. Data archiving and processing to determine the uncalibrated sensible heat flux density is described in Snyder et al (1996). Average flux densities were calculated for a 60 minute time interval (CR10X, CR23X) or a 30 minute interval (CR1000).

Sensible heat data from the EC systems were used to calibrate the SR method. The uncalibrated sensible heat flux determined by the SR system must be corrected for unequal heating between the ground and the measurement height using independent measurements of sensible heat flux such as the EC data.

RESULTS AND DISCUSSION

Fully-irrigated alfalfa evapotranspiration. Daily evapotranspiration of alfalfa was small, generally between 1.4 mm and 2.5 mm per day, at the start of the crop growing season, which varies depending on climate characteristics, increases with time of year to maximum values between 8 and 10 mm per day in June/July, and then decreases to small values at the end of the crop season, as shown in Figure 1 for Scott Valley, Sacramento Valley, and Imperial Valley sites. The growing season of Scott Valley is smaller than those of the Sacramento and Imperial Valley due to its altitude (823 m) and northerly location. In the Imperial Valley, alfalfa evapotranspiration from July to September in 2007 was affected by possible heat stress, reflected by daily ET values smaller than reference ET values. Similar behavior occurred in the Imperial Valley 2008 growing season (not shown). Daily ET decreased during the harvest, but increased rapidly with time after the first irrigation after harvest, reaching maximum values just before the next harvest.

Seasonal evapotranspiration ranged from 838 mm (Scott Valley 2008) to 1,651 mm (Imperial Valley 2008) (Table 1). Seasonal ET values of Scott Valley and Tulelake were greater than the historical ET commonly used for crop water use. Seasonal ET of the Sacramento Valley and Kern County sites was slightly higher than the historical ET, with an average of 1,346 mm for the three year period for the Sacramento Valley. The seasonal ET of the Imperial Valley was smaller than the historical value, possibly due to the heat stress.

Table 1. Seasonal ET of the fully-irrigated alfalfa and historical ET for the experimental sites.

Site		Seasonal ET (mm)	Historical ET (mm)
Imperial Valley	(2007)	1473	1930
	(2008)	1651	
Kern County	(2007)	1422	1245
Sacramento Valley	(2005)	1270	1245
	(2006)	1372	
	(2007)	1397	
Scott Valley	(2007)	991	838
	(2008)	838	
Tulelake	(2007)	1041	838
	(2008)	889	

Crop Coefficients. Crop coefficients were calculated as the ratio of the measured ET to the reference crop ET. Average alfalfa crop coefficients were calculated for each site and compared with the historical crop coefficients (Table 2). Coefficients were not calculated for Scott Valley, where reference crop ET was not available. Crop coefficients were the smallest just after a harvest and largest just before harvest. Values of the average, minimum, and maximum coefficients were similar to those in Doorenbos and Pruitt (1977) except for the Imperial Valley site.

Table 2. Crop coefficients of alfalfa.

Site	Average	Minimum	Maximum
Imperial Valley 2007	0.80	0.43	0.99
Kern County 2007	1.01	062	1.25
Sacramento Valley 2005	0.92	0.49	1.14
Sacramento Valley 2006	0.94	0.56	1.11
Sacramento Valley 2007	1.04	0.65	1.33
Tulelake 2007	0.99	0.50	1.30
Historical (Doorenbos and Pruitt, 1977)			
Humid[1]	0..85	0.50	1.05
Dry[1]	0.95	0.40	1.15
Strong wind	1.05	0.30	1.25

[1] light to moderate wind conditions

Mid-summer Deficit Irrigation. Mid-summer deficit irrigation reduced the ET, but the amount of reduction varied considerably between the experimental sites with differences between fully-and defict-irrigated alfalfa ranging from 5 mm (Tulelake 2007) to 238 mm (Sacramento Valley 2005) (Table 3). The 2007 value for Tulelake reflects the influence of shallow groundwater, which contributed to the ET of the deficit irrigated alfalfa. Only one month of deficit irrigation occurred for Kern County, which resulted in a small difference. The largest differences were found for Sacramento Valley. ET values of the fully-irrigated alfalfa during the period of deficit irrigation were similar for Imperial Valley, Sacramento Valley, and Tulelake.

Yield. Actual yield differences between fully–and deficit-irrigated alfalfa during the period of deficit irrigation ranged from 0.90 (Tulelake 2007) to 8.38 Mg ha^{-1} (Sacramento Valley 2007) (Table 4). The small Tulelake difference reflects the shallow ground water contribution. The differences for Kern County reflect the one month of deficit irrigation. However, experience has shown that a yield of 1.12 Mg ha^{-1} or smaller is not economical to harvest. Yields smaller than 1.12 Mg ha^{-1}were excluded in the practical yield differences. The practical yield differences represent the economical yield loss to the grower.

Table 3.ET differences between fully-and deficit-irrigated alfalfa and fully-irrigated ET during the periods of deficit irrigation.

Site		ET differences (mm)	Full ET during period of deficit irrigation (mm)
Imperial Valley	2007	61	572
Kern County	2006	46	226
	2007	43	356
Sacramento Valley	2005	239	594
	2006	168	538
	2007	119	475
Scott Valley	2007	51	269
	2008	79	320
Tulelake	2007	5	472
	2008	109	627

Table 4. Total yield difference between fully-and deficit-irrigated alfalfa.

Site		Actual yield difference (Mg ha^{-1})	Practical yield difference* (Mg ha^{-1})
Imperial Valley	2007	3.72	3.72
Kern County	2006	1.48	2.31
	2007	1.90	2.60
Sacramento Valley	2005	3.07	
	2006	6.23	8.85
	2007	8.38	10.28
Scott Valley	2007	1.84	3.09
Tulelake	2007	0.90	0/90

* adjusted for yields smaller than 1.12 Mg ha^{-1} not considered economical to harvest.

CONCLUSIONS

These ET measurements generally showed seasonal ET values that are higher than the historical seasonal ET values. The exception was Imperial Valley where the 2007 and 2008 seasonal values were considerably smaller than the historical value. Average crop coefficients were similar to the historical values except for Imperial Valley. Mid-summer deficit irrigation reduced the ET during the period of deficit irrigation, but the differences in ET between fully-irrigated and deficit-irrigated alfalfa were site specific. Yields were also reduced by deficit irrigation.

Water transfer amounts based on ET differences are not practical because of the site-specific responses, which cannot be predicted. Although ET occurred during the periods of deficit irrigation, the source of this water used by the crop was stored soil moisture from the earlier irrigations, prior to the start of deficit irrigation. Also,

this crop water use did not contribute to economical yield levels. The exception was at Tulelake where crop water use of the shallow ground water maintained high yields of the deficit-irrigated alfalfa. Water transfer amounts should be based on the ET of fully irrigated alfalfa during the period of mid-summer irrigation, which can be estimated as the product of crop coefficients and reference crop ET. This ET also more fully reflects the reduction in applied water during the deficit irrigation period.

REFERENCES

Doorenbos, J., and Pruitt, W.O. (1977). *Guidelines to Predicting Crop Water Requirements*. Irrigation and Drainage Paper (FAO), No. 24. United Nations, Rome, Italy.

Guitjens, J.C. (1993). "Alfalfa irrigation during drought." *Journal of Irrigation and Drainage Engineering*, 119(6), 1092-1098.

Ottman, M.J., Tickes, B.R., and Roth, R.L. (1996). "Alfalfa yield and stand response to irrigation termination in an arid environment." Agronomy Journal, 88, 44-48.

Paw U, K.T., Brunet, Y. (1991). "A surface renewal measure of sensible heat flux density." pp. 52-53. In preprints, 20th Conference on Agricultural and Forest Meteorology, September 10-13, 1991, Salt Lake City, Utah. American Meteorological Society, Boston, MA.

Paw U, K. T., Qiu, J., Su, H.B., Watanabe, T., and Brunet, Y. (1995). "Surface renewal analysis: a new method to obtain scalar fluxes without velocity data." *Agric. For. Meteorol.*, 74, 119-137.

Putnam, D., Takele, E., Kallenback, R., and Graves, W. (2000). "Irrigating alfalfa in the Low Desert: Can Summer Dry-down be Effective for Saving Water in Alfalfa?" Report submitted to the Bureau of Reclamation (USDI), Yuma, Arizona

Robinson, F.E., Teuber, L.R., and Gibbs, L.K. (1994). Alfalfa Water Stress Management During Summer in Imperial Valley for Water Conservation. Desert Research and Extension Center, El Centro, CA.

Snyder, R.L., Spano, D., and Paw U, K. T. (1996). "Surface Renewal analysis for sensible and latent heat flux density." *Boundary-Layer Meteorol.*, 77, 249-266.

Spano, D., Snyder, R.L., Duce, P., and Paw U, K.T. (1997.) "Surface renewal analysis for sensible heat flux density using structure functions." *Agricultural and Forest Meteorology*, 86, 259-271.

Tanner, B.D., Tanner, M.S., Dugas, W.A., Campbell, E.C., and Bland, B.L. (1985). "Evaluation of an operational eddy correlation system for evapotranspiration measurements." American Society of Agricultural Engineers National Conference on Advances in Evapotranspiration, December 16-17, 1985. Chicago, Ill.

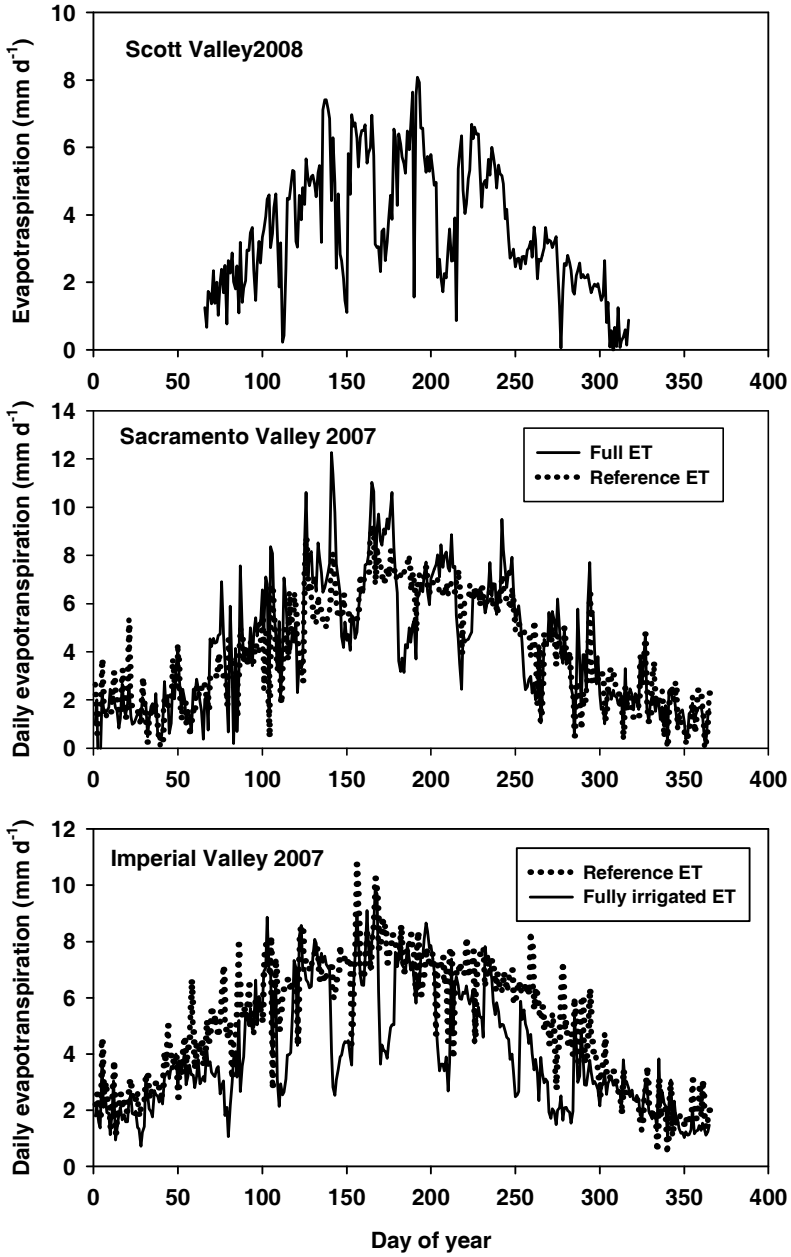

Figure 1. Daily evapotranspiration of alfalfa for Scott Valley (2008), Sacramento Valley (2007), and Imperial Valley (2007).

Recursive and Explicit Combination Methods for Calculating Reference Evapotranspiration

C. H. Hay[1] and S. Irmak[2]

[1]Postdoctoral Research Associate, Department of Biological Systems Engineering, University of Nebraska-Lincoln, 237 Chase Hall – East Campus, Lincoln, NE 68583-0726; PH (402) 472-4932; FAX (402) 472-6338; email: chay2@unl.edu
[2]Associate Professor, Department of Biological Systems Engineering, University of Nebraska-Lincoln, 241 Chase Hall – East Campus, Lincoln, NE 68583-0726; PH (402) 472-4865; FAX (402) 472-6338; email: sirmak2@unl.edu

The mention of trade names or commercial products is solely for the information of the reader and does not constitute an endorsement or recommendation for use by the authors or the University of Nebraska-Lincoln.

ABSTRACT

Efficient use of water in agroecosystems requires the accurate quantification of evapotranspiration (*ET*). Explicit combination method (ECM) equations (i.e., the Penman equation and its derivatives) have been widely used and tested. These equations rely on an assumption to remove the surface temperature from the calculation, and the validity of this assumption has been questioned as likely underestimating *ET*, particularly in semiarid and arid climates. Information on the validity of this assumption in subhumid regions is rare. Recursive combination methods (RCM), based on an equation proposed by Budyko, make no assumptions for the surface temperature, but they require iteration to arrive at a solution. The objective of this research was to compare daily *ET* calculated by the ECM and RCM and compare those values to Bowen ratio energy balance system (BREBS)-measured *ET* for a well-watered and maintained grassland near Central City, Nebraska. The results indicated that both equations were sensitive to the value chosen for the surface resistance (r_s). For equivalent values of r_s, *ET* predicted by the ECM was greater than *ET* predicted from the RCM. Using r_s values of 40 s m^{-1} for the ECM and 20 s m^{-1} for the RCM resulted in the best predictive performance for the two methods, and using these values, the ECM performed slightly better. While the RCM may potentially provide more accuracy under some conditions, it was no more accurate than the ECM under these experimental conditions.

INTRODUCTION

Accurate quantification of evapotranspiration (*ET*) is necessary for the efficient planning and use of water resources in agroecosystems. A number of different combination, temperature, and radiation-based equations have been

developed for estimating *ET*. The most accurate and reliable of these are the combination method equations which combine surface energy balance and mass transfer methods for calculating *ET*. The most popular of these are derivatives of the original Penman equation (Penman, 1948). Standardized versions of the Penman-Monteith formulation of the Penman equation have been developed, tested, and recommended for use in calculating *ET* (ASCE-EWRI, 2005).

The Penman equation and its derivatives rely on an approximation of the saturation vapor pressure vs. air temperature relation using the finite difference form of the Clausius-Clapeyron equation to remove the surface temperature from the equation (Sellers, 1965). This results in a single, explicit equation that is easily solved. This method is hereafter referred to as the explicit combination method (ECM). The validity of the assumption necessary to remove the surface temperature from the equation has been questioned (Lascano and van Bavel, 2007). The error due to the approximation is proportional to the difference between the surface and air temperatures, and errors are likely to be largest in arid and semiarid regions (Sellers, 1965). However, information on the validity of this assumption in subhumid areas is rare.

Budyko (1956), as cited in Sellers (1965), independently developed a combination equation that contains two unknowns, the surface temperature and the saturation vapor pressure at the surface temperature. It therefore, requires recursive iteration to arrive at a solution for the surface temperature to use to then calculate *ET*. This method is hereafter referred to as the recursive combination method (RCM). Because the RCM requires iteration to reach a solution, it is somewhat more cumbersome to use than the ECM. However, because it doesn't rely on the linear approximation of the saturation vapor pressure vs. temperature relation, it offers the potential for greater accuracy. Modern computer hardware and software makes the solution of the RCM trivial. The objective of this research was to compare daily *ET* calculated by the ECM and RCM and compare those values to Bowen ratio energy balance system (BREBS)-measured *ET* for an irrigated grassland.

METHODS

Study site and season. Measurements of *ET* and micrometeorological variables were made at an irrigated grassland near Central City, Nebraska (41°17'N, 97°56'W, 577 m MSL), which was maintained as a pasture. The study site is in a transition area from subhumid to semiarid zones. The grassland was approximately 64.7 ha and contained a mixture of cool season grasses [i.e., Tall Fescue (*Festuca arundinacea*) and Kentucky Bluegrass (*Poa pratensis*)]. Significant spring rains and irrigation in the summer kept the pasture well-watered. The pasture was irrigated, when needed, with a center pivot irrigation system and fertilized as needed. The pasture was grazed by cattle throughout most of the growing season, and the grass height varied between approximately 5 and 13 cm throughout the season. The data used for *ET* calculations were from the 2008 growing season, which was defined as May 1 (Day 122) to September 30 (Day 274).

Field instrumentation. Surface energy fluxes were measured using a deluxe version of a BREBS (Radiation and Energy Balance Systems (REBS), Inc., Bellevue, WA), and actual crop *ET* (ET_c) was calculated using the Bowen ratio method. The BREBS was installed near the middle of the study field but away from the pivot point of the center pivot. Fetch distances were at least 200 m or more in all directions. The BREBS included sensors to measure the following variables: air temperature and relative humidity gradients, incoming and outgoing shortwave radiation, net radiation, soil heat flux, soil temperature, soil water content every 30 cm up to 1.8 m in the soil profile, barometric pressure, precipitation, and wind speed and direction. A detailed description of the instrumentation may be found in Irmak and Irmak, (2008); Irmak and Mutiibwa (2008a); and Irmak and Mutiibwa (2008b). All variables were sampled at 30-s intervals and averaged and recorded every hour for energy balance calculations using a Model CR10X datalogger and AM416 Relay Multiplexer (Campbell Scientific, Inc., Logan, UT). The BREBS was closely supervised and general maintenance was provided at least biweekly. The BREBS data were downloaded from the datalogger weekly to biweekly and carefully screened.

Combination equations for calculation of *ET*. The ASCE Standardized Reference Evapotranspiration Equation (ASCE-EWRI, 2005) was used as the ECM for calculating *ET*. Calculations were carried out as described in ASCE-EWRI (2005) for calculation of daily reference *ET* for a grass surface with the exception that the denominator constant (C_d) was modified to allow for varying the surface resistance (r_s). The (Budyko, 1956) equation as cited in (Sellers, 1965) and applied by (Lascano and van Bavel, 2007) was used as the RCM for calculating *ET*. The RCM equation we used for daily *ET* calculations has the form:

$$R_n - G - \frac{0.622\rho\lambda K}{P(r_a + r_s)}(e_s - e_a) - \frac{\rho c_p K}{r_a}(T_s - T_a) = 0 \qquad (1)$$

where R_n is net radiation (MJ m^{-2} d^{-1}), G is soil heat flux (MJ m^{-2} d^{-1}), ρ is air density (kg m^{-3}), λ is the latent heat of vaporization (MJ kg^{-1}), P is air pressure (kPa), r_a is aerodynamic resistance (s m^{-1}), r_s is surface resistance (s m^{-1}), e_s is saturation vapor pressure at the effective surface temperature (kPa), e_a is actual vapor pressure (kPa), c_p is the specific heat of moist air (MJ kg^{-1} °C^{-1}), T_s is the surface temperature (°C), T_a is the air temperature (°C), and K is a unit conversion constant for daily calculations (86,400 s d^{-1}). To make the comparison with the ECM as consistent as possible, R_n, ρ, P, and r_a were all calculated as described in ASCE-EWRI (2005) for daily calculations except that net long-wave radiation, and ρ were calculated using T_s in place of T_a. G was assumed to be zero for daily calculations, and varying levels of r_s were used. Since T_s is not known, it must be solved for by finding the root of the RCM equation. T_s was solved for using the *uniroot* function of R v. 2.8.1 (R Development Core Team, 2008). However, root finding functions from other mathematical software or iterative spreadsheet solvers could also be used to solve the RCM equation for T_s. Once a value for T_s was found, *ET* was calculated from the latent heat flux term of the RCM.

Comparisons between the ECM and RCM. The primary difference between the ECM and the RCM is in the handling of T_s. The RCM uses iteration to solve for T_s, whereas the ECM uses a linear approximation of the saturation vapor pressure vs. air temperature relationship to eliminate surface temperature from the equation, which allows for an explicit solution for *ET*. To compare the impact of this assumption, effective T_s values as solved for in Equation 1 for the RCM and calculated for the ECM using the finite difference form of the Clausius-Clapeyron equation:

$$T_s - T_a = \frac{R_d T_a^{\,2}}{0.622 \lambda e_{sa}} \left(e_s - e_{sa} \right) \tag{2}$$

where R_d is the gas constant for dry air (287 J kg^{-1} K^{-1}), and e_{sa} is the saturation vapor pressure at the air temperature (kPa) (Sellers 1965) were compared. This was done with r_s set to zero in the RCM to remove the impact of the surface resistance term on the solved for T_s. *ET* values calculated using both the ECM and RCM, with the r_s term set to zero in both terms for consistency, were then compared. While the *ET* and micrometeorological data from the grassland were chosen to approximate the reference surface used in the ASCE Standardized Reference Evapotranspiration Equation, the actual surface of the grassland would be expected to vary somewhat over the length of the growing season. The grassland where this experiment was carried out was well-maintained, had relatively uniform height, and was composed of green and actively growing grass vegetation meeting the reference surface criteria. However, given the potential variations in vegetation during the season due to grazing, *ET* was also calculated with varying levels of r_s, using both the ECM and RCM, to evaluate the impact of r_s in both equations when compared with the measured *ET* of the grassland. The performance of the ECM and RCM equations was evaluated using root mean square deviation (RMSD) and two measures recommended by ASCE (1993), which were the cumulative deviation (D_V) and the Nash-Sutcliffe efficiency (NSE).

RESULTS AND DISCUSSION

The effective surface temperature from using the ECM was always greater than the air temperature, and the temperature difference remained fairly consistent over the growing season (Figure 1). The difference between T_s and T_a using the ECM ranged from 0.1 to 3.5°C with a mean difference of 1.1°C. Conversely, T_s calculated using the RCM method was not always greater than T_a, and the difference between T_s and T_a varied over the growing season. T_s and T_a were generally very similar during the early growing season. T_s generally began to exceed T_a around July 1 and generally exceeded the T_s values calculated using the ECM from mid-July to early September. T_s values, as calculated by the RCM, then declined during the remainder of the growing season and were generally less than T_a at the end of the growing season. $T_s - T_a$ using the RCM ranged from −5.1 to 7.6°C with a mean difference of 0.5°C.

ET calculated using the ECM (ET_{os}) was always greater than that calculated using the RCM (ET_{RCM}) when r_s was set to zero in both equations (Figure 2). The

difference ranged from 0.03 to 1.1 mm d^{-1} with a mean of 0.4 mm d^{-1}. ET_{os} and ET_{RCM} were generally much greater than ET_c during the early growing season. From late July through August both ET_{os} and ET_{RCM} were generally very similar to the measured ET_c, which indicates that, during this period, r_s was minimal. During September, ET_{os} and ET_{RCM} began to diverge from ET_c again. Lascano and van Bavel (2007) found that *ET* calculated using the RCM exceeded *ET* calculated with the ECM by 1 to 4 mm d^{-1} when *ET* exceeded 9 mm d^{-1} over a 45 day period during the summer at Lubbock, Texas. However, the regression equation that they developed indicates that ECM-calculated *ET* would exceed RCM-calculated *ET* for values less than 6 mm d^{-1}. Over 75% of the measured daily *ET* values in our study were less than 6 mm d^{-1}.

The value for r_s had a substantial impact on calculated *ET* values from both equations (Figures 3 and 4). ET_{os} exceeded ET_{RCM} for equivalent values of r_s, and thus the performance of the equations for predicting ET_c varied depending on the r_s value (Table 1). The results of this study indicate that an r_s value of approximately 40 s m^{-1} for the ECM and 20 s m^{-1} for the RCM resulted in the best performance for predicting ET_c of the grassland based on the BREBS-measured ET_c data. Using these values the ECM performed slightly better than the RCM with a lesser RMSD and greater NSE, although the D_V for the RCM was slightly less than that for the ECM. The ECM-calculated values generally had less scatter about the 1:1 line when compared with the measured ET_c. The results also indicate that the 70 s m^{-1} value of r_s used in the ASCE Standardized Reference Evapotranspiration Equation for a grass reference surface was too large and resulted in underpredictions of ET_c for the studied grassland. Although conditions of the studied grassland were representative of the standard surface, differences between the grassland and the hypothetical reference conditions and variations in conditions over the growing season may explain the underpredictions using the standard value for r_s.

CONCLUSIONS

ET values calculated using explicit and recursive combination methods were compared against each other and against measured *ET* from an irrigated and well-maintained grassland. The methods differ in their handling of the effective surface temperature, and while T_s was consistently greater than T_a for the ECM, T_s calculated from the RCM showed more variation over the growing season. In this study, *ET* calculated with the ECM exceeded *ET* calculated with the RCM for equivalent values of the surface resistance. The results indicated that an r_s of 40 s m^{-1} for the ECM and 20 s m^{-1} for the RCM resulted in the best predictive performance for estimating ET_c of the irrigated grassland. Using these values, the ECM method based on the ASCE Standardized Reference Evapotranspiration Equation performed slightly better than the RCM and exhibited less scatter. However, both methods performed extremely well, and the overall predicted *ET* for the growing season was within 1% of the overall measured ET_c using both methods. While the RCM may offer the potential of increased accuracy in situations where there are large differences between T_s and T_a, these results indicate that under the conditions of this study the ASCE equation was more accurate. However, both methods were sensitive to value chosen for r_s.

REFERENCES

ASCE. (1993). "Criteria for evaluation of watershed models." *J. Irrig. Drain. Eng.*, 119(3), 429-442.

ASCE-EWRI. (2005). *The ASCE Reference Evapotranspiration Equation*. (R. G. Allen, I. A. Walter, R. L. Elliott, T. A. Howell, D. Itenfisu, M. E. Jensen, and R. L. Snyder, eds.), ASCE, Reston, Virginia.

Budyko, M. I. (1956). *Teplovoi Balans Zemnoi Poverkhnosti*. Gidrometeorologicheskoe Izdatel'skoe, Leningrad. (English transl.: Stepanova, N. A. 1958. *The Heat Balance of the Earth's Surface*. Office of Technical Services, U.S. Dept. of Commerce, Washington).

Irmak, A., and Irmak, S. (2008). "Reference and crop evapotranspiration in south central Nebraska: II. Measurement and estimation of actual evapotranspiration for corn." *J. Irrig. Drain. Eng.*, 134(6), 690-699.

Irmak, S., and D. Mutiibwa. (2008a). Dynamics of photosynthetic photon flux density and light extinction coefficient for assessing radiant energy interactions for maize canopy. *T. ASABE,* 51(5), 1663-1673.

Irmak, S., and D. Mutiibwa. (2008b). On the dynamics of evaporative losses from Penman-Monteith with fixed and variable canopy resistance during partial and complete canopy. *T. ASABE*, (In review).

Lascano, R. J., and van Bavel, C. H. M. (2007). "Explicit and Recursive Calculation of Potential and Actual Evapotranspiration." *Agron. J.*, 99(2), 585-590.

Penman, H. L. (1948). "Natural Evaporation from Open Water, Bare Soil and Grass." *P. Roy. Soc. Lond. Ser.-A* 193(1032), 120-145.

R Development Core Team. (2008). *R: A Language and Environment for Statistical Computing*. R Foundation for Statistical Computing, Vienna, Austria.

Sellers, W. D. (1965). *Physical Climatology*. University of Chicago Press, Chicago.

Table 1. Performance statistics for *ET* estimates from the ASCE Standardized Reference Evapotranspiration Equation (ECM) and the recursive combination method (RCM) with varying levels of the surface resistance term (r_s) as compared to BREBS-measured ET_c. Included statistics are the root mean square deviation (RMSD), cumulative deviation (D_V), and the Nash-Sutcliffe efficiency (NSE).

	ECM			RCM		
r_s (s m^{-1})	RMSD (mm d^{-1})	D_v (%)	NSE	RMSD (mm d^{-1})	D_v (%)	NSE
0	1.32	-18.99	0.17	1.04	-10.28	0.49
20	0.87	-9.12	0.64	0.72	-0.88	0.75
40	0.64	-0.98	0.81	0.69	6.64	0.77
60	0.63	5.89	0.81	0.84	12.85	0.67
70	0.70	8.95	0.77	0.93	15.59	0.59
80	0.78	11.8	0.71	1.03	18.13	0.50
100	0.97	16.95	0.56	1.22	22.68	0.29

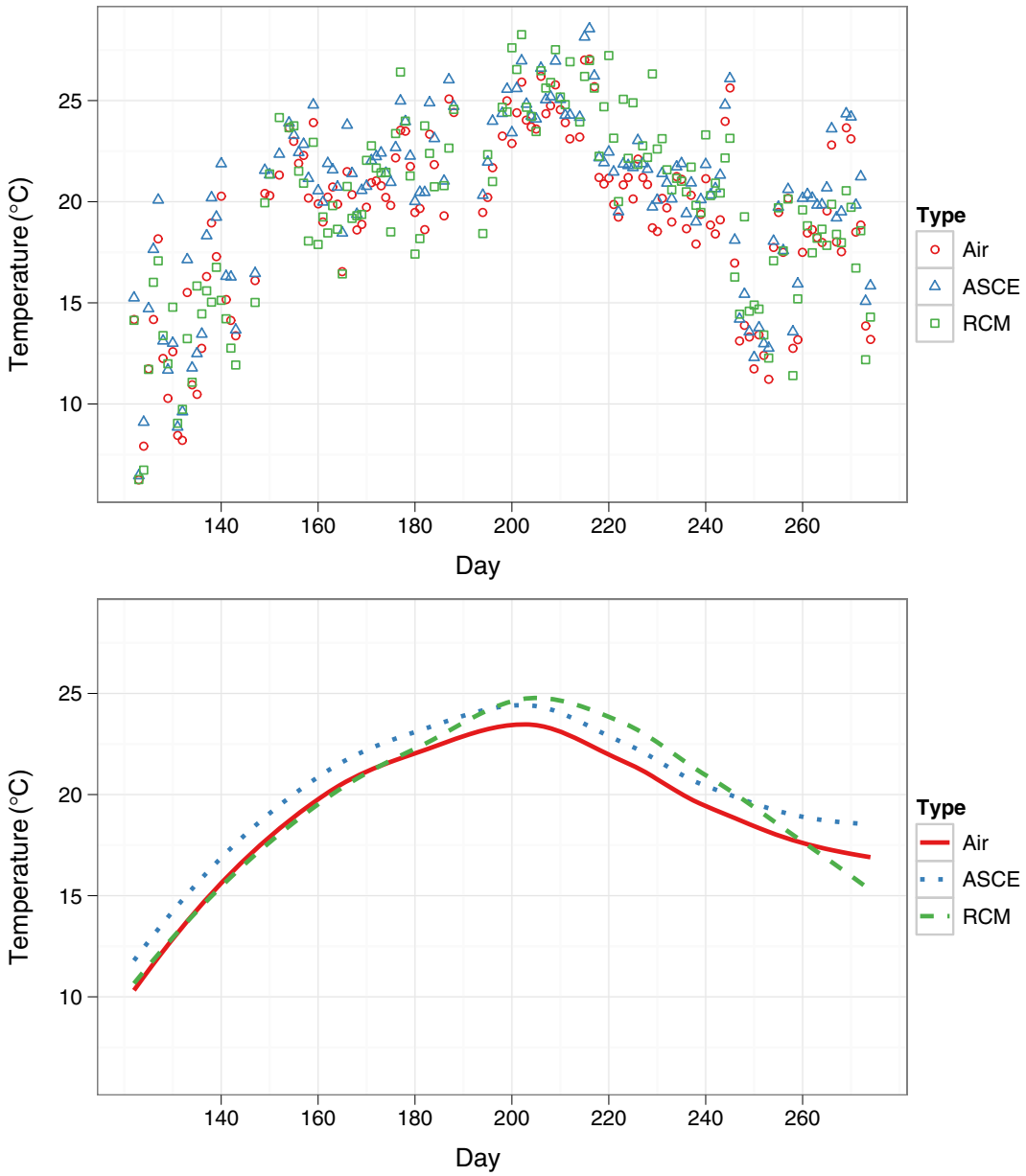

Figure 1. Effective surface temperatures from the ASCE Standardized Reference Evapotranspiration Equation (ASCE) and the recursive combination method (RCM) and measured air temperatures (Air). Actual data points are shown in the top plot and locally estimated (LOESS) regression lines are shown in the bottom plot.

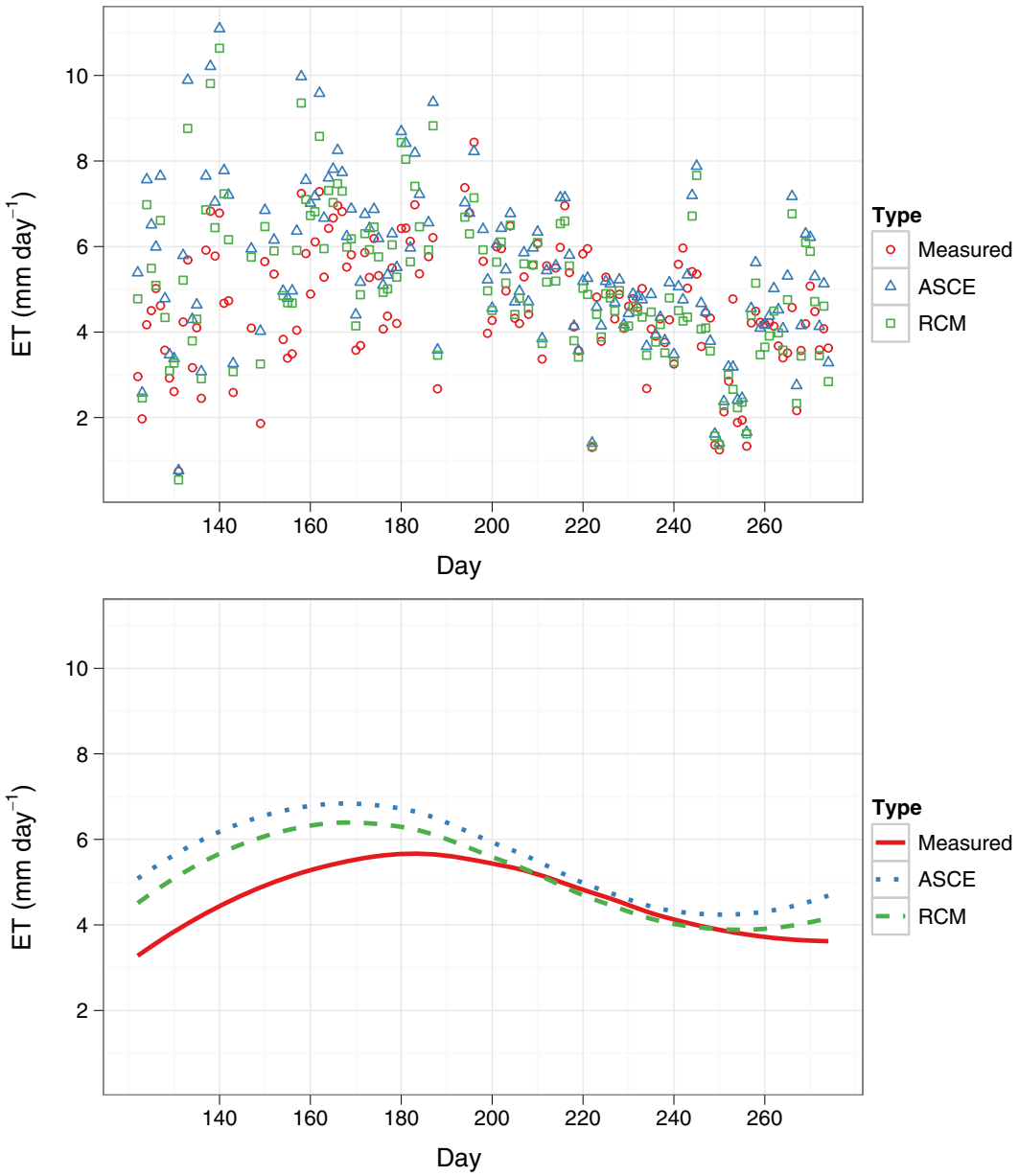

Figure 2. *ET* calculated using the ASCE Standardized Reference Evapotranspiration Equation (ASCE) and the recursive combination method (RCM) and BREBS-measured ET_c (Measured). The surface resistance (r_s) was set to zero in both equations. Actual data points are shown in the top plot and locally estimated (LOESS) regression lines are shown in the bottom plot.

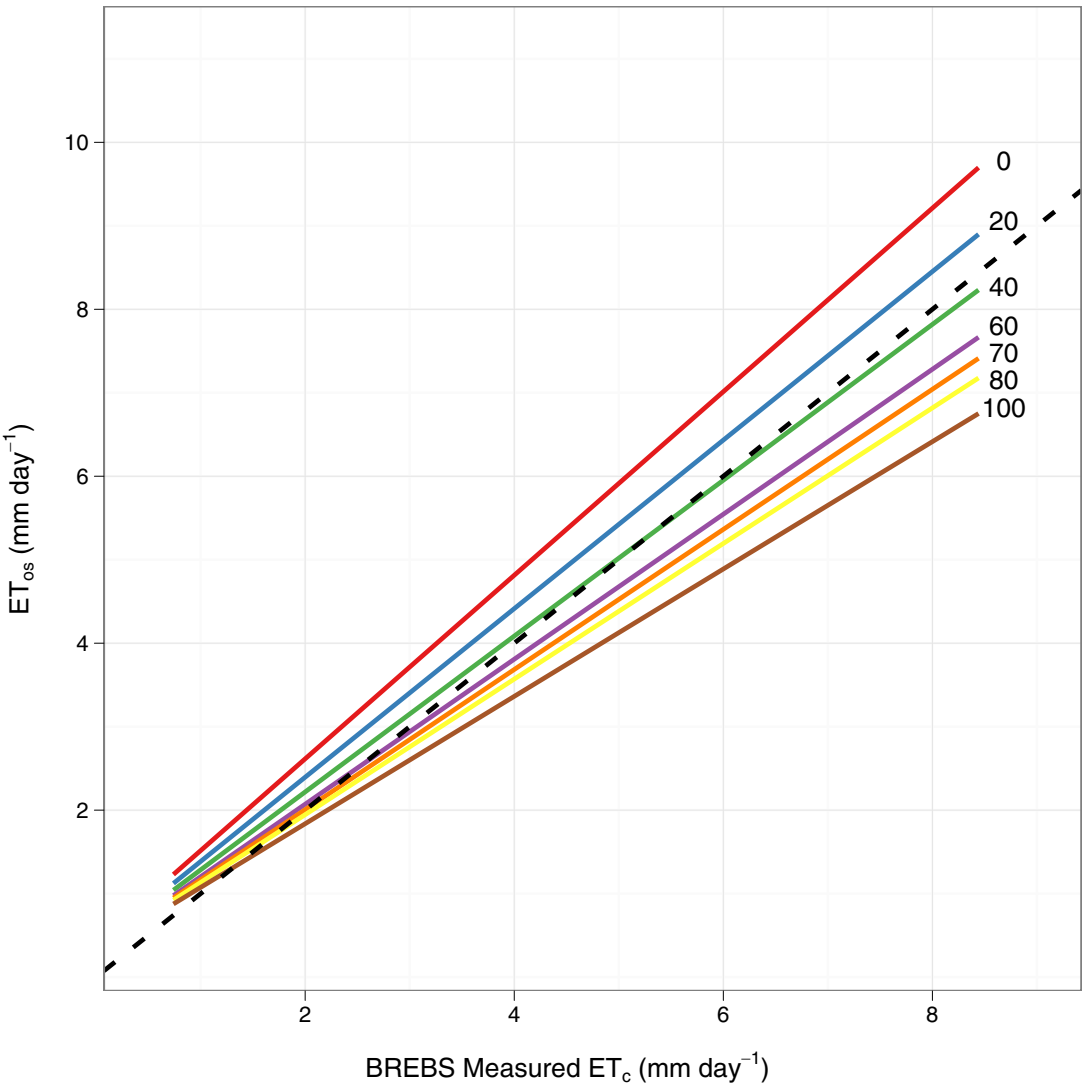

Figure 3. Linear regression lines of reference *ET* calculated using the ASCE Standardized Reference Evapotranspiration Equation (ET_{os}) versus the BREBS-measured ET_c with varying levels (0, 20, 40, 60, 70, 80, 100 s m^{-1}) of the surface resistance (r_s). The dashed line represents a 1:1 line.

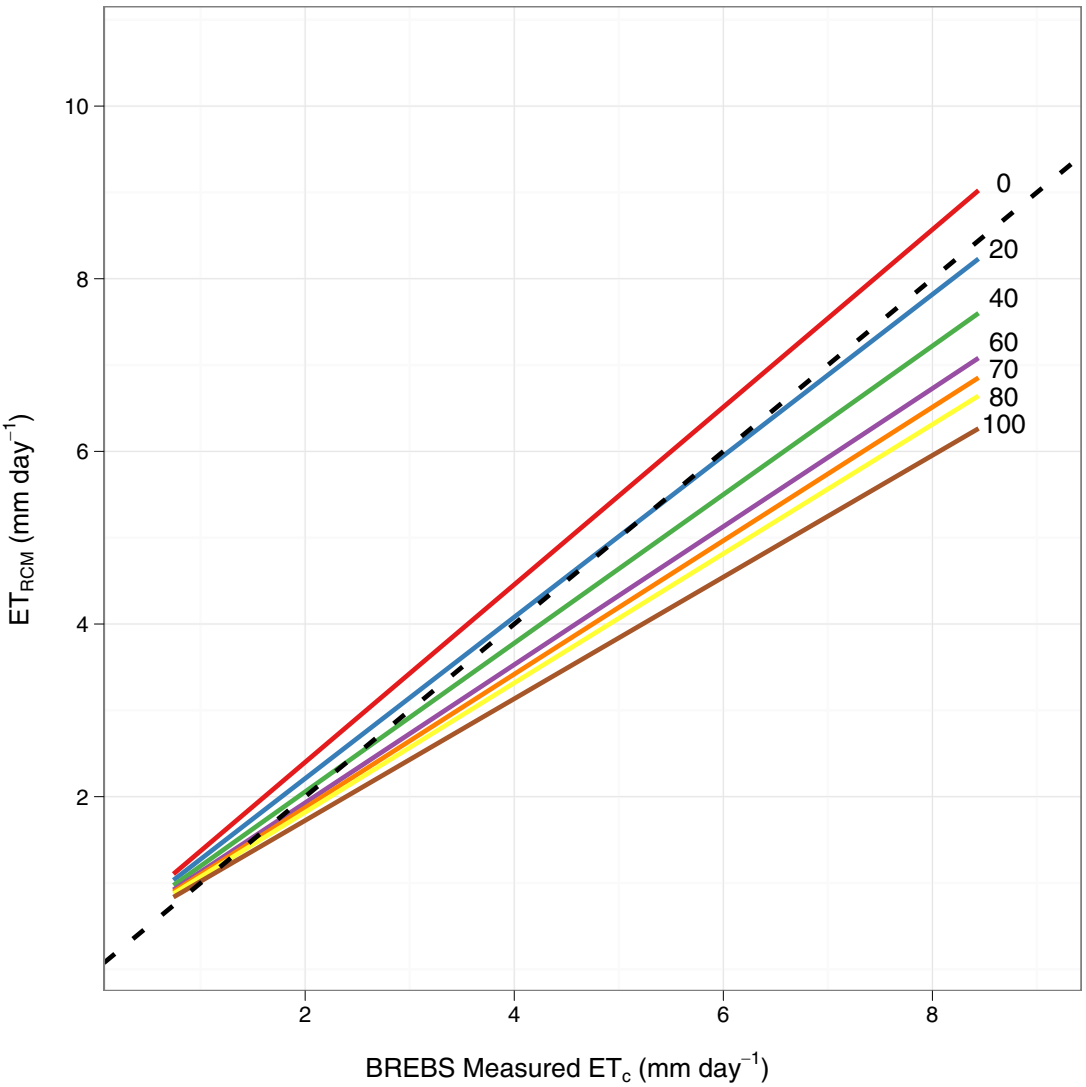

Figure 4. Linear regression lines of *ET* calculated using the recursive combination method of Budyko (1956) (ET_{RCM}) versus the BREBS-measured ET_c with varying levels (0, 20, 40, 60, 70, 80, 100 s m^{-1}) of the surface resistance (r_s). The dashed line represents a 1:1 line..

Some results of evapotranspiration measured by three weighing lysimeters in La Mancha, Spain.

López-Urrea, R[1]*., Montoro, A[1]., López-Fuster, P[1]., Martín de Santa Olalla, F[2].

[1]Instituto Técnico Agronómico Provincial, c/Gregorio Arcos s/n, PO Box 451, 02080, Albacete, Spain. *Corresponding author: E-mail address: rlu.itap@dipualba.es.
[2]University of Castilla-La Mancha. Campus Universitario s/n, E-02071, Albacete, Spain.

ABSTRACT

In semiarid environments with a shortage of water resources and a risk of overexplotation, it is essential to improve the accuracy of the estimation of crop water requirements to reduce water use and increase water productivity. For this reason, in 1999 three weighing lysimeters were installed in the experimental farm "Las Tiesas" located in Albacete (Central Spain). The facility has a lysimeter for measuring the grass reference evapotranspiration (ET_o), a second for rotating annual crops and third installed in a perennial vineyard for measuring grape water use. Each of lysimeter is surrounded by a one hectare square buffer plot planted to the lysimeter crop. The lysimeters are weighed with a balance beam and load cell configuration, with most of the weight being eliminated using counterweight. The overall resolution of the systems are 250 g or 0.04 mm of water. The measurement frequency is one second, and a reading is registered by a datalogger every 15 min. During the period 2002-2003 the FAO-56 Penman-Monteith (FAO-56 PM) and the ASCE "standardized" version of Penman-Monteith (ASCE PM) hourly equations were evaluated by comparing them with reference lysimeter measurements. In 2003 we measured the water use (ETc) of broccoli as a double crop. Records of grapevine ET were collected from 2002 to 2008 and detailed canopy development information was obtained from 2004 to 2008 growing seasons. In this paper, we present results of grapevine ET measured by a weighing lysimeter during 2008 growing season.

INTRODUCTION

The use of groundwater to supply large surfaces of irrigated land has been the key to agricultural development in a large number of countries over the past few years. In arid and semiarid areas, irrigation using groundwater has transformed good quality land with low productivity (due to drought) into areas of high productivity. Consequently, the income level of the farmers has increased and the rural population base has been maintained (Martín de Santa Olalla et al., 2003). This groundwater use must be sustainable, balancing the extractions with the recharge of the aquifer. Overexploitation of the system has often been practiced in the past, leading to serious environmental damage and contributing to the desertification process (Martín de Santa Olalla and de Juan, 2001).

In the Albacete province (Central Spain) water for irrigation and urban water supplies are still nearly exclusively from groundwater, although the implementation of the new state Water Plans provide for the substitution of some of this pumping by regulated surface water, which will allow a more rational and sustainable exploitation of the system (Montoro et al., 2002).

The semiarid climate of the south central plateau of Spain has limited water resources and recent irrigation development, primarily for maize production, is threatening the groundwater resource. Martín de Santa Olalla et al. (2003) have reported a decline in the water table of the aquifer 08.29 Mancha Oriental, and the problem seems to be increasing. This aquifer is located south-east of the Iberian peninsula, on the eastern side of the La Mancha plains, with a total surface area of 8,500 km^2. The aquifer supplies water to around 115,000 ha of irrigated lands provided with modern irrigation technology. The aquifer also supplies domestic and industrial water for a population of over 275,000. The annual water withdrawal for these purposes is about 500 hm^3 (Montoro, 2008).

In this situation, with a shortage of water resources and a risk of overexplotation, it is essential to improve accuracy in the estimation of crop water requirements to reduce water use and increase water productivity. For this reason, in 1999 three weighing lysimeters were installed in the experimental farm "Las Tiesas" located in Albacete (Central Spain). The facility has a lysimeter for measuring the grass reference evapotranspiration (ET_o), a second for rotating annual crops and third installed in a perennial vineyard.

Initially we conduced two studies to evaluate different equations to calculate daily and hourly ET_o using the measurements obtained by the reference lysimeter. In this research works, the FAO-56 Penman-Monteith method was the most accurate for calculating daily and hourly ET_o (López-Urrea et al., 2006a,b). During the period from 1999 to 2008 the annual crop lysimeter has been used to measure the water requirements of different agronomic crops (maize, sugar beet, barley, broccoli, sweet corn, canola, sorghum, etc.) (López-Urrea et al., 2004, 2006c, 2007, 2008). During the 2002 to 2008 growing seasons the water use of two grapevines (*Vitis vinifera* L. cv. Tempranillo) has been measured with the vineyard lysimeter (Montoro et al., 2008). In this paper, we present some results obtained by this lysimeter facility.

MATERIALS AND METHODS.

These studies were carried out during the period from 1999 to 2008 in the "Las Tiesas" farm, located near Albacete (Central Spain). Its geographical coordinates are: longitude 2º 5' 10" West, latitude 39º 14' 30" North, and its altitude is 695 m above sea level. The climate is semiarid, continental with 320 mm of annual rainfall, mostly concentrated in the spring and fall. Average mean, maximum and minimum temperatures are: 13.7, 24.0 and 4.5 ºC, respectively. For a more detailed description of the climate of the area see López-Urrea et al. (2006a).

The soil is classified as Petrocalcic Calcixerepts (Soil Survey Staff, 2006). Average soil depth of the experimental plot is 40 cm, and is limited by the development of a more or less fragmented petrocalcic horizon. Texture is silty-clay-loam, with 13.4% sand, 48.9% silt and 37.7% clay, with a basic pH. The soil is low in organic matter and in nitrogen, and has a high content of active limestone and potassium.

The reference lysimeter was used during the 2002 and 2003 growing season to evaluate the FAO-56 Penman-Monteith (FAO-56 PM) and the American Society of Civil Engineers version of Penman-Monteith (ASCE PM) equations to estimate hourly ET_o values in the semiarid environment of Albacete (Spain). The lysimeter was installed in the centre of a 10,000 m^2 grassy plot (*Festuca arundinacea* Schreb., cv. "Asterix") maintained in optimum growth conditions for the purpose of measuring reference evapotranspiration values (ET_o). An agro-meteorological station was installed next to

this lysimeter, which had the necessary sensors to record the meteorological data required for calculating ET_o.

To measure the ET_o, we used a weighing lysimeter with continuous electronic data recording (López-Urrea et al., 2006a). The ET_o values were calculated from hourly mass loss minus drainage loss and the mass added from irrigations and/or rainfall. The lysimeter is located in the center of a 100 x 100 m plot, where grass was sown in September, 1998. The whole plot has a permanent sprinkler irrigation system with sprinklers placed on a grid of 15 x 12.5 m that provide a precipitation rate of 8.6 mm h^{-1}. The lysimeter container is 2.7 m long, 2.3 m wide and 1.7 m deep, with an approximate total weight of 14.5 Mg. Efforts were made to keep the crop inside the lysimeter at the same growth rate and plant population as the crop outside to minimize edge effects. Two time domain reflectometry (TDR) soil moisture sensors (model CS615, Campbell Scientific Ltd., Leicestershire, UK) were installed in the lysimeter at the 0.30 and 0.60 cm depths for measurement of soil water content, and two soil temperature probes (model 107, Campbell Scientific Ltd., Leicestershire, UK) were placed at the 0.15 and 0.30 m depths. The lysimeter soil-containing tank sits on a system of scales and a counterweight that offset the dead weight of the soil and the tank. The de-multiplication factor of the system is 1000:1. A steel load cell (model SB2, Epelsa Ind., S.L.) is connected to the system of balances. The system allows measurement of ET_o in the lysimeter with a resolution of 0.04 mm water depth. Additional information about the technical features of the lysimeter may be found in Lopez-Urrea et al. (2006a). The lysimeter readings were checked daily to identify individual readings that could not be explained by natural processes of water input and loss. Data losses sometimes occurred during irrigation and precipitation events and during weight and calibration verifications.

The FAO-56 PM reference equation (hourly time step) evaluated was:

$$ET_o = \frac{0.408\Delta\left(Rn - G\right) + \gamma \frac{37}{T_{hr} + 273} U_2 \left(e^o\left(T_{hr}\right) - e_a\right)}{\Delta + \gamma\left(1 + 0.34U_2\right)}$$

where ET_o is the reference evapotranspiration (mm h^{-1}); Δ is the saturation slope vapour pressure curve at T_{hr} (kPa $ºC^{-1}$); Rn is net radiation at the grass surface (MJ m^{-2} h^{-1}); G is soil heat flux density (MJ m^{-2} h^{-1}); γ is the psychrometric constant (kPa $ºC^{-1}$); T_{hr} is the mean hourly air temperature (ºC); U_2 is the average hourly wind speed (m s^{-1}); $e_o(T_{hr})$ is the saturation vapour pressure at T_{hr} (kPa); and e_a is the average hourly actual vapour pressure (kPa).

The actual vapour pressure (e_a) is determined as:

$$e_a = e^o\left(T_{hr}\right)\frac{RH_{hr}}{100}$$

where RH_{hr} is the average hourly relative humidity (%). The saturation vapour pressure at T_{hr} ($e_o(T_{hr})$) is calculated from:

$$e^o\left((T_{hr}\right) = 0.6108\exp\left[\frac{17.27T_{hr}}{T_{hr} + 237.3}\right]$$

The ASCE PM equation for hourly time steps is expressed as (Walter et al., 2000; Temesgen et al., 2005):

$$ET_o = \frac{0.408\Delta(Rn - G) + \gamma \frac{37}{T_{hr} + 273} U_2 \left(e^o(T_{hr}) - e_a\right)}{\Delta + \gamma\left(1 + C_d U_2\right)}$$

The constant C_d in the denominator is a function of the time step representing bulk surface (r_s) and aerodynamic resistance (r_a), and varies with reference type and time of day. For hourly time steps, the ASCE PM equation has a C_d value of 0.24 during the daytime period (Rn > 0) and 0.96 during the nighttime period (Rn $\leqslant$ 0). All other terms and units are the same as for the FAO-56 PM equation.

Several comparisons were obtained through the simple linear regression analysis technique (Box et al., 1989) and a set of statistics proposed by Willmott (1982): the root mean square error (RMSE) and the index of agreement (d). The RMSE was calculated as:

$$RMSE = \left[N^{-1} \sum_{i=1}^{N} (Pi - Oi)^2 \right]^{0.5}$$

where N is the number of observations, Pi are estimated ET_o values, and Oi are observed ET_o values.

The index of agreement was computed as:

$$d = 1 - \left[\sum_{i=1}^{N} (Pi - Oi)^2 / \sum_{i=1}^{N} \left(|Pi - Oavg| + |Oi - Oavg| \right)^2 \right] \quad 0 \leq d \leq 1$$

Perfect agreement would exist between P and O if d = 1.

To determine actual broccoli ET, we used a weighing lysimeter with continuous electronic data recording. The ETc values were calculated from daily mass loss minus drainage loss and the mass added from irrigations and/or rainfall. The lysimeter is located in the center of a 100 x 100 m plot, where broccoli was transplanted on 4 August, 2003. Plant rows were 0.7 m apart with plants 0.25 m apart within the row. The lysimeter used for rotating annual crops has the similar characteristics as the reference lysimeter.

The 1 ha (100 x 100 m) vineyard was planted in 1999 with Vitis vinifera L. cv. 'Tempranillo' grafted to 110 Richter rootstock at a vine and row spacing of 1.5 and 3 m, respectively (4.5 m^2 per vine). During dormancy, grapevines were pruned to two, 10-node, fruiting canes. The trellis consisted of 1.7 m long aluminium posts driven 0.4 m into the soil and separated 6 m in the row with four vertical wires. The basal wire at 0.4 m above the soil supported the irrigation lateral, the next wire at 0.8 m above the soil supported the fruiting canes, and two more wires at 1.1 and 1.3 m above the soil supported the canopy. Vines were drip-irrigated with 3.5 L h^{-1} emitters spaced every one meter.

Water use of two grapevines was measured with a monolithic weighing lysimeter installed in the centre of the plot. The lysimeter dimensions were 3 x 3 m and 1.7 m deep and the total mass exceeded 18.5 Mg. The lysimeter was weighed with a balance beam and load cell configuration, with most of the weight being eliminated using counterweight. The overall resolution of the system was 250 g or 0.04 mm of

water. The sample frequency was 1 s, and a reading was registered by a datalogger (CR10X, Campbell Scientific Ltd., Logan, Utah, USA) every 15 min.

Two vines were planted in the lysimeter, each one occupying 4.5 m^2, the same as the vines in the rest of the plot. The vines were 1.5 m apart and 0.75 m from either end of the 3 m long lysimeter and 1.5 m from the sides of the lysimeter. The trellis for the vines in the lysimeter was self-contained and not attached to the trellis system used in the rest of the row, to ensure that it was part of the lysimeter mass.

The lysimeter's daily mass change was used to determine ETc. Irrigation (five hours) was always at night commencing at 2100 h and on irrigation days ETc was calculated omitting values during the irrigation period. No drainage was recorded during the study period. The data were downloaded daily for processing.

The ET_o and ETc were used to establish Kc for the grapevines in the lysimeter as a function of age and developmental stage. The Kc reported for 2008 was calculated with the ET_o values using the Penman-Monteith equation.

RESULTS AND DISCUSSION

Hourly reference evapotranspiration equations

Figure 1 presents the regression analysis of hourly values calculated from grass lysimeter measurements. This comparison was conducted from 696 observations from both years that the experimental work was carried out.

The hourly FAO-56 PM equation (Fig 1(a)) performs very well compared to lysimeter measurements. The slope of the straight line is very close to one, and neither overestimations nor underestimations are produced in the range of the values studied. These results differed from those obtained by Howell et al. (2000) who compared FAO-56 PM ET_o against lysimeter ET_o in Bushland, Texas, and observed tendencies in the FAO-56 PM equation to overestimate ET_o for low rates and to underestimate ET_o for high rates.

Figure 1b shows comparison of the hourly lysimeter ET_o values and ET_o calculated by the Standardized PM method. The data agree fairly well up to 0.45 mm h^{-1}, which indicates the good performance of this method for that range of values. However, above 0.45 mm h^{-1}, calculated values slightly overestimate lysimeter measurements.

Table 1 shows the results of this comparison, through simple regression analysis, between lysimeter measurements and the values calculated by both methods, and indicates the calculation of error and the index of agreement. Calculated reference valuaes were taken as dependent variables while the measurements made in the lysimeter, as the independent variable. The hourly FAO-56 PM equation showed very good performance when compared to values measured in the lysimeter. This method, with a RMSE of 0.0796 mm h^{-1} and a 0.9725 index of agreement, neither underestimates nor overestimates lysimetric measurements. These results are even better than in previous papers from the same area, where a comparison was made between daily measured and calculated ET_o values (López-Urrea, 2004; López-Urrea et al., 2006a).

The ASCE PM equation also performed well compared with lysimetric measurements, but produces a small overestimation (4%) with a RMSE of 0.0878 mm h^{-1} and a 0.9683 index of agreement. These results are slightly different from those obtained in a previous paper from Córdoba, Spain (Berenjena and Gavilán, 2005). In that paper hourly FAO-56 and ASCE PM equations were also evaluated and compared with weighing lysimeter data. Hourly ET_o values calculated by the ASCE PM equation underestimated lysimetric measurements by 2%, and had a RMSE of 0.032 mm h^{-1} and

a 0.997 index of agreement, while the FAO-56 PM method underestimated them by 3%, with a RMSE of 0.047 mm h^{-1} and a 0.993 index of agreement.

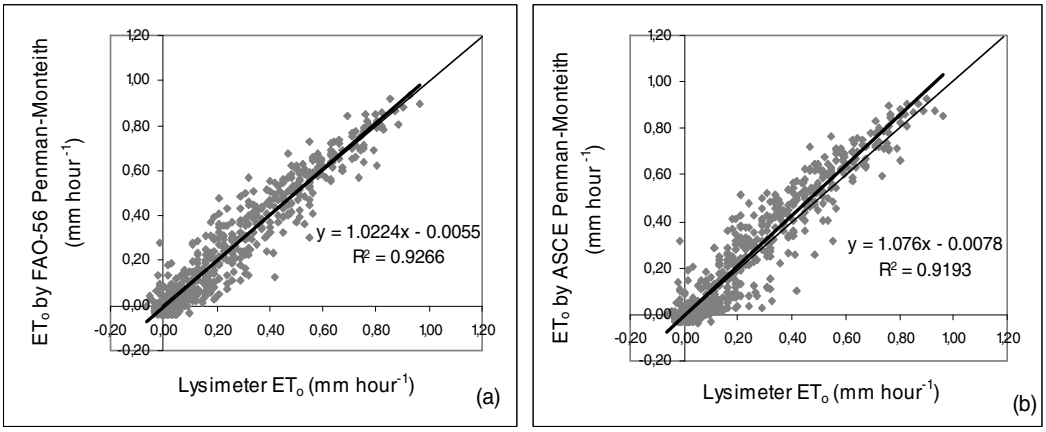

Figure 1. Hourly reference evapotranspiration comparison between the lysimeter and the FAO-56 (a) and ASCE Penman-Monteith (b) equations (hourly time step) during 13 days in 2002 and 16 days in 2003 (April-October).

Table 1. Lysimetric evaluation of hourly FAO-56 and ASCE Penman-Monteith equations.

Calculation method	N	Oavg (mm hour^{-1})	Pavg (mm hour^{-1})	Pavg/Oavg (%)	A (mm h^{-1})	B	R^2	RMSE (mm hour^{-1})	d
					ET_o(estimated) = A + B*ET_o(Lysimeter)				
FAO-56 Penman-Monteith	696	0.2033	0.2023	100	-0,0055	1.022	0.9266	0.0796	0.9725
ASCE Penman-Monteith	696	0.2033	0.2109	104	-0,0078	1.076	0.9193	0.0878	0.9683

N: observation number; Oavg: average of values measured in the lysimeter; Pavg: average of the values estimated by FAO-56 and ASCE Penman-Monteith (hourly time step); A: intercept; B: regression coefficient (slope); R^2: determination coefficient; RMSE: root mean square error; d: index of agreement. Values for A, B and R^2 were highly significant (P<0.01) in all cases.

Evapotranspiration and crop coefficient of broccoli

Figure 2 presents the daily broccoli ET data as well as the water input from irrigation and rainfall. Following transplanting, ETc was high due to daily applications of water, but then it decreased to low values around 15 August. ETc rose very rapidly after that date due to the fast canopy growth, facilitated by the favourable summer temperatures. Peak ETc was reached around 10 September and then declined following the general decrease in evaporative demand as the season advanced.

Figure 3 presents the Kc data, calculated as the ratio of the lysimeter measured ET and the ET_o, calculated with the FAO-56 PM equation. Previous lysimeter studies at the same location have reported a reasonably good performance of this equation (López-Urrea et al., 2006a). The minimum (0.39) and the maximum (1.31) Kc values were observed during the crop establishment stage and in the head emergence period, respectively. Because of the influence on ETc of the frequent surface wetting by irrigation, the Kc values are reported as 5-day averages which were fitted to a second degree polynomial function (Figure 3).

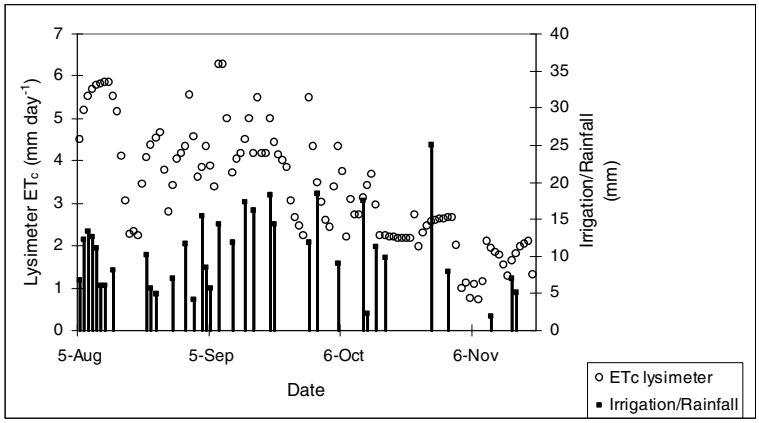

Figure 2. Daily evapotranspiration values measured in the lysimeter. Irrigation and rainfall during the experimental period is indicated with vertical bars.

The Kc curve fitted to the measured data does not follow the conventional shape of the crop coefficient curve recommended for broccoli (Figure 3). For the case of late summer plantings, the initial Kc results from the frequent watering following transplanting under the high seasonal ET_o conditions (Figure 3). Subsequently, the Kc drops and then increases again, reaching maximum values at commercial harvest, without the decline in Kc recommended in Allen et al. (1998) (also shown in Figure 3). In a recent paper, El-Shikha et al. (2007) used Kc values very similar to those in Allen et al. (1998) to compute broccoli ET in a remote sensing study of late fall plantings and spring harvest in Arizona. The slower Kc increase in the crop development phase of the data reported in Figure 3 compared to Allen et al. (1998) recommendations, reflects the sub-optimal autumn temperatures for broccoli canopy development. At any rate, the Kc measured values do not fit well the linear or even the curvilinear model, as there are significant fluctuations above and below the fitted lines (Figure 3).

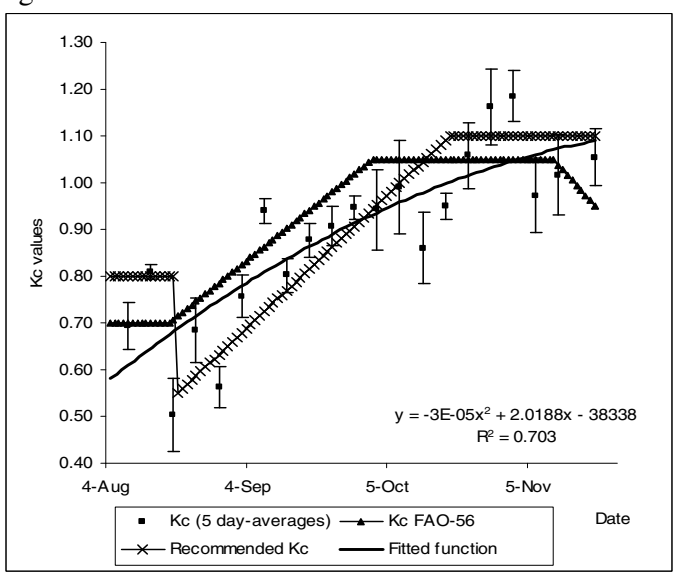

Figure 3. Crop coefficient curves: a) Recommended in Allen et al., (1998; triangles), b) recommended for fall plantings based on the data measured in the lysimeter (x). Squares indicate 5-day averages of measured values with the curve fitted. Bars indicate the standard error.

Evapotranspiration and crop coefficient of grapevine

The temporal variation in grapevine water use (ETc) during 2008 is shown in Figure 4. The observed values of daily ETc were similar to those measured by other authors (Lascano et al., 1992; Trambouze and Voltz, 2001). In 2008 maximum ETc occurred in August with 3.65 mm day^{-1} (Table 2).

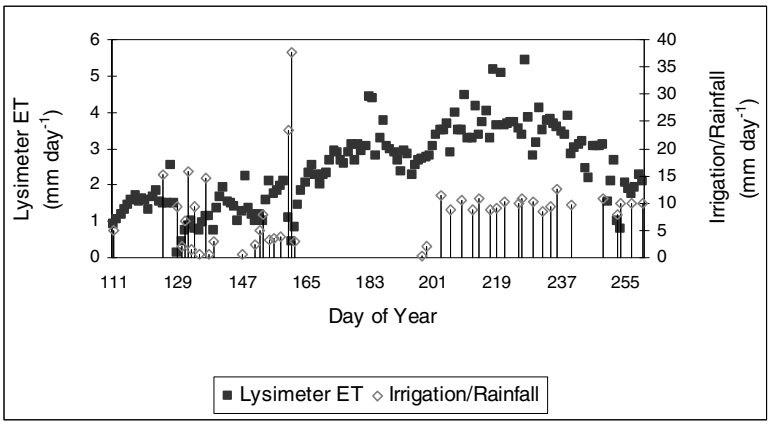

Figure 4. Daily evapotranspiration values measured in the vineyard lysimeter . Irrigation and rainfall during the experimental period is also indicated with vertical bars.

Monthly Kc values are shown in Table 2. The Kc values observed here are smaller than those found for Vitis vinifera cv. Thompson Seedless (Williams et al., 2003a, 2003b) but very similar to those reported for Vitis vinifera cv. Sultana (Yunusa et al., 2004).

Table 2. Irrigation, rainfall, reference evapotranspiration (ET_o), grapevine water use (ETc), and crop coefficient (Kc) in 2008.

2008						
	Irrigation and	ETo (mm)		ETc (mm)		
Month	rainfall (mm)	daily	monthly	daily	monthly	Kc
May	86	4.01	124	1.27	39	0.31
June	82	5.59	168	2.18	65	0.39
July	42	7.17	222	3.23	100	0.45
August	110	6.63	206	3.65	113	0.55
September	49	5.00	80	2.16	35	0.44
Total	369		800		352	

CONCLUSIONS

In a semiarid climate such as in this work area, the hourly FAO-56 and ASCE PM equations showed very good performance when compared to lysimetric measurements. In cold, semiarid environments, it is possible to take advantage of the late summer season and early fall for the production of vegetables, for which there is often a niche market. Our results for Central Spain showed that lysimeter ET for fall-grown broccoli amounted to 360 mm. The seasonal water use of the grapevines was 44% of ET_o in 2008, when the vines were nine years old. The experimental work

carried out during the period from 1999 to 2008 at the lysimeter station improve the accuracy in the estimation of crop water requirements.

ACKNOWLEDGEMENTS

We acknowledge the financial support of two projects: REN. 2001/0784/HID, funded by the Inter-Ministerial Commission for Science and Technology (CICYT), MEC, Spain and RTA2005-00038-C06-02 funded by INIA, Spain. The authors gratefully acknowledge to Thomas Trout the revision of this manuscript.

REFERENCES

Allen, R.G., Pereira, L.S., Raes, D., and Smith, M. (1998). "Crop evapotranspiration. Guidelines for computing crop water requirements." *FAO Irrigation and Drainage, paper nº. 56*, FAO, Rome.

Berengena, J., and Gavilán, P. (2005). "Reference evapotranspiration estimation in a highly advective semiarid environment." *J. Irrig. and Drain. Eng.,* ASCE 131(2), 147-163.

Box, G.E.P., Hunter, W.G., and Hunter, J.S. (1989). "Estadística para investigadores." Reverte, Barcelona, 675 pp.

El-Shikha, D.M., Walter, P., Hunsaker, D., Clarke, T., and Barnes, E. (2007). "Ground-based remote sensing for assessing water and nitrogen status of broccoli." *Agric. Water Manage.*, 92, 183-193.

Howell, T.A., Evett, S.R., Schneider, A.D., Dusek, D.A., and Copeland, K.S. (2000). "Irrigated fescue grass ET compared with calculated reference grass ET." *Proc., 4th National Irrigation Symposium*, ASAE, Phoenix, 228-242.

Lascano, R.J., Baumhardt, R.L., and Lipe, W.N. (1992). "Measurement of water flow in young grapevines using the stem heat balance method." *Am. J. Enol. Vitic.*, 43, 159-165.

López Urrea, R., Montoro Rodríguez, A., and López Fuster, P. (2004). "Seguimiento integral de las necesidades hídricas de la remolacha azucarera (*Beta vulgaris* L.) a través de ensayos de riego deficitario controlado, eficiencia en el uso del agua y medidas lisimétricas, en clima semiárido*." Actas XXII Congreso Nacional de Riegos*, Logroño, Spain.

López Urrea, R., Montoro Rodríguez, A., and López Fuster, P. (2006c). "Estudio de las necesidades hídricas de la cebada (*Hordeum vulgare* L.) cultivada en un clima semiárido." *Actas XXIV Congreso Nacional de Riegos*, Lugo, Spain.

López Urrea, R., Montoro Rodríguez, A., Martínez Molina, L., Martín de Santa Olalla, F., and López Fuster, P. (2008). "Medida de las necesidades hídricas (o evapotranspiración) del maíz dulce utilizando un lisímetro de pesada." *Actas XXVI Congreso Nacional de Riegos,* Huesca, Spain.

López Urrea, R., Montoro, A., Moratalla, A., and López Fuster, P. (2007). "Medida de la Evapotranspiración del Bróculi mediante Lisimetría de Pesada Cultivado en La Mancha Oriental." *Actas XI Congreso Nacional de Ciencias Hortícolas*, SECH, Albacete, Spain.

López-Urrea, R. (2004). "Evapotranspiración de referencia: métodos de cálculo y de medición directa en una estación lisimétrica en ambientes semiáridos." *Ph. D. Thesis,* Castilla-La Mancha University, Spain.

López-Urrea, R., Martín de Santa Olalla, F., Fabeiro, C., and Moratalla, A. (2006a). "Testing evapotranspiration equations using lysimeter observations in a semiarid climate." *Agric. Water Manage.,* 85, 15-26.

López-Urrea, R., Martín de Santa Olalla, F., Fabeiro, C., and Moratalla, A. (2006b). "An evaluation of two hourly reference evapotranspiration equations for semiarid conditions." *Agric. Water Manage.,* 86, 277-282.

Martín de Santa Olalla, F.J., and de Juan, A. (2001). "El uso del agua en una agricultura sostenible." In: F. Martín de Santa Olalla (Editor), *Agricultura y Desertificación*, Mundi-Prensa, Madrid, pp. 273-303.

Martín de Santa Olalla, F.J., Calera, A., and Domínguez, A. (2003). "Monitoring irrigation water use by combining Irrigation Advisory Service, and remote sensed data with a geographic information system." *Agric. Water Manage*., 61, 111-124.

Montoro, A. (2008). "Avances en el manejo del agua en la agricultura de riego." *Ph.D. Thesis,* University of Castilla-La Mancha, Spain.

Montoro, A., López Córcoles, H. and López Fuster, P. (2002). "An advisory service for irrigation in the plains of La Mancha, Spain." *Workshop: Irrigation advisory services and participatory extension in irrigation management*, FAO-ICID. Montreal, Canada.

Montoro, A., López-Urrea, R., Mañas, F., López Fuster, P., and Federes, E. (2008). "Evapotranspiration of grapevines measured by a weighing lysimeter in La Mancha, Spain." *Fifth International Symposium on Irrigation of Horticultural Crops, Book of Proceedings*, Mildura (Australia).

Soil Survey Staff, (2006). "Keys to Soil Taxonomy", *10th ed. USDA-Natural Resources Conservation Service*, Washington, DC.

Temesgen, B., Eching, S., Davidoff, B., and Frame, K. (2005). "Comparison of some reference evapotranspiration equations for California." *J. Irrig. and Drain. Eng*., ASCE 131(1), 73-84.

Trambouze, W., and Voltz, M. (2001). "Measurement and modelling of the transpiration of a Mediterranean vineyard." *Agric. For Meteororol.,* 107, 153-166.

Walter, I.A., Allen, R.G., Elliott, R., Jensen, M.E., Itenfisu, D., Mecham, B., Howell, T.A., Snyder, R., Brown, P., Echings, S., Spofford, T., Hattendorf, M., Cuenca, R.H. Wright, J.L., and Martin, D. (2000). "ASCE´s Standardized Reference Evapotranspiration Equation." *Proceedings of the 4th National Irrigation Symposium,* ASAE, Phoenix, AZ, Nov., 2000.

Williams, L.E., Phene, C.J., Grimes, D.W., and Trout, T.J. (2003a). "Water use of young Thompson Seedless grapevines in California." *Irrig. Sci*., 22, 1-9

Williams, L.E., Phene, C.J., Grimes, D.W., and Trout, T.J. (2003b). "Water use of mature Thompson Seedless grapevines in California." *Irrig. Sci.,* 22, 11-18.

Willmott, C.J. (1982). "Some comments on the evaluation of model performance." *Bulletin American Meteorological Society*, 63(11), 1309-1313.

Yunusa, I.A.M., Walker, R.R., and Lu, P. (2004). "Evapotranspiration components from energy balance, sapflow and microlysimetry techniques for an irrigated vineyard in inland Australia." *Agric. For. Meteorol.*, 127, 93-107.

Application of SIRMOD to Evaluate Potential Tailwater Reduction from Improved Irrigation Management

Byron Clark[1], Lindsay Hall[2], Grant Davids[3], Wynn Walker[4], and John Eckhardt[5]

[1]P.E., M.ASCE, Davids Engineering, Inc., 1772 Picasso Ave., Ste. A, Davis, CA 95618; PH: (530) 757-6107; FAX: (530) 757-6118; email: byron@de-water.com
[2]E.I.T., A.M.ASCE, Davids Engineering, Inc., 1772 Picasso Ave., Ste. A, Davis, CA 95618; PH: (530) 757-6107; FAX: (530) 757-6118; email: lindsay@de-water.com
[3]P.E., M.ASCE, Davids Engineering, Inc., 1772 Picasso Ave., Ste. A, Davis, CA 95618; PH: (530) 757-6107; FAX: (530) 757-6118; email: grant@de-water.com
[4]Ph.D., P.E., D.WRE, F.ASCE, Utah State University, Department of Biological and Irrigation Engineering, 4105 Old Main Hill, Logan, UT 84322; PH: (435) 797-2788; FAX: (435) 797-1248; email: wynnwalk@engineering.usu.edu
[5]Ph.D., P.E., D.WRE, M.ASCE, Imperial Irrigation District, P.O. Box 937, Imperial, CA 92251; PH: (760) 339-9736; email: jreckhardt@iid.com

ABSTRACT

The SIRMOD surface irrigation simulation, evaluation, and design software developed at Utah State University was applied to evaluate potential increases to irrigation performance from improved irrigation management within the Imperial Irrigation District of Southern California (IID). This study was conducted as part of a planning effort to develop strategies to satisfy the Colorado River Quantification Settlement Agreement and Related Agreements (QSA), which call for IID to generate more than 300,000 acre-feet annually through a combination of District and voluntary on-farm efficiency conservation savings.

Potential irrigation management performance increases were evaluated by calibrating the SIRMOD model for 34 selected border and furrow irrigation events for which delivery and tailwater hydrographs were measured. These events occurred at fields distributed throughout the Valley representing a range of crops, soils, run lengths, and tailwater production (surface runoff). For each event, simulations were conducted to identify potential reductions in tailwater resulting from different combinations of inflow rate and cutoff time. Simulations were constrained to minimize reductions in irrigation adequacy. Simulation results were detuned to represent practical, attainable performance based on an estimate of uncertainty in the soil moisture deficit prior to irrigation on the planning of an irrigation delivery.

BACKGROUND AND INTRODUCTION

The Imperial Irrigation District of Southern California (IID) is the nation's largest irrigation district, encompassing approximately 475,000 acres (190,000 ha) of irrigated agriculture.

Approximately 3.1 million acre-feet (3,800 MCM) of water is diverted annually for irrigation by IID from the Colorado River; the Colorado is IID's sole source of water for irrigation. Primary crops grown in IID include alfalfa, Bermuda hay, Sudan, sugar beets, wheat, carrots, onions, and lettuce. Soils range from heavy, cracking clay to sand with more than 80% of the service area consisting of cracking and heavy non-cracking clay soils. Primary irrigation methods employed by IID growers are graded border and graded furrow. Due to infiltration being relatively insensitive to intake opportunity time on many soils, high distribution uniformity and application efficiency are possible, with the primary on-farm loss being tailwater (surface runoff).

In 2003, IID entered the Quantification Settlement Agreement and Related Agreements (QSA), agreeing to the transfer of approximately 300,000 acre-feet (370 MCM) annually to other Southern California Colorado River water users through a combination of system and on-farm conservation projects aimed at increasing on-farm irrigation and distribution system efficiency. As a condition of the agreements, at least 130,000 acre-feet (160 MCM) must be generated through the implementation of on-farm conservation measures (CMs).

In 2007, IID completed its Efficiency Conservation Definite Plan (Plan), which identifies the most probable mix of on-farm and system improvements needed to satisfy transfer obligations while keeping costs below available transfer revenues. On-farm participants in the transfer program will be provided incentives to implement CMs to achieve conservation goals. The Plan identified numerous CMs that growers are likely to consider. Among those CMs growers expressed interest in implementing were management-based CMs aimed at increasing irrigation efficiency through decreased tailwater production. In particular, interest was expressed in improving surface irrigation methods through irrigation scheduling and event management.

Scientific Irrigation Scheduling (SIS), as evaluated under the Plan, includes decisions made prior to placing irrigation orders for individual fields including the timing, duration, and amount of water aimed at minimizing tailwater production while satisfying crop water requirements. Scientific Event Management (SEM), as evaluated under the Plan, includes decisions made after the start of an irrigation event based on observed advance, infiltration, and runoff aimed at minimizing tailwater production while providing adequate infiltration to meet crop water needs.

METHODOLOGY

Potential improvements in application efficiency from reduced tailwater production were estimated for individual irrigation events to gain insights into potential increases in irrigation efficiency through implementation of management-based CMs. Tailwater reduction potential was evaluated using the SIRMOD surface irrigation simulation, evaluation, and design software developed at Utah State University. First, the model was calibrated to determine infiltration characteristics for historical irrigation events. Next, parametric model runs varying inflow rate and set duration were completed for each event to determine the maximum application efficiency that could be attained while maintaining irrigation adequacy. Then, model results were detuned to allow for uncertainties or other considerations limiting the ability to optimize all irrigation

events over the course of a crop season. These estimates were used to parameterize a model estimating increases in irrigation performance from irrigation scheduling and event management of border and furrow irrigated fields. The model was applied district-wide across a range of crops and soils to estimate the total potential increase in irrigation performance from irrigation scheduling and event management (IID, 2007).

SIRMOD. SIRMOD is a surface irrigation software package providing simulation, evaluation, and design capabilities for border, basin, and furrow irrigation (Walker and Skogerboe, 1987; Walker, 1989; and Walker, 2004). The simulation of the hydraulics of surface irrigation systems at the field level uses hydrodynamic, zero-inertia, or kinematic-wave algorithms which can be used to identify the combination of event parameters (both management and physical) that optimize application efficiency. The evaluation algorithms utilize the two-point solution of the inverse problem allowing the computation of infiltration parameters from the input of advance data. The design algorithms utilize a standard volume balance procedure.

SIRMOD Calibration. Procedures for calibrating SIRMOD were developed based on available data, including delivery and tailwater hydrographs measured by IID's Irrigation Management and Monitoring Unit (IMMU). The delivery hydrograph is measured at the head gate, and the tailwater hydrograph is measured at the tailwater box at the lower corner of the field. Initially, an attempt was made to calibrate the model based on delivery and tailwater hydrographs for individual irrigation sets; however, upon close inspection of the hydrographs, it was determined that (1) the delay between the arrival of flows at the end of the set and arrival at the tailwater box and (2) overlapping of tailwater hydrographs from multiple irrigation sets limited the ability to calibrate the model based on data from a single set for some fields. To overcome this limitation, an alternative approach for model calibration was developed relying on advance time, tailwater production as a percentage of deliveries, and infiltrated depth determined from the IMMU dataset. Other input parameters used to calibrate the model were estimated from available data. Input parameters used in the calibration process are described in Table 1.

The 34 irrigation events simulated were selected from over 1300 events monitored by IMMU. Events were selected to cover the range of field configurations, cropping, soils, and tailwater production in IID.

Table 1. Input Parameters for SIRMOD Calibration.

Input/Calibration Parameter	Source	Method
Run Length	GIS	Visual Inspection of Aerial Photography
Field Width	GIS	Visual Inspection of Aerial Photography
Main Slope	GIS	Computation from Digital Elevation Model
Irrigation Method	IMMU	IID Staff Observation
Crop	IMMU	IID Staff Observation
Number of Sets	IMMU	Inferred from Tailwater Hydrograph
Furrow Geometry	Grower Consultation and Field Observations	Typical Geometry for Crop and Irrigation Method Simulated
Manning's n	Literature Values and Expert Judgment	Expected Values for Crop and Irrigation Method Simulated, Adjusted as a Calibration Parameter
Irrigation Cutoff Time	IMMU	Inferred from tailwater hydrograph
Infiltrated Depth	IMMU	(Delivered Volume – Tailwater Volume)/ Field Size
Percent Tailwater	IMMU	Tailwater Volume/Delivered Volume
Advance Time	IMMU	Inferred from tailwater hydrograph

Simulation of Irrigation Scheduling and Event Management. Following calibration, parametric SIRMOD runs were completed by varying inflow rates and set times to determine minimum tailwater production while maintaining observed infiltration and while maintaining distribution uniformity as estimated from the model through the calibration process. Thus, "optimized" irrigation events maintained irrigation adequacy.

For SIS, set durations from the original irrigation event were maintained, and the inflow rate was decreased to evaluate potential increases in irrigation performance. For each calibrated event, the inflow rate was reduced until the flow resulting in maximum application efficiency while maintaining the historical observed infiltration was found.

For SEM, the constraint imposed IID's delivery schedule was relaxed. IID regulations allow for growers to end deliveries early, provided that at least 3 hours advance notice is provided for the water to be shut off and backed out of the system. In the future, it is anticipated that growers will utilize available flexibility in shutoff time more often to reduce tailwater production.

Following the parametric model runs, inflow rates and set durations resulting in the least tailwater while maintaining irrigation adequacy were summarized for comparison to the observed event characteristics.

Note that changes to the infiltrated depth were not allowed in the model runs. This constraint results from limited flexibility in when irrigation events occur due to relatively firm irrigation timing resulting from the need for cultural practices. A good example of such constraints is the timing of cutting, drying, and baling for hay crops. Additionally, relatively low infiltration soils,

coupled with relatively high soil and water salinity in IID necessitates adequate infiltration to meet leaching requirements over the course of a crop season, or over a series of years in the case of perennial hay crops.

Estimated increases in irrigation performance represent idealized conditions in which the field is perfectly uniform. Additionally, it is unlikely that a grower could achieve optimum application efficiency across a series of event for a full crop season (or a full year in the case of hay crops). As a result, simulation results predicting a specific increase in application efficiency (translated to a percent decrease in tailwater production) for individual events were reduced based on an estimate of field nonuniformity and uncertainties faced by growers and irrigators in planning and conducting irrigation events.

RESULTS AND DISCUSSION

Selected Irrigation Events. As previously mentioned, a total of 34 irrigation events were selected for the SIRMOD analysis. Of these, 21 border irrigation events were selected and 13 furrow irrigation events were selected. Events were selected to represent a range of conditions affecting surface irrigation hydraulics. Characteristics of each event are summarized in Tables 1 and 2 for border and furrow irrigation, respectively.

Table 1. Border Event Characteristics Used in Calibration.

Field	Crop	Field Length (m)	Field Width (m)	Main Slope (%)	Border Inflow (L/s/m)	Cutoff Time (min)	Infiltrated Depth (cm)	Tailwater Percent	Advance Time (min)	Event Duration (hr)
B-1	Alfalfa	744	544	0.220	8.9	198	10.6	25%	320	40
B-2	Alfalfa	381	755	0.190	2.7	184	6.1	18%	250	25
B-3	Alfalfa	549	328	0.210	3.1	235	10.9	13%	310	16
B-4	Alfalfa	393	771	0.180	2.3	123	3.2	26%	270	23
B-5	Alfalfa	372	785	0.200	3.7	153	7.7	18%	210	23
B-6	Sudan	372	804	0.099	2.9	307	11.7	18%	500	31
B-7	Sudan	366	431	0.062	2.4	292	10.6	7%	750	24
B-8	Sorghum	357	401	0.540	2.7	235	7.3	32%	300	16
B-9	Sudan	338	797	0.024	1.6	336	7.6	20%	721	22
B-10	Sudan	384	778	0.710	1.7	574	13.5	14%	600	48
B-11	Wheat	375	743	0.085	4.2	147	8.7	14%	220	34
B-12	Wheat	381	775	0.250	3.6	216	9.5	23%	390	36
B-13	Wheat	387	784	0.210	2.0	498	13.5	14%	580	33
B-14	Alfalfa	366	792	0.264	2.8	210	6.7	28%	274	7
B-15	Alfalfa	786	375	0.268	2.9	720	12.7	20%	510	15
B-16	Alfalfa	421	750	0.193	5.2	150	9.3	14%	260	8
B-17	Alfalfa	405	750	0.264	4.6	170	9.9	0%	297	23
B-18	Bermuda	814	774	0.332	5.1	288	8.9	13%	645	15
B-19	Bermuda	366	863	0.156	1.3	390	6.6	20%	515	8
B-20	Bermuda	805	280	0.166	1.1	1455	9.5	6%	1712	7
B-21	Sudan	747	366	0.253	5.4	270	9.4	12%	424	7

Table 2. Furrow Event Characteristics Used in Calibration.

Field	Crop	Field Length (m)	Field Width (m)	Main Slope (%)	Furrow Spacing (m)	Furrow Inflow (L/s)	Cutoff Time (min)	Infiltrated Depth (cm)	Tailwater Percent	Advance Time (min)	Event Duration (hr)
F-1	Alfalfa	763	795	0.000	1.0	0.94	1410	9.7	8%	1440	74
F-2	Alfalfa	402	724	0.257	1.0	3.26	180	6.7	20%	186.4	24
F-3	Cotton	817	372	0.210	0.7	0.84	1450	4.7	29%	490	24
F-4	Corn	387	784	0.210	0.8	0.49	748	6.4	10%	415	25
F-5	Sugar Beets	387	760	0.090	0.7	0.50	1415	11.8	21%	950	47
F-6	Sugar Beets	774	746	0.260	0.7	0.54	1470	6.9	20%	1290	25
F-7	Asparagus	372	804	0.099	1.0	0.44	473	3.3	8%	430	24
F-8	Carrots	378	748	0.270	1.0	0.57	1465	8.5	34%	240	49
F-9	Tomatoes	384	632	0.150	1.0	0.53	503	2.3	43%	230	25
F-10	Carrots	756	369	0.240	1.0	0.99	1200	4.6	51%	90	48
F-11	Carrots	366	431	0.062	1.0	0.53	1440	7.4	40%	260	48
F-12	Onions	442	419	0.370	1.0	0.76	740	5.0	33%	320	25
F-13	Carrots	384	790	0.180	1.0	0.78	1180	11.4	20%	450	96

Calibration Results. The calibration procedure resulted in the soil intake curves displayed in Figures 1 and 2 for furrow and border irrigation events, respectively. Intake was modeled using the modified Kostiakov-Lewis equation to include a term for infiltration due to cracking. Soils at each field were assigned to a general soils class (light, heavy, or heavy cracking) based on the NRCS soil survey as indicated in the legend of each figure.

Figures 1 and 2 indicate that the soils in IID tend to behave like the heavier NRCS soil intake curves. The results for light soils in IID appear to be relatively heavy with respect to intake characteristics when compared to the standard NRCS curves.

The cracking term was utilized in the intake equation when adjustment of the Manning's n value within reasonable limits failed to match the observed advance time. The cracking term is modeled as an instantaneous infiltration as seen in the y-intercepts of the soil intake curves. Cracking was introduced for a majority of the calibrations, which is consistent with field observations and with the relatively high shrink/swell characteristics of Imperial Valley soils.

The range of soil intake curves are highly variable and overlapping. Infiltrated depths for row irrigated events ranged from 2.0 to 5.6 inches (5.1 to 14.2 cm) with an intake opportunity time of 24 hours. Infiltrated depths for border irrigated events ranged from 1.6 to 7.8 inches (4.1 to 19.8 cm) with an intake opportunity time of 12 hours. The NRCS curves used in the calibration (and subsequently refined for each specific event) ranged from heavy clay to sandy loam with the majority falling between silty clay and sandy clay. The representative NRCS intake curves are consistent with the soil textures described in the soil survey of the Imperial Valley.

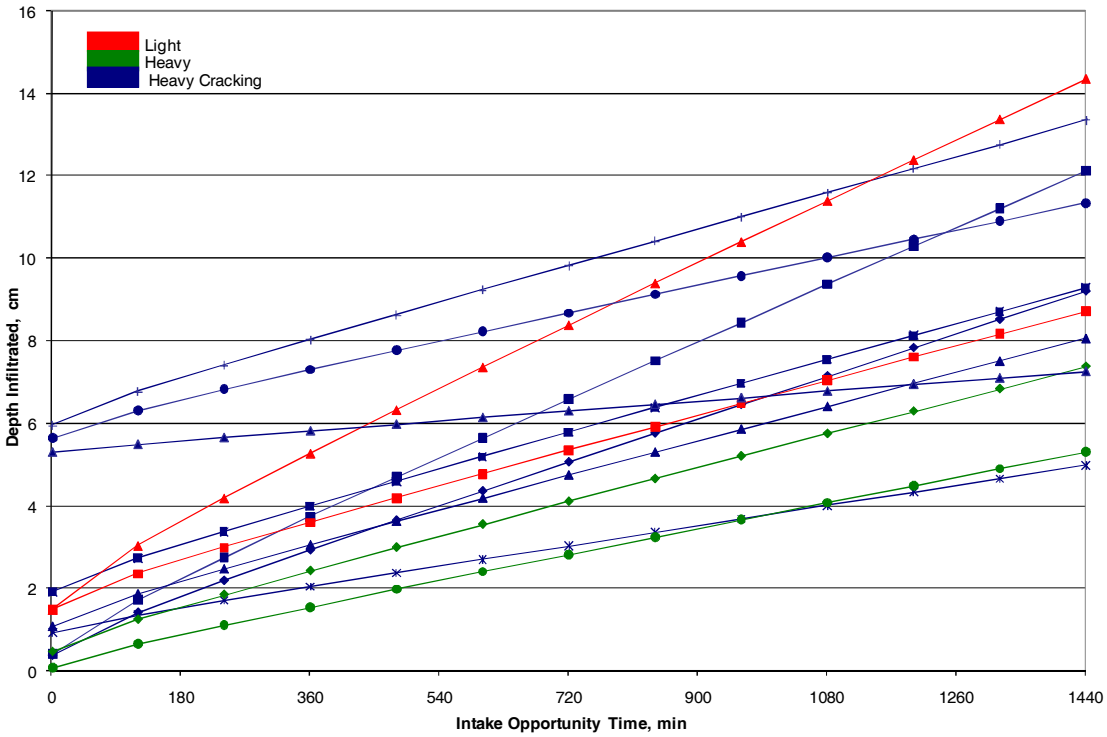

Figure 1. Calibrated Soil Intake Curves for Row Irrigated Events

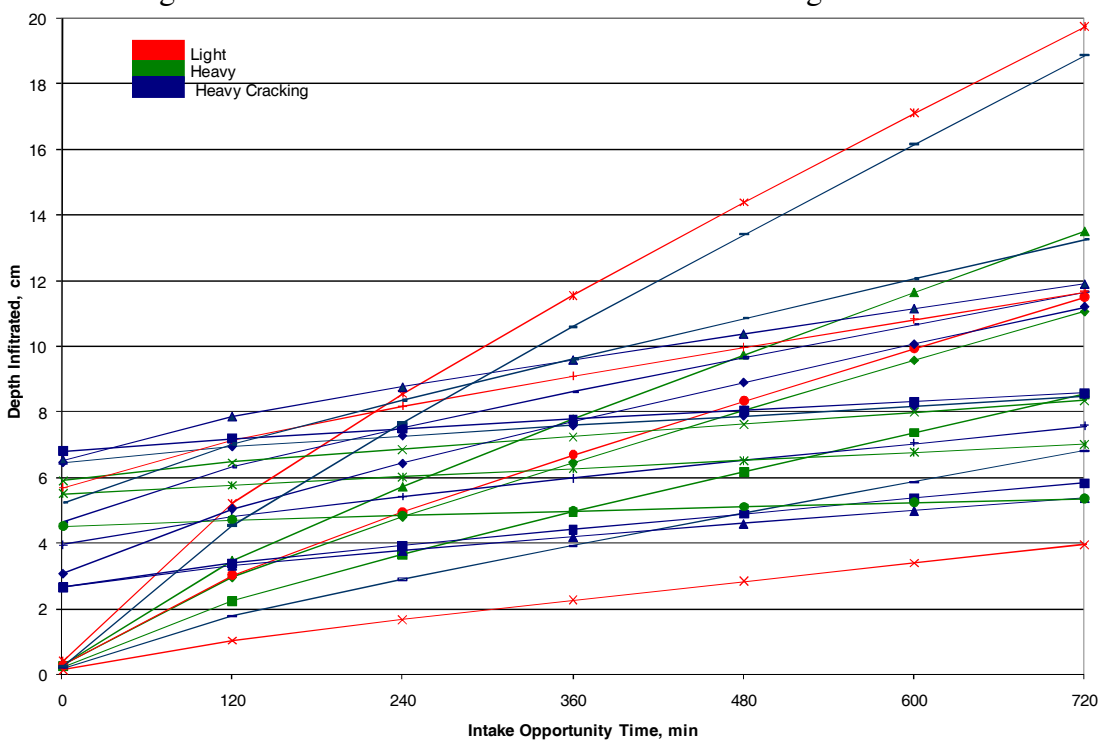

Figure 2. Calibrated Soil Intake Curves for Flat Irrigated Events

Simulation of Irrigation Scheduling and Event Management; Detuning of Model Results. As described previously, Scientific Irrigation Scheduling (SIS) and Scientific Event Management (SEM) are management-based conservation measures that were simulated by selecting flow, duration, and irrigation depth to optimize application efficiency. Optimum application efficiency (AE) was characterized as the maximum application efficiency attainable while meeting the desired total infiltrated depth (e.g., the estimated soil moisture deficit prior to irrigation).

Initially, a series of events was simulated representing SIS only. SIS was simulated by varying the ordered flow for each calibrated event to find the optimal AE while keeping the set duration fixed. Next, SEM was simulated by varying both the inflow and the set duration to find the optimal AE, thus removing the constraint that the delivery fit within the standard IID delivery cycle.

Optimal AE values were detuned to represent practical, attainable values of AE based on an approximation of the impact of uncertainty in soil moisture deficit prior to irrigation on the planning of an irrigation delivery. This uncertainty results from difficulty in quantifying the soil moisture depletion following the previous irrigation event, difficulty in quantifying crop ET since the last irrigation, and uncertainty of the availability of delivery on the requested day (carryovers). Additionally, within-field variability limits the ability to achieve uniformly high application efficiency for each irrigation set and over the course of multiple irrigation events. These uncertainties were represented by reducing the simulated soil moisture deficit by 5% and rerunning SIRMOD with the optimal flow (SIS and SEM) and duration (SEM only) to evaluate the impact on AE. The estimate of a 5% reduction in soil moisture deficit is representative of irrigating approximately one day earlier than the optimal date.

Detailed steps used to simulate optimal and detuned AE values for SIS and SEM are as follows:

1. Assign two soil deficits (z_{req}) that are less than the actual infiltrated depth for the furrow and the border irrigations. This assumes that the grower, on average, achieves more infiltration rather than less than the soil deficit. This assumption is supported by the fact that over time, adequate deep percolation must occur to maintain salt balance in the root zone and sustain production.

   Two depths were selected in order to bracket the estimated depletion prior to irrigation because the soil moisture depletion was not measured for the calibration events. The soil moisture deficits were selected to provide a representative range of application efficiencies for the calibration events. The soil moisture deficits were selected to be consistent with the observed range of estimated seasonal irrigation efficiencies developed as part of the Plan (IID, 2007).

2. Run SIRMOD using the inflow and duration from the calibration event at the two soil moisture deficits. Record the simulated AE, tailwater fraction, and tilewater fraction

(deep percolation as a fraction of delivered water) for each event and soil moisture deficit combination.

3. To simulate SIS, run SIRMOD again, decreasing the flow to maximize AE while limiting the deficit following the event to no more than 3% of the simulated deficit prior to the event. Record the simulated AE, tailwater fraction, and tilewater fraction for each event and soil moisture deficit combination. Thus, for each calibrated event, two optimal AE values under SIS are simulated.

4. To simulate SEM, rerun SIRMOD again, varying flow and duration to maximize AE while limiting the deficit following the event to no more than 3% of the simulated deficit prior to the event. Record the simulated AE, tailwater fraction, and tilewater fraction for each event and soil moisture deficit combination. Thus, for each calibrated event, two optimal AE values under SEM are simulated.

5. Decrease the soil moisture deficit by 5% for each optimized model run and rerun SIRMOD with the optimized flow (SIS and SEM) and duration (SEM only) to estimate the practical optimal application efficiency, tailwater fraction, and tilewater fraction.

Simulated application efficiencies are assumed to be representative of seasonal irrigation efficiency for purposes of evaluating the representative impact of SIS and SEM on on-farm water use. The cumulative distributions of application efficiency for the calibrated events, SIS, SEM, adjusted SIS, and adjusted SEM for furrow irrigated events are provided in Figure 3. Analagous distributions for border irrigated events are provided in Figure 4.

In Figures 3 and 4, application efficiencies for the calibration events ranged from 0.27 to 0.80 with an average of 0.62. For SIS, simulated application efficiencies ranged from approximately 0.48 to 0.89 with a mean of 0.74. Following adjustment, application efficiencies for SIS ranged from 0.53 to 0.85 with a mean of approximately 0.70. For SEM, simulated application efficiencies ranged from approximately 0.62 to 0.89 with a mean of 0.78. Following adjustment, application efficiencies for SEM ranged from 0.59 to 0.86 with a mean of approximately 0.75.

In general, for small soil deficits, and in some cases for soils with a large cracking term, large unit inflows with short set durations maximized application efficiency. The dynamics of these irrigations were such that the large flow was cut off before it reached the end of the field, and surface storage continued to drive advance to the end of the field, producing high uniformity and small quantities of tailwater. For large soil deficits, low flows with long durations maximized application efficiency.

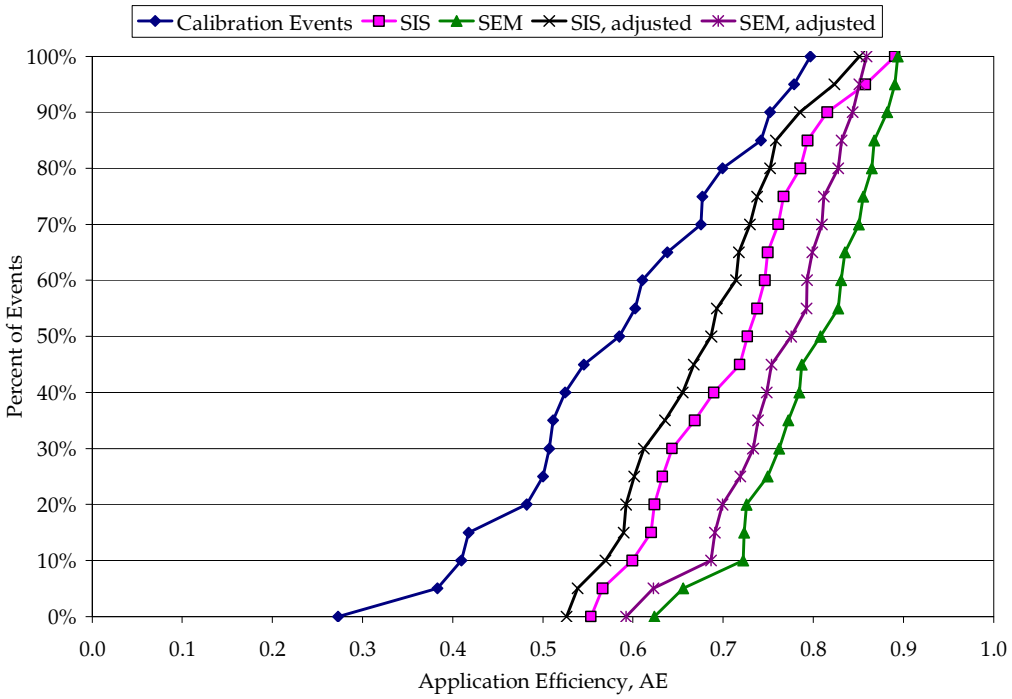

Figure 3. Cumulative Distributions of Application Efficiency for Calibrated Events, SIS, SEM, adjusted SIS, and adjusted SEM: Row Irrigated Events.

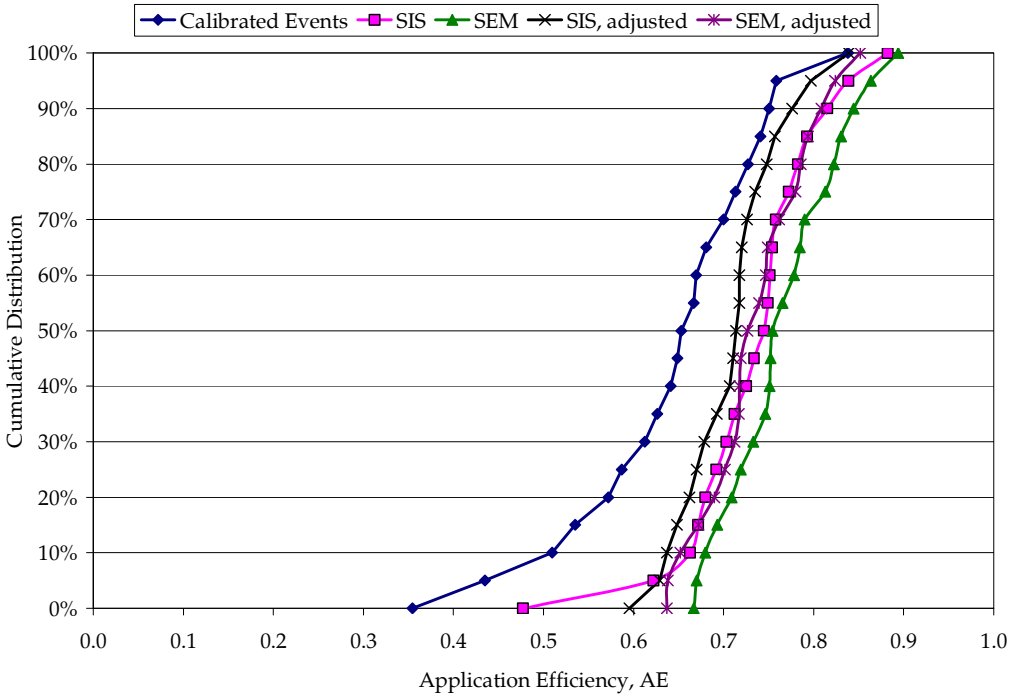

Figure 4. Cumulative Distributions of Application Efficiency for Calibrated Events, SIS, SEM, adjusted SIS, and adjusted SEM: Flat Irrigated Events

CONCLUSIONS

This study demonstrates that SIRMOD provides a useful tool for the evaluation of potential increases in irrigation performance from improved surface irrigation management. Additionally, SIRMOD evaluations of potential performance improvements can be completed with limited input data. Primary data requirements include delivery and tailwater amounts (from which infiltration depth is determined), general information describing field layout, slope, and surface roughness, advance rate, and set duration. SIRMOD could be applied as a management tool to provide near real-time feedback to growers regarding possible opportunities to reduce tailwater production while maintaining irrigation adequacy.

REFERENCES

IID Efficiency Conservation Definite Plan. 2007. Available at www.iid.com/Water/ EfficiencyConservationProgram.

Walker, W.R. and G.V. Skogerboe. 1987. Surface Irrigation: "Theory and Practice". Prentice-Hall Inc., Englewood Cliffs, New Jeresy. 386 pp.

Walker, W. R. 1989. Guidelines for designing and evaluating surface irrigation systems. FAO Irrigation and Drainage Paper 45, Food and Agriculture Organization of the United Nations, Rome, Italy. 137 pp.

Walker, W.R. 2004. Surface Irrigation Simulation, Evaluation, and Design. Utah State University, Logan, Utah. 155 pp.

ACKNOWLEDGEMENTS

The authors would like to thank the IID Irrigation Management and Monitoring Unit for their support and for providing the valuable data that enabled this analysis. Additionally, the authors would like to thank the members of IID's On-Farm Technical Advisory Committee who supported the analysis and the Plan as a whole through their insight and guidance.

Evaluation of Magnetic Meters for Irrigation Pipeline Measurement

Stuart W. Styles[1] and Bryan Busch[2]

[1] Assoc. Professor, Cal Poly State University BioResource and Agricultural Engineering Dept. and Director, Irrigation Training and Research Center. Phone: (805) 756-2429. Fax: (805) 756-2434. sstyles@calpoly.edu
[2] Irrigation Support Engineer, Cal Poly ITRC. Phone: (805) 756-2434. Fax: (805) 756-2434. bbusch@calpoly.edu

ABSTRACT

Magnetic flow meters are used to measure the flow rate of a liquid in a closed pipeline. This type of meter is becoming increasingly popular for measurement with agriculture applications. Electromagnetic meters were tested by the Irrigation Training and Research Center in pipelines located less than the 10 diameters upstream of disturbances with good results. Results show that location guidelines for placing a magnetic meter can be decreased even for turbulent conditions. This paper will discuss how a magnetic flow meter works, advantages and disadvantages of this type of meter, test results, and new guidelines for field applications.

INTRODUCTION

The accuracy and long-term success of any flow measurement program depends on many factors. Magnetic flow measurement is rapidly becoming the technique of choice in pipelines because of its simplicity and accuracy. However, the application of this technology has been limited in the past because of standard practice guidelines for magnetic flow meters, which have required installing the meters in a straight section of pipe at least 8-10 pipe diameters from any source of turbulence. In addition, standard practice recommends having at least two pipe diameters of straight unobstructed pipe downstream from the meter. However, in the case of many irrigation pumping plants, turnouts, and deliveries, these conditions can rarely be met without extensive and expensive modifications. Therefore, the Irrigation Training and Research Center (ITRC) at Cal Poly State University San Luis Obispo is currently investigating electromagnetic flow meters for potential applications under non-standard conditions.

Several current manufacturers claim that their magnetic meters can perform well even in locations where only two diameter lengths of straight pipe are available. Testing was done by the ITRC on several magnetic meters at the Cal Poly Water Resources Facility to evaluate comments by the manufacturers and to make recommendations to irrigation districts and growers interested in this new technology.

This research was conducted to determine:

- The accuracy of the magnetic meters in locations that are less than optimal
- The sensitivity of meters to increasing amounts of turbulence

Since this research was conducted, there have been numerous field installations of magnetic meters in various irrigation applications in California. The general consensus is that they are working well.

Magnetic Meters

According to Faraday's Law, a voltage will be induced proportional to the velocity of a conductor as it moves at right angles through a magnetic field. The water in the pipe is the conductor. By simply measuring the voltage, a magnetic meter is able to calculate the volume of the liquid passing through a controlled section.

Faraday's Formula: **E** is proportional to **V** x **B** x **D**

E = The voltage generated in a conductor
V = The velocity of the conductor
B = The magnetic field strength
D = The length of the conductor

This principle works for irrigation water passing through the magnetic field generated by the magnetic meter since the water acts as the conductor. The basic operating principle for magnetic meters is illustrated in **Figure 1**. Note that this discussion is limited to full-bore or in-line magnetic meters. There are several other types of meters on the market but this type is the one that was evaluated.

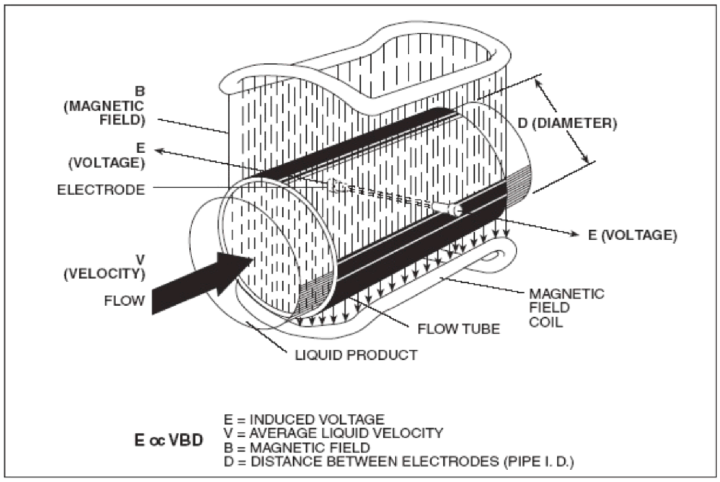

Figure 1. Operating principle for full-bore magnetic meter (Omega 2009)

As seen in **Figure 2**, there are two electrodes located inside the magnetic meter to measure the induced voltage. The flow rate/totalizer indicator is located on the top of the unit. These units can be placed at any angle. It is recommended that they be rotated so that one of the electrodes does not sit on the bottom of the pipe. This helps prevent problems from sediment covering the electrode. Note that on the unit in **Figure 2**, the magnetic field is generated by an insert unit into the pipeline. Some manufacturers install the coils to generate the magnetic field outside of the spool piece.

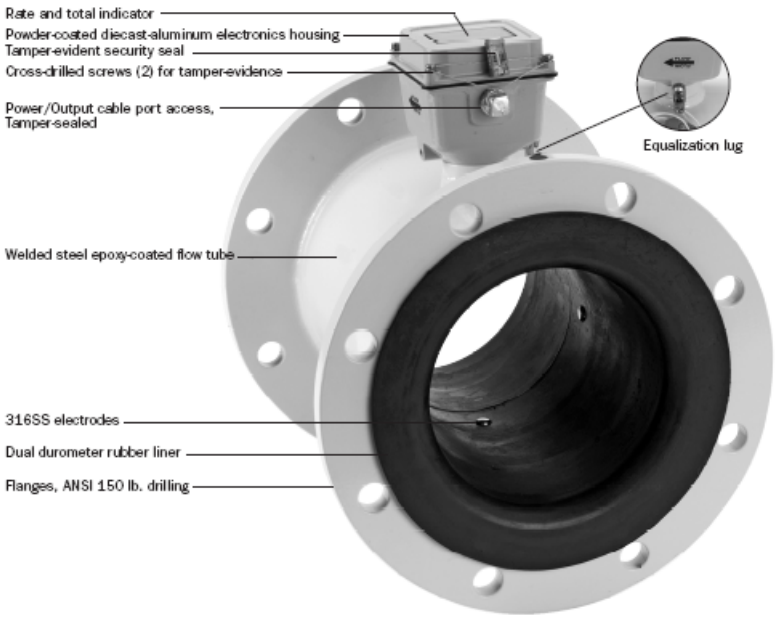

Figure 2. View of typical magnetic meter (SeaMetrics 2009)

Advantages of Magnetic Meters

- Highly accurate even with some flow disturbance.
- No headloss caused by meter.
- Is not impacted by trash, sediment, or sand.
- Can measure a wide range of velocity. This is a key criteria in areas that have seasonal high flows combined with very low flows.
- Has instantaneous and volumetric totalizing capability.
- Measurement accuracy is NOT affected by varying canal water levels.
- Minimal maintenance required.
- Temperature of the liquid has no effect on accuracy.

Disadvantages of Magnetic Meters

- Cost is a major constraint. Recently the cost has dropped dramatically, but this is still the most expensive option in some cases.
- Pipe must be full (as is the case in most agricultural applications).
- Installation into existing sites is often difficult and expensive.
- Sensitivity to turbulence.

Turbulence and Magnetic Meters

Magnetic meters have been considered particularly tricky for pumping plants and turnouts, because of the meter's sensitivity to turbulence. For example, one of the main problems associated with turnouts is the turbulence that occurs just downstream of the gate. **Figure 3** shows a typical turnout application with a magnetic meter.

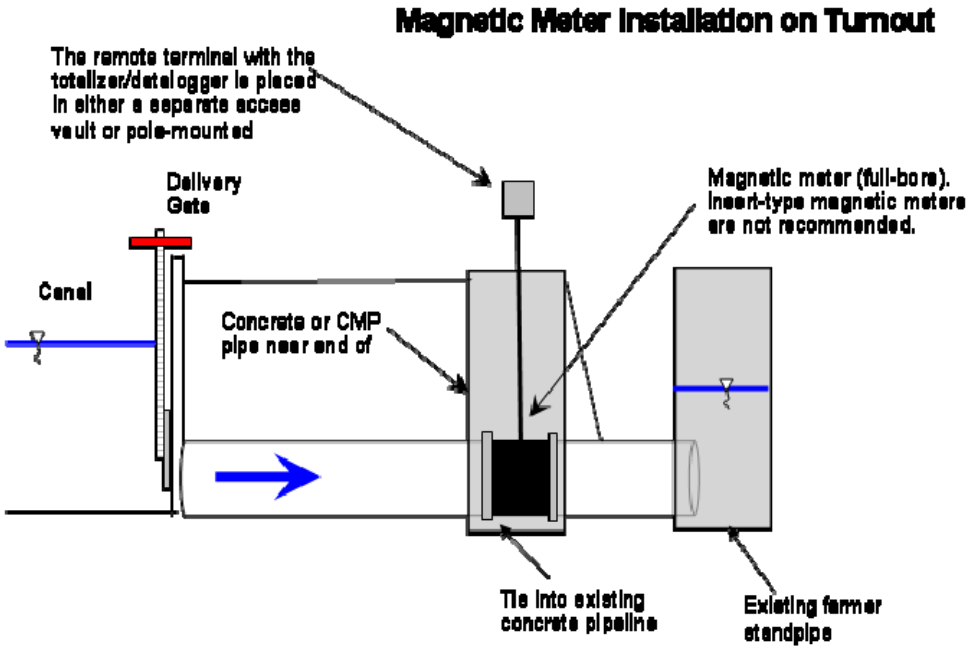

Figure 3. Conceptual sketch of magnetic meter installation for turnouts (not to scale)

In 1998, Hanson and Schwankl published results from non-optimal flow meter testing in their paper *Error Analysis of Flowmeter Measurements*. Pipeline measurements were taken with different types of flow meters to determine the effects on error resulting from different degrees of turbulence caused by elbows, check valves, and a partially opened check valve. Measurements were made at 2, 5, 10, and 15 pipe diameters downstream from the source of turbulence.

The results from Hanson and Schwankl (1998) indicated that for generally acceptable accuracy with propeller meters, pitot meters, and Doppler meters, measurements should be taken upstream of valves. The tests found that in some circumstances even with as little as 2 or 5 pipe diameters upstream of a flow meter, there were still large errors with all meters under conditions of severe turbulence.

Since most applications require the flow measurement downstream of a valve or turnout gate, manufacturers have recently claimed that their magnetic flow meter technology is now able to work effectively in situations where there is as little as two diameters of pipe length available. ITRC tested several magnetic meters at the Cal Poly Water Resources Facility to investigate these claims.

METHODOLOGY

Several manufacturers were tested in this study. The results are included here for one of the manufacturers[1]. Flow rates for the testing were measured with the SeaMetrics AG2000

[1] Reference to any specific product does not imply an endorsement or recommendation of use by the authors. The products names are included for completeness and clarifications in this paper.

Irrigation Magmeter in two different configurations at the Cal Poly Water Resources Facility. Two tests were conducted over a flow range of approximately 0.8 to 115 lps (12 to 1,800 gpm) using a second magnetic meter in optimal flow conditions as the control unit. **Figure 4** depicts the facilities used for testing.

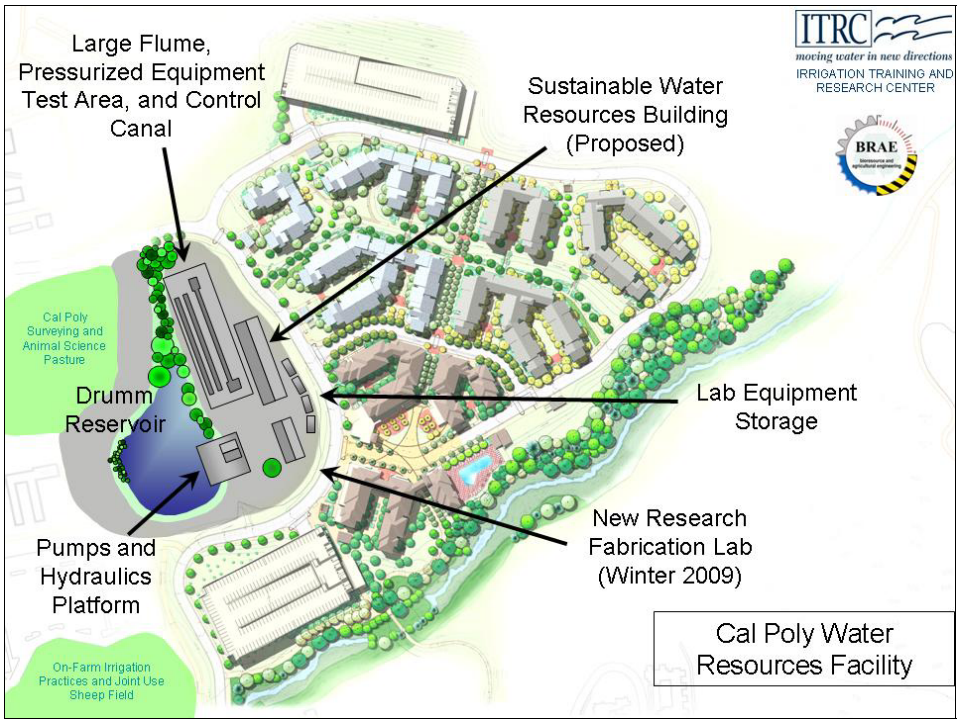

Figure 4. Cal Poly Water Resources Facility

The AG2000 flow meter readings were compared with the control unit to calculate the percent error in this paper as follows:

$$\% \text{ Error} = \frac{\text{AG2000 flow meter - Control unit}}{\text{Control unit}} \times 100$$

The AG2000 flow meter is an electromagnetic flow meter for use in 10 to 30 cm (4 to 12 inch) diameter pipelines. An optional 4-20 mA output module (AO55W) is available for remote monitoring applications with Supervisory Control and Data Acquisition Systems (SCADA) systems. The standard unit is battery powered and optional configurations are available for use with an external power source.

The control units used for the tests were a 10 cm (4 inch) and 30.5 cm (12 inch) McCrometer Ultra Mag flow meter, which had been calibrated using the weighing tank facility at the Water Resources Facility. ITRC did not attempt to verify the true accuracy of the AG2000 flow meter readings, only the percent error from the control units.

A magnetic flow meter was mounted on the Water Resources Facility Pump #2, downstream of a cast-iron concentric reducer, and immediately downstream of a butterfly valve (refer to **Figure 5**), designated as Test #1. The retail cost of this 25.4 cm (10 inch) magnetic meter is

$1,485, which is comparable to a standard propeller meter. This test configuration was designed to represent the "worst possible conditions imaginable" in an actual irrigation application.

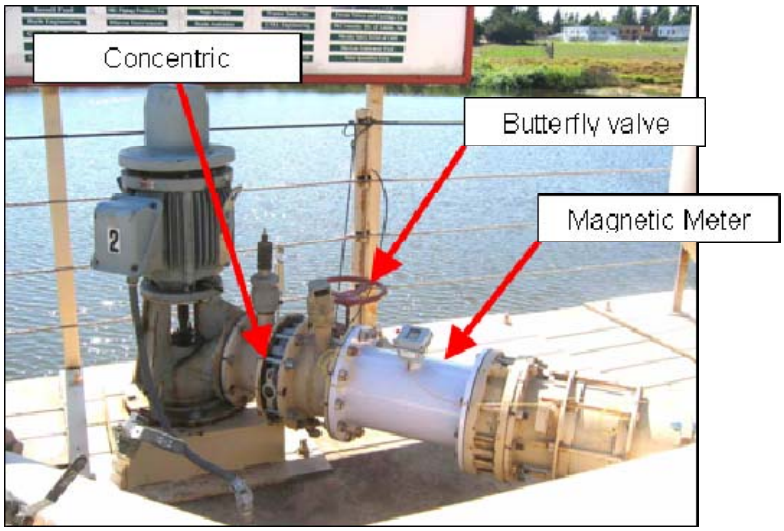

Figure 5. AG2000 test condition for Test #1 (10-inch)

A second AG2000 flow meter was mounted in a straight section of 10 cm (4 inch) pipeline only 20 centimeters (8 inches) downstream from a butterfly valve (equivalent to 2 pipe diameters), designated as Test #2 (see **Figure 6**). The retail cost of this 10 cm (4 inch) magnetic meter is $990, which is comparable to a standard propeller meter.

Once the initial flow rate was established, turbulence was introduced into the pipeline. The butterfly valves were adjusted during the tests from wide open to 75% and 90% closed in Tests #1 and #2, respectively. This testing would represent the worst possible case for irrigation applications.



Figure 6. AG 2000 test configuration for Test #2 (2 dia u/s & 0 dia d/s)

RESULTS

The error analysis of the AG2000 flow meter test results is summarized in **Table 1**. In Test #1, the percent error was less than **+2%** when the butterfly valve was partially closed up to 50%. The percent error was more than -10% when the butterfly valve was closed more than 75%. This increase in percent error may be attributed to the jetting effect of the cast-iron concentric reducer coupled immediately upstream of the butterfly valve.

Errors for this meter increased as the valve was closed and the flow rate was reduced. The AG2000 flow meter had a positive percent error (overestimating the flow rate) compared to the control unit when the butterfly valve was closed 50% or less. When the butterfly valve was closed more than 50% the AG2000 flow meter underestimated the flow rate by approximately 6-12%.

By comparison, the results reported by Hanson and Schwankl (1998) for partially closed butterfly valves with a propeller meter mounted two diameters downstream were ±14% at 42.7 lps (668 gpm), ±15% at 73.7 lps (1,153 gpm), and ±2% for flow rates of 139.9 lps (2,190 gpm). The valve was closed 10 degrees (out of 90 degrees) to provide the throttling effect. Based on the results of their study, it was recommended to always use a six vane straightening arrangement if measuring the flow rate downstream of a throttled butterfly valve.

The test results indicate that the AG2000 Irrigation Magmeter can be installed downstream of partially closed butterfly valves or other sources of turbulence without excessively degrading accuracy.

Table 1. AG2000 Test Results at Cal Poly ITRC Water Resources Facility

Test #	Valve Position	Ultra Mag Flow Rate (lps)	Ultra Mag Flow Rate (gpm)	AG2000 Flow Rate (lps)	AG2000 Flow Rate (gpm)	Error (%)
Test #1 25.4 cm (10") meter	Open	114.4	1,791	116.0	1,816	+1.4
	50% closed	102.1	1,597	102.4	1,603	+0.4
	60% closed	90.4	1,414	88.4	1,383	-2.2
	70% closed	81.2	1,271	72.8	1,140	-6.3
	75% closed	63.4	992	55.5	868	-12.5
Test #2 10 cm (4") meter	Open	25.6	401	25.6	401	0.0
	50% closed	21.6	338	21.6	338	0.0
	70% closed	7.9	124	7.9	123	-0.8
	80% closed	2.0	31	2.0	31	0.0
	≈ 90 % closed	0.8	12	0.8	12	0.0

In Test #2, the 10 cm (4 inch) AG2000 flow meter had a percent error of less than 1% even when the butterfly valve was 90% closed. Discrepancies were the same for conditions where the butterfly valve was wide open and when it was closed 80-90%. These results suggest that turbulence from a partially closed butterfly valve located two pipe diameters upstream had a negligible effect on the precision of the magnetic meter as compared to the control unit.

In summary, the test results indicated that under conditions of severe turbulence due to a partially closed butterfly valve, the 10 cm (4 inch) AG2000 flow meter readings were not adversely affected. For the 24.4 cm (10 inch) AG2000 flow meter, a partially closed butterfly valve coupled with a pump discharge caused errors of 1-2% up to 50% valve closure. The recorded percent error was generally reduced at the higher flow rates.

CONCLUSION

The test results indicate that the magnetic meter tested can be installed downstream of partially closed butterfly valves or other sources of turbulence without excessively degrading accuracy. Additionally, the magnetic meter is able to provide accurate readings to within ±2%, which is well within the limits expected for agricultural delivery. The costs of these units have also decreased to the point where they are competitive with traditional devices that cannot handle the turbulence associated with some irrigation applications.

REFERENCES

Hanson, B.R., and Schwankl, L.J. 1998. "Error Analysis of Flowmeter Measurements." *J. Irrig. and Drain. Engrg.*, ASCE 124(5), 248-256.

SeaMetrics, Inc. 2009. "Instructions: AG2000 Irrigation Magmeter." http://www.seametrics.com/flow_meter/agAG.html

OMEGA. 2009. Engineering Technical Reference, "Introduction to Magnetic Flow Meters." http://www.omega.com/prodinfo/magmeter.html

INCREASING FIELD WORK PRODUCTIVITY IN IRRIGATION EVALUATION PROCESSES THROUGH THE USE OF COMBINED IRRIGATION MODELS

Sergio Lecina[1], Christopher M.U. Neale[2], Gary P. Merkley[3], Carlos A.C. dos Santos[4]

[1] Visiting Post-doctoral Scholar, Dept. of Biological and Irrigation Engineering. Utah State University. 4105 Old Main Hill. Logan, UT 84322. USA. Phone: (435) 797 2476. E-mail: lecina@iies.es
[2] Professor, Dept. of Biological and Irrigation Engineering. Utah State University. 4105 Old Main Hill. Logan, UT 84322. USA. Phone: (435) 797 3689. E-mail: christopher.neale@usu.edu
[3] Professor, Dept. of Biological and Irrigation Engineering. Utah State University. 4105 Old Main Hill. Logan, UT 84322. USA. Phone: (435) 797 1139. E-mail: gary.merkley@usu.edu
[4] PhD Student, Dept. of Atmospheric Science. Federal University of Campina Grande. 882 Aprigio Veloso. Campina Grande, PB, 58429-900, Brazil. E-mail: carlostorm@gmail.com

ABSTRACT

A surface irrigation evaluation process in an irrigation project requires expensive field work. Models that reproduce irrigation events help to analyse the data obtained, and evaluate different scenarios of improvement. The use of combined models that reproduce the interaction between irrigation water and the conveyance and drainage network, agricultural production, and the environment can increase the productivity of the field work. Their results surpass the analyses based only on application efficiency, and provide a wide range of irrigation, hydrological and economic indicators. The application of one of these models (Ador-Simulation) in a study area of the Bear River irrigation project (UT) showed that an increase in irrigation efficiency from 56 to 77 % can be achieved optimizing current irrigation time. This results in a 27 % of water saving over the 2008 demand, and in a little increase in current low economic productivities.

INTRODUCTION

Irrigation is facing a time of changes. Some of the reasons behind these changes are the liberalization of trade in world agricultural commodity markets, the reductions in agricultural subsidies, the environmental restrictions, and the water scarcity in many areas of the world. Improving water management is a key factor for optimizing the use of this natural resource and achieving economic, social and environmental sustainability in the agricultural sector. Its application is user appreciated and cost effective, since its economic return (conserved water/investment) is often orders of magnitude larger than that obtained from improving the structures (Playán and Mateos, 2006).

Benchmarking is an important tool for improving water management in irrigation projects. It is a systematic process for securing continual improvement through comparison with relevant and achievable goals, norms, and standards (Malano and Burton, 2001). The rapid appraisal process (RAP) is a key part of benchmarking that allows for quickly determining key indicators of irrigation projects (Burt and Styles, 1999; Burt and Styles, 2004).

A more detailed diagnosis can be obtained through an irrigation evaluation process. This methodology combines field work and computer simulation. The data obtained in on-farm irrigation evaluations are used for applying simulation models. These models allow the assessment of the current irrigation performance, and identification of the main factor for improving water management. The models applied in this process have evolved from single on-farm irrigation simulation models (Playán et al., 2000; Dechmi et al., 2003; Lecina et al., 2005) to complex models that combine a number of integrated modules which permit us to simulate water flows in an irrigation district (Lecina and Playán, 2006a). This last kind of software has been designed to extend the insight on irrigation district performance gained through the process of irrigation evaluation.

In this paper we evaluate a surface irrigation area in the Bear River Basin (Utah) using the model Ador-Simulation. This model reproduces the interaction between irrigation water and the conveyance and drainage network, agricultural production, and the environment. It is composed of five simulation modules covering on-farm irrigation, crop growth, hydrosaline balance, water flow, and decision making in water allocation to farmers. Since the previous models and decision support systems do not include the simulation of the on-farm irrigation system (Merkley, 1994, Yamashita and Walker, 1994, Prajamwong et al. 1997, Mateos et al., 2002), Ador-Simulation presents the unique feature of analysing the interaction between on-farm and district irrigation management. A detailed description of this model can be found in Lecina and Playán (2006b).

The objective of this study is to show the capabilities of using such models, to improve water management by farmers and by Irrigation Districts/Companies water managers both on-farm and at irrigation project levels, and to support water resources decision making at basin level. This improvement takes into account the preference of the farmers of the study area to maintain current structures.

THE STUDY AREA

The study area is located close to the town of Tremonton, North Utah (Figure 1). The total irrigated area is 1,213 ha, all of them surface irrigated, and included in the Bear River irrigation project, that irrigates a total of 26.856 ha. This project was developed by a sugar beet company at the beginning of the twentieth century, and is currently managed by the Bear River Canal Co. (BRCC).

The climate is continental (the mean temperature is 10 ºC), with a large temperature difference between winter and summer. The mean annual precipitation is 441 mm (82 mm in summer).

According to the soil maps of the Natural Resources Conservation Service (NRCS), two main soil units can be distinguished in the study area, located in the terraces of the Malad river (Figure 1). The first unit correspond to Parleys soils (PdA). These

soils are deep, stone-free, and have a loam texture with no salinity problems. This unit occupies 530 ha in the study area. The second unit covers the remaining area and corresponds to Fielding soils (Fd), with similar characteristics, but with a silt-loam texture.

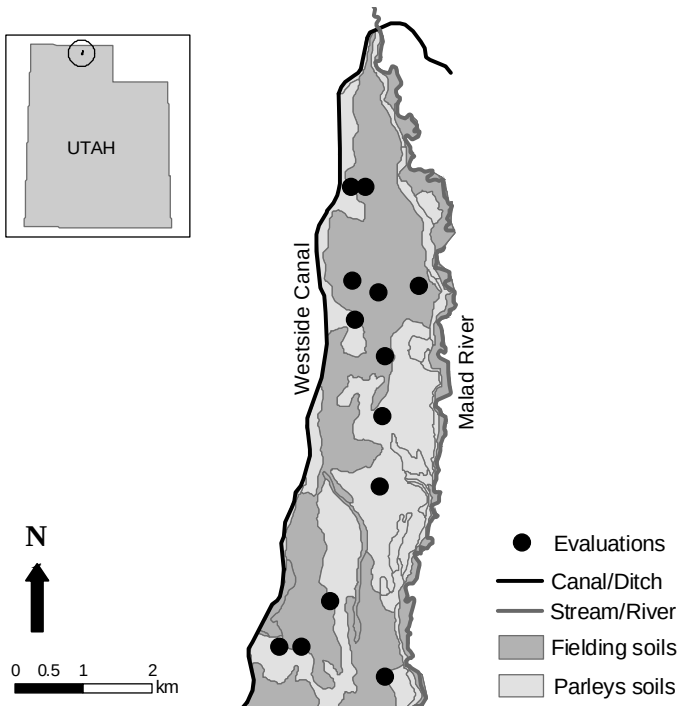

Figure 1. Location of the study area and irrigation evaluations. The background soil map has been adapted from NRCS.

A total of 79 land owners compose the study area, owning a total of 130 plots, according to the 2008 management database of the BRCC. The on-farm irrigation systems are, almost exclusively, blocked-end borders. Alfalfa (35 %) and corn (32 %) are predominant, and grass (11 %) and winter/spring grains (21 %) are also present in the cropping pattern of the area. Only 1 % of the irrigated is not cropped. The main destination of agricultural production is the livestock industry in the region.

Water conveyance structures consists of a network of unlined ditches which, starting at 24 headgates at the Westside canal, deliver water to the plots. Each headgate delivers the same discharge to all the plots within its irrigated command area. Irrigation return flows are collected and conveyed through buried drainage collectors that discharge into the Malad River, the natural drainage system of the area, and flow into the Great Salt Lake 25 km downstream.

Water deliveries is performed by the ditch riders of the BRCC. A rotation system is used applied with a daily irrigation period of 24 h. According to the classification system proposed by Clemmens (1987) for water delivery systems, the system is negotiated arranged, with fixed discharge. A fixed pricing structure (a specified fee per acre) is applied for water and services billing.

MATERIAL AND METHODS

On-farm irrigation evaluation

The purposes of the irrigation evaluations were to determine on-farm irrigation performance and to characterize soil infiltration. During 2008 a total of 13 irrigation evaluations were performed within the study area adopting the methodology proposed by Merriam and Keller (1978). Five of them were performed in the Parleys soils, and eigth evaluations were performed in the Fielding soils (Figure 1).

Borders were selected which were rectangular in shape. During the irrigation evaluation the farmer performed the normal irrigation practices. A measuring tape was used to determine the border dimensions. The slope and the standard deviation of soil surface elevation were determined from soil surface elevation measurements performed every 10-30 m along the border using a topographic level. Both parameters resulted from regression of elevation vs. distance along the border.

The inflow irrigation discharge was measured using a mini-propeller meter. The advance phase was determined from recordings of the advance time to reference points located along the border every 10-30 m. The flow depth at the upstream end of the border was measured shortly before cut off. A number of flow depth measurements were performed across the border, every 3-4 m. The average of all measurements was used to represent flow depth at this point and time.

Infiltration and roughness were determined from advance and flow depth using SIRMOD, a hydrodynamic one-dimensional surface irrigation model (Walker, 1993). Such a model was iteratively executed using tentative values of the coefficient k and the exponent a from the Kostiakov infiltration equation, and Manning n. The three parameters were adjusted until the model satisfactorily reproduced the experimental values of flow depth and irrigation advance for each evaluation.

The total available water (TAW, mm) (Allen et al, 1998) was determined by a soil survey carried out in the same field where the irrigation was evaluated. A soil sample was obtained in two holes in each plot for the top 0.15 m, and each subsequent 0.30 m until a depth of 1.20 m was reached. Field capacity, wilting point, and moisture content just before irrigation were determined (Soil Survey Division Staff, 1993). Bulk density was also determined at 0.20 m depth. The target irrigation depth (Zr) was determined as 50 % of TAW (Allen et al, 1998).

The next step was to determine the irrigation performance indices (Burt et al. 1997). These indices included the application efficiency (Ea) and the low-quarter distribution uniformity (DUlq). Ea expresses the percentage of irrigation water contributing to Zr. DUlq can be defined as the percentage of the average low-quarter infiltrated depth to the average infiltrated depth.

Model application

The basic data for the simulations were obtained from field work, the BRCC offices, and NRCS soil maps. Such data included on-farm irrigation water management, land tenure, morphology of the irrigation systems, water conveyance structures, crops and soil survey. Simulations were performed for the 2008 irrigation season on a daily basis (hourly for water delivery). The weather this growing season was slightly warmer and drier than the average.

In the Ador-Simulation model, the plot is the basic geographical unit. A typical irrigation unit (a border in this case) is characterized for each plot. Irrigation simulation is performed in the typical irrigation unit and extended to the whole plot area. In a large irrigation district it would be unmanageable to identify, characterize and simulate all borders in all cadastral plots. Therefore, a typical border was defined as characteristic of the irrigated area for each headgate (measured at the cartographical restitution of an aerial photograph, and taking into account the slopes determined in the on-farm evaluations). One of the two soil units of the study area was assigned to each plot according to the soil maps.

The initial soil water depletion at the onset of the simulation period was estimated from the meteorological conditions prevailing during the weeks preceding sowing. Depletion was established as a percent of TAW. The sowing date for each crop was statistically assigned, following the statistical distribution derived from farmers' interviews.

Each plot was related to a water conveyance network element (an irrigation ditch), and to the drainage network. In the case of the irrigation network, each element was characterized by a service and a conveyance discharge, which were obtained from the BRCC.

Crop growth and irrigation simulations were performed on the typical border of each plot. An irrigation was requested when 25 % of the border area was under water deficit (soil water depletion above allowable depletion). The duration of the phenological phases and the crop coefficients, the values of the thermal integral and the related temperature threshold, were derived from local experiences (Hill, 1994). The FAO methodology (Allen et al., 1998) was applied for computing the crop water requirements. The weather data was obtained from a weather station of the Utah State University Extension Service located in Tremonton. The Stewart coefficients for the determination of water stress sensitivity were obtained from the work by Doorembos and Kassam (1979). The common irrigation practices were gathered from farmers and BRCC manager interviews, and used to establish the relationship between agronomy and irrigation: pre-sowing irrigation, irrigation events following alfalfa and forage harvest. Yields, the economic value of crops, and costs were obtained from Government statistics.

The simulation of the current water performance was based on the cutoff time determined in the irrigation evaluations. In all evaluations, the cutoff time was longer than required to refill the soil water deficit. A simulation was performed in the typical border defined as characteristic of the irrigated area of each headgate to determine the optimum cutoff time. This optimum can be defined as the minimum cutoff time necessary in order to ensure that the average low-quarter infiltrated depth in the border attained at least Zr. The irrigation evaluations were equally optimized, and the ratio of real to optimum irrigation time was obtained for each soil type. This ratio was used to estimate the "real" irrigation time for each headgate under the current water management practices.

Two simulations of the water flows in the whole study area were carried out. The first simulated a representative **scenario of the current conditions** of on-farm irrigation practices in 2008. The second simulated the water flows for a **scenario of optimum irrigation time**. A number of irrigation quality, hydrological and

economic indicators were computed from the obtained results (Burt et al., 2007; Molden et al., 1998; Willardson et al., 1994).

RESULTS AND DISCUSSION

On-farm irrigation evaluation

Table 1 presents the aggregated results of the irrigation evaluations, distinguishing the two soil units. The evaluated crops were alfalfa and spring grains. The border size averaged about one and a half hectares, with a moderate variability. Borders are larger in Parleys soils than in Fielding soils. The field slope has a wide range of variation. On average, the slope was similar in both soil units (about 1.61 ‰). The standard deviation of soil surface elevation ranged between 10 and 22 mm, with an average value of 15 mm. These values indicate that laser levelling is often practiced in the study area.

Table 1. Results of the irrigation evaluations performed in the study area.

		Parleys soils	Fielding soils
Area (m^2)	Average	12,589	17,569
	CV (%)	47	21
Width (m)	Average	37	49
	CV (%)	17	20
Slope ($^0/_{00}$)	Average	1.89	1.48
	CV (%)	31	58
Standard deviation of soil	Average	13	16
surface elevation (mm)	CV (%)	38	22
Discharge (m3 s^{-1})	Average	0.091	0.091
	CV (%)	53	14
Irrigation time (h ha^{-1})	Average	5.70	7.18
	CV (%)	49	22
Irrigation depth (mm)	Average	144	230
	CV (%)	22	19
Manning *n*	Average	0.18	0.23
	CV (%)	20	13
Kostiakov *k* (m min^{-1})	Average	0.0145	0.0173
	CV (%)	15	18
Kostiakov *a*	Average	0.318	0.376
	CV (%)	4	5
Total Available Water (mm)	Average	204	228
	CV (%)	6	4
Application Efficiency (%)	Average	65	51
	CV (%)	18	18
Low Quarter Distribution	Average	66	74
Uniformity (%)	CV (%)	18	13

The irrigation discharges present a large variability –between 50 and 120 l s^{-1}- among irrigation ditches. Discharges were similar in both soil units, with an average of 91 l s^{-1}. The irrigation times, although largely variable as a function of the irrigation discharge, were long: about six hours per hectare in Parleys soils and seven hours per hectare in Fielding soils.

The irrigation application depth was generally high, with an average of 144 mm in Parleys soils, and 230 mm in Fielding soils. These irrigation depths were due to the available discharges, and to the irrigation scheduling influenced by soil physical characteristics and the presence of a water table. The TAW was high and uniform, with an average of 204 and 228 mm for Parleys and Fielding soils respectively. The seepage from the Westside canal resulted in the presence of a water table at a depth of about 1.30 and 1.50 m according to a piezometer network available in the area. The soil moisture of the vadose zone was used by crops for evapotranspiration, and constitutes a second source of water for this purpose. This effect was checked by the soil moisture determinations carried out just before the irrigation events. In an irrigation interval of about four weeks, the soil water depletion was about 55 % of the crop evapotranspiration.

Figure 2 presents the infiltration functions derived from the irrigation evaluations. The graphical representation has been grouped by soil unit. Based on these infiltration characteristics, two infiltration functions were derived and later applied to the simulation of irrigation in the study area. Infiltration in Fielding soils is larger than in Parleys soils. However, the geometry, slope, and discharge of the borders suggest that farmers have not taken soil infiltration rate differences into consideration. The main reason for that is the high spatial variability of the distribution of the soil units in the study area (Figure 1). Only in 9 of the 24 headgates contain a predominant soil unit occupying 85 % or more of the irrigated area.

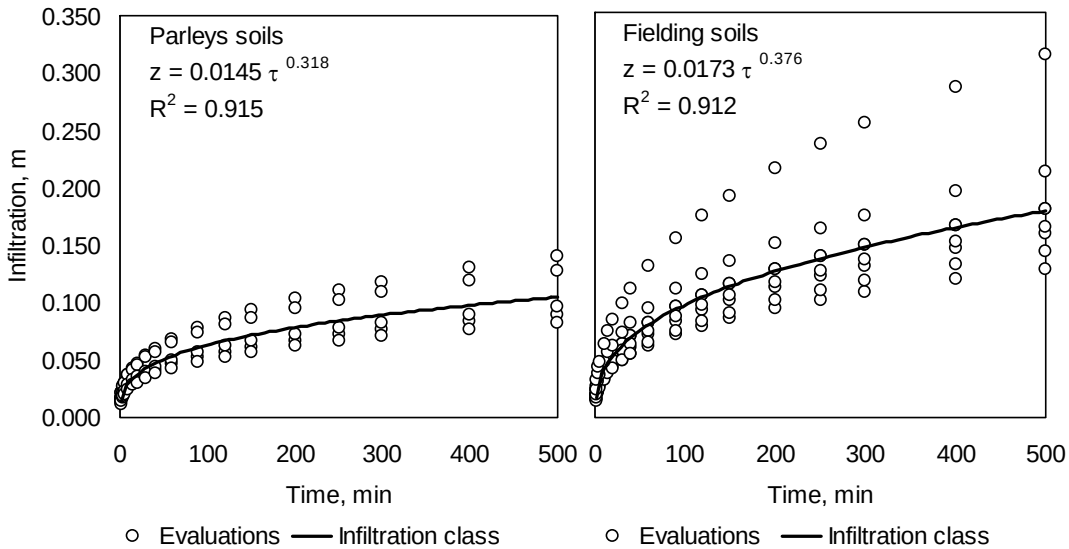

Figure 2. Infiltration functions corresponding to borders in Parleys and Fielding soils. The figures present results from the irrigation evaluations (symbols) and average infiltration curves (lines) and corresponding equations.

Application efficiency reached 65 % in Parleys soils, with uniform frequencies in a range of 54 to 87 %. In Fielding soils, the average application efficiency was 51 %, ranging from 35 to 63 %. These values of Ea can be classified as low, and the potential improvement for current irrigation pratices will be shown below.

The minimum DUlq was 55 %. In the Parleys soils the average uniformity was 66 %, while the average value for Fielding soils was 74 %. The accumulation of water at the end of the blocked-end borders is the main reason for these low values.

Model application

The first step was to optimize the cutoff time of the irrigation evaluations. The results showed that it is possible to reduce the irrigation time to an average of 5.2 h ha^{-1} ensuring that the average low-quarter infiltrated depth in the border attains at least Zr. This reduction allows for the increase of the application efficiencies to 72 % in Parleys soils, and 67 % in Fielding soils, with irrigation depths of 0.140 and 0.170 mm respectively.

The simulation of water flows in the whole study area for the **scenario of current conditions** of on-farm irrigation practices in 2008 considered the irrigation times determined in the evaluations. A number of parameters related to irrigation scheduling, conveyance network water losses, and evapotranspiration from the vadose zone were also considered in the simulation of the whole study area.

Irrigation scheduling parameters were the minimum interval between irrigations, and the maximum number of irrigations per crop. These parameters were provided by farmers and BRCC managers. Corn is irrigated between four and five times per season, with a minimum average interval of 14 days. Alfalfa and grass present the same number of irrigations but with an interval of about 28 days. Grains are irrigated three times per season in a minimum average interval of 21 days.

A previous study carried out by the BRCC determined that the average seepage and spills water losses in the conveyance network are about 10 % of the total water delivered from headgates.

A layer with constant moisture (field capacity) was considered in the model for reproducing the effect of the water table over the crop evapotranspiration. The depth of this layer was estimated at 0.70 m -over a root zone of 1.20 m- for obtaining similar water depletions just before irrigation to the depletions determined in the irrigation evaluations carried out during July and August.

Figure 3 shows the monthly water demand of the study area provided by the BRCC, and the demand simulated with the model. On a cumulative basis, the simulation results compare well with the BRCC data, with a seasonal difference of 3 %. On a monthly basis, during the peak of the season the differences vary between 2 and 10 %. In spring and autumn the differences are highly variable, reaching values between 8 and 35 %. These differences can be attributed to the agronomic practices of the farmers, which are difficult to establish and model. Additionally, soil infiltration during the first irrigation of the season is usually very large. Initial soil water content, temporal distribution of conveyance network water losses and water table depth oscillation are other factors which influence these monthly differences.

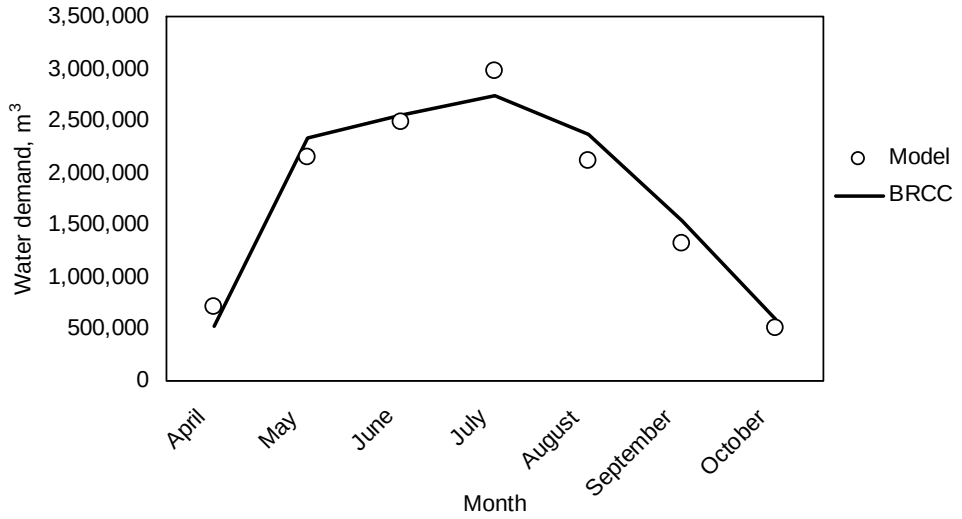

Figure 3. Water demands as registered by BRCC and simulated by Ador-Simulation in the study area.

The simulation of water flows in the whole study area for the **scenario of optimum irrigation practices** considered the optimized irrigation times determined for the evaluated irrigation events. The same values of irrigation intervals, percentage of conveyance network water losses and depth of the constant soil moisture layer were considered.

Table 2 shows the values of different indicators for the two simulated scenarios. The optimization of the cutoff time increase efficiencies about 20 %, to an average of 75 %, and DUlq from 62 to 75 %. The high TAW of the soils, the initial soil water content, and the vadose zone are the main factors that explain the reduced differences between application and irrigation efficiencies.

Improving on-farm irrigation practices would allow the reduction of water demand by 27 %, equivalent to a volume of 3,3 hm^3. The reduction could be higher if improvements in water delivery management are achieved, but this study did not have enough data for this estimation. This volume not only represents a water conservation, but also, a water saving due to the diminished irrigation returns flow to the nearby Great Salt Lake where this water can not be reused. For this reason, the consumptive fraction of the water demand is 100 %. The productive (crop evapotranspiration) consumptive fraction is increased from 60 to 77 % due to the reduction of return flows, and a minimal increase of the crop evapotransporation. The vadose zone contributes to this evapotranspiration with an estimated volume of 1,8 hm^3.

The difference between real and potential crop evapotranspiration is about 9 % in both scenarios, similar to other irrigation projects in the USA (Allen et al., 2005). This difference is mainly due to the effect of low DUlq, the optimization of cutoff time until the Zr is reached in the average low-quarter infiltrated depth in the borders, and the irrigation intervals applied. Although the capacity of the conveyance network allows for increasing the number of irrigation events with the irrigation times

adopted, the impact over crop evapotranspiration and yields are minimum, about 2 % (results not shown).

Table 2. Summary of simulation results obtained through the application of Ador-Simulation to the current scenario of the study area and an optimized scenario.

	Current Scenario	Optimized Scenario
IRRIGATION INDICATORS		
Irrigation time, h ha^{-1}	6.8	4.6
Average Application Efficiency, %	53	74
Average Irrigation Efficiency, %	56	77
Average LQ Distribution Uniformity, %	62	75
HIDROLOGICAL INDICATORS		
Canal Water Demand, hm^3	12.27	8.96
Precipitation, hm^3	1.25	1.25
Water Use from Vadose Zone	1.88	1.78
Crop Evapotranspiration, hm^3	9.55	9.59
Irrigation and Rain Return Flows, hm^3	6.25	2.90
Seasonal Soil Water Variation	-0.40	-0.51
Consumptive Fraction, %	100	100
Productive Consumptive Fraction, %	60	77
Crop Evapotranspiration Reduction, %	9	9
ECONOMIC INDICATORS		
Crop Yield Reduction, %	14	12
Crop Gross Value Reduction, %	12	10
Crop Gross Value, M$	1.488	1.516
Crop Net Value, M$	0.504	0.532
Gross Surface Productivity, $ ha^{-1}	1226	1249
Net Surface Productivity, $ ha^{-1}	416	439
Gross Consumptive Water Productivity, $ m^{-3}	0.092	0.117
Net Consumptive Water Productivity, $ m^{-3}	0.031	0.041

The crop evapotranspiration reductions imply a yield reduction of about 14 % in the current scenario, and 12 % in the optimized scenario, and consequently, a reduction in the gross crop production value of 12 and 10 % respectively. Due to these small differences between scenarios, and the low value of these field crops, the economic incentives for adopting a more careful control over irrigation time are negligible for the farmers. The net surface productivity is only increased by 23 $ ha^{-1}. Similar effects occur over low consumptive water productivities, whose value is lower than the average of US (Clemmens et al, 2008).

Nevertheless, the water saving obtained from improving on-farm irrigation practices can increase the water availability in drought years, and this fact can constitute a true incentive for farmers. In order to achieve the results shown in the Table 3 for the scenario of optimum irrigation practices, the farmers should apply the findings obtained in this study about irrigation time. For this purpose, a number of graphics like the one shown in Figure 4 were developed. These figures indicate the irrigation

time that optimizes the application efficiency considering different unitary discharge and slopes, and a Zr equivalent to 50 % of TAW. As Burt and Styles (2000) pointed out, technical assistance to farmers and districts/companies is a key factor form improving water management.

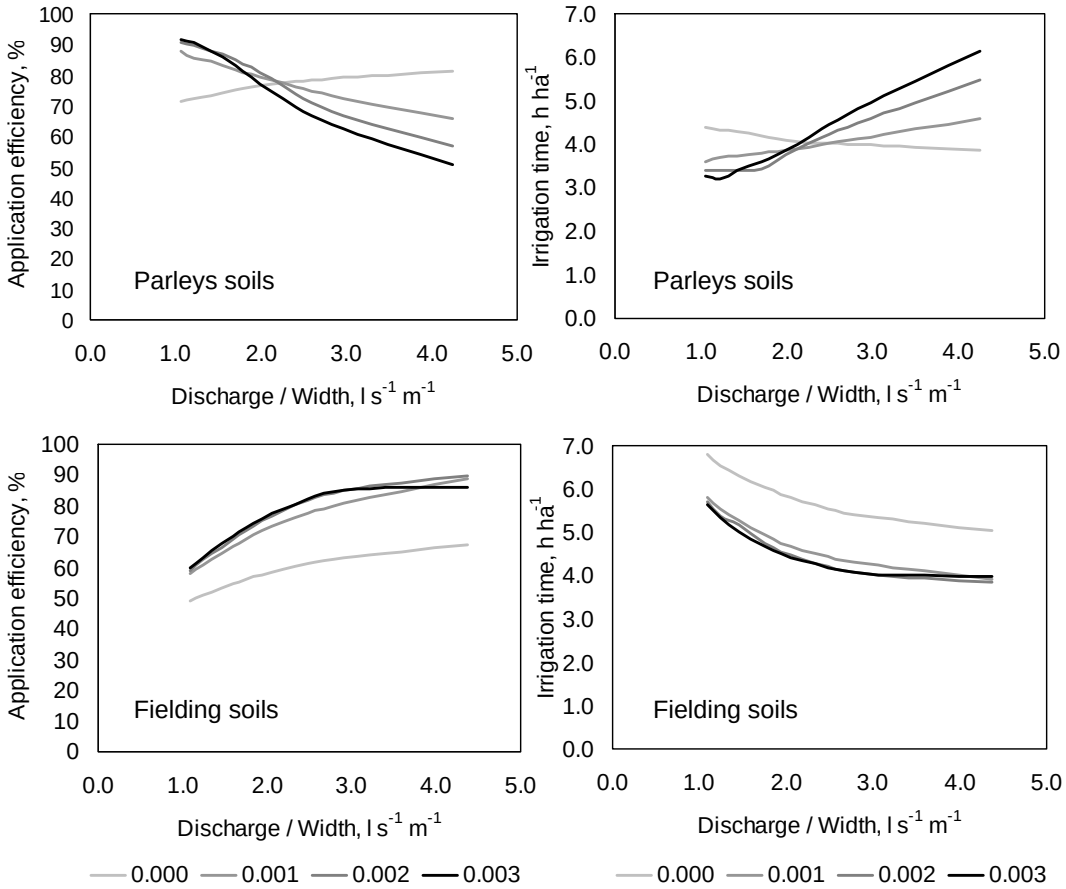

Figure 4. Application efficiencies for optimized irrigation times with a discharge of 85 l s^{-1} and different widths and slopes (m/m) in Parleys soils (with Zr of 102 mm) and Fielding soils (with Zr of 114 mm).

CONCLUSIONS

The productivity of irrigation evaluation field work processes can be notably increased by the use of combined models like Ador-Simulation. These models surpass the analyses based only on application efficiency, and provide a wide range of irrigation, hydrological and economic indicators.

The results can be useful for farmers and irrigation projects managers in order to improve on-farm irrigation practices, water delivery, and structures. River Basin Authorities managers can analyse potential water conservation and/or water saving in the agricultural water uses of the basin, and the economic and water security effects on farmers.

The application of this methodology to the study area in the Bear River irrigation project has shown that optimizing irrigation time can provide a potential of water

saving of about 27 % over the 2008 water demand. Although the effects of this improvement on the economic value of crop production and productivities are low, the water conserved could be important for reducing economic losses during drought years as the Bear River Canal Company could store some of that water in Bear Lake, upstream. The simulation can be easily applied to other years if managerial data are available, for example from RAPs, and using the data obtained from the field work performed in 2008.

ACKNOWLEDGEMENT

Thanks are due to the managers and farmers of the Bear River Canal Co., and technicians of the Utah State University Extension Service for their support. The postdoctoral contract of S. Lecina was funded by the Spanish Ministry of Science and Innovation and the Spanish Foundation for Science and Technology.

REFERENCES

Allen, R.G., Pereira, L.S., Raes, D., Smith, M. (1998). “Crop evapotranspiration. Guidelines for computing crop water requirements”. FAO Irrigation and Drainage Paper nº 56. FAO. Rome (Italy). 300 pp.

Allen, R.G., Clemmens, A.J., Burt, C.M., Solomon, K., O’Halloran, T. (2005). “Prediction accuracy for projectwide evapotranspiration using crop coefficients and reference evapotranspiration”. J. Irrig. Drain. Eng. 131(1):24-36.

Burt, C.M., Styles, S.W. (1999). “Modern water control and management practices in irrigation. Impact on performance”. FAO Water Reports No. 19. FAO. Rome (Italy). 223 pp.

Burt, C. M., Styles, S. W. (2000). "Irrigation district service in the western United States." Journal of Irrigation and Drainage Engineering-Asce, 126(5), 279-282.

Burt, C.M., Styles, S.W. (2004). “Conceptualizing irrigation project modernization through benchmarking and the rapid appraisal process”. Irrigation and Drainage, 53:145-154.

Burt, C.M., Clemmens, A.J., Strelkoff, T.S., Solomon, K.H., Bliesner, R.D., Hardy, L.A., Howell, T.A., Eisenhauer, D.E. (1997). “Irrigation performance measures: efficiency and uniformity”. J. Irrig. Drain. Engrg., ASCE, 123(6),423-442.

Clemmens, A.J. (1987). “Delivery system schedules and required capacities”. In: Planning, operation, rehabilitation and automation of irrigation water delivery systems. Portland, OR (USA). pp. 18-34.

Clemmens, A. J., Allen, R. G., and Burt, C. M. (2008). "Technical concepts related to conservation of irrigation and rainwater in agricultural systems." Water Resources Research, 44, 16.

Dechmi, F., Playán, E., Faci, J.M., Tejero, M., Bercero, A. (2003). “Analysis of an irrigation district in northeastern Spain: II: Irrigation evaluation, simulation and scheduling”. Agric. Wat. Manage., 61, 93-109.

Doorembos, J., Kassam, A.H. (1979). Yield response to water. FAO Irrig. and Drain. Paper nº 33. FAO. Rome (Italy). 212 pp.

Hill, R.W. (1994). “Consumptive use of irrigated crops in Utah”. Research Report 145. Utah Agricultural Experiment Station. Utah State University. Logan, UT (USA). 361 pp.

Lecina, S., Playán, E., Isidoro, D., Dechmi, F., Causapé, J., Faci, J.M. (2005). "Irrigation evaluation and simulation at the irrigation district V of Bardenas (Spain)". Agric. Wat. Manage., 73, 223-245.

Lecina, S., Playán, E. (2006a). "A model for the simulation of water flows in irrigation districts: II. Application". J. Irrig. and Drain. Engrg., ASCE, 132(4):322-331.

Lecina, S., Playán, E. (2006b). A model for the simulation of water flows in irrigation districts: I. Description. J. Irrig. and Drain. Engrg., ASCE, 132(4):310-321.

Malano, H., Burton M., (2001). "Guidelines for benchmarking performance in the irrigation and drainage sector". In: International Programme for Technology and Research in Irrigation and Drainage, 2001.

Mateos, L., López-Cortijo, I., Sagardoy, J.A. (2002). "SIMIS: the FAO decision support system for irrigation scheme management". Agric. Wat. Manage., 56, 193-206.

Merkley, G.P. (1994). "Planning Distribution Model. A simulation tool for water management planning in large-scale irrigation and drainage networks. User's Guide". Biological and Irrigation Engineering Department, Utah State University. Logan, UT (USA). 104 pp.

Merriam, J.L., Keller, J. (1978). "Farm irrigation system evaluation: A guide for management". Utah State University. Logan, UT (USA). 271 pp.

Molden, D.J., Sakthivadivel, R., Perry, J., Fraiture, C., Kloezen W.H. (1998). "Indicators for comparing performance of irrigated agricultural systems". Research Report 20, International Water Management Institute. Colombo, Sri Lanka. 26 pp.

Playán, E., Mateos, L., (2006). "Modernization and optimization of irrigation systems to increase water productivity". Agric. Wat. Manage., 80, 100-116.

Playán, E., Slatni, A., Castillo, R., Faci, J.M. (2000). "A case study for irrigation modernisation: II. Scenario Analysis". Agric. Wat. Manage., 42, 335-354.

Prajamwong, S., Merkley, G.P., Allen, R.G. (1997). "Decision support model for irrigation water management". J. Irrig. and Drain. Engrg., ASCE, 123(2), 106-113.

Soil Survey Division Staff. (1993). "Soil survey manual". United States Department of Agriculture. Handbook No. 18. Washington, D.C. (USA).

Yamashita, S., Walker, W.R. (1994). "Command area water demands. Part I. Validation and calibration of UCA model". J. Irrig. and Drain. Engrg., ASCE, 120(6), 1025-1042.

Walker, W.R. (1993). "SIRMOD, Surface irrigation simulation software". Utah State University. Logan, UT (USA). 27 pp.

Willardson, L.S., Allen, R.G., Frederiksen, H.D. 1994. "Elimination of irrigation efficiencies". In: 13th Tech. Conf. USCID, USCID (Ed.), 19-22 October, at Denver, CO (USA). 17 pp.

Neighborhood Channel is Redefined with Boulder Armoring

Ted Niemann, P.E., D.WRE[1] and John Loechle[2]

[1] Elizabeth Niemann & Associates, Inc., 3703 Taylorsville Rd, Louisville, KY 40205; PH (502)-458-0788; email: tlniemann_ena@bellsouth.net
[2] Louisville and Jefferson County Metropolitan Sewer District, 700 West Liberty Street, Louisville, KY 40203-1913; PH 502-540-6209; email: loechle@msdlouky.org

ABSTRACT

A channel through a neighborhood in Jefferson County, Kentucky was eroding and accumulating complaints of property damage and flooding. The channel, carrying an intermittent stream, had been filled by the developer of this neighborhood to be a grass channel flowing through the backyards. Development upstream increased the flows through this area and caused erosion of the grass channel. Efforts to armor the channel with gabion baskets and rip rap, and in some cases landscape timbers did not stem the tide of damage.

The length of channel being evaluated was approximately 1,800 feet. A solution for the entire length under review was desired. Armoring the banks with boulders was the preferred method to stabilize the stream banks. The SCS TR-55 program was utilized to calculate flows to size the proposed channel. The channel width was chosen to allow the channel to achieve bank full depth. The bank full depth was determined by field observation of sections of the entire length of the existing stream. The proposed channel alignment was arranged to closely resemble the existing and to minimize disruption to existing utilities as well as uses by the adjacent property owners.

Methodology of the hydraulic analysis and design of the stream bank armoring is discussed herein as a low tech solution for urban and suburban stream projects. Armoring the stream banks provided the protection needed while defining the stream and allowing movement of runoff through the project area without using a concrete channel. The use of boulders along the banks created a more "natural" channel appearance and satisfied the client (MSD) as well as the adjacent property owners.

BACKGROUND

In the late 1980's, the Saratoga Hills subdivision near Louisville Kentucky was developed. As a part of this development, a rock bottom intermittent stream was transformed into a grass swale. The grass swale made the backyards picture perfect for the new subdivision. In the years following this transformation, development upstream encouraged the retrenchment of the stream toward it original state. In 1997, a regional

flood event removed the remnants of the grass swale exposing the original rock bottom stream. What was a grass swale that neighbors could walk across turned into a stream spanning from inches to more than 20 feet in width. The transformation back to a natural system was causing soil erosion and property loss, including the exposure of several gravity sewer lines that were constructed parallel to the channel. The change was also threatening the adjacent homes with flooding along an 1,800 foot section of the stream. The problem impacted approximately 50 homes.

The local regulatory sewer and drainage authority, Louisville and Jefferson County Metropolitan Sewer District (MSD) started working with the Saratoga Hills Neighborhood Association in an effort to remediate the property loss and flooding concerns. In an effort to reduce or slow down erosion along the channel, remedial measures were installed. Rip rap, gabion baskets and property owner-installed landscape timbers slowed the inevitable erosion advance. Workshops were held to educate the neighborhood on green infrastructure solutions. Weekend native planting events were scheduled with material donated by MSD. These events continued the education of the neighborhood and get participation in reinforcing the stream banks using natural methods. The goal was to change the philosophy of the golf course, manicured lawn mindset; to develop a no-mow zone with plantings along the channel. However, most of the group that had purchased new homes with a nice grass swale in their backyards did not buy-in to the "no-mow" philosophy.

Improvements were needed to resolve soil erosion and potential property flood damage along the rear drainage system in the neighborhood. The subject channel is approximately 1,800 feet in length and runs between a 48-inch culvert at Saratoga Club Road and an existing storm water detention basin that eventually drains into Chenoweth Run Creek. Project goals were outlined as 1) stabilize the channel banks; 2) define the channel width the entire length; 3) provide a solution that will eventually blend with the neighborhood; 4) provide a "natural" look that will not look like an urban channelization project and 5) get the support of the neighborhood.

Boulder armoring was identified as the preferred method of remediation; providing a more natural appearance than poured concrete. It was anticipated that the channel would develop natural channel characteristics over time within the proposed defined channel. This method of protection would also allow the no-mow zones for the owners that chose to participate. Planting and native grass zones would be developed behind the boulder improvements. And for the owners not wanting to participate in the no-mow area, the boulders would give them erosion protection while allowing their 'golf course' mowing practices. The boulder protection would also provide the armoring needed for the storm velocities to which the channel is exposed.

There are multiple types of cross sections that exist within the project area due to variations of the existing terrain. Within the first few hundred feet, the stream is flat and covered with rip rap that has been placed to slow flows. The side slopes are slight and the channel width measures from 15 feet to just a few inches within this section. Within the

next several hundred feet the original rock bottom is evident and there are areas that have rock ledges that form cascades. The side slopes begin to increase and there are multiple methods of bank reinforcement in-place throughout this section. These range from gabion baskets to landscape timbers to large rip rap. The existing width increases to up to 20 feet in some areas. In the last section – several hundred feet leading into the existing drainage basin, the channel has eroded significantly and sediment has been deposited within the banks of the stream. In this area the channel width has gone beyond 20 feet in some areas but narrows down to just a few feet as it passes through the detention basin and outlets through an existing pipe and headwall.

DRAINAGE AREA AND DISCHARGE CALCULATION

The drainage area, depicted in Figure 1, above the culvert in Saratoga Club Road is approximately 82.6 acres and is made up of mostly residential lots with some undeveloped pasture land. The drainage area contributing directly to the channel identified for improvements is 74.0 acres, fully developed as residential lots. The total drainage area to the project is 156.6 acres. The MSD Design Manual recommends the Soil Conservation Service (SCS) method for runoff calculations is to be used when the drainage area exceeds 50 acres in size or is in need of a detention basin. The drainage area contributing to the subject channel meets this criterion.

In order to move forward with the design of the project, assumptions were made within the SCS – TR55 runoff model.

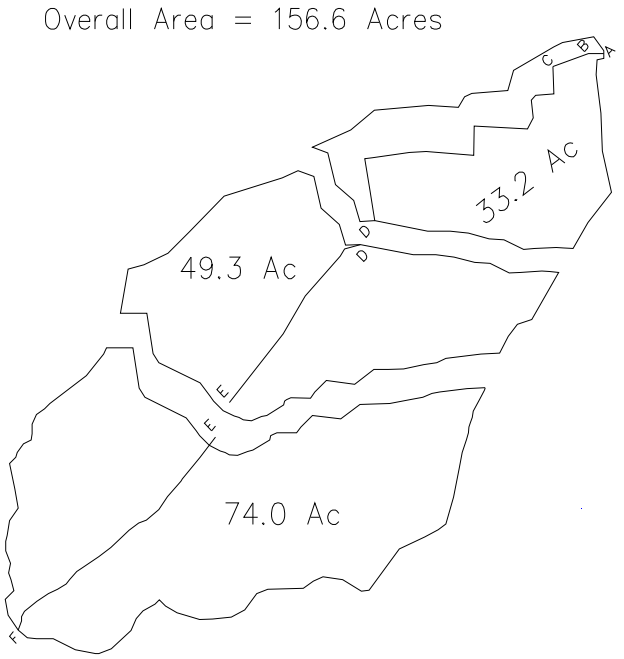

Figure 1. Drainage Area and Flow Path

To calculate the discharge for the upper portion of the water shed, the time of concentration had to be estimated. The time of concentration is the time it takes a drop of water to travel from the furthest point in the water shed to the outlet and is generally identified by T_c. The T_c is made up of the sum of three distinct components, summarized in table 1: 1) Overland (sheet) flow; 2) shallow concentrating flow; and 3) channel flow.

T_c = Tsheet+Tshallow+Tchannel

Table 1. Summary of Time of Concentration Calculation

Sub Area	Length (ft)	Slope (ft / ft)	Manning's n	Velocity (ft / sec)	Travel Time (hr)
Sheet	100	0.020	0.24		0.238
Shallow	239	0.029	0.05		0.024
Channel	2083	0.028	0.03	5.076	0.114
Channel	3004	0.026	0.04	7.320	0.114
				Total T_c	**0.49**

To design the channel improvements in this lower portion of the watershed, downstream of the culvert under Saratoga Club Road bank full flow was used. The bank full flow depth was observed in the field, and it varied within the different reaches with the deepest being approximately 1 foot. Bank full, or channel forming flow, can occur in the 0.8 to 2.0-year storm event. The channel width was chosen to allow space for the channel to achieve bank full depth. The flowrate was calculated using the SCS TR-55 model. Both the 2-year storm and the 10-year storm were analyzed with the existing upstream channel geometry.

The soil type and land use was evaluated for the drainage area to determine a curve number, which is similar to the rational formula's "C" factor. The land use for the area was observed to be a residential district (1/4 acre lots) with some undeveloped open space and pasture. The weighted curve number for the 156.6 drainage area was estimated to be 80.

- The peak flow calculated for a **2-Yr.** rainfall return period is **192.9 cfs**
- The peak flow calculated for a **10-Yr.** rainfall return period is **344.6 cfs**

The 100 year storm was not analyzed because there was no change in either the upstream conditions or the outlet conditions.

TOPOGRAPHIC SURVEY

A topographic survey of the project area was performed. This survey located existing topographic features as well as visible utilities in the area. The edges of the existing channel were located along with the existing planimetric and topographic information for the project area. Cross sections were taken at 50 foot intervals along the channel. This data was used to interpolate cross sections along the channel for use in the design.

PRELIMINARY DESIGN

Measurements were taken of the width of the existing channel in our project area as well as that of the section of channel directly upstream of the project area. These measurements, the bank full observations, along with the space restrictions that exist within the project boundary led to a proposed uniform channel width of 12 feet. This width was used in the drainage calculations when determining the flow into/through the project area.

The existing channel centerline was approximated based on the edge of channel determined by the land surveyor. A proposed channel alignment was laid out that attempted to follow the existing channel's path. Where existing natural features, (large trees, brushy banks, etc.), sanitary sewer features and other improvements such as fences and extensive landscaping were encountered, the channel alignment was adjusted to allow for protection of the feature. The proposed alignment was laid out to stay within the existing sanitary sewer and drainage easement, where possible.

Typical sections, as depicted in Figure 2, were developed to show the different scenarios for the rock boulder toe depending on the existing terrain. These typical sections were

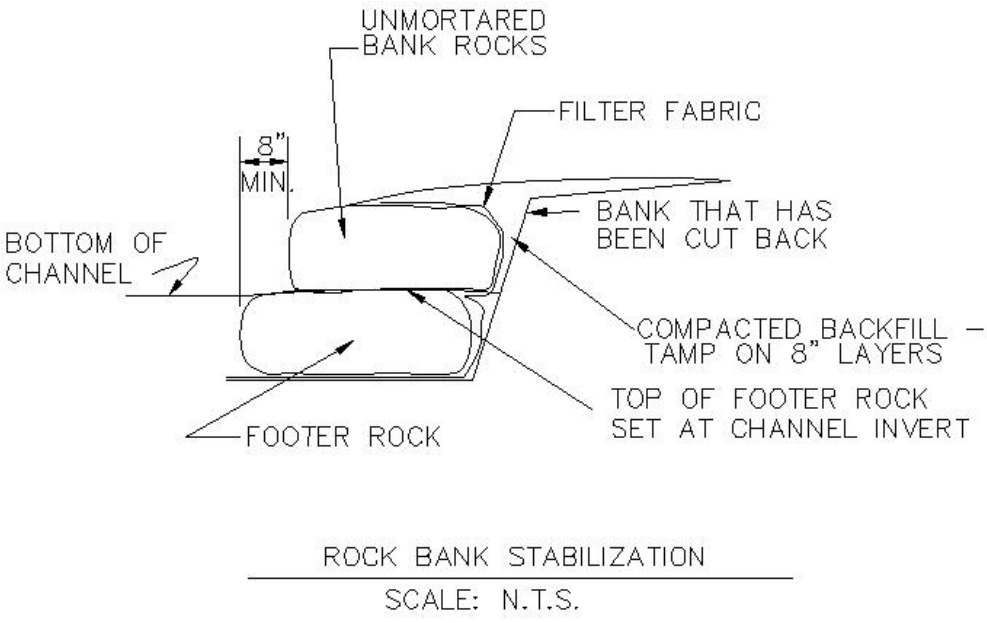

Figure 2. Typical Section Rock Stabilization

inserted into the cross sections to allow the designer to determine which section would fit best and how the rock boulder toe would transition from one section of channel to another. The cross sections were developed assuming a boulder height of one foot. The height the boulders would be stacked, or number of one foot courses, was determined from the existing terrain. The boulder "wall" course height was designed to have the soil behind the boulders at three to one grade or less. This would allow ease of maintenance for the property owners. A filter fabric was specified behind the boulders for prevention of soil loss.

A summary of the existing channel characteristics with velocities was presented in Table 1. The proposed channel geometry was evaluated for the 2 year and the 10 year storm events within the TR 55 software and the HYDRAIN software to get an idea of the proposed system performance. In the lower reaches of the channel velocities approached 7 feet per second (fps).

The maximum allowable velocity for a vegetative channel, with these characteristics, is approximately 2 fps. With the relatively steep slopes in the existing channel, grass lining could not withstand the shear stresses and would not be stable. Therefore, alternative methods were required.

The proposed channel could have been designed with larger rip rap. However, MSD's past experience with this type of installation suggested property owners would not be pleased with the irregular surface, vegetation (weeds) between the rock and the trash that sometimes get caught within the rock. The design needed to be able to withstand the high velocities and shear stresses that existed and appear more natural than man-made.

A standard channel width of 12 feet allows velocities to decrease to near 5 fps for a 2 year storm and also provides the capacity for sediment to be dropped during lower seasonal flows. The original channel's rock bottom that had been exposed provides a stable base for the higher velocities that sometimes occur. The boulders provide protection of the adjacent grass and soil during the typical bank-full flows and help maintain channel width definition as scouring velocities are reached.

PROPOSED PLANTINGS

After a site visit to the project area, the Biologist involved with this project suggested plantings that could be a part of the final restoration. Their suggestions included dividing the project area into two zones for plantings: Zone I is directly adjacent to the channel. Zone II is an area further back from the channel edge. In Zone I, fast growing trees and shrubs could be planted. Some of the possibilities in this area include: Flowering dogwood; Silky dogwood; Sycamore; Green Ash; Tulip Poplar and Persimmon. In Zone II some of the possibilities include: Northern Red Oak; White Oak; Black Oak and Black Walnut. Within areas that are determined to be a "no-mow" zone, a native seed mix could be planted that might consist of the following: Annual rye (if restoration occurs in the spring); winter wheat (if restoration occurs in the fall/winter); deer tongue panic grass; wild rye; switch grass; barnyard grass and creeping bentgrass.

CONSTRUCTION

PERMITTING

The channel is classified as an intermittent blue-line stream and required permits from two agencies associated with water and water quality.

Under the provision of Section 404 of the Clean Water Act, a Corp of Engineers permit was required. The project was judged to fall under the provisions of the Nationwide General Permit for Aquatic Habitat Restoration, Establishment and Enhancement Activities. Construction in the channel also required two permits from the Kentucky Department of Environmental Protection (KDEP). The first permit was a Stream Construction Permit – for restoration of a channel, the second a Water Quality Permit. There was more discussion than usual regarding the sediment control set up for the channel. Since the channel is classified as an intermittent Blue Line only one rock bag check dam was desired by the KDEP and that was an outlet protection measure. Originally, the design called for four rock bag check dams in the channel to catch sediment in the base flow. KDEP did not agree and the contractor was instructed to remove all but one rock bag check dam. Unusual treatment of the channel was thought to be justified since a detention basin existed at the channel outlet.

RELIANCE ON CONTRACTOR

The successful bidder was a contractor who had constructed other stream bank boulder revetments. Construction of the boulder toe walls is not much different than fitting together a child's building block set. Some pieces fit in one location better than they fit in another. Since fitting boulders of various sizes into a wall and providing positive drainage over or through the wall is a tedious process, having patience with this very hands-on approach can prove invaluable. When care is taken to think through the process the finished product will more than likely pass the test of time.

CONSTRUCTION

Construction began on the upstream end of the channel with transition stone laid from the existing 48-inch headwall to match the existing ground-line. Rip Rap was removed and boulders placed. The south side of the channel was higher than the north side and boulders were adjusted in the field to match existing ground line incorporating the proposed 50 foot cross sections detailed in the construction plans as closely as possible. Work proceeded downstream, first removing the rip rap or gabions, then placing the boulders and filter fabric and finally backfilling.

The Contractor provided a three man crew to perform the work. First, a mini-excavator operator removed rip rap and placed the boulders along the exposed banks. Second, a driver transported excavated rip rap and gabions to the staging area and carried selected boulders back to the work zone. The third member of the crew was a laborer who placed the filter fabric; fine tuned the backfill and trimmed the fabric once the backfilling was completed.

With work occurring in the actual channel, there was little that could be done to stop the transport of fine sediment. Efforts were made to keep rip rap in the stream and in other critical areas to help trap sediment during the low flows. The detention basin downstream was used as an erosion control measure allowing silt to be captured before discharge into the receiving stream.

Work was disrupted on a few occasions when sanitary sewer connections were encountered in a shallow trench, just under the excavated rip rap. These connections were much more shallow than anticipated and could be the result of the channel bed seeking its original level. Repair of a few connections were required after the equipment crushed the existing pipe.

ADJUSTMENTS

The channel was specified to be 12 feet in width. The Contractor and the MSD Inspector made the decision to adjust the alignments of the wall in certain locations to avoid removal of trees. The channel width was not compromised significantly and no ill effects are anticipated.

No geotechnical exploration was performed as part of the design. The Contractor chose to remove all of the rip rap / sediment from the original rock flow line. The restored channel is a rock bottom channel almost the entire length. Some pools exist and sediment is beginning to accumulate along the walls in portions of the channel creating a prototypical sand bar structure.

As the project progressed, additional thought was put into the restoration with native grasses, shrubs and trees. With the exception of the staging area that was located in the detention basin storage area, the disturbed foot print was quite small for the project. Occasionally, the disturbed limit was as close as 6-inches from the back of the installed boulder to as much as 10 feet. MSD reviewed the project site and recognized most of the properties abutting the project were maintained lawns. Experience on other projects led to the decision to restore in standard lawn grasses, rather than paying a premium for native seed. Although it would be more favorable to the stream to be surrounded by water favoring grasses and shrubs, there was a concern the property owners would see the native grasses and shrubs as “weeds”. When most moved into their homes it was a grass lined swale that they could walk across to visit their neighbors. Having the good intentions of a native restoration was not viewed as meeting the property owner’s perspective on the channel. A native restoration would likely be removed and reinstalled as lawn by the property owners. Three of the approximately 50 homeowners adjacent to the project have called MSD with concerns of not having the native restorations installed. MSD will work with these owners in the near future to establish a few native areas in the hope of providing an example of what these types of plantings could do for the rest of the neighbors. MSD is very interested in encouraging native restoration, where appropriate, throughout the entire Louisville Metro area.

LESSONS LEARNED

- Focus on the flow in the channel in order to match the channel to "normal" flow conditions
- Don't expect plans to be followed to the letter. Field conditions change. Materials used in construction vary which adds to the aesthetics of the project.
- Design should be flexible where possible. Communicate the areas that are not flexible.
- Understand as a designer, the boulders do not all come in the dimensions you called for. These are not toy blocks!
- Work with a Contractor, build a trust with them and make sure that they understand the intent of the project.
- Set expectations early for all involved, the local authority, the neighborhood, the Contractor and the Inspector.
- Make sure property owners understand intent, schedule and what they will be seeing.
- Match restoration as closely as possible to surrounding or get buy-in from the majority of property owners – don't throw your restoration money under the mower.
- Weather – understand how it will impact your construction and plan for it…. Because it will.

REFERENCES

Louisville and Jefferson County Metropolitan Sewer District (MSD), *MSD Design Manual; Chapter 10 Stormwater Facilities Design* , Revised Edition, January 2001. http://www.msdlouky.org/insidemsd/pdfs/designmanual02/Chapt10-2000.pdf

Natural Resources Conservation Service (2005); *TR-55 Small Watershed Hydrology Processing Program, Version 1.0.08.* United States Department of Agriculture

GKY and Associates, Inc. (1998). *HYDRAIN for Windows, Hydrologic and Hydraulic Modeling Software*

Evaluation of irrigation scheduling efficiency and adequacy by various control technologies compared to theoretical irrigation requirement

Mary McCready[1], Michael D. Dukes[2]

[1]University of Florida, Agricultural and Biological Engineering Dept., PO Box 110570, Gainesville, FL 32611, mlshedd@ufl.edu, mddukes@ufl.edu

Abstract

A variety of commercially available technologies for reducing residential irrigation water use are available to homeowners. These technologies include soil moisture sensors, rain sensors and evapotranspiration (ET) based controllers. The purpose of this research was to evaluate the effectiveness of these various technologies comparing the adequacy and efficiency of the irrigation schedules for each control device with an irrigation schedule developed using a theoretical soil water balance. Testing was performed on a soil moisture sensor (SMS, LawnLogic) at a low and a medium soil moisture threshold setting. Mini-Clik rain sensors (RS) comprised four treatments, with one treatment pre-set for 3 mm of rainfall and an irrigation frequency of 7 d/wk. The other three RS treatments had sensors pre-set to bypass irrigation for 6 mm of rainfall and irrigation schedules of either 1 or 2 d/wk. An ET controller was also tested, the Toro Intelli-Sense controller (TORO). A time-based treatment with irrigation 2 d/wk and no rain sensor (WOS) was established as a comparison. In general the irrigation schedule for all treatments was more adequate during the fall months of testing than the spring months. Efficiency decreased for most treatments in the fall months of testing. Adequacy values calculated for 30-day running totals tended to vary greatly during a testing period. During the spring months of testing the average range in 30-day adequacy ratings was 24% and during the fall months the average range was 21%. The range in adequacy was as high as 63% during testing for one treatment. Looking at only one 30-day testing period may not fully capture the adequacy of an irrigation control device.

Key Words Theoretical irrigation requirement, soil moisture sensor, rain sensor, ET controller, turfgrass

Introduction

Residential irrigation systems that are automated have been shown to use 47% more water on average than sprinkler systems that are not automated (Mayer et al., 1999). High water use with automated irrigation systems can be attributed to several factors, including the tendency to not adjust irrigation systems in response to

changing weather conditions. Another factor may be that the irrigation system is not uniform and/or the system irrigates all zones similarly regardless of soil and slope conditions. In an attempt to reduce the amount of water used for irrigation purposes, landscape irrigation has been regulated in most, if not all, areas in Florida. In the St. Johns River Water Management District (SJRWMD) irrigation is restricted to a maximum of two days/week between 4 pm and 10 am (SJRWMD, 2008).

Various irrigation control technologies are commercially available to optimize landscape irrigation. These technologies include; soil moisture sensor controllers, ET (evapotranspiration) controllers and rain sensors.

In a soil moisture based irrigation controller, data from the sensor is used to allow or bypass timed irrigation events. The sensor has an adjustable threshold setting and if the soil moisture content exceeds that setting the event is bypassed (Dukes, 2005). A single sensor can be used to control the irrigation for many zones or more than one sensor can be used to irrigate multiple zones. In the case of one sensor for several zones, the zone that is normally the driest, or most in need of irrigation, is selected for placement of the sensor in order to ensure adequate irrigation in all zones.

Evapotranspiration (ET)-based irrigation controllers ideally allow irrigation according to ET needs of the plant. ET is the water lost from the soil and plant surfaces by evaporation and from the plant by transpiration. Since the two processes occur simultaneously and are very difficult to separate, they are combined into one process (Allen et al., 1998). ET controllers can generally be programmed for various site specific conditions such as soil type, plant type, root depth, sun exposure, etc. ET controllers can be purchased as an addition to an existing irrigation timer or as a single component to replace the standard timer.

Rain sensors are devices designed to collect rainfall and after a certain depth of rainfall is collected the devices will interrupt scheduled irrigation events. These devices open the circuit between the irrigation timer and the irrigation valves (bypassing timed irrigation events) after a specific amount of rainfall has occurred. Rain sensors are attached to existing irrigation timers. An initial program is programmed into the timer and this program includes timing and depth of irrigation. The rain sensor then either bypasses or allows the programmed irrigation events based on local rainfall (Dukes and Haman, 2002a).

A soil water balance can be used to calculate the theoretical irrigation requirement. This approach sums inputs and outputs of water to the soil water profile based on a specified time step (Allen et al., 1998).

It was assumed that RO was equal to zero due to the high infiltration rate of sandy soils, which are present at the research site and capillary rise was neglected due to water table depth exceeding 10 m. The maximum amount of water that can be stored effectively in the root zone is equal to field capacity (FC), which is the soil water content 2 to 3 days after wetting event has occurred and the downward movement of water due to gravity is negligible (Soil Science Society of America SSSA, 2008). Any water that is applied in excess of FC is considered to contribute to deep percolation. Precipitation that does not lead to DP or RO is considered effective or counted in the soil water balance.

Reference ET (ET_o) is the transpiration and evaporation from a uniform surface of actively growing vegetation with a specified growing height and that is well-watered. Crop evapotranspiration was calculated by multiplying ET_o with the crop coefficient (Allen et al., 2005) as follows:

When scheduling irrigation, the availability of water in the soil profile has to be considered. The maximum amount of water that can be held in the soil profile is related to the soil type and root zone depth. The amount of water in the soil that is available for plant use is called available water (AW) and is the difference between field capacity and permanent wilting point over the plant root zone (Cassel and Nielsen, 1986). Irrigation should be applied before the soil water content is equal to the PWP, since permanent damage occurs to many plants before the soil water status reaches PWP. The portion of AW that is allowed to be depleted before irrigation occurs is known as the readily available water (RAW). Typically RAW is between 40 and 60% of AW for turfgrass irrigation purposes. The theoretical depth of irrigation required is the amount of water that needs to be applied to maintain the soil water content within the RAW moisture status.

As a soil dries, the potential energy of the water in the soil decreases. In dry soil, the water is more strongly bound to soil particles through capillary and absorptive forces. The increase in these forces make plant uptake of the water more difficult. Below a soil moisture level equal to RAW the crop is considered water stressed due to the decrease in water extractability from the soil. The effects of the water stress lead to a decrease in crop transpiration which is calculated using a water stress coefficient (K_s) as described in Allen et al (1998). When the soil water level is above RAW, the value of K_s is 1. As soil water depletion increases to a depth greater than RAW the value of K_s decreases linearly as described by the Allen et al. (1998).

The irrigation depth required to replace the water lost through ET_c that has not been replaced by rainfall is the net irrigation requirement. The actual application of water by the irrigation system is not perfectly uniform so the net irrigation requirement has to be increased to account for the inefficiency of the irrigation system. Gross irrigation is the total amount of water to be applied including the water which is required by the plant and the water which is lost during distribution of the water (Irrigation Association, 2005). Gross irrigation, therefore, accounts for water which is applied unevenly due to less than perfect distribution uniformity (DU). The efficiency factor ensures that all landscaped areas get the necessary amount of water. For irrigation scheduling purposes, the low half distribution uniformity (DU_{lh}) has been recommended (Irrigation Association, 2005). The gross irrigation depth is then calculated by multiplying the net irrigation requirement by the efficiency factor.

The objectives of this experiment were to evaluate the irrigation water applied using soil moisture sensors, ET controllers and rain sensors compared to the theoretical irrigation requirement.

Materials and Methods

This study was performed at the Plant Science Research and Education Unit in Citra, Florida. There were four treatment periods during April 22 2006 to June 30, 2006 (S06), September 23, 2006 to December 15, 2006 (F06) and May 1, 2007 to

August 31, 2007 (S07) and September 1, 2007 to November 30, 2007 (F07). The experimental area consists of 72 plots of 'Floratam' St. Augustinegrass (*Stenotaphrum secundatum*). Soil particle size analysis showed that the soil present at the field site consisted of 1.7% clay, 1.1% silt and 97.3% sand (Shedd, 2008). Treatments were established in a randomized block design due to increasing values of FC and PWP across the field. Both field capacity and permanent wilting point values varied across the experimental blocks; however, only the block with a soil moisture sensor controlling irrigation, where appropriate, was used in theoretical analysis. Based on the average DU_{lh} the calculated adjustment factor for the irrigation system was 0.8 (Shedd, 2008).

Irrigation applied by the various irrigation control technologies was compared to theoretical depth required to determine how adequate and efficient the irrigation applied was. The actual water applied was placed in a daily soil water balance along with ET_c and rainfall to determine the daily soil water level (mm). Adequacy (%) refers to whether or not the irrigation applied was sufficient for plant needs (SWAT, 2006) and was calculated as follows:

$$Adequacy = \left(\frac{ET_c - Deficit}{ET_c} \right) \times 100 \qquad [1]$$

where *Deficit* was calculated as the water that was needed by the plant, according to the calculated ET_c, that was not readily available. There were two scenarios that were considered when calculating the deficit. The first was when soil water at the beginning of the day was above the depth for RAW, but at the end of the day was below. The equation for this scenario was as follows:

$$IF\left[SW_{i-1} > (FC - RAW)\ and\ SW_i < (FC - RAW)\right]$$
$$then\ Deficit = (FC - RAW) - SW_i \qquad [2]$$

where SW_{i-1} is the soil water level (mm) at the start of the day and SW_i is the soil water level at the end of the day. The second scenario considered was when the soil water level at the beginning and end of the day were below the depth for RAW. If the soil water level at the beginning and end of the day were both below RAW often the soil water fell as low as PWP. Even though the soil water balance does not allow the soil water to fall below the PWP, there is still water that is needed by the plant that is not available. For these instances the *Deficit* had to be calculated using:

$$IF\left[SW_{i-1} < (FC - RAW)\ and\ SW_i < (FC - RAW)\right]$$
$$then\ Deficit = ET_c - I_{net} - P_e \qquad [3]$$

where I_{net} is the depth of water applied (mm) that actually reaches the root zone of the plant and P_e is the depth of rainfall that reaches the root zone.

Efficiency is a measure of how well irrigation depths were applied, preventing runoff and drainage as follows (SWAT, 2006):

$$Efficiency = \left(\frac{Net\ Irrigation - Scheduled\ Losses}{Net\ Irrigation} \right) \times 100 \qquad [4]$$

where *Scheduled Losses* (mm) is the amount of water applied that exceeded the FC of the soil, leading to drainage (deep percolation) or direct runoff. Due to the high infiltration rates at the test site runoff was assumed to be zero, meaning any over

irrigation lead to drainage below the root zone. Using the efficiency, the irrigation excess (%) was calculated as:

$$Irrigation\ Excess = 100 - Efficiency \quad [5]$$

where irrigation excess represents the water applied over the actual depth theoretically required for plant needs.

All three of these parameters were calculated as an average for the entire treatment period and as 30-day running totals. The value was only calculated for the 30 day period if rainfall totaled at least 10.2 mm and the ET_o was at least 63.5 mm based on SWAT (2006) methodology. The theoretical irrigation requirement was calculated using values of FC and PWP found during soil testing (Table 1). A summary of the various inputs used in the soil water balance is provided in Table 1.

Water use was monitored using pulse-type displacement flow meters, specifically AMCO PSMT 20 mm x 190 mm flow meters (Elster AMCO Water, Inc., Ocala, FL). Weather data was collected using an automated weather station (Campbell Scientific, Logan, UT) within 900 m of the experimental site. Rainfall data at the weather station was collected with both a tipping bucket rain gauge and with a manual rain gauge located at the research plots. Monthly values of K_c were calculated using warm season turfgrass (Jia et al., 2007).

Turfgrass quality was rated at least once every two weeks during S06 and F06 and at least once a month during S07 and F07 using National Turfgrass Evaluation Program (NTEP) procedures (Shearman and Morris, 1998). Ratings were on a 1 to 9 scale, with 1 representing dead or dormant grass and 9 representing grass with good color and density, and without weeds (Shearman and Morris, 1998). A quality rating of 5 was considered minimally acceptable for a homeowner lawn.

Table 2 gives a summary of experimental treatments reported here. The LawnLogic LL1004 (Alpine Automation, Inc., Aurora, CO.) was used for the SMS treatments. The LawnLogic, which uses site specific calibration methods, comprised two treatments, with low and medium levels of soil moisture threshold settings (LL Low and LL Med; Shedd, 2008). The thresholds of the LL controller are on a scale of 1 (dry) to 9 (wet). The settings used in this experiment were initially 2 (LL Low) and 5 (LL Med). In S06 turf quality was damaged in the LL Low plots so the setting was modified to 4 for the remaining testing periods (Table 3). The SMS treatments utilized one sensor buried in one of four experimental blocks to control the irrigation for all plots in the treatment. SMS-based treatments were restricted to irrigation two days per week. The Toro Intelli-sense (The Toro Company, Bloomington, MN) ET controller was installed at the test site in F06. The Toro Intelli-sense controller (TORO) calculates irrigation runtime and frequency of irrigation events. Rain sensor (RS) treatments, using the Mini-Clik rain sensor (Hunter Industries Inc., San Marcos, CA.), comprised three treatments. There were three irrigation frequencies 1, 2, and 7 d/wk (RS1, RS2, RS7) with a rainfall setting of 6 mm for the RS1 and RS2 treatments and a rainfall setting of 3 mm for the RS7 treatment.

Two comparison treatments were used; time-based treatment without a rain sensor (WOS) and a time based treatment with a rain sensor set at 6 mm and a schedule that was set to apply 60% of the possible depth scheduled for WOS and the other RS treatments (DWRS). The control was a non-irrigated treatment (NON).

The same total application depth per week was divided over the possible number of days of irrigation per week. Every treatment except for the TORO, DWRS and the NON treatments had the same possible total depth of irrigation application. The monthly irrigation schedule was based on recommendations by Dukes and Haman (2002b).

Results

Compared to the theoretical irrigation requirement calculated using the soil water balance (SWB) most of the treatments tended to over water during the F06 and F07 testing periods. In S06 none of the treatments applied more water than the cumulative theoretical irrigation requirement. In S07 only the DWRS treatment had a cumulative depth of water applied (383 mm) that was less than the SWB cumulative depth (456 mm).

The LL Low treatment was ended early in F06 and S07 due to poor turf quality (Shedd, 2008). In S06, the LL Low treatment applied less water cumulatively (111 mm) than the SWB requirement (290 mm) and produced less than acceptable turf quality (4.2). The 30-day adequacy ratings for the treatment were below 62% throughout the testing period and as low as 24% (Figure 1). The average adequacy rating for the LL Low treatment during S06 was 47.9%, while 69% of the 30-day adequacy ratings were below this value (Table 3).

The turf quality ratings for the LL Med treatment were higher than the LL Low treatment. In S06, the LL Med treatment had a turf quality rating of 6.5 (acceptable) and applied more water cumulatively (237 mm) than LL Low (Table 4). The depth applied for the LL med treatment was 53 mm less than the depth for the SWB in S06. The average adequacy rating for the LL med treatment in S06 was 72% and the 30-day adequacies ranged from 64% to 84% (Table 3 and Figure 1). The 30-day efficiency ratings of the treatment varied between 66% and 100% (Figure 1). The depth of water applied for the LL Med treatment was sufficient to promote good turf quality.

During S06 and S07, as adequacy increased, efficiency decreased. This trend can be seen in the adequacy and efficiency figures for the LL and the RS treatments (Figure 1 and Figure 2). Both testing periods were relatively dry, compared to typical Florida conditions. Due to the shallow depth of rainfall and the high values of ET_o during the two testing periods, irrigation was vital for turfgrass quality. According to the soil water balance, deficit occurred quickly in the root zone of the turfgrass (30 cm) due to the low water holding capacity of the soil. This meant that with one or two day-per-week water restrictions, the adequacy ratings were lower due to deficit occurring between irrigation events. This was especially true for the RS1 treatment, which only received irrigation a maximum of once per week (Figure 3). Deficit occurred as soon as the soil water content dropped below the RAW level, which happened between all of the irrigation events during the S06 testing period (Figure 3).

The RS 1 treatment had the lowest turf quality rating (5.3) in S06 compared to the RS 2 (6.1) and the RS 7 (6.2) treatments. The average adequacy rating of the RS 1 treatment was 63% with 30-day values ranging from 53% to 68% (Table 3). The lowest 30-day efficiency rating for the RS 1 treatment was 30%, compared to the RS 2 and RS 7 treatments with 63% and 88% (Figure 2). The RS 1 treatment had the

lowest average efficiency and adequacy ratings of the RS treatments during all testing periods (Table 3). During all of the testing periods the RS1 treatment had the largest range in 30-day adequacy values, with the exception of S06. The RS2 treatment received 30-day adequacy ratings ranging from 37% to 100% during S06, while RS1 received ratings ranging from 53% to 68%. The average adequacy rating for the RS2 (69%) was slightly higher than RS1 (63%). During the 30-day period where the RS2 treatment received a 37% adequacy rating only one irrigation event was bypassed and eight were allowed. During the same 30-day period the RS 1 treatment did not bypass any irrigation events. Between the irrigation events, during the months of April and May, the soil water content remained below the RAW level part of the time. The irrigation depth per event for the month of April was used for May in 2006 for all of the treatments. When irrigation was applied it was not deep enough to bring the soil water content up to FC (Figure 4). May 2006 was very dry compared to historical rainfall averages in the area. The depth of rainfall for May 2006 was only 16 mm which is much lower than the historical average for the area (102 mm). The depth of rainfall during June 2006 (142 mm) was much larger than May and closer to the historical average of 180 mm (NOAA, 2006). The irrigation schedule was calculated based on the historical net irrigation requirement, which takes into account historical rainfall. During June 2006 the soil water content never dropped below RAW. In S07 the proper irrigation schedule for the RS2 treatment was used and the water content never dropped below RAW. The treatment was less efficient during S07 (75%) than S06 (82%) due to drainage occurring from most of the irrigation events.

The RS7 treatment consistently had higher adequacy and efficiency ratings than the RS1 and RS2 treatments (Table 3). This treatment irrigated more frequently with shallower depths than RS1 and RS2. This meant that irrigation rarely caused deep percolation leading to higher efficiency scores. In S06, the RS7 treatment had only 4.6 mm of irrigation water lost to deep percolation compared to 32 mm for RS1 and 18 mm for RS2 (Figure 5). According to the soil water balance, the water content of the soil for the RS7 treatment dropped below the RAW level for an extended period of time in S06. The average adjusted ET_c for the S06 testing period was 3.5 which was the same depth as the average depth of water applied per irrigation event of 3.5 mm for the RS7 treatment. Without rainfall, irrigation applied only accounted for the depth that was generally lost during one day of ET_c. If an irrigation day was bypassed and no rainfall occurred than the soil water content dropped, and the irrigation the next day was only sufficient to maintain the soil water content for the previous day (Figure 5). Turf quality for the RS7 treatment in S06 was acceptable (6.2) even though the soil water content was below the level of RAW for almost an entire month (Figure 5). Some level of deficit irrigation was acceptable for maintaining adequate turf quality.

During F06 and F07 (cooler months) the average adequacy ratings increased for all treatments, except LL Low in F06, compared to S06 and S07 (Table 3). The LL Low treatment was ended early in F06 due to poor turf quality. In F06, there were seven 30-day periods which were not analyzed because the minimum weather parameters, cumulative rainfall depth of at least 10.2 mm and ET_o depth of at least 63.5 mm, were not met. Adequacy ratings increased in F06 compared to S06, due to lower values of ET_c during the F06 months and more rain during the 30-day periods.

For April and May cumulative rainfall during the running 30-day periods never exceeded 30 mm, while in F06 30-day rainfall always exceeded 30 mm after 10/28. Non-irrigated plots had average turf quality ratings that were acceptable in F07 (5.0; Table 4).

The TORO treatment had the lowest average adequacy rating for F06 (80%) and the highest efficiency rating (97%; Table 3). Turf quality for the TORO treatment was above minimally acceptable (6.5; Table 4). An adequacy rating of 100% proved unnecessary during all testing periods for producing good turf quality. Optimally, the irrigation schedule should provide adequacy and efficiency. In S07, the TORO controller received an adequacy rating of 91% which was less than the ratings for the LL Med (92%), RS2 (96%) and RS7 (100%) treatments. The TORO treatment applied between 35 mm (RS7) and 106 mm (RS2) less than these other treatments. The controller for the TORO treatment can reduce depth of irrigation applied based on a theoretical soil water balance performed in the controller. Only two treatments received higher efficiency scores in S07 than the TORO treatment (85%); DWRS (98%) and RS7 (87%; Table 3). Both DWRS and RS7 applied less water per irrigation event than the SMS or other RS based treatments and the controller for the TORO treatment generally irrigated a shallower depth than that of the RS and SMS based treatments (Figure 5, 6 and 7). The DWRS, RS7 and TORO treatments had acceptable turf quality ratings in S07 (ranging from 6.1 to 6.9; Table 4). Based on the soil water balance irrigating less per irrigation event can increase irrigation efficiency and provide good adequacy when scheduled correctly.

Summary and Conclusions

In general, adequacy of irrigation for all treatments improved in the fall months compared to the spring months of testing. This may be due to both a decrease in ET_c and in the case of F07 an increase in rainfall. Also, low adequacy ratings, based on the SWB were not always an indicator of damage to plant quality. This was seen in the DWRS treatment which received 30-day adequacy ratings during S06 and S07 as low as 34% (S06) and 58% (S07) however turf quality during these testing periods was always acceptable for the treatment (6.5 and 6.9 respectively; Shedd, 2008). In some instances, such as LL Low in S06 (adequacy rating of 48% and average turf quality of 4.2) the adequacy ratings were a good indicator of the need for a greater depth of irrigation application. According to the results, an average adequacy rating greater than 70% always ensured minimally acceptable turf quality ratings on St. Augustinegrass. A low adequacy rating; however, did not necessarily mean a low turf quality rating. The DWRS treatment had an adequacy rating of 60% in S06 and received a turf quality rating of 6.5.

Efficiency and adequacy ratings varied substantially for most treatments during spring testing periods compared the fall testing periods. Based on 30-day values, a range in adequacy of up to 63% was seen. An average range inadequacy including all treatments of 24% occurred during the four testing periods. The ranges in adequacy between 30-day values show that using an adequacy for just one 30-day time period or averaged over the entire time period may not give an accurate representation of the change in adequacy over time. For example, in F07 the LL Low treatment had an adequacy rating for the entire testing period of 95%, but during the testing period the

treatment had 30-day adequacy values as low as 58% and as high as 100%. The reported adequacy of the irrigation schedule would depend heavily on which 30-day period was used when testing occurred. Simply using adequacy alone or efficiency alone was not a good indicator of the accuracy of an irrigation schedule. Efficiency of irrigation may be high due to little drainage occurring, but this may be due to a decrease in irrigation applied. Some treatments received high efficiency scores but very low adequacy scores because irrigation was not sufficient for plant needs. For example, treatment LL Low produced an efficiency rating of 100% for all of the 30-day testing periods during S06. The adequacy ratings for the LL Low treatment however fell as low as 24% during S06 and average turf quality for the treatment was a 4.2 (Shedd, 2008). An efficiency rating of 100% can be achieved by simply not irrigating at all.

There were some limitations for the experimental treatments compared to the SWB. The SWB was allowed to irrigate whenever soil moisture dropped to RAW and it only irrigated to FC. The experimental treatments were scheduled for irrigation on specific days of the week (1, 2 or 7 d/wk) and irrigation depth was programmed into the timer, with the exception of TORO.

References

Allen, R.G., Pereira, L.S., Raes, D., and Smith, M., 1998. Crop evapotranspiration: Guidelines for computing crop requirements. Irrigation and Drainage Paper No. 56, FAO, Rome, Italy.

Allen, R.G., Walter, I.A., Elliot, R., Howell, T., Itenfisu, D., and Jensen, M. (eds)., 2005. The ASCE standardized reference evapotranspiration equation. American Society of Civil Engineers Environmental and Water Resource Institute (ASCE-EWRI). 59 pp.

Cassel, D. K., Nielsen, D. R., 1986. Field capacity and available water capacity. In Klute, A. (ed.), Methods of soil analysis. Part 1. Physical and mineralogical methods, 2nd ed. Soil Science Society of America, Madison, WI.

Dukes, M.D. 2005. Residential irrigation water use and control. Encyclopedia of Water Science. Marcel Dekker, New York, NY. DOI: 10.1081/E-EWS-120041736.

Dukes, M.D. and D.Z. Haman. 2002a. Residential irrigation system rainfall shutoff devices. ABE325, Institute of Food and Agricultural Sciences, University of Florida, Gainesville, FL. Available at: http://edis.ifas.ufl.edu/AE221. Accessed 4 January 2008.

Dukes, M.D. Haman, D. Z., 2002b. Operation of residential irrigation controllers. CIR1421, Institute of Food and Agricultural Sciences, University of Florida, Gainesville, FL. Available at: http://edis.ifas.ufl.edu/AE220. Accessed 20 April, 2006.

Irrigation Association., 2005. Landscape irrigation scheduling and water management. Irrigation Association Water Management Committee. Falls Church, VA. Available at: http://www.irrigation.org/gov/pdf/IA_LISWM_MARCH_2005.pdf. Accessed 17 January 2008.

Jia, X., Dukes, M.D., Jacobs, J.M., 2007. Development of bahiagrass crop coefficient in a humid climate. Proceedings from the American Society of Agricultural and Biological Engineers annual meeting, paper number 072151, 17-20 June 2007, Minneapolis, MI.

Mayer, P.W., DeOreo, W.B., Opitz, E.M., Kiefer, J.C., Davis, W.Y., Dziegielewski, B., and Nelson, J.O., 1999. Residential end uses of water. American Water Works Association Research Foundation. Denver, CO.

National Oceanic and Atmospheric Administration (NOAA). National Climatic Data Center. Surface Data. Available at: http://www.ncdc.noaa.gov/oa/ncdc.html. Accessed 14 December 2006.

Shearman. R. C. and Morris, K. N., 1998. NTEP Turfgrass Evaluation Workbook. NTEP Turfgrass Evaluation Workshop, October 17, 1998, Beltsville, MD.

Shedd, M.L. 2008. Irrigation of St. Augustinegrass with soil moisture and evapotranspiration controllers. MS thesis, Agricultural and Biological Engineering Department., University of Florida, Gainesville, FL.

Smart Water Application Technology (SWAT)., 2006. Climatologically based controllers; 7th draft testing protocol. The Irrigation Association, Falls Church, VA.

Soil Science Society of America (SSSA)., 2008. Glossary of soil science terms. Soil Science Society of America, Madison, WI. Available at: https://www.soils.org/sssagloss/. Accessed 15 September 2008.

St. Johns River Water Management District., 2008. Lawn and landscape irrigation rule. Palatka, FL. Available at: http://www.sjrwmd.com/irrigationrule/summary.html. Accessed 11 February 2008.

Table 1. Summary of input parameters used for calculating the theoretical irrigation requirement and evaluating the adequacy and efficiency of the actual irrigation applied by treatments.

Soil Water Balance Input	
Management Allowed Depletion, MAD	50%
Root Depth, RD	30 cm
Field Capacity, FC	8%
Permanent Wilting Point, PWP	3%
Readily Available Water, RAW	8 mm

Table 2. Summary of treatment codes and descriptions along with the frequency of the irrigation schedule.

Treatment code	Irrigation Frequency (d/wk)	Treatment description
LL Low	2	LawnLogic soil moisture sensor set at low setting[1]
LL Med	2	LawnLogic soil moisture sensor set at medium setting (#5)
TORO	2	Toro Intelli-Sense ET Controller
RS1	1	Rain sensor with 6mm rainfall threshold
RS2	2	Rain sensor with 6mm rainfall threshold
RS7	7	Rain sensor with 3mm rainfall threshold
WOS	2	Without sensor
NON	0	Non-irrigated
DWRS	2	Rain sensor with 6mm rainfall threshold Irrigation schedule 60% of WOS

[1]LL Low setting was #2 for S06 and then changed to #4 for F06, S07 and F07.

Table 3. Summary of average adequacy and efficiency ratings during the four testing periods.

	Average Adequacy (%)				Average Efficiency (%)			
Treatment	S06	F06	S07	F07	S06	F06	S07	F07
LL Low	48[2]	--[1]	--[1]	95	100[2]	--[1]	--[1]	60
LL Med	72	96	92	100	89	73	74	55
RS1	63	--[3]	78	97	68	--[3]	59	52
RS2	69	100	96	100	82	66	75	53
RS7	94	--[3]	100	100	95	--[3]	87	62
DWRS	60	90	78	100	90	92	98	86
TORO	--[4]	80	91	99	*NA*	97	85	87
WOS	73	100	96	100	77	61	67	41

[1]Ended before the treatment period was over due to poor turf quality
[2]Produced less than acceptable turf quality
[3]Irrigation system was malfunctioning
[4]Not installed until F06

Table 4. Average turf quality ratings during the four treatment periods. Turf quality is on a scale of 1 to 9, with a 1 representing dead turfgrass and a 9 representing perfect turfgrass quality. A rating of 5 was considered minimally acceptable for homeowners.

	Season Average Turf Quality			
Treatment	S06	F06	S07	F07
LL Low	4.2	--[1]	--[1]	6.2
LL Med	6.5	7.2	6.5	6.3
TORO	--[4]	6.5	6.1	6.4
RS1	5.3	--[2]	5.8	6.2
RS2	6.1	5.8	6.0	6.3
RS7	6.2	--[2]	6.5	6.8
DWRS	6.5	7.1	6.9	7.0
NON	1.4	--[1]	--[1]	5.0
WOS	5.6	6.1	6.5	6.3

[1]Ended before the treatment period was over due to poor turf quality
[2]Irrigation system was malfunctioning
[3]Not installed until F06

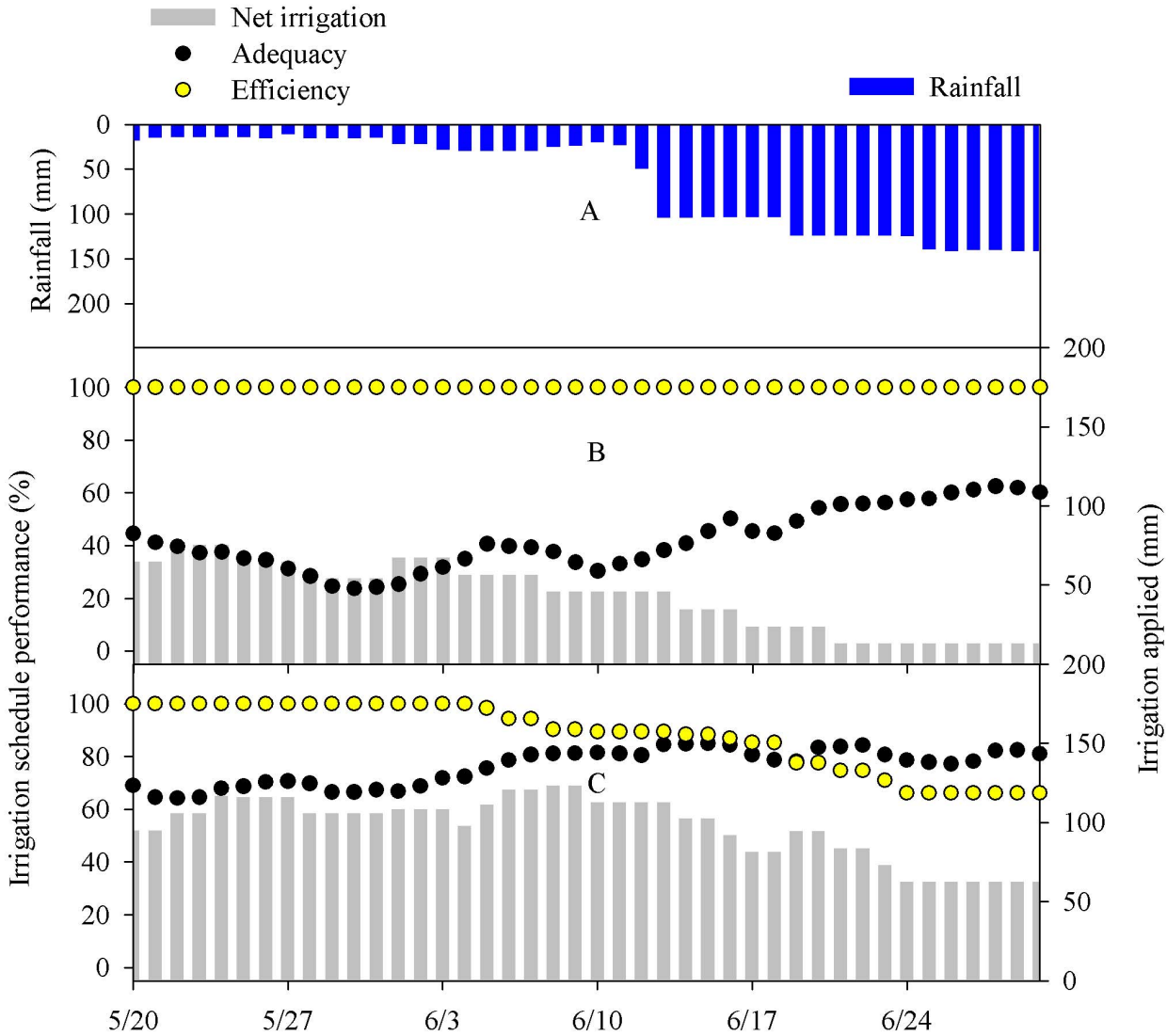

Figure 1. The adequacy ratings (dark circles) and efficiency ratings (light circles) alongside (A) rainfall and irrigation (gray bars) in running thirty day totals for SMS treatments (B) LL Low and (C) LL Med in S06.

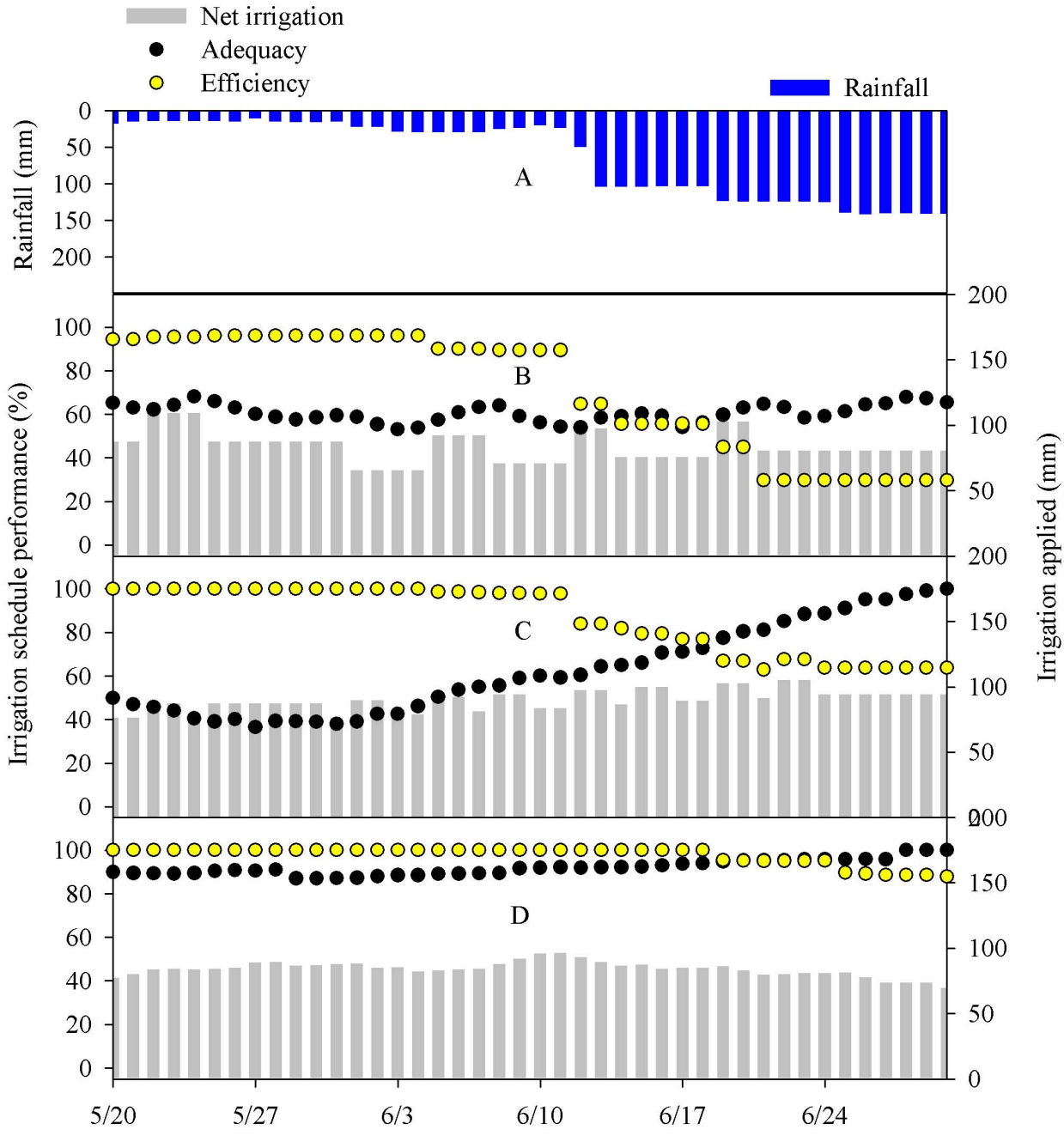

Figure 2. The adequacy ratings (dark circles) and efficiency ratings (light circles) alongside (A) rainfall and irrigation (gray columns) in running thirty day totals for RS treatments (B) RS1, (C) RS2 and (D) RS7 in S06.

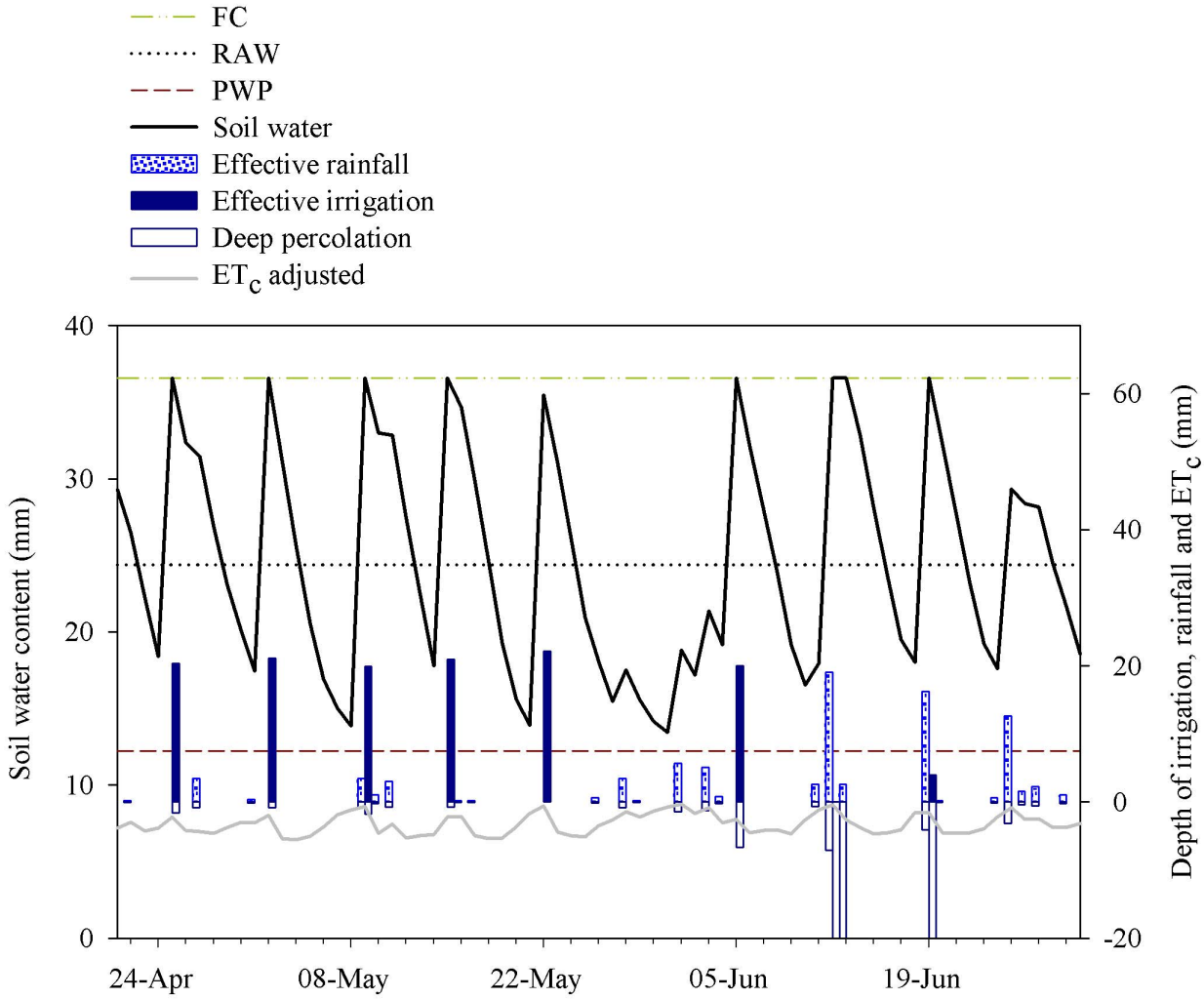

Figure 3. Soil water content (black line) for the RS1 treatment in S06 plotted along with field capacity, permanent wilting point and readily available water. The bar graph plotted using the y-axis on the right side of the graph, shows the depth of effective irrigation (net irrigation applied that did not lead to drainage) along with effective rainfall and deep percolation. The adjusted ET_c based on the stress coefficient K_s is shown also (gray line).

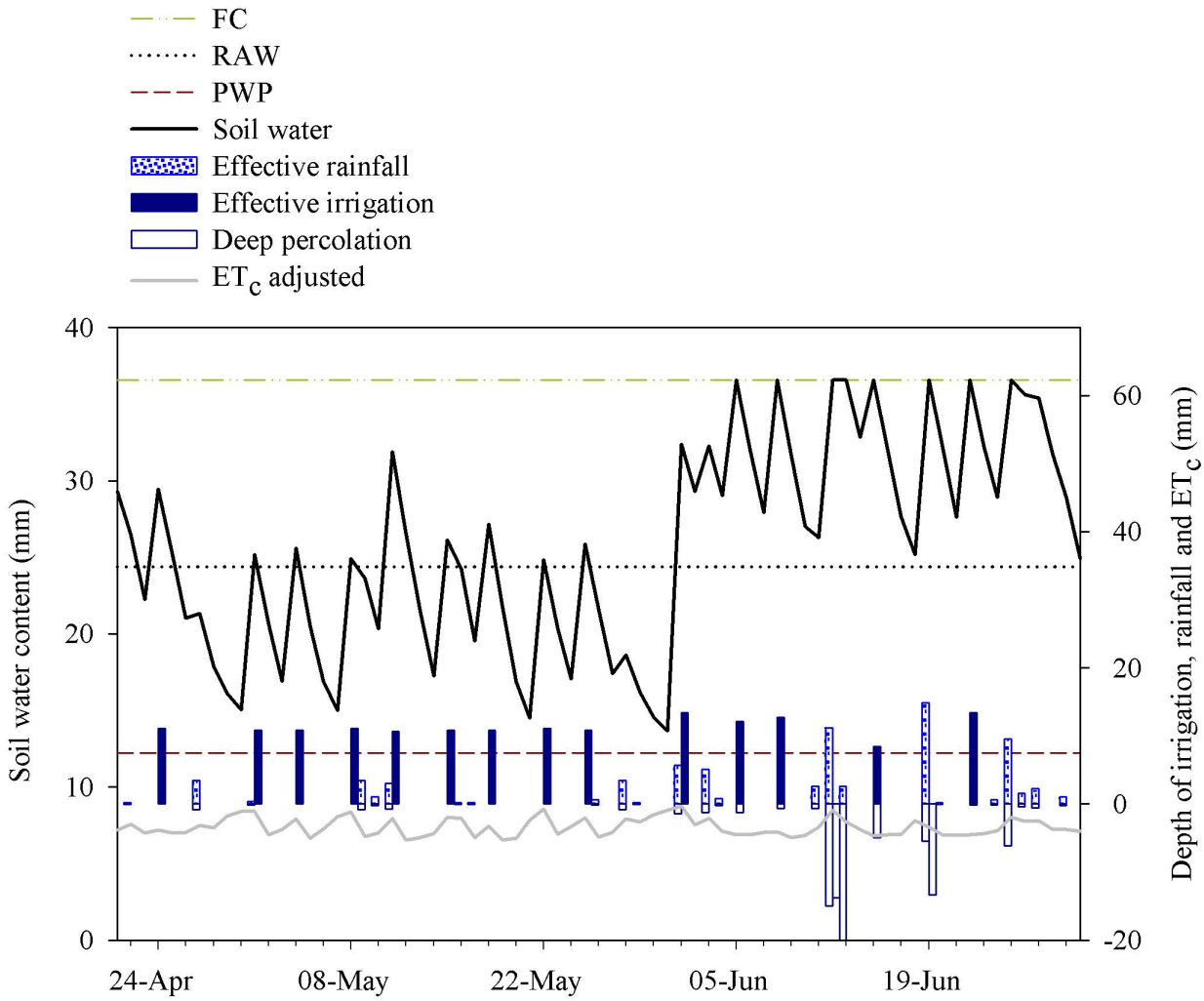

Figure 4. Soil water content (black line) for the RS2 treatment in S06 plotted along with field capacity, permanent wilting point and readily available water. The bar graph plotted using the y-axis on the right side of the graph, shows the depth of effective irrigation (net irrigation applied that did not lead to drainage) along with effective rainfall and deep percolation. The adjusted ET_c based on the stress coefficient K_s is shown also (gray line).

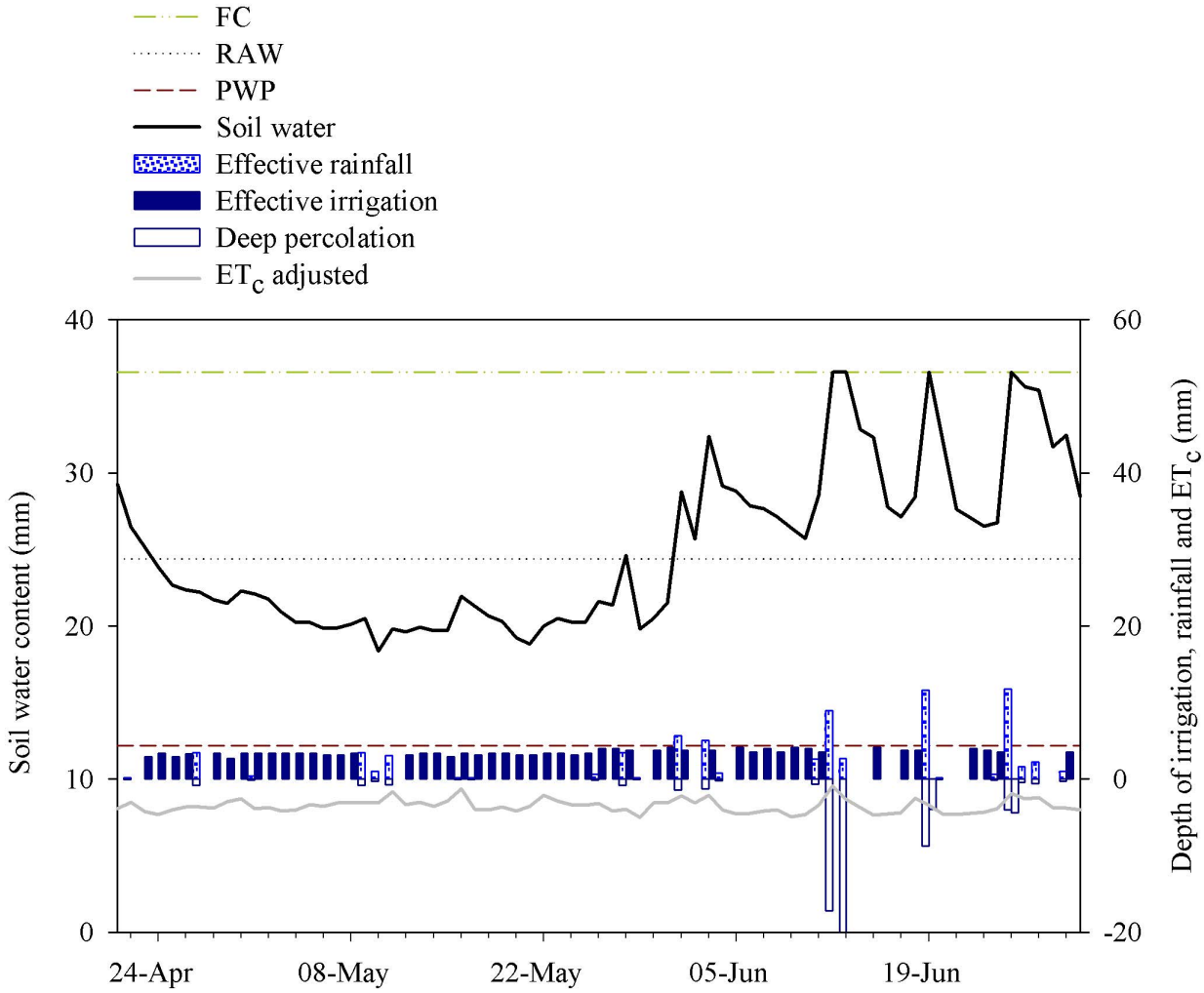

Figure 5. Soil water content (black line) for the RS7 treatment in S06 plotted along with field capacity, permanent wilting point and readily available water. The bar graph plotted using the y-axis on the right side of the graph, shows the depth of effective irrigation (net irrigation applied that did not lead to drainage) along with effective rainfall and deep percolation. The adjusted ET_c based on the stress coefficient K_s is shown also (gray line).

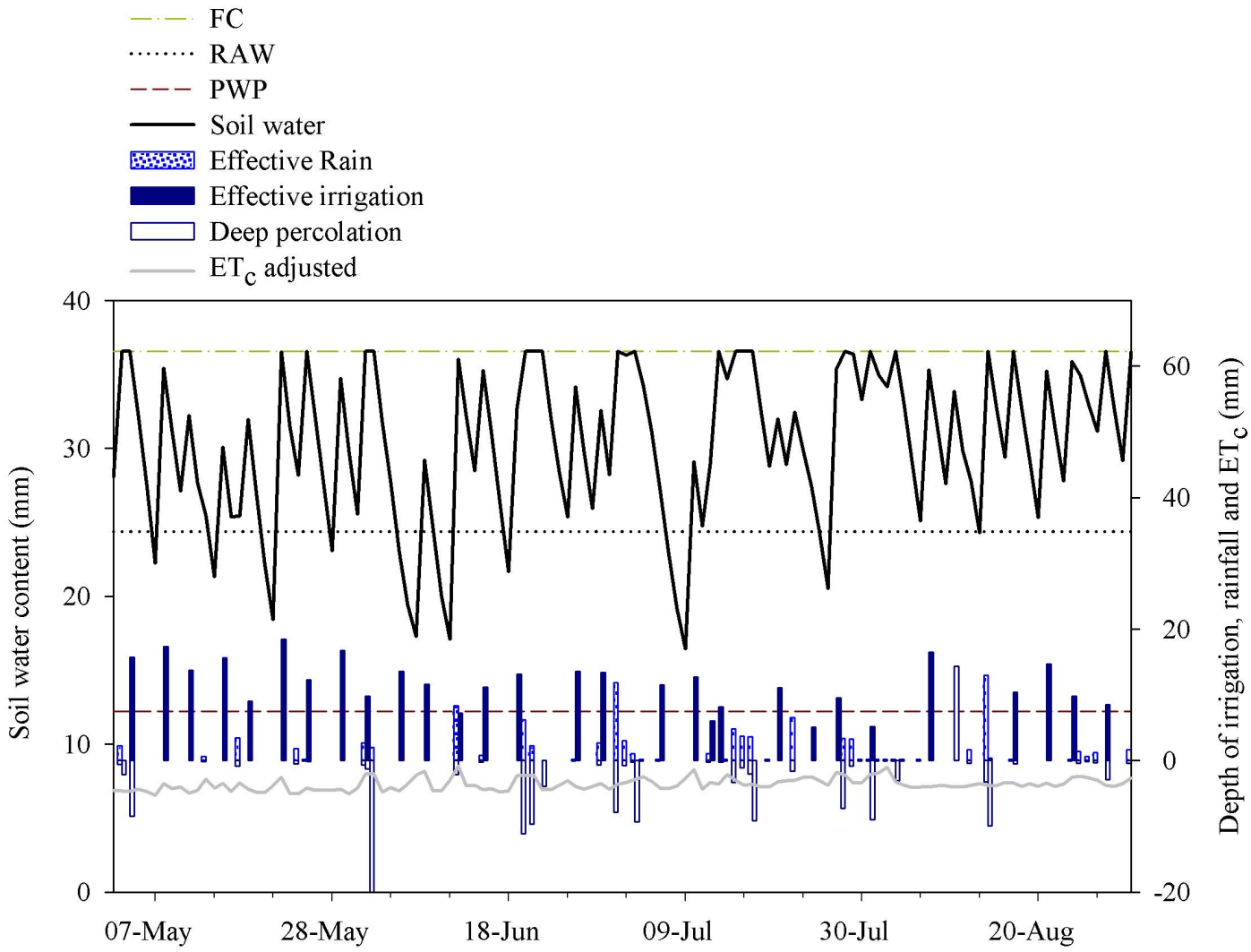

Figure 6. Soil water content (black line) for the TORO treatment in S07 plotted along with field capacity, permanent wilting point and readily available water. The bar graph plotted using the y-axis on the right side of the graph, shows the depth of effective irrigation (net irrigation applied that did not lead to drainage) along with effective rainfall and deep percolation. The adjusted ET_c based on the stress coefficient K_s is shown also (gray line).

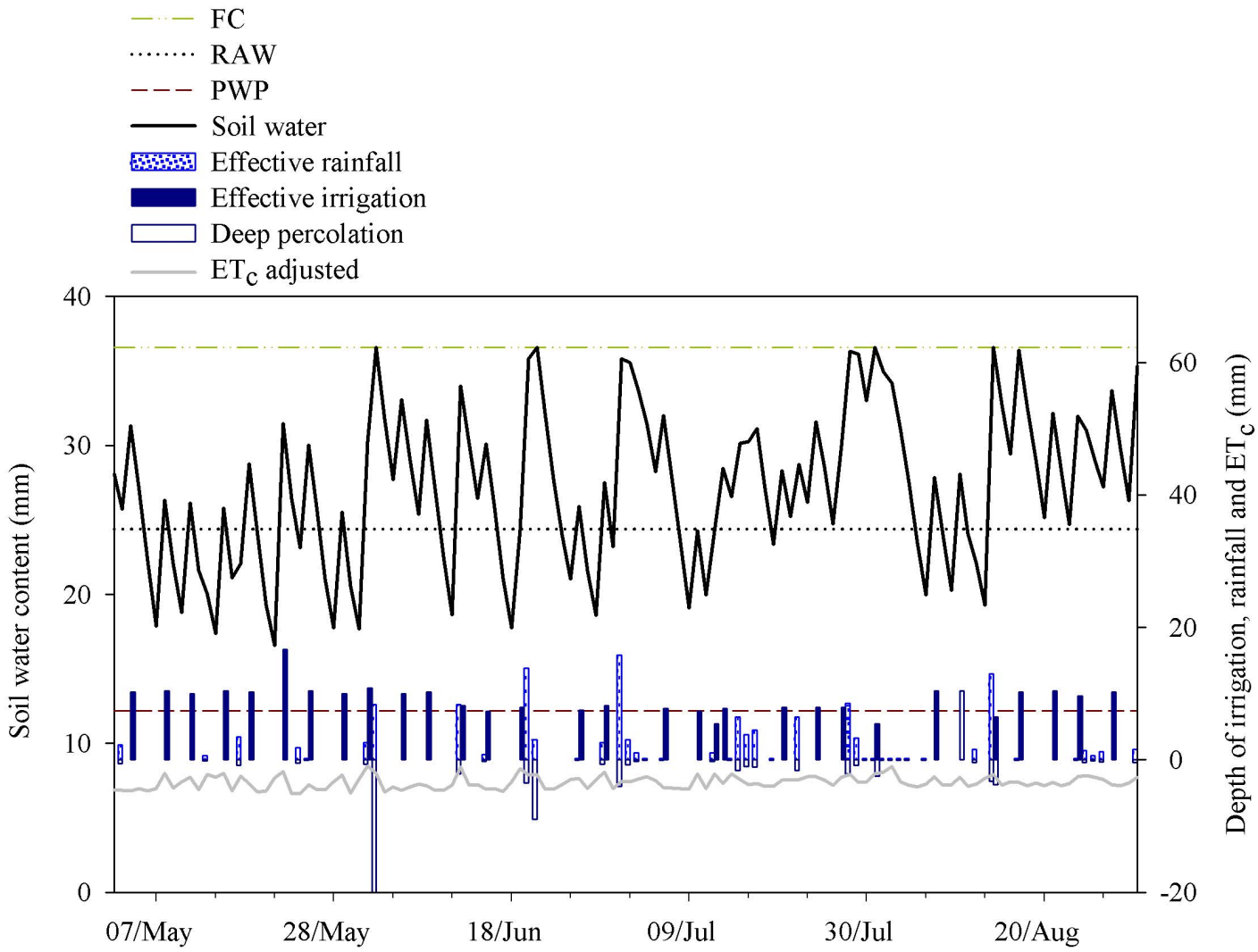

Figure 7. Soil water content (black line) for the DWRS treatment in S07 plotted along with field capacity, permanent wilting point and readily available water. The bar graph, plotted using the y-axis on the right side of the graph, shows the depth of effective irrigation (net irrigation applied that did not lead to drainage) along with effective rainfall and deep percolation. The adjusted ET_c based on the stress coefficient K_s is shown also (gray line).

Irrigation Rain Sensors Accuracy

B. Cardenas-Lailhacar[1], M. D. Dukes[2], P.E., and L. Meaks[3]

[1]Research Coordinator, Agricultural and Biological Engineering Dept., Univ. of Florida, Gainesville, FL 32611-0570. E-mail: bernardc@ufl.edu
[2]Corresponding author, Associate Professor, Agricultural and Biological Engineering Dept., Univ. of Florida, P.O. Box 110570, Gainesville, FL 32611-0570. E-mail: mddukes@ufl.edu , phone: 352-392-1864; fax: 352-392-4092.
[3]Graduate student, Agricultural and Biological Engineering Dept., Univ. of Florida, Gainesville, FL 32611-0570. E-mail: lmeeks@ufl.edu

ABSTRACT

In recent years, an increasing number of municipalities throughout the country have implemented mandates, rebates and/or cost-saving programs for the use of rain sensors (RSs). The objectives of this research were to evaluate two expanding disk RS types, Mini-Click (MC) and Wireless Rain-Click (WL), with respect to: a) the accuracy of their set point with respect to rainfall depth, b) the number of times in irrigation bypass mode, and c) the duration in irrigation bypass mode. For the MC treatments, rainfall set points of 3, 6, and 13 mm were established. Rain sensor models were monitored from 1 January 2006 to 31 July 2007, except for MC set at 6 mm which was monitored starting on 13 September 2006. The 576-day experimental period had rainfall frequency and cumulative amount below a historical year. The number of times that replicate units within a treatment switched to bypass mode tended to behave the same through time, for treatments WL and 3-MC, which ranged from 64 to 78 events and from 57 to 68 events, respectively. Treatment 6-MC was the most consistent between replicates, where three units switched to bypass mode on 39 occasions, and one unit did it on 34 times. Replicates from treatment 13-MC showed the most variable behavior, shutting off between 50 to 29 times. On average, treatment WL shut off after 2.8 mm of rain. Because this model does not have a specific set point, accuracy could not be calculated. Accuracies for the other treatments resulted in 73% for 3-MC, 30% for 6-MC, and 58% for 13-MC. Treatments WL, 3-MC, 6-MC, and 13-MC, remained in bypass mode 82, 80, 64, and 83% of the time, respectively, for less than 24 h.

INTRODUCTION

Rain sensors (RSs), are designed to interrupt a scheduled irrigation cycle on an automatic irrigation controller (i.e. time-clock or timer) when a specific amount of rainfall has occurred (Dukes and Haman 2002). During recent years, an increasing number of municipalities in seven states throughout the country have implemented mandates, rebates and/or cost-saving programs for the use of RSs because they appear to be a useful tool for irrigation water conservation, at a relatively low cost (Dewey 2008). Since 1991 Florida has had an overall RS statute, which requires an automatic

rain sensor shut-off device that is properly installed and functioning on all automatic irrigation systems (Florida Statutes, 2008).

The most common type of RSs employs hygroscopic disks to absorb water and expand proportionally to the rainfall amount. Then, a mechanical switch interrupts the system common wire, disabling the solenoid valves, until the sensor hygroscopic disks dry out. To adjust the drying rate of the disks, these sensors have an adjustable vent ring.

A version of these devices (also with hygroscopic disks inside) is a wireless RS, which has a sensor/transmitter installed in an area subject to rainfall and a receiver unit connected to the timer. According to the manufacturer, these RSs have a quick shut down of the irrigation system after it starts to rain (without preset adjustments for a certain precipitation amount). The wireless RSs can also be adjusted to keep the irrigation system off after the rain stops by setting the adjustable ventilation windows that control the dry-out time (Hunter Industries, Inc. 2006).

This research was based on the original work by Cardenas-Lailhacar and Dukes (2008), who studied the performance and reliability of some expanding disk RSs. The objectives of this experiment were to evaluate the reliability of two commercially available expanding disk RS-types with respect to: a) the accuracy of their set point with respect to rainfall depth, b) the number of times in irrigation bypass mode, and c) the duration in irrigation bypass mode.

MATERIALS AND METHODS

Twelve Mini-Click (MC) and four Wireless Rain-Click (WL) rain sensor models (Hunter Industries, Inc., San Marcos, CA) were placed at the University of Florida Agricultural and Biological Engineering Department turfgrass research facility in Gainesville. This experiment took place from 1 January 2006 to 31 July 2007. Four treatments with four replications each were established. For the MCs, three set points were established: 3, 6, and 13 mm thresholds (treatment codes 3-MC, 6-MC, and 13-MC, respectively). The dry-out ventilation windows of the MCs and WLs were kept completely open. All RSs in this study were 9 months old having been set up originally for the study reported by Cardenas-Lailhacar and Dukes (2008).

Each time an RS unit changed status (from allowing irrigation, to bypass mode, or vice versa), the date and time were automatically recorded, at a one-second sampling interval, by means of two AM16/32 multiplexers connected to a CR 10X model datalogger (Campbell Scientific, Logan, UT). Weather conditions were recorded by an automated weather station containing a CR 10X model data logger, located within 15 m of the experimental site. Rainfall was measured by means of a tipping bucket rain gauge, which was routinely checked against a manual rain gauge located nearby. Rainfall data were recorded at intervals of 0.25 mm (day of year, hour, minute, and second were logged). Until 13 September 2006, treatment 6-MC was not connected to the datalogger, so it was not considered for the calculations previous to that date. The total time that each RS remained in the irrigation bypass mode after the rain has stopped was computed (dry out period). Total rainfall before each RS switched to bypass mode was calculated, in order to evaluate the accuracy of

the rainfall thresholds. According to Figliola and Beasley (2000), the accuracy of an instrument refers to its ability to indicate a true value exactly. Accuracy is related to absolute error, ε, which is defined as the difference between the true value of a measurement and the indicated value of the instrument:

$$\varepsilon = \text{true value} - \text{indicated value} \quad [1]$$

from which the percent accuracy, A, is found by:

$$A = \left(1 - \frac{|\varepsilon|}{true\ value}\right) \times 100 \quad [2]$$

RESULTS AND DISCUSSION

Weather Conditions

Overall, the experimental period was drier than normal. During the 576-day experiment, 138 days exhibited rainfall (24%), including 28 days with more than 15 mm (3% of the days). These numbers could be considered below a historical year (1970 to 2000), which for the same period had 31% rainy days and 5% of rainfall events above 15 mm. The cumulative precipitation was 1,723 mm compared to a historical of 2,094 mm, or an 18% of deficit for the study period. Over the entire monitoring period, the tipping bucket rain gauge was very accurate (R^2= 0.99) compared to the manual rain gauge across a range of rainfall events from less than 1 mm up to 60 mm.

Number of Times in Bypass Mode

Figures 1 to 4 show the cumulative number of times in bypass mode of the replicates within treatments. It can be seen that this parameter was variable between the different replicates, with 13-MC the most variable treatment. Replicates at a particular set point sometimes responded properly according to their settings, sometimes did not detect rainfall events five or more times their set points, and sometimes they even shut off several hours after the rain had stopped (data not shown). This explains the range of variation in the number of times that individual RS units switched to bypass mode.

The four replications of the WL treatment (Figure 1) followed a similar pattern, with 64 to 78 events in bypass mode. However, these units were much more consistent when they were newer, varying between 78 and 83 bypassed events over a 282 day experimental period (Cardenas-Lailhacar and Dukes, 2008). Analogous to the WL units, all four 3-MC sensors (Figure 2) behaved similarly, with 57 to 68 times in bypass mode. In the case of the 6-MC treatment (Figure 3), the units were not set up until 13 September 2006. Therefore, the number of times in bypass mode were

smaller than the other treatments. However, these replicates were very consistent, where three of them switched to bypass mode on 39 occasions, and one unit did it on 34 times. The different replicates of treatment 13-MC showed an irregular performance (Figure 4). All replicates tended to behave similarly until 23 July 2006. After that date, one replicate switched to bypass mode more times (50) than the other units. Two other replicates operated similarly until 13 May 2007 (with 34 and 33 time in bypass mode), but afterwards they followed a different pattern and ended the testing period with 42 and 36 times in bypass mode. Finally, the last replication of treatment 13-MC shut off a fewer number of times than the other units after 23 July 2006, and ended with a total of only 29 times on bypass mode. No recorded weather data or physical evidence was found to explain the different performances between the 13-MC units after 23 July 2006.

Depth of Rainfall before Shut Off

The average depth of rainfall before the rain sensors switched to bypass mode, accuracy, and standard deviation for the different treatments is shown in Table 1. Treatment WL shut off after 2.8 mm of rain on average, with a standard deviation of 1.1. Because this model does not have a specific set point, accuracy could not be calculated. However, when these replicates were new they triggered the switch at an average of 1.4 mm of rainfall (Cardenas-Lailhacar and Dukes, 2008). Treatment 3-MC switched to bypass mode after an average of 2.2 mm of rainfall, resulting in an accuracy of 73%, with a standard deviation of 1.9. Unexpectedly, treatment 6-MC shut off on average after 1.8 mm of rainfall (even less rainfall than 3-MC), with a standard deviation of 1.2, and a resultant accuracy of just 30%. It should be noted that the different units were very consistent in their behavior (Figure 3). These sensors were previously set at 25 mm for almost two years, but no physical evidence was observed of any alteration on their expanding disks neither on their mechanism that could be related to this behavior. Treatment 13-MC switched to bypass mode after an average of 7.5 mm of rain, which corresponds to an accuracy of 58%, and resulted in the highest standard deviation (2.7). These average accuracies show that only 3-MC responded close to its set point and that all MC sensors became more sensitive to rainfall; whereas, WL sensors became less sensitive to rainfall compared to previous results (Cardenas-Lailhacar and Dukes, 2008).

Duration in Irrigation Bypass Mode (Dry-Out Period)

The time that it takes the RSs to reset for normal sprinkler operation after the rain has stopped is determined by weather conditions (temperature, wind, sunlight, relative humidity, etc.), which will determine how fast the hygroscopic disks dry out.

Figures 5 to 8 show histograms and frequency distribution for 6 h intervals in bypass mode for treatments WL, 3-MC, 6-MC, and 13-MC, respectively. Results showed that WL sensors remained in bypass mode 82% of the time for less than 24 h, and 23% of the time for less than 12 h (Figure 5). This result does not agree with manufacturer claims that the WL sensors will remain on that status shortly after the

rain stops (Hunter Industries, Inc. 2006). In previous work, WL sensors dried out 50% of the time before 12 hours (Cardenas-Lailhacar and Dukes, 2008). Similar to WL, the dry out period of treatment 3-MC (Figure 6) was 80% of the time less than 24 h, a higher frequency than the 51% found previously (Cardenas-Lailhacar and Dukes, 2008). Treatment 6-MC (Figure 7) also remained most of the time (64%) in bypass mode for less than 24 h, and 86% of the time for less than 36 h. Similar to the other treatments, the dry out period for 13-MC (Figure 8) was most of the time less than 24 h (83%). It is remarkable that the dry out period for all treatments occurred almost always in less than 48 h. Thus, it appears the MC sensors dried out faster with age, but the WL sensors dried out slower.

SUMMARY AND CONCLUSIONS

A study to evaluate and quantify the performance of RSs was carried out from 1 January 2006 to 31 July 2007. This testing period recorded a lower frequency and a lower amount of cumulative rainfall compared to historical records. Accuracy tests results suggested that the 3-MC responded close to its set point (73%), but 6-MC and 13-MC resulted in lower accuracies (30 and 58%). Replicates at a particular set point were variable, sometimes responding properly according to their settings, sometimes not detecting rainfall events five or more times their set points, and sometimes even shutting off several hours after the rain had stopped. This explains the accuracies and the range of variation in the number of times that individual RS units switched to bypass mode. Most of the time, treatments remained in bypass mode for less than 24 h, and almost all treatments dried out in less than 48 h during this testing period. Generally, MC sensors became more sensitive to rainfall and dried out quicker than when they were new; whereas, the WL sensors became less sensitive and dried out slower. In any case, after more than two years of continuous operation these devices still have the ability to bypass irrigation cycles during rainy weather; however, their accuracy appears to be degrading with time.

REFERENCES

Cardenas-Lailhacar, B. and Dukes, M. D. (2008). Expanding Disk Rain Sensor Performance and Potential Irrigation Water Savings." *J. Irrig. and Drain. Eng.*, 134 (1), 67-73.

Dewey, C. (2003). "Sensors at work." *Irrigation and Green Industry*, September 2003. <http://www.igin.com/Irrigation/0903sensors.html> (Dec. 4, 2006).

Dukes, M. D. and Haman, D. Z. (2002). "Residential irrigation system rainfall shutoff devices." *ABE325*, Institute of Food and Agricultural Sciences, University of Florida, Gainesville, Fla.

Figliola, R. S. and Beasley, D. E. (2000). *Theory and design for mechanical measurements*, 3rd Ed., John Wiley and Sons, Inc., N.Y.

Florida Statutes. (2008). "Chapter 373.62: Water conservation; automatic sprinkler systems." <http://www.leg.state.fl.us> (Jan. 26, 2009).

Hunter Industries, Inc. (2006). "Irrigation products."
<http://www.hunterindustries.com/Products/default.htm> (Jan. 26, 2009).

ACKNOWLEDGEMENTS

The authors wish to thank Engineer Larry Miller for his assistance on this project. This research was supported by the Pinellas-Anclotte Basin Board of the Southwest Water Management District, the Florida Department of Agriculture and Consumer Services, the Pinellas County Utilities, the Florida Nursery and Landscape Growers Association, and the Florida Agricultural Experiment Station.

Mention of a trade name, proprietary product, or specific equipment does not constitute a guarantee or warranty by the University of Florida and does not imply approval of a product or exclusion of others that may be suitable.

Table 1. Average depth of rainfall before rain sensors switched to bypass mode.

Treatment	Set point (mm)	Rainfall depth (mm)	Accuracy (%)	Standard Deviation (mm)
3-MC	3	2.2	73	1.9
6-MC	6	1.8	30	1.2
13-MC	13	7.5	58	2.7
WL	--	2.8	--[z]	1.1

[z] Because these instruments do not declare a specific set point, accuracy could not be calculated

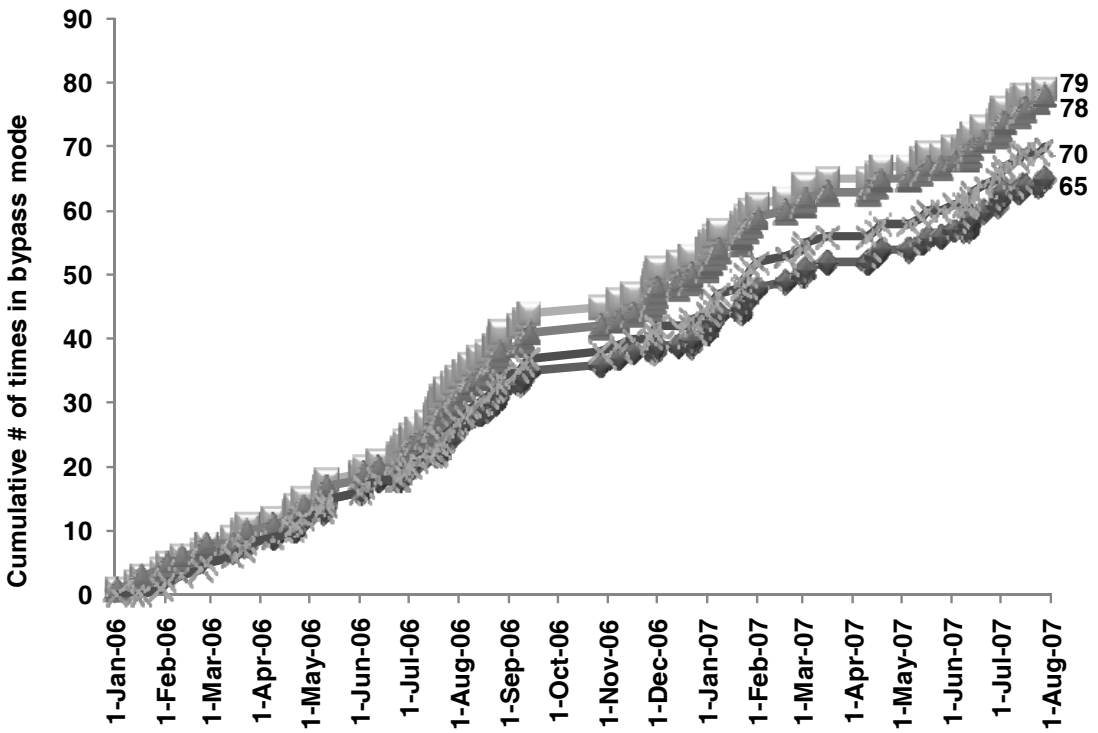

Figure 1. Cumulative number of times that replicates from wireless rain sensors (WL) switched to bypass mode.

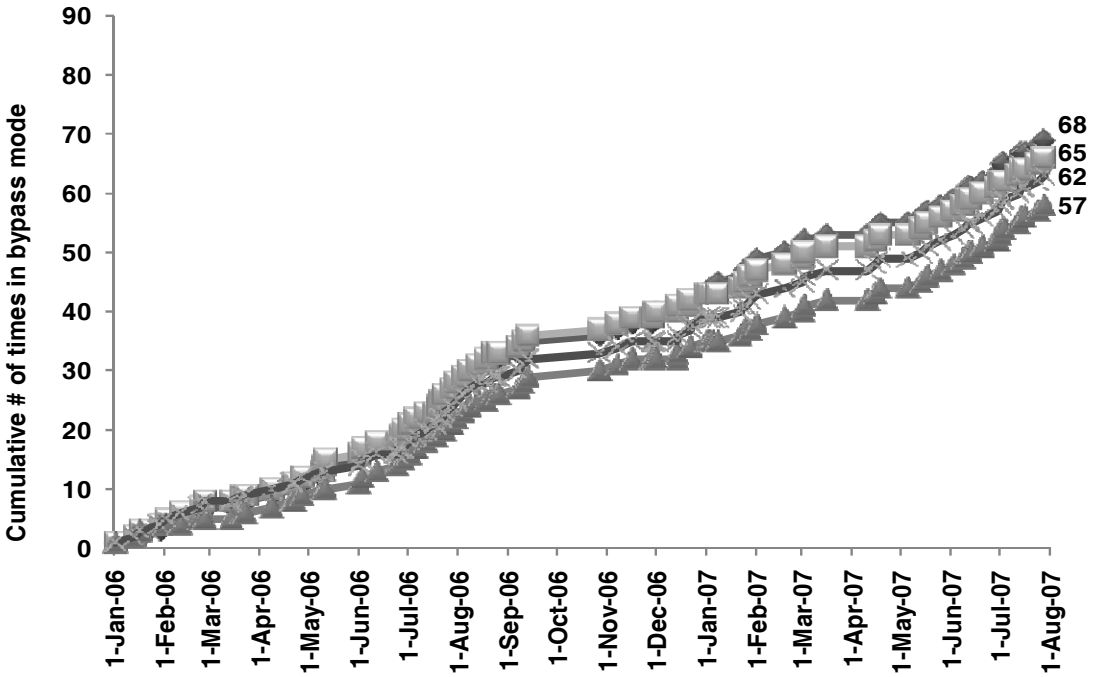

Figure 2. Cumulative number of times that replicates from Mini-Click rain sensors set at 3 mm (3-MC) switched to bypass mode.

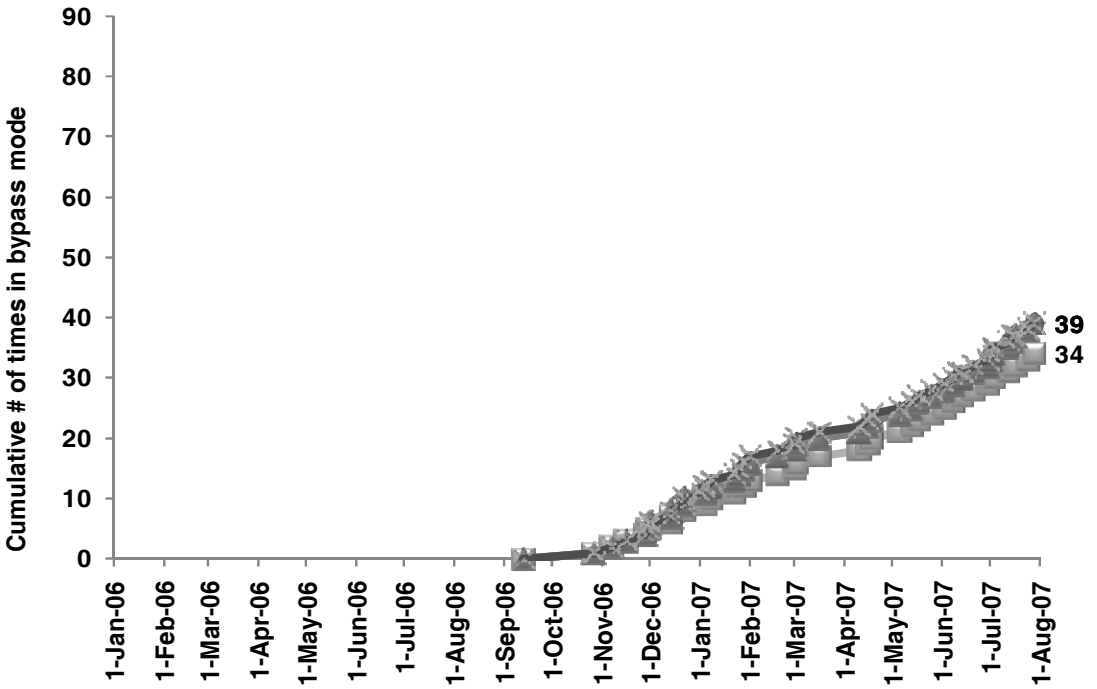

Figure 3. Cumulative number of times that replicates from Mini-Click rain sensors set at 6 mm (6-MC) switched to bypass mode.

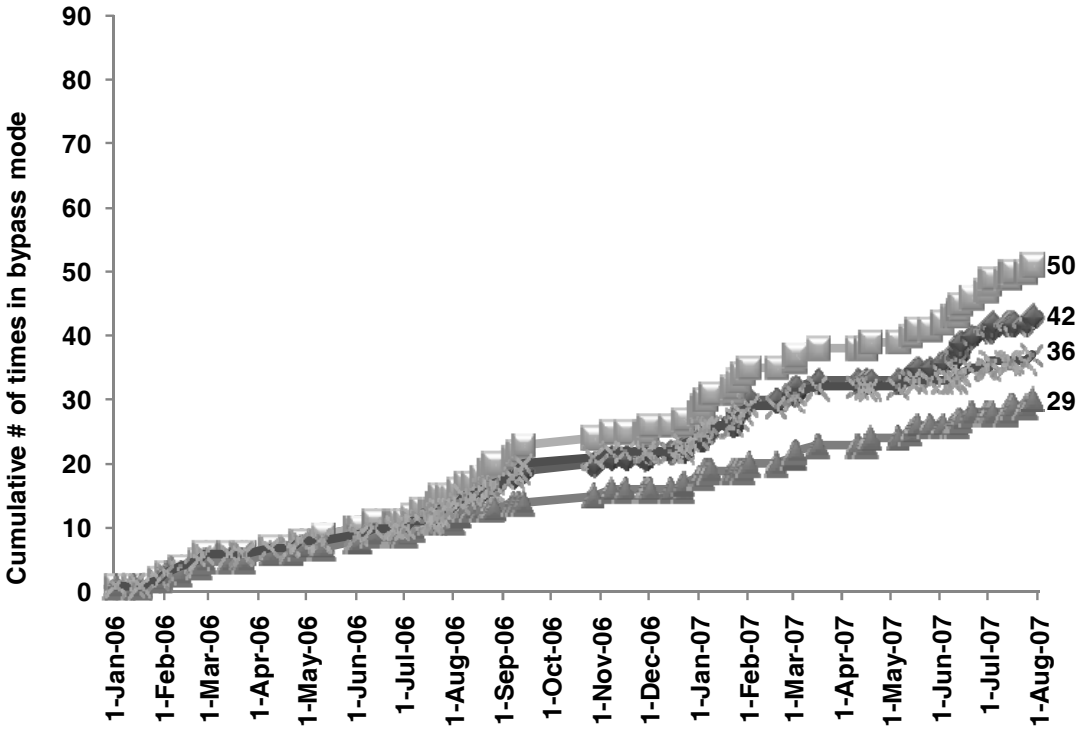

Figure 4. Cumulative number of times that replicates from Mini-Click rain sensors set at 13 mm (13-MC) switched to bypass mode.

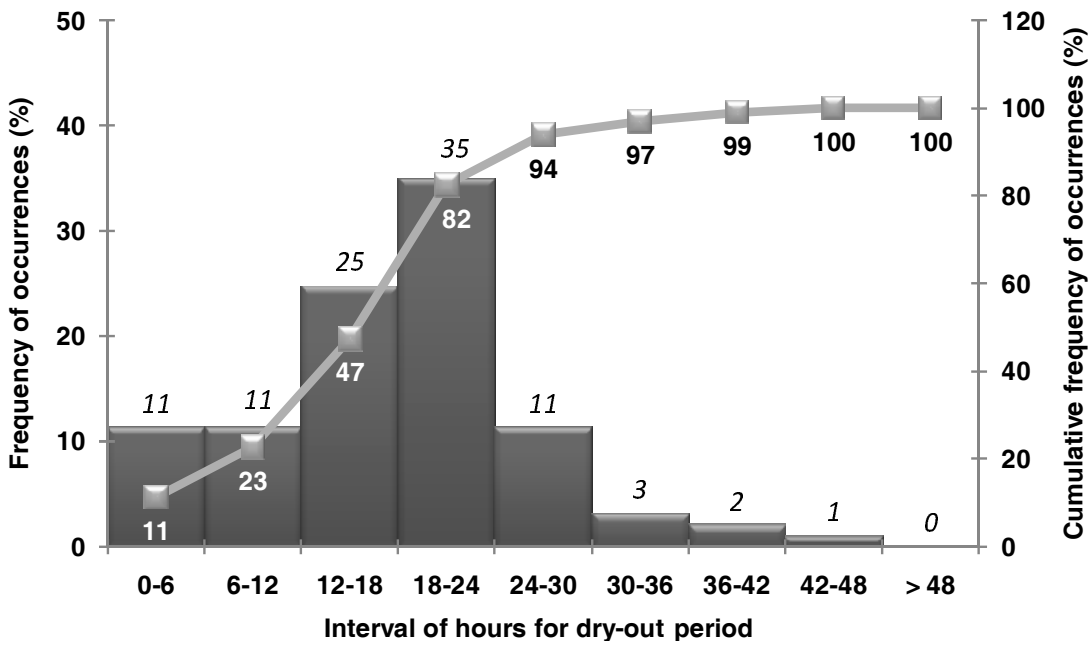

Figure 5. Average dry-out period of wireless rain sensors (WL); histogram and frequency distribution for 6-hour intervals.

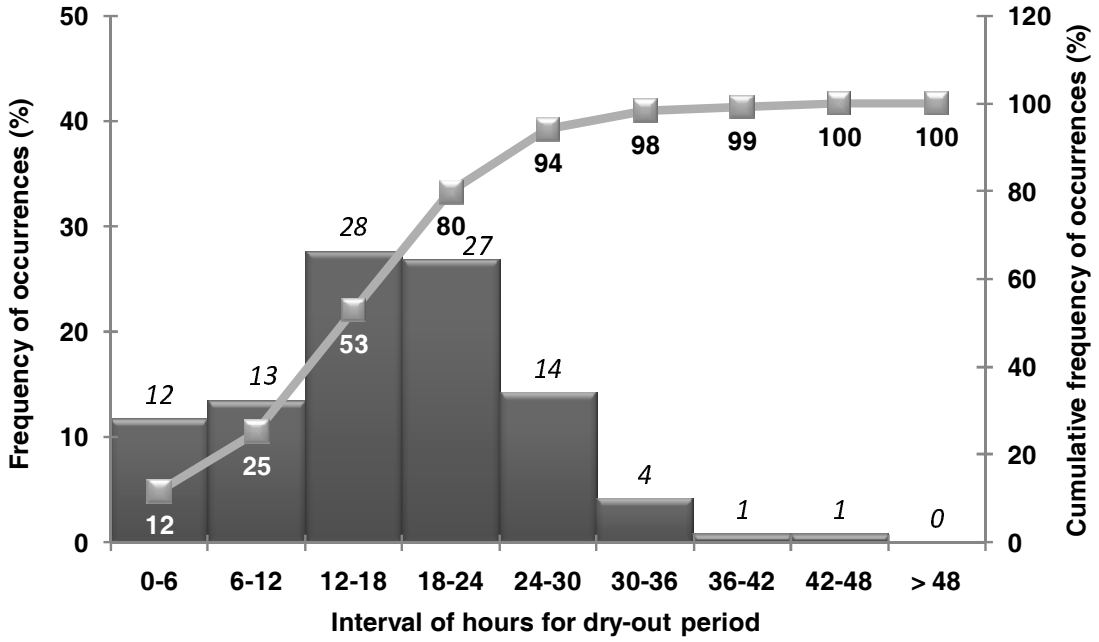

Figure 6. Average dry-out period of Mini-Click rain sensors set at 3 mm (3-MC); histogram and frequency distribution for 6-hour intervals.

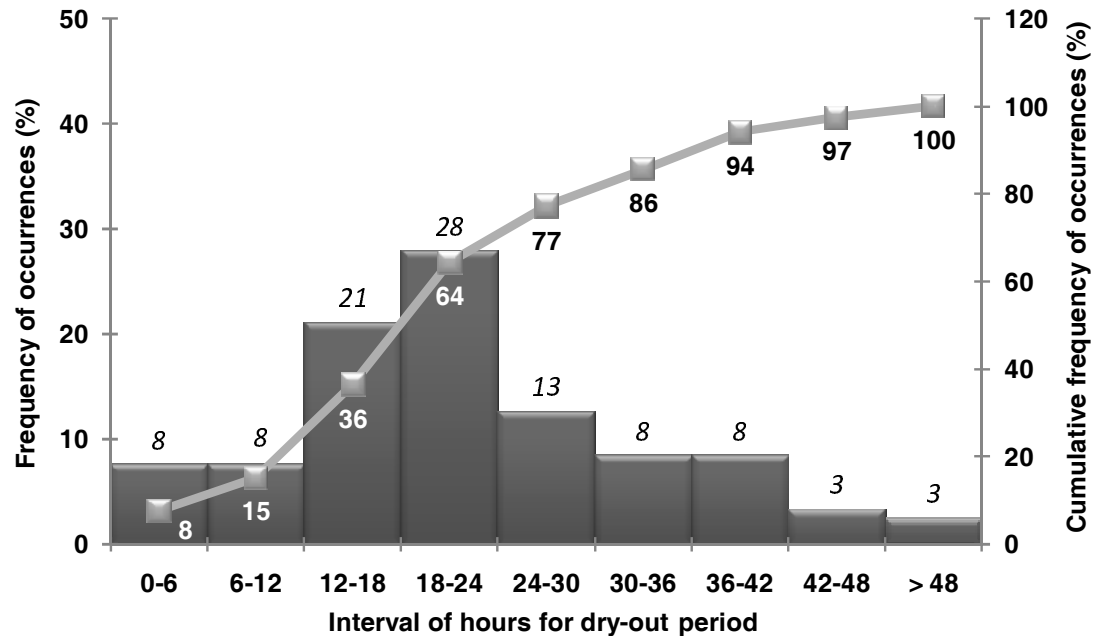

Figure 7. Average dry-out period of Mini-Click rain sensors set at 6 mm (6-MC); histogram and frequency distribution for 6-hour intervals.

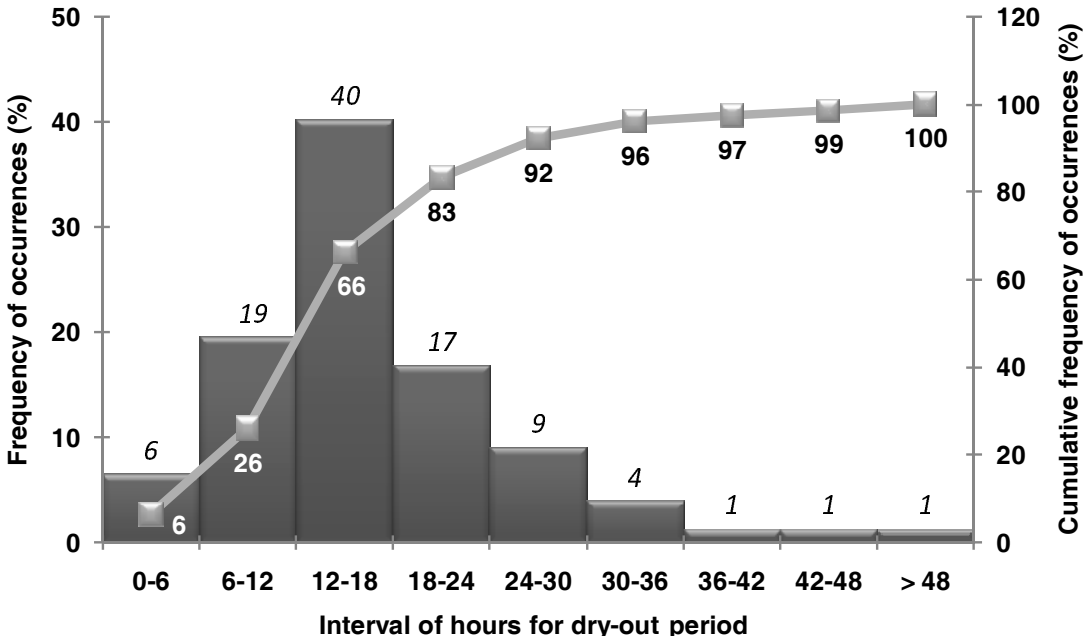

Figure 8. Average dry-out period of Mini-Click rain sensors set at 13 mm (13-MC); histogram and frequency distribution for 6-hour intervals.

Preliminary Results for Bench Testing of Evapotranspiration-based Irrigation Controllers In Florida

Stacia L. Davis[1] and Michael D. Dukes[2]

[1]Agricultural and Biological Engineering Department, University of Florida, P.O. Box 110570, Gainesville, FL 32611-0570; PH (352) 392-1864 ext. 266; FAX (352) 392-4092; email: stacia@ufl.edu
[2]Agricultural and Biological Engineering Department, University of Florida, P.O. Box 110570, Gainesville, FL 32611-0570; PH (352) 392-1864 ext. 205; FAX (352) 392-4092; email: mddukes@ufl.edu

ABSTRACT

The Irrigation Association has developed a smart water application technologies (SWAT) testing protocol for ET controllers that describes a procedure for testing the efficacy of ET controllers. The test requirements include a minimum of thirty consecutive days with 63.5 mm of reference evapotranspiration (ET_O) and 10.2 mm of rainfall. The objectives of this study are to duplicate the soil water balance calculations specified by the SWAT test and recreate the SWAT bench test in a humid region using ET controllers previously tested under the SWAT protocol in an arid climate. Three brands of ET controllers previously tested under the SWAT protocol by CIT were installed at the Agricultural and Biological Engineering campus research facility (Gainesville, FL). The controllers are as follows: Weathermatic SL1600 with SLW20 weather monitor, Toro Intelli-sense duplicates utilizing the WeatherTRAK ET Everywhere Service, and ETwater Smart Controller 100 duplicates. Duplicate controllers were distinguished by whether they utilized an additional Mini-clik rain sensor denoted with a rain sensor (WRS) or without a rain sensor (WORS). The study period for each controller received less ET_O and rainfall compared to historical averages by 40% and 56%, respectively. The results found during the 2008 SWAT test showed that the ET controllers generally scored well in SWAT performance scores of scheduling efficiency and irrigation adequacy. However, the controllers resulted in lower scheduling efficiency scores than the original published results: 2.5% for the ETwater controllers, 14% by the Toro controllers, and 5.6% by the Weathermatic. It is likely that manufacturers would have opted to not publish these results as a SWAT score and restarted the test with minor adjustments. The SWAT test determines whether the controllers have accurate irrigation scheduling capabilities and does not rate the potential for a controller to conserve water. The SWAT testing protocol should be clearly outlined and detailed enough for results to be reproducible if it will continue to be used as an industry standard.

INTRODUCTION

Water resources are limited in many areas of the United States. A recent study by Mayer et al. (1999) showed that 58% of total household water use was used for landscape irrigation. Of that outdoor water use, 40% was wasted by over-watering plant material (Mayer et al. 1999).

The increased demand for conservative irrigation practices has opened a market for technologies to aid in scheduling irrigation for the homeowner. One such technology, termed a smart controller, is defined by the Irrigation Association ([IA] 2008) as "…controllers [that] estimate or measure depletion of available plant soil moisture in order to operate an irrigation system, replenishing water as needed while minimizing excess water use...requires initial site specific set-up and will make irrigation schedule adjustments, including run times and required cycles throughout the irrigation season without human intervention." Smart controllers can come in many forms; one such controller is a climatologically-based controller, also known as an ET controller.

The Irrigation Association developed a smart water application technologies (SWAT) testing protocol for ET controllers (IA 2008). This testing protocol, currently under its 8th draft, describes a procedure for testing the efficacy of ET controllers and is performed solely by the Center for Irrigation Technology (CIT) at California State University (Fresno, CA). The test requirements include a minimum of thirty consecutive days with 63.5 mm of reference evapotranspiration (ET_O) and 10.2 mm of rainfall. Many of the tests performed to date required longer than 30 days to achieve 10.2 mm of rain. It is questionable whether these test limits are reasonable. For example, in humid climates the 10.2 mm rainfall limit is only a fraction of what might occur in a given growing season where amounts of 500 mm or more are common. Also, thirty days is a relatively short time period when testing an ET controller's ability to adjust irrigation over time.

As the industry progresses and new water conservation programs require ways to test smart technologies, the need for a formal, industry accepted procedure exists. The protocol is vague in various areas and the testing procedures cannot be fully duplicated as they are written. The objectives of this study are to duplicate the soil water balance calculations used by CIT as the SWAT test and recreate the SWAT bench test in a humid region using ET controllers previously tested under the SWAT protocol in California.

MATERIALS AND METHODS

SWAT Protocol. The SWAT test, as defined in the SWAT protocol document, uses a daily moisture balance to simulate the water dynamics of a landscape plant system. Six landscape scenarios are specified so that the controllers can be evaluated on their ability to schedule irrigation under different environmental conditions (Table 1). These landscape scenarios or "virtual irrigation zones" range from turfgrass to trees, drip to spray head irrigation, shady to sunny areas, loamy sand to clay soils, and 2% to 20% slopes. The daily balance is calculated by the following equation:

$$MB_i=MB_{i-1}-ET_C+R_E+I_E$$

where MB is the soil water content (mm) on day i or i-1, ET_C is the plant specific ET (mm) on day i, R_E is effective rainfall (mm) on day i, and I_E is effective irrigation (mm) on day i.

MB represents the water storage level in the soil profile on any given day. This level fluctuates from 0, or no readily available water in the soil profile, to a maximum value specified by the protocol for each zone termed root zone working water storage (RZWWS). A moisture balance level of 0 does not equate to the absence of water in the soil column. Therefore, MB does not represent the actual water level in the soil profile, but the level under which the plant material will no longer be considered well-watered.

Plant-specific evapotranspiration (ET_C) is calculated for any given plant material by applying a crop coefficient (K_C) using the following equation (Allen et al. 1998):

$$ET_C=K_C*ET_O$$

K_C values are specified by plant type and exposure expressed in the SWAT protocol (IA 2008).

Net rainfall is defined as the depth of total rainfall that enters the soil profile and is considered available for plant use. The protocol specifies that daily net rainfall is 80% of total daily rainfall. Effective rainfall is calculated from net rainfall and is the depth that causes the MB to reach RZWWS. Excess rainfall (that which exceeds soil storage capacity) is lost due to surface runoff or deep percolation.

ET controllers schedule irrigation by calculating the depth of irrigation required to reach RZWWS, termed net irrigation (I_{NET}). These controllers apply more irrigation than is scheduled to take into account system application inefficiencies (Table 1). The depth actually applied by the controllers, including efficiency adjustments, is considered gross irrigation. Effective irrigation is the portion of net irrigation that can be used by the plant. Effective irrigation can be less than net irrigation due to any combination of surplus and direct runoff. Surplus (S) is the depth of daily net irrigation exceeding RZWWS and is calculated as:

$$S=MB_{i-1}-ET_C+R_E+I_{NET}-RO_{DIR}-RO_{SOAK}-RZWWS$$

where RO_{DIR} is direct runoff (mm) for day i and RO_{SOAK} is soak runoff (mm) for day i. If the value of S is calculated as a negative value, then surplus is zero. Direct runoff is the depth of any one irrigation event exceeding the maximum runtime. It is calculated as:

$$RO_{DIR}=\left(I_{EVENT}-Rt_{MAX}\right)*E_{APP}*PR/60$$

where I_{EVENT} (min) is the irrigation occurring per event cycle, Rt_{MAX} (min) is the maximum runtime according to allowable surface accumulation and infiltration rate restrictions, E_{APP} is the application efficiency (Table 1), and PR (mm/hr) is the

precipitation rate (Table 1). Direct runoff is calculated for each event cycle and summed for a daily total. If I_{EVENT} does not exceed Rt_{MAX} , then RO_{DIR} is zero. Soak runoff is the depth of the next irrigation event during a cycle/soak irrigation schedule that occurs before the minimum soak time is complete. It is calculated as:

$$RO_{SOAK}=\left[\frac{I_{EVENT_a}*E_{APP}*PR}{IR*60}-Rt_{SOAK}\right]*\frac{PR}{60}$$

where I_{EVENTa} (min) is the event cycle runtime prior to Rt_{SOAK}, IR (mm/hr) is the infiltration rate defined by the soil type, and Rt_{SOAK} (min) is the soak cycle runtime between event cycles for a cycle/soak schedule. The RO_{SOAK} calculation is valid assuming $0<RO_{SOAK}<I_{EVENT_b}$, where I_{EVENTb} (min) is the event cycle runtime following the soak time. When RO_{SOAK} is calculated to be greater than I_{EVENTb}, then RO_{SOAK} equals I_{EVENTb}. Also, RO_{SOAK} is a positive value and is zero if found to be negative.

The SWAT protocol process "scores" the performance of the irrigation controllers with respect to over-irrigation and under-irrigation. As a result, scores of scheduling efficiency and irrigation adequacy are computed to represent measures of over-irrigation and under-irrigation, respectively. Scheduling efficiency is defined as the ability of a controller to schedule irrigation without applying excess irrigation that results in drainage or runoff (IA 2008). It is calculated in thirty day running totals or greater depending on the length of the test for any given controller with the following equation:

$$E=\frac{(I_{NET}-SL)}{I_{NET}}*100$$

where I_{NET} refers to the sum of net irrigation applied and SL refers to the scheduling losses summed over the time period. Scheduling losses include summed values of surplus, RO_{DIR}, and RO_{SOAK}. Irrigation adequacy quantifies the ability of the controller to supply sufficient irrigation to meet the plant water demand (IA 2008). It was also calculated in thirty day running totals using the following equation:

$$A=\frac{(ET_C-D)}{ET_C}*100$$

where D represents the deficit or the sum of the depth of water below the maximum allowable depletion over the time period (i.e. below RZWWS). Because the testing occurs for a virtual landscape, it is assumed that high irrigation adequacy results translate to acceptable landscape quality. Acceptable levels of irrigation adequacy and scheduling efficiency have not been specified by the protocol. Some discussion has indicated that respectively levels of 80% and 95% would be acceptable limits; however, evidence has not been made available to date to show that any particular level is an acceptable balance to meet plant water needs and to limit excessive watering.

Florida Test. Five ET controllers previously tested under the SWAT protocol by the Center for Irrigation Technology (CIT) in Fresno, California, were installed at the Agricultural and Biological Engineering campus research facility (Gainesville, FL). The controllers are as follows: Weathermatic SL1600 with SLW20 weather monitor (Weathermatic, Inc., Dallas, TX), Toro Intelli-sense duplicates (Toro Company, Inc., Riverside, CA) utilizing the WeatherTRAK ET Everywhere Service (Hydropoint Datasystems, Inc., Petaluma, CA), and ETwater Smart Controller 100 duplicates (ETwater Systems LLC, Corte Madera, CA). Duplicate controllers consisted of one with an additional Mini-clik rain sensor (Hunter Industries, Inc., San Marcos, CA) set at a 6.3 mm threshold, denoted with a rain sensor (WRS) or without a rain sensor (WORS). The Weathermatic gathers weather data from the on-site weather monitor and uses Hargreaves equation to calculate ET_O. The Weathermatic controller has an integrated expanding disk rain sensor similar to the devices used on the other controllers. The Toro and ETwater controllers are signal-based controllers that receive daily ET_O, calculated using the ASCE standardized ET_O equation (Allen et al. 2005), through remote signals.

Each controller was connected to a CR-10X datalogger (Campbell Scientific, Logan, UT) to record time and date at the beginning and end of each irrigation event for all active zones. Each controller was programmed by the manufacturer, or with the manufacturer's supervision, with settings identical to the original SWAT test performed by CIT. The official test began when the manufacturer determined that the controller(s) were programmed correctly.

Weather data were collected from two weather stations for this test. The first weather station was located on-site and managed by research personel. Values for reference evapotranspiration were calculated using the ASCE standardized reference evapotranspiration equation (Allen et al. 2005) as specified in the SWAT protocol (IA 2008) and used for the soil water balance model in association with the on-site controller. The second weather station was part of the Florida Automated Weather Network (FAWN) located in Citra, FL, approximately 20 miles from the study location. This station data were available via the internet. The ET_O and rainfall data were downloaded directly from the website and ET_O was calculated by FAWN using the IFAS Penman method. This weather data was used in the soil water balance model for the signal-based ET controllers.

The SWAT protocol specified that testing should occur over a minimum of thirty consecutive days (IA 2008). This test was performed for each ET controller for a minimum of ninety days to obtain multiple thirty day periods of results per controller. Thirty day results were reported only if they met the minimum requirements of 63.5 mm of ET_O and 10.2 mm of rainfall (IA 2008). Final results from the entire testing period were also calculated for each controller by averaging results from each zone. Preliminary results were given to the manufacturers periodically so they may update their settings if necessary. Updates made by the manufacturers to the program settings throughout the test did not affect results of the controllers.

RESULTS

The study period for each controller began in the fall season and continued through winter months. Historical ET_O and rainfall were reported from data collected at the Gainesville Regional Airport weather station operated by the National Oceanic and Atmospheric Administration using six years of data (Table 2). Cumulative ET_O was much less than historical totals for every controller in respective time periods by: 29% for the ETwater, 31% for the Toro, and 60% less for the Weathermatic. Rainfall was also less than historical totals by: 59% for the ETwater, 61% for the Toro, and 48% less than the Weathermatic.

Irrigation adequacy quantifies water deficit due to under-irrigation. The Weathermatic controller and both ETwater controllers always kept the moisture balance above zero for all zones, resulting in 100% average, maximum, and minimum irrigation adequacy scores (Tables 3 & 5). The Toro controllers both received slightly lower irrigation adequacy results with an average score of 98% and 97% for the WORS and WRS treatments, respectively (Table 3). Minimum scores for these controllers were 94% and some zones resulted in no under-irrigation due to the maximum irrigation adequacy result being 100%. Adding a rain sensor did not result in differences of irrigation adequacy. Also, there were no differences in irrigation adequacy results due to differences between methods of obtaining ET, whether calculated on-site or received by signal.

Scheduling efficiency is used to quantify over-irrigation. The ETwater WORS had results ranging from 80% to 100% with an average of 94% for the six zones (Table 3). The ETwater WRS performed better with results ranging from 92% to 100% with an average of 98%. In this case, the addition of a rain sensor to the controller caused irrigation scheduling to be more efficient. The Toro WORS and Toro WRS resulted in 86% and 85% averages for scheduling efficiency, respectively. These controllers had some zones that did not perform as well, with minimum scores reaching 67% and 62%, respectively, dropping the average results below the other controllers. In contrast to the ETwater controllers, scheduling efficiency results were reduced for the Toro controllers by using a rain sensor. The Weathermatic performed similarly to the ETwater WRS controller with results ranging from 92% to 100% and averaging 94% from the six zones. These results also show that there were no differences in results between controllers that use different methods for obtaining weather data.

The ETwater controllers, both with and without a rain sensor, began the SWAT test on 14 September 2008 with manufacturer permission and testing ended on 11 January 2009. Running totals for thirty, forty-five, and sixty day periods from the start date were calculated when totals for ET_O and rainfall were above the minimums specified by the protocol. The ETwater WORS and ETwater WRS consistently resulted in 100% irrigation adequacy for all thirty, sixty, and ninety day periods (Table 4). The ETwater controllers generally maintained scheduling efficiency results throughout the different time periods with average and maximum results slightly decreasing and minimum results slightly increasing over longer periods (Table 5). Results for these controllers differed by less than 2% between time periods.

The Weathermatic controller began the SWAT test on 23 September 2008. This controller consistently averaged 100% in irrigation adequacy for all zones and

over all time periods (Table 4). However, scheduling efficiency decreased as test length increased (Table 5). Minimum scheduling efficiency scores decreased by less than 2% indicating that lower averages occurred due to cumulative over-irrigation by individual zones when performing the SWAT test over time.

The Toro WORS and Toro WRS controllers began testing on 23 October 2008. The minimum requirements set by the SWAT testing protocol for ET_O were not met during the thirty day testing periods; results cannot be reported for thirty day running totals. Results from longer time periods indicate that irrigation adequacy was not affected by length of time period (Table 4). However, scheduling efficiency decreased for the Toro controllers, by 7-10% on average, by increasing the running time period by fifteen days (Table 5).

DISCUSSION

Irrigation scheduling by ET controllers occurs based on past weather information and do not have forecasting abilities. Therefore, the ET controllers schedule irrigation on the current day based on information from the previous day. Since it is not addressed in the testing protocol, it would be appropriate to assume that the SWAT program would also calculate the moisture balance in this way if the goal of the test is to verify the controller's ability to schedule irrigation. However, the SWAT program uses ET_O, rainfall, and irrigation on the same day to calculate the moisture balance. For optimum results, the ET controllers should be programmed to apply irrigation late in the day when running the SWAT test so that the controllers have the opportunity to gather weather information about the current day prior to the first irrigation cycle. However, in the "real world", typically irrigation is scheduled early in the day.

Priority of inputs and outputs to the daily moisture balance level were not specified prior to the current version of the protocol. It was unknown during the original testing of whether effective rainfall was calculated before or after irrigation. It was determined after working with the SWAT program that ET is removed prior to the calculation of effective rainfall and irrigation is applied after the effective rainfall calculation. By putting these inputs and outputs in this order, it assumes that rainfall occurs later in the day after most of the ET has left the soil profile. This allows for more rainfall, and consequently less irrigation, to be considered effective.

The SWAT protocol specifies in the newest version that a weather station must be on-site to perform the SWAT evaluation. However, irretrievable or inappropriate weather data is possible and can occur at any time. For the test performed in 2008, weather data was missing on 26 September 2008 to 28 September 2008. When using the data collected in the SWAT program, the missing data were replaced with zeros. However, the ET controllers would likely use the last ET_O value calculated or received by the controller until a signal was reestablished; this is what was done for the 2008 evaluation. It is likely that an official SWAT test would be restarted when this happens; however, the protocol does not specify a course of action.

The results presented for different time period lengths were averages of multiple periods within the study period. However, only one time period, or one data

point for irrigation adequacy and one data point for scheduling efficiency, is reported using the SWAT protocol. The manufacturer can continue to test their product until they decide to publish their scores. This can bias the validity of the test if the controller, over one short time period, can achieve one set of good scores by appropriate irrigation scheduling compared to a controller that consistently produces good scores.

Controller programming is the key to receiving good SWAT results. Controllers for the Florida test were programmed with settings that do not necessarily describe the landscape specified in the protocol. Typically, the changes create a smaller RZWWS than specified for the zone. This can be done by using a small root zone depth, increasing slopes, and using seasonal adjustments. Most settings were similar to the protocol for the ETwater controller with only minor adjustments. The Toro controllers were generally programmed with denser soil types, larger slopes, and smaller root zone depths than default values. The Weathermatic cannot adjust the root zone depth. As a result, precipitation rates were lowered to get the same effect. Also, denser soil types, larger slopes, and different landscape coefficients were sometimes used.

Inputting slightly different program settings can significantly impact SWAT scores. For example, the difference of a minute in gross irrigation can affect the scores by 5% to 10%. Events are scheduled so that they are short and frequent to ensure the soil profile receives enough water, but will not create direct or soak runoff. Short and frequent irrigation events will also minimize the penalty failing to properly predict rainfall. However, scheduling irrigation in this way is not consistent with standard irrigation practices, watering restrictions, or horticultural recommendations for healthy plant material. Small, frequent irrigation events occurring in the evening could increase the possibility of disease or fungi and may discourage deep root growth (Doss et al. 1960).

Since controller programming is extremely important to obtaining good SWAT results, manufacturers program the controllers based on how to get a good score rather than using the landscapes described in the protocol. The virtual landscape descriptions were provided so that manufacturers could program their controllers based on the landscape as would occur at a residential site. However, settings used for each zone do not necessarily coincide with the landscape descriptions. Also, there is a lack of standards for determining designations for each setting. Each controller may use a different reference for determining setting descriptions when designing the controller. It is misleading for presented results for a certain landscape when settings were incompatible to the landscape description.

PRELIMINARY CONCLUSIONS

The SWAT test determines whether the controllers have accurate irrigation scheduling capabilities and, despite some misconception, this test does not rate the potential for a controller to conserve water. The test does not include other areas of the controller's performance that could greatly hinder the success of implementation. These areas could include its ability to properly receive or calculate ET, ease of installation, ease of programming, and homeowner educational opportunities.

Cumulative totals for rainfall and ET_O over the study period were lower than the historical average, averaging 56% and 40%, respectively. The combination of low ET and rainfall suggests that irrigation wouldn't generally be required and plant material would be dormant during most of the time period.

The results found during the 2008 SWAT test showed that the ET controllers generally scored well in SWAT performance scores of scheduling efficiency and irrigation adequacy. However, the controllers resulted in slightly lower scores, mainly concerning scheduling efficiency, than what was published from the original SWAT test. Scheduling efficiency results were lower than the original published results by 2.5% for the ETwater controllers, 14% by the Toro controllers, and 5.6% by the Weathermatic. It is likely that manufacturers would have opted to not publish these results as a SWAT score and restarted the test with minor adjustments. The results also showed that there were no differences in results between controllers that use different methods for obtaining weather data.

The SWAT testing protocol should be clearly outlined and detailed enough for results to be reproducible if it will continue to be used as an industry standard. However, the testing procedures are not reproducible based on the current form of the protocol document.

REFERENCES

Allen, R. G., Pereira, L. S., Raes, D., and Smith, M. (1998). Crop evapotranspiration: Guidelines for computing crop requirements. Irrigation and Drainage Paper No. 56, FAO, Rome, Italy.

Allen, R. G., Walter, I. A., Elliot, R., Howell, T., Itenfisu, D., and Jensen, M. (eds). (2005). The ASCE standardized reference evapotranspiration equation. American Society of Civil Engineers Environmental and Water Resource Institute (ASCE-EWRI). 59 pp. Available at: http://www.kimberly.uidaho.edu/water/asceewri/ascestzdetmain2005.pdf. Accessed December 2, 2005.

Doss, B. D., Ashley, D. A., and Bennett, O. L. (1960). Effect of soil moisture regime on root distribution of warm season forage species. *Agronomy Journal.* 52:569-572.

Irrigation Association (IA). (2008). Smart Water Application Technology (SWAT) Turf and Landscape Irrigation Equipment Testing Protocol for Climatologically Based Controllers: 8th Draft. Irrigation Association, Falls Church, VA. Available at: www.irrigation.org. Accessed 20 September 2008.

Mayer, P. W., DeOreo, W. B., Opitz, E. M., Kiefer, J. C., Davis, W. Y., Dziegielewski, B., and Nelson, J. O. (1999). Residential end uses of water. American Water Works Association Research Foundation. Denver, CO.

Table 1. Landscape descriptions defined by the SWAT testing protocol used as guidelines to program each zone (IA 2008).

Description	Zone 1	Zone 2	Zone 3	Zone 4	Zone 5	Zone 6
Soil	Loam	Silty Clay	Loamy Sand	Sandy Loam	Clay Loam	Clay
Slope (%)	6	10	8	12	2	20
Exposure	75% Shade	Full Sun	Full Sun	50% Shade	Full Sun	Full Sun
RZWWS[1] (mm)	21.6	14.0	22.9	50.8	57.2	14.0
Vegetation	Tall Fescue	Bermuda	Ground Cover	Woody Shrubs	Trees and Ground Cover	Bermuda
Landscape Coefficient	Varies Monthly[2]	Varies Monthly	0.55	0.40	0.61	Varies Monthly
Precipitation Rate (mm/hr)	40.6	40.6	35.6	35.6	5.1	8.9
Application Efficiency (%)	55	60	70	75	80	65

[1]RZWWS represents the root zone working water storage or the depth of water readily available to the plant material.
[2]Turfgrass crop coefficients varied monthly depending on type of turfgrass and exposure effects (IA 2008).

Table 2. Measured and historical cumulative ET_O and rainfall over the study length for each controller.

Controller	Length (days)	ET_O (mm)		Rainfall (mm)	
		Measured	Historical	Measured	Historical
ETwater WORS	120	239	339	108	263
ETwater WRS	120	239	339	108	263
Toro WORS	81	122	176	52	132
Toro WRS	81	122	176	52	132
Weathermatic	110	278	301	116	224

Table 3. Irrigation adequacy and scheduling efficiency results for each controller during the 2008 SWAT test ending January 11, 2009.

Controller	Irrigation Adequacy (%)			Scheduling Efficiency (%)		
	Avg[1]	Max[2]	Min[3]	Avg	Max	Min
ETwater WORS	100	100	100	94	100	80
ETwater WRS	100	100	100	98	100	92
Toro WORS	98	100	94	86	100	67
Toro WRS	97	100	94	85	100	62
Weathermatic	100	100	100	94	100	92

[1]Denotes the average value.
[2]Denotes the maximum value.
[3]Denotes the minimum value.

Table 4. Irrigation adequacy results for each controller during the 2008 Florida test using the SWAT protocol over thirty, forty-five, and sixty day periods.

Controller	Irrigation Adequacy (%)								
	Mean			Maximum			Minimum		
Time (days)	30	45	60	30	45	60	30	45	60
ETwater WORS	100	100	100	100	100	100	100	100	100
ETwater WRS	100	100	100	100	100	100	100	100	100
Toro WORS	ND[1]	98	98	ND	98	98	ND	98	97
Toro WRS	ND	98	98	ND	98	98	ND	98	96
Weathermatic	100	100	100	100	100	100	100	100	100

[1]ND represents no data due to insufficient ET_O and rainfall totals for the time period resulting in no reportable scores.

Table 5. Scheduling efficiency results for each controller during the 2008 Florida test using the SWAT protocol over thirty, forty-five, and sixty day periods.

Controller	Scheduling Efficiency (%)								
	Mean			Maximum			Minimum		
Time (days)	30	45	60	30	45	60	30	45	60
ETwater WORS	96	95	95	99	98	97	91	89	92
ETwater WRS	98	97	97	99	98	98	95	95	96
Toro WORS	ND[1]	100	93	ND	100	100	ND	100	83
Toro WRS	ND	100	90	ND	100	100	ND	100	80
Weathermatic	97	93	93	100	100	99	90	88	88

[1]ND represents no data due to insufficient ET_O and rainfall totals for the time period resulting in no reportable scores.

The use of Soil-water Sensors in Turf Irrigation Control-How Effective are they?

Garry L.Grabow[1], Michael Dukes[2], and Bir Thapa[3]

[1]Department of Biological and Agricultural Engineering, North Carolina State University, Campus Box 7625 Raleigh, NC 27695 PH (919)513-7348; e-mail: Garry_Grabow@ncsu.edu
2 Agricultural and Biological Engineering Department, University of Florida, P.O. Box 110570 Gainesville, FL 32611-0570; PH (352)392-1864 ext. 107; e-mail: mddukes@ufl.edu
[3]Department of Crop Science, North Carolina State University
Campus Box 7620 Raleigh, NC 27695 PH (919) 515-8742; e-mail: bir_thapa@ncsu.edu

Abstract

Soil-Water sensor controllers have been used since the mid-1990s to manage turf irrigation. While evapotranspriation (ET) based controllers have been more widely adopted for turf and landscape irrigation, soil-water-sensor based systems hold some distinct advantages, particularly in humid regions where rainfall contributes significantly to turf water requirements and is highly spatially variable. Some perceived disadvantages of soil-water-sensor based systems are representativeness of whole landscapes when only one sensor is used; sensor accuracy and repeatability, and proper setting of soil-water setpoints. Several studies involving soil-moisture sensors have been done in Florida, and one study in North Carolina is near completion. These studies have looked at soil-water sensor based systems of various manufacturers in similar settings; have compared results between different moisture setting thresholds; have contrasted water usage with ET based controller systems; and have monitored root zone soil-water status in plots irrigated by soil-water based systems. Soil-water data has also been collected for replicates of sensor-based treatments in an effort to address the question of repeatability and sensor placement representativeness. Preliminary data from these studies have shown that there is wide variability between different sensor systems with respect to both applied water and turf quality. The data has also shown that soil water sensor based systems may in some cases apply less water than ET controllers. Consistent relationships between soil-water-content and controller settings has been found to be problematic. Analysis of soil-water data indicates that while there are differences in soil-water between replications of soil-water-based sensor treatments, soil-water trends are generally consistent between replications and turf quality is generally not substantially different between replications.

Introduction

Soil-water based controllers govern irrigation events using soil-water information. The concept is that all components of a water balance can be integrated into soil-water content. In essence, soil-water based controller systems measure soil-water while ET controller systems predict it. Most sensor-based systems require setting of one threshold (setpoint) moisture content, above which previously programmed irrigations are overridden. Some operate using two thresholds; one to initiate an irrigation event and the other to terminate the event. These thresholds are set to soil-water contents reflective of what is commonly termed an allowable depletion level (single setpoint for one-setpoint systems and lower setpoint for two setpoint systems) and field capacity (upper setpoint for two setpoint systems). While some products adjust baseline run times based on soil-water content, most do not adjust run time but simply allow or disallow a previously programmed irrigation. Some systems interrupt an irrigation cycle immediately when the soil-water content is above the threshold setting, while others allow completion of the irrigation event. Most systems are ‘‘add-on’’ systems meant to be added to an existing controller, while other are ‘‘stand alone’’ complete systems including a controller specifically designed for the system. The ‘‘add-on’’ systems are designed to operate with one sensor while some stand alone systems can accommodate multiple sensors corresponding to multiple irrigation zones. The soil-water sensors that come with these systems include tensiometric-based, conductivity-based and dielectric-based sensors. Setpoints vary from relative settings such as ‘‘wet’’ to ‘‘dry’’ to volumetric soil-water content.

Sensor based control of irrigation in turf began in the mid 1990s. Numerous systems have entered and left the market since then. In a recent review, eight soil-water sensor controllers design for turf and landscape irrigation were described (USBR, 2007). While the preponderance of research and testing has been done for ET controllers, research on these sensor-based systems dates back to the late 1990s. Most of these studies have compared water savings from soil-water sensor controllers versus ‘‘standard’’ timer based controllers with or without a rain shutoff device. In a study conducted in Utah, Allen (1997) found that the use of a simple automated device for overriding a standard electronic irrigation clock by monitoring soil-water can result in an average of 10% savings in water use and can still maintain healthy green lawns compared to a system without a rain sensor. In Florida Dukes et al. (2008) found that most SMS systems saved significant amounts of water when compared to time-based irrigation schedules typically used by homeowners. They recorded ‘‘wet weather’’ savings of 69% to 92% for three of the four systems tested and ‘‘dry weather’’ savings of 28% to 83% while maintaining turfgrass quality at acceptable levels (Cardenas-Lailhacar, et al., 2005).

Grabow, et al. (2008) found that soil-water sensor based systems saved from 12% to 50% of a timer treatment in a dry year when the sensor system was added to a controller programmed exactly as the timer treatment. Preliminary results from the subsequent year that had timely rain show a 24% to 58% savings for the same comparison. Turfgrass quality for both the timer-based and SMF systems suffered in

the first year of the study as the base controller for both was programmed for normal, rather than the dry conditions experienced that year.

Recently studies have been taken from controlled research facilities at universities and moved into residential settings. Haley et al., (2007) evaluated sensor based controller systems in a study conducted in Florida. Fifty-nine homes were included in the study that was divided into four groups, one of which had sensor based add-on systems and a standard timer controller. The residences with the sensor based technology saved 51% when compared to water use of the group using only standard controllers with no intentional guidance. This savings were more than those attained with a standard clock controller and rain sensor that saved 19% compared to the same group. Results of several studies done in Florida have led to the publication of a field guide on the use of soil-water based controller systems in Florida (Philpot et al., 2008).

Soil-Water sensor controller Performance Between Manufacturers

As soil-water sensor based controller systems vary with sensor type, threshold setting interfaces, and modes of operation, it follows that these systems do not all perform identically even when used on similar landscapes, soils and subjected to the same weather patterns. Cardenas-Lailhacar et al (2005) compared four sensor-based systems in irrigation of bermudagrass in Florida. The manufacturers and systems were: Acclima RS500 (Acclima,Inc., Meridian, ID), Watermark 200SS-5 (Irrometer Company, Inc., Glendora, CA), Rain Bird MS-100 (Rain Bird International, Inc., Glendora, CA), and Water Watcher DPS-100 (WaterWatcher, Inc., Logan, UT). The Rain Bird product is no longer on the market, and WaterWatcher is no longer in business. The study also looked at the effect of three irrigation frequencies; weekly, bi-weekly, and daily. While on average, the SMS systems saved 57% in terms of applied water compared to a timer based system set to replace 100% of historical evaportranspiration, individual systems varied widely in the amount of water applied. For the period 20 July to 14 December 2004, the average depth applied over all frequencies ranged from 100 mm to 420 mm. In the case of the system that applied 420 mm, only the weekly treatment resulted in a water savings when compared to the historical ET treatment (Cardena Lailhacar, et al., 2005). After two years of study at the same site, overall savings from 20% to 72% were reported by Dukes, et al,(2008).

Comparison with ET-based Systems

So-called “SMART” controllers can be placed into two broad categories; those that use weather data and site information to irrigate based on the evapotranspiration (ET) of the landscape and those that use soil-water sensors to control irrigation. More studies have been done with ET controllers, however some comparisons between the two types of systems have been made. Some relative comparisons can be made from studies in which the two types are not compared “side-by-side” but compared to a similar standard. Davis, et. al, (2007) in a study that evaluated three commercially available ET controllers, found water savings as much as 40% compared to the theoretical gross irrigation requirement, and water wastage by as

much as 63% depending upon the season. Much of the variation in the results in ET controllers is probably due not only to their ET estimation methods, but also to their ability (or lack thereof) to account for on-site rainfall. This is where the soil-water sensor based systems hold an advantage.

Vasanth et. al, (2007) and Grabow et al. (2008) found that two soil-water sensor systems applied less water than an ET controller in a study conducted in Raleigh, NC. As in the study done by Cardenas Lailhacar et. al. (2005) weekly, bi-weekly and daily irrigation frequencies were part of the experimental design. The two sensor based systems were manufactured by the same company, but one was a single setpoint "add-on" system, and the other was a two-setpoint or "on-demand" system. The on-demand sensor system was allowed to irrigate daily, but only did so when the soil-water level was below the lower setpoint. In the first year of the study, the single setpoint sensor system applied 46 - 48% less than the ET controller while the two-setpoint system applied from 31% less to 8% more depending upon irrigation frequency. Preliminary analysis of the second year's data show even more relative savings from the sensor based system, likely due to the increased rainfall and the system's ability to account for on-site rainfall. It should be noted that while the soil-water sensor systems afforded water savings in the first year of the study, turf quality suffered for the add-on systems. The on-demand sensor system has offered the best combination of water savings and turf quality in this study to date.

Representativeness and Repeatability

One argument against the soil-water based systems has been the perceived problems with representativeness of sensor location and repeatability of the sensor systems. Dukes and Miller (2005) evaluated the same four soil-water sensor systems as tested by Cardenas-Lailhacar et al (2005). They found that only one of the four sensors tested was highly predictable (repeatable) in its relationship between soil-water content and controller settings. Despite the lack of repeatability in three of the four systems, all but one system reduced applied water by 60-80% compared to a twice–a-week time based system. They noted that the slopes of the regression lines of controller setting vs. volumetric soil content varied by the irrigation frequency settings of the same controller. This was attributed to possible manufacturer variability or localized soil differences.

Studies in both North Carolina and Florida have looked at the difference in soil-water content over time in turf plots that are replications of one soil-water sensor treatment. This goes to addressing concern with sensor placement. In both of these studies, a sensor buried in one plot served as the "master" to "slaved" plots that served as replications. Figure 1 shows soil-water data over time in a study done in Florida. Three plots are slaves to the control plot (E04), i.e, plot EO4 has the control sensor and the other three have monitoring sensors. Note that while there are differences in the volumetric water content at any one time, soil-water trends the same in all plots. The differences are likely due to soil heterogeneity.

Figure 2 shows a similar plot that contains soil-water data from three soil-water-sensor controller systems and an ET controller and standard timer-based systems. These plots are in a clay soil located in Raleigh, North Carolina. Volumetric water

content was measured at four depths with a down-hole capacitance probe and an access tube. While not as in concert as the plots shown in Figure 1, soil water content of the replications for the soil-water sensor systems generally trend the same. The other treatments are shown for comparison. Variability is also evident in these other treatments, illustrating the fact the ET controllers are subject to the same variability as a soil-water sensor system. In this study done in North Carolina, differences in turf quality were noted in some of the soil-water sensor based replications in the first year (2007) but not in the second year.

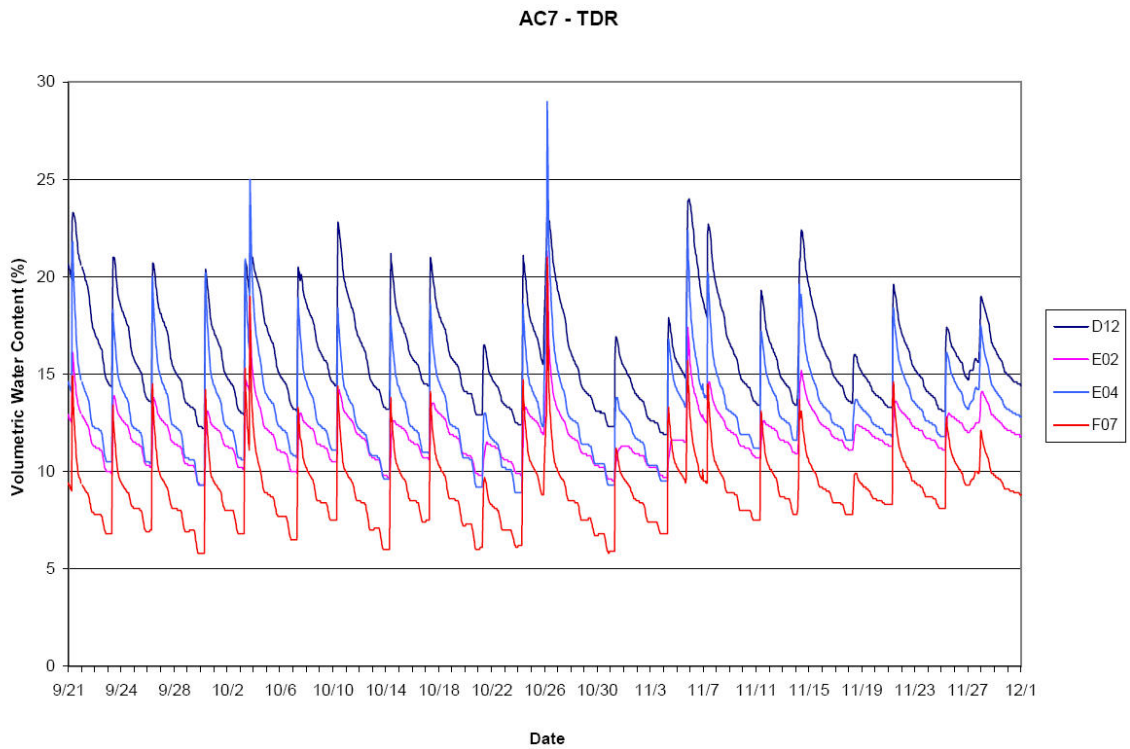

Figure 1. Volumetric Soil-Water Content for Four Replications of a Soil-Moisure Sensor Controller Treatment in Florida (2006). EO4 is the plot with the control sensor and the other three are slaves.

Summary And Conclusions

Soil-water sensor controller systems have conceptual advantages in irrigation control since they integrate all elements of a soil-water budget into the soil. Studies have shown the these systems consistently reduce water use when compared to standard controller systems set to irrigation on historical ET or historical gross irrigation requirement. They have also to been shown to apply less water than ET controllers in some instances while maintaining turf quality. The relative advantage of soil-water sensor systems to ET controllers may be enhanced in humid regions, as these systems can account for local effective precipitation. Sensor placement and representativeness may not be as problematic as first thought, and in fact spatial variability in soil, microclimate, plant and turf characteristics leads to spatial variability in soil-water content for ET systems as well. Sensor-bases systems that

allow for multiple sensors (e.g. one for each irrigation zone) would further address this concern.

As with any "SMART" irrigation system, proper installation and setup is critical. Guidance for this systems has been formulated in Florida and continuing research in other locations will aid in local guidance. It is imperative that for soil-water sensor based systems that run times be adequate to guard against periods of drought, yet not be longer than required to fill the root zone to field capacity. This is especially important for those systems that allow a complete irrigation rather than immediate termination of a cycle once the soil-water level has increased to above the threshold setting.

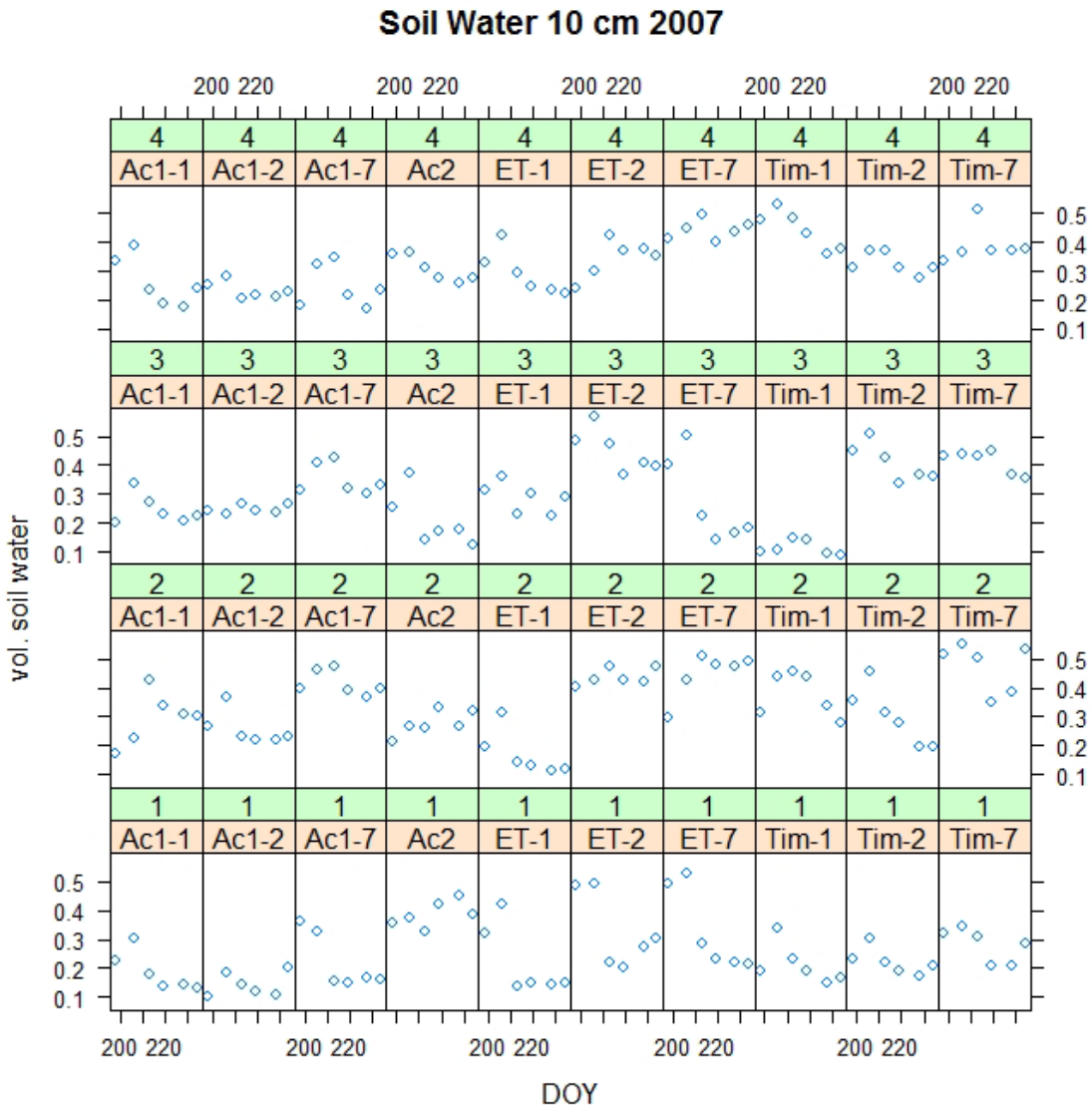

Figure 2. Volumetric Soil Water Content at 10 cm depth for 4 replications of four technology (Ac1, Ac2, ET, and Tim) and three irrigation frequencies (1-weekly, 2-bi-weekly, and 7-daily). The green band indicates rep (1,2, 3, and 4) and the brown band is treatment (technology x

frequency). DOY is day of year 2007. The Ac treatments are the sensor treatments and their control sensors are located in rep 2.

References

Allen, R. G. 1997. Demonstration of Potential for Residential Water Savings using a Soil-Moisture Controlled Irrigation Monitor. Project Completion Report for Project 6-FC-40-19490, United States Bureau of Reclamation, Provo, Utah office.

Cardenas-Lailhacar, B., M.D. Dukes, and G.L. Miller. 2005. Sensor-based control of irrigation inbermudagrass. ASAE Paper No. 05-2180. American Society of Agricultural Engineers, St.Joseph, MI.

Dukes, M.D. and G.L. Miller. 2005. Calibration and Testing of On-demand Irrigation Control Systems Final Project Report. Submitted to the Florida Nursery Growers and Landscape Association.

Grabow, G. L., Vasanth, A., D. Bowman, R.L. Huffman, and G. L. Miller. 2008. Evaluation of Evapotranspiration-Based and Soil-Moisture Based Irrigation Control in Turf. In: Proceedings of the 2008 World Environmental and Water Resources Congress, American Society of Civil Engineers, May 12-16, Honolulu, Hawaii. Babcock, R.W. and R. Walton editors. ISBN 978-0-7844-0976.

Haley, M.B., and M.D. Dukes. 2007. Evaluation of Sensor Based Residential Irrigation Water Application. ASABE Paper No. 072251, presented at the 2007 ASABE International Meeting, 17-20 June 2007.

Philpot, B.T. 2008. The Field Guide to Soil Moisture Sensor Use in Florida. IFAS, University of Florida. St. Johns River Water Management District, publisher.

USBR, 2007. Weather and Soil Moisture Based Landscape Irrigation Scheduling Devices. Technical Review Report, 2nd edition. Denver, Colorado.

Vasanth, A.*, G. Grabow, D. Bowman, R.L. Huffman, and G. L. Miller. 2007. Evaluation of Evapotranspiration-Based and Soil-Moisture Based Irrigation Control in Turf. In: Proceedings of the 28th Annual International Irrigation Show, Dec. 9-11, San Diego, Calif. ISBN: 9781605600987.

Application of SVMs Algorithms for Prediction of Evaporation in Reservoirs

Arun Goel[1]
[1]Assistant Professor, Civil Engineering Department, National Institute of Technology (Deemed University) Kurukshetra.136119. Haryana. INDIA. E mail: drarun_goel @yahoo. co. in., Fax: 91-1744-238050.

ABSTRACT

Assessment of water resource requires effective procedures for evaporation estimation involving measurable meteorological parameters and such approaches are rarely available in the literature. In the present work, the data of daily evaporation, temperature, solar radiation, relative humidity, wind speed are used to assess the potential and usefulness of SVM based modeling. The performance of the SVM algorithms (Rbf & Polynomial) is compared with the linear regression on the basis of performance parameters having different combinations of input parameters. The comparison of results showed that there is better agreement when more input parameters are considered for model building as compared to a single parameter. The outcome of study suggests that the SVM based modeling can be applied as an alternative approach for estimation of daily evaporation from the reservoirs.

Keywords: SVM, modeling, error, linear regression, evaporation, reservoir.

INTRODUCTION

Accurate estimation of evaporation influences water balance studies undertaken for efficient planning, design, construction, operation and management of water resources. The evaporation is considered to be most difficult to estimate in the hydrologic cycle due to complex interaction between components of land-plant-atmosphere system (Singh & Xu 1997). In the hydrological practice, the evaporation can be estimated by conventional approaches like direct or indirect methods involving use of empirical equations. The sole direct method is the U S weather Bureau Class A pan measurement. The indirect methods use meteorological data to estimate evaporation by the empirical based methods or statistical and stochastic approaches. The indirect methods are temperature based formula, radiation method, humidity based relation, Penman formula, energy balance approach etc. (Abtew 2001; Choudhury 1999; Vallet-Coulomb et al. 2001; Terz and Keskn 2005). All these approaches are although based on Penman formula but they are sensitive to site-specific evaporation parameters, which can vary form one place to other. Further it is not

possible to consider all the parameters affecting the evaporation estimation by any of the above approaches due to many assumptions and phenomenal constraints.
The literature review showed that these equations vary greatly in their ability to define the magnitude and variability of the evaporation from the reservoirs and the lakes. It is therefore necessary to develop alternate approaches to estimate the evaporation rates based on metrology variables, which are comparatively easier for measurements and estimation. One of the recent alternate approaches is to use of soft computing modelling techniques, which have better modelling flexibility & capability rather than previous empirical approaches where in each of the metrological parameter takes it share proportionally.
The ANN models have been applied to estimate the Pan evaporation by Terzi et al. 2006, Eskin and Terzi 2006) recently. Some studies by (Pal and Goel 2006, Pal 2006) have shown the SVM regression are working well in civil engineering applications in comparison to the neural network approach. However, very few studies have applied SVM modelling approach in this area of evaporation from reservoirs. Murthy and Gawande (2006) have applied linear regression approach for prediction of evaporation by using individual parameters form an Indian reservoir. They have used field data of air temperature (T), wind speed (U), sunshine hours (Sh) and relative humidity (Rh) to predict the evaporation loss (E) as individual parameters. This study has a major limitation that they have not considered the combined effect of all the input parameters in determining the evaporation losses. The average weekly evaporation and meteorological data of Manasgaon (from 1990 to 2004) are collected from a reservoir in Anand Sagar, Shegaon, India (Murthy and Gawande, 2006). Measured meteorological variables include daily observations of evaporation, mean air temperature, sunshine hours, mean relative humidity, and wind speed have been use in the present study.
The present study is aimed to check the potential and application of SVM modelling in predicting the evaporation loss along with linear regression models.

SUPPORT VECTOR MACHINES

Support vector machines (SVMs) are classification and regression methods, which have been derived from statistical learning theory (Vapnik, 1995, 1998). The SVMs classification methods are based on the principle of optimal separation of classes. If the two classes are separable - this method selects, from among the infinite number of linear classifiers, the one that minimize the generalization error, or at least an upper bound on this error, derived from structural risk minimization. Thus, the selected hyper plane will be one that leaves the maximum margin between the two classes, where margin is defined as the sum of the distances of the hyper plane from the closest point of the two classes (Vapnik 1995). The modelling techniques like support vector machines have the capability to reproduce the unknown relationship present between a set of input variables and the output of the system. Support vector machines performance was found to be better due to its use of the structural risk minimization principle in formulating cost functions and of quadratic programming during model optimization. These advantages lead to a unique optimal and global solution as compared to conventional neural network models.
If the two classes are non-separable, the SVMs tries to find the hyper plane that maximizes the margin and that, at the same time, minimizes a quantity proportional to the number of misclassification errors. The trade off between margin and misclassification error is

controlled by a positive constant that has to be chosen beforehand. This technique of designing SVMs can be extended to allow for non-linear decision surfaces. This can be achieved by projecting the original set of variables into a higher dimensional feature space and formulating a linear classification problem in the feature space (Vapnik, 1998). Support vector machines can be applied to regression problems and can be formulated as below:

Vapnik (1995) proposed ε-support vector regression (SVR) by introducing an alternative ε-insensitive loss function. The purpose of the SVR is to find a function having at most ε deviation from the actual target vectors (y_i) for all given training data and have to be as flat as possible (Smola, 1996). This can be put in other words as the error on any training data has to less than ε. For a given training data with k number of samples, represented by $(\mathrm{x}_1, y_1),.....,(\mathrm{x}_k, y_k)$ and a linear function $f(\mathrm{x}) = \langle \mathrm{w}, \mathrm{x} \rangle + d$ (1)

where $w \in \mathrm{R}^N$ and d $\in$ R. $\langle \mathrm{w}, \mathrm{x} \rangle$ represents the dot product in space R^N and N is the dimension of input space. A smaller value of w indicates the flatness of Equation 1, which can be achieved by minimizing the Euclidean norm as defined by $\|\mathrm{w}\|^2$ (Smola, 1996). Thus, an optimization problem for this can be written as: minimize $\frac{1}{2}\|\mathrm{w}\|^2$

$$\text{subject to } \begin{cases} y_i - \langle \mathrm{w}, \mathrm{x}_i \rangle - d \le \varepsilon \\ \langle \mathrm{w}, \mathrm{x}_i \rangle + d - y_i \le \varepsilon \end{cases} \quad (2)$$

The optimization problem in Equation 2 is based on the assumption that there exists a function that provides an error on all training pairs which is less than ε. In real life problems, there may be a situation like one defined for classification by Cortes and Vapnik (1995). So, to allow some more error slack variables ξ, ξ' can be introduced and the optimization problem defined in Equation 1 can be written as:

$$\text{minimize } \frac{1}{2}\|\mathrm{w}\|^2 + C\sum_{i=1}^{k}\left(\xi_i + \xi_i'\right)$$

$$\text{Subject to } y_i - \langle \mathrm{w}, \mathrm{x}_i \rangle - d \le \varepsilon + \xi_i$$

$$\langle \mathrm{w}, \mathrm{x}_i \rangle + d - y_i \le \varepsilon + \xi_i'$$

$$\text{and } \xi_i, \xi_i' \ge 0 \text{ for all } \mathrm{i} = 1, 2, \ldots\ldots, \mathrm{k}. \quad (3)$$

The parameter C is determined by the user and it determines the trade-off between the flatness of the function and the amount by which the deviations to the error more than ε can be tolerated. The optimization problem in Equation 3 can be solved by replacing the inequalities with a simpler form determined by transforming the problem to a dual space representation using Lagrange multipliers λ_i, λ_i', η_i, η_i' i = 1,….,k (Leunberger, 1984). The prediction problem can finally be written as:

$$f(\mathrm{x}, \alpha) = \sum_{i=1}^{k}\left(\lambda_i' - \lambda_i\right)\langle \mathrm{x}_i, \mathrm{x} \rangle + d \quad (4)$$

This technique can be extended to allow for non-linear support vector regression by introducing the concept of the kernel function (Vapnik, 1995). This is achieved by mapping the data into a higher dimensional feature space, thus performing linear regression in feature space. The regression problem in feature space can be written by replacing $x_i \cdot x_j$ with $\Phi(x_i) \cdot \Phi(x_j)$.

Where $K(x_i, x_j) \equiv \Phi(x_i) \cdot \Phi(x_j)$

The regression function for this can be written as:

$$f(x, \alpha) = \sum_{i=1}^{k} (\lambda_i^{'} - \lambda_i) K(x_i, x) + d \quad (5)$$

PERFORMANCE COMPARISON CRITERIA

Much success has already been achieved using neural network algorithms in lake water prediction (Eskin 2006), while the use of support vector machines is comparatively new to the field of hydraulics and water resource engineering (Khan and Coulibaly, 2006; Pao-shan et al., 2006, Pal 2006, Pal & Goel 2006). The SVMs, in addition to the choice of kernel require setting up of kernel specific parameters. The optimum values of the regularization parameter C and the size of the error-insensitive zone ε need to be determined. To select user-defined parameters i.e. (C, γ and d^*) a large number of trials were carried out by using different combination of these parameters on each of the data sets. Similarly, a number of trials were also carried out to find a suitable value of ε (error-insensitive zone) with a fixed value of C and kernel specific parameters. To reach at a suitable choice of these parameters, the correlation coefficients (CC), Root relative square error (RRSE), mean absolute error (MAE), relative absolute error (RAE) and Root Mean Square Error (RMSE) were compared and a combination of parameters providing smallest value of RMSE, MAE, RAE, RRSE and the highest value of correlation coefficient (CC) were selected for the final results. A number of trials were carried out with different data set to select a suitable value of regularization parameter C. Variation in the error-insensitive zone ε have no effect on the predicted scour so a value of 0.0010 was chosen for all experiments.

The data sets from Gawande and Murthy (2006) was used in the present study for model building and validation to assess the potential linear regression based modelling and RBF & Poly based kernels support vector machines in predicting the evaporation loss from the reservoir. Further, measured evaporation values were plotted against the computed values obtained with linear and SVMs algorithms. To study the scatter around the line of perfect agreement (i.e. a line at 45 degrees) was also plotted for the data set. Due to the availability of small data sets, a cross validation was used to train and test the performance of the SVMs. The cross-validation is a method of estimating the accuracy of a classification or regression model. The input data set is divided into several parts (a number defined by the user), with each part in turn used to test a model fitted to the remaining parts. In this study, the field data were used for both creating and testing the models. The choice of input parameters used in modeling the evaporation may influence the predicting capabilities of support vector machines. Graphs have been plotted for difference in actual and predicted values of the evaporation loss along with errors in results as shown in Figures 1-5.

ANALYSIS OF RESULTS

Scatter diagrams as well as error differences between actual and predicted daily pan evaporation values are plotted considering different input combinations of meteorological parameters. The results of the different methods obtained by using RBF & Polynomial kernels of SVM, and linear regression models, are compared with the actual pan evaporation values of the reservoir based on correlation coefficient, RMSE, MAE, RAE, and RASE. The examination of plotted figures 1 to 5 shows that there is better agreement of predicted results based on rbf kernel of SVM rather than for other modelling techniques like polynomial kernel of SVM and the linear regression.

The first set of analysis was carried out by using SVMs and linear regression with input as temperature and output as evaporation loss and the results are plotted as shown in Fig.1 (a). The SVMs determine a relationship (i.e. create a model) between the input and the output of the available data set of any system. These models are than used to predict the output from the known input values of the same system, thus requiring sufficient number of data to create and test the models. A 10 fold cross validation was used to create and test the models. A number of trials were carried out to reach at the various user-defined parameters required for The SVMs using both polynomial and RBF kernels and linear regression based algorithms using WEKA software. The Table 1 provides the value different user defined parameters and the (Table 2) shows the values of correlation coefficients, RMSE, MAE, RAE, RASE for the data set.

Similarly wind velocity, sun shine hours and relative humidity were taken as input parameters separately and evaporation loss were predicted and the results obtained are plotted as shown in Fig. 2 (a), 3(a) and 4(a) respectively. A graph shown as Fig.5 (a) is plotted when all four parameters were taken for model building and evaporation loss was predicted. Further, it is evident from Figure 1(a) to Figure 5(a) that more number of points are lying on the 45° line when the rbf kernel was used to predict the evaporation in comparison to polynomial kernel and linear regression based algorithm for any combination of input parameters. The error obtained between actual and predicted values of evaporation loss has been plotted in Fig. 1(b) to Fig. 5 (b). The figures indicate that there is larger variation of error in case of polynomial based kernel and linear regression approach as compared to radial basis function approach in the present study. It is evident from Fig 1(a) to 5(a) that the maximum value of correlation coefficient was obtained for air temperature followed by wind speed and relative humidity while, minimum values were obtained for sun shine hours (Table 2). Similarly minimum values of RMSE, MAE, RAE, RASE, were obtained for air temperature followed by wind speed and relative humidity and sunshine hours as shown in Table 2. However, all the factors influence concurrently, so it is pertinent to consider the combine influence of all the parameters in the evaporation loss estimation.

CONCLUSIONS

The study concludes that a combination of all input parameters provides better performance of model in estimating the evaporation loss rather than individual parameters. The study revealed that evaporation loss is best estimated by RBF-based SVM modelling rather than polynomial based SVM modelling and the linear regression techniques.

Further, the critical examination of three figures indicates that the performance of the SVM modeling is data dependent to a great extent. The outcome of the study provided an impetus to the potential use of RBF kernel based SVM approach in predicting the evaporation from the reservoirs.

ACKNOWLEGEMENTS

The author wishes to acknowledge Murthy and Gawande (2006) for their data set used in the present study.

REFERENCES

Abtew., W. (2001) Evaporation estimation of lake Okeechobee in south florida. J of irrigation and drainage, 127(3), 140-147.

Cortes, C., and Vapnik, V. N. (1995) Support vector networks, Machine Learning. Vol. 20, pp 273-297.

Choudhury, B. J. (1999) Evaluation of an empirical equation for annual evaporation using Field observations and results from biophysical model. J of Hydrology, 216, 99-110.

Eskin, M erol and erzi Ozlem (2006) Artificial neural network models of daily pan evaporation journal of Hydrologic Engg Vol. 11 no. 1., pp. 165-70.

Khan S. M. and Coulibaly P. (2006) Application of support vector machine in lake water level prediction. Journal of Hydrologic Engg., Vol. 11, No 3, pp.199-205.

Leunberger D. (1984), Linear and nonlinear programming. Addison-Wesley.

McKanzie, R. S. and Craig, A. R. (2001) Evaluation of river losses form the Orange river using hydraulic modelling, J of Hyrology, 241, 62-69.

Murthy, S. and Gawande, S. (2006) Effect of meterological parameters on evaporation in small reservoirs "Annad sagar" Shegaon - a case study. Journal of Perdushan Nimulan, Vol.3, No. 2 pp 52-56.

Pal, M. (2006) Support vector machines based modelling of seismic liquefaction potential. Int Journal of numerical and analytical methods in Geomechanics,Vol.30, 983-996.

Pal, M. and Goel, A. (2006) Prediction of end depth ratio and discharge in semi circular and circular shaped channels using SVM, J of flow measurement & instr, Vol. 17 pp. 50-57.

Pao-shan Y., Shien T. C. and I-Fan C. (2006) Support vector regression for real time flood stage forecasting. Journal of Hydrology, Vol. 328, pp. 704-716.

Singh, V. P. and C. Y. Xu, (1997), Evaluation and generalization of 13 mass transfer equations for determining free water evaporation. Hydrological Proce, 11:313-323

Smola, A. J. (1996), Regression estimation with support vector learning machines. Master's Thesis, Technische Universität München, Germany.

Terz, O. and Keskn, M. E. (2005) Modelling of daily pan evaporation, Applied science, Vol.5, pp 368-372.

Terzi Ozlem, Keskin M Erol and Taylan E Eliek (2006), Estimating evaporation using ANFIS Journal of Irrigation and drainage Engg, Vol. 132, No. 5, pp. 503-507.

Vapnik, V. N., (1995), The Nature of Statistical Learning Theory. NY: Springer-Verlag.

Vapnik, V. N. (1998) Statistical Learning Theory. New York: John Wiley and Sons.

Vallet-Coulomb, C. Legesse, D, Gasse,F Tavi and Chernet, T. (2001) Lake evaporation estimates in tropical africaa (lake Ziway, Ethopia). J of Hydrology, 245, pp.1-18.

Table 1. Values of kernel specific parameters of SVM based modelling

S.No.	Type of parameter	SVM(RBF)		SVM(POLY)	
		C	γ / d*	C	γ / d*
1	E with T	8	1.1	8	1
2	E with U	10	0.7	8	1
3	E with Sh	8	1	8	2
4	E with Rh	8	1	8	1
5	E with T+U+Sh+Rh	8	1	8	1

Table 2.Comparison of results

Input Parameter	Type of technique	Root relative squared error (RRSE)	Correlation coefficient (r)	Mean absolute error (MAE)	Root mean squared error (RMSE)	Relative absolute error (RAE)
T	SVM(RBF)	46.4285 %	0.8887	1.045	1.4435	42.9045 %
	SVM(POLY)	83.2174 %	0.5775	1.6679	2.5873	68.4772 %
	Linear	86.4156 %	0.5539	1.6755	2.6868	68.7895 %
U	SVM(RBF)	74.0648 %	0.6698	1.6972	2.3028	69.681 %
	SVM(POLY)	80.3536 %	0.5654	1.8114	2.4983	74.3694 %
	Linear	72.6388 %	0.6659	1.7026	2.2584	69.9022 %
Sh	SVM(RBF)	95.7248 %	0.3637	2.1307	2.9762	87.4761 %
	SVM(POLY)	102.9778 %	0.1803	2.1808	3.2017	89.5368 %
	Linear	94.0001 %	0.2678	2.3164	2.9226	95.1017 %
Rh	SVM(RBF)	87.1445 %	0.5338	1.5863	2.7094	65.1286 %
	SVM(POLY)	87.7811 %	0.5262	1.8554	2.7292	76.1741 %
	Linear	83.573 %	0.511	2.0088	2.5984	82.4746 %
All	SVM(RBF)	29.1492 %	0.9543	0.4939	0.9063	20.2768 %
	SVM(POLY)	41.0774 %	0.9099	0.8161	1.2772	33.5073 %
	Linear	43.0925 %	0.9022	0.8677	1.3398	35.6256 %

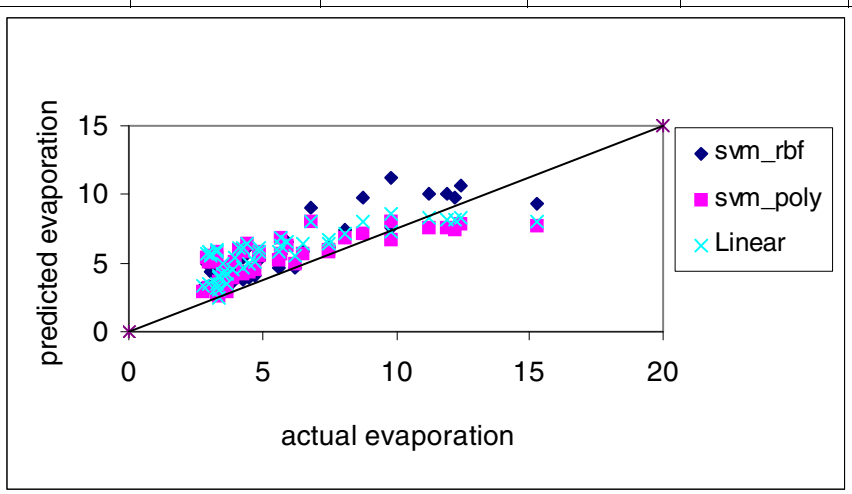

Fig1(a) Actual evaporation versus predicted evaporation with temp

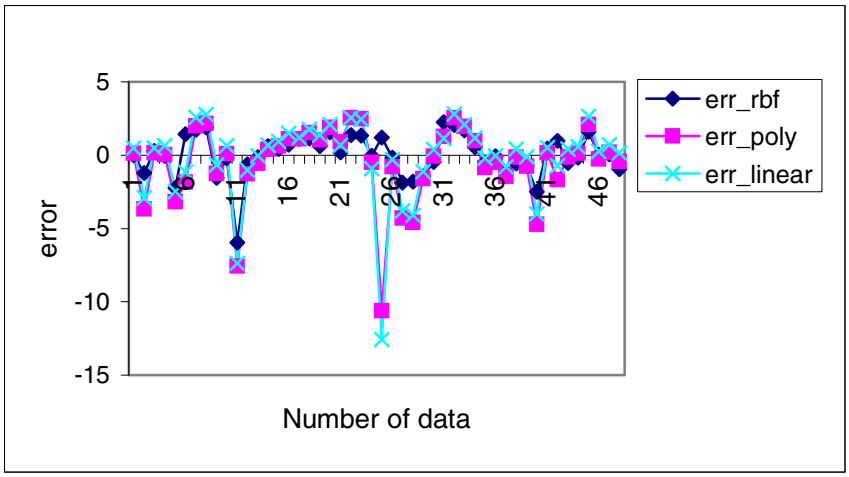

Fig.1(b) Variation of error with temperature

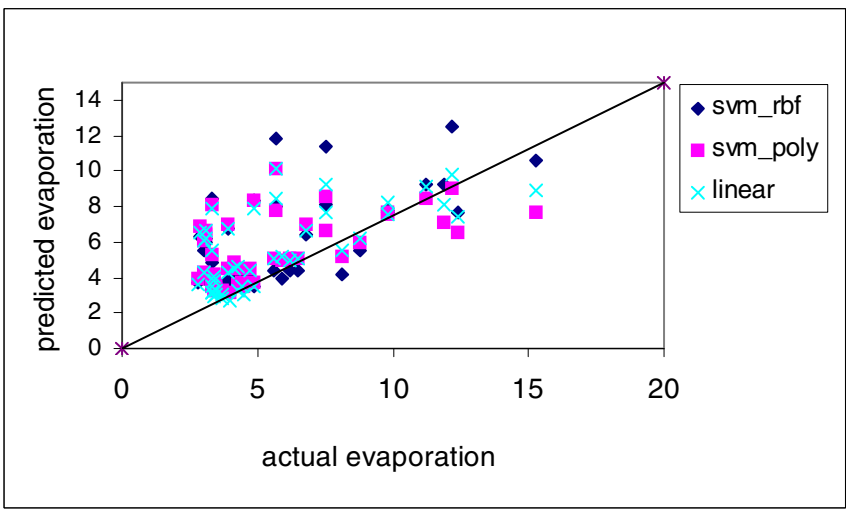

Fig2(a) Actual evaporation with predicted evaporation with wind velocity

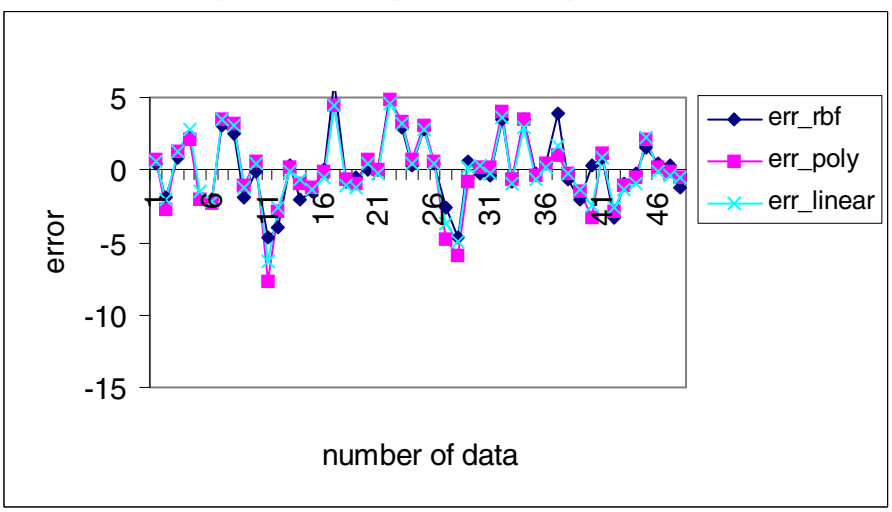

Fig.2(b) Variation of error with wind velocity

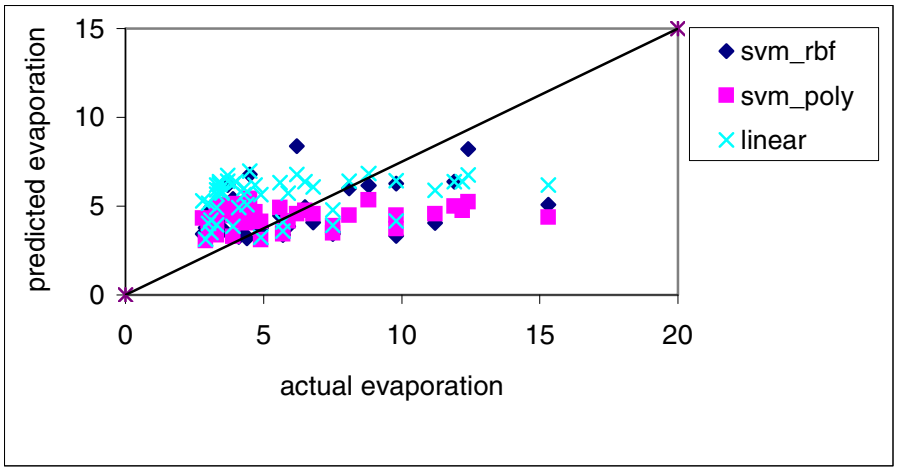

Fig3(a) Actual evaporation versus predicted evaporation with sun shine hours

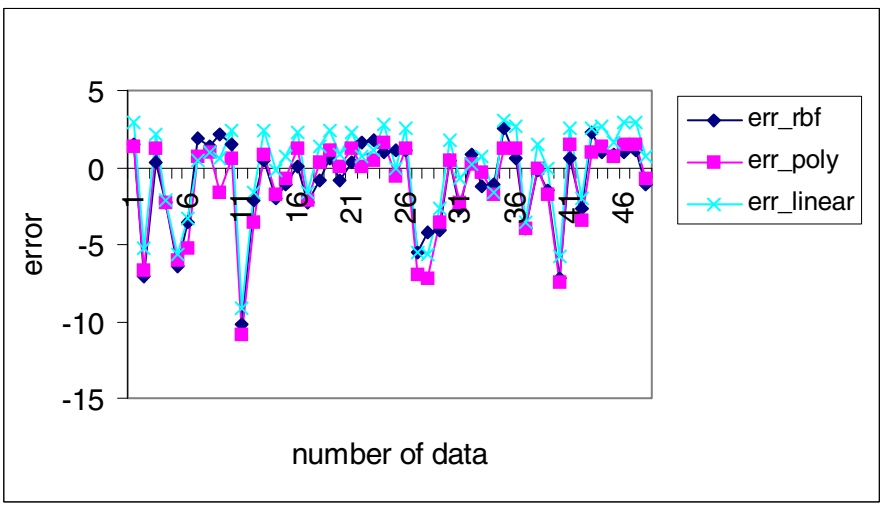

Fig.3(b) Variation of error with sun shine hours

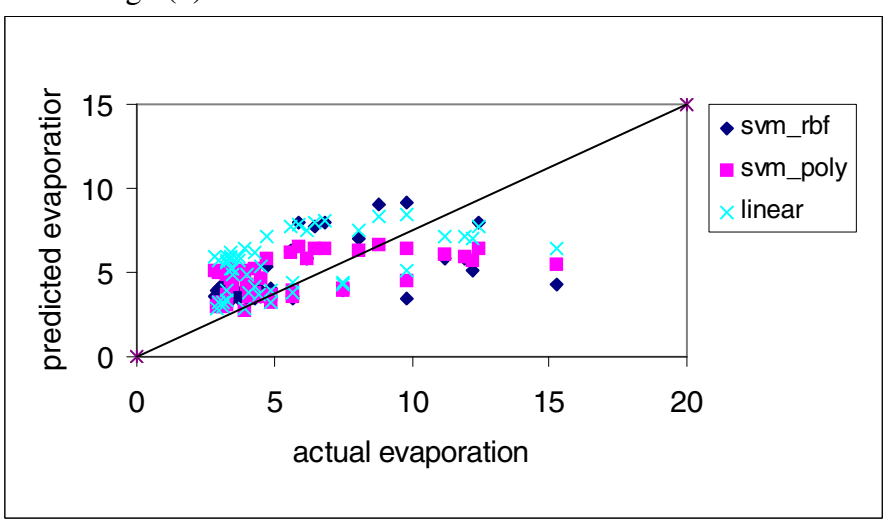

Fig4(a) Actual evaporation versus predicted evaporation with relative humidity

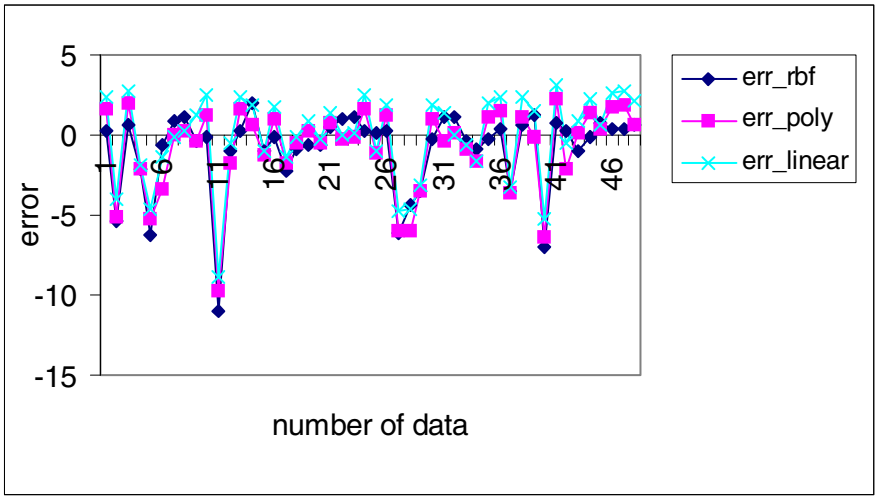

Fig.4(b) Variation of error with relative humidity

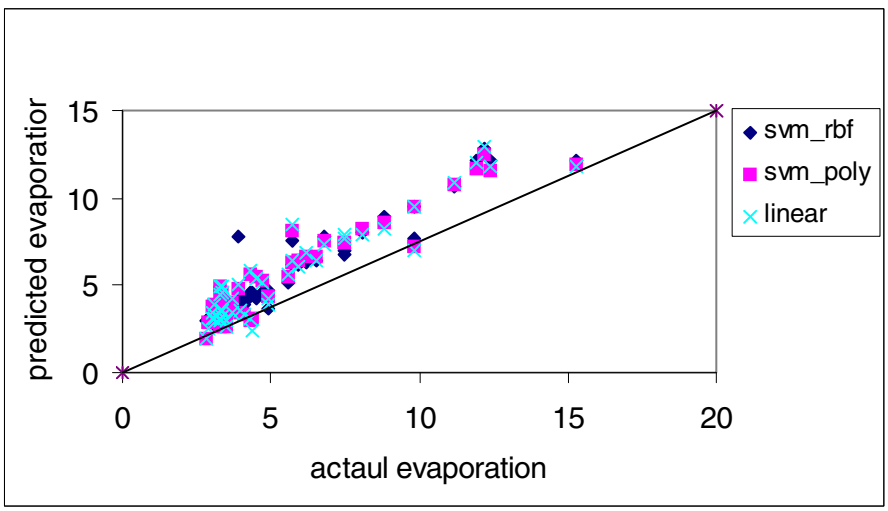

Fig5(a) Actual evaporation versus predicted evaporation with all parameters

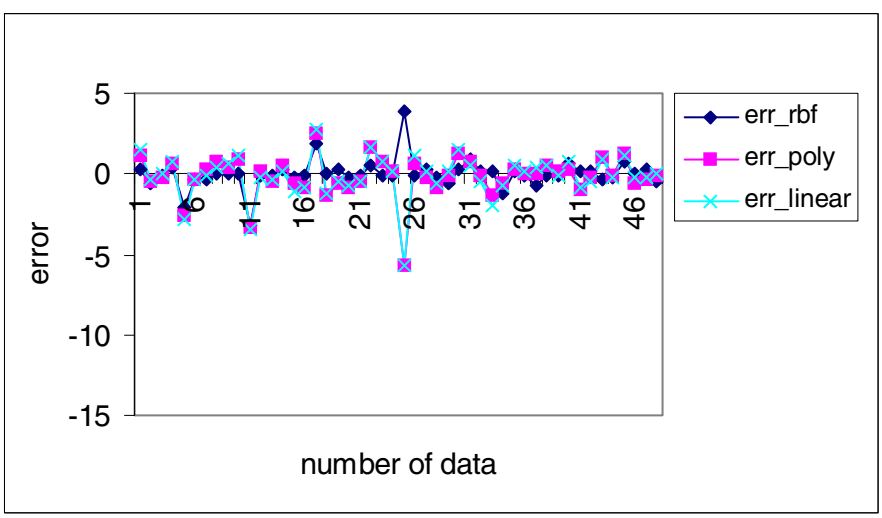

Fig.5(b) Variation of error with all parameters

Controlled drainage effects on crop yield and water use efficiency under semi-arid condition of Iran

Negar Sharifi Mood[1] and Masoud Parsinejad[2] and Farhad Mirzaei[2]

[1] Msc. Student of irrigation and drainage. Academy Center of Soil & Water Engineering, Department of Irrigation & Reclamation, Faculty of Agriculture & Natural Resources, University of Tehran, Faculty St., 31587-11167, Karaj, Iran (Email: negar.irr80@gmail.com)
[2] Assistant professor of irrigation and drainage. Academy Center of Soil & Water Engineering, Department of Irrigation & Reclamation, Faculty of Agriculture & Natural Resources, University of Tehran, Faculty St., 31587-11167, Karaj, Iran. PH(+98) 261-2241119; (Email: parsinejad@ut.ac.ir), (Email: fmirzaei@ut.ac.ir)

Abstract

Control of water table is one of the management processes in irrigation and drainage networks to reduce nitrogen, other salts and drainage water. Suitable depth of water table is decided upon based on the balance between effective root depth, capillary zone and upward flow. In addition sensitivity to water logging, soil water storage capacity, and electrical conductivity of irrigation water and soil stratification should also be taken into account.

If saline irrigation water is used, as a result of water loss through evaporation a salt stratification will result with the soil surface being more saline because of gradual accumulation of salts. The main effect of soluble salts on plants is osmosis effect because the presence of salts, adequate water absorption would be difficult for plants.

This study was conducted to examine the feasibility of implementing water table control technique (i.e., controlled drainage) in an arid and semi-arid region (e.g., Iran) with particular attention to its salinity management. Two water table control treatments including: free drainage (FD) and controlled drainage (CD) with 40 cm controlled water table and three different irrigation water salinity namely: 0.75, 3.4 and 4.8 dS/m were considered. The experimental setup included 6 treatments and three replications. Treatments were applied in 18 lysimeters (90 cm height, 55 cm diameter). The crop cultivated in lysimeters was sorghum. The results indicated that CD method can be used in arid and semi arid regions. The evidence showed that yield of the CD treatment is 2.5 times higher than FD treatment.

Keywords: Controlled drainage, free drainage, Water table management, Lysimeter, Salinity

1- Introduction

Irrigation and drainage management is a basic factor in soil's surface and subsurface flows in arid and semi arid areas. Since salt replacement occurs due to soil water flows, irrigation and drainage management quality represents salt flow quality in the soil to some extent. For example time of irrigation affects capillary rise in the root zone. Capillary rise causes to salt accumulation and irrigation reduction. With encouraging farmers to benefit from shallow water table to meet plant's water requirement and deficit irrigation, management of shallow water table would be possible. Although in this case, due to capillary rise, salinity risk and accumulation of poisonous elements in upper layer of the soil would be occurred. Root zone salinity increases osmosis pressure, therefore more energy should be spent by the plants to absorb the water in order to meet their evapotranspiration requirement. So in a certain viscosity rate, plant's roots are able to exert adequate force to absorb water from soil layers.

Meyer et al. (1980) showed that wheat extracted up to 28% to 38% of its ET from a water table of 1 meter in a loamy soil. Jia et al. showed the effectiveness of controlled drainage and vegetative buffers on reducing the transport of waste water nutrients from land applications filed in a 3 year field study. Positive effects of compatibility of controlled drainage in arid and semi arid areas through waste water reduction and irrigation water saving are presented in several researches by Abbott et al. (2001). Kahlown et al. (2005) concluded that water table depth of 1.5-2 m is the optimum water table depth for most crops except sugarcane which gave even higher yields with the water table at 2 m depths. Asad (2001) also concluded that high wheat yield could be obtained with 1–2 irrigations of 7.5 cm each when the water table depth was from 1 to 2 m. However, if the groundwater is saline generally more than 4.0 dS/m_1, the water table of 1–2 m or less results in decreased wheat and sugarcane yield.

It is clearly obvious that groundwater contribution as an important factor in water balance which provides ET of plants should be considered. Therefore it would be resulted in water and energy saving and also would be kept water level in a desired depth. At Karaj, Iran 18 lysimeters were constructed to evaluate controlled drainage and shallow water table effects on plants. Main objectives of this research are: (1) crop yield under controlled drainage system (2) groundwater contribution in meeting crop water requirements and (3) root distribution in shallow water table conditions.

2- Materials and methods

2-1- Model construction

In this research 18 lysimeters from PVC were used. To control water table, some pipes from PVC with 3cm diameter and 10cm length were applied. Some holes with the space of 2cm from each other and the diameter of 2mm were made on the pipes. To avoid from the entrance of soil particles to the pipe, a suitable filter like gunny fiber is used around the pipe. In the drainage outlet 5cm above bottom of the lysimeter one valve is installed which connected to the riser pipe beside the lysimeter. It acts as pisometer that made it possible to read the water level every time. In

controlled drainage treatments up to 40 cm of the lysimeter filled with sand and then the lysimeter fulfilled with soil. To avoid from the entrance of soil particles in sandy layer and mixture of soil with sand two layer of gunny fiber were used. In free drainage treatments, lysimeters were filled with sand just above the valve and then fulfilled with soil rest of it.

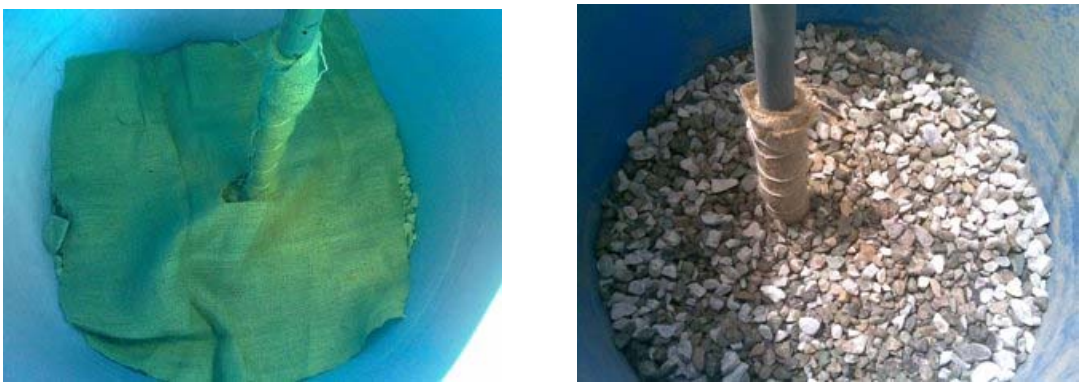

Figure 1- filling the lysimeters

2-2- water table control in the lysimeters

Water table control in controlled drainage treatments in 40 cm from the soil surface was done with the plant of sorghum simultaneously. After first irrigation event, rise and fall of the water table were read before and after irrigation. Hydraulic relation between riser and lysimeter follows the rule in which the water level in the lysimeter is equal to water level in the riser pipe. In other words water level in the riser shows the water level in the lysimeter. In figure 2 the fluctuations of water table for different treatments during the experiment are shown.

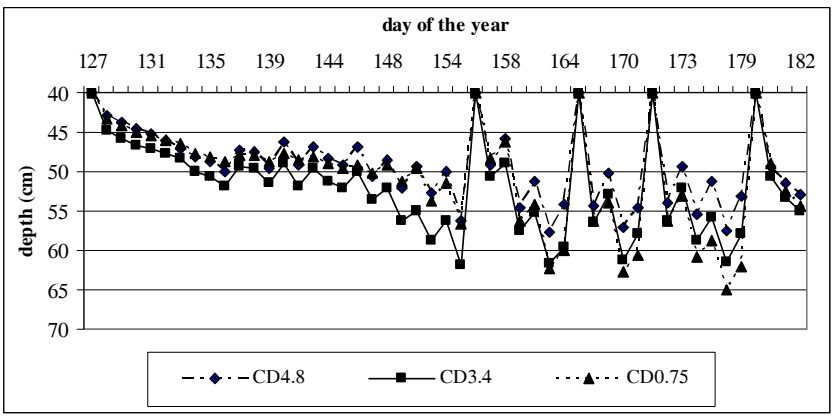

Figure2- water table fluctuations during the experiment period

2-3- Irrigation water

Three different quality of water included: 0.75 dS/m, 3.4 dS/m and 4.8 dS/m were used. In the beginning of the season for the sprouting of the seeds and establishment of roots, all treatments were irrigated with the same amount of

irrigation water. After that irrigation is done according to the NETWAT data for that specific area, considering two days for irrigation time. In controlled drainage treatments, total water volume is calculated through multiplying drop of the water table by area of the lysimetr and porosity. Total irrigation water for both kind of drainage is shown in the table 1 and 2.

Table 1- irrigation water for Free drainage

repetition	1	2	3	4	5	6	7	8	9	10	11	12	13	14	15	total	average
FD0/75-1	25	25	25	25	25	25	29	29	29	29	29	29	29	29	29	411	27/4
FD0/75-2	25	25	25	25	25	25	29	29	29	29	29	29	29	29	29	411	27/4
FD0/75-3	25	25	25	25	25	25	29	29	29	29	29	29	29	29	29	411	27/4
FD3/4-1	27	27	27	27	27	27	31	31	31	31	31	31	31	31	31	441	29/4
FD3/4-2	27	27	27	27	27	27	31	31	31	31	31	31	31	31	31	441	29/4
FD3/4-3	27	27	27	27	27	27	31	31	31	31	31	31	31	31	31	441	29/4
FD4/8-1	29	29	29	29	29	29	33	33	33	33	33	33	33	33	33	471	31/4
FD4/8-2	29	29	29	29	29	29	33	33	33	33	33	33	33	33	33	471	31/4
FD4/8-3	29	29	29	29	29	29	33	33	33	33	33	33	33	33	33	471	31/4

Table 2- irrigation water for controlled drainage

repetition	1	2	3	4	5	6	7	8	9	10	11	12	13	14	15	total	average
FD0/75-1	25	25	25	25	25	25	29	29	29	29	29	29	29	29	29	411	27/4
FD0/75-2	25	25	25	25	25	25	29	29	29	29	29	29	29	29	29	411	27/4
FD0/75-3	25	25	25	25	25	25	29	29	29	29	29	29	29	29	29	411	27/4
FD3/4-1	27	27	27	27	27	27	31	31	31	31	31	31	31	31	31	441	29/4
FD3/4-2	27	27	27	27	27	27	31	31	31	31	31	31	31	31	31	441	29/4
FD3/4-3	27	27	27	27	27	27	31	31	31	31	31	31	31	31	31	441	29/4
FD4/8-1	29	29	29	29	29	29	33	33	33	33	33	33	33	33	33	471	31/4
FD4/8-2	29	29	29	29	29	29	33	33	33	33	33	33	33	33	33	471	31/4
FD4/8-3	29	29	29	29	29	29	33	33	33	33	33	33	33	33	33	471	31/4

2-4- crop yield

2-4-1-Dry matter

Wet weight of the forage is measured and then by determining the dryness index, dry matter of the plant is calculated.

2-4-2-Water Use Efficiency

By considering the total volume of the water, water use efficiency for each treatment is also calculated.

2-4-2- Root weight

The roots were removed by washing the soil of the lysimetrs. Length of the roots were measured and then they were cut and weighted 10 cm by 10 cm. Surface roots based on the 40-30-20-10 rule absorb higher amount of water requirement.

3- Results and discussion

3-1- irrigation water

Although the amount of irrigation water was similar for the free and controlled drainage treatments, water use was found to be higher in controlled drainage. In controlled drainage plants can benefit from the presence of a nearby water table and compensate their ET requirement shortage. Capillary rise contribution and soil surface absorption were shown in table 3.

Table 4 - water use percent from capillary rise and soil surface absorption

treatment	Water use amount	
	Capillary rise	Soil surface absorption
CD0.75	28.21%	71.79%
CD3.4	33.21%	66.79%
CD4.8	27.91%	72.09%

Water use in controlled drainage treatments can be considered as nearly potential ET. Capillary rise has an important role on providing water requirement. Contrary to the case of Free Drainage that irrigation is just equal to compensate soil water depletion. The plant would gradually be faced with difficulty to absorb water after each irrigation and before the next irrigation. The rate of plant water use would then be less than potential in this case.

As the weather warms up and ET requirement is increased, more water is absorbed by the plant from the water table. This is just possible water table is controlled at an optimum depth that plant roots are able to extend to, easily. Higher rates of water extraction from the water table in controlled drainage treatments as the growing period progresses confirm this fact.

3-2- crop yield

Crop growth and development depend on the environmental conditions of root zone, root system depth, and crop sensitivity to salinity and drought. As we see from the figure 3 total dry matter of plant in the controlled drainage and free drainage

treatments indicated that production in CD was higher than in FD treatment. This is due to higher accessibility to moisture that lowered stress for the plants. We can actually propose that plants under the CD treatment, capillary rise of water could decrease the effect of salinity stress to some extent. Thus the yield of controlled drainage treatment with irrigation water of 0.75 dS/m (CD0.75) was higher than controlled drainage treatment with irrigation water of 3.4 dS/m (CD3.4) and higher than controlled drainage treatment with irrigation water of 4.8 dS/m (CD4.8).

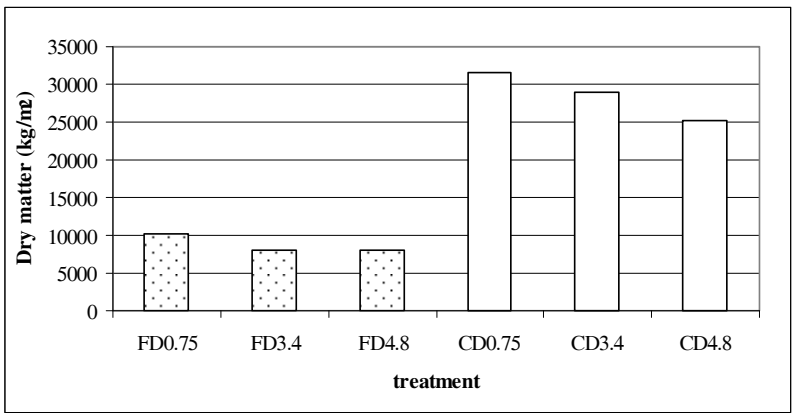

Figure 3 - crop yield of the treatments

3-3- Water use efficiency

The results presented in figure 4 clearly shows that water use efficiency in CD treatment is better than FD's but the more saline irrigation water the lower water use efficiency. Observation showed that salt accumulation in soil in CD treatment is more pronounced than what is in FD which would have a negative effect on the yield. Mutual effect of both saline irrigation water and water level indicated that better moisture condition in CD than in FD has decreased the salt accumulation effect which finally resulted in better yield.

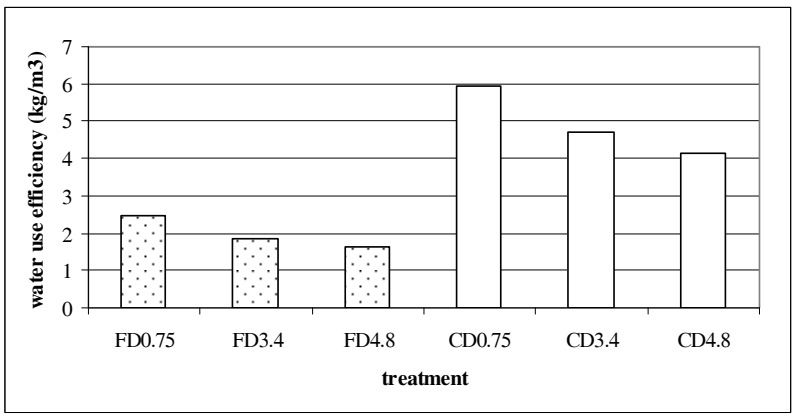

Figure 4 - water use efficiency of the treatments

3-4- Root weight

Root extension and development in the FD treatment is less than what is in CD, it is because access to adequate water in the root zone was limited. The results were shown in figure 5.

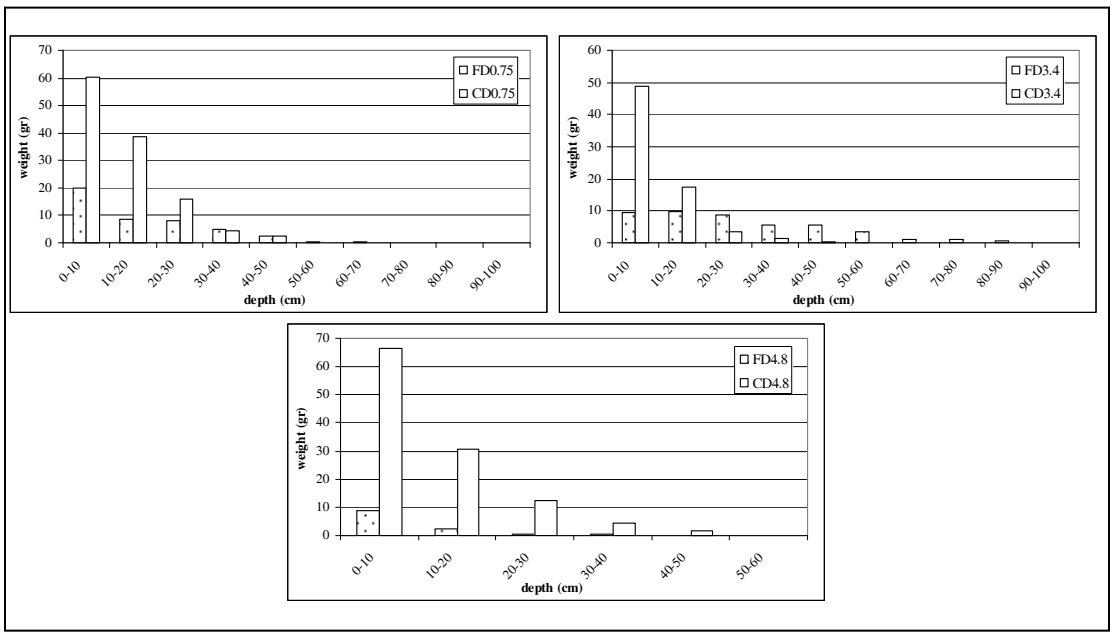

Figure5- root weight in soil profile

Root depth in CD treatment is limited to the level of water table, but in FD it has extended to even 80 cm depth. However the root development, distribution and volume are less than what is in CD treatments. By comparing salinity profile and root weight we can conclud that in lower layer of the soil there were lower salinity and root weight in both free and controlled drainage treatments.

4- Conclusion

Preservation of shallow water table using controlled drainage can provide water requirement from the groundwater in addition to what is applies at the surface. Crop yields can often be enhanced and the amount of irrigation applied can be reduced significantly. Controlled drainage has the potential to reduce drainage volumes and subsequently salt loads. This can help reduce negative downstream effects associated with subsurface drainage. The potential for root zone Salinization will be a major consideration when developing management practices to ensure the sustainability of controlled drainage. Careful monitoring and management will be required when implementing controlled drainage.

Finally the experimental results exhibited the potentials for environmental and economic benefits of the application of controlled drainage in semiarid regions like Iran.

Acknowledgments

The first author would like to thank Scientific Excellent center of "evaluation of irrigation and drainage networks" of Tehran University for providing fundings for the post graduate scholarship to support this study.

References

Abbott (2001) Review of the potential for Controlled Drainage Around the World.

Akram,M. Akram,S. (2008) Controlled drainage; appropriate method to better irrigation efficiency and enhancement of water use efficiency. 5th drainage and environment workshop.IRNCID:89-106

Agricultural drainage water management in arid and semi-arid areas-FAO irrigation and drainage papers: 61

Asad, S.Q., (2001). Irrigation requirements of wheat and cotton under different water table conditions. Sarhad J. Agric. 17, 7–13.

Kahlown. M.A., Ashraf. M. (2005) Effect of shallow groundwater table on crop water requirements and crop yields. Agricultural Water Management 76: 24–35.

Kahlown, M.A., Iqbal, M., Skogerboe, G.V., Rehman S.U., (1998). Water logging, salinity and crop yield relationships.Mona Reclamation Experimental Project, WAPDA, Report No. 233.

Meyer. W.S., Green (1980). Water use by wheat and plant indicators of available soil water. Agron. Journal 72:253-257.

Wesstrom, I. Messing,I (2007) Effects of Controlled drainage on N & P losses and N dynamics in a loamy sand with spring crops. Agri. Water manage. 87, 229-240.

Estimation of regional reference evapotranspiration from land surface temperature and co-kriging method at Tehran province, Iran

Mahdi Shahabifar, Maryam Chaichi and Mahdi Kouchakzadeh

Abstract

Evapotranspiration is the main factor of water cycle in nature and having the information of the amount of that is necessary to soil and water study. Estimation of this amount by using available equations indicates only the amount of evapotranspiration at the stations. Whereas in order to expansion water resources for irrigation and drainage, regional scale studied are required which geostatistical tools are used for achieving that. In this study reference evapotranspiration at 31 meteorology stations in Tehran province with Hargreaves-Samani method in January (wet) and July (dry) were estimated. To supply reference evapotranspiration maps in province that capable to be used at regional study, Co-Kriging was used. Land surface temperature was covariate in this method and has been determined by using image of NOAA14-16 at (1999-2003) and spilit window algorithms. Estimated temperature of images was compared with the temperature of 5cm depth of soil and Mean Absolute Error (MAE) was criterion for algorithms evaluation. Then land surface temperatures were determined from the network with 9200×7500m distance at area and were used for covariate of co-Kriging method and the maps of monthly reference evapotranspiration were drawn.

Keywords: Reference Evapotranspiration, Hargreaves-Samani, Geostatistics, Co-Kriging, Land Surface Temperature, NOAA Satellite.

1. Introduction

Evapotranspiration is the main factor of water cycle in nature, which causes water return from land surface into the atmosphere. In general, evapotranspiratuion is statement of crop water consumption and having information of the amount of that is necessary to soil and water studied. Also minute determination of this quantity and prediction ability of it is a valuable capital for water resources managers. Because the information about evapotranspiration was useful in expansion planting programming, climatology and hydrology studies.

Evapotranspiration is related to climate factors and is determined by using of meteorology data. In order to estimate it, so many methods were expanded. These methods used parameters such as air temperature, relative humidity, wind speed and sunshine. These are spatial data which strongly depend on special studied place. Therefore, evapotranspiration is a spatial variable.

Application of evapotranspiration estimation equations are only limited to meteorology stations and these estimations do not give any information for points without data. In water resources expansion studies which are done in large area, the information of the regional reference evapotranspiration amount is necessary and insufficient data of stations are not enough. Geostatistics is a suitable solution for this question because geostatistics is the collection of statistics methods for spatial variable estimation. Therefore, using of this method is limited in cases that spatial variable has been existed and interpolation is needed. In geostatistics, after estimation of a variable, interpolation methods are used in order to generalize these estimated amounts to a large scale [6]. Then the information of available stations is used to estimate unknown variable in the area and the related maps are provided.

In cases with insufficient data from a variable or the target variable for all the sampling network have not been measured, estimation process meets information shortage. Most of the time, measuring or collection of the target variable is time consuming and needs high cost; therefore, the estimators ,which are able to estimate by using a covariate and reciprocal correlation between target variable and covariate, are used. The covariate in evapotranspiration estimation could be a elevation, sunshine, or air temperature. It is worth using covariate which helps to estimation process; because, the estimation will be better and more precise by using more information. Remote sensing technique and using of satellite images are efficient methods that are provided the information from extensive area. Because of extensive covering of satellite images, these data are efficient in regional studies and research. Although using this method for collecting data seems to be more expensive than land method, in some conditions, which is needed distribution of variable at regional, is only the method for reaching the data. Therefore, covariate for geostatistical methods can be collected by using remote sensing. In this study, land surface temperature determined from noaa image has been applied for covariate.

So many researches have been done for generalization evapotranspiration in the world. For providing reference evapotranspiration map in Clorado, the climate

parameters were collected and meaning relations between climate parameters and elevation have been found by using correlation (Claessens et al (1994)). Reference evapotranspiration was calculated by using the data from 158 stations and Blleny-Kridel model and grnerallized into the all studied area by geostatistical tools (Martinez-cob (1996)). Dalezios et al (2002) were considered spatial variation in reference evapotranspiration in Greece. Reference evapotranspiration was interpolated by kriging method and kriging variance was estimated. Results were showed in the form of daily and yearly contour line maps which can be used for all the agriculture aims.

Remote sensing technique and Geostatistics were used by researchers in soil and water studies frequently. Recently, the determination of evapotranspiration as an effective factor in crop irrigation program by using of these techniques was also considered and it is increasing. But combining these techniques and using remote sensing data as a covariate of geostatistics estimators, has not been considered.

2. Methods and Material

Tehran province, the case study in this paper, with 19000 km^2 area situates in the north of Iran between northern latitude $34^{'}\ 46^{''}$ to $36^{'}\ 18^{''}$ and eastern longitude $50^{'}\ 14^{''}$ to $53^{'}\ 12^{''}$. Climate at north is moderate and hilly and in plains are semiarid. Average of annual rain, average of annual evapotranspiration and average of temperature are 187 mm, 2000 mm and 22.1 ^{o}C respectively. In this province, 31 meteorology stations exist.

For calculation reference evapotranspiration, Hargreaves-Samani method was used that explained with equation (1).

$$ET_o = 0.0023(T + 17.8)(T_{\max} - T_{\min})^{0.5} R_a \qquad (1)$$

Where,

ET_o, Reference evapotranspiration mm/day

T, Average of air temperature ^{o}C

$T_{\max}$, Average of maximum air temperature ^{o}C

$T_{\min}$, Average of minimum air temperature ^{o}C

And R_a, Average extraterrestrial radiation mm/day

In Hargreaves-Samani method, only required data is air temperature which is measured at all of the stations. Therefore, reference evapotranspiration in July and January (1999-2003) with this method were calculated at all the stations. July was selected for warm month that evapotranspiration has maximum amount and January was selected for cold month that evapotranspiration has minimum amount.

In order to determination of reference evapotranspiration in Tehran province, co-kriging method was used. In geostatistics interpolation methods, the estimation of a variable is done in two stages. At first, the semivariogram is drawn and the best model is fitted on it. Then according to model parameters, local structure of variable is considered. In the second stage, the estimation of a variable is done by interpolation methods which depend on parameters of the first model.

In geostatistics, correlation between various variables is estimated via co-kriging method that causes accuracy increasing and economizing on cost. In some cases which there are not enough data from one variable or the purpose is estimation with several variables, this type of kriging is used. In this method, the estimation is done with considering to a covariate in interpolation algorithm and on the basis of spatial relation between target variable and covariate. Target variable is the factor that measured in random points and covariate is the factor that amount of this is existed in most or all of the points. Using of this method is advised in the cases that high correlation coefficient between two variables is existed. Co-kriging equation for estimation of unknown point is stated with equation (2).

$$Z^*(x_i) = \sum_{i=1}^{n} \lambda_i Z(x_i) . \sum_{k=1}^{n} \lambda_k y(x_k) \quad (2)$$

Where,

$Z^*(x_i)$, Estimated amount for point x_i

λ_i , Weight for variable z

λ_k , Weight for covariate

$Z(x_i)$, Observed amount for target variable

And $y(x_k)$, Observed amount for covariate

In this study, covariate was land surface temperature (LST) that was determined by using remote sensing technique.

For determination LST by using noaa image, spilit window algorithm was used. At first, these algorithms were explained for sea surface temperature (SST) because sea surface emissivity was fixed and then used for land surface. SST determination equation is stated with relation (3).

$$SST = A.T_4 + B.(T_4 - T_5) + C \quad (3)$$

Where,

SST , Sea surface temperature ^{o}k

T_4, T_5 , Brightness temperature for channels 4 and 5 of AVHRR ^{o}k

And A, B, C are constants.

Determination of LST is more difficult than sea surface because of variation surface emissivity. The variation land surface emissivity is because of variation in structure, composition and moisture. Also specifications of vegetation and surface topography are effected on surface.

Price (1984) supposed that land surface emissivity was fixed and stated a spilit window equation for determination LST from noaa image that showed with equation (4).

$$LST = T_4 + 3.33(T_4 - T_5) \quad (4)$$

Where,

LST , Land surface temperature ^{o}k

However, other researchers such as Becker and Li (1990), Prata and Platt (1991) and Uliverir et al (1994) believe that variation of surface emissivity must be considered in spilit window algorithms. The effect of land surface emissivity in spilit window equations by using of channels 4 , 5 emissivity, average and these differences are considered. NDVI that showed accumulation of vegetation can be used instead of emissivity. NDVI determined by using of equation (5).

$$NDVI = \frac{\rho_2 - \rho_1}{\rho_2 + \rho_1} \quad (5)$$

Where,

ρ_2, ρ_1, Channels 1 and 2 reflectance of AVHRR

Cihlar et al (1997) proposed using of empirical equations on the basis of correlation between NDVI and emissivity channels 4 and 5 for considering land surface emissivity. Empirical equations between NDVI and emissivity channels 4 and 5 which is in the form of liner-logarithmic relation are stated equation (6) and (7).

$$\varepsilon_4 = 0.9897 + 0.029 Ln(NDVI) \quad (6)$$

$$\varepsilon_4 - \varepsilon_5 = 0.01019 + 0.01344.Ln(NDVI) \quad (7)$$

Where,

ε_4 , Emissivity for channel 4

And ε_5 , Emissivity for channel 5

On the basis of different options for LST determination and effect of land surface emissivity, many algorithms by researchers have been published. In recent 20 years, more than 17 spilit window algorithms have been published. These algorithms can be divided into four categories based on needed parameters: 1) emissivity-dependent models that set the atmospheric effects as constant and emphasized on LST change with ground emissivity. 2) two-factors models using only two essential parameters, ground emissivity and atmospheric transmittance or water vapor for determination of LST. 3) combined models that set other parameters as constant for the computation and 4) radiance models, directly using the observed radiance for the computation [15].

In this study, 10 algorithms from emissivity-dependent models were used for determination of LST: Price (1984), Mc Clain et al (1985), Becker and Li (1990), Prata and Platt (1991), Vidal (1991), Kerr et al (1992), Sobrino et al (1993), Coll et al (1994), Uliverir et al (1994) and Coll and Caselles (1997).

For evaluation of estimated LST from these algorithms, the temperature of 5 cm depth of soil, which was measured in synoptic stations, was used. At first it is required that

temperature of 5 cm depth of soil change to temperature at time of crossing satellite. Then Mean Absolute Error (MAE) as a criterion evaluation of algorithms is calculated by equation (8).

$$MAE = \frac{\sum_{i=1}^{n} \left| Z(e)_i - Z(m)_i \right|}{n} \quad (8)$$

$Z(e)_i$, Estimated amount by algorithm

$Z(m)_i$, Measured amount

n, Number of observation

The model with minimum amount of MAE was selected as the best algorithm to determine the LST in case study. After LST determination from each image, average of them for two investigated months in 5 years was calculated and the results were used in heads of a 9200×7500 m network in the area to covariate in co-kriging method.

For each of January and July during the investigation period (1999-2003) one images without any clouds was prepared by Noaa 14-16 satellite, so ten images were used to determine the LST.

3. Conclusion

Minimum of MAE in July was at Coll and Caselles algorithm (1997) with amount of $9.924\,^{o}C$ and in January with $7.767\,^{o}C$ at Mc Clain et al algorithm (1985). Therefore Coll & Caselles and Mc Clain et al algorithms were used for LST determination in July and January respectively. Estimated LST were used as covariate in co-kriging method. Table (1) shows results of fitting semivariogram on reference evapotranspiration - LST and also reciprocal semivariogram on LST - reference evapotranspiration in July and January.

TABLE 1- semivariogram and reciprocal semivariogram parameters

factor	model	C_0	$C_0 + C$	A_0	$\frac{C}{C_0 + C}$	R^2
$ET_0(july)$	*spherical*	110.00	7776.00	0.957	0.986	0.841
$LST(july)$	*spherical*	0.60	92.20	0.579	0.993	0.842
ET_0 & $LST(july)$	exp*otential*	31.20	120.10	0.050	0.740	0.001
$ET_0(january)$	*linear*	1.00	710.90	1.537	0.999	0.880
$LST(january)$	*spherical*	6.70	45.50	0.655	0.842	0.671
ET_0 & $LST(january)$	*spherical*	1.39	19.24	0.388	0.928	0.022

Amount of $\frac{C}{C_0 + C}$ represents the existence of suitable local structure. If this amount was more than 0.5 then local structure will be suitable. Results from table (2) showed that investigated variables in this study had a suitable local structure and by increasing distance, amount of semivariogram increased and met a fixed amount. This fixed or sill amount have been shown with $C_0 + C$ and after that by increasing distance,

semivariogram have not a noticeable change. Table (2) gives statistical parameters and RMSE that calculated by cross validation method.

TABLE 2- statistical parameters and RMSE at each month $^{mm}/_{month}$

factor	min	max	mean	Stder	RMSE
ET_0 & $LST(july)$	280.30	626.24	450.62	73.92	
ET_0 & $LSTco-kriging(july)$	355.53	586.15	449.00	53.73	47.99
ET_0 & $LST(january)$	32.66	98.95	79.92	15.77	
ET_0 & $LSTco-kriging(january)$	46.18	92.39	72.64	12.35	13.48

Minimum and maximum of reference evapotranspiration in July were 280.30 and 626.24 in Alodegi Firuzkouh and Zivan stations, respectively. In January, minimum of 32.66 was reported from Alodegi firuzkouh and maximum was in Mamloo station with 98.95. Figure (1) shows the maps of reference evapotranspiration in Tehran province in July and January that designed by co-kriging method. Maximum of reference evapotranspiration were observed in the south of province that had a semiarid climate. High temperature in the southern plains causes dryness of air and whereas reference evapotranspiration depends on temperature, it can be said that temperature is a factor of increasing the reference evapotranspiration.

Results, obtained from this study can be used in crop irrigation programming and local distribution of reference evapotranspiration maps are utilizable in soil and water project as a data layer.

July
Mm/month



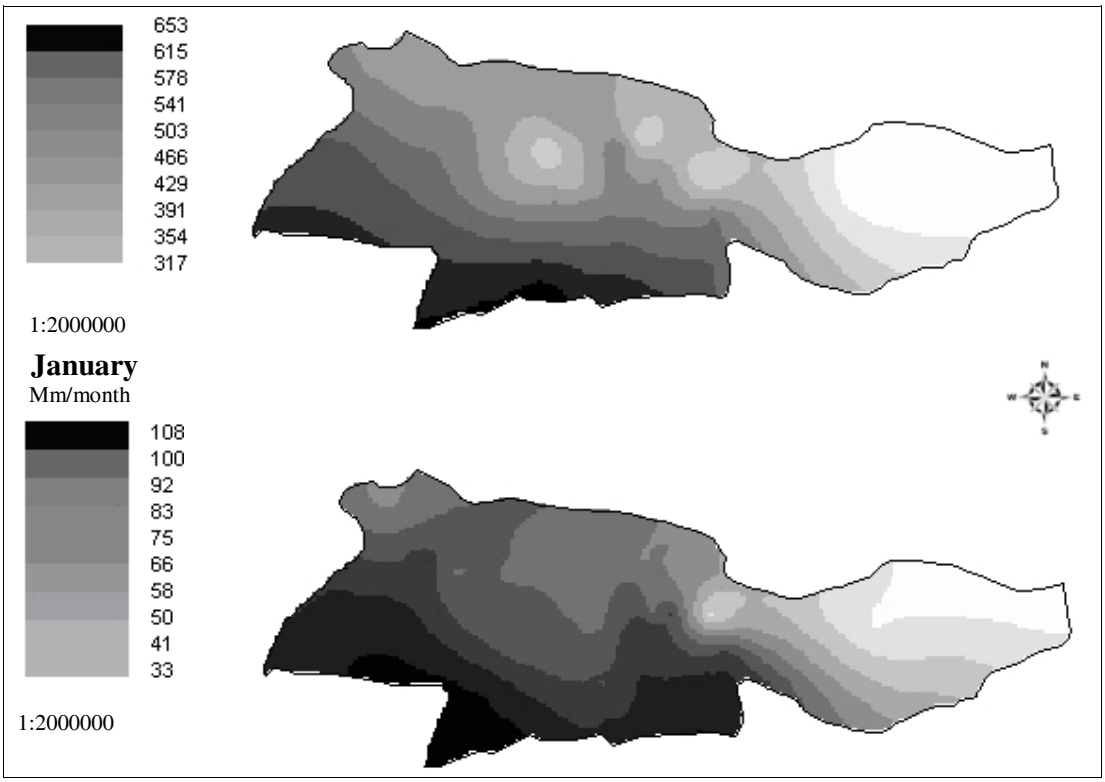

Figure 1- maps of reference evapotranspiration in Tehran province in July and January

4. References

[1] Becker, F. and Z. L. Li. 1990. Towards a local split window method over land surfaces. International Journal of Remote Sensing . 11 : 369-393.

[2] Cihlar, J., H., Ly, Z., Li , J. Chen, H. Pokrant and F. Huang. 1997. Multitemporal, multichannel AVHRR data sets for land biosphere stuies-artifacts ans corrections. Remote Sensing of Environment. 60: 35-57.

[3] Claessens L, Garcia LA, Jensen M, Lange RW 1994. Reference Evapotranspiration Maps for Colorado. Water Resources Research Ins., Completion Report No. 182.Fort Collins, Colorado .

[4] Coll, C., and Caselles, V. 1997. A spilit-window algorithm for land surface temperature from advanced very high resolution radiometer data: Validation and algorithm comparison. Journal of Geophisical Research. 102: 16697-16713.

[5] Coll, C., V., Casselles, J. A., Sobrino and E. Valor. 1994. On the atmospheric dependence of the split-window equation for land surface temperature. International Journal of Remote Sensing. 15:105-122.

[6] Dalezios, N.R., Loukas, A., Bampzelis, D. 2002. Spatial variability of refrence evapotranspiration in Greece. Physics and Chemistry of the Earth. 27:1031-1038.

[7] Deschamps, P. Y. and T., Phulpin. 1980. Atmospheric correction of infrared measurement of sea surface temperature using channels an 3, 7, 11 and 12 μm. Boundary-Layer Meteorol. 18:131-143.

[8] Hargreaves GH, Samani ZA 1985. Reference Crop Evapotranspiration from Temperature Appl. Eng. Agric., 1(2): 96-99.

[9] Kerr, Y. H., Lagouarde, J. P., and Imbernon, J., 1992. Accurate land surface temperature retrieval from AVHRR data with the use of an improved split-window algorithm. Remote

[10] McClain, E. P., W. G., Pichel, C. C., Walton, Z. Ahmad and J., Sutton. 1983. Multichannel improvements to satellite derived global sea surface temperatures. Advances in Space Research. 2: 43–47.

[11] Martinez-Cob A 1996. Multivariate Geostatistical Analysis of Evapotranspiration and Precipitation in Mountainous Terrain. Journal of Hydrology. 174: 19-35.

[12] Martinez-Cob,A and Cuenca,R.H 1992. Influence of elevation on regional evapotranspiration using multivariate geostatistics for various climatic in Oregon.Journal of Hydrology. 136: 353-380.

[13] Price, J. C. 1984. Land surface temperature measurements from the split window channels of the NOAA 7 Advanced Very High Resolution Radiometer. Journal of Geophysical Research. 89: 7231-7237.

[14] Prata, A. J. and C. M. R., Platt. 1991. Land surface temperature measurements from the AVHRR. Proceeding of The 5th AVHRR Data Users' Meeting, Tromso, Norway, 433-438.

[15] Qin, Z., Xu, B., Zhang, W., Li, W., and Zhang, H. 2004. Comparison of split window algorithms for land surface temperature retrieval from NOAA-AVHRR data. IEEE 2004 International Geosciences and Remote Sensing Symposium, VI, 3740-3743, September 20-24, 2004, Anchorage, Alaska, USA.

[16] Sobrino, J, A., Caselles, V., Coll, C. 1993. Theoretical spilit window algorithms for determininig the actual surface temperature, Il Nuovo Cimento, Verona, 16C(3): 219-236.

[17] Ulivieri, C., M. M., Castronouvo, R., Francioni and A., Cardillo. 1994. A split-window algorithm for estimating land surface temperature from satellites. Advances in Space Research. 14(3): 59-65.

[18] Vidal, A., 1991. Atmospheric and emissivity correction of land surface temperature measured from satellite using ground measurements or satellite data. International Journal of Remote Sensing. 12, 2449–2460.

Comparison of Evapotranspiration Estimates from Remote Sensing (SEBAL), Water Balance, and Crop Coefficient Approaches

Bryan Thoreson, Ph.D., P.E., M.ASCE[1], Byron Clark, P.E., M.ASCE[1], Richard Soppe, Ph.D.[2], Andy Keller, Ph.D., P.E., M.ASCE[3], Wim Bastiaanssen, Ph.D.[2], and John Eckhardt, Ph.D., P.E., M.ASCE[4]

[1] Davids Engineering, Inc., 1772 Picasso Avenue, Suite A, Davis, CA 95618, www.sebal.us.
[2] WaterWatch, Generaal Foulkesweg 28A, 6703 BS Wageningen, The Netherlands, www.waterwatch.nl.
[3] Keller-Bliesner Engineering, LLC, Vice President, 78 East Center, Logan, UT 84321, 435-753-5651; akeller@kelbli.com.
[4] Imperial Irrigation District, Executive Program Manager, QSA-IID/SDCWA Water Transfer, 333 East Barioni Boulevard, Imperial, CA 92251, 760-339-9736 JREckhardt@IID.com.

ABSTRACT

Three independent approaches were applied to estimate annual evapotranspiration (ET) for the Imperial Irrigation District of Southern California for the 1998 water year (October 1997 to September 1998). These approaches included remote sensing (Surface Energy Balance Algorithm for Land, SEBAL®), a district-wide water balance with ET as the closure term, and a dual crop coefficient approach based on the procedures of FAO Irrigation and Drainage Paper No. 56 with refinements to account for field-specific irrigation frequency. Differences between annual ET from each independent ET estimation approach are evaluated relative to estimated confidence intervals.

INTRODUCTION

To grow and produce food, plants must release water through the process of transpiration. When the soil surface is wet due to rainfall or irrigation, evaporation also occurs. These two processes together are termed evapotranspiration (ET). In irrigated areas, evapotranspiration is usually the largest consumer of water. Thus, accurate determination of evapotranspiration is important for water resources planning. This paper describes the methodology and compares the results of three independent methods to determine annual evapotranspiration from the Imperial Irrigation District (IID), a large irrigated area in the Southwestern United States.

The three approaches were an energy balance based on remote sensing, a water balance utilizing 15-minute flow measurements and a dual crop coefficient procedure (Allen, 1998 and Allen, et al 2005). The energy balance used was the Surface Energy Balance Algorithm for Land (SEBAL®) utilizing Landsat satellite images and the California Irrigation Management Information System (CIMIS). The water balance utilized 15-minute flow data collected by the Imperial Irrigation District. The dual crop coefficient procedure utilized crop areas and plant and harvest dates collected by the Imperial Irrigation District, reference ET obtained from CIMIS and crop coefficients from the Food and Agricultural Organization (FAO) (Allen, 1998) adjusted for local conditions as appropriate (Allen et al, 2005a).

This paper briefly outlines the physical setting, describes the input data and methodology used for each method, reports the results of each method and concludes with a discussion comparing and contrasting the results.

PHYSICAL AND INSTITUTIONAL SETTING

Established in 1911, IID is the nation's largest irrigation district, providing water to about 475,000 acres of diverse crops. The agricultural area lies in the Imperial Valley with much of the area below sea level. The lowest fields are just above the Salton Sea standing at 230 feet below sea level. The land slopes gradually northward from the Mexican border to the south shore of the Salton Sea. A shallow saline groundwater aquifer underlies the agricultural area. The four months of June through September have average high temperatures above 110 degrees Fahrenheit. Annual reference ET (ET_o) has averaged 74 inches ranging from 64 to 83 inches over the last 22 years. Annual precipitation has averaged 2.75 inches ranging from 0.2 to just over 5 inches over the last hundred years. ET_o was 71 inches and rainfall was 2.13 inches for the water year 1998 studied.

Soils underlying eighty-five percent of the cropped area contain a high percentage of clay with low infiltration rates and high water holding capacities. Annually about 100,000 acres of vegetable crops are grown throughout the area. Carrots, onions and lettuce are the most widely cultivated vegetable crops. The most common field crops include alfalfa, Bermuda grass, wheat, sugar beets and Sudan grass. Most of the vegetable area is double cropped, and roughly 350,000 acres is cropped year-round. In this climate, eight alfalfa cuttings are obtained in a typical year.

ET ESTIMATION METHODOLOGY

Three independent approaches were applied to estimate annual ET for the Imperial Irrigation District of Southern California for the 1998 water year (October 1997 to September 1998). These approaches included the remotely sensed energy balance SEBAL®, a district-wide water balance with ET as the closure term, and a dual crop coefficient approach based on the procedures of FAO Irrigation and Drainage Paper No. 56 with refinements to account for field-specific irrigation frequency. Input data and methods used are described in the following sections.

Remote Sensing Estimate of ET with SEBAL

The sun's net radiation reaching the Earth's surface balances with soil, sensible, and latent heat fluxes to conserve energy at the Earth's surface. Taking into account the latent heat of vaporization and density of water, latent heat flux can be converted into ET flux (volume of water per unit area per unit time). ET flux can be estimated as a closure term from estimates of the remaining fluxes (Equation 1).

$$ET_a = \frac{1}{\lambda \rho_w}\left[R_n - (G + H)\right] \qquad [1]$$

where λ is the latent heat of vaporization of water, ρ_w is the density of water, ET_a is the actual crop ET, R_n is the net radiation flux at the Earth's surface, G is the soil heat flux, and H is the sensible heat flux.

The SEBAL model estimates actual crop ET (ET_a) from the energy balance by applying radiative, aerodynamic, and energy balance physics in 25 computational steps. Multispectral satellite imagery with a thermal band is used to calculate ET_a at the pixel-scale. Required input data include radiances in the visible, near infrared, and thermal infrared regions sensed by earth observing satellites; ground based weather data from agricultural or other weather stations; and land use data describing general vegetation types, when available. Knowledge of specific crop types is not needed to solve the energy balance. SEBAL avoids the need for absolute calibration of the surface temperature of each pixel by utilizing a unique internal calibration for each image to estimate sensible heat flux between the surface and the atmosphere. A detailed explanation of the algorithm is provided by Bastiaanssen et al. (1998). Continuing refinements to the model include the use of digital elevation models for radiation balances in mountains (Allen et al., 2001), an improved albedo function (Tasumi et al., 2005), advection corrections, an improved soil heat flux relation, and an improved relation for surface roughness for momentum transport. Recent validations of SEBAL, summarized by Bastiaanssen et al. (2005), have shown seasonal ET_a results generally fall within five percent of seasonal ET_a determined from reliable ground-based measurements.

Input Data

A combination of satellite, ground based-meteorological, topographic, and land cover classification data are utilized to quantify spatially distributed ET_a. For this study, these datasets were obtained from the U.S. Geological Survey (USGS), CIMIS, and IID. These data are described in greater detail in the following paragraphs.

Satellite Images. Twelve Landsat 5TM multispectral images encompassing the period from October 1997 to September 1998 (Water Year 1998 or "WY 1998") for Path 37/Row 39 were obtained from USGS. Cloud-free images were selected to achieve a temporal frequency of one image per month for the WY 1998 period.

Meteorological Data. Measurements of incoming solar radiation (R_s), relative humidity (RH), air temperature (T_a) and wind speed (WS) were available as hourly averages for the time of image acquisition. Daily (average for the image date), and period (average for the days represented by an individual image) measurements were

also available. Five stations falling within or on the edge of the study area were used during image processing. The stations selected were Salton Sea West (Station 127), Salton Sea East (Station 128), Calipatria/Mulberry (Station 41), Meloland (Station 87), and Seeley (Station 68). Weather data were quality checked according to the guidelines specified in Appendix-D of the ASCE Task Committee Report on the Standardized Reference Evapotranspiration Equation (Allen et al., 2005).

Landuse Data and Digital Elevation Model (DEM). A generalized landuse map from the National Land Cover Dataset (NLCD) for 1992 was obtained from USGS and used to estimate obstacle heights for different surfaces within the study area. The NLCD data has been developed at a 30 meter pixel resolution using a series of Landsat images along with aerial photographs and ground-surveys.

A DEM of 1 arc-second resolution (approximately 30 meter resolution) was obtained from USGS and was used in SEBAL to incorporate the effects of the slope, aspect and elevation into the energy balance.

District-wide Water Balance Estimate of ET

IID's physical and climatic situation results in a unique opportunity to measure inflows and outflows accurately and develop a water balance that closes on ET with high accuracy. IID is unique in that a water balance can be performed based on measured surface flows (Figure 1) that solves for ET of the command area with a high degree of confidence. This is due to the following factors:

1. Location in an extremely arid environment with little annual rainfall,
2. Accurately measured single source of all surface water used for irrigation in the command area,
3. Accurate measurement of all surface water flows out of the command area (about 35 locations) ,
4. Tile drains convey deep percolation from about 95 percent of the command area into surface drains that are tributary to the 35 outflows,
5. Deep percolation not captured by the tile drains, enters the groundwater and is discharged into surface drains,
6. Groundwater is saline and unusable for irrigation (no pumping), and
7. Subsurface natural flows across the area boundaries into and out of groundwater are negligible.

Input Data

A water balance summarizes all the flows entering and leaving a defined area, specified by a closed boundary, within a defined time period. Water balances can be performed at various scales and for various time periods and are defined by equation 2.

$$\sum \text{Inflows} - \sum \text{Outflows} = \Delta \text{Storage} \qquad [2]$$

The next sections describe the boundaries and the flow measurements

Boundaries. The study area chosen for comparison is defined by the water balance boundaries. With the exception of small areas on the east and west, this area

is bounded by the All American Canal (AAC) on the south, the Westside Main Canal (WMC) on the west, the Salton Sea on the north and the East highline Canal on the east (Figure 1). These boundaries can be considered vertical planes and all subsurface and surface flows crossing the planes are considered in the water balance. ET flux and precipitation cross a horizontal plane imagined just above the crops within the vertical planes.



Figure 1. IID Water Balance Boundaries and Boundary Flow Measurements.

Inflows and Outflows. The inflows shown in Figure 2 include the AAC, Alamo and New Rivers from Mexico, rainfall, Mesa storm flows and subsurface inflows. The outflows going to the Salton Sea include the New and Alamo Rivers, drain flows to the Salton Sea (termed Direct to Sea flows) and subsurface outflow. Flows from the AAC and Direct to Sea measurement locations are transmitted to a central location at 15-minute intervals. The 15-minute data is loaded into a large database

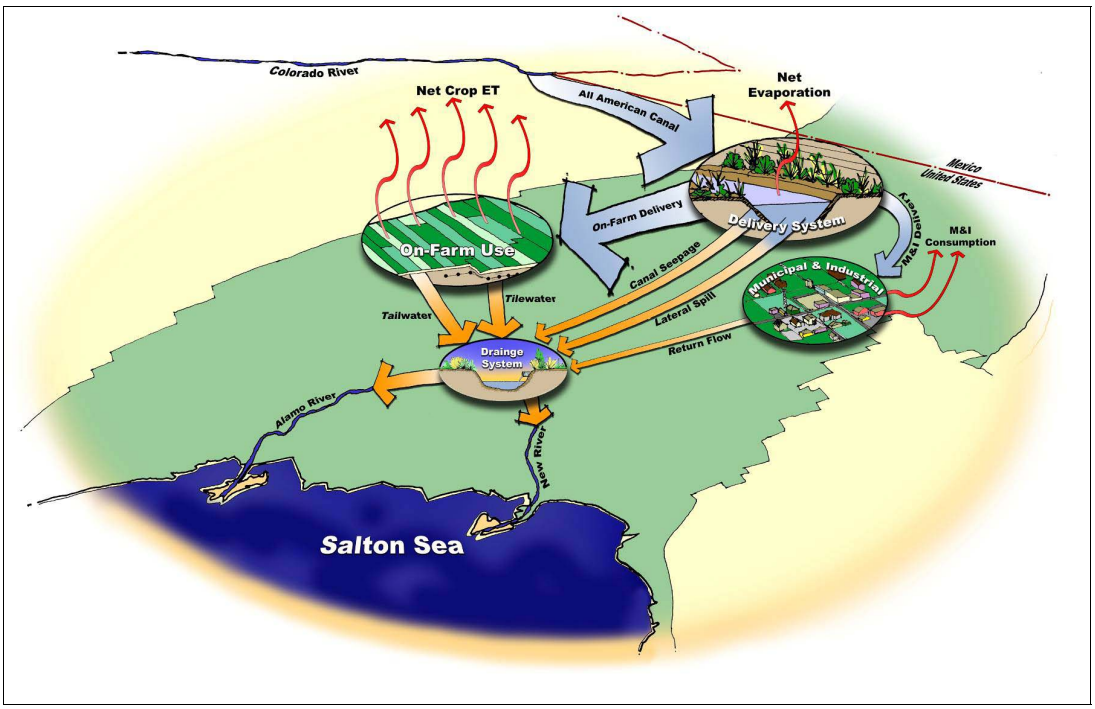

Figure 2. IID Water Balance Components and Flow Paths.

called the IID Water Information System (IID-WIS). In the WIS, the flow data is reviewed on daily, monthly and annual intervals. The 15-minute flows are summarized and reported as daily values. The New and Alamo River inflow and outflow measurements are conducted by the United States Geological Survey (USGS). Daily values from the USGS were used in this study. Rainfall is estimated based on the rainfall measured at three CIMIS stations (Calipatria/Mulberry, Meloland, and Seeley) within the water balance boundaries. Mesa storm inflows are estimated based on rainfall measurements. Small subsurface inflows and outflows estimated by groundwater studies are also included in the water balance.

Water Balance

A water balance was performed to determine total consumptive use (ET_a) within IID. The change in storage component of the water balance was limited to 50% of the available water content of the soils within the study area and estimated as a function of the monthly measured drain outflows relative to farm water deliveries. Given the factors listed above and the measurement accuracy of the surface inflows and outflows, the 95 percent confidence interval on ET_a, as the water balance closure term, was estimated to be 4.4 percent following the methodology of Clemmens and Burt (1997).

Crop Coefficient Estimate of ET

Potential crop evapotranspiration (ET_p) represents the total ET of a crop expected to occur under non-stressed growing conditions. Potential ET was estimated for each field-season by using the standardized dual crop coefficient approach described in FAO56 with planting and harvest dates recorded by IID. Total potential ET was

disaggregated into ET derived from precipitation and from applied irrigation water using a daily root zone water balance model (Allen et al, 2005a).

Input Data

Meteorological Data. The model uses daily weather data (relative humidity, wind speed, reference ET (ET_o), and precipitation) and crop and soil information for each identified field-crop season. Weather data parameters are calculated as a weighted average of quality controlled values from the Calipatria/Mulberry, Meloland, and Seeley CIMIS stations based on the area represented by each station determined using Thiessen polygons.

Crop Planting and Harvest Dates and Areas. IID zanjeros (ditch tenders) deliver water to growers and also record the crop plant and harvest dates and irrigated areas. This data is entered into IID's water order entry database and transferred to the IID-WIS.

Crop Coefficients. The crop coefficients used in the computations were based on FAO 56 and University of California Extension Leaflets 21427 and 21428 (Snyder et al., 1989a, 1989b). These crop coefficients were adjusted for local weather conditions using the FAO 56 recommended adjustment for extreme wind and humidity values.

Crop Water Use Computations

Effective (net) precipitation was estimated using a daily root zone water balance model developed in QuickBasic. Specified field-crop seasons were parameterized based on crop type, planting date, harvest date, and soil type (light or heavy).

The daily root zone water balance model was used to simulate the timing of irrigation applications, with irrigation triggered once the soil moisture depletion reached a crop and soil specific management allowed depletion. The model computes total potential ET (from both applied water and precipitation) by applying the standard dual crop coefficient approach described in FAO 56 (Allen, 1998). Daily values of reference evapotranspiration (ET_o) and precipitation were inputs to the root zone water balance.

The planting time period for many crops can span months due to the mild winters. For example, wheat can be planted anytime between October and January with a few plantings in February. To capture the variability in seasonal ET resulting from highly variable planting dates and resulting season length, root zone model runs were made for unique field-crop season plant and harvest date combinations.

ET ESTIMATION RESULTS

Remotely Sensed Surface Energy Balance Estimate of ET with SEBAL

The ET within the study area was estimated to be 2.010 million acre-feet by the remote sensing approach using SEBAL. The variation of ET across the study area is shown in Figure 3. The average ET for cropped areas within the IID is shown in Figure 4. Peak water consumption for the irrigated areas occurs in June. The average monthly actual ET (ET_a) is always less than the CIMIS reference ET.

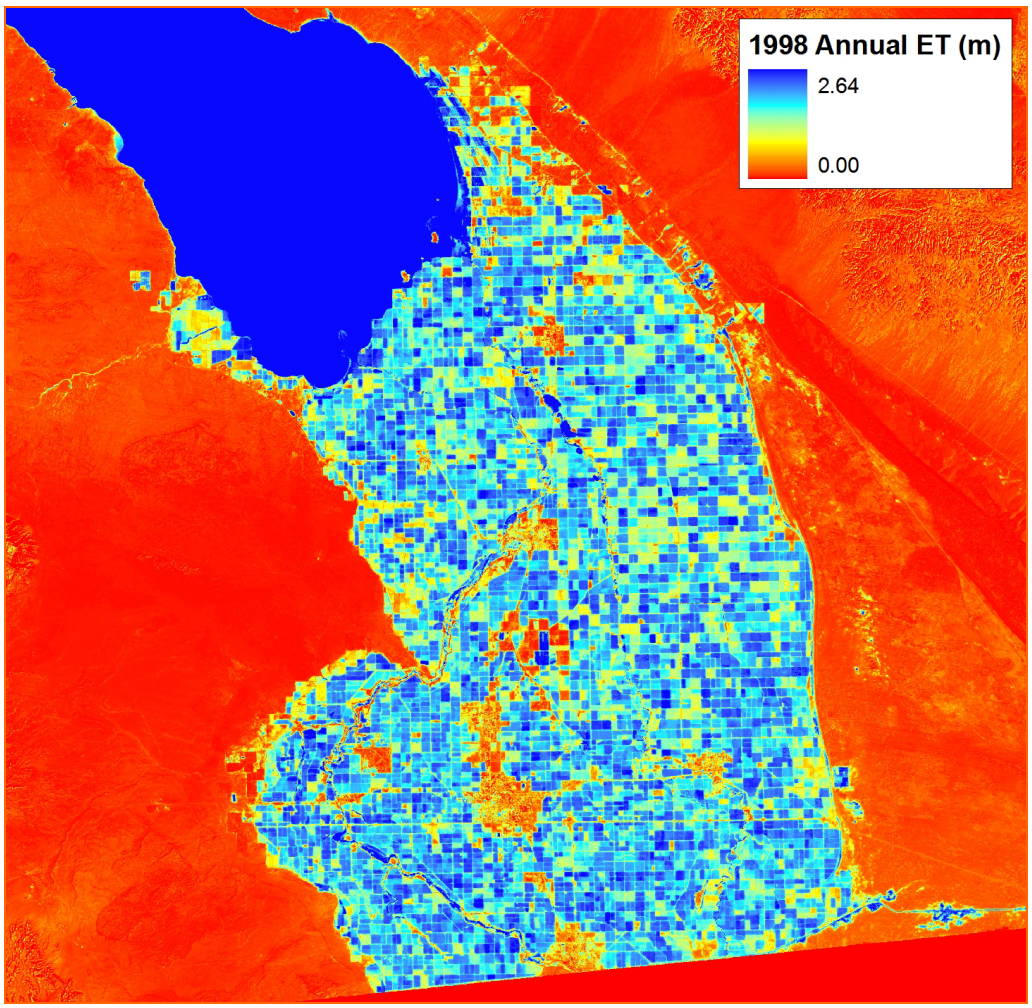

Figure 3. Water Year 1998 Seasonal ET_a Variation across IID Irrigated Area.

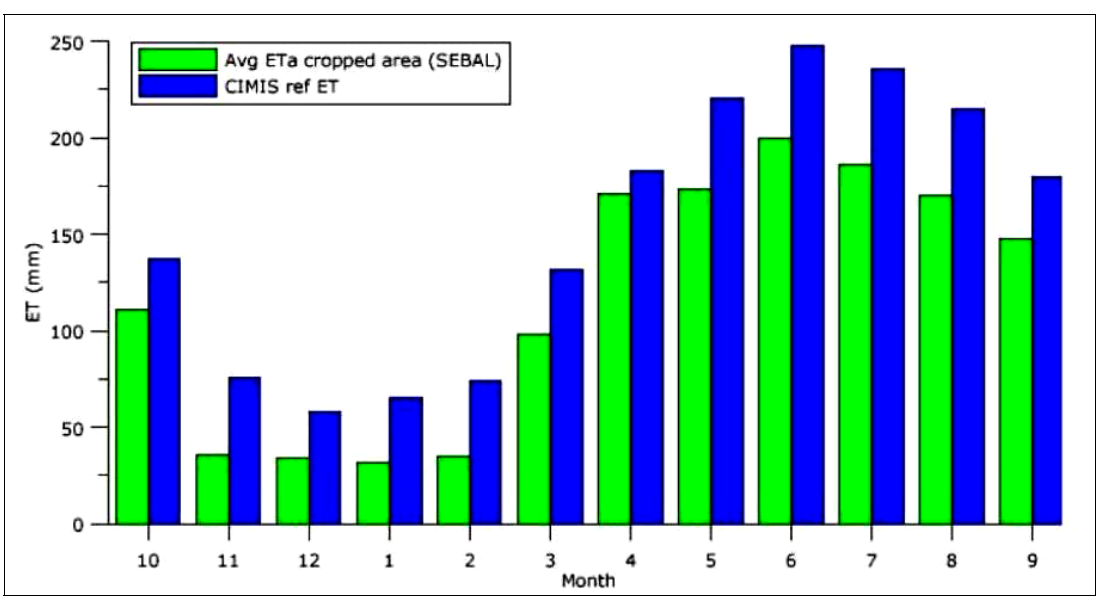

Figure 4. Average ET_a for Cropped Area in IID Compared with Average ET_o.

District-wide Water Balance Estimate of ET

The total inflow to the area from the AAC was 2.9197 million acre-feet. All the other inflows combined totaled 0.3116 million acre-feet. Outflows totaled 1.2327 million acre-feet, including a net depletion in soil water storage over the course of the year of 102 thousand acre-feet. The resulting estimate of ET within the study area is 1.9985 million acre-feet (Table 1).

The water balance quantifies all primary flow paths and associated water volumes within the study area. This improved understanding is important for water resources planning and management. However, the water balance itself provides no information on the variation of ET across the study area.

Table 1. Water Year 1998 IID Study Area Water Balance.

		Volume (1000 ac-ft)	
Location	**Data**	**1998**	**CI**
Total Inflows			
AAC Inflow at Mesa Lat. 5	Input	2,919.7	2.4%
Alamo River from Mexico	Input	1.5	2.0%
New River from Mexico	Input	181.0	2.0%
Total Rainfall	Calc.	103.2	22.4%
Mesa Storm Inflows	Calc.	5.9	100.0%
External Subsurface	Input	20.0	100.0%
Total Inflows	**Calc.**	**3,231.2**	**2.5%**
Total Outflows			
Alamo River to Salton Sea	Input	665.6	2.3%
New River to Salton Sea	Input	564.0	2.0%
Direct to Sea Drains	Input	104.1	20.0%
Subsurface to Sea	Input	1.0	100.0%
Change in Soil Storage	Input	-102.0	50.0%
Total Consumptive Use	Close	1,998.5	4.4%
Total Outflows	**Calc.**	**3,231.2**	**2.9%**

Crop Coefficient Estimate of ET

Computing ET for each field in the study area using a root zone water balance program with inputs of soil type, recorded plant and harvest dates, ET_o, rainfall, crop coefficients and related irrigation management parameters and summing the total across all fields resulted in a total ET of 2.280 million acre-feet. The climate in the study area allows for crops to be produced year-round and results in a wide range of possible plant and harvest dates for crops. For example, wheat can be planted any time from October through January and sometimes even in February and March. This results in a wide variation of seasonal ET totals for wheat as the later plantings extend into warmer weather before maturing (Figure 5).

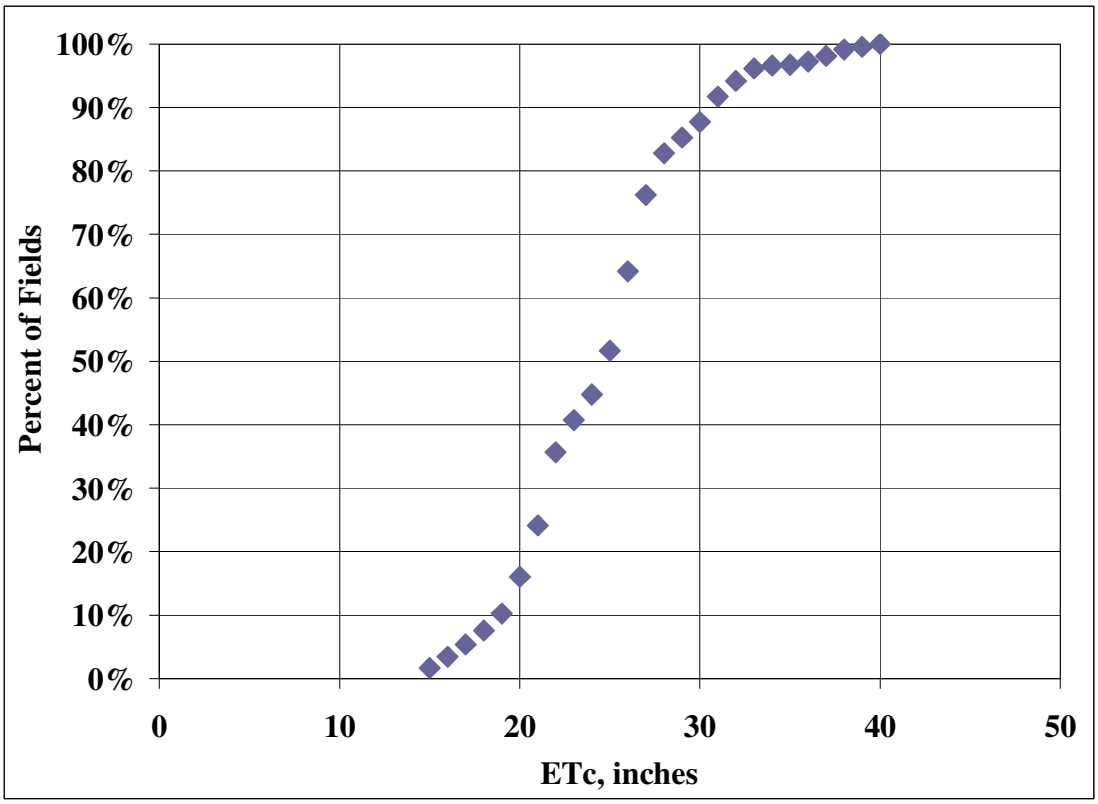

Figure 5. Cumulative Distribution of Wheat ET_c on Heavy Soil Using Reported Plant and Harvest Dates.

DISCUSSION

Annual ET in the study area was estimated using water balance closure, remote sensing energy balance and the FAO 56 crop coefficient approaches. Annual ET estimates varied from 1.999 million acre-feet to 2.280 million acre-feet for the water balance and FAO 56 crop coefficient approaches, respectively. The SEBAL remote sensing ET was very close to the water balance results at 2.010 million acre-feet. For this unique study area, the water balance estimate of ET was estimated to have a confidence interval of 4.4 percent based on the sum of variances method (Clemmens and Burt, 1997). The FAO 56 crop coefficient approach was expected to result in higher ET estimate than the other approaches due to unavoidable ET reducing heat and water stress experienced by crops during the extremely hot summers that is not accounted for in the crop coefficient approach. All estimates agreed within 15 percent (Table 2); however, the water balance and SEBAL approaches were within one percent of each other while the crop coefficient approach estimate was just over 14 percent greater than the water balance results.

Table 2. Comparison of the Three Approaches over the 1998 Water Year.

ET Estimation Approach	Water Year 1998 Total, kaf	Percent Difference (SEBAL-WB)/WB
Water Balance	1998.5	0.0%
SEBAL	2010.4	0.6%
Crop Coefficient	2280.2	14.1%

The monthly percent difference between the water balance and the SEBAL results varied from -2.7 percent to just over 30 percent in one month (Figure 6 and Table 3). Most of the difference is attributed to likely error in estimating the monthly change in soil water storage within the water balance computation. The annual estimate of change in soil water storage error is less error prone. Allen et al. (2005) discusses the month to month storage change and uncertainties in some detail.

The 30-m by 30-m pixel spatial resolution of the SEBAL results allow for a more complete understanding of ET among fields. Only a few alfalfa fields in the study area approach the potential ET computed by the FAO 56 crop coefficient procedures (Figure 7).

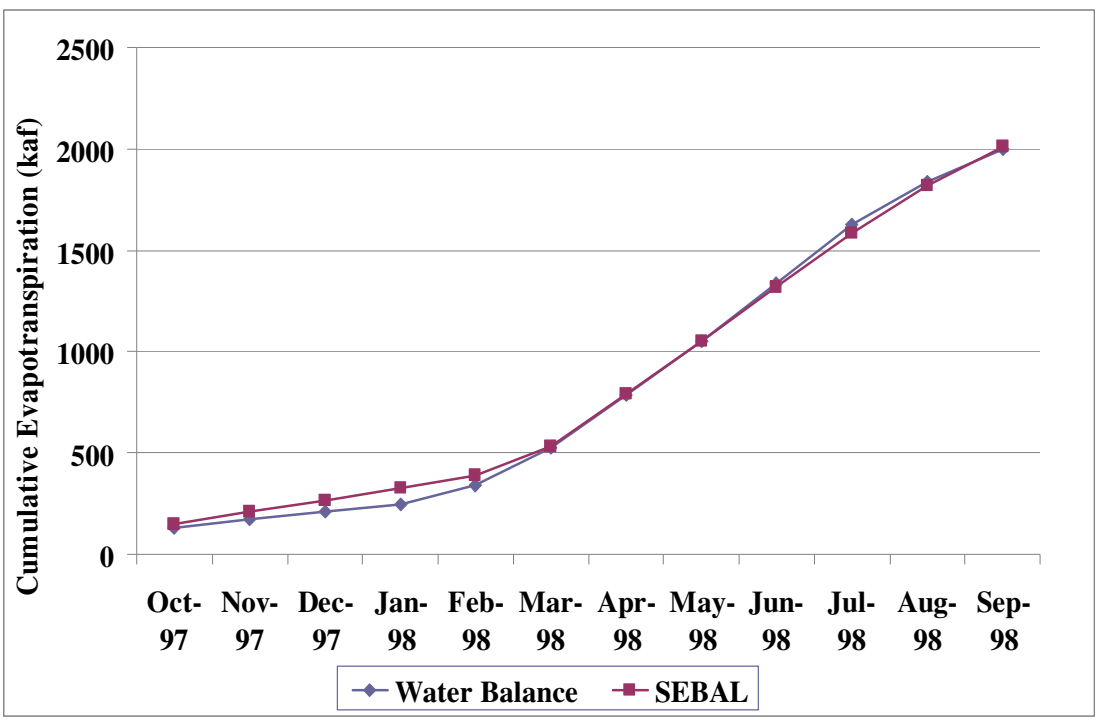

Figure 6. Cumulative ET from Water Balance and SEBAL Results.

Table 3. Comparison of Water Balance and SEBAL Cumulative Monthly Volumes.

Month	Cumulative, kaf		
	Water Balance	SEBAL	Percent Difference (SEBAL-WB)/WB
Oct-97	132.1	147.8	11.9%
Nov-97	173.0	208.6	20.6%
Dec-97	209.2	268.2	28.2%
Jan-98	249.5	326.1	30.7%
Feb-98	339.6	390.6	15.0%
Mar-98	525.8	531.7	1.1%
Apr-98	785.3	790.8	0.7%
May-98	1050.8	1049.4	-0.1%
Jun-98	1337.0	1316.2	-1.6%
Jul-98	1630.5	1585.7	-2.7%
Aug-98	1837.9	1820.9	-0.9%
Sep-98	1998.5	2010.4	0.6%

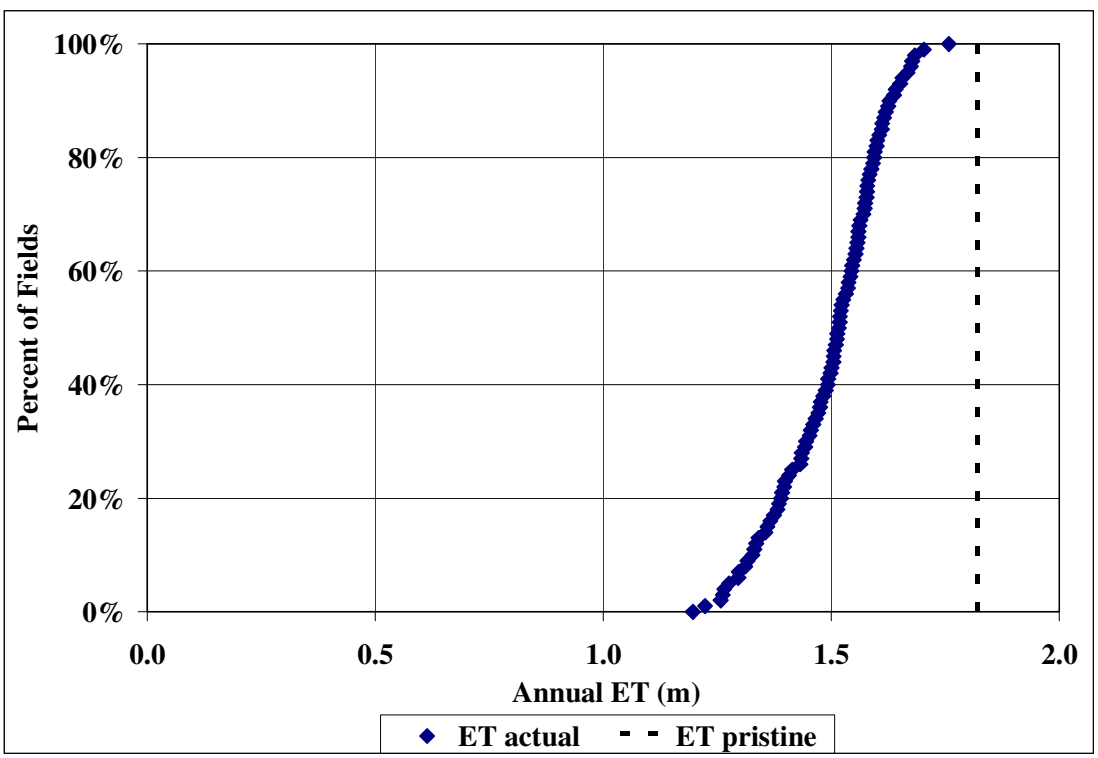

Figure 7. Cumulative Distribution of Water Year 1998 Field Scale ET for Flood Irrigated Alfalfa on Cracking Soils.

The SEBAL results allow for a more complete understanding of ET across time. Although a few fields exceed the monthly pristine ET in some months, the average monthly ET_a from the alfalfa fields in the study area is below the monthly pristine ET computed by the FAO 56 crop coefficient procedures (Figure 8). The low ET in the winter months is likely due to: 1) sheep grazing on some alfalfa fields lowers the averages and 2) 30-60 day periods in the winter when many alfalfa fields are not irrigated, remaining dormant for a couple months in the cooler part of the year.

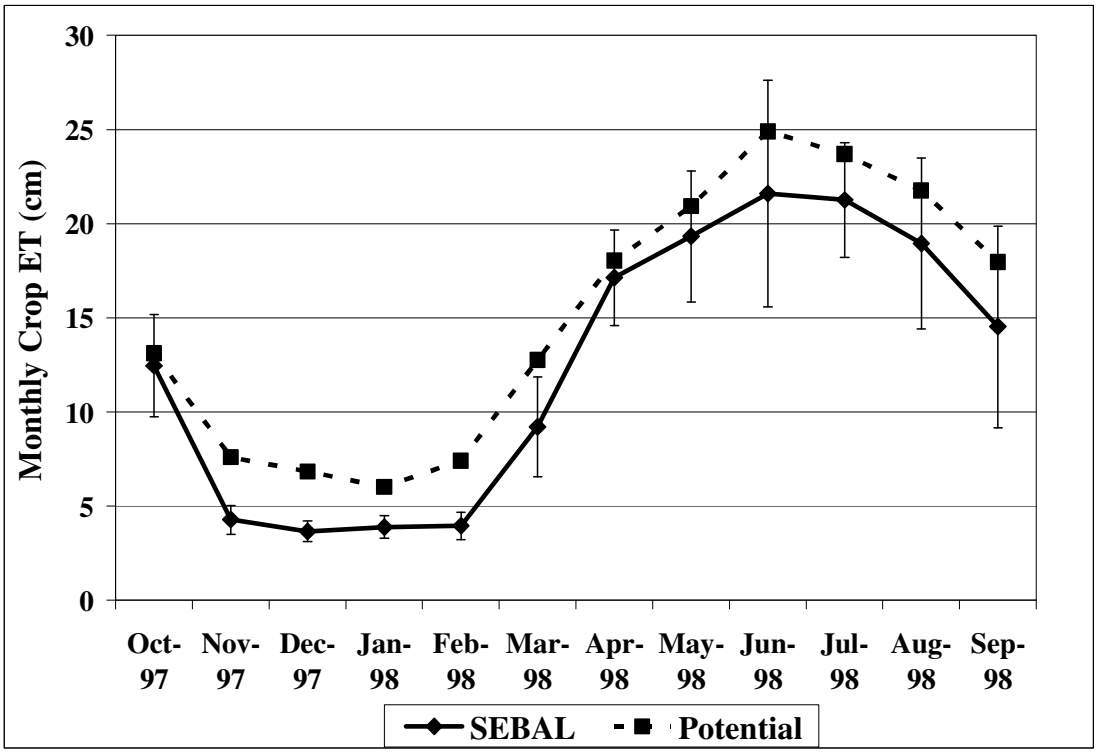

Figure 8. Comparison of Monthly Actual and Pristine ET for Flood Irrigated Alfalfa on Cracking Soils.

The SEBAL results allow for a more complete understanding of ET variation within fields. Six fields with boundaries superimposed on the July 98 SEBAL results are shown illustrating ET variability within fields (Figure 9). The largest field is ½ mile by ½ mile, 160 acres, 65 hectares, 720 pixels. Reduced ET often occurs uniformly and in concentrated areas. Fields with low uniformity may benefit from improved irrigation management to achieve ET (and yield) increases.

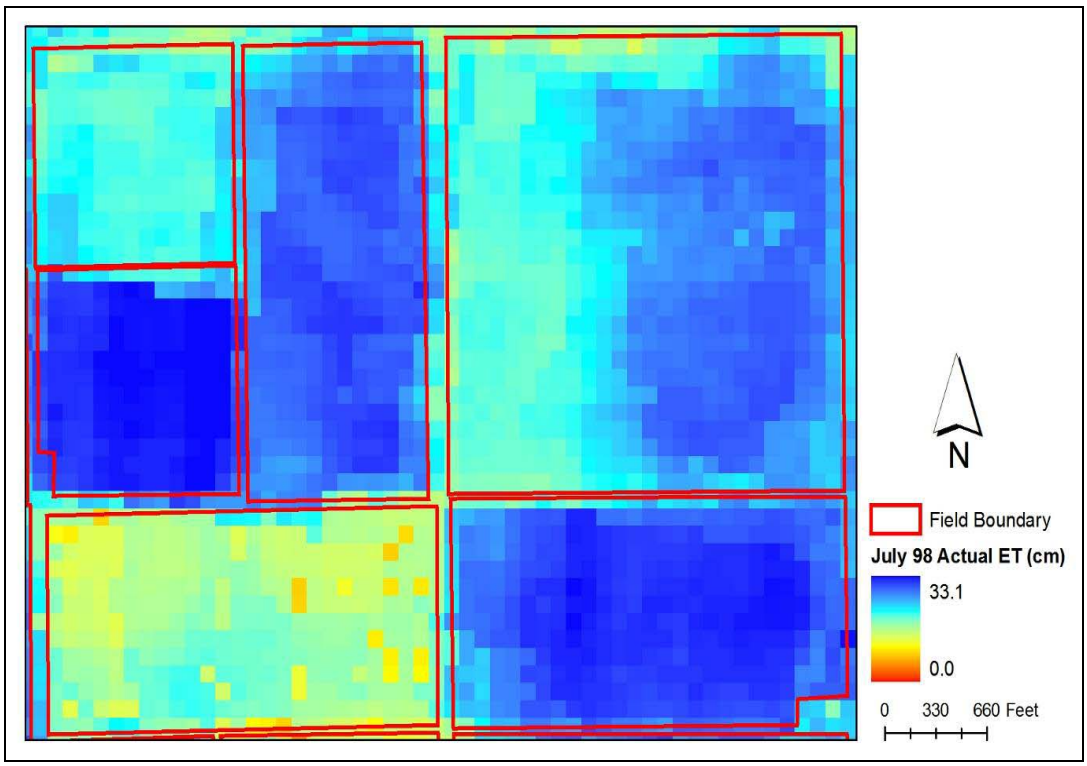

Figure 9. Example of ET Variation between Fields Identified through Remote Sensing.

CONCLUSIONS

Results of the district-wide water balance were compared to corresponding results from the remote sensing approach utilizing SEBAL for the 1998 water year (October 1997 to September 1998), resulting in a difference of less than one percent, providing a strong validation of SEBAL in arid, advective environments. The ET computed from the crop coefficient approach was 14 percent higher than the ET computed by the water balance approach.

The following additional conclusions are evident:

1. The 30-m by 30-m pixel spatial resolution of the remote sensing approach results allow for a more complete understanding of ET within and among fields.
2. The remote sensing approach results allow for a more complete understanding of ET across time.
3. Remote sensing of ET using thermal imagery plays an important role in the IID/SDCWA water transfer and, more broadly, water management in the West.
4. Remote sensing of ET provides opportunities for improved agricultural water management at field, farm, district, basin, state, and regional scales.

REFERENCES

Allen, R.G., Pereira, L.S., Raes, D., and Smith, M. (1998). Crop Evapotranspiration. *Irrigation and Drainage Paper No. 56. Food and Agriculture Organization of the United Nations.* Rome, Italy.

Allen, R.G., Bastiaanssen, W.G.M, Tasumi, M., and Morse, A. (2001). Evapotranspiration on the Watershed Scale Using the SEBAL Model and Landsat Images. ASAE Annual International Meeting, Sacramento, CA, 2001.

Allen, R.A., Walter, I.A., Elliot, R., Howell, T., Itenfisu, D. and Jensen, M. 2005. The ASCE Standardized Reference Evapotranspiration Equation. ASCE.Reston, VA.

Allen, R.A., Clemmens, A.J., Burt, C.M., Solomon, K. and O'Halloran, T. 2005. Prediction Accuracy for Projectwide Evapotranspiration Using Crop Coefficients and Reference Evapotranspiration. *Journal of Irrigation and Drainage Engineering.* 131(1), 24-36.

Bastiaanssen, W.G.M., Menenti, M., Feddes, R.A., and Holtslag, A.A.M. (1998). A Remote Sensing Surface Energy Balance Algorithm for Land (SEBAL): 1. Formulation. *Journal of Hydrology*, 212-213: 198-212.

Bastiaanssen, W.G.M., Noordman, E.J.M., Pelgrum, H., Davids, G., and Allen, R.G. (2005). SEBAL Model with Remotely Sensed Data to Improve Water Resources Management Under Actual Field Conditions. *Journal of Irrigation and Drainage Engineering.* 131(1), 85-93.

Clemmens, A.J. and Burt, C.M. (1997). Accuracy of Irrigation Efficiency Estimates. *Journal of Irrigation and Drainage Engineering.* 123(6), 443-453.

Snyder, R.L., Lanini, B.J., Shaw, D.A., and Pruitt, W.O. (1989a). Using Reference Evapotranspiration (ET_o) and Crop Coefficients to Estimate Crop Evapotranspiration (ET_c) for Agronomic Crops, Grasses and Vegetable Crops. *Leaflet No. 21427*, Cooperative Extension, University of California. Berkeley, California.

Snyder, R.L., Lanini, B.J., Shaw, D.A., and Pruitt, W.O. (1989b). Using Reference Evapotranspiration (ET_o) and Crop Coefficients to Estimate Crop Evapotranspiration (ET_c) for Trees and Vines. *Leaflet No. 21428*, Cooperative Extension, University of California. Berkeley, California.

Tasumi, M., Trezza, R., Allen, R.G., and Wright, J.L. (2005b). Operational aspects of satellite-based energy balance models for irrigated crops in the semi-arid U.S. *Irrig. Drain. Syst.*, 19, 355-376.

Independent Comparisons among Calibration and Output of Energy Balance Components Estimated by the METRIC Procedure

J. H. Kjaersgaard (member)[1], P. H. Gowda (member)[2], R. G. Allen (member)[3], T. A. Howell (member)[4]

[1]University of Idaho, Kimberly Research and Extension Center, 3792 N 3600 E, Kimberly, ID 83341; PH (208) 423 6672; email: jeppek@kimberly.uidaho.edu
[2]USDA-ARS, Conservation and Production Research Laboratory, P.O. Drawer 10, Bushland, TX 79012; PH (806) 356 5730; email: Prasanna.Gowda@ars.usda.gov
[3]University of Idaho, Kimberly Research and Extension Center, 3792 N 3600 E, Kimberly, ID 83341; PH (208) 423 6601; email: rallen@kimberly.uidaho.edu
[4]USDA-ARS, Conservation and Production Research Laboratory, P.O. Drawer 10, Bushland, TX 79012; PH (806) 356 5746; email: Terry.Howell@ars.usda.gov

ABSTRACT

An accurate estimation of evapotranspiration (ET) is an integral part of the hydrological cycle and is increasingly important in local and regional water resource management in central and western United States. Traditionally, estimation of ET included substantial uncertainties, but with the advent of algorithms applied to high resolution (30 m) satellite imagery, ET estimates from bare soil and vegetation can be obtained with greater accuracy. The METRIC image processing model estimates net radiation, soil heat flux and sensible heat flux through a series of steps before estimating ET as the residual from the energy balance. This paper describes a comparison of the METRIC surface energy balance model outputs produced by two different research groups when using the same two 2007 Landsat 5 images as input. One of the research groups is based at the USDA Conservation and Production Research Laboratory in Bushland, Texas where the images and ground-based data were captured, and the other group is from the Kimberly Research Center, University of Idaho where METRIC was developed.

INTRODUCTION

Considerable uncertainty exists regarding the spatial and temporal variability and distribution of the consumptive water use (CWU), not only for agricultural crops but also for rangeland, riparian zones and other areas with natural vegetation. The variability is caused by local and regional differences in weather, precipitation distribution and quantity, soil, land form and land use, vegetation type, cultivar and cropping system, irrigation application method and land management. Normally the vast majority of CWU is made up by evapotranspiration, ET. A common method to

estimate actual ET (ET_a) from the ground and vegetation include multiplying weather-based reference evapotranspiration (ET_r) with a crop coefficient (K_c) (Allen et al., 1998; ASCE-EWRI, 2005). Allen et al. (2007b) estimated ET with this procedure and is relatively accurate with an error of up to ± 20 %. Errors may arise from actual vegetation and growing conditions deviating from the idealized K_c values or results from undocumented water shortage in the vegetation. In addition, it is difficult to predict the correct crop growth stages for a large population of crops and fields.

Application of remote sensing algorithms solving the energy balance using high resolution satellite imagery has proven useful for establishing estimates of ET_a and K_c for large populations of fields and water users (Bastiaanssen et al., 1998; Tasumi et al., 2005, Allen et al. 2007a). The METRIC model (Mapping Evapotranspiration at high Resolution with Internalized Calibration) is a satellite image processing model which estimates ET as the residual of the energy balance (Tasumi et al., 2005, Allen et al., 2007b), Eq. 1.

$$LE = R_n - G - H \qquad (1)$$

where LE is latent heat flux density, R_n is net radiation, G is soil heat flux density and H is sensible heat flux density. In METRIC, R_n is calculated by solving the radiation balance as described by Allen et al. (2007b). Soil heat flux is the rate of heat being conducted into the soil and vegetation, and is estimated based on R_n, surface temperature and the Normalized Difference Vegetation Index, NDVI.

METRIC utilizes the *CIMEC* (calibration using inverse modeling of extreme conditions) procedure (Bastiaanssen, 1995, Bastiaanssen et al., 1998) procedure to calibrate the dT function based on a regression relationship between the dT and radiometric surface temperature of two "anchor" pixels. The advantage of the SEBAL approach to developing a dT vs. T_S relationship by inverting the energy balance at the two calibration points is that many biases in energy balance components are factored out, including those in T_S itself. In addition, the use of a dT that 'floats' above the surface may eliminate some of the issues with single source models (Allen et al., 2007b). The anchor pixels ideally represent the conditions of an agricultural field with full and actively transpiring vegetation cover and a bare agricultural field with no vegetation cover. The anchor pixel representing full vegetation cover has the characteristics of green vegetation and its dT is low due to evaporative cooling. This condition is often referred to as the "cold" condition. The anchor pixel representing a bare field has the characteristics of bare soil and its dT is high due to radiometric heating of the surface and is generally referred to as the "hot" condition.

METRIC uses alfalfa based ET_r to establish the energy balance at the cold pixel, thus establishing a ground reference for the satellite image based ET_a estimate. ET_r is calculated outside of METRIC using hourly (or shorter) weather data from a weather station preferably located toward the center of the study area. The use of ET_r is generally effective in tying down the energy balance calibration, especially in arid

and semiarid climates having advection. The use of ET_r for calibration and extrapolation of ET to longer time periods makes the METRIC process congruent with traditional ET_r based estimation methods. One of the outputs from METRIC is a map of the ET from each pixel stated as a fraction of ET_r, ET_rF. The ET_rF is synonymous with the well known K_c (for an alfalfa reference basis). Daily ET_a maps are calculated by multiplying the instantaneous ET_rF calculated for each pixel with the 24-h summed ET_r. The resulting high resolution maps of ET cover regions typically up to 150 km in scale. When used properly, METRIC provides a rapid and cost effective method to determine ET for focused regions.

The METRIC model can be set up to be nearly fully automated, but does require rather essential input from the user to define and interpret e.g. vegetation roughness, land use, and anchor pixels, during image calibration, representing fields with dry soil surface and with a vegetated, fully transpiring surface. Additionally, some of the algorithms for atmospheric attenuation and emission of radiation can benefit from further testing to be used with confidence over vide range of climates.

There is therefore merit in doing an inter-comparison of the output from METRIC produced individually by two independent groups. This paper describes a comparison of the preliminary results of METRIC outputs produced by two different research groups when processing the same two Landsat 5 images from 2007. The images were processed without contact between the two groups. Subsequently, following this comparison, the two groups will continue the collaboration and conduct an additional processing run, integrating local knowledge and experience about e.g. cropping patterns and land management, and long-term experience in METRIC application. Additionally, images from other times during the growing season and other years will be processed for inter-comparison purposes.

METHODS

One Landsat 5 scene from 07/10-2007 from path 31 row 36 have been selected. The scenes cover the central portion of the Texas panhandle, but were not geometrically corrected. To avoid errors caused by geometric incongruencies within the Landsat images and for the purpose of the initial comparison of METRIC output four square fields at the USDA-ARS, Conservation and Production Research Laboratory in Bushland was selected for the comparisons. The relative location of the fields in the Landsat image is shown in Fig. 1. The fields are equipped with four high precision weighing lysimeters each located at the center of each field (Howell et al., 1995). Each lysimeter (3 m length × 3 m width × 2.4 m depth) is located in the middle of 4.7-ha fields and all four lysimeters are arranged in a block pattern. Dryland cropping systems are managed on two lysimeter fields in the west and irrigated cropping systems are managed on two lysimeter fields in the east with a 10-span lateral move sprinkler system. The location of the fields and the 2007 crop cover is shown in Fig. 2.

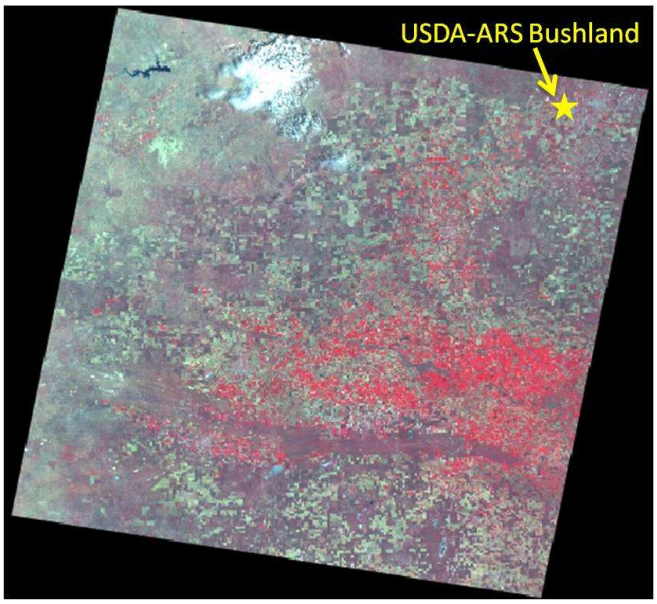

Figure 1. Location of the fields at USDA-ARS in Bushland used for the METRIC output comparison

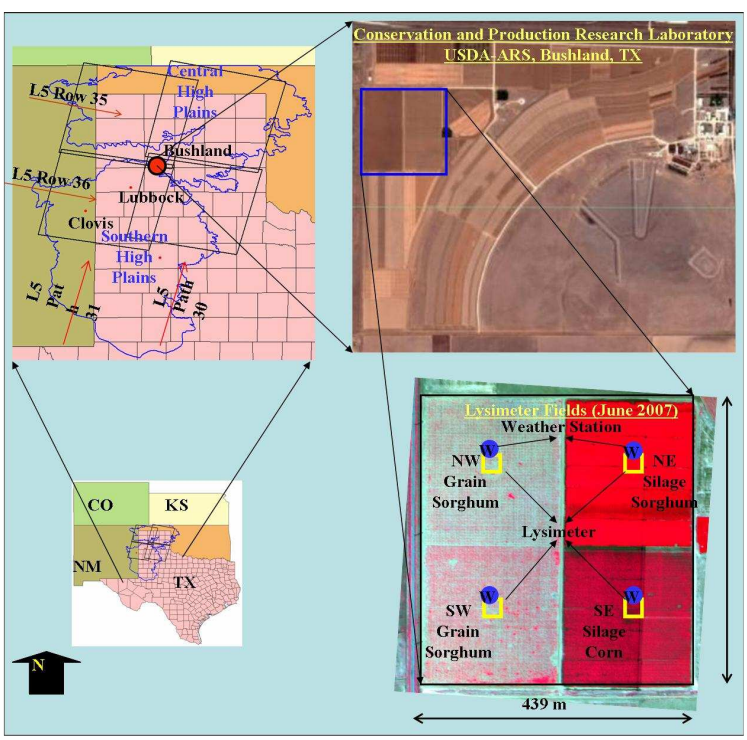

Figure 2. Location of the Bushland weighing lysimeters from. The geographic location of the SE lysimeter is shown in the lower right corner, 35° 11' 09.96'' N 102° 05' 43.35'' W.

The METRIC model was coded and processed using the ERDAS Imagine Spatial Modeler tool independently by each group. Reference ET was calculated using the RefET software (Allen, 2003) using meteorological data as input. Supporting input information, including a water balance to estimate residual evaporation from bare soil (for the hot pixel calibration) and the iterative numerical solution of the dT function equation based on the cold and hot anchor pixels, were carried out using a regular spreadsheet.

Weather data from the weather station located approximately one km from the fields were used during the processing. The station is part of the Texas High Plains Evapotranspiration network, operated by Texas A&M University. The quality of all meteorological data used in the METRIC processing were checked following the recommendations by Allen (1996), Allen et al. (1998) and ASCE-EWRI (2005). As ET_r was also used to establish a soil water balance several months before each image acquisition date, the integrity of the meteorological data for the entire year 2007 were evaluated. Hourly and daily values for solar radiation R_s were compared to computed clear sky solar radiation (R_{s0}). R_{so} was calculated based on atmospheric pressure, sun angle and precipitable water in the atmosphere. Generally a good agreement was found between observed R_s on days with clear sky conditions and the theoretical R_{s0} values, although the observed R_s values does run a few % higher than the R_{s0} curve during the winter period.

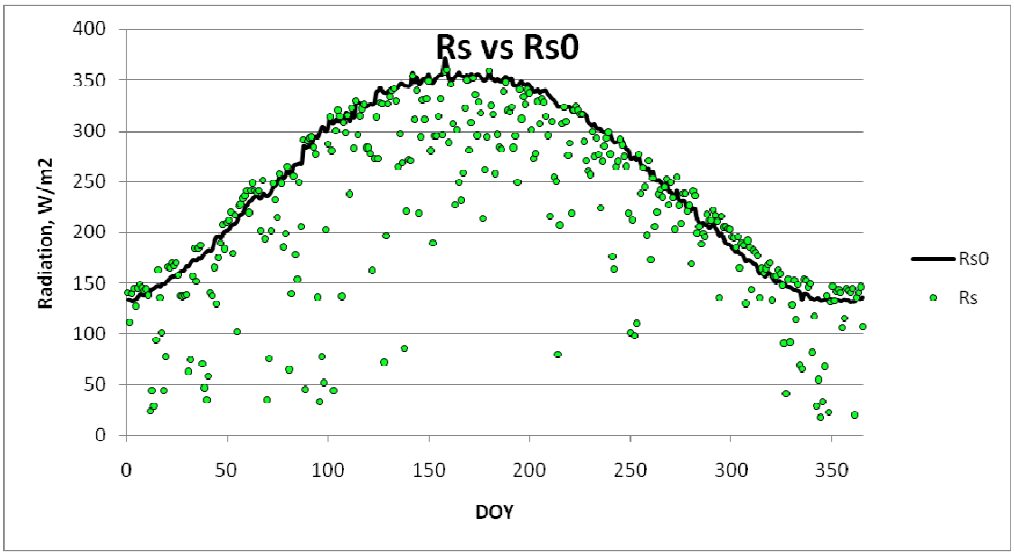

Figure 3. Daily solar radiation observed at the Bushland weather station versus theoretical clear sky solar radiation, R_{s0} during year 2007.

A range test was used to check daily minimum and maximum relative humidity. In addition, daily mean computed dewpoint temperature was compared against daily minimum air temperature following ASCE-EWRI (2005). The air temperature (T_a) was compared to nearby weather stations, and hourly T_a measurements were checked visually for sudden spikes and the expected diurnal

occurrence of minimum and maximum values. Wind speed was checked by calculating the gust factor (ASCE-EWRI, 2005) and comparing average daily wind speed to that of other nearby weather stations.

A daily water balance model based on Allen et al. (1998) was employed to estimate residual evaporation from the hot pixel (Fig. 4). The satellite overpass moment were obtained from the respective image header files and used to estimate the zenith angle of the sun and instantaneous values of wind speed at screen height and 200 m, air humidity and ET_r.

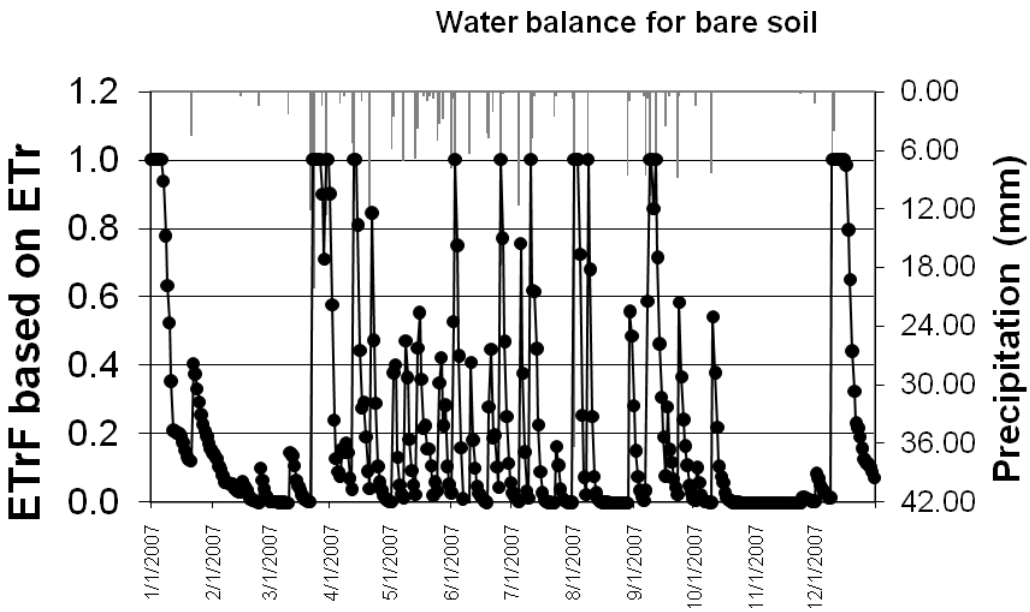

Figure 4. Soil water balance for bare soil calculated using meteorological data from Bushland, Texas 2007 and used to determine ET_rF for the hot pixel calibration.

PRELIMINARY RESULTS AND DISCUSSION

ET estimates from four 30-m pixels located towards the center of each of the four fields are sampled and averaged. Center pixels are generally selected to avoid sampling field edges where the vegetation cover is less due to e.g. traffic, insufficient irrigation and similar. The northwest and southwest fields were grown with grain sorghum under dryland conditions in 2007. Drought damaged the crop and by mid-summer the vegetation cover was relatively sparse. The northeast field was grown with a silage sorghum crop under irrigated conditions, while the southeast field had an irrigated silage corn crop. The crop pattern and the associated ET_rF values are recognized in Fig. 5. The crosshair is at the same geographic location at the four corners of the fields. The ET rates are highest for the corn being at full cover and under relatively good water supply.

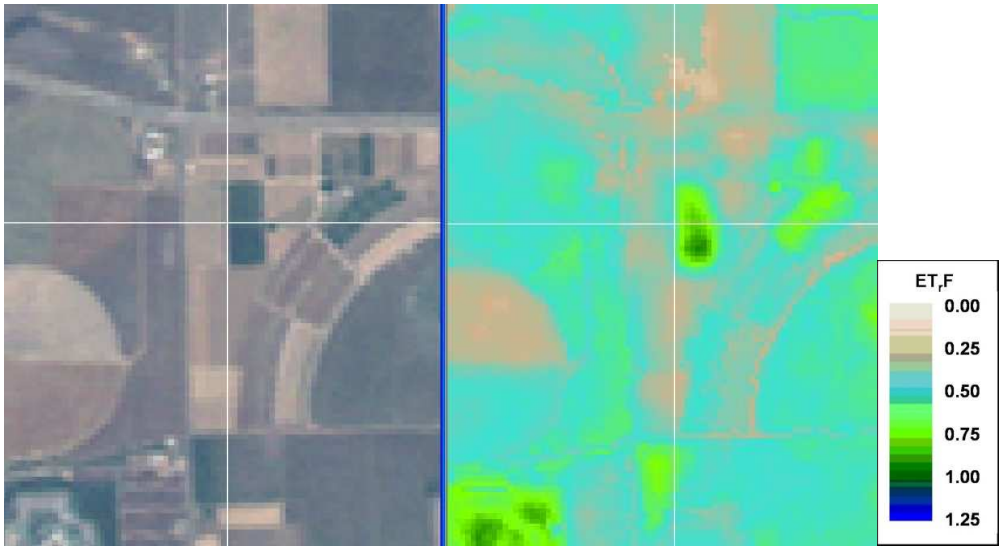

Figure 5. Satellite image in true color (left) and the corresponding resulting ET_rF map on July 10 2007, for the ARS station in Bushland, Tx. The crosshair is at the same geographic location.

A comparison of the instantaneous ET as measured by each of the four lysimeters and as predicted by each of the two research groups producing the estimates using METRIC is shown in Figure 6. The deviation in net radiation estimated by METRIC, Figure 7, is probably caused by differences in the estimation of atmospheric transmissivity and or emissivity of the surface or the atmosphere. For the field grown with silage corn the estimates of ET are close between the lysimeters, while more deviation is found for the two dryland fields. A thin layer of wilted plant material on the soil surface or the presence of senescenced standing crops may cause the differences between the lysimeter and the METRIC estimates. This may increase the "skin" temperature "seen" by the satellite causing H to be overestimated in METRIC and subsequently underestimate ET. A likely cause of the deviation between the estimates of ET between the two groups A and B is that the "hot" pixel selected by one (or both) of the groups does not entirely represent the conditions of a bare, dry field. This causes a deviation in the estimation of H, figure 8, possibly leading to an underestimation of H.

The scale of the fields used for the comparisons between the output produced by the two research groups adds additional uncertainty for the final result. Since each field has a side length of approximately 225 m there will likely only exist one thermal pixel (120 m) within each field. Since the thermal band has been resampled to 30 m resolution using cubic convolution (CC) resampling it is not possible to locate the original thermal pixel. There is therefore a risk that among the four pixels sampled for ET averaging one or more will be from a 120m thermal pixel that is not contained entirely within the field, or is located towards the edge of the field. Such thermal pixels may not be representative for a larger field, and may draw the ET estimates down. Additionally, meteorological sensors mounted on a bench are located near the

lysimeters, which may impact the amount of radiation reflected and emitted from that location.

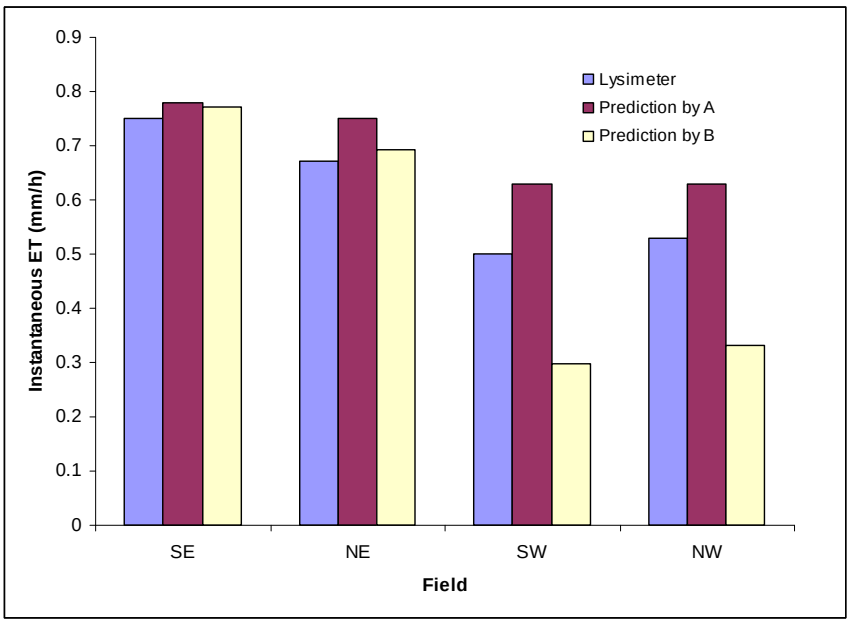

Figure 6. Comparison of instantaneous evapotranspiration (mm/hr) as measured by the four lysimers, and as predicted by user group A and user group B using METRIC.

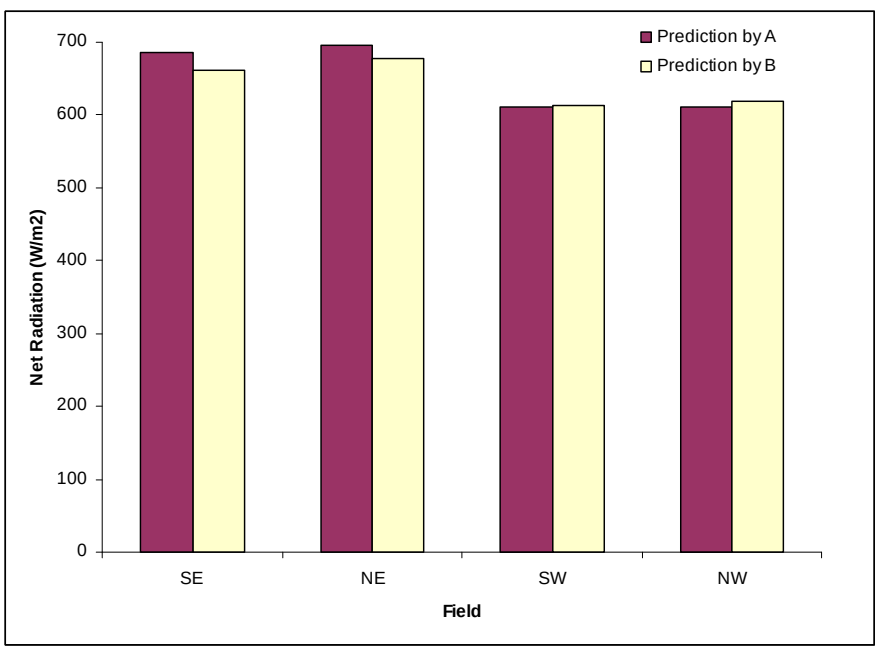

Figure 7. Comparison of net radiation as predicted by user group A and B using METRIC.

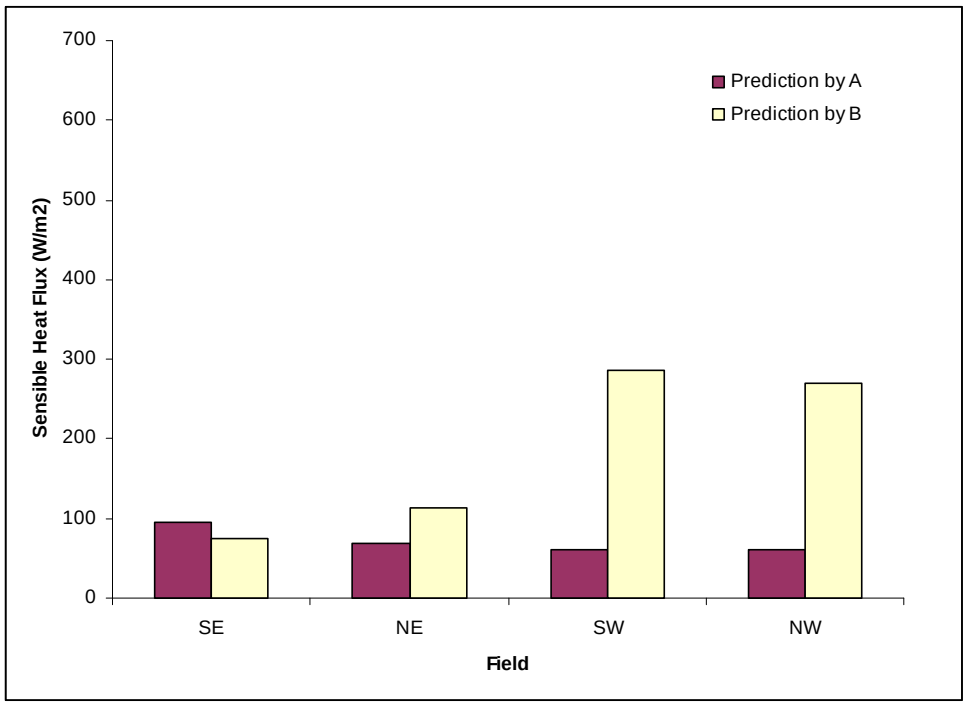

Figure 8. Comparison of sensible heat flux as predicted by user group A and B using METRIC.

Further investigation and comparisons, and through conducting an additional processing run the deviations should be minimized. The results obtained this far underlines the importance of the user being trained in the use of METRIC and having experience with running the model, including selection of hot and cold anchor pixels in order to obtain good and consistent results.

REFERENCES

Allen, R.G., 1996: Assessing integrity of weather data for reference evapotranspiration estimation. *J. Irrig. Drain. Engr*. 122(2), 97-106.

Allen, R.G., 2003: Ref-ET: Reference evapotranspiration calculation software for FAO and ASCE standardized equations. University of Idaho. 76 p. Downloaded May 1 2007 from www.kimberly.uidaho.edu/ref-et

Allen, R.G., Pereira, L.S., Raes, D., Smith, M., 1998: Crop evapotranspiration. Guidelines for computing crop water requirements. FAO Irrigation and Drainage Paper 56. Rome, Italy. 300 p.

Allen, R.G., Tasumi, M., Morse, A.T., Trezza, R., Kramber, W., Lorite, I., Robison, C.W., 2007a: Satellite-based energy balance for mapping evapotranspiration with internalized calibration (METRIC) – Applications. *J. Irrig. Drain. Engr*. 133(4), 395-406.

Allen, R.G., Tasumi, M., Trezza, R., 2007b: Satellite-based energy balance for mapping evapotranspiration with internalized calibration (METRIC) – Model. *J. Irrig. Drain. Engr*. 133(4), 380-394.

ASCE-EWRI, 2005: The ASCE Standardized reference evapotranspiration equation. ASCE-EWRI Standardization of Reference Evapotranspiration Task Committee Report. Reston, Virginia. 216 p.

Bastiaanssen, W.G.M., 1995: Regionalization of surface flux densities and moisture indicators in composite terrain: A remote sensing approach under clear skies in Mediterranean climates. PhD. Dissertation, CIP Data Koninklijke Bibliotheek, Den Haag, the Netherlands. 273 p.

Bastiaanssen, W.G.M., Menenti, M., Feddes, R.A., Holtslag, A.M.M., 1998: A remote sensing surface energy balance algorithm for land (SEBAL): 1. Formulation. *J. Hydrology* 212-213, 198-212.

Howell, T.A, Schneider, A.D., Dusek, D.A., Marek, T.H., Steiner, J.L.,. 1995. Calibration and scale performance of Bushland weighing lysimeters. Transactions of ASABE, 38(4):1019-1024.

Tasumi, M., Trezza, R., Allen, R.G., Wright, J.L., 2005: Operational aspects of satellite-based energy balance models for irrigated crops in the semi-arid U.S. *J. Irrig Drain. Systems*, 19, 355-376.

Measuring Soil Moisture in a Heterogeneous Field

Chadi Sayde[1], John Selker[1], and Marshall English[1]

[1]Department of Biological and Ecological Engineering, Oregon State University, 116 Gilmore hall,

Corvallis, OR 97331; PH (541) 737-2041; email: saydec@onid.orst.edu

ABSTRACT

Effective irrigation management commonly relies upon soil moisture measurements to ascertain crop water availability in field soils. But all such measurements are intrinsically uncertain, and even when individual soil moisture measurements are relatively accurate, estimates of crop water availability derived from those measurements may be quite uncertain due to the field scale variability of soil parameters and uneven distribution of applied water.

Replication of soil moisture measurements can reduce that uncertainty. Commonly, measurements at two or more sites in a field are averaged to reduce the variance of the estimate. Alternatively, multiple replications can be used to quantify the uncertainty of any single measurement. That quantitative uncertainty can then be used in a Bayesian decision model that combines soil moisture measurements with model estimates of cumulative ET. The result is an improved estimate of soil moisture.

Either approach depends upon replication of soil moisture measurements. But current measurement technology is such that the most accurate methods are expensive while the more affordable methods are relatively inaccurate and therefore require more replications. Either way replication is expensive.

This paper explores the theoretical basis, preliminary experimental results and potential benefits of using fiber optic technology for distributed measurement of field soil moisture. This technology determines soil moisture content by measurement of soil thermal response to a heat pulse. With a resolution of 1 m along a fiber optic cable this technique is capable of literally hundreds of measurements along a single cable installed at a specific depth. The technology is still under development at the time of this writing, but the indications are that it can quantify soil water variability with relatively high accuracy at moderate cost.

INTRODUCTION

Uncertainty in soil moisture measurements. The fundamental objective of scientific irrigation scheduling is accurate tracking of crop-available water in the soil. A variety of techniques are employed to measure soil water content, which is then used to calculate the amount of available water remaining in the root zone. But measurements of soil water content are inherently uncertain, and because crop water availability is defined in terms of the remaining 'available capacity' in the root zone the uncertainty of measured soil moisture is compounded by the natural variability of soil water holding characteristics and inexact knowledge of crop root zones and water uptake patterns.

The net effect is that estimates of field-wide crop water availability derived from soil moisture measurements are quite uncertain. Some degree of uncertainty is intrinsic to the measurement technique used. Additional uncertainty derives from soil heterogeneity and uneven distribution of applied water.

This paper is primarily concerned with the uncertainty of soil moisture measurements, and in particular, the uncertainty that derives from spatially variable factors illustrated in the following two Figures. Figure 1 shows a soil survey image of a 125 acre circle encompassing two different soil types. Using the indicated soil depths and holding capacities of these two soils, and assuming that local variations of both parameters have a standard deviation of 10%, a statistical simulation of total holding capacities generated the result indicated in the histogram. Figure 2 is a compelling indication of field scale variability that might be encountered under ordinary conditions.

Figure 3 illustrates small scale variations in the amount of irrigation water stored in a soil profile. The observed variability (from Scotter and Clothier, 1986) indicates the disposition of applied water to a depth of 60 cm over a 3.6 m span of a field following irrigations at two different application rates.

These figures confirm what most field managers have observed; that a point measurement of soil water content will often not be representative of average conditions, nor will it provide any information about the variability of soil water content. Additionally, the uncertainty of computed values of crop available water will be compounded by wide variations in total holding capacities.

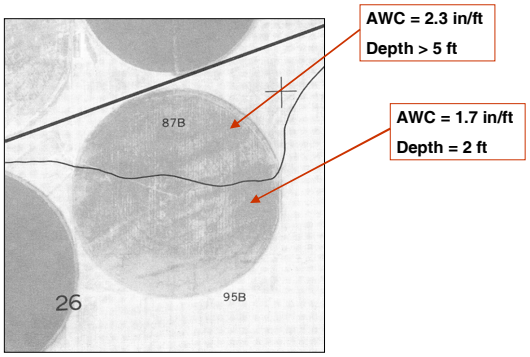

Figure 1: Field Scale Variations in total holding capacity

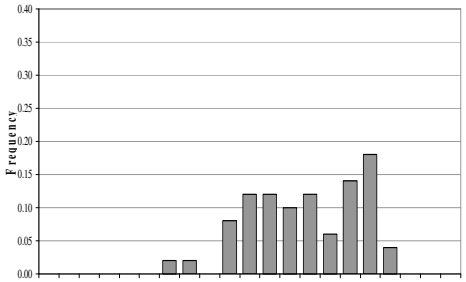

Figure 2: Variability of total available capacity

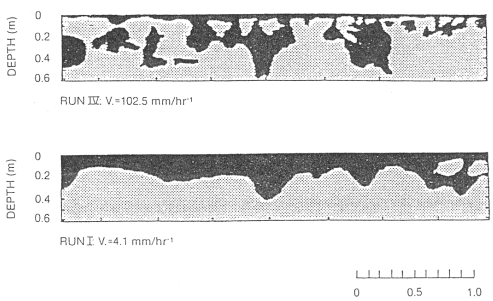

Figure 3: Local redistribution of applied water

Dealing with uncertainty. When water supplies are not limited the problem of measurement uncertainty is often circumvented by maintaining soil moisture at higher than critical levels, relying on point measurements of soil moisture to decide when to irrigate, and maintaining some soil water in reserve as a hedge against uncertainty. But with the accelerating competition for water and resulting increases in opportunity costs of water the practice of holding soil moisture in reserve will become progressively more expensive. That implies a need for more accurate ways of estimating crop water availability in heterogeneous fields.

More accurate determinations can be derived by replication, i.e. by taking measurements at several points in the field. The common assumption is that the variance of measured depletion is reduced inversely with the square of the number of

replicated measurements. However the validity of this assumption is limited by two factors:

- Individual measurements are not always statistically independent. Different soil types encompassed within a single field imply patterned variations in water holding characteristics (Figures 1 and 2).
- Non-uniform applications of irrigation water, compounded by redistribution of surface runoff and preferential subsurface flows may result in systematic variations in soil water distributions (Figure 3). Consequently, soil moisture measurements taken within definable sub-sectors of a field may be highly correlated.
- Uncertainties of crop root zone and uptake patterns are not reduced by replication of soil moisture measurements. The uncertainty of available capacity remains a confounding factor.

A proposed alternative approach to reduce the uncertainty of estimated crop available water would utilize a Bayesian decision model to integrate information embodied in estimates of ET with the information derived from soil moisture measurements (Sayde et al., 2008). Bringing additional information provided by another independent estimator (cumulative ET) into the analysis can reduce the overall uncertainty. The result is a maximum likelihood estimator of cumulative depletion. (The ET model may also compensate to some extent for the uncertainty of available capacity by indicating whether measured depletion is consistent with the assumed available capacity.) However, this Bayesian approach requires that the uncertainties of estimated ET and measured soil moisture must be quantified.

AN ALTERNATIVE APPROACH TO MEASURING SOIL MOISTURE

This paper presents an alternative soil moisture sampling technique that utilizes fiber optic cable and Distributed Temperature Sensing (DTS) technology to monitor soil response to a heat pulse. Though the method is still under development the indications are that this technology may offer two important advantages. One is that the marginal costs of replicated samples should be low. Because soil water content can be sampled at 1.0 meter increments along the length of cable, the number of sample sites increases as the length of cable is increased. Additionally the method can be automated and the results obtained by telemetry without routine human intervention.

Another important advantage is that soil water content can be sampled frequently. That makes it possible to observe peak water content (an indicator of available capacity), and to derive additional information about soil water dynamics by sampling the rates of change of soil moisture over relatively short intervals of time.

Distributed Temperature Sensing (DTS). DTS technology allows the measurement of temperature along a fiber optic cable with a spatial resolution < 1m. The principle behind temperature measurement along a fiber optic cable is based on the thermal sensitivity properties of the cable (Perzlmaier et al., 2006). Parts of a laser pulse injected into the fiber optic cable are reflected back at original energy, or absorbed and re-emitted at longer or shorter wave-length than the injected light. The reflection with a longer wavelength, called Stokes backscatter, is almost completely independent of temperature, while the reflection with a shorter wavelength, called anti-Stokes backscatter, is strongly dependent on the temperature at the point where it was reflected (Selker et al, 2006). By measuring the time of arrival of reflected light, the position along the cable from which the light was reflected can be obtained. Through calibration using sections of cable at known temperatures, temperature can be inferred by frequency analysis From the Stokes/Anti-Stokes ratio everywhere along the cable.

For a given DTS instrument and fiber optic sensing cable, the precision of a single temperature reading depends on two factors: 1) injection/reading cycle duration, and 2) distance from the light source.

In a longer cycle duration a higher number of light pulses are used to derive temperature, thus improving the temperature reading precision but only at the expense of high frequency readings rate.

The injected and reflected lights lose strength with distance, thus the signal-to-noise ratio decreases with distance from the light source.

The ability of fiber optic distributed temperature sensing (DTS) to measure temperature at high temporal frequency each meter along fiber optic cables several kilometers in length has opened many important opportunities in environmental monitoring. Selker et al. (2006) and Tyler et al. (2008) presented the basic methodology, and demonstrated its utility in a wide range of hydrologic applications.

DTS for soil moisture monitoring. Thermal properties of soils are a function of soil moisture content. Thus soil moisture content can be inferred by analysis of thermal responses of specific soils to a heat pulse. Available DTS technology can be used to monitor thermal responses of soil to a heat pulse, along a fiber optic cable with spatial resolution < 1 m. Many available fiber optic cables are composed of one or more optical fibers enclosed in stainless-steel tube and wrapped by stainless steel or other metallic wires. The metallic component of the fiber optic cable can be used as an electric resistance heater to inject heat into the surrounding soil, while the optical fiber is used as a thermal sensor to monitor temperature changes. This method, called the Actively Heated Fiber Optic (AHFO) method has been successfully used for subsurface water movement monitoring (e.g., Perzlmaier et al., 2004; Aufleger et al., 2005; and Perzlmaier et al., 2006). The application of AHFO method to determination of water content was reported to be only adequate to distinguish between dry, wet and saturated soil (Perzlmaier et al., 2006), but inadequate to

distinguish between small changes in volumetric soil moisture content above 6 % (Weiss, 2003). This is mainly due to the fact that the method of heat pulse analysis used in both articles is based on deriving the thermal conductivity (λ) of a soil from its thermal response to the slope and intercept of a line fit to the heat pulse signal with a log transformed time scale, then relating the obtained value of λ to soil moisture content by a data calibration equation. In fact, this method of heat pulses interpretation requires high frequency temperature readings, high signal-to-noise ratio, high energy input to accurately determine soil moisture content, mainly at high soil water content status. These requirements are not satisfied with the temperature and temporal resolutions provided by current DTS technology. Weiss (2003) concluded that only with dramatic improvement of the signal-to-noise ratio could the thermal conductivity be determined by a DTS heat pulse method with sufficient accuracy to quantify water content above 6%. In this context, a new method of data analysis that is suited to the nature of DTS readings is needed to allow better estimation of soil moisture content.

The Thermal Integral method. A new method of analyzing soil thermal responses to heat pulse is being developed at Oregon State University. Details and experimental results of this method can be found in Sayde et al. (2009). In summary, the thermal response of a soil to a heat pulse is quantified in the form of cumulative temperature increase over a certain period of time:

$$T_{cum} = \int_0^{t_0} \Delta T \, dt$$

Where T_{cum} is the integral of temperature increase over time [°C] as measured at the fiber optic cable, t_0 is the total time of integration, ΔT is the DTS reported temperature change from the pre-pulse temperature [°C].

Sayde et al. (2009) showed that T_{cum} monotonically decreases with water content. In fact, higher heat capacity and higher thermal conductivity, both monotonically increase with water content (θ), increase the rate at which heat is conducted away from the probe and reduce the integral (Figure 4).

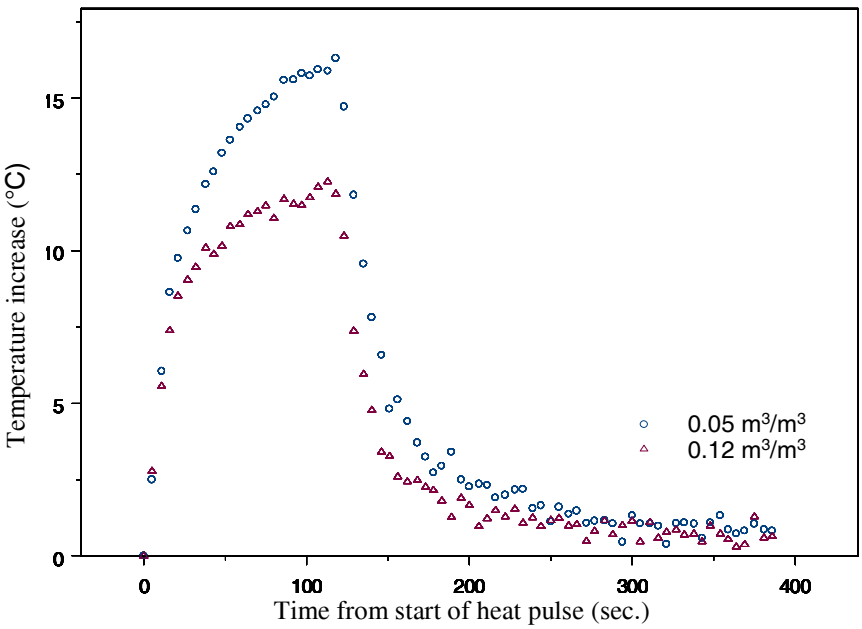

Figure 4: Thermal response of soil at two locations with different moisture content to a heat pulse of "2minutes - 20 W/m". $T_{cum,}$ The integral of temperature increase over the 2 minutes heating duration, was 1562°C and 1250°C for soil moisture contents of 0.05 m^3/m^3 and 0.12 m^3/m^3 respectively.

The use of the thermal integral method for interpretation of the AHFO heat pulses data has been tested under laboratory conditions where a 30 m section of a fiber optic cable was installed in a sand filled column, and several combinations of heat pulse durations and intensities were tested for the sand column under wide range of soil moisture content.

Sayde et al. (2009) demonstrated that for a 2 minute heat pulse at 20 W/m, the thermal integral method was able to distinguish water contents with coefficient of variation of 0.08 across volumetric water contents ranging from 4-41%. The highest error (0.033 m3/m3) is observed at saturation (θ = 0.41 m3/m3). This error can be further reduced by averaging several heat pulses results, or by increasing the heat pulse duration and integration time.

Another advantage of the integral method is that it requires much lower energy input and heating time than the methods described in Perzlmaier et al. (2006) and Weiss (2003), reducing the risk of water displacement from around the heated fiber optic cable and allowing more frequent heat pulses to be conducted. In fact, repeated measurements of soil moisture content under laboratory conditions have not shown any signs of water displacement.

Field application. A field trial of the technique was conducted in an agricultural field located near Hermiston, eastern Oregon. Three fiber optic cables, each of 250 m length, were installed at three different depths (30 cm, 60 cm, and 90 cm) to monitor spatial variability of soil moisture depletion.

A 45° angle, 2.54 cm thick plow designed specifically for this purpose was used to install the 3 fiber optic cables simultaneously at their respective depths with a minimum of soil disturbance (Figure 5). Soil moisture was monitored by the AHFO method with a rate of 1 heat pulse/hr. At this writing the data from this experiment are still under analysis.



(a) (b)

Figure 5. (a) 45-degree "lift-plow" showing cable insertion tubes, (b) in operation.

Challenges and concerns. In decreasing order of significance, the main concerns that can lead to substantial errors when applying the actively heated fiber optic method are: 1) the contact between soil and probe, 2) water displacement due to over-heating of the soil surrounding the cable, 3) spatial variability of soils properties, and 4) temperature dependence of soil thermal properties.

The biggest challenge during field installation is to minimize soil disturbance around the cable, and insure a good contact between the cable and the surrounding soil. A poor contact between the fiber optic cable and the surrounding soil at a particular point, caused by installation or by shrinking–swelling mechanics observed for some particular soils, will increase the thermal resistivity and reduces the thermal conductivity causing erroneous lower soil moisture estimation at this particular point. If those perturbation points are assumed to be randomly distributed along the fiber optic cable, a larger spatial scale for DTS measurement can be used to improve the accuracy of soil moisture estimation.

A large local temperature increase may cause water to evaporate and diffuse from a high temperature area toward a lower temperature area. Farouki (1986) showed that this moisture movement is a function of the interaction between the thermal gradient and the time of existence of this gradient. Therefore, it is crucial to reduce both the

magnitude and duration of the heat pulse.

Like any other heat pulse method, concerns regarding the accuracy of such methods remain related to soil bulk density (Tarara and Ham, 1997), soil mineralogy (Bristow, 1998) and total porosity (Ochsner et al., 2001). In fact, soil thermal properties are dependent on the volumetric fractions of solid, water, and air. (Ochsner et al., 2001). Those fractions vary greatly in space and time, and may substantially affect the thermal responses of soil along the fiber optic cable.

Heat pulse methods were found to be sensitive to ambient temperature due to the changes in the density and specific heat of water and specific heat of soil with respect to temperature (Olmanson et al., 2006). Diurnal cycling of soil thermal properties and moisture content is reported by Heitman et al. (2003), while Bristow et al. (2004) indicated that different initial temperature conditions, ranging from 24.20 °C to 38.53 °C, had negligible effect on measured thermal conductivity using a single probe heat pulse method.

CONCLUSION

The key findings of this work is that AHFO technique has a great potential to monitor soil moisture at temporal resolution under one hour, and spatial resolution of 1 m along cables exceeding several km in extent. Heat pulse method using coaxial heating and DTS sensing, when the results are interpreted using the Thermal Integral method, is feasible for determination of water content of soils across a much broader range of moisture contents than previously thought.

Such measurements are essential to quantify uncertainty and monitor spatial variability of soil water dynamics across m to km scales.

Many questions should be subject to further research efforts, mainly regarding the radius of influence of such measurements, optimal heating strategies, and errors that can be induced by soil disturbance during installation or by spatial variability of soil parameters.

REFERENCES

Aufleger, M., Conrad, M., Perzlmaier, S., and Porras, P. 2005. Improving a Fiber Optics Tool for Monitoring Leakage. HRW, 13(4):18-23.

Bristow, K. L., R. D. White, and G. J. Kluitenberg. 1994. Comparison of single and dual probes for measuring soil thermal properties with transient heating. *Australian Journal of Soil Research,* 32:447-464.

Bristow, K. L. 1998. Measurement of thermal properties and water content of unsaturated sandy soil using dual-probe heat-pulse probes. *Agricultural and Forest Meteorology*, 89:75-84.

Farouki, O.T. 1986. Thermal properties of soils. Series on rock and soil mechanics. Vol. 11. Trans Tech Publications, Clausthal-Zeller- feld, Germany.

Heitman, J.L., J.M. Basinger, G.J. Kluitenberg, J.M. Ham, J.M. Frank, and P.L. Barnes. 2003. Field evaluation of the dual-probe heatpulse method for measuring soil water content. *Vadose Zone J*. 2:552–560.

Ochsner, T.E., R. Horton, and T. Ren. 2001b. A new perspective on soil thermal properties. Soil Sci. Soc. Am. J. 65:1641–1647

Olmanson, O.K., and Ochsner, T.E. 2006. Comparing ambient temperature effects on heat pulse and time domain reflectometry soil water content measurements. *Vadose Zone* J., 5:751–756.

Perzlmaier, S., Aufleger, M., and Conrad, M. 2004. Distributed fibre optic temperature measurements in hydraulic engineering. - Prospects of the heat-up method. In: Proceedings of the 72nd ICOLD Annual Meeting - Workshop on Dam Safety Problems and Solutions-Sharing Experience, Seoul, South Korea, May 16-22, 2004, Korean National Committee on Large Dams (KNCOLD), Seoul.

Perzlmaier, S., Straßer, K.-H., Strobl, Th., and Aufleger, M. 2006. Integral Seepage Monitoring on Open Channel Embankment Dams by the DFOT Heat Pulse Method. 22nd ICOLD, Barcelona. Q. 86 – R. 12

Scotter, D.R., Clothier, B.E. 1986. The soil as a transport and storage medium for irrigation water. New *Zealand Agricultural Science* 20 (1), 23-28

Sayde, C., El Khoury, L., Gitelman, A., and English, M. 2008. Optimizing Estimates of Soil Moisture for Irrigation Scheduling. In: ASABE meeting, Providence, RI, 2008. (Paper # 084699)

Sayde, C., Gregory, C., Gil, M., Tufillaro, N., Tyler, S., van de Giesen, N., English, M., Cuenca, R., and Selker, J.S. 2009. Feasibility of Soil Moisture Monitoring with Fiber Optics. Submitted to *Wat. Resour. Res.*

Selker, J.S., Thévenaz, L., Huwald, H., Mallet, A., Luxemburg, W., van de Giesen, N., Stejskal, M., Zeman, J., Westhoff, M., and Parlange, M.B. 2006. Distributed Fiber Optic Temperature Sensing for Hydrologic Systems. *Wat. Resour. Res.,* 42, W12202, doi:10.1029/2006WR005326.

Tarara, J. M., and J. M. Ham. 1997. Measuring soil water content in the laboratory and field with dual-probe heat-capacity sensors. *Agronomy Journal*, 89:535-542.

Tyler, S., Burak, S., McNamara, J., Lamontagne, A., Dozier, J., Selker, J. 2008. Spatially Distributed Temperatures at the Base of Two Mountain Snowpacks Measured with Fiber Optic Sensors. Under review for publication in the Journal of Glaciology.

Weiss, J. D. 2003. Using Fiber Optics to Detect Moisture Intrusion into a Landfill Cap Consisting of a Vegetative Soil Barrier. *J. Air & Waste Manage. Assoc.*, 53:1130-1148.

Performance Evaluation of Soil Heat Flux Models in Great Plains

R. K. Singh[1], A. Irmak[2], E. A. Walter-Shea[3], and S. B.Verma[4]

[1]Dept. of Biological Systems Engineering, University of Nebraska-Lincoln, 249 Hardin Hall, Lincoln, NE 68583-0962; PH (402) 472-6826; FAX (402)472-3461; email: rsingh2@unl.edu

[2]School of Natural Resources and Dept. of Civil Engineering, University of Nebraska-Lincoln, 311 Hardin Hall, Lincoln, NE 68583-0973; PH (402) 472-8024; FAX (402)472-2946; email: airmak2@unl.edu

[3]School of Natural Resources, University of Nebraska-Lincoln, 803 Hardin Hall, Lincoln, NE 68583-0968; PH (402) 472-1553; FAX (402)472-2946; email: ewalter-shea1@unl.edu

[4]School of Natural Resources, University of Nebraska-Lincoln, 807 Hardin Hall, Lincoln, NE 68583-0978; PH (402) 472-6702; FAX (402)472-2946; email: sverma1@unl.edu

ABSTRACT

Soil heat flux plays an important role in land surface energy dynamics by constraining the amount of available energy for partitioning between latent heat flux and sensible heat flux. Thus accurate quantification of the soil heat flux is of key importance in energy balance studies. In this study, the performances of four different methods have been evaluated for the soil heat flux estimation in maize and soybean fields under irrigated and dryland conditions. Statistical analysis of the model performance has shown a wide variation in the ability of these models from site to site and from year to year. The RMSE for irrigated maize ranged from 15.16 W m^{-2} to 81.25 W m^{-2}, whereas the range for dryland maize was 14.99 W m^{-2} to 55.81 W m^{-2}. The RMSE between predicted and measured soil heat flux for irrigated soybean was between 19.36 W m^{-2} and 50.83 W m^{-2}. Relatively a narrow range (18.45-35.24 W m^{-2}) of RMSE was found for dryland soybean. In view of wide range of RMSE and negative model efficiency, it is recommended that the local calibration of the model should be carried out for remote estimation of soil heat flux.

Keywords: *Soil heat flux; Energy balance; Net radiation; NDVI; Nebraska*

INTRODUCTION

Soil heat flux (G) is a significant component of the daytime surface energy balance in many ecosystems. It can become a significant component in relatively sparse vegetation (Kustas et al., 2000) and predominant during night time (Murray and Verhoef, 2007a). In forest ecosystem, G usually accounts for 5% of net radiation ($R_{n)}$ (Beringer et al., 2005; Chen et al., 2002), while in grasslands, G can account for 25% of R_n (Wilson et al., 2002). In sparse canopy ecosystems in semi-arid or arid regions, G was found to account for up to 40% of R_n, which could be equal to or higher than LE (Verhoef et al., 1996). Shao et al. (2008) found that the spatial variability in G can account for 48 W m^{-2} (13% of R_n) during the day and 15 W m^{-2} (34% of R_n) at night, with an average of 28 W m^{-2} (24% of R_n) across three steppe ecosystems. An accurate quantification of *G* is of key importance in energy balance studies, particularly for energy balance closure assessment (Stannard et al., 1994) and for energy balance-based model output verification (Heusinkveld et al. 2004; Murray and Verhoef 2007a, b).

The remote sensing methods are increasingly used for estimating surface energy balance components including G. Kustas and Daughtry (1990) developed a method for estimating *G* based on measurements of R_n and ground-based reflectance in bare soil, alfalfa, and cotton fields in Arizona. They developed two G/R_n equations based on the ratio of ρ_{NIR}/ρ_R and NDVI. They

reported that the mid-day ratio of G and R_n (G/R_n) was linearly related to the ratio of ρ_{NIR}/ρ_R and NDVI as follows:

$$\frac{G}{R_n} = 0.294 - 0.0164\frac{\rho_{NIR}}{\rho_R} \qquad (r^2=0.74, n=11) \qquad (1)$$

$$\frac{G}{R_n} = 0.325 - 0.208 NDVI \qquad (r^2=0.86, n=11) \qquad (2)$$

Bastiaanssen et al. (1998) pooled together the G/R_n and NDVI data from Clothier et al. (1986), Choudhury (1989), Kustas and Daughtry (1990), and Oevelen (1991) and found the following relationship:

$$\frac{G}{R_n} = 0.30(1 - 0.98 NDVI^4) \qquad (r^2=0.61, n=35) \qquad (3)$$

Melesse and Nangia (2005) compared the measured and the estimated fluxes for local conditions using 10 Landsat Thematic Mapper (TM) and Enhanced Thematic Mapper (ETM) images in Montana and suggested a modified equation (Eq. 4) for estimating G as a function of R_n and NDVI.

$$\frac{G}{R_n} = 0.153(1 - 0.98 NDVI^4) \qquad (4)$$

Singh et al. (2008) found that the relationship used in Surface Energy Balance Algorithm for Land (SEBAL) prediction for soil heat flux (Equation 3) significantly overestimated G in a subsurface drip-irrigated maize field in south-central Nebraska with an r^2 of 0.055 and an RMSE of 79.8 W m^{-2}. Due to poor estimation of G, Singh et al. (2008) used measured G data to develop an exponential relation that utilizes NDVI and R_n as follows:

$$G = [0.3811\exp(-2.3187 NDVI)]R_n \qquad (5)$$

Although these equations have been shown to perform well for the conditions that they have been developed for, their applications to a different soil environments are not well known. Our overall objective is to apply and test aforementioned empirical equations for their ability to estimate G under maize (*Zea mays* L.) and soybean (*Glycine max* L.) cropping systems in the Great Plains environmental settings of the United States.

MATERIALS AND METHODS

Study Site: Mead, Nebraska

We used available data sets collected at three sites during 2003 to 2005 from an ongoing carbon sequestration research program at the University of Nebraska-Lincoln, Agricultural Research and Development Center (ARDC) near Mead, NE. The sites at ARDC represent three major cropping systems: a) irrigated continuous maize, b) irrigated maize-soybean rotation, and c) rainfed maize-soybean rotation. The first site (Site 1) (41° 9' 54.2"N, 96° 28' 35.9"W, 361 m above mean sea level) is irrigated with a center-pivot irrigation system and is about 48.7 ha in size. The second site (Site 2) (41° 9' 53.5"N, 96° 28' 12.3"W, 362 m above mean sea level) is also center-pivot irrigated and is 52.4 ha, while the third site (Site 3) (41° 10' 46.8"N, 96° 26' 22.7"W, 362 m above mean sea level) is rainfed and about 65.4 ha. These three sites are within 1.6 km of each other. The soils at all three sites are deep silty clay loams. The cropping details of the sites are presented in table 1. More details about these sites can be found in Verma et al. (2005) and Suyker et al. (2005).

Table1: Cropping details of the study sites

Site	Year	Crop/cultivar	Plant population (plants per Ha)	Planting date	Harvest date
Mead site1: Irrigated continuous maize	2003 2004 2005	Maize/Pioneer 33B51 Maize/Pioneer 33B51 Maize/DeKalb 63-75	77,000 79,800 69,200	May 15 May 3 May 4	October 27 October 13 October 12
Mead site2: Irrigated maize-soybean rotation	2003 2004 2005	Maize/Pioneer 33B51 Soybean/Pioneer 93B09 Maize/Pioneer 33B51	78,000 296,000 76,300	May 14 June 2 May 2	October 23 October 18 October 17
Mead site 3: Rainfed maize-soybean rotation	2003 2004 2005	Maize/Pioneer 33B51 Soybean/Pioneer 93B09 Maize/Pioneer 33G66	57,600 264,700 53,700	May 13 June 2 April 26	October 13 October 11 October 17
Clay Center: sub-surface drip irrigated	2005 2006 2007	Maize/Pioneer 33B51 Maize/ Pioneer 33B54 Soybean/ Pioneer 93M11	72,900 75,400 385,500	April 22 May 12 May 21	October 17 October 5-6 October 24

Net radiation was measured at 5.5 m above the ground using a Kipp & Zonen CNR1 net radiometer (Campbell Scientific Inc., Logan, Utah). Soil heat flux was measured at a depth of 0.06 m below the ground using soil heat flux plates (Radiation and Energy Balance Systems Inc., Seattle, WA). The soil heat flux was adjusted for soil moisture variation (Verma et al. 2005). Net radiation and soil heat flux were sampled at 0.1 sec intervals and averaged over 60 minutes using a Model CR10X datalogger and AM416 Relay Multiplexer (Campbell Scientific, Inc., Logan, UT). Spectral reflectance was measured in 2003, 2004, and 2005 with a pair of inter-calibrated SKR 1850 series four-channel light sensors (Model SKR 1850, Skye Instruments Ltd., Powys, UK) mounted at approximately 5 m on a mast located near the eddy covariance flux tower in the center of the fields. The SKYE radiometers measure in four narrow spectral bands: (1) 536-561 nm (green band), (2) 665-676 nm (red band), (3) 700 - 720 nm (red-edge band) and (4) 862-874 nm (near infrared band); all except the 700-720 nm red-edge band are comparable to MODIS bands. In the field, the SKYE instruments measured the same location, obtaining a 10 min average every half-hour between 11:30 am and 1:30 pm (Central Standard Time).

Study Site: Clay Center, Nebraska

A field experiment was conducted at the University of Nebraska-Lincoln, South Central Agricultural Laboratory (SCAL) during the 2005, 2006, and 2007 growing seasons. SCAL is located approximately 160 km west of Lincoln in the south central part of Nebraska near Clay Center, NE, U.S.A. (40°34′ N, 98°08′ W, 552 m above sea level). The soil at the experimental site is Hastings silt loam with a field capacity of 0.34 m^3 m^{-3} and permanent wilting point of 0.14 m^3 m^{-3}. Maize was planted during the 2005 and 2006 growing seasons, and soybean was planted in 2007 (Table 1). The experimental field (13 ha) was irrigated using a subsurface drip irrigation system. Measurements were made using a deluxe version of a Bowen Ratio Energy Balance System (BREBS) (Radiation and Energy Balance Systems, REBS, Inc., Bellevue, WA). Soil heat flux was measured using three REBS HFT-3.1 heat flux plates and three soil thermocouples. Each soil heat flux plate was placed at a depth of approximately 0.06 m below the mean ground

level. The REBS STP-1 soil thermocouple probes were installed in close proximity to each soil heat flux plate at depths of 0.02, 0.04, 0.06, 0.08, and 0.10 m below the soil surface. Measured soil heat flux values were adjusted to soil temperatures and soil water content as measured using three REBS SMP1R soil moisture probes. Net radiation was measured using a REBS Q*7.1 net radiometer that was installed approximately 4.5 m above the soil surface. All variables were sampled at a 30 sec interval and averaged and recorded on a hourly basis using a Model CR10X datalogger and AM416 Relay Multiplexer (Campbell Scientific, Inc., Logan, UT). More details about the measurements can be obtained from Irmak and Irmak 2008. The NDVI at the Clay Center site was calculated using cloud free Landsat5 and Landsat7 satellite images (Path 29, Row 32). The acquisition dates for Landsat5 and Landsat7 images are shown in table 2.

Table 2: Details of Landsat images (Path 29 Row 32) used for the study.

2005 Image Acquisition Date	DOY	Satellite/ Sensor	2006 Image Acquisition Date	DOY	Satellite/ Sensor	2007 Image Acquisition Date	DOY	Satellite/ Sensor
May 19	139	L5/TM	May 22	142	L5/TM	June 10	161	L5/TM
June 20	171	L5/TM	June 23	174	L5/TM	July 12	193	L5/TM
July 22	203	L5/TM	July 17	198	L7/ETM	August 13	225	L5/TM
August 07	219	L5/TM	July 25	206	L5/TM	September 22	265	L7/ETM
September 08	251	L5/TM	September 19	262	L7/ETM	September 30	273	L5/TM
September 16	259	L7/ETM	October 13	286	L5/TM			
October 18	291	L7/ETM	October 29	302	L5/TM			

RESULTS AND DISCUSSION

Comparison of empirical models for predicting G for irrigated and dryland maize cropping systems

Several models are available to estimate G from R_n and NDVI, and we compared some of those models to assess their performance at our study sites. We selected the Kustas and Daughtry (1990) (M1), Bastiaanssen et al. (1998) (M2), Melesse and Nangia (2005) (M3), and Singh et al. (2008) (M4) models for comparisons. Results are presented in the table 3.

Comparisons of measured and estimated G from the four models (M1-M4) for irrigated maize showed a wide variation from site to site and year to year (Fig. 1). At Mead site 1, M2 resulted in the highest mean absolute error (MAE) (44.14 W m^{-2}) and root mean square error (RMSE) (48.56 W m^{-2}) in 2005 (Table 3). The lowest values of MAE and RMSE at site 1 were 16.97 W m^{-2} and 24.43 W m^{-2}, respectively, using M3 during the 2004 cropping season. It is interesting to note that both M2 and M3 resulted in the same r^2 value as both equations have similar structures. However, M3 had a better model efficiency as compared with M2 during 2004 (0.51 vs. -0.75) and 2005 (0.43 vs. -0.74). The negative efficiencies of M2 indicated that the observed mean of G is a better predictor than the model.

Comparisons at Mead site 2 for irrigated maize showed that the M2 and M3 equations yielded the highest (46.65 W m^{-2}) and the lowest (13.51 W m^{-2}) values of MAE, respectively, in 2003. The maximum RMSE was 50.68 W m^{-2} (M2), and the minimum RMSE was 24.71 W m^{-2} for M3. Using the M1 model, G was overestimated by 38% in 2003 and 17% in 2005 at Mead site 2 (Fig. 1d-e). For the same site, M2 resulted in overestimation of G by 50% (2003) and 22% (2005). When compared with Mead site 1, the overestimation at Mead site 2 increased in 2003

but decreased in 2005. This decrease in 2005 may be due to less crop residue in 2005 as a result of the soybean crop in 2004.

Table 3: Statistical analysis results of the model validations using Kustas and Daughtry (1990) (M1), Bastiaanssen et al. (1998) (M2), Melesse and Nangia (2005) (M3), and Singh et al. (2008) (M4) equations.

Measure	Method	Mead Site 1			Mead Site 2			Mead Site 3			Clay center		
		2003	2004	2005	2003	2004	2005	2003	2004	2005	2005	2006	2007
MAE	M1	27.76	34.56	34.63	38.64	34.03	22.71	33.82	27.92	32.82	54.90	57.20	32.14
	M2	33.83	42.86	44.14	46.65	27.15	26.29	49.45	27.49	52.99	77.32	70.90	45.30
	M3	23.18	16.97	20.02	13.51	16.69	26.57	10.41	19.27	9.13	28.62	22.20	29.20
	M4	26.84	23.96	30.46	23.89	19.37	31.74	19.73	15.85	18.55	10.09	36.89	30.96
RMSE	M1	30.66	38.02	38.89	40.98	36.20	25.99	34.92	29.44	34.18	57.20	61.16	35.45
	M2	39.15	46.34	48.56	50.68	35.22	32.44	52.89	35.24	55.81	81.25	73.06	46.42
	M3	31.70	24.43	27.64	24.71	19.36	35.06	14.99	23.61	17.74	32.06	26.65	50.83
	M4	34.72	31.12	34.55	27.22	22.46	35.58	21.68	18.45	20.49	15.16	43.86	41.18
r^2	M1	0.76	0.71	0.72	0.82	0.90	0.83	0.91	0.96	0.93	0.94	0.41	0.94
	M2	0.77	0.79	0.78	0.75	0.89	0.69	0.78	0.90	0.81	0.57	0.61	0.88
	M3	0.77	0.79	0.78	0.75	0.89	0.69	0.78	0.90	0.81	0.57	0.61	0.88
	M4	0.62	0.56	0.54	0.77	0.83	0.79	0.89	0.95	0.93	0.88	0.03	0.72
E	M1	0.39	-0.18	-0.12	-0.24	-0.47	0.48	-1.24	0.36	-0.27	-1.59	-3.68	0.54
	M2	0.01	-0.75	-0.74	-0.89	-0.39	0.19	-4.14	0.08	-2.38	-4.22	-5.69	0.21
	M3	0.35	0.51	0.43	0.55	0.58	0.06	0.59	0.59	0.66	0.19	0.11	0.05
	M4	0.22	0.21	0.12	0.45	0.43	0.03	0.14	0.75	0.54	0.82	-1.41	0.38

The best performance at the Clay Center site for irrigated maize was obtained by using M4, because this model was calibrated at this site using data from the 2005 growing season. We excluded this model from our discussion here. The next best MAE and RMSE were obtained by using M3, whose minimum values were 28.62 W m^{-2} and 32.06 W m^{-2}, respectively. The corresponding r^2 and E values were 0.57 and 0.19, respectively. M1 had the highest r^2 (0.94), but its model efficiency was poor in both 2005 (-1.59) and 2006 (-3.68). The overall variation in G estimation during 2005 (Fig. 1f) ranged from -8% (M3) to 81% (M2). However during 2006 (Fig. 1g), all the models overestimated G at the Clay Center site, with M3 having the lowest (5%) and M2 having the highest (106%) values.

Dryland maize was grown at Mead site 3 during 2003 and 2005. The comparison of measured and estimated G for this cropping system showed similar distributions for 2003 and 2005 (Fig. 2). The M3 equation resulted in the lowest MAE during 2003 (10.41 W m^{-2}) and 2005 (9.13 W m^{-2}). In fact, these values were the best MAE achieved from among all the cropping systems in our analyses. The highest MAE was 49.45 W m^{-2} and 52.99 W m^{-2} during 2003 and 2005, respectively. These values were obtained from using M2. In 2003, the maximum RMSE was 52.89 W m^{-2} (M2), and the minimum RMSE was 14.99 W m^{-2} (M3). There was a slight increase in the minimum (17.74 W m^{-2}) and the maximum (55.81 W m^{-2}) RMSE in 2005. Though M1 had the highest correlation during 2003 (r^2 =0.91) and 2005 (r^2 =0.93), the model efficiency was negative during these two years (-1.24 in 2003 and -0.27 in 2005). Only M3 and M4 had positive model efficiency values for dryland maize. As similar to Mead sites 1 and 2, G

was overestimated at Mead site 3 using M1 and M2 and underestimated by M3 and M4 in 2003 (Fig. 2a) and 2005 (Fig.2b).

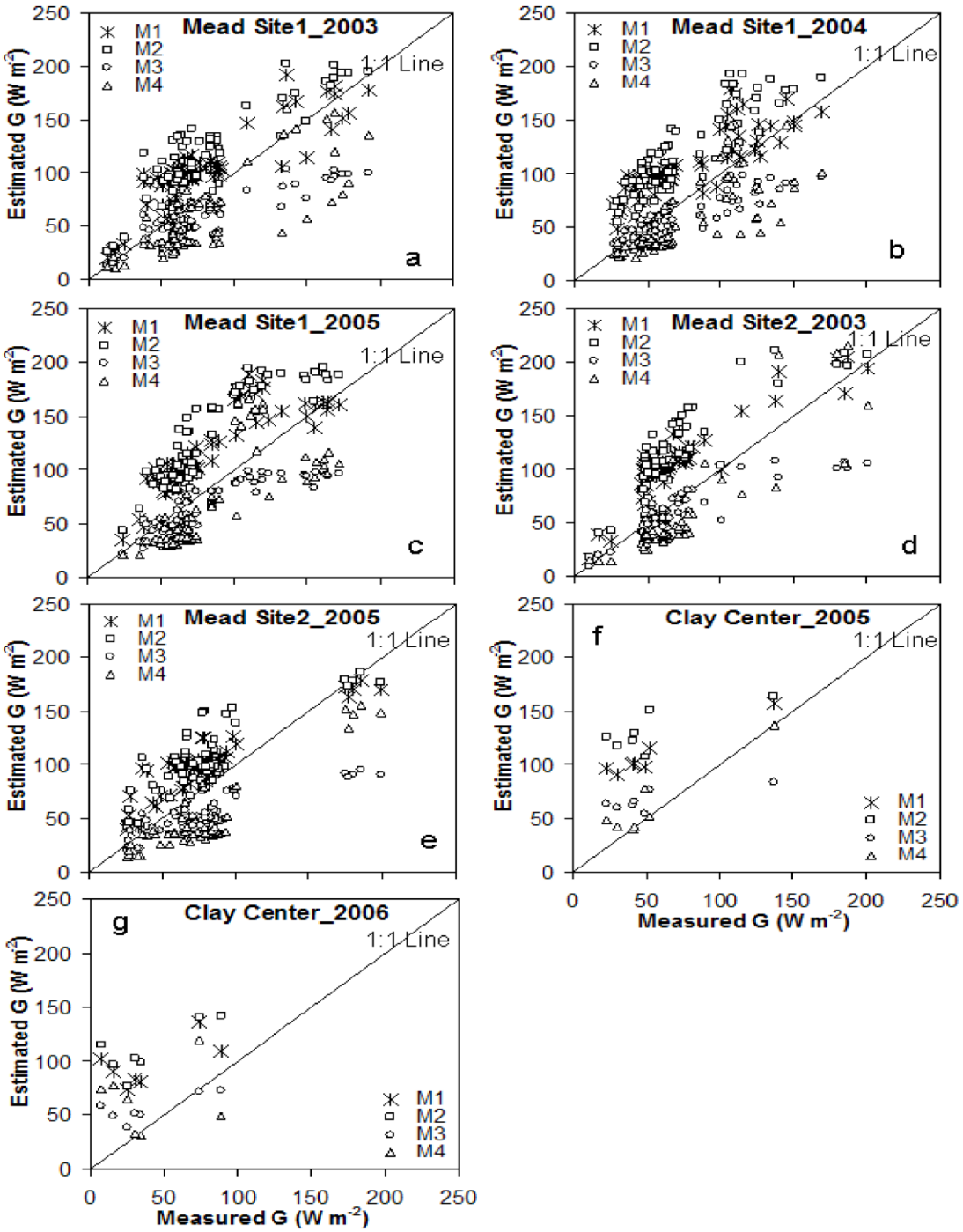

Figure 1. Model comparison for irrigated maize at Mead site 1 during (a) 2003, (b) 2004, (c) 2005, at Mead site 2 during (d) 2003 and (e) 2005 and at Clay Center site during (f) 2005 and (g) 2006 for estimation of G using the Kustas and Daughtry (1990) (M1), Bastiaanssen et al. (1998) (M2), Melesse and Nangia (2005) (M3), and Singh et al. (2008) (M4) equations.

Comparison of empirical* models *for predicting G for irrigated and dryland soybean cropping systems

The comparison of measured and estimated G for the irrigated soybean cropping systems is shown in figure 3. While M1 and M2 overestimated G, the other two equations (M3 and M4) underestimated G at Mead site 2 during 2004 (Fig. 3a). The overestimation was about 48% and 46% by M1 and M2, respectively. In contrast, M3 and M4 resulted in underestimation of G by 25% and 13%, respectively. The lowest MAE at Mead site 2 was 16.69 W m^{-2} using the M3 equation followed by M4 (19.37 W m^{-2}). The highest MAE obtained by M1 (34.03 W m^{-2}) was more than double that of the lowest MAE at Mead site 2. A very good correlation (r^2 =0.83-0.90) was obtained at this site for all four compared methods. However, only M3 (0.58) and M4 (0.43) had positive model efficiencies, indicating good model performance. Model efficacy for G estimation in subsurface drip-irrigated soybean at Clay Center site is shown in figure 3b. Comparison for irrigated soybean at Clay Center during the 2007 cropping season showed that, in general, the MAE and RMSE were higher at this site as compared with Mead site 2 (Table 3). We found that overall, the Kustas and Daughtry (1990) equation underestimated G by about 6%. The comparison of measured and estimated G for the dryland soybean cropping system is presented in figure 4.

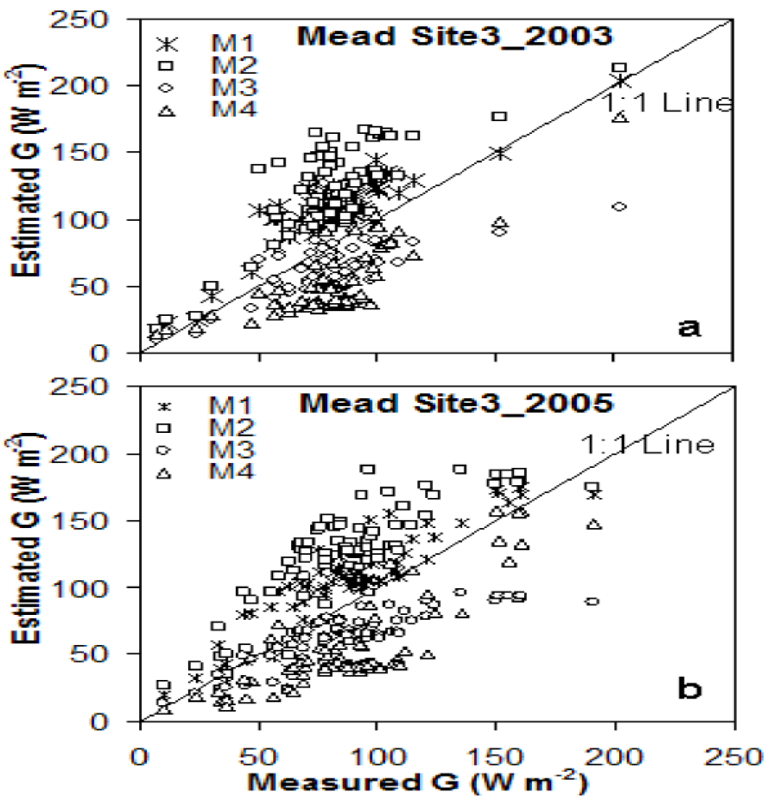

Figure 2. Model comparison for dryland maize at Mead site 3 during (a) 2003 and (b) 2005 for estimation of G using the Kustas and Daughtry (1990) (M1), Bastiaanssen et al. (1998) (M2), Melesse and Nangia (2005) (M3), and Singh et al. (2008) (M4) equations.

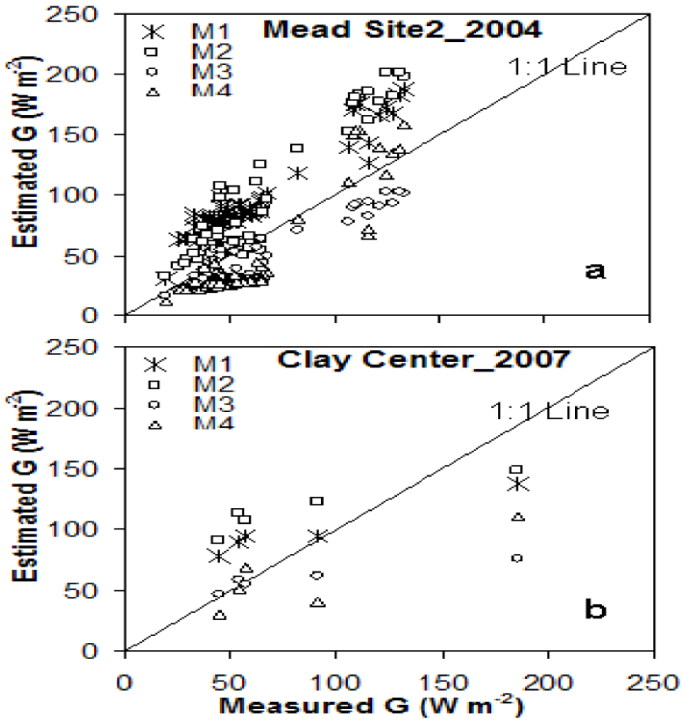

Figure 3. Model comparison for irrigated soybean at (a) Mead site 2 during 2004 and (b) Clay Center site during 2007 for estimation of G using the Kustas and Daughtry (1990) (M1), Bastiaanssen et al. (1998) (M2), Melesse and Nangia (2005) (M3), and Singh et al. (2008) (M4) equations.

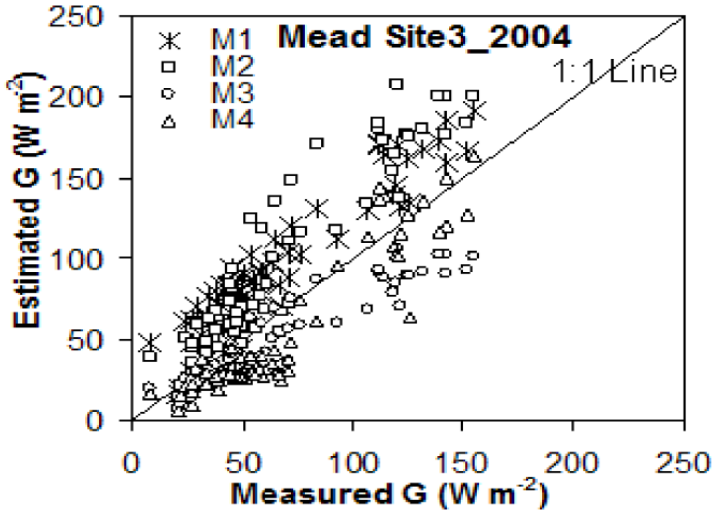

Figure 4. Model comparison for dryland soybean at Mead site 3 during 2004 for estimation of G using the Kustas and Daughtry (1990) (M1), Bastiaanssen et al. (1998) (M2), Melesse and Nangia (2005) (M3), and Singh et al. (2008) (M4) equations.

We observed considerable variations in model performance depending upon site, crop, and irrigation conditions. The differences in the performance of the models (M1-M5) may be attributed to various factors such as soil properties, measurement of G and R_n, band width for NDVI, NDVI measurement, model calibration procedures, and tillage and residue management

conditions. For example, in the case of Kustas and Daughtry (1990), the soil heat flux plate was buried at a depth of 5 cm. In the study reported in Singh et al. (2008), the soil heat flux plate was placed at a depth of 6 cm. Hence it is possible that the extra storage of the heat flux in the soil above the soil heat flux plate can cause differences in model performance. Meyers and Hollinger (2004) have discussed the impact of storage terms in the surface energy balance of maize and soybean. They showed that these components, taken together, can be about 14% for maize and 8% for soybean cropping systems. The NDVI for M1-M4 was calculated based on band widths similar to the Landsat satellite. In the present study, NDVI was calculated at the Mead sites based on band widths similar to MODIS and at Clay Center using Landsat data. Further, M3 and M4 were calibrated with NDVI calculated at the top of the atmosphere. However, in the present study, NDVI was calculated at the top of the surface at the Mead sites. Different methods of tillage and crop residue management can have an impact on G as well. All these differences may be a source for variations in the performance of the models used in this study.

CONCLUSIONS

Soil heat flux estimation is important in energy balance studies. The data collected from maize and soybean fields under irrigated and dryland conditions were used for models performance using different statistical measures. On an average, the soil heat flux was lower in soybean field as compared to heat flux in maize field due to higher NDVI of soybean. Overall, among the four evaluated models, the Melesse and Nangia (2005) model resulted in the best performance. However, in some cases this model also resulted in high RMSE (50.83 W m^{-2} at Clay Center in 2007) and low r^2 (0.57 at Clay Center in 2005). Based on the statistical analysis of the models performance, it can be concluded that local calibrations of soil heat flux models are essential for accurate and reliable soil heat flux estimation.

REFERENCES

Bastiaanssen, W. G. M., Menenti, M., Feddes, R. A., and Holtslag, A. A. M. (1998). "A remote sensing surface energy balance algorithm for land (SEBAL):1. Formulation." *J. Hydrol.,* 212-213, 198-212.

Beringer, J., Chapin, F. S., Thompson, C. C., and McGuire, A. D. (2005). "Surface energy exchanges along a tundra-forest transition and feedbacks to climate." *Agril. Forest Meteorol.,* 131, 143–161.

Chen, J. Q., Falk, M., Euskirchen, E., Paw U, K. T., Suchanek, T. H., Ustin, S. L., Bond, B. J., Brosofske, K. D., Phillips, N., and Bi, R.C. (2002). "Biophysical controls of carbon flows in three successional Douglas-fir stands based on Eddy-covariance measurements." *Tree Physiol.,* 22, 169–177.

Choudhury, B. J. (1989). "Estimating evaporation and carbon assimilation using infrared temperature data." In: Asrar, G. (Eds.), Vistas in modeling, in Theory and Applications of Optical Remote Sensing, Wiley, New York, 628-690.

Clothier, B. E., Clawson, K. L., Pinter, P. J., Moran, M. S., Reginato, R. J., and Jackson, R. D. (1986). "Estimation of soil heat flux from net radiation during the growth of alfalfa." *Agril. Forest Meteorol.,* 37, 319-329.

Heusinkveld, B. G., Jacobs, A. F. G., Holtslag, A. A. M., and Berkowicz, S. M. (2004). "Surface energy balance closure in an arid region: role of soil heat flux." *Agril. Forest Meteorol.,* 122, 21-37.

Irmak, A. and Irmak, S. (2008). "Reference and crop evapotranspiration in south central Nebraska: II Measurement and estimation of actual evapotranspiration for corn." *J. Irrig. Drain. Engr.,* 134(6), 700-715.

Kustas, W. P and Daughtry, C. S. T. (1990). "Estimation of the soil heat flux/net radiation ratio from spectral data." *Agril. Forest Meteorol.,* 49, 205-223.

Kustas, W. P., Prueger, J. H., Hatfield, J. l., Ramalingam, K., and Hipps, L. E. (2000). "Variability in soil heat flux from a mesquite dune site." *Agril. Forest Meteorol.*, 103 (3), 249-264.

Melesse, A. M., and Nangia, V. (2005). "Estimation of spatially distributed surface energy fluxes using remotely-sensed data for agricultural fields." *Hydrological Processes,* 19, 2653-2670.

Meyers, T. P., and Hollinger, S. E. (2004). "An assessment of storage terms in the surface energy balance of maize and soybean." *Agril. Forest Meteorol.,* 125, 105-116.

Murray, T. and Verhoef, A. (2007a). "Moving towards a more mechanistic approach in the determination of soil heat flux from remote measurements I. A universal approach to calculate thermal inertia." *Agril. Forest Meteorol.,* 147, 80-87.

Murray, T. and Verhoef, A. (2007b). "Moving towards a more mechanistic approach in the determination of soil heat flux from remote measurements II. Diurnal shape of soil heat flux." *Agril. Forest Meteorol.,* 147, 88-97.

Oevelen van, P. J. (1991). "Determination of the available energy for evapotranspiration with remote sensing," M. S. Thesis. Agricultural University of Wageningen, 68.

Shao, C., Chen, J., Li, L., Xu, W., Chen, S., Gwen, T., Xu, J., and Zhang, W. (2008). "Spatial variability in soil heat flux at three Inner Mongolia steppe ecosystems." *Agril. Forest Meteorol.,* 148, 1433-1443.

Singh, R. K., Irmak, A., Irmak, S., and Martin, D. L. (2008). "Application of SEBAL model for mapping evapotranspiration and estimating surface energy fluxes in south-central Nebraska." *J. Irrig. Drain. Eng*., 134(3), 273-285.

Stannard, D., Blanford, J., Kustas, W., Nichols, W., Amer, S., Schmugge, T., and Weltz, M. (1994). "Interpretation of surface flux measurements in heterogeneous terrain during the Monsson'90 experiment." *Water Resources Research,* 30, 1227-1239.

Suyker, A. E., Verma, S. B., Burba, G. G., and Arkebauer, T. J. (2005). "Gross primary production and ecosystem respiration of irrigated maize and irrigated soybean during a growing season." *Agril. Forest Meteorol.,* 131, 180-190.

Verhoef, A., vandenHurk, B. J. J. M., Jacobs, A. F. G., and Heusinkveld, B. G. (1996). "Thermal soil properties for vineyard (EFEDA-I) and savanna (HAPEX-Sahel) sites." *Agril. Forest Meteorol.,* 78, 1–18.

Verma, S. B., Dobermann, A., Cassman, K. G., Walters, D. T., Knops, J. M., Arkebauer, T. J., Suyker, A. E., Burba, G. G., Amos, B., Yang, H., Ginting, D., Hubbard, K. G., Gitelson, A. A., and Walter-Shea, E. A. (2005). "Annual carbon dioxide exchange in irrigated and rainfed maize-based agroecosystems." *Agril. Forest Meteorol.,* 131, 77-96.

Wilson, K.B., Goldstein, A., Falge, E., Aubinet, M., Baldocchi, D., Berbigier, P., Bernhofer, C., Ceulemans, R., Dolman, H., Field, C., Grelle, A., Ibrom, A., Law, B. E., Kowalski, A., Meyers, T., Moncrieff, J., Monson, R., Oechel, W., Tenhunen, J., Valentini, R., and Verma, S. (2002). "Energy balance closure at FLUXNET sites." *Agril. Forest Meteorol.,* 113, 223–243.

Application of remote sensing based tillage mapping technique to evaluate water quality impacts of tillage management decisions in Upper White River Basin

Shashank Singh[1], Indrajeet Chaubey[1], and Prasanna H. Gowda[2]

[1]Graduate Research Assistant, Department of Agricultural and Biological Engineering, Purdue University, West Lafayette, IN 47907
[1]Associate Professor, Departments of Agricultural and Biological Engineering, and Earth and Atmospheric Sciences, Purdue University, West Lafayette, IN 47907
[2]Agricultural Engineer, USDA-ARS Conservation and Production Research Laboratory, Bushland, TX 79012

ABSTRACT

Tillage practices directly impact runoff processes, erosion and water quality in agricultural watersheds. Consequently, environment models require tillage information for water quality modeling but often this information is not available at required spatial and temporal scales. Remote sensing approach facilitates tillage mapping at a larger scale than the conventional surveying methods. Models based on remote sensing can classify contrasting tillage practices with accuracy of 80% to 92%. The objectives of this study were to use reflectance based logistic regression models to classify contrasting tillage practices in agricultural watersheds using Landsat imagery. This study is conducted in the Upper White River Basin (7,000 km^2) located in central Indiana, an agricultural watershed with corn-soybean rotation. A single tillage practice can have different level of impact at different slope classes within the watershed therefore; the tillage system information is coupled with the slope classes within a watershed using geographic information system (GIS). This can identify the optimum slope class for a tillage system for minimum sediment loss. The tillage data derived are input in the Soil and Water Assessment Tool (SWAT) model to evaluate the distribution of tillage practices and their impacts on runoff, sediment, and pollutant losses.

INTRODUCTION

Tillage information is crucial in environmental and watershed modeling as it has a direct impact on soil and water quality but often this information are not available at required spatial and temporal scales. Remote sensing approach facilitates tillage mapping at a larger scale than the conventional surveying methods. The conventional method of crop residue cover and tillage practices assessment is done from roadside surveys in selected counties of the U.S. The survey is not done every year for each county and therefore leads into data inconsistency. Also, manual data collection from roadside surveys is often time-consuming, labor-intensive and costly. There is no program that can objectively monitor tillage over broad areas. Remote sensing can be an effective tool in differentiating contrasting tillage practices over a large spatial area in a time- and cost-effective manner.

Models based on remote sensing can classify contrasting tillage practices with an accuracy of 80% to 92%. Different tillage practices have different level of impact on runoff processes, erosion and water quality in agricultural watersheds. Sediment erosion from agricultural watershed is major pollutant for stream and river impairment. The U.S. Environmental Protection Agency and state agencies working on implementing Total Maximum Daily Loads (TMDLs) to address agricultural non-point source pollution require specific knowledge of prevailing tillage patterns as well as their location for adoption of conservation practices to reduce non-point source pollution. Watershed studies have shown that the adoption of conservation tillage (CT) methods can substantially reduce soil and phosphorus (P) losses compared with conventional tillage methods as they retain at least 30% of the soil surface covered with crop residue after a crop is planted. Conservation tillage includes no till, ridge till, strip till, mulch till and reduced till. The Conservation Technology Information Center (CTIC) has defined CT as any tillage and planting system that has >30% residue cover after planting, reduced tillage (RT) as 15 to 30% residue cover, and intensive tillage as <15% residue cover (CTIC, 2000). Conservation tillage system, or crop residual management, is recognized as a cost-effective means of significantly reducing soil erosion and maintaining productivity.

Logan and Adams (1981) found that conservation tillage practices were effective in reducing sediment and sediment-bound P losses by 89%. Similar results were observed by Angle et al. (1984) in their study on a Manor loam soil in Howard County, Maryland, where total P losses were 8 and 161 g/ha from corn plots with conservation and conventional tillage systems, respectively.

In recent years, numerous spectral models have been developed to measure crop residue cover or identify contrasting tillage practices. They exploit the characteristic shape of the green vegetation spectrum by combining the low reflectance of the visible with the high reflectance of the near infrared to identify and quantify green vegetation (Daughtry, 2004). Many spectral indices had been used to enhance the Landsat Thematic Mapper (TM) signal from crop residues which include Normalized Difference Tillage Index, Simple Vegetation Index (NDTI; STI; van Deventer et al., 1997) and Normalized Difference Index (NDI; McNairn and Protz, 1993). These indices utilize the relative difference in reflectance from soil and vegetative reflectance.

Daughtry et al. (2005) evaluated several spectral indices for crop residue cover using satellite multispectral and hyperspectral data and to categorize soil tillage intensity in agricultural fields. They found weak relationships between Landsat TM indices and crop residue cover. Similar results were reported in Minnesota (Thoma et al. 2004). However, these studies reported higher prediction accuracy when crop residue cover was classified into two categories (>30% and <30%), indicating that Landsat TM indices are useful in identifying contrasting tillage practices.

Van Deventer et al. (1997) developed a set of Landsat TM based probability models for discriminating conservation tillage from conventional tilled fields in Seneca County, northern Ohio. In their study, models using the ratio and the normalized

differences of TM bands 5 and 7 classified 93% of the tillage attributes correctly evaluated with independent data from 15 fields. The objective of this study was to evaluate a set of Landsat TM-based logistic regression models proposed by van Deventer et al. (1997) for their ability to identify tillage management practices.

STUDY AREA

This study is conducted in the Upper White River Basin (UWRB; 7,000 km^2) located in central Indiana, an agricultural watershed with corn-soybean rotation (Table 2). It extends across sixteen (16) counties including significant portions of Hancock, Marion, Hendricks, Johnson, Hamilton, Morgan, Boone, Tipton, Madison, Henry, Delaware, and Randolph Counties, as well as smaller portions of Owen, Monroe, Brown, and Clinton Counties. The city of Indianapolis is located in Marion County. Typical planting dates for major crops (Corn and Soybean) in the Indiana vary from May5 – May 20 for Corn to May 15 – June 5 for Soybean (NASS, 1997).

Annual average precipitation is about 1040.13 mm and 942 mm for Marion and Hamilton counties, respectively in UWRB. The dominant soil in UWRB is mainly Crosby-Treaty-Miami (headwaters areas) and Miami-Crosby-Treaty (downstream areas). These two soil type cover about 78% of the UWRB soil type. The most common conventional tillage system in Indiana for Corn crop is moldboard plowing.

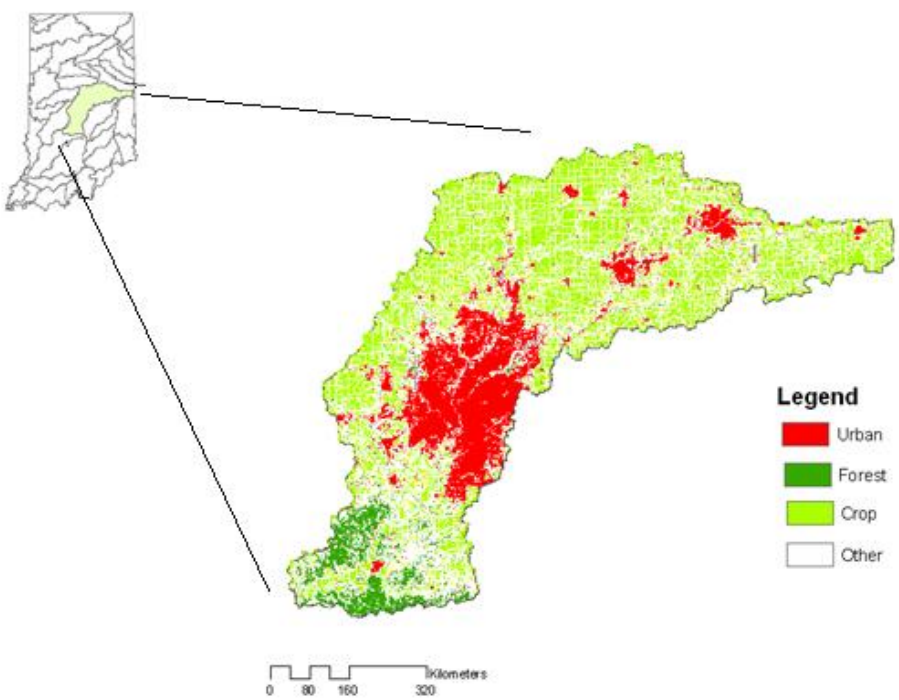

Figure 1 : Upper White River Basin (UWRB) in central Indiana with major land use classes.

MATERIALS AND METHODS

Table 1: Land use classification for Upper White River Basin

Land Use	Area
Agricultural Land	57.1%
Urban	23.9%
forest	14.4%
Water	0.4%
Other	4.1%

Developing and evaluating the tillage models consisted of four steps: (1) groundtruth data collection, (2) remote sensing data acquisition, (3) development of models using the linear logistic regression modeling technique, and (4) evaluation of models. Two Landsat TM scenes were acquired, one on 8th May 2003 for UWRB area (Path 21/Row 31-32) and the other on 25th July 2003 (Path 21/Row 31-32), for developing and evaluating Landsat TM-based tillage models. First image 8th May 2003 is during the time 70% of tillage was been done at central Indiana to prepare tillage classification maps (NASS, 2003) and the second image 25th July 2003 is during the crop growing season to classify land use (agricultural and non-agricultural land) in UWRB. Six TM based logistic regression models proposed by van Deventer et al. (1997) were used to identify contrasting tillage practices (Table 2). The Landsat TM-based logistic regression models (SAS, 1990) used in this study has the form:

$$\text{Logit}(\text{p}) = \ln\left(\frac{\text{p}}{1-\text{p}}\right) = \alpha + \beta\text{X} \quad (1)$$

$$p = \frac{e^{logit(p)}}{1+e^{logit(p)}} \quad (2)$$

Tillage practices were assigned a class value of 0 for conventional tillage and 1 for conservation tillage. In this study, the p in equation (1) is the conservation tillage probability. Therefore, the ideal p values for 100% conventional and 100% conservation tillage are 0 and 1, respectively. Logistic regression models require users to specify a cut-off response probability to classify the outcome of an event occurring. The p values below the cut-off value were classed as conservational tillage whereas values above cut-off value were classed as conservational tillage. Tillage classification was based on the percentage of the soil surface covered with crop residue. We defined conservation tillage systems as those that retained at least 30% of the soil surface covered with crop residue after a crop is planted.

Table 2 : Landsat TM-based logistic regression models proposed by van Deventer et al. (1997).

Model	Band	Intercept	Slope	Cut-off Tillage Probability
I	TM5	10.215	-0.072	0.62
II	R15	-19.404	29.949	0.56
III	M15	8.785	40.947	0.56
IV	D35	10.931	0.135	0.44
V	STI	45.218	-23.998	0.64
VI	NDTI	30.464	-99.483	0.62

Six logistic regression models were used with different values for abscissa in Eq. (1). Model I was derived from TM band 5. Model II was based on the ratio of TM bands 1 and 5 (R15). Model III was based on the normalized difference between TM bands 3 and 5 (M15). Model IV was based on the difference between TM bands 3 and 5 (D35). Model V was based on the ratio of TM bands 5 and 7 (Simple Tillage Index - STI). Model VI was based on the normalized difference between TM bands 5 and 7 (Normalized Difference Tillage Index - NDTI).

Tillage probability values (p) for each pixel in the TM image was calculated using model-builder module in ERDAS imagine, image processing software for 8th May 2003 image. The second image acquired on 25th July 2003 was used to classify land use class into agricultural and non- agricultural using ArcGIS software.

RESULTS AND DISCUSSION

Table 3 shows percentage of agricultural land in UWRB (county-wise) under conventional and conservational tillage practices (ISDA, 2004). This data was based on tillage survey conducted by the Indiana State Department of Agriculture (ISDA). Based on this survey data, about 56% of the fields surveyed adopted conventional tillage in the UWRB. The model results for percentage of conservational and conservational tillage in UWRB is shown in Figure 2. The Table 4 shows that model R15 and M15 has closer classification result than other models. The model STI and NDTI did not perform well in present study. This is consistent with results presented in Gowda et al. (2006) to Ochiltree County in the Texas Panhandle where they found that STI and NDTI models performed poor than other models which may be due to fact that TM Bands 5 and 7 are sensitive to organic matter content and soil water conditions. Also, in the same study, they found R15 and M15 models performed better than other models in classifying conservational and conservational tillage practices.

Table 3: Percentage area of Conventional tillage and Conservational tillage in UWRB counties (ISDA, 2004).

Counties UWRB	Conservational Tillage (%)	Conventional Tillage (%)
Randolph	74	26
Delaware	78	22
Hendricks	60	41
Hamilton	40	61
Morgan	33	68
Madison	19	81
Johnson	49	51
Henry	52	48
Tipton	4	95
Hancock	30	70
Average	**43.9**	**56.3**

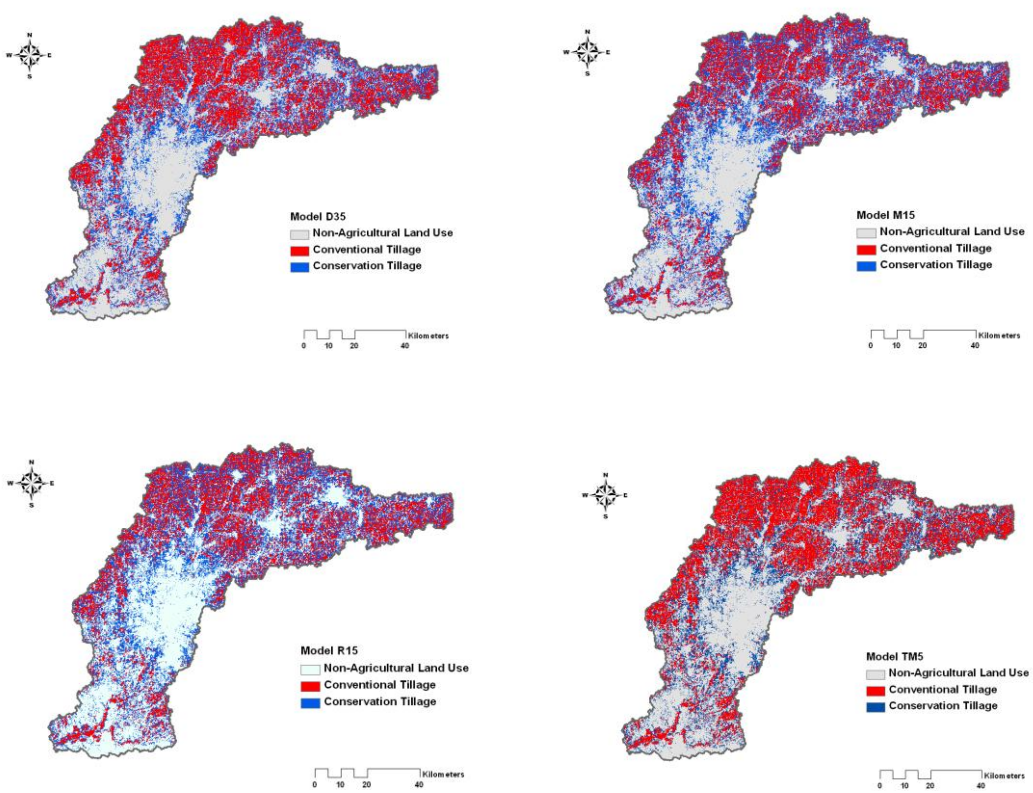

Figure 2 : Conventional tillage and Conservational tillage classification in UWRB obtained from logistic regression models D35 = Band 3 - Band 5, M15 = (Band 1 - Band 5) / (Band 1 + Band 5), R15 = (Band 1 / Band 5) and TM5.

Table 4: Percentage area of Conventional tillage and Conservational tillage in UWRB obtained from logistic regression models.

Model	Conservational Tillage (%)	Conventional Tillage (%)	Error Conventional Tillage (%)
TM5	59.5	40.4	15.8
R15	46.4	53.6	2.7
M15	45.8	54.2	2.1
D35	53.8	46.2	10.1

CONCLUSIONS

Tillage information is crucial in environmental and watershed modeling as it has a direct impact on soil erosion. A remote sensing approach is promising for the rapid collection of tillage information on individual fields over large areas. In this study, six Thematic Mapper (TM) - based logistic regression models proposed by van Deventer et al (1997) were used to distinguish conventional and conservation tillage practices in the UWRB located in central Indiana. Logistic regression models were easy to use, cost and time effective, and produced reasonably accurate tillage maps. The results were compared with county level data available from Indian State Department of Agriculture. This approach is useful in locating contrasting tillage information over large basin which can be applied to water quality models Soil and water Assessment Tool (SWAT) for more precise study for nonpoint source pollution from agricultural watersheds.

REFERENCES

Angle, J.S., Mcclung, G., Mcintosh, M.S., Thomas, P.M. and Wolf, D.C., (1984). *Nutrient losses in runoff from conventional and no-till corn watersheds.* Journal of Environmental Quality, 13, pp. 431–435.

CTIC, (2004). National Survey of Conservation Tillage Practices. Conservation technology Information Center, West Lafayette, IN., http://www.ctic.purdue.edu/CTIC/CRM.

Daughtry, C. S. T., Hunt, E. R., Jr., & McMurtrey, J. E., III (2004). *Assessing crop residue cover using shortwave infrared reflectance.* Remote Sensing of Environment, 90, 126−134.

Daughtry, C.S.T., Hunt Jr., E.R., Doraiswamy, P.C., McMurtrey III, J.E.,(2005). *Remote sensing the spatial distribution of crop residues*. Agron. J. 97, 864–871.

ISDA, (2008). *Conservation Tillage Program*. http://www.in.gov/isda/2354.htm#

Gowda P. H., Peters, R. T. Howell, T. A., (2006). *Mapping Contrasting Tillage Practices in the Texas Panhandle with Landsat Thematic Mapper (TM) Data*, ASCE Conf. Proc. 200, 298

Logan, T.J. and Adams, J.R., (1981). *The Effects of Conservation Tillage on Phosphate Transport from Agricultural Land, Corps of Engineers' Technical Report Series*. LakeErie Wastewater Management Study, Buffalo, NY, Bethesda: ASPRS.

Mcnairn, H., Boisvert, J.B., Major, D.J., Gwyn, Q.H.J., Brown, R.J. and Smith, A.M.,(1996). *Identification of agricultural tillage practices from C-band radar backscatter*. Canadian Journal of Remote Sensing, 22, pp. 154–162.

NASS, 2003. *Weekly Weather and Crop Bulletin*. http://usda.mannlib.cornell.edu/MannUsda/

SAS, (2005). *Categorical Data Analysis Using Logistic Regression Course Notes*, Book Code 60712 (Cary, NC: SAS Institute Inc.).

Van Deventer, A.P., Ward, A.D., Gowda, P.H. and Lyon, J.G., (1997). *Using Thematic Mapper data to identify contrasting soil plains and tillage practices.* Photogrammetric Engineering and Remote Sensing, 63, pp. 87–93.

Automated Selection of Anchor Pixels for Landsat based Evapotranspiration Estimation

J. H. Kjaersgaard (member)[1], R. G. Allen (member)[2], M. Garcia[3], W. Kramber[4], R. Trezza[5]

[1]University of Idaho, Kimberly Research and Extension Center, 3792 N 3600 E, Kimberly, ID 83341; PH (208) 423 6672; email: jeppek@kimberly.uidaho.edu
[2]University of Idaho, Kimberly Research and Extension Center, 3792 N 3600 E, Kimberly, ID 83341; PH (208) 423 6601; email: rallen@kimberly.uidaho.edu
[3]Universidad Mayor de San Andres, Heroes del Acre N[0] 1850, La Paz, Bolivia; email: magalygc1@yahoo.es
[4]Idaho Department of Water Resources, 322 E. Front St., Boise 83720; PH (208) 287 4800; email: bill.bramber@idwr.idaho.gov
[5]University of Idaho, Kimberly Research and Extension Center, 3792 N 3600 E, Kimberly, ID 83341; PH (208) 423 6640; email: rtrezza@kimberly.uidaho.edu

ABSTRACT

When managing local and regional water resources, the estimation of evapotranspiration is important and has generally been one of the components of the hydrological cycle that has the greatest uncertainty. With the development of suitable models and algorithms applied to high resolution (30 m) satellite imagery, evapotranspiration may be estimated with greater accuracy, and in a cost effective and time efficient manner. The METRIC image processing procedure calculates net radiation, soil heat flux and sensible heat flux through a number of steps before estimating evapotranspiration as the residual from the energy balance.
Sensible heat flux is calibrated using the so-called “cold” and “hot” anchor pixels. These pixels are selected by the user, which may introduce some operator dependency or human errors on the estimation of sensible heat flux and subsequently error in the final map of evapotranspiration. A procedure for automated selection of the anchor pixels is presented. The automated pixel selection procedure will reduce the user dependency of the estimations of sensible heat flux. Additionally, it may allow more novice users to obtain good results when applying METRIC.

INTRODUCTION

Application of remote sensing algorithms solving the energy balance using high resolution satellite imagery has proven useful for establishing estimates of actual evapotranspiration, ET_a and crop coefficients, K_c for large populations of fields and water users (Allen et al., 2007a). The METRIC model was developed for application with Landsat imagery to achieve high ET product resolution (30 m). This

resolution allows calculation of populations of ET within individual fields and along relatively narrow riparian systems along streams for the entire approximately 185 by 185 km Landsat scene.

The METRIC model (Mapping Evapotranspiration at high Resolution with Internalized Calibration) is a satellite image processing model which estimates ET as the residual of the energy balance (Tasumi et al., 2005, Allen et al., 2007b), Eq. 1,

$$LE = R_n - G - H \qquad (1)$$

where LE is latent heat flux density, R_n is net radiation, G is soil heat flux density and H is sensible heat flux density. In METRIC, R_n is calculated by solving the radiation balance as described by Allen et al. (2007b). Soil heat flux is estimated based on R_n, surface temperature and the Normalized Difference Vegetation Index ((NDVI).

Sensible heat flux is the rate of heat loss from the surface to the air due to a temperature difference. H is estimated in METRIC using a one-dimensional, aerodynamic, temperature gradient based equation for heat transport, Eq. 2,

$$H = \frac{\rho c_p dT}{r_{ah}} \qquad (2)$$

where ρ is air density (kg/m^3), c_p is air specific heat (J/kg/K), dT (K) is the temperature difference between two heights (z_1 and z_2) floating above the surface, and r_{ah} is the aerodynamic resistance to heat transport (s/m) between z_1 and z_2. METRIC utilizes the *CIMEC* (calibration using inverse modeling of extreme conditions) procedure (Bastiaanssen, 1995, Bastiaanssen et al., 1998) to calibrate the dT function. The *CIMEC* process is applied by inverting Eq. 2 for dT after solving Eq. 1 for H for two extreme conditions representing nearly full LE and nearly zero LE within the image. LE for the full LE condition is estimated using the ASCE-EWRI standardized alfalfa-based reference ET, ET_r, method (ASCE-EWRI, 2005) calculated using quality controlled hourly weather data (Allen, 1996, ASCE-EWRI, 2005). The weather station providing the weather data should preferably be located towards the center of the image or study area. LE for the low LE condition is estimated using a daily soil water balance evaporation model accounting for residual evaporation from antecedent precipitation events. Simulation results from the soil water balance model can be found in e.g. Kjaersgaard et al. (2008) and Allen et al. (2008). The dT for each remaining pixel in the Landsat scene is estimated as an indexed value based on a regression relationship between dT and the radiometric surface temperature from the satellite, T_s at two extreme conditions within the scene, Eq. 3,

$$dT = aT_{s\_dem} + b \qquad (3)$$

where a and b are calibration coefficients. T_s is lapse corrected to a common arbitrary elevation datum using a specified lapse rate. This correction adjusts for change in T_s caused by warming or cooling of air masses with elevation rather than change in evaporation and surface energy balance. The linearity of the dT vs T_s function is a major assumption of METRIC. Research by Bastiaanssen (1995) and comparisons of final ET estimates over a range of dT values (Tasumi et al., 2005, Allen et al., 2007b), indicate that this assumption fits a wide range of conditions.

Agricultural areas are generally selected for the extreme condition calibration because of their importance in water consumption and management. Also, the vegetation in intensively managed agricultural systems is normally more uniform at the 30 m scale compared to natural systems. For each satellite image the extremes are identified by the user through selection of two "anchor" pixels. The anchor pixels ideally represent the conditions of an agricultural field with full and actively transpiring vegetation, and a bare agricultural field with no vegetation cover and with little or no residual evaporation from the soil. The anchor pixel representing full vegetation cover has the characteristics of green vegetation and its dT is low due to evaporative cooling. This condition is often referred to as the "cold" condition. The anchor pixel representing a bare field has the characteristics of a bare soil and its dT is high due to radiometric heating of the surface. This condition is often referred to as the "hot" condition.

The use of ET_r in the estimation of LE at the cold anchor pixel is generally effective in "tying down" the energy balance calibration, especially in arid and semiarid climates having advection. Going through the extra efforts in selecting representative anchor pixels in METRIC may improve the accuracy of the resulting ET maps compared to other single source satellite based ET estimation methods (Allen et al., 2007b). It comes at a cost, however, as selecting representative anchor pixels is a time consuming and usually iterative process which requires an experienced operator. The anchor pixel selection process may also introduce some operator dependency or human errors on the estimation of sensible heat flux and subsequently the final map of evapotranspiration. An automated selection of the anchor pixels will greatly reduce the user dependency of the estimations of sensible heat flux, and allow more novice users to obtain good results when applying METRIC.

In this paper a procedure based on simple statistical procedures for automated selection of cold and hot anchor pixels to aid the user is presented. The set-up of the method in ERDAS Imagine Spatial Modeler is described as the procedure may be integrated with the METRIC model code. The procedure identifies a number of anchor pixel candidates from which the user can select which ones to use. A color coding directs the user towards more preferred pixels. Results from applications in Montana at different times during the growing season show the method identifies anchor pixels that compare relatively well to pixels selected independently by an experienced user.

METHODS

A statistical procedure to select the cold and hot anchor pixels was developed by Allen and Kelly (2004, unpublished). The method was tested by Burnett (2007) and Trezza (unpublished). The approach has been further refined in the current application. A summary of the statistical procedures is shown in Table 1.

Table 1. Summary of the statistical procedure for automated cold and hot anchor pixel selection

Anchor pixel	Step no	Procedure
Cold	1	Select the top 5 % NDVI pixels within a predefined and filtered Area of Interest (AOI).
	2	From the group in (1), calculate the average temperature among the coldest 20 % of T_s.
	3	Cold pixel candidates are pixels that have a T_s within ± 0.2 K of the average T_s from (2) and an albedo within ± 0.02 of Eq. 4.
	4	One pixel is selected from the group in 3) based on the homogeneity among its neighboring pixels.
Hot	1	Select the lowest 10 % NDVI pixels within a predefined and filtered Area of Interest (AOI).
	2	From the group in (1) calculate the average temperature among the hottest 20 % T_s. The average temperature is adjusted using Eq. 5.
	3	One pixel is selected from the group in (2) that has a T_s ± 0.2 K of the average T_s and has high homogeneity among neighboring pixels.

In addition to the criteria listed in Table 1, the anchor pixels should generally be:

- Located within 20 – 30 km of the weather station
- Located towards the center portion of an agricultural field with a homogenous surface
- Located on non-sloping terrain

The procedure to isolate reasonable cold and hot anchor pixel candidates is described below. From the resulting population of suitable cold and hot anchor pixel candidates, one cold and one hot pixel is selected by the user, and all attributes of the selected pixels are used during calibration of H.

Preprocessing. The first step is to delineate a cloud free Area of Interest (AOI) that lies completely within an irrigated agricultural project area. The hot and cold anchor pixels are found within this AOI and its outline should be relatively close to the weather station (generally, the cold and hot anchor pixels should be located within 20 – 30 km from the weather station). The AOI should be large enough to include a wide distribution of bare and vegetated fields (e.g. 10 by 10 km), and exclude significant areas of non-agricultural areas such as desert, forest, lakes, steep slopes or cities. In

desert areas it is important not to include large inclusions of non-irrigated land as this will bias the estimates. The AOI is a contiguous area that does include roads, farmsteads, etc. An example of an AOI is shown in Figure 1. Burnett (2007) discussed the relative importance of the outline of the AOI.

Step A: Identify homogenous fields. The 30 m pixels are grouped into clumps based on the DNs in band 6. The size of the clumps is defined by the user. Clumps are groups of contiguous pixels with the same value and are also called patches or raster polygons. The Coefficient of Variation (CV) within each clump is calculated by dividing the standard deviation by the mean of NDVI for each clump.The CV is used to determine whether the surface contained within the clump is relatively homogenous, and therefore, are pixel candidates from where the cold or hot anchor pixel can be selected.

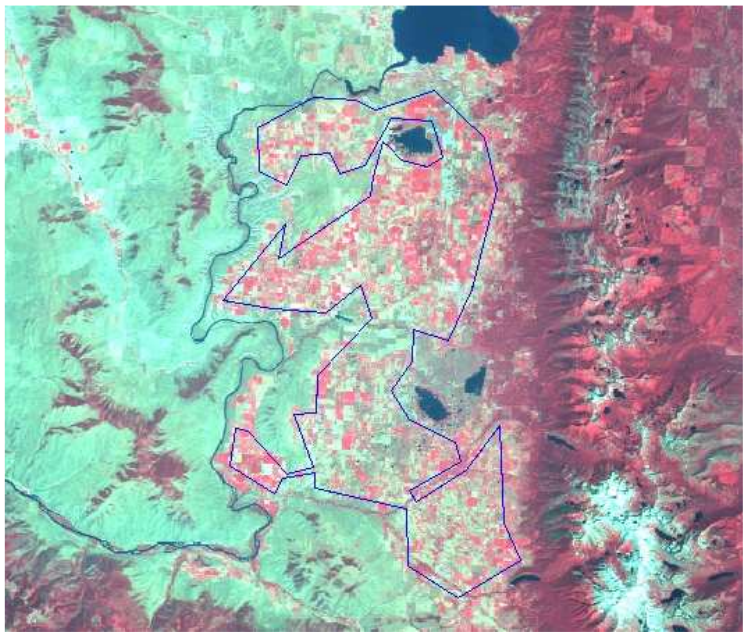

Figure 1. Example of the outline of an Area of Interest (blue line) delineating the area used for locating possible cold and hot pixel candidates.

If the CV of a particular clump is greater than a threshold value, it can be assumed that there is too much variation in NDVI within the clump and those pixels are rejected. A high CV may be due to the clump being located near e.g. a field edge, along a road, on top of a farmstead or in an area with a large spatial variation in the surface cover. In this application 240 m clumps and a CV threshold of 15 % were used to select clumps for sampling in steps B and C.

Step B: Cold pixel identification. From the subsample of homogenous pixels from Step A, the population of 30 m pixels having the top 5 % of NDVI is identified. From this 5 % subpopulation, the pixels that have a T_s in the bottom 20 % of the T_s are selected. This selection results in a pixel population of 1 % of the original sampled

and filtered (for homogeneity) population. This 1 % will have nearly the highest NDVI and the coolest T_s. From this 1 % population, the average T_s is calculated. Cold pixel candidates are selected among the pixels that meet all the following requirements:

- Lie in the interior of a homogenous field,
- Have a value of T_s that is within ± 0.2 K of the statistically identified average T_s
- Have an albedo that is within ± 0.02 of the albedo threshold calculated using Eq. 4,

$$\alpha = 0.001343\beta + 0.3281\exp(-0.0188\beta) \qquad (4)$$

where α is the albedo threshold, and β is the sun angle (°) above the horizon. Eq. 4 was developed by Dong at al. (1992) and parameterized by Trezza (2007) for Southern Idaho. The purpose of Eq. 4 is to compensate for effects of sun angle on albedo at the time of the image for full cover vegetation.

Step C: Hot pixel identification. From the subsample of homogenous pixels from step A, the population of 30 m pixels having the bottom 10 % of all NDVI is identified. From this 10 % subpopulation, the pixels that have a T_s in the top 20 % of the T_s are selected. This selection results in a pixel population of 2 % of the original sampled and filtered (for homogeneity) population. This 2 % will have nearly the lowest NDVI and nearly the warmest T_s. From this 2 % population, the average T_s is calculated. Burnett (2007) found that this average T_s required a modification for the "relative dryness" of bare soils late in the season. The T_s is modified by adding additional temperature computed as a function of the ratio of precipitation to reference ET the 60 days prior the image date, Eq. 5,

$$T_{fac} = 2.6 - 13\frac{precipitation_{60}}{referenceET_{60}} \qquad (5)$$

where T_{fac} is the adjustment factor and the ratio precipitation/reference ET is calculated for the 60 days prior to the image date. The ratio is limited to ≥ 0. When the ratio precipitation/reference ET is greater than about 0.2, no addition is needed. Eq. 5 was developed by Allen (unpublished) and tested by Burnett (2007) for Southern Idaho.

Hot pixel candidates are selected among the pixels that meet all the following requirements:

- Lie in the interior of a homogenous field and one that has bare soil, i.e. having no mulch or vegetation residue cover that may impact "skin" temperature
- Have a value of T_s that are within ± 0.2 K of the statistically identified average $T_s + T_{fac}$

Step D: Application of a colorization routine. A colorization routine can be implemented to indicate the relative appropriateness of pixels to select as cold and as hot anchor pixel. An example is shown in Fig. 2, where possible anchor pixels

identified by the statistical procedure are shown in non-black, while rejected pixels are black. Green indicates good/preferred pixels, while red indicates pixels that are unusable or pixels that need to be scrutinized before they are selected.

From the resulting population of suitable cold and hot anchor pixel candidates, a single cold and a single hot pixel is selected by the user, and all attributes of the selected pixels are used during calibration of H. Before selecting the anchor pixels, the user needs to review a possible candidate carefully by e.g. locating the pixel on the Landsat scene for a visual check of the pixel and its surroundings. This visual check is done to avoid selecting pixels located in near field edges, roads feedlots, construction areas, forests and similar non-agricultural settings.

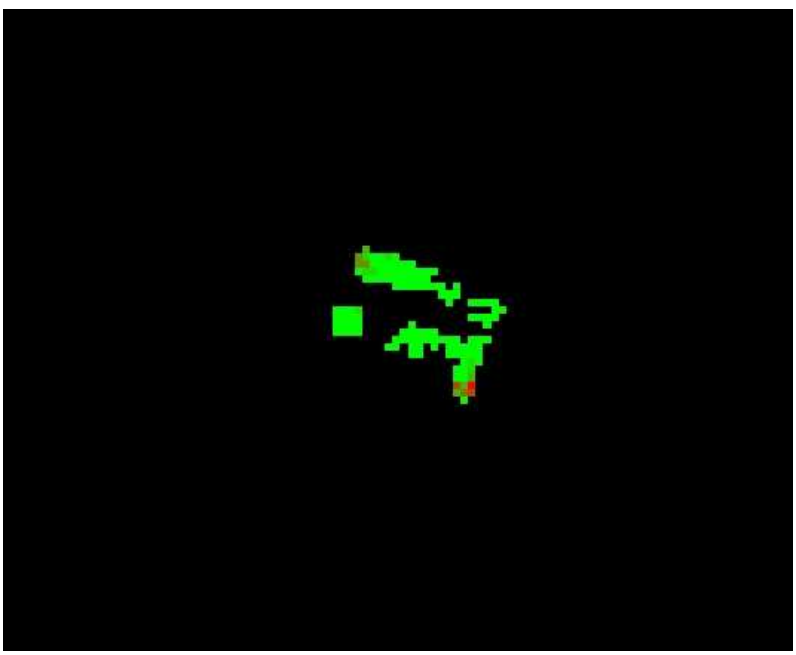

Figure 2. Example of the color scheme used to identify possible anchor pixels. Green indicates good/preferred pixels, while red indicates pixels that are unusable or pixels that need to be scrutinized before they are selected.

The procedures in steps A - D have been implemented into ERDAS Imagine Spatial Modeler as five separate sub-models. The models are summarized in Table 2.

STUDY AREA

The applicability of the automated anchor pixel selection routine was tested using seven Landsat 5 scenes from path 41, row 27, located in NW Montana. The Mission Valley, a basin about 20 km wide and 35 km long dominated by irrigated agriculture and surrounded by mountains, Fig. 1, are located in the center of the image. Weather data quality control and trends for weather data recorded in the basin were described by Kjaersgaard and Allen (2008).

Table 2. Procedures from steps A – D as implemented into ERDAS Imagine Spatial Modeler code.

Model	Input	Output	Description
1	Band 6 from Landsat	Four identical raster maps: Mean, SD, CV and CV15	In model 1 the pixels of the identified AOI are grouped into clumps. Each clump is assigned a unique number, starting from the upper left corner. Before running the model the model window must be set; select Model->Set Window from the menu bar of Spatial Modeler. The subsequent models may abort if the model window is not defined. The dimensions of the "Set Window" can be defined using an inquire box. The area defined in the Window is a rectangle that may include non-agricultural areas and must completely contain the AOI.
2	Maps of NDVI, Mean and SD	Attributes to Mean, SD, CV and CV15	In model 2 the mean, standard deviation and coefficient of variation of NDVI for each clump is calculated and attributed to the rasters created in model 1. A binary map indicating whether the CV in NDVI within each clump is above or below a threshold of 15% is created as the end product.
3	Maps of CV15, NDVI, T_s and albedo. Sun angle is input as scalar	Map of cold pixel candidates (no color)	Candidates for cold anchor pixels are calculated in model 3. The albedo threshold value is calculated using Eq. 4. Prior to processing the window must be set (same as when running model 1) and the AOI created in the preprocessing step invoked.
4	Maps of CV15, NDVI and Ts. T_{fac} is input as scalar	Map of hot pixel candidates (no color)	Candidates for hot anchor pixels are calculated in model 4. The T_{fac} adjustment calculated using Eq. 5 is included in the model. Prior to processing the window must be set (same as when running model 1) and the AOI created in the preprocessing step invoked.
5	Maps of cold and hot pixel candidates (no color)	Maps of cold and hot pixel candidates (in color)	A colorization routine is applied to indicate more or less representative anchor pixel candidates. The user must review these possible candidates and select a pixel located in the interior of a field with relatively homogeneous vegetation.

RESULTS

The typical T_s of the cold anchor pixel suggested by the statistical automated pixel selection system are compared to the T_s of the anchor pixels selected by an experienced METRIC user in Fig. 3. The absolute average deviation is 0.6 K which is slightly lower than the average deviation 0.8 K Burnett (2007) found for 11 images in Southern Idaho. Burnett (2007) estimated the deviation of 0.8 K would result in an error of 1.7 % in the average ET flux for the cold pixel. The good correlation on the first image date, April 13, is promising as there are very few fields at full vegetation cover at this early date.

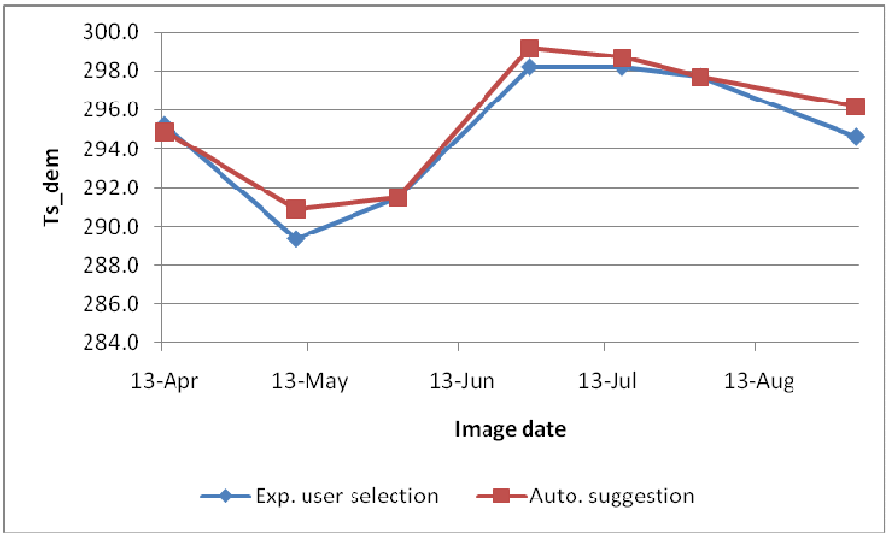

Figure 3. Surface temperature, $T_{s\ dem}$, of the cold anchor pixel selected by an experienced user and that of typical cold pixels candidates selected by the statistical routine.

The typical T_s of the hot anchor pixel suggested by the statistical automated pixel selection system are compared to the T_s of the anchor pixels selected by an experienced METRIC user in Fig. 4. The absolute average deviation is 1.0 K which is lower than the deviation of 2.0 K Burnett (2007) found for 11 images in Southern Idaho. Burnett (2007) estimated the 2.0 K deviation would produce an average error in H around 33 W/m^2 or 7 % of the average ET_r. The ratio of precipitation/reference ET for the 60 days before the image dates was well above 0.2 for all image dates where there is a bias in T_s, so that the $T_{fac} = 0$.

The biggest deviation in T_s between the pixels selected by an experienced user and the automated selection is found for two consecutive image dates in late June and late July. This may, in part, be caused by relatively few fields with no vegetation cover during the middle portion of the growing season. This causes the statistical procedure to include fields that with some vegetation cover, which is relatively colder than bare soil due to evaporative cooling thus biasing the average T_s downward. Further testing will show whether this phenomena is a random error, a systematic error that can be corrected, or is an artifact of an inadequate delineated AOI.

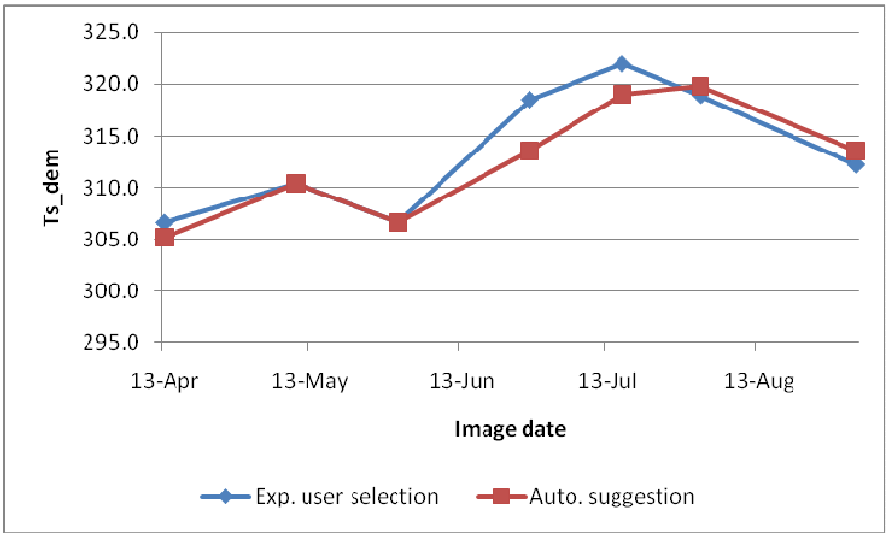

Figure 4. Surface temperature, $T_{s\ dem}$, of the hot anchor pixel selected by an experienced user and that of typical hot pixels candidates selected by the statistical routine.

REFERENCES

Allen, R.G., 1996: Assessing integrity of weather data for reference evapotranspiration estimation. *J. Irrig. Drain. Engr*. 122(2), 97-106.

Allen, R.G., Robison, C., Trezza, R., Garcia, M., Kjaersgaard J.H., 2008. Comparison of Evapotranspiration Images from MODIS and Landsat along the Middle Rio Grande of New Mexico. The 17th William T. Pecora Memorial Remote Sensing Symposium Proceedings, Denver, Colorado. 13 pp.

Allen, R.G., Tasumi, M., Morse, A.T., Trezza, R., Kramber, W., Lorite, I., Robison, C.W., 2007a: Satellite-based energy balance for mapping evapotranspiration with internalized calibration (METRIC) – Applications. *J. Irrig. Drain. Engr*. 133(4), 395-406.

Allen, R.G., Tasumi, M., Trezza, R., 2007b: Satellite-based energy balance for mapping evapotranspiration with internalized calibration (METRIC) – Model. *J. Irrig. Drain. Engr*. 133(4), 380-394.

ASCE-EWRI, 2005: The ASCE Standardized reference evapotranspiration equation. ASCE-EWRI Standardization of Reference Evapotranspiration Task Committee Report. Reston, Virginia. 216 p.

Bastiaanssen, W.G.M., 1995: Regionalization of surface flux densities and moisture indicators in composite terrain: A remote sensing approach under clear skies in Mediterranean climates. PhD. Dissertation, CIP Data Koninklijke Bibliotheek, Den Haag, the Netherlands. 273 p.

Bastiaanssen, W.G.M., Menenti, M., Feddes, R.A., Holtslag, A.M.M., 1998: A remote sensing surface energy balance algorithm for land (SEBAL): 1. Formulation. *J. Hydrology* 212-213, 198-212.

Burnett, B., 2007. A Procedure for Estimating Total Evapotranspiration using Satellite-Based Vegetation Indices with Separate Estimates from Bare Soil. Ms. Thesis, University of Idaho. 175 pp.

Dong, A., Grattan, S.R., Carrol, J.J., Prashar, C.R.K., 1992. Estimation of daytime net radiation over well-water grass. J. Irr. Drain. Engr. 188, 466-479.

Kjaersgaard, J.H., Allen, R.G., 2008. QA/QC of weather data from St. Ignatius, Round Butte and Creston Agrimet weather stations for 2006 – August 2008. Report, University of Idaho. 28 pp.

Kjaersgaard, J.H., Allen, R.G., Aggett, G.R., Schneider, C.A., Hattendorf, M.J., Irmak, A., Hergert, G.W., Robison., C., 2008. Computation of Landsat based Evapotranspiration Maps along the South Platte and North Platte Rivers. World Environmental & Water Resources Congress Proceedings, Honolulu, Hawaii. 10 pp.

Tasumi, M., Trezza, R., Allen, R.G., Wright, J.L., 2005: Operational aspects of satellite-based energy balance models for irrigated crops in the semi-arid U.S. *J. Irrig Drain. Systems*, 19, 355-376.

Trezza, R., 2007. METRIC albedo function. Technical Note, University of Idaho. 2 pp.

Mapping ET at High Resolution in an Advective Semi-Arid Environment with Airborne Multispectral Imagery

J.L. Chávez[1], Ph.D., A.M.ASCE, P.H. Gowda[2], Ph.D. A.M.ASCE, T.A. Howell[2], Ph.D., F. ASCE, L.A. Garcia[1], Ph.D., M.ASCE, and K.S. Copeland[2]

[1]Colorado State University, Department of Civil and Environmental Engineering, 1372 Campus Delivery, Fort Collins, Colorado 80523-1372; Ph: (970) 491-6095; Fax: (970) 491-7727; Email: Jose.Chavez@ColoState.edu, and Luis.Garcia@ColoState.edu

[2]USDA-ARS, Conservation and Production Research Laboratory, P.O. Drawer 10, Bushland, Texas 79012-0010; Ph: (806) 356-5724; Fax (806) 356-5750; prasanna.gowda@ars.usda.gov, terry.howell@ars.usda.gov, and karen.copeland@ars.usda.gov

Abstract

Periodic and accurate estimates of spatially distributed evapotranspiration (ET) are essential for managing water in irrigated regions and in hydrologic modeling. In this study, METRIC (Mapping ET at high Resolutions with Internal Calibration), an energy balance algorithm originally developed for application with Landsat imagery at a regional scale, was applied to very high resolution aircraft imagery (0.5-2 m pixels) in the Texas High Plains. ET predictions were evaluated using data from four large precision weighing lysimeters located in the USDA-ARS Conservation and Production Research Laboratory, Bushland, Texas. Statistical results indicated that METRIC worked better for crops with leaf area index greater than 2.5 m^2 m^{-2}. Potential limitations may have been the areal extent of the imagery, the surface roughness for the momentum transfer sub-model, and the lack of a cold pixel with characteristics similar to the reference crop, i.e. alfalfa.

Introduction

Remote sensing (RS) derived ET maps can potentially be used in the monitoring of spatially distributed crop water use, to schedule irrigations, and as input for hydrologic models. Also, spatially distributed seasonal ET may be used to assess the water use efficiency of irrigation projects. Spatially distributed ET has been estimated using land surface energy balance (EB) models using RS multispectral imagery and ground-based micro-meteorological data. Gowda et al. (2008) and Gowda et al. (2007) present a description and discussion on most of the RS-based EB models available in the literature. Most of these EB models are single source models, e.g. SEBI (Menenti and Choudhury, 1993), SEBAL (Bastiaanssen et al., 1998), SEBS (Su, 2002), METRIC (Allen et al., 2007a), ReSET (Elhaddad and Garcia, 2008).

Of all these algorithms, METRIC may have an advantage under advective conditions. METRIC's ET estimation errors were reported to be approximately 10 to 20% for

daily estimates and as low as 1 to 4% for seasonal ET estimates (Trezza, 2002; Allen et al., 2007b; Chávez et al., 2009) for a semi-arid environment. Therefore, the attributes presented by METRIC make it very attractive for mapping ET in the Southern High Plains (SHP) where advective conditions are regularly encountered. The SHP is a semi-arid region with heterogeneous landscapes in which irrigated fields are surrounded by dryland crops, fallow land, and/or rangeland. Therefore, the advection of hot air from dry surfaces is a significant source of energy that has a major impact on ET from irrigated areas. For example, Tolk et al. (2006) reported an average ET rate of 11.3 mm d^{-1}, measured with a large weighing lysimeter, for irrigated alfalfa in Bushland, Texas, with ET for some days exceeding 15 mm d^{-1} due to regional advection. However, METRIC has not been applied using very high resolution (0.5-2 m pixel) airborne imagery. METRIC was adapted from SEBAL (Surface Energy Balance Algorithm for Land) and was used with satellite imagery, Landsat 5/7, with pixel spatial resolutions in the order of 30-120 m.

In this study, the objectives were: a) to apply METRIC to the advective semi-arid SHP environment, using very high spatial resolution (0.5-2 m pixel) airborne RS imagery and ground-based meteorological data, and b) to evaluate METRIC estimated daily ET values using large precision weighing lysimeters.

Material and Methods

Study Area

This study was conducted at the USDA-ARS Conservation and Production Research Laboratory (CPRL) located in Bushland, Texas. The geographic coordinates of the CPRL are [35º 11' N, 102º 06' W], and its elevation is 1,170 m above mean sea level. Soils in and around Bushland are classified as slowly permeable Pullman clay loam. The major crops in the region are corn, sorghum, winter wheat, and cotton.

Remote Sensing System and Data

The RS system used in this study was the Utah State University (USU) airborne digital multispectral system. The USU RS system acquired high resolution imagery in the visible, near-infrared, and thermal-infrared portions of the electromagnetic spectrum. The USU multispectral system was comprised of three Kodak[1] Megaplus digital frame cameras (Eastman Kodak Company, Rochester, New York) with interference filters centered in the green (Gn) (0.545-0.560 μm), red (R) (0.665-0.680 μm), and near-infrared (NIR) (0.795-0.809 μm) portions of the electromagnetic spectrum. The fourth camera was an Inframetrics 760 (Inframetrics, N. Billerica, MA) thermal-infrared scanner radiometer (8-12 μm) that provides thermal-infrared (TIR) imagery, used to obtain surface radiometric temperature images. The USU airborne digital multispectral system flew at an altitude of about 1,000 m (above

[1] The mention of trade names of commercial products in this article is solely for the purpose of providing specific information and does not imply recommendation or endorsement by the U.S. Department of Agriculture or Colorado State University.

ground level), which resulted in a 0.5 m pixel resolution for the visible and NIR bands and 1.8 m for the TIR band.

Six airborne RS images acquired over the CPRL during the 2007 cropping season, on June 25 (DOY 176), July 3 (DOY 184), July 10 (DOY 191), July 11 (DOY 192), July 26 (DOY 207), and August 11 (233), were used in this study (e.g., Fig. 1). All images were acquired close to 11:30 AM CST, except on DOY 184 in which the image was acquired close to 9:00 AM CST. These images were calibrated and transformed into surface reflectance and temperature images for estimating reflected outgoing shortwave and longwave radiation, respectively, with both components required in the estimation of spatially distributed net radiation.

Radiometric and Atmospheric Calibration of Aircraft Data

The shortwave images were corrected for lens vignetting effects and geometric distortions using procedures similar to those described by Neale and Crowther (1994) and Sundararaman and Neale (1997). The individual R, Gn, and NIR images were registered into three band images and rectified to a digital orthophotoquad base map.

The digital numbers of the rectified multispectral image were converted to radiance using the system calibration method described in Neale and Crowther (1994). These radiances were divided by the incoming solar irradiance to obtain surface spectral reflectance. Solar irradiance in each spectral band was obtained from radiance measurements made concurrently to the flights with an Exotech radiometer placed over a barium sulfate standard reflectance panel with known bidirectional properties (Jackson et al., 1992).

The TIR imagery was rectified to the high-resolution three-band images described above. The digital numbers were transformed into apparent (at sensor or brightness) temperature values using the Inframetrics 760 thermal scanner system calibration bar at the bottom of each image. The surface brightness temperature images were corrected for atmospheric effects considering surface thermal emissivity and using the atmospheric radiative transfer model MODTRAN4 v3 (Berk et al., 2003). These corrections resulted in at-surface radiometric temperatures (T_s).

METRIC Model-based Remote Sensing ET

In METRIC, ET is computed as a residual from the surface EB equation as an instantaneous ET or latent heat flux (LE; Brown and Rosenberg, 1973; and Stone and Horton, 1974), Equation (1).

$$R_n = G + H + LE \tag{1}$$

where R_n is net radiation (W m^{-2}) calculated using T_s, near surface vapor pressure from a near-by weather station (WS), and R_s as explained below. G is soil heat flux (W m^{-2}), and H is sensible heat flux (W m^{-2}). R_n was computed using the following equation:

$$R_n = R_s \downarrow - \alpha R_s \downarrow + R_L \downarrow - R_L \uparrow - (1 - \varepsilon_o) R_L \downarrow \tag{2}$$

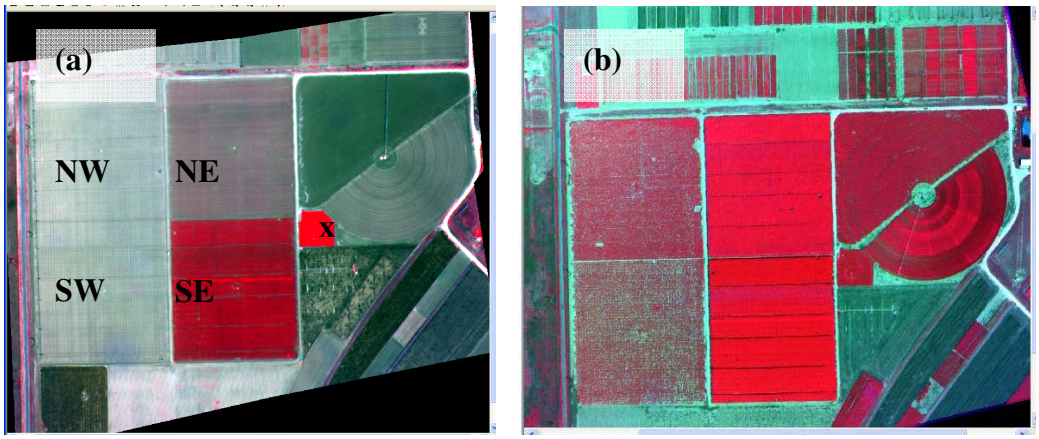

Figure 1. False color (NIR, R, Gn) composite reflectance images for (a) DOY 176 and (b) DOY 223. Lysimeter fields NW, NE, SE, and SW plus the weather station location (x) are shown in image (a) for DOY 176.

where $R_s\downarrow$ is incoming shortwave radiation (W m^{-2}). In this study, $R_s\downarrow$ was not estimated as indicated in Allen et al. (2002, 2007a) but rather measured with a pyranometer (model CMP 6, Kipp and Zonen, Bohemia, NY) installed at the USDA-ARS-CPRL weather station (TXHPET, 2006). Surface albedo, α, was estimated following Brest and Goward (1987). $R_L\downarrow$ is incoming long wave radiation (W m^{-2}) or downward thermal radiation flux originated from the atmosphere, which was estimated using the Stefan-Boltzmann equation and near surface air temperature as well as vapor pressure and sky emissivity. Sky/air/atmospheric thermal emissivity was estimated according to Brutsaert (1975). $R_L\uparrow$ is outgoing long wave radiation (W m^{-2}), a function of T_s and surface thermal emissivity (ε_o, dimensionless). The ε_o term was estimated according to Brunsell and Gillies (2002).

Soil heat flux (G) is a function of R_n, a vegetation index, T_s, and α (Bastiaanssen, 2000):

$$G = ((T_s - 273.15)\,(0.0038+0.0074\,\alpha)\,(1-0.98\,NDVI^4))\,R_n \qquad (3)$$

where NDVI is the Normalized Difference Vegetation Index [(R-NIR)/(R+NIR)], R is reflectance in the red band and NIR is reflectance in the near infrared band.

Sensible heat flux (H) is defined by the bulk aerodynamic resistance equation.

$$H = \rho_a Cp_a \frac{dT}{r_{ah}} \qquad (4)$$

where ρ_a is air density (kg m^{-3}), Cp_a is specific heat of dry air (1004 J kg^{-1} K^{-1}), dT (K) is a function of T_s, ($dT = a + b\,T_s$; Bastiaanssen, 1995) representing a near surface temperature difference between z_1 and z_2, and r_{ah} is aerodynamic resistance (s m^{-1}),

calculated between two near surface heights, z_1 and z_2 (0.1 and 2.0 m) using a wind speed extrapolated from a blending height above the ground surface (200 m) and an iterative stability correction scheme for atmospheric heat transfer based on the Monin-Obhukov stability length scale ($L_{\_MO}$, similarity theory; Foken, 2006).

The determination of *a* and *b* (in dT) involves locating a hot (dry) pixel in a fallow agricultural field with large T_s and a cold (wet) pixel with a small T_s (irrigated field) in the RS image. Then, the EB of Equation (1) can be solved for H_{cold} and H_{hot} as $\boldsymbol{H_{cold} = (R_n - G)_{cold} - LE_{cold}}$, and as $\boldsymbol{H_{hot} = (R_n - G)_{hot} - LE_{hot}}$, respectively. H_{hot} and H_{cold} are the sensible heat fluxes for the hot and cold pixels, respectively. The hot pixel is defined as having $LE_{hot} = 0$, which means that all available energy is partitioned to H. In METRIC, the cold pixel is assumed to have an LE value equal to 1.05 times that expected for a tall reference crop (i.e., alfalfa), thus LE_{cold} is set equal to 1.05 ET_r λ_{LE}, where ET_r is the hourly tall reference ET calculated using the standardized ASCE Penman-Monteith equation (ASCE-EWRI, 2005).

The hot pixel was chosen in a fallow agricultural field displaying high temperatures, high albedo and low biomass (low LAI). Thus, with the calculation of H_{hot} and $H_{cold,}$ Equation (4) was inverted to compute dT_{hot} and dT_{cold}. The *a* and *b* coefficients were then determined by fitting a line through the two pairs of values for dT and T_s from the hot and cold pixels. These *a* and *b* values were initial estimates that were used in an iterative stability correction scheme programmed in a Microsoft Excel™ spreadsheet, which after some iterations shows numerical convergence. The *a* and *b* coefficients for each iteration were then exported to a model in ERDAS IMAGINE® (ERDAS, Inc., Norcross, GA) to obtain the final stability corrected H image.

Instantaneous LE image values were obtained using Equation (1) and were converted to hourly ET (ET_i) in mm h^{-1} by dividing LE by λ_{LE} and ρ_w, as follows:

$$ET_i = 3600\ LE\ /\ \{[2.501 - 0.00236\ (T_s - 273.15)]\ (10^6)\ (1.0)\} \quad (5)$$

Reference ET fraction (ET_rF) is the ratio of ET_i to the alfalfa reference ET (ET_r) that is computed from WS data at overpass time (hourly average). Finally, the computation of daily or 24-h ET (ET_d), for each pixel, was performed as:

$$ET_d = ET_rF \times ET_r24 \quad (6)$$

where ET_r24 is the cumulative 24-h ET_r for the day (mm d^{-1}).

Verification of estimated daily ET values

Estimated daily ET values were verified by comparison with measured ET with four large monolithic weighing lysimeters located at the CPRL. The lysimeters (3×3×2.4 m) were situated in the middle of 4.7-ha fields. In 2007, the lysimeter fields, northeast (NE, Fig. 1) was planted to forage sorghum (planted on May 30), the southeast (SE, Fig. 1) was planted to corn (planted on May 17) both for silage production, the

northwest (NW, Fig. 1) was planted to grain sorghum in rows (planted on June 6), while the southwest (SW, Fig. 1) lysimeter field was planted to grain sorghum (planted on June 6) in clumps as part of another ongoing research project. Furthermore, the NE and SE lysimeter fields were irrigated while the NW and SW lysimeter fields were managed under dryland conditions. Each lysimeter field was equipped with one net radiometer [Q*7.1, Radiation and Energy Balance Systems (REBS), Bellevue, WA] and one infra-red thermometer, (Exergen, Watertown, MA) for measuring R_n and surface temperature, respectively.

Errors between estimated and observed ET values were reported as mean bias errors (MBE) and root mean square errors (RMSE). Besides ET, predicted instantaneous net radiation (R_n) was verified with measured data and differences were reported as MBE and RMSE.

Results and Discussion

Net Radiation Estimation

Remote sensing based R_n compared well with observed R_n as shown in Fig. 2. Net radiation was estimated with a small average under prediction error/bias of -17 W m^{-2} (-2.8%) and a RMSE of 48 W m^{-2} (7.9% of the observed mean); which shows a small error spread. Larger under estimation occurred when observed R_n values were larger than 700 W m^{-2} (Fig. 2). The error perhaps was due, in part, by error in the estimation of surface albedo for large biomass (LAI), closed canopy conditions. Nevertheless, it is an overall small error.

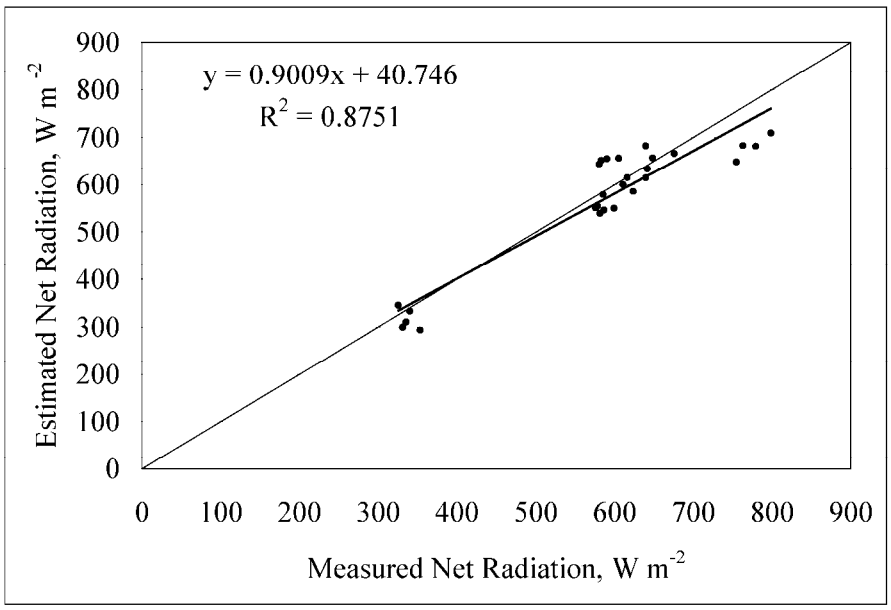

Figure 2. Estimated vs. observed instantaneous net radiation comparison.

Daily ET Estimation

METRIC underestimated daily ET with a MBE of -0.2 mm d^{-1} (-6.9%) and a RMSE of 1.9 mm d^{-1} (-40.1%). Although, Fig. (3) shows that the underestimation occurred on ET values ranging from 2 to 6 mm d^{-1} while an overestimation occurred for measured ET values larger than 6 mm d^{-1}. In part, errors in estimating ET may have been due to errors in locating true hot and cold pixels, i.e. true hot and cold pixels (extreme temperature pixels) may fall outside of the area covered by the aircraft overpasses. The areal extent of the airborne imagery used in this study was approximately 800 m (E-W direction) by 650 m (N-S direction) while a Landsat 5 Thematic Mapper (TM) scene covers an area of 170 km (N-S) by 183 km (E-W).

Errors associated with the selection of the cold pixel in the irrigated grass field of the ARS weather station location could have been another potential source of error. The grass height was kept at about 0.12 m; however, METRIC indicates selecting the cold pixel on a field with crop characteristics (height and LAI) similar to the alfalfa reference crop. This selection was not possible on DOY 176 and 184 because, all other fields covered in the airborne imagery were drier/warmer than the reference WS grass field.

The absolute differences (in %) between estimated and measured ET were plotted versus LAI in Fig. (4). As shown in Fig. (4), most large errors in ET (larger than 40%) occurred at LAI values smaller than 2.5 m^2 m^{-2}. Coincidently, most of these low LAI values showed the largest surface temperature. See Fig. (5). Although, there were some data points showing much cooler temperatures (circle) at low LAI values in Fig. (5). This latter fact may be attributed to an irrigation event (approx. 18 mm, to keep the sorghum alive) on DOY 184 on the NW and SW dryland lysimeter fields, and to a rainfall event on DOY 192 (approx. 15.5 mm) that lowered the temperature of these fields.

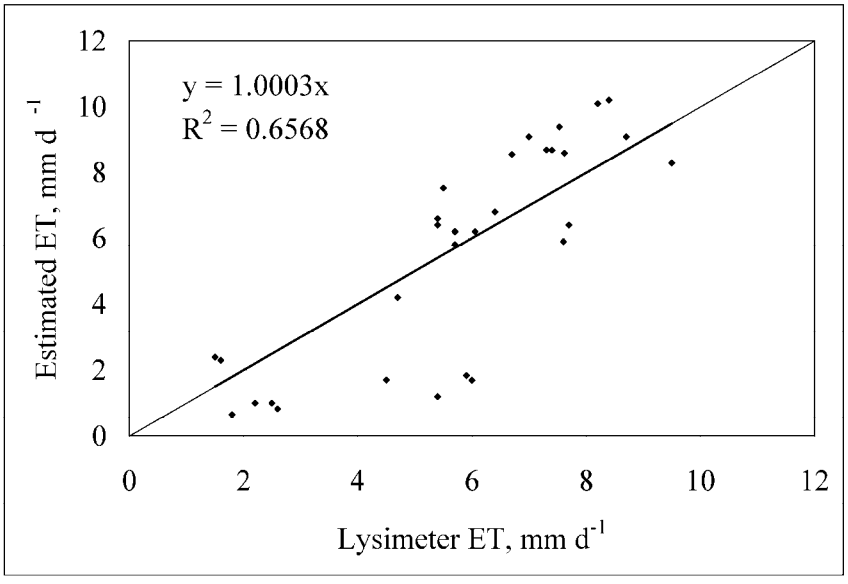

Figure 3. METRIC estimated ET vs. Lysimeter measured ET.

Therefore, the larger ET underestimation (circle in Fig. 4) occurred for LAI values smaller than 2.5 m^2 m^{-2} on DOY 184 and 192 when the sparse sorghum fields were wet. Under these conditions, the estimation of the roughness length for momentum transfer (Z_{om}), friction velocity (u_*), and aerodynamic resistance (r_{ah}) may have been compromised, resulting in errors in the estimation of H_{hot} and hence in ET.

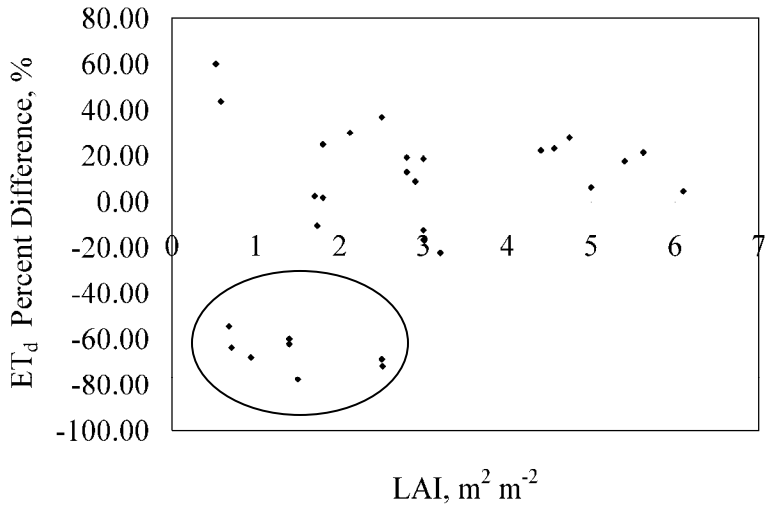

Figure 4. Percent ET error vs. LAI.

METRIC estimated ET with a MBE of 0.6 mm d^{-1} (10.8%) and a RMSE of 1.2 mm d^{-1} (16.5%) when estimated ET values from those fields/crops with LAI smaller than 2.5 m^2 m^{-2} were excluded from the analysis.

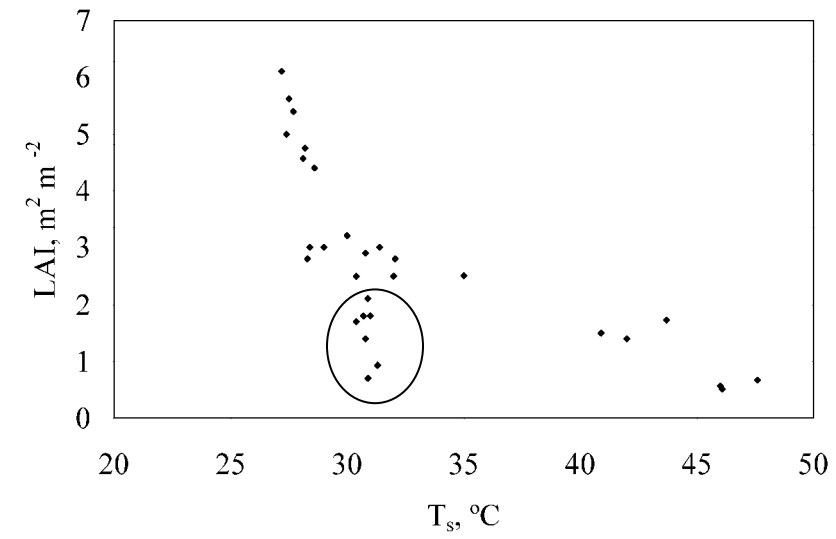

Figure 5. LAI vs. surface temperature (T_s).

Conclusions

METRIC was applied on six airborne RS images acquired over the CPRL during the 2007 cropping season over the semi-arid region of the Southern High Plains. There were large ET underestimation errors for crops with LAI values smaller than 2.5 m^2 m^{-2} under wet surface conditions. Removing ET values under those conditions reduced the error to 10.8±16.5% (an overestimation). It is hypothesized that the roughness length for momentum transfer (Z_{om}), friction velocity (u_*), and aerodynamic resistance (r_{ah}) may have not been well estimated under the conditions described above, resulting in errors in the estimation of H_{hot} and hence in ET. In addition, the areal extent covered by the airborne system may have prevented selecting true extreme cold and hot pixels. Moreover, selecting a cold pixel on a field with crop characteristics different from the alfalfa reference crop may result in a bias scaling of surface temperature in the dT function. Nonetheless, this result is encouraging. It is believed that by improving the Z_{om} sub-model and by enlarging the areal coverage of the airborne RS system, using multiple stitched images (mosaic), it may be possible to further improve the accuracy of ET estimates.

Acknowledgements

This study was possible thanks to funding provided through the Ogallala Aquifer Program. Our sincere appreciation goes to the following individuals who provided assistance: Donald A. Dusek, Kim Bush, and Dr. Christopher M.U. Neale.

References

Allen, R.G., M. Tasumi, and R. Trezza. 2007a. Satellite-based energy balance for mapping evapotranspiration with internalized calibration (METRIC)-model. *ASCE J. of Irrig. and Drain. Eng.* 133(4): 380-394.

Allen, R.G., M. Tasumi, A. Morse, R. Trezza, J.L. Wright, W. Bastiaanssen, W. Kramber, I. Lorite-Torres and C.W. Robison. 2007b. Satellite-based energy balance for mapping evapotranspiration with internalized calibration (METRIC)-Applications *ASCE J. of Irrig. and Drain. Eng.* 133(4): 395 - 406.

Allen, R.G., M. Tasumi, and R. Trezza. 2002. *METRIC^{TM}: mapping evapotranspiration at high resolution – application manual for Landsat satellite imagery*. University of Idaho, Moscow, ID.

ASCE-EWRI. 2005. The ASCE standardized reference evapotranspiration equation. Report by the American Society of Civil Engineers (ASCE) Task Committee on Standardization of Reference Evapotranspiration. Allen, R.G., I.A. Walter, R.L. Elliot, T.A. Howell, D. Itenfisu, M.E. Jensen, and R.L. Snyder (eds.), ASCE, 0-7844-0805-X, 204 pp., Reston, VA.

Bastiaanssen, W.G.M. 1995. Regionalization of surface flux densities and moisture indicators in composite terrain: A remote sensing approach under clear skies in Mediterranean climates. Ph.D. Dissertation, CIP Data Koninklijke Bibliotheek, Den Haag, The Netherlands, 273p.

Bastiaanssen, W.G.M., M. Menenti, R.A. Feddes, and A.A. Holtslang. 1998. A remote sensing surface energy balance algorithm for land (SEBAL): 1. Formulation. *J. of Hydrol.* 212-213:198-212.

Bastiaanssen, W.G.M. 2000. SEBAL-based sensible and latent heat fluxes in the irrigated Gediz Basin, Turkey. *J. of Hydrol.* 229:87-100.

Berk, A., G.P. Anderson, P.K. Acharya, M.L. Hoke, J.H. Chetwynd, L.S. Bernstein, E.P. Shettle, M.W. Matthew, and S.M. Adler-Golden. 2003. MODTRAN4 version 3 revision 1 user's manual. Air Force Research Laboratory, Space Vehicle Directorate, Air Force Materiel Command, Hanscom AFB, MA 01731-300, Hanscom.

Brest, C.L., and S.N. Goward. 1987. Driving surface albedo measurements from narrow band satellite data. *International Journal of Remote Sensing*, 8:351-367

Brown, K.W., and N.J. Rosenberg. 1973. A resistance model to predict evapotranspiration and its application to a sugar beet field. *Agron. J.* 65(3): 341-347.

Brunsell, N.A., and R. Gillies. 2002. Incorporating surface emissivity into a thermal atmospheric correction. *Photogramm. Eng. Remote Sens. J.* 68: 1263-1269.

Brutsaert, W., 1975. On a derivable formula for long-wave radiation from clear skies. Water Resour. Res. 11, 742-744.

Chávez, J.L., P.H. Gowda, T.A. Howell, and K.S. Copeland. 2009. Radiometric surface temperature calibration effects on satellite based evapotranspiration estimation. *Int'l J. of Remote Sens.* Accepted 21 June 2008. In Press.

Elhaddad, A., L.A. Garcia. 2008. Surface energy balance-based model to estimate evapotranspiration taking into account spatial variability in weather. *Journal of Irrigation and Drainage Engineering, ASCE*, 134(6): 681-689.

Foken, T. 2006. 50 Years of the Monin-Obukhov similarity theory. *Boundary-Layer Meteorol*. 119(3): 431-447.

Gowda, P.H., J.L. Chavez, P.D. Colaizzi, S.R. Evett, T.A. Howell, and J.A. Tolk. 2008. ET mapping for agricultural water management: Present status and challenges. *Irrig. Sci.* 26(3):223-237, DOI 10.1007/s00271-007-0088-6.

Gowda, P.H., J.L. Chávez, P.D. Colaizzi, S.R. Evett, T.A. Howell, and J.A. Tolk. 2007. Remote sensing based energy balance algorithms for mapping ET: Current status and future challenges. *Trans. ASABE* 50(5): 1639-1644.

Jackson, R.D., T.R. Clarke, and M.S. Moran. 1992. Bidirectional calibration results of 11 Spectralon and 16 BaSO4 reference reflectance panels. *Remote Sens. of Env*. 40: 231-239.

Menenti, M., and B.J. Choudhury. 1993. Parameterization of land surface evapotranspiration using a location dependent potential evapotranspiration and surface temperature range. In *Proc. Exchange Processes at the Land Surface for a Range of Space and Time Scales*. 561-568, Bolle HJ et al. (eds), IAHS Publ. 212.

Neale, C.M.U., and B. Crowther. 1994. An airborne multispectral video/radiometer remote sensing system: development and calibration. *Remote Sens. of Env.* 49(3): 187-194.

Stone, L.R., and M.L. Horton. 1974. Estimating evapotranspiration using canopy temperatures: Field evaluation. *Agron. J.* 66: 450-454.

Su, Z. 2002. The surface energy balance system (SEBS) for estimation of turbulent heat fluxes. *Hydrol. and Earth Syst. Sci.* 6:85-99.

Sundararaman, S., and C.M.U. Neale. 1997. Geometric calibration of the USU videography system. In *Proc. 16th Biennial Workshop in Videography and Color Photography for Resource Assessment*. American Society of Photogrammetry and Remote Sensing, Bethesda, MD.

Tolk, J.A., S.R. Evett, and T.A. Howell. 2006. Advection influences on evapotranspiration of alfalfa in a semiarid climate. *Agronomy Journal,* 98: 1646 - 1654.

Trezza, R. 2002. Evapotranspiration using a satellite-based surface energy balance with standardized ground control. PhD dissertation, Logan, Utah: Utah State University, Biological and Irrigation Engineering Department.

TXHPET. 2006. Texas High Plains Evapotranspiration Network. Available online at: http://txhighplainset.tamu.edu/index.jsp (accessed 4 September 2006).

Brentwood Stream Restoration Project
Lenexa, Kansas

Anthony Hall, P.E.[1] and Tom A. Jacobs, P.E., Member ASCE [2]

[1] CDM, 9200 Ward Parkway, Suite 500, Kansas City, Missouri 64114; PH (816) 444-8270; e-mail: hallad@cdm.com

[2] City of Lenexa, Kansas, 12350 West 87th Street Parkway, Lenexa, Kansas 66215; PH (913) 477-7680; e-mail: TomAJacobs@ci.lenexa.ks.us

Introduction

The City of Lenexa, Kansas (City) is a growing suburban community located in the Kansas City Metropolitan area. As with many growing communities, the City is regularly faced with various stormwater management challenges, including flooding, erosion, water quality impacts, regulatory requirements, and the ability to finance infrastructure improvements and new programs. To address these challenging issues, the City formed the Rain-to-Recreation Program.

The Rain to Recreation program is a proactive, integrated, watershed based approach to address stormwater quantity and quality. The goals of the program are to reduce flooding, protect water quality and natural habitat, and provide recreational and education opportunities. With the implementation of new development regulations, the City has created greenways and trails while protecting the environment and preserving wildlife. The long-term success of the program relies upon the support of individuals and businesses throughout the community. As such, the City builds community support through environmental education, and working together with local residents. Working together with the community, the program enhances the quality of the natural and built environments, ultimately conserving and even restoring our natural resources.

One of the recent challenges addressed by the City involves the flooding and severe erosion problems along the Brentwood stream, which is located in a fully urbanized residential watershed. The following paragraphs describe the project background and challenges associated with this stream reach.

Project Background

The Brentwood stream reach of Little Mill Creek, like many urban streams, has been a constant source of frustration over the past 20 years with severe bank erosion as well as home and street flooding. The stream reach extends from Brentwood to 87th Street, which migrates between the backyards of approximately 60 residential property owners. As development occurred in the watershed, the stream changed dramatically due to increased stormwater runoff volumes and velocities. This in turn caused street and home flooding along the stream, as well as streambank stability problems that adversely impacted the existing retaining walls, public utilities, and residential property.

The channel is bordered by mature trees, homeowner fences, and landscape features, located along the edge of the streambank. And this lack of open space along the channel for improvements and the desire to minimize property owner impacts was a major challenge during the design process. In addition, a limited number of existing easements exist along the channel, which required easement negotiations with nearly all of the local residents that live along the channel.

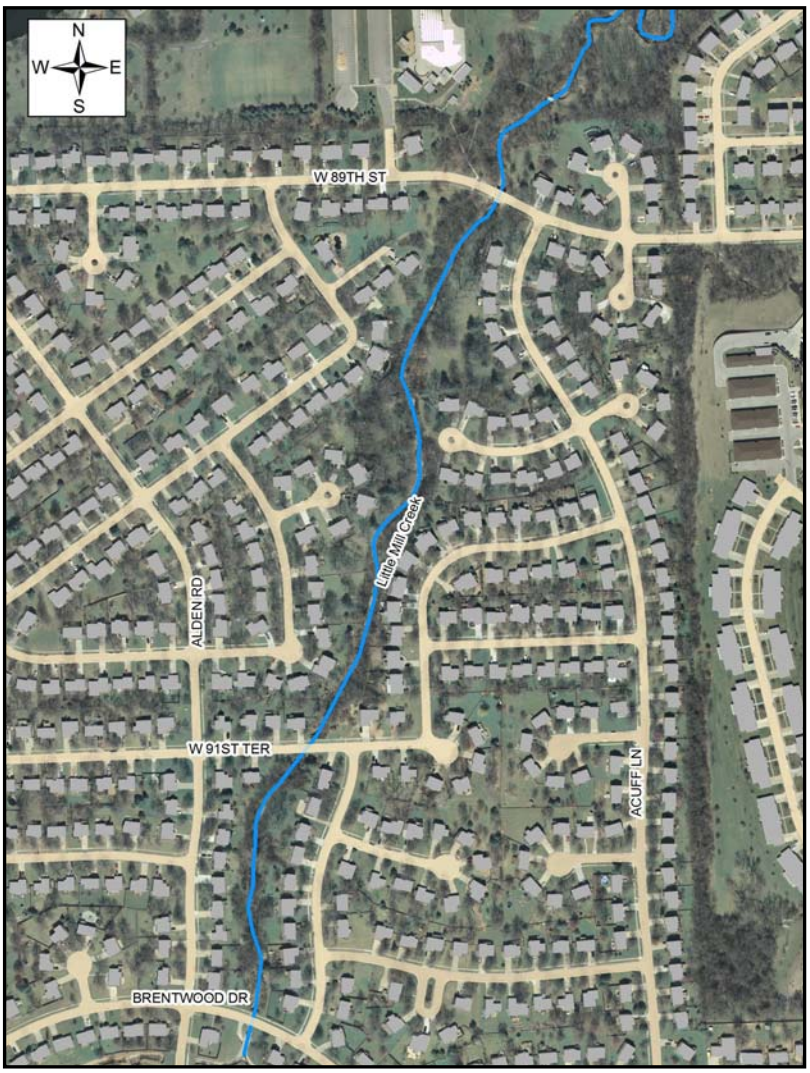

Project Location

The City's Rain to Recreation program partnered with the Johnson County Stormwater Management Program to correct the problems along the stream. The agencies retained Camp Dresser & McKee Inc. (CDM) to lead the design team and serve as the prime contractor using a design-build approach. CDM was responsible for the overall technical direction of the project, channel design, roadway improvements, and utility relocation components. Other design partners included Intuition & Logic which provided geomorphology technical support, and Patti Banks Associates, who assisted with the landscape plan and stakeholder involvement activities.

Project Goals and Objectives

The goals of the project were to improve safety, protect citizen's homes and property from flooding, reduce street flooding impacts, protect public utilities and property from damage due to erosion, and restore the stream as a neighborhood amenity. To achieve these goals, the following objectives were considered key components of the project:

- Select durable streambank protection materials to provide a long-term solution to the erosion problems
- Integrate natural features to enhance the aquatic and terrestrial habitat along the stream corridor
- Implement a comprehensive stakeholder involvement process to provide regular communication throughout the entire project

- Restore the stream back to neighborhood amenity

Major Design Elements

The following is brief discussion on the three major design elements of the project, including the streambank protection, in-stream grade controls, and the stream roadway crossings.

Streambank Protection

As result of the urbanization process, severe bank erosion existed along the majority of the channel. Using the HEC-RAS open channel hydraulic model, the Brentwood stream was evaluated in detail to determine the shear stress and velocity for this stream reach under various flow conditions. The results of this evaluation found that this stream segment is a high energy stream, with average velocities of over 5 feet per second (fps) and local peaks of over 10 fps. In addition, shear stress values average over 2 pounds per square foot (lbs/sq-ft) with localized areas of over 4 lbs/sq-ft. Shear stress is a measure of the erosive forces acting on the channel bed and banks and is a function of velocity and depth in the stream.



Examples of Channel Bank

To solve the erosion problem, the design team evaluated a wide range of armoring systems, including both natural and hard material options. The goal was to select a streambank protection system that would provide long-term stream stability, while providing an environmental benefits and aesthetically pleasing. The design team originally evaluated several options for armoring the lower and upper banks of the stream. Each of the armoring options was evaluated based on their shear stress resistance, and allowable stream velocity.

Bank Armoring Systemes Evaluated

- Coir Toe
- Turf Reinforced Mat (TRM)
- Vegetated Rip-Rap
- Composite Revetment
- Rock Gabions

Due to the high velocities and shear stress values, the lower part of the channel (below the 2-year design flow elevation), was designed with a retaining wall system. As part of the design process, several wall systems were considered, including Keystone™, Redi-Rock™, gabion baskets, and stacked limestone. All of the hard solutions were capable of meeting the design criteria, but each had a different appearance and cost. The Keystone™ wall system was eliminated because of the potential for movement during high stream flows without costly soil reinforcement. Upon the completion of an alternative analysis for the remaining options, the project team selected the Redi-rock wall system for the following reasons:

- Minimal long-term maintenance is required because of the size, mass, and durability of the Redi-Rock™ blocks.
- This system is well suited for steep embankments, which was required at a few specific locations
- Given the wide range of options available for face textures and color treatments, the Redi-Rock™ system provided a wall that is visually pleasing.



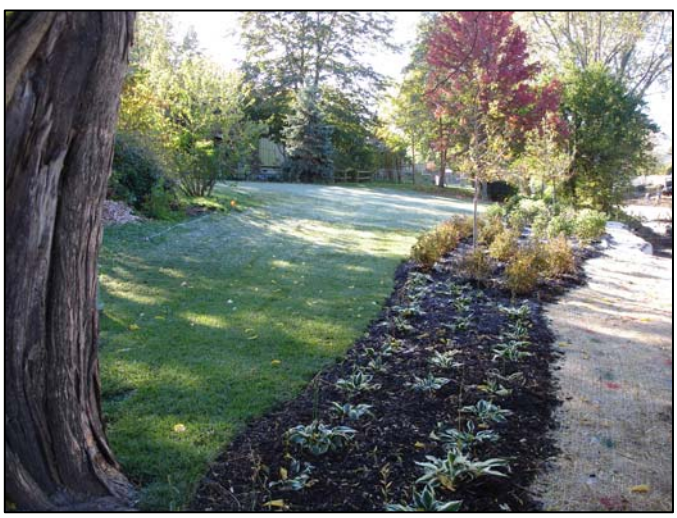

Retaining wall, TRM, and landscape transition

In areas where the shear stresses were not as severe, a TRM application with native plantings was installed.

The upper banks were treated with more green solutions. The upper banks had a landscaping TRM fabric with a dense plant cover that blended into the surrounding landscape. The purpose of the fabric and plant zones was to protect the upper banks from erosion, replace plant material that was removed during construction, and to reintroduce native plants to the stream corridor that have deeper roots to help support the streambank. In addition, the upper bank included a landscape transition zone between the stream corridor and the backyards.

In-stream Grade Controls

Another key component of the design was the integration of in-stream grade controls to properly manage the energy of the stream. With the selection of Redi-Rock™ material as the wall system, the project team utilized this same material to design customized in-stream drop structures. The in-stream drop structures reduce the slope along the stream reach which provides a stable bed slope and dissipates hydraulic energy. In addition, the drop structures are shaped to deflect scouring flows away from the streambank, which allows the channel bed and banks to become more stable over time. Prior to the construction effort the bed slopes ranged from 0.8 to 1.2 percent.



Culvert Improvements

This project also included the replacement of box culverts at three stream road crossings, due to insufficient capacity. The new box culverts were enlarged and redesigned to be a "two stage" culvert, also known as conservation culverts. This culvert configuration matches more closely the stream cross-section; with a low flow channel and higher overbank flow. The lower box is utilized to carry the more frequent storm events, while the box culvert placed at the higher elevation is only utilized during larger storm events.



Grade controls and culvert improvements

One of the benefits of this arrangement is that it reduces the amount of sediment and debris accumulation at the crossing. Each of the three street crossings have a rip-rap "stilling basin" downstream to help reduce energy as water exits the culverts.

Delivery Approach

As the design process was nearing completion, the City decided to utilize a design-build approach to expedite the schedule to complete the project. The Design/CM-at-Risk method was used, which provided the City with multiple additional benefits, including:

- An integrated design/construction team which streamlined coordination efforts between all parties.
- Provided an efficient vehicle for risk management
- Single point of responsibility reduced the City's administrative burden

- Discrete work packages maximized competition and provided lower subcontractor bid pricing
- Subcontractors were selected on both qualifications and price to deliver the best value to the City

By using the Design/CM-at-Risk approach, the overall schedule was reduced by 5 months. The time savings were realized by overlapping initial construction phases with final design, and by eliminating the traditional advertising and bidding process that follows the completion of a traditional design-bid-build approach. In addition, the construction professionals were involved early in the process to identify critical path portions of the project. Also, the constructability reviews focused on ease of construction and sequencing, which further accelerated the schedule and reduced the potential for delays.

Environmental Protection Measures

One of the main drivers for this project was to stabilize the existing channel by reducing the streambank erosion. However, to improve the channel it was necessary to remove existing vegetation and excavate in and around the stream. Therefore, steps were taking during the construction to limit impacts to the environment. Environmental considerations included special steps taken to preserve and protect the environment, wildlife, and habitat during the construction phase.

The biggest environmental challenge was sediment control. Sediment control measures included phasing the construction, maintaining "rock checks" that were inspected and maintained on a nearly daily basis. As areas were completed, the checks were removed or relocated. Streets were also swept in the evening after work activities. The other environmental issue was migratory bird habitat. Construction along the stream required the removal of several trees which had the potential for disturbing the nests of migratory birds. Removal of trees was completed prior to bird migration season which in Kansas was April 1.

Stakeholder Involvement

A comprehensive stakeholder involvement process was used to provide a forum for residents to voice their concerns about the project, and to be actively involved during the study, design and construction process. This required a fully integrated stakeholder involvement process which began during the study phase, and was intertwined throughout the design and construction process, through to the final ribbon cutting ceremony. Other community relation activities that were very important to this project and intertwined with the project are described below.

Neighborhood Meetings

The stakeholder involvement process began with local residents coming together for a series of three public meetings during the study phase. The first meeting was held to listen to the residents concerns and issues, which included:

- Regular flooding of homes, yards, and streets
- Streambank erosion that was impacting private property
- A strong desire for the corridor to remain as natural as possible
- The desire to protect the mature trees, landscape plantings and back yard amenities



The second and third meetings where held to obtain feedback on the proposed design concepts and anticipated project schedule. The messages consistently voiced by residents included the concern over losing their privacy and uniqueness of their backyards, and the preference to use materials that blended with the neighborhood to provide a natural appearance. The results of these three project meetings helped the CDM team understand the neighborhood issues which helped get the design phase off to a fast start.

During the design phase, two additional neighborhoods meetings were held to present the design details and to obtain the required easements necessary to construct the project. With nearly 60 property owners impacted by the project, securing the necessary easements in a timely manner was a major concern of the project team. To overcome this obstacle, easement specialists were present at the neighborhood meetings, to provide one-on-one consultation with the property owners to answer questions, and to review the necessary legal documents. This process proved to be very successful, which resulted in securing the majority of the easements, thus allowing the project to remain on schedule.

Results

The Brentwood Stream Restoration Project resulted in a final product that reduced flooding problems, addressed the severe erosion, integrated natural features to provide environmental benefits, and achieved stakeholder acceptance. As such, the project produced a sustainable solution that met the triple bottom line concept of economics, environmental, and social benefits.

Economics

This channel improvement project needed to meet the City's available budget and schedule. Therefore, the construction materials and delivery methods were evaluated to provide cost effective solutions that could be efficiently delivered. Using a Design/CM-at-Risk delivery method, the construction schedule was reduced by 5-months, while the selected materials matched the design requirements; which resulted in a project that completed under budget.

Environmental

One of the critical goals of this project was to improve the stream, by reducing the erosion of the banks and channel bottom, which would result in significantly improving improve water quality downstream. Using both engineered hard materials combined with green features, the

constructed solution provides a sustainable stream that meets the goals and objectives of the project.

Social

Streams tie neighborhoods together. The City is committed to the Rain to Recreation Program which uses stormwater challenges as an opportunity to enhance neighborhoods. For this project, the Brentwood stream corridor was transformed into a neighborhood amenity, and was fully embraced by the neighborhood. Throughout the project, the community was actively involved which resulted in project ownership. In essence, this was the biggest success of this project. As demonstrated by the enthusiasm during ribbon-cutting ceremony (insert graphic), the entire neighborhood community embraced the success of the project, which demonstrates the power of public and private partnerships working together for a common good.

References

Chang, H. 1998. *Fluvial Processes in River Engineering*. Krieger Publishing Company, Malabar, Florida.

Denver Metro Urban Drainage and Flood Control District. *2001. Urban Drainage Criteria Manual.*

Mid-America Regional Council and American Public Works Association. 2003. *Manual of Best Management Practices For Stormwater Quality*. September.

Nanson, G. C. and Hickin, E. J. 1983. Channel migration and incision of the Beaton River, American Society of Civil Engineers, Journal of Hydraulics Division, 109, 327-337.

Simon, A., A. Collison and E. J. Langendoen. 2002. ARS Bank-Stability Software Version 2.1. National Sedimentation Laboratory, U. S. Department of Agriculture.

U. S. Army Corps of Engineers. 1993. River Hydraulics, U. S. Army Corps of Engineers Engineering Manual EM 1110-2-1416.

United States Army Corps of Engineers - Engineer Research and Development Center. 1999. Channel Rehabilitation: Processes, Design, and Implementation

Ven Te Chow. 1959. *Open Channel Hydraulics*.

Watershed Management Institute, Inc. & EPA Office of Water, Operation Maintenance & Management of Stormwater Management. August 1997.

Golden Eagle – Brown County, Kansas
Emergency Streambank Stabilization

James M. Alexander[1]

[1]HNTB Corporation, Water Resources Engineer, 715 Kirk Drive, Kansas City, MO 64105; PH (816) 527-2208; FAX (816) 221-9016; email: malexander@hntb.com

ABSTRACT

The Kickapoo Water Intake Structure on the Delaware River is located on the Kickapoo Reservation in southern Brown County, Kansas, approximately 6 miles west of Horton, Kansas, and ½ mile south of Kansas 20. It is in section 32 of Township 4 South, Range 16 East. This paper addresses bank instability problems in the vicinity of a water intake structure owned/operated/maintained by the Kickapoo Tribe of Kansas. Eroding left and right banks around the concrete weir structure have undergone previous attempts at stabilization. Previous repairs have not performed successfully. Erosion has continued, both in the area that had been protected by previous revetments immediately downstream of the weir, and along both banks for approximately 200 feet farther downstream. Bank erosion continues to threaten the stability of the structure, water supply lines, and the access road to the site. The purpose of this paper is to assess the instability problems, provide and compare conceptual alternatives with respect to feasibility, and make a recommendation as to the preferred alternative to accomplish the repairs.

BACKGROUND INFORMATION

Intake Structure. The construction of the intake structure and weir dates to 1978; they were built as part of a water system construction project that included water lines, treatment facilities, a pump station, and the weir structure. The weir is located approximately in the middle of the straight channel reach. The construction plans showed the following elements:

- A concrete lined trapezoidal channel section 130-ft wide and 20-ft long, including 5-ft wide horizontal concrete slabs at the top of banks, concrete side slopes with a ratio of 2 horizontal to 1 vertical, and a concrete invert varying from 36 to 32-ft wide. The top portion of the slopes, and the adjacent slabs, are 12-in thick concrete; the lower portion of the slopes, and the invert, are 18-in thick. The tops of the slopes are shown at elevation 1005; the weir elevation is 990; the flowline at the upstream end of the invert is 984.
- A 6-ft high concrete weir located at the upstream face of the concrete channel section, with two 4-ft wide stop log slots in the center. The stop log slots are buttressed with triangular concrete supports.
- A continuous sheet pile cut-off wall located along the full width of the upstream face of the structure, plus an additional 20-ft to each side. The portions of the

sheet pile cut-off wall outside the limits of the paved channel section have a 4-ft high concrete cap wall. The sheet pile is shown extending a minimum of 30-ft below the sides of the paved channel section, and approximately 3-ft into shale, to elevation 958.

- A concrete cut-off wall along the downstream edge and top sides of the structure, extending 4-ft below the paved slopes, adjacent top slabs, and invert. The center portion of the concrete cutoff wall is shown as supported by timber or H-piles on 7-ft centers. The piles were to extend to elevation 953 or refusal.
- Two 8-in cast iron pipe intakes, on the upstream face of the weir, at elevations 985.33 and 987.66.
- A 2-ft layer of riprap, on a 6-in layer of bedding, extending 20-ft downstream of the channel paving and 25-ft past the top of banks (the entire width of the sheet pile cutoff wall). The riprap was to be placed flush with the surface of the structure; the downstream edge is shown as vertical, flush with the adjacent ground surface.

The plans did not show riprap or any other slope protection along the upstream face of the structure. The plans showed areas of grading disturbance adjacent to the structure significantly greater in extent than the coverage of the riprap. No information on riprap gradation was found in the plans; presumably it was defined by construction specifications. The plans showed a boring log for the structure site: it indicated a top layer consisting of 4½-ft of loose clayey silt, underlain by approximately 38-ft of silty clays and clayey silts, then by shale. The top of shale was shown at elevation 961.8.

Aerial Photographs. The Delaware River in the project reach appears to be a relatively recent, manmade channel. The 1954 aerial photo from the 1960 Brown County Soil Survey Report appeared to show the river channel not at the current location; rather it followed a meander to the north. The 1957 United States Geological Survey (USGS) map showed a new channel cut through the southern extent of the meander and running west to east generally straight for some 1000-ft.

Subsequent aerial photos dated 1981 and 1991 showed the river channel in the current location with the intake structure and weir in place. Both photos depicted the straight channel having some vegetation and trees on and adjacent to the bank. The 1981 aerial appeared to show the riprap indicated on the original plans; on the right bank and toe, that riprap seemed to be missing in the 1991 aerial photo. It was indeterminate whether riprap remained on the left bank in that picture. Two sandbars appeared on the 1991 aerial photo that were not evident on the 1981 image. The 1991 aerial photo showed a large bar deposit in the middle of the channel downstream of the structure. There also appeared to be a deposit of material along the left toe, just downstream of the original riprap location.

Site Inspection Photographs. The Corps of Engineers (COE) provided inspection photographs from several dates: June 24, 1987; June 30, 1993; November 9, 1993; and June 21, 1995. There was little or no rock protection remaining on the right bank slope downstream of the structure in the 1987, 1993 and 1995 photographs. It appeared that the rock was washed away leaving a near vertical, bare soil slope. There was a visible

washout beneath the right bank concrete sill/cutoff wall on the downstream side, which progressively worsened throughout the period covered by the 1987 to 1995 photographs.

Immediately upstream of the structure on the left side there was visible bank erosion in photographs prior to the 1996-1997 construction. For a few hundred feet upstream of the erosion adjacent to the weir structure, the photographs showed that the banks were generally vegetated down to the low flow channel. The photographs (1987 through 1999) consistently showed a steep, bare soil bank on the right bank at the outside of the first channel bend upstream of the structure. The appearance and apparent extent of that steep soil bank did not change much through the period covered by the pictures.

The progression of photographs did not as thoroughly cover the left bank downstream of the structure, but it generally appears that there was some rock slope protection covering the majority of the slope, with exposed soil areas visible near the structure. The pre-project (1996-1997 construction) rock protection appeared loose and not interlocked, had an irregular surface, and consisted of many long, flat rocks. Scattered tall weeds throughout the surface indicated the rock protection was probably thin. A June 1995 picture showed four square concrete slabs with manhole rings in the middle on the left slope downstream from the weir. Approximately 200-ft downstream of the structure, the succession of photographs showed a large sand/gravel bar situated in the middle of the channel. It appeared to be progressing downstream over time.

Previous Repairs. Repairs had been reportedly performed more than once, prior to the original (1996-1997) construction of the bank revetments. This is evidenced by 1987 photographs showing riprap on slopes downstream of what was included in original construction plans, and by some riprap that appeared on 1995 photographs of the right bank just downstream of the structure, where bare soil existed in 1993 photographs. The original streambank stabilization construction plans and documents were prepared in 1994-1995 and construction occurred in late 1996 and early 1997.

The stabilization efforts attempted to restore protection to the eroded downstream side slopes and channel bottom and add slope protection to the upstream slopes near the structure by placing a 3-ft minimum depth of rock stone revetment on 2:1 slopes with thickened toes. The stone protection extended for some 45-ft upstream to approximately 75-ft downstream of the structure, with 25-ft long transitions to existing at both ends. The irregular bank surface below the 3-ft revetment depth was to be filled with stone or concrete rubble. A 2-ft thickness of stone was placed on the bottom of the channel for a distance of 25-ft downstream of the intake. A washed-out area under the concrete sill/cut-off wall along the right side of the downstream edge of the structure was filled with gravel. Subsequent high flows in the channel, since the repairs, have caused damage to the rock slope protection.

Weir Raise. To remedy water supply shortages experienced during dry weather, the Kickapoo Tribe constructed a 2-ft temporary weir raise in July of 2000, but it collapsed within a month of construction. The supplementary structure was constructed of steel channels anchored to the existing concrete weir and removable wooden stoplogs.

In May of 2001 another 2-ft temporary weir raise constructed, this time designed and funded by the Bureau of Reclamation. The supplementary structure was constructed of welded steel channels and plates anchored to the existing concrete weir and removable wooden stoplogs. Plans for this raise stated that the stoplogs are to be removed during expected high flows and over winter months. Also, this weir raise was expected to be temporary, lasting only until an alternate water source could be implemented. During subsequent flood events (notably the May 2007 event), this raise suffered significant damaged and is no longer functional. The Federal Emergency Management Agency (FEMA) is currently in the process of replacing the structure.

ANALYSIS OF THE STREAMBANK EROSION PROBLEM

Flow Conditions. The erosion, bank instabilities, and riprap displacement that have occurred since the construction of the intake structure are mainly the result of the impact of the structure on flow conditions in that river reach. Velocity fluctuations that occur at the weir and paved channel section result in flow turbulence. The observed downstream erosion patterns, both in the riprap that was installed in 1996-1997 and in the left and right bank erosion areas, are likely the result of the flow turbulence. Prior experience with turbulent flow conditions at other sites has been that larger riprap than normally required is necessary for calculated velocities. A type of stilling basin has formed immediately downstream of the structure, consisting of a hole in the channel bottom and deposits of stone formerly located in riprap revetments on the channel sideslopes. For some discharges, there are probably secondary hydraulic impacts downstream of this stilling basin. Hydraulic analysis indicates the potential for a hydraulic jump occurring in the channel downstream of the structure; if this actually occurs, the resulting forces and turbulence may be beyond what any reasonable riprap gradation can withstand. The turbulent flow conditions and the stilling basin formation suggested that analysis should be performed using the COE Waterways Experimental Station (WES) Hydraulic Design Criteria 712-1.

Materials. It had been reported that much of the stone in the three-foot thick riprap layer installed in the previous stabilization project had been 6 to 8-inch stone. At the site investigations for this study, most of the stone remaining in place was estimated to be 4 inches to 6 inches in largest dimension. The specifications for the previous project apparently allowed shot rock, and the stone delivered and installed at the site was apparently too small to be stable for the velocities and turbulence that can occur.

The riprap installed upstream of the weir in the prior stabiliztion project is adequate in size, according to preliminary hydraulic analysis and preliminary Riprap15 results.

Photographs and observations of remnants of previous repairs were inconclusive. The material appeared to have been larger, but gradations may not have provided enough range of size to allow fully effective interlocking. The riprap installed with the original construction of the structure did not extend upstream of the structure, therefore providing

no protection for the acceleration of flow towards the weir. The original riprap also only extended 20 feet downstream of the weir, an inadequate distance for the increased velocities and turbulence resulting from the structure.

Geotechnical. Based on a review of available boring logs, the shale bedrock encountered at about elevation 960 is covered by a thick alluvial deposit of clay and silt with a few sand seams. The near-surface soils (those above about elevation 1000) are described on the National Resource Conservation Service (NRCS) soil survey as Kennebec silt loam, a moderately well drained material formed in the floodplain. These soils are considered susceptible to erosion, particularly the silty portions.

During the site visits described in this report, no scarps or other indicators of deep-seated slope instability were observed along the river banks upstream and downstream of the weir structure. Some of the remaining riprap from previous repairs was found to be highly friable, likely as a result of weathering. Downstream of the weir, bank instability is apparent with the observed vertical slopes and sloughing that is actively widening the channel on both sides. On the other hand, a vertical slope on the right bank upstream of the weir has not significantly sloughed for several years.

During site visits, the team did not observe any evidence of near surface slides on riprap covered 2(h):1(v) slopes, but this could be because subsequent or concurrent erosion removed slumped materials and other evidence.

Conclusions. It appears that energy dissipation downstream of the intake structure was not addressed by the original design. The original design also apparently did not consider the upstream effects of the acceleration of flow towards the weir. The riprap stone installed downstream of the structure in the initial stabilization work was too small for the velocities and turbulence that occur downstream of the intake structure. Stone installed previous to 1996 may have been of poor gradation that did not allow adequate interlocking of stones. The riprap stone installed upstream of the structure in the initial stabilization work appears to be adequate.

A hydraulic jump may occur in the channel downstream of the structure for a limited range of discharges. Occurrence of a hydraulic jump would have heavily damaged any of the previous revetments.

SITE HYDROLOGY AND HYDRAULICS

Discharges. The Delaware River has a drainage area of approximately 135 square miles at the project site. A USGS recording stream gage is located 14 miles downstream, near Muscotah, Kansas. The gage has been in operation since 1970. The drainage area at the gage is 431 square miles. The COE computer program HEC-FFA was used to determine expected probability discharges at the gage. Those discharges were then adjusted for the drainage area at the project site. Regression equations as developed for the state of Kansas by the USGS were also used to estimate discharges for various frequencies.

The table below shows the results of the hydrologic calculations for discharges at the project site.

Exceedance Probability	Return Frequency	Gage Analysis	USGS Regression
50%	2-Year	5,330 cfs	5,980 cfs
20%	5-Year	7,980 cfs	10,400 cfs
10%	10-Year	9,830 cfs	15,700 cfs
2%	50-Year	14,100 cfs	28,200 cfs

Normally, the results of gage analyses match regression results more closely. The procedure followed to adjust for the difference in drainage areas between the USGS gage site and the project location may have caused underestimation of the discharges at the intake structure. For expected discharges at the study site, the results of the regression analysis are assumed to be more accurate. Also, it was reported in 2001 by Bill Allen of the Kickapoo Environmental Office that a 2-in rain would cause the channel to flow half to two thirds full, and that bank-full conditions would result from 4 to 5-in of rain. This, in conjunction with the channel capacity calculations described in the following paragraph, supports the higher discharge results (by indicating that bank-full events are not extremely rare).

Hydraulic Modeling. To assess the flow conditions at the intake structure for a wide range of flow conditions, a HEC-RAS model was developed from the geometric information available from surveys. The model extended from about 4,400-ft downstream of the structure to 400-ft upstream. A wide range of discharges was analyzed (100 cfs to 16,000 cfs), and the model was run for mixed flow conditions, starting at both ends from an average channel slope determined from the USGS map. The hydraulics of the river was analyzed for different scenarios, as well as for sensitivity to varied conditions. The n-values were originally assigned relatively low values, for conservatism in hydraulic conditions, because higher downstream velocities would lessen the tailwater depth and increase the possibility for the occurrence of a hydraulic jump. As a result of photographs and field observations of significant flow events, a calibration exercise was performed that increased the n-values.

Results of the Hydraulic Analysis. The weir raise conditions should not have a significant effect on the proposed protection, although the plunge pool design was based on the long term existing plunge pool configuration. HNTB's analysis of the weir raise indicates that the proposed streambank stabilization design (designed for the pre-weir raise condition) will also provide adequate protection for the 2-ft raise as shown in the Bureau of Reclamation plans (RFQ NO. 01SQ600089). This analysis is based on all stoplogs in-place at an equal elevation across the structure. Weir raise effects become unpredictable if weir raise stoplogs are out of place, debris

accumulates on the weir, or other undesirable situations (such as an ice jam) arise that cause non-uniform flow patterns across the weir raise. Sustained non-uniform flow has the capability to jeopardize the function and integrity of the proposed stabilization protection. For this reason, proper flow conditions across the weir raise need to be monitored and maintained by water plant personnel as part of ongoing plant operations.

The true size of the existing plunge pool is likely heavily dependent on the major and abrupt drop from the end of the concrete section to the adjacent downstream channel, once the channel slopes have eroded. This has been the predominant condition for many years at the site, except for brief periods subsequent to previous repairs. This abrupt drop will not exist after construction of the proposed bank stabilization project. The impact of the weir raise on the size of the plunge pool is expected to be more than counter-balanced by the elimination of the abrupt drop at the end of the structure.

CONCEPT DESIGN ALTERNATIVES

In order to meet the goals of an emergency streambank stabilization project at this site, five (5) alternatives were considered. Exhibits showing a schematic drawing for each alternative can be found in the Golden Eagle Feasibility Analysis dated May 29, 2008. Typical sections for the various improvements discussed can also be found in Exhibit 9 of the Feasibility Assessment.

Alternative 1 Riprap Stilling Basin, LPSTP (Longitudinal Peaked Stone Toe Protection), and Slope Revetment (Page 11)

The first 60-ft downstream of the weir would be protected by a 54-in thick large diameter rock blanket. It would match the geometry of the downstream section of the concrete drop structure, with a top elevation of 1004.00 and 2:1 sloping sides. On the left bank, a 90-ft slope revetment transitioning from full bank height (elevation 1004.00) upstream to half bank height (elevation 995.00) downstream would be installed. It would have a thickness of 24-in on the 2:1 side slope. The first 40-ft of slope revetment would be supported at the bottom with a toe blanket and the remaining 50-ft would be supported with an incised section of toe rock. This incised toe would be an inverted trapezoidal section, 36-in thick with a 10-ft flat bottom. The 48-in thick toe blanket would provide toe support for the left bank slope revetment and protect the channel bottom from the transition out of the large riprap blanket plunge pool.

LPSTP would be placed along both the left and right banks. The left bank protection would match the end of the slope revetment on the upstream end with a top elevation of 995.00 and a 2:1 riverward side slope and will have a 1.5:1 landward side slope. It would transition for the first 60-ft in length, down to top elevation 992.00 and a 1.5:1 riverward side slope. The LPSTP would continue downstream for 120-ft on a linear alignment, where it would tie into the existing bank. The right bank would have a combination of slope revetment and LPSTP protection. It would match the end of the

large riprap blanket on the upstream end with a top elevation of 995.00 and a 2:1 riverward side slope and would have a 1.5:1 landward side slope. It would transition for the first 40-ft in length, down to top elevation 992.00 and a 1.5:1 riverward side slope. The LPSTP would continue downstream for 195-ft with a linear alignment, where it would tie into the existing bank. Overall, the left bank protection would extend 30-ft further downstream than the right bank protection.

Within the protective works area, the channel would be graded to a flat flowline elevation of 985.00, with the exception of the invert within the large riprap blanket plunge pool. Downstream of the proposed protective works for a length of approximately 200-ft, the existing channel has dual thalwegs and an island accretion of rocky material. The excess material in the center of the channel would be moved toward the split channels near the left and right banks, and graded to drain toward the center and downstream in the channel to an elevation of 984.50 at its terminus.

Alternative 2 Concrete Stilling Basin, LPSTP, and Slope Revetment
The stilling basin in this alternative would have the first 45-ft downstream of the weir protected by a concrete stilling basin with 11-foot high walls instead of the riprap stilling basin. The other features of this alternative are identical to Alternative 1.

Alternative 3 Sheet Pile Stilling Basin, LPSTP, and Slope Revetment
The stilling basin in this alternative would have the first 45-ft downstream of the weir protected by an 11-foot high sheet pile stilling basin with a concrete lined bottom instead of the riprap stilling basin. The other features of this alternative are identical to Alternative 1.

Alternative 4 Sheet Pile Wall
Another alternative that was further assessed subsequent to detailed hydraulic analysis was the usage of sheet piling. For this variation, riprap revetments would not be used for armoring the presently unprotected eroding banks. The sheet piling would be driven along the downstream edge of the intake structure (existing sheet pile only provides formwork for grout work and protection for interface between grout and soil) and down the left bank to protect the waterline. There would also be some sheet pile driven for a short distance down the right bank to prevent the existing concrete weir from being flanked. The scour hole would remain as is and the stream would be left to run its natural course. The scour hole would be allowed to expand, to serve as an energy dissipater.

Alternative 5 Riprap Stilling Basin with Stabilized Slopes
The soils behind the large riprap blanket and the slope revetment would be stabilized to provide slopes that satisfy criteria specified in EM 1110-2-1913. Horizontal layers of geogrid reinforcement vertically spaced at 4-ft are proposed. The geogrid would be embedded in 12-in layers of sand (6-in above and 6-in below). The remaining 3-ft of material between sand layers would be soil fill from the site. Filter fabric wrapped around the riverward face of these 3-ft layers would prevent migration of fines into the gravel bedding layer below the riprap. The top elevation of the stabilized slopes

would match the top of the faced rock protection. A rock layer would be placed below the soil, sand and geogrid stabilization. The displaced existing riprap on the site would be recovered for this rock layer. The bottom of this rock layer would be at elevation 980.00 for the large riprap blanket and slope revetment with toe blanket, and elevation 981.00 for the slope revetment with incised toe.

CONCLUSIONS AND RECOMMENDATIONS

Protection of the site is technically and economically feasible. The first priority is to protect the water line and intake structure. The second priority is to stabilize the left bank downstream, to protect the access road. The third priority, while not required by the project, is to stabilize the right bank downstream in order to help control flow conditions at the intake structure. Protection on the right bank would help prevent an asymmetrical scour hole and potential flanking of the weir structure, so it is felt to be important.

A "No Action" alternative would likely result in eventual damage to the structure and require its complete replacement, as it is not believed that the piling at the structure would be adequate for its support if most of the underlying soil washes out. Replacing the structure is a viable alternative, especially if the new structure incorporated an energy dissipater; however, replacement would be far more expensive than stabilizing the downstream channel.

Biostabilization techniques were determined not to be a feasible option for this project based upon the turbulent flow conditions and excessive velocities through the proposed stabilization area. In addition, the scour hole that is already present needs to be addressed by the chosen solution.

The hydraulic analysis shows that unstable conditions (potential hydraulic jump) may exist downstream of the weir due to the abrupt drop from the end of the concrete section to the adjacent downstream channel. All alternatives except Alternative 4 address this issue. The sheet pile wall protects the road and water line, but it does nothing for the existing scour hole or erosion elsewhere. Alternative 4 is also significantly more expensive than the other alternatives.

Alternatives 2 and 3 could have safety issues because the sheetpile or concrete will leave high vertical walls. As people have been known to fish the area, safety measures such as railing and/or barriers would be needed at a minimum. That cost is not currently included in the estimates, which already show higher costs than Alternatives 1 and 5.

The geotechnical investigation performed in 2000 included slope stability analysis. Results indicated that the slope stabilization measures described in Alternative 5 are needed to meet the design criteria specified in EM 1110-2-1913 for levee slopes. Because (1) site observations to date have found no evidence of deep slides and (2) the consequences of a bank failure downstream of the intake weir are not commensurate with failure of a levee, the additional costs associated with Alternative 5 do not appear to be warranted.

Alternative 1 is the recommended solution for the site. This riprap stilling basin, along with the LPSTP and slope revetment meets all of the priorities of the proposed project and is the most economical.

SOURCES OF INFORMATION

Aerial photographs were acquired from the NRCS Brown County Field Office in Hiawatha, Kansas. Plans for the intake structure, previous site inspection photographs, and the 1995 bank stabilization plans were provided by the Kansas City District (KCD) COE.

The following is a list of the information used for this paper:

- USGS Horton NW Quadrangle, 1:24,000 (based on 1957 aerial photography).
- USGS Kansas City 1 x 2-Degree Series Map, 1:250,000 (based on 1951-1952 and 1973 aerial photography).
- Aerial Photographs dated 1981 and 1991.
- NRCS Soil Survey aerial photograph, dated 1954.
- Brown County NRCS soil properties description sheet.
- Construction plans for Kickapoo Water Supply System, including Water Intake Structure plans.
- KCD COE Bank Protection plans (dated 1994-1995).
- USGS stream gage data, Delaware River.
- Detailed Project Report: Delaware River, Water Intake Weir, Kickapoo Tribe of Kansas, Brown County Kansas; CWIS Number 92942; March 1994; KCD COE.

Golden Eagle Section 14 Emergency Streambank Protection Feasibility Assessment; May 2008; Kansas City District Corps of Engineers; Eric Lynn, Project Manager.

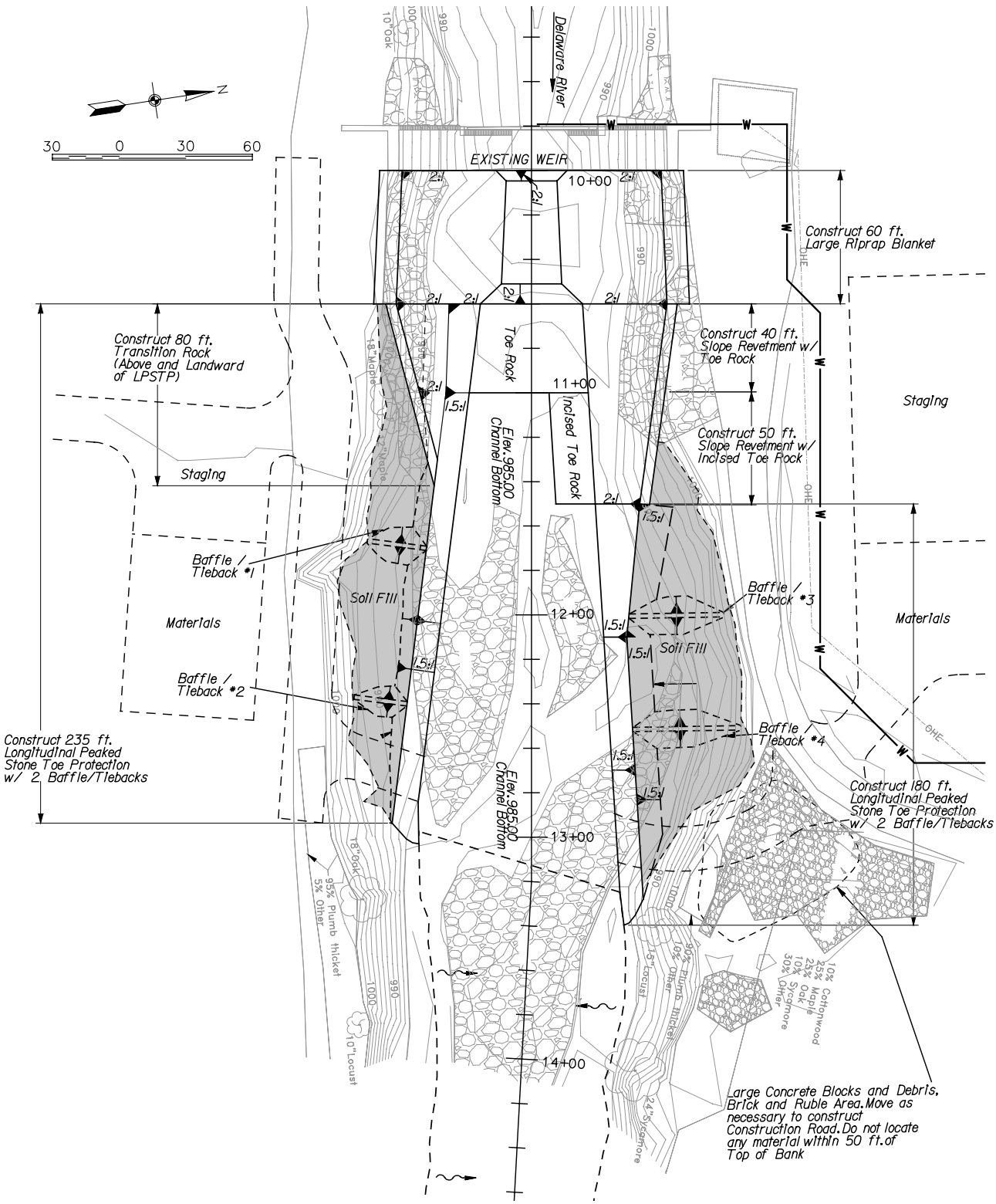
N
30 0 30 60
Delaware River
EXISTING WEIR
10+00
11+00
12+00
13+00
14+00
Construct 60 ft. Large Riprap Blanket
Construct 40 ft. Slope Revetment w/ Toe Rock
Construct 50 ft. Slope Revetment w/ Incised Toe Rock
Construct 80 ft. Transition Rock (Above and Landward of LPSTP)
Construct 235 ft. Longitudinal Peaked Stone Toe Protection w/ 2, Baffle/Tiebacks
Construct 180 ft. Longitudinal Peaked Stone Toe Protection w/ 2 Baffle/Tiebacks
Toe Rock
Incised Toe Rock
Elev. 985.00 Channel Bottom
Staging
Materials
Soil Fill
Baffle / Tieback #1
Baffle / Tieback #2
Baffle / Tieback #3
Baffle / Tieback #4
2:1
1.5:1
OHE
Large Concrete Blocks and Debris, Brick and Ruble Area. Move as necessary to construct Construction Road. Do not locate any material within 50 ft. of Top of Bank



4-30-08: Looking across weir North to South.



4-30-08: Facing SE from top of bank. Downstream erosion along right bank.



4-30-08: Facing SE from top of bank. Downstream erosion along right bank.



4-30-08: Facing East from top of bank. Downstream erosion along left bank.

Hutchinson, KS – 4th and Carey Groundwater Remediation and Reverse Osmosis Water Treatment Facility Project

Danita S. Boettner, P.E.[1], Don Koci, P.G.[2], Darren L. Brown, P.G[3], Bruce Allman, P.E.[4]

[1]CDM, 6000 Uptown Blvd NE, Suite 200, Albuquerque, NM 87110; PH (505)243-3200; FAX (505)243-2700; email: BoettnerDS@cdm.com
[2]City of Hutchinson, Public Works Department, 1500 S. Plum, Hutchinson, KS 67501; PH (620)694-1900; FAX (620)694-1980; email: donk@hutchgov.com
[3]CDM, 345 Riverview, Suite 520, Wichita, KS 67204; PH (316)660-6700; FAX (316)264-3025; email: BrownDL@cdm.com
[4]Professional Engineering Consultants, P.A. (PEC), 303 S. Topeka, Wichita, KS 67202; PH (316)262-2691; FAX (316)262-3003; email: Bruce.Allman@pec1.com

Abstract

In the early 1980s, the 4th and Carey groundwater contamination site was discovered when the U.S. Environmental Protection Agency (EPA) began testing public water supply wells. A city of Hutchinson well located at the intersection of 4th Avenue and Carey Street was found to be contaminated with volatile organic compounds (VOCs). The groundwater contamination findings issued as a result of EPA and Kansas Department of Health and Environment (KDHE) investigations led to the establishment of the 4th and Carey Site. Strong proactive efforts by the city and local industry leaders prevented the site from being placed on EPA's National Priority List (NPL, or Superfund). The city signed a consent agreement with KDHE in 1994, assuming responsibility to clean up the site. At that time, the city contracted with CDM for remedial assistance. Impacts by high chloride levels in groundwater areas to be treated left the city faced with discharge restrictions due to total maximum daily load requirements for chloride in Cow Creek. The city evaluated alternatives that included beneficial reuse of contaminated water, including a regional solution that addressed the site's contamination, the high chloride waters, water appropriation issues, and other industrial groundwater contamination in the area. Implementation of the approved regional plan included the following activities: delineation of soil and groundwater contamination; installation of source area air sparge and soil vapor extraction systems; soil excavation; installation of a groundwater remediation well system for downgradient capture of regional contamination; water appropriations permitting; two Class I non-hazardous underground injection control (UIC) wells; and construction of a fully automated 6-million-gallon-per-day (mgd) reverse osmosis (RO) water treatment facility. The facility blends treated water with 4 mgd of existing municipal water, producing 10 mgd of higher quality water for potable water use. The RO water treatment facility design and construction management was performed by Professional Engineering Consultants, P.A. (PEC).

The source area and downgradient remediation systems, Class I non-hazardous UIC wells, and portions of the buried waterlines are operational and are being monitored under the direction of KDHE. The RO water treatment facility is currently under construction and is anticipated to be fully operational in spring 2009. Funding for the project was obtained utilizing the potential responsible party settlement money, third-party negotiated funds, tax increment financing, KDHE low-interest loans, and water utility capital improvement project funding. The project was estimated to cost approximately $33 to $35 million and has cost approximately $34.5 million to date.

Introduction

The 4th and Carey Site, U.S. Environmental Protection Agency (EPA) Identification Number KSD061608006, is located in Hutchinson, Kansas, in Reno County. The site encompasses approximately 1,240 acres. Groundwater contamination at the site was discovered in the early 1980s, when the EPA and Kansas Department of Health and Environment (KDHE) began testing public water supply wells. A city of Hutchinson well located at the intersection of 4th Avenue and Carey Street was found to be contaminated with volatile organic compounds (VOCs). The groundwater contamination findings issued as a result of EPA and the KDHE investigations led to the establishment of the 4th and

Carey Site in 1994, with the city of Hutchinson assuming the lead role, in order to keep the site from being placed on EPA's National Priority List (NPL, or Superfund). Agreements were reached with potential responsible parties (PRPs) for the contamination. The city of Hutchinson contracted with CDM to provide remedial assistance, including KDHE coordination, investigations, planning, remedial design, and associated construction to address the VOC contamination of the site. Professional Engineering Consultants, P.A. (PEC) was the engineer of record associated with the design and construction for the reuse component of the project.

The site is generally bounded by Lorraine Street to the west, Carey Street to the south, Corey Road to the east, and 11th Avenue to the north, with an extension north to 17th Avenue west of Halstead Street. The general site layout is shown in Figure 1.

Figure 1: Overall Remediation, Containment, and Concentrate Disposal

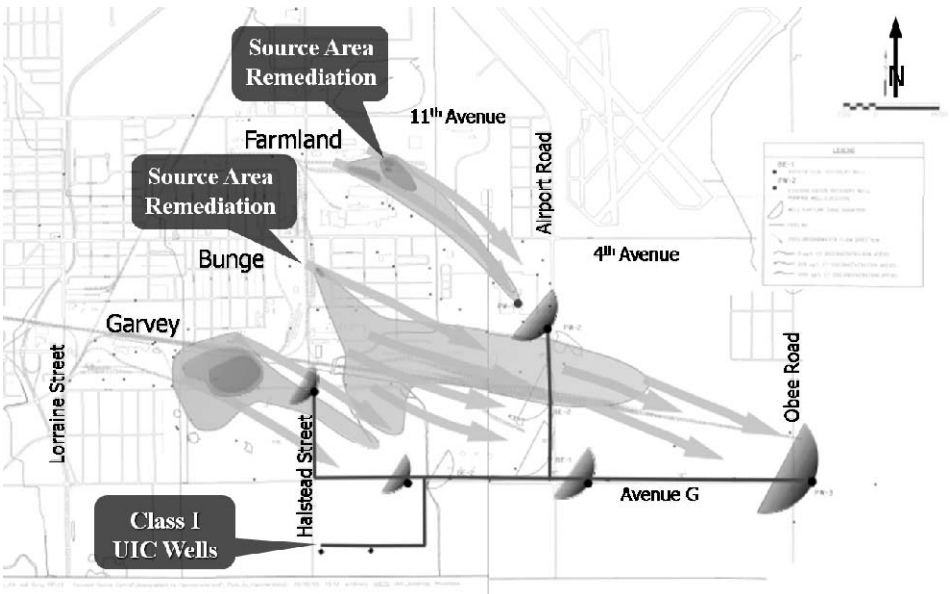

The 4th and Carey site is named for the location of public water supply (PWS) well #8 at the intersection of Carey Street and East 4th Avenue in Hutchinson. VOCs were detected in groundwater samples collected from this well in 1982. Carbon tetrachloride (CT) was first detected at a concentration of 1.6 micrograms per liter (µg/L) in a sample collected from PWS well #8 on June 7, 1982, and increased in concentration until the city removed PWS #8 from service on April 20, 1985, at KDHE's request.

The site has been subject to a series of investigations beginning in 1984. Following completion of a Listing Site Investigation in 1991, EPA scored the site using the Hazard Ranking System (HRS) for inclusion of the site on the NPL in January 1993. The city and CDM, with the PRP group's assistance, took the lead on the remedial investigation and feasibility study (RI/FS), because of the potential threat to public health and because property values could be adversely affected if the site was in the Superfund Program. This resulted in EPA transferring oversight of the RI/FS to KDHE. KDHE outlined the requirements of the RI/FS and defined the site boundaries in a Consent Agreement and Consent Order (CACO) between the city and KDHE on April 25, 1994.

Remedial Investigation and Source Control Investigation Results

CDM conducted the 4th and Carey RI field activities between August 1994 and January 1997. KDHE approved the resulting RI Report as final on February 12, 1998. Upon completion of the RI, CDM conducted source control investigations (SCIs) at the former Farmland Elevator J, Bunge Elevator, and Garvey Elevator. The SCIs at these elevators were completed and approved by KDHE on October 26, 2001.

Site Characteristics

The site is generally flat with a gentle topographic dip to the south and southeast. The land use within the site is diversified and includes commercial, industrial, recreational, and residential properties. The geology of the study area primarily consists of Arkansas River Valley alluvium, Pleistocene-age glacial outwash, and associated terrace deposits overlying the Permian-aged Ninnescah and Wellington Formation bedrock. Both formations primarily consist of shales with salt deposits present within the Wellington Formation. Depth to bedrock averages approximately 60 feet below ground surface. The aquifer at the site consists of sands and gravels with an average thickness of 43 to 55 feet. In general, the sediments in the water-bearing zone appear to be coarser (more permeable) with depth. The upper 12 to 15 feet consist of interbedded silts and clays, with some minor sand stringers.

Aquifer testing in the area indicates a hydraulic conductivity ranging between 517 to 771 feet per day. Storativity ranges from 0.019 to 0.065. Groundwater flows principally to the southeast, although local flow directions vary considerably with localized aquifer stresses (e.g., pumping wells). The hydraulic gradient also varies locally, ranging from 0.0006 to 0.003 feet/foot with the hydraulic gradient and groundwater velocity increasing near pumping wells.

Contaminant Distribution

Two shallow groundwater CT plumes were identified as emanating from three source areas at the former Farmland Elevator J facility. One shallow groundwater CT plume was identified as emanating from the former Bunge Elevator. A CT plume was also identified as emanating from the former Garvey Elevator. Several additional plumes have been identified in the area and are being managed by KDHE under separate CACOs. Three offsite groundwater plumes (two perchloroethelyene [PCE] and one PCE and trichloroethelyene [TCE]) were observed migrating onto the western portion of the site**.** In addition, chloride contamination was discovered at the site. Three sources of chloride contamination were identified by KDHE. The chloride-impacted areas are generally in the south central portion of the site, as well as south of the site.

At the Farmland and Bunge elevator source areas, the CT contamination is primarily situated in the upper portion of the aquifer and then migrates into the middle and lower portion of the aquifer as it progresses downgradient. VOC contamination in the groundwater at the former Garvey Elevator is present both in the shallow and the deep aquifer; it is characterized by shallow and deep plumes in the alluvial sediments. In general, the shallow plumes originate in the source areas and are of limited horizontal extent and contaminants move from shallow to deeper groundwater away from the source areas, as the deeper sediments appear to be more permeable than the shallow sediments. The downgradient groundwater plumes are more extensive than the shallow source area plumes.

Corrective Action Decision

KDHE issued a final interim corrective action decision (CAD) for source area remediation at the 4th and Carey site in June 2002. The final interim CAD summarized the RI/FS report for the 4th and Carey site and established selected remedial alternatives. The selected remedial alternative specific to the Bunge and Farmland source areas was focused air sparging (AS) and soil vapor extraction (SVE). The final interim CAD revised the plan to include the preferred remedial alternative for downgradient containment in November 2004 and became the final CAD for the site on May 9, 2005. The presence of significant chloride contamination in the area of the downgradient containment systems impacted the choice of the selected remedy for the site. As a result, the downgradient system would need to be

configured in a way that isolated the anticipated high-chloride contaminated groundwater from future reuse through the installation of a reverse osmosis (RO) water treatment facility.

Cleanup goals for groundwater at the 4th and Carey Site follow the federal maximum contaminant levels (MCLs) associated with the Safe Drinking Water Act. Cleanup goals for soil are the Kansas Risk-Based Standards for the residential migration to groundwater pathway. The city of Hutchinson is responsible for the remediation activities at three CT source areas at the former Farmland J Elevator; one CT source area at the former Bunge Elevator; and a fifth CT source area at the former Garvey Elevator. Other VOC source areas are being addressed by other responsible parties.

Several controls have been instituted with the intent to prevent exposure to contaminated groundwater. These controls consist of: (1) groundwater use restrictions; (2) deed restrictions; (3) public education, such as mailings and public meetings; and (4) provision of alternate water supply. The city of Hutchinson monitors and maintains these controls on an annual basis to ensure protection of human health and the environment. Changes of land use in impacted areas are also monitored.

Pre-Design Data Acquisition (PDA)

Data collected by CDM during the PDA field work included AS/SVE pilot testing and groundwater pumping tests. These data provided a basis for sizing the equipment, piping, and wells; for designing the placement of AS, SVE, monitoring, and extraction wells; and for optimizing system cycling needs to minimize the impacts of groundwater mounding associated with air sparge operations at the former Farmland J and Bunge elevators. The PDA established water level and contaminant concentration information to serve as a basis for measurement of remedial effectiveness for the site.

During 2004, the shallow source area at the former Garvey Elevator was remediated by excavating and properly disposing of shallow soils in the vicinity of the former CT tank. The deep groundwater at the former Garvey Elevator is being monitored to ensure that no CT concentrations re-occur, which could trigger the implementation of source control measures.

Source Area Remediation (Farmland J and Bunge Elevators)

The selected remedy for the remediation of the shallow soil and groundwater source areas at the former Farmland J (Farmland NE, Farmland SE, and Farmland SW) and Bunge Elevators was AS/SVE. Several site conditions impacted the CDM design of the AS/SVE systems.

- The PRP properties are currently owned and operated by separate parties. Therefore, work in these areas required access agreements and associated design approvals by the respective party, in addition to the PRPs.
- Facility-owned rail lines located at the north and south sides of Farmland limited the placement of wells and associated piping.
- SVE and AS wells had to be completed below grade to accommodate elevator operations.
- The AS wells were divided into operating zones with each zone operating individually to accommodate a pulsing operation for groundwater mounding and collapse.
- Clayey soils with intermingled silt and sand lenses identified at Bunge, Farmland SW, and Farmland SE required an alternate SVE design to capture as much sparged air as possible. SVE wells operate continuously at all four locations.
- Vapor monitoring points (VMP) were installed to monitor vacuum in the vadose zone created by the system.

Startup for the AS/SVE systems was January 9, 2006, with final acceptance of the system by the city of Hutchinson on October 10, 2007.

Downgradient Remediation

Based on the downgradient modeling results performed by CDM, the settlement agreement with PRPs, and the water-supply needs of the city, a downgradient preferred alternative was developed. It

integrated the hydraulic containment of the contaminant-impacted groundwater with a treatment process that provides a beneficial reuse of the water. The alternative involves hydraulically containing the plumes with extraction wells and piping the contaminated groundwater to a treatment facility that would use RO membranes to treat elevated chloride and VOC levels. An air stripper will be installed as a polishing process for removing VOCs and carbon dioxide from the treated water. Additional inorganic compounds from the groundwater would also be removed through this process. The RO concentrate that contains the rejected organic and inorganic compounds will be disposed of via Class I non-hazardous underground injection control (UIC) wells upon completion of the RO treatment facility discussed later in this paper.

The preferred alternative was developed incorporating two third-party pumping systems in conjunction with the new city-constructed pumping system. In April 2007, five extraction wells in the southern portion of the site began operation as part of chloride plume containment efforts of a third party. Groundwater flow in the southeastern portion of the site is also impacted by groundwater extraction efforts of a separate third-party remedial containment system for a TCE groundwater plume. These regional systems provided additional benefits to the CT remediation, as shown in Figure 1. Therefore, the city of Hutchinson and the two third-party entities entered into agreement for addressing the regional concerns of KDHE. In addition to the third-party systems, the city of Hutchinson installed three downgradient extractions wells to address migration of CT within the central region of the downgradient contamination. Two of the three southeastern downgradient third-party wells provide containment of the eastern most portions of the CT plume, along with other VOCs in the region. These wells will ultimately become the city's responsibility and be pumped directly to the RO treatment facility upon completion of the pipeline and RO treatment facility.

The downgradient containment system designed and installed by the city of Hutchinson and CDM is described in further detail below:

- Piping was installed to accommodate 500 gallons per minute (gpm) of high-chloride water from the neighboring former salt facility property, as agreed upon between the city and the associated third-party owner. Groundwater from one city extraction well, which has a pumping rate of approximately 100 gpm, will also be continually sent to the Class I non-hazardous UIC wells.
- Two additional city extraction wells were installed and completed in March 2006. Both wells are pumped at a design pumping rate of approximately 300 to 400 gpm.
- Connection point and associated valving was installed for ease in transition to the future RO treatment facility.

As a result of water from the wells being injected down the Class I non-hazardous UIC wells (and eventually to the RO treatment facility), the extraction wells were designed and developed such that minimal turbidity and suspended solids were produced.

Extraction wells EW-1 and EW-3 were fully operational on July 24, 2006, while operation of extraction well EW-2 was delayed until April 16, 2007. Operation of EW-2 was delayed until the five extraction wells for the third-party chloride plume containment began operation. Final acceptance of the downgradient system occurred on October 16, 2006.

Water Appropriations

The remediation project required that permits be obtained from the Kansas Department of Agriculture's Division of Water Resources for the five groundwater extraction wells (EW-1, EW-2, EW-3 and two third-party wells). Groundwater appropriations for the remediation wells total approximately 4,188 acre-feet per year (afy) (1,365 million gallons per year [mgy]) resulting in groundwater withdrawals of nearly 3.75 mgd at maximum capacity.

Due to the unique nature of the project and the beneficial use of the treated groundwater in the public water supply, the quantity of water permitted from the remedial wells shall be limited to the quantity of water previously authorized for the city's municipal wellfield—consisting of 20 wells permitted for a

total withdrawal quantity of 11,666 afy (3,801 mgy). Therefore, the additional groundwater appropriations required for the contamination remediation use did not increase the total pre-existing appropriations amount for the area. This is both an important regulatory and environmental element of the project, as aquifer appropriations had previously reached or exceeded maximum development limitations under the state's safe-yield regulation, which seeks to balance groundwater withdrawals with natural aquifer recharge to prevent groundwater mining.

The additional treatment and use of the contaminated groundwater for beneficial purposes allow the city to remediate the aquifer without significantly increasing groundwater usage from the area. The quantity of water withdrawn from the remedial wells will offset or reduce the amount of water pumped from existing municipal wells. As a result, it is the city's intent to apply the annual water use for the remediation project to the city's prior municipal water permits that have not yet been certified by the state of Kansas.

Class I Non-Hazardous Underground Injection Control Wells

Implementing the downgradient containment system in a timely manner is critical to prevent ongoing migration of the contaminant plumes. Therefore, it was determined that the best option was to proceed with construction of the extraction wellfield as soon as possible. This required implementing a disposal option for the high-chloride groundwater and VOCs by using an environmentally acceptable method while the RO water treatment facility is being designed and constructed. To this end, untreated groundwater from the downgradient wellfield is being injected directly into the Class I non-hazardous UIC wells, designed and constructed by CDM (shown in Figure 1), until the RO water treatment facility is operational. Once the facility and all associated transfer piping are constructed, water from the downgradient wellfield will be treated for distribution to the potable water supply system.

Flow to the Class I non-hazardous UIC wells currently consists of the 700 to 900 gpm of groundwater from the proposed extraction wells and an additional 500 gpm from the neighboring chloride remediation efforts. After construction of the RO treatment facility, the Class I non-hazardous UIC wells will accept rejected concentrate water from the RO process, approximately 100 gpm from the city's extraction well, and 500 gpm from the neighboring chloride remediation system. Ultimately, approximately 2 million gallons per day (mgd) of RO membrane concentrate water will require disposal through these wells.

Permitting was performed for the installation of three Class I non-hazardous UIC wells; however, the city proceeded with construction of two wells to meet the demand of the remediation and RO treatment facility. The third well was permitted for additional future capacity, should it be necessary. A siting study was performed to minimize design impacts, permitting delays, and costs by identifying key issues that could affect the project prior to submitting the permit application documents to KDHE-Bureau of Water (BOW) (UIC) and subsequent public notice. The KDHE-BOW Class I UIC permits became effective May 9, 2005. The two constructed injection wells were fully operational on July 24, 2006.

Reverse Osmosis (RO) Water Treatment

Professional Engineering Consultants, P.A. (PEC) designed and provided construction management services associated with the RO water treatment system. The reuse portion of the preferred remedial alternative calls for the blending of RO membrane treated water from the downgradient remediation wellfield with water from the Northwest (NW) wellfield. Because the two wellfields are at opposite sides of the city, the decision was made to pipe the raw water to the RO water treatment facility located near the center of town. The associated raw water piping was constructed primarily during the year 2008.

The water treatment system consists of several key components, including remedial and raw water collection, the RO water treatment facility, concentrate waste piping, Class I non-hazardous UIC well disposal, and the distribution system. The RO product water will be blended with the NW wellfield water for the city of Hutchinson's drinking water supply. The water from the NW wellfield is not

contaminated with VOCs; however, it contains elevated levels of hardness, chlorides, iron, and manganese. By blending this water with RO-treated water, the city will produce a higher quality of water for its citizens. The concentrated brine stream produced by the RO system will be sent to the Class I non-hazardous UIC wells for disposal. A schematic of this system is shown in Figure 2.

Figure 2: Proposed Hutchinson Water Treatment System Schematic

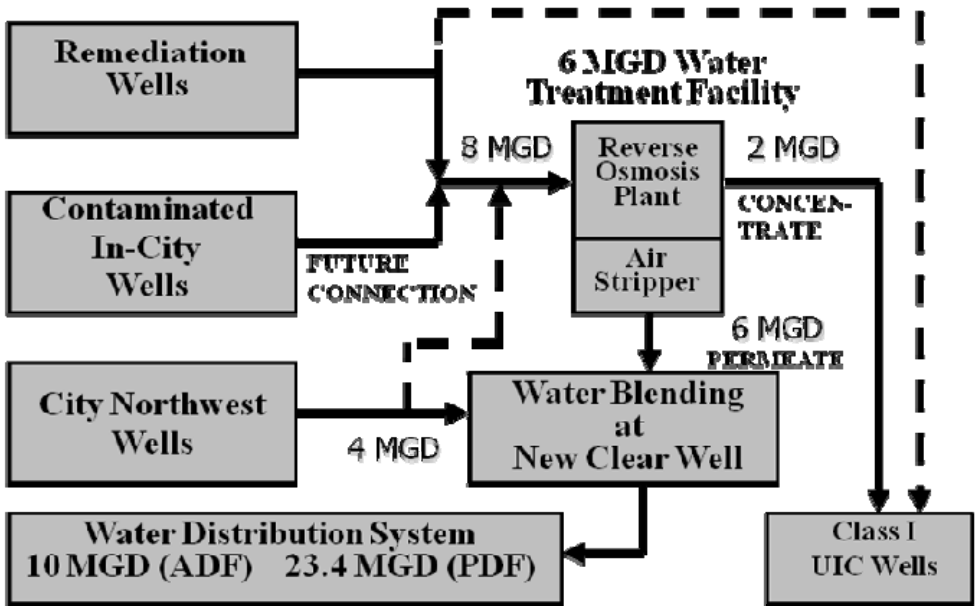

Raw Water and Finished Quality Goals

Currently, the raw water supply for the city of Hutchinson is entirely groundwater from the Equus Beds aquifer, which is primarily composed of saturated sand and silt. The city of Hutchinson's public water supply system consists of 16 active groundwater wells, which are divided into two geographic regions of the city: the NW wellfield and the In-City wellfield (southeast areas). The NW wellfield consists of higher quality groundwater and will be used to blend with the RO-treated water. The In-City wellfield, including several wells in the central portion of the city, consists of poorer quality groundwater. The water from these wells will not be used or treated by the RO treatment facility under the initial design plan; however, these wells may be brought online and treated in the future.

Currently, it is intended for only the NW wellfield and the remediation wellfield to supply water to the RO facility for treatment. The facility is designed for varying raw water blends of the two water sources to accommodate the overall water usage by the city. Current water quality data associated with these blends were obtained through existing and pilot plant programs. The treatment goal for the RO water treatment facility is to produce a finished water quality that meets and exceeds current and foreseeable future regulations. The result will be water with lower naturally occurring chloride, hardness, iron, and manganese levels, which will be more aesthetically pleasing to consumers. Table 1 shows the raw and finished water quality desired by the city of Hutchinson.

TABLE 1.
RAW AND FINISHED WATER QUALITY

Parameter	Unit	Raw Water	Finished Water
Alkalinity	mg/L	234 ~ 350	120 ~ 150
Chloride	mg/L	135 ~1420	80 ~ 120
Hardness	mg/L	315 ~ 517	100 ~ 150
Iron	mg/L	0.23 ~ 5.21	0.05 ~ 0.15
Langelier Index (L.I.)	-	-0.60 ~ +0.44	0.10 ~ 0.55
Manganese	mg/L	0.09 ~ 0.52	0.01 ~ 0.03
Nitrate nitrogen	mg/L	1.34 ~ 6.85	1.00 ~ 3.50
pH	-	6.8 ~ 7.7	7.8 ~ 8.2
Sulfate	mg/L	134 ~ 304	60 ~ 100
Temperature	Deg. C	12.8 ~ 18.3	12.8 ~ 18.3

The finished water quality presented in Table 1 is achieved by blending 60-percent RO-treated water with 40-percent NW wellfield water. Sodium hydroxide and chlorine are added for final water pH stability and for disinfection credits and residuals.

Reverse Osmosis Water Treatment Facility

The RO water treatment facility is currently under construction and scheduled to be operational in spring 2009. The facility has been designed and sized to meet the projected flow demands for the average daily flow projection of 10 mgd in the year 2030 by producing 6 mgd of RO-treated water to be blended with 4 mgd of NW wellfield water. Additionally, the facility is designed to support a peak pumping capacity of 23.4 mgd to meet projected peak-day demands using modified RO-treated water and NW wellfield water blends. The RO water treatment facility will consist of several distinct components used to meet the requirements for treatment, blending, distribution, and wastes. All components will be located at the same treatment site and will be automatically controlled with online water quality instrumentation and a centralized computer and radio telemetry system.

The influent wetwell will consist of two 50,000-gallon concrete reservoirs used to collect and blend raw water for treatment. Four vertical turbine pumps on variable frequency drives (VFDs) are used to pump raw water through the facility for treatment. Six greensand and anthracite pressure filters are provided to remove iron and manganese from the raw water, which include chlorine and potassium permanganate chemical feed systems for oxidation of the iron and manganese and for recharge of the filter media.

The RO treatment system consists of pretreatment, RO membranes, and post stabilization subsystems. The pretreatment system consists of sodium bisulfate feed to eliminate any residual chlorine, antiscalant chemical feed to protect the membranes from particulate formation, cartridge filters to protect the membranes from particulate carryover, and online instrumentation. The RO membrane system includes a manual clean-in-place system for acid and caustic chemical feed and pumping. Following the RO membranes, the permeate water is further treated by a degasification tower to strip any dissolved gases, carbon dioxide, and VOC compounds. This process leaves the water unstable with a low pH. Therefore, caustic soda chemical feed systems are provided to raise the pH to desired levels and to stabilize the water and make it less corrosive.

The RO-treated water is blended with NW wellfield water to meet the desired quantity and quality of water needed. Blending takes place within the piping, and chlorine disinfection is accomplished in a disinfection basin. The disinfection basin leads to two 300,000-gallon clearwells to store the treated water prior to distribution. Six VFD-driven high-service pumps are used to send clearwell water to the city distribution system. Clearwell water is also used by two VFD-driven pressure filter backwash pumps.

Concentrate wastes from the RO membranes are collected onsite and pumped approximately 5 miles to the Class I non-hazardous UIC wells. A wetwell of approximately 150,000 gallons is designed to provide for flexibility in operations and controls between the RO treatment facility pumps and the Class I wells.

Distribution System

With the construction of the RO water treatment facility, several improvements to the distribution system are required, including additions to the distribution system piping and upgrades to the water tower control system to accommodate varying flow directions, pressures, and water chemistry. The distribution piping modifications were completed in 2007 and 2008, during early RO water treatment facility construction and other city capital improvement projects.

Conclusions and Project Status

To date, the source area remediation at the former Farmland J and Bunge Elevators has resulted in significant reduction in the contaminant concentrations at the source areas. CT concentrations at the source areas have been reduced from several hundred µg/L to less than 5 µg/L (MCL), and in several cases less than the laboratory reporting limit of 1 µg/L. The AS/SVE system at the former Bunge Elevator was shut down shortly before the third quarter sampling and remained down during the fourth quarter of 2008 to monitor for possible rebound effects. The Bunge source area monitoring results have shown a minor rebound effect of CT above MCLs. Therefore, the Bunge AS/SVE system was restarted for the first quarter of 2009. All other source area systems remain in operation. The downgradient and Class I non-hazardous UIC wells have been in continuous operation since startup and are anticipating full operation of the RO treatment facility in spring 2009. At that time, the city will work toward taking over the third-party wells associated with downgradient capture and send this water to the RO treatment facility.

A collaborative effort between all parties involved in planning, design, and startup have worked to make this project a success, while remaining within the planned budget of $33 to $35 million. Key project components, costs, and funding are estimated as follows:

Project Components:

- Source remediation components; 4 AS/SVE source area systems, 1 soil source excavation.
- 3 extraction wells and 13,600 linear feet of 6" through 18" collection piping.
- 2 Class I UIC wells and equalization for remedial and RO concentrate disposal.
- 10-mgd average daily flow RO membrane water treatment facility.
- 90,300 linear feet of 12" through 36" raw water, concentrate, and distribution piping.

Project Funding:

Payments from companies responsible for contamination (PRPs)	$10,547,000
TCE and chloride remediation party agreement payments	$ 1,675,000
TIF district tax proceeds and interest earned	$ 1,086,000
Federal grants ($3.5 million less grant admin. costs)	$ 3,372,000
KDHE low interest loans – city funds	$16,650,000
Water utility capital improvement project (CIP) funds – city funds	$ 1,350,000
Total	$34,680,000

Project Cost:

Groundwater contamination source remediation	$ 740,000
RO Concentrate and Class I non-hazardous UIC wells)	$ 4,095,000
Groundwater remediation wells and pipelines	$ 2,610,000
RO water treatment facility	$17,660,000
RO raw water, concentrate and distribution system pipelines	$ 9,340,000
Total	$34,445,000

The city of Hutchinson, CDM, and PEC continue to work toward meeting the goals of remediation of the site, while minimizing design, construction, and operational costs associated with groundwater treatment and the RO water treatment facility.

Hutchinson, KS – 4th and Carey Site
Groundwater and Source Control Measures at Two Grain Elevators

Darren L. Brown, P.G[1], Danita S. Boettner, P.E.[2], Don Koci, P.G.[3],

[1]CDM, 345 Riverview, Suite 520, Wichita, KS 67204; PH (316) 660-6700; FAX (316)264-3025; email: BrownDL@cdm.com
[2]CDM, 6000 Uptown Blvd NE, Suite 200, Albuquerque, NM 87110; PH (505) 243-3200; FAX (505)243-2700; email: BoettnerDS@cdm.com
[3]City of Hutchinson, Public Works Department, 1500 S. Plum, Hutchinson, KS 67501; PH (620) 694-1900; FAX (620)694-1980; email: donk@hutchgov.com

Abstract
The 4th and Carey Site, U.S. Environmental Protection Agency (EPA) Identification Number KSD061608006, is located in Hutchinson, Kansas in Reno County. The site encompasses approximately 1,240 acres. Groundwater contamination at the site was discovered in the early 1980s when the EPA and Kansas Department of Health and Environment (KDHE) began testing public water supply wells. A city of Hutchinson well, located at the intersection of 4th Avenue and Carey Street, was found to be contaminated with volatile organic compounds (VOCs). The groundwater contamination findings conducted by EPA and the KDHE led to the establishment of the 4th and Carey site in 1994 with the city of Hutchinson assuming the lead role in order to keep the site from being placed on EPA's National Priority List (Superfund). Agreements were reached with potential responsible parties (PRPs) for the contamination.

Investigations at the site conducted by CDM for the city resulted in the identification of six carbon tetrachloride (CT) source areas; one trichloroethene (TCE) source area; one tetrachloroethene (PCE) and TCE source area; and two areas impacted by petroleum hydrocarbons. The TCE and PCE/TCE source areas are being addressed by the property owners under KDHE oversight. The areas impacted by petroleum hydrocarbons and one of the CT source areas are being monitored by the city. The remaining CT source areas required the implementation of source control measures for CT and its degradation products, primarily chloroform (CFM).

Source area investigation activities determined that the contaminant distribution at the five remaining CT source areas was predominantly located in the unsaturated soils and the top ten feet of the aquifer. The soils at the source area consist of 10 to 12 feet of silty clays underlain by 45 to 50 feet of sands and gravels. A shale formation serves as the base of the alluvial aquifer at the site. The water table at the CT source areas is generally within a couple feet of the base of the silty clays. The five CT source areas are located adjacent to grain elevators that used a CT-based compound as a fumigant prior to its banning by EPA in 1985.

Contamination at one of the CT source areas was addressed by a limited excavation program in 2004. The selected remedial alternative for the remaining four CT source areas was a combination of air sparging (AS) and soil vapor extraction (SVE). The AS/SVE remedial system was selected because of concerns that excavation efforts could impact the stability of the adjacent grain elevator bins and the operation of the elevators. With the water table at or near the base of the clays, the subsurface conditions were not ideal for an effective SVE collection system. Special construction techniques were required for the installation of SVE collection points to ensure that air sparge vapors could be collected.

The startup date for the AS/SVE systems was January 9, 2006. The AS/SVE systems in groundwater at the source areas have resulted in the reduction of CT concentrations from greater than 1,000 micrograms per liter (µg/L) to less than 5 µg/L without impacting the operations at the grain elevators.

Introduction

The site is located in south central Kansas in the city of Hutchinson, within Reno County and encompasses approximately 1,240 acres. Groundwater contamination at the site was discovered in the early 1980s when the EPA and Kansas Department of Health and Environment (KDHE) began testing public water supply wells. A city of Hutchinson well located at the intersection of 4th Avenue and Carey Street was found to be contaminated with volatile organic compounds (VOCs). The groundwater contamination findings conducted by EPA and the KDHE led to the establishment of the 4th and Carey site in 1994 with the city of Hutchinson assuming the lead role in order to keep the site from being placed on the U.S. Environmental Protection Agency's (EPA) National Priority List (Superfund). The site, EPA Identification Number is KSD061608006, is shown on **Figure 1**.

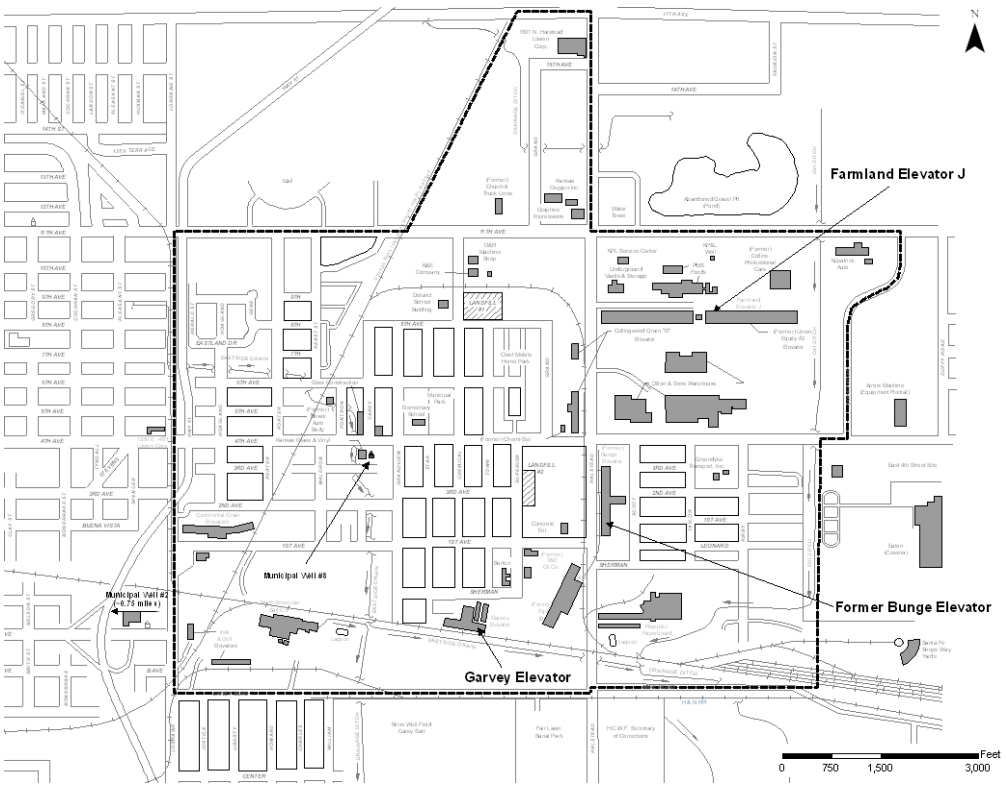

Figure 1 – Site Map – 4th and Carey Site, Hutchinson, Kansas

Carbon tetrachloride was first detected at a concentration of 1.6 µg/L in a sample collected from public water supply well #8 (PWS #8) on June 7, 1982 and increased in concentration until the city removed PWS #8 from service on April 20, 1985 at KDHE's request.

The site has been subject to a series of investigations beginning in 1984. Following completion of a Listing Site Investigation in 1991, EPA scored the site using the Hazard Ranking System (HRS) for inclusion of the site on the National Priorities List (NPL) in January, 1993. The city, with the Potentially Responsible Party (PRP) Group's assistance, took the lead on the Remedial Investigation (RI) and Feasibility Study (RI/FS) because of the potential threat to public health and because property values could be adversely affected if the site were enrolled into the Superfund Program. This resulted in EPA transferring oversight of the RI/FS to KDHE. KDHE outlined the requirements of the RI/FS and defined the site boundaries in a Consent Agreement and Consent Order (CACO) between the city and KDHE on April 25, 1994.

The 4th and Carey remedial investigation (RI) field activities were conducted by CDM for the city between August 1994 and January 1997. The RI report was approved as final by KDHE on February

12, 1998. Upon completion of the RI, source control investigations (SCIs) were conducted at the former Farmland Elevator J, former Bunge Elevator, and former Garvey Elevator. The SCIs at these elevators were completed and approved by KDHE on October 26, 2001.

Site Characteristics

The site is generally flat with a gentle topographic dip to the south and southeast. The land use within the site is diversified and includes commercial, industrial, recreational, and residential properties. The geology of the study area primarily consists of Arkansas River Valley alluvium, Pleistocene-age glacial outwash, and associated terrace deposits overlying the Permian-aged Ninnescah and Wellington Formation bedrock. Both formations primarily consist of shales with salt deposits present within the Wellington Formation. Depth to bedrock averages approximately 60 feet below ground surface. The aquifer at the site consists of sands and gravels with an average thickness of 43 to 55 feet. In general, the sediments in the water bearing zone appear to be coarser (more permeable) with depth. The upper 12 to 15 feet consists of interbedded silts and clays, with some sand stringers.

Aquifer testing in the area indicates a hydraulic conductivity ranging between 517 to 771 feet per day. Storativity ranges from 0.019 to 0.065. Groundwater flows principally to the southeast, though local flow directions vary considerably with localized aquifer stresses (e.g., pumping wells). The hydraulic gradient also varies locally, ranging from 0.0006 to 0.003 feet per foot. Based upon the above information, the groundwater velocity is estimated to range between 0.3 to 2.3 feet per day. The hydraulic gradient and groundwater velocity increase near pumping wells. In April 2007, a private third party (third party #1) began operating five extraction wells with a planned total extraction rate of 500 gallons per minute (gpm) in the south central portion of the site as well as south of the site as part of their chloride plume containment efforts. The extracted groundwater is discharged at two Class I non-hazardous underground injection (UIC) wells installed by the city as part of the final corrective action decision (CAD). Groundwater flow in the southeastern portion of the site is also impacted by groundwater extraction efforts of another third party (third party #2) as part of their remedial containment system for their TCE groundwater plume. Third party #2 operates three groundwater extraction wells with total rate of approximately 1700 gpm. The groundwater extracted by third party #2 is currently treated by air stripping and discharge to a surface water drainage ditch. **Figure 2** shows a potentiometric map as of September 2008.

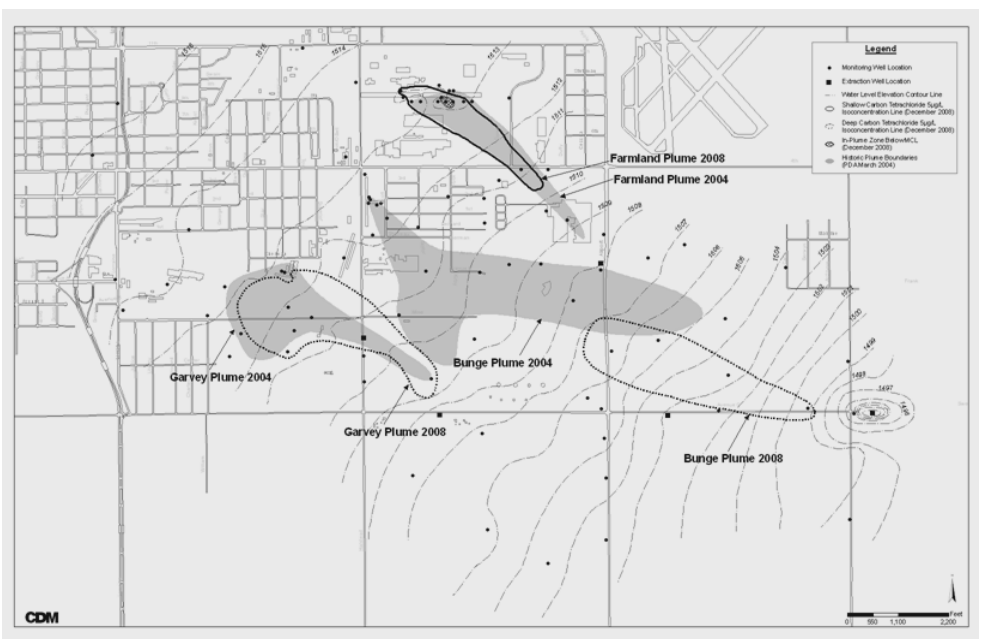

Figure 2 – September 2008 Potentiometric Surface Map and CT Plume Distribution

Contaminant Distribution

Investigations at the site conducted by CDM for the city resulted in the identification of six CT source areas; one TCE source area; one PCE and TCE source area; and two areas impacted by petroleum hydrocarbons. The TCE and PCE/TCE source areas are being addressed by the property owners under separate CACOs with KDHE oversight. The areas impacted by petroleum hydrocarbons and one of the CT source areas are being monitored by the city. The remaining CT source areas required the implementation of source control measures. Three offsite groundwater plumes (two PCE and one PCE and TCE) were observed migrating onto the western portion of the site. These plumes are being addressed by outside parties under KDHE oversight.

Through its own investigations, KDHE identified three areas with chloride impacts within the site. The sources of chloride impacts include a former salt mining and production facility; a former soda ash mining operation; and a former tanning operation. The majority of the chloride impact is in the south central portion of the site, as well as south of the site. The chloride impacts on the groundwater are significant in that extracted and VOC-treated groundwater could not be discharged to surface waters due to the total maximum daily limit (TMDL) restrictions associated with total dissolved solids.

Two shallow groundwater carbon tetrachloride (CT) plumes were identified as emanating from three source areas at the Farmland Elevator J facility. One shallow groundwater CT plume was identified as emanating from the former Bunge Elevator. A CT plume was also identified as emanating from the Garvey Elevator.

VOC contamination at the former Farmland J and former Bunge Elevator is characterized by soil impacts at the release areas, which extend down to the water table interface. CT is a dense non-aqueous phase liquid (DNAPL) and as a pure product can migrate vertically through an aquifer and accumulate as a free phase product at the base of an aquifer. At the former Farmland J and Bunge Elevators, the data indicates that the CT product migrated downward to the water table but appeared to be of insufficient mass or density to overcome the capillary pressure in the sediments at the water table interface. The CT contamination appears to have spread laterally over a relatively small area on top of the water table surface. Groundwater testing at these source areas indicated that the bulk of the CT contamination was confined to the upper few feet of the aquifer. The identified releases at the former Farmland J Elevator are referred to as farmland J southeast (SE), farmland J southwest (SW), and farmland J northeast (NE). Maximum CT concentrations in groundwater at the three Farmland J SE, SW, and NE source areas, collected by direct-push technology (DPT), were 7,700; 2,000; and 5,300 µg/L; respectively. It appears that the monitoring wells installed at the source areas had lower concentrations as a result of dilution effects due to a larger sensing zone compared to the direct-push sensing zones. The maximum CT concentrations observed in groundwater at the Bunge source area, collected by DPT, were 8,000 µg/L. As with the farmland source areas, the monitoring well installed at the Bunge source area was lower than the DPT results. At the Farmland and Bunge elevator source areas, the CT contamination is primarily situated in the upper portion of the aquifer and then migrates down into the middle and lower portions of the aquifer.

VOC contamination at the former Garvey Elevator had two components. The shallow soils at the former CT storage tank pad were impacted by CT. Additionally, the RI investigation identified significant CT groundwater contamination (in the milligrams per liter range) at the base of the aquifer at the former Garvey Elevator. Groundwater testing did not identify significant CT impact in the middle portion of the aquifer and the mechanism of the CT release for the deep groundwater contamination was not identified. Subsequent source control investigation (SCI) work conducted between 1998 and 2002 indicated that the high levels of deep CT contamination at the former Garvey Elevator had apparently migrated downgradient with only minimal CT concentrations remaining in the deep groundwater at the apparent source area. VOC contamination in groundwater associated with the Garvey source areas is characterized by shallow and deep plumes in the alluvial sediments.

In general, the shallow plumes originate in the source areas and are of limited horizontal extent as the contaminants tend to move from shallow to deeper groundwater away from the source areas due to

apparent increased permeability with depth in the shallow sediments. Thus, the downgradient groundwater plumes are more extensive than the shallow source area plumes.

Corrective Action Decision

The KDHE issued a final interim CAD for source area remediation at the 4th and Carey site in June 2002. The final interim CAD summarized the RI/FS report for the 4th and Carey site and established selected remedial alternatives for the site. The selected remedial alternative specific to the Bunge and Farmland J source areas was air sparging (AS) and soil vapor extraction (SVE). Excavation at these four source areas was screened as a remedial action due to concerns over the stability of the adjacent grain bins. The final interim CAD was revised to include the preferred remedial alternative for downgradient containment in November 2004 and became the final CAD for the site on May 9, 2005.

Cleanup goals for groundwater at the 4th and Carey Site are 5 µg/L for CT, 80 µg/L for CFM—the federal maximum contaminant levels (MCLs) associated with the Safe Drinking Water Act. Cleanup goals for soil are the Kansas Risk-Based Standards for the residential migration to groundwater pathway (0.2 milligrams per kilogram (mg/kg) for CT and 0.96 mg/kg for CFM).

The city of Hutchinson is responsible for the remediation activities at three CT source areas at the former Farmland J Elevator; one CT source area at the Bunge Elevator; and a fifth CT source area at the former Garvey Elevator. Other VOC source areas are being addressed by other responsible parties.

Several controls have been instituted with the intent to prevent exposure to contaminated groundwater. These controls consist of: 1) groundwater use restrictions, 2) deed restrictions, 3) public education (such as mailings and public meetings), and 4) provision of alternate water supply. The city monitors and maintains these controls on an annual basis to ensure protection of human health and the environment. Changes of land use in impacted areas are also monitored.

Source Area Remediation

Pre-design data acquisition (PDA) activities were conducted in accordance with the KDHE's Interim CAD for Source Area Remediation established on July 9, 2002 between them and the city. Data collected during the PDA field work provided a basis for sizing the equipment, pipes, and wells, and for designing the placement of AS and SVE systems, as well as the monitoring and extraction wells. Additionally, the PDA provided water-level and contaminant-concentration information to serve as a basis for measurement of remedial effectiveness.

Based on the findings of the PDA, it was concluded that AS can effectively reduce VOC concentrations in groundwater at the source areas. The air sparge zone of influence (ZOI) with a radius of 20 feet was established at a pressure of 14 pound-force per square inch gauge (psig). Pilot testing indicated a 4-hour air sparging interval was sufficient to produce mounding and collapse of the groundwater. The data also indicated that two hours with no air sparging was sufficient time to allow the water table to return to static conditions between AS pulses.

The SVE testing showed no minimal effect in the shallow vadose zone soils at the former Farmland J Elevator. The former Bunge Elevator testing showed one well with no vapor flow while the other well produced vacuum. The SVE ZOI was established to be between 40 and 57 feet at 25 inches of water vacuum based upon the pilot test at Farmland J Northeast. Other design considerations based on PDA data include SVE well designs customized for local lithology (in cases where limited unsaturated sands are present for vapor collection) and related engineering controls to capture as much AS air as possible.

During 2004, the shallow source area at the former Garvey Elevator was remediated by excavating the shallow soils in the vicinity of the former CT tank. The excavated soils were properly disposed at a KDHE-approved landfill. The deep groundwater at the former Garvey Elevator is being monitored to ensure that no CT concentrations re-occur, which could trigger the implementation of source control measures.

Source Area Remediation at the Former Farmland and Bunge Elevators

The selected remedy for the remediation of the shallow soil and groundwater source areas at the former Farmland J (NE, SE, and SW) and Bunge Elevators was AS/SVE. Several site conditions affected the design of the AS/SVE systems.

- The PRP properties are currently owned and operated by separate parties. Therefore, work in these areas required access agreements and associated design approvals by the respective party, in addition to the PRPs.
- Facility-owned rail lines located at the north and south sides of Farmland limited the placement of wells and associated piping.
- SVE and AS wells had to be completed below grade to accommodate elevator operations.
- The AS wells were divided into operating zones with each zone operating individually to accommodate a pulsing operation, groundwater mounding, and collapse.
- The presence of clayey soils with intermingled silt and sand lenses at the Bunge, Farmland SW, and SE source areas at or just above the water table required an alternate SVE design to capture as much AS air as possible.
- SVE wells operate continuously at all four locations.
- Vapor monitoring points (VMP) were installed to monitoring vacuum in the vadose zone created by the system.

Startup for the AS/SVE systems began on January 9, 2006. A description of each AS/SVE system is provided below.

Bunge

The AS/SVE system installed at the former Bunge Elevator consists of four AS wells and two SVE wells. The AS/SVE system is described below.

- Two sets of two, 2-inch diameter AS wells were installed with 35 foot spacing. One set was installed on the north side of the elevator and the second set was installed on the south side of the elevator.
- The four AS wells were divided into two operating zones (two north wells in one zone, two south wells in the second zone) with each zone (two wells) operating individually to accommodate a pulsing operation. A total flow per zone of 30 standard cubic feet per minute (scfm) is provided to each zone in operation.
- Two, 4-inch diameter SVE wells were installed within 6-foot diameter boreholes due to an insufficient thickness of vadose-sand interval above the water table to capture vapor from the AS systems. One well between each AS well set spaced approximately 15 to 20 feet from each AS well. SVE wells operate continuously to capture as much AS air as possible.
- Two vapor monitoring points (VMP) were installed to monitor vacuum in the vadose zone created by the system.

Farmland NE

- Seven, 2-inch diameter AS wells were installed, including two wells north of the railroad tracks spaced 40 feet apart east to west and five wells south of the railroad tracks spaced 40 feet apart, extending 160 feet east to west. One existing AS well, constructed for the pilot test and located between the railroad tracks, was also incorporated into the AS system.
- The eight AS wells were divided into three operating zones (two to three wells in each zone) with one zone (two to three wells) operating at one time translating to a total flow per zone of 30 to 45 scfm.
- Three, four-inch diameter SVE wells were spaced 60 to 70 feet apart over 130 feet, between the two sets of railroad tracks.
- Three vapor monitoring point (VMP) wells were installed to monitor the vacuum in the vadose zone exerted by the SVE system.

Farmland SE

- Five, 2-inch diameter AS wells, including three wells north of the railroad tracks spaced 40 feet apart, extending 80 feet east to west, and two wells are between the railroad tracks spaced 40 feet apart east to west.
- The five AS wells are divided into two operating zones (the three northern wells in the first zone, the two southern wells in the second zone) with one zone (two to three wells) operating at one time translating to a total flow per zone of 30 to 45 scfm.
- Two, 4-inch diameter SVE wells were installed within 6-foot boreholes evenly spaced between the northern AS wells.
- Two VMP well was installed to monitor the vacuum created by the SVE system.

Farmland SW

- Six, 2-inch diameter AS wells are spaced 35 feet apart and extend 175 feet east to west between the railroad tracks and the Farmland J Elevator west wing.
- The six AS wells are divided into three operating zones (two wells in each zone) with one zone (two wells) operating at one time translating to a flow of total flow per zone of 30 scfm.
- Three, 4-inch diameter SVE wells are installed within 6-foot boreholes spaced approximately 70 feet extending 140 feet east to west, approximately five feet south of the AS well line and beginning 17.5 feet east of the westernmost AS well.
- Three VMPs were installed to monitor the vacuum in the vadose zone exerted by the SVE system.

The AS wells were installed using an 8.25-inch outside diameter (OD) hollow stem auger and drill rig. Each well was constructed with two-inch diameter, Schedule 40 PVC with a five-foot, 0.010-inch slotted screen set at the bottom five feet of the well. The wells were completed by placing filter sand from the bottom of the borehole to approximately 2 feet above the screened interval, a two-to-four foot-thick filter pack seal of ¼-inch coated bentonite pellets above the filter pack, and an annular space seal of neat cement grout from the top of the filter pack seal to approximately 5 feet below ground surface (bgs). The total depth of the AS wells was 40 feet bgs (approximately 26 feet below the water table) with five foot of screen at the base of the well.

In order to compensate for the lack of sufficient permeable sand material in the vadose zone above the water table at the Bunge, Farmland SE, and Farmland SW source areas, SVE wells at these source areas were installed using a bucket auger rig to create a six-foot diameter borehole. A temporary 8-inch plastic casing was lowered to the bottom of the borehole and centered within the borehole. A 4-inch diameter PVC well with a 5-foot, 0.010-inch slotted screen was placed inside the temporary casing. The bucket auger borehole was filled to 8 feet bgs with crushed rock material. The annulus between the temporary casing and the 4-inch well was filled with filter sand from the bottom of the borehole to 8 feet bgs (approximately 2 feet above the screened interval). Following placement of the filter pack, the temporary casing was removed. Approximately 2 to 4 feet of 3/8-inch diameter bentonite chips were placed above the crushed rock and filter pack material. The screen interval of these SVE wells is 10 to 15 feet bgs. **Figure 3** shows a generalized cross-section of the AS/SVE system at the former Bunge Elevator.

SVE wells installed at the Farmland NE source area were installed using an 8.25-inch OD hollow stem auger and drill rig. Each well was constructed with 2-inch diameter, Schedule 40 PVC with a 5-foot, 0.010-inch slotted screen set at the bottom 5 feet of the well. The wells were completed by placing filter sand from the bottom of the borehole to approximately 2 feet above the screened interval, placing a 2-to-4-foot-thick filter pack seal of 3/8-inch bentonite chips above the filter pack, and placing an annular space seal of neat cement grout from the top of the filter pack seal to approximately 4 feet bgs. The screen intervals for the Farmland NE SVE wells are 9 to 14 feet bgs.

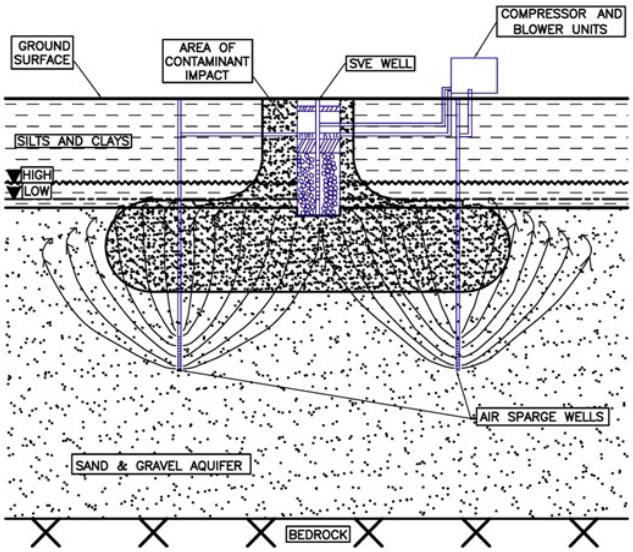

Figure 3 – Generalized Cross-Section of AS/SVE System at the Bunge Source Area

Generally, the AS systems operate at approximately 12 to 15 psi pressure with a typical flow of approximately 12 to 18 scfm per well at the manifold. The AS manifold timers are set to operate on a staggered on/off cycle to reduce the potential of sparge bubbles from setting up preferential pathways and potentially failing to effectively strip VOCs out of the aquifer. The AS wells are connected to the compressors via manifolds with a combination of two or three wells per manifold. The SVE system operates at approximately 10 to 50 inches of water (IOW) vacuum pressure, depending on the system, and a typical flow of 22 to 32 scfm for the individual wells. The SVE wells are connected to the blower via a manifold. The SVE system is in continuous operation and the blowers operate at approximately 150 percent of the AS flow rate. The piping is buried at a minimum of 42 inches for freeze protection and has been slightly sloped towards either the wells or condensate knockouts to minimize condensate collection in pipelines. Buried and trailer mounted condensate knockouts are pumped into a temporary storage tank for off-site disposal, when necessary.

System Operation and Monitoring

Groundwater monitoring for the 4th and Carey Site is required under the Final Corrective Action Decision dated May 17, 2005 and is as follows:

- The site monitoring network was selected from existing monitoring wells for the purposes of monitoring volatile organic compound (VOC) concentrations within the existing plumes and at or in the vicinity of the MCL boundaries, and to monitor contaminant transport from shallow to deep groundwater. Site monitoring network locations were selected to provide data for evaluating changes in site-wide contaminant transport and contaminant mass, as well as monitoring site-wide plume boundaries.

- Source area remediation performance monitoring measures the effectiveness of the air sparge/soil vapor extraction (AS/SVE) systems at the former Bunge and Farmland J elevators and documents contaminant levels at each source area. The startup date for the AS/SVE systems was January 9, 2006 with final acceptance on October 10, 2007. Groundwater monitoring and air monitoring of VOC concentrations are conducted on a quarterly basis for these source areas. The shallow Garvey source area was addressed by limited soil excavation activities in 2004. Currently, remediation activities at the Garvey source area consist of quarterly groundwater monitoring of VOC concentrations to verify continued reduction in contaminant concentrations.

The former Garvey Elevator was demolished and the resulting debris removed in 2008. The other elevators continue to remain operational.

To date, the source area remediation at the former Farmland J and Bunge Elevators has resulted in significant reduction in the groundwater concentrations at the source areas. **Figure 2** shows the plume configuration as of December 2008. CT and CFM concentrations at the source area monitoring wells have been reduced from several hundred µg/L to less than MCLs and in several cases less than the laboratory reporting limit of 1 µg/L. The monitoring wells immediately downgradient of the source areas have also shown significant reductions in CT concentrations. **Figures 5 through 8** show the CT trends at the Farmland and Bunge source areas. There are two charts shown for each source area. The above chart shows the concentrations at the source area monitoring well. The lower chart shows the concentrations at the nearest downgradient monitoring well located outside of the direct influence of the AS/SVE system. The AS/SVE system at the former Bunge Elevator was shut down shortly before the third quarter sampling and remained down during the fourth quarter of 2008 to monitor for possible rebound effects. The Bunge source area monitoring well results do show a minor rebound effect of CT above MCLs. The Bunge AS/SVE system was restarted for the first quarter of 2009. Based upon the available data, CDM anticipates shut down of all four AS/SVE systems by late 2009 or early 2010

Summary and Conclusions

The 4th and Carey Site has been impacted by a number of chlorinated VOCs. Groundwater has also been contaminated by elevated chloride concentrations from three sources. The chloride impacts are significant enough that discharge of groundwater only treated for VOCs to surface waters would not be permitted by KDHE. The city of Hutchinson is responsible for the remediation activities at three CT source areas at the former Farmland J Elevator; one CT source area at the Bunge Elevator; and a fifth CT source area at the former Garvey Elevator. Other VOC source areas are being addressed by other responsible parties. Source area remediation at the former Farmland J Elevator and the former Bunge Elevator is being implemented through AS/SVE systems. The AS/SVE systems have been in operation since January 2006. CT and CFM concentrations in the source area monitoring wells have been reduced from several hundred µg/L to less than MCLs and in several cases less than the laboratory reporting limit of 1 µg/L. The Bunge AS/SVE system was shut down during the fourth quarter of 2008 and did show a minor rebound (CT <20 µg/L). All four systems are currently operating. Shut down of all four AS/SVE systems is anticipated to occur in late 2009 or early 2010.

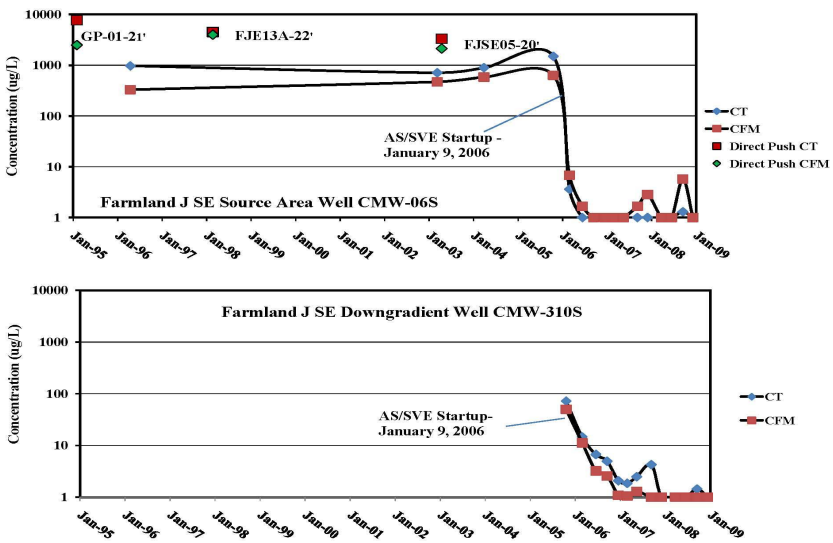

Figure 5 – Farmland J SE Source Area Groundwater Trends

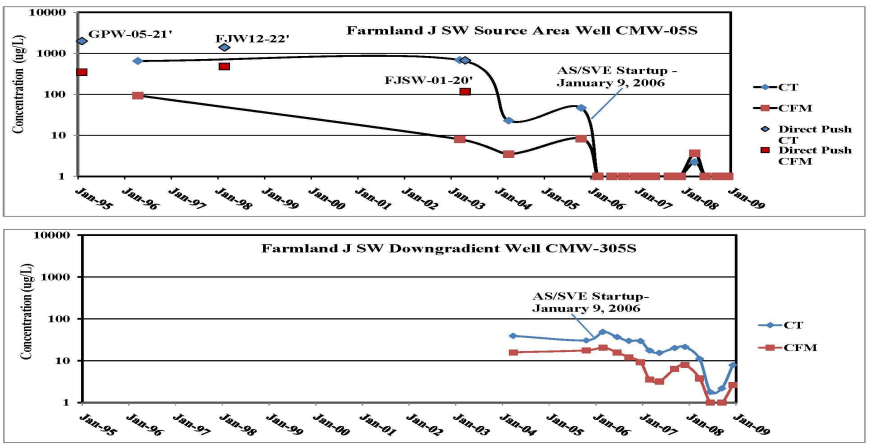

Figure 6 – Farmland J SW Source Area Groundwater Trends

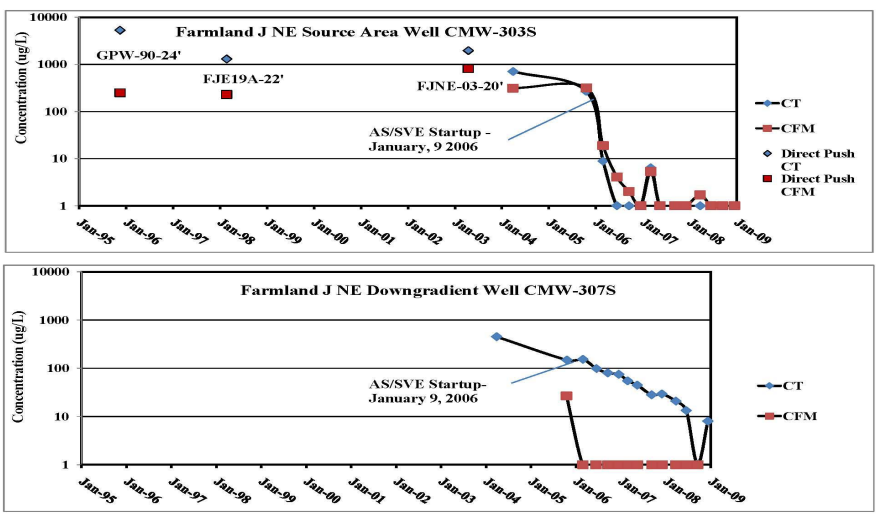

Figure 7 – Farmland J NE Source Area Groundwater

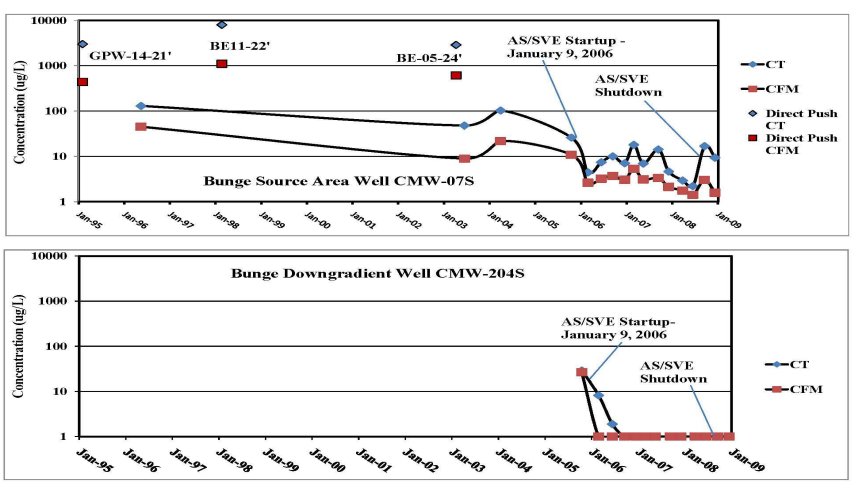

Figure 8 – Bunge Source Area Groundwater Trends

Impacts of Biota on Bioretention Cell Performance during Establishment in the Midwest

A. M. Greene[1, 2], S. L. Hutchinson[3], R. Christianson[4], T.L. Moore[5]

[1]Department of Biological and Agricultural Engineering, Kansas State University, 129 Seaton Hall, Manhattan, KS 66506; PH (785) 532-2900
[2]Water Resources Division, Camp Dresser McKee, 9200 Ward Parkway Suite 500, Kansas City, MO 64114; PH (816) 444-8270; email: greeneam@cdm.com
[3]Department of Biological and Agricultural Engineering, Kansas State University, 147 Seaton Hall, Manhattan, KS 66502; PH (785) 532-2943; email: sllhutch@ksu.edu
[4]Department of Agricultural and Biosystems Engineering, 215 Davidson Hall, Iowa State University, Ames, Iowa 50011; PH (515) 294-1230; email: reiddc@gmail.com
[5]Department of Biological and Agricultural Engineering, 208 D.S. Weaver Labs, North Carolina State University, Raleigh, NC 27695; PH (919) 515-2694; email: trish.culbertson@gmail.com

ABSTRACT

To understand the region-specific effects of biota on function of bioretention cells, a lysimeter study was conducted at Kansas State University to determine how earthworms and native Kansas grasses impact runoff treatment and hydraulic function of a bioretention cell. This study also employed the Comprehensive Bioretention Cell (BRC) model to demonstrate how three seasons of growth could impact bioretention cell function. The model results of the first season of growth were then compared to field data. Results indicate that the interaction of plant roots and soil macrofauna over one growing season improved several aspects of bioretention cell function. The greatest increase in saturated hydraulic conductivity was in the treatment that included both plants and macrofauna. The presence of vegetation reduced ponding effects and increased water storage. Earthworm treatments had a lesser ability to store water. All treatments were effective in reducing the concentration of P in effluent. A large amount of N was released during all events from all treatments probably because of a high initial N content of the bioretention media. No treatment performed significantly better in improving water quality, indicating that macropore flow in the earthworm treatments did not induce a higher rate of pollutant transport.

INTRODUCTION

Urban stormwater management is receiving increased attention as a result of the National Pollutant Discharge Elimination System (NPDES) Permit Program and growing awareness of stormwater runoff impacts on surface and groundwater source quality and quantity. To alleviate stormwater impacts on receiving waters, a number of Stormwater Best Management Practices (BMPs) have been developed. BMPs can be used in conjunction with, or as an alternative to, traditional stormwater practices and facilitate water treatment through natural processes.

A bioretention cell is a recessed area of vegetation designed to accept and treat stormwater runoff through infiltration into layers of plant roots and growing medium, and is just one example of a BMP. The conventional design has been found to significantly

reduce concentrations of heavy metals (copper, lead, and zinc), oils and grease, Total Kjeldahl Nitrogen (TKN), ammonium, and total phosphorus from stormwater runoff (Davis et al., 2001; Davis et al. 2003; Sharkley and Hunt, 2005). However, design limitations arise from the lack of understanding of the influence of ecological factors on the function and longevity of bioretention cells.

Previous bioretention research has focused on engineering the cell for hydraulic properties and has thus neglected the important role that plants and belowground processes play in improving infiltration and pollutant removal. Bioretention cell research has also primarily been conducted on the east and west coasts of North America, leaving few applicable standards for other regions. A functioning bioretention design must mimic a natural, functioning ecosystem. This "ecosystem" must be regionally appropriate and site-specific. By incorporating native vegetation and fauna, a bioretention cell will establish more rapidly and be more stable during changes in runoff volumes and pollutant concentrations.

A lysimeter study was conducted on the Agronomy Research farm at Kansas State University to assess the impacts of vegetation and microfauna, particularly a native Tallgrass Prairie mixture and *Lumbricus terrestris* (Canadian nightcrawlers), on the pollutant removal and hydraulic function in a bioretention cell. The objectives of this lysimeter study were; (1) to quantify overall water quality improvements, (2) to quantify overall changes in runoff quantity, (3) to quantify how earthworms and plants influence infiltration rates, and (4) to employ a model showing impacts of earthworms and soil fauna on soil macroporosity, and compare results to field data.

METHODS AND MATERIALS

Study Site

The study was conducted using twelve lysimeter cells (75 cm wide, 230 cm long, and 230 cm deep) located on the Kansas State University North Agronomy Research farm. The average high temperature range is from 4-32°C and the average low temperature ranges from -10-20°C. The mean annual precipitation is 835 mm (LTER, 2008). Three-fourths of the annual precipitation falls during the growing season from April-June with intense thunderstorms. This is followed by periods of drought during hot summer months (Hayden and Davis, 1998).

Experimental Design

The study consisted of four treatments in a completely randomized design; (1) earthworms only, (2) vegetation only, (3) earthworms and vegetation, and (4) control (see Figure 1). The cells were installed belowground with a 5 cm drainage pipe to allow water to drain from the cell. The lysimeter cells were used for previous water quality studies and were left with a 1 m layer of silt-loam soil. The remaining 100 cm were filled with a similar silt-loam soil (48% sand, 43.5% silt, 8.5% clay).

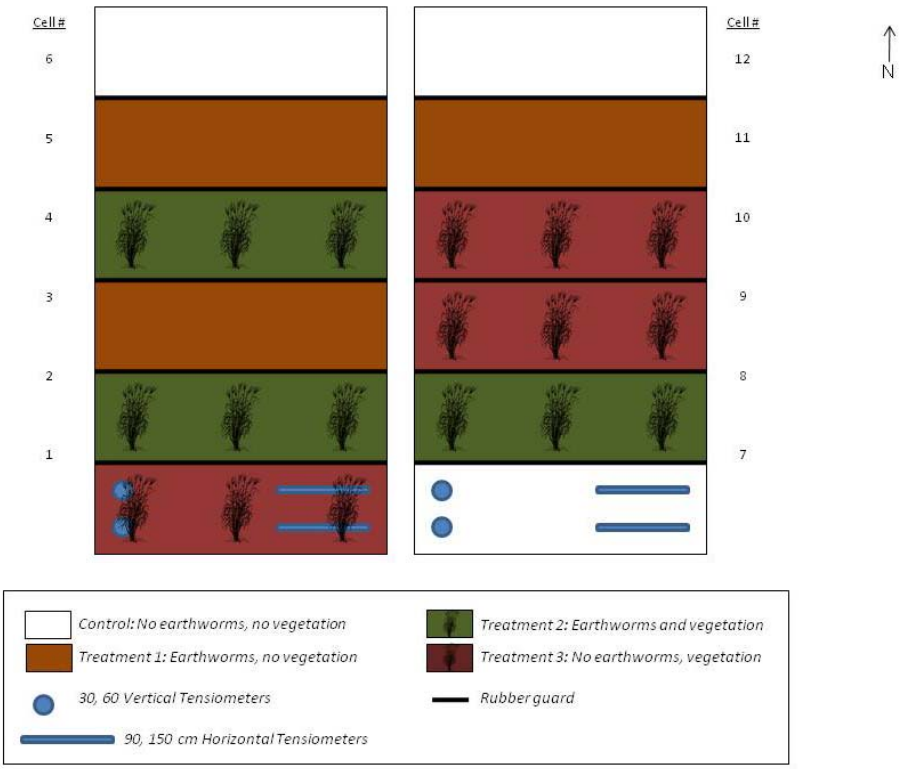

Figure 1. Configuration of lysimeter cells in completely randomized design.

To track changes in nutrient and metal content, five 30 cm (1 ft) deep soil cores were taken after weathering over the winter and after the conclusion of the growing season. Soil samples were analyzed for pH, nutrients, and metals. Synthetic stormwater and irrigation water was applied via a gravity-fed PVC pipe system. The chemicals used for the synthetic stormwater were mixed with potable water from the North Farm in 100 gallon tanks that drained into the PVC pipe system. Outflow was measured to the nearest liter.

On April 15, 2008 lysimeters cells 2, 3, 4, 8, and 10 (see Figure 1) were planted at with *S.* scoparium, Tripsacum *dactyloides*, *Sorghastrum nutans*, and *Bouteloua curtipendula*. These grasses were chosen because of their dense root structure and their ability to withstand the climatic variability. The root formation provides paths for water to flow into the soil, and thus may increase the storage capacity of a bioretention cell. Plant growth was monitored throughout the season and biomass was measured at the conclusion of the season by removing all aboveground biomass 5 cm above ground level. Roughly 10% (by weight) of removed biomass was dried overnight at 105°C and weighed to determine the dry-weight of aboveground biomass.

On April 1, 2008, 72 Canadian Nightcrawlers (*Lumbricus terrestris,* Figure 3.3) from Derick's Bait and Tackle (of unknown origin) in Manhattan, KS were introduced to cells 2, 5, 8, 9, 10, and 11 (see Figure 1). The burrowing activity of earthworms facilitates water movement via macropore flow. *L. terrestris* form vertical burrows that can be up 2.4 m deep (Shipitalo and Butt, 1999) that remain intact in an undisturbed soil system.

Synthetic Stormwater Tests

Each cell received natural precipitation as well as synthetic stormwater treatments. Table 1 shows the components of the synthetic stormwater. Water samples were collected for quality analysis either during synthetic stormwater application or at 48 hours after application, depending on the storm duration. Water pooled at the cell bottom for 48 hours may induce anaerobic conditions, and thus may impact nitrate removal through denitrification.

Table 1. Chemical components of synthetic stormwater

Pollutant Source	Mass (mg $10L^{-1}$)	Pollutant	Conc. (mg L^{-1})
Cupric Sulfate $CuSO_4 \cdot 5H_2O$	0.8	Copper	0.13
Sieved Soil	1	Total Suspended Solids	100
DAP $(NH_4)_2 \cdot HPO_4$	26	Nitrogen	0.47
		Total Phosphorus	1.2
Urea $(NH_2)_2 \cdot CO$	63	Nitrogen	2.83
		Total Nitrogen	3.3

Two different types of synthetic stormwater treatments were applied to the lysimeter cells. The first type of treatment, TREAT1, consisted of the water quality volume (WQv) generated from a representative watershed of 11.7 m^2 (MARC, 2008). Based on this procedure, 0.38 m^3 (100 gal.) of synthetic stormwater was applied to each cell for TREAT1. In the second treatment, TREAT2, 1.5 m^3 (400 gal.) of synthetic stormwater was applied to each cell. Results from the second treatment provided minimum size requirements for a bioretention cell to effectively treat an area.

All stormwater treatments were applied within 48 hours of each significant (> 13 mm) natural rainfall event from August to October 2008. There were no synthetic stormwater applications prior to August 2008 to demonstrate a potential bioretention cell management technique: routing stormwater runoff away from the cell during vegetation establishment.

Infiltration Tests

Cell soil moisture was measured prior to synthetic stormwater applications using vertical tensiometers located at 30 and 60 cm depths to note the impact of soil moisture on infiltration. Cell soil moisture was recorded weekly from August to October 2008 to note fluctuations in moisture. Infiltration rates were measured using a double ring infiltrometer prior to planting in March and again in October at the completion of this study. Infiltration during synthetic stormwater application was measured by noting the difference in time between whole-cell application and complete infiltration of the water front.

Comprehensive Bioretention Cell Model

The Comprehensive Bioretention Cell (BRC) Model was used to predict how a bioretention cell functions under a single storm event. The model allows cell designers to determine appropriate dimensions for bioretention layers based on desired pollutant

trapping efficiency and effluent water quality (Christianson, 2005, Christianson et al., 2004). Three parameter inputs, fractal dimension (Dv), macropore size (MAC), and layer depth, were manipulated to represent earthworm and vegetation impacts on infiltration; all other parameters were held at default values. Estimates for the parameters were based on the rates of macropore formation by earthworms and vegetation and the resulting macropore densities. This information was taken from previous research on earthworm dynamics and soil physical properties (Binet and Curmi, 1992, Butt and Nuutenin, 1998, Edwards et al., 1988, Edwards et al., 1990, Lee and Foster, 1991, Rice et al., 1998, Shipitalo and Butt, 1999, Weaver, 1946, Weaver, 1958, Weaver and Rowland, 1952)

It is very difficult to model the development of a living system over time as many different environmental factors control the progression of growth. The complex process was simplified for use in the BRC model by first compiling information on earthworm burrow and plant root size, population density, depth, and season of activity from ecological literature. Table 3 shows estimates for the D_v, MAC, and layer depth parameters in the BRC model based on ecological data. These values were used to model cell performance over the first three years of growth.

Table 2. Ecological data for BRC model parameters with sources

	Growing Season 1							
	D_v	**MAC**	**Layer 1**	**Layer 2**	**D_v**	**MAC**	**Layer 1**	**Layer 2**
	April				*September*			
EW	1.72	0.02	75	199	1.76	0.7	100	100
PL	1.72	0.02	1	199	1.74	0.05	30	170
EW + PL	1.72	0.02	1	199	1.75	0.9	100	100
Control	1.72	0.02	1	199	1.73	0.02	5	195
	Growing Season 2							
	D_v	**MAC**	**Layer 1**	**Layer 2**	**D_v**	**MAC**	**Layer 1**	**Layer 2**
	April				*September*			
EW	1.78	0.9	120	80	1.8	1	120	80
PL	1.74	0.05	50	150	1.75	0.1	70	130
EW + PL	1.76	1	120	80	1.76	1	120	80
Control	1.73	0.02	5	195	1.75	0.02	10	190
	Growing Season 3							
	D_v	**MAC**	**Layer 1**	**Layer 2**	**D_v**	**MAC**	**Layer 1**	**Layer 2**
	April				*September*			
EW	1.8	1	120	80	1.8	1	120	80
PL	1.75	0.1	80	120	1.75	0.1	90	110
EW + PL	1.76	1	120	80	1.76	1	120	80
Control	1.75	0.02	10	190	1.75	0.02	10	190

RESULTS AND DISCUSSION

Establishment of Ecological System

The maximum vegetation density (visual) occurred in late August and began to decline near the close of September and into October. The system was very productive compared to the Konza Prairie (Table 3). On average, cells treated with both vegetation and earthworms had higher densities of biomass and roots ($P > 0.6384$), possibly due to the symbiotic interaction between earthworms and plants (Baker *et al.,* 2006 and Kirkham,

1982). The high productivity rates were likely due to the high amount of nutrients available, particularly N, concentrated sunlight, and the lack of competition. The successful establishment of the grasses and earthworms may have been due in part to the management technique of routing the stormwater runoff away from the cell during the first few months of growth.

Table 3 Dry weight (g/m^2) of aboveground biomass

Treatment*	Biomass Density (g/m^2)	Estimated Root Density** (g/m^2)
VEG1	942.19	753.76
VEG2	940.65	752.52
VEG3	839.53	671.62
AVE	*907.46*	*725.97*
VEGEW 1	473.81	379.05
VEGEW 2	1611.51	1289.21
VEGEW 3	1196.03	956.82
AVE	*1093.78*	*875.03*

* VEG is vegetation treatment and VEGEW is vegetation + earthworm treatment
** Assumed ratio of roots to tops was 0.8 (Weaver and Zink, 1946)

Infiltration

On a seasonal-basis, the conductive ability of soil was enhanced by the introduction of vegetation and earthworms (Table 4). The effective saturated hydraulic conductivity (K_{eff}) is indicative of the ability of the soil profile to infiltrate water. The seasonal change in K_{eff} was significant in the earthworm only treatment and vegetation and earthworm combination treatment ($P > 0.0281$ and $P > 0.0046$, respectively).

Table 4. K_{eff} (cm/hr) by cell type

	Apr-08	Oct-08		Apr-08	Oct-08		Apr-08	Oct-08
VEG*	0.76	11.1	**EW**	0.7	18.3	***Overall Ave.***	*1.07*	*20.82*
VEG	0.9	1	**EW**	0	10.2	***Overall Std. Dev.***	*0.78*	*14.54*
VEG	0	21.5	**EW**	1.6	19.2			
Ave.	0.55	11.20	*Ave.*	1.15	15.90	***Treatment Ave.***	*1.32*	*20.94*
Std. Dev.	0.48	10.25	*Std. Dev.*	0.64	4.96	***Treatment Std. Dev.***	*0.73*	*13.63*
VEGEW	1.7	24.4	**CONT**	1.8	22.4			
VEGEW	0.9	38.5	**CONT**	0.6	4.9	***Control Ave.***	*1.20*	*11.47*
VEGEW	2.7	44.3	**CONT**	0	7.1	***Control Std. Dev.***	*0.92*	*9.53*
Ave.	1.77	35.73	*Ave.*	0.80	11.47			
Std. Dev.	0.90	10.23	*Std. Dev.*	0.92	9.53			

*VEG is vegetation treatment, VEGEW is vegetation + earthworm treatment, EW is earthworm treatment, and CONT is control

It is important to note that the typical K_{eff} for a silt loam is 0.65 cm/hr. In April 2008, the overall average saturated hydraulic conductivity for all cells was close to this K_{eff} value, at 1 cm/hr. The average infiltration rates of all treatment cells in October 2008 were around 20 cm/hr, almost double that of the control. The considerable increase in infiltration rates in all treatment types reflects the degree of establishment of the soil matrix, vegetation, and earthworms over the growing season. The greatest increase in K_{eff}

was in the most biologically diverse treatment (vegetation/earthworm) implying that earthworm and vegetation interactions in the combination treatment enhanced infiltration rates over vegetation or earthworm only treatments.

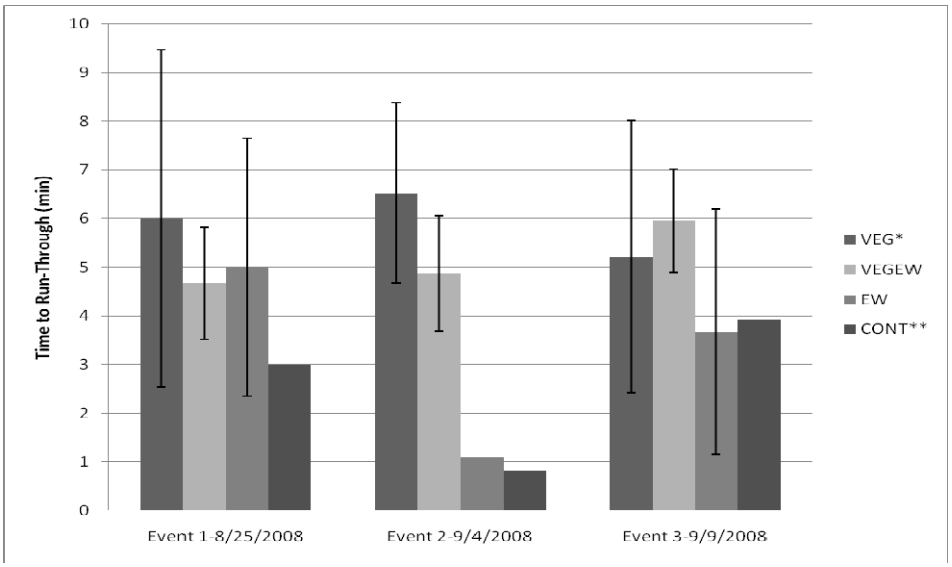

Figure 2. Time to run-through averaged by treatment for each storm event

On an event-basis (Figure 2), the treatments had an interesting impact on infiltration. Vegetation and vegetation/earthworm treatments generally had greater run-through times, while the earthworm and control treatments generally had shorter run through times. This may be explained by the presence of roots and the maintenance of the fine structure of the soil (Hino et al., 1987) which results in fewer macropores and an ability to remove water from the top soil via uptake and evapotranspiration. Detainment of runoff in the soil profile dissipates runoff energy and allows time for filtration and pollutant removal. The control and earthworm treatment do not detain water; water was instead readily conducted through the soil matrix.

Soil Moisture Fluctuations

Soil moisture fluctuations reflected how the presence of vegetation and earthworm impacts on long-term bioretention cell function. During the growing season, vegetation activity utilized water for growth and maintenance. Their influence continued in the off season through the macropores created during the active season that remained intact in the soil profile. The drying effect was evident in the tensiometer data at both 30 and 60 cm depths (Figures 3 a, b) because the tension of the control cell remained lower (wetter) than all other treatments.

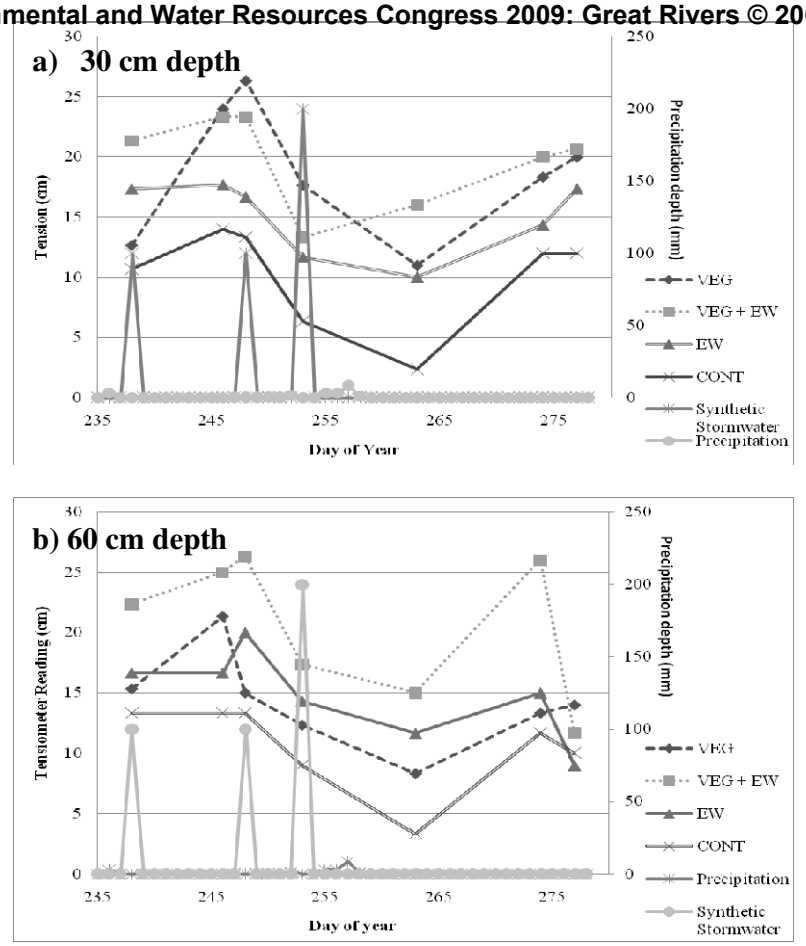

Figure 3. Tensiometer readings taken from August-October 2008 given in cm at a) 30 cm depth and b) 60 cm depth

In the top 30 cm of the soil profile, tension readings taken near the end of the growing season followed predicted trends of cells with more biological activity (VEG + EW > VEG > EW) drying out quicker. This was likely due to evapotranspiration and vegetation utilizing water for growth. However, the effect of the treatments on the soil moisture fluctuation was less pronounced at a 60 cm depth. This may be due to the fact that the roots of the vegetation had not yet reached the 60 cm depth in the first growing season.

Soil Quality

The media composition analysis (Table 4.2) of the cells in November 2007 prior to plant and earthworm inoculation showed high levels of N and P, a relatively neutral pH, and varying levels of chloride (from 0.5-12.5 ppm). The elevated levels of nutrients and chloride was likely a residual from the last experiment conducted in the lysimeter cells (Roberts, 2007).

Table 5. Summary of average percent change in soil quality by treatment type

	Mehlich-3 P	NH4-N	NO3-N	Total N	Total P	Chloride	pH
				VEG			
Ave.	3838	-13	207	283	118	1181	0
Std. Dev.	324.97	8.49	93.31	116.57	17.48	315.12	1.75
				VEGEW			
Ave.	4606	-10	140	331	150	744	1
Std. Dev.	104.10	2.33	73.55	58.54	22.25	708.19	1.79
				EW			
Ave.	4352	-33	145	323	141	633	-1
Std. Dev.	1057.48	9.85	266.36	104.45	42.07	1050.01	1.00
				CONT			
Ave.	4543	-37	412	380	157	779	-2
Std. Dev.	1691.74	19.74	323.40	173.39	66.15	470.43	2.68

These large increases in P, N, and chloride indicate that plant uptake of water and nutrients did not sufficiently decrease the concentrations of pollutants in the topsoil. However, trapping pollutants in the top 30 cm of soil prevents pollutants from exiting the cells as effluent. With continued establishment, mature grass should utilize excess N and reduce export over time. These results show that plant processes minimally affected the uptake of nutrients and salts in the top 30 cm of soil. However, retention of the pollutants in the top soil reduced the concentration of pollutants in outflow.

Water Quality

All treatments reduced P by 84-96%. A large amount of N was released during all events from all treatments probably because of a high initial N content and consequent leaching potential of the bioretention media. It was difficult to analyze the results of Cu and TSS; the percent trapping efficiency was highly variable in the VEG, EW, and VEGEW treatments. With continued establishment, the mature grass will use more N and reduce the export of the nutrient with outflow over time.

Table 1. Percent trapping efficiency for each pollutant averaged for storm events

	Total N		Total P		Cu		TSS	
	Ave	Std Dev	Ave	Std Dev	Ave	Std Dev	Ave	Std Dev
VEG	-1205	1143	85	17	-171	452	-94	322
EW	-1541	710	84	4	-124	341	77	20
VEGEW	-2590	2512	85	4	62	53	28	62
CONT	-736	323	96	3	93	9	95	5

It is important to note that there was no significant difference among the treatments in transporting pollutants. Past studies have suggested that macropore flow increases the movement of pollutants, particularly with the transport of herbicides and in tile-drained agricultural fields (Nuutinen and Butt, 2002, Shipitalo et al., 1994). However, results from this study did not support these findings.

Model Results

Functional parameters investigated in this study included hydraulic conductivity, ponding depth, drawdown time, infiltration depth, storage, and volume outflow. The model results validated the hypothesis that the introduction of an ecologically diverse system improves bioretention function during the first two years of establishment by improving

infiltration, increasing infiltration depth, storage capacity, and reducing drawdown time. The model results for Season 1 reflected data collected from the first season of the field study. By the end of the first growing season, the vegetation and earthworm combination treatment exhibited the greatest impact on bioretention cell function. The maximum impact of vegetation on bioretention cell function occurred at the end of the second growing season, reflecting the fact that Tallgrass prairie root systems reach their greatest density after the second year of growth.

As depicted in Table 4.7, the earthworm treatment had an immediate impact on the ponding and storage in April of the first growing season. Without earthworm burrows, soils would likely be dominated by smaller, more uniform pores that would restrict infiltration to saturated flow only. Treatments with earthworms permitted unsaturated water flow via macropores and reduced the ponding drawdown to 24 hours within the first growing season. In the field, treatments with only earthworms actually restricted water movement due to surface sealing effects. Although the model results indicate that the control treatment drawdown time was always greater than 48 hours, the effects of surface sealing in the earthworm treatments were accurately characterized.

Table 2 Results from BRC model analysis for the first three growing seasons

	EW	VEG	VEGEW	CONT	EW	VEG	VEGEW	CONT
	Season 1							
	April				September			
Hyd. Cond. (cm/hr)	8.5	8.5	8.5	8.5	101.9	8.5	470	8.5
Max. Pond (m)	10.1	26.5	26.5	26.5	3.5	19.1	3.4	25.2
Drawdown (hrs)	30.1	Ponded	Ponded	Ponded	24	42.4	24	Ponded
Infil. Depth (cm)	195.1	163.1	163.1	163.1	201.6	183.2	202.1	169.3
Storage (m^3)	0.9	0.8	0.8	0.8	0.9	0.9	0.9	0.8
Volume out (m^3)	0.9	0.8	0.8	0.8	0.9	0.9	0.9	0.8
% Storage Inc. from Control	7.7	No inc	No inc		4.4	4.4	4.4	
	Season 2							
	April				September			
Hyd. Cond. (cm/hr)	225.9	8.5	636.2	8.5	248	8.5	636.2	8.5
Max. Pond (m)	0.2	14.8	0.2	25.2	0.2	10.9	0.2	23.9
Drawdown (hrs)	24.0	36.2	24	Ponded	24	31.2	24	Ponded
Infil. Depth (cm)	207.1	188.5	219.1	169.3	211.3	193.8	219.1	176.7
Storage (m^3)	0.9	0.9	0.9	0.8	0.9	0.9	0.9	0.9
Volume out (m^3)	0.9	0.9	0.9	0.8	0.9	0.9	0.9	0.9
% Storage Inc. from Control	4.4	4.2	4.2		0.5	0.5	0.5	
	Season 3							
	April				September			
Hyd. Cond. (cm/hr)	248	8.5	636.2	8.5	248	8.5	636.2	8.5
Max. Pond (m)	0.2	9.0	0.2	23.9	0.2	7.2	0.2	23.9
Drawdown (hrs)	24.0	29.1	24.0	Ponded	24.0	27.2	24.0	Ponded
Infil. Depth (cm)	211.3	196.4	219.1	176.7	211.3	199	219.1	176.7
Storage (m^3)	0.9	0.9	0.9	0.9	0.9	0.9	0.9	0.9
Volume out (m^3)	0.9	0.9	0.9	0.9	0.9	0.9	0.9	0.9
% Storage Inc. from Control	0.5	0.5	0.5		0.5	0.5	0.5	

CONCLUSIONS

Despite poor initial growing conditions, the tallgrass plants and earthworms became well established over the course of the study and had interesting impacts on bioretention cell function. Perhaps the most notable impact was the considerable increase in infiltration rates in all treatments. As predicted, the greatest increase in saturated hydraulic conductivity was in the treatment with both vegetation and earthworms. It is also apparent from similar improvements in all cell types that ecological succession occurs to a certain extent despite ecological additions made prior to establishment. This was reflected in model results. When operated within the valid bounds of fractal dimension and macropore size, the BRC model can be an informative tool for bioretention cell design providing estimates for desired outcomes.

Other findings illustrate the important balance between biology and function: cells with biological components, such as earthworms and native vegetation, behave more like a natural system. Soil moisture fluctuations determined from tensiometer readings indicate a drying effect in treatments with biological activity. The control treatment (little to no macro-biology) consistently had a lower tension reading over time, indicating that the soil profile remained wetter longer than other treatments. Tensiometer readings taken at the end of the growing season (after day 265) followed the trend that higher levels of biology had a greater impact on soil moisture regimes. The trend was not as pronounced in the 60 cm deep tensiometers. This demonstrated that soil moisture fluctuations reflect the level of ecological establishment not only in the time it takes to dry the soil profile, but also in the depth of activity. With continued development, it is expected that the plant roots will have a greater impact deeper in the soil profile.

The results of this study show that ecological development is improved with diverse inputs. More biologically diverse bioretention cells experienced enhanced grass/root development, a decrease in drawdown time, reduced ponding, and an increase in infiltration rates. Cells with vegetation and earthworms also were more effective in drying out the soil profile, improving the ability of the cell to function in subsequent stormwater events. By conducting research in the Midwest utilizing native plants, fauna, and soil, the results of this study contribute to a growing pool of information which developers can use to guide effective BMP design. It is critical to continue developing our understanding of NPS pollution generation, transport, and mitigation in the urban environment. This will enhance our ability to develop and implement BMPs that have initial and long term viability and sustainability.

REFERENCES

Baker, G.H., Brown, G., Butt, K., Curry, J.P., Scullion, J. 2006. Introduced earthworms in agricultural and reclaimed land: their ecology and influences on soil properties, plant production and other soil biota. *Biol. Invasions* 8(6): 1301-1316.

Binet, F. and Curmi, P. 1992. Structural effects of *Lumbricus Terrestris* on the soil-organic matter system: micromorphological observations and autoradiographs. *Soil Biol. Biochem.* 24: 1519-1523.

Christianson, R., Barfield, B., Hayes, J., and Brown, G. 2005. Comprehensive Bioretention Cell Model Draft Manual

Christianson, R. D., B. J. Barfield, J. C. Hayes, K. Gasem, G. O. Brown, 2004. Modeling Effectiveness of Bioretention Cells for Control of Stormwater Quantity and Quality. Proceedings of the 2004 World Water and Environmental Resources Congress June 27 to July 1, Salt Lake City, Utah (edited by G. Sehlke, D. F. Hayes, and D. K. Stevens).

Edwards, W.M., Shipitalo, M.J., Owens, L.B., and Nortan, L.D. 1990. Effect of *Lumbricus terrestris* burrows on hydrology of continuous no-tell corn fields. *Geoderma*. 46: 73-84.

Edwards, W.M., Shipitalo, M.J., Traina, S.J., Edwards, C.A., and Owens, L.B. 1992. Role of *Lumbricis Terretris* (L.) burrows on the quality of infiltrating water. *Soil Biol. Biochem.* (24) 12: 1555-1561.

EPA. 1999a. Stormwater technologies fact sheet-bioretention.EPA 832-F99_012. Available at: www.epa.gov/owm/mtb/bioretn.pdf. Accessed 15 May 2007.

Hino, M., Fujita, K., and Shutto, K. 1987. A laboratory experiment on the role of grass for infiltration and runoff processes. *J. of Hydrology*. 90: 303-325.

Kirkham, M.B. 1982. Water and air conductance in soil with earthworms: An electrical-analogue study. *Pedobiologica*. 23:367-371.

Lee, K.E. and Foster, R.C. 1991. Soil fauna and soil structure. *Australian Journal of Soil Research*. 29 (6): 745-775.

Long Term Ecological Research Network. 2007. Konza prairie-LTER Description. Available at: www.lternet.edu/sites/knz/fulldescription.php?site=KNZ Accessed 20 October 2007.

MARC Regional Water Quality Education Program. 2008. Manual of best management practices for stormwater quality. Available at: www.marc.org/environment/Water/bmp_manual.htm. Accessed 20 October 2007.

Nuutinen, V. and Butt, K. 2002. Interaction of *Lumbricus terrestris* burrows with field subdrains. *Pedobiologica*. 47 (5) 578-581.

Shipitalo, M. and Butt, K. 1999. Occupancy and geometrical properties of *Lumbricus terrestris* L. burrows affecting infiltration. *Pedobiologia.* 43:782-794.

Shipitalo, M.J., Edwards, W.M., and Redmond, C.E. 1994. Comparison of Water Movement and Quality in Earthworm burrows and Pan Lysimeters. *J. Environ. Qual.* 23: 1345-1351.

Weaver, J.E. and Rowland, N.W. 1952. Effects of excessive natural mulch on development, yield, and structure of native grassland. *Botanical Gazette* 114:1-19.

Weaver, J.E. and Zink, E. 1946. Annual increase of underground materials in three range grasses. *Ecology* 27:115-127.

Weaver, J.E. and Zink, E. 1947. Length of life of roots of ten species of perennial range and pasture grasses. *Plant Physiology*. 21:201-217.

Importance of Levees in the Kansas City Area

David W. Renetzky[1], P.E., M.ASCE and John Grothaus[2]

[1]HNTB Corporation, Project Manager - Water Resources Group, 715 Kirk Drive, Kansas City, MO 64105; PH (816) 527-2313; FAX (816) 221-9016; email: drenetzky@hntb.com
[2]U.S. Army Corps of Engineers, Kansas City District, Chief - Planning Section, 601 E. 12th Street, Kansas City, MO 64106; PH (816) 389-3110; FAX (816) 389-2025; email: John.J.Grothaus@usace.army.mil

ABSTRACT

Kansas City's deliberate location along the Missouri River at the confluence of the Kansas River played a key part in the city's rich history and prosperity. From the city's beginnings, the river was a way to link one part of the country to another through transportation and trade. It provided a means to westward expansion and free enterprise. From early on, though, the river demonstrated its power over those that settled along its banks. That brought rise to federal flood control which originated in the early 1900s as a coordinated attempt to provide flood protection. As flood control evolved, the Flood Control Acts of 1936 and 1944 allowed the construction of the existing protection system in Kansas City. The Kansas City metropolitan system of seven flood protection levee units protect vital infrastructure while the rivers continue to provide an important asset to the area. Major flood events in 1951 and 1993 proved the potential devastation to the areas along the Missouri and Kansas Rivers. The 1951 flood led to improvements on many of the levee units. An ongoing feasibility study as a result of the 1993 flood will determine what beneficial changes can be made for the future. Billions of dollars have been saved over the years through property damage prevention, along with an unknown number of lives. As the river continues to be an important part of Kansas City, so too does the flood protection system that surrounds it.

ESTABLISHMENT OF A RIVER CITY

The Kansa, or Kaw, Native Americans were the first occupants of the area now known as Kansas City. Following the Louisiana Purchase, Meriwether Lewis and William Clark became the first people of European descent to come to the area. Lewis and Clark camped at the confluence of the rivers for three days in 1804 during their expedition. They mapped the area now known as Quality Hill calling it "a fine place for a fort." That declaration drew some interest for the area, but it was not until several years later that a Frenchman from St. Louis named Francois Chouteau settled along the river. He established a depot in 1821 for the American Fur Company about three miles below the large bend in the Missouri River (the current Northeast

Industrial District). Within five years after setting up the depot, however, Chouteau's warehouse was destroyed in a flood. When he decided to rebuild on slightly higher ground, several other French families joined him and the town of Kansas developed.

The appeal of the Missouri River also brought John Calvin McCoy to the Kansas City area in hopes of a successful selling and trading business. He set up a store in 1832 a few miles inland of Chouteau on the Santa Fe Trail. McCoy called this area south of the river Westport, as he considered it a portal to the West. At the same time, McCoy established a rock ledge area on the south shore of the Missouri as a landing area for river boats. Travelers soon found that the water route was faster and easier than shipping by land. Even with the four mile trip overland to Westport, the land travel reduction was substantial because the previous transfer point was about 22 miles farther east in Independence, Missouri. By 1845, Westport had replaced Independence as a source of supplies and point of departure for wagons headed west (see Exhibit 1).

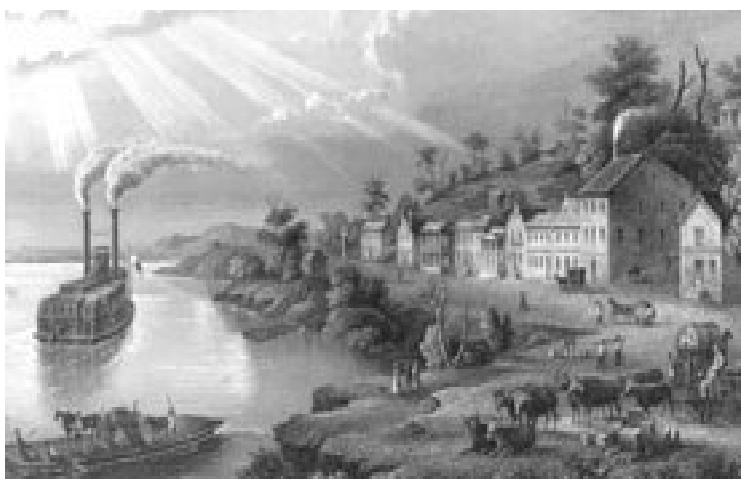

Exhibit 1: Depiction of Kansas City around 1850

Both the town of Kansas and Westport prospered under western migration for several years until a cholera epidemic threatened that in 1849. The epidemic took half of the population and drove business out of town. It took several years for the town of Kansas to recover, but it stayed viable and was incorporated as the City of Kansas in 1853. Westport survived as well and overland trade returned to the area. The settlements began to prosper again just in time for conflicts over slavery and the outbreak of the Civil War to disrupt the trend. Following some years of turmoil, the Missouri River came to the rescue once again for the Kansas City area. The Missouri Pacific Railroad arrived in 1865 and decided that the confluence of the Missouri and Kansas Rivers was the perfect spot for its railroad distribution center. The City of Kansas emerged as a wheat and grain exchange center. This led to the bridging of the Kansas River in 1866 and the construction of the Hannibal Bridge across the Missouri River in 1869. The first stockyards opened in 1870, setting the stage for the area to become known as a "cowtown." Kansas City adopted its current name in 1889 and annexed Westport in 1897.

ORIGINS OF FEDERAL FLOOD PROTECTION

As development and prosperity continued beyond the turn of the century in the Kansas City area, the Missouri River periodically reminded those living along its entire corridor that it remained an untamed force of nature. Major floods occurred along the Missouri River in 1903, 1915, 1926, and 1934. The 1903 flood inundated Kansas City, as seen in Exhibits 2 and 3. It is evident that the Kansas City area already had a vast amount of infrastructure that needed protection from the river.



Exhibit 2: 1903 photo of flooded business area in Kansas City



Exhibit 3: Photo of 1903 flooding at the old Union Station

Levees were constructed by locals in the early 1900s in what are now the Argentine, Armourdale, Central Industrial District, North Kansas City, and

Birmingham units (see Exhibit 4 in next section). Similar local and agricultural levees were being constructed in many parts of the country.

The failures of an uncoordinated levee system throughout the country were recognized in the late 1800s when the Mississippi River Commission was created to undertake flood control planning on the lower Mississippi. Despite this Commission, though, the existing levee-based flood control system was proven to be inadequate. When over 16 million acres in the lower Mississippi River valley were flooded in 1928, Congress passed flood control legislation and gave a role to the Corps of Engineers in its implementation. Congress eventually followed with the 1936 Flood Control Act which created a strong role for the federal government in floodplain management. This act declared flood control to be an acceptable federal government activity and authorized the expenditure of $310 million for more than 200 flood control projects, including several in Kansas City (Government Printing Office, 1940). Expenditure was conditioned on local interest participation and long-term operation and maintenance.

The Flood Control Act of 1944 allowed for expansion of the levee system and construction of multiple-purpose reservoirs for irrigation, navigation, water supply, hydropower, and recreation in the Missouri River basin. The development of the plan passed as part of this Act began as more flooding occurred in the early 1940s. Three floods in 1943 were particularly severe in the Omaha, Nebraska area. As Omaha's airport was vital to the war effort at the time, the flooding brought unprecedented congressional and public attention to the Missouri River basin.

The Corps of Engineers was authorized by the House Committee on Flood Control to produce a plan for the Missouri River basin that would provide flood control and other benefits. Colonel Lewis A. Pick, then division engineer in the Corps' Omaha office, was in charge of preparing the plan. On March 2, 1944, just 90 days after authorization, Pick submitted his plan which included major provisions for dams and levees along the river and its tributaries. It called for five dams on the Missouri River below Fort Peck, Montana, over a dozen reservoirs on tributaries, and 1,500 miles of levees on both sides of the river from Sioux City to the confluence of the Mississippi River (National Park Service, 2009). The plan was heavily focused on flood control and navigation, without much substance for irrigation benefits.

During the same timeframe, the Department of Interior's Bureau of Reclamation had been performing a multi-year study of the basin's water needs with the goal of producing a comprehensive plan by 1945. The impetus behind the Bureau's study was unsustainable agricultural practices, economic depression, and prolonged drought in the basin. Submission of the Pick Plan caught the Bureau by surprise and prompted the rapid completion of their plan. It was submitted to the Senate Committee on Commerce on May 5, 1944 and called for 17 power plants, 90 reservoirs, and the irrigation of nearly five million acres of the Great Plains (National Park Service, 2009). The focus of the Bureau's plan, known as the Sloan Plan, was irrigation and reclamation.

With two differing plans, a debate ensued in Washington. There were strong supporters on both sides, along with a growing idea of creating a Missouri River Authority that would manage efforts in the basin. President Roosevelt requested that the agencies develop a unified plan. Aided by the fact that the Corps and the Bureau

agreed on their dislike of the potential for a Missouri River Authority, they ultimately reached a compromise plan. The resulting Pick-Sloan Plan included the majority of provisions outlined by the individual plans and was ratified by Congress in the Flood Control Act of 1944. President Roosevelt signed the Flood Control Act on December 22, 1944 which also authorized appropriations to each of the two agencies for construction of the initial stages.

KANSAS CITYS FLOOD CONTROL IMPROVEMENTS

The combined 1936 and 1944 Flood Control Acts provided authorization and funding that led to the emergence of a focused protection system for the Kansas City area. The existing system is known as the Kansas Citys Flood Damage Reduction Project, as it provides local flood protection for the metropolitan areas of Kansas City, Missouri and Kansas City, Kansas. The project consists of seven levee units along reaches of the Kansas and Missouri Rivers:

- Argentine Unit
- Armourdale Unit
- Birmingham Unit
- Central Industrial District Unit
- East Bottoms Unit
- Fairfax-Jersey Creek Unit
- North Kansas City Unit

The existing project extends over the lower 10 miles of the Kansas River and, on the Missouri River, from 6.5 miles upstream to 12.5 miles downstream of the mouth of the Kansas River. The seven units of the flood protection system were designed and constructed in conjunction with each other, but are independently operated to some extent. The total protected area covers about 32 square miles and is characterized by dense industrial and commercial development. Some limited residential habitation is also present. Communities (or portions thereof) within the area include Kansas City, North Kansas City, Randolph, and Birmingham all in Missouri; and Kansas City, Kansas.

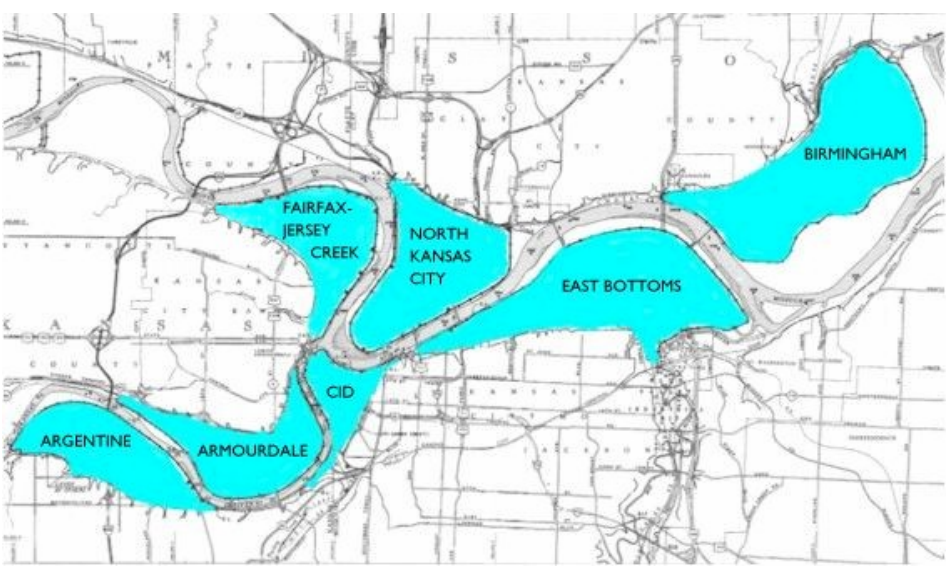

Exhibit 4: Overview map of the Kansas Citys Levee System

The **Argentine Unit** is located in Wyandotte County, Kansas, on the right bank of the Kansas River. The unit begins at the Santa Fe Railroad embankment upstream from the Turner Bridge at a point approximately 4,000 feet east of the mouth of Barber Creek. The beginning portion of the levee unit parallels the Santa Fe Railroad embankment before turning northwesterly toward the Barber Creek mouth. At about Kansas River Mile (RM) 10.1, the unit turns to follow the course of the Kansas River. The levee unit ends on the Kansas River at a point about 2,000 feet downstream of the 18th Street Bridge (Kansas RM 4.7). A floodwall containing two stoplog gaps crosses the train tracks to the south and ties into high ground.

Modification and strengthening of works originally constructed by the Kaw Valley Drainage District began in May, 1951 and were completed in November, 1955 by the Corps of Engineers. More recent improvements, separately authorized as the 1962 Modification, were completed in April, 1978.

The flood protection facilities consist of levees, stability berms, floodwalls, underseepage control, 2 stoplog gaps, 6 pumping plants and 18 drainage structures. The levees total approximately 5.2 miles long. The floodwalls total about 1,350 feet.

The **Armourdale Unit** is located along the left bank of the Kansas River from RM 7.0 to RM 0.3, near the confluence of the Kansas and Missouri River. The original levees and floodwalls were constructed under the jurisdiction of the Kaw Valley Drainage District. The protection is separated into three sections totaling about 5.8 miles in length. The uppermost levee section is a tieback from high ground west of Mattoon Creek, then heads downstream to the Union Pacific Railroad tracks. From the Union Pacific Railroad tracks, the levee extends from the railroad embankment near the mouth of Mattoon Creek downstream along the left bank of the Kansas River to the floodwall. The second portion is a floodwall that begins north of the Chicago, Rock Island, and Pacific Railroad Bridge and extends downstream to connect with the third levee section. The third levee section ties back into high ground at the embankment of the Lewis and Clark Viaduct.

Construction of the Federal project began in May, 1949 and was completed in February, 1951. More recent improvements, separately authorized as the 1962 Modification, were completed in April 1976.

The flood protection unit consists of levees, stability berms, retaining walls, floodwalls, underseepage control including 45 relief wells, 2 sandbag gaps and 2 stoplog gaps, 10 pump plants, and 36 drainage structures. The levees stretch about 5.7 miles through the Armourdale Unit and the floodwalls total approximately 6,600 feet.

The **Birmingham Unit** is located on the left bank of the Missouri River, approximately 12.4 miles downstream from the mouth of the Kansas River. The original construction was done under the jurisdiction of the Birmingham Drainage District allowed by a resolution dated February 18, 1946. The upstream section of the levee was raised and strengthened in 1952 by the Federal Government. The downstream section was strengthened and modified in 1954 and 1955. The levee begins at the bluff southeast of Randolph, Missouri and extends southwest along an abandoned railroad fill. It continues south to the Missouri River and downstream until it turns north and west along the left bank of the old Liberty Bend channel to the

old Wabash Railroad. From there, the levee goes upstream along the right bank of Shoal Creek to high ground at Liberty Road.

The flood protection works include a levee, stability berms, floodwalls, underseepage control, 3 sandbag gaps, 2 stoplog gaps, 2 pump plants, and 4 drainage structures. The levee is about 11.0 miles long and the floodwalls total approximately 430 feet.

The Kansas portion of the **Central Industrial District Unit** is located in Wyandotte County and extends from the Kansas/Missouri state line along the right bank of the Missouri River to the mouth of the Kansas River. It then continues upstream along the right bank of the Kansas River to RM 3.4. The Kaw Valley Drainage District is the local agency responsible for operation and maintenance. The original unit was constructed by the Kaw Valley Drainage District prior to May, 1948, when initial Federal improvements began. The bulk of the improvements were completed by November, 1955. The most recent improvements were completed in December, 1979.

The unit consists of a system of levees and floodwalls, underseepage control including 17 relief wells, a stoplog gap, a sandbag gap, 10 pump plants, and 23 drainage structures. The levee is approximately 1.7 miles long and the floodwalls total about 7,900 feet.

The Missouri portion of the Central Industrial District flood protection unit is located in Kansas City within Jackson County. The unit extends along the right bank of the Missouri River, upstream from the Grand Avenue Viaduct (RM 365.7), to the Kansas/Missouri state line (RM 367.2). The initial construction took place in March, 1946 and was completed in September, 1947. Significant improvements and repair of 1951 flood damage followed the initial construction and were completed in November, 1955.

The unit consists of a system of levees, floodwalls, underseepage control, 1 sandbag and 7 stoplog gaps, 7 pump plants, and 5 conduits. The levees total about 430 feet in length and the floodwalls are about 1.5 miles long.

The **East Bottoms Unit** is located in Kansas City, Missouri within Jackson County. The unit extends downstream along the right bank of the Missouri River from the Armour-Swift-Burlington (A.S.B.) Bridge, RM 365.6 (adjusted 1960) to the mouth of the Blue River, RM 357.7 (adjusted 1960). Then the levee turns and heads west upstream along the left bank of the Blue River to the Union Pacific Railroad embankment.

The initial construction was completed in September, 1950, and the City of Kansas City formally accepted the project on July 30, 1951. The most recent work on the East Bottoms Unit was completed in August, 1974.

The unit consists of a system of levees, floodwalls, stability berms, retaining walls, underseepage control including 28 relief wells, 3 stoplog gaps, 11 pump plants, and 17 drainage structures. The levee portion is about 9.2 miles long. The floodwall portion is approximately 2,190 feet long.

The **Fairfax-Jersey Creek Unit** is located on the left bank of the Kansas River from the Union Pacific Railroad Bridge (Kansas RM 0.3) downstream to the mouth of the Kansas River. It then extends along the right bank of the Missouri River from Missouri RM 367.5 to RM 373.9 (1960 adjusted mileage).

Initial construction occurred in April, 1940 and was completed in May, 1941. Numerous modifications and improvements were constructed in the late 1940s, early 1950s, and 1955, with the most recent completed in June 1955.

The flood protection facilities consist of levees, floodwalls, underseepage control including 113 relief wells, 4 stoplog gaps, 1 sandbag gap, 13 pump plants, and 23 drainage structures. The total length of levees is about 5.3 miles and the floodwalls are approximately 4,040 feet. The Fairfax Drainage District provides operation and maintenance from levee Sta. 31+50 (boundary line with Kaw Valley Drainage District) to Sta. 313+72 (bluff at upstream end of unit).

The Airport Section of the **North Kansas City Unit** is located in Kansas City, Missouri within Clay County. The protection lies along the left bank of the Missouri River from a few feet beyond the city boundary with North Kansas City, Missouri (RM 369.6, 1960 adjusted) to the downstream floodwall at the Hannibal Bridge (RM 366.2, 1960 adjusted).

Construction began in May, 1946 and Kansas City, Missouri accepted the unit in October, 1947. Several improvements have been made since the initial construction, with the most recent work being completed in June, 1955.

The flood protection facilities consist of levees, floodwalls, underseepage control including 48 relief wells, 3 pump plants, and 3 drainage structures. Total lengths of levee and floodwall are approximately 2.5 miles and 530 feet, respectively.

The portions of the North Kansas City Unit maintained by the North Kansas City Levee District are located in both North Kansas City and in Kansas City, Missouri. These portions include a short upper section extending downstream along the left bank of the Missouri River from the bluff just north of the Kansas City, Missouri Waterworks intake to where the Airport section (described above) begins. After the Airport Section ends, the North Kansas City Levee District portion continues in an easterly direction. It follows along the left bank of the Missouri River to a point where the North Kansas City hillside ditch exits to the Missouri River near the Missouri River Chouteau Bridge. At the hillside ditch outlet, a long hillside tieback turns back sharply to the Northwest and runs to a termination point just west of the North Cherry Street Bridge. Construction began in 1946. Several improvements have been made since initial construction, with the most recent work being completed in June, 1955.

The unit consists of a system of levees, floodwalls, underseepage control, 3 stoplog gaps and 1 sandbag gap, 6 pump plants and 6 conduits. The North Kansas City Unit portion maintained by the North Kansas City Levee District has approximately 6.2 miles of levees and about 310 feet of floodwalls.

One can observe from the descriptions above that the protection system for the Kansas City metropolitan area is somewhat complex. It involves two states, two major rivers, and seven levee units operating together with multiple local sponsors. There are over 50 miles of flood protection works including 46 miles of earthen levee (typically over 12 ft. high) and 6 miles of floodwall (heights ranging from 2 ft. to 22 ft.). The estimated fixed investment within the protected area is over $16 billion. It protects about 5,000 structures (business and residential) and about 20,000 residents. About 90,000 people are employed within the protected area, where there are

extensive road and rail systems of regional and national importance. A municipal airport and several vital utilities also exist.

IMPACT OF MAJOR FLOODS

The Missouri River natural valley floodplain is approximately 2 to 2½ miles wide, while the main channel averages about 1,000 feet wide throughout the protected reaches. Bank-full discharge is approximately 140,000 cubic feet per second (cfs) for the reach of the Missouri River upstream of the mouth of the Kansas River. For the reach of the Missouri River downstream of the mouth of the Kansas River, the bank-full discharge is approximately 180,000 cfs. The drainage area of the Missouri River just upstream of the confluence with the Kansas River is 425,100 square miles.

The Kansas River natural valley flood plain is approximately 1¼ miles wide, while the main channel averages about 600 feet wide throughout the protected reaches. Bank-full discharge is approximately 60,000 cfs. The drainage area of the Kansas River basin is 60,060 square miles.

Two major floods stand out in the history of the modern Kansas Citys flood protection system. The Great Flood of 1951 was mainly a Kansas River event, while the Great Flood of 1993 was primarily a Missouri River event. The peak flow on the Missouri River downstream of the confluence of the Kansas was estimated to be about 573,000 cfs for the 1951 event, the highest discharge on record. The 1993 event was slightly lower at about 543,000 cfs and ranks third behind the 1903 event mentioned earlier.

At the time of The Great Flood of 1951, only one reservoir (Kanopolis Lake) of the several that were planned was in operation on the Kansas River. The peak on the Kansas River was estimated to be about 510,000 cfs. The protection system was in its early stages of completion and the flood overtopped all three of the levee units along the Kansas River – Argentine, Armourdale, and the Central Industrial District. An estimated 15,000 people were evacuated from the area and five people lost their lives to the flood. The damages were approximately $870 million in 1951 dollars, which would be almost $10 billion today.



Exhibit 5: Kansas City newspaper photo from The Great Flood of 1951

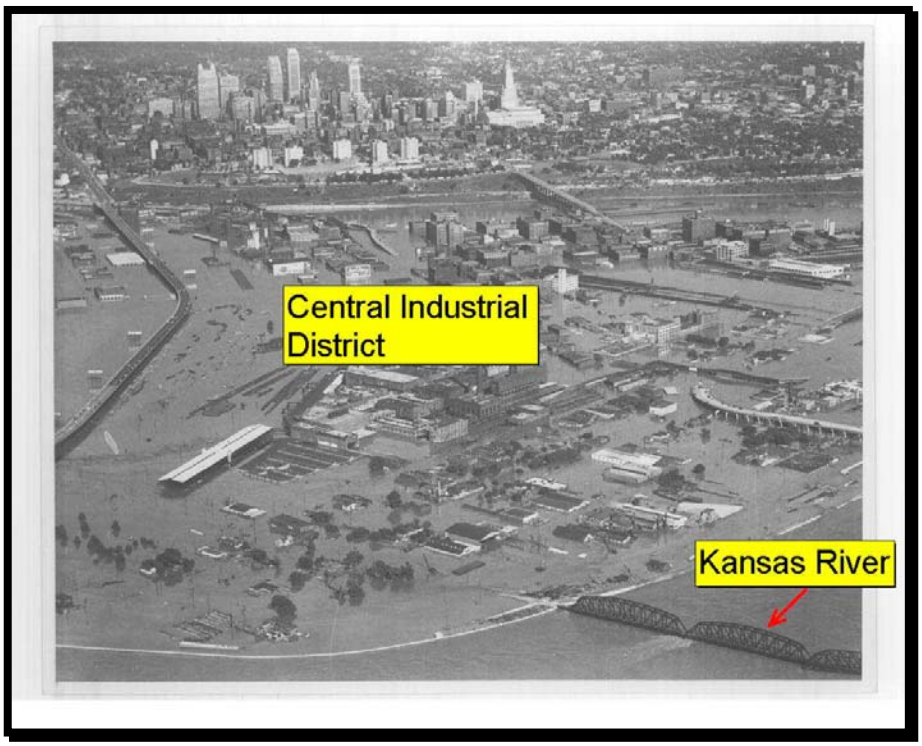

Exhibit 6: Photo of Central Industrial District during 1951 flood

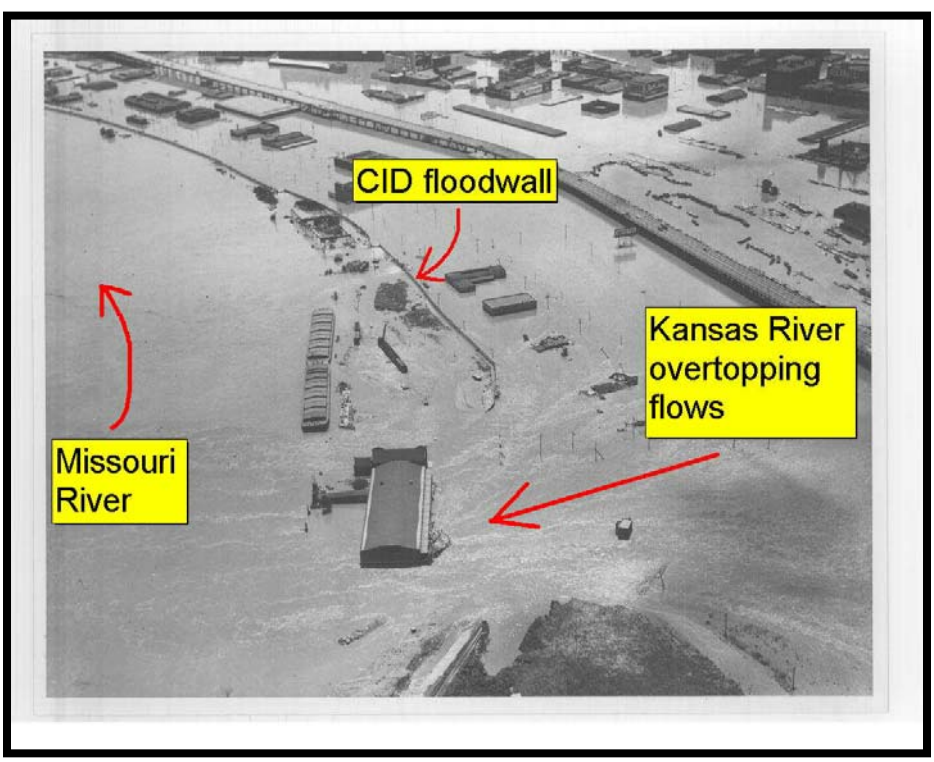

Exhibit 7: 1951 flood photo of overtopping in the Central Industrial District

Examination of the 1951 flood and associated peak discharges led to the 1962 modified design flows and ultimately the "1962 Modification" that raised the Kansas

River levees. It also expanded the control system by authorizing more upstream reservoirs, including Milford, Perry, and eventually Clinton Lake in the Kansas River basin.

Upstream flood control lakes and levee raises in Kansas City were in place in 1993, when the new benchmark flood on the Missouri River occurred. The Great Flood of 1993 was a major test of the Kansas Citys levee system. The Kansas River reservoirs utilized all of their flood control storage volume and greatly reduced the flows down the Kansas River. The Missouri River mainstem dams were operating to greatly reduce flows on the Missouri as well. The entire protection system passed the flood without failing, but the water crested close to the levee tops on the lower Kansas River. The flood peaked about three to five feet below the top of levee on most of the Missouri River units. It is estimated that about $4.5 billion in damages were prevented.

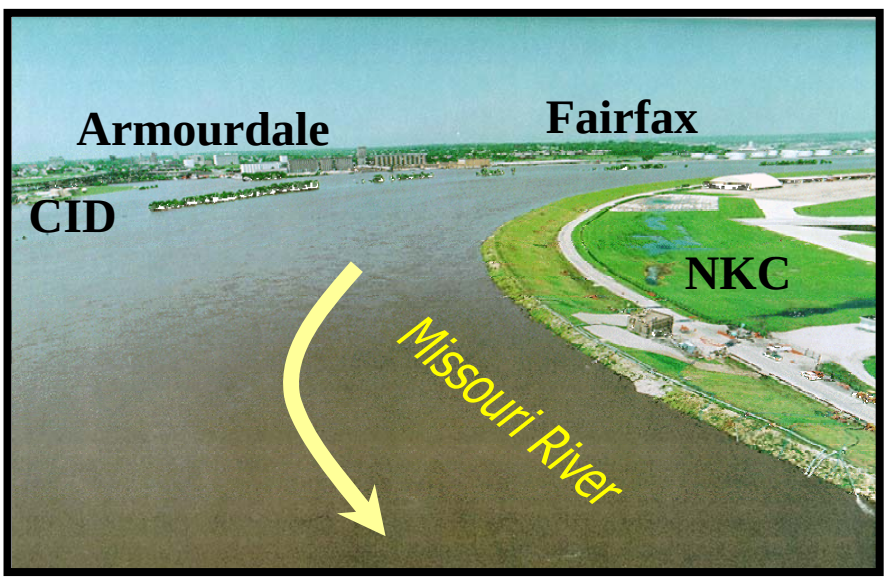

Exhibit 8: Flood stage photo from 1993 flood event

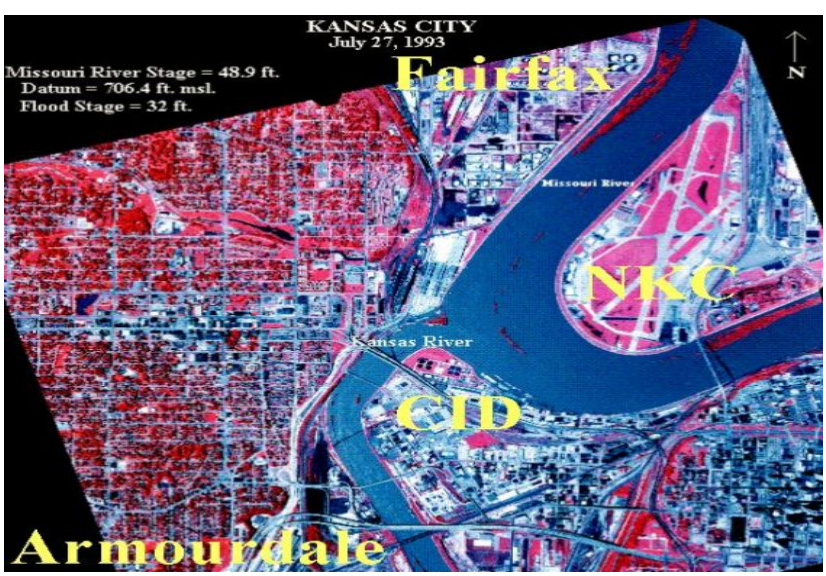

Exhibit 9: Aerial photograph of 1993 flood

CURRENT CORPS OF ENGINEERS FEASIBILITY STUDY

From a hydraulic overtopping standpoint, each of the Kansas Citys seven levee units passed the 1993 flood event. Some minor repairs to the flood protection system were needed after the waters receded, but that was not unexpected. Based upon observations from the 1993 flood, some questions were raised regarding the system's performance relative to the original design intent, and regarding the geotechnical and structural components. The levee unit owners (also known as "sponsors") requested a reevaluation of the Kansas Citys Levee System. In 1999 the Kansas City District, Corps of Engineers initiated a comprehensive $8 million investigation of the Kansas Citys Levee System, called a "feasibility study".

The feasibility study is authorized by Section 216 of the Flood Control Act of 1970, which provides general authority to review completed projects as follows:

> *The Secretary of the Army, acting through the Chief of Engineers, is authorized to review the operation of projects the construction of which has been completed and which were constructed by the Corps of Engineers in the interest of navigation, flood control, water supply, and related purposes, when found advisable due to the significantly changed physical or economic conditions, and to report thereon to Congress with recommendations on the advisability of modifying the structures or their operation, and for improving the quality of the environment in the overall public interest.*

The City of Kansas City, Missouri, the North Kansas City Levee District, the Fairfax Drainage District, and the Kaw Valley Drainage District are the study sponsors. Their share of the feasibility study costs is 50 percent.

The feasibility study is evaluating modifications to increase the system reliability, reduce flood damages and reduce the flood risks for six of the seven levee units within the existing Kansas Citys Levee System. These include the Argentine Levee Unit, the North Kansas City Levee Unit, the East Bottoms Levee Unit, the Fairfax-Jersey Creek Levee Unit, the Armourdale Unit, and the Central Industrial District Unit. The Argentine, Amourdale, and the Kansas portion of the Central Industrial District levee units are owned by the Kaw Valley Drainage District. The Fairfax-Jersey Creek Unit is owned by the Fairfax Drainage District. The City of Kansas City, Missouri owns the Missouri portion of the Central Industrial District Unit and the East Bottoms Unit. The Birmingham Levee Unit was not deemed to need improvements.

In 2006, an Interim Report was completed and submitted, and subsequently approved by the Headquarters, U.S. Army Corps of Engineers (HQUSACE). The interim or "Phase I" report recommended site specific improvements to structural and foundation features for the units located on the Missouri River, but no Missouri River units were recommended to be raised in height. The report found that the Argentine

Unit on the Kansas River does not provide the nominal 500-year level of protection originally anticipated by the authorization, and the Phase I Report has recommended a levee raise for that unit of 5 feet on average. The feasibility study is continuing, with detailed evaluations of the Armourdale and Central Industrial District units to be published in a final or "Phase II" report in 2010. The recommended plan modifications from Phase I of the report are summarized below:

Argentine Levee Unit: Approximately 5.5 miles of levee would be raised an average of about 5 feet. The levee unit raise includes modifying earthen levee and berms, about 1,340 feet of flood wall, stop log gaps, and other necessary line of protection features. Fourteen utility crossings would be relocated over the levee, including pressure pipelines that currently pass under the levee. Three pump stations would be modified or replaced to retain the reliability of the line of protection.

Fairfax Jersey Creek Levee Unit – Fairfax-Jersey Creek Sheetpile Wall: The modifications would include reconstructing about 870 feet of sheetpile wall to ensure the wall's stability and construction of about 600 feet of new sheetpile wall to reduce the risk of levee failure.

East Bottoms Levee Unit: Modifications would include installing approximately seventeen pressure relief wells to reduce underseepage and reduce the risk of failure and constructing approximately 2,100 linear feet of 30-inch pipe system to transfer collected seepage from the wells to the proximity of the Hawthorne pump plant.

North Kansas City Levee Unit – Harlem Area: Modifications would include constructing a new buried collector system about 2,600-feet long and 18-inches in diameter with seepage collection vaults to enable pumping during flood events. This would control underseepage pressures at the interior toe of the existing levee.

North Kansas City Levee Unit – National Starch Area: Modifications would include installing approximately 20 pressure relief wells, an approximately 2,000-feet long and 30-inch diameter pipeline, and a new pump station to collect, move and remove water in order to control underseepage at the interior toe of the existing levee.

Fairfax Jersey Creek Levee Unit – Fairfax-BPU Floodwall: The modifications would include strengthening about 1,450 feet of floodwall using approximately 50-foot deep; 24-inch diameter piles about seven feet apart**.**

The table on the next page (Exhibit 10) shows the estimated total costs and cost sharing associated with the levee modifications recommended in the Phase I Report. Construction of features recommended in a feasibility report is cost shared 65 percent by Federal, and 35 percent by the local sponsor. Currently, as funding becomes available, design work has been initiated on several of the project features approved in the Phase I Report.

Levee Unit and Site	Price Level Estimate ($1000)		
	Total By Site	Federal (65%)	Sponsor (35%)
Argentine 5 ft levee raise	52,873	34,367	18,506
Fairfax/BPU floodwall modification	7,879	5,121	2,758
Fairfax-Jersey Creek sheetpile wall	4,984	3,240	1,744
NKC-Harlem buried collector	1,549	1,007	542
NKC National Starch area wells & pump	6,621	4,304	2,317
East Bottoms pressure relief wells	1,644	1,069	575
Totals	75,550	49,107	26,443

Exhibit 10: Summary of levee modification costs recommended in the Phase 1 Report

CONCLUSIONS

The history of the Kansas City metropolitan area is tied very closely to the Missouri and Kansas Rivers, and the Kansas Citys Levee System that protects much of the commercial, industrial, and residential development in the very heart of the area. If we had the ability to turn back the clock 200 years, certainly all would agree that development in the floodplain should have been avoided. However, the evolution of history and man's interaction with nature does not often have the full benefit of hindsight. Meanwhile, the areas protected by the levee system provide critical manufacturing, transportation, and other essential services for the region and the entire Nation. Our responsibility now, along with pursuing wise policies in floodplain management and risk communication, is also to reduce the exposure to flood risk whereever justified and affordable. The Army Corps of Engineers, along with its many partners, is now embarking upon the challenge of the next century and the next millennium - striking the proper balance between multiple goals in water resources, effective risk management, and maintaining a viable levee protection system prepared to meet the future challenges of a dynamic and changing river system.

REFERENCES

Kansas City Historical Information: Kansas City Museum, 3218 Gladstone Boulevard, Kansas City, MO 64123; University of Missouri, Western Historical Manuscript Collection, 302 Newcomb Hall, 5100 Rockhill Road, Kansas City, MO 64110

Kansas City Flood Photos: Missouri Valley Special Collections, Kansas City Public Library, 14 West Tenth Street, Kansas City, MO 64105

Government Printing Office (1940), Laws of the United States Relating to the Improvement of Rivers and Harbors from August 11, 1790 to January 2, 1939, 3 volumes, Washington, DC

Kansas City District, Northwestern Division (2006), Review of Completed Project, Kansas Citys Levees, Missouri and Kansas, Interim Feasibility Report and Environmental Impact Statement, http://www.nwk.usace.army.mil/projects/7levees/

National Parks Service (2009), "Overview of the Pick-Sloan Plan", U.S. Department of the Interior, Missouri National Recreational River, P.O. Box 591, O'Neill, NE 68763

KANSAS CITY, MISSOURI WET WEATHER SOLUTIONS PROGRAM A TWELVE STEP PROGRAM

Erin Ollig and Sheila Shockey

Shockey Consulting Services, LLC, 7611 Park Street, Lenexa, Kansas 66216; PH (913) 248-9585; FAX (913) 248-9581; EMAIL: Erin@shockeyconsulting.com; Sheila@shockeyconsulting.com

ABSTRACT

The measure of a successful public participation effort is not only sharing information, and gathering public input but also in changing behaviors on a larger scale. The Wet Weather Solutions Program was created by the City of Kansas City Missouri to reduce flooding, improve water quality and protect and restore the natural environment. To prepare the long-rang plan, a large scale public participation process was employed. It resulted in an innovative plan but also drove significant changes to the culture of an entire city organization; and introduced and promoted sustainability throughout all aspects of the City. As a result of the public participation process, Kansas City is destined to be one of the greenest cities in the United States over the next 25 years. A unique perspective from inside the public participation process of a $4.0 billion public infrastructure project is outlined from the lead public participation consultants for the Program.

INTRODUCTION & BACKGROUND

In 2001, the Kansas City Missouri Water Services Department began to develop a Combined Sewer Overflow (CSO) Plan as required by state and federal regulators. That effort evolved into a Wet Weather Solutions Program primarily as recommended by stakeholders during a large scale public participation process. The stakeholders further drove significant changes to the culture of an entire city organization, introducing and promoting sustainability, starting with management of water resources and moving throughout all aspects of the city services. As a result of the public participation process, Kansas City is destined to be one of the greenest cities in the United States over the next 25 years.

Born out of the regulatory and financial drivers, the Overflow Control Program (OCP), a division of the Kansas City Missouri Water Services Department, moved beyond the traditional management of wastewater facilities and started to manage wet weather in a more integrated way. The Wet Weather Solutions Program's mission was to manage the City's water resources in a sustainable way. The City's Water Services Department had previously never involved the public until this program demonstrated successful public participation efforts. Now, several citizen committees work on policy issues and participation at the project level.

But things didn't change overnight. Over a span of five years, a variety of methods were used to involve the public. Some methods worked, others didn't. The methods that did succeed were the reasons why the Plan ultimately received broad stakeholder support.

WHO WANTS TO TALK ABOUT SEWERS?

Citizen leadership was very important, however it was not all sunshine and daisies. Many bumps and roadblocks set progress back and moved progress in a different direction. At the end of the day, citizen leadership made the difference. It is not always easy to get people to give up their time to talk about sewers.

Community Panel Chairperson

The heart of the public participation program for the Wet Weather Solutions Program was the Wet Weather Community Panel. A strong chairperson who had a passion for improving Kansas City and a capacity to learn new and complicated information was very important. Carol Grimaldi, President of Brush Creek Community Partners, was the Chairperson of the Panel the entire five years. She never missed one of the forty-five meetings that were held and attended many of the subcommittee meetings as well as meetings with the consultant team and staff. She was able to help the program team understand what was not being said out loud or behind the scenes. Her meeting management style was inclusive but firm. She often let the other Panelists' air their concerns, while making sure the message stayed on task. She became the spokesperson for the program and the Overflow Control Plan.

In 2005, the Panel nearly fell apart because the Panelists felt like they were not allowed to get to the "meat" of the discussion. The staff and project team had not gathered all the data and information needed yet so the meetings were primarily basic education. They were worn out. The turning point was in late 2005 and early 2006 when the Panelists revolted. Finally, the Panelists were allowed to provide important input. They began to develop Guiding Principles and Goals and Objectives that eventually helped to define the Panelists' purpose and the entire Wet Weather Solutions Program. The data was not available to discuss alternatives so the Panel focused on values and a general strategy. They finally had the "meat" that they wanted and felt like their time was being used wisely.

Subcommittees

The subcommittees of the Community Panel were developed to discuss specifics of the recommendations in more detail. These subcommittees were found to be an invaluable method to work on the details of important issues. Some members of the Community Panel were more interested in certain subjects than others. When opportunities arose to discuss some of those subjects in more detail, they were encouraged to participate in the subcommittee meetings. The subcommittees would meet and often make recommendations that would be forwarded on to the entire Community Panel for further discussion. Many complicated discussions took place in the subcommittee meetings, discussions that couldn't have taken place in the time constraint of the two-hour long Community Panel meetings.

Funding Task Force

The Wet Weather Community Panel did not discuss funding for the program as part of their scope. Instead, a separate Mayoral-appointed committee was formed in January 2008. The Water Services Utility Funding Task Force was tasked with helping to integrate community values into forming a funding strategy for the City's water, sewer and stormwater utilities. The Task Force developed guiding principles for the development of user charges and fees that are fair, equitable and sufficient to meet revenue requirements. In addition, the Task Force provided guidance on how to fund the Overflow Control Program. The Task Force provided the Mayor and City Council written recommendations regarding funding issues. A resolution was passed endorsing their recommendations in December 2008.

Council Participation

In May 2007, Councilwoman Jan Marcason was made the point person for sewers for Kansas City. Eventually deemed the "Sewer Queen", Councilwoman Marcason attended most of the Community Panel meetings after she came to office and was the Chairperson for the Funding Task Force. Once the draft Plan was submitted to the City Council for approval in May 2008, Councilwoman took the heat because many didn't think the Plan was "green" enough. She began to educate her fellow council members and worked with staff to educate them. Eventually, in December 2008 when the Plan was approved by the City Council, Councilwoman Marcason was praised by her peers for her on-going commitment and dedication.

Lessons Learned

1. It is important to be able to include people with varying interests in the conversations, particularly those with different perspectives and dissenting views. Getting the right people involved and asking them to discuss the right questions at the right time is key.

2. People talk about what they know. Distribute materials ahead of the meeting is a good idea, but most participants won't read it if there is too much or if the information is highly technical. It's hard to grasp the nuances of the technical details of such a project such as levels of control and the magnitude of the costs. Don't be surprised is someone nontechnical is the one to change the entire conversation because they simplify the topic and say something very profound around their basic values. That type of thinking and conversation is how you build consensus.

3. Don't start too early with advisory groups or citizen committees. Wait to convene stakeholder committees when you have recommendations for them to develop or input that is needed.

IT'S ABOUT THE SEWERS STUPID!

Let's be honest, sewers aren't sexy. It's hard to peak interest in something that is out of sight, out of mind, as they say, but it is after all about the sewers. You need to talk

about pollution, public health and explain the risks and tradeoffs. This was difficult for some team members initially. They didn't want to say what the problem was and that something needed to be done about it because then the regulators may force them to fix it. This created an "elephant in the room" that no one would talk about. This seemed silly because the agency folks were going to make the city do something about overflows and we needed citizens to feel good about paying for it. If people couldn't talk about sewage in streams, how were they going to help to figure out how to address it or feel good about paying to fix it? We needed to help them understand how it all affected them or how they would benefit from solutions and investment. The public was told that there was a problem, yet the details were very vague. The local newspaper even said it wasn't a story.

In 2006, the City began to shift its thinking and began to tell people that fixing the sewers will relieve basement backups, remove diluted sewage from the streams and that the Plan will be very expensive to implement. Interest began to pick up. Consultants were allowed to use different language than before such as "sewage" and "billion" to describe the problems. The program was tagged as the "largest infrastructure improvement in Kansas City's history." Then sewers became the sexy story and people wanted to talk about them.

When funding began to be discussed in detail in early 2008, the newspapers became very interested. Interest peaked in other aspects of the Program as well. One reporter who came to the funding meetings began to write more about water quality too. Sometimes the news was inaccurate or negative, but the City felt that any coverage on the Program would be good coverage- this was a way to get the word out to the larger public. As the media became more and more interested, we developed a good working relationship with reporters and an editor in particular who really began to understand the issue and therefore reported the facts and figures accurately.

Lessons Learned:

4. Tell people why they should care! It is important to be blunt about what the problem is when you are trying to get the public's interest. People don't understand that sewage goes into the streams. People don't understand that dog poop and geese droppings make more of an impact on water quality than they do. Be upfront and forthcoming and the interest and trust will increase.

SPAGHETTI DINNERS AND FISH FRIES

Successful public education is not just about counting the number of cookies that have been eaten at a meeting, but about the number of people that have been educated. Again, sewers aren't sexy, so sometimes innovative methods need to be used to get the word out.

In 2006 and 2007, Basin Coordinating Committees were formed throughout the City. There were a total of 57 meetings and 11 open houses that took place as part of this process. A lot of time and money went in to the preparation of these meetings. After

all is said and done, it may have been more efficient to reach out to existing groups at existing meetings than trying to get people to come to a meeting about sewers.

To increase attendance at one of the open houses in the inner city, spaghetti dinner and fish were served. A couple of pancake breakfasts were held to draw people in and to get them to listen to staff speak about the problem. The turn out at the events was high. We are uncertain whether the people in attendance really learned anything about the issues and there was little input provided. It was, however, a positive event to reach out to the public.

Kansas City is divided up into many small neighborhood associations, block groups, and homes associations. The City decided to reach out to the neighborhood leaders and ask if they could speak at one of their meetings. This was well-received. To date, over 2,300 people with 92 organizations have received a road show presentation. There was great interaction and discussion at the meetings.

Lessons Learned:

5. Serve food, and they will come but not necessarily pay attention and participate.

6. Go to where people already gather to get the best collaboration.

YOU CAN'T SAY IT TOO MANY TIMES OR TOO MANY DIFFERENT WAYS

The average person needs to hear something five (5) times before they internalize the message and act on it. Using multiple communication techniques and methods with the same message really helps build understanding.

One of the most used tools was a short video about the issues and plan. In 2006, a video was created primarily for the Overflow Control Program to visually demonstrate what the sewer system looks like and describe the problem Kansas City faces. In 2008, the video was updated to include elements about stormwater as well as educating people on the way the City will fix the problems and what they can do to help.

Other methods included water bill newsletter inserts that are distributed to over 450,000 persons, television programming on the local access channel, a 10,000 Rain Gardens Campaign that was advertised through television and radio media, two public opinion surveys that were randomly distributed throughout Kansas City, and a Wet Weather Solutions Program website that contains information on what citizens can do as well as information on meeting dates and materials.

A lot of money was spent on public education and participation and that was criticized by the City Council, but many felt there was not enough. At many Community Panel meetings, we heard "we need more public education," "we need to get the word out," and "my neighbor has not heard anything about this problem."

This was really frustrating for us but we feel like we should have communicated better to people what we had been doing to educate and involve the public more and invite them to participate in the education process.

Lessons Learned:

7. Repetition is the key.

8. Use multiple methods and techniques.

9. Try to be efficient in your use of resources.

10. Communicate to stakeholders what you are doing and involve them in the education and outreach as much as possible to build buy in.

DON'T BLAME ME, IT'S GOT TO BE SOMEONE ELSES FAULT

As people became more and more educated about how watersheds work, the neighbor upstream, Johnson County, Kansas became a target. Johnson County is at the top of the Blue River watershed- a watershed that is a central focus of the problem and proposed improvements.

Johnson County officials came to a majority of the Community Panel meetings and twice gave presentations on what their County and municipalities are doing to improve water quality on their part. Despite all of that, some Community Panelists pointed fingers upstream and pressed for ways to get them to pay for it. The result of this conversation was the inclusion of the Blue River Watershed Plan in the Overflow Control Plan. It is a commitment to continue to work with neighbors in the watershed to solve problems jointly.

Lessons Learned:

11. Involve stakeholders beyond city limits to solve watershed issues.

GREEN TAKES ON A LIFE OF ITS OWN

In late 2006 and early 2007, a shift took place. Green solutions became a purposeful and intentional part of discussions, particularly amongst Community Panelists. It is hard to determine how the movement began, but when it did, it took on a life of its own. For various reasons, whether it was a business opportunity, personal interest, interest in finding ways to reduce the cost of the Program, or interest in improving the City as a whole, many people thought green solutions were the answer. The conflict came about when people thought green solutions were the only answer.

Green solutions and technologies for combined sewer overflow control is not the typical strategy. The project team wanted to accommodate stakeholders' desire for green solutions but they wanted to make sure it would be accepted by the agencies and not just be an add-on to the program. Sustainable thinking considers people, prosperity and the planet and there was concern about green solutions costing more

up front. This program was already going to cost billons. A subcommittee of the Community Panel was formed in January 2007 to discuss green solutions as part of the Plan in more detail. This became an impassioned group that produced a Position Paper that eventually was endorsed by the entire City Council and Mayor. This interest peaked interest by other City departments and the regulators. The U.S. Environmental Protection Agency's Deputy Director, Benjamin Grumbles, became a rock star to Community Panelists when he distributed a memorandum touting the benefits of green solutions for combined sewers.

The project team was never against green solutions, although some may disagree. There was a lot of discussion about whether green technologies were the silver bullet, the miracle cure, or simply one tool in the tool box. The project team felt green solutions was an important tool in the tool box. They were working with regulators to accept green in Kansas City but that was perceived by some proponents of green as not having enough support for green. Some community participants and even City Council members didn't think the project team was truly committed to green. It began to feel like two people were in the same room saying the same thing but neither one hears the other. Everyone was talking past each other. Outside forces were feeding the misunderstanding and mistrust. It was frustrating.

Because of the on-going discussions on green solutions, the City was granted a six-month extension on submitting its Plan to determine if more green solutions could be added to the Plan. The City will spend the first ten years on green solutions and committed to some more specific plans for green pilot projects.

Lessons Learned:

12. Public participation can sometimes be messy but in the end, it is completely worth it.

SUMMARY

As a result of the public participation process of the Wet Weather Solutions Program for Kansas City Missouri, a shift has taken place. Not just green solutions, but also about how and when to involve the public. The Water Services Department did not involve the public in developing plans in the past, but as a result of this process, the staff and consultants have developed a new respect for citizens. Ultimately, the City's partnership with citizens resulted in a better plan and that partnership will be vital for the implementation of this long-term plan.

Kansas City, MO Overflow Control Program: Line Creek/Rock Creek Sanitary Sewer Study

Jeffrey W. Davies, P.E.

HNTB Corporation, 715 Kirk Drive, Kansas City, MO 64105; PH (816) 527-2838; FAX (816) 221-9016; email: jwdavies@hntb.com

ABSTRACT

Kansas City's Water Services Department (WSD) prepared a Long Term Control Plan (LTCP) to provide a roadmap to reduce the magnitude, frequency, and duration of combined sewer overflows (CSOs), and for the rehabilitation and improvement of the sanitary sewer system (SSS) to prevent sanitary sewer overflows (SSOs) and basement backups.

The study area for this project includes the sanitary sewer system within the Line Creek, Rock Creek, Buckeye Creek, and Searcy Creek watersheds. The drainage area of these watersheds is approximately 25 square miles north of the Missouri River and contain 8-in to 72-in diameter sanitary sewers.

A hydraulic model was developed using XP-SWMM based on data collected from the City's Geographical Information System. Recommended improvements were evaluated to prevent SSOs, and preliminary cost estimates were developed.

HYDRAULIC MODEL

The collection system hydraulic model was developed based on the Kansas City, MO *Hydrologic and Hydraulic Model Protocol* and included pipelines with a diameter of 24 inches or greater, associated manholes, diversion structures, and pump stations. Inclusion of 24-inch and greater diameter pipelines served the purpose of minimizing model analysis run time while retaining the hydraulic integrity of the collection system. A summary of the modeled pipe diameter and length is provided in Table 1 and can be seen in Figure 1.

Table 1 Summary of Modeled Pipe Diameter & Length

Diameter (in)	Length (ft)		Diameter (in)	Length (ft)
24	41,615		48	8,071
27	9,762		54	6,596
30	16,630		60	2,704
33	4,265		66	3,495
36	26,874		72	3,195
42	2,209		Total	125,416

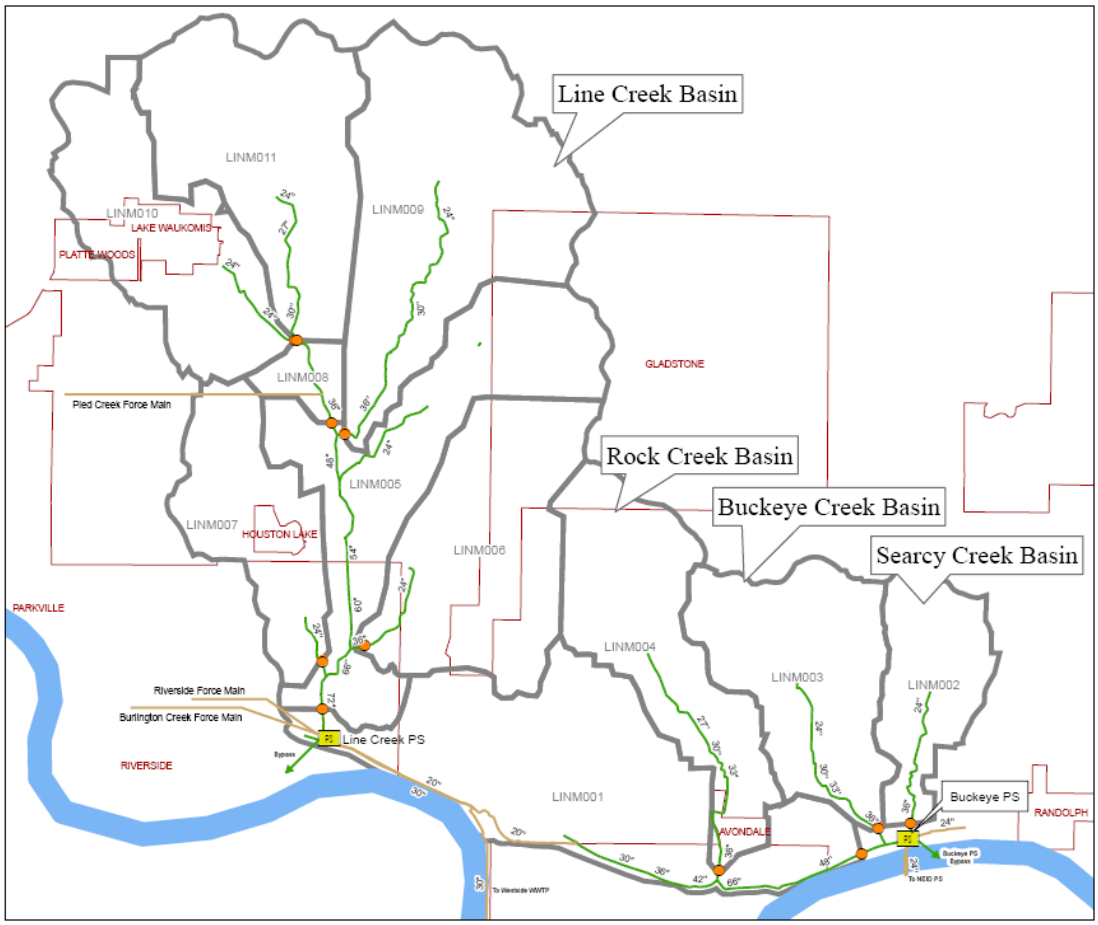

Figure 1 Basin Locations & Modeled System

The development and calibration of the wastewater collection system model proceeded in four phases:

Phase 1 - Data Collection
Phase 2 - Network Development
Phase 3 - Flow Projection
Phase 4 - Dry and Wet Weather Calibration

Data Collection

The data collection phase consisted of gathering the City's best available data on the sewer collection and conveyance system. For the existing sanitary sewer system, information on pump stations, pipes, manholes, and control structures which served as the physical foundation of the sewer model was developed from the City's GIS database and available reports. In addition to the physical data, current and future sewer loads were needed. Data from the pump stations, wastewater treatment plant influent data, and data from the 2005 flow monitoring program were gathered and analyzed to assist in model development and calibration.

Network Development

Pipe network attribute data was verified through quality control procedures in an effort to minimize the amount of erroneous information incorporated into the model. The manhole database was checked for quality control first, by following the procedures below:

- Verified XY coordinates through GIS
- Checked for duplicate manhole IDs
- Checked for manholes with duplicate XY coordinates
- Ensured that rim elevations were greater than manhole invert elevation
- Verified that appropriate manholes were referenced in the pipe database

After verifying the manhole database, the following procedures were used to provide quality control for the information in the pipe database:

- Checked for duplicate pipe IDs
- Verified pipe lengths using a GIS

Once the quality control checks were performed, manholes and pipes with missing data (i.e., IDs, elevations, sizes, lengths, etc.) were documented and provided to the field investigation team. The field investigation included:

- Locate manhole and provide global positioning coordinates (GPS) of the manhole lid (northing, easting, top elevation).
- Open manhole and provide depth to flow lines, pipe diameters, pipe material, manhole size, assessment of manhole condition, etc.
- Complete manhole inspection form.
- Photograph manhole exterior and interior.

Flow Projection

During model development, existing and future land use data was used to generate sanitary base flows at the sewer system manholes. Using the GIS, the sanitary base flows at each manhole were computed by taking the sewer flows for various land uses in the sewer service area and assigning sewer flows to the nearest manhole. The Line Creek GIS sewer layer and hydraulic model network of the sewer system were used to as the basis for delineating the existing sewer service area.

Dry and Wet Weather Calibration

The calibration process consisted of calibrating both dry and wet weather flow events. Dry weather flow calibration ensured an accurate depiction of base flow generated within the study area. The wet weather flow calibration consisted of calibrating the hydraulic model to a specific set of storm events to quantify the peak flow and volume of rainfall dependent inflow and infiltration (RDII) entering the collection system. The amount of RDII allowed to enter the collection system is essentially the difference between the wet weather flow and dry weather flow components.

DESIGN STORM ANALYSIS

The City provided information regarding the storm event used for the design storm event analysis. For this project, the U.S. Soil Conservation Service (SCS) Type II 24-hour distribution was used as the design storm. Analysis of the existing system and future system requirements was based on the 5 year storm event. Table 2 summarizes the rainfall totals for the 5 year storm event.

Table 2 SCS 24-hour Type II Rainfall Distribution

Return Frequency (years)	5
Rainfall Depth (inch)	4.68
Peak Hour (inch)	2.34
Peak 30 Minute (inch)	2.00
Peak 15 Minute (inch)	1.29

Existing wastewater production was based on data acquired during the 2005 City wide flow monitoring program. Wastewater production associated with future development was based on 100 gallons per capita per day. Collection system and facility requirements for existing conditions were determined using the previously calibrated model as a starting point. The City stipulated the operation of the Line Creek pump station during design model simulations. After a detailed investigation into the existing operation of the Line Creek pump station, the dry weather models were configured to send 60-70% of flow up to a maximum of 8 MGD to the Hillside Levee Interceptor and the remaining portion of the flow to the Westside WWTP.

The wet weather flow consists of dry weather wastewater production in addition to infiltration and inflow, also known as rain dependent inflow and infiltration (RDII). The limited capacities of the existing Line Creek and Buckeye Creek pump stations caused extensive backup into the collection system. The pump stations were removed from the design storm models and the inlets to the pump stations were modeled under free outfall conditions.

Results of the analysis show that parts of the system contain bottlenecks that become overloaded during large rain events. To establish the location of these flow restrictions, the results from the model were broken into five (5) separate sections. These sections represent the four (4) major watersheds included in the project area and the Hillside Levee Interceptor. To better understand the existing level of service in each one of the watersheds, the number of manholes and length of pipe which are not currently adequate for the desired level of service was summarized. To develop a better understanding of existing system performance, each line segment included in the model was put into one of five (5) categories of percent utilization. When Q refers to the maximum simulated flow and C refers to the design capacity of each pipe segment, the categories are defined as follows:

1. **<100%** - if Q/C*100<100%
2. **Backup** - if Q/C*100<100% and downstream manhole is surcharged
3. **>100%** - if 150% > Q/C*100 > 100%
4. **>150%** - if 200% > Q/C*100 > 150%
5. **>200%** - if Q/C*100 > 200%

The results from this analysis are summarized in Table 3, Table 4, and Table 5.

Table 3 Summary of Existing Conditions Model Results

Model Segment	Length of Sewer (ft)					
	Included in Model	Percent Utilization				
		<100%	Backup	> 100%	>150%	>200%
Buckeye Creek	10,600	2,800	1,000	6,000	700	0
Line Creek	64,800	42,300	2,800	17,200	1,500	1,100
Rock Creek	13,200	0	2,200	10,000	400	700
Hillside Levee Interceptor	17,500	900	2,400	3,800	6,500	3,800
Searcy Creek	8,400	8,400	0	0	0	0
Total	114,500	54,400	8,400	37,000	9,100	5,600

Table 4 Summary of Year 2030 Model Results

Model Segment	Length of Sewer (ft)					
	Included in Model	Percent Utilization				
		<100%	Backup	> 100%	>150%	>200%
Buckeye Creek	10,600	2,800	1,000	6,000	700	0
Line Creek	64,800	38,500	4,600	18,300	1,500	1,800
Rock Creek	13,200	0	2,000	10,000	600	700
Hillside Levee Interceptor	17,500	1,700	2,000	3,500	6,500	3,800
Searcy Creek	8,400	8,400	0	0	0	0
Total	114,500	51,400	9,600	37,800	9,300	6,300

Table 5 Summary of Ultimate Build-Out Model Results

Model Segment	Length of Sewer (ft)					
	Included in Model	Percent Utilization				
		<100%	Backup	> 100%	>150%	>200%
Buckeye Creek	10,600	2,700	1,100	5,800	900	0
Line Creek	64,800	23,400	8,900	27,400	2,600	2,600
Rock Creek	13,200	0	2,000	9,700	900	700
Hillside Levee Interceptor	17,500	1,000	2,000	4,200	5,900	4,400
Searcy Creek	8,400	8,400	0	0	0	0
Total	114,500	35,500	14,000	47,000	10,300	7,700

ALTERNATIVE DEVELOPMENT

The Line Creek Drainage Basin was divided into seven (7) sub-basins for I/I flow monitoring. The Rock Creek/Searcy Creek/Buckeye Creek Drainage Basin was divided into four (4) sub-basins. Refer to Figure 1 for the location of the various sub-basins within the overall Drainage Basins.

Inflow & Infiltration (I/I) Removal Plan

Flow was monitored in each sub-basin and an estimate of the cost required to remove I/I flow was developed for each Sub-Basin. The Unit I/I Removal Costs ($/gpd) ranged from $0.48 to $2.09. Total I/I rehab costs ranged from $0.2M to $6.5M per basin being improved. An I/I reduction program known as the "Nashville Approach" was used to determine if there was a cost-effective point for these improvements. This approach begins with the assumption that I/I improvements will be needed in 20% of the total length of the sewers in each sub-basin and that a reduction of I/I flow of 50% will be achieved by the improvements.

Based on this method, it was determined that it is cost effective to remove I/I flow from every basin. A few basin improvement scenarios were selected that will allow a large percentage of I/I reduction to be achieved without removing I/I flow from every basin. Additional basins could be added to the improvement plan in the future to gain extra capacity for the treatment units.

Relief Sewers

Relief sewer improvement costs were also calculated for the number and size of pipes that were required to be replaced or upgraded after I/I improvements were made to each basin. Relief sewer improvement costs ranged from $33.9M if no I/I improvements were made to $9.5M if all the basins received I/I improvements. A summary of the I/I removal costs and the relief sewer improvement cost for the basin improvements scenarios selected for evaluation is shown in Table 6.

Table 6 I/I Removal and Relief Sewer Improvement Cost Summary

Selected Basins for I/I Improvements	Basins 010, 009, 006, 005, and 004	Basins 010, 009, 006, 005, 004, and 003	All Basins
Expected Reduction in Total Flow	28%	35%	41%
Total I/I Removal Cost ($M)	34.3	44.4	70.9
Total Relief Sewer Improvement Costs ($M)	15.7	12.4	9.5

Wet Weather Solutions

Several types of storage, transport, and treatment technologies were compared and evaluated. The types which were most applicable to this project included lift stations/force mains, tunnels for both storage and transport, above ground storage facilities, a new wastewater treatment facility to be built near the current Line Creek Lift Station, and upgrades to the existing Birmingham wastewater treatment facility to treat the additional flows rerouted there.

Selection of Alternatives for Evaluation

Three (3) alternatives utilizing the various technologies were chosen for evaluation:

1. New wastewater treatment facility near Line Creek Lift Station for the Line Creek Basin flow transport of the wastewater (by tunnel) from the

Buckeye Lift Station (Rock Creek/Searcy Creek/Buckeye Creek Basin Flow) to the Birmingham Wastewater Treatment Facility.
2. New force main from the Line Creek Lift Station to the Buckeye Lift Station to the Birmingham Wastewater Treatment Facility.
3. New tunnel from the Line Creek Lift Station to the Buckeye Lift Station to the Birmingham Wastewater Treatment Facility.

Each Alternative was further analyzed under four (4) options involving how flow was split between new and existing treatment facilities:

A Up to 12 MGD of flow is pumped to the Westside Treatment Plant. Up to 10 MGD is pumped to the Blue River Treatment Plant. All remaining flow is treated north of the river.
B. Up to 12 MGD of flow is pumped to the Westside Treatment Plant. All remaining flow is treated north of the river.
C. Up to 10 MGD is pumped to the Blue River Treatment Plant. All remaining flow is treated north of the river.
D. All flow is treated north of the river.

Each Option was further evaluated under the following Basin I/I Improvement Scenarios:

a. No I/I reduction in any basin. No relief sewer improvements.
b. No I/I reduction in any basin. Relief sewer improvements only.
c. I/I reduction in basins 10, 9, 6, 5, and 4. Relief sewer improvements.
d. I/I reduction in basins 10, 9, 6, 5, 4, and 3. Relief sewer improvements.
e. I/I reduction in all basins. Relief sewer improvements.

Design Criteria

The following design criteria were also used in determining the required equipment sizing:

- Pump Stations were sized to handle the peak flow.
- Storage Facilities, including Tunnels and Evacuation Pumps, were sized to fill during peak flow events and to be emptied over a period of 48 hours.
- Treatment Facilities were sized with a 2.5 peak to average ratio. The required pump rate to empty the Storage Facilities in 48 hours was considered the sustained peak flow that the treatment plant must handle, and the plant size (based on the average flow) was calculated based on the ratio listed above.
- Force Mains were sized for a minimum velocity of 2 ft/sec and a maximum velocity of 5 - 6 ft/sec.
- Gravity Outfall sewers were sized to flow up to 75% full at peak flow at an assumed slope of 0.005 ft/ft.
- A minimum slope of 0.1% is assumed for tunnels. A minimum of 3 ft/sec is needed for proper flushing in the tunnel system.

Cost Analysis

All of the Alternatives/Options were analyzed for costs using the Kansas City, MO *Basis of Cost Manual*. Table 7 (Table ES-1 from that Manual), which summarizes the construction cost and O&M cost equations used in this evaluation.

The following values were used for the variables required in the equations:

- C = calculated value
- A = calculated value
- V = calculated value
- N = 6 uses per year
- N_s = based on one shaft every 3,333'
- D = calculated value
- L = Line Creek Lift Station to Buckeye Lift Station – 29,000 ft; Buckeye Lift Station to Birmingham WWTP – 21,000 ft; Total Length – 50,000 ft
- Q = calculated value
- Hr = calculated value
- Q_{ave} = calculated value

The following cost data was used in addition to the cost formulas given in the Basis of Cost Manual:

- Odor Control costs were included in the pump station, storage tank, and tunnel costs as follows: Pump Stations - $1,000 per MGD pumping capacity; Storage Tanks - $11,000 per MG; Tunnels - $200,000 per access shaft.
- Wastewater Treatment Plant costs were estimated at $5 per MGD treatment capacity (average flow).
- O&M costs for existing facilities remaining in operation were not included in the alternative analysis.
- O&M costs for tunnels in continuous operation were assumed to be the same as wet-weather tunnels (N=6).

Replacement Costs were estimated assuming a 50 year design period. Process equipment associated with treatment facilities was assumed to have a service life of 20 years and have a replacement cost of 35% of the original construction cost. Mechanical and electrical systems associated with pumping facilities were assumed to have a service life of 10 years and have a replacement cost of 35% of the original construction cost.

The Present Worth and Equivalent Uniform Annual Cost for the capital, O & M, and replacement costs of each Alternative/Option were calculated using the formulas given in the *Basis of Cost Manual*. A 50 year life cycle and a discount rate of 5% were used.

Table 7 Summary of Construction and O&M Cost Equations

Control Technology	Construction Cost (million $)	Annual O&M Cost ($1,000)
Storage Tanks[5]	$C = 8.367\ V^{0.5546}$	$A = 1.2\ N + 2.5\ C$
Tunnels		
Hard Rock[6]	$C = 1154.4\ e^{0.0721\ D} \times L/10^6$	$A = 2.24 \times 10^{-4}\ L + 6\ N_s +$
Soft Ground[7]	$C = 981.4\ e^{0.1121\ D} \times L/10^6$	$1.2NxL/10{,}000+2.5C$
Swirl Concentrators	$C = 0.310\ Q^{0.611}$	$A = 0.6\ N + 20\ C$
Screens	$C = 0.1275\ Q^{0.843}$	$A = 0.6\ N + 20\ C$
Sedimentation Basins	$C = 0.398\ Q^{0.688}$	$A = 0.9\ N + 20\ C$
High Rate Treatment[8]	$C = 0.2846\ Q$	$A = 0.350V + 20C$
Chlorination/Dechlorination	$C = 0.228\ Q^{0.464}$	$A = 0.3\ N + 20\ C + 0.251\ V_{avg}$
Ultraviolet Disinfection	$C = 0.536 + 0.072\ Q$	$A = 0.3\ N + 1.062\ Q + 0.00043\ Q*Hr$
Sewer Construction	Use cost estimator	Minimal[3]
Pump Station		
Intermittent Service	$C = 0.3437\ Q$	$A = 0.6\ N + 20\ C + 0.372$ $+ 0.419Q + 0.00069Q*Hr$
Continuous Service	$C = 0.3437\ Q$	$A = 219.4 + 20\ C + 0.477\ Q + 5.93\ Q_{avg}$
Combined Sewer Separation[4]		
Residential	$C = 0.036\ S$	None[3]
Commercial/Mixed Use	$C = 0.085\ S$	
Downtown Area	$C = 0.130\ S$	

1. ENRCCI = 8500
2. Cost variables: C=Construction cost (million $); A=Annual O&M cost ($1000); V= Storage volume (million gallons); N=Average annual number of uses; N_s=Number of access shafts; D=Finished tunnel diameter (feet); L= Tunnel length (feet); Q=Design flow rate (MGD); V= Overflow volume treated per year (MG); V_{avg}=Average annual treatment volume (MG); Hr=Average annual operating hours; Q_{avg}=Average annual discharge rate (MGD); and S=Total sewer basin area (acres). The variable "e" is the base of the natural logarithm.
3. The annual O&M cost for new sewers is assumed to be minimal. O&M consist of video inspection and cleaning once every 10-15 years.
4. Unit costs of sewer separation considered valid for basins less than 250 acres only.
5. The unit cost equation for storage tanks is considered applicable for tanks with volumes ranging from 2 million gallons to 30 million gallons.
6. The unit cost equation for hard rock tunnels is considered applicable for diameters of 10 to 35 feet.
7. The unit cost equation for soft ground tunnels is considered applicable for diameters of 5 to 20 feet.
8. The unit cost equation for high rate treatment facilities is considered applicable to facilities with capacities less than or equal to 100 MGD.

RESULTS

The alternative analysis produced total capital costs ranging from $344.2M to $607.3M, and total present worth values ranging from $391.5M to $751.4M.

Based on the results of this analysis, Alternative 3, Option A, I/I Reduction in All Basins was determined to have the lowest present worth value. Alternative 3, Option A, with I/I Reduction in Basins 010, 009, 006, 005, 004, and 003 produced very comparable numbers, and does not rely on achieving a large I/I reduction from every single basin. A summary of the costs associated with these two alternatives is located in Table 8.

Table 8 Alternative Cost Summary

	Alternative 3, Option A I/I Reduction in All Basins	Alternative 3, Option A I/I Reduction in Basins 10, 9, 6, 5, 4, and 3
Expected Reduction in Total Flow (%)	41	35
Required Equipment Sizing Summary		
-Line Creek Basin		
-Tunnel Diameter (ft)	8	9
-Rock/SearcyBuckeye Creek Basins		
-Tunnel Diameter (ft)	8	9
-Pumping Facilities (MGD)	23	26
-Birmingham WWTP Upgrades		
-Treatment Plant (MGD)	10	11
Total Capital Cost ($M)	345.5	344.2
Present Worth Operation and Maintenance Costs ($M)	32.9	35.2
Present Worth Replacement Cost ($M)	13.1	14.5
Total Present Worth ($M)	391.5	393.9
Equivalent Uniform Annual Equivalent Cost ($M)	21.4	21.6

ACKNOWLEDGEMENT

George Butler & Associates was a sub-consultant to HNTB Corporation for this project and provided flow monitoring, hydraulic modeling, and design storm analysis.

REFERENCES

Basis of Cost Manual, Kansas City Missouri - Water Services Department, Overflow Control Program, December 19, 2006.

Hydrologic and Hydraulic Model Protocol, Kansas City, Missouri - Water Services Department, Overflow Control Program, November 9, 2004.

LAKE WINNEBAGO DAM RELOCATION PROJECT

Jonathan L. Polak[1] and Shannon W. Tyree[2]

[1]Environmental Engineer, Olsson Associates, 7301 W. 133rd Street, Suite 200, Overland Park, Kansas 66213; PH 913.381.1170; FAX 913.381.1174; email: jpolak@oaconsulting.com

[2]Restoration Ecologist, Olsson Associates, 7301 W. 133rd Street, Suite 200, Overland Park, Kansas 66213; PH 913.381.1170; FAX 913.381.1174; email: styree@oaconsulting.com

ABSTRACT

The City of Lake Winnebago, Missouri, is a tight-knit community focused on providing residents with water-based recreational opportunities on the existing 244-acre lake. The original master plan for the community involved building two lakes; however, bankruptcy by the developer limited the community to one lake. Residents never lost their desire to complete the original lake plan and have partnered with South Winnebago Partners, LLC to complete the vision for the city.

The project proposes to construct a new earthen filled dam downstream of the existing lake. The proposed dam is 65 feet tall and 1,440 feet long. Relocating the dam will expand the surface area of the lake from 244 acres to approximately 416 acres. The proposed project would result in placing fill material into jurisdictional waters of the United States, causing the unavoidable impact to 15,879 linear feet of stream and 16.57 acres of wetlands. Because this project is one of the largest regulated Corps of Engineers activities within the Kansas City metropolitan area, Olsson Associates was hired to complete Section 404 Permitting and mitigation planning.

Mitigation measures are proposed at two locations within the South Grand River watershed. Mitigation is consistent with the project goals of using a watershed-based approach, providing self-sustaining ecological units, protecting rare and unique habitats, and constructing complementary habitats within the existing landscape. Mitigation activities include preserving and restoring 118 acres of the Middle Big Creek floodplain. Restoration includes planting approximately 5,500 trees to restore 25.4 acres and enhance 11.3 acres of riparian woodland. The plan also includes restoring 8.1 acres of native grass buffer, enhancing 8.1 acres of mesic prairie buffer, enhancing 4.3 acres of prairie buffer, and the enhancing 6.0 acres of wetland prairie. Approximately 750 linear feet of tributary will be created to reconnect historic flows to 2,400 linear feet of tributary. To compensate for wetland impacts, 15.28 acres of emergent wetlands will be restored, and 6.45 acres of existing forested wetlands will be preserved.

PROJECT BACKGROUND AND HISTORY

The Lake Winnebago dam relocation project proposes to increase the size of an existing community-based recreational lake to stimulate new residential and commercial development. However, the full breadth of benefits the proposed project offers the local community must also be recognized. The primary driver for this project is the partnership of the City of Lake Winnebago and a local group of development investors, South Winnebago Partners, LLC, to ensure the long term viability of the city. This community, with approximately 485 homes, has focused on providing residents with recreational lake living. Yet, the financial and social livelihood of the community has continually been challenged since the community's conception and the subsequent bankruptcy by the original development group.

In 1964, Mr. Robert Steinhilber established a development company and a master plan to build two phases of a lake community in northern Cass County. The original master plan included constructing the existing Lake Winnebago and the uncompleted Lake Winnebago South. Constructing both phases would have ultimately included residential development surrounding two separate lakes and a commercial retail component located along Missouri Highway 291. Following construction of the first phase of the community in 1968, in 1970 the development company operated by Mr. Steinhilber filed for bankruptcy, leaving the residents to absorb a large debt resulting from unpaid bonds sold to fund the construction of sewers, waterlines, and other infrastructure.

After filing for bankruptcy in 1970, Mr. Steinhilber once again organized a second development company to sell lots around the proposed south lake. Between 1970 and 1972, Mr. Steinhilber sold approximately 400 lots in the second phase before a receivership was filed against his company. The developer once again defaulted on obligations, and the property was held in receivership for over 27 years. All 400 lots sold before the receivership was filed were never deeded to the original purchasers, and only a partial repayment was made following the legal settlement with Mr. Steinhilber's development group.

The financial burden to the residents from the original bankruptcy in 1970, in addition to necessary repairs to the existing dam over the last 40 years, depleted the available financial resources of the community, prohibiting the purchase of the phase two properties when the receivership ended. The properties were ultimately purchased by the current landowner, whom the city approached to complete the development as originally promised by Mr. Steinhilber in 1964.

The city has needed the proposed lake expansion since 1968 due to insufficient economic resources to support the daily operations of the city, maintain important infrastructure, and manage lake maintenance. This large financial burden has resulted in high taxation and financial assessments to community residents. The cooperation with by the existing land owner and the partnership with South Winnebago Partners, LLC provide an opportunity to change the community's future. The project will increase the number of residential properties to almost 900 homes and will add a

commercial district to generate desperately needed tax revenues. The additional revenue stream will provide available funds for significant improvements to the city's infrastructure including roads, sewer lines, waterlines, and more.

PROJECT DESCRIPTION AND LOCATION

South Winnebago Partners, LLC, in partnership with the City of Lake Winnebago, is planning to construct a new earthen filled dam south of the existing Lake Winnebago Dam. The project would expand the surface area of the lake from 244 acres to approximately 416 acres. The overall project site consists of approximately 450 acres located in Cass County, Missouri, immediately south of the City of Lake Winnebago. The project area incorporates the main stem of Middle Big Creek, which is a tributary to Big Creek, in Cass County, Missouri.

The proposed dam would be 65 feet tall and 1,440 feet long and would have a top width of 38 feet to accommodate a roadway surface. The top of dam would be located at an elevation of 930.00 feet, National Geodetic Vertical Datum (NGVD), while the lake's normal pool elevation would be 918.50 feet, NGVD. The proposed flood elevation is 923.00 feet, NGVD, which is six inches lower than the lake's existing flood elevation. Reducing the flood elevation will provide added protection to homes, the existing civic building, and local streets that currently experience flooding. Additional benefits to the community include relocating 167th Street, which is currently closed due to safety concerns from the deteriorated roadway.

The final component of the project includes concurrently developing residential and commercial lots in the uplands adjacent to the expanded lake. The proposed development plan identifies approximately 400 residential lots, including lakefront lots and second and third tier homes without lakefront property. Areas have been set aside to create open green space, an amenity center for the community, and commercial development along the frontage of Missouri Highway 291.

PERMITTING APPROACH

Olsson Associates (Olsson) began working with South Winnebago Partners, LLC and the City of Lake Winnebago during the summer of 2005. Initial efforts focused on developing a new master plan to identify preliminary dam sizing, dam location, available residential and commercial tracts, and available infrastructure to serve the future project area. Understanding the regulatory complexities and agency coordination required to expand the existing 244-acre lake to approximately 416 acres, Olsson's environmental staff completed a comprehensive environmental inventory of the 450-acre project area. The Jurisdictional Wetland Evaluation and Functional Assessment (Olsson, 2005) classified tributaries within the project area as ephemeral, intermittent, and perennial tributaries and identified wetland areas as open water, emergent wetlands, and forested wetlands. Olsson worked closely with the Kansas City District Corps of Engineers to ensure compliance with newly issued guidance addressing significant nexus and reclassifying tributaries to permanent, relatively permanent, and non-relatively permanent tributaries (U.S. Army Corps of Engineers, 2007).

Olsson also coordinated a review with the U.S. Fish and Wildlife and the Missouri Department of Conservation regarding the potential for threatened and endangered species occurrences in the project area. Olsson's review for species and critical habitat included a field survey for the Indiana bat's (*Myotis sodalis*) suitable habitat (Olsson, 2007). No endangered species were identified during the field survey, and the percent of suitable habitat for the Indiana bat was determined to be insufficient for further investigation. A final step completed as part of the environmental inventory included coordinating cultural resources with the State Historic Preservation Office through the Missouri Department of Natural Resources. A section 106 application was submitted, and a Phase I Cultural Resource Investigation was completed for Olsson (Environmental Research Center of Missouri, Inc., 2006). No archaeological or historic resources were identified within the project area.

Project Purpose and Need

The critical component to the Section 404 application is the ability for the applicant to demonstrate a clear and concise project purpose and need. For the Lake Winnebago dam relocation project, Olsson identified three codependent purposes and needs. The project purpose and need included the following components:

1) Expand the City of Lake Winnebago in general accordance with the master plan commitment made to the community over 40 years ago to create development that helps ensure the future economic viability of the city.

2) Reduce the increasing flood risk to residents of Lake Winnebago.

3) Replace an aging 42-year-old high hazard dam with a new structure designed to meet current dam construction standards.

The opportunity for revenue to be generated by the proposed development provides an economically viable option to resolve current and long-term flooding issues, address long-term dam safety issues, and provide a reasonable assurance of long-term economic viability for the community.

Evaluating Alternatives

Olsson coordinated with the applicant to evaluate alternatives pursuant to [40 CFR 230.10]. The National Environmental Policy Act (NEPA) and implementing regulations at [40 CFR 1502.14] require that a range of reasonable alternatives, including the No-Action alternative, be evaluated. To address the three components of the purpose and need, the following four alternatives were considered for the Lake Winnebago project:

1) No Action Alternative - This alternative would not resolve the uncertain economic viability of the community; the City of Lake Winnebago would continue to experience flooding on local streets, residential homes and the civic center; and the aging dam would need continued maintenance for repairs necessary to maintain the community's primary amenity.

2) Dam Removal Alternative - The dam removal alternative would resolve the concerns associated with dam failure for the aging dam; however, it would not address the city's economic stability. Removing the existing dam would cause significant societal and environmental concerns such as land ownership, property values, and maintaining the exposed mudflat. Removing the dam would also be detrimental to the existing aquatic ecosystem and stream corridor. Completely removing the existing dam is not in the public's best interest and would not meet the need for increased protection from flooding and economic stimulus to the city.

3) Dam Reconditioning and Watershed Planning Alternative - Dam reconditioning and watershed planning alternatives focused on structural improvements to reduce flood elevations and protect the integrity of the dam. This alternative considered lowering the permanent pool elevation to increase flood storage, constructing small impoundments upstream to help attenuate storm events, and reconditioning the existing spillway to manage larger storm events. Due to the difficulties of reconstructing the existing dam, the risk of failure as the structure ages, the lack of increased flood protection this alternative did not meet the purpose and need for the project.

4) Dam Relocation (Preferred) Alternative - Constructing a new dam downstream of the existing dam would increase the lake size while maintaining the same permanent pool elevation of the existing lake. The increased storage area would provide increased flood control, protection of aquatic resources, and protection of the health and safety of residents. Constructing the new dam downstream in a similar location to the original master plan serves both the purpose and the need of the project.

Impacts to Waters of the U.S.

The preferred alternative includes constructing an earthen filled dam south of the existing Lake Winnebago Dam. The surface area of Lake Winnebago will be expanded from 244 acres to approximately 416 acres. The preferred alternative for relocating the Lake Winnebago Dam will result in unavoidable impacts to 15,879 linear feet of tributary, including 4,067 linear feet of perennial tributary, 7,864 linear feet of intermittent tributary, and 3,948 linear feet of ephemeral tributary. Approximately 16.57 acres of wetlands, including 1.29 acres of forested wetlands and 15.28 acres of emergent wetlands, will also be affected by the project.

MITIGATION REQUIREMENTS

To determine the appropriate mitigation requirements, Olsson used guidance from the U.S. Army Corps of Engineers Regulatory Guidance Letter 02-2 (U.S. Army Corps of Engineers, 2008) and the Missouri Department of Natural Resources: State of Missouri Aquatic Resources Mitigation Guidelines (MDNR, 1998). Due to agency requirements, wetlands and tributaries were assessed independently to determine the appropriate mitigation measure required of impacted tributaries and wetlands.

Wetlands

Olsson completed a functional assessment of impacted wetlands to provide the background data needed for the Corps to determine an appropriate mitigation ratio for wetland impacts. Given the condition of existing wetlands, it was determined that a 1:1 ratio (15.28 acres) would be appropriate to mitigate emergent wetlands and a 5:1 ratio (6.45 acres) for forested wetlands, assuming a preservation credit.

Tributaries

The Department of the Army and State of Missouri approved Stream Mitigation Method (Department of Army, 2007) was used as a basis to determine tributary impacts (debits) and mitigation credits. The Adverse Impact Factors for Riverine Systems Worksheet was completed to determine the total mitigation credits required to mitigate project impacts. Based on the worksheet and coordination with the Corps of Engineers, it was determined that a total of 77,020 credits were needed to fully mitigate project impacts.

MITIGATION APPROACH

Olsson's approach to mitigation considered a watershed based approach to mitigating resource impacts. Olsson developed a mitigation plan that would fully replace the ecological functions and values as a result of project impacts. The plan incorporated a concept known as habitat architecture into the design process. Habitat architecture is the process of combining independent wildlife habitats, such as prairie, wetlands, forest, etc., into a self-sustaining ecological unit. Habitat creation, restoration, enhancement, and preservation of natural resources were all included as components to the mitigation plan.

Mitigation Site Selection

The single and most difficult component to successful mitigation is location. Mitigation measures completed outside the context of the existing landscape will undoubtedly fail. Olsson invested considerable time and effort into identifying suitable mitigation sites that would complement existing natural resources and ensure mitigation site success.

A mitigation matrix and alternatives mitigation site map was developed for properties within the watershed that appeared to have the potential to provide mitigation opportunities. The mitigation matrix included such criteria as perceived site conditions based on aerial reviews, length of degraded stream, availability, land cost, etc. Once the in-house review was completed, field site visits to each property were completed to further refine the potential for mitigation and to select the most viable mitigation options.

FINAL MITIGATION SITES

Two mitigation sites were ultimately selected: 1) the Ingles Floodplain and Tributary Mitigation Site, and 2) the Pintail Pastures (Urich, Missouri) Wetland Mitigation Site. Both sites were consistent with the project goals listed below of using a watershed based approach, providing self sustaining ecological units, protecting rare and unique habitats, and constructing complementary habitats within the existing landscape.

Goals of Mitigation

The primary goals for the Lake Winnebago mitigation included the following:

Goal 1: Use a watershed based approach. – Mitigation activities and site selection were considered based on protecting aquatic resources and enhancing the entire watershed. Both mitigation sites are located within the South Grand River Watershed.

Goal 2: Provide a comprehensive and sustainable ecological unit. – Providing a sustainable ecological unit is an important goal of the mitigation plan. The mitigation plan encompasses restoration, enhancement, creation, and preservation that work together to provide a long-term sustainable ecological unit.

Goal 3: Protect rare and unique habitats. – A rare and unique habitat, in the form of an undisturbed wet prairie/fen, exists on the "Ingles Floodplain Restoration and Tributary Mitigation Site." An undocumented occurrence for closed gentian (*Gentiana andrewsii*), a flowering plant, was identified during initial site investigations. A primary goal with any mitigation site is to provide long-term protection to rare and unique habitats when possible. The wet prairie on the site has been incorporated into the mitigation plan as a tributary buffer and is permanently protected by legal restrictions on the property.

Goal 4: Constructing complementary habitats within the existing landscape context. – Mitigation activities will be completed within the context of the existing landscape. Planting plans were developed based on existing vegetative communities, while site grading was based on avoiding over-engineered structures. A landscape context is an essential element to meeting the goal of providing a comprehensive and sustainable ecological unit.

Ingles Floodplain Restoration and Tributary Mitigation Site

The Ingles Floodplain Restoration and Tributary Mitigation Site is an approximately 243-acre site located two miles downstream of Lake Winnebago and three miles west of the Town of Pleasant Hill. The site provided a unique opportunity to restore multiple habitats within the watershed and floodplain of Middle Big Creek. The site had been owned by the same family as a working farm for over 100 years. Most of the site had been heavily affected by grazing cattle. However, in areas restricted to cattle, the site was diverse and provided baseline reference habitats for the results restoration could achieve on the site.

To assess mitigation measures relative to the mitigation credits, the site was divided into net benefit areas. Each net benefit area included its own suite of habitats, mitigation opportunities, and generated mitigation credits (see Table 1).

The unique combination creating, restoring, enhancing, and preserving site resources resulted in a total of 78,465 credits and exceeded the 77,020 required credits. Table 1 summarizes mitigation activities relative to net benefit areas and the total mitigation credits achieved on the Ingles Floodplain and Tributary Mitigation Site.

Table 1: Ingles Floodplain and Tributary Mitigation Site Debits/Credits and Net Benefits

Tributary Impacts		
Tributary Type	**Linear Feet**	**Missouri Stream Mitigation Method (Credits Required)**
Perennial	4,067 linear feet	17,175
Intermittent	7,864 linear feet	42,869
Ephemeral	3,948 linear feet	16,976
Total	**15,879 linear feet**	**77,020 debits**

Tributary Mitigation (Net Benefit Areas)		
Tributary Type	**Mitigation Activities**	**Missouri Stream Mitigation Method (Credits Generated)**
Net Benefit Area 1	• Restore 25.4 acres of riparian corridor. • Enhance 11.3 acres of riparian corridor. • Enhance 4.3 acres of native prairie. • Preserve a 300-foot buffer of Middle Big Creek.	58,746
Net Benefit Area 2	• Create 750 linear feet of tributary, and re-connect 1,150 linear feet of historic channel. • Restore part of 8.1 acres of native prairie. • Enhance part of 8.1 acres of mesic prairie. • Preserve a 300-foot tributary buffer.	4,620
Net Benefit Area 3	• Enhance 2.0 acres of rare and unique existing wetland prairie habitat. • Restore part of 8.1 acres of native prairie. • Enhance part of 8.1 acres of mesic prairie. • Preserve a 300-foot tributary buffer.	9,499
Net Benefit Area 4	• Enhance 4.0 acres of rare and unique existing wetland prairie habitat. • Reconnect 1,250 linear feet of historic channel. • Preserve a 300-foot tributary buffer.	5,600
Total	**118 acres of preserved mitigation activities**	**78,465 credits**

Pintail Pastures Wetland Mitigation Site

The Pintail Pastures Wetland Mitigation Site is an approximately 35-acre site located just east of Urich, Missouri. The site is located in the floodplain of the South Grand River and provided a unique opportunity to restore historic wetland conditions to the site. The site was designated by the Natural Resource Conservation Service as a *Prior Converted* wetland. The designation gives a strong indication that restoring historic conditions to the site would result in successfully restoring the wetland. However, the site was not as straightforward as reconnecting historic hydrology. Years of agricultural use and drainage ditches had greatly influenced site conditions. In addition, the site was located within the Truman Lake flowage easement, which restricted constructing any structures or losing flood storage. Working on the site required a complex combination of multiple disciplines, including survey, hydrology, soils, biology, ecology, and engineering.

The final wetland design included restoring historic hydrologic conditions on the site by removing the man-made drainage ditches. Hydrology was then restricted on the site by installing low berms, which increased the residence time and frequency of hydrology on the site. The restored hydrology and low berms, less than six inches in places, provided the hydrology necessary to restore the wetland to its historic and sustainable condition. In addition, the short berms, coupled with seasonal transpiration and evaporation, limited inundation without recharge to less than thirty days. Design criteria were mandated by the Truman Lake flowage easement on the property.

The Pintail Pastures Wetland Mitigation Site restored approximately 20 acres of wetlands and preserved 6.45 acres of existing forested wetlands. A total of 15.28 acres of the restored wetland and all 6.45 acres of forested wetland have been deed restricted. Table 2 summarizes project impacts and mitigation credits achieved on the Pintail Pastures Wetland Mitigation Site.

Table 2: Pintail Pastures Wetland Impacts and Mitigation

Wetland Impacts	
Wetland Type	**Acreage**
Forested	1.29
Emergent	15.28

Wetland Mitigation		
Mitigation Type	**Acreage**	**Ratio**
Preserving existing forested wetland	6.45	5:1
Restoring prior converted wetlands	15.28	1:1
Total Deed Restricted Area	**21.73**	

Olsson continues to provide maintenance and monitoring services for the project and anticipates compliance certification by the Corps at the end of the five year monitoring period.

REFERENCES

Department of the Army Corps of Engineers and State of Missouri (2007). *Stream Mitigation Method.*

Environmental Research Center of Missouri, Inc. (2006). *Cultural Resource Investigations, Phase I Survey; Middle Big Creek Development Project, Cass County, MO.*

Missouri Department of Natural Resources (MDNR) (1998). *State of Missouri Aquatic Resources Mitigation Guidelines*, Water Pollution Control Program.

Olsson Associates (2005). *Jurisdictional Wetland Evaluation and Functional Assessment.*

Olsson Associates (2007). *Preliminary Site Assessment and Field Survey.*

U.S. Army Corps of Engineers (2007). "Practices for Documenting Jurisdiction under Section 9 *& Section 10 of the Rivers & Harbors Acr (RHA) of 1899 and Section 404 of the Clean Water Act (CWA)." *Regulatory Guidance Letter No. 07-01.*

U.S. Army Corps of Engineers (2008). "Compensatory Mitigation for Losses of Aquatic Resources." *33 CFR part 332*, 73 FR 19670.

Zona Rosa & Rush Creek Conservation Area – Applied Ecology in a Mixed-Used Development

J. J. Dremsa[1] and D. M. Mensing[2]

[1] Applied Ecological Services, Inc., Regional Contracting Manager, 701 East 22nd Street, Lawrence, KS 66046; PH (785) 842-3300; FAX (785) 842-3313; email: jason.dremsa@appliedeco.com

[2]Applied Ecological Services, Inc., Senior Ecologist, 21938 Mushtown Road, Prior Lake, MN 55372; PH (952) 447-1919; FAX (952) 447-1920; email: dougm@appliedeco.com

ABSTRACT

In 2001, Applied Ecological Services, Inc. (AES) was asked to assist in the design and installation of restored native ecosystems and a restored stream and riparian corridor on the 200-acre property proposed as the Zona Rosa mixed-use development, located in Kansas City, Missouri. Following our analysis of over 1,950 linear feet of Rush Creek, a degraded stream within the property, AES designed restoration and bioengineering strategies for a variety of ecological zones, requiring various treatments.

Design strategies were based on extensive hydrologic modeling and environmental engineering. Ecological restoration treatments along the Rush Creek Conservation Area (RCCA) included: native riparian buffer plantings, restoration of upland prairie, savanna and forest buffers, created in-stream pools and riffles, and a variety of bank stabilization strategies using bioengineering techniques. These included brush layering, installation of live stakes and willow posts, and toe protection using biologs. Parking lot BMPs were selected to reduce runoff into the stream, and stormwater management treatments necessary to success of the project were also designed and constructed upstream of the site. Five-year monitoring programs were developed to document water quality, vegetation success, erosion control, and stability of the stream system.

AES installed and has maintained all aspects of this innovative ecological restoration project. The restored riparian corridor represents a healthy mosaic of native plant communities and aquatic habitats, providing a functional and attractive centerpiece to the Zona Rosa development.

INTRODUCTION

The Zona Rosa development is located along Rush Creek at I-29 and Barry Road in Kansas City, Missouri in Platte County. It is a multi-use development, which includes apartments, a movie theater, restaurants, and retail stores in close proximity. The goals of restoring the Rush Creek Conservation Area (RCCA) included: restoring native ecosystems, restoring stream and riparian corridor, stabilize creek and minimize erosion, detain and control runoff from the upstream areas and the development, and mitigate for wetland impacts.

METHODOLOGY

Ecological Design

Existing site data were gathered, reviewed, ground-truthed, and augmented through fieldwork and data collected by AES ecologists and engineers. Based on our site findings, conceptual plans were developed to stabilize the degraded Rush Creek, restore native ecosystems along the stream, and mitigate impacts proposed to occur as a result of the development. U.S. Army Corps of Engineers, Missouri DNR, and City of Kansas City permits were obtained for construction of the project.

Design strategies were based on extensive hydrologic modeling and environmental engineering. AES investigations suggested that the severe erosion of the creek could not be effectively stabilized unless upstream tributary waters were regulated. To store and control runoff from the upstream areas owned by Missouri DOT, AES successfully proposed the establishment of a depressional wetland with outlet controls within the MODOT property.

Various ecological restoration zones were designed, based largely on hydrologic regime and ecosystem function. Customized native plant species lists were developed for each restoration zone, and local ecotype seed and plant materials were specified to maintain ecological integrity of the project. Deep-rooted native plants were selected to provide diverse native habitats, stable soils, and increased infiltration (to reduce runoff). Ecological restoration treatments on-site included: native riparian woodland and grassland buffer plantings, restoration of upland prairie, created in-stream pools and riffles, wetland detention basin, and bank stabilization strategies such as live stake installation and toe protection using four-inch diameter limestone rock and cross veins (Figures 1 and 2).

An Ecological Management Plan and monitoring program is in place for the RCCA to: guide management efforts (e.g., spot herbiciding and periodic mowing); document native vegetation establishment success; assess overall stream stability, erosion control, and ecosystem health; and develop remedial measures when needed. Short-term management efforts (2009 to 2010) will be focused on newly planted areas in the RCCA, followed by a less intensive, long-term management regime in perpetuity for the entire RCCA.

The end of 2008 marks the completion of a fifth full year of restoration/maintenance activities related to native plant installations along the RCCA. During 2008, AES's Contracting Division focused on repairing/restoring areas along the north side of Rush Creek that were damaged during Phase II site development.

Erosion Control Monitoring

Ongoing development activities in Phase II of the Zona Rosa site necessitated erosion control inspections in this portion of the property. Per the project's Missouri DNR permit and its associated Stormwater Pollution Prevention Plan (SWPPP), site inspections were typically conducted weekly and/or within 48 hours of a 0.25-inch rain event. Special attention was focused on unstabilized areas, stormwater BMPs, outfalls, and areas 50 feet downstream from outfalls. During inspections, personnel from AES or Norman Ecological Consulting documented the presence of erosion, turbidity in surface waters, sedimentation, and other erosion-related issues. They also determined if existing erosion control measures were adequate and whether additional measures were required. Photographs were taken to document conditions during erosion control inspections. Inspection results and recommended corrective actions were summarized in weekly reports and submitted to the developer.

Vegetation Monitoring

The purpose of vegetation monitoring at Zona Rosa is to determine if restoration efforts along the RCCA meet the Missouri DNR's minimum requirement of ≥70% vegetation cover noted in the permit for the project. This criterion applies to the entire riparian corridor disturbed by construction, and is required for the termination of the permit. Vegetation monitoring also addresses the Corps' mitigation monitoring requirements. The Corps permit for the Zona Rosa site states that perpetual stewardship must be conducted along the RCCA.

Vegetation along the RCCA was monitored using a qualitative approach, which consisted of a pedestrian survey of the entire RCCA riparian corridor from the upper reaches of Rush Creek at the MODOT embankment downstream to the outlet structure below the wetland detention basin. During the assessment, several parameters were documented, including the general condition and extent of established native vegetation, number of native species observed, location and extent of non-native/invasive species, and other information pertinent to the restoration effort. 2008 monitoring data were collected during one intensive vegetation monitoring effort (June 25-26) in combination with numerous other efforts conducted during erosion control inspections/water quality monitoring during the 2008 growing season.

Photographs were taken to document field conditions during monitoring activities. In addition, communication with AES maintenance staff and project managers provided regular updates and prompt issue identification and resolution during 2008.

RESULTS

Ecological Design

Construction began in 2002 and continued into Winter 2008. Phase I of the Zona Rosa development was completed in 2006, at which time all of Phase I had been stabilized. In October 2003, ecological restoration began along the 1,950-foot stretch of Rush Creek that bisects the Zona Rosa development (the RCCA). Ecological management tasks (management mowing and spot herbiciding of non-native/invasive plants) has been conducted at the site since installation.

During Phase II construction of the Zona Rosa development, some portions of the RCCA were damaged from construction activities. Restoration of Phase II impacts was conducted from July 15 to September 15, 2008, and included the installation of erosion control mat, straw mulch, live native plants, and native seed. Restoration activities covered approximately 0.67 acre of uplands, on which 21,780 native plants (live plugs) and 110 pounds of native seed were installed.

Erosion Control Monitoring

During 2008, regular erosion control inspections were performed from March through November in the Phase II portion of the site. Erosion control issues were identified quickly by AES and/or Norman Ecological Consulting and then addressed by the developer's contractors. The developer's contractors regularly swept roadways, blocked and cleaned storm drains, and installed and/or repaired damaged silt fence and other best management practices (BMPs) to control erosion. Despite these efforts, turbidity was occasionally observed in site surface waters, underscoring the importance of constant vigilance with regard to erosion and sediment control practices.

As of winter 2008, the majority of the Phase II construction areas were stabilized with either impervious surfaces (e.g., sidewalks, buildings, roads) or dense vegetation (e.g., turf, native plantings, or mulched beds). Only a few areas lacked the ≥70 % vegetative cover criteria required to terminate the Missouri DNR permit. Areas that did not meet this criterion included young restoration areas along the north side of Rush Creek, turf areas planted late in the fall, and bare areas stabilized with erosion control mat and mulch that have experienced limited seed germination and vegetative cover. Monthly erosion control inspections are being performed over the winter, and more frequent inspections will likely resume during Spring 2009.

Vegetation Monitoring at RCCA

Our 2008 monitoring indicates that the RCCA generally consists of healthy, maturing native plant communities. The main exception is the areas recently restored after Phase II construction damage. These areas should be well-vegetated by late Spring 2009; however, the young native plantings will probably not be native-dominated

until 2010. While the entire RCCA will be managed in the coming years, these young restoration areas will be the focus of AES's 2009 and 2010 ecological management activities.

CONCLUSIONS

The restoration design of Zona Rosa's Rush Creek Conservation Area was based on thorough data review, field assessment, and detailed modeling and engineering. The restoration is progressing well, based on the observations that most of the riparian corridor is vegetated by a dense stand of native vegetation approaching or above the 70% cover threshold. Portions of the RCCA impacted by Phase II construction activities were repaired/restored by mid-September 2008. These newly restored areas will likely take several years before a thick cover of native vegetation is established. Construction of Phase II of Zona Rosa was mostly complete as of November 2008, with most of the site being stabilized and vegetated. Only a few places remain in Phase II that require more vegetative cover, which should be accomplished with the onset of warmer temperatures in Spring 2009.

Regular erosion control inspections, prompt reporting, and remedial actions have been essential to protecting the site and Rush Creek from the adverse effects of erosion and sedimentation resulting from site development. Vegetation monitoring has provided a critical feedback loop to not only assess existing conditions, but also to guide subsequent ecological management activities. Pursuant to Corps permit requirements, the entire RCCA will continue to be managed in perpetuity, following the site's Ecological Management Plan and associated ecological monitoring program.

The Zona Rosa and Rush Creek Conservation Area restoration project is a showcase example of how a degraded riparian corridor can be restored and how water resources can be protected through thoughtful ecological design and execution. The restoration was designed to grow, evolve, and adapt to the changing conditions in the environment, providing a natural, sustainable, functional, and attractive riparian corridor through a high-use development. The RCCA (including its design, construction, perpetual management, and monitoring) will help to insure that the valuable water resources in the Rush Creek watershed will be protected for future generations.


MATCHLINE A-SEE SHEET 4
Legend
Aquatic Biofilter with Low Flow Channel .50 Ac.
Emergent Wetland Biofilter 1.92 Ac.
Sediment Trap/Plunge Pool .33 Ac.
Flower Bed 50-2" Wildflower Plugs/100 sq. ft.-26 Ac.
Stream Bank Side Slope .80 Ac.
Riffle Bottom .31 Ac.
Upland Prairie Restoration 6.41 Ac.
Forested Buffer .58 Ac.
Shrub/Flower Beds .21 Ac.
Aquatic Zone .12 Ac.
Channel Rock .17 Ac.
Channel Rock with Live Stakes .11 Ac.
Sod .09 Ac.
Shade Tree (avg cal 2 1/2") Qty -48
NOTE:
FLOWER BED & SHRUB/FLOWER BED ZONES
After planting, broadcast/1,000 sq. ft.:
1/4 oz. Rattlesnake pinnata
1/4 oz. Rudbeckia hirta
1/4 oz. Monarda fistulosa
1 oz. Andropogon scoparius
Upland prairie mix at specified rate then
mulch with 1/2" clean oat straw.
SCALE: 1"= 40'
NORTH
Zona Rosa
Kansas City, Missouri
As-Built Planting Plans
Stream Restoration, Protection and Enhancement
TranSystems Corporation
2400 Pershing Road, Suite 400
Kansas City, Missouri 64108
Steiner & Associates
10100 N. Ambassador Drive
Kansas City, Missouri 64153
As-Built Planting Plan-
East Section
Drawn By: t.e.g.
AES Project No.: 01-276
Checked:
File Name: asbuilt062904.dwg
Approved:
Date: 06-29-2004
Sheet Number
2 of 2

Figure 1.

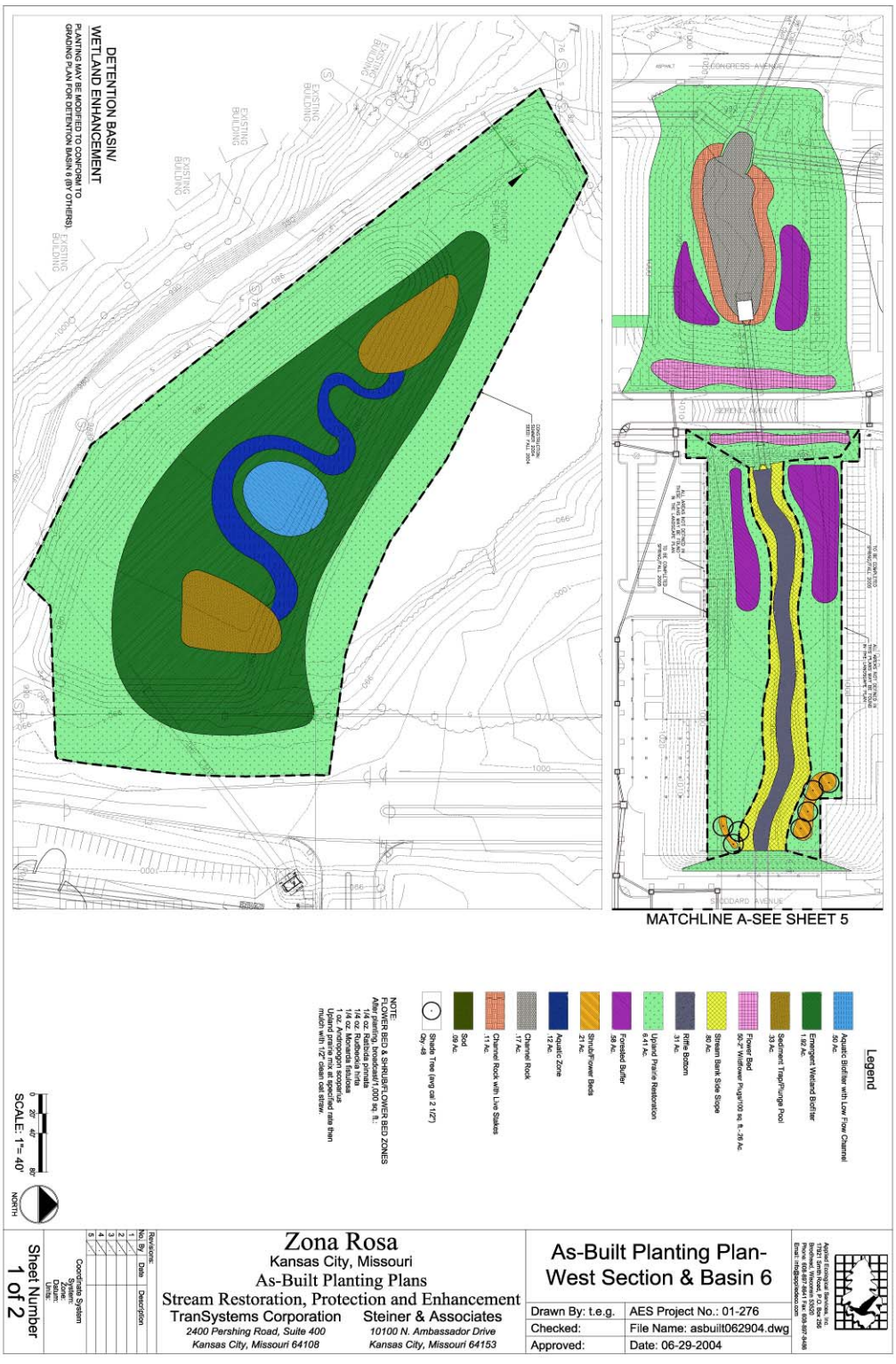
DETENTION BASIN/
WETLAND ENHANCEMENT
PLANTING MAY BE MODIFIED TO CONFORM TO GRADING PLAN FOR DETENTION BASIN 6 (BY OTHERS)
MATCHLINE A-SEE SHEET 5
Legend
Aquatic Biofilter with Low Flow Channel 80 Ac
Emergent Wetland Biofilter 1.60 Ac.
Sediment Trap/Plunge Pool 33 Ac.
Flower Bed 90-3" Wildflower Plugs/100 sq. ft - 26 Ac
Stream Bank Side Slope 80 Ac.
Riffle Bottom 31 Ac
Upland Prairie Restoration 6.41 Ac.
Forested Buffer 56 Ac.
Shrub/Flower Beds 21 Ac.
Aquatic Zone 12 Ac.
Channel Rock 17 Ac.
Channel Rock with Live Stakes 11 Ac.
Sod 09 Ac.
Shade Tree (reg cal 2 1/2") Qty. 48
NOTE:
FLOWER BED & SHRUB/FLOWER BED ZONES
After planting, broadcast/1,000 sq. ft.
1/4 oz. Rabula pinnata
1/4 oz. Rudbeckia hirta
1/4 oz. Monarda fistulosa
1 oz. Andropogon scoparius
Upland prairie mix at specified rate then mulch with 1/2" clean oat straw.
SCALE: 1"= 40'
NORTH
Zona Rosa
Kansas City, Missouri
As-Built Planting Plans
Stream Restoration, Protection and Enhancement
TranSystems Corporation
2400 Pershing Road, Suite 400
Kansas City, Missouri 64108
Steiner & Associates
10100 N. Ambassador Drive
Kansas City, Missouri 64153
As-Built Planting Plan-
West Section & Basin 6
Drawn By: t.e.g.
Checked:
Approved:
AES Project No.: 01-276
File Name: asbuilt062904.dwg
Date: 06-29-2004
Sheet Number
1 of 2
Revisions:
No. By Date Description
Coordinate System
Zone:
Datum:

Figure 2.

Modeling Impacts of Conventional and Low Impact Stormwater Controls on Receiving Streams

By: Elise Ibendahl Author[1], PE and Dan Medina, PhD, PE C.O. Author[2]
CH2M HILL

[1]CH2M HILL, 1034 South Brentwood Blvd, Suite 2300, Saint Louis, MO 63117; PH (314) 335-3022; FAX (414) 454-8720; email: elise.ibendahl@ch2m.com

[2]CH2M HILL, 1100 Wayne Ave., Suite 670, Silver Spring, MD 20910; PH: (301) 495-8840 x 41017; FAX: (703) 376-5935; email: Daniel.Medina@ch2m.com

1. Abstract

This paper presents a methodology to measure the impact of stormwater controls on the receiving stream using a series of discrete events to represent the long-term hydrologic regime as a simpler alternative to continuous simulation. Hydromodification impacts on channel morphology are best evaluated using flow and shear stress duration curves, which typically require continuous simulation. The methodology proposed herein allows the development of these duration curves using discrete events.

The methodology was tested in a hypothetical development in the City of Columbia, Missouri. Design assumptions were made for a typical residential development and a typical stream. Various stormwater controls were designed for this site, including conventional detention, a water quality volume and channel protection volume basin, and bioretention. The outflow from each design scenario was analyzed to determine the effectiveness of different levels of stormwater controls. The objective was to compare the effect of each scenario using duration curves to measure its ability of mimic the original hydrology. The study indicates that LID most closely replicates the original regime and that detention provides some benefits when water quality and channel protection are included, although its effect does not reproduce the original hydrology. Detention criteria based on extreme events, such as the 100-year storm event, are ineffective for this purpose.

2. Detention Requirement

The City of Columbia, Missouri Stormwater Management and Water Quality Manual currently requires that *"the maximum release rate from any development and redevelopment shall be controlled by limiting the stormwater release rates for the 1%, 10%, 50%, and 100% storms to the predevelopment peak flow rates for the 1%, 10%, 50%, and 100% storms respectively."* This requirement was examined to determine effectiveness at preventing potential channel erosion.

Assumptions were made for a typical residential development in the City of Columbia and a typical stream. Stormwater controls for the development were designed using three different scenarios: a detention pond meeting the Manual requirements for the typical development; ponds meeting water quality volume and channel protection volume requirements; and low impact development (LID) technologies. The outflow from the site was analyzed under these development scenarios to determine the effectiveness of different levels of stormwater control. Conclusions based on general effectiveness and levels of protection were then made.

2.1 Pre- and Post-Development Conditions

Table 1 lists the assumptions for the pre- and post-development scenarios. These assumptions represent a typical headwaters development in the City of Columbia, Missouri.

TABLE 1.
Typical development hydrologic parameter assumptions

	Pre-Development	**Post-Development**
Area (Acres)	25	25
Hydrologic Soil Group	C	D
Land Use	Agricultural (Pasture), 0% Impervious	¼ Acre Lots, 35% Impervious
Curve Number	74	89
Runoff Calculation Method	NRCS Unit Hydrograph Method	NRCS Unit Hydrograph Method
Time of Concentration	20	15

2.2 Typical Detention Pond Designs

Detention ponds meeting the Manual requirements for the typical development were designed as well as ponds meeting water quality volume and channel protection volume requirements. All ponds were designed to have 4:1 side slopes and a 4-foot depth without freeboard.

2.2.1 Detention Pond Design

A detention pond was designed to meet the Manual's requirements, which is to match the pre- and post- development runoff rates for the 1-, 2-, 10-, and 100-year 24-hour design storm events. A stair step weir configuration was used for the four-stage pond outlet.

A pond meeting the requirements of the Manual with a 4:1 side slope would have a footprint of 1.09 Acres, which increases to 1.35 acres of space when freeboard and the required access strip are included.

1-Year Storm Event Summary

Post-Development Peak Inflow:	54	cfs
Post-Development Peak Outflow:	16	cfs
Pre-Development Peak Flow:	22	cfs
Total Volume:	3.9	Ac-ft
Peak Storage:	1.5	Ac-ft

10-Year Storm Event Summary

Post-Development Peak Inflow:	111	cfs
Post-Development Peak Outflow:	54	cfs
Pre-Development Peak Flow:	66	cfs
Total Volume:	8.2	Ac-ft
Peak Storage:	2.8	Ac-ft

2-Year Storm Event Summary

Post-Development Peak Inflow:	67	cfs
Post-Development Peak Outflow:	20	cfs
Pre-Development Peak Flow:	34	cfs
Total Volume:	4.9	Ac-ft
Peak Storage:	1.9	Ac-ft

100-Year Storm Event Summary

Post-Development Peak Inflow:	164	cfs
Post-Development Peak Outflow:	111	cfs
Pre-Development Peak Flow:	113	cfs
Total Volume:	12.5	Ac-ft
Peak Storage:	3.6	Ac-ft

Peak flows for the pond configurations are shown above. The Total Volume represents the total runoff volume generated by the storm event, while the Peak Storage represents the maximum runoff volume in the detention facility.

2.2.2 Water Quality Storm and Channel Protection Pond Design

A second pond was sized based on the water quality volume specified by the Manual and a channel protection volume. Because the City's manual does not contain guidance on incorporating water quality detention into a traditional detention facility, the pond was sized to release the water quality volume over a 40-hour period per the newly updated March 2008 Mid-America Regional Council Manual of Best Management Practices for Stormwater Quality (MARC) manual. The volume required for a 40-hour release of the water quality volume was 0.5 acre-feet.

The channel protection volume is pond storage added to the water quality volume. Because the City does not currently have a channel protection requirement, criteria from the Metropolitan St. Louis Sewer District (MSD) were used. MSD requires the 1-year, 24-hour storm to be released with 24-hour extended detention. The 24-hour detention time is defined as the interval between the center of mass of the inflow hydrograph and the center of mass of the outflow hydrograph. The volume required for detention of the channel protection volume is 2.6 acre-feet.

A pond designed to meet only the water quality and channel protection criteria would have a footprint of 0.85 acres, with a 4:1 side slope, which increases to 1.04 acres of space when freeboard and the required access strip are included.

2.2.3 Low Impact Development Stormwater Controls

The third stormwater control scenario assumed the entire site was developed with LID controls such as bioretention and bioswales. The City's Manual states that 90% of all rainfall is less than or equal to 1.30 inches for storms less than 24 hours. It was assumed that up to the first 1.30 inches of each storm event would be retained on-site in the LID controls and any additional rainfall would become direct runoff from the site. The LID storage volume to meet this requirement is approximately 1.0 acre-

foot. This storage can be achieved with approximately 2 acres of total bioretention area, with a depth of 6 inches. This storage represents about 8 percent of the site area and can be incorporated into landscaping and other green space requirements.

TABLE 2.
Stormwater Controls Summary

	Conventional Detention (1-, 2-, 10- and 100-year Design Storm)	**Water Quality and Channel Protection Volume Detention (No additional design storm detention)**	**Bioretention (First 1.3" of each rain event)**
Depth without freeboard (ft)	4	4	0.5
Side slopes	4:1	4:1	Varies
Bottom length (ft)	443	243	Varies
Bottom width (ft)	68	103	Varies
Top length (ft)	475	275	Varies
Top width (ft)	100	135	Varies
Area (no freeboard)	1.09 Acres	0.85 Acres	2
Maximum area with freeboard	1.41 Acres	1.04 Acres	N/A
Maximum storage volume (ac-ft)	3.6 (100-yr)	2.6 (Channel Protection and Water Quality)	1.0 Ac-ft (1.3")
Storage Volume Destination	Receiving stream	Receiving stream (with 40-hr release)	Baseflow

2.3 Channel Shear Effects

Open channels in the City are subject to severe erosion problems. The shear stress created by the flow acting on the channel bed and bank materials is the parameter often used as a measure of a stream's ability to retain the soil particles in the channel bed and banks. Critical shear stress is the shear stress required to mobilize sediments stored on the channel bed and banks and delivered to the channel from upstream. When the shear stress is greater than the critical shear stress for the bank material, erosion ensues and channel degradation will likely result. Assumptions were made to represent a typical channel in the City of Columbia and the shear stress resulting from a variety of flow conditions was calculated. Typical channel characteristics are shown in Table 3.

TABLE 3
Typical channel physical parameters

Parameter	Value	Description
side slope	2H:1V	channel side slope
bottom width	1.56	feet
slope (ft/ft)	0.040	slope along flow line of channel
Manning's n	0.035	Manning's roughness factor

2.3.1 Precipitation Analysis

Precipitation data that recorded at the Columbia Municipal Airport (1948-1969) and Columbia Regional Airport (1969-2007) were used to determine an average year of rainfall. Approximately 59 years of hourly precipitation data (September 1, 1948 through August 1, 2007) were run through the XP-SWMM rainfall utility to determine individual storm events. A minimum six-hour dry period was used to separate precipitation into discrete storm events. A total of 5,916 storm events ranging from 0.01 inches to 5.97 inches were determined.

The storm event data were sorted into several 'bins' based on the total volume of precipitation in the event. This breakdown provides an annual average summary of the rainfall record in terms of depth, duration, and number of events per year. Table 4 displays the results of this summary.

TABLE 4
Annual storm event summary

Bin ID	Lower Limit (in)	Upper Limit (in)	# Storms	Mean Rainfall Depth (in)	Mean Number storms per year	Percent of Total Rainfall in Bin[1]	Mean Annual Rainfall (in)	Mean Duration (h)
1	0.00	0.25	3655	0.078	60.92	13.3%	4.74	3.6
2	0.25	0.50	957	0.366	15.95	16.4%	5.84	7.8
3	0.50	0.75	441	0.620	7.35	12.8%	4.56	9.6
4	0.75	1.00	282	0.869	4.70	11.5%	4.08	12.0
5	1.00	1.25	184	1.122	3.07	9.7%	3.44	12.5
6	1.25	1.50	128	1.379	2.13	8.3%	2.94	14.7

TABLE 4
Annual storm event summary

Bin ID	Lower Limit (in)	Upper Limit (in)	# Storms	Mean Rainfall Depth (in)	Mean Number storms per year	Percent of Total Rainfall in Bin[1]	Mean Annual Rainfall (in)	Mean Duration (h)
7	1.50	1.75	94	1.623	1.57	7.1%	2.54	15.9
8	1.75	2.00	52	1.871	0.87	4.6%	1.62	17.3
9	2.00	2.25	32	2.137	0.53	3.2%	1.14	15.8
10	2.25	2.50	24	2.402	0.40	2.7%	0.96	14.5
11	2.50	2.75	19	2.587	0.32	2.3%	0.82	20.8
12	2.75	3.00	18	2.879	0.3	2.4%	0.86	23.9
13	3.00	6.00	30	4.044	0.5	5.7%	2.02	28.7

[1]Represents the fraction of the total rainfall depth in this bin that fell over the entire period of record.

The mean rain depth for each bin was then used to determine the runoff that would be produced during each 'typical' event. Because only hourly rainfall data was available for the period of record, the total volume was distributed into 15-minute increments using comparable storm durations and appropriate quartile distributions for Columbia from "*Bulletin 71: Rainfall frequency Atlas of the Midwest*" by Huff and Angel.

2.3.2 Runoff Calculation

A model was created using the HEC-HMS version 3.1.0 software. The model incorporated the average annual rainfall series discussed in Section 2.3.1 as well as several design storm events with the SCS Type II distribution to calculate runoff from the watershed. An exceedence curve for the historical rainfall data against the rainfall amounts for the various design storm events shows that the design storms are much larger than the rain events that occur most often in a typical year.

In addition to the pre- and post-development conditions, three additional scenarios evaluate the post-development conditions including the effect of two different detention ponds: the first designed according to the Manual, and the second designed based only on management of the water quality volume and for channel protection. The third scenario evaluates the effectiveness of bioretention.

The pre-development and post-development scenarios have the runoff flow into the trapezoidal channel described at the beginning of this section downstream of the detention pond. In the bioretention scenario, the captured volume is infiltrated and reaches the receiving stream as baseflow. Excess stormwater overflowing the bioretention facilities reaches the stream as direct runoff.

2.3.3 Shear Stress and Erosion Potential

The maximum shear stress acting on the bottom of a channel is given by

$$\tau_b = \gamma S_e R_h$$

where γ is the specific weight of water, S_e the energy slope, and R_h the hydraulic radius. For a trapezoidal channel, the maximum shear stress acting on the side slopes is approximately 80 percent of the maximum on the bottom.

The flows in the trapezoidal channel calculated with the HEC-HMS model were used to determine the normal depth of flow in the channel. The results of the model simulations were compiled and the shear stress was calculated for each scenario.

To understand the long-term effects of excess shear stress, it is necessary to examine behavior of a continuous record of flows, typically resulting from continuous simulation. However, single-event modeling is more commonly known as a design technique. The analysis depicted in Table 4 can be used as a surrogate of long-term behavior based on the individual storm events and their frequency and characteristics. Therefore, the shear stress was calculated for each of the bin storm events in Table 4 and a shear stress exceedence curve was developed based upon the average number of storm events occurring for each bin per year. A summary of this analysis is presented in Figure 1.

Several critical shear stresses are shown in Figure 1 and are listed below in Table 6. The categories shown represent typical channel conditions that may be encountered for a headwaters development in the City of Columbia. Bed material is typically silt loam, but incised channels typically expose stiff clay material. Typical channel critical shear stress in most cases will be between 0.048 psf and 2.16 psf. In a state of dynamic equilibrium, critical stress is exceeded and material is mobilized some of the time. However, the quantity of interest is the work performed by the stream, which is the area under the shear stress duration curve. If a development scenario results in stream work greater than the original conditions, channel degradation will occur.

TABLE 6
Critical Shear Stress

Description	Critical Shear Stress (psf)
Silt Loam, Noncolloidal (ML), clear water	0.048 psf
Stiff Clay, very colloidal, CL, clear water	0.260 psf
Well-established dense vegetation to the normal low water	2.16 psf

3. Results

From Figure 2, it can be seen that a conventional detention pond does little to improve the shear stress. If the pond were designed for water quality and channel protection as described in Section 2.2.2, the figure shows that the stress is below than the pre-development conditions for a range of low-frequency flows but is above for more frequent flows. If the site is designed with LID controls the shear stress curve best approximates the shape of the pre-development curve. The lower levels of shear stress suggest that the LID design could be optimized to better match the target condition.

It should be noted that even under the pre-development conditions, the critical shear stress is exceeded some of the time, which is consistent with the natural dynamic geomorphic processes taking place in the stream. This is observable throughout the City where bare soil and exposed roots can be seen in channel bottoms. The important criterion to consider is how different the post-development conditions are from the pre-development state. When higher shear stresses are experienced over time in a given channel, sediment is lost and erosion begins to occur. If the shear stresses are not mitigated and continue at higher levels over time or are allowed to increase, more sediment is lost in the channel bed and erosion worsens. Eventually, the channel becomes bare of vegetation and the erosion problem continues to move upstream and worsen.

The threshold shear stress values shown in Figure 1 assume that there is no vegetation or armoring of the stream bed material. This explains why channel erosion is such a large problem in Columbia (where bare channels and exposed tree roots already exist throughout the system) and shows the need for citywide stream assessment and restoration. All scenarios modeled produced annual shear stresses well below the critical shear stress for well-established, densely vegetated channels.

Although the shear stress curve for the channel protection criterion is well below the pre-development conditions, it should be pointed out that a lower target should be selected to mitigate current rates of erosion and channel degradation. The 1-year design storm event was selected for this analysis

because it is commonly used for channel protection design. For example, this is the nearby criteria for MSD in the St. Louis metropolitan area and the State of Maryland. Due to the lack of 15-minute rainfall data, the annual period of record was approximated using Huff rainfall distribution and assumptions were made to represent a typical residential development. While these assumptions produce valuable results and verify that channel protection technology or the use of LID controls are valuable tools for the City, the true channel protection target should be closer to the critical shear stress frequency regime that existed during the original conditions, which do not necessarily coincide with the pre-development state. In practice, it is virtually impossible to return stream channels in urban or urbanizing watersheds to a pristine state; therefore, a sensible target is probably somewhere between the original and pre-development conditions.

A detailed analysis encompassing a more detailed approximation of the rainfall record and multiple land use scenarios is necessary to pinpoint the design event criteria most appropriate to replicate pre-development shear stress conditions. Most jurisdictions in the United States have not performed this detailed analysis, which requires development of allowable shear stress curves for a variety of development scenarios and possible customization for different watersheds. Some jurisdictions in the state of California are moving toward developing these curves, and Western Washington State has completed such an analysis. Western Washington State has developed a stand-alone software application that designers can use to meet shear stress criteria for a wide range of conditions.

4. References

City of Columbia, Missouri, 2007, *Stormwater Management and Water Quality Manual*.

Huff, F.A., and Angel, J.R., 1992, *Rainfall Frequency Atlas of the Midwest,* Midwestern Climate Center and Illinois State Water Survey.

Metropolitan St. Louis Sewer District, 2006, *Rules and Regulations and Engineering Design Requirements for Sanitary Sewer and Stormwater Drainage Facilities*.

Mid-America Regional Council and American Public Works Association, 2008, *Manual of Best Management Practices for Stormwater Quality*.

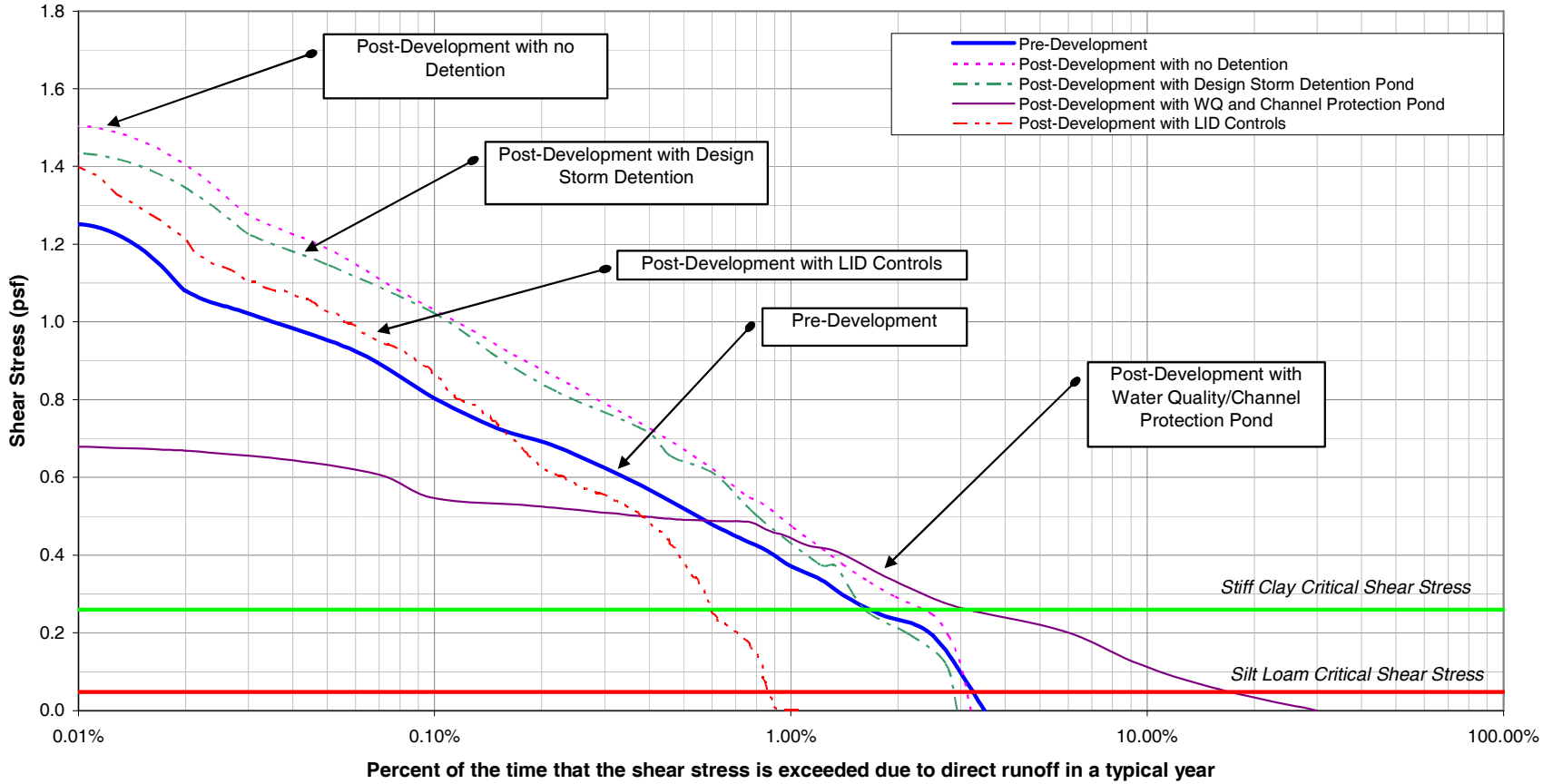

Figure 1. Shear stress duration curves comparing several stormwater management scenarios.

Potable Water from a Superfund Site?

Marc Schlebusch, P.E.

CDM, 9200 Ward Parkway, Suite 500, Kansas City, Missouri 64114; PH (816) 444-8270; FAX (816) 444-8232; email: schlebuschm@cdm.com

ABSTRACT

This paper will describe the beneficial use of contaminated groundwater after treatment to supplement a local potable water supply. Contaminated groundwater from Superfund sites is usually treated and discharged to a stream or storm sewer or conveyed to a wastewater treatment plant. Discharge of treated water is seen by many as a waste of resources, particularly in areas affected by drought. Beneficial reuse of this treated water as potable water is an attractive alternative, and can become a considerable asset, provided that community stakeholders are assured of the quality of the treated water and that treatment operations meet or exceed federal, state, and local requirements.

INTRODUCTION

At a Superfund site in Nebraska, tetrachloroethene (PCE) and trichloroethene (TCE) contamination in groundwater exceeded the federal maximum contaminant level (MCL) of 5 µg/L and threatened the local potable water system. As an interim remedy, a series of extraction wells were planned upgradient of the city's southern municipal well field to capture contaminated water before it entered the potable water system. During the early planning of the interim remedy, the reuse of treated groundwater as potable water was identified as a goal by the Environmental Protection Agency (EPA). Although the Nebraska Department of Environmental Quality (NDEQ) and the city supported the idea of reuse, the Nebraska Department of Health and Human Services (NDHHS) expressed skepticism. Reuse of treated water from a Superfund site had never been done in Nebraska.

To help allay NDHHS's concerns, the design process began with careful review of Nebraska regulations concerning potable water treatment plants. Based on this review, the design was developed to address such diverse issues as cross connections, backflow prevention, impacts of materials and chemicals on potable water quality, the ability of the potable water system to accept the volume of treated water, the locations of groundwater extraction wells, well vaults, and piping systems, and post-operation sampling.

BACKGROUND

The Superfund site consists of a volatile organic compound (VOC)-contaminated groundwater plume located beneath commercial and residential properties in the southwest, central, and north central portion of the city.

The Superfund site comprises two operable units (OUs). OU1 includes an area in the southern portion of the city and the southern municipal well field where groundwater contamination was originally identified. The contamination was originally traced to two dry cleaning operations located south of the railroad tracks. Subsequent groundwater sampling events indicated an extended area of contamination existed upgradient of the original site area. Additional investigations conducted between 1998 and 2000 showed the plume extended to a third primary source area, a dry cleaning facility, located over ½ mile north of OU1. This extended site area constitutes OU2. Additional areas of contamination not associated with the Superfund site were also identified: a former manufactured gas plant and a former aboveground oil storage facility. Figure 1 shows the site and the locations of the potential source areas with respect to the southern municipal well field.

The southern well field consists of seven wells located near the city's water treatment plant. VOC contaminants have been detected in five of the seven municipal wells in the southern well field and in the city's water distribution system. The city has two additional areas from which it can draw groundwater: five municipal wells in a northern well field and two other municipal wells used mainly for emergency purposes. The entire water collection and distribution system is controlled by a supervisory control and data acquisition (SCADA) system at the southern municipal water treatment plant. The water treatment processes used by the city include chlorination for disinfection, fluoridation, and the addition of a copper sequestrant.

An interim Record of Decision (ROD) for OU2 was signed in September 2001. The selected remedy for the interim action at the site included extraction of contaminated groundwater at one of the municipal wells in the city's southern well field and plume interception by extraction of contaminated groundwater upgradient of the city's southern well field. The primary objective of the interim remedial action was to reduce PCE- and TCE-contaminated groundwater reaching the city's southern municipal well field.

A design package for the groundwater extraction and treatment (GET) system with a packed column air stripper was prepared between 2001 and 2002. Construction of the GET system began in August 2003 and was completed in April 2004. The GET system initially consisted of three extraction wells and one municipal well for a total design flow rate of 1,250 gallons per minute (gpm) or 1.8 millions gallons per day (mgd). In 2005, a fourth extraction well was added to increase the design flow rate of the GET system to 1,400 gpm (2 mgd).

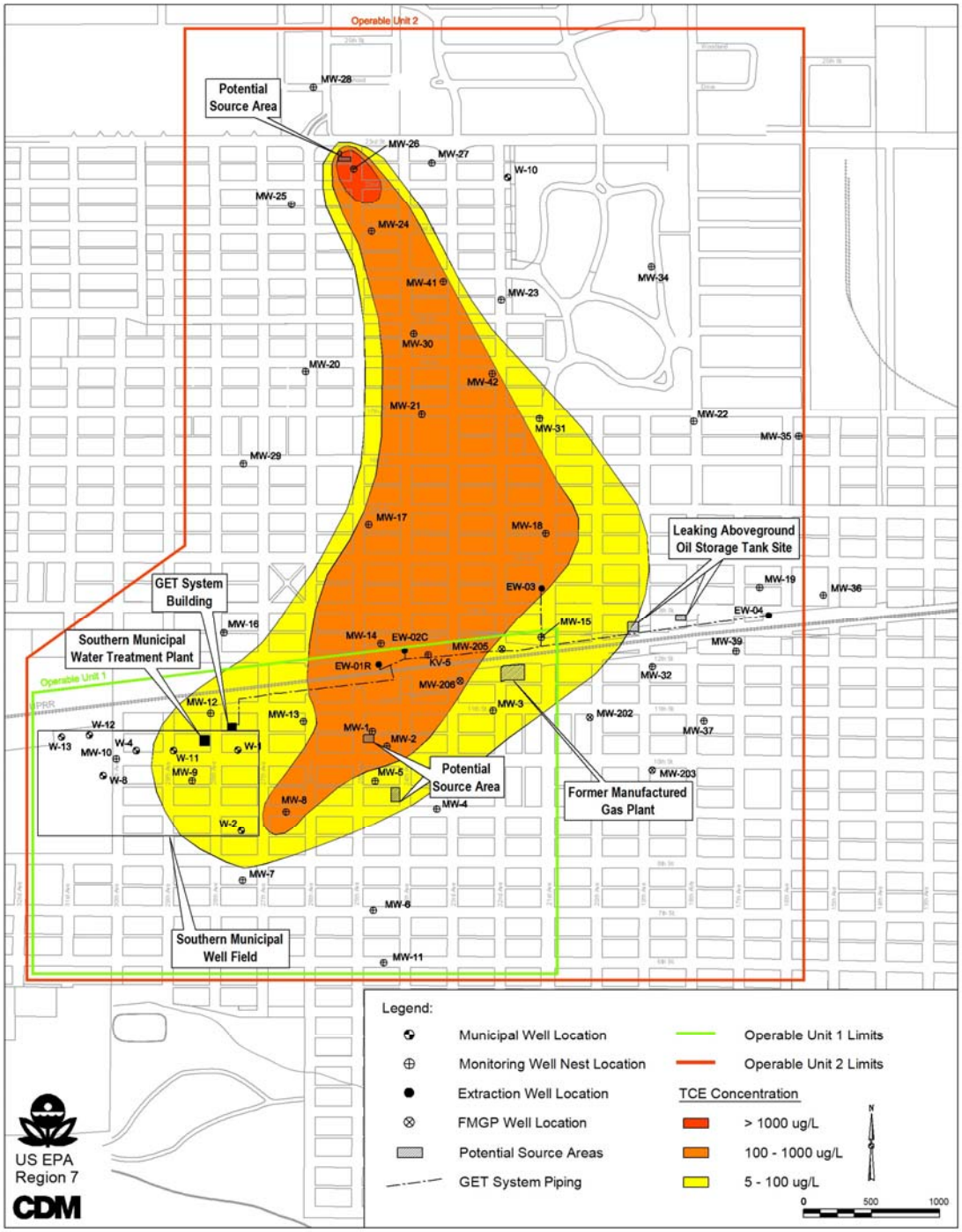

Figure 1. Site Map

DISCHARGE OPTIONS

A discharge system consistent with the interim ROD was developed and approved by the EPA and NDEQ.

The interim ROD for OU2 provided for three discharge options for groundwater:

- Discharge of extracted groundwater to the city's municipal water treatment plant
- Discharge to surface water through the city's storm sewer system
- Reuse options

The option of discharging to the municipal wastewater treatment plant was not selected because the existing wastewater treatment system did not have the capacity to treat the extracted groundwater at the estimated flow rates. Extracted groundwater would first be treated to meet federal MCLs prior to being discharged to the municipal water treatment plant. The municipal water treatment plant would provide chlorination for disinfection and fluoridation. Only during periods of high demand, however, would the municipal plant be able to accept 100 percent of the treated groundwater. In evening hours and winter months, when demand is less, water storage capacity limits would prevent the city from accepting the full volume of treated groundwater. Because the GET system would not run consistently, contaminated groundwater would not be captured at a rate consistent with the ROD.

Discharging to surface water through the city's storm sewer system would allow for consistent operation of the GET system.

The reuse options that were evaluated included a combination of the first two discharge options: potable water reuse and surface water discharge. Reuse would help to conserve water resources. Supplementing reuse with occasional discharge to surface water through the city's storm sewer would allow for consistent operation of the plume interception extraction wells and municipal well W-1 during periods of low demand.

The combination of the two discharge options had the advantage of providing the city with groundwater consistently meeting MCLs without unnecessarily burdening the city's storm sewer system with non-rain event water. The preferred discharge option called for a single treatment facility, which would reduce capital, operation, maintenance, and monitoring costs.

TWO REGULATORY BODIES, ONE GOAL

The solution combining potable water reuse with discharge to the storm sewer required design of a groundwater treatment system that met or exceeded the state requirements of two different agencies. The discharge of treated water to the storm sewer is regulated by the NDEQ and the Nebraska Pollutant Discharge Elimination System (NPDES). The discharge of treated water to the city's southern municipal water treatment plant is regulated by the NDHHS. The design requirements for potable water reuse were the more stringent of the two.

As mentioned above, this project was unique to the state of Nebraska. Officials from NDHHS and NDEQ were consulted early in the design process to ensure that the design met all pertinent design requirements. At first, NDHHS seemed reluctant to perform reviews for designs from EPA and its consultants. Because NDHHS generally works directly with the municipalities that they regulate, they were unaccustomed to providing a high level of review for deliverables from EPA. Eventually, however, NDHHS became a key member of the project team, vital to the overall success.

Design Requirements. Because treated groundwater is discharged to the municipal water treatment plant, the plume interception extraction wells are considered water supply wells and the groundwater treatment system is considered an adjunct potable water treatment plant. Therefore, the following NDHHS-specific requirements (Title 179) pertained to the design and construction of the GET system:

- Wells must be constructed according to the EPA document *Manual of Well Construction Practices*, 1977.
- The groundwater treatment plant must be constructed in accordance with NDHHS Title 179 requirements and the Great Lakes - Upper Mississippi River Board of State and Provincial Public Health and Environmental Managers document *Recommended Standards for Water Works (10 State Standards)*, 2007.
- Each extraction well must be tested for VOCs, semi-volatile organic compounds (SVOCs), pesticides, herbicides, inorganic compounds, dioxin, asbestos in water, radioactive contaminants, general water quality parameters, and total coliform.
- Water supply wells shown to be under the influence of surface water must be screened below 50 feet below ground surface (bgs) and must be further than 50 horizontal feet from any sanitary sewers.
- A Nebraska Class 1 operator must be on call during operation of the groundwater treatment system.

Because treated groundwater is discharged to the storm sewer and ultimately to the river, the following NDEQ-specific requirements pertained:

- Effluent discharge requirements are based on Nebraska MCLs (Title 118, Chapter 4) for potable water, Nebraska National Pollutant Discharge Elimination System (NPDES) limits, and Nebraska surface water discharge limits (Title 117, Chapter 4) for water discharged to the storm sewer/river.
- Applicable standards and requirements of Title 117: Nebraska Surface Water Quality Standards; Title 118: Nebraska Groundwater Quality Standards; Title 119: Rules and Regulations Pertaining to the Issuance of Permits under the National Pollutant Discharge Elimination System; Title 121: Effluent Guidelines and Standards; and Title 129: Nebraska Air Quality Regulations

Installation of Extraction Wells. Groundwater contamination at the Superfund site extends across the upper aquifer from 15 feet bgs to approximately 70 feet bgs. Wells screened above 50 feet bgs are considered under the influence of surface water unless testing proves otherwise. Tests required by the NDHHS in the use of such wells are a microscopic particulate analysis (MPA) for the presence of Giardia and Cryptosporidium and monthly examination of turbidity, pH, and temperature. If the well is determined to be under the influence of surface water, an increased chlorine contact time for disinfection is required by the NDHHS.

The municipal water treatment plant was not designed to provide the required chlorine contact time and modification of the municipal water treatment system was deemed cost prohibitive. All extraction wells were installed with the top of the screen set at 50 feet bgs or greater. Groundwater modeling was conducted to verify the shorter and deeper screened interval would still capture the contaminated groundwater. Modeling results guided the placement of the wells to capture VOCs while avoiding groundwater contamination from a former manufactured gas plant and fuel site.

Materials of Construction and Sequestrant. Materials of construction for a typical Superfund treatment plant are generally selected based on the contamination and the treatment processes used. Because the intent of this treatment plant was to discharge treated water to the city's southern municipal water treatment plant, the materials used in construction needed to be appropriate for contact with a potable water supply.

The *Recommended Standards for Water Works* (also known as the 10 State Standards) are the only standards cited by the state of Nebraska in Title 179, Chapter 2, Attachment 1 for the design and construction of potable water treatment plants. Nebraska regulations do not cite specific National Sanitation Foundation (NSF) and American Water Works Association (AWWA) standards/specifications outside of the 10 State Standards.

According to the 10 State Standards, the two major standards to be followed in the design and construction of potable water treatment plants are from the NSF and AWWA. The 10 State Standards stipulate that "chemicals and water contact materials shall meet ANSI/AWWA quality standards and ANSI/NSF standard 60 or 61 specifications." The 10 State Standards further state that "pipe, fittings, valves, and fire hydrants shall conform to the latest standards issued by the AWWA and/or NSF, if such standards exist, and be acceptable to the reviewing authority. In the absence of such standards, materials meeting applicable Product Standards and acceptable to the reviewing authority may be selected. Special attention shall be given to selecting pipe materials which will protect against both internal and external pipe corrosion."

During the construction of the GET system, the materials used were reviewed for compliance with the appropriate AWWA and NSF requirements. The piping, valve, and gasket materials were reviewed to ensure that they were compatible with the contaminants being treated and complied with the AWWA and NSF requirements.

The influent groundwater was naturally high in calcium, iron and magnesium. These metals precipitate easily in the turbulent environment of an air stripper, creating scale on packing material and the internal works of the air stripper. This precipitation of metals would necessitate frequent acid washing of the packing material, thus increasing operation and maintenance costs and diminishing operating time. A sequestrant was recommended to keep the calcium and magnesium in solution, reducing scale in the air stripper. The sequestrant chosen was a polyphosphate-based material that was NSF-approved. Bench-scale tests were conducted to identify any chemical incompatibility with the copper sequestrant used in the municipal water treatment plant.

Other Design and Construction Issues. Several other design and construction issues developed during construction and subsequent inspections.

Exhaust Vent. To reduce the risk of contamination by birds, NNHSS requested that the air stripper vent not be constructed as a straight vertical shaft, as is typical. A screen had already been designed into the discharge end of the vent. The vent was redesigned to include a 180-degrees turn. Air emissions modeling determined the appropriate height of the air stripper vent to keep below risk levels any vapors discharged toward nearby homes. Air sampling at nearby homes was conducted during startup testing to verify that discharge vapors were below risk levels.

Storm Sewer Discharge. During periods of high potable water demand, the city may accept all the water from the GET system. However, in times of low demand, the GET system discharges by gravity to the storm sewer. One of the main design concerns was ensuring an appropriate air gap between the gravity discharge and potable water transfer components of the GET system to prevent the potential for a backflow in the event of a storm sewer backup. The original design called for the gravity discharge end to flow into a large concrete box with walls extending several feet above grade surface. The water would fall approximately 10 feet from the discharge end to the bottom of the concrete box. The NDHHS insisted that the end of the discharge pipe be cut off to maintain the appropriate air gap between the bottom of the pipe and the top of the walls of the concrete box.

Operating Challenges. During the first six months of operation, the differential pressure across the air stripper increased, necessitating acid cleaning of the packing material. This maintenance requirement was not unexpected as acid cleaning is a routine part of the operation of a packed tower air stripper. However, the acid cleaning was ineffective. Upon inspection, the air stripper packing material was found to be severely coated and clogged with deposits that appeared to be a combination of inorganic precipitates and organic biomass. It was later determined that the packing media was fouled to the extent that it would need to be replaced by new media. The existing fouled media was subsequently removed and disposed.

Prior influent and effluent water sample analyses (pre- and post-stripper) demonstrated that as much as 93 percent of the dissolved iron in the groundwater was

being removed/oxidized in the air stripper. This high percentage was consistent with the high levels of iron oxide and iron phosphate found in the bulk sample from the air stripper deposits. The findings also suggested that the NSF-approved polyphosphate sequestrant was not effective in keeping iron in solution through the air stripper. The high level of phosphate in deposits indicated that the polyphosphate sequestrant was breaking down to orthophosphate. In addition, the orthophosphate appeared to be reacting with iron and calcium in the groundwater to form phosphate precipitates. The presence of phosphate in the deposits (nearly 40 percent by weight) further suggested that the residence time of groundwater in the air stripper was sufficient for polyphosphate degradation. The phosphate contributed by the sequestrant was likely serving as nutrient source for the naturally occurring bacteria in the groundwater.

An NSF-approved, low-molecular weight polymer dispersant (product formulation was based on sodium salts) was identified to replace the polyphosphate sequestrant. The polymer dispersant proved more effective at inhibiting the formation of metal precipitates. Although the polymer dispersant reduced the likelihood of the packing material from becoming fouled to the extent that it needed replacement, the high natural iron levels in the influent groundwater still create iron staining of the packing media. As a precautionary measure, the GET system is shut down every 3 months and the air stripper is acid cleaned.

POST-OPERATION SAMPLING

Representatives of the EPA, NDEQ, and NDHHS participated in pre-final and final inspections of the GET system and provided recommendations for system improvements. Before granting approval to use the treated groundwater in the city's potable water system, NDHHS required proof of the GET system's effectiveness in treating the contaminants of concern. The contaminants of concern and water quality parameters such as pH, turbidity, and metals were monitored. The NDHHS reviewed monitoring results and granted approval for reuse of the treated groundwater in the city's potable water system contingent on additional monitoring.

Initial Startup Testing. Extensive monitoring of the influent and effluent of the GET system has been conducted since the system began operation in February 2004. Samples have also been collected at the system influent, post-chemical addition, and effluent points in the GET system for quantifying the percent loss of metals and hardness across the air stripper. Samples also provided an indicator of how well chemical additives were inhibiting scale formation. A thorough analysis of the GET system was conducted during 14-day and 8-week Operational and Functional (O&F) periods.

Water samples were collected during the 14-day and 8-week O&F periods to confirm GET system performance with regard to contaminant removal and ability to meet effluent discharge limits. In addition, field monitoring using direct reading instruments and HACH test kit analyses was performed onsite by the system operator. Furthermore, the system operator recorded the residual chlorine readings for the

potable water taps at the southern water treatment plant and wastewater treatment plant locations. Samples were collected from the following locations:

- Groundwater influent to the treatment plant
- Treated water effluent from the air stripper
- Within the city distribution system (via taps inside the southern municipal water treatment plant building and city wastewater treatment plant)

Water samples collected during the O&F periods were analyzed for the following parameters:

- VOCs
- Metals
- Total coliform bacteria
- Total organic carbon

Analyses of water samples collected from the GET system effluent and the city distribution system indicated no significant detections of VOCs other than TCE, cis-1,2-dichloroethene (DCE), and low levels of chloroform (periodically detected in the samples from the southern municipal treatment plant). The concentrations for all detected VOCs were well below MCLs. Overall, the air stripper achieved a 97 to 99 percent removal of TCE and 100 percent removal of PCE. Contaminants in the effluent water were consistently below MCLs.

Blending treated water from the GET system with the city's potable water supply had no apparent impact on residual chlorine in the city's distribution system. Residual chlorine values recorded at the city wastewater treatment plant (representing the most remote point in the city's distribution system) were consistently greater than 0.1 mg/L as required. The values were generally higher at the southern municipal water treatment plant.

Quarterly Sampling. The GET system is sampled quarterly at a minimum for compliance with Nebraska Discharge Elimination System (NPDES) permit requirements and to verify that the contaminants in the treated water are either not detected or below the MCLs. Effluent water is also sampled quarterly for VOC analysis at the NDHHS laboratory. This sampling provides an ongoing measure of the treatment system's effectiveness at meeting the MCLs.

PUBLIC MEETINGS AND PUBLIC COMMUNICATION

Before, during, and after construction, EPA and the city held public meetings inform the community of the GET system and the planned reuse of the treated groundwater. Community awareness and acceptance are essential for successful implementation of beneficial water reuse from a Superfund site.

LESSONS LEARNED

The design, construction, and approval of a Superfund site groundwater treatment plant with the intent of potable water reuse led to some valuable lessons learned including:

- Engage the regulator(s) early. Understand the expectations of the regulator and understand who the regulator(s) will engage during design, construction, and operation. In the case of this project, the NDHHS preferred to work through the city who was receiving the treated water and would be the Class 1 operator, and not through the EPA who was constructing the project.
- Understand the drivers of stricter potable treatment standards. The contamination of the shallow aquifer necessitated shallow extraction wells. However, wells with a screened interval of 50 feet bgs or shallower are considered under the influence of surface water unless extensive testing and monitoring show otherwise. A system under the influence of surface water is subject to more rigorous treatment methods than one that is not.
- Understand that the treatment plant will be considered a potable water treatment plant, requiring that all materials and chemicals used must be suitable for a potable water supply. These requirements also apply to the extraction wells, which are considered potable wells.
- Communicate the intentions of the reuse project with the public before design begins, during construction, and before discharging water to the municipal water treatment plant. Water quality and quantity is an important issue with many people. Explaining the beneficial reuse aspects of the project is critical for public acceptance. In the case of this project, there was no public resistance.
- Conduct extensive post-operation sampling to assure the regulatory agencies and the public that the treatment system will consistently exceed state and federal treatment standards.

CONCLUSIONS

Initially, the city only used 26 percent, on average, of the total available treated groundwater. This amount has since increased to more than 70 percent of the treated flow being reused as potable water after the city decreased the amount of water pumped from its other wells. During times of high potable water demand, the city has reused nearly 100 percent of the flow from the GET system. The remainder is discharged to the city's storm sewer system.

Careful planning and extensive communication have been crucial to the success of the project. Between April 2005 and December 2008, the GET system has provided over one billion gallons of treated water that has been reused by the city's potable water system.

RIVERSIDE-QUINDARO BEND LEVEE (L-385) ON THE MISSOURI RIVER: THE ESSENTIAL ROLE OF O&M AND DOCUMENTATION

Gary W. Creason, P.E.

Affinis Corp, 7401 West 129th Street, Overland Park, KS 66213; PH (913) 239-1100; FAX (913) 239-1111; email: gcreason@affinis.us

ABSTRACT

RIVERSIDE-QUINDARO BEND LEVEE (L-385) ON THE MISSOURI RIVER: THE ESSENTIAL ROLE OF O&M AND DOCUMENTATION

The Riverside-Quindaro Bend levee (L-385 in the Missouri River levee system) was originally built as an agricultural levee in the 1920s, was authorized for study by the Flood Control Act of 1944, and drew heightened interest after 1993's major floods in the Midwest. Authorized for final design and construction in September 1997, construction was essentially completed in May 2005. Since then, there has been one high water event, and the levee performed as intended.

The paper provides a brief history of the project, including organizational, legal, and regulatory requirements (including funding, floodplain management plan, operation and maintenance (O&M), flood fight planning, and recertification).

The discussion of L-385 highlights design considerations, key features, and details about levee construction. The discussion emphasizes the basic importance of operation and maintenance and the overwhelming importance of sound documentation for 1) qualifying for federal funds for repairs and rehabilitation after a flood event, and 2) recently mandated levee recertification. Prudently operated and maintained according to existing federal regulations administered by the Corps of Engineers, levees should serve the community and safeguard public investment for many years.

INTRODUCTION

In *Rising Tide*, John Barry's book on the Great Mississippi Flood of 1927, the author observes that major riverine levees designed to absorb phenomenal hydrostatic pressures can fall victim to small flaws:

> "A dozen things can cause a levee to collapse. A single piece of wood, a branch, left in a levee during construction could cause disaster if it rots and creates a cavity. Burrowing animals, even crawfish nests, also create cavities.

> The river will find such flaws and can enlarge them enough to cause a massive levee to collapse…."
>
> "But the biggest danger is simply pressure, constant unrelenting pressure…."
>
> "Each of these dangers could be handled, at least in theory. But men had to do everything right, and they had to do so twenty-four hours a day. As long as a flood lasted, the river could only grow stronger, the levees weaker. Since the river was relentless, men had to be relentless. Since nature missed nothing, made no mistakes, and was perfect, men had to miss nothing, make no mistakes, and be perfect."

To successfully design and construct levees we must first understand and respect the river itself. This requires study and analysis of the floodplain's hydraulics, hydrology, geotechnical, structural, and environmental factors; historic events; and the effects of existing infrastructure on the levee system. Levees can do their work only when engineers and scientists do their work to understand the nature of the river.

To the naked eye, levees look like large, simple, grass-covered embankments built to hold back water. In reality, levee design relies on many engineering disciplines. Beneath that grassy mound, levees are hardworking structures that involve complex engineered systems.

Levees are part of the public infrastructure system. Prudently operated and maintained according to federal regulations administered by the Corps of Engineers, levees should serve the community and safeguard public investment for many years.

This paper uses the L-385 Levee on the Missouri River to illustrate key factors in the life of a levee, most notably operation and maintenance (O&M). It provides a brief historical overview; organization as a political subdivision; general design considerations; construction; O&M; floodplain management plan; flood fight plan; and recertification requirements.

HISTORIC OVERVIEW OF L-385 LEVEE ON THE MISSOURI RIVER

Levee projects typically begin with a singular idea: "We need flood protection." The process from idea to reality can be complex and may take years. Consider L-385: Tired of flooded fields, lost crops, and other damage, the local community organized as a levee district in 1918. Shortly thereafter, they built an agricultural levee. Construction of the levee as it exists today didn't start for another 84 years.

Missouri River Levee System – Unit L-385 was first authorized for study as part of the Missouri River levee system by the Flood Control Act of 1944 (P.L. 534).

The very name of the levee is a good illustration of the impact of the built environment and time: L-385 indicates that the levee is on the left bank of the river (as one faces downstream), 385 miles upstream from the confluence of the Missouri with the Mississippi River in St. Louis. As the result of various federal Missouri River channel projects over the years, the levee is actually located along the river from mile 372 to 376.

Interest in constructing and expanding the levee heightened in the aftermath of major flooding that hit the Midwest in 1993 (see Figure 1). Flooding that approached the 500-year event impacted approximately 1,300 acres of developed and undeveloped land, closing nearly 70 businesses, putting more than 5,000 people out of work for months. Total cost to repair damage to property and infrastructure was approximately $27 million.



Figure 1: Riverside, Missouri, July 1993.

The legal instrument (Project Cooperation Agreement, or PCA) between the U.S. Army Corps of Engineers (USACE) and Riverside-Quindaro Bend Levee District of Platte County, Missouri (referred to as RQBLD) to build the levee was signed in September 1997. Construction began in March 2002. The intent of L-385 is to protect the community located within the city limits of Riverside, Missouri (see Figure 2).

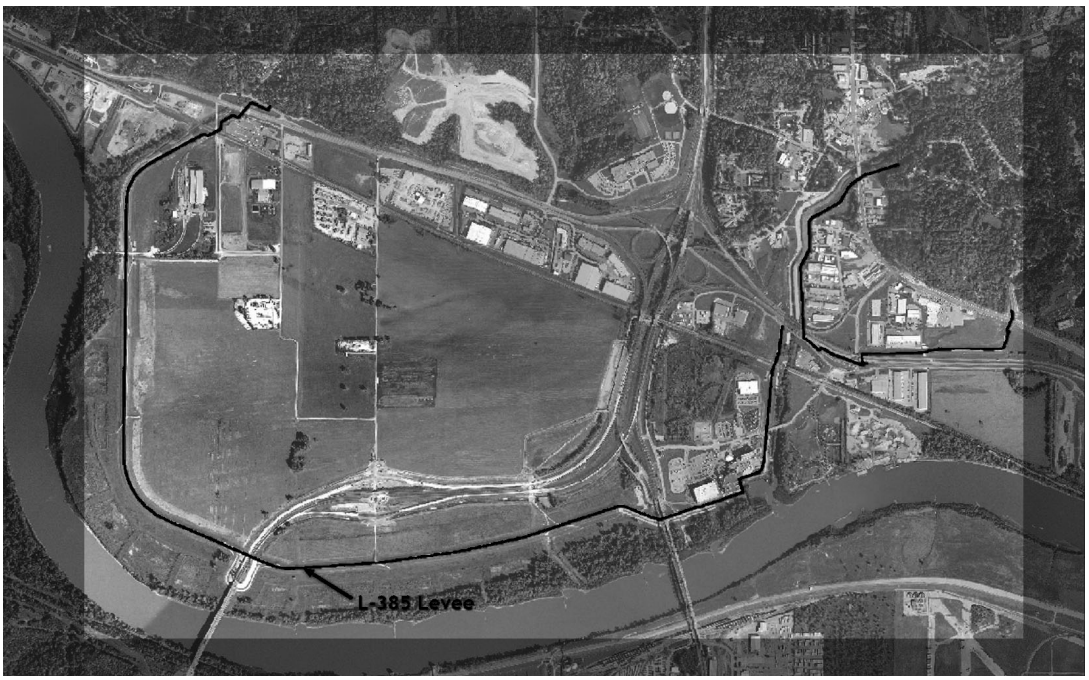

Figure 2. Aerial View of L-385's Location on the Missouri River.

L-385 is the first new Missouri River levee in the U.S. Army Corps of Engineers Kansas City District (KCD) in nearly 30 years. Construction essentially was completed in May 2005. Since then, there has been one high water event, and the levee performed as intended, protecting homes, infrastructure, undeveloped acreage, and business development from floodwaters.

The levee district is actively performing O&M tasks in strict accordance with the *Code of Federal Regulations* Title 33, Pt. 208.10 (33CFR208.10). This document lays out, in detail, the O&M requirements for federally authorized levees.

The technical details of L-385's design are specific to its location on the Missouri River (soils, hydrology, etc.), and its alignment must integrate with existing area roads and utilities. Everything from the organization of the levee district, to a complex engineering design process, to O&M of the system follows the same legal and regulatory process required of any federal levee.

ORGANIZATIONAL, LEGAL AND REGULATORY REQUIREMENTS

Levees as political subdivisions. Levee districts (also known as local sponsors) are political subdivisions, organized under and subject to state statutes, and every state has its own requirements. In the case of L-385, Missouri Statutes Chapter 245 drove the reorganization of two separate districts into the Riverside-Quindaro Bend Levee District in 1988. The statute dictates such things as number of board members, meeting protocol, requirements for attorney-of-record and engineer-of-record, procedures for issuance of bonds for land acquisition and construction, and levying of taxes for O&M, and ultimately adoption of the plan of reclamation.

Funding. Design and construction of federal levees are funded via a cost-sharing agreement between the Corps of Engineers and the local sponsor. Essentially, prior to 1986, the local sponsor's only responsibility was to provide all required lands, easements, and rights-of-way. The Water Resources Development Act of 1986 (P.L. 99-662) (WRDA 1986) also required the local sponsor to provide relocations and disposal of excavated materials. Together, these costs are referred to as LERRDs. For L-385, LERRDs were approximately $25 million.

Rivers exist in political, economic, and public opinion environments. WRDA 1986 marked a significant shift in the cost sharing structure, and local sponsors were required to assume a greater portion of the costs. WRDA 1986 established the cost-sharing split as 75 percent federal/25 percent local sponsor.

> "Congress fundamentally transformed the ground rules for Corps water project planning and funding through WRDA 1986 (33 U.S.C. 2211) by establishing new cost-share formulas, resulting in greater financial and decision-making roles for local stakeholders." (Congressional Research Service 20866, 2006)

In the case of L-385, due to the amount of undeveloped land in the Quindaro Bend portion of the levee district, the final cost-sharing was approximately 50/50 of the total $80 million project cost.

Type of Cost: First costs typically include LERRDs, construction of gatewell structures, closure structures, pump stations, floodwalls, embankment, relief wells, etc. Through a rigorous economic evaluation, the project must demonstrate that the benefits exceed the costs.

Once the levee is built, ongoing costs primarily include both administrative and O&M costs – levees require routine maintenance, whether or not there is a flood. L-385 budgets about $500,000 a year for O&M.

Project Authorization and Contractual Agreements. With the levee district in place, its president signed the PCA with the Corps to formally authorize the plan of reclamation for final design and construction. The PCA establishes the contractual linkages between all players. Under the PCA, the Corps has a contractual linkage with the local sponsor and a contractual relationship with the general contractor. There is no such linkage between the local sponsor and the contractor.

DESIGN CONSIDERATIONS

In general, a levee is a structural system (earthen embankment and other structures) typically on an alluvial fill (materials deposited by the actions of the river over tens of thousands of years). A levee is a significant civil engineering project whose sole purpose is to control and withstand an enormous amount of kinetic energy produced by the swollen river.

Thus, the focus of levee design and (by extension) ultimately O&M is managing the enormous hydrostatic pressure from the river on the levee structure, its foundation soils, and the adjacent ground. The key parameter is the hydraulic grade line (see Figure 3).

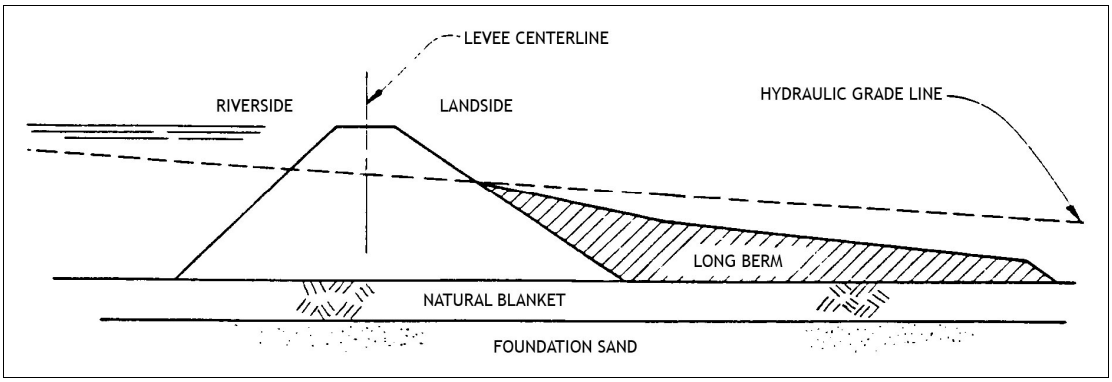

Figure 3. Typical Levee Section.

Suffice it to say that the design process encompasses multiple engineering disciples and involves complex hydraulic, hydrologic, geotechnical, and structural analysis. The process also draws on years of empirical data collected by the Corps for a given river and locale. Each Corps district publishes design standards or guidelines for projects. The standards address such things as slope stability and underseepage.

The output of the design process determines the final alignment and height of the levee, as well as location of stability and underseepage berms, riprap, and other features such as rolling gates, gatewells, stoplog closure structures, pump station, and relief wells (see Figure 4).

- Quindaro Bend levee: 4.1 miles of earthen levee
- Riverside levee: 0.9 miles of earthen levee
- Height: Up to 21 feet
- Concrete floodwall: 1,535 feet
- Two rolling gates
- Four stoplog closure structures
- Pumping station discharge capacity: 75 cfs
- Thirteen gatewells, ranging in diameter from 36 to 108 inches
- Argosy Casino flood door
- Sandbag gaps: 1,043 feet on Quindaro side, 181 feet on Riverside

Figure 4. Features and Structures of L-385 Levee.

In addition to designing the levee to meet the goal of protecting land from flood damage, design considerations also include mitigation of displaced wetlands. In the case of L-385, borrow pits used as a source of material for the levee embankment were designed to address this wetlands mitigation.

As noted in KCD's final environmental assessment for the project, the mitigation provided "appropriate and substantial compensation":

"Establishing functioning wetlands in the remaining 88 acres of borrow area would be a greater than 4-to-1 replacement ratio for wetland mitigation, more than adequate mitigation for the less than 20 acres of wetlands affected by the L-385 levee." (Environmental Assessment: Missouri River Levee System, Levee Unit No. L-385, 2001)

CONSTRUCTION

As agreed to by the PCA, the Corps is responsible not only for design, it also is responsible for levee construction.

There are unique things about the construction of a levee that differentiate this activity from other infrastructure projects. The contractor always has to be aware of the river (its actual and forecasted stage); pipe bedding has to be on direct soil as opposed to granular material; and the contractor must maintain the soil stratigraphy (stratification of materials) during underground excavation and backfill operations.

The newly constructed L-385 levee protects the community from a 500-year Missouri River flood, dwarfing the old 1920s-era agricultural levee by three times the height.

OPERATION & MAINTENANCE

The often tedious process to organize the levee district, request assistance from the federal government, develop a plan of reclamation, secure funding, and complete final design and construction is a huge undertaking. However, it has an endpoint. In contrast, operation and maintenance run for the life of the levee. The integrity of the levee – and thus its ability to perform as intended during a flood – depends on rigorous O&M practices. Poorly operated and maintained, the levee and its many features, may not function well and could lose the battle with the river during a flood.

Whether self-performed by the local sponsor or contracted out to others, effective O&M is similar to setting up and running a small business. For example, the district must hire good people; purchase equipment; develop an accounting system; establish an inspection protocol (another example of the value of the Corps' empirical knowledge base); and conscientiously perform inspections and maintenance on a defined, periodic basis.

As with design standards, the Corps' requirements for O&M, Title 33 (33CFR208.10) contains the standards for federal levees. The Corps develops a unique operation, maintenance, repair, replacement and rehabilitation (OMRR&R) manual for each levee unit. This manual becomes the basic "how to" document for each particular levee unit.

RQBLD employees perform routine maintenance tasks for the Riverside-Quindaro Bend Levee year round. Some tasks occur seasonally, some on a calendar basis, others as needed. The list includes mowing, fertilizing, burrowing animal control, weed control, erosion repair; levee crown rock blading and rolling; and equipment maintenance (gatewells, rolling gates, fences, etc.). For RQBLD these tasks have been itemized and scheduled resulting in a list of 79 items. The documentation to verify that these tasks have been performed is an important piece of levee O&M process.

The Corps defines an important area adjacent to the levee called the levee critical area (LCA). It is defined as that area from 300 feet riverward of the levee center line to 500 feet landward of the levee center line. RQBLD's responsibilities also include coordination and communication with other entities, such as utilities, located in the LCA. Some of the coordination is simply good practice. Maintaining an up-to-date contact list, for example, is one of those activities. Other activity, however, requires RQBLD's engineer-of-record and the Corps to be involved. For example, if Kansas City Power & Light wants to work on buried power lines within the LCA, the

levee district must approve the work (the Corps provides technical guidance) and be able to certify that it was done in accordance with the approved plans.

Conscientious, well-documented O&M is not only a good idea for the levee to provide protection, it is legally required by the Corps, through Title 33 (33CFR208.10). Also, as discussed later, this documentation is important in complying with the new recertification mandate issued by the Federal Emergency Management Agency (FEMA).

FLOODPLAIN MANAGEMENT PLAN

Since October 12, 1996, the Corps has required a local sponsor of a project to develop a floodplain management plan. This condition was a part of the Water Resources Development Act of 1996 (P.L. 104-303) (WRDA 1996). Among other things the plan calls for the local sponsor to implement measures, practices, and policies to reduce loss of life, injuries, and damages to property and facilities brought about by residual flooding. Clearly the development and implementation of the plan requires close coordination with the local community. An example is a reverse 911 call to warn all entities located in the protected area of the need for evacuation in the event the flood is forecasted to exceed the designed capacity of the levee.

FIGHTING THE FLOOD

L-385 was essentially completed in May 2005. Since then there has been one flood event, in May 2007. During what was considered a 15-year event, the levee performed as designed.

Obviously, successful flood fighting will demonstrate the value of the levee. To be successful, flood fighting depends on a detailed flood fight plan. This plan is part of the OMRR&R manual. L-385's plan has 82 specific items. The backbone of its plan is a series of four action levels (see Table 1). These action levels are linked to actual or forecasted river elevations. Each action level dictates procedures to commence at progressively higher river stage.

Table 1. Action Levels in L-385's Flood Fight Plan.

Action Level	Description
1 – Normal operations	Routine duties to be performed regardless of river stage.
2 – Flood season	April 1–July 31, as defined by KCD.
3 – Hannibal gauge of 15	River is capable of reaching appreciable flooding at L-385 within a day-and-a-half from this stage.
4 – Hannibal gauge forecasted gauge of 35 or higher	The river stage that represents the start of appreciable flooding at L-385.

Those responsible for the levee can never turn their backs on the river. These action levels enable RQBLD board members and maintenance staff to be aware of the condition of the river and react appropriately when conditions warrant.

Major flooding will likely take its toll on a levee, no matter how well maintained. After the waters have receded, major repairs or rehabilitation of the levee system may be required. Congress recognizes this and provides for it in the Flood Control and Coastal Emergency Act (P.L. 84-99). This law essentially says that the federal government will pay 100 percent of these costs, provided that the levee unit has been maintained in accordance with the Corps' established procedures (33CFR208.10). This is yet another example of why continual documentation of maintenance is so important.

FEMA RECERTIFICATION

The basic policy governing levee certification for the National Flood Insurance Program (NFIP) was issued by FEMA in 1986 as Part 65.10 of *Code of Federal Regulations* Title 44 (44CFR65.10).

Subsequently, on August 22, 2005, FEMA issued "Procedural Memorandum 34 – Interim Guidance for Studies Including Levees." On June 23, 2006, the Corps responded with the following statement: "[I]f local governments wish areas behind levees to be shown on FEMA's new Digital Flood Insurance Maps (DFIRMs) as protected to at least the one percent change of flood using FEMA's guidance on certification, they must arrange for certification documentation to be provided to FEMA." (USACE, 2006) Furthermore, FEMA requires this recertification to be performed every 10 years.

Although FEMA requires recertification it does not perform recertification. In anticipation of being tasked to do so, the Corps is establishing guidelines for performing levee recertification. Circular EC-1110-2-6067, *Certification of Levee Systems for the National Flood Insurance Program (NFIP)* contains the guidelines (USACE, 2008). (At the time of this writing, the circular is in draft review form.)

This engineering circular makes it clear that documentation is key to this recertification process. This documentation includes both the original design as well as documentation of the design of any repair, rehabilitation, or work performed by others in the LCA. Once again, documentation of O&M and implementation of the floodplain management plan are integral to this recertification process.

The L-385 levee district maintains extensive documentation, which will be one of the most critical activities related to recertification requirements so that when directed to recertify it should be able to do so in a straightforward way.

CONCLUSIONS

Rivers behave according to the laws of physics. We can calculate hydraulic pressures and water velocities. We can study historical weather patterns and analyze the current season's weather, although we can't predict when a flood will come and how hard it will hit. Therefore, we must be ready at all times to react to nature's forces.

As this paper illustrates with the example of the Riverside-Quindaro Bend levee on the Missouri River (L-385), there are myriad state and federal policies and regulations that cover a levee project from the initial awareness of a need for flood protection to the inevitable requirement to successfully fight a flood. Although some of these requirements (such as FEMA's requirement for levee recertification) are relatively new, most of these regulations have existed for many years. They don't need to be changed or added to, they just need to be complied with. Awareness and understanding of these regulations will serve a local sponsor well, to paraphrase John Barry in doing everything right, 24 hours a day:

> "Since nature missed nothing, made no mistakes, and was perfect, men had to miss nothing, make no mistakes, and be perfect." (Barry, 1997)

REFERENCES

Barry, John M. (1997) *Rising Tide: The Great Mississippi Flood of 1927 and How It Changed America*, Simon & Schuster.

Congressional Research Service. *The Civil Works Program of the Army Corps of Engineers: A Primer*. RS20866. (Sept. 20, 2006) Nicole T. Carter and Betsy A. Cody. Available: http://www.nationalaglawcenter.org (Dec. 31, 2008).

"Environmental Assessment: Missouri River Levee System, Levee Unit No. L-385," Volume 1, Section 2.2.4(b). June 2001. Kansas City District, U.S. Army, Corps of Engineers.

"Flood Control and Coastal Emergencies Act." P.L. 84-99 (33 U.S.C. 701n). Available: http://www.spd.usace.army.mil/rehab.html (Apr. 22, 2003).

"Levee Districts." Missouri Code Title XV, Chapter 245. Available: http://law.justia.com/missouri/codes/t15/c245.html (Jan. 5, 2009).

"Local Flood Protection Works; Maintenance and Operation of Structures and Facilities." *Code of Federal Regulations* Title 33, Pt. 208.10, 2003 ed. Available: http://www.nww.usace.army.mil/ (Jan. 9, 2004)

"Mapping of Areas Protected by Levee Systems." *Code of Federal Regulations* Title 44, Pt. 65.10, 2002 ed. Available: http://frwebgate.access.gpo.gov/cgi-bin/get-cfr.cgi (Sept. 11, 2007).

U.S. Army Corps of Engineers. "Guidance on Levee Certification for the National Flood Insurance Program – FEMA Map Modernization Program Issues" (memorandum, Major General Don T. Riley). June 23, 2006.

U.S. Army Corps of Engineers. *Certification of Levee Systems for the National Flood Insurance Program (NFIP)*. Circular EC-1110-2-6067. Sept. 30, 2008.

Protecting Infrastructure: Emergency Streambank Stabilization

John Grothaus[1], Ken Markwell, PE [2], Pete Jarchow PE [3] and John Blancett PE [4]

[1]Planning Branch, U.S. Army Corps of Engineers, Kansas City District, 700 Federal Building, 601 East 12th Street, Kansas City, Missouri 64106-2896; PH (816) 389-3110; FAX (816) 389-2025; email: John.J.Grothaus@usace.army.mil
[2]Northwest District, Missouri Department of Transportation, 3602 North Belt Highway, St. Joseph, MO 64105-1399; PH (816) 387-2441; FAX (816) 387-2359; e-mail: MARKWK@mail.modot.state.mo.us
[3]Water Resources Engineering Department, HNTB Corporation, , Kansas City, MO 64105; PH (816) 527-2248; FAX (816) 221-9016; email: pjarchow@hntb.com
[4]Water Resources Engineering Department, HNTB Corporation, , Kansas City, MO 64105; PH (816) 527-2539; FAX (816) 221-9016; email: jblancett@hntb.com

ABSTRACT

The Emergency Streambank Stabilization program has been a vital part of protecting local infrastructure, including bridges and other utilities, from the dynamic rivers and streams in Missouri. The U.S. Army Corps of Engineers, Kansas City District has a long-established emergency streambank stabilization program, carried out under Section 14 of the 1946 Flood Control Act. The program is cost shared 65 percent Federal, 35 percent local, and after construction, projects are turned over to the local partners, or "sponsors" for ownership and maintenance. In the region surrounding Kansas City, the program has consistently provided for projects which protect critical infrastructure such as roadways, bridges, and utilities, from severely eroding stream banks. Sponsors include counties, cities, Indian Tribes, and state departments of transportation. This paper presents two of ten projects built in the last ten years that have served two sponsors very well: the City of Parkville, Missouri and the Missouri Department of Transportation. Section 14 projects are developed and constructed in a multi-stage process. This process includes evaluation of multiple stabilization techniques, including longitudinal peak stone toe protection (LPSTP), bank armoring, bendway weirs, dikes, jetties, sheet piling, bioengineering, and windrow revetments. The Section 14 program plays a key role in protecting rural and urban transportation and water infrastructure. It assists states and local governments in diligently monitoring and maintaining their infrastructure, supports economic health and development, and contributes to sustainable water resources in the community. Finally, Section 14 program is an example of a highly beneficial partnership between a Federal agency and state and local governments.

INTRODUCTION

The U.S. Army Corps of Engineers (USACE) has a long-established emergency streambank stabilization program, initially implemented under specific Congressional authorities, but since 1947 carried out under Section 14 of the 1946 Flood Control Act. Many districts of the USACE participate in this program, but the Kansas City District is one of the most active and effective practitioners. The District has designed many Section 14 projects. In recent years, due to staff being prioritized to levee, dam safety and Missouri River work, the District has found it very effective to contract with HNTB, taking advantage of their expertise in streambank stabilization projects.

In the past ten years, ten Section 14 emergency bank stabilization projects have been constructed in eastern Kansas and central, western and northwestern Missouri. Five additional projects are in various phases of design and are expected to be constructed by 2011. Another five are planning phase and could be built within the next 2 to 5 years. These projects typically protect infrastructure such as roadways, bridges, utility lines, water intakes, and recreation facilities from rapidly eroding streambanks and degrading stream beds. Five of these completed projects have been constructed with the Missouri Department of Transportation (MoDOT) as the sponsor, including four with MoDOT District 1.

SECTION 14 PROGRAM BACKGROUND

Kansas City District Section 14 projects are generally conducted in a five step process:

- The potential sponsor submits a request and supporting data to the Kansas City District.

- The Kansas City District contracts a task order with HNTB. HNTB visits the project location with their experienced Section 14 team, consisting of a Project Manager, Civil Engineer, Geotechnical Engineer and a Water Resources Engineer. The team reports their observations and conclusions from this site visit with a Site Reconnaissance Report, with a recommendation of whether to proceed to the next step. The site visit generally includes a visit to the local offices of the Nation Resources Conservation Service (NRCS) and Farm Service Agency (FSA), who typically have historic photos available that can be used to track the progress of the problem over a span of anywhere from 10 to 70 years.

- Based upon the recommendations of the Site Reconnaissance Report, an alternatives analysis is conducted, assessing up to four possible solutions. Preliminary field surveys are used to estimate construction quantities and costs, and a matrix is developed comparing potential maintenance and

anticipated performance of the alternatives. The resulting Concept Design Alternatives Report is submitted, with a recommendation for proceeding further.

- Final design is then performed for the recommended solution from the Concept Design Alternatives Report, with preparation of construction plans and specifications. When necessary, additional field surveys are performed for more accurate plans and quantities, and to provide a basis for right of way and easement acquisition. Environmental permitting, easement acquisition and right of way acquisition are also accomplished during this step.

- A contractor is then selected, either through some form of competitive bidding or a negotiation process, and then construction is initiated. The ideal construction season is either January through March, or mid-July through September, which tend to be drier, with less risk of significant flow events. Depending upon the size of the project and weather, construction can take less than one month or up to 3 to 6 months on larger projects.

The majority of the completed Section 14 projects use a stabilization method known as Longitudinal Peak Stone Toe Protection (LPSTP). Other methods used include flow directing stone jetties, stone and sheet pile grade control weirs, and stone slope revetment. Other techniques considered during the alternatives analysis steps include sheet pile revetments, bendway weirs, bioengineered vegetative banks, and windrow revetments (both surface and buried). All constructed projects include a planting component. Due to the rural nature of the majority of projects, and the need to provide rapidly installed and highly reliable projects, measures relying solely or heavily on vegetation have been avoided. The reliance on riprap stone solutions allows a significant design life, and provides better assurance of success under extreme conditions such as droughts or frequent floods, and through extended periods of inundation that could heavily damage a project relying largely on vegetative methods.

The LPSTP solution in particular is very flexible in its installed condition. LPSTPs are generally used where banks are subject to collapse after flow events. Often, sandy banks are present that collapse under their own weight when water levels drop after the flow peak. The LPSTP is placed either at the toe of the bank, or along a smooth alignment out from the bank and linked back to the bank with baffles/tiebacks. It works by forcing the thalweg of the stream out away from the bank, and by reducing the velocity of the flow adjacent to the bank. Therefore, when banks collapse, the slumping soil no longer falls into the deepest, fastest flowing portion of the stream to wash downstream; instead the slumped soil stays in place, buttressing the bank and helping the bank reach an equilibrium slope that will no longer collapse when wetted. The slope is then further reinforced as natural vegetation is established. The overall area between the LPSTP and the bank eventually fills with sediment and also vegetates.

The top of the LPSTP is generally set at a third to a half of the bank height. Because many of the projects have been on streams that were channelized and oversized many years ago, that height of LPSTP generally equates to an annual or slightly greater high water event. The LPSTP is constructed by dumping a specified weight of rock per unit length (tons per foot) along its centerline. The riprap stone ends up at its angle of repose. If the stream thalweg deepens adjacent to the LPSTP, then the stone launches and the mass of the LPSTP shifts. However, if the initial height of the LPSTP is adequate, then the revetment is essentially self-healing, with the mass of rock providing long term protection and stability. Adjacent banks, if left undisturbed during construction, will continue to collapse until a stable slope develops. Often, the banks are flattened during construction so that they can be included in the project vegetation planting step.

The following two sections describe examples that demonstrate the range of recent Section 14 projects in the Kansas City area. One is a rural project with a simple cause and one specific protection objective, and the other is an urban project, with multiple contributing factors for the instability and numerous potential impacted features.



Middle Fork Grand River



Rush Creek

MIDDLE FORK GRAND RIVER AT US 169

This project is located in Gentry County, Missouri. The project sponsor was the Missouri Department of Transportation (MoDOT), District 1. The initial site visit occurred in March 2001, and the project was constructed in the summer of 2003.

Like many rivers in northwest Missouri, the Middle Fork Grand River was reportedly straightened and channelized around 1920 to reduce flooding impacts on agriculture. Over time, a series of meanders has formed and begun progressing downstream. One of these meanders was threatening the east abutment and roadway approach on US Highway 169, near Gentry, Missouri. The existing bridge was constructed in 1961 as part of a new highway project; there was no bridge at the location prior to its construction.

The Middle Fork Grand River floodplain is nearly one mile (1.6 km) wide at the project site. The river's drainage basin at that location is 162 square miles (39,400 hectares). There is minimal urbanization in the watershed, with the predominant land use being agricultural. The channel top width at the bridge is approximately 150 feet (46 m). The bridge has five spans and a total length of 428 feet (130 m). The bridge and its substructure were configured at a 35 degree angle to the channel when it was constructed; that angle had increased to 56 degrees by 2001. The active channel was nearing the east abutment of the bridge, which is constructed on a relatively shallow pile foundation. MoDOT had dumped riprap under and adjacent to the bridge within their right of way, but the eroding bank upstream of the bridge was pushing eastward, resulting in the concern that the meander might threaten the roadway embankment if unchecked. Photo 1 shows the eroding bank and MoDOT's riprap. MoDOT requested that the Kansas City District initiate a Section 14 project, and in February 2001, they contracted the site visit step to HNTB Corporation located in Kansas City, Missouri. HNTB sent their design team with experience from several previous Corps of Engineers Section 14 projects to the site.

Aerial photos from 1940, 1965, 1981, 1990, 1993 and 1996 were acquired at the time of the site visit. The 1940 photo (north at the top, typical) shows a low water channel gently meandering within the limits of what was likely the original channel excavation; sands bars were small and few in number. The 1965 photo depicts a regular series of meanders pushing slightly outside the limits of the original straightened channel, with much larger sand bars. Several hundred feet upstream of the highway crossing, four jetties had been constructed on the left side of the river. The 1981 photo showed significant meanders had formed upstream and directly across from the jetties. The 1990s photos showed these meanders pushing progressively farther out from the original channel alignment, and showed the approach flow angle into the bridge worsening as a meander formed between the jetty area and the highway.

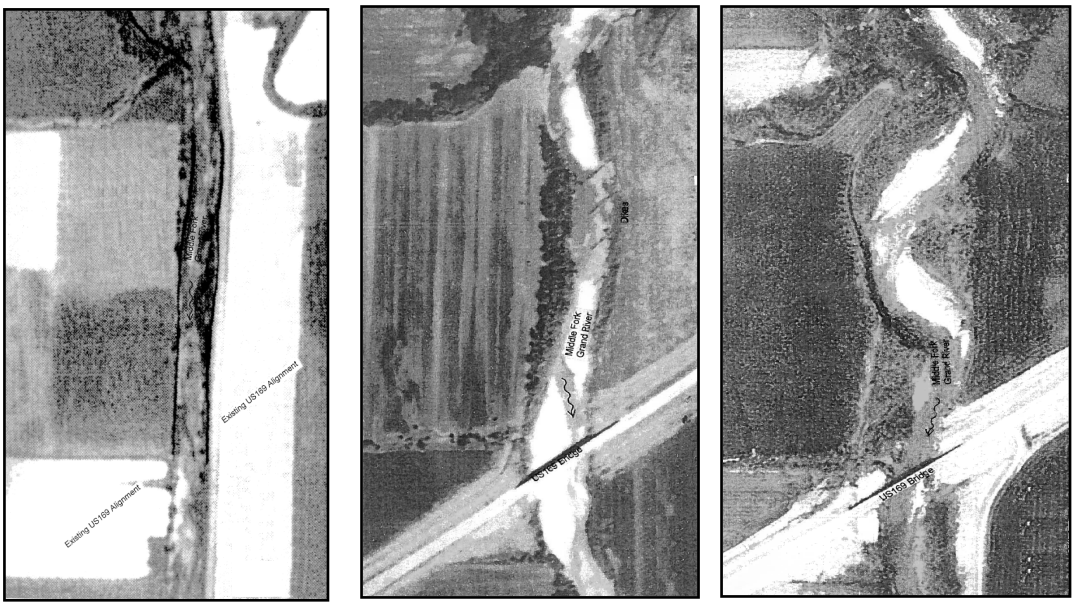

Middle Fork Grand River Erosion Progression, 1940, 1965 & 1996

After receiving their Site Visit and Preliminary Assessment Report, the Kansas City District asked HNTB to conduct an alternatives analysis study and then to perform final design and preparation of construction plans and documents. HNTB subcontracted site surveys to Torres Consulting Engineers, Inc. The Concept Design and Alternatives Report presented four alternatives: bank aligned LPSTP; out-from-bank LPSTP; bank aligned sheet piling; and three rock jetties. After meetings with the Kansas City District and MoDOT, the out-from-bank LPSTP alternative was selected for final design. It was anticipated to be the most cost effective method of halting the bank movement and also improve the angle of flow into the bridge opening.

In final design, it was decided to remove some material from the point bar on the inside of the bend, across from the LPSTP. The LPSTP itself was aligned in virtually a straight line, from 400 feet (122 m) upstream of the bridge to 250 feet (76 m) downstream of the bridge. A total of six baffles, up to 40 feet (12 m) in length, were used to tie the LPSTP into the bank.

Stone toe revetment was included along the right bank, a short distance downstream of the bridge, to protect a portion of a slightly bending outside bank where the proposed LPSTP could conceivably increase the chance of new bank movement. This downstream right bank revetment was connected to new riprap on the west abutment slope of the bridge by use of a buried windrow. This buried windrow consisted of a mass of riprap with four feet (1.3 m) of soil cover. The intent of the windrow was to provide a mass of rock that would launch and create a barrier to further bank movement, if heavy erosion were to eventually occur on the west side of the bridge opening.

In addition to installing new riprap on the west abutment slope of the bridge, a west embankment protection revetment was included for 120 feet (37 m) westward of the abutment riprap on the upstream side of the bridge. The riprap was installed as protection against the possibility of eventual movement of an upstream right bank meander all the way to the bridge. The project budget could not justify LPSTP protection at the location of the meander; it was believed that it would take many years before this meander could progress downstream through a 400 foot (122 m) long wooded area. The west embankment protection revetment was designed to consist of a large mass of riprap stone placed as a wide, thick toe along the existing roadway embank. In the event that the right bank meander eventually progressed downstream through the wooded area to the roadway, this revetment would be expected to launch and provide at least short term protection to the roadway.

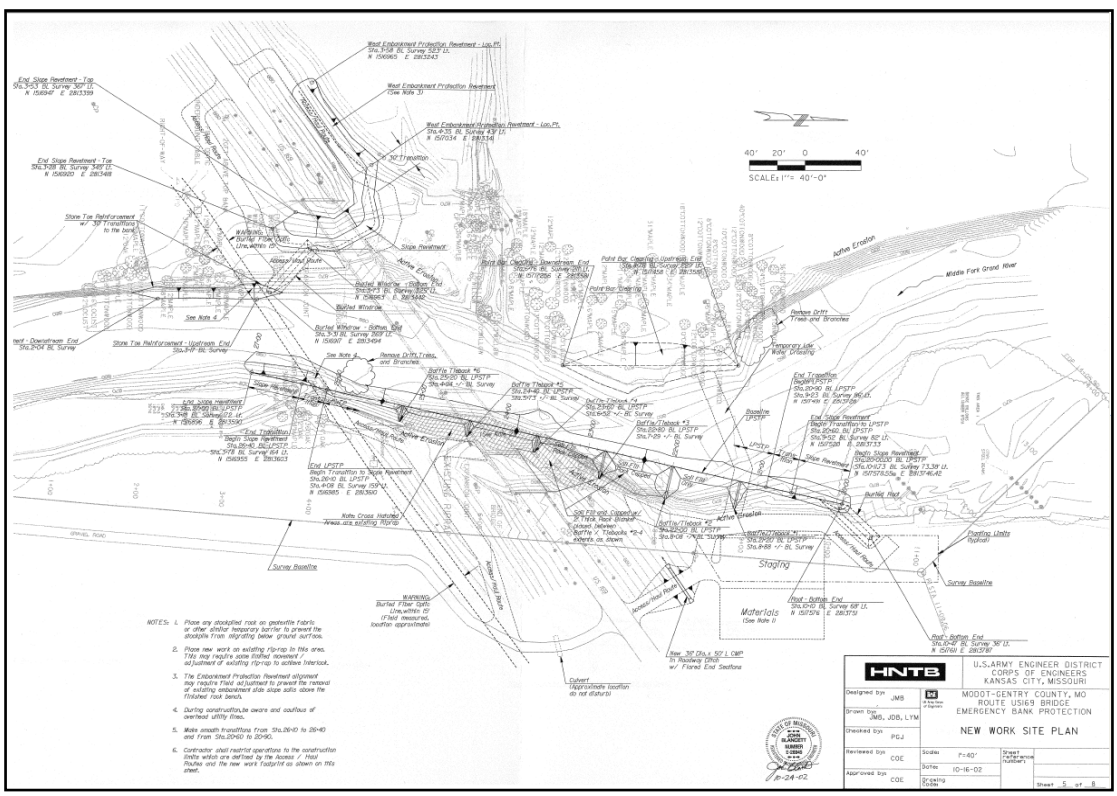

Middle Fork Grand River at US 169 Construction Plan

Construction was completed in September, 2003. Photo 1 shows the severity of the erosion and threat to the road and bridge abutment. (MoDOT dumped rock is seen in the photo, intended only as a stopgap measure.) Photos 2 and 3 show the upstream left bank LPSTP during and immediately after construction. Tree plantings in the buffer area are visible in Photo 3. Photo 4 shows the project a few years subsequent to construction.



Photo 1: March 13, 2001



Photo 2: September 8, 2003



Photo 3: September 24, 2003



Photo 4: March 6, 2006

The construction contractor was Pangea Group, and the construction cost was approximately $225,000. The Middle Fork Grand River at US 169 is representative of the typical rural Section 14 project, providing important transportation infrastructure reliable and cost-effective protection from stream bank movements.

RUSH CREEK AT ENGLISH LANDING

This project is located in the City of Parkville, in Platte County, Missouri. The City was the project sponsor. The initial site reconnaissance occurred in February 2003, and the project was constructed starting in February 2007. The delay from initiation of the project to construction was due in large part to funding for Corps civil works projects being constrained after 2003 due to the war. However, this particular project was also much larger and more complicated than the typical Section 14 project.

Rush Creek at English Landing Park is located immediately south of downtown Parkville, Missouri. The City's wastewater treatment plant is located near the creek, and main sanitary and water lines cross under the streambed. This urban park, a major regional destination, is heavily used, with ball fields, pavilions, boat ramps and a city market nearby.

Rush Creek has a drainage area of 18 square miles (4700 hectares), most of which is steeply sloped land along the north bluff line of the Missouri River. There are two major lakes in the basin: Weatherby Lake is on the main branch of Rush Creek, over five miles (8.0 km) upstream of the project site; and Riss Lake, approximately one mile (1.6 km) upstream on White Aloe Branch, a tributary that joins Rush Creek about half way through the project reach. There is a roadway/pedestrian bridge (Main Street) at the upstream end of the project reach, which is used mainly for public and equipment access to the southern portion of the park.

There is a notable pedestrian bridge in the downstream portion of the project reach (see photos 7 and 8); this structure is a historic relocated railroad bridge that is one of the last two remaining examples of an A-Frame truss as designed by J.A.L. Waddell. The bridge was originally constructed in 1898 in Trimble, Missouri. It was removed in 1984 by the USACE to prevent it being permanently inundated by Smithville Lake on the Platte River, and was installed in English Landing Park in the late 1980s. HNTB contributed some of the design expertise in re-assembling the bridge on Rush Creek.

At the time that the Waddell Bridge was relocated in the park, plans for its installation showed a channel less than 10 feet (3 m) deep at the new location. By early 2003, when the Site Visit and Preliminary Assessment Report were prepared, the channel depth at the bridge had approximately doubled. Most of the banks between the outlet to the Missouri River and the Main Street bridge were showing signs of movement, with numerous trees either having collapsed into the channel or having been undercut by erosion and threatening collapse. An unsightly broken concrete rubble revetment provided some stability to the right (south) bank of the channel adjacent. Adjacent to the channel on this bank was Grigsby Field, a very new and valuable baseball field. On the opposite side of the channel, a bank failure had caused a fence and a portion of a grandstand to collapse into the creek. There was an exposed pipe that had undermined just upstream of the confluence with White Aloe Branch, and an eroding, nearly vertical left bank was getting close to the north abutment of the Waddell Bridge. Very rapid channel erosion and degradation were threatening the City's critical infrastructure and the bridges.

After agreeing to include Rush Creek in the Section 14 program with the City of Parkville as the Sponsor, the Kansas City District contracted with HNTB in 2003 to perform the site visit and prepare a preliminary assessment report.

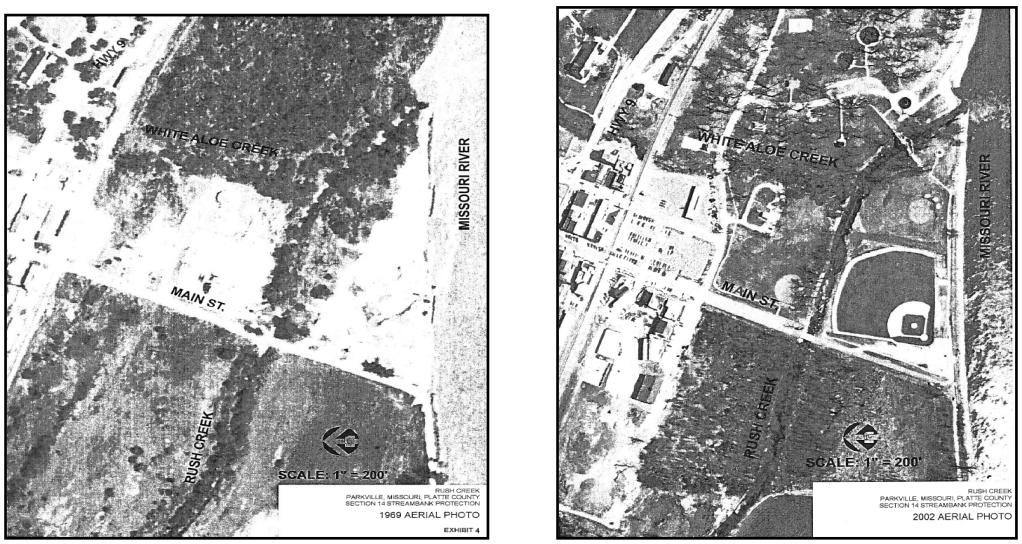

Rush Creek Aerial Photos, 1969 & 2002

During the Site Visit step, numerous constraints along the creek in the project reach were identified. Primary of those were the two bridges, three ball fields (including Grigsby Field), utility line crossings, a boat landing, a vehicular turn-around area, the sewage treatment plant, the park trail system, benches, parking areas, and numerous large trees. White Aloe Branch was also identified as a concern, although it was not part of the project scope. It was obvious that the headcutting that had already occurred on Rush Creek would very like soon progress upwards on White Aloe Branch. Aesthetics and environmental compatibility of the project were also identified as important issues by the City.

After the site reconnaissance and considerable coordination with the Kansas City District, Parkville and others, HNTB submitted the Site Visit and Preliminary Assessment Report in November 2003. Due to the high visibility of the project because of its location, more numerous and more detailed alternatives were evaluated for the initial report. Five were considered and presented in the report: an LPSTP alternative, a full channel lining/sideslope revetment alternative with sheetpile cut-off walls, a structural planting wall alternative, and two bioengineering alternatives, one with large rock or gabion slope protection, and one with reinforced earth slopes. At a subsequent meeting with the KCD and the sponsor, the full channel lining alternative was eliminated, mainly due to its anticipated impact on adjacent trees.

On proceeding into the Concept Design Alternatives step, considerable effort was spent assessing the causes of the instability including hydrology, geotechnical, and geomorphology. Several factors were found to be significant contributors.

- There is significant recent and ongoing development in the rapidly urbanizing watershed. This results in larger runoff peaks and volumes. A limited number of upstream detention ponds, plus the two large (non-flood control) lakes in the watershed, also impact the hydrology, by increasing the length of

time that bankfull discharges occur. The net result is that flow peaks are larger and of significantly greater durations than would have occurred from the same rainfalls historically. These larger and longer flows impact the stream geomorphology, in essence changing the magnitude of the channel forming event.

- The two major lakes in the watershed, particularly the nearer Riss Lake on White Aloe Branch, probably impact the sediment loading of the stream by discharging relatively sediment starved water.

- The existing channel in the study reach passes through an old land fill area. This suggests that the channel may not be in its natural location. A prior relocation may not have replicated the slopes and meanders of the original stream.

- The Missouri River flow line has reportedly dropped approximately 10 feet (3 m) in the Kansas City reach. This has resulted in headcutting on the lower end of many local streams, including Rush Creek.

- Geotechnical information and investigations identified that the surface material at the project site consisted of clays, silts and loams. Including top soil, the silt-clay layer tended to be 13.5 feet to 15.5 feet (4.1 to 4.7 m) deep in the project reach. This cohesive layer is underlain by sandy material. One result of the lowering of the Missouri River bed is that the downstream end of Rush Creek subsequently penetrated through the silt-clay material into the sand. The sandy material is highly erodible and has led to relatively rapid deepening and widening of the channel throughout the project reach.

The geotechnical factor, related to the presence of the sand layer along the new channel thalweg, adversely impacted the feasibility of several of the alternatives presented in the Site Visit and Preliminary Assessment Report. Therefore, burying and isolating the sand layer from active flows became a major emphasis of the design. This eliminated the bio-engineering solutions from further consideration, because those alternatives did not provide for filling the lower portion of the existing streambed that had degraded into the sand layer. Also, cost estimates developed in the alternatives analysis step indicated that most of the bio-engineering alternatives assessed in the site visit phase were prohibitively expensive.

After additional meetings with the Kansas City District and the City of Parkville, a new alternative was developed and scoped for final design. This new alternative incorporated a grade control structure downstream of the Waddell Bridge, with the intent of restoring the flowline at the bridge and at the upstream confluence with White Aloe Branch back to near its elevation prior to the headcut and degradation of the channel bottom into the sand layer. The design included filling the channel bottom upstream of the grade control, and included use of LPSTP along the new channel toes, extending along both sides of the channel to the Main Street bridge. Work on the upper sideslopes of the channel, in the silt-clay material, was specifically

excluded, with the intent that the city would eventually provide selected vegetation. Virtually all constraints would be avoided, and many of the larger trees along the channel bank would be left in place, albeit with steep adjacent slopes between them and the project's reconstruction of the lower portion of the channel. This design was completed and bid in late 2006. At the time of the potential letting, market pressures from the aftermath of Hurricane Katrina had heavily impacted the costs of steel and concrete, and therefore the proposed grade control structure. In addition, due to heavy area-wide construction activity, only one responsive bid was received. As a result, the one bid significantly exceeded the project cost estimate and the available funds. Having only received one responsive bid, the Kansas City District and the City were able to enter into intensive negotiations with the contractor to value engineer the project to meet the established goals within the project budget.

The Kansas City District, HNTB and Parkville reevaluated the design function, conducted a series of meetings with the contractor who had submitted the responsive bid, and discussed various methods of accomplishing the project goals of stabilizing the stream without impact the numerous adjacent facilities. Ultimately, the decision was made to return to a design concept that had been screened out earlier. It was decided to use a series of four grade control structures, each with sheet piling driven to a minimum depth of 12 feet (4m) below ground, projecting above grade 3 feet (1 m) high or less, to raise the channel flowline above the sand layer. This necessitated compromises on the desired channel elevation and sideslopes at the Waddell Bridge, because it was only possible to construct two of the drops between the bridge and the Missouri River. However, the desired channel bottom raise was achieved slightly downstream of the confluence with White Aloe Branch. The new design also included rock armoring of the banks and bed of the stream at various levels throughout the channel reach. Once consensus was reached with all parties regarding the new approach, HNTB quickly revised the design and plans, and an affordable price was negotiated with the contractor.

The project was constructed in early 2007, by ESI Contracting of Kansas City. Photos 6 and 8 depict the constructed project in direct comparison to the pre-construction conditions in Photos 5 and 7. To this date, periodic monitoring indicates that the project is performing as expected. The City's infrastructure and the English Landing Park have been protected from extremely rapid and destructive erosion. The City and community have generally indicated great satisfaction with the project. The new design required the removal of a few trees that were not initially expected to be removed, which caused concern among some Park visitors. However, left without a project, all of the trees that were removed by construction, and many that were saved by the project, would have fallen victim to the erosion in a very short time.

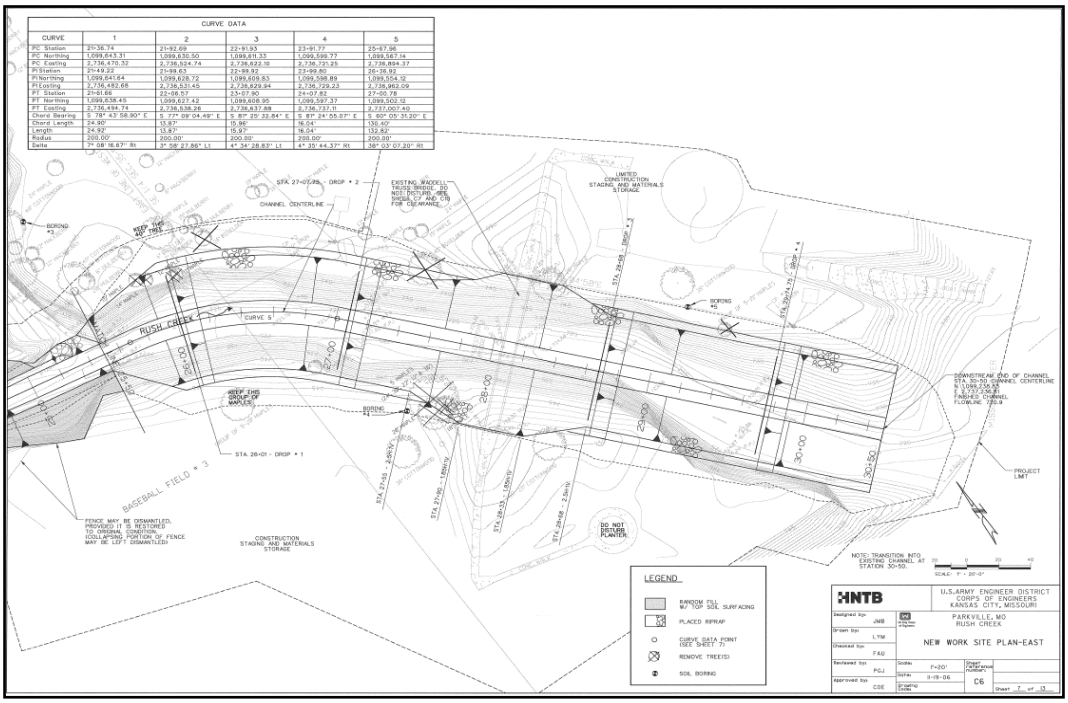

Rush Creek at English Landing Park Construction Plan



Photo 5: March 12, 2005



Photo 6: August 14, 2007



Photo 7: March 13, 2006



Photo 8: August 14, 2007

LONG TERM PERFORMANCE

Another Section 14 project with MoDOT was the bridge over the Grand River at Route A. This project was constructed in March-April, 2001. It has withstood numerous bank full events, including one that occurred during construction, and has proven to be quite stable. It arrested a rapidly moving bank, and has accumulated significant sediments both in the voids of the riprap, and in the open cells between the bank, the LPSTP, and the baffles. These sediments support vegetation that traps more sediment, enhancing both the protective function of the project, and providing natural cover that helps reduce the potential negative impacts of riprap. Photos 9 through 14 show a progression over time, looking upstream from the Route A bridge.



Photo 9: January 20, 1999



Photo 10: April 18, 2001



Photo 11: March 29, 2002



Photo 12: September 5, 2002



Photo 13: March 6, 2006



Photo 14: May 23, 2007

A large flood in 2006 removed some the vegetation that had covered over the silted baffles, and over time it is expected to be restored. Also of note in the photographs is the successful use of a vegetative buffer along the field adjacent to the bank stabilization project. This feature, included in all similar Section 14 projects, involves attaining a permanent easement, combined with selective plantings. The Route A project is typical of the Section 14 projects where the stabilized project fills in with sediment, and then natural vegetation eventually covers the project features, tying in with the riparian zone on the original bank.

CONCLUSION

The Section 14 program in the Kansas City District of the U.S. Army Corps of Engineers has been an excellent example of a Federal agency, local and state agencies, consulting firms, and private contractors coming together in partnership to provide much needed protection to an important segment of the Nation's infrastructure. Dozens of projects have been constructed over the decades, especially on the dynamic and active rivers of Northwest Missouri. Periodic site visits indicate that all of the projects constructed in this region have performed as designed, not only in protecting infrastructure, but also serving to repair scarred streams. Using established construction techniques applied with sound engineering principles, along with the combined experience of the Kansas City District and HNTB Corporation, the Section 14 program is truly a tool that will continue to be highly relevant and valuable in the 21st century in addressing our daunting infrastructure challenges.

REFERENCES

Design Criteria:

- EM 1110-2-1416 River Hydraulics, 15 Oct 93
- EC 1105-2-211 Continuing Authorities Program Procedures
- EM 1110-2-1601 Hydraulic Design of Flood Control Channels
- ER 1105-2-100 Appendix F—Continuing Authorities Program Procedures
- http://www.hnd.usace.army.mil/techinfo
- General Design Considerations for Streambank Protection Measures, Charles M. Elliot, as published by USAWES (undated)

Ground photographs by John Blancett, HNTB Corporation
Aerial photographs courtesy of U.S. Department of Agriculture Farm Service Agency
Construction plans courtesy of the U.S. Army Corps of Engineers

The Impact of Smaller Detention Basins on Flood Hazard Areas in Lenexa, Kansas

Elangovan Karuppasamy, P.E. [1], Natalie Postel, P.E. [2], Christine A. Pomeroy, Ph.D., P.E. [3] and Tom A. Jacobs, P.E.[4]

[1] CDM, 9200 Ward Parkway, Suite 500, Kansas City, Missouri 64114; PH (816) 444-8270; e-mail: Karuppasamye@cdm.com

[2] CDM, 9200 Ward Parkway, Suite 500, Kansas City, Missouri 64114; PH (816) 444-8270; e-mail: postelNA@cdm.com

[3] Department of Civil and Environmental Engineering, University of Utah, 122 S. Central Campus Drive Room 104, Salt Lake City, UT 84112; PH (801) 585-7300; e-mail: Christine.Pomeroy@utah.edu

[4] City of Lenexa, Kansas, 12350 West 87th Street Parkway, Lenexa, Kansas 66215; PH (913) 477-7680; e-mail: TomAJacobs@ci.lenexa.ks.us

Abstract

In the early 1990s, the City of Lenexa, Kansas (City) adopted a flood control standard which required new developments to limit post-construction 1-percent-annual-chance flow rates to 2.79 cubic feet per second (cfs) per acre. In 2003, the City adopted new standards (American Public Works Association Specification 5600) that removed the 1-percent-annual-chance requirement but included matching the 100-percent-annual-chance and 10-percent-annual-chance post-development flow rates to pre-development flow rates (Lenexa City Code, January 2008). As a result of these requirements, many detention basins have been constructed in the past two decades have not been included as part of a city-wide flood hazard analysis. To remedy this omission, the City initiated the East Lenexa Detention Study (ELDS) to quantify the effect of the small detention basins on peak flow rates and water surface elevations.

The purpose of this study was to evaluate the impacts of the smaller detention basins on flood hazard areas in Lenexa using HEC-HMS and HEC-RAS models. For the hydrologic analysis, HEC-HMS models were used to simulate peak runoff from the 50 percent, 10 percent, and 1 percent annual chance storms. For the hydraulic analysis, HEC-RAS models were used to estimate water surface elevations using the peak flow rates estimated by the HEC-HMS model.

The 1-percent-annual-chance peak flows within the Study Area increased as much as 57 percent in one location (Mill Creek) and decreased as much as 32 percent at another location (Indian Creek) to the existing FEMA models as a result of identified detention basins and updated landuse characteristics. The 1-percent-annual-chance peak water surface elevation decreased as much as 6.1 feet in one location and increased as much as 10.9 feet in another location due to refinement of HEC-RAS model input. As a result, 11 buildings within the ELDS Area were removed from the floodplain limits.

Background

Detailed floodplain mapping efforts within the City of Lenexa, Kansas (City), were recently completed by the Johnson County Stormwater Management Program, and the updated Flood Insurance Rate Maps (FIRMs) are currently adopted by the Federal Emergency Management Agency (FEMA). The hydrologic modeling for the mapping effort was accomplished using the U. S. Army Corps of Engineers (USACE) Hydrologic Engineering Center's (HEC) Flood Hydrograph Package (HEC-1). As part of the analysis, large stormwater detention basins that receive significant drainage were included in the evaluation. However, smaller basins that were often designed specifically to detain flood flows from smaller areas were not included in the hydrologic modeling effort. This level of detail was beyond the requirements for the FIRM updates.

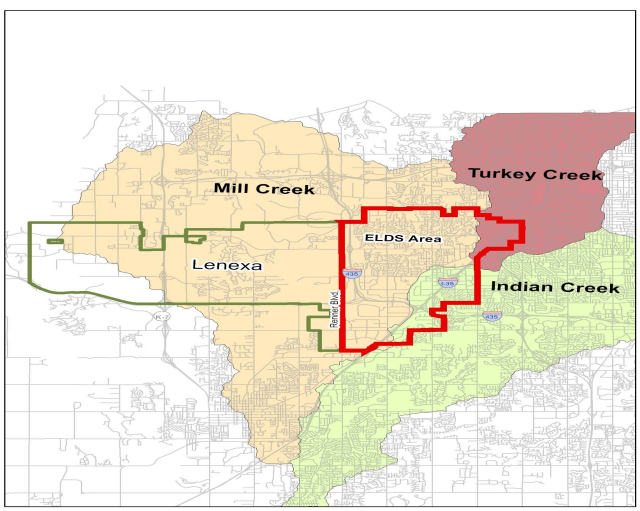

Figure 1. East Lenexa Detention Study Area

In the early 1990s, the City adopted the Kansas City Metropolitan Chapter of the American Public Works Association (APWA) standards for flood control, which required developments to limit post-construction 1-percent-annual-chance unit flow rates to 2.79 cubic feet per second (cfs) per acre. In 2003, the City worked in parallel with the Kansas City Metropolitan Chapter of APWA and adopted new requirements that are more specific to the region. The new standards replace the 1-percent-annual-chance requirement with matching the 100- and 10-percent-annual-chance post- to pre-development flow rates. In addition, the new standard requires implementing best management practices (BMPs) to control the smaller rainfall events (Lenexa City Code, January 2008). As a result of these requirements, many detention basins have been constructed in the past two decades that are specifically designed to detain low probability flows in local drainage ways, but have not been included as part of a city-wide flood hazard analysis. To remedy this omission, the City initiated the East Lenexa Detention Study (ELDS) to quantify the effect of the small detention basins on peak flow rates and water surface elevations.

The ELDS Area includes the area in eastern Lenexa east of Renner Boulevard to the City limits, encompassing approximately 15 square miles (Figure 1). The Study Area land use is mostly residential, commercial, and open space and includes 148 detention basins (Figure 2) distributed throughout three major watersheds: Mill Creek, Indian Creek and Turkey Creek.

Methods

Hydrologic Evaluation

Quantifying the effects of these smaller basins on peak flow rates and water surface elevations required the creation of a hydrologic model (HEC-HMS 3.1.0) with sufficient detail to evaluate the impacts of detention basins. A refined hydraulic model (HEC-RAS 3.1.3) to evaluate the impacts of detention basins on peak water surface elevations was also needed. This section provides a detailed description of the methodology used to estimate the hydrologic effects of incorporating the 148 detention basins.

Following are the steps used to create a refined hydrologic model:

1. Obtaining the FEMA Preliminary Effective Models (HEC-1 Version 4.0)
2. Converting the FEMA Preliminary Effective Models from HEC-1 version 4.0 to the Hydrologic Engineering Center's Hydrologic Modeling System (HEC-HMS) version 3.1.0, creating the FEMA Converted Model
3. Refining the FEMA Converted Model to include subarea and routing refinements to create the Converted Refined Model
4. Modifying the Converted Refined Model to include storage nodes for all identified detention basins to create the Existing with Detention Model

Each step is summarized in the following paragraphs.

FEMA Preliminary Effective Models

The updated FIRMs are identified as FEMA's "preliminary effective FIRMs" until they become effective in 2009. The hydrologic models (HEC-1) used to create the preliminary effective FIRMs (using HEC-RAS 3.1.1) were used as the starting point for the hydrologic model.

The results from three watershed studies (HEC-1 models) were obtained for the ELDS project. The watershed studies included:

- Mill Creek Watershed Study (Mill Creek Watershed Study, 2006)
- Indian Creek Watershed Study (Indian Creek Watershed Study, 2006)
- Northeast Johnson County Watershed Study (Northeast Watershed Study, 2006)

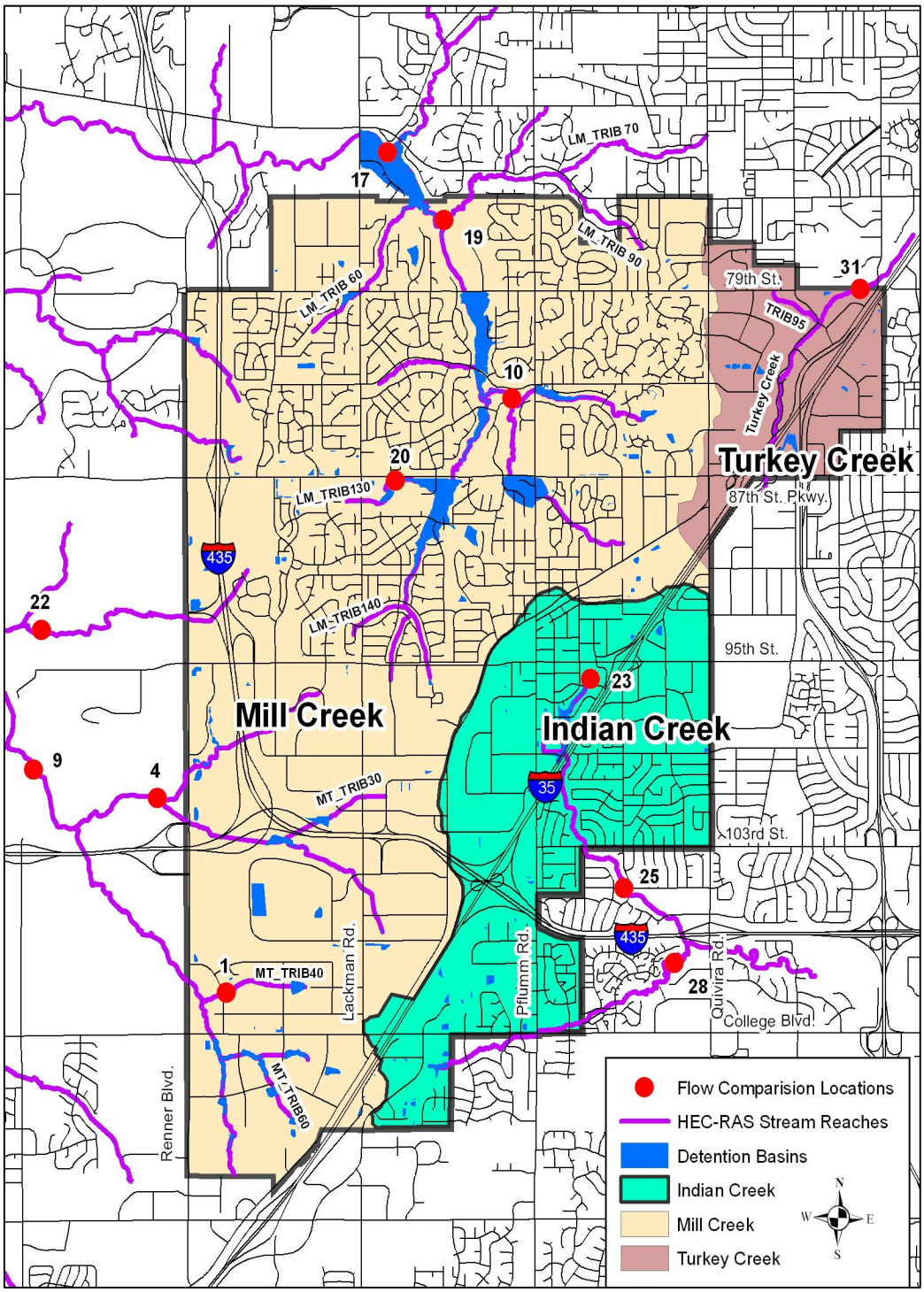

Figure 2. ELDS Area

FEMA Converted Model

The FEMA Converted Model was created by converting the FEMA Preliminary Effective HEC-1 models to HEC-HMS version 3.1.0. HEC-HMS version 3.1.0 was used for this study because it is the currently HEC-supported software and the hydrologic models produced as part of this study are intended to be tools that the City will use in future analyses. The primary purpose of creating the FEMA Converted Model is to isolate the effects of the refined models from changes in the model results associated with software version differences.

Table 1 includes a comparison of the FEMA Preliminary Effective Model to the FEMA Converted Model for 1-, 10-, and 50-percent-annual-chance peak flows along the study reaches at select locations (shown on Figure 2).

Table 1: FEMA Converted Model Flow Comparisons

Mill Creek Watershed

Reach Name	Location ID	FEMA Preliminary Effective			FEMA Converted Model			Percent Difference		
		50%	10%	1%	50%	10%	1%	50%	10%	1%
MT_TRIB40	1	331	568	931	278	527	928	-16	-7	-<1
MT_TRIB10	4	1320	2284	3788	1130	2225	3849	-14	-3	2
MillCreekTrib1	9	1950	3598	6248	1721	3695	6468	-12	3	4
LM_TRIB110	10	986	1990	3520	928	2135	3610	-6	7	3
Little Mill Crk	17	3532	7772	14215	3492	8579	15078	-1	10	6
LM_TRIB70	19	906	2178	4279	833	2252	4348	-8	3	2
LM_TRIB130	20	178	354	654	149	354	661	-16	<1	1
MCTRIB60	22	649	1436	2644	526	1369	2630	-19	-5	-1

Indian Creek Watershed

Reach Name	Location ID	FEMA Preliminary Effective			FEMA Converted Model			Percent Difference		
		50%	10%	1%	50%	10%	1%	50%	10%	1%
Nth_Brch	25	1637	3038	4780	1351	2953	4780	-17	-3	0
NB_Tribb	28	926	1969	3552	759	1971	3651	-18	<1	3

Turkey Creek Watershed

Reach Name	Location ID	FEMA Preliminary Effective			FEMA Converted Model			Percent Difference		
		50%	10%	1%	50%	10%	1%	50%	10%	1%
Turkey Creek	31	N/A	3273	5665	2248	3647	5932	N/A	11	5

Converting the HEC-1 model to HEC-HMS caused the 1-percent-annual-chance peak flows to increase by a maximum of 6 percent at certain locations. The conversion to HEC-HMS generally increased flow rates compared to HEC-1 for the 1-percent-annual-chance event. However, for the 50-percent-annual-chance event, the peak flow rates generally decreased with the HEC-HMS conversion. The 10-percent-annual-chance peak flow rates tended to increase or decrease depending upon the location, within a maximum increase of 11 percent and maximum decrease of 9 percent. This

increase or decrease in flows was due to different computation routines between the HEC-1 and HEC-HMS models (HEC, February, 2001).

Converted Refined Model

The inclusion of the detention basins in the hydrologic model required refining the subbasin boundaries, calculating new hydrologic characteristics, and incorporating new routing reaches. To quantify the impacts of these model refinements on peak flow values, a Converted Refined Model was created. The Converted Refined Model includes all subbasin refinements necessary with the exception of the 148 detention basins. Comparing the results of the Converted Refined Model to those of the FEMA Converted Model identified changes in flow rates due solely to subarea refinement.

Existing with Detention Model

The Converted Refined Model was modified to include information relating to 148 detention basins surveyed within the ELDS Area to create the Existing with Detention Model. Table 2 shows flow comparison between FEMA preliminary effective model and Existing with Detention Model. The difference in peak outflow between these models is discussed in results section.

Table 2 Existing with Detention Model Flow Comparisons

Mill Creek Watershed

Reach Name	Location ID	FEMA Preliminary Effective			Existing with Detention Model			Percent Difference		
		50%	10%	1%	50%	10%	1%	50%	10%	1%
MT_TRIB40	1	331	568	931	230	470	799	-31	-17	-14
MT_TRIB10	4	1320	2284	3788	1048	2042	3281	-21	-11	-13
MillCreekTrib1	9	1950	3598	6248	1750	3705	6112	-10	3	-2
LM_TRIB110	10	986	1990	3520	845	1933	3153	-14	-3	-10
Little Mill Crk	17	3532	7772	14215	3409	8587	14798	-3	10	4
LM_TRIB70	19	906	2178	4279	897	2342	4364	<-1	8	2
LM_TRIB130	20	178	354	654	221	568	1025	24	60	57
MCTRIB60	22	649	1436	2644	575	1441	2582	-11	<1	-2

Indian Creek Watershed

Reach Name	Location ID	FEMA Preliminary Effective			Existing with Detention Model			Percent Difference		
		50%	10%	1%	50%	10%	1%	50%	10%	1%
Nth_Brch	23	304	499	787	150	319	537	-51	-36	-32
Nth_Brch	25	1637	3038	4780	1337	2998	4876	-18	<-1	2
NB_Tribb	28	926	1969	3552	679	1762	3293	-27	-11	-7

Turkey Creek Watershed

Reach Name	Location ID	FEMA Preliminary Effective			Existing with Detention Model			Percent Difference		
		50%	10%	1%	50%	10%	1%	50%	10%	1%
Turkey Creek	31	N/A	3273	5665	2063	3332	5239	N/A	2	-8

Hydraulic Evaluation

This section provides a detailed description of the methodology used to estimate the floodplain elevations within the ELDS Area using the refined peak flow rates from the Existing with Detention Hydrologic Model.

As with the hydrologic model refinement, hydraulic models used to create the preliminary effective FIRMs were used as the starting point for the hydraulic model refinements. These models will be referred to as the FEMA Preliminary Effective Models.

The following steps used to create a refined hydraulic model:

1. Obtaining the FEMA Preliminary Effective Models (HEC-RAS version 3.1.1)
2. Running the FEMA Preliminary Effective Models in HEC-RAS version 3.1.3, to create the FEMA Duplicate Effective Model
3. Revising the FEMA Duplicate Effective Model to create the Existing with Detention Model

The FEMA Duplicate Effective Models resulting water surface elevations were compared with the FEMA Preliminary Effective Models, which showed a negligible (plus or minus 0.50 feet) change in water surface elevations at all but four cross sections. All four cross sections are located along Mill Creek Tributary 60.

Existing with Detention Model

The Existing with Detention Model was created from the Duplicate Effective Model. Peak flow rates from Existing with Detention Hydrologic Model were input into the HEC-RAS model

Results and Discussions

Hydrologic Results

The results of the hydrologic model refinements showed an increase in 1-percent-annual-chance peak flows at some locations (with the maximum of 57%) within the ELDS Area. The reasons for the peak flow increase are:

- The FEMA Preliminary Effective Models were run using a 5-minute computation time step. When the models were converted to HEC-HMS, a 1-minute computation time step was used. Use of the 1-minute time step in the computer model resulted in increased flow rates at locations where the 5-minute time step did not capture the hydrograph time to peak.
- Percentage imperviousness was increased throughout the ELDS Area, with the Mill Creek Watershed increasing an average from 22 percent to 38 percent by the largest percentage.

- Refinement of the hydrologic models included refining the drainage area delineations using more detailed storm sewer and drainage information than was available at the time the FEMA Preliminary Effective Models were developed. Slight increases in drainage areas to downstream locations result in increases in peak flow rates.

- Refinement of the rating curves for storage areas modeled in the FEMA Preliminary Effective Model resulted in increased peak flows at the location of the basin and for some distance downstream.

The results of the hydrologic model refinements showed decreases in 1-percent-annual-chance peak flows at many of the locations (with the maximum of 32%) within the ELDS Area. The reasons for the peak flow decrease include the following:

- The detention basin performance in Mill Creek and Indian Creek averaged 25 and 23 percent reduction respectively in the 1-percent-annual chance peak flow rates, and detention basins in Turkey Creek averaged 34 percent reduction. Many areas with reduction in peak flow rates can be attributed to the inclusion of upstream detention.

- Refinement of the hydrologic models included refining the drainage area delineations using more detailed storm sewer and drainage information than was available at the time the FEMA Preliminary Effective Models were developed. Slight decreases in drainage areas to downstream locations show decreases in peak flow rates.

- Refinement of the rating curves for storage areas modeled in the FEMA Preliminary Effective Model resulted in decreased peak flows at the location of the basin and for some distance downstream.

Some of the detention basins analyzed showed zero reduction in the 1-percent annual chance peak flow rates. Closer inspection of these basins indicated that although the basins were identified as detention basins for the purpose of this study, most appear to be drainage features that were not specifically designed for stormwater detention.

Hydraulic Results

The following paragraphs summarize the results for the Mill Creek, Indian Creek, and Turkey Creek Watersheds.

Mill Creek Watershed

The results show a reduction in the 1-percent-annual-chance peak water surface elevation at 193 of the 489 cross sections modeled within the Mill Creek Watershed as part of this study. Increases in peak water surface elevations were observed at 286 of the cross sections. Peak water surface elevations at 10 of the cross sections matched the peak water surface elevation in the FEMA Duplicate Effective Model.

The maximum reduction in 1-percent-annual-chance peak water surface elevation was approximately 6.1 feet. This reduction appears to be a result of the decrease in peak flow rates due to upstream detention.

The maximum increase in the 1-percent-annual-chance peak water surface elevation was approximately 10.9 feet. This increase in water surface elevation resulted from adding the rating curve to define discharge from the in-line detention basin.

As part of the Mill Creek Watershed Study, the lowest adjacent grade (LAG) elevation for 33 buildings located adjacent to the floodplain boundary and within the ELDS Area were surveyed and compared to the 1-percent-annual-chance water surface calculated as part of the study. The LAG is defined by FEMA as the lowest ground elevation touching the building. Of the 33 buildings surveyed, 12 were found to be outside the floodplain (i.e., the LAG was at or above the water surface elevation calculated during the study).

The LAG for the existing 31 buildings was compared to the Existing with Detention 1-percent-annual-chance water surface elevation. Comparing the LAG with Existing with Detention water surface elevations resulted in an additional nine buildings found to be outside the floodplain.

Indian Creek Watershed

Comparison of the FEMA Duplicate Effective Model with the Existing with Detention Model shows a reduction in the 1-percent-annual-chance peak water surface elevation at 70 of the 100 cross sections modeled within the Indian Creek Watershed. Increases in peak water surface elevations were observed at 28 of the cross sections. Peak water surface elevations at two of the cross sections matched the peak water surface elevation in the Duplicate Effective Model.

The maximum reduction in 1-percent-annual-chance peak water surface elevation was approximately 1.7 feet. This reduction appears to be a result of the reduction in peak flow rates due to upstream detention.

The maximum increase in the 1-percent-annual-chance peak water surface elevation was approximately 0.2 feet. This small increase in water surface elevation at this location appears to be the result of adding the rating curve for in-line detention basin.

During the Indian Creek Watershed Study, the LAG elevation for 32 buildings located adjacent to the floodplain boundary and within the ELDS Area were surveyed and compared to the 1-percent-annual-chance water surface calculated as part of the watershed study. Of the 32 buildings surveyed, 17 were found to be outside the floodplain.

The LAG elevations for the 32 buildings were compared to the Existing with Detention 1-percent-annual-chance water surface elevation resulting in one additional building found to be outside the floodplain.

Turkey Creek Watershed

The results from the Existing with Detention Model shows a reduction in the 1-percent-annual-chance peak water surface elevation at 36 of the cross sections modeled. Increases in 1-percent-annual-chance peak water surface elevations were observed at 25 of the cross sections. Peak water surface elevations at one of the cross sections matched the peak water surface elevation in the Duplicate Effective Model. The maximum reduction in 1-percent-annual-chance peak water surface elevation was approximately 1.9 feet. This reduction appears to be a result of the reduction in peak flow rates due to upstream detention.

The maximum increase in the 1-percent-annual-chance peak water surface elevation was approximately 2.8 feet. This increase in water surface elevation appears to be a result of increases in peak flows at this location.

During the Turkey Creek Watershed Study, the LAG elevations for four buildings located adjacent to the floodplain boundary and within the ELDS Area were surveyed and compared to the 1-percent-annual-chance water surface calculated as part of the watershed study. Of the four buildings surveyed, all were found to be within the floodplain.

The LAG elevations for the four buildings were compared to the Existing with Detention 1-percent-annual-chance water surface elevation. Even though the water surface elevations at each of the buildings decreased, the decrease was not enough to change the status of the buildings.

Conclusions

The model refinements that were made to account for existing detention facilities in the study area reduced the estimated 1-percent-annual-chance floodplain elevations in some locations. As a result, 11 buildings within the ELDS Area were removed from the 1-percent-annual-chance floodplain limits.

References

US Army Corps of Engineers, February, 2001, *Hydrologic Modeling System Version 2.1.1 Release Notes*, Page 6.

Johnson County, KS, Stormwater Management Program, 2006, *Mill Creek Watershed Study*, Section 7, page 1.

Johnson County, KS, Stormwater Management Program, 2006, *Northeast Johnson County Watershed Study*, Section 6, page 65.

Johnson County, KS, Stormwater Management Program, 2006, *Indian Creek Watershed Study*, Section 7, page 1.

Lenexa, KS, January, 2008, *Lenexa City Code Article 4-5-E Storm Water Management Regulations*, Section 4-5-E-15, pages 1.

Water Quality of Streams in Johnson County, Kansas, 2002-07

T.J. Rasmussen[1]

[1]U.S. Geological Survey, 4821 Quail Crest Place, Lawrence, KS 66049; PH (785) 832-3576; email: *rasmuss@usgs.gov*

This paper is a reprint of U.S. Geological Survey Fact Sheet 2008-3090, October 2008.

ABSTRACT

Water quality of streams in Johnson County, Kansas was evaluated from October 2002 through December 2007 in a cooperative study between the U.S. Geological Survey and the Johnson County Stormwater Management Program. Water quality at 42 stream sites, representing urban and rural basins, was characterized by evaluating benthic macroinvertebrates, water (discrete and continuous data), and/or streambed sediment. Point and nonpoint sources and transport were described for water-quality constituents including suspended sediment, dissolved solids and major ions, nutrients (nitrogen and phosphorus), indicator bacteria, pesticides, and organic wastewater and pharmaceutical compounds. The information obtained from this study is being used by city and county officials to develop effective management plans for protecting and improving stream quality. This fact sheet summarizes important results from three comprehensive reports published as part of the study and available on the World Wide Web at http://ks.water.usgs.gov/Kansas/studies/qw/joco/.

INTRODUCTION

Rapid population growth and urbanization in Johnson County in northeast Kansas has affected stream quality. Urbanization results in more residential, commercial, and industrial developments, and generally affects streams by altering hydrology, geomorphology, chemistry, and biology (Paul and Meyer, 2001). Consequently, these changes affect aquatic communities. Contamination entering streams in rural and urban areas can originate from point sources (such as wastewater treatment discharges) and nonpoint sources (such as stormwater runoff, leaking sewer lines, septic tanks, and atmospheric deposition). Water quality in Johnson County streams affects communities in the Kansas City metropolitan area because basins covering about one-third of the county flow northeast into Missouri. Water quality and the effects of combined sewer overflows in Kansas City, Missouri, have been the subject of previous studies (Wilkison and others, 2006).

Streams in Johnson County are important for human and environmental health, water supply, recreation, and aesthetic value. The information obtained during this study is useful for defining current water-quality conditions, understanding

variability in conditions, evaluating effects of urbanization, developing effective water-quality management plans, documenting changes in water quality, and evaluating conditions relative to total maximum daily loads (TMDLs), National Pollutant Discharge Elimination System (NPDES) requirements, and water-quality standards.

Stream quality was evaluated from October 2002 through December 2007 using benthic macroinvertebrate, discrete water and streambed sediment samples, and continuous water-quality monitoring. Macroinvertebrate samples were collected to assess biological conditions, an indication of how well water bodies support aquatic life and, therefore, a measure of overall stream quality. Macroinvertebrates were collected from 15 stream sites in Johnson County and evaluated along with data from seven additional sites collected as part of a separate study with similar objectives in Missouri (Wilkison and others, 2006). Various aspects of macroinvertebrate communities, including organism diversity (number and variety of species), composition, tolerance, and feeding characteristics also were used to evaluate and compare stream quality. Water samples were collected from 42 stream sites representing all of the major basins in the County (Figure 1, some sites represent multiple sampling locations). Water samples were analyzed for suspended sediment, dissolved solids and major ions, nutrients (nitrogen and phosphorus species), indicator bacteria, pesticides, and organic wastewater and pharmaceutical compounds. Samples were collected during base-flow (unaffected by storm runoff, when streamflow is sustained by ground-water inflow, springs, and, in some locations, wastewater discharge) and storm-flow conditions. Constituent concentrations, loads (amount of constituent transported in a stream during a specified period of time), and yields (load divided by drainage area for comparing basins) were determined for five major basins of Johnson County using continuous monitoring (hourly in-stream measurements) and statistical regression models. Streambed-sediment samples were collected from 15 sites and analyzed for major ions, nutrients, trace elements, bacteria, pesticides, and organic wastewater compounds. Unless otherwise referenced, the information summarized here is included in publications by Lee and others (2005), Poulton and others (2007), and Rasmussen and others (2008); additional explanation and results can be found in those reports.

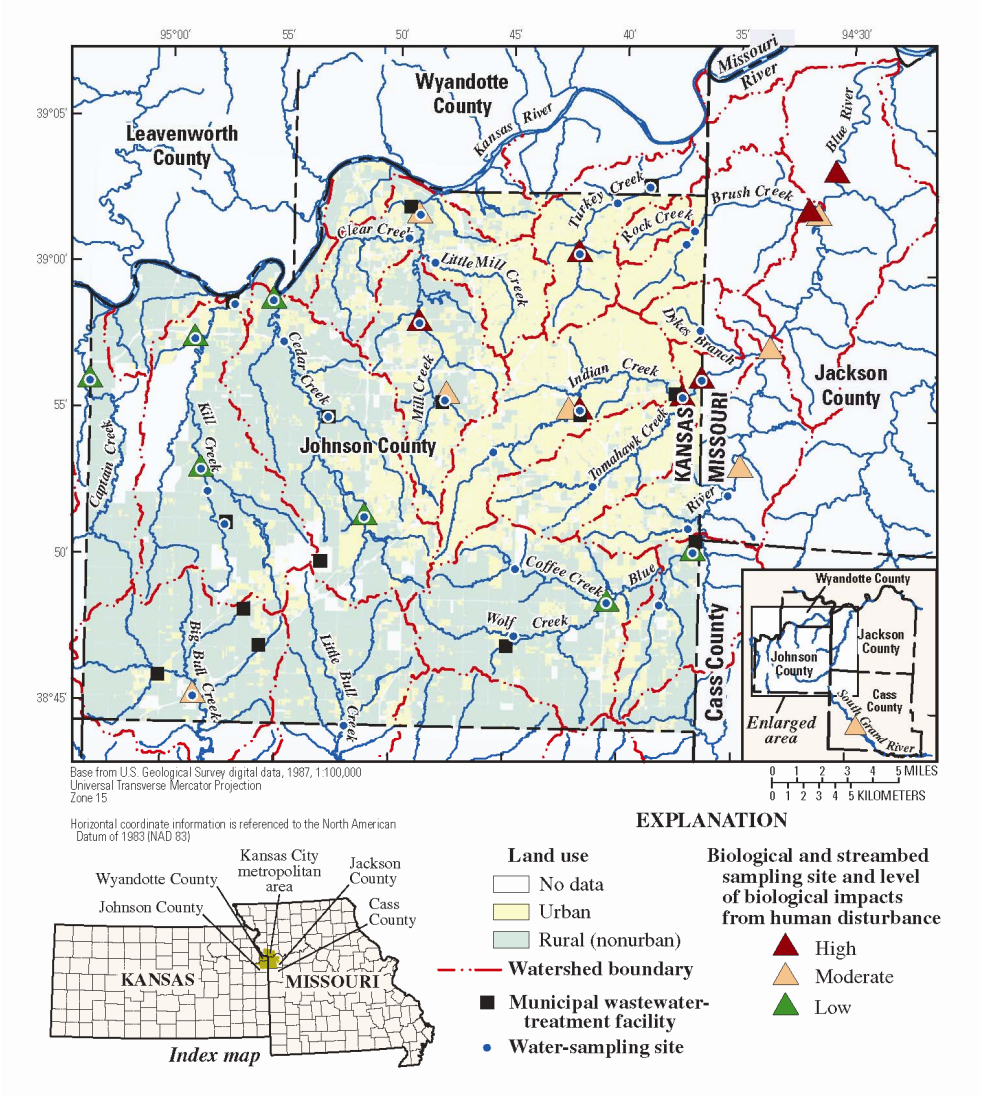

Figure 1. Location of stream sampling sites, urban and rural land use, and relative biological impacts (negative responses associated with human-induced disturbance or stress) in Johnson County, Kansas.

BIOLOGICAL CONDITIONS – AN OVERVIEW OF STREAM QUALITY

- During 2003 and 2004 when biological samples were collected, no sites, including the reference site on Captain Creek, met State criteria (Kansas Department of Health and Environment, 2006) for full support of aquatic life. Reference streams are streams designated by the State as being minimally disturbed by human activity, and generally serve as a basis for comparison in stream evaluations.
- The least impacted stream sites predominantly were in rural areas. As impervious surface area (a general indication of urbanization) increased, biological quality generally decreased.

- Sites in Johnson County that were least impacted by human disturbance included upstream Blue River (Figure 2), Cedar, Kill, and Captain Creek sites (Figure 1). Indian, Tomahawk, and Turkey Creek sites in Johnson County, and downstream Blue River and Brush Creek sites in Missouri were most impacted by human disturbance.



Figure 2. Example of a stream site in Johnson County, Kansas, showing minimal impacts from human disturbance and some macroinvertebrates generally associated with healthy streams (macroinvertebrate photographs from http://www.epa.gov/bioindicators/html/photos_invertebrates.html).

- In the Blue River basin where biological conditions were least impacted, biological quality was strongly correlated with upstream land cover consisting of forests and grasslands. Biological quality declined with increases in impervious land cover, nutrient enrichment, and prevalence of organic wastewater compounds and pharmaceuticals (Wilkison and others, 2006).

SUSPENDED SEDIMENT

- Of the total suspended-sediment load transported in 2005-06, 90 percent or more occurred during less than 2 percent of the time (the equivalent of about 7 days per year), generally during large streamflows, at all five monitoring sites. Therefore, management practices designed to control sediment during large streamflows can substantially reduce annual loads.
- About 35 percent larger average annual precipitation in 2005 compared to 2006 resulted in an average of four times the suspended sediment load.
- Annual sediment yields in the urban basins (Indian and Mill Creeks) were 50 percent larger than in rural basins (Cedar and Kill Creeks, Blue River) in 2005.

- About 70 percent of the time (generally when there was little or no storm runoff), suspended-sediment concentrations in Indian Creek were smaller than in other basins partly because of the large contribution of treated water discharged from upstream wastewater-treatment facilities. However, total annual sediment load and yield in Indian Creek were larger than other basins because of disproportional loading that occurred during large streamflow at that site.
- Sediment transport in Johnson County streams and, therefore, management practices implemented to control sediment are especially important because other contaminants such as nutrients and bacteria frequently are associated with sediment particles.

NUTRIENTS AND DISSOLVED OXYGEN

- In Johnson County stream reaches during 2005 and 2007, about two-thirds of the Indian Creek total nitrogen load and one-third of the Blue River total nitrogen load originated from wastewater treatment facilities (WWTFs) (Figure 3). Nitrogen from WWTFs primarily occurred in the form of nitrate. In 2006, when total annual rainfall was about 65 percent of the total rainfall that occurred in 2005 or 2007 (resulting in less nonpoint-source nutrient load), total nitrogen originating from WWTFs accounted for a larger percentage (about three-fourths) of the total load in Johnson County reaches of both Indian Creek and the Blue River. Wilkison and others (2006) determined that during 2002-04, about 60 percent of the total nitrogen and total phosphorus loads in the lower Blue River in Missouri originated from Indian Creek.

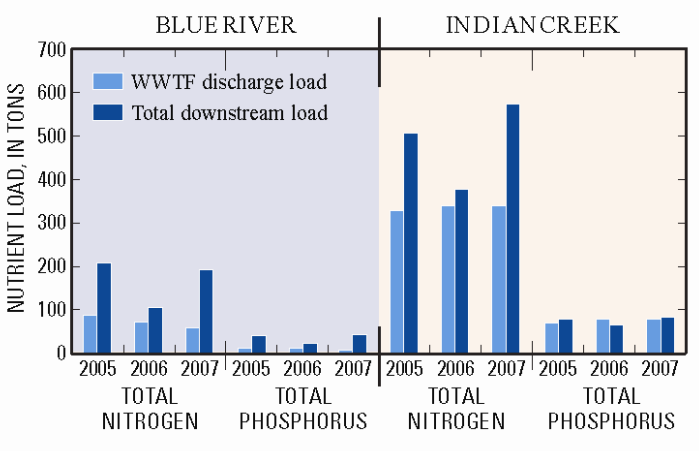

Figure 3. Annual estimated total nitrogen and total phosphorus loads and loads originating from wastewater treatment facility (WWTF) discharges in the Blue River and Indian Creek, Johnson County, Kansas, 2005-07. WWTF discharges were a primary contributor to downstream nutrient loads.

- From March 2004 through December 2007, dissolved oxygen (important to sustain aquatic life) was less than the minimum state criterion of 5 mg/L (Kansas Department of Health and Environment, 2005) less than 5 percent of the time at the 5 continuous monitoring sites except Blue River (8 percent) and Indian Creek (15 percent) (Figure 4). Low dissolved oxygen concentrations primarily occurred during the summer.

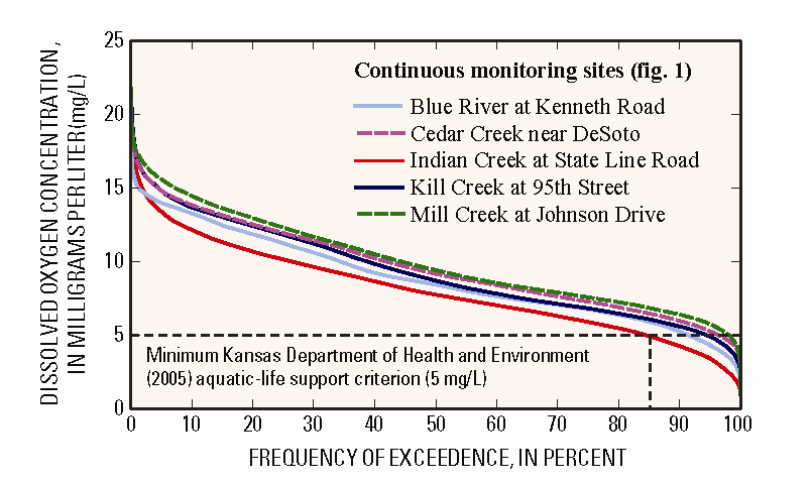

Figure 4. Measured dissolved oxygen (DO) and frequency of exceedence (percentage of time a given value is equaled or exceeded) at five continuous monitoring sites in Johnson County, Kansas, March 2004-December 2007. DO was less than the state criterion about 15 percent of the time at the Indian Creek site.

INDICATOR BACTERIA

- *Escherichia coli (E. coli)* bacteria density at the Indian Creek site, located in the most urban basin, was nearly always largest with a median density more than double that of any other site. *E. coli* is used as an indicator of pathogens in streams that may cause illness in humans who come into contact with the water.
- During base flow, the largest bacteria densities occurred upstream from WWTFs indicating that wastewater discharges generally do not contribute substantially to bacteria densities in streams.
- During 2005-07, less than 3 percent of the total annual fecal coliform bacteria load in Indian Creek and the Blue River originated from WWTFs. Wilkison and others (2006) also reported that bacteria in streams originated primarily from nonpoint sources during storm runoff.
- Water-quality conditions in streams often change rapidly during storm runoff. For example, *E. coli* bacteria density in Kill Creek during May 2007 increased

from about 180 colonies per 100 milliliters of water (col/100mL) to about 100,000 col/100mL during a 12-hour period (Figure 5).

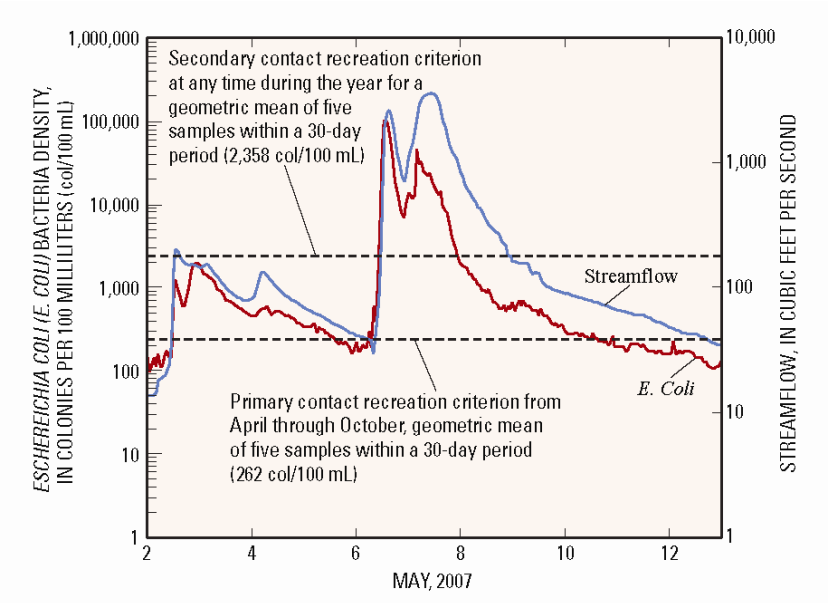

Figure 5. Streamflow and estimated *E. coli* bacteria density at the Kill Creek monitoring site, Johnson County, Kansas, in May 2007. Bacteria density increased from about 180 col/100 mL to about 100,000 col/100 mL during a 12-hour period.

ORGANIC COMPOUNDS

- Atrazine was detected in nearly all water samples, including base flow samples, and had the largest concentrations of all pesticides sampled. Atrazine concentrations, however, did not exceed the state chronic aquatic-life criterion of 3.0 micrograms per liter (µg/L) as an annual average (Kansas Department of Health and Environment, 2005).
- During base flow, water samples from urban stream sites had the largest number of pesticide compounds detected, and water samples from rural sites had the largest total concentration of pesticides.
- The largest total concentrations of organic wastewater compounds occurred in base-flow samples from sites at or immediately downstream from WWTFs. The most common compounds were AHTN (acetyl-hexamethyl-tetrahydro-napthalene, a musk fragrance), caffeine, DEET (mosquito repellant), a detergent surfactant (nonylphenol-diethoxylate), and a flame retardant and plasticizer (tris(2-butoxyethyl) phosphate), which together comprised more than one-half of the total organic wastewater compound concentrations in 80 percent of the base flow samples.

- In streambed sediment samples, the largest organic compound concentrations included chlordane (an insecticide banned in 1988), dichloro-diphenyl-trichloroethane (DDT, a pesticide banned in 1972), and polyaromatic hydrocarbons (PAHs, likely carcinogens that originate from combustion of fossil fuels and are used as an ingredient in asphalt), and were present in urban basins but were not closely linked to WWTF discharges.

ADDITIONAL FACTORS AFFECTING WATER QUALITY

- Water contaminants including sediment, total nitrogen and phosphorus, bacteria, and pesticides (particularly during spring) at urban and rural sites originated primarily from nonpoint sources during storm runoff. As a consequence, climate (precipitation and resulting runoff) had a substantial effect on water quality, and larger amounts of rainfall resulted in larger amounts of contaminants. In addition, the probability that water-quality criteria are exceeded is substantially larger during storm runoff.
- Wastewater discharges were the primary source of streamflow at sites downstream from WWTFs during base-flow conditions. This is true not just immediately downstream, but many miles downstream, from the WWTF.
- About 10 percent of the time chloride concentrations in Indian and Mill Creeks were elevated as a result of runoff from road salt application; however, the acute aquatic life criterion of 860 milligrams per liter (mg/L) (Kansas Department of Health and Environment, 2005) was exceeded less than 1 percent of the time.

CONCLUSION

Water quality of streams in Johnson County, Kansas, varied according to climate (precipitation and resulting runoff conditions), degree of urbanization, and contribution from and proximity to wastewater discharges. Results from the Johnson County water-quality studies generally were consistent with results on Blue River water quality reported by Wilkison and others (2006). Information from these studies is being used by municipal and county officials to address water-quality concerns, particularly those related to expected increases in population and urban land use leading to additional demands on streams. For example, wastewater treatment facilities on Indian Creek and the Blue River are undergoing major upgrades to increase capacity and reduce nutrients in discharges to streams. In addition, the information is being used for public education about stormwater runoff and water quality. It also is being used to enhance and monitor programs to protect streams, such as construction runoff controls and stream setback programs. Ongoing monitoring of water quality and stream health will provide information about trends with time and effectiveness of management plans.

REFERENCES

Kansas Department of Health and Environment (2005). Kansas Administrative Regulations (KAR), Title 28, Article 16, Surface water quality standards 2005: Topeka, Kansas, Secretary of State.

Kansas Department of Health and Environment (2006). Kansas section (303(d) list of impaired surface waters, http://www.kdheks.gov/tmdl/methodology.htm.

Lee, C.J., Mau, D.P., and Rasmussen, T.J. (2005). Effects of point and nonpoint sources on water quality and relation to land use in Johnson County, northeastern Kansas, October 2002 through June 2004: *U.S. Geological Survey Scientific Investigations Report 2005-5144*, 104 p.

Paul, M.J., and Meyer, J.L. (2001). Streams in the urban landscape, *Annual Review of Ecological Systems,* v. 32, p. 333-365.

Poulton, B.C., Rasmussen, T.J., and Lee, C.J. (2007). Assessment of biological conditions at selected stream sites in Johnson County, Kansas, and Cass and Jackson Counties, Missouri, 2003 and 2004: *U.S. Geological Survey Scientific Investigations Report 2007-5108*, 68 p.

Rasmussen, T.J., Lee, C.J., and Ziegler, A.C. (2008). Estimation of constituent concentrations, loads, and yields in streams of Johnson County, northeast Kansas, using continuous water-quality monitoring and regression models, October 2002 through December 2006: *U.S. Geological Survey Scientific Investigations Report 2008-5014*, 103 p.

Wilkison, D.H., Armstrong, D.J., Norman, R.D., Poulton, B.C., Furlong, E.T., and Zaugg, S.D. (2006). Water-quality in the Blue River Basin, Kansas City metropolitan area, July 1989 to October 2004: *U.S. Geological Survey Scientific Investigations Report 06-5147*, 170 p.

Water-quality assessment of the largely urban Blue River Basin, Metropolitan Kansas City, USA, 1998 to 2007

Donald H. Wilkison[1], Daniel J. Armstrong[2], and Sarah A. Hampton[2]

[1]U.S. Geological Survey, Missouri Water Science Center-Kansas City, 401 N.W. Capital Drive, Lee's Summit, MO 64086; PH (816) 554-3489 x205; email: wilkison@usgs.gov
[2]U.S. Geological Survey, Missouri Water Science Center-Kansas City, 401 N.W. Capital Drive, Lee's Summit, MO 64086; PH (816) 554-3489x210; email: armstron@usgs.gov; shampton@usgs.gov

ABSTRACT

From 1998 through 2007, over 750 surface-water or bed-sediment samples in the Blue River Basin – a largely urban basin in metropolitan Kansas City - were analyzed for more than 100 anthropogenic compounds. Compounds analyzed included nutrients, fecal-indicator bacteria, suspended sediment, pharmaceuticals and personal care products.

Non-point source runoff, hydrologic alterations, and numerous waste-water discharge points resulted in the routine detection of complex mixtures of anthropogenic compounds in samples from basin stream sites. Temporal and spatial variations in concentrations and loads of nutrients, pharmaceuticals, and organic wastewater compounds were observed, primarily related to a site's proximity to point-source discharges and stream-flow dynamics.

Total nitrogen concentrations were frequently greater than 10 milligrams per liter in surface-water samples and total phosphorous concentrations were routinely greater than 1 milligram per liter. Non-point source runoff accounted for the majority of bacteria in basin streams. Pharmaceutical and personal-care compound concentrations in water samples typically were less than 1 microgram per liter but mixture concentrations were frequently 30 to 50 times greater. More than 75 percent of samples analyzed had detections of the antimicrobial compound triclosan, the insect repellent DEET (n, n-diethyl-meta-toluamide), metabolites of detergent surfactants, caffeine, and the nicotine metabolite cotinine. More than one-half of stream samples had detections of pharmaceutical compounds; however, over-the-counter drugs accounted for more than 90 percent of the total mass of pharmaceuticals measured.

In effluent-dominated reaches, increased caffeine and cholesterol plus coprostanol contributions to streams occurred during the winter when colder temperatures may have reduced wastewater removal rates; constituent contribution declines coincided with increased summer temperatures. For stream reaches that received only combined sewer overflows, seasonal load patterns more closely followed seasonal precipitation patterns because overflows were controlled by rainfall events. One exception was DEET, for which June to August accounted for the largest percentage of seasonal contributions at all sites.

Biogeochemical processes in bottom sediments reduced some constituent concentrations by approximately two-thirds during a 6 to 8-month period. Bioassessments, indicated substantial declines in macroinvertebrate communities along an urbanization gradient. Declines correlated with increased upstream urban land-use and increased concentrations of anthropogenic compounds at stream sites.

Introduction

Stream-water quality in the Blue River Basin is influenced by a variety of factors including urbanization, point and non-point source pollution, physical stream conditions, and complex water-quality processes. The Blue River Basin encompasses 280 square miles and roughly one-half of the Kansas City metropolitan area. Fifty-four percent of the basin is located in Kansas and 46 percent is located in Missouri. The U.S. Geological Survey (USGS), in cooperation with the City of Kansas City, Missouri, Water Services Department collected water-quality data from 1998 through 2007 to provide an assessment of the chemical, bacteriological, and biological conditions of basin streams, identify sources of selected constituents, and provide an understanding of factors affecting water quality.

Kansas City, Missouri, is 1 of approximately 750 municipalities in the United States with a combined sewer system. Such systems carry sanitary wastewater and stormwater runoff and function differently during dry and wet weather conditions. In dry weather, combined systems convey sewage from homes, businesses, and industry to a wastewater-treatment plant (WWTP). After treatment, the water is discharged to a receiving stream in accordance with applicable water-quality standards. During wet weather, runoff from streets, rooftops, parking lots, and lawns enters the combined system and is delivered to the WWTP for treatment and discharge. However, if runoff and sewage volumes exceed the pipe or treatment plant capacity then excess flow (a mixture of stormwater and untreated sewage) is diverted and discharged to receiving streams, events referred to as combined sewer overflows (CSOs). Roughly ninety percent of the CSO outfall points in Kansas City, Missouri, are located within the Blue River Basin.

Communities with combined sewer systems are required under federal and state regulations to develop a plan to control overflows and to monitor their impacts on receiving waters. Control plans include analysis of current water-quality conditions based on a watershed perspective and characterization of other pollutant sources that might inhibit the attainment of applicable water-quality standards (U.S. Environmental Protection Agency, 1999). To support development of a control plan and to understand the effects of wastewater on urban receiving streams, laboratory and hydrologic analysis of stream samples from the Blue River Basin collected during base flow (defined as streamflow unaffected by storm runoff) and stormflow events included physical properties, nutrients, selected organic wastewater compounds (OWCs), selected prescription and over-the-counter pharmaceutical compounds, *Escherichia coli* (*E. coli)* and fecal coliform bacteria, and benthic macroinvertebrates (fig. 1). Selected base-flow *E. coli* samples were analyzed for host-source using genotypic, geographic-specific, library-based methods (Dombek and others, 2000; Carson and others, 2003). Vertical water-quality profiles were determined for selected impounded reaches of Brush Creek.

Sample locations were determined based on a variety of factors including proximity to tributaries, the combined sewer system area, and WWTPs (fig. 1). Six sites on the main stem of the Blue River (sites 1, 2, 7, 8, 13, and 14), four sites on the tributary Brush Creek (sites 9 to 12), and three sites on the tributary Indian Creek (sites 3, 4, and 6) were sampled. Two stream sites, one in the basin (site 5, Tomahawk Creek) and one

outside of the basin (site 19, South Grand River) were sampled as controls for aquatic-biota measurements. Data from three WWTPs (sites 15 to 17) that discharge in the basin also were analyzed.

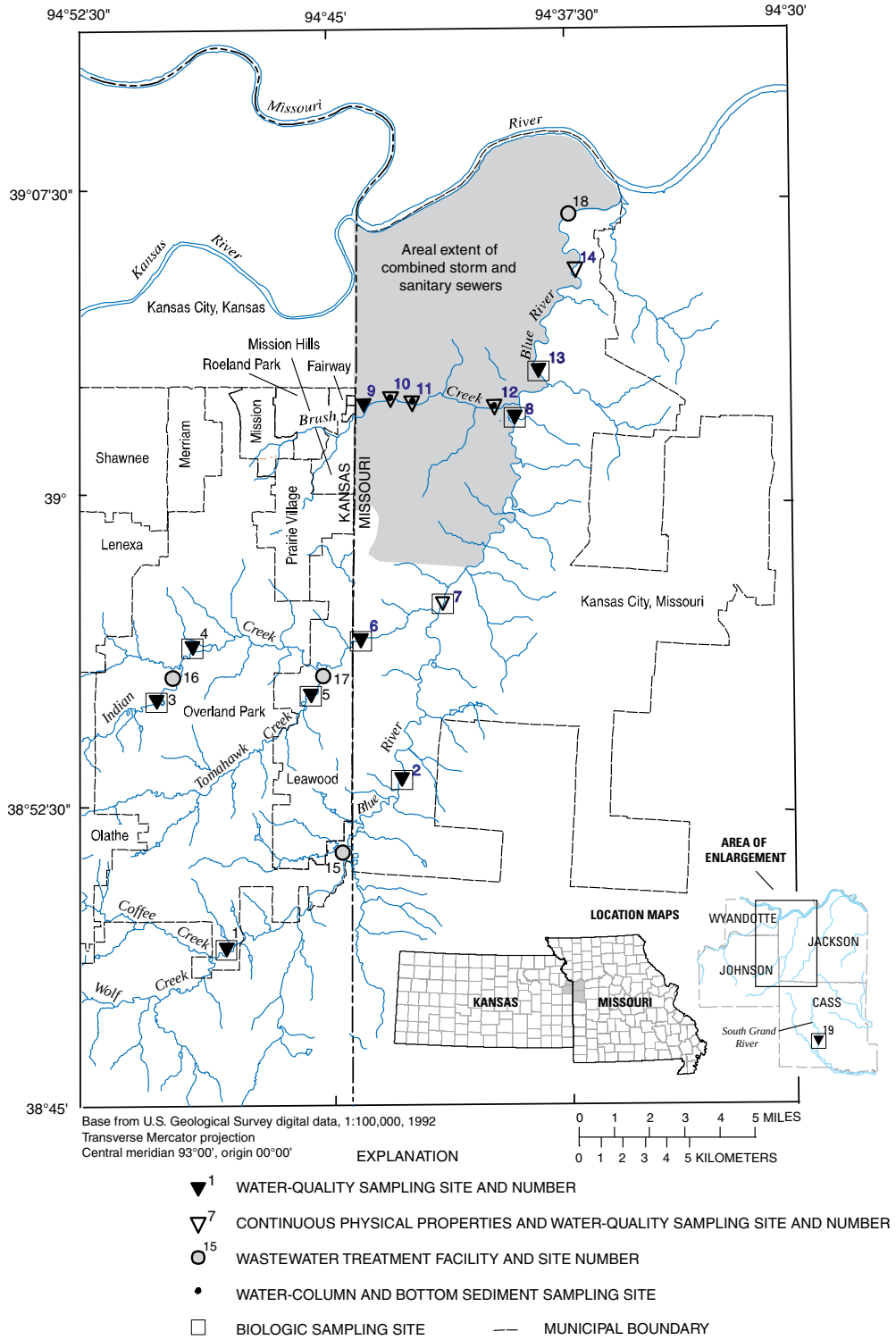

Figure 1. Map showing location of study area, sampling sites, wastewater treatment facilities, and area of combined storm and sanitary sewers. [Site numbers shown in blue are storm sampling sites]

Major Factors Affecting Stream-Water Quality

The combination of numerous over-lapping, urban-related factors has adversely affected on water quality and the ecological condition of several stream reaches in the Blue River Basin. Urbanization and flood-control projects have resulted in substantial loss of riparian vegetation, degraded stream habitat through stream channelization and stream-bank armoring, and resulted in extensive loss of native pool and riffle sequences, and altered flow regimes. Urban nonpoint-source runoff contributed a substantial part of the contaminant load in the basin. In areas served by a combined sewer system and WWTPs, discharges of treated and untreated wastewater additionally contributed nutrients, OWCs, and pharmaceuticals to streams. Nutrient enrichment was common at many stream sites with concentrations greater than expected background, non-urban concentrations (Smith and others, 2003). Deleterious water-quality effects were most pronounced in lower Indian Creek (below site 4), the lower and middle reaches of the Blue River (below site 7), and lower Brush Creek (below site 11).

Although there was some daily and seasonal variability, WWTPs provided the dominant source of streamflow, nutrients, and OWCs and pharmaceutical compounds to the middle and lower Indian Creek and the Blue River during base flow. Downstream of WWTPs, effluent can comprise greater than 95 percent of base flow. Only a small part of effluent nutrients were removed by in-stream nutrient assimilation and transformation processes an indication that such contributions frequently exceed the ecological assimilation capacity of many reaches. During storms, the predominant source of nutrients shifted from point sources to non-point sources. Examples of nonpoint sources that may contribute nutrients to streams include runoff from fields, parks, golf courses, lawns, impervious surfaces, storm sewers, compromised sewer lines, and ground- and surface-water interactions with these sources. As flows increased, the concentration of dissolved nutrients declined (figs. 2a and 2b) while concentrations of suspended nutrients, sediment and fecal-indicator bacteria increased (fig. 2c-2f). Suspended sediment and fecal-indicator bacteria loads (concentration times flow) increased substantially over those measured in base-flow samples at all stream sites.

In Brush Creek, wet weather events provided the dominant source of nutrients. Storm-event nutrient loads, a combination of non-point and CSO sources, were 200 to 300 times greater than base flow loads. Because of hydrologic alterations to Brush Creek, particulate nutrients were trapped in impounded reaches - a process that facilitated algal growth and eutrophication in these reaches.

Nutrients

Total nitrogen and total phosphorus loads and yields (load divided by drainage area) were estimated at four basin sites to allow comparison between sites and to those estimated at sites outside of the basin (fig. 3). Approximately 60 percent of the total nitrogen and total phosphorus in the middle and lower Blue River originated from Indian Creek, smaller amounts from the upper Blue River (from 16 to 28 percent), and less than 5 percent from Brush Creek. Nutrient yields from the lower Indian Creek (site 6) and the middle Blue River (site 7) were significantly greater than yields from the upper Blue River (site 2), lower Brush Creek (site 11) and sites outside the basin (fig. 4). Total

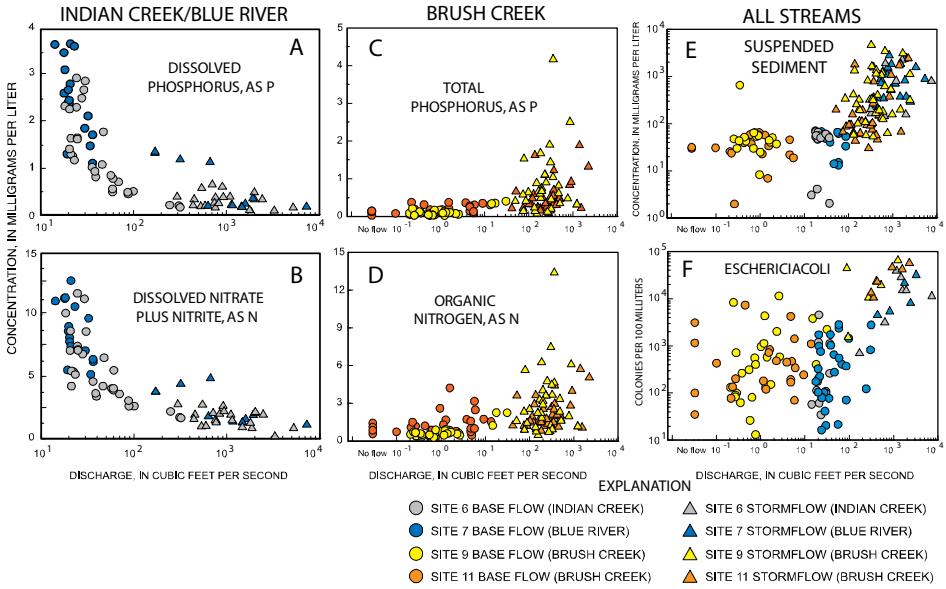

Figure 2. Concentrations of selected water-quality constituents in relation to discharge.

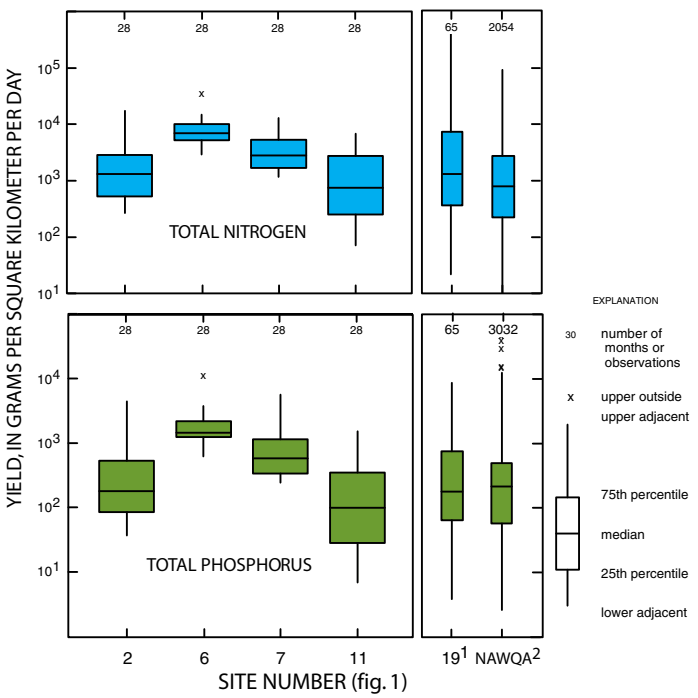

Figure 3. Estimated total nitrogen and total phosphorus yields at sites in the Blue River Basin for the period July 2002 through September 2004, left panels, and yields estimated at sites outside the basin, right panels. [NAWQA, data from 13 urban National Water-Quality Assessment sites (U. S. Geological Survey, 2005]. [1]Upper detached values not plotted. [2]Upper detached, lower outside, and lower detached values not plotted.

nitrogen and total phosphorus yields from the upper Blue River and lower Brush Creek were not significantly different from one another.

Organic wastewater and pharmaceutical compounds

Organic wastewater compounds analyzed included a suite of organic chemicals common to household, industrial, and personal care products, including, but not limited to, detergent by-products, disinfectants, antimicrobials, plasticizers, musk, and fragrance compounds. Pharmaceutical compounds included analgesics (acetaminophen and ibuprofen), an anti-convulsant (carbemazepine), antibiotics (sulfamethoxazole and trimethoprim), cardiac and anti-clotting medications (dehydronifedipine, diltiazem, and warfarin), a cholesterol-regulator (gemfibrozil), a narcotic (codeine), and stimulants (caffeine and cotinine, a metabolite of nicotine).

At sites on Indian Creek and the Blue River, organic wastewater and pharmaceutical compounds were largely attributable to WWTP discharges during base flow (figs. 4 and 5). Two classes of OWCs, defined operationally as detergents (consisting of surfactants and by-products) and sterols (consisting of plant and animal sources such as cholesterol and coprostanol) comprised the majority of OWCs. Over-the-counter medications constituted the bulk of the pharmaceuticals. Concentrations of most OWCs and pharmaceuticals declined in stormflow samples except for two classes of OWCs—pesticides and residues from hydrocarbon combustion and petroleum products — which increased during storms indicating significant non-point source contributions of these compounds during runoff events.

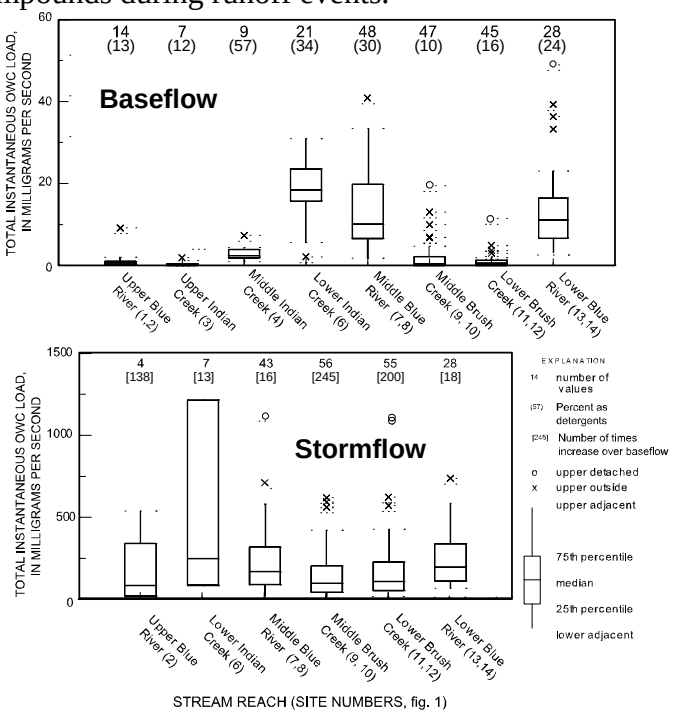

Figure 4. Total instantaneous organic wastewater compound (OWC) load by stream reach in samples collected between August 1998 and September 2004.

On Brush Creek, sources of OWCs and pharmaceuticals were largely attributable to a combination of wet-weather nonpoint and CSO sources as evidenced by general increases in contaminant concentrations with flow. Increased OWC concentrations and streamflow resulted in OWC storm loads several orders of magnitude greater than in base flows (fig. 4). Frequent detections of wastewater compounds at site 9 (upstream from most CSOs) during base flow and stormflows indicated that other factors may be as important as CSOs in the occurrence of these compounds in Brush Creek.

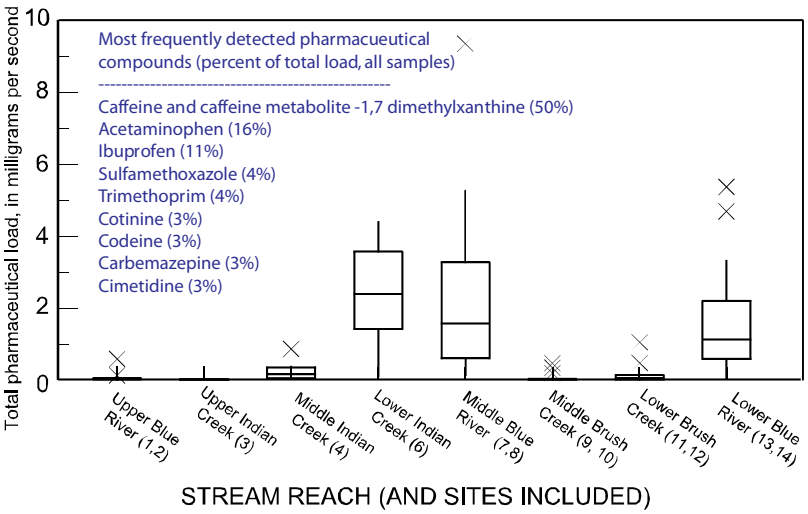

Figure 5. Total pharmaceutical load in baseflow stream samples collected between May 1999 and June 2004, most frequently detected compounds, and percent of total load.

Organic wastewater and pharmaceutical compounds

Organic wastewater compounds analyzed included a suite of organic chemicals common to household, industrial, and personal care products, including, but not limited to, detergent by-products, disinfectants, antimicrobials, plasticizers, musk, and fragrance compounds. Pharmaceutical compounds included analgesics (acetaminophen and ibuprofen), an anti-convulsant (carbemazepine), antibiotics (sulfamethoxazole and trimethoprim), cardiac and anti-clotting medications (dehydronifedipine, diltiazem, and warfarin), a cholesterol-regulator (gemfibrozil), a narcotic (codeine), and stimulants (caffeine and cotinine, a metabolite of nicotine).

At sites on Indian Creek and the Blue River, organic wastewater and pharmaceutical compounds were largely attributable to WWTP discharges during base flow (figs. 4 and 5). Two classes of OWCs, defined operationally as detergents (consisting of surfactants and by-products) and sterols (consisting of plant and animal sources such as cholesterol and coprostanol) comprised the majority of OWCs. Over-the-counter medications constituted the bulk of the pharmaceuticals. Concentrations of most OWCs and pharmaceuticals declined in stormflow samples except for two classes of

OWCs—pesticides and residues from hydrocarbon combustion and petroleum products — which increased during storms indicating significant non-point source contributions of these compounds during runoff events.

On Brush Creek, sources of OWCs and pharmaceuticals were largely attributable to a combination of wet-weather nonpoint and CSO sources as evidenced by general increases in contaminant concentrations with flow. Increased OWC concentrations and streamflow resulted in OWC storm loads several orders of magnitude greater than in base flows (fig. 4). Frequent detections of wastewater compounds at site 9 (upstream from most CSOs) during base flow and stormflows indicated that other factors may be as important as CSOs in the occurrence of these compounds in Brush Creek.

Macroinvertebrate Community Assessment

The diversity and abundance of stream fauna measured at upper Blue River sites (sites 1 and 2) consistently scored at, or above, the control site (site 19) indicating that stream-water quality was sufficient to support a diverse biological component in the upper Blue River (fig. 6). Aquatic community integrity declined downstream in the basin in response to increases in several inter-related urbanization factors including declines in vegetative cover, increases in percent impervious cover, increased nutrient enrichment, and increased wastewater inputs.

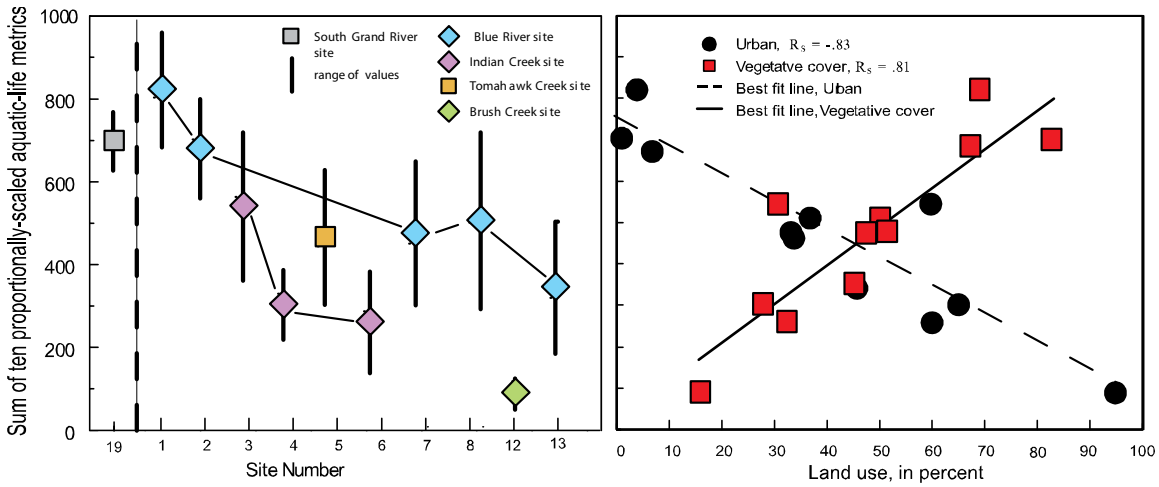

Figure 6. Sum of ten proportionally-scaled aquatic-life metrics by site (left panel) and relation between proportional metric score and the percent of vegetative cover and urban land use at sites (right panel) [Rs, Spearman's correlation coefficient].

References

Carson, A.C., Shear, B.L., Ellersieck, M.R., and Schnell, J.D. (2003) Comparison of ribotyping and repetitive extragenic palindromic-PCR for identification of fecal Escherichia coli from humans and animals: *App. Eniv. Microbiology*, v. 3, 1,836–1,839.

Dombek, P.E., Johnson, L.K., Zimmerley, S.T., and Sadowsky, M.J. (2000) Use of repetitive DNA sequences and the PCR to differentiate Escherichia coli isolates from human and animal sources: *App. Eniv. Microbiology*, v. 66, 2,572–2,577.

Smith, R.A., Alexander, R.B., and Schwartz, G.E. (2003) Natural background concentrations of nutrients in streams and rivers of the coterminous United States: *Eniv. Sci. and Technology*. 37 (14), 3,039–3,047.

U.S. Environmental Protection Agency (1999) Combined sewer overflows—Guidance for monitoring and modeling: Washington, D.C., Office of Water, EPA 832-B-99-002.

U.S. Geological Survey (2005) National Water-Quality Assessment Program retrospective database for nutrients in ground and surface water, http://water.usgs.gov/nawqa/nutrients/dataset/ retro.data.sw>(Sept., 2005).

Runkel, R.L., Crawford, C.G., and Cohn, T.A. (2004) Load estimator (LOADEST): A FORTRAN program for estimating constituent loads in streams and rivers: USGS TRWI Book 4, Chap. A5.

Wilkison, D.H., Armstrong, D.J., and Blevins, D.B. (2002) Effects of wastewater and combined sewer overflows on water quality in the Blue River Basin, Kansas City, Missouri and Kansas, July 1998–October 2000: USGS WRIR 02–4107.

Wilkison, D.H., Armstrong, D.J., Brown, R.E., Poulton, B.C., Cahill, J.D., and Zaugg, S.D. (2005) Water-Quality and biologic data for the Blue River Basin, Kansas City Metropolitan Area, October 2000 to October 2004: USGS DS Report 127.

Wilkison, D.H., Armstrong, D.J., Norman, R.D., Poulton, B.C., Furlong, E.T., and Zaugg, S.D., (2006) Water-Quality in the Blue River Basin, Kansas City Metropolitan Area, July 1998 to October 2004: USGS SIR 2006-5147.

A Bayesian Framework for Cost Effective Management of Sediment Reduction in the Minnesota River Basin.

Sarah K. Jacobi, Pearl Zheng, Benjamin F. Hobbs, Peter R. Wilcock

Department of Geography and Environmental Engineering, 313 Ames Hall, Johns Hopkins University, Baltimore, Maryland 21218, email: skjacobi@jhu.edu

Abstract

Water quality impairments remain a pressing concern in the United States. Selecting appropriate management actions (i.e., best management practices) to improve water quality involves tradeoffs between cost and effectiveness, both of which are prone to uncertainty. In addition, significant uncertainties exist in the scientific understanding of the natural system. To address these concerns, we have developed a framework to identify the optimal set of actions to reduce turbidity and sedimentation in the Minnesota River Basin, while explicitly incorporating uncertainty. The framework combines Bayesian inference with multiobjective programming models to select the optimal combination of research actions, which improve our understanding of the natural system, and management actions, which reduce sediment contributions to the river basin. We also evaluate the value of information of each research action, to identify where further study is warranted. Our results communicate the general nature of the tradeoffs and complex interactions among sediment loadings, best management practices, and the possible research projects. More important, our results indicate that explicit consideration of uncertainty can lead to improved selection of management actions that most accurately address the complexity of the problem.

Problem Background

Despite the passage of the Clean Water Act amendments to the Federal Water Pollution Control Act in 1977, many river basins throughout the United States are still impaired, meaning that they do not meet state or federal water quality standards. According to the Environmental Protection Agency, as of the year 2000, "39% of assessed stream miles, 45% of assessed lake acres, and 51% of assessed estuary acres are impaired (US Environmental Protection Agency 2003)". Impairments are due to primarily to nonpoint source pollution, with nearly 48% of the impacts on impaired rivers and streams due to agricultural activities (US Environmental Protection Agency 2003).

The Minnesota River frequently violates federal or state water quality standards for a variety of pollutants including nutrients and turbidity (Mallawatantri 1999). In 2001, the Minnesota Pollution Control Agency published the Minnesota River Basin Plan (Minnesota Pollution Control Agency 2001), which described the state of the river basin and identified priorities for addressing water quality impairments. The plan described a basin management approach that addressed water pollutants by aiming to achieve environmental objectives using an integrated management approach to address both point and non-point sources of pollution while encouraging the involvement of stakeholders.

One focus of the Minnesota River Basin Plan is to reduce sediment loading from nonpoint sources to the Minnesota River, its tributaries, and Lake Pepin. Runoff from

agricultural lands is likely to be a major cause of sediment and water quality impairments. Additionally, stream bank and bed erosion may contribute significantly. The sedimentation of waterways in the Minnesota Basin causes significant problems. Turbidity limits light penetration, causing changes in primary production. Conditions for primary producers can shift from nutrient-limited to light-limited, ultimately affecting dissolved oxygen and stream metabolism. Excess sediment can lead to habitat loss, changes in predation success, and alteration of food web dynamics. Additionally, the amount of sediment originating from each source is highly uncertain.

Sediment reduction in the Minnesota River Basin is addressed here using an efficient framework that considers uncertainty in the system and the benefits of information acquisition. A potentially useful way to address the sedimentation problems in the Minnesota River is to use a systems approach. The uncertainty-based methodology developed here combines a Bayesian approach with a multiobjective programming to select the optimal suite of information acquisition and management actions.

Previous research regarding sediment reduction began with deterministic optimization approaches to nonpoint source pollution reduction dating back to the 1970s. That research aimed to determine the effects of different soil erosion control policies on the agricultural industry. Seitz et al (1979) summarized several studies that maximize social welfare subject to constraints on resources, consumer demand, soil loss, sediment transport and environmental standards. The decision variables described the crop rotation, tillage, and conservation practices needed to meet different policy requirements. The problems were modeled as deterministic linear programs. Sediment transport was described by fixed transport coefficients with constant sediment delivery ratios describing the amount of sediment reaching a targeted area. No uncertainties were considered.

Kramer et al. (1984)also developed a linear program (LP) to evaluate agricultural policies for reducing nonpoint pollution. Their model, like the one I propose, included BMPs not tied to specific agricultural activities, such as grass waterways. Braden et al. (1989)improved on the models described by Seitz et al. (1979)by incorporating spatial sediment movement functions that allow variable sediment delivery ratios. The problem was solved using a dynamic programming nonlinear model. Bouzaher et al. (1990)also developed a dynamic programming model. Their model minimized the cost of achieving a sediment standard by identifying the best set of management alternatives for each sediment delivery path.

Schleich and White (1997) developed an LP that minimizes total phosphorus reduction costs such that a target total phosphorus standard is met. Veith et al. (2003)developed a deterministic integer-programming model for locating BMPs at the watershed level. A genetic algorithm was combined with a geographic information system to determine the most cost effective placement of BMPs. Gitau et al. (2004)built upon the work by Veith et al. (2003)and also determined optimal BMP placement using a genetic algorithm.

Deterministic models described above assume that loadings and control effectiveness are known with certainty. However, the actual values are highly uncertain and even

controversial, as in the Minnesota basin. To address these uncertainties, several stochastic programming models have been developed to address sediment reduction. Chance constrained programming models were developed by several authors. Milon (1987) and Zhu et al. (1994)maximized net economic returns to landowners subject to constraints requiring environmental standards be met with certain user specified frequencies. The loadings of pollutants (Milon 1987) or soil loss (Zhu et al. 1994) to receiving waters were assumed to be uncertain due to variability in precipitation. Kampas and White (2003) and Lacroix et al.(2005) combined chance constrained programming models with simulation models to addressing nonpoint source pollution. Instead of chance constrained programming, Luo et al. (2006) developed an interval two-stage stochastic program that minimized total system costs by choosing cropland to retire.

Yulianti et al.(1999), on the other hand, considered the effects of uncertainty in input parameters to a simulation/optimization model for selecting agricultural management actions to control sediment transported to surface waters. The authors considered two uncertain inputs – uncertainty in soil and land characteristics due to insufficient data, and uncertainty in meteorological and cost data that is inherently variable. Monte Carlo simulation, generalized sensitivity analysis and regret analysis were used to determine management practices that were most and least sensitive to uncertainties considered. Nicklow and Muleta (2001) addressed sediment reduction using a discrete-time optimal control framework. The research determined farm management decisions over a three-year period. Uncertain sediment yield over the time period was simulated and a genetic algorithm was used to determine the set of land cover and tillage practices that result in the minimum sediment yield from the watershed.

Both Farzin and Kaplin (1998) and Borisova et al. (2005)considered the value of information with regards to sediment loading. Farzin and Kaplin (1998) developed a method for addressing uncertainty in site-specific characteristics of pollution sources. A nonlinear model was developed to minimize the cost of environmental damages subject to a budget constraint. The manager must determine the frequency with which to collect data on sediment loading and stream flow, as well as the abatement effort at each source. The data is used to update the manager's prior probability of sediment loading using a Bayesian approach. The authors also consider the expected value of perfect information (EVPI). The value of perfect information is defined as the difference in environmental damages incurred if the manager knows the future stream flows with certainty and if the manager is uniformed.

Similarly, Borisova et al. (2005) calculated the EVPI of various types of information for reducing nitrogen loads from agricultural land to the Chesapeake Bay. The objective was to maximize net benefits of pollution control subject to a variety of policy constraints. A simulation model, composed of an economic agricultural production submodel and a physical submodel, considered three sources of uncertainty: 1) uncertainty about economic costs of changes in agricultural production to reduce nitrogen loads; 2) uncertainties in nitrogen loads due to changes in agricultural practices; and 3) uncertainty in economic benefits from nitrogen load reductions. Both quantity and price control policies were examined.

The research proposed here is most closely related to the research by Farzin and Kaplin (1998)and Borisova et al.(2005). The impacts of uncertainty in sediment load are explicitly considered and the benefits from considering this uncertainty are calculated. However, the research here considers different types of actions for reducing uncertainty regarding sediment loads and combines this information with an optimization program to choose among management actions to reduce sediment loadings. In contrast to previous work, the management actions considered here include actions aimed at stream restoration, not only agricultural BMPs.

Methodology

To determine the optimal set of information acquisition and management actions for controlling sediment loadings in the Minnesota River Basin, we develop a framework combining Bayesian analysis with multiobjective programming. Sediment loadings from each source in each watershed are highly uncertain. To improve our understanding of these loadings, information acquisition or research actions can be performed. Each action has an associated likelihood function that describes the probability of observing a particular research outcome given the true, though unknown, sediment loadings. Starting with a prior joint probability of the sediment loadings from each sediment source in each watershed, Bayes' law is used to combine this prior information with the likelihood function to determine the information acquired from each research action. The application of Bayes' law produces a posterior distribution of sediment loadings. The mean values from the posterior distribution are then input into a multiobjective linear program that determines the optimal set of BMPs that minimizes the expected cost and expected sediment remaining. The framework produces a tradeoff curve describing the non-inferior set of research and management actions that achieve the cost and sediment reduction objectives.

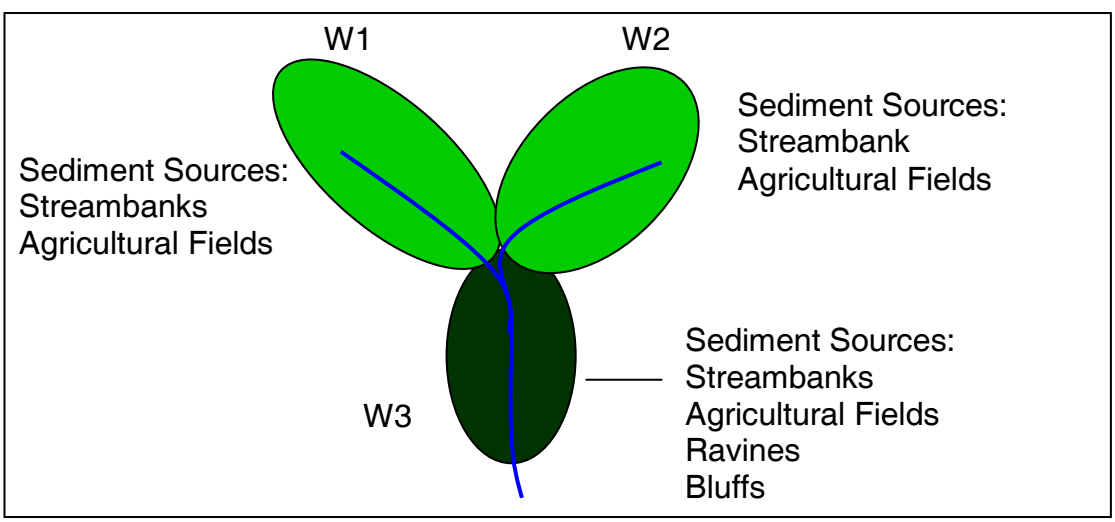

Figure 1: Three watershed model. Watersheds W1 & W2 are upstream of watershed W3

The framework is applied to a three watershed model, representative of the Maple River watershed within the Minnesota River Basin (Figure 1). Watersheds W1 and W2 drain into watershed W3. The upper two watersheds have two major sources of sediment:

streambank and agricultural fields, and the lower watershed has four sources: streambanks, fields, ravines and bluffs.

The framework for selecting information acquisition and management actions is summarized in Figure 2. Before any information acquisition action is chosen, a prior joint probability of the sediment loadings from each source in each watershed is determined by conversations with experts. The eight sediment loadings displayed in Figure 1 are assumed to follow a joint log-normal prior distribution.

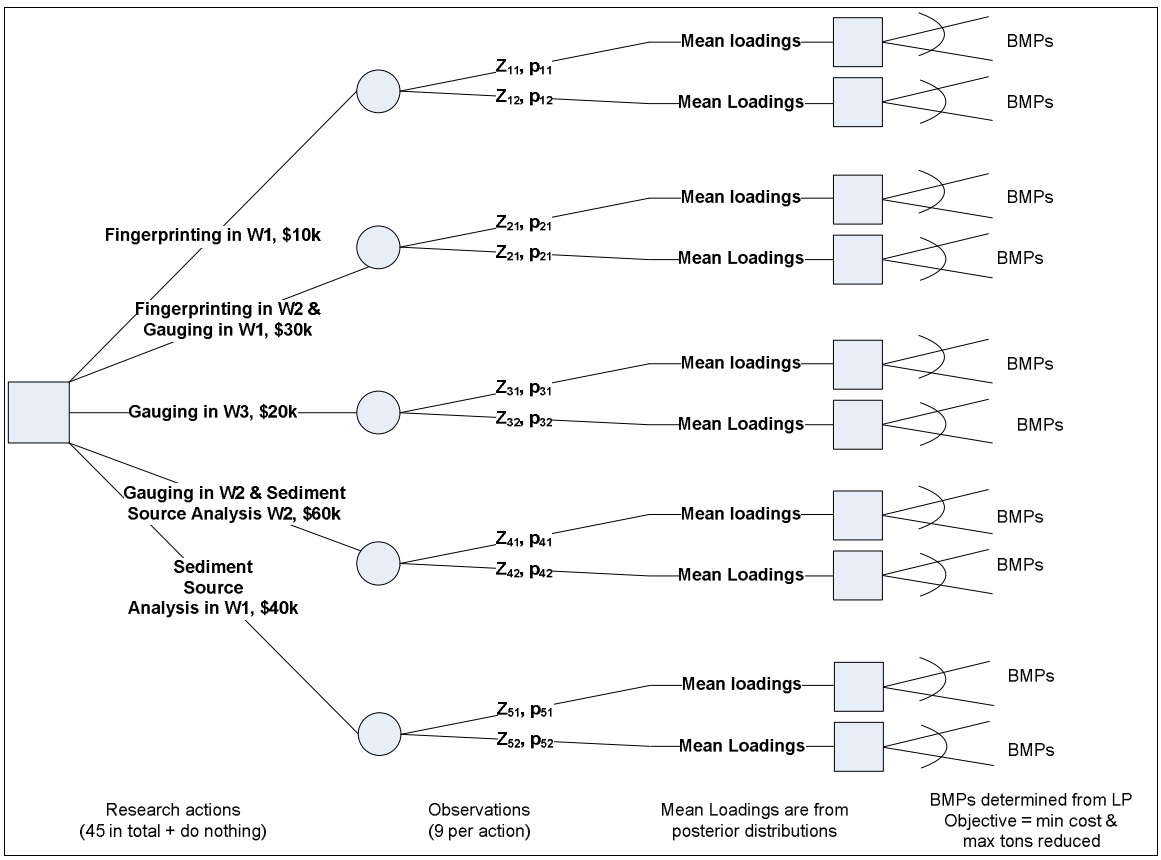

Figure 2: Decision Framework

For each watershed, three information acquisition actions can be performed: gauging, sediment fingerprinting or a sediment source analysis. Gauging involves using stream gauges to determine the total annual average sediment loading at the outlet of the watershed. Sediment fingerprinting involves using atmospherically deposited radionuclides as tracers for sediment sources. The approach determines the annual average ratio of sediment from agricultural fields to all other sediment sources. The sediment source analysis action is similar to a full sediment budget, but excludes the use of gauging data. This action produces estimates of the loading from each source in each watershed. In total, 46 actions are considered, with a limit of at most two concurrent actions. This limit was chosen to allow for a manageable number of information acquisition actions to illustrate the framework. Figure 2 shows a sampling of only five of the 46 possible actions, in order to keep the figure readable.

For each information acquisition action, nine possible observations are considered. Figure 2 displays a sampling of two of the nine observations for each action, to allow for readability. Each observation is written as Z_{ij}, where i is the action number (i = 1, 2,…,46) and j is the observation number (j=1,2,…,9). The probability associated with each of the observations is written as p_{ij}. The likelihood function for each research action is assumed to be log-normal.

For each of the 45 research actions and nine observations, a posterior distribution was generated using WinBUGS (Lunn et al. 2000) with two Markov chains. The results of this Bayesian analysis will then used to choose among management actions using a linear multiobjective program for each of the resulting posterior distributions. The linear program seeks the set of management actions that minimize cost and maximize sediment reduction. The set of selected actions are subject to the constraint that the area placed under each management action cannot exceed the area available for that action. The linear multiobjective program is run multiple times using different objective function weights, producing a tradeoff curve.

The management actions under consideration address all sources of sediment. In particular, for each sediment source (fields, streambanks, ravines and bluffs), three different BMPs will be considered. Field BMPs under consideration are critical area planting, filter strips and conservation tillage. Critical area planting addresses areas of high erosion and involves establishing permanent vegetation, such as perennial grasses, perennial legumes, trees, shrubs, vines or mixture on these sites (USDA NRCS 2009). Filter strips are areas of "herbaceous vegetation situated between cropland, grazing land, or disturbed land (including forestland) and environmentally sensitive areas (USDA NRCS 2006a)." Conservation tillage is an agricultural practice that manages the "the amount, orientation, and distribution of crop and other plant residue on the soil surface year round while limiting soil-disturbing activities to only those necessary to place nutrients, condition residue, and plant crops (USDA NRCS 2006b)."

The three BMPs being considered for stream restoration include streambank and Shoreline protection, stream barbs and rock riprap. Streambank and shoreline protection involves stabilizing and protecting stream banks or shorelines using treatments such as redirecting stream flows, reshaping slopes, and vegetation of streambanks (USDA NRCS 2009). Stream barbs are used to redirect streamflow away from an eroding bank and are defined by NRCS as "low rock sills which project out from a streambank and across the stream's thalweg (USDA NRCS 1999)." Rock riprap involves installing a blanket of graded rocks on a streambank in order to protect the slope by reducing erosion (USDA NRCS 2009).

To reduce erosion from ravines, three BMPs are under consideration: water and sediment control basins, grade stabilization structures, and tile drainage pipes. Water and sediment control structures are earthen embankments that are installed to form a sediment trap (USDA NRCS 2009). A grade stabilization structure is used to grade back the slope of a ravine and often involves the placement of a retaining wall and drainage pipes. Tile

drainage pipes are laid along the bottom of the ravine to direct the flow from the ravine to the stream channel, thus reducing erosion along the bottom of the ravine.

Lastly, the three BMPs under consideration for address soil loss from bluffs are stream barbs, rock riprap and complete stabilization of the bluff.

Preliminary Results and Future Work

At this time, the Bayesian analysis component of the framework has been completed. Figure 3 shows the prior marginal distributions and posterior marginal distributions for one observation from a sediment source analysis in watershed W3, as an example. The prior distribution is shown in blue and the posterior distribution is shown in red and green, one of each chain.

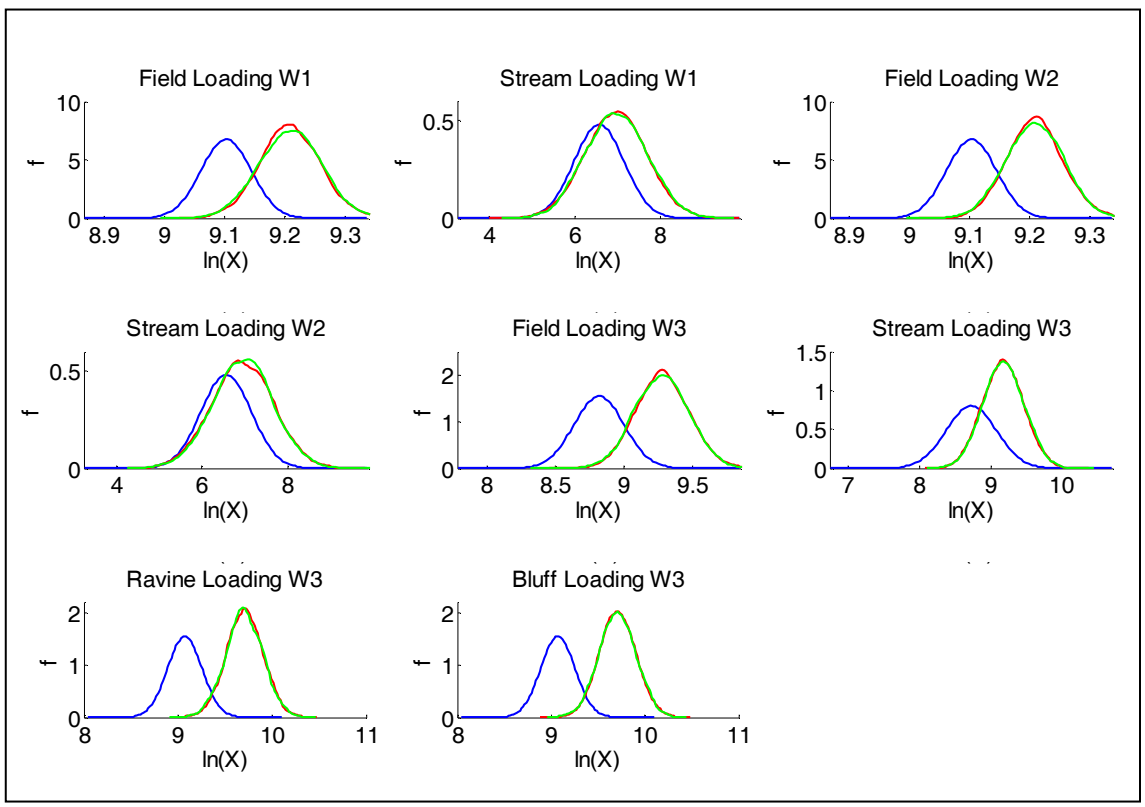

Figure 3: Prior (Blue) and Posterior (Red & Green) Marginal Distributions

The remaining work involves running multiobjective linear programs using the mean posterior loadings as inputs. The results of the linear programs will indicate the non-inferior set of management actions that simultaneously minimize cost and maximize sediment reduction. These results will then be weighted based on the probability of the research observation leading to the posterior sediment loading. Thus, an overall tradeoff curve will be created relating expect cost minimization to expected sediment reduction. In addition, a value of information analysis will also be completed to determine the value of each research action.

References

Borisova, T., Shortle, J., Horan, R. D., and Abler, D. (2005). "Value of information for water quality management." *Water Resour.Res.,* 41(6), W06004.

Bouzaher, A., Braden, J. B., and Johnson, G. V. (1990). "A Dynamic-Programming Approach to a Class of Nonpoint Source Pollution-Control Problems." *Management Science,* 36(1), 1-15.

Braden, J. B., Johnson, G. V., Bouzaher, A., and Miltz, D. (1989). "Optimal Spatial Management of Agricultural Pollution." *Am.J.Agric.Econ.,* 71(2), 404-413.

Farzin, Y. H., and Kaplan, J. D. (1998). "Optimal management of nonpoint source pollution control under incomplete and costly information." *Am.J.Agric.Econ.,* 80(5), 1193-1193.

Gitau, M. W., Veith, T. L., and Gburek, W. J. (2004). "Farm-level optimization of BMP placement for cost-effective pollution reduction." *Trans.ASAE,* 47(6), 1923-1931.

Kampas, A., and White, B. (2003). "Probabilistic programming for nitrate pollution control: Comparing different probabilistic constraint approximations." *Eur.J.Oper.Res.,* 147(1), 217-228.

Kramer, R. A., McSweeny, W. T., Kerns, W. R., and Stavros, R. W. (1984). "Evaluation of Alternative Policies for Controlling Agricultural Nonpoint Source Pollution." *Water Resour Bull,* 20(6),.

Lacroix, A., Beaudoin, N., and Makowski, D. (2005). "Agricultural water nonpoint pollution control under uncertainty and climate variability." *Ecol.Econ.,* 53(1), 115-127.

Lunn, D. J., Thomas, A., Best, N., and Spiegelhalter, D. (2000). "WinBUGS -- a Bayesian modelling framework: concepts, structure, and extensibility ." *Statistics and Computing,* 10 325-337.

Luo, B., Li, J. B., Huang, G. H., and Li, H. L. (2006). "A simulation-based interval two-stage stochastic model for agricultural nonpoint source pollution control through land retirement." *Sci.Total Environ.,* 361(1-3), 38-56.

A. Mallawatantri. (1999). "Minnesota River Basin Information Page." http://www.soils.umn. edu/ research/mn-river/doc /intro.html (1/30, 2009).

Milon, J. W. (1987). "Optimizing Nonpoint Source Controls in Water-Quality Regulation." *Water Resour Bull,* 23(3), 387-396.

Minnesota Pollution Control Agency. (2001). "Minnesota River Basin Plan." Minnesota Pollution Control Agency, St. Paul, MN.

Nicklow, J. W., and Muleta, M. K. (2001). "Watershed management technique to control sediment yield in agriculturally dominated areas." *Water Int.,* 26(3), 435-443.

Schleich, J., and White, D. (1997). "Cost minimization of nutrient reduction in watershed management using linear programming." *J.Am.Water Resour.Assoc.,* 33(1), 135-142.

Seitz, W. D., Taylor, C. R., Spirze, R. G. F., Osteen, C., and Nelson, M. C. (1979). "Economic-Impacts of Soil Erosion Control." *Land Econ.,* 55(1), 28-42.

US Environmental Protection Agency. (2003). "National Management Measures to Control Nonpoint Source Pollution from Agriculture." *Rep. No. EPA 841-B-03-004,* .

US Department of Agriculture (USDA) Natural Resource Conservation Service (NRCS). (2009). "Electronic Field Office Technical Guide." http://efotg.nrcs.usda.gov (1.30, 2009).

USDA NRCS. (2006a). "Conservation Practice Standard - Filter Strip Code 393." http://efotg.nrcs.usda.gov/references/public/NE/NE393.pdf (1/30, 2009).

USDA NRCS. (2006b). "Conservation Practice Standard - Residue and Tillage Management No Till/Strip Till/Direct Seed Code 329." http://efotg.nrcs.usda.gov/references/public/TN/Residue_and_Tillage_Mgt_No-till_Strip_Till_Direct_(329)_Standard_FINAL_2006.pdf (1/30, 2009).

USDA NRCS. (2004). "Conservation Practice Standard - Critical Area Planting Code 342." http://efotg.nrcs.usda.gov/references/public/AL/342rev04.pdf (1/30, 2009).

USDA NRCS. (1999). "Stream Barbs." http://www.abe.msstate.edu/csd/NRCS-BMPs/pdf/streams/bank/streambarbs.pdf (1.30, 2009).

Veith, T. L., Wolfe, M. L., and Heatwole, C. D. (2003). "Optimization procedure for cost effective BMP placement at a watershed scale." *J.Am.Water Resour.Assoc.,* 39(6), 1331-1343.

Yulianti, J. S., Lence, B. J., Johnson, G. V., and Takyi, A. K. (1999). "Non-point source water quality management under input information uncertainty." *J.Environ.Manage.,* 55(3), 199-217.

Zhu, M., Taylor, D. B., Sarin, S. C., and Kramer, R. A. (1994). "Chance Constrained Programming Models for Risk-Based Economic and Policy Analysis of Soil Conservation." *Agric.Resour.Econ.Rev.,* 23(1), 58-65.

A Decentralized Optimization Algorithm for Multi-Agent System Based Watershed Management

Yi-Chen E. Yang [1], Ximing Cai[1] and Dušan M. Stipanović[2]
[1]Department of Civil and Environmental Engineering, [2]Department of Industrial and Enterprise Systems Engineering, University of Illinois at Urbana-Champaign, e-mail: yang24@illinois.edu, xmcai@illinois.edu, dusan@illinois.edu

Abstract

A watershed can be considered a multi-agent system (MAS) composed of water users (agents) spatially distributed in a distinct manner within a common defined environment from which they can all access a particular resource. The watershed system is characterized by distributed decision processes at the agent level and a coordination mechanism organizing the interactions among individual decision processes. This paper presents a decentralized optimization method known as constraint-based reasoning, which allows individual agents in a multi-agent system to optimize their behaviors. The method incorporates the optimization of all agents' objectives through a bargaining scheme, in which the ith agent optimizes its objective with a selected priority for collaboration and sends the solution back to all agents that interact with it. This methodology allows agents to determine how important their own objectives are in comparison to the constraints, using a *local interest factor* (β_i). A large β_i value indicates a selfish agent who puts high priority on its own local benefit and ignores constraints. This analysis is applied to a hypothetical watershed with three offstream human agents (city and farms), one instream human agent (reservoir) and two ecological agents (fish habitat in the river). The proposed approach takes the objectives of individual agents into account and balances them through interactions among the agents. This bottom-up problem-solving approach mimics real-world watershed management problems better than conventional "top-down" optimization methods in which it is assumed that individual agents will completely comply with any recommendations that the coordinator makes.

Keywords: Multi-agent systems, watershed management, ecohydrology, penalty-based methods, decentralized optimization

Introduction

Watershed systems consist of many interdependent water users (Loucks, 2003) and each one of them will have their own decision process. Traditional water resources management practice usually fragmented by production sectors without holistic resource allocation procedures and divided among land and water management. These practices tend to focus on human needs without sufficient consideration of ecosystem requirements. Sustainable watershed management needs a comprehensive approach and treats watersheds as coupled human-nature systems (Liu et al., 2007). Specific concerns for watershed management should include the balance of human needs which are offstream, with instream environmental needs. Moreover, management of the coupled human-nature system requires the participation of local stakeholders. Therefore, facilitating the transfer of modeling technology to provide information to stakeholders and managers is requested by government agencies (EPA, 1996; NRC, 1999). The stakeholders' participation can transition the traditional top-down management of water resources to bottom-up management (Parker and Tsur, 1997; NRC, 1999).

Conventional watershed management models use a centralized approach to explore the system-wide optimal solution, assuming that (1) there is a top-down management process in

which all watershed stakeholders completely obey a "super brain," such as watershed management coordinator, (2) complete information exchange exists among the stakeholders in different locations and production sectors and (3) perfect economic efficiency is realized, i.e., the marginal welfare of water use is identical for all agents. These assumptions are usually unrealistic in real-world watershed management situations. This paper presents a decentralized modeling approach, which is at least partially free of those assumptions.

New modeling techniques for watershed management have been postulated (Wolf, 2007). The theory of MAS has emerged from the field of distributed artificial intelligence (Sycara, 1998). Under the definition of MAS, an agent is an object that interacts with others and its environment, and the interactions are characterized by behavioral rules of individual agents. Several characteristics define agents: They are autonomous, (i.e., they have control over their actions), they have different and possibly conflicting goals, they share a common environment, and they each make decisions that impact the common environment (Dooley and Corman, 2002).

In this study, we examine the application of a MAS model to a watershed, which can be naturally described as an MAS. Agents in a watershed MAS include offstream land and water user and instream or in-situ water "users," such as riparian aquatic ecosystems. The environment of the MAS is composed of static geomorphologic features (e.g., the natural drainage network) and temporally dynamic attributes such as flow regimes and water quality. Advances in water-related disciplines, including hydrology, ecology, biology and economics have paved the way for modeling the environment of watersheds. In the MAS framework, agents are defined as autonomous computational units. Stakeholder participation associates the computational units with human agents (Drougoul et al. 2003), including land owners and representatives for land and water use agents. Reservoir managers are considered as instream human agents, and government or citizen organizations as ecosystem agents. In this context, a watershed is characterized by disaggregated but interactive decision processes at the agent level, and with a coordination mechanism among individual decision processes.

MAS are increasingly used in the field of environmental and natural resource management issues (Barreteau et al, 2004; Chen et al., 2008), such as ecological modeling (Bousquet and Le Page, 2004), basin land use management (Parker et al., 2003; Jaziri and Paquet, 2006), and urban catchment problems (Pahl-Wostl, 2005). Some researchers have recently begun to use MAS on water resource planning and management issues. It is widely accepted that water resource management demands an integrated assessment of resource use options, including local and regional impacts on the environment and stakeholders (Loucks et al., 2005**;** Croke et al, 2007). MAS can be a suitable approach to dealing the water resource planning and management issue.

However, despite the existing applications of MAS models, mathematical formulation of the framework and development of solution algorithms remain a great challenge for specific MAS problems, including watershed management. This paper adapts a MAS model from decentralized control theory to analyze the water allocation among various water users. Offstream human agents, instream human agents, and ecosystem agents are defined in the spatial domain of a watershed. The behavior of each agent is assumed to be driven by an economic benefit objective. The focus of this paper is to model the interactions among agents and illustrate how the behaviors of individual agents affect the overall performance of the system. Indicators of system performance will be derived from agents' decisions and their consequences. In the rest

of this paper, the description of the methodology is first given, followed by the description and discussion of results and then, finally, conclusions.

Methodology

Penalty-based optimization methods (Luenberger, 1984) provide a convenient way to solve a decentralized problem such as MAS. A modified penalty-based decentralized method (İnalhan et al., 2002) is used in this study. Each agent has its own decision framework that captures only the local dynamics and the interconnecting constraints associated with these dynamics. The method achieves optimization among agents with a bargaining scheme, by which the ith agent optimizes its objective with a selected priority for collaboration and sends the solution back to all other agents with which it interacts. All agents do this simultaneously, and their solutions are evaluated together by a "central processor," from which information, such as system cost and the degree of constraint violation, is sent back to agents for the next round of bargaining. The method is based on a formula that allows agents to deal with infeasible constraints that different subsystems impose. The idea of this method is not to directly seek the optimal solution of a formulated problem, but to use a two-step approach – first finding out a solution based on the choices of all individual agents, allowing the violation of some constraints defined with the optimization models for individual agents, and then trying to reduce the constraint violation at the system level. This follows the bottom-up problem-solving procedures, in which individual agents make decisions and interact with other agents and then the coordinator resolves conflicts by balancing the decisions of different agents.

The mathematical formulation of typical optimization problem is given as follows:

$$\max_{x_i} f_i(x_i) \tag{1}$$

$$subject\ \ to\ \ g_i(x_i|\{x_j\}_i)\begin{cases} g_{li}(x_i) \le 0 \\ g_{gi}(x_i|\{x_j\}_i) \le 0 \end{cases} \tag{2}$$

This optimization procedure has both local constraints $g_{li}(x_i)$ and interconnected constraints $g_{gi}(x_i|\{x_j\}_i)$. An interconnected constraint specifies that agent i receives the value of $\{x_j\}_i$ from agent j and needs to accept the value. Following İnalhan et al. (2002), the penalty-based objective function for agent i is:

$$\max F_i(x_i, \beta_i|\{x_j\}_i) = \max\{\beta_i \cdot f_i(x_i) - P_i(x_i|\{x_j\}_i)\}, \text{ for } \beta_i > 0 \tag{3}$$

where $\beta_i>0$ is a *local interest factor,* f_i is the original objective function, and P_i is the penalty function that penalizes any violation of the constraints in the formulation of equation (3). A larger β_i will result in a larger f_i. According to the proof by İnalhan et al. (2002), a larger β_i will also lead to a larger penalty item, P_i. This scheme allows each agent to use local β_i selection as a tool to search for a solution which increases local benefit (f_i) as much as possible while violating fewer constraints.

The first and second order conditions are used to solve this penalty-based mathematical problem as described in equation (3). The final differential equation for each agent is

$$\frac{\partial F_i}{\partial x_i} = \beta_i \frac{\partial f_i(x_i)}{\partial x_i} - \sum_{k=1}^{k_i} \frac{\partial g_{i,k}}{\partial x_i} \max(0, g_{i,k}(x_i|\{x_j\}_i)^{\gamma-1} \cdot \gamma = 0 \tag{4}$$

where $\gamma \geq 2$ is assumed to ensure the second order differentiability. The number of constraints corresponding to the ith agent is k_i. The most important advantage of this solving process is that it allows each agent to use local β_i selection as a tool to search for a solution which violates fewer constraints while not resulting in the decrease of F_i.

This scheme allows the ith agent to optimize equation (4) by using a local search for β_i. The result of ith agent will then be sent to neighboring agents. The global performance of the entire system is treated as public information that is accessible to all agents. İnalhan et al. (2002) suggested that the sum of the objective function (F_{total}) and the total violation (P_{total}) could serve as a global performance metric since the selection of β_i gives each agent a tool with which to "bargain." With a large value of β_i, the solution ends with a better objective function [$f_i(x_i)$] but a larger constraint violation than it would with a small β_i.

Results

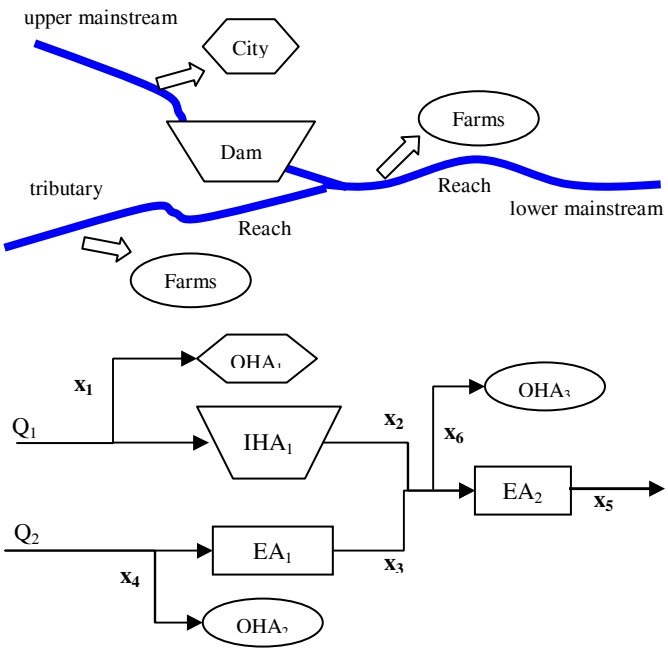

Fig 1. Hypothetical watershed for MAS framework

The MAS framework was applied to solve a hypothetical watershed as in Fig 1. Six agents are identified in this watershed. There are three offstream human agents, OHA_1 as the city, and OHA_2 and OHA_3 as the farms. The objectives of offstream human agents are consuming water to maximize their economic profits. The dam on the upper mainstream is defined as an instream human agent (IHA_1) with the objective to release water for hydropower generation. The general objective functions for OHAs and IHAs were obtained from the literature (Cai et al., 2003 and Loucks et al., 2005). The fish habitats located at the tributary and the lower mainstream are identified as ecosystem agents, EA_1 and EA_2, respectively. The objective functions of EAs can use the results Yang et al. (2008). An assumption is made here that the unit of EAs' objectives is the same with human agents which is the economic benefit. This assumption can make the following analysis easier and provides clearer demonstration of the emergence pattern due to agents' behaviors.

The quadratic objective function, the constraints and the parameters for OHA_1 are provided in Table 1 as an example. The decision models of all agents are inter-connected by the

Table 1. The objective function and constraints of OHA_1

$\max_{x1} f_1(x_1) = a_1 x_1^2 + b_1 x_1 + c_1$ st. $\begin{cases} \alpha_1 - x_1 \leq 0 \\ \alpha_2 - Q_1 + x_1 \leq 0 \end{cases}$	$f(x) = a_1 x^2 + b_1 x + c_1$: the benefit from municipal and industrial water use x_1: water withdraw for municipal water use Q_1: the monthly inflow of mainstream α_1: the minimum water demand for the city α_2: the minimum flow requirement for the dam

water sharing or the upstream – downstream relationships. When one agent seeks its optimal solution, it might violate the constraints with others. Both analytical and numerical results are presented for this hypothetical watershed management problem in the following section.

Penalty-based method is applied to solving the formulated MAS problem. The formulation of a penalty-based objective function and the effect of the local interest parameter (β_i) on the decisions of various agents are demonstrated by equation (5) and Fig 2. Equation (5) shows the penalty-based format of this individual agent's objection function and the value of β_1 indicates "how far" the agent can explore its solutions within the infeasible region (Fig 2).

$$F_1(x_1) = \max_{x_1} \left[\beta_1 \cdot f_1(x_1) - P_1(x_1)\right]$$
$$= \max_{x_1}\left\{\beta_1 \cdot (a_1 x_1^2 + b_1 x_1 + c_1) - [\max(\alpha_1 - x_1, 0)]^2 - [\max(\alpha_2 - Q_1 + x_1, 0)]^2\right\} \quad (5)$$

With a given value of β_1, OHA_1 will search local optimal solutions (x_1) result in maximum benefit ($f_1(x_1)$) inside and outside of the feasible region (gray area in Fig 2, which represent the solutions are $\alpha_1 \le x_1 \le Q_1-\alpha_2$) of the solution space (the entire x-axis). When β_1 is set at zero, all possible solutions (agent's decisions) will locate within the feasible region, if it exists. Under this situation, the violation of the constraints will be minimal (violation will be zero if the feasible region exists). When β_1 is greater than zero, agents may explore solutions in the infeasible region. The value of β_1 indicates how far the exploration can go in the whole solution space. When β_1 approaching infinity, OHA_1 can search the entire space and find the optimum solution without considering any interconnection constraints. In other words, the benefit of OHA_1 changes from point ***I*** to point ***II*** in Fig 2. However, since the optimum solution (point ***III*** in Fig 2) is in the infeasible region, the violation of the constraints caused by the solution may be large.

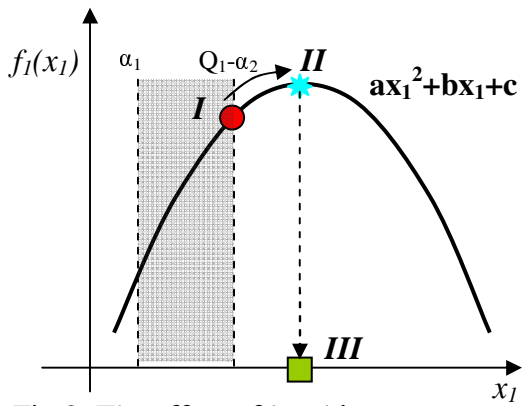

Fig 2. The effect of local interest parameter: β_i

The numerical results of agents' benefit at a given inflow condition are shown in Fig 3(a) for all active agent scenario and in Fig 3(b) for reactive ecosystem agent scenario. The β_i for all agents are set at the same value to simply the problem. In Fig 3(a), since all agents are active which means they all have the power to make their own decision, their benefit will all increase with increasing β_i. When β_i larger than "10" in this case, OHA_2 and OHA_3's benefit will become constant which means that they already achieve their local optimum just like point ***II*** in Fig 2. Fig 3 (b) shows the reactive ecosystem agent scenario, which means that ecosystem agents have no power to make any decision and they can only use the water after human agents' decision. This scenario is similar to the traditional watershed management. The results show that when β_i increases, the benefits for human agent will still increase. The benefits will increase to optimum value when β_i are larger than "10", which is consistent with all active agent scenario. Consequently, the benefits for the ecosystem agents (EA_1 and EA_2) decrease when OHAs withdraw more water from the river. Note that changing β_i has no effect on EAs since the benefits of EAs fully depend on the connected OHAs. These figures illustrate the decentralized results at agent level and also effect of β_i at a given fix flow condition.

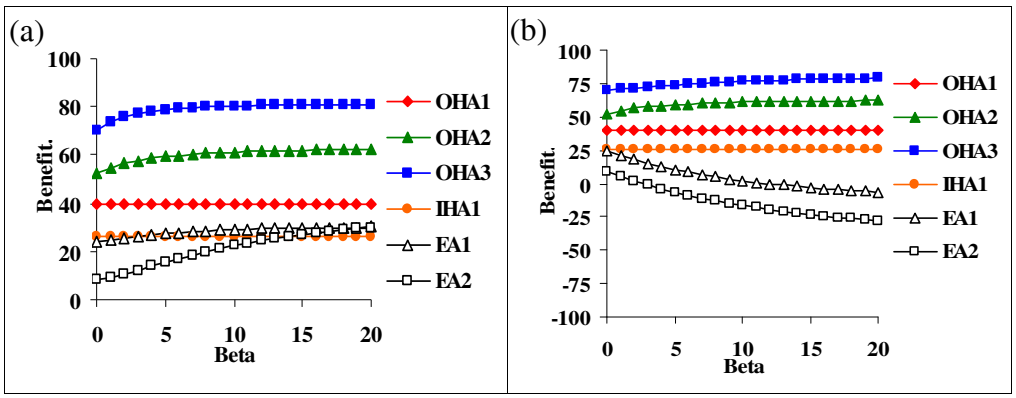

Fig 3. The numerical results of all agent s' benefit change with β_i

The results of Fig 3 can be summed together for the system benefit and we can also compute the system violation by aggregate agents' violation. Meanwhile, the results from different inflow conditions can be evaluated. The inflows are treated as available resource and the agent's behavior is represented by β_i. The concept of β_i can extend the conventional water management issue from a 2D (inflow and benefit) to a 3D (inflow, benefit and agents' behavior) problem. A 3-dimensional figure is given in Fig 4 shows the (a) system benefit (sum of all agents' benefits) and (b) system constraints violation (sum of all agents' violation) due to different agents' behavior (β_i) and available resources (inflow). Notice that the axis orders are different in Fig 4(a) and (b) to clearly show the shapes of two surfaces. The change of benefit with inflow is affected by the value of β_i (Fig 4a). When β_i=0 (the square-symbol line), the benefit increases with inflow, while the violation is zero when inflow is greater than 45 and increases when inflow decreases beyond 45 (Fig 4b). It can also be seen that when inflow is greater than 110 the change of β_i does not affect the benefit and violation, since all agents can achieve their local optimums.

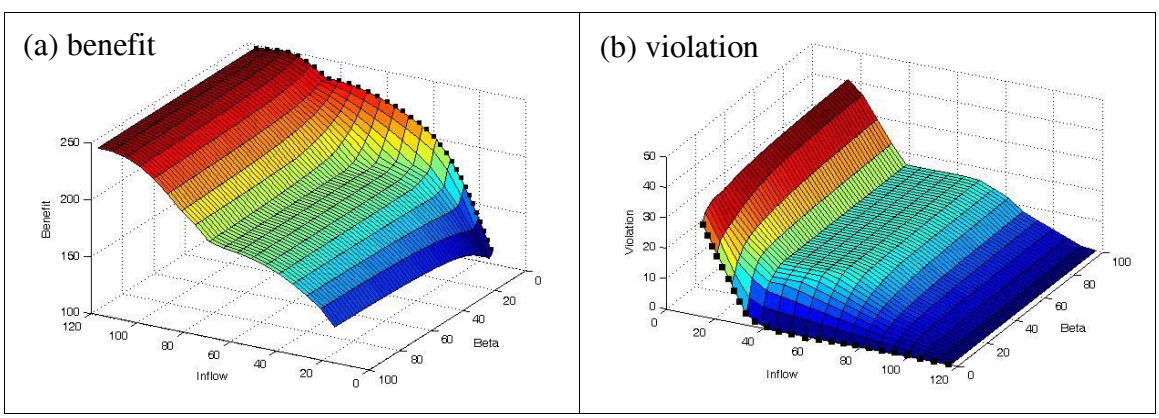

Fig 4. The crossover effect of local interest parameter: β_i and inflow.

Discussion and Conclusion

This study applied a penalty-based decentralized optimization algorithm to solving a watershed MAS problem. The demonstration on a hypothetical case study indicated that the concept of local interest parameter (β_i) can explicitly represent the water user's behavior in the management practice. The value of β_i and associated system violation can be useful in two aspects. First, water users can adjust their behavior (by changing β_i values) to achieve a minimum system violation while maintaining the optimum for system benefit. An ideal situation

is that different values of β_i are identified for different agents so that the system violation is reduced to minimum while all agents are satisfied with their own behavior. Second, for the planning purposes, the violation of constraints, particularly caused by the violation of physical constraints, can be explained as the necessary amount of water imported into the system, or how much supply capacity increase is needed to sustain a certain level of benefit.

References

Barreteau, O., Bousquet, F., Millier, C. and Weber, J. 2004. Suitability of Multi-Agent Simulations to study irrigated system viability: application to case studies in the Senegal River Valley. *Agricultural Systems*, 80: 255–275.

Bousquet, F. and Le Page, C. 2004. Multi-agent simulations and ecosystem management: a review. *Ecological Modelling*, 176: 313–332.

Cai, X., McKinney, D.C. and Lasdon, L.S. 2003. An integrated hydrologic-agronomic-economic model for river basin management, *Journal of Water Resources Planning and Management-ASCE*, 129 (1): 4-17.

Chen, S. H., Jakeman, A. J. and Norton, J. P. 2008. Artificial Intelligence techniques: An introduction to their use for modelling environmental systems. *Mathematics and Computers in Simulation*, 78: 379–400.

Croke, B. E. W., Ticehurst, J. L., Letcher, R. A., Norton, J. P., Newham, L.T. H. and Jakeman, A. J. 2007. Integrated assessment of water resources: Australian experiences. *Water Resources Management*, 21: 351–373.

Dooley, K., and Corman, S. 2002. Agent-based, genetic, and emergent computational models of complex systems, in *Encyclopedia of Life Support Systems* (EOLSS), L.D. Kiel (ed.), Oxford, U.K.: UNESCO/EOLSS Publishers.

Drougoul A., Vanbergue, D. and Merrisse, T. 2003. Multi-agent based simulation: Where are the agents? In J.S. Sichman, F. Bousquet, and P. Davidsson (eds), *MABS* 2002 LNAI 2581, pp. 1-15.

United States Environmental Protection Agency (U.S. EPA) 1996. *National Water Quality Inventory*, U.S. EPA, Washington D.C.

İnalhan, G., Stipanović, D. M. and Tomlin, C. J. 2002. Decentralized optimization, with application to multiple aircraft coordination, *Proceedings of the 41st IEEE Conference on Decision and Control*, December 2002, Las Vegas, NV, USA.

Jaziri, W. and Paquet, T. 2006. A Multi-Agent Model and Tabu search Optimization to Manage Agricultural Territories*, GeoInformatica*, 10:337-357.

Liu, J. et al. 2007. Complexity of coupled human and natural systems. *Science*, 317: 1513-1516.

Loucks, D. P. 2003. Managing America's rivers: Who's doing it? *The International Journal of River Basin Management*, 1(1): 21–31.

Loucks, D. P., van Beek, E. Stedinger, J. R., Dijkman J. P. M. and Villars, M. T. 2005. *Water Resources Systems Planning and Management: An Introduction to Methods, Models and Applications*. Paris-UNESCO.

Luenberger, D. G. 1984. *Linear and Nonlinear Programming*. Reading, MA: Addison Wesley, second ed., New York, USA.

National Research Council (NRC). 1999. *New strategies for America's watersheds*, Committee on Watershed Management, National Academy Press, Washington, D.C.

Parker, D. C., Manson, S. M., Janssen, M. A., Hoffmann, M. J. and Deadman, P. 2003. Multi-Agent Systems for the simulation of land-use and land-cover change: A review. *Annals of the Association of American Geographers*, 93(2): 314–337.

Parker, D. D. and Tsur, Y. (ed) 1997. D*ecentralization and Coordination of Water Resource Management*. Kluwer Academic Publishers, Boston, USA

Pahl-Wostl, C. 2005. Information, public empowerment, and the management of urban watersheds. *Environmental Modelling and Software*, 20: 457-467.

Sycara, K. 1998. Multi-Agent Systems. *AI Magazine*, 19(2): 79-92.

Wolf, A. T. 2007. Shared waters: Conflict and cooperation, *Annu. Rev. Environ. Resour.*, 32: 241-269.

Yang, Y. C. E., Cai, X. and Herricks, E. E. 2008. Identification of hydrologic indicators related to fish diversity and abundance: A data mining approach for fish community analysis. *Water Resources Research*, 44, W04412, doi:10.1029/2006WR005764.

A Decision Support System for Water Resources Planning and Management for the North Slope of Alaska

Amy C. Tidwell[1], Kelly Brumbelow[2], Stephen F. Bourne[3], William E. Schnabel[4]

[1] Research Assistant Professor, Univ. of Alaska-Fairbanks, Water and Environmental Research Center, PO Box 755860, Fairbanks, AK 99775-5860, a.tidwell@uaf.edu
[2] Assistant Professor, Texas A&M Univ., Zachry Dept. of Civil Engineering, 3136 TAMU, College Station, TX 77845-3136
[3] Senior Project Manager, Applied Technologies Group, PBS&J, Inc., 1800 Parkway Place, Suite 1200, Marietta, GA 30067, SFBourne@pbsj.com
[4] Research Assistant Professor, Univ. of Alaska-Fairbanks, Water and Environmental Research Center, PO Box 755860, Fairbanks, AK 99775-5860, Bill.Schnabel@uaf.edu

Abstract

Alaska's North Slope hosts a phenomenal wealth of natural, cultural, and economic resources. It represents a complex system, not only in terms of the biophysical system and its global importance but also from the standpoint of its social dynamic. A major challenge at the forefront of domestic energy development on the North Slope is the need for best management practices that will ensure benefits for all stakeholders. To do so requires stakeholder cooperation that enables cost-effective development strategies that fit within a broader context of long term cultural, economic, and environmental sustainability.

Ice roads and ice pads provide a cost-effective means of oil and gas exploration with minimal impact to the sensitive underlying tundra. Consequently, these ice structures have become integral to oil and gas exploration activities on the North Slope. Their widespread use represents a challenge to water resource managers, however, due to the large volume of water required to construct and maintain them. Crucial questions on water balance and ecosystem impact must be considered in the state regulatory process that permits construction of these ice structures.

The North Slope Decision Support System (DSS) is currently under development as a technology in support of oil and gas exploration and development that explicitly considers optimal water use, direct and cumulative environmental impacts, and multiple objectives and values among stakeholders. Major modules of the DSS include information systems, natural system models, planning and management functions, and regulation workflow. Development of the DSS is a collaborative effort of academic and industry personnel with significant stakeholder involvement from multiple agencies of local, state, and federal government, private energy companies, and non-governmental organizations.



Fig. 1. North Slope of Alaska (Geographic Information Network of Alaska [GINA] SwathViewer).

Introduction

The North Slope of Alaska lies between the Brooks mountain range and the Arctic Ocean (see Fig. 1). Water is an essential component of the North Slope environment. Local communities use lakes and rivers for access to subsistence resources and to sustain those same resources and requisite habitat. As well, energy development in the region is inextricably tied to water resources. Oil and gas exploration and development require a great deal of freshwater to support ice road and ice pad construction, for drilling muds, domestic water supply, and to implement emerging enhanced oil recovery (EOR) methods.

Due to the fundamental role of water in natural and human systems, successful management of this resource is indeed essential to the broader issue of environmental protection and responsible energy development on the North Slope. The challenges of developing best management practices for water resources include the following: resource planning and management for efficient and sustainable water use; understanding and explicitly considering environmental impacts and protection; and developing and implementing effective participatory management strategies with representative stakeholder participation from all sectors.

Ice roads and ice pads provide a cost-effective means of oil and gas exploration with minimal impact to the sensitive underlying tundra. Consequently, such ice structures have become integral to oil and gas exploration activities on the North Slope. Their widespread use represents a challenge to water resource managers, however, due to the large volume of water required to construct and maintain them. As the proximity of

available water sources has a significant impact on the planned location of ice roads and ice pads, changes in water resource management strategies could significantly impact oil and gas exploration activities. At present, water withdrawals require lake-specific permits that specify the maximum volume of water that may be pumped from each lake. Withdrawal limits are set by the Alaska Department of Natural Resources (ADNR) and depend on the presence and species of fish, total lake storage, and under-ice volume at the time of maximum ice thickness.

Additional water withdrawal considerations include the potential for water withdrawals to impact the annual and interannual lake water balance. Such changes could in turn impact local and regional wildlife habitat, permafrost thermal balance, or other biophysical systems.

How can we identify exploration scenarios that maximize water access and minimize exploration costs, environmental impact, and economic/environmental risk? On the North Slope, limited data is generally understood to be the greatest impediment to tackling problems such as this. Indeed, there are relatively few observational data available for the North Slope to support resource planning and management. This is due to the vast area of the region as well as the extreme, logistically-challenging climate. The majority of data that does exist has evolved over decades of individual and disjointed research efforts undertaken by various agencies, researchers, and private companies. The overwhelming effort required to locate, let alone retrieve, these data is prohibitive to its use and has greatly diminished its effective value. Moreover, drawing conclusions from and basing decisions on only a small fraction of the available data fundamentally increases uncertainty and risk. Therefore, the problem of best management practices inherently includes the problem of locating as much existing data as possible and making it readily accessible. This is also a necessary first step to prioritizing future data investment.

The institutional challenges to participatory resource management are just as important as the physical system analysis. There are many stakeholders of North Slope oil and gas resources. Here and throughout this document, the term stakeholders refers to groups and representatives from local, state, and federal government, North Slope residents, and oil and gas companies. The stakeholder group encompasses a broad range of values with respect to economic development and environmental resources. Furthermore, water uses and management objectives, as with other resources, are not the same for all stakeholders. Traditional approaches to resource development have generally not been inclusive of all stakeholders and, consequently, have not promoted a real sense of shared resource ownership and responsibility. This often leads to mistrust in regulatory and development processes and frequently results in adversarial relationships among stakeholders.

The overarching challenge being addressed in this project relates to North Slope water resource management. ***Specifically, are developing a water resources management solution in support of oil and gas exploration that explicitly considers optimal water use, direct and cumulative environmental impacts, and multiple objectives and values among stakeholders.*** The solution will consist of an information system, software tools for decision support, and methodologies for facilitating stakeholder involvement in the decision making process. The tools developed in this work will not only be applicable to the water management issues considered here, but will also be applicable to broader environmental management issues and industry development applications.

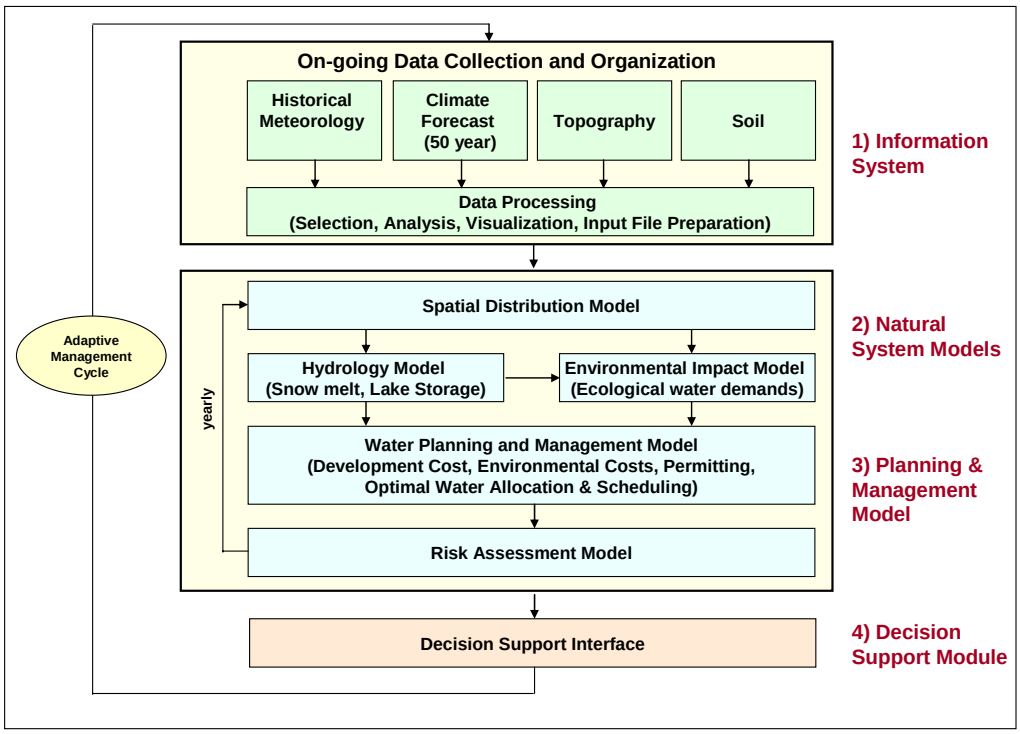

Fig. 2. Conceptual design of the NSDSS.

Design of the NSDSS

Conceptual design of the North Slope DSS structure and its major components is presented in Fig. 2. The DSS will be built on a state-of-the-art GIS-based information system that fully integrates both geospatial and time series data into a comprehensive database. The information system will serve as a workbench for importing, exporting, and quality controlling data. It will also control data flow between DSS modules. The information system will accept ongoing updates to the database as more data become available through field stations, remote sensing, stakeholder workshops, continuing research, etc.

Natural system models will accept user-specified input and simulate hydrologic and environmental responses to meteorological and anthropogenic forcing. The water resources planning and management model will interact with the natural system model to evaluate the costs and benefits associated with potential management scenarios. The interaction can be in the form of scenario exploration (i.e. define a water use scenario and evaluate the impact to a project) or as part of an optimization algorithm that suggests a set of favorable water use scenarios to meet user-defined objectives (e.g., minimize costs and maintain environmental compliance). Uncertainty in the natural and management model results will also be quantified and presented in the form of risk assessment.

The user interacts with the planning and management model through the decision support module. This feature will allow the user to look at operational scale analyses (e.g., water schedules over days, weeks, or months), seasonal planning and management (e.g., ice road planning, source lake selection, permitting support), or long term planning (e.g., multi-year exploration planning and climate change impact assessments.) At the operational scale, the decision support module will allow adaptive management of water resources by reengaging models with newly entered data. This data will be ingested through the information system and

may include updated weather forecasts, observed lake ice, lake depths, or changes in water demand for ice road construction and/or maintenance.

One of the innovations of the NSDSS will be its operational integration of a distributed cyber-infrastructure as part of its information system (Fig. 3). A central, enterprise, geographic database will be installed at the University of Alaska-Fairbanks. The structure of this database will be designed to ensure the database can act as a common foundation for all required data, findings, and management scenarios. The data collection process will add existing data stores – from both Alaskan and national data sources – to the central database. Ongoing data collection from field stations and remote sources will be continually fed into the central database.

The DSS workbench will be developed as a GIS-based application that connects to the central database, downloads user-selected data for analysis, and uploads assessment results. Probable locations for workbench installation include: UAF for research, on the North Slope for stakeholder involvement and outreach, at field sites for adaptive management, and at oil company headquarters in Anchorage for planning.

The central database will house the entire North Slope data inventory collected as part of this specific project. Some of the data types that will be accepted include traditional GIS data layers, such as shape files; point-based station data, such as precipitation and temperature from meteorological stations; remotely sensed data; and gridded data, such as reanalysis data from international climate centers, GCM data, or spatially distributed observational fields (e.g., gridded surface temperature). An important part of the information system design process will be to organize the existing data into a formal geographic database design that captures the spatial relationships from one dataset to another, thereby creating a digital depiction of the physical world.

While the complete central database will be publicly available through an online ArcGIS server, users may select subsets of data for download and off-line access on their individual workbenches. Data will be directly accessible through a GIS interface. The information system will also be designed to communicate with efforts such as the GIS database being developed and maintained by the Geographic Information Network of Alaska (GINA) as contracted by the North Slope Science Initiative. In this way, both systems will have access to data and functionality from the other, and efforts will be neither duplicated nor disregarded. Private data sets will also be accommodated within individual users' desktop environments.

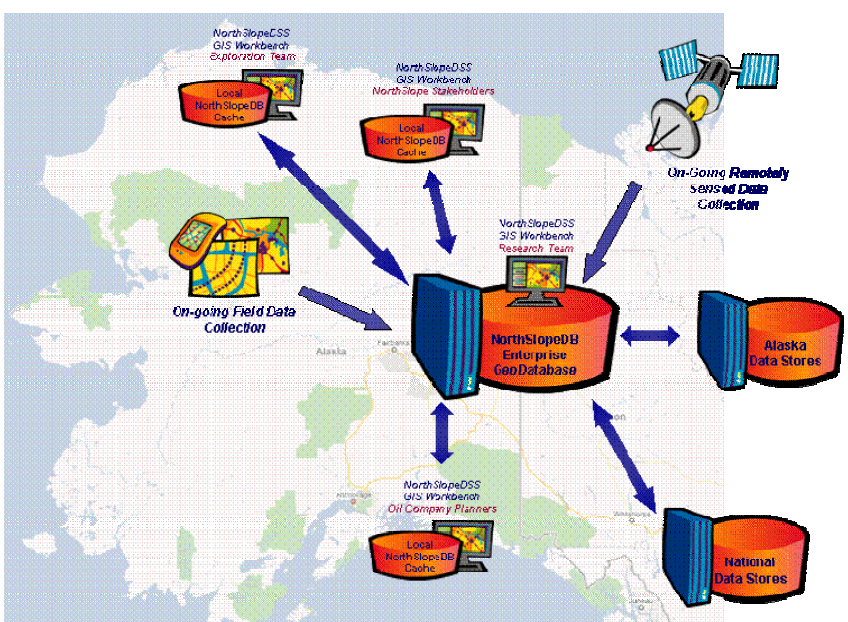

Fig. 3. The physical architecture of North Slope DSS information solution.

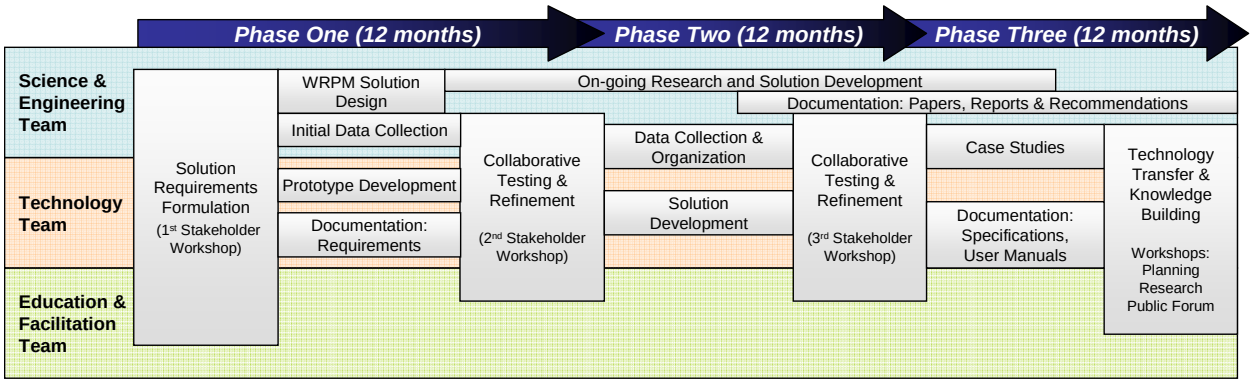

Fig. 4. Project phases and solution development.

Stakeholder Participation and Solution Development

The success of the North Slope DSS depends on its ability to meet existing and future needs of North Slope stakeholders as well as effective technology transfer to promote its use. Therefore, the proposed solution also includes significant stakeholder input during the design, testing, and application (case studies) of the DSS. A series of stakeholder workshops will be held (1) at the beginning of the project to solicit design recommendations from stakeholders; (2) at the end of year one to distribute a prototype DSS for stakeholder testing and feedback; (3) at the end of year two to distribute, test, and refine the full scale DSS; and (4) during year three for hands-on workshops focused on planning/management, research, and public DSS applications. These workshops bound the three major project phases, each one year in length (Fig. 4).

Phase I (October 2008 – September 2009) is focused on DSS prototype development. An initial stakeholder workshop was held in January 2009 to introduce stakeholders to the state-of-the-science in decision support technology and shared vision resource management and to solicit input on workbench design to meet stakeholder needs. This workshop included 28 attendees representing 4 state government agencies, 4 federal agencies, 1 local government, 3 private companies, 1 non-governmental organization, and 4 academic partners (project team excluded from this listing). The workshop involved discussion of multiple "usage scenarios" for the NSDSS that were used to develop functional, non-function, and institutional requirements for the system. The project team is now using these requirements to drive rapid development of a prototype workbench. The prototype will be a focused on a pilot area of the North Slope and will employ simple versions of the suite of models necessary for water resources management.

The prototype system will be delivered to stakeholders during a second workshop at the end of Phase I. This forum will provide an opportunity to present and discuss prototype capabilities in a hands-on fashion, whereby cooperators may test the system and provide feedback for improvements and outstanding needs. The benefits of this approach are two fold. First, the open and engaging format develops trust among scientists, stakeholders, and regulators. Second, the approach ensures that the system is truly designed to meet the North Slope community needs.

Phase II (October 2009 – September 2010) encompasses full scale DSS development. The workbench and information system will be extended to the complete North Slope region and will be upgraded with more comprehensive versions of the natural system and management models. Natural system and planning models will be refined, calibrated, and verified. This phase of work will also address climate change scenarios as well as develop an adaptive management methodology. Phase II will conclude with a third stakeholder workshop where the full-scale system will be presented to stakeholders and regulators for final testing and refining. At this time, case studies will be selected for applying the North Slope DSS to pressing stakeholder water management problems.

Phase III (October 2010 – September 2011) will focus on technology transfer and knowledge building. Case studies will be conducted for North Slope DSS applications, such as water planning and scheduling to support oil exploration and water management for enhanced oil recovery. Technology transfer during this phase will include a series of workshops aimed at various user groups. A planning workshop will be held for stakeholders and regulators and will focus on water planning and management scenario exploration. A second workshop will be held with a focus towards using the North Slope DSS in research applications by university and agency scientists. Participants will be able to formulate questions and explore solutions and scenarios with the tool during these workshops. Finally, a public forum will be held in Barrow to introduce the North Slope community to the tool, research results, and how the system can also be used to explore the existing and future North Slope environment.

A Framework for determining the Possible Impacts of a Changing Climate on Water Supply

MARK SUMMERTON[1] AND ROLAND SCHULZE[2]

[1]Umgeni Water, P.O.Box 9, Pietermaritzburg, 3200, South Africa
Mark.Summerton@umgeni.co.za
[2] School of Bioresources Engineering and Environmental Hydrology, University of KwaZulu-Natal, Private Bag X01, Scottsville, 3209, South Africa.

ABSTRACT

For effective water resources management, all "stressors" that may impact on balancing future water supply and demand must be assessed. Hydrologists have recently begun making headway towards assessing a previously ignored "stressor", *viz*. the impact of a changing climate. At Umgeni Water, a bulk water utility in South Africa, a process has been initiated to quantify potential impacts, initially on strategic catchments using daily physical-conceptual hydrological modelling. Preliminary results indicate that streamflow could increase by up to 2.6 and 5.3 fold by the year 2065 and 2100 respectively, mostly in the currently dry winter months. Furthermore, inter-annual variability could decrease. This could increase risks of flooding and compromise dam safety. Should additional streamflow improve water yields, climate change could potentially benefit cash flows by delaying capital expenditure on projects to improve assurance of supply. Regardless, it is imperative that the hydrological consequences of a changing climate be included in water development, disaster risk and system operating plans.

Keywords: *Climate Change, Water Resources Management and Planning, sustainable economic development, ACRU Agro-hydrological model, adaptation, Mgeni catchment in KwaZulu-Natal.*

1. INTRODUCTION

A water utility must provide a sustainable bulk supply of potable water to maintain livelihoods and sustain economic development in its region of supply. Sustainability implies that the risks associated with not being able to supply water are managed to maintain an acceptable assurance of supply. Numerous "stressors" that impact on the ability to supply water are considered when balancing water supply and demand. These stressors include, most importantly, the demand for water in the future. However, it has only recently become apparent in South Africa and elsewhere that many water resource managers have yet to include the impacts of climate change on water availability in their future scenario planning, this despite having being sensitised to the potential impacts since *ca*. 1988, as indicated by Schulze *et al*. (2005). The dire reality is that most water resource managers still rely on historic, sometimes vastly outdated hydrology on which to base decisions about future water resources in their development plans and risk management initiatives.

Clear evidence exists to support the notion that the climate is changing globally and that this will have an impact on water resources. Furthermore, contemporary assessments using General Circulation Models (GCMs) which provide an indication of possible future climates are starting to show a degree of consensus in their regional predictions. Changes in climate will be amplified in the water environment, where a relatively small change in precipitation will see average river flows and water availability increasing by 10-40% in some areas, while in others they will decrease by 10 – 30% (Muller, 2007). Africa is seen as one of several regions that will be most severely impacted where, according to the Intergovernmental Panel on Climate Change (IPCC) in its Fourth Assessment Report (IPCC, 2007), between 75 and 250 million people are projected to be exposed to increased water stress due to climate change by 2020. Climate change is projected to alter the magnitude and timing of rainfall and consequently runoff, thereby impacting on the reliability of current water management systems and water related infrastructure. This should be of primary concern to water utilities, along with possible secondary, although no less severe, risks which could include those related to disaster risk management such as droughts and floods.

In response to this, Umgeni Water in the province of KwaZulu-Natal in South Africa, the second largest water utility in that country, has developed a modelling framework to determine the possible impacts of a changing climate on water resources (Figure 1). An initial workshop (Umgeni Water, 2006a) was held to introduce the water utility to climate change and the potential effects on, *inter alia*, water resources. Several recommendations, including the need to model the impact of climate change on water resources emanated from this workshop. The potential risks associated with climate change also began to feature prominently at a corporate level and have been officially included in the top 3 risks facing the utility in its corporate business plan for 2008/9 – 2012/13.

This paper provides a preliminary assessment of the impacts of a changing climate on the water resources of the main water supply catchment, *viz.* the Mgeni catchment, thereby addressing steps 1 to 3 of the framework in Figure 1. This involved setting up a daily hydrological model to simulate the impact of current and future climate scenarios on the water resources of the Mgeni catchment. To enable this, data describing rainfall patterns, land cover and its different water use patterns, other water uses such as irrigation, reservoir abstractions, wetlands, soils, and evaporation were configured as a base scenario in the *ACRU* Agrohydrological model. Simulated streamflows from this base scenario are compared with observed streamflows at 4 weirs in the upper catchments to verify the model's accuracy. Three rainfall simulations from a GCM, and increased evaporation rates have been added to the base scenario to simulate future water resource scenarios. These findings are summarised and discussed in light of contemporary research. Based on these findings, some options for adaptation in order to minimise the consequences are introduced. The paper follows work by Summerton and Gillham (2007) and is largely based on an internal report (Summerton, 2008) by the water utility.

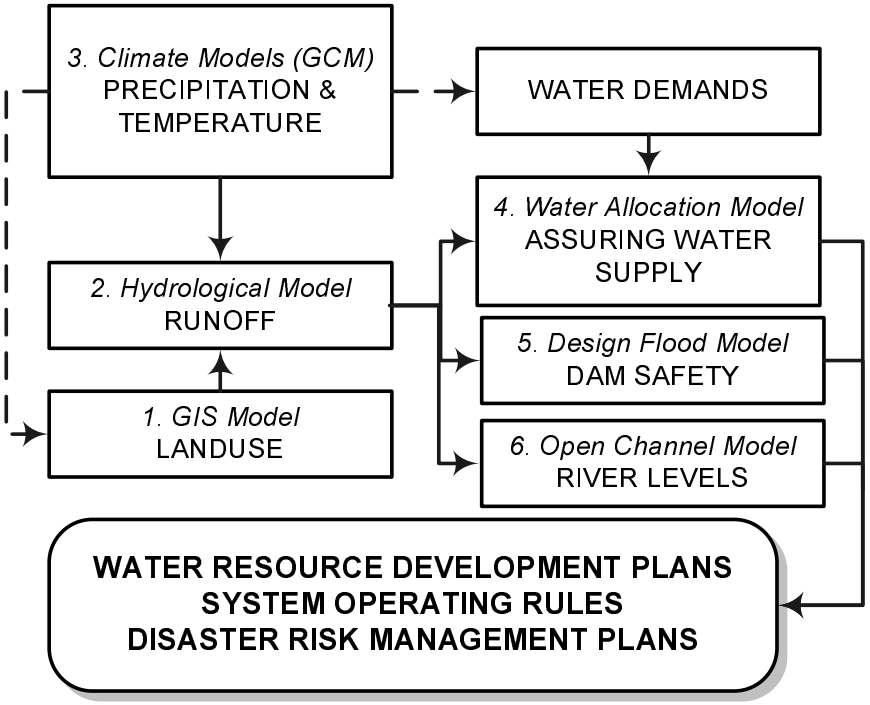

Figure 1. Modelling framework to determine the impacts of a changing climate on water resources.

2. THE MGENI CATCHMENT AND ITS WATER RESOURCES

The 4400km^2 Mgeni catchment provides water resources to the economic hub of Pietermaritzburg and Durban in KwaZulu-Natal, South Africa (Figure 2). Although the Mgeni catchment constitutes only 0.33% of South Africa, it supplies water to nearly 15% of South Africa's population and produces *ca*. 20% of the gross domestic product (Schulze *et al*., 2004). The area can be described as having a warm, sub-tropical climate. Summer (December – March) is generally hot and humid with daily maximum temperatures averaging 28˚C, and currently experiences the majority of the highly variable annual rainfall, while winter, with average daily maxima of 23˚C, is generally dry. Mean Annual Precipitation (MAP) ranges from more than 1200 mm in the upper parts of the Drakensberg mountains in the west, to around 700 mm towards the Indian ocean in the east.

During the 2006/07 financial year ending in June 2007, a total of 363.63 million m^3 of water was treated and supplied to some 5 million people in this area by Umgeni Water. The risks associated with the supply of water are currently based on a 99% level of assurance; however in recent years this has periodically not been achievable due to several "stressors" on the water resource. The main stressor has been an increasing demand for water since 2002 due mainly to development in the area. Indications are that this demand will continue to increase at between 2 - 5% per annum until 2011. These forecasts however do not include the impacts of a changing climate and consequential rainfall patterns which have started becoming anecdotally evident. Sound management of this catchment's water resource is therefore critical to the sustainability of the utility's operations, hence the need to build sound hydrological modelling systems to determine the likely impacts of stressors such as climate change on the water resources of the future.

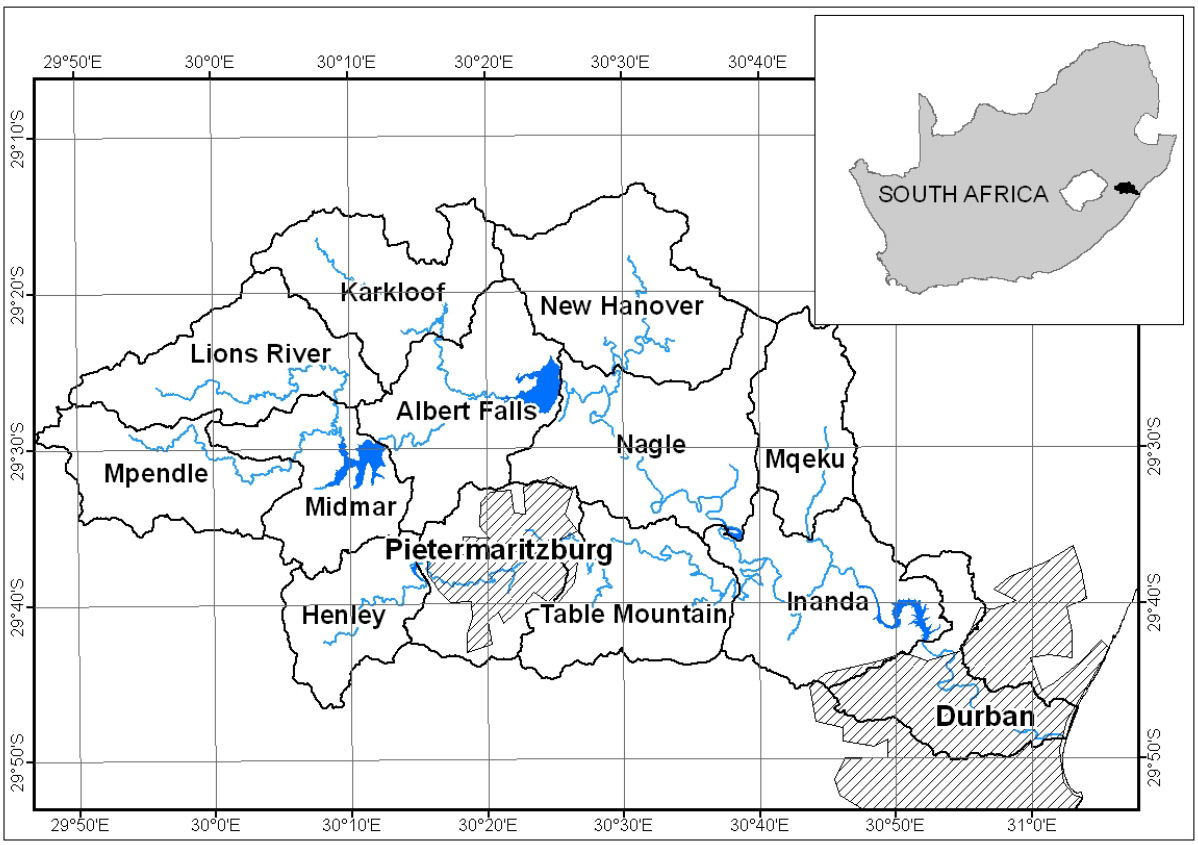

Figure 2. The Mgeni catchment, KwaZulu-Natal, including its 13 management catchments.

3. CONFIGURATION OF THE HYDROLOGICAL MODELLING SYSTEM

Assumptions

Owing to the complexities associated with hydrological modelling, several assumptions were necessary to obtain a model that would realistically simulate natural conditions but not be too cumbersome to apply. These include:

(a) Water demands are not dynamically changed, and 2007 levels are used for all future scenarios,
(b) Water use by land cover remains static for the entire simulation period since the accurate prediction of future land covers is almost impossible, and consequently, and
(c) Any feed-backs or –forwards that would be associated with land cover changes due to a changing climate have not been modelled.

Model Selection

Because of the strategic importance of the Mgeni catchment it was deemed necessary to invest in a model that could not only fulfil the requirements of this project, but of future hydrological studies as well. Furthermore, when modelling the impacts of climate change on hydrological responses, the model should, according to Schulze (2005):

(a) explicitly model the dynamics of the runoff generating mechanisms,
(b) distinguish between channel-based and landscape-based processes,
(c) be verified for a range of climatic regimes, land use practices and spatial scales, and
(d) simulate at a daily time step.

Consequently, based on a high degree of confidence in its ability to successfully model impacts of climate change on water resources in other simulations, the more complex *ACRU* Agrohydrological Modelling System (AAHMS) (Schulze, 1995 and updates) was selected for this study. The Amalgamation of Agro-Hydrological Modelling Groups (AAMG) application (Pott *et al*, 2007), was invaluable in the initial setup and configuration, particularly when data were available in a GIS format, as with all data sourced from Schulze (1997).

Base Data

Using base data such as daily rainfall from Lynch (2004), a detailed land cover map (Summerton, 2008) and associated water use parameters, irrigation and reservoir data based largely on the Department of Water Affairs and Forestry's (DWAF) Water Act Resources Management Service (WARMS) database, evaporation and soils information from the South African Atlas of Agrohydrology and – Climatology (Schulze, 1997) and abstraction and return flows from Umgeni Water's Water Resources Management (WRM) database as input, the base configuration was constructed by delineating the 13 management catchments into 1450 modelling subcatchments for the years 1960 – 2000 in order to run with the daily time step *ACRU* model.

Verification of Streamflow

Simulated streamflows were verified against observed data at the 4 management catchments with streamflow records. Criteria of R^2 values of at least 0.75 and an average error in daily flow of less than 0.2 mm equivalent were met at all 4 subcatchments. At these gauging weirs, highly acceptable simulations were achieved with R^2 values between 0.75 and 0.90 and average errors in flows of between -0.07 and 0.13 mm/day.

4. RAINFALL AND EVAPORATION AS DRIVERS OF CLIMATE CHANGE

For the purposes of predicting future water resources scenarios, future rainfall and temperature patterns are derived from GCMs and are used in hydrological modelling. For the purposes of this project, the Geophysical Fluid Dynamics Laboratory (GFDL) GCM was selected based on the premise that of the six GCMs from the IPCC's Fourth Assessment Report (IPCC, 2007) assessed for southern Africa by Lumsden and Schulze (2007), the GFDL was considered the "middle of the road" scenario. The GFDL GCM is based on the SRES A2 emissions scenario defined by the IPCC (2001), where efforts to reduce global emissions this century are assumed to be relatively ineffective. The Climate Systems Analysis Group (CSAG) at the University of Cape Town used empirical downscaling techniques to downscale the GCM data to a quarter of a degree (*ca*. 25 km^2) resolution. In order to represent the regional climate scenarios at a Quaternary Catchment scale, pixels were selected by Lumsden and Schulze (2007) from regional scenario grids to represent each of the 1946 Quaternary Catchments covering southern Africa. These same pixels and their associated rainfall time series were assigned to each of the 1450 modelling catchments in the Mgeni. For temperature and evaporation changes, plausible estimates were derived from discussions with Schulze (2008). Subsequently, simulations on three climate scenarios were performed, *viz*:

(a) Current Climate Scenario (1960 – 1990) - Based on model configuration with rainfall input from the GFDL GCM replacing *de facto* rainfall data,
(b) Intermediate Future Climate Scenario (2046 – 2065) - Based on Scenario (a), but for an intermediate climate by using GFDL rainfall, and a plausible increase in reference potential evaporation of 6% to mimic a temperature increase of 1.5˚C, and
(c) Distant Future Climate Scenario (2081 – 2100) - Based on Scenario (b), but for a future climate by using GFDL rainfall, a temperature increase of 2.7˚C and a potential evaporation increase of 11%.

Although the GFDL GCM was used for this preliminary study, discussions with Tadross (2008) confirmed that it is imperative that the remaining GCM models be assessed before reaching a conclusive decision on future impacts. Future work should also include advances in the downscaling process to individual station level (as opposed to pixels) available at some 2600 rainfall and 409 daily minimum and maximum temperature stations throughout the country.

5. STREAMFLOW AS A RESPONSE TO CLIMATE CHANGE

For this preliminary assessment, the focus is on accumulated streamflows as the main response to a changing climate. The magnitudes of accumulated streamflows are assessed by means of ratios between intermediate future and current, and distant future and current streamflows. The use of ratios is considered prudent until such time as convergence is shown between several different GCMs, and confidence is built up in the ability of GCMs to predict magnitudes of changes more accurately. In a similar manner the coefficient of variation (CV %) has been used to depict variations about the mean as an indicator of climatic and hydrological risk. Furthermore, to obtain an indication of whether any shifts in accumulated streamflows patterns occurred, monthly patterns were analysed at 4 key locations in the catchment *viz.* the Midmar, Albert Falls, Nagle and Inanda dams.

Magnitude of streamflow change

Figures 3 and 4 contain mapped ratios of mean annual streamflows for intermediate future to present climates and distant future to present climates, respectively. Using the GFDL GCM, indications are that it is likely that streamflows will increase between 1.3 and 2.6 fold by 2065, and 1.7 and 5.3 fold by 2100. Higher increases are observed in catchments on main rivers and major tributaries due to accumulation of water throughout the catchment, particularly the Nagle management catchment. The lowest increase is *ca.* 1.35 and 1.7 fold by 2065 and 2100 respectively for those catchments not on the main channel where accumulation of streamflow is less. These results add overwhelming support to contemporary indications of a wetter eastern South Africa in future climates, although the magnitudes may be excessive and require further investigation.

Inter-annual variability

Figures 5 and 6, displaying ratios for intermediate and distant future to the present climate's annual coefficient of variation, indicate that generally there will be less year-on-year variation in flows under future GFDL climate scenarios. This suggests that in future climates, streamflows are projected to become less variable, and therefore more predictable, especially in the key Nagle management catchment. This projected decline in variability could be partly attributable to lower variability in intra-annual streamflows as a result of increases in streamflows in the low flow winter months. The exceptions are the Lions and Mpendle management catchments where in the intermediate climate, variability could increase.

Distribution of monthly streamflows

Figures 7 and 8 contain ratios of intermediate future to present as well as distant future to present mean streamflows into the 4 key dams for each of the 12 months. Streamflows are predicted to be generally greater in all months of the year. This is especially true during the winter period with ratios of around 3 and 6 for 2065 and 2100 respectively, but above 10 for Nagle Dam. Winter is generally the period of low flows and consequently these results allude to a possible reduction in intra-annual variability. In some respects this is a beneficial result since the increased streamflow could be distributed better over the year rather than occurring during the already wet summer periods with increased possibility of flooding. Figures 9 and 10 contain ratios of intermediate future to present and distant future to present streamflows (95th percentile) for the 12 months of the year. Peak flows are predicted to increase during the winter months, especially into Nagle dam which, depending on actual streamflow volumes, may present issues concerning dam safety. During the summer months, some peak flows may even be lower than under current climatic conditions.

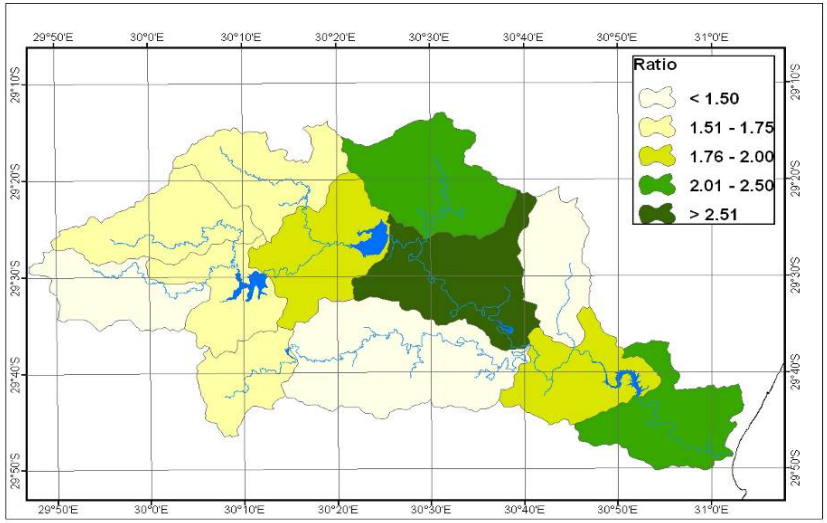

Figure 3. Ratios of intermediate future to present climate Mean Annual Accumulated Streamflows per management catchment.

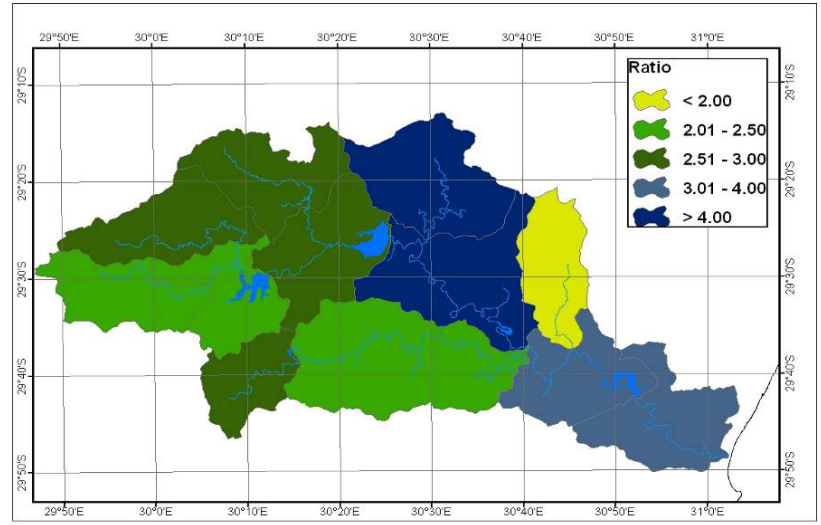

Figure 4. Ratios of distant future to present climate Mean Annual Accumulated Streamflows per management catchment.

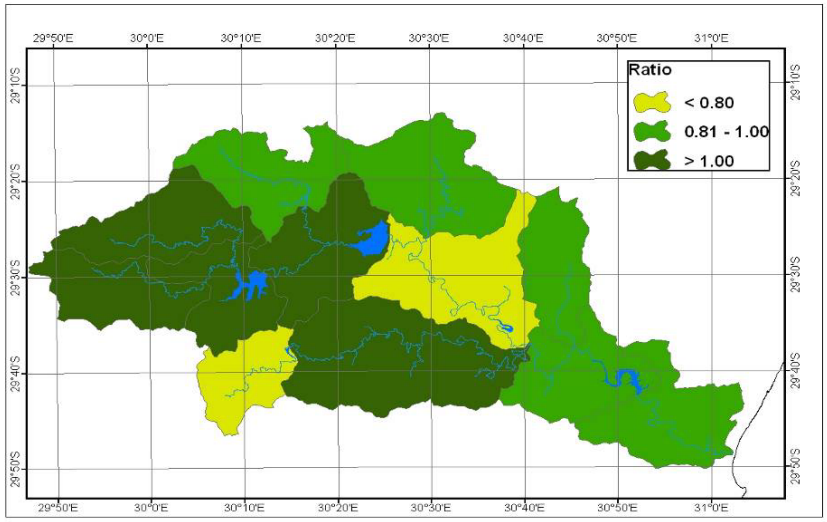

Figure 5. Ratios of intermediate future to present climate Inter Annual CV of Accumulated Streamflows per management catchment.

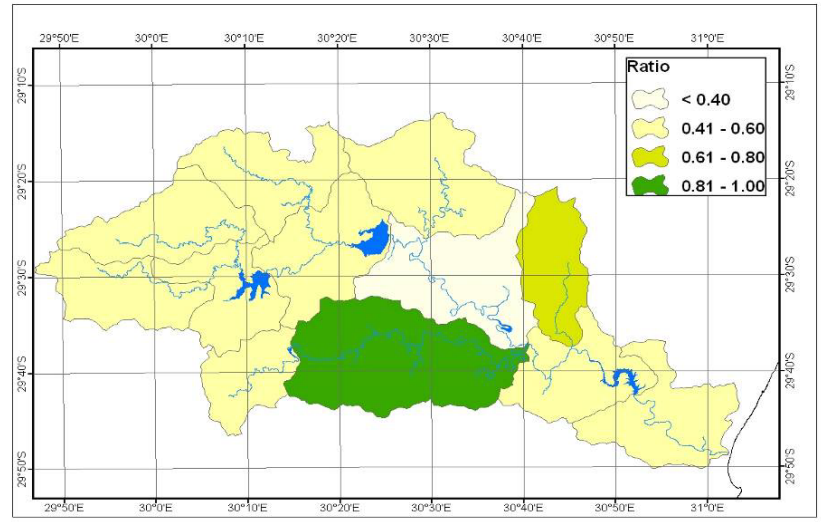

Figure 6. Ratios of distant future to present climate Inter Annual CV of Accumulated Streamflows per management catchment.

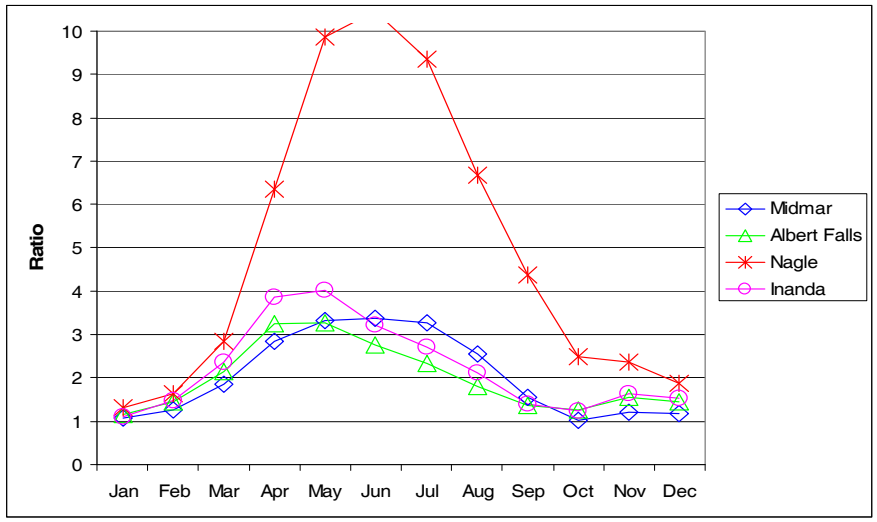

Figure 7. Ratios of intermediate future to present climate means of monthly streamflows.

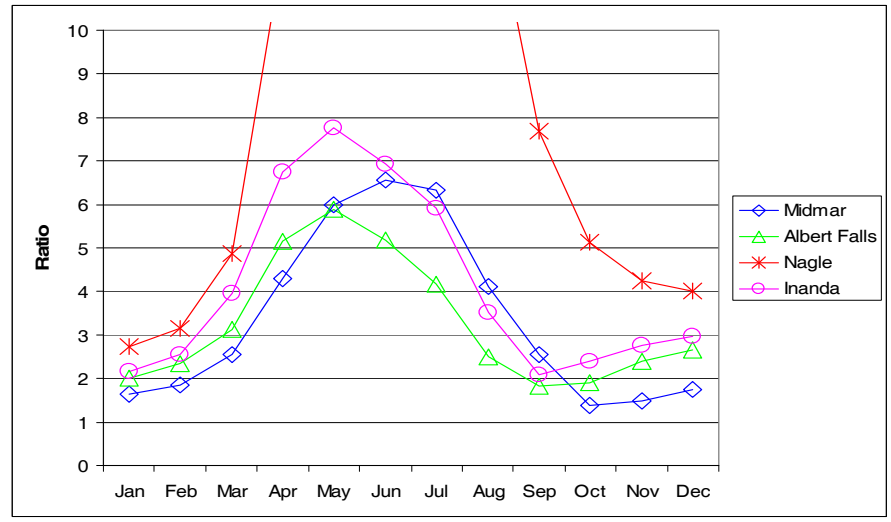

Figure 8. Ratios of distant future to present climate means of monthly streamflows.

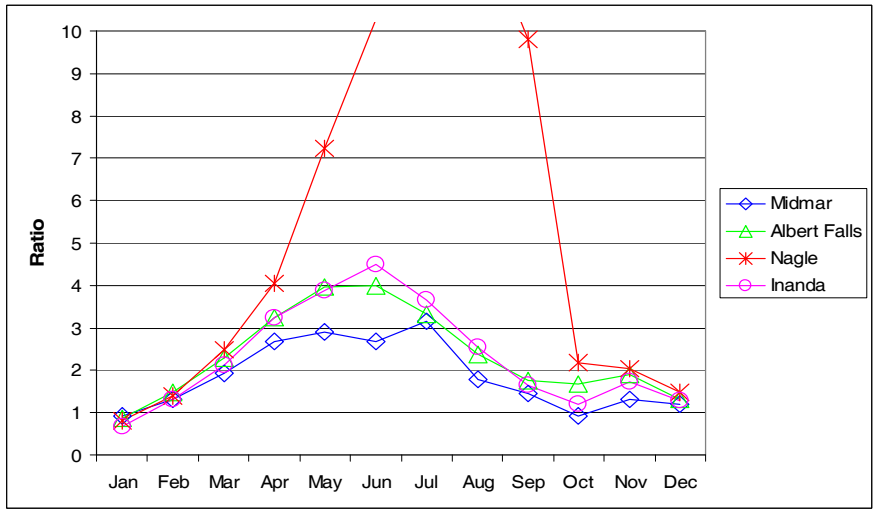

Figure 9. Ratios of intermediate future to present climate 95th percentiles of monthly streamflows.

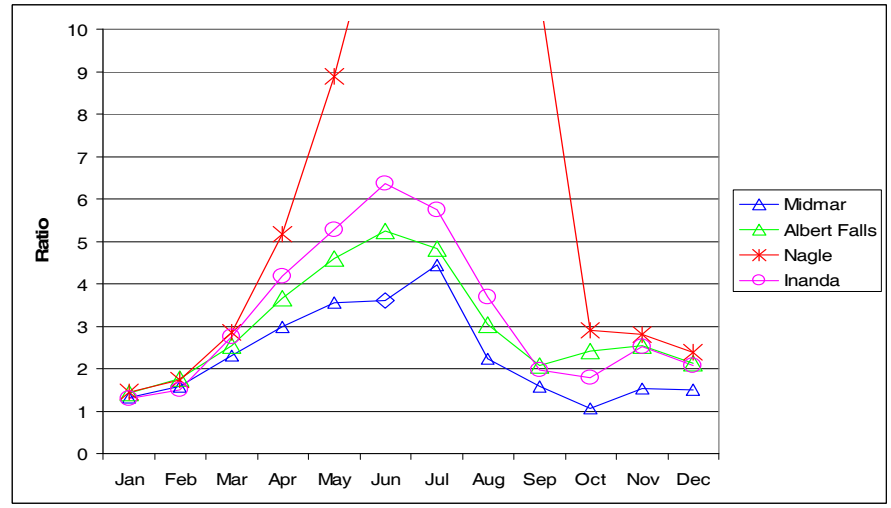

Figure 10. Ratios of distant future to present climate 95th percentiles of monthly streamflows.

6. CONCLUSIONS

A daily hydrological modelling system for the Mgeni catchment in KwaZulu-Natal, South Africa has been configured at a finer resolution than ever before. The potential applications of this system are vast. However, this initial application has focused on a preliminary assessment of the impacts of a changing climate on streamflows using the GFDL GCM. Notwithstanding the acknowledgement that several aspects of the modelling process are still rudimentary and need improvement, the results do indicate several trends.

Indications are that streamflow will generally increase in the currently relatively drier, low flow winter months by up to 2.6 and even 5.3 fold by 2065 and 2100 respectively, thereby resulting in a smooth supply of streamflow all year round. Inter-annual variability could decrease. Generally, the potential impacts that require further attention would be that of flooding and dam safety. Furthermore, although it would seem that additional streamflow should be beneficial to the supply of water at particular assurance of supply levels, the current capacity of the dams may not be appropriate to harness this extra capacity. If sizing is adequate, there may be benefits in terms of delayed capital expenditure on future water resource supply projects. It is this seasonal shift that could also impact on water quality both in the rivers and in dams due to decreased variability.

In addition to the generalised potential impacts presented above, there are several hotspot catchments within the Mgeni catchment that will require closer attention. Most critical is the Nagle catchment where future mean and peak streamflows have the potential to increase the most. In addition, the Lions and Mpendle catchment where in the intermediate future climate, variability could increase, may require closer observation and management.

7. THE WAY FORWARD

It is imperative that the integrity of the configuration, and therefore the confidence in these results be improved. Key to this requirement is the inclusion of other readily available GCM scenarios that output daily rainfall and temperature values at a climate station (rather than averaged pixel) level. These only became available recently, after the end of this study. Other improvements to the configuration could include using physically based reference potential evaporation calculations, modelling land cover in a dynamic manner with feedback loops from hydrological modelling, and making dynamic changes to the water demands.

Secondly, the hydrological scenarios presented here should be included in the utility's water yield and assurance of supply assessments to identify whether the existing system is capable of harnessing the additional water resources, were these to materialise. Key to this process will be the use of GCM output for the period up to 2040, i.e. the horizon which is influenced by current planning, Should additional streamflow result in additional yield and assurance of supply, the potential benefit of climate change is that capital projects could be delayed.

Additional streamflow could well increase the risks associated with flooding and compromise dam safety, particularly in catchments already prone to flooding. Areas with higher risk include the Nagle management catchment where future mean and peak streamflows have the potential to increase the most, as well as the Lions and Mpendle management catchments where in the intermediate future climate, variability could increase. These areas may require closer observation and management and possibly even a need to consider real time water management systems.

Lastly, in order for the results of this study to be effective, it is imperative that climate change be included water resource development plans, operating rules and disaster risk management plans. These should include adaptation strategies and risk management practices to maximise resilience

against the impacts of climate change on water resources. A framework for this approach is readily available in Umgeni Water (2006b). Mitigation measures, including revision of antecedent precipitation indices to enhance forecasts of flood impacts, reviewing of engineering design criteria and dam safety issues, should be addressed.

8. REFERENCES

IPCC, 2001. Climate Change 2001: Impacts, Adaptation and Vulnerability. Intergovernmental Panel on Climate Change, Working Group II Contribution to the Third Assessment Report of the IPCC. Geneva, Switzerland.

IPCC, 2007. Climate Change 2007: Synthesis Report, Contribution of Working Groups I, II and III to the Fourth Assessment Report of the IPCC, Geneva, Switzerland.

Lumsden, T.G. and Schulze, R.E., 2007. Evaluation of potential changes in Hydrologically Relevant statistics of rainfall in southern Africa under conditions of climate change. *In:* Proceedings of the Thirteenth South African National Hydrological Symposium. Cape Town, RSA.

Lynch, S.D., 2004. Development of a Raster Database of Annual, Monthly and Daily Rainfall for Southern Africa. Water Research Commission, Pretoria, RSA, Water Research Commission Report 1156/1/04. pp 78.

Muller, M., 2007. Climate Change Adaptation and Integrated Water Resource Management. Global. Water Partnership, policy brief number 5.

Pott, A.J., van der Merwe, R.J., Meier, K.B. and Summerton, M.J., 2007. GIS Integrated linking of the *ACRU* and Mike Basin model. *In:* Proceedings of the Thirteenth South African National Hydrological Symposium. Cape Town, RSA.

Schulze, R.E., 1995. Hydrology and Agrohydrology: A Text to Accompany the *ACRU* 3.00 Agrohydrological Modelling System. Water Research Commission, Pretoria, RSA, Report TT 69/9/95. pp 552.

Schulze, R.E., 1997. South African Atlas of Agrohydrology and -Climatology. Water Research Commission Report, Pretoria, RSA, Report, TT82/96. pp 276.

Schulze, RE, Lorentz, SA, Kienzle, SW and Perks, L., 2004. Case Study 3: Modelling the Impacts Of Land Use And Climate Change On Hydrological Response In The Mixed, Underdeveloped/Developed Mgeni Catchment, Southern Africa. *In*: Kabat, P., Claussen, M., Dirmeyer, P.A., Gash, J.H.C., Bravo de Guenni, L., Meybeck, M., Pielke, Sr., R.A., Vörösmarty, C.J., Hutjes, R.W.A. and Lütkenmeier, S. (eds.), Vegetation, Water, Humans and the Climate: A New Perspective on an Interactive System. Springer, Heidelberg, Germany.

Schulze, R.E., Lumsden, T.G., Horan, M.J.C., Warburton, M. and Maharaj, M., 2005. An Assessment of Impacts of climate change on Agrohydrological Responses over Southern Africa. *In*: Schulze, R.E. (Ed) climate change and Water Resources in Southern Africa: Studies on Scenarios, Impacts, Vulnerabilities and Adaptation. Water Research Commission, Pretoria, RSA, Water Research Commission Report 1430/1/05. Chapter 9, 141 - 189.

Schulze, R.E. (Ed), 2005. Climate Change and Water Resources in Southern Africa: Studies on Scenarios, Impacts, Vulnerabilities and Adaptation. Water Research Commission, Pretoria, RSA, Water Research Commission Report 1430/1/05.

Schulze, R.E., 2008. School of Bioresources Engineering and Environmental Hydrology. University of Natal, Private Bag X01, Scottsville, 3209, South Africa. Personal communication.

Summerton, M.J. and Gillham, S.W., 2007. A Water Utility's approach to addressing the potential impacts of Climate Change. *In*: Proceedings of the Thirteenth South African National Hydrological Symposium. Cape Town, RSA.

Summerton, M.J., 2008. A Preliminary Assessment of the Impact of Climate Change on the Water Resources of the Mgeni Catchment. Umgeni Water, Planning Services, Engineering and Scientific Services, Pietermaritzburg, RSA. Report Number 160.8/R001/2008.

Tadross, M., 2008. Climate Systems Analysis Group, University of Cape Town, Private Bag X3, Rondebosch, 7701. Personal communication.

Umgeni Water, 2006a. Recommendations for addressing Climate Change at Umgeni Water, Planning Services, Engineering and Scientific Services, Pietermaritzburg, RSA. Version 9 January 2006.

Umgeni Water, 2006b. A Framework for Disaster Risk Management. Prepared for the Umgeni Water Risk Committee by Planning Services, Engineering and Scientific Services, Pietermaritzburg, RSA. Version 1, November 2006.

A GIS-Based Decision-Making Methodology for Evaluation of Environmental Justice Impacts of Community Infrastructure Projects

James S. Cole[1], M.ASCE, Kathleen M.Trauth[2], Ph.D., P.E., M.ASCE, Yingkui Li[3], Ph.D.

[1]Dept of Civil & Environmental Engineering, University of Missouri, E2509 Lafferre Hall, Columbia, MO 65211; PH (573) 884-7859; FAX 573-882-4784; email: jscole@mizzou.edu
[2]Dept of Civil & Environmental Engineering, University of Missouri, E2509 Lafferre Hall, Columbia, MO 65211; PH (573) 882-5843; FAX 573-882-4784; email: trauthk@missouri.edu
[3]Dept of Geography, University of Missouri, 8 Stewart Hall, Columbia, MO 65211; PH (573) 882-8370; FAX (573) 884-4239; email: liyk@mizzou.edu

Advances in geospatial analysis technology have resulted in new data-gathering techniques for environmental justice (EJ) assessments. Frequently investigated metrics relate to race and income due to relatively easy availability of census data. Geographic information systems (GIS) offer the ability to embed these data in maps in order to better recognize patterns that may designate discriminatory practices. Many other indicators of disproportionate negative effects exist and can be assessed using GIS. Map-based analysis results can also provide data on proximity for various phenomena. However, expert human analysis is required to interpret images which may lead to arbitrary or subjective conclusions. Researchers at the University of Missouri have developed a GIS methodology to overcome the limitations of image-based analyses for evaluating spatial relationships in community infrastructure by employing metrics such as travel time and distance to jobs, education, healthcare, and food markets in order to move beyond identification of those affected to quantification of the impacts on their lives. That is, to quantify the answers to the questions: How does daily life change as a result of infrastructure improvements? How do the impacts on these parameters compare to the impacts of alternative projects? Manifestations of these impacts have been transformed into quantifiable data that will offer planners greater decision-making confidence. Mathematical representations in the form of indices have been developed to offer a consistent approach to infrastructure problems as they relate to EJ.

INTRODUCTION

The Bill Emerson Memorial Bridge project, linking southeast Missouri with southern Illinois across the Mississippi River, was analyzed as a demonstration of the methodology used to study community impacts resulting from transportation infrastructure. The bridge's western approach, located in Cape Girardeau, Missouri, has bisected the immediate community, altering mobility and access to various elements of the neighborhood (Perry 2003). A GIS was used to create quantifiable parameters describing changes in inhabitants' daily life in terms of access to transportation, education, healthcare and food that result from the impacts of this

transportation infrastructure project. Quantification of impacts has not been widely integrated into planning processes (Perry 2003). Identification of these impacts within their spatial context and expression through a numerical representation provides a framework for robust EJ impact analysis and the ability to incorporate this system for other community infrastructure projects.

BACKGROUND

The methodology for evaluating EJ impacts was adapted from a GIS-based analysis of nuclear materials transportation conducted by University of Missouri Researchers. The following steps were identified in the existing methodology: (1) identification of potential parameters for analysis (2) collection and analysis of spatial information (3) assessment of the utility of the spatial information for decision-making (4) assessment of the completeness of the set of parameters (and the subsequent identification, collection, and analysis of additional data, as appropriate), (5) data standardization, (6) weighting of parameters, and (7) aggregation of parameters (Divate et al. 2007a, b). This framework was applied to aid in identifying parameters and quantifying social impact analyses to aid in decision-making for infrastructure planners.

METHODS

The area of interest includes the low-income and minority demographics described in Executive Order 12898 (Clinton 1994). The lowest income and highest minority population percentages coincide in the neighborhood where the bridge approach has been constructed (Figure 1, 2). These census block groups were selected to evaluate possible changes in pedestrian travel as a result of the highway improvements.

One goal of this decision-making tool is to quantify impacts so that individuals can attempt to avoid locales susceptible to disproportionate adverse affects in route planning. Therefore, the parameters selected must be measurable and be expressible in a non-subjective numerical format. As a demonstration of one set of parameters, travel distance and time were selected. The parameters are actually two representations of one metric. Pedestrian travel time simply represents travel distance as a rate per unit time. Thus, the ratio of each parameter change, before and after infrastructure improvements, is identical. Travel time is calculated as:

$$T = (D / S) * (60 \text{ min} / 1 \text{ hr})$$

where T = travel time (min)
D = travel distance (mi)
S = travel rate (mph)

The pedestrian travel rate, S was approximated at 3 mph which is a value between that of average foot travel for men and women (Noland 1996).

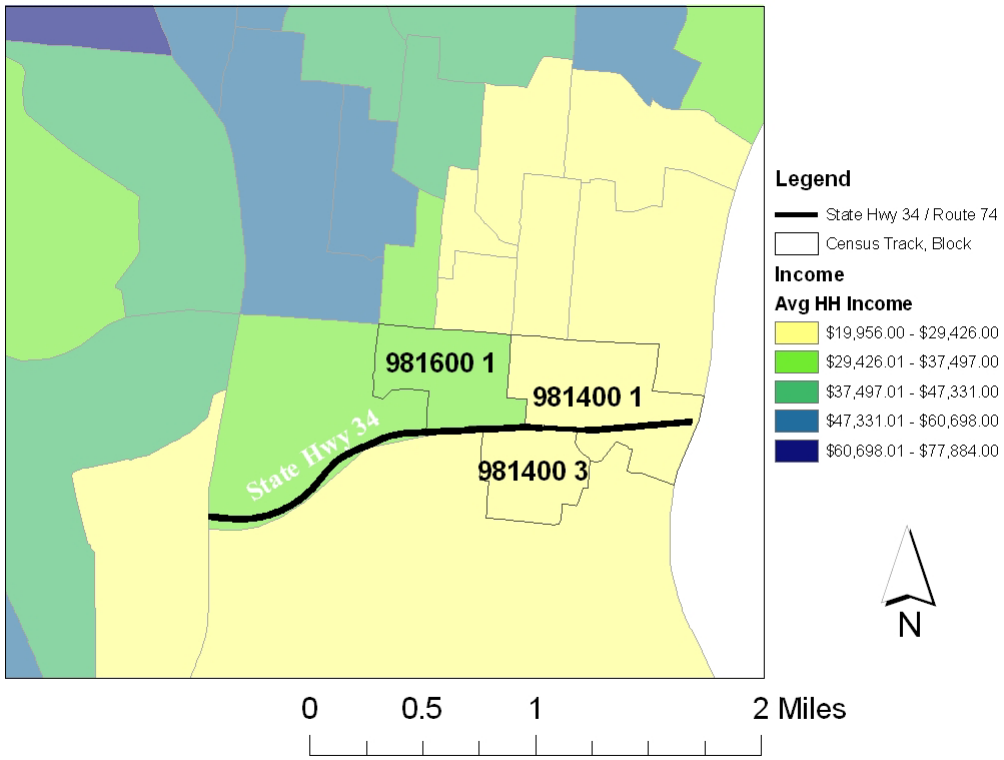

Figure 1. Map of Cape Girardeau income distribution.

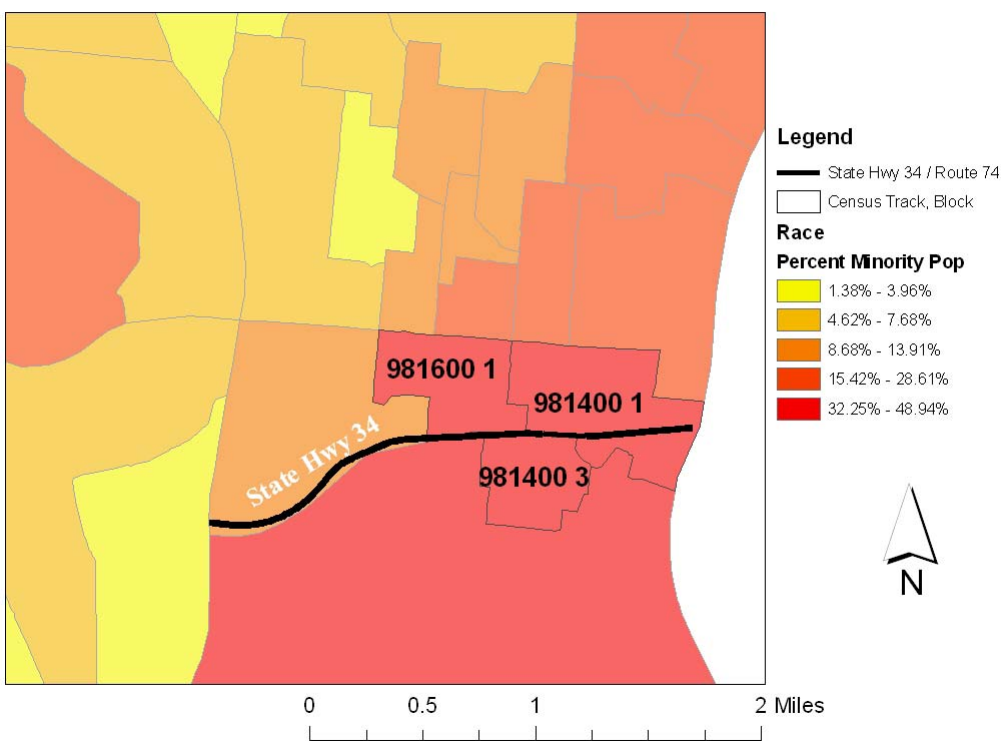

Figure 2. Map of Cape Girardeau minority population distribution.

Spatial information was collected online from the Center for Applied Research and Environmental Systems at the University of Missouri (CARES 2008). Data collected includes aerial images, maps, transportation routes, administrative and political boundaries, socioeconomic and census data (US Census 2000), and site spatial locations. GIS software was used to analyze distance measurements (ESRI 2006). Pedestrian travel was determined by measuring the straight-line distance on the centerline of street travel routes. Measurements begin at the centroid of census blocks and proceed to a destination by either the shortest previously available street path or the shortest path available after completion of the highway project. An alternative approach involves reducing the block group to quadrants to further identify areas most vulnerable to modified mobility. Aerial maps of the selected areas show the census blocks, the highway route and example site locations (Figure 3, 4).

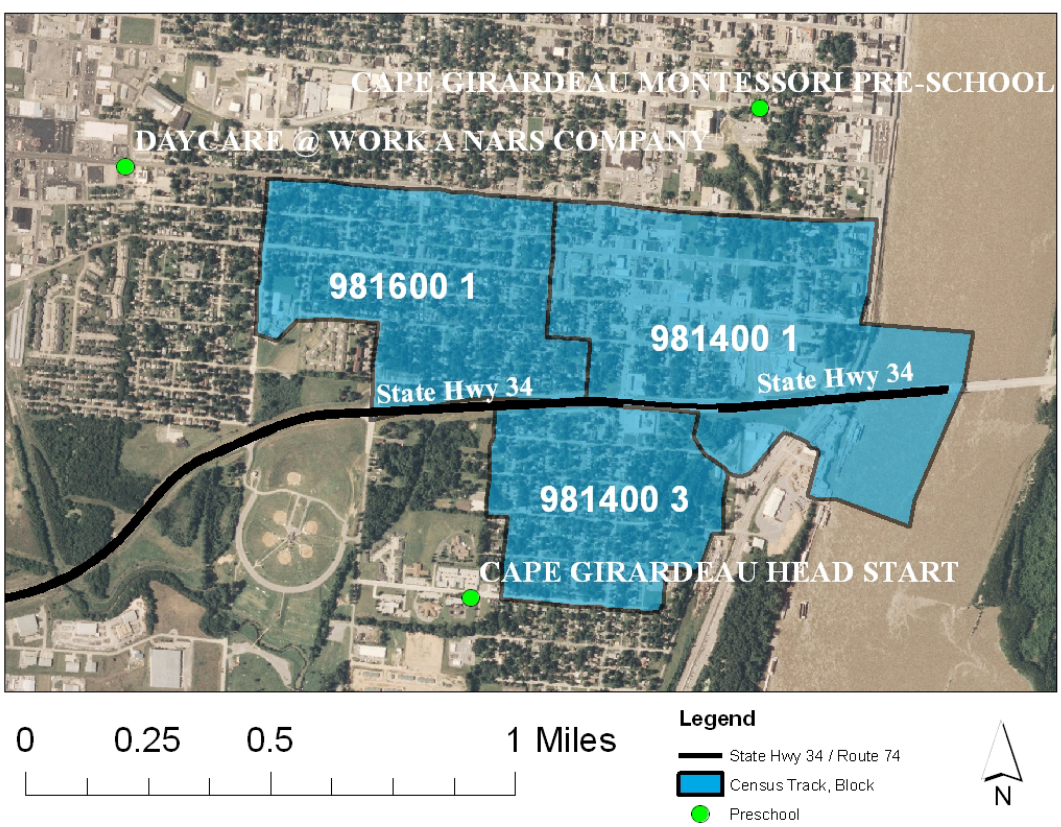

Figure 3. Aerial map of Cape Girardeau and area of interest.

This analysis may fit well within the social impact assessment portion of the design process particularly if it is not addressed along with motorized traffic engineering. Pedestrian traffic patterns have traditionally played a minor role in transportation infrastructure planning and adding this approach may help to eliminate some human impacts during the planning process (Noland 1996).



Figure 4. Close up aerial image of the highway and neighborhood.

Values are normalized using an index ranging from 0 to 1. Pedestrian Travel Index Value, N is calculated as:

$$N = (X_i - X_{min}) / (X_{min} - X_{max})$$

where N = Pedestrian travel index
X_i = the original travel value
X_{min} = the lowest travel change percentage for destination in a category (e.g. healthcare) for all block groups.
X_{max} = the greatest travel change percentage for destination in a category (e.g. healthcare) for all block groups.

These index scores can be compared for various alternative projects in a large array of categories to evaluate impacts and assist in selecting a proposal with the smallest overall impact. Alternatively, the process of comparison could be used to guide the formulation and evaluation of alternative proposals that address the specific impacts identified.

Results

Trip distance, D, travel time, T, percent difference, and the pedestrian travel impact index value, N, for Block Group 9814003 are shown in Table 1. Index results for all three block groups are displayed in Table 2.

The healthcare destinations selected include the three nearest hospitals and the county health clinic. Pedestrian routes to these locations remained unchanged with the highway construction, so travel was not impacted because the shortest pedestrian travel path did not change for any of the block groups.

However, access to some education sites was impacted. The nearest elementary, middle and high schools were selected along with the neighborhood Head Start preschool. The elementary and middle schools travel routes were modestly impacted for one block group. The schools are located northwest of Block Group 9814003 and previously the shortest route to the schools occurred along side streets that are no longer contiguous. Instead, pedestrians must now first travel due north from the center of the block group in order to cross Highway 34 before heading west.

Two large chain food stores and two smaller local groceries were selected to evaluate access to food. Again, only Block Group 9814003 appeared to be impacted by changes in pedestrian travel. Perhaps because nearly all food stores in the area are located northwest of the area of interest. In an online Yellow Pages search, 16 out of 17 grocery outlets listed in the zip code were located northeast of the block group and all were positioned outside of it. One grocer, Cauble & Fields, was located on a side street in Block Group 9814001, north of the highway. Access to this store was only impacted for Block Group 9814003 by a small distance (approximately 0.11 miles). However, its proximity relative to other stores (on average 2 miles away) may indicate that any changes in access to this store could prove significant, particularly to elderly or disabled pedestrians.

Table 1. Example of inputs for Pedestrian Travel Impact Index for census block group 9814003.

Block 9814003 **Destination**	**Before / After Trip Distance, D (mi)**	**Before / After Travel Time, T (min)**	**Travel Time Change (%)**	**Pedestrian Travel Impact Index Value, N**
Healthcare				
SE MO Hospital	2.02	40.40		
	2.02	40.40	0.00%	0.00
Landmark Hospital	2.18	43.60		
	2.18	43.60	0.00%	0.00
St. Francis	3.24	64.80		

Medical Center	3.24	64.80	0.00%	0.00
Cape Giradeau Rural	0.49	9.80		
County Health Clinic	0.49	9.80	0.00%	0.00
Education				
Cape Girardeau	0.46	9.20		
Head Start	0.46	9.20	0.00%	0.00
Jefferson Elementary	1.37	27.40		
School	1.41	28.20	2.92%	0.44
Jackson Middle	1.45	29.00		
School	1.53	30.60	5.52%	0.83
Cape Central	2.83	56.60		
High School	2.83	56.60	0.00%	0.00
Groceries				
Albertson's	1.96	39.20		
	2.02	40.40	3.06%	0.14
ALDI	1.97	39.40		
	2.03	40.60	3.05%	0.14
Cauble & Field	0.52	10.40		
Fruits, Veg & Groc	0.63	12.60	21.15%	1.00
Fenny's Mexican	1.95	39.00		
Grocery	2.03	40.60	4.10%	0.19

Table 2. Comparison of Pedestrian Travel Impact Index by Block Group.

Destination	**9814001**	**9814003**	**9816001**
Healthcare	**N**	**N**	**N**
SEMO Univeristy Hospital	0.00	0.00	0.00
Landmark Hospital	0.00	0.00	0.00
St. Francis Medical Center	0.00	0.00	0.00
Cape Girad. Rural Cnty Health Clinic	0.00	0.00	0.00
Education			
Cape Girardeau Head Start	0.00	0.00	1.00
Jefferson Elementary School	0.00	0.44	0.00
Jackson Middle School	0.00	0.83	0.00
Cape Central High School	0.00	0.00	0.00
Groceries			
Albertson's	0.00	0.14	0.00
ALDI	0.00	0.14	0.00
Cauble & Field Fruits, Veg & Groc	0.00	1.00	0.00
Fenny's Mexican Grocery	0.00	0.19	0.00

Because possible impacts on Block Group 9814003 were identified during a first analysis, a second investigation was conducted on this block group. It was divided into quadrants and distance measurements were performed starting from the street intersection nearest the centroid of each quadrant. Index values were developed using only minimum and maximum values from block group 9814003 quadrants. This moved the distance measurement start point from Sprigg St, the only path for highway crossing in 9814003, to various smaller neighborhood streets (Figure 4).

Each block group quadrant was impacted differently. The greatest impacts occurred at the NW and SW quadrants. Figures 3 and 4 show that the western portion of the block group is bound by the highway on the north and parkland and an undeveloped area on the west. Access to food and educational destinations to the northwest is significantly impacted. For instance, the schools are located northwest of Block Group 9814003 but pedestrians are now required to first travel east in order to cross Highway 34 before traveling back to the west towards the elementary and middle school.

Table 3. Index values by quadrant for block group 9814003.

Block Group 9814003	**Pedestrian Travel Impact Index Value by Block Quadrant**			
Destination	**NE**	**NW**	**SW**	**SE**
Healthcare				
SEMO Univeristy Hospital	0.00	1.00	0.78	0.00
Landmark Hospital	0.00	0.00	0.00	0.00
St. Francis Medical Center	0.00	0.69	0.46	0.00
Cape Girad. Rural Cnty Health Clinic	0.00	0.00	0.00	0.00
Education				
Cape Girardeau Head Start	0.00	0.00	0.00	0.00
Jefferson Elementary School	0.00	0.87	0.43	0.00
Jackson Middle School	0.00	1.00	0.26	0.00
Cape Central High School	0.00	0.00	0.00	0.00
Groceries				
Albertson's	0.00	0.49	0.29	0.00
ALDI	0.00	0.50	0.30	0.00
Cauble & Field Fruits, Veg & Groc	1.00	0.00	0.00	0.83
Fenny's Mexican Grocery	0.37	0.37	0.21	0.00

CONCLUSION

This methodology offers the potential for enhanced evaluation of EJ impacts. Determining sites for travel distance measurements are particularly important. In block group 9814003, the centroid aligned with the major street that crosses the highway, allowing for access to the education and grocery outlets in the northeast area of the neighborhood and revealing little, if any, change in travel time. However, those most likely to be adversely affected by the highway project, live in the western two quadrants of the block group. When measurements are taken from the centroids of the northwestern and southwestern quadrants, impact index values increase dramatically. These areas and those in the adjacent block group 9816001 that have seen their previously linked streets severed by the highway expansion experienced the largest changes in travel time (Figure 4).

Greater impacts may exist on smaller streets or more remote parts of neighborhoods. Hospitals and other large amenities may presumable exist on major thoroughfares, while neighborhood grocers, individual healthcare offices, other small businesses or schools may be more likely to be located on smaller streets. Block groups that demonstrated no impacts when travel paths were measured from the block group's center, may indeed reveal potential pedestrians impacts when population density and distribution, existing pedestrian travel patterns, street layout, neighborhood geometry and arrangement relative to other spatial factors are included in the determination of a point of origin for measurement and analysis.

Future work in data collection and analysis methods for enhancing social impact assessments may include greater public involvement. An identified shortfall of the social impact assessment process is the lack of primary data collection (direct public involvement) while secondary data (e.g., census data) is relied upon greatly (Perry 2003). One means of increasing community involvement may be to survey or interview potentially impacted individuals in order to prioritize the importance of access to various elements in a neighborhood. Parameters could be weighted and used to guide planning alternatives and estimate potential impacts during a project design phase.

REFERENCES

CARES Interactive Maps. (2008). Cape Girardeau County. http://ims.missouri.edu/maproom/missouri/viewer.htm>(Dec 2, 2008)

Clinton, W. J. (President) (1994). "Federal actions to address environmental justice in minority and low-income populations." Executive Order 12898.

Divate, M., Trauth, K.M., and Li, Y. 2007a. "Methodology for quantifying risk factors impacting the transportation of nuclear materials utilizing GIS." 48th

Annual Meeting of the Institute of Nuclear Materials Management, Tucson, AZ, July 8-12.

Divate, M., Trauth, K.M., and Li, Y. 2007b. "Demonstration of a geographic information system methodology to quantify risk factors for the transportation of nuclear materials." 15th Int. Symposium on the Packaging and Transportation of Radioactive Materials, Miami, FL, October 21-26.

ESRI ArcMap, ArcCatalog. (2006). http://www.esri.com.

Noland, R. B. (1996). "Pedestrian travel times and motor vehicle traffic signals." Transportation Research Record, (1553), 28-33.

Perry, E. B. (2003). "Integration, status, and potential of environmental justice and the social impact assessment process in transportation development in Missouri." Dissertation. University of Missouri-Columbia.

Romero, M., Trauth, K.M., Li, K., Marrero, T.R. "A GIS-based analysis of wind speed, frequency, and direction on route selection for the transportation of nuclear materials." INMM 49th Ann. 200X.

United States Census (2000). U.S. Census Bureau, Dept. of Commerce.

Yellowpages.com. (2009). Online search. http://www.yellowpages.com/Cape-Girardeau-MO/Grocery-Stores/city-Cape-Girardeau?search_terms=grocery

A Pragmatic Cycle for Ongoing Water Resources Research and Management

Thomas L. Singleton[1], Stephen Bourne, P.E.[2], and Jack Hampson[3]

[1]PBS&J, 2639 North Monroe Street, Building C, Tallahassee, FL 32303; PH (850) 580-7929; FAX (850) 574-0251; email: tlsingleton@pbsj.com
[2]PBS&J, 2198 Goodwood Blvd, Smyrna, GA 30080; PH (404) 895-0753; FAX (770) 426-5316; email: sfbourne@pbsj.com
[3]PBS&J, 5300 W. Cypress, Suite 300, Tampa, FL 33607; PH (813) 281-8368; FAX (813) 281-0954; email: jchampson@pbsj.com

ABSTRACT

Organizations focused on managing water resources are recognizing the need to have tools for literature review, data integration, modeling, and decision support. Decision support systems (DSS) can help to meet these needs because they are aimed at integrating data and knowledge, evaluating management options in terms of organizational objectives and risk, and facilitating multiple-stakeholder decision making where competing objectives and risk preferences must be reconciled. Using the internet, organizations can share the costs and benefits of existing and newly developed information, theories, and technologies among a broad, diverse user group.

This paper discusses an approach, based on experience, to developing DSSs through a larger, iterative cycle of ongoing, collaborative environmental research and development. Multiple stakeholders with multiple conflicting objectives need insightful, often novel, models of environmental systems. The answers developed to new research questions contribute to requirements and specifications for new tools and technology, and the technology is then built to facilitate the collaborative management process. Information added at any point can influence the collaborative management–research–technology cycle in both directions.

Stakeholder workshops to specify the DSS requirements, formulate its design, and review its use are critical. The DSS must be built progressively, first focusing on pilot areas and tractable research problems and eventually moving to a national scope. To motivate continued development, rapid prototyping is an ideal tool for achieving early success. The DSS—and the entire cycle—must also be self-maintaining. Two case studies illustrate these concepts.

INTRODUCTION

Organizations focused on managing water resources are recognizing the need to have tools for literature review, data integration, modeling, and decision support. Decision support systems (DSS) can help to meet these needs because they are aimed at integrating data and knowledge, evaluating management options in terms of

organizational objectives and risk, and facilitating multiple-stakeholder decision making where competing objectives and risk preferences must be reconciled.

Using the internet, geographically separated organizations with similar objectives can benefit from sharing experiences, data, and models. The development of enterprise- and nationwide DSSs enables organizations to share the costs and benefits of existing and newly developed information, theories, and technologies among a broad, diverse user group.

While DSSs are desirable, it is not very clear how to go about building them. This paper discusses an approach to developing DSSs by focusing on a larger cycle of ongoing environmental research that starts with the need to manage natural environments collaboratively. Environments, such as estuaries, are the focus of multiple stakeholders, each with multiple objectives that are often opposed; thus there is a need for insightful, and often novel, models of these systems. As more insight is sought, new research questions are continually raised. The answers developed to new research questions contribute to requirements and specifications for new tools and technology, which is then built to facilitate the collaborative management process. New information added at any point can influence the collaborative management–research–technology cycle in both directions, as illustrated in Figure 1.

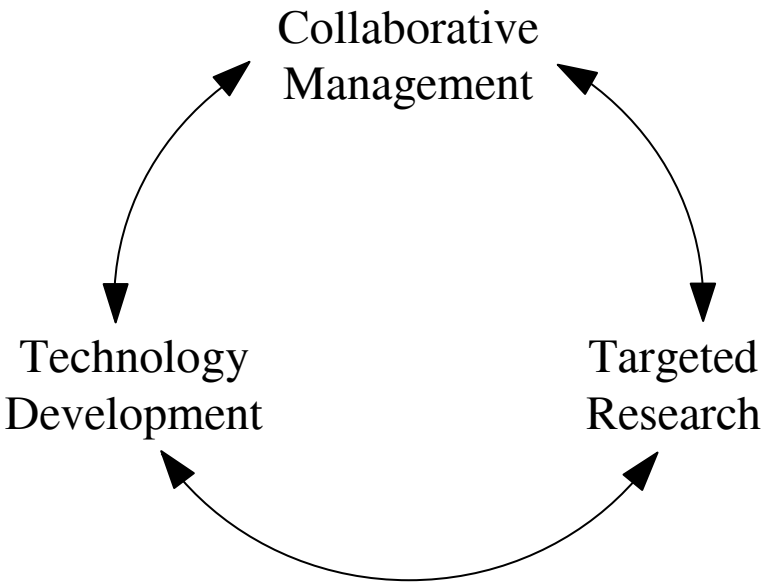

Figure 1. Collaborative management–research–technology cycle.

Establishing the cycle requires a pragmatic approach. First, the community must build the DSS to ensure community adoption. Stakeholder workshops to specify the DSS requirements, formulate its design, and review its use are critical. Second, the DSS must be built progressively—first focusing on pilot areas and tractable research problems and eventually moving to a national scope. Third, the DSS must be built with early success in mind to motivate continued development. Rapid prototyping is an ideal tool for achieving such success. Finally, the DSS—and

the entire cycle—must be self-maintaining. These concepts are illustrated in two case studies, the Northslope DSS, a tool in development for collaborative management of the North Slope in Alaska under proposed oil exploration, and a proposed DSS for management and research of the National Estuarine Research Reserve (NERR) System, under the National Coastal and Estuarine Research Technology (NCERT) Program. The proposed NCERT DSS provides a large-scale, practical example of how the collaborative management-research-technology cycle would be applied to a real-world problem.

NATIONAL COASTAL ESTUARINE RESEARCH AND TECHNOLOGY PROGRAM DSS

In establishing the NCERT Program in partnership with the NERR System, NOAA is seeking to stimulate research and scientific collaboration between the NERRs and their state agency, local governmental, and university partners to develop and implement new and innovative tools, in order to help coastal managers detect, prevent, and reverse the impacts of coastal pollution and habitat degradation. The primary focus of the effort is to address land use, habitat, contamination, and stormwater issues related to coastal development.

The challenge of establishing the NCERT Program, in partnership with the NERR System, to fund collaborative research to assist coastal managers in detecting, preventing, and reversing coastal pollution and habitat degradation, is extraordinarily complex but necessary. The program, therefore, must serve as a catalyst for a diverse array of activities that range from collecting, analyzing, interpreting, and using data to identify significant empirical and mechanistic relationships and develop new and innovative tools for resource protection and management. Developing appropriate management approaches and actions that affect public policy and influence human behavior is possible through stakeholder interactions linked to database analyses.

The skills required to do this work cut across many disciplines and areas of specialization, including biologists (marine, estuarine, riverine, coastal wetland, and upland biologists); geologists; hydrologists; hydrogeologists; geophysicists; statisticians; geographers; climatologists; modelers; coastal engineers; drinking water, stormwater, and wastewater engineers and regulators; highway and land use planners and engineers; and local and regional planning commissions. The coastal watersheds are just as diverse, ranging from very small watersheds (first-order streams) encompassing less than 50 acres (small neighborhoods), to enormous watersheds (tenth-order streams) that encompass more than a million square miles and cover more than half of the country (Mississippi River).

It is hard, then, to identify, let alone choose, a research program or suite of assessment tools that will meet the needs of a single estuarine system, let alone serve the needs of a network of estuaries such as the NERR System. This will not simply happen by creating a program, bringing people together, or sponsoring collaborative research. The approach must connect the *stakeholders* to the *science* and the

technology that they need and thus enable individual stakeholders to help themselves and each other. Each NERR watershed has both unique and generic problems and solutions. The proposed NCERT Program DSS will share knowledge, experience, and expertise and build a base of knowledge and a set of tools that will serve NERR sites individually and collectively.

Each part of the program is highly dependent on the other parts, *i.e.*, each part affects and is affected by the other parts in a highly interactive and adaptive management process, as illustrated in Figure 2. This approach will achieve the desired NCERT Program objectives by actively involving stakeholders in the development of an information system to facilitate and target future research through a collaborative decision-making and management process among NERR stakeholders.

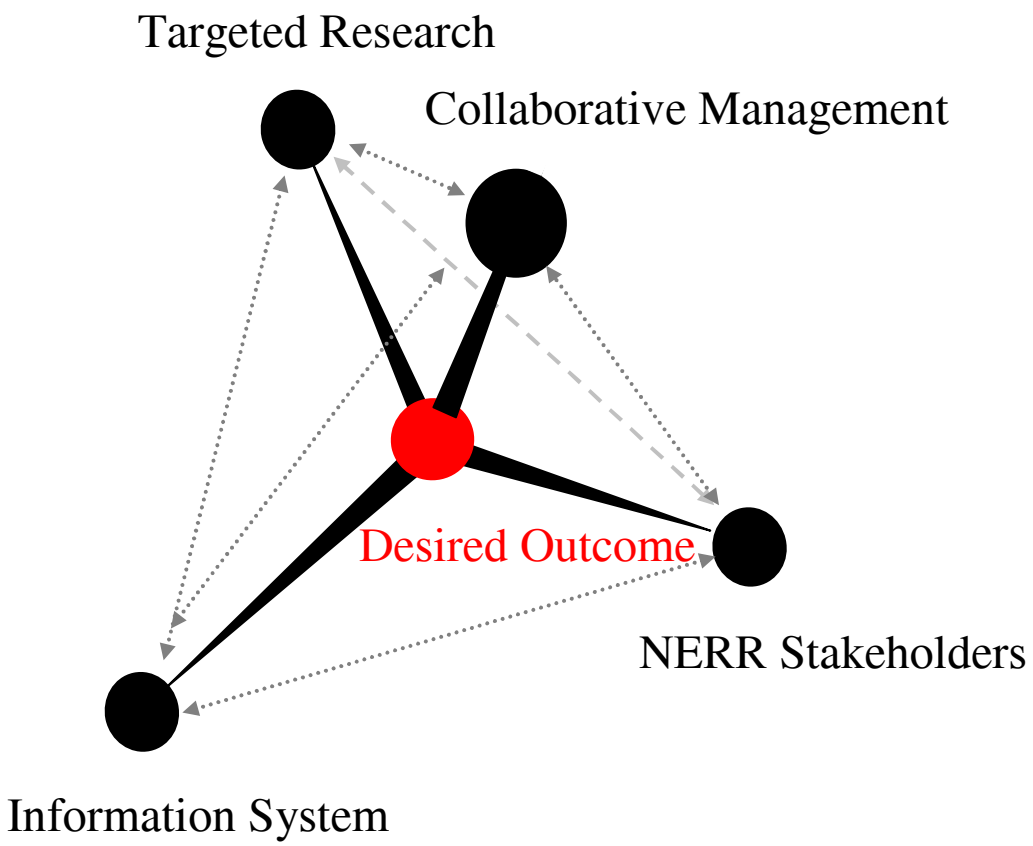

Figure 2. A model for achieving the NCERT Program objectives.

Collaborative Decision-Making Process

Conflict is a natural part of human relationships and reaching consensus is not always possible; however, when properly managed, conflict can be a positive force that leads to new ideas and new ways of doing things. It can also be a catalyst for strengthening stakeholders' relationships and developing better, longer-lasting outcomes.

The project team will coordinate and direct a collaborative process with the NERRs and their state agency, local governmental, and university partners to (a) gain

consensus on critical data needs and research tools for enhancing estuarine assessment and (b) identify appropriate management approaches and actions for restoring and protecting estuarine health. This collaborative process will be implemented using a tiered approach that will facilitate information sharing between the project team and the individual NERRs and their associated stakeholders on a local, regional, and national level.

The results of these interactions will be used to develop an information system, through existing technologies and databases, to link researchers and stakeholders participating in the NCERT Program through a central, online, federated database system via web-based and desktop applications, including NCERT.org. The proposed collaborative process and information system will support estuarine data collection and analysis, and strengthen land and water resource decision making. The end product of this effort will be a data-driven research and technology program that will allow management to incorporate trade-offs that support NERRs into the decision-making process.

A working prototype of this information system, the Analytical Framework for Coastal and Estuarine Study (ACES), has been developed and fully documented by the St. Johns River Water Management District (SJRWMD) and PBS&J. It uses a geographic information system (GIS)–based database of spatial and temporal data to describe the environment and a suite of modeling tools, based on first principles, to evaluate different management scenarios. With ACES, estuarine bulk parameters related to shape, residence time, and flushing potential can be derived, and the influence of tide and terrestrial drainage on estuarine water quality can be assessed using regression and other approaches. ACES was created through a collaborative and rapid-prototype development process involving national estuarine experts that was similar to the process proposed for the NCERT Program DSS.

Annual national NCERT Summits will be held to promote collaboration between NERR stakeholders. These meetings, used as part of a tiered approach—including local "listen-and-learn" meetings with individual NERRs and their governmental and university partners, as well as regional workshops—will engage stakeholders at all levels in the process of developing the information system and building consensus on data needs, assessment tools, and research priorities. Research priorities identified through this process will be funded through targeted grants to participating NERRs, universities, and state and local governments.

Technology Development

As the collaborative management process is implemented, stakeholders will need information to define problems, clarify objectives, and assess the effectiveness of management activities and strategies. The specific information that stakeholders require for planning and management decisions should drive which information is collected. The major challenge to stakeholders will not be collecting information—for there will be an overwhelming amount even if they gather only the specific information needed—but processing data to obtain exactly the required information.

Furthermore, the quality of the information collected is most important, rather than the quantity. Obviously, good information results in better management decisions.

Effective and sustainable management requires an estuary-by-estuary study approach. On the other hand, the NCERT goals of collaboration and efficiency through data-, model-, technology-, and idea-sharing necessitate a communal approach in which a single technological framework is used by all.

These two requirements—estuary-specific study and a single technological framework—are not mutually exclusive. The national, community-based solution proposed will enrich the understanding gained through estuary-specific studies by identifying and focusing on similarities in the research and decision-making processes. That is, while two estuaries may be largely different in their geomorphology, water chemistry, hydrodynamics, etc., the processes undertaken to identify how to model the estuary, collect the data, develop the management alternatives, and ensure stakeholder approval are largely similar. Building a nationally applicable information solution that facilitates these processes is therefore not only possible, but will bring a whole new level of data access, research finding access, and collaboration to the fore.

The project team will develop a comprehensive information system. Existing databases containing data, models, research findings, and management policy documents for all 27 NERRs will be linked to form a national cyberinfrastructure network. This network will form the foundation for storing and communicating the results of the on-going research program. Access to the network will be provided via two methods. First, a GIS-based website called NCERT.org will be created that provides a broadly accessible view of all data, models, and scientific findings. Second, a GIS-based software workbench for analyzing estuaries will be built. This workbench will form the means of conducting new research, and will be stocked with a growing set of models created as the research process continues. As new results and models are created, the user will be able to publish them directly to the national network for review by the NERR community. The research will be driven by the process of building decision support systems for estuarine management, which in turn will drive the development of natural systems models to assess the effect of management plans. The modular design of the software workbench allows researchers to submit their newly developed natural systems and decision support models to the national network so that the entire community can use them.

The NCERT DSS is an ambitious information solution that will serve the needs of a growing and diverse estuarine science community. Certainly, to build the solution from the ground up would be a large effort and would exceed the time and funding available. Fortunately, several national emerging role models and technologies can be leveraged to quickly arrive at an operational NCERT DSS Framework. The proposed framework is based on the following building blocks, as illustrated in Figure 3 on the next page:

- *A national cyber-infrastructure that enables real-time, communitywide communication.*
- *A national standard for storing estuarine information, including GIS-based data, observations data, models, and research findings.*
- *A means of including existing databases, models, and research findings in the national cyber-infrastructure and ensuring they can optionally remain in their current format, or be converted to the national standard, or some hybrid of the two.*
- *A workbench tool that works with data from the national cyber-infrastructure and enables a range of estuary analysis—from first principles to complex, systemwide modeling.*
- *A modular tool framework that allows for the development and incorporation of new tools for estuarine analysis into the national toolset—an openly available suite of tools for all NERRs to use.*
- *A broadly accessible, web and virtual globe–based tool that focuses on serving the estuarine community with user-friendly, ergonomically driven methods for learning about, analyzing, and documenting findings about estuaries.*

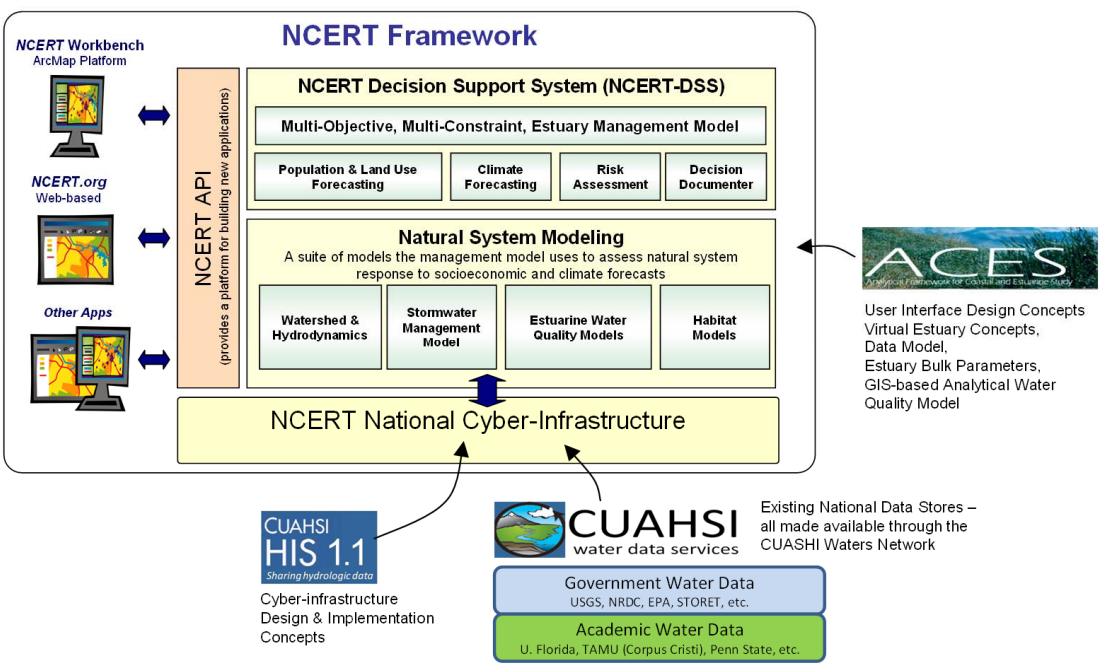

Figure 3. Proposed NCERT DSS framework.

These building blocks are each being developed in some form for efforts similar to NCERT. For example, the water resources and hydrology world is currently experiencing a leap forward in technological innovation with the continued development of the Hydrologic Information System (HIS) concept, a cyber-infrastructure based approach to making available the nation's water data (Maidment 2008). Another example is map-based web technologies, which have exploded in

recent years with the introduction of virtual globe browsers such as Google Earth. These technologies have focused heavily on making the experience the user has with a tool an intuitive one that ensures the user reaches the desired information quickly, without being required to adopt new technology concept models along the way.

Having identified the building blocks for the NCERT information solution and the emerging technologies that will be used to quickly build the solution, it is important to consider the way in which the solution will be built. A strong pragmatism is required in the process of solution development to ensure that adequate proof-of-concept is established early in the process and that sufficient developmental momentum is maintained. Sequencing of tasks and goals is paramount.

The technology developmental approach centers on the following:

- *Starting small and expanding to quickly identify challenges and ensure early success,*
- *Driving the development of technology with a realistic problem, and*
- *Establishing ownership of the solution and the design process throughout development.*

Targeted Research on Impacts of Climate Change and Population Growth

Given their wide geographic distribution across the U.S., the size, geomorphology, hydrology, and ecology of the 27 NERRs vary significantly. In addition, the degree of anthropogenic alteration and watershed development (e.g., dredge and fill, point sources, stormwater runoff) also varies widely among the NERRs. Despite this inherent variability, there are two common stressors that threaten the integrity of all the NERRs: climate change (and associated sea-level rise) and population growth (and associated impacts such as increased pollutant loading).

While each of the NERRs may have unique local and site-specific research priorities, we propose that, as part of the development of the NCERT Program, targeted research be implemented with the common focus of assessing the existing and potential future impacts of these stressors on the estuarine system integrity of each of the NERRs. Assessing and mitigating their effects are clear national priorities, and the implementation of a common thematic research platform will complement the collaborative process proposed for developing a comprehensive information system linking researchers and stakeholders participating in the NCERT Program. The targeted research results will be significantly leveraged, both through collaborative efforts and the dissemination of scientific findings nationally.

Existing data, and data collection needs, will vary widely among the NERRs. Therefore, the first step in the targeted research will be to conduct a complete inventory of available data. Data gaps will then be identified, thus establishing the first tier of research priorities. Furthermore, appropriate spatial and temporal analytical scales will need to be determined for each of the NERRs in accordance with the availability of existing data as well as locally specific management issues.

NORTH SLOPE DSS

The collaborative decision-making and management process for building a DSS described in the NCERT proposal is being implemented in the Northslope DSS, a tool for collaborative management of the North Slope in Alaska under proposed oil exploration. The Northslope DSS will support the construction of ice roads and ice pads to provide a cost-effective means of oil and gas exploration on Alaska's North Slope with minimal impact to the sensitive underlying tundra. Such ice structures have become integral to oil and gas exploration. Their widespread use represents a challenge to water resource managers, however, due to the large volume of water necessary to construct and maintain them. As the proximity of available fresh water sources has a significant impact on the planned location of ice roads and ice pads, changes in water resource management strategies could significantly impact oil and gas exploration activities.

Due to the fundamental role of water in natural and human systems, successful management of this resource is indeed essential to the broader issue of environmental protection and responsible energy development on the North Slope. The challenges of developing best management practices for water resources include the following: resource planning and management for efficient and sustainable water use; understanding and explicitly considering environmental impacts and protection; and developing and implementing effective participatory management strategies with representative stakeholder participation from all sectors.

This project is developing a water resources management solution in support of oil and gas exploration that explicitly considers optimal water use, direct and cumulative environmental impacts, and multiple objectives and values among stakeholders. The solution consists of an information system, software tools for decisions support, and methodologies for facilitating stakeholder involvement in the decision making process. The tools developed in this work will not only apply to the water management issues considered here, but will also be applicable to broader environmental management issues and industry development applications.

CONCLUSION

The challenge in building a DSS is to apply the needed resources for determining the appropriate types of research, without forcing a "one size fits all" product onto the System as a whole. **For this reason, an adaptive management process for identifying data and information needs and a mechanism for targeting and funding the necessary research are major elements of the DSS Program solution.**

Water resources management crosses many boundaries, including political, institutional, and natural. The complexity involved in the management of resources that includes inputs from all participants can be overwhelming. **Thus the proposed DSS solution provides for an inclusive, collaborative management process to**

assist in the understanding of these complexities and to arrive at better, scientifically sound management decisions.

Information management issues lie at the heart of many difficulties in making land and water resource decisions. Resolving certain information management problems—including too much information, a lack of information, data of uncertain quality, and difficulty connecting information from different sources and disciplines—can be addressed with existing technology. Other information management issues, however, must also be addressed, including a lack of standardized technology, resolving multiple data formats, easily accessing available information, and accessing data used to produce published literature and scientific reports.

The challenges of sharing data, models, and research findings must be overcome for stakeholders to fully benefit from their collaborative research efforts. In resolving these challenges, new tools must also be developed to enhance the interpretation of data and information and promote further collaboration between researchers. **For this reason, the development of a comprehensive solution for managing, sharing, and using information is a major element of a DSS solution.**

REFERENCES

Bourne, Stephen, Singleton, Thomas L., and Hackney, Courtney (2008). *National Coastal and Estuarine Research and Technology (NCERT) Program: A Collaborative Approach to Managing Estuarine Resources Through Technology Development and Targeted Research*. National Ocean Service, National Oceanic and Atmospheric Administration, US Department of Commerce, National Coastal and Estuarine Research and Technology Program grant.

Hampson, Jack, Bourne, Stephen, and Brumbelow, Kelly (2008). *The Digital Watershed For Dynamic Decision Support.* Proceedings of the AWRA Spring Specialty Conference, San Mateo, CA.

Maidment, David R. (2008). CUAHSI Hydrologic Information System: Overview of Version 1.1. Consortium of Universities for the Advancement of Hydrologic Science, Inc.

Singleton, Thomas L. and Lord, Linda (2000). *Making Community Decisions Using a Model for Integrated Water Resource Management*. Unpublished manuscript.

Tidwell, Amy, Brumbelow, Kelly, Bourne, Stephen, and Schnabel, William (2008). *North Slope Decision Support System for Water Resources Planning and Management*. US Department of Energy, National Energy Technology Laboratory, Environmental and Unconventional Oil-Technology Solutions for Oil and Gas Resource Development grant.

A Spatio-Temporal Drought Analysis for the Midwestern US

Shih-Chieh Kao[1], Rao S. Govindaraju[2], and Dev Niyogi[3]

[1] Computational Sciences and Engineering Division, Oak Ridge National Laboratory, Oak Ridge 37831-6017, USA; email: kaos@ornl.gov
[2] Civil Engineering, Purdue University, West Lafayette, IN 47907, USA; email: govind@purdue.edu
[3] Agronomy and Earth and Atmospheric Sciences, Indiana State Climate Office, Purdue University, West Lafayette, IN 47907, USA; email: climate@purdue.edu

ABSTRACT

Droughts are prolonged abnormalities of moisture deficits that vary widely across temporal and spatial scales. Many hydrometeorologic variables are used to monitor the status of a drought. However, because of the dependence structure between all affecting variables under various temporal windows, an integrated spatio-temporal analysis of droughts cannot be easily achieved. In this study, a copula-based drought analysis was performed by using long-term monthly precipitation dataset for the upper Midwest United States. The spatio-temporal dependence relationships between various drought variables were investigated, and their joint probability distribution was constructed by combining drought marginals and the dependence structure. A copula-based joint deficit index (JDI) was adopted for an objective (probability-based) description of the overall drought status and compared to the Palmer drought severity index results. Results from the copula-based JDI provide information for drought identification, and further allow a month-by-month assessment for future drought recovery.

KEY WORDS: Copulas, Drought, Standardized Precipitation Index, Palmer Drought Severity Index

INTRODUCTION

Drought has been a challenging topic in water resources management. It is perceived as one of the most expensive and least understood natural disasters. Drought impacts tend to be more severe in areas such as the mid-western United States, where agriculture is the major economic driver. Droughts are categorized based on their impacts and duration. For example, meteorological droughts consider deficits in precipitation, agricultural droughts primarily consider deficits in soil moisture, and hydrologic droughts respond to streamflow deficits (Dracup *et al.*, 1980). Though these different types of deficits are generally positively correlated and are likely responding to the same trigger, they exhibit diverse temporal and spatial scales. An integrated drought indicator, that covers multiple types of deficits over different temporal scales, is therefore difficult to develop owing to the complicated dependencies in the variables that are used to characterize droughts.

Given their somewhat nebulous nature, the status of droughts is often assessed by various indices that are derived from hydrometorologic variables. Palmer (1965) proposed a moisture index (Palmer Drought Severity Index, PDSI) based on water budget accounting using precipitation and temperature data. PDSI soon became a popular choice for drought assessment and is widely used even today (Dalezios *et al.*, 2000; Kim *et al.*, 2003). Another popular index - Standardized Precipitation Index (SPI) was introduced by McKee *et al.* (1993). Based on a given window size, the rainfall depth is transformed to its corresponding cumulative probability, and then mapped onto the standard normal scale. The probabilistic nature of SPI allows it to be comparable among various locations and variables, and it can be further interpreted in terms of recurrence intervals (return periods). Nevertheless, to judge an overall drought status, different SPIs with multiple temporal scales (e.g. 3-, 6-, 9-, 12-month) need to be examined.

Despite the availability of different drought indices, no single index is ideal for characterizing droughts. The drought status that is assessed from one indicator often does not correspond well with that obtained from another. Therefore, to successfully assess the various drought characteristics, information from various sources need to be examined simultaneously. This is currently successfully managed by the US Drought Monitor where the severity of a drought (D0 ~ D4) is determined based on various indicators (PDSI, CPC Soil Moisture, USGS weekly, Percent of normal, SPI, and VCI), and from human input as described by Svoboda *et al.* (2002). Nevertheless, though an Objective Blend of Drought Indicators (OBDI, a linear weighted average of several indicators) is adopted as a measure of the overall severity, the decision of final drought status relies heavily on the subjective judgment of many people, instead of invariant objective standards. Because of the subjective intervention in specification of drought status, a rigorous analysis of the physical and probabilistic characterization of droughts is challenging.

There is a need to develop objective standards for analyzing records and specifying drought status based on multiple variables. So far, one of the major stumbling blocks to such an approach has been our inability to describe the complicated dependent relationships between various drought-related variables. To accomplish this goal, this study employed copulas to identify and construct the dependence structure of droughts. Building on the analysis, we propose a new copula-based drought indicator that enables the computation of a probability-based overall water deficit index from multiple drought-related quantities (or indices). By invoking copulas, we construct joint distributions of droughts so that marginal distributions of relevant variables and their dependence structures can be fully preserved. The joint distribution affords an objective description of the overall deficit, and assists the computation of probabilistic quantities such as return period and associated risk of a drought.

COPULAS

Over the last decade, copulas have emerged as a powerful approach in simplifying multivariate stochastic analysis. Sklar (1959) showed that for *d*-dimensional continuous random variables $\{X_1,...,X_d\}$ with marginal cumulative distribution functions (CDFs) $u_j = F_{X_j}(x_j)$, $j = 1,...,d$, there exists one unique

d-copula $C_{U_1,...,U_d}$ such that:

$$H_{X_1,...,X_d}(x_1,...,x_d) = C_{U_1,...,U_d}(u_1,...,u_d) \quad (1)$$

where u_j is the jth marginal and $H_{X_1,...,X_d}$ is the joint-CDF of $\{X_1,...,X_d\}$. Copulas $C_{U_1,...,U_d}$ can be regarded as a transformation of $H_{X_1,...,X_d}$ from $[-\infty,\infty]^d$ to $[0,1]^d$, in which the marginal distributions are segregated from $H_{X_1,...,X_d}$. Hence, $C_{U_1,...,U_d}$ becomes only relevant to the association between variables, and it gives a complete description of the entire dependence structure. This approach is available for all existing joint distributions, and it further provides a general method for constructing suitable joint distributions. Kao and Govindaraju (2007) showed that copulas allow for easier computation of probabilistic quantities such as means and standard deviations of rainfall excess. The detailed theoretical background and descriptions for the use of copulas can be found in Nelsen (2006). Specific properties that are central to the implementation of study are described below.

Choices of Copulas for Higher Dimensional Joint Distributions

Previous studies have indicated that copulas perform well for bivariate problems, and in particular Archimedean copulas have been a popular choice. However, the direct extension of Archimedean copulas to higher orders (>2) is very limited because they impose severe restrictions on the pair-wise mutual dependencies that can be accommodated, and compatibility conditions are far more difficult to satisfy in higher dimensional problems (Kao and Govindaraju, 2008). Only few parametric copula families with general applicability such as meta-elliptical copulas are available at higher dimensions (Genest *et al.*, 2007). Nevertheless, the computational burden associated with meta-elliptical copulas increases rapidly with increasing dimensions since explicit expressions exist only for the copula densities and not for the copulas themselves. The dimension of drought dependence structure is expected to be quite large to capture the temporal behavior, and consequently nonparametric empirical copulas are chosen in this study.

Similar to the concept of plotting position formula used in univariate statistical analysis (e.g. Weibull formula), empirical copulas are rank-based empirical joint cumulative probability measures (Nelsen, 2006). For sample size *n*, the *d*-dimensional empirical copula C_n is:

$$C_n\left(k_1/n, k_2/n, ..., k_d/n\right) = a/n \quad (2)$$

where a is the number of samples $\{x_1,...,x_d\}$ with $x_1 \le x_{1(k_1)}$, …, $x_d \le x_{d(k_d)}$, and $x_{1(k_1)}$, …, $x_{d(k_d)}$ with $1 \le k_1,...,k_d \le n$ are the order statistics from the sample. Empirical copulas are mostly used for model verification and are treated as the observed (real) dependence structure. When a sufficiently large sample size is available, empirical copulas can be used to construct non-parametric joint empirical probability distributions, which tend to be more computationally efficient. This is a

desirable feature for drought analysis.

Distribution Function of Copulas - K_C

For given *d*-variate sample marginals $\{u_{1x},...,u_{dx}\}$, a copula $C_{U_1,...,U_d}(u_{1x},...,u_{dx})$ is the cumulative probability measure $P[U_1 \le u_{1x},...,U_d \le u_{dx}] = q$. One can expect that there exist other sample marginals $\{u_{1y},...,u_{dy}\}$ with the same value of cumulative probability $C_{U_1,...,U_d}(u_{1y},...,u_{dy}) = q$. If this cumulative probability q is treated as an indicator, i.e. events with same value q are assumed to cause similar impact (e.g. in drought analysis it can be defined as joint deficit status, a smaller q implying overall drier conditions), then it will be of interest to know what the probability of random event $\{U_1,...,U_d\}$ with $C_{U_1,...,U_d}(U_1,...,U_d) = q$, or $C_{U_1,...,U_d}(U_1,...,U_d) \le q$. In this context, the distribution function K_C of copulas can be defined as the probability measure of the set $\{(U_1,...,U_d) \in [0,1]^d \mid C_{U_1,...,U_d}(U_1, ...,U_d) \le q\}$:

$$K_C(q) = P[C_{U_1,...,U_d}(U_1,...,U_d) \le q] \quad (3)$$

Salvadori and De Michele (2004) adopted K_C for defining a secondary return period for bivariate Archimedean copulas. The most appealing feature of K_C is that it can help project multivariate information onto a single axis. Though an analytical expression of K_C might not exist for non-Archimedean copulas, it can be numerically constructed from Monte Carlo simulations, and then the empirical distribution function K_C may be constructed as (example shown in Kao and Govindaraju, 2008):

$$K_{C_n}(l/n) = b/n \quad (4)$$

where b is the number of samples $\{x_1,...,x_d\}$ with $C_n(k_1/n,...,k_d/n) \le l/n$. K_C allows us to compute the probabilistic measure of the joint deficit status, which can be further translated to a joint drought index.

DATA USED IN THIS STUDY

To construct reliable multivariate statistical models, sufficiently long observations are desirable. In the proposed study, the Time Bias Corrected Divisional Dataset (TD-9640, http://www7.ncdc.noaa.gov/CDO/CDODivisionalSelect.jsp#) is adopted for the mid-western US (including states of IL, IN, IA, KS, MI, MN, MO, NE, ND, OH, SD, and WI). The data consists of monthly average temperature, precipitation, SPI and PDSI of each climate division within US from January 1895 to present (see Karl (1986) and Karl *et al.* (1986) for more details), and also provides an areal averaged value of the drought status. To investigate the droughts on a finer scale, the precipitation records over Indiana were obtained from the daily surface dataset (TD 3200) of cooperative stations (COOP) from National Climate Data Center (NCDC). After data processing (such as quality assuring with neighboring stations), a

total number of 73 stations with record lengths greater than 80 years were used in the analysis discussed ahead. Monthly precipitation was computed based on aggregated daily values. In cases where data was missing for the entire month (around 1.22% of the entire precipitation dataset), it was replaced by the historic mean of that specific month (assuming normal moisture status for that unknown month). We adopted copulas for conducting at-site analyses to capture temporal evolution of droughts, and used spatial interpolation for assessing the behavior over the regional scale.

COPULA-BASED JOINT DROUGHT DEFICIT INDEX

In this study, the standardized precipitation index (SPI) introduced by McKee *et al.* (1993) was adopted for developing a copula-based joint drought deficit index. There are several reasons for adopting SPI: (1) it can be applied to precipitation, streamflow, and other variables as well, (2) it does not incur model assumptions that are typical for other indices such as PDSI, and (3) it is a probability measure of cumulative precipitation by definition. Therefore, drought severity (dryness) is normalized in terms of probabilities that can be compared between various temporal scales, locations and variables. Since the current SPI approach cannot account for seasonal variability, an amendment proposed by Kao and Govindaraju (2009) was adopted in order to obtain a more statistically sound SPI. For a *w*-month SPI, the corresponding *w*-month marginal u_w can be expressed as

$$u_w = \phi(\mathrm{SPI}_w) \tag{5}$$

in which ϕ is the standard Gaussian CDF. Referring to the definition of drought categories used in US Drought Monitor (Svoboda *et al.*, 2002), Table 1 shows the range of SPI values along with their probabilities of occurrence and corresponding drought conditions.

Table 1. The categories used in US Drought Monitor along with the corresponding SPI values.

SPI Values	Prob. of Occurrence (%)	Drought Condition	Drought Monitor Category
-0.84 ~ -0.52	20 ~ 30	Abnormally dry	D0
-1.28 ~ -0.84	10 ~ 20	Drought - moderate	D1
-1.64 ~ -1.28	5 ~ 10	Drought - severe	D2
-2.05 ~ -1.64	2 ~ 5	Drought - extreme	D3
< -2.05	< 2	Drought - exceptional	D4

Droughts have varying durations and a single SPI cannot capture the overall status. By invoking copulas, the dependence structure of selected SPIs was constructed, and the overall deficit status was expressed as joint cumulative probability (a lower probability measure corresponds to overall dry conditions) thus allowing for a more comprehensive assessment of droughts. To capture the short- as well a the long-term droughts, window sizes from 1-, 2- to 12-month ($w = 1, 2, \ldots, 12$) were selected. Empirical copulas (Eq. 2) were adopted to construct the dependence structure for precipitation marginals $\{u_1, u_2, ..., u_{12}\}$. Since the record lengths are quite large (>1000 data points for most of stations and climate divisions), empirical copulas were assumed to provide reliable results. The choice of $\{u_1, u_2, ..., u_{12}\}$ in forming

high dimensional copulas increases the complexity of the dependence model. Nevertheless, it was needed because drought durations exhibit wide temporal variations, and only by encompassing various durations (e.g., from 1- to 12-month) the drought characteristics can be analyzed. An annual cycle also accounts for seasonal effects naturally. Moreover, this construct allows for a month-by-month assessment for future conditions, as will be shown later.

After a copula has been constructed, it yields the cumulative probability $P[U_1 \le u_1,...,U_{12} \le u_{12}] = q$. Clearly, when a drought occurs, most of the marginals u_w will be small and result in a small value of *q*. Therefore, the cumulative probability *q* can be viewed as the *joint deficit status* with a smaller *q* implying overall drought conditions while a higher *q* would imply overall wet conditions. We note that the joint deficit status *q* is linked to the given set of marginals and is only comparable to other *q* with the same set of marginals. For instance, q_1 for $\{u_1, u_2,..., u_{12}\}$ and q_2 for $\{u_1, u_2,..., u_{11}\}$ are not comparable. Therefore, a more general index derived from *q* is desirable. By assuming that events with the same value of *q* will have similar joint drought severity, it will be of interest to know the cumulative probability for events with joint deficit status less than or equal to a given threshold *q* (i.e., $P[C_{U_1,...,U_{12}}(U_1,...,U_{12}) \le q]$). The distribution function of copulas K_C (Eq. 3) provides this probability. Therefore, a *joint deficit index* (JDI) can be defined analogously to SPI:

$$\text{JDI} = \phi^{-1}(K_C(q)) = \phi^{-1}(P[C_{U_1,...,U_{12}}(U_1,...,U_{12}) \le q]) \quad (6)$$

where positive JDI ($0.5 < K_C < 1$) implies overall wet conditions, negative JDI ($0 < K_C < 0.5$) indicates overall dry conditions, and JDI zero ($K_C = 0$) indicates normal conditions. In other words, JDI is based on the cumulative probability of joint deficit status *q*. An extreme drought will result in a small *q*, and the JDI will correspondingly yield a low probability. Since JDI is on an inverse normal scale (same as SPI), the classifications listed in Table 1 can be adopted for JDI as well.

An illustration of the JDI using precipitation marginals of station Alpine 2 NE in Indiana (COOPID: 120132) is shown in Figure 1. JDI, SPI_w, $w = 1, 2, \ldots, 12$ and the corresponding 12-month precipitation values are presented for four select cases. In Fig. 1(a), SPI_w values observed in all window sizes for June 1988 report large precipitation deficits indicating a severe drought, which is also noted in the JDI. Nevertheless, only by invoking JDI can the overall deficit status be expressed as a probability-based index. Fig. 1(b) shows an opposite case, in which JDI and SPI_w observed in all window sizes for August 1985 report sufficient precipitation. One can notice that JDI is slightly higher than all other SPI_w in this instance. Since JDI is based on the joint probability of all SPI_w, it suggests that the joint behavior of a drought cannot be assessed by a simple weighted average of SPI_w due to the effect of dependence structure. Fig. 1(c) shows a case of emerging drought in February 1978, in which SPI_w is quite small due to the large precipitation deficit in February while

other SPI_w are above normal. This case is difficult to interpret since most of the indices do not capture droughts in a timely manner. The JDI reflects a drought condition based on the entire dependence structure. Fig. 1(d) shows a prolonged drought in Oct. 1988, in which SPI_1 and SPI_2 report sufficient precipitation in September and October while other SPI_w report precipitation deficit due to the preceding drought. Therefore, an important feature of JDI is that the overall deficit status is based on the dependence structure of deficit indices with various temporal windows. When the deficit indices are found to be uniformly low, the resulting joint drought index will be extremized due to its rareness.

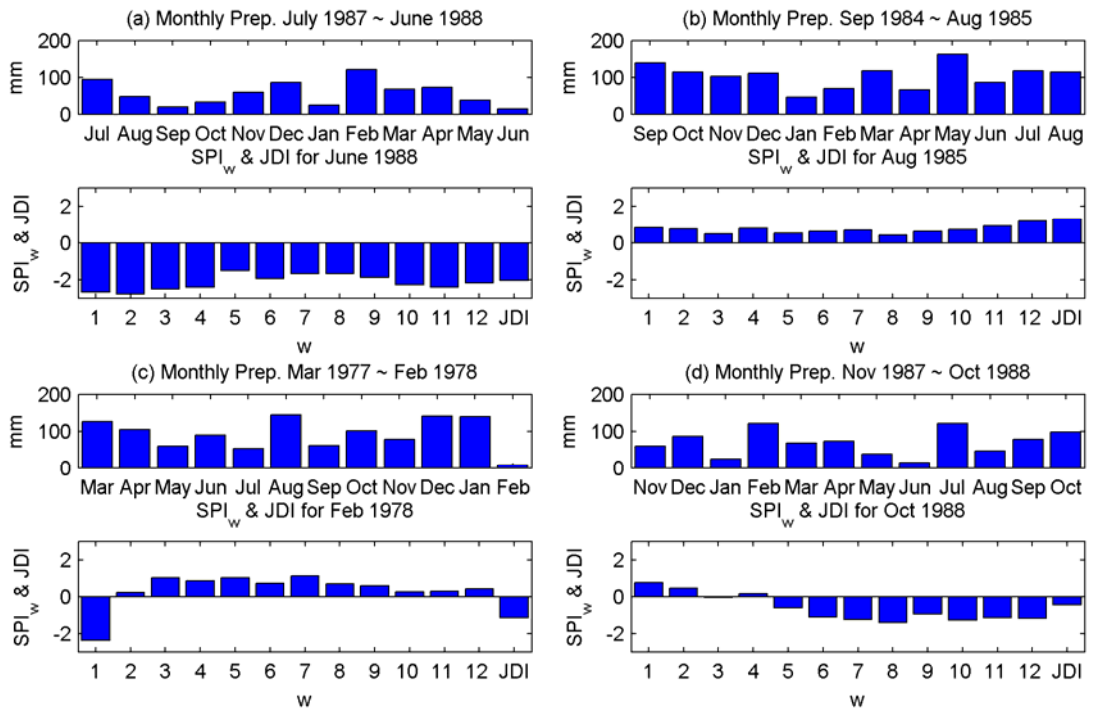

Figure 1. Illustration of JDI and SPI_w, w = 1, 2,…, 12 of precipitation station Alpine 2 NE, Indiana (COOPID: 120132) for four selected cases.

COMPARISON BETWEEN VARIOUS DROUGHT INDICES

To gain more insights into the proposed drought index, a comparison between JDI, SPI_1, SPI_3, SPI_6, SPI_9, SPI_{12} and PDSI was performed using the TD-9640 dataset for the Midwest. Since PDSI has been included in TD-9640, only JDI and modified SPIs were computed for each climate division. Spearman's rank correlation coefficients between different indices were constructed and are shown in Table 2.

Table 2. Average Spearman's rank correlation coefficient between various drought indices of the entire Midwest

	SPI_1	SPI_3	SPI_6	SPI_9	SPI_{12}	JDI
JDI	0.72	0.80	0.79	0.76	0.70	
PDSI	0.45	0.66	0.75	0.77	0.76	0.79

The comparison indicates that the correlation between JDI and SPIs are

generally high (0.7 ~ 0.8). This is anticipated since JDI is built on SPIs with various window sizes. In other words, JDI represents the overall drought status with respect to different temporal scales. We then compare both JDI and SPI to the commonly used PDSI, which is based on a somewhat different water accounting approach. While the correlation between PDSI and SPIs increases with window sizes, it is of interest to note that the JDI shows good similarity to PDSI, especially for the eastern part of Midwestern US as illustrated in Figure 2. Though a more in-depth analysis should be conducted to see why these two different approaches can independently produce similar results, it indicates that JDI can effectively combine SPIs to form an overall drought index. The JDI approach can also be applied to other mixtures of indices, and is worthy for further investigation.

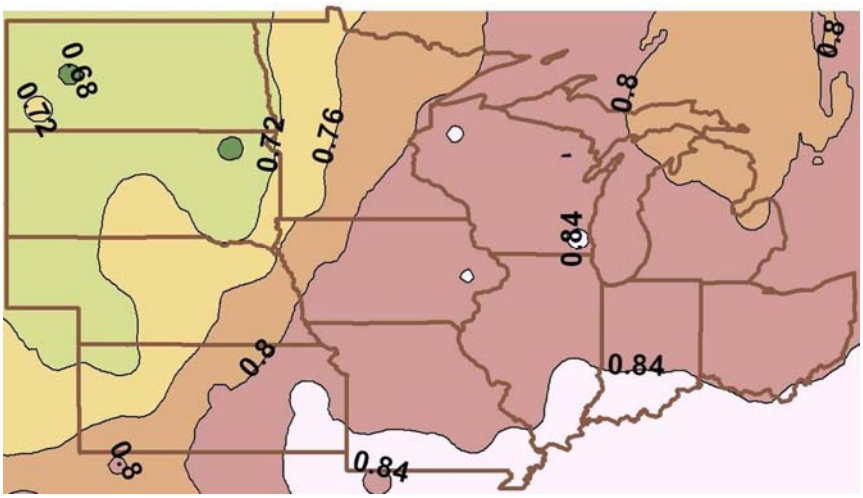

Figure 2. Spearman's rank correlation between JDI and PDSI of the Midwest

USING JDI TO ASSESS THE POTENTIAL OF FUTURE DROUGHTS

The adoption of high dimensional marginals facilitates a month-by-month future drought potential assessment since JDI is based on temporal dependence structure of deficits. Therefore, it will be of interest to know under given current conditions, what amount of precipitation is required in the following months to bring the joint deficit status to normal (JDI = 0 or $K_C = 0.5$). In other words, how much precipitation is required in a future time horizon to recover from an existing drought? This can be achieved via an iterative procedure described in Kao and Govindaraju (2009). A regional illustration of the required precipitation for July 1988 to achieve normality based on the observations made from August 1987 to June 1988 and the corresponding probability of exceedance is shown in Figure 3. As indicated in Fig. 3, a majority of Indiana would have needed over 150-mm of rain in July 1988. Based on historical July precipitation, this information can be further transformed into exceedance probability, and it suggests that the probability for recovering to normal conditions is small (less than 0.1 for most of the state). Such drought maps can be an effective way of relaying drought information, as most of the current indices are not amenable to statistical interpretation and are artificially converted into drought severity levels.

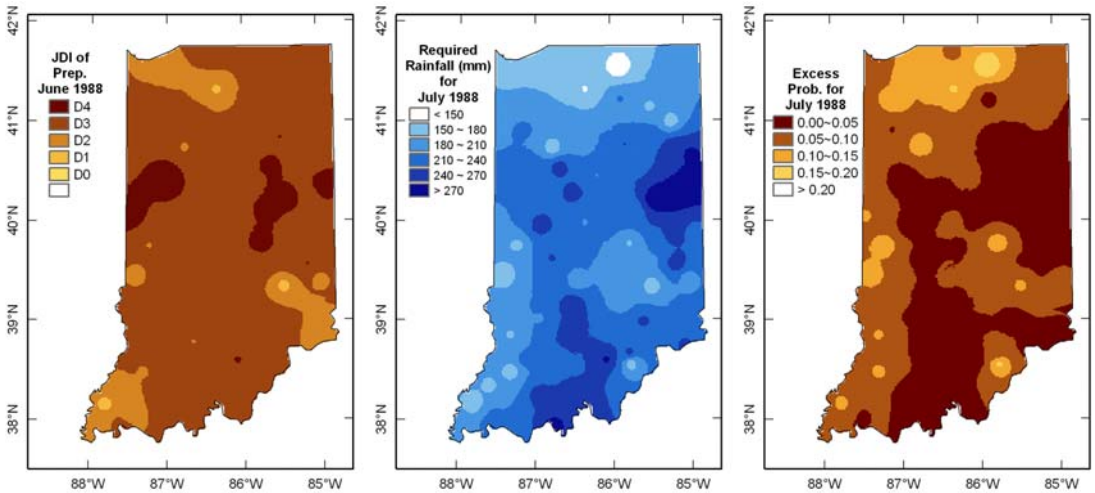

Figure 3. Illustration of (a) left: JDI for June 1988, (b) center: required precipitation for July 1988 to achieve normal status ($K_C = 0.5$ or JDI = 0), and (c) right: the corresponding excess probability of Indiana based on the observations made from Aug 1987 to June 1988

CONCLUSIONS

The complex relationships between drought-related variables have hindered characterization of overall drought status in the past. However, copulas provide a promising method for characterizing the complicated dependence structure by using a modified SI based on observed rainfall and streamflow data. The dependence structures of precipitation marginals with window sizes varying from 1- to 12-months were constructed via empirical copulas. The reliability of empirical copulas was founded on the large sample sizes adopted in this study. Study results can be summarized as follows:

(1) A joint deficit index (JDI) was proposed in this study using the distribution function K_C of copulas. The JDI offers a probability-based drought index from a set of SPIs with various temporal window sizes. This is an improvement over conventional drought status indices that could be estimated through subjective judgments or by linear weighted SPIs. Besides providing objective description of the overall drought status, the JDI was shown to be capable of capturing both emerging and prolonged droughts in a timely manner.

(2) Comparing to SPIs with various window sizes, the JDI is found to resemble behavior of PDSI especially for the eastern part of Midwestern US. Thus, JDI can effectively combine drought status with various temporal scales to form an overall deficit index. The similarity in the performance of two independently derived indices (PDSI and JDI) deserves further investigations.

(3) Drought severity can be assessed through the proposed JDI approach. For instance, the required precipitation for achieving normal conditions (JDI = 0) can be estimated. The required rainfall depth along with its exceedance probability provides good interpretation of drought status and mitigation needs.

The utilization of copulas in drought characterization was demonstrated in this study. Copulas can play an important role in drought analysis and perhaps in other hydrometeorological studies as they enable multidimensional stochastic analysis.

ACKNOWLEDGEMENTS

Support for this study was provided by National Science Foundation (grant numbers OCI:0815811 and DBI:0619086). Any opinions, findings, and conclusions or recommendations expressed in this material are those of the author(s) and do not necessarily reflect the views of the National Science Foundation.

REFERENCES

Dalezios, N. R., A. Loukas, L. Vasiliades, and E. Liakopoulos (2000), Severity-duration- frequency analysis of droughts and wet periods in Greece, *Hydrol. Sci. J.*, 45(5), 751-770.

Dracup, J. A., K. S. Lee, and E. G. Paulson, Jr. (1980), On the definition of droughts, *Water Resour. Res.*, *16*(2), 297-302.

Genest, C., A.-C. Favre, J. Béliveau, and C. Jacques (2007), Metaelliptical copulas and their use in frequency analysis of multivariate hydrological data, *Water Resour. Res.*, *43*, W09401.

Kao, S.-C., and R. S. Govindaraju (2007), Probabilistic structure of storm surface runoff considering the dependence between average intensity and storm duration, *Water Resour. Res.*, *43*, W06410.

Kao, S.-C. and R. S. Govindaraju (2008), Trivariate statistical analysis of extreme rainfall events via Plackett family of copulas, *Water Resour. Res.*, *44*, W02415.

Kao, S.-C. and R. S. Govindaraju (2009), A copula-based joint deficit index for droughts, submitted to *J. Hydrol.*, in revision.

Karl, T. R. (1986), The sensitivity of the Palmer drought severity index and Palmer's Z-index to their calibration coefficients including potential evapotranspiration, *J. Appl. Meteorol.*, *25*(1), 77-78.

Karl, T. R., C. N. Williams Jr., P. J. Young, and W. M. Wendland (1986), A model to estimate the time of observation bias associated with monthly mean maximum, minimum and mean temperatures for the United States, *J. Appl. Meteorol.*, *25*(2), 145-160.

Kim, T.-W., J. B. Valdés, and C. Yoo (2003), Nonparametric approach for estimating return periods of droughts in arid regions, *J. Hydrol. Eng.*, *8*(5), 237-246.

McKee, T. B., N. J. Doeskin, and J. Kleist (1993), The relationship of drought frequency and duration to time scales, in Proceedings of the 8th Conference on Applied Climatology, 179-184, January 17-22, Anaheim, California.

Nelsen, R. B. (2006), *An Introduction to Copulas*, Springer, New York.

Palmer, W. C. (1965), Meteorological drought, Res. Paper No. 45, Weather Bureau, Washington, D. C.

Salvadori, G., and C. De Michele (2004), Frequency analysis via copulas: Theoretical aspects and applications to hydrological events, *Water Resour. Res.*, 40, W12511.

Sklar, A. (1959), Fonctions de répartition à *n* dimensions et leurs marges, *Publ. Inst. Statist. Univ. Paris*, *8*, 229-231.

Svoboda, M., D. LeComte, M. Hayes, R. Heim, K. Gleason, J. Angel, B. Rippey, R. Tinker, M. Palecki, D. Stooksbury, D. Miskus, and S. Stephens (2002), The drought monitor, *B. Am. Meteorol. Soc.*, *83*(8), 1181-1190.

AGENT BASED MODELS FOR SIMULATION OF WATERSHARING IN A RIVER BASIN

S. Mohan
Professor

K. Santhosh Kumar
Graduate Student

Department of Civil Engineering
Indian Institute of Technology Madras
Chennai – 600 036, India

Abstract

Water-sharing in a river basin by different users as well as between different stakeholders along the river basin has been a serious problem and becomes more complex when there is an acute shortage of supply in the river basin. Many negotiations and interactions take place between the farmers as well as between the watersupplier and the farmers before the actual water allocation takes place. This paper presents a novel approach of agent based modeling for solving the water allocation problem. Agent based modeling using a multi-agent approach has been used to represent the various interactions between stakeholders during the process of water allocation. The spatial multi-agent programming model has been used for assessing the performance of the water allocation strategies. It is found that the developed model could provide the various possible scenarios and their consequences to the decision makers. The developed model is very generic and consists of a group of farmers with different farm sizes and crops, and a water supplier who does the allocation. The water allocation rules are built into the functioning of the models and are used to evaluate the performance of the developed rules. The performance indicators adopted in this model include individual farmers view point where one could observe the water needs and water allocated per unit area, global viewpoint with the overall yield, and the ethical viewpoint with disparities in water allocation and yields. It is found that the developed model has been proved to be successful to evolve a compromise and effective solution for the water allocation problem, when the model was applied to a case-study in Tamilnadu, India.

INTRODUCTION

Water Resources Management is the concept integrating the different aspects of water resource systems namely a number of water sub-sectors such as hydropower, water supply and sanitation, irrigation and drainage, and environment. An integrated water resources management perspective ensures that social, economic, environmental and technical dimensions are taken into account in the management and development of water resources (Lee and Dinar, 1995).

In this paper, a tool for water resources infrastructure planning has been developed by applying agent-based modeling to integrate physical, hydrological, social and economic aspects of water resource management. This tool is proved to provide insights into the social processes of water management, leading to consideration of a wider range of the environment in decision-making.

The main objective of the paper was set to evaluate the applicability of agent-based modeling of problems of water resources planning and management. For doing this, agent-based models are developed which are applied for assessing the economic, social, and environmental effects of alternative management policies. The situation of water sharing between different farmers is considered; and models are developed to evaluate the performance of different water allocation rules. Using these models it is shown to the policy makers the possible consequences of different water allocation rules.

Using **SeSAm** software, generic multi-agent models have been developed to test the efficiency of the four different sets of water allocation rules. The four different sets of water allocation rules are simulated using the four models and their performance is compared with respect to each other, based on different criteria such as realization of individual water needs, disparities between farmers, and global outputs.

Berger (2000) attempted to develop a new mathematical programming approach for prediction of diffusion processes, natural resource changes, and policy responses. The model class developed used a multi-agent/cellular automata approach by using heterogeneous farm-household models and capturing their social and spatial interactions explicitly. The individual choice of the farm-household among available production, consumption, investment and marketing alternatives is represented in recursive linear programming models. The models applicability is tested on an empirical policy-related research question in Chile.(Le Bars, 2007) in which the use of farm-based linear programming within a Cellular Automata framework was proved to be successful.

A tremendous amount of work has been accomplished during the past three decades in developing computer models for use in water resources planning and management. Powerful generalized software packages are playing an increasingly important role in all aspects of water management. With recent advances in computer technology, essentially everyone working in the water resources and environmental field now has convenient access to desktop computers providing all the hardware capabilities needed to execute a mighty arsenal of available models. Computer modeling is no longer limited solely to organizations that can afford expensive mainframe computers.

Mathematical models have been used in agriculture and water resource economies for almost half a century (Srbljinovic and Ognjen, 2003). Organizing data and processes in input and output vectors has proven to be the appropriate format for merging rather multidisciplinary information from farmers, agronomists and

agricultural engineers. In combination with a properly defined objective function, mathematical programming provides a way of integrating/including human decision making into agricultural production and resource use models.

However, if the portrayed real-world situations are characterized by spatial and behavioral heterogeneity together with economic and ecological instability, such models are often poor predictors of human behavior and might therefore fail to provide reliable information for policy analysis (Claudia, 2002). Since they largely neglect the complexity of human interactions and spatial relations, they are especially weak in analyzing the role of technological change and human organization.

AGENT-BASED MODELS FOR WATER RESOURCES PLANNING

Models associated with water resources planning and management; generally have various components which are spatially adjacent and generally interrelated. If one considers the situation of water sharing between farmers for example, during the process of water distribution a lot of interaction and negotiation takes place between all stakeholders, namely the farmers and the water supplier. The advantages of using agents-based models in such situation as well as the few limitations are discussed in the following sections.

Multi-Agent Systems (MAS) or Agent based models are computer systems composed of autonomous entities or agents which have only limited knowledge and information processing capabilities. While agents can b as simple as subroutines of a computer program, typically they are larger entities with some sort of persistent control. Good examples are personal electronic assistants that search for information on the Internet, arrange their owner's time schedules, and assist car drivers. Accordingly, on a more abstract level, their purpose is to solve larger, complex problems that one centralized unit cannot tackle, because too much information and computation power would be required. In MAS, agents instead interact and exchange information in a decentralized and somewhat 'social' manner, which explains why the term 'Distributed Artificial Intelligence' was coined. Particularly, this last aspect makes MAS an interesting tool for the social sciences. The idea is to use computer simulations with humanlike agents in order to study how an aggregation of individuals leads to complex macro behavior. These *in silico* experiments will help to test hypotheses on the fundamental social mechanisms in human societies. Typically, the agents occupy positions on a two-dimensional grid of cells and distances between them influence their interactions.

SeSAm model is the agent based model platform used in this study for the development of agent-based models. **S**e**SA**m stands for Shell for Simulated Agent Systems. SeSAm was and is further developed at the Universität Würzburg and can be freely distributed. It provides a generic environment for modelling and experimenting with agent-based simulation. It is a tool for the easy construction of complex models. The important features of SeSAm are:

- Agents consist of a body that contains a set of state variables and a behavior that is implemented in form of UML-like activity diagrams.
- Activities are seen as simple scripts that are initiated and terminated based on rules.
- The actions and conditions can be composed of an extensive number of primitive building blocks; a user is able to design visually a simulation without programming in a traditional language.
- User functions, features (set of variables and functions) and user defined data types provide a possibility to construct higher level building blocks.
- A component for evolutionary adaptation of parameters is also integrated. All is implemented visually in form of quasi declarative descriptions. These are executable in the same environment.
- Dynamics of this simulation may be observed in form of animation or user configured, autonomously updating curves.
- As there are freely configurable instruments for gathering data and scripting options for constructing simulation experiments, SeSAm is a highly valuable tool for MAS simulations especially for complex models with flexible agent behavior and interactions.

For running the simulation one has to choose the appropriate situation and analysis list and create a simulation. Now the simulation is ready for running. Before running one can choose to run to run it continuously or in pre-specified step sizes. After building the model one can run the simulation and observe the animation and on-line evaluation curves. All steps can be assessed in a visual way.

METHODOLOGY

The objective of the model is to show the evolution of a group of farmers over a number of years who use a limited water resource. A water supplier manages the resource and allocates the water to different farmers based on the water allocation rules of the system.

The current model is generic one and does not correspond to a local situation. The aim is not to provide the optimal solution but only to show the negotiators the possible consequences of the water allocation rules they decide to use. For this four different sets of water allocation rules are simulated using models and compared with each other, according to different criteria such as realization of individual water needs, disparities between farmers, and global outputs. However, in this paper one water allocation model has been demonstrated with an illustrative example. The model is mainly conceptualized on the Water allocation rules based on fair water requests by the farmers. In this model, **a**ll farmers evaluate their water requirements based on the farm sizes and type of crop being cultivated and send the requests based on the actual water requirement. All the farmers request only for the actual water requirement, as per the area of their farms and type of crop being cultivated.

If the total water available (with the water supplier) is more than the sum of all the water requests, then each farmer gets the amount of water he requested for i.e., the

water request. Otherwise, the water supplier water supplier allocates the available water to the farmers in proportion of the individual water requests.

For the model development, the suitable reasoning engine of the farmer agents needs to be adopted. The water supplier agent/water supplier-farmer as well as the test situation world are same, as the reasoning engine of the Farmer Agents takes care of all the interactions and information exchanges. In the simulation, each year consists of a sequence of four information exchanges which are:

- Each farmer determines the type of crop to be cultivated. The model considers two types of crops: crop 1 and crop 2. Each of these crops has its own water requirements and yield. The type of crop is decided based on the performance of farmers of each crop type in the previous year. For the first year the farmers are manually assigned to one type.
- The farmers send information to the water supplier based on which the water supplier has to allocate the water resource. The nature of this information depends on the rule being simulated. This information can either be as a direct water request or information about farm sizes, etc.
- The water supplier receives the information (the water requests on farm sizes information) from the individual farmers. Now he allocates water to the farmers in accordance with the water allocation rules and the amount of water available with him.
- The farmers receive the information about the amount of water that is allocated to them. Based on this the yield of each farmer can be calculated.

The model was run for 5 years and at the end of each year, farmers who perform badly change their crops. At the end of the simulations one can analyze the performance of the rules based on different criteria-individual farmers view point where we observe the water needs and water allocated per unit area, global view point with the overall yield, ethical view point with disparities in water allocation and yields. Also, the water allocation rules basically describe the interaction between the farmers (Farmers Agents) and the water supplier (Water Supplier Agent/WaterSupplier- Farmers World) which eventually leads to the water allocation. So, the reasoning engine for the Farmer Agents will be different for the four models accordingly.

The following set of variables which describe the state of the Farmer Agents. The state of the Farmer Agents in the four models is described using a combination of this set of variables. The main variables considered are Farm size, type of crop, Water Requirement per Unit Area, Water Requested by the Farmer, Informed Water Request by the Farmer, Water Allocated to the Farmer, Water Allocated to the Farmer per Unit Area, Yield of the Farmer, Ratio 1, Ratio2, and the change in the crop type. The functioning of models is based on the interaction between the Farmer Agents and Water Supplier Agent & Water Supplier-Farmers World. This interaction depends primarily on the reasoning engines of the Farmer Agents. The reasoning engines consist of a series of activities, which are performed when certain rules are satisfied. Each of the activity takes on time step of the simulation to complete.

- **Initialization:** Based on the Test Situation configuration the farmer agents will know their respective Size of Farm. For the first year the Type of Crop for each of the farmer agent is manually assigned randomly. For subsequent years, the each farmer agent first compare their Ratio1 and Ratio2 with those of a neighboring farmer (chosen randomly), if both ratios of the farmer are lesser than those of the neighbour the farmer switches to crop type, otherwise he continues with the same crop. Once the farmer agent decides the crop type, the total Water Requirement and Water Requirement per Unit Area will be evaluated.

- **Activity 1 – Sending the Water Request to the Water Supplier Agent:** In this model all the farmer agents request only for the required amount of water. Thus the amount of Water Requested by the Farmer will be the same as the water requirement. This information is sent in the following manner-all the farmer agents increment the value of Sum of all Water Requests (which is a variable of the Water Supplier/Water Supplier Farmers World) by the amount of their respective water requests.

- **Activity 2 – Water Allocation by the Water Supplier Agent:** As per the allocation Rule 1, the water supplier has to distribute the Total Available Water to the farmers in proportion of their individual Water Requested by the Farmer. The water allocated to each farmer will be the product of Water Requested by the Farmer and Alpha..

- **Activity 3 – Receiving the Water Allocation information by the Farmers:** The farmer agents receive the value of Alpha and based on that the each farmer knows the amount of water allocated to him. All the farmer agents evaluate the values of Water Allocated to the Farmer, Water Allocated to the Farmer per Unit Area and Yield of the Farmer.

Then the simulation elements namely the test situation and the analysis list are to be contrived.. It is to be noted that the configuration of the simulation elements, it is proposed to simulate the performance of the water allocation rules in the given environment, with the same configuration of map, with number of farmers placed in the same manner.

RESULTS AND DISCUSSIONS

For the demonstration of the proposed methodology, a 10 × 10 map is used as the world (Fig. 1). A total of 100 farmer agents have been considered, one for each of the hundred grids. Among these 100 farmers there are 10 big farmers, 30 medium farmers and 60 small farmers. These 100 farmers are placed on the map manually in a random manner. Then each of these farmers is assigned a crop type manually (Fig. 2). Then the value of total available water (MCM) for the world was given as the input and this completes the configuration of the test situation.

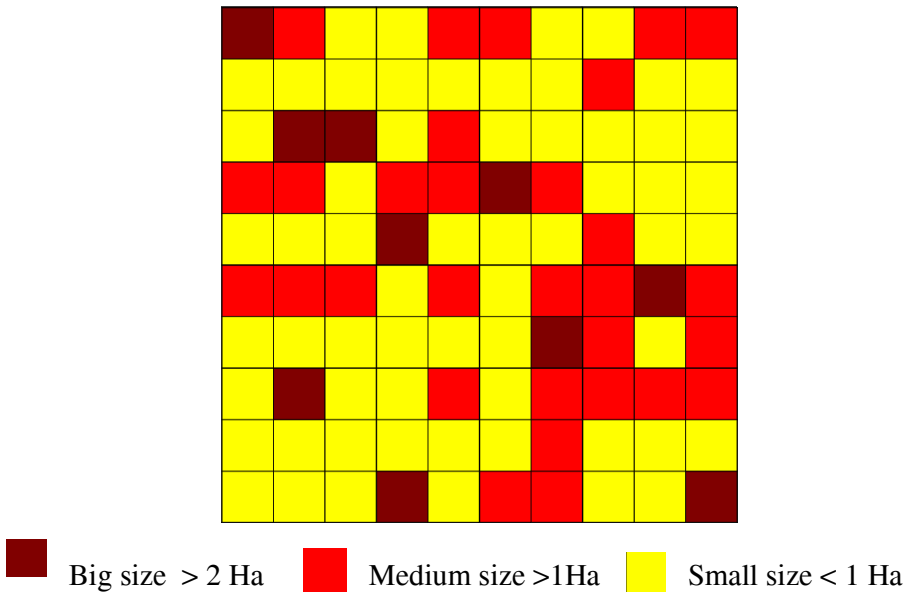

Fig 1. Map Configurations – Placement of Farmers

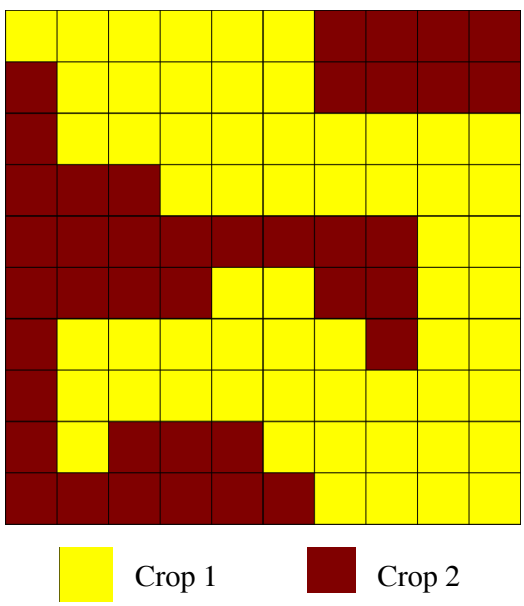

Fig.2 Crop types at the beginning of the first year

The analysis list can be used to specify what data is to be exported and in what format. We transfer the values of all the variables for each of the farmer agents to an excel spreadsheet, where we use to evaluate the performance of the four water allocation rules with respect to certain criteria. In the model, one year consists of initialization followed by three and the simulation was run for 5 such years, to see the performance of the rules both in the short term and long term. In our simulation

one step consists of one activity being performed, so four steps of the simulation make up one year (except the first year which has only three steps). The performance at the end of every fourth step starting from step three (3, 7, 11, 15 and 19 have been presented here.

For the first year the crop type of each farmer is manually assigned during configuration of the test situation. After the first year is over the values of the entire set of variables defined are calculated for the world and all the farmer agents.Then each farmer looks around selects one neighbor and compares his performance (in terms of yield) with the neighbors as well as the equitability of the water distribution process. If he performs badly, he will change his crop type otherwise he will continue with the same crop. So as the simulation continues, farmers who perform badly switch crop types. The criteria used for evaluating and comparing the performance of the water allocation rules are: global view point with the overall yield, individual farmers view point where we observe the water needs and water allocated per unit area, ethical view point with disparities in water allocation and yields.

During the simulation run, the change in the cropping pattern can be observed in the form of animation. At the end of the year the cropping patterns are captured in the form of image files for all the four models. Using these one can observe the behavior of farmers with respect to crop selection. The variations of overall yield of all the farmers with time for each model are shown in Fig. 3. It can be seen that there is a gradual increase in overall yield as time passes. This is because more and more farmers switch to Crop Type 1 as years pass by, and Crop Type 1 is more responsive to additional increments of water than Crop Type 2. The changes in crop pattern for the developed model are shown in Figure 4. It can be seen that as years pass by most of the crop 2 farmers change to Crop 1. This is because all Crop 2 farmers have higher water allocated per unit area and also productivity of Crop 2 is higher and more responsive to additional water. So, if Rule 1 is applied it is possible that after sometime all the farmers change to Crop 1 and totally abandon Crop 2.

CONCLUSIONS

The models developed are applied to the hypothetical case study and performance of the the typical water allocation rules is analyzed. It is found that Rule 1 leads to a fair satisfaction of all the farmers water needs, whereas all the other three rules result in inequitable situations with some of the farmers getting more than the required amount of water. If one looks at the equitability of the rules in terms of individual farmer yields, Rules 1 and 3 perform very well. Rule 3 results in the most inequitable distribution of individual farmer yields, with Rule 4 performing slightly better than Rule 3. It is concluded that the same rules may perform differently in a different situation, based on the configuration of farm placement, farm behavior, etc. Though the models developed are generic in nature, one can apply them to any situation and any set of water allocation rules by making changes in the agent behavior and configuration of the world. The present study also firmly establishes that agent-based

modeling is an appropriate modeling framework for testing water allocation rules. This is because, agent-based modeling is well adapted to modeling many types of agents with different rationalities. Further, multi-agent systems provide adequate structure to represent multiple and complex interactions between various kinds of agents (like farmers and water supplier) that have an important place in the process of water allocation

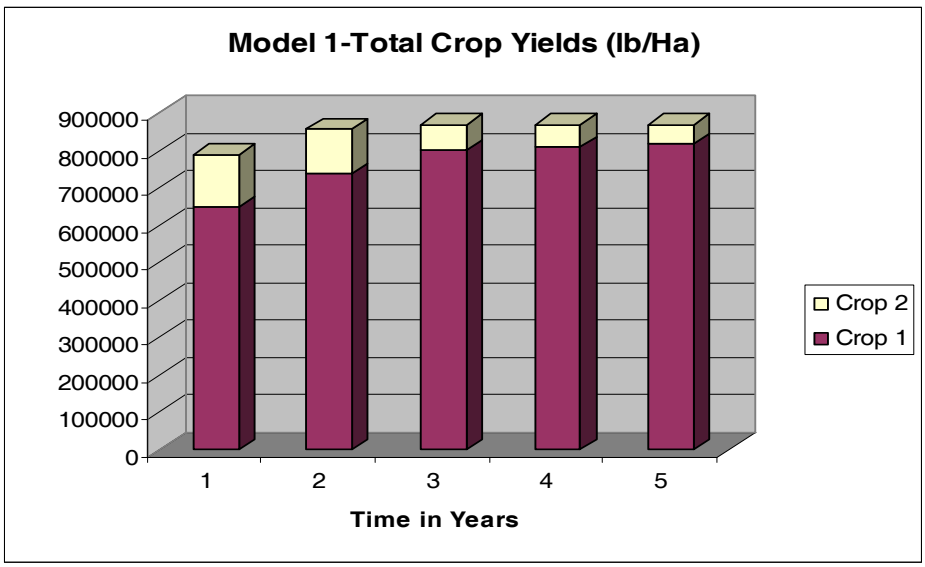

Figure 3 Total Crop yield of all farmers for Model 1

REFERENCES

Berger, T. 2000, *"Multiple –Agent Modelling Applied to Agro-Ecological Development"*. Centre for Development Research, University of Bonn.

Le Bars, M., J. M. Attonaty and S. Pinson, 2002, *"Agent-based Simulation for Water Sharing Between Different Users"*. AAMAS'02, July 15-19, Bologna, Italy.

Donna J. Lee, Ariel Dinar, 1995, *"Review of Integerated approaches to river basin planning, development and management"*. Agriculture policies division, World Bank.

Srbljinovic, A., and Ognjen, S., 2003, *"An introduction to agent based modelling and simulation of social processes"*. Interdisciplinary Description of Complex Systems 1 (1-2), 1-8.

Claudia, P.W., (2002) *"Agent Based Simulation in Integerated Assessment and Resources Management"*. Institute for Environmental Systems Research, University of Osnabrück.

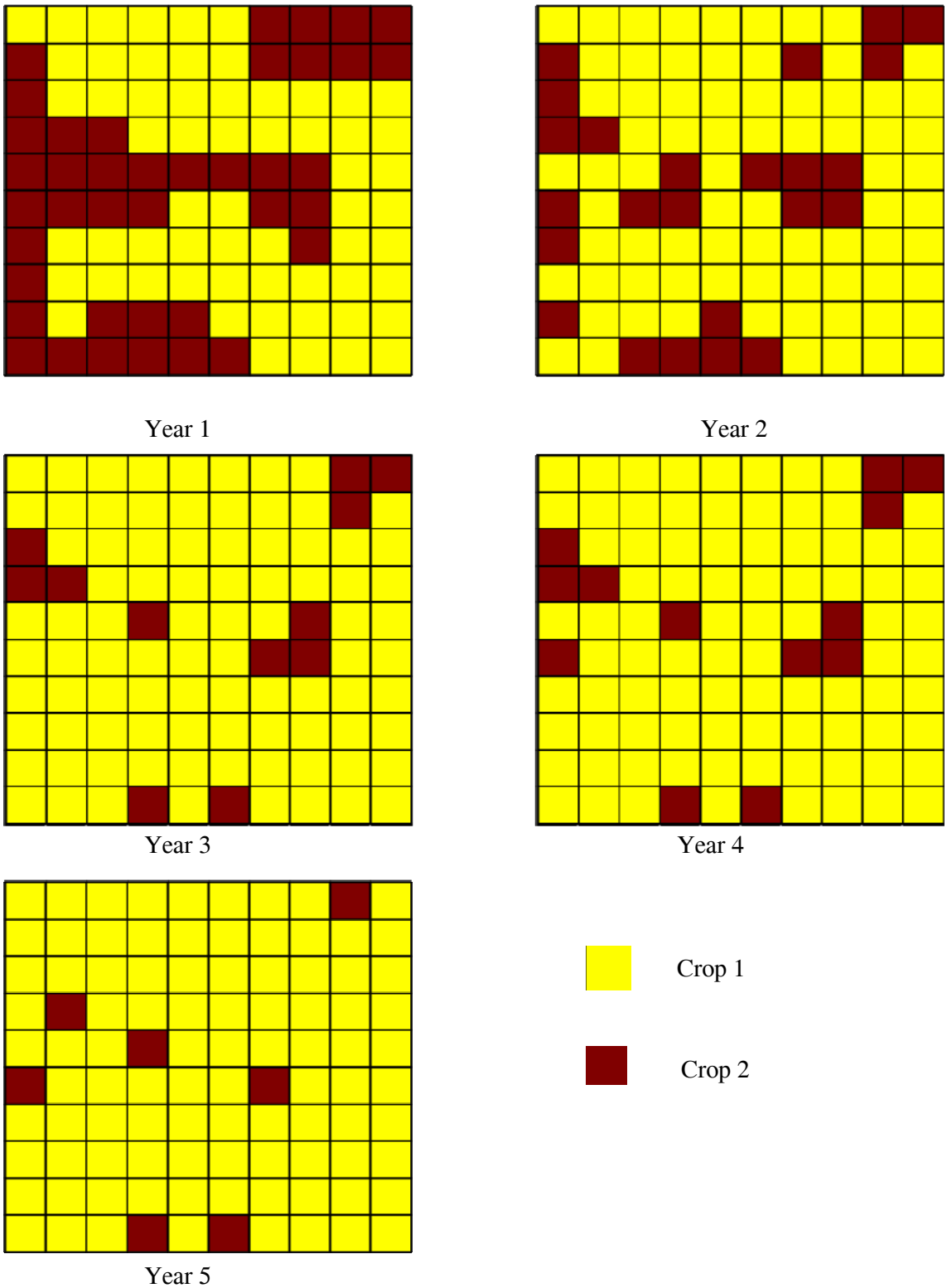

Figure 4. Year wise change in cropping pattern

Analysis on effect to EVW from policy intervention

(Ruan Ben-qing Zhang Chun-ling Wang Cheng-li Xu Feng-ran)
(China Institute of Water Resources and Hydropower Research, Beijing, China, 100038)

Abstract: High benefit utility of water is one of the main goals on water management activity. Calculational economic value of water (EVW) of industry by appropriate method can express the benefit of water use, which may be intervened by some policies, such as industry structure adjusting, water pricing, and product techniques innovating ect. The effects to EVW from the policies intervention in Beijing are discussed, which will be propitious to perfect policy on water use.

Key Words: EVW Industry Structure Water Price Techniques Innovation Sensitivity

1 . Introduction

In addressing serious water scarcity in the Hai basin in China, one of goals of water resources management is to use water more efficiently by improving industries and policy interventions within the national macro-policy framework in accordance with resources conditions.

The national policy intervention is aimed at the maximization of the national interests as a whole rather than the maximization of EVW alone. In this section, by linking EVW with the national goals and policy orientation, major policy interventions with considerable influences on productivity, water use efficiency and EVW are analyzed to proposes recommendations on promoting rational water resources allocation and increasing EVW under the premise of maximizing the national interests.

2. Effect from Readjustment of Industrial Structure

In recent years, the governments at various levels have timely been readjusting the regional industrial structure by discouraging development of industries with high energy and water consumptions and serious pollution, encouraging clean and resources-conserved productions, raising production efficiency and benefit in accordance with local resources condition to increase social output and improve people's living quality for attaining the goal of establishing well-to-do and harmonious society. Taking Beijing for example, where targets of readjusting structure of three industry are clearly defined in the Eleventh Five-year Plan although no detailed data of sub-sectors and the primary industry are available, to analyze the impacts of readjustment of the secondary and tertiary industrial structures on economic value of water quantitatively.

In the 1990s, Beijing was focused on development of the secondary industry, when the proportions of outputs of the primary, secondary and tertiary industries in GDP were 8:52:40. As industrial structure adjusted from then, in 2004, Beijing has the proportions of outputs of the three industries in GDP of 2:38:60 with the tertiary industry dominant. According to the Overall Plan for the Development of Beijing Municipality, by 2020, the proportion of the tertiary industry will further increase, GDP of Beijing will reach 1,500 billion yuan (at 2000 price), or over 10,000 US$ per capita on the average, and the proportions of outputs of the three industries will be readjusted to 1:29:70.

In order to analyze the impacts of readjustment of industrial structure on EVW, with the output value of Beijing in 2004 (base year) as the basis, the EVW is calculated for the secondary and tertiary industries based on the industrial structures at the end of 1990s and in 2020, and the results are compared with the base year. Assuming that total output and water use per unit output do not change, readjustment of industrial structure will cause changes in the input, net benefit and water abstraction of each sector. The EVW for the secondary and tertiary industries and the integrated one are listed in Table1. The results indicate:

Table 1 Economic Value of Water for Different Industrial Structures in Beijing

Year	PI:SI:TI	Secondary		Tertiary		Integrated	
		EVW (yuan/m^3)	Change range(%)	EVW (yuan/m^3)	Change range(%)	EVW (yuan/m^3)	Change range(%)
1990s	8 : 52 : 40	33.65	-0.95	37.18	0.22	34.63	-1.85
2004	2 : 38 : 60	33.97	0	37.10	0	35.28	0
2020	1 : 29 : 70	35.47	4.4	37.02	-0.21	36.7	4.02

If the proportions of the three industries are readjusted to 1:29:70 from 2:38:60 in the base year, with the same social output value, the output value of the secondary industry decreases, associated with decrease in water abstraction and increase in EVW as compared with the base year. At the same time, the output value of the tertiary industry increases with its development, associated with increase in water abstraction and less change in EVW. As a result, with unchanged total output value of the secondary and tertiary industries and decrease in the total water abstraction, the integrated EVW increases by 4.02% over the base year (Table 1).

If the proportions of the three industries are readjusted to 8:52:40 from 2:38:60 in the base year, the integrated EVW decreases by 1.85% as compared with the base year, indicating an adverse impact on EVW (see Table 1).

According to the information on the proportion of full cost of water supply in total cost by industries of Beijing in 2004 (see Table 4.5 in Appendix 4), the proportion of the secondary industry (2.6%) is bigger than that of the tertiary industry (2.4%). Because the profit&tax to cost ratio of the tertiary industry is high, the water use per unit output is small, the economic value per m^3 of water is also high, and the pollution produced is low. Therefore the increase of proportion of the tertiary industry with high EVW is favorable to the increase of regional integrated EVW.

The future readjustment of industrial structure in Beijing Municipality will further decrease the proportion of the primary industry, thus decreasing the water consumption dramatically, favoring the relief of pressure on water supply. The saved water may be used to develop industries with high EVW, thus promoting the overall increase of regional EVW.

Based on the above analysis, for the Hai Basin with serious water scarcity and for the purpose of achieving efficient use of water resources, the regional industrial structure should be readjusted by further developing the tertiary industry, putting rational limitation to the secondary industry and reducing the primary industry, thus fully tapping the potential of regional EVW through actively developing industries or sectors of efficient use of water resources.

3.Effcet from Reformation of water pricing

The major indicator of inefficiency influencing EVW of the Hai Basin is water productivity, with the lower water price as the main reason. Water price directly affects productive cost and the benefit sharing coefficient of water supply. The impacts of water pricing reform on EVW occur in the pattern of "raising water price – encouraging water saving - improving EVW". Because of the economic leverage role of price, raising water price within the users' ability to pay will promote water users to save water and reduce water abstraction per unit of output value, thus improving water use efficiency.

As the basic industry of national economy, the primary industry has a low level of development and a weak bearing capacity and is related to national grain security. As price elasticity is small for the primary industry under a series of protection policies, the impacts of water pricing reform on EVW for the secondary and tertiary industries are analyzed in this study by taking Beijing for example.

By fitting the 1995-2001 relationship between water price and water use in Beijing, a price elasticity coefficient of water use of 0.462[1] is derived and, based on this coefficient, water use norms are adjusted for different sectors, then with the increase of water price, water use norms decrease. When water price doubles, the water use norms decrease by 46 % (Table 2). Then EVW is analyzed for all industries.

Table 2 Water Use Norms by Sector after Adjustment of Water Price in Beijing

% of Price Change	SI			TI			Integrated water use norm	
	Price	Water use norm		Price	Water use norm			
	(yuan/m^3)	($m^3/10^4$yuan)	Change (%)	(yuan/m^3)	($m^3/10^4$yuan)	Change (%)	($m^3/10^4$yuan)	Change (%)
-20	4.5	25.48	9.08	4.8	26.45	9.07	26.10	9.07
Base year[A]	**5.6**	**23.36**		**6.1**	**24.25**		**23.93**	
20	6.8	21.05	-9.89	7.3	21.85	-9.90	21.56	-9.90
100	11.2	12.57	-46.19	12.2	13.05	-46.19	12.87	-46.22

Note: A stands for the year of 2004

The water price of base year in Beijing was 5.6 yuan/m^3 for the secondary industry and 6.1 yuan/m^3 for the tertiary industry. Impacts of changes of water price on EVW are analyzed for the scenarios of varying water price by ±20% and +100% over the base year.

With increased water price by 20% and 100%, respectively, based on the base year, EVW increases for all sectors to a varying extent. The increases of EVW are 1.21% and 1.71% for the secondary industry, 0.12% and 0.74% for the tertiary industry, and 4.27% and 4.86% for combination of the secondary and tertiary industries, respectively (Table 3).

When water price decreases by 20% based on the base year for all the sectors, the integrated EVW decreases by 2.42%.

Table 3 EVW for Different Scenarios of Water Price Adjustment in Beijing

[1] Ni Hongzhen, A Study of Value and Price of Water Resources based on Green Accounting, Doctorate Thesis of IWHR, Oct., 2004

% of Price Change	SI		TI		Integrated	
	EVW (yuan/m^3)	Change (%)	EVW (yuan/m^3)	Change (%)	EVW (yuan/m^3)	Change (%)
-20	32.83	-3.36	37.07	-0.07	34.43	-2.42
The base year[A]	**33.97**		**37.1**		**35.28**	
20	34.39	1.21	37.14	0.12	36.79	4.27
100	34.56	1.71	37.37	0.74	36.99	4.86

Note: A stands for the year of 2004

The analytical results show that EVW is not sensitive to the change of water price. Even water price doubles, integrated EVW only increases by 4.86%. Because of the increase of water price, water using sectors have to reduce water abstraction, their expenditures on water charge and their net benefits also change accordingly, thus causing changes to EVW. EVW increases only if the impact of decrease of water abstraction on cost and benefit exceeds that of increase of water price on cost and benefit, or vice versa. Therefore, only if all sectors realize water saving and improvement of water use efficiency through water saving actions with the increase of water price, can their EVW increases. But the increase of water price has obvious influence on decreasing water use norms (Table 3), therefore a proper rise of water price may encourage water conservancy and efficient water use.

4.Effcet from Decrease of Water use norms

With the improvement and perfection of water use technologies, the water abstraction per unit of output value, i.e., water use norm, declines and EVW increases. Take Beijing as an example for analyzing impacts of improved water use efficiency on EVW for the secondary and tertiary industries.

The changes of EVW are analyzed for different sectors in Beijing for the scenarios of 10%, 30% and 50% decreases in water use norms with those in 2004 taken as the baseline value. Calculation shows that EVW by sectors and the integrated one for all sectors increase with the decrease of water use norms. As compared with the base year, if water user norm is decreased by 10%, 30% and 50%, EVW is increased by 0.40%, 1.05% and 3.14% for the secondary industry, by 0.22%, 0.68% and 1.13% for the tertiary industry, and the integrated EVW is increased by 1.87%, 3.88% and 6.07%, respectively (see Table4).

Table4 Economic Value of Water for Different Water Use Norms in Beijing

Change range of water use norm (%)	SI		TI		Integrated	
	EVW (yuan/m^3)	Change (%)	EVW (yuan/m^3)	Change (%)	EVW (yuan/m^3)	Change (%)
The base year[A]	**33.97**		**37.10**		**35.28**	
10	34.11	0.40	37.18	0.22	35.94	1.87
30	34.33	1.05	37.35	0.68	36.65	3.88
50	34.70	2.14	37.52	1.14	37.42	6.07

Note: A stands for the year of 2004

The analytical results show that, with the same output value, total water use decreases significantly with the improvement of water use efficiency, thus resulting in reduction of water use cost and the total cost, and increase of net returns, hence increase of EVW for different sectors.

Because the water use norms change to the same extent for different sectors, EVW also practically changes to the same extent. Therefore, to formulate effective policies for water use, promote all sectors to improve productive technologies and processes, enhance water reuse rate and water use management level and reduce productive water abstraction can increase EVW and promote water saving greatly.

5. Notes

It should be noted that the above analysis of impacts of policies for the readjustment of industrial structure, change of water price and improvement of water use efficiency is all based on particular assumptions, which are quite different from realities. In realities, multiple influential factors for EVW usually change and act jointly, exerting impacts more significantly and effectively than the results of above analysis. Productive water abstraction and consumption of water resources can be effectively reduced by rationally readjusting industrial structure, appropriately increasing water price and actively improving productive water use technologies. Saved water may be used for expanding production and increasing output properly, or for improving the regional ecology and environment to bring about huge ecological and environmental benefits, which represents great significance for the Hai Basin with serious scarcity of water resources. As limited by data and time for the study, benefit of water saving is not evaluated, therefore, the EVW as affected by policy impacts on water saving is underestimated and that as affected by increased water use overestimated, and the sensitivity of EVW to policy impacts thus reflected is biased to the low side.

References

[1] Economic Valuation of Water and Policy Intervention in the Hai Basin, IWHR,2008
[2] Zhang Jinshui, Mathematic Economics – Theory and Application, Tsinghua University Pubilisher, 1992
[3] Ministry of Water Resources, Criterion of Economic Evaluation for Water Project, 1966
[4] Xu Zhifan and Shen Peijun, Economics of Water Project, Beijing, China Water Press, 1987

APPLICATION OF GENETIC ALGORITHMS FOR ESTIMATION OF FLOOD ROUTING MODEL PARAMETERS.

S. MOHAN
Professor
Environmental and Water Resources Engineering
Department of Civil Engineering
Indian Institute of Technology Madras
Chennai – 600 036
(email: smohan@iitm.ac.in)

ABSTRACT

Flood routing through rivers and channels is an essential activity in hydrological analysis and this is particularly important because of the increasing emphasis that has been placed on dam-safety worldwide and due to the increasing urbanization near river channels. The routing of flood through river channels may be accomplished using two basic approaches namely hydrologic routing approach and hydraulic routing approach. There are different methods currently in usage and the Muskingum method is the most popular method and generally used by hydrologists and engineers. However, the reliability of this method is heavily depends upon the accuracy of the parameters namely K and x or C_0, C_1 and C_2 of the model. These parameters are usually estimated by trial and error procedure. Muskingum model together with the Model proposed by Loucks (1989) have been considered for the present study and the parameters of these models were estimated using genetic algorithms, new search procedures for function optimization that apply the mechanics of natural genetics and natural selection to explore a given search space. This paper presents the results of the study of application of genetic algorithm for optimal parameter estimation of both linear and non-linear flood routing models to a case study. The sensitivity analysis of these estimated parameters was also carried out. The results had clearly depicted that the genetic algorithm is an efficient and robust means for estimation of flood routing model parameters.
.

INTRODUCTION

Flood routing through rivers and channels is an essential activity in hydrological analysis and this is particularly important because of the increasing emphasis that has been placed on dam-safety worldwide and due to the increasing urbanization near river channels. The routing of flood through river channels may be accomplished using two basic approaches namely hydrologic routing approach and hydraulic routing approach. There are different methods currently in usage and the Muskingum method is the most popular method and generally used by hydrologists and engineers. However, the reliability of this method is heavily depends upon the accuracy of the parameters namely K and x or C_0, C_1 and C_2 of the model. These

parameters are usually estimated by trial and error procedure (Viessman et al. 1977). Muskingum model together with the Model proposed by Loucks (1989) have been considered for the present study. Genetic algorithms are used because they are able to quickly optimize the parameters of functions involving multivariate. The resultant parameter values are accurate and can be used for reliable routing and thus avoiding the difficult task of estimation of routing parameters. The details of genetic algorithms are presented in this context.

GENETIC ALGORITHMS

Genetic Algorithms (GAs) are adaptive algorithms with a probabilistic component, which may be used to solve search and optimization problems. They provide a means to search poorly understood, irregular spaces. Genetic algorithms have successfully been applied to a variety of function optimization, parameter searches and machine learning applications. The basic principles of GA were first laid down rigorously by Holland (1975) and are well described in many texts, for example Goldberg(1989). GA was developed to simulate some of the processes observed in natural evolution, a process that operates on chromosomes. Natural selection links chromosomes with the performance of their decoded structure. The process of natural selection cause those chromosomes that encode successful structures to reproduce more often than those that do not. Recombination processes create different chromosomes in children by combining material from the chromosomes of two parents, and this process is referred as reproduction. Mutation may cause the chromosomes of children to be different from those of their parents.

GA appropriately incorporates these features of natural evolution in computer algorithms to solve difficult problems in the way that nature has been doing, namely through evolution. GA requires the problem to be maximized in the form of an objective function. In GA, a set of variables for a given problem is encoded into a binary string or any other coding structure, analogous to a chromosome in nature. These strings are converted to a numerical value and then linearly mapped over the range allowed for the variable. This value is then used to evaluate the objective function, yielding the "fitness." GA selects parents from a pool of strings (population) according to the basic criteria of survival of the fittest. It reproduces new strings by recombining the parts of selected parents in a random manner. The population of the next generation is done using three methods: reproduction, crossover, and mutation. Reproduction means simply those strings with highest fitness should receive the multiple copies in the next generation while the strings with low fitness receive a lower number of copies or even none at all. Crossover refers to splitting a string into two parts at a randomly generated crossover point and recombining it with another string that has been split at the same crossover point. This procedure serves to promote changes in the best strings that will give them even higher fitness. Mutation is the random alteration of a bit in the string. This assists in keeping diversity in the population.

Genetic algorithms have many advantages over other methods. Currently most literature defines three main types of search methods: calculus-based, enumerative, and random (Goldberg, 1989). Calculus based methods can be divided into two classes: indirect and direct. In indirect methods, local extreme are determined by finding where the gradient of the objective function is equal to zero. Direct methods follow along the objective function in a direction related to the local gradient. Both classes share two main disadvantages that greatly limit their usefulness. First, both are local in scope; that is, if a function has multiple local maxima, these methods may drive toward one of these values without approaching the global maxima. The second deficiency of calculus-based methods is their dependence on the existence of their derivatives. However, many real-world functions are discontinuous and noisy, and therefore do not work well with a method that prefers smooth and continuous functions. Enumerative methods are very simple but one has to carry out enormous number of iterations to locate the maxima, thus carries a high cost. This method takes a discretized search space and examines the objective function at every point. Thus, even though this method is simple, it is quite inefficient, and its execution time becomes too long when the search space becomes larger. The random search method can perform as poorly as the enumerative methods in many respects because of its inefficiency. Randomly searching through a space and saving the best results can become time-consuming as the space becomes large.

The power of GA comes from the fact that the technique is robust, and can deal successfully with a wide range of problem areas, including those which are difficult for other methods to solve. GA works through function evaluation, not through differentiation and uses probabilistic rather than deterministic transition rules. Although GA begins with a randomly generated set of points, it exploits the information contained in those points to drive it through search space. Because GA is based on function evaluation, it can be applied to all types of optimization problems as long as they are properly coded.

GA has been used in optimization problems as diverse as image analysis by Grefenstette and Fitzpatrick (1985) and gaming strategy by Axelrod (1987). The first practical engineering example of GA's application is Goldberg's study of a system of 10 pipes and 10 pumping stations (Goldberg, 1986). Expert systems have also been improved by using GA, as shown by Davis and Coombs (1987). Wang (1991) has used GA for calibrating a conceptual rainfall-runoff model and proved that GA is robust and efficient in parameter estimation. Simpson et al. (1994) have used genetic algorithm for pipe network optimization and reported that GA resulted in efficient estimation of the design variables based on a comparison with the traditional optimization techniques.

The software used for this paper was developed in C++ language. The program allows evaluation of multiple parameters and multiple objective functions. Multiple parameters are incorporated by letting each string be divided into substrings that represent different variables. The substrings length need not be equal in order to

allow a smaller substring length for integer parameters. For example, if the problem has three floating point variables and one integer variable, a string length of 28 could be used to represent three substrings of length 8, and one substring of length 4 for integer variable may be used to have an acceptable precision. The precision of each substring is determined from the equation

$$p = \frac{V_{max} - V_{min}}{2^{l} - 1}$$

where p is the precision of the parameter, V_{max} and V_{min} are the maximum and minimum of the allowed value of the parameter, and l is the length of the substring. Obviously, longer string lengths are required if each variable or parameter is to have an acceptable precision.

FLOOD ROUTING MODELS

As already mentioned, two flood routing models namely Muskingum model and the Loucks model are considered for this study. These models are explained briefly in this section for completeness.

Muskingum Method

This method is one of the sophisticated of the hydrologic flood routing procedures. This method stems from an assumption of relating storage within a routing reach to outflows at each end of the reach, which results in the basic equation:

$$S = K [x I + O (1-x)] = KO + Kx (I-O)$$

where : i

S = storage in the reach,

K and x = routing constants and

I and O = simultaneous inflow and outflow, respectively, for the reach .

For any time period t , the above equation may be written as

$$O_t = C_0 I_t + C_1 I_{t-1} + C_2 O_t$$

The C_0, C_1,and C_2 are the three parameters that may be determined from the values of K and x, and this equation is commonly used in practice.

The values of K and x are determined using past records of I and O. These values are then assumed to be characteristic values for the channel reach in future flood routing. The commonly used procedure for determining the value of x is by trial and error. Assuming a value of x, the values of x I + (1-x) O are computed and plotted against the corresponding values of storage, S. The value of x for which the width of the loop is reduced to minimum (determined by visual judgment) is considered as best value. The coefficient K is the reciprocal of the slope of the line (Cudsworth, 1989). Although using this method, a reasonable value of x may be determined

within four or five trials, the method is subjected to criticism due to its tentativeness. For instance, commenting on this method, Kulandaiswamy (1966) observed that using this method, no two investigators may get the same value of x and K for a given flood movement. The other criticism is that this procedure is time-consuming and prone to subjective interpretation. The visual judgment may not correctly identify the best among several nearly collapsed loops when all may appear acceptable (Yoon and Padmanabhan, 1992). Thus, a better and wholly objective method of determining these parameters is warranted to reduce the bias. GA offers an excellent means for estimation of these parameters.

Loucks model

In case where the storage versus weighted flow relationship is not linear as implied in the original Muskingum model, using a linear form of the model may introduce considerable error. To consider this effect, two forms of non-linear Muskingum models may be used (Yoon and Padmanabhan, 1992). Loucks (1989) proposed another nonlinear routing model and used in the general Multipurpose, multireservoir simulation model namely IRAS, and this model is used in this study. The model is given by the following three equations:

$$R_{it} = (A \,.\, S_{it} + B \,.\, Q_{it})^{C}$$

$$S_{i,t+1} = S_{it} + Q_{it} - R_{it}$$

$$Q_{it} = R_{i-1,t}$$

where,

i = 1,2 , ...N: Number of reaches or stages

t = 1,2, ...T : Time periods

R_{it} = Outflow from reach i at time t.

S_{it} = Storage in reach i at the time t

A, B, C and N: Model Parameters.

It can be proved that as the parameter A decreases, the outflow is decreased and when it is equal to zero the reach tends to keep all the storage produced in the previous stage. The parameter B does not affect the amount of outflow from the reach, but causes the lag of outflow. On the other hand, the parameter C is the most sensitive and the outflow will be significantly decreased and lagged as its value decreases. It may be noted, the value of unity for C indicates a linear reach or linear reservoir as in the other models. Care must be exercised to see that the resulted value inside the bracket should be more than one, by adopting suitable units for the flows.

APPLICATION OF GA FOR PARAMETER ESTIMATION

The main purpose of this computational experiment is to examine the ability of GA to perform a multi-parameter function optimization of a flood routing problem. One linear routing model and one non-linear routing model are considered in this study. The parameter estimation through GA is explained with reference to two examples. The first example is taken from Hoggen (1989) and the second example is from the "Flood Hydrology Manual" by Cudsworth (1989).

There are three parameters in the Muskingum model and four parameters in the Loucks model and these parameters are estimated by GA. All these parameters are to be calibrated by minimizing the function F^2 defined as the sum of squares of differences between computed and observed discharges. The model efficiency is measured by the proportion of the variance accounted for by the model and is given by the following equation

$$R^2 = 1.0 - \sqrt{}(F^2 / n)$$

where n is the total number of values. A value of R^2 =1.0 indicates that the estimated parameters are equal to their true values.

In the Muskingum model the parameters C_0, C_1 and C_2 are the three continous decision variables ranging from 0 to 1. In the Loucks non-linear routing model, parameters A, B and C are the three continous variables ranging from 0 to 1 and the parameter N is an integer variable ranging from 0 to 15. In order to encode all these continous variables into binary code, three chromosomes strings, whose length is 8,10 or 12 bits are used in each model. This binary code represents each continous variable with a minimum precision of 0.004, which is considered to be enough for the routing models. In the case of the integer variable namely N, the number of fictitious reaches along the channel or reservoirs along the river, it was considered that a 4 bit string which can produce 16 distinct integer values. Thus each string corresponds to a parameter value with one-to-one scheme ranging from 0 to 15. The GA requires that the objective function needs to be maximized. To fulfill this requirement, it is considered that the inverse of F^2 is maximized, which in turn minimize the F^2 . In order to avoid too rapid dominance and too slow improvement, the linear scaling method (Goldberg, 1989) is used in evaluating the fitness values.

For the flood data reported by Hoggen (1989), runs were made with a population size of 100, cross-over probability of 0.9 and a mutation probability of 0.1 for different string lengths of 12,18,24,30 and 36. The lower string lengths were also considered to check the variation of objective function with these values. Each run was made with 200 function evaluations or in other words the number of iterations were used is 200. It was found for the flood routing problem the increased number of iterations does not produce the increase in accuracy. Since GA is initiated

randomly, the runs were repeated with 20 different seeds and the best value of the objective function was taken as the optimal value of the objective function. When the variation of minimum sum of squares with the different string lengths was analyzed, it was found that the sum of square value has been improved with increased string (chromosome) length and a minimum of 24 is necessary to estimate the parameters with reasonable accuracy. With the string length of 36 and the crossover probability of 0.9, and the mutation probability remaining at 0.1, the sensitivity of the results to the population size was explored. For this purpose the population size is varied from 50 to 250 in steps of 50. Here again, the runs were repeated 20 times with different seeds and the best value was taken as the optimal one. The results showed that the optimum value of the objective function was achieved both at population sizes of 100 and 250. However, the corresponding values at population sizes of 150 and 200 are not much different from these values. Perhaps contrary to expectations, there appears that increased number of populations may not result in better estimation, at least with the structure of problem addressed here. It is interesting to note that similar observations were made by Koumousis and Georgiou (1994) as the population size of 50 gave better optimum and was more stable in the optimization of steel truss roofs. For the population size of 100, the results converged within 45-65 iterations, notably lower when compared to 130-185 iterations with the population size of 250. A population size of 100 was therefore adopted in examining the sensitivity of the results to cross-over probability.

Retaining the string length of 36, mutation probability of 0.1 and the population size of 100, the cross-over probability was varied from 0.6 to 1.0 in steps of 0.1. The results of this analysis proved that the lowest value of the objective function was achieved with the cross-over probability of 0.9. Similarly, with the string length of 36, population size of 100 and with the cross-over probability of 0.9, the sensitivity of the mutation probability with the optimal value of the objective function was examined. The mutation probability was varied from 0.02 to 0.1 in steps of 0.02. From the results of these runs it was found that the variation of the objective function with the mutation probability was not very significant. The lowest value of the objective function was obtained with the mutation probability of 0.04. Thus the parameters of the genetic algorithm were identified as: population size=100; string length = 36; cross-over probability = 0.9; and the mutation probability = 0.04. However, the other values of the population size = 150, 200, 250; string length = 24, 30; cross-over probability = 0.6, 0.7, 0.8; and mutation probability of 0.02, 0.06, 0.08, 0.1 can also be adopted without much loss of the global optimal value of the objective function but perhaps with more number of iterations.

The estimated values of C_0, C_1, and C_2 through the genetic algorithm are listed along with the reported values in Table 1. The corresponding F^2 and R^2 values are also reported in the same table and one could see that the parameter values are almost same and the R^2 values are also higher. The computed outflow hydrograph with the genetic algorithm when plotted along with the reported values as shown in Fig. 3, reveals that the estimated values by the genetic algorithm exactly match with each

other. This proves that the genetic algorithm is robust in estimating flood routing parameters thus avoiding the subjective and inefficient trial and error procedure. More so, this algorithm simultaneously estimates all the parameters and doesn't require the assumption of x value before estimating the other parameter K as in the calibration procedures adopted by other researchers (Gill, 1978).

The optimal values of the genetic algorithm parameters namely population size, stringlength, cross-over probability and mutation probability were obtained for the Loucks model, for the first example, in the sameline as explained above. They are Population size =100; Stringlength = 40; Crossover probability = 0.9 and the mutation probability = 0.06. The resulted values of the parameters of Loucks model are also listed in Table 1. The computed outflow hydrograph from Loucks model was also shown in Fig. 1 and are indistinguishable from the reported outflows. This is also evident from the higher values of R^2. From the above discussions it can be said that the results obtained by applying GA are practically indistinguishable from the actuals and thus offers as an efficient tool in flood routing parameters estimation.

CONCLUSIONS

In this study, genetic algorithms have been applied to flood routing parameters estimation problem. Even though in most methods routing parameters estimation would be considered as a cumbersome procedure and also to yield only approximate values, GA handled the task quite successfully. Although the model used here to estimate the flood routing parameters consist only four parameters, the procedure would be exactly same with a more elaborate hydrological model with more parameters. Results of assorted runs agreed with actual data. The ability of GA to handle a problem of this nature could make it a very important tool in the future of water resources research.

REFERENCES

1. **Axelord, R**., (1987). "The evolution of strategies in the iterated prisoner's dilemma ". ***Genetic Algorithms and Simulated Annealing***, ed. L. Davis, Pitman, London, and Morgan Kaufmann Publishers.

2. **Cudsworth, A.G**.,(1989). " Flood Hydrology Manual ", A Water Resources Publication, United States Department of the Interior, Bureau of Reclamation, Denver, Co., U.S.A.

3. **Davis,L., and Coombs,S.,** (1987) Optimizing Network Link Sizes with Genetic Algorithms, *Proc. Conferenece on Computer Simulation and Modeling*, Tucson, AZ.

4. **Gill, M.A**.,(1978), " Flood Routing by Muskingum Method ", Jl. of Hydrol.,36,253-363.

5. **Goldberg, D.E.,** (1986) Computer-aided gas pipeline operation using Genetic Algorithms and Rule Learning, Ph.D Thesis, University of Alabama.

6. **Goldberg, D.E**., (1989). Genetic algorithms in Search, Optimization and Machine Learning. Reading: Addison Wesley, Mass., U.S.A.

7. **Grefenstette, J.J., and Fitzpatrick, J.M**., (1985) Genetic Search with approximate function evaluation ", *Proc. International Conference on Genetic Algorithms and their Applications*, ed., J.J. Grefenstette, Pittsburg, U.S.A.

8. **Holland,J.** 1975. Adaptation in natural and artificial systems, Ann Arbor : Univ. Michigan Press., MI., U.S.A.

9. **Hoogen,** (1989). " Computer Assisted Flood Plain Computations ", Hydrologic Engineering Centre, California, U.S.A.

10. **Koumousis, V.K.**, and **P.G.Georgiou**, (1994) " Genetic Algorithms in Discrete Optimization of Steel Truss Roofs, Jl. of Computing in Civil Engg., ASCE., 8(3), 309-325.

11. **Kulandaiswamy,V.C**., (1966) " A Note on Muskingum Method of Flood Routing", Jl. of Hydrol., 4(2), 273-276.

12. **Loucks, D.P**., (1989), Integrated River and Aquifer Simulation (IRAS) : User's Manual, Cornell University, Ithaca, N.Y.

13. **Simpson**, **A.R, G.C.Dandy., and L.J.Murphy**, (1994) Genetic Algorithms compared to other techniques for Pipe Optimization, Jl. of Water Resources Planning and Management, ASCE, 120(4), 423-443.

14. **Viessman,W., Knapp, J.W., Lewis, G.L., and Harbaugh, T.E.,** (1977) Introduction to Hydrology, IEP Publishers, N.Y.

15. **Wang,Q.J**., (1991). The Genetic Algorithm and Its Application to Calibrating Conceptual Rainfall-Runoff models, Water Resour. Res., 27(9),pp2467-2471.

16. **Wilson,E.M**., (1974) Engineering Hydrology,MacMillan Company, London, England.

17. **Yoon,J., and Padmanabhan,G**., (1993) " Parameter Estimation of Linear and Nonlinear Muskingum Models", Jl. of Water Resources Planning and Management, ASCE, 119(5), 600-610.

Table 1. Estimated and Reported Parameters of Different models

Loucks Model				Muskingum Model		
A	**B**	**C**	**N**	**C_0**	**C_1**	**C_2**
0.033236	0.125122	0.749756	12	0.015686	0.709804	0.909804
SSE = 16331.1				SSE = 8773.5		

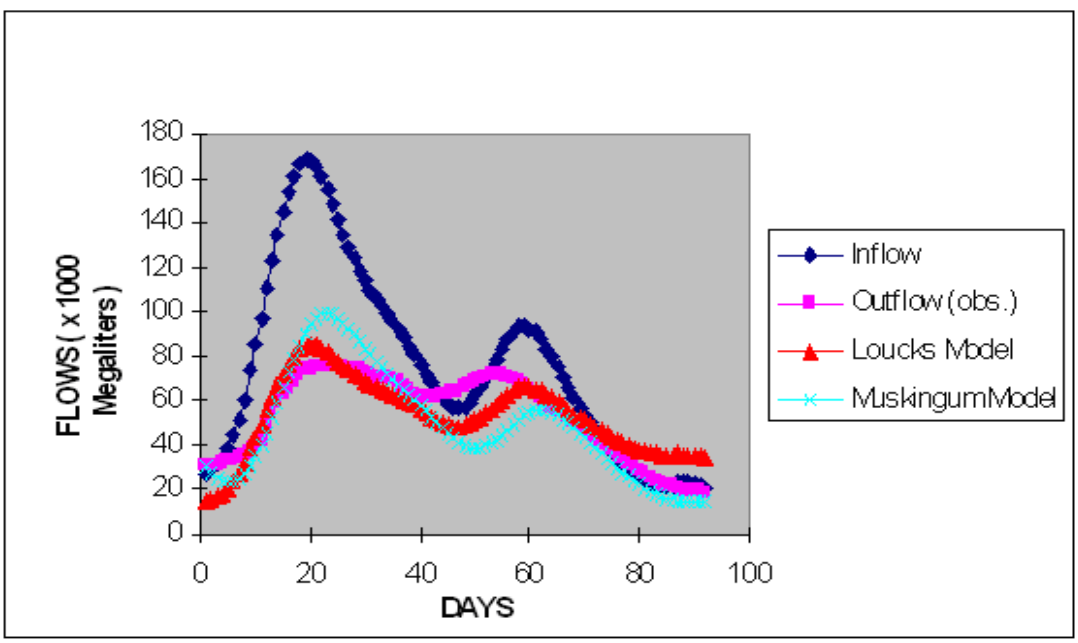

Fig.1. Comparison of Computed and Observed Flows

Application of multi-objective differential evolution algorithm (MDEA) to irrigation planning

Josiah Adeyemo* and Fred Otieno
Civil Engineering Department, Tshwane University of Technology, Private Bag X680, Pretoria, 0001, South Africa. Fax Number: +27123825226
Emails: Adeyemoja@tut.ac.za; Otienofao@tut.ac.za

ABSTRACT

Farmers in a water scarce environment have a problem of maximizing total income from farming. Irrigation planning is very important to prevent crop failures. DE, an evolutionary algorithm, which is a stochastic parallel direct search evolution algorithm known to be fast and robust in numerical optimization, is extended to multi-objective problems in this study. The new algorithm named multi-objective differential evolution algorithm (MDEA) adjusts the selection scheme of traditional DE to solve multi-objective problems. The algorithm also modifies the domination criteria for the population. The offspring generated in subsequent generations are improved before domination check is performed on the population in the final generation. MDEA is tested on three benchmark problems and later applied to an irrigation planning. The algorithm achieves the two goals in multi-objective optimization algorithm which are to discover solutions as close to the Pareto-front as possible and to find solutions as diverse as possible in the obtained non-dominated front.

Keywords: irrigation planning, differential evolution; multi-objective; optimization; evolutionary algorithm

INTRODUCTION

Optimization is a procedure of finding and comparing feasible solutions until no better solution can be found. It also refers to finding one or more feasible solutions which correspond to extreme values of one or more objectives (Deb, 2001). In engineering designs, it may be necessary to find the optimal solutions in a problem. There may be a problem of designing for minimum cost, or for maximum benefit. There may be optimization problem that involves one objective function. It is always called single-objective optimization. The procedures for solving this kind of problem are gradient-based and heuristic-based search techniques. If optimization problem involves more than one objective functions, then the problem is known as multi-objective optimization. Mostly real-world search and optimization problems naturally involve multiple objectives. All the objectives in a multi-objective problem are all important. Single objective problem involves finding the minimum and maximum of a single-variable function. The method used may be the techniques of finding an optimum of a first and second order derivative of a function. Also it may be the technique of finding an optimum in a multi-variable function. The optimization may also involve finding the true optimum in the presence of

constraints. The real world problems involve restricting some properties of the system to lie within some ranges. These constitute the constraints of the problem. Constrained optimization techniques include Lagrange multipliers, linear and non-linear programming, dynamic programming, quadratic programming, fractional programming, geometric programming, etc. The mathematical structure of the model will determine the application of each these constrained optimization procedure.

In multi-objective optimization, there may not exist a solution that is best with respect to all objectives, instead, there are equally good solutions which are known as Pareto optimal solutions (Deb, 2001). A Pareto optimal set of solutions is such that when we go from any one point to another in the set, at least one objective function improves and at least one other worsens (Babu and Jehan, 2003). Neither of the solution dominates over each other and all the sets of decision variables on the Pareto are equally good.

Evolutionary algorithms (EAs) have the ability to find multiple Pareto optimal solutions in one single simulation run because of their population-approach. EAs are general purpose stochastic search methods simulating natural selection and biological evolution (Salman, Engelbrecht, and Omran, 2007). EAs maintain a population of potential (or candidate) solutions to a problem. They are biologically-inspired optimization algorithms, imitating the process of natural evolution, and are becoming important optimization tool for several real world applications. They use a set of solutions called population to converge to the optimal solution. They are robust optimization method. They are less susceptible to problem dependent characteristics, such as the shape of the Pareto front (convex, concave or even discontinuous), and the mathematical properties of the search space, whereas these issues are of concerns for mathematical programming techniques for mathematical tractability (Angira and Babu, 2005).

Several studies have extended evolutionary algorithm to solve multi-objective numerical optimization problems (Angira and Babu, 2005; Babu and Jehan, 2003; Babu, Mubeen, and Pallavi, 2005; Deb, 2001; Deb, Agrawal, Pratap, and Meyarivan, 2001; Deb, Pratap, Agarwal, and Meyarivan, 2002; Fan, Lampinen, and Levy, 2006; Madavan, 2002; Reddy and Kumar, 2007; Robic and Filipic, 2005; Santana-Quintero and Coello, 2005; Xue, Sanderson, and Graves, 2003). Over the past decade, a number of multi-objectives evolutionary algorithms (MOEAs) have been suggested (Deb *et al.*, 2001).

Differential evolution (DE) is a very simple population-based, stochastic function minimizer which is very powerful at the same time (Price and Storn, 2008). It is a family of EAs and has the advantages of simple structure, ease of use, speed and robustness. Unlike other EAs, DE does not make use of some probability distribution function in order to introduce variations into the population (Salman *et al.*, 2007). Instead, DE uses the differences between randomly selected factors (individuals) as the source of random variations for a third vector (individual), referred to as the target vector. Hence, the trial solutions which will compete with the parent solution are generated by adding the weighted difference vectors to the target vector (Price and Storn, 2008).

Multi-objective differential evolution algorithm (MDEA)

Multi-objective differential evolution (MODE) is proposed by (Babu and Jehan, 2003; Babu *et al.*, 2005). In the algorithm, the dominated solutions are removed from the population in each generation. Only the non-dominated solutions are allowed to undergo DE operations of mutation, crossover and selection. The offspring are placed into the population if they dominate the parents. The algorithm worked well on the test problems but the number of non-dominated solutions generated is few. The dominated solutions that are removed from the population can still be improved using the DE operations. During mutation stage, they may be combined with other vectors to produce offspring that may replace them instead of just removing them. In this way, at the end of the generation, the number of non-dominated solutions is increased with quality members giving wider Pareto optimal fronts. In the original DE with single objective, most of the initial generated solutions are infeasible. They undergo mutation and crossover before they are improved to be feasible. In the same way, the solutions in each generation should be allowed to mutate, recombined and undergo crossover. The final solutions are the only one to be checked for domination. Therefore, domination check is done once instead of doing it in all the generations.

The algorithm proposed by (Fan *et al.*, 2006) is implemented by modifying the selection scheme of DE. In their selection scheme, the trial population is compared with its counterpart in the current population. If the trial candidate dominates the current population member it will survive from the tournament selection to the population of the next generation and replaces the current population otherwise the current population is retained. They suggest that if the trial solution is worse than the target solution in all the objectives, it should be discarded.

A new DE algorithm for multi-objective optimization problems (MOOPs) is proposed in this study and it is called multi-objective differential evolution algorithm (MDEA). The DE algorithm proposed is based on the existing DE algorithm proposed by (Price and Storn, 1997). The only difference is its implementation of multi-objectives. Though the proposed MDEA can be used on any strategy, the strategy used in this study is DE/rand/1/bin which is the most widely used of all the ten strategies of DE. MDEA combines the advantages of both algorithms described above while overcoming the shortcomings of the algorithms. In this way, MDEA runs faster with more quality Pareto optimal solutions. The description of the MDEA is as follows. The vectors are randomly generated to create initial vectors and solutions to the problem. The generated solutions are allowed to undergo mutation, crossover and selection for the number of generations. The solutions that evolve are checked for domination and the dominated solutions are removed. The selection procedure of (Fan *et al.*, 2006) is used. The trial solution survives to the next generation if its objective function is better or equal in all the objective. MDEA will produce many non-dominated solutions on the Pareto front than the algorithm by (Fan *et al.*, 2006) and (Babu *et al.*, 2005). Moreover, the algorithm by them has not been modified to handle constraints except bound constraints. Our algorithm can handle multiple constraints. If any of the constraints is violated, a high value (10^8) is added to the objective function to make the solution infeasible (Deb, 2001). In this

way, the solution will not be selected when compared with other solutions because of high value.

The pseudo code of MDEA is presented below. The proposed MDEA methodology can be summarized in the following steps.

1. Input the required DE parameters like population size, crossover constant, scaling factor, maximum generation, number of objectives, bound constraints etc.
2. Initialize all the vectors randomly in the limit of bound constraints.
3. Set the generation counter, G =0.
4. Perform mutation and crossover operations as explained in the DE algorithm above on all the population members
    a. For each parent, select three distinct vectors randomly from the current population. The selected vectors must not be parent vector.
    b. Calculate new mutation vector using the expression, $V_i(g) = X_{i3}(g) + F*(X_{i1}(g) - X_{i2}(g))$
    c. Perform crossover using any of the two crossover method. Binary crossover method is used because of the strategy DE/ran/1/bin used in MDEA in this study.
5. Evaluate each member of the population and check the offspring for domination. Replace the parents with offspring in the next generation if the offspring dominate the parents otherwise, the parents proceed to the next generation.
6. Increase the generation counter, G, by 1. i.e. G = G+1 and check if G = GMAX. If G < GMAX, then go to step 4 above and repeat mutation, crossover and selection. If G = GMAX, then goto step 7.
7. Remove the dominated solutions in the last generation. A solution is dominated if there is another solution which is better than it in all the objectives. The method used here is naïve and slow suggested by (Deb, 2001).
8. Output the non-dominated solutions

The steps above are followed, using the pseudo code below, to code the algorithm in MATLAB 7.0 (The MathWorks Inc., USA) and is executed on a 1.7GHz, 2GB RAM PC and tested on some test problems below to demonstrate its ability to solve linear and non-linear constrained multi-objective optimization problems. The results are presented in Figures 1, 2 and 3. The DE parameters used are population size(NP) = 50, crossover constant(Cr) = 0.5, scaling factor (F)=0.5 as suggested by (Price and Storn, 2008). The description of each of the three test problems are presented below.

The Pseudo code for multi-objective differential evolution algorithm (MDEA)

**Initialize the values of D, NP, Cr, F, k (number of objective functions) & maximum generation (MAXGEN)*
**input the boundary constraints of the problem*
**Initialize all the vectors of the population randomly*

For i = 1 to NP
For j = 1 to D
$X_{i,j}$ = $Dlower_j$ + *random number[0,1] * [*$Dupper_j$-$Dlower_j$*]*
Next j
Next i
**Initialize gen = 1*
for gen = 1 to MAXGEN
for i = 1 to NP
For m = 1 to k
Evaluate the objective function values
Next k
Check the constraints violation
*If violated objective function value = objective function value + 8*10*^{8} *(Deb K, 2001)*
For j = 1 to D
(Mutation stage)
Select 3 different vectors for perturbation different from i such that i≠r1≠r2≠r3
$V_{i,gen} = X_{r3,gen} + F(X_{r1,gen} - X_{r2,gen})$
(Crossover Stage)

$$u_{j,i,gen} = \begin{cases} v_{j,i,gen} & \text{if randj} \le \text{Cr or j} = \text{n} \\ \text{x}_{\text{j,i,gen}} & \text{otherwise} \end{cases}$$

and n ∈{1, …,D}
next j
(Selection stage)
Start comparing vectors $U_{i,gen}$ *and* $X_{i,gen}$
For m = 1 to k
evaluate kth objective function, $f_k(U_{i,gen})$
If $f_k(U_{i,gen}) \le f_k(X_{i,gen})$
Select vector $U_{i,gen}$*, the trial vector*
$(X_{i,gen+1}) = (U_{i,gen})$
goto next step
Else
Next m
endif
select $X_{i,gen}$ *the current population member for the next generation*
$(X_{i,gen+1}) = (X_{i,gen})$
next m
next i
next gen
**remove the dominated solutions from the last generation using naïve and slow method proposed by (Deb, 2001)*
print the results

Test Problems

Problem 1 (Lampinen, 2000):

Minimize $f1(x) = x_1^2 + x_2$,
$f2(x) = x_1 + x^2_2$
$-10 \le x_1, x_2 \le 10$

Problem 2 (Deb, 2001)

Minimize $f1(x) = 4x_1^2 + 4x_2^2$
$f2(x) = (x_1 - 5)^2 + (x_2 - 5)^2$
Subject to $C_1(x) = (x_1 - 5)^2 + x_2^2 \le 25$
$C_2(x) = (x_1 - 8)^2 + (x_2 + 3)^2 \ge 7.7$
$0 \le x_1 \le 5,$
$0 \le x_2 \le 3.$

Problem 3

Minimize $f1(x) = x_1$
$f2(x) = \frac{1+x_2}{x_1}$
subject to $g_1(x) \equiv x_2 + 9x_1 \ge 6$
$g_2(x) \equiv -x_2 + 9x_1 \ge 1$
$0.1 \le x_1 \le 1,$
$0 \le x_2 \le 5$

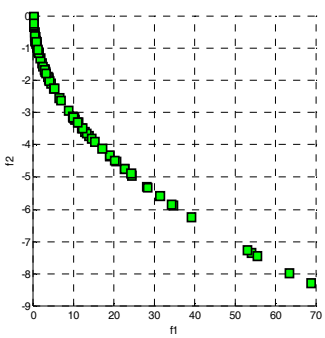

Figure 1. The non dominated solutions for test problem 1.

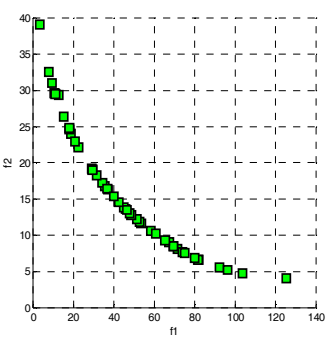

Figure 2. The non dominated solutions for test problem 2.

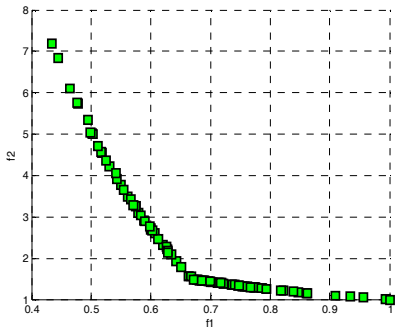

Figure 3. The result of the convergence of test problem 3.

IRRIGATION PLANNING MODEL

MDEA is further extended to irrigation planning where the aim is to minimize the area of land cultivated and to maximize the total farm income. There are 8 crops to be planted on the cultivated area. The crops are carrot, potato, water melon, pea, maize, wheat, bean and onion. The model is presented below:

Objective function 1: Minimize the cultivated land

The cultivated land area available for irrigation is minimized to reduce the number of employee that will be working on the farm. This will also reduce the complexity of management on the farm.

$$\text{Minimize } CA = \sum_{i=1}^{N} A_i$$

where CA is the total cultivated area in hectares and A_i is the cultivated area for $crop_i$.

Objective function 2: Maximize the total farm income

The total farm income in South African Rand (ZAR) on the total cultivate land is maximized.

$$\text{Maximize } FINC = \sum_{i=1}^{N} (\text{Price}_i * Yield_i) * A_i$$

Where,
FINC = total farm income
$Price_i$ = price of crop planted on land A_i
$Yield_i$ = yield of $crop_i$ on land A_i

The above objectives are subjected to the following constraints:

Constraint 1: Minimum and maximum cultivated areas
Each crop in the command area is planted on minimum and maximum cultivated areas. The minimum for all the crops is 500 ha and the maximum vary from crop to crop.

$$500 \leq A_i \leq A_{i\max}$$

Constraint 2: Canal capacity
Irrigation release in any month can not be more than the canal capacity.

$V_i \leq canal$ capacity $\forall$ i = 1 to 12

Constraint 3: Total volume of water
The total volume of water in the whole year should be less than the annual allocated irrigation water in the area.

$$TVOL \leq 10\ Mm^3$$

Constraint 4: Crop water requirement
The monthly irrigation release must meet the crop water requirements for all the crops in the month.

$V_i \geq (CWR_i * A_i) \quad \forall$ i = 1 to 12

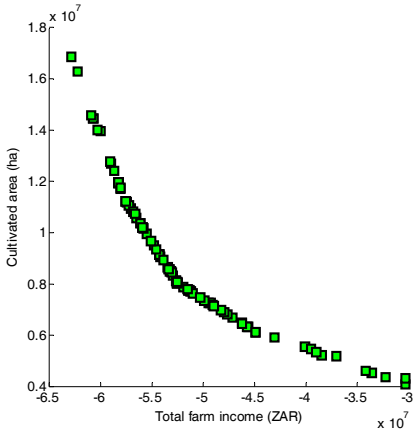

Figure 4. The non dominated solutions for the irrigation planning

Results and discussions

MDEA is used to solve the multi-objective problems above. Figures 1, 2, 3 and 4 above present the non dominated solutions for the test problems 1, 2, 3 and irrigation planning model. It is found that the solutions converge to Pareto front. It can also be found that MDEA achieved the two goals in multiobjective optimization problem. The goals are to discover solutions as close to the Pareto-front as possible and to find solutions as diverse as possible in the obtained non-dominated front. A good multi-

objective evolutionary algorithm will be known if both goals are satisfied (Deb, 2001). The non-dominated solutions will be evaluated using higher level knowledge to determine the appropriate solution to be chosen at a particular time.

In all the test problems and irrigation planning model, the number of non dominated solutions generated are 50. This shows that all the solutions become non-dominated after undergoing the operations of DE which are mutation, crossover and selection. The otherwise solutions that would have been infeasible or dominated produce offspring to replace themselves. All the problems converge to Pareto optimal front in less than 200 iterations.

Conclusions

Multi-objective differential evolution algorithm (MDEA) is illustrated in this paper. The selection scheme in the original DE is improved to be able to solve multi-objective problems. Also, dominated solutions are removed in the last generation only instead of removing them in all the generations. This saves us lots of simulation runs and also increases the number of non-dominated solutions giving us wider Pareto optimal fronts. The test problems used to validate the algorithm show that MDEA is a good optimizer. The algorithm gives good spread of solutions maintaining diversity and convergence. The algorithm is further applied to irrigation planning problem and the results are encouraging. Therefore, MDEA is a good alternative for solving water resources management problems and other engineering problems.

REFERENCES

Angira, R., and Babu, B. V. (2005). Non-dominated sorting differential evolution for multi-objective optimization. *2nd Indian international conference on Artificial intelligence (IICAI-05)*, 1428-1443.

Babu, B. V., and Jehan, M. M. (2003). December 8 - 12. *Differential evolution for multi-objective optimization.* Paper presented at the Congress on Evolutionary Computation (CEC-2003), Canberra, Australia.

Babu, B. V., Mubeen, J. H. S., and Pallavi, G. C. (2005). Multi-objective differential evolution (MODE) for optimization of adiabatic styrene Reactor. . *Chemical Engineering Science, 60*, 4824-4839.

Deb, K. (2001). *Multi-Objective Optimization using Evolutionary Algorithms*: John Wiley and Sons, Chichester, UK.

Deb, K., Agrawal, S., Pratap, A., and Meyarivan, T. (2001). *A Fast Elistist Non-Dominated Sorting Genetic Algorithm for Multi-Objective Optimization: NSGA-II* (No. 200001): Kanpur Genetic Algorithms Laboratory(KanGAL) Indian Institute of Technology Kanpur.

Deb, K., Pratap, A., Agarwal, S., and Meyarivan, T. (2002). *A fast and elitist multi-objective genetic algorithm: NSGA-II.* Paper presented at the IEEE Transaction on Evolutionary computation.

Fan, H. Y., Lampinen, J., and Levy, Y. (2006). An easy-to-implement differential evolution approach for multi-objective optimizations. *Engineering Computations: International Journal for Computer-Aided Engineering and Software, 23*(2), 124-138.

Lampinen, J. (2000). *Multi-objective nonlinear Pareto-optimization: a pre-investigation report, Technical Report*: Laboratory on Information Processing, Lappeenranta University of Technology, Lappeenranta.

Madavan, N. K. (2002). *Multi-objective optimization using a Pareto differential evolution approach.* Paper presented at the Congress on Evolutionary Computation (CEC '2002).

Price, K., and Storn, R. (1997). Differential evolution. *Dr Dobb's Journal*(April 97,), 18 - 24.

Price, K., and Storn, R. (2008). Differential evolution homepage (web site of Price and Storn) as at 2008. http:\\www.ICSI.Berkeley.edu/~storn/code.html. [Online]. Available from: 2008.

Reddy, M. J., and Kumar, D. N. (2007). Multiobjective Differential Evolution with Application to Reservoir System Optimization. *Journal of Computing in Civil Engineering @ ASCE, 21*(2), 136-147.

Robic, T., and Filipic, B. (2005). *DEMO: Differential evolution for multiobjective optimization.* Paper presented at the 3rd Int. Conf. on Evolutionary Multi-Criterion Optimization, EMO 2005.

Salman, A., Engelbrecht, A. P., and Omran, M. G. H. (2007). Empirical analysis of self-adaptive differential evolution. *European Journal of Operational Research, 183*, 785-804.

Santana-Quintero, L. V., and Coello, C. A. C. (2005). An algorithm based on differential evolution for multi-objective problems. *International journal of computational intelligence research, 1*(2), 151-169.

Xue, F., Sanderson, A. C., and Graves, R. J. (2003). *Pareto-based multi-objective evolution.* Paper presented at the Congress on Evolutionary Computation, Canberra, Australia.

Assessing Potential Implications of Climate Change for Long-Term Water Resources Planning in the Lower Colorado River Basin

Susan Butler, AICP*, Armin Munevar, P.E.*, Ron Anderson, P.E. **, Joseph Rippole, P.E. ***
*CH2M HILL
12301 Research Boulevard, Building 4, Suite 250
Austin, Texas 78759
Lower Colorado River Authority * San Antonio Water System

Abstract

The Lower Colorado River Authority (LCRA) – San Antonio Water System (SAWS) Water Project is being studied to conserve water, develop conjunctive groundwater supplies, and capture excess and unused river flows to meet future water needs for two neighboring regions in Texas. Agricultural and other rural water needs would be met on a more reliable basis in the lower Colorado River basin through water conservation, surface water development and limited groundwater production. Surface water would be transferred to the San Antonio area to meet municipal needs in quantities still being evaluated. The project is in its sixth year of detailed studies addressing environmental, agricultural, socioeconomic, and engineering aspects of the project. Tools are being developed and used in project planning including instream flow criteria, water quality assessments, bay freshwater inflow criteria, surface water availability models and operating approaches, agricultural conservation measures, groundwater models, and economic models.

Models used to calculate water availability and environmental flow requirements have been developed largely within existing frameworks based on hydrologic data available from historical events. This is a standard approach used by water planners across the country as well as by many regulatory agencies for permit review. In view of the project's eighty-year planning horizon, contractual obligations associated with this particular project, comments from the project's Science Review Panel and increased public and regulatory awareness of climate change issues, the project team is exploring predictions of climate change in the region and methods to assess potential impacts on the LCRA-SAWS Water Project during the project's expected life.

After qualitatively assessing system vulnerabilities potentially resulting from changed climate conditions, the project team initiated a quantitative evaluation of possible future climate scenarios. Using a scenario approach identifies a broad range of possible future implications for the watershed and its various systems. Two atmosphere-ocean general circulation models and two carbon emission scenarios were selected from which to generate potential climate scenarios for future time periods of 2050 and 2080. Global-scale changes in key climate parameters (i.e., temperature, precipitation, evaporation and sea level rise) were then translated to the local watershed scale. The Variable Infiltration Capacity hydrology model was then used to simulate historical runoff, river flow and evaporation under future climate

conditions and to generate "perturbation ratios" (adjustment factors) to be applied to historical data.

Climate-change adjusted hydrologic data sets were produced for use in simulating water availability that could result if the climate scenarios were to occur. Simulations using the "new" hydrologic flows were generated using the surface water model for project planning. Potential changes throughout the system including water availability, river water quality, affects to riverine habitat, and affects to Matagorda Bay were analyzed. Additionally, projected changes to agricultural water demand due to changes in atmospheric carbon dioxide levels, temperatures and precipitation were projected.

Introduction

The Lower Colorado River Authority (LCRA)-San Antonio Water System (SAWS) Project (LSWP) is a water sharing proposal to develop alternative supplies that could help meet long-term needs in the lower Colorado River basin and the San Antonio area. The LSWP contains three strategies that would conserve and develop water in the lower Colorado River basin for both regions:



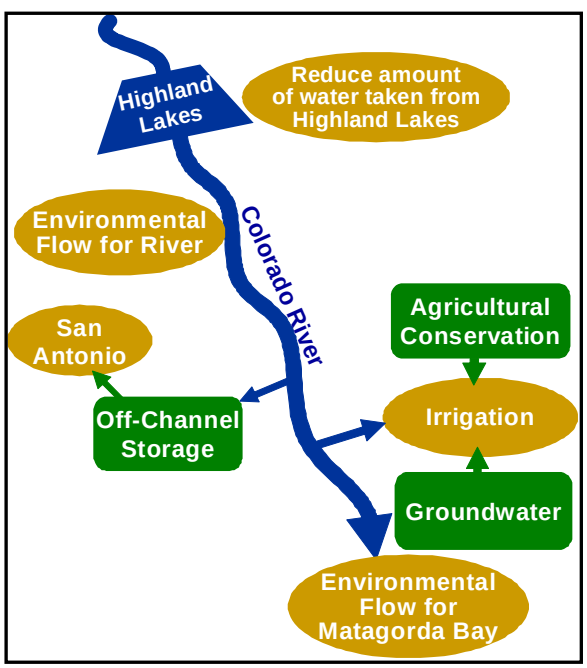

1. Reduce agricultural irrigation demands for water with conservation practices and measures, such as laser-leveling fields, improving canals and growing more water-efficient rice,
2. Capture and store unused and excess river flows in an off-channel storage facility and,
3. Use a limited amount of groundwater for agriculture during dry periods when an adequate volume of surface water is not available.

LCRA and SAWS agree the project will not proceed if studies show the costs are too high, not enough water is

available, or if the project does not meet specific requirements adopted by the Texas Legislature to protect the lower Colorado River basin.

Climate change was considered a key aspect to overall project risk due to its potential effects on water availability, agricultural water use, and the Matagorda Bay system.

Framework for Evaluating Climate Change Risk

Climate change risk assessment is used to systematically evaluate the vulnerability of water systems to climate changes. A dual analytical framework consisting of both qualitative and quantitative approaches was applied in this assessment. The qualitative assessment involved focused workshops with experts in each of the key system component areas. Through guided discussions, the climate sensitivity, adaptive capacity, and vulnerability of various system components was explored, documented into a vulnerability matrix, and the most critical areas were identified.

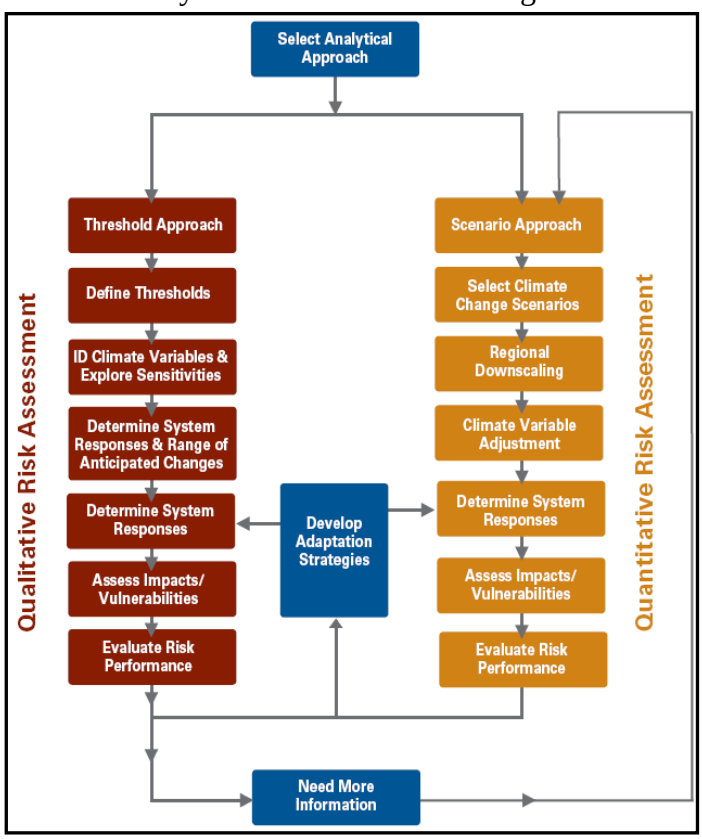

Following the identification of key areas, a quantitative scenario approach was initiated. The scenario approach involved the selection of climate change scenarios, scaling global climate projections to the regional scale (downscaling), application of techniques to statistically-adjust historical climatology, assessment of water supply and ecological system responses to various changes in climate parameters and, finally, an assessment of the system vulnerability and risk.

Climate Scenario Development

Methods

Given the uncertainty associated with future climate change projections and models, it was desirable to bracket a range of future conditions. Climate scenarios were developed by selecting a combination of future emission scenarios developed by the Intergovernmental Panel on Climate Change (IPCC) and simulated climate projections from coupled atmosphere-ocean general circulation models (AOGCMs).

Five basic criteria were considered in the selection of climate change projections for use in the project including:

- Climate parameters and metrics (annual mean temperature and precipitation)
- Future climate periods (2050 and 2080)
- Locations across the watershed (upper, mid, and lower basin)
- Range of projections (bracketed range to extent possible)
- Consistency of global circulation models and emission scenarios

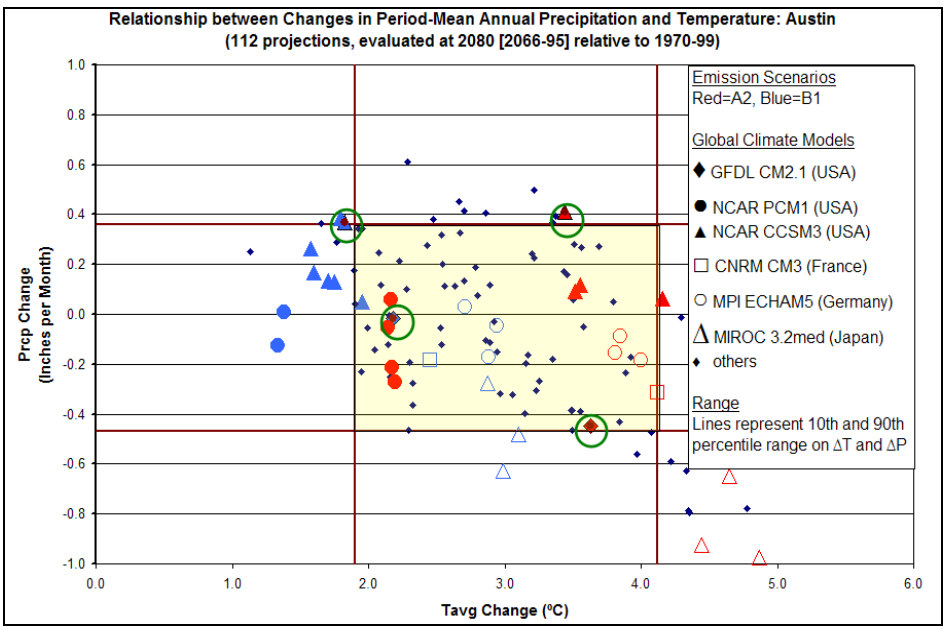

A total of 112 future projections developed for the IPCC, subsequently bias-corrected and statistically downscaled to 1/8th degree, were obtained from Lawrence Livermore National Laboratory (LLNL) under the World Climate Research Program's (WCRP) Coupled Model Intercomparison Project Phase 3 (CMIP3). The model projections were computed for several points in the Colorado River basin for two future periods: 2050 and 2080. Analysis bracketing the 10th and 90th percentile range of temperature and precipitation projections was developed and judged suitable for evaluating the range of future conditions. Two models were selected for the analysis: (1) the U.S. Department of Commerce National Oceanographic and Atmospheric Administration Geophysical Fluid Dynamics Laboratory (GFDL) model and (2) the National Center for Atmospheric Research model (CCSM). Simulations for relatively high and relatively low carbon emission scenarios (A2 and B1, respectively) were selected to create four scenarios that broadly captured the range of potential future climate conditions.

Results

The "A2" climate scenarios represent conditions with emissions of greenhouse gases somewhat higher than others developed by the IPCC and thus represent a warmer future climate. Under these scenarios, basin-wide annual average temperatures are

projected to increase by more than 2 degrees C (3.6° F) by 2050 and nearly 4 degrees C (7.2° F) by 2080. More modest warming is projected under the "B1" scenarios, with warming around 2 degrees C (3.6° F) by 2080. Precipitation trends, however, are more variable among the scenarios. The GFDL model consistently projects moderate to high drying conditions, while the CCSM model consistently projects wetter conditions. Regardless of the direction of the precipitation change, the annual projected changes are small by year 2050 [from a drying of 4.2 centimeters per year (1.7 inches per year) to a wetting of 2.9 centimeters per year (1.1 inches per year)]. The greatest warming is projected for the upper portion of the basin, but the precipitation projections appear more dependent on the general circulation model than on the emission scenario.

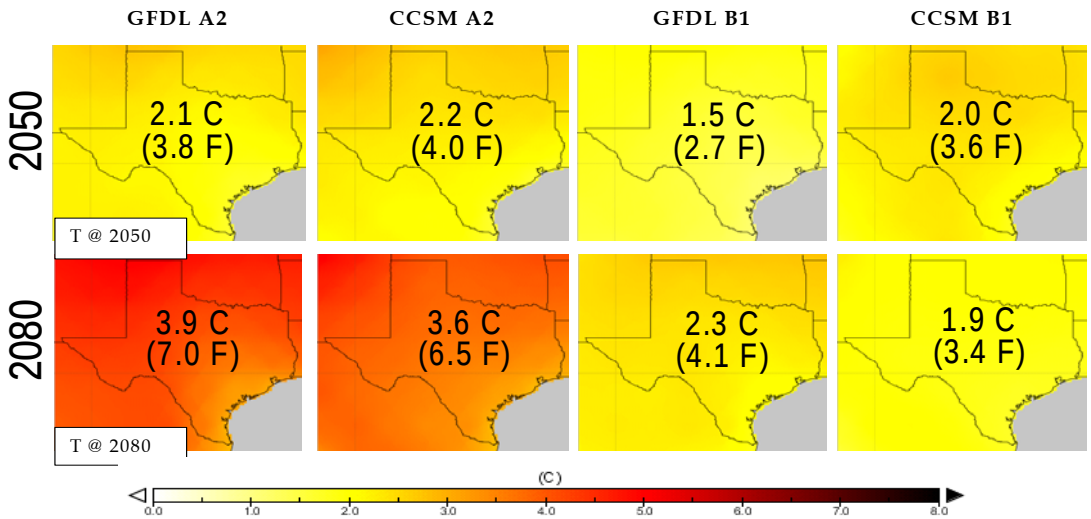

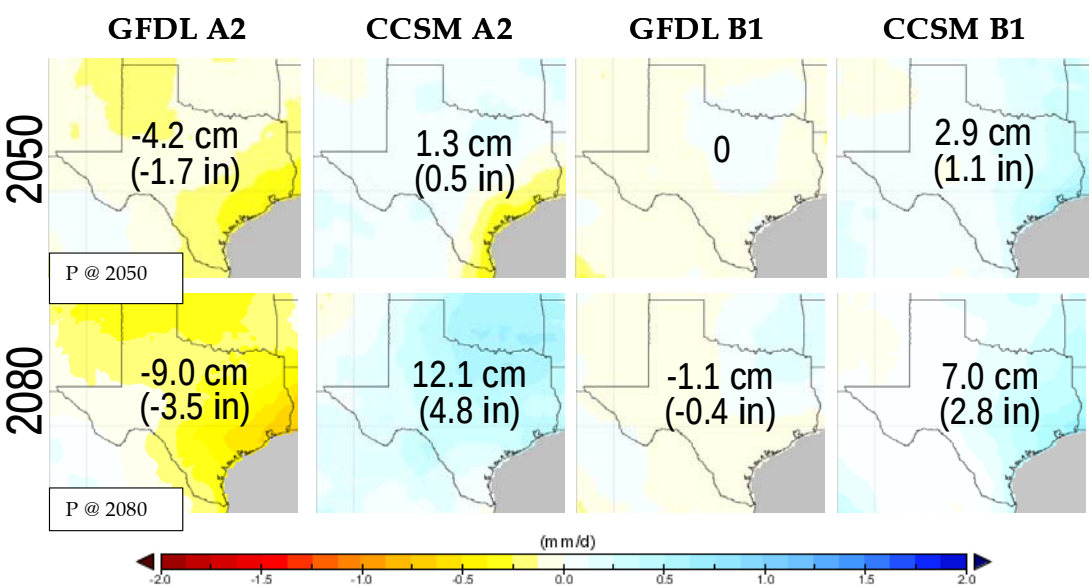

Hydrologic Modeling

Methods

While climate, primarily temperature and precipitation, is where changes are manifested, it is the interaction of climate and the land processes that are of greatest importance to surface water availability analysis. A survey of hydrologic models was performed to identify the most suitable physically-based model that could translate the changes in climate to changes in runoff, evaporation, evapotranspiration, and soil moisture. The Variable Infiltration Capacity (VIC) model application for the Gulf region was obtained from University of Washington's Climate Impacts Group (CIG) and was adapted for this study. The VIC model was calibrated for the Colorado River basin "naturalized" flows based on observed 1950-1999 climate. Future (2050 and 2080) simulations were developed for the four climate change scenarios: GFDL A2, GFDL B1, CCSM A1 and CCSM A2.

One difficulty that arises in implementing climate change into long-term water resources planning is that natural hydrologic variability is often greater than the magnitude of change expected over several decades. To effectively integrate the natural variability and climate change signal, modified historical temperature and precipitation time series were created by applying a "quantile map" approach. This approach maps the statistical properties of climate change data set onto the longer observed data set. This approach can reconcile shifts in the probabilities, where little change occurs in January, a consistent drying in May, and redistribution of rainfall in September.

Results

In each of the climate change scenarios for 2050, Colorado River streamflow was projected to decrease. Decreases were most substantial in the upper portion of the basin above the City of Llano and occurred even under modestly wet climate scenarios due to the overwhelming effect of increased evapotranspiration. Overall annual projected streamflow reductions ranged from 17 percent to 38 percent at Lake Travis (near Austin). However, the change in streamflow downstream of Lake Travis ranged from very small reductions to increases. The lower portion of the basin is more sensitive to the precipitation projections as the annual rainfall generally exceeds evapotranspiration. The projected changes in stream flow for each of the scenarios are compared in the figure below.

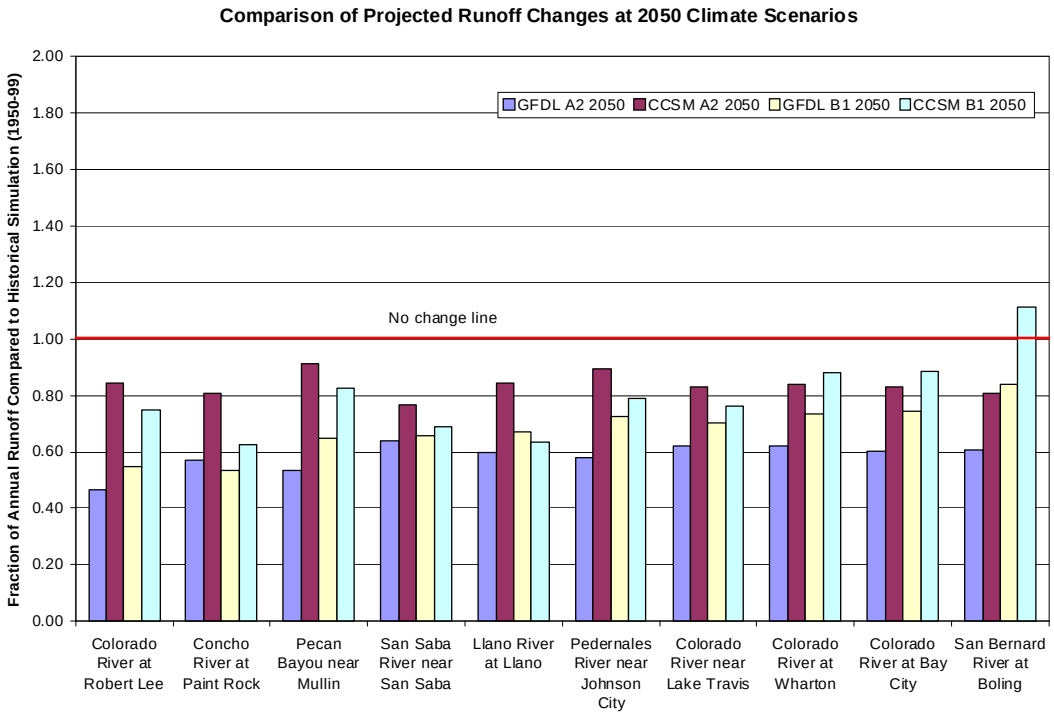

The results of the hydrologic modeling were consolidated into a time series of adjustments to the historical naturalized hydrology. This process is necessary since most of the assessment tools are configured to evaluate future changes under historical hydrology. Bias-correction was performed to the hydrologic simulation results to compensate for errors in calibration, gage records, climate data sets, or other errors. The changes, along with changes in non-hydrologic parameters, will be provided to the various impact assessment teams for evaluation of climate impacts on riverine and ecological systems.

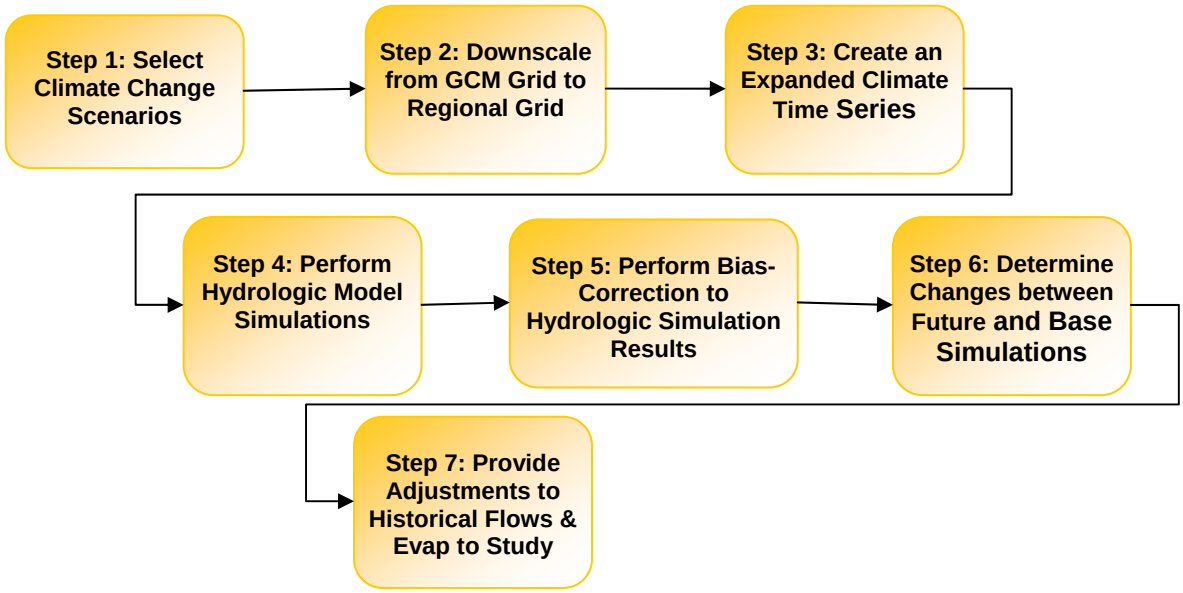

Impact and Risk

The current phase of the climate change study is assessing possible impacts on key aspects of the LSWP. Projected changes in climate parameters, streamflow, evaporation and evapotranspiration, sea level rise, and carbon dioxide concentrations are being incorporated into assessments related to:

- Surface Water Availability
- Groundwater for Agriculture
- Agricultural Water Use and Conservation
- River Water Quality and Aquatic Habitat
- Matagorda Bay Health (Temperature, Salinity, Freshwater Flows)

Surface Water Availability

The projects surface water availability teams is evaluating changes in reservoir operations, deliveries to various water users, hydropower generation, and general feasibility of the LSWP.



Groundwater and Agriculture

Project teams are evaluating the impact of climate change on rice yields, planting dates, groundwater recharge and water levels, water demands, and conservation potential.

Aquatic habitat and Matagorda Bay Health



Teams are evaluating changes to river water quality and habitat and estuarine ecosystems due to changes in temperature, flow, and sea level rise. Changes in coastal erosion, barrier islands, and salinity intrusion are being evaluated along with changes to freshwater flows to evaluate effects to Matagorda Bay.

A Comprehensive Risk Analysis

The next step planned for the climate change assessment includes comprehensive analyses that will consider the major identified areas of risk to the project. Climate change is only one, albeit important, factor being considered in this structured analysis. In 2009, the LSWP is expected to

complete its principal evaluations and will be able to understand risks associated with the project and causal mechanisms for the major areas of uncertainty.

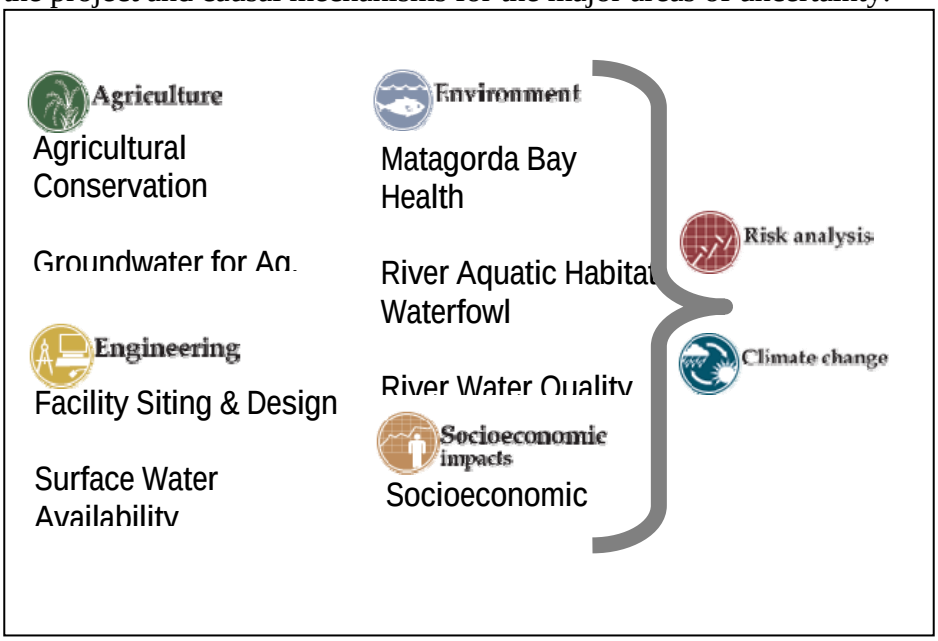

Conclusion

The Lower Colorado River Authority and the San Antonio Water System are leading the efforts to assess the potential long-range implications of climate change on water resources. The approach comprehensively incorporates major elements of the river system including projected water demands, supply availability from groundwater and surface water sources and aquatic and marine ecosystems. While the results of the analyses from individual studies are not yet complete, the application of climate projections on historical hydrology data sets provides a strong foundation for understanding the range of uncertainty in future riverine and ecological systems.

ASYMPTOTIC VARIANCE OF REGIONAL GROWTH CURVE FOR GENERALIZED LOGISTIC DISTRIBUTION

Shin, Hongjoon[1], Nam, Woosung[2], Jung, Younghun[3], and Heo, Jun-Haeng[4]

[1] Ph.D. Candidate, School of Civil and Environmental Engineering, Yonsei University, Seoul, Korea; TEL +82-2-393-1597; email : sinong@yonsei.ac.kr
[2] Ph.D. Candidate, School of Civil and Environmental Engineering, Yonsei University, Seoul, Korea; TEL +82-2-393-1597; email : nws77@yonsei.ac.kr
[3] Ph.D. Candidate, School of Civil and Environmental Engineering, Yonsei University, Seoul, Korea; TEL +82-2-393-1597; email : yhjung2000@yonsei.ac.kr
[4] Ph.D. & Professor, School of Civil and Environmental Engineering, Yonsei University, Seoul, Korea; TEL +82-2-393-1597; email : jhheo@yonsei.ac.kr

ABSTRACT

The index flood method was introduced by Dalrymple to overcome the difficulties to obtain reliable estimates of the quantiles from relatively short record length. However, the application of index flood method must account for the additional uncertainty due to estimation of index flood at site. One must account for the uncertainties of the quantile estimates and those associated with the index flood. In this study, the generalized logistic distribution is considered as a an appropriate model for regional frequency analysis in Korea based on the method of probability weighted moments under the assumption that the regional quantiles and the index flood at site are independent. An approximate formulation of the variance of the quantile is introduced to evaluate the uncertainty of the estimated growth curve.

INTRODUCTION

Statistical quantiles of frequency analysis are influenced by increasing uncertainty with frequency occurrence as those are estimated from relatively short record length. It is difficult to obtain reliable quantile estimates with small exceedance probabilities because the frequency analysis generally used annual maximum series of 30-50 years of observations.

Benson (1962) showed that reliable quantile estimates can be obtained when the return period is less than twice of the record length, while reliable quantile estimates are obtained only for that nonexceedance probability is less than 1-1/T by Hosking et al. (1984). Regional frequency analysis is a method which tries to overcome these difficulties by using space to increase time, and this is done by normalizing annual maximum series in a region using index flood. The regional frequency analysis provides a reliable quantile estimate of the normalized sample for return periods for design purposes. However, the application of index flood method should be considered additional uncertainty from the estimation of index flood as well as the uncertainties of the normalized quantile estimates in a specified site.

The index flood method has been applied and provided appropriate procedures for estimating quantile in many countries; however, there have been not many studies about the uncertainty of quantile estimates.

Assuming a two-parameter regional Weibull model, Boes et al. (1989) derived an exact simple formula for the Cramer–Rao lower bound for the variance of unbiased estimator of the quantile and quantified the gain of regional flood frequency analysis over single-site analysis via this formula. Lu and Stedinger (1992) provided simple formulas based on PWM quantile estimator for estimating the sampling variances of the GEV distribution. Heo et al. (2001) derived and compared the asymptotic variances on a population quantile for the three-parameter Weibull model based on the methods of moments, maximum likelihood, and probability weighted moments. De Michele and Rosso (2001) evaluated the variance of quantile estimator for the regional probability distribution of normalized flood flows when the GEV distribution is used with the parameters estimated by the PWM method. They combined this with the variance of index flood estimator to obtain an uncertainty model for evaluating the variance of at-site flood estimators, and introduced an efficiency index to discriminate between single-site analysis and the regional analysis. In this paper, the variance of quantile estimates obtained from the index flood method was proposed to assess the uncertainty in regional frequency analysis following the procedures presented by De Michele and Rosso (2001).

The method of the probability weighted moments was considered for parameter estimation and the generalized logistic distribution recently recommended as an appropriate model for regional frequency analysis in Korea was used. Finally, we joined the variance of the normalized quantile estimator to that of the estimated index flood at a given site so as to yield the variance of the regional quantile estimator.

VARIANCE OF THE QUANTILE ESTIMATOR

Generalized Logistic (GL) Distribution

The GL distribution is a generalization of the 2-parameter logistic distribution and is also a special case of the kappa distribution. This generalization of the logistic distribution differs from other distributions defined in the literature. It is a reparameterized version of the log-logistic distribution presented by Ahmad et al. (1988). The name reflects the distribution's similarity to the generalized Pareto and generalized extreme value distributions (Hosking and Wallis, 1997). The cumulative distribution function and the probability density function of the GL distribution are defined respectively as (Hosking, 1986). Figure 1 shows some examples of the PDF of the GL distribution with $\beta = \mp 0.185, \mp 0.114, 0$ (corresponding to skewness coefficients $\gamma = \pm 2, \pm 1, 0$) for $x_0 = 0$ and $\alpha = 1$.

$$F(x) = \left[1 + \left\{ 1 - \frac{\beta}{\alpha}\left(x - x_0\right) \right\}^{1/\beta} \right]^{-1} \tag{1}$$

$$f(x)=\frac{1}{\alpha}\left\{1-\frac{\beta}{\alpha}(x-x_0)\right\}^{1/\beta-1}\left[1+\left\{1-\frac{\beta}{\alpha}(x-x_0)\right\}^{1/\beta}\right]^{-2} \tag{2}$$

where x_0, α, and β are the location, scale, and shape parameter, respectively.

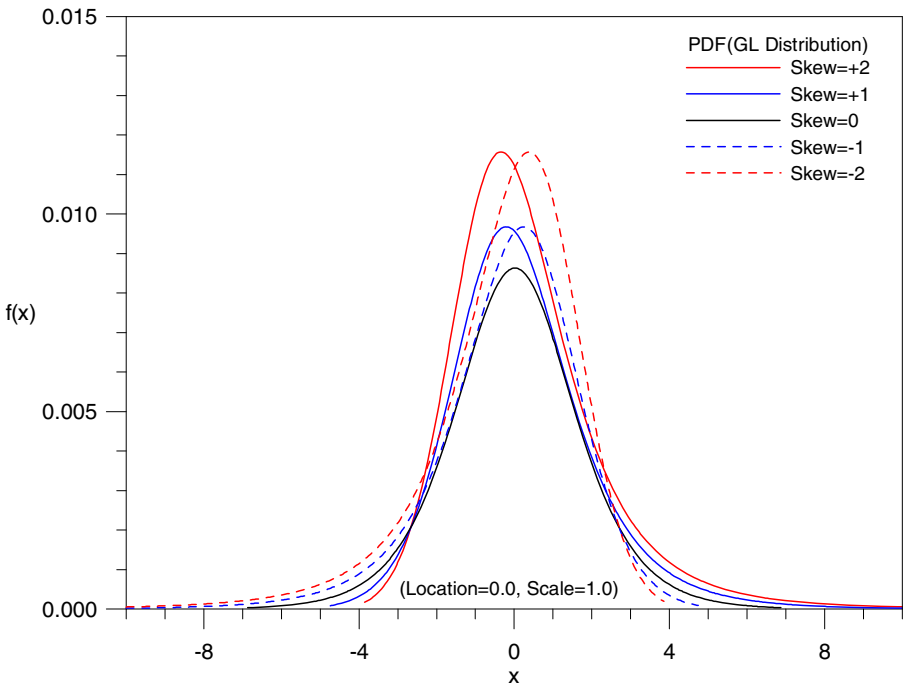

Figure 1. PDFs of the generalized logistic distribution ($x_0=0, \alpha=1$)

In this paper, the variance of quantile was estimated using the method of probability weighted moments as described below.

$$\begin{aligned}Var(\hat{x}_T)=&Var(\hat{x}_0)+Var(\hat{\alpha})\left(\frac{1-(T-1)^{-\hat{\beta}}}{\hat{\beta}}\right)^2+Var(\hat{\beta})\left(\frac{\hat{\alpha}}{\hat{\beta}}\frac{\log(T-1)}{(T-1)^{\hat{\beta}}}-\frac{\hat{\alpha}}{\hat{\beta}^2}\left(1-\frac{1}{(T-1)^{\hat{\beta}}}\right)\right)^2\\&+2Cov(\hat{x}_0,\hat{\alpha})\left(\frac{1-(T-1)^{-\hat{\beta}}}{\hat{\beta}}\right)+2Cov(\hat{x}_0,\hat{\beta})\left(\frac{\hat{\alpha}}{\hat{\beta}}\frac{\log(T-1)}{(T-1)^{\hat{\beta}}}-\frac{\hat{\alpha}}{\hat{\beta}^2}\left(1-\frac{1}{(T-1)^{\hat{\beta}}}\right)\right)\\&+2Cov(\hat{\alpha},\hat{\beta})\left(\frac{1-(T-1)^{-\hat{\beta}}}{\hat{\beta}}\right)\left(\frac{\hat{\alpha}}{\hat{\beta}}\frac{\log(T-1)}{(T-1)^{\beta}}-\frac{\hat{\alpha}}{\hat{\beta}^2}\left(1-\frac{1}{(T-1)^{\hat{\beta}}}\right)\right)\\&=\frac{\alpha^2}{n}v(\beta,T)\end{aligned} \tag{3}$$

where

$$Var(\hat{x}_0) = \frac{1}{n}\left[g_{00}{}^2 V_{00} + g_{01}{}^2 V_{11} + g_{02}{}^2 V_{22} + 2g_{00}g_{01}V_{01} + 2g_{00}g_{02}V_{02} + 2g_{01}g_{02}V_{12} \right] \quad (0.d)$$

$$Var(\hat{\alpha}) = \frac{1}{n}\left[g_{10}{}^2 V_{00} + g_{11}{}^2 V_{11} + g_{12}{}^2 V_{22} + 2g_{10}g_{11}V_{01} + 2g_{10}g_{12}V_{02} + 2g_{11}g_{12}V_{12} \right] \quad (0.e)$$

$$Var(\hat{\beta}) = \frac{1}{n}\left[g_{20}{}^2 V_{00} + g_{21}{}^2 V_{11} + g_{22}{}^2 V_{22} + 2g_{20}g_{21}V_{01} + 2g_{20}g_{22}V_{02} + 2g_{21}g_{22}V_{12} \right] \quad (0.f)$$

$$Cov(\hat{x}_0, \hat{\alpha}) = \frac{1}{n}\left[g_{10}g_{00}V_{00} + g_{11}g_{01}V_{11} + g_{12}g_{02}V_{22} + (g_{10}g_{01} + g_{11}g_{00})V_{01} + (g_{10}g_{02} + g_{12}g_{00})V_{02} + (g_{11}g_{02} + g_{12}g_{01})V_{12} \right] \quad (0.g)$$

$$Cov(\hat{x}_0, \hat{\beta}) = \frac{1}{n}\left[g_{20}g_{00}V_{00} + g_{21}g_{01}V_{11} + g_{22}g_{02}V_{22} + (g_{20}g_{01} + g_{21}g_{00})V_{01} + (g_{20}g_{02} + g_{22}g_{00})V_{02} + (g_{21}g_{02} + g_{22}g_{01})V_{12} \right] \quad (0.h)$$

$$Cov(\hat{\alpha}, \hat{\beta}) = \frac{1}{n}\left[g_{20}g_{10}V_{00} + g_{21}g_{11}V_{11} + g_{22}g_{12}V_{22} + (g_{20}g_{11} + g_{21}g_{10})V_{01} + (g_{20}g_{12} + g_{22}g_{10})V_{02} + (g_{21}g_{12} + g_{22}g_{11})V_{12} \right] \quad (0.i)$$

and $d_1 = \psi(1+\beta) - \psi(1-\beta)$, $g_1 = \Gamma(1+\beta)\Gamma(1-\beta)$, $g_{00} = \frac{1}{g_1}\left\{ \frac{(1-\beta)^2(g_1-1)}{\beta^2} + 1 - \frac{1-\beta}{\beta}d_1 \right\}$,

$g_{01} = \frac{2}{g_1}\left\{ \frac{(2\beta-3)(g_1-1)}{\beta^2} + \frac{(3-\beta)}{\beta}d_1 \right\}$, $g_{02} = \frac{6}{g_1}\left\{ \frac{(g_1-1)}{\beta^2} - \frac{d_1}{\beta} \right\}$, $g_{10} = \frac{1}{g_1}\{(1-\beta)d_1 - 1\}$,

$g_{11} = \frac{2}{g_1}\{1-(3-\beta)d_1\}$, $g_{12} = \frac{1}{g_1}\{6d_1\}$, $g_{20} = \frac{1}{g_1}\left\{ \frac{\beta-1}{\alpha} \right\}$, $g_{21} = \frac{2}{g_1}\left\{ \frac{(3-\beta)}{\alpha} \right\}$, $g_{22} = \frac{1}{g_1}\left\{ -\frac{6}{\alpha} \right\}$.

Index Flood Method

Regional frequency analysis is a procedure that used the all available data in a region that approximately satisfy hydrological homogeneity condition, thus the reliable quantile estimate for relatively large return period could be obtained. It is assumed that a statistically homogeneous region is defined as that region where the underlying data at each site have identical frequency distribution apart from the index flood. Index flood method is generally used in the regional frequency analysis and the sample data in a homogeneous region normalized by dividing the at-site index flood follows a growth curve that is identical for all sites. Therefore, the quantile at a certain site is estimated by multiplying the quantile of the growth curve by the mean annual data at the site. This procedure could be expressed following equation.

$$q_T = q_{index} \cdot x_T \quad (5)$$

where q_T is the T-year quantile at a certain site, x_T is the T-year normalized quantile in the region, q_{index} is index flood at a certain site.

The T-year quantile estimate is given by Eq. (6).

$$\hat{x}_T = \hat{x}_0 + \frac{\hat{\alpha}}{\hat{\beta}}\left[1-\left(T-1\right)^{-\hat{\beta}}\right] \tag{6}$$

From Eqs. (6) and (5), one gets

$$q_T = q_{index} \cdot \left[\hat{x}_0 + \frac{\hat{\alpha}}{\hat{\beta}}\left\{1-\left(T-1\right)^{-\hat{\beta}}\right\}\right] \tag{7}$$

The sampling variability of the quantile estimate can be investigated by assuming that $\hat{q}_T$ is a random variable, which is product of two variates, $\hat{q}_{index}$ and $\hat{x}_T$ with mean $E[\hat{q}_{index}]$ and $E[\hat{x}_T]$, respectively, and variance $Var[\hat{q}_{index}]$ and $Var[\hat{x}_T]$, respectively (Stedinger et al., 1992).

Although the procedure of estimating q_{index} is somewhat independent from that used to evaluate the regional growth curve, this does not make $\hat{q}_{index}$ and $\hat{x}_T$ statistically independent. However, it is assumed here that $\hat{q}_{index}$ and $\hat{x}_T$ are statistically independent in order to derive an uncertainty model useful for practical application. Accordingly

$$E[\hat{q}_T] = E[\hat{q}_{index}]E[\hat{x}_T] \tag{8}$$

$$\begin{aligned}
Var(\hat{q}_T) &= E\left[\left(\hat{q}_{index}\hat{x}_T\right)^2\right] - E^2[\hat{q}_{index}\hat{x}_T] \\
&= E\left[\hat{q}_{index}{}^2\right]E\left[\hat{x}_T{}^2\right] - E^2[\hat{q}_{index}]E^2[\hat{x}_T] \\
&= E\left[\hat{q}_{index}{}^2\right]E\left[\hat{x}_T{}^2\right] - E^2[\hat{q}_{index}]E\left[\hat{x}_T{}^2\right] + E^2[\hat{q}_{index}]E\left[\hat{x}_T{}^2\right] - E^2[\hat{q}_{index}]E^2[\hat{x}_T] \\
&= Var(\hat{q}_{index})E\left[\hat{x}_T{}^2\right] + E^2[\hat{q}_{index}]Var(\hat{x}_T) \\
&= Var(\hat{q}_{index})\left\{E\left[\hat{x}_T{}^2\right] - E^2[\hat{x}_T] + E^2[\hat{x}_T]\right\} + E^2[\hat{q}_{index}]Var(\hat{x}_T) \\
&= Var(\hat{q}_{index})\left\{E\left[\hat{x}_T{}^2\right] - E^2[\hat{x}_T]\right\} + Var(\hat{q}_{index})E^2[\hat{x}_T] + E^2[\hat{q}_{index}]Var(\hat{x}_T) \\
&= Var(\hat{q}_{index})Var(\hat{x}_T) + Var(\hat{q}_{index})E^2[\hat{x}_T] + E^2[\hat{q}_{index}]Var(\hat{x}_T)
\end{aligned} \tag{9}$$

If annual maximum series of length n' is available for a given site, one can estimate q_{index} as the sample mean of the observed series, hence the sampling variance of $\hat{q}_{index}$ is given by

$$\begin{aligned}
Var(\hat{q}_{index}) &= Var(\hat{\mu}_Q) \\
&= Var\left(\frac{1}{n'}\sum_{i=1}^{n'} Q_i\right) = \frac{1}{n'^2}Var\left(\sum_{i=1}^{n'} Q_i\right) \\
&= \frac{1}{n'^2}\sum_{i=1}^{n'} Var\left(Q_i\right) = \frac{1}{n'^2}n'Var\left(Q\right) = \frac{1}{n'}Var\left(Q\right)
\end{aligned} \tag{10}$$

APPLICATION

In this paper, the regional frequency analysis was performed with annual maximum 24hr rainfall data of 378 sites in Korea based on the method of forming homogeneous regions by Nam et al. (2005). And 378 sites were divided into 14 homogeneous regions by Fuzzy technique. The site characteristics were used in the cluster analysis as follows: longitude, latitude, altitude, annual mean precipitation over 12 months, and annual mean precipitation over rainy season.
The homogeneous regions divided by cluster analysis and the heterogeneity measures (H) of Hosking and Wallis (1997) of each region were summarized in Table 1. Table 1 showed that all regions were homogeneous except for NAK2. On the other hand, according to studies of Nam et al. (2005), the generalized logistic distribution was selected as an appropriate regional frequency distribution of Korea.

Table 1. Results of Regional Frequency Analysis (Nam et al., 2005)

Region	Sub Region	Number of Site	Number of Data	Location Parameter	Scale Parameter	Shape Parameter	Homogeneity
Hangang	HAN1	55	1209	0.899	0.246	-0.235	Hom.[1]
	HAN2	25	422	0.920	0.242	-0.192	Hom.
	HAN3	42	756	0.887	0.249	-0.254	Hom.
Kumgang	KUM1	12	255	0.911	0.209	-0.241	Hom.
	KUM2	18	345	0.898	0.223	-0.257	Hom.
	KUM3	20	273	0.951	0.204	-0.141	Hom.
Nakdonggang	NAK1	37	587	0.920	0.201	-0.227	Hom.
	NAK2	55	989	0.928	0.204	-0.205	Poss. Hom.[2]
	NAK3	26	423	0.928	0.193	-0.214	Hom.
Namhaean	NAM1	14	436	0.898	0.220	-0.260	Hom.
Sumjingang	SUM1	10	161	0.928	0.210	-0.199	Hom.
Tonghaean	TON1	9	298	0.893	0.220	-0.272	Hom.
Youngsangang	YOU1	28	427	0.968	0.180	-0.107	Hom.
	YOU2	27	598	0.932	0.200	-0.199	Hom.

Figure 2 showed the quantile estimates and the corresponding 95% confidence intervals of 14 homogeneous regions with the normalized data, the index flood method, and the asymptotic variance. In Fig.2, KUM01, KUM02, NAM01, SUM01, and TON01 regions have relatively wide intervals for other regions. It may be caused by the relatively short record length and the small number of site of those regions.

[1] Hom : Homogeneous

[2] Poss. Hom. : Possibly Homogeneous

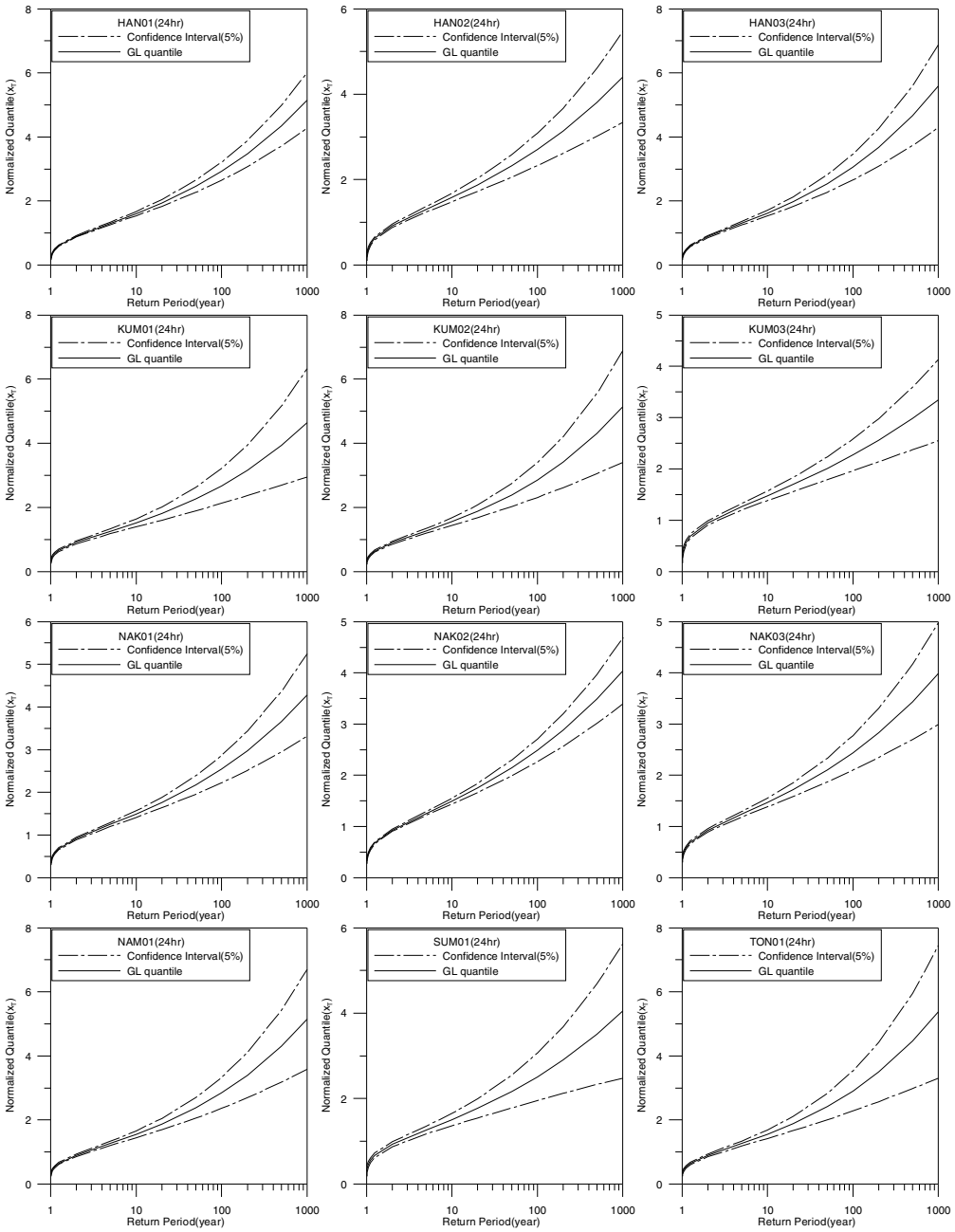
HAN01(24hr)
HAN02(24hr)
HAN03(24hr)
KUM01(24hr)
KUM02(24hr)
KUM03(24hr)
NAK01(24hr)
NAK02(24hr)
NAK03(24hr)
NAM01(24hr)
SUM01(24hr)
TON01(24hr)
Confidence Interval(5%)
GL quantile
Normalized Quantile(x_T)
Return Period(year)

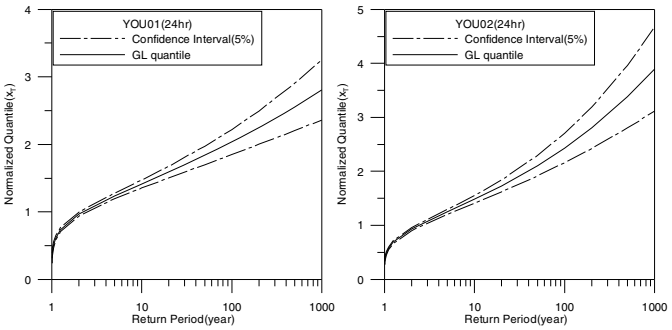

Figure 2. Growth Curves and Confidence Intervals for 14 Regions

CONCLUSIONS

The variance of regional quantiles for the generalized logistic distribution were introduced to assess the uncertainty of index flood method as a regional frequency analysis to overcome difficulties to obtain reliable estimates of the quantiles from relatively short record length. The asymptotic variance of quantile estimator for the generalized logistic distribution was introduced to evaluate confidence intervals and it was assumed here that the index floods and quantile estimates are statistically independent in order to derive an uncertainty model useful for practical application. In this study, the generalized logistic distribution is considered as a an appropriate model for regional frequency analysis in Korea based on the method of probability weighted moments under the assumption that the regional quantiles and the index flood at site are independent. An approximate formulation of the variance of quantile is introduced to evaluate the uncertainty of the estimated growth curve.

REFERENCES

Benson, M.A. (1962) Evolution of methods for evaluating the occurrence of floods. USGS Water Supply Paper, 1580A.

Boes, D.C., Heo, J.H., and Salas, J.D. (1989) Regional flood quantile estimation for a Weibull model. Water Resources Research, Vol.25, No.5, pp.979-990.

De Michele, C. and Rosso, R. (2001) Uncertainty assessment of regionalized flood frequency estimates. Journal of Hydrology Engineering, Vol.6, No.6, pp.453-459.

Heo, J.H., Boes, D.C., and Salas, J.D. (2001a) Regional flood frequency analysis based on a Weibull model : part 1. Estimation and asymptotic variances. Journal of Hydrology, Vol.242, No.3-4, pp.157-170.

Heo, J.H., Salas, J.D., and Boes, D.C. (2001b) Regional flood frequency analysis based on a Weibull model : part 2. Simulations and applications. Journal of Hydrology, Vol.242, No.3-4, pp.171-182.

Hosking, J.R.M., Wallis, J.R., and Wood, E.F. (1984) Estimation of the generalized extreme value distribution by the method of probability weighted moments. Technometrics, Vol.27, No.3, pp.251-261.

Hosking, J. R. M. and Wallis, J. R. (1997) Regional frequency analysis: An approach based on L-moments, Cambridge University Press.

Lu, L.H. and Stedinger, J.R. (1992) Variance of two- and three- parameter GEV/PWM quantile estimators and a regional homogeneity test. Journal of Hydrology, Vol.138, pp.247-267.

Nam, W.S., Shin, H.J., Heo, J.H., and Kim, K.D. (2005) Regional Rainfall Frequency Analysis Based on Generalized Logistic Model, 2005 World Water & Environmental Resources Congress, Alaska,US

Stedinger, J.R., Vogel, R.M., and Foufoula-Georgiu, E. (1992) Frequency analysis of extreme events, Handbook of Hydrology, Ch18., McGraw-Hill, New York.

Balancing the Budget: A Limited Detail Approach to Flood Studies

Andrew J. Bonner[1], P.E., CFM

[1]AECOM Water, 2405 Grand Blvd, Suite 1000, Kansas City, MO 64108; PH (816) 502-9420 ext. 4958; FAX (816) 502-9497; email: andrew.bonner@aecom.com

ABSTRACT

Floodplain or inundation mapping studies are performed for a variety of reasons, and are many times only one phase of a larger engineering or mapping project. As is often the case, many communities and agencies write their scope so that their project's flood studies are performed in accordance with FEMA guidelines, with the intention of incorporating those studies onto FEMA's flood maps in the future. More times than not, this results in the development of a project scope that would fit FEMA's definition of a "detailed study" – field survey, development of the 10-, 50-, 100-, and 500-year flood profiles, etc. However, in certain instances, it may be appropriate to apply a more "limited" detail approach to the study area, while still being able to meet project objectives.

This paper will focus on the various floodplain study methodologies that have been accepted by FEMA (approximate, limited detail, and detailed), when and where each study type can be used, and the similarities and differences between the three. The limited detail approach will specifically be explained and highlighted as a potential solution to bridge the gap that often exists between budget and accuracy needs. Several case studies will be presented to show the difference in steady flow HEC-RAS modeling and mapping results between the study types.

INTRODUCTION

Floodplain and/or inundation mapping studies are performed for numerous reasons. They are performed as a floodplain management tool and as a predecessor to flood hazard mitigation actions. They are often undertaken during the initial phases of larger construction projects to more accurately analyze the risk at the project site, or to compare the risk between pre- and post-construction plans. Flood studies help developers and business or home owners determine the water surface levels at which they must elevate their property in order to reduce the flood risk to which they are susceptible. They are also often important parts of emergency action plans, environmental impact statements, and comprehensive watershed master plans.

As the overseer of the National Flood Insurance Program (NFIP), the Federal Emergency Management Agency (FEMA) undertakes and incorporates flood studies onto their maps in an effort to provide the most accurate product to states, communities, and citizens to use for flood hazard identification and mitigation purposes. Because of floodplain management ordinances and regulations in NFIP communities, many of these non-FEMA-funded flood studies are nevertheless scoped in accordance with FEMA's guidelines so that they can be incorporated onto FEMA's maps at a later time,

either as part of FEMA's routine map updates, or through their Letter of Map Revision (LOMR) process.

FEMA FLOOD STUDY BACKGROUND

Flood insurance rates for any home, building, or habitable structure are determined in large part by two factors: (1) what flood zone the structure is mapped in, and (2) how the ground floor elevation of the structure compares to the 1%-annual-chance water surface elevations (known as base flood elevations, or BFEs) published in the Flood Insurance Study (FIS). With the exception of coastal flooding, shallow flooding, or flooding in areas protected by manmade structures, flood zones are most often mapped on FEMA's Flood Insurance Rate Maps (FIRMs) as either Zone A or Zone AE.

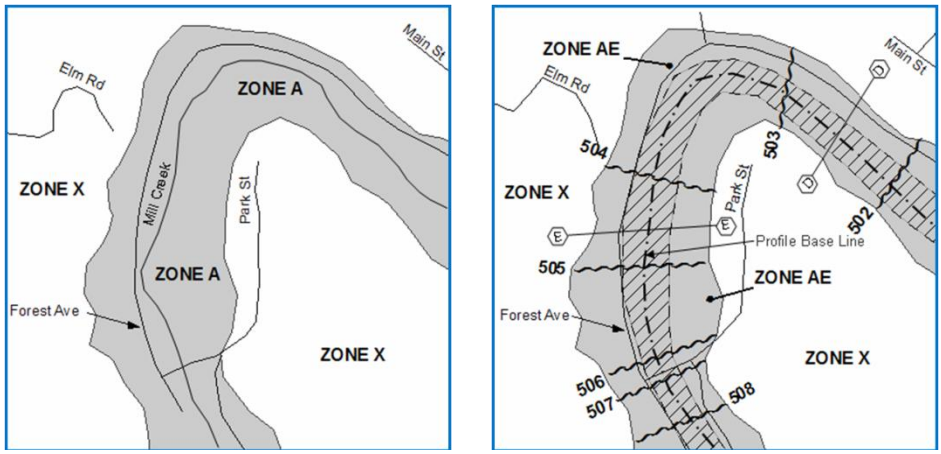

Figure 1. Comparison of Features Shown on Zone A vs. Zone AE Maps

Zone A floodplains on FEMA's maps are used to depict studies that are performed using approximate methods of analysis, and/or where the accuracy of the available topographic data used to develop the floodplain delineations is deemed too coarse to support published BFEs. Zone AE floodplains are used for studies that are performed using detailed methods of analysis. BFEs are published on FEMA's maps for Zone AE streams and are used by flood determination companies for flood insurance rating purposes. Because the flood elevations on Zone A-mapped streams are unknown, flood insurance premiums are often higher for structures in the Zone A floodplain than in the Zone AE floodplain, all things being equal. Therefore, in addition to the improved accuracy that the detailed methodologies provide, there are also insurance premium benefits to performing a study worthy of Zone AE mapping. The decision to do Zone A vs. Zone AE studies in the past has most often been based on budget, accuracy of the available data, and/or flood risk.

FLOOD STUDY TYPES

Historically, most riverine floodplain studies were performed with one of two methodologies. While tools and procedures may have varied from study to study, the general approach followed either the approximate or the detailed path.

Approximate Study. The approximate riverine study is the least rigorous and least expensive of the study types and is most often represented as a Zone A on FEMA's maps. Zone A floodplains have been determined using methodologies ranging from delineations of flood-prone areas using soils and wetlands maps, to simplified normal depth calculations at cross-sections, to actual hydraulic models developed through automated tools. As the name implies, the approximate study is an approximation of the floodplain using best available data, although as technology has improved, it has become more cost-effective to perform new approximate studies using acceptable hydraulic models, which has improved the accuracy of these studies.

Hydraulic structures such as culverts, bridges, and dams are typically not included in approximate models. The 1% annual chance flood (100-year) discharges are most often calculated through the use of regression equations. A regulatory floodway, or the area of the floodplain that must be reserved to be able to pass the base (or 1% annual chance) flood without increasing the water surface elevation by more than a specific height designated by the community, is also not computed for an approximate stream. Approximate studies are most often performed in rural areas, although they can also be useful elsewhere. Flood profiles showing the water surface elevations along each approximate stream are not included in the FIS report that accompanies the flood maps.

Detailed Study. The detailed riverine study, as FEMA terms it, is the study type that most closely translates to hydrologic and hydraulic (H&H) studies performed on other types of non-FEMA projects. The resultant floodplains from a detailed study are most often displayed as Zone AE with BFEs on FEMA's maps, although FEMA has other zone designations that can be used, depending on the circumstance. Cross-sections and hydraulic structures are surveyed in the field for a detailed study. Discharges are often estimated by hydrologic models or more in-depth analysis, although regression equations can be used as well. Regulatory floodways are typically computed for detail-studied streams, and the 10%, 2%, 1%, and 0.2% annual chance flood profiles are all calculated and published in the FIS report.

Until recently, new riverine flood studies undertaken for FEMA purposes followed one of these two paths. However, FEMA now recognizes a blend of these two methodologies, called the limited detail study, as an acceptable approach for updating their flood maps. The limited detail study is a cost-effective alternative to the traditional detailed study and, in areas where high quality topographic data is available (such as LiDAR or aerial surveys), has been shown to be compatible with publishing BFEs on FEMA's flood maps.

LIMITED DETAIL STUDY METHODOLOGY

In the early 2000s, as part of its statewide floodplain mapping program, North Carolina began funding what they termed "limited detail studies" to update the thousands of miles of Zone A riverine floodplain within their state and map them as a Zone AE with published BFEs. As one of the state's original floodplain study contractors, AECOM's Watershed Concepts group played an integral role in working with the state to define the limited detailed methodology and to begin implementing it throughout numerous

counties and watersheds within the state. Since then, thousands of miles of limited detail studies have been performed in multiple states throughout the nation for FEMA floodplain mapping projects in addition to North Carolina, including South Carolina, Georgia, Kentucky, Tennessee, Mississippi, Louisiana, Oklahoma, and New Mexico to name a few.

The decision to publish BFEs on the maps for limited detail studies is left to the discretion of the communities, states, and FEMA. One of the important distinctions between a limited detail study and a detail study is that floodways are typically not mapped for the limited detail study. According to Title 44 of the Code of Federal Regulations, part 60.3, communities where floodways have not been designated but BFEs have been provided are required that "until a regulatory floodway is designated, that no new construction, substantial improvement, or other development… shall be permitted… unless it is demonstrated that the cumulative effect of the proposed development, when combined with all other existing and anticipated development, will not increase the water surface elevation of the base flood more than one foot at any point within the community." [44 CFR Part 60.3(c)(10)] This is an important factor for communities to consider when performing limited detail studies. Because of this, several communities have actually determined floodways, or non-encroachment areas, for their limited detail study streams to satisfy these requirements and provide better information for their residents.

Limited detail studies have been used effectively in situations where a more detailed analysis has been necessary, but where budget constraints have prevented a full detailed analysis. In an economy where greater scrutiny is required for all spending, the limited detail approach has been an excellent balance between the need to produce a better estimate of flood risk than an approximate study can accomplish, but at a reduced cost of a full detailed study

The limited detail study is similar in many ways to a traditional detail study, although there are also several distinct differences between the two. The main difference exists in how survey data is collected and used in the model. Unlike detailed studies where hydraulic structure data are collected in the field using traditional survey methods, structures are only "measured" in the field for the limited detailed approach. Rather than establishing vertical control using published benchmarks, the survey crew for limited detail studies collects structure measurements, such as the stream invert from the top of the road, channel top and bottom widths, top width and toe width of bridge abutments, and culvert opening sizes, among others (see FEMA's *Guidelines & Specifications, Appendix N: Data Capture Guidelines*, pages N-51 – N-54 for full list of measurements collected; http://www.fema.gov/library/viewRecord.do?id=2206). Surveyors will often use a hand or automatic level to get more exact measurements, as shown in Figure 2. Once the size and shape of the hydraulic structure opening is measured, "vertical control" for the limited detail structure uses the elevation at the point from which the measurements were recorded, and all other associated structure elevations are referenced to that "vertical control elevation", or VCE, to come up with the placement and alignment of the structure in the model. The horizontal location of the VCE point is most often collected by GPS, and then the vertical elevation is

extracted from the underlying topography. Thus, the more accurate the available topographic data, the more "in-line" the structures will appear in the model. Advancements have also been made in the vertical accuracy that some types of GPS receivers and methods can achieve (RTK, Virtual Reference System network, etc.). As this technology continues to advance and become more efficient, it may become a useful and efficient alternative to obtain the vertical control elevation for limited detail measurements.

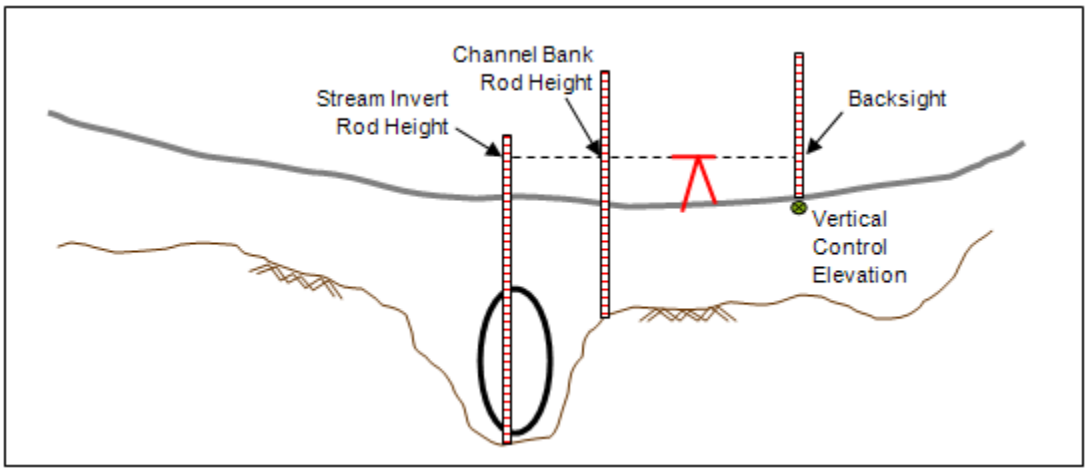

Figure 2. Limited Detail Structure Measurement

In addition to the differences in the way hydraulic structure geometry is estimated in the hydraulic model, the stream channel of the cross-section in the limited detail model is estimated as a trapezoid, as opposed to most detailed models, where the channel and possibly a few points on the overbanks are surveyed (with cross-section geometry supplemented by topographic data where the survey data stops). At limited detail structures, the top and bottom widths of the trapezoidal channel are measured in the field. In between structures at natural floodplain cross-sections, the trapezoidal channel geometry is estimated based on user-defined top width vs. drainage area curves and the channel depth is manually estimated prior to creating the model. The accuracy of the topographic data plays an important role in helping the modeler estimate channel widths once within the limited detail model. Channel depths can often be estimated using nearby measurements from limited detail structures.

Part of the theory behind the limited detail methodology is that the majority of the conveyance is in the overbanks, so having detailed survey dimensions of the actual channel often has little impact on the water surface. Because of this, it may be more appropriate to perform studies of streams that have wide channels or very narrow floodplains, or where the accuracy of the model at lower recurrence intervals (i.e. the 25% or 10% annual chance flood) is critical, using traditional detailed study methods.

Although the cost of a limited detail study is significantly less than that of a full detail study, it is nevertheless important to understand how the difference in approach affects model results, and how the calculated water surface elevations (WSELs) compare to one another based on different factors.

CASE STUDIES

Several detail streams throughout the country that had recently been studied and incorporated onto FEMA's maps were selected as case studies to evaluate how a limited detail version of the stream would compare to the detailed model results. For the purpose of this paper, streams were only considered that had been studied using steady flow HEC-RAS. The other criteria that was used in selecting streams for comparison is outlined as follows:

- Detail stream must have been completed, reviewed, approved, and incorporated onto FEMA's maps
- Detailed model must be available
- Topographic data used in the study must be available and be of high quality

In order to isolate the true differences between limited detail and detail studies, the only parameter that was varied in the limited detail model representation was the survey data. The survey data used within the detailed model was, in essence, "thrown out" and not used, and field measurements and trapezoid size/shape were estimated for the structure and channel geometry, respectively. All other model components (discharges, n-values and associated breaks, topographic data points, cross-section alignment and stationing, starting conditions, etc.) were kept the same between the detailed model and its limited detail equivalent. Ineffective areas were kept the same wherever possible, with the only exceptions being at a few structures, where they were changed according to modeling guidelines because of slight changes in measurements as compared to the detailed models. In the case study results that follow, the thicker, red lines in the profile figures represent the water surface elevations calculated in the original detail model, whereas the blue, filled-in water surface corresponds to the limited detail model results.

CASE STUDY #1: BROWN CREEK (North Carolina)

Table 1. Brown Creek Model Background

Reach Info		Other	
Length	4.1 mi.	Drainage Area	105.5 mi^2
# Structures	2	Discharge Methodology	Regression Equations
# Cross-sections	42	Topographic Data	LiDAR
Average Slope	0.0013 ft/ft	Starting Conditions	Known WSEL

Table 2. Brown Creek Comparison Statistics

Statistic	Value
Average Absolute WSEL Error	0.14 ft
Maximum WSEL Error	0.33 ft
% Cross-Sections within 0.1ft Error	43%
% Cross-Sections within 0.3ft Error	96%
% Cross-Sections within 0.5ft Error	100%

As Table 2 and Figure 3 indicate, the Brown Creek limited detail model results compare very closely with those in the detail model. As one would expect, the differences in channel geometry and at structures comprise the majority of the actual

error. The term "error" as mentioned here indicates how the limited detail model's WSELs compared to those in the detail model.

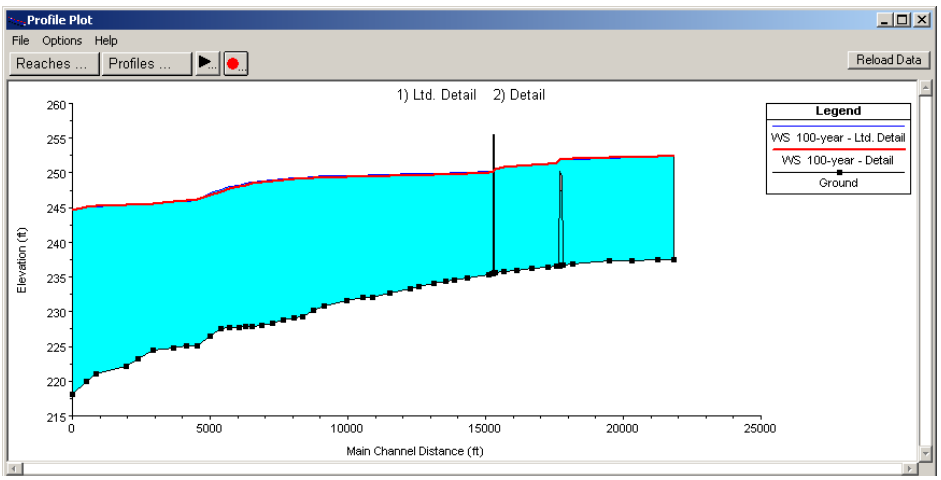

Figure 3. Brown Creek Profile Comparison

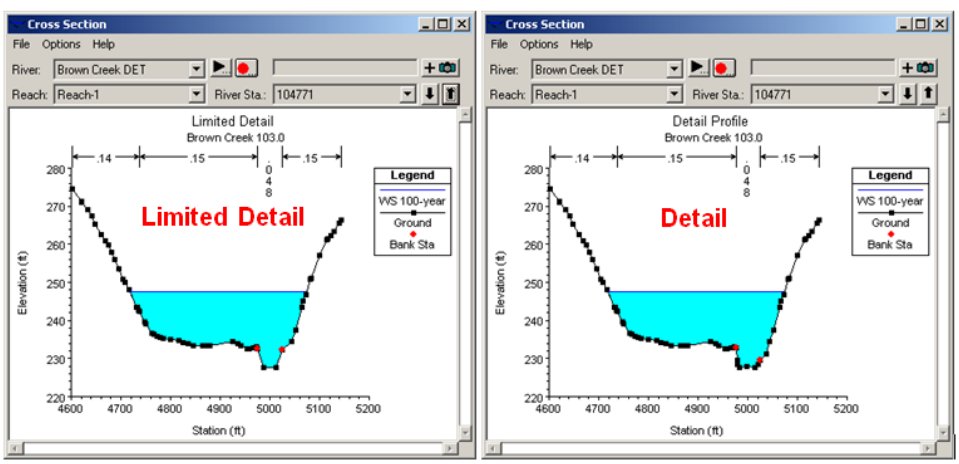

Figure 4. Brown Creek XS Geometry Comparison at Largest WSEL Error

CASE STUDY #2: BUCKNERS CREEK (Texas)

Table 3. Buckners Creek Model Background

Reach Info		Other	
Length	4.8 mi.	Drainage Area	185.4 mi^2
# Structures	2	Discharge Methodology	HEC-HMS
# Cross-sections	28	Topographic Data	2ft contours
Average Slope	0.00074 ft/ft	Starting Conditions	Known WSEL

Table 4. Buckners Creek Comparison Statistics

Statistic	Value
Average Absolute WSEL Error	0.28 ft
Maximum WSEL Error	-0.65 ft
% Cross-Sections within 0.1ft Error	13%
% Cross-Sections within 0.3ft Error	53%
% Cross-Sections within 0.5ft Error	94%

The error in the limited detail model of Buckners Creek as compared to its detailed model version is due to a difference in channel widths. Buckners Creek has fairly steep banks. Since channel bank locations in hydraulic models are often open to interpretation (especially on deeper channels), there were several cross-sections where the engineer performing the limited detailed model estimated a slightly wider channel than what was estimated in the detailed model. The cumulative effect of this resulted in a limited detailed WSEL profile that was on average 0.3ft less than that of the detailed model profile. The largest WSEL error in the Buckners Creek model occurred at the downstream face of the downstream-most bridge in the model. Figure 6 shows how the hydraulic structure using the limited detail representation can often differ from the field surveyed data, which in the case of the Buckners Creek model also had an impact on the overall WSEL difference.

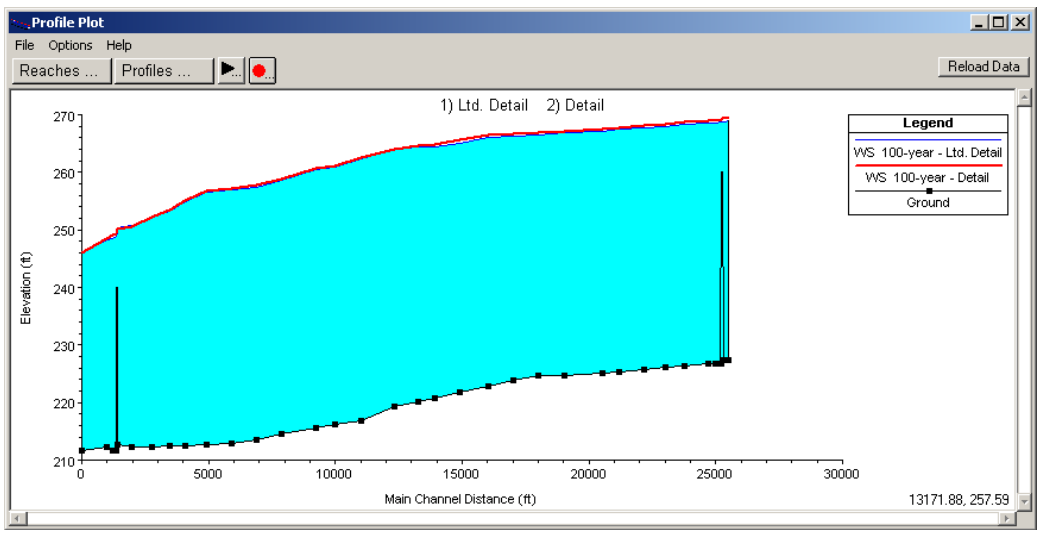

Figure 5. Buckners Creek Profile Comparison

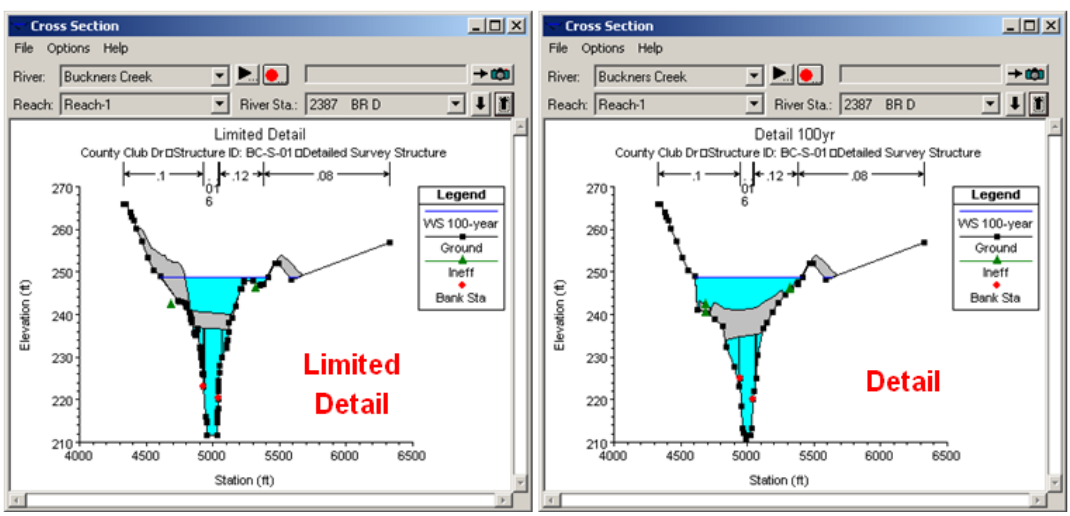

Figure 6. Buckners Creek XS Geometry Comparison at Largest WSEL Error

CASE STUDY #3: CHOUDRANT CREEK (Louisiana)

Table 5. Choudrant Creek Model Background

Reach Info		Other	
Length	5.6 mi.	Drainage Area	21.5 mi^2
# Structures	7	Discharge Methodology	Regression Equations
# Cross-sections	41	Topographic Data	LiDAR
Average Slope	0.0022 ft/ft	Starting Conditions	Normal Depth/Slope

Table 6. Choudrant Creek Comparison Statistics

Statistic	Value
Average Absolute WSEL Error	0.16 ft
Maximum WSEL Error	0.66 ft
% Cross-Sections within 0.1ft Error	42%
% Cross-Sections within 0.3ft Error	87%
% Cross-Sections within 0.5ft Error	96%

Similar to Buckners Creek, the source of the largest "error" as compared to the Choudrant Creek detail model was a result of several cross-sections where the channel width in the limited detail model was estimated to be narrower, as shown in Figure 8. However, once again, the water surface elevations between the two study types are very comparable, even with the inclusion of several additional structures as compared to the previous two case studies.

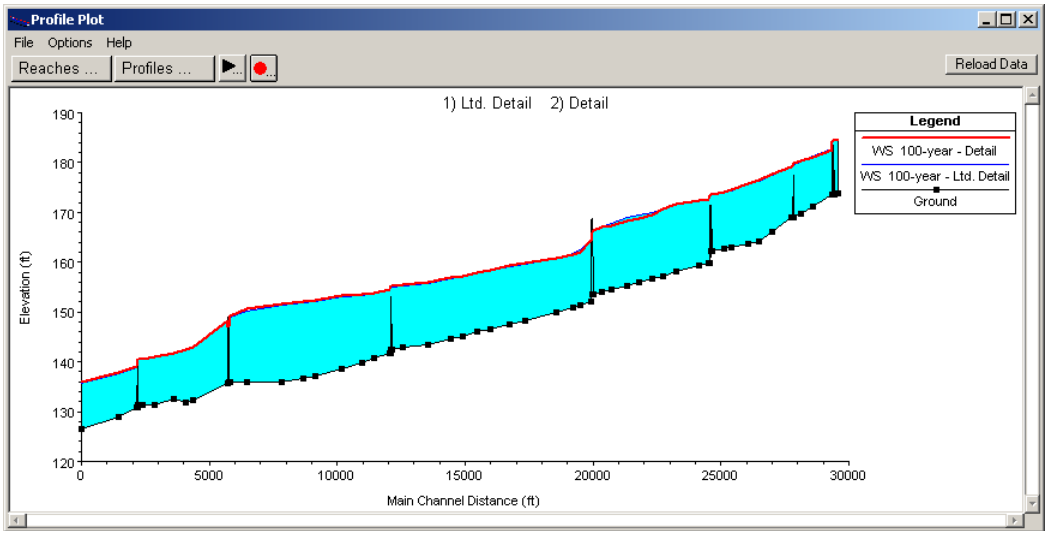

Figure 7. Choudrant Creek Profile Comparison

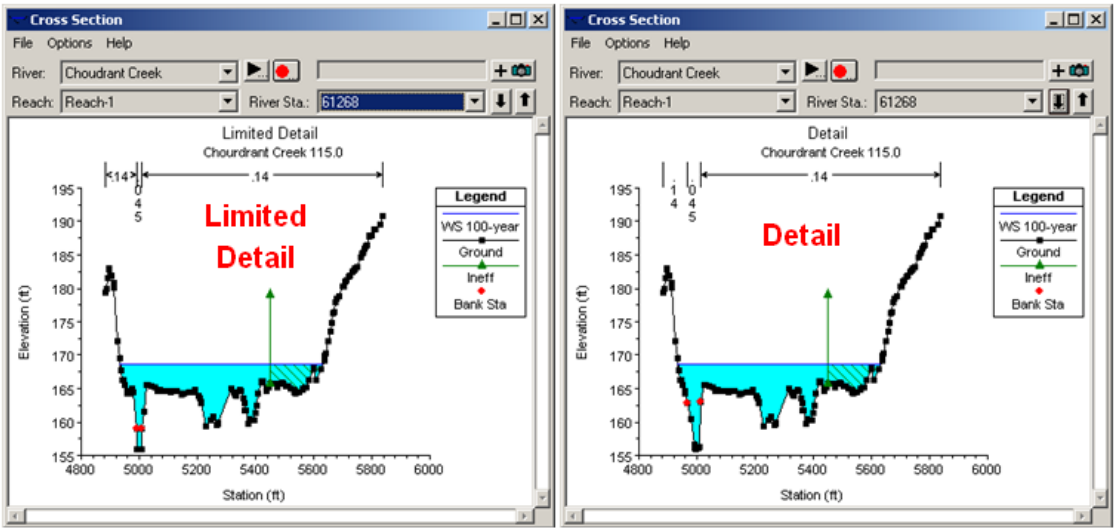

Figure 8. Choudrant Creek XS Geometry Comparison at Largest WSEL Error

CONCLUSIONS

Although the results of these particular three streams that were randomly selected show a very favorable comparison between the limited detail and detail modeling results, further investigation is warranted into other types of streams (i.e. smaller, steeper streams). As previously discussed, smaller streams (with lower discharges) or streams with very narrow floodplains may be more sensitive to the slight changes in geometry between the two different approaches.

However, it should be noted that none of these three streams had any historical data available to use for calibration purposes. Calibration of a limited detail hydraulic model to high water marks, stage-discharge information at gages, or other published data would be performed in a similar manner as it would for a detail model. Therefore, when calibration data is available, a limited detail study can be just as effective at establishing a defendable hydraulic model as a detail model could.

Since the limited detail approach is dependent upon topographic data for establishing its "vertical control" for hydraulic structures in the model, a limited detail study worthy of publishing BFEs on FEMA's maps may not be appropriate in areas where coarser topographic data is the best that is available. However, it is an option that should be considered when budget is a concern, but more accuracy is needed than an approximate study can provide.

Climate Flow Forecast Model for the Brazilian Hydropower System

by

Mario T. L. Barros[1], João E. G. Lopes[2], Renato C. Zambon[3], Alberto L. Francato[4], Paulo S. F. Barbosa[5], Fabio R. Zanfelice[6]

ABSTRACT --- The Brazilian Hydropower System (SIN) is composed today by 107 hydropower plants with 81,036 MW of installed capacity. The system is completely connected due to the Brazilian heterogeneous hydrology. The flow forecast is a very important tool to operate SIN and to other decisions involved in the Brazilian electrical sector. This paper aims to present a model for SIN flow forecasting done in a climate basis, in a monthly basis considering rainfall forecasts for six months ahead. The rainfall forecasts are done by the Brazilian Center for Weather Forecast and Climate Studies (CPTEC). The CPTEC climate forecasting model covers the South America continent and produces forecasts in two grids, 200 by 200 Km and 40 by 40 Km. The flow forecast is done by two hydrological methods. One is the rainfall-flow model SMAP (Soil Moisture Accounting Procedure) by (Lopes et al., 1982) and the other a stochastic linear model (MEL). The final forecasts are defined by a weigh function considering SMAP and MEL forecasts. The flow forecast model is called GERAVAZ and was design using a decision support system frame in order to be practical to users. GERAVAZ was applied to twenty basins covering the main Brazilian rivers. These twenty forecasts are the reference to produce the inflow forecasts to all SIN reservoirs. Preliminary results are quite promising and have great evidences of the potential application of this modeling tool.

LOPES J.E.G., BRAGA B.P.F., CONEJO J.G.L. (1982), SMAP - A Simplified Hydrological Model, Applied Modeling in Catchment Hydrology, ed. V.P.Singh, Water Resources Publications.

[1] Professor, University of São Paulo Brazil; e-mail: mtbarros@usp.br; ASCE Member
[2] Consulting Engineer; e-mail: jelopes@dglnet.com.br
[3] Researcher, University of São Paulo; e-mail: rczambon@usp.br
[4] Associate Professor, University of Campinas; e-mail: francato@fec.unicamp.br
[5] Professor, University of Campinas; e-mail: franco@fec.unicamp.br
[6] Manager, CPFL Energy Inc.; e-mail: fabio@cpfl.com.br

Introduction

Short-term and long-term reservoir inflow forecasts represent a big challenge to operation managers of large hydropower systems. When considering the large-scale of the Brazilian Interconnected Power System, the availability of river flow forecasts is still more relevant for hydrothermal operation planning since the annual hydropower production is nearly 91% of the total electricity production. The stochastic modeling of river flows based on time series approach (e.g. Box-Jenkins methodologies) is too complex for practitioners at real time reservoir operation. Also, the quality of the resulting forecasts has been pointed out as a source of criticisms. In addition to potential impacts on operation planning, inflow forecasts can also be a source of great volatility for marginal operational costs, which are linked to electricity spot price formation in hydrothermal systems. Therefore, reservoir inflow forecasts have important impact on commercial strategies of hydropower generation companies.

This work presents a mathematical model with two methodologies for climate flow forecast, the SMAP model (Soil Moisture Accounting Procedure) and the MEL model (Linear Stochastic Model), both based on rainfall forecasts provided by CPTEC- Brazilian Centre of Weather and Climate Forecasting, as described by Sampaio and Nobre (2006). These monthly rainfall forecasts are distributed in a grid of 200 x 200 km, with a time horizon of 6 months ahead. The monthly rainfall forecasts are transformed in reservoir inflows by using rainfall-runoff models. The natural hydro-energy inflows (ENAs) are calculated taking the reservoir inflows (m3/s) multiplied by the unit turbine efficiency parameters (MW/m3/s), thus forming the basic input for hydrothermal system operation in use both by NEWAVE and DECOMP optimal dispatching models. This forecast information is also important for other sectors of power generation companies, including the power trading and the maintenance planning divisions, among other ones.

Methodology of the Forecasting Models

The rainfall forecast is provided by an atmosphere numeric model (oceanic) using approximate numeric representation of the fundamental mathematic equations that govern the air and water at atmosphere, and their corresponding interactions with Earth surface. The atmosphere is divided in millions of volumes (200 km x 200 km x 0.5 km) with calculation of the air moisture and temperature, wind velocity and pressure for future time intervals (Sampaio and Nobre, 2006).

The rainfall-runoff methodology is implemented by using two distinct modeling approaches:

- Physically based modeling for the rainfall-runoff process, with the SMAP model, which was developed by Lopes et al (1982);
- Linear stochastic model, using mixed models (Beven, 2001)

The SMAP (Soil Moisture Accounting Procedure) model is a simple monthly time step based rainfall runoff model of the lumped conceptual type. It is particular useful if only monthly input data is available. This is often the case in overall water resources planning or for analyses of long-term reservoir operations.

The model accounts for the water storage in two linear reservoirs representing the root zone and the groundwater reservoirs respectively. It has five calibration parameters and four transfer functions, with monthly up-to-dating of the four state variables. The main components of SMAP are shown in Fig.1.

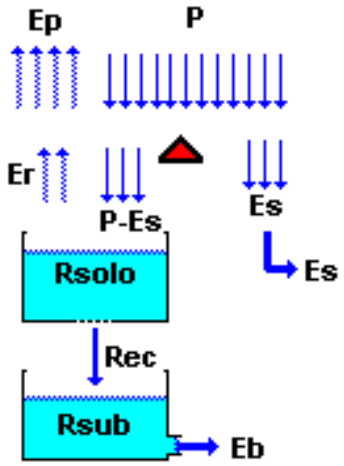

Figure 1 – Main components of the SMAP model
(Lopes et al, 1982)

The Stochastic Linear Model (MEL) is a mixed model, using as input both observed river flows and rainfalls on upstream areas of each reservoir. ARIMA models are used for forecasting purposes. The minimization of square sum of errors is used at calibration stage (Box and Jenkins, 1976).

Forecasting Models Applied to the Brazilian Interconnected Power System

The forecasting models described before were applied to selected river basins of the Brazilian Hydropower System (SIN). Specific river stations were selected in order to define the forecasts of inflow reservoirs. The main river basins of the SIN are shown at Fig. 2.

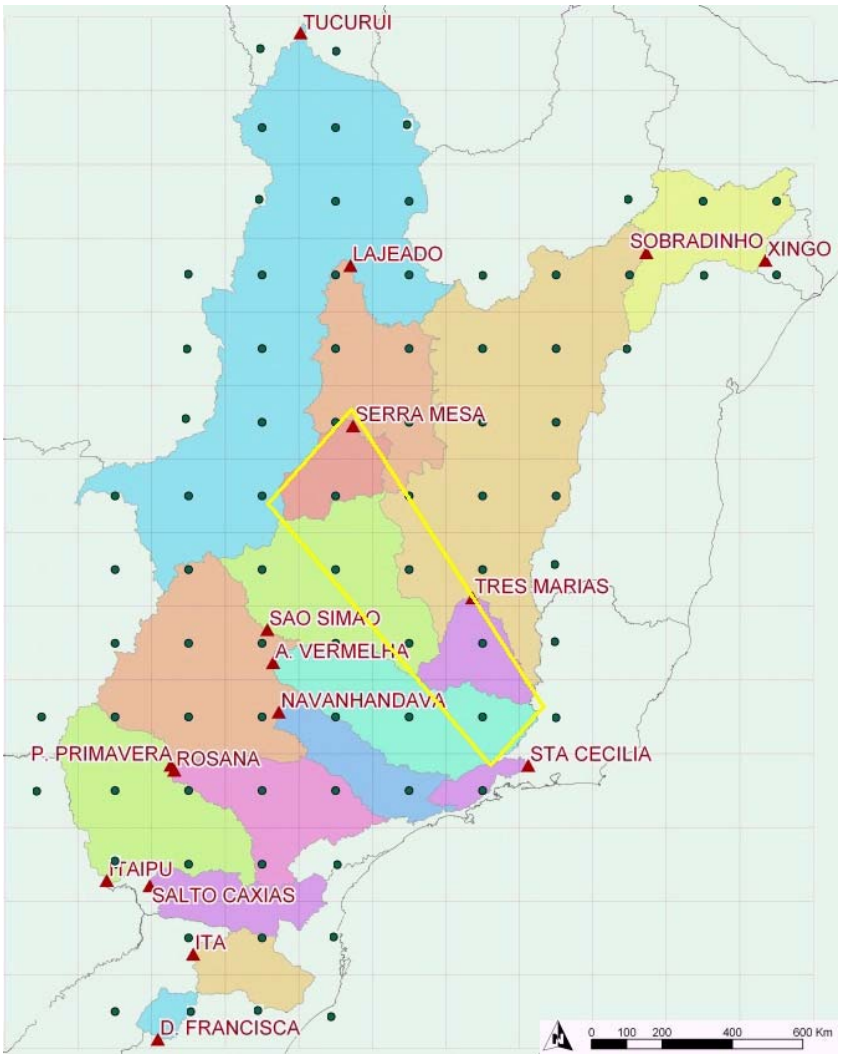

Figure 2 – Strategical Stations for Forecasting

Using the ArcView software, the axis of dams for each reservoir was taken as a reference to define the corresponding watershed polygonal limits of the drainage area, taking maps available at ANA (National Regulatory Agency of Water Resources). The grid defined by CPTEC for rainfall forecast was launched over the river basins that compose the Brazilian Hydropower System (SIN), as shown in Fig.2, where the black points represent the center of the corresponding cell for rainfall forecasting purpose, and the triangles represent the position of reservoirs.

The following river basins and sub-catchments areas are the main parts of the Brazilian Hydropower System (SIN), representing almost the total of inflows to the SIN:

• Paraná river basin upstream Itaipú hydropower plant, with 822.000 km2 (divided into 6 sub-catchments areas)

- Tocantins river basin upstream Tucuruí hydropower plant, with 758.000 km² (divided into 3 sub-catchments areas)
- São Francisco river basin upstream Xingó hydropower plant, with 609.000 km² (divided into 3 sub-catchments areas)
- Iguaçu river basin upstream Salto Caxias hydropower plant, with 57.000 km²
- Uruguai river basin upstream Ita hydropower plant, with 45.000 km²
- Jacuí river basin upstream D. Francisca hydropower plant, with 14.000 km²
- Paraíba do Sul upstream Sta Cecília hydropower plant, with com 17.000 km²

The following data were used for model calibration and validation purposes:

- Historical series of monthly rainfall (mm) in grids of 200 km x 200 km, for all the selected river basins and sub-catchments areas, from January 1995 to May 2007, available of CPTEC database;
- Historical series of monthly river flows (m3/s), for selected (16) stations corresponding to the drainage are upstream each hydropower plant, from January 1931 to May 2007,available at ONS (Independent Operator System) database;
- Long term mean of potential evaporation for the 16 river basins, available at database of DAEE (Dept. of Water and Power), CESP (Power Generation Company of State of Sao Paulo) and INMET(National Institute of Meteorology).

The results of the SMAP and MEL models calibration and validation processes are shown at Fig. 3 to Fig. 6.

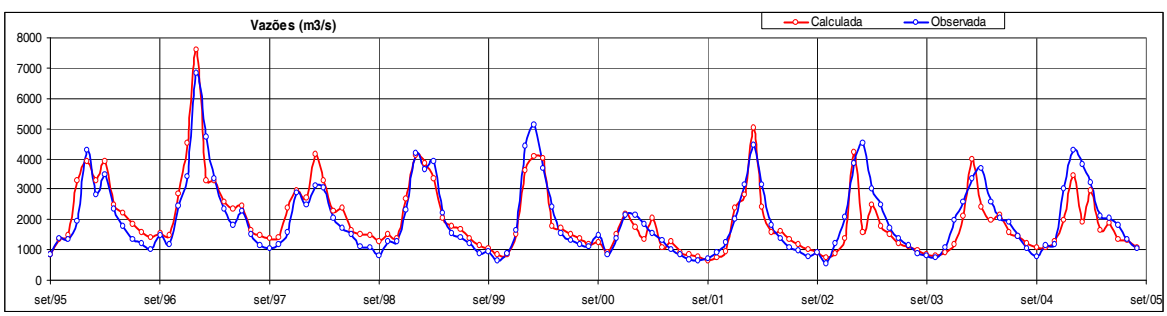

Figure 3 – Calibration of the SMAP model at Água Vermelha flow station (m3/s) (Red: SMAP flow calculations, blue: historical flow)

As can be seen from Fig. 3 to Fig. 6, the application results at Agua Vermelha station reveals good fit to both SMAP and MEL models. The Akaike criteria (1973) were adopted in the assessment of the fit goodness to avoid systematic errors in the rainfall-runoff modeling processes.

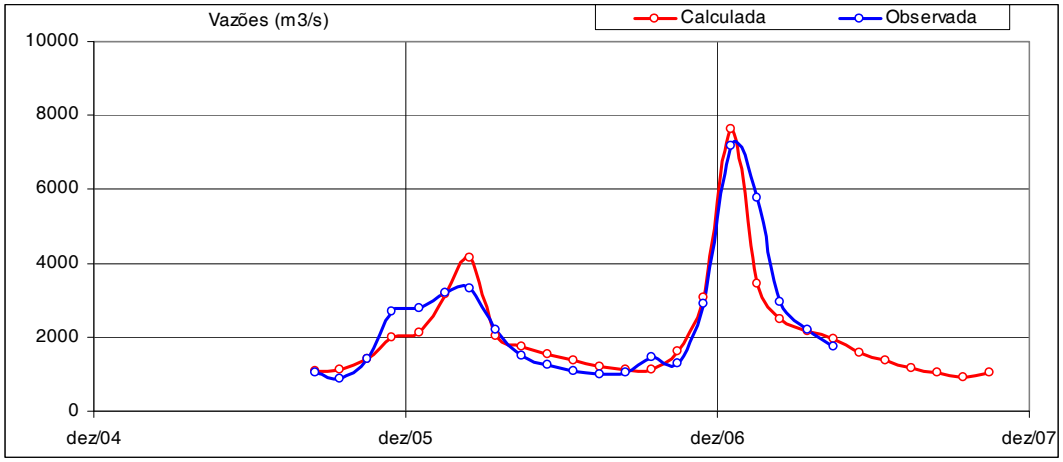

Figure 4 – Validation of the SMAP model at Água Vermelha flow station (m3/s)
(Red: SMAP flow calculations, blue: historical flow)

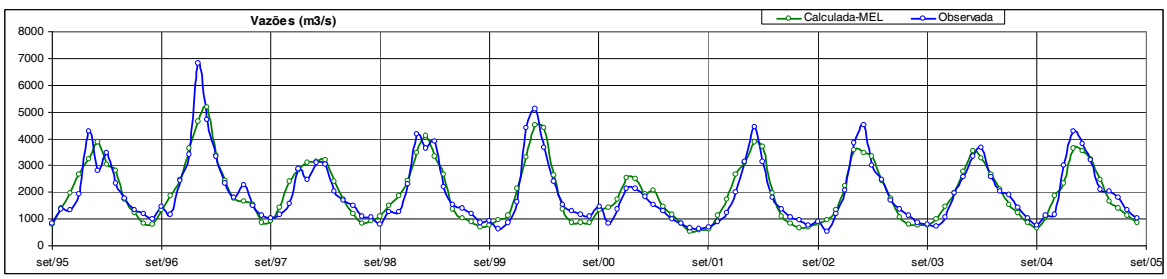

Figure 5 - Calibration of the MEL model at Água Vermelha flow station (m3/s)
(Green: MEL flow calculations, blue: historical flow)

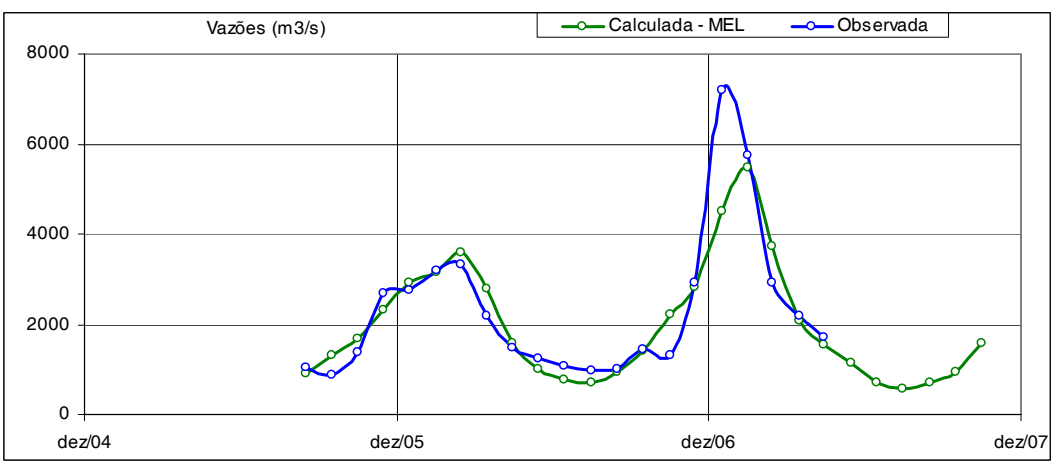

Figure 6 – Validation of the MEL model at Água Vermelha flow station (m3/s)
(Green: MEL flow calculations, blue: historical flow)

The GERAVAZ software

The GERAVAZ software was developed based on general concepts of decision support systems (DSS). As described by Porto et al (1997), DSS are computational systems especially designed to help taking decisions on problems with a not well defined structure or with a partially structured framework. There is no previously defined algorithm for solving such kind of problems, thus requiring intense interaction between man and machine (computers). A DSS typically requires a mix of data base, mathematical models and interfaces. An important aspect of a DSS is to provide multiple solutions to allow broader assessment and insight of the problem being studied. A DSS is not a substitute for decision makers, but a helpful tool to improve a decision making process.

The GERAVAZ decision support system is composed by a data base, interfaces and the SMAP and MEL forecasting models. The interface was developed with the Borland Delphi devices to be processed coupled with the Microsoft Windows operational system. It was designed using multiple pages and screens with options that allow data visualization, river basin maps, SMAP and MEL runs, and output results. Two examples of interface screens of GERAVAZ are shown in Figure 7.

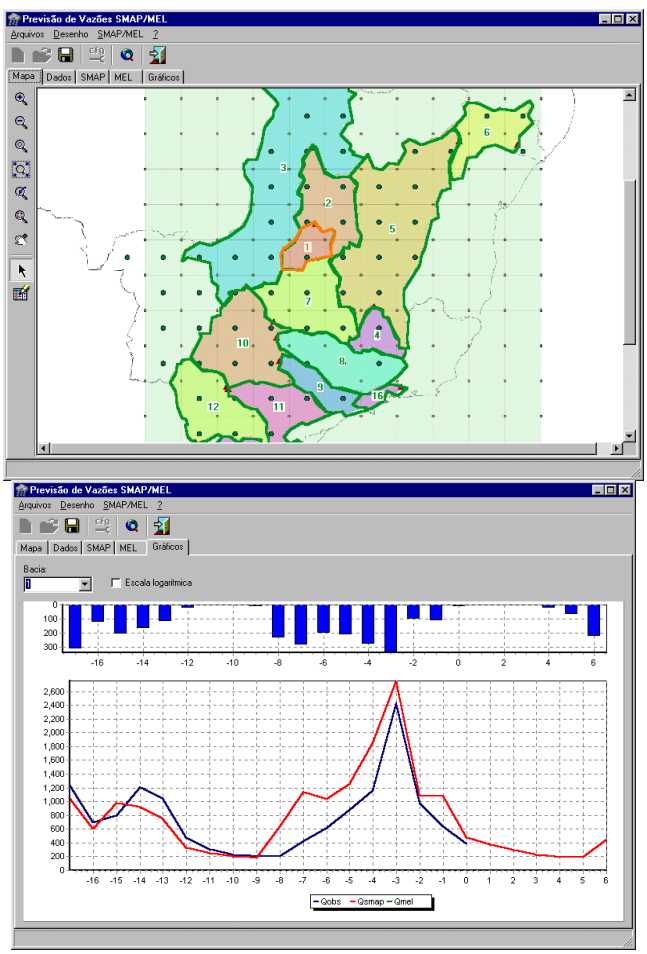

Figure 7 – Illustrative examples of GERAVAZ interface screens

Input and output data are stored in a Microsoft Access data base. It stores data of historical rainfall and river flows, rainfall forecasts, forecasting data generated by SMAP and MEL, potential evapotranspiration, long term means, cells of grid, parameters of the rainfall-runoff calibration process and hydropower plants that compose the Brazilian Hydropower System (SIN).

The GERAVAZ interface allows selecting rainfall forecasting options, by using outputs of both rainfall-runoff models or long term mean values of historical observations. In addition, rainfall scenarios can be constructed from the previous ones by multiplying specific factors to the original rainfall forecast values.

At the final stage of GERAVAZ use, after generating the river flow forecasts, specific routines prepare these flow output to be used as input to the NEWAVE and DECOMP optimal power dispatching models.

Conclusion

The development and results of the GERAVAZ decision support system, with the rainfall-runoff SMAP and MEL models, reveals its full success as a tool to provide river flow estimates for the main river basins of the Brazilian Hydropower System. From several applications it can be recognized that errors on rainfall forecast have significant impact on river flow forecasts. Actually, these errors are big when the regional rainfall forecasting model (ETA model, developed by CPTEC) was used.

As someone could expect, comparisons between GERAVAZ river flow forecasts and observed flows reveals smaller errors at the first time interval (monthly) ahead, when compared to the next five months. This suggest the use of GERAVAZ model in a dynamic fashion, with monthly up-to-dating (rolling horizon), or even at intervals smaller than one month wherever new climate information become available.

It should be highlighted the broad potential to improve river flow forecasts as a result of additional improvements on rainfall forecasts throughout river basins that compose the Brazilian Hydropower System. A possible alternative to be investigated is a further reduction of the cell size in the grid for rainfall forecasting, thus allowing better description of the precipitation process.

As a final comment, this work showed the potential for future scientific development and collaboration between researchers of hydrological sciences and meteorological sciences as an important aid to improve the quality of river flow forecasting.

Acknowledgements

The authors recognize the helpful participation of the technical staff of CPFL Energia, Inc., providing useful data and support for developing this work.

References

Aitken, A.P. (1973) Assessing Systematic Errors in Rainfall-Runoff Models. Journal of Hydrology, v.20, p.121-136.

Beven, K.J. (2001) Rainfall-Runoff Modelling: The Primer, John Wiley & Sons.

Box, G.E.P, Jenkins, G.M. (1976) Times Series Analysis: Forecasting and Control. San Francisco: Holden Day.

Lopes J.E.G., Braga B.P.F., Conejo J.G.L. (1982), SMAP - A Simplified Hydrological Model, Applied Modeling in Catchment Hydrology, ed. V.P.Singh, Water Resources Publications.

Porto, R.L.L.; Lanna, A.E.L.; Braga Jr., B.P.F.; Cirilo, J.A.; Zahed Filho, K.; Gobetti, L.; Azevedo, L.G.T.; Barros, M.T.L.; Barbosa, P.S.F. (1997) Técnicas Quantitativas para o Gerenciamento de Recursos Hídricos. Coleção da ABRH, UFRGS. *(in Portuguese)*

Sampaio, G.; Nobre, C. A. (2006) Previsões Experimentais de Precipitação e Temperatura Médias Mensais. CPTEC. *(in Portuguese)*

Collaborative Groundwater Model Development

David W. Barfield[1]

[1]Chief Engineer, Division of Water Resources, Kansas Department of Agriculture, 109 SW 9th Street, Topeka, KS 66612-1283; PH (785) 296-3710; FAX (785) 293-1176; email: david.barfield@kda.ks.gov

ABSTRACT

In our day of increasing conflicts for water resources, water management decisions require the understanding of the hydrologic nature of the interactions between water use and the water resources. In Kansas, conflicts for water resources occur at both the interstate and intrastate level, and have led to the development of groundwater models as tools for water management decision-making.

In the past, groundwater model construction has typically been the responsibility of a single entity, with limited technical input from agencies and/or interested constituents, and peer review generally at the end of the model construction process. This has led to models with limited buy-in from the regulated community, limiting their usefulness in difficult and contested water management decisions.

A robust, collaborative model development process was used in the development of the Republican River Compact Administration groundwater model by the states of Colorado, Kansas and Nebraska as part of their settlement of their compact litigation in 2002. More recently this model development process was used to build the Middle Arkansas River Basin groundwater model in south-central Kansas. The model development process used allowed multiple experts to review model datasets and calibration targets, test modeling assumptions, explore various modeling approaches, and determine when model construction was complete.

While the process requires greater commitment of total resources, in both cases the process led to good, practical, defendable models, which are being used as tools to guide important water management decisions.

INTRODUCTION

In Kansas, as in other regions where dependable water supplies are less than demands, water resource conflicts occur at both the intrastate and interstate level. This has led us to develop and rely on groundwater models as a tool in guiding water management decisions. In the model development process, understanding of the

hydrologic system and its various components is increased and a tool to evaluate the impact of future management of the system is provided.

NEED FOR AN IMPROVED MODEL DEVELOPMENT PROCESS

However, this application of groundwater modeling is subject to legal and other challenges and past model development processes have been insufficient to withstand this scrutiny. In an effort to build better models able to significantly increase acceptance by the regulated community and to withstand legal challenges, Kansas has adopted a new model development approach that includes on-going collaboration of the lead contractor developing the model, a peer review modeler, stakeholders, and other experts in a given area. The approach's use of robust, on-going review of the model development has improved resulting models and buy-in from stakeholders.

The process provides for early decisions being made on model targets (groundwater levels, streamflows), rigorous joint data development and review, testing of alternate modeling processes to determine the most appropriate methodology and aids in eliminating bias. Kansas currently has completed two modeling projects using this approach: 1) interstate - Republican River Compact Administration and 2) intrastate - Middle Arkansas River. The state is at different levels of progress on four additional models being developed using this approach.

REPUBLICAN RIVER COMPACT ADMINISTRATION GROUNDWATER MODEL

The Republican River Compact Administration groundwater model was constructed as part of a comprehensive settlement of litigation among the states of Colorado, Kansas, and Nebraska regarding the Republican River Compact. The model is used as a significant input into the Compact accounting used to determine compact compliance. The model is run annually to determine streamflow depletions due to groundwater pumping and streamflow accretions to the Republican River basin from the Platte River. As a consequence, the model is also used by the States to target its activities to achieve compliance with Compact requirements.

The model was developed using the processes advocated here, except model development was not an open process since it was done as part of settlement discussions. Each state was represented by a team of modeling and other experts and state officials, with federal modelers also participating. This modeling committee

collaboratively gathered and agreed to calibration target data (groundwater levels and historic baseflows), developed and reviewed model data, and tested alternative model processes to develop a defendable model.

MIDDLE ARKANSAS RIVER GROUNDWATER MODEL

The Middle Arkansas River groundwater model was constructed to provide a tool for quantifying historical groundwater conditions and to evaluate how future changes might impact groundwater levels and streamflow conditions. The model development process used allowed for improvements to boundary conditions, refining model methods to develop recharge estimates and reducing model bias. The process resulted in a more reliable and defendable model and increased stakeholder. With an agreed-upon model, the focus of our remaining work will now shift from adequacy of a model to water management objectives and means to achieve them.

CONCLUSION

Groundwater models being constructed for water resource management decision-making require additional attention to detail via on-going robust participation by experts and stakeholders to withstand scrutiny associated with their application to such decision-making. Such model development needs a clearly defined purpose; a diverse team with multiple modelers, data experts and stakeholders; and joint testing of alternate model processes with robust data development and review. This process enhances model performance and acceptance by the regulated community.

REFERENCES

Republican River Ground Water Modeling Committee (2003). *Republican River Compact Administration Ground Water Model Documentation*, http://www.republicanrivercompact.org/v12p/RRCAModelDocumentation.pdf

Whittemore, Donald O. and Sophocleous, Marios A (2006). *Numerical Model Of The Middle Arkansas River Subbasin,* http://www.kgs.ku.edu/HighPlains/Mid_Ark_model_report_all_071206.pdf

Communicating drought severity and re-evaluating firm yield – Cumberland County, Tennessee as a case study

Lars Hanson[1] and Stuart Stein[2]
1 Water Resources Engineer. GKY & Associates, 4229 Lafayette Center Dr, Suite 1850, Chantilly, VA 20151 (ph) 703-870-7000 Email: lhanson@gky.com
2 President, GKY & Associates.

Abstract: The 2007 drought in Cumberland County, Tennessee greatly strained the three reservoirs that provide the large majority of the county's water supply and prompted a new analysis of the reservoirs' firm yield. With the reservoirs lacking long term streamflow and operations records, traditional yield analysis could not be performed directly. A multi-scale Standardized Precipitation Index (SPI) analysis was conducted, and the resulting multi-scale SPI plot was found to be a highly effective tool for communicating the drought severity of the current drought relative to past droughts. A simple, continuous-simulation HEC-HMS model was used to generate a synthetic streamflow record, and determine the critical drought period for each reservoir using the traditional sequent peak algorithm. Using the sequent peak algorithm, storage-yield relationships a multiple yield cumulative deficit plot were created as useful tools for explaining reservoir behavior. This is part of a County-wide water supply plan being developed by the US Army Corps of Engineers, which includes projecting future water demand, evaluating potential conservation measures, and evaluating sources to meet the growing demand.

1. Introduction

Estimating firm-yield of a small reservoir can be a relatively straightforward process when high quality records of inflows, withdrawals, and lake levels are available. Often, though, these data are incomplete or lacking entirely. The firm-yield can still be estimated, provided that sufficient information is available to estimate the water balance to the reservoir.

Cumberland County, Tennessee, located in the East-Central part of the state endured a severe drought from 2007 to the early part of 2008. Though its reservoirs did not fail, Cumberland County, with its rapidly increasing population, decided to restudy its estimates of firm yield in light of the recent drought. The county located on top of the Cumberland Plateau is entirely a headwater area, and gets nearly all of its water from three small reservoirs. Two of the reservoirs, Meadow Park Lake and Lake Holiday, are controlled by the City of Crossville Utility District and the third, Otter Creek Lake is controlled by the Crab Orchard Utility district. Figure 1 shows Cumberland County, the three reservoirs and their watersheds.

There are several challenges that complicate the calculation of firm yield in Cumberland County, which are typical to counties with relatively small water distribution systems. Due to Cumberland County's small population and relatively wet climate, water has always been plentiful, and has only recently been a concern. As a result, records of the reservoir levels and streamflow monitoring have been

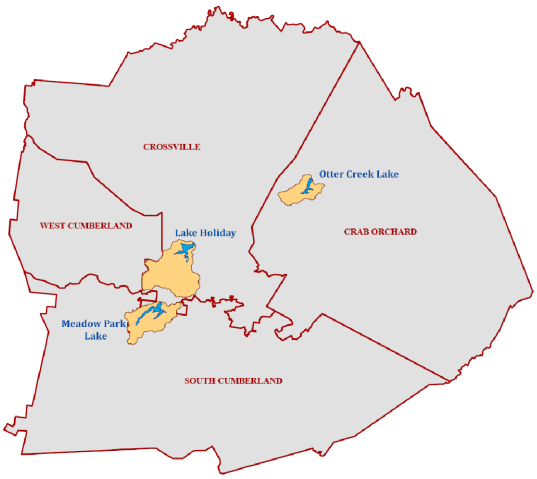

Figure 1. Cumberland County, utility district boundaries (red), and three reservoirs with catchments

largely absent except for in the last few years. While firm-yield can still be calculated through other methods, the resulting estimates are subject to more uncertainty than if long term reservoir or streamflow records were available. Further complicating the situation is that there is little consensus on the total available storage in each reservoir due to conflicting estimates and unknown rates of sedimentation. For small water systems in relatively humid environments, this is not an uncommon scenario.

The goal of this study was to use all available data to investigate the relative magnitude of the 2007 drought, establish solid estimates of firm-yield for the three reservoirs, and explain the results as clearly as possible to the stakeholders in Cumberland County.

2. Methods

This study was completed in three stages. First, historical precipitation records were analyzed to determine the most severe drought periods in the County over the last 95 years. Second, the historical inflow to the reservoirs was simulated using the Hydrologic Engineering Center's Hydrologic Modeling System (HEC-HMS) rainfall runoff model. The simulated historic inflow sequence was then used in the traditional sequent peak algorithm to estimate the critical drought sequence.

Drought Analysis with the Standardized Precipitation Index

To analyze the relative magnitude of the current drought, a drought metric had to be selected to compare droughts from different periods. Aside from temperature and precipitation, each of which has a 95-year record length in Cumberland County, hydrologic indicators such as soil moisture, evaporation, solar insolation, and others were not available. As a result, many of the most common drought indicators and indices (Palmer indices) were rejected. The Standardized Precipitation Index (SPI) was chosen because it only requires monthly precipitation as an input, and can be computed at multiple time scales.

The SPI index value reflects the probability of certain rainfall totals occurring for the given analysis duration. Instead of reporting this probability as a percentile, the SPI index uses a standard normal variate (or Z-score). The rainfall totals are fitted to a gamma distribution and then transformed to a normal distribution, and the score is roughly analogous to the number of standard deviations the rainfall total falls from the median. Below average precipitation, therefore, has a negative index value. A

drought occurs when the index value falls below -1, and a severe drought is triggered when the index drops to -2. (McKee et al., 1993)

The Crossville Exp Stn precipitation gage, with a 95-year record length was used to compute the SPI at durations of 3, 6, 9, 12, 15, 18, 24, 30, 36, 42 and 48 months. Viewed through the lens of the SPI (or likely any other metric), it is difficult to declare any single drought as the most severe. Table 1 displays critical SPI values from seven droughts at various durations, with the highest SPI value for each duration in bold, and the highest value within each drought in italics. Unfortunately, several droughts could be considered the most severe, depending on the duration of interest.

Table 1 - Critical 3 to 48 months duration SPI values for droughts at Crossville Exp Stn

Drought	3	6	9	12	15	18	24	30	36	42	48
1924-1926	-2.49	-2.71	-2.73	**-2.83**	***-2.86***	-2.53	-2.69	-2.49	-2.41	-2.22	-2.01
1930-1934	-2.18	-2.25	-2.38	-2.55	***-2.86***	**-2.81**	**-2.77**	-2.45	-2.39	-2.28	**-2.59**
1940-1942	**-2.66**	***-2.92***	-2.53	-2.48	-2.37	-2.57	-2.48	**-2.59**	**-2.62**	-2.16	-2.14
1952-1953	-2.54	-2.89	***-2.95***	-2.21	-1.78	-2.14	-1.93	-1.94	-	-	-
1980-1982	-2.1	-2.44	*-2.82*	-2.51	-2.03	-1.83	-	-	-	-	-
1986-1988	-1.8	-1.99	*-2.35*	-2.11	-2.18	-2.25	-1.74	-2.03	-1.94	**-2.33**	-2
2006-2008	-2	-2.17	-2.55	*-2.56*	-2.18	-2.18	-1.91	-1.83	-1.9	-	-

Table 1 demonstrates there is uncertainty in declaring one drought as most severe, but communicating that uncertainty to clients and stakeholders can be difficult. To better explain the uncertainty in severity and duration of droughts, a surface plot (Figure A1 in the Appendix) was devised to show the SPI value as contours on surface plot with base axes showing time versus SPI analysis duration. Drought periods appear as yellow, orange and red. Figure A1 very effectively illustrates how droughts evolve over time with some severe droughts starting as long mild dry spells, and other severe droughts rapidly abated with months.

HEC-HMS Modeling

The HEC-HMS (Hydrologic Engineering Center – Hydrologic Modeling System) model is used for a very limited and specific purpose in this application. The HEC-HMS model is often used to compute peak flows, but this study has no use for them, as droughts are the hydrologic phenomenon of interest, and the model is used only to transform historical rainfall values into the most representative daily streamflow sequence possible for the three catchments. As a result, the model is run in an atypical fashion, as a long-term simulation rather than a single storm event.

Precipitation and Basin Model

The HEC-HMS model requires precipitation data at a daily or finer scale. The Crossville Exp Stn precipitation gage has been recoding daily precipitation values nearly continuously for over 95 years. A record length from September 1, 1913 to August 31, 2008 is used in this model. Data gaps were filled with daily precipitation values from nearby stations with concurrent records. Wherever, possible, the nearby Crossville Mem Ap station was used to substitute values. In the HEC-HMS model, the rainfall data is entered as a precipitation gage in the time series data editor.

Constant monthly evaporation was chosen as the evaporation method in the meteorological model ("Met model" in HEC-HMS). Expressed in inches per month, the evaporation rate (in addition to the constant infiltration rate) controls the rate at which water exits the single soil layer. The rate can be specified by month, but each month has a constant rate for the entire simulation period. Pan evaporation data (1978-2005) for the Crossville Exp Stn gage were used to determine the average monthly rates. The pan coefficient was assumed to be 0.7.

There are a limited number of options for running long term simulations at a daily time step. Essentially, the Deficit and Constant Loss method and the Soil Moisture Accounting method are the only potential loss methods for this study. The soil moisture accounting method is a complex model that requires a large number of parameters that are difficult to estimate with available data in the Cumberland County area. Therefore, the Deficit and Constant Loss method is chosen.

The Deficit and Constant Loss method is a very simple soil moisture tracking model. The surface soil layer is treated as a simple reservoir with two losses and one input. The soil layer is assumed to cover the entire subbasin. The soil layer thickness is characterized by the maximum depth, which is assumed to represent the available void space in the soil layer for flow to pass. **Error! Reference source not found.** shows a conceptual model of the single soil layer model. The soil layer loses water to deeper soil layers through infiltration. The soil layer can also lose water to evapo-transpiration (ET). And of course, the soil layer receives water only through precipitation. When the soil layer is full, runoff occurs.

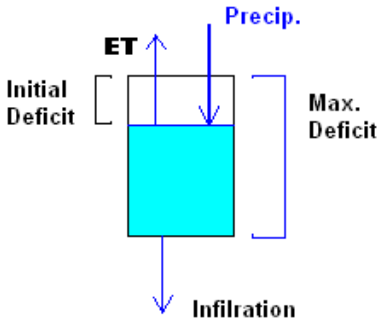

Figure 2. Conceptual model of single soil layer Deficit and Constant Loss method

In the HEC-HMS model, the constant baseflow method was selected as most applicable for this study. This method assumes constant baseflow within each month. While Eastern Tennessee has relatively little seasonality in its rainfall totals, there is a strong seasonal pattern in its baseflow pattern. While there are no stream gages on the streams that feed the reservoirs of interest, streamflow data from several stream gages on other streams in Cumberland County and surrounding counties were downloaded from the United States Geological Survey (USGS). Using the streamflow records, the USGS's PART program was run to determine the baseflow, expressed as specific discharge (flow per unit of drainage area). (Ries, 2006)

Watershed times of concentration (Tc) for the three reservoirs' catchments were computed via the Kerby, Kirpich, and SCS equations and were found in all cases to be less than five hours. With the model time step of one day, this factor becomes insignificant, and the model has to automatically extend Tc to allow the model to run. Therefore, the routing and storage option was turned off as it proved insignificant. Since the HEC-HMS model is only used to compute volume of runoff and not within-day timing or peak values, this is acceptable.

Calibration of the HEC-HMS model

Since long term, high-quality records of the reservoirs could not be obtained, calibrating to the reservoirs' actual data could not be performed. USGS's PART model, in addition to computing baseflow, also computes the monthly streamflow as specific discharge. The mean and median discharge for each month were computed from the stations whose records were used for the baseflow estimation. Though the streamflow records are fairly well distributed through the simulation time period, they are not uniformly distributed enough to assume that the computed average (or quantile values) of discharge are good estimators of the true average because differences in rainfall have a large effect on the quantity of discharge. Therefore, to normalize these statistics, the runoff ratio is used instead of specific discharge. Runoff ratio is calculated by dividing a month's specific discharge by the total precipitation for the same month. Thus, the discharge from the stream gages, which are all near Cumberland County, is divided by precipitation from the Crossville Exp Stn.

The calibration strategy is to get the model's monthly mean and median discharge to match that of the streamflow gages as closely as possible. As an example, **Figure 3** displays the calibration results for Meadow Park Lake in comparison to the monthly median and average runoff ratio for the USGS streamflow gages. The model calibration was completed by adjusting the loss parameters for the watersheds and lakes. **Figure 3** shows the calibration is generally good, especially considering the limitations of the modeling options chosen. Most notably, the runoff ratio for the entire period of record (PoR on the graph) was nearly a perfect match between the model and gage data. On the whole, the model values follow the general pattern of the runoff ratios month to month fairly well. The model medians drop below the model averages in the summer much as the gage medians and gage averages. The winter months tend to somewhat under-estimate the runoff ratios, while the summer months tend to overestimate, though by a lesser amount. The red and blue dotted lines indicate the 40th and 60th percentiles of the runoff ratios of the monthly USGS streamflow data to give some indication of the monthly variation in values.

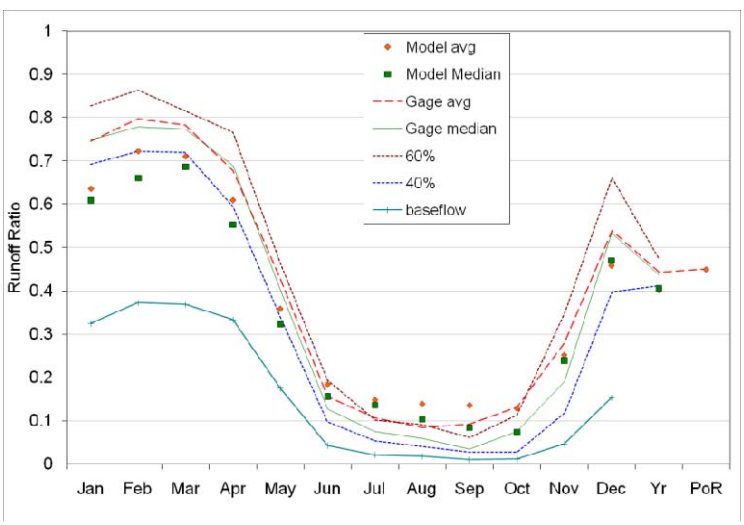

Figure 3. Calibration chart comparing monthly average runoff ratio from the model and stream gages

The next section goes over the calibrated parameter values for the loss method, and the monthly climate parameters.

3. Sequent Peak Algorithm to Identify Critical Drought

The HEC-HMS model provides daily runoff as an output, and from this, the sequent peak algorithm can be used to develop an estimate for the yield the reservoir can support. The sequent peak algorithm (based on the work of Rippl, 1883; Thomas and Burden, 1963) tracks the daily (or monthly, yearly, etc) water balance for a real or theoretical reservoir with known inflow and a specified demand pattern. For this study, the sequent peak algorithm is computed on a daily time step, as the HEC-HMS model output is also daily.

The sequent peak algorithm is based on Equation 1.

$$K_t = (D_t - Q_t) + K_{t-1} \qquad \text{if } K_t>0, \text{ else } K_t=0 \qquad \textbf{Equation 1}$$

Where:

K_t is the cumulative deficit at time t
D_t is the demand at time t
Q_t is the inflow at time t
K_{t-1} is the cumulative deficit at time (t-1)

Essentially, equation 1 tracks the cumulative deficit at each time step. The rate of change in the deficit for each day is equal to the demand minus the inflow for that day. Adding that difference to the cumulative deficit of the previous day (K_{t-1}) gives the current day cumulative deficit (K_t). Typically, demand is assumed to be constant each day, though the algorithm allows for the demand to vary with time. For a firm yield study such as this one, demand remains constant. The firm yield is the yield at which the maximum value of K is equal to the reservoir storage.

The sequent peak algorithm is useful because it generates an estimate of the storage required for a no-failure condition at a given yield. Running the sequent peak algorithm at many different demand levels (yields) generates a relationship between storage and yield for a 100% reliability condition. This relationship, when plotted with yield on the x-axis and required storage (i.e. maximum deficit) on the y-axis produces a smoothly increasing curve called the Storage-Yield curve. **Figure 4** displays the storage yield curves for the three reservoirs in Cumberland County. The yield in MGD is displayed on the x-axis and the required storage to support that yield on the y-axis.

The red diamonds on each curve show the best estimate of actual storage in each reservoir. Many of these estimates are old, and may not reflect actual storage available for use in the treatment plants. Fortunately, the Storage-Yield curves are an excellent tool for analyzing the uncertainty in these estimates. For example, if Meadow Park Lake's storage estimate was 100 million gallons too high, the yield would be reduced to about 3.75 from 4.02. Otter Creek Lake would not see such a big reduction from the same decrease as the curve is steeper at its current storage estimate. In similar ways, these curves can guide management decisions. If one wanted to raise a dam, for instance, Lake Holiday and Meadow Park would make the most sense, as the current storage is on the flat part of the storage-yield and there is substantial increase in yield to be gained. The storage-yield curves in **Figure 4** also have a short blue vertical line at the end of each curve, with the yield at that point labeled. These lines indicate where the yield becomes equal to the average total

inflow to the lake. This is a practical limit to the yield since withdrawals cannot sustainably exceed inputs.

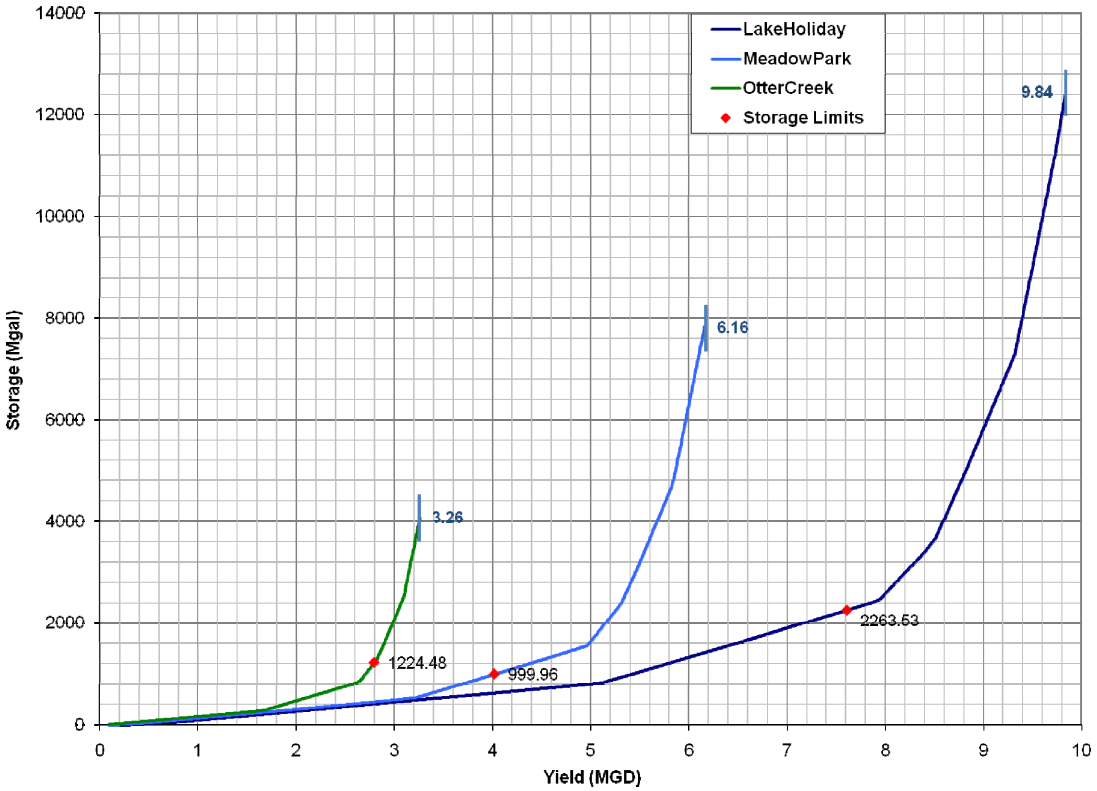

Figure 4. Storage-Yield Curves for the three Cumberland County reservoirs

The total inflow also controls the overall size of the curve, which is clearly demonstrated by the three curves. While the firm yield estimates of 2.80, 4.02, and 7.61 MGD for Otter Creek Lake, Meadow Park Lake, and Lake Holiday, respectively, could have been simply delivered to the stakeholders, the Storage-Yield curves are a much more valuable tool. It would be yet more valuable, however, to relate the storage yield relationships to the drought analysis already completed.

4. Relating Drought Analysis to Firm Yield

When the daily sequent peak algorithm is run at the firm yield, the critical drought length can be computed relatively easily by plotting the cumulative deficit versus time. The length of the critical drought sequence is simply the time difference between the maximum deficit and the last time the cumulative deficit was zero. Figure 4 displays a short sequence of the sequent peak algorithm's cumulative deficit values for Meadow Park, and contains the critical drought sequence. It is relatively easy to calculate the critical drought length as 19 months. Suppose, however, that the storage volume was calculated incorrectly, or a stakeholder wants to know which drought will lead to a maximum deficit at a current yield level. Instead of replotting Figure 4, plotting cumulative deficit at multiple yields simultaneously can answer these question and explain much more about the reservoir's behavior.

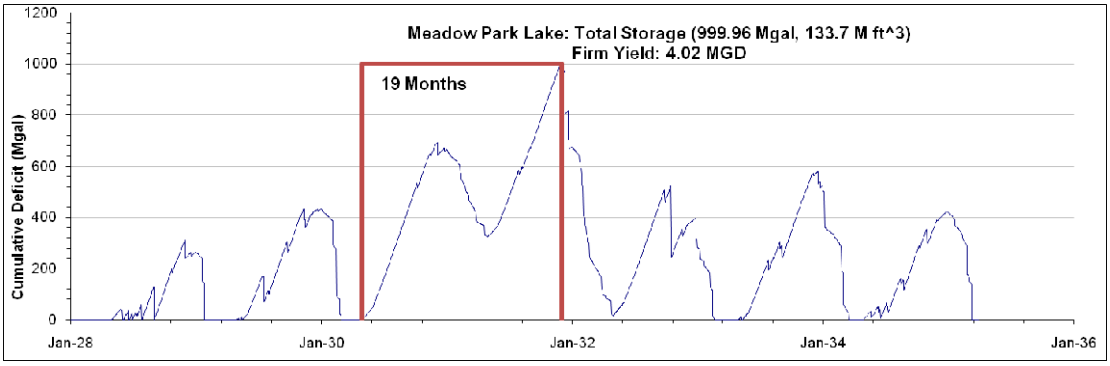

Figure 5. Cumulative Deficit plot showing critical drought sequence of Meadow Park Lake

Figure A2 in the Appendix plots the cumulative deficit at multiple yields as surface plot with yields across the x-axis and time down the y-axis. To normalize the plot, the cumulative deficit is plotted as the percentage of the maximum deficit for the given yield. Additionally, the monthly maximum series of cumulative deficit is plotted instead of the daily series to smooth the plot. Since the peaks of the cumulative deficit plot are of the greatest concern, cumulative deficits less than 68% of the maximum deficit are not plotted. The peaks are plotted in orange, red, with the absolute maxima shown in black. Figure A2 shows quite clearly that the 1930-1931 drought is clearly the critical one for a range of yields from 3 MGD to over 4.75 MGD. The 1952-1953 drought, however, is the most critical when yield is between 2 and 3 MGD. At 5 MGD and beyond, the peaks begin blending together and the maximum moves steadily later in time. This is a fairly clear indication that the critical drought sequence is lengthening significantly. Increasing yield further simply moves the peak later as the refill amounts aren't enough to bring the deficit down to zero. After a break in the plot, the 2007 drought is shown at the bottom. The red coloration indicates a clear peak, but with no black, 2007 does not show evidence of being the critical drought.

Placing the cumulative deficit plot next to the multiple duration SPI plot, some very interesting parallels emerge. Consider the firm yield of 4.02 on the cumulative deficit plot. A green arrow drops down to find the maximum deficit occurs during the 1930-1931 drought. A second arrow crosses over to the SPI plot to locate a wide patch of dark red, indicating a severe drought period. Two green arrows extend upward from the edges of this patch to cross the duration axis at 15 and 24 months. Logically, this would seem to indicate that 15 to 24 months is a good estimate for the length of the critical drought sequence. Not surprisingly, Figure 4 showed that the actual length is 19 months. If the firm yield were instead 2.5 MGD, a similar method shows the critical drought length of the 1952-1953 as 3 to 9 months. At the higher yields, the SPI plot is not wide enough to perform the same procedure.

5. Conclusion

Computing the firm yield of a small reservoir is often difficult because they often lack the long records that larger reservoirs have, and are nearly always located on ungaged streams. Cumberland County is a perfect example of a community that

depends on small reservoirs, and due to population pressures and recent drought experience needs a better understanding of it reservoirs.

This study falls back on standard hydrologic methods to study the behavior of Cumberland County's reservoirs. Drought identification is performed using the Standardized Precipitation Index. Lacking a long, high quality streamflow record, we used a very common rainfall-runoff model (HEC-HMS) to generate a synthetic streamflow sequence using rainfall as an input. Nearby evaporation, soil survey, and baseflow data were used to parameterize the model. Once the streamflow sequence is generated, the well-known sequent peak algorithm is used to complete the analysis. These methods can generate reasonable approximation of the reservoirs' behavior relatively quickly and within a modest budget.

By carefully considering the presentation of results, however, a great deal more information about the reservoirs can be given to the stakeholders. The (100% reliability) Storage-Yield relationships provide a very useful tool for reservoir management and can make up for uncertainty about the available storage in the reservoir. The multiple duration SPI plot was found to be a tremendously useful communication tool for showing how droughts evolve over time. The multiple yield cumulative deficit plot was found to be useful in showing when the critical drought sequence occurs at any yield. When the two are placed next to each other, we discovered a quick and convenient method of estimating critical drought length. All of these items can be created with minimal additional computation, but the value added for the client and stakeholders in comprehending reservoir behavior is considerable.

Acknowledgements

Walter Green, Ben Rohrbach, Parvathi Gaddipatti, (USACE- Nashville District);
City of Crossville; Crab Orchard Utility District; West Cumberland Utility District;
South Cumberland Utility District;
Lyle Bentley, Tennessee Dept. of Environment and Conservation-Safe Dams Section;
James LaRosa, National Weather Service

References

McKee, T.B.; N.J. Doesken; and J. Kleist. 1993. The relationship of drought frequency and duration to time scales. Preprints, 8th Conference on Applied Climatology, pp. 179–184. January 17–22, Anaheim, California.

Ries, K.G., 2006, The National Streamflow Statistics Program, Version 3: A Computer Program for Estimating Streamflow Statistics for Ungaged Sites: U.S. Geological Survey Techniques and methods Report TM 4-A6, 42 p.

Rippl, W., 1883. The capacity of storage-reservoirs for water-supply. Minutes Proc. Inst. Civ. Eng., 71: 270-278.

Thomas Jr., H.A. and Burden, R.P., 1963. Operations Research in Water Quality Management. Harv. Water Resource. Group, Cambridge, Mass., pp. 1-17.

Appendix A. Time series surface plots of climate and reservoir behavior

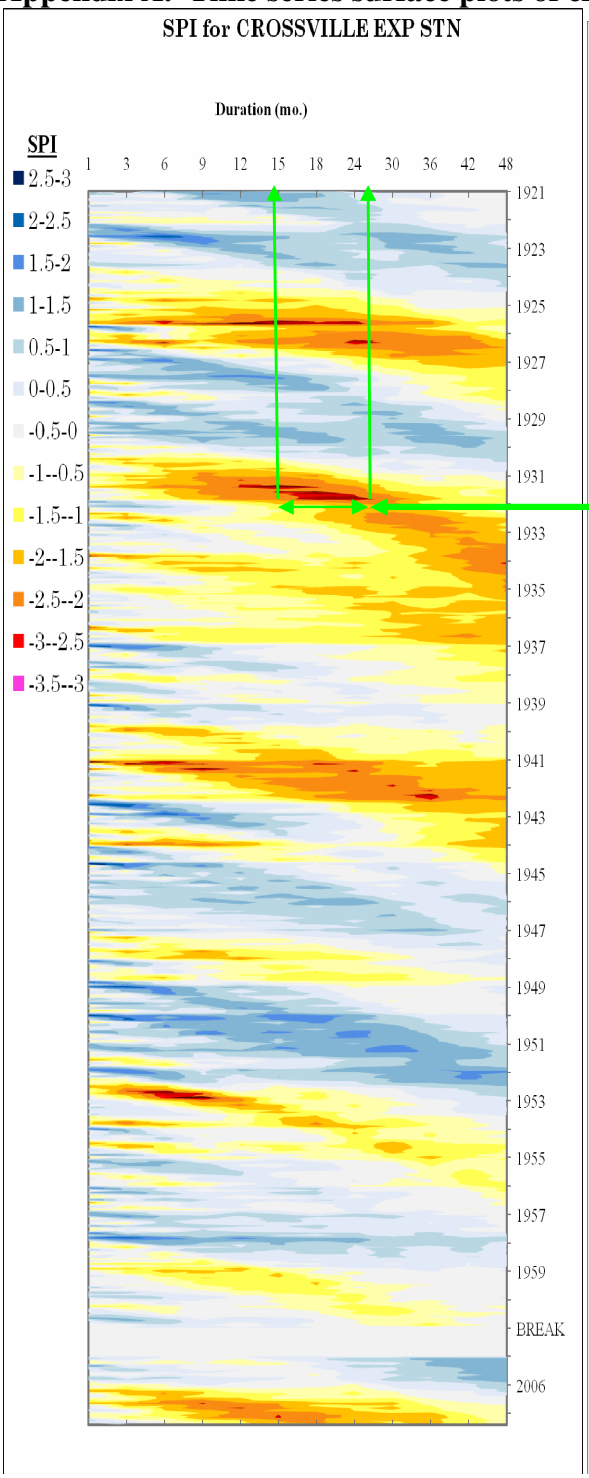

Figure A1. Surface plot of SPI index values over time at several analysis durations (1-48 months). Especially wet periods are shown by dark blue and extreme droughts are depicted in red and fuschia.

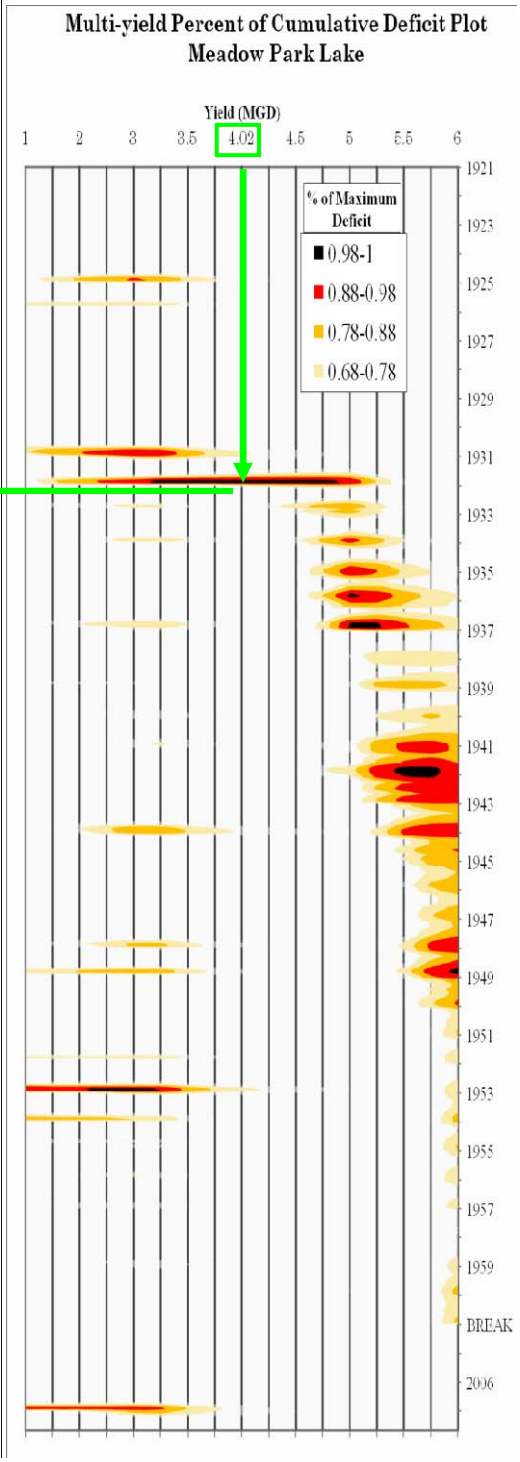

Figure A2. Surface plot of monthly maximum cumulative deficit over time at several yield values for Meadow Park Lake. Deficit is expressed as % of maximum for the given yield. Max deficits shown in black.

Computer Aided System for Managing, Controlling and Analyzing Data from Hydroelectric Plants

Ieda G. Hidalgo[1], Darrell G. Fontane[2], Secundino Soares Filho[3] and Marcelo Augusto Cicogna[4]

[1] Ph.D. Candidate, Department of Electrical and Computer Engineering, State University of Campinas (UNICAMP) – Brazil and Department of Civil and Environment Engineering, Colorado State University (CSU) – EUA; email: iedahidalgo@gmail.com
[2] Professor, Department of Civil and Environment Engineering, Colorado State University (CSU) – EUA; email: fontane@engr.colostate.edu
[3] Professor, Department of Electrical and Computer Engineering, State University of Campinas (UNICAMP) – Brazil; email: dino@cose.fee.unicamp.br
[4] Ph.D. Electrical Engineering, Anhanguera Educacional (AESA) – Brazil; email: marcelocicogna@gmail.com

ABSTRACT

This paper presents a computer aided system for managing, controlling and analyzing data from hydroelectric plants. The proposed system consists of three modules. The first is a relational database that organizes, standardizes and manages data from hydroelectric plants. The second module allows a user to build, store and manage advanced queries on this or certain other databases. The third is a simulator of the hydroelectric plants operation which can be used for planning the future operation or reproducing the past operation. The computational implementation of these modules uses the Object-Oriented Paradigm, the C++ Programming Language and the Structured Query Language *(SQL)***.** The data manager, the queries builder and the simulator were tested with data from Brazilian hydroelectric plants and the results show the potential of this system for the analysis and consistency evaluation of data from hydroelectric plants.

INTRODUCTION

The hydroelectric operation planning of a plant involves the manipulation of the static and dynamic data recorded by the plant. Static data are those that do not vary with the operation, while dynamic data depend on the operation interval and can be measured or calculated. The quality of these data has great importance to the operation planning because they supply the mathematical models of the computational tools developed for optimization, simulation and streamflow forecasting.

However, all measurements are prone to errors that can be either systematic or random. Systematic errors are caused by imperfect calibration of measurement instruments, imperfect methods of observation, or changes in the environment which

interfere with the measurement process. Sources of random errors may be unpredictable fluctuations in the readings of a measurement apparatus, or in the experimenter's interpretation of the instrument's reading (Lind et al. 2006).

The objective of the system presented in this paper is to aid, in different ways, the managing, controlling and analyzing data from hydroelectric plants. It consists of three modules: a data manager, a queries builder and a simulator of the hydroelectric plants operation. This paper is organized as follows: the first section presents the Brazilian model for hydroelectric operation planning; the second describes the three modules that make up the system presented and the third shows some case studies to assess the performance of the system.

BRAZILIAN MODEL FOR HYDROELECTRIC OPERATION PLANNING

The most common formulations of the Brazilian system for hydroelectric operation planning include: the production function and the water balance equation (Barros et al. 2003; Vinhal 1998; Pereira and Pinto 1985).

Production Function

The goal of the production function, Eq. (1), is to quantify the power generation of a hydroelectric plant.

$$p = k.\eta_t.\eta_g.[h_{fb}(x) - h_{tr}(u) - h_{pl}].q \qquad (1)$$

where:

- p Is the instantaneous power obtained in the conversion process of the hydraulic potential energy to electric energy (MW).
- k Is the gravity constant, multiplied by the water specific weight and divided by 10^6. Its value is 0.00981 (MW/(m³/s)/m).
- η_t . η_g Is the efficiency of the turbine-generator set in the conversion process of the mechanical energy to electrical energy.
- x Is the water storage in the reservoir of the plant (hm³).
- $h_{fb}(x)$ Is the forebay elevation which is function of the water storage x (m).
- u Is the water release of the plant, that is, the sum of the water discharge and the water spillage (m³/s).
- $h_{tr}(u)$ Is the tailrace elevation which is function of the water release u (m).
- h_{pl} Is the penstock head loss which is function of the water discharge (m).
- q Is the water discharge by the turbines of the powerhouse (m³/s).

Water Balance Equation

The water balance equation, Eq. (2), is used to calculate the water mass conservation balance of the reservoir.

$$x = x_0 + \left(y + \sum_{j \in \Omega} u_j - (q + s + ev + uc) \right) \frac{\Delta t}{10^6} \qquad (2)$$

where:

- x_0 Is the reservoir volume at the beginning of period t (hm³).

y Is the incremental water inflow during the period t (m^3/s).
Ω Is the upstream plants index set from the analyzed plant.
s Is the water spillage during the period t (m^3/s).
ev Is the reservoir evaporation during the period t (m^3/s).
uc Is the reservoir water advisory use during the period t (m^3/s).
Δt Is the size of the period t (s).

In order to aid the calculation of the parameters involved in the equations presented above are used eight static functions: polynomial area x level, polynomial level x volume, polynomial level x release, function maximum power, function maximum water discharge, function turbine-generator efficiency and function penstock head loss (Arce et al. 2002).

MODULES THAT MAKE UP THE SYSTEM

The computer aided system for managing, controlling and analyzing data from hydroelectric plants consists of three modules: a data manager, a queries builder and a simulator of the operation. The software project and the computational implementation of these modules use the Object-Oriented Paradigm (Cicogna 1999; Horstmann 1997), the C++ Programming Language (Hollingworth et al. 2001; Josuttis 1999) and the Structured Query Language (SQL) (Elmasri and Navathe 2000; Bowman et al. 1996). However, the use of the tools does not require specific software knowledge by the user.

Data Manager

The data manager is used for the organization, standardization and management of data from hydroelectric plants. Its graphical resources allow a critical view of the quality of the information it contains. It is possible, for example, to graphically view the polynomials that relate: reservoir area x forebay level, forebay level x reservoir volume and tailrace level x water release. Additionally, the functions related to the plant's operational limits, such as maximum power and maximum water discharge can be graphically analyzed. In relation to turbine efficiency hill curve, it is possible to do cuts, either horizontally or vertically, across the three dimensions to create two-dimensional planes in order to assess the quality of the information. This module also has a calculator that allows a user to provide the plant's reservoir volume and water release and obtain its power, turbine-generator efficiency, spillage and forebay and tailrace levels. Finally, this module shows graphics and tables with the dynamic data of a hydroelectric plant (Cicogna 2003).

Queries Builder

The queries builder allows a user to build, store and manage advanced queries on databases from hydroelectric plants. It does not require knowledge of the SQL Language and the analyzed database structure. Its queries can be applied for all plants at one time; therefore, it facilitates keeping track of data for an entire

hydroelectric system. This module can also be used as a generator of reports and as a viewer of the database. It enables one to manipulate the data from the query's result using mathematical operations. For this, there is a specific button that sends the data to electronic spreadsheets, like Excel. This module has two other capabilities. One of them is the possibility of exporting queries from database to a text file and the other is the possibility of importing queries from a text file to the database of the module. That means that the queries managed by this application can be easily transported from one machine to another because, in general, text files are smaller than database files. In addition, the text files created by this module can be stored as backup or easily interchanged by the users (Hidalgo 2004).

Simulator of the Hydroelectric Plants Operation

The simulator of the hydroelectric plants operation can be used for planning the future operation or reproducing the past operation for a hydroelectric plant. It has two major modules. One module can represent in detail the active operational restrictions on medium and long term horizons. The other module can represent a large collection of restrictions related to operating conditions in short term horizons. The simulation process is based on Eq. (1) and Eq. (2). It was created for the computational representation of several operating rules for hydrothermal systems (Cicogna 2003). Among the set of available operating rules, this study uses a short term rule that allows simulating the reservoir operation from the initial volume, the trajectories of generation, water spillage and inflow. The choice of this operating policy is due to the fact that the forebay and tailrace levels, the electric generation and the water spillage in a plant are measured variables. Water inflow is calculated based on the polynomial level *x* volume (Cicogna et al. 2009).

CASE STUDIES

In this section the data manager, the queries builder and the simulator will be used as tools for controlling of the data which have major influence on the hydroelectric operation planning. A detailed analysis of the production function, Eq. (1), and the water balance equation, Eq. (2), shows that there is a relationship of dependency between static and dynamic data. For example, the calculation that converts the forebay water level in storage volume uses the inverse function of the polynomial level *x* volume, which is static information. However, the data involved in the representation of storage, the level and the volume, are dynamic. In the same way, the function maximum water discharge is static; however the gross head and the water discharge related to this function are dynamic. It may be said that all the dynamic variables that are not measured depend on the static data to be calculated.

Thus, the computer aided system proposed in this paper will have as focus the managing, controlling and analyzing of the following static data: polynomial area *x* level, polynomial level *x* volume, polynomial level *x* release, function maximum power, function maximum water discharge and function turbine-generator efficiency. This system has been applied to more than 110 Brazilian hydroelectric plants. These plants are under the coordination of the Brazilian Electric System National Operator.

Polynomials area x level, level x volume and level x release

The analysis of the polynomials area *x* level, level *x* volume and level *x* release can be made using either the data manager or the queries builder.

Although the data manager has as main goal to organize and standardize the data from hydroelectric plants, the bulk of its graphical resources allows this module to also be used as a tool to evaluate data consistency. For example, the polynomial that describes forebay level *x* volume is expected to have a shape that looks like Fig. 1. However, if there is some simplification of this historical information, then the graph will be presented as in Fig. 2.

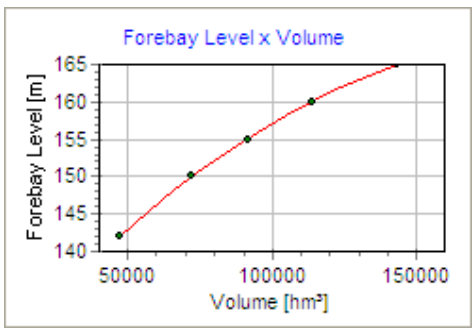

Fig. 1. Variable polynomial

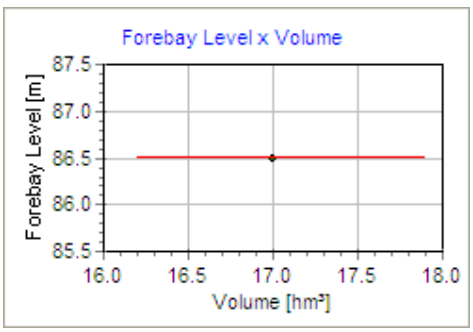

Fig. 2. Constant polynomial

If the objective is to analyze this information for all the plants at one time it is better to make use of the queries builder. Using the queries builder it is possible to list all the recorded plants which do not have a representation of the forebay level variation as a function of the water storage in the reservoir.

As an illustration, Fig. 3 shows the SQL command automatically built by the queries builder to this example query. This query lists the fields: cod, name and coef0 (rows 1, 2 and 3). These fields belong to tables "plant" and "polevo" (rows 4 and 5). The rows 6 and 7 relate the tables of this query. The filters of this query are: coef1, coef2, coef3 and coef4 equal to null because this mark a constant function (rows 8, 9, 10 and 11). These filters are connected by the conjunction operator "AND". The order to show the result of this query is ascending name (rows 12 and 13). Fig. 4 displays an example of result for the SQL command shown in Fig. 3.

```
1  SELECT
2    plant.cod, plant.name,
3    polevo.coef0
4  FROM
5    plant, polevo
6  WHERE
7    plant.cod = polevo.cod AND
8    polevo.coef1 is null AND
9    polevo.coef2 is null AND
10   polevo.coef3 is null AND
11   polevo.coef4 is null
12 ORDER BY
13   plant.name
```

Fig. 3. SQL command automatically built by the queries builder

Cod	Name	Coef0
59308182	Fontes Nova	415
60878070	Foz do Rio Claro	354
80310080	Henry Borden	728
66099001	Itiquira II	320
73500080	Monjolinho	328
64278080	Ourinhos	398
59309080	Pereira Passos	86
64219080	Pirajú	531
60878210	Salto	446
28544080	Santa Isabel	125
65925600	São João	692
75310100	São José	153

Fig. 4. Example of result for the SQL command of Fig. 3

Functions maximum power and maximum water discharge

The analysis of the functions maximum power and maximum water discharge can be made using the data manager and the queries builder at the same time. For example, in order to analyze the maximum power function, Fig. 5, the data manager is responsible for providing the graph of this function (broken line). The queries builder is responsible for retrieving from the database the gross head and the power output for a certain plant operation period (small circles). According to Fig. 5, this maximum power function is coherent with the post-operation data of the analyzed plant, that is, there is no value above the function limit.

The same comparison can be done for the maximum water discharge function, Fig. 6. Again, the data manager provides the graph of the function (broken line) and the queries builder provides the post-operation data (small circles). However, for this example, the post-operation data of the analyzed plant are not coherent with the function because some values exceeded its limit. It is necessary to check the measuring process of water discharge and the graph recorded in the database that relates maximum water discharge to gross head.

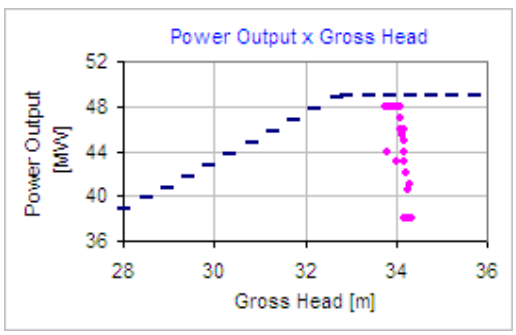

Fig. 5. Maximum power function *x* post-operation data

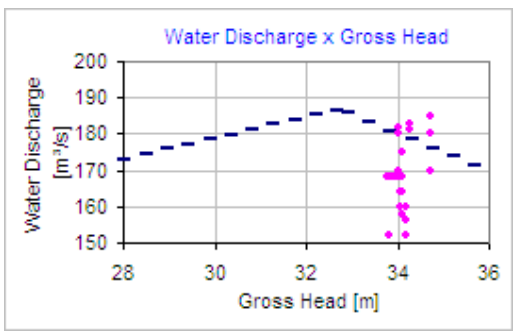

Fig. 6. Maximum water discharge function *x* post-operation data

Function turbine-generator efficiency

The function turbine-generator efficiency can also be graphically examined using the data manager or it can be numerically analyzed using the queries builder. Data manager shows it as a graph in three dimensions, as illustrated in Fig. 7. It is possible to do cuts across the three dimensions to create two-dimensional planes in order to assess the quality of the information. Fig. 8 illustrates a horizontal cut over an efficiency hill curve. It is easy to realize that this cut was done over a hill curve with data problems because the resulting line is not smooth.

Similar to what was done for the polynomials, using the queries builder it is possible to check all the recorded plants to see if there is some incoherence with respect to the efficiency of the turbine-generator sets, that is, if at some moment the value of efficiency of these sets was higher than 94%.

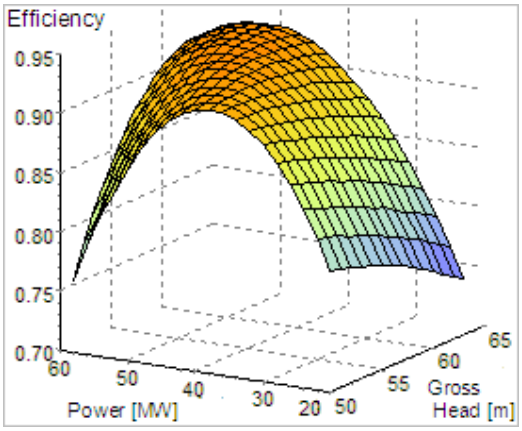

Fig. 7. Example of efficiency hill curve presented by data manager

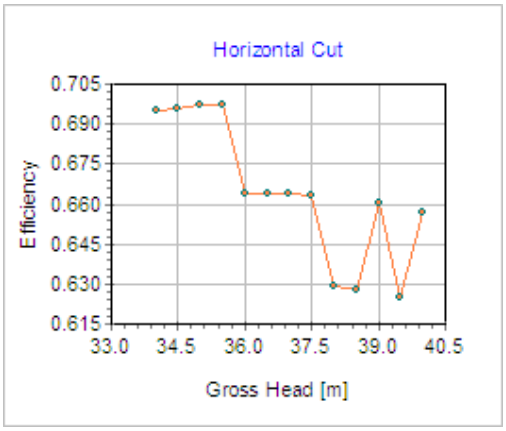

Fig. 8. Horizontal cut over a hill curve with problem

Analysis of data using the simulator

All the static data mentioned above can be analyzed together using the simulator of the hydroelectric plant operation. This simulator becomes a tool for analyzing of data when it is used for reproducing the past operation. If the simulated trajectories move away from verified trajectories, as illustrated in Fig. 9, means that the static data recorded by the plant are not coherent with the real operating.

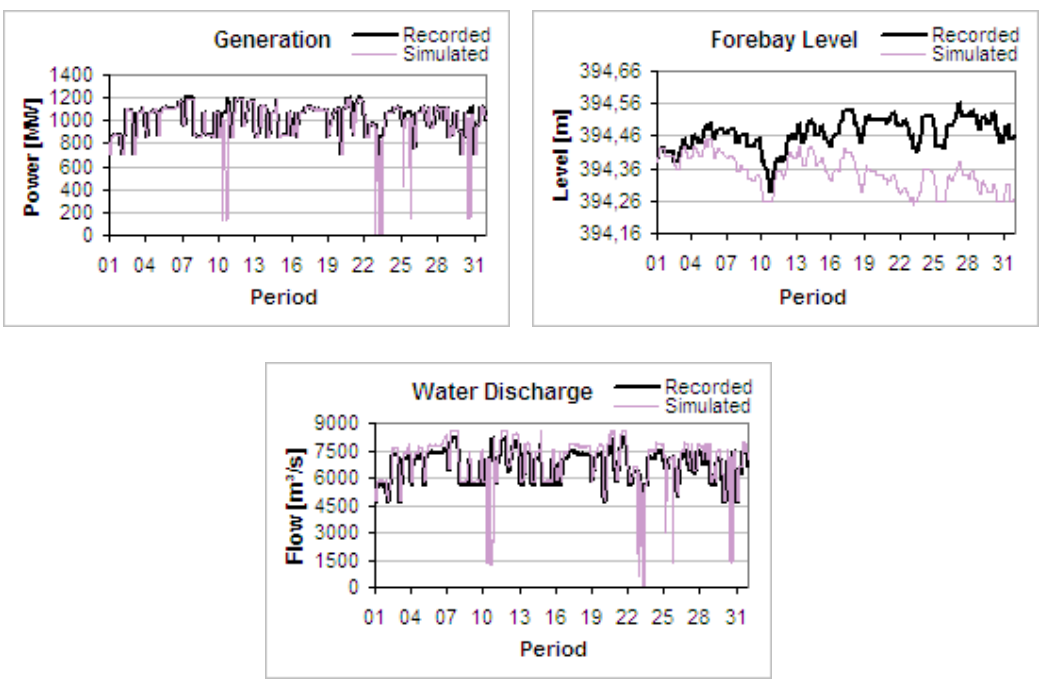

Fig. 9. Recorded data *x* simulated data with information not coherent with the plant's real operating

Otherwise, the proximity of the simulated and verified trajectories, shown in Fig. 10, indicates that the plant's static data are consistent with its operation.

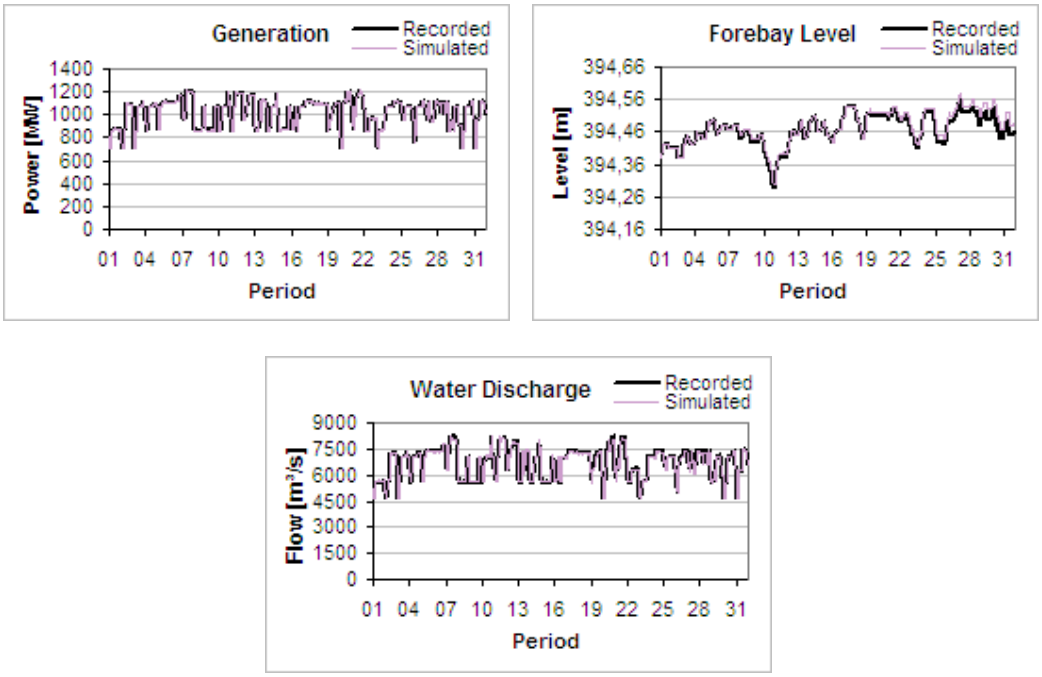

Fig. 10. Recorded data *x* simulated data with information consistent with the plant's real operating

CONCLUSIONS

Each of the modules that makes up the system presented in this paper has a specific objective. In summary, the data manager organizes information from hydroelectric plants, the queries builder extracts information from database and the simulator predicts the plant's operation under a given set of conditions. However, they all can be used as tool for managing, controlling and analyzing data. The data manager enables the graphic data analysis for a plant, the queries builder facilitates the numerical data analysis for a whole hydroelectric system and the simulator shows, at one time, the quality of the data involved in the operating planning when it is used for reproducing the plant's past operation.

Besides the applications mentioned in Case Studies section, the modules of the presented system allow others analyses. For example, the data manager can also be used for assessing the quality of the post-operation variables. The queries builder enables testing the limits of reservoir, tailrace, water discharge and spillage. The simulator is also capable of checking the water balance of the plants.

The computational models used by the energy sector for optimization, simulation and streamflow forecasting depend on data quality to provide reliable results. Therefore, the critical view of the quality of the information allowed by these modules can bring a significant improvement in terms of efficiency to the operational planning of electric power systems.

REFERENCES

Arce, A., Ohishi, T. and Soares, S. (2002). "Optimal dispatch of generating units of the Itaipu hydroelectric plant." J. IEEE *Transactions on Power Delivery*, 17(1).

Barros, M. T. L., Tsai, F. T-C., Yang,S-L, Lopes, J. E. G. and Yeh, W. W-G. (2003). "Optimization of large-scale hydropower system operations." *J. of Water Resources Planning and Management*, 129(3), 178-188.

Bowman, J. S., Emerson, S. L. and Darnovsky, M. (1996). "The practical SQL handbook – Using Structured Query Language." *Addison Wesley Professional*, MA, EUA.

Cicogna, M. A. (1999). "Model for energetic operation planning of hydrothermal systems using object oriented programming." MS thesis, State University of Campinas, SP, Brazil.

Cicogna, M. A. (2003). "Support decision system to short and long term planning of hydroelectric power system." Ph.D thesis, State University of Campinas, SP, Brazil.

Cicogna, M. A., Fontane D. G., Hidalgo, I. G and Lopes, J. E. G. (2009). "Multiple Reservoir Simulation Using Multi-Criterion Restrictions and Object-Oriented Software Design". Accepted for the *World Environmental & Water Resources Congress (ASCE-2009)*, Kansas City, Missouri, USA.

Hidalgo, I. G. (2004). "Search system for data analysis from hydroelectric plants." MS thesis, State University of Campinas, SP, Brazil.

Elmasri, R. and Navathe, S. (2000). "Fundamentals of database systems." *Addison Wesley Professional*, MA, EUA.

Horstmann, C. S. (1997). "Practical object-oriented development in C++ and Java." *John Wiley & Sons, Inc,* NY, EUA.

Hollingworth, J., Butterfield, D., Swart, B. and Allsop, J. (2001). "C++ Builder 5 developer's guide." *Sams Publishing*, EUA.

Josuttis, N. M. (1999). "The C++ standard library – A tutorial and reference." *Addison Wesley Professional*, MA, EUA.

Lind, D. A., Marchal, W. G. and Wathen, S. A. (2006). "Statistical techniques in business and economic." *McGraw-Hill College* , MA, EUA.

Pereira, M. V. F. and Pinto, L. M. V. G. (1985). "Stochastic optimization of a multireservoir hydroelectric system: a decomposition approach." *J. Water Resources Research*, 21(6), 779-792.

Vinhal, C. D. N. (1998). "Decision support system for energetic operation planning of electrical systems." PhD thesis, State University of Campinas, SP, Brazil.

Copula Approach for Reducing Uncertainty in Design Flood Estimates in Insufficient Data Situations

Hemant Chowdhary[1], Vijay P Singh[2]

[1] Graduate Research Assistant, Department of Civil and Environmental Engineering, Louisiana State University, Baton Rouge, LA 70803-6405; email: hchowd1@lsu.edu

[2] Caroline & William N. Lehrer Distinguished Chair in Water Engineering and Professor, Department of Biological and Agricultural Engineering, Texas A and M University, College Station, Texas 77843-2117; email: vsingh@tamu.edu

ABSTRACT

Sufficiently long period of data is required for making sound flood estimates corresponding to the design return periods. Such long-term and good quality flow data is often a difficult proposition, especially in developing and under-developed countries. Most watersheds in these countries that are of immediate interest and concern are either completely ungauged or are insufficiently gauged. Flood estimates in situations of inadequate length of data invariably involve large amounts of uncertainties. There is a growing interest in investigating if these uncertainties in flow estimates can be reduced by supplementing the limited flow data with that available at adjoining river gauging station(s) on the same river or that in the adjoining river basins. It is expected that additional information can be derived from the dependence among flow characteristics at these adjoining flow stations when they are considered together. The maximum likelihood procedure, with likelihood function involving univariate and joint probabilities corresponding to exclusive and concurrent periods of data availability, is employed for estimating parameters of flood frequency distributions. Copula-based bivariate distribution approach offers advantage over conventional functional forms by admitting arbitrary marginal types that are dictated by the nature of the flow regimes at these river stations under consideration. This paper presents a comparison of uncertainties in the estimated flood quantiles at a station with limited data, as obtained from the univariate consideration and that from the simultaneous consideration of additional flow data from a neighboring river gauging station. A significant reduction in uncertainty achieved by this approach indicates that substantial improvements in the accuracy of flood estimates can be made by multivariate consideration of flood frequency analysis that is facilitated by copula approach.

INTRODUCTION

Flood frequency analysis typically involves fitting univariate distributions to annual maximum (AM) flows or to peak over threshold (PoT) flows observed at a location of interest along a river. Commonly employed distributions include 2 and 3-parameter lognormal (LN and LN3), 2-paramter gamma (G2), Pearson type III (P3), log-Pearson type III (LP3), the extreme value type I (EV1) or largest extreme value

(LEV) or Gumbel, the generalized extreme value (GEV), and Wakeby distribution, among others. The main objective of various hydrological designs, e.g., for dam spillways, bridges, etc., is to estimate a flow that shall have an average inter-arrival period more than a specified design (return) period. Sufficiently long period of data is normally required for estimating design flood values with desirable narrower confidence widths. Availability of such long-term data is an exception in many cases, especially in developing and under-developed countries. Most watersheds in these countries that are of immediate interest and concern, owing to ever-increasing human activity and development, are either completely ungauged or are insufficiently gauged. Flood estimates in situations of inadequate length of data invariably involve large amounts of uncertainties. There is a growing interest in investigating if these uncertainties in flow estimates can be reduced by supplementing the limited data at a flow station with that available at adjoining river gauging station(s) on the same river or that in the adjoining river basins. Simultaneous consideration of data from two or more stations or variables that exhibit certain level of interdependence requires undertaking bivariate or multivariate frequency distribution analysis. A variety of bivariate distributions, such as bivariate normal, lognormal, exponential, or Gumbel (called mixed Gumbel) distributions have been traditionally applied for hydrological variables such as flood peaks, and associated flood volume and duration. These distributions are generally limited to having same type of marginals. A newer approach in multivariate frequency analysis, called copula approach, facilitates admittance of arbitrary marginals in the distributional forms and thus provide tremendous flexibility. This study demonstrates achieving substantial reduction in uncertainty of the parameter estimates and consequently of the design flood estimates at a station, by way of augmenting it with data at a neighboring station and including a copula-based bivariate distribution in the likelihood function.

Several studies in the past, even as early as 1950s, aimed at utilizing inter-station dependence or inter-variable dependence for augmenting limited data available at a station. Most of these studies assumed the involved random variables to be jointly normally distributed. Anderson (1957) presented maximum likelihood estimates of bivariate normal distribution when some data for one of the variables were missing. It involved linearly regressing the missing data with the help of additional data of the other variable. This note also listed similar contributions by Lord (1955) and Edgett (1956) that handled trivariate normally distributed variables, with a different arrangement of the missing data. Fiering (1960) extended these works by introducing the random errors about the simple and multiple linear regressed flow values. The paper also presented exact and asymptotic maximum likelihood formulations for relative information corresponding to small and large samples, based on results obtained by other researchers (Cochran, W.G. and Thomas, H.A. Jr.) cited therein. It was concluded that for most cases of large sample sizes and adequate correlation there is a gain in information with respect to mean and variance estimates. However, for very small sample sizes and/or having very small correlation, there sometimes can be loss of information and in such cases univariate consideration with short data record is better than bivariate or trivariate analysis. Graphical results were given and tabular results cited in this study in order to know if a certain combination of correlation and length of short and long records will result in improvement in

relative information. Matalas and Jacobs (1964) concluded that for the two cases when the noise component to the regressed estimates is added or not added a minimum correlation coefficient of 0.5 and 0.85, respectively, is required for reducing uncertainty in mean and variance estimation.

Extending investigation of reduction in uncertainty of parameter estimates to non-Gaussian distributions, Clarke (1980) considered augmenting shorter annual flood records with longer precipitation records that were assumed to be bivariate Gamma distributed. A significant gain in information by way of employing bivariate over univariate distribution was reported. Reuda (1981) worked with the cases of bivariate normal distribution as well as two forms of bivariate extreme value Gumbel distributions. This study concluded that the information gain for the parameter estimates of the shorter series depends upon the ratio of sizes of longer series and the concurrent data period, for both normal and Gumbel distribution types. This gain was not found for the bivariate normal case when the size of the concurrent period was very small (i.e., when the ratio was close to unity) or when there was very low correlation. Another important result was that whereas for the bivariate normal case there was no information gain for the estimated parameters of the longer series there was such significant gain in the two cases of bivariate Gumbel distributions. It was also inferred that the information gain for the two Gumbel distributions was larger for higher correlation between the two series. Furthermore, for the shorter series it was higher when the abovementioned ratio was larger whereas for longer series it was higher when the ratio was closer to unity. The applicability of the asymptotic formulations in the above cases was also confirmed for small sample size of 10 on the basis of simulation studies. It was conjectured that further information gain may be possible by multivariate considerations as compared to bivariate cases and also recommended similar studies with other distributions, involving for instance the gamma and the log-Pearson III distributions. Raynal (1985) also employed three types of bivariate extreme value distributions and found that there was reduction of uncertainty in the flood estimates even when the sample sizes of the marginals were equal.

Escalante and Raynal (1998) employed trivariate distributions, with extreme value Type I (Gumbel) marginals, to regional flood frequency analysis in a region of Mexico, in order to investigate if there was reduction in uncertainty of estimated parameters. The conclusions made were similar to those by Rueda (1981), with respect to gain in information for shorter and longer series. It was also reported that the gain of information was more for quantile estimates of larger return periods. The study also confirmed appropriateness of maximum likelihood based asymptotic estimates for small sample sizes of 20 by conducting simulation analysis. Similar conclusions of uncertainty reduction were drawn by Escalante (2007) and Escalante and Raynal (2008) with respect to the use of bivariate Weibull, and mixed Weibull and trivariate general extreme value (GEV) distributions respectively. Comparisons of standard error of fit (SEF) and mean absolute relative deviations (MARD) was made by Raynal and Salas (2008) for two pairs of flood data series with unequal sizes and employing univariate and bivariate forms of general extreme value distribution. Univariate procedure was found to be better in one case whereas obtaining parameter estimates by bivariate consideration was better in the second case.

In all of the above studies the involved bivariate or multivariate distributions had the same type of marginals, such as normal or extreme value type I (Gumbel) or general extreme value or Weibull or mixed Weibull. Intuitively, the choice of marginal must be dictated by the type of distribution that best represents the data under consideration. And in many cases the multivariate data may involve different types of marginal distributions to be best suiting the data. The conventional bivariate or multivariate distribution forms do not admit arbitrary marginals. In such cases where arbitrary marginals are desired to be included in the multivariate distributions, copula-based formulations have distinct advantage and may offer many possibilities. This paper employs a copula-based bivariate distribution that involves largest extreme value (LEV) and log-Pearson Type III (LP3) as marginals and shows that the estimated quantiles for the shorter series have lesser uncertainty as compared to when they are obtained on a purely univariate basis.

COPULA-BASED DISTRIBUTION FOR CASES OF INCOMPLETE DATA

Copula is a simple concept wherein bivariate or multivariate probabilities are expressed in terms of marginal probabilities and more advantageously in terms of uniform marginals. This theory has been in vogue for some time, especially with respect to actuarial science and finance applications. In recent years, this approach has also made an impressive beginning in the field of hydrological engineering. Several illustrative and review studies, such as Favre et al. (2004), Salvadori and De Michele (2004), De Michele et al. (2005), Genest and Favre (2007), Poulin et al. (2007), Salvadori and De Michele (2007), Serinaldi and Grimaldi (2007), Zhang and Singh (2007) provide elaborate discussion on copula applications related to flow variables and explain its advantages and limitations. There are several other studies that have also been reported recently covering applications related to rainfall variables. In simple terms the copula-based joint distribution function for any random variable (X,Y) may be written as

$$F(x,y) = C[F_X(x), F_Y(y)], \qquad x,y \in R$$

where $F_X(x)$ and $F_Y(y)$ are marginal probability distributions and $C:[0,1]\times[0,1]\rightarrow[0,1]$, a mapping function, is the "copula". In turn, it means that a valid model for (X,Y) is obtained whenever the three constituents (C, F_X, and F_Y) are chosen from given parametric families, viz.

$$F_X(x;\boldsymbol{\delta}), \quad F_Y(y;\boldsymbol{\eta}), \quad C(u,v;\boldsymbol{\theta})$$

where $\boldsymbol{\delta}$ and $\boldsymbol{\eta}$ are the parameter vectors of marginal distributions and $\boldsymbol{\theta}$ is the parameter vector for the dependence structure. u and v are the quantiles of the uniformly distributed variables $U = F_X(X)$ and $V = F_Y(Y)$ respectively.

Several classes and families of copulas, such as the meta-elliptic copulas, extreme value copulas, and Archimedean copula, exist. Of the several families that exist, the one that has been frequently applied in the field of hydrology is the Archimedean family. This copula family has the following form

$$\phi[F(x,y)] = \phi\{C[F_X(x), F_Y(y)]\} = \phi[F_X(x)] + \phi[F_Y(y)]$$

where ϕ, a continuous and strictly decreasing function, from $I\,[0,1]\rightarrow[0,\infty]$ and $\phi(1)=0$, is called a generating function. The joint probability function can then be written as

$$\begin{aligned} F_{X,Y}(x,y) &= C\left[F_X(x),F_Y(y)\right] = \phi^{[-1]}\left\{\phi\left[F_X(x)\right]+\phi\left[F_Y(y)\right]\right\} \\ &= C(u,v) = \phi^{[-1]}\left\{\phi(u)+\phi(v)\right\} \end{aligned} \tag{1}$$

Parameter θ is hidden in the generating function. For example, the generating function of the Gumbel-Hougaard copula family involves θ in the form

$$\phi(t)=(-\ln t)^{\theta}\ , \quad \theta\in[1,\infty)$$

Employing the above generating function and the form of Archimedean copulas given in Eq. (4), the bivariate cumulative probability distribution is obtained as

$$\begin{aligned} F_{X,Y}(x,y) &= \exp\left\langle-\left\{\left[-\ln F_X(x)\right]^{\theta}+\left[-\ln F_Y(y)\right]^{\theta}\right\}^{1/\theta}\right\rangle \\ &= \exp\left\{-\left[(-\ln u)^{\theta}+(-\ln v)^{\theta}\right]^{1/\theta}\right\} \\ &= \exp\left[-\left(\tilde{u}^{\theta}+\tilde{v}^{\theta}\right)^{1/\theta}\right] = C(u,v) \end{aligned}$$

where $\tilde{u}=-\ln u=-\ln F_X(\mathrm{x})$ and $\tilde{v}=-\ln v=-\ln F_Y(\mathrm{y})$. Here, $C(u,v)$ is called the copula probability. Double differentiating the above bivariate probability function results in the joint density function as

$$\begin{aligned} f_{X,Y}(x,y) &= f_X(x)f_Y(y)\left\{\frac{1}{uv}\frac{(\tilde{u}\,\tilde{v})^{\theta-1}\left[\left(\tilde{u}^{\theta}+\tilde{v}^{\theta}\right)^{1/\theta}+\theta-1\right]}{\left(\tilde{u}^{\theta}+\tilde{v}^{\theta}\right)^{\left(2-\frac{1}{\theta}\right)}}C(u,v)\right\} \\ &= f_X(x)f_Y(y)\ c_{\theta}(u,v) \end{aligned} \tag{2}$$

where $f_X(x)$ and $f_Y(y)$ are the marginal probability densities and $c_{\theta}(u,v)$ is the copula density. Chowdhary and Singh (2008) lists expressions for probabilities of few more commonly used copula families and their corresponding parameter space and generating functions.

The present study considers a bivariate data set (X,Y) having some concurrent period and some individual data series availability as depicted in Figure 1. Here, N_X and N_Y are respectively the total number of data in the two data series individually. Of these lengths, the concurrent period has n_{XY} elements. Similarly, n_X and n_Y are respectively the number of elements when series X or Y is exclusively available. Presence of these exclusive and concurrent periods of data lengths n_X, n_Y and n_{XY} is expressed by the indicator variables I_X, I_Y and I_{XY}. A value of 1 or 0 is assigned to these indicator variables as per the presence or absence of the corresponding part of the two series. The maximum likelihood parameter estimates of a univariate flood frequency distribution, say of series Y, are conventionally obtained using the likelihood or log-likelihood functions as

$$L_U = \prod_{1}^{N_Y} f_Y(y) \text{ or } LL_U = \sum_{1}^{N_Y} \log f_Y(y) \quad (3)$$

The objective of the study here is to know if, in order improve the accuracy of parameter estimates as obtained from the above likelihood function, is it advantageous to consider a composite likelihood function L_C of the form

$$L_C = \left[\prod_{1}^{n_X} f_X(x)\right]^{I_X} \left[\prod_{1}^{n_{XY}} f_{X,Y}(x,y)\right]^{I_{XY}} \left[\prod_{1}^{n_Y} f_Y(y)\right]^{I_Y}$$

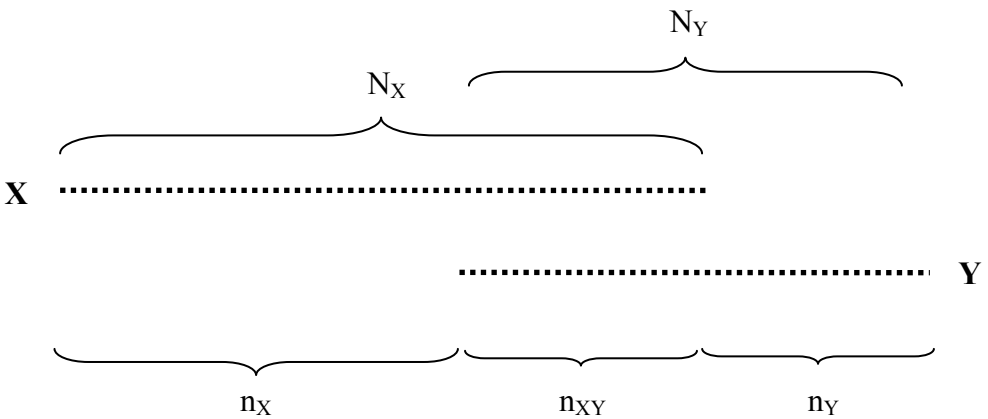

Figure 1 Arrangement of occurrence of series X and Y.

The above composite likelihood function incorporate both, the bivariate nature of the process (X,Y) and the exclusive occurrences of X or Y in the remaining periods. The univariate densities for the exclusive periods are given by the marginal densities $f_X(x)$ and $f_Y(y)$. And the choice of these distributions is dictated by the nature of the two processes. The bivariate probability density $f_{X,Y}(x,y)$ is based on copula-based distribution function, e.g., the one given in Eq. (2), allowing arbitrary marginals to be considered as per the nature of the individual processes. The simpler composite log-likelihood function LL_C can be expressed as

$$LL_C = I_X\left(\sum_{1}^{n_X} f_X(x)\right) + I_{XY}\left(\sum_{1}^{n_{XY}} f_{X,Y}(x,y)\right) + I_Y\left(\sum_{1}^{n_Y} f_Y(y)\right) \quad (4)$$

As is apparent from the above composite log-likelihood function, if any one or both of the exclusive period lengths n_X and n_Y are non-existent then the value of the indicator variables I_X and I_Y will correspondingly take a value of 0. In that case such part(s) will not be present in the above likelihood function. It may also be noted here that there is no requirement for the individual or concurrent portions of the data series to be contiguous. In other words, there can be any number of gaps at arbitrary points of time within the exclusive or the concurrent portions. Furthermore, the exclusive periods of the two series may lie on one or both sides of the concurrent period, unlike on only one side as schematized in Figure 1.

PARAMETER AND UNCERTAINTY ESTIMATION

The maximum likelihood approach is considered for obtaining parameter estimates based on the composite log-likelihood function (LL_C) given in Eq. (4). A numerical solution for maximizing the log-likelihood function will be sought, as obtaining and solving the score equations would be a formidable task when likelihood function includes mathematically involved function such as $f_{X,Y}(x,y)$ given in Eq. (2). The numerical solution is obtained by employing "BFGS" method, published simultaneously by Broyden, Fletcher, Goldfarb and Shannon (Goldfarb, 1970). In cases when this method results a local minima, the simulated annealing algorithm (Belisle, 1992) is used instead.

The reduction in uncertainty of quantile estimates is reflective of reduction in uncertainty of parameter estimates. The standard errors of the quantile estimates would be compared for the two cases, when distribution parameters are obtained: (a) on the basis of the composite likelihood function LL_C given in Eq. (4), and (b) on a purely univariate basis, i.e., using likelihood function LL_U given in Eq. (3). Letting $\boldsymbol{\psi} = \{\boldsymbol{\delta}, \boldsymbol{\eta}, \boldsymbol{\theta}\}$ imply a combined vector of the three parameter vectors $\boldsymbol{\delta}$, $\boldsymbol{\eta}$ and $\boldsymbol{\theta}$ defined earlier. The variance of the quantile estimate, based on parameters that are estimated by composite likelihood (LL_C) approach, using the Cramer-Rao lower bound limit for large samples, is given as

$$\mathrm{Var}\left[q_{CY}(\boldsymbol{\eta}|T)\right] \approx -\left(\frac{\partial q_{CY}}{\partial \boldsymbol{\eta}}\right)' \left[\frac{\partial^2 LL_C(\boldsymbol{\psi}|\mathbf{x},\mathbf{y})}{\partial \boldsymbol{\psi}\,\partial \boldsymbol{\psi}'}\right]^{-1} \left(\frac{\partial q_{CY}}{\partial \boldsymbol{\eta}}\right)$$

where $q_{CY}(\boldsymbol{\eta}|T) \Rightarrow$ the quantile function for the series Y, for a given value of return period T. The derivatives of q_{CY} and the information matrix are evaluated at the estimated values of parameters, say $\hat{\boldsymbol{\psi}}_C$, and the standard error is thereby given as

$$\mathrm{S.E.}(q_{CY}) = \sqrt{\mathrm{Var}\left[q_{CY}(\boldsymbol{\eta}|T)\right]}\,@\,\hat{\boldsymbol{\psi}}_C$$

Similar procedure is followed for obtaining the uncertainty estimates of quantile estimates obtained for the case when distribution parameters are obtained purely on univariate basis as

$$\mathrm{S.E.}(q_{UY}) = \sqrt{\mathrm{Var}\left[q_{UY}(\boldsymbol{\eta}|T)\right]} \approx \sqrt{-\left(\frac{\partial q_{UY}}{\partial \boldsymbol{\eta}}\right)' \left[\frac{\partial^2 LL_U(\boldsymbol{\eta}|\mathbf{y})}{\partial \boldsymbol{\eta}\,\partial \boldsymbol{\eta}'}\right]^{-1} \left(\frac{\partial q_{UY}}{\partial \boldsymbol{\eta}}\right)}\,@\,\hat{\boldsymbol{\eta}}_U$$

where $\hat{\boldsymbol{\eta}}_U \Rightarrow$ the vector of parameters estimated purely on the basis of univariate likelihood given in Eq. (3). It may be noted that the functional form of the quantile and its gradient in the above two equations are essentially the same. These are subscripted differently only to indicate that they are evaluated at different sets of parameters obtained from two approaches.

APPLICATION

An application is presented here with the objective of investigating if indeed there is some reduction in uncertainty in parameter estimates when a neighboring flow data series, having some inter-dependence with the series under investigation, is simultaneously considered. Composite likelihood function, as outlined previously, combines the concurrent and exclusive periods of the two data series. A copula-based bivariate distribution function represents the concurrent period whereas the best distributions fitting the marginals are chosen to represent the exclusive parts of the two series. As copula-based probability density functions are expressed in terms of marginal densities, the parameters are estimated commonly for exclusive and concurrent parts of the two series.

Data Set

The Annual peak flows of Greenbrier River at Alderson (USGS station # 03183500) and Buckeye (USGS station # 03182500) stations in West Virginia State are obtained from USGS website. The Greenbrier River is a tributary of the New River in southeastern part of the state and is approximately 165 mi long. Through the New, Kanawha and Ohio Rivers, it is part of the Mississippi River watershed. River gauging station at Alderson is located at Latitude 37°43'27" and Longitude 80°38'30" and Buckeye at Latitude 38°11'09" and Longitude 80°07'51". These command drainage areas and contributing areas of 1,364 and 540 square miles respectively. The datum of the gages at the two stations is respectively at 1,529.42 and 2,085.69 feet above sea level. A length of 112 years of data for Alderson, from 1896 to 2007, and 78 years for Buckeye, from 1930 to 2007, is considered for this analysis. The bivariate scatter plot of time series of these two data sets, in 103 cusec, is given in Figure 2.

Potential Marginal Distributions

Several candidate distributions, such as 2 and 3-parameter lognormal (LN2 and LN3), 2-paramter gamma (G2), Pearson type III (P3), log-Pearson type III (LP3), largest extreme value (LEV), and Weibull are considered for fitting the annual peak flows of Alderson (series X) and Buckeye (series Y) stations on univariate basis. On the basis of Kolmogorov-Smirnov, Anderson Darling, and Chi-Squared fit statistics and overall fit of the Q-Q plots, LEV and LP3 distributions were taken to be better representing the flood peak distributions at the two stations, respectively. The overlay of density curves of these distributions and the corresponding histograms is shown in Figure 3. The probability and density functions for LEV (for X) and LP3 (for Y) are given as

$$F_X(x) = \Phi_{\text{LEV}}\left(\frac{x-\mu}{\sigma}\right) \quad \text{with} \quad \Phi_{\text{LEV}}(z) = \exp[-\exp(-z)]$$

$$f_X(x) = \frac{1}{\sigma}\phi_{\text{LEV}}\left(\frac{x-\mu}{\sigma}\right) \quad \text{with} \quad \phi_{\text{LEV}}(z) = \exp[-z-\exp(-z)]$$

$$f_Y(y) = \frac{1}{\alpha\, y\, \Gamma(\beta)} \left(\frac{\log(y) - \gamma}{\alpha} \right)^{\beta - 1} \exp\left[-\left(\frac{\log(y) - \gamma}{\alpha} \right) \right]$$

$$F_Y(y) = \frac{1}{\alpha\, \Gamma(\beta)} \int_{\gamma}^{y} \frac{1}{y} \left(\frac{\log(y) - \gamma}{\alpha} \right)^{\beta - 1} \exp\left[-\left(\frac{\log(y) - \gamma}{\alpha} \right) \right] dy$$

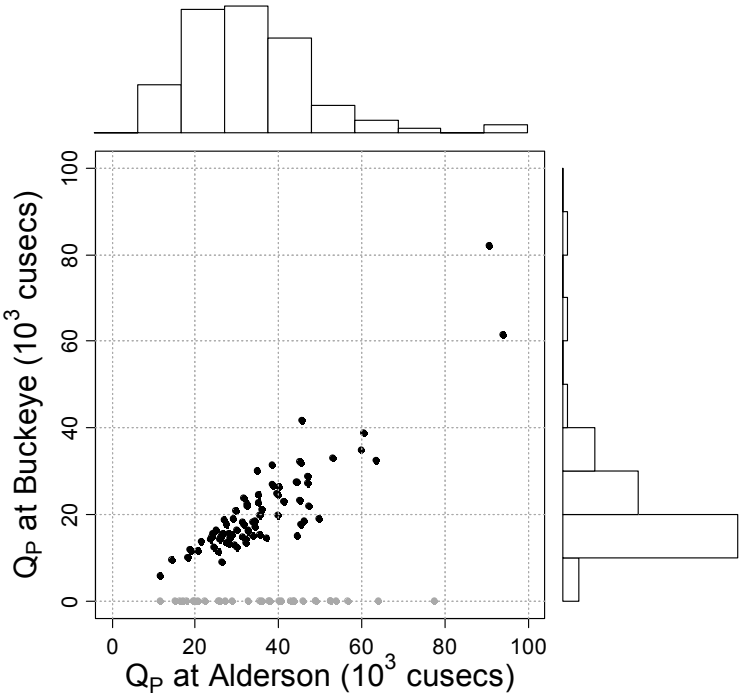

Figure 2 Scatter plot of peak flows at Alderson and Buckeye river gauging stations. Data from concurrent period are plotted in black whereas those from the exclusive period of Alderson are plotted on the x-axis in grey.

Comparison of Univariate and Composite Likelihood Approaches

The flow peak data series at Alderson is for a period of 112 years and that for Buckeye station is for 78 years. The last 78 years is the concurrent period between the two series. Normally, such data availability is considered more than adequate for making sound parameter estimates on the basis of purely univariate consideration. However, these two data series are used here for demonstrating if accuracy of parameter estimates for Buckeye station improves when data of Alderson station is also used and composite likelihood approach employed. Moreover, the effect of relative sizes of the two series is seen by artificially blanking out certain period of Buckeye station data. Six such cases are considered for which number of elements and values of indicator variables for both series are given in Table 1.

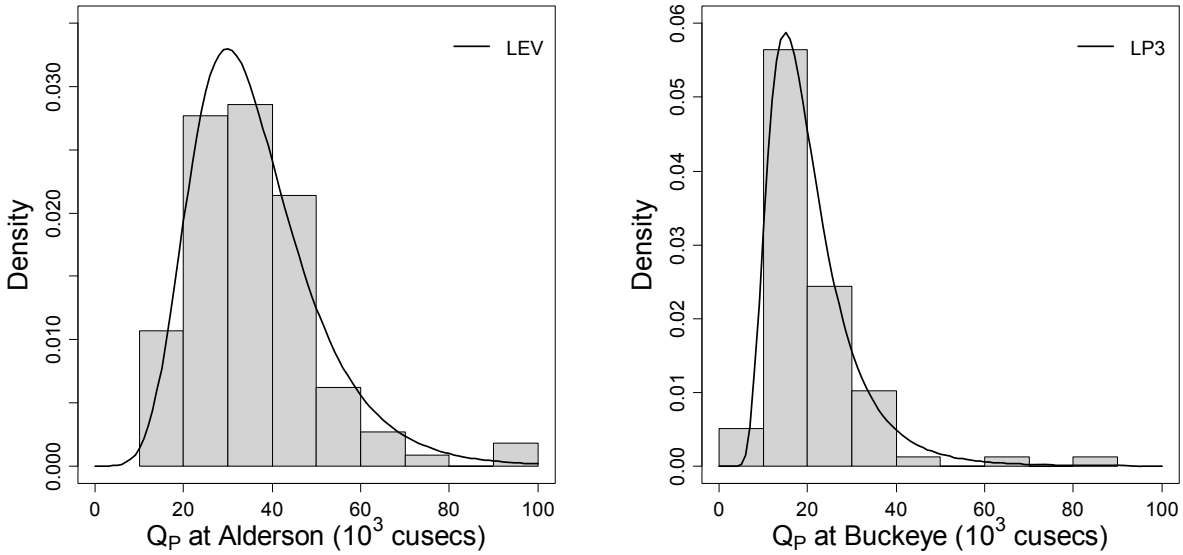

Figure 3 Histograms and plausible probability density functions for peak flows at Alderson and Buckeye river gauging stations.

Parameter estimates and variance covariance matrices are obtained for the Buckeye data series (Y) on the basis of maximum likelihood method employing the two approaches: (a) on a purely univariate basis using LL_U, and (b) on the basis of the composite likelihood function LL_C. The comparison of probability plots resulting from these two approaches for Buckeye station is shown for cases I, III, and V in Figure 4. Other cases also show similar pattern of reduction in widths of confidence intervals. As LP3 is the assumed distribution for this station, the plots are drawn on log-gamma probability papers. The quantile estimates and the associated standard errors are computed with respect to return periods equal to 50, 100, 200, 300, 500, 1000 years. These quantile estimates, associated standard errors, and widths of 95% confidence intervals for both these approaches are given for return periods of 100, 200 and 500 years in Table 2. The percent reduction in uncertainty, in terms of standard error and confidence interval, is also given. Apart from the computation of reduction of uncertainty based on standard errors of quantile estimates and widths of confidence intervals, few more error statistics, such as root mean square error (RMSE), standard error of fit, bias (BIAS), and mean absolute relative deviations (MARD) are also computed for the two approaches and are given in Table 3. The reductions based on these error statistics is also given in the table.

Table 1 Lengths and indicator variables for different lengths of Buckeye series

Case	Alderson Data Series (X)				Buckeye Data Series (Y)				Concurrent Period	
	Years	N_X	n_X	I_X	Years	N_Y	n_Y	I_Y	n_{XY}	I_{XY}
I	1896-2007	112	82	1	1930-1959	30	0	0	30	1
II	1896-2007	112	72	1	1930-1969	40	0	0	40	1
III	1896-2007	112	62	1	1930-1979	50	0	0	50	1
IV	1896-2007	112	52	1	1930-1989	60	0	0	60	1
V	1896-2007	112	42	1	1930-1999	70	0	0	70	1
VI	1896-2007	112	32	1	1930-2007	78	0	0	78	1

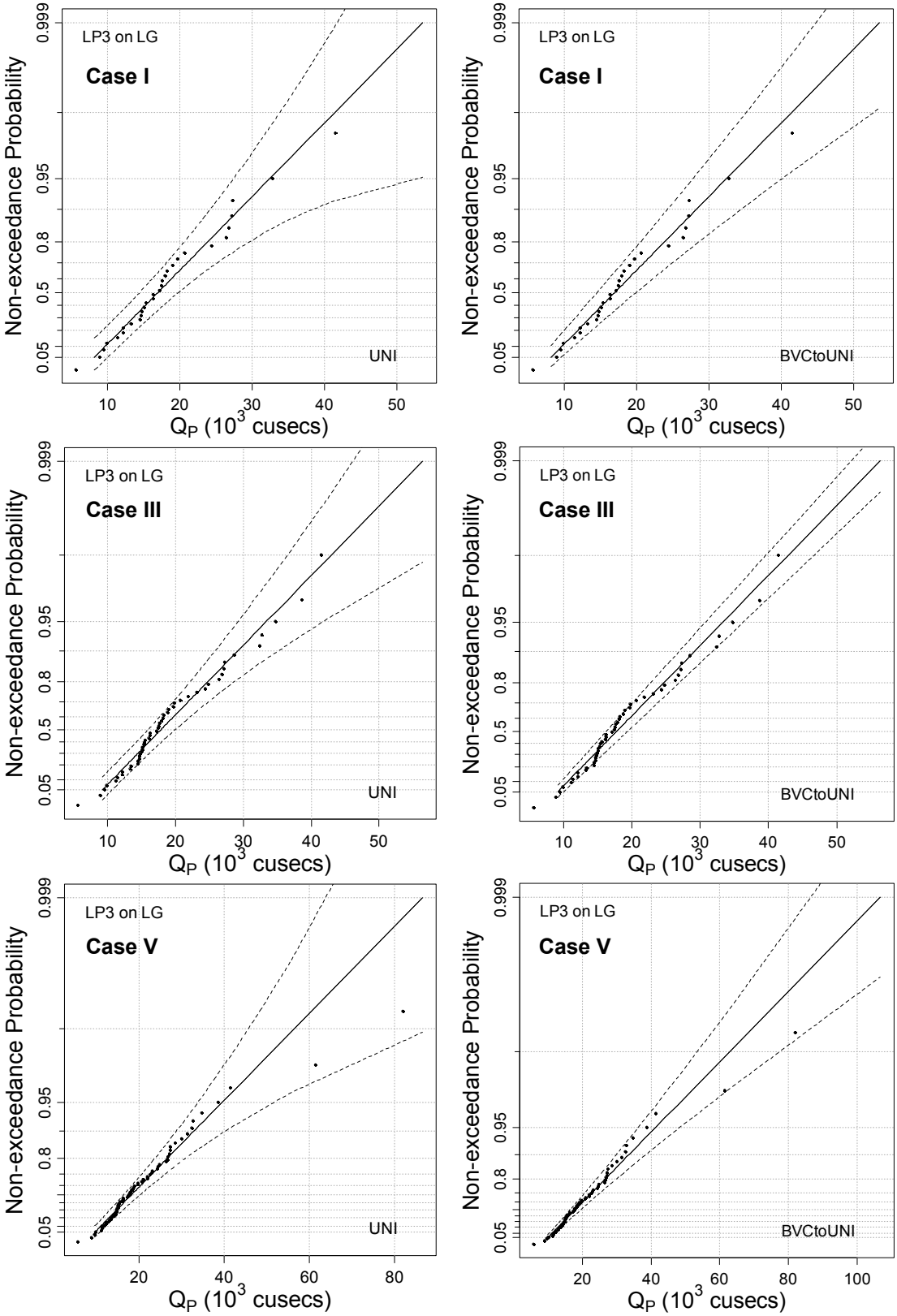

Figure 4. Comparison of LP3 probability plots for Buckeye river gauging station for cases I, III, and V. Left-side plots, annotated as "UNI", are based on LL_U and right-side plots, annotated as "BVCtoUNI", are based on LL_C.

Table 2 Comparison of peak flow quantiles and corresponding error statistics, computed based on univariate fitting and composite bivariate copula fitting

Case	Return Period (years)	Computed Quantiles and Error Statistics (10^3 cusecs)						% Decrease (10^3 cusecs)		
		LL_U Based			LL_C Based					
		Quantile	Standard Error	Confidence Width	Quantile	Standard Error	Confidence Width	Quantile	Standard Error	Confidence Width
I	100	41.4	6.0	23.7	41.4	4.0	16.0	0.0	32.3	32.8
I	200	45.1	7.2	28.7	45.1	4.6	18.0	0.0	36.6	37.2
I	500	50.0	9.0	35.9	50.0	5.3	20.9	0.0	41.2	42.0
II	100	41.7	4.9	19.5	41.7	1.3	5.3	0.0	72.8	73.0
II	200	45.6	5.9	23.2	45.6	1.5	5.8	0.0	74.8	75.0
II	500	50.9	7.2	28.5	50.9	1.7	6.6	0.0	76.4	76.7
III	100	42.9	4.5	17.8	42.9	1.8	7.0	0.0	60.5	60.7
III	200	46.9	5.3	21.1	46.9	1.9	7.6	0.0	63.7	63.9
III	500	52.3	6.5	25.8	52.3	2.1	8.4	0.0	67.0	67.3
IV	100	54.2	8.1	32.2	60.0	5.8	22.8	-10.8	28.5	29.1
IV	200	62.0	10.6	42.2	70.7	7.4	29.2	-14.1	30.0	30.8
IV	500	73.3	14.6	58.5	86.9	10.0	39.5	-18.6	31.4	32.5
V	100	56.4	8.0	31.6	62.8	5.8	22.8	-11.3	27.3	27.8
V	200	64.7	10.4	41.6	74.2	7.5	29.5	-14.7	28.5	29.2
V	500	76.7	14.5	58.0	91.6	10.2	40.4	-19.5	29.3	30.3
VI	100	55.9	7.2	28.3	60.6	5.2	20.5	-8.4	27.3	27.7
VI	200	64.0	9.3	36.9	71.0	6.6	26.0	-11.0	29.1	29.7
VI	500	75.6	12.7	50.9	86.6	8.8	34.8	-14.6	30.8	31.6
Min.		41.4	4.5	17.8	41.4	1.3	5.3	-19.5	27.3	27.7
Max.		76.7	14.6	58.5	91.6	10.2	40.4	0.0	76.4	76.7

Table 3 Comparison of goodness-of-fit and other error statistics with respect to univariate (UNI) and composite bivariate copula (BVC) fitting

Error Statistic	Error Estimates for Various Cases Based on											
	I		II		III		IV		V		VI	
	LL_U	LL_C	LL_U	LL_C	LL_U	LL_C	LL_U	LL_C	LL_U	LL_C	LL_U	LL_C
RMSE	1.14	1.14	1.31	1.31	1.07	1.07	3.53	2.84	3.19	2.29	2.94	2.31
SEF	1.18	1.18	1.35	1.35	1.1	1.1	3.59	2.89	3.23	2.33	2.98	2.34
BIAS	-0.07	-0.07	-0.11	-0.11	-0.1	-0.1	-0.16	-0.13	-0.15	-0.1	-0.15	-0.12
MARD	4.90	4.9	5.77	5.77	5.12	5.12	5.8	5.5	4.89	4.32	4.58	4.11
	% Differences [100*(LL_U Based- LL_C Based)/ LL_U Based**]**											
RMSE	0.0		0.0		0.0		19.4		28.0		21.6	
SEF	0.0		0.0		0.0		19.4		28.0		21.6	
BIAS	-0.3		0.0		0.0		21.5		29.5		19.6	
MARD	0.0		0.0		0.0		5.3		11.7		10.2	

DISCUSSIONS

It is apparent from the narrower confidence intervals in the probability plots of composite likelihood approach of Figure 4 (right side plots) that there is visible reduction in uncertainty of the quantile estimates, in all the three cases I, II, and III for most ranges of return periods. Table 2 shows this improvement in accuracy in quantitative terms. There is across-the-board substantial reduction of about 25 to 75% in the standard error or the confidence width, when parameter estimation is done by employing composite log-likelihood in place of univariate log-likelihood. The improvement in all six cases is slightly more for increasing return periods. Furthermore, baring one of cases (Case I) the relative improvement is greater for shorter period of concurrent period for the same length of the exclusive period of series X. In the first three cases the quantile estimates are same for both approaches whereas for the last three cases the estimates from composite approach are conservative up to about 20%. Besides improvement in accuracy of the quantile estimates, there is marked improvement in the four error statistics considered, i.e., RMSE, SEF, BIAS, and MARD. The absolute values of these error statistics and the percent improvements are given in Table 3. The improvement is of the order of 5 to 30% with respect to the last three cases whereas there is no change in the first three cases. Overall, it can be stated that substantial gain by bivariate consideration of data and making use of the composite likelihood approach instead of the pure univariate approach.

CONCLUSIONS

The results of this study show that there is substantial gain in information and consequent reduction of uncertainty in design flood estimates by considering data from inter-dependent stations. The reduction in uncertainty of estimated quantiles is quite substantial and ranges from 25 to 75% for this particular case study. It is also found that the relative gain in information is higher for increasing return periods. Also, that there is a general trend of gain being higher for smaller length of concurrent period for the same length of exclusive period of the additional station considered. Another interesting result of the study is that not only there is reduction in uncertainty of the estimated quantiles, the other error statistics such as root mean square error, standard error of fit, bias, and mean absolute relative deviations also show significant improvement. Thus, it is concluded that composite likelihood approach, which simultaneously considers bivariate and univariate occurrences of inter-dependent data, provides encouraging avenues for reducing the uncertainty in design flood estimation. Furthermore, copula-based joint distribution functions included in the composite likelihood functions provide desired flexibility for choosing the required distribution types for representing the marginals. It is opined that this approach is not only valid for extending incomplete data in one of the series but may also be equally useful where both series are of equal but limited lengths.

REFERENCES

Anderson, T. W. (1957). "Maximum likelihood estimates for a multivariate normal distribution when some observations are missing." Journal of American Statistical Association, 52(278): 200-203.

Chowdhary, H. and Singh V.P. (2008). “Gains from copula-based multivariate distribution functions for rainfall processes.” World Environmental and Water Resources Congress, Hawaii, ASCE.

Clarke, R. T. (1980). "Bivariate gamma distributions for extending annual streamflow records from precipitation: Some large-sample results." Water Resources Research, 16(5): 863-870.

Edgett, G. L. (1956). "Multiple regression with missing observations among the independent variables." Journal of American Statistical Association, 51: 122-31.

Escalante, C. (2007). "Application of bivariate extreme value distribution to flood frequency analysis: A case study of Northwestern Mexico " Natural Hazards, 42: 37-46.

Escalante, C. and J. A. Raynal (1998). "Multivariate estimation of floods - The trivariate Gumbel distribution." Journal of Statistical Computational Simulation, 61(4): 313-340.

Escalante, C. and J. A. Raynal (2008). "Trivariate generalized extreme value distribution in flood frequency analysis." Hydrological Sciences, 53(3): 550-567.

Fiering, M. B. (1962). "On the use of correlation to augment data." Journal of American Statistical Association, 57(297): 20-32.

Goldfarb, D., A Family of Variable Metric Updates Derived by Variational Means, Mathematics of Computation 1970, 24: 23-26.

Lord, F. M. (1955). "Estimation of parameters from incomplete data." Journal of American Statistical Association, 50: 870-876.

Matalas, N. C. and B. Jacobs (1964). A correlation procedure for augmenting hydrologic data. U.S.G.S. Professional Paper, 434-E.

Raynal, J. A. (1985). Bivariate extreme value distributions applied to flood frequency analysis. Ph.D. Dissertation, Civil Engineering Department, Colorado State University, Colorado.

Raynal, J. A. and J. D. Salas (1987). “A multivariate stochastic flood analysis using entropy.” Hydrologic frequency modeling: Proceedings of the International Symposium on Flood Frequency and Risk Analyses, Baton Rouge, U.S.A., Reidel, Dordrecht, The Netherlands.

Raynal, J. A. and J. D. Salas (2008). Using bivariate distributions for flood frequency analysis based on incomplete data. World Environmental and Water Resources Congress, Hawaii, ASCE.

Rueda, E. (1981). Transfer of information for flood related variables. M.S. Thesis, Civil Engineering Department, Fort Collins, Colorado State University.

Deriving Rule Curve for Hydropower Reservoirs; Seymareh Experience

F. Sharifi[1], M.R. Jalali[1] and R. Afzali[1]

[1]Department of Water Resource Management, Mahab Ghodss Consulting Engineering, 17 Takharestan, Vahdid Dastgerdi, Tehran, Iran, 1918781185

Emails: fsharifi@iust.ac.ir, mrjalali@iust.ac.ir, raheleh_afzali@hotmail.com

Abstract

A common method of design and operation of hydropower dams in Iran is based on peaking hours. In other words, monthly network demand (peak hours multiplied in install capacity) will be fully produced if the water level of reservoir in that month is between Minimum Operating Level (MOL) and Normal Water Level (NWL). If it is located under MOL or above NWL, the water level will be fixed on MOL or NWL and energy production will be lowered or increased, respectively. In order to take into account different monthly values of energy, implementing of an operating policy and rule curve is indispensable. The main goal of this study is to derive a set of monthly target storage elevation as a rule curve to operate the powerplant of Seymareh reservoir in West-South of Iran. The main simulation model of Seymareh reservoir and powerplant is developed in Vensim Environment using System Dynamics (SD) approach. In this process, all the technical and practical details of this reservoir are taken into account. Relations between discharge and turbine efficiency and tail water, volume-area-elevation relations, reservoir evaporation, overload coefficient and maximum and minimum allowable head and turbine discharge are some of these details. Energy production will be occurred if the water elevation of a particular month of reservoir is located above the defined target elevation of that month. This process is performed on historical time series aiming to maximize mean annual value of generated energy. In the next part of this study, to avoid the trial and error process of target elevation selection of above discussed simulation model, a simple ACO algorithm with an embedded coded simulation model is implemented. Results show the ability of this algorithm in defining a rule curve for an absolutely practical case study.

INTRODUCTION

Nowadays in the world, especially in developed countries, water resources planning and management is one of the most controversial tasks and its benefits justify tendency and studies in this area. The limitations in the use of fossil fuels and the benefits of use of the clean and renewable hydro-energy have led to the increased development of hydroelectric projects. In order to design and construct hydroelectric systems, their operation should be analyzed over a representative hydrologic period.

(Afzali et al, 2008). This may be done by using mathematical modelling and system analysis tools. Mathematical simulation and optimization models are extensively used in hydropower reservoir systems analysis. Descriptive simulation models, due to their computational advantages, are able to consider more details of real systems than optimization models. However, they require that the model builder specifies an operating policy. Use of rule curves (Loucks and Sigvaldason 1982), heuristic rules such as space rule (Bower et al. 1962), New York City (NYC) rule (Clark 1950, 1956) and hedging rules (Tu et al. 2003) are common ways of defining operating policies required in simulation models.

The main goal of this study is to derive a set of monthly target storage elevations as a rule curve to operate the powerplant of Seymareh reservoir in West-South of Iran. A system dynamics approach is used for assessing the energy potential of hydroelectric system. In order to find a set of initial solutions, a simple simulation-optimization model is used. The main prepared simulation model in Vensim environment enhances us to see the variation of desired objectives like total generated energy, energy value and summer energy to choose the best combination of 12 monthly target elevation of reservoir. In order to maximize the total energy value and because of the trial and error nature of selecting end-of-month target elevations in Vensim simulation environment, in the next part of this study, Ant Colony Optimization (ACO) algorithm is used to determine these end-of-month target elevations. To do so, an embedded monthly hydropower simulation model is used to operate Seymareh reservoir by any proposed rule curve of each ant. Using this approach, it is expected to find better target storages in comparison with trial-error method of Vensim simulation. In this study, all the practical functions and parameters of a real powerplant is taken into account.

ELECTRICAL ENERGY CONSUMPTION

Reservation of electrical energy, especially in large scale, is impossible. So, the production of hydropower energy should be adjusted to the current demand of network. In the peak time of energy consumption, all the powerplants of system have to work with their maximum power. In short term, the electrical energy consumption is affected by environmental parameters like temperature, humidity and wind velocity and varies by time period like hours of weak, month and even especial ceremonies. In long term, it is affected by social and economical improvements and population growth. In general, the electrical energy load varies by hour, day, weak, month and year, but the trend of energy demand variation is constant over the time period. Energy demand variation curve in Iran's electrical network, in 24 hours of a day, is a curve with two peaks. The second and biggest peak starts around sunset and continues to around 10 or 11 at night. The other information regarding energy demand variation in Iran which is out of scope of this paper result in:

- 24 hour electrical energy demand curve in Iran has two local peaks.
- The peak time length of daily consumption varies by season. Maximum length occurs in summer and minimum length occurs in spring.

- Generally, beginning of the spring has the minimum energy demand in contrast with late July.
- Monthly consumption shows the maximum demand for summer months and the minimum demand for March and April.
- The long peak of summer days shows the great value of energy in these months.

According to the above discussion, two basic parameters of operation of hydropower reservoirs are as follows.

Value of energy in different months

Introducing different energy values for different months of a year enhance us to operate the hydropower reservoirs and their powerplants more efficiently. In order to do so and according to the above information, different proportional energy values are assigned to each month (Table 1).

Minimum peak energy generation

The peaking capability of powerplant in current study is as shown in table 1. Different monthly energy values for base, intermediate and peak load emerges us to develop an operating rule to optimally operate hydropower reservoirs. The aim of this study is to derive a rule curve consisting of 12 end-of-month target elevations considering different energy values which leads us to maximum energy value.

Table 1. Monthly distribution of electrical relative energy value and minimum peak hours

	Jan.	Feb.	Mar.	Apr.	May	Jun.	Jul.	Agu.	Sep.	Oct.	Nov.	Dec.
Relative Energy Value	8	9.5	5	3.5	5	11	14.5	16	12.5	3.5	5	6.5
Minimum Peak Hours	2	2	2	3	4	5	6	6	5	3	2	2

CASE STUDY; SEYMAREH DAM

The Seymareh concrete dam, currently under construction on Seymareh river (main branch of Karkheh river), is located in Ilam province, south-west of Iran. According to the latest information, the NWL and MOL of dam are fixed to 720 and 705 masl, respectively. Seymareh powerplant is consists of 3 units of 160 MW with design inflow of 153.5 cms which can conduct 156.1 cms in its critical period. In the phase of design, all the calculations were made on the basis of 4 peak hour operation. In this study, peaking hours of powerplant is calculated using proposed rule curve, considering different monthly energy values.

SIMULATION-OPTIMIZATION; DERIVING INITIAL SOLUTIONS

Hydropower rule curve consists of two main parameters: 1) End-of-month reservoir target elevation, 2) Minimum peak hour operation of hydropower plants.

According to the energy value in Iran, the minimum peak hours of Seymareh powerplant is fixed as shown in table 1. In order to define the end month target elevation, a simple simulation-optimization model is developed. The 12 month end target storages obtained from the model is considered as an initial solution for the main simulation model using system dynamics approach. To develop the discussed simple simulation-optimization model the following objective function are taken into account: 1) Maximization of long term energy production, 2) Maximization of flood control volume of reservoir in flooding months, 3) Minimization of energy production deficit in comparison with monthly minimum peak hours of operation (table 1), and 4) Minimization of spill.

As it can be seen, the first two objectives are completely in conflict. The first objective is trying to maximize storage and net head and the second one is trying to keep water elevation near to minimum operation level. The total relative energy value is calculated by long term summarization of produced energy multiplied in monthly relative energy value. For the second objective function, the sum of long term free storage of reservoir in flood control months (December to April) are taken into account. In addition, the following constraints are implemented to the prepared model: 1) Mass balance equation, 2) Inflow to powerplants, 3) Elevation-Area-Volume of the reservoir, 4) Outflow and tail water elevation, 5) Energy production, 6) Minimum and Maximum Storage of reservoir, 7) maximum 24 hours of energy production, and some more constraints. The previously discussed simulation-optimization model is prepared by Lingo and the derived end target elevations are considered as an initial solution for the main system dynamics simulation model. Table 2 shows the derived target elevation of the reservoir.

Table 2. Initial end-of-month target elevation values derived from simulation-optimization model

	Jan.	Feb.	Mar.	Apr.	May	Jun.	Jul.	Agu.	Sep.	Oct.	Nov.	Dec.
Target Elevation	709.5	710	713.5	718	720	720	717	709.5	705	705	707	709

HYDROPOWER RESERVOIR OPERATION WITH RULE CURVE

In order to start the main simulation process, an estimation of installed capacity is needed. As mentioned before, our case study, Seymareh dam, is currently under construction and its install capacity is fixed to 3*160 MW. In the next step, an initial storage of reservoir is needed. In this study, an average of minimum and maximum operation storage of reservoir is assumed as an initial storage capacity. In long term reservoir operation, the value of initial storage has no major influence on total generated energy except few first time periods. In absence of power market and network analysis, it may be desirable to maximize the system's energy yield that can reliably be produced. The following equations show the generated energy as a term of reservoir release and powerplant's firm energy.

$$E(t) = 2.73 \times R(t) \times H(t) \times e_p \quad (1)$$

$$H(t) = h(t) - h_{tail}(t) - h_f(t) \quad (2)$$

$$FE(t) = IC \times hours \times PF(t) \quad (3)$$

Where E(t) is the generated energy of month t, ep is powerplant efficiency in month t, R(t) is turbine release of month t, H(t) is the net head on the turbine, h(t), $h_{tail}(t)$ and $h_f(t)$ are storage level of reservoir, tail water level and total minor and frictional losses in conveyance structures all in month t, respectively. IC is install capacity of powerplant, hours is number of hours in month t, FE(t) is system's monthly firm energy and PF(t) is powerplant's plant factor. The monthly turbine release would then be calculated as follows:

$$R(t) = \frac{FE(t)}{2.73 \times \left(0.5 \times \left(h_2(t) + h_1(t)\right) - h_{tail}(t) - h_f(t)\right) \times e_p(t)} \quad (4)$$

In the above equation, $h_2(t)$, $h_{tail}(t)$ and $h_f(t)$ depend on the turbine release making the equation implicit with respect to R(t). Therefore it has to be solved iteratively. Assume an end-of-month reservoir storage that that yields the initial R(t) from above equation. The new end-of-month reservoir storage is then determined from the mass balance equation of reservoir. The new end-of-month storage is compared with the one initially assumed. If they are not the same, the next estimation of the turbine release is determined from the new end-of-month storage. The procedure is repeated to get the end-of-month storages and releases converged to same values in two successive iterations.

The result end-of-month storage is checked with end target storages of the same month. In the case that the end-of-month storage is less than end target storage, the energy production of powerplant will be reduced. If the end-of-month storage is more than end target storage, the turbine discharge and energy production will be increased until the storage of reservoir will fixed to target storage. In this case if there is more water than powerplant's energy production capacity, the excess water will be spilled to the river.

SYSTEM DYNAMICS APPROACH

Dynamic simulation allows us to observe the behaviour of a modelled system and its response to interventions over time. Dynamic simulation models consist of equations describing dynamic changes. If system state conditions are known at one point in time, the system state at the next point in time can be computed. Repeating this process one can move through time step-by-step over any desired interval. Simulation aids our capacity to make predictions of future states. In System Dynamics Methodology (SDM) the underlying premise is that the structure of a system gives rise to its observable and thus predictable behaviour (Forrester, 1968, 1987). Using the Vensim software, one can easily develop complicated simulation models with various numbers of variables and interrelation among them. The user can define the relations of variables in various pages. In addition, there are some sliders which help users to see the influence of each variable changes on predefined parameters. Generally, system dynamics prepares a forum to analyze the complicated

systems. In this study, some of the basic assumptions of prepared model are as follow: 1) Simulation time step is monthly, 2) Energy demand is defined as the installed capacity of powerplant multiplied to minimum operation hours, 3) After each time period operation of powerplant, if the target elevation of reservoir is between MOL and NWL, the end month storage will be fixed to the end target elevation by lowering the energy production. In the case of locating the storage elevation above the target elevation, again, the end month storage will be fixed to the end target elevation by releasing more water up to 24 hours of energy production. In this case, the excess water will release from reservoir directly to the river, 4) In addition to the limitation of energy production according to the maximum and minimum storage volume, there are some other constrains like minimum and maximum head and inflow to the powerplant. If the inflow to the powerplant is more than allowable, the inflow will be limited to the maximum allowable flow of powerplant. 5) In addition to the discussed basics and constraints, the generated power in time step is limited to the installed capacity of powerplant multiplied in an overload factor.

DERIVING RULE CURVE; SD APPROACH

As it mentioned, the result of simple simulation-optimization model is entered to the main simulation model as an initial solution. In this step, the main goal is précising the target elevation values using graphical and sensitivity analyses abilities of Vensim. In order to perform sensitivity analysis of different target elevation and because of the importance of generated summer energy, this factor is also taken into account as an important operative factor. In addition, because of the different monthly energy values for low, medium and high peak energy, the mean total annual energy value is considered as another operative factor other than total generated energy. Table 3 and 4 shows the relative energy values and variation of low, medium and high peak hours of a year.

Table 3. Relative energy value in different hours and month of the year

	Jan.	Feb.	Mar.	Apr.	May	Jun.	Jul.	Agu.	Sep.	Oct.	Nov.	Dec.
Low Peak Hours	1.2	1.2	1	1	1	1.6	1.6	1.6	1.6	1	1	1.2
Medium Peak Hours	1.9	1.9	1.6	1.6	1.6	2.5	2.5	2.5	2.5	1.6	1.6	1.9
High Peak Hours	8	8	6.6	6.6	6.6	10.6	10.6	10.6	10.6	6.6	6.6	8

Table 4. variation of low, medium and high peak hours during a year

	Jan.	Feb.	Mar.	Apr.	May	Jun.	Jul.	Agu.	Sep.	Oct.	Nov.	Dec.
Low Peak Hours	6	5.5	5	6	5	5	5	4	5	8	7	6
Medium Peak Hours	16	16.5	17	15	15	14	13	14	14	13	15	16
High Peak Hours	2	2	2	3	4	5	6	6	5	3	2	2

The definition of peak, medium and low bar enhanced us to calculate the long term mean relative energy value in simulation model. So, the other operative factor is

mean annual relative energy value. Finally, the following three operative parameters are taken into account in sensitivity analysis of different monthly storage target elevation: 1) Total energy, 2) Summer energy (four months), 3) Annual relative energy value. In this study, the annual relative energy value is considered as the first and most important operative objective. The summer and total energy are considered following to the first one, respectively. According to the preferences of decision makers and stakeholders, in some cases a trade off analysis is needed to select a monthly target elevation series. The final monthly target elevation is derived by trial and error using previously discussed initial solutions (obtained from simulation-optimization model).

In order to find 12 monthly target elevations a sensitivity analysis process is performed. To do so, all the end-of-month target elevations are first set to their initial values. Starting from October (a non critical month regarding to the flood and high energy demand), all the possible end-of-month target elevations of this month (705 masl to 720 masl, 0.5m discrete) is checked while the end-of-month target elevations of other months are fixed to their initial values. Total energy values are calculated for all 31 possible combinations and the optimum end-of-month target elevation is derived. As soon as the précised end-of-month target elevation of October is fixed to its optimum value (705 masl), the same process starts for November. Again in this step, the end-of-month target elevation of all months are fixed to their initial values except fixed target elevation of October (705 masl) and varying target elevation of November (705 masl to 720 masl). Figure 1 shows the discussed process for the month of March. In this figure, the relative energy value of all 31 possible combinations of end-of-month target elevations to the first combination of this month is plotted against 31 different values of end-of-month elevations. As it can be seen, the target elevation of 710.5 is selected for this month. Table 5 shows the target elevations.

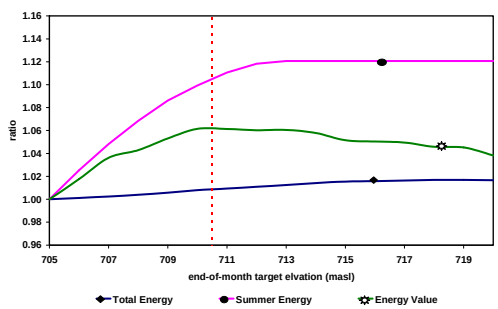

Figure 1. Results of sensitivity analysis of energy value, total energy and summer energy to the end-of-month target elevation of reservoir in March

Table 5. Final values of end-of-month target elevation of Seymareh reservoir of each month

	Jan.	Feb.	Mar.	Apr.	May	Jun.	Jul.	Agu.	Sep.	Oct.	Nov.	Dec.
Target Elevation	708	708.5	710.5	716	720	720	715	709	705	705	706	708

As mentioned before, in the various phase of designing of Seymareh dam, the operation peak hours of its powerplant was set to 4 hours. In addition, there is not any rule curve for target storages of reservoir. In this study, by introducing different monthly peak operation hours, some changes are occurred in operation of reservoir and powerplant. Although the amount of 6 GWH reduction is occurred in the case of using derived rule curve, 110 GWH energy is added to the 4 month more valuable summer energy. These changes results in about 400 million dollars of increased mean annual energy value.

DERIVING RULE CURVE; ACO APPROACH

As mentioned before, the task of a part of ACO algorithm, ants generate trial monthly target elevation by choosing a target elevation for end of each month. The probability that a particular target elevation will be chosen from the set of available options at a particular decision point is a function of the pheromone and the local desirability of that option based on heuristic information, as shown in Equation 5:

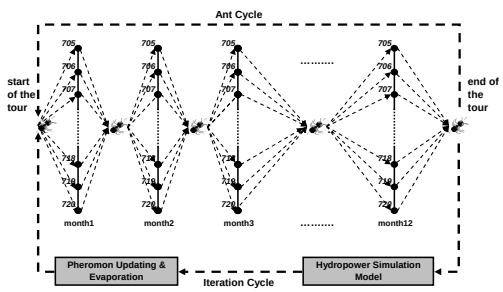

Figure 2. ACO algorithm applied to hydropower rule curve problem

$$P_{ij}(t) = \frac{[\tau_{ij}(t)]^{\alpha}[\eta_{ij}(t)]^{\beta}}{\sum_{j=1}^{n}[\tau_{ij}(t)]^{\alpha}[\eta_{ij}(t)]^{\beta}} \quad (5)$$

where $P_{ij}(t)$ is the probability that target elevation j is chosen of month i in iteration t; $\tau ij(t)$ is the pheromone intensity deposited on target elevation j of month i in iteration t; ηij is the heuristic value for target elevation j of month i in iteration t; n is the total number of target elevation choices available for month t; α is the relative importance of pheromone intensity; β is the relative importance of the heuristic which was set to 0 in this study. The pheromone level associated with a particular option (i.e. target elevation level of a particular month) is a reflection of the quality of the 12 target storage elevations that have been generated that contains this particular option. Once a trial target elevation has been constructed by choosing a target elevation at each decision point, taking into account pheromone levels, one ant-cycle has been completed (Figure 2). After r ant-cycles, where r equals the

number of ants used, the ACO algorithm enters the iteration-cycle (Figure 2). During this stage, the quality of the r trial solutions is evaluated using a simulation model coded according to the process discussed in former sections, as part of which the objective function values, such as energy value, summer energy and total energy calculated and violations of any constraints are identified. The objective function value which is taken into account in this study is energy value. In contrast with trial and error method of system dynamics approach, all the process of seeking best target elevation is done by artificial ants. In the proposed ACO algorithm, a single colony of 75 ants is used. In order to attain acceptable values for decision variables, total number of 200 iterations is used. Next, pheromone is updated in a way that reinforces good solutions. Generally, in metaheuristic algorithms, constraints are implemented to the optimization model as a penalty function. Here in this study, some limitations regarding to the mean monthly generating hours of Seymareh powerplants should be introduced. Three kind of limitations studied here are as follows and table 6 shows the final energy value, summer energy and total energy of each case:

1- No limitation

If there are no limitations regarding to the mean monthly generated hours of powerplants, in consequence, the penalty function would then set to zero for any chosen target elevation. It is expected to attain maximum energy value (see ACO1 in table 6).

2- Limited to the mean generating hour of Vensim simulation

If the mean monthly generating hours of Seymareh powerplants are limited to the mean monthly generating hours derived from Vensim simulation, the penalty function would then be calculated by summarizing the 12 constraint violations of a year. Because of the nature of ACO algorithm (see ACO 2 in table 6), it is expected to find better set of target elevations in comparison to Vensim simulation considering annual energy value.

Tabele 6. Annual energy value, summer energy, total energy and monthly generated hours of powerplant

	Mean Annual Energy Value	Summer Energy (GWH)	Total Energy (GWH)	Mean Monthly Generated (hr)											
				Jan.	Feb.	Mar.	Apr.	May	Jun.	Jul.	Agu.	Sep.	Oct.	Nov.	Dec.
Design	5803	221	832												
Vensim	6700	331.3	826.1	4.9	5.8	6.8	5.7	6.6	2.5	6.3	7.5	5.1	1.0	1.7	2.0
ACO 1	6765	334.7	832.7	7.8	7.0	5.6	5.6	6.9	2.6	5.3	7.4	6.3	0.0	0.2	0.9
ACO 2	6706	331.3	826.8	4.9	5.9	6.9	5.7	6.6	2.5	6.3	7.5	5.1	1.0	1.7	2.0

CONCLUSION

In practical powerplant's operation of hydropower reservoirs, operating policies or operation rule curves may be employed considering objectives like

maximum annual total energy or value. The main objective of this study is to find a rule curve (consisting of 12 end-of-month target elevations) for operating Seymareh reservoir in order to maximize mean annual energy value. Dynamic and graphical enhancements of system dynamics approach and Vensim software convince us to develop the main simulation model of hydropower operation in this environment. In order to have an estimation of these target elevations, a simple simulation-optimization model is prepared. Final target elevations (rule curve) are derived from the main simulation model using trial and error. It should be mentioned that in this study, all the practical parameters and equations of a real powerplant is implemented. In the next part of this study, because of the trial and error nature of using system dynamics approach, a metaheuristic algorithm is developed and used for deriving target elevation of Seymareh reservoir. Results show the performance of ACO algorithm in finding end-of-month target elevations.

REFERENCES

Afzali, R., Mousavi, S.J., and Ghaheri, A., (2008), "Reliability-Based Simulation-Optimization Model for Multireservoir Hydropower Systems Operations: Khersan Experience", J. Water Resour. Plng. and Mgmt. 134, 24.

Bower, L., Hufschmidt, M. M., and Reedy, W. H. (1962). "Operating procedures: Their role in the design and implementation of water resource systems by simulation analysis" Design of water resource systems, A. Maass et al., eds., Harvard Univ. Press, Cambridge, Mass., 443–458.

Clark, E. J. (1950). "New York control curves." J. Am. Water Works Assoc., 42(9), 823–827.

Clark, E. J. (1956). "Impounding reservoirs." J. Am. Water Works Assoc., 48(4), 349–354.

Forrester, J. W., (1968) "Principles of Systems". Productivity Press, Portland, Oregon, USA.

Forrester, J. W., (1987) "Lessons from system dynamics modeling" System Dynamics Review, 3(2):136–149.

Loucks, D. P., and Sigvaldason, O. T. (1982). "Multiple-reservoir operation in North America." In the Operation of Multiple Reservoir Systems, Proc. IIASA Collaborative Proc. Ser. CP-82-53, Z. Kaczmarek and J. Kindler, eds., International Institute for Applied Systems Analysis, Laxenburg, Austria, 1–103.

ReVelle, C. (1999). Optimizing reservoir resources, including a new model for reservoir reliability, John Wiley & Sons, New York.

Tavanir Company (www.tavanir.org.ir)

Tu, M.-Y., Hsu, N. S., and Yeh, W. W.-G. (2003). "Optimization of reservoir management and operation with hedging rules." J. Water Resource Planning and Management, 129(2), 86–97.

Wolstenholme, E., (2004) "Using generic system archetypes to support thinking and modeling System Dynamics Review", 20(4):341–356, doi: 10.1002/sdr.302.

Detection of Streamflow Trends and Variability in Karun River-Iran as parts of Climate Change and Climate variability

Alireza Farrokhi [a], Ahmad Abrishamchi [b]

[a] *Graduate Student of Water Resources Engineering,* [b] *Professor.*
Department of Civil Engineering, Sharif University of Technology, Tehran, Iran.

Abstract

This paper describes the application of statistical and spectral procedures that identifies trends and periodicity in streamflow time series. The results of Mann-Kendall and seasonal Kendall tests (non-parametric tests which are known as appropriate tools in detecting linear trends of hydrological time series) shows negative trends especially during low water months (August to November). This downward trend is more significant in October. But these methods can not interpret periodic behavior. Hence spectral procedures were applied on data series to investigate periodicities in streamflow data series. Fourier and Continuous Wavelet Transform (**CWT**) analyses produce evidence of interannual variability (3-4 and 5-6 years), especially in Karun River. These oscillations can be related to **ENSO** phenomenon. Also we observed near decadal, PDO-related variability. However, the short length of the streamflow series can obscure such these results.

Keyword**:** Climate change, Trend detection, Streamflow variability, Wavelet analysis

1. Introduction

Today there is not any doubt that Global warming as the result of human-induced 'greenhouse effect' will lead regional water resources and hydrological cycles to the changes in different spatial and temporal manners (Qader, 2002; Labat et al., 2004).
Climate change and climate variability may affect human society and enforce them to undergo much harm in their life. Of all of the elements of the hydrologic cycle, streamflow may be the most consequential to human life, especially as the primary source of drinking water in arid areas. Also streamflow time series have advantage, over precipitation records, that they integrate the influences of many variables over a watershed like of rainfall, evapotranspiration, vegetation cover and topography.

Consequently accurate forecasts of streamflow are very valuable for planning water supplies and managing demands. But without recognition and perception of these changes and variations, we are not able to determine any long-term water policy for our future.

Historical streamflow data may not always serve as the best tool for prediction of the future. Some fluctuations in the streamflow records from year to year may correspond to phases of large-scale global atmospheric circulation patterns. In particular, the El Nino Southern Oscillation (ENSO) is an irregular oscillation with a period and amplitude that have undergone a considerable change over the last century and has become a leading focus of research involving earth-atmosphere relationships (e.g., Ropelowski and Halpert, 1987; Cayan and Peterson, 1989; Cayan and Webb, 1992; Kahya and Dracup, 1993).

Establishing the connectivity between such low-frequency climate events (ENSO and PDO) and local hydrology (i.e., streamflows), with correlation and spectral analysis, can increase our knowledge about interannual, decadal and multidecadal variation of land surface hydrological cycle in regional scale and make it possible to predict streamflow for time periods greater than a few days or weeks. Labat, 2005 showed Asian annual runoff comport low-intensity but statistically significant 5- to 6-y ENSOrelated interannual variability and multidecadal 30-y oscillations. Timing is another valuable characteristic of streamflow, especially for snowmelt dominated basins. Any shift in streamflow timing can increase the conflict between water supply and demand.

Therefore in this paper we have investigated and detected streamflow trends and periodicity, both aspects of runoff variability, during the past years.

2. Study Area

The Karun River basin (Fig. 1), with an area of approximately 67,000 km2, is Iran's most effluent, and the only navigable, river with 450 miles (720 km) long. It is located in the southwest (from 30º 16´ to 32º 40´ N latitude and 49º 33´ to 52º 0´ E longitude) of Iran and rises in the ZardKuh mountains district in the Zagros range, receiving many tributaries, such as the Dez and the Kuhrang, before passing through the Ahvaz, capital of the Khuzestan province. The Karun continues toward the Persian Gulf, forking into two primary branches on its delta: the Bahmanshir and the Haffar that joins the Arvand Rud, emptying into the Persian Gulf. Also lower Mesopotamia basin has been affected form Karun and Karkeh rivers by the buildup of sediment brought from the Zagros (Mesopotamia is a trench in front of the Zagros mountains, partly occupied by the sea and gradually being infilled by sediments brought down by the Tigris and Euphrates rivers).

More climatologist confirm that the basin covers three climatic zones, with elevations between 800 and 4400 m,: a high mountain zone containing the dam site and reservoir basin, a foothill and inland desert zone containing the irrigation areas, and a coastal desert zone containing the downstream water use areas. The climate of the region varies from an extremely hot, dry summer accompanied by air temperatures as

high as 54°C to mild winter with sub-zero temperatures for most areas of the region (Khodjeini 1994).

Total annual precipitation, occurring mainly in the November through April or May ranges from 100 to 1200 mm/y in the plain and high mountains respectively, and the low flow season generally begins in July and ends in November. Agriculture (especially sugar production) is by far the biggest user of the Karun River, consuming around 10 billion m3 per year.

Drinking water and other subsistence demands of 1.5 million inhabitant populations in cities of Khoramshahr and Abadan, extremely depend on this river. Excessive use of water by Iran and Iraq, urgency of need for electricity and thereupon operation of inordinate hydropower dams on upstream and brittle ecosystem of the region has intensified conflictions in recent year (Ghadiri 2005).

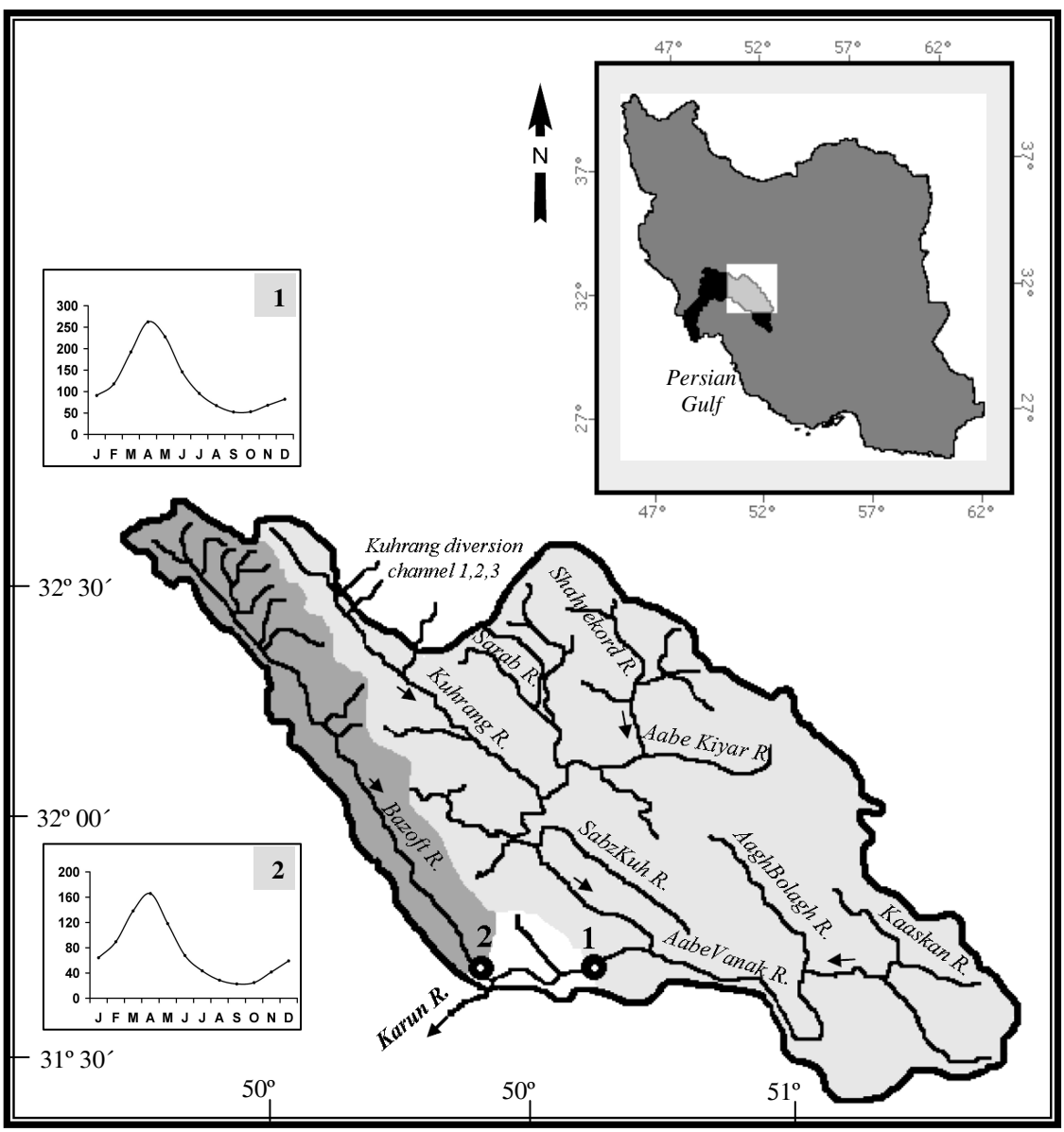

Figure 1 Map of the Karun River basin (full-black area) and Karun-4 sub-basin showing the location of selected stations (shown by numbers keyed in Table 1) and corresponding typical hydrographs.

Whereas climate change and variability can unbalance such system and consequently make many problems, we have decided to investigate discharge characteristics of Karun River in this research. Any research on the basis of detection of climate change and variability, require intact and unregulated flows. Hence we choose one of the most important sub-basins of vast Karun basin, called Karun-4 (Fig. 1) that located on up-stream of Karun-4 dam in Chaharmahal province. This basin (from 31º 20´ to 32º 40´ N latitude and 49º 35´ to 51º 50´ E longitude) covers an area of approximately 12,800 km2. Recent years unfortunately several harmful and inclement floods have occurred in this region and affected the construction of Karun-4 dam and its hydro-electric power plant (Karimi 2006).

3. Data and Methods

In this study we used daily, monthly and annual streamflow records (will remark accurately on the next section), in a period of thirty years from 1975 to 2004, were gathered from Water Resources Research Organization (TAMAB Co.). Table 1 lists two major analyzed stations located throughout the Karun-4 basin. Fig. 1 shows the location of each station and the areas were covered by each sub-basin.
To identify characteristics of observed streamflow data, we have employed statistical and mathematical analysis. Existing any relation between streamflow and known climatic indices (such as the Pacific Decadal Oscillation and the El Nino–Southern Oscillation) were investigated by statistical and spectral analysis. The outline of methods were employed in this research, are described in the sections that flows.

3.1. Trend Detection Test

Tests for trend have been of keen interest in environmental sciences during the last century. Trend analyses in this study were conducted by the nonparametric Mann–Kendall (MK) family tests (Mann, 1945; Kendall, 1975). These tests are widely used for hydrologic data analysis, because of their robustness towards non-normally distributed data, missing values and values below detection limit, and can detect

Table 1 Main characteristics of studied discharge stations

Drainage basin	No. of station	Name of station	Latitude (N)	Longitude (E)	Record period	Elevation (m a.s.l.)	Area (km^2)	Ave. annual runoff (m3/s)
Karun-4	1	Armnad	31º 41´	50º 46´	1975-2004	1050	9986	121.28
	2	Morghak	31º 39´	50º 28´	1975-2004	860	2355	72.26

The numbers of stations correspond to stations in Fig. 1

trends that are monotonic but not necessarily linear (Burn and Elnur, 2002; Yue et al., 2003). We have used the Mann–Kendall test to analyze annual streamflow data, whereas we have employed the seasonal Kendall test (Hirsch et al., 1982) to examine monthly trends. The computational procedure for Mann-Kendall test is described below.

In these tests, the null hypothesis Ho states that the data (x1;…; xn) are independent and identically distributed random variables (Yu et al.,1993) and the alternative hypothesis H1 says that there is a trend in the records. Let the time series consist of n data points and Xi and Xj are two sub-sets of data where i=1, 2, 3, . . . , n−1 and j=i+1, i+2, i+3, . . . , n. Each data point Xi is used as a reference point and is compared with all the Xj data points. The Kendall's S-statistic is computed by Eqs. (1) and (2), then variance for the S-statistic is defined by Eq. (3) which:

$$S = \sum_{k=1}^{n-1} \sum_{i=k+1}^{n} \mathrm{sgn}(x_i - x_j) \tag{1}$$

$$\mathrm{sgn}(x_i - x_j) = \begin{cases} +1 & if \quad (x_i - x_j) > 0 \\ 0 & if \quad (x_i - x_j) = 0 \\ -1 & if \quad (x_i - x_j) < 0 \end{cases} \tag{2}$$

$$Var(S) = \frac{1}{18}\left[n(n-1)(2n+5) - \sum_{p=1}^{q} t_p (t_p - 1)(2t_p + 5) \right] \tag{3}$$

In witch tp denotes the number of ties for the pth value and q is the number of tied values. For the cases that n is larger than 10, the standard normal variable z is computed by using the following equation (Douglas et al., 2000).

$$Z = \begin{cases} \dfrac{S-1}{\sqrt{Var(S)}} & S > 0 \\ 0 & S = 0 \\ \dfrac{S+1}{\sqrt{Var(S)}} & S < 0 \end{cases} \tag{4}$$

This test statistic is used to test the null hypothesis (Ho). If $|Z|$ is greater than $Z_{1-\alpha/2}$, where α represents the chosen significance level (usually 5%, with $Z_{1-\alpha/2}$=1.65), then the null hypothesis is invalid, meaning that the trend is significant. A positive value of S indicates an 'upward trend' and a negative value indicates a 'downward trend'. The slope of the trend was estimated using Sen's slope estimator (Sen, 1968). The Sen Slope is the median of the slopes calculated from all pairs of values in the data series, a method that is little affected by data outliers and missing data (Salmi, 2002).

The Seasonal Kendall (SK) test for trend (Hirsch, 1982 and Slack, 1984) was developed by the U.S. Geological Survey (USGS) in the 1980s to analyze trends in surface-water quality throughout the United States. This test performs the Mann-Kendall (MK) trend test for individual seasons of the year, where season is defined by the user. It then combines the individual results into one overall test for whether the dependent (Y) variable changes in a consistent direction (monotonic trend) over

time. When serial correlation occurs, p-values for significance tests will be too small, and trends may be incorrectly found (we know, so the smaller the p, the more significant the trend). Thus adjusted p-value was suggested in the presence of serial correlation. Recently the test was modified to form the Regional Kendall (RK) test for trend. In this form, trends at numerous locations within a region are tested to determine whether the direction of trend is consistent across the entire region. (USGS Report 2005 Helsel, Mueller and Slack).

In this research Seasonal Kendall test was developed to examine monthly trends. The test statistic is a sum of the Mann-Kendall statistic (S; similar to that in Eq. (1)) computed for each month. But serial correlation between months can lead to overestimation of the significance level when the test statistic is summed by month to test for the overall trend. Hence we have calculated and showed each monthly test statistic separately.

3.2. Spectral analysis for flow dynamics

Spectral analysis of long-term climatic records has been widely used to identify quasi-oscillatory signals and their connections across large-scale circulation indices and hydroclimatic variables throughout the world (see Trenberth, 1990; Ghil and Mo, 1991; Mann and Park, 1993, 1994; Mann et al., 1995). In this study we have used two spectral procedures to investigate periodicities in streamflow time series: Fourier analysis and wavelet transform.

These methods were used to analyze the deseasonalized streamflow records that obtained by subtracting the monthly historical means from monthly means. The traditional Fourier transform uses sine and cosine base functions that have infinite span and are globally uniform in time. It does not contain any time dependence of the periodicity, and only reveals what spectral component is present in the signal (Lau and Weng, 1995). Thus Fourier analysis allows a preliminary determination of the characteristic periods in land surface runoff.

Wavelet transform is a powerful way to characterize the frequency, the intensity, the time position, and the duration of variations in a climate data series (Jiang et al., 1997), which reveals the localized time and frequency information without requiring the time series to be stationary unlike the Fourier transform and other spectral methods (most of the climatic oscillations are nonstationary and do not persist for the entire span of the time series (Labat 2005)). The basic objective of the wavelet transform is to detect the temporal changing characteristics of the streamflow and their correlation with climatic indices. Continues wavelet transform (CWT) was used to determine the temporal variation of frequency content of signals. The coefficients of the wavelet transform of a continuous-time signal $x(t)$ are defined by the linear integral operator:

$$C_x(a,\tau) = \int_{-\infty}^{+\infty} x(t)\ \psi^*_{a,\tau}(t)dt \qquad with$$
$$\psi_{a,\tau}(t) = \frac{1}{\sqrt{a}}\psi\left(\frac{t-\tau}{a}\right) \tag{5}$$

where * corresponds to the complex conjugate. The parameter a can be interpreted as a dilation (a >1) or contraction (a <1) factor of the wavelet function $\psi(t)$, corresponding to different scales of observation. The parameter τ can be interpreted as a temporal translation or shift of the function $\psi(t)$, which allows the study of the signal $x(t)$ locally around the time τ. The wavelet spectrum $W_x(a,\tau)$ of a continuous-time signal $x(t)$ is defined, by analogy with the Fourier analysis, by

$$W_x(a,\tau) = C_x(a,\tau)C_x^*(a,\tau) = \left|C_x(a,\tau)\right|^2 \tag{6}$$

Additional explanations of wavelet and Fourier transform are abundant in the literature (e.g. Torrence and Compo, 1998; Labat, 2005).

4. Results

4.1. Trend detection

Fig. 1 shows a map of the Karun-4 basin along with two hydrographs of selected stations, which we have used here to investigate their historical streamflow trends. According to hydrographs, we can distinguish dominant regime in the region: in both sub-basins (Armand and Morghak), high water month occur during March to May (approximately in the spring), with peak flow in April and low waters during August to October (approximately in summer and autumn).

Fig. 2 shows average annual rainfall and temperature in the region with their linear trends. Obviously increasing trends were observed in annual temperature series, especially in the period of 1992-2004, while most regional rainfall has decreased significantly during the period of 1975-2004 and have been pointed out by several researchers (e.g., Saghafian et al., 2006; Raziei et al., 2005; Rahimzadeh et al., 2002).

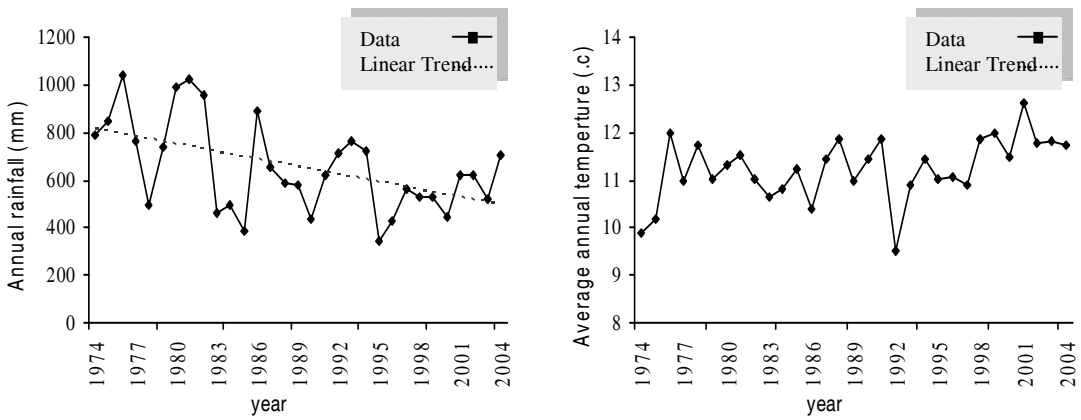

Figure 2 average regional rainfall and temperature with their linear trends.

Table 2 Mann–Kendall trend test results for mean annual discharge series

River	station	Latitude (N)	Longitude (E)	Record period	No. of years	Test Z	*p* value	Sen's slope
Karun	Armnad	31º 41´	50º 46´	1975-2004	30	-1.677	< 0.05	-0.63
Baazoft	Morghak	31º 39´	50º 28´	1975-2004	30	-0.535	n.s.	-0.13

n.s.: not statistically significant.
Positive Z values indicate increasing trend, negative values would indicate decreasing trend.

Table 2 shows the resulting of Mann–Kendall trend test for two annual streamflow time series. All test Z parameter indicate decreasing trends, but only significant at $p<0.05$ in Armand station. Also Sen's slope estimator represents the trend's true slope (change per unit time (i.e. one year)). Insignificant trend in Baazoft River can probably due to its short length records (30 years) and small area of its sub-basin (9986 km2). The seasonal Kendall test (Hirsch et al., 1982) was applied to monthly streamflow time series of Karun-4 basin and summarized in Table 3. The results show significant decreasing trends during low water months (August to November), especially in October. The shaded areas in Table 3 indicate different levels of statistical significance (99% to 90% levels with darkest to lightest gray), where algebraic signs (''+'' and ''_'') denote positive and negative trends respectively. For most months, the results of trend test are negative, consistent with the annual analysis (however not significant in high water months).
There were operated several dams and hydraulics structures in the Karun River basin, which can affect on natural flows and consequently unsettle our analysis. For example Kuhrang diversion channels (located on up-stream of Kuhrang River), convey high volume of annual flows to its main neighbor basin (ZayandehRUD River basin).

Table 3 Seasonal–Kendall test results for monthly mean streamflow time series

River	Station	Seasonal–Kendall test											
		Jan	Feb	Mar	Apr	May	Jun	Jul	Aug	Sep	Oct	Nov	Dec
Karun	Armand	1.36	0.86	0.32	0.61	0.68	0.82	1.18	2.71	3.14	3.18	2.14	1.18
		-	-	+	-	-	-	-	-	-	-	-	-
Baazoft	Morghak	0.07	0.09	0.05	0.37	0.41	1.02	1.05	0.66	1.95	1.98	0.27	0.48
		-	+	+	-	-	-	-	-	-	-	-	+

The shaded cells indicate different confidence levels, from 99% (darkest gray) to 90% (lightest gray) and white cells indicate not statistically significant results.

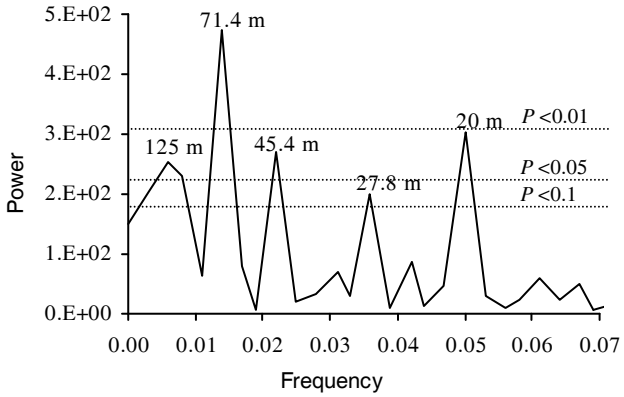

Figure 3 Fourier periodogram of averaged deseasonalized monthly streamflow.

This irregular transmission has produced uncertainties and doubts on accuracy of results. Moreover some factors can determine the variability of the tests results (e.g. increasing use of ground water supplies and deforestation).

4.2. Spectral analysis

During the recent years, many researchers have focused on connection between river discharge and ENSO for achieving better prediction systems (e.g. Tajrishi and Abrishamchi 2006, Labat et al. 2005, Ames 1998). Summarized results of these researches, show interannual oscillations in the range of 2-7 years, which apparently correspond to ENSO phenomenon (especially streamflow decreases during La Nin˜a (cold event of ENSO)). However there are some evidences of decadal and quasi-decadal fluctuations that have been linked to PDO (Barton and Ramirez, 2000). Spectral analysis was used to investigate the main periodicities in streamflow series. Fig.3 shows Fourier periodogram of deseasonalized monthly streamflow time series. Because of consistent behavior in the rivers, we have represented only one chart for whole region. Our Fourier spectral analysis shows 4 peaks (confidence levels > 90%) at interannual scale (6, 3.8, 2.3 and 1.7 years) and 1 peak at decadal scale (10.4 years). The power of spectrum is low because we have short length records.

Fig. 4 shows the Fourier periodogram of the 1975–2004 series of the SOI (Southern Oscillation Index) and PDO (Pacific Decadal Oscillation) index. It shows series of significant peaks that seem to be correlated with regional flows, especially at interannual scale. The results represent one important fact: that the ENSO is an effective driver in Karun River basin. Moreover, coherency spectral analysis of streamflow with SOI index shows good significant coherency at the interannual frequencies. For example, there were observed ENSO-related variation with 5.3, 3.5 and 2.5 years peaks.

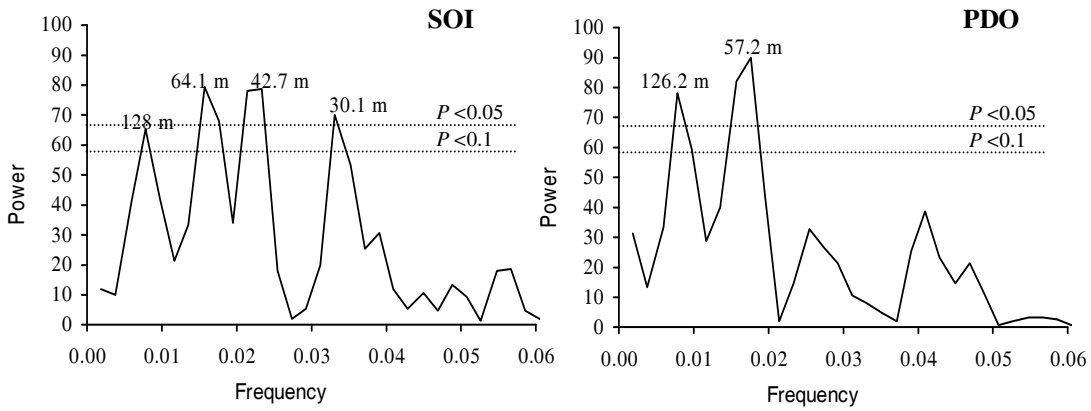

Figure 4 Fourier periodogram of the 1975–2004 series of SOI and PDO.

We have used wavelet spectral analysis to represent temporal variability of periodic signals on deseasonalized monthly streamflow time series. This method has been used for various studies, especially in hydrologic and atmospheric sciences. Torrence and Compo 1997 and Labat 2005 are considerable studies that focused on climatic index, specifically on SOI index. Labat 2005 showed low-intensity but statistically significant 6-y ENSOrelated interannual variability corresponding to the Pacific Coast Rivers in global asian rivers. Fig.5 shows Karun River 3-4 and 5-6 years interannual variability with maximum power peaks on 1991 (corresponds to the 95% statistical confidence level). Whereas Bazoft River shows weak 3-4 years but strong 2-3 years variability (restricted from 1991 to 1996). Such oscillations may be related to the already ENSO occurrences. It is also evident in Fig. 5, the decadal (and near decadal) signal that could be related to PDO phenomenon.

5. Conclusions

In this paper, appropriate analyses of streamflow variability are exposed. Both statistical and spectral analyses highlight existence of trends and oscillations in different state. Mann-Kendall and seasonal Kendall analyses showed downward direction of trends in general. However, negative flow trends vary in significance through the region. Karun River exhibits powerful and significant decreasing trend, especially during low water months (August to November). Such behavior is obvious in Bazoft River, although with low intensity. These negative trends (especially during summer and autumn) are probably corresponding to temperature increasing, specifically in snowmelt season (due to global warming).

Our spectral analysis has produced evidence of interannual variability (3-4 and 5-6 years), especially in Karun River. Connection between these impermanent variations

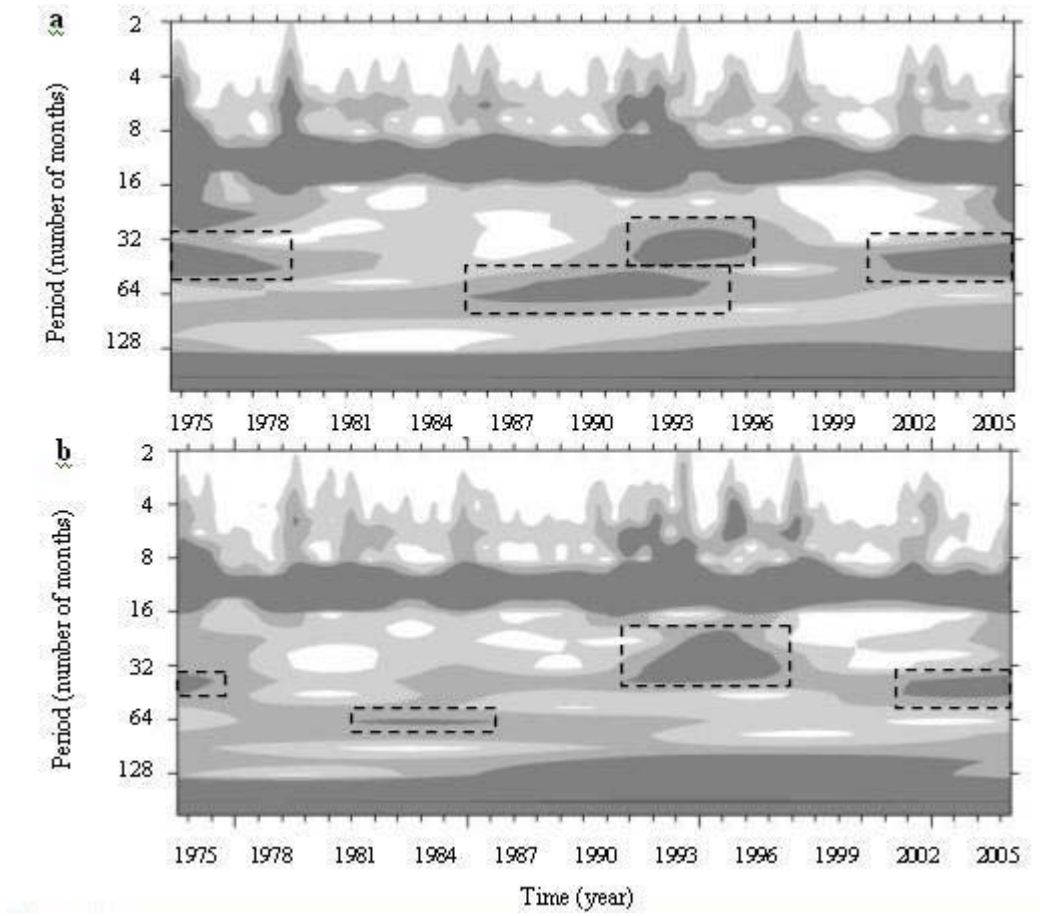

Figure 5 Wavelet spectrum of deseasonalized monthly streamflow time series at Armand (a) and Morghak (b) stations.

and ENSO is clearly discernible and useful for long-term fluctuations prediction in this arid region. Also we observed near decadal variability. However, the short length of the streamflow series can obscure such these results (quasi-decadal and decadal results).

Our results show that changes of the streamflow regime in this region were partly complex and need to be reanalyzed with inclusion of the influences of precipitation and temperature variables to be better understood. Therefore it will be plausible to investigate whether relations exist between trend and periodicity.

6. References

Ames, D.p., (1998). "Seasonal to Interannual Stream Flow Forecasts Using Nonlinear Time Series Methods and Climate Information". A Thesis of Master of Science, Utah State University, Logan, Utah.

Andrea I. Pasquini *, Pedro J. Depetris, (2006). "Discharge trends and flow dynamics of South American rivers draining the southern Atlantic seaboard." Journal of Hydrology 333, 385– 399.

Donald H. Born, Mohamed A. Hagh Elnur, (2000). "Detection of hydrologic Trend and Variability." Jurnal of hydrology 255, 107-122.

Ercan Kahya, Serdar Kalaycı, (2004). "Trend analysis of streamflow in Turkey." Journal of Hydrology 289, 128–144.

Hirsch, R.M., Slack, J.R., Smith, R.A., (1982). "Techniques of trend analysis for monthly water quality data." Water Resources 20, 107–121.

Karimi, Saman, (2006). "Short term flood prediction, in Karun River, IRAN." A Thesis of Master of Science, Sharif University of Technology, Tehran, Iran.

Kendall, M.G., (1975). "Rank Correlation Methods." Griffin, London, (202pp.).

Labat, D., (2005). "Recent advances in wavelet analyses: Part 1. A review of concepts." Journal of Hydrology 314, 275–288.

Labat, D., (2005). "Oscillations in land surface hydrological cycle." Earth and Planetary Science Letters 242, 143– 154.

Mann, H.B., (1945). "Nonparametric tests against trend." Econometrica 13, 245–259.

Qiang Zhang, Chunling Liu, Chong-yu Xu, Youpeng Xu, Tong Jiang, (2006). "Observed trends of annual maximum water level and streamflow during past 130 years in the Yangtze River basin, China." Journal of Hydrology 324, 255–265.

Sen, P.K., (1968). "Estimates of the regression coefficient based on Kendall's tau." Journal of American Statistical Association 39, 1379–1389.

Torrence, C., Compo, G.P., (1998). "A practical guide to wavelet analysis." Journal of American Meteorological Society 79 (1), 61–78.

Zhang, X., Harvey, K.D., Hogg, W.D., Yuzyk, T.R., (2001). "Trends in Canadian streamflow." Water Resour. Res. 37 (4), 987–998.

Developing Artificial Neural Networks to Represent Salinity Intrusions in the Delta

Francis I Chung [1] and Sanjaya A. Seneviratne[2]

[1] Modeling Support Branch, California Department of Water Resources, P.O Box 942836, Sacramento, 1416 Ninth Street; PH (916) 653-5924; FAX (916) 653-9574; email: chung@water.ca.gov
[2] Modeling Support Branch, California Department of Water Resources, P.O Box 942836, Sacramento, 1416 Ninth Street; PH (916) 654-5345; FAX (916) 653-9574; email: sanjaya@water.ca.gov

ABSTRACT

Impacts of 1 ft and 2ft sea level rise on Delta operations and salinity increases at export locations are quantified in this memo. California Department of Water Resources (DWR) uses many numerical models to study the Sacramento- San Joaquin Delta operations. Delta Simulation Model (DSM2) was used to calculate the salinity at some key locations in the Delta and to train Artificial Neural Networks (ANN) for each of the sea level rise scenarios. ANNs generated here are flow salinity relationships that calculate electrical conductivity (EC) at a given location using Delta boundary flows. CalSim II (Central Valley Project and State Water Project operation model) was used to determine the extra cost of water to mitigate the sea level rise. In this study current operation rules specified in State Water Resources Control Board's (SWRCB) Water Right Decision 1641 (D 1641) were assumed unchanged.

INTRODUCTION

Sacramento San Joaquin Delta

Sacramento-San Joaquin Delta (Delta) covers 738,000 acres interlaced with hundreds of mile of waterways. Much of the land is below sea level and relies on more than 1,000 miles of levees for protection against flooding. The Delta is unique and valuable resource and an integral part of California's water system. It receives runoff from 40 percent of the State's land area including Sacramento, San Joaquin and east side streams (DWR, 1987). Its land and waterways support communities, agriculture, and recreation and is the focal point for water distribution throughout the State.

The Sacramento-San Joaquin Delta is a tidal estuary. Water levels vary greatly during each tidal cycle, from less than foot near Sacramento to more than five feet at Martinez (down stream end of Figure 1). During the tidal cycle flows can vary in direction and amount. Tidal action and Delta outflow creates a gradual salinity gradient from the Pacific Ocean into the interior Delta.

Two major water export facilities are dependent on Delta waterways and the levees. Banks pumping plant provides water to the State Water Project (SWP) via the California Aqueduct while the Tracy (renamed Jones) pumping plant provides water to the Central Valley Project (CVP) via the Delta Mendota Canal. These water projects are operated under strict guide lines spelled out in D1641 (SWRCB, 2000). Upstream reservoir releases, Delta cross channel operation, amount of pumping are controlled to satisfy the standards in D1641.

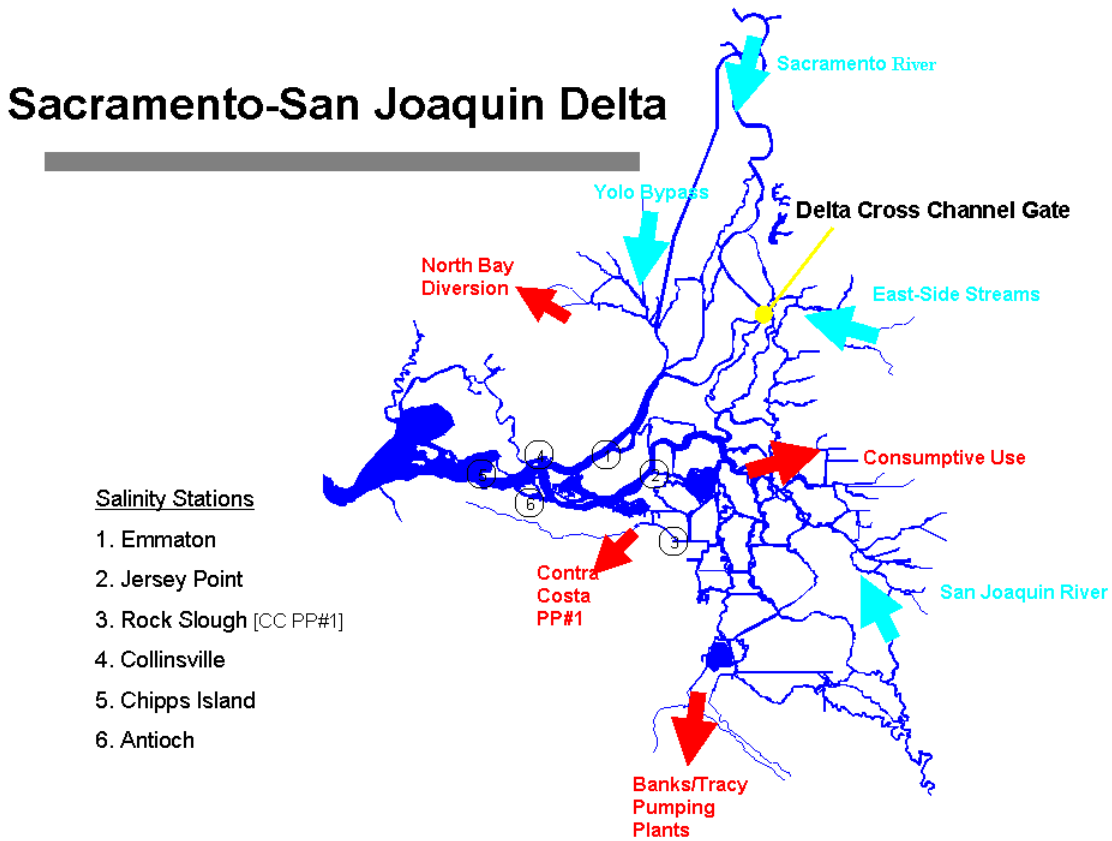

Figure 1: Locations where Delta salinity Standards are specified

Numerical Models

California Department of Water Resources (DWR) uses the following models for long term planning of SWP and CVP operations. Field data and outputs from many other models are used to derive inputs to these models.

Water Resources Integrated Modeling System (WRIMS), is a generalized water resources simulation model for evaluating alternatives in a Water Resources System. CalSim II is the application of WRIMS, and specifically used as a planning tool to simulate the State Water Project (SWP) and the Central Valley Project (CVP). CalSim II (DWR, 2002a) model has been applied to simulate the CVP and SWP systems at various levels of development, system configurations, and demand scenarios and operations rules. One such operation rule is the

salinity standards imposed at various locations in the Delta to protect the environment of the Delta. Currently the controlling locations in CalSim II are Rock Slough, Jersey Point, Emmaton, Collinsville, Chipps Island and Antioch. In addition to these 6 stations X2 (approximate location of 2000 parts per million total dissolved solids) locations are specified during certain months of the year. An 82 year simulation of CalSim II takes approximately 30 minutes.

Delta Simulation model (DWR, 2002b) is one dimensional hydro dynamics and water quality model. The model can calculate stages, flows, velocities; many mass transport processes, including salts, multiple non-conservative water quality constituents, temperature, and tracking of individual particles for given upstream flow boundary condition and downstream stage boundary. Conceptually DSM2 simulates flow conditions and concentration of water quality constituents (conservative and non-conservative mass) and tracks movements of individual particles in a network of channels. To simulate 1 year of salinity in the Delta, DSM2 takes about 1 hour of computing time in a 3.0 GHz windows XP machine. Therefore due to extensive computing time using DSM2 to calculate salinity at controlling locations in CalSim II would not be feasible.

Artificial Neural Networks (ANN) was used to develop flow salinity relationships (Sandhu et al., 1999) in the Delta enabling fast predictions of salinity at the controlling locations. ANN is considered a universal approximator and it is capable of theoretically modeling any continuous nonlinear function. With a proper network setup and training, an ANN can be reasonably accurate and robust on new data.

Sea Level Rise Estimates

Most mainstream scientists agree that global climate change causes an increase in temperature, thus an increase in global sea level rise. What is uncertain is the extent of the sea level rise at a given future time. Sea level rise increases the threat of salinity intrusion, floods, levee failure, coastal inundation and habitat changes.

Acceleration of global sea level changes has been observed in both tide gauge and satellite altimeter data. Ranges of future sea level changes have been projected by international climate change panel and several leading scientists. However, there have been no previous reports on designing probability curve for practical planning purposes.

Rising sea levels would enter the Delta though San Francisco Bay and would bring higher water levels and salinity concentrations. Water managers need methods for quantifying the increased salinity intrusion to develop strategies for protecting the Delta's future water quality and California's future water supply. The California Department of Water Resources (DWR) has developed a methodology for creating Artificial Neural Networks to estimate salinity intrusion for sea level rise scenarios. The ANNs can be incorporated into decision making tools to assess potential impacts of sea level rise on water project operations.

As shown in Figure 2 (Roos, 2004) sea level at the Golden Gate of California has been increasing by 0.08 inches per year over last century. If the historical rate of sea level rise were to

continue in the future additional 0.3 ft rises occur at mid century and 0.7 ft increase at the end of the 21st century.

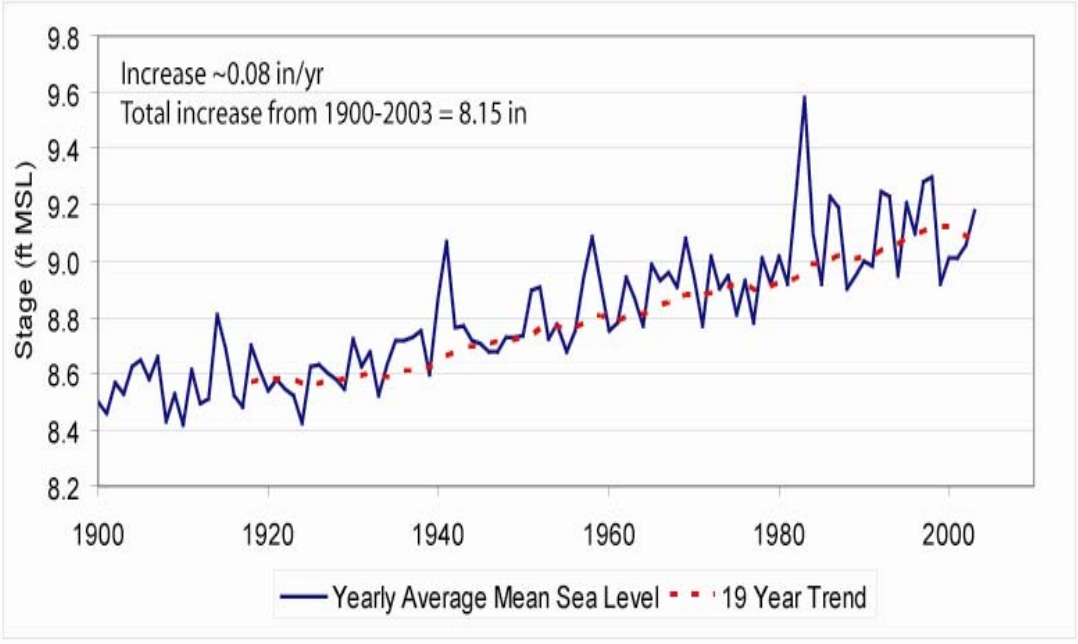

Figure3: Historical sea level at Golden Gate Bridge, San Francisco

The Third Assessment report of the Intergovernmental Panel on Climate Change (IPCC 2001) projected a global mean sea rise by 0.3 ft to 2.9 ft between 1990 and 2100 for the full range of greenhouse gas emissions described in IPCC Special Report on Emission Scenarios (IPCC SRES, 1996). The IPCC Fourth Assessment Report (IPCC 2007) projected a sea level increase from 0.6 ft to 1.93 ft for this century (2000 to 2100) depending on selected emission scenarios. Compared to the third assessment, the fourth assessment reduces the estimated projection of sea level rise by nearly 1 foot. CalFed Independent Science Board (Mount) using Rahmstorf's semi empirical approach predicted an increased uncertainty of projections in sea level rise. Figure 3 summarizes the sea level rise estimates from 3 different sources.

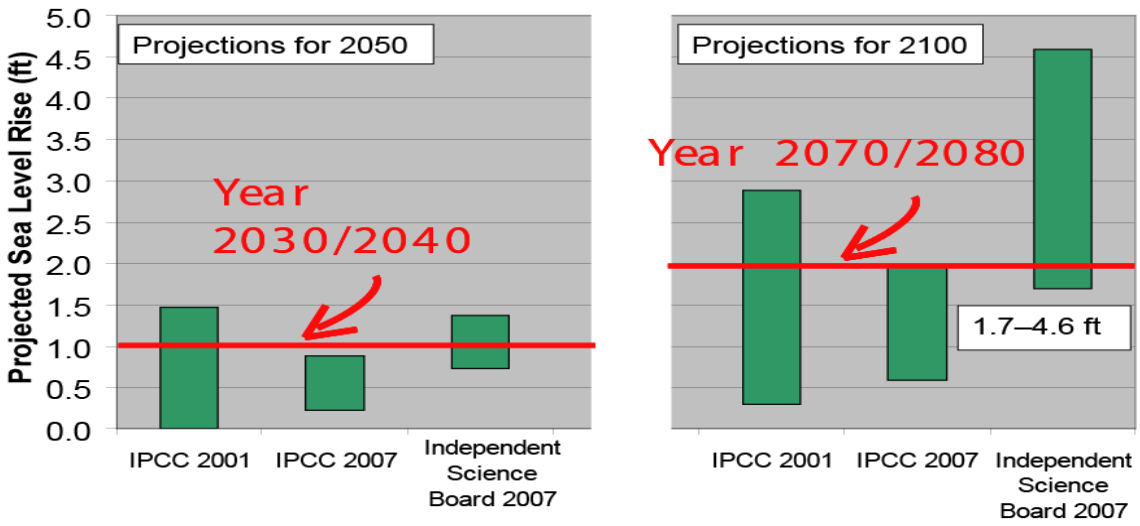

Figure 3: Mid and End of century sea level rise projections

MODELING

Delta Simulation Model assumes that Delta levees are high enough to prevent water overflowing the banks at peak sea level rise (two feet sea level rise). To prevent any tidal reflection from the upstream boundary both Sacramento river and the San Joaquin river were extend upstream by about 10 miles to gain an elevation increase of 3 feet.

DSM2 uses Martinez as its seaward boundary condition which is 54 km away from the ocean. At present for 16 year planning tide Martinez EC is calculated using a complex relationship between several EC stations and net Delta outflow. However with changes in sea level this relationship cannot be used to compute Martinez EC. A preliminary study was done to measure the sensitivity of salinity changes at export locations for different values of boundary (Martinez) salinity. Assuming zero sea level rise, Martinez salinity was increased by 2%, 5%, 7% and 9%. DSM2 model was used to model the salinity increase at the export locations.

DSM2 being a one dimensional model cannot handle vertical dispersion that arises due to sea level rise. Hence salt propagation into the Delta modeled by DSM2 is much less than salt propagation by multi dimensional models. Therefore in order to propagate salt in DSM2 tidal amplitude had to be artificially increased. A study for the Public Policy Institute of California report (PPIC, 2008) used a one dimensional tidally averaged model called WAM (water analysis module) developed by Resources Management Associates to explore the effects of 1 ft and 3 ft sea level rise. WAM uses dispersion algorithms developed from three dimensional modeling work (Gross et al, 2007). From the WAM studies (URS, 2007) it was found that Martinez EC for 1ft and 2ft is approximately 6% and 11% higher than the DSM2 base study. Jersey Point is considered the gateway for salt intrusion into interior Delta. Tidal amplitude was increased in DSM2 studies to match the percent increase of salt from WAM study outputs at Jersey Point. It was found that incorporating a 4" (9%) and 8" (18%) tidal increase propagated enough salt. In reality it is unclear whether the amplitude will change with the sea level rise. For the last century

San Francisco tidal amplitude increase by 2.5 inches while at Monterey the tidal amplitude reduced over 6 inches (Flick et al., 2003).

ANN tool in MATLAB was picked to develop flow salinity relationships mainly because of better graphics and plotting capabilities. Five different hydrologic scenarios were used in the training process. These 5 scenarios were picked to ensure that training data (calibration data) encompasses a wide range of hydrology. For the purpose of training ANN, 117 antecedent conditions were used with the following inputs. Inflows into the Delta from the north, Inflows from the south, channel depletions, exports, cross channel operation and tidal range. Each study was randomly perturbed with a maximum limit of ±30% to ensure that the training data captures extreme events. 80% of all results were used for training ANN and the remaining 20% were used as verification. The data used for training was randomly selected. Results obtained from ANN were compared with DSM2 results to ensure validity of using ANN in CalSim II (Seneviratne and Wu, 2007)

At present CalSim II uses Kimmerer-Monismith (KM) (Jassby et al., 1995) equations to calculate X2 locations in the Delta for a given Delta outflow. The empirical formula developed by KM used real time data. This equation ceases to be valid when down stream boundary elevation (mean sea level) is different from historical conditions. DSM2 model was used to develop new ANNs for X2 for the base case and different sea level scenarios and these were implemented in CalSim II. CalSim II model had to be restructured to accommodate this feature.

RESULTS

ANN development

ANN predicted salinity and DSM2 generated Salinity were compared at salinity controlled stations. Figure 4 shows a very good comparison between ANN and DSM2 at Jersey Point for the base case. All control stations had a similar good fit between ANN and DSM2.

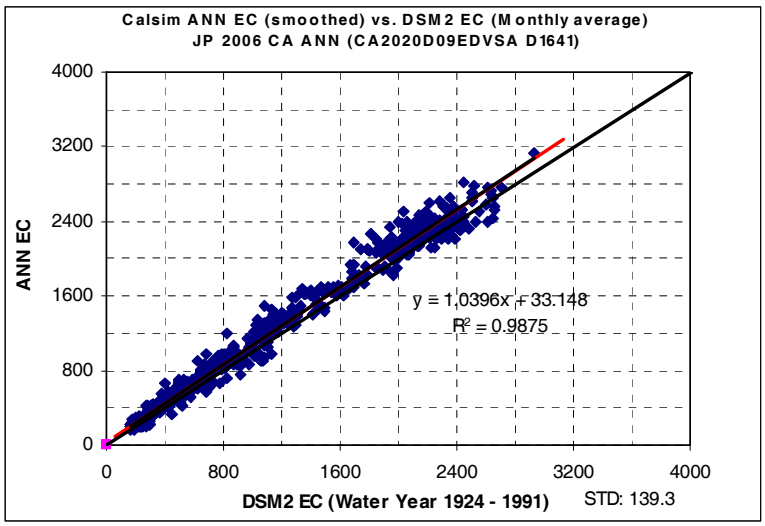

Figure 4: Comparison between DSM2 and ANN predicted salinity.

Sensitivity Analysis of Boundary salinity

Table 1 shows the average monthly sensitivity of Martinez EC at some key export locations in the Delta. The table below shows the increase in EC at Banks and Jones (Tracy) export locations purely due to a hypothetical increase in EC at Martinez. For the six month period between February and July the impact due to an increase in Martinez EC is negligible. This is because during this period high Delta outflows tend to push the ocean salt away from the Delta. For the period between August to January the Delta outflow is at its lowest. Even during this period the salinity impact at the pumping locations are not highly sensitive to changes in the boundary EC.

Table 1: Sensitivity Analysis of Boundary salinity.

Martinez	SWP Intake		CVP Intake	
(EC increase)	(Aug-Jan)	(Feb-July)	(Aug-Jan)	(Feb-July)
2%	0.75%	0.19%	0.64%	0.16%
5%	1.88%	0.47%	1.60%	0.41%
7%	2.63%	0.66%	2.23%	0.57%
9%	3.38%	0.85%	2.87%	0.73%

Salinity Increase due to Sea level Rise

Without changing any operations (Inflows to Delta, Exports and Delta Cross Channel operation) DSM2 studies were conducted for base case (zero sea level rise), 1ft and 2ft sea level rise scenarios. The following table shows a summary of EC impacts at SWP and CVP export locations in the Delta for the 2 different sea level rise scenarios.

Table 2: Sensitivity Analysis of Boundary salinity.

Alternatives	CCFB Intake		CVP Intake	
	(Aug-Jan)	(Feb-July)	(Aug-Jan)	(Feb-July)
1 ft Mean sea level rise	23%	8%	20%	7%
2 ft Mean sea level rise	53%	20%	45%	16%

As discussed before for periods of high Delta outflow (February through July) the increase in salinity is lower than for low outflow periods (August through January). Impacts at CVP intake is a little less than the SWP intake because the CVP intake is further away from the ocean influence.

Reduction in Exports

CalSim II model was run for a period of 82 years. The following tables show the reduction in the ability to deliver water due to sea level rise scenarios for three significantly important periods, long term average (1921-1994), long term drought periods (1928-1934 and 1986-1992) and the most severe drought (1976-1977).

Table 3: Reduction in Exports due to 1ft sea level rise.

	Exports		
Periods	Base	change	%change
1928-1934	3553	-117	-3.3%
1976-1977	3598	-59	-1.6%
1986-1992	3941	-305	-7.7%
1922-1993	5939	-130	-2.2%

Table 4: Reduction in Exports due to 2ft sea level rise.

	Exports		
Periods	Base	change	%change
1928-1934	3553	-489	-13.8%
1976-1977	3598	-341	-9.5%
1986-1992	3941	-647	-16.42%
1922-1993	5939	-472	-7.9%

CONCLUSIONS

a) Successful ANNs were developed for all salinity controlled stations in the Delta for base case and the 2 sea level rise scenarios.
b) Sensitivity of salinity at export locations due to changes in Martinez salinity is low. Hence for the existing Delta boundary conditions any error in computing the Martinez boundary EC becomes insignificant. This is especially so during the period February – July when Delta outflow is high. For the period between August-January where ocean salt tends to dominate the estuary rather minimal impact is observed due changes in Martinez salinity.
c) For sea level rise scenarios the water quality at export locations increase approximately 50% during certain periods of the year. This will increase the treatment cost for the end user to meet the drinking water standards. In addition to lower water quality the amount of water that can be delivered is reduced significantly during drought years. For example for 2ft sea level rise, the ability to export due to sea level rise dropped by 16% during the recent prolonged dry years.

REFERENCES

California Department of Water Resources. (1987). "Sacramento-San Joaquin DELTA ATLAS"

California Department of Water Resources. (2002a). "CalSim Water Resources Simulation Model II"
http://modeling.water.ca.gov/hydro/model/index.html

California Department of Water Resources. (2002b). "An Introduction to the Delta Simulation Model II for simulation of hydrodynamics and water quality of the Sacramento-San Joaquin Delta"
http://baydeltaoffice.water.ca.gov/modeling/deltamodeling/models/dsm2

California State Water Resources Control Board. (2000). Revised Decision 1641. "Decision implementing flow objectives for the Bay-Delta estuary. Revised accordance with order WR2000-02"

Flick, R.E., J.F. Murray, C.E Lesley. (2003). "Trends in United States Tidal Datum Statistics and Tide Range." *Journal of Waterway, Port, Coastal, and Ocean Engineering*, 129:4. July 1.

Roos M. (2004). Maury Roos, California State Hydrologist, California Department of Water Resources, personal communication.

Gross, E.S., M.L. MacWilliams, and N. Nidzieko. (2007). "Three-Dimensional Salinity Simulations of Sea Level Rise Scenarios," Delta Risk Management Strategy, California Department of Water Resources

Intergovernmental Panel on Climate Change. (2001). "Climate Change 2001: IPCC Third Assessment Report."

Intergovernmental Panel on Climate Change. (2007). "Climate Change 2007: IPCC Fourth Assessment Report."

Intergovernmental Panel on Climate Change Special Report on Emission Scenarios. (1996)
http://www.ipcc.ch/ipccreports/sres/emission/index.htm

Jassby A.D., W.J. Kimmerer, S.G. Monismith, C.Armor, J.E. Cloern, T.M. Powell, J.R. Schubel, T.J. Vendlinski. (1995). "Isohaline position as a habitat indicator for estuarine populations." Ecological Applications 5:272-289

Mount Jeffrey Dr. (2007) "RE: Sea Level Rise and Delta Planning." Memorandum to Michael Healey, Lead Scientist, CALFED Bay-Delta Program fro chair of the CALFED Independent Science Board. 6 Sep 2007.

Public Policy Institute of California. (2008). "Comparing Futures for Sacramento-San Joaquin Delta".

Rahmstorf S. (2007). "A semi-empirical approach to projecting future seal level rise" *Science, V.315*

Sandhu, N., D.Wilson, R. Finch, and F. Chung. (1999). "Modeling Flow Salinity Relationships in the Sacramento-San Joaquin delta using Artificial Neural Networks" Technical Information Record OSP-99-1, California Department of Water Resources.

Seneviratne S., S Wu. (2007). Chapter 3: "Enhanced Development of Flow Salinity Relationships in the Delta using Artificial Neural Networks: Incorporating Tidal Influence." In: *Methodology for flow and salinity Estimates in the Sacramento-san Joaquin Delta and Suisun marsh. 28th Annual Progress Report to the SWRCB*. California Department of Water Resources.

URS Corporation/Jack R. Benjamin & Associates Inc. (2007). Technical Memorandum: Delta Risk Management Strategy (DRMS) Phase 1, Topical area: Water Analysis Module (WAM) Draft 2, June 15 2007. Prepared for California Department of Water Resources.

Developing Best Practices for Computer Aided Dispute Resolution

S. Langsdale[1] and L. Bourget[2]

[1]Institute for Water Resources, U.S. Army Corps of Engineers, 7701 Telegraph Road, Alexandria, VA 22315; PH (703) 428-7245; FAX (703) 428-8171; email: slangsdale@gmail.com
[2]Institute for Water Resources, U.S. Army Corps of Engineers, 7701 Telegraph Road, Alexandria, VA 22315; PH (715) 386-0124; FAX (715) 386-0124; email: elizabeth.c.bourget@usace.army.mil

ABSTRACT

Computer aided dispute resolution (also known as collaborative modeling or shared vision planning) combines technical analysis and modeling with collaboration and traditional planning principles in order to address complexity, manage conflict, promote learning and understanding, and build relationships among stakeholders. The participatory process enhances model credibility, while the model supports the decision-making process and promotes group learning. Computer aided dispute resolution is a relatively new field, and current practitioners generally have a unique mix of technical and process skills that enable them to conduct this groundbreaking work. To train the next generation of practitioners and to ensure high quality work, we must identify and communicate the necessary skills and practices that support successful processes. With this objective, in the fall of 2008, the Environmental and Water Resources Planning and Management Committee established a task committee to formulate and document best practices in this developing field. The task committee will deliberate and advise which elements of the case study context, team member skills, process design elements, and modeling approaches are critical for incorporating computer aided dispute resolution into water resources planning and management successfully. The products of this task committee will include a written monograph, dissemination of results at conferences, and an evaluation of next steps. In this presentation, we will share progress to date and invite audience feedback and participation.

INTRODUCTION

In a recent editorial in the Journal of Water Resources Planning and Management, Werick and Palmer called for a new Standards of Practice in Water Resources Planning, stating that "now is an excellent time to assemble the emerging approaches that have universal appeal to planners and that can be applied to a broad range of problems." They also note that they "are not alone in the belief that water planners should publish best practices" (Werick and Palmer, 2008). The Environment and Water Resources Institute (EWRI) has established a Best Practices in Collaborative Modeling task committee to produce a manuscript that will help meet this need regarding the use of computer aided

dispute resolution (CADRe) in water resources planning and management for the next generation of practitioners.

CADRe is a relatively new field, and current practitioners generally have a unique mix of technical and process skills that enable them to conduct this groundbreaking work. To train the next generation of practitioners and to ensure high quality work, we must identify and communicate the necessary skills and practices that support successful processes.

CADRe DEFINED

Computer Aided Dispute Resolution (CADRe) is a general title for the methodology used by a number of agencies, university researchers and private consultants who have been marrying technical decision support tools with collaborative processes. In CADRe, the technical tools are collaboratively developed by actively engaged stakeholders, so that all parties are aware of and in agreement about the system characterization and data used to support it. The approach addresses complexity, manages conflict, promotes learning and understanding, and builds relationships among stakeholders. The participatory process enhances model credibility and helps ensure that the full breadth of stakeholder concerns are reflected, while the model supports the decision-making process and promotes group learning. Consensus is not the single goal of the process; however, CADRe may increase the chance of identifying win-win alternatives.

CADRe IN USE

CADRe traces its roots to water supply planning for the Washington DC region in the mid-1970s. CADRe has been applied to the full spectrum of stages in the planning process. A recent collection of case studies (Stephenson, Shabman, et al., 2008) shows CADRe being used in situations as varied as anticipatory processes intended to lay the groundwork for future exercises, to examination of alternatives for changing dam operations. CADRe is being utilized within both the public and private sector. For example, the Corps of Engineers' path in developing CADRe began with Drought Preparedness Studies in the early 1990's, which evolved into Shared Vision Planning: a process that uses traditional Corps planning principles but modified to include earlier and more intensive collaboration with a wide variety of stakeholders. Sandia National Laboratories has also developed models through collaborative processes to support watershed planning. In recent years, the U.S. Institute for Environmental Conflict Resolution, which supports Alternative Dispute Resolution, is exploring and fostering the use of technical tools to support their collaborative processes. CADRe has also been employed by private firms to solve complex water resources issues. Its growing use by a variety of practitioners creates an expanding body of expertise and knowledge.

CHALLENGES TO FUTURE AND IMPROVED USE

Although CADRe has been used successfully in numerous projects, challenges exist to increasing and improving future use. Perhaps first and foremost is awareness.

Computer modeling provides a common basis for decision-making, but the deliberate early and continuing integration of public participation with computer modeling is not widely used, and the potential benefits of this deliberate integration are not always readily apparent. Furthermore, terminology and practice can be confusing or misleading. There is a wide spectrum of public involvement, ranging from broad-based early and ongoing collaboration to more limited back-end information sharing with an opportunity to submit comment. There is also a wide spectrum in the adaptability of computer models or systems of computer models, ranging from the application of standard single-purpose models with pre-determined input and output to relational models (or suites of linked models) capable of being adjusted to incorporate new input, new relationships, and new ways of displaying output. CADRe strives for early and iterative collaboration with key stakeholders using adaptable computer models. So while some may say that they use computer aided dispute resolution, and may in fact both involve the public and use computer models, the degree to which the two facets are integrated may be limited, possibly with consequent limits in potential benefits (see Figure 1.)

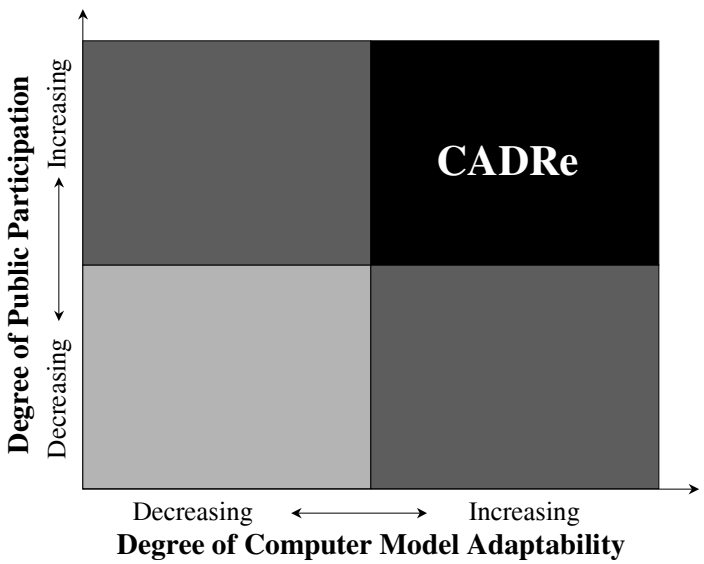

Figure 1. Integration in CADRe

The unique skill sets required to implement CADRe pose a second challenge to its further use and improvement. Computer modelers abound, but more are comfortable with applying existing models than with changing the models themselves, and fewer still have skills so important to involving the public: listening skills, the ability to communicate effectively with both technical and non-technical partners, and an understanding of how the process itself can support successful participation. Professional facilitators are trained in these important skills but may lack access either to appropriate technical tools, or to those with the expertise to adjust models in response to changing expectations and understanding. Opportunities to learn the full suite of needed skills, or to connect experts that in partnership encompass effectively the full suite of needed skills, have to date been limited.

Uncertainty regarding CADRe processes and their outcomes can also pose challenges to its further use and improvement. Modelers may wonder why they should consider adjustments to models they may have used for years, or may question how participation by non-technical partners might improve technical models. Organizations may raise concerns about the time needed up-front to understand various participants' concerns and how that time fits with their more standard processes and expectations. They may worry that including unaccustomed partners, particularly early in the process but also throughout, may lead to some loss of control. There may be comfort with historical approaches, uncertainty regarding what the results may be if change is instituted, and questions as to whether the risk inherent in those changes is worth undertaking them. While many case studies exist, and some have been documented, there is limited systematic documentation of what works, what doesn't, and what it all means.

EWRI TASK COMMITTEE ON CADRe BEST PRACTICES

A Task Committee under the Environment and Water Resources Institute (EWRI) of the American Society of Civil Engineers is an ideal vehicle for helping overcome the challenges to further CADRe use and improvement in water resources planning. EWRI's vision includes the integration of technical expertise and public policy for planning related to water resources, and it is committed to accomplishing this vision through a diverse membership, excellence in products and services, collaborative partnerships, and innovative programs and solutions. Its 22,000-strong membership encompasses its foundation within its traditional civil engineering base, but also includes non-civil engineer allied professionals. And EWRI's committee structure provides a way to establish an interested team of professionals and to give that team some organizational support so that it can help advance and serve the profession through such means as publications, reports, conferences, and continuing education seminars.

Goals and Products. Seeking to share the lessons learned by CADRe practitioners, increase awareness, and raise the bar for CADRe's further use, a group formed an EWRI Task Committee in the fall of 2008 entitled "Best Practices for Collaborative Modeling." The Task Committee, housed under the Environmental and Water Resources Planning and Management Committee, will focus on developing best practices for incorporating computer aided dispute resolution processes into participatory water resource planning, documenting the results, and summarizing key findings. Its efforts can yield increased level of detail over what is now available, provide guidance on when and how to use computer aided dispute resolution processes, and offer ways to evaluate the success of participatory processes in water resources planning. Work by the Task Committee will take note of cutting-edge efforts now underway by the U.S. Army Corps of Engineers' Institute for Water Resources to develop means to evaluate the success of CADRe processes.

The Task Committee's primary product will be a monograph that documents and summarizes key findings, with anticipated completion in 2010. The monograph will help address the need for systematic documentation of high-caliber CADRe practices and their

evaluation. Dissemination of the monograph will increase awareness of CADRe process goals and benefits, and will help ensure high quality work as the relatively new field develops and matures. The Task Committee will also seek to disseminate information in other ways as appropriate and feasible, such as at conferences. At the conclusion of its work, the Task Committee will evaluate what further steps may be appropriate.

Next Steps. Reaching out to partners and practitioners is important for ensuring a high quality product. The Task Committee continues to welcome new members interested in participating. Possible contributions range from providing references, to writing a short case study that illustrates a "best practice," to presenting Task Committee results.

The Task Committee has established a core group of anticipated monograph authors, and has begun to frame a conceptual monograph outline, to be discussed by contributors. We anticipate later identifying a select group to review the draft monograph.

CONCLUSION

The EWRI Task Committee on Best Practices for Collaborative Modeling provides a valuable role in furthering the use of CADRe in water resources planning. The Task Committee is in its early stages and welcomes feedback on its plans, additional information from CADRe practitioners regarding best practices, and participation by those interested in helping to advance this developing field.

REFERENCES

Stephenson, K., Shabman, L., et al. (2008). "Computer Aided Dispute Resolution: Proceedings from the CADRe Workshop." Institute for Water Resources. IWR Report 07-R-6.

Werick, William J., and Palmer, Richard N. (2008). "It's Time for Standards of Practice in Water Resources Planning." *Journal of Water Resources Planning and Management*, ASCE, 1-2.

Development of a Fuzzy Based Pipe Condition Assessment Model Using PROMETHEE

Yi Zhou[1]; Kala Vairavamoorthy[2]; Frank Grimshaw[3]

[1.] Dept. of Urban Water and Sanitation, UNESCO-IHE, P.O. Box 3015, 2601DA Delft, the Netherlands; Wuhan University, Wuhan, 430072, China; email: yzhou@unesco-ihe.org

[2.] Dept. of Urban Water and Sanitation, UNESCO-IHE, P.O. Box 3015, 2601DA Delft, the Netherlands; School of Civil Engineering, the University of Birmingham, Edgbaston, Birmingham, B15 2TT, UK; Tel: +44 (0)121 4145147, email: k.vairavamoorthy@bham.ac.uk

[3.] Severn Trent Water Limited, 2297 Coventry Road, Birmingham, B26 3PU, UK, Tel: +44 (0)121 722 4117; email: frank.grimshaw@severntrent.co.uk

ABSTRACT

The deterioration of pipes in water distribution systems is a serious problem for water utilities. In order to rehabilitate the deteriorated pipes in a planned and proactive way, there is a need to have a better understanding of pipe condition assessment.

Pipe condition assessment can be regarded as a multiple criteria decision making problem. A new model for pipe condition assessment is developed using fuzzy PROMETHEE II. The model processes four first-level and seven second-level pipe condition indicators and then generates a pipe condition index for each pipe in the system. The weight for each indicator is generated by using Analytic Hierarchy Process (AHP).

The paper presents the application of the new method to some pipes in a water distribution system. This application demonstrates both the stability of the new method and its ability to generate results that will greatly assist decision makers in the development of their rehabilitation strategies.

KEY WORDS:

Pipe condition assessment; Multi-criteria decision making; PROMETHEE; Water distribution system

INTRODUCTION

Pipe breakage is caused by numerous human and natural factors. Proactive rehabilitation and replacement is an effective way to avoid excessive financial losses.

Budgetary constraints make prioritizing pipe rehabilitation and/or replacement essential. An important component of the prioritization process is pipe condition

assessment that should be based on available and reliable data.

Pipe condition assessment models can be generally classified into three categories: physical based models, statistic based models and data mining models (Kleiner and Rajani 2001).

Physical based models usually involve several main influence factors of pipe deterioration, and their limitation is the requirement of extensive data and a detailed understanding of the various deterioration mechanisms. Statistical models also rely on an abundance of data but have more adaptability. Data mining models utilize both objective data and also experts' experience. For example, Yan and Vairavamoorthy (2003), applied the Fuzzy Compromise Programming techniques for pipe condition assessment, where the most important influence factors were identified and combined through a hierarchical process. Geldermann et al. (2000) proposed the use of a fuzzy algebra throughout PROMETHEE algorithm, which is flexible.

Pipe condition assessment involves several components such as breakage rate, water loss, water quality deterioration in distribution system etc. Pipe breakage rate is one of the main indicators to reflect pipe condition and also influence several other aspects. Therefore, pipe breakage risk (possibility of pipe breakage in the future), can be considered as a useful surrogate of pipe condition.

In this paper a new techniques for pipe condition assessment is proposed. The method is based on PROMETHEE, an outranking method, which brings together flexibility and simplicity for user. It includes two phases: the first one is the construction of an outranking relation on a criterion/indictor, and the second one is the exploitation of this relation in order to give a rank to each pipe.(Brans and Vincke 1985; Brans, Vincke et al. 1986),

In the first phase, a preference function is defined and a valued outranking graph, representing the preference of the decision maker, is obtained.

The exploitation of the outranking relation is realized by considering for each pipe a multi-criteria preference index (in terms of a leaving and an entering flow) in the valued outranking graph.

The main requirement of PROMETHEE is the weight and preference function of each criterion (Figueira, Greco et al. 2005). The proposed method falls into the category of data mining models. Compared with pervious data mining models, the model in this paper has several improvements. It places greater emphasis on the data that can be expected to be available. Another one is that only a few parameters are to be fixed in this method and they all have a pipe breakage signification so that expert is able to determine their values easily. Furthermore, the stability analysis at the end of this paper shows that some small deviations in the determination of weights do not often induce important modifications of the obtained rankings.

In this paper the PROMETHHEE method is first described and then demonstrated by means of a simple application.

MODEL ESTABLISHMENT AND SOLUTION

Influence factors. Numerous factors influence pipe breakage, e.g. ground load, pipe material, soil corrosion, pipe age, construction quality, pipe length, soil condition, breakage history, etc. Generally, the data available from water utilities include pipe diameter, pipe age, pipe material, length, and record of rehabilitation, and incident repair records (Boxall, O'Hagan et al. 2007). Data requirement of this model mainly rely on the generally available data from water utilities.

Structure of the model. The structure of the proposed model is shown in Figure 1.

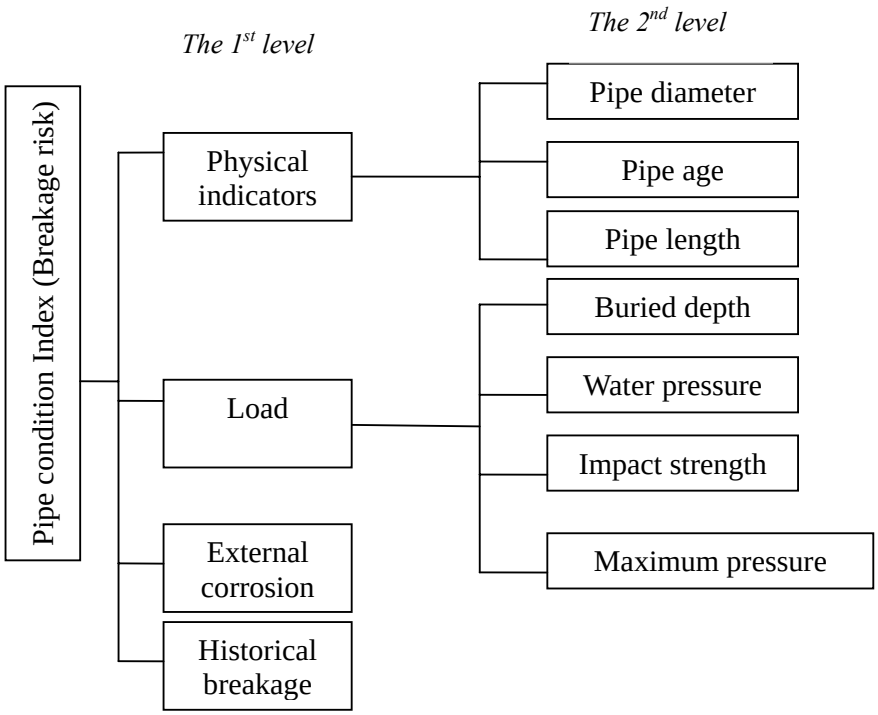

Figure 1 Structure of pipe breakage risk assessment model

As shown in Figure 1, two of the first level indicators (load and physical indicators), are aggregated indicators (from the 2nd level). Most of the 2nd level indicators used to generate these 1st level indicators can be obtained from water utilities. In addition, the 1st level indicator, historical breakage data can also be obtained from the water utility.

The external corrosion indicator is determined by a combination of soil corrosion and pipe material corrosion resistance(Vairavamoorthy, Sunil D. Gorantiwar et al. 2006). This method involves normalizing the score of soil corrosion and material resistance and then combining to generate an external corrosion indicator (that is then further normalized).

It should be noted that high values in the indictors: pipe age; buried depth; water pressure; external corrosion; and historical breakage rate; all suggest a higher

breakage risk for a pipe. These indicators are termed high risk indicators for the purpose of this paper. In contrast, the remaining indicators suggest a lower breakage risk (termed low risk indicators in this paper).

Weight for each indicator. The weights associated with different indicators reflect their relative importance to other indicators.

In the proposed method, the weights for the indicators are generated using Analytic Hierarchy Process (AHP). The foundation of this subjective weight method is experts' experience and opinion. As this is subjective, the weights can be regarded as fuzzy numbers that are distributed randomly in the neighborhood around the mean value of weights. The uncertainties associated with these weights are described later on in the paper.

Preference function. A key aspect of the PROMETHEE method is the preference function that is defined for each indicator. This function is used to compute the degree of preference associated to the high breakage risk in case of the pair-wise comparisons. It is often a function of the difference between two pipes. Brans and Vincke (1985) put forwards six basic types of PROMETHEE preference functions. In this research, the type and parameters of the functions are usually obtained from expert according to the specified indicator's influence to pipe breakage.

The linear preference function is continuous and easy to understand. Hence this type of preference function is used in this model. The function expression is as follow:

$$p(d) = \begin{cases} 0 & (d \le 0) \\ d & (d > 0)) \end{cases} \tag{1}$$

Where, d is two pipe's normalized difference in a specific criterion, $|d| \le 1$.

Calculation steps.

Let's consider the multi-criteria problem: ranking all pipe condition assessment with the finite set of pipes K, if there are k criteria f_i, ($i=1,2, \ldots,k$).

The basic steps of PROMETHEE are as follows:

1. Normalization

In order to compare and calculate, data must be first normalized before inputting into the RPOMOTHEE model.

For the high risk indicators the normalization formula is as follows:

$$y_{ij} = \frac{x_{ij} - x_{i\min}}{x_{i\max} - x_{i\min}} \tag{2}$$

For low risk indicators the normalization formula is as follows:

$$y_{ij} = \frac{x_{ij} - x_{i\max}}{x_{i\min} - x_{i\max}} \tag{3}$$

where, y is the normalized value, i, j is the ID of criteria and pipe; x_{ij} is the *j-th* pipe's

data in the *i-th* criteria/indicator; x_{imax} and x_{imin} is the maximum and minimum value in the *i-th* criterion.

2. Calculate multi-criteria preference index $\pi\ (a, b)$

Suppose that experts have specified a preference function p_i and weight w_i for each criterion f_i *(i=1, 2,…, k)*. The multi-criteria preference index $\pi\ (a, b)$ is defined as weighted average of the preference function $p_i\ (a, b)$:

$$\pi(a,b) = \frac{\sum_{i=1}^{k}(w_i \cdot p_i(a,b))}{\sum_{i=1}^{k} w_i} \tag{4}$$

$\pi\ (a, b)$ represents the experts preference intensity that Pipe *a* over Pipe *b*, when considering simultaneously all the criteria. It is a figure between 0 and 1 and:

If $\pi\ (a, b) \approx 0$, denote a weak preference of *a* over *b* for all the criteria.

If $\pi\ (a, b) \approx 1$, denote a strong preference of *a* over *b* for all the criteria.

These weights are fuzzy and are generated using the AHP (as mentioned earlier). Preference function $p_i\ (a, b)$ are obtained through expert's experience and knowledge. In this research,

$$p_i(a,b) = p_i(f_i(a) - f_i(b)) = \begin{cases} 0 & (f_i(a) \le f_i(b)) \\ f_i(a) - f_i(b) & (f_i(a) > f_i(b)) \end{cases} \tag{5}$$

where, $f_i(a)$ and $f_i(b)$ are the degree of preference for the comparison of pipes *a* and *b* in the *i-th* criterion respectively.

This preference index determines a valued outranking relation on the set *K* of pipes. This relation can be represented as a *valued outranking graph*, the nodes of which are the pipes of *K* (see Figure 2). Between two pipes (nodes in Figure 2), *a* and *b*, there are two arcs having values $\pi(a, b)$ and $\pi(b, a)$ (there is no particular relation between $\pi(a, b)$ and $\pi(b, a)$).

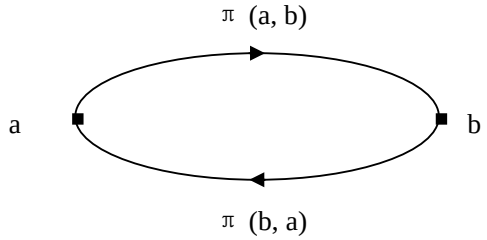

Figure 2 Flows in the valued outranking graph

3. Calculate net flow $\phi^{net}(a)$

For the node *a* in the valued outranking graph, the *leaving flow* can be defined as

$$\phi^{+}(a) = \sum_{b \in K} \pi(a,b) \tag{6}$$

The leaving flow is the sum of the values of the arcs leaving node *a* and provides a measure of the outranking character of *a*.

Similarly, the entering flow can be defined by:

$$\phi^{-}(a) = \sum_{b \in K} \pi(b,a) \tag{7}$$

The entering flow measures the outranked character of *a*.

Then the *net flow* of pipe *a* is as follow:

$$\phi^{net}(a) = \phi^{+}(a) - \phi^{-}(a) \tag{8}$$

Basically, the higher the leaving flow and the lower the entering flow, the higher breakage risks this pipe.

4. Rank all the pipe condition

The last step is to sort the order of each pipe's net flow by a complete preorder:

a outranks *b* , if $\phi^{net}(a) > \phi^{net}(b)$;

a is indifferent to *b* , if $\phi^{net}(a) = \phi^{net}(b)$

Stability of model. Because this model involves weights, whose influence to the ranking under minor changes always concerned by decision makers. Therefore, the model stability analysis is very important(Brans, Vincke et al. 1986). In this research, model stability analysis is needed due to weights from subjective uncertainty. Moderate stabilization is necessary for a good model. An unstable model's conclusion will change greatly due to some parameters' minor variations. Some random changes in a small interval will be applied for weights to simulate expert opinion's uncertainty. Then the variation's effect will be tested.

APPLICATION OF THE MODEL

The model has been applied to a sample of eight pipes, of four materials, with diameters varying from 200 to 900 mm. Table 1 shows the 10 indicators for each of the 8 pipes in the sample.

The value of parameters. The mean values of criterions' weights are generated using the AHP and are shown in Table 2, 3 and 4. As described in previous section, a liner preference function (Equation (5)) is used and the results of applying the PROMTHEE II are given in Table 5.

From the results shown in Table 5, it is clear that the net flow of Pipe 3 is the highest. This suggests that Pipe 3 has the highest breakage risk in this sample. Similarly, Pipe 6 has the lowest breakage risk. One of the main benefits associated with the calculated net flows, is that they indicate the sensitivity of the rank order of pipes in

relation to pipe breakage risks. This sensitivity can be analyzed by considering the interval size of net flow between adjacently ranked pipes. Where this interval is large, this indicates that a pipe's ranking position will not be affected by changes in the weights used (and where intervals are small then the rankings will be affected).

For example, in Table 5, the difference of net flow between Pipe 3 and 4 is 0.022, which is the smallest. And the difference of net flow between Pipe 6 and 8 is 0.082, which is the secondly smallest. This implies that these pipes' rank is easy to be affected by weights because the net flow is very close to that of its adjacent rank pipes.

To demonstrate the sensitivity of the rank order to changes in weights, and to highlight the role that the net flow can play in predicting changes in rank order, several applications of the PROMTHEE method were undertaken where the weights were varied between ±30% of mean value of weights.

The test calculation repeated numerous times. Table 6 shows the calculation results in five tests. If the result in Table 5 is a benchmark, Pipe 3 and 4 exchanges position three times, and Pipe 6 and 8 exchanges position twice. For most of the other pipes, their rank in this pipe set is stable because their net flows have a greater difference with other pipes. If more test calculations are taken, these two pairs of pipes often exchange their rank positions while others seldom do. These results agree with the previous analysis.

This example proves that the pipes with close net flow of other pipes are sensitive to the change of weights. It is difficult to make a fixed rank of pipe condition with close net flows. The general rank for all the pipes will not be greatly affected by the weight's variation. So the model has good stability though weights change within a small variation.

On the other aspect, in order to examine the validity of the model, test calculation of changing some variables' value (e.g. historical breakage rate) sometimes result the change of the pipe's rank of position. If such test calculation is done one indicator by one indicator, the results show that all the variables changing tendencies agree with that of general experience. For example, according to experience and statistic analysis, pipe condition is good if historical breakage rate is low and without any changes in other variables. If the breakage rate in Pipe 1 change from 0.329 to 0.20, its rank of position also change from 6 to 4. This denotes that this pipe's breakage risk decrease, which agree with general experience.

Table 1 Input data

No.	Criterion	Pipe ID							
		1	2	3	4	5	6	7	8
1	Pipe material	DI	DI	CI	CI	PVC	PVC	AC	AC
2	Diameter（mm）	500	700	900	600	300	200	400	500
3	Pipe age（year）	17	20	34	29	10	8	30	25
4	Pipe length (m)	530	565	698	974	1733	1509	1097	1462
5	Buried depth （m）	1.01	1.00	2.01	1.18	1.00	0.54	2.37	1.61
6	Water pressure （m）	33.82	31.23	42.35	32.56	50.5	49.88	51.5	38.37
7	Impact strength (m-kg/m)	102.5	102.5	150	150	4.4	4.4	23.5	23.5
8	Maximum pressure (Kg/cm^3)	54.87	54.87	56.1	56.1	11.73	11.73	20.4	20.4
9	External corrosion *	0.613	0.715	1.000	0.945	0.162	0.000	0.523	0.358
10	Historical breakage ($(yr•km)^{-1}$)	0.329	0.171	0.254	0.227	0.316	0.288	0.220	0.124

* External corrosion is determined by soil corrosion and pipe material together. And normalization has been done.

Table 2 Weight for physical indicators

Physical indicators	weight
Diameter	0.240
Pipe age	0.550
Pipe length	0.210

Table 3 Weight for load

Load	weight
Buried depth	0.239
Water pressure	0.207
Impact strength	0.229
Maximum pressure	0.324

Table 4 Weight for the 1st level indicators

The 1st level indicators	weight
Physical indicators	0.263
Load	0.186
External corrosion	0.322
Historical breakage	0.228

Table 5 The calculation results based on fuzzy PROMETHEE II

Rank	1	2	3	4	5	6	7	8
Pipe ID	6	8	5	2	7	1	4	3
Net flow	-0.907	-0.825	-0.504	-0.053	0.091	0.538	0.819	0.841
Difference of net flow	0.082	0.321	0.451	0.144	0.447	0.281	0.022	

Table 6 Pipe condition rank with weights change within ±30% variation

Pipe ID	1	2	3	4	5	6	7	8
The rank in the 1st test	6	4	8	7	3	1	5	2
The rank in the 2nd test	6	4	7	8	3	1	5	2
The rank in the 3rd test	6	4	8	7	3	1	5	2
The rank in the 4th test	6	4	7	8	3	2	5	1
The rank in the 5th test	6	4	7	8	3	2	5	1

CONCLUSION

In this paper, the new method, fuzzy PROMETHEE II is proposed for the problem of pipe condition assessment. The method calculates pipe breakage risk to reflect the condition assessment. The proposed model is different from previous model in that it only requires usually available data, and that it gives an insight into expert opinion's uncertainty and preference that has a pipe breakage signification in each criterion. By including these components into the condition assessment process, we are able to achieve better understand. This is the improvement of previous method as they failed to account for these uncertainty and preference.

In PROMETHEE method, there are only a few parameters to be determined in each criterion (e.g. one parameter if linear preference function is applied). And these parameters all have a pipe breakage signification so that experts are able to determine their values easily.

An interesting aspect of the proposed method is the net flow values generated. This net flow reflects each pipe's relative condition. The utility of net flow is that it provides a strong indication of sensitivity of pipe rank position in relation to the subjective weights which are obtained from experts' opinion. The benefit of net flow is that two adjacent ranking pipes with larger difference of net flow are not so affected by these weights.

REFERENCES:

Boxall, J. B., A. O'Hagan, et al. (2007). "Estimation of burst rates in water distribution mains." *Water Management* 160: 73-82.

Brans, J. P. and P. Vincke (1985). "A preference ranking organisation method: the PROMETHEE method for multiple criteria decision-making)." *Management science* 31(6): 647-656.

Brans, J. P., P. Vincke, et al. (1986). "How to select and how to rank projects: The PROMETHEE method." *European Journal of Operational Research* 24(2): 228-238.

Figueira, J., S. Greco, et al. (2005). *Multiple Criteria Decision Analysis: State of the Art Surveys*, Springer.

Geldermann, J., T. Spengler, et al. (2000). "Fuzzy outranking for environmental assessment. Case study: Iron and steel making industry." *Fuzzy Sets and Systems* 115(1): 45-65.

Kleiner, Y. and B. Rajani (2001). "Comprehensive review of structural deterioration of water mains: statistical models." *Urban Water* 3(3): 131-150.

Vairavamoorthy, K., Sunil D. Gorantiwar, et al. (2006). *Water Safety Plans: Risk Assessment of Contaminant Intrusion Into Water Distribution Systems*, Water, Engineering and Development Centre, Loughborough University.

Development of Regression Models to Estimate Flow Duration Statistics at Ungaged Streams in Oklahoma Using a Regional Approach

Rachel A. Esralew, US Geological Survey Oklahoma Water Science Center, Oklahoma City, Oklahoma; email: resralew@usgs.gov Tel. 405-810-4425

Abstract

Multiple-regression analysis was used to develop equations for estimating annual and seasonal flow-duration statistics at ungaged streams in and near Oklahoma that are not substantially affected by human alteration. Ordinary least-squares and left-censored (Tobit) multiple-regression techniques were used to develop equations that relate these statistics, from continuous streamflow data at gaged locations with 10 or more years of record, to physical and climatic basin characteristics. Separate equations were developed to estimate these statistics for stations within similar hydrologic and geologic regions. Use of separate regressions by region substantially improved the accuracy of the estimate for streams in eastern and central Oklahoma when compared with estimating equations developed for the entire State, especially for regressions estimating lower flow duration values. For all regions, the equations were more reliable for estimating higher flow duration values. The accuracy of regressions for estimating flow duration statistics in western Oklahoma was very poor, especially for lower flow duration values.

Introduction

Effective planning in water resources management requires knowledge of streamflow conditions on streams which are to be regulated for water-supply permitting, water-quality regulation, and other water-rights issues. Successful management of reservoir operations, permitting for stream withdrawals, and maintenance of water quality standards is supported by knowledge of the magnitude of flow that can be expected in a stream at any given time. Flow duration statistics, which describe the percentage of time a stream discharge value is equaled or exceededare commonly used by the Oklahoma Water Resources Board (OWRB) as a guideline for making informed decisions regarding water resources planning and management.

The long-term historical continuous daily streamflow information collected at streamflow gaging stations by the U.S. Geological Survey provides a valuable resource for estimating streamflow values that are expected to be equaled or exceeded for a given percentage of time under a range of temporal conditions, including annual and seasonal time periods. However, most streams in Oklahoma are ungaged.

Because of the need for flow duration statistics at ungaged stations that describe annual and seasonal flow conditions, the USGS, in cooperation with the OWRB began a study to develop techniques for estimating long-term streamflow statistics at ungaged locations based on data from gaged locations. The OWRB had identified several statistics that are effective in water resources planning, including developing estimates of daily mean discharge at ungaged locations that are exceeded 20, 50, 80, 90, and 95% of the time (referred to as the Q20, Q50, Q80, Q90, and Q95, respectively) on an annual and seasonal basis.

Statistics calculated at streamflow gaging stations with long-term daily mean streamflow record are highly variable among stream locations, but are strongly related to physical characteristics of the drainage basin such as size, topography, geology, land-use and climate. Statistical models that describe these relations for gaging stations can be developed in order to estimate streamflow statistics, including annual and seasonal flow duration values, at ungaged locations that are not in close proximity to gaged stream locations. Regression estimates of these statistics at ungaged locations using easily obtainable physical basin characteristics provide a low cost and efficient means for assessing flow conditions at ungaged locations when obtaining

direct or nearby flow measurements or developing site-specific digital models is too costly or infeasible.

One of the challenges involved with development of regression equations that accurately describe flow conditions at ungaged sites is selecting appropriate basin characteristics for the model that adequately account for the annual and season variability of streamflow. Differences in the response of streamflow to climate, landscape, and geologic diversity can increase the error and decrease the accuracy of the regression model estimates.

Oklahoma has diverse physical and climatic characteristics which can affect streamflow. Oklahoma contains a variable topography and physiography, including vast plains, extensive alluvial deposits, elevated karst plateaus, and folded, low mountains. Annual precipitation increases gradually eastward (figure 1), but variability in rainfall duration and frequency increases westward. Basin characteristics such as annual and seasonal precipitation, basin or channel slope, landcover, and soil characteristics, and the response of streamflow to these basin characteristics, can vary across Oklahoma. This regional variability can pose challenges to selecting optimal explanatory variables for use in regression equations to produce equally accurate estimates of flow duration and mean annual flow conditions for streams throughout Oklahoma.

In order to utilize model parameters that are easy to obtain while minimizing the error of the streamflow estimate, regression equations can be developed for smaller, more homogeneous regions as long as there are enough sample locations (Haan, 1977). This method has been applied to other states with distinct regional geologic and climatic diversity, such as Idaho (Hortness and Berenbrock, 2001) and Oregon (Risley and others, 2008). While physical and climatic diversity can be observed in Oklahoma, the topographic relief is generally low, and the variability of precipitation changes gradually throughout the state (figure 1), making regions more difficult to define solely by use of observational analysis of spatial characteristics. There are 12 ecoregions in Oklahoma which can be used to define regions (figure 2), however, a lack of streamflow gaging stations with long-term streamflow data within certain ecoregions of Oklahoma may limit the size and number of regions that can be used to produce meaningful regressions for those regions.

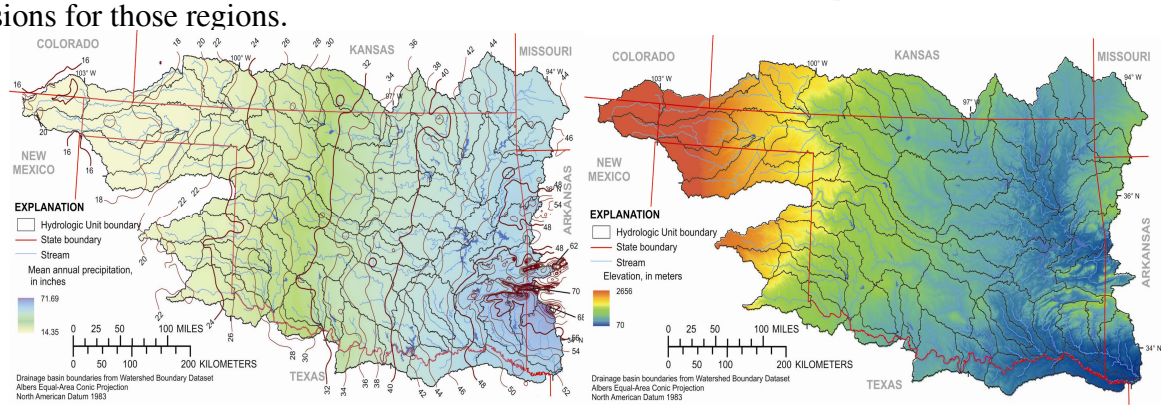

Figure 1. A.) Mean annual precipitation, in inches, and B.) elevation, in meter, in and near Oklahoma

As an alternative, statistical methods can be used to group gages with similar physical drainage characteristics (Hortness and Berenbrock, 2001). Statistical groupings of streams with similar characteristics can be supplemented by visual analysis of spatial characteristics to define regression regions for Oklahoma. Comparison of the regression models developed for each region can be used to observe differences in the response of streamflow to basin characteristics throughout Oklahoma. The results from the statistical analysis can also be used to evaluate of hydrologic variability across the state.

Purpose and Scope

Statistical analyses were used to develop regression models to estimate annual and seasonal flow duration statistics at ungaged sites throughout Oklahoma. The ungaged sites selected for analyses are not affected by water-supply regulation. This report provides a discussion of a) the methods used to develop the regional regression equations, b) variables used in the regression equations, including the accuracy of the regressions and how these results varied between models, and c) the limitations to the application of the regional regression equations.

Methods

Selection of Data for Regression Equations

Streamflow-gaging stations selected for use in constructing the regression equations had a minimum of 10 years of record and were not substantially affected by water-supply reservoirs or large-scale groundwater or surfacewater withdrawals. Additionally, the data set included all gage sites contained within USGS 8-digit hydrologic boundaries (HUC 8) that touch the Oklahoma border.

Periods of record for gages that were significantly affected by diversion and withdrawals for irrigation and other water use were determined by historical hydrographer remarks, analysis notes from previous publications (Tortorelli and Wahl 1997, Smith and Wahl 1993), and supported by inspection and analysis of the annual hydrograph. A streamflow gage was considered significantly affected by regulation if 20% or more of the drainage basin upstream from the gage was regulated by a major water supply reservoir. The year in which a reservoir was constructed and which resulted in this threshold being met was considered the cut-off year for defining an unregulated period of record. Floodwater retention structures were not considered an act of regulation for purposes of this study because these structures are unlikely to have a significant effect on median flows (Tortorelli and Bergman, 1985).

Flow duration and mean annual flow statistics from gages in the Beaver/North Canadian River Basin and Upper Cimarron River Basin of Oklahoma and the eastern panhandle of Texas were not included in the final regression analysis because streams in this region are significantly affected by irrigation withdrawals and diversions. (Tortorelli and Wahl 1997; Dale Boyle, oral and written communication). The effects of these activities on the hydrology of the area cannot be appropriately characterized by a regional regression approach. Figure 3 shows gages considered for analysis.

Calculation of Flow Duration and Mean Annual Flow Statistics

A flow-duration curve (FDC) is a graphical representation of the percentage of time that streamflow for a given time step (in this case, a daily time step) is equaled or exceeded during a specified period. Flow duration statistics are points along the FDC. For example, the 95-percent flow duration streamflow is equaled or exceeded 95 percent of the time, whereas the 50-percent duration streamflow (median) is equaled or exceeded 50 percent of the time. Strictly interpreted, flow duration statistics reflect only the period for which they are calculated; however, when the period of record used to compute the statistics is sufficiently long, the statistics can be used as an indicator of probable future conditions (Searcy, 1959). The period of record used for flow-duration curve calculation can be for the complete period of record, or daily flows during a specified period within the period of record, such as for a group of months (or a season).

The computer software program SWSTAT was used to format input data and complete the flow-duration statistics and mean annual flow analysis (Lumb and others, 1990). Flow duration curves were constructed for daily flow data in SWSTAT for annual flow duration curve (all daily flow data in the period of record), and seasonal flow duration curves (daily flow occurring the summer-fall period, June 1st through October 31st; and daily flow occurring during

the winter-spring period, November 1st through May 31st), resulting in 15 values (5 values for three FDCs) for each gage.

Computation of Drainage Basin Characteristics

Climatic and physical characteristics of the drainage basins upstream of the streamflow-gaging stations were used as independent variables in the regression equations to predict streamflow statistics. Using Geographic Information System (GIS) techniques, 23 different basin characteristics initially were computed for 167 streamflow-gaging stations (121 of which were included in the final regression analysis). The final selection of 9 basin characteristics that were used in the regression equations are listed in table 1. The computations were made using Arc Macro Language (AML) scripts run in ArcInfo, version 9.2 (Environmental Systems Research Institute, 2007). Data sources include the National Hydrography Dataset Plus (NRD) (http://nhdgeo. usgs.gov/viewer.htm, accessed July, 2008), Parameter-elevation Regressions on Independent Slopes Model (PRISM) (http://www.prism.oregonstate.edu/, accessed July, 2008), U.S. Natural Resources Conservation Service (NRCS) State Soil Geographic (STATSGO) datasets, and USGS National Land Cover Dataset (NLCD) (http:// landcover.usgs.gov/ natllandcover.php, accessed July, 2008).

Development of Regions

In regional streamflow frequency analyses, attempts are made to define regions that are hydrologically similar in terms of physical characteristics being studied (Haan, 1977). The climate and geology of Oklahoma vary greatly across the state, mostly with respect to longitude (see figures 1 and 2). A k-means cluster analysis was performed in SPlus (Insightful Corporation, 2007) using selected basin characteristics obtained for all gaging stations used in this study, including those which were later removed because they were considered substantially altered by anthropogenic activities. The results of the cluster analysis are a grouping of datapoints, in this case stations, that are similar to each other with respect to the variables used in the algorithm. Basin characteristics that were used as variables in the cluster analysis were those that were not related to drainage size or specific to gage location (such as channel slope, mean basin slope, or mean and outlet elevation). Final basin characteristics included in the cluster analysis were forested area, soil permeability, and mean annual precipitation at the gage location.

Description of Regions

On the basis of the cluster analysis, the state was divided into three regions and separate equations were developed for stream locations within each region. Regional boundaries were determined spatially by manual delineation, and are shown in figure 2. Delineated boundaries were determined on the basis of the following 5 factors: (1) the grouping of similar basin characteristics at gaged locations as a result of the cluster analysis; (2) hydrologic boundaries such as the HUC 8; (3) geographic features, such as mountains, geologically heterogeneous areas, or other distinct geologic divides; (4) ecoregion boundaries (Woods and others, 2005) which are helpful in delineating a combination of climate and geologic distinctions between areas; and (5) author's judgement based on general knowledge of the area. Hydrologic boundaries (such as the HUC 8 and smaller subcatchments) were used where possible to delineate regions in order to avoid arbitrary boundaries that cut across natural drainages.

This analysis revealed several unique groupings of basin characteristics across Oklahoma. Figure 4 and 5 show locations of the regions with respect to forested area and soil permeability. Figure 6 shows the Regions with respect to Ecoregions and large topographic and hydrologic features in Oklahoma.

Gages in Region 1, the western region, had little to no forested area, and higher average soil permeability. Region 1 contains most of the Central Great Plains Ecoregion, the western slopes of the Wichita Mountains, and eastern edges of the High Plains Ecoregion. Note that

Region 1 in figure 2 contains the panhandle region, but this region was excluded from the Region 1 regression because streamflow is impacted by irrigation.

Region 2, the North and South Central Region, was divided into two parts (Region 2A and Region 2B). Region 2A, in the Arkansas River Basin, is separated on the eastern border by the Neosho River and contains the Central Irregular Plains and the Flint Hills ecoregions, as well as a portion of the Cross Timbers Ecoregion. Region 2B, in the Red River Basin, was divided on the eastern slopes of the Wichita Mountainsand contain the Arbuckle Mountains Region. Gages in Region 2 had lower average soil permeability than Region 1 or Region 3. Gages in Region 2 also had intermediate forested area and intermediate annual precipitation.

Region 3, the Eastern and Central Region, included the Ozark Highlands ecoregion east of the Neosho River and the Ouachita Mountains to the south. Region 3 contains more forested area, greater annual rainfall, and more variability of annual rainfall in the southeastern mountain region, compared to Regions 1 and 2.

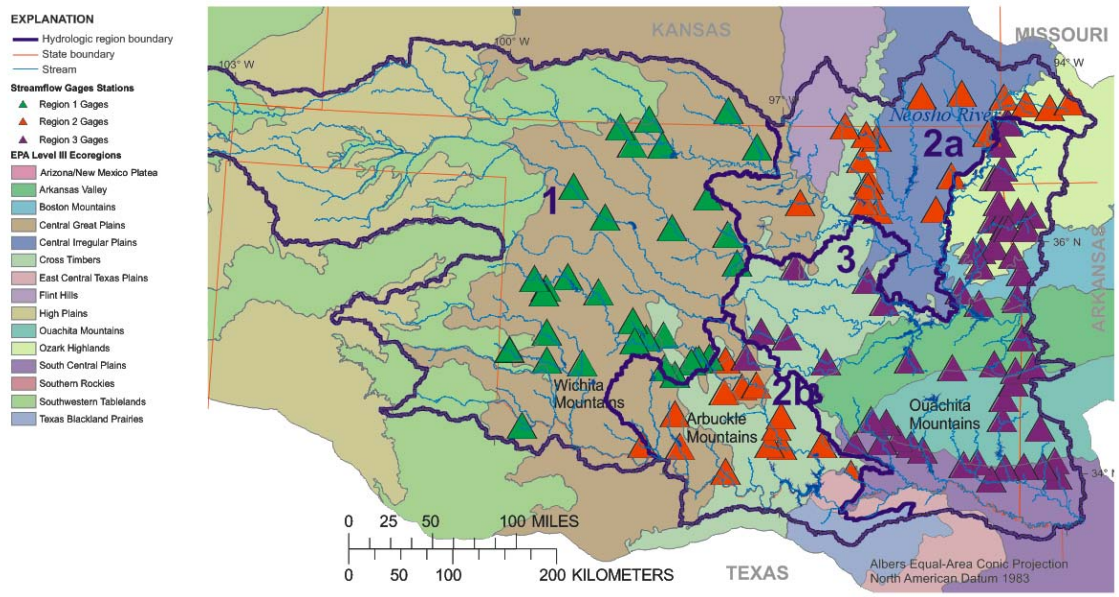

Figure 2. Study area showing regional boundaries, EPA Ecoregion boundaries, and streamflow gaging stations selected for regression analysis.

The distribution of streamflow values also varied for gages in each Region. Gages in all three regions had similar distributions for the Q20 and Q50 flow duration values. The summer flow duration values were lower for all three regions. However, for the Q80, Q90, and Q95, Region 2 had the lowest flows compared to Region 1 and Region 3. Region 2 also had the highest frequency of zero flows. Figure 7 shows a comparison of the logarithmic distributions of flow duration statistics for gages in all three regions. Zero flows were set equal to the log of 0.004 so that they could be plotted.

Development of Regression Equations for Each Region

The development of regressions and selection of explanatory variables, or basin characteristics, for each regression equation was determined using a combination of automated and manual techniques. An outline of the process is shown in figure 5. An effort was made to ensure that the explanatory variables had a physical or hydrologic reason to be used to predict flow duration values.

Regressions were developed separately for both annual and seasonal flow duration statistics. Regression equations for each annual, summer, and winter flow duration statistic (5 flow duration statistics, each on 3 FDCs) were developed separately for each of the three regions.

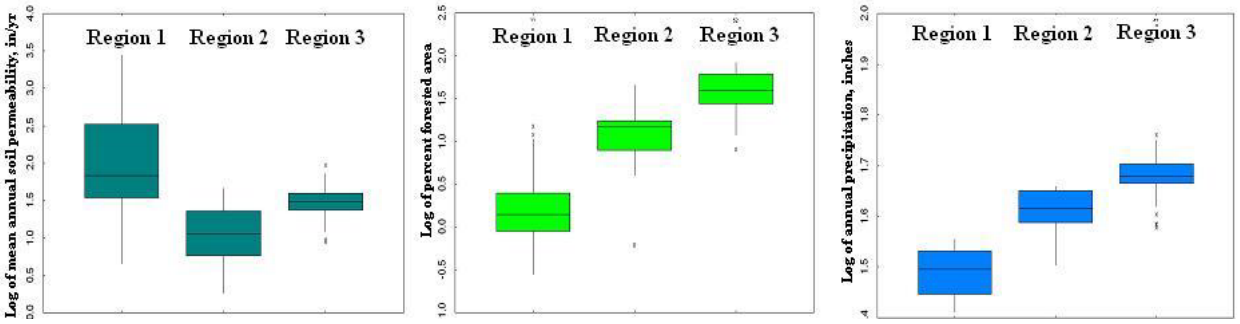

Figure 3. Comparison of logarithmic distributions of basin characteristics for three regions in Oklahoma

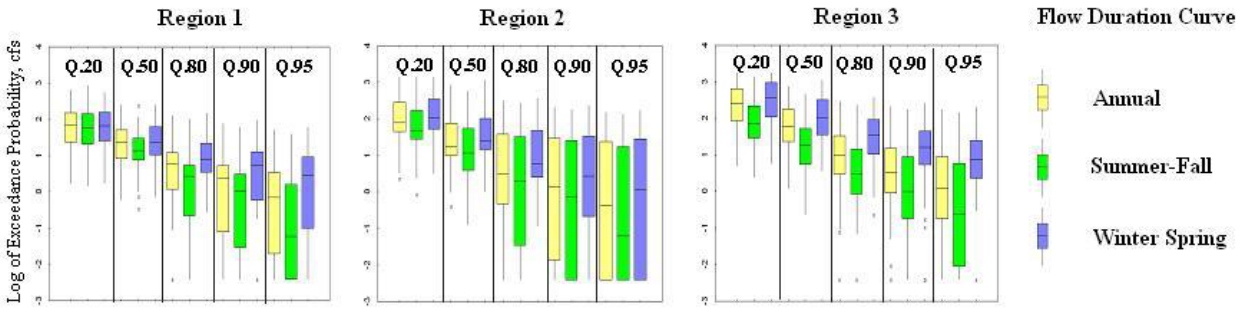

Figure 4. Comparison of flow duration values along three flow duration curves (annual, summer-fall, and winter-spring) in three regions

This produced 45 separate regression equations. A summary of the variables used in the models and the standard error and coefficient of determination are presented in table 1. Final regression equations will be reported in a US Geological Survey Scientific Investigations Report, "Estimating Flow-Duration and Mean Annual Flow Statistics at Ungaged Streams in and near Oklahoma" (Esralew and Smith, in press).

Regression Equation Format

To develop regression equations, all streamflow and basin characteristic data were transformed to base-10 logarithms. This transformation was performed to develop a linear regression model with equal variance about the regression line. Streamflow statistics with values of zero were commonly observed for flow duration statistic datasets, especially for the Q90 and Q95 datasets in Region 2. The log of zero cannot be taken. To avoid this, any dataset that had an occurrence of a flow statistic equal to zero had a small delta value added to all values in the dataset prior to log transformation. When testing possible regression equations (described in the next section), the delta constant was varied until the standard error was minimized and the adjusted R^2 was maximized. The delta constant can be subtracted from the final regression equation after retransformation from log-space to real-space has been performed.

Final regression equations will be reported in the following form:

$$Q = aB^{b1} * C^{b2} \ldots . N^{bn} - D$$

where Q is the desired dependent variable (streamflow statistic); a is the multiple regression constant; $b1$, $b2$,..bn are the regression coefficients; and B, C,…N are the values of the required explanatory variables (basin characteristics). D is the delta constant.

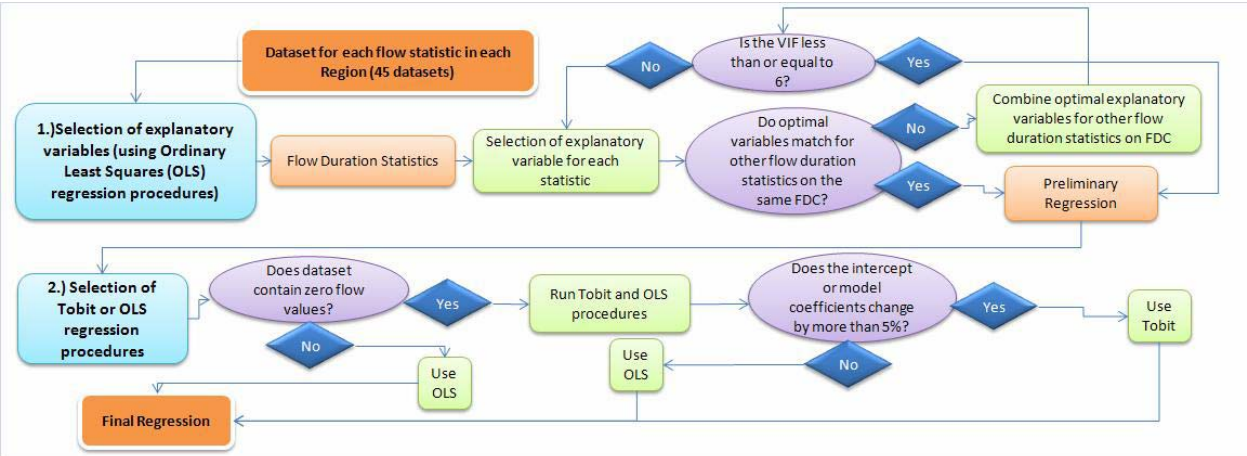

Figure 5. Flow chart outlining procedure used to develop regression equations to estimate streamflow statistics using physical basin characteristics.

Selection of Explanatory Variables from Drainage Basin Characteristics

To select optimal explanatory variables for the regression equations, a step-wise procedure and an overall method (Helsel and Hirsch, 1992) were used. The possible explanatory variables included each of the 23 basin characteristics selected for potential inclusion in the final regression models. Common diagnostic statistics were used to evaluate and select the final regression equations. These diagnostic statistics include the PRESS, Mallow's Cp, variance inflation factor (VIF), root mean standard error (*RMSE*) adjusted coefficient of determination (R^2), and results of partial t-tests. Further documentation on these regression selection methods can be found in Helsel and Hirsch (1992). If PRESS statistics and Mallow's Cp values were similar for models including a variable number of explanatory variables, the model with the least number of explanatory variables was selected. The VIF, which is a measure of correlation between explanatory variables, was minimized for any possible combination of explanatory variables to avoid multi-collinearity in the regression. Multi-collinearity can result in unreasonable slope coefficients. Combinations of explanatory variables were not accepted if the VIF was greater than 6.

An effort was made to use the same explanatory variables in the regression equations for flow duration statistics on the same FDC in each region. For any given FDC for any given region, if the explanatory variables were different between flow duration statistics on the curve, the explanatory variables were combined in the final equation as long as the variance inflation factor for the explanatory variables did not exceed 6. This ensures that the correlation structure between streamflow for each FDC is preserved. This procedure resulted in stable and consistent estimates of the statistics (Haan, 1977; Hortness and Berenbrock, 2002). For example, for the summer FDC in Region 1, contributing drainage area and annual mean precipitation at the gage were the best variables to estimate the Q20, Q50, and Q80, but mean June precipitation and channel slope were the best variables to estimate the Q90 and Q95. The variance inflation factor for the combined variables did not exceed 6, and so the variables were combined for the final regression equation.

Selection of the Modeling Procedure

Various approaches can be used to develop regressions that have zero flow values. One approach involves treating zero flow values as "censored" at or below zero. At times the streamflow may actually be zero, while in other cases flow values may be nonzero but too small to be measured and therefore reported as zero.

If there is a sufficient number of dependent variables that are censored (in this case, a sufficient number of streamflow values equal to zero), it is possible to use a Tobit regression (Ludwig and Tasker, 1993). A Tobit regression is a model in which the dependent variable is censored, and the model supposes that there is a latent (i.e. unobservable) variable below the censor. The Tobit procedure uses an MLE to assume a distribution of values below the lowest censored value, which in this case would be the delta value which was added to all values prior to log transformation. (Tobin 1958).

Kroll and Stedinger (1999) found that use of an OLS model, under conditions where there are left-censored data (data where values below a minimum value are considered latent variables), did not perform as well as a Tobit model. The error residuals for an OLS model using left-censored data will be biased higher, especially at the lower end of the linear regression. According to their study, for small amounts of censoring, however, an OLS is acceptable.

If there are no censored values, Tobit model procedures will result in the same model coefficients as an OLS. As more values are censored, or equal to the censoring value of zero, the resulting model coefficients and intercept will start to differ between OLS and Tobit procedures. A Tobit model is more computationally intensive than an OLS. For ease of reporting and data processing, a Tobit model was only applied if the regression determination procedure resulted in an intercept that was 5% different from the model that was developed using OLS procedures.

Results

A summary of the 45 final regression equations are presented in table 1. To test whether the regional regressions offered improved estimates of flow duration statistics compared with a regression equation developed for the entire study area, the adjusted R^2 and standard errors were compared between the regional regression equations and a regression equation, using the same procedures outlined above, for all regions combined (121 gages), as shown in figure 7.

Basin characteristics used in the final regressions include contributing drainage area; mean annual, summer-fall, winter-spring, and June precipitation; channel slope, elevation of the stream location, mean basin elevation, and forested area.

Average soil permeability was not selected as an explanatory variable for any regression, or the regression using all sites. This result was unexpected. Lower soil permeability should reduce low-flow duration values because contributions from shallow groundwater during baseflow would be reduced; the Region with the lowest permeability, Region 2, had the highest frequency of flow duration values equal to zero.

Differences between resulting explanatory variables for regression estimates

The importance of explanatory variables in each of the resulting regressions differed between regions and flow duration curves. This difference can be evaluated using results from a partial t-test. A partial t-test can be used to indicate whether or not an explanatory variable is accounting for a significant amount of variation of the dependent variable when other explanatory variables are present (Helsel and Hirsch, 1992). Using a two-sided t-test with $\alpha = 0.05$ and the number of variables being greater than 20, the critical value of t is greater than 2 or less than -2 for the null hypothesis (which states that the variable does not account for variation in the dependent variable). If the t-value for an explanatory variable is in this range when used in a regression with other variables, then the null hypothesis can be rejected and an assumption can be made that thethe variable is accounts for a significant amount of variation of the dependent variable; when comparing t-values, an assumption can be made that variables with higher absolute t-values are more important to the regression.

[Q.xx, daily mean discharge which is exceeded xx percent of the time during the specified time period, in cubic feet per second; Qa, mean annual discharge; DA, contributing drainage area; SL, channel slope between points 10 and 85 percent of the stream length s tarting from the stream location and along the longest flow path; OE, station elevation; ME; mean basin elevation; FR, percent of forested area in the drainage basin; PRC, mean annual precipitation at the gage location, PRC_J, mean precipitation during June, at the gage location; PRC_{JO}, mean summer-fall precipitation from June to October, at the gage location; R^2_A, adjusted R2, SEE, standard error of the estimate]

FDC	Flow Statistic	Region 1				Region 2				Region 3				All Regions			
		Explanatory Variables	Model Type	Standard Error	R^2_A	Explanatory Variables	Model Type	SEE	R^2_A	Explanatory Variables	Model Type	SE E	R^2_A	Explanatory Variables	Model Type	SEE	R^2_A
Annual	Q.20	DA, ME, PRC_{JO}	OLS	0.18	91.5	DA, SL, OE, PRC_{NM}	OLS	0.19	92.6	DA, FR, ME, PRC	OLS	0.11	96.8	DA, PRC_J, PRC, ME	OLS	0.19	92.7
	Q.50		OLS	0.24	84.2		OLS	0.23	91.5		OLS	0.18	90.4		OLS	0.30	81.9
	Q.80		OLS	0.56	51.1		OLS	0.36	87.4		OLS	0.28	82.9		OLS	0.68	48.3
	Q.90		Tobit	0.57	48.7		Tobit	0.59	81.4		Tobit	0.39	74.9		Tobit	0.75	45.7
	Q.95		Tobit	0.75	37.9		Tobit	0.44	79.9		Tobit	0.57	69.5		Tobit	0.74	44.3
Summer-Fall	Q.20	DA, SL, PRC_J, PRC_{JO}	OLS	0.19	91.8	DA, SL, OE, PRC_{NM}	OLS	0.17	94.5	DA, FR, ME, PRC_{JO}	OLS	0.13	96.1	DA, ME, PRC_J	OLS	0.25	87
	Q.50		OLS	0.24	84.2		OLS	0.29	90.2		OLS	0.23	84.3		OLS	0.42	69.6
	Q.80		Tobit	0.67	52.9		OLS	0.47	81.1		Tobit	0.43	80.3		OLS	0.74	43.1
	Q.90		Tobit	0.69	52.7		Tobit	0.49	82.5		Tobit	0.68	72.5		Tobit	0.94	42.8
	Q.95		Tobit	0.86	53.5		Tobit	0.68	79.2		Tobit	0.72	75.8		Tobit	0.75	42.2
Winter-Spring	Q.20	DA, SL, ME, PRC	OLS	0.18	90.8	DA, SL, OE, PRC_{NM}	OLS	0.21	90.6	DA, FR, ME, PRC	OLS	0.12	96.7	DA, ME, PRC	OLS	0.19	92.8
	Q.50		OLS	0.24	84.2		OLS	0.23	89.8		OLS	0.18	92.3		OLS	0.30	82.1
	Q.80		OLS	0.35	69.9		OLS	0.34	86.0		OLS	0.24	88.6		OLS	0.46	66
	Q.90		OLS	0.55	53.8		OLS	0.52	79.9		OLS	0.25	87.0		OLS	0.62	48.7
	Q.95		Tobit	0.76	53.0		Tobit	0.38	75.9		Tobit	0.33	80.2		Tobit	0.75	41.4

Table 1. Summary of results from determination of regression equations developed to estimate flow duration statistics for three regions and combined regions in and near Oklahoma.

Figure 5 shows an example comparison of t-values for annual FDC regressions for all three regions. Because optimal explanatory variables may have been different for statistics along the same FDC, and those variables were combined in the final regressions, some regressions contained explanatory variables where the critical t-value was between 2 and negative 2.

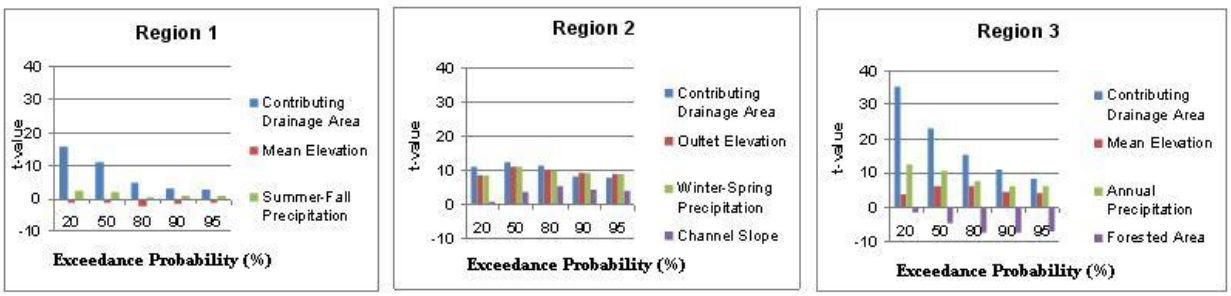

Figure 6. Comparison of t-values for explanatory variables for regressions estimating flow duration statistics on an annual flow duration curve.

For almost all regression equations, drainage area and precipitation (annual and seasonal) were more important for determining higher flow estimates than they were for lower flow while forested area, channel slope, and June precipitation were increasingly important for determining lower flows. For Region 3, forested area was increasingly important for lower flows and had a negative relation to flow (the more forested area, the lower the flow). An explanation to support this observation is increased evapotranspiration from vegetation, which can lower baseflow. Forested area was not included in other regressions, which contained less forested area than Region 3.

Elevation parameters (outlet and mean elevation) were equally important for most flow statistics in Region 2 and 3, but were not overly important. There is no direct hydrologic explanation for inclusion of this variable aside from the possibility that streams that are closer to one another (and thus have an increased probably of having similar hydrologic characteristics)

may be similar in elevation. Inclusion of this parameter typically decreased the standard error by more than 20% for most regressions, and so a decision was made to use these variables in the final regressions.

Comparison of Performance of Regressions between Regions and Flow Duration Curves

For all three flow duration curves, the regional regression equations improved the estimates for the Q50, Q80, Q90, and Q95 for gages in Region 2 and Region 3. However, use of regional regressions instead of a combined regression did not substantially improve the estimates for Region 1 at the low flow portion of the flow duration curve (Q80, Q90, and Q95), which were also very poor.

The performance of most regional regressions showed improvement over a regression developed using all gages, which can be seen by looking at the standard error and adjusted R^2 in table 1 and the plot of R^2 values in figure 7. The regression estimate using all gages was extremely poor for estimates of low-flow (Q80, Q90, and Q95).

For Regions 2 and 3, the winter-spring flow duration regressions produced slightly better estimates than the summer and annual flow duration regressions. A possible explanation for an increased uncertainty associated with estimating summer flow may be increased water-use for agricultural activities during the growing season or increased evapotranspiration which can affect low flow. For Region 1, the summer and winter estimates were slightly more accurate than the annual flow duration regressions, but all regression equations estimating low-flow values (the Q80, Q90, and Q95) were extremely poor.

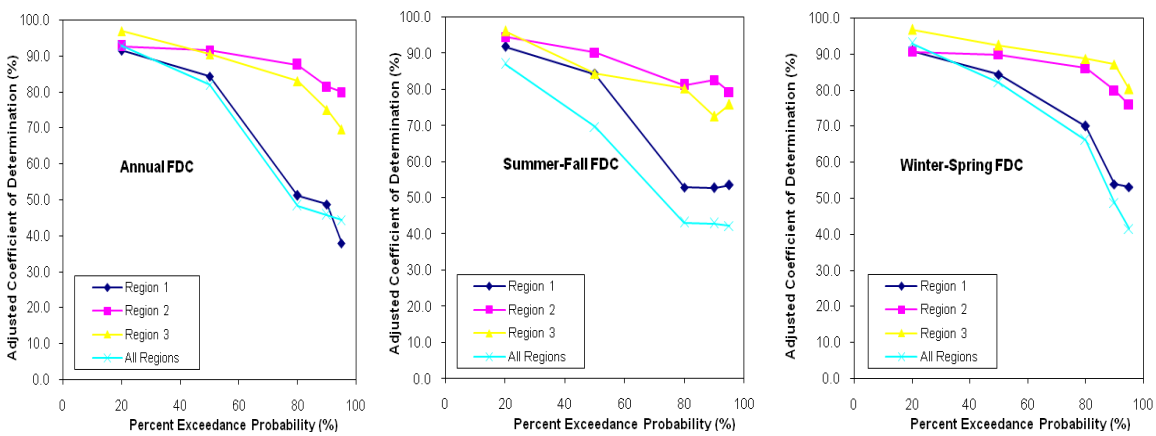

Figure 7. Comparison the adjusted coefficient of determination (R^2) for regressions developed for annual, summer-fall, and winter-spring flow duration curves for three separate regions compared to regressions developed using all sites.

For all three regions, the regressions for lower flow duration values tended to have decreased accuracy compared with higher flow duration values along the same flow duration curve. Low-flow estimates are less accurate than high-flow estimates most likely because streamflows are largely affected by localized geology that cannot be easily quantified (Riggs, 1972).

Region 1 low-flow estimates were extremely poor compared to low-flow estimates for Regions 2 and 3, which suggests that there is a high uncertainty associated with low-flow estimates in Region 1 and that the basin characteristics selected for regression analysis do not adequately describe the variability in low-flow estimates in Region 1. A possible source of variability in low-flow estimates in this region could be regional alteration from irrigation activities. Figure 8 shows how irrigation water-uses vary across Oklahoma (Tortorelli, 2009, in press) and are more pronounced in the western portion of the state. Irrigation water-use, whether water is derived from groundwater or surface-water sources, can have a significant effect on the

variability of low-flow due to nearby withdrawals and irrigation returns. Although an attempt was made to eliminate gages that were affected by local or regional irrigation and other water-use activities, these activities may not be sufficiently documented or were hard to detect from hydrograph inspection if they occurred during the entire period of record used for analysis.

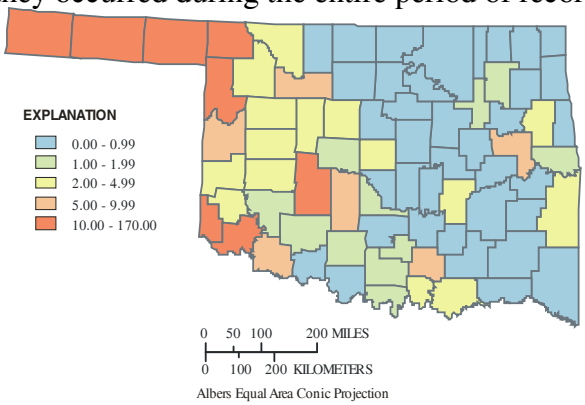

Figure 8. Map showing irrigation withdrawals from surface water and groundwater, in millions of gallons per day (adapted from Tortorelli, 2009, in press)

Another source of uncertainty for estimating low-flows in Western Oklahoma may be associated with increased variability of precipitation in west-central Oklahoma. Garbrecht (2009) found that the variability of mean precipitation between wet and dry periods in this region had a pronounced effect on the variability of annual water yield. The minimum period of record for inclusion of gages was 10 years, which may not have been a long enough period to encompass climate variability in this region. However, a requirement of a longer period of record for gages would have substantially reduced the number of gages that could be included in the analysis.

Limitations

Regressions for regions should only be applied to streams located in that region. If a drainage basin extends outside of a region, regressions from both regions can be used to estimate the flow statistic by using an average of the estimated values weighted by the percent of drainage area located in each region.

Regression equations may not be reliable for sites where the basin characteristics are outside the range of values of explanatory variables that were used to develop the equations. Use of regressions for streams with basin characteristics more than or near extremes of values used in the regression might result in unreliable estimates as well. Maximum and minimum values of basin characteristics used in each regression region will be published in Esralew and Smith (2009, in press).

Summary and Conclusion

The U.S. Geological Survey used multiple-regression analysis to develop equations for estimating daily-mean discharge exceeded 20, 50, 80, 90, and 95 percent of the time annually and seasonally (June through October and November through May). The equations were developed in order to estimate these statistics at ungaged streams in and near Oklahoma.

Separate equations were developed to estimate each of these statistics for stations within similar hydrologic regions in Oklahoma. Three groups of streamflow gaging stations were determined using a k-means cluster analysis to group gages that had similar soil permeability, annual precipitation, and forested area. Gages tended to fall in spatial regions that were distinguishable along longitudinal, hydrologic, and geologic boundaries. Based on the clustering

of gages and a delineation of distinguishable boundaries, three regions were developed.: 1.) western, 2.) north and south central, and 3.) eastern and central Oklahoma.

Ordinary least-squares and left-censored (Tobit) multiple-regression techniques were used to develop estimating equations that relate these statistics at gaged locations with 10 or more years of record to physical and climatic basin characteristics. Basin characteristics found to be significant independent variables in the regression analyses were contributing drainage area, mean annual, seasonal, and monthly precipitation, stream elevation at the outlet, mean basin elevation, channel slope, and percent forested area.

Basin characteristics selected for the final regressions varied significantly by region. Drainage area was the only basin characteristic included in all regressions for all regions. For all three regions, drainage area was more important for determining higher flows than lower flows. Depending on region, forested area, channel slope, and June precipitation were more important for determining lower flows. Forested area was important for low flows in the eastern region while it was not included in the regressions for other regions.

The equations were more reliable for estimating higher streamflow exceedance probabilities (Q20 and Q50) than for estimating low streamflow statistics (Q80, Q90, and Q95). This may have occurred because low streamflows are largely affected by localized geology which was not quantified by the basin characteristics selected for use in the regression equations.

Use of separate regressions by region significantly improved the accuracy of the estimate for streams in eastern and central Oklahoma when compared with estimating equations developed for the entire State, although no significant improvement of the models were observed in western Oklahoma and no significant improvement of the models were observed for any of the regions for regressions estimating the Q20.

The standard errors of estimate of equations for western Oklahoma were significantly larger than those for other regions, especially for lower flow durations. This could be a result of greater variability in low flow because of increased irrigation activities in the basin and lower and more intermittent precipitation in this region compared with other regions.

The equations are not accurate for streams regulated by water-supply reservoirs or streams that are significantly affected by local irrigation withdrawals and diversions from groundwater or surface water.

References

Esralew, R.A., Smith, S.J., Estimating Flow Duration and Mean Annual Flow at Ungaged Streams in and near Oklahoma. U.S. Geological Survey Water Resources-Investigations Report (in press)

Garbrecht, J.D., Multi-Year Precipitation Variations and Water Resources in West-Central Oklahoma, abstract of oral presentation for Geological Society of America South-Central Section 43rd Annual Meeting, March 2009.

Haan, C.T., 1977, Statistical methods in hydrology: Ames, Iowa State University Press, 378 p

Hortness, J. E., and Berenbrock, Charles, 2001, Estimating Monthly and Annual Streamflow Statistics at Ungaged Sites in Idaho : U.S. Geological Survey Water Resources-Investigations Report 01-4093, 36 p.

Helsel, D.R., and Hirsch, R.M., 2002, Statistical methods in water resources: U.S. Geological Survey Techniques of Water-Resources Investigations, book 4, chap. A3, 510 p.

Insightful Corporation, 2002, S-PLUS Version 6.1 for Windows Professional Edition, Release 1: Copyright, Lucent Technologies, Inc.

Kroll, C.N., and Stedinger, J.R., 1999, Development of regional regression relationships with censored data: Water Resources Research, v. 35, no. 3, p. 775-784.

Ludwig, R.H., and Tasker, G.D., 1993, Regionalization of low-flow characteristics of Arkansas streams: U.S. Geological Survey Water-Resources Investigations Report 93-4013, 32 p.

Lumb, A.M., Kittle, J.L., Jr., and Flynn, K.M., 1990, Users manual for ANNIE, a computer program for interactive\hydrologic analyses and data management: U.S. Geological Survey Water-Resources Investigations Report 89-4080, 236 p.

Perry, C.A., Wolock, D.M., Artman, J.C., 2002, Estimates of Median Flows for Streams on the Kansas Surface Water Register U.S. Geological Survey Water Resources-Investigations Report 02-4292

Riggs, H.C., 1972, Low-flow investigations: U.S. Geological Survey Techniques of Water-Resources Investigations, book 4, chap. B1, 18 p.

Risley, J., Stonewall, Ad. Haluska, T., 2008, Estimating Flow-Duration and Low-Flow Frequency Statistics for Unregulated Streams in Oregon, U.S. Geological Survey Water Resources-Investigations Report 08-5126

Searcy, J.K., 1959, Flow-duration curves, Manual of hydrology—Part 2. Low-flow techniques: U.S. Geological Survey Water-Supply Paper 1542-A, 33 p.

Smith, S.J., and Wahl, K.L., 2003, Changes in streamflow and summary of major-ion chemistry and loads in the North Fork Red River basin upstream from Lake Altus, northwestern Texas and western Oklahoma, 1945-1999: U.S. Geological Survey Water-Resources Investigations Report 03-4086, 36 p.

Tobin, J., 1958, Estimation of relationships for limited dependent variables: Eonometrica, v. 26, p. 24-36.

Tortorelli, R.L., and Bergman, D.L., 1985, Techniques for estimating flood peak discharges for unregulated streams and streams regulated by small floodwater retarding structures in Oklahoma: U.S. Geological Survey Water Resources Investigations Report 84-4358

Wahl, Kenneth L., and Tortorelli, Robert L., 1997, Changes in flow in the Beaver-North Canadian River basin upstream from Canton Lake, western Oklahoma: U.S. Geological Survey Water-Resources Investigations Report 96-4304, 58 p.

Woods, A.J., Omernik, J.M., Butler, D.R., Ford, J.G., Henley, J.E., Hoagland, B.W., Arndt, D.S., and Moran, B.C., 2005, Ecoregions of Oklahoma: Reston, Virginia, U.S. Geological Survey (map scale 1:1,250,000).

Development of Sustainable Water Supply Scheme in Reservoir Operation: Case Study

M. Karamouz[1], S. Nazif[2], S. Mohammadi[3]

[1] Professor, School of Civil Engineering, University of Tehran, Tehran, Iran. PH: +98 21 88 555 884, FAX: +98 21 88 701 507, Email: karamouz@ut.ac.ir
[2] Ph.D. Candidate, School of Civil Engineering, University of Tehran, Tehran, Iran. Email: saranazif@yahoo.com
[3] M.Sc. Student, Amirkabir University (Polythechnic), School of Civil Engineering, Tehran, Iran. Email: soulmaz.mo@aut.ac.ir

ABSTRACT:

The development of societies is dependent upon the sustainable water supply through sound management of resources. It is important to determine the sustainable capacity of the water resources if further development is needed. Reservoirs play an important role in water supply of basins in arid and semi-arid regions. In this paper a methodology is proposed to find a sustainable water supply scheme in reservoir operation considering the impacts of climate change on inflow and water demand variations. Different approaches such as deterministic and chance constraint optimization models are utilized for this purpose in both monthly and annual time scales. The objective function of the optimization model is to maximize the minimum reservoir release. As extreme dry or wet years can highly affect the model results, their effects on the reliable water supply are also evaluated. The proposed method has been applied to the Sattarkhan Reservoir located in Ahar-chay basin in northwest Iran. Through the probabilistic approach, the reservoir operation can be managed with different risk levels and potential hazards. The results show that the reservoir has been overdesigned and it could carry only 60% of its capacity. Furthermore, the potential water resources in the studied basin are decreasing.

Keywords: Reservoir Operation, Reliable Water Supply, Climate Change, Sustainability.

INTRODUCTION

The main factors that cause changes in water resources availability and also water demand should be considered in developing long-lead water resources development strategies. Climate change has caused considerable changes in the global water cycle in recent years. Assessment of regional hydrologic characteristics shows significant

variations due to climate change impacts which should be considered in evaluation of water resources and demand. Determining the reliable water supply could help diminish undesirable effects of dry years and provide a view of water resources for future planning.

Brekke (2008) has assessed reservoir operation risks under climate change. He used the risk analysis to study climate change effects on California's Central Valley Project (CVP). Burn and Simonovic (1996) have assessed the sensitivity of reservoir operation performance to climatic change. Wolock and McCabe1 (1999) proved warming may create substantial water supply shortages in the Colorado River basin. The results of all of these studies demonstrate the increasing risk in operation of water resources under the effects of climate change. They have concluded that the effects of these phenomena should be considered in developing water resources operation schemes.

In this study an algorithm is proposed for assessment of reliable water supply from the Sattarkhan reservoir located at Ahar-chay basin in the north-western part of Iran. An agricultural development project is underway in this region and for maximizing the benefits of this project and avoiding unexpected situations, a precise water allocation scheme is necessary. Different deterministic and probabilistic approaches are considered in order to establish meaningful results of monthly reliable water supply. Also the effects of climate changes and project progress on reliable water supply and water demand in a 5-year periods are considered.

The paper is followed by the description of the methodology. Then the study area is introduced. The results of study are discussed in the next section and finally a summary and conclusion is given.

METHODOLOGY

For evaluation of reliable water supply as the first step, it is important to provide a vision of probable future condition of the system. For this purpose, the effects of climate change on reservoir input is evaluated using downscaled GCM output data; moreover, the changes on water demands are simulated in the planning horizon. Even though global climate models in the future are run at a low resolution, the need will remain to "downscale" the results from such models to individual sites or localities for impact studies (Department of the Environment, 1996). There are enormous downscaling methods that are used due to site characteristics and data availability. In situations where low-cost, rapid assessments of localized climate change impacts are required, statistical downscaling (currently) is more effective. In this study, SDSM (Statistical DownScaling Model) developed by Wilby et al. (2002) has been used for long-lead rainfall simulation for an individual site at daily time–scales using grid resolution GCM output. In downscaling with the SDSM, a multiple linear regression model is developed between selected large-scale predictors and local precipitation based on some statistical analysis.

The downscaled rainfall data are imported into a rainfall-runoff simulation model called IHACRES developed by Jakeman and Hoernberger (1993). This model needs limited data including basin area, historical series of basin rainfall and temperature and a meteorological parameter such as evaporation or temperature. The general

structure of the model is illustrated in Figure 1. The model includes two modules: first a non-linear loss module that simulates the effective rainfall, and second a linear unit hydrograph module that estimates the stream flow.

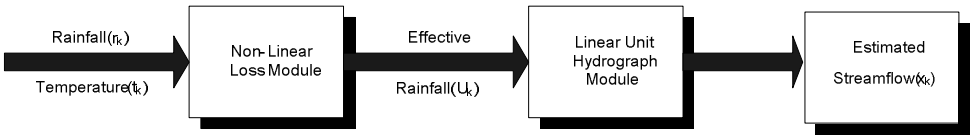

Figure 1: The structure of the IHACRES model (Jakeman and Hornberger, 1993)

Then the simulated long-lead reservoir inputs are employed as optimization model input to determine the reliable water supply of the future under climate change effects. The optimization model maximizes the minimum yearly water supply of the reservoir using deterministic and probabilistic approaches.

Deterministic Approach

In this approach linear programming is applied to maximize the minimum yearly water supply (R_{Min}) from reservoir which is considered as the available water in yearly development and allocation projects. The model is formulated as follows:

Maximize (R_{Min}) (1)

Subject to:

$$S_t + I_t - R_t - S_{t+1} = 0, \quad t \in \{1,...,T\} \tag{2}$$

$$S_{\min} \le S_t \le S_{\max} \tag{3}$$

$$R_t \ge R_{Min} \tag{4}$$

where I_t is the yearly reservoir inflow, S_t is the reservoir storage at the beginning of the year, R_t is yearly reservoir outflow, T is reservoir operation lifespan and $S_{\min}$ and $S_{\max}$ are the maximum and minimum possible reservoirs water storages in the planning horizon.

Probabilistic Approach

In this approach chance-constraint modeling is applied for determining R_{Min}. LP structure with probabilistic constraints is used in this paper. Normal distribution functions fitted to the reservoir inflow are used for conversion of the probabilistic constraints to deterministic equivalent. For this purpose Eq.s 2 and 4 are presented as follows:

$$P(S_t - S_{t+1} + I_t \geq R_{\min}) \geq p_\alpha \quad (5)$$

where p_α corresponds to the desired level of reliability in determining the reliable water supply. For example if p_α has been considered equal to 0.9, Eq. 5 can be rewritten as follows:

$$\begin{aligned} &P(S_{t+1} - S_t + R_{\min} \leq I_t) \geq 0.9 \\ &P(I_t \leq S_{t+1} - S_t + R_{\min}) \leq 0.1 \end{aligned} \quad (6)$$

CASE STUDY

The Aharchay river basin in northwestern Iran (Figure 1) has been selected as the case study of this paper. Aharchay river basin is located between 47° 20' and 47° 30' north longitude and 38° 20' and 38°45' east latitude. The Sattarkhan dam is the only available water storage resource in the study area. There are two meteorological stations, namely Kasanagh and Ahar, and a hydrometeorological station, Orang, just upstream of the Sattarkhan dam, whose recorded data is considered in this study. The stations' characteristics are presented in Table 1.

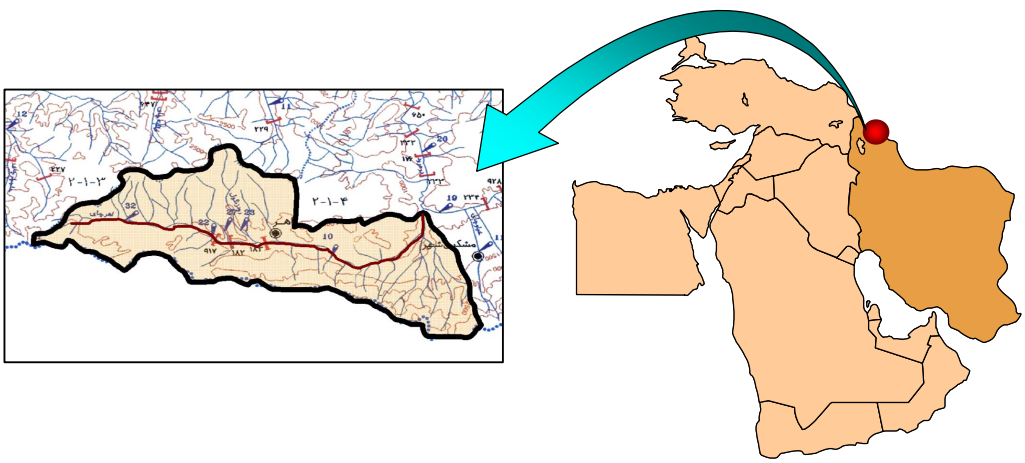

Figure 1: The location of the study area on the map of Iran

Table 1: The characteristics of hydrological and meteorological stations in the Aharchay basin

Station	Kasanagh	Ahar	Orang
Longitude	46° -51′	47°-04′	46°-52′
Latitude	38°-31′	38°-26′	38°-28′
Type of station	Rain gage	Synoptic	Hydrometer
Operation time periods (year)	1971-2000	1986-2003	1983-2004

Water supply in this part of Iran depends on seasonal rainfall, temperature and resulting runoff. Assessing the climate change and water availability, is therefore important in sustainable development of this region. The demand of the Aharchay basin is currently 68.28 MCM/year. There is an agricultural development program in this area that will increase future water demand of the basin. The monthly Aharchay streamflow variations with long lead average streamflow (6.8 MCM) are shown in Figure 2. This figure shows that this region has experienced a drought during years 1998-2006. In these years most of the months have an inflow less than 5 MCM and the yearly peak inflows which are about 20 MCM in normal years don't exceed 15 MCM. The minimum and maximum values of the reservoir storage are 18.2 and 131 MCM. The monthly variations of reservoir storage have been depicted in Figure 3. The results demonstrate that the reservoir is overestimated since at the present situation the largest storage of the reservoir does not exceed 75 MCM (60% of reservoir maximum storage capacity). So the reservoir capability to supply reliable water should be reassessed.

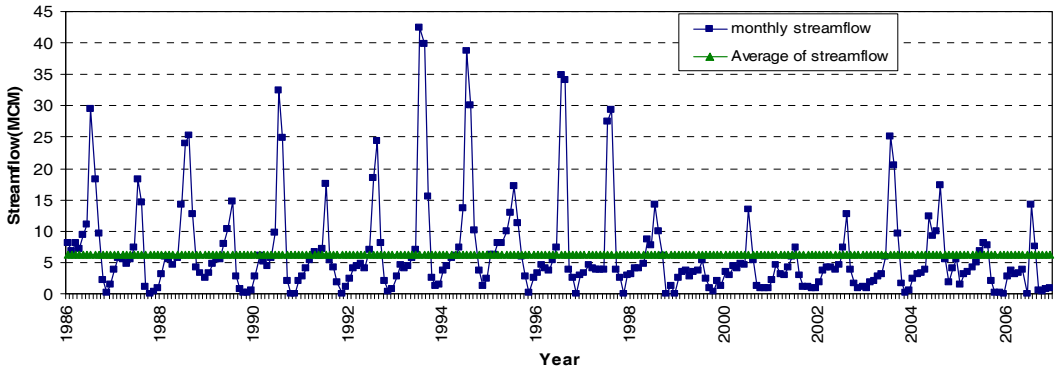

Figure 2: Monthly variation of Ahar river streamflow

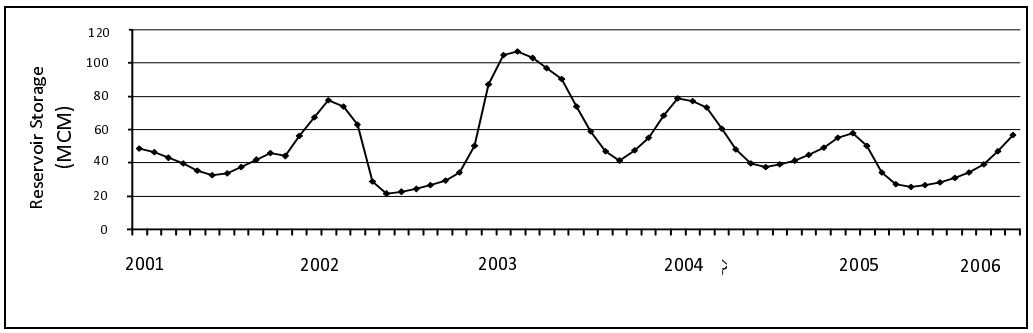

Figure 3: Monthly average storage of Sattarkhan dam

RESULTS

The simulated Sattarkhan inflow under climate change effects, within the next 35 years, is illustrated in Figure 4 (Karamouz et al., 2007). As can be seen, there is a considerable change in the basin runoff regime. In the next 10 years, the yearly

streamflow considerably decreases and is less than 30 MCM, the long term average. An interesting point is that in the first years there are high variations in yearly streamflow (about 10 MCM) which show intense dry and wet periods, however in time the difference between dry and wet years' streamflow decreases.

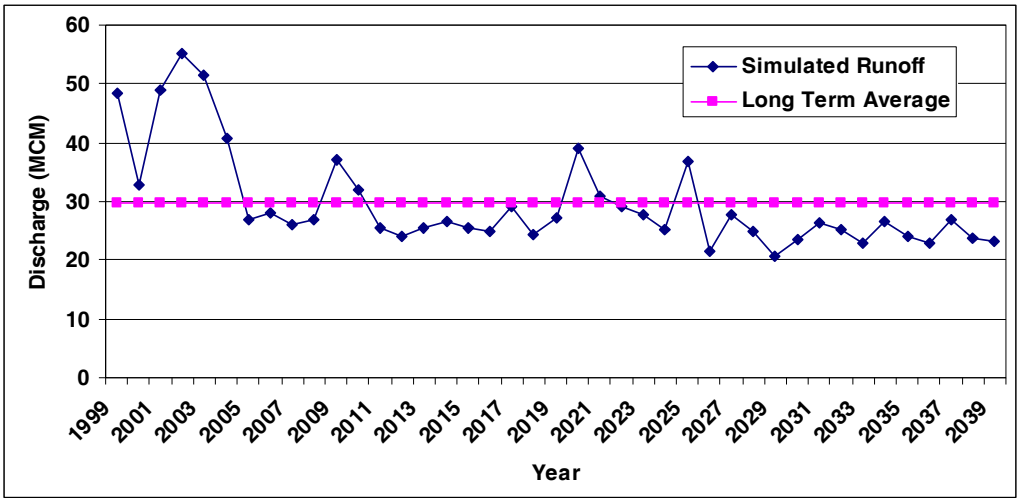

Figure 4: Simulated runoff of the Aharchay basin under climate change effect

Two approaches are considered in this study for evaluation of reliable water supply: In the first approach, the data for all years are considered, in the second approach, however, the years are divided into dry, wet and normal periods in order to evaluate reliable water supply for each condition. In other words, in the second case the two most optimistic and pessimistic scenarios of reservoir operation are evaluated.

First Approach

Using the simulated runoff, the reservoir reliable water supply is determined as presented in Table 2. It should be noted that the initial reservoir has been considered equal to 40 MCM. The reliable water supply is about 20.5 MCM in a year in the reservoir operation period. There are some fluctuations in reliable water supply value in different wet and dry periods but its value decreases with time. The minimum simulated reliable water supply is about 18 MCM in period of 2019-2025. By comparing the yearly water demand of basin which is about 69 MCM and about 40% of it is vital for continuing basin life; the initial water shortage is about 7 MCM (25%) which by considering a fix demand will increase up to 32%.

The probabilistic approach has also been applied in this study to estimate reliable water supply. Different probability thresholds have been considered including 95%, 90%, 80% and 60%. The results are given in Table 3 for different time periods. By decreasing the considered probability threshold the risk of not satisfying the reliable water supply in the year increases so that the reliable water supply would increase as it is obvious in Table 3. But the percentage of variation depending on the humidity situation of the different periods (inflow condition) is considerably different. For

example, the difference between reliable water supply with 60% and 95% of reliability, in periods 2012-2018 and 1999-2004 are 7% and 22%, respectively.

Table 2. The reservoir deterministic reliable water supply

Period	Average inflow (MCM)	Reliable water (MCM)	Average reliable water (MCM)
1999-2004	46.264	24.70	20.51
2005-2011	28.97	19.2	
2012-2018	25.70	23.69	
2019-2025	30.85	17.96	
2026-2032	24.27	19.47	
2033-2039	24.37	22.25	

Table 3. The reservoir probabilistic reliable water supply

Period	Average inflow (MCM)	Reliable water (MCM)			
		60%	80%	90%	95%
1999-2004	46.264	44.82	41.88	38.95	36.47
2005-2011	28.97	30.01	28.54	26.75	25.22
2012-2018	25.70	27.96	27.38	26.69	26.08
2019-2025	30.85	31.15	29.37	27.34	25.44
2026-2032	24.27	25.83	24.92	24.06	23.17
2033-2039	24.37	26.58	26.04	25.32	24.70

However the water demand of the region is not fixed and it changes because of development projects as well as climate change effects. Based on the estimation of Karamouz et al. (2007), the water demand of the region will increase by an average rate of 2% per year, which will make the situation much worse. In this case, managerial solutions such as conjunctive use of surface and ground water and demand management could help reduce the water shortage severity.

Second Approach

The reliable water supply for each of the considered scenarios for wet, dry and normal situations are given in Table 4. The wet, normal and dry situations are determined based on the reservoir inflow. The water supply in normal situations is about 10% more than the deterministic water supply achieved in the previous approach. Although the average input in wet periods is considerably higher than other periods, it seems that dry seasons have affected the reliable water supply because the number of dry years is much more than wet years. In this way different water allocation strategies could be employed in wet and dry years and it helps decrease the possible damages using on-time strategies to deal with extreme events.

SUMMARY AND CONCLUSION

In this study a process for the evaluation of reliable water supplies in probabilistic and deterministic approaches are presented. The effects of climate change on the

future basin runoff are simulated using SDSM and IHACRES to obtain more sound results. The proposed algorithm is applied to the Sattarkhan reservoir in Aharchay basin. The reservoir capability is assessed in order to modify the reservoir operation scheme in the coming situation considering the changes in water availability of the region. Since different levels of risk are considered for different water allocation purposes, the reliable water supplies with different probabilities are determined using chance-constraint optimization model. Also for considering the effects of inflow variations in dry, normal and wet years, the reservoir reliable water supply has been determined for characterized wet, normal and dry periods.

The reliable water supply fluctuates in different periods up to 15% from the long term average which is 20.51 MCM. The results show the significant effect of climate change on reliable water supplies. Also, there is considerable difference between reliable water supply of wet years and other years. In this way the high potential of water resources in normal and especially wet years could be employed for further development of the basin and better management of dry seasons through appropriate methods.

Table 4. The reservoir probabilistic reliable water supply

Period	Average inflow (MCM)	Reliable water (MCM)				Deterministic reliable water (MCM)
		60%	80%	90%	95%	
Wet period	44.72	43.05	40.98	38.32	35.72	25.41
Normal period	26.82	26.33	25.54	24.64	23.79	22.62
Dry period	22.47	25.38	25.00	24.60	24.25	20.41

REFRENCES

Burn, D.H., Simonovic, S.P., (1996), "Sensitivity of reservoir operation performance to climatic change", *J. Water Resources Management*, 10, 463-478.

Brekke, L., (2008), "Assessing reservoir operations risks under climate change", *J. hydrology*, 5(4), 125-140.

Department of the Environment, (1996), "Review of the potential effects of climate change in the United Kingdom", *HMSO*, London, 247-260.

Jakeman, A., Hornberger, G.M., (1993), "How much complexity is warranted in a rainfall- runoff model?", *J. Water Resources Research*, 28, 2637-2649.

Karamouz, M., Imen, S., Nazif, S., (2007), "Climate change and water availability", Second International Conference on Earth Systems Modeling (ICESM), 1, ICESM2007-A-0043.

Wilby, R.L., Dawson, C.W., Barrow, E.M., (2002), "SDSM- A decision support tool for the assessment of regional climate change impacts", *J. Environmental Modeling and Software*, 17, 147-159.

Wolock, D.M., McCabe, G.J., (1999), "Effects of potential climatic change on annual runoff in the conterminous United States", *J. American Water Resource Association*, 35, 1341–1350.

Developments on Stochastic Analysis, Modeling, and Simulation (SAMS 2009)

J.D. Salas[1], O. Sveinsson[2], T.S. Lee[3], W. Lane[4] and D. Frevert[5]

Abstract

Stochastic Analysis Modeling and Simulation (SAMS) is a software where stochastic techniques are utilized for simulating synthetic water resources data such as monthly streamflows. The current version, SAMS 2007, includes alternative modeling approaches and data analysis features. The stochastic models included in SAMS 2007 are parametric models such as multivariate autoregressive and disaggregation linear models. SAMS 2009 is now available. Various alternatives and options have been added particularly nonparametric techniques. The main purpose of this paper is to summarize the capabilities of SAMS 2009.

Introduction

Stochastic simulation of water resources time series, in particular hydrologic time series, has been widely used for several decades for various problems related to planning and management of water resources systems. Typical examples are determining the storage capacity of a reservoir, evaluating the reliability of a reservoir with a given capacity, evaluating the adequacy of a water resources management strategy under potential hydrologic scenarios, and evaluating the performance of an irrigation system under uncertain irrigation water deliveries. Stochastic simulation has been performed through the built-in functions of general software packages such as S-PLUS, SAS, SPSS, R, and Matlab, etc. While these built-in functions for general time series simulation are useful, they are often meant for general purpose and do not reproduce features inherent in hydrological data. Therefore, specialized software for stochastic simulation and data analysis of hydrology data is attractive because they are built in such a way as to reproduce the special features that are characteristic in hydrologic time series such as long memory, periodicity, skewed marginal distributions, and intermittency. In addition, river network systems generally involve spatial dependency and connectivity requiring special modeling concepts and schemes such as aggregation and disaggregation.

The LAST package was developed during 1977-1979 by the U.S. Bureau of Reclamation

[1] Department of Civil and Environmental Engineering, Colorado State University, Fort Collins, CO 80523. Phone (970) 491-6057 and Email address: jsalas@engr.colostate.edu

[2] Director of Research, Electric Power Company, Iceland.

[3] Institute National de la Research Scientifique, Eau Tarre Environment, 490 Rue de Couronne Quebec, QC G1K 9A9, Canada.

[4] Consulting Engineer, Golden, CO

[5] Retired, Bureau of Reclamation, Lakewood, CO, Phone (303) 989-4270, Email address: dkfrevert@netzero.net

(USBR). Originally, the package was designed to run on a mainframe computer but later it was modified for use on personal computers (Lane and Frevert, 1990). While various additions and modifications have been made to LAST in the late 1970's and the 1980's, the package has not kept pace with either advances in time series modeling or advances in computer technology. Thus USBR in collaboration with Colorado State University developed the SAMS software. SAMS is a computer software package that deals with the stochastic analysis, modeling, and simulation of hydrologic time series. The main purpose of SAMS is to generate synthetic hydrologic data. It is not built for hydrologic forecasting although data generation for some of the models can be conditioned on most recent historical observations.

The basic concepts and procedures of stochastic simulation are discussed in the next section. And the capabilities of SAMS 2009 are described in a later section.

Brief review of basic concepts and procedures of stochastic simulation

Stochastic simulation of hydrologic time series hinges on a mathematical model that is built in such a way that the synthetic records derived from such a model reproduce key statistical properties observed in the historical records. For this purpose alternative parametric models and nonparametric algorithms have been suggested. The autoregressive moving average (ARMA) model is likely the most popular parametric model for simulating stationary processes such as yearly streamflows at a single site (e.g. Salas, 1980; Loucks et al., 1981). ARMA models assume that the distribution of the underlying variable is normal, and in most cases this requires that the hydrologic variable under consideration is transformed (to normal) prior to fitting the model. As an alternative to avoid this process of transformation a limited class of gamma autoregressive models has been suggested (e.g. Fernandez and Salas, 1987; 1990). Also shifting mean models have been developed to reproduce the patterns of shifting means that may be observed in some hydrologic records (Salas and Boes, 1980; Sveinsson et al., 2003). Likewise, to account for periodicity in hydrologic time series, periodic ARMA (PARMA) models have been developed (e.g. Salas 1993) for single site. In addition, multivariate ARMA, contemporaneous multivariate ARMA (CARMA), and contemporaneous PARMA (CPARMA) are also available for stationary and periodic series such as monthly streamflows (e.g. Salas 1993; Stedinger et al. 1985). Furthermore, to model large river basin networks such as the Colorado River system, aggregation and disaggregation models have been developed (Valencia and Schaake 1973; Mejia and Rousselle 1976; Stedinger and Vogel 1984; Lane and Frevert, 1990). All the models summarized above represent a class of parametric models that are defined by one or more mathematical equations involving a set of variables and parameters (to be estimated from observations.)

Besides parametric models alternative nonparametric algorithms and procedures (also denoted here as "models") have been developed in literature. For example, the index sequential method (ISM) has been employed by the Bureau of Reclamation (Ouarda et al. 1997; Prairie et al. 2005) because of its simplicity. Block bootstrapping (BB) is a useful resampling technique that has been popularly employed in literature (e,g, Vogel and Shallcross, 1996). The k-nearest neighbor resampling (KNN) has been originally developed by Lall and Sharma (1996). It has been modified and widely employed in hydrologic and environmental systems (Gangopadhyay et al. 2005; Prairie et al. 2007; Prairie et al. 2006; Rajagopalan and Lall 1999). Recently, Salas and Lee (2009) developed a resampling technique employing KNN and gamma kernel perturbation (KGK) for a single site variable. Also a multivariate nonparametric model using BB and genetic algorithm (Lee and Salas, 2009) and a nonparametric disaggregation model (NPD) (Lee et al. 2009) have been developed recently. The foregoing parametric and nonparametric models are

available in the current software SAMS 2009.

Using one type of model or another for a particular case depends on several factors such as physical and statistical characteristics of the process under consideration, data availability, the complexity of the system, and the overall purpose of the simulation study. Given the historical record, one would like the model to reproduce important historical statistics. This is why a standard step in streamflow simulation studies is determining the historical statistics. Once a model has been selected, the next step is to estimate the model parameters, then to test whether the model represents reasonably well the process under consideration. This may be accomplished through goodness of fit tests such as the Akaike information criterion (AIC), and by comparing the statistics obtained from the generated data with those obtained from the historical data.

Capabilities of SAMS 2009

The procedures of stochastic simulation mentioned above are included in SAMS 2009. The main menu of SAMS 2009 is summarized in Fig. 1 and the capabilities for each menu item are briefly indicated. Here we will explain them in some detail. To illustrate some of the key features we use monthly data of the Colorado River System. The historical gaged data at 29 sites have been naturalized (Prairie and Callejo, 2005) for the period 1906-2003 and part of the data have been extended by Lee and Salas (2006) back to 1906 employing linear regression and nonparametric bootstrapping with trace selection method.

File

Firstly the historical data must be imported into SAMS. There are two ways to import historical data: by reading the data directly from a text file and by copying the data from a table (e.g. from Excel). In the first case the user must prepare a data file (*.dat) with the format readable by SAMS. This is a common way to upload data into SAMS, but formatting the data readable by the program may lead to errors especially for a new user. The second way of importing data is easier and more reliable. In this case the user needs to insert some basic information such as, the record length, the number of stations (sites), and starting year, as shown in Fig. 2 and to paste the data that the user may have in Excel (or an equivalent format/program) into the table that will be prompted by SAMS. In addition, the information about data transformation that is performed in the module Data Analysis can be saved and imported in the File menu bar. This is useful especially when working with complex systems involving a large number of sites and large number of seasons in the year (e.g. 12 seasons) and the user may want to preserve the data transformation parameters for future operations.

Data Analysis

Generally hydrologic data are significantly skewed especially for seasonal data while parametric models (with some exceptions) generally assume that observed data are normally distributed. Therefore, the data must be transformed into normal prior to fitting stochastic models. Various transformations are included in SAMS 2009 such as logarithm, power, Box-Cox, and gamma. Test statistics such as skewness and Filliben tests as well as graphical displays are available to check whether the transformed data are normally distributed.

The statistical characterization of hydrologic data is useful for selecting the type of model to be fitted and the model order as the case may be. In addition, it is useful for comparing against statistics that are derived from generated data. For this purpose, SAMS 2009 has various tools to investigate the characteristics of historical data such as plotting time series, visual and tabular representation of key statistics (e.g. mean, standard deviation, skewness, and correlations), spectrum analysis, histogram and kernel density estimation (KDE), and operational statistics

such as drought, surplus, and storage related statistics. An example of the histogram and KDE is shown in Fig. 3 for the monthly streamflows (May) of the Colorado River at Lees Ferry (site 20). Also a three-dimensional plot of the lag-0 cross-correlation coefficients of annual streamflows is illustrated in Fig. 4 for the 29 sites of the Colorado River system.

Model Fitting

As indicated above, alternative parametric and nonparametric models have been suggested in literature for stochastic streamflow generation. The various stochastic models that are available in SAMS 2009 are summarized in Table 1. The parametric models include: ARMA, GAR, PARMA, MPARMA, CSM-CARMA, PMC-ARMA, and linear disaggregation. One of the major improvements in SAMS 2009 is the addition of nonparametric models such as ISM, BB, KNN, and KGK for both annual and seasonal data as well as disaggregation approaches, as shown in Table 1. In some cases the parametric and nonparametric models that are available in SAMS 2009 may be combined to tackle the generation of complex water resources systems.

An example of parametric and nonparametric model selection is shown in Fig. 5 where menu options for the PARMA(p,q) model (left in Fig. 5), and KNN with gamma KDE and pilot variable (nonparametric KGKP) model (right in Fig. 5) are shown. Note that Fig. 5 (right panel) shows how a parametric model (ARMA) and a nonparametric model (KGKP) are combined.

Fitted Model

After fitting a model, the user may like to see a summary of the fitted model, the parameters, as well as some results of goodness-of-fit tests of the fitted model. Some test statistics are available only for some of the parametric models. However, for all models the tests of the fitted model can be done by comparing the historical and generated statistics. For this purpose, tables of the mean and standard deviation of various key statistics obtained from the generated samples are displayed along the historical statistics. Also box plots of the generated statistics along with the historical statistics are available.

Generate Series

The stochastic generation option is activated by entering a number of parameters such as the generation length, the number of samples, and additional information pertaining to the output. Once data are generated, the fitted model can be tested by comparing the statistics of generated data and the historical data. For example, the comparisons of the generated and historical annual key statistics are shown in the boxplots in Fig. 6 for a SKGKA model fitted to the Colorado River at the Lees Ferry station, and similarly in Figs. 7-8 for a SKGKP model. In the boxplots, the triangles in Figs. 6 and 8 and the line of segments in Fig. 7 represent the historical statistics. And the end lines of the box are the 25 and 75 percentiles while the cross lines above the box on the whisker correspond to the 90 percentile and the maximum, while the cross lines below the box on the whisker represent the 10 percentile and the minimum. In Fig. 6 there is indication of a significant underestimation of the annual standard deviation when using the SKGKA model, while analyses of the generated data based on a SKGKP model (refer to Fig. 8) indicate a better performance of the SKGKP than SKGKA with regards to reproduction of the annual key statistics. Additionally, Fig. 7 shows that the monthly data generated using model SKGKP reproduce the monthly statistics reasonably well.

Final Remarks

SAMS 2009 is a versatile software that may be applicable for any number of seasons in the year. While in principle it may be applicable all the way to daily series it is advisable not to apply it for more than 26 seasons (biweekly). Modeling weekly time series may require smoothing weekly statistics using Fourier series. Alternatively modeling weekly and daily time series may be done using disaggregation techniques. But up to now these capabilities are not available. Plans are to add further features as soon as practicable.

Acknowledgments. Thanks are due to the U.S. Bureau of Reclamation (Denver Office and Lower Colorado Office) for the financial support through a number of projects that allowed us the development and further updates to SAMS. In addition, the support of HydroQuebec (Canada) and the Great Lakes Environmental Research Laboratory, NOAA are acknowledged.

References

Fernandez, B. and Salas, J.D., 1986, "Periodic Gamma Autoregressive Processes for Operational Hydrology," Water Resour. Res., 22(10):1385-1396.

Fernandez, B. and Salas, J.D. 1990, "Gamma-Autoregressive Models for Streamflow Simulation," ASCE J. Hydr. Eng., 116(11): 1403-1414.

Gangopadhyay, S., Clark, M., and Rajagopalan, B. (2005). "Statistical downscaling using K-nearest neighbors." *Water Resources Research*, 41(2), -.

Lane, W and Frevert, D. (1990) "Applied Stochastic Techniques Users Manual", Bureau of Reclamation, Denver, CO.

Lee, T., Salas, J.D. and Prairie, J. (2009). "Nonparametric Streamflow Disaggregation Model" submitted to *Water Resources Research*.

Loucks, D.P., Stedinger J.R., and Haith D.A. (1981), *Water Resources Systems Planning And Analysis*, Prentice-Hall, Englewood Cliffs, NJ, 559 pages

Mejia, J.M., and Rousselle, J. (1976). "Disaggregation Models in Hydrology Revisited." *Water Resources Research*, 12(2), 185-186.

Ouarda, T.B. M.J., Labadie, J.W., and Fontane, D.G. (1997). "Indexed sequential hydrologic modeling for hydropower capacity estimation." *Journal of the American Water Resources Association*, 33(6), 1337-1349.

Prairie, J., and Callejo, R. (2005). "Natural flow and salt computation methods." Bur. of Reclam., U.S. Dep. of the Inter., Salt Lake City, Utah.

Prairie, J., Rajagopalan, B., Lall, U., and Fulp, T. (2007). "A stochastic nonparametric technique for space-time disaggregation of streamflows." *Water Resources Research*, 43(3), -.

Prairie, J.R., Rajagopalan, B., Fulp, T.J., and Zagona, E.A. (2005). "Statistical nonparametric model for natural salt estimation." *Journal of Environmental Engineering-Asce*, 131(1), 130-138.

Prairie, J.R., Rajagopalan, B., Fulp, T.J., and Zagona, E.A. (2006). "Modified K-NN model for stochastic streamflow simulation." *Journal of Hydrologic Engineering*, 11(4), 371-378.

Rajagopalan, B., and Lall, U. (1999). "A k-nearest-neighbor simulator for daily precipitation and other weather variables." *Water Resources Research*, 35(10), 3089-3101.

Salas, J.D. (1993). "Analysis and Modeling of Hydrologic Time Series", chapter 19 in *Handbook of Hydrology*, D.R. Maidment, Editor, McGraw-Hill.

Salas, J.D., D.C. Boes. (1980). "Shifting level modeling of hydrologic series." *Advances in Water Resources*, 3, 59-63.

Salas, J.D. and Lee, T. (2009). "Nonparametric model for streamflow simulation", submitted to ASCE *J. Hydrologic Engr.*

Stedinger, J.R., Lettenmaier, D.P., and Vogel, R.M. (1985). "Multisite Arma(1,1) and Disaggregation Models for Annual Streamflow Generation." *Water Resources Research*, 21(4), 497-509.

Stedinger, J.R., and Vogel, R.M. (1984). "Disaggregation Procedures for Generating Serially Correlated Flow Vectors." *Water Resources Research*, 20(1), 47-56.

Sveinsson, O.G.B., Salas, J.D., Boes, D.C., and Pielke, R.A. (2003). "Modeling the dynamics of long-term variability of hydroclimatic processes." *Journal of Hydrometeorology*, 4(3), 489-505.

Valencia, D., and Schaake, J.C. (1973). "Disaggregation Processes in Stochastic Hydrology." *Water Resources Research*, 9(3), 580-585.

Vogel, R.M., and Shallcross, A.L. (1996). "The moving blocks bootstrap versus parametric time series models." *Water Resources Research*, 32(6), 1875-1882.

Table 1 Models Included in SAMS 2009

		Annual Data	Seasonal Data
Univariate	P*	- Autoregressive Moving Average: ARMA(p,q) - Gamma Autoregressive: GAR(1) - Shifting Mean: SM	- Periodic ARMA: PARMA(p,q) - Periodic Markov chain - ARMA: PMC-ARMA(p,q) - Temporal Disaggregation
	NP**	- Index Sequential Method: ISM - Block Bootstrapping: BB - K-Nearest Neighbors Resampling: KNN - KNN with Gamma Kernel Density Estimate: KGK	- Seasonal ISM: SISM - Seasonal BB: SBB - Seasonal KNN: SKNN - Seasonal KGK: SKGK - SKGK with yearly dependence: SKGKA - SKGK including pilot variable: SKGKP - Temporal disaggregation
Multivariate	P	- Multivariate Autoregressive: MAR(p) - Contemporaneous ARMA: CARMA (p,q) - Contemporaneous SM-ARMA: CSM-CARMAR(p,q) - Spatial Disaggregation Model	- Multivariate Periodic AR(p): MPAR(p) - Spatial-Temporal Disaggregation - Temporal-Spatial Disaggregation
	NP	- Multivariate ISM: MISM - Multivariate BB with KNN and Genetic Algorithm: MBKG - Spatial Disaggregation Model	- Multivariate ISM: MISM - Multivariate BB with KNN and Genetic Algorithm: MBKG - Temporal Disaggregation Model

* Parametric Models, ** Nonparametric Models

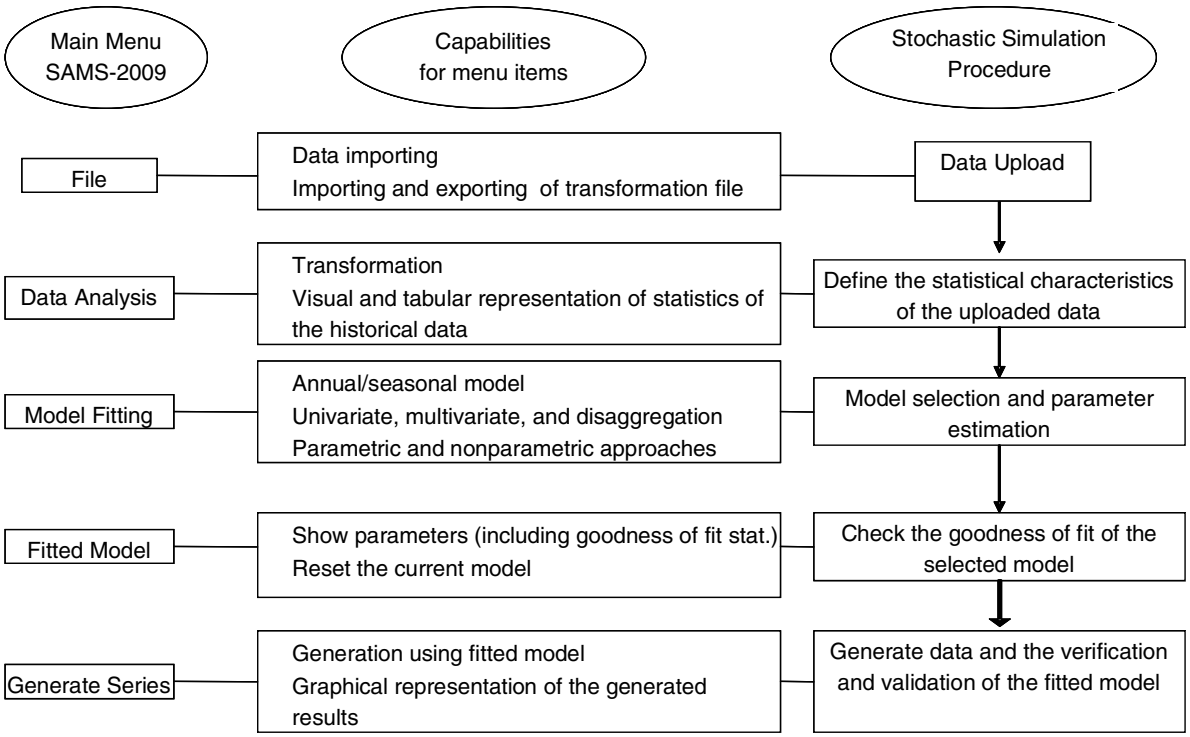

Fig. 1 Summarized description of the capabilities of SAMS 2009

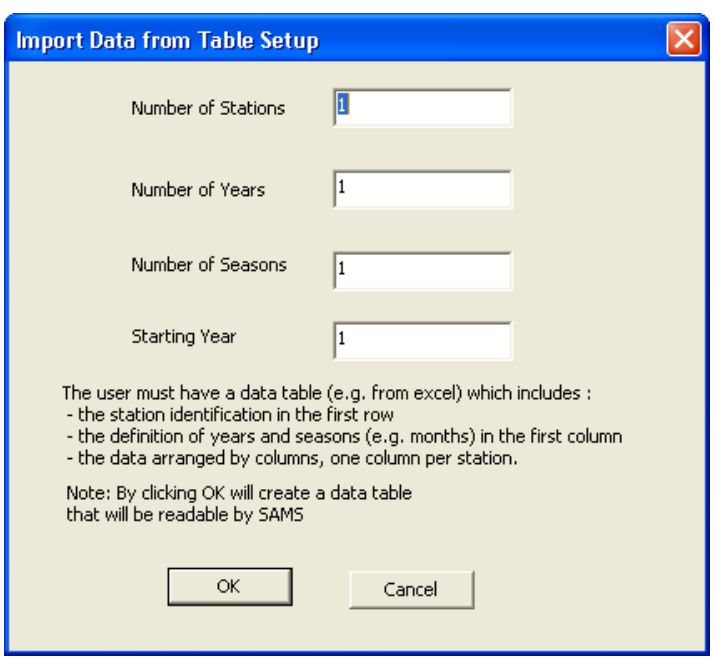

Fig. 1 Option dialog box after clicking “Importing data from Table”

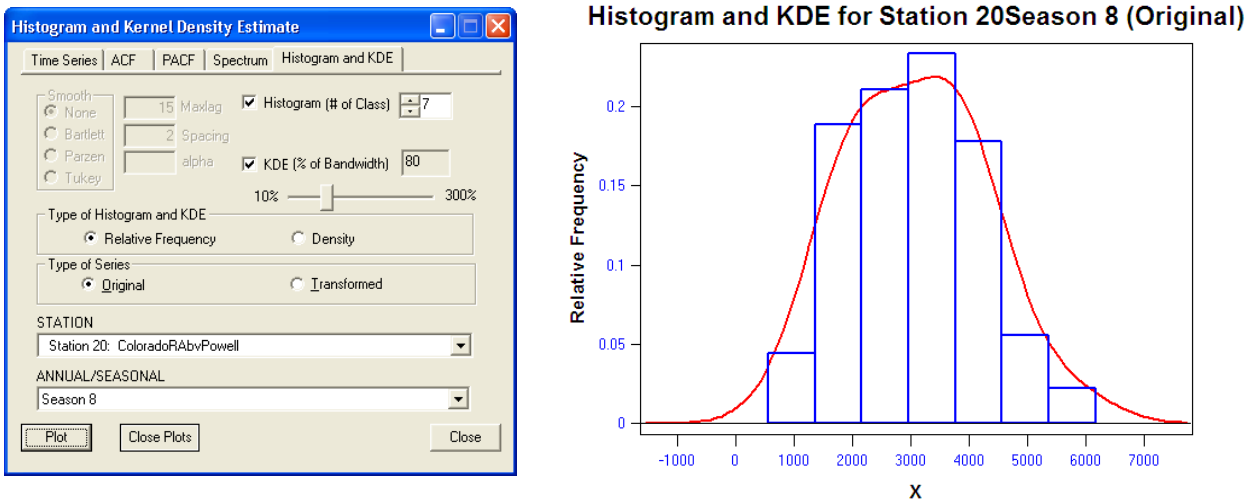

Fig. 2 The dialog box for plotting the Histogram and Kernel Density Estimate (left) and corresponding graphs (right) for the Colorado River at Lees Ferry streamflows for the month of May.

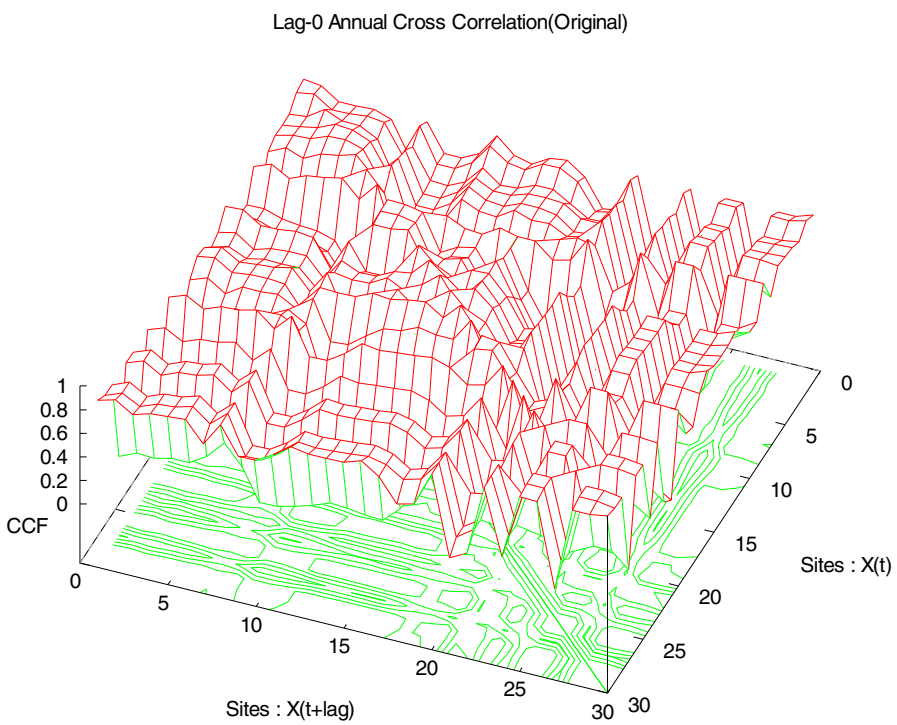

Fig. 3 Lag-0 cross-correlation coefficients of the annual streamflows for 29 stations of the Colorado River system.

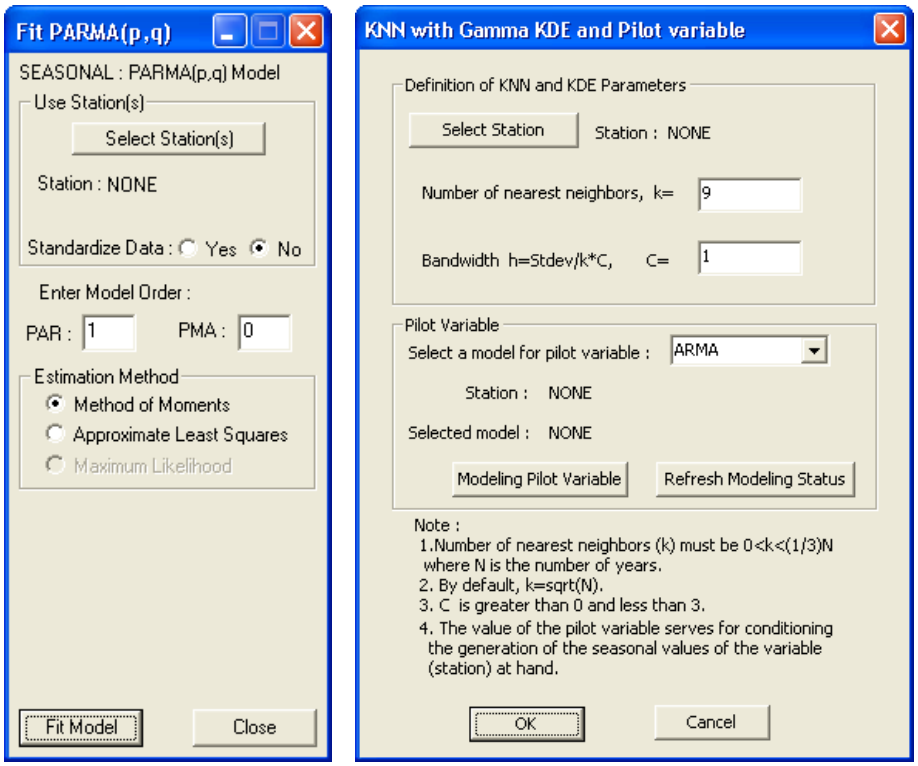

Fig. 4 Menu bars for model fitting based on the PARMA (p,q) model (left) and nonparametric SKGKP model (right)

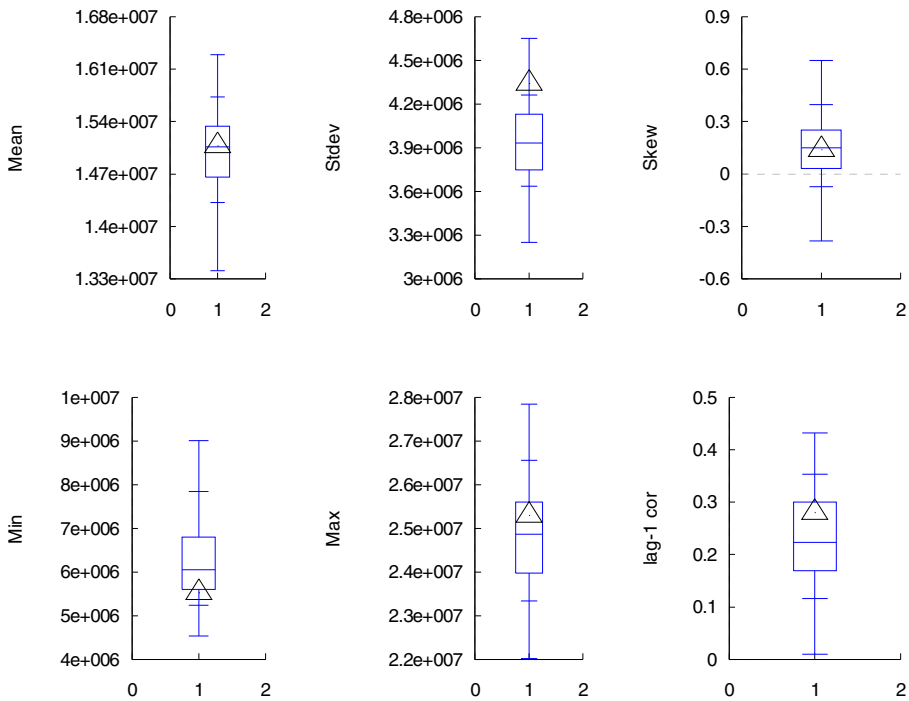

Fig. 5 Basic statistics of yearly statistics obtained from the historical and generated data (from 100 samples) using model SKGKA for the Colorado River at Lees Ferry

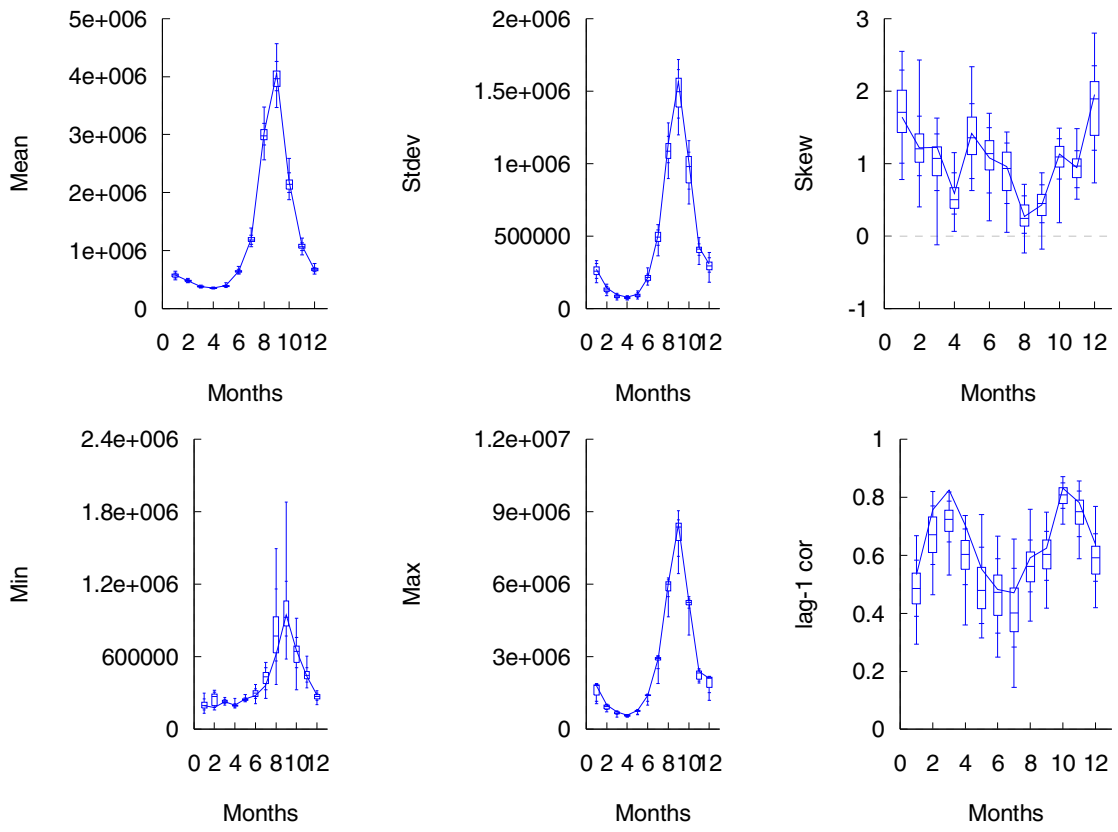

Fig. 6 Boxplots of monthly basic statistics obtained from the generated data using model SKGKP for the Colorado River at Lees Ferry. The line represents the historical statistics.

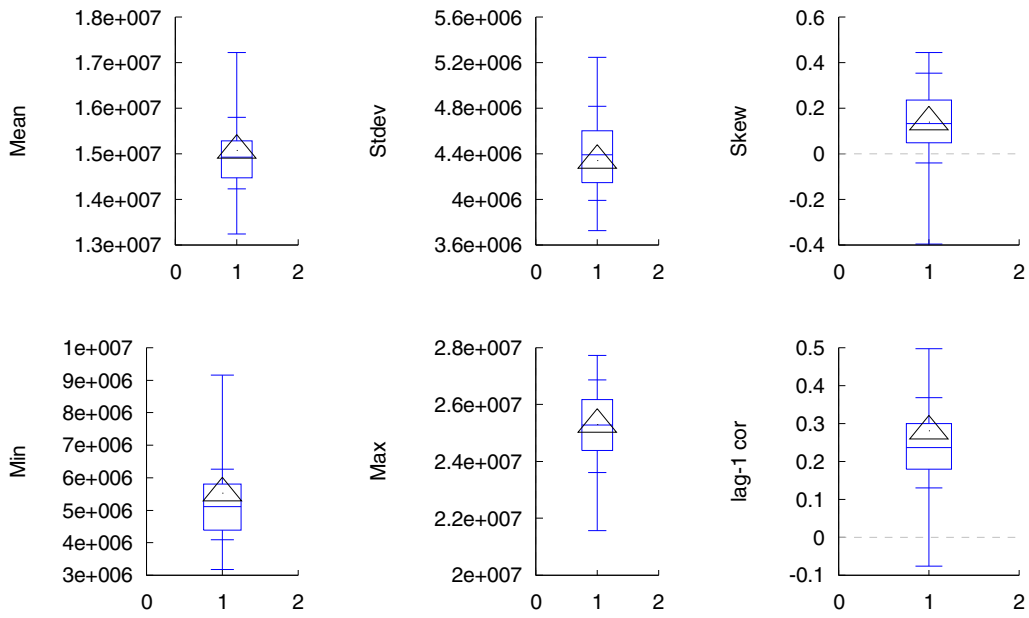

Fig. 7 Boxplots of annual basic statistics obtained from the generated data (100 samples) based on the model SKGKP for the Colorado River at Lees Ferry. The triangle symbol represents the historical statistics.

Does Collaborative Modeling Lead to Better Management of Our Water Resources?

S. Langsdale[1] and W. Michaud[2]

[1] Institute for Water Resources, U.S. Army Corps of Engineers, 7701 Telegraph Road, Alexandria, VA 22315; PH (703) 428-7245; FAX (703) 428-8171; email: slangsdale@gmail.com
[2] SRA, International, Inc., 3434 Washington Boulevard, Arlington, VA 22201; PH (860) 738-7501; FAX (860) 738-7550; e-mail: bill_michaud@sra.com

ABSTRACT

Shared Vision Planning (also known as Collaborative Modeling or Computer Aided Dispute Resolution) is a relatively new but growing field. Advocates claim that the method increases the quality of decisions and policies in a way that is "cheaper, better, and faster" than traditional decision making or dispute resolution without computers. But can we prove this? In an attempt to find out, the Corps of Engineers' Institute for Water Resources and SRA International developed an array of performance measures to see if the benefits of shared learning and better policies are achieved, as well as to explore what factors (e.g., transparent model, trusted facilitator) are critical for producing the intended outcomes. The performance measures seek to characterize the quality of the participatory process, the quality of the resulting model, what impact the model had on the process and any policy recommendations, and if the process produced any longer-term impacts such as building institutional capacity and social capital. Results of assessing case studies using the performance measures will be presented.

INTRODUCTION

Collaborative modeling as an approach to resource management has evolved from several different fields, as technological developments have allowed us to generate transparent, integrated models through a collaborative process. Current practitioners include representatives of federal agencies, academia, and private consulting. The Institute for Water Resources at the Army Corps of Engineers has developed a version they named "Shared Vision Planning" and refers to the process more generally as "Computer Aided Dispute Resolution." Many claim that collaborative modeling is a means to better water management; that it is "cheaper, better, and faster" than traditional planning approaches. However, the question arises, do people just feel better for having participated in a process that fosters shared understanding, trust, and social capital, or does it really have the potential to improve resource management?

Many of the benefits achieved by collaborative modeling processes are intangible. However, without some concrete measurement of benefits, government agencies have trouble justifying choosing a collaborative modeling process that may be viewed as riskier and that requires more upfront investment of resources than the status quo. Documenting measurable benefits from collaborative modeling processes will not only encourage resource managers and agencies to consider the approach more seriously, but

will give them the ability to weigh whether the option is appropriate given their particular circumstances and justify it to those to whom they are held accountable.

To fill this need, the Institute for Water Resources began developing performance measures and related survey instruments in fall 2007. The surveys will be used for both retrospective case study analysis and for future case studies. In addition to providing evidence of benefits, the results will provide insight as to which context and process design factors are critical for increasing the chances of a successful outcome.

MEASURING THE PERFORMANCE OF COLLABORATIVE MODELING

To develop an approach for evaluating the effect of collaborative modeling on resource management decisions, IWR and SRA identified elements and outcomes of the planning process that would be useful to measure. We mapped these elements and outcomes to an existing approach used by the U.S. Institute for Environmental Conflict Resolution (USIECR) and developed a survey instrument to be used to gather systematic data regarding collaborative modeling processes.

To start, IWR and SRA developed a logic model describing the manner in which Shared Vision Planning is intended to improve resource management decisions. With the logic model as a framework, we identified six areas where systematic data collection could prove useful for measuring the effect of collaborative modeling:

- *Planning setting* – characteristics of the setting within which water resources planning processes are convened, including factors such as the type of resource management issue being addressed, level of conflict at the outset of the process, institutional constraints, etc.
- *Stakeholder participation process* – qualities of the design and implementation of the overall stakeholder participation process, including factors such as the degree to which stakeholders participating in the process represented all key interests, opportunities provided for influencing the process design, conflict resolution processes, etc.
- *Model setting and modeling* – qualities of the design and implementation of collaborative modeling processes, including level of stakeholder participation in developing the model, model type, quality of the modeling team, etc.
- *Model-level outcomes* – the performance of the model itself, including the degree to which the model integrates available information, the handling of stakeholder interests, model transparency, capability of the model to support the timely evaluation of alternatives, etc.
- *Modeling process-level outcomes* – the performance of the modeling process in terms of its effects on stakeholders' awareness and understanding of others' interests, trust in the planning process, evolution and clarity of resource management objectives, etc.
- *Planning-level outcomes* – the effect of the collaborative modeling and planning processes on resource management decisions, including the extent to which the

process influenced the ultimate outcome, the quality of the resource management decision, institutional changes that could improve future decisions, etc.

As the performance measures strategy took shape, IWR and SRA noted that several of the areas of interest aligned with the Multi-Agency Evaluation Study (MAES) developed by USIECR. IWR recognized the potential benefits of building on the USIECR work – use of tried and tested survey questions, the possibility of being able to extrapolate the IWR findings to a broader set of circumstances, and the value of exposing the concepts of collaborative modeling to a wider policy/process dialogue – and decided to pursue an integrated approach.

The existing survey instruments developed under the MAES project are focused on evaluating collaborative processes used for alternative dispute resolution in general. We built on the MAES questions to achieve a specific focus on collaborative modeling. We also explored alternatives for measuring the effect of a collaborative process on not only the quality of the agreement, decision, or recommendation but also the effect of the process on the actual management of a resource.

With regard to the latter issue – evaluating the effect of collaborative planning and modeling processes – IWR and SRA identified the types of measures that would be required to attribute resource management outcomes to specific processes. However, we recognized that a survey approach alone would likely not achieve this objective. More intensive explorations such as mixed-method evaluation or a "constructed counterfactual" approach such as the Systematic Evaluation of Environmental and Economic Results (SEEER) method developed by US Environmental Protection Agency (EPA) and US Department of Interior (DOI) could provide useful alternatives. The logic model and strategy developed by IWR and SRA provide a useful framework for pursuing such alternatives.

DEVELOPMENT OF A SURVEY INSTRUMENT

To take advantage of the potential benefits of integrating IWR and USIECR data, we adopted the MAES mediation process "participant" questionnaire in its entirety. To the 15 multi-part questions included in the MAES questionnaire, we added 10 questions focused on collaborative modeling and related areas. Other than questions designed to collect descriptive information, the majority of the questions ask the respondent to rate their agreement to statements about the collaborative process and resulting outcomes.

While the draft survey organizes questions according to logical subject groupings (e.g., all questions about the design of the collaborative process are lumped together), each of the questions is mapped to a specific performance measure identified through the logic modeling process. In this way, the survey is efficiently focused on information that will be useful for assessing performance. The mapping will also facilitate the compilation of survey data into meaningful performance measures in the future.

To test the instrument, IWR and SRA selected a range of Shared Vision Planning case studies at or near completion that represent a variety of settings, project sizes, and approaches to applying collaborative methods. We invited representatives of those case studies to participate, and a total of eight participants (all of those contacted) agreed to complete the survey and participate in follow-up interviews to provide feedback on their

experience. As of this writing (January 2009), six of the participants completed the test survey, and SRA is currently conducting the interviews. After completion of this review stage, we will make final modifications to the survey questions as required.

PLANNED USE OF THE TOOL

In spring 2009, IWR will apply for full approval of the survey instrument from the Office of Management and Budget (OMB) to use this survey on future Shared Vision Planning and related collaborative modeling projects. In order to measure participant learning and changes in views, IWR is pursuing approval to administer preliminary as well as post surveys, and, for multi-year processes, interim surveys. In the near term, IWR's focus will be on using the survey as new projects arise.

IWR and SRA have discussed the tool with other federal agencies (USIECR, DOI, EPA) who may be interested in using this survey as they increase their use of technical tools in their agreement seeking processes.

EXPECTED RESULTS

The results of the survey will provide both short-term and long term insights. For each case study for which we are able to use the survey, the tool will provide insight as to the level of success achieved. It will give indication as to how satisfied participants were with both the process (their level of involvement, learning experience, trust in the model, the quality of facilitation, and if the frequency of meetings and attendance was appropriate); and the outcome (were the goals achieved, did the group reach consensus on a decision, was a policy implemented). When interim surveys are given, the information will provide feedback to the facilitators who may choose to modify the process or procedures.

Over the longer term, follow up surveys or interviews will help us to track the success of implementation and success of the policy while minding other external factors that influence outcomes.

Once we accumulate results for enough case studies (over time or through a retrospective study), we will analyze the data more holistically and identify critical factors for success. Although each case study is different, once enough case studies are included, we may be able to provide evidence of the specific benefits of collaborative modeling over traditional collaborative alternative dispute resolution approaches and the circumstances under which collaborative modeling is most suitable.

In addition, by creating a close linkage with the MAES study, we may be able to draw conclusions about the broader universe of cases that might benefit from collaborative modeling processes. For example, if the IWR data suggest that collaborative modeling is particularly beneficial in certain settings that are common to both the IWR and USIECR cases, this could provide insights for the broader application of this approach.

It is hoped that the systematic evaluation of collaborative modeling processes and the interactions created by working with other agencies in this area will help improve our understanding of the benefits of collaborative modeling and expand its appropriate use within the resource management and dispute resolution fields.

Flow Augmentation for Dissolved Oxygen Improvement in Chicago Waterways

Emre Alp[1], Charles S. Melching[2], M. ASCE, and Richard Lanyon[3]

[1]Instructor, Department of Environmental Engineering, Middle East Technical University, Ankara 06531, Turkey, PH (+90) 312 210-5853, FAX (+90) 312 210 2646, email: emrealp@metu.edu.tr
[2]Associate Professor, Department of Civil and Environmental Engineering, Marquette University, P.O. Box 1881, Milwaukee, WI, 53201-1881, PH (414) 288-6080, FAX (414) 288-7521, email: charles.melching@marquette.edu
[3]Metropolitan Water Reclamation District of Greater Chicago, 100 E. Erie St., Chicago, IL, 60611-2903, email: richard.lanyon@mwrd.org)

ABSTRACT

Even though treatment plant (water reclamation plant [WRP]) effluent concentrations meet the applicable standards and most reaches of the Chicago Waterway System (CWS) meet applicable water quality standards, dissolved oxygen (DO) standards are not met in the CWS during some periods. DO deficiencies particularly result in reaches subject to periods of limited flow, such as the upper North Shore Channel (NSC). Thus, an Use Attainability Analysis was initiated to evaluate what water-quality standards can be achieved in the CWS. Flow augmentation practices evaluated for the upper NSC included: i) a portion of the North Side WRP (NSWRP) effluent was transferred to the upstream end of the NSC, ii) the flow was transferred to and divided between two discharge points—one at the upstream end of the NSC and the other at 2.80 km upstream from the NSWRP. It was found that shifting the entire NSWRP effluent flow to the upstream end of the NSC could not achieve 100 percent compliance with a 4 mg/L DO criterion along the upper NSC. Another augmentation alternative was to add oxygen to the NSWRP effluent in the force main, and this transfer of oxygenated effluent was found to effectively improve DO in the upper NSC.

INTRODUCTION

The Chicago Waterway System (CWS) is composed of the Chicago Sanitary and Ship Canal (CSSC), Calumet-Sag Channel, North Shore Channel (NSC), lower portion of the North Branch Chicago River (NBCR), South Branch Chicago River (SBCR), Chicago River Main Stem, and Little Calumet River (north). The CWS is a 122.8 km branching network of navigable waterways controlled by hydraulic structures in which the majority of flow is treated sewage effluent from 3 of the largest wastewater treatment plants in the world. The dominant uses of the CWS are for commercial and recreational navigation and for urban drainage, i.e. draining combined sewer overflows (CSOs), stormwater runoff, and treated wastewater from the Chicago area

away from Lake Michigan, which is the water supply for Chicago. The Calumet and Chicago River Systems are shown in Figure 1.

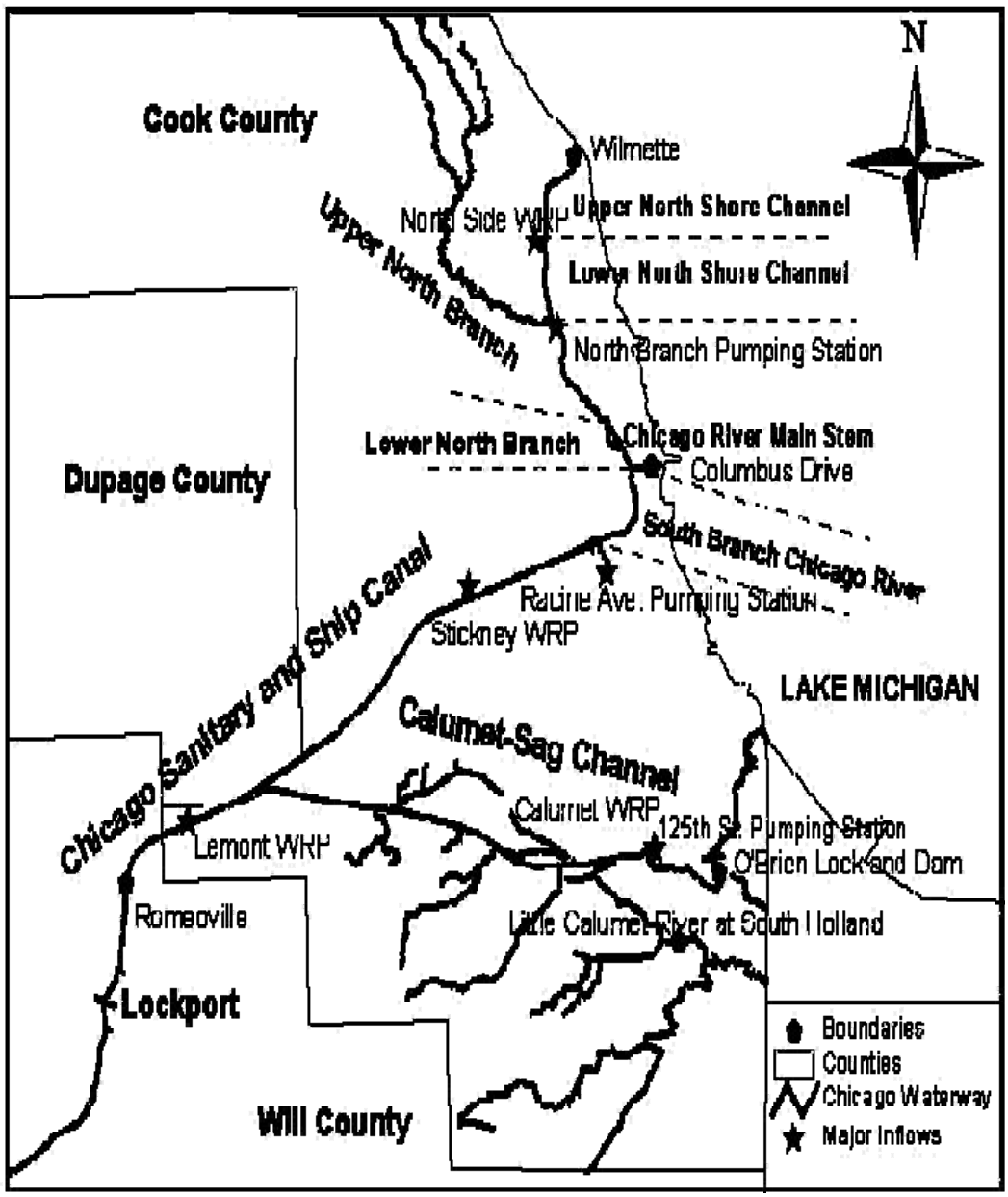

Figure 1. Schematic diagram of the Calumet and the Chicago River Systems.

The Illinois Pollution Control Board regulations (Title 35, Section 302.206 and Section 302.405) state that for General Use waters the dissolved oxygen (DO) concentration shall not be less than 6 mg/L during at least 16 hours of any 24 hour period, nor less than 5 mg/L at any time. In the CWS, only the upper NSC and the Chicago River Main Stem are considered General Use waters. The remainder of the CWS is considered Secondary Use waters wherein the DO concentration shall not be less than 4 mg/L at any time except that the Calumet-Sag Channel shall not be less than 3 mg/L at any time. This regulation was established in 1972 with a modification

for the Calumet-Sag Channel in 1988, and since that time the Metropolitan Water Reclamation District of Greater Chicago (MWRDGC) has made many improvements to the wastewater treatment plants (water reclamation plants, WRPs), CSOs, and aeration resources of the CWS. Thus, in 2003 the Illinois Environmental Protection Agency initiated an Use Attainability Analysis (UAA) for the CWS to see if DO in the CWS could be brought closer to the General Use standard at a reasonable cost. In anticipation of this UAA and to meet other water-quality management needs the MWRDGC began an intensive sampling of hourly DO and temperature throughout the CWS in 1998, and entered into an agreement with Marquette University in 2000 to develop a water-quality model for the CWS that was suitable for simulating constituent concentrations during unsteady-flow conditions. The DUFLOW (2000) water-quality model developed in the Netherlands was selected for this study for the following reasons.

1) Includes several options for water quality simulation, one that is identical to the WASP4 model of the U.S. Environmental Protection Agency (Ambrose et al., 1988) and another that adds the DiToro and Fitzpatrick (1993) sediment flux model to the WASP formulation.
2) Compatible with Geographical Information Systems.
3) Microsoft Windows based including a powerful graphical user interface.
4) Low license cost.
5) Low computational time.
6) Successfully applied to several European rivers (e.g., Manache and Melching, 2004).

DUFLOW was calibrated and verified for the periods of July 12 to November 9, 2001, and May 1-September 23, 2002, respectively. An extensive data set including hourly in-stream DO data at 25 locations, monthly in-stream water-quality measurements at 18 locations, daily treatment plant effluent measurements, and detailed hydraulic data were used to calibrate and verify the model at a 1-hour output time step. Details of the calibration procedure and results are given in Alp and Melching (2006) and Melching et al. (2004).

The UAA (CDM, 2007) found that although treatment plant effluent concentrations meet the applicable standards and most reaches of the CWS meet the applicable water-quality standards, periods occur when DO standards are not met in the CWS, especially during and after wet-weather periods with CSOs. The upper NSC is particularly prone to low DO concentrations because the flow upstream of the North Side WRP (NSWRP) typically is less than 1 m^3/s during dry weather periods allowing effluent from the WRP to back up into the upper NSC and stagnate because of the low hydraulic gradient throughout the CWS. Further, 21 major gravity CSOs discharge to the upper NSC during storm periods, leaving substantial benthic deposits of organic material. Thus, the UAA (CDM, 2007) recommended that one way to solve the problems related to stagnant/low flow in the upper NSC channel would be to pump a portion of the effluent from the NSWRP 6.6 km to the upstream end of the NSC to create a substantial dry weather flow and to dilute CSO flows such that DO concentrations could be substantially improved. This paper reports the results of different flow augmentation scenarios for the upper NSC.

SCENARIOS EVALUATED

Three classes of flow augmentation scenarios were evaluated: (1) NSWRP effluent pumped effluent pumped to the upstream end (50%) and to a mid-point (50%) of the upper NSC, and (3) aerated NSWRP effluent pumped to the upstream end of the NSC. The UAA found that reaching the General Use standard would be unrealistic for the upper NSC, and the model was used to determine what would be needed to achieve DO standards of 4, 5, and 6 mg/L. The results for these three cases are summarized in the following sections.

Flow Augmentation to the Upstream End of the NSC. For this case two types of flow transfer were considered—the transfer of (1) a fixed amount (2.19 or 4.38 m^3/s) and (2) a percentage (10, 50, 75, or 100%) of the NSWRP effluent—for the period July 12–November 9, 2001. The minimum one hour flow from the NSWRP was 4.81 m^3/s. Thus, it was necessary to consider a percentage flow transfer rather than a fixed amount transfer to evaluate higher transfer levels. In Alp and Melching (2006) the performance of flow augmentation in improving DO concentrations was considered at two DO monitoring sites on the upper NSC—Simpson Street and Main Street. Main Street generally had lower DO concentrations, and, thus, only results for Main Street are reported in detail here due to space limitations. The percentage of hours that target dissolved oxygen (DO) concentrations of 3, 4, 5, and 6 mg/L are equaled or exceeded for July 12–November 9, 2001 are listed in Table 1 for Main Street. The wet periods listed in the tables in this paper correspond to times when flows at the downstream boundary at Romeoville were higher than typical dry weather flows (i.e. greater than 100 m^3/s).

Table 1. Percentage of time that dissolved oxygen concentrations are higher than the target concentrations at Main Street for July 12 – November 9, 2001 for different transfers of the North Side Water Reclamation Plant effluent

	3 mg/L		4 mg/L		5 mg/L		6 mg/L	
Scenario	dry	wet	Dry	wet	dry	Wet	dry	wet
Measured	42.8	13.8	33.7	7.7	22.9	4.4	12.5	3.0
Calibrated	47.2	22.1	36.2	15.4	19.7	6.3	9.2	0.0
2.19 m^3/s	72.0	35.2	48.3	9.6	27.0	3.8	6.1	0.0
4.38 m^3/s	90.6	88.9	74.6	73.3	35.0	8.9	13.4	0.0
10 %	61.7	28.3	41.6	7.8	24.2	0.0	5.8	0.0
50 %	94.8	99.7	86.0	89.1	47.3	62.9	17.9	19.0
75 %	98.0	100.0	90.6	97.7	64.8	79.7	26.6	42.0
100 %	98.7	100.0	94.5	99.8	74.1	87.0	31.3	49.3

The simulation results in Table 1 and Figure 2 show the improvement of DO concentrations in the upper NSC resulting from the flow transfer. It can be seen that even transferring the complete NSWRP flow does not result in attainment of DO concentrations in excess of 3 mg/L at Main Street during dry weather 100 percent of the time. This target DO concentration is achieved 100 percent of the time during wet

weather. Surprisingly, for nearly all target DO concentrations and all transfer scenarios higher percentages of compliance are achieved for wet weather than for dry weather. Thus, extra flow for dilution of CSOs is effective in improving DO concentrations in the upper NSC during storms. The simulation results at Addison Street on the NBCR 9.0 km downstream of the NSWRP showed only small decreases in DO concentrations resulting from the transfer because the operation of the Devon Avenue Instream Aeration Station reduces the negative impacts of the flow transfer (Alp and Melching, 2006).

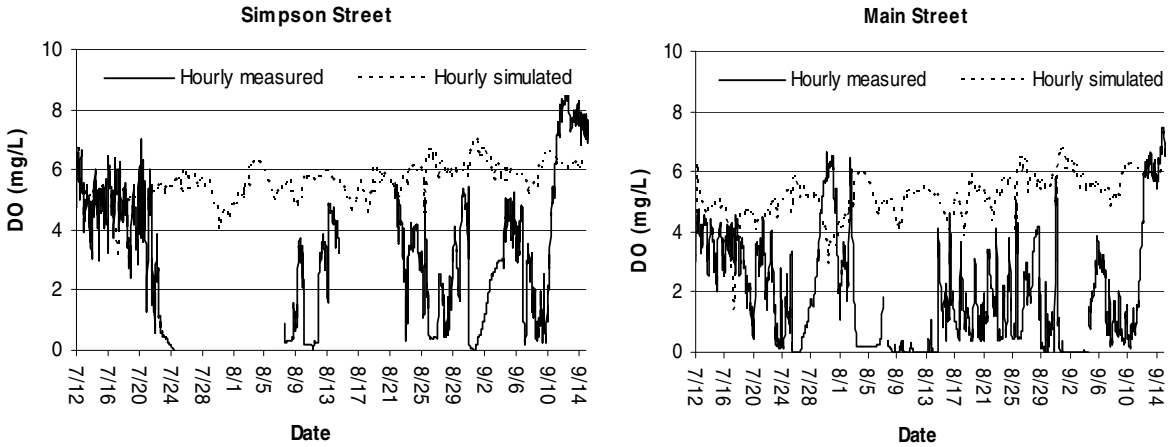

Figure 2. Simulated hourly dissolved oxygen concentrations at Simpson Street and Main Street on the North Shore Channel for a 100 percent transfer of the effluent of the North Side Water Reclamation Plant to the upstream end of the North Shore Channel compared with measured concentrations for July 12 to September 14, 2001.

The surprising result that transferring the entire flow from the NSWRP to the upstream end of the NSC does not result in DO concentrations greater than 4 mg/L at all times during dry weather flow is because of two causes. The first is that for most days in July and August 2001 the DO concentration in the NSWRP effluent is 6 mg/L or less (Figure 3). Thus, there is a small margin between the effluent DO concentration and the 4 mg/L target, and the carbonaceous biochemical oxygen demand (CBOD) and ammonia loads and sediment oxygen demand are sufficient to reduce DO concentrations below the 4 mg/L target. The second is that occasionally higher concentrations of CBOD and ammonia are present in the NSWRP effluent. Figure 2 shows the simulated hourly DO concentrations at Simpson Street and Main Street on the upper NSC resulting from a 100 percent transfer of the NSWRP effluent to the upstream end of the NSC for July 12-September 14, 2001. The occasional instances of low DO concentrations are the result of periods with relatively higher CBOD and ammonia concentrations in the NSWRP effluent. For example, on July 17, 2001, the daily mean CBOD and ammonia concentrations in the NSWRP effluent were 10.0 and 3.49 mg/L, respectively (and the daily mean DO concentration was 5.4 mg/L). Whereas, these concentrations are not high relative to the NSWRP permit limitations and general performance of wastewater treatment plants in the U.S., they are more than double and triple, respectively, the CBOD and ammonia concentrations

in the NSWRP effluent on most days. Thus, occasional higher concentrations in the effluent, and the small difference between the effluent DO concentration and DO concentration targets means that 100 percent compliance with targets will be difficult to achieve.

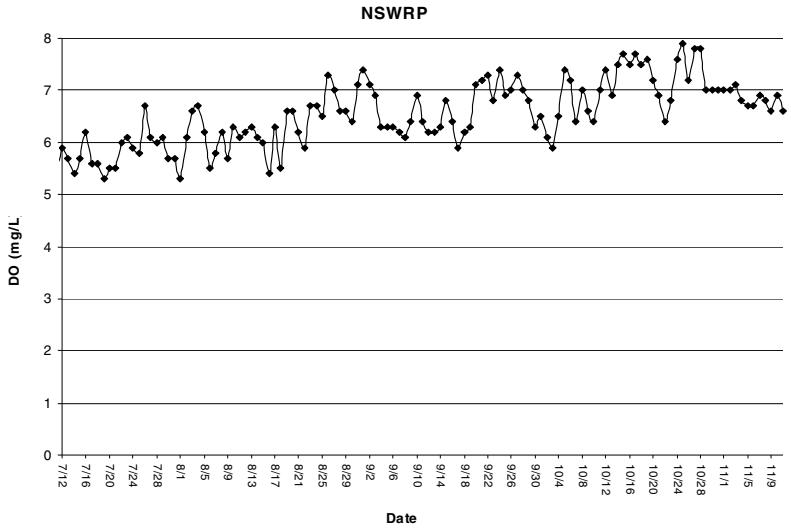

Figure 3. Daily mean dissolved oxygen concentration in the North Side Water Reclamation Plant Effluent for July 12 – November 9, 2001.

One final aspect of the results that requires discussion is the reduction in the percentage of the time in compliance with various target DO concentrations when small amounts of effluent (2.19 m^3/s or 10 percent) are transferred to the upstream end of the NSC relative to the no transfer (calibrated model) case. For the no transfer case compliance with the various target DO concentrations is achieved at certain times. For some of these times the addition of a CBOD and ammonia load in the transferred effluent may result in a decrease in DO concentrations below the targets. For small flow transfers the number of hours with reduced DO may be greater than the number of hours improved by the effluent transfer. At higher levels of flow transfer, the number of hours improved is substantially more than those that are adversely affected.

Flow Augmentation with Two Discharge Points. In this case, the NSWRP effluent is transferred to and divided between two discharge points: one at the upstream end of the NSC and the other 2.80 km upstream from the NSWRP. Again results were obtained for the period of July 12 to November 9, 2001, and the results for Main Street are listed in Table 2.

For flow transfers less than 100 percent, splitting the flow results in slightly worse (a few percentage points less) percentages of compliance with the various target DO concentrations at Simpson Street (Alp and Melching, 2006), but substantially improved percentages of compliance at Main Street. For complete (100 %) flow transfers the results with one or two outlets are nearly identical in terms of percentage of compliance. These results indicate that if a transfer of NSWRP effluent is utilized a final design with multiple outlets would be most efficient as it would

yield nearly identical (or even improved) DO concentrations at smaller construction and operation costs.

Table 2. The percentage of time that dissolved oxygen concentrations are higher than the target concentrations at Main Street on the North Shore Channel for July 12 – November 9, 2001 for different transfers of the North Side Water Reclamation Plant effluent with two discharge points

	3 mg/L		4 mg/L		5 mg/L		6 mg/L	
Scenario	Dry	Wet	Dry	Wet	Dry	Wet	Dry	Wet
Measured	53.1	20.6	41.7	11.5	28.8	6.6	25.5	4.4
Calibrated	46.7	22.1	35.7	15.5	19.6	6.3	9.2	0.0
4.38 m^3/s	99.3	100.0	95.9	100.0	75.9	87.8	31.7	48.2
50 %	99.2	100.0	95.5	100.0	76.0	87.6	31.4	49.3
75 %	99.1	100.0	94.9	99.9	74.9	87.6	31.3	49.5
100 %	98.7	100.0	94.5	99.8	74.2	87.2	31.3	49.5

Flow Augmentation with Aeration. It was previously found that even shifting the entire NSWRP effluent discharge to the upstream end of the NSC could not achieve 100 percent compliance with a 4 mg/L DO criterion at Main Street during the period July 12 to November 9, 2001. It was speculated that this resulted because DO concentrations in the NSWRP effluent often were relatively low (between 5 and 6 mg/L) in July and August 2001. The review of aeration technologies by CTE (2007) as part of the UAA alternatives review found that it would be relatively easy to bring the flow to saturation in the force main used to transfer flow from the NSWRP to the upstream end of the NSC. Thus, it was decided to consider a case of flow augmentation wherein oxygen would be added to the NSWRP effluent in the force main.

Daily mean temperature data for the NSWRP effluent for the periods July 12 to November 9, 2001 and May 1 to September 23, 2002 were used to determine the saturation DO concentration in the force main. Some of this DO would be consumed during travel from the NSWRP to the upstream end of the NSC, but this would be matched by a decrease in the CBOD. Thus, for simplicity the quality of the transferred flow was taken as that of the NSWRP effluent with the DO concentration raised to saturation. The transfer amount was taken as the lesser of the selected transfer value or the actual effluent flow for a particular hour.

In the charge to CTE for the NSWRP Facility Plan a target of 90 percent compliance with DO criteria of 4, 5, and 6 mg/L over all flows was set for developing cost estimates. Thus, the aerated transfer amount necessary to meet 90 percent compliance with the DO criteria during the simulated periods is evaluated. The simulated periods are dominated by summer (July-September) conditions during which temperature stresses on DO concentrations are greatest. Thus, 90 percent compliance in the summer implies much higher compliance over an entire year, and the transfer amounts determined are conservative relative to 90 percent compliance over the entire 2 year period. Figure 4 shows the overall percentage compliance with the 4, 5, and 6 mg/L DO criteria resulting from different amounts of flow transfer from the NSWRP to the upstream end of the NSC. Ninety percent compliance with

the 4, 5, and 6 mg/L criteria is achieved at Main Street with a transfer of approximately 2.85, 3.94, and 5.69 m^3/s, respectively, of aerated effluent (Figure 4). As part of the UAA, CTE (2007) estimated that transferring 4.38 m^3/s of aerated NSWRP effluent to the upstream end of the NSC, where U-tubes (Speece, 1969) are used for aeration, would involve a capital cost of US$60 million and an annual operational cost of US$744,000. The higher flow rate than derived from Figure 4 is necessary to ensure 90% compliance throughout the upper NSC.

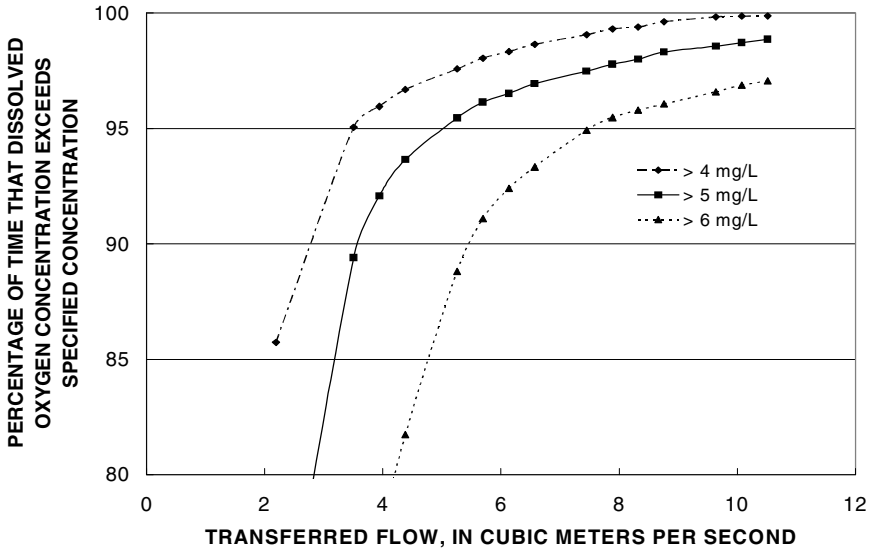

Figure 4. Relation between aerated North Side Water Reclamation Plant effluent and percentage compliance at Main Street with dissolved oxygen concentration criteria of 4, 5, and 6 mg/L for the periods of July 12-November 9, 2001 and May 1-September 23, 2002.

The overall percentage compliance with the 4, 5, and 6 mg/L DO criteria resulting from transfer of 3.50, 5.26, 7.45, and 8.32 m^3/s NSWRP flow to the upstream end of the NSC at the locations downstream from NSWRP are shown in Tables 3 and 4. Even though the increase in DO is not as drastic as that observed along the NSC, at least 10% improvement is achieved by transferring 8.32 m^3/s compared to 3.50 m^3/s at Addison Street, 9.0 km downstream from the NSWRP, for the 6 mg/L DO criterion (Table 3). The DO criterion of 5 mg/L could be met 95 and 94.1 percent of the time for dry and wet weather periods, respectively, at Addison Street by a transfer of 3.50 m^3/s. However, even a transfer of 8.32 m^3/s aerated NSWRP flow could not result in 90 % compliance with a 5 mg/L criterion at Fullerton Avenue, 12.1 km downstream from the NSWRP (Table 4).

Thus, additional instream aeration stations would be needed to achieve 90% compliance with a 5 mg/L DO standard on the NBCR downstream from Addison Street. Results show that the effect of flow augmentation with aeration decreases considerably at locations downstream from the junction of the NBCR and SBCR (Alp and Melching, 2006).

Table 3. The percentage of time that dissolved oxygen (DO) concentrations are greater than the target concentrations at Addison Street on the North Branch Chicago River for July 12-November 9, 2001 and May 1-September 23, 2002 for different transfers of North Side Water Reclamation Plant effluent brought to saturation DO concentration.

	>4 mg/L		>5 mg/L		>6 mg/L	
Scenario	Dry	Wet	Dry	Wet	Dry	Wet
Baseline	99.0	99.8	89.9	91.3	55.4	62.2
3.50 m^3/s	99.6	99.8	95.0	94.1	68.8	67.2
5.26 m^3/s	99.6	99.7	96.6	94.9	74.2	71.0
7.45 m^3/s	99.7	99.7	97.7	96.4	81.5	75.6
8.32 m^3/s	99.8	99.7	98.1	96.8	83.9	78.3

Table 4. The percentage of time that dissolved oxygen (DO) concentrations are greater than the target concentrations at Fullerton Avenue on the North Branch Chicago River for July 12-November 9, 2001 and May 1-September 23, 2002 for different transfers of North Side Water Reclamation Plant effluent brought to saturation DO concentration.

	>4 mg/L		>5 mg/L		>6 mg/L	
Scenario	Dry	Wet	Dry	Wet	Dry	Wet
Baseline	89.5	95.5	54.1	72.3	18.6	38.6
3.50 m^3/s	93.8	95.8	70.2	80.3	28.6	46.7
5.26 m^3/s	96.2	96.0	75.5	84.1	32.3	49.5
7.45 m^3/s	97.5	96.8	79.6	86.7	41.5	54.3
8.32 m^3/s	97.9	97.2	81.2	87.5	44.7	56.9

CONCLUSIONS

Simulation of the period July 12-November 9, 2001 with the DUFLOW model calibrated and verified for the CWS found that transfer of even the entire flow from the NSWRP to the upstream end of the NSC would not result in 90% compliance with the 5 mg/L DO criterion. Splitting the transferred effluent between the upstream end of the NSC and a point 2.80 km upstream of the NSWRP yielded similar results to the case of transferring all the flow to the upstream end of the NSC at a potentially reduced cost. Aeration of the transferred effluent in the force main was found to be an effective and efficient means to improve the DO concentrations to acceptable levels (5 mg/L, 90% of the time) in the upper NSC with estimated construction and operation costs of US$ 60 million and 744,000/year, respectively. The benefits of this aeration also allow compliance with target DO criteria for about 10 km downstream of the NSWRP, whereas, compliance further downstream will require supplemental aeration stations.

Refined design of the flow augmentation for the upper NSC channel is currently under study as part of the development of an integrated strategy for water

quality improvement throughout the CWS. This design will test flow augmentation performance against new dissolved oxygen standards proposed by the Illinois Environmental Protection Agency for selected representative wet and dry years for the CWS. Single and multiple discharge points for the transferred flow will be considered. Combination of the aerated flow augmentation with addition of instream aeration stations will also be considered.

REFERENCES

Alp, E. and Melching, C.S. (2006). Calibration of a model for simulation of water quality during unsteady flow in the Chicago Waterway System and application to evaluate use attainability analysis remedial actions. *Technical Report 18*, Institute of Urban Environmental Risk Management, Marquette University, Milwaukee, WI.

Ambrose, R.B., Wool, T.A., Connolly, J.P., and Schanz, R.W. (1988). WASP4, a hydrodynamic and water quality model—model theory, User's manual, and programmer's guide. U.S. Environmental Protection Agency, *EPA/600/3-87-039*, Athens, GA.

Camp Dresser and McKee (CDM), 2007, Chicago Area Waterway System Use Attainability Analysis (UAA), report submitted to the Illinois Environmental Protection Agency, available on line at http://www.chicagoareawaterways.org/documents/CAWS-UAA-Final-Report.pdf.

Consoer Townsend Envirodyne (CTE), 2007, Flow Augmentation of the Upper North Shore Channel, *Technical Memorandum 5WQ*, report submitted to the Metropolitan Water Reclamation District of Greater Chicago, Chicago, Ill.

Di Toro, D. M. and Fitzpatrick, J. (1993). *Chesapeake Bay Sediment Flux Model*. HydroQual, Inc. Mahwah, NJ. Prepared for U.S. Army Engineer Waterway experiment Station, Vicksburg, MS. Contract Report EL-93-2

DUFLOW (2000). *DUFLOW for Windows V3.3: DUFLOW modelling studio: user's guide, reference guide DUFLOW, and reference guide RAM*, EDS/STOWA, Utrecht, The Netherlands.

Manache, G. and Melching, C.S. (2004). Sensitivity analysis of a water-quality model using Latin hypercube sampling. *Journal of Water Resources Planning and Management*, **130**(3), 232-242.

Melching, C.S., Alp, E., Shrestha, R.L., and Lanyon, R. (2004). Simulation of water quality during unsteady flow in the Chicago Waterway System. *Proceedings CD-ROM*, *Watershed 2004*, July 11-14, 2004, Dearborn, MI, Water Environment Fedaration.

Neugebauer, A. and Melching, C.S. (2005). Verification of a continuous water quality model under uncertain storm loads in the Chicago Waterway System, *Technical Report 17*, Institute of Urban Environmental Risk Management, Marquette University, Milwaukee, WI.

Speece, R. (1969). U-tube stream reaeration, *Public Works*, 100, 111-113.

Examining the Flow Regime Alteration and Its Potential Impacts to Freshwater Ecosystems under Changing Climate Conditions

Jian-Ping Suen[1]

[1] Department of Hydraulic and Ocean Engineering, National Cheng Kung University, No.1 University Road, Tainan 701, TAIWAN; Phone 886-6-2757575-63243; Fax 886-6-2741463; Emails: jpsuen@mail.ncku.edu.tw

Abstract

This paper uses observed daily streamflow data to examine the flow regime alteration and how these changes might potentially affect freshwater ecosystems. The earth surface temperature has been observed gradually increase and associate with precipitation and atmospheric moisture changes over space and time. Climate induced flow regime changes are examined by Indicators of Hydrologic Alteration approach. The annual extreme water conditions (1-, 3-, 7-, 30-, 90- day annual minima or maxima) reveal larger alteration from analyzing twenty-three gauging stations throughout Taiwan. More severe flood and drought events happen in the period of after 1991 than the period of 1961-1990. Frequency and duration of the flood and drought events also reveal high fluctuation. Flow regime is being altered and is going to continue into the foreseeable future. The aquatic organisms not only need to defend themselves from the anthropogenic damage to the river system but also are facing the on-going threat from thermal and flow regime altering under changing climate. This paper tries to raise this issue to allow water resources managers taking some precautionary measures to reduce the cumulative effects from anthropogenic influence and changing climate.

Introduction

Water in a river system provides aquatic ecosystems maintaining with fisheries, wildlife habitat, recreations, and other tremendous values. The different quantities of the water at different locations and different timing affect aquatic ecosystems significantly. Over the thousands of years, the river system sustains some level of natural and seasonal patterns of rising and falling water levels that shape the instream and riparian habitat, provide cues for organisms breeding and migration, and allow the aquatic ecosystems to function properly (Poff et al., 1997). Many aquatic organisms have adapted to the predictable flow variation associated with natural fluctuations; deviation from these patterns may increase the threat for their survival in the rivers (Poff and Ward, 1989; Bunn and Arthington, 2002). Altering the natural flow patterns may strongly affect the aquatic organisms that depending on them. Streamflow has been considered as a dominated variable that influences many fundamental ecological processes in aquatic ecosystems.

In the past century, the earth surface temperature has been observed approximately 0.56 to 0.92 ℃ increases in average in the world (IPCC, 2007) and 1.0 to 1.4 ℃ increases in Taiwan (Hsu and Chen, 2002). It is expected this increasing trend is going to continue into the foreseeable future. Ecosystem responses to the recent global warming trends have been widely observed and documented (Walter et al., 2002). In addition to the direct warming effect, the increasing temperature may cause changes in global atmospheric circulation, and affect precipitation and atmospheric moisture over space and time. Streamflow is more or less reflecting the changing precipitation patterns and reveal a certain level of alteration. The alteration including changes in the magnitude and timing of extreme flow events, frequency and duration of high or low flow events, and magnitude of monthly or yearly flow may result in a severely altered river system which will threaten to native aquatic ecosystems in it. Climate change is perhaps one of the greatest on-going threats to the aquatic ecosystems. Although aquatic organisms are commonly resilient to most of the anthropogenic disturbance, current environmental condition changes caused by climate change are probably too rapid for some of the organisms to adapt (Dudgeon et al., 2006; Angeler, 2007).

Most recent climate change impact analysis on water resources or streamflow management focus on the trend determination (Yu et al., 2002; Burns et al., 2007; Novotny and Stefan, 2007) with paying special attentions on extreme water conditions (e.g. flood, drought) (Milly et al., 2002; Lehner et al, 2006), and very few of them consider the changes of whole flow regimes. The trend of water quantity is very important for water resources management purpose, but the changes of whole flow regime characteristics are rather crucial, especially in aquatic ecosystems. In this paper, the Indicators of Hydrologic Alteration (IHA) developed by The Nature Conservancy (Richter et al., 1996) will be used as a tool to assess streamflow alteration potentially caused by the changing climate in Taiwan. The aim is to examine these changes and understand possible effects on aquatic organisms. Unlike most climate change research using global circulation models (GCMs) to project future climatic conditions (e.g. Caballero et al. 2007), this paper uses observed daily streamflow data to examine the flow regime alteration happened in the past. By realizing the hydrologic alteration and the potential impact to freshwater ecosystems, new management strategies could be developed to mitigate the impact and benefit to aquatic ecosystems.

Method

Streamflow Alteration and Ecological Responses

In a natural stream, the aquatic organisms evolve strategies for surviving in different kinds of environmental conditions, particularly driven by the magnitude, frequency, duration and timing of flow (Poff et al., 1997). There is a large and rapidly growing literature trying to identify the connection of hydrologic conditions to the organisms (e.g. Poff et al., 1997; Petts et al., 2006). Engineers and system

analysts are trying to use numerical models to simulate hydrologic variability and river hydrodynamics in relation to species populations or biological indexes (e.g. biodiversity index) (Yang et al., with editor). These models built the mathematical relationships between the inputs (hydrologic valuables) and outputs (biological/ecological parameters). Then engineers and system analysts can manipulate the hydrologic variables to predict the biological/ecological responses. On the other hand, ecologists and biologists continue to develop understanding how organisms interact with these hydrologic variables, paying special attention on life history requirements, microhabitat conditions, and movement behaviors. Experimental designs and field work samplings are conducted to provide more solid scientific basis at a holistic level over different temporal and spatial scales (Herbert and Gelwick, 2003; Jowett et al., 2005). Both attempts from engineers and ecologists are reflecting the importance of the connections between streamflow and aquatic organisms. Due to the highly stochastic characteristics of hydrologic variables and extremely complicated responses of aquatic ecosystems, the connections between hydrology and ecology still focus on target or dominant species and are still site specific in most cases.

Station Selection and Data

Taiwan is an island located at east of Mainland China and south of Japan in the Western Pacific with a total area of 36,000km^2. The island is long and narrow with the Central Mountain Range in the middle. The annual rainfall in Taiwan reaches about 2,500 mm which is around 2.6 times the world average, but rainfall concentrates in the period from May through October with an amount of 3/4 of annual average, which is wet season. Rivers are basically short but steep in Taiwan with large runoff differences in wet and dry seasons. Discharges respond rapidly with rainfall intensity and flood flows. Because of the subtropical climate and high elevation gradient change, Taiwan has very plentiful aquatic ecosystems from upstream high mountain stream to downstream estuary.

Gauging stations throughout Taiwan are considered based on the available length of daily streamflow data and natural flow condition. The length of data is very crucial in climate change research. Longer period of data can reduce the effects caused by short term natural fluctuations and show trend (if there is any) developed by climate change. Unfortunately the streamflow data of most gauging stations in Taiwan are either relatively short or are affected by upstream hydraulic constructions (e.g. dams). Therefore only twenty-three stations with minimal anthropogenic influence are considered suitable for this analysis. The drainage area ranges from 82 to 812 and the elevation ranges from 20 to 1,630 m.

Indicators of Hydrologic Alteration

Hydrologic indicators have been widely applied in ecological water resources management (Suen and Eheart 2006). Those indicators are recognized having highly ecological relevance and can be easily calculated (e.g. Richter et al., 1996; Poff et al., 1997; Suen and Herricks, in reviewing). One of the most frequently used methods is the Indicators of Hydrologic Alteration (IHA) approach (Richter et al., 1996). The

IHA uses daily streamflow data to characterize flow regimes in terms of five ecological significant aspects: magnitude, frequency, duration, timing, and rate of change. Thirty-one hydrologic parameters are categorized in five groups: magnitude of monthly water conditions, magnitude and duration of annual extreme water conditions, timing of annual extreme water conditions, frequency and duration of high and low pulses, and rate and frequency of water consecutive daily means condition. These parameters can be easily calculated by a Windows-based computer software developed by The Nature Conservancy, USA. Olden and Poff (2003) review 171 currently applied hydrologic indicators and suggest that the IHA could adequately represent the majority of the variation of the flow regime for hydroecological studies. The detailed IHA development, please refer to Richter et al. (1996).

In this research, the observed daily streamflow data are transferred to the whole set of hydrologic indicators by IHA for examination. There is no justification can be found to show one IHA group is more important or can replace other groups. Therefore, whole suite of IHA is considered equal weight in the analysis in terms of each group or each indicator. Altering any of the groups or indicators will affect the flow regimes in various ways.

The Range of Variability Approach

The primary function of the IHA is to examine changes in flow regimes caused by hydraulic constructions. By comparing data between pre- and post-impact periods, the percentage change in each ecological relevant statistics shows the degrees of hydrologic alteration and it can be applied to assess potential impact to the aquatic ecosystems. The Range of Variability Approach (RVA), proposed by Richter et al. (1997), offers a more quantitative way to evaluate the degree of alteration by giving a target range for each hydrologic indicator. In this research, the percentage change between the 25th- and 75th-percentile pre-impact baseline indicator values is set as a target for alteration assessment. The post-impact values should have similar frequency as that which occurred in the natural or pre-impact baseline flow regimes if there is no obvious climate change happening. The measure of hydrologic alteration A, expressed as a percentage, is defined as:

$$A = \left| \frac{Y_o - Y_e}{Y_e} \right| \times 100\% \quad (1)$$

where Y_o is the observed count of post-impact years for which the value of the hydrologic indicator falls within the RVA target range, and Y_e is the expected count of post-impact years for which the value of the hydrologic indicator falls within the RVA target range.

Results and discussion

The daily streamflow data of twenty-three gauging stations are calculated by Indicators of Hydrologic Alteration software. In order to determine the flow regime alteration under changing climate, historical daily streamflow data over the period of

November 1960 to October 1990 (1961-1990) are used as the baseline condition based on the IPCC guidelines (IPCC-TGCIA, 1999), and streamflow data after November 1990 (after 1991) are used to assess the potential impact on climate change influence. For each of the thirty-one hydrologic parameters, the absolute percentage changes both in mean and in coefficient of variation (CV) between baseline and post-baseline periods are calculated. Table 1 shows the mean absolute percentage changes of twenty-three gauging stations calculated from whole Taiwan Island and separated in four sub-regions. Noted that the absolute percentage changes of Julian date of annual 1-day minimum and maximum (IHA group 3) should consider to be neglected because the value of the Julian date is not the magnitude of the parameters. Besides that, the annual 1-day minimum in Taiwan usually happens in dry season, which is from November to next April, so the value of Julian date of annual 1-day minimum may have a large variation because it may happen in November and December (large Julian date number) or from January to April (small Julian date number).

In order to compare how much hydrologic alteration happened between 1961-1990 and after 1991 periods, the before 1990 data are divided into two periods for further analysis. Data over the period of 1976 to 1990 are used as the *post-impact* condition to test the hydrologic alteration to the *pre-impact* period (before 1975). Table 2 shows the comparisons of the mean absolute percentage changes between baseline and post-baseline periods and between two sub-periods within the baseline period. Table 2 also shows the probability of post-baseline value larger than baseline value of twenty-three gauging stations in mean and in CV. A close to 100% probability value means the post-baseline value is larger than the baseline value in most observed gauging stations. In other words, it is very likely having an increasing tendency in this hydrologic parameter.

The differences of mean absolute percentage changes between baseline and post-baseline periods and between two sub-periods within the baseline period are not so obvious. Only the annual extreme water conditions (IHA group 2) shows consistently larger absolute changes. It means these extreme water conditions (1-, 3-, 7-, 30-, 90-day annual minima or maxima) alter more in period of after 1991 than in period of 1961-1990.

The RVA method is originally used to guild the streamflow management strategies for sustaining native aquatic ecosystem biodiversity and integrity after a hydraulic construction was built (Richter et al., 1997). In this research, the RVA is adapted to measure the hydrologic alteration between two periods of streamflow data under changing climate. The full range of pre-impact period data for each hydrologic indicator is divided into three categories: middle, high, and low. The middle RVA category expresses the value of each hydrologic indicator of post-baseline period lies between 25th- and 75th-percentile pre-impact baseline indicator values, i.e. the RVA target. The high or low RVA category expresses the value of each hydrologic indicator of post-baseline period lies above 75th-percentile or below 25th-percentile pre-impact baseline indicator values, respectively. For each gauging station, the hydrologic alteration A can be calculated by equation (1). Richter et al. (1998)

suggested that the value of A ranging between 0 and 33.3 % represents low alteration, 33.3-66.6 % represents moderate alteration, and 66.6-100 % represents high alteration. If the percentage value of low alteration in the middle RVA category is low, it means fewer stations can reach the RVA target, i.e. hydrologic alteration is higher. Again, the annual extreme water conditions (IHA group 2) show smaller percentage values in low alteration in the middle RVA category. The values of "Frequency and duration of high and low pulses (IHA group 4)" and "Rate and frequency of water consecutive daily means condition (IHA group 5)" have similar results as the IHA group 2. Hydrologic alteration is much more in period of after 1991 than in period of 1961-1990.

The annual extreme water conditions show more alteration both in magnitude and in CV of each extreme hydrologic parameter. Most of these parameters show smaller mean values with larger fluctuation within years (i.e. low predictability) in post-baseline period than they are in baseline period. Increased incidents of flooding and drought events may threaten to the aquatic ecosystems. Invertebrate community might be impacted by increased frequency of drought events at some locations that will be swapped by drought-resistant fauna (Hogg and Williams, 1996). Increased frequency of flood events will interrupt riparian plant succession and reduce available low-energy, backwater habitat for aquatic organisms (Poff, 2002). High magnitude, short duration events may create high velocity and turbulence that lead to injury or death of fish (Harvey, 1987). Correspondingly extended duration of low flows are expected to reduce available channel habitat and increase the risk of loss of organisms due to changing water quality or increased predation risk (Magoulick and Kobza, 2003). Altered annual extreme water conditions change original flood and drought patterns and their primary functions for the aquatic ecosystems.

An important impact to aquatic ecosystems under changing climate is the temperature alteration and it has been widely discussed in worldwide and in Taiwan (Meyer et al., 1999; Han et al., 2007). This paper raises another issue, flow regime alteration, which might have strong potential impact to aquatic ecosystems. The complexity in determining responses of aquatic ecosystems to climate change is mixed from above concerns and moreover will be intensified by the direct or indirect interactions with other forms of anthropogenic impacts (e.g. landuse change) (Meyer et al.,1999; Gibson et al., 2005). It is almost impossible to precisely predict the impact of climate change to freshwater ecosystems, even in the near future (Malmqvist and Rundle, 2002). People in Taiwan have suffered from strong competition for limited water resources between agricultural, municipal, and industrial water demands right now and hydrologic alteration caused by climate change will make the situation more complicated. Proper actions should immediately be applied to reduce future harm to nature and to human society. More flexible management strategies that could effectively response to both long term and short term flow regime change need to be developed for water resources management. These strategies also need to preserve the potential capacity in adapting streamflow change to maintain healthy aquatic ecosystems.

Table 1 The mean absolute percentage changes of gauging stations calculated from whole Taiwan Island and separated in four sub regions

Hydrologic parameters	*Taiwan Island*		*North Region*		*Central Region*		*South Region*		*East Region*	
	Absolute change (%)									
	Mean	*CV*	*Mean*	*CV*	*Mean*	*CV*	*Mean*	*CV*	*Mean*	*CV*
Parameter Group #1										
November mean flow	18.5	79.8	17.2	43.2	11.2	46.7	46.7	294.8	16.3	88.2
December mean flow	16.9	45.6	16.5	37.6	11.2	44.0	59.5	70.6	7.1	43.4
January mean flow	20.5	42.6	19.6	26.2	9.0	30.2	86.9	115.3	9.5	50.1
February mean flow	28.6	75.5	21.6	101.6	29.1	42.2	101.3	83.7	9.3	59.7
March mean flow	25.0	53.8	10.6	42.0	24.3	21.1	120.5	57.5	11.4	99.3
April mean flow	19.7	28.2	12.6	27.6	17.5	28.2	75.2	32.8	11.1	22.7
May mean flow	16.9	42.6	19.5	54.3	17.7	32.3	15.8	42.4	9.7	30.1
June mean flow	28.1	27.8	24.5	25.3	27.9	25.4	39.9	46.8	25.2	23.3
July mean flow	15.2	28.6	15.2	20.1	14.7	43.8	3.8	14.2	17.0	23.9
August mean flow	19.1	32.8	18.3	30.7	20.9	38.1	14.3	39.2	16.5	22.0
September mean flow	15.3	37.5	12.7	28.7	19.4	55.7	20.7	54.1	10.0	17.8
October mean flow	21.3	48.2	16.0	68.7	23.5	27.7	36.5	55.9	18.0	31.0
Group average	20.4	45.2	17.0	42.2	18.9	36.3	51.8	75.6	13.4	42.6
Parameter Group #2										
1-day minimum	23.1	81.2	32.3	45.3	8.3	106.8	28.1	86.5	21.1	89.7
3-day minimum	23.2	88.7	30.5	38.3	6.0	95.9	45.6	153.2	21.3	119.8
7-day minimum	21.0	78.4	25.9	40.3	5.6	84.8	45.8	146.6	19.9	92.3
30-day minimum	18.4	65.6	18.9	41.2	6.2	74.6	51.9	95.3	17.4	70.9
90-day minimum	17.5	56.2	13.5	33.0	14.8	52.2	57.0	63.9	10.7	83.8
1-day maximum	29.7	100.4	30.0	100.8	23.2	100.8	51.6	291.8	24.8	18.7
3-day maximum	25.3	87.9	21.9	84.2	22.8	105.4	48.2	227.3	21.5	11.7
7-day maximum	21.7	78.6	23.4	64.6	21.4	103.4	46.3	171.6	7.6	26.7
30-day maximum	18.1	62.0	14.6	73.6	17.1	52.4	33.4	76.5	16.2	40.6
90-day maximum	17.6	61.9	14.7	77.1	15.1	67.2	26.9	14.4	18.7	38.5
Group average	21.6	76.1	22.6	59.8	14.0	84.3	43.5	132.7	17.9	59.3
Parameter Group #3										
Date of minimum	19.5	25.6	25.2	27.0	11.5	27.0	11.5	0.0	19.7	26.2
Date of maximum	6.1	55.2	6.1	90.0	5.3	35.3	1.3	28.6	7.6	25.8
Group average										
Parameter Group #4										
Low pulse count	21.0	60.3	17.0	58.7	23.0	60.0	29.2	144.0	18.6	25.0
Low pulse duration	35.5	59.0	32.0	39.1	39.3	112.3	31.2	19.4	31.9	30.1
High pulse count	10.4	49.9	7.5	56.2	10.4	39.9	5.0	97.5	14.9	28.0
High pulse duration	22.2	40.7	12.2	33.5	35.3	28.8	21.7	100.1	18.5	38.5
Group average	22.3	52.5	17.2	46.9	27.0	60.3	21.7	90.3	21.0	30.4
Parameter Group #5										
Rise rate	32.5	52.4	20.7	33.6	39.6	76.5	48.2	43.8	31.5	46.4
Fall rate	19.2	39.5	12.8	40.0	27.0	44.4	21.4	44.9	15.9	24.6
Number of reversals	12.8	78.9	7.7	20.7	17.7	101.5	1.8	268.6	16.4	63.5
Group average	21.5	56.9	13.7	31.5	28.1	74.1	23.8	119.1	21.3	44.8

Table 2 The comparisons between baseline and post-baseline periods and between two sub-periods within baseline period

Hydrologic parameters	*Base:1961-90 Post: after 1991*		*Base: before 1975 Post:1976-90*		*Base:1961-90 Post: after 1991*		*Base: before 1975 Post:1976-90*	
	Absolute change (%)				*Probability of increasing (%)*			
	Mean	*CV*	*Mean*	*CV*	*Mean*	*CV*	*Mean*	*CV*
Parameter Group #1								
November mean flow	18.5	79.8	11.5	27.2	8.7	78.3	56.3	37.5
December mean flow	16.9	45.6	15.4	26.9	30.4	78.3	12.5	50.0
January mean flow	20.5	42.6	11.1	29.8	21.7	69.6	50.0	43.8
February mean flow	28.6	75.5	13.5	26.8	65.2	87.0	68.8	12.5
March mean flow	25.0	53.8	23.0	54.8	52.2	65.2	62.5	87.5
April mean flow	19.7	28.2	51.5	84.7	60.9	43.5	56.3	81.3
May mean flow	16.9	42.6	38.0	39.8	34.8	69.6	81.3	43.8
June mean flow	28.1	27.8	21.2	31.0	0.0	60.9	56.3	37.5
July mean flow	15.2	28.6	12.6	44.3	43.5	60.9	50.0	68.8
August mean flow	19.1	32.8	14.6	42.4	30.4	26.1	43.8	68.8
September mean flow	15.3	37.5	12.8	28.0	21.7	60.9	62.5	18.8
October mean flow	21.3	48.2	29.5	31.9	26.1	65.2	0.0	25.0
Group average	20.4	45.2	21.2	39.0	33.0	63.8	50.0	47.9
Parameter Group #2								
1-day minimum	23.1	81.2	9.9	33.9	43.5	78.3	31.3	81.3
3-day minimum	23.2	88.7	7.4	37.5	43.5	78.3	37.5	56.3
7-day minimum	21.0	78.4	8.1	27.7	39.1	82.6	37.5	56.3
30-day minimum	18.4	65.6	11.0	35.5	34.8	82.6	31.3	43.8
90-day minimum	17.5	56.2	12.5	19.3	39.1	69.6	37.5	37.5
1-day maximum	29.7	100.4	26.6	31.0	21.7	78.3	56.3	25.0
3-day maximum	25.3	87.9	24.0	23.6	26.1	78.3	68.8	18.8
7-day maximum	21.7	78.6	21.1	29.0	21.7	87.0	62.5	12.5
30-day maximum	18.1	62.0	13.9	31.7	13.0	82.6	31.3	43.8
90-day maximum	17.6	61.9	14.0	36.2	8.7	95.7	43.8	37.5
Group average	21.6	76.1	14.8	30.6	29.1	81.3	43.8	41.3
Parameter Group #3								
Date of minimum	19.5	25.6	19.6	31.9	34.8	60.9	56.3	37.5
Date of maximum	6.1	55.2	9.1	36.7	39.1	82.6	18.8	37.5
Group average								
Parameter Group #4								
Low pulse count	21.0	60.3	23.3	43.4	39.1	69.6	37.5	25.0
Low pulse duration	35.5	59.0	28.4	30.2	52.2	52.2	62.5	50.0
High pulse count	10.4	49.9	16.3	51.0	30.4	73.9	56.3	43.8
High pulse duration	22.2	40.7	37.9	37.4	34.8	39.1	56.3	50.0
Group average	22.3	52.5	26.5	40.5	39.1	58.7	53.1	42.2
Parameter Group #5								
Rise rate	32.5	52.4	17.3	29.2	26.1	65.2	50.0	37.5
Fall rate	19.2	39.5	18.8	34.4	26.1	82.6	43.8	37.5
Number of reversals	12.8	78.9	6.6	56.5	69.6	56.5	50.0	62.5
Group average	21.5	56.9	14.2	40.0	40.6	68.1	47.9	45.8

Summary

This study examines the flow regime alteration in Taiwan and the potential impact to freshwater ecosystems since 1961. The annual extreme water conditions, frequency and duration of the flood and drought events, rising rate and hydrograph reversal reveal more alteration from the IHA analysis by using current available historical data. Unlike using GCMs to project future climate scenarios, the results show what kind of hydrologic changes are current happening in a full range of flow regime type analysis. The potential threat caused by flow regime alteration can be analyzed as precautionary information for water resources and aquatic ecosystems management.

It is important that policy makers and water resources managers recognize the potential impact to freshwater ecosystems caused by changing climate and develop prompt strategies to maintain healthy aquatic ecosystems that will preserve their ability to adapt to the changing climate. Engineers and ecologists need to collaborate for better defining the influence of hydrologic alteration to aquatic ecosystems. New polices and water resources management strategies need to reduce anthropogenic influence and climate changing effects in a river system to sustain a healthy freshwater ecosystem.

Acknowledgements

The research supporting this paper was supported by National Cheng Kung University under grant number R046 and by the Taiwan National Science Council under Contract No. 96-2221-E-006-264-MY3. The author acknowledges the assistance of Dr. Pao-Shan Yu and Dr. Cathy Marcinkevage in the various aspects of this work.

References

Angeler DG. 2007. Resurrection ecology and global climate change research in freshwater ecosystems, *Journal of the North American Benthological Society* 26(1): 12-22.

Black AR, Rowan JS, Duck RW, Bragg OM, Clelland BE. 2005. DHRAM: a method for classifying river flow regime alterations for the EC Water Framework Directive, *Aquatic Conservation: Marine and Freshwater Ecosystems* 15(5): 427-446.

Bunn SE, Arthington AH. 2002. Basic principles and ecological consequences of altered flow regimes for aquatic biodiversity, *Environmental Management* 30(4): 492-507.

Burns DA, Klaus J, McHale MR. 2007. Recent climate trends and implications for water resources in the Catskill Mountain region, New York, USA, *Journal of Hydrology* 336(1-2): 155-170.

Caballero C, Voirin-Morel S. Habets F, Noilhan J, LeMoigne P, Lehenaff A, Boone A. 2007. Hydrological sensitivity of the Adour-Garonne river basin to climate change, *Water Resources Research* 43(7): W07448.

Dudgeon D, Arthington AH, Gessner MO, Kawabata ZI, Knowler DJ, Leveque C, Naiman RJ, Prieur-Richard AH, Soto D, Stiassny MLJ, Sullivan CA. 2006. Freshwater biodiversity: importance, threats, status and conservation challenges, *Biological Reviews* 81(2): 163-182.

Gibson CA, Meyer JL, Poff NL, Hay LE, Georgakakos A. 2005. Flow regime alterations under changing climate in two river basins: Implications for freshwater ecosystems, *River Research and Applications* 21(8): 849-864.

Han CC, Tew KS, Fang LS. 2007. Spatial and temporal variations of two cyprinids in a subtropical mountain reserve - a result of habitat disturbance, *Ecology of Freshwater Fish* 16(3): 395-403.

Harvey BC. 1987. Susceptibility of young-of-the-year fishes to downstream displacement by flooding. *Transactions of the American Fisheries Society* 116(6): 851-855.

Herbert ME, Gelwick FP. 2003. Spatial variation of headwater fish assemblages explained by hydrologic variability and upstream effects of impoundment, *Copeia* 2003(2): 273-284.

Hogg ID, Williams DD. 1996. Response of stream invertebrates to a global warming thermal regime: an ecosystem-level manipulation, *Ecology* 77(2): 395-407.

Hsu HH, Chen CT. 2002. Observed and projected climate change in Taiwan, *Meteorology and Atmospheric Physics* 79(1-2): 87-104.

IPCC. 2007. *Climate Change 2007: The Physical Science Basis, Summary for Policymakers*, IPCC Secretariat, WMO, Geneva. [On the web at www.ipcc.ch/SPM2feb07.pdf].

IPCC-TGCIA. 1999. *Guidelines on the use of scenario data for climate impact and adaptation assessment, version 1*. Prepared by Carter TR, Hulme M, Lal M. Intergovernmental Panel on Climate Change, Task Group on Scenarios for Climate Impact Assessment, 69 pp.

Jowett IG, Richardson J, Bonnett ML. 2005. Relationship between flow regime and fish abundances in a gravel-bed river, New Zealand, *Journal of Fish Biology* 66(5): 1419-1436.

Koel TM, Sparks RE. 2002. Historical patterns of river stage and fish communities as criteria for operations of dams on the Illinois River, *River Research and Applications* 18(1): 3-19.

Lehner B, Droll P, Alcamo J, Henrichs T, Kaspar F. 2006. Estimating the impact of global change on flood and drought risks in Europe: A continental, integrated analysis, *Climatic Change* 75(3): 273-299.

Magoulick DD, Kobza RM. 2003. The role of refugia for fishes during drought: a review and synthesis, *Freshwater Biology* 48(7): 1186-1198.

Malmqvist B, Rundle S. 2002. Threats to the running water ecosystems of the world, *Environmental Conservation* 29(2): 134-153.

Meyer JL, Sale MJ, Mulholland PJ, Poff NL. 1999. Impacts of climate change on aquatic ecosystem functioning and health, *Journal of the American Water Resources Association* 35(6): 1373-1386.

Milly PCD, Wetherald RT, Dunne KA, Delworth TL. 2002. Increasing risk of great floods in a changing climate, *Nature* 415(6871): 514-517.

Novotny EV, Stefan HG. 2007. Stream flow in Minnesota: Indicator of climate change, *Journal of Hydrology* 334(3-4): 319-333.

Olden JD, Poff NL. 2003. Redundancy and the choice of hydrologic indices for characterizing streamflow regimes, *River Research and Applications* 19(2): 101-121.

Petts GE, Morales Y, Sadler J. 2006. Linking hydrology and biology to assess the water needs of river ecosystems, *Hydrological Processes* 20(10): 2247-2251.

Poff NL. 2002. Ecological response to and management of increased flooding caused by climate change, *Philosophical Transactions of the Royal Society of London Series A - Mathematical Physical and Engineering Sciences* 360(1796): 1497-1510.

Poff NL, Allan JD, Bain MB, Karr JR, Prestegaard KL, Richter BD, Sparks RE, Stromberg JC. 1997. The natural flow regime. *Bioscience* 47(11): 769-784.

Poff NL, Ward JV. 1989. Implications of streamflow variability and predictability for lotic community structure: a regional analysis of streamflow patterns, *Canadian Journal of Fisheries and Aquatic Sciences* 46: 1805-1818.

Richter BD, Baumgartner JV, Powell J, Braun DP. 1996. A method for assessing hydrologic alteration within ecosystems, *Conservation Biology* 10(4): 1163-1174.

Richter BD, Baumgartner JV, Wigington R, Braun DP. 1997. How much water does a river need? *Freshwater Biology* 37(1): 231-249.

Richter BD, Baumgartner JV, Braun DP, Powell J. 1998. A spatial assessment of hydrologic alternation within a river network, *Regulated Rivers: Research & Management* 14(4): 329-340.

Suen JP, Eheart JW. 2006. Reservoir management to balance ecosystem and human needs: incorporating the paradigm of the ecological flow regime, Water Resources Research 42(3): W03417.

Suen JP, Herricks EE. In Reviewing. Developing fish community based ecohydrological indicators for water resources management, submitted to *Hydrological Science Journal*.

Walther GR, Post E, Convey P, Menzel A, Parmesan C, Beebee TJC, Fromentin JM, Hoegh-Guldberg O, Bairlein F. 2002. Ecological responses to recent climate change, *Nature* 416: 389-395

Yang YCE, Cai XM, Herricks EE. With editor. Identification of hydrologic indicators related to fish population: comparative study of three approaches, *Water Resources Research*.

Yu PS, Yang TC, Wu CK. 2002. Impact of climate change on water resources in southern Taiwan, *Journal of hydrology* 260(1-4): 161-175.

FEMA Flood Map Accuracy

David R. Maidment[1]

Director, Center for Research in Water Resources, University of Texas, Austin Tx 78712. Tel: (512) 471-0065. Email: maidment@mail.utexas.edu

ABSTRACT

FEMA is completing $1 billion 5-year program to modernize its flood insurance rate maps and convert them to digital form. At the request of FEMA, the National Academies of Science and Engineering have established a Committee on FEMA Flood Maps to review the accuracy of these maps and to recommend cost-effective improvements to them. The Committee's report "Mapping the Zone: Improving Flood Map Accuracy" was released in January 2009. The Committee examined the relative effects of accuracy of hydrologic, hydraulic and terrain information on riverine flood maps, the factors affecting the accuracy of coastal flood mapping, and the costs and benefits of various levels of detail of flood mapping and modeling, using case studies set in North Carolina. This paper focuses on the riverine flood map accuracy portion of the report, and concludes that accuracy of the terrain data is the most important factor influencing riverine flood map accuracy.

INTRODUCTION

From 2003 to 2008, the Federal Emergency Management Agency (FEMA) conducted a Map Modernization program. The goal of this program was to upgrade and convert to digital form the Flood Insurance Rate Maps of the nation. The budget for this effort was $200 million per year, or $1 billion total in federal funds. Many state and local communities contributed additional matching funds for improved base map input data and flood modeling. During these years, this was the nation's largest investment in new hydrologic information, and it spawned new innovations in automated hydrology and hydraulics and in Lidar measurement of land surface terrain.

---

[1] This paper summarizes a report of National Research Council Committee on FEMA Flood Maps, of which the author served as Chairman. The other members of the Committee were David S. Brookshire, J. William Brown, John Dorman, Gerald E. Galloway, Bisher Imam, Wendy Lathrop, David Maune, Burrell E. Montz, Spencer Rogers, Karen L. Schuckman, Y. Peter Sheng and Juan B. Valdes. The NRC Study Director was Anne Linn. The author wishes to acknowledge the contribution of these colleagues to the Committee's study and conclusions.

As the program evolved, it became clear that the original goal of achieving complete digital flood map coverage of the nation could not be accomplished within the existing budget, and there were concerns about the quality of some of the digital flood maps being produced. This led to a "mid-course adjustment" (FEMA, 2006), during which the mapping goal was changed to ensure that 92% of the nation's population and 65% of the land area would have a modernized map. In addition, more formal procedures were introduced to ensure that the floodplain boundaries match available topography within a tolerable error, and that adequate engineering studies underlie flood maps. As of March 31, 2008, 21% of the population had a flood map meeting those standards, and new maps continue to be produced. Figure 1 shows a typical riverine flood map. Zone A is the Special Flood Hazard Area within the 100 year floodplain, while Zone X is outside the 100 year floodplain but inside the 500 year floodplain.

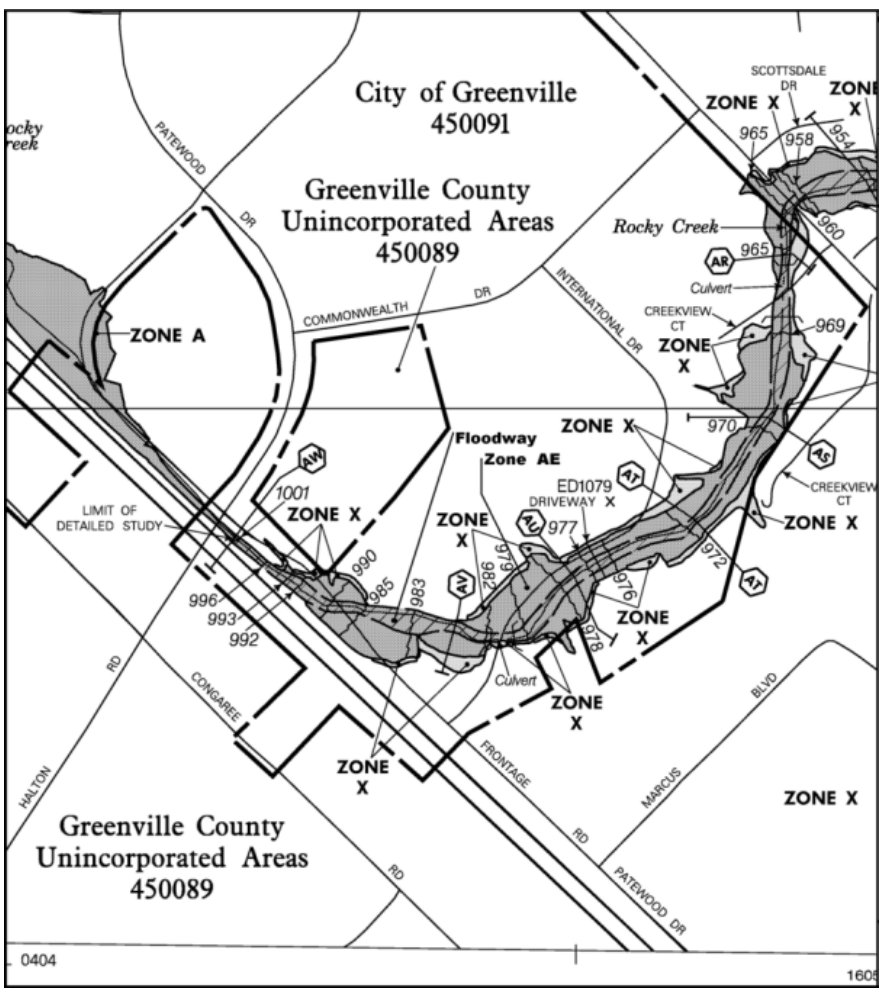

Figure 1. A portion of a floodplan map for Greenville, SC.

FEMA flood maps are produced to support identification of properties to be covered under the National Flood Insurance Program. Since the NFIP does not operate on federal lands, this means that about 1 million of the nation's 4 million miles of rivers and streams are not covered under this program. In addition, about 60,000 miles of coastlines need flood maps.

FEMA and NOAA commissioned a study conducted by the National Academies to examine flood map accuracy, and to make recommendations for its improvement. While the Committee's Report (NRC, 2009) also covers coastal flood mapping, economic analysis of mapping alternatives, and risk communication, this paper focuses on the portion of the Committee's report dealing with the effects of accuracy of hydrologic, hydraulic and terrain information on riverine flood map accuracy. Coastal flood mapping is more complicated than riverine flood mapping, because coastal mapping is more dependent on predictive models of flood storm surge and wave action, and less on observed data on historical floods.

RIVERINE FLOOD MAP ACCURACY

A continual challenge for FEMA Map Modernization is how investment in flood mapping can be matched to the degree of flood risk in the floodplain area. Several alternative mapping methods are available:

- *Detailed* studies in which extensive land surveying of structures is combined with accurate terrain information measured by lidar or aerial photogrammetry and hydraulic models are constructed;
- *Limited Detailed* studies, similar to detailed studies but less land surveying information is acquired;
- *Redelineation* studies where the base flood elevation from an existing study is remapped onto new terrain information;
- *Approximate* studies where flood maps are constructed using best available data.

The costs of these studies may vary from $250 per stream mile for an approximate study to $25,000 per stream mile for a detailed study, but are typically in the range of $900 to $13,500 per stream mile.

It is understood that while the edge of the floodplain boundary is drawn as a line, it actually represents a zone of some unknown width because the base flood elevation used to create the floodplain boundary is not known precisely, and neither is the terrain or land surface representation upon which the floodplain is drawn. The

relative role of uncertainties in hydrology, hydraulics and terrain information contributing to uncertainties in floodplain mapping has been unclear.

There are two aspects of riverine flood map accuracy – the *base flood elevation*, which is the elevation of the water surface during a flood event equaled or exceeded on average once every 100 years, and the *special flood hazard area*, which is the area of inundation around a stream, river or coastline resulting from this flood event. Both of these items are important. The base flood elevation is used in floodplain regulations by local communities who limit construction so that first floor elevation of structures is at or above the base flood elevation. The special flood hazard area is used by insurance companies to define which properties are eligible or required to have federal flood insurance under the National Flood Insurance Program.

CASE STUDIES

In an attempt to quantify the effect of uncertainties on flood mapping and flood risk, the Committee collaborated with the North Carolina Floodplain Mapping Program to conduct several case studies of riverine flood mapping in North Carolina. As shown in Figure 2, representative counties and river reaches were chosen from mountainous Western North Carolina (City of Asheville and Buncombe County), from the hilly Piedmont (City of Charlotte and Mecklenburg County), and from the flat coastal plain (Pasquotank and Hertford Counties for economic and hydraulic studies, respectively.

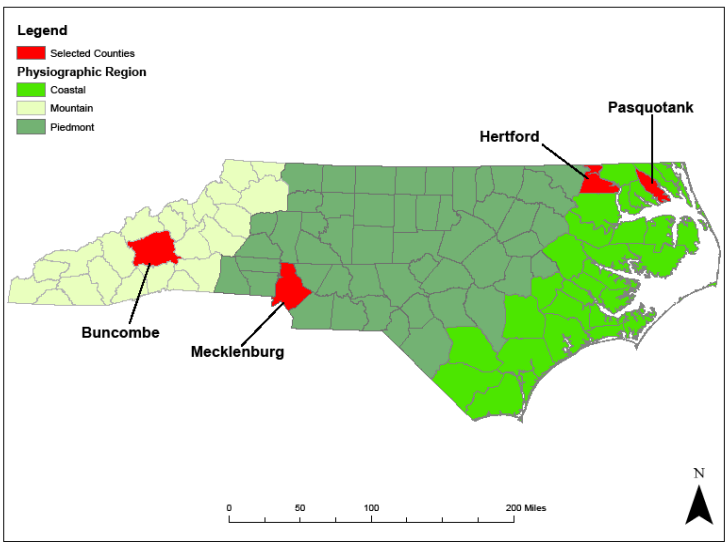

Figure 2. Location of flood mapping case studies in North Carolina. Source: NCFMP (2009). Used with permission.

These studies cover a range of topography and enable detailed study of the effects of alternative choices in floodplain mapping and modeling. A representative river reach from 5 to 7 miles long was selected in each of the three regions. These river reaches were on the Swannanoa River (Mountains), Long Creek (Piedmont), and Ahoskie Creek (Coastal).

UNCERTAINTY IN FLOOD STAGE

The nation has no repository of historical flood inundation maps, and the only place where flood elevation has been measured consistently over a long period of time is at USGS streamflow gaging stations. Flood frequency analysis is normally carried out over the record of annual maximum flood discharges, but the USGS also records the annual maximum flood stage at each gage, regardless of whether it occurred at the same time as the peak discharge or not. Annual maximum flood stages were subjected to frequency analysis at 31 long-term streamgaging sites in North Carolina and Florida. Data from Florida were studied in addition to those in North Carolina to assess whether the pitted landscape and karst terrain in Florida lead to different peak stage uncertainties. The Corps of Engineers HEC-SSP program was used for these analyses, and for each stream gage site, a flood discharge frequency curve and a flood stage frequency curve were generated. The two curves were similar to each other in appearance at all sites.

The HEC-SSP program provides 5% and 95% confidence limits on these extreme value estimates, and from this confidence interval, the sampling uncertainty in the peak flood stage, can be defined. This is approximately equivalent to the standard error of estimate of the base flood elevation because the only difference between the flood stage and the flood elevation is that one is determined with reference to a gage datum and other to a geodetic datum. As shown in Figure 3, there is no discernable pattern in the distribution of these sampling errors either with size of the drainage area, or with topography, or whether the landscape was pitted with sinkholes in karst terrain or not. This is a quite remarkable result because it suggests that there is some underlying unifying mechanism that makes the sampling uncertainty of extreme stage heights consistent across landscape types that otherwise might be considered to have very different flood flow processes.

One gage site has a very large sampling error because of a highly skewed frequency curve there. Leaving aside this site, the average sampling error of extreme flood stages at 30 of the 31 USGS gage sites is approximately 1 foot with a range from 0.3 to 2.4 feet. The results of this stream gage study should be considered representative only of the gage sites studied – it is possible that an exhaustive analysis of the more than 27,000 sites at which the USGS documents peak discharge

data might reveal patterns in the sampling uncertainty of peak stage heights for different landscape types.

Three of the stream gages analyzed lie within the three river reaches used in the flood mapping case studies. For these reaches, detailed flood studies using HEC-RAS models were available, and from these the lateral slope at the edge of the floodplain can be estimated from the HEC-RAS cross-section data. These data showed that a one foot uncertainty in the base flood elevation translates to a horizontal uncertainty of from 8 feet in the mountains to 40 feet in the coastal plain. These estimates are lower bounds on the true uncertainty in the floodplain boundary at ungaged locations where more approximate modeling and mapping methods are used.

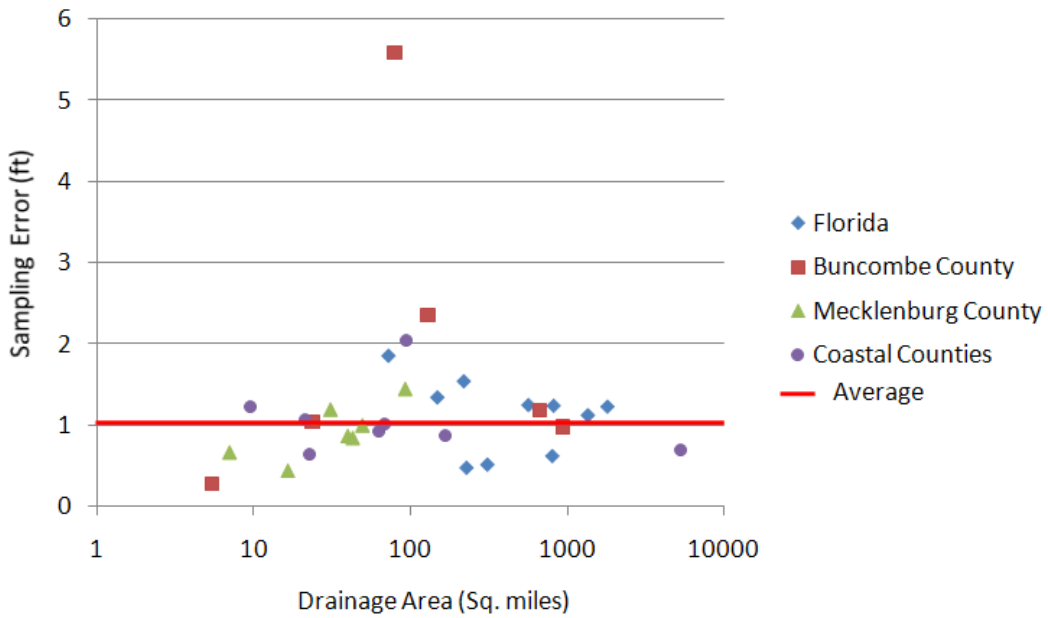

Figure 3. Sampling error in peak stage at 31 gages in North Carolina and Florida. Source: NRC (2009) Reprinted with permission from the National Academy of Sciences, Washington, D.C.

HYDROLOGIC UNCERTAINTY

Three approaches are used to define the peak discharge in FEMA flood mapping studies: rainfall-runoff modeling, flood frequency analysis, and the USGS Regional Regression equations. The latter two methods can be combined by adjusting the regional regression equation results so that they are consistent with the flood frequency results at gage locations. In each of the three study reaches, the sensitivity of the base flood elevation to alternative choices of hydrologic method

was examined. A typical result is shown in Figure 4, which shows the base flood elevation profiles at Long Creek, in Mecklenburg County. The only hydrologic method which produced significant variations in base flood elevation is to take the regional regression equations and choose the discharge at the upper and lower limits (+/- 47% of the estimated flow). This produces an effect of from one to three feet in the base flood elevation.

It is possible that these results are biased by the fact that it is a standard practice in FEMA flood mapping studies to calibrate the results of all methods to the flood frequency curve produced at stream gages, and all three study reaches had a stream gage in them, so this calibration dominated the results and diminished the variation in discharges among alternative methods that might otherwise have resulted.

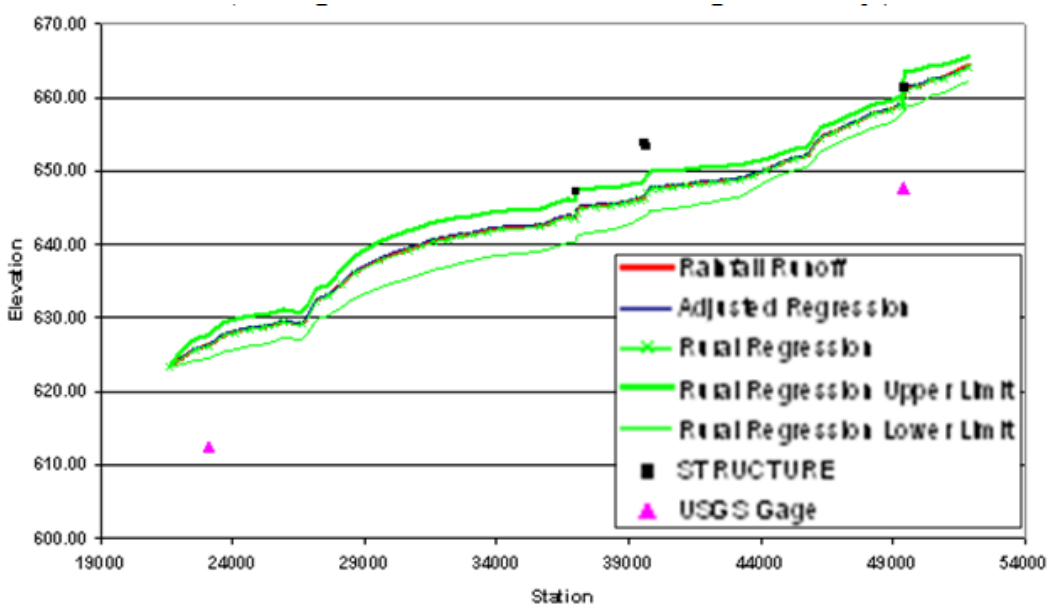

Figure 4. Effect of alternative hydrologic methods on base flood elevation at Long Creek (Mecklenburg County). Source: NCFMP (2009). Used with permission.

HYDRAULIC AND TERRAIN UNCERTAINTY

Similar to the hydrologic studies, several alternative combinations of hydraulic modeling and terrain data were examined. The North Carolina Floodplain Mapping Program has a comprehensive Lidar program for mapping the terrain of the state and these data are available at our study sites. An alternative is to use the 30m Digital Elevation Models available as part of the National Elevation Dataset, which with its associated tagged vector contour data from USGS topographic maps, is used in many Approximate floodplain mapping studies. Similarly, three alternatives were examined for surveyed structure information: full surveys as used in Detailed

Studies, limited surveys as used in the North Carolina Limited Detailed Studies, and no surveys in a method called Limited Detailed Studies National approach. Figure 5 shows the effects of these alternatives at Long Creek. There is little difference among any of the alternatives (a standard deviation of 1 to 3 feet), except for the alternative of approximate modeling on the National Elevation Dataset, which here produces a base flood elevation on average 21 feet higher than that produced by a Detailed Study. This large systematic discrepancy is produced because of a similar difference between the mean elevation of the Lidar and NED data at Long Creek and because of differences in the location of the stream centerline between these two data sources.

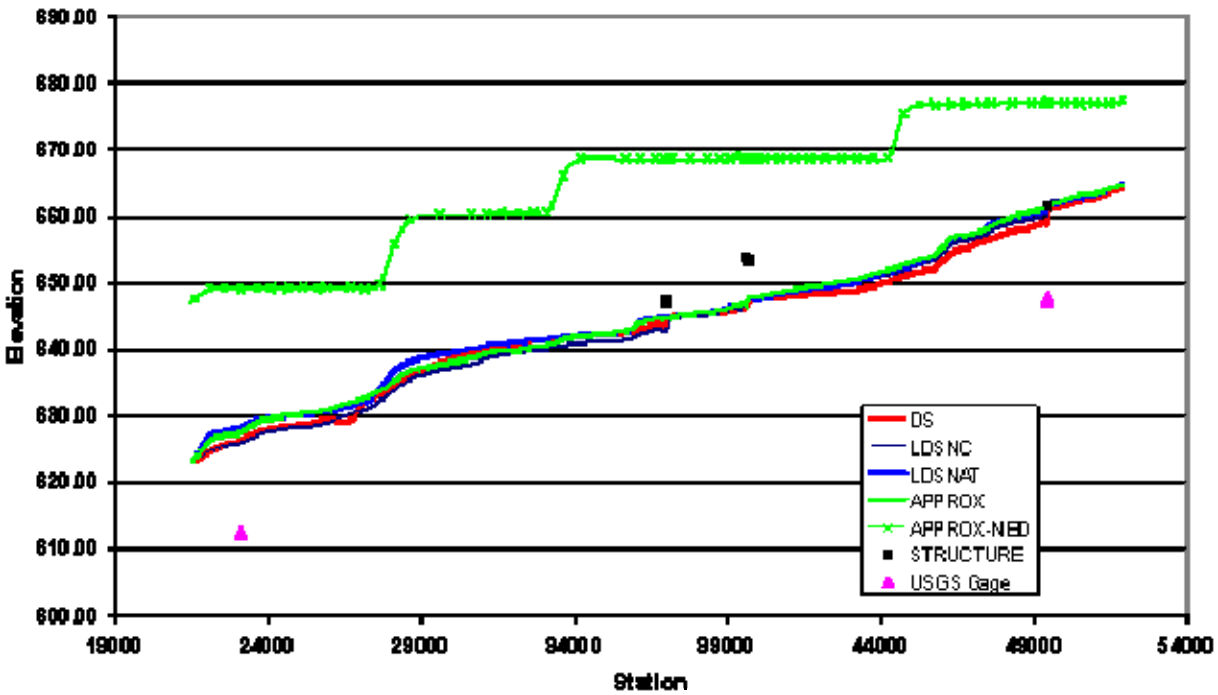

Figure 5. Effect of hydraulic and terrain data alternatives on base flood elevation at Long Creek. Source: NCFMP (2009). Used with permission.

Differences in elevation information between Lidar and the NED in the floodplain zone of our three study reaches are large, as illustrated in Table 1, which shows that besides the large systematic difference at Long Creek, there are random differences of the order of tens of feet at all locations. These differences are much larger than any differences induced by variations in hydrologic and hydraulic methods at these locations.

Stream	Mean (feet)	Standard Deviation (feet)	Minimum (feet)	Maximum (feet)
Ahoskie Creek (Coastal Plain)	0.5	3.9	34.8	−25.3
Long Creek (Piedmont)	14.7	15.6	81.5	−46.0
Swannanoa River (Mountains)	−2.0	17.5	89.7	−139.3

Table 1. Differences in elevation information (NED-Lidar) in the three study reaches. Source: NRC (2009) Reprinted with permission from the National Academy of Sciences, Washington, D.C.

DISCUSSION

The relative role of hydrologic, hydraulic and terrain information accuracy on the accuracy of base flood elevation and floodplain mapping has long been uncertain. From the viewpoint of the hydrologist, the size of floods that nature can generate seems so uncertain that it is hard to conceive of why this is not the dominant uncertainty in the picture. Terrain information seems so fixed and immutable, that it cannot be uncertain. It turns out, however, that the National Elevation Dataset has an elevation error when compared to survey bench marks at the same locations of 14.9 feet at the 95% confidence level (NRC, 2007). Thus, the statistical variations between the National Elevation Dataset and Lidar mapping of the same terrain shown in Table 1 are not unexpected. It might also be argued that it is not the absolute elevation compared to a geodetic datum that matters but rather the height of the water relative to the elevation of the channel in which it flows. The problem with this approach is that base flood elevations, as shown in Figures 4 and 5, are established with respect to a geodetic datum (the North American Vertical Datum of 1988), and these elevations govern all subsequent land development in the area, which is also referenced to this geodetic datum.

The result of this study (NRC, 2009) confirms in greater detail the insight that was presented in a previous study of the accuracy of flood map input information (NRC, 2007). That study concluded the average USGS topographic map was completed in 1970, that the terrain information in the 30m National Elevation Dataset are an order of magnitude less accurate than is called for by FEMA's standards for terrain data accuracy, and thus that a remapping of the nation using Lidar is called for. This proposed program is termed "Elevation for the

Nation", by analogy with the existing "Imagery for the Nation" program for updating digital orthophoto coverage of the United States. As Lidar from existing mapping programs like the one in North Carolina, are incorporated into the National Elevation Dataset, its accuracy will improve.

CONCLUSIONS

The key to accuracy of base flood elevation is accurate data on the elevation of the land surface that underlies the flooded landscape. The 30m National Elevation Dataset is about an order of magnitude less accurate than is needed for floodplain mapping. New terrain mapping of the nation is needed. When Lidar data are available, the relative effects of hydrologic, hydraulic and terrain data are much more balanced, with variations within reasonable ranges producing effects on the base flood elevation of from one to three feet. A lower bound on the uncertainty of the base flood elevation of approximately one foot is established by analysis of extreme stage heights measured at gages in North Carolina and Florida. This translates to a horizontal uncertainty in the location of the floodplain boundary of from 8 feet in mountains to approximately 40 feet in a flat coastal plain area. There is no discernable pattern in the distribution of these sampling errors either with size of the drainage area, or with topography, or whether the landscape was pitted with sinkholes in karst terrain or not.

REFERENCES

FEMA (2006). *Flood Map Modernization, Mid-Course Adjustment*, available at <http://www.fema.gov/library/viewRecord.do?id=2195>.

NCFMP (2009). *North Carolina Floodplain Mapping Program: 2000-2008 Program Review*, http://www.ncfloodmaps.com/program_review.htm

NRC (2007). *Elevation Data for Floodplain Mapping*, Report of the National Research Council Committee on Floodplain Mapping Technologies, National Academies Press, Washington DC, http://www.nap.edu/catalog.php?record_id=11829

NRC (2009). *Mapping the Zone: Improving Flood Map Accuracy*, Report of the National Research Council Committee on FEMA Flood Maps, National Academy Press, Washington, DC.

Generating different scenarios of BMP designs in a watershed scale by combining NSGA-II with SWAT

P. Kaini[1], K. Artita[2] and J. W. Nicklow[3]

[1] Graduate Research Associate, Department of Civil and Environmental Engineering, Southern Illinois University Carbondale (SIUC), Mail Code 6603 Carbondale, IL 62901; Ph: (618) 536-2368; Fax: (618) 453-3044 Email: pkaini@siu.edu
[2] Graduate Research Associate, Department of Civil and Environmental Engineering, SIUC, Email: kartita@gmail.com
[3] Associate Dean and Professor, College of Engineering, SIUC, Email: nicklow@engr.siu.edu

Abstract. A multi-objective optimization technique, Non-dominated Sorting Genetic Algorithm (NSGA-II), is coupled with a semi-distributed hydrological model, Soil and Water Assessment Tool (SWAT) with the objective of generating a set of non-dominated solutions. The model is formulated to optimize two conflicting objectives: the cost of structural Best Management Practices (BMPs) and the treatment goal. The cost of the BMPs is the function of type, size, and location of BMPs; whereas, the treatment goal considered is the reduction in annual sediment load the watershed outlet. Structural BMPs included in the modeling include detention ponds, infiltration type detention ponds, parallel terraces, filter strips, and grade stabilization structures which are applicable in agricultural watersheds. The model is demonstrated on Silver Creek watershed, a sub watershed of Lower Kaskaskia in Illinois. SWAT delineates watershed into 159 subbasins and are considered as potential locations of BMPs. The model came up with a Pareto front, which comprises a set of non-dominated solutions, a set of least cost solutions for different level of annual sediment load reduction.

Keywords. NSGA-II, watershed modeling, treatment goals, SWAT, Silver Creek, BMPs.

Introduction

Structural best management practices (BMPs) are often used to control runoff, sediments and nutrients, both in urban and rural or agricultural watersheds. Structural BMPs generally applicable in agricultural watersheds include detention and retention basins, filter strips, grade stabilization structures, grassed waterways, and field terraces. The current practice is to design an individual BMP structure where required on-site. Few recent studies have pointed out that the on-site practice could lead to the implementation of many BMPs in the watershed, and still could not assure that the

treatment goals at the watershed outlet are achieved. An on-site approach is not particularly effective in collectively reducing watershed-wide peak flows, and can potentially increase peak flow rates for detention-based systems by negatively impacting each other (Emerson et al., 2005). Harrell and Ranjithan (2003) emphasized that fewer regional basins can be implemented in place of many on-site basins to achieve the same treatment goals when they are implemented at a watershed scale. To address the watershed scale design of BMPs, Kaini et al. (2008) developed a single objective optimal control model which can optimize the cost of BMPs for user specified level of annual sediment load and peak flow reduction. In this study, a multi-objective optimization model is formulated which can find a set of optimal or near optimal solutions for various level of treatment goals. The multi-objective model generates various cost effective solutions for different level of water quality goal at the same time. This can serve as a valuable tool in formulating a watershed management plan.

A multi-objective optimal control model (OCM) is developed by coupling a semi-distributed hydrological model, the Soil and Water Assessment Tool (SWAT), with the contemporary multi-objective algorithm, Non-Dominated Sorting Genetic Algorithm-II (NSGA-II), to identify the optimal designs (sizes, types, and locations) of structural BMPs for varying level of annual sediment load reduction goals at a watershed-scale. A multi-objective optimal control model (MO-OCM) has been developed which optimizes the cost of BMPs (by selecting type, size, and location) and the environmental goal (e.g.annual sediment load) simultaneously.

Problem Formulation

The current problem can be stated as the design of BMPs (type, size and location) at a watershed scale that:

Minimize: Total cost of BMPs
Annual sediment load at the watershed outlet

Subject to the following constraints:

(1) Water balance in the watershed
(2) BMP size constraints
(3) Landuse constraints

Mathematically, this can be expressed as

Minimize:

$$1)\ BMPC = \sum_i \sum_j BMPC_{ij}$$

$$2)\ SedL_{annual}$$

Subject to:

$$\sum_{k=1}^{n} A_k \le A_{\max}$$

$$A_k = A_{k,sb} \times fr$$

$$Sj \leqslant Sj_{\max}$$
$$SedL_{\max} = g_2(x,u,t)$$

where, *BMPC* is the total cost of BMPs implemented in a watershed. $BMPC_{ij}$ is the cost of a *j* type of BMP implemented in a subbasin *i*. A_k is the area of the pond in subbasin *k* whose value lies within the user-defined maximum and minimum limits, A_{max} is the maximum limit of the total pond area assigned to the watershed, $A_{k,sb}$ is the area of subbasin *k*, and *fr* is the fraction of the subbasin area that drains to the pond. *Sj* is the size of *j* type of BMP and Sj_{max} is the maximum size limit of the corresponding BMP. The final two relationships represent simulation constraints, where *g* generally represents all pertinent hydrologic and hydraulic relationships, as a function of dependent (state) and independent (decision) variables, *x* and *u,* respectively, and time, *t*. BMPs are not implemented in a subbasin where the dominated land use is either forest or water body.

Silver Creek Watershed

The model is developed and applied to the 1,189 km^2 (459 sq. miles) Silver Creek watershed (Figure 1). The primary landuses in the watershed are cropland, grassland, and forest; however, the area is currently experiencing moderate to high levels of urbanization (Kaini et al., 2008).

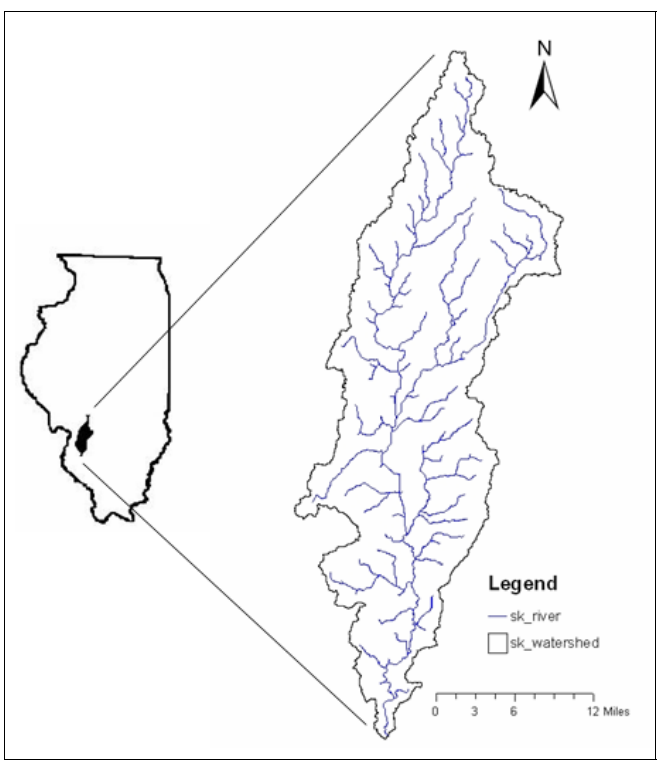

Figure 1 Location of Silver Creek Watershed, Illinois

The basic data required to run SWAT were obtained from various government agencies. Climate data for the study area, which include the daily precipitation and

maximum and minimum daily temperatures, were obtained from the National Climate Data Center (NCDC). A 30-m resolution Digital Elevation Model (DEM) and hydrologic data (daily flow) for the hydrological station USGS-05594800, located near Freeburg (St Clair County) in Illinois were obtained from US Geological Survey (USGS). The digital soil map and the land use map were obtained from the Natural Resources Conservation Service (NRCS).

SWAT

SWAT is a physically based, spatially-distributed, continuous-time watershed model that operates on an ArcView GIS (i.e., AVSWAT) platform. It was developed by the US Department of Agriculture (USDA) to predict the impact of land management practices on water, sediment and agricultural chemical yields in large complex watersheds with varying soils, land use and management conditions over long periods of time (Neitsch et al., 2002). The main purpose of SWAT is the computation of runoff, sediment and nutrient loads from a watershed. SWAT requires specific information about climate, topography, soil properties, land use and management of a watershed for simulation (Neitsch et al., 2002). To account for the spatial heterogeneity of climate, topography, land use and soil, SWAT delineates the watershed into spatially defined sub basins by using Digital Elevation Model (DEM). Each subbasin is further sub-divided into hydrologic response units (HRUs). A HRU is the total area in a subbasin with a particular land-use, management and soil type. SWAT simulates the surface and subsurface flow accounting for rainfall/snowfall and snow melt and sub surface flow processes. SWAT employs Modified Universal Soil Loss Equation (MUSLE) to evaluate sediment load from HRUs.

Calibration of SWAT

SWAT is calibrated for the Silver Creek watershed using mean daily flow and daily sediment load, observed at station USGS 05594800, located near Freeberg, Illinois. The station lies just upstream of the Silver Creek River and Kaskaskia River confluence. SWAT is simulated for the period of 1990 through 1996, and calibration is performed for the period of 1992 through 1994. Simulation from 1990 through 1991 is considered as a warm-up period to reduce the initial condition impacts, whereas the simulation from 1995 through 1996 is used for verification. Daily measured sediment data were available only for 134 days for calibration within the calibration period (1/1/1992 to 12/31/1994) and 113 days of data were available for validation within the validation period (1/1/1995 to 12/31/1996). Therefore, statistical evaluations of sediment calibration are based on these limited data. Only the data of the particular days where the measured data were available, were used. This is one of the major data limitations in model calibration. Considering the complexity due to large number of parameters in a distributed model with 159 subbasins, and with reference to Neitsch et al. (2002), Muleta and Nicklow (2005) and Bekele and Nicklow (2007), only 19 important parameters for stream flow and 7 important parameters for sediment load are considered in calibration.

A genetic algorithm is coupled with SWAT to set up an automatic calibration model. The objective function of the calibration routine is the Root Mean Square Error (RMSE) between the observed and the simulated flow. The objective of the

calibration is to search a set of parameter values having minimum RMSE between the mean daily observed and the simulated output.

The results obtained here, Nash and Sutcliffe Efficiency (NSE) equal to 0.703 for flow calibration and 0.826 for flow validation based on daily data, are higher than the generally acceptable minimum NSE value (0.5) for flow calibration (Moriasi et al., 2007). NSE values for sediment calibration and validation obtained are 0.502 and 0.512, respectively, which are within the acceptable limits.

Structural BMPs

Detention pond, filter strip, parallel terrace and grade stabilization structure are implemented in the model as solutions to reduce sediment load from the watershed. Different sets of SWAT model parameters and their values are identified to represent these BMPs (Bracmort et al., 2006; Kaini et al., 2008). A detention pond is employed by adjusting appropriate parameters including the pond area, volume, subbasin area draining to the pond, and the permeability coefficient in the pond subroutine. A pond reduces suspended sediments, metals and dissolved nutrients by sedimentation and biological processes. In this study, the infiltration type of detention pond is represented with the bottom permeability coefficient (K) of 1.0 mm/hr where as normal detention pond is represented with the value of K equal to 0.0 mm/hr.
A filter strip, also known as field border, is a uniformly graded and densely vegetated area at the border of the field where excessive sheet and rill erosion is likely to occur. A filter strip is represented by the width of the edge of field filter strip (FILTERW). The value of FILTERW is 0.0 m for no filter strip and 5.0 m if a filter strip is applied (Bracmort et al., 2006). The trapping efficiency of the strip is a function of the filter width (Neitsch et al., 2002).

Terraces are formed by earthen embankments or channels or a combination of the two to reduce the sheet and rill erosion, peak flow, retain moisture and reform the farm to increase the productivity. Bracmort et al. (2006) identified parameters initial SCS runoff curve number for moisture condition II (CN2), USLE equation support practice factor (USLE_P) and average slope length (SLSUBBSN) to represent the effects of parallel terrace in a HRU scale in SWAT. Neitsch et al. (2002) recommends the adjustment of CN2 for parallel terraces. USLE_P for the terrace implemented case is recommended to be 0.4 (Bracmort et al., 2006), whereas the initial value is 1.0 (without parallel terrace). To represent the parallel terrace, SLSUBBSN is defined as (ASAE, 2003):

$$SLSUBBSN = (X \times S + Y)\frac{100}{S}$$

where, X and Y are constants. X depends on location of the watershed; it is 0.21 for the watershed considered (ASAE, 2003). The value of Y depends on the soil erodibility, cropping system and management and the value varies from 0.3 to 1.2 (ASAE, 2003), with lower values for more erodible soil. It is assumed to be 0.9 for the case considered.

A grade stabilization structure is a structure designed to reduce the channel grade in natural or constructed water course. It reduces or prevents the erosion due to higher grade on the channel bed. This practice is applicable where structures are required to prevent head cutting or stabilize gully erosion and also where the intersecting channels have different elevations. They may be vertical drop, weir spillways, chutes, or pipe drop structures and may be made of reinforced concrete, steel sheet piling, concrete block, riprap, corrugated metal, plastic, or concrete pipe, depending on-site conditions. The structure is represented by a CH_EROD value equal to zero and by reducing the average slope of a subbasin main channel (CH_S2) by 10%.

Non-dominated Sorting Genetic Algorithm (NSGA-II)

Non-dominated Sorting Genetic Algorithm (NSGA-II), developed by Deb et al. (2002), is an improved version of the original NSGA (Srinivas and Deb, 1994). NSGA-II is recognized as one of the high-performing contemporary multi-objective EAs, and has been successfully applied in various disciplines (Reed et al., 2003). Deb et al. (2002) demonstrated that NSGA-II outperformed two other contemporary multi-objective evolutionary algorithms, Strength Pareto Evolutionary Algorithm (SPEA) and Pareto Achieved Evolutionary Algorithm (PAES), in terms of finding a diverse set of Pareto optimal solutions close to the true Pareto front in a number of test functions. The stepwise procedure of NSGA-II, as outlined by Deb (2001), is as follows:

(a) An initial population of P is randomly generated which is considered as the set of parent solutions (P_t) with population size N.

(b) The offspring population, Q_t, with population size N, is generated from P_t solutions applying GA operation. The GA operation includes crowded tournament selection, crossover and mutation operators.

(c) Parent and offspring solutions are combined to create combined population of R_t of population size 2N.

(d) Combined solutions (R_t) are then sorted into different non-dominated fronts (F_i)

(e) The new generation solutions are selected starting from the best Non-dominated fronts until the N number of solutions are found. Since R_t contains 2N solutions, all the solutions will not be accommodated in the new generation.

(f) All fronts which are not accommodated in the new generation are simply deleted.

(g) In the last allowed front, it may have more than required solutions. Solutions are selected based on their crowding distance. The crowding distance criteria make sure that the most diverse solutions are selected from the last front.

(h) The step (b) through (g) is repeated until the termination criterion is met.

NSGA-II assures elitism by including the best parent solutions and best offspring solutions obtained in a population, whereas the diversity of solutions is preserved by the crowding tournament selection operator. The operator, on the basis of non-domination ranking and local crowding distance, selects solutions in the non-

domination ranking. The crowding distance is the average distance between an individual solution and those solutions nearest to it in the objective space (Deb, 2001). Binary tournament selection and uniform crossover are considered as genetic operators because the decision variables in the problem considered are represented by integers.

Methodology

A multi-objective OCM is developed by coupling SWAT with NSGA-II to generate alternate designs of BMPs at a watershed scale. SWAT is run for a 2 years, from 2001 through 2002. SWAT delineates the watershed into 159 subbasins, and each subbasin is considered as a HRU. Types of structural BMPs considered in the study are detention ponds, infiltration ponds, filter strips, grade stabilization structures and parallel terraces. The NSGA-II operation starts with a random generation of an initial set of solutions which consists of a combination of different BMPs located in different sub basins. The decision parameters include the area of detention pond, part of subbasin area draining to the detention pond, permeability coefficient of the pond bottom, size of filter strip, subbasin length and curve number (for terracing), and height of the grade stabilization structure. Two objective functions considered are the total cost of the BMPs implemented and the annual sediment load at the watershed outlet. The schematic representation of optimal control model is presented in Figure 2.

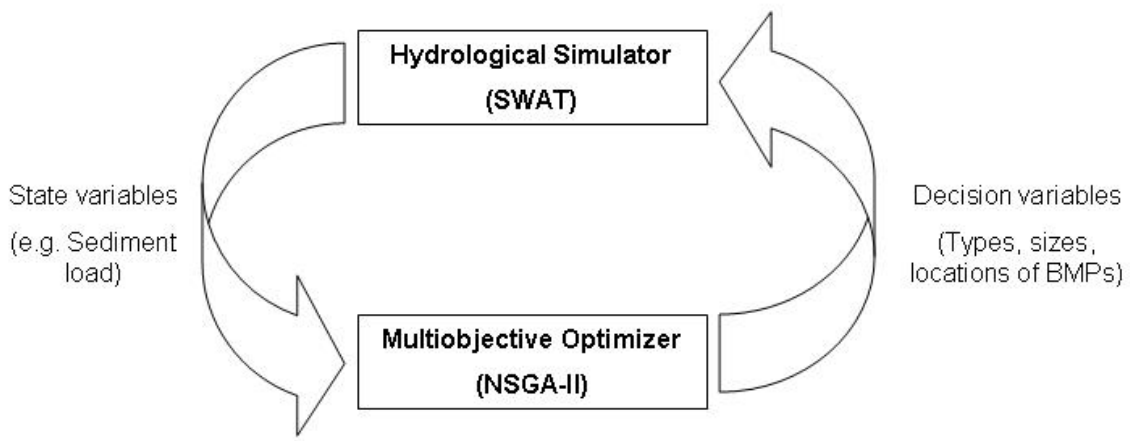

Figure 2 Schematic representation of Optimal Control Model

The costs of BMPs are evaluated based on the unit costs presented in Table 1.

Table 1 Unit Costs of BMPs

SN	BMP	Unit	Unit Cost (US$)
1	Detention pond	Acre- ft	500.00
2	Filter strip	Acre	250.00
3	Parallel terrace	Acre	500.00
4	Grade stabilization structure	Number	6000.00

Results and Discussion

As an example, the OCM is run with a population of 50 chromosomes and for the maximum generation of 50. Figure 3 shows the results found in the 20th and 50th generation. The default value of annual sediment load at the watershed outlet is 48177 tons. With the implementation of BMPs, the model found the set of solutions for various levels of sediment reduction criteria. The maximum reduction of 18% was found with the cost of 77 million USD which corresponds to the implementation of 119 detention ponds, 79 filter strips, 71 parallel terraces, and 44 grade stabilization structures. The minimum reduction (9%) corresponds to the cost of 42 million USD which requires 76 detention ponds, 52 filter strips, 47 parallel terraces, and 44 grade stabilization structures. The results show that the Pareto front should further extend on either side of the curve. By extending towards higher values on y-axis, it should hit the solutions with much lower cost and higher sediment load; and similarly on the other extent of the curve, solutions with further reduced sediment loads can be expected.

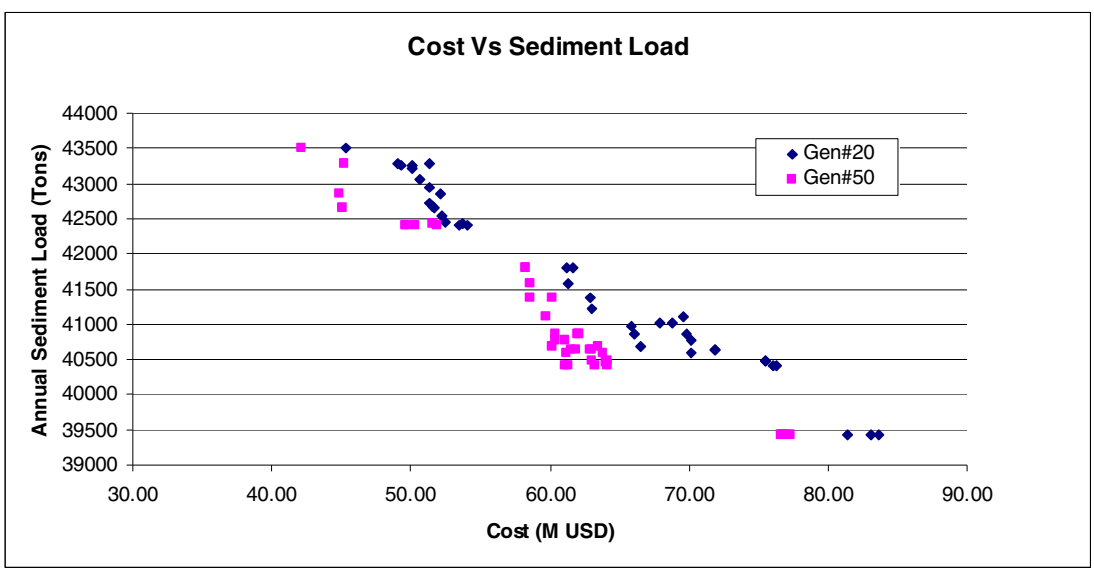

Figure 3 Pareto Curve for 20th and 50th generation

Conclusion

The results on Figure 3 shows the trend of the Pareto curve, but these results may not represent true optimal solutions. It can be expected that the curve can extend on either side: reduction on cost and reduction on sediment load. The future work will further improve the algorithm as well increase the number of population and generation. The costs are based on the unit costs for the example watershed considered. Therefore the results are site specific; however, with the specific model data and unit costs, OCM can be applied to other similar watersheds.

References

ASAE (2003). *Design, Layout, Construction and Maintenance of Terraces System*s. ASABE, 1950 Niles Road, St Joseph, MI, 49085-9659.

Bekele, E. and Nicklow, J. W. (2007). "Multiobjective Automatic Calibration of SWAT using NSGA-II" *J. Hydrol.,* 341, 165-176.

Bracmort, K. S., Arabi M., Frankenberger J. R., Engel B. A., Arnold J. G. (2006). "Modeling Long Term Water Quality Impact of Structural BMPS" *American Society of Agricultural and Biological Engineers ISSN,* 49(2), 367–374.

Deb, K. (2001). *Multi-Objective Optimization Using Evolutionary Algorithms*. John Wiley and Sons Ltd., Chichester, UK.

Deb, K., Pratap, A., Agarwal, S., and Meyarivan, T. (2002). "A Fast and Elitist Multi-objective Genetic Algorithm: NSGA–II." *IEEE Trans. on Evolutionary Computation*, 6(2): 182- 197.

Emerson, C. H., Welty, C., and Traver, R. G. (2005). "Watershed-scale evaluation of a system of storm water detention basins." *J. Hydrol. Eng.,* 10(3), 237-242.

Harrell, L. J., and Ranjithan, S. R. (2003). "Detention Pond Design and Land Use Planning for Watershed Management." *J. Water Resour. Plan. Mgmt.* 129(2), 98-106.

Kaini P., Artita K., and Nicklow J. W. (2007). "Evaluating Optimal Detention Pond Locations at a watershed scale." *World Environment and Water Res. Congress, Tampa, FL.*

Moriasi, D. N., Arnold, J. G., Van Liew, M. W., Binger, R. L., Harmel, R. D. & Veith, T. L. (2007). "Model Evaluation Guidelines for Systematic Quantification of Accuracy in Watershed Simulations" *American Society of Agricultural and Biological Engineers ISSN,* 50(3), 885-900.

Muleta, M. K. and Nicklow, J. W. (2005). "Sensitivity and Uncertainty Analysis coupled with Automatic Calibration for a Distributed Watershed Model" *J. Hydrol.,* 306, 127-145.

Neitsch, S.L., Arnold, J.G., Kiniry, Williams, J.R, and King, K. W. (2002). *Soil and Water Assessment Tool, Theoretical Documentation Version 2000.* Temple, Texas, USA: USDA-ARS.

Reed, P., and Minsker, B. S. (2004). "Striking the Balance: Long-Term Groundwater Monitoring Design for Conflicting Objectives." *J. Water Resour. Plng. Mgmt.* 130(2), 140- 149.

Reed. P., Minsker, B. S., and Goldberg, D. E. (2003). "Simplifying Multiobjective Optimization: An Automated Design Methodology for the Nondominated Sorted Genetic Algorithm-II." *Water Resour. Res.,* AGU 39 (7),

Scott Knight, E.I.T., Engineer
Aurora Water
15151 E. Alameda Parkway, Ste. 3600
Aurora, CO 80012
sknight@auroragov.org
Ph: 303-739-7367
Fax: 303-739-7604

Hardening a Great and Growing City's Water Supply

Abstract

Cities across the West face the threat of dwindling water supplies. Issues such as climate change, competing supplies, and litigation threaten water availability for municipal uses. In Colorado, where approximately 86 percent of water is used for agriculture (CFWE 2005) and the system of administration is prior appropriation, adequate water supply in an increasingly competitive market is no longer a certainty. Many municipalities whose systems are based on junior water rights have been forced to turn to innovative – and expensive – projects to develop the water supplies of the future.

The City of Aurora, Colorado is a suburb to Denver and the third largest city in the state, with a 2008 population of nearly 312,000. For Aurora Water, meeting the increased thirst of a burgeoning city is a challenge. Continued growth and a possibly dwindling water supply have necessitated an evaluation of the city's water infrastructure and "out-of-the-box" planning to ensure that a reliable water supply is available for the future. In 2002, low rainfall and runoff brought the system's vulnerability to attention. With seemingly no water available to increase storage levels, reservoir levels fell to 25 percent full in March 2003, well below the desired minimum level and an adequate supply for only six months of indoor use in the City. This situation made perfectly clear the need for guaranteed reliability in the face of continued pressure on available water supplies.

To meet these needs and enhance the ability to protect against prolonged drought many projects are being undertaken. The Prairie Waters Project, slated for completion in mid-2010, is an example of insightful planning that is taking place in Aurora. When completed, this project will deliver reusable water from approximately 35 miles away, pumping the supply back to the City for treatment and incorporation in the City's water system. An additional effort being undertaken is the acquisition of senior agricultural water rights along the South Platte River for increased water supply. The City is also purchasing and negotiating with several mining companies to develop large sub-surface open water storage reservoirs to improve operational flexibility and increase the ability to capture every drop of reusable water before it is permanently lost from the system. This paper will examine these projects and other ways Aurora is "hardening" its water supply to protect existing users and provide for future citizens.

Colorado is unique among western states because of its large water exports to other states. Because the Rocky Mountains are situated in the center of the state, Colorado receives significant amounts of precipitation which is then used in-state and exported based on a series of Interstate Compacts as shown in Figure 1. The Rocky Mountains also serve as the Continental Divide splitting the eastern and western United States hydrologically. To further complicate issues more than 80% of the states population lives on the eastern, "Front Range" side of the mountains (State of Colorado, 2009), and the greatest water supply is located on the western side of the mountains.

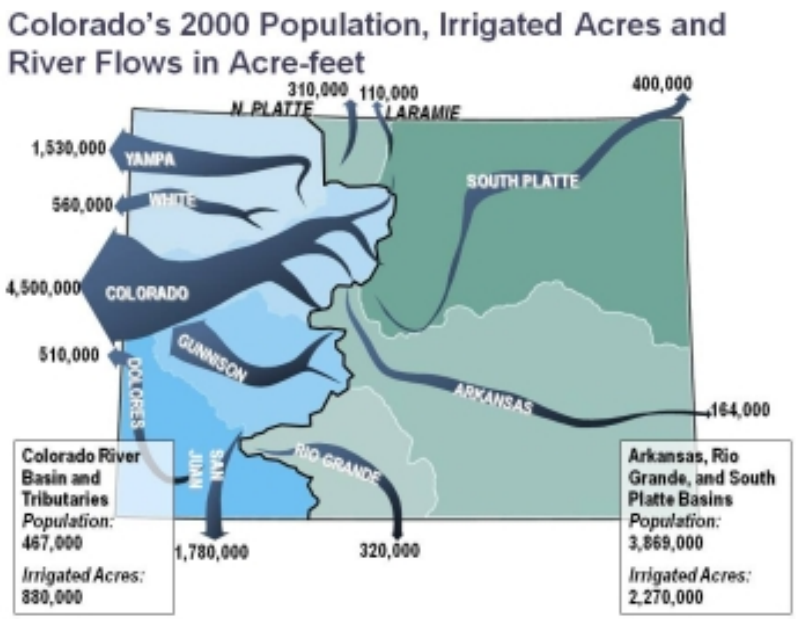

Figure 1 – Colorado Water Exports (CWCB 2009)

To maintain a prosperous and thriving population it has become necessary to develop and maintain a vast water distribution system. Beginning in the 1850s a water system was developed to capture, divert, and use the water. By the mid- to late-1800s, the prior appropriation system had been developed to manage the ownership and use of water in Colorado. The prior appropriation doctrine in its simplest form is that the first person to divert and use the water has a right to continued use of the resource into the future. It is also defined by the colloquial sayings, "Use it or lose it" and "First in time, first in right." Over time and with increasing technological improvements and demand for water, the prior appropriation system has evolved and increased in complexity.

City of Aurora Water Supply

The City of Aurora is the third largest city in the state of Colorado, behind Denver and Colorado Springs, with a 2008 population of about 312,000 people. The city has had difficulties with water from the start. Formed in the 1890's and founded in 1928, the City of Aurora is relatively new compared to the City of Denver which was founded in 1861. Beginning in the early 1890's the suburb had inadequate water supplies for its residents.

Aurora was heavily reliant on Denver for water supply. This changed when in the 1950s, Aurora began its major quests to develop independent water supplies.

Since its creation, but especially beginning in the 1950s, Aurora has striven to maintain an adequate and independent water supply to support its development and population. This has included the development of new water rights and reservoirs as well as the purchase and transfer of existing water rights. Beginning in the 1960s, the City developed a series of reservoirs including Homestake, Spinney Mountain, and Strontia Springs (Mehls et al., 1985). During this period the City also acquired water rights in the South Park area, upstream of Spinney Mountain Reservoir. Figure 2 below shows a simplified schematic of Aurora's water supply system.

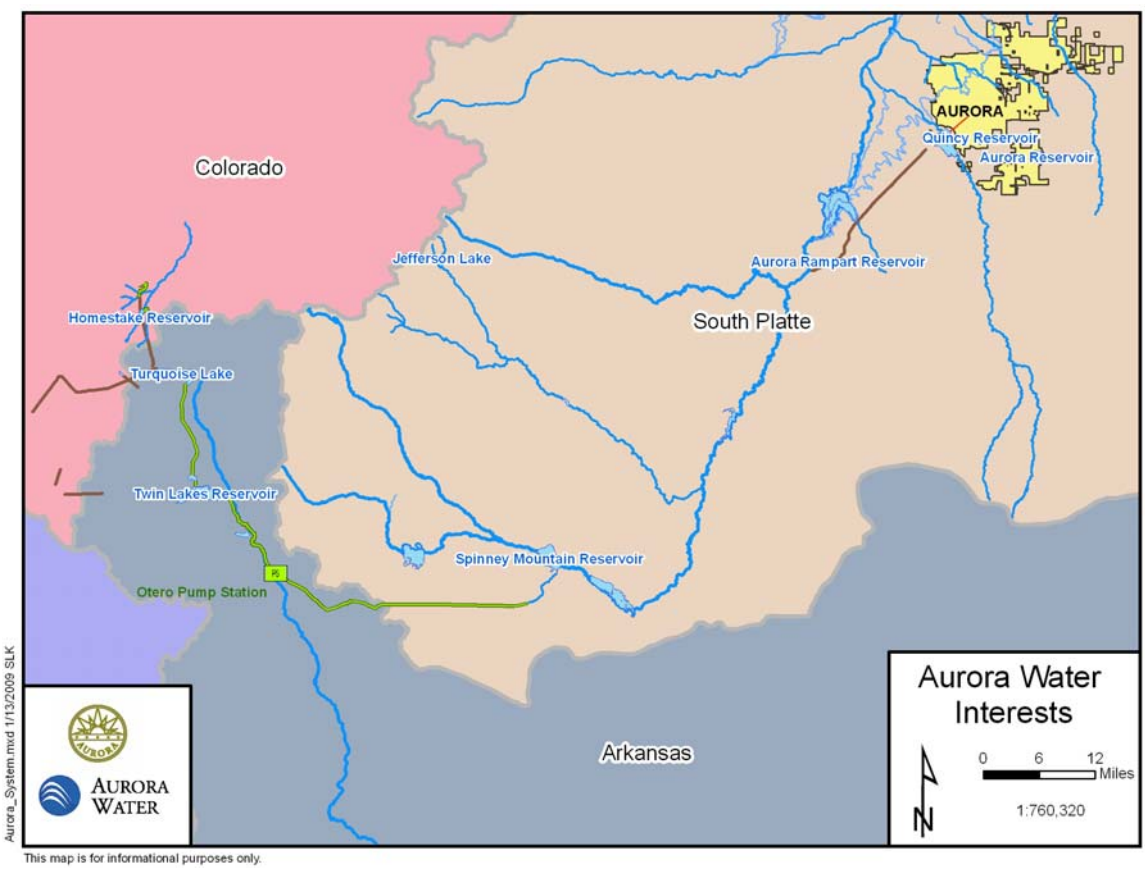

Figure 2 – Aurora Water System Schematic

With the development of additional water rights and storage the City helped ease some of the problems of the past by ensuring a reliable water supply. However, in 2002 one of the worst droughts in recent history occurred. This caused nearly all water providers to struggle to meet the needs of their citizens while also preserving water in storage to protect against a worsening drought. During this period the City of Aurora had its water reservoir storage plunge to 37,576 acre-feet or 25% of its total capacity. This volume of water represented only six months of supply for indoor water uses in the City. Once again, the City found itself in a position where water could dictate its future development

As a result of this drought and the realization of what a multiple year drought could do, the City began to consider ways to increase their water portfolio and "harden" the system by ensuring that all water the City owned could be used. This effort has led to new and novel thinking that has helped keep the City of Aurora active in pursuing its mission to "enhance and protect the quality of life for Aurora citizens" (Aurora Water, 2009).

Hardening the City's Water Supply

To improve the reliability of the City's water supply several methods have been applied. A multi-faceted approach has appeared to be the most likely for success because of the changing conditions for the City, water in Colorado and the nation as a whole. The methods under consideration and use include: cooperation with other municipalities, conservation, water rights acquisition, increased operational flexibility, and investing in new and improved infrastructure. Each of these areas has become a focus for the City in a well-rounded approach to address diminishing water supplies and increased competition.

Cooperation and Collaboration

While the City of Aurora is working to meet its future municipal needs it is certainly not alone. Many municipalities are struggling to find the water to ensure a healthy and prosperous future for their citizens. This has led to struggles and increased competition for available water supplies. Several Front Range municipalities have relied almost solely on groundwater. This reliance has led to decreased groundwater levels in the aquifers and increases in pumping cost because of increased drawdown. These municipalities have now begun to look to other sources for renewable water supplies.

Because competition serves no purpose, but to drive up prices, efforts are now being made to work collaboratively and collectively with other municipalities. These efforts allow money to be spent more effectively and water to be used more efficiently through design and construction of regional projects that can squeeze more use out of every drop of water. Examples of these efforts include the formation of the South Metro Water Supply Authority, of which Aurora is not a member. This group was formed by 13 individual water providers to allow for collaboratively developing long-term water supplies (South Metro, 2009). These projects are typically expensive; therefore, having members with similar interests can help make a project that is too expensive for one member affordable for the group.

In addition to guaranteeing a water supply there is also a desire to examine and predict future water supplies. This has become even more important with the recent national focus on climate change. To better understand the potential effects of climate change on their water supplies, the City of Aurora and several other municipalities have started the Joint Front Range Climate Vulnerability Study. This project is examining the potential impacts on stream flow as a result of increased temperatures and decreased precipitation.

The City of Aurora has also joined with agricultural and wildlife interests to examine the potential for leasing water to municipalities. This project is discussed further in the section on Water Rights Acquisition.

Conservation

In an effort to make every drop of water go further, Aurora has consistently employed an aggressive conservation program. This has included the use of restrictions, rebates, education, and certifications. Beginning as early as 1896 the town enacted watering restrictions on outdoor vegetation (Mehls et al., 1985). This has continued throughout the history of Aurora and exists to this day. More recently, the City has also begun other methods of encouraging citizens to conserve water. These have included rebates on toilets and washing machines that meet certain efficiency requirements, tiered water rates, education on alternative landscaping methods, and rebates on alternative landscaping methods. Rebates have proven very successful in Aurora where more than 1254 people have taken advantage of the rebates on toilets, 1797 on washing machines, and 145 on xeriscape landscaping in 2008. Tiered water rates have also helped cut down on water wasting in the City. The rates were set up to encourage conservation by increasing the price per 1,000 gallons as more water was used. The current residential water rates are shown in the table below.

	Gallons	Rate
Tier 1	**≤ 20,000**	**$4.90**
Tier 2	**20,001 – 40,000**	**$5.58**
Tier 3	**≥ 40,001**	**$6.98**

Table 1 – City of Aurora 2009 Water Rates (Aurora Water, 2009)

Water Rights Acquisition

To further add to the City's water supply, additional water rights are being purchased. Water sources that are available include new water rights, transferring agricultural water rights, and water rights trades. New water rights in the South Platte Basin can be adjudicated if a need is shown and water is shown as being available. However, the South Platte River Basin is over appropriated, meaning that in any given year not all water rights holders will be able to withdraw their allotment. Adjudication, therefore, is not a preferred method of acquiring new rights since the water rights are so far down (junior) in priority that they are unlikely to yield much, if any, water.

In addition to new water rights, Aurora is also acquiring water rights on the Lower South Platte. The primary source of water in this area is agricultural water from mutual ditches. These water rights are purchased from interested sellers. To negotiate a value for the shares of ditch water the City develops a consumptive use model. This looks at farming practices, crops grown, irrigation method, historic weather patterns, and mutual ditch

right that can be changed to municipal use in court. This water, once decreed for municipal use, can be used by the City to increase their available water supply. The decreed consumptive use portion of this water can also be reused to extinction. The remainder of the water right is assumed to return to the stream system for the benefit of other water rights holders.

To use these water rights, generally, the water must be removed at or downstream of the historic place of use. This ensures that water can be delivered to the users on the ditch who relied on the hydraulic head from that water right. This means that to deliver the water right from the ditch requires an augmentation station, or a diversion. On one of the ditches that the City of Aurora has an interest, the Brighton Ditch, the City owns four augmentation stations and a diversion that allows their shares to be delivered either back to the South Platte River or to one of their storage reservoirs.

Since 2000, the City of Aurora has acquired water on six ditch systems. These shares amount to approximately 2,700 acre-feet of water in an average year. Figure 3 below shows ditches that the City of Aurora owns or leases shares in, on the Lower South Platte River.

An unfortunate side effect of the transfer of water from agricultural to municipal uses is the dry-up of the farm. This means that water from the purchased ditch can no longer be used to irrigate the property (e.g. a farm that sells water from the Brighton Ditch can no longer use water from the Brighton Ditch for irrigation). In general this means that the farm goes out of production. This has caused these transactions to be termed “buy and dry” and has led to a negative view of municipalities as “water buffaloes” taking all the water from “poor” farmers.

To combat the loss of farm land and “agricultural heritage” the City of Aurora has begun cooperating with the Colorado Corn Growers Association and several other entities to look at a rotational fallowing and leasing program. These types of programs can be beneficial to farmers and cities because they allow farmers to lease their water in years when there is water needed by the cities due to a drought or a lack of yield. This is also beneficial to farmers because during these “bad” water years they may have difficulty successfully growing a crop because of weather conditions or water availability.

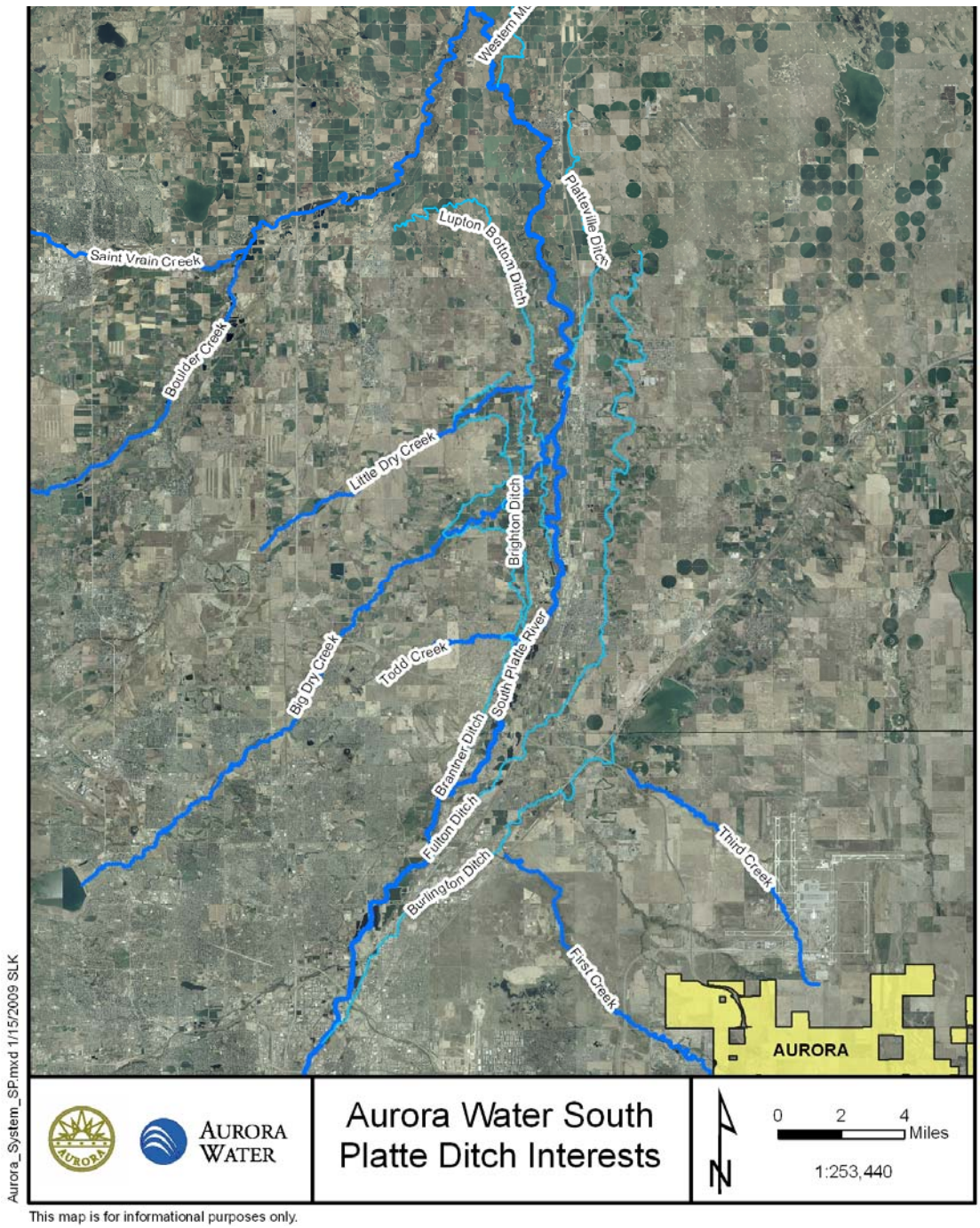

Figure 3 – Aurora Water South Platte Ditch Interests

System Flexibility

In an effort to develop a robust water system, Aurora has a significant amount of flexibility in its system. This includes multiple reservoirs, multiple pipelines, and two treatment plants. This redundancy makes it easier to adjust if a problem in one portion of the system takes down a component. This flexibility also ensures that when possible,

storage where it can be delivered to the city by gravity. This operational flexibility also allows for infrastructure to be taken off-line to allow for maintenance without affecting the overall delivery to the City.

Infrastructure

The final piece of the puzzle to improve the reliability of the water system and harden it against adverse conditions has been the construction of infrastructure in key locations. This infrastructure will allow for durability of the water supply in the face of prolonged drought, and use of the City's existing water rights to the fullest extent. A majority of this infrastructure is being developed in the Lower South Platte River Basin north of the City of Aurora. The infrastructure in these areas includes large in-ground reservoirs, wells, pumps, and pipelines. This infrastructure is being developed to move water from areas where it is being purchased back to the City, and to transfer its reusable water back to the City. In Colorado, some water can be reused to extinction. Water that meets this reusability standard is: water transferred from another River Basin (imported/foreign water), the consumptive use portion of transferred water rights, some groundwater rights, and water that is decreed to be reusable (newly decreed water rights). Water from these sources can be used and any portion of that water which is not consumed (removed from surface or groundwater basins) can be captured and reused successively to extinction.

This also applies to outdoor irrigation. When areas are irrigated, some portion of the water applied is not fully consumed. These lawn irrigation return flows (LIRFs) are allowed to be captured and reused in the City's water system. LIRFs in the City were decreed in Caser No. 02CW341 in 2008 and allow for approximately 14% of the water applied in outdoor irrigation to be reclaimed based on their lagged timing to the receiving water body. Specific LIRF percentages were developed for each of the City's receiving basins. The percentages can fluctuate based on continued monitoring.

As of January 2009, the City of Aurora has approximately 10,000 acre-feet of storage on the Lower South Platte River. These sites are in-ground reservoirs that are constructed as a byproduct to the mining of sand and gravel. These sand and gravel mines remove the aggregate from the historic river bed and leave large holes which are then isolated from the alluvial groundwater with clay-slurry cutoff walls. These reservoirs can then be used to store City water for augmentation, direct use, or repayment of obligations. The location of the City's future Lower South Platte reservoirs is shown in Figure 3.

The reservoirs shown in Figure 4 are Walker, Everist, Kirby-Dersham, and Aquifer Recharge and Recovery Site A (ARR-A). Walker, Everist, and Kirby-Dersham will be in-ground excavated reservoirs like those described above. ARR-A is a portion of the Prairie Waters Project, discussed in more detail below. This site, in the near term, will serve as a cutoff wall isolated, insitu storage basin that will provide water quality improvements through infiltration.

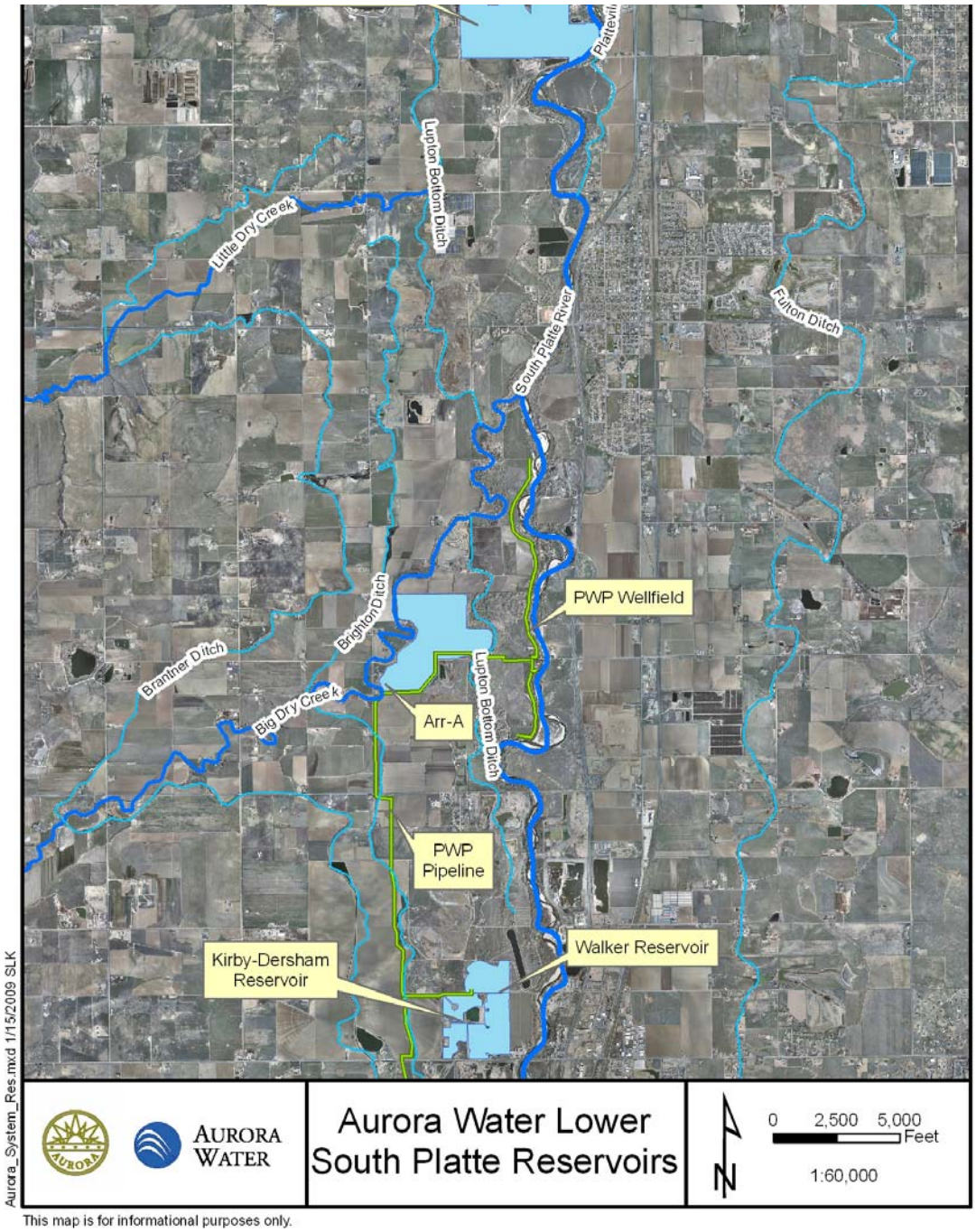

Figure 3 – Aurora Water Lower South Platte Reservoirs

The largest infrastructure project the City has ever built is currently under construction. This project, termed the “Prairie Waters Project” (PWP) pumps water from about 30 miles north of the City back to Aurora where it is treated in a cutting-edge water purification facility. The idea for this project was developed after the drought of 2002 and the project was quickly initiated and moved forward. Final completion for the project is scheduled for 2010. The PWP is designed to pump water from alluvial wells on the banks of the South Platte River, near Fort Lupton, Colorado, into infiltration basins located within ARR-A. These infiltration basins in concert with the riverbank filtration at the

From this in-ground reservoir, pumps will draw the water out and put it in a pipeline back to the City. This pipeline is capable of moving 10,000 acre-feet per year, or about 9 million gallons per day. The water from the pipeline is then treated in a state-of-the-art water purification facility and blended with the rest of the City's supply. Figure 4 shows the location of the well field parallel to the river and the beginning of the pipeline.

This project is being completed at a cost of nearly $750 million and will, when completed, allow the City to reuse its return flows in the South Platte River. The water available for reuse will include the agricultural water rights being purchased, LIRF credits, reusable effluent discharged from the Metro Wastewater Treatment Plant, any lease water acquired on the South Platte, and any other water sources decreed for use in the City. This project is also being designed to allow for expansion in the future with a larger pipe running most of the distance to the City. This large infrastructure project will also provide the potential for partnering with other entities in the future that need a firm water supply.

Conclusion

Aurora is just one of many cities in Colorado that have a concern over future water supply. With more people moving to the state every year and a population expected to double by about 2050, water supply issues are here to stay. To further exacerbate the problem there are predictions that climate change could lower the amount of streamflow the state currently enjoys or significantly alter the runoff pattern. There is also increasing competition for what water is available. This has pitted municipalities against eachother as well as municipalities against agricultural water users. Steps are starting to be made in the right direction, and Aurora is on the forefront of several of these efforts. To combat the dwindling water supplies Aurora has employed a multi-faceted approach. Cooperation is helping Aurora work better with its neighbors in a less hostile setting; conservation is helping preserve what water the City already has; new water is being acquired through leases and purchases to ensure an adequate supply; and new infrastructure is being built to allow the City to maximize the use of its new and existing water rights. With these novel approaches the City of Aurora can "harden" its supply and help ensure that services to citizens are always adequate to maintain the high quality of life that keeps people moving to the state.

References

Aurora Water. About Us. (2009). Retrieved January 16, 2009, from Aurora Water Web Site: http://www.auroragov.org/AuroraGov/Departments/AuroraWater/AboutUs/index.htm

Aurora Water. Rate Information. (2009). Retrieved January 15, 2009, from Aurora Water Web Site: http://www.auroragov.org/AuroraGov/Departments/AuroraWater/CustomerService/RateInformation/046356?ssSourceNodeId=602&ssSourceSiteId=621

Colorado Foundation for Water Education. (2005). Citizen's Guide to Where Your Water Comes From. Denver, CO: CFWE

Colorado Water Conservation Board. (2009). Retrieved January 21, 2009, from Colorado Water Conservation Board Web Site: http://cwcb.state.co.us/IWMD/

Mehls, S. M., Drake, C. J., and Fell Jr., J. E. (1985). Aurora: Gateway to the Rockies. Evergreen, CO: Cordillera Press, Inc.

South Metro Water Supply Authority. About SMWSA. (2009). Retrieved January 15, 2009, from South Metro Water Supply Authority Web Site: http://www.southmetrowater.org/index.html

State of Colorado, State Demography Office. Final Colorado Population Estimates. (2009). Retrieved January 15, 2009, from Colorado Department of Local Affairs: Division of Local Government: State Demography Office Web Site: http://dola.colorado.gov/dlg/demog/population/estimates/table1_07final.pdf

High Resolution Radar Precipitation Evaluation

Dennis Miller[1], Shaorong Wu[1], David Kitzmiller[1], and Feng Ding[1]

[1]NOAA, National Weather Service, Office of Hydrologic Development, 1325 East-West Highway, Silver Spring, MD, 20910; phone: (301) 713-0640 x190; email: Dennis.Miller@noaa.gov

Abstract

A series of experiments were undertaken to determine if any operational benefit might be realized from an upgrade of WSR-88D hourly precipitation products to the highest spatial resolution now possible, namely 0.5º x 250 m. The precipitation products are currently disseminated in arrays of 1.0 º x 1000 m spacing. Reflectivity from the NCAR S-Pol S-band radar (a radar with similar characteristics to the WSR-88D) in east-central Florida during the summer of 1998 were converted into precipitation estimates and collated with 1-hour gauge accumulations collected from several high-density rain gauge networks that were deployed simultaneously in the region. Radar-gauge correlations were calculated for several degrees of spatial aggregation, ranging from 1.0º x 150 m to 1.0º x 900 m. Correlations were estimated from over 8000 radar-gauge pairs, for both single points and areal averages. It appears that the degree of spatial aggregation of the radar estimates has little effect on radar-gauge correlations.

Overview and Problem Investigation

An enhanced version of the Weather Surveillance Radar-1988 Doppler (WSR-88D) that was phased in to operation beginning in the summer of 2008 will provide base reflectivity data at an 8x higher spatial resolution (i.e. 0.25 km x 0.5°) than that which was the standard (1 km x 1°) during the first nearly twenty years of operation of the legacy system. This very high resolution (termed "Super Res") data may provide an opportunity for achieving greater refinement in the discretization of rainfall to delineated stream and river basins and hence, to improved accuracy in radar-based, quantitative precipitation estimates and forecasts (QPE and QPF). However, sub-beam factors that could cause gauge-radar discrepancies, such as advection, evaporation, and hydrometeor interactions may be magnified at higher spatial resolutions.

The goal of this research is to investigate the potential for realizing improved accuracy in radar-based precipitation estimates – and subsequently, improved results in hydrological applications – from the processing of radar reflectivity data at higher spatial resolutions than previously available. Focus herein will be on the exploration of this question via performance of gauge-radar statistical evaluations.

Approach

The basic methodology employed is to compute quantitative rainfall estimates for selected hours from an S-band radar similar in characteristics to the operational WSR-88D, using an independently-implemented QPE algorithm modeled after the present WSR-88D Precipitation Processing System (PPS). The rainfall estimates are determined through a span of discrete spatial resolutions, ranging from approximately that used in the PPS to approximately that now becoming available operationally. These estimates are then compared against co-located, hourly, rain gauge reports and – after quality control (QC) measures are taken – statistical results are determined for the resultant set of "gauge-radar pairs" (G-R pairs) at each discrete radar resolution. Furthermore, this basic approach is undertaken for three distinct configurations of the rain gauges within the radar umbrella: (1) all (quality-controlled) individual gauge reports under the entire radar umbrella; (2) clusters (sub-sets) of more densely-packed gauges covering areas < 20 km^2 (representing multiple, idealized small basins of a theoretical stream network); and (3) gauge-reported mean-areal precipitation (MAP) in the same clusters, over areas < 20 km^2.

In order to conduct this study, good datasets of both high-resolution reflectivity data from an S-band radar (similar to the WSR-88D) and rain gauge reports from dense rain gauge network, gathered simultaneously, had to be available. The most suitable combination of datasets found consisted of the National Center for Atmospheric Research (NCAR)'s S-band, dual polar, Doppler radar (known as "S-Pol") while it was located in the vicinity of Melbourne, Florida during the summer of 1998 (July 20 to Sept. 29), coincidentally with deployment of the National Aeronautics and Space Administration (NASA)'s dense (as closely spaced as 1-km) Tropical Rainfall Measurement Mission Ground Validation (TRMM-GV) rain gauge network.

Studies with related goals were reported by Habib and Krajewski (2002) and by Gebremichael and Krajewski (2004), though their primary focus was on spatial variability of rainfall and its relationship to gauge-radar correlations in general.

While the NCAR S-Pol radar has dual-polar capability, the study here is confined to evaluations of radar-rainfall estimates derived from the traditional, single-polar "Z-R" relationship, for consistency with legacy QPE analyses. The finest spatial resolution of the S-Pol data is 0.15 km x 1.0°, and although not the same as the new NEXRAD "Super Res" data (i.e. 0.25 km x 0.5°), those resolutions are close to one another (e.g. at 57.5 km from the radar, a sample bin in "Super Res" NEXRAD will have an area of .125 km^2 while one in S-Pol has an area of .150 km^2 - just 20% larger). Furthermore, S-Pol sample bins can be successively aggregated (i.e. averaged, by rain rate) in the radial direction, in multiples of 150 m, to simulate discrete resolutions ranging from the future to the present WSR-88D. This is done for each of the following levels of aggregation: 150m; 300m; 450m; 600m; 750m; and 900m.

In each of the three analysis phases described above and at each of the above spatial

resolutions, some or all of the following statistical parameters are determined: Radar Mean Accumulation (after correction for Mean Field Bias (MFB) - i.e. ratio of gauge-mean to radar-mean accumulations among all co-located pairs at all aggregation levels); Ratio of (bias-corrected) radar accumulation to gauge accumulation (for each radar aggregation level); Correlation Coefficient (CC); Mean Absolute Error (MAE); and Root Mean Square Error (RMSE).

Data Processing

Determination of the gauge-radar pair datasets

Both the TRMM-GV rain gauge reports and the precipitation estimates from the S-Pol radar were assembled for one-hour ("clock-hourly") blocks, i.e. beginning/ ending at the 'top' of an hour (and also matching the accumulation periods of the DPA products from the nearby WSR-88D KMLB (Melbourne, FL) radar).. In order for a set of gauge-radar pairs for a given hour to be included in our analysis dataset, either the rain gauge report or the radar estimate determined at one (of the six) spatial resolutions would have to be non-zero. The number of hours for which gauge-radar pairs were found for the principal dataset used in our study was 96.

Rain gauge data and Quality Control

The distribution of gauges within a radius of 171 km from the S-Pol unit is shown in Figure 1. The figure shows only the 125 gauges retained after the QC procedures explained below. Because part of our study dealt with the ability of the radar to represent small-scale spatial variability in rainfall, attention was also focused on several sub-networks shown in Fig. 1

Several steps of quality control (QC) were performed before the rain gauge data could be used. The first step was about consistency of the gauge locations, as reported by two sources: the header lines of each gauge data file and a list file showing latitude/longitude information of all gauges within the network. Differences between the two of up to 0.8km were found; those gauges with differences greater than 100 meters were discarded.

The second step of QC was to identify and remove suspect gauge reports by comparing the rainfall records of nearby gauges with one another, as well as with the estimate from the corresponding 4x4 km grid box of the Digital Precipitation Array (DPA) 1-hour rainfall product from the nearby KMLB radar. We focused our efforts on situations of multiple gauges located in the same DPA grid box. To perform this analysis, time series depictions of hourly rainfall accumulation data from pairs of closely located gauges were compared first against each other, and then against the time series from the corresponding DPA grid box.

For example, Figure 2 shows the time series of hourly rainfall accumulation data of TFB0112 (in green) and TFB0115 (in red). The X-axis is the time index, in hours,

when at least one record from each of the gauges in the DPA grid box was non-zero. Rainfall values (Y-axis) of one gauge were plotted upside-down to better show the differences or similarities between the two gauges. The series from the two gauges are seen to match each other very well until around 09/04/98 14:00Z (time index of about 90). After then, reports from TFB0115 appear to have been shifted about 39 hours earlier.

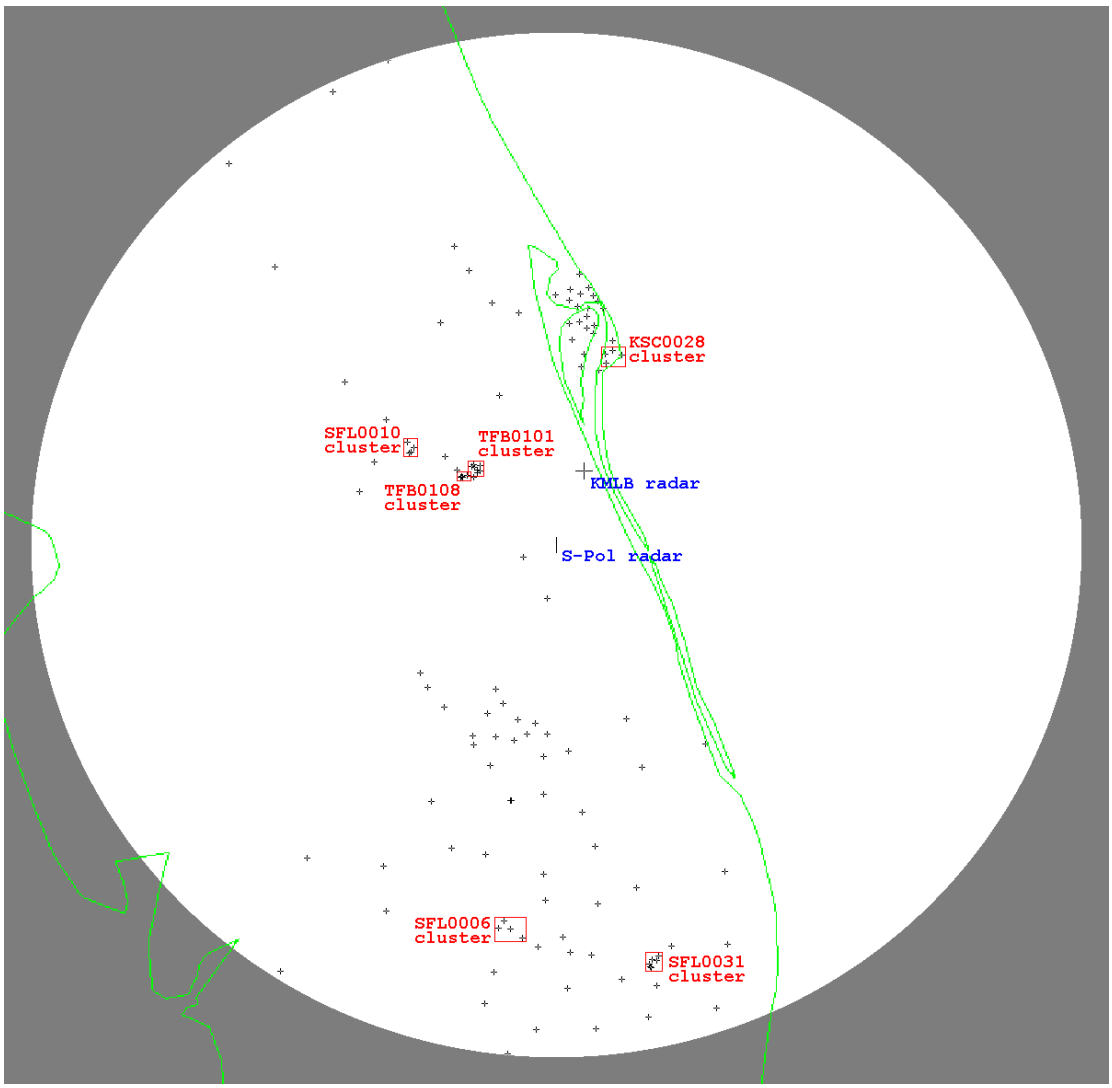

Figure 1. Distribution of gauge sites (small crosses) relative to S-pol radar site (large cross at center). Six sub-networks or 'clusters' of closely-located gauges are shown in red. The white circle indicates a radius of 171 km. WSR-88D Melbourne radar (KMLB) also shown.

Similar time series accumulation depictions were formulated for each of TFB0112 and TFB0115 against the DPA product for the grid box in which they were both located. Gauge TFB0112 matched the DPA product very well throughout, while TFB0115 did so during the early hours, then revealed significant differences in the latter hours. In this instance, the latter part of the record of TFB0115 was removed

from the ensuing analysis.

The third step of QC was to deal with gaps (i.e. prolonged periods of no reported rain) in the gauge data. Since we have no simple means of distinguishing between missing data and true 'no rain' data, we would assume the presence of a gap simply to mean 'no rain' for most situations. However, for gaps at the end of the PRECIP98 (or TEFLUN-B) experimental period, we treat them as missing data and remove them from our study, feeling it is reasonable to assume that gauges might stop operating at the end of the field experiment.

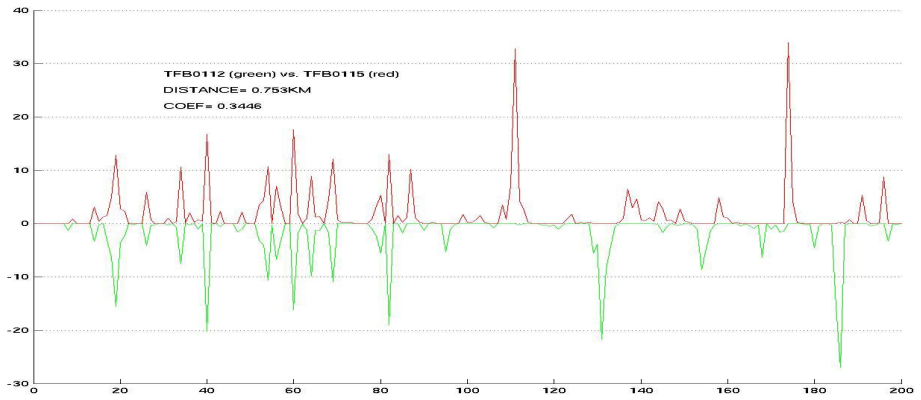

Figure 2. Time series of hourly precipitation rates at rain gauge sites TFB0115 (above horizontal axis; red) and TFB0112 (below the axis; green). Serial hours are indicated. Note close correlation through beginning of analysis period, then lack of correlation after ~hour 90.

A fourth QC operation was performed after the gauge data had been paired with radar data. On one occasion, the S-Pol radar data at one or more resolutions corresponding to a gauge location appeared to be contaminated by ground clutter; in this instance, the gauge was removed (i.e. no gauge-radar pairs were included at any of the trial resolutions).

Radar data - one-hour rainfall estimates from S-Pol

Radar rainfall estimates from the S-Pol data were calculated using an independently-implemented, in-house, QPE algorithm modeled after the WSR-88D Precipitation Processing System (PPS) (Fulton et al. 1998). Time intervals between S-Pol volume scans were approximately 5 minutes, corresponding well with WSR-88D scanning strategies. Therefore, data from ~13 volume scans were typically used to calculate the one-hour radar-rainfall accumulation estimates.

The reflectivity field from the 0.5° elevation scan was used to calculate the rainfall rates by employing the default (i.e. 'Convective') Z-R relationship from NEXRAD (i.e. $Z = a R^b$, where Z = backscattered Reflectivity Power (mm^6/m^3); R = Rainfall Rate (mm/hr); a = 300; and b = 1.4). To get rainfall rates at the aggregated 300m to

900m resolutions, the rates from 2 to 6 contiguous radar bins at 150m resolution were averaged along the radial direction.

Overview of weather during test period and significant events

The weather situation during the course of the experiment (20 July to 29 September 1998) was typical of mid-to-late summer over Florida, with some intense local rainfall and some cases with mesoscale organization of precipitation features. Data from 27 days were utilized. Overall, approximately 37% of the hourly gauge reports indicated measurable rainfall ≥ 0.25 mm rainfall; 11% had ≥ 2.5 mm, and about 0.7% had ≥ 25 mm.

Findings

Phase 1 – all G-R pairs considered

In this phase, correlation and error statistics were calculated based on radar-gauge pairs meeting the criterion that either a gauge or radar value must be non-zero. This was done first for all G-R pairs under the radar umbrella (8211 pairs were found), then for subsets of those pairs falling within three discrete range-bands. Our aim was to test the effect of spatial aggregation of radar data on radar-gauge correlation in general, when rainfall was measured by rain gauges at individual points (this methodology is one that has been used in correction of radar bias and in validation of radar rainfall). A conceptual depiction of this phase of the analysis is shown in Figure 3.

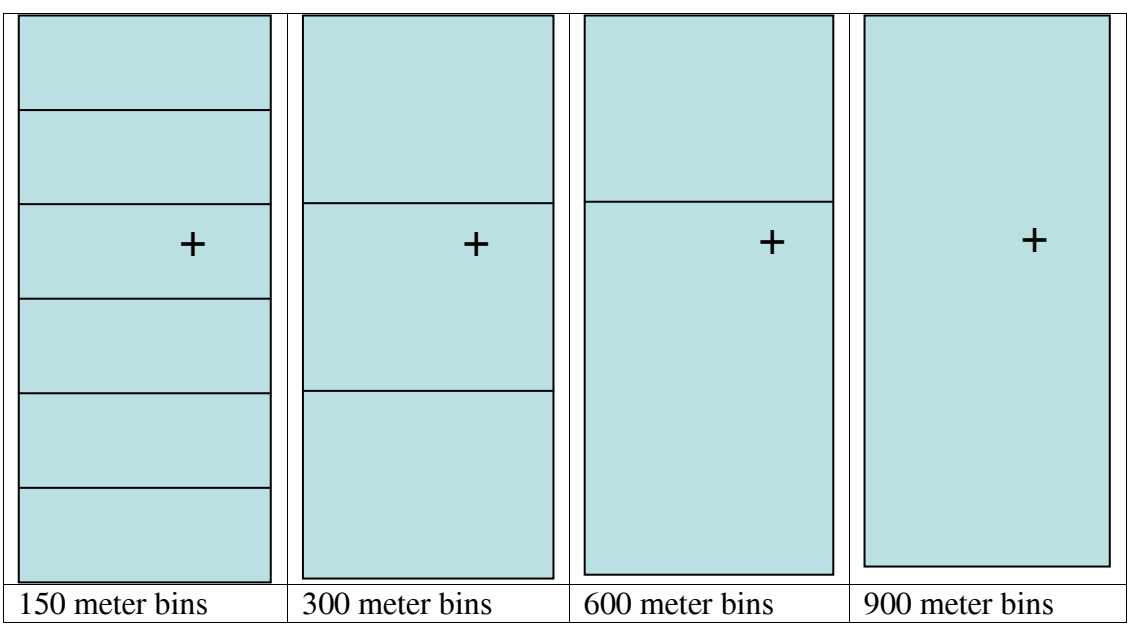

Figure 3. Schematic diagram for radar QPE aggregation in radial direction, PHASE 1 (+ indicates rain gauge location). Note that aggregation volumes are

not necessarily symmetric about the gauge point – the location of the grid volumes is arbitrary, as is the case in operations.

Results for the various G-R statistical measures are shown in Table 1, first for all G-R pairs under the radar umbrella, then for the pairs stratified by distance from the radar (i.e. near: 0-67 km; middle: 67-106km; far: 106-171 km). For each statistic in each set, the "best" result is depicted in **bold** (i.e. highest CC; lowest MAE or RMSE) and the "worst" result in ***bold italics*** (opposite criteria).

Table 1. Gauge-radar correlation coefficients, mean absolute errors, and root-mean-squared errors listed by spatial aggregation distance for radar data. All gauge-radar pairs considered together (1a); then stratified by range from the radar (1b-1d). Gauge or radar value must be non-zero for a G-R pair to qualify. For each statistical measure, the 'best' result among all spatial resolutions (aggregation distances) is shown in **bold** and the 'worst' in ***bold-italics***.

Table 1a - All ranges: # R/G-data-pairs: 82; Gauge mean: 1.92(mm)

Radar:	Mean(mm)	R/G Ratio	CorCoef	MAE(mm)	RMSE(mm)
150m-res	1.89	0.98	0.78	**1.15**	3.23
300m-res	1.91	0.99	***0.77***	1.16	***3.30***
450m-res	1.91	1.00	0.78	1.16	3.23
600m-res	1.94	1.01	0.78	***1.17***	3.27
750m-res	1.93	1.01	0.79	1.17	3.17
900m-res	1.94	1.01	**0.80**	1.17	**3.16**

Table 1b - 0-67 km: # R/G-data-pairs: 32; Gauge mean: 1.64(mm)

150m-res	1.73	1.05	0.74	**1.03**	3.35
300m-res	1.77	1.08	***0.72***	1.06	***3.54***
450m-res	1.76	1.07	0.74	1.04	3.37
600m-res	1.82	1.11	0.73	***1.08***	3.49
750m-res	1.78	1.09	**0.76**	1.05	**3.20**
900m-res	1.80	1.10	0.76	1.06	3.22

Table 1c - 67-106 km: # R/G-data-pairs: 27; Gauge mean: 1.98(mm)

150m-res	1.82	0.92	0.85	1.07	3.12
300m-res	1.83	0.92	**0.85**	**1.07**	**3.11**
450m-res	1.83	0.93	0.85	1.07	3.12
600m-res	1.86	0.94	0.84	1.08	3.12
750m-res	1.86	0.94	***0.84***	1.09	***3.14***
900m-res	1.87	0.95	0.84	***1.09***	3.13

Table 1d - 106-171 km: # R/G-data-pairs: 23; Gauge mean: 2.23(mm)

150m-res	2.18	0.98	***0.78***	1.42	***3.18***
300m-res	2.19	0.98	0.78	1.42	3.17
450m-res	2.21	0.99	0.78	***1.43***	3.16
600m-res	2.20	0.98	0.79	1.41	3.12
750m-res	2.21	0.99	0.78	1.42	3.15
900m-res	2.21	0.99	**0.79**	**1.40**	**3.10**

It is apparent that in each instance, the results across all resolutions are quite similar. For example, with all G-R pairs within the radar umbrella included, the difference between the lowest Correlation Coefficient (i.e. 0.7742) and the highest (i.e. .7951) is only 2.7%. However, within the narrow range in each instance, it is seen that the 'better' statistical results are more often than not found at the coarser resolutions and

the 'lesser' results at the finer resolutions. In the top part of the table, it is seen that the 'best' results for two of the three statistical measures (i.e. CC and RMSE) are found at the coarsest resolution of 900m and the 2nd best results at the 2nd coarsest of 750m; only for MAE are the better results found at the finer resolutions.

When stratified by distance from the radar, the better/lesser results in both the near range band (0-67 km) and the far range band (106-171 km) are also found at the coarser/finer resolutions for all statistical measures (except MAE at the near range). However, in the middle range band (67-106 km), the opposite holds – i.e. the better/lesser results are found at the finer/coarser resolutions.

These results may indicate that there could be an advantage in achieving more accurate rainfall estimates when base radar data are available – and analyzed – at finer resolutions, but only in certain circumstances. Sub-beam effects, for example, could play a significant role. Near to the radar, biota and/or radar side lobes could play a role in contaminating radar estimates and hence, obscuring gauge-radar correlations. At the far ranges, where the radar beam is more elevated, wind advection would have a longer time to act upon falling hydrometeors, causing them to drift to adjacent locations from where they were first sampled aloft; the relative impact of this effect being greater when overlaid on a finer-resolution grid than a coarser one. Perhaps only at the mid ranges would neither of these effects predominate and would an advantage (in accuracy of QPE) be gained in performing the analysis at finer resolution.

Phase 2 – Gauge-radar spatial correlation within small gauge networks

The second phase of the experiment was designed to determine if spatial aggregation of the radar data had an effect on representation of the spatial rainfall pattern, and not necessarily the absolute amount. This question is important because some NWS operational practices are based on the assumption that the radar can properly depict sharp spatial gradients in rainfall and differentiate between rain amounts over adjacent, small basins. Therefore, we examined the spatial correlations between radar and gauge estimates within small sub-networks or clusters of four-to-seven closely-located gauges, occupying only a few tens of km^2. A conceptual depiction of this phase of the analysis is shown in Figure 4.

Six such 'clusters' were identified (refer to Fig. 1). An individual hour's data was included when the difference between the largest and smallest 1-h gauge report was at least 2.5 mm, to insure some appreciable variability in the small-scale rainfall pattern. The gauge and radar estimates for that hour were ranked by order of amount and then correlated We found (not shown) that, for most clusters in individual hours, the radar did show appreciable skill in depicting the rainfall distribution over these very small areas. That is, for 1-h rainfall, in many cases the gauge-radar correlation (across all levels of aggregation) within the gauge network was ≥ 0.7 (indicating ~50% reduction of variance).

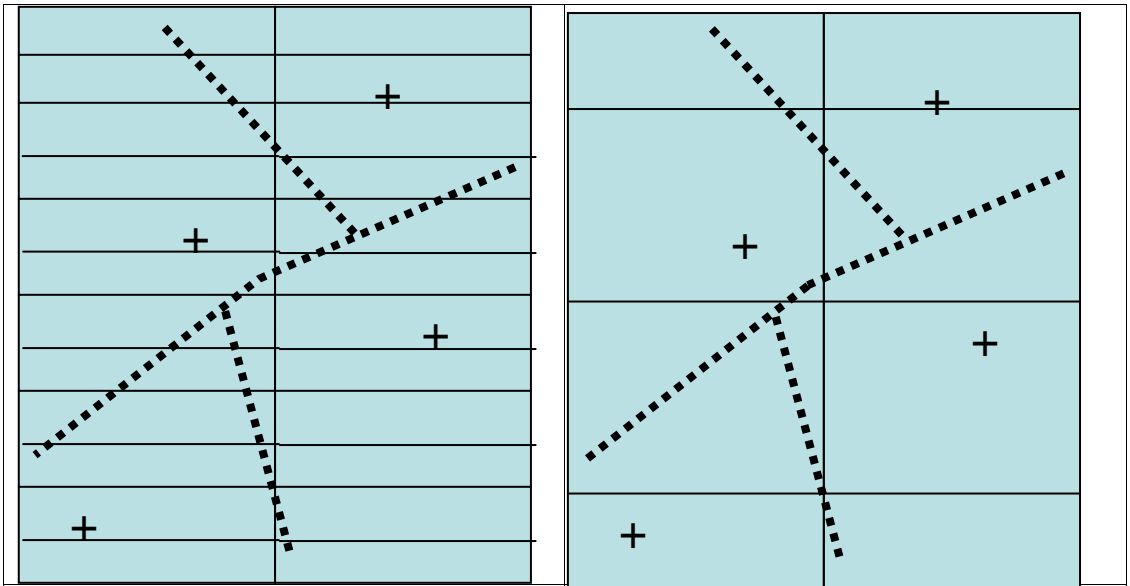

Figure 4. Schematic diagram for radar QPE aggregation - patterns, PHASE 2. (+ indicates rain gauge locations). Dashed lines indicate basin boundaries. Note: radar sample bins correlating with rain gauges change with radar spatial resolution.

Shown in Table 2 are the Mean Correlations as a function of aggregation distance over all qualifying hours, and the Fraction of Hours for which the gauge-radar correlation was ≥ 0.7, with the clusters ordered from highest to lowest in terms of overall correlation (i.e. average of the Mean Correlations). (Note that for each cluster, the Mean Separation Distance among the gauges and the Mean Range of the gauges from the radar are also shown.)

Findings overall were quite similar to those of Phase 1 when all G-R pairs under the radar umbrella were considered – i.e. the higher mean correlations were found at the larger aggregation distances (i.e. 600 to 900 m) while the lower correlations were found at the smaller aggregation distances (i.e. 150 to 450 m). This was pretty much a universal finding among the six 'clusters', indicating again that the spatial aggregation of the radar data had relatively little effect on the correlations to rain gauge reports. (It should be noted that the variations in correlation statistics within clusters as a function of aggregation distance tended to be relatively minor compared to other factors concerning the clusters as a whole, such as the distance of their centroids from the radar or the average separation distance among their constituent gauges.)

Table 2. Mean value of gauge-radar linear correlation coefficients within individual rain gauge clusters (subnetworks), averaged over multiple 1-h events, and number of hours in which the gauge-radar correlation was ≥ 0.7. Highest and lowest values of any given field across the range of spatial aggregation are indicated as in Table 1 (in cases of "ties", all are so indicated). The clusters are shown in order of highest to lowest Mean Correlation (averaged over all aggregation distances).

	Aggregation distance (m)						
Cluster KSC0028 (15 hours)							
Gauges: 3 or 4; Mean separation 2.99 km; Mean range 65.9 km							
	150	300	450	600	750	900	[Avg]
Mean Correlation	0.73	***0.67***	0.71	0.72	0.77	**0.78**	[0.73]
Fraction ≥ 0.7	0.67	***0.60***	0.67	0.73	**0.80**	**0.80**	
Cluster SFL0010 (11 hours)							
Gauges: 4; Mean separation 1.47 km; Mean range 57.6 km							
	150	300	450	600	750	900	[Avg]
Mean Correlation	***0.58***	0.69	0.67	0.63	**0.70**	0.60	[0.64]
Fraction ≥ 0.7	0.73	0.73	***0.64***	**0.82**	**0.82**	***0.64***	
Cluster TFB0101 (14 hours)							
Gauges: 5 to 7; Mean separation 0.99 km; Mean range 36.8 km							
	150	300	450	600	750	900	[Avg]
Mean Correlation	***0.60***	0.62	0.62	**0.66**	0.62	**0.66**	[0.63]
Fraction ≥ 0.7	***0.64***	***0.64***	***0.64***	**0.79**	0.71	0.71	
Cluster SFL0031 (19 hours)							
Gauges: 6; Mean separation 1.04 km; Mean range 143.2 km							
	150	300	450	600	750	900	[Avg]
Mean Correlation	0.49	***0.48***	0.49	0.49	**0.55**	***0.48***	[0.50]
Fraction ≥ 0.7	0.47	***0.42***	0.47	**0.53**	***0.42***	**0.53**	
Cluster SFL0006 (18 hours)							
Gauges: 4; Mean separation 3.53 km; Mean range 129.4 km							
	150	300	450	600	750	900	[Avg]
Mean Correlation	**0.50**	***0.43***	0.47	0.47	**0.50**	0.48	[0.48]
Fraction ≥ 0.7	**0.67**	***0.61***	***0.61***	**0.67**	**0.67**	**0.67**	
Cluster TFB0108 (14 hours)							
Gauges: 4; Mean separation 0.76 km; Mean range 38.1 km							
	150	300	450	600	750	900	[Avg]
Mean Correlation	0.13	0.23	***0.07***	**0.30**	0.18	**0.30**	[0.20]
Fraction ≥ 0.7	***0.14***	***0.14***	***0.14***	**0.50**	0.21	**0.50**	

Phase 3 – G-R correlation for small-area hourly mean precipitation

In the final phase of the experiment, gauge and radar values for individual gauge points were each separately aggregated within network clusters. These values approximate gauge and radar mean-areal precipitation (MAP) such as might be

observed over small stream basins. Spatial aggregation might have some effect on radar MAPs because with greater aggregation, precipitation immediately outside the area would be included. A conceptual depiction of this phase of the analysis is shown in Figure 5.

Once more, the degree of radar spatial aggregation generally was found to have little, effect on the gauge-radar MAP correlation or error, though again, an overall tendency was seen toward higher/lower correlations at the coarser/finer resolutions (i.e. for all but one of the clusters, the highest gauge-radar correlations were realized at aggregation ranges of 600 - 900 m).

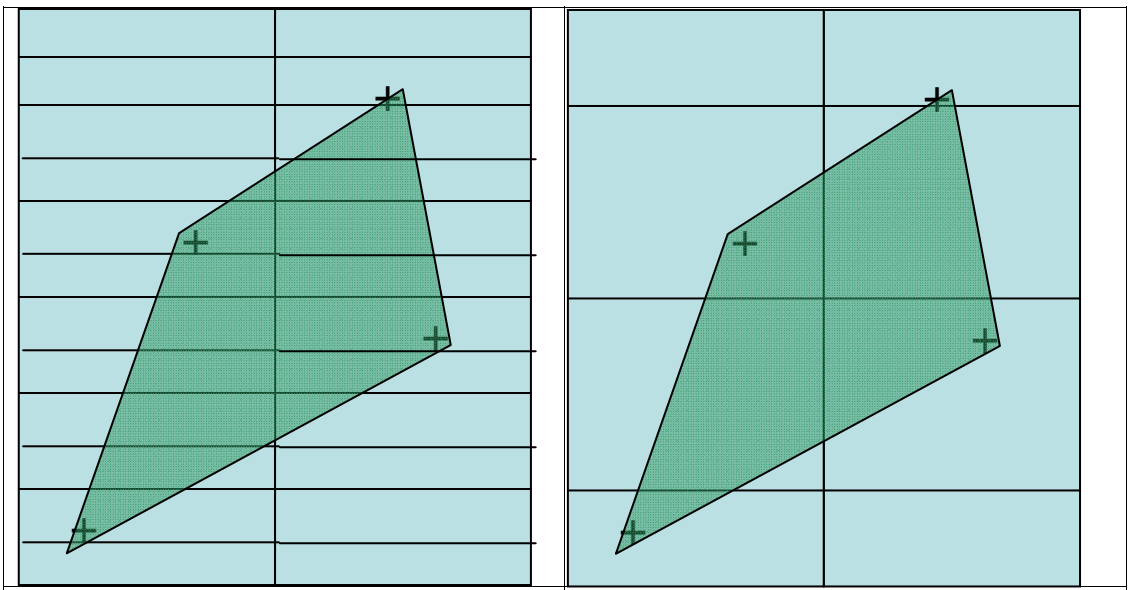

150 meter bins Approximation to Mean Areal Precip is from 4 radar data points.	900 meter bins Approximation to Mean Areal Precip is from 4 different, larger radar data points.

Figure 5. Schematic diagram for radar QPE aggregation – Mean Areal Precipitation (MAP), PHASE 3. (+ indicates rain gauge locations). Shaded area represents a basin over which gauges are averaged for MAP.

Summary, Conclusions, and Future Work

Overall, in the three phases of analysis of gauge-radar statistical correlation that we performed, we generally found no appreciable difference among gauge/radar correlation statistics computed at the various radar spatial resolutions, which ranged from 150 to 900 m. Indeed, we found slightly better results at the coarser, rather than the finer, resolutions overall. However, in one circumstance – i.e. with all G-R pairs included in the middle range of our analysis (i.e. 67-106 km from the radar), we did find the best statistical correlations at the finest resolution. This suggests that, perhaps, the availability of base radar data at finer resolution could result in more

accurate measures of one-hour QPE, but only in certain circumstances, as iterated above (i.e. 'Findings – Phase 1' section).

One potential avenue for future study would be to attempt to factor in sub-beam wind effects on falling hydrometeors by performing statistical correlations of individual rain gauges not just with rainfall estimates from the immediately-corresponding sample bin (in which that gauge is contained), but rather, with surrounding sample bins in all directions and within a prescribed distance. If an offset distance and direction (i.e. vector) could be identified that would yield superior results, that vector could then be analyzed against ambient wind conditions (as recorded by ground or upper-air measuring devices or estimated by model). Ultimately, it may prove possible to incorporate ambient wind conditions in a predictive capacity in relating rainfall estimates determined at high spatial resolution, aloft, to distribution of rainfall at the surface.

Another potential future pursuit would be to perform a similar analysis to the above, but with rainfall estimates derived via a dual polar methodology such as that which is to be implemented within WSR-88D operational radars in future years (Ryzhkov et al, 2005b).

Acknowledgements

We are indebted to Scott Ellis and the NCAR staff for assistance with obtaining and interpreting the S-pol radar data. As noted above, rain gauge reports were obtained from the TRMM SVO office.

References

Fulton, R. A., J. P. Breidenbach, D. J. Seo, D. A. Miller, and T. O'Bannon, 1998: The WSR-88D rainfall algorithm. *Weather and Forecasting*, **13**, 377-395.

Gebremichael, M., and W.F. Krajewski, 2004: Assessment of the statistical characterization of small-scale rainfall variability from radar: analysis of TRMM ground validation datasets. *J. Appl. Meteor.*, **43**, 1180–1199.

Habib, E., and W.F. Krajewski, 2002: Uncertainty analysis of the TRMM ground-validation radar-rainfall products: application to the TEFLUN-B field campaign. *J. Appl. Meteor.*, **41**, 558–572.

Ryzhkov, A., Giangrande, S., and Schuur, T., 2005b: Rainfall estimation with a polarimetric prototype of WSR-88D. *J of Appl. Meteor.*, **44**, 502-515.

Hydrologic Modeling for Assessing Climate Change Impacts on the Water Resources of the Rio Conchos Basin

Eusebio Ingol-Blanco[1] and Daene C. McKinney[2]

[1]Center for Research in Water Resources, University of Texas at Austin, Austin, TX 78712; PH (512) 471-0031; FAX (512) 471-0072; email: ingrecurhid@mail.utexas.edu
[2] Center for Research in Water Resources, University of Texas at Austin, Austin, TX 78712; PH (512) 471-5644; FAX (512) 471-0072; email: daene@aol.com

Abstract

This paper presents a hydrologic modeling application to assess climate change impacts on the water resources of the Rio Conchos basin, especially for agriculture and domestic water uses. The study basin is located in the Mexican State of Chihuahua, with a drainage area around 67,862 km2. It is one of the most important Mexican tributaries of the binational Rio Grande basin and contributes major water deliveries (about 55%) to US through the 1944 treaty between Mexico and the US. However, during period of drought, for instance in the 1990s, there has been conflict and competition for the water resources in the basin, and as a consequence Mexico accumulated an important water debt to the US. In addition, the hydrological behavior of the basin has recurrent periods of water stress, problems with long drought periods, allocation and release, and water pollution. Under this reality, it is important to evaluate and predict the available water resources in the next 50 or 100 years taking account of possible climate change impacts in the basin as well as assessing the policies to be implemented in order to face drought periods and preserve the agreements treaty between Mexico and the US. For this purpose, the Water Evaluation and Planning (WEAP) model is used. The model was calibrated and validated comparing the simulated flows resulting from the input of climatic time series with naturalized flows. Monthly climate time series from 1980-1999 (20 years) were used and some soil parameters were adjusted for calibration. Also, comparisons between simulated and naturalized flows were performed for different stations. In addition to this, calibration considering all water management infrastructures, such as, reservoirs, operation rules, canals, and diversions, was also carried out. The results show good correlation between simulated and observed flows which indicates that the model reproduces the hydrologic behavior of the basin, including, natural and historical flows, storage in reservoirs, water supplies, and water demands for agriculture and urban activities.

Key words: Hydrological modeling, Water Management, Climate Change

1. Introduction

Changes in temperature and precipitation patterns as a consequence of increasing greenhouse gas concentrations may affect the hydrology process, water resources availability, and water uses for agriculture, population, and mining industry, aquatic life in rivers and lakes, and hydropower. Climate changes will accelerate the global hydrological cycle, with increase in the surface temperature, changes in precipitation patterns, and evapotranspiration rate. The spatial change in amount, intensity and frequency of the precipitation will affect the magnitude and frequency of stream flows; consequently, it will increase the intensity of floods and droughts, with substantial impacts on the water resources at local and regional levels. In addition to this, global climate simulations indicate that precipitation will decrease in lower and mid latitudes and increase in high latitudes (IPCC, 2008). Results indicate that precipitation will decrease in part of North American (Mexico), central America and South America, Caribbean regions, sub tropical western coasts, and over the Mediterranean. Evaporation, soils moisture content, and groundwater recharge will also affected. Consequently, drought conditions are projected in summer for sub tropics, low and mid latitudes. These facts arouse the interest of many researchers to analyze basin-wide (local scale) effects. In addition, to evaluate and quantify these impacts at local scale, several tasks must be carried out. One of them is hydrological modeling of the basin. This paper focuses on the hydrological modeling in the Rio Conchos basin (67,862 km2), a main Mexican tributary of the Bi-national Rio Grande (Figure 1) . It contributes water deliveries to the USA according to a 1944 water sharing treaty. Several hydrological studies have been carried out in the different places of the world such as in the Nile basin (Yates and Kenneth, 1998), Sacrament Valley in California (Joyce, Sebastian Vicuna, Larry Dale, 2006); however, there are few studies related to this issue in the study area. The main goal of this research is to perform the hydrological modeling to assess climate change impacts on the basin, using the Soil Moisture Method incorporated into the Water Evaluation and Planning Model (WEAP) (SEI, 2007).

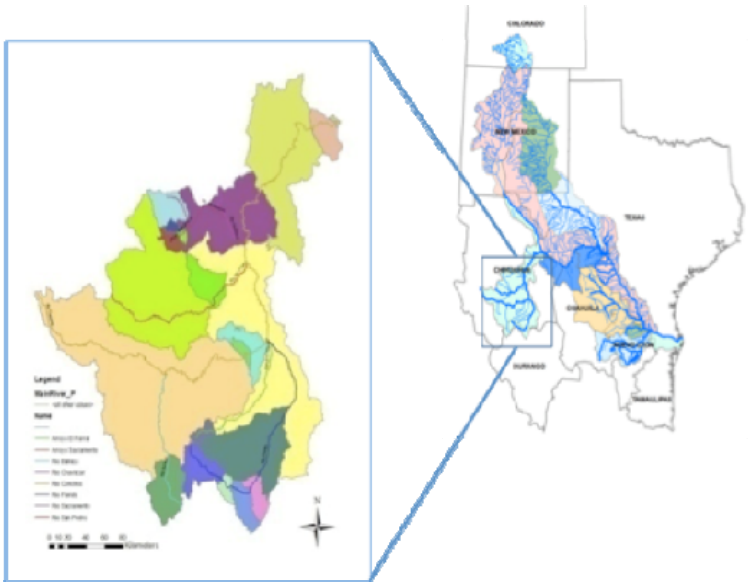

Figure 1. Location of the Rio Conchos basin

2. Climate and Land Use Data

Precipitation - Daily precipitation from 1980 to 1999 was used to calibrate and validate a WEAP model of the Rio Conchos basin as well as to analyze its temporal behavior. These data were collected for control stations in each sub-catchment, and monthly cumulative values were calculated. Monthly maximum values observed range of 200 to 310 mm and, the annual average is 425 mm/year with seasonal variation indicating that the rainy period is from June to September. On the other hand, spatial variation shows that the rainfall varies with altitude, with higher values in the Llanitos subbasin, 740 mm/year on the average lower values in the Luis Leon and Peguis subbasins located in the lower basin, with annual average of 325 mm.

Temperature - Surface temperature in the basin was obtained from the North American Regional Reanalyis (NARR) (NOAA, 2008) for the period 1980 -1999. First, these data were processed using GIS in order to estimate the monthly averages in each sub-catchment. Maximum temperatures occur from June to August and minimum from November to February. Spatial variation indicates that, high values occur in the lower basin (desert region), with values around 32 ^{o}C for Ojinaga and Peguis, and 21 ^{o}C for Llanitos and Puente. Lower values vary from 7–11 ^{o}C and 12-16 ^{o}C. On the other hand, temperature and precipitation showed a negative correlation during the period of analysis, which means that the temperature tends to rise and rainfall to decrease.

Relative Humidity - Data for 1980 to 1999 was obtained from the NARR. In addition to this, GIS tools were used to compute the monthly average of each sub-catchment. Spatial variation indicates that lowest values in Fco Leon, Pegui, and Ojinaga catchments located in the lower basin, and the highest values are in the upper basin. The average for the whole basin is around 42 % and the temporal variation indicates that maximum values are recorded from July to September.

Wind Velocity - In the Rio Conchos, the dominant winds come from Southwest to Northeast. Two components of velocity were obtained from the NARR for different sub catchments of the basin and processed in order to get the wind velocity. There is a seasonal variation with high values in November to April, with an average of 12 km/h for the whole basin. In the upper basin the wind speed is greater than the lower basin, with 18 km/h and 6 km/h, respectively.

Land Use Data - Twenty sub-basins were identified by soil groups and land use categories (Amato and McKinney, 2006) and were applied for using the Soil Moisture Method in the WEAP model.

3. Methodology

Model calibration was carried out using historical observed data inputs (precipitation, temperature, relative humidity, and wind velocity) to obtain stream flow outputs. Naturalized flows (TCEQ, 2001) for a period of 10 years (1980 - 1989) were used to compare to model outputs. The calibrated model was then validated for a period of ten years more from 1990 to 1999.

Soil Moisture Method - Land use data are used in this method considering the movement of water through the soil composed for two simple layers: (1) water retained near the surface and available for plants, and (2) a deep layer that can transmit water as base flow or groundwater storage.

Root zone water capacity - Initially 900 mm of root zone water capacity were considered for irrigated areas, small pastures grasses, and cultivated grassland, and 2500 mm for forest. Adjustments of this parameter were carried out taking account the depth of soils in the basin (Pro Fauna, 2003) with variation due to type and formation of soils located in each zone.

Root zone conductivity - This parameter controls the transmission of flow to the lower layer as well as interflow. Interflow depends of the preferred flow direction; in this case, ranging from 0.05 to 0.20 and zero in other subbasins.

Root zone water capacity - Estimated values of the root zone capacity vary from 5 to 30 % in some sub basins with lower values in the sub catchments Luis L. Leon, Peguis, and Ojinaga located in the lower basin where less relative storage of water in the first layer exist (desert area).

Lower zone water capacity - Lower zone water capacity values are higher in some subbasin where deep aquifers exist. Large values of this parameter can result in high base flow.

Lower zone conductivity - Deep conductivity, together with lower zone water capacity, controls the transmission of base flow in each subbasin. Rough calculations of the base flow were made using the straight line method.

Initial deep storage - Storage to the lower soil layer were also calibrated, which also has a large effect on base flow.

4. Results

In this part, results simulated in WEAP model are compared with the naturalized flows observed in each control station. For this research, stream flow data from 6 streamflow – gaging stations located along to the basin were used to compare the results of the model; the location can be seen in figure….). In general, the results indicate that the model built in WEAP can be able to reproduce the hydrological dynamic of basin as is shown in the calibration and validation processes. Table 1 and 2 show the soil parameter values calibrated for the period from 1980 to 1989 whose stream flow results were validated with the period 1990 to 1999 (10 years), noting that in the validation process, some adjustments have been carried out basically in the second layer. Small depths proposed for this layer reproduced high base flows at the end of the simulation period.

4.1 Calibration

Monthly stream flows simulated and observed for the calibration period (1980 - 1989) can be seen in figures 2a-b for stations Ojinagaand la Boquilla, respectively. It is

observed that in most months, the simulated flows look very close to the observed, with a volumetric error 2 - 19 % for the simulation period, for Ojinaga (lower basin) and La Boquilla (middle basin), respectively. Maximum errors produced in the upper basin are due to the important differences between simulated and observed base flows. For instance, for the La Boquilla station, simulated base flows are generally lower than the simulated values from January to May. Probably, the uncertainties in naturalized flow calculations and a more accurate representation of the groundwater system in the middle and upper basin would improve the estimations. Despite this, the model reproduces the hydrological response of the basin, with simulated stream flows representing between 85 to 95 % of naturalized flows.

The trend of the model to reproduce the observed values is also seen in Figures 3a-d. Relationships between monthly simulated and observed streamflows indicate a high correlation ranging from 91% to 95% for La Boquilla and Ojinaga, respectively. The spatial variation indicates that the model is more accurate in reproducing the streamflows in the lower basin. Special conditions such as the topography in the middle and upper basin (high slope), size of sub division catchments (for instance La Boquilla), and other factors mentioned above could be influencing in this behavior. Similarly, calibrated annual flows show slight differences with the annual naturalized flows, with an error in volume around 10 % on average. The biggest error is in the Jimenez station located in the upper basin.

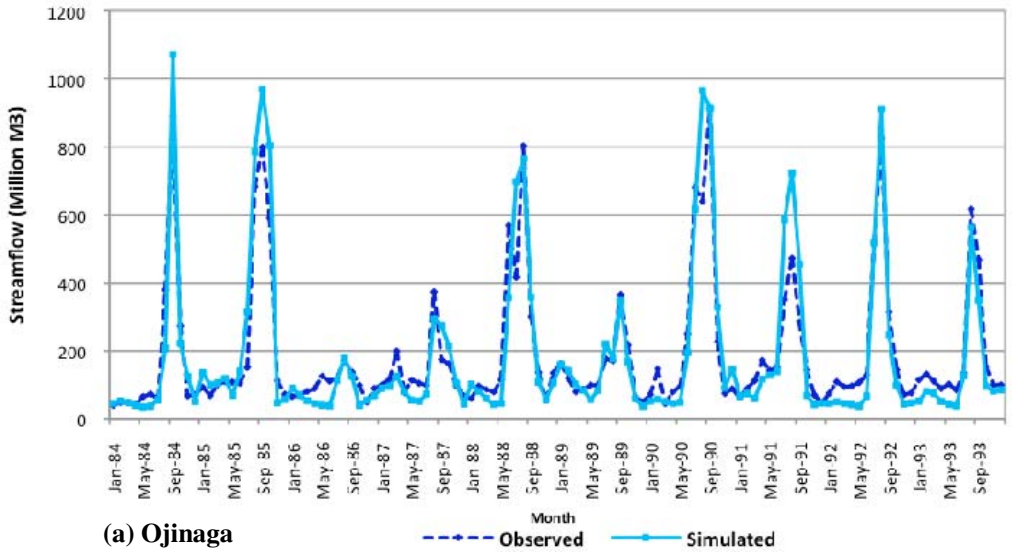

(a) Ojinaga

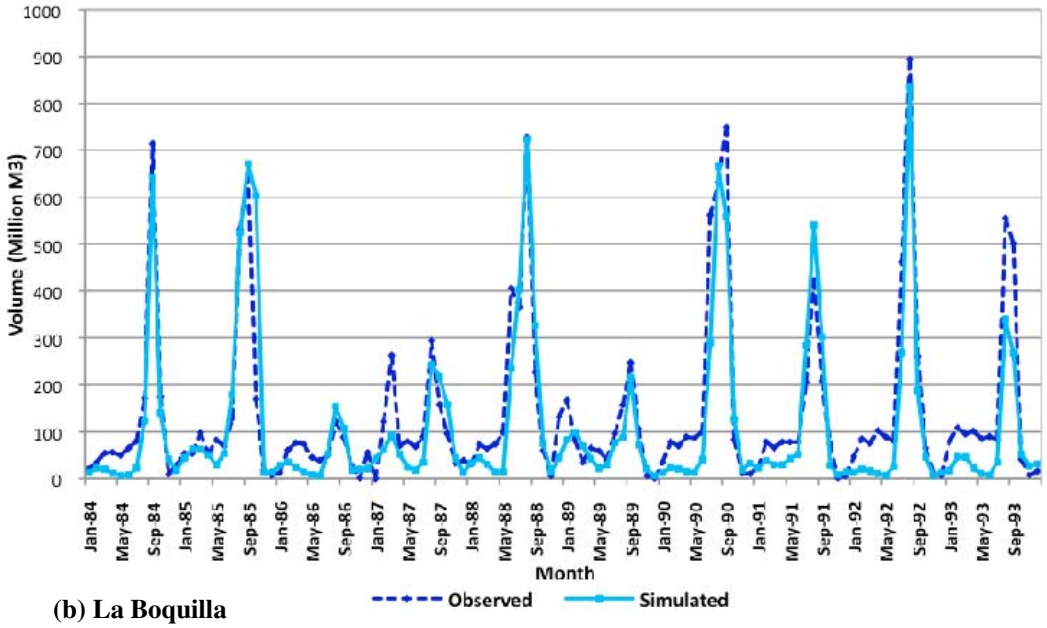

(b) La Boquilla

Figure 2. Monthly variation of observed and simulated streamflows in control stations in the Conchos river basin. (a) Ojinaga and (d) La Boquilla.

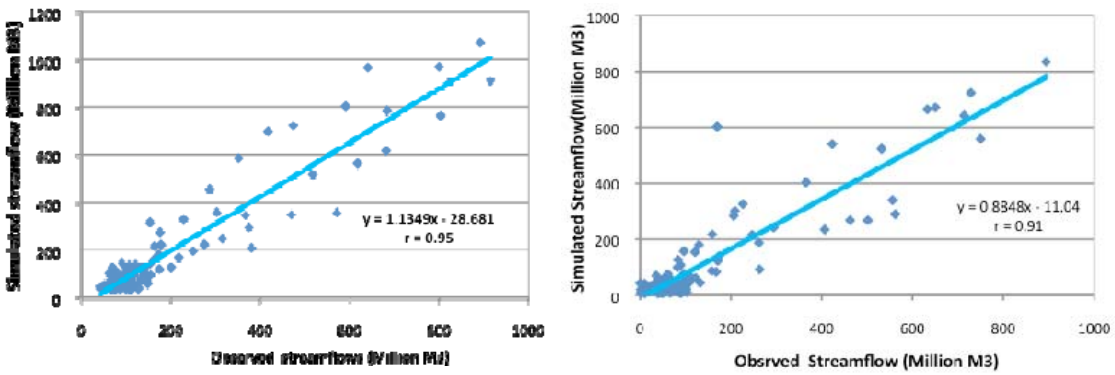

(a) Ojinaga **(b) La Boquilla**

Figure 3. Relationship between monthly observed and simulated streamflows in control stations: (a) Ojinaga and (d) La Boquilla.

4.2 Validation

In order to evaluate the calibration of the hydrological model, it was run for a time period out of the calibration period; from 1990 to 1999 (10 years). The results of the model validation are present in Figures 4a-b. For all the stations, the simulated monthly results are quite good compared to the naturalized flows. On the other hand, the relationship between these flows indicates a high correlation for the Ojinaga, Granero, and Granero, with rates higher than 0.94 (Figures 5a-b). Additionally, the model shows a good performance in reproduce the flows in the control stations La Boquiilla, Villalba, and Jimenez. For all cases, the model calculates efficiently the peak and base flows.

Likewise, from the seasonal analysis, the model tends to be more accurate for the summer and fall flows.

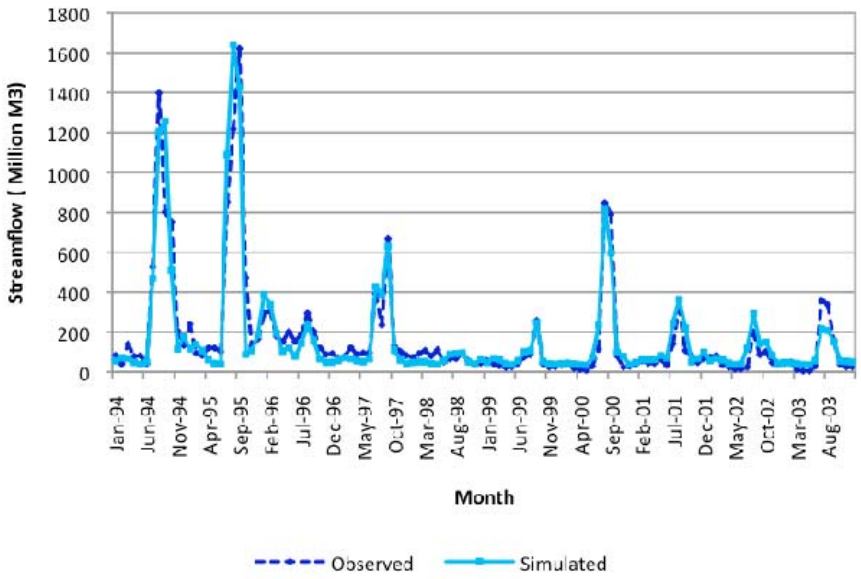

(a) Ojinaga

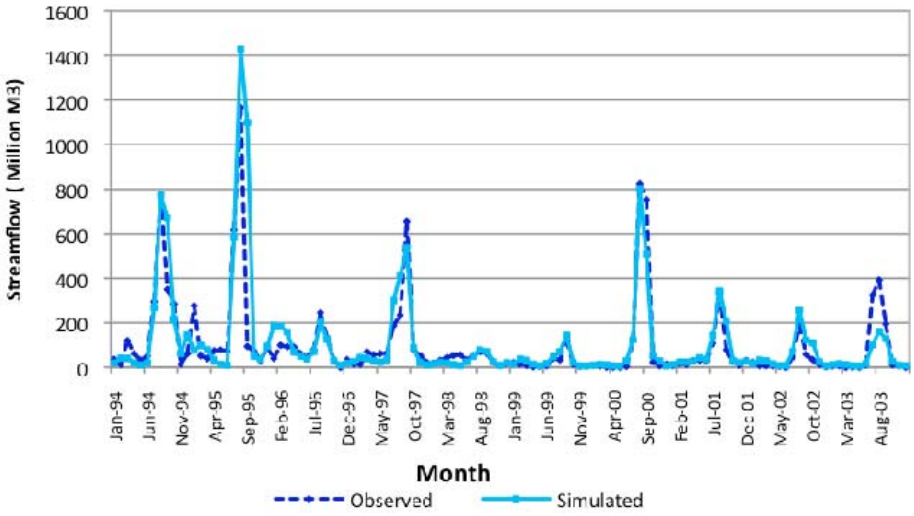

(b) La Boquilla

Figure 4. Monthly variation of observed and simulated stream flows for the validation period (a) Ojinaga and (b) La Boquilla.

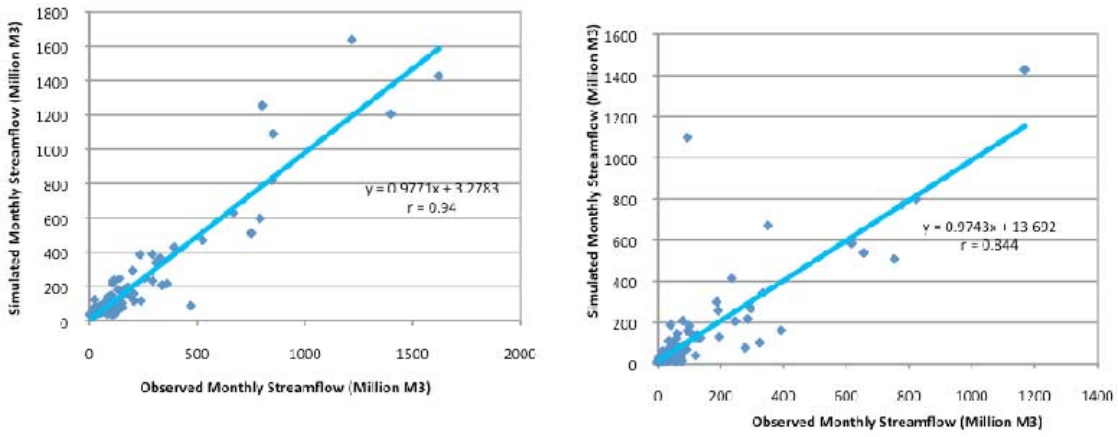

(a) Ojinaga **(b) La Boquilla**

Figure 5. Relationship between monthly observed and simulated streamflows for the validation period in the control stations: (a) Ojinaga and (b) La Boquilla.

4.3 Statistic Analysis

Table 1 shows a summary of the comparison statistics between simulated and naturalized values. The root mean square error (RMSE) and the mean absolute error were used to measure the deviation between the model outputs with the naturalized flows. Likewise, the error in volume measures the deviation between the naturalized and simulated flows, expressed in percentage. The biggest differences between the naturalized flows and the simulated flows are at the La Boquilla, Jimenez, and Las Burras stations, with errors in volume from 6.3%, -6.4%, and 9.0 %, respectively. Negative error indicates the model overestimate the stream flows in that control station. The overall correlation coefficient varies from 0.87 to 0.94, indicating a strong correlation between simulated and naturalized flows. The correlation is bigger in the stations in the lower basin such as Las Burras, El Granero, and Ojinaga. Uncertainties in the naturalized flows, averaged climatology data used for each sub-catchment as well as the complex hydrological characteristics of the upper basin influence this behavior.

Table 1. Summary of Statistical Results for Monthly Comparison in Simulated and Naturalized Flows.

Statistic	Rio San Pedro at Villalba	Rio Conchos at Presa La Boquilla	Rio Florido at Cd. Jimenez	Rio Conchos at Las Burras	Rio Conchos at El Granero	Rio Conchos at Ojinaga
Number months	240	240	240	240	240	240
Mean observed flow (m3/s)	12.0	44.7	5.6	75.1	73.4	68.1
Mean simulated flow (m3/s)	11.5	41.9	6.0	68.4	73.1	67.9
Root Mean Square Error (m3/s)	10.1	29.4	4.7	30.7	32.4	28.1
Mean Absolute Error (m3/s)	2.5	11.1	2.1	10.8	9.4	7.7
Error volume (%)	3.7	6.3	-6.4	9.0	0.4	0.2
Coeficient of determination(r^2)	0.80	0.75	0.78	0.89	0.89	0.89
Coeficient of correlation(r)	0.89	0.87	0.88	0.94	0.94	0.95

References:

Amato, C. C., D. C. McKinney, E. Ingol-Blanco, and R. L. Teasley, M.S. December 2006. Center for Research in Water Resources. Bureau of Engineering Research, the University of Texas at Austin.

Brandes, R.J. 2003.. Water Availability Modeling for the Rio Grande Basin, Naturalized Stremflow Data. Texas Commission on Environmental Quality. Final Report

Intergovernmental Panel on Climate Change (IPCC), 2008: Climate Change and Water. IPCC technical paper VI. http://www.ipcc.ch/ipccreports/tp-climate-change-water.htm

Intergovernmental Panel on Climate Change (IPCC), 2001: The Scientific Basis. "Regional Climate Information – Evaluation and Projections" http://www.ipcc.ch/ipccreports/tar/wg1/index.htm

Joyce, B., S. Vicuna, L. Dale, D. Purkey, and D. Yates. 2006. Climate Change Impacts on Water for Agriculture in California: A case Study in the Sacrament Valley. California Energy Commission and the California Environmental Protection Agency (EPA).

Kim, T.W., and J. Valdes, 2005. Synthetic Generation of Hydrology time Series Based on Nonparmetric Random Generation. Journal of Hydrology Engineering. ASCE, 10(5), 395-404.

Kim, T.W., J. Valdés, and J. Aparicio, 2002. Frequency and Spatial Characteristics of Droughts in the Conchos River Basin, Mexico. International Water Resources Association. 27(3), 420-430.

North American Regional Reanalysis. NARR. http://www.emc.ncep.noaa.gov/mmb/rreanl/

Pro Fauna, Physical and Hydrological Condition Indicators of the Rio Conchos, Chihuahua. Mexico, 2003

Stockholm Environment Institute's Boston Center, 2007. Water Evaluation and Planning System, WEAP.

Yates, D., Purkey, D., Sieber, J., Huber-Lee, A., West, J., and Galbraith, H. 2006. A Physically-based, Water Resources Planning Model of the Sacrament Basin, California. ASCE J. of Water Resources Management.

Yates, D., and Strzepek, K. 1998. Modeling the Nile Basin under Climate Change. Journal of Hydrology Engineering. ASCE, 20(3), 98-108.

Hydrological Feasibility of Environmental Flows in the Rio Grande/Bravo Basin

Samuel Sandoval-Solis[1] and Daene C. McKinney[2]

[1]Center for Research in Water Resources, University of Texas at Austin, Austin, TX 78712; PH (512) 471-0071; FAX (512) 471-0072;
email: samuel.sandoval@mail.utexas.edu
[2]Center for Research in Water Resources, University of Texas at Austin, Austin, TX 78712; PH (512) 471-5644; FAX (512) 471-0072; email: daene@aol.com

Abstract

Due to high water demand, the scarcity of water resources, and the complexity of water allocation in the Rio Grande/Bravo basin, environmental flows have not been considered as an integral part of the water management in this basin. Important environmental habitats such as the Big Bend National Park in the US, the Northern Chihuahuan desert, the Maderas del Carmen and the Cañon de Santa Elena natural reserves in Mexico are ecologically threatened because of the lack of environmental water management policies in the basin. Several efforts have been undertaken by government agencies and non-governmental organizations in order to determine the environmental flows requirements for the basin. Even though environmental flows in several locations along the basin have been determined (e.g., the Rio Conchos tributary), the quantification and availability of the water necessary to provide these environmental flows has not been determined. In this paper we evaluate the hydrological feasibility of environmental flows in the Rio Conchos tributary to the Rio Grande. This evaluation is done in a basin model constructed in the Water Evaluation and Planning system (WEAP) software. An analysis of the available water has been defined to determine the amount of water required to provide the environmental flows. The description and evaluation of the environmental flows are presented along with a comparison against the current water management policies.

Introduction

The Rio Grande/Bravo basin is a transboundary basin between Mexico and the United States (U.S.). Historically, this basin has been manipulated in an exclusive human water resource management mode (Enriquez-Coyro, 1976), not considering the environmental needs of the native ecosystems. The Convention of 1906 signed between Mexico and the U.S. (IBWC 1906) and the Rio Grande Compact (TCEQ 1939) ratified in 1939 between the States of Colorado, New Mexico and Texas prove the fact that the water in this basin was thought to be used exclusively for human benefit. The water allocation in these agreements obeys exclusively the human concerns, leaving out the natural water requirements of the basin. As a result of the previous agreements, the quantity of water in the Rio Grande/Bravo reach between El Paso to Presidio Texas were reduced so dramatically, that this reach is now referred

as the "forgotten river" where almost no water flows. Another example is the signature of the treaty of 1944 between Mexico and the U.S. (IBWC 1944). In this treaty, the environmental issues are not considered and the priority assigned to the environment is not even specified, leaving it in disadvantage with respect to the other water uses. In addition, because of the water scarcity in the basin and the high competition among water users for the resource, the environmental requirements has been denied or not even considered for a long time.

In 2002, a consortium of eight institutions integrated by universities, non-governmental organizations (NGO's) and governmental research agencies from both countries was formed to assess the hydro-physical opportunities to improve the water management in the Rio Grande/Bravo basin. By conducting extensive interviews with water users, planning agencies, research institutes, NGO's and local, state and national government institutions the consortium defined a set of 33 scenarios that have some possibility to improve the water management in the basin (NHI 2001 and 2006, PAP 2006).

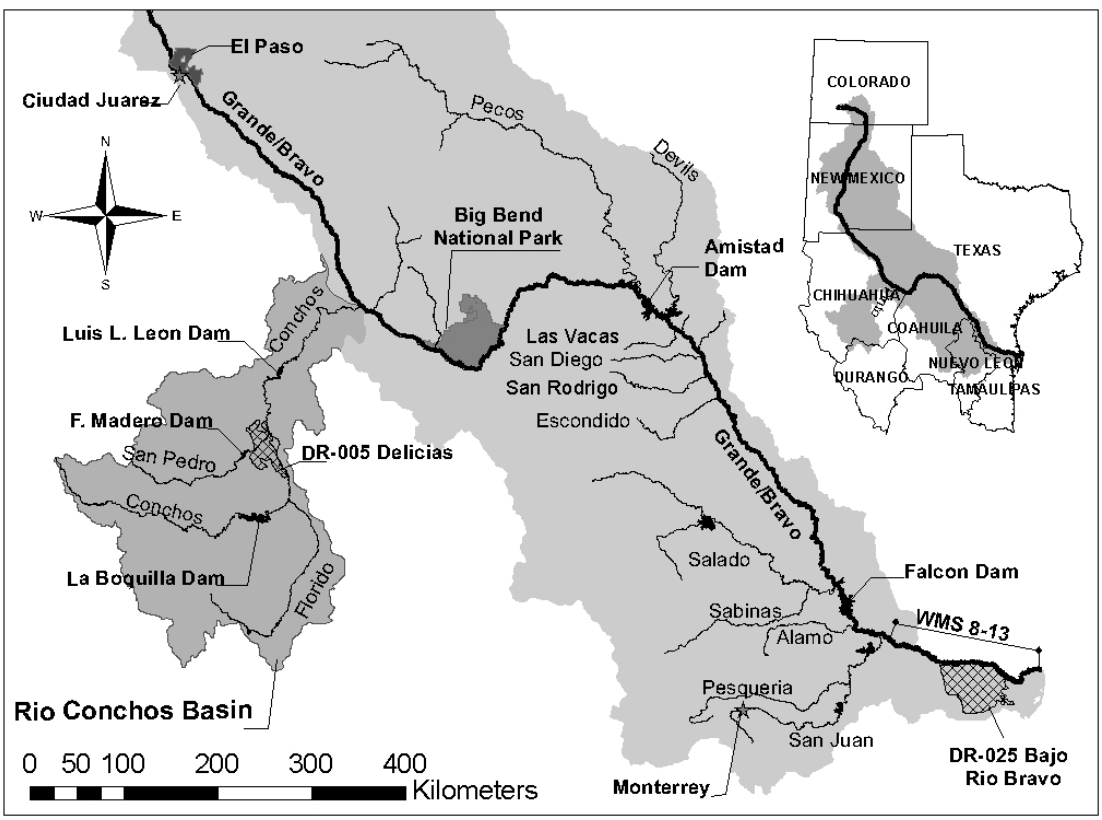

Figure 1. Rio Grande/Bravo Basin.

The aim of this paper is to present the results of one scenario that evaluates the hydrological feasibility of environmental flows in the Rio Conchos, a tributary of the Rio Grande/Bravo. This evaluation is done in a basin model constructed in the Water Evaluation and Planning system (WEAP) software. The description and

evaluation of the environmental flows are presented along with a comparison against the current water management policies.

Environmental flows in the Río Conchos Basin

The Rio Conchos basin is a sub-basin of the Rio Grande/Bravo Basin, it has an area of 25,872 square miles (67,008 Km^2) (Patiño-Gomez and McKinney 2005) and is the main tributary to the Rio Grande/Bravo. Downstream the *forgotten river* reach, where almost no water flows in the Rio Grande/Bravo, Rio Conchos' waters revitalizes Rio Grande/Bravo at their confluence in Ojinaga/Presidio. Environmental flows downstream this point, such as the ones for the Big Bend National park, Maderas del Carmen and Cañon de Santa Elena natural reserves, depends on the water coming from the Rio Conchos.

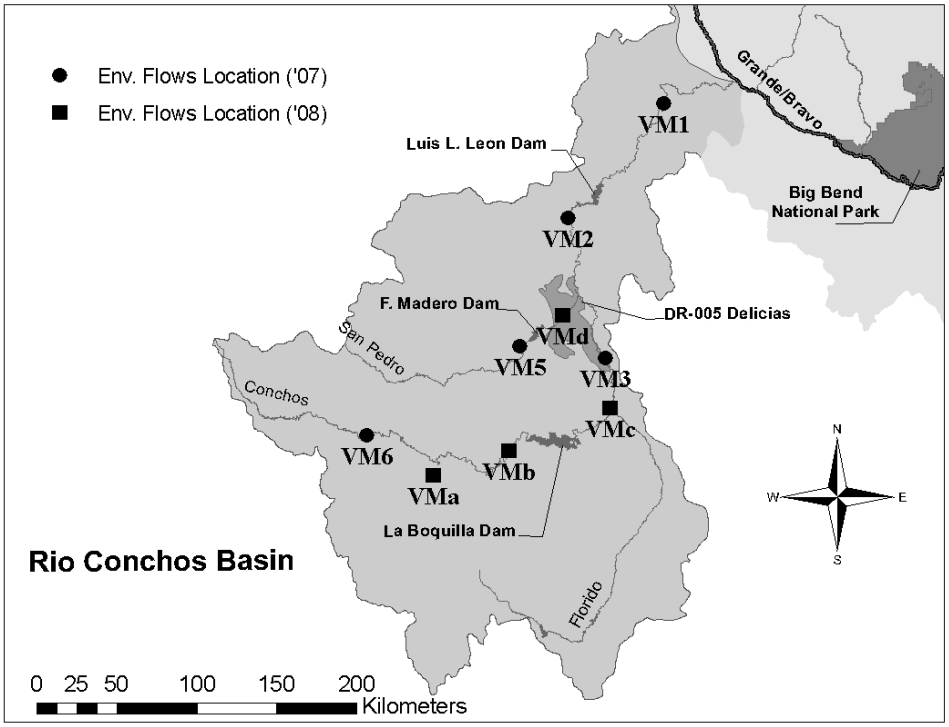

Figure 2. Environmental Flows Locations in the Rio Conchos Basin.

As part of an environmental flow assessment for the Rio Conchos, the World Wildlife Fund estimated the environmental flows in 9 locations along the Rio Conchos basin through the use of the Building Block Method (WWF 2006). The geomorphology, flora and fauna (fish and invertebrates) were considered to determine the maintenance and drought flows necessary to meet the environmental requirements. Figure 2 shows the location where the environmental flows were determined. Table 1 shows the name, stream and annual volume required for each location where environmental flows were defined. A monthly variation for each condition, maintenance or drought, was determined for each location.

Table 1. Location of Environmental flow control points

Site	Name	River	Environmental Flow Maintenance ($1X10^6$ m^3/year)	Drought ($1X10^6$ m^3/year)
VM1	Cuchillo Parado	Conchos	381.5	47.7
VM2	El Potrero	Conchos	323.6	36.2
VM3	Estación Conchos	Conchos	27.1	14.2
VM5	San Pedro de Conchos	San Pedro	114.2	34.1
VM6	Agua Caliente	Conchos	134.5	24.4
VMc	Camargo	Conchos	50.6	23.6
VMd	C. Ortíz	San Pedro	60.8	45.3

One of the goals in this research is to determine if there is enough water in the basin to satisfy the environmental requirements at the locations selected and how much it affects other users in the basin. Ideally, we are looking for an alternative policy that meet the environmental needs without harming other water users, in other words, an alternative policy that is hydrologically feasible. In reality, it is necessary to evaluate several alternative water management policies and chose the one that brings the best tradeoffs between the delivery of water to the environment and the damages to other water users. Once the alternative policy is determined, more detailed operation policies must be developed to assess the facilities operation to meet the environmental flows in time, volume and space. The last assignment is out of the present research.

For this paper, 5 control points were selected to evaluate the environmental flow compliance at these locations: VM1 Cuchillo Parado, VM2 El Potrero, VM3 Estacion Conchos, VMc Camargo and VMd C. Ortiz. These control points were selected because they are spatially located downstream control structures, such as dams, that made available the intentional delivery of environmental flows to these locations. The control points VMa and VMb do not have any control structure that made possible the intentional delivery of environmental flows.

Methodology

The following methodology is proposed to evaluate the hydrological feasibility of environmental flows in the Rio Conchos basin.

1. An evaluation of the environmental flows proposed with the actual water management policies is done to identify the conflict points where the environmental requirements are more threatened.
2. An alternative operation policy is proposed.
3. The alternative operation policy is evaluated to determine if it improves the environmental requirements and how much this policy affects or benefits other water users in the basin.

The Rio Grande/Bravo WEAP model was used to evaluate the actual and proposed water management policies in the Rio Conchos basin. The model has an hydrologic period of analysis of 60 years, form October 1940- to September 2000, it has been calibrated, validated (Danner et al. 2006) and it has been used to evaluate other alternative water managements policies (Sandoval-Solis et al. 2008).

Status Quo of the Environmental flows in the Rio Conchos Basin

A Baseline scenario that follows the actual policies of water management in the basin was constructed in the Rio Grande/Bravo WEAP model. The alternative water management policies will be compared with the Baseline scenario to evaluate the improvements in the system. Three performance criteria are used to evaluate the environmental flow compliance at each location: Reliability, Resilience and Vulnerability (Loucks and van Beek 2006). Reliability refers to the frequency in time an event is successful in relation to the total period of time analyzed (Hashimoto et al. 1982 and Klemes et al. 1981). We define a successful event as the event when there is no deficit in the delivery of environmental flows to the location in concern. Resilience is the probability that once the system is in a deficit, the next period the system recover to a successful event (Hashimoto et al. 1982). Vulnerability is the expected value of the deficits, in other words, it is the average deficit of environmental flows experienced (Hashimoto et al. 1982). For this paper, we are going to use the dimensionless vulnerability by dividing the average annual deficit by the environmental annual requirement (McMahon et al. 2006). These three performance criteria we are used to analyze the environmental flows.

Table 2. Reliability Resilience and Vulnerability for the Baseline Scenario

Location	Reliability (%)	Resilience (%)	Vulnerability (%)
VM1	60	58	3
VM2	42	37	9
VM3	2	0	69
VMc	2	0	70
VMd	2	0	74

Table 2 shows the reliability, resilience and vulnerability for the 5 control points selected with the actual water management conditions. For VM1, 60 percent of the time the environmental flows were met properly (Reliability); the average annual deficit to meet the environmental requirements is 3% (Vulnerability), and the probability of coming back from a deficit is 58% (Resilience). For VM2, 42% of the time the environmental needs were delivered properly (Reliability), the average annual deficit is 9% of the environmental flow requirements and the probability of coming back from a deficit is 37%. Notice that these two control points, which are located in the lower part of the Conchos basin, have the best results among the 5

control points evaluated. For the control points VM3, VMc and VMd, located in the middle of the Conchos basin, only 2% of the time the environmental flows were met among the 60 year period of analysis, the average deficit to meet the environmental requirements was 69, 70 and 74% respectively, and when the system fall into a deficit, it never come back again, 0% of Resilience. From these results is possible to affirm that the environmental flow are better accomplished in the lower Rio Conchos basin than in the middle and upper region.

Environmental Flow Scenario

The previous results showed that the conflict zones are located in the middle Conchos basin, at the control points VM3, VMc and VMd. As an initial approach, we propose an alternative water management policy that delivers water to the control points VMc and VMd. These control points are the most upstream control points to be analyzed and they are located just downstream La Boquilla and F. Madero reservoirs. Two reasons were considered for this decision. First, these are locations where water can be delivered properly from the dams in time and quantity, making the alternative policy operationally feasible. Second, we would like to evaluate if meeting the environmental requirements in the most upstream sites, it will provoke the rest of the control points downstream also meet their environmental requirements.

An analysis of La Boquilla–Francisco I. Madero reservoir system was done, in order to decide what kind of environmental flows, maintenance or drought, is allocated each year to the environment. First, at the beginning of each hydrological 0) in the reservoir system is estimated as the sum of the available storage in La FM). The available storage for each reservoir is calculated by subtracting the storage $+Losses$).

FM
$+Losses$
$+Losses$

Second, the *diversion* required to satisfy all the users from this reservoirs system is estimated. The *diversion* is calculated dividing the surface water right (SW) from these reservoirs by the conveyance efficiency ($Conv.Eff.$) from the reservoir to the delivery point.

$Conv.Eff.$

Finally, the *available storage* is compared with the *diversion*. Based on this comparison a decision is made:

1. If the *available storage* is larger than the *diversion*, the maintenance flow is assigned,

$$Maintenance$$

2. If the *available storage* is less than the *diversion*, the drought flow is assigned.

$$Droug\square t$$

The philosophy of this decision is that if the water users are expecting a shortage in their water supply, it is reasonable to ask only for the minimum volume of water for the environment, that in this case is the drought volume. If there is enough water in the reservoir system to supply properly all the water users, it is reasonable to ask for the normal flow for the environment than in this case is maintenance flow.

Evaluation of the Environmental Flow Scenario

Table 3 shows a comparison of the reliability, resilience and vulnerability between the Baseline and the Env. Flow scenario for the 5 control points selected. As can be seen, all the performance criteria were improved significantly. The reliability for all the points except of VMd is almost 100%. This means that almost all the time the environmental flows were delivered at these locations. Similarly, the resilience follows in all the control points, except VMd, has a value of 100%. This means that when a deficit happens in the environmental requirements, the next period the system recovers delivering the adequate water quantity to the environment. In addition, the vulnerability also decreased significantly almost to 0%. This means that when a deficit in the environmental requirements happens, the quantity of the deficit is small, 0% in almost all locations and 4.6% at VMd downstream F. Madero.

Table 3. Comparison of the Reliability Resilience and Vulnerability between the Baseline and the Environmental Flow Scenario

	Reliability		Resilience		Vulnerability	
	Baseline	Env. Flows	Baseline	Env. Flows	Baseline	Env. Flows
Location	(%)	(%)	(%)	(%)	(%)	(%)
VM1	60	100	58	100	3	0
VM2	42	100	37	100	9	0
VM3	2	97	0	100	69	0.3
VMc	2	97	0	100	70	0.2
VMd	2	78	0	46	74	4.6

Even thought there is a significant improvement in the delivery of environmental flows in all the locations, the three points located in the middle Rio Conchos basin will not meet all the times the environmental requirements. For VM3 and VMc, the failures may be ignored since it has a reliability of 97% and an average deficit (Vulnerability) close to 0% (0.3% and 0.2% respectively). In contrast, the failures for VMd cannot be ignored, since 22% of the time the environmental flows will not be meet by an average of 5%. These results show that during drought periods,

there is not enough water in the La Boquilla – F. Madero reservoir system to satisfy the environmental minimum request that is the drought flow volume.

Now, let's evaluate how the implementation of the Environmental Flow scenario may affect or benefit other water users along the basin. For this purpose, the three biggest water user consumers were selected, two irrigation districts from Mexico, DR-005 Delicias and DR-025 Bajo Rio Bravo; and one irrigation district from the U.S., WMS-8-13 Agriculture "A". Table 4 shows the performance criteria results for these water users.

As can be seen, irrigation district DR-005 Delicias will be affected by the alternative policy proposed since the period of time this user was supplied properly (Reliability) will be reduced from 72% to 65%. Besides, its average deficit (Vulnerability) increases from 36% to 48 %. These results were expected since DR-005 Delicias relies on La Boquilla and F. Madero dams as its main source of water. In contrast, the performance of irrigation district DR-025 Bajo Rio Bravo improved since its reliability increases from 93 to 95%. However, the Environmental scenario also increased the vulnerability for DR-025 Bajo Rio Bravo.

Table 4. Performance criteria for main water users

	Reliability		Resilience		Vulnerability	
	Baseline	Env. Flows	Baseline	Env. Flows	Baseline	Env. Flows
WaterUser	(%)	(%)	(%)	(%)	(%)	(%)
DR-005	**72**	**65**	29	29	**36**	**48**
DR-025	**93**	**95**	25	25	**25**	**29**
WMS 8-13	85	85	22	22	15	15
Treaty Obligations	83	83	50	50	**38**	**33**

Considering the distribution of water between Mexico and the U.S., the Treaty of 1944 (IBWC 1944) specifies the water distributions and allocation among both countries. In summary, for the Rio Grande/Bravo, Mexico has the obligation to deliver a volume of $431.721X10^6$ m^3 to the U.S. on average, per year in cycles of 5 consecutive years; this means a total of $2158.605\ X10^6$ m^3 per cycle. This volume must be achieved by 1/3 of the waters reaching the main channel of the Rio Grande/Bravo from 6 Mexican tributaries (Rio Conchos, San Diego, San Rodrigo, Escondido, Salado and Arroyo Las Vacas). Results for the treaty obligations presented in Table 4 showed that the number of deficits will not be reduced (Reliability doesn't change), and the system will recover as fast as it does with the actual policy (Resilience does not change), however, there is an improvement in the reduction of the expected deficit amount (Vulnerability), from 38% estimated with the actual policy to 33% estimated with the policies proposed in the Environmental Scenario. These results show that as a consequence of the policies proposed in the Environmental Scenario, the delivery of treaty obligation from Mexico to the U.S. will be improved.

Conclusions

Results presented in this paper show the alarming situation of the environment in the Rio Grande/Bravo basin, specifically at the Conchos basin. The actual water management does not meet the environmental requirements by far. Results obtained in the Environmental Flow scenario showed a significant increase in meeting the environmental requirements in the Rio Conchos basin. Besides, the policies proposed also benefit the treaty obligations and water users located in the lower Rio Grande/Bravo basin, such as irrigation district 025 Bajo Rio Bravo. In contrast, the application of the Environmental Flow scenario will affect irrigation district 005 Delicias. These conclusions are discussed in detail as follows:

1. The actual environmental conditions in the basin are unsustainable. Results for the 5 control points evaluated with the actual water management show the lack of compliance of the environmental flows in the Rio Conchos basin. The area more affected is the middle Rio Conchos basin, where the environmental requirements are almost never met. In the lower Rio Conchos basin, the situation is better than in the middle basin but is still worrying. The analysis of the actual conditions let us determine the where the conflicts areas are in order to propose actions to solve the situation in these locations.
2. Results from the policies proposed in the Environmental Scenarios showed a significant improvement in the environmental situation for the entire basin. Meeting the environmental flows in the most upstream control points, VMc and VMd, increases significantly the environmental flows in all the control points evaluated. The improvements can be listed as follows:
   a) Increase in the period of time the environmental needs are met (Reliability);
   b) Increase in the resilience of the environmental flows; the system was able to recover faster when it fails; and
   c) Decrease in the environmental flows deficit (Vulnerability). When the system was not able to deliver the environmental requirements, the failure was smaller than in the actual conditions.
3. Even though the environmental requirements can be improved significantly, it will not be satisfied completely by the alternative policies proposed. The results showed that not all the times the environmental requirements will be met because during drought periods, there is not enough water in the reservoirs systems to supply the water users and the environmental needs.
4. The policies proposed in the environmental scenario will affect irrigation district 005 Delicias with a decrease in the time this irrigation district is supplied properly and an increase in the amount of the deficits. On the contrary, the Environmental scenario will benefit the Treaty obligations by reducing the volume of the deficits and irrigation district 025 Bajo Rio Bravo by increasing the period of time this water user is supplied properly.

Recommendations

The policies proposed in the Environmental scenario are recommended because they will improve the environmental situation of the Rio Conchos basin. However, further research is need to find out a policy that mitigates the ravages provoked to DR-005 Delicias, one of this policies may be the delivery of the water savings established in Minute 309 in an environmental pattern.

Besides, it is also necessary to determine the environmental flow requirements in other parts of the Rio Grande/Bravo basin, such as the Big Bend area. The determination of these flow requirements in other regions will make possible the evaluation of the environmental faith with the actual water management policies and will also make possible the proposition of alternative water management policies that can improve the environment situation of the basin.

Acknowledgments

Special acknowledgement is given to Rebecca L. Teasley, Carlos Patiño Gomez, Ivonne Muñoz Gonzalez and the National Council of Science and Technology of Mexico, CONACYT. Partial funding for this research has been provided by the World Wildlife Fund of Chihuahua.

References

Danner, C. L., McKinney, D. C., and Teasley, R. L. (2006). "Documentation and Testing of the WEAP Model for the Rio Grande/Bravo Basin." CRWR Online Report 06-08.

Enriquez-Coyro, E., (1976) "El Tratado entre México y los Estados Unidos de América sobre Ríos Internacionales." Facultad de Ciencias Políticas y Sociales. Universidad Nacional Autónoma de México.

Hashimoto, T., Stedinger, J.R., and D.P. Loucks (1982). *Reliability, resiliency and vulnerability criteria for water resource system performance evaluation.* Water Resources Research 18 (1), 14-20.

International Boundary and Water Commission (IBWC) (1906). "Convention between the United States and Mexico. Equitable distribution of the Waters of the Rio Grande" http://www.ibwc.state.gov/Files/1906Conv.pdf

International Boundary and Water Commission (IBWC) (1944). "Treaty between the Unites States of America and Mexico." www.ibwc.state.gov/Files/1944Treaty.pdf

Loucks D. P. and E. van Beek (2005). *Water Resources Systems Planning and Management*. UNESCO

Natural Heritage Institute (2001). "A Physical Assessment of the Opportunities for Improved Management of the Water Resources of the Bi-National River Basin" (December 28, 2006)

McMahon, T. A., Adoloye, A.J. and S. Zhou (2006). *Understanding performance measures of reservoirs* Jounal of Hydrology 324 (2006) 359-382.

Natural Heritage Institute (2006). "Water Management Scenarios for the Rio Grande/Bravo basin from the Rio Conchos to the Gulf." San Francisco CA. (October 3rd, 2006)

Patiño-Gomez, C., and D. McKinney (2005). "GIS for Large-Scale Watershed Observational Data Model." CRWR Online Report 05-07, Center for Research in Water Resources, University of Texas at Austin.

Pegasys Consulting (2007). The Rio Conchos Basin – Basin Allocation Assessment. January 2007.

Physical Assessment Project (PAP 2006), A Physical Assessment of the Opportunities for Improved Management of the Water Resources of the Bi-National Rio Grande/Rio Bravo Basin: Recent Project Accomplishments, 2006, www.riogrande-riobravo.org/Documents/Project%20Accomplishments.pdf

Sandoval-Solis, S., McKinnaey, D.C. and H. Sanvicente-Sanchez. *Evaluation of Water Management Scenarios for the Rio Grande/Bravo*. Proceedings World Environmental and Water Resources Congress 2008. Honolulu Hawaii.

Texas Commission on Environmental Quality (TCEQ) (1939). Rio Grande Compact. Water Code, Title 3, Chapter 41. http://tlo2.tlc.state.tx.us/statutes/docs/WA/content/pdf/wa.003.00.000041.00.pdf

World Wildlife Fund (2006). "Conclussions from the Building Block Method specialist work session Rio Conchos" February 27th to March 1st, 2006.

Impacts of the Upstream Storage Reservoirs on Itaipu Hydropower Plant Operation

by
Mario T. L. Barros[1], Renato C. Zambon[2], João Eduardo G. Lopes[3], Paulo S. F. Barbosa[4], Alberto L. Francato[5] and William W-G. Yeh[6]

Abstract

This paper presents some results related to the operation of the Itaipu hydropower plant. Itaipu is one of the largest hydropower plants in the world. It is a binational undertaking run by Brazil and Paraguay at the Paraná River on the border section between the two countries. Each country owns 50% of the installed capacity (14,000 MW). This study evaluates the impacts of the upstream storage reservoirs on the hydropower production of Itaipu. The analysis involves a system of 55 hydropower plants. Itaipu hydropower plant operates as a run-of-river reservoir and itself does not have storage capacity. However, there are many upstream storage reservoirs located in Brazil. The analysis is conducted using the HIDROTERM decision support system (DSS), which is basically an optimization model. HIDROTERM is designed for the management and operation of large hydrothermal systems. In its formulation the hydro plants are considered individually and the thermal plants are aggregated into subsystems. The optimization model is capable of handling different types of constraints, such as water transfers, multiple purposes and environmental requirements. Its objective function is to produce energy at a minimum cost. HIDROTERM integrates a database with basic information (hydrological and technical) to run the model and an interface to manage input and output data. The optimization model is written using the General Algebraic Modeling System (GAMS) package and so it can run with different nonlinear programming (NLP) routines. The results from the analysis show that the upstream reservoirs located in Brazil have significant impacts on the hydropower production of Itaipu.

[1] Professor, University of São Paulo, Brazil; e-mail: mtbarros@usp.br; ASCE Member
[2] Professor, University of São Paulo; e-mail: rczambon@usp.br
[3] Consulting Engineer; e-mail: jelopes@dglnet.com.br
[4] Professor, University of Campinas; e-mail: franco@fec.unicamp.br
[5] Professor, University of Campinas; e-mail: francato@fec.unicamp.br
[6] Distinguished Professor, UCLA; e-mail: williamy@seas.ucla.edu; ASCE Honorary Member

Introduction

This paper presents some results related to the operation of the Itaipu hydropower plant. The Itaipu dam was built from 1971 to 1982 and the first generating unit started running in 1984. Two or three units were installed per year until 1991 and the last two units in 2006 and 2007, completing the today installed capacity of 14,000 MW, with 20 generating units of 700 MW each. The total length of the dam is 7,235 m. The reservoir area is 1,350 Km², with a storage capacity of 29,000 hm³ and an average head of 120 m. It is a binational undertaking run by Brazil and Paraguay at the Paraná River on the border section between the two countries. Each country owns 50% of the installed capacity, but Brazil uses most part of it, buying the surplus produced by Paraguay. While Brazil consumes its entire half, Paraguay only consumes five percent of its share and sells the rest back to Brazil. In 2008, Itaipu produced 94,684 GWh which supplied 90% of the energy consumed by Paraguay and 19% of the energy consumed by Brazil. Note that, in terms of annual energy production, Itaipu ranks number one in the world, but it is second only to the Three Gorges plant in terms of installed capacity.

Itaipu hydropower plant operates as a run-of-river reservoir and itself does not have storage capacity. However, there are many upstream storage reservoirs located in Brazil. The Paraná river basin has a system of 55 hydropower plants, the most important basin in the Brazilian electrical system.

The Brazilian electrical system is one of the largest in the world due to its hydro and thermal plants. The system is completely linked and called SIN (*Sistema Interligado Nacional*). Recent data from ANEEL (2009) indicates that during the period from 2005 to 2008, on average, 91% of the electricity was produced by the hydro system and 9% by the complementary thermal system, which includes natural gas, nuclear, biomass and other sources. Brazil has, including hydro, thermal and other systems, 2,019 power plants with 110,979 MW of installed capacity, Itaipu contributing 13% of it.

This study evaluates the impacts of the upstream storage reservoirs on the hydropower production of Itaipu.

The analysis is conducted using the HIDROTERM decision support system (DSS) developed by Barros et al (2008), which is basically an optimization model. HIDROTERM is designed for the management and operation of large hydrothermal systems. In its formulation the hydro plants are considered individually and the thermal plants are aggregated into subsystems. The optimization model is capable of handling different types of constraints, such as water transfers, multiple purposes and environmental requirements. Its objective function is to produce energy at a minimum cost. HIDROTERM integrates a database with basic information (hydrological and technical) to run the model and an interface to manage input and output data. The

optimization model is written using the General Algebraic Modeling System (GAMS, 2008) package and so it can run with different nonlinear programming (NLP) routines.

Optimization models have been developed for reservoir management and operation. Yeh (1985), Simonovic (1992), Wurbs (1993), Momoh et al (1999a,b), and Labadie (2004) have reviewed and evaluated various optimization methods and their corresponding models. In Brazil the ACQUANET model developed by Porto et al. (2005) and the SISOPT model developed by Barros et al (2003, 2005) are being used to optimize large-scale and complex reservoir systems.

Yeh et al. (1992) developed a real-time optimization model for hydrothermal system operation in China. The model considered the seasonal variations of inflow to the reservoirs, the variation of transmission losses with hydro and thermal plant loadings, and thermal unit commitment and dispatch.

HIDROTERM Model Methodology

The HIDROTERM model consists of a hydro module/model (HIDRO) and a thermal module/model (TERM). These two modules are connected. The optimization process can proceed in different combinations: with the HIDRO module alone, the TERM module alone, the HIDRO and TERM connected by an iterative process, and the automatically coupled HIDRO and TERM. In this paper only the HIDRO module was used.

The HIDRO module employs an operation policy that considers individualized hydropower plants producing electrical energy with maximum efficiency: reservoirs empty or fill, keeping the maximum value of the energy production factor and following the demand curve variation in time so that the thermal complement is minimum. In mathematical terms the problem lends itself to nonlinear programming (NLP) with the following objective function and subject to a set of constraints:

$$\min ZH = \sum_{t=1}^{nt} dt_t \cdot \left[D_t - \sum_{i=1}^{ni} P_{i,t} \right]^2 \qquad (1)$$

where:
i = hydropower plant/reservoir index
ni = number of hydropower plants/reservoirs
nt = number of time periods
t = time period index
dt_t = time period duration (10^6 s)
D_t = objective demand, usually the total demand minus the fixed generation, though it can be defined arbitrarily by the user (for example, as the maximum installed power capacity MW)
ZH= HIDRO model objective (10^6 s.MW²)

The HIDRO model is subject to the following set of constraints:

Total release is the summation of the turbine release and non-power release or spill:

$$R_{i,t} = R'_{i,t} + R''_{i,t} \tag{2}$$

Continuity equation:

$$S_{i,t} = S_{i,t-1} + dt_t \left[\sum_{m_i=1}^{nm_i} R_{m_i,t} + I_{i,t} - R_{i,t} - UC_{i,t} - DT_{i,t} \right] - E_{i,t} \tag{3}$$

Evaporation:

$$E_{i,t} = \frac{A_{i,t} + A_{i,t-1}}{2} \cdot IE_{i,t} \tag{4}$$

Storage limits, with time-varying flood control:

$$S_i^{\min} \le S_{i,t} \le S_{i,t}^{\max} \tag{5}$$

Power generation capacity:

$$P_{i,t} \le P_i^{\max} \cdot ID_{i,t} \tag{6}$$

Ending storage:

$$S_{i,t=nt} \ge S_{i,final} \tag{7}$$

Total, turbine and non power release limits:

$$R_{i,t} \ge R^{\min}{}_i \tag{8}$$

$$R'^{\min}_i . ID_{i,t} \le R'_{i,t} \le R'^{\max}_{i,t} . ID_{i,t} \tag{9}$$

$$R''_{i,t} \ge 0 \tag{10}$$

Water head:

$$Hg_{i,t} = \frac{H_{i,t} + H_{i,t-1}}{2} - HT_{i,t} \tag{11}$$

Power generation:

$$P_{i,t} = \eta_i \cdot Hg_{i,t} \cdot R'_{i,t} \tag{12}$$

Forebay water level:

$$H_{i,t} = a_{0i} + a_{1i} \cdot S_{i,t} + a_{2i} \cdot S_{i,t}^2 + a_{3i} \cdot S_{i,t}^3 + a_{4i} \cdot S_{i,t}^4 \tag{13}$$

Tailrace water level:

$$HT_{i,t} = b_{0i} + b_{1i} \cdot R_{i,t} + b_{2i} \cdot R_{i,t}^2 + b_{3i} \cdot R_{i,t}^3 + b_{4i} \cdot R_{i,t}^4 \tag{14}$$

Reservoir area:

$$A_{i,t} = c_{0i} + c_{1i} \cdot H_{i,t} + c_{2i} \cdot H_{i,t}^2 + c_{3i} \cdot H_{i,t}^3 + c_{4i} \cdot H_{i,t}^4 \tag{15}$$

Turbine flow maximum limit:

$$R_{i,t}^{\acute{}\max} = d_{0i} + d_{1i} \cdot Hg_{i,t} + d_{2i} \cdot Hg_{i,t}^2 + d_{3i} \cdot Hg_{i,t}^3 + d_{4i} \cdot Hg_{i,t}^4 \tag{16}$$

where:

j_k = hydropower plant/reservoir index in subsystem k
k = subsystem index
m_i = index for upstream hydropower plants/reservoirs to i
nj_k = number of hydropower plants/reservoirs in subsystem k

nm_i = number of upstream hydropower plants/reservoirs to i
$A_{i,t}$ = reservoir forebay area (Km²)
$DT_{i,t}$ = deviation or transposition uses (m³/s)
$E_{i,t}$ = evaporation (10^6 m³)
$Hg_{i,t}$ = water head (m)
η_i = power generation efficiency ($0 \leq \eta_i \leq 1$) (-)
$H_{i,t}$ = reservoir forebay water level (m)
$HT_{i,t}$ = reservoir tailrace water level (m)
$ID_{i,t}$ = availability index due to maintenance and system expansion ($0 \leq ID_{i,t} \leq 1$) (-)
$IE_{i,t}$ = evaporation rate during time period t (m)
$I_{i,t}$ = natural inflow (m³/s)
$P_{i,t}$ = energy production (MW)
$P^{max}{}_i$ = maximum energy production (MW)
$R''_{i,t}$ = spill or non-power release (m³/s)
$R'_{i,t}$ = power release (m³/s)
$R'^{max}{}_{i,t}$ = maximum power release (m³/s)
$R'^{min}{}_i$ = minimum power release (m³/s)
$R_{i,t}$ = total release (m³/s)
$R^{min}{}_i$ = minimum total release (m³/s)
$S_{i,t}$ = storage (10^6 m³)
$S^{max}{}_{i,t}$ = time-varying maximum storage for flood control (10^6 m³)
$S^{min}{}_i$ = minimum storage (10^6 m³)
$UC_{i,t}$ = consumptive use (m³/s)

Case study: Itaipu Dam and Upstream Reservoirs

The input data for the case was based on the official data from ONS published in July 2008 (ONS, 2008). The data set includes the existing system and planned expansion for the next five years. But in this study only the existing system and subsystem of 55 hydropower plants and reservoirs in the Paraná river basin are used, which include Itaipu, as shown in figure 1. Out of the 55 plants, 31 are run-of-river and 24 have storage to regulate flows in the basin.

To evaluate the impacts of the upstream storage reservoirs on the hydropower production of Itaipu two operation scenarios were used: first, operating the system in a simulation mode with run-of-river operation and natural inflow; that is, without the effect of the upstream storage reservoirs; and second, optimizing the system to minimize the hydropower quadratic complementation for the entire basin, with the 55 hydropower plants. The optimization was applied to obtain the best results for the entire basin production. The historical natural inflow series from 1940 to 1999 was divided into six segments (one for each decade) and used as inputs to the optimization model.

One important aspect as shown in figure 2 is that the historical series is non-stationary. This is mainly due to changes in soil use in the last decades which were

basically from forests to agricultural occupation, thus reducing evapotranspiration and increasing the runoff.

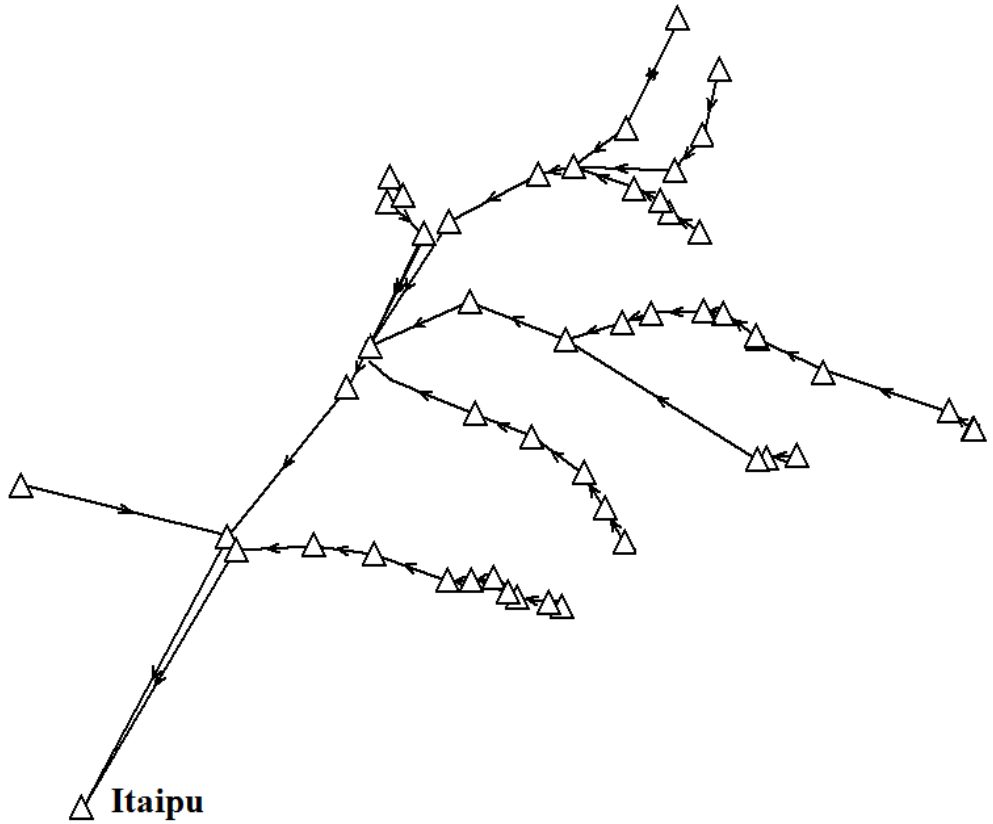

Figure 1 - Network of hydropower plants in the Paraná river basin, including Itaipu

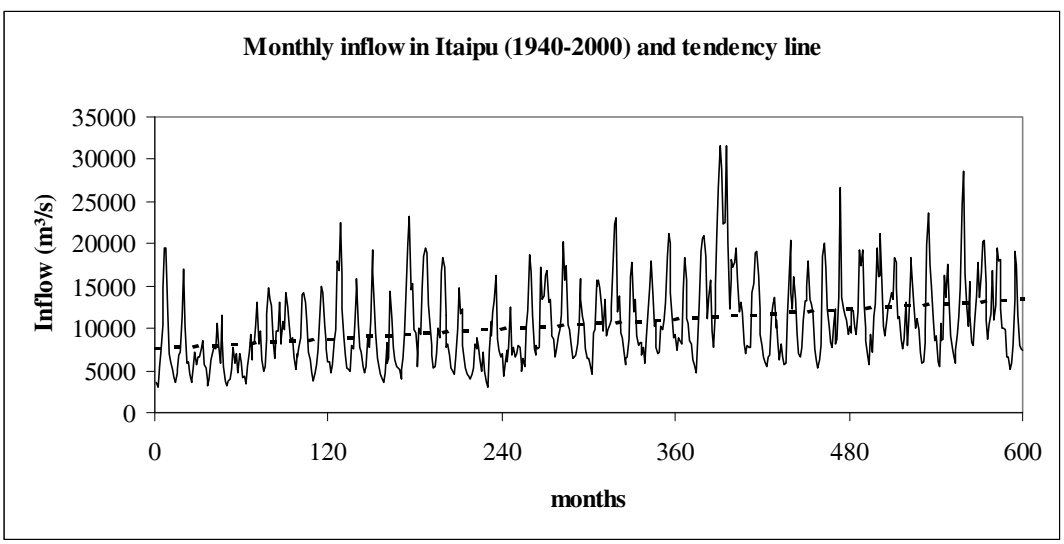

Figure 2 - Natural inflow at Itaipu

Table 1 and figure 3 show the results of Itaipu average production with run-of-river operation and natural inflow as well as the optimized results with upstream regularization. In all six scenarios of inflow the production in Itaipu was significantly increased due to the regularization of the upstream reservoirs in the basin.

Table 1 - Itaipu average production with run-of-river operation and natural inflow (Pror) as well as with upstream regularization (Pres)

decade	Pror(MW)	Pres(MW)	Δ(%)	Δ(MW)
1940	8186	9123	11.4%	937
1950	7839	8315	6.1%	476
1960	8499	9771	15.0%	1272
1970	9822	11283	14.9%	1460
1980	10398	11851	14.0%	1453
1990	10613	11977	12.8%	1363

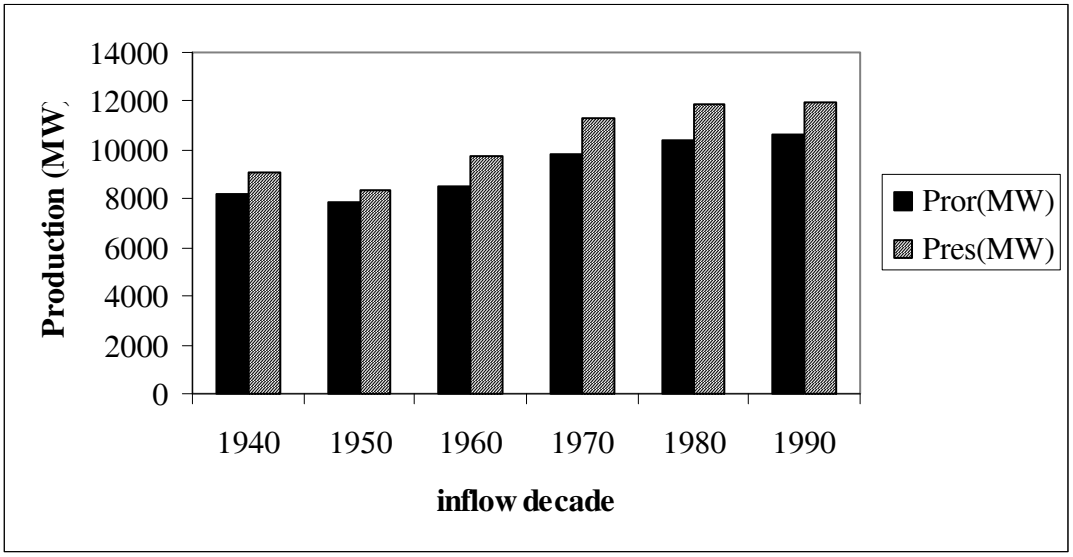

Figure 3 - Itaipu average production with run-of-river operation and natural inflow (Pror) as well as with upstream regularization (Pres)

In this example the HIDRO problem size was reasonably large, with 15,360 decision variables. The optimization was done using MINOS, a nonlinear programming routine. The process required from 17 to 24 minutes on a notebook with an AMD Turion64 X2 TL-58 (1.9GHz) processor to run each decade scenario (55 hydropower plants and 120 time steps).

Final Comments

This paper has presented an application of the HIDROTERM DSS to evaluate the impacts of the upstream storage reservoirs on the hydropower production of Itaipu. Using the last three decades of historical inflow data, the optimized power production when considering the upstream regularization was on average 14% or 1426 MW higher than the power production obtained without upstream regulation. This conparasion indicates that there are significant impacts and benefit of the upstream regularization not only for the entire system but also for the Itaipu power production.

The methodology presented is suitable to different applications, such as planning operation and studies of reliability, capacity expansion, environmental constraints, operational rules, tradeoff between multiple uses of water and other technical aspects related to hydrothermal systems.

References

ANEEL - Agência Nacional de Energia Elétrica (2009). <http://www.aneel.gov.br>.

Barros, M.T.L., Tsai, F., Lopes, J.E.G., Yeh, W. (2003). "Optimization of Large-Scale Hydropower System Operations." *J. Water Resources Plan. Manage.*, 129(3), 178-188.

Barros, M.T.L., Zambon, R.C., Lopes, J.E.G. (2005). "Sistema de Suporte a Decisão para o Planejamento da Operação Hidráulica de Sistemas Hidroenergéticos." *Proc., III Simpósio de Recursos Hídricos Del Cono Sur*, Mendoza.

Barros, M.T.L., Zambon, R.C., Lopes, J.E.G., Barbosa, P.S.F., Francato, A.L.F., Yeh, W. (2008). "Model to Optimize Large Hydrothermal System Operation Considering Water and Environment Sustainability." *Proc., World Environmental & Water Resources Congress 2008*, Honolulu.

GAMS - General Algebraic Modeling System (2008). <http://www.gams.com>.

Labadie, J. (2004). "Optimal Operation of Multireservoir Systems: State of Art Review." *J. Water Resources Plan. Manage.*, 130(2), 93-111.

Momoh, J. A., El-Hawary, M. E., and Adapa, R. (1999a). "A review of selected optimal power flow literature to 1993, Part I: Nonlinear and quadratic programming approaches." *IEEE Trans. Syst.*, 14(1), 96-104.

Momoh, J. A., El-Hawary, M. E., and Adapa, R. (1999b). "A review of selected optimal power flow literature to 1993, Part II: Newton, linear programming and interior point methods." *IEEE Trans. Syst.*, 14(1), 105-111.

ONS - Operador Nacional do Sistema Elétrico (2008). <http://www.ons.org.br>.

Porto, R.L.L., Mello, A.V., Roberto, A.N., Palos, J.C. (2005). "ACQUANET: Arquitetura, Estratégias e Ferramentas." *Proc., XVI Simpósio Brasileiro de Recursos Hídricos*, João Pessoa.

Simonovic, S. P. (1992). "Reservoir systems analysis: Closing gap between theory and practice." *J. Water Resources Plan. Manage.*, 118(3), 262-280.

Wurbs, R. A. (1993). "Reservoir-system simulation and optimization models." *J. Water Resources Plan. Manage.,* 119(4), 455-472.

Yeh, W.W-G. (1985). "Reservoir management and operation models: A state-of-the-art review." *Water Resources Research*, 21(12), 1797-1818.

Yeh, W.W-G., Becker, L., Hua, S-Q., Wen, D-P., and Liu, J-M. (1992) "Optimization of Real-Time Hydrothermal System Operation." *J. Water Resources Plan. Manage*, 118(6), 636-653.

Inflow Forecasting for Real-time Reservoir Operation Using Artificial Neural Network

Taesoon Kim[1], Gian Choi[2], Jun-Haeng Heo[3]

1 Research Professor, School of Civil and Environmental Engineering, Yonsei University, Seoul 120-749, South Korea (e-mail: chaucer@yonsei.ac.kr)
2 Graduate Student, School of Civil and Environmental Engineering, Yonsei University, Seoul 120-749, South Korea (e-mail: gian@yonsei.ac.kr)
3 Professor, School of Civil and Environmental Engineering, Yonsei University, Seoul 120-749, South Korea (email: jhheo@yonsei.ac.kr)

ABSTRACT

Artificial neural network (ANN) is used for inflow forecasting of reservoir up to the next 12 hours. Numerical weather forecasting information (RDAPS), recorded rainfall data, water level of upstream dam and stream gauge site, and inflow of the current time are employed as input layer's training values, and target value is +3, +6, +9, and +12 hours later inflow to Hwacheon reservoir in South Korea. Comparison result between ANN with RDAPS and without RDAPS shows that RDAPS information is useful for forecasting inflow of reservoir.

INTRODUCTION

Accurate inflow forecasting for reservoir operation is essential for proper and reliable operation (Labadie 2004). Especially for flood season operation in order to prevent flooding from downstream area, at most next 12 hours inflow should be forecasted with accuracy. However, most of physically based rainfall-runoff model such as HEC-1 in real-time reservoir operation show very poor model performance and they need a lot of time and effort to be modified for incorporate rainfall forecasting information which is able to be acquired by numerical weather forecasting model that is a common tool for weather forecasts.

Artificial neural network (ANN) has been adopted widely to forecast lots of hydrological variables like runoff, water-level, or occasionally rainfall amount itself (Dibike and Solomatine 2001; Tokar and Markus 2000; Wu et al. 2005). It has strong

points to compute a response resulted from many nonlinear impact factors, and this nonlinearity is very common phenomenon in hydrologic modeling. Moreover, hydrologic model should consider the lack of data by malfunction of recording device or disconnection from network in real-time operation. Therefore, the conventional physically based hydrologic model would not be proper to applied to real-time operation, especially for reservoir operation.

In addition, the recent advanced numerical weather forecasting model (Guo and Senior 2006) like RDAPS (Regional Data Assimilation and Prediction System) of South Korea show reliable prediction result with regard to qualitative analysis that forecast "on and off" of rainfall in the next 24 hours, thus the rainfall forecasting information from RDAPS could be used for inflow forecasting although quantitative analysis result shows very poor performance.

The goal of this study is to evaluate the usefulness of RDAPS data into reservoir inflow forecasting in real-time operation. A short length of data confines a limited evaluation of ANN using only training data set without calibration, and verification data sets, however, comparison study of two cases with- and without-RDAPS information simply shows the advantage of ANN with numerical weather forecasting data.

ANN AND RDAPS

ANN has been widely used for inflow or runoff forecasting from lots of researches. The ANN model here has very simple structure that has only one hidden layer with 4 hidden nodes, and backpropagation, one of the most implemented error propagating method, is applied also (Bishop 1995). As mentioned before, we have very short record lengths of RDAPS, namely at most 4 years, and during this period only one rainfall-runoff event can be used for evaluation of ANN. Therefore, only training process can be applied here, and if the more RDAPS data and corresponding rainfall-runoff events are gathered, whole procedure of evaluation for ANN would be employed.

RDAPS data are computed by Korea Meteorological Administration (KMA) and its data format is GRIB that is popular in meteorological science field. It has 191 by 171 grids with 30km distance and is projected on Lambert Conformal surface. RDAPS has been calculated at 00UTC and 12UTC that is 09:00 and 21:00 local time with 3-hours interval, and forecasting time horizon is 66 hours. Usually, next 48 hours forecasting information which is 16 time steps is used for operational use. Fig. 1 shows APCP variable layer at the ground level with GrADS software.

INFLOW FORECASTING FOR REAL-TIME RESERVOIR OPERATION

Inflow forecasting with artificial neural network and regional numerical weather forecasting model, namely RDAPS mentioned in the previous section, is applied to Hwacheon reservoir basin in South Korea (Fig. 2). The basin area of Hwacheon reservoir is about 3,845 km^2 and there are two local streams in the basin. Peace dam that is located at the very upstream of Hwacheon reservoir has four tunnels for releasing water downstream and it has no spillway with gate. Peace dam is in the lake of Paroho that is made by Hwacheon dam, thus water level of Peace dam is one of the measuring tools for forecasting inflow of Hwacheon reservoir. The other water level gauge located at YangGu SeoChun that is another local stream in Hwacheon reservoir basin is used also for inflow forecasting.

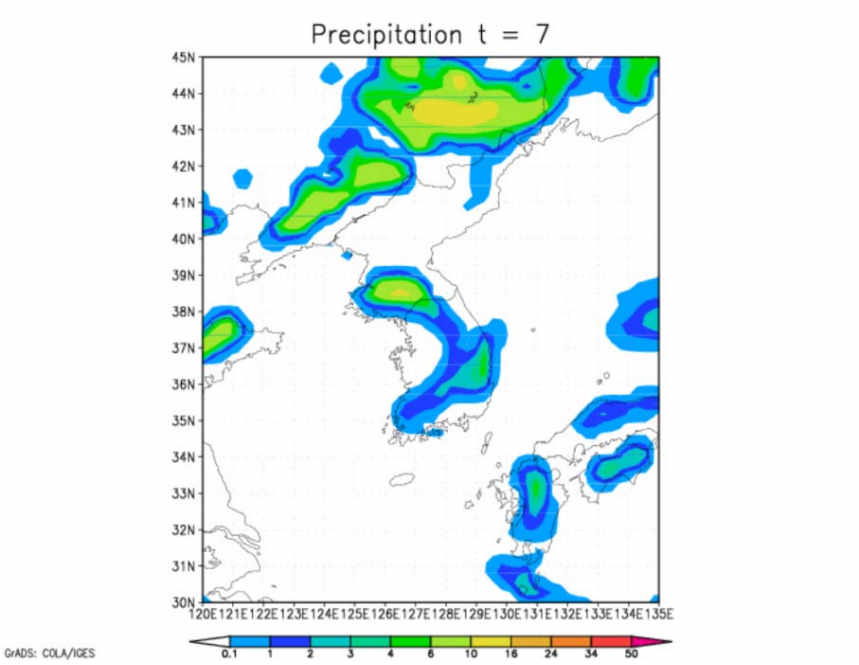

Fig. 1 Surface precipitation data extracted from RDAPS 30km

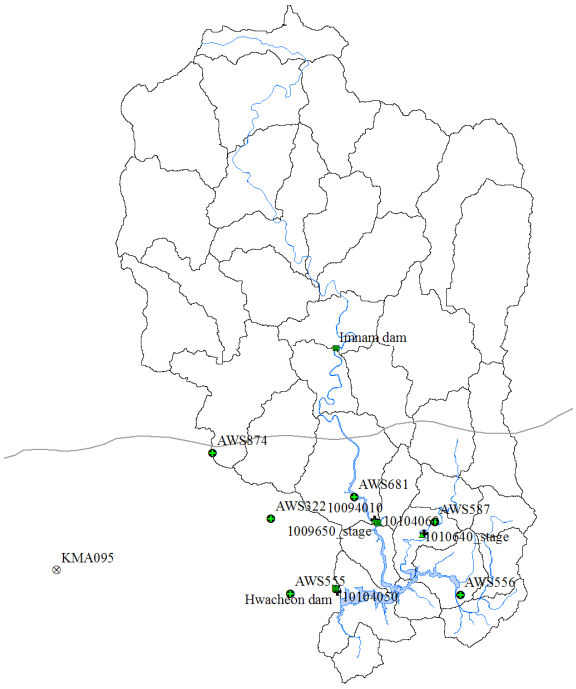

Fig. 2 Hwacheon and Peace dam basin and rainfall and water level recording sites

The experiment is performed with two cases. The first one uses rainfall data gathered from total 10 rainfall recording sites. Seven sites are inside of Hwacheon reservoir basin and the other are in the west outside region of basin. Because Korea Peninsula is located in the westerly wind area, the rainfall that is recorded at the west side of basin can be used to forecast the future time's rainfall. The second one applies only RDAPS data as rainfall input of ANN model. None of any rainfall data from recording sites is employed in this case. All of these two experiment use inflow data of Hwacheon reservoir at the current time as additional input of ANN model. Therefore, the first case has 13 input data that are 10 rainfall data, 2 water level data, and 1 inflow data, and the second one has only 4 input data such as 2 water level data, 1 RDAPS data, and 1 inflow data.

RDAPS data can be acquired during only about 4 years from January 1 of 2005 to September 30 of 2008, and corresponding inflow data of Hwacheon reservoir that are relatively large enough to release water through spillway can be achieved only in July 2006. Thus, the experiment is performed with a rainfall-runoff event which was occurred in between July 12 and 18 of 2006 (Fig. 3). This event has a maximum inflow as 5,254 m^3/sec at 1:00 pm, July 15 and has a smaller peak (978 m^3/sec) at 21:00 pm, July 12.

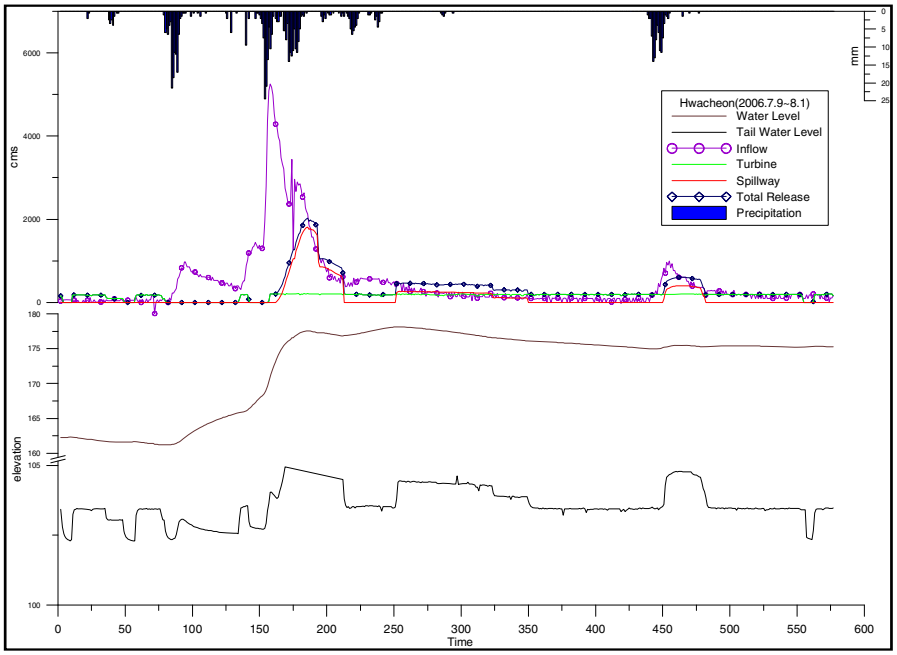

Fig. 3 Rainfall-runoff event in July 12 and 18 of 2006 at Hwacheon basin

Since RDAPS model computes results twice a day at 00UTC and 12UTC, only 14 data sets can be achieved during July 12 and 18 of 2006 and this is very insufficient number of data sets for verification and calibration, thus all data sets should be used as training data set and comparison between case 1 that uses only gauged rainfall data inside and outside of basin, and case 2 which uses numerical weather forecasting model's output is performed in order to evaluate the effect of numerical weather forecasting model into improvement of accuracy for reservoir inflow forecasting

Table 1 shows rainfall data from 10 recording sites, water level data from 2 gauges at local streams in the basin and inflow at the current time and next 3, 6, 9, 12 hours. 4 ANN models are formulated for the sake of forecasting next 3, 6, 9, and 12 hours inflow to Hwacheon reservoir. Each ANN model has 1 hidden layer and 4 hidden nodes, and trained using back-propagation with delta-rule. All training procedure has 10,000 epochs and error tolerance is set to 0.001. Since rainfall, runoff and water level data has very different data units, normalization should be introduced. All input and output layer data are normalized not to be over 0.99.

Table 1. Rainfall, water level and inflow data

date	hour	KMA 095	AWS 874	AWS 322	AWS 681	AWS 587	AWS 556	AWS 555	1009 4010	1010 4060	1010 4050	1009650_ stage	1010640_ stage	HC_ Inflow	+3	+6	+9	+12
2006-07-12	9	24.5	28.5	16.5	7.0	17.5	18.5	19.5	9.0	9.0	12.0	163.37	0.71	0	222	333	722	978
2006-07-12	21	102.5	78.5	119.0	39.0	80.5	131.0	109.0	87.0	92.0	112.0	164.63	1.96	978	856	733	672	672
2006-07-13	9	28.0	9.0	14.5	0.0	1.5	2.5	4.5	5.0	2.0	3.0	167.14	1.54	672	611	600	600	533
2006-07-13	21	5.5	3.0	10.5	0.0	8.0	2.5	2.0	7.0	8.0	2.0	166.99	1.37	533	467	400	400	333
2006-07-14	9	0.5	10.5	3.5	1.5	4.0	1.0	16.0	1.0	2.0	10.0	166.49	1.26	333	400	319	519	1189
2006-07-14	21	9.0	44.5	30.0	19.5	82.5	12.0	3.5	98.0	40.0	11.0	170.60	2.71	1189	1319	1372	1300	1950
2006-07-15	9	27.5	27.5	87.5	86.5	87.5	38.0	44.0	56.0	29.0	26.0	174.30	2.95	1950	5090	4989	4224	3483
2006-07-15	21	76.5	70.5	85.0	65.5	76.0	87.0	56.5	124.0	90.0	90.0	179.88	2.64	3483	2741	2366	1263	2892
2006-07-16	9	111.0	77.5	101.0	13.0	89.5	90.5	98.0	92.0	91.0	82.0	178.01	2.81	2892	2698	2278	1858	1566
2006-07-16	21	18.5	7.5	19.5	0.0	16.5	25.0	22.5	22.0	25.0	32.0	178.13	2.20	1566	1234	958	846	593
2006-07-17	9	12.5	4.0	7.5	2.5	5.5	8.0	10.0	5.0	5.0	8.0	177.14	1.71	593	547	504	642	379
2006-07-17	21	8.0	2.5	5.0	2.0	3.5	5.0	6.0	4.0	4.0	7.0	176.76	1.41	379	386	582	570	587
2006-07-18	9	33.0	25.5	29.5	24.0	28.0	34.5	30.5	33.0	34.0	33.0	177.10	1.44	587	567	567	568	568
2006-07-18	21	4.5	7.5	11.0	7.5	9.5	9.5	8.0	11.0	10.0	8.0	177.58	1.42	568	534	471	480	496

* KMA is rainfall recording sites managed by Korea Meteorological Administration. AWS is automatic weather system also by KMA. Next 8-digit means the identical number for rainfall recording sites by Korea Government. “stage” means water-level recording sites. +3, +6, +9, and +12 hours are lead-time from the current time at the most left side column.

Training results from case 1 and 2 show good agreement to the observed data (Fig. 4). X-axis means 3-hours interval since the minimum time interval of RDAPS is 3-hours. The first x-axis value that is 3 means +3 hours forecasted inflow using case 1 and 2, and corresponding observed data. The starting time of experiment is 09:00 of July 12, thus this first value is for 12:00 pm which is +3 hours from 09:00. Because a new RDAPS data can be acquired after next 12 hours later that is 21:00 pm, 5th value in Fig. 2 whose x-axis’ value is 15 can be computed using 2nd RDAPS data which is made at 21:00 pm. Therefore 5th value is actually +3 hours forecasted value from 2nd RDAPS data.

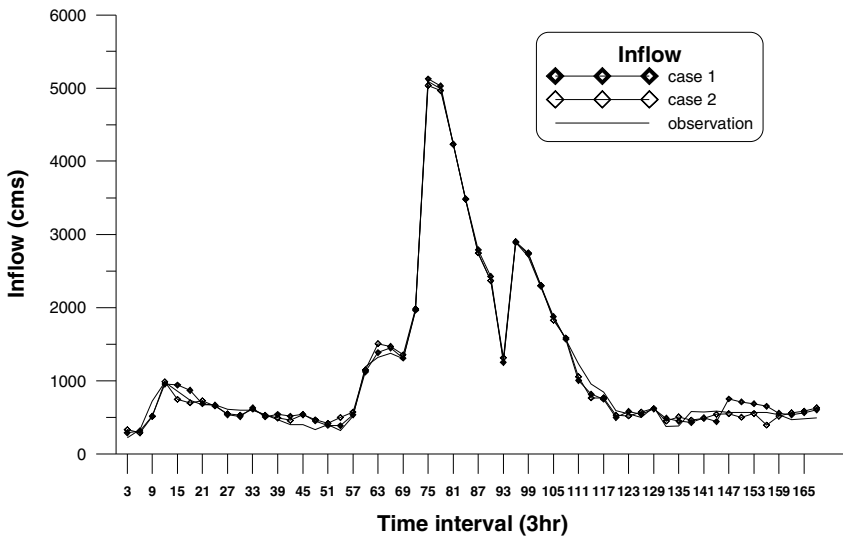

Fig. 4 Training result and observed data from case 1 and 2. All data points mean serial 3-hours interval values from July 12 at 12:00 to 18 at 21:00.

Next figures (Fig. 5) show another analysis result of ANN model. The first graph whose title is "3-HR_INFLOW" shows comparison between forecasted inflows from case 1 and 2, and observed inflow of Hwacheon reservoir. The x-axis values are 7 00UTC and 12UTC, respectively. Since experiment period is only 7 days, 14 data sets can be computed. All of these 4 graphs show the results from ANN are very similar to the observed data even though forecasting time horizon is expanded to 12 hours.

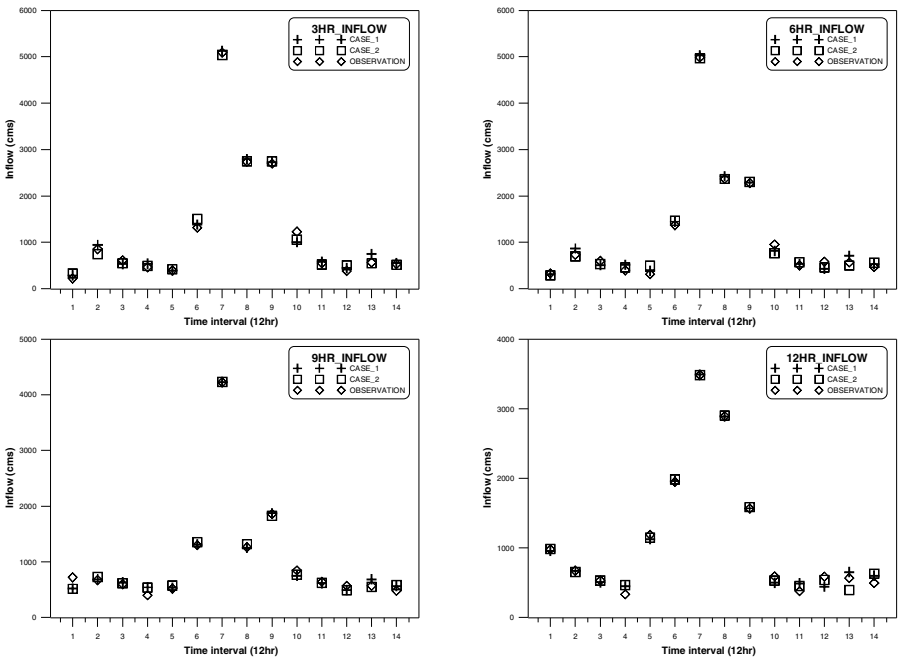

Fig. 5 Comparison between training and observed data sets. Each point is for 00UTC or 12UTC of July 12 to 18.

Another comparison results (Table 2) show the observed data and computed data using ANN model, and RMSE (root mean square error) value also. RMSE of case 2 in 3, 6, 9-hours lead-time are smaller than that of case 1. However RMSE of 12 hours lead-time show the opposite result. This could mean that the accuracy of RDAPS become deteriorated after 12 hours lead-time. On the other hand, it is noted that the results from case 2 that uses only RDAPS data as rainfall information are better than those from case 1 which apply much more information with regard to rainfall.

Table 2. Inflows from ANN and observed data. Case 1 uses all the rainfall data from recording sites; Case 2 apply RDPAS information as input layer. Three RMSE of case 2 out of total 4 different lead-time values are smaller than that of case 1.

Lead-time		case 1	case 2	observed			case 1	case 2	observed
3-Hour	1	289	332	222	6-Hour	1	315	288	333
	2	943	746	856		2	870	699	733
	3	536	549	611		3	509	532	600
	4	541	492	467		4	517	461	400
	5	393	420	400		5	387	500	319
	6	1386	1508	1319		6	1447	1469	1372
	7	5126	5035	5090		7	5029	4967	4989
	8	2792	2747	2741		8	2426	2369	2366
	9	2731	2747	2698		9	2293	2305	2278
	10	1006	1058	1234		10	818	767	958
	11	581	521	547		11	540	573	504
	12	448	507	386		12	430	461	582
	13	753	550	567		13	711	502	567
	14	557	517	534		14	533	562	471
	RMSE	**94.361**	**91.369**			**RMSE**	**94.661**	**93.821**	
		case 1	case 2	observed			case 1	case 2	observed
9-Hour	1	518	514	722	12-Hour	1	955	986	978
	2	686	726	672		2	667	656	672
	3	629	614	600		3	507	532	533
	4	542	537	400		4	451	467	333
	5	535	573	519		5	1123	1147	1189
	6	1310	1353	1300		6	1963	1982	1950
	7	4229	4232	4224		7	3490	3481	3483
	8	1253	1317	1263		8	2889	2901	2892
	9	1877	1827	1858		9	1568	1586	1566
	10	749	767	846		10	500	530	593
	11	616	620	642		11	491	453	379
	12	493	488	570		12	442	541	587
	13	686	551	568		13	652	394	568
	14	565	584	480		14	602	629	496
	RMSE	**84.771**	**84.175**			**RMSE**	**75.702**	**76.119**	

CONCLUSION

ANN is useful to forecast inflow of reservoir especially for the real-time operation since it can be used in case of input data missing. In this study, two ANN model are formulated using recorded rainfall data and numerical weather forecasting data. Owing to very short record length of RDAPS data, only one rainfall-runoff event can be used, thus training data set is just examined. The first case uses 13 input variables for input layer and one output layer's target like Hwacheon reservoir's +3, +6, +9 and +12 next hours inflow. And, the other case has only RDAPS data as rainfall information and no recorded rainfall data is used. All of these two models

show good performance comparing with the observed records. However, the accuracy of ANN model using only RDAPS data is generally smaller than that of ANN model with recorded rainfall data.

This study is a kind of preliminary research. The performance of ANN model is largely affected by a method of selecting training data sets, and it is also important to maintain accuracy and reliability of training process through verification and calibration processes. All of these processes need a lot of data sets including a various different input and output patterns. However, even though a very short record length is applied comparison study shows that including numerical weather forecasting data like RDAPS is somewhat promising for inflow forecasting.

REFERENCES

Bishop, C. M. (1995). *Neural networks for pattern recognition*, Oxford University Press, Oxford.

Dibike, Y. B., and Solomatine, D. P. (2001). "River flow forecasting using artificial neural networks." *Physics and Chemistry of the Earth, Part B: Hydrology, Oceans and Atmosphere*, 26, 1-7.

Guo, Y., and Senior, M. J. (2006). "Climate model simulation of point rainfall frequency characteristics." *Journal of Hydrologic Engineering*, 11(6), 547-554.

Labadie, J. W. (2004). "Optimal operation of multireservoir systems: state-of-the-art review." *Journal of Water Resources Planning and Management*, 130(2), 93-111.

Tokar, A. S., and Markus, M. (2000). "Precipitation-runoff modeling using artificial neural networks and conceptual models." *Journal of Hydrologic Engineering*, 5(2), 156-161.

Wu, J. S., Han, J., Annambhotla, S., and Bryant, S. (2005). "Artificial neural networks for forecasting watershed runoff and stream flows." *Journal of Hydrologic Engineering*, 10(3), 216-222.

Integrated Management of a Finite Water Supply in the Desert

Daniel Wendell, Steve Shultz, and Aditya Tyagi

CH2M HILL, 155 Grand Ave, Suite 1000, Oakland, CA 94611; PH (510) 251-2888

ABSTRACT

Fort Irwin is located in California's Mojave Desert, adjacent to Death Valley, and receives about five inches of rain per year. Local water supply comes from three separate groundwater basins that have no significant natural recharge and therefore provide a finite supply of water. The base is an important Army training facility and extending the life of water supplies is of critical importance. This work was undertaken to maximize the "lifespan" of local water supplies, minimize costs, and avoid adverse impacts to the extent possible.

To meet the needs of this project, the entire water cycle of the area was evaluated in an integrated and quantitative manner, including: modeling local groundwater supplies; evaluating potential development of remote water supplies and associated costs; conducting an end-use water demand and conservation analysis; developing a recycled water irrigation program; implementing an indirect wastewater reuse (i.e., recharge) program; developing an operations program designed to mitigate adverse impacts such as land subsidence; and assessing cost, power consumption, and greenhouse gas emissions from the various alternatives.

This work effort was integrated in a quantitative fashion using the system dynamics model "GoldSim". Use of Goldsim allowed modeling the entire water system in an integrated fashion while assessing feedback relationships in the various water management alternatives that might have otherwise been lost. For example, water demand management yields less available wastewater for groundwater recharge, which in turn affects the lifespan of the local groundwater basins. GoldSim was used to optimize lifespan of the basins, cost, and greenhouse gas emissions by varying the water management alternatives. Key output included: "lifespan" of each of the three local groundwater basins; timing of projected onset of land subsidence; water savings and costs of water demand management alternatives; and greenhouse gas emissions. A key advantage of the model is that it is packaged into a "player" version that can be used by planners without detailed understanding of the feedback loops.

INTRODUCTION

Fort Irwin currently has a population of approximately 19,300 people composed of 10,000 resident soldiers and dependents, 3,500 civilian and contractor day-workers and a monthly average of 5,800 rotational trainee forces. Local water supplies for Fort Irwin are very limited. To best manage this critical resource and help meet

potential growth in water demand, the Army assessed potential benefits of water conservation measures.

In most respects, military installations are much like small cities in that they contain many of the same services and recreational opportunities needed by Post residents as do civilian communities. However, one key difference between military installations and civilian communities is the typical lack of on-Post water meters. Fort Irwin is no exception.

Effectively determining water use and conservation potential requires professional experience and judgment to supplement available meter data. Professional judgment was especially critical in this case due to the limited amount of meter data. Base Command highlighted the fact that all proposed water conservation measures, as well as the overall Fort Irwin Water Demand Management Plan, meet the following criteria:

- Fully support, and not interfere with, Fort Irwin's mission.
- Maintain the existing quality of life for Fort Irwin residents and employees.
- Allow for "smart growth" of residential and commercial activities.
- Be fiscally prudent.

BACKGROUND

The water cycle at Fort Irwin is relatively unique in that it is essentially a closed system; that is, there is negligible outflow from the system by streams or other methods. The water consumed by humans in homes, at work, and in commercial operations is collected, sent to the wastewater treatment plant (WWTP) and, except for evaporation losses and reclaimed water uses, is returned to the groundwater by percolation. The only water lost from the system is through evaporation and evapotranspiration. Accordingly, reducing water loss by reducing evaporation and irrigation is the most meaningful way to conserve water and the only way to extend the life of the local groundwater basins. However, there are other benefits to reducing overall water use and, therefore, groundwater extraction, including:

- Increasing lifespan of local groundwater resources.
- Providing additional water to help meet future growth.
- Reducing overall cost by reducing pumping, transmission, and treatment costs.
- Lowering the rate of TDS increase in local basins by reducing cycling of water.
- Reducing buildup of nitrogen and other compounds in groundwater with less irrigation.
- Delaying need for capacity upgrades to water and wastewater treatment facilities.
- Reducing greenhouse gas emissions from reduced energy usage.
- Providing a public showcase of water conservation measures and an example for others.

Water Supply

Groundwater is the only source of water supply to Fort Irwin. Currently, production comes from the three local groundwater basins present on the Post: the Irwin,

Bicycle, and Langford Basins. Production well meter readings from 2003 to 2007 indicate that past average annual pumpage is about 2.5 million gallons per day (mgd). This is equivalent (less transmission and distribution system losses) to average annual demand for 2003-2007. However, due to the new WTP, "annual average year" irrigation requirements, and changes to residential neighborhoods and associated irrigation, the future annual average demand is expected to be 2.57 mgd. Monthly average pumpage varies seasonally from about 1 mgd in the winter to over 3 mgd in the summer, with daily pumpage as high as 5 mgd. Allocation of pumpage amongst the three basins is variable and changes frequently. For the purposes of evaluating the lifespan of local basins, pumping distribution was assumed to be 46 percent from Bicycle Basin, 32 percent from Langford Basin, and 22 percent from Irwin Basin.

Water Treatment and Distribution

The potable water distribution systems at Fort Irwin currently consist of two separate networks. Treated drinking water is provided across the cantonment from an existing reverse osmosis (RO) WTP. This RO plant will soon be replaced by a new WTP facility, scheduled to be online in late 2009. The existing RO plant produces about 0.09 mgd, with product brine averaging about 0.08 mgd. A second, separate "domestic water" (DO) network provides disinfected groundwater throughout the Post that is used for fire protection, irrigation, toilets, and bathing. There are a total of nine storage tanks on the two systems that provide water to meet peak demands, maintain system pressure, and provide emergency supplies. These storage tanks have a combined capacity of approximately 5 million gallons (MG).

The new WTP will provide water to the existing DO distribution system, which will become the single source of drinking water and water for all other uses (except those areas irrigated by reclaimed water). Data from the existing RO and DO water systems were used to determine baseline 2004-2005 water production rates. However, in the future the water system will be operated in an integrated fashion, and therefore projected future water budgets are based on the new WTP, with effectively zero brine, and combined water distribution system.

Wastewater

All wastewater from Fort Irwin is processed at a secondary wastewater facility located within the cantonment. Metered influent to the WWTP from January 2003 to November 2006 indicates average flows of about 1 mgd, with very little seasonal fluctuation. Treated water effluent from the WWTP is reclaimed and used to irrigate the pitch-and-putt golf course. The reclaimed water distribution system is planned to be expanded into the cantonment to provide irrigation to selected recreation and parade fields. The WWTP has been modified to allow for tertiary treatment of the wastewater but these facilities have not yet been brought online.

Total Water Demand and End-use Categories

Projected potable water demand at Fort Irwin is assumed to be equal to total pumpage (2.57 mgd), minus a small amount of water exported to a satellite facility

("Goldstone", 0.08 mgd). This leaves a total onsite demand estimate of 2.49 mgd. An additional 0.06 mgd of reclaimed water is currently used to irrigate the pitch-and-putt golf course. To assess the feasibility of specific conservation measures, indoor and outdoor demands for each user type were quantified according to end use. End uses for indoor demands consist of toilets, laundry, showers, dishwashers, faucets, baths, leakage, and "other." End uses for outdoor demands consist of irrigation, air conditioning, car washes, leakage, and "other."

ANALYTICAL APPROACH AND MODEL DEVELOPMENT

To assess costs and benefits of various conservation options a "system dynamics" model of the water cycle at the base was developed using the "GoldSim" code. The model was developed to provide a general-purpose, probabilistic simulation framework used for planning and risk management. The GoldSim model was developed to simulate all aspects of the Fort Irwin water system, including water demand, water supply, managing water supply to meet demand and evaluate longevity of the water supply, and to evaluate cost and water demand savings associated with conservation measures and combinations of measures. The model was used to evaluate effectiveness of conservation measures and develop a recommended Water Demand Management Plan based on: total water savings; 5-year cost (referenced to present value); ongoing O&M costs, following implementation of scenario; 20-year cost-benefit ratio; and basin life.

Water demand is broken down into user type and end use. A total of 35 end uses were identified in the following categories: indoor residential, outdoor residential, indoor commercial, and outdoor commercial. The model is set up for the user to specify the percentage of total demand that is satisfied by each of eight local groundwater basins. The first three already have infrastructure built. If any of the other basins is pumped, a capital cost developed is added. Each groundwater basin is simulated as a separate "reservoir" in GoldSim. Inflow to and outflow from the basins are specified. All basins except Irwin were assumed to be closed basins, i.e., there is no natural recharge or discharge. Based on results of previous groundwater modeling, lookup tables were utilized to track groundwater levels in the basins. A minimum water level is set by the user, below which the basin can no longer be utilized. At that time, pumpage is reallocated evenly amongst the other basins.

The model calculates wastewater production as a specified percentage of all indoor water use, which is currently set to 90 percent. A percentage of the wastewater is assumed to be lost at the wastewater treatment plant. The user specifies the annual average of reclaimed water that can be used to satisfy demand. If there is a deficit (i.e., non-potable demand exceeds reclaimed supply with current infrastructure), then the excess non-potable demand is supplied by potable water. Whatever reclaimed water that is not used to satisfy demand gets routed to wastewater ponds. A mass transport calculation is run on the wastewater ponds, based on evaporation and percolation rates. Whatever is not evaporated is assumed to percolate into the groundwater system. The user specifies both the infiltration rate of the ponds, and the basin where the ponds are located.

Conservation Measure Evaluation

Costs and related water demand savings were calculated for a wide range of conservation measures. The impact of interactions between conservation measures was considered within each scenario. Overlapping measures do not have a cumulative effect on indoor or outdoor end uses and are therefore not included in percent reductions. This evaluation targeted the end use and cumulative effect of measures impacting the same end use within an alternative were reduced based on a calculation of the total combined effect of each measure, refereed to as "Net Effect."

For the purposes of cost evaluation, it is assumed that the cost of water is $3.67 per 1,000 gallons. This cost was estimated based on cost of water and wastewater services ($1.20/1,000 gallons), total energy used in the water and wastewater system (including raw water supply, conveyance, treatment, and distribution, as well as wastewater collection, treatment, and discharge), and an assumed average energy cost of $0.14/kilowatt-hour (kWh) (total $2.46/1,000 gallons). Present worth costs assume a nominal rate of 3 percent (6 percent interest rate less 3 percent inflation rate).

Energy and Greenhouse Gas Evaluation

Energy usage in the water system at Fort Irwin includes: Raw water supply and conveyance, water treatment, water distribution, wastewater collection and treatment, wastewater treatment plant discharge, reclaimed water distribution, and energy associated with end use. Because energy usage for these components are not metered, energy rates were estimated based on previous experience and figures referenced by the California Energy Commission (CEC 2005). Greenhouse gas emissions (CO2, N2O, and CH4) were calculated based on region-specific factors from the Climate Leaders GHG Protocol (October 2004), a method sanctioned by the EPA. Energy consumption, and associated greenhouse gas emissions, are tracked by the model and presented in the results of all management scenarios.

Model Input

Inputs to the model include: number of accounts; basin pumping allocations; minimum allowable basin water levels; average annual reclaimed water usage (the model calculates seasonal usage); cost functions, including the cost of water, inflation and interest rate for present-worth analysis, and year for benefit/cost ratio analysis; irrigation recharge, which is the percent of applied irrigation water that recharges the basin; wastewater recharge; and WTP capacity, which is the maximum rate of water supply.

Model inputs related to demand rates include check boxes to "turn on" any number of 13 pre-defined conservation programs, and optional input of any number of additional user-defined conservation programs. Each conservation program uses the following input: a base water usage rate by fixture type (gpd per account), cost parameters for conservation, implementation schedule for conservation program, and water savings. Implementation and water savings are both time series data. Several other types of

data are input as a time-series, including number of accounts and "suppliable reclaimed demand."

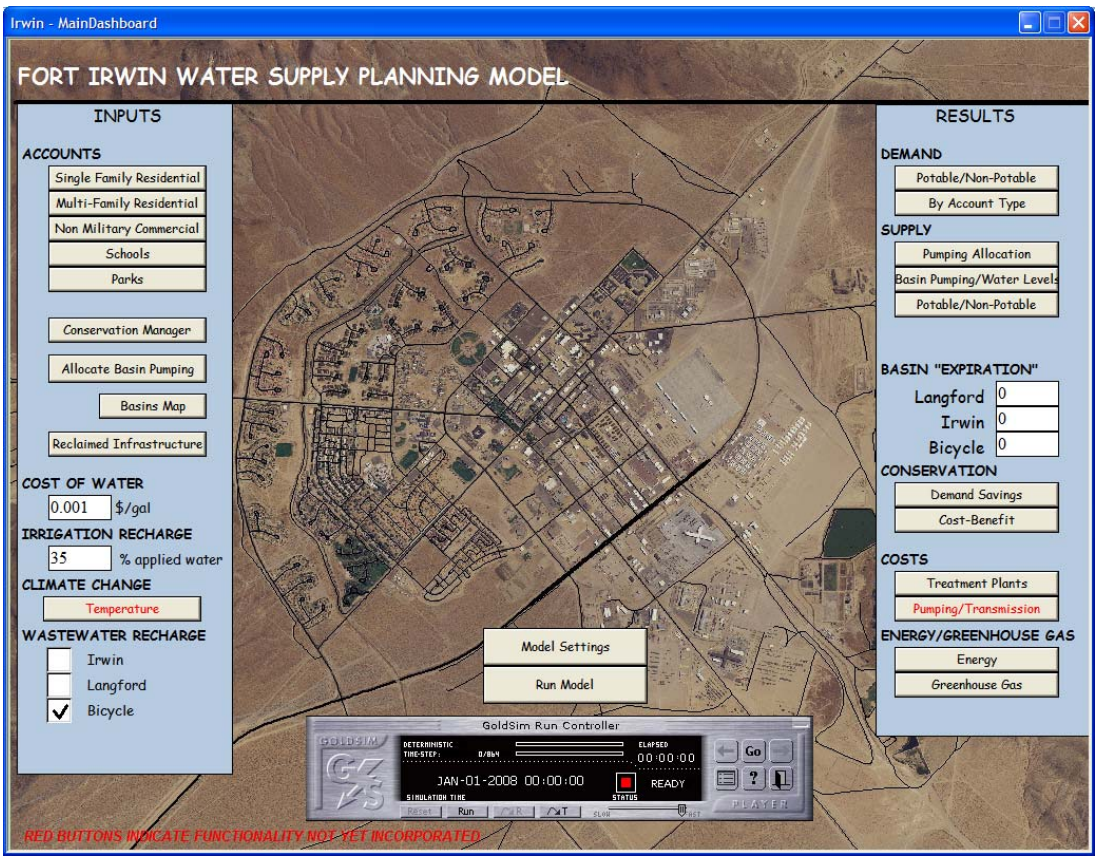

Model Output

Model output provides detailed plots of water supply and demand, water demand savings due to conservation measures, available reclaimed water supply, "expiration" dates for basins, and costs and benefits of water conservation. An example of the cost-benefit analysis is presented below,

In addition, greenhouse gas emissions and greenhouse gas savings due to implementation of conservation measures are output (see example plot below).

Model Calibration

The model was calibrated to 2004 water demand. Total water demand at Fort Irwin is assumed to be equal to total pumpage (2.46 mgd in 2004) minus RO treatment plant brine discharge (0.08 mgd) and export water to Goldstone (0.08 mgd). This leaves a total demand estimate of 2.3 mgd. Total average annual outdoor water use is estimated to be 1.23 mgd in 2004, based on a total demand of 2.3 mgd minus an indoor water demand of 1.07 mgd. The model was calibrated against the primary sources of available data: total water supply, and total indoor use.

SUMMARY MODEL RESULTS

Improvements in irrigation management practices provide the greatest potential for water savings, both in terms of quantity of water saved and ratio of benefit to cost. If all irrigation measures with quantified savings are implemented, total savings could be on the order of 0.5 mgd, or about 20 percent of total water used at the site (note that overlapping measures result in non-additive savings, due to "net effect"). Some of these measures have relatively insignificant capital costs, relatively minimal O&M costs, and yet save significant amounts of water. These measures represent "low hanging fruit".

A key indicator of the financial benefit of conservation measures is the payback period. This indicator shows that irrigation management and replacement, education, and faucet aerators offer the quickest payback periods and greatest return on investment. The payback period is less than ten years for all seven of these measures. The same seven measures have the highest benefit/cost ratio.

In addition to evaluation of conservation measures based on financial benefit, it is also worthwhile to consider total water savings. Five measures stand out as having very high water savings potential, all greater than 0.1 mgd: replace turf and trees, replace toilets, education, frequent irrigation schedule changes, and rate structure. All other measures have potential water savings of less than 0.05 mgd. The measures with the highest water savings are not all financially favorable, particularly the financial incentives, since it involves an expensive meter-reading and replacement program.

Impact of Assumed Projected Growth

Water demand and cost analyses assumed that Fort Irwin will grow by 50 percent in the future. It was assumed that the all types of accounts would grow at the same rate (i.e., residential units, commercial units, schools, and athletic fields). It was also assumed that all new development would use water-efficient fixtures, specifically: toilets, faucets, laundry machines, dishwashers, and urinals. This is consistent with practice at the newest development. Accordingly, the water savings during the Plan phases would not be expected to increase proportionally to the growth at the Post.

Reclaimed Water Options

Use of reclaimed water for irrigation, in place of potable water, is both a good and established water resource management practice. It reduces groundwater pumping, along with its associated power costs and carbon emissions, and provides a direct offset of potable water, allowing the potable water to be used for other, higher needs. A small "pitch-and-putt" golf course is currently the only area irrigated with reclaimed water at Fort Irwin. Plans are in place for facilities needed to transmit reclaimed water to athletic fields and parade grounds for irrigation.

Although a reduction in groundwater pumpage will occur as a result of expanding the reclaimed irrigation system, the life of local groundwater basins would not be

significantly extended by this action. This is because a high percentage of treated wastewater already percolates back into the local aquifer. As more reclaimed water is used for irrigation, a decrease in this recharge will occur, thus counteracting the effect of reduced groundwater pumping. This does not mean that the basin does not realize a significant benefit from these activities. There are the cost and carbon emission benefits noted above, as well as a decrease in the cycling of water through the basin that results in reduced TDS and nitrate buildup in the underlying aquifer.

In order to evaluate the combined effect of water conservation and irrigation with reclaimed water, the model was used to assess affects of decreased groundwater pumpage and extension of local groundwater resources for the various reuse options and Plan phases. With the planned expansion of the reclaimed system, annual average groundwater pumping would be reduced by between 0.13 and 0.19 mgd, as compared with the current reclaimed irrigation system. This results in an extension of basin lifespan of about three years. If the reclaimed system were expanded to include about 45 irrigated acres, pumping would be reduced by an additional 0.18 to 0.26 mgd, extending the basin lifespan an additional three to five years. These results suggest that expansion of the reclaimed system, combined with the Plan, would be an effective strategy to reduce groundwater pumpage and, to a lesser extent, to increase lifespan of local groundwater resources.

RECOMMENDED WATER DEMAND MANAGEMENT PLAN

Results of this investigation indicated that improvements in irrigation management practices provide the greatest potential for water savings at Fort Irwin, both in terms of quantity of water saved and ratio of benefit to cost. If all irrigation measures with quantified savings were implemented, total savings could be on the order of 0.5 mgd, or about 20 percent of total water used at the Post. These measures also provide the greatest effect on extending the life of the local water resource.

The recommended Water Demand Management Plan is divided into three phases designed to be implemented in sequence. This phased approach places work that achieves relatively large water savings at a low cost in the immediate future. More costly measures are then phased in over time as experience and greater understanding of water demand characteristics of the Post are obtained. This is especially important at Fort Irwin given the lack of meter data for many critical uses. The three phases are:

- **Phase-1: Measures with No Capital Costs.** This phase consists of projects with zero capital costs and a benefit/cost ratio greater than one at 10 years. It represents “low-hanging fruit.” Phase-1 total average annual water savings are estimated to amount to about 0.26 mgd with zero capital costs and an estimated O&M cost of $77,000 per year. The calculated benefit/cost ratio is 4.5 at year 10. Phase-1 measures should extend the lifespan of local groundwater supplies by about 2 years.
- **Phase-2: Measures with Payback of <10 Years.** Phase-2 consists of conservation measures with capital costs that have a payback period of less than

10 years. These are the most cost-effective conservation measures that are not otherwise included in Phase-1. The average annual incremental water savings achieved by implementation of Phase-2 is estimated to be about 0.45 mgd at a capital cost of about $1.9 million, and no additional O&M costs. The benefit/cost ratio for these incremental measures is 2.7 at year 10. Phase-2 measures would extend the life of local groundwater supplies an estimated 16 additional years, which, in combination with Phase-1, results in an overall increase in basin lifespan of 18 years.

- **Phase-3: Meter Installation and Reading Measures**. Phase-3 consists of conservation measures that require water meters to be installed and a meter reading and replacement program implemented. The average annual incremental water savings achieved by implementation of Phase-3 is estimated to be about 0.18 mgd at a capital cost of about $500,000 and additional O&M costs of $180,000 per year. The benefit/cost ratio of these incremental measures is 1.0 at year 10. Phase-3 measures should extend the life of local groundwater supplies an estimated four additional years which, in combination with Phase-1 and Phase-2, results in an overall increase in basin lifespan of 22 years.

Because there are no capital costs associated with Phase-1, it was recommended that these measures be implemented as soon as possible. Phase-2 measures have relatively nominal capital costs, realize significant water savings, have a payback period of about four years, and significantly increase the life of local groundwater basins. Accordingly, it was recommended that Phase-2 measures be implemented as soon as is practicable. Phase-3 water savings are about 25 percent of those realized in Phase-2, with a payback period of about nine years. Although these conditions are not as favorable as Phase-1 or Phase-2, a key benefit of Phase-3 is that the metering associated with this phase will help better quantify benefits of all conservation measures. Accordingly, it was recommended that Phase-3 be implemented as soon as adequate funds are available.

While the above Plan focuses on reduction of demand, use of reclaimed water for irrigation, which provides a direct offset of potable water requirements, could be performed in conjunction with the Plan. With the planned expansion of the reclaimed irrigation system (17 acres, in addition to the current system of 6 acres), annual average groundwater pumpage would be reduced by an additional 0.13 to 0.19 mgd and basin lifespan could be extended by an additional three years. Model results suggest that the maximum area that could be serviced by reclaimed irrigation is about 45 acres (about 35 percent of total irrigation on the Post), without demand exceeding reclaimed supply during peak periods. This would reduce groundwater pumpage by about 0.3 mgd and extend basin lifespan by about seven years, as compared with the existing 6-acre reclaimed irrigation system.

Long-lead Forecasting of Monthly Rainfall Using Large Scale Climate Signals and Statistical Disaggregation Models

Azadeh Ahmadi[1], Mohammad Karamouz[2], Sara Nazif[3], Navideh Noori[4]

[1] Ph.D. Candidate, School of Civil Engineering, University of Tehran, Tehran, Iran. Email: azadehahmadi@ut.ac.ir
[2] Professor, School of Civil Engineering, University of Tehran, Tehran, Iran. Email: karamouz@ut.ac.ir
[3] Ph.D. Candidate, School of Civil Engineering, University of Tehran, Tehran, Iran. Email: saranazif@yahoo.com
[4] M.Sc., School of Civil Engineering, University of Tehran, Tehran, Iran. Email: navide_noori@yahoo.com

ABSTRACT

Monsoon, one of the most dynamic climate systems, controls rainfall variation in some countries in Asia such as India, Bangladesh, Pakistan, and Iran. It delivers the main component of annual rainfall in these regions. In this study, the relationship between Iran monsoon rainfalls and some large scale climate signals such as SLP (Sea Level Pressure) and SLP differences over certain effective regions have been examined. The correlation coefficient between various combinations of climate signals with the rainfall at different time lags demonstrates some significant correlations which are used to identify the predictors for the rainfall forecasting.
In this paper, a fuzzy rule model has been developed to predict the six-month rainfall in the southeastern part of Iran. Then the long-lead forecasting rainfall is disaggregated to a monthly scale using statistical disaggregation models and by considering the historical share of each month from total 6 month precipitations. In real time, the predicted value of each month during the 6 month time horizon is modified once the observed precipitation in any of the prior months becomes available using the Bayesian Theory. This way the accuracy of prediction will be significantly increased as we approach the last 3 months of the forecast period. The proposed model makes adequate lead time for estimation of the water resources potential for mid-term planning. Since the planning scale of water resources planning is usually monthly, disaggregated rainfall could increase the accuracy of operating schemes in the study area.

Keywords: Climate Signals, Fuzzy Rule, Disaggregation, Forecasting, Bayesian Theory

INTRODUCTION

Different optimization techniques are developed in order to define operating policies for operation of water resources systems and facilities. Forecasts of precipitation and streamflow in the next few months or even seasons are necessary for the real-time operation of water resources systems such as reservoirs. Different methods have been widely used for precipitation prediction. These methods followed different approaches ranging from pure statistical methods to methods that are mostly based

on the conceptual modeling of meteorological conditions.

The summer monsoon is one of the dynamic climate systems and the livelihood of more than 60 percent of the world's population depends on them. Furthermore, the Asian summer monsoon is a key component of the earth's climate system, having important teleconnections with global weather and climate in Iran and delivers a component of annual rainfall in the southeastern part of Iran. The sum of rainfall during the month of July, August and September is the seasonal monsoon in the southeastern part of Iran. Many investigations have been done to understand the relation between monsoons and other global phenomenas and large scale climate signals such as El Nino southern oscillation, (SST), (SLP) and other large scale climate signals. (Karamouz et al., 2004)

Following the great Indian drought of 1877, Blanford, who established the Indian Meteorological Department in 1875, forecasted Indian monsoon rainfall in 1884. Later, in the early part of the 20th century, Walker initiated extensive studies of global teleconnections which led him to the discovery of Southern Oscillation. Walker introduced the concept of correlation for long-range forecasting of Asian summer monsoon and his findings are relevant even today (Krishna Kumar et al., 2004). The models established later by Gowariker et al. (1989), Thapliyal (1990), and Sahai et al. (2003) belong to the category of Walker's studies. Among these, the model of Sahai et al. (2003), which links global SST with Indian monsoon seasonal data, appears to be the most successful.

In recent years, many efforts have been devoted to development of mid to long-term (monthly and seasonal) precipitation forecasting models for major river basins in different parts of the world. Most of these models incorporate the effects of large scale climate signals. Chiew et al. (1998) studied the correlation between the El-Nino Southern Oscillation (ENSO) events and the precipitation in Australia. Nicholson and Selato (2000) studied the effects of La-Nina events on the precipitation in Africa. Mariotti et al. (2002) studied the effects of ENSO on the Mediterranean precipitation in Europe.

In this study, a method for predicting the range of probable precipitation for two season in southwest of Iran is developed. These seasons are defined based on dry and wet periods of the year. The wet season is considered during December to May and the dry season is considered during June to November. In this method, Fuzzy Set Theory (FST) is used to develop the fuzzy rules for predicting the precipitation.

Fuzzy logic provides a framework for dealing with imprecise, vague and/or linguistic information in modeling. Fuzzy logic accepts overlapping boundaries. In other word, instead of assigning one as the degree of belonging and zero as the degree of not belonging to an element within a set (Classical Set Theory), partial membership (degree of belonging) in any given set is possible (Ozelkan et al., 1996). Karamouz and Mousavi (2003) have developed a Fuzzy Stochastic Dynamic Programming Model for reservoir operation optimization. Results of application of their model to Karoon and Dez reservoirs in Iran have shown significant improvement of operating policies of these two major reservoirs in the Middle East.

In this study, attempts have been made to explore the relationship between the rainfall in the south western part of the Iran and some large scale climate signals such as SLP (Sea Level Pressure) and SLP differences over certain effective regions all

over the world to find the appropriate predictors for forecasting precipitation. Then a fuzzy rule model has been developed to predict the rainfall at wet (Dec-May) and dry (June-Nov) seasons in the southeastern part of Iran from six months before. The proposed model makes adequate lead time for estimation of the water resources potential for long-term planning. Since the planning scale of water resources planning is usually monthly, disaggregated rainfall could increase the accuracy of operating schemes in the study area. Therefore the 6-month predicted rainfalls are disaggregated into included months using statistical disaggregation models considering the historical share of each month from total six month precipitations in different seasons. The disaggregated predictions are modified by using real time observations to make the necessary changes in reservoir operation if it is needed.
The paper is followed by an introduction to the study area and then the methodology applied for rainfall prediction and desegregation of the results are described. The results of applying the method in the study are presented in the next section and finally a summary and conclusion is given.

STUDY AREA

The study area including South Baloochestan, Kerman and Hormozgan provinces are located between 53° and 63° northern latitude and 25° and 32° eastern longitude, in the south-east part of Iran (Figure 1). The area of the considered watershed is about 25000 square kilometers and the mean annual precipitation is about 218 millimeters.

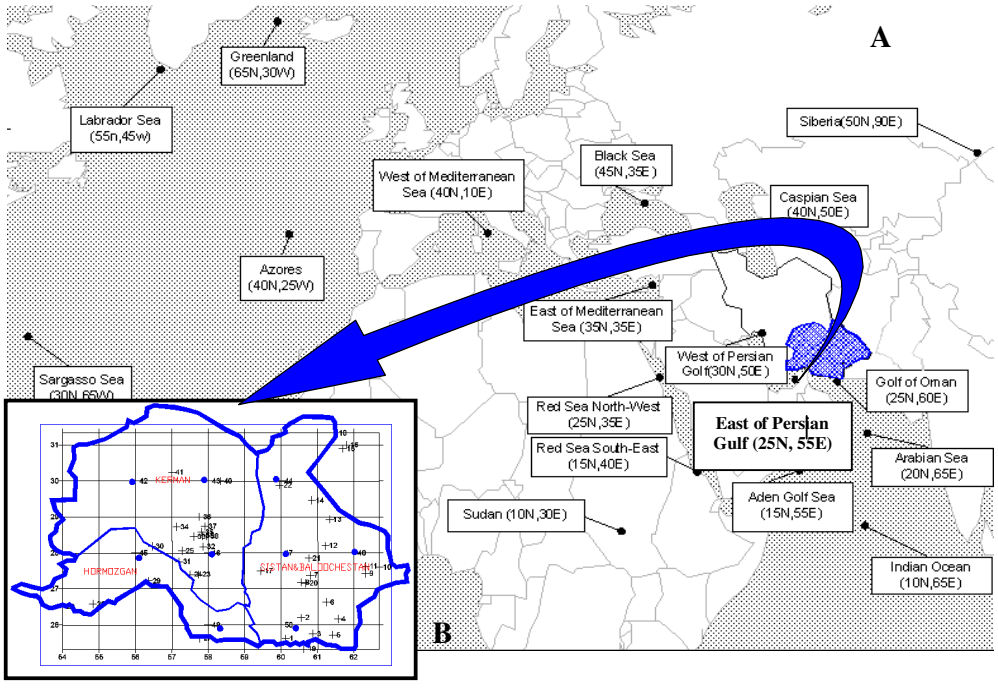

Figure 1: Location of the study area in Iran and the key points affecting its climate

The spatial variation of precipitation of this region is estimated using a multivariate geostatistical algorithm in forms of the Kriging method. In order to estimate the average precipitation of the region using the Kriging method, the stations with more than 30 years recorded data out of 41 stations shown in Figure 1-b are selected.
The average precipitation of the region is estimated to be about 155.1 mm in which 87% of the annual precipitation occurred during the wet season. Precipitation in the dry season is usually flash flood which causes flood damages. Therefore in order to use the flood potential and to estimate the water availabilities for water resources planning, precipitation forecasting is requisite.
The precipitation is forecasted considering some large scale climate signals such as SLP (Sea Level Pressure), SST (Sea Surface Temperature) and SLP differences over certain regions. These points, shown in Figure 1-a, have been determined to be effective signals on Iran's climate in previous studies by Karamouz et al. (2004).
SLP data between the years 1973 to 2004, which is estimated for the National Science Foundation by the National Center for Atmospheric Research (NCAR) in USA, has been used in this study. Monthly SST data is also derived from NOAA Advanced Very High Resolution Radiometer (AVHRR). The spatial resolution is approximately 5.689 pixels per degree.
The effective signals on the case study climate are determined considering correlation coefficient between average precipitation and all of the considered signals, and scatter plots for accuracy control. The selected signals are considered as the fuzzy inputs for six month precipitation forecast, then the forecasted results are disaggregate to monthly values. In the next section the Fuzzy Rule and statistical disaggregation models are explained.

MATERIALS AND METHODS

Fuzzy Rule Model

In this study, a method for seasonal precipitation prediction using the FST (Fuzzy Set Theory) is developed. In general, a fuzzy set consists of a set of explanatory variables called premises, $A_{i,n}$, given in the form of fuzzy numbers with membership functions $\mu_{A_{i,n}}(a_n)$ and a consequence B_i also in the form of a fuzzy number:

$$If\ a_1 \in A_{i,1} \Theta\ a_2 \in A_{i,2} \Theta \ldots a_n \in A_{i,n}, Then\ b \in B_i \quad (1)$$

where Θ is a logical operator that can be selected based on the application. The membership function $\mu_{A_{i,n}}(a_n)$ measures how much each observed data a_n belongs to the set $A_{i,n}$. In contrast to the crisp rules, fuzzy rules allow partial and simultaneous degree of fulfillment of rules. The following steps should be taken for development of fuzzy rules (Karamouz and Zahraie, 2004):

- Divide input-output space into fuzzy regions (intervals)
- Generate fuzzy rules from given data
- Calculate the degree of fulfillment for each rule (see Zimmerman, 1996)
- Assign a weight to each rule

- Predict using the rule-based system

The following structure has been used for defining fuzzy rules:
Rule number z:

$$If \quad G_1(t) \in G_i^f \otimes G_2(t) \in G_j^f \otimes G_3(t) \in G_k^f \otimes G_4(t) \in G_l^f \otimes G_5(t) \in G_m^f \otimes G_6(t) \in G_n^f \quad (2)$$
$$Then \quad P(t+1) = P_h^f$$

where:
$G_i(t)$: i^{th} SLP index in season 2 of the year t
$P(t+1)$: Average precipitation in season 1 of the year t+1
G_k^f : k^{th} fuzzy interval defined for standardized SLP and SLP gradient
P_h^f : characteristic value of the hth fuzzy interval defined for precipitation
Then the degree of fulfillment of rule z is calculated using the following equation:

$$v_z(t) = \mu_{G_i^f}[G_1(t)] \cdot \mu_{G_j^f}[G_2(t)] \cdot \mu_{G_k^f}[G_3(t)] \cdot \mu_{G_l^f}[G_4(t)] \cdot \mu_{G_m^f}[G_5(t)] \cdot \mu_{G_n^f}[G_6(t)] \quad (3)$$

where $\mu_{G_i^f}[G_k(t)]$ is the value of the membership function of related fuzzy intervals. To show which portion of the data is explained by a given rule, the weight associated with each rule (ξ_z) can be estimated as:

$$\xi_z = v_z(t) \cdot \mu_{P_h^f}[P(t+1)] \quad (4)$$

where $\mu_{P_h^f}[P(t+1)]$ is the value of the membership function of related fuzzy interval for the precipitation in each season of the year t+1. Elimination of the rules can be done if desired, by setting a threshold so that the rules having weights below or equal to that limit are not considered. In this study, a 10 percent threshold is considered.

Statistical Disaggregation

The basic goal of any disaggregation model is to allow the preservation of statistical properties at more than one level. Disaggregation facilitates the use of long-term persistence levels, particularly in multi sites, multi seasons time series modeling. Salas et al. (1980) classified disaggregation models into temporal and spatial disaggregation models. In the case of seasonal disaggregation, the sub-series (seasonal data) sum exactly to give the original series (annual data). In this study, the basic disaggregation model proposed by Valensia and Schaake (1973) is used. The linear dependence model is as follows:

$$Y_t = AX_t + B\varepsilon_t \quad (5)$$
$$\hat{A} = S_{YX} S_{XX}^{-1}$$
$$\hat{B}\hat{B}^T = S_{YY} - \hat{A} \cdot S_{XY}$$

where X_t is the annual rainfall matrix of year t, Y_t is the current observation of the series being generated, ε is the matrix of the independent random variables, A, B are the parameters matrix, and S_{YX} is the matrix of covariances' between the seasonal series.

Modification of Monthly Data

Because of high uncertainties in long lead rainfall prediction, the observed value may be completely different from what has been forecasted. Therefore modification of the rainfall forecasts based on the recorded data in each coming month could help in achieving more reliable results to be applied in water resources management practices.

In this study for modifying the disaggregated rainfalls a similarity based approach has been applied. For this purpose at first, the Equilidian distance between the observed rainfall values in the present year and the historical years (D_{ij}) is calculated as follows:

$$D_{ij} = \sqrt{\sum_{n=1}^{m} (R_{ni} - R_{nj})^2} \quad (6)$$

where R_{ni} and R_{nj} are the rainfall value in month n in the present year and year j, respectively. m is equal to the number of the observed months plus one because the situation of the last month before starting the forecasting season is also considered in rainfall modification.

The year with the minimum distance from the present situation has been considered for monthly rainfall modification. The monthly weight for rainfall in the subject year are calculated and averaged with the weights obtained by disaggregation. The monthly rainfall predictions are modified based on the resulting weights as follows:

$$R_{\mathrm{mod}\,k} = R_k \frac{W_{\mathrm{mod}\,k}}{W_{dk}} \quad (7)$$

where R_{modk} and R_k correspond to the modified and disaggregated rainfall in month k respectively. W_{modk} is the modified weight of month k and W_{dk} is the resulting weight of month k from disaggrigation.

RESULT

The effective signals on the case study climate are determined for two seasons. The used signals for June to November (dry season) are:

- SLP difference of west of the Persian Gulf and the Aden Gulf
- SLP difference of east of the Persian Gulf and the Oman Gulf
- SLP difference of east of the Persian Gulf and the Aden Gulf
- SLP of the Caspian Sea
- SST of the Oman Gulf
- SST of west of P the Persian Gulf

The selected signals for December to May (wet season) are:

- SLP difference of Siberia and Sudan
- SLP of west of Mediterranean Sea
- SLP difference of east of the Persian Gulf and Arabian sea
- SST of Black Sea

- SLP difference of the Aden Gulf and the Arabian Sea

The results show that during the dry season, effective signals are local such as the Persian Gulf, Oman Gulf, Aden Gulf and the Caspian Sea and close to the case study. For more accurate results, more studies are needed to investigate the effects of local signals in finer grids on the model performance.

One of the effective signals during the wet season is SLP the difference of the Siberia high pressure zone and Sudan low pressure zone on the precipitation over the study area. The Sudanese system is formed over Sudan when the air pressure is low. This system can absorb the water vapor due to the high temperature of its air mass. The humidity of this system is significantly increased after moving toward east over the Red sea. Some times, this system becomes over humid after movement over the Persian Gulf and it can create heavy rainfalls in the study area. In some cases, both Mediterranean and Sudanese Systems enter the country contemporaneously.

After a sensitivity analysis to find the number of fuzzy regions, the precipitation standardized SLP and SLP gradient are descritized into five fuzzy regions. The extents of fuzzy regions are defined based on the variability of the observed signals and precipitation data in the historical records. The fuzzy regions are used to classify the data into very low, low, normal, high, and very high categories as shown in Figure 2.

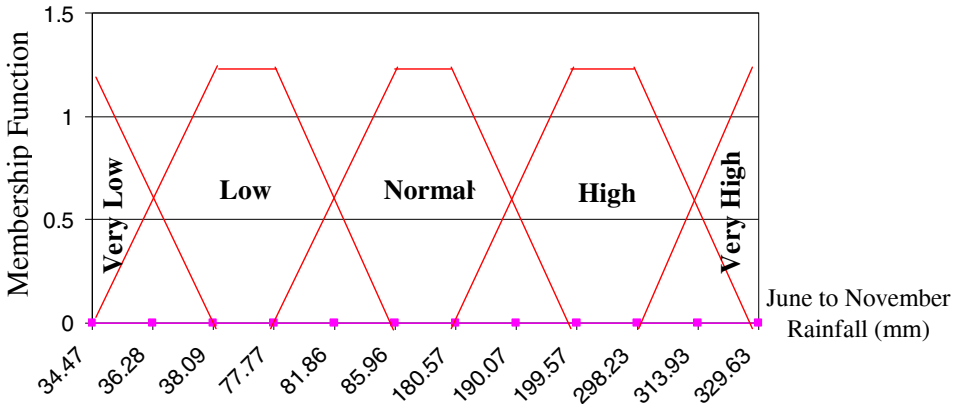

Figure 2: The fuzzy classification for observed rainfall

After developing the structure of fuzzy rules, the rules are used for reproducing the historical records. The effectiveness of the rule structures were tested in order to reproduce the actual observations for 21 years of historical records (calibration period) and then simulate and validate them for 11 years. The forecasting results are presented in Table 1 and show even though the average of low and high bounds for each year is not exactly the same as observed data, but the forecasted bounds include the observed value.

Disaggregation is used to obtain the monthly precipitation. Matrix A includes 0.08, 0.17, 0.19, 0.05, 0.22, 0.28 values for June to November respectively. The results show the share of July and August is relatively high and it is because of the flash flood in the study area.

Table 1: The results of forecasting model for dry and wet seasons

Year	Forecasted precipitation (June- November)		Observed	Forecasted precipitation (December- May)		Observed
	Low Bound	High Bound		Low Bound	High Bound	
1996	8.73	39.83	38.2	77	170	122.1
1997	18.16	47.60	42.18	126	272	142.9
1998	8.52	36.31	11.29	77	170	110.8
1999	7.58	35.86	10.46	82	116	93.7
2000	11.24	41.90	15.33	82	116	98.5
2001	6.80	38.24	15.36	74	209	91.9
2002	8.02	39.24	20.42	24	90	42
2003	8.61	36.90	11.58	79	147	124.8
2004	7.43	38.76	24.64	77	170	172.3

Table 2: The observed (obs) and disaggregated forecasts (dis) for June to November (mm)

	June		July		August		September		October		November	
	obs	dis	obs	dis	obs	dis	obs	dis	obs	dis	obs	dis
1996	3.99	3.26	2.88	2.09	3.20	3.09	2.09	0.95	9.91	4.8	16.13	10.09
1997	0.72	0.00	2.04	3.52	5.01	3.3	2.86	1.87	16.34	16.0	15.21	8.19
1998	1.29	1.19	3.30	4.78	2.70	2.49	4.00	5.13	0.00	2.02	0.00	6.81
1999	1.04	3.56	1.68	5.64	2.33	4.07	0.25	0.00	0.00	0.00	5.17	8.45
2000	1.11	0.54	1.09	1.85	0.13	3.11	0.48	0.95	2.47	2.58	10.05	17.54
2001	4.91	5.68	0.54	5.13	0.78	3.06	4.26	4.37	1.72	1.17	3.16	3.11
2002	2.09	2.65	7.65	7.89	6.36	5.65	0.11	3.8	0.00	0.12	4.21	4.53
2003	4.56	4.27	0.79	1.41	4.43	4.85	0.18	0.49	0.60	1.67	1.02	10.08
2004	14.16	13.21	6.12	3.0	1.39	2.82	2.97	2.11	0.00	1.18	0.00	0.78
RMSE	1.03		2.42		1.59		1.43		1.92		5.60	

The Root Mean Squared Error (RMSE) is used to evaluate prediction accuracy:

$$RMSE = \sqrt{\frac{\sum_{t=1}^{n}(y_t - \hat{y}_t)^2}{n}} \qquad (6)$$

where y_t is the observed data, $\hat{y}_t$ is the associated modeled value and n is the total number of data. The RMSE for the forecasted model in dry season is about 2.4 mm. Because of local phenomena that cause perturbations in monthly rainfall variations, the downscaled data are not well compatible with the observed data. Therefore the modification process has been employed to achieve more reliable results in monthly time scale.

The modified monthly rainfall forecasts from year 1996 to year 2004 are tabulated in Table 3. As can be seen by using the modification method the forecasted monthly rainfall data becomes more similar to the observed values. The results show the most important period in forecast modification is from June to September and after that the modification does not result in high variations in monthly forecasted values. Considering more local parameters in rainfall forecast modification could considerably help in increasing forecasts reliability.

Table 3. Comparison between modified (mod) and monthly observed (obs) rainfalls (mm)

	July		August		September		October		November	
	obs	mod	obs	mod	obs	mod	obs	mod	obs	mod
1996	2.88	2.63	3.20	3.19	2.09	1.30	9.91	6.11	16.13	18.92
1997	2.04	3.31	5.01	5.44	2.86	3.34	16.34	15.34	15.21	13.08
1998	3.30	4.09	2.70	2.84	4.00	4.42	0.00	1.26	0.00	0.00
1999	1.68	2.93	2.33	2.13	0.25	0.40	0.00	0.00	5.17	6.41
2000	1.09	1.81	0.13	0.73	0.48	0.79	2.47	2.29	10.05	11.33
2001	0.54	2.33	0.78	1.84	4.26	4.35	1.72	1.59	3.16	3.55
2002	7.65	7.83	6.36	5.46	0.11	2.18	0.00	0.06	4.21	4.10
2003	0.79	1.10	4.43	4.46	0.18	0.40	0.60	0.83	1.02	3.66
2004	6.12	5.91	1.39	1.99	2.97	3.26	0.00	0.00	0.00	0.00
RMSE	0.93		0.57		0.78		1.38		1.59	

SUMMARY AND CONCLUSION

The long lead rainfall forecasting plays an important role in developing reliable water resources management schemes. Since there are different sources of uncertainties affecting the rainfall variations, applying the methods that could incorporate these uncertainties could help achieve reliable results. In this study, Fuzzy set theory has been employed for forecasting rainfall in two seasons (Jun-Nov and Dec-May) in the south-eastern part of Iran. The most correlated climatic signals with rainfall of the study area have been considered as predictors and the 6 month rainfall is considered as the predictant. The considered signals include SLP, SST and SLP difference.

The observed values of the six month rainfall are in the forecasted interval of rainfall by Fuzzy model but in some cases they are near boundaries. The six month forecasted values are disaggregated using statistical models to monthly time steps to be applied for practical purposes. The best results are obtained for September and the worse correspond to November. The perturbations in the results are related to local climatic variability that effects the rainfall variations. For employing these effects in rainfall forecasting a modification method has been developed based on the similarity of the present year to historical data. The forecasts reliability has been improved up to 50% by this method. This improvement could result in more

flexibility in water resources operation.

REFERENCES

Chiew, F. H. S., Piechota, T. C., Dracup, J. A., and T. A. McMahon (1998). "El Nino/Southern Oscillation and Australian rainfall, streamflow and drought: links and potential for forecasting." *Journal of Hydrology*, 204, 138-149.

Gowariker, V., Thapliyal, V., Sarker, R. P., Mandal, G. S. and Sikka, D. R., (1989). "Parametric and powe regression models: new approach to long range forecasting of monsoon in India." Mausam, 42, 115-122.

Karamouz, M. and Mousavi, S. J., (2003). "Uncertainty Based Operation of Large Scale Reservoir Systems." *J. of Water Resources Association*, 961-975.

Karamouz, M., Zahraie, B., and Eghdami, S. (2004). "Effects of Large Scale Climate Signal on Regional Dry and Wet Spells." Proceedings *of the 6th International Conference on Hydroinformatics* - Liong, Phoon & Babovic (eds).

Karamouz, M., Zahraie, B., (2004), "Seasonal Streamflow Forecasting using Snow Budget and Enso Climate Signal: Application in Salt River Basin in Arizona", ASCE, Journal of Hydrologic Engineering, 9(6), 117-130.

Krishna Kumar, K., Soman, M.K., Rupa, Kumar, K., (2004), "Seasonal Forecasting of Indian Summer Monsoon Rainfall: A review", Indian Institute of Tropical Meteorology.

Mariotti, A., Zeng, N. and Lau, K. M. (2002). "Euro-Mediterranean Rainfall and ENSO – a Seasonally Varying Relationship." *Geophysical Research Letters*, 29(10), 59.1-59.4.

Nicholson, S. E. and Selato, J. C. (2000). "The Influence of La-Nina on African Rainfall." *International Journal of Climatology*, 20, 1761-1776.

Ozelkan, E. C., Ni, F., and Duckstein, L. (1996). "Relationship between monthly atmospheric circulation patters and precipitation: Fuzzy logic and regression approach." *Journal of Water Resources Research*, 32(7).

Sahai, A. K., Grrimm, A. M., Satyan, V. and Pant, G. B. (2003). "Long lead prediction of Indian Summer monsoon rainfall from global SST evolution." climate Dyn, 20, 855-863.

Tapliyal, V. (1990). "Long range prediction of summer monsoon rainfall over India: Evolution and development of new models." Mausam, 91, 339-346.

LOOKING FOR A SOLUTION – JOINT FRONT RANGE CLIMATE CHANGE VULNERABILITY STUDY

Alfredo Rodriguez[i], Laurna Kaatz[1]

[1] Sr. Water Resources Engineer, Aurora Water, Aurora Colorado 80012 (303)739-7334 email: drodrigu@auroragov.org
[2] Climate Scientist, Denver Water, Denver Colorado 80204 (303)628-6424 email: Laurna.kaatz@denverwater.org

Abstract

This paper summarizes ongoing efforts by Colorado's Front Range water providers to assess changes in the timing and volume of hydrologic runoff that might be expected from selected climate change scenarios for the years 2040 and 2070. Many utilities across the United States believe that climate change poses a threat to their water supplies, and have a desire to evaluate potential impacts. This cooperative research will provide water utilities in the Rocky Mountain Front Range with the knowledge and methodology necessary to evaluate potential climate change impacts on their water supplies. Furthermore, this study will set the stage for future advances in procedures and technologies.

1. Introduction

Water is essential for the continued economic development of the western United States. With the increasing recognition of global and regional climate changes, Metropolitan water providers along Colorado's Front Range are concerned about the possible impacts these changes may have on their future water supply availability. This is of particular concern given that recent studies indicate global warming may lead to unprecedented drought conditions in the Southwest U.S. (IPCC 2007). Several Front Range water providers including the City of Aurora, City of Boulder, Colorado Springs Utilities, Denver Water, City of Ft. Collins, and Northern Colorado Water Conservancy District have come together to participate in a study intended to provide the education, tools, and methodology necessary to examine the possible effects of climate change on several shared watersheds.

The study area that includes the service area of the Front Range providers is shown in Figure 1.



Figure 1. Project Study region over which temperature and precipitation offsets will be are derived. Boundaries of the study region are 107.526-104.4375 W and 38.5625-40.5625 N. This area in the data set contains 17 N-S grid points by 26 E-W grid points.

This study is designed to enable entities that obtain their water supplies from the upper Colorado, South Platte, Arkansas, Cache la Poudre, St. Vrain, Boulder Creek, Big Thompson, and other similar river basins to examine potential effects climate change may have on those supplies. This regional unified approach is intended to help Colorado water providers communicate with their customers and the media cohesively by working with the same historic and projected hydrometeorological data, historic natural streamflow, and methodology. Lessons learned from this collaborative approach can be used to encourage and establish other regional efforts in Colorado and throughout the country.

The central objective of this project is to assess changes in the timing and volume of hydrologic runoff that might be expected from selected climate change scenarios for the years 2040 and 2070. Two hydrologic models will be calibrated and implemented in this study including the WEAP (Water Evaluation and Planning) Model run by Dr. David Yates of NCAR, and the linked Sacramento Soil Moisture model with the Snow-17 model (hence forth called the "Sacramento Model") run by Riverside Technology, inc. The Colorado Water Conservation Board (CWCB) will aid in the compilation of historic naturalized streamflow sequences (1950-2005) for use as a baseline comparison for river basin gauge locations of primary interest to the participants. Based on regionally downscaled temperature and precipitation projections (developed by the Bureau of Reclamation and others) and discussions with the Western Water Assessment (WWA),

the future temperature and precipitation scenarios to be used to generate corresponding future streamflow have been established. These future scenarios of temperature and precipitation are based on the results of 16 global climate models (GCMs) driven by three future greenhouse gas emissions scenarios, A2, A1b, and B1. The streamflows obtained by running perturbed sequences of temperature and precipitation through the hydrologic models will be compared to historic streamflows to estimate the sensitivity of water supplies to climate change. The outputs from this research will include climate-adjusted natural-flow time series at selected locations, and statistical evaluations of differences between these and historic natural flows for water availability assessments.

2. Project Description

Metropolitan water providers along Colorado's Front Range are concerned about the impact climate change may have on their future water supply availability. To better understand the possible impacts of climate change several Front Range providers are working together to provide the education, tools, and methodology needed to study these effects. This project is designed to enable entities that obtain their water supplies from the upper Colorado, South Platte, Arkansas, Cache la Poudre, St. Vrain, Boulder Creek, and Big Thompson River Basins to examine potential effects climate change may have on these supplies. The participating group, called the Project Steering Committee (PSC), consists of representatives from Aurora Water (Aurora), City of Boulder (Boulder), City of Fort Collins (Fort Collins), Colorado Spring Utilities (Colorado Springs), Denver Water (Denver), and Northern Water (Northern). The role of the PSC is to ensure the study meets each provider's needs. Additional expert resources have been and will continue to be utilized through the help of the Western Water Assessment (WWA) and the Colorado Water Conservation Board (CWCB). The WWA aids the PSC in selection of greenhouse gas emission scenarios used to drive Global Climate Models (GCMs), and interpreting and selecting downscaled GCMs temperature and precipitation output data. The selected datasets will be used to drive the hydrologic models necessary to assess the sensitivity of streamflow to changes in climate. The CWCB is working with the PSC to establish the sets of historic naturalized streamflow data on a daily timestep for use in the hydrologic models: these datasets will be useful to all study participants. This unified approach is intended to help Front Range water providers communicate with their customers and the media cohesively, through use of the same hydrometeorological data and use of the same methods and climate change scenarios. Lessons learned from this unified approach could also be used to encourage and establish further regional efforts in Colorado and throughout the country.

The goal of this study is a streamflow sensitivity analysis of the PSC's watersheds focused on the development of future naturalized streamflow data using selected climate change scenarios. Each provider can use these future streamflow scenarios in conjunction with their water rights allocation assumptions to estimate the impacts of various climate change scenarios on their water supply. Throughout this process each participant will have the opportunity for education in:

- climate variables and modeling techniques (including emissions scenarios, global climate models (GCMs), and downscaling approaches) through educational sessions with the WWA,
- the standardization process of historic naturalized streamflow sequence development with oversight from the CWCB,
- two hydrology models calibrated for several river basins in Colorado,
- the procedures required for this type of sensitivity analysis, and
- correctly interpreting study results with guidance from WWA.

Scientific understanding of the Earth's long-term and short-term climate trends has increased over the past several years. In parallel with this increased understanding, have been improvements in modeling techniques used to project current changes, past trends, and future possibilities at the global, regional, and local levels. Future global climate projections have been modeled using different emission scenarios determined by variables including economic growth, population growth, varying energy sources, and environmental sustainability. These models consistently predict that global average surface temperatures will rise. The most current quantitative results predict that the mean global surface temperature will increase by 0.8 to 4ºC by 2099 (these values are considered "Best estimates" in the IPCC 2007 AR4).

Possible changes in North America's climate include greater annual warming across the continent as compared with global projections, decreases in snow depth and season length, and across the southwest United States in particular, a decrease in annual precipitation and an increase in average summer temperatures (IPCC 2007 AR4). Though this information comes from the latest scientific studies, it is important to note that the uncertainty in these projections is large and the stated results should be considered only as possibilities.

Snowpack is the most important water source in the western U.S., and thus it is critical that water managers be provided with, 1) estimates of changes in future snowpack under various scenarios; and 2) an improved understanding of the mechanisms that give rise to snowpack variability from year-to-year. Previous climate studies have shown a wide variety of possible impacts, from no change (Duffy et al. 2006), to significant reductions in snowpack (Leung et al. 2003). Observations over the past 50 years of winter precipitation and temperature in the Western United States are shown in Figure 1 (Edwards and Redmond, 2005). The figure shows no obvious trend in winter precipitation but indicates that winter temperatures are on the rise. A recent analysis of the 2007 IPCC Fourth Assessment global models by Hoerling and Eischeid (2006) indicates that the combination of increased temperature and a weak to non-existent trend in snowpack may produce unprecedented drought conditions over the next 50 years in the Southwestern United States due to a strong increase in evapotranspiration resulting from increased temperature. Seager et al. (2007) came to similar conclusions regarding future runoff in the Southwest through an independent analysis of the IPCC Fourth Assessment global models. This study suggested that drought conditions will be unlike any previously observed in this region because of significant drying in sub-tropical

regions due to shifts of the Hadley cell circulation and extratropical jet stream pattern northward combined with El Niño events.

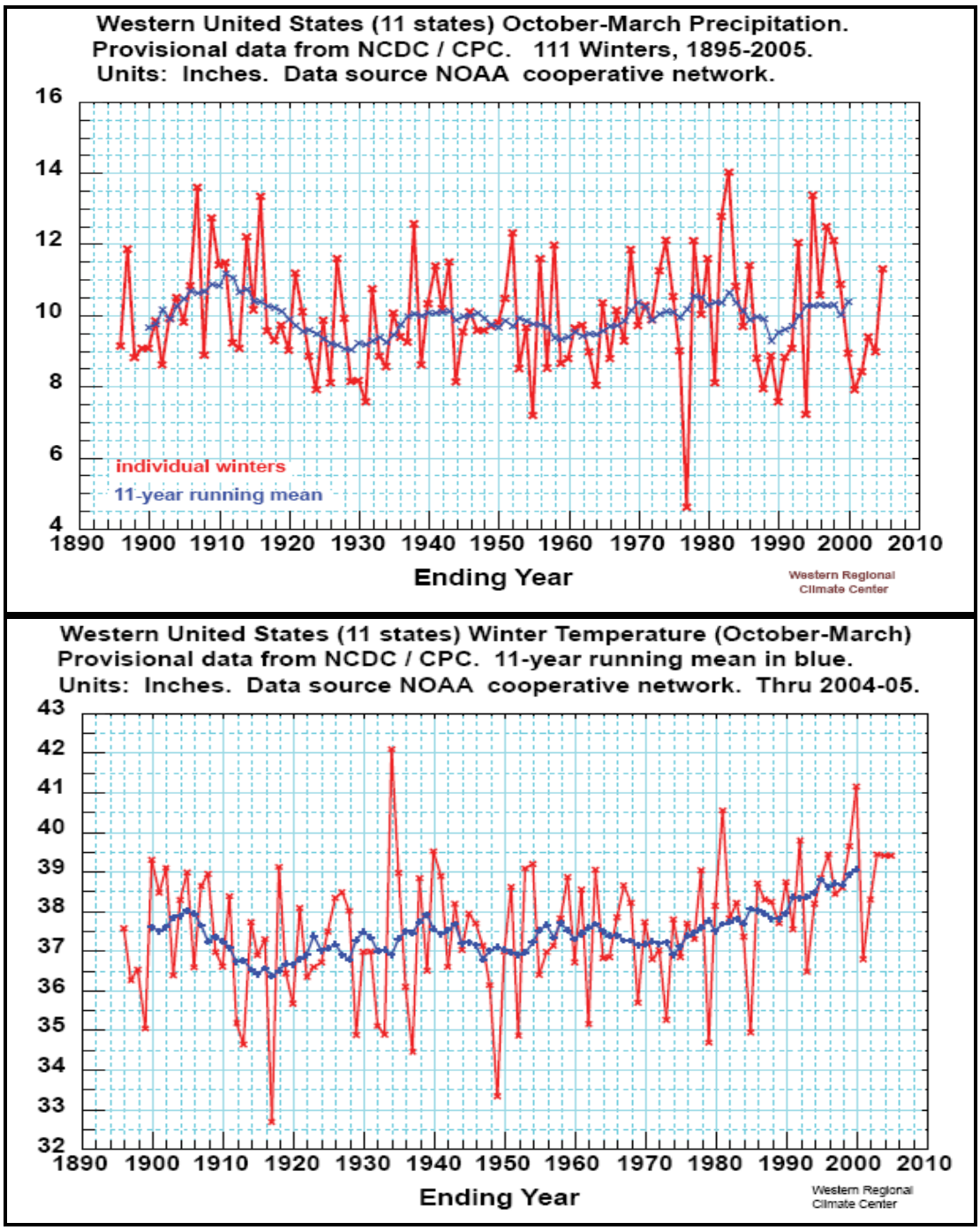

Figure 1. Western U.S. winter precipitation (Oct.-March; left) and western U.S. winter temperature for October-March from 1895-2005 (note: units on right graph are °F not inches, which is mislabeled). From Edwards and Redmond, 2005.

Scientific studies have shown that hydrologic systems and water resources are sensitive to climate change and variability, and that such changes add further stress to already over-allocated river basins. The June 2006 Western Governor's Association Report stated that average temperatures in the West have risen 2-5º F during the 1900s and are predicted to continue rising. The possible vulnerabilities to river basins in Colorado due to the previously described climate change include:

- Changes in precipitation including:
  - frequency and intensity,
  - phase (rain vs. snow),
  - temporal distribution (seasonality), and
  - spatial distribution (location),
- Increases in water use,
- Decreases in snowpack,
- Earlier snowpack melt-off,
- Increases in evaporation,
- Changes in soil moisture,
- Frequent and extended extreme conditions (droughts and floods),
- Increases in the frequency and duration of wildfires,
- Erosion and sedimentation changes,
- Water quality changes, and
- Recreational and environmental impacts

Such impacts are likely to change the historic timing and yield of water systems throughout Colorado. This study will aid in the understanding of how some of these changes may impact water supplies for Front Range users.

3. Project Duration and Cost.

This project is being co-funded by all of the participating entities with a matching research fund from the American Water Works- Research Foundation (AwwaRF). The following values and Table 1 below indicate the amount of contributions made by all of the participants in the project.

The total cost of this 13-month project has been estimated to be $379,900.

AwwaRF Funds Requested:	$80,000
Amount of Funds eligible for AwwaRF match:	$82,400
Amount of Funds not eligible for AwwaRF match:	$37,600
Total Cash Budget (AwwaRF Funds + All Co-Funding Cash):	$200,000
Total In-kind Contributions:	$179,900
Total Project Budget (Cash + In-kind):	**$379,900**

Table 1 - Joint Front Range Study Participant Cost

Organization Name	Cash Co-fund Amount	In-Kind* Contribution Amount
City of Aurora	$48,000	$14,000
City of Boulder	$8,000	$5,500
Colorado Springs Utilities	$10,000	$16,000
Denver Water	$24,000	$16,000
City of Fort Collins	$10,000	$5,500
Northern Colorado Water Conservancy District	$20,000	$10,500
Western Water Assessment		$22,400
National Center of Atmospheric Research		$54,000
Riverside Technology, Inc.		$36,000
TOTAL	**$120,000**	**$179,900**

Overall, we envision the project to take 13 months, as shown in **Table 2**. This schedule assumes a project start date of November 1, 2008.

Objective	Start	Finish	2008 Nov	Dec	Jan	Feb*	Mar	Apr	May*	2009 Jun	Jul	Aug*	Sep	Oct	Nov
Streamflow Accumulation	11/1/08	3/31/09	■	■	■	■	■								
Model Development	11/1/08	3/31/09	■	■	■	■	■								
Model Bias Adjustment	2/1/09	3/31/09				■	■								
Preliminary Investigation	4/1/09	4/30/09						■							
Delta TP Development	4/1/09	4/30/09						■							
Sensitivity Evaluation	4/1/09	7/31/09						■	■	■					
Results and Training	8/1/09	8/31/09										■			
Draft Report	6/1/09	8/31/09								■	■	■			
AwwaRF Review	9/1/09	9/30/09											■		
Final Report	10/1/09	11/30/09												■	■

* Depicts the beginning of every month a quarterly report is due.

Table 2. Joint Front Range Climate Change Vulnerability Study Schedule. Regular progress and communication meetings will occur at the end of every month.

4. Conclusions

As of the date this document was written, the Joint Front Range Study is in its third month and results have not been obtained. Data continue to be gather and models being

calibrated. It is expected that by the time of the conference, the authors will be able to show preliminary results.

One of the most important aspects of this project relates to education. Although climate change has been documented and advertised intensively, this phenomenon and its effects need to be really understood in order to make sound decisions in the water supply arena, especially at the regional and local level.

The cost of building projects to ameliorate the effects of climate change appear to be prohibitive but with the proper education and sound policy decisions, adaptation seems to be a more reasonable approach, but in order to adapt one needs to understand the cause and effects of a phenomena such as climate change.

REFERENCES

Duffy, P.B., R.W. Arritt, J. Coquard, W. Gutowski, J. Han, J. Iorio, J. Kim, L.R. Leung, J. Roads, and E. Zeledon, 2006, *J. Climate*, **19**, 873 – 895.

Edwards, L.M., and K. T. Redmond, 2005: Climate factors on Colorado River Basin water supply. Colorado River Basin Climate, Special publication for Association of California Water Agencies and Colorado River Water Users Associations Conference, November 2005, 14 – 22.

Hoerling, M. and J. Eischeid, 2006: Past Peak Water in the Southwest. *Southwest Hydrology*, January/February, **35**,18-19.

IPCC (2007). "Contribution of Working Group I to the Fourth Assessment Report of the IPCC." Report can be found at: http://ipcc-wg1.ucar.edu/index.html

Leung, L. R., Y. Qian, J. Han, J. Roads, 2003: Intercomparison of global reanalyses and regional simulations of cold season water budgets in the Western United States, *J. Hydromet*., **4**, 1067 – 1087.

Leung, L.R. and Y. Qian, 2003: The sensitivity of precipitation and snowpack simulations to model resolution via nesting in regions of complex terrain. *J. Hydromet*., **4**, 1025 – 1043.

Seager, R., M. Ting, I.Held, Y. Kushnir, J. Lu, G. Vecchi, H-P. Huang, H. Harnik, A. Leetmaa, N-C Lau, C. Li, J. Velez, and N. Naik (2007): Model projections of an imminent transition to a more arid climate in Southwestern North America. *Science*, **316**, 1181 – 1184.

Managing Salinity in the Upper Santa Clara River System of California

Nathan Brown[1], Brian Louie[2], Frank Guerrero[3], Terry Foreman[4], Sorab Panday[5], Vivek Bedekar[6], and Jagjit Kaur[7]

[1]CH2M HILL, 2525 Airpark Drive, Redding, CA 96001; PH (530)229-3254; email: nate.brown@ch2m.com
[2]Sanitation Districts of Los Angeles County, 1955 Workman Mill Road, Whittier, CA 90601; PH (562)908-4288, x2802; email: blouie@lacsd.org
[3]Sanitation Districts of Los Angeles County, 1955 Workman Mill Road, Whittier, CA 90601; PH (562)908-4288, x2832; email: fguerrero@lacsd.org
[4]CH2M HILL, 325 E. Hillcrest Drive, Suite 125, Thousand Oaks, CA 91360; PH (805)371-7817, x38065; email: terry.foreman@ch2m.com
[5]AMEC Geomatrix Consultants (formerly with HydroGeoLogic), 620 Herndon Parkway, Suite 200, Herndon, VA 20170; PH (703)483-6468; email: sorab.panday@amec.com
[6]S.S. Papadopulos & Associates (formerly with HydroGeoLogic), 7944 Wisconsin Avenue, Bethesda, MD, 20814; PH (301)718-8900, x233; email: vivekb@sspa.com
[7]CH2M HILL, 1000 Wilshire, 21st Floor, Los Angeles, CA 90017; PH (213)538-1392, x35429; email: jagjit.kaur@ch2m.com

ABSTRACT

The Santa Clara River in Southern California provides beneficial uses that include agricultural water supply, groundwater recharge, and rare and endangered species habitat. Significant urbanization has contributed to elevated chloride concentrations along portions of the river in the Santa Clarita Valley and downstream areas. The affected reaches of the Santa Clara River are included on California's list of impaired waters with respect to chloride. A total maximum daily load for chloride, which was originally adopted by the Los Angeles Regional Water Quality Control Board in 2002 and later amended in 2004 and 2006, required special studies to provide the technical basis for establishing appropriate chloride water quality objectives. As part of these studies, a fully integrated groundwater/surface-water numerical model was developed to facilitate the implementation of the chloride total maximum daily load. Modeling results indicated that implementation of expensive water treatment alternatives at two water reclamation plants would not likely lead to consistent compliance with existing chloride objectives in local streams or underlying groundwater basins. Accordingly, the model was used to develop a cooperative alternative water resources management approach. Once implemented, this approach could protect beneficial uses, aid in managing salinity (specifically chloride concentrations) in the Santa Clara River system, improve salt exportation from the study area, and provide enhanced water-supply benefits to water users in affected areas, while providing flexibility and more feasible chloride compliance solutions.

INTRODUCTION

Hydrologic Setting

The Santa Clara River (SCR) is the largest river system in Southern California that flows in a relatively natural state (Los Angeles Regional Water Quality Control Board [Regional Board], 2006). This river originates in the San Gabriel Mountains in Los Angeles County and flows into the Pacific Ocean in Ventura County. The SCR provides beneficial uses including agricultural water supply, groundwater recharge, and rare and endangered species habitat. The study area includes Reaches 7, 6, 5, and 4 (as designated by the Regional Board) of the SCR near the Santa Clarita Valley and Piru Subbasin (Figure 1).

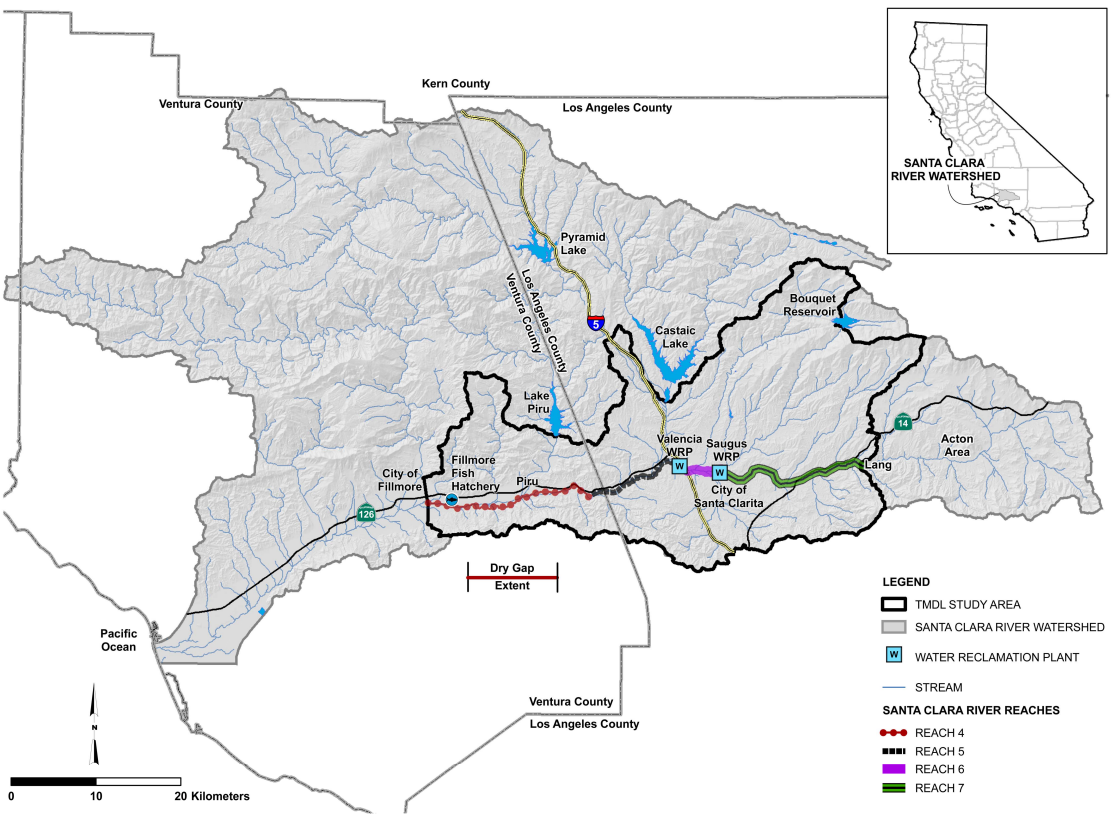

Figure 1. Map of Study Area and Surrounding Vicinity.

The Santa Clarita Valley is a thriving urbanized area located in Los Angeles County, 56 kilometers (km) (35 miles [mi]) north of downtown Los Angeles along Reaches 7, 6, and 5 of the SCR. The Santa Clarita Valley Sanitation District of Los Angeles County (SCVSD) owns and operates the Saugus and Valencia Water Reclamation Plants (WRPs), which provide primary, secondary, and tertiary treatment of domestic wastewater from residential, commercial, and industrial areas in the Santa Clarita Valley. These WRPs discharge tertiary-treated recycled water to Reaches 6 and 5 of the SCR, respectively. The Piru Subbasin is located in Ventura County, downstream and west of the Santa Clarita Valley along Reach 4 of the SCR. The Piru Subbasin is predominantly an agricultural area that includes cultivation of salt-sensitive crops,

such as strawberries, avocadoes, and nursery crops. Significant surface-water reservoirs exist upstream and north of the Santa Clarita Valley and Piru Subbasin, including Bouquet Reservoir, Pyramid Lake, and Castaic Lake in Los Angeles County, and Lake Piru in Ventura County (Figure 1).

The only location of perennial streamflow in the study area includes Reaches 6 and 5 of the SCR, located downstream of the Saugus and Valencia WRPs, and an eastern portion of Reach 4 of the SCR (Figure 1). This section of perennial flow in the SCR results from groundwater discharge and discharge from the WRPs.

Water Use

Potable water in the Santa Clarita Valley is either imported (mostly from the State Water Project [SWP]) or pumped from local groundwater basins. Water from the SWP is transported to the Santa Clarita Valley via the California Aqueduct and stored in Castaic Lake (Figure 1). The stored SWP water is delivered by Castaic Lake Water Agency (CLWA) to retail water purveyors known as the Upper Basin Water Purveyors[1], who also operate groundwater production facilities. These purveyors sell their potable supplies to users in their respective service areas of the Santa Clarita Valley and surrounding communities. The sources of irrigation water in the Santa Clarita Valley include potable water provided by the Upper Basin Water Purveyors and minor amounts of recycled water from the Valencia WRP.

Potable water in the Piru Subbasin comes solely from locally pumped groundwater from private wells. Irrigation water in the Piru Subbasin is mostly derived from groundwater, but a few surface-water diversions on the SCR and Piru Creek are also operated to supplement irrigation water supply.

Regulatory Background

The Santa Clarita Valley and Piru Subbasin are both semiarid regions with an average annual precipitation of less than 50 centimeters per year (less than 20 inches per year) and managing salinity in such regions is challenging. Chloride concentrations in imported water from the SWP have historically exceeded local chloride water quality objectives (WQOs) during drier-than-normal climate conditions (WQOs were established in the Basin Plan [Regional Board, 1994]). Increased urbanization in the Santa Clarita Valley and the prevalent use of self-regenerating water softeners in local residences and commercial and industrial facilities have also exacerbated salinity problems in portions of the SCR and underlying groundwater basins.

Portions of the SCR receiving discharge from the WRPs and downstream agricultural areas are included on California's list of impaired waters with respect to chloride. This listing occurred in response to claims of impairments to beneficial uses in agricultural areas downstream of the WRPs and led to the Regional Board's adoption of the Upper Santa Clara River Chloride Total Maximum Daily Load (TMDL) in 2002. Implementation of this TMDL would have required the Saugus and Valencia WRPs to meet a chloride WQO of 100 milligrams per liter (mg/L). This would have

[1] The Upper Basin Water Purveyors consist of Los Angeles County Waterworks District #36, Newhall County Water District, Santa Clarita Water Division of CLWA, and Valencia Water Company.

required construction and operation of advanced-treatment facilities at both WRPs and a 69 km (43 mi) brine conveyance pipeline to a new ocean outfall costing nearly a half-billion dollars. Recognizing the potentially costly implementation and time required for construction of such measures, the Regional Board amended this TMDL in 2004 and 2006 to require special studies to help provide a scientific basis for implementation of the chloride TMDL. The SCVSD provided funding for these special studies, which were managed jointly by the SCVSD and the Regional Board.

Scope

This paper describes results of the groundwater/surface-water interaction model required by the special TMDL studies. The purpose of developing the model was to improve the understanding of the interaction between surface water and groundwater and the linkage between surface-water quality and groundwater quality with respect to chloride. Particular emphasis was placed on evaluating the impact of the WRP recycled water discharges to the SCR on downstream surface water and groundwater chloride concentrations. The project also required significant collaboration among members of a TMDL stakeholder group consisting of individuals representing SCVSD, the Regional Board, local utilities, city and county entities, state and federal agencies, academia, contractor organizations, environmental groups, and the general public.

The outcome of this TMDL study included development of a cooperative alternative water resources management approach to comply with the TMDL that, once implemented, could protect beneficial uses and aid in managing salinity (specifically chloride concentrations) in the SCR system. Modeling results also indicated that implementation of this management approach could provide enhanced water-supply benefits to water users along the SCR in portions of Los Angeles and Ventura Counties.

METHODOLOGY

Code Selection

This TMDL study required a modeling code that could simulate the flow of water and solutes over the land surface and through the subsurface. This model was built using a proprietary code called MODHMS (HydroGeoLogic [HGL], 2007), which has its origins in the popular United States Geological Survey (USGS) Modflow model (McDonald and Harbaugh, 1988). MODHMS has been enhanced and further developed by HGL to include numerous features that are not included in the original USGS code. MODHMS is a physically based, spatially distributed numerical model that includes several packages for simulating fully integrated groundwater and surface-water flow (including three-dimensional saturated and unsaturated flow) and solute transport. This code was selected for the following reasons:

- Project scope required a code that is capable of simulating unconfined subsurface flow interacting with a stream channel flow domain, and the associated solute transport therein. The code also needed to be capable of simulating drying and re-

wetting of both surface and subsurface domains. MODHMS meets these requirements.

- The SCR watershed is characterized by complex hydrogeology, mixed and evolving land uses, dynamic groundwater/surface-water interactions (including gaining and losing river reaches), and variable climatic conditions. These factors would challenge the applicability of most readily available numerical codes, but MODHMS is well suited to address these factors.
- MODHMS treats the flow of water and transport of solutes in a rigorous and mechanistic manner by mathematically representing surface and subsurface domains as one holistic system. Thus, it is neither necessary to estimate locations of losing or gaining stream reaches outside of the model, nor to manually link numerical solutions of the groundwater and surface-water systems separately.
- MODHMS is the product of more than 15 years of development and is built on the USGS Modflow model. Modflow has been used extensively in groundwater evaluations worldwide for more than 20 years.
- MODHMS has been benchmarked and verified (HGL, 2007).

Model Development

MODHMS mathematically separates the field problem into two hydrologic flow and solute transport regimes: surface and subsurface. The surface flow regime includes an overland flow (OLF) domain and channel flow (CHF) domain. The subsurface flow regime includes the unsaturated and saturated groundwater flow (GWF) domains of the materials underlying the OLF and CHF domains.

A grid that mathematically represents an area of 1,083 square kilometers (418 square miles) was developed for this study and is illustrated on Figure 2. The domain boundaries were debated and selected collaboratively by the stakeholder group to coincide with natural hydrologic divides around an area downstream of Bouquet Reservoir, Castaic Lake, and Lake Piru. A curvilinear grid type was selected for this model because of its ability to be warped along nonlinear features of interest, such as the domain boundaries and the SCR. Use of a curvilinear grid also facilitated assignment of smaller cell spacings (i.e., finer discretization) within areas of interest along Reaches 6, 5, and 4 of the SCR. Grid resolution varies in the x-direction from 15 to 915 meters (m) (50 to 3,000 feet [ft]) and in the y-direction from 15 to 3,353 m (50 to 11,000 ft). The surface regime was discretized using an OLF grid and CHF grid. The subsurface regime was discretized into nine GWF layers using an extension of the OLF grid with depth to provide a three-dimensional representation of the surface and subsurface system. The OLF grid has a two-dimensional connectivity and represents the land surface within the domain. The CHF grid consists of a network of interconnected one-dimensional channel segments, which vary in length between 52 and 134 m (170 and 440 ft), with most of the segments being approximately 91 m (300 ft) long.

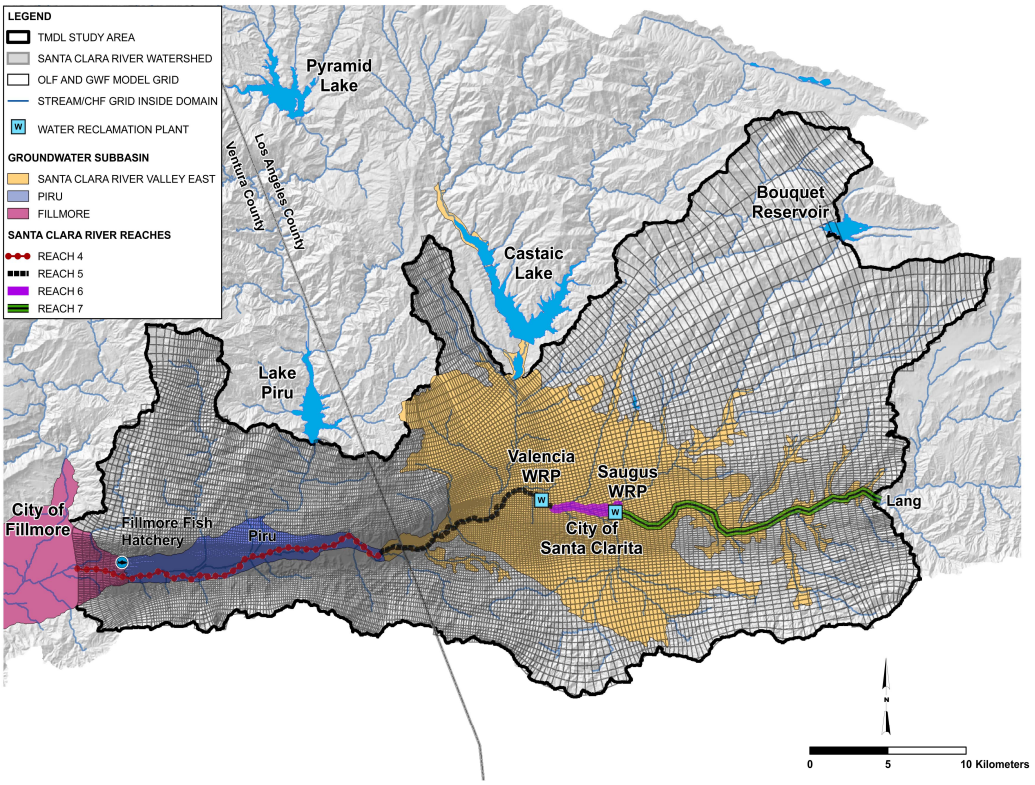

Figure 2. Map of Curvilinear Model Grid.

The model was initially developed using parameters and assumptions from previously developed models of the area (Systech Engineering, 2002a and 2002b; USGS, 2003; CH2M HILL, 2004 and 2005). Additional details related to the spatial discretization and parameterization of the groundwater/surface-water interaction model can be found in CH2M HILL-HGL (2008).

To fulfill the modeling objectives, the model was developed and calibrated using daily input data over a historical period including calendar years 1975 through 2005 (CY 1975-2005). This historical period and the requirement of model output at a daily frequency were debated and selected collaboratively by the stakeholder group. The available data and conceptual model that provided the basis for model development can be found in CH2M HILL-HGL (2006a, 2006b).

RESULTS

Model Calibration

The Modeling Team selected qualitative and quantitative calibration targets for the surface and subsurface flow of water and chloride in the model. Calibration targets selected for this study included 88 groundwater-level locations, 50 groundwater-chloride locations, 6 streamflow locations, and 12 surface-water quality locations, as well as general patterns and characteristics of the hydrologic system.

Calibrating the model to daily streamflow data and available groundwater elevation and chloride concentration data over the CY 1975-2005 period resulted in a model

that was suitable for its intended applications. Following are the primary attributes that made the model appropriate for its intended uses:

- It can simulate historical short-term and long-term trends in groundwater elevations, groundwater discharge, streamflows, dry gap locations, and chloride concentrations over a 3-decade period that reflects increased urbanization, increased SWP water imports, wet and dry periods, and associated changes in land use and water use.
- It can simulate the interacting surface and subsurface flow regimes, the transport of chlorides throughout these regimes, and the complex process of evapotranspiration and evapoconcentration of chlorides.
- The numerical solution is adequately constrained by the many, and sufficiently distributed, calibration targets that include flow rates, flow volumes, groundwater elevations, and surface and subsurface chloride concentrations.
- The modeling results are consistent with the conceptual model that was described in CH2M HILL-HGL (2006b).

Additional details regarding model calibration can be found in CH2M HILL-HGL (2008).

Model Application

Although it is impossible to predict future hydrology, land use, and water use conditions with certainty, future water use and WRP waste load allocation assumptions for calendar years 2007 through 2030 (CY 2007-2030) were developed collaboratively by the stakeholder group. Following calibration, the model was used to evaluate future site-specific hydrologic system and chloride transport behavior resulting from implementation of assumed chloride management activities. Twenty-one scenarios of future conditions were ultimately evaluated using the model, which incorporated a variety of technical and policy-related considerations. The range of assumptions included in these scenarios of future conditions fall into five general categories including (1) level of recycled water use in the Santa Clarita Valley; (2) level of wastewater treatment at the Saugus and Valencia WRPs; (3) timing related to the removal of self-regenerating water softeners from the Santa Clarita Valley; (4) alternative WRP discharge locations in the SCR; and (5) alternative water resources management options. Several of the scenarios of future conditions included assumptions from multiple categories.

Results from the first 20 scenarios of future conditions included elements from the first four categories listed above. These results indicated that compliance with groundwater and surface water WQOs for chloride would not be consistently achieved at all locations and under all climatic conditions, especially during drought periods. Thus, the 21st scenario incorporated an alternative water resources management approach in conjunction with developing proposed chloride site-specific objectives (SSOs) ranging from 117 to 150 mg/L in the SCR for consideration by the Regional Board. This scenario was designed to achieve compliance with chloride SSOs at all times at receiving water locations with mitigation measures established to

protect downstream agricultural beneficial uses as needed (Geomatrix Consultants, 2008b). This alternative water resources management approach was developed jointly by the SCVSD and the Upper Basin Water Purveyors in Los Angeles County, and stakeholders representing downstream water users in Ventura County. A Memorandum of Understanding among these entities is being developed to provide a more feasible regional solution as an alternative for compliance with the existing chloride WQO of 100 mg/L in the SCR. The alternative water resources management scenario included the following elements:

- Implementing measures to reduce chloride in the recycled water at the WRPs by removing self-regenerating water softeners from the Santa Clarita Valley and incorporating ultraviolet disinfection technology at the WRPs
- Incorporating advanced treatment measures for a portion of the recycled water from the Valencia WRP to further reduce chloride concentrations in recycled water when needed
- Procuring local groundwater or an alternative water supply to be either discharged to the SCR as supplemental water supply or otherwise provided to protect salt-sensitive agricultural beneficial uses of the SCR
- Constructing and operating groundwater extraction wells in eastern Ventura County to facilitate exportation of groundwater with elevated chloride concentrations from the Piru Subbasin
- Expanding recycled water uses in the Santa Clarita Valley
- Revising groundwater and surface-water WQOs to support all of these elements

DISCUSSION

Results from the 21 scenarios of future conditions indicated that there is no simple solution to managing salinity in the TMDL study area. Use of the groundwater/surface-water interaction model for this collaborative study promoted an enhanced understanding of how chloride is routed between the surface and subsurface flow systems, as compared to previously developed models. This enhanced understanding of the hydrologic system has led to improved collaboration among stakeholders. Implementation of an alternative water resources management program could protect beneficial uses, increase salt exportation from the TMDL study area, and enhance water-supply benefits to water users in affected areas, while providing flexibility and more feasible chloride TMDL compliance solutions.

Results of this study were subject to significant scrutiny including discussions over the site conceptual model, level of protection required for downstream beneficial uses, and competing interests from a diverse stakeholder group. The degree of collaboration required in such a challenging hydrologic study area made this TMDL study very complex and often contentious. However, the advanced modeling capabilities of the code and modeling team facilitated constructive dispute resolution on the basis of objective scientific analyses. Additional details of this study can be

found in CH2M HILL-HGL (2006a, 2006b, 2007, and 2008) and Geomatrix Consultants (2008a and 2008b).

ACKNOWLEDGEMENTS

The authors gratefully acknowledge the organizations that provided hydrologic, well construction, climatic, and operational input data for the model development effort. These organizations include, but are not limited to the Santa Clarita Valley Sanitation District, Los Angeles Regional Water Quality Control Board, Ventura County Watershed Protection District, United Water Conservation District, Systech Engineering, United States Geological Survey, Upper Basin Water Purveyors, Newhall Land and Farming Company, Los Angeles County Department of Public Works, Fillmore Fish Hatchery, United States Army Corps of Engineers, Ventura Regional Sanitation District, Los Angeles Department of Water and Power, Southern California Association of Governments, and United States Environmental Protection Agency.

REFERENCES

CH2M HILL. 2004. *Regional Groundwater Flow Model for the Santa Clarita Valley. Model Development and Calibration.* Prepared for the Upper Basin Water Purveyors including Castaic Lake Water Agency, Newhall County Water District, Santa Clarita Division of Castaic Lake Water Agency, and Valencia Water Company. April.

CH2M HILL. 2005. *Calibration Update of the Regional Groundwater Flow Model for the Santa Clarita Valley, Santa Clarita, California.* Prepared for the Santa Clarita Valley Water Purveyors. August.

CH2M HILL, in association with HydroGeoLogic (CH2M HILL-HGL). 2006a. *Literature Review and Data Acquisition. Task 1A – Evaluate Existing Models, Literature, and Data. Upper Santa Clara River Chloride TMDL Collaborative Process.* Draft Report. Prepared for Sanitation Districts of Los Angeles County and Los Angeles Regional Water Quality Control Board. March.

CH2M HILL, in association with HydroGeoLogic (CH2M HILL-HGL). 2006b. *Task 2A – Conceptual Model Development, East and Piru Subbasins. Upper Santa Clara River Chloride TMDL Collaborative Process.* Prepared for Sanitation Districts of Los Angeles County and Los Angeles Regional Water Quality Control Board. October.

CH2M HILL, in association with HydroGeoLogic (CH2M HILL-HGL). 2007. *Task 3 – Public Review Strategy for the Groundwater/Surface-water Interaction Model. Upper Santa Clara River Chloride TMDL Collaborative Process.* Draft Report. Prepared for Sanitation Districts of Los Angeles County and Los Angeles Regional Water Quality Control Board. February.

CH2M HILL, in association with HydroGeoLogic (CH2M HILL-HGL). 2008. *Task 2B-1–Numerical Model Development and Scenario Results. East and Piru Subbasins. Upper Santa Clara River Chloride TMDL Collaborative Process.* Final Report. Prepared for the Sanitation Districts of Los Angeles County and Los Angeles County Regional Water Quality Control Board. March.

Geomatrix Consultants. 2008a. *Supplement to Task 2B-1 – Numerical Model Development and Scenario Results, East and Piru Subbasins. Upper Santa Clara River Chloride TMDL Collaborative Process.* Prepared for Sanitation Districts of Los Angeles County and Los Angeles Regional Water Quality Control Board. March.

Geomatrix Consultants. 2008b. *Task 2B-2 Report–Assessment of Alternatives for Compliance Options Using the Groundwater/Surface Water Interaction Model. Upper Santa Clara River Chloride TMDL Collaborative Process.* Draft Report. Prepared for the Santa Clarita Valley Sanitation District of Los Angeles County. June.

HydroGeoLogic (HGL). 2007. MODHMS: A Comprehensive Modflow-based Hydrologic Modeling System, Version 3.0, Documentation and Users Guide.

Los Angeles Regional Water Quality Control Board (Regional Board). 1994. *Water Quality Control Plan – Los Angeles Region. Basin Plan for the Coastal Watersheds of Los Angeles and Ventura Counties.*

Los Angeles Regional Water Quality Control Board (Regional Board). 2006. *Draft State of the Watershed–Report on Surface Water Quality. The Santa Clara River Watershed.* April.

McDonald, M.G., and A.W. Harbaugh. 1988. "A Modular Three-Dimensional Finite-Difference Groundwater Flow Model." U.S. Geological Survey Techniques for Water-Resources Investigation. Book 6, Chapter A1.

Systech Engineering. 2002a. *Final Task 1 Report for Santa Clara River Nutrient TMDL Analysis: Source Identification and Characterization.* Prepared for Santa Clara Nutrient TMDL Steering Committee. July.

Systech Engineering. 2002b. *Linkage Analysis For Santa Clara River Nutrient TMDL Analysis Parts I and II: Hydrology and Water Quality.* Prepared for Santa Clara Nutrient TMDL Steering Committee. September 1.

United States Geological Survey (USGS). 2003. *Simulation of Ground-Water/Surface-Water Flow in the Santa Clara-Calleguas Ground-Water Basin, Ventura County, California.* Water-Resources Investigations Report 02-4136. A contribution of the Southern California Regional Aquifer-System Analysis Program.

Modeling Techniques to Incorporate Low Impact Development Features into Detention Analyses

Kristin White, P.E., CFM, LEED AP[1] and Jennifer J. Walker, P.E., CFM[1]

ABSTRACT

Developments that include Low Impact Development (LID) features or integrated management practices (IMP)s can achieve both storm water quality and quantity benefits. The greatest quantity and quality benefits may be achieved when the site is designed with a holistic approach to LID from the beginning. To maximize the benefits of the LID features, it is often beneficial to integrate the volume and infiltration capacities into the detention analysis. This paper examines various modeling techniques to incorporate IMPs into detention analyses. Simplistic analysis as well as complex modeling techniques are included.

INTRODUCTION

Low impact development (LID), a term coined by Prince George's County (PGC), Maryland, is a method of designing and planning stormwater management systems using integrated management practices (IMPs) to minimize the effects of development on rainfall runoff. In particular, the goal is to limit the post-development runoff conditions (volume and quality) to the pre-development runoff conditions. LID methods either focus on retaining the runoff for future non-potable use, ground water recharge or detaining for a delayed slower release to a larger system. Significant water quality benefits are commonly associated with both the retention and detention of runoff. Water quality benefits occur either as an integral part of the design or a beneficial side effect. In general, water released from any LID configuration has improved water quality over the raw stormwater even if the LID device is only a grassed separation of impervious areas.

The intent of LID is to focus collection and pollutant removal efficiency on smaller, more frequent storm events rather than large, infrequent events. Although certain LID devices may provide enough storage volume for a larger design storm event, the design intent is to collect and/or treat common wet weather events.

LID technology is widely used in the northeastern, mid-Atlantic and Pacific Northwestern parts of the Country. Some Texas communities are beginning to analyze these methodologies to determine if they provide sufficient protection from common large floods. Below are some of the major conceptual-level benefits and disadvantages of using LID; however, true benefits and disadvantages vary by the type of LID device as well as site and region specific characteristics:

[1]Dodson & Associates, Inc. 5629 FM 1960 West, Suite 314 Houston, Texas 77069-4216
281-440-3787 (phone) 281-440-4742 (fax)

Advantages	Disadvantages
Lower or no impact on community resources such as regional detention or collection systems	May require a direct connection to a traditional system to handle large flood volumes
Encourages groundwater recharge through significant infiltration	Effectiveness is significantly reduced when soil or pavement is completely saturated
Improves water quality of discharge by collecting debris and absorbing pollutants before releasing	Large storage volumes will be required for design storms
Space efficient for small, urban areas such as rooftops and smaller parking lots	Not space efficient for larger, heavily impervious sites such as warehouses or airports
For smaller sites, cost is often lower than updates to a larger collection or detention	For larger sites, cost is typically higher than updates to a larger system due to required land
Focuses on managing frequent stormwater events to limit all peak flows rather than only the design storm peak flow	IMPs will require regular maintenance since they are used for frequent storm events

COMMON LID IMP EXAMPLES

Listed below are several LID IMP examples with their description and suggested use. These devices are all different; however are all used similarly on a site to lower the total impervious area, separate the impervious areas and increase the time of concentration. The applicability of each device depends on the intended project and desired result.

Integrated Management Practice	Description	Suggested Use
Bioretention	Depressed landscaping feature with soil and ponding storage volume	Runoff storage for small sites or use overflow or underdrain system for larger storm events
Filter Strips	Vegetated strip of land along side an impervious cover to accept and sometimes store sheet flow	Along the side of a road or highway to treat and sometimes collect impervious runoff
Wet and Dry Vegetated Swales	Vegetated, linear depressed area to collect, store and sometimes convey runoff	Runoff collection on smaller sites. Dry systems may have a second recreational use
Trees	Grouping or line of trees to intercept rainfall and separate impervious areas	As separation of streets from sidewalks or similar

Porous Pavement	Surface with large pore volume to infiltrate and store initial rain fall, not runoff	As driveways, parking lots or lightly traveled roads
Rain Cisterns	Cistern to collect runoff directly from impervious areas	Collect runoff from roofs of houses or commercial buildings
Underground Detention	Local system to collect runoff through inlets and store underground for infiltration, future non-potable use or later release	Collect runoff from large commercial sites with minimal available pervious area
Green Roof	Roof structure with soil and planted vegetation to limit runoff from roof surface	Commercial buildings and business centers
Blue Roof	Roof structure to collect rainfall for future non-potable use or release	Commercial buildings, centers and warehouses

METHODOLOGY

Conceptual Differences Between LID Planning and Traditional Stormwater Management

LID planning typically involves breaking the development area down to micro-drainage areas or individual development pieces such as driveways, parking lots, roof tops, etc whereas traditional methods analyze the development with larger drainage areas. LID IMPs are most effective when used to capture and treat runoff from these smaller, concentrated areas. In particular, LID planning relies on separating the impervious areas from each other.

Traditional methods are designed to collect combined runoff from larger areas through conveyance systems and/or regional detention. This type of system works to capture and convey the runoff from the entire site. Therefore, the conveyance system is designed to collect all of the rainfall (after the initial abstraction) that falls on the site.

Modeling and Sizing

The modeling of LID IMPs is based both on a retention/detention storage volume as well as a peak flow. For this reason, the Rational Method is typically not recommended when assessing LID features due to its reliance on peak flow rather than total volume. Accounting for LID IMPs can be accomplished using several basic methodologies:

- Manipulate the post-development hydrograph to account for LID IMPs
- Analyze and plan IMPs using the PGC methodology
- Enter IMP design and layout into a hydrologic model with LID capability

Modifying the Post-Development Hydrograph

Modifying the post-development hydrograph can be done in a variety of ways, depending on the analysis method used. If using the National Resources Conservation Service (NRCS) TR-55 method, the IMP storage volume can be accounted for as conventional detention, or by altering the curve number, runoff or rainfall. Alternatively, the conventional post-development hydrograph can be directly manipulated.

IMPs accounted for as conventional detention use the available ponding storage only. This is done by subtracting the total storage volume from the total runoff volume. This method will be equivalent to using a conventional detention pond. This method is simple to follow and uses commonly followed hydrologic calculations; however the resulting required ponding volume will be oversized due to no exfiltration calculations.

Modification of the key terms in the NRCS runoff depth equation, shown below, can also be used to account for LID IMPs:

$$Q = (P-I_a)^2 / (P-I_a)+S$$

Where Q = Runoff Depth
P = Rainfall Depth
I_a = Initial Abstraction
S = 1000/CN – 10
CN = Composite Site Curve Number

The curve number can be adjusted to account for similarly sized, evenly distributed LID features. This method can be completed by determining the total detention volume offered by the LID arrangement, including estimated soil volume, and subtracting that volume from the total runoff volume. With the adjusted runoff volume, a new curve number can be solved for and used to develop the LID post-development hydrograph.

The runoff volume can be adjusted by subtracting the total retention volume from the $(P-I_a)$ term. This method alters the rainfall volume prior to incorporating the soil or ground cover type. This creates a post-development hydrograph that accounts for all IMP storage as complete retention or infiltration with no runoff leaving the site.

The post-development hydrograph may be altered directly by taking the conventionally calculated post-development hydrograph with no detention and removing the total provided IMP retention volume from the curve, starting at the leading edge. This results in a new perpendicular leading edge rather than a standard curve. Alternatively, the hydrograph may be altered by reducing the amplitude by a percentage of retention volume provided. For example, the total

flow at each point in the hydrograph would be lowered by the percentage of LID storage volume to total runoff volume. This method will reduce the height of the hydrograph, however the base duration will remain the same.

These methods can be employed in conventional models (such as HEC-HMS or SWMM) by modeling the site with no LID features, exporting the conventional resulting runoff hydrograph, altering the hydrograph using one of the above methods and then importing the altered hydrograph back into the model for routing. In some cases, this may require an iterative effort to provide the appropriate retention volume within the LID IMPs. These methods will not be able to assess the compared effectiveness of separate LID methods, or disconnected impervious areas but will provide an estimated comparison between using an LID system over a more traditional system.

PGC Methodology

The PCG method focuses on minimizing the impervious area, disconnecting the impervious area and increasing the post-development time of concentration to meet the pre-development time. Accomplishing these goals results in a post-development hydrograph with a lower peak flow (when compared to conventional methods) with a peak time equal to the pre-development time. Assuming the LID design peak flow and runoff volume are still greater than the pre-development conditions, the volume difference must be retained to meet the pre-development conditions. The PGC methodology was developed to determine this volume using a more accurate LID design hydrograph that accounts for disconnected impervious areas, IMP retention volume and evenly dispersed IMPs. In addition, this method can also be used for IMP sizing.

The method follows the below basic steps:

1. Calculate the pre-development time of concentration (T_c) and curve number using the TR-55 (SCS, 1986) method. These values should be determined assuming the pre-development conditions are woods in good condition.
2. Prepare a preliminary layout with estimated LID surface areas and disconnected impervious areas.
3. Calculate the proposed curve number as a weighted area average rather than using a standard TR-55 value for the development type. The PGC method also includes a refined CN equation to account for disconnected impervious areas. This equation is shown below:
    a. $CN_c = CN_p + (P_{imp}/100) * (98 - CN_p) * (1 - 0.5*R)$

        Where CN_c = the weighted average CN from the preliminary layout

        CN_p = the weighted average CN from the pervious areas only

        P_{imp} = the percent of the impervious area to the entire site

        R = the ratio of unconnected impervious area to the total impervious area

4. Calculate the proposed Tc. If this value is greater than the pre-development Tc, the preliminary layout should be revised to increase the Tc at least to the pre-development time.
5. Determine the design storm event by calculating the rainfall required to initiate direct runoff during pre-development (well wooded) conditions and multiplying it by 1.5. This formula is shown below:
    a. Design Rainfall Depth = 1.5 * (0.2 * [1000/CN_c – 10]) where CN_c is the composite (weighted average) pre-development curve number.
6. Use PGC design charts to determine required IMP retention volume to maintain the existing CN. This chart is based on the design rainfall, geographic region, the pre-development and post-development CN.
7. Calculate required volume for water quality based on local regulations. This is typically the first 0.5-inch or 1.0-inch of rainfall.
8. Use the higher of the 2 values in steps 6 and 7 as the required retention volume.
9. Use PGC design charts to determine required IMP detention volume to maintain the pre-development peak discharge. This chart is also based on the design rainfall, geographic region, the pre-development and post-development CN.
10. If the retention volume (step 8) is higher than the detention volume (step 9) then use the retention volume as total required LID volume and size the LID IMPs. This may be an iterative process if IMP surface areas need to be resized as they will change the composite CN.
11. If the retention volume (step 8) is lower than the detention volume (step 9) then a hybrid of retention and detention must be used. The detention volume is calculated using the PGC design charts based on the design rainfall, geographic region, the pre-development and post-development CN. The hybrid ratio of retention to detention volume is determined by creating a linear relationship between the two storage values and assessing the reasonably available retention volume on the design site. This will be an iterative process if the IMP surface areas are resized as they will change the composite CN.

Computational Models

Certain models have been either specially created or retrofitted to account for the use of LID IMPs. Several common hydrology models have been retrofitted with ex-filtration and water quality volume calculation options to help in the modeling with an LID feature. These require advanced knowledge of exfiltration rates for the design site for a hydrologic analysis. Conventional models which have not been retrofitted, such as HEC-HMS, should not be used for modeling LID, but rather only for developing a conventional hydrograph.

More complex hydrologic models have been developed or enhanced specifically to design and model LID IMPs within a watershed. These models have the capability to analyze the effectiveness of specific IMPs and size them based on set requirements. The following table

outlines common and complex models with their suggested use. Two specific models, CH2M HILL's LIFE™ and PGC's BMP Module and discussed in more detail.

Model	Brief Description	Recommended Use for LID
EPA's SWMM	Hydrologic, hydraulic and water quality model with optional continuous simulation	Detailed analysis of watershed with storage-focused LID IMPs Does not account for impervious separation
XP SWMM	Enhanced hydrologic, hydraulic and water quality model with optional continuous simulation	Detailed analysis of a watershed with different IMPs where removal efficiency of each device is known
Bentley's Pond Pack	Hydrologic model to design and analyze detention ponds with optional exfiltration option	Analysis of larger storage and exfiltration based IMPs within a watershed
Hydro-CAD	Hydrologic model to calculate runoff and detention pond routing with exfiltration option	Analysis of storage and infiltration based IMPs within a watershed
Hydrologic Simulation Program-Fortran (HSPF)	EPA model to analyze water quality effects based on continuous rainfall	General continuous analysis of LID water quality benefits, not for flood control design
Western Washington Hydrologic Model (WWHM3 PRO)	HSPF-based model to analyze hydrology and water quality of particular IMPs in WA	Continuous analysis of a watershed with multiple, different IMPs Can be modified for areas outside of WA
Bay Area Hydrology Model (BAHM)	Created for west coast hydrology for sizing detention and water quality systems	Sizing particular IMPs: bioretention swales, gravel trench beds, sand beds or irregularly shaped ponds
HEC-HMS	Model to develop standard hydrograph based on precipitation input	Obtaining standard, non-adjusted hydrographs. Not recommended for modeling IMPs
LIFE™	CH2M HILL model to analyze and design IMPs using continuous simulation	Continuous analysis of a watershed with multiple, different IMPs or design of a specific IMP
PGC BMP Module	PGC model to analyze effectiveness of IMPs or size IMPs	Continuous analysis of an IMP or network of IMPs, each with detention rate > 1 hour IMPs should all be similarly sized and equally distributed

Prince George County's BMP Module

The Prince George's County BMP Module (the module) is a tool developed to evaluate the effect of a particular LID Best Management Practice (BMP) on the resulting water quality and outflow for a general area. The model was developed between 1999 and 2000 by Prince George's County and Tetra Tech, Inc. In general, this model is best for site-level analysis or evaluating small watersheds. It can be used for a single LID device or with an LID network. The module takes the following factors into consideration for evaluation:

- Evapotranspiration
- Infiltration
- Orifice outflow
- Weir controlled overflow
- Underdrain capacity and flow
- Feature design (sloping and shape)
- Roughness of device
- Soil media filtration capacity for particular pollutants
- First order loss or decay of pollutants

This model requires a separate hydrologic input on an hourly time series for computation. The time series may come from a conventional model such as HSPF, HEC-HMS or SWMM. Because of the hourly time step requirement, this model would not be effective for an LID device with a retention/detention time less than one-hour. The results of the model provide hourly pollutant load and flow discharge data. If using the module to incorporate an LID device in a detention analysis, a series of models would need to be used. A possible flow chart for the model set up is shown below in Figure 1. Due to its emphasis on water quality and the LID design method of designing for more common storms, this module is most effective when run over a long-term period or multiple storm simulation.

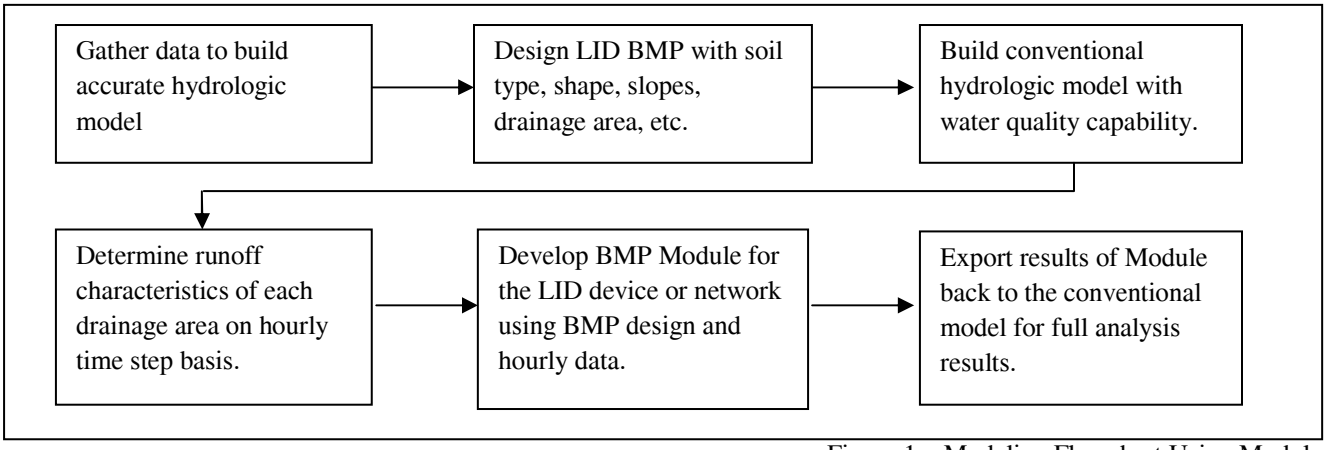

Figure 1 – Modeling Flowchart Using Module

LIFE™ Model by CH2M HILL

The LIFE™ model developed by CH2M Hill uses very similar inputs to the BMP module however the LIFE™ model is a full analysis and design model with the capability to determine runoff volumes and water quality characteristics as well as optimize designs. It is also a continuous simulation model but includes the option to have a time step less than one hour, making it suitable for devices with shorter detention or retention times. A flow chart of the model process is shown below in Figure 2.

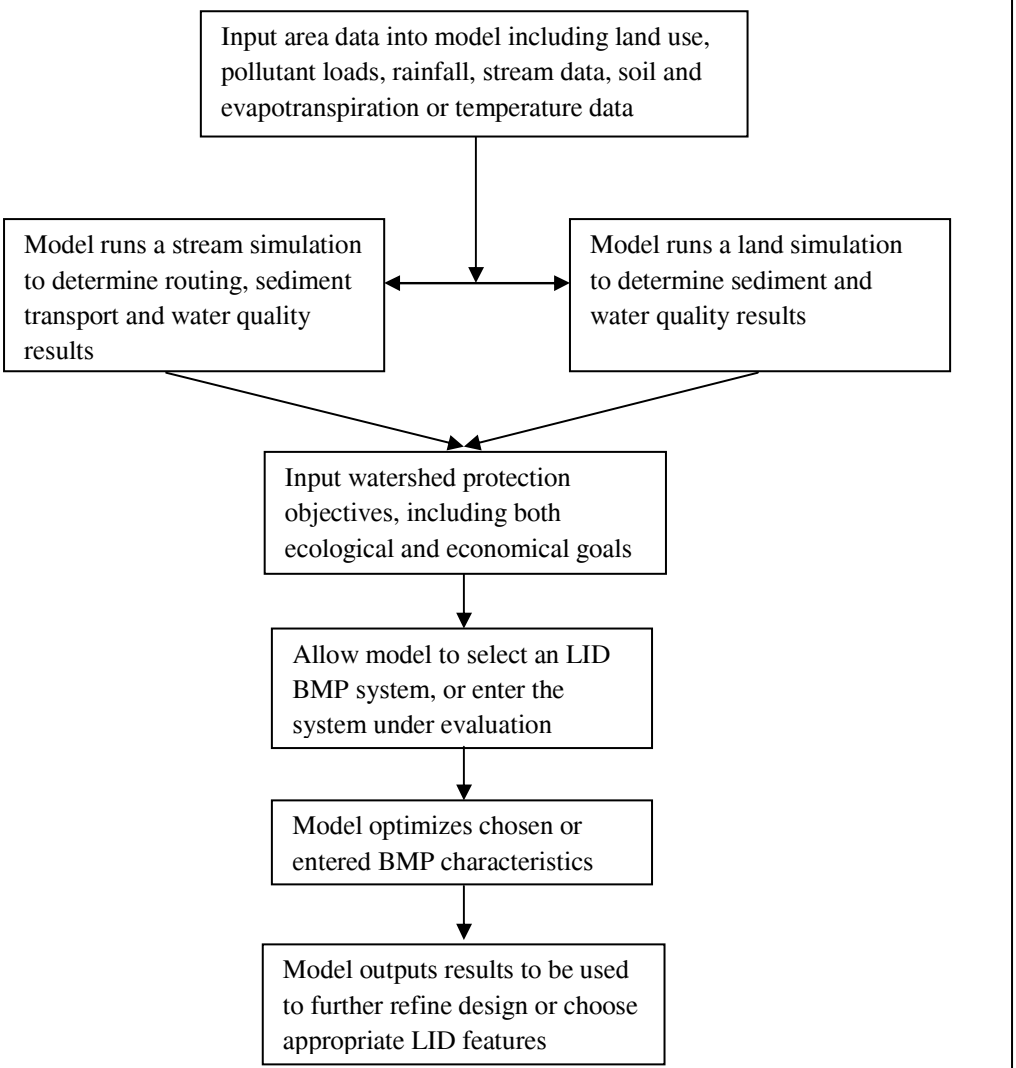

Figure 2 – Modeling Flowchart Using LIFE™

CONCLUSION

Low Impact Development planning techniques are very beneficial for stormwater collection, storage and treatment in smaller areas with new impervious cover added. LID methodology is continuously growing and improving as it becomes a more accepted method for treating and collecting stormwater runoff. LID analysis may be done by estimating the storage effectiveness of IMPs through standard calculations, using the PGC developed algorithm or by using complex modeling system to model a detailed design. Sizing LID components can be done either through direct volume calculations or by using a more complex model. The following table summarizes the discussed models with their recommended hydrologic and hydraulic (H&H) analysis, water quality (WQ) analysis, specific analysis concentration and sizing availability.

Analysis Goal	IMP as Detention	Altering NRCS	Altering Hydrograph	PGC Method	HEC-HMS	SWMM	XP SWMM	Hydro-CAD	Pond Pack	HSPF	BAHM	WWHM 3 PRO	LIFE™	BMP Module w/HSPF
H&H Analysis with All Similar IMPs		●	●	●		●	●	●	●	●	●	●	●	●
H&H Analysis with All Varied IMPs							●				●	●	●	
H&H Analysis with Few IMPs		●	●	●		●	●	●	●	●	●	●	●	●
H&H Analysis with Significant IMPs				●		●	●			●	●	●	●	●
H&H Analysis with Storage IMPs	●	●	●	●		●	●	●	●	●	●	●	●	●
H&H Analysis with Non-Storage IMPs				●			●			●		●	●	●
H&H Analysis w/ Continuous Rainfall						●	●			●	●	●	●	●
H&H Analysis for Large Events	●	●	●	●		●	●	●	●		●	●	●	●
Account for Disconnected Impervious				●						●		●	●	●
Account for Exfiltration in IMP(s)		●		●		●	●	●	●	●	●	●	●	●
WQ Analysis for Single IMP						●	●			●	●	●	●	●
WQ Analysis for IMP Network						●	●			●	●	●	●	●
WQ Analysis w/ Continuous Rainfall						●	●			●	●	●	●	●
Sizing Single IMP				●			●				●	●	●	●
Sizing IMP Network-All Similar				●			●				●	●	●	●
Sizing IMP Network-All Varied							●				●	●	●	

REFERENCES

Koch, Paul R. 2005. A Milwaukee Model for LID Hydrologic Analysis. ASCE Watershed.

Wright, Leonard, Heaney, James P, and Weinstein, Neil. 2004. Micro-Scale Modeling of Low-Impact Development. ASCE Water Resources 2004.

Cheng, Mow-Soung, et. al. 2004. BMP Model for Low-Impact Development. ASCE World Water Congress 2004.

Cheng, Mow-Soung. 2005. PGC – BMP Module: Prince George's County BMP Module. Appendix A: Model Fact Sheets from TMDL Model Evaluation and Research Needs.

Patwardhan, Avinash, Haden, Joel. 2005. LID Solutions for an Industrial Site. ASCE EWRI.

CH2M HILL, Inc. 2004. LIFE™ Model pamphlet online.

Prince George's County. 1999. Low-Impact Development Hydrologic Analysis. Department of Environmental Resources Programs and Planning Division, Prince George's County, Maryland.

MOPSO in multipurpose operation of single-reservoir system

E. Fallah-Mehdipour[1], O. Bozorg Haddad[1], and M. A. Mariño[2]

[1] Department of Irrigation & Reclamation Engineering, Faculty of Soil & water Engineering, College of Agriculture & Natural Resources, University of Tehran, Karaj, Tehran, Iran. PH (FAX) +98-261-2241119;
E-mail: Falah@ut.ac.ir, OBhaddad@ut.ac.ir

[2] Departments of Land, Air & Water Resources, Civil & Environmental Engineering, and Biological & Agricultural Engineering, 139Veihmeyer Hall, University of California, Davis, CA 95616-8628, USA. PH (530) 752-0684; FAX (530) 752-5262;
E-mail: MAMarino@ucdavis.edu

Abstract

Complexity of engineering problems, especially in the field of water resources, makes traditional optimization tools less efficient and enhances the popularity of evolutionary algorithms. Traditional optimization methods present just a single point as the optimal solution even in multi-objective problems. Thus, the main necessity to apply evolutionary algorithms is to present a set of nondominated solutions/Pareto-fronts as the optimal/near-optimal solutions, whereas most of problems in the field of water resources management are considered as a compromise between several objectives. In this paper, the Multi-Objective Particle Swarm Optimization (MOPSO) is applied to the operation of a multipurpose reservoir system. The objectives are: (1) maximization of reliability; (2) minimization of vulnerability; and (3) minimization of resiliency of the reservoir system, satisfying the downstream demand. The proposed algorithm is compared to a traditional method (weighting method). Results show that the MOPSO algorithm is successful in finding near-optimal, Pareto-front solutions.

Keywords: Multi-objective particle swarm optimization (MOPSO); multipurpose; reservoir operation.

1. Introduction

Reservoirs are one of the main sources of surface water and are commonly operated with several conflicting objectives. To determine the optimal operation of a reservoir, simulation and optimization models have been used. Simulation models do not provide an optimal operation policy, but optimization models use mathematical relations to archieve optimal/near-optimal solutions. Labadie (2004) presented a list of reasons which causes a continuing gap between theoretical development and real-world implementation for optimal operation of reservoir systems which include: (1) many reservoir system operators are skeptical about models purporting to replace their judgment and prescribe solution strategies and feel more comfortable with use of existing simulation models; (2) computer hardware and software limitations in the past have required simplifications and approximations that operators are unwilling to accept; (3) optimization models are generally more mathematically complex than

simulation models, and therefore more difficult to comprehend; (4) many optimization models are not conducive to incorporating risk and uncertainty; (5) the enormous range and varieties of optimization methods create confusion as to which to select for a particular application; (6) some optimization methods, such as dynamic programming, often require customized program development; and (7) many optimization methods can only produce optimal period-of-record solutions rather than more useful conditional operating rules. In addition, there are difficulties in solving large-scale, convex optimization models. To find an optimal or near-optimal solution to those problems, evolutionary algorithms and metaheuristic methods have been considered.

Evolutionary algorithms are stochastic search methods that mimic the natural biological evolution and/or the social behavior of species. Examples include how ants find the shortest route to a source of food and how birds find their destination during migration (Elbeltagi et al., 2005). Most applications of evolutionary algorithms have been to mathematical benchmark problems. Cieniawski et al. (1995) applied genetic algorithm (GA) to solve a multi-objective groundwater monitoring problem under uncertainty conditions. Prasad and Park (2004) presented multi-objective GA for design of water distribution networks, considering minimization of the network cost and maximization of reliability measure. Prasad et al. (2004) applied multi-objective GA in booster disinfection of water supply networks. Baltar and Fontane (2006) applied Multi-Objective Particle Swarm Optimization (MOPSO) algorithm proposed by Coello and Lechuga (2002) in single-reservoir operation to find nondominated solutions. MOPSO results were compared with results of the ε-constraint method as the optimal Pareto-front. Kumar and Reddy (2007) used Particle Swarm Optimization (PSO) algorithm to solve a multipurpose, multireservoir operation problem. The weighting method was used to handle multi-objective problem to the single objective and then the PSO algorithm was used as the optimization tools.

In this paper, the MOPSO algorithm is applied in the operation of a multipurpose reservoir system. Results from the MOPSO algorithm, as the nondominated solutions/Pareto-fronts, are compared with the results of the weighting method.

2. Multi-Objective PSO Algorithm

Particle swarm optimization (PSO) is a swarm intelligence algorithm based on the social behavior of birds. In the real world, the birds' movement toward food/destination is based on the position of each bird in the swarm during the time movement. Thus, each bird moves using its best position and the position of the one which has the minimum distance from the food/destination. In the PSO algorithm, each bird is presented as the particle and a set of the birds (particles) is identified as the swarm. The steps of the PSO algorithm are as follows:

1. Producing the random particles ($X_{N\times D}$) as the initial solutions in which N = the number of particles; and D = the number of decision variables.
2. Calculating the velocity particles ($V_{N\times D}$) by Eq. 1:

$$v_{id}^{t+1} = \alpha\left(w^t.v_{id}^t + c_1.r_1^t\left(Pbest_{id}^t - x_{id}^t\right) + c_1.r_2^t\left(Gbest_d^t - x_{id}^t\right)\right) \quad (1)$$

for $i = 1,2,...,N \qquad d = 1,2,...,D$

in which v_{id}^{t+1} = velocity of *i*th particle for *d*th dimension in (*t+1*)th iteration; α = constriction factor which is a fixed value that controls the velocity movement toward an optimal point; w^t = inertia weight parameter which is calculated by Eq. 2:

$$w^t = w_{Max} - \frac{(w_{Max} - w_{Min}) \times t}{iter_{Max}} \tag{2}$$

This parameter starts from the maximum value (w_{Max}) in the first iteration to the minimum value in the last iteration ($iter_{Max}$); v_{id}^t = velocity of *i*th particle for *d*th dimension in (*t*)th iteration; c_1 , c_2 = cognitive and social parameters which divide the velocity between the best position of the particle and swarm; r_1^t, r_2^t = random numbers in [0,1] with uniform distribution in the (*t*)th iteration; $Pbest_{id}^t$ = best position of the *i*th particle for the *d*th dimension in the (*t*)th iteration; and $Gbest_d^t$ = best position of the swarm for the *d*th dimension in the (*t*)th iteration.

Each particle (bird) moves in decision space by two vectors which are the distance between *Pbest*/*Gbest* and the current position of a particle.

3. Limiting the calculated velocity to the lower (v_{Min}) and upper (v_{Max}) of velocity bounds.

$$v_{\min} \le v_{id}^{t+1} \le v_{\max} \tag{3}$$

4. Updating particles' position using Eq. 4:

$$x_{id}^{t+1} = x_{id}^t + v_{id}^{t+1} \tag{4}$$

The movement toward an optimal point in single-objective PSO (SOPSO) depends on the objective function value. However, the number of objectives is more than one in the MOPSO. Thus, some technique such as multi-swarm can be used. The vector evaluated PSO (VEPSO) is a MOPSO algorithm which links each objective to a swarm. In this algorithm, each particle uses its best potion as the *Pbest* and the best particle of the other swarms as the *Gbest*.

In this paper, the proposed algorithm (Parsopoulos and Vrahatis, 2002) with an external archive is used. All particles are transferred to the archive in each iteration. Nondominated solutions are stored and the others are removed. Thus, the final members of the archive are reported as the Pareto-front. Moreover, in this paper, a technique called warm up is applied to improve the quality of the Pareto-front. This technique allocates a swarm to each objective which leads each swarm to move toward optimal/near-optimal solutions. Then, the resulting solutions are used as the initial swarm in the search process of the MOPSO algorithm.

According to the previous steps, the MOPSO algorithm is based on the stochastic method in the search process. Thus, different Pareto-fronts can be found in the several runs. To compare Pareto-fronts and select the best one, generational distance (*GD*) has been considered as the comparison criterion. *GD* is a metric value proposed by Veldhuizen (1999) in which the average distance between the found nondominated solutions and the optimal Pareto-front, is:

$$GD = \frac{1}{NS}\sqrt{\sum_{i=1}^{NS} d_i^2} \tag{5}$$

where GD = generational distance; NS = number of solutions found; and d_i = the Euclidean distance (in the objective space) between each nondominated solution and the nearest member of the optimal Pareto-front.
In this paper, there is no predefined optimal Pareto-front. Thus, the intersection of the best value of all objective functions is used as the comparative point/optimal Pareto-front.

3. Weighting method

The weighting method is a multi-objective optimization method in which a vector of weights is allocated to the objectives and a multi-objective problem is transferred to a single-objective one.

$$Max./Min.\ \ Z(x) = \sum_{j=1}^{n} w_j . Z_j(x) \tag{6}$$

$$\sum_{j=1}^{n} w_j = 1 \tag{7}$$

where n = number of objectives; w_j = allocated weight to the jth objective; $Z_j(x)$ = jth objective function; and $Z(x)$ = objective function.

To find different points of the Pareto-front, different combinations of weights are used in Eqs. 6-7.

4. Reservoir System Simulation

Application of the MOPSO algorithm is tested in a single-reservoir system with three objectives. Eqs. 8-10 illustrate the maximization of reliability, and the minimization the vulnerability and resiliency of the system with respect to supply and demand as follows:

$$Max.\ \ Z_1 = \frac{\sum_{t=1}^{T} Min.(R_t, D_t)}{\sum_{t=1}^{T} D_t} \tag{8}$$

$$Min.\ \ Z_2 = \frac{N.D}{N.C.D} \tag{9}$$

$$Min.\ \ Z_3 = Max.\left(\frac{D_t - R_t}{D_t}\right) \quad for \quad t = 1,2,\ldots,T \tag{10}$$

where Z_1 = reliability of system; T = number of operational periods; R_t = release at period t; D_t = downstream demand at period t; Z_2 = vulnerability of system; $N.D$ = number of periods in which there is deficit (the value of release is less than

demand); $N.C.D$ = number of periods with continuing deficit; and Z_3 = resiliency of the system.

In the operational model, reliability and resiliency of the system are presented as the quality values, and vulnerability of the system is identified as the quantity value.

The model formulation is constrained by the following relations:

$$S_{t+1} = S_t + Q_t + R_t - Loss_t \tag{11}$$

$$Loss_t = f_1\left(Ev_t, \overline{A_t}\right) \tag{12}$$

$$\overline{A_t} = \left(A_t + A_{t+1}\right)/2 \tag{13}$$

$$A_t = f_2\left(S_t\right) \tag{14}$$

$$S_{Min} \le S_t \le S_{Max} \tag{15}$$

$$S_1 = S_{T+1} \tag{16}$$

in which S_t and S_{t+1} = storage volume at the start of periods t and $t+1$ respectively; Q_t = inflow to the reservoir at period t; $Loss_t$ = volume of losses water from reservoir at period t; Ev_t = evaporation depth of reservoir at period t; $\overline{A_t}$ = average surface of reservoir at period t; A_t and A_{t+1} = water surface of reservoir at the start of periods t and $t+1$, respectively; S_{Min} = minimum storage of reservoir; and S_{Max} = maximum storage of reservoir.

To use the weighing method as the optimization tool in this problem, the objective function is calculated by Eqs. 17-18:

$$Min.\ \ Z(x) = -w_1.Z_1(x) + w_2.Z_2(x) + w_3.Z_3(x) \tag{17}$$

$$\sum_{j=1}^{3} w_j = 1 \tag{18}$$

In this problem, the first objective is maximization of the reliability of the system. To apply all objectives in the minimization form, $Z_1(x)$ is used with the opposite sign.

5. Algorithm Application

To apply the MOPSO algorithm and weighting method, a single-reservoir system is considered. This reservoir is located in the southwest of Iran with a volume of $308.15\times10^6\,m^3$. Monthly releases and initial storage of reservoir have been considered as the decision variables. Thus, the number of decision variables for a five-year operational period is 61.

The weighting method is an optimization tool which solves the introduced model by using nonlinear programming (NLP) and Lingo8 software. To find different points of Pareto-front, 25 weighting vectors have been used and the objective functions are calculated. The Lingo8 software takes lots of time to find a global optimal solution for the proposed problem. To have the same base in different

runs (problem) using each weighting vector, each run is interrupted in the fifth minute of run by using Lingo8. Thus, the time for finding the Pareto-front is 125 (5×25) minutes. Finally, 25 points have been found and just 5 of those points were in nondominated state. The other points which are removed have the worst situation in all objectives (Z_1, Z_2, and $Z3$). The best value for each objective has been calculated by Lingo8 and the comparative point is (0.761, 1.944, 0.500).

To find the best Pareto-front by using the MOPSO algorithm, *GD* criteria is calculated for five different runs. The time of finding the Pareto-front is 125 minutes which is equal to solving model by the weighting method. Table. 1 shows the *GD* criteria and its statistical measures. According to results, the Pareto-front of the fifth run is the best one with the minimum value of *GD*.

Table 1. *GD* criteria and its statistical measures for five runs

Run number					Statistical Parameter				
1	2	3	4	5	Minimum	Average	Maximum	Standard Deviation	Coefficient of Variation
14.481	18.215	13.682	13.423	11.215	11.215	14.203	18.215	2.549	0.179

Fig. 1. shows the best Pareto-front in three and two dimensions.

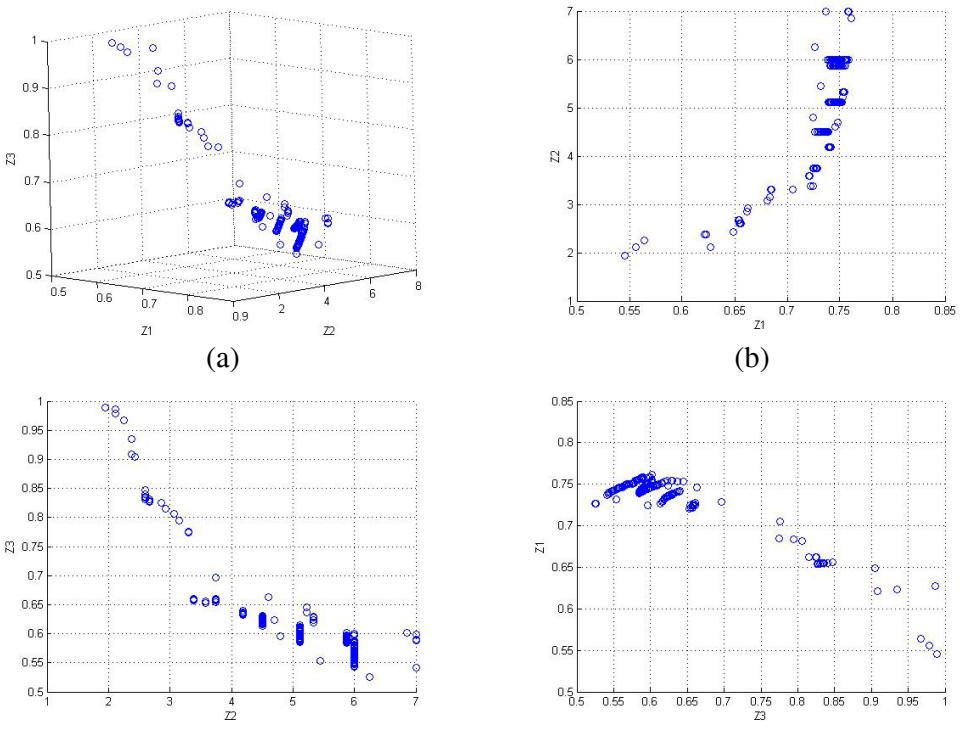

Figure 1. The best Pareto-front: (a) in three dimensions; (b) in two dimensions for the first and second objectives; (c) in two dimensions for the second and third objectives; and (d) in two dimensions for the first and third objectives

According to Fig.1(b), the first objective (Z_1) changes from 0.546 to 0.761. Fig.1(c) shows the best values of the second (Z_2) and third (Z_3) objective are 1.944 and 0.500, and the worst ones are 7.000 and 0.989, respectively. To demonstrate the best objective functions of the best Pareto-front, monthly releases for each of them have been considered in Figs. 2-4.

Figs. 2 and 4 show amounts of release for the best value of Z_1 and Z_3 in the best Pareto-front having a smaller difference from demands. In the first objective (Z_1), the larger value of release in each period, the better value of Z_1. In the third objective (Z_3), to reduce the maximum value of $\left(\left(R_t - D_t\right)/D_t\right)$ in the operational period, the values of release increase in all periods. However, Fig. 3 shows that releases for the best value of the second objective (Z_2) have a lot of fluctuation. In this state, to decrease the number of periods with continuing deficit, the amounts of release have been presented without considering any difference from demands. It means that if there is not enough water to supply demand at a period, the water should be stored in the reservoir and the demand is supplied at the next period.

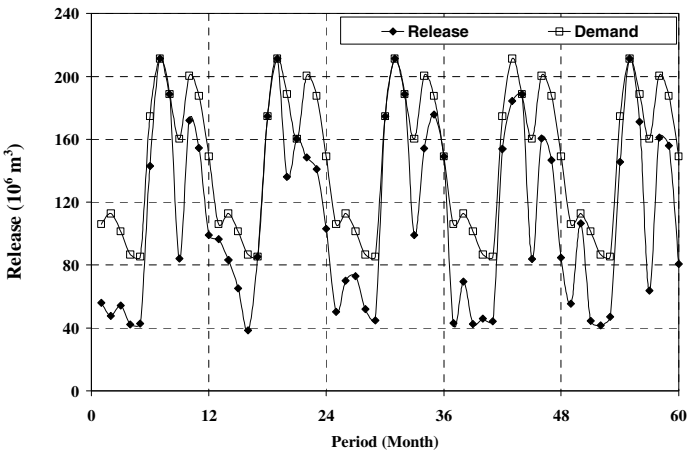

Figure 2. Monthly releases for the best value of Z_1 in the best Pareto-front

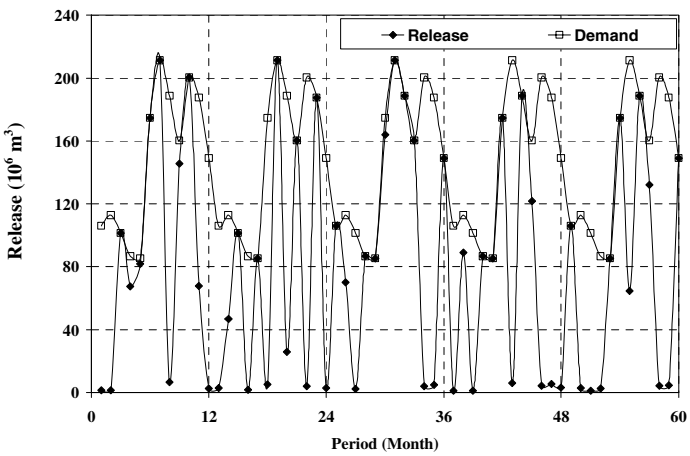

Figure 3. Monthly releases for the best value of Z_2 in the best Pareto-front

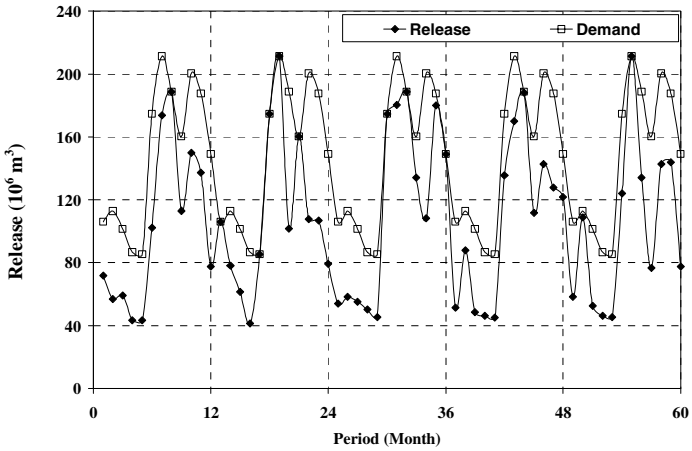

Figure 4. Monthly releases for the best value of Z_3 in the best Pareto-front

To demonstrate the capability of different algorithms, the best values of each objective are presented in Table 2.

Table 2. The best objective functions for different algorithms

Algorithm	Objective Function		
	Z_1	Z_2	Z_3
NLP	0.761	1.944	0.500
Weighting Method	0.728	2.111	0.500
MOPSO	0.754	1.944	0.500

According to results, in the first objective (Z_1), the MOPSO and weighting method are respectively 0.920% and 4.366%, less than the found solution by NLP algorithm. In the second objective (Z_2), the MOPSO algorithm has produced the best value (1.944) but the weighting method has 8.591% difference. In the third objective (Z_3), results of the all algorithms are the same. On the other hand, the MOPSO algorithm in a same time of run (125 minutes) has produced 215 nondominated solutions, whereas the weighting method has produced five nondominated solutions.

Thus, the capability of the MOPSO algorithm to find optimal/near-optimal Pareto-front is more than in the weighting method.

6. Concluding Remarks

In this paper, application of multi-objective particle swarm optimization (MOPSO) algorithm was presented. To show the capability of the MOPSO algorithm, a single-reservoir operation with three objectives (maximization of reliability; minimization vulnerability; and minimization of resiliency of system) was used. Results of the MOPSO algorithm can be presented as a set of nondominated solutions/Pareto-front. The weighting method is another multi-objective optimization tool which is searching for an optimal point by transferring a multi-objective problem to a single-objective one. To compare the results of the weighting method

and MOPSO algorithm, *GD* criteria was used. Results show that the MOPSO can find optimal solutions with a suitable distribution in much less time.

7. References

Balter, A. M., and Fontane, D. G. (2006). "A Multiobjective Particle Swarm Optimization Model for Reservoir Operations and Planning." International Conference on Computing and Decision Making in Civil and Building Eng. Montreal, Canada. June 2006. 1544-1552.

Cieniawski, S. E., Eheart, J. W., and Ranjithan, S., (1995). "Using Genetic Algorithms to Solve a Multiobjective Groundwater Monitoring Problem." Water Resource Research, 31(2), 399-409.

Coello, C. A., and Lechuga, M. S. (2002). "MOPSO:A Proposal for Multiple Objective Particle Swarm Optimization." Proceedings of the IEEE Congress on Evolutionary Computation (CEC'2002). IEEE Service Center. Piscataway, New Jersey. May 2002. Vol. 2, 1677-1681.

Elbeltagi, E., Hegazy, T., and Grierson, G., (2005). "Comparison Among Five Evolutionary-Based Optimization Algorithms." Journal of Advanced Engineering Informatics., 19(1), 43-53.

Kumar, D., and Reddy, J. (2007). "Multipurpose Reservoir Operation Using Particle Swarm Optimization." Journal of Water Resource Planning and Management. ASCE, 133(3), 192-202.

Labadie, J. W., (2004). "Optimal Operation of Multireservoir Systems: State-of-the-Art Review." Journal of Water Resource Planning and Management. ASCE, 133(2), 93-110.

Parsopoulos, K. E., and Vrahatis, M. N., (2002). "Particle Swarm Optimization Method in Multiobjective Problems." In Proceedings of the 2002 ACM Symposium on Applied Computing, Madrid, Spain. March 2002. 603-607.

Prasad, T. D., and Park, N. S., (2004). "Multiobjective Genetin Algorithms for Design of Water Distribution Networks." Journal of Water Resource Planning and Management. ASCE, 130(1), 73-82.

Prasad, T. D., Walter, G. A., and Savic, D. A., (2003). "Booster Disinfection of Water Supply Networks: Multiobjective Approach." Journal of Water Resource Planning and Management. ASCE, 130(5), 367-376.

Veldhuizen, D. (1999). "Multiobjective Evolutionary Algorithms: Classification, Analyses, and New Innovations." Ph.D. thesis. Department of Electrical and Computer Engineering, Air Force Institute of Technology, Dayton., Ohio.

Multi-criteria Decision Making under Uncertainty in Rainfall-Runoff Calibration: A Fuzzy Compromise Programming Approach Based on Alpha Level sets

M. Shafii[1] and F. De Smedt[1]

[1]Department of Hydrology and Hydraulic Engineering, Vrije Universiteit Brussel, Pleinlaan 2, 1050, Elsene, Brussels, Belgium, FAX: (32) 2-629-3022, emails: mshafiih@ub.ac.be, fdesmedt@vub.ac.be

Abstract

This paper involves a methodology developed for multi-criteria decision making and to reduce the number of Pareto optimal solutions. The technique is a Fuzzy Compromise Programming (FCP) coupled to a Genetic Algorithm (GA) applied for a case study on multi-objective rainfall-runoff calibration. The uncertainty associated with probable preferences of decision-makers has also been dealt with by the fuzzy extension principle and alpha-cut levels (i.e. considering the importance of the criteria by triangular fuzzy weights). The problem, therefore, becomes to solve a set of non-linear programming problems using GA, which results in ranking the alternatives based on a distance metrics. The obtained results show that the proposed hybrid FCP-GA approach performs well as a means to sieve among the Pareto optimal parameter sets of the problem. It would also help to choose the most preferable solutions, especially in cases where one is obliged to give a limited number of best solutions.

INTRODUCTION

Calibration of rainfall-runoff (RR) models is a process in which parameter adjustment are made so as to match (as closely as possible) the dynamic behaviour of the RR model to the observed behaviour of the catchment. Because of the multi-objective nature of RR calibration processes, and due to advances in computational power as well as population-based optimization techniques, automatic calibration routines for hydrologic models with multiple objective capabilities are becoming increasingly popular. These approaches have shown to lead to better characterization of complex behaviour of the catchments. Gupta et al. (1998) discussed for the first time the advantages of multiple-objective model calibration and showed that such schemes are applicable and desirable. Subsequently, more research has been focused on multi-objective approaches for calibration of RR models (Yapo et al., 1998; Boyle et al., 2000; Madsen, 2000). There are also an increasing number of recent studies focusing on developing multi-objective calibration strategies for distributed hydrologic models (Madsen, 2003; Ajami et al., 2004; Shafii and De Smedt, 2009).

It should be, though, noted that as more objective functions are included in the calibration, the number of optimal solutions (Pareto-optimal parameter sets, Pareto (1986)) increases and the calibration issue quickly becomes a decision-making problem. In a practical sense, attention is focused towards choosing a suitable

parameter set among the Pareto-optimal solutions. One of the approaches to handle this problem, as proposed by Khu and Madsen (2005), can be the development of a calibration procedure that will result in a small number of preferred solutions. Khu and Madsen (2005) combined an optimization routine, based on multi-objective genetic algorithms (MOEAs), and Pareto preference ordering. In their case, the Pareto-optimal solutions which are also Pareto-optimal in different subspace combinations of the objective functions are preferred.

Another approach that can be applied in this context is Multi-Criteria Decision Making (MCDM). Multi-criteria techniques help in evaluation and ranking of alternatives based on the objective function values associated with each of the alternatives and preference of the various decision-makers. Compromise programming (CP), proposed for the first time by Zeleny (1973), is a MCDM technique which resolves multiple criteria into a commensurable, unitless, distance metric measured from an ideal point (for each alternative). The result is a direct ranking of alternatives, valid for the selected weights and the chosen form of distance measurement, whereby the closest solutions to the ideal point determined by some measure of distance are identified as the most preferable solutions.

Due to different uncertainties associated with MCDM, CP methods need to be combined with an uncertainty assessment routine. Bender and Simonovic (2000) introduced the Fuzzy Compromise Programming (FCP) approach and used it in water resources systems planning. Their proposed method involves the transformation of a distance metric into a fuzzy set by changing all inputs from crisp to fuzzy and applying the fuzzy extension principle. Although some further applications of this technique are reported in decision making for water resources management (Tkach and Simonovic, 1997; Simonovic and Nirupama, 2005), one can hardly find any CP application for RR calibration problem.

Hence, this paper involves two major issues: (i) application of FCP technique to multi-objective rainfall-runoff calibration, i.e. finding the most preferable solution among the Pareto optimal solutions of the problem, and (ii) coupling this method to alpha-cut-level-based extension principle (EP) and evolutionary optimization algorithm to handle the issue of uncertainty. Multi-objective calibration of a distributed hydrological model (WetSpa) on a catchment located in Slovakia forms the case study of this paper. The method is used to sieve through the Pareto-optimal solutions (alternatives) of the problem obtained by a multi-objective genetic algorithm (NSGA-II, Deb, et al., 2002) and select a smaller number of preferred solutions. In this way, alternatives which tend to be closest to the ideal point, as determined by some measure of distance, are called compromise solutions and are preferred. The distance metric is transformed to a fuzzy set by FCP technique through changing all inputs from crisp to fuzzy based on alpha level sets and the fuzzy extension principle. This approach turns out to be a nonlinear programming (NLP) problem which can be solved applying an evolutionary algorithm, in this case Genetic Algorithm (GA). FCP ranks alternatives based on the membership functions of their metrics to select the most suitable parameter set.

This paper is organized as follows. Basic concepts and terminology of multi-criteria decision making analysis are briefly presented in Section 2, followed by the

proposed methodology of this study in Section 3 as a combination of an FCP approach and a GA optimization routine. Section 4 provides the case study addressed in this paper, and the implementation of the FCP technique to solve the problem is discussed in Section 5. Results and discussions are provided in Section 6, and conclusions are presented in Section 7.

MULTI-CRITERIA DECISION MAKING (MCDM) ANALYSIS

MCDM analysis is a discipline aimed at supporting decision makers who are faced with making conflicting evaluations. MCDM aims at highlighting these conflicts and deriving a way to come to a compromise in a transparent process. The general formulation of a multi-criteria decision problem is based on: (a) a set of potential alternatives, (b) a set of objectives or criteria, (c) a number of decision-makers, (d) a preference structure or weights, and (e) a set of performance evaluations of alternatives for each objective. In a mathematical form a multi-objective decision problem can be presented as:

$$\min\left\{ f_1(x), f_2(x),..., f_n(x) \right\} \quad (1)$$

Where $f_i(x), i = 1,2,...,n$ are n different objective functions and x is a set of decision variables such that $x \in X$ while X is a feasible region defined as:

$$X = \left\{ x : x \in R^n, g_i(x) \le 0 \right\} \quad (2)$$

Where R^n is a set of real numbers, and $g_i(x)$ is a set of constraints. Every feasible solution to the problem (1) implies particular values for different objective function. The n-dimensional objective function maps the feasible region in decision space into the feasible region in objective space, defined on the n-dimensional vector space.

For a Multi-criteria optimization problem like the one presented by Eq. (1), it is significant to note that multiple criteria are often non-commensurable and cannot be combined into a single criterion. The criteria usually conflict with each other and any improvement in one can be achieved only at the expense of another. Hence, there is no ‘‘optimal” solution for the Multi-criteria optimization as in case of a single criterion problem. For the solution of problem (1) only a set of non-dominated, Pareto optimal, solutions can be obtained. However, decisions represented by the Pareto set are not uniquely determined (different preferences associated with each of the objectives result in a different Pareto optimal solution). The final decision must include a selection among the set of Pareto optimal solutions, generally considering outranking relationships, distance metrics, and/or utility theory (Bender and Simonovic, 2000). For instance, CP as a Multi-criteria technique, revolves criteria into a unitless, distance metric measured from an ideal point (for each alternative), as discussed in following section.

FUZZY COMPROMISE PROGRAMMING BASED ON ALPHA CUTS

As already mentioned, multi-objective optimization problems deal with decision-making through which more appropriate solutions among Pareto optimal solutions

can be selected. The CP method, proposed by Zeleny (1973), is such an approach. The basic idea of the CP method is to define the scalarized objective function by a metric form, which is non-linear in terms of constitutive criteria. Mathematically, this metric is a sort of evaluation index measuring the minimum distance between the Pareto optimum to be sought and the global unattainable optimal point where all criteria take their optimum value simultaneously. The following mathematical formulation is used to compute the distance metric values (L_j) for a set of n criteria and m alternatives (i.e. in our case Pareto solutions):

$$L_j = \left[\sum_{i=1}^{n} w_i^{\,p} \left| \frac{f_i^* - f_{i,j}}{f_i^* - f_{i,w}} \right|^p \right]^{1/p} \tag{3}$$

where L_j is the distance metric for alternative $j = 1,2,...,m$, f_i^* is the optimal value of the ith criterion, $f_{i,j}$ is the value of the ith criteria for alternative j, $f_{i,w}$ is the worst value of the ith criterion, w_i are weights indicating decision-maker preferences with respect to different criterion, and p is the distance metric exponent ($1 \le p \le \infty$). As it is seen, L_j is directly dependent on p, as well as on the criteria weights the sum of which is assumed to equal unity (i.e. $\sum wi=1$). The CP method of Zeleny (1973) does not consider the uncertainties associated with these judgements of preferences. The combination of a CP technique with fuzzy sets, as an example of a hybrid decision making tool, has been shown to be a proper methodology for uncertainty assessment (Bender and Simonovic, 2000).

The Fuzzy Compromise Programming (FCP) technique developed by Bender and Simonovic (2000) transforms a CP distance metric to a fuzzy set by changing all inputs from crisp to fuzzy through the application of the fuzzy extension principle. This approach can address various uncertainties that are associated with the elements of their case study, i.e. flood management. This paper extends the FCP method of Bender and Simonovic (2000) considering the criteria weights as fuzzy numbers, as well as coupling this technique to a GA to solve the non-linear optimization problem contained in determination of distance metric membership function, as follows.

Assuming a fuzzy definition for the criteria weights (w_i) in Eq. (1), and given an exponent p, the resulting fuzzy distance metrics (L_j) possesses a particular membership function for each alternative. The most commonly used fuzzy numbers have triangular shape membership functions defined as,

$$\mu_{\bar{A}}(x) = \begin{cases} (x-a)/(b-a), & a \le x \le b, \\ (d-x)/(d-b), & b \le x \le d, \\ 0, & otherwise, \end{cases} \tag{4}$$

A triangular fuzzy number is usually denoted as (a, b, d). According to Zadeh's extension principle (Zimmermann, 1991), a fuzzy number/set $\bar{A}$ can also be expressed by its intervals, namely

$$\bar{A} = \bigcup_{\alpha} \alpha A_{\alpha}, \quad 0 < \alpha \le 1 \tag{5}$$

Where

$$A_\alpha = \left\{ x \in X \middle| \mu_{\bar{A}}(x) \geq \alpha \right\} = \left\{ \min\ [x \in X \middle| \mu_{\bar{A}}(x) \geq \alpha],\ \max\ [x \in X \middle| \mu_{\bar{A}}(x) \geq \alpha] \right\} \quad (6)$$

A_α is referred to as α-level sets or α-cuts of the fuzzy number/set $\bar{A}$. Transformation of a distance metric into a fuzzy set is possible by applying the fuzzy extension principle and aforementioned α-level-based method. In this way, choosing the shortest distance to the ideal solution is no longer a straightforward ordering of distance metrics, and it is required to compare fuzzy sets corresponding to different solutions. Let $(w_i)_\alpha = \left[(w_i)_\alpha^L, (w_i)_\alpha^U\right]$ be alpha-level sets of the weights (w_i). The resulting fuzzy distance metric has the following form:

$$\bar{L}_j = \left[\sum_{i=1}^{n} \bar{w}_i^p \left| \frac{f_i^* - \bar{f}_{i,j}}{f_i^* - f_{i,w}} \right|^p \right]^{1/p} \quad (7)$$

Subject to $(w_i)_\alpha^L \leq \bar{w}_i \leq (w_i)_\alpha^U$, where $\bar{L}_j$ and $\bar{w}_i$ are the fuzzified distance metric and criteria weights indicating decision-maker preferences, respectively, of which the latter satisfies $0 \leq w_j \leq 1$, and $\sum w_j = 1$, $i = 1,...,n$ criteria and $j = 1,...,m$ alternatives. Obviously, $\bar{L}_j$ is an interval in this situation, whose lower and upper bounds can be captured by the following pair of fractional programming models:

$$(\bar{L}_j)_\alpha^L = \min \left[\sum_{i=1}^{n} \bar{w}_i^p \left| \frac{f_i^* - \bar{f}_{i,j}}{f_i^* - f_{i,w}} \right|^p \right]^{1/p} \quad (8)$$

$$(\bar{L}_j)_\alpha^L = \max \left[\sum_{i=1}^{n} \bar{w}_i^p \left| \frac{f_i^* - \bar{f}_{i,j}}{f_i^* - f_{i,w}} \right|^p \right]^{1/p} \quad (9)$$

Both subject to $(w_i)_\alpha^L \leq \bar{w}_i \leq (w_i)_\alpha^U$, and $\sum \bar{w}_i = 1$. This is actually a pair of non-linear programming problems that can be solved using appropriate optimization procedures. In this study, a GA optimization procedure is used to search for the optimal values of this distance metric. Given a particular p, different alpha sets $(\bar{L}_i)_\alpha = \left[(L_i)_\alpha^L, (L_i)_\alpha^U\right]$ can be generated by setting different alpha-levels and solving above mentioned optimization problems.

For n alternatives, we have n fuzzy relative closeness values, which are all expressed by their alpha-level sets and are usually no longer triangular. In order to select a best alternative or rank m alternatives, these fuzzy relative closeness values need to be defuzzified. The averaging level cuts (ALC) suggested by Dubois and Parade (1978) is perhaps the simplest defuzzification method based on alpha-level sets and is therefore used in this study. The defuzzified values of $\bar{L}_j$ can be determined by,

$$(L_j)^*_{ALC} = \frac{1}{N}\sum_{i=1}^{N}\left(\frac{(L_j)^L_{\alpha_i} + (L_j)^U_{\alpha_i}}{2}\right) \quad (10)$$

In order to apply this methodology, it is first required to determine the different items of the multi-criteria decision making problem. Initial data requirements include: (a) a set of alternatives, (b) a set of relevant criteria/objective values, (c) the best and the worst criteria values to compute the distance metrics, and (d) fuzzy membership functions for the weights.

CASE STUDY

The case study addressed in this paper is the calibration problem studied by Shafiei and De Smedt (2009) that used a Non-Dominated Sorting Genetic Algorithm (NSGA-II) to calibrate a distributed hydrological model (WetSpa) within a multi-objective formulation for simulation of river discharge in the Hornad catchment, located in Slovakia. Detailed information about the model, the optimization routine, the study area, and the obtained results are provided in Bahremand et al. (2007) and Shafiei and De Smedt (2009). A brief description of the different elements of the problem is provided as follows.

WetSpa is a grid-based distributed hydrologic model to predict peak discharges and hydrographs in a river basin. The WetSpa model potentially involves a large number of model parameters most of which can be assessed from field data. However, some model parameters are of a more conceptual nature and cannot be directly assessed. Hence, these have to be determined through a calibration process. NSGA-II (Deb et al., 2002) is an evolutionary-based population-based multi-objective optimization algorithm used by Shafiei and De Smedt (2009) to calibrate WetSpa. The considered criteria are the model bias (CR_1), the model efficiency to reproduce stream flows, known to be biased for peak flows (CR_2), and a logarithmic transformed model efficiency, giving more emphasize to low-flow values (CR_3). Table 1 provides the mathematical representation of these criteria and the corresponding best and the worst feasible quantities, where Qo_i is the observed discharge at time i, Qs_i the simulated discharge, the bar stands for average, and N is the total number of time steps in the calibration period.

IMPLEMENTATION OF FCP APPROACH BASED ON ALPHA-CUTS

The Pareto optimal front obtained for aforementioned problem includes 27 different parameter sets which are all considered as the calibration outcome alternatives. Table 2 gives the corresponding objective function values. Nonetheless, as already mentioned, it is better to apply a post-processing analysis to reduce the number of the most appropriate solutions. The proposed FCP approach of this paper deals with this issue based on distance metric.

Consideration of the criteria weights as fuzzy numbers takes the uncertainty associated with the preferences of stake-holders into account through the extension principle and alpha-cut levels. The fuzzy weights have a triangular shape (0,1/3,1); notice that the peak is set to 1/3 due to the number of objective functions (i.e. 3). In

order to obtain accurate fuzzy distance metric for each alternative, 11 alpha levels are set for computation, i.e. from 0 to 1with steps of 0.1. For each alpha-cut, the optimization problems determined by (8) and (9) are solved to obtain the extreme values for the distance metric and to build the corresponding membership function. These problems are all solved using GA optimization. As a huge body of literature can be found regarding GA and its concepts, it is not discussed again in this paper.

Table 1. Model evaluation criteria and their range.

Code	Criterion	Description	Best value	Worst value
CR_1	$\left\| 1-\sum_{i=1}^{N} Qs_i \Big/ \sum_{i=1}^{N} Qo_i \right\|$	Model bias for evaluating the ability of reproducing the observed streamflow volume	0	1
CR_2	$1-\frac{\sum_{i=1}^{N}(Qs_i - Qo_i)^2}{\sum_{i=1}^{N}(Qo_i - \overline{Qo})^2}$	Model efficiency for evaluating the ability of the model to reproduce all streamflows	1	0
CR_3	$1-\frac{\sum_{i=1}^{N}[\ln(Qs_i)-\ln(Qo_i)]^2}{\sum_{i=1}^{N}[\ln(Qo_i)-\overline{\ln(Q_0)}]^2}$	Model efficiency for evaluating the ability of the model to reproduce low flows	1	0

Table 2. Evaluation criteria values of the Pareto optimal solutions.

No.	CR_1	CR_2	CR_3	*Continued*			
1	0.003	0.737	0.701	No.	CR_1	CR_2	CR_3
2	0.006	0.748	0.697	15	0.005	0.755	0.574
3	0.002	0.740	0.691	16	0.001	0.728	0.688
4	0.008	0.753	0.667	17	0.043	0.757	0.635
5	0.005	0.748	0.687	18	0.008	0.758	0.624
6	0.014	0.726	0.715	19	0.033	0.741	0.700
7	0.014	0.739	0.705	20	0.020	0.755	0.640
8	0.001	0.734	0.713	21	0.003	0.754	0.614
9	0.003	0.722	0.714	22	0.051	0.755	0.642
10	0.001	0.749	0.649	23	0.002	0.745	0.671
11	0.001	0.745	0.659	24	0.025	0.708	0.716
12	0.012	0.753	0.678	25	0.008	0.753	0.637
13	0.017	0.749	0.687	26	0.042	0.754	0.656
14	0.034	0.715	0.718	27	0.007	0.758	0.592

RESULTS AND DISCUSSION

The results obtained through application of our FCP approach to above mentioned problem include the quantification of the fuzzy distance metrics and corresponding

ranking of the Pareto optimal solutions. Given different values between 2 and 5 for *p* in Eq. (8), extreme values of the distance metric along different alpha-cut levels were calculated. The defuzzified values computed by Eq. (10) and the corresponding ranking of alternatives were subsequently determined as shown in Table 3. Moreover, the corresponding membership functions of the different alternatives in case of *p=2* are illustrated in Figure. 1.

As it is observed for *p=2*, the solution No. 9 is shown to be superior to all other parameter sets. Likewise, solution No. 8 is more desirable when *p* is 3, 4, and 5. Hence, these solutions can be considered as the best compromise and, hence, the most preferable parameter sets. Obviously, as the results of our proposed hybrid FCP-GA methodology are obtained through consideration of different criteria importance weights, all preferences of future stake-holders would be probably covered. In other words, if we would be obliged to give only a limited number of optimal parameter sets, solutions No. 8 and No. 9 would be the most preferable choices.

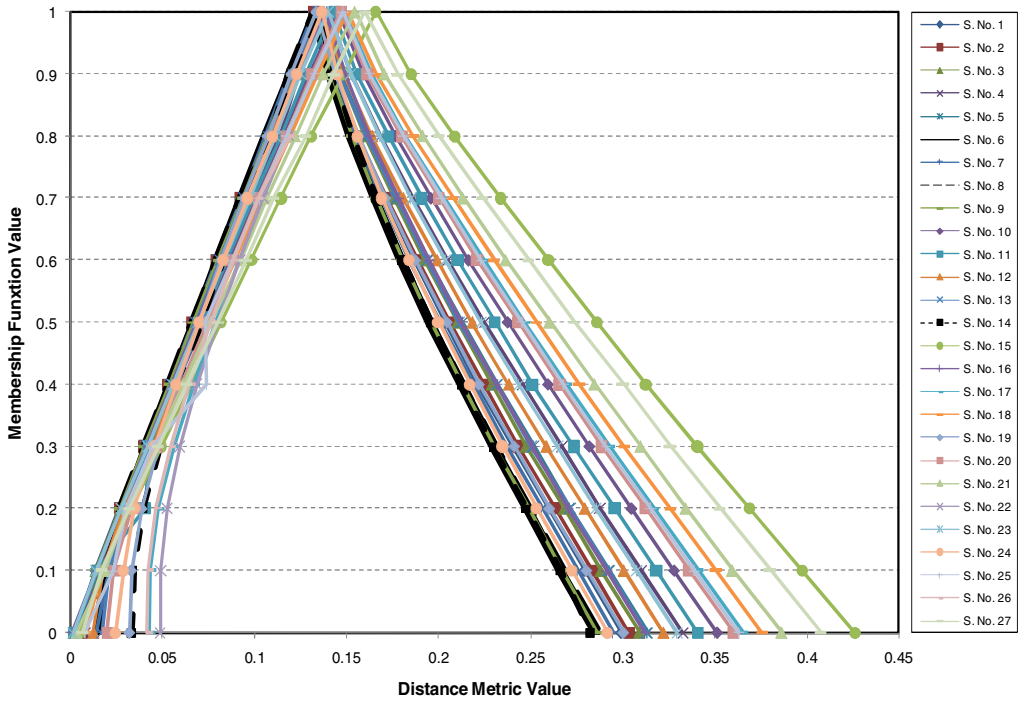

Figure. 1. Distance metric membership functions for different solutions (*p=2*).

CONCLUSIONS

This paper presents an application of an FCP approach coupled to a GA optimization routine to Multi-criteria decision making in a multi-objective rainfall-runoff calibration problem. The goal is to find the most preferable solutions among the Pareto optimal solutions of the problem. The uncertainty associated with probable preferences of decision-makers has been taken into account through the fuzzy extension principle and alpha-cut levels. The technique deals with selecting the most preferred solutions that are closest to the ideal point, as determined by some measure

of distance. Considering the importance of the criteria by triangular fuzzy weights, the distance metric is also a fuzzy number which can be evaluated along different alpha-cuts. The extreme values of distance metric membership function for each alpha-cut are determined by GA solving a pair of NLP problems. Finally, the alternatives can be ranked based on a simple defuzzification of the distance measure.

The obtained results show that the proposed methodology performs well as a means to sieve among the Pareto optimal solutions of the multi-objective optimization problem and to choose the most preferable solutions. In case one is obliged to give a limited number of "best" solutions, application of our hybrid FCP-GA approach would be promising.

Table 3. Defuzzified distance metric values and alternatives ranking for different p.

Solution No.	*P=2*		*P=3*		*P=4*		*P=5*	
	$(L)^*_{ALC}$	Rank Number	$(L)^*_{ALC}$	Rank Number	$(L)^*_{ALC}$	Rank Number	$(L)^*_{ALC}$	Rank Number
1	0.1256	5	0.1204	6	0.1186	7	0.1176	7
2	0.1267	7	0.1215	8	0.1196	8	0.1189	8
3	0.1290	9	0.1238	10	0.1219	10	0.1209	10
4	0.1372	16	0.1322	16	0.1304	16	0.1297	16
5	0.1302	11	0.1256	12	0.1236	11	0.1229	12
6	0.1225	3	0.1168	3	0.1146	3	0.1136	2
7	0.1250	4	0.1196	5	0.1175	5	0.1165	5
8	0.1221	2	0.1164	1	0.1144	1	0.1134	1
9	0.1221	1	0.1167	2	0.1145	2	0.1137	3
10	0.1438	18	0.1392	18	0.1372	18	0.1366	18
11	0.1406	17	0.1351	17	0.1337	17	0.1325	17
12	0.1339	14	0.1286	14	0.1267	14	0.1259	14
13	0.1310	13	0.1259	13	0.1239	13	0.1231	13
14	0.1259	6	0.1195	4	0.1172	4	0.1160	4
15	0.1710	27	0.1666	27	0.1652	27	0.1654	27
16	0.1307	12	0.1255	11	0.1237	12	0.1225	11
17	0.1538	24	0.1480	23	0.1459	23	0.1451	23
18	0.1525	22	0.1483	24	0.1465	24	0.1462	24
19	0.1296	10	0.1237	9	0.1214	9	0.1208	9
20	0.1485	20	0.1435	20	0.1416	20	0.1408	20
21	0.1565	25	0.1520	25	0.1507	25	0.1497	25
22	0.1528	23	0.1465	22	0.1444	22	0.1434	22
23	0.1360	15	0.1310	15	0.1293	15	0.1286	15
24	0.1271	8	0.1208	7	0.1185	6	0.1173	6
25	0.1492	21	0.1437	21	0.1417	21	0.1411	21
26	0.1466	19	0.1405	19	0.1383	19	0.1374	19
27	0.1643	26	0.1600	26	0.1584	26	0.1580	26

REFERENCES

Ajami, N.K., Gupta, H.V., Wagener, T., and Sorooshian, S.: Calibration of a semi-distributed hydrologic model for streamflow estimation along a river system, J. Hydrol., 298, 112–135, 2004.

Bahremand, A., De Smedt, F., Corluy, J., and Liu, Y.B.: WetSpa Model Application for Assessing Reforestation Impacts on Floods in Margecany–Hornad Watershed, Slovakia, Water Resources Management, 21, 1373-1391, 2007.

Bender, M., Simonovic, S.P.: A fuzzy compromise approach to water resource systems planning under uncertainty, Fuzzy Sets Syst., 115(1), 35–44, 2000.

Boyle, D.P., Gupta, H.V., and Sorooshian, S.: Toward improved calibration of hydrologic models: Combining the strengths of manual and automatic methods, Water Resour. Res., 36, 3663–3674, 2000.

Deb, K., Pratap, A., Agarwal, S., and Meyarivan, T.: A Fast and Elitist Multiobjective Genetic Algorithm: NSGA-II, IEEE Trans. Evol. Computation, 6, 182-197, 2002.

Dubois, D., Prade, H.: Operations on fuzzy numbers, Int. J. Systems Sci., 9(6), 613-626, 1978.

Gen, M., Cheng, R.: Genetic algorithms and engineering optimization, New York: John Wiley &Sons, 2000.

Goldberg, D.E.: Genetic Algorithms in Search, Optimization and Machine Learning, Addison-Wesley Publishing Co., Inc., Redwood City, CA, USA, 1989.

Gupta, H.V., Sorooshian, S., Yapo, P.O.: Toward improved calibration of hydrological models: multiple and noncommensurable measures of information, Water Resour. Res., 34 (4), 751–763, 1998.

Khu, S.T., Madsen, H.: Multiobjective calibration with Pareto preference ordering: an application to rainfall–runoff model calibration, Water Resources Research, 41, W03004, 2005.

Madsen, H.: Parameter estimation in distributed hydrological catchment modeling using automatic calibration with multiple objectives, Adv. Water Resour., 26, 205–216, 2003.

Madsen, H.: Automatic calibration of a conceptual rainfall-runoff model using multiple objectives, J. Hydrol., 235, 276-288, 2000.

Pareto, V.: The Rise and Fall of the Elites, Totowa, N.J.: Bedminster Press, 1968.

Simonovic, S.P., Nirupama: A spatial multi-objective decision making under uncertainty for water resources management, Journal of Hydroinformatics, 7(2), 117–133, 2005.

Shafii, M. and De Smedt, F.: Multi-objective calibration of a distributed hydrological model (WetSpa) using a genetic algorithm, Hydrol. Earth Syst. Sci. Discuss., 6, 243-271, 2009.

Tkach, R.J., Simonovic, S.: A new approach to multi-criteria decision making in water resources, J. Geog. Inf. Dec. Anal., 1(1), 25–43, 1997.

Yapo, P.O., Gupta, H.V., Sorooshian, S.: Multi-objective global optimization of hydrological models. J. Hydrol. 204, 83–97, 1998.

Zadeh, L.: Fuzzy sets, Inform. Control, 8, 338-353, 1965.

Zeleny, M.: Compromise programming, in: J. Cochrane, M. Zeleny (Eds.), Multiple Criteria Decision Making, University of South Carolina Press, Columbia, USA, 1973.

Zimmermann, H.J.: Fuzzy set theory and its applications (2nd ed.), Boston, MA: Kluwer-Nijhoff, 1991.

Multiobjective Differential Evolution and Differential Evolution for Irrigation Planning

Piyush Gupta[1], A. Vasan[2] and K. Srinivasa Raju[3]

[1]Civil Engineering Group, Birla Institute of Technology and Science, Pilani, Rajasthan 333031, India; PH (+91) 9413057555;
email: coolpiyush2005@gmail.com
[2]Civil Engineering Group, Birla Institute of Technology and Science-Pilani, Hyderabad campus, Andhra Pradesh, India; PH (+91) 040-66303510;
email: vasan.arunachalam@gmail.com
[3]Civil Engineering Group, Birla Institute of Technology and Science-Pilani, Hyderabad campus, Andhra Pradesh, India; PH (+91) 040-66303519;
email: saiksraju@gmail.com

ABSTRACT

The present paper discusses the applicability of Multiobjective Differential Evolution (MODE) and single objective Differential Evolution (DE) to a case study of Mahi Bajaj Sagar Project, Rajasthan, India. Three objectives, namely, net benefits, agricultural production and labour employment are analyzed in the multiobjective framework using MODE. Four variations (strategies) of Differential Evolution, namely, DE/rand/1/bin, DE/rand/1/exp, DE/best/1/bin and DE/best/1/exp are explored. Population size, crossover and mutation probabilities and number of generations are the parameters that are required as input to MODE. In order to have a better insight on the performance of the strategies, DE in single objective framework is also employed with the same four strategies for all the three objectives with the above settings. In addition, a comparative analysis is also made for all the four strategies in both single and multiobjective framework.

INTRODUCTION

Water resources for irrigation in many countries are facing acute shortage due to increasing demand from irrigation, municipal, industrial etc. This makes irrigation planning, that involves cropping pattern, storage, release and water allocation policies, rather more complex. In addition, the problem becomes more complex when multiobjective planning is necessitated for the given situation. However, most of the traditional multiobjective optimization methods such as weightage and constraint method require huge computational requirements that lead to complexity while analyzing the solution (Deb, 2001). This is mainly due to the limitation of the methods to generate one solution at a time. This requires efficient solution methodologies that can handle irrigation planning in multiobjective framework in a systematic and sustainable way (Janga Reddy and Nagesh Kumar, 2007).

In the present study evolutionary algorithm, namely Differential Evolution both in single objective and multiobjective framework is employed for a case study of Mahi Bajaj Sagar Project (MBSP), Rajasthan, India. Important parameters that affect the planning problem are population size, number of generations, crossover and mutation probabilities and chosen DE strategy. Present paper is divided into

literature review, brief description about MODE algorithm, case study and mathematical modeling, results and discussion followed by conclusions.

LITERATURE REVIEW

Differential Evolution (DE) algorithm was introduced by Storn and Price in 1995 (Price and Storn 1997; Price and Storn, 2009). DE has advantages in terms of its simple structure, efficiency, robustness and use of floating point encoding instead of binary numbers. DE draws its inspiration from evolutionary algorithm in a way that it has random initial population, which is then improved using selection, mutation, and crossover operations. A predefined upper limit for the number of generations or computed function evaluations provides an appropriate stopping criterion.

Lampinen and Storn (2004) explained Differential Evolution with three numerical examples. They performed sensitivity analysis on various parameters such as population size, crossover constant and weighting factor. It is concluded that the method is easy to implement and use, effective, efficient and robust. Ali and Törn (2004) proposed new versions of the Differential Evolution algorithm to improve its efficiency and robustness. They introduced an auxiliary population of *NP* individuals alongside the original population and proposed a rule for calculating the control parameter *F*, automatically. Liu and Lampinen (2005) proposed a version of DE, where the mutation control parameter and the crossover control parameter are adaptive.

Ranjithan (2005) stressed on the role of evolutionary computation in environmental, water resources systems analysis and discussed the various methods in brief, namely, Simulated Annealing, Tabu Search, Genetic Algorithm, Evolutionary Strategies, Particle Swarm technique and Ant Colony Optimization. He concluded that new areas that shape the direction of a beneficial integration of evolutionary computation into environmental and water resources systems are essential. Vasan and Raju (2007) employed Differential Evolution for single objective, namely, net benefits for the case study of Mahi Bajaj Sagar Project, India in irrigation planning scenario. Janga Reddy and Nagesh Kumar (2007) presented Multiobjective Differential Evolution (MODE) with an application to a case study of Hirakud Reservoir, Orissa with two objectives. The developed algorithm is first tested on a few bench-mark test problems with standard performance measures by comparing them with non dominated Sorting Genetic Algorithm-II.

The following are the inferences from the literature review (1) most studies involve only two objectives and the number of constraints and variables involved are limited (2) Very little work has been reported in the field of irrigation planning in multiobjective evolutionary algorithm framework involving three objectives with extensive sensitivity analysis.

MODE ALGORITHM

MODE methodology can be summarized in the following steps:

1. Input the required DE parameters. Generate the initial population P randomly within the limits of each decision variable.
2. Evaluate the initial population P and perform mutation and crossover to create new children vectors from all the members of the population, i.e., for each parent vector.
3. Evaluate each children vector. Determine the nondominated set by merging the children and parent population according to fast sort algorithm.
4. To maintain the uniformly spread pareto optimal front, select the vectors to next generation based on non domination rank and crowding distance (Deb et al., 2002).

MATLAB code for NSGA-II, developed by Seshadri (2008), has been suitably modified for the working of MODE. Penalty function approach is employed in the present study to handle the constraints. More information on Differential Evolution and Multiobjective Differential Evolution are available in Price and Storn (2009), Janga Reddy and Nagesh Kumar (2007).

CASE STUDY

The Mahi Bajaj Sagar Project (MBSP) is situated near a village Borkhera about 16 km northeast of Banswara town in southern part of Rajasthan state. The project includes a dam, Kagdi pick up weir, a system of canals and two hydroelectric power houses, *PH 1* located near Banswara with installed capacity of 2x25 MW, and *PH 2* near Lilvani village with installed capacity of 2x45 MW. Gross and live storage capacity of the reservoir is 2180.39 Mm^3 (here $Mm^3=10^6$ m^3) and 1829.27 Mm^3 respectively. Culturable Command Area (CCA) of the project is 80,000 ha. Out of this, already 57,531 ha has been opened for irrigation (MBSP Report on Status June 2002 at a Glance, 2002; Vasan and Raju, 2007). The MBSP has three main canal systems namely, Left Main Canal (LMC), Right Main Canal (RMC) and Bhungra Canal (BC). The mathematical modelling of the irrigation planning problem of MBSP command area is explained below. Three conflicting objectives (Raju and Nagesh Kumar, 1999) namely, maximization of net benefits, agricultural production and labour employment are considered.

Mathematical Modeling

Objective 1

The objective of the model is that annual net benefits (*BE*) from planning region under different crops after meeting the costs of seeds, fertilizer, labour, surface water, ground water and plant protection are to be maximized. Mathematically it can be expressed as

$$Max \quad BE = \sum_{il=1}^{12} B_{il}.A_{il} + \sum_{ir=1}^{12} B_{ir}.A_{lr} + \sum_{ib=1}^{12} B_{ib}.A_{lb} - P_{GW} \sum_{t=1}^{12} GW_t$$

where *il* = Crop index for Left Main Canal [1=maize, 2=paddy, 3=cotton, 4=pulses, 5=sugarcane, 6=zaid crop, 7=wheat, 8=barley, 9=gram, 10=barseen, 11=mustard, 12=fruits and vegetables], *ir* = Crop index for Right Main Canal [1=maize, 2=paddy, 3=cotton, 4=pulses, 5=sugarcane, 6=zaid crop, 7=wheat, 8=barley, 9=gram, 10=barseen, 11=mustard, 12=fruits and vegetables], *ib* = Crop

index for Bhungra Canal [1=maize, 2=paddy, 3=cotton, 4=pulses, 5=sugarcane, 6=zaid crop, 7=wheat, 8=barley, 9=gram, 10=barseen, 11=mustard, 12=fruits and vegetables], *t*=Time index (1=January, ... 12=December). *BE* = Net benefits from the whole planning region (Rs.); B_{il}, B_{ir}, B_{ib} =Net benefits from $il^{th}, ir^{th}, ib^{th}$ crop including ground water cost (Rs./ha); A_{il}, A_{ir}, A_{ib} = Area of crop $il^{th}, ir^{th}, ib^{th}$ grown in the command area of LMC, RMC and BC (ha); P_{GW} =Ground water cost (Rs./Mm^3); GW_t =Monthly ground water withdrawal (Mm^3). Here Rs. indicates Indian Rupees.

Objective 2
Agricultural production (PR) of all the crops, for the whole planning area, is to be maximized and can be expressed as

$$PR = \sum_{il=1}^{12} Y_{il}.A_{il} + \sum_{ir=1}^{12} Y_{ir}.A_{lr} + \sum_{ib=1}^{12} Y_{ib}.A_{lb}$$

Where *PR* = Agricultural production (Tons); Y_{il}, Y_{ir}, Y_{ib} = Yield of the crop *il, ir* and ib respectively (Tons / ha).

Objective 3
Labour employment for each crop i, for the whole year for the whole planning area is to be maximized and can expressed as

$$LM = \sum_{il=1}^{12} L_{il}.A_{il} + \sum_{ir=1}^{12} L_{ir}.A_{lr} + \sum_{ib=1}^{12} L_{ib}.A_{lb}$$

where *LM* = Labour requirement for whole planning horizon (Man-Days); L_{il}, L_{ir}, L_{ib} = Labour requirement for crop *il*, *ir* and *ib* respectively in month t (Man-Days) per hectare.

The model is subjected to the constraints such as continuity equation for reservoir storage; crop area restrictions; water releases from the reservoir; storage capacity restriction of reservoir; canal capacity restrictions; monthly releases for hydropower production; crop diversification; monthly ground water pumping restriction (Vasan, 2005).

RESULTS AND DISCUSSION

MODE algorithm is validated using test examples (Deb, 2001) and is then applied to case study of MBSP. Inflow levels of seventy five percent dependability are considered for the planning problem. The model is validated for culturable command area that is opened for irrigation (57, 531 ha) and proposed (80,000 ha) as per phase 1. Accordingly, all the lower and upper bounds were determined for the decision variables. The model includes 67 constraints and 121 variables.

MODE is run for 500 generations with population size of 100, crossover and mutation probability as 0.9 and 0.1 respectively. Figure 1, Figure 2, Figure 3 and Figure 4 presents the result for DE/rand/1/bin, DE/rand/1/exp, DE/best/1/bin and

DE/best/1/exp respectively. It can be observed from Figure 1 and Figure 2 that the pareto optimal curve is fairly continuous while Figure 3 shows that the strategy DE/best/1/bin is converging to a point. Figure 4 shows a discontinuous pareto optimal front and that also with fairly low values of fitness functions. The annual net benefits are varying from Rs.1.134 x 10^9 to Rs.1.1355 x 10^9;agricultural production from 2.62 x 10^6 to 2.645 x 10^6 tonnes and labour employment from 4.96x 10^6 to 4.985 x 10^6 Man-days for strategy DE/rand/1/bin. It is inferred that there is reasonably good variation. The annual net benefits are varying from Rs.9.1 x 10^8 to Rs.9.25 x 10^8;agricultural production from 1 x 10^6 to 1.3 x 10^6 tonnes and labour employment from 3.25x 10^6 to 3.5 x 10^6 Man-days for strategy DE/rand/1/exp. Although the variation is more when compared to DE/rand/1/bin but the fitness function values are very low for all the three objectives. It was inferred that the former strategy is superior to the latter. There is no variation in all the three objective functions in terms of their values for strategy DE/best/1/bin, thus inferring that the strategy is not able to maintain diversity and is not suitable for the problem. Similarly the last strategy DE/best/1/exp is not able to maintain diversity as well as the preferred optimal values when compared to the DE/rand/1/bin. Thus it can be easily inferred that for the chosen case study, strategy DE/rand/1/bin is suitable than the other three.

The annual net benefits, agricultural production and labour employment for all the four strategies namely DE/rand/1/bin, DE/rand/1/exp, DE/best/1/bin and DE/best/1/exp are compared for both MODE and DE scenarios in Table 1. It is observed from Table 1 (MODE result) that values shown for MODE are for 1st member of 1st front having an infinite crowding distance value; however the results of DE are computed after running the algorithm for each individual objective. The table shows that the strategy DE/rand/1/bin has outperformed all the other strategies in terms of all the three objective function values. But in the case of DE strategy DE/best/1/exp is performing the best among the four strategies. However, the values for DE/best/1/bin are very close to that of DE/best/1/exp.

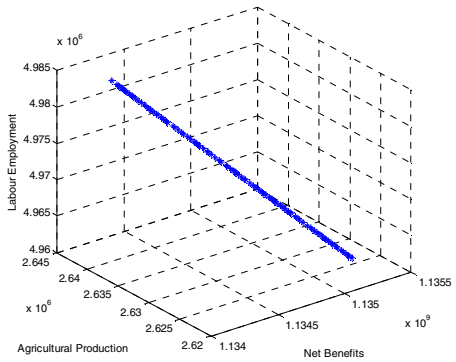

Figure 1. Pareto-optimal front (fitness function) after 500 generations (DE/rand/1/bin) for MODE

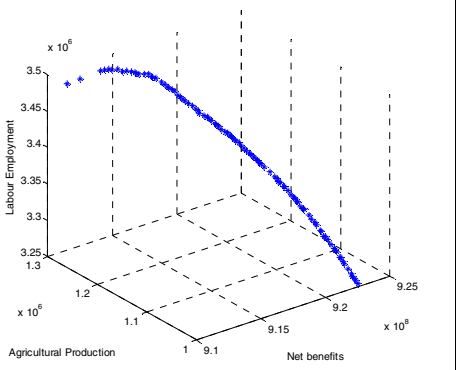

Figure 2. Pareto-optimal front (fitness function) after 500 generations (DE/rand/1/exp) for MODE

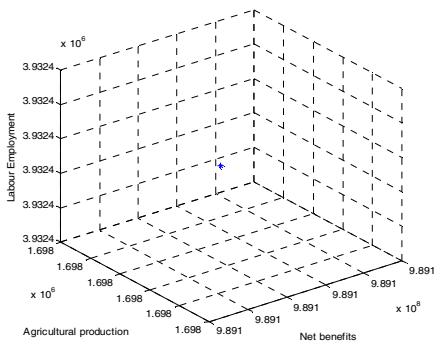

Figure 3. Pareto-optimal front (fitness function) after 500 generations (DE/best/1/bin) for MODE

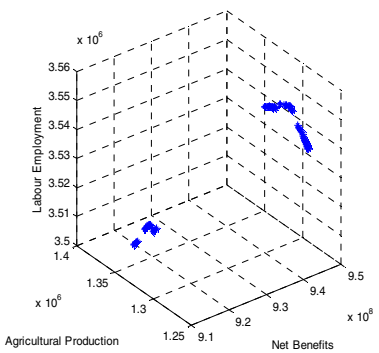

Figure 4. Pareto-optimal front (fitness function) after 500 generations (DE/best/1/exp) for MODE

Table 1: Comparison of objective function values for MODE and DE for all the four strategies

Strategy	Scenario	Objective 1 Net Benefits	Objective 2 Agricultural Production	Objective 3 Labour Employment
DE/rand/1/bin	MODE	$1.172 * 10^9$	$2.789 * 10^6$	$5.109 * 10^6$
	DE	$1.195 * 10^9$	$2.986 * 10^6$	$5.249 * 10^6$
DE/rand/1/exp	MODE	$9.68 * 10^8$	$1.38 * 10^6$	$3.5 * 10^6$
	DE	$1.192 * 10^9$	$3.05 * 10^6$	$5.305\ 10^6$
DE/best/1/bin	MODE	$9.997 * 10^8$	$1.786 * 10^6$	$4.035 * 10^6$
	DE	$1.201 * 10^9$	$3.09 * 10^6$	$5.324 * 10^6$
DE/best/1/exp	MODE	$9.78 * 10^8$	$1.32 * 10^6$	$3.67 * 10^6$
	DE	$1.195 * 10^9$	$3.14 * 10^6$	$5.313 * 10^6$

In single objective environment, out of the three objectives, the maximum value for two namely, net benefits and labour employment, are shown by strategy DE/best/1/bin whilst for the third objective agricultural production maximum value is shown by DE/best/1/exp and also the values for both the strategies are almost same.

While comparing the strategies for MODE and DE for performance analysis, an entirely conflicting situation is observed. In MODE "rand" strategies are performing better while in DE "best" strategies are performed better. There is no clear pattern while comparing strategies on "bin" or "exp" criterion in MODE scenario while in case of DE "exp" strategies are far better than "bin" strategies. However, it is inferred from the analysis made in the present paper that the "best" strategies are performing better in case of DE because in case of single objective optimization maintaining the diversity is not required. On the other hand it is required to find only one optimal solution which is further facilitated by preserving the best member of the generation and then using that particular member for crossover and mutation to develop the new population. This will

eventually help in reaching to the optimum much faster and the search for the member will be concentrated in particular objective space as compared to "rand" strategies where a random member is used for mutation and crossover. But when these "best" strategies are applied to MODE scenario, they do not possess the property of maintaining the diversity and thus finally converge to a point rather than searching for the optimal front in a rather larger objective space; however "rand" strategy keep searching the solution in whole objective space and thus result in a rather continuous pareto front. Also the algorithm developed uses crowding distance and distributing the whole population in number of fronts which support the "rand" strategies more for the same reasons mentioned above. Also in case of DE "rand" strategies values of objective function are constantly improving and are trying to reach further to optimal values thus stating the need to increase the number of generations as compared to almost stable values for "best" strategies. In this regard, more studies are in progress to analyze the strategies with more number of parameter settings and various inflow scenarios.

CONCLUSIONS

Multiobjective Differential Evolution and Differential Evolution is applied for a case study of Mahi Bajaj Sagar Project (MBSP) and following conclusions are drawn based on chosen set of parameters and case study:

1. DE/rand/1/bin generated better pareto-optimal curve as compared to that of DE/rand/1/exp, DE/best/1/bin and DE/best/1/exp when MODE scenario is considered.
2. It is observed that "best" strategies have performed better as compared to "rand" strategies in the case of single objective optimization.
3. It is also observed that "exp" strategies have performed slightly better in the case of DE when compared to "bin" strategies.

It is inferred that MODE with DE/rand/1/bin can be used as an efficient multiobjective optimization solver and also any of the strategies mentioned can be used for single objective optimization given enough number of generations to converge the value.

ACKNOWLEDGEMENTS

This work is supported by Council of Scientific and Industrial Research (CSIR) through project 22(0407)/06/EMR-II dated 12.10.06. Authors are grateful to authorities and farmers of Mahi Bajaj Sagar Project for providing necessary information.

REFERENCES

Ali, M.M., and Törn, A. (2004). "Population set-based global optimization, algorithms: some modifications and numerical studies." *Compu. Oper. Res.*, 31(10), 1703–1725.

Deb, K. (2001) *Multiobjective Optimization using Evolutionary Algorithms*, Wiley, Chichester, U.K.

Deb, K., Pratap, A., Agarwal, S., and Meyarivan, T. (2002). "A fast and elitist multi-objective genetic algorithm: NSGA-II." *IEEE Trans. Evol. Comput.,* 6(2), 182–197.

Janga Reddy, M., and Nagesh Kumar, D. (2007). "Multiobjective differential evolution with application to reservoir system optimization.", *J. of Comput. in Civ. Engrg.*, ASCE, 21(2), 136 – 146.

Lampinen, J., and Storn, R. (2004). "Differential Evolution" in G.C. Onwubolu, and B.V. Babu, "*New Optimization Techniques in Engineering*", Springer-Verlag, Germany.

Liu, J., and Lampinen, J. (2005). "A fuzzy adaptive differential evolution Algorithm." *Soft Comput. Fusion Found. Methodol. Appl*, 9(6), 448–462.

MBSP Report on Status June 2002 at a Glance. (2002), Government of Rajasthan, Banswara, Rajasthan, India.

Price, K., and Storn, R., (1997). "Differential evolution - a simple evolution strategy for fast optimization." *Dr. Dobb's Journal*, 22, 18-24 and 78.

Price, K., and Storn, R., (2009). Home page of differential evolution, URL: *http://www.icsi.Berkeley.edu/~storn/code.html*.

Raju, K.S., and D. Nagesh Kumar. (1999). "Multicriterion decision making in irrigation planning." *Agri. Sys.* , 62 (2), 117-129.

Ranjithan, S. R. (2005). "Role of evolutionary computation in environmental and water resources systems analysis." *J. Water Resour. Plng. and Mgmt.*, ASCE, 131(1), 1-2.

Seshadri, A. (2008). "A fast elitist multiobjective genetic algorithm - NSGA-II." MATLAB central, file exchange, Mathworks, http://www.mathworks.com/matlabcentral/fileexchange.

Vasan, A. (2005). "*Studies on Advanced Modeling Techniques for Optimal Reservoir Operation and Performance Evaluation of an Irrigation System*", PhD Thesis, Birla Institute of Technology and Science, Pilani, India.

Vasan, A, and Raju, K.S. (2007). Application of differential evolution for irrigation planning: An Indian case study, *Water Resour. Mgmt. ,* 21(8), pp.1393-1407.

Multireservoir Simulation Using Multipurpose Constraints and Object-Oriented Software Design

Marcelo A. Cicogna[1], Darrell G. Fontane[2], Ieda G. Hidalgo[2] and João E. Lopes[3]

[1] Anhanguera Educacional S.A., Alameda Maria Tereza, 2.000, Valinhos, São Paulo, Brasil; PH 55 (19) 3512-1715; email: marcelocicogna@gmail.com.
[2] Dept. of Civil Engineering, Colorado State University, Ft. Collins, CO 80523; email: {darrell.fontane, ieda.hidalgo}@colostate.edu.
[3] Duke Energy International Geração Paranapanema, Av. Das Nações Unidas, 12.901, São Paulo, SP, Brasil; email: jelopes@dglnet.com.br

ABSTRACT

The hydroelectric short term planning is quite challenging in order to respect all the operational restrictions concerned with hydropower generation. A detailed simulation model combining multipurpose constraints and object-oriented software design is presented for short term decision support. The object-oriented design permits a mathematical structure that divides the decisions tasks from the regular hydroelectric computation. The main operational policy allows users to validate a hydro generation schedule towards an inflow forecasting. In other words, the simulator can accept hydro generation as data input and convert it to water flow variables (turbines discharge and spillage), using the inflow forecast and the initial reservoirs storage. The water balance equation, hydro generation and efficiency calculation modules are synchronized with the state-of-the-art of multireservoir operation. As an important result, this simulator can automatically correct the input data of the operational policy, saving substantially time into decision-making process. A test problem on 94-reservoir from Brazilian Integrated Hydropower Generation System was simulated over an hourly one-week horizon with fine performance, evidencing the simulation model capabilities against large scale hydropower operation problem.

SIMULATION MODEL

In reservoir management practices, a simulation model can be used as a valuable planning tool to evaluate the impact of changes to the system's configuration or operational objectives. The desired generation or release scheduling can be checked towards inflow forecasting in order to satisfy the entire set of operational constraints feasibility. At the real time operation stage, a simulation tool can be used to quickly check operational alternatives due to emergency events or planning and real-time incongruence. In post-operation studies, a simulator can be applied as data consolidation tool in exhaustive inspection of recorded trajectories feasibility (Hidalgo et al., 2009).

Inserted in a computer-aided scenario, Yeh (1985) cites simulation as a modeling technique that is used to approximate the behavior of a system on the computer, representing all the characteristic of the system by a mathematical description. Wurbs (1993) provided extensive list of simulation computer models for reservoir system analysis. Using the classification presented by Wurbs, the model here presented can be classified as a conventional simulation model in the sense that no formal optimization or mathematical programming algorithms are

used. However, it will be shown that the data structure for hydro plants joint operation is based on network flow modeling resources and this design can hold a detailed hydroelectric mathematical model.

The simulation of multipurpose reservoir operation is also presented. Fontane (1997) provided a relevant reservoir operations planning model through fuzzy and dynamic programming to deal with imprecise objectives. This model guides the multipurpose implementation of the present simulation model.

This research work aims to present a simulation model that implements such resources and capabilities variety. The mathematical model and software design are detailed presented with emphasis on practical application for further researches become able to reproduce these results. The authors believe that any kind of optimization model for reservoir operation has limitations (Labadie, 2004). Also, it is hard to see comparison studies among different models and their results. In this sense, different operational policies can be checked in a detailed simulation model, with a particular object-oriented design, to address performance analyses and to evaluate distance between model results and real problem aspects.

A test study on 94-reservoir Brazilian hydro plants is presented as demonstration of simulation model capabilities and computational performance. The user interface is outlined to present useful software resources for multireservoir operation analysis. The concluding section discusses design and implementation experience and future development.

Reservoir Model

The reservoir operation has limits and constraints associated to the maximum and minimum water levels, as described in Figure 1. For reservoirs with hydroelectric powerhouses, the minimum level takes into account the minimum head that permits generation. The z^c level represents the dam crest elevation.

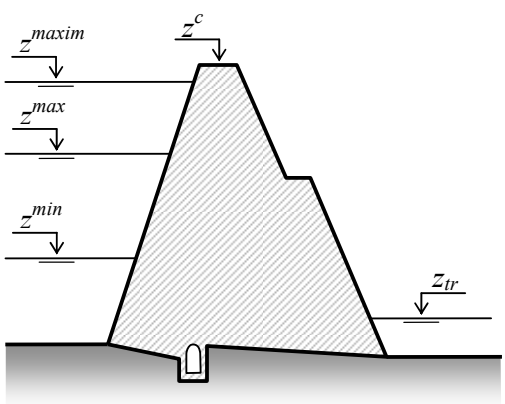

Figure 1. Reservoir operational water levels.

Over the maximum operational level, there is a *maximorum* level related to the dam security purpose. The simulation model presented here has a particular computation module that automatically deals with reservoir constraints under emergency situations, as will be described into the software's design section.

Hydroelectric Model

The simulation model has detailed representation of hydro plants, focused on a complete set of operation constraints and nonlinear equations. In Figure 2 is shown an arrangement of main operational variables. This paper uses the SI units

standard for convenience of Brazilian hydro plants data presentation, although modeling resources are presented for other standards and general application.

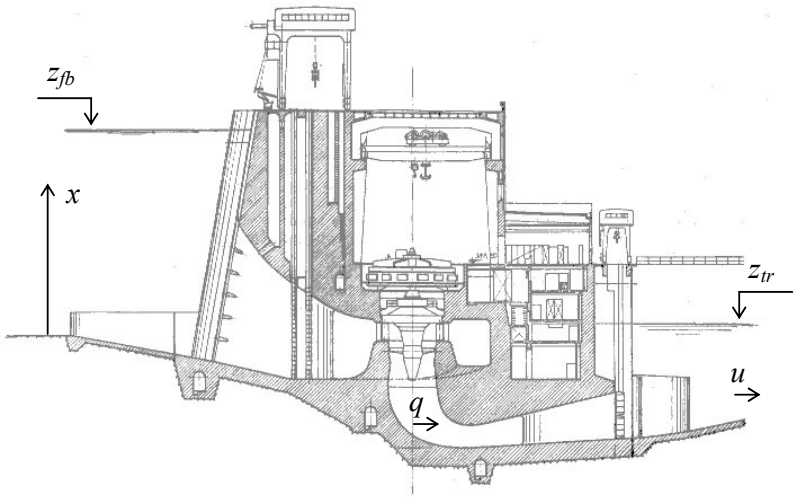

Figure 2. Hydro plant's main variables arrangement.

Hydroelectric power availability is direct related to the potential energy created by a dam, i.e. it depends on the difference between upstream and downstream water levels. Therefore the gross head is directly calculated as:

$$h_g = z_{fb}(x) - z_{tr}(u) \tag{1}$$

where:

h_g is the gross head (m).
x is the water storage in the reservoir of the plant (10^6 m³ or hm³).
u is the total water release (outflow), that is, the sum of the discharge q and the spillage s (m³/s).
$z_{fb}(x)$ is the forebay elevation (m) as a function of the water storage x.
$z_{tr}(u)$ is the tailrace elevation (m) as a function of the water release u.

The forebay and tailrace equations could be expressed as any function of reservoir storage and total outflow, respectively. In the case of Brazilian hydroelectric plants, those functions are commonly represented by polynomials.

There are also losses from the potential energy due to friction of flow through raceways, racks and gateways (Mead, 1908). These losses can be estimated as a quadratic function of turbine discharges, as expressed in Equation (2). Therefore, the penstock head losses are measured in length units.

$$h_{pl} = c.q^2 \tag{2}$$

where:

h_{pl} is the penstock head losses (m).
c is a hydraulic loss parameter (s²/m⁵).
q is the total turbines water discharge (m³/s).

After the head and losses description, the kernel of hydro plant operation is the hydropower production function. This model details the hydro production as shown in Equation (3).

$$p = k.\eta_T.\eta_G.(h_g - h_{pl}).q \quad (3)$$

where:

- p is the instantaneous power obtained in the conversion process of the hydraulic potential energy to electric energy (MW).
- k is the gravity constant, multiplied by the water specific weight and divided by 10^6. This constant manages the power output in MW. Its value is 0.00981 (MW/(m³/s)/m). This constant can also embed unit transformation factors.
- η_T is the efficiency parameter of the turbine in the conversion process of the potential energy to mechanical energy.
- η_G is the efficiency parameter of the generator in the conversion process of the mechanical energy to electrical energy.

The turbine efficiency can be expressed as function of head and hydro power. Some machinery projects have head and discharge as basic input data for efficiency computation. This simulation model accepts any combination from gross or net head and power or discharge. Due to its shape, this function is also known as the efficiency's *hill curve* and an example could be noted in Figure 3a. Also, efficiency contour lines are commonly part of turbines project (Figure 3b).

The turbine and generator mechanic set has operational limits expressed as functions of gross or net water head. The maximum hydro power limit depends on head in two stages (Figure 3b): a) for head smaller than h^{ef} , the power is direct proportional to the head, since it is limited by hydraulic available energy; b) when head is bigger than h^{ef} , the power transferred to the turbine-generator's shaft can damage the equipment, so valves or wicket gates gearing are necessary to keep the output power constant and beneath the electrical damage limit. The h^{ef} head is called *effective head*. A minimum hydro power limit can be imposed and expressed as a function of water head as well (Figure 3b).

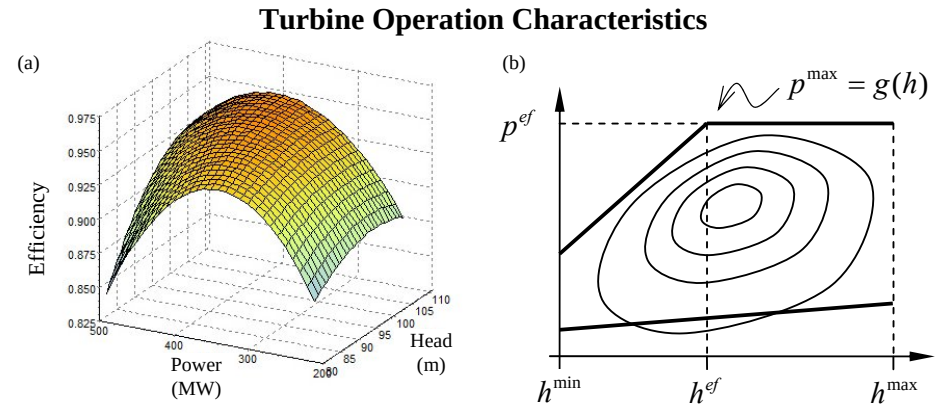

Figure 3. Example of the turbine efficiency function - hill curve - and maximum and minimum power productions functions.

The maximum spill capacity s^{max} can be expressed as a function of reservoir water level z_{fb}. Depending on gates existence, two spillway operations are possible: controlled and uncontrolled. In Figures 4a and 4b are shown examples of these functions, respectively. The term s^{prj} is related to the capacity projected to the spillway. The forebay z^{sc} is the water level on the spillway crest.

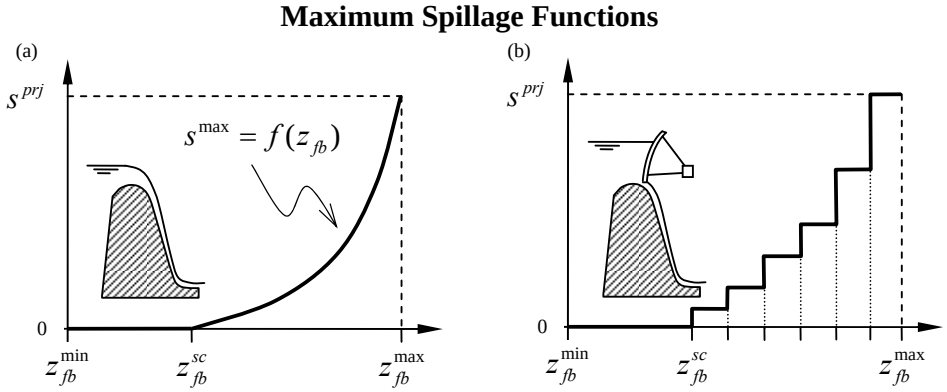

Figure 4. Uncontrolled and controlled maximum spill functions.

As can be seen, the simulation model has a detailed reservoir and hydro power operation representation. In next section, it will be shown the multireservoir model and the adopted implementation structure and design.

Multireservoir Simulation

This section presents a network flow formulation for the multireservoir simulation problem as a temporally expanded arborescence (Rosenthal, 1981). In Figure 5 are shown the hydro elements represented by the simulation model. The model assumes that the exogenous inflows y to the reservoir system are deterministic or provided by inflow forecasting models. Reservoirs could be simple water storage as node number 3 or could have powerhouses working as hydro plants. Special river stream flow control stations can be simulated as well (node 7). Diversions structures, as channels and tunnels, are able to be simulated, as illustrated by the linked-reservoir 3 and 4 example. The practical 94-reservoirs study present later is a bigger replication of the hydro elements example shown in Figure 5. Also, this study simulates two real diversion structures from Brazilian hydroelectric system: the Pereira Barreto's channel that links the Ilha Solteira and Três Irmãos reservoirs located in Paraná River basin and a diversion tunnel linking the reservoirs Jordão and Segredo in Iguaçu River basin. These water diversions are governed by the communicating vessels hydraulic rules.

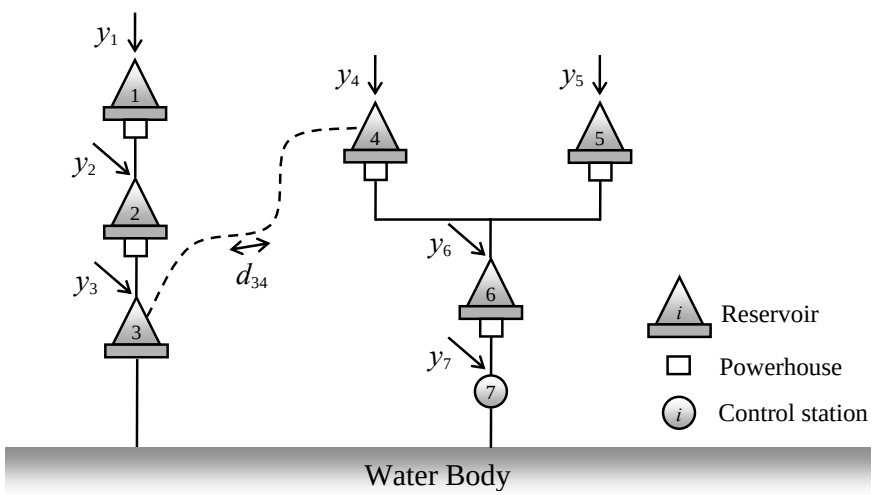

Figure 5. Hydro elements available for multireservoir simulation.

Rosenthal's representation, since a deterministic network flow optimization model, imposes that no reservoir has more than one other reservoir directly downstream from it. This constraint is quite true for all 94-reservoir Brazilian hydropower system. However, the diversion variable was created to overcome this restriction, since a simulation model has more space for structural expansions. The second imposition was related to the routing effect between adjacent reservoirs. This restriction was overcome with adaptations in the expanded arborescence structure, as shown in Figure 6.

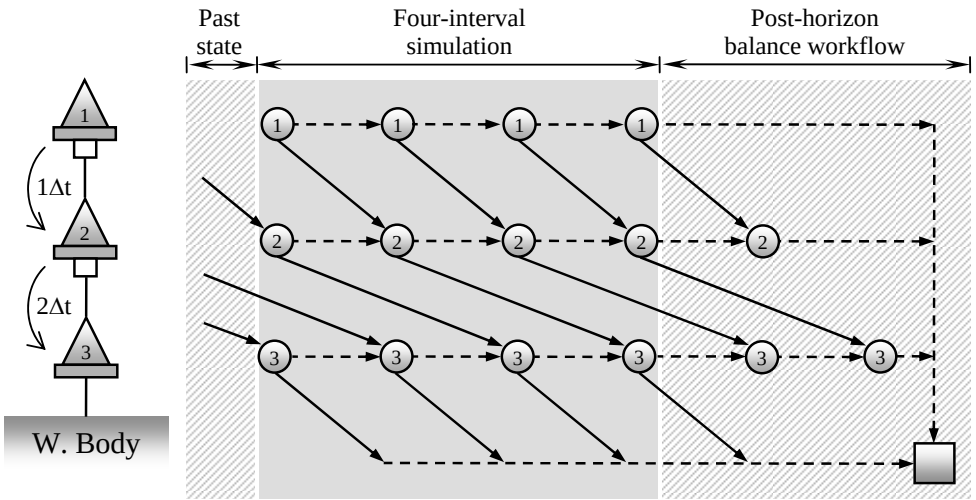

Figure 6. Three-reservoir and four-interval hydro system as a temporally expanded arborescence with routing effect representation.

In the routing effect representation illustrated in Figure 6, solid arrows represent releases and broken-line arrows represent storages transported between time intervals. These storage arcs form the temporally expanded network structure from the arborescence. Note that two additional arc-node sets are necessary to complete the structure: left represents the recent past releases before the first simulation time interval; and right are the post-horizon arcs and nodes, without release arcs, that are necessary to complete and maintain mass balance.

The reservoir mass balance equation (4) is very detailed in terms of multipurpose constraints.

$$x_{i,t} = x_{i,t-1} + \left(y_{i,t} + \sum_{k \in \Omega_i} f(u_{k,t-tr}) - \left(q_{i,t} + s_{i,t} + ev_{i,t} + mu_{i,t} + d_{i,t} \right) \right) . f_{uc} \qquad (4)$$

where:

- i,t are plant and time indexes, respectively. There are N reservoirs and T intervals. The storage variables x are indexed as time instants (initial t-1 and final t). The flow variables are averages during the time interval.
- y is the reservoir inflow (m³/s).
- Ω is the direct upstream reservoirs index set. With the tr time lag, the sum of upstream releases represents the routing effect computation.
- s is the spillage flow (m³/s).
- ev is the reservoir evaporation calculated as a water flow (m³/s). It takes into account the reservoir area at the average volume $(x_t + x_{t-1})/2$, leading to an iterative calculus.

mu represents the reservoir multiple-uses expressed as water flows (m^3/s). As example, irrigation and water supply associated with one reservoir could be simulated with this variable.

d represents the water diversions from reservoir *i*, also expressed as water flow (m^3/s). The diversion can be reach another reservoir, river or an external hydro element not present into the study configuration.

f_{uc} is the unit conversion factor between flow and storage variables.

As a powerful modeling resource, the unit conversion factor f_{uc} embeds into the simulation model the ability of dealing with any kind of time interval. This model can compute studies with monthly, daily, hourly, half hour or even any combination that composes a mixed interval horizon. Considering Brazilian general units hm^3 for storage and m^3/s for streamflows, this factor became:

$$f_{uc} = \frac{\Delta t}{10^6} \tag{5}$$

The multireservoir model ends with the operational constraints related to storage, minimum and maximum releases, maximum discharge as a function of gross head and maximum spill as a function of reservoir storage level.

$$x_{i,t}^{\min} \le x_{i,t} \le x_{i,t}^{\max} \tag{6}$$

$$u_{i,t}^{\min} \le u_{i,t} \le u_{i,t}^{\max} \tag{7}$$

$$p_i^{\min}(h) \le p_{i,t} \le p_i^{\max}(h) \tag{8}$$

$$q_{i,t} \le q_{i,t}^{\max}(h) \tag{9}$$

$$s_{i,t} \le s_i^{\max}(z_{fb}) \tag{10}$$

It is important to note that constraints (6) to (10) have interval indexing for multipurpose constraints representation, as presented in next subsection.

Multipurpose Constraints

Typically, reservoir multipurposes may include a combination of requisites like hydroelectric power generation, water supply for irrigation, domestic and industrial use, water quality improvement, flood control, wildlife and environment maintenance, navigation and recreation (Yeh and Becker, 1982).

The hydroelectric purpose was described in previous subsections. Through multiple-use *mu* and water diversion *d* variables from Equation (4) it is possible to simulate water supply and irrigation purposes. A seasonal minimum water level or storage may be imposed to guarantee water supply impounding, navigation and recreation purposes as well. The releases constraints from Equation (7) permit simulating fish-wildlife maintenance and navigation operational limits. Flood control is generally achieved by maintaining reserve storage in each of the many reservoirs as an anticipation control procedure on high-flow periods. This can be achieved with temporary upper bound storage limits, but smaller than the reservoir maximum, as expressed in Equation (6).

SOFTWARE DESIGN

This section is dedicated on the use of object-oriented modeling as a powerful approach for designing a multireservoir simulator. Slobodan et al. (1997)

present object-oriented design as a successful modeling tool to the Egyptian water resources planning. The natural object-oriented partition between policy commitment and data permits the construction of "what-if" search scenarios in an easier level to the decision-making process. Another interesting object-oriented experience is detailed presented by Belkhouche (1999) and can be used as a guide to object-oriented design of database and software resources to water quality systems. Also, Horstmann (1997) provides a didactical introduction to object-oriented software development.

The present simulation model was implemented using the object-oriented software design. As expected, the software was built using classes to represent all multireservoir simulation aspects. There are classes to represent the hydro plants main components and the network flow elements. Also, there are extra classes to support the software organization, such as horizon description and database connectors and data providers. The whole class diagram is omitted for article's length convenience. However, some important details from the object-oriented design are shown to guide further researches.

Data Structures

The key step for a computational implementation of the simulation model is to interpret the mass balance equation (4) as a network flow node (Rosenthal, 1981). The node flow equilibrium has equivalence with the mass balance using canalized arcs to represent operational constraints, as presented in Figure 7. The *tr* time delay represents the routing effect of upstream releases.

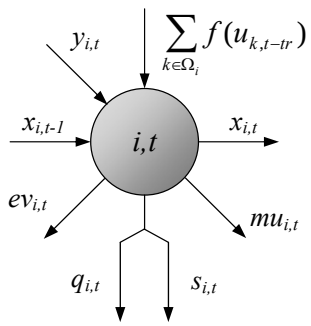

Figure 7. Mass balance equation equivalence with a network node.

The whole network nodes can be simple stored as a bi-dimensional matrix M_{NxT} representing the operation variables from the reservoir *i* during the time interval *t*. Other data structures using node's linked lists can be used as well, but a rectangular matrix provides good performance and reasonable size storage. The arcs are implemented as links between nodes and stored as nodes properties.

Object-Oriented Design

The simulation model uses an object-oriented resource called *polymorphism* to reach a mathematical structure that splits the decisions tasks from the hydroelectric computing tasks in different software components. As a direct result, the simulation model accepts different operational policies, keeping apart the hydro computational kernel composed by the operational restrictions, water balance equation, power generation and efficiency functions. A simulation algorithm flowchart is shown in Figure 8 in order to illustrate the polymorphic composition of the operational policy and the hydro computational kernel. Note

that hydro kernel has a special resource to correct decisions that can lead the reservoir to an infeasible state.

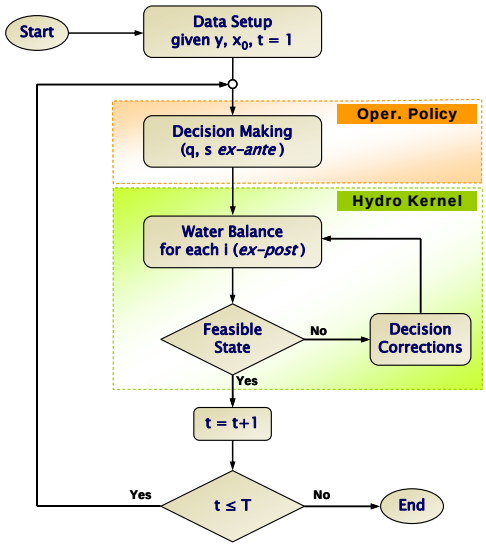

Figure 8. Simulation algorithm with object-oriented polymorphism applied to partition of operational policy and the hydro computational kernel.

The polymorphism concept has many definitions but to this simulation model it will means that *the same operation may behave differently on different classes* (Horstmann, 1997). In other words, the polymorphism will be used to promote a partition between operation policy and hydroelectric and reservoir computations. This object-oriented concept permits that the resultant simulation software to have an expandable and adaptable collection of operation policies.

Operational Policies

The operation policy object is responsible to determine the reservoir total water release. In case of powerhouse existence, the amount of turbines discharge is also necessary. Mathematically, the operational policy can be expressed as a function f_p of the available policy variables from Equation (4):

$$[q_{i,t}, s_{i,t}] = f_p(x_{i,t-1}, x^*_{i,t}, y_{i,t}, \sum_{k \in \Omega_i} f(u_{k,t-tr}), ev^*_{i,t}, mu_{i,t}, d^*_{i,t}) \qquad (11)$$

where the * denotes variables that are not directly available for policy analyses and may be estimated. For example, the final storage at interval t and evaporation can be estimate in function of the release determined by the operational policy. Any external operational policy that has in its results the release and spillage variables can be simulated with this model.

From this polymorphic structure, a particular operational policy was implemented to transform hydro generation dispatch, composed by generation goals and turbines unit commitment, into the discharge and spillage decisions variables. The generation-release transformation is based on iterative and detailed procedure over the hydro production equation (3), where the power is given and the release and spillage are calculated recursively. This policy aims to check generation scheduling towards an inflow forecasting, given the initial reservoir storage states and keeping the hydroelectric kernel intact. As one can see, this polymorphic design can accomplish other types of policies, including the decision results from optimization models (Wurbs, 1993).

CASE STUDY

This section briefly shows a test on 94-reservoir Brazilian hydro plants that demonstrates the simulator capabilities and performance. The generation system has 75.944 MW as installed capacity and a one-week horizon generation scheduling was checked in terms of hydroelectric constraints feasibility.



Simulation Study Main Characteristics		
Reservoirs	94	
Basin/Rivers	8/33	
Drainage area	2,621,243	km²
Installed capacity	75,944	MW
Diversion structures	2	
Control stations	2	
Horizon	7	days
Intervals	168	hours

Figure 9. The 94-reservoir map from Brazilian Integrated Hydropower Generation System and its main characteristics.

The test checks, for each reservoir, an hourly one-week horizon generation scheduling towards a daily inflow forecasting provided by a external hydrologic model. All the variables trajectories (see section about multireservoir model) are available in singular tabs as charts or grid presentation. In Figure 10 are outlined the software and user interface for study's data input and result analyses. The left frame is a study navigator resource that shows studies in a tree view items organization. The data and results access are provided by tabs switch.

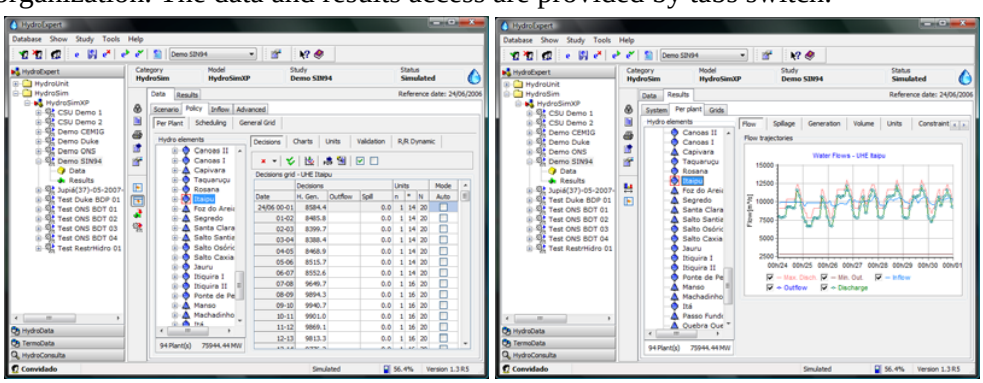

Figure 10. Simulation software and its user interface.

The test was run in computer with a 3.0 GHz Pentium IV processor and 2 GB of RAM. The 94-reservoir and 168-hour horizon study takes 2.4 seconds in average to be simulated. As one can note, this is a relevant computational performance for a simulation model with the operational policy that converts generation goals into release and spillage trajectories with auto constraint feasibility checking.

CONCLUSION

It was presented a multireservoir simulation system with detailed hydroelectric modeling and multipurpose constraints. The software is based on network flow with canalized arcs as data structure to represent multireservoir joint

operation. Two simple but powerful model resources were presented to permit general simulation application: unit conversion factor on hydropower production function and multi and mixed time intervals factor on mass balance equation. Due to the object-oriented design, the operational policies and hydro computational kernel were divided in different software components. With this design it is possible to check different and external operational policies in a detailed simulation model. Also is suitable to address performance analyses and evaluating the distance between computer-aided model results and real problem aspects.

A test study on 94-reservoir Brazilian hydro plants with a one-week horizon generation scheduling was checked toward an inflow forecasting with focus on the operational constraints feasibility. It is distinguished the simulation model performance in terms of reservoir operation accuracy and computational consumed time. The mathematical model and software design were presented with emphasis on practical application for further researches become able to reproduce these results.

REFERENCES

Belkhouche, B., Demtchouk, I., and Steinberg, L. J. (1999). "Design of object-oriented water quality software system." *J. Water Resour. Plan. Manage.*, ASCE, 125(5), 289-296.

Fontane, D. G., Gates, T. K., and Moncada E. (1997). "Planning reservoir operations with imprecise objectives." *J. Water Resour. Plan. Manage.*, ASCE, 123(3) 154-162.

Hidalgo, I. G., Fontane, D. G., Soares Filho, S., and Cicogna, M. A. (2009). "A simulator of the hydroelectric plants operation as tool for analyzing data." Accepted for the *2009 World Congress on Computer Science and Information Engineering* (CSIE), Los Angeles/Anaheim, California, USA.

Horstmann C. S. (1997). *Practical Object-Oriented Development in C++ and Java*. John Wiley & Sons.

Labadie J. W. (2004). "Optimal operation of multireservoir systems: state-of-the-art review". *J. Water Resour. Plan. Manage.*, ASCE, 130(2), 93-111.

Mead, D. W. (1908). "Chapter II - Hydraulics." *Water Power Engineering: The theory, investigation and development of water powers*, First Edition, McGraw-Hill, New York, 42-78.

Rosenthal, R. (1981). "A nonlinear network flow algorithm for maximization of benefits in a hydroelectric power system." *Operation Research*. 29(4), 763-786.

Sigvaldason, O. T. (1976). "A simulation model for operating a multipurpose multireservoir system." *Water Resources Research*, 12(2), 263-278.

Slobodan, P. S., Hussam, F., and Amin, E.-S. (1997). "The use of object-oriented modeling for water resources planning in Egypt." *Water Resources Management*, Kluwer Academic Publishers, 11, 243–261.

Yeh, W. W-G., and Becker L. (1982). "Multiobjective analysis of multireservoir operations." *Water Resources Research*, 18(5), 1326-1336.

Yeh, W. W-G. (1985). "Reservoir management and operations models: A state-of-the-art review." *Water Resources Research*, 21(12), 1797-1818.

Wurbs, R.A. (1993). "Reservoir-system simulation and optimization models." *J. Water Resour. Plan. Manage.*, ASCE, 119(4), 455-472.

Nonlinear Dependence in Hydrologic Time Series

H. S. Kim[1], B. Sivakumar[2] and E. T. Lee[3]

[1]Department of Civil Engineering, Inha University, Incheon, 402-751, South Korea; PH +82-(0)32-860-7572; FAX +82-(0)32-876-9783; email: sookim@inha.ac.kr
[2]Department of Land, Air and Water Resources, University of California, Davis, CA 95616; (530) 752-8577; FAX (530) 752-5262; email: sbellie@ucdavis.edu
[3]Department of Civil Engineering, KyungHee University, Suwon, South Korea; PH +82-(0)31-201-2549; email: etlee@khu.ac.kr

ABSTRACT

Studies investigating the chaotic nature of hydrologic processes commonly employ the correlation dimension method. Although this method is generally reliable, it may also have some limitations, influenced by a host of factors. One such factor is the delay time for reconstruction of the phase-space to represent the underlying dynamics. There is also an increasing realization that fixing the delay time window rather than just the delay time itself may be more appropriate. An attempt is made in this study to test the C-C method towards fixing the delay time window and assessing the nonlinear and chaotic dynamic characteristics of hydrologic time series. Three data sets are studied: daily flow from St. Johns River, Florida; biweekly volume from the Great Salk Lake; and daily rainfall from Seoul. The results from this method are also compared with those obtained using the autocorrelation function method.

INTRODUCTION

In recent years, studies investigating the nonlinear deterministic nature of hydrologic processes have gained momentum [see Sivakumar (2000) for a review]. Such studies have employed a host of methods for identification and prediction, including correlation dimension, Lyapunov exponents, false nearest neighbors, and local approximation. Among these, the correlation dimension method has been most widely used, and the presence of a low correlation dimension has generally been treated as an indicator of nonlinear determinism. Regardless of the method, a necessary first step is the reconstruction of the observed data in a multi-dimensional

space for representation of the system dynamics. This multi-dimensional phase-space reconstruction often involves the 'rearrangement' of a single-variable time series that reliably represents the system. Among the many available methods, the method of delays (e.g. Takens, 1981) is the most commonly used one. According to this method, using its history and an appropriate delay time, a single-variable series $\{x_i\}$where $i = 1, 2, ..., N$, can be reconstructed in an m-dimensional phase space, as follows:

$$\vec{x}_i = (x_i, x_{i+1}, \ldots, x_{i+(m-1)t}), \vec{x}_i \in R^m \quad (1)$$

where t is the index lag. If the sampling time is τ_s, then the delay time is $\tau_d = t\tau_s$.

It is clear that the delay time τ_d is a crucial parameter to reliably represent the 'attractor' of the underlying dynamics. However, the effectiveness of implementation of Takens' theorem is not limited by the delay time, because the theorem is based on the assumption that the time series is infinite and noise-free and that any arbitrary delay time would be reliable. This, however, is not the case in real data (which are always finite, often short, and contaminated with noise), for which an appropriate delay time is necessary because only an optimum selection of τ_d gives the best separation of neighboring trajectories within the minimum embedding phase-space.

Many researchers have addressed the delay time selection and proposed different methods, popular among which are: autocorrelation function (ACF), mutual information (MI), and correlation integral (CI). In the ACF method, τ_d is chosen as the lag time (or index lag) at which the ACF first crosses the zero line (Holzfuss and Mayer-Kress, 1986) or attains a certain value (0.1 or 0.5). In the MI method, τ_d is chosen to coincide with the first (local) minimum of the mutual information (Frazer and Swinney, 1986). In the CI method, the first minimum of the logarithm of the generalized correlation integral is considered to provide a proper choice of τ_d (Liebert and Schuster, 1989). Each of these methods has its own advantages and disadvantages and none provides a definitive guideline for choosing the delay time.

A reliable alternative to address the delay time selection is to try to fix the delay time window $\tau_w = \tau (m - 1)$, since τ_w is the one that is of actual interest to represent the dynamics. One such attempt was made by Martinerie et al. (l992), who compared the delay time window and the delay times estimated using the ACF and MI methods but did not observe a consistent agreement between them. This is because, τ_w is basically the optimal time for representing the independence of the data, whereas the ACF and MI methods determine only the first local optimal times in their estimation of τ_d. Kim et al. (l998) showed (through analysis of synthetic time series) that, with an increase in the embedding dimension m, the correlation dimension

converges more rapidly for the case of τ_w held fixed than for the case of τ_d held fixed (especially so for small data sets). Based on this distinction between τ_d and τ_w, Kim et al. (l999) developed a new technique to estimate both τ_d and τ_w. This technique, called the C-C method [see below], uses the BDS (Brock-Dechert-Scheinkman) statistic (Brock et al., 1991, 1996), which has its base on the correlation integral for testing nonlinearity in a time series. The main difference between the BDS method and the C-C method is as follows. The BDS method uses the statistic $S(m,N,r) = C(m,N,r) - C^m(1,N,r)$, where $C(m,N,r)$ is the correlation integral [see Eq.(2) below for details], whereas the C-C method uses the statistic $S(m,N,r,t) = C(m,N,r,t) - C^m(1,N,r,t)$, involving an additional parameter in the form of the index lag t. The study by Kim et al. (1999) reveals that preliminary results of the application of C-C method for determination of delay window τ_w are reliable.

Encouraged by these results, an attempt is made in the present study to estimate the general dependence of hydrologic time series using the C-C method, and hence to assess their nonlinear deterministic characteristics. To this effect, three hydrologic time series are studied: (1) daily flow from St. Johns River near Cocoa, Florida; (2) biweekly volume from the Great Salt Lake; and (3) daily rainfall from Seoul. Interpretations regarding nonlinear determinism in these series are made based on the results for the artificial time series reported by Kim et al. (1998, 1999).

MEASURE OF NONLINEAR DEPENDENCE

Correlation integral and BDS statistic. After the attractor has been reconstructed in the phase-space [Eq. (1)], quantitative characteristic measures or invariants of the system can be determined. The correlation dimension method (Grassberger and Procaccia, l983) is arguably the most basic method for estimation of these invariants and for identification of chaotic behavior. The correlation integral or function with index lag t, which is used in this method for distinguishing between chaotic and stochastic systems, is given by (Kim et al., 1998):

$$C(m,N,r,t) = \frac{2}{M(M-1)} \sum \Theta(r - \|\bar{x}_i - \bar{x}_j\|), \qquad r > 0 \qquad (2)$$

where $\Theta(a) = 0$, if $a < 0$,

$\Theta(a) = 1$, if $a \geq 0$,

N is the size of the data set, $M = N - (m-1)t$ is the number of embedded vectors (or points) in the m-dimensional space, $\| \ \|$ denotes the sup-norm, and Θ(a) is the Heaviside step function. The function $C(m,N,r,t)$ measures the fraction of the pairs of

points $\vec{x}_i$, i = 1,2,…,M, whose sup-norm separation is no greater than r. If the limit of $C(m,N,r,t)$ for N $\rightarrow \infty$ exists for each r, then the fraction of all vector points that are within r of each other is given by $C(m,N,r,t) = \lim_{N\to\infty} C(m,N,r,t)$, and the correlation dimension is given by $D_2(m,t) = \lim_{r\to 0}[\log C(m,r,t)/\log r]$. However, since N remains finite (often small) in real situations, r cannot go to zero. Therefore, a linear 'scaling region' in the log $C(m,N,r,t)$ vs. log r plot is identified for estimation of correlation dimension $D_2(m,t)$; i.e. the slope of the scaling region.

Brock et al. (l991, 1996) used the BDS statistic to test for the presence of nonlinearity in time series. More specifically, the BDS statistic was used to reject the null hypothesis that the data are independent and identically distributed (iid). Under this null hypothesis, the BDS statistic for $m > 1$ is defined as:

$$BDS(m,M,r) = \frac{\sqrt{M}}{\sigma}[C(m,M,r) - C^m(1,M,r)] \tag{3}$$

and the statistic converges to a standard normal distribution as M $\rightarrow \infty$. The asymptotic variance $\sigma^2(m,M,r)$ of the BDS statistic can be estimated as:

$$\sigma^2(m,M,r) = 4\{m(m-1)C^{2(m-1)}(K-C^2) + K^m - C^{2m} + 2\sum_{i=1}^{m-1}[C^{2i}(K^{m-i} - C^{2(m-i)} - mC^{2(m-i)},(K-C^2)]\}, \tag{4}$$

$$C(m,M,r) = \frac{2}{M(M-1)}\sum_{1\le i\le j\le M}\Theta(r - \|\bar{x}_i - \bar{x}_j\|), \tag{5}$$

$$K(m,M,r) = \frac{6}{M(M-1)(M-2)}\sum_{1\le i\le j\le k\le M}[\Theta(r - \|\bar{x}_i - \bar{x}_j\|)\Theta(r - \|\bar{x}_j - \bar{x}_k\|)], \tag{6}$$

Since the BDS statistic originates from the statistical properties of the correlation integral, it measures the statistical significance of the correlation dimension estimation. Although the statistic cannot be used to distinguish between a nonlinear deterministic system and a nonlinear stochastic system, it is still a powerful tool for distinguishing between a linear stochastic (random) time series and a time series generated by a chaotic or nonlinear stochastic process.

The C-C method. The present study is particularly concerned with the properties of the statistic $S(m,N,r,t) = C(m,N,r,t) - C^m(1,N,r,t)$, proposed by Kim et al. (1998). According to Brock et al. (l991), if a stochastic process $\{x_i\}$ is *iid*, it can be shown that $C(m,r) = C^m(1,r)$ for all m and r; i.e. the correlation integral behaves much like the characteristic function of a serial string. This led Kim et al. (1998) to interpret the

statistic $S(m,N,r,t)$ as the serial correlation of a nonlinear series. The statistic can thus be regarded as a dimensionless measure of nonlinear dependence, and can also be used to determine an appropriate index lag t. In other words, for fixed m, N, and r, the $S(m,N,r,t)$ versus t plot is a nonlinear analog of the ACF versus t plot.

In order to study the nonlinear dependence (and eliminate the spurious temporal correlations), the time series $\{x_i\}$, $i = 1,2,\ldots,N$, is first subdivided into t disjoint time series of size N/t, and the statistic $S(m,N,r,t)$ is then computed from these t disjoint time series. The procedure is as follows. For $t = 1$, there exists only a single time series $\{x_1, x_2,\ldots,x_N\}$, and the statistic $S(m,N,r,t)$ is given by:

$$S(m,N,r,1) = C_1(m,N,r,1) - C_1^m(1,N,r,1) \tag{7}$$

For $t = 2$, two disjoint time series $\{x_1, x_2,\ldots,x_{N-1}\}$ and $\{x_2, x_4,\ldots,x_N\}$ are obtained, each of length $N/2$, and $S(m,N,r,t)$ is given by the average of the two as:

$$S(m,N,r,2) = \frac{1}{2}\{[C_1(m,N/2,r,2) - C_1^m(1,N/2,r,2)] + C_2(m,N/2,r,2)] - C_2^m(1,N/2,r,2)]\} \tag{8}$$

In general, for a given t, the statistic is given by:

$$S(m,N,r,t) = \frac{1}{t}\sum_{s=1}^{t}[C_s(m,N/t,r,t) - C_s^m(1,N/t,r,t)] \tag{9}$$

Finally, for $N \to \infty$, the statistic becomes

$$S(m,r,t) = \frac{1}{t}\sum_{s=1}[C_s(m,r,t) - C_s^m(1,r,t)], \qquad m = 2,3... \tag{10}$$

For fixed m and t, $S(m,r,t)$ will be identically equal to zero for all r, provided the data is *iid* and $N \to \infty$. However, since real series are always finite (and often serially correlated), $S(m,r,t) \neq 0$. Consequently, the locally optimal times may be either the zero crossings of $S(m,r,t)$ or the times at which $S(m,r,t)$ shows the least variation with r, as such only indicates a nearly uniform distribution of points. To account for this, several representative values r_j are selected, and the quantity $\Delta S(m,t)$ defined as:

$$\Delta S(m,t) = \max\{S(m,r_j,t)\} - \min\{S(m,r_j,t)\} \tag{11}$$

which is a measure of the variation of $S(m,r,t)$ with r. The locally optimal times t are thus the zero crossings of $S(m,r,t)$ and the minima of $\Delta S(m,t)$. The delay time τ_d will then correspond to the first of these locally optimal times.

Determination of the nonlinear dependence of a finite time series using the statistic $S(m,N,r,t)$ requires some kind of criteria for appropriate selection of m and r. In general, neither m nor r should be too large; the role of the sample size N is also

important. For a fixed value of N, since the data become very sparse for large values of m, $C(m,N,r,t)$ will become vanishingly small. Also, when r exceeds the size of the attractor (since most pairs of points are within r), $C(m,N,r,t)$ will attain saturation. According to Broke et al. (1991), results are better for m ranging between 2 and 5 and r between $\sigma/2$ and 2σ; and also $N \geq 500$ provide good approximations.

Brock et al. (l991) investigated the BDS statistic for time series generated from six asymptotic distributions in order to determine the appropriate values of m and r. They studied three different sample sizes (with N = 100, 500, and 1000) of time series generated through Monte Carlo simulation from the following asymptotic distributions: standard normal, student-t with three degrees of freedom, double exponential, Chi-square with four degrees of freedom, uniform distribution, and bimodal mixture of normals. Their analyses revealed that the results were better when m ranged between 2 and 5 and r between $\sigma/2$ and 2σ. All the asymptotic distributions were also well approximated by finite time series with $N \geq 500$. In light of these, Kim et al. (1998) selected four different values of r in the range $\sigma/2 \leq r \leq 2\sigma$ as representative values, with $r_1 = (0.5)\sigma$, $r_2 = (1.0)\sigma$, $r_3 = (1.5)\sigma$, and $r_4 = (2.0)$. They examined the averages of the quantities in Eqs. (10) and (11), which are given by:

$$\overline{S}(t) = \frac{1}{16}\sum_{m=2}^{5}\sum_{j=1}^{4} S(m, r_j, t) \tag{12}$$

$$\Delta\overline{S}(t) = \frac{1}{4}\sum_{m=2}^{5} \Delta S(m,t) \tag{13}$$

The first zero crossing of $\overline{S}(t)$ or the first local minimum of $\Delta\overline{S}(t)$ for selecting the first locally optimal time data independence were found, which also provided the delay time $\tau_d = t\tau_s$, with τ_s being the sampling time. The optimal time was found from the index lag t for which $\overline{S}(t)$ and $\Delta\overline{S}(t)$ were both closest to zero. If equal importance to these two quantities are assigned, then the minimum of the quantity

$$S_{cor}(t) = \Delta\overline{S}(t) + \left|\overline{S}(t)\right|, \tag{14}$$

can simply be found, which will provide the delay time window $\tau_w = t\tau_s$.

APPLICATIONS TO HYDROLOGIC TIME SERIES

In the persent study, the C-C method is applied to three hydrologic time series to measure their general dependence and assess nonlinear characteristics: daily flow

from St. Johns River, Florida (1979-1988); biweekly volume from the Great Salt Lake (1847-1992); and daily rainfall from Seoul (1987-1996). Figure 1 shows variations of these series. Since the ACF method is widely used in nonlinear dynamic and chaos studies, results from the C-C are also compared with those obtained from the ACF method. The ACF analysis is presented first.

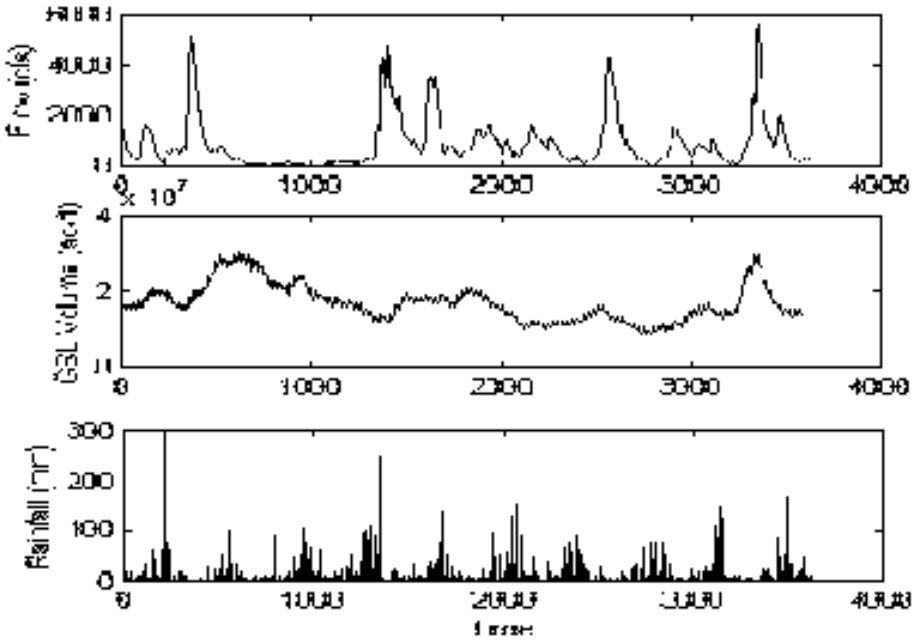

Figure 1 Time series plots: (a) daily streamflow from the St. Johns River; (b) biweekly volume from the GSL; and (c) daily rainfall from Seoul

Delay time estimation using ACF method. As for the selection of τ_d, the guidelines are: if the ACF decays exponentially with index lag t, then τ_d is taken as the index lag at which the ACF drops to 1/e; otherwise, τ_d is chosen as the index lag at which the ACF first crosses the zero line or its first local minimum, whichever occurs first. The ACFs for the flow and lake volume exhibit temporal persistence, while for the rainfall it fluctuates about zero [Figures not shown]. These observations indicate that the flow and lake volume are not random, but the rainfall is probably random. The τ_d values for these three series are 51 (days), 14 (biweeks), and 3 (days), respectively.

Delay time and delay window estimation using the C-C method. In the C-C method, the nonlinear dependence is measured using the statistic $S(m,N,r,t)$. As N is fixed for a given series, this statistic reduces to $S(m,r,t)$, and thus can be estimated with appropriate selection of only the parameters m and r, for a given t. Following the guidelines provided by Kim et al. (1998), four different (representative) values of r in

the range $\sigma/2 \le r \le 2\sigma$ are selected, with $r_1 = (0.5)\sigma$, $r_2 = (1.0)\sigma$, $r_3 = (1.5)\sigma$, and $r_4 = (2.0)\sigma$. Similarly, four different values of m are used, with $m = 2$, 3, 4, and 5. Figure 2 presents the $S(m,r,t)$ estimates obtained for the daily flow from the St. Johns River. It is clear that, for a given m, the index lag t at which the statistic $S(m,r,t)$ first crosses the zero line (τ_d) is different for the four different values of r. The average of these four values is $\tau_d = 89\,\tau_s$. Similarly, τ_d for the biweekly GSL volume is found to be $\tau_d = 11\,\tau_s$, and that for daily rainfall from Seoul is $\tau_d = 3\,\tau_s$ [Figures not shown].

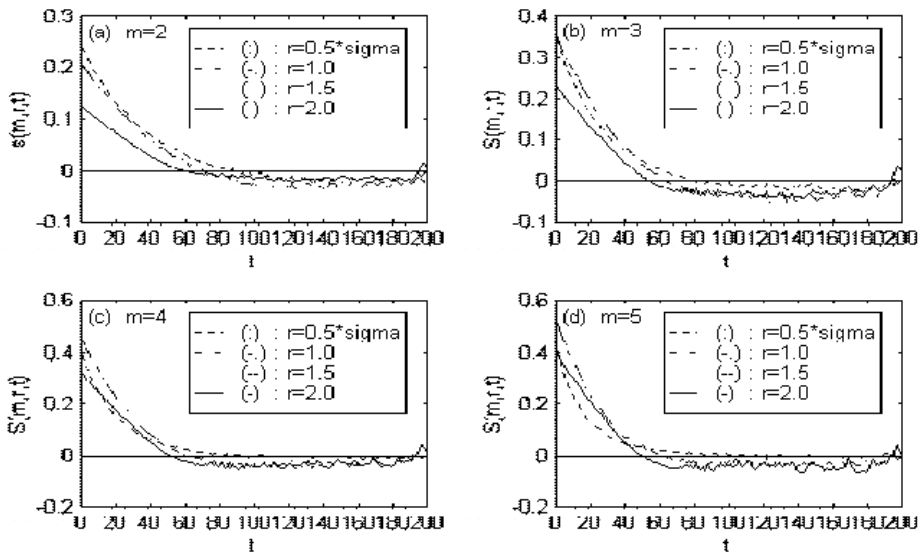

Figure 2 Results from the C-C method to flow series from the St. Johns River. The statistic $S(m,r,t)$ for: (a) $m = 1$; (b) $m = 2$; (c) $m = 3$; (d) $m = 4$

Figure 3 presents further results from the C-C analysis of the daily flow from the St. Johns River: (a) $\Delta S(m,t)$ for m = 2, 3, 4, and 5; (b) $\overline{S}(t)$ and $\Delta\overline{S}(t)$; and (c) $S_{cor}(t)$. The τ_w value is found to be $\tau_w = 194\,\tau_s$. The τ_w values for the GSL volume and the daily rainfall from Seoul are $\tau_w = 223\,\tau_s$ and $\tau_w = 48\,\tau_s$ [Figures not shown].

Comparison of results from ACF and C-C methods. For the daily flow from the St. Johns River and also for the biweekly GSL volume, the τ_d values from the two methods are different: 51 (days) and 14 (weeks) from the ACF method, whereas 89 (days) and 11 (weeks) from the C-C method. However, for the daily rainfall from Seoul, both the methods yield the same value, with $\tau_d = 3$ (days). These results seem

to indicate that: (1) both the methods perform equally well when the time series is the outcome of a linear stochastic process; and (2) the C-C method performs better than the ACF method when the time series is the outcome of a nonlinear process. The fact that the biweekly GSL volume has been shown to exhibit nonlinear deterministic behavior (e.g., Abarbanel and Lall, 1996), the present results are confirmation on the inadequacy of the ACF method for τ_d selection in nonlinear time series.

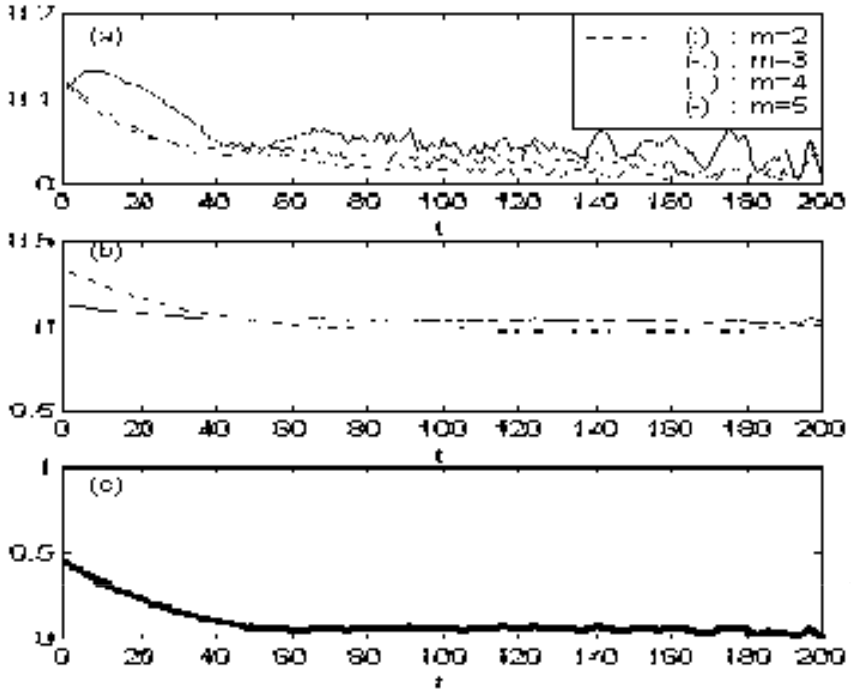

Figure 3 Results from the C-C method to the daily flow series from the St. Johns River: (a) $\Delta S(m,t)$ **; (b) (-):** $\overline{S}(t)$ **and (--):** $\Delta\overline{S}(t)$ **; and (c)** $S_{cor}(t)$

CONCLUSION

This study tested the effectiveness of the C-C method, proposed by Kim et al. (1998), for the selection of delay time and delay window for phase-space reconstruction of hydrologic data. Three hydrologic time series were studied: (a) daily flow from the St. Johns River, Florida; (b) biweekly volume of the GSL; and (c) daily rainfall from Seoul, Korea. The results indicate the ability of the C-C method to represent the general dependence of these series, against only the linear dependence represented by the autocorrelation function method. The results also suggest presence of nonlinear determinism in the daily flow from the St. Johns River and the biweekly GSL volume, while the nature of the daily rainfall in Seoul seem to be linear stochastic.

ACKNOWLEDGMENTS

This study was supported by the 2007 SOC Project (07-GIBANGUCHUK-D03-01) through the Design Criteria Research Center of Abnormal Weather-Disaster Prevention in KICTTEP of MOCT.

REFERENCES

Abarbanel, H. D. I., and Lall, U. (1996). "Nonlinear dynamics of the Great Salt Lake: System identification and prediction." *Climate Dyn.*, 12, 287-297.

Brock, W. A., Hsieh, D. A., and Lebaron, B. (l991). *Nonlinear dynamics, chaos, and instability: Statistical theory and economic evidence*, MIT Press, Cambridge.

Brock, W. A., Dechert, W. A., Scheinkman, J. A., and LeBaron, B. (l996). "A test for independence based on the correlation dimension." *Econ. Rev.*, 15(3), 197-235.

Frazer, A. M., and Swinney, H. L. (1986). "Independent coordinates for strange attractors from mutual information." *Phys. Rev. A*, 55, 1134-1140.

Grassberger, P., and Procaccia, I. (l983). "Measuring the strangeness of strange attractors." *Physica D*, 7, 153-180.

Holzfuss, J., and Mayer-Kress, G. (l986). "An approach to error-estimation in the application of dimension algorithms." *Dimensions and entropies in chaotic systems*, Springer-Verlag, New York.

Kim, H. S., Eykholt, R., and Salas, J. D. (l998). "Delay time window and plateau onset of the correlation dimension for small data sets." *Phys. Rev. E*, 58(5), 5676-5682.

Kim, H. S., Eykholt, R., and Salas, J. D. (l999). "Nonlinear dynamics, delay times, and embedding windows." *Physica D*, l27(1-2), 48-60.

Liebert, W., and Schuster, H. G. (1989). "Proper choice of the time delay for the analysis of chaotic time series." *Phys. Lett. A*, 141, 386-390.

Martinerie, J. M., Albano, A. M., Mees, A. I., and Rapp, P. E. (l992). "Mutual information, strange attractors, and the optimal estimation of dimension." *Phys. Rev. A*, 45, 7058-7064.

Sivakumar, B. (2000). "Chaos theory in hydrology: Important issues and interpretations." *J. Hydrol.*, 227(1-4), 1-20.

Takens, F. (1981). "Detecting strange attractors in turbulence." *Dynamical systems and turbulence*, Springer-Verlag, Berlin, Germany, 366-381.

Paleo Pacific Ocean Sea Surface Temperature Variability and Upper Colorado River Basin Streamflow

Oubeidillah A. Aziz[1] and Glenn A. Tootle[2]

[1]Graduate Research Assistant, University of Tennessee, Department of Civil and Environmental Engineering, 73F Perkins Hall, Knoxville, TN, 37996-2010; email: oaziz@utk.edu

[2]Assistant Professor, University of Tennessee, Department of Civil and Environmental Engineering, 73F Perkins Hall, Knoxville, TN, 37996-2010; email: gtootle@utk.edu

ABSTRACT

A study of the influences of Paleo Pacific Ocean Sea Surface Temperature (SST) variability and water-year Upper Colorado River Basin (UCRB) reconstructed streamflow is presented. Reconstructed streamflow data is available from several sources in the UCRB. The proxy records (streamflow) are derived from tree ring chronologies and these streamflow reconstructions provide an effective way to analyze patterns of variability (including drought) over a period of time extending beyond any instrumental record in UCRB.

Yearly proxy and coral based Pacific Ocean SST reconstructions, consisting of five by five degree cells, are available from 1590 to 1990. The range selected for the study is from Latitude 20° South to 60° North and 120° East to 80° West and 40° West to 2° West. A "lag" analysis is performed such that the SST dataset is for the year prior to the streamflow dataset. Additionally, epochal variability of climate signals [e.g., El Niño-Southern Oscillation (ENSO) and the Pacific Decadal Oscillation (PDO)] will be examined to determine if ENSO or PDO has strengthened (or weakened) over time.

The Singular Value Decomposition (SVD) statistical method has been identified as the preferable statistical method to identify coupled relationships between two, spatial-temporal fields. While SVD has been applied to SSTs and various hydrologic variables (e.g., Palmer Drought Severity Index – PDSI, precipitation, streamflow), this represents the first such application to reconstructed (paleo) datasets. The use of SVD with Pacific Ocean SSTs eliminates any spatial bias as to which SST region (or regions) may impact streamflow. This will assist in the identification of a SST region (or regions) that may not be represented in existing Pacific Ocean climate variability (e.g., ENSO, PDO) and could display the impacts of climate change.

INTRODUCTION

Numerous investigations have evaluated oceanic-atmospheric variability and continental U.S. hydrologic (e.g., snowpack, streamflow and precipitation) response [*Hunter et al., 2006; Tootle et al.*, 2005; *Gershunov*, 1998]. These studies show strong sub-continental impacts linked to particular phases (e.g. cold or warm) of

Pacific Ocean climate variability [e.g., El Niño-Southern Oscillation (ENSO) and the Pacific Decadal Oscillation (PDO)]. However, a limitation of these studies was that they focused on pre-defined (e.g., ENSO, PDO) regions of climate variability and the resulting hydrologic response to phases (e.g., warm or cold) of these climate signals. An alternative to evaluating known climate signals is to utilize entire regions of sea surface temperature variability. *Bretherton et al.* [1992] concluded that Singular Value Decomposition (SVD) was simple to use and preferable for general use while *Wallace et al.* [1992] found that SVD isolates the most important modes of variability. SVD has been utilized to evaluate SST and hydrologic variability [*Tootle and Piechota*, 2006; *Rajagaopalan et al.*, 2000; *Wang and Ting*, 2000]. However, a limitation of these and the previous climate signal studies is that they utilize (only) instrumental records of hydrologic response. Therefore, only one to three phases of the interdecadal (PDO) signal can be evaluated.

The proposed research represents the first time application of SVD to reconstructed Pacific Ocean SSTs and reconstructed UCRB streamflow. Initially, a "testing or verification" period is used such that three Pacific Ocean SST datasets (instrumental, tree-based and coral-based) and instrumental streamflow are evaluated. Since instrumental SSTs and instrumental streamflow have been utilized in past research efforts, this will allow for the comparison of the results between the instrumental SST dataset and the reconstructed SST datasets. Next, the period of record is extended and tree-based reconstructed Pacific Ocean SSTs and UCRB reconstructed streamflow is used. Finally, for the extended period of record, epochal (approximately 100 year periods) periods are evaluated to determine variability in SSTs and streamflow regions.

DATA

The available datasets used include instrumental and reconstructed streamflow, and instrumental and reconstructed (tree-ring based and coral based) Pacific Ocean SSTs.

Instrumental Streamflow Data

Data from unimpaired UCRB streamflow stations (Figure 1) were obtained from the U.S. Geological Survey (USGS) National Water Information System (NWIS). The average monthly streamflow rate in cfs were summed and converted into water-year streamflow volumes using appropriate conversions.

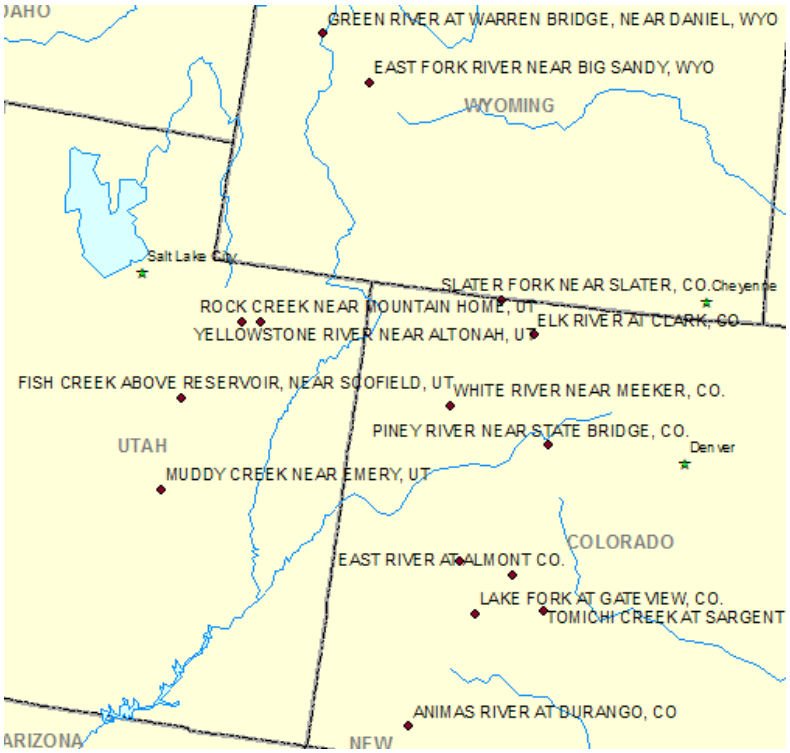

Figure 1: Location Map of UCRB instrumental streamflow gages.

Reconstructed Streamflow Data

Reconstructed water-year streamflow volumes for the UCRB were obtained from several sources including *Woodhouse, et al.* [2006] and *Barnett et al.* [2009] (Figure 2).



Figure 2: Location Map of UCRB reconstructed streamflow gages.

Instrumental Pacific Ocean SST Data

Instrumental Pacific Ocean SST data was obtained from the National Climatic Data Center website (http://www.cdc.noaa.gov/cdc/data.noaa.ersst.html). This dataset consists of monthly average values at a resolution of 2° by 2°. Average yearly values for each grid cell were determined and used in the current research.

Reconstructed (Tree-ring and Coral) Pacific Ocean SST Data

The reconstructed (Tree-ring and Coral) Pacific Ocean SST datasets, at a resolution of 5° by 5°, were obtained from the World Data Center for Paleoclimatology Climate reconstructions website (ftp://ftp.ncdc.noaa.gov/pub/data/paleo/coral/east_pacific/sst_evans2002). The yearly values represent the water-year (Oct to Sep).

Instrumental and Reconstructed ENSO and PDO Indices

The instrumental and reconstructed ENSO and PDO indices were obtained from the Working Group on Surface Pressure website (http://www.cdc.noaa.gov/Pressure/Timeseries), the NCAR Climate and Dynamics website (http://www.cgd.ucar.edu/cas/catalog/climind/TNI_N34/) and the JIASO website (http://jisao.washington.edu/pdo/PDO.latest).

METHODOLOGY

Singular Value Decomposition (SVD)

SVD is a powerful statistical tool for identifying coupled relationships between two, spatial-temporal fields. While *Bretherton et al.* [1992] provide a detailed discussion of the theory of SVD, a brief description of SVD as applied in this study, is provided. Initially, a matrix of standardized SST anomalies and a matrix of standardized water year streamflow anomalies were developed. The time dimension of each matrix must be equal while the spatial component (i.e., the number of SST cells and the number of streamflow stations) can vary in dimension. The cross-covariance matrix was then computed for the two spatio-temporal matrices and SVD was applied to the cross-covariance matrix and "teleconnection" information regarding the relationship between the two was obtained.

The resulting SVD of each cross-covariance matrix created two matrices of singular vectors and one matrix of singular values. The singular values were ordered such that the first singular value (1st mode) was greater than the second singular value and so on. *Bretherton et al.* [1992] defines the squared covariance fraction (SCF) as a useful measurement for comparing the relative importance of modes in the decomposition. Each singular value was squared and divided by the sum of all the squared singular values to produce a fraction (or percentage) of squared covariance for each mode. In applying SVD, the SCF is somewhat analogous to the percent of explained variance (by components) when applying PCA.

Finally, the two matrices of singular vectors were examined, generally referred to as the left (i.e., SST) matrix and the right (i.e., streamflow) matrix. The first column of the left matrix (1st mode) was projected onto the standardized SST anomalies matrix and the first column of the right matrix (1st mode) was projected onto the standardized

streamflow anomalies matrix. This resulted in the 1st temporal expansion series (TES) of the left and right fields, respectively. The left heterogeneous correlation field (for the 1st mode) was determined by correlating the SST values of the left matrix with 1st temporal expansion series of the right field and the right heterogeneous correlation field (for the 1st mode) was determined by correlating the streamflow values of the right matrix with the 1st temporal expansion series of the left field. The left temporal expansion series have a physical meaning since they represent SST variability that may not already be included in existing SST indices and could represent a new index of SST variability.

Utilizing an approach similar to *Tootle et al.* [2008], *Rajagopalan et al.* [2000] and *Uvo et al.* [1998], maps displaying significant (90%) correlation values for streamflow regions were reported while contour maps (displaying all correlation values) were provided for the Pacific Ocean SSTs. If the Pacific Ocean SST and streamflow significant regions have the same sign, then they behave similarly [i.e., higher (lower) SST temperatures result in higher (lower) streamflow] while opposite signs result in opposite behavior [i.e., lower (higher) SST temperatures result in higher (lower) steamflow]. Please note, the "switching" of the signs is inherent to SVD and the importance of the results is the positive/negative relationships between SSTs regions and streamflow stations, as displayed by the figures. For each analysis, the previous year SSTs are used with the current water-year streamflow and (only) the 1st mode of variability is reported.

Proposed Research Approach

Verification of Instrumental, Tree-ring based and Coral based Pacific Ocean SST datasets with Instrumental Streamflow

The first analysis compares the SVD results of instrumental Pacific Ocean SSTs and instrumental streamflow to tree-ring based and coral based Pacific Ocean SSTs and instrumental streamflow. Instrumental records typically have less uncertainty than records developed from biological factors. Also, instrumental SST and instrumental streamflow datasets have been previously evaluated in past research efforts and will provide a "benchmark" for comparison to the tree-ring and coral based SST datasets. Therefore, the same period of record (1950 – 1989 for SSTs and 1951-1990 for streamflow) was selected.

Evaluation of Tree-ring based Pacific Ocean SSTs and Reconstructed Streamflow (Entire Record 1615 – 1989 for SSTs and 1616 – 1990 for Streamflow)

After the verification step, the previous year Pacific Ocean SSTs and the current water-year streamflow were evaluated for the entire period of record.

Evaluation of Tree-ring based Pacific Ocean SSTs and Reconstructed Streamflow (Epochal Analysis 1700 – 1799 for SSTs and 1701 – 1800 for Streamflow; 1800 – 1899 for SSTs and 1801 – 1900 for Streamflow; 1900 – 1989 for SSTs and 1901 – 1900 for Streamflow)

The final analysis divides the entire period of record dataset into three, 100-year periods. Each period (epoch) is evaluated to determine if climate signals have varied over time.

RESULTS

Verification of Instrumental, Tree-ring based and Coral based Pacific Ocean SST datasets with Instrumental Streamflow

When comparing the three Pacific Ocean SST datasets with instrumental streamflow for the same period of record, similar spatial Pacific Ocean SST patterns were observed (Figure 3). First, the instrumental SSTs (Figure 3a) display a well defined equatorial region (i.e., ENSO) and a region south of Alaska (i.e., PDO). Both of these "red" regions display positive correlation values. When observing the streamflow stations, approximately eight "red" (positive correlation) stations were significant in Utah and Colorado. The "black" stations are not significant while one "blue" station was identified. This displays the "classic" southwestern U.S. ENSO signal in which increased (decreased) equatorial SSTs results in increased (decreased) streamflow. The tree-ring based reconstructed SSTs (Figure 3b) display a similar ENSO pattern ("blue" or negatively correlated region) and six "blue" (negative correlation) stations are identified in Utah and Colorado. As previously stated, the "switching" of signs is inherent in SVD and the same relationship [increased (decreased) SSTs results in increased (decreased) streamflow] was maintained. Perhaps the most interesting result was the coral-based reconstructed SSTs (Figure 3c). While a similar spatial pattern was displayed for the SSTs, only two stations (blue) were identified with a "positive" relationship to ENSO. It appears that the coral-based reconstructed SSTs do not "capture" SST variability (i.e., more uncertainty and "noise" in the dataset) when compared to the instrumental and tree-based SST datasets. Additionally, both the reconstructed SST datasets have a larger grid size (5 degree) when compared to the instrumental dataset (2 degree).

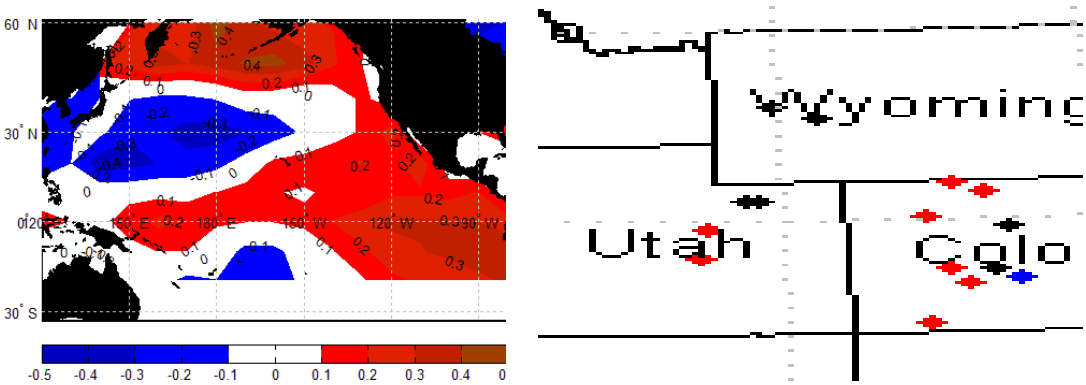

(a)

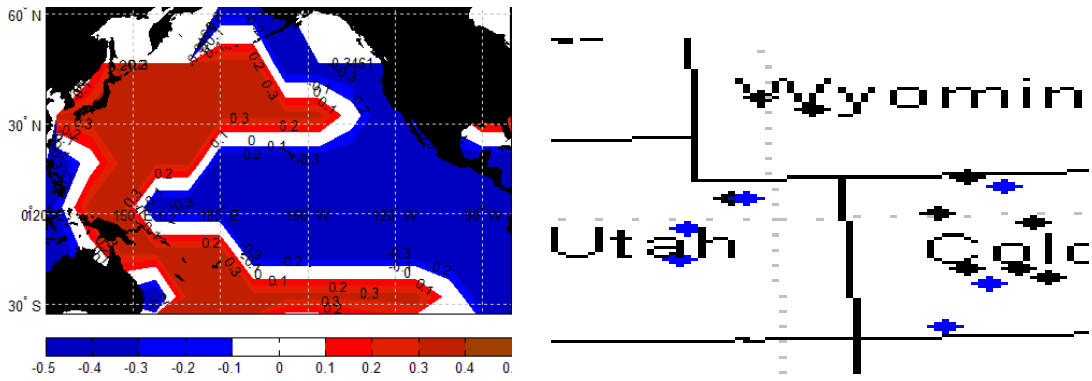

(b)

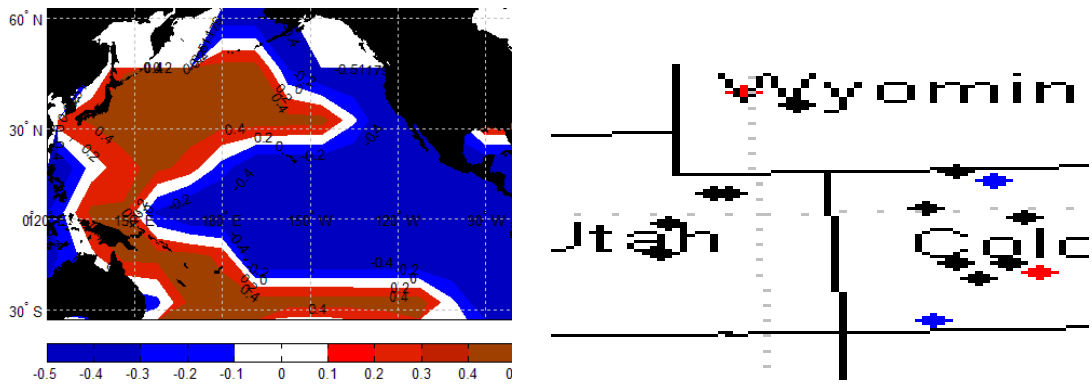

(c)

Figure 3: Results of SVD analysis (1st mode) of Pacific Ocean SSTs (a) instrumental (b) tree-ring based (c) coral based and instrumental streamflow.

Evaluation of Tree-ring based Pacific Ocean SSTs and Streamflow (Entire Record)
When evaluating the tree-based SSTs and reconstructed streamflow for the entire period of record, a similar spatial SST pattern in addition to a similar spatial streamflow station pattern was observed (Figure 4). It appears that equatorial SSTs (i.e., ENSO) are the primary climatic driver of UCRB streamflow. However, it appears the signal weakens as you move north into the basin (i.e., Green River Basin of Wyoming). Also, there is a consistent "opposite sign" (red) spatial SST pattern southeast of Japan that consistently shows up in this and past research efforts. This pattern may well influence streamflow variability, in addition to ENSO. Interestingly, the "PDO like" SST region is not well defined in any of the reconstructed SST patterns (Figures 3b & 3c and Figure 4). This may be attributed to the larger grid size.

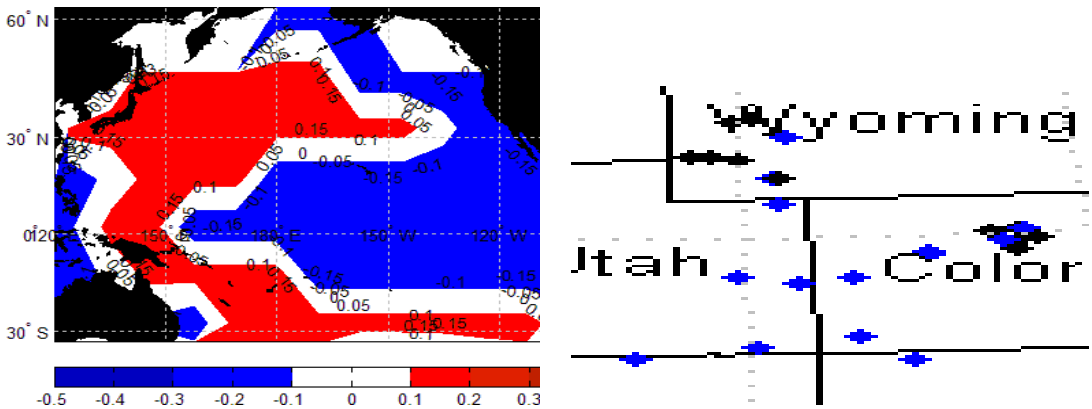

Figure 4: Results of SVD analysis (1st mode) of tree-ring based Pacific Ocean SSTs and reconstructed streamflow.

Evaluation of Tree-ring based Pacific Ocean SSTs and Streamflow (Epochal Analysis)

The epochal analysis provided some interesting results (Figure 5). The 1700's (Figure 5a) results in almost all streamflow stations being significant while the opposite occurs for the 1800's (Figure 5b). The 1900's (Figure 5c) closely matches the previous analysis (Figure 3b), which, given the similar time periods, confirms those results. A closer evaluation shows that the ENSO-like SST pattern in the 1700's has a stronger correlation value when compared to the pattern in the 1800's. Perhaps a stronger, more defined ENSO-like signal was present during that epoch, which resulted in a stronger streamflow response throughout the UCRB.

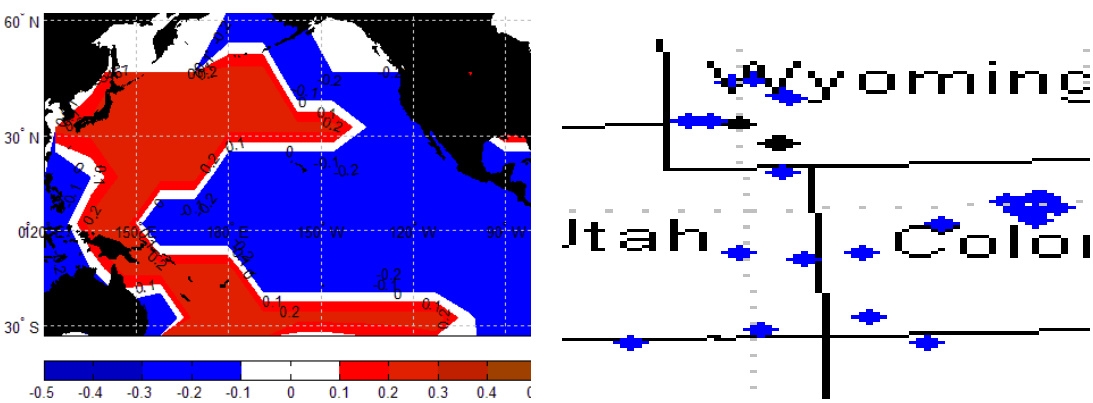

(a)

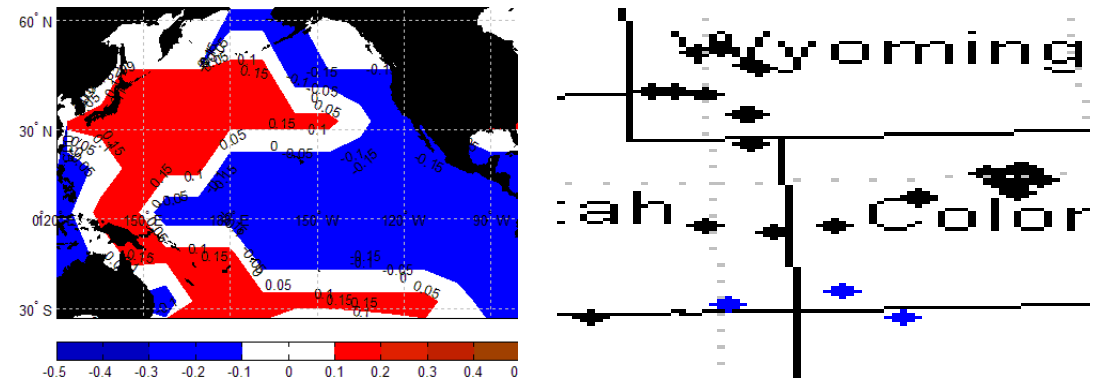

(b)

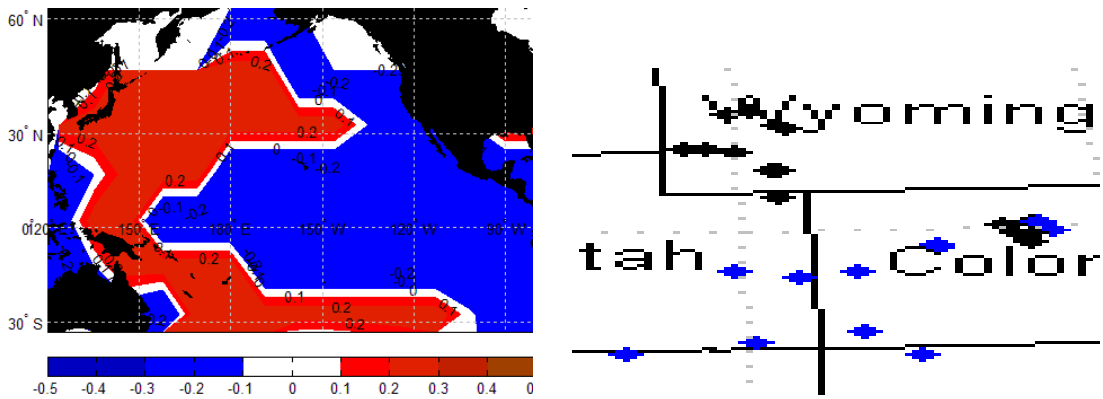

(c)

Figure 5: Results of SVD analysis (1st mode) of tree-ring based Pacific Ocean SSTs and reconstructed streamflow (a) 1700-1799 (b) 1800-1899 (c) 1900-1989.

CONCLUSIONS & FUTURE WORK

ENSO appears to be the dominant signal in UCRB streamflow, based on the consistent ENSO-like equatorial SST pattern present in the current research. However, it appears the strength of this signal varies over time which results in UCRB streamflow variability. Future research will evaluate ENSO (and PDO) signal strength during the various epochal periods. Additionally, rather than selecting "arbitrary" 100-year epochal periods, periods may be selected based on cycles of the PDO (25 to 50 years). Also, an important next step in these research efforts is to attempt to relate droughts (or mega-droughts) with these cycles and to determine if ENSO (and PDO) signal strength is changing (strengthening or weakening) and if this change is related to climate change.

REFERENCES

Barnett, F.A., T. Watson, S. Gray and G. Tootle (2009). Upper Green River Basin Streamflow Reconstructions and Drought Analysis. Submitted to *American Society of Civil Engineers Journal of Hydrologic Engineering* (under 1st review).

Bretherton, C.S., C. Smith, and J.M. Wallace (1992). An Intercomparison of Methods for Finding Coupled Patterns in Climate Data. *Journal of Climate*, 5, 541-560.

Gershunov, A. (1998). ENSO influence on influence on intraseasonal extreme rainfall and temperature frequencies in the contiguous United States: implications for long-range predicitability. *Journal of Climate*, 11, 3192-3203.

Hunter, T., Tootle, G.A., and T.C. Piechota (2006). Oceanic-atmospheric variability and western U.S. snowfall. *Geophysical Research Letters*, 33, L13706.

Rajagopalan B., E. Cook, U. Lall, and B.K. Ray (2000). Spatiotemporal variability of ENSO and SST teleconnections to summer drought over the United States during the twentieth century. *Journal of Climate*, 13, 4244-4255.

Tootle, G.A., T.C. Piechota and F. Gutierrez (2008). The Relationships between Pacific and Atlantic Ocean Sea Surface Temperatures and Colombian Streamflow Variability. *Journal of Hydrology*, 349(3-4), 268-276.

Tootle, G. A., and T. C. Piechota (2006). Relationships between Pacific and Atlantic ocean sea surface temperatures and U.S. streamflow variability, *Water Resources Research*, 42, W07411.

Tootle, G.A., T.C. Piechota and A.K. Singh (2005). Coupled Oceanic / Atmospheric Variability and United States Streamflow. *Water Resources Research*, 41, W12408.

Uvo, C.B., C.A. Repelli, S.E. Zebiak, and Y. Kushnir (1998). The relationships between tropical Pacific and Atlantic SST and northeast Brazil monthly precipitation. *Journal of Climate*, 11, 551-562.

Wang, H. and M. Ting (2000). Covariabilities of winter U.S. precipitation and Pacific sea surface temperatures. *Journal of Climate*, 13, 3711-3719.

Wallace, J.M., D.S. Gutzler, and C.S. Bretheron (1992). Singular Value Decomposition of Wintertime Sea Surface Temperature and 500-mb Height Anomalies. *Journal of Climate*, 5, 561-576.

Woodhouse, C.A., S.T. Gray, and D.M. Meko (2006), Updated streamflow reconstructions for the Upper Colorado River Basin, *Water Resources Research*, 42, W05415, doi:10.1029/2005WR004455.

Planning for Climate Change

John A. Kliem, PE

Commander, Civil Engineer Corps, U.S. Navy, Graduate, Industrial College of the Armed Forces, National Defense University, Fort McNair, Washington D.C. 20340. PH (703) 571-9780; email john.kliem@js.pentagon.mil. The information contained in this paper is solely the opinion of the author and in no way reflect the policy of the United States Department of Defense or any other agency of the U.S. Government.

Abstract

Climate change is upon us. Models used to predict climate change lack the granularity to allow communities to be accurately predicting the impacts of climate change. Federal Funding of Climate change research can barely keep pace with inflation much less provide the research required for local communities to develop climate change plans. Local governments need to develop a strategy to resource the modeling of climate change for their community. Regions could band together to source the modeling or solicit help from their congressional representatives. Next, leaders need to develop an action plan that addresses possible impacts to the community's industrial base or other natural resources.

Introduction

The world's climate is changing and the vast majority of the world is unprepared to handle the effects of these changes. Our Federal government has taken only modest steps to ensure our country is prepared for climate change. These measures include the creation of an interagency structure of Federal Agencies formed to synthesis and coordinate government climate change research and modest investments were made into modeling climate change. The results of this research, while beneficial at the global and national level, falls short of providing information needed by local governments to assess and make action plans to be ready for the effects of climate change. Local government leaders must assume a larger role in planning for climate change to include developing strategies for resourcing and executing climate change action plans for their communities.

Climate Change Research and Development Funding

Government spending on Research and Development (R&D) for climate change is limited and lacks the focus to get the results required for local leaders. According to the American Association of the Advancement of Sciences, overall federally funded R&D declined during fiscal year 2008. Total Federal investment in R&D increased only 1.2 percent and below the inflation rate (AAAS, 2008). The Department of Energy (DOE), Office of Science, The National Science Foundation (NSF) and the National Institute of Standards and Technology (NIST) budgets were cut to fund continued medical research, Energy R&D, and environmental research that including climate change research (AAAS, 2008). The increase in Environmental R&D and climate change

research only resulted in a rise of four percent to $2.1 billion (AAAS, 2008). The Climate Change research Agencies benefiting from this small increase include the U.S. Geological Survey (USGS), the National Aeronautics and Space Administration (NASA), and the National Oceanic and Atmospheric Administration (AAAS, 2008).

The Budget for fiscal year 2009 is not complete most agencies maintained their 2008 funding levels under the continuing resolution passed by Congress this includes the agencies involved in climate change research. Even if the Democratic Congress and President Obama's administration managed to increase funding for Climate change sciences, it is doubtful in the amount of time remaining in this fiscal year that the government will be able to develop a climate change strategy that will have an effect on local governments.

Climate Modeling Efforts

The Climate Change Science Program created in 2002 coordinate's climate change research within the federal government. This program cuts across executive agencies and assimilates research within the U.S. Global Change Research Program that was established under the Global Change Research Act of 1990 and the Climate Change Research Initiative created by President Bush in 2001 (Bodman; et al, 2007). The Climate Change Science Program orchestrates research on climate and global change amongst 13 Federal Agencies and Departments (Bodman; et al, 2007). Topics within climate that are studied include atmospheric composition, climate variability and change, the global water cycle, land use and land cover effects, the global carbon cycle, ecosystems, and human contributions and responses to environmental change (Bodman; et al, 2007). The Climate Change Science Program ensures unity of effort amongst all the agencies by ensuring a consistent approach to modeling and measurements keeping all agencies focused on the same climate change research and development objectives (Bodman; et al, 2007).

Climate change modeling requires a vast infrastructure of satellites, ocean buoys and land based temperature gauges. These instruments upload measurements of a variety of atmospheric parameters such as green house gasses, temperature and air particulates to super computers loaded with historical climate measurements. This data is the processed through a number of physical, chemical and climate science algorithms (Glass, 2008). One of the more popular climate models is used by NASA's Goddard Space Flight Center along with other government agencies and research institutions created four super computer simulations that simultaneously model the ocean, atmosphere, land surface and sea ice. These simulations comprise the Earth System Modeling Framework this climate model will allow scientists to make climate change projections into the next century (Gutro, 2005). Earth Systems Modeling Framework has unified the climate modeling community making it easier to share data and eliminates the expense of each agency need to develop their own model or coupling software (Gutro, 2005).

Future models being developed will allow climatologists to simulate reactions in the atmosphere. One of these models is a Carbon Cycle model to predict the transport and fate of carbon within our climate. Additionally, two models are being simultaneously developed to look at chemistry in the troposphere and stratosphere.

These models will be coupled to allow better prediction of impacts to air quality and water quality which would then be tied to human health (Glass, 2008).

These Climate models are enabling scientists to make important climate impact predictions on an international or global level as reported in the Climate Change Science Program's annual report. These results have been widely reported and include observations that higher latitudes are experiencing shorter winters and longer summers. Measurements and Modeling indicate that the seasonal changes are the result of human activity vice climate variability (U.S. Fed News Service, 2007). The output of climate models like the one described above makes as reported by David Talbot in *Technology Review* is that these climate predictions are for a large grid square of about 150 kilometers by 190 kilometers (Talbot, 2007). This causes problems since weather patterns can be created by urban centers or mountain ranges within the grid skewing the results. Researchers are working to "nest" regional climate models into larger global climate models to give results more clarity (Talbot, 2007). The creation of regional "nested" models is a new research area that the Federal Government has not focused on to date.

Planning

State and local governments need to start now to develop a strategy for the creation of an action plan for climate change preparedness. We still do not understand all of the potential impacts to climate change and local governments cannot afford to wait for the federal government to push out actionable information for local government leaders. The first step should be to determine potential vulnerabilities within their community. Paying particular attention to major community components that could be impacted by significant changes in the climate. For example, Louisiana and Texas would be impacted by climate change with an increase in size and severity of hurricanes affecting the petro-chemical industry. Local leaders need to develop specific plans to ensure the survival of the region's economic base as well as their communities. Likewise we need to understand and plan for climate change impacts affecting an infrastructure or economic base that is essential to our national security like the example mentioned above. Additionally, local leaders need to also study the impact of climate change on major resources like water.

Resourcing the Plan

There are some reports of Federal Grants being awarded to local communities to implement climate change planning at the local level. These efforts are largely hit or miss and we certainly lack a national strategy for the development of climate change mitigation plans. Notably, the National Science Foundation in fiscal year 2007 and 2008 awarded ten grants to researchers to investigate climate change issues involving urban areas and coastal barrier islands (Dybus, 2008). This is a small but necessary step to encourage and develop the research infrastructure to be prepared to take on a larger role in climate change planning and development. The Federal Government will most likely continue to make modest investments in the short term but will likely lack the emphasis

or focus to lead the comprehensive development of a national strategy for the development of climate change planning.

Industry will not take the lead in planning for climate change. It is difficult for individual industries to take the initiative and begin planning for the impacts of climate change that may not be felt for a few decades. Much of our countries industrial base is developing business plans to positively affect their balance sheet in the next quarter much less planning for the long term future.

This leaves our local leaders to develop ways to resource their climate changing efforts. Some state governments have already taken the initiative to develop and issue climate change planning grants. For example, Aspen, Colorado invested $145,000 to develop climate predictions for their own town (Talbot, 2007). At the end of the spectrum the state of California is investing $4 million in a regional climate model (Talbot, 2007). These local or regional plans will allow local governments to begin detailed planning to mitigate the forecasted climate change (Talbot, 2007). However, most communities will not be able to resource climate change planning efforts on their own. They will need to build a partnership base with other local governments along with state and federal governments. In some cases it may be appropriate to issue a carbon tax or carbon trading program to generate funds for climate change planning. A tax on fuel consumption is another option that would elevate the cost of fuel but local government could remove the tax if the cost of fuel were to rise again. Local governments could also work with the Department of Homeland Security if they can relate local climate change to national security. This could be an effective way of getting a Federal partner to investigate local climate change impacts. The key partner to the local leader to developing a resourcing strategy will be state and federal representatives. It is essential that elected leaders understand that Federal Climate Change research lacks the granularity to allow for local planning and what the potential impacts of lack of planning would be to their state or district. Without their help it is doubtful that the local leader will get the momentum and assistance required to fully develop the plan.

Strategy implications

Local planning efforts need to take the long view. What will the future of climate change bring? It is possible that certain communities may identify the loss of an economic base such as a fishery or a tourist attraction. Through early planning local leaders can take steps to mitigate these losses and even encourage the development of industry that would not be impacted by climate change. It would be a monumental undertaking for a region to shift to a different economic base and will take a great deal of time. This is why local governments cannot afford to wait to begin climate change planning efforts. In most cases it will take decades to implement climate change practices.

It is very likely that local climate change models will identify zoning issues within communities. For example, local climate change models may identify regions that will be more likely to be impacted by flooding. These communities located in climate change impacted zones should be identified early. Assistance will have to be provided in some cases to encourage relocation. Property taxes could also be used to drive a change

in zoning. Effective land use plans would have to be developed for impacted areas. Viable land re-use plans could include space for parks or environmental mitigation zones.

Conclusion

Federal government funding for climate change sciences has been lack luster. Existing climate change models lack the granularity required for local planning and mitigation. Communities need to act now to develop local climate change plans. Communities should identify possible impacts of climate change based on current climate change modeling efforts. Since, local climate change models are expensive local leaders will need to find partners or some fund source through taxation to create their plan. Possible strategic partners with communities could be local industry, state officials, the Department of Homeland Security (if local climate change poses a threat to national security). Once a plan is developed and the climate change impact is identified leaders need to take the long view in implementing the plan taking necessary steps to rezone land and or shift economic bases as required. Planning for climate change will not be easy. However, current climate change predictions indicate radical shifts in climate over the coming decades and it will take communities at least that long to get ready.

Bibliography

"Congress Wraps Up another Disappointing Year for Federal R&D Funding." American Association for the Advancement of Science (AAAS). http://www.aaas.org/spp/rd/upd1207.htm (accessed March 17, 2008, 2008).

Congress Wraps Up another Disappointing Year for Federal R&D Funding. Washington D.C.: AAAS R&D Budget and Policy Program, 2008, http://www.aaas.org/spp/rd/upd1207.htm (accessed January 16, 2008).

"Third U.S. Climate Change Science Program Report Issued." *US Fed News Service, Including US State News* (Oct 18, 2007).

Bodman, Samuel W., Gutierrez, Carlos M., Marburger III, John H. *Our Changing Planet*. Washington D.C.: Climate Change Science Program, 2007.

Dybas, Cheryl. "NSF Awards 10 Grants for Studies of Coupled Natural and Human Systems." National Science Foundation. http://www.nsf.gov/news/news_summljsp?cntn_id=112346 (accessed January 11, 2009).

Gass, James. "NASA Goddard Space Flight Center, Global Modeling and Assimilation Office." National Aeronautical Space Administration. http://gmao.gsfc.nasa.gov/overview.php (accessed March 19, 2008, 2008).

Gutro, Rob. "**Field Tests Unite Weather and Climate Models**." NASA. http://www.nasa.gov/centers/goddard/news/topstory/2005/esmf.html (accessed March 16, 2008, 2008).

Talbot, David. "Planning for a Climate-Changed World." *Technology Review* 110, no. 3 (May/Jun, 2007): 62.

Probabilistic Streamflow Forecasts Based on Hydrologic Persistence in Central Texas

Wenge Wei[1] and David W. Watkins, Jr.[2]

[1] Graduate Student, Department of Civil and Environmental Engineering, Michigan Technological University, Houghton, MI 49931. E-mail: wewei@mtu.edu
[2] Associate Professor, Department of Civil and Environmental Engineering, Michigan Technological University, Houghton, MI 49931. E-mail: dwatkins@mtu.edu

Abstract

In many cases, streamflow persistence (month-to-month or season-to-season correlation) can be used in place of climate forecasts to provide useful forecast information to water managers. In this study, an ordinal polytomous logistic regression model is proposed to generate tercile probability stream flow forecasts (i.e., probability of low, medium, and high categories) based on persistence for the Lower Colorado River system in central Texas. Forecast performance is evaluated by cross-validation using the Brier skill score (BSS) and the Ranked probability skill score (RPSS). The results show that stream flow persistence can provide significant forecast skill during the winter and spring seasons, when water allocation decisions are being made for the coming summer growing season.

Introduction

Reliable streamflow forecasts with lead times of one season can have a significant effect on the performance of reservoir operation policies and operation efficiency (Karamouz, et al, 2004). In recent years, much effort has been made to develop mid- to long-term hydroclimatic and streamflow forecasting models for major rivers in the United States. For example, the NOAA Climate Prediction Center issues seasonal forecasts of temperature, precipitation, and soil moisture, as well as a drought outlook, for the entire U.S. In the western U.S., the USDA Natural Resources Conservation Service forecasts streamflows in the first half of the year based on observed snowpack conditions. At many stream gage locations throughout the U.S., the National Weather Service provides probabilistic seasonal flow forecasts through a procedure known as Ensemble Streamflow Prediction, or ESP (Day, 1985; Smith et al., 1992). Traditionally, each of the meteorology traces has been assumed to represent an equally likely scenario for the future; recently, methods have been developed to condition the probabilities of the historical meteorological traces based on seasonal climate forecasts (e.g., Croley 2000). On a global scale, the NOAA/Columbia University International Research Institute for Climate and Society (IRI) is one institution that issues seasonal forecasts of temperature and precipitation.

Significant progress has been made in understanding the influence of large-scale ocean-atmospheric patterns, such as El Niño–Southern Oscillation (ENSO), Pacific Decadal Oscillation (PDO), the North Atlantic Oscillation (NAO), and Atlantic Multidecadal Oscillation (AMO), on regional climate anomalies around world. Recent studies have shown that incorporation of large-scale ocean-atmospheric patterns can improve the ability to forecast streamflow in long lead time (Hamlet and Lettenmaier, 1999; Sharma, 2000; Tootle, et al, 2006). At least three previous studies have identified teleconnections for central Texas. Piechota and Dracup (1996) found strong correlation between the Southern Oscillation Index (SOI) and the Palmer Drought Severity Index (PDSI), indicating the potential of improved climate forecasts, up to a year in

advance, for the region. However, a strong relationship between SOI and streamflow was not found. One possible reason for this is that PDSI is a mathematical function of temperature and precipitation and provides a general indication of drought, whereas streamflow tends to integrate climatic processes over interseasonal time scales, and this seasonal averaging may limit forecast accuracy. For instance, streamflow is a function of both surface runoff and groundwater discharge, and groundwater recharge and discharge processes often exhibit lag times markedly longer than those of rainfall-runoff processes. Furthermore, groundwater basins seldom align directly with surface watersheds, which may confound statistical analyses of climate and streamflow variables measured at specific gage locations.

In another study, Rajagopalan et al. (2000) found correlation between summer PDSI and winter Pacific Ocean sea surface temperature anomalies. However, they also found epochal variations in this correlation, with the period of 1963-1995 showing weaker teleconnections than the period 1895-1962. Of course, without a means of predicting these epochal shifts in teleconnections, such variation tends to confound statistical forecasting methods based on the entire historical record. It is widely hypothesized that interdecadal North Pacific variability modulates ENSO-precipitation teleconnections (e.g., Gershunov and Barnett, 1998), but Rajagopalan et al. (2000) were not able to conclude that either NAO or PDO has any effect on ENSO-precipitation teleconnections in central Texas.

Finally, Tootle et al. (2005) completed a study of the influence of interdecadal, decadal, and interannual oceanic-atmospheric influences on streamflow in the United States. Unimpaired streamflow was identified for 639 stations for the period 1951–2002, and the phases (cold/negative or warm/positive) of ENSO, PDO, NAO, and AMO were identified for the year prior to the streamflow year (i.e., long lead time). Statistical significance testing of streamflow, based on the interdecadal, decadal, and interannual oceanic-atmospheric phase (warm/positive or cold/negative), indicated no spatially coherent teleconnections for central Texas. Although this study focused on a specific annual period (October-September) and forecast lead time, it provides an indication that long-lead climate forecasts may not be useful to water managers in this region.

Streamflow forecasts may be either deterministic or probabilistic, but probabilistic methods are often preferable for water management because they can provide more information about uncertainty. Categorical streamflow forecasts are common, providing the probabilities of flow being in each of a number of categories (e.g., low, medium, high). Probabilities of each category could be generated directly or indirectly. Piechota et al. (1998) proposed linear discriminant analysis to produce the probabilities of each category of streamflow directly. This method involves nonparametric kernel density estimation of the probability density function for each flow category. Regonda et al. (2006) employed logistic regression to directly predict the probability of streamflow above a given threshold. They applied this approach to categorical forecasts of the spring (April-June) streamflow at six locations in the Gunnison River Basin. However, this approach treats the response variable as binary, i.e., 1 if streamflow value exceeds a given threshold and zero otherwise. A drawback of this approach for multiple categories is that the logistic regression needs to be repeated multiple times to obtain the probability corresponding to each category threshold, and sum of probabilities is not guaranteed equal to 1.

In this paper, a statistical method called polytomous logistic regression for ordinal response (Kutner et al. 2004) is proposed to generate tercile probability forecasts (monthly to seasonal lead times) for the Highland Lakes system in central Texas. Because large-scale climate signals do not demonstrate great potential for skillful forecasts, hydrologic persistence will be examined as only predictor variable. In many cases, streamflow persistence (month-to-month or season-to-season correlation) is strong enough to provide useful forecast skill. The performance of forecasts is evaluated by cross-validation using the Brier skill score (BSS) and the ranked probability skill score (RPSS).

Case study

The Lower Colorado River Authority (LCRA) operates the Highland Lakes system in central Texas, a series of six lakes on the watershed of the Lower Colorado River. As a water conservation and reclamation district, the LCRA provides water supply and flood control to a 33-county area, including the City of Austin and several rice irrigation districts along the Texas Gulf Coast (see Figure 1). In addition, the LCRA produces wholesale power for a 53-county service area and provides water resources for lake recreation activities and in-stream flow maintenance. To meet rapidly growing demands, reservoir inflow forecasts with seasonal lead times would be very beneficial; however, hydrologic forecasts are not used by the LCRA for a number of reasons, including high seasonal and annual variability of stream flow, the absence of easily measured hydrologic indicators such as snowpack, and a lack of experience with probabilistic planning methods.

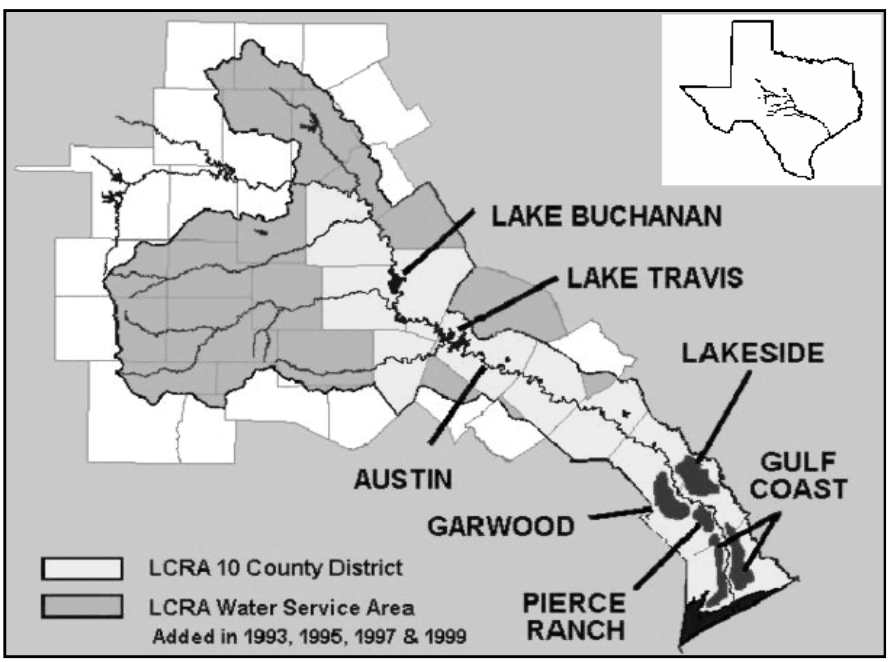

Figure 1. Lower Colorado River Authority District

The data used in the analyses come from two sources: 1) aggregate Highland Lakes inflows based on USGS gage measurements and adjustments made by LCRA staff to account for inflows from ungaged areas; and 2) unregulated flows downstream of the Highland Lakes, as determined by the Texas Water Availability Model (WAM). A total of 57 years of monthly flow data covering from 1950 to 2006 are used in this study. For most of the analyses, the raw flow data are normalized through a two-step process—first a logarithmic transformation, then conversion to a standardized anomaly by subtraction of the mean (of the log values) and division of the standard deviation (of the log values). While this transforms the data so that the statistical assumption of normality is more valid, it should be noted that the correlation coefficients are then inflated (due to the log-transform), and thus an effort is made to illustrate the results in terms of the raw flow data.

Estimates of monthly reservoir inflows may be based on measured flows at three USGS gage sites—Colorado River near San Saba, Pedernales River near Johnson City, and Llano River near Llano. LCRA staff have adjusted these flows to account for ungaged portions of the drainage area, as well as precipitation falling directly onto the lakes. Figure 2 shows the monthly autocorrelations of this time series, ranging from a high of nearly 0.8 for February and March flows to a low of -0.02 for July and August flows. Figure 3 shows seasonal correlations, which again peak in the winter season with a correlation coefficient of 0.66. The correlation coefficient that is significant at the $p = 0.05$ level is 0.20. It may be surprising that the seasonal correlation between OND and JFM flows is higher than the average of monthly correlation coefficients during this period. One reason for this may be that averaging over a three-month period reduces the "noise" that results from individual storm events which have a significant effect on monthly flow totals.

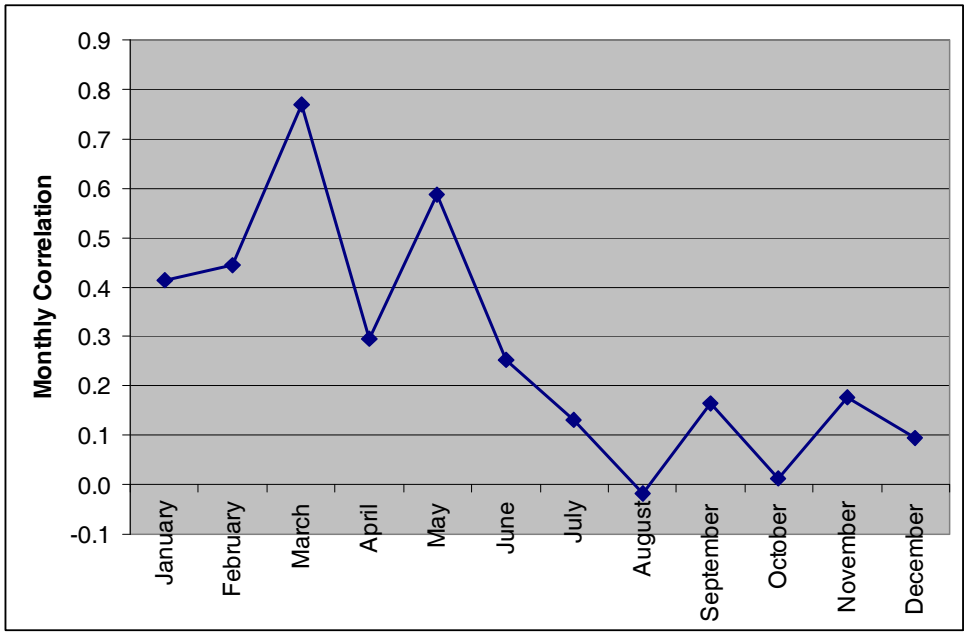

Figure 2. Monthly autocorrelations for aggregate inflows to the Highland Lakes. Correlation coefficients are computed using raw flow data.

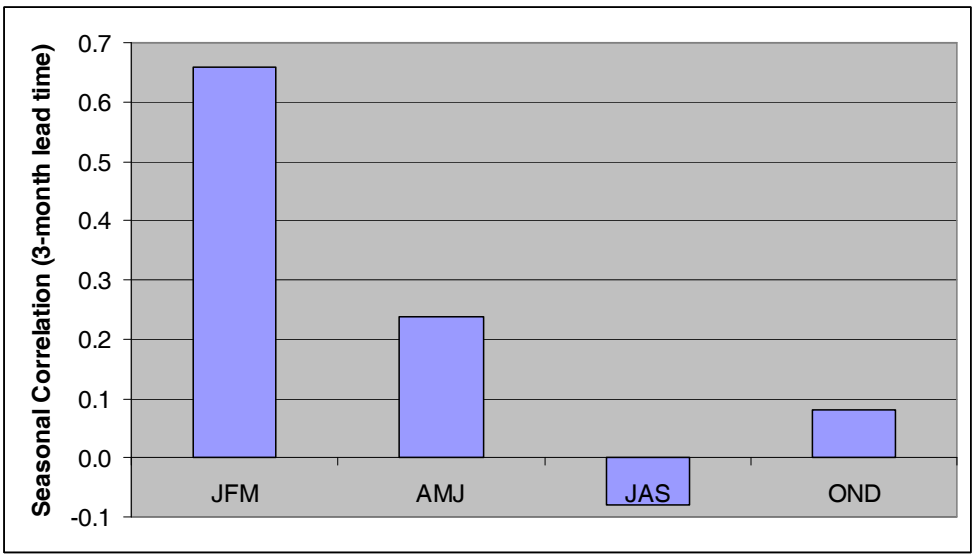

Figure 3. Seasonal autocorrelations for aggregate inflows to the Highland Lakes. Correlation coefficients are computed using raw flow data.

Methodology

Logistic regression is most frequently used to model the relationship between a binary response variable and a set of predictor variables. If the response variable has more than two levels, logistic regression can still be employed by means of a polytomous or multicategory logistic regression model (Kutner et al., 2004). The goal of this study is to develop a framework for developing categorical forecasts of streamflows. The polytomous logistic regression method is used to produce tercile probability forecasts (below normal, normal, and above normal categories). Since these categories may be treated as ordered, and the ordinal polytomous logistic regression model may be more effective, yielding a more parsimonious model with easily interpreted results. The basic principle is described below.

In general, a linear logistic regression with a binary response variable Y, logit(p) can be expressed as a function of one (simple linear logistic regression) or more than one predictor variables (multiple linear logistic regression) as follows:

$$\text{logit}(p) = \log(p/(1-p)) = \beta_0 + \beta_1 x_1 + \cdots\cdots \beta_k x_k \qquad (1)$$

where $p = \Pr(Y = 1)$ denotes the probability of success. The parameters β_j are usually estimated using maximum likelihood theory.

In the binary logistic case, logit(p) compares the probability of a category-1 response (success) to the probability of a category-2 response (failure). For a response variable with J categories, it is necessary to develop J - 1 logistic regression models. One category will be chosen as the baseline or reference category, and then all other categories will be compared to it. The choice of reference category is arbitrary. Frequently the last category is chosen.

Using category J to denote the reference category, only J - 1 logits need to be developed. For a nominal response, the jth logit expression for the ith observation is given as:

$$\log\left[\frac{p_{ij}}{p_{iJ}}\right] = X_i^T \beta_j \qquad \text{for} \quad j = 1, 2, \ldots J-1 \tag{2}$$

where $\beta_j = \left[\beta_{0j} \quad \beta_{1j} \quad \cdots \quad \beta_{kj}\right]^T$ and $X_i = \left[1 \quad X_{i1} \quad \cdots \quad X_{ik}\right]^T$

(Note that vectors β_j are different for each category j.)

If multiple response categories are treated as ordered, the logistic regression model could be reduced to J - 1 cumulative logits as follows:

$$\log\left[\frac{p(Y_i \le j)}{1-p(Y_i \le j)}\right] = \alpha_j + X_i^T \beta \qquad \text{for} \quad j = 1, 2, \ldots J-1 \tag{3}$$

The difference between the ordinal response logits and the nominal response logits is that each of the J - 1 parameter vectors β_j is unique for the nominal case; for ordinal response, the slope coefficient vector β is identical for each of the J - 1 cumulative logits, and only the intercepts α_i differ. Finally, the cumulative probabilities $p(Y_i \le j)$ for the ordinal logistic regression model is given as follows:

$$p(Y_i \le j) = \frac{\exp(\alpha_i + X_i^T \beta)}{1+\exp(\alpha_i + X_i^T \beta)} \qquad \text{for} \quad j = 1, 2, \ldots J-1 \tag{4}$$

The maximum likelihood method is used to estimate the unknown parameters. The package VGAM developed by Yee in R (http://www.r-project.org) was used to develop the ordinal polytomous logistic regression model.

Forecast verification

Forecast verification aims to evaluate the agreement between forecasts and observations (Katz and Murphy, 1997; Stephenson, 2003). The Brier skill score (BSS) and the ranked probability skill score (RPSS) are common statistics used to measure the improvement in the accuracy of multicategory probability forecasts over a naïve forecasting method such as climatology.

The Brier skill score (BSS) (Dogget, 1998) is defined as

$$BSS = 1 - BS / BSC \tag{5}$$

where BS is the Brier score, and is defined as

$$BS = (1/n)\Sigma(f_i - l(\text{obs}_i))^2 \tag{6}$$

where f_i is the forecast probability of event i occurring; $l(\text{obs}_i)$ is an indicator variable (1 if event in category i occurs, else 0); n is the number of events; and BSC is the climatologically expected

value of *BS*, and is defined as $BSC = P_i * (1 - P_i)$, where P_i is the climatological probability of the event. The Brier score is often applied to events that exceed a given threshold, but it can also be applied to categorical events. In this study, we consider three tercile categories, i.e., below normal, normal and above normal. Accordingly, $BSC = (1/3)*(1-1/3) = 0.222$ for each category. A perfect forecast has a value of BSS of 1; positive values between zero and one indicate forecast performance better than climatology, and negative values indicate forecast performance worse than climatology.

The ranked probability score (*RPS*) evaluates the sum of the squared differences in the cumulative probability space, so that

$$RPS = \frac{1}{K-1}\sum_{m=1}^{K}\left[\left(\sum_{k=1}^{m} f_k\right) - \left(\sum_{k=1}^{m} o_K\right)\right]^2 \tag{7}$$

where K is the number of forecast categories (below normal, normal and above normal), f_k is the forecast probability for the kth point, and o_k equals zero or one to indicate whether or not the observed flow is in the kth category. The use of *RPS* results in higher penalties for forecasts farther away from actual outcomes, rather than scoring based on only hit and miss. The *RPS* can assume a number between zero and one, with a perfect forecast scoring zero. The *RPSS* then measures the relative improvement of using a forecast over climatology alone, and is given by

$$RPSS = \frac{\overline{RPS} - \overline{RPS}_{climatology}}{o - \overline{RPS}_{climatology}} = 1 - \frac{\overline{RPS}}{\overline{RPS}_{climatology}} \tag{8}$$

The probabilities of streamflow in each category in the climatology forecast (i.e., prior probabilities) are the same and equal 1/3 due to the definition of the flow regimes. Thus, the *RPS* values of the three categories (below normal, normal and above normal) in the climatology forecast are 0.278, 0.111 and 0.278, respectively. A perfect *RPSS* is 1, and negative scores indicate that forecasts performed worse than climatology.

Results

The polytomous logistic regression model for ordinal response described above was applied for forecasting flows in the Highland Lakes system in central Texas. In the model, streamflow persistence (month-to-month, month-to-season or season-to-season correlation) was used as potential predictor variable. The probabilities of three tercile categories of streamflow with one month or one season lead time were predicted. For example, the winter (JFM) streamflow was forecasted based on the previous fall (OND(-1)) streamflow (one season lead time). The January streamflow was predicted using the previous December streamflow (one month lead time), and so on. Performance metrics are based on the leave-one-out cross-validation method, which selects a single data point of the sample for validation and the remaining data points for training data until each data point in the sample is used once as the validation data.

A summary of the results for reservoir inflow forecasts is presented in Tables 1 and 2. Table 1 shows the regression coefficients of streamflow persistence with different lead times, along with the corresponding Wald test p-values. The hypothesis in the Wald test is:

$$H_0: \beta_k = 0 : \ H_a: \ \beta_k \neq 0 \quad \text{for } k = 1, \ldots. 5. \tag{9}$$

Wald test p-values are all much less than 0.05, indicating that the regression coefficients are statistically significant at the 0.05 level and corresponding predictor (streamflow with one to three months lead time) should be retained in the model. Table 2 presents the values of BSS and RPSS, which are consistence with the above analysis. The BSS values show that winter (JFM) streamflow forecast with one month and one season lead times have 19.7% and 31.6% improvement over the climatology, respectively. Monthly streamflow forecasts with one month lead time during winter have an average 37.8% improvement over the climatology. The RPSS values indicate that forecasts have 16.7% and 29.3% improvement over climatology for one month and one season lead times, respectively. According to the RPSS values, the monthly streamflow forecasts with one month lead during winter period have a 34.9% improvement over climatology, on average.

Table 1. Ordinal polytomous logistic regression coefficients and significance test for reservoir inflow forecast models based on persistence.

OND(-1)-JFM		Dec(-1)-JFM		Dec(-1)-Jan		Jan-Feb		Feb-Mar	
Coef.	P	Coef.	P	Coef.	P	Coef.	P	Coef.	P
-2.07	<0.001	-2.70	<0.001	-2.32	<0.001	-2.56	<0.001	-2.50	<0.001

Table 2. Brier Skill Score (BSS) and Ranked Probability Skill Score (RPSS) for monthly and seasonal forecasts of reservoir inflows.

Category	OND(-1)-JFM		Dec(-1)-JFM		Dec(-1)-Jan		Jan-Feb		Feb-Mar	
	BSS	RPSS	BSS	RPSS	BSS	RPSS	BSS	RPSS	BSS	RPSS
Below Normal	0.284	0.463	0.411	0.587	0.555	0.696	0.503	0.643	0.405	0.564
Normal	-0.013	-0.403	0.083	-0.282	0.183	-0.153	0.212	-0.047	0.122	-0.248
Above normal	0.320	0.440	0.454	0.574	0.431	0.495	0.606	0.706	0.386	0.485
AVE	**0.197**	**0.167**	**0.316**	**0.293**	**0.390**	**0.346**	**0.440**	**0.434**	**0.305**	**0.267**

Summary

This work aimed to improve the long-term (from monthly to seasonal) streamflow forecasts for the Highland Lakes system in central Texas. A direct and effective method for producing the probabilistic categorical streamflow forecast using ordinal polytomous logistic regression is presented, with hydrological persistence (month-to-month, month-to-season and season-to-season) examined as the basis for streamflow forecasts. Results indicate that persistence is a very useful predictor for monthly and seasonal streamflow forecasts during winter period. The Brier Skill Score (BSS) and Ranked Probability Skill Score (RPSS), in particular, indicate a significant improvement over climatology. The method presented here is fully transferable to other regions where significant hydrologic persistence exists.

This method is also applicable for other predictors, including large-scale climate signals such as ENSO, PDO, NAO and AMO. These will be investigated in future work for their potential to

improve long-term (seasonal or annual) streamflow prediction. To this end, a higher order polytomous logistic regression model, called polynomial logistic regression, may be developed to incorporate the large-scale climate signals and their interactions into the forecast model.

Acknowledgment

Adjusted flow data and helpful advice was provided by Ron Anderson of the Lower Colorado River Authority.

References

Araghinejad, S., D. H. Brun , and M. Karamouz (2006). Long-lead probabilistic forecasting of streamflow using oceanic-atmospheric and hydrological predictors. *Water Resour. Res.,* 42, W07411, doi:10.1029/2004WR003853

Croley, T. E., II (2000). *Using Meteorology Probability Forecasts in Operational Hydrology*. ASCE Press, Reston, VA.

Day, G.N. (1985). Extending streamflow forecasting using NWSRFS. *J. Water Resour. Plng. & Mgmt*, 111(2), 157-170.

Gershunov A. and T. P. Barnet (1998). ENSO influence on intraseasonal extreme rainfall and temperature frequencies in the contiguous United States: Observations and model results. *Journal of Climate*, 11(7), 1575-1586.

Hamlet, A. F., and Lettenmeier, D.P. (1999). Columbia River streamflow forecasting based on ENSO and PDO climate signals. *J. Water Resour. Plng. & Mgmt*., 125(6), 333-334.

Karamouz, M. F., and Zahraie, B. (2004). Seasonal streamflow forecasting using snow budget and El Niño-Southern Oscillation climate signals: Application to the Salt River Basin in Arizona. *J. Hydrologic Engrg*. 9(6), 523-533.

Katz, R. W., and A. H. Murphy (1997). *Economic Value of Weather and Climate Forecasts*, Cambridge University Press, Cambridge, United Kingdom, Ch. 2, pp. 19-74.

Kutner, M. H., Nachtsheim, C. J., and Neter, J. (2004). *Applied Linear Regression Models*. McGraw-Hill, Irwin, CA.

Piechota, T. C., F. H. S. Chiew, J. A. Dracup, and T. A. McMahon (1998), Seasonal streamflow forecasting in eastern Australia and the El Nino–Southern Oscillation, *Water. Resour. Res*., 34, 3035– 3044.

Piechota, T.C. and J.A. Dracup (1996). Drought and regional hydrologic variation in the United States: Associations with the EI Niño-Southern Oscillation. *Water Resour. Res.,* 32 (5), 1359-1373.

Rajagopalan, B., E. Cook, U. Lall and B. K. Ray (2000). Spatiotemporal variability of ENSO and SST teleconnections to summer drought over the United States during the twentieth century. *Journal of Climate*, 13(24), 4244-4255.

Regonda, S. K., B. Rajagopalan, and M. Clark (2006). A new method to produce categorical streamflow forecasts. *Water Resour. Res*., 42, W09501, doi:10.1029/2006WR004984.

Salas, J. D., Delleur, J. W., Yevjevich, V., and Lane, W. L. (1988). *Applied Modeling of Hydrologic Time Series*, Water Resources Publications, Littleton, CO.

Sharma, A. (2000). Seasonal to interannual rainfall probabilistic forecasts for improved water supply management: 1. A strategy for system predictor identification. *J. Hydrol*., 239, 249-258.

Smith, J., G. N. Day, and M. D. Kane (1992). Nonparametric framework for long range streamflow forecasting, *J. Water Resour. Plng. and Mgmt.*, 118(1), 82-92.

Stephenson, D. B. (2003). "Glossary," in Jolliffe, I. T., and D. B. Stephenson (eds.) *Forecast Verification: A Practitioner's Guide in Atmospheric Science*, Wiley and Sons Ltd., UK.

Tootle, G. A., and T. C. Piechota (2006). Relation ships between Pacific and Atlantic Ocean sea surface temperatures and U.S. streamflow variability. *Water Resour. Res.,* 42, W07411, doi:10.1029/2005WR004184.

Tootle, G. A., T. C. Piechota and A. Singh (2005). Coupled oceanic-atmospheric variability and U.S. streamflow. *Water Resour. Res*., 41, W12408.

Providing a Physical Basis for Statistical Homogeneity in Regional Frequency Analyses

Fredline Ilorme[1] and Veronica W. Griffis[2]

[1]Graduate Research Assistant; [2]Assistant Professor, Dept. of Civil & Environ. Engr., Michigan Technological University, 1400 Townsend Drive, Houghton, MI 49931-1295. vgriffis@mtu.edu

Abstract

To estimate the magnitude and frequency of flood flows at ungauged sites, space is traded for time using a regional frequency analysis. This requires the delineation of homogeneous regions in which the flood regime is sufficiently similar to allow the spatial transfer of information to ungauged sites. However, the ability to do so with adequate precision is hindered by our limited knowledge of the physical properties and mechanisms that produce flood flows. In addition, the actual delineation of regions is highly dependent on the similarity measures and classification techniques employed. It is generally accepted that similarity in the flood regime is indicated by similarity in basin characteristics, and thus these basin characteristics can be used to delineate regions and to classify ungauged sites. However, recent evidence suggests this is not the case. The objective of this research is to evaluate whether or not regions which are statistically homogeneous are also physically homogeneous. Preliminary results using data for 480 sites in the Southeastern U.S. are presented in this paper. Multivariate statistical methods were employed to delineate regions based on physical basin characteristics and at-site flood statistics. The delineated regions were then assessed from both a physical and statistical viewpoint.

Introduction

Accurate estimates of flood quantiles are necessary for floodplain definition and management, and for the design of water-use and water-control projects, as well as transportation infrastructure such as bridges and roads. Obtaining such estimates, however, is problematic because of the uncertainty in estimates based on individual station records shorter than the return period of interest, and is even more troublesome when the site of interest is ungauged. To compensate for limited or unavailable data, one solution is to trade space for time using a regional frequency analysis, wherein the characterization of flood flows at sites of interest is derived using information pooled from nearby hydrologically similar gauged sites (NRC 1988). Common approaches are the Index Flood procedure (e.g. Dalrymple 1960; Hosking and Wallis 1988, 1997; Stedinger and Lu 1995; Kjeldsen and Rosberg 2002), and regional regression procedures, such as weighted and generalized least squares regression (e.g. Tasker and Stedinger 1989; Tasker et al. 1996; Madsen and Rosberg 1997; Eng et al. 2007ab; Griffis and Stedinger 2007).

An important component of regional flood frequency analysis is the delineation of homogeneous regions (or groups of sites) in which the flood regime is deemed sufficiently similar to allow the spatial transfer of information to ungauged sites (see for example, Stedinger and Lu 1995, and citations therein). The flood regime includes the magnitude, timing, duration, frequency, and inter-annual variability of flood events. It is generally assumed that the flood regime, or hydrologic response, is similar at sites with comparable basin characteristics (e.g. physiographic characteristics and meteorologic inputs). More recent studies have observed, however, that similar hydrologic response is not guaranteed simply by similar basin characteristics because of complex interactions among those characteristics (Zrinji and Burn 1994; Burn 1997; Burn et al. 1997).

Regional quantile models and flood frequency analyses in general are based on superficial relationships between flood quantiles and physiographic characteristics (Potter 1987; Gupta et al. 1994). These models are hindered by our limited knowledge of the physical properties and mechanisms producing flood flows. Typically only log-log and log-linear relationships between flood quantiles and basin characteristics are employed, and in most cases only drainage area is determined to be useful for estimating flood quantiles at ungauged sites (Eng et al. 2007b; Griffis and Stedinger 2007). More complex relationships and interactions between basin characteristics are generally not considered because the current understanding of hydrology is not advanced enough to know if such a model is reasonable (Eng et al. 2007b; Griffis and Stedinger 2007). Thus, models of flood quantiles and other statistics at ungauged sites can be improved by increasing our knowledge of what basin characteristics, or interactions among basin characteristics, predominantly contribute to flood flows.

For regional regression analyses, regions are often formed as a matter of convenience, such as using state boundaries. In regards to index flood procedures, the delineation of homogeneous regions involves three major steps: (1) selection of an appropriate set of attributes; (2) application of a statistical classification technique; and (3) tests of the homogeneity of delineated regions. A variety of attributes and classification techniques have been employed in the hydrologic literature (for example, GREHYS 1996a; Burn 1997; Burn et al. 1997; Hosking and Wallis 1997; Chiang et al. 2002a,b; Isik and Singh 2008). The delineated regions are dependent on the choice of similarity measures and the classification technique employed (see for example, GREHYS 19961b; Castellarin et al. 2001).

Burn (1997) and Burn et al. (1997) observe that the selection of appropriate catchment similarity measures is complicated by the need to employ measurable features that are indicative of hydrologic response, and allow classification of an ungauged site within a delineated region, as well as the development of a regional quantile estimator for use at ungauged sites. Thus, similarity measures derived from the observed flood series, such as at-site flood statistics and measures related to the timing and seasonality of flood peaks, should not be employed. Use of at-site flood statistics as similarity measures is also not appropriate because subsequent tests to verify the homogeneity of delineated regions are based on the same statistics (Burn

1990, 1997). As a result, the delineated regions may appear homogeneous, but would be inefficient for developing regional quantile estimators.

Further, current techniques for delineating regions do not guarantee statistical homogeneity in terms of the probability distributions representing annual maximum flood series and the subsequent quantile relations. These methods also only superficially provide homogeneity from a physical viewpoint. Rao and Srinivas (2006) observe that regions identified using a variety of clustering algorithms are generally not statistically homogeneous; however, the regions do tend to align with geographical features and soil characteristics. Potentially more informative sets of similarity measures which include the composite effects on flood quantiles due to complex interactions among the basin characteristics have yet to be considered.

The primary objective of this research is to determine if regions which are statistically homogeneous are also homogeneous from a physical viewpoint. In the context of this research, a statistically homogeneous region is defined as one in which the flood response at gauging stations are deemed sufficiently similar on the basis of statistics of the at-site flood distribution. Physically homogeneous regions are those in which the physical basin characteristics are reasonably similar. Preliminary results for 480 sites in the Southeastern United States are presented below.

Study Area and Data Employed

The study area considered in this paper is defined by the watershed spanning the Southeastern United States (Alabama, Tennessee, Florida, Georgia, South Carolina, North Carolina and Virgina). A total of 480 unimpaired U.S. Geological Survey (USGS) gauging stations were considered in this analysis (see Figure 1). These sites were identified using the Hydro-Climatic Data Network (Slack et al. 1993). Annual maximum peak streamflow data were collected for each gauging station from the USGS website (http://nwis.waterdata.usgs.gov/usa/nwis/peak). Summary statistics for the flood series are presented in Table 1 by state.

Table 1: Number of sites per state and record length statistics

State	Number of sites	Minimum record length	Maximum record length	Average record length
Alabama	25	25	77	49
Florida	19	27	81	50
Georgia	169	25	115	43
N. Carolina	118	19	111	55
S. Carolina	38	26	79	51
Tennessee	64	16	131	47
Virginia	47	25	108	53

A number of basin characteristics are considered in this study. For each site, Gruber and Stedinger (2007) provided data on the following ten characteristics: drainage area (A), main channel slope (S_{Ch}), main basin slope (S_B), basin shape (Sh)

computed as a ratio of the main channel length squared to the drainage area, mean basin elevation (E), mean annual precipitation (Pr), percent impervious surface (Imp), percent forest cover (F), average soil drainage index (SI) as a measure of soil moisture, and average hydrologic soil index (Inf) as a measure of infiltration.

Methodology

The methodology employed to evaluate the statistical and physical homogeneity of delineated regions will include five main steps:

1. Delineate statistically homogeneous regions based on at-site flood statistics.
2. Assess the similarity of basin characteristics (i.e. physical homogeneity) within the statistically homogeneous regions delineated in step (1).
3. Assess the dissimilarity of basin characteristics among the statistically homogeneous regions delineated in step (1).
4. Delineate regions on the basis of observable basin characteristics.
5. Assess the statistical homogeneity of the physically homogeneous regions delineated in step (4).

These steps are described in more detail below.

Statistically homogeneous regions in which the flood regime is sufficiently similar from site to site could be delineated on the basis of at-site flood statistics such as the 100-year event (Q_{100}), L-moments, or a measure of the seasonality of flood peaks. The preliminary results presented in this paper consider regions delineated based on the Coefficient of L-Variation (L-CV). Use of the L-CV is advantageous as it is a distribution free measure of the shape of the at-site distribution (Hosking and Wallis 1997).

Regions will be delineated using the Ward clustering algorithm (Johnson and Wichern 2002, pp. 690-692). Each delineated region will be evaluated to determine if criteria for statistical homogeneity have been met. These criteria indicate whether or not the sites in a region have similar probability distributions representing the observed annual maximum flood series. For regional flood frequency analysis, Hosking and Wallis (1997) compare sample L-moments among sites as a means of region validation. In particular, they propose a set of H-statistics, which measure the average distance from the individual site statistics (L-moments and L-moment ratios) to the regional average values. If a region is not deemed sufficiently homogeneous, then the sites therein will be scrutinized further to see if particular sites are influencing the results using a discordancy measure (Hosking and Wallis 1997).

The physical homogeneity of each statistically homogeneous region will be assessed using techniques such as cluster analysis (CA) and principal component analysis (PCA). These techniques will assist in identifying common basin characteristics within a delineated region. For each statistically homogeneous region, CA and PCA will be applied to the ten basin characteristics listed above.

Alternatively, the dissimilarities in the basin characteristics in different statistically homogeneous regions will be identified using canonical correlation

analysis (CCA). In general, CCA results in a series of discriminant functions (or canonical variates) which separate the groups (or delineated regions) as much as possible. The discriminant functions are formed for optimal combinations of variables, such that the first discriminant function provides the most information pertaining to the differences between groups; subsequent discriminant functions provide successively less information pertaining to the differences. In addition, the discriminant functions are orthogonal such that their individual contributions to our understanding of the differences between groups do not overlap. The first few discriminant functions resulting from the CCA should reveal the primary physical differences between the delineated regions. The extent to which the basin characteristics of sites identified as discordant differ from the remaining sites will also be investigated.

In addition, regions will be delineated on the basis of the ten basin characteristics using the Ward clustering algorithm. The statistical homogeneity of these physically homogenous regions with then be assessed using the H-statistics and discordancy measure of Hosking and Wallis (1997).

Preliminary Results

Using the ward clustering algorithm, six statistically homogeneous regions were delineated on the basis of the L-CV and sis physically homogeneous regions were delineated on the basis of the ten basin characteristics under consideration. The resulting regions are illustrated in Figures 1 and 2 for the L-CV and the basin characteristics, respectively. The number of regions delineated in each case was optimized according to the pseudo F-test which maximizes the differences between the regions (Fovell and Fovell, 1993). Although it is difficult to discern any patterns in the delineated regions, a quick comparison of the two figures indicates that regions delineated using physical basin characteristics are not consistent with those delineated based on the L-CV.

Tables 2 and 3 provide the mean and standard deviation of the basin characteristics and the L-CV for the regions illustrated in Figures 1 and 2, respectively. Overall, the results in Table 2 reveal that there is very little difference between the statistically homogeneous regions in terms of the basin shape (Sh), mean annual precipitation (Pr), percent impervious surface (Imp), percent forest cover (F), average soil drainage index (SI), and average hydrologic soil index (Inf). This suggests that these basin characteristics do not contribute significantly to the hydrologic regime of annual maximum flood series. The differences among the statistically homogeneous regions in terms of the remaining basin characteristics are unclear because the standard deviation of each characteristic is quite large relative to the mean. However, the average of the drainage area (A), main basin slope (S_B), and mean basin elevation (E) tends to be inversely related to the magnitude of the L-CV.

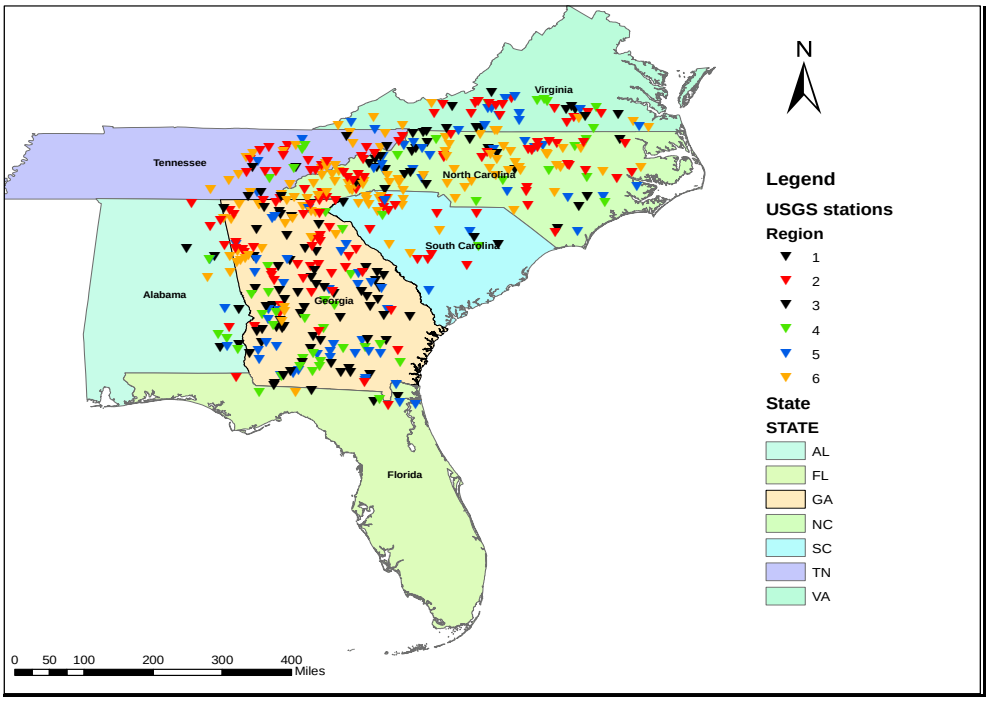

Figure 1: Location of unimpaired gauging stations in the Southeastern U.S. and statistically homogeneous regions delineated based on L-CV

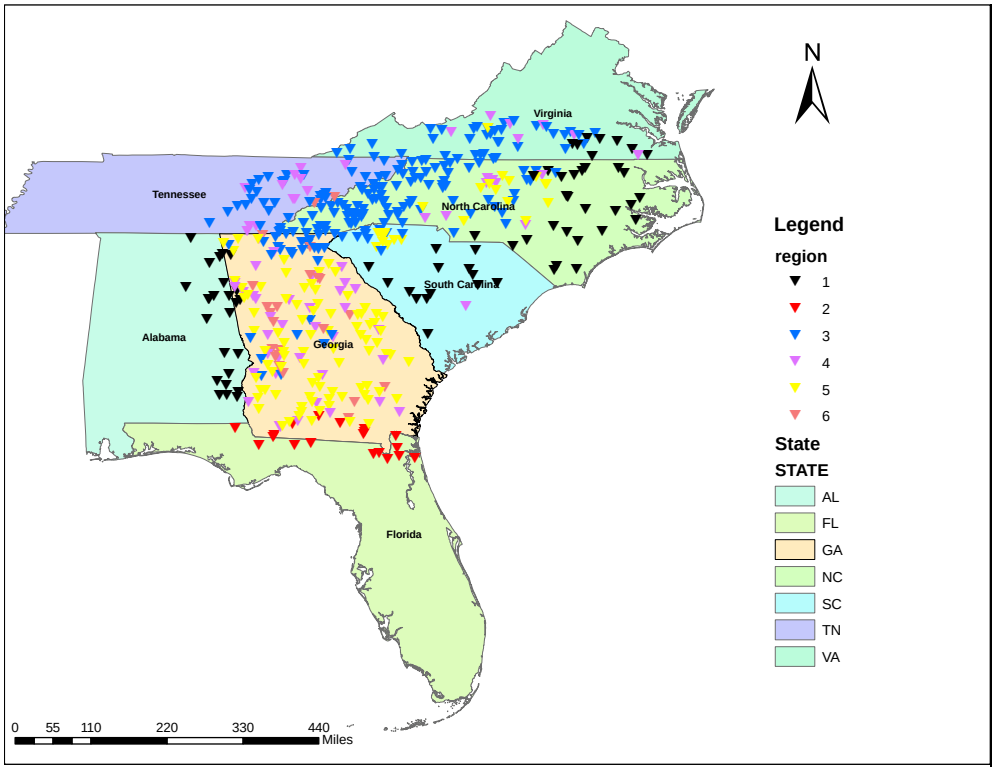

Figure 2: Location of unimpaired gauging stations in the Southeastern U.S. and physically homogeneous regions delineated based on basin characteristics

Table 2: Mean and standard deviation of basin characteristics and the L-CV for regions delineated based on the L-CV

	A	S_{Ch}	S_B	Sh	E	Pr	Imp	F	SI	Inf	L-CV
						Region 1					
Mean	567	23.0	11.1	7.02	989	52.1	4.15	54.6	3.46	2.44	0.35
Stdev	1683	44.7	10.6	3.88	936	6.09	6.56	24.2	0.81	0.43	0.01
						Region 2					
Mean	686	25.8	13.6	8.15	1109	52.2	3.29	55.6	3.23	2.40	0.32
Stdev	1624	58.3	12.2	4.16	973	7.44	4.15	22.5	0.67	0.42	0.01
						Region 3					
Mean	131	73.2	9.59	5.39	796	50.1	3.39	47.1	3.55	2.41	0.54
Stdev	166	167	13.62	2.83	978	3.80	3.47	25.7	0.80	0.41	0.06
						Region 4					
Mean	244	29.2	6.74	7.97	549	50.4	3.06	46.7	3.57	2.49	0.45
Stdev	408	68.6	7.12	5.37	570	3.89	2.81	23.1	0.77	0.39	0.01
						Region 5					
Mean	487	51.7	10.0	7.00	840	51.1	3.68	50.2	3.61	2.49	0.40
Stdev	1116	133	11.3	5.15	918	4.83	5.48	23.5	0.90	0.47	0.01
						Region 6					
Mean	929	28.9	17.4	8.65	1302	54.8	3.07	61.2	3.11	2.37	0.26
Stdev	2318	62.8	13.0	4.67	1100	8.33	4.57	20.3	0.39	0.33	0.03

Fewer observations can be made based on the results in Table 3 for regions delineated based on watershed characteristics. Overall, there is very little difference between the delineated regions in terms of the basin characteristics basin shape (Sh), mean annual precipitation (Pr), average soil drainage index (SI), and average hydrologic soil index (Inf). Thus, these characteristics are not responsible for the clustering of sites. However, it is unclear which of the remaining characteristics governed the clustering. Simple two-sample t-tests performed on a pairwise basis suggest significant differences between the delineated regions in terms of the average values of the main channel slope (S_{Ch}), main basin length (S_B), percent impervious surface (Imp), and percent forest cover (F). The use of multivariate statistical techniques in future analyses should reveal more conclusive results.

Table 3: Mean and standard deviation of basin characteristics and the L-CV of regions delineated based on the watershed characteristics

	A	S_{Ch}	S_B	Sh	E	Pr	Imp	F	SI	Inf	L-CV
						Region 1					
Mean	353	5.03	5.22	8.53	139	50.7	0.96	50.6	3.70	2.56	0.35
Stdev	357	3.69	3.56	4.26	120	4.21	0.62	16.6	0.86	0.45	0.08
						Region 2					
Mean	1113	360	0.05	5.39	151	54.7	2.12	32.6	5.05	3.17	0.41
Stdev	1677	237	0.05	2.23	66.5	1.19	3.18	20.4	0.95	0.58	0.07
						Region 3					
Mean	671	31.3	22.8	8.41	1788	54.6	1.59	71.2	2.99	2.32	0.33
Stdev	2093	47.2	12.2	5.18	1038	8.85	1.69	15.4	0.22	0.28	0.08
						Region 4					
Mean	32.2	36.9	6.98	3.94	758	50.1	6.19	41.9	3.26	2.36	0.40
Stdev	151	35.8	5.08	1.84	417	4.19	6.08	22.3	0.50	0.34	0.10
						Region 5					
Mean	807	4.47	4.96	8.52	506	49.8	7.52	45.0	3.57	2.44	0.37
Stdev	1330	2.15	3.24	4.04	301	3.09	6.00	12.0	0.69	0.38	0.09
						Region 6					
Mean	869	33.0	9.70	6.56	943	52.9	0.00	18.5	3.33	2.40	0.38
Stdev	2380	101	12.5	2.51	840	6.08	0.00	33.6	0.94	0.58	0.09

Summary

The significance of this research lies in the fact that more accurate estimators of quantiles and the associated flood risk are needed at ungauged sites and sites with limited data. To this end, available data must be used more efficiently, and our understanding of the underlying relationships between basin characteristics and the flood regime must be improved. As a start in the movement to address this issue, this research will ultimately assess the value of using physical basin characteristics to delineate regions which are sufficiently statistically homogeneous for the transfer of information to data limited and ungauged sites.

Preliminary results indicate that basin characteristics such as the drainage area, main basin slope, and mean basin elevation tend to be inversely related to the magnitude of the L-CV. Thus, these basin characteristics may serve as appropriate attributes for use in delineating regions which are statistically homogeneous.

Admittedly, the results presented herein do not provide much insight as to how the basin characteristics differ among the statistically homogeneous regions. More definitive results are expected from future analyses using multivariate statistical methods such as cluster analysis, principal component analysis, and canonical correlation analysis as outlined in the Methodology section above.

Future work will also include an assessment of the impact on quantile estimates due to differences in region delineation resulting from the use of at-site flood statistics such as the L-CV for clustering versus physical basin characteristics. In addition, the same methodology will be applied to the U.S. portion of the Great Lakes basin in order to consider a wider range of geographic locales and potentially a wider variety of flood generating mechanisms (e.g., snowpack).

References

Burn, D. H. (1990). Evaluation of regional flood frequency analysis with a region of influence approach, *Water Resour. Res.*, 26(10), 2257-2265.

Burn, D. H. (1997). Catchment similarity for regional flood frequency analysis using seasonality measures, *J. of Hydrology*, 202, 212-230.

Burn, D. H., Z. Zrinji, and M. Kowalchuk (1997). Regionalization of catchments for regional flood frequency analysis, *J. of Hydrologic Engineering*, 2(2), 76-82.

Castellarin, A., D. H. Burn, and A. Brath (2001). Assessing the effectiveness of hydrological similarity measures for flood frequency analysis, *J. of Hydrology*, 241, 270-285.

Chiang, S. M., T. K. Tsay, and S. J. Nix (2002a). Hydrologic regionalization of watersheds, I. Methodology Development, *J. of Water Resour. Plan. and Manage.*, 128(1), 3-11.

Chiang, S. M., T. K. Tsay, and S. J. Nix (2002b). Hydrologic regionalization of watersheds, II. Applications, *J. of Water Resour. Plan. and Manage.*, 128(1), 12-20.

Dalrymple, T. (1960). Flood-frequency analyses, Water Supply Paper 1543-A, U. S. Geological Survey, Washington, D.C.

Eng, K., J. R. Stedinger, and A. M. Gruber (2007a). Regionalization of streamflow characteristics for the Gulf-Atlantic rolling plains using leverage-guided region-of-influence regression, World Environmental & Water Resources Conference - Restoring our Natural Habitat, K.C. Kabbes ed., Tampa, Florida, May 15-18, 2007.

Eng, K., P. C. D. Milly, and G. D. Tasker (2007b). Flood regionalization: A hybrid geographic and predictor-variable region-of-influence regression method, *J. of Hydrologic Engineering*, 12(6), 585-591.

Fovell, R. G. and M.-Y. C Fovell, 1993. Climate zones of the conterminous United States defined using cluster analysis. *Journal of Climate*, 11, 2103-2135.

Griffis, V. W. and J. R. Stedinger (2007). The use of GLS regression in regional hydrologic analyses, *J. of Hydrology*, 344, 82-95.

Groupe de Recherche en Hydrologie Statistique (GREHYS) (1996a). Presentation and review of some methods for regional flood frequency analysis, *J. of Hydrology*, 186, 63-84.

Groupe de Recherche en Hydrologie Statistique (GREHYS) (1996b). Inter-comparison of regional flood frequency procedures for Canadian rivers, *J. of Hydrology*, 186, 85-103.

Gruber, A. M. and J. R. Stedinger, Models of LP3 regional skew, data selection, and Bayesian GLS regression, World Environmental & Water Resources Conference 2008 AHUPUA'A, paper 596, R. Babcock and R. Walton (eds.), Amer. Soc. of Civil Engineers, Hawaii, May 12-16, 2008.

Gupta, V. K., O. J. Mesa, and D. R. Dawdy (1994). Multiscaling theory of flood peaks: Regional quantile analysis, *Water Resour. Res.*, 30(12), 3405-3421.

Hosking, J. R. M. and J. R. Wallis (1988). The effect of intersite dependence on regional flood frequency analysis, *Water Resour. Res.*, 24(4), 588-600.

Hosking, J. R. M. and J. R. Wallis (1997). Regional Frequency Analysis: An Approach Based on L-Moments, Cambridge University Press, New York, New York, 224 pp.

Isik, S. and V. P. Singh (2008). Hydrologic regionalization of watersheds in Turkey, *J. of Hydrologic Engineering*, 13(9), 824-834.

Johnson, R. A. and D. W. Wichern, 2002. *Applied Multivariate Statistical Analysis*. 5th Edition, Prentice Hall, Upper Saddle River, NJ, 767 pp.

Kjeldsen, T. R., and D. Rosbjerg (2002). Comparison of regional index flood estimation procedures based on the extreme value type I distribution, *Stochastic Environmental Research and Risk Assessment*, 16, 358-373.

Madsen, H. and D. Rosbjerg (1997). Generalized least squares and empirical Bayes estimation in regional partial duration series index-flood modeling, *Water Resour. Res.*, 33(4), 771-782.

National Research Council (1988). Estimating Probabilities of Extreme Floods, National Academy Press, Washington, D.C., 141 pp.

Potter, K. W. (1987). Research on flood frequency analysis: 1983-1986, *U.S. Natl. Rep. Int. Union Geod. Geophys*, 25(2), 113-118.

Slack, J. R., A. M. Lumb, and J. M. Landwehr (1993). Hydro-Climactic Data Network (HCDN), Water-Resource Investigations Report 93-4076, USGS, Washington, D.C.

Stedinger, J. R. and L. Lu (1995). Appraisal of regional and index flood quantile estimators, *Stochastic Hydrology and Hydraulics*, 9(1), 49-75.

Tasker, G. D. and J. R. Stedinger (1989). An operational GLS model for hydrologic regression, *J. of Hydrology*, 111, 361-375.

Tasker, G. D., S. A. Hodge, and C. S. Barks (1996). Region of influence regression for estimating the 50-year flood at ungauged sites, *Water Resour. Bulletin*, 32(1), 163-170.

Zrinji, Z. and D. H. Burn (1994). Flood frequency analysis for ungauged sites using a region of influence approach, *J. of Hydrology*, 153, 1-21.

Reducing Uncertainty of Continuous Streamflow Predictions in Ungauged Basins (PUB) using Regional Constraints: Using regional constraints for PUB

T. Wagener

Department of Civil and Environmental Engineering, The Pennsylvania State University, Sackett Building, University Park, PA16801, USA; PH (814) 865-5673; FAX (814) 863-7304; email: tuw4@psu.edu

ABSTRACT

Our environment is changing rapidly in many regions of the world, with often-significant implications for current and future water resources. Disturbances to the current environmental system include land cover change, and the increasing impacts of a changing climate. The potential of developing successful strategies to respond to these changes lies in our capacity to anticipate their impact. One important question in this context is the potential change to streamflow characteristics at the watershed scale. However, most watersheds in the US and elsewhere are ungauged, leading to large uncertainty in our hydrological predictions to establish benchmarks, which are often the basis for the development of water resources management strategies. How can we obtain a reliable and continuous spatio-temporal picture of regional environmental status, trends and long-term projections to identify information gaps – and thus monitoring needs – and likely hot spots and hot moments where for example critical ecosystem thresholds are exceeded or will be exceeded in the future? This paper presents a methodology to formalize regional information on streamflow characteristics using a Mixture of Gaussians approach, which provides constraints on continuous watershed simulations. US examples show how this approach leads to reduced uncertainty in continuous streamflow predictions for water management in ungauged basins and in terms of potential change impacts.

INTRODUCTION

"*The United States is facing unprecedented environmental changes, but decision makers do not have the information they need to understand and respond to these changes in a timely fashion*" (Heinz Center, 2008; see also The White House, 2008). Stresses to the environment include land cover change (DeWalle et al., 2000; Poff et al., 2006a;b), and the increasing impacts of changing climate (U.S. Climate Change Science Program, 2008). The potential of developing successful strategies to deal with these changes lies in our capacity to anticipate their impact (Clark et al., 2001; U.S. Government Accountability Office, 2007). Watersheds collect, store and release incoming precipitation and thus provide important freshwater (watershed)

services for aquatic ecosystems and for people (Wagener et al., 2008; see also Brauman et al., 2007). Headwaters (Poff et al., 2006a;b) are increasingly recognized for their importance in controlling ecological and water quality functions throughout river basins (Lowe and Likens, 2005). Headwaters contain over 50% of the total strength length in the US – excluding Alaska (Nadeau and Rains, 2007), and a much higher percentage in certain regions, for example in most of the Eastern US. They are however severely under-represented in operational gauging (Freeman et al., 2007), where nearly 95% of smaller streams are poorly characterized with less than 3% of all gauges (Poff et al., 2006a;b). At the same time, processes and ecosystem habitats in headwaters are particularly sensitive to atmospheric and terrestrial disturbances (Buttle and Meatcalf, 2000). The National Research Council (NRC, 2004) stresses that the lack of gauges in small streams requires research into better modeling tools for streamflow simulations across hydroclimatic and geologic settings. "… *for the majority of streams that support aquatic life, a systematic understanding is lacking on water quality, habitat, biota, specific discharge*, …" (Bishop et al., 2008). How can we obtain a continuous spatio-temporal picture of regional environmental status, trends and long-term projections? Since "… *protecting the long-term ecological integrity and ecosystem services of natural systems, whether aquatic or terrestrial, cannot succeed without a foundation of intact and functional headwaters*" (Lowe and Likens, 2005). The maintenance of these services will require significant advances in our understanding and in our ability to predict natural system response patterns and their controls (Palmer et al., 2004). We need to address the "… *increasingly evident need for regional-scale interdisciplinary investigations that integrate observations, data and information systems, process studies, and models with the process detail and spatial resolution necessary to advance scientific understanding of ecosystem processes and the impacts of multiple interlinked environmental stresses*" (NCAR, 2002).

Models of watershed hydrology are the tools used to quantify our state of knowledge about the underlying system and to predict future watershed behavior. The unavoidable uncertainty present provides an indicator of the state of our science (Beven, 2006), and quantifies our degree of confidence for decision-making (Reckhow, 1994). In gauged watersheds, conditioning the model on available observations of the response variable can reduce uncertainty. In ungauged watersheds, model application has so far meant reducing the uncertainty on *a priori* parameter estimates (Atkinson et al., 2003; Koren et al., 2003) or on regionalized parameter sets (Lamb, 2000; Bloeschl, 2005). Both approaches still result in significant uncertainties (McIntyre et al., 2005) and are ultimately limited by our current lack of ability to observe bulk hydraulic properties of the environment at the model element scale (Wagener and Wheater, 2006; Beven, 2001), even if the model is physically-based (Parkin et al., 1996). "*Given the increasingly widespread usage of watershed models for solving environmental problems, the regionalization of watershed models may be one of the most challenging and fundamental problems within the entire field of hydrology*" (Vogel, 2006). However, current streamflow predictions are uncertain if local observations of the watershed response are not available for model calibration (Sivapalan et al., 2003), as is the case for most headwater streams (Freeman et al., 2007), a situation that is even worse in the global

context where existing monitoring networks are declining (Stockstad, 1999). Thus significantly limiting the possible assessment of conditions and trends in ecosystem services (e.g. Millennium Ecosystem Assessment (MEA, 2005)), and for water resources applications especially in those regions of the world where resources for hazard mitigation and adaptation are extremely poor (GRDC, 2004; Widen-Nillson et al., 2007). Advancement in this area is most likely to come from the synthesis of state-of-the-art observations, models and theory (Kirchner, 2006; Bloeschl, 2006).

Our ability to predict the hydrologic response behavior of watersheds is crucial for operational applications such as flood and drought prediction, and it is evidence of our degree of understanding (or lack thereof) of hydrologic systems. In this paper we discuss a new approach to derive continuous ensemble predictions in ungauged basins. Watersheds form a landscape element (at various scales) that integrates all aspects of the hydrological cycle within a defined area that can be studied, quantified and acted upon. The hydrologic response (e.g. streamflow) is depending on the functions that a specific watershed exerts on the precipitation it collects. Those functions include the partitioning of water into different pathways at the land surface, the storage of water (in fluid or solid form) in different stores with different residence times, and the release of water through different pathways for example as streamflow or evaporation (Wagener et al., 2007). The watershed also transmits water between hillslopes, the riparian zone and the river network; and it acts as a conveyance system for mass and energy (Brutsaert, 2005). These functional characteristics of watershed are reflected in the observed response behavior, i.e. the response provides a signature of the specific functional behavior of a watershed. Being able to link functional behavior and signatures, and being able to predict the functional behavior based on knowledge of physical watershed characteristics and the regional climatic regime would provide a significant advancement to the current state of hydrologic science. Winter (2001) for example suggests that *"... areas having similar land slopes, surficial geology, and climate will result in similar hydrologic flow paths regardless of the geographic location of the site"*. Such behavioral characteristics or signatures typically include characteristics of streamflow, but could also be extended to evaporation, groundwater dynamics, soil moisture dynamics, snow cover, distributions of residence time and water age, isotopic composition, concentrations of chemicals such as chloride and nitrate (Sivapalan 2005). In this paper we discuss how such regional relationships can be established and used in an optimization framework to reduce the uncertainty in predictions in ungauged basins. We close with a brief discussion of how such a prediction in ungauged basins (PUB) framework can be linked with the concept of watershed services to explicitly address water resource management issues.

CONDITIONING WATERSHED MODELS ON REGIONAL CONSTRAINTS

As identified above, a problem common to all watershed models is that they require some degree of parameter calibration to achieve reliable predictions, i.e. a process in which the model parameters are adjusted (manually or automatically) until observed and simulated watershed responses match as closely as possible. This calibration step is by definition not possible if the watershed is ungauged or went through significant

changes, e.g. land use. As discussed, two main approaches have been used to compensate this lack of calibration – estimation of parameters directly from local physical characteristics or through regional equations. Reducing the uncertainty on predictions in ungauged basins from which both approaches suffer is a current focal point of the hydrologic community (Sivapalan et al., 2003).

An alternative to the derivation of *a priori* model parameter estimates from physical watershed characteristics lies in the regionalization of streamflow signatures. Prior studies have found that the correlation between streamflow signatures and physical watershed characteristics is often significantly higher than between model parameters and watershed characteristics (e.g. Poff et al., 2006a;b; Yadav et al., 2007). Although the correlation between streamflow and watershed characteristics does not directly provide predictions of the continuous streamflow hydrograph, regionalized flow signatures provide dynamic aspects of the watershed system that can be used to constrain hydrologic model predictions, even if they are only known with some degree of uncertainty. Yadav et al. (2007) revised the regionalization of flow characteristics by including estimates of uncertainty in the regression equations. Uncertainty ranges, in addition to the expected values of flow characteristics, are valuable sources of information for constraining a model and thus for creating ensemble predictions at ungauged locations. Yadav et al. (2007) showed in a pilot study using 30 UK watersheds how this regionalized information can be used to constrain ensemble predictions of any model at ungauged sites. Dominant controlling characteristics were found to be climate (wetness index), topography (slope), and hydrogeology. Main streamflow signatures were high pulse count (defined as how many times the flow exceeded three-times the mean flow per year), runoff ratio (the long term ratio of streamflow to precipitation), and the slope of the flow duration curve (between the 33rd and 66th percentiles). Streamflow ensembles from *a priori* (unconstrained) feasible parameter sets produced very uncertain predictions at ungauged locations. This uncertainty was significantly reduced when ensemble members that conflicted with the regionalized flow signatures (i.e. the constraints) were rejected. The work of Yadav et al. (2008) provides an avenue to assimilate regional information to reduce the uncertainty in continuous predictions of streamflow at ungauged locations, and could possibly be used to assess the impact of change (Wagener, 2007).

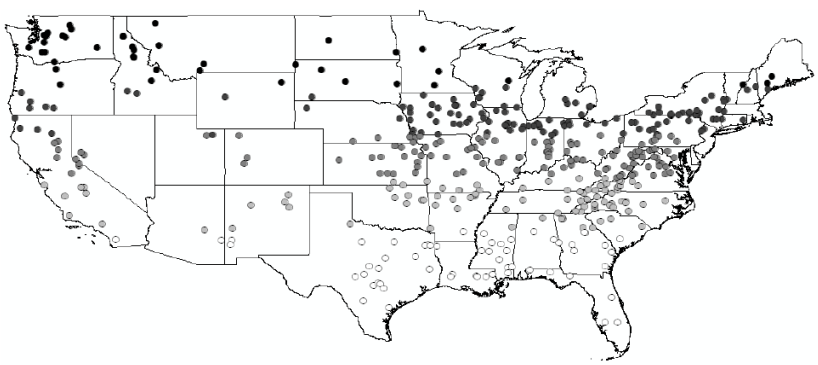

Figure 1. Over 400 watersheds with daily hydro-meteorological data were used to derive the joint PDF shown in Figure 2.

Recently, we started working on replacing the regression based definition of regional constraints with a Mixtures of Gaussian approach (Wojcik et al., 2006). Gaussian Mixture Models (GMMs) are linear combinations of Gaussian densities and provide a nonparametric approach to deriving PDFs. Combared to regression analysis, GMMs do not require potentially restrictive assumptions about the PDF underlying the data (e.g. Gaussian). Rather, they can approximate any continuous density to any precision while adapting even to complex geometries (McLachlan and Peel, 2000). A preliminary result of this approach to derive regional PDFs is shown in Figure 2.

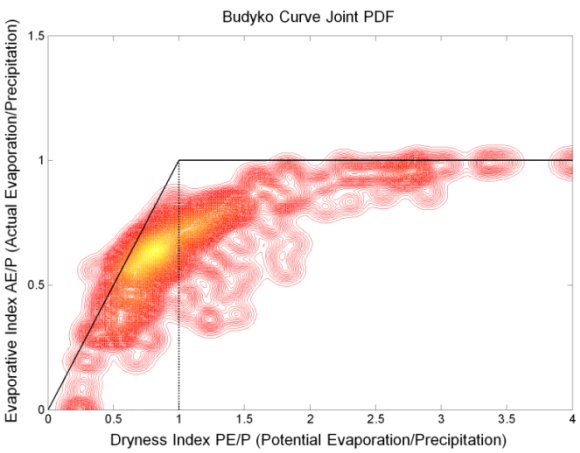

Figure 2. Preliminary result showing a joint probability density function (PDF) of evaporative and dryness indices derived using Mixtures of Gaussians. This graph is often referred to as Budyko curve (Budyko, 1974). The PDF is based on an analysis of over 400 watersheds distributed across the US (MOPEX database). Conditional PDFs of the evaporative index in ungauged watersheds can be derived from knowledge of long-term precipitation and potential evaporation of the specific location. Knowledge of the evaporative index provides an estimate of the expected long-term runoff ratio (a signature) of the ungauged location, and thus a constraint on the watershed yield.

However, the search for parameter sets providing simulations that fall within the regional behavioral signature space has proven to be very cumbersome in many cases (Zhang et al., 2008). At the same time, there have been decades of research into developing powerful global optimization algorithms (Wagener and Gupta, 2005) that, as yet, are unused in ungauged circumstances. Zhang et al. (2008) recently suggested a solution to this problem by introducing a novel multiobjective framework for identifying behavioral parameter ensembles for ungauged basins using suites of regionalized hydrologic signatures, i.e. constraints (Figure 3). The new formulation enables, for the first time, the use of multiobjective optimization algorithms for the identification of model ensembles (i.e. parameter sets within a selected model structure) for predictions in ungauged basins. In this approach, the behavioral signature space is assumed to be spherical. The objective is to find solutions (i.e. parameter sets that produce signatures consistent with the constraints) that fill the sphere, since all solutions on the inside are considered equally likely (in this

formulation). A trade-off is created by defining objective functions that search for solutions close to the centre of the sphere and close to the edge. Application of the new formulation to the 30 watersheds of Yadav et al. (2007) in a three constraints problem, and a comparison of the results with the previously used Monte Carlo approach demonstrated that the new formulation significantly advances our ability to reduce the uncertainty of PUB. The high efficiency and robustness of the ε-NSGAII (the multiobjective Genetic Algorithm used in their study, for details see Tang et al., 2006) in finding behavioral parameter sets indicates that (1) more complex (incl. distributed) hydrologic model decision spaces can be searched using the multi-objective PUB framework presented in this study, and (2) an increasing number of hydrologic indices can be tested for constraining ensemble predictions for ungauged basins. Zhang et al. (2008) demonstrate that PUB can be viewed as a new class of multiobjective search problems. Reformulating the PUB problem as a multiobjective search for behavioral model parameter sets, generalizes our ability to test a wide range and number of hydrologic signatures to maximize our use of the information available in streamflow datasets. The PUB problem formulation contributed in their study can be easily adapted to solve larger, more computationally demanding model identification problems. This will have particular value for future studies seeking to develop high fidelity, probabilistic scenarios for environmental change under uncertainty (Wagener, 2007).

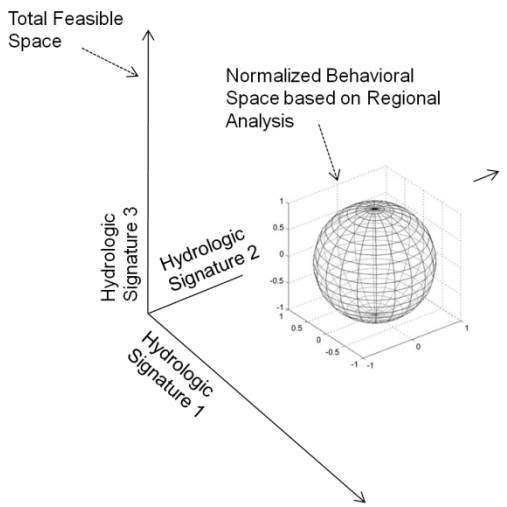

Figure 3. Conceptual representation of a three constraint (signature) search space including the behavioral solutions' sphere as defined by Zhang et al. (2008).

CONCLUSIONS AND OUTLOOK

In conclusion, it is important to look towards how this discussion on PUB can ultimately advance our ability to better use models in support of water management for water security of humans and ecosystems from water scarcity or excess. While hydrologic signatures describe hydrologically relevant characteristics of the watershed response, it is crucial to explicitly include the implication of the values of

different streamflow characteristics for humans and ecosystems. Such an inclusion would explicitly define the societal relevance of watershed behavior. We can distinguish positive and negative implications of watershed functions for humans and ecosystems. Benefits received by humans supplied by resources and processes of natural ecosystems have become known as ecosystem services (e.g. Daily, 1997). Here, we are concerned with the positive impacts or benefits received by nature (ecosystems) and humans from resources and processes supplied by watersheds, and will therefore refer to these as ***watershed services*** (Wagener et al., 2008). The PUB approach discussed, based on physical characteristics, climatic characteristics and signatures, can provide significant advances to our ability to predict the continuous streamflow response of ungauged basins. These ensembles predictions subsequently enable us to extract any (streamflow related) indicator that relates to watershed services (or disservices) provided to humans or ecosystems.

ACKNOWLEDGEMENTS

Partial support for this work was provided by the National Science Foundation under grant EAR-0635998. Any opinions, findings, and conclusions or recommendations expressed in this paper are those of the authors and do not necessarily reflect the views of the National Science Foundation.

REFERENCES

Atkinson, S., Sivapalan, M., Viney, N.R. and Woods, R.A. (2003). Physical controls of space-time variability of hourly streamflows and the role of climate seasonality: Mahurangi catchment, New Zealand. *Hydrological Processes*, 17, 2171-2193, doi: 10.1002/hyp.1327.

Beven K. (2001). How far can we go in distributed hydrological modeling? *Hydrology and Earth System Sciences*, 5, 1-12.

Beven, K. (2006). On undermining the science? *Hydrological Processes*, 20(14), 3141-3146.

Bishop, K., Buffam, I., Erlandsson, M., Foelster, J., Laudon, H., Seibert, J. and Temnerud, J. 2008. Aqua Incognita: the unknown headwaters. *Hydrological Processes*, 22, 1239-1242.

Bloeschl G. (2005). Rainfall-runoff modelling of ungauged catchments. Article 133 in: *Encyclopedia of Hydrological Sciences*, M. G. Anderson (Managing Editor), J. Wiley & Sons, Chichester, 2061-2080.

Bloeschl G. (2006). Hydrologic synthesis: across processes, places, and scales. *Water Resources Research*, 42, W03S02 Doi:10·1029/2005WR-004319.

Brauman, K.A., Daily, G.C., Duarte, K. and Mooney, H.A. (2007). The nature and value of ecosystem services: An overview highlighting hydrologic services. *Annual Review of Environment and Resources*, 32, 67-98. doi:10.1146/ annurev.energy. 32.031306.102758

Brutsaert, W. (2005). *Hydrology – An Introduction*. Cambridge University Press, Cambridge, UK.

Buttle, J.M. and Meatcalfe, R.A. (2000). Boreal forest disturbance and streamflow response, northeastern Ontario. *Canadian Journal of Fisheries and Aquatic Sciences*, 57, 5-18.

Budyko, M.I. (1974). *Climate and Life*. Academic Press (Translated by Miller D.H.).

Clark, J.S. et al. (2001). Ecological forecasts: An emerging paradigm. *Science*, 293, 657-660.

Daily, G.C. (1997). *Nature's services: Societal dependence on natural ecosystems*. Island Press, Washington. 392pp.

DeWalle DR, Swistock BR, Johnson TE, and McGuire KJ. (2000). Potential effects of climate change and urbanization on mean annual streamflow in the United States. *Water Resources Research* 36: 2655–2664, 10·1029/2000WR900134.

Freeman, M.C., Pringle, C.M. abd Jackson, C.R. (2007). Hydrologic connectivity and the contribution of stream headwaters to ecological integrity at regional scales. *Journal of the American Water Resources Association*, 43(1), 5-14.

Global Runoff Data Centre (GRDC) (2004). Long term mean annual freshwater surface water fluxes into the world oceans. – Comparison of GRDC freshwater flux estimate with the literature. http://grdc.bafg.de/servlet/is/7083/, Accessed June 2007.

Heinz Center (2008). *Environmental information: A road map to the future*. Heinz Center Report, Washington D.C.

Jones, D.A. and Kay, A.L. (2007). Uncertainty analysis for estimating flood frequencies for ungauged catchments using rainfall-runoff models. *Advances in Water Resources*, 30, 1190-1204.

Kirchner, J.W. (2006). Getting the right answers for the right reasons: Linking measurements, analyses, and models to advance the science of hydrology. *Water Resources Research* 42: W03S04 Doi:10·1029/2005WR004362.

Koren, V., Smith, M. and Duan, Q. (2003). Use of *a priori* parameter estimates in the derivation of spatially consistent parameter sets of rainfall–runoff models. In Duan, Q., Sorooshian, S., Gupta, H., Rosseau, H. and Turcotte, H. (eds.). *Calibration of Watershed Models*. Water Science and Applications 6, AGU, 239–254.

Lamb, R. (2000). An approach to the calibration of a conceptual rainfall-runoff model for flood frequency estimation by continuous simulation. *Water Resources Research*, 35, 3103-3114.

Lowe, W.H. and Likens, G.E. (2005). Moving headwater streams to the head of the class. *Bioscience*, 55(3), 196-197.

McIntyre, N., Lee, H., Wheater, H.S., Young, A. and Wagener, T. (2005). Ensemble prediction of runoff in ungauged watersheds. *Water Resources Research*, 41, W12434, doi: 10.1029/2005WR004289.

McLachlan, G. and Peel, D.A. (2000). *Finite mixture models*. Wiley Interscience, New York, NY, US.

Millennium Ecosystem Assessment (MEA) (2005). *Ecosystems and Human Well-being: Synthesis*. Island Press, Washington, DC.

Nadeau, T.-L. and Rains, M.C. 2007. Hydrological connectivity between headwater streams and downstream waters: How science can inform policy. *Journal of the*

American Water Resources Association, 43, doi: 10.1111/j.1752-1688.2007.00010.x.

NCAR (2002). *Cyberinfrastructure for Environmental Research and Education*. Report from a workshop held at the National Center for Atmospheric Research October 30 - November 1, 2002.

NRC (National Research Council) 2004. *Assessing the national streamflow information program*. National Academy Press, Washington, D.C.

Palmer, E. et al. (2004). Ecology for a crowded planet. *Science*, 304, 1251-1252.

Parkin, G., O'Donnell, G., Ewen, J., Bathurst, J.C., O'Connell, P.E. and Lavabre, J. (1996). Validation of catchment models for predicting land-use and climate change impacts. 1. Case study for a Mediterranean catchment. *Journal of Hydrology*, 175: 595-613.

Poff, N.L., B.D. Bledsoe, and C.O. Cuhaciyan (2006a), Hydrologic variation with land use across the contiguous United States: geomorphic and ecological consequences for stream ecosystems, *Geomorphology*, 79, 264-285.

Poff, N.L., J.D. Olden, D.M. Pepin and B.P. Bledsoe. (2006b), Placing global stream flow variability in geographic and geomorphic contexts, *River Res. Applications*, 22(2), 149-166.

Reckhow, K.H. (1994). Importance of scientific uncertainty in decision-making. *Environmental Management*, 18, 161-166.

Sivapalan, M. (2005). Pattern, Process and Function: Elements of a Unified Theory of Hydrology at the Watershed Scale. In *Encyclopedia of Hydrological Sciences* Part 1. Theory, Organization and Scale. Copyright © 2005 John Wiley & Sons, Ltd DOI: 10.1002/0470848944.hsa012.

Sivapalan, M., K. Takeuchi, S.W. Franks, V.K. Gupta, H. Karambiri, V. Lakshmi, et al. (2003), IAHS decade on predictions in ungauged basins (PUB), 2003-2012: shaping an exciting future for the hydrological sciences, *Hydrol. Sci. J.*, 48(6), 857–80.

Sivapalan, M., Takeuchi, K., Franks, S.W., Gupta, V.K., Karambiri, H., Lakshmi, V., X. Liang, J. J. McDonnell, E. M. Mendiondo, P. E. O'Connell, T. Oki, J. W. Pomeroy, D. Schertzer, S. Uhlenbrook, and E. Zehe (2003). IAHS Decade on Predictions in Ungauged Basins (PUB), 2003-2012: Shaping an exciting future for the hydrological sciences. *Hydrological Sciences Journal*, 48(6), 857-880.

Smakhtin, V. (2007). Environmental flows: a call for hydrology. *Hydrological Processes*, 21, 701-703.

Stockstad, E. (1999). Scarcity of rain, stream gages threatens forecasts. *Science*, 285, 1199-1200. Doi: 10.1126/science.285.5431.1199

Tang, Y., Reed, P.M. and Wagener, T. (2006), How effective and efficient are multiobjective evolutionary algorithms at hydrologic model calibration? *Hydrology and Earth System Science*, 10, 289-307.

The White House 2008. www.whitehouse.gov/ceq/NEST-Indicators-Letter.pdf (Accessed July 2008)

U.S. Climate Change Science Program (2008). *Scientific assessment of the effects of global change on the United States*. A Report of the Committee on Environmental and Natural Resources National Science and Technology Council, U.S. Climate Change Science Program, Washington, DC.

U.S. Government Accountability Office (2007). *Climate change: Agencies should develop guidance for addressing the effects on federal land and water resources*. GAO-07-863.

Vogel, R.M. (2006). Regional calibration of watershed models. In Singh, V.P. and Frevert, D.K. (eds.) *Watershed models*. CRC Press, 549-567.

Wagener, T. (2007). Can we model the hydrologic impacts of environmental change? *Hydrological Processes*, 21(23), 3233-3236.

Wagener, T. and Gupta, H.V. (2005). Model identification for hydrological forecasting under uncertainty. *Stochastic Environmental Research and Risk Assessment*, 19(6), 378-387. doi: 10.1007/s00477-005-0006-5.

Wagener, T. and Wheater, H.S. (2006). Parameter estimation and regionalization for continuous rainfall-runoff models including uncertainty. *Journal of Hydrology*, 320(1-2), 132-154.

Wagener, T. and Wheater, H.S. (2006). Parameter estimation and regionalization for continuous rainfall-runoff models including uncertainty. *Journal of Hydrology*, 320(1-2), 132-154.

Wagener, T., Sivapalan, M. and McGlynn, B.M. (2008). Catchment classification and services – Towards a new paradigm for catchment hydrology driven by societal needs. In Anderson, M. (ed.) *Encyclopedia of Hydrological Sciences*, John Wiley and Sons, Chichester, UK.

Wagener, T., Sivapalan, M., Troch, P. and Woods, R. (2007). Catchment classification and hydrologic similarity. *Geography Compass*, 1(4), 901, doi:10.1111/j.1749-8198.2007.00039.x.

Weiskel, P.K., Vogel, R.M., Steeves, P.A., Zarriello, P.J., DeSimone, L.A. and Ries III, K.G. (2007). Water use regimes: Characterizing direct human interaction with hydrologic systems. *Water Resources Research*, 43, W04402, doi:10.1029/2006WR005062.

Widen-Nilsson, E., Halldin, S. and Xu, C.-Y. (2007). Global water-balance modelling with WASMOD-M: Parameter estimation and regionalization. *Journal of Hydrology*, 340, 105-118.

Winter, T.C. (2001). The concept of hydrologic landscapes. *Journal of the American Water Resources Association*, 37, 335–349.

Wojcik, R., Troch, P.A., Stricker, H. and Torfs, P. (2006). Mixtures of Gaussians for Uncertainty Description in Bivariate Latent Heat Flux Proxies. *Journal of Hydrometeorology*. 7, 330-345.

Yadav, M., Wagener, T. and Gupta, H.V. (2007). Regionalization of constraints on expected watershed response behavior for improved predictions in ungauged basins. *Advances in Water Resources*, 30(8), 1756-1774. doi:10.1016/j.advwatres.2007.01.005.

Yilmaz, K.K. (2007). *Towards improved modeling for hydrologic predictions in poorly gauged basins*. PhD Dissertation, Department of Hydrology and Water Resources, University of Arizona, USA.

Zhang, Z., Wagener, T., Reed, P. and Bushan, R. (2008). Ensemble streamflow predictions in ungauged basins combining hydrologic indices regionalization and multiobjective optimization. *Water Resources Research*, 44, W00B04, doi:10.1029/2008WR006833.

San Joaquin River Restoration Program Monitoring and Management Plans

J. Payne[1] and D. Mooney[2]

[1]MWH Americas, 3321Power Inn Road, Sacramento, CA 95826; PH (916) 924.8844; email: Jeffrey.T.Payne@mwhglobal.com
[2]Bureau of Reclamation, U.S. Department of the Interior, 2800 Cottage Way (MP-170), Sacramento, CA 95825; PH (916) 978.5458; email: dmooney@mp.usbr.gov

ABSTRACT

The San Joaquin River is a prominent and important feature of California's Central Valley. Historically, spring runoff from Sierra streams would spread over a valley floor covered by marshes and seasonal wetlands. In 1942, Reclamation completed construction of Friant Dam, ceasing flow to some portions of the river and ultimately led to the extirpation of salmon runs in the San Joaquin. In 1988, a coalition of environmental groups challenged renewal of long-term water service contracts to the CVP Friant Division contractors. On September 13, 2006, after more than 18 years of litigation, all litigants signed onto a Stipulation of Settlement.

A significant challenge to the implementation of the Settlement will be creating an adaptive management plan for a river which has not provided a connected ecosystem in over fifty years. The monitoring plan discussed in this paper is being developed to assist in the adaptive management of the Settlement.

INTRODUCTION

The San Joaquin River is a prominent and important feature of California's Central Valley. Originating in Sierra Nevada Mountains, the San Joaquin conveys high mountain snowmelt to the valley floor before turning north and becoming the second largest river in California and the backbone of a multiple-river system draining the southern half of the Central Valley. The river's water feeds the Sacramento-San Joaquin Delta and ultimately flows to the Pacific Ocean under the Golden Gate Bridge in San Francisco Bay.

Historically, spring runoff from Sierra streams would spread over a valley floor covered by marshes and seasonal wetlands. These marshes would slowly drain to the Delta, providing rich habitat that supported numerous aquatic and wildlife species, including Chinook salmon. Over the past two centuries, water resource development has dramatically transformed the San Joaquin River. In the late 1880s, the valley lowlands were drained for agriculture, and a series of diversion dams and canals was constructed to support small farms. Over time, hydroelectric development harnessed power in upper portions of the San Joaquin watershed, further modifying the river.

In 1942, Reclamation completed construction of Friant Dam, thereby diverting a substantial amount of the San Joaquin River for agriculture. Today, over 1

million acres of highly productive farmlands along the eastern portion of the San Joaquin Valley rely upon Friant Dam for irrigation. Operation of the dam ceased flow to some portions of the river and ultimately led to the extirpation of salmon runs in the San Joaquin River above its confluence with the Merced River.

OVERVIEW OF THE SETTLEMENT

In 1988, a coalition of environmental groups led by the Natural Resources Defense Council (NRDC), filed a lawsuit challenging the renewal of long-term water service contracts between the United States and the Central Valley Project (CVP) Friant Division contractors, *NRDC et al. v. Kirk Rodgers et al*. On September 13, 2006, after more than 18 years of litigation, NRDC, Friant Water Users Authority (FWUA), and the U.S. Departments of the Interior and Commerce agreed on terms and conditions for a Stipulation of Settlement which was subsequently approved by the U.S. Eastern District Court of California (Court) on October 23, 2006. The Settlement establishes two goals:

- **Restoration Goal –** To restore and maintain fish populations in "good condition" in the mainstem San Joaquin River below Friant Dam to the confluence of the Merced River, including naturally reproducing and self-sustaining populations of salmon and other fish.
- **Water Management Goal –** To reduce or avoid adverse water supply impacts on all of the Friant Division long-term contractors that may result from the Interim Flows and Restoration Flows provided for in the Settlement.

To achieve the Restoration Goal, the Settlement establishes releases of water from Friant Dam and flow targets to the confluence of the Merced River. Additionally, the Settlement calls for a combination of channel and structural modifications along the San Joaquin River below Friant Dam and the reintroduction of Chinook salmon.

To achieve the Restoration Goal, the Settlement establishes releases of water from Friant Dam and flow targets to the confluence of the Merced River. Additionally, the Settlement calls for a combination of channel and structural modifications along the San Joaquin River below Friant Dam and the reintroduction of Chinook salmon.

The activities undertaken to implement the Water Management Goal revolve around water supply arrangements and strategies, and thus fall outside the scope of this paper.

THE SAN JOAQUIN RIVER RESTORATION PROGRAM

The San Joaquin River Restoration Program, SJRRP consists of a multi-agency interdisciplinary team with a co-located office in Sacramento, CA. State and Federal agencies, led by the U.S. Bureau of Reclamation (Reclamation) formed the SJRRP to implement the Stipulation of Settlement. Implementing Agencies are Reclamation, U.S. Fish and Wildlife Service (USFWS), National Marine Fisheries Service (NMFS), California Department of Water Resources (DWR), California Department of Fish and Game (DFG), and California Environmental Protection Agency (CalEPA).

The Settlement includes a detailed timeline for developing and implementing SJRRP actions, as shown Table 1-1.

Table 1-1. Key Settlement and SJRRP Milestones.

Date	Milestone
September 2009	Complete program-level NEPA, NHPA, ESA, CEQA reviews
October 2009	Initiate Interim Flows and Monitoring Program
September 2010	USFWS submits a completed permit application to NMFS for reintroduction of spring-run Chinook salmon
April 2012	NMFS issues a decision on the permit application for reintroduction of spring-run Chinook salmon
December 2012	Reintroduce spring-run and fall-run Chinook salmon
December 2013	Complete Phase 1 improvements Secretary of the Interior, in consultation with the Settling Parties, develops operational guidelines
January 2014	Initiate full Restoration Flows
December 2016	Complete Phase 2 improvements
December 2024	Secretary of Commerce reports to Congress on the progress made in reintroducing spring-run and fall-run Chinook and discusses plans for future implementation of the Settlement
December 2025	Review and revise Restoration Flows, if necessary
January – July 2026	Any party to the Settlement may file a motion to request an increase, decrease, or material change in the quantity and/or timing of the Restoration Flows

Key:
CEQA = California Environmental Quality Act
ESA = Federal Endangered Species Act
NEPA = National Environmental Policy Act
NHPA = National Historic Preservation Act
NMFS = National Marine Fisheries Services
USFWS = U.S. Fish and Wildlife Service

Federal Role in Implementing Settlement

The Settlement identifies the Department of the Interior, through Reclamation, as the lead Federal agency responsible for implementation and the lead National Environmental Policy Act (NEPA) agency in preparing a Program Environmental Impact Statement / Report (PEIS/R). USFWS is the lead Federal agency responsible for reintroduction of spring-run and fall-run Chinook salmon. The Settlement also identifies the Secretary of the U.S. Department of Commerce, through NMFS, as a necessary participant for the reintroduction of spring-run Chinook salmon. Implementation will require federal authorization from the U.S. Congress.

State Role in Implementing Settlement

The Settlement also calls for participation by the State of California (State) through the Natural Resources Agency's DWR and DFG, and through CalEPA. DWR will assist in the Settlement identified physical improvements including flood protection, levee relocation, and modifications to and maintenance of channel facilities. DFG will provide technical assistance on the release of flows and the reintroduction and monitoring of fish, and planning, designing, and constructing facilities to provide fish passage. DWR is the lead California Environmental Quality Act (CEQA) agency in preparing a PEIS/R.

PURPOSE, NEED AND OBJECTIVES OF THE SJRRP

The purpose of the SJRPP is to implement the Settlement. The need for action is to establish changes to the operation of Friant Dam to support achievement of the Restoration Goal, while reducing or avoiding adverse impacts to water deliveries to the Friant Division long-term contractors. The Implementing Agencies identified several objectives that need to be met to successfully achieve the purpose of the SJRRP, including: Release Interim and Restoration flows from Friant Dam, Implementation of channel and structure modifications, Reintroduciton of spring-run and fall-run Chinook salmon, and Development and implementation of monitoring and management plans to incorporate adaptive management into implementation of the Settlement.

Geography of the SJRRP

Much of the restoration effort focuses on a 150-mile reach of the San Joaquin River between Friant Dam and its confluence with the Merced River. This stretch defines the SJRRP's Restoration Area. A significant challenge to the Restoration effort will be redesigning the existing Restoration Area, which contains several physically and operationally distinct reaches, into something which provides a naturally self-sustaining population of salmon. Figure 1 and the following descriptions provide context for the fragmented state of the Restoration Area, today.

Reach 1 begins at Friant Dam and ends at Gravelly Ford, about 39 miles downstream from Friant Dam. An average of about 117,000 acre-feet of water per year is released from Friant Dam for riparian water users. This is the only reach with existing gravel and a river gradient suitable for Chinook salmon spawning. Gravel mining has left many pits, some connected to the river, within the historic floodplain. Reach 1 has become heavily incised since completion of Friant Dam.

Reach 2 meanders across the alluvial fan of the San Joaquin River between Gravelly Ford and Mendota Dam. The channel for Reach 2 and downstream reaches primarily has a sand bed. Sand moving downstream from Reach 1 affects channel capacity in Reach 2.

Except during times of floods, water passing Gravelly Ford typically infiltrates before reaching the Chowchilla Bypass Bifurcation Structure, and therefore, Reach 2B normally does not convey water. Many of the levees in Reach 2

seep water into adjacent fields during flood events. Portions of Reach 2A have become heavily incised since completion of Friant Dam.

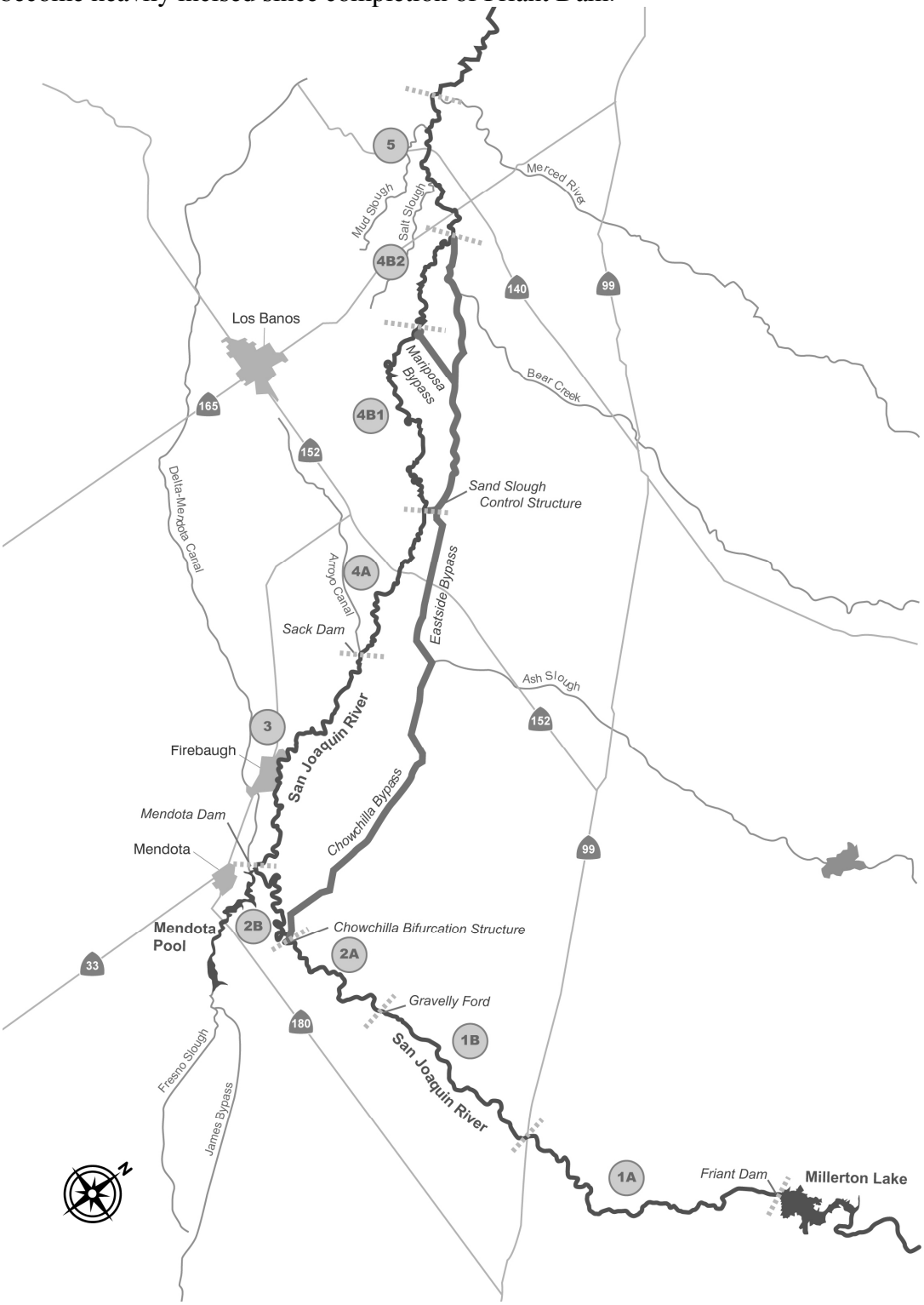

Figure 1 – Reaches of the San Joaquin River within the Restoration Area.

Reach 3 conveys flows of up to 800 cfs for water deliveries from the Delta-Mendota Canal (DMC), through the mainstem San Joaquin River, and to Sack Dam for diversion to Arroyo Canal. For most of its length, this reach is bounded on both sides by irrigation canals.

Reach 4 has been divided into several sub-reaches, but overall extends from Sack Dam to the confluence with Bear Creek and the Eastside Bypass. Except for times of high flows, Reach 4A only carries seepage water from Sack Dam and from adjacent agricultural areas. At the downstream end of Reach 4A, any water in the channel flows into the Eastside Bypass through Sand Slough. Reach 4B1 has not carried flow in many years, and channel capacity has been greatly reduced by vegetation, road crossings, and other obstructions. Although Reach 4B1 was designed to carry 1,500 cfs, portions of Reach 4B1 may have a flow capacity of less than 20 cfs. Downstream from the Mariposa Bypass, Reach 4B2 has greater capacity than Reach 4B1 and regularly conveys agricultural return flows and runoff.

Reach 5 includes levees that are part of the Federal/State flood control project for the San Joaquin River. Reach 5 is bounded on the west bank by Federal/State levees downstream to the Salt Slough confluence and on the east bank to the Merced River confluence. Reach 5 has become incised since completion of Friant Dam.

Chowchilla, Eastside, and Mariposa bypasses were designed to conveys water during high-water conditions to prevent flooding. Currently, water at the downstream end of Reach 4A flows to the bypasses rather than into Reach 4B. Many of the levees along the bypasses seep water into adjacent fields during flood events. During floods, sand from Reach 2 is conveyed into the bypass.

The Eastside Bypass extends from Ash Slough to the head of Reach 5. The Eastside Bypass receives flows from the Chowchilla Bypass, Sand Slough, the Chowchilla River, the Mariposa Bypass, and Deadman, Owens and Bear creeks.

Management Plan Structure

The Restoration Area has changed dramatically since the completion of Friant Dam, and the conditions which the Settlement provides for restoration of salmon runs to the San Joaquin River are considerably different than what may have existed 200 years ago. As a result, Restoration will be guided by adaptation to information collected by several management plans.

Settlement stipulates the restoration Spring-run Chinook salmon, and monitoring of releases to do so. Additional monitoring requirements will be needed for flood control, and the avoidance of seepage impacts to third parties and biological conditions within the river. Seepage impacts result when the Restoration Flows raise groundwater tables in adjacent farm lands. These complex physical and biological monitoring efforts have been divided among management plans for Flow, Seepage, Vegetation, Sediment and Fisheries.

The management plans group actions by timeframe, decisions, and subject matter. Implementation of the various plans will be coordinated by the multi-agency SJRRP office. The SJRRP uses a simplified structure for each management plan. The following outline presents the common components of each management plan:

- **Objectives**: description of desired outcomes
- **Thresholds**: measurement which indicates an outcome or initiates an action.
- **Monitoring**: network of instrumentation, sampling schedule, and reporting.
- **Short-term Actions**: responses to reduce or avoid immediate impacts.
- **Long-term Institutional and Structural Modifications**: policy documents, construction, or mitigation activities to increase operation flexibility where goals cannot be reached.

Experimentation will play a key role in implementation of the Restoration Program. The SJRRP management plans do not prescribe how the program will adapt and change. Changes to Program implementation are expected to come from the review and recommendation of the SJRRP workgroups with representatives from all implementing agencies.

Monitoring Programs

Monitoring objectives contribute toward known needs for meeting the Restoration and Water Management goals, and in avoiding adverse impacts to Third Parties. A physical monitoring plan has been drafted for measuring flow, water quality, groundwater and seepage, sediment transport and morphology, and vegetation growth resulting from implementation of Interim Flows and Restoration Flows. A Fisheries Management Plan (FMP) includes objectives in monitoring for fisheries benefits. New information and changing objectives through time may result in alteration to the monitoring plan. This paper describes the long-term monitoring efforts. Implementation may require numerous studies with shorter-term objectives beyond the scope of this document.

Flow Monitoring

The Settlement requires that flows be measured at six locations between Friant Dam and the Merced River (e.g., Friant Dam release, Gravelly Ford, below the Chowchilla Bifurcation Structure, below Sack Dam, Top of Reach 4B, and Merced River confluence). A combination of existing gages, retrofitted gages, and newly constructed gages will be used to satisfy the requirement.

Water Quality Monitoring

Adverse impacts to water quality may limit the operation of the SJRRP. Water quality monitoring is planned for 10 locations along the San Joaquin River (e.g., Friant Dam, below Friant Dam, Gravelly Ford, below the Chowchilla Bifurcation Structure, Mendota, below Sack Dam, top of Reach 4B, Fremont Ford Bridge, Hills Ferry, and Crows Landing). The SJRRP will coordinate with water quality data being collected for the Central Valley Project Baseline Water Quality Monitoring Program (full Title 22 organic and inorganic compounds, plus bacterial) and Grassland Bypass Project (nitrate, ammonia, total kjeldahl nitrogen, total phosphate, and ortho phosphate). Other water quality parameters to be measured include: electrical conductivity (salinity), temperature, pH, dissolved oxygen, turbidity, and chlorophyll. Future efforts will include a list of short term monitoring.

Groundwater and Seepage Monitoring

Monitoring of seepage includes combining data from surface water discharges, diversions, groundwater conditions, and groundwater extractions in the vicinity of the San Joaquin River. Monitoring of groundwater levels, streamflow, river stage, land use, and geophysical data provide information to understand surface–ground- water interactions by capturing the variability in groundwater levels. Monitoring of groundwater levels and river stage will help to determine whether seepage losses increase and result in impacts to areas with productive lands. To meet river losses and bank seepage monitoring requirements, a series of monitoring wells will be used to measure groundwater levels along selected transects through the San Joaquin River. A total of 144 new groundwater wells are planned, including: nine in Reach 1A, twenty-one in Reach 1B, thirty-four along six transects in Reach 2A, seven along one transect in Reach 2B, nineteen along three transects in Reach 3, eighteen along three transects in Reach 4A, eighteen along three transects in Reach 4B, eighteen along three transects in Reach 5.

Sediment Monitoring

Adverse impacts of sediment displacement may limit the operation of the program to meet the Restoration Goal of a self-sustaining Chinook salmon population. The sediment impacts include reduced channel capacity due to deposition, and infrastructure risk due to systemic scour. Maintenance of habitat also depends on sediment transport rates. Suspended and bed load sampling is planned at twelve locations, including: three sites in Reach 1A, one in Reach 1B, one in Reach 2A, two in Reach 2B, one in Reach 3, one in Reach 4A, two in Reach 4B, and one in Reach 5.

Measurements of bank erosion and river bed profile is planned at areas of high mobility and includes surveyed transects.

Vegetation Monitoring

Vegetation monitoring seeks to establish habitat conducive to fish and avoid the spread of invasive species. A component of the Restoration Flows includes a volume of water for shaping to recruit native willow and cottonwood species. Vegetation monitoring includes observing seed dispersal to determine the likely timing. Transects to monitor seedling establishment will identify the risk of desiccation. Regular aerial flights will record the growth of vegetation and potential encroachment on flood conveyance capacity.

FISHERIES MONITORING PROGRAM

Monitoring is a critical component in the adaptive management process and will be used to assess the performance in terms of meeting the Restoration Goal. The monitoring and evaluation methods were developed to assess the performance of the SJRRP through monitoring in accordance with guidance developed by the CALFED Performances Measures Report, Phase 1 (CALFED 2007). The FMP identifies three types of monitoring needs, each useful at a separate stage of the Adaptive Management Approach. Limiting factor monitoring and assessment is a necessary precursor to the development of potential actions, and is used to verify the

prioritization of limiting factors and goals of the conceptual models. This type of monitoring also is useful to fill important life history information gaps, which are in turn useful for the development of quantitative models. Action-specific monitoring is used to determine the effectiveness of all types of restoration actions to identify the success of actions and incorporate new information into the SJRRP Adaptive Management Approach. Program-level monitoring is designed to measure the success of the program in meeting the Restoration Goal. Program-level monitoring is generally at the fisheries population-level, and consists of the measurement of elements such as escapement levels, viability values, and genetic fitness.

Table 2 summarizes monitoring activities and objectives from the FMP.

Table 2. Summary of the SJRRP Fisheries Monitoring Elements.

Monitoring Element	Performance Measure
Migration timing for Chinook salmon	Temporal and spatial occurrence of adult and juvenile fish
Adult Chinook salmon escapement	Number of spawning Chinook salmon
Egg survival and emergence	Early life history survival (e.g., egg survival, number of fry per redd)
Chinook salmon juvenile recruitment	Number of outmigrating smolts
Fish health	Fish body condition and survival rate
Genetic fitness	Genetic diversity and effective population size
Food supply	Maximized growth rates and accelerated smoltification
Predation	Egg, juvenile and adult Chinook salmon predation rates
Harvest	Impact of harvest on salmonid populations
Straying	Number of adult Chinook salmon that stray into false migration diversions
Entrainment	Number of juvenile Chinook salmon entrained in diversions
Juvenile stranding	Stranding rate
Migration and passage of other fish	Passage for other fish at structures
Individual, community and population condition	Fish community condition
Streamflow	Meet at least minimum passage requirements for adult Chinook salmon; Number of successful outmigrants; Holding pool habitat capacity and quality; Depth, velocity and flow conditions during spawning; Spawning gravel quality and quantity in Reach 1
Gravel recruitment	Spawning habitat quality and quantity in Reach 1
Holding pool habitat	Holding pool capacity and quality
Water temperature	Maintain sufficient water temperature for adult passage Maintain sufficient water temperature for juvenile and adult

	salmonids to meet the Restoration Goal
Water quality	Maintain suitable water quality to meet the Restoration Goal
Instream habitat, floodplain inundation, and riparian vegetation	Floodplain inundation frequency and accessibility for Chinook salmon and other fish; Instream habitat and riparian vegetation quality

Next Steps

The Stipulation of Settlement provides a framework to return flows and fish to the San Joaquin River but left considerable flexibility in implementation. Restoration will require rebuilding a substantial portion of the river while learning how to operate a new system within the confines of agency authority. A dramatic change from historical conditions and limited information will require innovative solutions which develop and improve through time. Monitoring provides information to support operational decisions and hypotheses on how to make the most of available water for river restoration while providing water supply to the rich agricultural lands of the Southern Central Valley, CA. The Program maintains a web site for public information at www.restoresjr.net. The monitoring program begins with the first release of flows in October 2009.

References

CALFED Bay-Delta Program (CALFED). 2001. 2001 Strategic Plan for Ecosystem Restoration.

CALFED. 2007. _____p. 6-1_____.California Data Exchange Center (CDEC). 2008. Available at: http://cdec.water.ca.gov/.

California Department of Fish and Game (DFG). 2001. San Joaquin River chinook salmon enhancement. Annual Report, Fiscal Year 1999-2000, Sport Fish Restoration Act, Project F-51-R-6, Project No. 26, Jobs 1 through 6. California Department of Fish and Game, San Joaquin Valley and Southern Sierra Region, Fresno.

DWR. 2006. Final Report: Progress on Incorporating Climate Change into Management of California Water Resources, Technical Memorandum Report.

McBain & Trush (eds), 2002. San Joaquin River Restoration Study Background Report, prepared for Friant Water Users Authority, Lindsay, CA, and Natural Resources Defense Council, San Francisco, CA.

Natural Resources Defense Council et al. (NRDC). 2006. Notice of Lodgment of Stipulation of Settlement. E.D. Cal. No. Civ. S-88-1658 LKK/GGH. NRDC v. Rodgers. September 13.

SJRRP. 2008. Initial Program Alternatives Report. June 2008.

U.S. Department of the Interior, Bureau of Reclamation and San Joaquin River Group Authority (Reclamation and San Joaquin River Group Authority). 1999. Meeting Flow Objectives for the San Joaquin River Agreement 1999 – 2010: Environmental impact Statement and Environmental Impact Report. January.

Water Education Foundation. 1992. Layperson's guide to California rivers and streams: Sacramento, California.

Selection of Overflow Control Strategies for the Austin Clean Water Program

Joseph D. Smith[1] and Eric D. Loucks[2]

[1] AECOM Water, 811 Barton Springs Rd., Suite 400, Austin, TX 78704; PH 512-479-1615; joseph.smith@aecom.com.
[2] AECOM Water, 811 Barton Springs Rd., Suite 400, Austin, TX 78704; PH 512-479-1648; eric.loucks@aecom.com.

ABSTRACT

The Austin Clean Water Program (ACWP or Program) was created in 2001 to assist the City of Austin in meeting the terms of a USEPA Administrative Order that required the City to address its overflow problems by 2009. With a database of more than two thousand defects and overflows, it was not immediately obvious how the City should proceed. The City and the Program were under significant time constraints with less than eight years available to establish a course of action and then design and build the needed improvements. This paper describes the decision making process used to identify the improvements included in the program. A flow down approach was employed to systematically identify the system deficiencies and associated remedies that were likely to accomplish the objectives of the Program. The final Program now consists of one hundred collection system rehabilitation, repair or replacement projects with a total cost of 350 million dollars.

BACKGROUND

Austin Texas is the 16th largest city in the United States with a 2000 census population of 656,562 and an estimated 2007 population of 743,074. The city is situated along the Colorado River at the boundary between the Texas coastal plain and the Edwards Plateau formed by the Balcones Escarpment. The Austin Water Utility provides water and wastewater services to the City of Austin and a few adjacent communities and independent systems. The city's first wastewater treatment facility was built in 1917 on the banks of the Lower Colorado River. The facility used a tank for the settling of wastewater solids. In 1937, the tank system was replaced by the Govalle Wastewater Treatment Plant, a revolutionary facility utilizing a relatively new treatment process using activated sludge. As the City grew, the sanitary sewer system evolved along the natural gravity paths that followed the different creeks. As was common practice early in building sanitary sewers, many were located within the creek beds.

Today, the city's sewersheds are delineated along the 47 different watershed boundaries. The Govalle plant was recently taken off line and there are two newer, major wastewater treatment plants in operation; the South Austin Regional and

Walnut Creek Treatment Plants. With growth driving the sewer treatment needs, the South Austin Regional and Walnut Creek plants were built along with large diameter interceptor sewers that flow west to east picking up the flows from the different watersheds. Besides treating the sanitary flows, the City also reuses the sludge created by the plants to generate a compost product called "Dillo Dirt" at the Hornsby Bend Biosolids facility.

Currently, the city owns and operates its water and wastewater system providing service to a population of 820,765 (766,428 retail and 54,337 wholesale) through 187,000 service connections. The city's utility service area of 538 square miles consists of 2,500 miles of pipelines, 124 city maintained wastewater lift stations, over 45,000 manholes, two major wastewater treatment plants with a total treatment capacity of 135 million gallons per day (MGD) and one central biosolids processing plant.

In 1998, a lightning-induced failure at a wastewater lift station just north of Austin resulted in a discharge into Brushy Creek. The episode drew attention to wastewater overflows and resulted in the United States Environmental Protection Agency (USEPA) issuing an Administrative Order (AO) on September 11, 1998. The AO included a finding of violation and an order for compliance noting that the City had also reported 129 unauthorized discharges in the preceding three years. While the September 1998 AO was specific to the violation on Brushy Creek, a subsequent AO was issued in 1999 that required the City to eliminate sanitary sewer overflows by 2009.

APPROACH

The task was tackled by in a step by step flow down process that started by looking at the entire City, then looking closer at areas of the highest inflow and infiltration (I&I) to identify and prioritize specific problems and finally to replace or make improvements to deficient parts of the wastewater system. The City-wide portion of the analysis was accomplished with three large scale I&I studies. A sanitary sewer evaluation survey (SSES) was completed for the areas of the highest I&I. Findings from the SSES were clarified, studied, and used to make recommendations for improvements in Technical Memorandums and grouped into construction projects in Administrative Order Reports. The steps in this process are described in more detail in the following paragraphs.

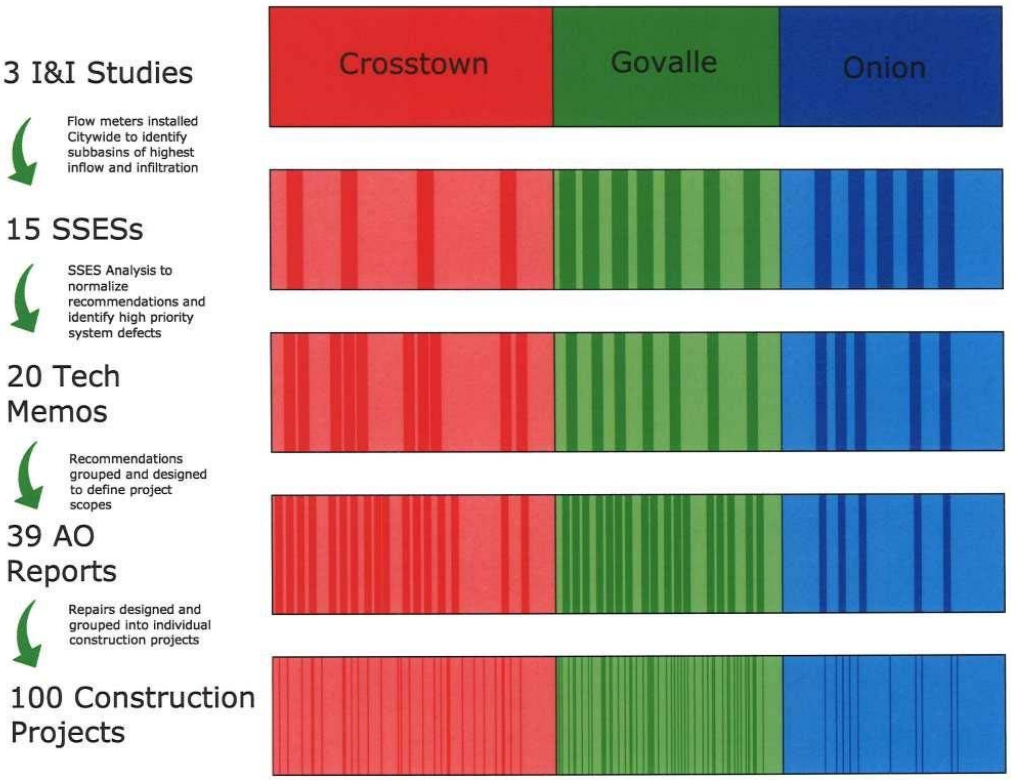

Figure 1. Process of Identifying and Replacing Priority Wastewater Deficiencies.

INFLOW AND INFILTRATION STUDIES

To begin to approach the Sanitary Sewer Overflow question in Austin, Inflow and Infiltration Studies were conducted to determine the areas of the City most impacted by I&I. The City is divided into three major sewer basins by sewer network configuration and topology. There is a main tunnel draining each of the major sewer basins.

North – Crosstown Basin (Crosstown Tunnel)
Central – Govalle Basin (Govalle Tunnel)
South – Onion Basin (Onion Creek Tunnel)

The extent and locations of the major sewer basins is shown in Figure 2.

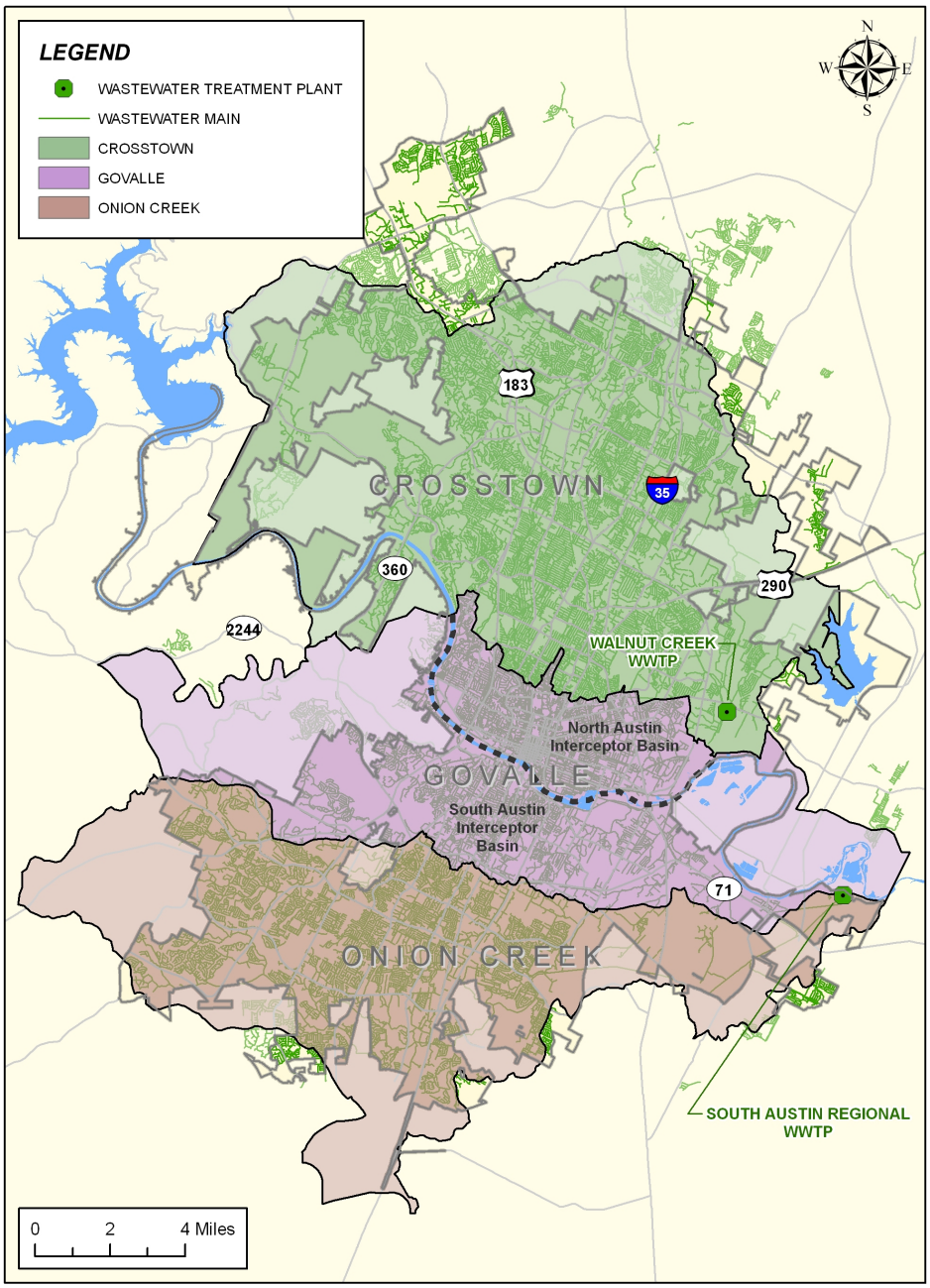

Figure 2. Austin Water Utility Wastewater Basins

An I&I study was performed in each of the three major sewer basins by monitoring flow at all of the major interceptors in each major basin. This divided the City's sewer system into sewer basins that were tributary to each interceptor. The I&I studies ranked the sewer basins based on evidence of high I&I in the sewer basin using flow monitoring studies. The sewer basins with the highest evidence of I&I were identified to be studied more thorough with an SSES study. The I&I studies monitored flows in approximately 94 basins and approximately 28 basins were recommended to be studied further.

SANITARY SEWER EVALUATION SURVEY STUDIES

The SSES studies were used to derive Capital Improvements Program (CIP) projects to address problems and minimize overflows. The SSES studies were conducted by consulting engineers hired directly by the City. Each SSES report included:

Hydraulic Modeling
Flow Monitoring
Smoke testing
CCTV investigation
Manhole inspections
Survey and Mapping of the Wastewater Collection System

A typical SSES report usually included a project area description, results of field investigations, a hydraulic model, a prioritization of suggested improvements, and recommended improvements with cost estimates.

The SSES studies were to prioritize recommended improvements with the following prioritization scheme.
Priority 1 - SSO Elimination, including hydraulic deficiencies and structural defects that result in overflows.
Priority 2 - Rehabilitation of assets with moderate to severe structural defects and I/I deficiencies not attributable to SSOs.
Priority 3 - Scheduled Preventive Maintenance, including the evaluation of all remaining pipe segments on a phased schedule.
Priority 4 - Rehabilitation of infrastructure identified in Priority 3.

Oversight and a clear understanding of the scope of the SSES studies appeared to be lacking and several of the SSES studies were not ready to be used for their intended purpose as submitted. In some sub-basins, supporting documentation and detail was omitted. Most hydraulic models prepared by the SSES consultants did not account for future growth in their evaluation and recommendations and had limited flow meter data. Very few of the SSES recommendations gave consideration to systems planning or moving wastewater pipes out of creeks. Some the SSES recommended improvements were not very cost effective. It was determined that the information in the SSES studies needed to be refined to best determine which improvements were Priority 1 and needed to be fixed during the ACWP.

TECHNICAL MEMORANDUMS AND AO REPORTS

As the SSES studies were performed by various consultants without a lot of specific direction the reports varied. The ACWP Team performed an in depth review of each SSES studies to develop Technical Memorandums (TM) to normalize the SSES reports. This process involved

- hydraulic model review and recalibration
- application of a consistent design storm to the hydraulic models

- application of 2020 future population to the hydraulic models
- re-evaluation of CCTV tapes to look at them critically with a better understanding of the overall condition of the wastewater collection system
- field visits to verify and investigate unresolved questions

A TM was prepared for each SSES basin to summarize recommended Priority 1 improvements based on further investigation and normalizing the findings of the SSES studies. During the preparation of the TMs some suggested improvements that were not identified by the SSES consultant but were known to be trouble spots in the collection system by City staff or were identified as causing a recent overflow were added to the list of suggested improvements. Alternative, more cost effective solutions such as CIPP lining, spot repairs and manhole replacements were also suggested as part of the TMs prepared for each basin.

Suggested Priority 1 improvements from the TMs were grouped together to form construction projects that were to be designed by consulting engineers. Suggested improvements were grouped together in the form of an AO report that was intended to outline each design project. The AO reports further clarified and suggested the improvements that were needed for each repair. Projects were usually grouped geographically when possible with approximate dollar amounts in mind that were appropriate size for a construction project. During the preparation of the AOs further recommendations by the City Staff and SSO investigation staff was also added to the list of Priority 1 improvements. The AO reports contained preliminary engineering analysis, cost estimates, environmental constraints maps and suggestions for coordination with other projects and improvements being planned in the City (water lines, street resurfacing, and channel stabilization). These reports were used as scoping documents in the COA's task of bidding CIP Projects.

CONSTRUCTION PROJECTS

By 2004 the Priority 1 Construction Projects had been identified from the process. These projects were designed by separate consulting engineers with oversight from the City and ACWP staff starting in 2002 with the last design completed in the fall of 2007. These projects total $350 million in design and construction fees and 75 miles of improvements to the wastewater system. The locations of these projects within Austin are indicated in Figure 3. The program is on track for final completion of all construction by April 30, 2009. The ACWP was the largest construction program ever taken on by the City and it has accomplished many much needed improvements the wastewater collection system. The Priority 2-4 problems with the system remain or will develop and are planned to be improved as part of an ongoing maintenance program.

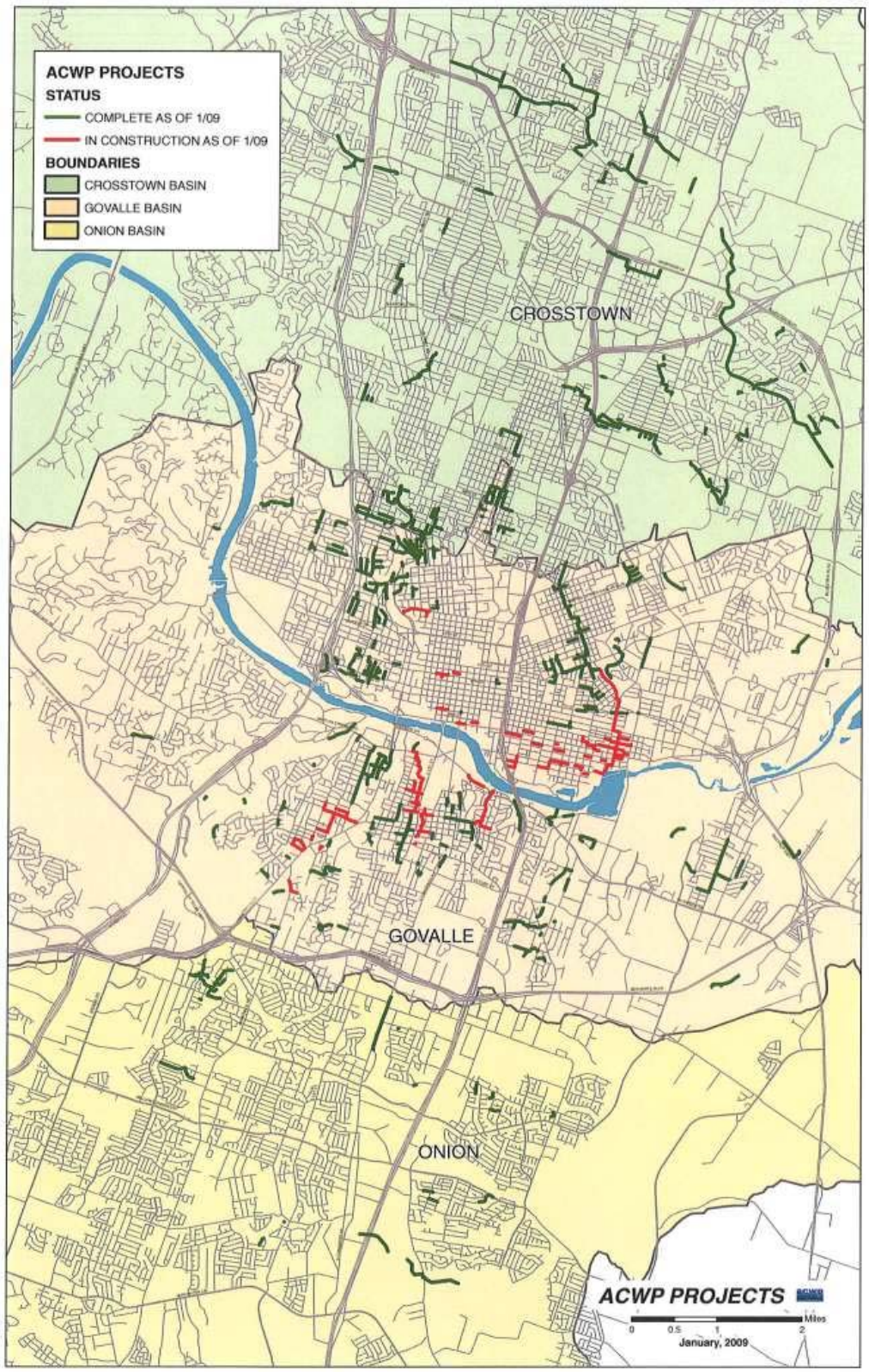

Figure 3. ACWP Construction Project Status Map (January 2009)

CONCLUSION

In 2001, the City of Austin and the Austin Clean Water Program was faced with the daunting task of determining how to eliminate a pervasive sewer overflow problem within its wastewater collection system. The terms of its USEPA Administrative Order required quick and decisive action. The analysis started at the major basin level and drilled down to the construction project level through a logical sequence of steps. The ACWP employed a systematic process of analyzing flow data, field surveys, CCTV, smoke testing, computer modeling, and inspection to determine the highest priority wastewater improvements that would maximize the reduction in sanitary sewer overflows. This process led to one hundred construction projects that have already lead to a remarkable reduction in recorded overflows. This decision making approach could be applied in any City facing a similar mandate and should be considered as a possible procedure for addressing widespread sewer overflows elsewhere.

Spatial Evolutionary Algorithms for Characterizing Large-scale Spatial Groundwater-Vegetation Dynamics in Arid Region

Jihua Wang, Ximing Cai, Albert J. Valocchi

Hydrosystems Laboratory, Civil and Environmental Engineering, University of Illinois at Urbana-Champaign, Urbana, 61801. E-mail: xmcai@uiuc.edu, jwang41@uiuc.edu, valocchi@uiuc.edu

Abstract

Vegetation in arid riparian zones heavily depends on groundwater, meanwhile the distribution of vegetation impacts the groundwater flow in the area. This study describes a methodology to characterize groundwater-vegetation dynamics using a spatial evolutionary algorithm (SEA). It incorporates spatial knowledge of groundwater and vegetation to facilitate the optimal search of vegetation distribution compatible to groundwater flow. Unlike a regular EA for spatial models, the SEA employs a hierarchical tree structure to represent spatial variables in a more efficient way. Furthermore, special crossover and mutation operators are designed in accordance with the tree representation. In this paper, the SEA is applied to searching for the maximum vegetation coverage associated with a distributed groundwater system in an arid region. The results of computational experiments demonstrate the efficiency of SEA for large-scale spatial optimization problems. Extension of the algorithm for other water resources management problems is discussed.

Keywords: spatial evolutionary algorithms (SEA); large-scale; vegetation-groundwater interactions; spatial optimization; ecosystem management

1 Introduction

In many arid regions of the world, surface water-groundwater interactions are critically important for the health of the riparian ecosystem (Grimm et al., 1997; Le Maitre et al., 1999; Zhu et al., 2004). The main scientific issues relevant to the study of riparian ecosystem include the nonlinear feedback and interactions among the surface water, groundwater and vegetation system. In arid regions where plant growth is limited by groundwater availability, the spatial pattern of vegetation is the result of preexisting environmental heterogeneity, such as groundwater depth. Meanwhile, the distribution of vegetation impacts the groundwater flow in the area.

The groundwater-vegetation dynamics is essentially characterized with spatial patterns of groundwater and vegetation. The simulation of the dynamics as well as the decisions on optimal human controls for groundwater management and vegetation maintenance has a significant spatial dimension. This motivates a modeling analysis of vegetation management within a spatial analytical framework. This study describes a methodology to characterize the large-scale, groundwater-vegetation dynamics using a spatial evolutionary algorithm (SEA). The SEA uses spatial knowledge of groundwater and vegetation to support the optimal search of vegetation distribution compatible to groundwater flow. A computational experiment shows the effectiveness and efficiency of this approach for large-scale spatial optimization problems.

In this paper, a conceptual model of the research problem is proposed and the

assumptions discussed. The components of the SEA are then addressed in detail, including the hierarchical encoding scheme, the formulation of the spatial fitness function, and the enhanced crossover and mutation operators. Both the newly-developed SEA and the regular evolutionary algorithms (REA) are applied to the ground water in the computational experiments and the performances are compared. At the end, the differences between SEA and REA are summarized.

2 Conceptual model of the study problem

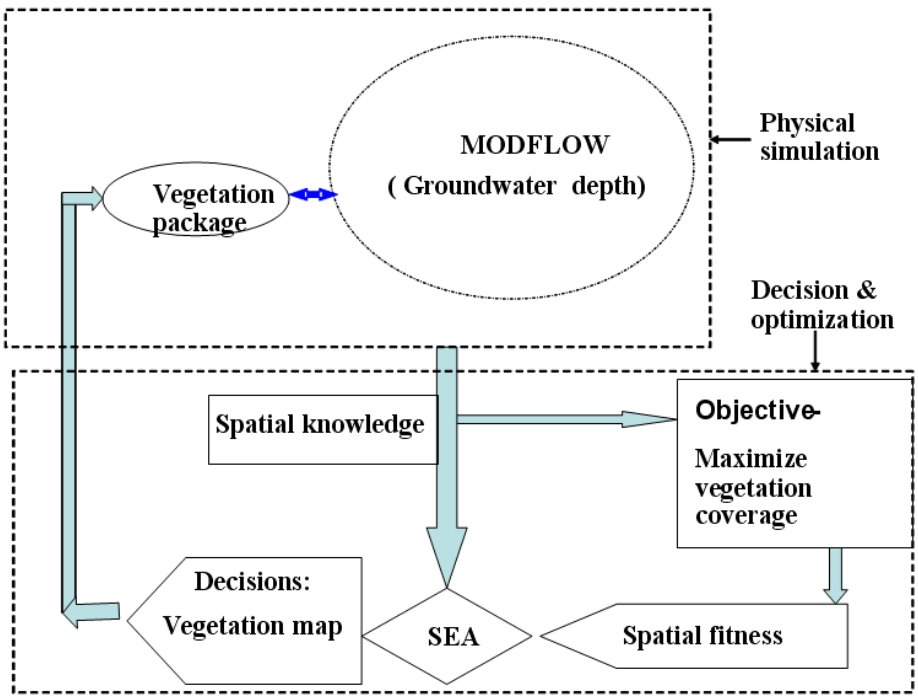

Fig1. Conceptual model of the study problem

The study problem can be formulated as an integrated simulation and optimization model as shown in Fig. 1. The assumption is, in arid regions with little precipitation, vegetation is mainly sustained by ground water. Where there is more ground water, there is more vegetation. Fig. 1 shows the systematic combination of models, management objectives and decision variables.

The spatial parameters to be assessed, such as the distributions of vegetation and groundwater and their dynamic interactions, distinguish this problem from regular optimization-simulation problems. The developed methodology will subsequently focus on exploring the interactions of the spatial patterns of vegetation and groundwater, and further on how to take advantage of these to solve the large-scale optimization-simulation problem.

3 Overview of SEA

Water resources systems contain numerous hydrological features which are inherently spatial and as such can be considered “large-scale spatial systems”. They present challenges because large-scale problems are computationally expensive for traditional

optimization methods and spatial patterns are not easily represented in the quantitative models. Meanwhile large-scale spatial systems provide some opportunities for the optimization method. This presents a motivation to design SEA to meet the challenges and take advantages of the specialty of the systems. The tree structure is employed to depict the interesting subsets of the whole system, which could save much computational time for large-scale problem. Meanwhile the spatial knowledge of a system is incorporated into the SEA framework to improve the performance of the optimal search.

3.1 Flowchart of SEA

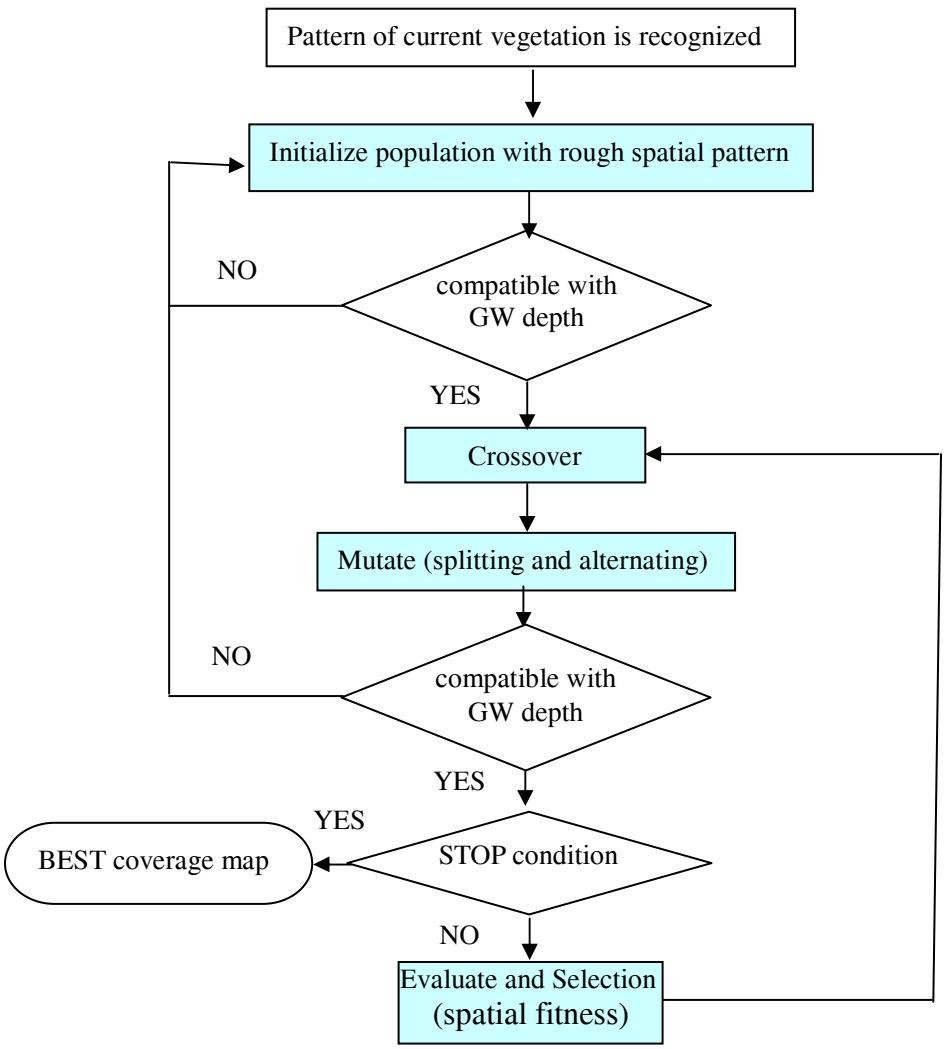

Fig. 2. Flowchart of SEA

As shown in Fig. 2., SEA starts from initialization of population and then moves to crossover, mutation, selection and terminates when the stop condition is satisfied. The enhanced components have been marked in blue and will be discussed in more detail later. The left loop of the flowchart checks the feasibility of the solution using the physical simulation model to determine whether groundwater can support this coverage solution.

The right loop represents the generations of SEA, and the evolution will not stop until (1) generation reaches the maximum generations, (2) there is no improvement within a specified number of generations, and (3) a specified percentage of the population reaches the maximum depth of the tree structure. The third stop condition is designed specifically for the hierarchical tree structure of SEA. The maximum level can be determined by the modeler's experience or by the constraints of the simulation model. Taking the vegetation for example, since the simulation model is constructed with Modflow, maximum depth depends on the grid numbers used in Modflow. The evolution will stop when specified percentage of population reaches the maximum depth.

3.2 The hierarchical encoding scheme

Encoding schemes for decision variables are fundamental to all EAs. In a regular EA, solutions are encoded with binary strings (Holland, 1975), real numbers (De Jong, 1998) or finite state machines (Fogel, 2000). Generally, the encoding method of the solutions is dependent on the context of the problem: EA designers normally select the most suitable encoding scheme for their problems.

To solve large-scale spatial optimization problems, two essential requirements present for the design of the encoding scheme. Firstly, since large-scale problems are computationally expensive if every grid of a map is encoded as a decision variable, it is necessary for the encoding of the population to represent the spatial characters with limited data volume. Secondly, the spatial solutions must be represented by a well-defined spatial data structure that can be easily handled by the EA operators.

To meet these requirements, the tree structure is employed to represent the spatial population solution because it has been shown to capture spatial characters with reduced data volume (Samet, 1990). In addition, the operators of crossover and mutation can be easily manipulated on the tree structure. More details about operators will be given in the following subsections. In this paper, I use a quadtree to represent the map of vegetation converge. For other water resources applications, the tree structure can be modified in accordance with the specialty of those spatial problems.

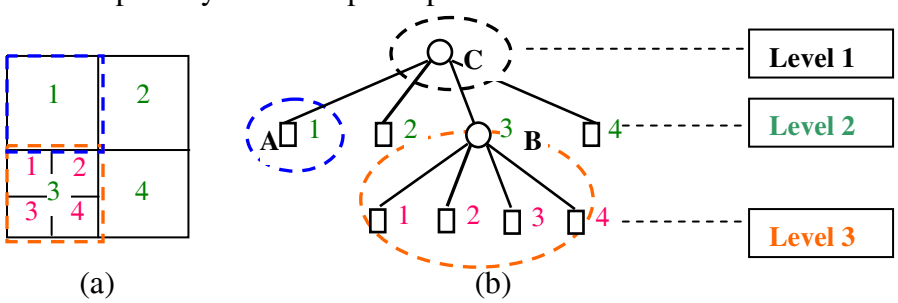

Fig. 3. Encoding a spatial population (a) with a quadtree (b)

Taking the vegetation coverage for example, every population of the coverage is encoded as a quadtree. Every leaf without a predecessor in the quadtree (like A in Fig. 3(b)) is for a uniform coverage in the population map(orange square in Fig. 3(a)) while a node (like B in Fig. 3(b)) represents 4 different coverages(blue square in Fig. 3(a)).

The tree structure of SEA offers flexibility for modelers to get various degrees of accuracy of the optimization solution for a large-scale spatial problem. The quadtree starts from a rough pattern and then further refines the map. The quadtree in Fig. 3(b), for

example, starts from a uniform map and is constructed from level 1, as node C shows. If the refinement of the map leads to an improvement of the optimization objective, node C splits, and the depth of quadtree goes to level 2 and leads to more variations in the corresponding map. If we want to increase the accuracy further, node B in level 2 splits again, the depth of quadtree goes to level 3, and the corresponding map shows more details(Fig. 3(a)). Refinement is prohibited unless necessary, and hence SEA is computationally efficient for large-scale problems.

SEA works like a top-down method: it starts from a rough pattern and then further refines the map. It is flexible and efficient for large-scale problems since the accuracy depends on what you need. This top-down method can balance the tradeoff between accuracy and computation.

3.3 Initial Population generation

To solve the vegetation problem, a rough pattern of the current vegetation coverage is used as the basis for initialization because vegetation coverage is relatively consistent and there is no abrupt change. Since the final result should be much closer to the current coverage than to a randomized coverage map, significantly fewer generations are required to reach the optimized coverage from the current coverage.

3.4 Spatial fitness

Spatial patterns of the study problem contain much important information about the specialties and characters of the problem. So it is essential to incorporate them into the model. However, one challenge for spatial optimization problems is that it is usually difficult to represent spatial patterns explicitly in the models. Hence, it is the modelers' responsibility to apply their professional experience and insight when they try to recognize the spatial patterns, interpret them as spatial knowledge and incorporate the knowledge into quantitative models.

In arid regions with little precipitation, we assume that vegetation is mainly supported by groundwater and hence the distribution of the vegetation coverage is highly correlated with that of the saturated thickness of groundwater. The spatial pattern of the correlation is further interpreted by a quantitative index like the spatial cross-covariance between vegetation coverage and groundwater depth. The spatial fitness of the vegetation problem can then be defined as

$$\text{Max} \underbrace{\text{total coverage}}_{(a)} + \lambda * \underbrace{(\text{cross-covariance})}_{(b)} \qquad \text{Equation (1)}$$

Besides the original objective (a), the spatial fitness has an extra component (b) to incorporate spatial patterns into the optimization models. Lambda (λ), the Lagrange multiplier, can be determined by modeler's experiences. With spatial fitness it is relatively easy to incorporate spatial patterns into the optimization models.

In this paper, spatial patterns are incorporated into the spatial fitness function to represent the preference for the compatible vegetation coverage. It must be mentioned that spatial knowledge can be incorporated into fitness or work as a strict spatial constraint like the boundary of locations for a site selection problem. Since the preference for specific

vegetation coverage is implicit and not as strict as the boundary condition, the spatial knowledge is incorporated into the fitness to guide the search for compatible vegetation.

3.5 Crossover operator

Since we encoded the solution with a quadtree rather than the conventional string, the crossover and mutation operators must also be modified to meet the spatial specialty of the tree structure and guarantee that the results from the two operations are still legal quadtrees. Swapping has been widely used in genetic programming (GP) to exchange the nodes, and has been shown to be efficient in many applications. In this paper, swapping is employed to change the nodes within the same area between individuals.

The crossover of SEA is operated on the nodes of a tree rather than on the grid of a map as in regular EA, which is computationally efficient for large-scale problems. Unlike the crossover in GP which can be operated at different areas or within the same individual, the crossover in SEA swaps nodes within the same area and is only applied between individuals. The main benefit of this operational constraint in SEA is that the swap of the nodes within the same area between individuals can pass the locally good information to the next generation. Since a good neighborhood or distribution in one location may not make sense for another location, the crossover is only applied between individuals and not within the same individual.

3.6 Mutation operator

Mutation is important to introduce new information into a population. The conventional mutation is not efficient for large-scale problem size because randomly changing some parts of the population without the guidance of spatial knowledge may be computational expensive before convergence for a large-scale problem.

Three criteria are used for designing the mutation operator of SEA. First of all, the mutation is able to be efficiently implemented on the large-scale problem with the help of spatial knowledge extracted from the study problem. Secondly, some randomness must be included to keep the diversity of the population and balance exploration and exploitation. Thirdly, the resultant offspring is required to be a legal quadtree for the consistency of the encoding in the next generation.

SEA employs two kinds of mutation: splitting and alternating. Both are operated on the leaves of a tree. Similar to the conventional mutation operator, alternating randomly selects a number of leaves and changes their values. Splitting, which is based on the sensitivity of the leaves to the fitness improvement, focuses the computations on interesting subsets of the whole large volume of data.

Similar to the promising index in nested partition methods (Shi et al, 1999), sensitivity, a good quantifiable index of spatial knowledge, works as a guide for concentrated computations on the most promising parts of the large volume of data and saves computations on those insensitive/insignificant parts. Fortunately the hierarchical character of the tree structure offers the flexibility of focus and concentration. As discussed in 2.3, splitting, together with the tree structure, make computational efficiency and flexibility possible for large-scale problems.

However, splitting is not totally dependent on sensitivity: some insensitive regions are also selected randomly for splitting to maintain the diversity of the population and reduce the risks of pre-convergence. More diversity of the leaves is also introduced by randomly alternating some leaves based on the specific probability. Both the splitting and alternating will obviously preserve the quadtree structure.

4 Computational experiment

To test the efficiency of this algorithm, both SEA and REA are applied to the same conceptual GW model. All the shared parameters of these two algorithms and the initialized maps (starting point for evolution) are the same for SEA and REA in order to get a fair comparison. The same GW model is used as the test issue and the GW constraints are also the same.

The specific aim of this experiment is to examine whether SEA sustains its effectiveness as problem sizes increases. Five different resolutions of the same GW model are designed for the experiment. As the problem sizes increases, the grid size of the GW models decreases and the number of decision variables (complexity of optimization model) increase.

Three scenarios are tested: (1) to compare the optimized pattern of vegetation coverage, run both algorithms with unlimited computational time until model converges. (2) Run algorithms with similar computational time and compare the fitness and (3) compare the computational time when both models reach the same fitness.

4.1.Run algorithms until model converges

As the problem size increases, both SEA and REA takes more time to converge because GW model needs more simulation time and the number of decision variables also increases. However, SEA reaches a better fitness with less total generations than REA. Table 1 and Fig. 4 show that SEA obtains nearly twice fitness using about 60% of the computational time with the REA.

Fig. 5 shows SEA finds a more compatible vegetation pattern with GW depth for 128*128 grids: the vegetation coverage is higher nearing the river since river is the main water supplier recharging this aquifer under arid climate. The optimized vegetation converge with REA has no clear pattern and may be dominated by randomness because of the huge computational complexity caused by decision variables.

Table 1. Comparison of computational time and fitness when model converges

	Generations		Time[min]		Max Fitness (Average density)		SEA/REA	
Size	REA	SEA	REA	SEA	REA	SEA	time ratio	fitness ratio
8*8	601	330	77	47	0.33	0.70	**0.61**	**2.12**
16*16	601	329	103	53	0.41	0.62	**0.51**	**1.51**
32*32	601	301	163	89	0.38	0.59	**0.55**	**1.55**
64*64	601	301	287	150	0.28	0.66	**0.52**	**2.36**
128*128	481	301	670	452	0.23	0.63	**0.67**	**2.74**

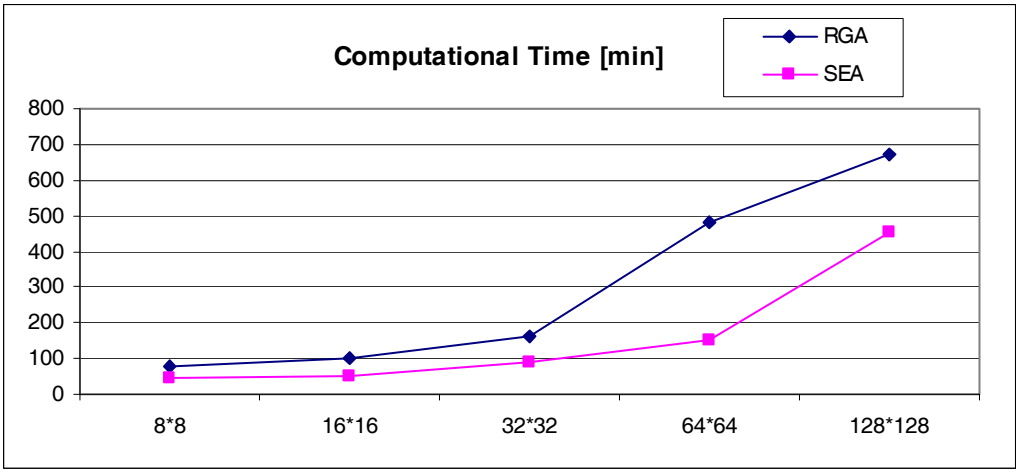

Fig. 4. Comparison of computational time when model converges

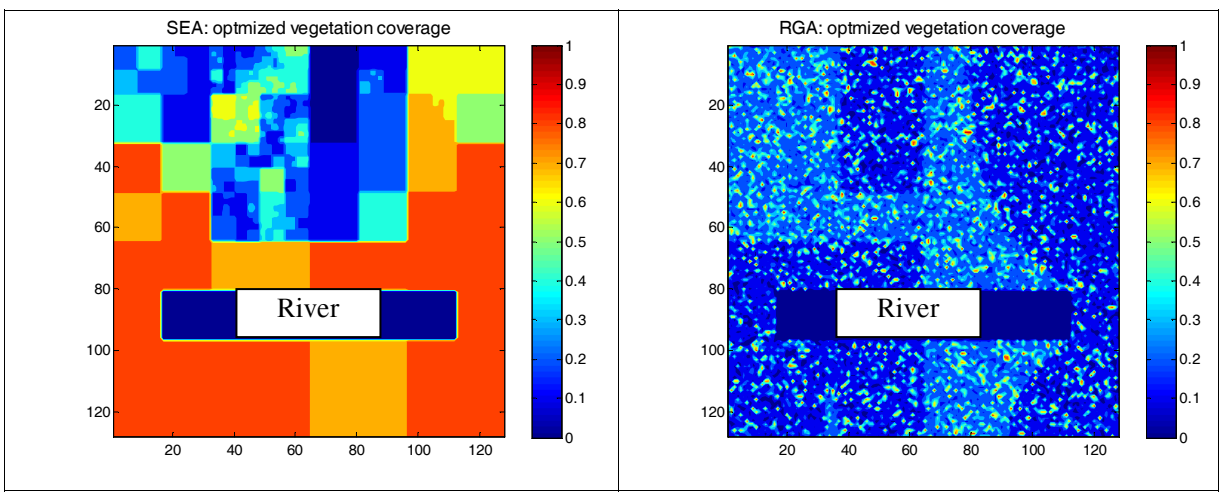

Fig. 5. Optimized vegetation converge when model converges

4.2.Run algorithms with similar computational time

With similar computational time, SEA obtains twice fitness as REA, which shows SEA is more efficient for large-scale optimization problem.

Table 2. Comparison of fitness with similar computational time

Problem Size	Generations		Time[min]		Max Fitness		SEA/REA	
	REA	SEA	REA	SEA	REA	SEA	time ratio	fitness ratio
8*8	99	101	13	13	0.29	0.57	0.99	**1.98**
16*16	110	101	17	17	0.23	0.63	0.99	**2.80**
32*32	107	101	25	25	0.29	0.55	1.00	**1.93**
64*64	120	101	48	47	0.27	0.59	0.99	**2.17**
128*128	113	101	131	130	0.23	0.60	0.99	**2.66**

4.3.Run algorithms when both reach similar fitness

When both algorithms reach the similar fitness, SEA takes no more than 1% computational time as REA. This time ratio is reasonable since REA evolves slowly when the model has a large number of decision variables.

Table 3. Comparison computational time when both algorithms reach similar fitness

Problem Size	Generations		Time[min]		Max Fitness		SEA/REA	
	REA	SEA	REA	SEA	REA	SEA	time ratio	fitness ratio
8*8	5001	5	684	2	0.47	0.53	0.002	1.11
16*16	5001	3	841	2	0.42	0.46	0.002	1.10
32*32	3691	4	1062	6	0.41	0.43	0.006	1.04
64*64	3001	4	1387	6	0.45	0.48	0.004	1.06
128*128	1021	2	1477	14	0.46	0.48	0.009	1.04

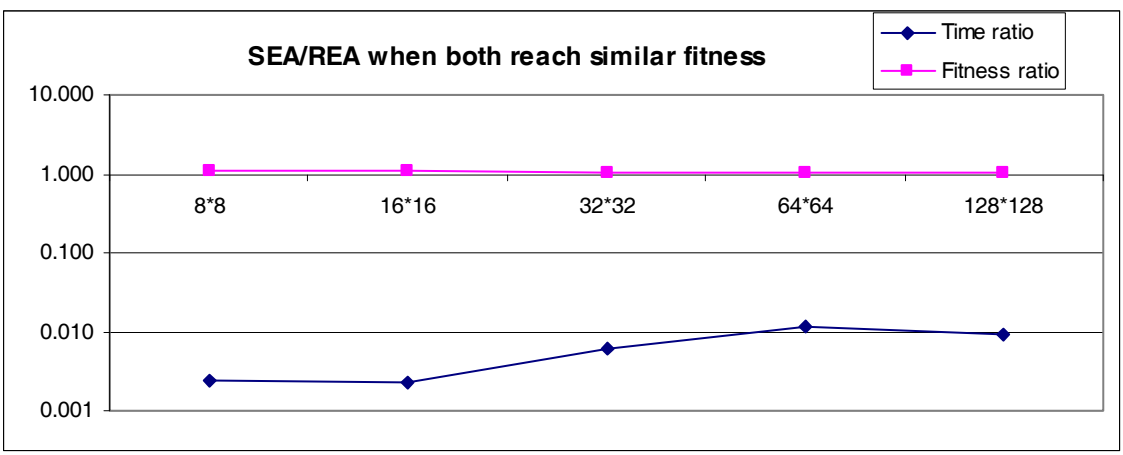

Fig. 6. Optimized vegetation converge when model converges

5 Conclusion

The main components of SEA, encoding, initialization, fitness and operators, have been modified to meet the challenges and also to make use of the characters of large-scale spatial problems. The spatial knowledge used in crossover, mutation and fitness together with a tree structure for encoding, distinguishes the SEA from a regular EA and increases flexibility and computational efficiency for large-scale spatial problems. In summary, the SEA has the following merits:

- The tree structure and initialization procedure increase the computational efficiency for large-scale spatial problems;
- Splitting, based on sensitivity in the mutation operation, introduces more exploitation into mutation and helps to speed up the optimal search for solutions to large-scale problems;
- Crossover swaps the nodes within the same area between individuals, maintains locally good information and passes it on to future generations;
- Spatial knowledge is interpreted from the spatial patterns of the study problem and helps to modify the crossover, mutation and fitness function of SEA.

References

De Jong K A, 1998, Evolutionary computation: where we are and where we're headed. Fundamenta Informaticae, (35): 247 -259

Fogel D B, 2000. Evolutionary Computation: Toward a New Philosophy of Machine Intelligence, IEEE Press, Piscataway, NJ.

Gong M. and and Yang Y., 2004. Quadtree-based genetic algorithm and its applications to computer vision. Pattern Recognition. (37): 1723 -1733

Grimm, N. B., A. Chacon, C. N. Dahm, S. W. Hostetler, O. W. Lind, P. L. Starkweather, and W. W. Wurtsbaugh. (1997). "Sensitivity of aquatic ecosystems to climatic and anthropogenic changes: The basin and range, American Southwest and Mexico." Hydrological Processes, 11:1023–1041.

Holland J H, 1975. Adaptations in Natural and Artificial Systems, University of Michigan Press, Ann Arbor, MI.

Le Maitre, D. C., D. F. Scott, and C. Colvin. (1999). "A review of information on interactions between vegetation and groundwater." Water SA, 25(2):137–152.

Samet H., 1990. The Design and Analysis of Spatial Data Structures, Addison-Wesley, New York.

Shi L et al, 1999. A new hybrid optimization algorithm, Computers & Industrial Engineering. (36): 409-426

Zhu, Y., Y. Wu, and S. Drake. (2004). "A survey: obstacles and strategies for the development of ground-water resources in arid inland river basins of Western China." *Journal of Arid Environments,* 59:351–367.

Study on the Water Value Conversion between Economy and Ecology and Countermeasures of Water Resources Distribution for Coordinated Development of Economy and Ecology

Hongzhen Ni[1], Hao Wang[1], Bo Zhao[1], Dangxian Wang[1]

[1]China institute of water resources and hydropower research, Fuxing road, Haidian district, Beijing, 100038 ; PH (86)010-68785703; FAX (86)010-68483367; email:nihongzhen@163.com

Abstracts: Taking Beijing as an example, the paper studies response mechanisms to water quantity and quality of economy and environment, calculates water value and studies the conversion law of water value, measuring the gains and losses of the water conversion between economy and ecology. On this basis of analysis, the paper tries to give some suggestions for water sustainable utilization. The example gives us some conclusions: (1) in Beijing 2000, the water value of economy is more than ecologic, and in the low level of life, the man could pay more attention to economic water use; (2)if 4.04×10^9 m^3 used by social economy in 2000 are reallocated between environment and economy, following utility maximum principle, 24.76 million m^3 could be used by economy which is far less than actual, comprehensive water price is RMB 8.01/m^3 which is more than actual price 2.81, present water price cannot promote water reasonable allocation and sustainable utilization.

The social economy fast development caused the economical water consumption sharply increased. It has gone beyond the natural water resources bearing capacity, which occupied the natural ecosystem water used, broke the natural biosphere water demand balance, and then initiated the humanity to live the interdependence ecological environment worsening. However, with the economics growing and the material wealth increasing, the human energetic culture demand promotes quickly, so the higher qualities of life pursue needs support of superior environment. Therefore how to rationally allocate the limited water resources between economic society and the ecological environment, and how to make water resources utility value most superior display, has now become an extremely thorny pair of contradictory in water resources management.

Beijing is China's capital, located at Huabei Plain, where is serious scarcity of water.

In this article, we take Beijing as an example; analyze the water value and influence factors and the countermeasure of water resources reasonable distribution.

1 Basic data of study region

In 2000, the Beijing GDP reached 2478.76 hundred million Yuan, the total population achieved 12,779,000 people, the land area was 16807.8 square kilometers, the waters area was 9.70 square kilometers, and the urban garden greening area was 20600 hectare [1]. According to 2000 Beijing water resources bulletin[2], in 2000, the total water use in economic and society in Beijing is 40.40 hundred million m^3, went far beyond water resources supply quantity 16.86 hundred million m^3 in the same year. Compared last year the surface water resources depletion quantity approximately was 6.91 hundred million m^3, and the groundwater resources depletion quantity approximately was 5.89 hundred million m^3. In 2000 the total sewage discharge was 13.55 hundred million m^3, in which the industrial sewage discharge reached 5.79 hundred million m^3, and the domestic sewage (including the tertiary industry) reached 7.76 hundred million m^3. Conversions [3] according to the water quality condition is that the comprehensive surface water quality rank weakened from 3.58 to 3.62 by the beginning of the year, and corresponding the synthesis ground water from 3.46 to 3.6. Calculating according to the 2000 year price, Beijing investment costs per year on water resources management, maintenance, plan, and water source projects was 0.6 Yuan /m^3; The tap water supply volume is totally 7.54 hundred million m^3,and its total cost is12.54 hundred million Yuan.

2 The eco-environment value accounting of water resources

2.1 The eco-environment value of surface water

(1) The eco-environmental water demand and deficit calculation of surface water

In Beijing, the eco-environmental water demand is mainly influenced by the eco-environmental water demand inside the rivers, the lake's eco-environmental water demand in the city and the eco-environmental water demand of the urban green spaces.

① Eco-environmental water demand inside the rivers

There are five main rivers in Beijing, in turn from west to east is Juma River, Yongding river, northern canal, Chaobai River and Ju river, and they separately belong to Daqing river system、Yongding river system、northern canal system、Chaobai river system and Ji canal system.

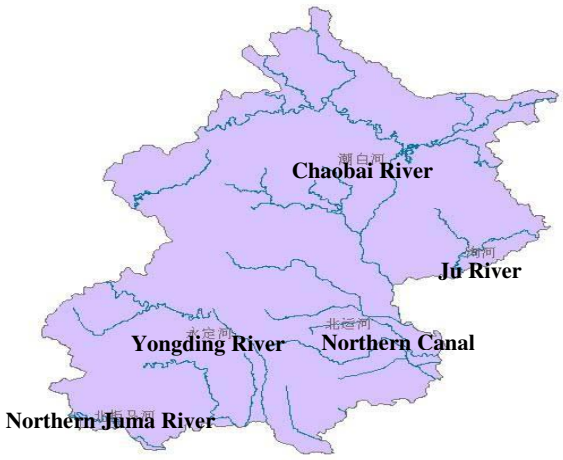

Figure 1. Distribution map of main rivers in Beijing

Here the calculating is directed towards to the five rivers in Beijing, and the eco-environmental water demand inside the river should meet three requirements: 1) to maintain the minimum flow of river; 2) to satisfy the water surface evaporation in river; 3) for the groundwater level in Beijing now falls generally and seriously, the water demand should also contains the channel leakage.

$$Q = Q_1 + Q_2 + Q_3 \quad (1)$$

which: Q Stands for the minimum eco-environmental water demand inside river;

Q_1 Stands for the water volume to maintain the minimum flow of river;

Q_2 stands for the water volume to satisfy the surface evaporation;

Q_3 stands for the water volume to satisfy the channel leakage;

The calculation of Q_1, take Guanting, Tongxian and Suzhuang stations as the controlling stations of Yongding River, Northern canal and Chaobai river systems. For the three stations locate on the main streams, they can stands for the changes of each water systems in Beijing. And other three stations, as shown in Table 1, Zhangfang station use the extrapolate formula in Hai river project; Ju river is a sub steam of Ji Canal, so here take the average flow in minimum month of Ju river's Sanhe station in the 1960s. The results are shown in Table1. The water volume to maintain the minimum flow of river in Beijing is 0.124 hundred million.

Q_2 The annual average surface evaporation in Beijing is 1100mm, according to the relationship between surface water wide and flow, we can obtain the water surface wide to each water system's minimum flow. So the total surface evaporation volume in Beijing is 6.473 hundred million. The results are shown in Table 1.

Q_3's calculation formula :

$$Q_3 = K\ F \quad (2)$$

K is empirical coefficient, F stands for water surface area.

Considering Beijing area is in the plain before the mountain, seepage property is worse

from west to east, therefore take Northern Juma River and the Yongding River's K value as 1.5, take northern canal and Chaobaihe River as 1, and take Ji Canal as 0.8. After computation the year river leakage quantity is 6.389 hundred million m^3, see Table 1.

Table 1. The eco-environmental water demand and water deficit of river

River name	Northern Juma River	Yongding River	Northern Canal	Chaobai River	Ju River	Total
River system	Daqing River	Yongding River	Northern Canal	Chaobai River	Ji Canal	
Control stations	Zhangfang	Guanting	Tongxian	Songzhuange	Sanhe	
River length（km）	51	240	339	680	85	
River water surface wide(m)	40	35	50	45	10	
Minimum ecological flow(m^3/s)	1.67	4.46	1.42	6.37	0.4	
Flow percentage (%)	7.22	7.4	12.1	10.5		
Water volume to maintain the minimum flow of river Q_1 (hundred million m^3)	0.014	0.039	0.012	0.055	0.004	0.124
Water volume to satisfy the surface evaporation Q_2 (hundred million m^3)	0.224	0.924	1.865	3.366	0.094	6.473
Water volume to satisfy the channel leakage Q_3 (hundred million m^3)	0.306	1.26	1.695	3.06	0.068	6.389
Total (hundred million m^3)	0.545	2.223	3.572	6.481	0.165	12.986
Status water volume （hundred million m^3）	0.40	1.64	2.64	2.98	0.12	7.78
Water deficit (hundred million m^3)	0.14	0.58	0.94	3.51	0.04	5.21

According to major achievement of the tenth five-year plan projects torch-plan countries -- China's regional ecological water use standard research, by 2000 correlation controlling stations' actual flow analysis, calculated that the rivers' extant water volume is 7.78 hundred million m^3, and get the result in the present situation that rivers ecological environment water deficit finally is 5.2 hundred million m^3.

② Eco-environmental water demand of the urban green spaces

According to each kind of material, Beijing city green space vegetation water used fixed quantity: Yearly average $1m^3/m^2$, so calculated that the urban vegetation green space need man-power water supply 2.06 hundred million m^3. According to investigates Beijing city green space vegetation's real water supply is $0.25m^3/m^2$, and the urban green space actual water used total quantity is 0.52 m^3, so the water scarcity is 1.54 hundred million m^3.

③ The lake eco-environmental water demand in the city

According to "Ecological environmental Water demand Theory, Method And Practice" (Yang Zhifeng and so on, Scientific Publishing house, 2003) (in city limit's lake and artificial river) the smallest eco-environmental water demand is 0.70 hundred million m^3.See Table 2.

Table 2. the minimum lake eco-environmental water demand in Beijing in 2000 (hundred million m^3)

Evaporation	Seepage	Habitat	Water recharge	Based flow	Total
0.0328	0.0064	0.0205	0.0137	0.6307	0.7041

In 2000, the actual water supply is 0.43 hundred million m^3, water storage capacity is

0.980 hundred million m^3 in the beginning, and the ecological environment water scarcity is 0.17 hundred million m^3.

Table3. the minimum surface water eco-environmental demand in Beijing in 2000(hundred million m^3)

	Channel	River and lake	Green vegetation	Total
Water demand	12.98	0.70	2.06	15.74
Water consumption	7.78	0.53	0.52	8.83
Water scarcity	5.20	0.17	1.54	6.91

(2) Surface water eco-environmental demand value and water scarcity loss accounting

①Value of eco-environmental water demanded and water scarcity loss accounting in channel

Use Haihe river's basin data 1.35 Yuan /m^3 to calculate the Beijing rivers' dilution value, the result is 17.52 hundred million Yuan /a.

According to Costanza etc.（1997），and if according to the price index in 2000 the conversion price is 3488.26 Yuan /hm^2, considered that the ecological environment value's increment effect, take the growth factor is 3%, then it results in 3811.72 Yuan /hm^2, then Beijing river eco-environmental water for biodiversity value is 0.21 hundred million Yuan /a, converted 0.02 Yuan /m^3.The surface water can adjustment temperature and saves the energy, the parameter is 56.67 Yuan /m^3.a, so Beijing's rivers adjustment climate and save energy 366.63 hundred million Yuan /a.

②Value of rivers and lakes eco-environmental water demanded and water scarcity loss accounting

According to the dilution ability[3] (1.35 Yuan /m^3) and the channel cleanout effect (refers to "15" research projects " Key technologies of Ecology Water Computation Research", 5.12 Yuan /m^3) the water's value is 6.47 Yuan /m^3, the river-lake eco-environmental water demand value is 4.53hundred million Yuan, and the water scarcity loses 1.10 hundred million Yuan.

③Value of the urban green vegetation eco-environmental water demanded and water scarcity loss accounting

The country "85" research project "Beijing City Botanical garden Ecological benefit's Research" indicate that vegetation can absorb CO_2 228.72t/hm^2, and release O_2 159.13t/hm^2 and so on, so the urban green vegetation eco-environmental water demand value and water scarcity loss is as Table 4.

About the green space water holding capacity, through the former experiments take 25% as the proportion of interception rainfall. With the shadow project method to calculate the water conservation value computation, the investment which namely the construction same storage capacity's storage facility (for example reservoir) needs, the value = water-holding capacity×the unit storage capacity cost. According to 2000's price the reservoir's cost to construct is 5.714 Yuan /m^3 , converted by Beijing city green space area, Beijing green space for water conservation's value can reach 0.295 hundred million Yuan.

According to related green vegetation improvement mass of atmosphere value correlation data: Antiseptic value 875 Yuan / hm^2•a, increases negative oxygen ion

value is 55.0 Yuan / hm^2•a, the storage preserves soil moisture value is 1065.6 Yuan / hm^2•a, humidification and adjusting temperature value is 278.0 Yuan / hm^2•a, so Beijing green vegetation value that make purification mass of atmosphere is 0.47 hundred million Yuan (in 2000 price).

Through the accounting, the green space eco-environmental water value is as Table4. According to normal water demand 2.06 hundred million m^3 of existing construction area green space in Beijing in 2000, the value converts for 5.92 Yuan/ m^3. And there are also large green spaces need artificially recharge water, so green space water scarcity loss is 9.12 hundred million Yuan. According to the value contribution, of water resources to the green space, takes the water used benefit sharing coefficient as 0.5, so the net value of green space's eco-environmental water used was 6.1 hundred million Yuan in 2000 in Beijing, and per m^3 water's value contribute to green vegetations is 2.96 Yuan, the green space water scarcity creates loss 4.56 hundred million Yuan.

Table 4. Eco-environmental water use value of green spaces in Beijing

Function	Amount of dust absorption	Absorb CO_2	Release O_2	Improve Air quality	Water conservation	Total
Value(hundred million Yuan)	0.19	7.95	3.28	0.47	0.30	12.19

According to the ecological and environmental experts' opinion, municipal reservoir constructions in Beijing destroyed the natural river 's ecological equilibrium, the reservoir's eco-environmental benefit did not arrive at original natural river system displaying the ecological environment benefits as river mouth, therefore did not calculate the value of reservoir's ecology water used adding to the total eco-environmental value in Beijing. And based on the water resources disposition, the surface water eco-environmental demand value and water scarcity loss accounting is as Table 5. The conversion for per m^3 water's value is 23.11 Yuan /m^3.

Table 5. The value and water scarcity loss on the satisfaction to minimum surface water eco-environmental demand in 2000 in Beijing

Classification	Channel	River and lake	Green spaces	Sum
Value (Yuan/m^3)	29.61	6.47	2.56	
Total value(Hundred million Yuan)	384.36	4.53	6.10	394.99
Water scarcity loss (Hundred million Yuan)	154.27	1.1	4.56	159.93

2.2 Eco-environmental value of ground water

Beijing ground water's ecological environment value can be calculate mainly through the value which prevent the surface subsidence and the value maintaining the bearing pressure of water-bearing to prevent the ground water form being polluted. As a result of the material limit, the ground water ecological environment's value is taken by: max {economic loss which avoids reducing ground water ultra exploitation, ground water recharging cost}.

According to Chinese Geology University's "City Groundwater resources Sustainable Mining Model Study" report, that in 2000 Beijing land subsidence surpassed 0.15m, and average economic loss of unit area will reach 4.5 Yuan /m^2. In 2000 in Beijing the most greatly land subsidence surpassed 0.59m, the area of influence surpassed 600km^2.Estimating from this, the eco-environmental loss which for the ground water ultra exploitation creates 27 hundred million Yuan in 2000 in Beijing. And in 2000 the

ground water ultra exploitation is 11.97 hundred million m^3, ultra exploitation the per m^3 water loss is 2.26 Yuan /m^3. (If according to the multi-annual means 24.55, in 2000 the ground water ultra exploitation is 2.6 hundred million m^3, and the unit water loss is 10.38 Yuan /m^3.)

Beijing is in Huabei region, if take the Shandong Province cost which recharges ground water to restores the ground water's eco-environment as references, considering the price factor and the time effect, the eco-environmental value in 2000 in Beijing is 4.43 Yuan /m^3.

2.3 Ecological environment value of water resources

The eco-environmental water used value in Beijing in 2000 is: surface water is 23.11 Yuan/m^3,ground water is 4.43Yuan/m^3，and the comprehensive value is 10.56 Yuan/m^3。

3 Value accounting of economic water use

The water resources' social and economy value calculation includes the effective and the disadvantageous consequence which caused by all social economy water use, which embody the advantageous and disadvantageous effect or the utility that the water resources produce in economic society (including ecological environment loss and water pollution economic loss).

3.1 Economic society water use accounting

The total water use volume of economic society in 2000 in Beijing is 40.40 hundred million m^3， including 13.25 hundred million m^3 surface water and 27.15 hundred million m^3 groundwater，which far beyond the water supply volume 16.86hundred million m^3。According to the basic data of Beijing, the accounting results are as shown in Table 6.

Table 6. Water resources use condition in 2000 in Beijing (Hundred million m^3)

Sub item		Industry	City life	River and lake	Agricultural use	Sum
Water use volume		10.52	9.76	0.43	19.69	40.4
Water source classification	Surface water	5.27	4.45	0.43	3.1	13.25
	Ground water	5.25	5.31		16.59	27.15

3.2 Positive effectiveness of economic society water use

The effectiveness economic society water use manifests in water used benefit shares among various departments. Because the lack on data information, it is difficult to establish the detailed relations between water use volume and production volume in minute department, so from the entire society national economy production angle, established Douglas production function which take capital, labor force and water as the essential factors, to analyze the production water supply utility value.

The total water volume in 2000 year in Beijing is 40.4 hundred million m^3, GDP is

2478.76 hundred million Yuan. The value that unit water shared in GDP is 61.355 Yuan /m^3. By the total water consumption, GDP, total capital and employed population during 1988~2002 year economic society, when caring about factor in which the water used efficiency, the capital enhance use efficiency and the labor force level developing along with the time, obtains the entire social product function through fitting as follows:

$$GDP = 0.0023K^{0.528}L^{0.545}W^{0.242} \quad (3)$$

By the functional relations, in the situation which capital, labor force and so on essential factors are invariable, increasing per m^3 water used value in the economic society to GDP is 14.73 Yuan /m3.

3.3 The water polluted cost caused by economy society water use

(1) Surface water polluted cost caused by economy society water use

According to the water quality ~ economical loss factor function in economic society water use [3], the surface water polluted cost caused by economy society water use in 2000 in Beijing is 112.32 hundred million Yuan; the estimate result is as shown in Table 7.

Table7. Water polluted cost caused by economy society water use in 2000 in Beijing

Sub item	Agriculture	Industry	City life	Tourist industry	Town planning	Sum	Total water (hundred million m^3)	Per m^3 water loss (Yuan/m^3)
Loss(hundred million Yuan)	12.59	8.43	43.99	23.94	23.36	112.32	40.4	2.78

(2)Ground water polluted cost caused by economy society water use

Ground water polluted cost caused by economy society water use in 2000 in Beijing is 2.25 hundred million Yuan[3], and the per m^3 water loss is 0.06 Yuan/m^3。

Generalized analyzing, the ecological environmental loss caused by the economic society water use sums as 114.57 hundred million Yuan, according to same year economic society water use 40.4 hundred million m^3,the shared per m^3 water use cost is 2.84 Yuan /m^3.

3.4 Value and loss of economic society water use

Considering each loss calculation achievement, the accounting results are as shown in Table 8. The total ecological environmental loss caused by the economic society water use sums as 327.95 hundred million Yuan, the shared per m^3 water use cost is 8.11 Yuan /m^3.

Table 8 Environment and resources accounting evaluation indexes of economic society water use

Idem	Total (hundred million Yuan)	Percentage of GDP	Per capital volume (Ten thousand Yuan)
1. Environment loss index	114.57	4.62%	0.090
Surface water polluted loss	112.32	4.53%	0.088
Ground water polluted loss	2.25	0.09%	0.002
2. Resources depletion index	213.02	8.59%	0.167
Surface water depletion loss	159.93	6.45%	0.125
Ground water depletion loss	53.09	2.14%	0.042
Sum of two index	327.59	13.21%	0.257

Through the green account of water resources, the eco-environmental synthesized water used value was 10.56 Yuan /m^3 in 2000 in Beijing, the economic society synthesized water used value is 14.73 Yuan /m^3, and the environment economy synthesis loss was 8.11 Yuan /m^3.

4. The conversion of water value and analysis of gains and loss

If ignoring the negative effect or loss caused by economy water use, Driven by interest, the economic man should be in the pursuit of economic development as a main goal because of the water use benefits of economy outweighing environment. Furthermore, the local people are still in the low level life, and the role and value of water used in ecological environment is still in the senses, not completely and deeply. Similarly, now many propaganda material also just stay in scattered, rather than the profound information, could not to hit and shock the theory of driven by interest which is in the souls deeply. The economic man only values the positive benefits of economic water use, not from the overall social welfare including direct and indirect, tangible and intangible, positive and negative, short-term and long-term, economy and natural environment, to study and evaluate, and make an optimal decision. Therefore, in the life level below or at the primary stage of rich, especially in state of paying less attention to high quality requirements in ecological environment and its demand weakening, or the destruction of ecological environment due to water scarce not endangering the survival, the economic man will be yet driven by interest to consider economic water use at first, although the ecological environment water use and benefits can get attention gradually, it is also in secondary demand status.

At present, people's knowledge is not enough to calculate the value of ecological water use completely. From the simple arithmetic, social welfare value of economic water use is still positive, namely 6.62 yuan/m^3. If seeing the problem in a shortsighted view, it is profitable to economic occupying ecological water. But 6.62 yuan/m^3 < 10.56 yuan/m^3, the net benefits of economic water use are less than the value of environmental water use; water does not reach the optimal allocation and utilization.

5 Economical regulation analysis of water resources optimal allocation

In the view of social welfare, put environment and economy into a virtual water market (not exist yet), use the market water price mechanism to study the allocation of Beijing economic water use in 2000, according to the optimal allocation principle. Applying the theory of partial equilibrium analysis, studies the effect of water price.

5.1 Water demand equation

The budgetary expenditures of water consumption *M*, according to the coefficients of development stage [5] and the international average standard: the charge of living water is about 3% of water incomes; the charge of industrial water could be 5% of total industrial output value.

According to the 2000 Engel's coefficient 36.3% [1], Beijing economic development stage coefficient $l = \frac{1}{1+e^{-1/0.363+3}}$=0.44. The proportion of expenditure budget of living water consumption for income: 3%×0.44＝1.32%; The proportion of expenditure budget of industrial water use for total industrial output value: 5%×0.44=2.2%. In 2000, the second industrial output value of Beijing is 3878.35 billion Yuan [1], the budgetary expenditures of water consumption are for 85.324 billion Yuan; According to the 6.5% (international rate) of output value of the tertiary industry and the coefficient of development stage, budgetary expenditures of the tertiary industry water consumption are: 3952.92[1]×6.5%×0.44＝113.05 billion Yuan; Income of resident is 695.5 billion Yuan [1], the budgetary expenditures of the water consumption are for 9.18 billion Yuan; According to 1.32% of GDP (same as living), the budgetary expenditures of the agriculture water consumption are for 195.18 [1] ×1.32%＝2.58 billion Yuan. The budgetary expenditures of whole society total up to 210.14 billion Yuan, namely 8.5% of GDP.

According to value, economic water utility preference coefficient set as 0.6, the ecological environment water utility preference coefficient set as 0.4.

Based on the analysis of water use in 2000, the ecological environment basic water demanded cannot be guaranteed and lack 6.91 billion m^3. According to the basic human "water" (BRW) 50L for each day [7], the basic water of life to safeguard should be 230 million m^3/a. To establish the utility maximization equation of water demand.

$$\begin{cases} \max U = 0.6\ln(Q_s - 2.3) + 0.4\ln(Q_e) \\ p_s Q_s = M = 0.085GDP = 210.14 \\ 2.3 \le Q_s + Q_e \le 40.4 \\ Q_s, Q_e, p_s \ge 0 \end{cases} \tag{4}$$

U is the utility of total water use, Q_S is the water demanded by economic society, Q_e is water demanded by ecological environment, p_s is the price of economic water use.

5.2 Water supply equation

From the water supply, according to the market mechanism, take the profit maximization of water supply as an aim, the equation is as follow:

$$\begin{aligned} \max\ \pi &= v_e Q_e + p_s Q_s - C \\ &= 10.56 \times (40.4 - Q_s) + p_s Q_s - C \end{aligned} \tag{5}$$

π is the profits of water supply, v_e is the value of ecological water use, C is the total cost of water supply to economy and ecological loss due to economic water use not rationally.

When to meet the basic water demanded by ecological environment, the water 40.4-6.91 =33.49 billion m^3 might be use by economy. With the whole cost accounting of economic society water use, setting the quantity of tap water supply as a constant, by the analysis of the financial costs in Beijing 2000, the relationship between whole cost of social economic water use and water consumption is as bellow:

$$\begin{cases} C = 8.11 Q_s + 0.6(Q_s - 7.54) + 12.54 & Q_s > 33.49 \\ C = 2.84 Q_s + 0.6(Q_s - 7.54) + 12.54 & Q_s \le 33.49 \end{cases} \tag{6}$$

Taking the simultaneous equations of water supply and demand, do the iterative computation. In 2000, the total water 40.4 billion m^3 used by social economy are reallocated between ecological environment and social economy, the result is that comprehensive water price is RMB 8.01/m^3 under maximum utility of water use, 24.76 million m^3 could be used by social economy, water quantity available for ecological environment is 15.64 billion m^3, the optimal comprehensive benefits of economic and environmental water use is 440 billion Yuan. Through analysis, it can be found if the ecological basic water demanded can not be satisfied, with the bear ability of social economy, all the cost caused by social economy water use would not be recovered.

In 2000, Beijing actual comprehensive price is 2.81 yuan/m^3 that cannot promote reasonable allocation and sustainable utilization of water resources.

6 Counter measures of water reasonable allocation

Beijing water failed to reach optimal allocation, the main reason is not only market failure, such as water price etc., but also water management and macro-control measures problems. Therefore, for the optimal allocation of water resources rationally, many kinds of methods combined are necessary. Overall, mainly these points should be taken seriously as following.

(1) To strengthen ecological water right management. Considering the ecological benefits enjoyed by the human as a right, set up the water resources management control system which rights and obligation is peer to peer. The basic standard of ecological environment water demanded should be taken scientifically, to ensure social economy and ecological environment coordinated development.

(2) Use the preferential policy encouraged, promote economic sectors saving water, and then protect the ecological water use. Through the priority development, tax cuts and subsidies, encourage cleaning production and saving water.

(3) Fully exert the market mechanism, scientifically make water price to allocating water rationally and optimally. With the passage of time, the ability to shoulder economically cost of water use and scarce degree of water resources will change, water price must dynamically be adjusted accordingly, in order to guarantee their normal adjustment ability of supply and demand of water resources. With the water became restriction of production and life environment beautification more and more seriously, it can be consider to gradually set price of ecological environment water use relating to human welfare, changes the view of ignoring value of ecological water use, promote to value ecological water use as well as economics'.

REFRENCES

[1] Beijing Municipal Bureau of Statistics. (2001). Beijing Statistical Annual on the 2000[M]. Beijing: China Statistics Press

[2] Beijing Water Authority. (2001).Water Resources Communiqué of Beijing [J], Beijing: Water publication Press

[3] China Institute of Water Resources and Hydropower Research. (2004). Coordinated Development analysis of Water Resources and National Economy. 155~156.

[4] Ni Hongzhen.(2004). A Study on Water Resources Value and Price Based on the System of Integrated Environmental and Economic Accounting（D）, Beijing : China Institute of Water Resources and Hydropower Research

[5] LI Jinchang. (1999). Ecological Axiology(M), Chongqing: Chongqing University Press,95～106

[6] Wang Hao, Ruan Benqing, Shen Dajun. (2003).The Theory and Practice of Water Pricing Face to Sustainable Development（M）, 38~89

[7] Peter H·Gleick.(2000).The World's Water (M), Beijing: China Agricultural University Press, 32~36.

The implications of discretizing continuous random variables: An example using the U.S. Geological Survey reporting standards for streamflow data

By Stacey A. Archfield[1] and Richard M. Vogel[2]

[1]Department of Civil and Environmental Engineering, Tufts University, Medford, MA, 01255. Phone: 508-490-5072, Email: stacey.archfield@tufts.edu
[2]Department of Civil and Environmental Engineering, Tufts University, Medford, MA, 02155. Phone: 617-627-4260, Email: richard.vogel@tufts.edu

ABSTRACT

One of the most fundamental assumptions in statistical analysis is whether the random variable of interest is continuous or discrete. Natural processes such as streamflow are considered to be continuous random variables, able to take on an unlimited number of possible values. However, to reflect data accuracy, reported streamflow values are generally rounded. For example, the U.S. Geological Survey (USGS) reports mean daily streamflow values less than 1 cubic foot per second (ft^3/s) to the nearest hundredth place (0.01), resulting in only 99 possible values for streamflows between 0 and 1 ft^3/s available for statistical analyses. The limits of the data subsequently result in the discretization of a continuous variable; the effects of discretization on the statistical properties of the data could affect applications such as moment estimation, regional frequency analysis, and distribution fitting, particularly for low flows where rounding could substantially reduce the number of possible values. In an effort to determine the effects of discretization, large samples of independent data were generated from a generalized probability distribution to the sixteenth decimal place. The synthesized data was then rounded according to USGS streamflow-reporting standards. Initial comparisons of the original synthesized data and the rounded data show that estimates of the sample mean and standard deviation only differed slightly. Additional experiments will explore the effects of rounded data in other statistical analyses as well as for autocorrelated data.

INTRODUCTION

A common technique to estimate flow-duration-curve quantiles at ungaged locations is to develop regional regression equations that relate measurable basin characteristics to streamflows

at the quantiles of interest. In southern New England, it is a well-documented feature of these regional-regression equations that the prediction error and uncertainty in the regression equations increase with increasing exceedance probability (see Reis and Friesz, 2000 and Archfield and others, 2007). It is commonly hypothesized that this phenomenon occurs because there does not yet exist a set of explanatory variables capable of adequately estimating low flows. The purpose of this paper is to explore the streamflow estimates themselves as an alternative explanation for the increased prediction error and uncertainty in low-flow regional-regression equations. In particular, this paper begins to explore the effect that U.S. Geological Survey (USGS) reporting standards for streamflow have on the estimation of streamflow quantiles.

U.S. GEOLOGICAL SURVEY STANDARDS FOR REPORTING STREAMFLOW DATA

The USGS rules for reporting streamflow values are given in table 1 (U.S. Geological Survey, 2009). Given those reporting rules, there are only a limited number of values that exist for streamflows less than 1,000. Notably, there are only 99 possible unique values for streamflows less than 1 cubic foot per second and 90 possible unique values for streamflows between 1.0 and 10 cubic foot per second. The reporting rules have the effect of discretizing streamflow - a continuous random variable - into a discrete random variable. Because the effects of this reporting standard are most pronounced for streamflows less than 10 cubic feet per second, it is hypothesized that the reporting standard has some effect on any statistical analysis performed with the discretized values.

Table 1. U.S. Geological Survey rules for reporting streamflow values

Range of streamflow values, in cubic feet per second	Reporting rule for streamflow values
Less than 1	Nearest hundredth
Between 1.0 and 10	Nearest tenth
Between 10 and 1,000	Whole numbers
Greater than 1,000	Three significant figures

STUDY AREA AND STREAMFLOW-GAGING STATIONS

We begin by exploring the impact of the reporting rules in Table 1 on actual streamflow records. We consider the 66 gaged basins shown in Figure 1 all of which do not contain major water withdrawals or return flows and the predominant land cover in the basin is forest; however, the presence of dams within the basins was not considered in the identification of minimally-impacted sites. Daily, continuous streamflow observations at the gages ranged from 10 to 86 years, with 47 gages containing greater than 20 years of continuous record and the drought of the 1960s, which is considered to be the drought-of-record in New England (fig. 1). Armstrong and others (2008) provide a detailed description of the geologic, hydrologic and climatic conditions of the study area as well as information on water use, land cover, and the presence of dams within the study basins.

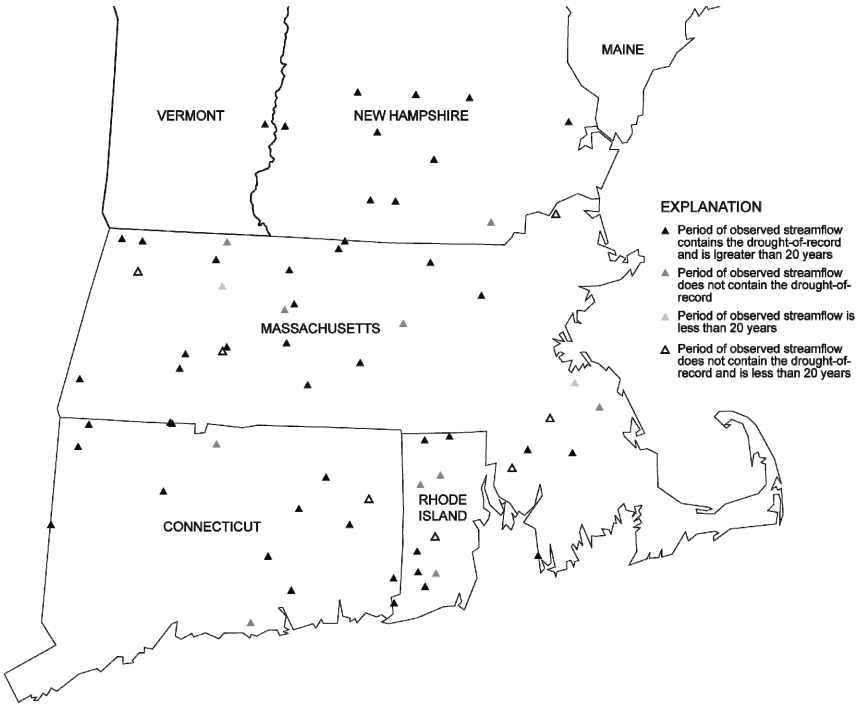

Figure 1. Locations of 66 minimally-impacted streamflow gages in southern New England.

CHARACTERIZATION OF STREAMFLOW DATA

The effects of the USGS reporting standard (table 1) is evident from a simple count of the number of unique values that occur in each of the streamflow records at the 66 study gages shown in figure 1. The average record length of the study gages is 15,655 daily streamflow values; however, the average number of unique streamflow values is only 547. One of the more dramatic cases is the Moss Brook at Wendell Depot, MA streamflow gage, which has over 24,400 daily streamflow observations but only 361 unique streamflow values. In general, at most only 8 percent of the reported observed flow values across all of the study gages were unique values and the number of unique values in a particular streamflow record tends to increases with the median streamflow computed from the gage's period of record as shown in fig. 2.

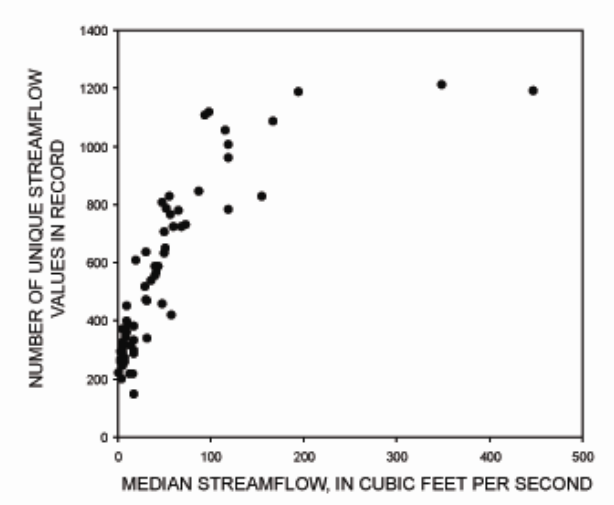

Figure 2. Relation between the numbers of unique streamflow values and the median streamflow for 66 study gages in southern New England.

SIMULATION EXPERIMENT AND RESULTS

To begin to understand the effects of the USGS reporting standard on quantiles and moments of streamflow estimated from the discretized streamflow values, 66 samples of 20,000 independent streamflow values were generated from a 3-parameter generalized Pareto (GP) distribution using the parameter sets estimated from the 66 observed streamflow records (fig. 1). Vogel and Fennessey (1993) found that a GP distribution provides a good approximation to the distribution of daily streamflows in Massachusetts. More recently Archfield et al. (2007) determined a kappa distribution to be a more appropriate distribution than the GP for representing the distribution of daily streamflow, however, the GP distribution was used in this analysis to avoid complications in parameter estimation that is introduced by use of the kappa distribution.

Simulated data were then rounded according to the USGS reporting rules shown in table 1. The mean, median and standard deviation of the simulated data and simulated-then-rounded data were compared. Differences in the estimated means and standard deviations varied only slightly; however, it is interesting to note the USGS reporting rules do not preserve the sample mean and variance of the data. When the median values were compared, the simulated data and simulated-then-rounded data differed by as much as 4 percent. A difference of up to 4 percent was also observed when a comparison of the data at the 90- and 95-percent exceedence probabilities was made. Such large exceedance probabilities, associated with low streamflows are where we expected the most significant differences to occur. The difference is more pronounced when one takes the natural log of the streamflows, as is commonly done in regional-regression analysis. In fact, more than a 15-percent difference was observed when comparing the log-transformed simulated data and rounded-simulated data for 3 samples.

DISCUSSION

Reported values are rounded based solely on the magnitude of the streamflows; independent of the measurement or rating errors. The reporting rules do not appear to be based on any error or uncertainty analyses, making it unclear why these rules are practiced. The experiment presented in this paper only considers an independent random variable; whereas, daily streamflow is highly autocorrelated. The autocorrelation in daily streamflow will only exacerbate the number of non-unique values, particularly for low flows where the number of possible values is much smaller. In the experiment presented in this paper, we were unable to simulate a record that contained a similar number of non-unique values as the observed streamflow records; this is because the samples we generated were independently generated. Future experiments will generate daily streamflow data based on an autocorrelated process. Additional work will explore the effects of this reporting standard in other statistical analyses, such as distribution fitting and regional frequency analysis. Future work will also explore the use and utility of quantile estimators presented in Vogel and Fennessey (1994). These estimators show promise in smoothing the flow-duration curve and thus converting discretized data into a continuous streamflow series. . It is also unclear if the effects of this reporting standard are more pronounced for smaller sample sizes than the 20,000 used here. We expect to report on all of the above issues in much greater detail at our oral presentation at the 2009 EWRI conference in Kansas City.

REFERENCES

Armstrong, D.S., Parker, G.W., and Richards, T.A. (2008). Characteristics and classification of least altered streamflows in Massachusetts: *U.S. Geological Survey Scientific Investigations Report* 2007–5291, 113 p., plus CD-ROM.

Archfield, S.A., and Vogel, R.M. (2008). A decision-support system to assess surface-water resources in Massachusetts, *Proceedings of the American Society of Civil Engineers World Water and Environmental Resources Congress*, Honolulu, Hawaii, 2008.

Archfield, S.A., Vogel, R.M. and Brandt, S.B. (2007). Estimation of flow-duration curves at ungaged sites in southern New England, *Proceedings of the American Society of Civil Engineers World Water and Environmental Resources Congress*, Tampa, Florida, 2007.

Vogel, R.M. and N.M. Fennessey, (1993). L-Moment Diagrams Should Replace Product-Moment Diagrams, *Water Resources Research*, Vol. 29, No. 6, pp 1745-1752.

Vogel, R.M. and Fennessey, N.M. (1994). Flow Duration Curves I: A New Interpretation and Confidence Intervals, ASCE, *Journal of Water Resources Planning and Management*, Vol. 120, No. 4, 1994.

Ries, K.G. and Friesz, P.J. (2000). Methods for Estimating Low-Flow Statistics for Massachusetts Streams, US Geological Survey WRIR 00-4135.

U.S. Geological Survey (2009) Documentation for the 2005 Annual Water Data Report located at http://wdr.water.usgs.gov/wy2005/documentation.html#stage accessed on January 26, 2009.

ACKNOWLEDGEMENTS

The authors would like to thank the Massachusetts Department of Environmental Protection and the U.S. Geological Survey Cooperative Water Program for their funding and support of this work.

Uncertainty Analysis: You Need to Know What You Don't Know

Presented by:

David T. Williams[1], Ph.D., P.E., CFM, D.WRE, F.ASCE, P.H.
Joseph D. Countryman[2], P.E., D.WRE

[1] Senior Technical Advisor, Water Resources, PBS&J, 2032 Lowe St., Suite 202, Fort Collins, CO 80525, dtwilliams@pbsj.com
[2] Principal, MBK Engineers, 2450 Alhambra Boulevard, 2nd Floor, Sacramento, CA 95817, countryman@mbkengineers.com

Whose Idea Was This to Use Risk and Uncertainty Analysis in Water Resources?

Many of the ideas presented in this paper have been around for numerous years. The main proponent of this approach for use in water resources subjects is the U.S. Army Corps of Engineers (COE) and it use is mandated for COE flood control projects. In the early 1990s, the COE and other entities re-examined the concept of freeboard for their flood control projects and felt that the use of Risk and Uncertainty concepts would help quantify the additional required protection above the design elevation instead of adding a somewhat arbitrary value (NRC, 2000). This paper presents the concepts of Risk and Uncertainty Analysis (affectionately termed as RU) as applicable to floodplain management and issues. It also goes over some of the important aspects of RU analysis that should be understood by water resources engineers and floodplain managers. Within about 5 years, floodplain managers will be required to be knowledgeable on the subject of Risk and Uncertainty!

Types of Uncertainties (adapted from Pappenberger, et.al., 2006; NRC, 2000)

1. Natural Uncertainty (Variability) - Refers to inherent variability in the physical world
2. Uncertainties that stem from the assumed inherent randomness and basic unpredictability in the natural world
3. Characterized by the variability in known or observable populations
4. Knowledge Uncertainty - Lack of scientific understanding of natural processes and events in a physical system.

   - Process model uncertainty – Models (e.g., HEC-RAS and HEC-HMS) are an abstraction of reality and can never be considered true. Measured data versus modeled data gives an insight into the extent of model uncertainty.
   - Statistical inference uncertainty - Quantification of the uncertainty of estimating the population from a sample. The uncertainty is related to the extent of data and variability of the data that make up the sample.

5. Statistical model uncertainty - Associated with the data fitting of a statistical model. If two different models fit a set of data equally well but have different extrapolations/interpolations, then it is not valid - statistical model uncertainty.

Some Definitions used in Uncertainty Analysis

1. Deterministic Analysis: Uses single values for key variables, e.g., use of an expected flow to determine a single water surface elevation.
2. Probabilistic Analysis: Uses a probability distribution rather than a single value for key variables - captures and describes uncertainty of the variable, e.g., expected flow including a range of possible flows to determine a range of possible water surface elevations.
3. Annual Exceedance Probability (AEP): Measures "the probability of getting flooded" in any given year, considering the full range of floods that can occur – uses only the peak discharge of each year.
4. Conditional Annual Non-Exceedance Probability - CNP (Assurance): The probability that a project will provide protection from a possible distribution of a specified event. For levees, includes the chance of capacity exceedance and the chance of failure at lesser stages. CNP is computed by determining the expected exceedance/failures at top of levee (levee will not fail before overtopping); or application of levee elevation failure probability curve (chance of failure prior to overtopping).

Who is Monte Carlo and Why are We Afraid of Him?

The Monte Carlo techniques are integral to RU analyses. Monte Carlo methods are a class of computational algorithms that iteratively evaluates deterministic model results using input of random numbers. The methods are used when it is infeasible or impossible to compute an exact result with a deterministic algorithm. There is no single Monte Carlo method; instead, the term describes a large and widely-used class of approaches. These approaches tend to follow a particular pattern:

1. Define a domain of possible inputs (e.g., average and standard deviation).
2. Generate inputs randomly from the domain, and perform a deterministic computation on them.
3. Aggregate the results of the individual computations into the final result.

Example of the Monte Carlo Techniques: Determine π by Random Darts

A simple example of the Monte Carlo method can be seen in a classic experiment, using random dart throws to determine an approximate value of π. First, take a quarter of a circle and place it within a square (see Figure 1). If one randomly throws darts at that square (disregard any that fell out of the square), some would land within the circle, and some would land outside. The proportion of darts that landed in the circle to darts that landed outside would be roughly one-fourth of π (see equations below).

$$\frac{\#\text{ darts hitting shaded area}}{\#\text{ darts hitting inside square}} = \frac{\frac{1}{4}\pi r^2}{r^2} = \frac{1}{4}\pi$$

or

$$\pi = 4\frac{\#\text{ darts hitting shaded area}}{\#\text{ darts hitting inside square}}$$

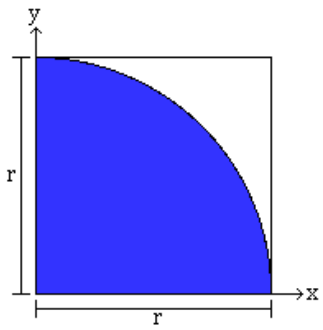

Figure 1. ¼ Circle Within a Square

If only a few darts are thrown, the results of the throws would not lead to a very accurate value for π. As in most Monte Carlo simulations, thousands or millions of trials must be made so that outliers do not affect the accuracy of the results.

Parameter Value and Possible Range

To perform a Monte Carlo simulation, the parameter(s) of interest must be valued and the variation of that value determined. This is illustrated in Figure 2 in which a parameter can have a "best guess" value and a probability of its range of values. This is termed a probability density function (PDF). This PDF can be transformed into a Cumulative Probability Distribution Function (CDF) as illustrated in Figure 3.

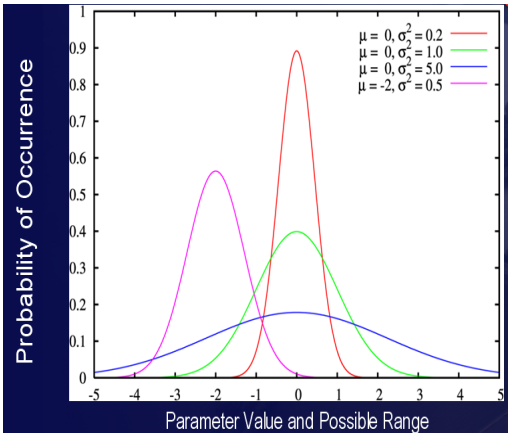

Figure 2, Example of a Probability Density Function

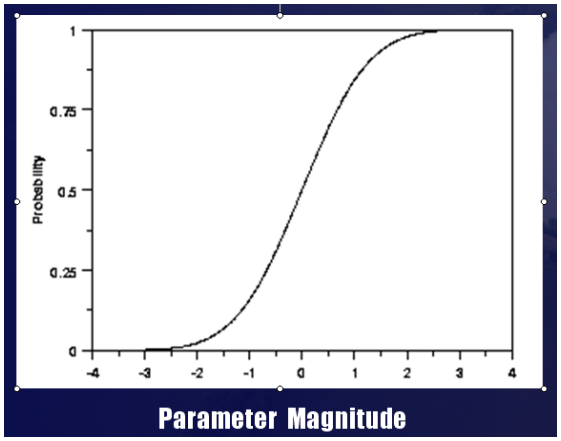

Figure 3. Example of a Cumulative Probability Distribution Function

Determining the Answer Using Monte Carlo

Once the CDF of a parameter is determined, it is randomly sampled and each sample value and its associated probability are noted. These values can be input to a model for simulation (e.g., precipitation depth in HEC-HMS) and the result of the simulation (e.g., peak discharge) has the associated probability of the input value, resulting in another CPD. In this example, the probability distribution of the peak

discharge. The following procedure is applicable to Hydrology and Hydraulics using RU Analysis. Results can be used for a variety of floodplain management strategies.

1. Determine the CDF for a given discharge
2. Determine the CDF of the parameters affecting the water surface elevations in a hydraulic model
3. Use Monte Carlo to develop a CDF of the water surface elevation versus discharge relationship, combining the hydrologic and hydraulic CDFs
4. Results are associated probability for each water surface elevations for the given discharge

How Do We Determine the Hydrologic Parameters and Their Variations?

For hydrology, frequency analysis of discharges can be used from gage data and statistically determine the mean and variation of the peak annual discharge. The standard error of flood discharges from gaging station data can be determined as described by Kite (1988). The standard error of gaging station estimates can also be determined using the 84-percent one-sided confidence limits as described in Bulletin 17B (WRC, 1981). The approach by Kite (1988) is favored because it considers the uncertainty in the skew coefficient while the Bulletin 17B approach does not.

The standard errors of estimate or prediction of the USGS regression equations can also be obtained from regional flood frequency reports (e.g., Dillow, 1996). The standard error of rainfall-runoff model estimates is not usually known. WRC report (1981) suggested that it is larger then the standard error of regression estimates in part because rainfall-runoff models based on a single-event design storm are not usually calibrated to regional data.

Confidence limits or standard errors of flood discharges from rainfall-runoff models can be estimated if an equivalent years of record is assumed for the flood discharges - USACE (1996b). However, no established practice of estimating the uncertainty of flood estimates from rainfall-runoff models.

How Do We Determine the Hydraulic Parameters and Their Variations?

Variations in water stage can be done by observation of the stage vs. discharge relationship. The uncertainty in stage for ungaged locations can be estimated by the following (COE, 1996b):

$$S = [0.07208 + 0.04936\ I_{Bed} - 2.2626x10^{-7}A_{Basin} + 0.02164\ H_{Range} + 1.4194 \times 10^{-5}Q_{100}]^2$$

Table 5-1
Bed Identifiers

Material	Identifier
Rock/Resistant Clay	0
Boulders	1
Cobbles	2
Gravels	3
Sands	4

Where: S = standard deviation in meters, H = maximum expected stage
A = basin area in sq km, Q = 100 year discharge, I = from Table 5-1

Hydraulic models can be used and the parameters that could be varied are:

- Expansion and contraction ratios (usually important only at bridges and culverts)
- Other parameters influences on the stage vs. discharge relationship are very small
- Manning's "n" values – requires a mean value, maximum and minimum, and an assumed distribution (usually a normal "Gaussian" distribution): this is the most common parameter to be varied. See Figure 4 for example.

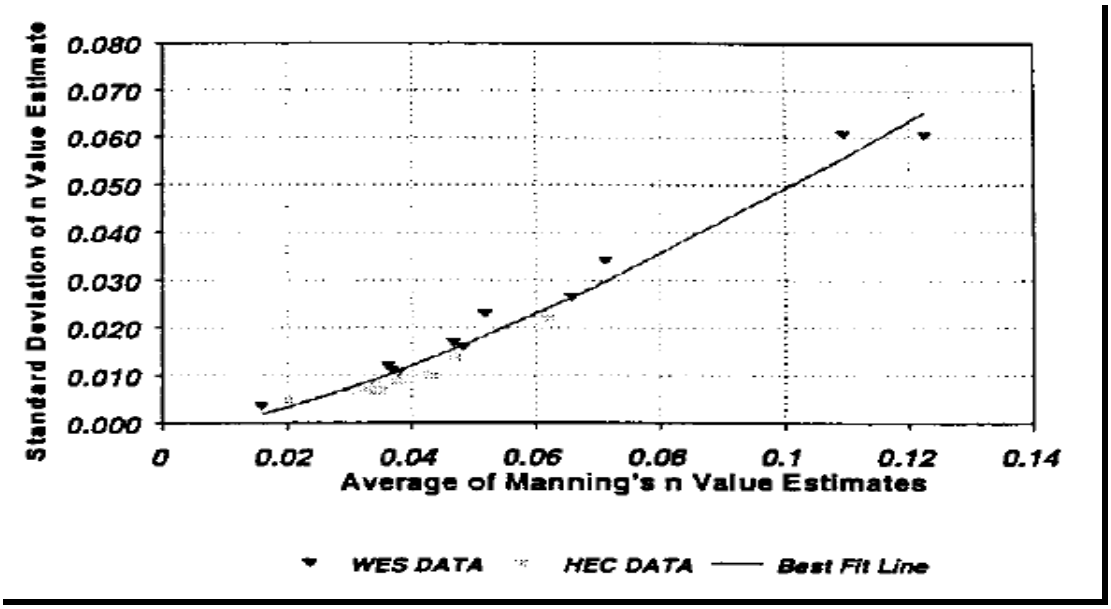

Figure 4. Estimation of the variation in Manning's "n" (COE, 1996b)

What Does The Results Look Like?

The variation in discharge can be used to determine the variation in stage (with in-bedded Monte Carlo simulation in the hydraulic model) and then used to determine the variation in stage, as illustrated in Figure 5. The variation of the stage for a single probability is illustrated in Figure 6.

Hydrologic and Hydraulic Model Linkages and Stochastic Modeling

The Corps of Engineers' Engineering and Research and Development Center (ERDC) sponsors the development of WMS 7.0, which is an interface of various hydrologic models. Within WMS 7.0, the ability to link an HEC-1 hydrologic analysis to a HEC-RAS model has been developed. HEC-HMS is planned for later. The user defines certain modeling parameters for both models within a range of probable values and then runs the linked simulations. Only CN and Precipitation are currently

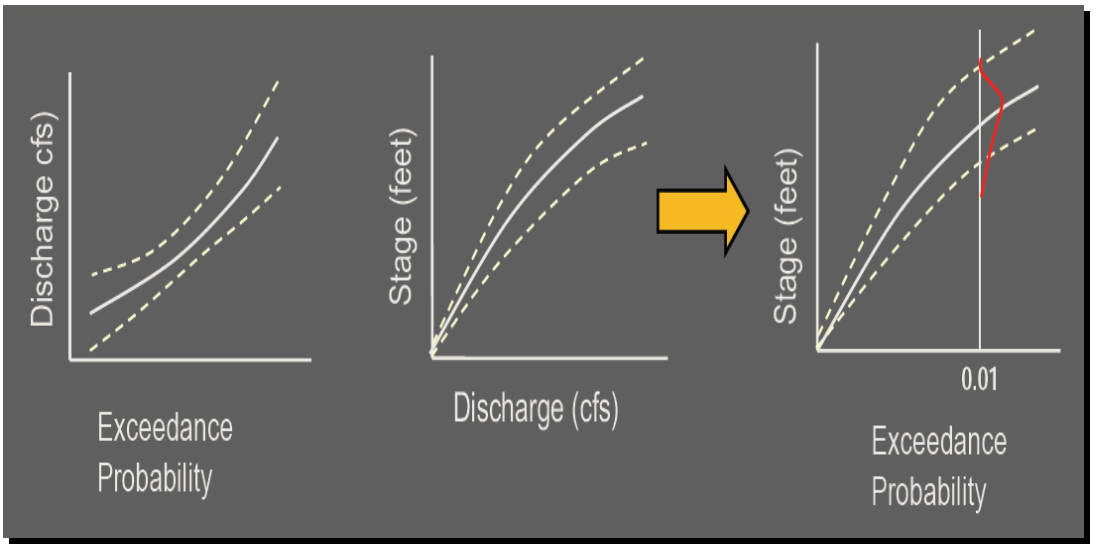

Figure 5. Determination of Stage Uncertainty (Deering, 2007

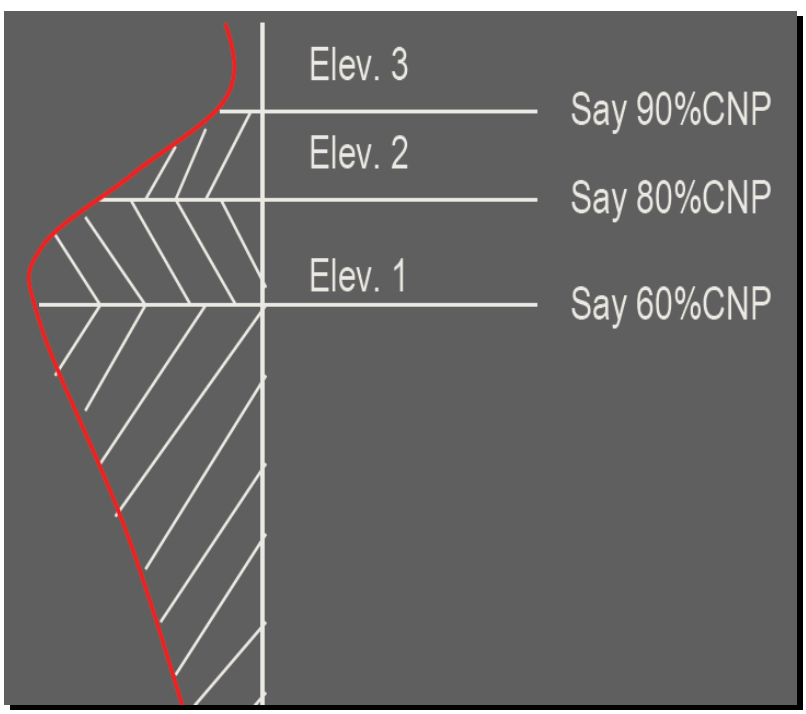

Figure 6. Stage Variation for a Single Probability (Deering, 2007)

the possible parameters for HEC-1 models and Mannings roughness for HEC-RAS models. Additional parameters will be added to both models.

What Are Some Applications of RU to Levees?

The traditional design for top of levees includes freeboard (to account for uncertainties) added to the design water surface elevations. If the uncertainties can be quantified as a range of probabilities, the freeboard can be determined if a certain

CNP can be agreed upon (say 90 or 95% CNP). The lower the acceptable risk (want less risk of failure), the higher the CNP and the higher the top of levee above the traditional deterministic water surface elevation.

What is the Corps policy on RU and Levees?

The US Army Corps of Engineers (COE) has guidelines for computing an aggregated annual exceedance probability (AEP) in the floodplain for levee certification (see USACE, 1996a, 1996b and NRC, 2000). The COE (since 1996) does not use "freeboard" but uses the concept of the CNP elevation above the deterministic elevation. In the NRC (2000) report, it states that the COE approach to levee certification is well thought out, but is still lacking in certain areas. Two recommendations for improving the current methods (NRC 2000) are: (1) consider spatial variability in flood studies and (2) use the AEP more widely as the measure of levee performance for both COE and FEMA.

What about FEMA, Corps, Levees and RU?

In 1996, FEMA and the Corps proposal combined FEMA's old criteria with the Corps RU methodology. This supplements 44 CFR 65.10. The Corps and FEMA agreed to certify a levee if its elevation was at least:

- (1) at the 90 percent CNP elevation if it is greater than 3 feet.
- (2) at the 95 percent CNP elevation if it is greater than 2 feet
- (3) at 3 feet if it is between the CNP of 90 percent and 95 percent.

Why bother with RU for levees? (Davis, 2007)

Consider these situations:

Situation 1. Flat gradient, flow/stage variability low, long flow/stage record, high integrity existing levee.
Situation 2. Steep gradient, flow/stage variability high, short record, uncertain integrity existing levee.

Traditional methods would give one value for freeboard, but risk analysis explicitly quantifies difference between these situations and reflects residual risk. From an HEC study of 13 levee systems, the following observations were made:

- FEMA standard of 3 feet of freeboard provides a median expected level of protection of approximately 230 years, range of <100 years to >10,000 years
- Corps – FEMA 90% - 3ft - 95% criterion provides an average of 3.3 feet of freeboard and yields a median expected level of protection of approximately 250 years, range of 190 to 10,000 years
- The 90 percent CNP has an average of 3.0 feet of freeboard and a median expected level of protection of approximately 230 years, range of 170 to 5,000 years
- The 95 percent CNP has an average of 4.0 feet of freeboard and a median expected level of protection of approximately 370 years, range of 210 to 10,000 years.

Use of RU and CNP for Levee Elevation Determinations

We can use the results of the RU analysis to determine inundation extents for any CNP. From the CNP elevations for a given AEP (say 100 year event), we can map the floodplain inundation areas for a given CNP. Smemoe (2004) has proposed using uncertainty analysis for this purpose. This can aid the floodplain managers in regulation of the floodplain. Flood insurance rates within contour intervals could be determined by a more realistic and physically based methodology

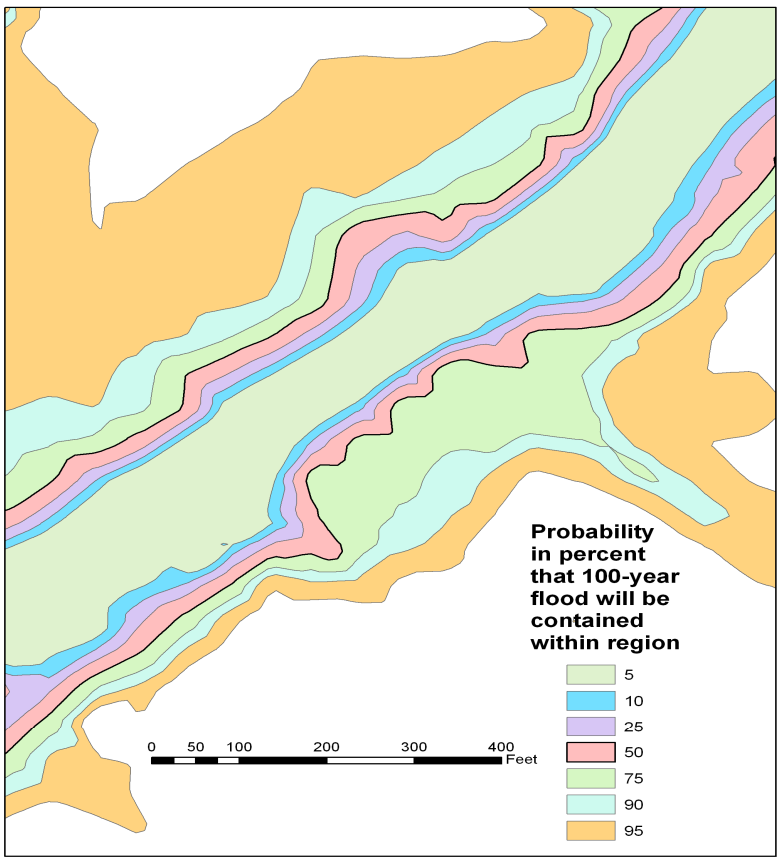

Figure 7. Example Floodplain Probability Contours

RU Design Issues

Much of the uncertainty that is required for an R&U analysis is difficult to define with any accuracy; e.g., standard deviation of the water surface elevation for a given flow, coincident probabilities of stage and wind for a wave calculation, coincident timing of flood peaks for two different size drainage areas upstream from the project, etc. Deterministic assumptions are made on these items and because designers have been trained to analyze "worse" case conditions, they establish "Base" case or most likely conditions that are far more extreme than the most likely. The RU analysis therefore begins with a significant bias that is unrecognized.

In flood control, the greatest uncertainty lies in the estimation of the flow frequency curve and/or stage frequency function. Engineers and Hydrologists have relied upon Confidence Interval calculations found in Bulletin 17B (WRC 1981b) to estimate this uncertainty. It has been shown that this procedure can vastly overestimate the uncertainty because it does not recognize physical limitations of a watershed (PMF, etc). Therefore, the assurance level calculations based on Bulletin 17B Confidence Interval calculation can be extremely misleading.

Current procedures used by the Corps to establish "90% Assurance" levels that are not based on Bulletin 17B are quite sensitive to changes in the 1.1 and 2-year flood levels when calculating the 200-year 90% Assurance level. This is unexplainable.

A levee project designed with R&U will have a design top of levee but no design water surface elevation. This makes operation and maintenance requirements for the channel unknowable.

Levee system performance assumptions for an R&U analysis have not been determined. If there is 1100 miles of levee upstream from the project, a true RU analysis must consider the possibility that upstream levees will fail. Upstream levee failure will impact the stage frequency function at the project location. A deterministic design may assume upstream levees do not fail and this assumption becomes just another of the "worse case" assumptions associated with deterministic design. A no failure assumption destroys the basic assumption of RU analysis.

In the Sacramento Valley, numerous levee failures have occurred over the years and before the levees overtop. Is it reasonable to assume for instance that 80+ miles of levee would overtop during a 500-year flood and not fail? A "No Failure" assumption for an R&U analysis would vastly overestimate the flood risk.

There is a requirement to determine "when" and "how" a levee will fail. A levee that fails after the peak flows and stages have occurred has a much different impact on flood stages than a levee that fails before or at the peak flow and stage condition. History has provided numerous examples of all three failure conditions.

The "How" assumption is also significant. A 25 foot wide levee break has a different impact than a 1000 foot wide break. It is necessary that a hydraulic model can be programmed to execute the desired failure scenarios. At this time, the models are limited in their capability to simulate varying assumptions of this type.

A Risk Analysis methodology that incorporates "Worse" case assumptions as the base case significantly overstate the risks associated with a project and could potentially lead to bad decision making.

A requirement to use RU procedures when correcting project defects has been stated as a Corps 408 permit requirement but with no definitive guidance provided. What does it mean and how to implement it is a very significant policy issue.

References

1. Davis, Darryl (2006), "Risk Analysis and Levee Certification," FEMA Levee Policy Review Task Committee, Washington, DC
2. Deering, Michael (2007), "Certification of Levee Systems for the National Flood Insurance Program Certification Program," USACE Infrastructure Conference, Detroit, MI
3. Dillow, J. A. (1996), "Techniques for Estimating Magnitude and Frequency of Peak Flows in Maryland," U.S. Geological Survey Water-Resources Investigations Report 95-4154, p. 55
4. Kite, G. W. (1988), "Frequency and Risk Analysis in Hydrology," Water Resources Publications, Littleton, Colorado, p. 257
5. National Research Council (2000), "Risk Analysis and Uncertainty in Flood Damage Reduction Studies," National Academy Press
6. Pappenberger, F., Harvey, H., Beven, K. J., Hall, J., Romanowicz, R., and Smith, P. J. (2006), "Risk and Uncertainty – Tools and Implementation," UK Flood Risk Management Research Consortium, Lancaster University, Lancaster, UK
7. Sehlke, Gerald, Hayes, D. F., Stevens, D. K. – Editors (2004), "Critical Transitions in Water and Environmental Resources Management," World Water and Environmental Resources Congress, June 27 – July 1, 2004, Salt Lake City, Utah, USA
8. Smemoe, Christopher, Nelson, J., and Zundel, A. (2004), "Risk Analysis Using Spatial Data in Flood Damage Reduction Studies," World Water Congress, ASCE, 2004
9. Thomas, Wilbur O., Grimm, M., and McCuen, R. (1999), "Evaluation of Flood Frequency Estimates for Ungaged Watersheds," Hydrologic Frequency Analysis Work Group, Hydrology Subcommittee of the Advisory Committee on Water Information (ACWI)
10. U.S. Army Corps of Engineers (2007), Engineer Technical Letter (ETL) 1110-2-570, "Certification of Levee Systems for the National Flood Insurance Program (NFIP)," Washington, DC., September 2007
11. U.S. Army Corps of Engineers (2000), ER 1105-22-100, "Guidance for Conducting Civil Works Planning Studies," Washington, DC., April 2000
12. U.S. Army Corps of Engineers (1996a), ER 1105-22-101, "Risked-Based Analysis for Evaluation of Hydrology/Hydraulics, Geotechnical Stability, and Economics in Flood Damage Reduction Studies," Washington, DC., March 1996
13. U.S. Army Corps of Engineers (1996b), EM 1110-2-1619, "Risk-Based Analysis for Flood Damage Reduction Studies," Washington, DC., 1996
14. Water Resources Council (1981a), "Estimating Peak Flow Frequencies for Natural Ungaged Watersheds – A Proposed Nationwide Test," Hydrology Subcommittee, U.S. Water Resources Council, 346 p.
15. Water Resources Council (1981b), "Guidelines for Determining Flood Flow Frequency, Bulletin 17B," Hydrology Subcommittee, U.S. Water Resources Council

Uncertainty and Sensitivity Analysis for Models with Calibrated Parameters

Seung Uk Lee[1]and Jery R. Stedinger[2]

[1]School of Civil and Environmental Engineering, Cornell University, Ithaca, NY, 14853-3501, Email: sl673@cornell.edu,
[2]School of Civil and Environmental Engineering, Cornell University, Ithaca, NY, 14853-3501, Email: jrs5@cornell.edu

Abstract

Traditional measures of sensitivity in watershed modeling are based upon a framework wherein parameters are specified externally to a model, so one can independently investigate the impact of uncertainty in each parameter on model output. However, when parameter estimates results from a joint calibration to observed data, the resulting parameter estimators are interdependent and different procedures should be employed. For example, over some range, evaporation rates may be adjusted to correct for changes in a runoff coefficient, and vice versa. As a result, descriptions of the precision of such parameters may be very large individually, even though their joint response is well defined by the calibration data. These issues are illustrated with the simple abc rainfall-runoff model. In fitting the abc model to data from the Pigeon River Watershed (North Carolina), our analysis explicitly accounts for rainfall measurement errors so as to adequately rpresent the likelihood function for the data given the major source of errors causing lack of fit.

1. Introduction

Traditionally the parameters of most watershed and ecological models were estimated as part of an extensive calibration process conducted by experienced models. Currently, the trend in the profession is to make much greater use of automated calibration procedures (Yapo et al., 1996; Boyle et al., 2000; Duan et al., 2003; Bekele and Nicklow, 2007). This eliminates the tedious and subjective trial-and-error exercises that modelers conducted in earlier years. However, without the need to conduct such trial-and-error analyses, a modeler can lose the previous insight into how well different parameters can be resolved, and how they interact. Uncertainty and sensitivity analyses need to provide such insight for model development and calibration, and well as the appropriate confidence to attach to model predictions.

How to obtain appropriate parameters for any modeling study is an issue which has faced considerable attention within the hydrologic community and has motivated many studies. Gupta et al. (2003) offer an interesting reflection on recent advances in automatic calibration of watershed models. Attractive algorithms of uncertainty analysis for highly non-linear models with multi-dimensional parameter spaces are presented in Mugunthan and Shoemaker (2006) and Blasone et al. (2008a). A multi-step automatic scheme (MACS) that emulates the thought processes of expert-manual calibration of Sacramento model is described by Hogue et al. (2003). The combined impacts of

parameter uncertainty and model error have been well documented (Kuzcera et al., 2006; Clark and Vrugt, 2006; Ajami et al., 2007).

Many hydrological studies have embraced the Bayesian credo and have derived different model specification schemes that characterize uncertainties and which reflect such uncertainties in prediction limits on the simulated model outputs. These approaches include classical Bayesian schemes (Kuczera and Parent, 1998; Bates and Campbell, 2001; Thiemann et al., 2001; Thyer and Kuczera, 2003; Marshall et al., 2005a; Choi and Beven, 2007; Yang et al., 2007; Stedinger et al., 2008).

In this study, we review the sensitivity analysis for watershed models when parameters are calibrated. In Section 2, we discuss traditional sensitivity and uncertainty analyses measures. Sections 3, 4 and 5 discuss the appropriated definitions of parameter uncertainty when data is used to calibrate several parameters jointly. Finally, Section 6 uses the abc model with a likelihood function that reflects the critical rainfall estimation errors to illustrate different sensitivity analysis approaches and a posterior Bayesian evaluation of parameter uncertainty.

2. Traditional Measures of Sensitivity

Morgan and Henrion (1990) provide definitions and motivation for traditional sensitivity analysis and uncertainty analysis:

"It is usually not immediately obvious which assumptions and uncertainties may significantly affect the conclusions. The purpose of sensitivity and uncertainty analysis is to find out. *Sensitivity analysis* is the computation of the effect of changes in input values or assumptions (including boundaries and model functional form) on the outputs. *Uncertainty analysis* is the computation of the total uncertainty induced in the output by quantified uncertainty in the inputs and models, and the attributes of the relative importance of the input uncertainty in terms of their contributions. Failure to engage in systematic sensitivity and uncertainty analysis leaves both analysts and users unable to judge the adequacy of the analysis, and the conclusions reached."

Several metrics have been employed by different investigators for sensitivity and uncertainty analysis; they include:

- one-at-a-time analysis of each factor
- joint analysis changing several factors at a time
- parametric analysis of selected parameter ranges
- probabilistic analysis that can use correlation, regression, or other approaches to examine how much of the uncertainty in the output is attributable to uncertainty in each parameter input.

Morgan and Henrion (1990, pp. 174-176) describe metrics used to quantitative describe sensitivity, as do Loucks and Stedinger (1994); Saltelli et al. (2000); Frey and Patil (2002); Loucks et al. (2005); and Benaman et al. (2005).

3. Sensitivity Analysis with Calibrated Parameters

The traditional measures of sensitivity described in Section 2 are based upon the concept that parameters are determined externally to a model, so one can independently

investigate the impact of uncertainty in those parameters on the output of the model. Figure 1 represents a conceptualization of a modeling process when this is appropriate.

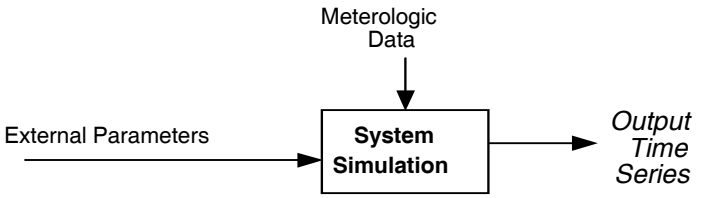

Figure 1: Simple conceptualization of modeling process.

However, it is important to recognize that hydrologic models have many key parameters that are estimated in the calibration process. That means that these "calibrated parameters" are estimated as best one can to make the model output time series match observed flow and stage series when the model is run with the corresponding historical meteorological data. This is important for at least three reasons (Madsen, 2000; Kavetski et al. 2003):

1. Any errors in external parameters may have been compensated for by adjustment of calibrated parameters so that the model output matches observed values. For example, if depression storage is over-estimated, the runoff coefficient may be underestimated in the calibration process so that the resulting model better estimates observed runoff. Thus calibrated parameters may have errors that compensate for errors in external parameters.

2. Because calibrated parameters are estimated jointly, errors may be interdependent. For example, it may be difficult for the model to exactly estimate a detention storage parameter and a runoff coefficient: over some range almost the same model output can be obtained with a higher detention storage parameter and a lower runoff coefficient, and visa versa. Thus when the calibration procedure attaches to detentions storage a standard deviation σ_d, that value implicitly assumes that such variations in detentions storage goes with corresponding and compensating variations in the runoff coefficient. Thus it is no longer appropriate in a sensitivity analysis to independently vary detention storage by ± 2 σ_d without making the corresponding adjustments in other parameters.

3. The mathematical model is not a perfect representation of reality. The calibration set providing flow and stage data and some groundwater elevations is not without measurement error and does not exactly match the spatial and time averages with which it is compared. Thus the match between the model predictions and the calibration data will not be perfect making it impossible to precisely resolve the values of calibrated parameters.

Initially, before serious calibration of the model, traditional sensitivity analysis that varies one parameter at a time can have an important role revealing or documenting when, where, and which parameters have a large impact on model predictions. Benaman et al. (2005) discuss such procedures. However, after a model is calibrated, a different concept of sensitivity analysis is appropriate that reflects the interdependence among possible errors that remain after the calibration process.

4. Calibration and Parameter Uncertainty

Figure 2 presents an appropriate conceptualization of the modeling process when parameters are calibrated with available data describing watershed behavior .

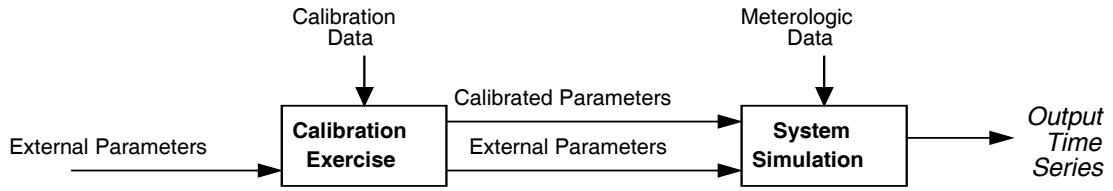

Figure 2: Conceptualization of modeling process when calibration data is employed to estimate some parameters.

Given the values of external parameters, calibration data is never sufficient to accurately resolve all of the parameters of complex watershed and environmental models. Thus in considering the conceptualization of the modeling process above, one recognizes that conditional on the assumed model structure and the external parameter values, there can be significant uncertainty in the calibrated parameters. Furthermore, errors in different parameters of complex models are often interrelated. Thus we desire to consider the uncertainty in the calibrated parameters, and the resulting uncertainty in the simulation model output time series and statistics based upon that time series.

5. Bayesian Approach

Figure 3 describes a Bayesian conceptualization of the modeling process. Here no distinction need be made between external and calibrated parameters. What were before external parameters are now parameters for which external data is thought to provide very precise information; as a result their values will not change during the calibration process: the size of canals, the dimension of cells, and the area of land in different crops would be examples. Still the values of these parameters could be adjusted during the calibration process if a much better fit could be obtained, though it is also possible to prohibit such adjustments.

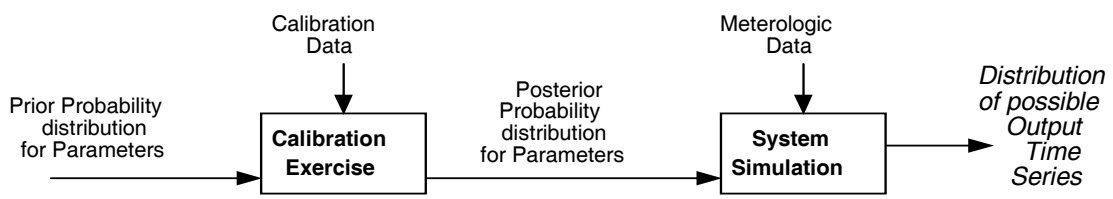

Figure 3: Bayesian conceptualization of modeling process when calibration data is employed to improve the understanding of the likely values of the parameters.

Moreover, there are now no internal parameters whose values are only determined by calibration. Such calibrated parameters initially have some prior distribution representing conceptual reasonableness, physical appropriateness, and experience elsewhere with similar natural systems. However, if such prior information does not result in a relatively precise resolution of the values of such parameters, then the information about system performance introduced in the calibration process is likely to be the major determinant of the value of such parameters.

In Figure 3, having derived the posterior distribution for the model parameters, the results of system simulation is a distribution of possible system performance time series. This distribution represents how the system might operate with the ranges of parameters that are reasonable given both prior information and the information added in the calibration process. In practice the distribution of parameters is described by a large number of generated values, perhaps with different weights (probabilities), which yield an equal number of simulation time series, with the same weights (probabilities). Stedinger et al. (2008) cite examples.

6. Case Study

6.1 The abc model

This study focuses on the abc model introduced by Fiering (1967) as a pedagogical tool. See also Kuczera and Parent (1998). The abc model uses two linear equations with only three parameters to describe a water balance between precipitation, evaportranspiration, groundwater storage and streamflow. The initial value S_0 of the aquifer storage variable S_t must be specified. The model is driven by the rainfall P_t:

$$Q_t = (1-a-b)P_t + cS_{t-1} \quad (1)$$
$$S_t = (1-c)S_{t-1} + aP_t$$

Here Q_t is the streamflow output and S_t is the groundwater storage at given time t. The abc model partitions rainfall P_t into evapotranspiration bP_t, recharge to the groundwater store aP_t, and quickflow to the stream $(1\text{-}a\text{-}b)P_t$. The parameter c is the fraction of groundwater storage released as baseflow in each period.

6.2 Data

A 2-year record (water year: 1 Jan. 2003-31 Dec. 2004) for the Pigeon watershed, North Carolina (USGS Cataloging Unit: 06010106), was employed consisting of daily precipitation from a rainfall USGS raingage station 03455773, and mean daily streamflow discharge rate from USGS streamflow station 03456500. Some precipitation was shifted a day to obtain a better fit to the daily flow data.

6.3 Calibration and rainfall errors

With just a single point-rainfall gage, or even the average of several gages in or near a watershed, there will exist a potentially large error in basin-wide average precipitation. This is especially important for large storm events which provide the bulk of the water entering this hydrologic system. Errors in this storm rainfall input can be very important, resulting in misrepresentation of streamflows, and yield correlated residual errors as observed in the calibration process. In order to reflect likely rainfall errors in large storms, the abc model was rewritten to include errors as:

$$Q_t = (1-a-b)P_t \exp(\delta_i) + cS_{t-1} \quad (2)$$
$$S_t = (1-c)S_{t-1} + aP_t \exp(\delta_i)$$

where δ_i is a normally distributed error for storm event P_t ; δ_i has mean 0 and standard deviation σ_δ.

In this study, the objective function is to minimize the sum-of-squared errors so as to identify maximum likelihood estimators (MLE); based on the assumption that the flow

and rainfall measurement errors are lognormally distributed, the negative of the log-likelihood function is:

$$L = \sum_{t=1}^{n} \frac{(\ln Q_t - \ln \hat{Q}_t)^2}{2\sigma_e^2} + \frac{n}{2} \ln 2\pi\sigma_e^2 + \sum_{i=1}^{I} \frac{\delta_i^2}{2\sigma_\delta^2} + \frac{I}{2} \ln 2\pi\sigma_\delta^2 \qquad (3)$$

where n is the number of days of data available for calibration, I is the number of storm events modeled as having an error, and σ_e^2 is a constant model error variance.

Figure 4 shows that the match between observed and simulated streamflow. Here one observes that the rainfall error calibration approach produces nearly identical results to the observed streamflow data using 4 estimated parameters, and 26 storm errors for the days with the largest precipitation totals. The correlation between the observed and predicted streamflows is 0.918. Without the 26 precipitation errors, the best calibration yields a correlation between observed and predicted flows of 0.820. With precipitation errors, the autocorrelation of the prediction errors was 0.206, whereas without precipitation errors, the autocorrelation of the prediction errors as 0.301.

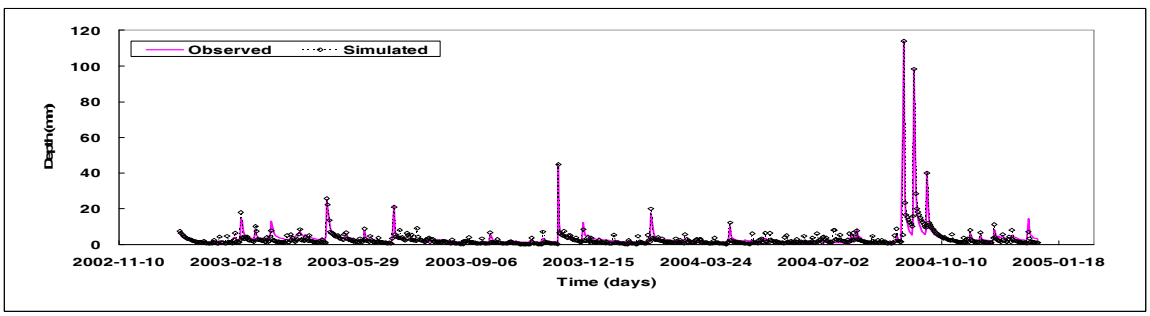

Figure 4: Observed streamflow and the simulated flow at calibration period.

6.4 Parameter uncertainty through MCMC

In this study the Bayesian posterior distribution of the model parameters was represented using 10,000 iterations of a Monte Carlo Markov Chain Gibbs sampler algorithm (Geman and Geman, 1984); the first 1,000 samples generated were removed to forget the initial parameter set. Figure 5 describes the relationships between two pairs of parameters, a and b, and b and c. From the scatter plot of b and c, one sees that the evapotranspiration parameter, b, has a wider range for small baseflow parameter c. It means that the uncertainty of parameter c is smaller than the others with small standard deviation. We also see that there is a strong linear relationship between the recharge and evapotranspiration parameters, a and b. These scatter plots show the relationships among parameters when calibrated parameters are estimated jointly. Table 1 summarizes posterior correlations among the three estimated parameters.

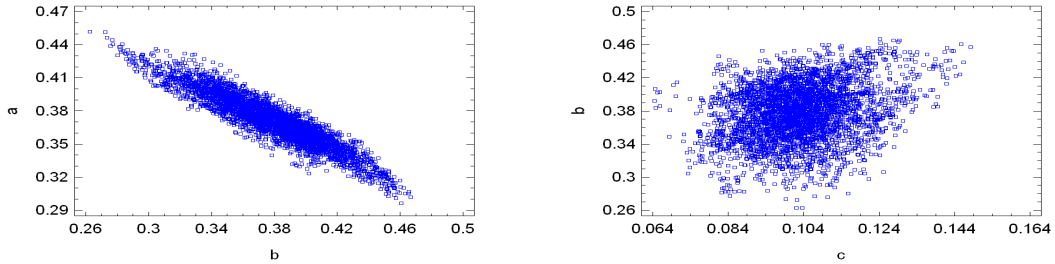

Figure 5: Scatter plots of parameter pairs generated by the Bayesian MCMC analysis.

Table 1. Correlations between the estimated parameters and MCMC posterior moments.

Parameter	Correlation			Mean	St. Dev.	MLE*
	a	*b*	*c*			
a	1			0.371	0.023	0.394
b	-0.930	1		0.379	0.034	0.349
c	-0.435	0.232	1	0.103	0.012	0.095

* Values of maximum likelihood estimators; σ_δ=0.135 and σ_e= 0.074.

6.5 The sensitivity index

Two sets of sensitivity indices were evaluated to illustrate the important of reflecting interdependences in calibrated parameters in a sensitivity analysis.

1) *Simple sensitivity index:* This represents a simple conceptualization of a sensitivity analysis as described in Figure 1. A dimensionless one-at-a-time sensitivity index for each parameter β_i is

$$e = \beta_i / Flow \,.\, \partial Flow / \partial \beta_i \Big|_{\beta_j \, fixed} \tag{4}$$

where $\partial\beta_i$ is a change in parameter *i* from the nominal value and $\partial Flow_i$ is the corresponding change in flow, or some other output value of our interest. In this study, the outputs of interest were the lowest streamflow, the mean streamflow, the peak flow, and the sum of square errors. For the total sum of square errors, sensitivity index (4) is generally not of interest, because at the optimized parameter, equation (4) is zero. Thus a critical statistic that would be of interest is the normalized second derivative

$$d_{SS}^2 = \beta_i^2 / SS \,.\, \partial^2 SS / \partial \beta_i^2 \tag{5}$$

where ∂SS is the change of sum of square errors which describes how well a model fits a calibration data set.

2) *Sensitivity index with parameter interaction:* A sensitivity index for when parameters are calibrated as described in Figure 2 is:

$$e_C = \beta_i / Flow \,.\, \partial Flow / \partial \beta_i \Big|_{\beta_j optimized} \tag{6}$$

This index describes the sensitivity of parameter β_i when other parameters β_j (j≠i) are adjusted to retain the best fit possible; thus other parameters β_j will be re-optimized to consider the interrelation of different parameters of the model. One can also compute the value of d_{SS}^2 when the other parameters are simultaneously re-optimized.

6.6 Sensitivity analysis

Sensitivity analysis can consider basic input data, model structure, initial conditions (S_0) or weather parameters. Here our focus is on calibrated model parameters, specifically *a*, *b* and *c*. Figure 6 provides the results of the two sensitivity analyses for the 3 parameters. The sensitivity analyses consider the lowest flow, mean flow, the peak flow, and the sum of squares. The lowest and peak flows were considered as the averages of the lowest and highest in each of the two years respectively. The indices of sensitivity were measured with +/-1 % changes in each parameter. Both sensitivity analysis statistics

indicate that *a* (recharge from rainfall) is potentially the most important parameter. Both statistics indicate *a* is critical to low flows, though the new statistic attributes to *a* twice the impact; however, they disagree about *a*'s impact on high flow. The traditional statistics indicate *a* is important to floods, as a simplistic analysis would indicate. But recalibration of *b* compensates for variations in *a* so that model predictions of floods are little effected by errors in *a*. However, such changes in *a* have a critical impact on low flows and also the mean flow. The traditional sensitivity analysis indices miss entirely the link between errors in *a* and the mean flow. Parameter *c* (base flow from storage) is the next most important, and both statistics indicate that it has a critical impact on low flows. Overall, as shown by the sensitivity analysis indices for the sum of squares, *a* is the most important parameter, *c* is next most critical, and *b* (evapotranspiration) has the smallest impact on model performance. The sensitivity analysis index for the sum of squares without recalibration ranks *b* before *c*, but this makes little sense. These results show that the simple sensitivity analysis that does not reflect parameter interactions when parameters are calibrated fails to capture several critical issues.

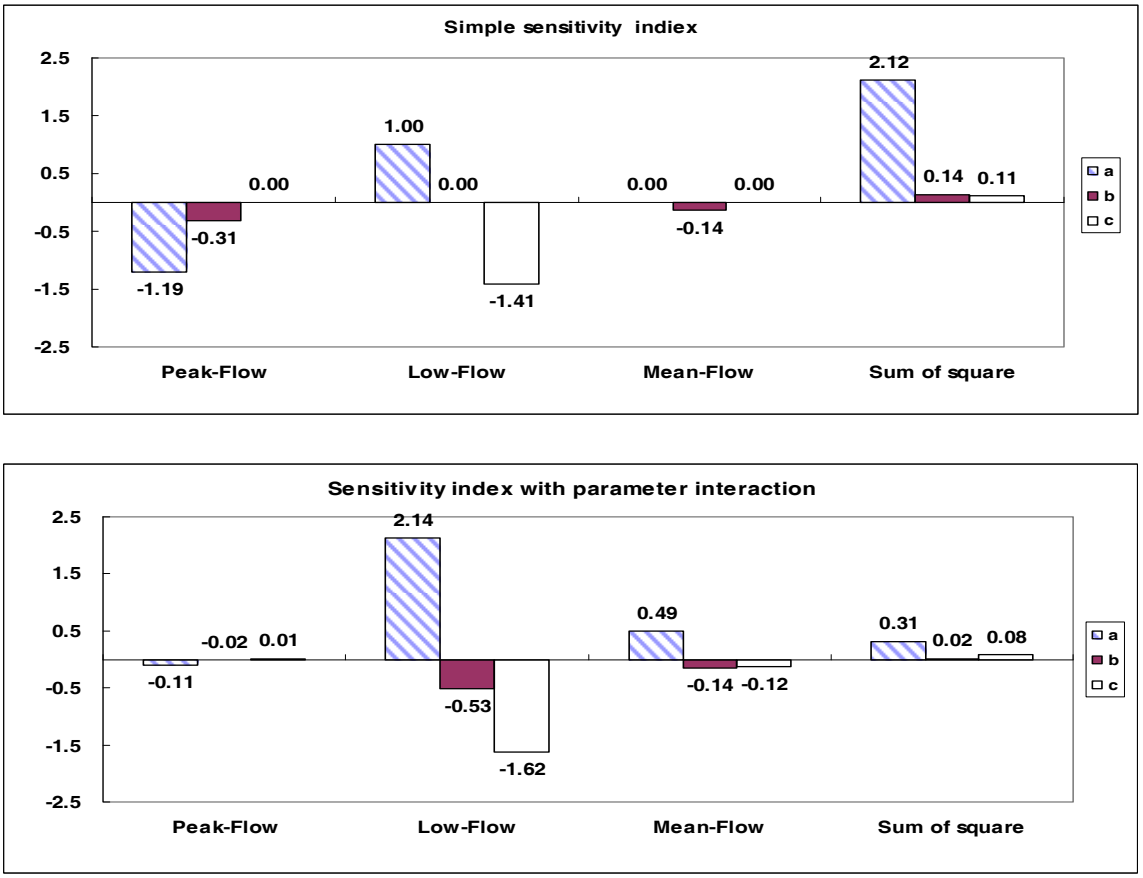

Figure 6: Sensitivity results with two different sensitivity indices.

7. Conclusions

In this study, we analyzed the importance of watershed parameters using one-at-a-time sensitivity index and sensitivity index considering parameter interactions. The one-at-a-time sensitivity analysis can misrepresent critical issues when parameters are jointly

calibrated. For this example, the new sensitivity analysis indices capture critical issues reflecting the interaction among the parameters in the calibration process.

To improve the reliability of a model and its ability to be understood, it is important to be explicit about precision and uncertainty throughout the model calibration and verification processes. This includes recognizing the precision of data, which are generally point measurements used to represent spatial and time averages. Clearly the daily precipitation from one gauge employed in this study provided an imperfect description of basin precipitation, and precipitation errors resulted in correlation among flow errors and degraded the goodness of fit. As part of the calibration process, quantitative measures of the precision of estimated parameters should be developed. Similarly, sensitivity and uncertainty analyses can be used to quantify the impact of parameter uncertainty on the precision of simulated measures of system performance.

References

Ajami, N., Q. Duan, and S. Sorooshian (2007). "An integrated multi-model ensemble prediction approach to account for total uncertainty." *Water Resour. Res*., 43, W01403, doi:10.1029/2005WR004745.

Bates, B.C., and E.P. Campbell (2001). "A Markov chain Monte Carlo scheme for parameter estimation and inference in conceptual rainfall-runoff modeling." *Water Resour. Res., 37*(4), 937-947.

Bekele, E. G., and J. W. Nicklow (2007). "Multi-objective automatic calibration of SWAT using NSGA-II." *J. of Hydrol.*, 341, 165-176.

Benaman, J., C.A. Shoemaker, and D.A. Haith (2005). "Calibration and Validation of the Soil and Water Assessment Tool on the Cannonsville Reservoir Watershed." *J. of Hydrologic Engineering, 10*(5), pp. 363-374.

Blasone, R-S., J.A. Vrugt, H. Madsen, D. Rosbjerg, B.A. Robinson, and G.A. Zyvoloski (2008a). "Generalized likelihood uncertainty estimation (GLUE) using adaptive Markov chain Monte Carlo sampling." *Advances in Water Resour., 31,* 630–648.

Boyle, D. P., H. Gupta, V. Hoshin, and S. Sorooshian (2000). "Toward improved calibration of hydrologic models: combining the strengths of manual and automatic methods." *Water Resour. Res.*, 36, 3663-3674.

Choi, H.T., and K. Beven (2007). "Multi-period and multi-criteria model conditioning to reduce prediction uncertainty in an application of TOPMODEL within the GLUE framework." *Jour. of Hydrol*., 332, 316-336.

Clark, M. P., and J. A. Vrugt (2006). "Unraveling uncertainties in hydrologic model calibration: Addressing the problem of compensatory parameters." *Geophys. Res. Lett., 33,* L06406, doi:10.1029/2005GL025604.

Duan, Q., H. Gupta, S. Sorooshian, A. N. Rousseau, and R. Turcotte (2003) *Calibration of Watershed Models*, AGU Books, Washington.

Fiering, M.B. (1967) *Streamflow Synthesis, Harvard University Press*, Cambridge, MA.

Frey, H.C., and S.R. Patil (2002). "Identification and Review of Sensitivity Analysis Methods." *Risk Analysis, 23*(3), 553-578.

Geman, S., and D. Geman (1984). "Stochastic relaxation, Gibbs distributions and the Bayesian restoration of images." *IEEE Transactions PAMI*, 6, pp.721-741.

Gupta, H.V., S. Soroooshian, T. S. Hogue, and D. P. Boyle (2003). "Advances in automatic calibration of watershed models." in *Calibration of Watershed Models*, edited by Duan Q et al., pp. 9-28, AGU.

Hogue, T. S., H. V. Gupta, S. Sorooshian, and C. D. Tomkins (2003). "A multi-step automatic calibration scheme for watershed models." in *Calibration of Watershed Models*, edited by Duan Q et al., pp. 165-174, AGU.

Kavetski, D.N., Franks, S.W., and Kuczera, G.. (2003). "Confronting input uncertainty in environmental modeling." in *Calibration of Watershed Models*, edited by Q. Duan, H. Gupta, S. Sorooshian, A. N. Rousseau, and R. Turcotte, pp. 49-68, AGU Books.

Kuczera, G., and E. Parent (1998). "Monte Carlo assessment of parameter uncertainty in conceptual catachment models: the Metropolis algorithm." *J. of Hydrol.*, 211, 69-85.

Kuczera, G., D. Kavetski, S. Franks, and M. Thyer (2006). "Towards a Bayesian total error analysis of conceptual rainfall-runoff models: Characterizing model error using storm-dependent parameters." *Jour. of Hydrol*., 331, 161-177.

Loucks, D. P., and E. van Beek, (with contributions by Jery R. Stedinger [chapters 7-8-9]) (2005), Jozef P.M. Dijkman, Monique T. Villars, *Water Resources Systems Planning and Management An Introduction to Methods, Models and Applications,* Studies and Reports in Hydrology, UNESCO PUBLISHING, Paris, France.

Loucks, D.P., and J.R. Stedinger (1994). "Sensitivity and Uncertainty Analysis in Hydrologic Simulation Modeling of the South Florida Water Management District." Report of the Workshop on Reduction of Uncertainties in Regional *Hydrologic Simulation Models*, 10 June.

Madsen, H. (2000). "Automatic calibration of a conceptual rainfall-runoff model using multiple objectives." *J. of Hydrol., 235,* 276–288.

Marshall, L. D. Nott, and A. Sharma (2005a). "Hydrological model selection: a Bayesian alternative." *Water Resour. Res.*, Vol. 41.

Morgan, M. G., and M. Henrion (1990) *Uncertainty: A Guide to Dealing with Uncertainty in Quantitative Risk and Policy Analysis*, Cambridge Univ. Press, NY.

Mugunthan, P., and C.A. Shoemaker (2006). "Assessing the impacts of parameter uncertainty for computationally expensive groundwater models." *Water Resour. Res.*, 42, W10428, doi:10.1029/2005WR004640.

Saltelli, A., K. Chan, and E.M. Scott (2000) *Sensitivity Analysis,* J. Wiley and Sons, Ltd, Chichester, England.

Stedinger, J.R., R.M. Vogel, S.U. Lee, and R. Batchelder (2008). "Appraisal of Generalized Likelihood Uncertainty Estimation (GLUE) Methodology." *Water Resour. Res.*, 44, WOOB06, doi:10.1029/2008WR006822.

Thiemann, M. et al. (2001). "Bayesian recursive parameter estimation for hydrologic models." *Water Resour. Res.*, 37, 2521-2535.

Thyer, M., and G.. Kuczera (2003). "A hidden Markov model for modeling long-term persistence in multi-site rainfall time series 1. Model calibration using a Bayesian approach." *J. of Hydrol.*, Volume 275, Pages 12-26.

Yang, J., P. Reichert, K. C. Abbaspour, and H. Yang (2007). "Hydrological modelling of the Chaohe Basin in China: Statistical model formulation and Bayesian inference." *J. of Hydrol.*, Vol. 340, Pages 167-182.

Yapo, P. H. Gupta, and S. Sorooshian (1996). "Automatic calibration of conceptual rainfall-runoff modes: sensitivity to calibration data." *J. of Hydrol.*, 181, 23-48.

VULNERABILITY OF THE HYDRAULIC RESOURCES OF THE RIVER BASIN OF THE SAN JUAN-BRAVE RIVER WITH THE GLOBAL CLIMATIC CHANGE

Rodríguez García José Luis[1] y Cardoso Landa Guillermo[1]

[1]Land Sciences Department, Instituto Tecnológico de Chilpancingo, Av. J. F. Ruiz Massieu # 5, Col. Villa Moderna, C. P. 39000, Chilpancingo, Gro., México; PH (747)4725899; e-mail: gclanda@prodigy.net.mx

ABSTRACT

All the countries are exposed the devastating consequences of the climatic change. For such reason it is necessary to implement political that not only they help to resist the phenomenon but that also help to adapt to the new climatic conditions and to diminish the vulnerability to extreme the climatic events such as droughts, floods, changes in precipitation regimes, among others. This global problem has local solutions. For the analysis and effects of this one phenomenon a region of the barren zone has been selected to the North of our country that is the river basin of the Bravo river, in where the pressures become more evident on the resource water due to different factors on the one hand from their shortage and on the other hand from the demand by the use of the water, situations that difficult the diverse uses of the water. Specifically the river basin of the San Juan-Brave River was studied, that is a sub river basin of the river basin of the Bravo River.

A general diagnosis of the River basin of the San Juan-Brave River appears, showing its basic characteristics as they are: geographic location, physical frame, climate, physiographic, edafology, geology, orography, pluvial precipitation, evaporation, temperature, flora, fauna, economic policy and industrialization, hydraulic infrastructure, cattle agriculture, activities, forest activities, quality of the superficial water, pick up, problematic, in addition a general explanation to integration and operation of a GIS based on Internet at the moment in operation.

10 stations by their distribution in the river basin were selected and its greater number of years of registry and is used the method of polygons of Thiessen in addition of which the maximum precipitations in 24 calculate hours for different periods from return by means of 8 functions of probability and the one of smaller error is chosen to use it in the method of the Triangular Unitary Hidrogram.

The precipitation regimes are quantified and analyzed that will in the future appear due to the global climatic change for the 4 different scenes proposed by Intergovernmental Group of Experts on Climatic Change for years 2050 and 2080. The equations of the variation of the percentage of diminution of the cost with respect to the percentage of diminution of the precipitation are obtained doing a regression analysis.

INTRODUCTION

The evolution of the activities of the man has brought like result important modifications of the means in which it lives and it is developed, the atmosphere as it leaves from this one is not the exception. The phenomenon of the effect conservatory is the main cause of the global heating, although several gases exist that produce the effect conservatory such as they are the water steam, ozone (O_3), nitrous oxide (N_2O), methane (CH_4), the chlorofluorocarbons (CFCs) and mainly carbon dioxide (CO_2) which the hypothesis more widely accepted at the present time is come off that talks about to that we journeyed by a period of heating, due to the increasing carbon dioxide concentration (CO_2) in the atmosphere.

As a result of the global heating they have come appearing effects such as the increase of temperature, the increase in the mean sea level, the variation in the precipitation regimes, and in addition the extreme phenomena have been become serious such as the calls El Niño, La Niña, the prolonged droughts, the intense precipitations, the hurricanes, among others with potential catastrophic effects in many regions of the planet. The incidence of these phenomena and their different levels from affectation, the currents contamination of and channel are aggravated by, and the low productivity and inefficiencies in the use of the water in agriculture and the urban services. These effects hit in the resource water in the hydrological river basins, in individual in those sensible river basins to these changes like the located ones in the arid zones or the coasts, as it is the case of the river basin of the Bravo River and in individual one of his sub river basins the river basin of the San Juan River.

Intergovernmental panel on climatic change (IPCC)

During the decade of the Eighties the scientific evidence of the possibility of the global climatic change grew, bringing a great concern between governmental scientists and heads, by its possible consequences. Recognizing the problem of the potential global climatic change World Meteorological Organization (WMO) and the Program of the Nations United for Ambient (PNUMA) established the Panel Intergovernmental on Climatic Change (IPCC) in 1988, with the purpose of:

a. To evaluate the information available on climatic change,
b. To evaluate the environmental and socioeconomic impacts of the climatic change and
c. To formulate answer strategies.

The IPCC has three work groups and one significant task that next it is explained:

- ✓ Work group I, evaluates the scientific aspects of the climatic system and climatic change.
- ✓ Work group II, analyzes the negative and positive vulnerability of socioeconomic and natural systems before the climatic change, consequences of the climatic change, and options of adaptation.
- ✓ Work group III, evaluates options to limit the emissions of effect gases conservatory and to mitigate the climatic change on the other hand.

- ✓ The significant task in National Gas Inventories of Effect Conservatory consists of watching the National Program of Inventory of Gases of Effect Conservatory.

Models of general circulation

At the present time, the most reliable tool for the investigation of the climate, their fluctuations and variations, is the models of general circulation of the atmosphere (MGC). A MGC is approximated a space and temporary representation of the main physical processes that happen in the atmosphere and of its interactions with the other components of environment . Essentially, it is constituted by a system of equations derived differentials in partial. These equations express the physical laws that govern the system. Most important they are 7 and they are: Canadian Climate Center Model (CCCM), United Kingdom Meteorological Office Model (UKMO), United Kingdom Office Model run 1989 (UK89), Goddard for Institute Space Studies (GISS), Geophysical Fluid Dynamics Laboratory (GFDL), Harley Centre Models (HADCMGHG and HADCMGHS).

BOUNDARY AND BASIC CHARACTERISTICS OF THE ZONE OF STUDY

Geographic location

This affluent of the Bravo River is the second in importance of the Mexican effluents to that international current. Its confluence happens to 58 km waters underneath the curtain of the Imprisoned Falcon, 38 km waters underneath the entrance of the Álamo River, 25 km waters underneath the City Miguel Alemán and 383 km waters above of the opening in the Gulf of Mexico.

The extreme limits of the river basin are confined inside of parallels 24° the 50' and 26° 25' of North latitude and by the meridians 98° 45' and 101° 59' of length WG.

This river is one of most important of the Northeast region of the country, by the category of the zone in which this nailed, including the territory of three states that are: Coahuila with 13.123 km^2, Nuevo León with 18.860 km^2 and Tamaulipas with 989 km^2. Within its river basin several important cities have left such as Forecastle, Coahuila, Monterrey, Nuevo León and Camargo, Tamaulipas. They excel the following advantages in its river basin: Dam Rodrigo Gómez (the Mouth), Dam Marte R. Gómez, Dam "El Cuchillo" and System of Potable Water Dowry to Monterrey.

Given to its location the river basin of the San Juan River it is exposed to strong cyclonal disturbances of the Gulf, those that periodically they have caused increasing of importance between most remarkable is the one of year 1967.

Physical Marco

The River basin of the San Juan River - Brave it has a surface of 32, 763,43 km^2 and it is located in parts of three States of the Republic: Coahuila, Nuevo León and Tamaulipas, but the greater area belongs again to the State Leon, so that it is possible to be affirmed that the dominant policy in the zone is certain reason why it occurs in this organization.

43 Municipalities are in the zone, of which 35 are in Nuevo León and registering the greater number of inhabitants of the economically active population and of services and industries of the River basin, in addition to the 4 Municipalities of Coahuila and the 4 Municipalities of Tamaulipas. This zone of the River basin of the San Juan River is constituted by the Metropolitan Area of Monterrey whose economic dynamics turns it one of the five strategic zones for the growth of the country.

Climate

The climatic characterization has to be considered under the vision of the climatic classification of Köpen modified by Enriqueta García. The great climate groups that cover to the River basin; the tempering, happening through semiwarm subhumid (A) the C (Wo) until subhumid semicold C (E) X'; and the dry one from the semidry Bs1Kw tempering to the very dry BWhw.

Physiographic

More significant the physiographic rank constitutes the folding that undergoes the Mountain range Eastern Mother to the height of the city of Monterrey, from which acquires a general direction East-West. To the north of this folding the orographic elements become spaced and the less narrow geologic structures more, in addition the relief diminishes gradually to the east, until constituting the coastal plain of the Gulf.

Edaphologhy

The present types of ground in the area of study and its zone of influence are: Xerosol Háplico, and Lúvico, Vertisol Calcárico, Fluvisol Calcárico, Yermosoles Háplicos and Cálcicos, Castañozems Calcic, Regosol Eútrico, Rendzina, Planosol Mólico and Litosoles.

Pluvial precipitation, evaporation, temperature

Taking solely from reference the 10 selected climatologic stations, the precipitation is low and irregular with an annual average value of 524,31 mm; the temperature it has an average value of 17.27 °C, and the evaporation it has an annual average value of 1.812 mm.

Flora

In general terms it can say that there are two types of predominant vegetation: the forests and the scrubs; in the first case it dominates the pine forest, with some species like: Pinus cembroides (piñonero Pine), Pinus sp (Pine), Pinus pseudostrobus (Pine), Pinus teocote (Pine), combined with Shrubs jalapensis (madroño), Quercus polymorpha (encino), Mexican Quercus (encino) among others.

Fauna

In the Mountain ranges is puma (concolor Felis), the Texan deer white tail (Odocoileus virginianus), the wild cat (Lynx rufus), as well as some squirrels (Ammospermophilus leucurus, Scirus alleni, Spermophilus mexicanus, Spermophilus

spilósoma). In the little mountains and plains small mammals like coyote exist (Canis latrans), four species of rabbit, between these the rabbit of the desert (Silvilagus audubonii), the raccoon (lotor Portion), six species of tlacuaches, three species of thorny mice, 17 species of mice and rates of field, three species of zorrillo and pecari of necklace (Dicotyles tajacu). As far as the birds, in the zone corresponding to Tamaulipas there are several anátidos species of, like the texano duck (Anas fulvigula), duck of necklace (platyrnynchos Anas), and mainly doves like: the one of white wings (Asian Zenaida), the arroyera dove (Leptotila verreauxi), the dove huilota (Zenaida macrcura) among others.

Economic policy and industrialization

In general terms politically speaking, in the country there is a tendency to industrialization, but focused that industry of high exportability since the country is interested in the currency pick up; this has given like result that the North border strip of the country becomes more interesting the geographic place for the industrial investment, by its proximity with the great potential market that represents the United States of North America and thanks to the Free Trade Agreement.

Agriculture

The weather agriculture is disperses in all the River basin. In this type of agriculture, the maize and the sorghum are the annual culture that emphasize more in the States of Tamaulipas and Nuevo León, in the State of Coahuila is the wheat the most important culture. The irrigation agriculture is located essentially in the States again Leon and Tamaulipas. It is possible to mention that in addition to the maize and sorghum, perennial cultures in the State Leon are registered again. The Municipalities of Montemorelos and Terán General are accountants, since they represent one of the more important citric zones of the country.

GIS based on Internet

It was helpful the consultations of the GIS for the river basin of the San Juan River that has been modeled under the model Relational of Data bases, and introduced in tables with different attributes according to which it is wanted to present/display and the requirements of each data set, as well as the sobreposition of maps of different characteristics before mentioned that they were put simultaneously in different layers up to three.

DEVELOPMENT

10 stations by their distribution in the river basin were selected and their greater number of years of registry and their areas of influence by means of the method of polygons of Thiessen calculate in addition of which the maximum precipitations in 24 calculate hrs. for different periods from return by means of 8 functions of probability among them they are: Exponential, Range 2 parameters, Gumbel, Gumbel two populations, Log-Normal, Nash, Normal and Pearson III, the distribution Gumbel, takes the best model, taking into account its smaller standard error of adjustment and applying the factors of adjustment of the precipitation per

fixed period of observation (Fd) and by area (Fa) to each one of the climatologic stations and is used the method of the Triangular Unitary Hydrogram.

Next the process of calculation of the crescents of design of the river basin of the site in study is described.

Table 1 Characteristics and parameters of the river basin of the San Juan River

Area of river basin (km^2)	32763.43	One calculated by means of AutoCAD.
Length of the main channel (km)	295.75	The main channel calculated by means of the measurement of a thread following and applying the scale.
Slope of the channel (Taylor-Schwarz)	0.00631068	One calculated removing to the pending average dividing the length overall between the difference from unevennesses.
Time of concentration (h), Kirpich	37.22	One calculated by means of the application of the propose formula by Kirpich.
Number of draining	77	It is considered according to the type of ground.
Constant ***e*** of Kuichling	0.5225	One calculated by means of the propose formula by Kuichling.
Constant ***n*** of the HUT	22.54	One calculated previously with the described formula.
Adopted model of Distribution	Several	One calculated depending on that it had less error.

In Table 2 are the maximum expenses, assigned to different periods from return, using the weighted average by means of the polygons of Thiessen of the Maxim precipitation in 24 hours.

Table 2 Calculation of maximum expenses assigned to different return periods

San Juan River basin	**Tr=2**	**5**	**10**	**20**	**50**	**80**	**100**	**500**
Average HP 24h	59.79	97.80	130.44	159.42	196.40	215.37	224.19	286.88
Cte k Kuichlig	6.3	10.2	13.7	16.7	20.6	22.5	23.5	30.0
Average HP for tc	73.73	120.60	160.85	196.59	242.19	265.57	276.45	353.76
Effective HP for tc	25.51	61.31	95.79	127.92	170.15	192.17	202.48	276.60
Tp, time tip	28.43	28.43	28.43	28.43	28.43	28.43	28.43	28.43
Qp (m^3/s)	**738.16**	**1774.27**	**2772.09**	**3701.93**	**4924.13**	**5561.55**	**5859.91**	**8004.98**

The precipitation regimes are quantified and analyzed that will appear in the future due to the global climatic change for the 4 different scenes proposed by Intergovernmental Panel on the Climatic Change for years 2050 and 2080. The results of the presented/displayed variation of the precipitation for our country they were obtained from the average answer of a sample of ten recent models of simulation for global climates. These simulations were made by seven located climatic laboratories in 6 different countries. Most of the climatic models they indicate a drought process on the continental part of Central America and in the islands of the Caribbean, being the most significant changes for the continent that stops the islands. Giving as result for the zone of study the following percentage of variation: -4%, -5%, -7%, -8% and -12%.

Applying these percentages to the Maxima precipitation in 24 hours the following results presented in tables 3, 4, 5, 6 and 7 are obtained:

Table 3 Calculation of maximum expenses with diminution of 4% for the return per.

San Juan River basin	**Tr=2**	**5**	**10**	**20**	**50**	**80**	**100**	**500**
Average HP 24h	57.40	93.89	125.22	153.04	188.55	206.75	215.22	275.40
Cte k Kuichling	6.0	9.8	13.1	16.0	19.7	21.6	22.5	28.8
Average HP for tc	70.78	115.78	154.41	188.72	232.50	254.95	265.39	339.61
Effective HP for tc	23.52	57.35	90.13	120.76	161.09	182.14	192.00	262.94
Tp, time tip	28.43	28.43	28.43	28.43	28.43	28.43	28.43	28.43
Qp (m^3/s)	**680.61**	**1659.78**	**2608.38**	**3494.77**	**4661.94**	**5271.30**	**5556.64**	**7609.67**

Table 4 Calculation of maximum expenses with diminution of 5% for the return per.

San Juan River basin	**Tr=2**	**5**	**10**	**20**	**50**	**80**	**100**	**500**
Average HP 24h	56.80	92.91	123.92	151.45	186.58	204.60	212.98	272.54
Cte k Kuichling	5.9	9.7	13.0	15.9	19.5	21.4	22.3	28.5
Average HP for tc	70.04	114.57	152.81	186.76	230.08	252.30	262.63	336.07
Effective HP for tc	23.03	56.37	88.72	118.97	158.83	179.64	189.39	259.53
Tp, time tip	28.43	28.43	28.43	28.43	28.43	28.43	28.43	28.43
Qp (m^3/s)	**666.42**	**1631.37**	**2567.67**	**3443.18**	**4596.58**	**5198.92**	**5481.00**	**7511.01**

Table 5. Calculation of maximum expenses with diminution of 7% for the return per.

San Juan River basin	**Tr=2**	**5**	**10**	**20**	**50**	**80**	**100**	**500**
Average HP 24h	55.61	90.96	121.31	148.26	182.65	200.29	208.50	266.80
Cte k Kuichling	5.8	9.5	12.7	15.5	19.1	21.0	21.8	27.9
Average HP for tc	68.57	112.16	149.59	182.83	225.23	246.98	257.10	328.99
Effective HP for tc	22.05	54.42	85.92	115.42	154.32	174.65	184.17	252.72
Tp, time tip	28.43	28.43	28.43	28.43	28.43	28.43	28.43	28.43
Qp (m^3/s)	**638.28**	**1574.83**	**2486.50**	**3340.26**	**4466.11**	**5054.40**	**5329.95**	**7313.87**

Table 6 Calculation of maximum expenses with diminution of 8% for the return per.

San Juan River basin	**Tr=2**	**5**	**10**	**20**	**50**	**80**	**100**	**500**
San Juan river								
Average HP 24h	55.01	89.98	120.00	146.67	180.69	198.14	206.25	263.93
Cte k Kuichling	5.8	9.4	12.6	15.4	18.9	20.7	21.6	27.6
Average HP for tc	67.83	110.95	147.98	180.86	222.81	244.33	254.34	325.46
Effective HP for tc	21.57	53.44	84.52	113.65	152.07	172.16	181.56	249.32
Tp, time tip	28.43	28.43	28.43	28.43	28.43	28.43	28.43	28.43
Qp (m^3/s)	**624.33**	**1546.70**	**2446.06**	**3288.94**	**4401.00**	**4982.25**	**5254.55**	**7215.41**

Table 7 Calculation of maximum expenses with diminution of 8% for the return per.

River basin	**Tr=2**	**5**	**10**	**20**	**50**	**80**	**100**	**500**
Average HP 24h	52.62	86.07	114.79	140.29	172.83	189.52	197.29	252.45
Cte k Kuichling	5.5	9.0	12.0	14.7	18.1	19.8	20.7	26.4
Average HP for tc	64.88	106.13	141.55	173.00	213.12	233.71	243.28	311.31

Effective HP for tc	19.68	49.59	78.96	106.58	143.10	162.21	171.17	235.74
Tp, time tip	28.43	28.43	28.43	28.43	28.43	28.43	28.43	28.43
Qp (m^3/s)	**569.42**	**1435.15**	**2285.26**	**3084.57**	**4141.43**	**4694.53**	**4953.76**	**6822.30**

CONCLUSIONS

As it is appraised in the results, the waited for global climatic change for years 2050 and 2080 and the 4 different scenes proposed in relation to the precipitation does not leave to the margin the area drained by the fluvial system of the San Juan River, their hydrologic cycle will even be affected of significant way in the availability of the resource water, in individual due to the influence of the city of Monterrey. Therefore still it is time to take, at least, some local measures as the ecological conservation of the geographic space and a more rational use of the vital liquid in order that this change repels with smaller severity.

Making an analysis of correlation and regression with the method of square minimums, with the percentage of resulting variation of the precipitation the following equations of variation of the percentage of diminution of the cost with respect to the percentage of diminution of the precipitation was obtained:

· For a period of return of 2 years:
%VQ = (1.882) (%VP) + 0.3147 (Linear)
%VQ = (- 0,0058) $(\%VP)^2$ + (1.9752) (%VP) - 0,012 (Polynomial of second degree)
· For a period of return of 5 years:
%VQ = (1.5822) (%VP) + 0.1459 (Linear)
%VQ = (- 0,0027) $(\%VP)^2$ + (1.6257) (%VP) - 0,0068 (Polynomial of second degree)
· For a period of return of 10 years:
%VQ = (1.4568) (%VP) + 0.092 (Linear)
%VQ = (- 0,0017) $(\%VP)^2$ + (1.4844) (%VP) - 0,0047 (Polynomial of second degree)
· For a period of return of 20 years:
%VQ = (1.3849) (%VP) + 0.0662 (Linear)
%VQ = (- 0,0012) $(\%VP)^2$ + (1.4048) (%VP) - 0,0036 (Polynomial of second degree)
· Para un periodo de retorno de 50 años:
%VQ = (1.3212) (%VP) + 0.0466 (Linear)
%VQ = (- 0,0009) $(\%VP)^2$ + (1.3352) (%VP) - 0,0026 (Polynomial of second degree)
· For a period of return of 80 years:
%VQ = (1.2963) (%VP) + 0.0398 (Linear)
%VQ = (- 0,0007) $(\%VP)^2$ + (1.3082) (%VP) - 0,0023 (Polynomial of second degree)

· For a period of return of 100 years:
%VQ = (1.2859) (%VP) + 0.0371 (Linear)
%VQ = (- 0,007) (%VP) ^{2} + (1.2971) (%VP) - 0,0022 (Polynomial of second degree)
· For a period of return of 500 years:
%VQ = (1.2294) (%VP) + 0.0241 (Linear)
%VQ = (- 0,005) (%VP) ^{2} + (1.2367) (%VP) - 0,0015 (Polynomial of second degree)

Where:
%VQ = Percentage of diminution of the cost.
%VP = Percentage of diminution of the precipitation.

The regression with less error is the polynomial of second degree; nevertheless the linear regression gives very acceptable results. As it is possible to be appreciated in the results, the effects that the diminution of the precipitation produces magnify in relation to the cost.

REFERENCES

Aparicio Mijares F. J., (1997), *Foundations of superficial hydrology*. Limusa Noriega Publishing.

Aparicio Mijares F. J., (1990), *Hydrological Modeling.* Hydraulic Engineering in Mexico.

Brater et al., (1963), *Hidrology*. John Wiley & Sons, Inc.

Campos Aranda D.F., (1992), *Processes of the hydrologic cycle*. University of San Luis Potosí.

Domínguez R. et al, (1981), Federal Commission of Electricity. *Manual of civil works*, Hydrotechnics, Relation between precipitation and draining. A.1.5 volume.

Martinez A. P., (1993), Molina M. M., *Climatic change: possible consequences and some suggestions to diminish its effect in Mexico.* Magazine Hydraulic Engineering in Mexico, Bowl. VIII, number 1, January-April, 1993.

Martinez A. P., Molina M. M., (1994), *Climatic Change and its potential effects in the hydric resources and the agriculture of the Valley of the Yaqui.* Hydraulic Engineering in Mexico. IX, núm. 1, January-April, 1994.

Navarro P., Lacy T., (1987), Ecological *Ordering of the river basin of the San Juan River*. Date of beginning: 31 of October of 1986. Date of completion: 30 of April of 1987.

Water Demand Forecasting for the City of the Future against the Uncertainties and the Global Change Pressures: Case of Birmingham

K.B. Khatri[1] and K. Vairavamoorthy[1]

School of Civil Engineering, College of Engineering and Physical Sciences, B15 2TT Edgbaston, Birmingham, UK, PH (+44) 121 414 5152; email: khatrikb@bham.ac.uk

School of Civil Engineering, College of Engineering and Physical Sciences, B15 2TT Edgbaston, Birmingham, UK, PH (+44) 121 414 5147; email: k.vairavamoorthy@bham.ac.uk

ABSTRACT

In order to ensure the adequate and sustainable water management for the city of the future, the impact of the global change pressures and sources of uncertainties should be analyzed appropriately. This paper presents a model for forecasting the future water demand addressing the uncertainties associated to the climate change, population and economic growth. It uses the historic time series records of water consumption for forecasting the future water demand, and applies the Monte Carlo sampling, Latin hypercube sampling and bootstrap methods to describe the associated uncertainties. The model was applied in Birmingham, UK to analyse the water demand for year 2035. Results showed that future water demand in Birmingham will be governed by the socio-economic factors not by the climate change impact. There is a very high likely risk of not meeting the future water demand from the existing supply sources.

Key words: Global change pressures, uncertainties, scenarios, forecasting, sampling

INTRODUCTION

Forecasting of water demand is a crucial component in the successful operation of water supply system. Accurately forecasted water demand either in short-term, or medium-term, or long-term time horizons can be very useful for capacity planning, scheduling of maintenance, future financial planning and rate adjustment, and optimization of the operations of a water system In addition, adequately forecasted demand will be a basis for the strategically decision making on future water sources selection, upgrading of the available water sources and designing for the future water demand management options, so that water resources are not exhausted, and competing users have adequate access to those resources.

Most of the previous studies on water demand forecasting are based on the three approaches: end-use forecasting, econometric forecasting, and time series forecasting. End use forecasting is an approach that bases the forecast of water demand on a forecast of uses for water, which requires tremendous amounts of data and assumptions. The econometric approach is based on statistically estimating historical

relationships between different factors (independent variables) and water consumption (the dependent variable) assuming that those relationships will continue into the future. Time series approach forecasts water consumption directly, without having to forecast other factors on which water consumption depends (Zhou *et al.*, 2000).

Many climatic variables, such as rainfall, air temperature, sunshine duration, relative humidity, wind speed, historical water uses were considered for developing a linear regression to the artificial neural network model for forecasting the water demand studies. Linear regression models developed by Jain et al. (2001) uses weekly maximum air temperature, weekly rainfall amount, weekly past water demand, and the occurrence and non-occurrence of rainfall as dependent parameters. The linear regression models developed by Graeser (1958) have the number of previous days with maximum air temperature above 100°F, and the number of weeks from last occurrence of one inch of rainfall as dependent variables. Box and Jenkins models were developed by Maidment *et al*. (1985) to predict the daily municipal water use. In more recent studies, artificial neural network (ANN) model are becoming prominent for water demand forecast as the neural network was found to outperform the regression and time-series models in some studies (Bougadis *et al.*, 2005; Ghiassi *et al.*, 2008). Similarly, a Takagi Sugeno fuzzy method for predicting future monthly water consumption values from three antecedent water consumption amounts was developed by Altukaynak *et al.,* (2005) for future demand forecasting.

Some other studies have included economic, demographic, and weather factors in their water demand models. Billings & Agthe (1998) used the marginal price of water and personal income per capita in their model. Zhoua *et al* (2000) modelled daily water consumption by splitting it into two components: base (weather-insensitive) and seasonal (weather-sensitive) uses for Melbourne water supply. Arbués *et al* (2003) have reviewed the main variables that can affect demand and highlighted the water price, income, or household composition as the crucial determinants of residential consumption. Moreover, there are many studies done on water demand forecasting and impacts analysis in urban scale, catchments scale & regional scale, for examples see (Arnell, 2004; Arnell & Delaney, 2006; Bradley, 2004; Ruth *et al.*, 2007; Sophocleous, 2004; Vörösmarty *et al.*, 2000).

Most of those studies are focusing on the future demand forecasting without considering the uncertainties associated to the future change pressures. The future changes pressures; such as climate changes and variability, population growth and urbanisation, changes in public behaviours and socio-economic condition, ageing and deterioration of buried infrastructures, increased rate of leakage, technological development, increased demand for water to maintain in stream ecosystems, alter in water quality, and (Khatri & Vairavamoorthy, 2007) and their impacts are highly uncertain. Consequently, without dealing with these future change drivers and associated uncertainties, the predicted forecast will not be reliable and sufficient for the planning and management of water supply system.

The objective of this paper is to explore the different sources of uncertainties in future water demand forecasting due to climate changes, population growth, and changes in public behaviour, and assess the risks. We apply the computing tool to describe,

propagate and forecast the domestic demand considering these change variables, and apply in the real case of Birmingham, UK. It also attempts to assess the main governing drivers' for the future water demand (i.e. climatic or socioeconomic) in Birmingham city.

The paper is organized to address each of these topics in six sections. The second section presents the main sources of uncertainties associated to these change pressures. Third section presents the methodology applied for describing the uncertainties during the demand forecasting process. The fourth section introduces the case study area, and fifth section will present the current and potential future climatic and social condition of the Birmingham city followed by analysis. Finally, a brief discussion and conclusions of the study will be presented in the sixth section.

SOURCES OF UNCERTAINTIES

The sources of uncertainty refer to the causes that give rise to uncertainty in the forecasted state of the system that is modelled (Krzysztofowciz, 2001; Mannina *et al.*, 2006; McIntyre *et al.*, 2003; Paté-Cornell, 1996). A complete assessment of impacts caused by the future change pressures in water demand forecasting is being impossible either due to the complexities, or incomplete knowledge, or unknowable knowledge leading to a range of uncertainties. It may be either data uncertainty, or model uncertainty, or parameter uncertainty, or natural and operational uncertainty, or all. Here, we are exploring the sources of parameters uncertainties subjected to the future water demand forecasting.

Climate Change

Most of the climate change studies including IPCC (2007) had already concluded the greater impacts of climate change on water resources. Climate variability and change affect the availability of demand and quality of water, and runoff or temperature extremes. Different sources of uncertainties stemming from the climate change; such as future temperature, precipitation, sunshine duration, wind speed, relative humidity, evaporation rate, transpiration rate, soil moisture content will have significant impact on future water consumption. The extreme events (drought or frequent flood) will have also considerable impact on future demand. Therefore, how these climatic parameters changes in future will govern to water demand forecasting.

However, prediction of future climate change and impacts contains the series of uncertainties, which cascades from scenarios to impacts studies. Such as future scenarios of how the future (complex non-linear dynamic system) will be; emission generated, natural process, and variability; different global climatic models for the prediction and their capacity; downscaling and error; uncertainties associated to hydrological modelling; and finally uncertainties associated to the impact model. These associated uncertainties are due to the incomplete knowledge or unknowable knowledge to be articulate and quantified (Berliner, 2003; Carter *et al.*, 1999; New & Hulme, 2000). Planning for the future with less or no regret strategy against climate change impact, will be possible only if associated uncertainties are well described.

Population Growth

Urbanisation and population growth follow a very complex process and affected by a range of economic, political, social, cultural, and environmental factors. Traditional population forecasting techniques are based on the assumption that three components (fertility, mortality and migration) of population growth will be smooth and follow a monotonic path for future trends. However, demographic situation is neither known perfectly in the present, nor future trends in births, deaths, and net migrants are predictable. Future population growth can be influenced by affecting birth, death, or migration rates due to social, economic, political, technological, and scientific developments. We do not know whether new diseases, or drug-resistant strains of old diseases, will raise mortality in the future. We do not know whether migration toward industrial countries will accelerate or abate (Lee & Tuljapurkar, 1994; O'Neill *et al.*, 2001).

The two approaches commonly used for characterizing uncertainty in demographic forecasting are scenario and probabilistic. Scenario uses to describe its projections in consistent story in which fertility, mortality, and migration assumptions are embedded to provide a comprehensive picture of what the future might be. Building alternative scenarios to assess and communicate the uncertainty associated with their projections, is common in national forecasts. An alternative to scenarios as a means of communicating uncertainty is probability distributions. It explicitly accounts for uncertainty in projected trends of fertility, mortality, and migration; and derives the resulting probability distributions for projected population size and age structure. Further details on these areas can be found elsewhere (Keilman *et al.*, 2002; Lee & Tuljapurkar, 1994; National Research Council (NRC), 2000; Wilson & Bell, 2004).

Socio-economic Changes

Many previous studies have revealed that there is a strong correlation between water consumption and socio-economic changes. Examples are changing life style, changing housing type and household size, acceptability, and market penetration of water efficient appliances alternative sources of water, economic development, employment opportunities, education level, and water pricing (Bradley, 2004; Clarke *et al.*, 1997; Schneider & Whitlatch, 1991). Forecasting and describing these parameters are subjected to uncertainties.

It has been recognised that economic prosperity, type of housing, occupancy, climate and technical developments in water-using devices influences the micro-components of water uses (Herrington, 1995). Micro-components of water demand typically uses water for the devices; such as toilets, showers, bath, washing machines, dishwashers, internal and external taps are considered and assessed separately. Future domestic water consumption will be decided by how these micro-component changes, which will be based on change in life styles, emerging new technology, ecological awareness and economic reason (Hensher *et al.*, 2005).

DESCRIPTION OF UNCERTAINTY

In this study, we purpose a risk based approach for analysing the uncertainties while forecasting the future water demand. We are applying, therefore scenario approach,

random sampling techniques (Monte Carlo simulation and Latin Hypercube sampling), and bootstrapping techniques for describing the uncertainties. Domestic water demand will be forecasted based on the micro-components of water demand analysis and total population in the future. Impacts of climatic variables will be assessed using the regression models developed from historic time series records.

Monte Carlo Simulation (MCS) will be applied for prediction of total future population with uncertainty. MCS is a well established and tested method of overall assessment of the uncertainty relies on the central limit theorem. MCS technique generates an estimate of the overall uncertainty in the predictions due to all the uncertainties in the input parameters (Macdonald & Strachan, 2001). Time series population data will be used for trend analysis, moving average technique for the smoothing in forecasting, and lognormal distribution for the future probabilistic simulation of total population using MC simulation (see section 5). Population forecasted with a large numbers of random simulations and predicted population in 95% confidence interval will describe the uncertainty ranges in total future population.

Latin Hypercube Sampling (LHS) technique will be used to analyse the micro - components of water demand and to get the distribution for per capita water consumption. Latin Hypercube Sampling (LHS) is a stratified sampling procedure, and converges more quickly than other stratified sampling procedures. It produces the more precise results than MCS results for same numbers of model runs in case of linear and monotonic problems (Ferson *et al.*, 2004; McKay, 1992). Uniform distribution will be developed for per capita water consumption considering the occupant numbers and ACRON (see section 5), and get the present water demand distribution. Secondly, micro-component of water demand will be classified in 8 – groups with uniform probability distribution. Future per capita water use will be obtained after LHS sampling. The ranges of micro-components water demand values were selected based on UK study results.

Bootstrap technique will be applied to describe the uncertainties in future average temperature and precipitation. The bootstrap is the simplest technique for simulating the probability distribution of any statistic, without making any assumptions or estimating any parameters. Bootstrapping amounts to re-sampling a record, with replacement, to generate (B) bootstrap samples, from which one can simulate B estimates of a given statistic, leading to an empirical probability distribution of the statistic. In order to resample the records assuring the temporal and spatial covariance structure of the original time series, moving block bootstrap techniques is applied. In a moving-blocks bootstrap, one chooses a block length $\lambda \approx n/k$, where n is the record length and k is the number of blocks to resample. The idea is to choose a large enough block length λ, so that observations more than λ time units apart will be nearly independent. Details on bootstrap and moving block bootstrap can be found in (Efron & R. J. Tibshirani, 1993; Hidalgo, 2003; Ku¨nsch, 1989; Vogel, 1996).

Similarly, scenario approach will be considered for the climate change impacts analysis. We considered the different emission scenarios and predicted climatic variables. Wide spectrum of possible climate change scenarios, prediction and their

impact in water demand will cover the associated uncertainties. We have used the predicted results obtained after downscaling from climate impact study UKCIP02.

CASE STUDY: BIRMINGHAM

Birmingham is the second most populated British city after London. It is situated in 52° 29′ 1″ N, 1° 54′ 23″ W, having total area 267.77 km2; average elevation of 150 to 350 m; and population 1113600 (city council, 2008 estimate). The City of Birmingham forms part of the larger West Midlands conurbation and includes several neighbouring towns and cities; such as Solihull, Wolver Hampton and the towns of the Black Country. Although Birmingham's industrial importance has declined, it has developed into a national commercial centre, being named as the third best place in the UK to locate a business, and the 21st best in Europe and fourth most visited city by foreign visitors in the UK.

Severn Trent Water Limited (STWL) and South Staffordshire Water (SSW) Company are responsible for supplying drinking water, managing waste water and environment within the Birmingham. STWL provides water from the Birmingham water resource zone (WRZ) - one of the six water resource zone (Figure 1). The Birmingham WRZ includes most of the city of Birmingham, which is principally supplied from the Elan Valley reservoirs in mid Wales, via a 70 mile long aqueduct. The estimated total population within this zone was 1125183 in 2007. There is no raw water abstracted from within this resource zone. The deployable output of this zone is approximately 329.6 Mega liters per day (ML/d), and there is approximately 314.9 ML/d of water available for use. The service area has an average occupancy rate of 2.2 per household, and per capita water consumption of 146.98 litres (STWL, 2008).

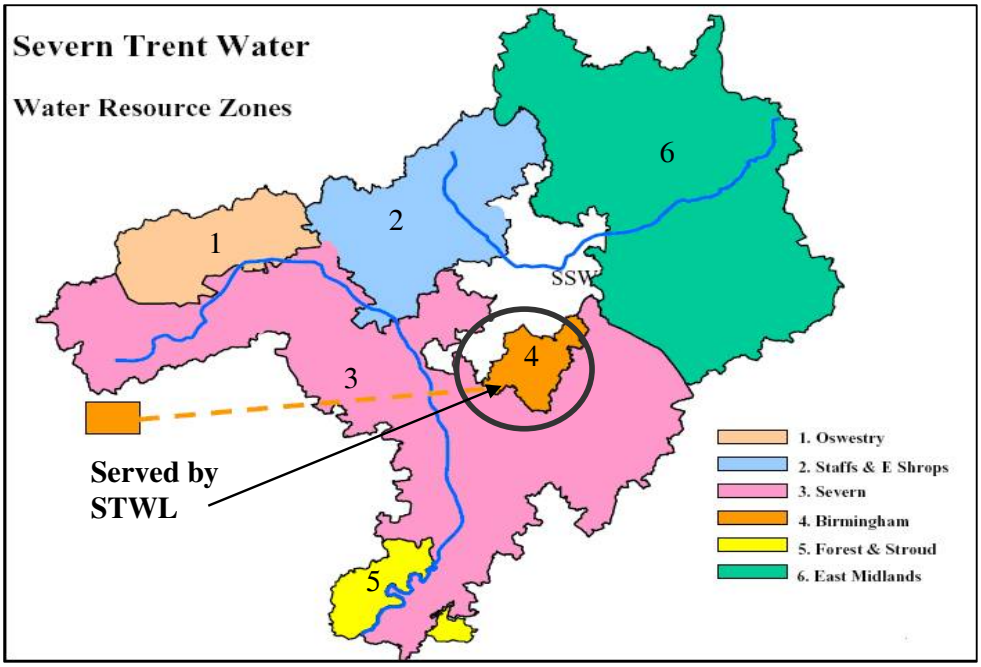

Fig. 1. Severn Trent Water resource Zones and supply area for Birmingham

DATA, LIMITATION AND ANALYSIS

Water Demand

We obtained water consumption data for this analysis from STWL from Jan 1996 to March 2005 (see Figure 2). We have only total consumption data, so we are unable to distinguish water use for residential, commercial, and industrial sectors. For the monthly analysis, we aggregated the data into monthly totals, normalizing each total for the length of the month so that all data assume a 30.416 day month. We don't have sufficient data on total population served from year 1996, so adjustment for water consumption to a per capita basis was not possible.

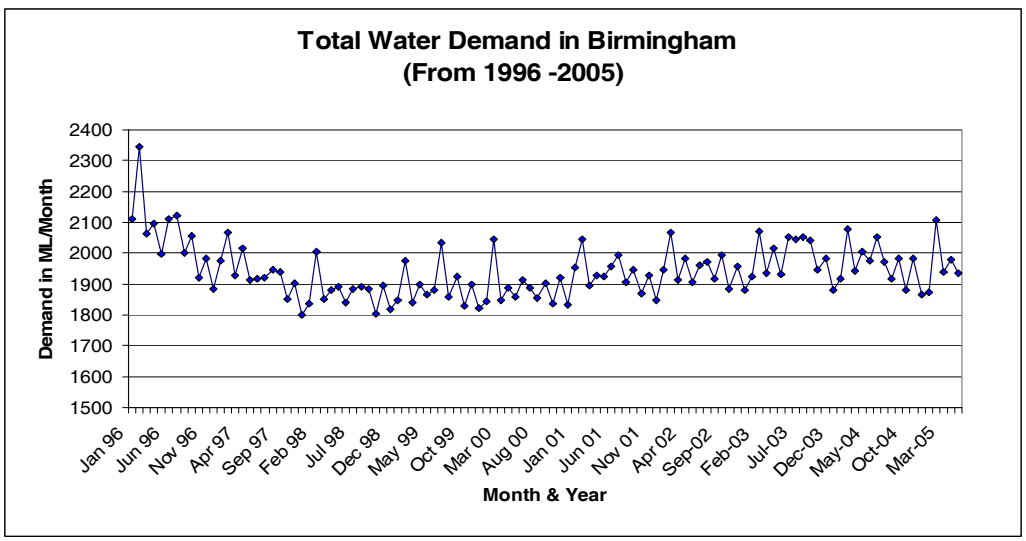

Fig. 2. Total Water consumption per month in Birmingham served by STWL

In the time series records, water demand is decreasing from 2111 ML/Month in January 1996 to 1837 ML/Month in January 1998. Although, we lack the data on water demand by sector, the reduction in demand might be due to decreasing numbers of industries. From 1998 to 2001, there is no considerable increase in water demand with average rate of 1943 ML/month. Average water consumption during the winter appears fairly consistent and summer time consumption figures are well above normal. Apparently, the peak demand is increasing in a warmest summer month of the year compared to normal year, such as year 1996.

Historical and Future Climate Change Scenarios

Historical time series records for the temperature and precipitation parameters for two rain gauge stations (Sutton Bonnington, Nottingham shire and Penkridge, Shropshire) was provided by STWL. The average value of the two stations was used for the case of Birmingham. Although water demand has direct affect of rainfall patterns, air temperature, sunshine duration, relative humidity and wind speed, we are limiting our work only on temperature and precipitation due to unavailability of data.

In order to correlate the temperature and precipitation affect on water demand, a linear regression model was developed from year 2001 as shown in Figure 3 (a) & (b). From the regression results, water demand is negatively correlated with precipitation $Y = 1.9934 * 1000000 - 0.0006 * P$ with adjusted regression coefficient of R^2 = 0.26, having standard error in repressors of 0.3369. Temperature is positively correlated $Y = 1.9389 * 1000000 + 0.0021 * T$ with adjusted coefficient of R^2 = 0.19, standard error of 0.0533. Although there is lower correlation of variables to the prediction, we have applied here single linear regression technique to estimate the future implication in water demand from available information.

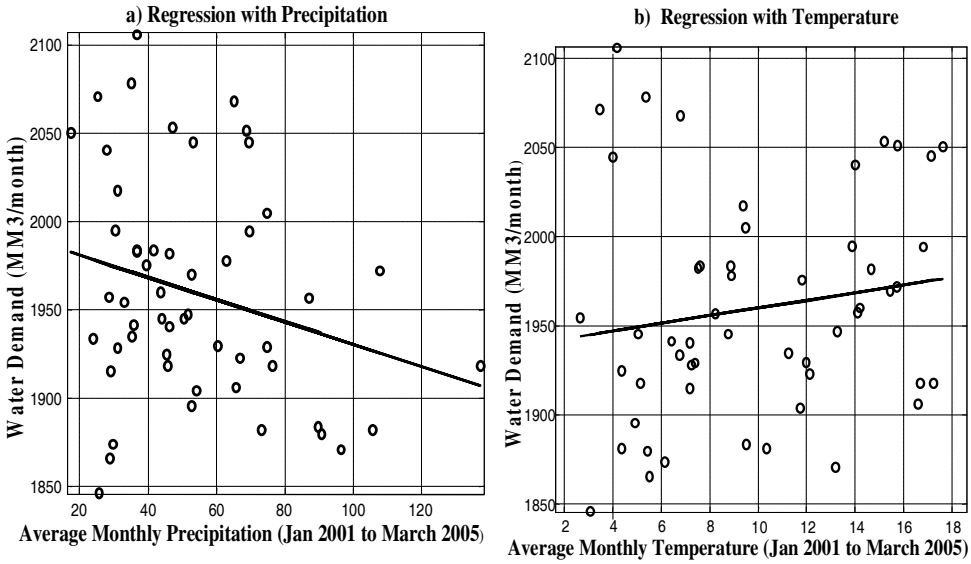

Fig.3 Regression results on water demand and average precipitation (a) and temperature (b)

Future climate change scenarios for Birmingham are based on the scenarios developed and studied by the UK Climate Impacts Programme-2002 (UKCIP02). UKCIP02 uses the Hadley Global Climate Model (GCM) of the atmosphere including a dynamic ocean circulation model (see www.ukcip.org.uk). It provides climate change database for three time slices 2020s (predictions for 2011 to 2040), 2050s (predictions for 2041 to 2070), 2080s (predictions for 2071 to 2100) and for four core emissions scenarios (Low, Medium-Low, Medium-High, and High) at both 50Km and 5Km resolutions. In this case, we are using the temperature and precipitation parameters for four emissions scenarios for time 2020s at 50Km resolutions (Table 1 & 2).

For the future water demand prediction, we are considering the two cases of climatic variables. Firstly, average monthly temperature and total change in precipitation for four scenarios (Table: 1&2) was analysed using moving block bootstrapping. We grouped data of the predicted values in three months (block length) time periods for the four scenarios. After bootstrapping by moving block for 1000 times, a seasonal average value with 95% confidence intervals was estimated (see Table 3). It embeds a wide range of possible intra - and inter-annual variation in climate. Average future demand will be predicted with respect to these mean values. There are uncertainties in

future extreme events of drought; however the average values will provide a sufficient base for the future planning.

Table 1. Monthly average temperature and changes in daily mean temperature simulated by HadRM3 with SRES A2 for time slice 2020

Scenarios	Dec	Jan	Feb	March	April	May	Jun	July	Aug	Sep	Oct	Nov
Base case Average Temp ° C	4.55	4.85	5.89	8.21	11.41	14.34	16	15.8	13.4	9.87	6.75	4.98
Low	0.69	0.63	0.6	0.63	0.69	0.77	0.89	1.05	1.15	1.1	0.95	0.8
Medium to Low	0.77	0.7	0.67	0.71	0.77	0.86	1	1.17	1.28	1.23	1.06	0.89
Medium to High	0.77	0.7	0.67	0.71	0.77	0.86	1	1.17	1.28	1.23	1.06	0.89
High	0.82	0.75	0.72	0.75	0.82	0.92	1.06	1.25	1.36	1.31	1.14	0.95

Table 2. Monthly average precipitation rate (mm/month) and changes in total precipitation rate (%) simulated by HadRM3 with SRES A2 for time slice 2020

Scenarios	Dec	Jan	Feb	March	April	May	Jun	July	Aug	Sep	Oct	Nov
Base case Average	48.12	44.32	45.72	55.98	53.08	45.67	40	40.73	47.5	52.79	52.29	48.17
Low	4.93	5.41	3.68	0.91	-2.25	-5.41	-8.34	-10.4	-9.98	-6.64	-2.16	2.02
Medium to Low	4.09	1.01	-2.5	-6.02	-9.29	-11.59	-11.1	-7.4	-2.4	2.25	5.49	6.03
Medium to High	4.09	1.01	-2.5	-6.02	-9.29	-11.59	-11.1	-7.4	-2.4	2.25	5.49	6.03
High	5.87	6.44	4.37	1.08	-2.67	-6.43	-9.92	-12.38	-11.9	-7.9	-2.57	2.4

Table: 3 Seasonal average changes in temperature and total precipitation rate (%) after bootstrap sampling

Parameters	Dec	Jan	Feb	March	April	May	Jun	July	Aug	Sep	Oct	Nov
Lower 95% Tempt °C		0.6			0.63			0.89			0.8	
Precipitation %		-2.5			-11.59			-12.38			-7.9	
Mean Value Tempt °C		0.7073			0.7743			1.1405			1.0528	
Precipitation %		2.2894			-6.8608			-8.1021			2.2608	
Upper 95% Tempt °C		0.82			0.92			1.36			1.31	
Precipitation %		6.44			0.91			-2.4			6.03	

Population Growth and Socio-economic Changes

Population trends of Birmingham city was obtained from the Birmingham City council. However, STWL covers the partial area of Birmingham, and includes the additional neighbouring area, so population figures obtained from STWL is different than total city population. For the probabilistic population forecasting, demographic data of total population obtained from city council was used to find the best distribution of total population growth. The lognormal distribution was obtained as the best fit from total population and applied for the population forecasting in STWL

service area. Future forecasted population was smoothened by moving average method with 5- year time steps. Sufficient MCS was run (1000 times) to get the future total population for STWL area with 95% confidence interval (see Figure 4).

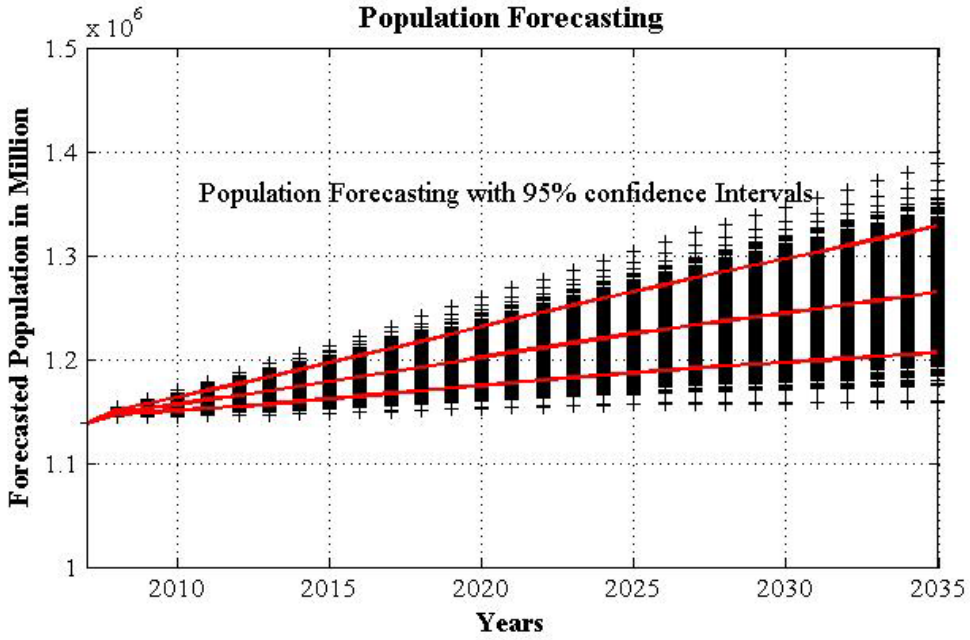

Fig. 4. Total population forecasted for Birmingham (served by STWL)

We consider the micro-component of water demand and geo-demographic classification to assess the future water demand. ACRON is a geo-demographic classification of population used in UK. It groups the entire UK population into 5 categories, 17 groups and 56 types using more than 400 variables (see www.caci.co.uk). The water consumption according to the ACRON number (1 to 5) and family size (1 to 5) obtained from STWL was used for the analysis. Water consumption patterns per capita, for different ACRON types for Birmingham is shown in Figure 5.

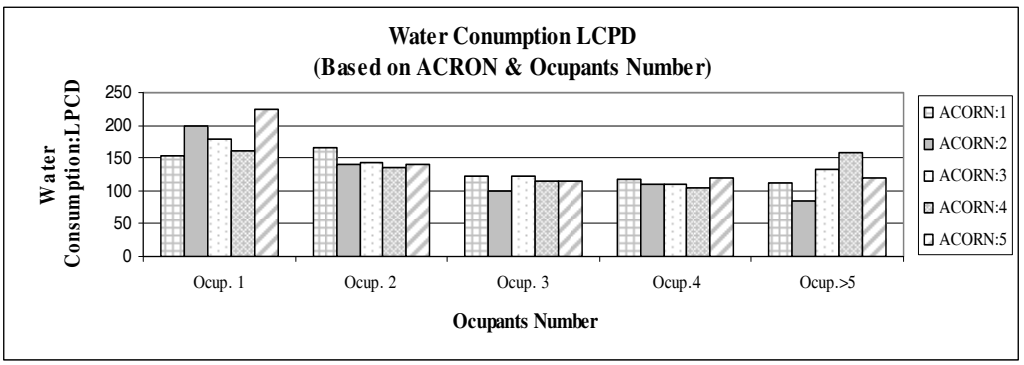

Fig. 5. Per capita water consumption based on ACRON

From the water consumption for ACRON (1 to 5), we assumed uniform distribution for different occupants' numbers (ACRON: 1(120-167); ACRON: 2(85-200) ACRON: 3(110-178): ACRON: 4(104-160): ACRON: 5(115-226)). Using LHS, we sampled random samples (1000 simulations) and finally, we got a distribution, which gives the most likely value 146.50 LPCD, and 95% confidence intervals (see Figure 6(A)).

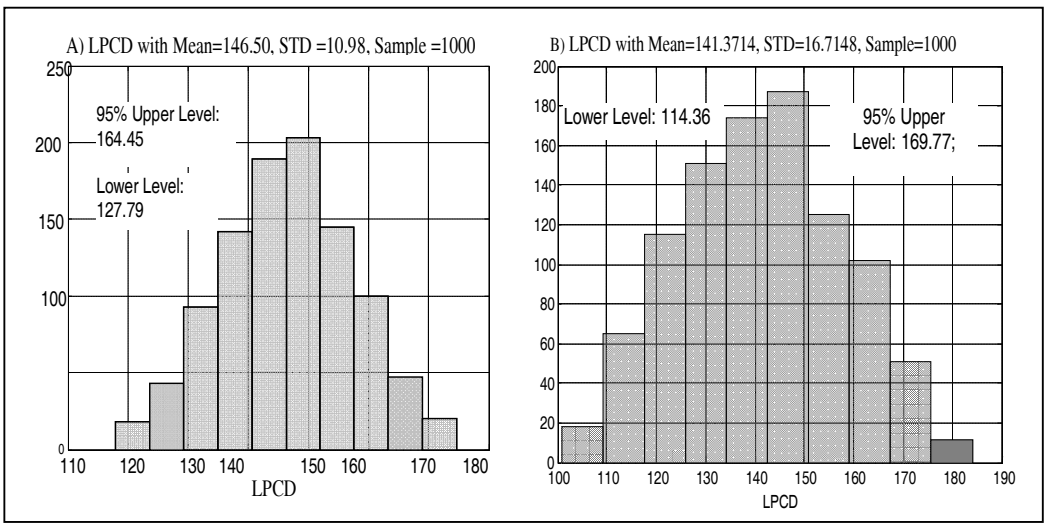

Fig. 6. Water consumption based on ACRON for preset (A) and for the future (B)

We divide the micro-components of water consumption in 8-groups (WC:(10-40%), Washing Machine(10-20%), Dish wash:(5-8%), Bath(10-20%), Shower: (4-8%), Sink Kitchen:(8-20%), Wash basin: (4-12%), and outside and losses(10-15%) as a uniform distribution of present LPCD, and future water per capita was forecasted in terms of distribution applying the LHS techniques (see Figure 6(b)). The range of micro-components was considered based on the STWL survey results and Environmental Agency study in UK.

Future Water Consumption

We have population forecasted with confidence intervals, LPCD forecasted for the future (considering the micro-components of the water demand) which will give the future domestic demand. Regression models on temperature and precipitation shows-there will be 2.10% increase and 0.06 % reduction in total monthly demand, if temperature increases by 1ºC, and rainfall increases by 1mm/Month. We are forecasting the climatic affect for year 2035, considering the average value obtained in Table 3. We have no detailed data base on non - domestic demand, and leakage but we are using information available from STWL. From this analysis, water demand situation in Birmingham for year 2035 is shown in Figure 7.

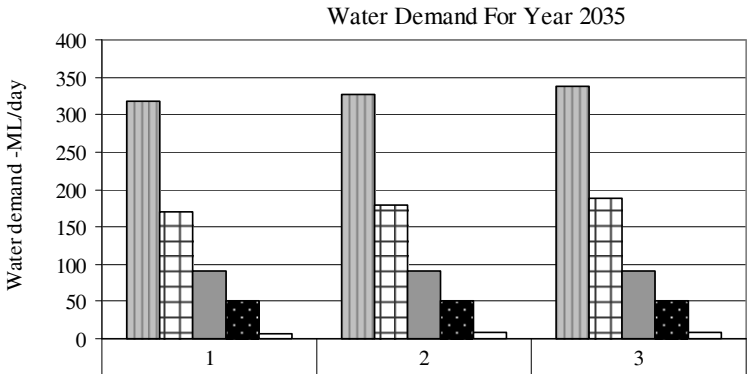

	1	2	3
Total demand	318.0717	327.8076	338.0925
Domestic	170.5629	178.7765	187.7676
Leakage	90.0000	90.0000	90.0000
Non domestic	50.7500	50.7500	50.7500
Climatic	6.7588	8.2811	9.5748

Fig. 7. Future water demand for three scenarios (minimum, average and maximum)

DISCUSSION AND CONCLUSIONS

This study is limited by numbers of constraints. First, the unavailability of sector-specific data, social data (exact population coverage and GDP rate), water price data, leakage rate, and climatic data in smaller time scale lacks the better understanding of these variables and representation into the model including description and propagation of the uncertainties. As a reason, we limited our analysis only in domestic demand, which is most uncertain part for the future water demand. We could not be able to assess the water demand affect due to climate change. Second, the monthly time step does not allow us to see whether climate characteristics that occur within months (which most extreme events are likely to be) will threaten the city's ability to maintain adequate reserves of drinking water. Regardless, this paper demonstrates and emphasises on uncertainties associated to the future and future change pressures. We cannot describe the future water demand deterministically as those change pressures are highly uncertain, and new study on demand forecasting should have significant emphasise on associated uncertainties description, which can be described either by scenarios approach, or probabilistically. Our efforts in this regards will be new insights for the future planning for the Birmingham or similar cities.

From the analysis, it is clear that future water demand (at the monthly aggregate level) is largely driven by change in population and socio-economic changes rather than climate changes. From the analysis, we found average water demand for year 2035 318.07<327.87<338.09 ML/day having supply side risk of not meeting the future demand from present sources of 314.9 ML/day (water available for use). The role of Birmingham is changing from industrial city to commercial city, which will have different demand characteristics in the future than simply projected by Water Company. We recommend for the further detailed analysis on future water demand

forecasting in Birmingham, and apply appropriate planning options for maintaining the sustainable management of future water demand in Birmingham STWL service area.

ACKNOWLEDGEMENT

The authors would like to express their kind appreciation for the useful data and information provided by the Severn Trent Water Limited, Birmingham, UK, especially to Business Strategy Manager Frank Grimshaw.

REFERENCES

Altukaynak, A. S., Özger, M., & Çakmakci, M. (2005). Water consumption Prediction of Istanbul city by using Fuzzy logic approach. *Water Resources Management 19*, 641-654.

Arbués, F., Garc´ıa-Valiñas, M. ı. Á., & Mart´ınez-Espiñeira, R. (2003). Estimation of residential water demand: a state-of-the-art review. *Journal of Socio-Economics, 32* 81–102.

Arnell, N. W. (2004). Climate change and global water resources: SRES emissions and socio-economic scenarios. *Global Environmental Change 14*, 31-52.

Arnell, N. W., & Delaney, E. K. (2006). Adapting to Climate Change: Public Water Supply in England and Wales. *Climate Change, Springer Link, 78*(2-4), 227-255.

Berliner, L. M. (2003). Uncertainty and Climate Change. *Statistical Science, 18*(4), 430-435.

Billings, R. B., & Agthe, D. E. (1998). State-space versus multiple regressions for forecasting urban water demand. *Journal of Water Resources Planning and Management, 124*(2), 113–117.

Bougadis, J., Adamowski, K., & Diduch, R. (2005). Short-term municipal water demand forecasting. *Hydrological Process, 19*(1), 137–148

Bradley, R. M. (2004). Forecasting Domestic Water Use in Rapidly Urbanizing Areas in Asia. *Journal of Environmental Engineering, 130*(4), 465-471.

Carter, T. R., Hulme, M., & Viner, D. (1999). *Representing Uncertainty in Climate Change Scenarios and Impact Studies*: Climatic Research Unit, UEA, Norwich, UK.

Clarke, G. P., Kashti, A., McDonald, A., & Williamson, P. (1997). Estimating Small Area Demand for Water: A New Methodology. *Water and Environment Journal, 11* (3), 186 - 192.

Efron, B., & R. J. Tibshirani. (1993). *An Introduction to the Bootstrap*. New York: Chapman and Hall.

Ferson, S., Joslyn, C. A., Helton, J. C., Oberkampf, W. L., & Sentz, K. (2004). Summary from the epistemic uncertainty workshop: consensus amid diversity *Reliability Engineering & System Safety, 85*(1-3), 355-369

Ghiassi, M., Zimbra, D. K., & Saidane, H. (2008). Urban Water Demand Forecasting with a Dynamic Artificial Neural Network Model. *Journal of Water Resources Planning and Management, 134*(2), 138-146.

Graser, H.J. (1958). Meter records in system planning. *Journal of American Water Works Association 50(11)*, 1395-1402.

Herrington, P., (1995). *Climate change and the demand for water*. Final report to the Institute of Hydrology and the Department of the Environment. London, April 1995.

Hensher, D., Shore, N., & Train, K. (2005). Households' Willingness to pay for water service attributes. *Environmental and Resource Economics, 32*(4), 509-531.

Hidalgo, J. (2003). An alternative bootstrap to moving blocks for time series regression models. *Journal of Econometrics, 117* 369 – 399.

Intergovernmental Panel on Climate Change (IPCC). (2007). *Working Group II: Impacts, Adaptation and Vulnerability, Summary for Policymakers*: The Fourth Assessment Report of the Intergovernmental Panel on Climate Change

Jain, A., Varshney, A.K., and Joshi, U.C. (2001). Short-term water demand forecast modelling at IIT Kanpur using artificial neural networks. *Water Resources Management* 15, 299-321.

Keilman, N., Pham, D. Q., & Hetland, A. (2002). Why population forecasts should be probabilistic - illustrated by the case of Norway. *Demographic Research, 6*(15), 409-454.

Khatri, K., & Vairavamoorthy, K. (2007). *Challenges for urban water supply and sanitation in the developing countries.* Water for changing world-Enhancing local knowledge and capacity, (13-15 June), UNESCO-IHE, Delft.

Krzysztofowciz, R. (2001). The case for probabilistic forecasting in hydrology. *Journal of hydrology, 249*(1), 2-9.

Ku¨nsch, H. R. (1989). The Jacknife and the bootstrap for general stationary observations. *The Annals of Statistics, 17*(3), 1217–1241.

Lee, R. D., & Tuljapurkar, S. (1994). Stochastic population forecasts for the United States: Beyond high, medium, and low. *Journal of the American Statistical Association, 89*, 1175– 1189.

Macdonald, I., & Strachan, P. (2001). Practical application of uncertainty analysis. *Energy and Buildings 33*, 219-227

Maidment, D.R., Miaou, S.P., and Crawford M.M. (1985). Transfer function models of daily urban water use. *Water Resources Research* 21(4): 425-432.

Mannina, G., Freni, G., Viviani, G., Sægrov, S., & Hafskjold, L. S. (2006). Integrated urban water modelling with uncertainty analysis. *Water Science & Technology, 54*(6), 379-386.

McIntyre, N. R., Wagener, T., Wheater, H. S., & Yu, Z. S. (2003). Uncertainty and risk in water quality modelling and management. *Journal of Hydro-informatics, 5*(4), 259-274.

McKay, M. D. (1992, December 13-16, 1992). *Latin hypercube sampling as a tool in uncertainty analysis of computer models.* Paper presented at the Proceedings of the 24th conference on Winter simulation, Arlington, Virginia,.

National Research Council (NRC). (2000). *Beyond Six Billion: Forecasting the World's Population. Panel on Population Projections.* Washington, DC: Committee on Population, Commission on Behavioural and Social Sciences and Education, National Academy Press.

New, M., & Hulme, M. (2000). Representing Uncertainty in Climate Change Scenarios: a Monte-Carlo approach. *Integrated Assessment, Springer, 1*, 203-213.

O'Neill, B. C., Balk, D., Brickman, M., & Ezra, M. (2001). A guide to global population projections. *Demographic Research 4*(8), 203-288.

Paté-Cornell, M. E. (1996). Uncertainties in risk analysis: Six levels of treatment *Reliability Engineering and System Safety, 54*(2), 95-111.

Ruth, M., Bernier, C., Jollands, N., & Golubiewski, N. (2007). Adaptation of urban water supply infrastructure to impacts from climate and socioeconomic changes: The case of Hamilton, New Zealand. *Water Resource Management, 21*, 1031–1045.

Schneider, M. L., & Whitlatch, E. E. (1991). User-specific water demand elasticise. *Journal of Water Resources Planning and Management, 117*(1), 52-73.

Severn Trent Water Limited (STWL). (2008). *Severn Trent Water - Water Resources Management Plan 2009*.

Sophocleous, M. (2004). Global and Regional Water Availability and Demand: Prospects for the Future. *Natural Resources Research, 13*(2), 61-75.

Vogel, R. M. (1996). The moving blocks bootstrap versus parametric time series models. *Water Resources Research 32*(6), 1875–1882.

Vörösmarty, C. J., Green, P., Salisbury, J., & Lammers, R. B. (2000). Global Water Resources: Vulnerability from Climate Change and Population Growth. *Science 289*, 284-287.

Wilson, T., & Bell, M. (2004). Australia's uncertain demographic future. *Demograhpic Research, 11*(8), 195-234

Zhou, S. L., McMahona, T. A., Waltonb, A., & Lewisb, J. (2000). Forecasting daily urban water demand: a case study of Melbourne. *Journal of Hydrology 236*, 153-164.

Water Quality Effects of Varying Crop, Fertilizer and Carbon Prices

T. L. Ng[1], J. W. Eheart[2] and X. Cai[3]

[1]Department of Civil and Environmental Engineering, University of Illinois at Urbana-Champaign, 205 N Mathews Ave, Urbana, IL 61801-2352; PH (217) 333-6850; email: tng@illinois.edu
[2]Department of Civil and Environmental Engineering, University of Illinois at Urbana-Champaign, 205 N Mathews Ave, Urbana, IL 61801-2352; PH (217) 333-6962; email: weheart@illinois.edu
[3]Department of Civil and Environmental Engineering, University of Illinois at Urbana-Champaign, 205 N Mathews Ave, Urbana, IL 61801-2352; PH (217) 333-4935; email: xmcai@illinois.edu

ABSTRACT

Crop and fertilizer prices have increased dramatically in the past few years. These prices, together with existing demand for carbon trading allowances, affect farmers' decisions. It is useful to assess the effect of varying crop, fertilizer and carbon prices on farmers' decisions, and in turn, the effect of these decisions on surface water quality, specifically the nitrate load from the watershed. To achieve the objectives of this study, a mixed integer optimization model incorporating a hydrologic model of a test site is developed. The Salt Creek watershed in East Central Illinois has been selected as the test site for this study. Simulation results indicate that there is a higher tendency for farmers to produce corn in 2007 and 2008 than in previous years. Consequently, the average fertilizer use in that period is relatively high, causing greater levels of nitrate runoff. Results also indicate that at current carbon prices, carbon trading is ineffective in reducing nitrate runoff.

INTRODUCTION

With the growing demand for biofuels and general worldwide pressure on cereal grain supplies, crop prices have increased dramatically in the past few years. At the same time, fertilizer prices have also been increasing due to rising energy costs. These prices, together with existing demand for carbon trading allowances, affect farmers' decisions. On one hand, high crop prices create greater motivation for farmers to adopt more aggressive production practices. On the other hand, rising fertilizer prices cause farmers to be more conservative in their use of fertilizer. Similarly, carbon trading gives incentive for farmers to implement certain best management practices (BMPs) that may negatively affect crop production. In this study, carbon trading is modeled after the Illinois Conservation and Climate Initiative (ICCI) (www.illinoisclimate.org) program, through which farmers may sell carbon credits on the Chicago Climate Exchange (CCX) (www.chicagoclimatex.com).

It is useful to assess the effect of varying crop, fertilizer and carbon prices on farmers' decisions, and in turn, the effect of these decisions on surface water quality. A better understanding of this will facilitate the formulation of more informed

policies to control agricultural runoff, which is a major source of nutrient loading in surface waters and a direct contributor to hypoxia in many coastal ecosystems.

The Salt Creek watershed in East Central Illinois has been selected as the test site for this study. It is typical of most Midwestern agricultural watersheds and like many of these systems, experiences excessive nutrient loads in its waters.

METHOD

To meet the objective of this study, a hydrologic model of the Salt Creek watershed in East-Central Illinois is developed and linked to an economic model to estimate farmers' decisions- subject to crop, fertilizer and carbon prices- and subsequently, the effect of those decisions on water quality.

Hydrologic model

The Salt Creek watershed model is developed using the Soil and Water Assessment Tool (SWAT) (www.brc.tamus.edu/swat/). SWAT is a watershed-scale hydrologic model to simulate the environmental effects of land and agricultural practices. It is public domain software supported by the US Department of Agriculture (USDA) Agricultural Research Service (ARS) and is widely accepted in both academia and government (Gassman et al., 2007).

Input data for the watershed model include elevation, land use, soil type, temperature and precipitation data, which are obtained from online databases maintained by the USDA, US Geological Survey (USGS) and National Oceanic and Atmospheric Administration (NOAA).

The watershed is delineated into a hundred subbasins of varying sizes with the average being 48 km^2. The soil type and land use within each subbasin is assumed homogenous throughout it. Two of the subbasins representing the area in and around the City of Bloomington are urban, while the remaining subbasins are agricultural with corn and soybean as their primary crops.

The watershed model is calibrated and validated against observed data for daily stream flow, monthly riverine nitrate load and annual corn and soybean yields. The observed data are from various sources including the USGS, Illinois Environmental Protection Agency (IEPA) and USDA National Agricultural Statistics Service (NASS). Results show a good fit between simulated and observed values based on their coefficients of determination (R^2) and Nash-Sutcliffe coefficients (NSE).

Economic model

The economic model to predict farmers' decisions as a function of crop, fertilizer and carbon prices can be described as follows. A farmer has to choose the right crop (corn or soybean), best level of fertilizer input and/or whether or not to adopt certain BMPs to generate carbon offsets for sale. In this study, two types of BMPs are considered, i.e. grass planting and conservation tillage.

The farmer stands to gain from crop sales. He also stands to gain from selling carbon credits should he choose to participate in that. However, he has to weigh these potential gains against the costs of fertilizer, pesticide, labor, energy, equipment etc. To identify the most optimal balance that maximizes his overall profit, he will have to refer to the current year's crop, carbon and fertilizer prices.

In making his decisions, the farmer also has to consider the "rotation effect", where a crop planted continuously is more vulnerable to pest and disease than if planted in rotation with another crop (Turco et al., 1990; Katsvairo and Cox, 2000). Thus, it is generally costlier to plant a crop after itself than after another crop.

If assuming rational behavior and perfect information on the part of the farmer, the problem can be framed as a mixed integer optimization model and linked to the SWAT hydrologic model to obtain predictions of the farmer's decisions.

RESULTS AND DISCUSSION

Simulations are carried out to estimate farmers' decisions for the years 1999 to 2008 and the effect of those decisions on riverine nitrate load at the outlet of the Salt Creek watershed. For each of the agricultural subbasins in the SWAT watershed model of the system, the optimal combination of crop choice, fertilizer input and BMP application is computed.

To maintain a common basis for comparison, all simulations are carried out using the same set of climate data (2002 data). For the same reason, the initial condition of the system is also maintained constant across the years. Here, the initial condition refers to the previous year's crop and BMP selection; and is assumed as approximately half the watershed cultivating corn and half soybean with zero implementation of conservation tillage or grass planting.

Preliminary simulation results show that there is a greater tendency for farmers to plant corn in 2007 and 2008 than in previous years. This is due to record high corn prices in those years; and is in spite of the rotation effect. Corn acreage in both years exceeds 80% of the watershed, which is high considering that the ten-year average is 56%.

These results are a cause of concern as corn is a more polluting crop than soybean. Corn requires greater levels of fertilizer input that causes serious water quality problems when washed into surface waters. Indeed, the simulated average fertilizer use in 2007 and 2008 is relatively high and correspondingly, so is the nitrate load coming out of the watershed. This is the case even though fertilizer prices for those years are unusually high when compared to historical values.

Another item of interest is the price of a carbon dioxide equivalent. At current carbon prices (as determined by the CCX), carbon trading does provide some additional incentive, on top of the savings they gain, to farmers to practice conservation tillage. However, the prices are not competitive enough to provide any incentive to farmers to adopt grass planting, which requires them to give up their crops. This means that at current prices, carbon trading is not a viable policy instrument to mitigate nitrogen runoff from agriculture; as conservation tillage is ineffective in reducing nitrogen loss where there is subsurface drainage (Bjorneberg et al., 1996) (as is the case of the Salt Creek watershed and much of the Midwest).

CONCLUSIONS

A hydrologic model of the Salt Creek watershed in East Central Illinois is developed and linked to a mixed integer economic model to predict farmers' decisions subject to crop, fertilizer and carbon prices; and the effect of those decisions on water quality, specifically the nitrate load from the watershed. The results obtained indicate that there is a greater tendency for farmers to produce corn (versus soybean) in 2007 and 2008 than in previous years. Consequently, the average fertilizer use in that period is relatively high, causing greater levels of nitrate runoff. Results also indicate that at current carbon prices, carbon trading is ineffective in reducing nitrate runoff.

All this suggests that should 2007 or 2008 conditions prevail, there is a real possibility of farmers switching from their current corn-soybean rotation schedule to a continuous corn schedule permanently; at the expense of the environment. Suitable policies, beside or on top of carbon trading, will have to be implemented to control the increases in nitrate runoff that will be inevitable.

ACKNOWLEDGMENTS

This work is funded by the Energy Biosciences Institute, which is supported by BP.

REFERENCES

Bjorneberg, D. L.; Kanwar, R. S. and Melvin, S. W. (1996). Seasonal changes in flow and nitrate-N loss from subsurface drains. Transactions of the ASAE, 39(3), 961-976.

Gassman, P. W.; Reyes, M. R.; Green, C. H. and Arnold, J. G. (2007). The soil and water assessment tool: historical development, applications, and future research directions. Transactions of the ASABE, 50(4), 1211-1250.

Katsvairo, T. W. and Cox, W. J. (2000). Tillage × Rotation Management × Interactions in Corn. Agronomy Journal, 92, 493-500.

Turco, R. F.; Bischoff, M.; Breakwell, D. P. and Griffith, D. R. (1990). Contribution of soil-borne bacteria to the rotation effect in corn. Plant and Soil, 122, 115-120.

Water Resources Planning under Non-stationary Hydroclimate in a Snow Dominant Watershed

Francis I Chung [1], Tariq N. Kadir[2] and Jefferey K. Galef[3]

[1] Modeling Support Branch, California Department of Water Resources, P.O Box 942836, Sacramento, 1416 Ninth Street; PH (916) 653-5924; FAX (916) 653-9574; email: chung@water.ca.gov
[2] Modeling Support Branch, California Department of Water Resources, P.O Box 942836, Sacramento, 1416 Ninth Street; PH (916) 653-3513; FAX (916) 653-9574; email: kadir@water.ca.gov
[3] Specialized Areas Branch, California Department of Water Resources, P.O Box 942836, Sacramento, 1416 Ninth Street; PH (916) 651-0889; FAX (916) 651-9678; email: jgalef@water.ca.gov

ABSTRACT

Milly et al. in a recent article (Science, Vol319, 1February, 2008, pp573-574) declared that "stationarity is dead and should no longer serve as a central, default assumption in water-resources risk assessment and planning." They went on stating, "Finding a suitable successor is crucial for human adaptation to changing climate." Noting that the fundamental cause of this climatic change is the warming temperature and further noting no apparent change in the runoff volume for the last century, the authors hypothesize that a temperature based hydrology can explain most of the non-stationary behavior of the runoff in a snow dominant watershed like the Upper Feather Basin in California. The observation of the historical temperature data suggests that this region is warming consistent with the global trend. The projections of precipitation by various GCM's are wide spread and uncertainties on the wetness (or dryness) abound whereas the future temperature projections, through also widely spread, are unanimous in directional sense—going up or getting warmer over time. Noting this robust nature of the future temperature projections and also noting that the cause of the future precipitation changes between rain and snow is due to the rising temperature, the authors take an approach that the temperature, rather than the precipitation, should be the commencing point in the development of the changing future hydrology. We claim that the main cause of the "death" of the stationarity in a snow dominant watershed may be the warming temperature. Therefore, by commencing with the temperature in the hydrologic process, either the form of precipitation or the melting of the accumulated snow can be simulated and the non-stationary aspects of the future hydrology can be captured for more adequate water resources planning and management. The USGS under a contract to the California Department of Water Resources completed development of the Precipitation-Runoff Modeling System (PRMS) application for simulating daily streamflow for the Upper Feather River Basin. PRMS simulates all the major snowmelt/precipitation related physical processes including snowpack accumulation/melting, sublimation, evapotranspiration, surface runoff, subsurface flow, and ground water flow. The calibrated model simulates Water Years 1971-2001. This analysis perturbs the historical period daily minimum and maximum

temperatures by 1°C, 2°C, 3°C, and 4°C, respectively, to determine the impact on snowmelt/runoff processes and ultimately streamflow at Oroville; all other parameters were unchanged from the historical simulation (Base Case). Precipitation spatial and temporal distribution was unchanged. Model output parameters studied include evapotranspiration, groundwater flow, groundwater recharge, interception evaporation, precipitation (rain/snow), runoff, snow cover percent, snow evaporation/sublimation, snowmelt, snowpack water equivalent, surface streamflow, subsurface flow, and subsurface recharge. For these varying degrees of warming, the outflows of the Basin were examined and compared to the base historical simulation. The timing of the center of the mass, the April through July runoff as a percent of the annual runoff, and the April snowpack water equivalent are shown to change appreciably with rising temperature.

INTRODUCTION

The assumption of stationarity of a hydrological time series is fundamental to long term water resources planning. In a snow dominant watershed, hydrological series such as temperature and precipitation (both snow and rainfall) have a direct impact on snowmelt and rainfall-runoff processes impacting stream flows which is crucial for planning and operating large surface water reservoirs receiving such flows. Global climate change studies suggest that such an implicit assumption of stationarity may not be true anymore. Milly et al. in a recent article (Milly et al, 2008) declared that "stationarity is dead and should no longer serve as a central, default assumption in water-resources risk assessment and planning." They went on stating, "Finding a suitable successor is crucial for human adaptation to changing climate."

Noting that the fundamental cause of this climatic change is the warming temperature and further noting no apparent change in the runoff volume for the last century, the authors hypothesize that a temperature based hydrology can explain most of the non-stationary behavior of the runoff in snow dominant watersheds in California. The observation of the historical temperature data suggests that these regions are warming consistent with the global trend. The projections of precipitation by various GCM's are wide spread and uncertainties on the wetness (or dryness) abound whereas the future temperature projections, through also widely spread, are unanimous in directional sense—going up or getting warmer over time (Figure 1 and Figure 2).

Noting this robust nature of the future temperature projections and also noting that the cause of the future precipitation changes between rain and snow is due to the rising temperature, the authors take an approach that the temperature, rather than the precipitation, should be the commencing point in the development of the changing future hydrology. We claim that the main cause of the "death" of the stationarity in a snow dominant watershed may be the warming temperature. Therefore, by commencing with the temperature in the hydrologic process, either the form of precipitation or the melting of the accumulated snow can be simulated and the non-stationary aspects of the future hydrology can be captured for more adequate water resources planning and management.

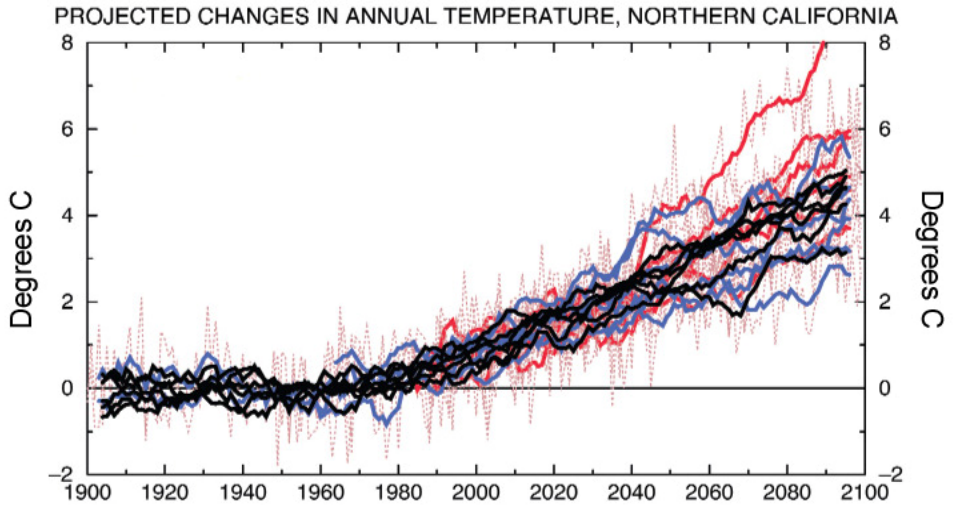

nger, 2005)

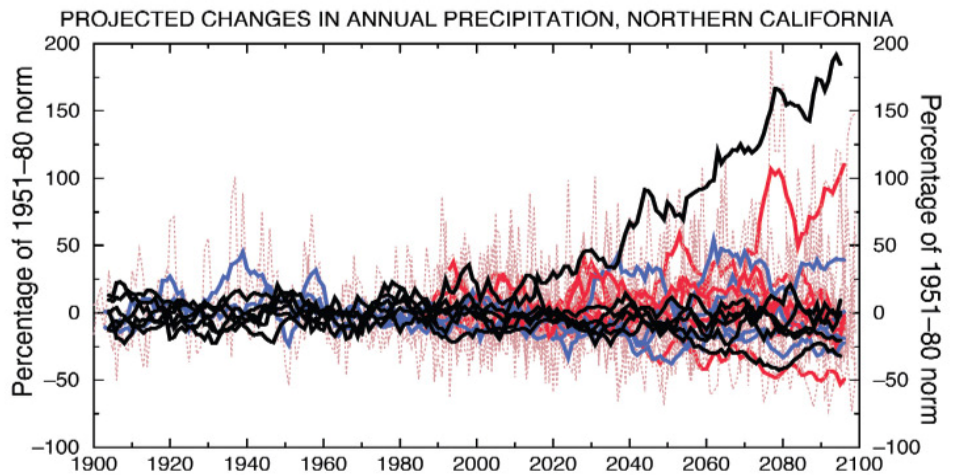

)05)

UPPER FEATHER RIVER BASIN

The Upper Feather River Basin is a 3600 square mile drainage area whose runoff flows into Oroville reservoir, a key component of California's State Water Project (Figure 3 and Figure 4). Altitudes for the basin range from 843 feet (above Mean Sea Level) at Oroville to 9525 feet near Mount Lassen. The average snowline altitude is 5500 feet. The geology is volcanic rocks in the north and west, and granitic sedimentary rocks in the south. The climate is Mediterranean with warm dry summers and cool wet winters and springs. Most of the basin lies at altitudes where winter temperature can easily vary from below to above freezing. Daily temperatures at the lowest station range from 46°F to 71°F, whereas at the highest station it ranges from 33°F to 60°F. The lapse rate is approximately 3.6°F per 1000 feet of altitude change. The average April through July runoff for the watershed for water years 1922 through 2003 averages 1992 thousand acre-feet (TAF) and is approximately 45% of the total annual runoff of 4394 TAF. Lake Oroville, the backbone of the SWP, receives much of its inflow from the upper Feather River

basin in the Sierra Nevada mountain range. Sierra Nevada means “snowy mountains” in Spanish, and, true to this name, snowpack that accumulates from October through March in the upper Feather Basin provides the majority of the spring and summer runoff that eventually flows into Lake Oroville. Because snow melting and sublimation is heavily dependant on temperatures, it is important to the operation of Lake Oroville to know how projected future climate conditions can affect both the timing and quantity of flows arriving there. This study uses a physical model of the upper Feather Basin to better understand the effects of increasing air temperature on precipitation, snowpack, and runoff.



Figure 3: Upper Feather River Basin and State Water Project

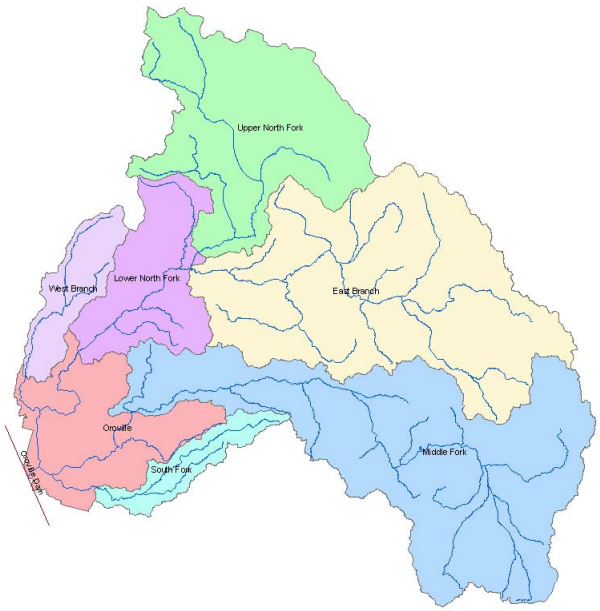

Figure 4: Major Sub-basins within the Upper Feather River Basin

A key hydrological parameter to note for the basin is the snow indices measured for the historical period and shown in Figure 5.

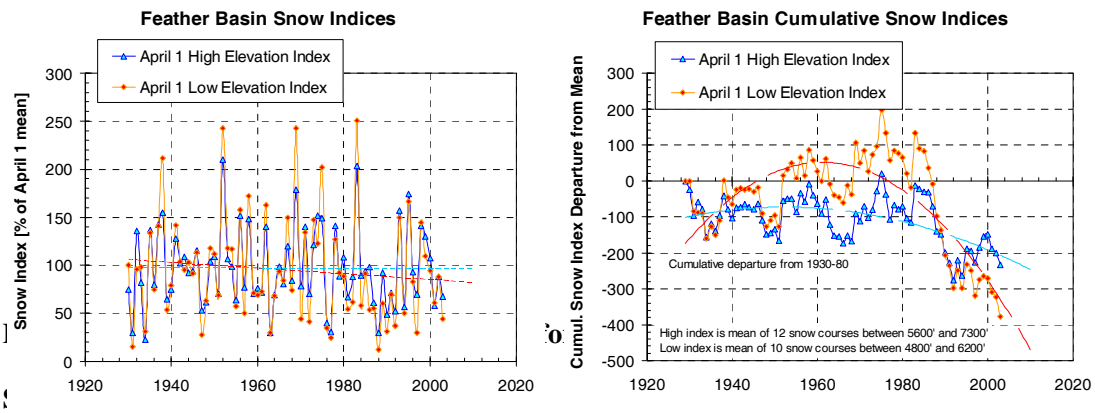

The Precipitation-Runoff Modeling System PRMS is a physically based precipitation-runoff model developed by the USGS (Figure 6). The model simulates all the major snowmelt and precipitation-related physical processes, including snowpack accumulation or melting, sublimation, evapotranspiration, surface runoff, subsurface flow, and groundwater flow. It was applied to the Upper Feather River Basin in a study by the USGS for the California Department of Water Resources DWR (Koczot et al. 2004). The model simulates the historical period water

years 1972–1997 (which is also the calibration period), and has since been extended through water year 2001.

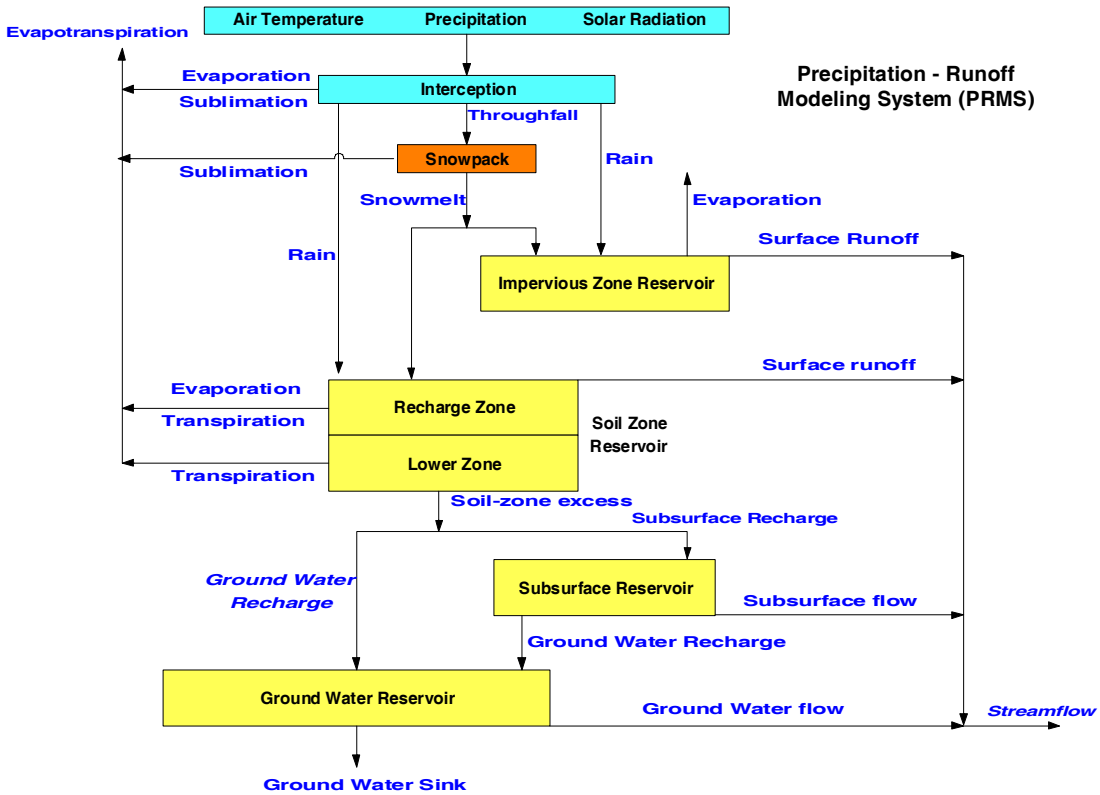

Figure 6: The Precipitation-Runoff Modeling System by USGS

A sensitivity analysis was conducted using the PRMS for the Upper Feather River Basin to quantify the effects of increasing daily minimum and maximum ambient air temperature by 1°C, 2°C, 3°C, and 4°C (1.8°F, 3.6°F, 5.4°F, and 7.2°F) on snowmelt and runoff processes in the basin and impact on inflow into Oroville reservoir. The daily minimum and maximum temperatures for the 324 Hydrologic Response Units over the 30-year historical period (water years 1972-2001) were increased and impacts on the hydrological components, including streamflow and base flow were analyzed by comparing the alternative scenarios with the historical base scenario.Air temperature was the only parameter that changed for each simulation. Spatial and temporal distributions of precipitation and all other model parameters were the same for each simulation. The results below compared alternative air temperature scenarios with the historical base scenario.

KEY FINDINGS

In California, April has traditionally been considered as the time when snowpack is at its peak. The majority of the snowmelt runoff is assumed to occur in April through July. As air

temperatures increase, these traditional assumptions may no longer be valid, and water planning practices may need to be revised**.** Figure 7 shows the dramatic decrease in the April Snow Water Equivalent with increasing temperatures.

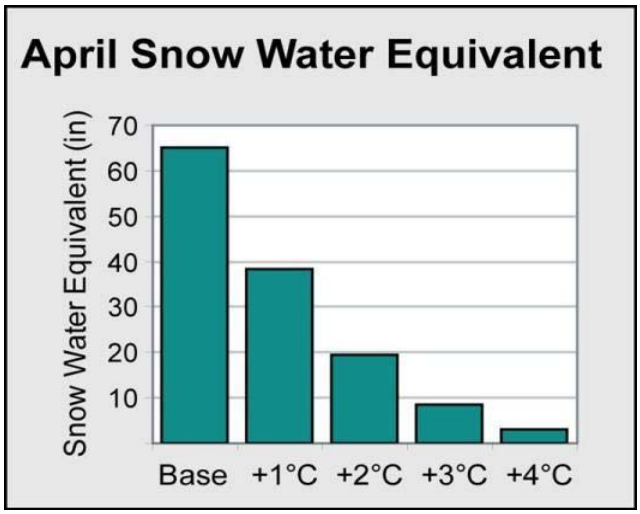

Figure 7: April Snow Water Equivalent for Upper Feather River Basin

Figure 8 shows how the day in the water year when 50% of the annual inflow arrives in Lake Oroville moves earlier in the year as air temperature increases. Figure 9 shows the fraction of annual runoff that occurs during the traditional runoff period of April through July decreases through time for all scenarios (including the base scenario) and decreases as air temperatures increase. These changes can have important impacts on current Water Year classifications (e.g., Sacramento Valley Water Year Type Index) and associated regulatory standards.

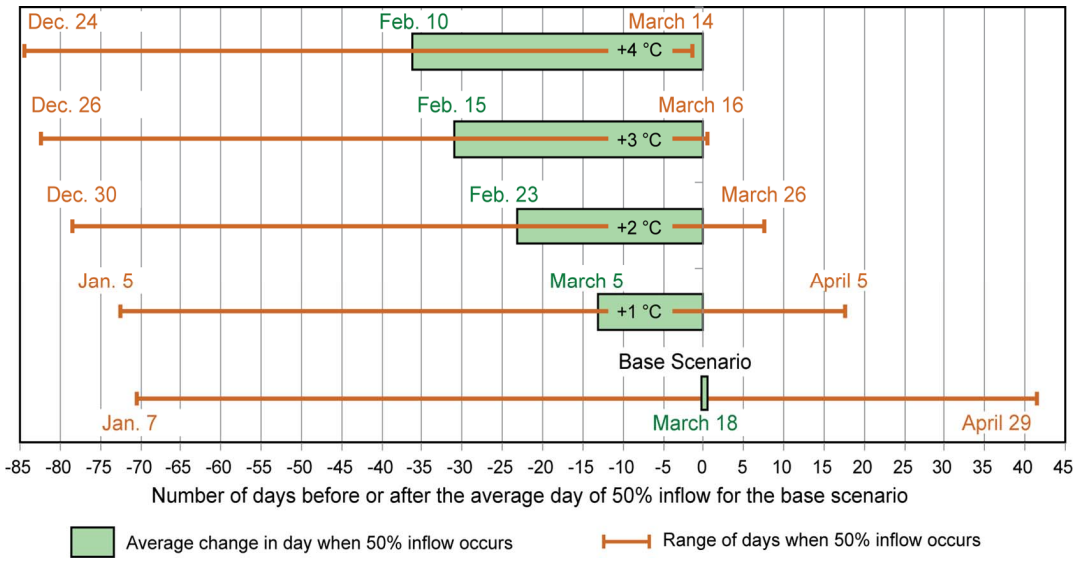

Figure 8: Impact on Center of Mass for Flow Into Oroville for Upper Feather River Basin

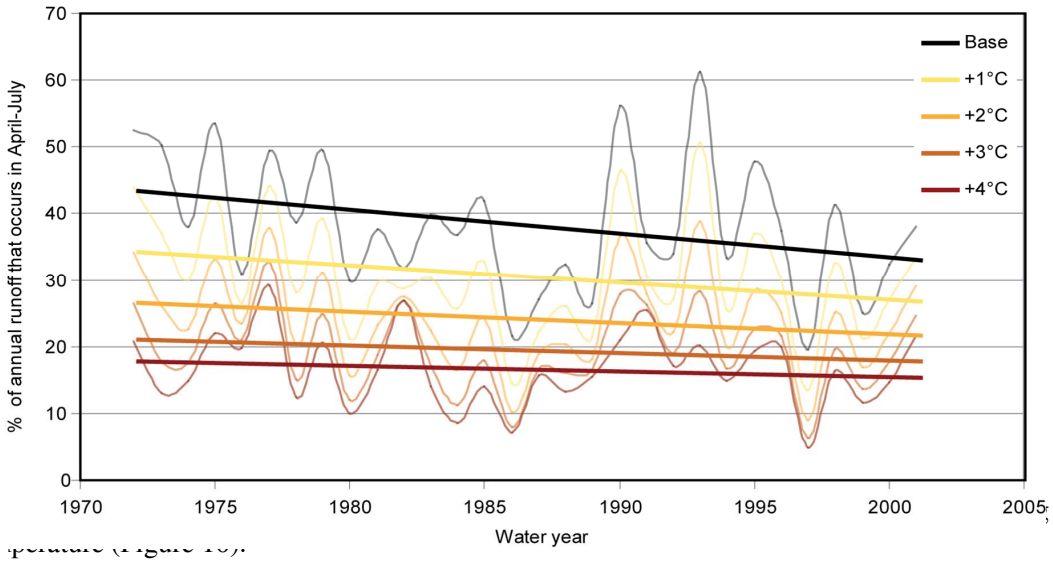

perature (Figure 10).

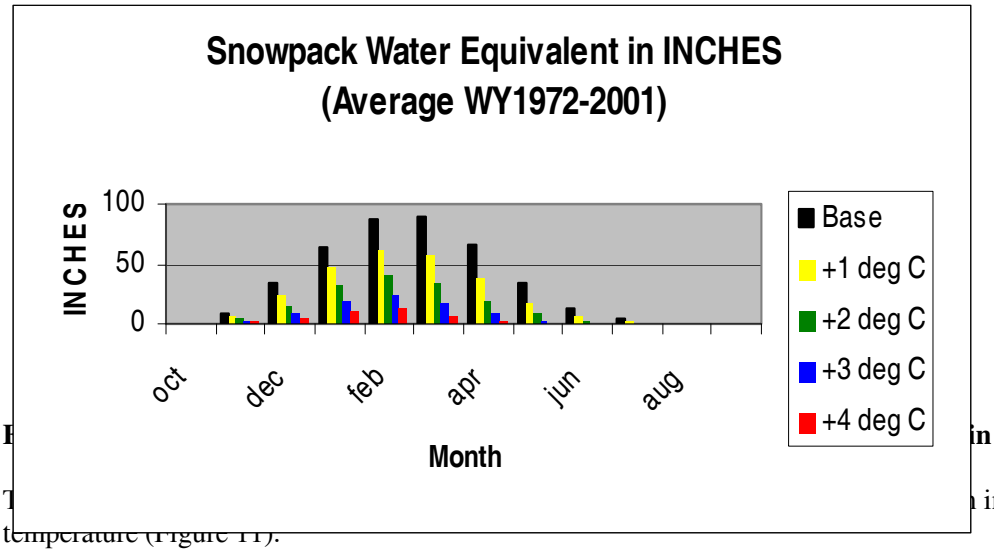

F **in**

T increasing temperature (Figure 11).

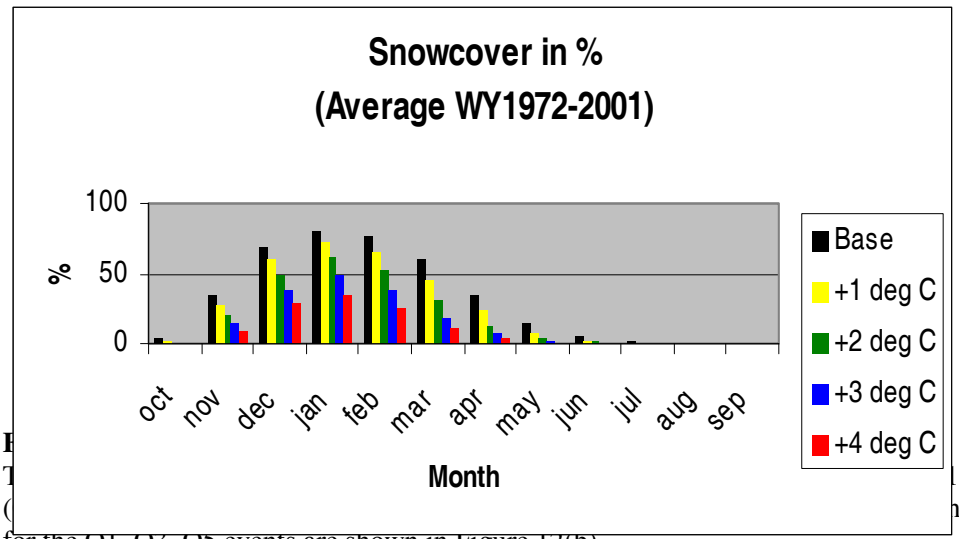

), 3-day
e peak flows
for the Q1, Q3, Q5 events are shown in Figure 12(b).

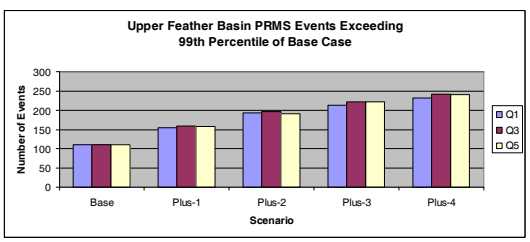

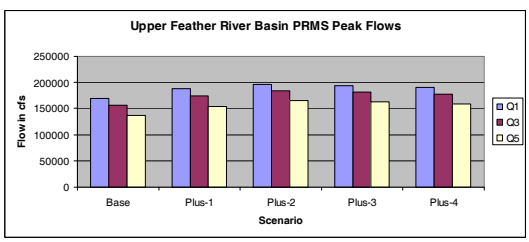

Figure 12: Impact on Q1, Q3, and Q5 Events and Peak Flows Exceeding 99th Percentile for Upper Feather River Basin

CONCLUSIONS

Using global climate change studies indications of increasing trends in temperature but with uncertain trends in precipitation, the sensitivity analysis of increasing ambient air temperatures conducted using PRMS on the Upper Feather River Basin in California to determine impacts of increasing ambient air temperatures showed significant impacts on hydrological processes such as April snow water equivalent, % snow cover, timing of center of mass for flow into Oroville, snowpack water equivalent, and Q1, Q3, Q5 events exceeding 99th percentile flow for Oroville. Use of the physically based PRMS model is superior to empirical based approaches from downscaled GCM results though more expensive to conduct and more resource intensive.

REFERENCES

Department of Water Resources (DWR). (2006). Progress on incorporating climate change into management of California's water resources. http://water.ca.gov/climatechange/docs/DWRClimateChangeJuly06.pdf.

Department of Water Resources (DWR). (2008). John Pierre Stevens (personal communication).
Dettinger, M.D. (2005). "From Climate-Change Spaghetti to Climate-Change Distributions for 21st Century California", San Francisco Estuary and Watershed Science, Vol.3, Issue 1, March 2005.

Koczot, K., A. Jeton, B. McGurk, and M.Dettinger. (2004). "Precipitation-Runoff Processes in the Feather River Basin, Northeastern California, with Prospects for Streamflow Predictability, Water Years 1971–97." USGS Scientific Investigations Report 2004-5205.

Milly, P. C. D., J. Betancourt, M. Falkenmark, R.M. Hirsch, Z.W. Kundzewicz, D.P. Lettenmaier, and R.J. Stouffer. (2008). "Stationarity Is Dead: Whither Water Management?" Science 319(5863): 573 – 574. February 1, 2008. DOI: 10.1126/science.1151915. www.sciencemag.org/cgi/content/short/319/5863/573

ACKNOWLEDGEMENTS

The authors wish to acknowledge contributions of the following. From the California Department of Water Resources: Michael Anderson, Jamie Anderson, and John Pierre Stevens; and from the US Geological Survey: Kathryn Koczot and Steve Markstrom.

Water Supply and Energy Generation

L. K. Lampe[1], L. M. Adams[2] and D. G. Jensen[3]

[1, 2] Black & Veatch Water Resources and Sustainable Planning Practice, 8400 Ward Parkway, Kansas City MO, 64114; PH (913) 458-3363; email: LampeLK@bv.com
[3] Metropolitan Energy Center, 3808 Paseo Boulevard, Kansas City, MO 64109

ABSTRACT

Energy and water resources are inextricably linked: the production of energy requires large volumes of water; and reciprocally, the treatment and distribution of water relies on available, affordable energy. This paper reviews technology trends, identifies regulatory and technical challenges to the electrical energy industry, provides case studies based on work by Black & Veatch that explores methods for the sustainable provision of energy and water to communities, and discusses the ongoing research and development efforts as related to utilities and regional stakeholders.

INTRODUCTION

Water and energy resources have stimulated unprecedented economic growth and development in the United States. A growing population has also contributed to competition for resources; together these demands affect the value and availability of energy and water. The Census Bureau projects US population will grow by about 70 million, from just over 300 million, in the next 25 years. During that time, electricity demands are estimated to increase by 50% (EIA, 2006). Energy and water resources are inextricably linked. The production of energy requires large volumes of water, and reciprocally, the treatment and distribution of water relies on available, affordable energy.

In the United States, the USGS estimates that 136 billion gallons of freshwater are withdrawn and 10 billion gallons of freshwater are consumed each day for thermoelectric generation (Hutson, 2004). Approximately 3% of overall electrical usage, 56 billion kilowatt-hours, is used for water and wastewater treatment and distribution annually (EPRI, 2001). Municipal electrical usage, however, is largely connected to a community's need for water infrastructure. For the City of Kansas City, Missouri, municipal water and wastewater treatment and distribution accounts for approximately 29% of the City's annual energy budget (Kansas City, 2007). The health of economies and populations in developed and developing countries around the world will hinge on the availability of clean and cost-effective energy and water resources.

TECHNOLOGY TRENDS

Water is integral to the production of energy. Water is used during resource extraction, refining, processing, and transportation, and water systems dominate the cooling and emissions scrubbing in thermoelectric power plants. Thermoelectric power plants, such as coal, oil, natural gas, and nuclear fueled power generators that use a steam turbine system based on the Rankine thermodynamic cycle, require significant quantities of water for generating electrical energy. The thermoelectric power generation market is the single largest user of freshwater in the US, accounting for 48% of the freshwater withdrawals in

the country annually. Most of the water that is withdrawn is returned at the end of the process at a higher temperature and with other changes in quality; however, it is available for subsequent use. Water consumption data refers to the loss of water as an available resource, often through evaporation. Figure 1 illustrates the water processes within a thermoelectric power plant, demonstrating that cooling is the most water consumptive process.

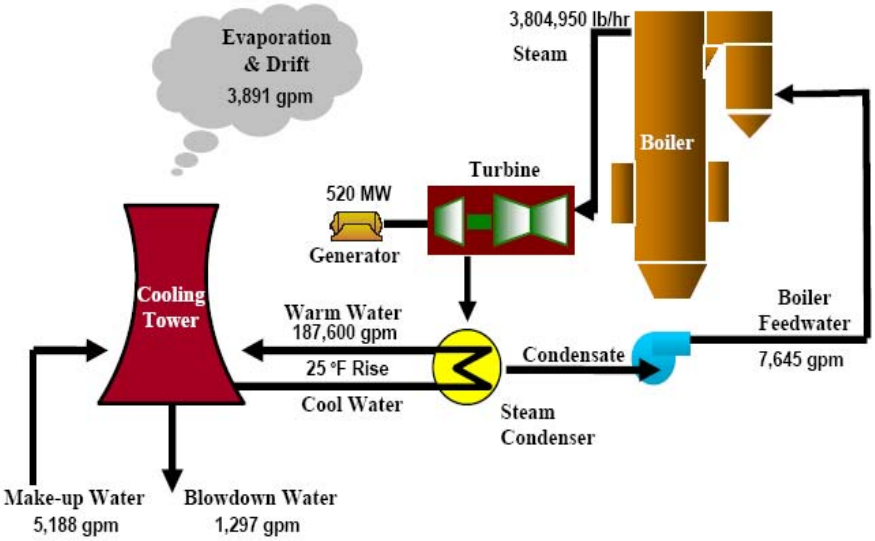

Figure 1. Thermoelectric Power Plant Schematic (Feeley, 2007)

Water for thermoelectric plants is withdrawn primarily from large volume sources, such as reservoirs, rivers, oceans, or underground aquifers. Approximately 70% of withdrawals are from freshwater sources. The volume of water withdrawn and consumed is dependent on the allowable temperature rise of the cooling water and the cooling technology. Industry typically uses three cooling water system designs: once-through, wet recirculating, and dry recirculating. In once-through cooling systems, water is withdrawn from a local water source and returned after passing through a condenser. On average, these systems withdraw a relatively high volume of water, but they consume only a small percentage, 0.25% of water withdrawn, in evaporative losses (Feeley, 2005). Wet recirculating systems recycle cooling water after dissipating the heat from warmed cooling water to the ambient air. The systems incorporate cooling towers, ponds, or canals for heat dissipation. On average, wet recirculating systems withdraw less water than once-through systems, but lose a larger percentage to evaporation, 92% of water withdrawn (Feeley, 2005). Dry recirculating cooling systems prevent evaporative losses by integrating a closed-loop heat exchanger to conduct heat from the used cooling water to the ambient air. These systems are not frequently constructed due to high capital and operating costs, and slowed energy generation is the trade-off for greater water efficiency. Figure 2 shows the number of existing cooling systems at US steam plants for 2005 and average total cost. Environmental regulations and permitting will continue to drive developers to choose options that are less water intensive.

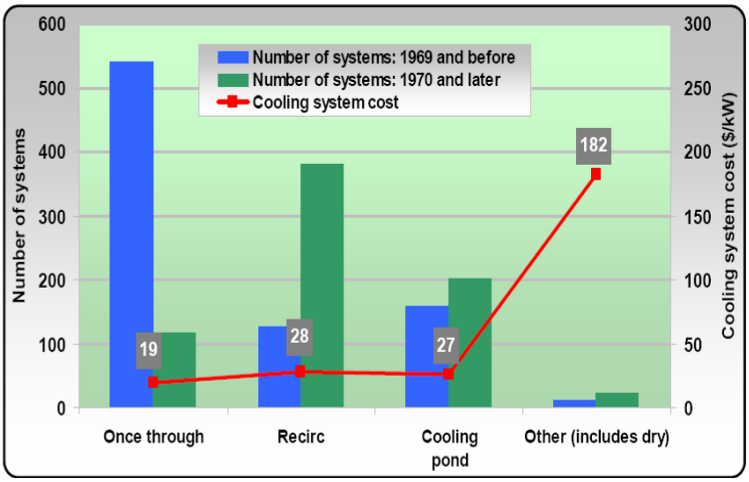

Figure 2. Cooling Technology Trends (Gerdes, 2008)

The cooling water system has the most substantial effect on the water requirements of a generation technology. Flue gas desulfurization (FGD) in coal-fired power plants also affects the withdrawal and consumption of water. The National Energy Technology Laboratory (NETL) developed national average water withdrawal and consumption factors for model thermoelectric power plants based on 2005 data. The team compared five types of generation: coal, nuclear, oil and natural gas, natural gas combined cycle, and integrated combined cycle systems. Their results also demonstrate the water efficiency of alternative cooling systems, boiler types, and FGD methods. A condensed summary of their results is presented in Table 1.

Table 1. Average Water Withdrawal and Consumption (Feeley, 2008)

Generation Type	Cooling water system type	Withdrawal factor (gal/kWh)	Consumption factor (gal/kWh)
Coal	Once-through	24.83	0.102
	Wet cooling tower	0.57	0.461
	Cooling Pond	16.46	0.405
Nuclear	Once-through	31.49	0.137
	Wet cooling tower	1.01	0.624
Oil & NG	Once through	22.74	0.09
	Wet cooling tower	0.25	0.16
	Cooling pond	7.89	0.11
NGCC	Once through	9.01	0.002
NGCC	Wet cooling tower	0.15	0.13
	Cooling pond	5.95	0.24
	Air cooled	0.004	0.004
IGCC	Wet cooling tower	0.226	0.173

The comprehensive assessment of withdrawal and consumption presented above is based on national averages; however, consumption rates and prevalent technology vary significantly by region. There are two major alternating current power grids in North America: the Eastern Connection and the Western Connection. The separation provides a

way to assess the water intensity of power generation on a regional basis, as presented in Table 2.

Table 2. Water Consumption by Region (Torcellini, 2003)

Power Provider	Thermoelectric *Gallons Evaporated per kWh*	Hydroelectric Plants *Gallons Evaporated per kWh*	Aggregate *Gallons Evaporated per kWh*
Western Interconnect	0.38	12.40	4.42
Eastern Interconnect	0.49	55.10	2.33
Texas Interconnect	0.44	0.00	0.43
U.S. Aggregate	**0.47**	**18.00**	**2.00**

If practices go unchanged, thermoelectric power plants will increasingly compete for freshwater with other sectors such as domestic, commercial, agricultural, industrial, and in-stream use – particularly in regions of the country with limited freshwater supplies. At times, energy generation is competing against protection of drinking water resources. Thermoelectric generating capacity is expected to increase by nearly 22% between 2005 and 2040, based on the Energy Information Administrations Annual Energy Outlook 2007 projections.

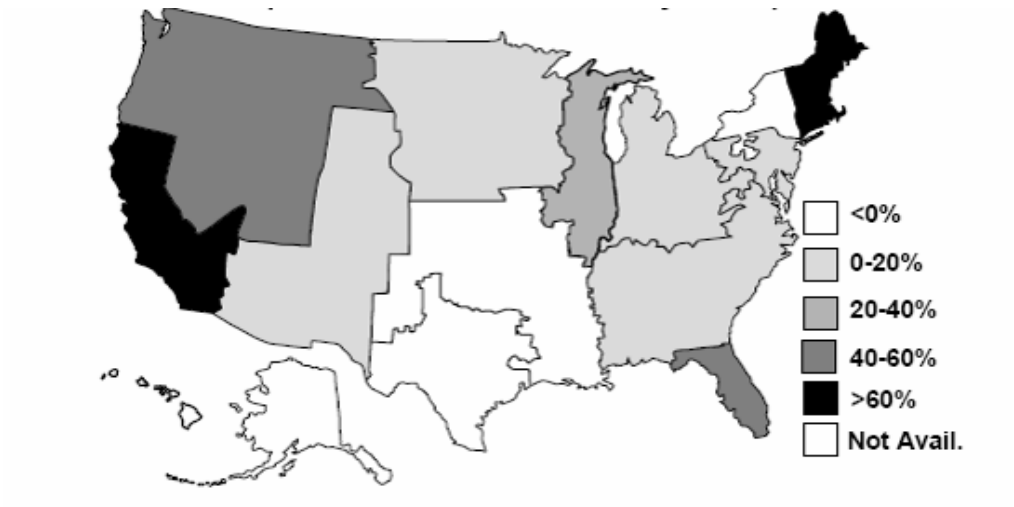

Figure 3. Percentage Increase in Power Plant Water Consumption (EPRI, 2002)

A water needs analysis conducted by NETL suggests that regional water demands may be significant as freshwater consumption increases. Figure 3, suggests that regions with very constrained water resources, such as the west coast and southeast, project the largest increases in power plant water consumption between 2000 and 2020.

OPPORTUNITIES FOR INTEGRATION

Overall, the existing thermoelectric power plant industry operates, on average, at 32% efficiency (Nichols, 2008). The designed efficiency of a power plant partially reflects the price of fuel at the time of construction. As fuel prices and operating costs have increased, greater consideration has been given to the efficiency of generation and transmission. Improvements in efficiency, alternative system designs, and demand side

management to reduce peak loading have implications for the water requirements of a power generation facility.

The following Black & Veatch projects demonstrate a broad range of options for integrated decision making, regional planning, and technological innovation:

Energy Recovery Opportunities in Water Infrastructure

San Diego County Water Authority: Rancho Penasquitos Hydroelectric Facility

The public San Diego County Water Authority serves the San Diego region as a wholesale supplier of water from the Colorado River and Northern California. The Rancho Penasquitos Pressure Control and Hydroelectric Facility (PCHF), located in the City of San Diego, was designed to facilitate delivery of untreated water to Authority member agency facilities. The RPPCHF is part of the extensive water distribution system that the Water Authority owns and operates in San Diego County. Located along a major aqueduct and connected to a 108-inch-diameter untreated-water pipeline, the facility was designed not only to control water pressure and flow but also to generate renewable energy through a turbine-generator sized at 4.5 megawatts, enough power for approximately 5,000 homes. The San Diego community benefits from this green renewable energy, which takes full advantage of the excess pressure at the project site. Planning, designing, and constructing a single facility that serves dual purposes was a challenge, because different processes, equipment, and engineering skills were needed to control water pressure and flow and simultaneously generate electricity in an environmentally responsible manner.

Decentralized Power Generation Options for Water Processes

Hybrid Water and Power Innovation (HWPi) Desalination Plant

Desalination of sea or brackish water often involves a power plant and a water plant. To increase efficiency and reduce the cost of this traditional approach, the project team incorporated product innovations and plant design improvements resulting from an integrated facility. GE's newest and most efficient gas turbine, the LMS100, was united with Black & Veatch's innovation in integrated thermal desalination. The gas turbine employs off-engine intercooling technology with an external heat exchanger, making it an efficient simple cycle turbine. It provides enough power to operate the 10 MGD desalination plants and simultaneously provide 105 MW of electricity to consumers. Paired with the advanced membrane technology and flexible modes of operation, this hybrid solution provides safe and reliable water and power to growing communities with a smaller carbon and water footprint.

A variety of renewable technologies may be utilized for decentralized applications as well. For example, wastewater utilities, as well as being a consumer of energy, can use anaerobic digesters to generate reliable, cost effective power. Biogas from these digesters can be used in a combined heat and power (CHP) system as "free" fuel to generate reliable electricity and power. Renewable energy represents about 2.4% of the fuel source mix in the United States and non-hydroelectric renewable electricity generation is expected to quadruple by 2030 (EIA, 2008). The operation of non-

hydroelectric renewable energy generation is dependent on very little, if any, water withdrawal and consumption.

Progressing the Understanding of Wastewater Recovery for Energy Generation Processes

Western Corridor Water Recycling

As a result of a long-standing drought in South East Queensland, Australia, diversifying water supply sources, including the advanced treatment of wastewater, is integral to ensuring sustainable water availability in the region. However, alternative treatment technologies and transport of water supplies increase the energy intensity of water. Historically, the region has depended on dams and other low-energy infrastructure for water supply. The program focus is to guarantee water supplies by managing demand effectively, resolving regional supply gaps, and carefully addressing agricultural and industrial needs.

The Bundamba Advanced Water Treatment (AWT) plant, designed by Black & Veatch in 2008, produces nearly 20ML per day of purified recycled water, replacing a facility that previously discharged a lower quality effluent into the nearby river. The purified recycled water from Bundamba AWT plant is piped from the plant via a 7.3 kilometre, 800 millimetre diameter pipeline into a lake at the CS Energy Swanbank Power Station near Ipswich. The continual water flow reduces the power station's reliance on the drought-affected Wivenhoe Dam and ensures that the power station remains available to support Southeast Queensland's growing electricity needs in the midst of severe water shortages. The design incorporated the latest membrane and advanced oxidation technologies to provide purified recycled water for both municipal water supply and cooling demands at the Swanbank Power Station. Main treatment steps – ultra-filtration membranes, reverse osmosis membranes followed by advanced oxidation using ultra-violet irradiation and hydrogen peroxide employed at the plant – present a high standard for water reclamation. The Bundamba plant is part of the Western Corridor project, a network of 200 kilometres of underground pipelines and three new advanced water treatment plants. The diversified supply plan will help secure water resources in Queensland into the future, while moving forward the discussion and practical applications of waste recovery technology.

Regional Water and Energy Resource Planning

Colorado River Long-Term Augmentation

Drought conditions on the Colorado River coupled with population growth in the region are driving long-range measures to manage the River water supply and augment its flow. Colorado River water allocations are regulated by a series of interstate and national contracts, approved in 1922, that specify a base river flow. The River has the most complete allocation of water resources of any river in the world and a highly-complex regulatory environment.

In 2007, Black & Veatch utilized extensive stakeholder outreach to provide a strategic plan for the long-term management and augmentation of the Colorado River water supply. Twelve potential long-term options were developed and evaluated by these standards: water quality, technical implementation, environmental considerations, permitting, relative costs, and projected water yield. The expert panel documented that

large volumes of water were withdrawn from the river system for cooling water at conventional thermoelectric power generation facilities. Their study evaluated the potential water saving if power plants withdrawing from the Colorado River water supply would convert existing cooling processes to non-evaporative systems. The team projected a potential savings as great as 160,000 acre-feet per year – demonstrating both the effectiveness of regional infrastructure planning and the significance of technological innovation to preserve water supplies while maintaining energy production.

In the past, water supply planning focused on identifying quality surface or groundwater supplies to meet needs for a specific community or small region. In managing water scarcity, however, a larger regional and holistic approach can integrate alternative water supplies and needs into a plan that optimizes the water balance of a region for a wide range of stakeholders. This project demonstrates the benefits of regional water planning, decision support, and technology selection.



Figure 4. Colorado River Valley

ONGOING RESEARCH AND INTERESTING CHALLENGES

Multiple agencies and associations across the nation are conducting research and development regarding the energy-water nexus. NETL, as part of the Department of Energy (DOE), hosts an integrated expansive energy-water research and development program. The Water Energy Technology Team (WETT) at Lawrence Berkeley National Laboratory is promoting new technologies and practices for key players by comparing technical feasibility and economic efficiency of newly developing technologies, practices, and policies to existing ones, and optimizing new technologies that promote water and energy sustainability. The Sandia National Laboratories support a program that integrates three components: prediction and decision support, science and technological innovation, and technology transfer and implementation. Decision support tools rely on access to information and the development of high-performance computer models that link the many systems that influence water and energy resources, including climate changes, land uses, regional hydrology, population growth, energy use, and regulatory constraints. These systems are meant to provide an unprecedented level of detail to optimize the balance of water use among stakeholders. The DOE drive toward technological innovation will focus on minimizing the impact of energy production on water quality and availability and in parallel, reducing the amount of energy necessary for the treatment and distribution of water. Stakeholder teams will provide real world feedback by testing decision support systems and prototyping technological innovations. The program's short term goal is to reduce freshwater consumption and withdrawal, in terms of gallons/kWh: 50% by 2015 and 70% by 2020. Many organizations supplement this research endeavor, providing forums for discussion of applications. These programs

share a common goal of ensuring sustainable supplies of energy and water by reducing impact on the environment and engaging in regionally based planning.

Resource Planning

The 2006 DOE Report to Congress on the Interdependency of Energy and Water highlights collaboration in resource planning to ensure proper evaluation and valuation of water resources for all needs regionally (inclusive of energy development and generation, agriculture, domestic, etc.). The report emphasizes that significant improvements in conservation and efficiency can be achieved through energy water infrastructure synergies – innovative processes or technologies, co-location of energy/water facilities, and improvements to infrastructure.

In addition to technological innovation and regional planning, the broad application of sustainability assessments across sectors may provide a comprehensive resource and tool for both water and energy utilities. As energy utilities experience increased regulatory requirements and consumer demand for responsible resource management, they are recognizing that environmental performance is linked to financial success (DeBono, 2004). Energy utilities are given the challenging task of powering a community while simultaneously supporting emissions reductions. Increasingly, the energy industry has shifted focus from supply management to demand management and increasing efficiency. Similarly, efficient water utilities must anticipate the need to improve treatment capacity while decreasing energy consumption during the process. Sustainability assessments and metrics provide a useful tool for benchmarking and determining success.

Reducing Carbon Emissions

In 2007, nearly half of the total generation of the United States was produced by coal-fired power plants. These plants are associated with 82% of the power sector carbon dioxide emissions and are expected to continue servicing communities over the next few decades. Utilities may reduce emissions by improving plant efficiency with additional technology, operational practices, maintenance, and by augmenting carbon dioxide recovery processes (CDR). The most widely applied CDR process at coal-fired power plants and natural gas combined cycle plants is a monoethanolamine (MEA) recovery unit.

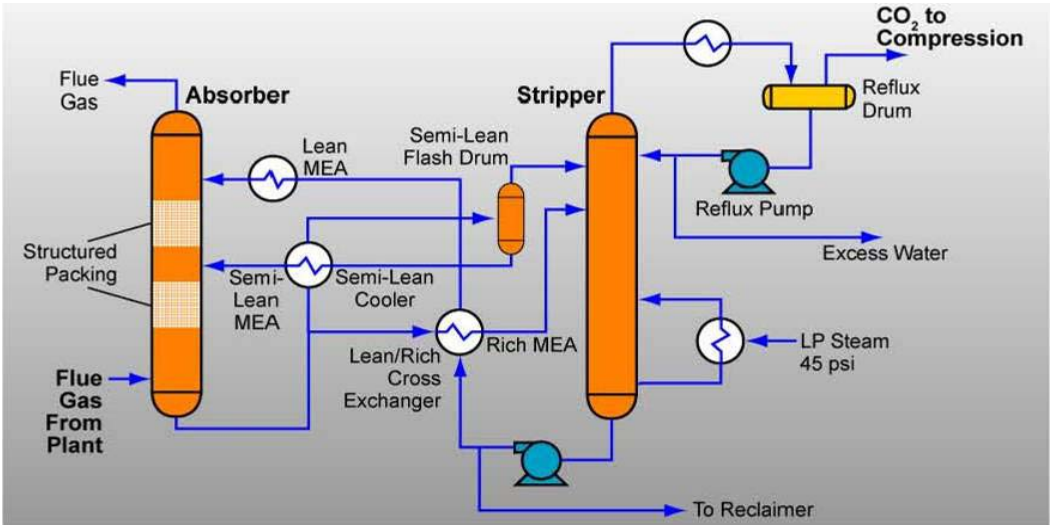

Figure 5. MEA Carbon Recovery Process (Gerdes, DOE)

This chemical process, illustrated in Figure 5, is based on cooling flue gases, allowing the MEA to absorb CO_2, and steam-heating the CO_2-laden MEA to release the CO_2 for compression and shipment. Each of the sub-processes requires significant volumes of cooling water (Gerdes, 2008). A greater concentration of CO_2 increases the efficiency of the process in an integrated gasification combined cycle facility. Other technologies to recover CO_2 include water shift reactors and physical absorption based scrubbers. Similar to FGD, installation of CDR processes in a thermoelectric power plant actually decreases plant efficiency. Much like the energy intensity of advanced treatment of pollutants in water, the need for carbon-capture technology comes with an energy and water penalty.

CONCLUSIONS

Despite the claims of others, the provision of energy and water resources to a society is perhaps the oldest profession. The significance of research and investment in systems that appreciate and optimize the energy-water nexus is critical. Future projections suggest the reality of resource scarcity. Current technology often demands a compromise between the efficient uses of available resources. Yet, research institutions and engineering firms have demonstrated that thoughtful applications of technology and broad-based resource planning can result in solutions that sustain a community. With growing concerns about the effects that greenhouse gases, such as carbon dioxide from fossil fuel combustion, are having and will continue to have on the climate, the attention given to synergies between energy and water resources is timely.

REFERENCES

Energy Information Administration. (2008). Annual Energy Outlook 2008. Energy Information Administration. DOE/EIA-0383 (2008) June 2008.

Energy Information Administration. (2007). Annual Energy Outlook 2007. Energy Information Administration. DOE/EIA-0383 (2007) February 2007.

Energy Information Administration. (2006). Annual Energy Outlook 2006. Energy Information Administration. DOE/EIA-0383 (2006) February 2006.

DeBono, Teresa. (2004). Integrating Sustainability Practices into Power Generation Operations. *Global Market Institute*. 46.

Department of Energy, (2006). Energy Demands on Water Resources: Report to Congress on the Interdependency of Energy and Water.

EPRI, 2002. Water & Sustainability (Volume 3): U.S. Water Consumption for Power Production – The Next Half Century, EPRI, Palo Alto, CA: 2002. 1006786. Feeley III, T. J. et al. (2005) "Addressing the Critical Link between Fossil Energy and Water" Department of Energy/Office of Fossil energy's Water-Related Research, Development, and Demonstration Programs. NETL. October 2005.

Feeley III, T. J. et al. (2008). "Reducing CO2 Emissions by Improving the Efficiency of the Exiting Coal-fired Power Plant Fleet." DOE/NETL-2008/1329.

Feeley III, T. J. et al. (2008). "Water: a critical resource in the thermoelectric power industry." *Energy: The International Journal*, Elsevier, 33(1), 1-11.

Gerdes, Kristin et al. (2008). "Water Requirements for Existing and Emerging Thermoelectric Plant Technologies." DOE/NETL-402/080108

Hoffman, Jeffrey. (2004). "Estimating Freshwater Needs to Meet 2025 Electricity Generating Capacity Forecasts. DOE/NETL.

Hutson, Susan et al. (2004). Estimated Use of Water in the United States in 2000. USGS Circular 1268. United States Geological Survey.

Kansas City Water Services Department. (2007) Software Database for the Progress Report on Climate Protection and Phase 1 Recommendations. City of Kansas City, Missouri. 12 April 2007.

Torcellini, P. et al. (2003). "Consumptive Water Use for U.S. Power Production." Technical Report. National Renewable Energy Laboratory/TP-550-33905.

WATERSHED MANAGEMENT IN THE INDIAN HIMALAYAN REGION: ISSUES AND CHALLENGES

Samagra Rana [1], Vaibhav Gupta [1]
[1]G. B. Pant University of Agriculture and Technology

Abstract

Indian population constitutes about 15 % of the world's population, whereas its land area and water resources are about 2 % and 4 % of the world's total, respectively. In the last 50 years, the per capita availability of fresh water has been reduced by about 90 %, and the same trend is still going on with the increase in population, urbanization, and industrialization. At the national level, the irrigation alone consumes about 83 % of the available water resources. About 30 % of the total geographical area is drought prone due to erratic pattern of rainfall and out of about 148 million hectare cultivable land about 72 % is rain fed.

The economy of the Himalayan region is predominantly agrarian. More than 4/5th of the working population is directly engaged in agriculture. Though Himalayan region gave birth to several perennial rivers and streams, the inhabitants face the problems of drinking water and irrigation. Even though only 12.5% of the total land area is under agriculture, only 11% of the cultivable area is irrigated, almost 64% of which is fed by natural springs. The topography of the region is steep; the average annual rainfall is high (1200-1600 mm) and the soils range from sandy to sandy loam causing very high percolation losses of rainwater from individual farmers' terraced fields. The soil does not hold water for long and consequently in the absence of available soil moisture, the crops suffer badly due to moisture stresses at different stages of crop growth during post-monsoon period. About 60 % population in hilly region depends on natural water springs to fulfill their day to day water needs for drinking, sanitation, irrigation etc. About half of the perennial springs have either dried-up or have become seasonal due to ecological imbalance and environmental degradation during last two decades. Nearly 8000 villages mostly located in upper and mid hills have been facing acute shortage of drinking water.

Keeping the above facts in mind, the only way to enhance socio-economic status of the inhabitants of the Himalayan region is to adopt appropriate strategies on a watershed basis, which ensures proper utilization of land, water and vegetative resources in a rational manner. From the engineering point of view, the land and water resources development and management strategies must emphasize application of appropriate technical measures for the development of watershed. Using GIS and remote sensing digital analysis for the land use and terrain analysis will have to be incorporated; such data provides an important link between intensive, localized ecological research and management of biological diversity. Studies conducted in the mid- and high-hills have revealed that the land has to be used as per its capability and sincere efforts have to be made to develop and conserve the existing water resources on sustainable basis. Hence, the adopted technologies have to be location specific, cost effective and easily maintainable by the farmers themselves.

Introduction

The Himalayas are amongst one of the youngest folded mountainous formations of the world, and the youngest in India. The Aravallis, Nilgiris, and the Eastern Ghats are 1500 to 2500 million years old, and the Vindhyachals around 1000 million years old (Swaminathan, 1992). By comparison the Himalayas date back to only 40-45 million years. They traverse an arc for about 2500 km between the Indus and the Brahmaputra. The average width of this mountain range along the entire longitudinal extension ranges from 100 to 400 km. Upadhyay (1995) estimated that the Himalayas cover an area of 4.6 million sq. km. above 1500 m, 3.2 million sq. km. above 3000 m and 0.56 million sq. km. above 5400 m. The Himalayas extend from west to east, from the Pamit Knot in the northwest to the valley of the Brahmaputra River in the east. The range passes through Afghanistan, Pakistan, India (Jammu and Kashmir, Himachal Pradesh, Uttaranchal, Sikkim, Assam, Arunachal Pradesh, Manipur, Meghalaya, Mizoram, Nagaland, Tripura and Darjeeling district of West Bengal), China, Nepal, Bhutan, Bangladesh and Myanmar.

The birth of the Himalayas is the result of a calamitous event of break-up of the peninsular part of present India (the Deccan Plateau) from the supercontinent Gondwanaland, 140 million years ago. The peninsular Indian Plate, having its original locale proximal to Madagascar and South Africa, started drifting northward about 15 cm per year, across what is now the Indian Ocean. Around 15 million years ago, it collided into the Asian continent near the present state of Assam in India. This crashing of the peninsular Plate against the

Southern edge of the Asian continental plate led to the rise of the Himalayas (Khoshoo, 1992). The Indian Plate continues to move northward at the rate of 2 cm per year. The Himalayas are still geologically active and structurally unstable. For this reason, earthquakes continue to be a frequent occurrence in the entire Himalayan region. Being the worlds' highest mountain chain, the Himalayas is characterized by a complex geologic structure, snowcapped peaks, large valley glaciers, deep river gorges and rich vegetation. A complex interplay of climatic and geological processes, patterns of resource use and economic conditions have led to resource degradation and associated environmental consequences in the Himalayan ecosystem (Jodha, 2001).

The paper is an attempt towards an analysis of the major ecological concerns, the underlying driving factors (both human and natural processes), socio-economic impacts and the responses in trying to cope with these, both at the micro/community level and at the national or international levels. We begin with a glimpse of the social and economic structure of the Himalayan region, which constitutes a critical basis for the ensuing analyses. This is followed by an overview of the state of the environment in the region and a detailed analysis of key environmental issues: water resources and their sharing, biodiversity loss, glacier recession, deforestation, land degradation and agriculture systems, natural disasters and solid waste management.

Socio-economic background

The Himalayan mountainous belt is inhabited by 51 million people, covering 18% of the geographical area and 6% of population of India. The mountain range, with its richness of resources, has been contributing to the economic development of

mainland India since times immemorial. However, conventional parameters of development are not the best measures for understanding the social and economic status of the hill communities. The prevalence of traditional lifestyles, barter trade and common property resources
tend to hide the level of poverty or prosperity of the highland people. The following discussion is structured around the key social and economic themes that have had ramifications for the state of environment and ecology of the mountain belt.
The trade-off between meeting subsistence needs and commercial interests is engendering newer forms of social tensions. The privatization of the traditionally common property land along the " fruit-belt" of the Mussoorie-Chamba road in Tehri Garhwal district has led to commoditization of local activities, use of migrant labor and changing working relationships.

Overview of the state of the environment

The Himalayan region is characterized not only by ecological fragility but also by a deep and historical geopolitical sensitivity (Stone, 1992). An ecosystem based natural resource management approach is difficult to achieve as many countries share the resources of this mountain system.

The Himalayas are full of natural wealth, both renewable and non-renewable resources. Amongst its non-renewable resources are deposits of boron, lead, lithium, coal, chromium, ores of iron, copper, tungsten, zinc and deposits of building material like limestone, dolomite and marble. These deposits occur across the length and breadth of the Himalayas cutting across international boundaries. Though the Himalayas have substantial mineral wealth, the common image of resources there is that of water and forests (Stone, 1992). The Himalayas present a storehouse of bio-diversity, where flora and fauna vary extensively with climate diversity from one region to the other. If an attempt is made to divide the forests types based on the standard classification of tropical, sub-tropical, temperate and alpine, it becomes difficult to describe the rich diversity of the Himalayan forests. However, extensive commercial felling of forest for timber has been reported in the region, especially in the last few decades when urban centers began to grow in areas near the forests. While the forests, farmlands and grasslands are of extreme importance for the a grip a store economy within the Himalayan region, the other renewable resource, water, has always been crucial for thickly populated plains further down in the south and east. The Himalayas has one of the highest hydropower potentials of the world which includes three of the mightiest rivers of the world, i.e. Indus, Ganga and Brahmaputra. Besides, water resources, vast extended grasslands and dense forests in some highland parts and in the foothills of the Himalayas have certain specific advantages such as a tremendous potential for tourism. However, extreme climate variations and inaccessible terrain make it difficult to exploit and utilize all the natural resources of the great Himalayas. Climatic extremes like cloudbursts, hailstorms and earthquakes play a critical role as an environmental constraint. Global warming is effecting ice and glacier cover in the region. Furthermore, due to inaccessibility of the region, it is difficult to quantify and assess the damage caused by these natural events. The environmental constraints against the exploitation of natural resource also include other natural phenomena like mass wasting, high seismic activity, landslides, glacial lake outburst floods, erosion and sedimentation. Soil erosion is one of the major environmental constraints, which results in frequent

flooding in the plains downstream and damage to agriculture, life and infrastructure. The livestock population in the region has also increased during the recent past and problem of grazing in the high altitudes has acquired serious dimension, as a result the vegetative cover is decreasing which has resulted in the loss of top soil due to excessive erosion. The relatively soft rocks and favorable climatic conditions are the factors behind quick weathering followed by mass wasting and landslides. Intense monsoon rainfall also accelerates soil erosion in the region. The Himalayan Rivers also carry a very heavy sediment load especially during summer and rainy season, which provides conditions for river shifting.

Water resources

This section assesses the water resources of the Himalayan region, the impact of climate change on hydrological balance and stresses on the crucial issue of water sharing between countries in the South Asian region. Finally, the mechanisms for management of water resources in the Himalayan region, at the national, regional and international level are discussed. The term “Himalaya” has been derived from a Sanskrit word meaning “the Abode of snow”. The region is characterized by intense rainfall in the east and heavy snowfall in the western reaches, which feed some of the longest glacier systems in the world and are the source of major rivers (Stone, 1992). The region is home to Cherrapunji, the second highest rainfall region in the world. The water resources of the Himalayan region are a crucial part of the lives of millions of people living in the hills and the plains. Rivers originating in the Himalayas bring fertile silt and irrigation water, which is essential to the development of the agro-economy in the plains. This dependence of the neighboring plains on mountain water resources has led to the description of the South Asian civilization as a 'hydraulic society' (Stone, 1992). The Himalayas contain over half the permanent snow and ice-fields outside the Polar Regions and it is estimated that roughly 50,000 sq. km of glaciers feed into the world’s largest water drainage system of the Indus, Ganga and Brahmaputra rivers. This perennial river system of the Himalayas is fed by melt water contributions from snow cover, glaciers and permafrost regions. The total amount of water flowing from the Himalayas to the plains of the Indian subcontinent is estimated to be about 8.6 x 106 m3 per year (IPCC, 2001). The contribution of snow to the runoff of major rivers in the eastern Himalayas is about 10% (Sharma, 1993) but more than 60% in the Western Himalayas (Vohra, 1981). Natural lakes exist at high altitude regions ranging from 600-5600 m, and are of freshwater as well as saline in nature. Two of the world’s largest rivers, the Indus and Brahmaputra originate from these glacial lake systems. The average annual run-off of Indus, Ganga and Brahmaputra rivers is 208, 494 and 510 km3 per year, respectively. Varying estimates of water resources in the Himalayan region have been made. Murthy (1978) estimated Himalayan water resources around 245 km3 per year, Gupta (1983) and Kawosa (1988) estimated the total amount of water flowing from the Himalayas to the plains to be around 8643 km3 per year. Bahadur (1998a) re-evaluated his earlier estimates of 200–500 km3 per year as 400-800 km3 per year as melt water contributions from the snow and glacier fields in the high mountain region. Despite these widely differing estimates of the water resource of the Himalayan region, the

water output could be the highest from any single mountain range in the world (Stone, 1992). In recent decades the hydrological characteristics of watersheds in the Himalayan region have undergone substantial changes due to land use changes leading to more frequent hydrological disasters, enhanced variability in rainfall and runoff, extensive reservoir sedimentation and pollution of lakes (Ives and Messerli, 1989). Water availability, in terms of temporal as well as spatial distribution, is expected to be highly vulnerable to anticipated climate change (IPCC, 2001). Changes in the snowfall pattern have been observed in the Himalayas (Verghese and Iyer, 1993). These changes will have a marked impact on the monsoon regime, seasonal run-off and vegetation cover, including agriculture (IPCC, 2001). Because the melting season of snow coincides with the summer monsoon season, any intensification of the monsoon is likely to contribute to flood disasters in the Himalayan catchments (IPCC, 2001). Such impacts will be observed more in the Western Himalayas than in the Eastern Himalayas because of the higher contribution of snowmelt runoff in the west (Sharma, K P 1997).

The effect of climate change on hydrology of the region will be multifaceted: ranging from regional variations in precipitation characteristics, glacial shifts, mean run-off frequency and intensity of droughts and floods, soil moisture, water supplies for irrigation and hydroelectric generation. The Himalayas play a critical role in providing water to continental monsoon Asia. Increased temperatures and enhanced seasonal variability in precipitation are expected to result in glacier recession and increasing danger from glacier lake outburst floods. A reduction in average flow of snow-fed rivers, together with increase in peak flows and sediment yields would have a major impact on hydropower generation, urban water supply and agriculture. Studies of one catchment in the Western Himalayas (the Chenab, a tributary of the Indus) show that the average snowmelt and glacier-melt contribution to the annual flow of water is 49.1%; a significant proportion of run-off is derived from snow in the dry season, when water demand is highest (Singh et al., 1997).

If the rainfall pattern in the Himalayas changes due to climate change, the impact could be felt in downstream countries such as Bangladesh. The water and agriculture sectors are likely to be most sensitive to climate change-induced impacts in Himalayas. Catchments in Nepal supply about 70% of the dry-season flow of the Ganges River, and the tributaries of the Brahmaputra river originating in Bhutan supply around 15% of the total annual flow of that river. If climate change disrupts these resources and alters mountain hydrological regimes, the effect will be felt not only in the montane core of Tropical Asia but also downstream, in countries that are dependent on this water resource.

Water Resource Management for sustainable agriculture production in Himalayan Region

Water resources hold the key for socio-economic development mountain region. Indian Himalayan has two distinct geopolitical sub regions, viz., north east hills and north west hills. Despite adequate rainfall in both the flanks of Himalayas, there is a shortage of water not only for raising the crop but also for drinking. Against this backdrop, it becomes imperative to study various options for increasing the crop water productivity i.e. more crop per drop, and also for meeting the basic

requirements of water to the community for various purposes. So, there is a need for various technological options for the betterment of the water supply and conservation, restoration of links between forests and water, construction of water harvesting structure, agronomical measures for improving water use efficiency, watershed approach for water management.

The Watershed Concept

The watershed approach enables planners to harmonize the use of soil, water and vegetation in a way that conserves these resources and maximize their productivity. The watershed is the appropriate hydrological unit for technical efforts to manage water and soil resources for production and conservation. But watershed management is complicated by the fact that watersheds rarely correspond to human-defined boundaries. The fundamental social problem of watershed development is that it often distributes benefits and costs unevenly, making it a likely source of disagreement and conflict. Mostly, watershed projects distribute costs and benefits unevenly, with costs incurred disproportionately upstream, typically among the poorer farmers, and benefits realized disproportionately downstream, where water use is concentrated and richer farmers own most of the land. The challenge is to internalize the costs and the benefits in such a way that all the stakeholders are part of a win-win scenario.

The impact and control of water Erosion and natural soil resources

Soil erosion is critical issue on hills due to steep slopes. Soil loss from cultivated slopes is quite high particularly during first two to three years of cultivation. It has been expected that concerning 6 million hectare of land require careful conservation measures in Himalayan and sub Himalayan regions. The havoc of erosion has been becoming a burning problem due to accelerated activities against nature by human beings viz. Cutting of hillocks, deforestation etc.

Natural resources management and control of erosion on hills

1. **Contour Farming**: The ridges of same depth are called as contours. The crop is sown on the ridges and water is provided through the furrows. This encourages more water infiltration into the soil the soil profile.
2. **Conservation Tillage**: Now days, the concept of conservation tillage (zero tillage, no tillage) is coming up to overcome the problem of soil erosion.
3. **Riparian Fencing**: Fencing of waterways will prevent grazing of land and trampling of river banks by herbivores. Moreover, tree plantation on river sides also reduces river bank erosion.
4. **Grassed Waterways**: Grassing over the shallow waterways, in most cases is found to be effective in preventing soil loss from it. Grass leaves act as a barrier against the speed of water current and reduce the erodibility of soil.
5. **Shelterbelts:** They provide roots at the boundaries of the fields, sheltering the soil and supply organic matter.
6. **Spaced Tree Planting:** Trees provide deep roots that hold the soil; Cycle

deep nutrients and loss nutrients also provide good amount of organic matter to the soil. Trees must compete with highly metabolizing grassland, thus should be fast growing and deciduous.

7. **Retirement Fencing:** Fencing is an absolute must to encourage natural growth and to protect tree planting.
8. **Topdressing:** Fertilizing of soil leads to rapid growth of vegetations, is the best remedy against soil erosion.
9. **Forest Fire Control**: Forest Fire destroys vegetation cover up to various extent. There is also change in the amount of light, pH of soil and destruction of soil organism. As a result soil productivity is reduced.
10. **Cultivation of fruits**: Fruits such as oranges, pineapple, Jack fruit, banana and papaya reduce soil erosion as well as provide income to the people of this region.
11. **Bench Terracing**: On steeply sloping (16% to 33%) and undulated land, intensive farming is possible. The field is made into a series of benches by excavating of the soil from upper part of the terrace and felling in the lower part.
12. **Anti-seep Collar**: An impermeable diaphragm of sheet metal or concrete constructed at intervals within the zone of saturation along the conduit of a principle spillway to increase the seepage length along the conduit thereby preventing piping and seepage.
13. **Debris Dams:** They check the movement of water in steep gullies. They should not be used in slow flowing waterways. Any kind of debris would do but natural products such as tree stumps, braches, planting are better.

Judicious Use of Excess Water in Hilly Regions

Himalayas are considered as the source of water but rain or the availability of water for irrigation purpose is not up to the mark in adjoining regions as many places are either rain-fed or having heavy rain with temporal and spatial variability. Dry spells are direct consequences of spatial and temporal variability, and these hamper the success of rain-fed agriculture by causing crop yield reduction and crop failure in many regions a number of times. Water conservations and storage techniques are essential in these regions for sustainable agriculture. Water harvesting is not a new concept however generally the water harvesting techniques are used to harvest only rain water which is not available throughout the year. Therefore an attempt has been made to study the applicability of poly tanks for water harvesting in the region. The construction of poly tank is very cheap and successful to save the crop at the time of acute water shortage if they are constructed at proper site.

Present Scenario In the region

Though most areas receive good annual rainfall, its intensity and distribution is quite erratic and causes severe drought spells to hamper the growth of timely sown winter crops and subsequent planting of spring crops due to lack of soil moisture. This

situation forces the farmers to risk their winter crops at germination and ripening stages of growth. The average annual rainfall in this region varies from 700 mm to 3000 mm of which about 70 % occurs during monsoon months of June to September. The existing rivers, streams and natural springs have been drying up fast due to systematic environmental degradation by humans and natural calamities. Presently, only few perennial natural springs exist in the mid-Himalayan region, while most springs have become seasonal due to lack of continuous recharge. Therefore, the inhabitants generally suffer from shortage of water for drinking and household activities, and to irrigate their crops at critical times. The crops suffer badly due to moisture stresses at different stages of crop growth during post-monsoon period and long dry spells during rainy season. Because of lack of sufficient moisture, the seeds remain dormant from October to December until winter rainfall/snowfall occurs. Usually, the amount and distribution of rainfall does not coincide with the water requirements at critical stages of crop growth. Frequent and long dry spells also retard the growth, fruit size and yield of important fruit crops like apple, plum, peach, apricot etc.

Agricultural Scenario in Uttarakhand Hills

- Population engaged in agriculture > 90 %
- Status of agriculture
  - Irrigated 11 % (Valleys)
  - Rainfed 89 %
  - Land holding
    - Marginal (< 1 ha) 70 % (Scattered)
    - Small (1 – 2 ha) 17 %
  - Cropping intensity 102 %
- Frequent natural/man-made hazards Soil erosion, landslide, drought, cloud-burst, forest fire.

- About 60 % population in hilly region depends on natural water springs to fulfill their day to day water needs.
- About half of the perennial springs have either dried-up or have become seasonal due to ecological imbalance and environmental degradation during last two decades.
- Nearly 8000 villages mostly located in upper and mid hills have been facing acute shortage of drinking water.
- If scientifically appropriate biological and engineering measures to rejuvenate the existing springs are not taken in time, the remaining springs will also die sooner than later.
- Low spring discharge, if collected and stored in a suitable tank/pond, will create a huge water resource for use by the local people to fulfill their household and agricultural needs.
- Flowing rivers (24), streams, lakes (16) and glaciers (38)
- Flowing natural water springs (perennial & seasonal)

- Overland runoff during rainfall

Runoff through roof-tops of houses during rainfall

Modernizing irrigation water management

FAO has defined modernization as "a process of technical and managerial upgrading of irrigation schemes combined with institutional reforms, if required, with the objective to improve resource utilization and water delivery service to farms" (Facon and Renault, 1999). In this sense, modernization offers a means of institutional reform with a purpose, not just reform for its own sake. It is systemic and practical without asking that all institutional elements change and it needs to be applied where irrigated agriculture has a clear comparative advantage.

Irrigation institutions need to adopt a service orientation and improve their performance in economic and environmental terms. This entails: adopting new technologies; modernizing infrastructure; applying improved administrative principles and techniques; and promoting the participation of water users. Irrigation-sector institutions need to link their central task of providing irrigation services to agricultural production and to integrate their water demands and uses with other users at basin level. An enhanced appreciation of the water cascades and flows across landscapes and the circulation of groundwater within aquifers will lead to informed decisions on the use and reuse of agricultural water.

Development of Small Hydropower System in the region and GIS applications in Energy Sector

Hydropower, hydraulic power or water power is power that is derived from the force or energy of moving water, which may be harnessed for useful purposes. Prior to the widespread availability of commercial electric power, hydropower was used for irrigation, and operation of various machines, such as watermills, textile machines, and sawmills. A tromp produces compressed air from falling water, which could then be used to power other machinery at a distance from the water. Small scale hydro has been increasingly used as an alternative energy source, especially in remote areas where other power sources are not viable. Small scale hydro power systems can be installed in small rivers or streams with little or no discernible environmental effect on things such as fish migration. Most small scale hydro power systems make no use of a dam or major water diversion, but rather use water wheels.

There are some considerations in a small-hydro system installation. The amount of water flow available on a consistent basis, since lack of rain can affect plant

operation. Head, or the amount of drop between the intake and the exit. The more head, the more power that can be generated. There can be legal and regulatory issues, since most countries, cities, and states have regulations about water rights and easements. Over the last few years, the Government of India has increased support for alternative power generation. Many resources such as grants, loans, and tax benefits are available for small scale hydro systems. Small-hydro power can be used directly as "shaft power" for many industrial applications. Alternatively, the preferred option for domestic energy supply is to generate electricity with a generator or a reversed electric motor which, while less efficient, is likely to be available locally and cheaply. Small-scale hydropower systems are those that generate between .01 to 30 MW of electricity.

Application of Geographical Information System in Small Hydropower

The technology of GIS provides a means of introducing information and knowledge from various data sources in to the decision-making process and help in handling and manipulating the classified remotely sensed data. Entire information is stored in the database in GIS environment as separate thematic layers and hence it becomes easy to handle the entire data.

A GIS stores a representation of the world in the form of layers connected by a common geographical frame of reference. Each of the features required for hydropower projects, has a unique identifier, which distinguishes it from the rest of the features on the layer, and allow us to relate it to relevant information stored in external databases, etc and to capture only those elements of the world that are of interest to us, like catchment area, under forestation, covered under snow etc. GIS is also used to input, store, retrieve, manipulate, analyze and output geographically referenced data or geospatial data, in order to support decision making for planning and management of land use, natural resources, environment, transportation, urban facilities, and other administrative records.

GIS based Watershed Management System

GIS and Remote sensing techniques are used to generate action plans for conservation of land and water resources. Spatial database on soils, land use, contours, geology, drainage etc. is created using Survey of India topographical maps, cadastral maps, ground truth and remotely sensed data obtained from various sources using state of art GIS software. This primary resource data is used to derive secondary vector layers and quad trees (data structures) corresponding to slope, erosion class, soil depth, land capability etc. Rules are framed to arrive at certain suitable solutions to each of the area-specific problems identified for the watershed. Further a number of macro-level and location-specific action plan maps are generated based on the secondary derived maps and the action plans framed.

A resource inventory towards the development of an efficient and an effective Watershed Management System is created. Suitable decision rules are framed and the same are used in conjunction with the resource inventory to arrive at certain suitable solutions in the form of action-plan and treatment-plan maps to each of the area-specific problems identified for the Watershed.

Conclusion

Environmental sustainability of the Himalayan region is critical to the well being of millions of people in the Indian subcontinent who are directly or indirectly dependent on its resources. Increased accessibility, population pressures, economic development and the concomitant excessive utilization of the regions resources have resulted in a threat to the health of this mountain ecosystem and its inhabitants.

Integrated watershed management in these regions requires adoption of innovative soil conservation and crop management techniques to prevent land degradation, maintain soil fertility and ensure environmental security for achieving sustainable productivity. Experience of integrated watershed development programs in hilly and valley regions has indicated that they greatly helped in moderating floods in downstream areas, improve in-situ moisture conservation and groundwater recharge for increased biomass production and were economically viable with tremendous environmental externalities.

Water harvesting and groundwater recharge, location-specific and cost-effective technologies for erosion control and flood moderation, suitable plant materials and integrated farming systems for higher production and conservation of natural resources, contingency planning for undertaking calamity relief works for generating productive employment and diversification for new market opportunities based on demand-driven growth need to be promoted. Modern tools and procedures should be deployed for planning of watersheds and provide better opportunities to the marginalized and inaccessible hilly situations.

References

1. J.S. Singh, Sustainable development of the Indian Himalayan region: Linking ecological and economic concerns, CURRENT SCIENCE, VOL. 90, NO. 6, 25 MARCH 2006.
2. R. K. Mall, Akhilesh Gupta, Ranjeet Singh, R. S. Singh, L. S. Rathore, Water resources and climate change: An Indian perspective, CURRENT SCIENCE, VOL. 90, NO. 12, 25 JUNE 2006.
3. Badhani, K.N, 1998. Enterprise-based transformation of hill agriculture: a case study of vegetable growing farmers in Garampani area, Nainital District, India. Discussion Paper, Series No. MEI 98/5, Kathmandu, Nepal, ICIMOD.
4. Bahadur, J, 1998a. Himalayan eco-hydrology - an emerging topic. Journal. Indian Association of Hydrologists, Roorkee.
5. Bahadur, J, 2000. *Water resources management in the Himalayan region*. Proceedings

of the Internal Conference on Managing natural resources for sustainable agricultural production in the 21st Century, New Delhi, Feb 14-18, 2000, pp. 459-461.

6. Dhar, U, 1996. *Overview of Himalayan biodiversity*. Changing perspective of biodiversity status in the Himalaya, New Delhi. The British Council.
7. Fujita, Koji, Masayoshi Nakawo, Yoshiyuki Fuji and Prem Paudyal, 1997. Changes in glaciers in Hidden valley, Mukut Himal, Nepal Himalayas, from 1974 to 1994. Journal Of Glaciology, Vol. 43, No. 145, pp. 583-588.
8. Gupta, R D and Banerjee, S K, 1991. Problems and management of soil and forest resources of north-west Himalayas. Mahajan Book Center and Publishers, Jammu. 162p.
9. Samagra Rana, Small Hydropower and GIS applications in energy sector, Agriculture Technology For Hills, Oct,2008.
10. P.V. Singh, Judicious Use of Excess water in Uttarakhand Hills, Agriculture Technology for Hills, Oct, 2008.
11. Negi, S.S., 1991. Himalayan rivers, lakes and glaciers. Indus Publishing Co. New Delhi, 182p.

WHATEVER IT TAKES
FROM WATER AVAILABILITY MODEL TO COST OF WATER

Alfredo Rodriguez[1]

[1] Sr. Water Resources Engineer, Water Resources Division, Aurora Water, Aurora, Colorado 80012 (303) 739-7334; email: drodrigu@auroragov.org

Abstract. This paper summarizes ongoing efforts by the Water Resources Division at Aurora Water to determine the cost of Raw Water for the City of Aurora. Aurora is currently developing, at a cost of approximately 700 million dollars, a new water supply and delivery system, the Prairie Waters Project (PWP). This project will act as an additional source of water supply. The project is designed to divert Aurora's reusable return flows from the lower South Platte River, pump them back to the City, and, after suitable treatment, reintroduce them into the City's potable water system. In addition, Aurora Water staff is diligently pursuing the acquisition of storage and agricultural water rights in the South Platte River north of the Denver Metropolitan Area. Purchased agricultural water will be transferred to municipal use to supplement reclaimed water in order to provide for future population growth. Using results from the water availability model, and established budgeting procedures, staff at Aurora Water is taking the necessary steps to determine the cost of raw water.

This complex system of water supply raises the following question: What is the actual cost of water? Finding the answer to that question is not a small task.

Information to establish the cost of water is obtained by combining data from the Aurora Water adopted budget, the proposed construction costs and the cost of acquiring water rights and storage in the lower South Platte River.

1. Introduction

The City of Aurora encompasses a service area of approximately 151 square miles directly east of the City and County of Denver. Aurora Water has a complex water supply system and water rights portfolio.

Water is delivered to the City from the Arkansas, Colorado, and South Platte River basins and treated at two 80 MGD treatment facilities before distribution to the end users (see Figure 1.) In addition, the City is building the Prairie Waters Project and diligently pursuing the acquisition of additional water rights in the lower South Platte River Basin (Figure 2).

Water diverted through the Prairie Water Project to the City will be treated at a 50 MGD treatment facility (Prairie Water WPF) as indicated in Figure 2

[1] DISCLAIMER: **Cost values shown in this document are for illustrational purposes only and are not intended to reflect actual City of Aurora water costs.**

Population growth has been estimated at a constant rate of 1.75% per year. Table 1 summarizes the long-range official growth projections through the year 2055. At this rate, the population of Aurora is expected to more than double in the next 50 years.

Portions of the water supply system are built and have been debt free for a while, some have been built and are being paid off either through revenue bonds or through general obligation bonds, and other portions of the system are under construction and will be paid off through the issuance of bonds. In addition, there are a series of other proposed projects being considered for future expansions.

Table 1 – City of Aurora Long-Range Population Projection

Year	Official Population Projection
2000	276,393
2005	303,833
2010	323,777
2015	351,967
2020	382,612
2025	415,924
2030	452,137
2035	491,503
2040	534,296
2045	580,815
2050	631,384
2055	686,356

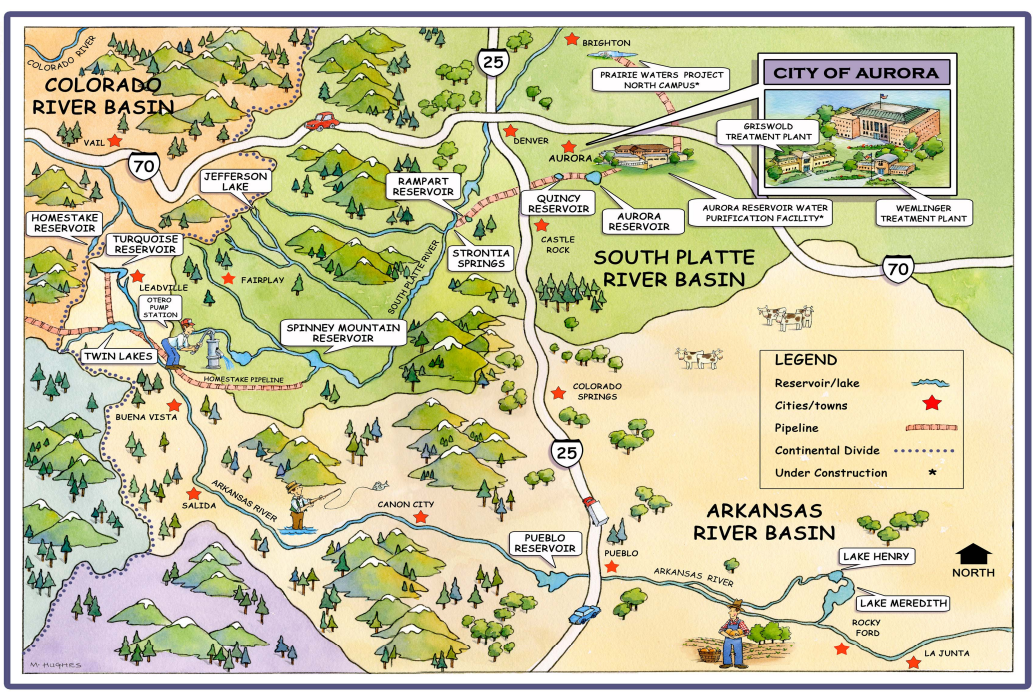

Figure 1 - City of Aurora Water Supply System



Figure 2 - Prairie Waters Project

Because of the complexity of the system, the cost of water in the Arkansas and Colorado basins is calculated by facility (i.e. a reservoir) and by water right as explained below. In the South Platte Basin, the cost of water is determined by facility and by type of water (i.e. reusable water).

The Aurora Water Availability Model is used to determine the amount of water yielded by the City using pre-established conditions (i.e. expected infrastructure during the year 2015). and the price

Results from the Aurora Water Availability Model are copied into an Excel Workbook and the cost of water is calculated using adopted City budgets for existing facilities and proposed construction and operational costs for future facilities.

The cost of water per acre-foot in the Economic Model is based on the amount of water yielded by the system and not on the total amount of water moved through each facility. In addition, the cost is calculated for both the raw portion and the treated portion as explained in the following sections.

ARKANSAS/COLORADO BASIN COSTS

Cost of Water by Facility

Cost of water per acre-feet for each of the facilities (i.e. Colorado Canal, Homestake Reservoir) is determined based on the amount of water coming into (inflows) and leaving (outflows) a particular facility.

In each facility, the main component is the water that is either yielded or moved through that facility via exchanges or leases.

The Colorado/Arkansas basin has the following water supply systems as shown in Table 2, some of which are proposed projects as noted:

Table 2 – Arkansas/Colorado Water Supply Systems

Facility Name	Size/Amount/Capacity	Condition
Holbrook Reservoir	4,000 AF	Existing
Timpas Creek Reservoir	4,000 AF	Proposed
Valco Gravel Pit	10,000 AF	Proposed
Colorado Canal	9,117	Existing
LaFarge Gravel Pit	10,000 AF	Proposed
Pueblo Reservoir	10,000 AF	Existing (Lease)
Otero Pump Station	75 cfs	Existing
Twin Lakes	2,724 AF	Existing
Box Creek Reservoir	20,000 AF	Proposed
Turquoise Reservoir	20,000 AF	Existing
Homestake Collection	21,441 AF	Existing

The following table shows an example of a calculated average cost of water from the Arkansas/Colorado Basin by facility. In this example, the average annual cost of water was estimated at $906.87 per acre-foot.

Table 3 – Average Annual Cost of Water for the Colorado/ Arkansas System by Facility.

ECONOMIC OPTIMIZATION MODEL
AURORA WATER COST SUMMARY BY FACILITY

WATER SYSTEM	INFLOW TO SYSTEM (AF)	COST PER ACRE-FOOT ($/AF)	TOTAL COST
BOX CREEK RESERVOIR SYSTEM	0	$0.00	$0
HOLBROOK RESERVOIR SYSTEM	4,804	$268.92	$1,291,841
TIMPAS CREEK RESERVOIR SYSTEM	0	$0.00	$0
ROCKY FORD SYSTEM	14,181	$237.85	$3,373,078
RIG YIELD	**8,755**		**$2,082,463**
RFII YIELD	**5,426**		**$1,290,615**
ROCKY FORD (VALCO) GRAVEL PIT SYST	0	$0.00	$0
HIGHLINE CANAL SYSTEM	534	$2,719.24	$1,453,122
COLORADO CANAL SYSTEM	10,788	$238.97	$2,578,087
LAFARGE/RICH GRAVEL PIT SYSTEM	0	$0.00	$0
PUEBLO RESERVOIR SYSTEM	15,276	$273.39	$4,176,203
WATER FROM PUEBLO	10,711	$0.00	$0
OTERO PUMP STATION SYSTEM	30,829	$210.11	$6,477,493
FROM TURQUOISE H/S ACCOUNT	**6,021**		**$1,265,138**
FROM TURQUOISE CF&I ACCOUNT	**8,424**		**$1,769,900**
FROM TWIN LAKES	**16,384**		**$3,442,456**
FROM BOX CREEK RESERVOIR	**0**		**$0**
TWIN LAKES COLLECTION SYSTEM	16,416	$193.33	$3,173,669
NATIVE YIELD	**1,047**		**$202,419**
TOTAL WATER LEASES	**2,196**		**$424,609**
OTHER SOURCES OF WATER	**13,173**		**$2,546,641**
TURQUOISE CF&I ACCOUNT	8,570	$196.94	$1,687,693
HOMESTAKE SYSTEM	**6,165**		**$1,214,191**
BUSK-IVANHOE SYSTEM	**1,411**		**$277,907**
EXCHANGES AND LEASES	**993**		**$195,596**
HOMESTAKE COLLECTION SYSTEM	13,579	$275.95	$3,746,981
COLUMBINE/WURTZ/EWING DITCH SYSTE	0	$0.00	$0
TOTAL ANNUAL COST OF THE COLORADO/ARKANSAS SYSTEM			**$27,958,167**
AVERAGE ANNUAL COST OF WATER PER AF FOR THE COL/ARK SYSTEM			**$906.87**
COST OF WATER FOR THE COL/ARK SYSTEM ($/1,000 Gallons)			**$2.78**

The methodology used throughout the Aurora Water system is shown in the following example.

Example: Pueblo Reservoir System

In the following example, the cost per acre-foot of water at Pueblo Reservoir was estimated at $273.39. The following graph shows the Pueblo Reservoir Facility.

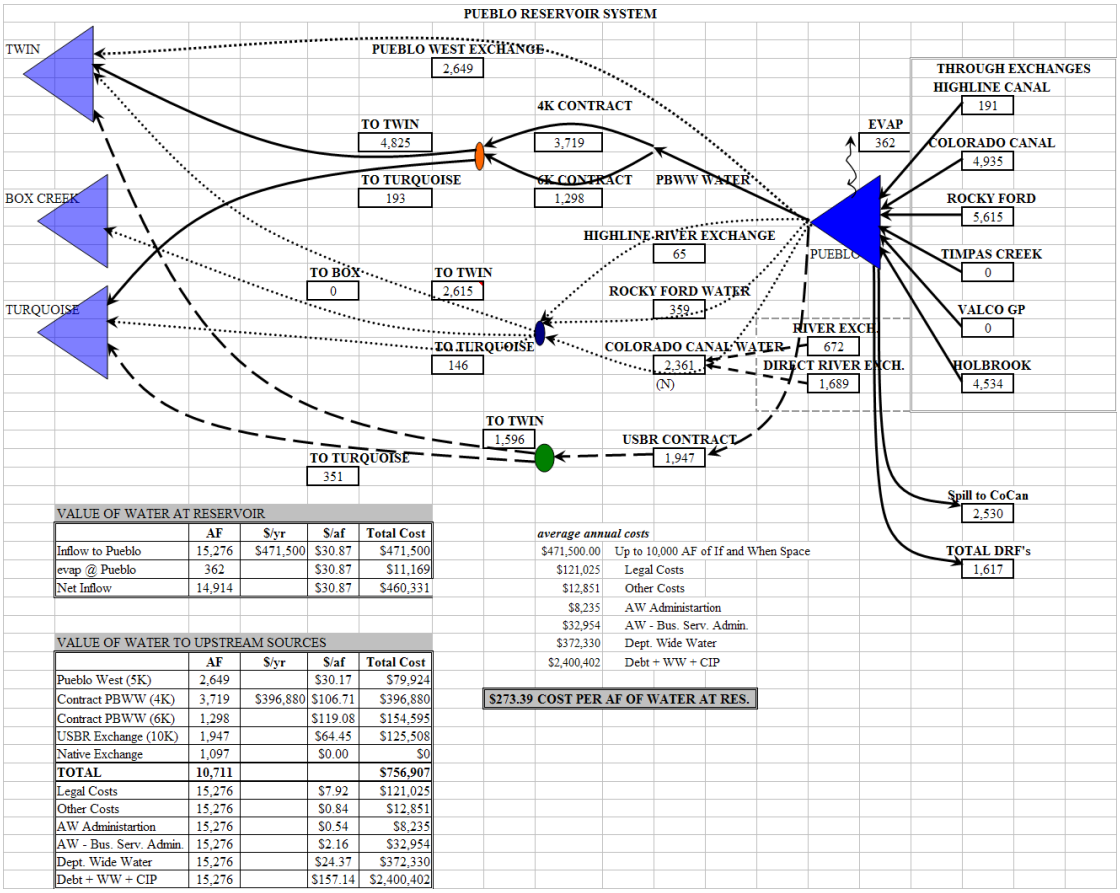

Figure 3 - Pueblo Reservoir System - Cost Calculation

Inflows to Pueblo:

The cost of moving water into the Reservoir is calculated to be $30.87 per acre-foot as follows:

The total estimated average annual amount of Aurora water moved, via exchanges, from the different sources into the reservoir is 15,275 AF as follows:

1. 4,935 AF from the Colorado Canal
2. 5,615 AF from the Rocky Ford Ditch
3. 4,434 AF from the Holbrook Reservoir
4. 191 AF from the Highline Canal Lease

Aurora Water pays an annual assessment of $471,500 for the right to used 10,000 AF of **If-and-When** space in the reservoir. Therefore, $471,500/15,275 AF = $30.87.

Outflows from the System:

The cost of moving water out of the Reservoir has been estimated as $70.67 per acre-foot as follows:

1. 2,649 AF of water is moved through the Pueblo West Contract exchange at $30.17 per acre-foot.
2. 3,719 AF of water is moved through a 4,000 AF contract exchange with the Pueblo Board of Water Works. The annual payment for the right to exchange this water is $396,880. The cost per acre-foot is estimated at $106.71.
3. 1,298 AF of water is moved through a 6,000 AF contract exchange with the Pueblo Board of Water Works. The cost of this contract exchange is $119.08 per acre-foot.
4. 1,947 AF of water is moved through a 10,000 AF contract exchange with the U.S. Bureau of Reclamation. The cost of this contract exchange is $64.45 per acre-foot.
5. 1,097 AF of water was moved via a Native Exchange for which there is no cost to Aurora Water.

Therefore, $756,907/10,711 AF = $70.67

Other Costs at Pueblo Reservoir:

In addition to the cost of moving water through a reservoir, there are additional cost such as Legal, Administrative and other costs that the City incurs due to its day to day operations.

In the case of this example, Total Other costs at Pueblo Reservoir were estimated at $192.97 per acre-foot

Cost of Water by Water Right

Cost of water per acre-foot for each of Aurora's Water Rights (i.e. decreed or contracted) is estimated based on the total amount of water moved through the Otero Pump facility for each water right or water contract.

Aurora Water has the following water rights in the Colorado/Arkansas basin:

Table 4 –Aurora's Water Rights in the Colorado/Arkansas River Basins

Water Right	Type
Homestake	Decreed
Busk-Ivanhoe	Decreed
Twin Lakes	Decreed
Upper Ranches	Decreed
Rocky Ford	Decreed
Colorado Canal	Decreed
Lake Creek Ranch Lease	Contract
Eagle River Lease	Contract
Climax Water Lease	Contract
Pueblo West Lease	Contract
PBWW Lease	Contract
Highline Canal	Contract
Columbine/Ewing/Wurtz Ditches	Contract

The following table shows the average cost of water from the Arkansas/Colorado Basin by water right. In this example, the average annual cost of water in the Colorado/Arkansas basins is estimated to be $906.93 per acre-foot

Table 5 – Average Annual Cost of Water for the Colorado/ Arkansas System by Water Right.

AURORA WATER

ECONOMIC OPTIMIZATION MODEL
AURORA WATER COST SUMMARY BY WATER RIGHT

WATER RIGHT	AMOUNT DELIVERED TO OTERO (AF)	COST PER ACRE-FOOT ($/AF)	TOTAL COST
Homestake	12,082	$587.48	$7,097,786
Busk-Ivanhoe	1,387	$429.52	$595,796
Twin Lakes	1,045	$407.63	$425,973
Upper Ranches	1,485	$403.55	$599,259
Rocky Ford	6,471	$1,402.01	$9,073,047
Colorado Canal	5,638	$1,254.12	$7,070,541
Lake Cr Ranch lease	0	$0.00	$0
Eagle River lease	0	$0.00	$0
Climax lease	0	$0.00	$0
Pueblo West lease	0	$0.00	$0
PBWW 2500 af lease	2,491	$556.13	$1,385,084
Highline lease	233	$7,332.36	$1,711,928
Columbine/Ewing/Wurtz Leases	0	$0.00	$0
TOTAL ANNUAL COST OF THE COLORADO/ARKANSAS SYSTEM			**$27,959,414**
AVERAGE ANNUAL COST OF WATER PER AF FOR THE COL/ARK SYSTEM			**$906.83**
COST OF WATER FOR THE COL/ARK SYSTEM ($/1,000 Gallons)			**$2.78**

SOUTH PLATTE BASIN COSTS

Costs in the South Platte Basin are divided into two components, the first one includes the existing system (from Spinney Mountain Reservoir to the City's Treatment Facilities), and the second one includes the Prairie Waters Project (from the Metro Wastewater Treatment Plant to the Aurora Reservoir Water Purification Facility) presently under construction and the costs of acquiring agricultural water rights.

In addition, costs are divided into Raw Water costs (from source to treatment) and Treated Water costs (from a treatment plant to the end consumer), see example below.

In the calculation of treated water from the City treatment facilities, the following annual organizational budget and account numbers are included:

Cost of Water by Facility

Cost of water per acre-feet for each of the facilities in the South Platte Basin, as in the case of the Arkansas/Colorado basins, were determined based on the amount of water coming into (inflows) and leaving (outflows) at a particular facility (i.e. Wemlinger Treatment Plant, Aurora Reservoir, etc.)

Table 6 below shows the summary of the cost of raw water in the South Platte Basin. In this example, the cost per acre-foot of raw water was estimated at $4,160.76.

The example shown below, includes the calculation of raw water cost and treated water cost for one of the water treatment facilities at the City of Aurora.

Example: Wemlinger Water Treatment Facility

The following example, shown on Figure 4, includes the calculation of the raw water and the treated water portions of the system at the Wemlinger Treatment Facility.

The cost of raw water at the Treatment Facility has been estimated to be $248.79 per acre-foot while the cost of treated water from the facility has been estimated to be $458.68 per acre-foot.

Table 6 – Average Annual Cost of Water for the South Platte System by Facility.

ECONOMIC OPTIMIZATION MODEL
AURORA WATER COST SUMMARY BY SYSTEM

WATER SYSTEM	FLOW THROUGH SYSTEM (AF)	COST PER ACRE-FOOT ($/AF)	AVERAGE ANNUAL RAW WATER COST
UPPER SOUTH PLATTE RIVER BASIN			
SPINNEY MOUNTAIN RESERVOIR SYSTEM	53,833	$202.20	$10,884,997
JEFFERSON LAKE / TARRYALL CREEK SYSTEM	668	$1,800.52	$1,202,052
STRONTIA / RAMPART SPRINGS RESERVOIR SYSTEM	116,283	$208.90	$24,291,986
STRONTIA RESERVOIR SYSTEM	70,288	$209.09	$14,696,595
RAMPART RESERVOIR SYSTEM	45,995	$208.62	$9,595,391
QUINCY RESERVOIR SYSTEM	1,071	$240.49	$257,608
AURORA RESERVOIR SYSTEM	2,122	$216.49	$459,328
GROUND WATER WELLS	5,142	$371.33	$1,909,402
GRISWOLD WATER TREATMENT SYSTEM	28,828	$169.41	$4,883,881
WEMLINGER WATER TREATMENT SYSTEM	19,212	$248.79	$4,779,710
PRAIRIE WATERS PROJECT			
NORTH CAMPUS FACILITY	27,095	$809.81	$21,942,142
FROM WELLS TO CITY	0	$0.00	$0
NORTH CAMPUS THROUGH PS-1	0	$0.00	$0
THROUGH PS-2 AND PS-3	0	$0.00	$0
BRIGHTON CAMPUS	0	$0.00	$0
EAST RESERVOIR	0	$0.00	$0
AURORA RESERVOIR WATER PURIFICATION FACILITY SYSTEM	0	$0.00	$0
EVERIST GRAVEL PIT	0	$0.00	$0
ANNUAL SOUTH PLATTE YIELD	16,971		
TOTAL ANNUAL COST OF THE SOUTH PLATTE RIVER BASIN SYSTEM			**$70,611,106**

AVERAGE ANNUAL COST OF WATER FOR THE SOUTH PLATTE SYSTEM ($/AF)	**$4,160.76**
AVERAGE ANNUAL COST OF WATER FOR THE SOUTH PLATTE SYSTEM ($/1,000 Gallons)	**$12.77**

WEMLINGER WATER TREATMENT SYSTEM

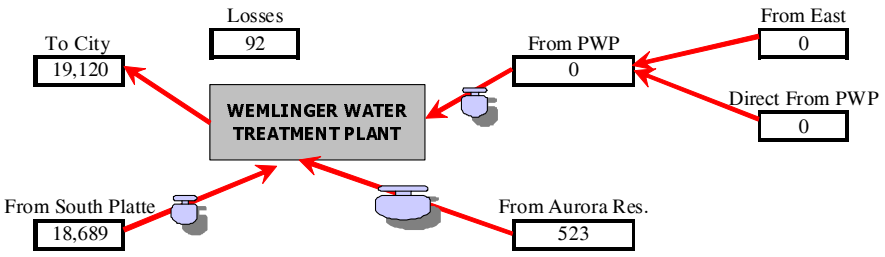

$248.79 ANNUAL COST PER AF OF RAW WATER AT WEMLINGER

Wemlinger WTP

	AF	$/yr	$/af	Total Cost
From South Platte	18,689		$119.02	$2,224,338
From Aurora Res.	523		$119.02	$62,287
From PWP	0		$119.02	$0
Total Flow	**19,212**		**$119.02**	**$2,286,625**
SPWRAP Portion	19,212		$0.86	$16,430
Legal Costs	19,212		$6.98	$134,146
Other Costs	19,212		$0.42	$8,100
AW Administartion	19,212		$0.27	$5,191
AW - Bus. Serv. Admin	19,212		$1.08	$20,772
Dept. Wide Water	19,212		$12.22	$234,698
Debt + WW + CIP	19,212		$78.76	$1,513,089
Pumping from Rampar	18,689		$30.00	$560,660

average annual costs	
2,286,625	Annual Treatment Cost
16,430	SPWRAP Portion
134,146	Legal Costs
8,100	Other Costs
5,191	AW Administartion
20,772	AW - Bus. Serv. Admin.
234,698	Dept. Wide Water
30	Pumping from Rampart Line
1,513,089	Debt + WW + CIP

$458.68 ANNUAL COST PER AF OF TREATED WATER AT WEMLINGER

Treated and Distributed (NOT RAW WATER COST)

	AF	$/yr	$/af	Total Cost
Pumping Station Wate	19,120		$7.22	$138,068
Billing Services	19,120		$20.59	$393,636
Plans Review	19,120		$13.83	$264,455
P.I & Conservation	19,120		$31.13	$595,112
Utility Quality Control-	19,120		$24.61	$470,481
Customer Services	19,120		$57.22	$1,094,033
T&D Flow	19,120		$109.55	$2,094,612
CIP	19,120		$26.95	$515,308
Aurora Water Ops Adr	19,120		$14.55	$278,244
Aurora Water Services	19,120		$22.12	$422,982
Technical Operations -	19,120		$15.49	$296,247
Water Conservation	19,120		$15.69	$299,926
Legal Costs	19,120		$6.98	$133,503
Other Costs	19,120		$0.42	$8,062
AW Administartion	19,120		$0.27	$5,166
AW - Bus. Serv. Admin	19,120		$1.08	$20,673
Dept. Wide Water	19,120		$12.22	$233,574
Debt + WW + CIP	19,120		$78.76	$1,505,843
Total OutFlow	**19,120**		**$458.68**	**$8,769,923**

$138,068	Pumping Station Water
$393,636	Billing Services
$264,455	Plans Review
$595,112	P.I. and Conservation
$470,481	Utility Quality Control-Water
$1,094,033	Customer Services
$2,094,612	T&D Cost
$515,308	CIP
$278,244	Aurora Water Ops Admin-Water
$422,982	Aurora Water Services - Water
$296,247	Technical Operations - Water
$299,926	Water Conservation
$133,503	Legal Costs
$8,062	Other Costs
$5,166	AW Administartion
$20,673	AW - Bus. Serv. Admin.
$233,574	Dept. Wide Water
$1,505,843	Debt + WW + CIP

Figure 4 - Wemlinger Water Treatment Plant System Cost Calculation

Cost of Water by Type of Water

Water in the South Platte basin is accounted for by type (i.e. Single Use Storable and Reusable). Using the same example and shown in Table 7 below, the cost of water by type in the South Platte Basin was estimated at $4,160.57 per acre-foot.

Table 7 - South Platte Basin Cost of Water by Water Type

ECONOMIC OPTIMIZATION MODEL
AURORA WATER COST SUMMARY BY TYPE OF WATER

WATER TYPE			TOTAL ANNUAL COST
Last chance single use			$1,327,943
Last chance CU			$131,273
Last chance DRF			$287,363
1964 strontia (single use)			$2,135,011
2004 strontia (CU)			$4,081,878
Tarryall Creek CU			$2,382,807
Tarryall Creek single use			$1,442,705
Tarryall Creek DRF			$0
Ranches above spinney CU			$11,213,565
Ranches above spinney DRF			$669,899
Spinney right			$2,830,066
Transmountain from Otero			$7,337,956
Transmountain via Spinney			$11,933,180
Transmountain via Antero			$0
Ground Water			
Cherry creek deep wells (wc)			$1,148,865
Cherry creek single use			$1,447,968
Senac CU (aurora resv. only)			$298,483
Prairie Waters Project			
Reusable Indoor water usage			$19,015,723
Reusable Ground Water return flow			$0
East Cherry Creek Valley source			$2,915,619
Chatfield releases			$0
New Ag rights below metro			
Platteville Ditch			$2,592
Fulton Ditch			$34
New Brantner			$225
Brighton Ditch			$3,500
Lupton Bottom Ditch			$1,050
Lupton Meadows Ditch			$18
Farmer's Independent Ditch			$0
Western Mutual Ditch			$150
South Platte JR water rights			$0
Everist reservoir release			
Reusable Indoor water usage			$0
Reusable Ground Water return flow			$0
East Cherry Creek Valley source			$0
Chatfield releases			$0
New Ag rights below metro			
Platteville Ditch			$0
Fulton Ditch			$0
New Brantner			$0
Brighton Ditch			$0
Lupton Bottom Ditch			$0
Lupton Meadows Ditch			$0
Farmer's Independent Ditch			$0
Western Mutual Ditch			$0
South Platte JR water rights			$0
TOTAL ANNUAL COST OF THE SOUTH PLATTE RIVER BASIN SYSTEM			**$70,607,876**
AVERAGE ANNUAL COST OF WATER FOR THE SOUTH PLATTE SYSTEM ($/AF)			**$4,160.57**
AVERAGE ANNUAL COST OF WATER FOR THE SOUTH PLATTE SYSTEM ($/1,000 Gallons)			**$12.77**

AURORA WATER TOTAL WATER SYSTEM COSTS

Having determined the cost of raw water for both the Arkansas/Colorado and the South Platte River Basins, as well as the cost of treatment and distribution of the treated portion, then the total water system cost con be calculated as shown on Table 8.

Using the example in this document, the total cost of the system for the City of Aurora has been calculated to be $2,516 per acre-foot, of which $2062 per acre-foot is the cost of raw water and $454 per acre-foot the cost of treated water

Table 8 – Aurora Water System Cost Summary

ECONOMIC OPTIMIZATION MODEL
AURORA WATER SYSTEM COST SUMMARY

Aurora Water System	Total Yield (AF)	Total Cost ($)	Cost of Water ($/AF)	Cost of Water ($/1,000 Gal.)
South Platte River Basin Raw Water Cost	16,971	70,611,106	$4,161	$12.77
Arkansas/Colorado River Basins Raw Water Cost	30,829	27,958,167	$907	$2.78
Total Aurora Water Annual Cost of Raw Water	**47,800**	**98,569,272**	**$2,062**	**$6.33**
Aurora Water Treated Water Cost	47,798	$21,689,293	$454	$1.39
Annual Cost of Water for Aurora Water System	**47,800**	**120,258,566**	**$2,516**	**$7.72**

Final Remarks

Aurora Water's Water Resources Division recognizes that this is a continuous project and that the results will vary according to an specific condition or conditions set in its water availability model.

Additional work needs to be accomplished to include electrical cost for the operation of the Prairie Waters Project.

The results of this project can be used to determined the base charge for water in case of a potential sale of water to a third party.

CURRENT WATER MANAGEMENT PRACTICES AND THE EFFECTS OF CLIMATE CHANGE ON THE COLORADO RIVER BASIN

J. Brandon Klenzendorf, Student Member

Graduate Student, Civil Engineering Department, University of Texas at Austin, Austin, TX, jbklenz@mail.utexas.edu

ABSTRACT

The Colorado River Basin (CRB) reservoir system is one of the most over-allocated systems in the world. Due to recent drought conditions within the past decade, reservoir storage has been decreasing and shows no sign of increasing in the near future. The allocated demands from the system are greater than the average streamflow into the system. Furthermore, it is expected that climate change will only make the situation more severe in the near future. Various modeling techniques show that climate change will decrease precipitation in the CRB while increasing evaporation. This combination results in decreased runoff and streamflow which provides the majority of water in the CRB. However, the more significant problem is the over-allocation of the river. The allocations and water usage can be controlled much easier and have a much greater impact on the reliability of the reservoir system than global climate change. This paper will highlight some of the major flaws in the water allocations utilized in the CRB and reasons for mistakes made in the past. Previous studies on the reliability of the CRB reservoir system are investigated, and the general impacts of climate change on the hydrologic cycle are briefly discussed.

INTRODUCTION

The reservoir system of the Colorado River Basin (CRB) consists of over 90 reservoirs, of which Lake Mead (created by the Hoover Dam) and Lake Powell (created by the Glen Canyon Dam) account for 51.9 million acre-feet (MAF) of storage, or roughly 85% of the total CRB reservoir storage volume (Christensen et al., 2004). Lake Mead is the largest man-made reservoir in the United States and is the main focus of this study. The lake is located in the Lower CRB and provides water to roughly 8 million people in the southwestern United States and parts of Mexico. It contains about 16 MAF of capacity for the joint use of water supply, irrigation and power, and 10 MAF for inactive storage (USBR, 2008b). Figure 1 shows the water surface elevation of Lake Mead through time since its construction in 1936. Several important elevations are listed to give an idea of when the lake will no longer produce hydropower and

when water can no longer be extracted by gravity for municipal use. A water level below 1,125 feet is considered to be drought conditions; Lake Mead has experienced three significant droughts during its life. The short drought around 1965 was impacted by the construction and subsequent filling of Lake Powell (in the Upper CRB) upstream of Lake Mead. The lake is currently experiencing drought conditions.

The following statistics and characteristics of the CRB were taken from Christensen et al. (2004). The total drainage area of the CRB is 243,000 square miles. The annual average streamflow is around 15.1 MAF based on gage data collected since 1906. Of this streamflow value, 90% of the flow is generated in the Upper Basin, which is designated as the area upstream of Lees Ferry, Arizona. 70% of the flow generated in the Upper Basin comes from snow pack which also controls the seasonal timing of streamflow. The average annual precipitation of the entire CRB is 14.0 inches, of which approximately 12.2 in. evaporates, which leaves 1.8 in. of water available for runoff. Therefore, only 13% of the precipitation becomes runoff and contributes to streamflow and water storage. This low runoff value, together with the low precipitation and high water demands show why water resources are a major concern in this part of the country.

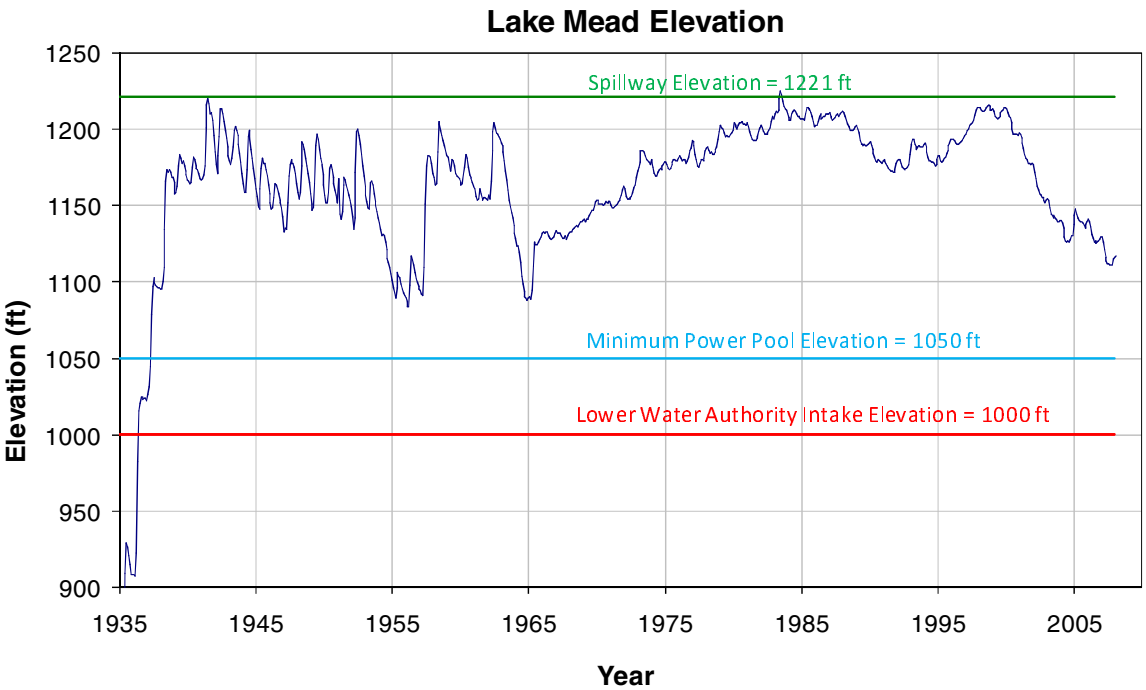

Figure 1 – Lake Mead water surface elevation (data: USBR, 2008a)

OBJECTIVES

The main objective of this paper is to investigate the surface water availability and management practices within the CRB, which is currently experiencing drought conditions. Lake Mead will be used as an indicator of the total water availability issues in the CRB due to its large storage volume. A brief inspection of the reliability of the CRB reservoir system is provided based on previous studies available in the literature. Furthermore, the possible impacts

of global climate change are investigated based on projected changes to the hydrologic cycle. Specifically, the influence of climate change on precipitation, evaporation, and runoff are necessary to determine surface water availability in the future. Finally, the overall water availability within the CRB is summarized based on current water management practices and the possible impacts of global climate change.

WATER AVAILABILITY AND MANAGEMENT PRACTICES

Water resources management in the CRB is governed by the "Law of the River", which is a collection of over 50 international treaties, interstate compacts, court decisions, and other legislation that has occurred over the years (Harding et al., 1995). The Law of the River allocates an annual amount of water of 7.5 MAF for the Upper Basin, 7.5 MAF for the Lower Basin with an additional 1.0 MAF if needed, and 1.5 MAF for Mexico. This combines for an allocated annual streamflow total of up to 17.5 MAF. However, this does not account for the minor water rights that are reserved for such uses as endangered fishes and Indian tribes (MacDonnell et al., 1995). Therefore, the total allocated water in the entire basin is approximately 18 MAF per year.

The value of annual allocated water must be provided by the combination of reservoir storage and streamflow. The average annual streamflow varies depending on what data source is considered. Gage streamflow data taken beginning in 1906 by the United States Bureau of Reclamation (USBR) estimate an annual average streamflow of 15.1 MAF. However, historical streamflow records have been estimated based on tree ring reconstructions dating back to the early 1500s. The tree ring records suggest an average annual streamflow as low as 13.5 MAF (Christensen et al., 2004). Figure 2 shows one collection of tree ring reconstructions at the location of Lees Ferry, Arizona presented as 10-year averaged streamflow values (Woodhouse et al., 2006) together with the averaged gage data monitored since 1906. Lees Ferry is the dividing point between the Upper and Lower Basins, and is a good representation of the total water in the entire CRB since the Upper Basin accounts for 90% of the total flow. The important point of these data is to point out that the observed streamflow values since 1906 show a higher average annual streamflow value than suggested by the tree ring reconstructions. Furthermore, allocations of water in the CRB, governed by Law of the River, total up to 18 MAF per year. When these allocations were made in the 1920s, the CRB was experiencing a high annual average streamflow value equal to this allocation value, possibly the highest streamflow over the past 500 years. Therefore, allocations were made based on the observed 18 MAF annual average at the time, as opposed to the more likely 13.5 MAF annual average suggested by the tree ring reconstructions. Currently, 90% of the allocated water is actually being utilized, so that roughly 16 MAF of water each year is being used by the residents in the CRB, with little indication of this number decreasing in the future unless changes to the water resources management practices are made. Clearly, this over-allocation of water is the major problem associated with water resources management in the southwest United States. As shown in Figure 2, there have been only four possible times when an annual allocation of 18 MAF could actually be provided by streamflow alone.

The CRB is one of the most over-allocated river systems in the world. An annual allocation of 18 MAF is provided by the Law of the River. Over 16 MAF of water is actually being used each

year. The average annual streamflow of record is 15.1 MAF, with a possible average closer to 13.5 MAF as suggested by tree ring reconstructions. Therefore, since the outflow to water users is greater than the inflow to the reservoir system, the reservoirs have been consistently draining in recent years with no indication of filling in the near future. This suggests that the entire system is destined to fail in the future unless drastic water resources management changes are made.

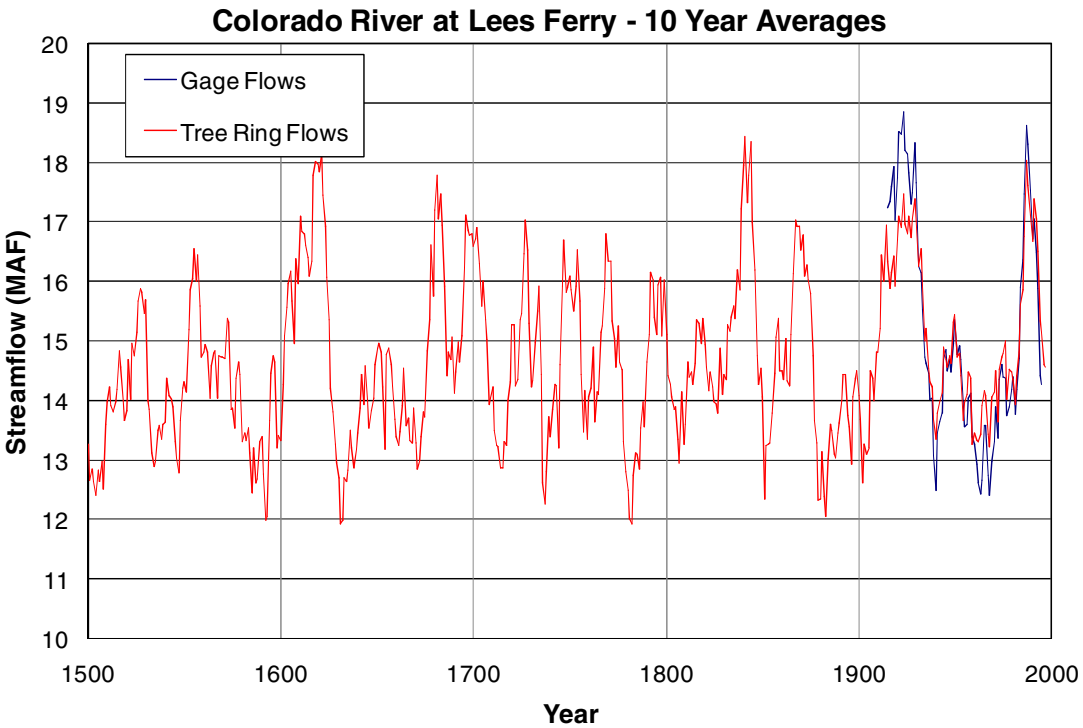

Figure 2 – 10-year average annual streamflow values in the CRB (data: NOAA, 2008)

RELIABILITY OF RESERVOIR SYSTEM

Many previous studies have investigated the reliability of the reservoir system in the CRB. This issue has been important due to the fact that the system supplies water to a large population. Previous studies prior to the current drought conditions have shown that the reservoir system is very reliable. However, more recent studies suggest the reservoir system is not as reliable and likely could go dry in the future.

Tarboton (1995) examined the impacts of three scenarios of severe sustained droughts on the CRB. The first drought scenario is the "Colorado Drought of Historic Record" which occurred from 1943 to 1964 and is likely to occur again. The second scenario is the "Colorado Severe Drought" which is the worst drought from tree ring reconstructed flows and occurred from 1579 to 1600. The third drought is the "Colorado Rearranged Severe Drought" where the annual flows in the "Colorado Severe Drought" are rearranged in descending order so that this is a worst case scenario. The major finding is that only the most severe drought ("Colorado Rearranged Severe Drought") must take place before any extreme consequences are felt. Therefore, the

other two scenarios will not significantly impact the water resources in the region in the long run. This study did not take into account any climate effects but only considered actual streamflow values that have occurred in the CRB. In a similar study, Harding et al. (1995) found that a severe sustained drought would have little impact on the Lower Basin, but would heavily strain the water resources on the Upper Basin. These studies prior to the recent drought showed that the reservoir system of the CRB is very resilient to severe sustained drought.

More recent studies suggest the reservoir system is likely to go dry in the future. Barnett and Pierce (2008) are the first to attempt to predict the time at which decreased water availability will begin to impact the residents of the CRB. They looked at various scenarios and developed cumulative distribution functions of when the active storage in Lakes Mead and Powell will disappear based on Monte Carlo simulations of a water balance model for the entire basin. They found that the net inflow (inflow minus outflow) for the year 2008 is -0.2 MAF per year based on the average inflow of 15.1 MAF. This is consistent with the above description in the previous section of the outflow from the system being greater than the inflow. The simulations of current conditions, with no impact of climate change, showed that by the year 2060 the net inflow would be -1.2 MAF per year. This suggests that even without the impacts of climate change, the system is destined to fail under current conditions due to continued increased water demand. However, these values are based on the higher observed annual streamflow average. If the lower tree ring reconstruction flows are used, the actual net inflow for the year 2008 may be closer to -1.0 MAF. The current value of negative net inflow for the CRB reservoir system is what distinguishes the results from more recent studies when compared to older studies. In the older studies, the reservoir system was experiencing positive net inflow which suggested that the system could withstand large droughts. Due to the recent shift to negative net inflow as a result of over-allocation of the available water, the system is much more likely to fail in the future.

One major finding in Barnett and Pierce (2008) is that in the early twenty-first century, the probability that the reservoir system will run dry is more likely than the chance that the reservoir system will fill back up. This is shown in Figure 3 (taken from Barnett and Pierce, 2008), where the curves show the probability of the system going dry or filling within the following 20 years. For example, in the year 1960, around the construction of Lake Powell, there was virtually no chance of the system going dry by the year 1980. On the other hand, around 2005, there is about a 25% chance that the system will go dry by 2025, and similarly a 25% chance the system will fill up by 2025. Beyond this year, the probability of going dry is greater than the probability that the system will fill back up. This shift, corresponding with the change to negative net inflow, again shows why earlier studies on the CRB determined that the reservoir system was very reliable.

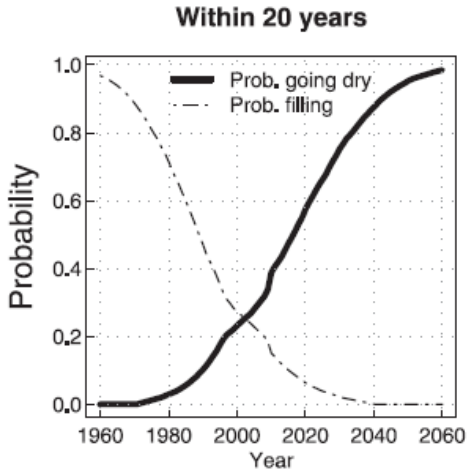

Figure 3 – Probability of system running dry or filling up in the following 20 years (source: Barnett and Pierce, 2008)

All of these studies show that the current allocations and water management practices in the CRB, together with possible decreases in runoff due to climate change, are destined to fail the reservoir system. Therefore, drastic change in reservoir operating policies is necessary in order to ensure the longevity of the system. However, this does not include other possible water sources of water such as groundwater and importing water from other basins. These could be two possible courses of action in order to maintain the surface water use in the CRB. This problem has become even more strained due to the possible impacts of climate change on the region. Assuming that the global temperature will increase in the future, this change will impact both the timing and amount of water in the CRB. Increased temperatures will impact the amount of snowfall that occurs in the Colorado River headwaters. Since snow pack accounts for 70% of the annual streamflow, this change can have major effects. Increased temperatures will cause more precipitation to fall as rain as opposed to snow. Also, the higher temperatures will cause the snow packs to melt earlier in the spring, which will alter the timing of streamflow downstream. Finally, increased temperatures will result in higher evaporation, which will cause an even greater loss of water to the atmosphere than in the past. This increase in temperature will, in turn, increase the demand of water for such uses as irrigation and hydropower.

IMPACTS OF CLIMATE CHANGE

The issue of global climate change has been a concern for many years. However, this issue has gained more attention in recent years. The possibility of increasing global temperatures can have a drastic effect on the hydrologic cycle which controls much of the water resources throughout the world. A very brief description of the mechanics of climate change deal with the continued increase in emissions of CO_2 and other greenhouse gases, such as water vapor, that have been shown to absorb infrared thermal radiation emitted from the surface of the Earth and radiate it back towards the surface where it is reabsorbed. This leads to an increase in infrared radiation at the surface that must be balanced by the loss of energy through increased latent heat and sensible heat (Boer, 1993). Increased latent heat results in an increased evaporation rate at the surface, whereas increased sensible heat results in increased temperature at the surface.

The most important impact of climate change for the CRB is the impact on evaporation and precipitation. As mentioned above, evaporation is expected to increase globally due to climate change. However, the impact on precipitation is more difficult to determine. Boer (1993) found that the precipitation over land does not increase as much as evaporation. Therefore, more rain will fall over the oceans, which will result in a decrease in runoff of 5.2% on land. Multiple studies have attempted to model the change in runoff (precipitation minus evaporation) over the entire Earth. Figure 4 (modified from Held and Soden, 2006) shows the average percent change of runoff, δ(P-E), based on latitude. This is for a scenario of twice the current concentrations of CO_2 in the atmosphere using two separate modeling techniques. Over the tropics near the equator, runoff increases drastically. Runoff is expected to decrease over the mid-latitudes where the CRB is located. Finally, runoff increases over the high latitudes. These trends follow the predications associated with changes in precipitation, which correspond to the current distribution of precipitation over the Earth. This suggests that precipitation will increase where it is already high and decrease where it is already low. The reason for this trend is that the locations of high precipitation are controlled by the air circulation in the atmosphere, which is not expected to change considerably due to global climate change. In general, precipitation is likely to occur where there is a rising air mass, such as at the equator and high latitudes. At the mid-latitudes, there is in general a falling dry air mass, so precipitation is expected to decrease. Overall, the pattern of runoff is exaggerated with increased temperatures. This means that current areas of low runoff are expected to have even lower runoff, and areas of high runoff are expected to have even higher runoff with increased temperature.

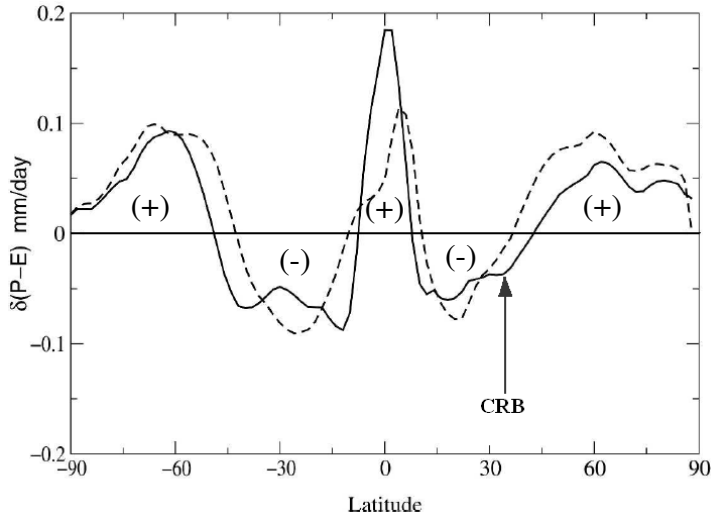

Figure 4 – Change in runoff versus latitude (modified from: Held and Soden, 2006)

Various studies have attempted to model the impacts of global climate change using general circulation models. Studies such as Christensen et al. (2004), Milly et al. (2005), Christensen and Lettenmaier (2007), and McCabe and Wolock (2007), among others, have investigated these changes either on a global scale, or specifically for the CRB. There are common trends seen in all of these studies which suggest an increase in temperature and evaporation, resulting in a decrease in runoff available for streamflow within the CRB.

SUMMARY AND CONCLUSIONS

The Colorado River Basin reservoir system is one of the most over-allocated systems in the world. It supports a very large population and is the major source of water for much of the southwestern United States. Due to the large demands placed on the system and recent drought conditions, reservoir storage has been decreasing for the past decade and shows no sign of increasing in the near future. The water allocation demands from the system are greater than the average streamflow into the system. Therefore, if decreases in allocations are not made in the near future, the system will eventually run dry and fail to provide water even if drought conditions decline. The recent change to negative net inflow has made the system more vulnerable than ever before.

In addition to these problems, it is expected that climate change will only make the situation more severe. Various modeling techniques show that climate change will decrease precipitation in the CRB and increase evaporation. This combination results in a decrease in runoff and streamflow in the CRB. Therefore, not only is water use in the CRB currently greater than the supply by streamflow, but climate change is expected to decrease the available streamflow.

In conclusion, climate change is expected to further decrease the reliability of the reservoir system in the CRB. However, the more significant problem is the over-allocation of the river. The allocations and water usage can be controlled much easier and have a much greater impact on the reliability of the reservoir system than global climate change does. The high water usage and over-allocation is the first problem that should be addressed in order to maintain a reliable water supply in the CRB. The current allocations were made during an unusually wet period, and therefore are not representative of the actual amount of water available for distribution. Reallocating the water, together with obtaining water from different sources is necessary to ensure the longevity of a reliable water system in the Colorado River Basin.

REFERENCES

Barnett, T.P. and D.W. Pierce (2008): "When Will Lake Mead Go Dry?", *Water Resources Research*, Vol. 44, W03201.

Boer, G.J. (1993): "Climate Change and the Regulation of the Surface Moisture and Energy Budgets", *Climate Dynamics*, Vol. 8, pg. 225-239.

Christensen, N.S., A.W. Wood, N. Voisin, D.P. Lettenmaier, and R.N. Palmer (2004): "The Effects of Climate Change on the Hydrology and Water Resources of the Colorado River Basin", *Climatic Change*, Vol. 62, pg. 337-363.

Christensen, N.S. and D.P. Lettenmaier (2007): "A Multimodel Ensemble Approach to Assessment of Climate Change Impacts on the Hydrology and Water Resources of the Colorado River Basin", *Hydrology and Earth System Sciences*, Vol. 11, pg. 1417-1434.

Harding, B.L., T.B. Sangoyomi, and E.A. Payton (1995): "Impacts of a Severe Sustained Drought on Colorado River Water Resources", *Water Resources Bulletin*, Vol. 31, No. 5, pg. 815-824.

Held, I.M. and B.J. Soden (2006): "Robust Responses of the Hydrological Cycle to Global Warming", *Journal of Climate*, Vol. 19, pg. 5686-5699.

MacDonnell, L.J., D.H. Getches, and W.C. Hugenberg Jr. (1995): "The Law of the Colorado River: Coping with Severe Sustained Drought", *Water Resources Bulletin*, Vol. 31, No. 5, pg. 825-836.

McCabe, G.J. and D.M. Wolock (2007): "Warming may Create Substantial Water Supply Shortages in the Colorado River Basin", *Geophysical Research Letters*, Vol. 34, L22708.

Milly, P.C.D., K.A. Dunne, and A.V. Vecchia (2005): "Global Pattern of Trends in Streamflow and Water Availability in a Changing Climate", *Nature*, Vol. 438, pg. 347-350.

NOAA (2008): *NOAA Paleoclimatology Program – Woodhouse et al. 2006 Upper Colorado River Basin Streamflow Rec*, 19 March 2008, National Oceanic and Atmospheric Administration Satellite and Information Service, <http://www.ncdc.noaa.gov/paleo/pubs/woodhouse2006/woodhouse2006.html>

Tarboton, D.G. (1995): "Hydrologic Scenarios for Severe Sustained Drought in the Southwestern United States", *Water Resources Bulletin*, Vol. 31, No. 5, pg. 803-813.

USBR (2008a): *Bureau of Reclamation: Lower Colorado Region*, 5 March 2008, United States Department of the Interior, Bureau of Reclamation, <http://www.usbr.gov/lc/region/g4000/hourly/mead-elv.html>

USBR (2008b): *Bureau of Reclamation: Lower Colorado Region – Hoover Dam: Lake Mead FAQs*, 16 April 2008, United States Department of the Interior, Bureau of Reclamation, <http://www.usbr.gov/lc/hooverdam/faqs/lakefaqs.html>

Woodhouse, C.A., S.T. Gray, and D.M. Meko (2006): "Updated Streamflow Reconstructions for the Upper Colorado River Basin", *Water Resources Research*, Vol. 42, W05415.

DOES POLYMER HAVE AN EFFECT ON BACTERIAL REGROWTH IN ANAEROBICALLY DIGESTED BIOSOLIDS?

Jean M. Ryan, Student Member

Undergraduate Student, Environmental Engineering Department, Penn State, Harrisburg, PA, jmr5190@psu.edu

ABSTRACT

Recently more attention is being given to the regrowth of bacteria in treated biosolids. It has been found that in many anaerobically treated biosolids, bacterial regrowth occurs between digestion and the point in which the biosolids are disposed of or used for land application. This experiment examines the possible effect of polymer usage on bacterial regrowth in anaerobically digested biosolids. In order to examine this possible effect, a control sample, a sample with newly-reconstituted polymer, and a sample with pre-constituted polymer (several days old) were compared for their effects on bacterial regrowth using an MPN test. Each sample was 300mL, and a weight ratio of 1mg: 185kg, assuming 2% solids, was used to add polymer to all of the samples, excluding the controls. These samples were then compared at 0, 1, and 2 days of incubation. As a whole, the MPN values increased with one and two days of incubation at room temperature. However it was also found that the control samples had a higher MPN than the samples treated with the old and new polymer after one and two days of incubation, which suggests that polymer does not have an effect on the increase of fecal coliforms in biosolids.

INTRODUCTION

The proper treatment and disposal of sewage sludge has not always been common practice. Years ago, the effects that sludge may have caused on the environment were not considered. However as people became more aware of environmental issues, attention was directed towards the importance of properly handling and disposing of sewage sludge. Because of this attention, many countries, including the United States, have regulations that are required for the treatment of sewage sludge. In the United States, the Environmental Protection Agency (EPA) issued the "Standards for the Use or Disposal of Sewage Sludge" which lays out general requirements, pollutant limits, operation standards, and management practices, as well as frequency of monitoring, record keeping, and reporting requirements (U.S.

EPA, 1994). These regulations serve to classify biosolids by their level of treatment and describe their future use in an environmentally safe manner.

Some of the regulations that are in place deal directly with sludge stabilization and the amount of pathogen reduction that is required in the treatment of sludge (U.S. EPA, 1994). Pathogen reduction is considered to be one of the parameters used to determine sewage sludge quality (U.S. EPA, 1994). This pathogen reduction is done so that biosolids can be designated as either Class A or Class B biosolids. The EPA's Part 503 regulation contains two classes of pathogen reduction, which are Class A and Class B biosolids (U.S. EPA, 1994). Class A biosolids are considered to be nearly pathogen free and must have a fecal coliform density of less than 1000MPN per gram of biosolids (dry weight basis) after they are treated (U.S. EPA, 2003). On the other hand, biosolids must have a fecal coliform density of less than 2 million MPN per gram of biosolids to be classified as Class B biosolids (U.S. EPA, 2003). Therefore it is necessary that Class B biosolids require further regulations in order to prevent any sort of harmful contamination.

There are three ways for pathogen requirements to be met so that biosolids can be considered Class B biosolids (U.S. EPA, 2003). These methods are the monitoring of fecal coliform, using a process to significantly reduce pathogens (PSRP), or using a process that is equivalent to a PSRP (U.S. EPA, 2003). There are five types of PSRPs that are used for pathogen reduction. They are aerobic digestion, air drying, anaerobic digestion, composting, and lime stabilization (U.S. EPA, 2007). Of these five PSRPs, anaerobic digestion is the most commonly used in treatment facilities (Qi et al., 2007). By treating biosolids at a certain temperature and for a given length of time, anaerobic digestion can meet the proper criteria for pathogen reduction (U.S. EPA, 2003). Once this criterion is met, the treated biosolids are considered to be Class B solids and can be used for land application.

The problem with these requirements is that treated biosolids are characterized immediately after digestion rather than when they are used or disposed of (Qi et al., 2007). Between the digestion process and the disposal of biosolids, processes such as conditioning and dewatering occur (Qi et al., 2007). While these processes have not been expected to have any effect on bacterial density, recent studies suggest that this is not the case (Higgins et al., 2007). Over the past several years research has shown that after mechanical dewatering, there are higher concentrations of fecal coliforms than there are after the anaerobic digestion step (Higgins et al., 2007). This creates a problem in that the regrowth of fecal indicators in the treated biosolids may no longer fall within the U.S. EPA's standards (Chen et al., 2007). By failing to meet the set regulations, these biosolids are no longer eligible for land application (Chen et al., 2007). These biosolids must then be disposed of, which in turn is more costly than if they had been applied to the land.

There have been several different theories presented in order to explain the increase of fecal coliforms in dewatered sludge. One potential explanation is the regrowth of fecal coliforms (Higgins et al., 2007). It has also been suggested that the difference

in enumeration between the liquid and cake was due to sample matrix effects. This idea is similar to the idea that the shearing effect on solids that are exposed to high solids centrifugation, improves the "release" of bacteria from the floc matrix (Higgins et al., 2007). Because of this, the amount of bacteria that can be cultured will increase when compared to the amount of culturable bacteria before the dewatering process (Higgins et al., 2007). It has also been suggested that contamination with fecal coliforms could also explain the high counts that are found after dewatering (Higgins et al., 2007). Finally it has also been proposed that bacteria enter a nonculturable state during digestion, and that dewatering can "resuscitate" the bacteria allowing them to grow once again (Higgins et al., 2007).

It has also been shown that the regrowth of fecal coliforms in anaerobically digested biosolids is associated with odor production (Chen et al., 2007). This odor production is a result of food release and oxygen exposure that occurs during centrifuge dewatering (Chen et al., 2007). However, it is also possible that polymer, which is a chemical coagulant composed mainly of hydrocarbons, used for dewatering can serve as food source for regrowth. The use of polymer in dewatering has been common in the treatment process in order to improve the efficiency and reduce the cost of both transporting and handling sludge (Wu et al., 1997). Still any link between the addition of polymer and bacterial regrowth is still unclear. While it has been proposed that polymer is indeed partially biodegradable and therefore a possible food source for bacterial regrowth, it has yet to proven. Therefore the goal of this paper is to examine the possible relationship between the addition of polymer and bacterial regrowth in anaerobically digested biosolids, and see whether or not polymer is being used as a food source for bacterial regrowth.

METHODOLOGY

Sample Collection

The biosolids used were from the Highspire (Pennsylvania) Wastewater Treatment Plant, a conventional municipal activated sludge plant (Figure 2). The biosolids were collected after digestion and storage and before centrifuge dewatering. The biosolids were anaerobically digested at a temperature of 95-98°F for a period of approximately 35 days. They were stored (for approximately three days) in sterilized and sealed plastic containers at room temperature until just before experimentation.

Polymer Addition Testing

The biosolids were separated into nine plastic containers, which had been sterilized with bleach and sterile water, with 300mL in each of the containers. Three containers were used for controls (no polymer added), three were treated with three day old polymer, and three were treated with newly constituted polymer. The polymer used was Claifloc NE-1200 from Polydyne Inc. located in Riceboro, GA, and it is a

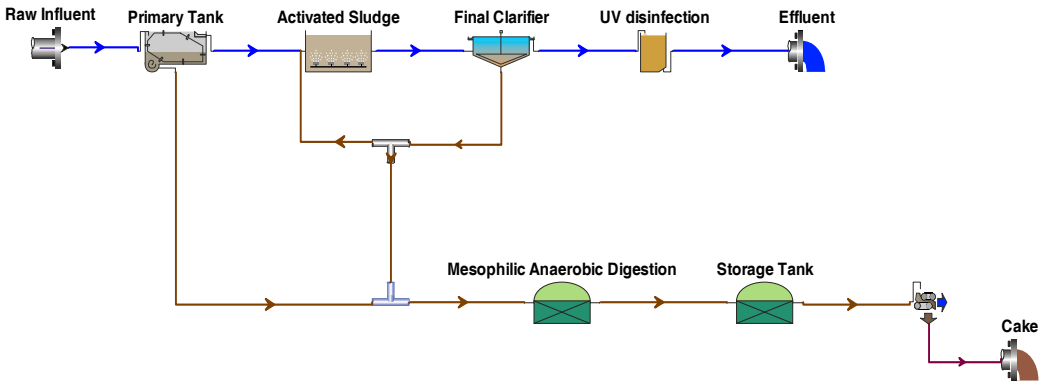

Figure 1. Flow Chart of Highspire Wastewater Treatment Plant completed using BioWin

medium charge cationic polyacrylamide. The polymer, which was made using a ratio of 2.7g to 500mL of tap water, was added to the biosolids at a dry weight ratio of 1mg of polymer per 185kg of sludge. The identical ratio was also used to add distilled water to the control samples in order to keep the volumes of each sample the same. Testing was done on the biosolids immediately and at one and two days of incubation at room temperature by using one of each type of sample- a control, a sample treated with old polymer, and a sample treated with new polymer- at each different day of incubation.

MPN Enumeration of Fecal Coliform

The three samples of biosolids that were to be tested immediately were individually placed into autoclaved blenders and blended on high for two minutes as laid out by the U.S. EPA under 40 CFR Part 503 (U.S. EPA, 2003). Each sample was then diluted using a dilution buffer to obtain five separate dilutions. A traditional Most Probable Number (MPN) test, which was based on the U.S. EPA Method 1680, was performed for each of the each of the samples with five trials done for each serial dilution. (U.S. EPA, 2006). The MPN tubes were stored in an incubator at 37°C for two days. The positive results, which can be determined by the color change from purple to yellow of the Lauryl Tryptose Broth, were then transferred using a sterile transfer loop to a MPN tube containing EC Medium and a Durham tube. The Durham tubes were used in order to examine the gas production in the test tubes after one day in a warm water bath. Calculations were then based off of the Standard Methods table (U.S. EPA, 2006).

RESULTS AND DISCUSSION:

The hypothesis of this experiment was that polymer addition affected bacterial regrowth in biosolids. It was expected that there would be higher bacterial densities in biosolids treated with old polymer compared to those treated with new polymer and the control samples used in the experiment. It also was expected that incubation of the biosolids would also increase the bacterial density in the sludge.

The results of the experiment can be found in Figure 2. The MPN values of the samples of biosolids at their various days of incubation were plotted using a bar graph to allow for visual comparison. As expected it can be seen that the MPN in all of the samples increased with incubation. Yet, the differences between the control, the new polymer, and the old polymer samples, were not what they were hypothesized to be. While initially (no incubation), the old polymer sample had a slightly higher MPN than both the control and new polymer samples, after just one day of incubation the control had a higher MPN than both the new and old polymer. This was also the case for two days of incubation. However these differences were not significant and the error bars on the graph account for the differences between the samples. Given these results it could be suggested that polymer does not have an effect on bacterial regrowth in anaerobically digested biosolids.

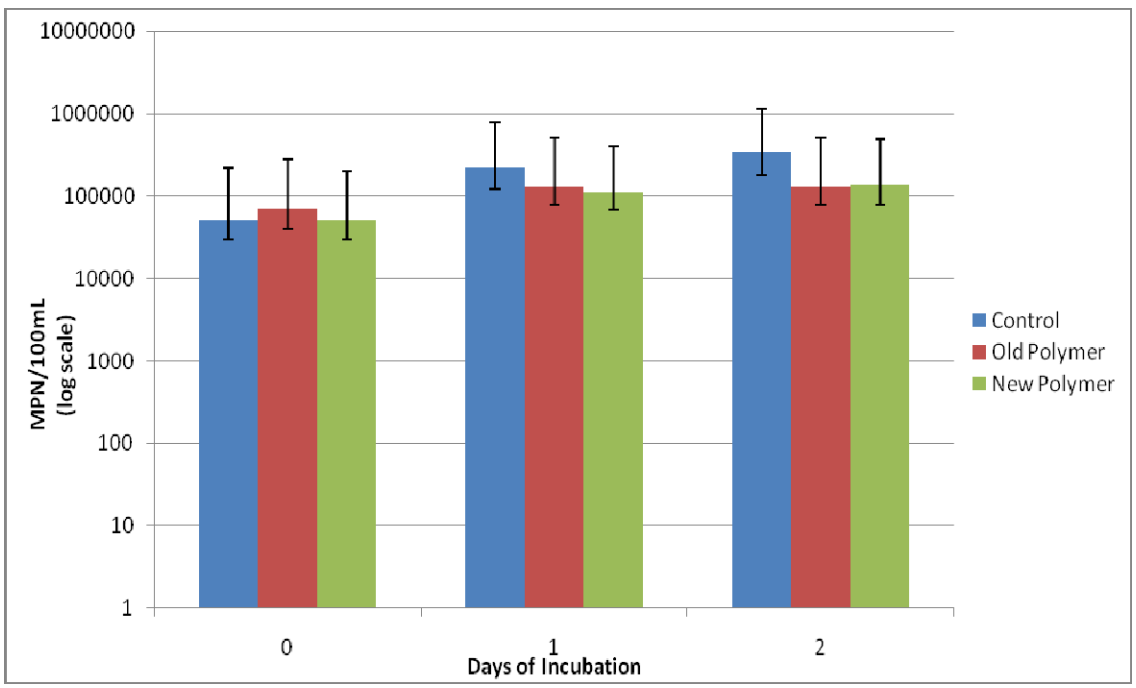

Figure 2. Represents the MPN/100mL of fecal coliform bacteria in anaerobically digested biosolids at various days of incubation. The error bars represent the 95% confidence interval

A study in which it is shown that polymer may contribute significantly to bacterial regrowth is the study done by Qi et al. In this study it was suggested that a higher polymer dosage led to an increase in the number of fecal coliforms and therefore a larger MPN value (Qi et al., 2007). In that study a weight ratio of 1:100 and 1:10 were experimented with (Qi et al., 2007). In the biosolids treated with a 1:10 ratio of polymer, a significant increase of two orders of magnitude in the MPN value was found. There was also a slight increase in MPN in the biosolids treated with the ratio of 1:100. It is also important to note that in the Qi et al. study, the treated biosolids were incubated at 37°C versus the room temperature in which the biosolids were incubated at in this experiment. The increase in temperature would allow for the bacteria to grow more quickly as it is a temperature in which they tend to thrive.

The main problem with this study is that while it shows a significant increase in biosolids treated at a 1:10 ratio, these biosolids are overdosed with polymer. Polymer overdosing can lead to an increase in the bound water content of the biosolids (Wu et al., 1997). Treating biosolids with excess amounts of polymer can also lead to a significant increase in the diameter of a conditioned sludge floc as well as a decrease in floc density (Wu et al., 1997). This is because when biosolids are overdosed with polymer, the flocs of bacteria that have been formed can actually separate back into single cells (Wu et al., 1997). It is therefore possible that overdosing with polymer can lead to an observed increase in the MPN values of the biosolids. This is because more bacteria cells are available to culture in the MPN media.

In this experiment a ratio of 1:184 was used to treat the biosolids, which is around the typical dosage used in conditioning. As stated previously, no significant increases in the biosolids treated with polymer both before and after incubation were shown. This suggests that polymer is not being used as a food source for bacterial regrowth. It would also suggest that the results of the Qi et al. study were the result of polymer overdosing, in which the bacterial cells were separated from their flocs to individual cells, rather than polymer being used as a food source for the bacteria. This would then serve to explain the difference in MPN values observed in the treated biosolids of that study.

In this experiment it was also found that after incubation the control had higher MPN values though these increases were not significant. This is most likely because polymer is a coagulant and as previously mentioned causes bacteria to form flocs. In the control samples no polymer was added and therefore the bacteria did not form flocs and showed higher MPN values as the bacteria cells were more readily available like they are in biosolids that have been overdosed with polymer. Running the experiment again could be useful to verify these results and see if the controls have higher MPN values than the treated samples or if once again the results are insignificant. Performing the experiment again would also help to verify the results that polymer does not contribute to the regrowth of bacteria.

Further research should be done to verify these results aside from the possibility of running the experiment again. A Bushnell-Haas test on a pure culture could be done to see if fecal coliform can grow on polymer. Comparing their growth on polymer to their growth on a known carbon source such as Dextrose would allow for another observation on whether or not polymer can be used as a possible food source for the bacteria. Further research could also be done in order to examine the possible effects that treating biosolids with excess polymer may have. In order to do this the same type of experimental procedure could be used though various polymer dosages should be tested in the samples rather than the old and new polymer dosages which were done in this experiment.

CONCLUSION

From the results of this seed project it can not be said that the addition of polymer increases the number of fecal coliforms present in anaerobically digested biosolids. The results of the experiment suggest that polymer does not have an effect on bacterial regrowth and that polymer is not used as a food source for bacteria in treated biosolids. However, further testing is required in order to verify these results. By performing the experiment again the results can be verified to make sure there was no error in the experimental procedure. Another type of test such as the Bushnell-Haas test can also be done in order to determine if polymer can be used as a food source for bacteria. Further research on the possible effects of polymer overdosing may also prove of interest by observing the effect that it has on the regrowth of bacteria in treated biosolids.

REFERENCES

U.S. Environmental Protection Agency (1994) *Land Application of Sewage Sludge;* EPA 831-B-93-002b.

U.S. Environmental Protection Agency (2003) *Environmental Regulations and Technology: Control of Pathogens and Vector Attraction in Sewage Sludge;* EPA 625-R-92-013.

U.S. Environmental Protection Agency (2006) *Method 1680: Fecal Coliforms in Sewage Sludge (Biosolids) by Multiple-Tube Fermentation using Lauryl Tryptose Broth (LTB) and EC Medium;* EPA 821-R-04-026.

Qi, Yinan, Dentel; Steven K.; Herson, Diane S. (2007). *Increases in fecal coliform bacteria resulting from centrifugal dewatering of digested biosolids.* Water Research. Vol 41. Issue 3; Elsevier, Amsterdam, Netherlands; 571-80.

Higgins, Matthew J.; Chen, Yen-Chih; Murthy, Sudhir N.; Hendrickson, Donald; Farrel, Joseph; Schafer, Perry. (2007). *Reactivation and growth of non-culturable indicator bacteria in anaerobically digested biosolids after centrifuge dewatering*. Water Research. Vol 41. Issue 3; Elsevier, Amsterdam, Netherlands; 665-73.

Wu, Chih Chao; Huanu, Chihpin; Lee, D.J. (1997). *Effects of polymer dosage on alum sludge dewatering characteristics and physical properties.* Colloids and Surfaces A:Physicochemical and Engineering Aspects. 122. Elsevier, Amsterdam, Netherlands; 89-96.

Chen, Y; Higgins, M.J.; Beightol, S.M.; Araujo, G.C.; Murthy, S.N.; Barben, E.J.; Toffey, W.E. (2007). *Odour Generation and Pathogen Indicator Regrowth after Dewatering: Are The Related?*. Proceedings of The IWA Moving Forward Wastewater Biosolids Sustainability: Technical, Managerial and Public Synergy Conference. Moncton, Canada.

EFFECT OF ACID MINE DRAINAGE ON ALUMINUM RELEASE FROM CLAY MINERALS

Oscar Vazquez, Student Member

Civil and Environmental Engineering Department, University of Pittsburgh, Pittsburgh, PA, ocv1+@pitt.edu

ABSTRACT

Aluminum is an environmentally toxic material found in some acid mine drainage (AMD) locations. Data reported from over 150 different mine drainage samples across USA showed that over 30% of these locations presented minimum dissolved aluminum concentrations of 50 mg/L, elucidating that aluminum pollution must be taken seriously. Research underway at the University of Pittsburgh involves an AMD site where a former trout fishery stream has been ruined. The evolution of the aluminum in this AMD, released from a subsurface environment, suggested a first stage dominated by first order kinetics of exchange reactions on clay surfaces, followed by a second stage dominated by dissolution processes with lower rates that exist over a long term. Results from a batch experiment involving synthetic AMD and kaolin minerals were in concordance with this analysis.

Further research, taking into consideration factors such as pH, AMD characteristics, type of clay minerals and retention time, is necessary in order to better understand the effect of AMD on the aluminum release from clay minerals. Such understanding is necessary for prediction of short-term and long-term impacts of AMD on aquatic ecosystems and will assist in the design and selection of treatment systems leading to practical remediation strategies.

INTRODUCTION

Aluminum is an environmentally toxic material found in some acid mine drainage (AMD) locations. Data reported from over 150 different mine drainage samples across USA showed that over 30% of these locations presented minimum dissolved aluminum concentrations of 50 mg/L (Watzlaf, 2004). Aluminum is typically found in AMD when the underground geology is characterized by the presence of clay and other aluminum bearing minerals. The problem is aggravated at low pH values, as reported by Cravotta (2006), who showed the median aluminum concentrations in mine discharge samples from 140 abandoned coal mines collected

in Pennsylvania in summer and fall 1999. Over 50% of the 140 abandoned mine discharges sampled presented median dissolved aluminum concentrations over 1 mg/L. The highest concentrations of aluminum were found in the acidic range of pH 2-5 with values between 1-50 mg/L of aluminum.

Elevated aluminum levels in AMD often occur when subsurface soils contain high concentrations of aluminum. Typical of such soils include clays containing the mineral kaolinite [$Al_2Si_2O_5(OH)_4$] (Smoke, 2007; Sidenko et al, 2005). Galan et al (1999) showed that kaolinite could be a possible reaction product of the dissolution of unstable smectite under acidic conditions. Smectite [$(Ca, Na, H)(Al, Mg, Fe, Zn)_2(Si, Al)_4O_{10}(OH)_2 - xH_2O$] is another clay mineral present worldwide, particularly extended in the northern hemisphere and commonly found in US soils (Astudillo, 2004). The Appalachian region including Pennsylvania and West Virginia historically support high mining activities and have elevated potentials for the generation of AMD with high concentrations of aluminum due to the abundance of smectite, and possibly other clay minerals.

In the scenario of AMD generation, when the oxidation of pyrite takes place in a location with a high presence of alumino-silicate materials (clays) and under strong acidic conditions (pH<5), the release of aluminum may typically be caused by ion-exchange (Tan, 2000) and dissolution of clay processes (Essington, 2004).

The purpose of this study was to explore the interactions between AMD and clay minerals under conditions typically found in the Pennsylvanian and Appalachian region. The study was focused on the effect of AMD cations including iron, Fe, and brackish groundwater with sodium, Na^+, and potassium, K^+, salts on the release of aluminum, Al, from clay minerals. In order to accomplish this goal the following objectives were set forth: (1) evaluate the evolution of aluminum in AMD released from aluminum-bearing soils after interaction with AMD; (2) explore the effect of synthetic AMD, including iron and sodium and potassium salts on the release of aluminum from clay minerals.

METHODS AND MATERIALS

The following tasks were performed to accomplish these goals: (1) analysis of the field data from an actual case of AMD pollution; (2) batch experiments to explore the effect of synthetic AMD on the release of aluminum from clay minerals.

A previous study at the University of Pittsburgh (Smoke, 2007), reported low concentrations of dissolved iron, high concentrations of dissolved aluminum and minimal concentrations of particulate aluminum in AMD affecting the Jonathan Run stream in Centre County, PA. Field data from this AMD discharge, which was sampled and tested from 1999-2008 (Hedin, 2003; GAI, 2007; Neufeld et al, 2007), was collected and further analyzed.

Two different weights of kaolin samples, $Al_2Si_2O_5(OH)_4$, (2 g and 16 g) were shook for a 67-hour period with a prepared pH 2.6 solution and two synthetic AMD solutions with different characteristics (Table 1) and further analyzed. The kaolin powder sample used to conduct this experiment was supplied by Fisher Scientific Company. $FeSO_4$ $7H_2O$ and H_2SO_4, also supplied by Fisher Scientific Company, were used to prepare the synthetic AMD solutions. KCl and NaCl used to prepare the synthetic AMD 2 solution were supplied by Mallinchrod. The suspensions were shaken for 67 hours and then centrifuged. The pH was determined before filtration by using a pH meter. Afterwards the centrifuged samples were filtrated through 0.45 µm nitrocellulose membrane filters supplied by Millipore Corporation and the extracts were stored at 4°C for further analysis. Standard Methods (2005) was used to determine the concentrations of Al, Fe, K^+ and Na^+. The concentrations of Al, Fe, K^+ and Na^+ were determined by flame atomic absorption spectrometry.

RESULTS

Data showing the aluminum concentration from the major surface seep polluting the Jonathan Run stream in Centre County, PA, from 1999 to 2008, is shown on Figure 1. The values represented in this figure are quarterly aluminum averaged values. The data appear to follow two different trends from 1999-2003 and from 2003-2008. The averaged aluminum concentrations released from the main source of pollution, as shown in Table 2, were 104.6 mg/L and 47.6 mg/L for the stages 1999-2003 and 2003-2008, respectively, with the second stage reaching and apparent steady state of about 48 mg/L. The field pH values averaged 4.1 and 3.5, as shown in Table 2, for the stages 1999-2003 and 2003-2008, respectively, and were rather consistent in each period, as shown in Figure 2.

The results of the release of aluminum from the kaolin mineral when exposed to solutions with different characteristics for a 67-hour period are shown in Table 1. The release of aluminum from the clay mineral, when exposed to an acid solution (pH 2.6), was not detectable. Conversely, when the clay mineral was exposed to synthetic AMD 1 with Fe concentrations over 600 mg/L, the release of aluminum was significant, reaching 6.3 mg/L when the soil(g):solution(ml) ratio was 16:40. The release of aluminum from the clay mineral increased up to 12.2 mg/L when the soil (g): solution (ml) ratio was 16:40 and the solution (AMD2) contained K^+ and Na^+. The initial iron concentration in AMD 1 was 660 mg/L, as shown in Table 1. After 67 hours of interaction with the clay mineral, a decrease in the iron concentration was observed; 555 mg/L and 335 mg/L for the 2:40 and 16:40 suspensions (susp.), respectively. In a similar way, the initial K^+ concentration in AMD 2 was 600 mg/L. After 67 hours of interaction with the clay mineral, a decrease in the K^+ concentration was observed; 400 mg/L and 400 mg/L for the 2:40 and 16:40 susp., respectively. The concentrations of Na^+ in the soil solution remained constant, 1000 mg/L, as shown in Table 1.

Table 1. pH, Al, Fe, Na^+ and K^+ concentrations in the initial synthetic AMD and pH 2.6 solutions and in the soil solution after 67 hours of experiment.

	pH	Al(mg/L)	Fe (mg/L)	Na^+ (mg/L)	K^+ (mg/L)
pH 6 solution	2.6	[1]N.D.	N.D.	N.D.	N.D.
AMD 1	2.6	N.D.	660	N.D.	N.D.
AMD 2	2.6	N.D.	630	1000	600
pH6 Susp. (2g:40ml)	3.2	N.D.	N.D.	N.D.	N.D.
pH6 Susp. (16g:40ml)	3.2	N.D.	N.D.	N.D.	N.D.
AMD1 Susp. (2g:40ml)	3.3	3.5	555	N.D.	N.D.
AMD1 Susp. (16g:40ml)	3.0	6.3	335	N.D.	N.D.
AMD 2 Susp. (2g:40ml)	3.4	4.5	565	1000	400
AMD 2 Susp. (16 g:40ml)	3.3	12.2	420	1000	400

[1]N.D. Non Detectable

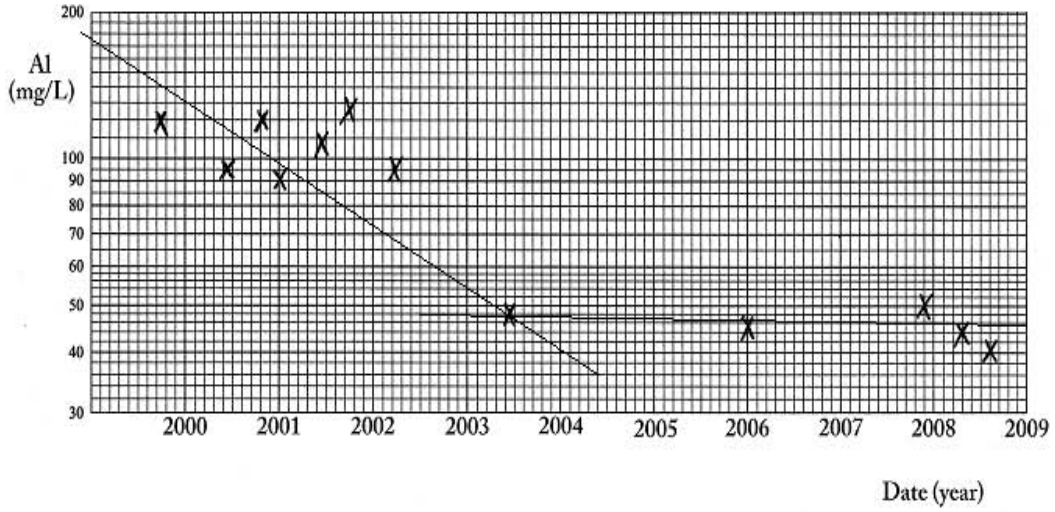

Figure 1. Evolution of aluminum released from the main source polluting the Jonathan Run Stream, Centre County, PA (1999-2008). Data from Hedin (2003), GAI (2007) and Neufeld et al (2007).

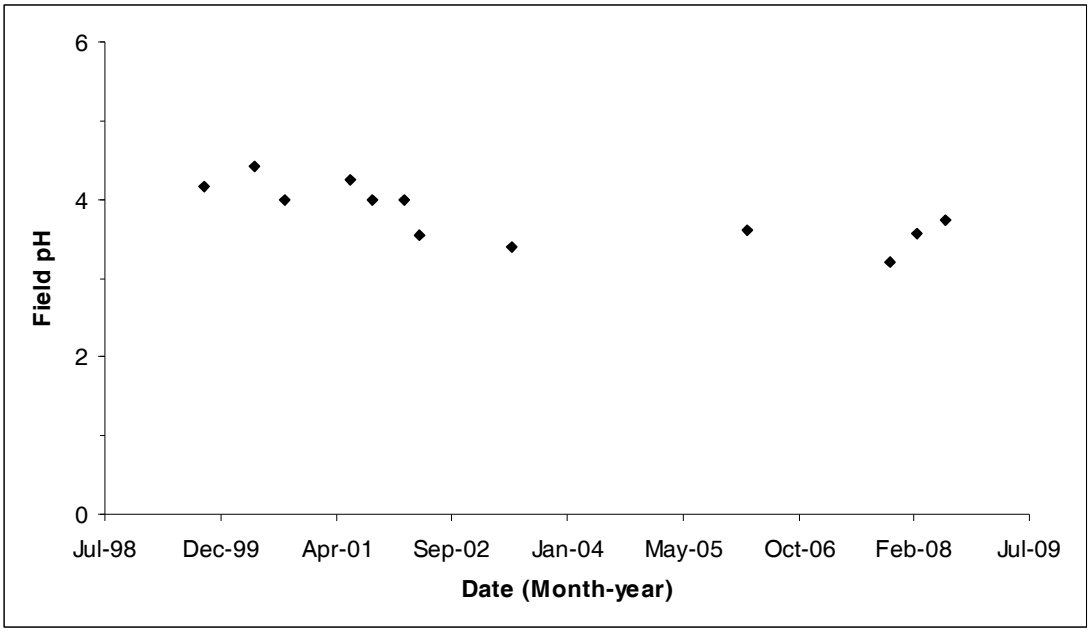

Figure 2. Evolution of field pH from the main source polluting the Jonathan Run Stream, Centre County, PA (1999-2008). Data from Hedin (2003), GAI (2007) and Neufeld et al (2007).

Table 2. Average values for Field pH and aluminum concentrations from the main source polluting the Jonathan Run Stream, Centre County, PA. Periods 1999-2003 and 2003-2008.

	Field pH	pH Sd. Dev.	Al (mg/L)	Al Sd. Dev.
Period 1999-2003	4.1	0.4	104.6	28.9
Period 2003-2008	3.5	0.3	47.6	6.4

DISCUSSION

The dissolution reaction rates of clay minerals are generally slow in contrast to the exchange reactions rates which are typically fast (Li, 2006). Huertas (1999) studied the proton-promoted dissolution kinetics of kaolinite using batch reactors at 25°C in the pH range 1-13. In his experiment, 80 mg of kaolinite and 40 ml of solution were placed in continuously shaken reaction vessels to maintain the solid phase in suspension. At pH 3, after more than 400 days of experiment, the concentration of aluminum released from the clay mineral was below 35 μM. This slow rate of release of aluminum seems to follow a similar pattern to the second stage illustrated in Figure 1, which appear to follow a zero order rate expression once the aqueous aluminum concentration reached an apparent steady-state of about 48 mg/L in the field. Likewise, the first stage of aluminum release shown in Figure 1 may be approximated by a first order differential equation:

$$d[Al]/dt = - 0.29\ [Al]$$

where [Al] = aluminum concentration (mg/L) and
t = time (years)

These results suggest that an early stage of aluminum release could be dominated by exchange reaction processes with high rates of aluminum release appearing to be first order with time, and a second stage of aluminum release dominated by longer term dissolution processes, with lower rates of aluminum release.

The results from the batch experiments involving synthetic AMD and kaolin minerals seemed to be in concordance with the analysis of the field data from the actual case of AMD pollution. The release of aluminum from the kaolin mineral, when exposed to the acidic solution (pH 2.6), was slow (not detectable) if compared with the release of aluminum when exposed to the synthetic AMD, with iron concentrations of about 600 mg/L, at the same pH value of 2.6 (Table 1). The release of aluminum from the clay mineral seemed to be influenced by the content of iron and potassium cations in the synthetic AMD. The decreases in K^+ and Fe concentrations in the soil solution after a 67-hour period were a common feature. This was presumable due to adsorption and/or cation exchange between the solutions and the kaolin mineral. The potassium concentration in the soil solution decreased over 30% after the 67-hour period. Despite of this change, the potassium remained constant with the

soil(g):solution(ml) ratio and thus seemed not to play a role in the change of aluminum release when changing the soil(g):solution(ml) ratio. Sodium ions seemed not to cause any effect on the aluminum release within the experimental conditions. The sodium concentrations remained constant, 1000 mg/L throughout the experiment. The adsorption and exchange behavior of the alkali metals in soils and other exchange media is strongly a function of their hydrated radii, according to the selectivity rule for the same valence cations. This resulted in K^+ being retained in preference to Na^+. The ratio of soil (g): solution (ml) seemed to play a significant role in the release of aluminum from the clay. The results suggested that the aluminum released increased with increasing the amount of kaolin in the solution.

CONCLUSIONS

When a clay mineral interacted with a synthetic AMD, it influenced the chemical composition of the synthetic AMD. Processes such as ion exchange, adsorption, hydrolysis and dissolution took place. The release of aluminum from the clay mineral when exposed to an acidic solution (pH 2.6) was not detectable after 67 hours of experiment but when the clay mineral was exposed to synthetic AMD solutions, with iron and potassium concentrations in equivalent conditions of pH (around 2.6), the release of aluminum became significant. Although the results of this experiment may differ in the magnitude of the impacts that would occur in the field environment, qualitatively, they seem to be in concordance with the evolution of the aluminum concentrations, as shown in Figure 1, for an actual case of pollution of a stream by aluminum-containing AMD. These results suggested that two types of processes, cation exchange and dissolution processes, may take place when AMD meets an argillic area. In order to better understand the effect of AMD on the aluminum release from clay minerals and the resulting AMD characteristics, further research taking into consideration factors such as pH and content of AMD, type and amounts of aluminum bearing minerals and retention time, need to be conducted . Such understanding is necessary for prediction of short-term and long-term impacts of AMD on aquatic and terrestrial ecosystems and will assist in the design and selection of treatment systems leading to practical remediation systems and ultimately, to a better management of AMD in locations where the underground geology, due to the presence of clay and another aluminum bearing minerals, is right for the in-situ generation of aluminum discharges.

REFERENCES

Astudillo, M.R. 2004. Mecanismo y velocidad de dissolution de la Montmorillonita en soluciones de electrolitos inertes. Influencia del pH y de la Temperatura. PhD Dissertation. Universidad de Granada. Facultad de Ciencias.

Cravotta, C.A. 2006. Relations among pH, sulfate, and metals concentrations in anthracite and bituminous coal-mine discharges, Pennsylvania. International Conference of Acid Rock Drainage, St. Louis, MO.

Essington, M.E. 2004. Soil and Water Chemistry. CRC Press, Boca Raton, FL.

Galan et al. 1999. Effects of acid mine drainage on clay minerals suspended in the Tinto River (Rio Tinto, Spain). An experimental approach. Clay minerals 34, 99-108.

GAI Consultants. 2007. Jonathan Run Acid Rock Discharge Mitigation Strategies. Prepared for Pennsylvania Department of Transportation. Research Division.

Hedin Environmental. 2003. Assessment of Pollution Sources to the Headwaters of Jonathan Run and Recommended Remediation Actions. Prepared for the Beech Creek Watershed Association.

Huertas, J. 1999. Mechanism of kaolinite dissolution at room temperature and pressure. Part II: kinetic study. Geochimica et Cosmochimica Acta, Vol.63, No. 19/20, pp. 3261-3275.

Li, J. 2006. Mechanism of aluminum release from variable charge soils induced by low-molecular-weight organic acids: Kinetic study. Geochimica et Cosmochimica Acta 70, 2755-2764.

Neufeld, R. D., Gray, T., Monnell, J., Smoke, J. 2007. "Jonathan Run Acid Rock Discharge Mitigation Strategies" FHWA-PA-2007-010-04011 March, 2007 (available from NTIS as PB2007-107284) 134 pages.

Sidenko et al. 2005. Characterization of Aluminu-Rich Phases in Heap-Leach Pads at the Landusky Gold Mine, Montana, USA. The Canadian Mineralogist, 43, pp. 1157-1170.

Smoke, J.D. 2007. Preliminary design of a treatment system to remediate acid rock drainage into Jonathan Run. M.S.Thesis, Department of Civil and Environmental Engineering, University of Pittsburgh.

"Standard Methods for the Examination of Water and Wastewater". 2005. 21st Edition. APHA-AWWA-WPCF, Washington.

Tan, Kim H. 2000. Environmental Soil Science, 2nd edition. Marcel Dekker, Inc, New York, pp: 187-191.

Watzlaf, G.R. et al. 2004. The passive treatment of Coal Mine Drainage. DOE/NETL-2004/1202.

SENSITIVITY ANALYSIS OF HEC-HMS HYDROLOGIC MODEL TO THE NUMBER OF SUB-BASINS: CASE STUDY

Osama Z. Al-Hamdan, Student Member

Graduate Student, Civil and Environmental Engineering Department, University of Alabama in Huntsville, Huntsville, AL, alo@uah.edu

ABSTRACT

This paper presents a sensitivity analysis of the hydrologic model HEC-HMS to the number of sub-basins for the McDonald Creek watershed in Huntsville, Alabama. ArcGIS was used to estimate the parameters needed for the model. The sensitivity analysis of HEC-HMS runoff results was evaluated for two cases, namely, Case 1 and Case 2. The number of sub-basins of the watershed was 3 and 5 for Case 1 and 2, respectively. This study implements kinematic wave method to model the overland flow transform and Muskingum-Cunge method for channel routing. The loss rate was estimated using both Green-Ampt and SCS curve number methods. The results demonstrated that the number of sub-basins did not significantly affect the discharge results. However, increasing the number of sub-basins changed the discharge peak values. The results also showed that HEC-HMS model was sensitive to the input slope parameter when the SCS method was used, while it was not in case of using the Green-Ampt method.

INTRODUCTION

Watershed models have become an essential tool for water resources planning, development, and management (Singh and Woolhiser, 2002). There are several well known watershed models in current use in the United States and one of these models is the Hydraulic Engineering Center Hydrologic Modeling System (HEC-HMS). HEC-HMS is considered the standard model in the private sector in the United States for the design of drainage systems and quantifying the effect of land use change on flooding (Singh and Woolhiser, 2002).

HEC-HMS was developed by the U.S. Army Corps of Engineers for rainfall-runoff simulation processes of networking watershed systems. HEC-HMS consists of meteorological, hydrologic and hydraulic functional components, including losses, runoff transform, open-channel routing, analysis of meteorological data, rainfall-runoff simulation, and parameter estimation. In order to estimate the runoff and basin

outflow, the hydrologic elements of HEC-HMS, including sub-basins, reaches, junctions, reservoirs, diversions, sources, and sinks are connected in a network. HEC-HMS utilizes several methods for transforming excess precipitation into surface runoff such as unit hydrograph and the kinematic wave method with multiple planes and channels. The runoff computation in HEC-HMS proceeds from upstream elements in a downstream direction. For infiltration losses simulations, HEC-HMS utilizes several methods including the initial constant, Soil Conservation Service (SCS) curve number, and Green-Ampt. For more details about the model, see U.S. Army Corps of Engineers HEC-HMS user's manual (2005).

In HEC-HMS, the watershed can be represented in hydrologic elements. These elements are used to break the watershed into manageable pieces that are connected together in a network to form a representation of a stream system. By creating multiple representations of the same watershed, different development scenarios or management alternatives can be evaluated. Hence, HEC-HMS simulation results could be sensitive to the number of sub-basins that assemble the representations as the sub-basin hydrologic parameters might vary in each representation. Therefore, this paper studies the effect of number of sub-basins on the outflow discharge by using two different representations of a watershed.

METHODOLOGY

The study area belongs to the watershed of McDonald Creek in Huntsville, Alabama. The drainage basin area is 2.16 square mile and consists of a second order main stream. The drainage basin is mostly of urban type, covered sparsely with lawn-type vegetation. The average annual precipitation of the watershed is 57.5 inch.

In order to evaluate the sensitivity of HEC-HMS model to the number of sub-basins, the model was used to estimate the runoff discharge of McDonald Creek for two cases. The watershed was divided into 3 and 5 sub-basins for Case 1 and 2, respectively. In Case 1, the sub-basin areas are 0.937, 0.543, and 0.680 square mile for Sub-basin I, II, and III, respectively. In Case 2, the sub-basin areas are 0.301, 0.637, 0.246, 0.296 and 0.680 square mile for Sub-basin I, II, III, IV, and V, respectively. In both cases, the sub-basins were divided to two planes as seen in Figure 1. HEC-HMS simulation discharge results were studied at the exit of the watershed as well as at the conjunction point of sub-basins I and II for Case 1, and sub-basins I, II, III and IV for Case 2.

This study implements kinematic wave method to model the overland flow transform and Muskingum-Cunge method for channel routing. The loss rate was estimated using both Green-Ampt and SCS curve number methods with the assumption of no base flow. In order to study the sensitivity of the discharge results to the input watershed parameters, the model was also run for both cases for the following four conditions: (1) all parameters in Case 2 are different than the corresponding parameters in Case 1 (i.e., smaller planes in Case 2 than in Case 1); (2) all parameters in Case 2 are same as the corresponding parameters in Case 1 except for the slope; (3) all parameters in Case 2 are same as the corresponding parameters in Case 1 except

for the imperviousness; and (4) all parameters in Case 2 are same as the corresponding parameters in Case 1 except for the soil type. The discharge results of Case 1 and 2 were statistically compared for all four conditions.

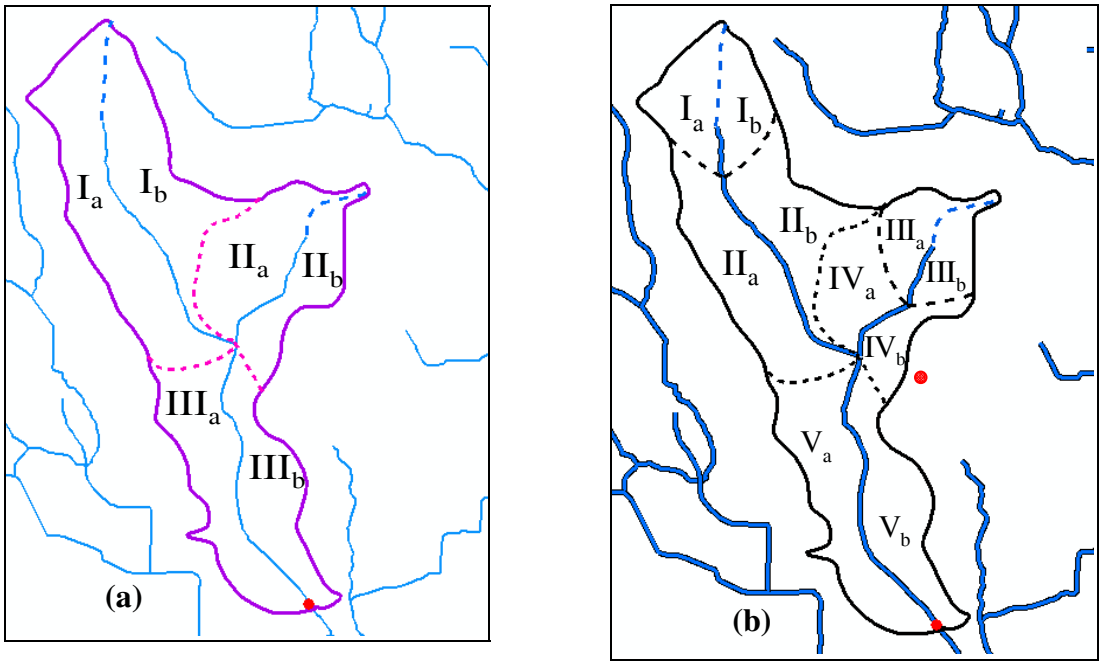

Figure 1. McDonald Creek watershed: (a) Case 1 (b) Case 2.

Data Collection

In order to determine the runoff discharges using HEC-HMS, the model requires different types of watershed data, such as precipitation, soil type, topography, and land cover. The rainfall hyetograph used in this study is depicted in Figure 2 (USGS, 2005). The topographical data were obtained from the digital elevation model (DEM) files downloaded from the US Geological Survey website (USGS, 2004). The soil types of the watershed were obtained from the Soil Survey Geographic (SSURGO) database of the National Resources Conservation Service (NRCS) (NRCS, 2004). The land cover data were obtained from the NRCS website (NRCS, 2004).

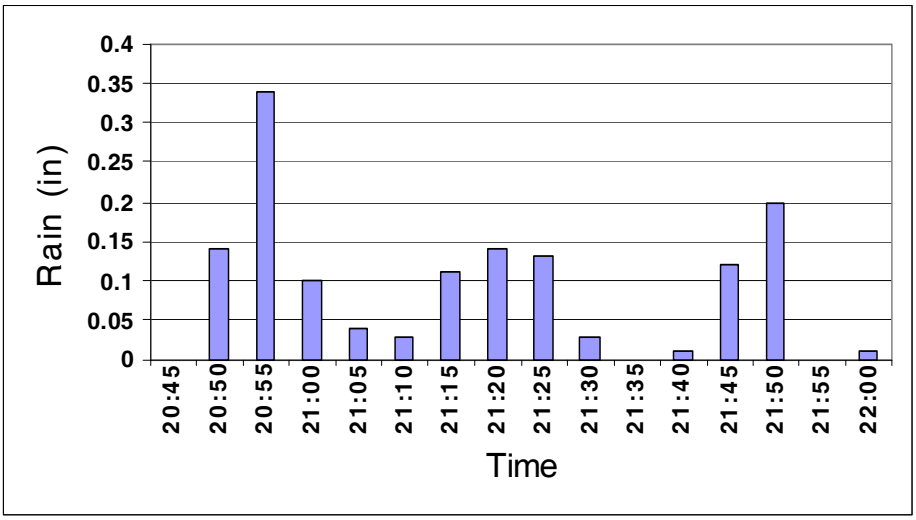

Figure 2. Hyetograph of the selected storm used in this study (USGS, 2005a).

The collected input data were then imported into ArcGIS software to estimate the parameters required for running the HEC-HMS model. The watershed was delineated using ArcGIS. The slopes of the watershed planes and streams were calculated using ArcGIS as seen in Figure 3a. The estimated physical properties data of McDonald Creek planes and streams are illustrated in Table 1 and 2, respectively. The soil properties (hydraulic conductivity and head suction), imperviousness, Manning's n values, and the land use SCS curve numbers were obtained from Chow (1959) and Chow et al. (1988) based on the SSURGO soil and land cove maps. The SSURGO map classifies the soil to more than 50 types. In this study, the soil types were simplified and classified based on the soil texture into eight major groups, namely, clay, clay loam, loam, loamy sand, sandy loam, silt loam, silty clay, and silty clay loam (Figure 3b). In order to determine the SCS curve number, the soil groups were categorized using ArcGIS into four SCS hydrologic soil groups as seen in Figure 4. The calculated soil properties data and the land use SCS curve numbers of the studied watershed are presented in Table 3. The values in Table 3 represent the weighted average properties of each plane. For calibration purposes, the Manning's n value of the planes was assumed to be 0.1.

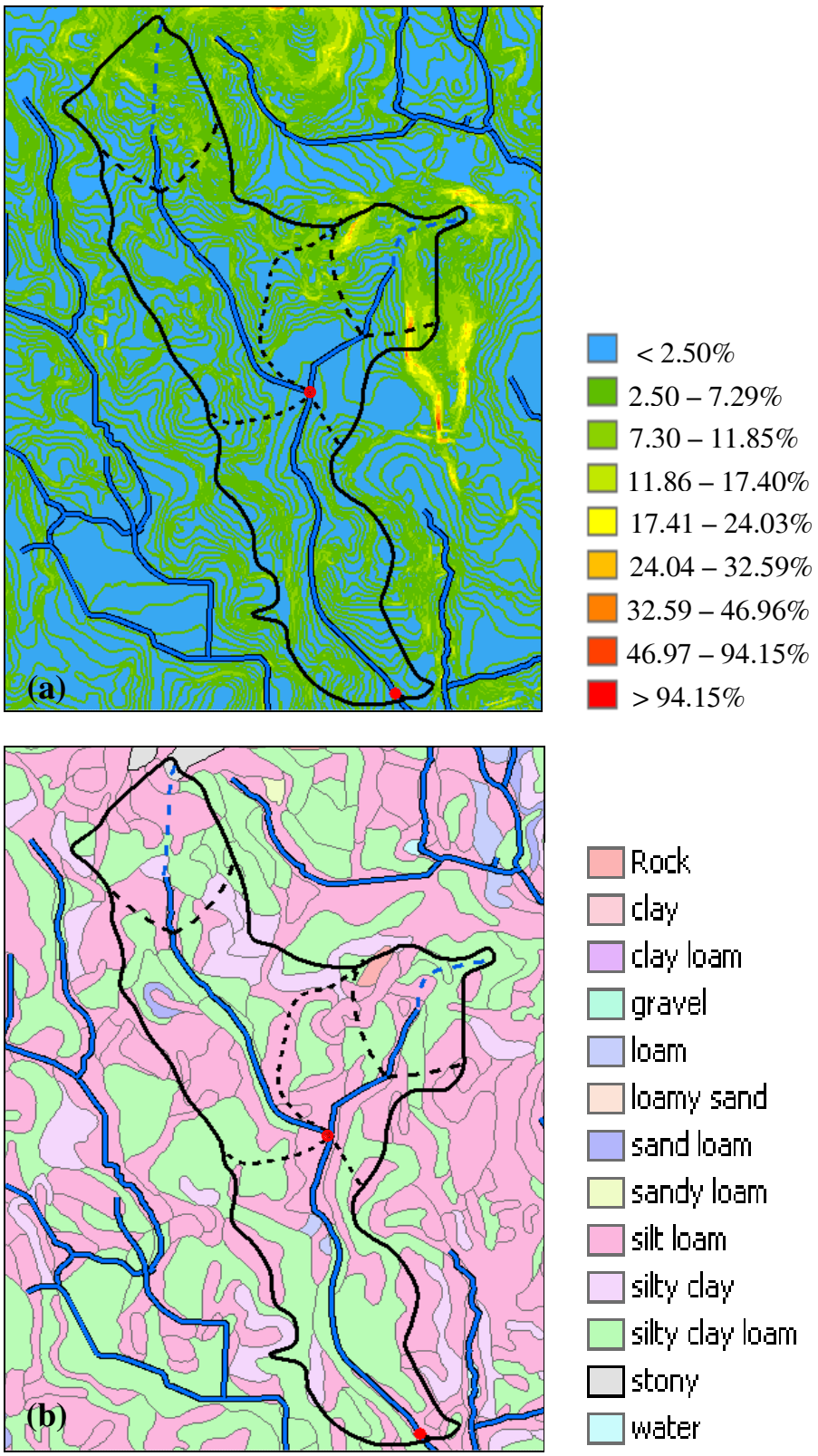

Figure 3. ArcGIS data (a) Plane slopes map (b) Soil texture map

Table 1. Physical Prosperities of the watershed planes.

Case No.	Sub-basin Number		Area (mi^2)	Plane Slope	Plane Length (ft)	Manning's n
1	I	a	0.5469	0.0244	1780	0.1
		b	0.3906	0.0373	2500	0.1
	II	a	0.3164	0.0391	2320	0.1
		b	0.2266	0.0402	1800	0.1
	III	a	0.3789	0.0283	1200	0.1
		b	0.3008	0.0273	2000	0.1
2	I	a	0.1680	0.0397	1780	0.1
		b	0.1328	0.0569	2500	0.1
	II	a	0.3789	0.0200	1780	0.1
		b	0.2578	0.0324	2500	0.1
	III	a	0.1289	0.0731	2320	0.1
		b	0.1172	0.0669	1800	0.1
	IV	a	0.1875	0.0255	2320	0.1
		b	0.1094	0.0231	1800	0.1
	V	a	0.3789	0.0283	1200	0.1
		b	0.3008	0.0273	2000	0.1

Table 2. Physical Properties of streams.

Case Number	Sub-basin Number	Stream width (ft)	Stream Length (ft)	Stream Slope	Manning's n
1	I	6	7750	0.0063	0.02
	II	6	3800	0.0086	0.02
	III	15	8200	0.0040	0.03
2	I	6	1370	0.0022	0.02
	II	6	6380	0.00048	0.02
	III	6	1760	0.0017	0.02
	IV	6	2040	0.00075	0.02
	V	15	8200	0.0040	0.03

Table 3. Soil Properties and SCS curve number data of the watershed.

Case No.	Sub- basin Number		Water Suction (in)	Hydraulic Conductivity (in/hr)	SCS Curve Number	Imperviousness (%)
1	I	a	8.055	0.183	83	37.5
		b	9.736	0.098	78.5	7.5
	II	a	8.941	0.1348	83.3	41.35
		b	8.657	0.148	88.4	51.75
	III	a	7.874	0.106	86.75	51
		b	9.285	0.115	83.53	34
2	I	a	8.44	0.162	79.85	22.5
		b	9.19	0.123	74.98	0
	II	a	7.68	0.204	85.15	45
		b	10.04	0.085	81.06	12.65
	III	a	8.96	0.134	81.95	29.25
		b	9.49	0.104	89.9	60.5
	IV	a	8.92	0.135	88.35	49
		b	7.82	0.191	85.45	34
	V	a	7.874	0.106	86.75	51
		b	9.285	0.115	83.53	34

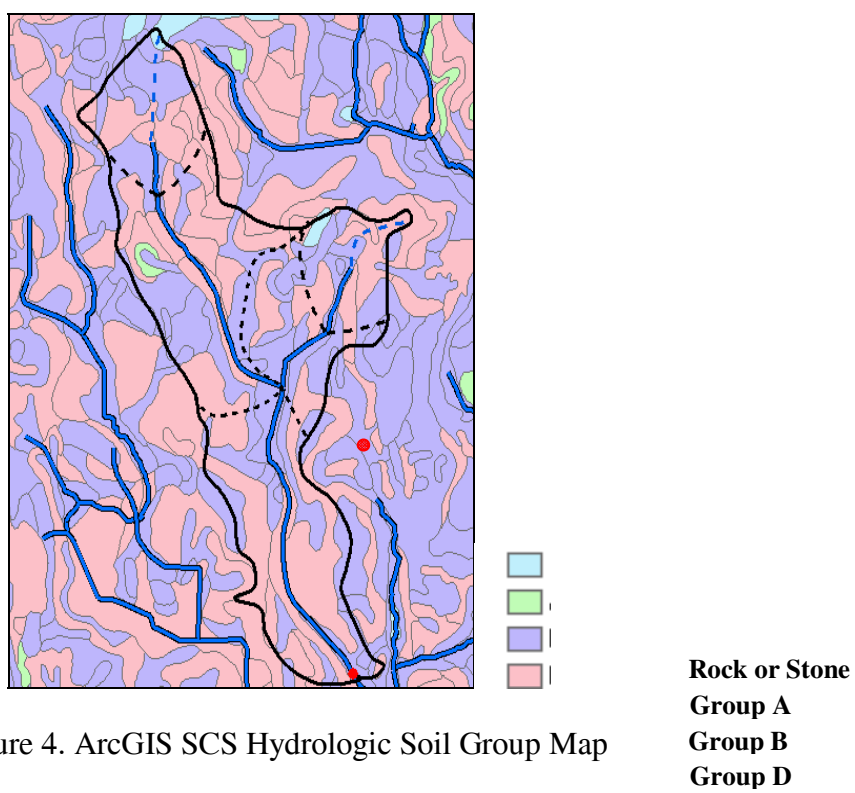

Figure 4. ArcGIS SCS Hydrologic Soil Group Map

RESULTS

The HEC-HMS discharge results of Case 1 and 2 for all conditions as described above were statistically compared using paired T-test. The analysis was also performed using two different methods for rate loss determinations, namely, Green-Ampt method and SCS method. The null hypothesis in the T-test is that the means of the modeled discharges are equal for both cases. The differences in peak discharge values, concentration times to the peak, and the total discharge volumes were also measured for each studied condition. The statistical analysis results are shown in Tables 4 and 5.

Table 4. P-value and differences of discharge results at the watershed exist and the conjunction point using Green-Ampt method.

Outflow point	Condition	P-value	Peak value Difference (%)	Difference in Time of peak (min)	Difference in Volume (%)
Watershed Exit	1	0.768	-4.5	0	-0.7
	2	0.858	-4.2	0	-0.4
	3	0.633	-0.4	0	-0.2
	4	0.856	-2.8	0	-0.4
Conjunction Point	1	0.758	-6.2	0	-1.0
	2	0.854	-5.6	0	-0.6
	3	0.636	-1.1	0	-0.3
	4	0.85	-3.4	0	-0.6

Table 5. P-value and differences of discharge results for at the watershed exit and conjunction point using SCS method.

Outflow point	Condition	P-value	Peak value Difference (%)	Difference in Time of peak (min)	Difference in Volume (%)
Watershed Exit	1	0.875	-5.9	+ 5	0.3
	2	0.912	-7.1	+5	-0.2
	3	0.072	0.3	0	0.6
Conjunction Point	1	0.872	-6.0	+ 5	0.5
	2	0.911	-8.0	+5	-0.3
	3	0.095	-1.6	0	-0.9

For all conditions at the watershed exit and conjunction point, the T-test results show that the null hypothesis with an α-level of 0.05 could not be rejected (i.e., p-value > 0.05). In other words, the means of the discharge values for Case 1 and 2 are likely the same. Moreover, the number of sub-basins does not significantly affect the discharge results. However, the number of sub-basins changed the discharge peak values in all conditions.

The results also demonstrate that the discharge peak difference increased from 4.5% at the watershed exit to 6.2% at the conjunction point. Also, the difference in the total discharge volume increased from 0.7% at the watershed exit to 1% at the conjunction point. The increase in these differences indicates that the effect of sub-basin number increase from 2 to 4 is higher than from 3 to 5 as Sub-basin III in Case 1 and Sub-basin V in Case 2 are identical.

In case of implementing the SCS method in HEC-HMS model, the results of the peak difference values and the difference in time of peak for condition 1 and 2 at the watershed exit and conjunction point are almost the same; indicating that that HEC-HMS model is more sensitive to the input slope parameter than the imperviousness when using the SCS method. While in case of implementing the Green-Ampt method in HEC-HMS model, the results show that the time of the peak did not change for all conditions; indicating that HEC-HMS is not likely sensitive to the slope parameter when using Green-Ampt method.

CONCLUSIONS

This study shows that ArcGIS facilitates the estimation of the parameters that needed for running the hydrologic model and makes it faster in creating representations of the same watershed in larger number of sub-basins. The results of this study demonstrate that the number of sub-basins did not significantly affect the discharge results. This study also shows that HEC-HMS model was sensitive to the input slope parameter when the SCS method was used, while it was not in case of using the Green-Ampt method.

REFERENCES

Chow, V.T. (1959). “Open channel flow.” McGraw-Hill, New York, NY.

Chow, V.T., Maidment D.R., and Mays, L.W. (1988). "Applied Hydrology." McGraw-Hill, New York, NY.

National Resources Conservation Service (NRCS) (2004). “The Soil Data Mart.” <http://soildatamart.nrcs.usda.gov> (Nov. 20, 2004).

Singh, V. P., and Woolhiser, D.A. (2002). “Mathematical modeling of watershed hydrology." *Journal of Hydrologic Engineering*, 7, 270-292.

U.S. Army Corps of Engineers, Hydrologic Engineering Center (HEC), “Hydrologic Modeling System, User’s Manual.” (2005). <http://www.hec.usace.army.mil/software/hec-hms/-documentation/CPD-74A_2005Dec.pdf> (Oct. 10, 2008).

US Geological Survey (USGS), (2004). Geographic Data Download, <http://edc.usgs.gov/geodata/> (Nov. 04, 2004).

US Geological Survey (USGS) (2005). “National Water Information System.”, NWIS Web Data for the Nation, <http://nwis.waterdata.usgs.gov/nwis> (Jul. 15, 2005).

STUDY OF LOW DOSAGE PRE-OZONATION ON SAND FILTRATION EFFICIENCY

Walter Lee Ellenburg, Student Member

Undergraduate Student, Civil and Environmental Engineering Department, University of Alabama in Huntsville, Huntsville, lee.ellenburg@uah.edu

ABSTRACT

The most traditional method for water filtration is the sand filter. Sand filters consist of sand, some type of activated carbon, and a more coarse aggregate such as gravel. Particles too large are then filtered out. Suspended particles too small for sand to catch are thus the problem, therefore different techniques are used to increase the efficiency of sand filters, these techniques are called pre-filtration. The goal of pre treatment is to coagulate, or clump together; the small suspended solids so that they may be caught in the filter. Current water treatment plants use many different types of pre-filtration: ferric, aluminum salts, or cationic polymers.

One form of pre-treatment is ozonation. By electrically charging oxygen and allowing a third molecule to join, ozone, (O_3), is created. Ozonation is the process of applying ozone to cause the small suspended particles in a given sample to coagulate. It has been studied and experimented for many years, proving a significant increase in coagulation and thus allowing the sand filtration to be more effective. As longer treatments of ozone are applied, the taste and odor may also be neutralized. In addition to the benefits previously stated, ozone may also be used as a disinfectant. In fact ozone oxidizes thousands times faster than that of chlorine. However, the production of ozone is somewhat energy intensive, and therefore an option that is sometimes over looked.

In this experiment, pre-ozonation will be examined in low dosages to see if the effects of coagulation are as beneficial as those exposed to longer periods of time. These smaller exposures would be more economical and a more realistic alternative for coagulation. If this hypothesis proves correct, the pre-treatment of ozone may be more appealing than other alternatives such as Alum and other chemical treatments which may stay longer in the water thus causing rising concerns in health related issues.

The result of this experiment proved that compared to previous tests with high amounts of ozone, small amounts of ozone will also reduce the suspended solids with time. The suspended solids were reduced by 1% with a five minute exposure and rapidly increased to a reduction of 7% over a 45 minute time period. From 45 minutes on the percent of decreased suspended solids slowly increased to 8%.

BACKGROUND

Direct filtration is a filtration process that treats direct surface runoff. This process usually includes the adding of a coagulant, rapid mixing, flocculation and filtration. Flocculation however, can usually be sidestepped. When the flocculation tank is omitted, it is usually called direct in line filtration, where the flocculation occurs in the filter itself. In the direct filtration process there is no need for sediment tanks, and it usually requires less chemical coagulant. These, among others, are key factors in the popularity of direct filtration. Direct filtration appears to be the most economical form of surface water filtration; however its inability to handle waters with high turbidity and operating challenges provides room for other filtration methods. The most common of these direct filtration methods are those using sand as the primary filter and therefore will be the direct filtration method used in this experiment. Larger aggregates and activated carbon will also be used as ingredients of the filter to best mimic the local Huntsville city water treatment system [Pontius, 1990].

Coagulation is the interaction of colloids and particulate with a destabilization agent. To agglomerate these particles and colloids is the central purpose for coagulation. These small particulates and colloids are also referred to as suspended solids. Suspended solids range in size and weight and can settle quite quickly, in a matter of hours or could take years. This bundling process is referred to as the destabilization of colloidal systems. These suspended solids usually have a maximum diameter of 10μm. Their rate of settling is usually no more than 10^{-2}cm/s [Faust, et al., 1982]. To achieve an increase the sedimentation of these suspended solids, a chemical coagulant is added. Ozone is one of many different types of coagulants used in water treatments. This process of pre-treating water with ozone before it is filtered is called Pre-Ozonation. Pre-Ozonation is a technique using Ozone, O_3, to cause the small suspended particles in the water sample to coagulate. Once these particles begin to coagulate, or bundle together, they begin to gain mass and surface area and therefore gain in sedimentation velocity and start to sink to the bottom of the container. Since direct in line filtration will be used in this experiment, the ability to sediment the particles is trivial. However, as the suspended particles begin to agglomerate; their surface area begins to increase, thus allowing more of the suspended solids to be filtered out [Gottschalk, et al., 2000].

When comparing a sample of ozonated water and un-treated filtered water, there should be a noticeable difference in the visible suspended solids and turbidity, along with the color and odor. This can be observed due to the oxidizing capability of ozone. Ozone is a gas that is unstable and therefore must be generated at the point of

use. Ozone can be created by a number of different methods. These methods include electrical, electrochemical, photochemical, thermal, and by radiation. The electrical discharge ozone generator is the most common used and will be used in this experiment. This process of generating ozone begins with first producing ionized molecular oxygen by applying high powered alternating current to oxygen. Ozone is then formed by the recombination of the ionized oxygen atoms and the unionized oxygen. Basically, the oxygen atom is charged and a third oxygen is combined then to create O_3, ozone. Differing amounts are capable of production depending on the air pressure and the pureness. The ozone generator used in this experiment produces 2.5 mg every 30 minutes.

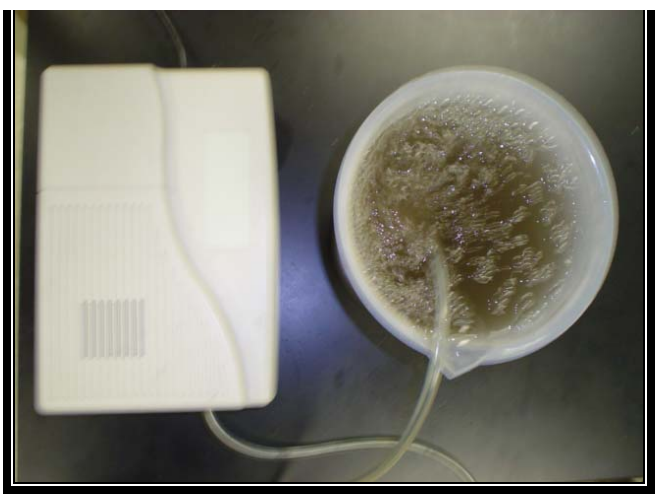

Figure1: Ozone generator
Source: Image taken by author

For this study, inline direct filtration was used to examine the effects of ozone as a coagulant aid in low dosages. Specifically, this experiment will compare several doses to examine how pre-ozonation affects coagulation. These smaller doses would be more economical and a more realistic alternative for chemical coagulation. Tests for suspended solids, TSS, will be conducted to determine the effectiveness of the proposed pre-filtration method [Faust, et al., 1982]

EXPERIMENTAL

In this experiment a simulated surface water model sample was prepared. The simulated water sample was mixed exactly the same for each experiment of differing ozone levels. The sample was created by mixing a commercially available composted cow manure, which is naturally high in organic matter, in water. It was mixed with de-ionized water at 150 grams per liter. The mixture was then mixed thoroughly and allowed to settle for two hours. Before filtration a small net was skimmed over the surface to remove large floating suspended solids to keep the filters from clogging. Once the surface water sample was allowed to settle, the control sample was then passed through the sand filter without any ozone exposure. Once the control was

established differing amounts of ozone were applied then filtered. First a small exposure of 5 minutes per 5 liter container was measured for a dosage of 1 mg/L. The next experiment conducted was an ozone exposure of 10 minutes for a 2 mg/L dose. Next increments of 15 minutes were test up to 45 minutes. Then one, two and three hours of exposure were tested. In each of these tests, TSS were conducted in accordance with standard methods for the examination of water and wastewater. Four different samples were taken from each sample before exposure and four after the ozone exposure to obtain a valid average analytical result for each parameter studied.

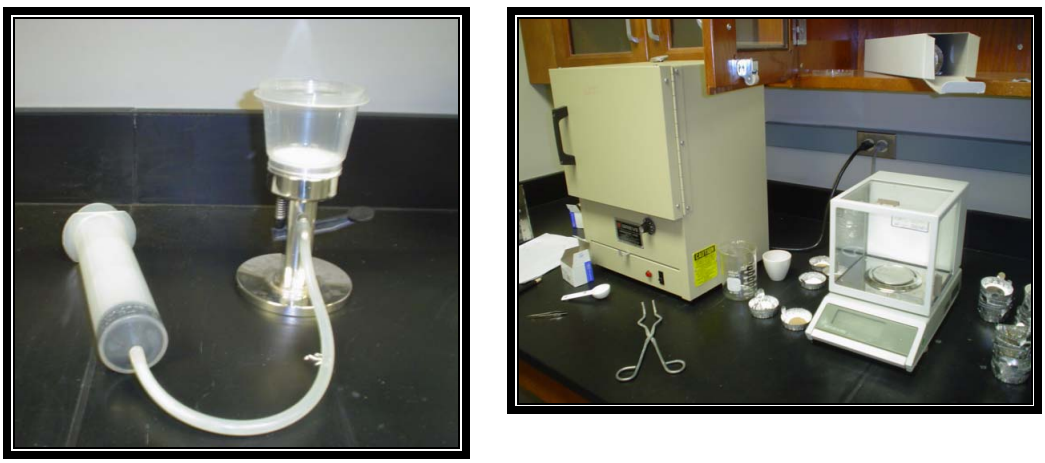

Figure 2: Suspended solids apparatus used (left); Oven and scale (right)
Source: Image taken by author.

The filter used was built to model the sand filtration water treatment plant currently used by the City of Huntsville. The laboratory sand column was built using a 4 inch diameter, 2 foot long, polyethylene tube with six holes drilled out of the bottom to allow for the water sample to percolate steadily through. The media consisted of a two inch (2") layer of large aggregate at the bottom, a two inch (2") layer of activated carbon and eighteen inches (18") of sand. The sand was obtained from the water treatment plant so that the experiment would be as realistic as possible. The sand was first washed and layered out to dry, then placed into the tubes on the larger rock and activated carbon layers. As designed, the water will first percolate though the sand, then the activated carbon, and finally though the large rocks, which is similar to the configuration at the actual plant.



Figure 3: Filtration apparatus Source: Image taken by author

DISCUSSION

The results of this experiment proved the initial hypothesis correct. Specifically, the amount of suspended solids in the sand filter effluent decreased with the amount of ozone applied as shown in Figure 4. However the decline was not linear and the results seem to hit a minimum increasing dosage.

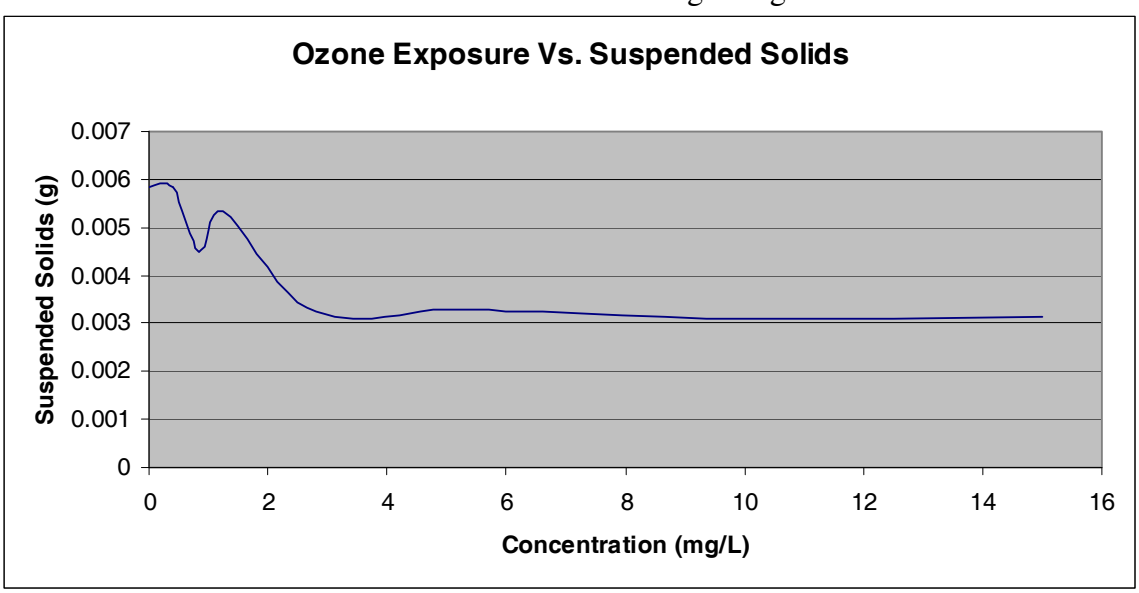

Figure 4: Ozone Exposure Vs. Suspended Solids

As one can clearly see the suspended solids dropped rapidly with the 1 mg/L dose. After 4 mg/L the suspended solids in the effluent remained relatively constant. When the percent of decrease of the suspended solids were analyzed a similar trend resulted, however the rapid increase occurred with the 0.83 mg/L dose. This data is the more accurate, since the percentage is considered. This trend can be seen below in

Figure 5.

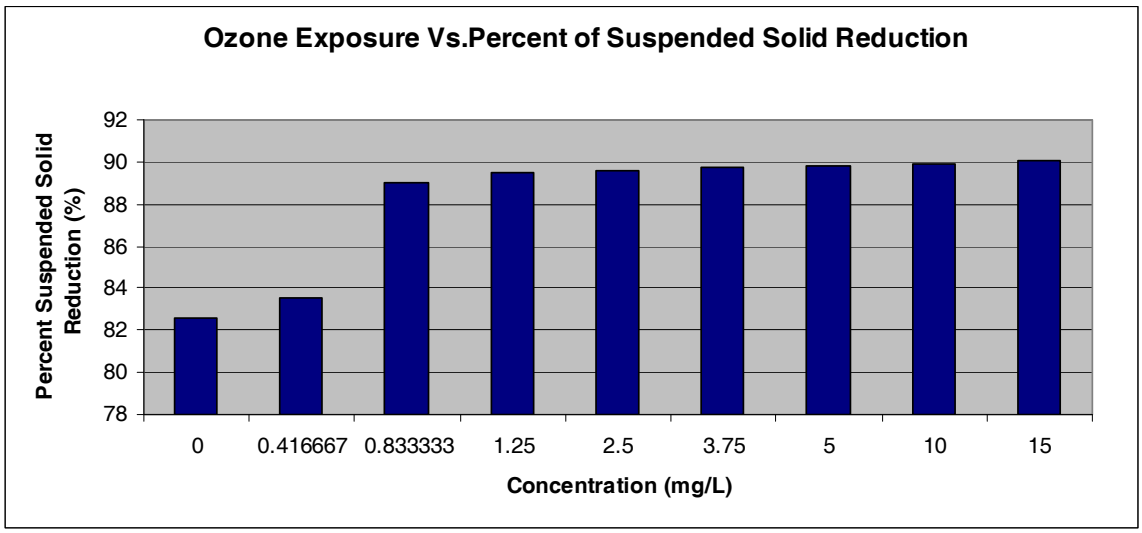

Figure 5: Ozone Exposure Vs. Percent of Suspended Solid Reduction

From simple visual observation, see Figure 6, one can see the reduction of suspended solids and the reduction in color. It was also noticed that the water became clearer throughout the experiment as the ozone concentrations increased. However, as the data suggest, it's only in the first few small concentrations of ozone that a significant reduction in suspended solids were measured. It is noted that sand filtration depends greatly on the type of surface water that is to be filtered. As stated previously, direct filtration cannot handle waters with high turbidity or color.

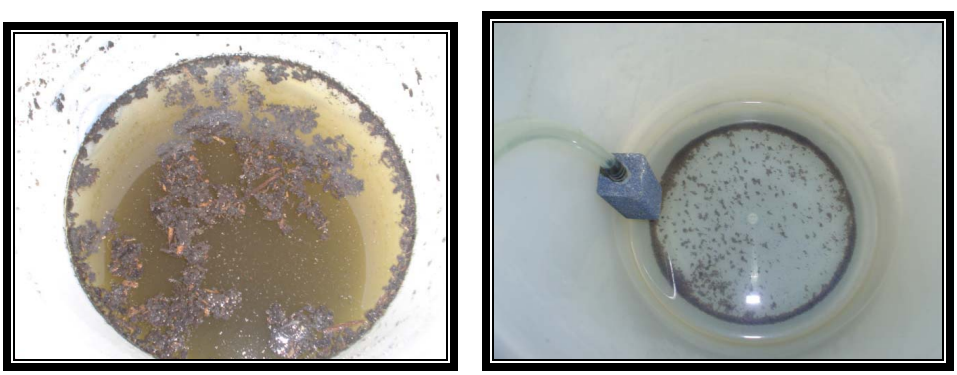

Figure 6: Before (left) and after (right) of Pre-Ozonation.

CONCLUSION

This experiment was successful in learning that small amount of ozone as a pre-treatment will reduce the suspended solids. The experiment analyzing the effects of low amounts of ozone exposure prior to sand filters resulted in a marked decrease in suspended solids. The best results occurred at approximately 0.83 to 1.0 mg/L dose. Higher doses did not seem to make any difference in this study. The maximum

reduction in suspended solids was 89 percent. The control sample of reduced suspended solids by simple filtration was 82 percent. Thus pre-ozonation removed over 7% of additional SS than the traditional sand filters.

It is recommended that further studies should be pursued to develop more exact results on optimizing ozone dosages. If turbidity were examined along with the suspended solids and compared, more conclusions could be made. Also, when this experiment was conducted small variations in the organic matter that simulated the surface water could have taken place. If the experiment used an actual surface sample and was conducted in a concentrated time, more accurate results may be obtained.

REFERENCES

Faust, Samuel D.; Aly, Osman M., Chemisty of Water Treatment, Butter Worths, 1983

Gottschalk, C., Libra, J.A., Saupe, A., Ozonation of Water and Waste Water, Wiley-vch, 1st Edition, 2000.

Pontius, Frederick W., Water Quality and Treatment, McGraw-Hill, 4th Edition, 1990.

THE DUBAI PALMS: CONSTRUCTION AND ENVIRONMENTAL CONSEQUENCES

Ethan Poole, Student Member

Undergraduate Student, University of Tennessee, Knoxville, Knoxville, TN
epoole1@utk.edu

ABSTRACT

Virtually every western news agency and even the Discovery Chanel have produced ever growing pieces about the engineering accomplishments of the small Middle Eastern country of The United Arab Emirates (UAE). In an attempt to create tourism, Dubai, UAE, has created some impressive structures, but now, it is creating land itself. Five artificial islands are being reclaimed from the Persian Gulf — one of which, the Palm Jumeirah, takes the shape of a date palm, and will be the focus of this paper. Reaching several hundred meters into the gulf, and standing several above the water line, the Palm Jumeirah is so large it can be seen from space. While an impressive creation, a reclamation project of this size could easily have a negative effect on the environment. Upon researching the project, it became clear that the UAE was in such a rush to build the islands that the proper planning and environmental studies were not conducted, thus resulting in the destruction of the Persian Gulf's eco-system. While most projects do tend to negatively effect the surrounding environment in some form, the islands, due to their shear size, have completely destroyed an already fragile eco-system in a manner that may be irreversible. After introducing the reader to some basic information regarding the construction of Dubai's Palm Jumeirah, this paper will examine some of the major environmental effects that have occurred as a result of the Palm Jumeirah project.

INTRODUCTION

In the late twentieth century, the Middle Eastern nation of the United Arab Emirates (UAE) began to make plans to distance itself from the petroleum industry that dominates most of the Persia. Driven by the fact that internal experts believe the country's oil reserves will be depleted by the year 2012, the UAE is attempting to transition to a service industry, with a major focus on tourism, retail, and entertainment. In order to transform its economy, the UAE is first focusing of the

already advanced city of Dubai, which is the first tax free, centrally-planned, free-market capitalist society in the Middle East (1). With an economy valued at over forty six billion dollars, the city of Dubai is, by far, the most economically powerful city in that part of the world. Yet it has virtually no ties to the commanding petroleum industry (2).

The UAE is in the process of spending trillions of dollars transforming Dubai into an engineering marvel. Of all of the structures that the emirate has recently created, including the tallest structure in the world and a revolving skyscraper, this report will focus on the largest land reclamation project to date, the manmade island formed in the shape of a date palm. The island, which Dubai has already termed "the eighth wonder of the world," adds almost 1,600 km (1,000 mi) of additional coastline to Dubai, and is formally called the Palm Jumeirah (3). While it is an engineering marvel, without extensive research and planning, the creation of such an island chain could have severely affected the local environment and coastal eco-system. Unfortunately, the UAE did not have time or patience for such research and planning, and therefore, the repercussions of such a large scale project have been devastating. This report will first give the reader some background on the Palm Jumeirah project and will then discuss some of the environmental repercussions of this large land reclamation project.

Palm Jumeirah Background

The Palm Jumeirah was designed and created by the state owned development company, The Nakheel Corporation. Formed in the shape of a Date Palm, Jumeirah consists of a trunk measuring 457 m (1500 ft) wide, 2.5 km (1.6 miles) long, and surrounded by an expansive canopy of seventeen fronds. Once complete, the palm will support over sixty luxury hotels, over 5,000 residential villas and apartments, several marinas, and various forms of entertainment (4).

Engineering Information

The engineering of this island was done in four major steps, first the breakwater was raised from the gulf. Next the center crescent was created, followed by the fronds. Currently, the newly formed dry land is being populated with amazing structures. Preliminary plans did not call for the large protective breakwater, but fortunately the executives realized the palm island must be protected by such a structure in order to abate the flow of the gulf.

Constructing the Breakwater

The breakwater was constructed where the water had a depth greater than 10 m (33 ft). It is 11 km (6.8 mi) long and 200 m (656 ft) wide, and rises 4 m (13 ft) out of the water. The barrier was made up of reclaimed sand from the bed of the surrounding area. In order to stop erosion, a cap structure was added. Engineers topped the breakwaters with two separate layers of massive rocks on the top, and three layers for the subsurface sections. Each rock was precisely sanded, shaped, and individually placed to form a wall-type structure that would remain sturdy (5).

Creating the Actual Palm

The island itself was created in a similar fashion. In order to provide support for the immense weight that will be added upon completion, the ground layer consists of enormous rocks blasted from far away mountains. Next, layers of soft sea sand that was covered with an erosive-preventing water-permeable geo-textile formed the bulk of the structure (6). This sand was, for the most part, dredged from the bottom of the gulf about 35 m (115 ft) from the breakwater. One-ton rocks sit atop this sand layer and create a cap that breaches the surface of the water.

At this point, the island began to show shape, but rose only several feet above the surface of the water. The final step was to dredge over 8,500,000 m^3 (302,000,000 ft^3) of ocean sand onto the top of the base structure in order to create habitable islands. This sea sand increased the island's height to 4 m (13 ft) above low tide (6). In order to quickly, yet precisely acquire and distribute the sand, fleets of dredging vessels and massive transport/delivery ships were brought from a European manufacturer.

Dredging

In dredging millions of cubic meters of sea bed, the project used specialized cutter suction dredgers in order to apply the sand to the desired surface. A cutter suction dredger, according to the European Dredging Association (EuDA), is a large rig with a powerful underwater suction tube generally 10 - 100 cm in diameter extended angularly from the centroid of the vessel with a large crane extending from the rear of the ship to stabilize the tube (7). Due to the dense makeup of the Persian Gulf, the dredgers had a cutting head at the base of the tube. This head chews through the rock bed with over 5,000kW cutting power. It was equipped with a massive jet dredge system powered by a submerged pump attached to the tube to help pull the destroyed bedrock into the ship (8 & 9). The jet dredge systems create an extreme negative pressure in the pipe, which creates a basic Bernoulli venturie tube effect. The negative tube pressure created uses the weight of the surrounding sea to force the debris up the tube and into the vessel at an incredible rate (Hughes 8).

Environmental Effects: Introduction

As the island was being built, global praise and awe far outweighed environmental concern, but once the initial amazement had worn off, many critics began voicing their concerns. In response, Nakheel continually issued publications from their scientific board and assertions stating that the ecosystem was not, and would not be, adversely affected. In many reports, they even claimed that the ecosystem would benefit from the construction (10). While the company did make some concessions, which are described below, the project ultimately resulted in extreme environmental destruction. The new archipelago not only completely changed the shape and makeup of the gulf, but the dredging and construction itself had even worse effects on the local environment.

The Positive Environmental Points

The company's environmental impact plan did have some positive points. They did modify the breakwater by adding two 3 m (9.8 ft) deep channels cut about a quarter of the way into the structure on each side. This design change allows additional currents to enter the island's channels, thus greatly reducing the internal water renewal time to about fifteen days (11). It also provides nutrients to the inner ecosystem and reduces the occurrence of stagnation which would allow bacteria to thrive. The company also spent two months transplanting 1,869 marine animals from an area where the sub-sea transit tunnel was to be placed (12). In addition, they employed two oceanographic experts to study the effects of the new islands on the environment and help design several different kinds of artificial reefs throughout the archipelago in order to replace the original habitat.

Impact on Construction on the Pre-Existing Landscape

While some considerations toward the environment were made, the result of creating a land mass with an area of 25,000 m^2 (270,000 ft^2) at an average depth of 10 m (33 ft) was nothing short of catastrophic for the environment. The creation of the Palm Jumeirah has influenced the ecosystem enough to alter the landscape of the preexisting beaches. Stable beaches go through transformations every day. As alluvial sand is relatively unconsolidated, the sand is constantly eroding with each undercurrent, but that erosion is usually counteracted as the natural currents and waves regularly re-deposit sand lifted off of the sea floor. Once the island was constructed, it disrupted the natural currents that move along the coast of the UAE, essentially acting as a large jetty. By dampening the force of the waves several miles out, the island current is not able to deposit enough sand on the natural beaches. This causes severe depletion of the beach soil. According to Dr. Tom Williams, Nakheel's Former Senior Technical Advisor, by 2006, the Palm Island had drastically reduced sediment deposits along almost 41 km (25 mi) of Dubai's shoreline (4).

The Direct Impact of Construction on the Marine Life

In addition to damaging the existing coastline, the Palm Jumeirah has proved deadly to most of the marine species in the area. Due to its extreme temperatures, salinity, and fierce storms, the Persian Gulf is already a high stress ecosystem with the marine life that exists there held in a delicate balance. The plentiful yet fragile sea grass, biota, algae, and microorganisms form the basis of life as they are one of the few stable food sources in the region. This food source attracts varieties of small fish that have limited territories. They are restricted to areas with ample food and protection from predators. Generally, the only form of protection in the coastal areas of the Persian Gulf is coral reefs. Obviously, it is these small fish that then in turn attract the larger, more mobile and nomadic predatory marine life.

Creating an intricate island chain like the Palm Jumeirah was a slow process and Nakheel reasoned that most of the aquatic life would have adequate time to relocate. This proved to be an accurate assumption for most of the larger organisms. However, the majority of the immobile flora, algae and coral reefs that support life, as well as those fauna that lived within the reefs were either dredged, permanently dislodged, or completely buried under the new island itself. Nakheel's environmental impact study found that about 10% of the area under and around the Palm contained

coral reefs. While that may sound like a small amount, given the shear size of the project, it totals to over 1.2 km^2 (300 acres) of coral, and all life sustained therein, directly destroyed (4). In addition, much of the sea grass and microorganisms located on the perimeter of the construction zone would have easily been sucked up by the jet pumps, ripped out of the sea floor by the excessive turbulence, or just choked out by the immense disturbance. Even those species originally located in the construction site that attempted to flee would have had to travel over 4.8 km (3 mi) into the gulf or almost 35.5 km (22 mi) along the coast to escape the construction.

The Indirect Impact of Construction on Marine Life

While the direct impact of the construction site decimated the marine population located in or close to the construction site, the indirect impact was far worse. Since the majority of the islands were formed using either bedrock or sea sand, the dredgers and transport vessels pulled up hundreds of millions of tons of sand and sprayed it back into the sea in a technique called rainbowing, which, according to a Dubai environmental protection agency, resulted in "substantial re-suspension of finer sediments, and the consequent siltation of [marine] communities in the general region of each development" (13). Plumes of sedimentation from the sprayed sand and the disrupted bed spread more than 25,000 m^2 (6 acres) acres in each direction, thus making the total area affected by over-sedimentation greater than 75,000 m^2 (18.5 acres): an area larger than the state of West Virginia. Nakheel stated that the silt would settle in a few months, but that was not the case as the construction and rainbowing lasted several years. The result was the burial or asphyxiation of any organism that could not travel that distance in time.

CONCLUSION

The creation of the Palm Jumeirah island community is an undeniable marvel of engineering. The Nakheel Corporation was able to successfully create an immense and intricately designed island that required accuracy to the centimeter. It is a testament to the fact that with proper design techniques and an attention to detail, a trained engineer can create awe inspiring structures. However, it is also a prime example of how unguided ambition can have catastrophic windfall. The damage to the local aquatic environment, and possibly that of the entire Persian Gulf may be permanent. Today, seven years after construction began, the water around the Palm Jumeirah is still murky and the fine sediments become re-suspended every time a storm comes through. The coastal beaches, which historically lost 10,000 – 15,000 m^3 per year of sand due to natural erosion, have already lost over 3,500,000 m^3 (14). According to fish counts, less than half of the 35 species of fish have returned to the site. Every single species of fauna that once existed at the site were destroyed during construction, and fewer than 30 of the original 106 species have returned. The Palm Jumeirah may be a structure that will stand the test of time and revolutionize coastal development, but the loss of a unique ecosystem may prove to have been too high of a price to pay.

REFERENCES

"United Arab Emirates" The CIA World Factbook. 20 April 2006. Central Intelligence Agency. <http://www.cia.gov/cia/publications/factbook/geos/ae.html> (10 Jan. 2008).

Economist Intelligence Unit (EIU) (2005). Country Report: United Arab Emirates, (Nov 2008).

Conference Board and Groningen Growth and Development Centre, The. Total Economy Database. Jan. 2006. <http://www.qqdc.net> (02 Feb. 2008).

Salahuddin, Bayyinah. The Marine Environmental Impacts of Artificial Island Construction: Dubai, UAE. The Nicholas School of The Environmental and Earth Sciences at Duke Universty. 2006.

Sale, Peter et al. – International Network on Water Environment and Health (UNU-INWEH). "Building a Management Program fir an Effective and Sustainable Environment for the Palm Island Project – Dubai: Phase I – Pilot Study: Final report to Nakheel." 2004. Appendix C. Integrated Environemental Impact Assessment. By Nakheel

Dowdey, Sarah. "Why is the World's Largest Artificial Island in the Shape of a Palm Tree?" How Stuff Works Online, < http://travel.howstuffworks.com/dubai-palm1.htm> (08 Jan. 2008).

"What About Dredging." The European Dredging Association (EuDA). 2006. <http://www.european-dredging.info/ab7.html> (10 Feb. 2008).

Hughes, T. H.; B. White. Effect of the Environment on Processing and Handling Materials at Sea [and Discussion]. Philosophical Transactions of the Royal Society of London. Series A, Mathematical and Physical Sciences, Vol. 290, No. 1366, Sea Floor Development: Moving into Deep Water. (Aug. 21, 1978), pp. 161-177.

Jan De Nul. "Dredging, Civil, Heavy Lift and Environmental Project." <http://www.jandenul.com/jdn.html> (12 Jan. 2009).

Palm Jumeirah. <http://www.thepalm.ae/jumeirah/environment/the-palm-jumeirah - ecosystem/> (28 Jan. 2009).

Stamou, A.I., Memos, C., Spanoudaki, K. (2007). "Estimating water renewal time in semi-enclosed costal areas of complicated geometry using a hydrodynamic model." Journal of Coastal Research., SI 50, 282-286.

Palm Jumeirah. <http://www.thepalm.ae/jumeirah/environment/case-study-1> (28 Jan. 2009).

Dubai Municipality Environment Department Environment Protection and Safety Section. "Technical Guideline No.53 Environmental Impact Assessment Procedures."

Van Oord "Project: Beach Replenishment and Shore Protection Dubai." <http://www.vanoord.com> (10 Jan. 2008).

Developing Green Streets Prototypes to Reduce Combined Sewer Overflows for Cincinnati, Ohio

Brian Marengo[1], Thomas Cahill[1], Daniel Wible[1], Courtney Marm[1], Ralph Johnstone[2]
[1]CH2M HILL, 1717 Arch St., Philadelphia, PA 19103; (215)-640-4220;
brian.marengo@ch2m.com , [2]Cincinnati Stormwater Management Utility, 1600 Gest St # 2
Cincinnati, OH 45204; (513) 557-7167; Ralph.Johnstone@cincinnati-oh.gov

ABSTRACT

The purpose of this study was to evaluate the feasibility of developing stormwater management retrofit demonstration projects for application in the public right-of-way (ROW) in form of "Green Streets." This study responded a motion issued by the City Council of Cincinnati to create a plan for a Green Streets Pilot Project, targeting specific downtown streets for the implementation of methods to address stormwater runoff generated by the public right-of-way and to assess their feasibility to reduce combined sewer overflows.

The study developed conceptual prototype stormwater controls to fit into common features in the public right-of-way and adjacent impervious features for four (4) street segments in the central business district of Cincinnati, Ohio. CH2M HILL's Low Impact Feasibility and Evaluation (LIFE) model was applied to evaluate each of the BMP concepts in terms of runoff reductions resulting from the planned level of storage, infiltration into the subsurface soils, and evapotranspiration. Cost estimates were developed to assess runoff reduction efficiency.

Introduction Background and Purpose

Many urban communities served by combined sewers have struggled for years to find an economically viable solution to mitigate the impacts of wet weather overflows. Most of the applied technology has focused on increasing the capacity of the conveyance system, adding storage to detain storm flows until treatment capacity returns, or providing some form of water quality treatment to the overflow discharges.

Alternate approaches seek to reduce the volume of stormwater runoff entering the combined sewer system. Various stormwater management technologies developed over the past three decades have been given closer consideration for application in the urban environment. Measures that infiltrate (porous pavements, linear infiltration systems, and tree trenches); measures that transpire and reduce energy demand (vegetated roofs); measures that infiltrate and transpire (rain gardens and planter boxes); and measures that capture and reuse rainfall (rain barrels and grey water systems) have all evolved in different regions around the globe, depending on the local ecology and water resource requirements or limitations.

This study responded to the City of Cincinnati Council Motion of May 29, 2007, which required "that the administration create a plan for a Green Streets Pilot Project, targeting specific Downtown Streets for the implementation of methods to address stormwater runoff." The purpose of this study was to evaluate the feasibility of these measures for application in the public right-of-way in the form of "Green Streets." Various terms have evolved to describe the application of such solutions in the urban environment, with the word "green"

providing a popular and acceptable label. In fact, the use of vegetative systems as an integral part of the engineered designs provides hydrologic, hydraulic, water quality, and aesthetic benefits.

Project Area

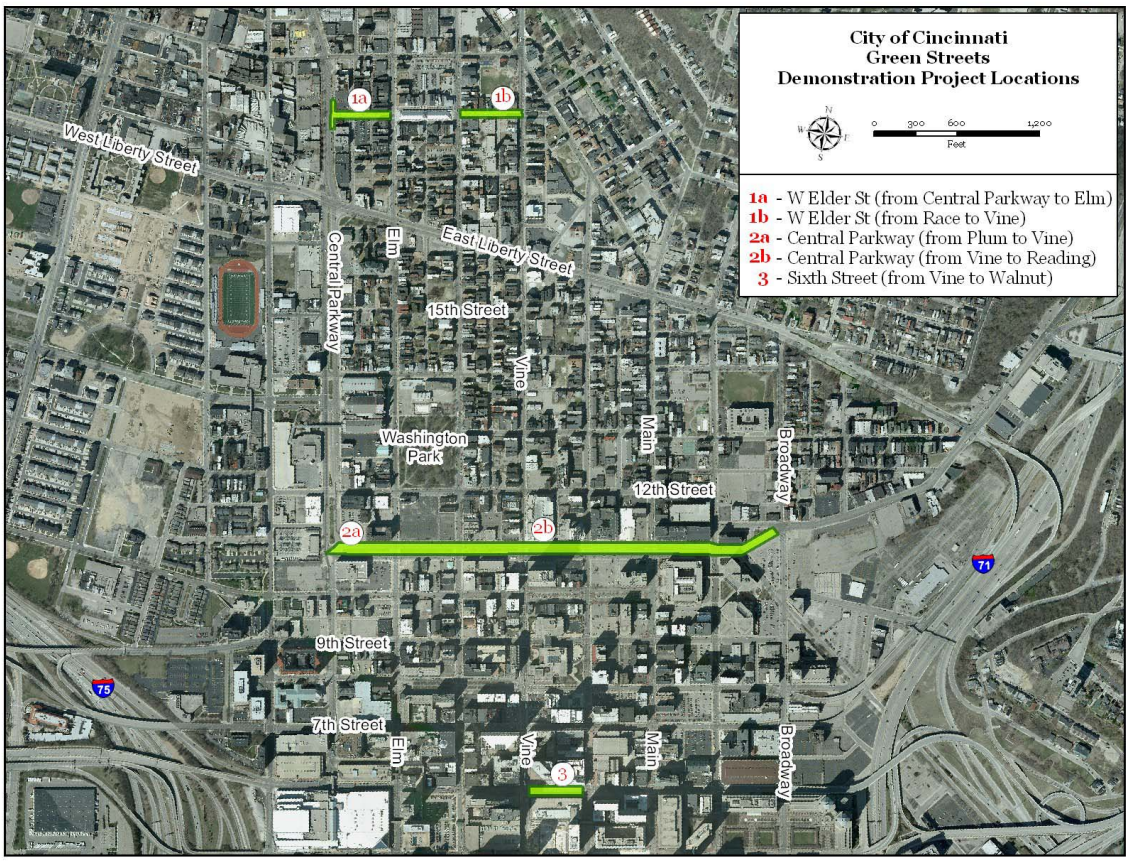

Figure 1 - Street Areas Selected for Feasibility Analysis

The Stormwater Management Utility (SMU), the Department of Transportation Engineering (DOTE), and the Parks Department collaborated to develop a set of ranking criteria to select viable street segments for the feasibility study. Based upon this criteria, the streets shown in the project area map in Figure 1 were selected for the feasibility analysis.

BMP Concept Development

Early on the process, the project team held a workshop meeting with SMU, the Parks Department, and DOTE to develop evaluation criteria, to conduct onsite reconnaissance of the proposed project areas, and to discuss potential concepts with City staff in the field. The workshop presented and critiqued relevant stormwater control technologies and their potential applicability to the City streetscape. The technologies drew from case studies that had been successfully implemented in other areas of the country, many with similar hydrologic characteristics to those found in Cincinnati. The technologies that were considered for application in the Green Streets program include the following:

- Porous pavements
- Subsurface infiltration
- Infiltration trench
- Bioretention
- Vegetated planter box
- Vegetated (green) roof

Using the knowledge obtained at the initial field visit and through analysis of the available source data (CAGIS, anecdotal observations from key staff, soil survey data), opportunities and constraints were identified for the street sections. The basic procedure entailed developing generic Green Street "retrofit" concepts or prototypes, as well as additional low impact development (LID) concepts for sustainable stormwater management in the adjacent areas, including concepts that managed runoff from adjacent parcels. While the focus of this work effort was clearly on the streets themselves, it is important to understand opportunities to further reduce runoff by "retrofitting" the adjacent areas, which included some publicly-owned impervious areas. Concepts were also developed for a limited number of these areas for comparison purposes.

In order to organize the various Green Street "retrofit" concepts into a framework specific to the City of Cincinnati, the project team developed a classification system of prototypes. This prototype classification is unique to this project and allowed the project team to group different "green" stormwater practices and technologies into unified Green Street concepts. Specifically, the following five Prototypes were developed:

- Prototype 1: vegetated curb extensions, infiltration under standard pavement parking lane, continuous tree trench, and porous concrete sidewalk with infiltration
- Prototype 2: vegetated curb extensions, infiltration under standard pavement parking lane, and continuous tree trench
- Prototype 3: vegetated curb extensions and infiltration under standard pavement parking lane
- Prototype 4: vegetated curb extensions
- Prototype 5: porous pavement parking lane and tree trench

Prototype 1 included all four elements of a comprehensive Green Street design that seeks to maximize runoff capture by using all available elements of the streetscape. Prototypes 2, 3 and 4 represent variations on Prototype 1, by subtracting one element from the preceding design prototype. The common elements in these four Prototypes are the vegetated curb extensions, which represents the minimum level of stormwater treatment. Prototype 5 provides a variation on Prototype 4 by substituting porous pavement with a stone infiltration bed for the vegetated curb extensions in the parking lane. Green Street design is most efficient when it utilizes either vegetated

curb extensions or porous pavement parking lanes, rather than using the two practices in combination. With porous pavement parking lanes, little runoff, if any, would ever reach the vegetated areas, which allows for direct comparison of vegetated measures with the porous pavement technologies.

For Prototypes 1 through 4, the vegetated curb extensions (or bioretention areas) will receive runoff from the streets and, in some cases, adjacent impervious areas (sidewalks, awnings, etc.) and allow it to be filtered, treated, and evapotranspired prior to it draining into a subsurface aggregate infiltration system. In this way, the curb extensions will serve at least three stormwater treatment functions: pretreatment, evapotranspiration, and infiltration. The underlying aggregate infiltration system will actually extend beneath all elements in the particular prototype. (For the purpose of this study, these prototypes were considered as unified "systems", as opposed to separate, individual elements.) In addition, it has been previously demonstrated at other locations that these measures can provide traffic calming benefits and soften the aesthetics of the streetscape.

For Prototype 5, runoff from the streets and, in some cases, adjacent impervious areas will drain directly through the porous pavement, which will have to be vacuum-swept on a biannual basis to maintain porosity, and into the subsurface infiltration system. For all the prototypes, runoff will be temporarily stored both on the surface and in the voids of the underlying aggregate (typically 40 percent) until it has had an opportunity to exfiltrate into the subsoil. In the event of a larger rain events (> 1 inch), the full design of the prototype would incorporate controlled overflow mechanisms (weirs, constricted outlet orifices, overflow pipes, etc.) to allow for excess flows to pass on to the existing combined sewer system.

Drainage Areas for the four streets were delineated digital aerial photos, site photographs, field notes, and utility information obtained from CAGIS (Cincinnati Area Geographic Information System). The drainage areas tributary to each BMP concept were delineated using a combination of GIS features (inlets, manholes, catchments, contours, etc.) and field investigation (verification of street crown, inferred ground slope). Estimates of the pervious and impervious areas to each BMP were recorded in summary tables. In several cases, it was assumed that minor modifications could be made to existing street inlets either to allow more runoff to enter the various concepts or to allow runoff to overflow from the concepts into the existing sewer system. This provided a comparison of how Green Street features could be used to capture additional runoff and at what cost.

Using the drainage area delineations, runoff volumes were calculated from the 0.5 inch, 0.75 inch, and 1.0 inch rainfall events. Based on these volumes, the various BMP concepts were sized to hold the runoff volume resulting from a 1.0 inch storm as "dead storage" either on the surface or in the aggregate voids (typically 40 percent) in the case of a gravel bed. Infiltration and evapotranspiration were not considered at this conceptual sizing stage.

The benefits of these hydrologic functions were evaluated as part of the modeling evaluation of the BMP performance. Based upon the results of the modeling analysis, it is likely that some of these concepts could be downsized and still provide capture for the first inch of rainfall. It should be noted that in situ soil permeability testing should be used as the basis for the final design sizing. Tables 1 and 2 provide an example of the BMP Sizing analysis, in this case for West Elder Street.

For all rain events, the impact of stormwater runoff on the combined sewer system (and overflows) will be reduced through the application of these prototypes. The runoff reductions associated with each prototype were quantified in this study, but the simulation of the specific overflow reductions occurring at the downstream CSO were beyond the scope of this effort. It is also important to note that the five prototypes and other LID concepts considered for this project are only conceptual in nature and would require full engineering and detailed site investigation prior to implementation. Soil permeability testing, deep pit excavations, utilities investigation, and topographic surveying would have to be performed to ensure the effectiveness of the various designs and the minimization of risks to adjacent structures.

This effort also considered demonstrating the use of porous concrete at several bus stop locations throughout the project area. Based upon input from DOTE, concrete bus stop pads were indicated to be failing in some locations throughout the City and in need of replacement. Thus, the project team evaluated the potential stormwater benefit of an existing transportation feature that inherently possesses a large, deep stone bed for structural stability. This 18-inch stone base could also provide useful stormwater storage that can be utilized in one of two ways: porous pavement or connection of an inlet or area drain to the stone void space (typically 40%).

Table 1 - BMP Sizing and Storage Volume Estimates - West Elder St. at Findlay Market

Location	Option Priority	BMP ID	BMP Type	Impervious Area (ft^2)	Pervious Area (ft^2)	1.0" Capture Volume (ft^3)
North side W. Elder St. - 3 blocks	Primary	1a	Prototype 1	41,818	3,330	3,275
North side W. Elder St. - 3 blocks	Primary	1b	Prototype 1	45,378	3,330	3,542
South side W. Elder St. - 3 blocks	Primary	2	Prototype 3	4,962	-	372
North Side - Pavement adjacent to Parking lot	Primary	3	Bioretention	15,406	-	1,155
South Side - adjacent parking lot	Secondary	4	Porous pavement	27,743	-	2,081
North Side - New Building	Secondary	5	Vegetated roof	12,452	-	934

Table 2 - BMP Sizing and Storage Volume Estimates - West Elder St. at Findlay Market

		Surface			Subsurface			
Location	BMP ID	BMP Area (ft^2)	Depth (in)	Storage Volume (ft^3)	BMP Area (ft^2)	Depth (in)	Storage Volume (ft^3)	Total Storage Volume (ft^3)
North side W. Elder St. - 3 blocks	1a	1,500	6	750	6,423	12	2,569	3,319
North side W. Elder St. - 3 blocks	1b	1,500	6	750	6,423	14	2,997	3,747
South side W. Elder St. - 3 blocks	2	1,500	6	750	3,240	6	648	1,398
North Side - Pavement adjacent to Parking lot	3	1,751	8	1,167	1,751	6	-	1,167
South Side - adjacent parking lot	4	-	-	-	21,660	12	8,664	8,664
North Side - New Building	5	12,452	1	1,038	-	-	-	1,038

Prototype 1 - Vegetated curb extensions, infiltration under parking, tree trenches, porous sidewalk
Prototype 2 - Vegetated curb extensions, infiltration under parking, tree trenches
Prototype 3 - Vegetated curb extensions, infiltration under parking
Prototype 4 - Vegetated curb extensions
Prototype 5 - Porous parking spaces and tree trenches
BMP ID - Scenario b - Denotes an alternative where an available adjacent impervious area (roof leader, parking lot, etc.) was routed to the BMP

LIFE™ Model

CH2M HILL's Low Impact Feasibility and Evaluation (LIFE) model was applied to evaluate each of the BMP concepts in terms of runoff reductions resulting from the planned level of storage, infiltration into the subsurface soils, and evapotranspiration for measures that had a vegetative component. The LIFE™ model is a physically-based hydrologic and water quality simulation tool that was developed to evaluate the performance of various LID techniques (e.g., bioretention, infiltration systems, rainwater capture/reuse systems, permeable pavement, green roofs, etc). It is well suited to site-level analysis of spatially distributed stormwater source controls (i.e., LID techniques).

Table 3 - LIFE™ Model Evaluation of Runoff Reduction and Cost Efficiency - West Elder Street - Findlay Market

			Annual Runoff Volumes				Unit Runoff Reduction Cost	
Location	BMP ID	BMP Type	Existing Condition (ft^3)	With BMP (ft^3)	Volume Reduction (ft^3)	Percent Reduction	$ / Gallon (Low)	$ / Gallon (High)
North side W. Elder St. - 3 blocks	1a	Prototype 1	148,533	99,135	49,398	33%	$0.23	$0.33
North side W. Elder St. - 3 blocks	1b	Prototype 1	171,659	123,566	48,093	28%	$0.24	$0.34
South side W. Elder St. - 3 blocks	2a	Prototype 3	5,029	144	4,885	97%	$1.48	$1.72
South side W. Elder St. - 3 blocks	2b	Prototype 3	11,563	286	11,277	98%	$0.33	$0.33
North Side - Pavement adjacent to Parking lot	3	Bioretention	49,923	28,956	20,967	42%	$0.33	$0.33
South Side - adjacent parking lot	4	Porous pavement	94,349	0	94,349	100%	$0.71	$0.96
North Side - New Building	5	Vegetated roof	42,347	18,810	23,537	56%	$0.21	$0.21
Scenario A Total			340,181	147,045	193,136	57%	$0.30	$0.35
Scenario B Total			369,841	171,618	198,223	54%	$0.25	$0.30

NOTES

Prototype 1 - Vegetated curb extensions, infiltration under parking, tree trenches, porous sidewalk
Prototype 2 - Vegetated curb extensions, infiltration under parking, tree trenches
Prototype 3 - Vegetated curb extensions, infiltration under parking
Prototype 4 - Vegetated curb extensions
Prototype 5 - Porous parking spaces and tree trenches
BMP ID - Scenario b - Denotes an alternative where an available adjacent impervious area (roof leader, parking lot, etc.) was routed to the BMP

The LIFE™ model provides a continuous simulation of the runoff, interflow, infiltration, and baseflow from a developed area given the following inputs:

- *Continuous rainfall data* (typically in time increments of one hour or less) and *evapotranspiration data* (daily), typically for a time period of one year or more. Evapotranspiration (ET) can also be calculated from temperature data.
- *Site design parameters and land cover characteristics* for each land use type being modeled (e.g., road width, rooftop coverage, surface parking coverage).

- *Information on LID techniques* that are applied for each land use type, including:
  - Extent of source control application (e.g., fractions of road and of building coverage with certain types of source controls)
  - Source control design parameters (e.g., area and depth of infiltration facilities, soil depth for green roofs or absorbent landscaping, volume of rainwater re-use cisterns)
- *Soils information, including:*
  - Surface soil parameters (e.g., maximum water content, vegetation rooting depth)
  - Sub-surface soil parameters (e.g., saturated hydraulic conductivity)

LIFE™ calculates runoff and pollutant loads under a variety of weather conditions, land uses, and soil types and has more robust representation of infiltration processes than commonly applied planning models such as the U.S. Environmental Protection Agency's (EPA) Stormwater Management Model (SWMM). Final LIFE™ hydrographs for the Green Streets project scenarios can be fully incorporated into the City's EPA SWMM models of the combined sewer system to scale site benefits for evaluating the impact of system-wide implementation. These benefits would typically be reflected in runoff volume, recharge, peak flow, and water quality.

In the case of some project locations, such as West Elder Street, two scenarios were tested. In Scenario A, the proposed control measures were modeled as if they would treat only their immediate drainage areas. In Scenario B, additional impervious area was added to these control measures, given the assumption that nearby inlets and pipes could be practically modified. Table 3 and Figure 2 provide an example of the LIFE™ model results and corresponding cost estimates ($/Gallon reduction), in this case for West Elder Street.

According to the results summarized in Figure 2, the three primary BMPs (represented as DA1 Scenario A, DA1 Scenario B, DA2 Scenario A, DA2 Scenario B, and DA3) reduced total runoff volumes by 22 to 31 percent. These represent the best opportunities for retrofits based on public ownership of and access to their proposed locations. If two additional "secondary" BMPs were added (DA 4 and DA 5), the annual runoff volumes could be reduced an additional 32 to 36 percent. The LIFE™ model also indicates that several control measures are probably over-sized either in terms of surface area or storage depth. The proposed BMPs for both DA 2 and DA 4 removed all but 286 ft^3 of their combined annual runoff volume. Sizing of individual control measures was not part of the modeling process and should be revisited in any future design process.

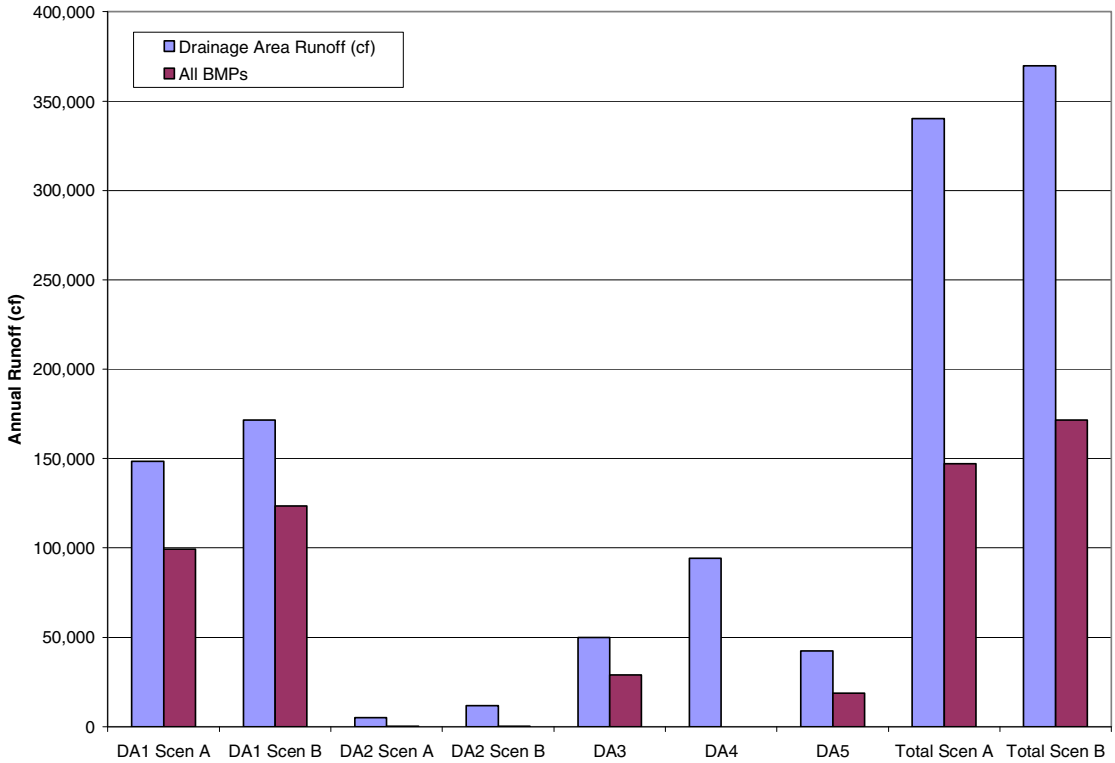

Figure 2 - Comparison of Runoff Reduction for each Drainage Area – BMP Combination - West Elder St. Cincinnati, OH.

Cost Analysis

After selecting and sizing the various Green Street and LID concepts described above, conceptual cost estimates were developed both for construction and ongoing operation and maintenance (O&M). For each concept, the project team specifically considered the following probable cost items: pavement demolition, excavation, aggregate, geotextile, standard pavement, porous pavement (asphalt or concrete), pipes and cleanouts/catch basins, existing inlet modifications, planting soil, curbing, bioretention vegetation, street trees, tree grates, and vegetated roof material. Unit costs for these various items were based on several sources, including the project team's recent construction experiences, the latest version of "R.S. Means Construction Costs", and other published data. A 20 percent contingency was applied to the total cost of each concept.

Two construction cost scenarios were developed to provide a "high" and "low" cost for each project concept. For the "high" cost scenario, all of the line items listed above were included. For comparison, the "low" cost scenario considered the case where several line items are not directly related to stormwater management. In other words, these components would have to undergo some level of routine maintenance and rehabilitation as part of maintaining the street infrastructure. These items included the following: standard asphalt pavement, porous asphalt and concrete pavement (only the cost increase over standard asphalt and concrete was considered),

curbing, street trees, and tree grates. The "low" cost estimate would illustrate the benefit of integrating the timing of green streets projects with renewal of the street ROW as part of a broader infrastructure renewal need.

The expected primary maintenance tasks for the various Green Street and LID Concepts include the following: cleaning out cleanouts/catch basins, pruning/weeding/watering/etc of bioretention vegetation during establishment period (if and when required), removing trash/sediment/debris from bioretention curb extensions and planter boxes, vacuum-sweeping the porous pavement, and irrigating the vegetated roof material during the establishment period. It is important to note that the O&M cost analysis did not factor in the current costs of drainage maintenance (removal of trash/sediment/debris from inlets and gutter lines) incurred by the City, in so much as they exist and would presumably continue with or without the Green Streets project. Therefore, the costs summarized in the tables below, either as actual dollar amounts or as "high", "medium", or "low", are likely to be rather conservative.

Project Implementation Plan

A basic prioritization scheme was developed to select projects for implementation. The projects were ranked according to a set of criteria and criteria weights that reflected the goals adopted by the project team. The project concepts were evaluated with respect to the above evaluation criteria. Weighting factors were developed for each of the main ranking criteria as follows:

- Community Amenity / Education (40%)
- Reduction of Runoff and CSO volume (90%)
- Complements / Integrates Multiple Existing Projects (70%)
- Constructability - How easy is it to build? (50%)

The projects were then ranked according to the criteria and weighting scores and the top ranked projects were recommended to move on to design development and were incorporated into the Long Term Control Plan Strategy for the Metropolitan Sewer District of Greater Cincinnati. The next phase of this effort is expected to occur in 2009 and will entail implementation of one or more of the proposed Green Street projects.

Implementation and Performance of Stormwater Best Management Practice Retrofits in Wilmington, NC

J. D. Wright[1], W. F. Hunt[1], M. R. Burchell II[1], C. A. Perrin[2] E.R. McCoy[3]

Abstract. *Burnt Mill Creek, located within downtown Wilmington, NC, is on the EPA's 303(d) list for impairment due in large part to urban stormwater runoff. The urban nature of the watershed presents challenges for restoration because of the varying land uses including single and multi-family residential areas, recreational parks, and commercial and industrial areas. Restoration efforts are multiplying in Burnt Mill Creek as a result of passionate involvement from local community leaders, and partnerships with state organizations. The Watershed Education for Communities and Local Officials (WECO) coordinated a partnership, with NCSU BAE, the City of Wilmington, as well as several other key state and local organizations and citizens groups, to obtain an EPA 319 grant that addresses stormwater management in the watershed. Community involvement has led to several retrofit BMP opportunities, including pervious pavement and rain gardens at a local YMCA, two bioretention cells installed in the parking lot at Port City Java's corporate headquarters, a stormwater wetland in a city owned communal area, and several residential scale rain gardens in an urban low income community. Twelve rain gardens and twenty four rain barrels were installed at citizen's private residences in an urban neighborhood in downtown Wilmington. Although restoration takes time, momentum continues to build in the Burnt Mill Creek watershed as resources are devoted to thoughtful education and engagement with the public.*

Keywords. Stormwater, BMPs, Urban Retrofits, Bioretention, Wetlands, Permeable Pavement

Introduction

Burnt Mill Creek watershed is located in downtown Wilmington in New Hanover County, North Carolina, and is on the EPA 303(d) list of impaired streams for impacts from stormwater runoff. In 2002, the NC Ecosystem Enhancement Program completed a watershed plan for Burnt Mill Creek and adjacent Smith Creek. The NCEEP plan indicated general impacts resulting from increased stormwater discharges and associated pollutants. More recently, NCDWQ's Assessment Report (2004) of the Burnt Mill Creek watershed identified toxic impacts from polycyclic aromatic hydrocarbons (PAHs) as the primary cause of biological impairment, with secondary and cumulative causes being sedimentation, and nutrient enrichment. Research conducted by the University of North Carolina at Wilmington (UNC-W) found all PAH samples exceeded concentrations that would cause harmful effects in aquatic communities (Mallin, et al; 2006). The same report identifies fecal coliform counts well in excess of the State standard for human contact waters at all but one sampling station. Stormwater runoff generated by development will continue to degrade the creek unless measures are taken to manage stormwater runoff.

WECO coordinated a partnership including the North Carolina State University Department of Biological and Agricultural Engineering, City of Wilmington Stormwater Services, Cape

[1] Department of Biological and Agricultural Engineering, North Carolina State University, Campus Box 7625, Raleigh, NC 27695
[2] Agricultural and Resource Economics, North Carolina State University, Campus Box 8109, Raleigh, NC 27695
[3] Department of Landscape Architecture, College of Design, North Carolina State University, Campus Box 7701, Raleigh, NC 27695

Fear Riverwatch, UNC-Wilmington, New Hanover County Planning Department and Soil and Water Conservation District, NCEEP, and citizens that received an EPA 319 grant to address stormwater management in the watershed. The focus of the grant was to install six BMPs throughout the Burnt Mill Creek Watershed, involve the community through education and involvement installing several residential BMPs, and water quality monitoring. BMP sites were identified by project cooperators and concerned citizens through community meetings and workshops.

BMP retrofits were installed at seven sites in the Burnt Mill Creek Watershed, four of which are described herein. A gravel parking lot at the Wilmington Family YMCA was a substantial source of sediment into Burnt Mill Creek. The gravel was replaced with porous concrete, two rain gardens, and grassed landscaping. The porous concrete and rain gardens improved infiltration and the rain gardens provided some pollutant removal trough filtration and plant uptake. Runoff from the parking lot at the Port City Java headquarters was intercepted by a sod bioretention area designed to reduce peak flow and improve water quality through filtration and plant uptake. A stormwater wetland was constructed to treat a 5.5 acre watershed, comprised mainly of single family residential, that drains through City of Wilmington owned open space, referred to as Mary Bridgers' Park, on the banks of Burnt Mill Creek. The wetland will reduce peak flow and provide treatment for the design storm.

The Bottom Neighborhood Empowerment Association (BNEA) is a group of citizens living in the bottom area who are striving to improve the quality of life in their neighborhood. The bottom area, called the bottom because it is one of the lowest points in the watershed, is a dense urban neighborhood where many residents have incomes lower than the median income of Wilmington and New Hanover County (Wilmington median income is $42,000, New Hanover County $41,000; areas in BMC between $22,000 and $34,000 depending on census tract) (NC Census, 2000). Cooperation with BNEA has led to several educational and LID retrofit opportunities including three educational workshops held in the community, installation of twelve rain gardens in community areas and private residences, and distribution of twenty-four 246 L (65 gallon) rain barrels.

Methods

Wilmington Family YMCA

Site Description

A gravel area at the Wilmington Family YMCA was being used as an overflow parking area for members of the YMCA (Figure 1). Because of the areas use for parking the gravel had become compacted such that is was nearly impermeable. Roof top runoff from half of the roof was also directed into the parking lot causing runoff from rain events to wash a substantial amount of sediment into the stormwater system. Two best management practices were used as a treatment system to manage stormwater on this site. Porous concrete was installed to stabilize the site and two rain gardens were used to treat the roof top runoff (Figure 2). Porous concrete will allow the rainfall that falls on the surface to infiltrate preventing runoff. Some storage is also available within and in the materials below the porous concrete. Rain gardens serve to store and infiltrate the stormwater removing pollutants through filtration and plant uptake.

Porous Concrete

The site was excavated 30 cm (1 ft) below the existing grade. Due to the concern for the rain fall infiltrating through the porous concrete impacting the foundation of the building, a buffer of at least 2.4 m (8 ft) was maintained between the building and the edge of the porous concrete. Typically a buffer of 3 m (10 ft) would be recommended, however, because of the extremely high infiltration rates it was determined that 2.4 m would be sufficient. Because



Figure 1 Gravel Parking Area

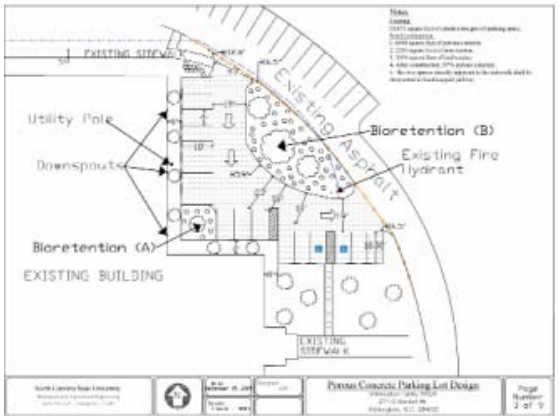

Figure 2 YMCA Design

the site was extremely sandy there was no concern about compacting the insitu soils. Fifteen cm (6 in) of washed no 57 stone was spread through the bottom of the excavated area. Thirty cm (12 in) curb and gutter was used to separate the porous concrete from the rain gardens and prevent vehicles from driving into the rain gardens. Two curb cuts were installed in the curb and gutter around each of the rain gardens to allow for over flow into the parking area utilizing the storage capacity of the porous concrete. Each load of porous concrete was inspected to verify that the moisture content of the porous concrete was at an optimum level. The porous concrete was then covered in plastic overnight to retain moisture and prevent it from drying to quickly. Immediately after the porous concrete was in place sod was installed around the edges of the parking area to stabilize the site and prevent soil from washing onto and potentially clogging the porous concrete (Figure 3). A standard concrete strip was installed between the asphalt and the porous concrete to provide a sturdy transition between the two materials. The porous concrete area was closed to all vehicles for 14 days as recommended by the Carolina Ready Mix Concrete Association (2004) to allow adequate time for the porous concrete to cure. The parking lot was then marked in accordance with standards enforced by the City of Wilmington.

Rain Gardens

Two rain gardens were installed to capture the runoff from half of the roof of the YMCA. Three downspouts were connected with 10 cm (4 in) plastic corrugated pipe to a drop inlet installed in the porous concrete parking area. The drop inlet was installed below the bottom of the downspouts so that water will not back up into the downspouts if the capacity of the rain garden is exceeded. The run off was gravity fed from the drop inlet into the rain garden through a 20 cm (8 in) smooth walled corrugated pipe. The rain garden was excavated in a bowl shape with the lowest elevation being 25 cm (10 in) below the level of the porous concrete parking area. The larger rain garden was 200 m^2 (1255 ft^2) and the smaller rain garden was 36 m^2 (390 ft^2). The two rain gardens are large enough to store and treat 2.5 cm (1 in) of rain fall from the roof. The rain gardens were both filled with 5 cm (2 in) of topsoil that was mixed into the top 20 cm (8 in) of the existing soil. Triple shredded hardwood mulch was spread 7.5 cm (3 in) deep and appropriate vegetation was added (Figure 4). Table 1 shows the vegetation that was planted in the rain gardens.

Port City Java (PCJ)

Site Description

Port City Java corporate headquarters were located on the bank of Burnt Mill Creek. The stormwater from the 1,435 m^2 (15,450 ft^2) parking lot drains directly into the creek. Two bioretention cells 110 m^2 (1180 ft^2) total were installed in the parking lot to intercept the stormwater before it flowed into existing storm inlets (Figure 5). The bioretention areas were



Figure 3 Finished Porous Concrete with Sod Strip



Figure 4 Larger Rain Garden

Table 1 Rain Garden Vegetation

Common Name	*Scientific Name*
Coneflower	*Rudbeckia laciniata*
Muhly Grass	*Muhlenbergia capillaris*
Panic Grass	*Panicum virgatum*
Maiden Grass	*Miscanthus*
Southern Magnolia	*Magnolia grandiflora*
Dwarf Yaupon	*Ilex vomitoria*
Virginia Sweetspire	*Itea virginica*
Holly	*Ilex*

designed to store runoff from 2.5 cm (1 in) of rainfall. Bioretention areas have been shown to reducing peak flows (Davis, 2007, Hunt et al. 2008) and reduce pollutant concentrations and loads (Hunt et al., 2006, Dietz and Clausen 2006).

Bioretention Areas

Two bioretention cells were installed as a retrofit in an existing parking lot, therefore, 123.5 m^2 (1,330 ft^2) of asphalt had to be removed from the parking area (Figure 6). The cells were each in the shape of a "T." The tail was 1.5 m (5 ft) wide and expanded at the end to an area equivalent to two parking spaces. Because this was a retrofit, the parking lot had to meet city standards requiring that the distance between curb stops installed between spaces be no more

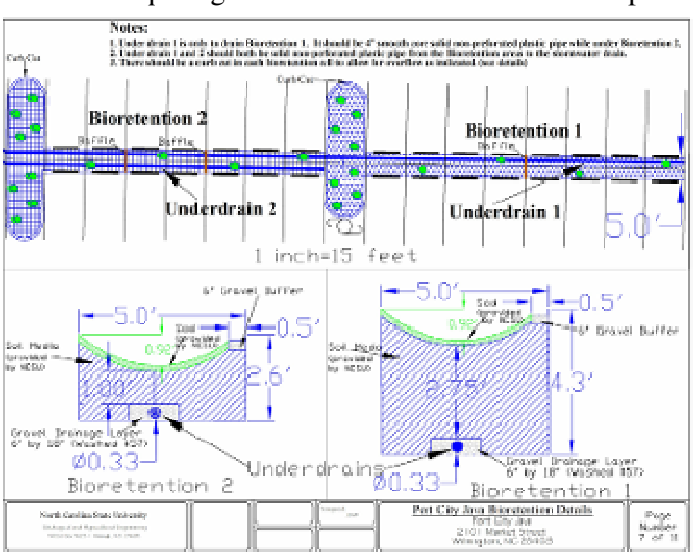

Figure 5 Bioretention Design



Figure 6 Asphalt Removal

than 1.5 m. The existing soil was sandy and was removed and temporarily stored on site to be later used in the bioretention area. Underdrains were installed in the cells at two different depths to collect filtered samples after rain events. The underdrains were installed 84 cm (2.75 ft.) and 30 cm (1 ft) below the surface of the bioretention area in the cells named PCJ Deep and PCJ Shallow, respectively. The underdrains were installed in a gravel layer 15 cm (6 in) deep and 45 cm (18 in) wide and were covered in a soil stabilization fabric (Figure 7). The underdrains were connected to the existing stormwater inlet.The soil removed from the cells was replaced to an elevation within 30 cm (1 ft) of the parking lot. A linear storage zone was formed and zenith zoysia sod was installed. A sodden verge was installed to slow the runoff from the parking lot and allow for pretreatment. Curb stops were installed along the edge of the cells to prevent vehicles from driving into the bioretention areas. The curb stops on the upper side of the bioretention areas were raised 6 mm (1/4 in) to allow runoff to pass beneath them, minimizing concentrated flow that may lead to erosion of the bioretention areas. Curb and gutter surrounded the top of the "T" of the bioretention areas to delineate the cells and prevent vehicles from accidentally driving into the bioretention areas. A curb cut was installed in the curb and gutter to allow for overflow into the existing storm drains when the capacity of the cells was exceeded. Footbridges were also installed across the bioretention cells to allow customers and employees easy access to both sides of the bioretention areas (Figure 8). A dwarf variety of wax myrtle was planted in the cells to provide some woody vegetation for diversity and aesthetic purposes. The dwarf variety was chosen so that the view of the Port City Java building would not be obstructed.



Figure 7 Underdrains



Figure 8 Bioretention Cells

Mary Bridgers Stormwater Wetland (MB)

Site Description

Mary Bridgers Park is an area owned by the City of Wilmington that is classified as open space by the city. A 2.2 ha (5.5 acre) drainage area consisting of single family residential drains through the park before entering Burnt Mill Creek. Because the area was designated by the city as open space, there were no design constraints for the size of the wetland and, therefore, was sized appropriately to treat runoff from the 2.5 cm (1 inch) rain event. The 800 m^2 (8,605 ft^2) stormwater wetland consisted of 22% deep pools, 29% shallow water, and 49% temporary inundation zone (Hunt et al. 2007). The pools were 0.75 m (2.5 ft) deep and the shallow water areas were 10 cm (4 inches) to 15 cm (6 in) deep at normal pool. Burnt Mill Creek has had elevated bacteria levels in the area of Mary Bridgers Park (Mallin et al. 2006); therefore, the shallow water and temporary inundation areas were increased to promote bacteria removal (Figure 9). The level of the water in the wetland was controlled by an adjustable outlet control structure. Weir boards were installed in the outlet structure such that water is ponded to a depth of 30 cm (12 inches) in the wetland following rain events.

Wetland Construction

Construction began at the outlet structure and progressed to the inlet taking precautions to ensure that the equipment did not compact the finished surfaces. The banks and all disturbed areas outside the wetland banks were covered with a straw mat with a biodegradable net and seeded with a Bermuda mix (Figure 10). More than 3,500 plants were planted by volunteers from the surrounding neighborhoods including 4 cypress tress.





Figure 9 MB Stormwater Wetland Design Figure 10 MB Wetland After Construction

Residential Practices

Two residential practices, rain gardens and rain barrels, were installed at residences throughout the bottom area. Home owners interested in installing stormwater practices at their homes were initially identified at a workshop held in the bottom neighborhood. Site visits were conducted by NCSU and Cape Fear River Watch employees to evaluate the site and determine if a rain garden and/or rain barrel were appropriate.

Rain Garden Installation

Rain gardens were installed at eleven homes in the bottom area and at an assisted living home. Site visits were conducted to evaluate the impervious area that could be captured in a rain garden. The rain gardens were then sized and installed by the Cape Fear River Watch and their volunteers. A variety of vegetation was planted in the rain gardens. Rain gardens were installed to collect surface runoff in low spots on the property or roof runoff was routed into the rain garden by connecting the downspout using plastic corrugated pipe. An example of the rain gardens that were installed is presented in Figure 11.

Rain Barrel Installation

Rain barrels can be utilized to collect roof top runoff during rain events and can be used for irrigation between storms. Twenty four 246 L (65 gallon) rain barrels were distributed to home owners throughout the bottom area. Gutters were required for the rain barrels and were not covered by the grant funding. Homeowners had to demonstrate a demand for the water in order to qualify for the rain barrels. The rain barrels were installed by the homeowners at the end of an existing downspout (Figure 12).

Data Collection

Port City Java

Inflow volume was calculated based upon watershed characteristics and rainfall data recorded at the site. An ISCO rain gage was used to measure rainfall and trigger an ISCO 6712 sampler. The sampler was enabled and began taking samples when water was detected and took samples with every 3.8 mm (0.15 in.) of rain. A steel “trough” was constructed to pool a small amount of water at the edge of the parking lot so a sample could be taken. The location of the inlet sample was selected so that an area representative of the watersheds of



Figure 11 Residential Rain Garden



Figure 12 Residential Rain Barrels

both bioretention systems could be intercepted. To monitor outflow from the underdrains, steel weir boxes were constructed and mounted inside the concrete drop inlet, where underdrains daylighted, for both bioretention systems. Effluent flowed over a 30-degree weir plate for measurement.

ISCO 730 bubbler modules were used to measure the depth of flow over the weirs and calculate flow rate. The bubblers triggered ISCO 6712 automatic samplers to take flow-weighted composite samples for the storm. The sampler received pulses from the bubbler each time a pre-defined volume of water passed over the weir and then took a sample. Runoff from storm events up to 25 mm (1 inch) in size was expected to be fully captured by the bioretention cells.

Results and Discussion

Port City Java

Water quality results from the Port City Java Bioretention area are presented in Table 2. The bioretention cells showed some pollutant reduction except for fecal coliforms, Enterococcus, nitrate nitrite (referred to subsequently as nitrate), and ortho phosphorus (OP). The concentrations of OP entering the bioretention area are relatively low, and it is difficult to obtain significant reductions from these concentrations. The increase in nitrate is somewhat

Table 2 Concentrations and Removal Efficiencies for PCJ

Concentration	Median Influent	Median Effluent (Shallow n=7)	Reduction Efficiency	Median Effluent (Deep n=8)	Reduction Efficiency
Fecal (CFU/100mL)	5650	6132	-9%	2737	52%
Entericoccus (MPN)	272	692	-155%	460	-69%
TKN (mg/L)	1.88	0.56	70%	0.42	77%
NO_3&NO_2 (mg/L)	0.17	0.31	-81%	0.47	-176%
TN (mg/L)	2.05	0.87	58%	0.90	56%
NH_3-N (mg/L)	0.10	0.04	59%	0.03	68%
TP (mg/L)	0.28	0.19	34%	0.12	59%
Ortho P (mg/L)	0.03	0.07	-112%	0.02	22%
TSS (mg/L)	157.71	17.69	89%	11.00	93%
PAH (ng)	459	112	76%	39	91%

expected due to the fact that the bioretention is designed to dry and remain in an aerobic state.

The fact that there is an increase in fecal coliform bacteria and Enterococcus indicates that the bioretention area may not be drying out completely as bacteria thrive in damp environments. This is somewhat contradictory to the explanation for the increase in nitrate. The effluent water could also be contaminated by water from Burnt Mill Creek, although there is no data to show that the creek impacts the outlet of the bioretention. The bioretention areas did perform well in the area of TSS removal as expected. There was also a significant reduction of PAH's. Concentrations of PAH's were only detected in the first two storms and were undetectable in the remaining storm events. The parking lot was seal coated immediately prior to the completion of the bioretention project. Any PAH's in the seal coat may have been flushed during the first few events. There were also some differences in the concentration reduction efficiencies between the shallow and deep cells. The deep cells showed greater reduction efficiencies for each pollutant except for nitrate and TN. The greater reduction in fecal bacteria and increase in nitrates indicates that the deeper cell dries out at the surface more often than the shallow cell. Because of the proximity to Burnt Mill Creek it is possible that the water from the creek influenced the outlet of the shallower cell although there are no data to support this theory.

When the effect of the reduction in volume from the shallow bioretention is considered there is a reduction in each pollutant except for Ortho P (Table 3). Similar results were found in the load reductions form PCJ Deep (Table 4). The deeper cell showed a slightly greater volume reduction. This, in conjunction with greater concentration reductions, showed reductions in each pollutant in the bioretention cell.

Table 3 Pollutant Load from PCJ Shallow

Shallow Load (n=10)	Median Influent	Median Effluent	Reduction Efficiency
TKN (g)	15.0	2.8	81%
NO_3&NO_2 (g)	2.6	1.7	34%
TN (g)	17.7	4.5	74%
NH_3-N (g)	0.8	0.2	71%
TP (g)	2.4	1.0	58%
Ortho P (g)	0.2	0.3	-44%
TSS (g)	1551.7	87.3	94%
PAH(mg)	7.6861	0.2323	97%
Water Volume (L)	125248	61250	51%

Residential Practices

The rain garden and rain barrels were offered to home owners in the bottom neighborhood at no cost to them; however, their property had to be suitable for one of the practices, and they had to agree to maintain them after the grant ended. There had to be a defined drainage path where runoff could be intercepted by a rain garden or gutters where a downspout could be routed into the rain garden. Wilmington, being in the coastal plain, is very flat and several of the homes did not initially meet the criteria. Many residents in the bottom made the financial investment ($100 to $300) to install gutters on their homes in order to meet the criteria to receive a rain garden or a rain barrel. Home owners have taken ownership of their rain gardens in a variety of ways including adding decorative borders and supplementing the vegetation that was provided with additional plants from their surrounding landscaping.

Table 4 Pollutant Load from PCJ Deep

Deep Load (n=11)	Median Influent	Median Effluent	Reduction Efficiency
TKN (g)	28.4	5.0	82%
NO3&NO2 (g)	6.5	4.8	26%
TN (g)	34.9	9.8	72%
NH3-N (g)	2.1	0.4	80%
TP (g)	5.0	1.6	69%
Ortho P (g)	0.5	0.3	34%
TSS (g)	2,352.0	134.3	94%
PAH(mg)	19.57	0.6045	97%
Water Volume (L)	313580	138742	56%

A survey conducted by a graduate student in the College of Design Landscape Architecture Department at NC State University found that all of the residents involved in the residential project who responded to the survey were educated about stormwater runoff and water quality as a result of their involvement in the residential project. The survey revealed that the majority of the survey respondents involved in the Bottom Neighborhood Empowerment Association and the project were women above the age of 55 and long time residents of the community. It is important to note that the residential project generally excluded people who did not own their homes (100% of respondents owned their homes). Many of the respondents indicated that they shared what they learned with their neighbors, a significant accomplishment in accordance with the goals of the overall project. The survey also indicated that the residents responded to the emphasis placed on the beautification of their property using rain gardens rather than just stormwater management. According to the survey, word-of-mouth was the most effective tool for informing the residents about the BNEA and the residential program. Many of the homeowners who requested a rain garden or a rain barrel did so after seeing the practice installed at a neighbor's home. Also, visual information, such as fliers, captured people's attention. All of the respondents that participated in the residential program had some affiliation with the BNEA and three of the respondents became involved in the BNEA after they first became involved in the residential stormwater retrofit program (McCoy, 2007)

Conclusion

The Port City Java Bioretention area appears to be performing as expected based on the load reductions. There were higher than expected loads with respect to ortho phosphorus, however, the concentrations where low enough that reduction efficiencies may be difficult. The deeper cell showed greater load reductions indicating that the deeper media is more effective for pollutant removal including TSS, PAH, and pathogens where the pollutant removal generally occurs at the surface. The deeper cell may have greater capacity for infiltration allowing the surface to dry more than the surface of the shallower cell. Moisture probes have been added at the surface of both cells to determine if moisture content at the surface is a factor in pathogen removal.

Each of the stormwater BMPs installed has been well received by each of the land owners. All of the land owners have agreed to maintain the BMPs on their property, and have been provided BMP management guidebooks that were published by the City of Wilmington's Stormwater Services. All of the landowners were aware that stormwater runoff is an issue that must be addressed but were uncertain of how to proceed. The survey that was conducted

revealed the necessity of public education in the community. One of the main goals of the project, public education, was most widely accomplished by focusing on the BNEA. A greater impact on stormwater can be made at a residential scale if an emphasis is placed on stormwater treatment practices that provide beautification rather than just stormwater impacts.

Acknowledgements

The authors would like to thank the Burnt Mill Creek action team for the continued efforts in the Burnt Mill Creek watershed. They would like to thank the USEPA and NC DENR for funding the project. They would also like to thank the City of Wilmington Stormwater Services and Alicia Herrmann for her efforts in data collection and the Cape Fear River Watch and Joseph Abbate for his efforts in coordinating the rain garden and rain barrel installations.

References

Davis, A.P. (2007) "Field Performance of Bioretention: Water Quality," *Environ. Engg. Sci.,* 24(8) 1048-1063.

Dietz, M.E., and Clausen, J.C. (2006). Saturation to Improve Pollutant Retention in a Rain Garden. *Environ. Sci. Technol.*, 40, 1335-1340.

Grant, D.M. and B.D. Dawson. 2001. *Isco Open Channel Flow Measurement Handbook, Fifth Edition*. Isco, Inc. (Lincoln, NE).

Hunt, W.F., A.R. Jarrett, J.T. Smith, and L.J. Sharkey. (2006). "Evaluating bioretention hydrology and nutrient removal at three field sites in North Carolina. *J. Irrig. Drain. Eng*., 132(6):600-608

Hunt, W.F., M.R. Burchell, J.D. Wright, and K. L. Bass. 2007. Urban Waterways – Stormwater Wetland Design Update: Zones, Vegetation, Soil, and Outlet Guidance. AG-588-12. North Carolina Cooperative Extension Service.

Hunt, W.F., J.T. Smith, S.J. Jadlocki, J.M. Hathaway, and P.R. Eubanks. (2008). "Pollutant removal and peak flow mitigation by a bioretention cell in urban Charlotte, NC," *J. Environ. Eng*. (in press)

Mallin, M.A., L.B. Cahoon, Posey, M.H., Johnson, V.L., Parsons, D.C., Alphin, T.D., Toothman, B.R., Ortwine, M.L., Merit, J.F. 2006. Environmental Quality of Wilmington and New Hanover County Watersheds 2004-2005. CMS Report 06-01. Center for Marine Science, UNC-Wilmington.

McCoy, E.R. 2007. Choreographing Urban Sustainability with Communities: How can community building and the improvement of stormwater management systems support one another in low-income, urban neighborhoods?. A thesis submitted to the Graduate Faculty of North Carolina State University in partial fulfillment of the requirements for the Degree of Master of Science. Landscape Architecture. Raleigh, North Carolina.

NCDENR DWQ Planning Branch. 2004. *Assessment Report: Biological Impairment in the Burnt Mill Creek Watershed*. Collaborative Assessment of Watersheds and Streams (CAWS) project.110 pp.

NCDENR NC Wetlands Restoration Program (current Ecosystem Enhancement Program). 2002. New Hanover County Local Watershed Planning Initiative: Causes and sources of Water Quality Degradation in Burnt Mill Creek, Lower Smith, and Prince George Creeks. Prepared by KCI Associates of NC for NCWRP.

Modeling Stormwater Basins for Potential Retrofit Designs

R.R. Headley[1] and J.R. Wyrick[2]

[1]Undergraduate Research Assistant, Department of Civil and Environmental Engineering, Rowan University, 201 Mullica Hill Rd., Glassboro, NJ 08028; PH (609) 774-4277; FAX (856) 256-5242; email: headle74@students.rowan.edu
[2]Assistant Professor, Department of Civil and Environmental Engineering, Rowan University, 201 Mullica Hill Rd., Glassboro, NJ 08028; PH (856) 256-5380; FAX (856) 256-5242; email: wyrick@rowan.edu

ABSTRACT

Outflow structures for stormwater detention basins can vary widely within a single watershed. The designs are often left to the whim of the local engineer. Why should there be such differences? This research attempts to discern the performance and efficiency of various typical and atypical weir shapes. To accomplish this task, a scale model of a stormwater detention basin was constructed with removable outlet weirs. The physical model was calibrated using typical weir structures (e.g. rectangular, V-notch, submerged orifice, etc.) in which accepted numerical models exist to calculate outflow discharge. Empirical stage-discharge relationships were then calculated for the atypical weir structures (e.g. stepped notch, combinations of typical shapes, etc.). The atypical weirs simulated herein represent the range of outlet structure designs located in the Upper Mantua Creek watershed, Gloucester County, New Jersey. This area of New Jersey has experienced large urban growth in the past 40 years, and many of the existing basins were not designed for the current runoff volumes they experience. Within this 7.3 square mile watershed, there are currently 61 stormwater basins and more than 50 different outlet structure designs. The ability of each stormwater basin to pass or detain a given flow event can now be determined empirically. From these data, appropriate retrofit designs can be implemented.

INTRODUCTION

As urbanization increases within watershed boundaries, the effectiveness of stormwater detention basins to attenuate peak-flow rates also becomes increasingly more important. Common characteristics of the outlet structures within the detention basins include a low-flow orifice near the base of the structure, a weir or orifice opening above that for attenuating normal runoff volumes, and emergency overflow spillway to pass the extreme events. (Akan and Houghtalen 2003). The shape and size of the weir or orifice outlets for the normal runoff events can vary widely within a single watershed. As new outlets are designed and built, or old outlets re-tested for their efficiency at passing the newer, higher runoff volumes, a simple model is needed to accurately assess their capability. This research describes an effort to create a physical scale model of a detention basin with varying weir configurations to analyze the performance of any outflow structure.

The basin outlets modeled in this study are examples of the range of designs found within the Upper Mantua Creek watershed (Fig. 1). There are currently 61

stormwater basins and more than 50 different outlet structure designs within this watershed. Located in southwest New Jersey, Mantua Creek flows northwest towards its junction with the Delaware River. The study area encompasses about 7.3 square miles and is contained within five municipalities: Washington Township, Glassboro Borough, Pitman Borough, Mantua Township, and Monroe Township. The topography of the watershed is relatively flat with a few rolling hills at the headwaters. Prior to the 1970's, the land use was dominated by agriculture. Based upon land use data from the New Jersey Department of Environmental Protection (NJDEP), over the past forty years, urban development has increased from 45% to 67% of the watershed while agriculture has decreased from almost 30% to less than 10%. This decrease in pervious land cover has led to increases in peak runoff volumes in Mantua Creek.



Figure 1. Location of the Upper Mantua Creek Watershed (in black) in New Jersey

RELEVANT THEORY

Most outflow structures in detention basins can be considered as sharp-crested weirs (SCW). For typical SCW configurations, theoretical numeric solutions for discharge relationships exist in the literature (e.g., Ackers, et al. 1978). These discharge relationships are dependent on the depth of ponding above the weir crest. For a rectangular SCW, the outflow discharge is a function of the depth to the 3/2 power (Eq. 1a) and the effective width of the over-fall (Eq. 1b). For a V-notch SCW, the discharge is a function of the depth to the 5/2 and the internal angle (Eq. 2). Flow through a submerged orifice is a function of depth to the 1/2 power and the size of the orifice (Eq. 3).

$$Q = C_d \frac{2}{3} \sqrt{2g} B' H^{3/2} \tag{1a}$$

$$B' = B - 0.1nH \tag{1b}$$

$$Q = C_d \frac{8}{15}\sqrt{2g}\tan\left(\frac{\theta}{2}\right)H^{5/2} \tag{2}$$

$$Q = C_d\sqrt{2gH}\,A \tag{3}$$

Where, Q is the discharge, C_d the discharge coefficient, g the acceleration due to gravity, B' the effective width of the weir, B the channel width, n the number of contracted sides (0, 1, or 2), H the depth of the flow above the weir crest, Θ the internal angle of the V-notch in the weir, and A the cross-sectional area of the orifice.

For all theoretical discharge solutions, a discharge coefficient (C_d) is used to amend the flow calculations. This discharge coefficient can vary with the type of weir structure, and accounts for errors in the theoretical derivations due to assumptions about the pressure distributions, water surface profile, and viscous effects (Chin 2006). For a rectangular SCW, the discharge coefficient is a function of the flow depth and weir height (Eq. 5). For a triangular SCW, the discharge coefficient (Eq. 6a) is a function of the Reynolds Number (Eq. 6b) and the Weber Number (Eq. 6c) (Chin 2006).

$$C_d = 0.611 + 0.075\frac{H}{H_w} \tag{5}$$

$$C_d = 0.583 + \frac{1.19}{(Re\,We)^{1/6}} \tag{6a}$$

$$Re = \frac{g^{1/2}H^{1/2}}{\upsilon} \tag{6b}$$

$$We = \frac{\rho g H^2}{\sigma} \tag{6c}$$

Where, H_w is the height of the weir crest above the channel bottom, Re the Reynolds Number, We the Weber Number, υ the kinematic viscosity of the fluids, ρ the fluid density, and σ the surface tension of the fluid.

For submerged orifices, the discharge coefficient is required because of the vena contracta phenomenon, which is due to the fluid's inability to turn a sharp corner (Munson, et al. 2006). This value is usually assumed to be 0.61 for the type of model outflow structure present in the experimental basin (Mays 2005). Often, discharge equations for weirs may combine the gravitational and numeric constants with the discharge coefficient to create an all-encompassing weir coefficient, C_w. It is this weir coefficient that will be compared and calibrated for the physical model presented herein, and discussed in the following sections.

EXPERIMENTAL METHODOLOGY

Outflow discharges for basin outlet weirs are typically determined using numerical models.

In order to accurately depict the outflow through the weirs in this study, a scale model detention basin was built with replaceable weir configurations (Fig. 2). The walls of the model basin were constructed out of Plexiglas and the weirs from 0.25-in thick aluminum plates. The dimensions of the model basin are 36-in x 36-in x 22-in with a 6-in high weir structure, which provides a basis for varying length scales for comparisons to actual stormwater basins. The comparatively over-sized side walls (22 inches) prevented losses from splashing and spills (Fig. 2).

.

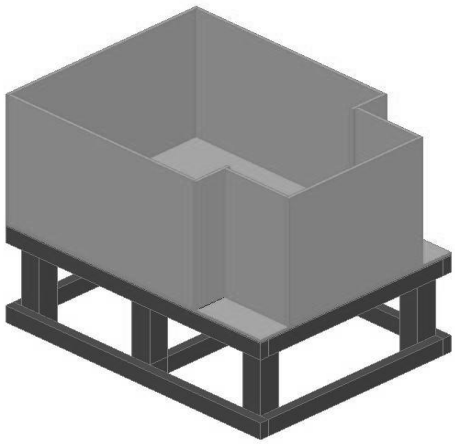

Figure 2a. Computer Rendering of Model Detention Basin.

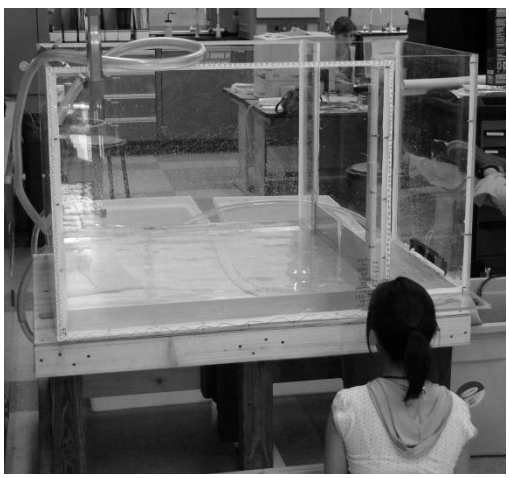

Figure 2b. Measuring Discharges in Model Detention Basin.

Of the 61 stormwater basin designs in the Upper Mantua Creek, six distinct outflow weir configurations were chosen to be modeled for this study. Some of the weirs chosen represent typical configurations, such as a contracted rectangle, V-notch, and a submerged circular orifice (Fig. 3). These "typical" configurations were chosen to validate the model using accepted numeric equations (Eqs. 1, 2, and 3). The other weir shapes modeled here represent atypical configurations (Fig. 4) that do not have simple numeric solutions.

Most basin outflow weirs are also equipped with low-flow orifices (e.g., Fig 3 a-c). These allow for small runoff events to pass through the basin unabated, while larger events will pond behind the outlets. The theoretical discharge calculations accounted for these low-flow outlets, and thus used a combination of Equation 3 with either Equation 1 or 2.

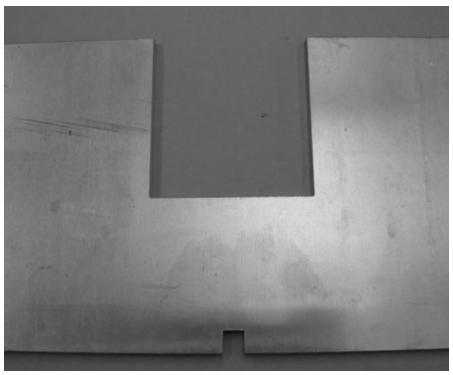


3a. Contracted Rectangular Weir

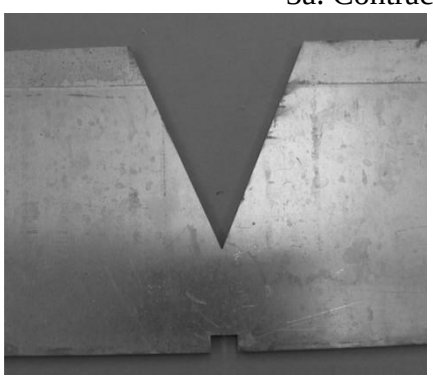
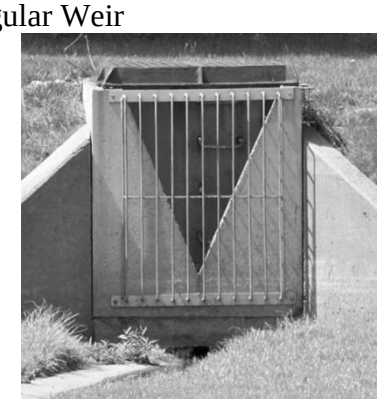

3b. 49° V-notch Weir

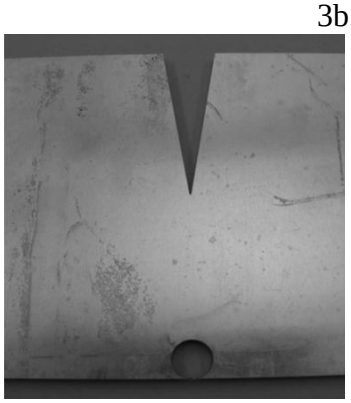
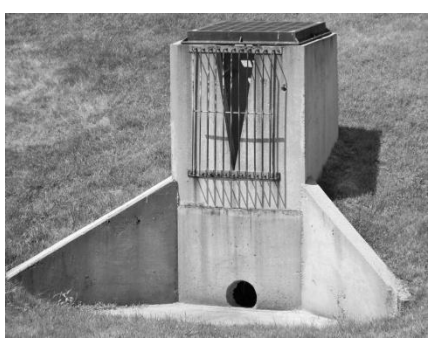

3c. Perched 22° V-notch Weir

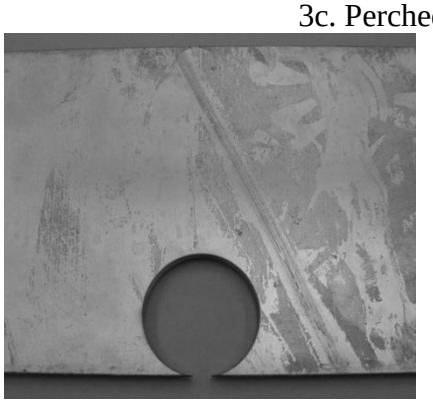


3d. Circular Orifice

Figure 1. Typical Outlet Weir Configurations Used in the Scale Model.

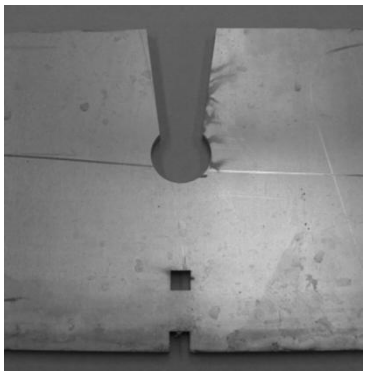


4a. Keyhole Combination Weir

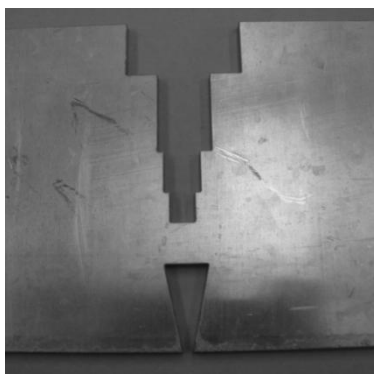


4b. Stepped Notch Weir

Figure 4. Atypical Weir Configurations used in the Scale Model

The flowpath through the model includes water being pumped from a reserve reservoir into the model basin, over or through the weir, and out an exit orifice into a catchment basin. To quantify the discharge rate of each weir structure, the incremental changes in storage volume behind the weir were measured visually over time with a depth gauge and a stopwatch (Fig. 2b). Each weir and discharge rate was modeled at least five times to ensure accuracy.

RESULTS & DISCUSSION

To calibrate the physical model, theoretical flows for the typical weir configurations (Fig. 3) were modeled using Equations 1-3. The empirical depth-discharge data measured for each scale model weir was then compared, and was modified with a varying discharge coefficient until the theoretical and experimental data matched. The overall shape of the empirical data fits very well with the theoretical data (Figs. 5 and 6), thus the coefficient modification only resulted in a shift of the data points.

Figure 5 represents the comparison of the theoretical depth-discharge relationship for a contracted rectangular weir (Fig. 3a) to the empirically collected

model data after the sensitivity analysis was performed on the discharge coefficient. Figure 6 represents the comparison for the wide V-notch weir (Fig. 3b).

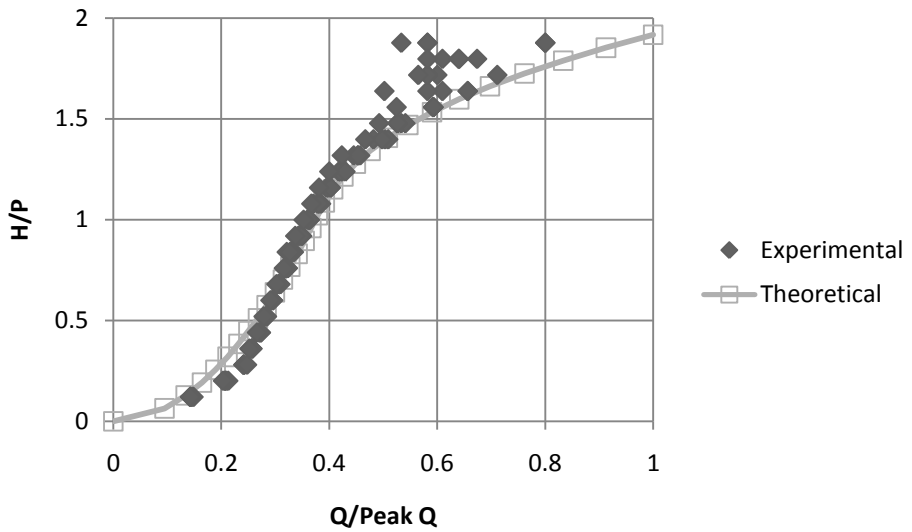

Figure 5. Relationship of Depth (normalized by weir height) to Discharge (normalized by peak discharge) for the Contracted Rectangular Weir (Fig. 3a)

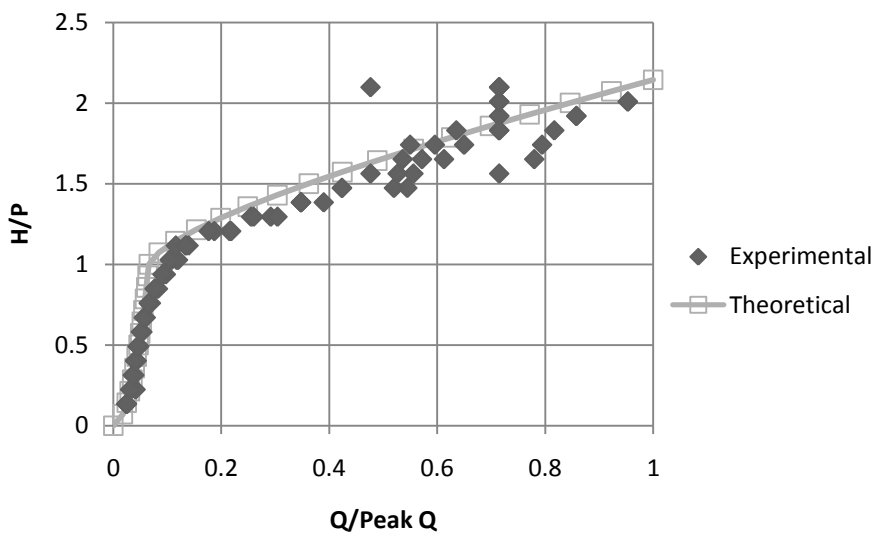

Figure 6. Relationship of Depth (normalized by weir height) to Discharge (normalized by peak discharge) for the Perched V-notch Weir (Fig. 3c)

A sensitivity analysis was performed on each of the typical weir configurations to determine their empirically-derived discharge coefficients (Table 1). The sensitivity analysis included the altering of only the discharge coefficient for the lower orifice of the outflow structure. This was done because the data for the theoretical and experimental outflow in the upper sections of each weir were in relative agreement already.

Table 1. Discharge Coefficients for Lower Orifices after Sensitivity Analysis.

Weir	C_d *Value*
Rectangular	2
Perched V-notch	1
Wide V-notch	2
Circular Orifice	0.61

The empirically-solved discharge coefficients listed in Table 1 are greater than normal expected values, which typically range from 0.5-0.7. Several factors could be the cause for this discrepancy. The first is that the available material constrained the width of the model weir plate to be 0.25 inches and the typical widths of the actual outflow structures are 6 – 8 inches. For the length scale factor based on the weir heights, the model weir width should be about 0.07 inches. It is unclear whether this factor is providing a significant difference in experimentation but will be further researched. Another factor that could potentially be skewing the experimental data is the material used for the model. The aluminum used in the model does not exhibit the equivalent scaled roughness compared to the concrete used in the actual outflow structures. The variable roughness's of these materials could cause some discrepancies and also need to be further researched.

Table 1 at least provides a range of C_d values with which to calculate the depth-discharge relationships for the atypical weir configurations (Fig. 4). Figure 7 represents the empirical data for the keyhole-shaped weir (Fig. 4a). Superimposed onto the data are the original design calculations provided by the local soil conservation district. The methodology for the original design values is unavailable, but the data do correspond fairly well to the empirical model data.

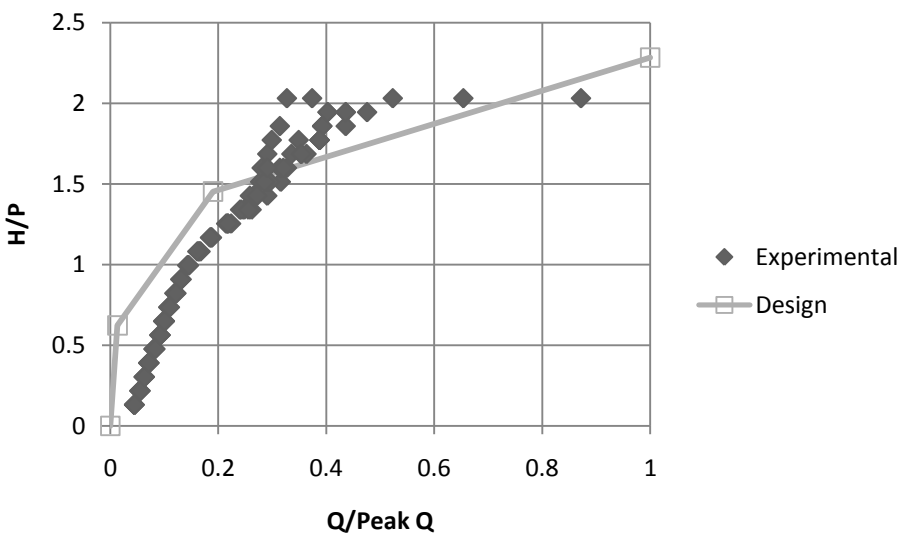

Figure 7. Relationship of Depth (normalized by weir height) to Discharge (normalized by peak discharge) for the Keyhole Weir (Fig. 4a)

Once the data presented in Figure 7 are determined to be accurate enough, a weir coefficient (C_w) for the upper section of the weir can be derived (i.e. the "keyhole" section). To determine this weir coefficient, the general weir equation, $Q = C_w\sqrt{H^3}$, is used. A plot of discharge versus $\sqrt{H^3}$ was created for each of the atypical weir structures. The slope of a linear trendline fitted to the data provides the weir coefficient for the upper section of the weir (Fig. 8). The depth, H, used for these analyses represent only the depth of flow above the upper weir crest, thus the non-zero value for H=0 accounts for the low-flow orifice.

The weir coefficient calculated for the Keyhole weir was determined to be 0.09 (Fig. 8) and for the Stepped Notch it was 0.12. These values may be lower than expected, but they might be offset due to the previously described theoretical discrepancies in the low-flow outlets.

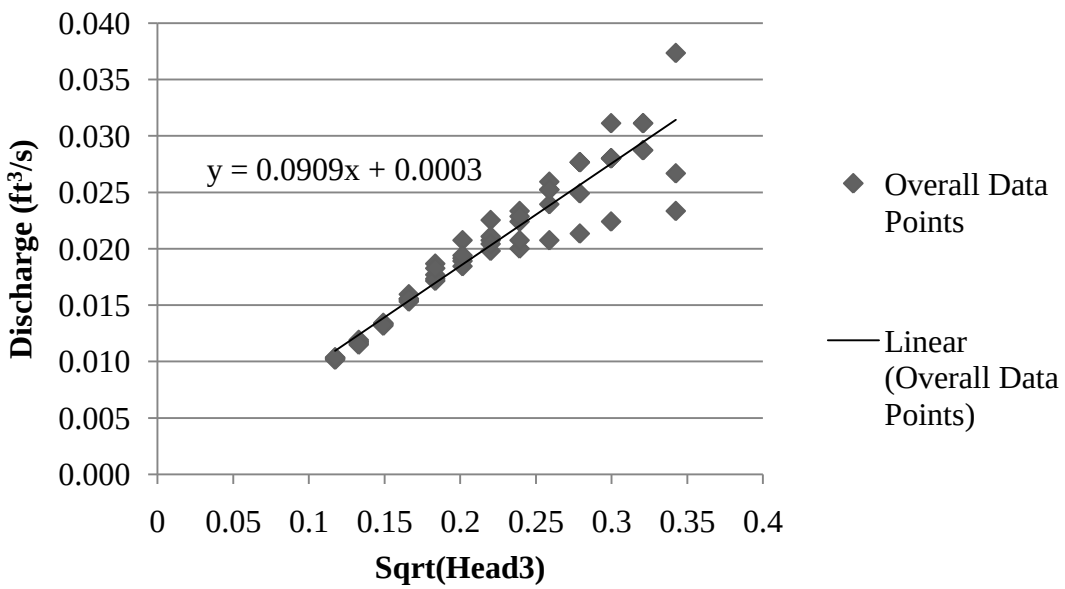

Figure 8. Experimental Data used to determine Discharge Coefficient for the Keyhole Weir.

CONCLUSIONS AND FUTURE WORK

Physically-based models of detention basin outlet structures are rare in hydrology research experiments. However, they could be a quick and effective method to predict their performance, especially if older structures are tasked to handle new and greater runoff inflow volumes. Using a physical model can help determine the efficiency of any new or old structure, and help to determine if any retro-fits are required for older structures.

The model presented herein represents a step forward in physically-based scale models. The calibration and validation of the model may not yet be perfect, but

overall results are in relative agreement, and any model discrepancies will likely be resolved soon.

Because the most common method for modeling detention basin outlets is the use of numerical models such as HEC-HMS (e.g., Emerson et al. 2005), the obvious future for this model study is to compare the physical scale model data to the numerical, computer-derived data. That study is currently underway.

REFERENCES

Ackers, P., White, W., and Perkins, J. (1978). *Weirs and Flumes for Flow Measurement*. John Wiley & Sons, Inc.

Akan, A and Houghtalen, R (2003). *Urban Hydrology, Hydraulics, and Stormwater Quality*. John Wiley & Sons, Inc.

Emerson, C., Welty, C., and Traver, R. (2005). Watershed-scale evaluation of a system of stormwater detention basins. *Journal of Hydraulic Engineering, 10 (3)*, 237-242.

Mays, L (2005). *Water Resources Engineering*. John Wiley & Sons, Inc.

Munson, B., Young, D., and Okiishi, T. (2006). *Fundamentals of Fluid Mechanics*. John Wiley & Sons, Inc.

Chin, D (2006). *Water-Resources Engineering*. Pearson Prentice Hall.

Stormwater Infiltration Retrofits
Experience Gained Through Long Term Monitoring

R. G. Traver

Professor, Dept of Civil & Environmental Engineering, Villanova University, Villanova, 19085; PH (610)519-6754; email: Robert.Traver@Villanova.edu

ABSTRACT

This paper presents an overview of the experience gained through the design, construction and extended monitoring of multiple retrofit stormwater infiltration best management practices (BMP). Common design issues for retrofit infiltration BMPs include utilities, hydraulic inflow and outflow paths, and compacted urban soils. Assuming these constraints are addressed, the resulting project should work at least as well as any newly constructed BMP.

The experience of long term monitoring of multiple BMPs allows the researcher to contrast performance and design features for both individual storms and seasons. Simply building new BMPs in a public setting introduces this concept to the professional community and the public. Findings from a suite of project reports, journal and conference proceedings, and student work is presented.

INTRODUCTION

While information on the design of stormwater infiltration Best Management Practices (BMP) for newly urbanizing sites is becoming available, retrofitting existing sites is still somewhat of a mystery. Compacted soils, limited hydraulic pathways, existing utilities all complicate the design requiring the designer to be innovative, and to understand the opportunities that are available. Additional perspective of the character and performance of these infiltration BMPs has been gained through long term monitoring of the sites through the Commonwealth of Pennsylvania's 319 non point source program (Emerson and Traver 2008, Traver 2008). A major benefit of continual monitoring is the marriage of observation and performance data, and a continuum of research, with each component building upon the past. This paper will first review three individual infiltration BMPs, and conclude with overall conclusions based upon the body of work.

RETROFIT INFILTRATION BMPS

Funding for developing the BMP park concept, as well as for construction of the BMPs was provided by Pennsylvania Department of Environmental Protection through Section 319 Nonpoint Source Pollution Program, Pennsylvania's Growing Greener initiative, and donations from the Villanova Urban Stormwater Partnership (VUSP) corporate partners (Traver 2002a, 202b, 2004, 2005). As of the submittal date of this publication, the park includes a stormwater wetland, two green roofs, an infiltration trench, two bioinfiltration BMPs, three pervious pavement sites, and a

historic seepage pit. Construction is expected in the immediate future on several bioretention / bioinfiltration type BMPS to include a bioswale. Each of these sites with the exception of the historic seepage pit are retrofits, each with its own set of challenges and lessons learned. Information on each project can be found through the VUSP website (http://www.villanova.edu/VUSP).

Bioinfiltration BMP Two Bioinfiltration BMPs are now on campus. The first was constructed in the summer of 2001 from an existing traffic island (Traver 2002b). Funded by the Pennsylvania Growing Greener program, the site has been monitored since 2003. The facility was designed to capture and infiltrate the initial first 2.5 cms of rainfall from the site, but routinely exceeds those performance criteria. A second newer bioinfiltration site has been built as part of a university expansion of the Villanova Pavilion. It was built to meet state requirements for stormwater management, and to partially replace an existing detention basin.

Retrofit lessons learned on this site included hydraulics of how to get the flows into the bowl of the traffic island, outflow, utilities, and compacted soils. First and foremost the existing utilities were located. Utility lines, and lighting, are routinely included in green strips in existing parking areas. These also can be an asset to the project for monitoring (communications / power). The hydraulics of the site was the second challenge. Clearly the capture of flows off the impervious surface is key. This first flush is the most frequent and dominate source of runoff, and capturing it maximizes the capture efficiency of the BMP (Batroney 2007).

For the traffic island site, two methods of ingress were used. First adjacent runoff was directed into the site using curb cuts, located through observation during storm events. As part of this process, an inlet was filled with rock and paved over to capture more surface inflow. A second inlet was located adjacent to the site that carried flows from multiple inlets upstream. By insuring that the bottom of the inlet was lower than the BMP bowl, flow was redirected by cutting through the back of the inlet, installing a culvert into the BMP, and constructing a redirection barrier within the inlet. The barrier also acts as a weir, allowing overflow to be directed through the original site drainage system to a detention basin. Similar concepts were used for the Pavilion site, except an inlet structure was used for overflow, connected by piping to a new underground detention structure. Note that in both cases, the great majority of runoff is infiltrated and never reaches the detention structure.

In both cases, compacted soils were a design consideration. By insuring that the depth of excavation was deeper then the compacted layer, no difficulties were encountered. The excavation needed for the bowl and made soils was well below any compacted layers.




Figure 1 - VU Bioinfiltration BMPs (Traffic Island Left – Pavilion Right)

Infiltration Trench Constructed in August 2004, the project is designed to capture runoff from an elevated parking deck and then infiltrate it through a rock bed into the ground (Traver 2002b). Funded through the state / EPA 319 program, this BMP presents some unique possibilities. It is the only site available with a 100% impervious drainage area, and is purposely undersized to speed aging of the site. The void space in the rock is filled quickly at around 0.5 cms. It is postulated that the bottom of the trench has sealed and all infiltration occurs through the sides (Emerson 2007, Emerson and Traver 2008)

Retrofit lessons learned on this site again included hydraulics of how to get the flows into the bowl of the traffic island, outflow, utilities, and depth to bedrock. In this case depth to bedrock dictated the location. As the site was in between two separate buildings that were constructed at different times, and had legacy utilities, locations of water, power, telephone, sanitary and storm sewer dictated the footprint precisely. An adjacent tree was expected to be damaged, but in the long run benefited from the runoff infiltration. Depth to bedrock also drove the site selection. Core samples at the original site showed rock close to the surface. By moving only 20 feet down slope, the depth to bedrock tripled enabling the project. Compaction was not an issue due to the depth if the infiltration trench.

As the runoff was captured from an elevated parking garage, it was relatively simple to reroute the piping under the parking deck to the infiltration trench, and to create measurement points. Overflow though was more of a challenge. A small pipe was routed close to the surface exiting to an adjacent inlet. Larger storms exit as sheet flow rising through the EP Henry Ecopavers that are the cover of the Infiltration Trench. Note that these pavers are designed to permit infiltration.

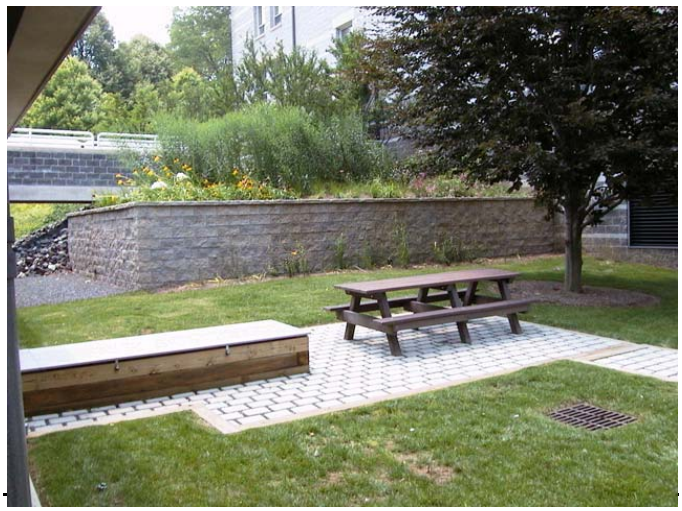

Figure 2 - VU Infiltration Trench BMP

Pervious Pavements

The original Porous Concrete site has been joined by two other pervious pavement sites to include a pervious asphalt site, and a Porous Concrete / Pervious Asphalt. This discussion focuses on the original site constructed through the 319 program in summer 2002 (Traver 2004). Note that due to the size of this project it had to be constructed in the summer as it is a pedestrian mall in the center of the campus. Noise and service interruption are a concern for retrofit projects. The grant was to create a porous concrete infiltration facility in an existing central paved area on the Villanova University campus. The site is much larger than the previous two projects, capturing flows from the roof top and the pervious surface. The retrofit design issues of utilities, compacted soils, and hydraulics was actually much simpler due to the scale of the project. There was much less uncertainty over utilities as in general they were relocated, and the depth of the beds was well below any compacted layer.

The hydraulics of the collection system was again the prime design feature. As the site was surrounded by buildings, runoff was directly connected to the underground rock bed, plus of course the infiltration through the porous surface. Due to the slope of the site, the rock bed was designed as three rock beds each separated by an earthen dike. The design engineer installed a collection system immediately below the surface to prevent overflow which was routed to the existing downstream stormwater collection system. Note that the designer also included an under drain which in hindsight was either not needed, or should have included a valve to restrict flows between beds. Note that there were several surface materials issues at the site that have previously been reported (Traver 2004). Since that time the pervious concrete industry has matured, and our second site had no similar issues.



Figure 3 - VU Pervious Pavement BMPs

PROJECT FINDINGS

When researching the performance of multiple BMPs monitored continuously over multiple years, the resulting findings are greater than the sum of the parts. The ability to contrast observations and results, plus the ability to compare past work provides insight into the mechanisms and characteristics of the BMPs. The below findings from the 319 program are an overview of the results from multiple student and faculty research projects over the last 5 – 7 years. Note: These findings are the author's interpretation of accumulated results from the combined research projects support through the 319 EPA National Monitoring Program, Growing Greener, and CiCEET funding, as presented in journal articles, masters thesis's, and research project reports as listed in the references.

Major Findings

- Proof of Concept: Results from constructing, operating, and monitoring infiltration practices has proven that these devices are an effective Stormwater Management Practice in removing pollutants and volume from the surface stream.

- Effectiveness of Small Storm Capture: The efficiencies of designing for small storms has been proven. Results from the infiltration trench, pervious concrete, and bioinfiltration traffic island have shown that because the majority of the regions rainfall is produced by smaller storms, BMPS designed for smaller storms are extremely effective in reducing runoff volume and capturing surface pollutants. If has also been shown that infiltration occurs throughout the storm event, and should be included when estimating removals.

- Variability of Infiltration Rate: Results from all three sites have shown that while the rate of infiltration is consistent over an individual storm event, it is dependent on season / temperature and thus considerable variation is seen

when looking across a year of events. Several papers have been published that relate at least part of this variation to the change in viscosity of the water. Note that on a yearly basis, this variation has not diminished the BMP's performance, but does impact municipal inspection / monitoring programs.

- Variation in Pollutant Loading Rate / First Flush: One result has been that the runoff from contributing areas has been found to vary considerably in quality. For example, roof top runoff from taller buildings has been found to be remarkably free of TSS, which makes it an ideal candidate for infiltration. The same was found for the Pervious Concrete site which is a pedestrian area. Contrasting the Infiltration Trench has extremely high loading of pollutants.

- Longevity: A study based upon the results of this project has shown that there is no statistical reduction in performance for the BioInfiltration Traffic Island after 7 years, or from the pervious concrete site after 4 years. In fact there is every expectation that these sites will remain effective for a very long time. Longevity is supported through proper design, construction, and location (characteristics of the drainage area). For the bioinfiltration BMP, freeze thaw, and vegetation are aiding in maintaining the infiltration capacity. For the pervious concrete BMP, the lack of suspended sediments in the rooftop runoff, the filtering through the pervious concrete, and the large bottom area support its longevity. Conversely a considerable change in performance has been seen at the infiltration trench due to the theorized clogging of the bottom layer. It should be noted, that it is estimated that when compared to the design recommendations of the Pennsylvania BMP manual, the infiltration trench has experienced a pollutant load closer to over 80 years when compared to the Pennsylvania BMP Manual specifications, and remains extremely effective (Emerson 2008, Emerson and Traver 2008).

Indirect Benefits

Besides the engineering research findings, the construction and research on the performance of BMPs has multiple indirect benefits.

- Introduction to the Profession: These sites have introduced the concept of infiltration BMP's to both the profession and the public across Pennsylvania and beyond. Lessons Learned as to design, maintenance, and expected performance are disseminated through publications, presentations, tours, and the project internet site.

- Catalyst for Advanced Studies: Through the continuing data stream, more advanced studies are using this data. Projects with CICEET sharing data with University of Maryland and NC State are underway, as are funded projects with William Penn working with Temple University.

- Catalyst for Studies by others: The data submitted to the ASCE – EPA BMP National Database is supporting other studies nationwide on BMP Performance.

- Education: The graduate and undergraduate students who are supported on these grants enter the workforce as engineers with advanced understanding of stormwater design to mitigate nonpoint source pollution. In addition, these results are used in undergraduate and graduate engineering classes at Villanova, supporting the advancement of the profession, and aiding in the protection of the water resources of the Commonwealth.

CONCLUSION

Retrofitting infiltration BMPs in the urban environment is clearly possible and is an effective strategy to reduce the impact of past urbanization. While the fundamental engineering design principals are the same as for new construction, the site design may be limited by hydraulic gradients and utilities. This may also be an opportunity as the existing drainage structure can be incorporated as inflow / outflow to the infiltration BMP. Note that in some cases retrofit designs may actually be an easier process, especially compared to new projects with large cuts and fills.

The value of multiple continuously monitored sites is clear. The variability of performance, longevity, effects on the surrounding environs, and issues to include maintenance and longevity can only be addressed with long term records. The multiple sites allow direct comparison of design components.

These results confirm the need to continue studying the operation of these BMPs. The relations between site characteristics, load and volume to BMP design are still poorly understood. As the understanding of the processed involved advance, the VUSP expects that the design methods used for these BMPS will change, to more accurately represent the hydrologic, chemical and biological processes involved.

REFERENCES

Batroney, T., The Implications of the First Flush Phenomenon on Infiltration BMP Design, Civil and Environmental Engineering. Villanova, PA, Villanova University.

Davis, A. Hunt, W. Traver, R., "Bioretention Technology: An Overview of Current Practice and Future Needs." ASCE Journal of Environmental Engineering – (in press)

Braga, A., Horst, M., Traver, R. "Temperature Effects on the Infiltration Rate through an Infiltration Basin BMP", Journal of Irrigation and Drainage, ASCE 2007 Nov/Dec 2007

Emerson, C. (2008). Evaluation of Infiltration Practices as a Means to Control Stormwater Runoff. Civil and Environmental Engineering. Villanova, Villanova. **Doctor of Philosophy:** 331.

Emerson, C., Traver R., "Long-Term and Seasonal Variation of Stormwater Infiltration Best Management Practices," Journal of Irrigation and Drainage – ASCE Sep/Oct 2008

Ermilio, J. R. (2005). Characterization Study of a Bio-Infiltration Stormwater BMP. Civil and Environmental Engineering. Villanova, PA, Villanova University. **Master of Civil Engineering:** 238.

Heasom, W., *et al.* (2006). "Hydrologic Modeling of a Bioinfiltration Best Management Practice." Journal of the American Water Resources Association **42**(5): 1329-1347.

Kwiatkowski, M, Welker, A., Traver, R., Vanacore, M., Ladd, T. "Evaluation of an Infiltration Best Management Practice (BMP) Utilizing Pervious Concrete", AWRA, Oct 2007

Prokop, M. J. (2003). Determining the Effectiveness of the Villanova Bio-Infiltration Traffic Island in Infiltrating Annual Runoff. Civil and Environmental Engineering. Villanova, PA, Villanova University. **Master of Civil Engineering:** 103.

Traver, R. G. (2002a). Villanova Stormwater Best Management Practice Demonstration Park - Phase 1 - Planning. PaDEP Growing Greener Program Project Report, Villanova University.

Traver, R. G. (2002b). Villanova Stormwater Bioinfiltration Traffic Island Growing Greener Grant Final Project Report, Villanova University.

Traver, R. G. (2004). Villanova Stormwater Best Management Practice Porous Concrete Demonstration Project. PaDEP 319 Program Project Report, Villanova University.

Traver, R. G. (2005). Villanova Stormwater Best Management Practice Infiltration Trench Demonstration Project. PaDEP 319 Program Project Report, Villanova University.

Traver, R. G., *et al.* (2007). "Bioretention and Bioinfiltration BMPs: Three researchers experience." Stormwater **8**(7).

Traver, R. G. (2008). VUSP ~ PaDEP - Best Management Practice National Monitoring Site- Year 5 PaDEP 319 Program Yearly Project Report, Villanova University.

Welker, A., Gore, M.,Traver, R. "Evaluation Of The Long Term Impacts Of An Infiltration Bmp", ICHE The 7th In. Conf. on Hydroscience and Engineering (ICHE-2006)R. G. (2008).

A Tool for Determining Effectiveness and Whole Life Costs of BMPs

C.C. Olson[1], L.A. Roesner[1] and B.R. Urbonas[2]

[1]Department of Civil and Environmental Engineering, Colorado State University, Fort Collins, CO 80523; PH (970) 491-2838; FAX (970) 491-7727; Email: colson23@engr.colostate.edu, Larry.Roesner@colostate.edu

[2]Urban Watersheds Research Institute; PH (303) 728-4449; Email: burbonas@urbanwatersheds.org

ABSTRACT

This paper describes the development of a tool that can be used to determine cost effective stormwater management strategies on a watershed scale, using various structural stormwater best management practices (BMPs). The tool is designed for application at the planning level and is simple enough to be used and understand by both technical and non-technical personnel in the stormwater management field. With relatively few required user inputs, the tool estimates the following:

- BMP effectiveness; reported in terms of the reduction of annual pollutant loading to the receiving water
- BMP whole life cycle costs; reported as the net present value of all costs incurred over the economic life of the BMP
- BMP cost effectiveness, reported in terms of cost per mass of pollutant removed from the receiving water

The tool is applied to a theoretical problem where a municipality must reduce pollutant loads from an existing, highly-developed urban setting. Several scenarios that meet the regulatory objectives are determined using different BMP technologies, and the differences in whole life cycle costs for each scenario are presented. The results show how the tool is useful in making better decisions based on the cost effectiveness of BMPs. In addition, the results show the importance of including long-term costs of maintenance and rehabilitation in evaluating cost effectiveness. *NOTE*: *At the time of writing this paper and preparing the example application, the tool was still in "beta" version. The results and methods used here may differ from those presented at the conference and in subsequent versions of the tool. Please contact the authors for the most up-to-date versions of the tool and documentation.*

INTRODUCTION

Structural best management practices (BMP) are constructed facilities that prevent, capture and/or treat stormwater runoff. There are many types of structural BMPs available, each with their own advantages and disadvantages. Over the past 20-30 years, hundreds of thousands (perhaps even millions) of BMPs have been constructed throughout the United States at a considerable cost to the public. In most cases, the decision to select one BMP over another in a given situation was based on site-

specific and/or short-term constraints such as construction costs, land availability and/or the acceptance level of a BMP by the regulating authority (based on "proven" BMP performance). However, the state of the stormwater management planning practice is evolving, and it is becoming better understood that the decisions made to select certain BMPs will have broader, more long-term ramifications that include (1) the effectiveness in the protection of the receiving waters, (2) long-term costs of operating and maintaining the BMPs, and (3) administrative costs that the municipality will need to budget for over the years to make sure that the BMPs deployed within its boundaries continue to function as originally designed.

The primary objective of this tool is to provide professionals and decision makers with facts and fiscal information on what effects their decisions will have on the financial and environmental resources of the owners and/or municipality in which the BMPs are deployed, over the long-term. The tool, developed in Microsoft Excel® specifically for use in communities on the Front Range of Colorado, allows the user to efficiently determine the expected effectiveness and whole life costs (capital plus long-term maintenance/administration) of various BMPs when implemented within a watershed. The user enters watershed data (i.e. land use, contributing area, slope, etc.) into the tool, and then selects what types and sizes of BMPs will be implemented within the watershed. The model generates outputs for: average annual pollutant emissions from the watershed (without BMPs), average annual pollutant loading to receiving waters (with BMPs), average annual runoff volume generated from watershed (without BMPs), average annual runoff volume entering receiving waters (with BMPs), and net present value of all initial and future costs. The user can test different scenarios of BMP application in a watershed to determine which scenario most cost effectively removes pollutants from stormwater discharges on an average annual basis.

The tool can be used to evaluate the cost effectiveness of 12 structural BMPs; constructed wetland basin (CWB), constructed wetland channel (CWC), extended detention basin (EDB), hydrodynamic separator (HS), inlet insert (II), media filter vault (MFV), porous landscape detention (PLD), retention pond (RP), sand filter basin (SFB), sand filter vault (SFV), sediment/oil/grease separator (SOG), vault with capture volume (VCV).

METHODS

The methods used to quantify whole life cycle costs and BMP effectiveness are described in the following sections.

Whole Life Cycle Costs

Whole life cycle costs associated with constructed facilities typically include; 1) capital costs, 2) land costs, 3) annual operation and maintenance (O&M) costs, 4) infrequent rehabilitation/replacement costs, and 5) salvage value. In addition, Urbonas (pers. comm.) recommends that the administrative costs of operating a stormwater management agency also be included as an annual cost.

Capital Costs

Capital costs are the costs of planning, designing and constructing a facility. There have been many studies conducted over the past 20-30 years to identify the construction costs of BMPs. Table 1 summarizes the BMP construction cost estimates used in the tool. The original cost estimates were adjusted to May 2008 costs using the Engineering News Record Construction Cost Index (ENRCCI)[1].

Table 1: BMP construction cost estimates provided in the literature

BMP	Construction Cost ($2008)	Source	Notes
CWB	34,973(A) - 75,893(A)	USEPA, 1999a	
CWC	17,487(A) – 37,946(A)		Assume 50% of CWB costs, no better information available
EDB	$15.94(V)^{0.694}$	Wiegand et al, 1986	
HS	2,200(F) - 18,333(F)	USEPA, 1999b	
II	145(E) - 2,173(E)	USDOT, 2008a	
MFV	$58,231(IA)^{0.882}$	Wossink and Hunt, 2003	Assumed same as sand filter vault.
PLD	$6,178(IA)^{0.796}$	Wossink and Hunt, 2003	
RP	35,592 + 0.45(V)	SEWRPC, 1991	
SFB	30,390 + 0.63(V)	SEWRPC, 1991	
SFV	$58,231(IA)^{0.882}$	Wossink and Hunt, 2003	
SOG	3,266(IA) – 4,899(IA)	APWA, 1992	
VCV	$56.69(V)^{0.681}$	USDOT, 2008b	For concrete structure

Notes:
E - each
F – design flowrate of BMP (cfs)
IA – contributing area to BMP (impervious acres)
SA – surface area of BMP (acres)
V – storage volume of BMP (ft^3)

In addition to the construction costs, other costs associated with planning, designing and unexpected costs (i.e. contingencies) are incurred. Typically, these can be estimated as a percentage of the construction costs. Urbonas (pers. comm.) suggested a 40% increase in construction costs to account for these other costs.

Capital costs are computed using the equation;

$$CapitalCosts = (1 + CEA) * (B + XU^{\alpha})$$

Where,

CEA = percentage to account for contingencies/engineering/administration
B = base cost
X = unit cost

[1] The 20-city averaged ENRCCI value for May 2008 was 8,141.

U = number of units (i.e. size of BMP)
α = economy of scale factor

Land Costs

There are two components to estimating the land costs associated with structural BMPs. One is the cost of the land itself ($/acre) and the second is the area of land (acres) required for the BMP. Land costs can vary considerably from site to site. If a BMP is to be constructed within an area of open space, easement, public park, etc; then that land may be considered "free". But if the land consumed by the BMP could have been developed, then the land cost could be considered equal to the market value of that land (Strecker et al, 2005) or the opportunity costs (future returns) that are foregone from not developing the land (Sample et al, 2003).

Estimates of urban land costs as a function of land use are provided in Strecker et al (2005) and presented in Table 2.

Table 2: Land cost estimates as function of land use

Land Use	Land Cost ($/acre)
Unimproved Land	$25,000 – 50,000
Residential	$75,000 – 200,000
Commercial	$100,000 – 300,000
High Density	$500,000 – 3,000,000

The authors have estimated the area of land consumed by various BMPs, as a factor of the total size of the BMP (LCFCTR) (Table 3).

Table 3: Land consumed by BMPs

BMP	LCFCTR (acres/unit)	Units	Notes
EDB	0.5	acre-feet (storage volume)	
RP	0.5	acre-feet (storage volume)	
SFB	0.33	acre-feet (storage volume)	
VCV	0	-	underground
SFV	0	-	underground
MFV	0	-	underground
CWB	1	acres (surface area)	
PLD	0	-	assume that PLDs are assimilated into existing landscaping
HS	0	-	underground
SOG	0	-	underground
II	0	-	underground
CWC	1	acres (surface area)	

Land costs are computed using the equation

$$LandCosts = UnitCost * BMPSize * LCFCTR$$

O&M Costs

Annual operation and maintenance (O&M) costs were estimated using information collected from several stormwater agencies in the Denver, Colorado region and the RSMeans 2005 Site Work & Landscape Cost Data Guide (RSMeans, 2005). All costs were adjusted to May 2008 dollars using the ENRCCI. Table 4 presents the equations developed to estimate O&M costs as a function of the size of the BMP.

Table 4: Annual O&M cost equations

BMP	O&M Cost Equations ($2008)	Units
EDB	1,420 + 3,502(AF)	AF = acre-feet storage
RP	1,809 + 2,825(AF)	AF = acre-feet storage
SFB	3,948(AF)	AF = acre-feet storage
VCV	0.29(CF)	CF = cubic feet storage
SFV	0.54(CF)	CF = cubic feet storage
MFV	0.55(CF)	CF = cubic feet storage
CWB	3,152(AF)	AF = acre-feet storage
PLD	0.37(CF)	CF = cubic feet storage
HS	493(cfs)	cfs = cubic feet per second flowrate
SOG	1,368(cfs)	cfs = cubic feet per second flowrate
II	561(E)	E = each
CWC	534(A)	A = acres surface area

Rehabilitation/Replacement Costs

These costs represent the costs associated with major rehabilitation and/or replacement activities that occur infrequently during the life of a BMP, such as inlet/outlet and headwall replacements on storage basins or baffle replacement in hydrodynamic separators and sediment/oil/grease separators. Urbonas (pers. comm.) suggested the following costs (as a percentage of initial capital costs) and frequencies of rehabilitation/replacement costs for each BMP included in the tool (Table 5).

Table 5: Rehabilitation/Replacement cost and frequency estimates

BMP	Frequency (years)	Cost (as % of capital costs)
EDB	25	80%
RP	25	80%
CWB	40	80%
CWC	20	20%
SFV	0	0%
MFV	0	0%
SOG	10	50%
PLD	0	0%

VCV	20	50%
HS	25	50%
SFB	25	80%
II	0	0%

Salvage Value

Strecker et al, in a similar work to compute whole life cycle costs of BMPs, suggested that estimating the future salvage value is too difficult and therefore were assumed to be zero (2005). In this tool, salvage value is also assumed to be zero.

Administrative Costs

Administrative costs account of the additional costs of operating a stormwater management program, including the costs of maintenance planning and oversight, regulatory reporting, compliance inspections, etc. Urbonas (pers. comm.) suggested an estimate of administrative costs as 12% of the annual O&M costs. In addition, separate compliance inspection costs were estimated to be approximately $27 per BMP.

Net Present Value Costs

The net present value (NPV) of all costs is computed using the equation (Newnan, 1996);

$$NPV = F(1+ROR)^{-n}$$

Where,

NPV = net present value of cost
F = future cost ($) in year "n"
n = year in which cost/return occurs (i.e., years from present)
ROR = average rate of return (%) over period of analysis

BMP Sizing

The size of a BMP refers to the quantity of its design storage volume (expressed in acre-feet, cubic feet, etc.) or its design flowrate (expressed in cubic feet per second). "Volume-based" BMPs are designed to capture and treat a specified volume of runoff and "flow-based" BMPs are designed to convey and treat a specified peak flowrate of runoff. Table 6 lists the BMPs and their design classification.

Table 6: BMP design classification

Volume-Based BMPs	EDB, RP, SFB, VCV, SFV, CWB, MFV, PLD
Flow-Based BMPs	HS, SOG, II, CWC

Volume-based BMPs are sized to capture and treat the water quality capture volume (WQCV) (approximately 0.43 watershed inches near Denver, CO), based on design criteria published in the Urban Drainage Flood Control District's (UDFCD) Urban Storm Drainage Criteria Manual (UDFCD, 2004). **Note**: The design volume computed for each BMP does not account for additional storage required for larger storms or flood control.

Flow-based BMPs are sized to convey the 2-peak flow rate. The peak flow rate is computed using the Rational Method, using UDFCD methods for estimating time of concentration and design rainfall intensity.

BMP Effectiveness

BMP "effectiveness" is defined as a "measure of how well a BMP system meets its goals in relation to all stormwater flows" and a "BMP system" is defined as "a BMP and any related bypass or overflow" (Geosyntec and ASCE, 2002). Therefore, BMP effectiveness accounts not only for how well a BMP removes pollutants from runoff that is captured, but also for how much runoff is not captured (i.e. bypassed) and what pollutant quantity is in the bypassed runoff. It is recommended that BMP effectiveness be assessed by determining the following (Strecker et al, 2001);

1. How much stormwater runoff is prevented by evapotranspiration, infiltration, source controls, etc.
2. How much stormwater runoff is treated by the BMP and how much bypasses?
3. What is the effluent quality leaving the BMP?

In this tool, BMP effectiveness is reported in terms of reduced annual pollutant loading to the receiving water. The tool estimates annual pollutant loads with and without BMPs implemented in the watershed. When BMPs are implemented, it is assumed that 85% of annual runoff is effectively "treated" by the BMP and 15% "bypasses" the BMP.

Annual Pollutant Load without BMPs

$$AnnLoad_{WO} = LUEMC * Runoff$$

Where,

$AnnLoad_{WO}$ = average annual pollutant loading (mass/year) without BMPs
LUEMC = "land use" event mean concentration (concentration)
Runoff = average annual runoff (volume)

The "land use" event mean concentrations are provided in the appendix.

Runoff volume is computed by The Simple Method (Schueler, 1987);

$$V = P \bullet Pj \bullet RC$$

Where,

V = annual runoff (volume)
P = annual precipitation (depth)
Pj = percentage of annual storms producing runoff (0.9)
RC = runoff coefficient

Annual Pollutant Load with BMPs

$$AnnLoad_{W} = (EffEMC * Discharge) + (LUEMC * Runoff * 0.15)$$

Where,

$AnnLoad_{W}$ = average annual pollutant loading (mass/year) with BMPs
EffEMC = "effluent" event mean concentration (concentration)

Discharge = average annual discharge from BMP (volume)

The "effluent" event mean concentrations are provided in the appendix.

Discharge is computed by;

$$Discharge = (Runoff * 0.85 - \Delta S)Z$$

Where,

Discharge = volume of effluent
ΔS = change in storage (assumed to be zero)
Z = ratio of measured outflow/measured inflow (Table 7)

Table 7: Ratio of measured outflow/measured inflow for various BMPs

BMP Type	Outflow/Inflow
Detention Basins	0.70
Biofilters	0.62
Media Filters	1.00
Hydrodynamic Separators	1.00
Wetland Basins	0.95
Retention Ponds	0.93
Wetland Channels	1.00

Source: Strecker et al (2004)

The difference between the two loads is the annual mass of pollutant removed from the receiving water.

$$\Delta AnnLoad = AnnLoad_{WO} - AnnLoad_{W}$$

BMP Cost Effectiveness

The cost effectiveness of a structural BMP (reported in terms of the total cost to remove a unit of pollutant) is computed using the following equation;

$$CostEff = \frac{NPV}{\Delta AnnLoad}$$

Where,

CostEff = cost per unit of pollutant removed ($/mass)

APPLICATION

This application demonstrates how the tool can be used to quickly evaluate multiple different scenarios for an urban BMP retrofit project.

Watershed Information

Assume the area is already developed with no BMPs currently in place. The stormwater agency must reduce TSS loading to the receiving water by 60%, however because the area is already developed, there is very little land available for BMPs. The following information is available to the user.

- The 55 acre area has a land use density similar to "commercial" land uses and has average slope <1%.
- The agency has determined that some portions of existing right-of-ways (roadways, sidewalks, alleyways) could be used for long, narrow-type BMPs, such as porous landscape detention or sand filter vaults. There would be no land costs associated with these areas (the city already owns them).
- For other BMPs that consume land area, the land and demolition costs of $300,000 per acre.
- Soils in the area are NRCS Type D and are NOT adequate for infiltration-type BMPs.
- The economic life of the BMPs is assumed to be 50 years (i.e. whole life cycle costs are computed for 50 years)

Although the watershed can be considered homogeneous, in some scenarios it was subdivided to allow for applying BMPs to some areas and leaving other areas "untreated".

BMP Scenario 1
For this scenario, the use of hydrodynamic separators will be evaluated. Typically, the contributing area to each device should not exceed 5 impervious acres. It was found that implementing 10 hydrodynamic separators with treatment capacity of 1.5 cfs, each treating 5 acres, would reduce TSS loading approximately 60%. The 50-year NPV of all costs for this scenario is $1,420,000. These are underground structures; therefore no land costs are incurred by these projects.

BMP Scenario 2
For this scenario, the use of porous landscape detention will be evaluated. It was found that approximately 8 PLDs, each capturing runoff from 5 impervious acres, would reduce TSS loading by approximately 60%. The 50-year NPV of all costs for this scenario is $1,578,000. These costs neglect land costs, as it is assumed that the PLDs could be constructed within the right-of-ways as discussed in the problem statement.

BMP Scenario 3
For this scenario, underground sand filter vaults will be evaluated. To reduce TSS loading by 60%, 8 SFVs capturing runoff from 5 impervious acres and 1 SFV capturing runoff from 2 impervious acres would be required. The 50-year NPV of all costs for this scenario is $6,442,000. These costs neglect land costs, as it is assumed that the SFVs could be constructed within the right-of-ways as discussed in the problem statement.

BMP Scenario 4
The cost effectiveness of constructing a single, extended detention basin is evaluated in this scenario. It was found that a single EDB treating 43 impervious acres would

reduce TSS loading by 60%. The 50-year NPV of all costs for this scenario is $1,481,000.

BMP Scenario 5

This scenario will evaluate the use of a single, constructed wetland basin. It was found that a single CWB treating 43 impervious acres would reduce TSS loading by approximately 60%. The 50-year NPV of all costs for this scenario is $1,326,000.

RESULTS AND DISCUSSION

Table 8 summarizes the results of each of the 5 scenarios evaluated. Each scenario was optimized to reduce TSS loading by approximately 60% (9000 kg).

Table 8: Summary table of results for Application #2

	Scenario				
	1	**2**	**3**	**4**	**5**
BMP	HS	PLD	SFV	EDB	CWB
Treated Area (acres)	50	40	42	43	43
NPV Costs	$1,420,000	$1,578,000	$6,442,000	$1,481,000	$1,326,000
Capital Costs	$1,043,000	$529,000	$3,477,000	$1,047,000	$1,081,000
O&M Costs	$325,000	$927,000	$2,638,000	$387,000	$218,000
Admin. Costs	$51,000	$121,000	$327,000	$48,000	$27,000
Cost/Kg TSS Removed	$158	$175	$716	$165	$147

CONCLUSIONS

Several important conclusions can be made from the results of this application. First, it shows how the tool can be used to develop a cost-effective plan for achieving reductions in pollutant loadings to receiving waters. Second, it shows the importance of including maintenance and administrative costs in evaluating the cost effectiveness of a BMP plan. One can see that if BMPs were planned solely based on capital costs alone that PLDs would have been found to be considerably more cost effective. Lastly, this evaluation took only 1 hour for an experienced user to conduct, which shows how the tool will enable effective decisions to be made in an efficient manner.

ACKNOWLEDGEMENTS

This project was funded by Urban Drainage and Flood Control District, the Colorado Stormwater Council, the Urban Watersheds Research Institute and the member agencies that support each of those entities. The authors appreciate the cooperation of many agencies in the Denver metropolitan region that provided cost information for this project.

REFERENCES

American Public Works Association (APWA). (1992). “A study of nationwide costs to implement municipal storm water best management practices.” *Rep.*, Southern California Chapter, Water Resource Committee, APWA, Washington, D.C.

Engineering News Record (ENR), 2008. Construction Cost Index History. http://www.economics.nrcs.usda.gov/cost/priceindexes/index.html [Accessed May 2008].

Means, R.S. 2005. Site Work and Landscape Cost Data. 24th Edition.

Newnan, Donald, G. 1996. Engineering Economic Analysis. Sixth Edition.

GeoSyntec Consultants Urban Drainage and Flood Control District and Urban Water Resources Council of ASCE (GeoSyntec and ASCE). (2002). Urban stormwater BMP performance monitoring: a guidance manual for meeting the national stormwater BMP database requirements. EPA 821/B-02/001. U.S. Environmental Protection Agency, Office of Water, Washington, DC.

Sample, D. J; Heaney, J.P; Wright, L.T; Fan, C; Lai, F; and Field, R. 2003. Costs of Best Management Practices and Associated Land for Urban Stormwater Control. Journal of Water Resources Planning and Management, Vol. 129, No. 1. January.

Schueler, T. 1987. Controlling Urban Runoff: A Practical Manual for Planning and Designing Urban Best Management Practices. MWCOG. Washington, D.C.

Southeast Wisconsin Regional Planning Committee (SEWRPC). 1991. Costs of Urban Nonpoint Source Water Pollution Control Measures. Technical Report Number 31.

Strecker, E., Huber, W., Heaney, J., Bodine, D., Sansalone, J., Quigley, M., Leisenring, M., Pankani, D., and Thayumanavan, A. 2005. Critical Assessment of Stormwater Treatment and Control Selection Issues. Water Environment Research Foundation, 02-SW-1.

UDFCD, 2004. Urban Storm Drainage Criteria Manual – Volumes 1-3.

Urbonas, Ben. 2008. Personal Communication.

United States Department of Transportation (USDOT), 2008a. Stormwater Best Management Practices in an Ultra-Urban Setting – Catch Basin Inserts Fact Sheet. Federal Highway Administration.
[http://www.fhwa.dot.gov/environment/ultraurb/3fs13.htm] Accessed June 2008.

United States Department of Transportation (USDOT),, 2008b. Stormwater Best Management Practices in an Ultra-Urban Setting – Detention Tanks and Vault Fact Sheet. Federal Highway Administration.
[http://www.fhwa.dot.gov/environment/ultraurb/3fs6.htm] Accessed June 2008.

United States Environmental Protection Agency (USEPA), 1999a. Stormwater Technology Fact Sheet – Stormwater Wetlands. EPA 832-F-99-025. Office of Water.

United States Environmental Protection Agency (USEPA), 1999b. Stormwater Technology Fact Sheet – Hydrodynamic Separators. EPA 832-F-99-017. Office of Water.

Wiegand, C.: Schueler, T.: Chittenden, W. and Jellick, D. 1986. Cost of Urban Runoff Quality Controls. Proceedings from: Urban Runoff Quality. Engineering Foundation Conference. American Society of Civil Engineers.

Wossink, A. and Hunt, B. 2003. The Economics of Structural Stormwater BMPs in North Carolina. North Carolina State University, Raleigh, NC. Report UNC-WRRI-2003-344. May.

Appendix

Constituent	ABR
Total Suspended Solids	TSS
Total Phosphorus	TP
Total Nitrogen	TN
Total Kjeldahl Nitrogen	TKN
Total Zinc	TZ
Dissolved Zinc	DZ
Total Lead	TL
Dissolved Lead	DL
Total Copper	TC
Dissolved Copper	DC

Land use average EMCs in stormwater runoff for Denver, CO metropolitan region

Constituent	Units	Industrial	Commercial	Residential	Undeveloped
TSS	mg/L	399	225	240	400
TP	mg/L	0.43	0.42	0.65	0.40
TN	mg/L	2.7	3.3	3.4	3.4
TKN	mg/L	1.8	2.3	1.8	2.9
TZ	mg/L	0.5200	0.2400	0.1800	0.1000
DZ	mg/L	**0.3224**	**0.1488**	**0.1116**	**0.0620**
TL	mg/L	0.1300	0.0590	0.0530	0.1000
DL	mg/L	**0.0195**	**0.0089**	**0.0080**	**0.0150**
TC	mg/L	0.0840	0.0430	0.0290	0.0400
DC	mg/L	**0.0420**	**0.0215**	**0.0145**	**0.0200**

Source: Table SQ-5 (UDFCD, 2004)
Bold – indicates assumed values based on ratios presented in Table SQ-6 (UDFCD, 2004)

BMP Effluent EMCs

BMP	TSS	TP	TN	TKN	TZ	DZ	TL	DL	TC	DC
	mg/L									
EDB	31.04	0.19	2.72	1.89	0.060	0.026	0.016	0.002	0.012	0.007
SFB	15.86	0.14	0.76	1.55	0.038	0.051	0.004	0.001	0.010	0.009
RP	13.37	0.12	1.43	1.09	0.029	0.033	0.005	0.002	0.006	0.005
CWB	17.77	0.14	1.15	1.05	0.031	**0.023**	0.003	0.001	0.004	**0.002**
CWC	37.25	0.37	1.91	1.35	**0.031**	**0.023**	0.009	**0.001**	**0.004**	**0.002**
SFV	15.86	0.14	0.76	1.55	0.038	0.051	0.004	0.001	0.010	0.009
MFV	15.86	0.14	0.76	1.55	0.038	0.051	0.004	0.001	0.010	0.009
SOG	41.80	1.27	2.07	1.48	0.140	0.192	0.012	0.002	0.013	0.014
PLD	23.92	0.34	0.78	1.51	0.040	0.025	0.007	0.002	0.011	0.008
VCV	31.04	0.19	2.72	1.89	0.060	0.026	0.016	0.002	0.012	0.007
HS	49.96	0.28	1.48	0.94	0.072	0.055	0.004	0.002	0.012	0.024
II	38.00	0.12	0.70	1.90	0.099	0.069	0.007	0.001	0.014	0.009

Source: International BMP Database, June 2008
Bold – indicates assumed values based on ratios presented in Table SQ-6 (UDFCD, 2004)

Controlled Full-Scale Field Testing of an Up-Flow Filtration Device

Noboru Togawa[1] and Robert Pitt[2]

[1]Department of Civil, Construction, & Environmental Engineering, The University of Alabama, P.O.Box 863307 Tuscaloosa, AL 35486-0030, CELL: (205) 239-9666, natogawa@bama.ua.edu
[2]Department of Civil, Construction, & Environmental Engineering, The University of Alabama, P.O.Box: Box 870205 Tuscaloosa, AL 35487, PH: (205) 348-2684, Rpitt@eng.ua.edu

ABSTRACT
The objective of this research is to examine the removal capacities of a recently developed stormwater filtration device, in part developed by engineers at the University of Alabama through a Small Business Innovative Research (SBIR) grant from the U.S. Environmental Protection Agency. The UpFlo™ Filter is an efficient high-rate stormwater filtration technology designed for the removal of trash, sediments, nutrients, metals and hydrocarbons from stormwater runoff. Compared with the traditional downflow filtration treatment, the upflow filtration method reduces clogging and was developed to remove a broad range of stormwater pollutants, especially those associated with particulates. The high flow rate capacities of the upflow filter are accomplished through controlled fluidization of the filtration media, while still capturing very small particulates through a flexible, but constraining, media container. The upflow filter also drains down between rain events which minimizes anaerobic conditions in the media and which also partially flushes captured particulates from the media to the storage sump, decreasing clogging and increasing run times between maintenance. Gross floatables are captured through the use of an angled screen before the media and a hood on the overflow siphon, while the sump captures bed load particulates.

INTRODUCTION
Many types of stormwater controls are available, but most are relatively large or insufficient in their treatment capacity. Adequate treatment of runoff requires the removal of many types of pollutants as well as large amounts of debris and floatable materials, over a wide range of flows. Traditional downflow filters, which can provide high levels of treatment, can quickly clog, reducing their treatment flow rate and overall treatment capacity. They also usually operate at a low treatment flow rate requiring a large area to treat substantial portions of the runoff from a site. The UpFlo filter is designed to treat stormwater runoff from critical source areas that discharge especially high levels of pollutants. The commercialized UpFlo filter minimizes clogging and was developed to remove a broad range of stormwater pollutants at a relatively high rate, and can be retrofitted into existing stormwater drainage. This presentation will present the results from a controlled full-scale field evaluation located at a parking lot in Tuscaloosa, AL. Treatment flow rates, particle size controls, and SSC reductions will be stressed in this presentation.

LOCATION AND SIZE OF FILTER

A 7-foot tall 4-foot diameter standard inlet containing a six module UpFlo™ Filter has been installed at the Riverwalk parking lot near the Bama Belle on the Black Warrior River in Tuscaloosa, Alabama. The chamber is a conventional concrete manhole with a sump, with the UpFlo™ filter components installed. The filter receives surface runoff from a parking lot, road, sidewalks, and a small landscaped area, as shown in Table 1. The total drainage area tributary to the device is approximately 0.9 acres. Figure 1 shows the drainage area and the location of the test site.

Table 1. Drainage Area Land Use

Land Use	Area (ft^2)	Area (acre)	% of Land Use
Parking Area	11,800	0.27	30.5
Other Paved	1,300	0.03	3.4
Side Walks	2,100	0.05	5.4
Entrance Road	10,990	0.25	28. 5
Green Space	12,400	0.29	32.2
Total	**38,610**	**0.89**	**100.0**



Figure 1. Site map and drainage area.

DESCRIPTION OF FILTER

The full-scale filter system (having a full complement of 6 filter modules) was installed and is being tested to confirm laboratory and the initial pilot-scale test results under actual rain conditions. Hydraulic capacity and pollutant removal capabilities in the full-scale field installation are being monitored under both controlled and actual runoff conditions. Figure 2 shows the main features of the UpFlo™ filter, while Figure 3 shows the installation of the full-scale test filter at Tuscaloosa. Depending on the selected media, the filtration treatment flow rate varies from 15 to 25 gal/min/ft^2. With 6 modules, each having about 1ft^2 of filter surface,

the total treatment flow rate for this installation is expected to be at least 100 gallons/minute.

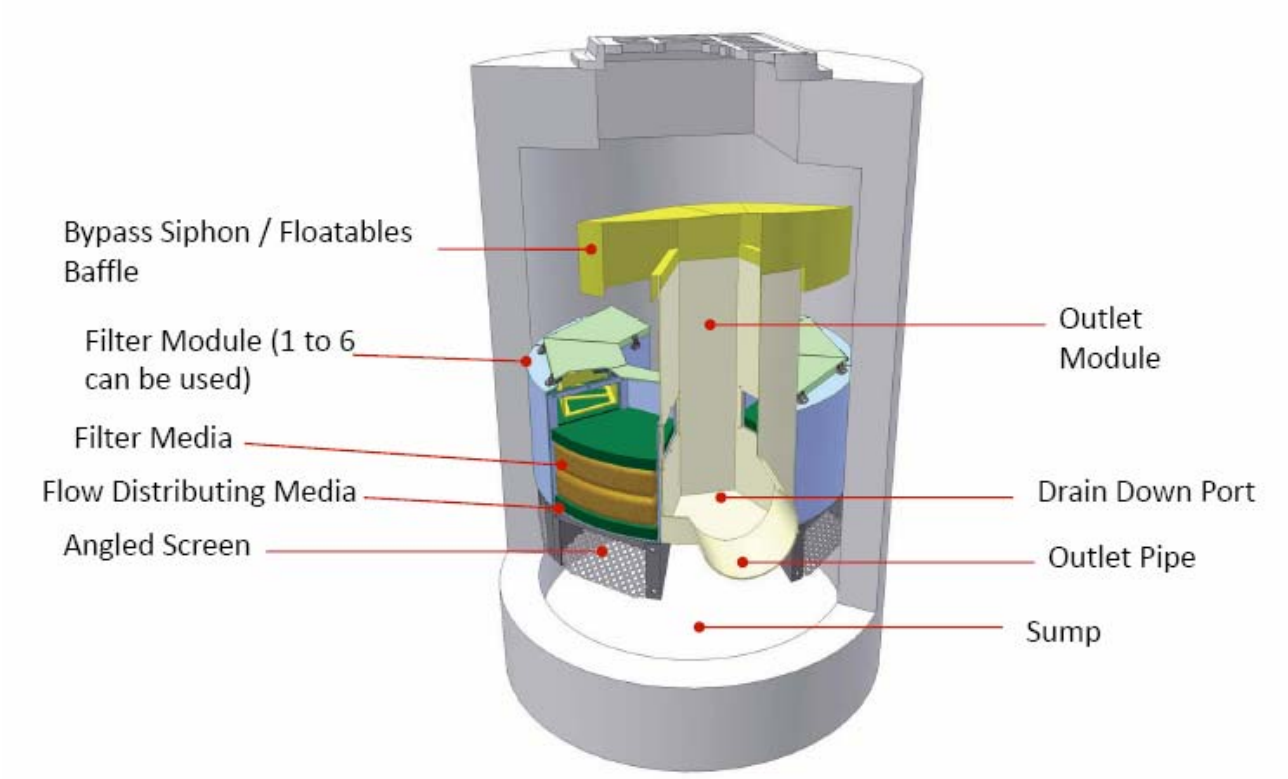

Figure 2. UpFlo™ Filter components.



Figure 3. Installation of Tuscaloosa UpFlo™ filter.

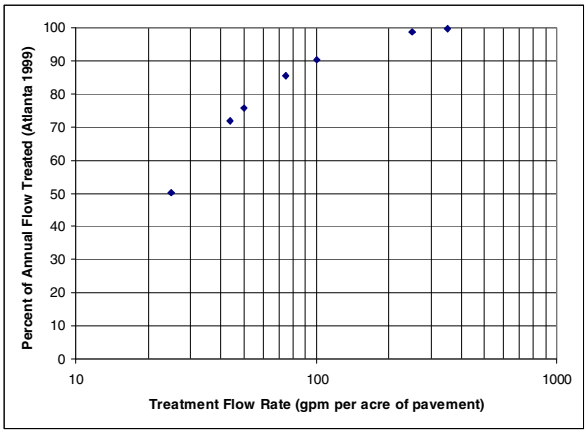

Figure 4. Treatment flow rate requirements for southeast US paved conditions (Example shown for continuous simulation results for Atlanta, GA).

Figure 4 shows the treatment flow rate requirements for typical southeastern US conditions, based on continuous simulations (Pitt and Khambhammettu 2006). The 100 gal/min for the test site is expected to treat about 90 percent of the annual flow for a typical rain year, with about 10 percent of the annual flow bypassing filtration.

CONTROLLED FLOW TEST & CONTROLLED PARTICLE CAPTURE TEST

This paper describes the initial controlled performance monitoring that is being conducted at the Riverwalk parking lot near the Bama Belle in Tuscaloosa, Alabama. The first flow test was conducted for the purpose of determining the hydraulic capacity and the pollutant removal capabilities in a full-scale field installation under controlled conditions. In the test, the filtration rate of the CPZ Mix™ filter media, a proprietary mixture of bone char activated carbon, peat moss, and manganese coated zeolite was evaluated. Based on results of prior lab scale testing, the mixed media is expected to have high pollutant removal at relatively high filtration rates. The UpFlo™ Filter was fitted with two media bags in each of the 6 chambers, for a total of 12 bags, as well as the flow distribution material placed above and below the media bags.

METHODOLOGY FOR THE EVALUATION OF FILTRATION RATE

Flow tests were conducted in the field with the cooperation of the Tuscaloosa Department of Transportation by using a pump to deliver river water to a flow splitter/flow controlling barrel. The water flow rate was measured by measuring the time needed to fill a measured volume (Figure 5). When the rate was established, the volume tray was removed, directing the known and steady flow to the gutter immediately above the Up-Flo intake. For each flow rate, measurements were taken of the steady-stage water depth in the filter and the reported flow rate from the area-velocity sensor that will be used to monitor the flow during rain events. The measurements were repeated 5 times for each flow to reduce the errors. Figure 6 shows an example flow vs. head graph developed during these tests.



Figure 5. Pumped River water is discharged from splitter barrel to the 11 gallon plastic tray.

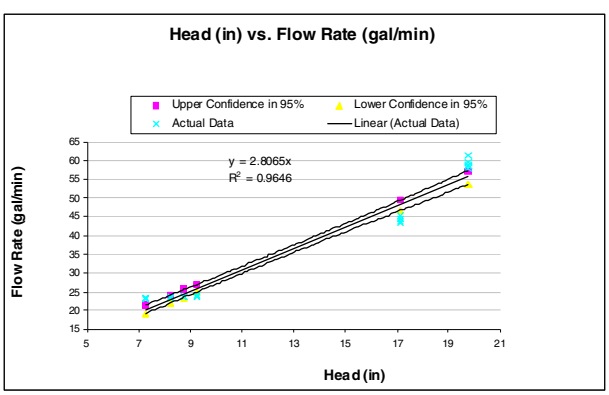

Figure 6. Example flow vs. head graph for mixed media, showing highly repeatable measurements.

PARTICLE SIZE DISTRIBUTION OF TESTED MEDIA AND TEST SEDIMENT

The test sediment in the stormwater stimulant used a mixture Sil-Co-Sil 250, Sil-Co-Sil 106 (both from U.S. Silica Co.), and coarse and fine concrete sands. The mixture was made by mixing the four components with different ratios to obtain a relatively even particle size distribution representing the complete range from about 20 to 2,000µm. This mixture was not intended to represent actual stormwater (which usually has a smaller median size), but to ensure sufficient amounts of large particles so they could be accurately monitored to quantify their removal. As shown later, all of the results of these controlled tests were presented based on many narrow particle size ranges so they could be applied to any expected particle size distribution of the flowing water. Since the samples were all analyzed using sieves and a Coulter Counter, the results are much more useful than if individual SSC analyses were conducted representing all sizes combined. If a single analysis was conducted, then the psd of the challenge water would have to match the stormwater psd, a difficult objective given the highly variable particle size characteristics of stormwater. Figure 7 shows the particle size distributions of two test mixtures that were used during the tests.

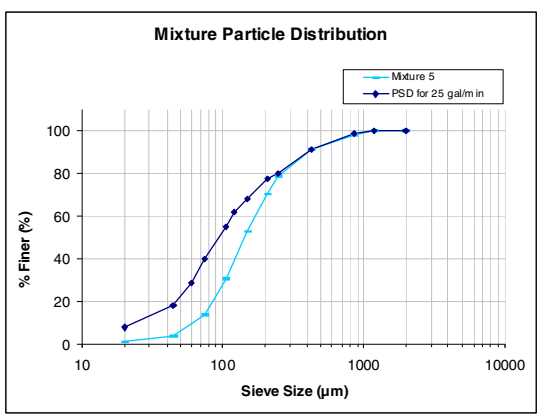

Figure 7. Particle size distribution of mixture used for the flow test.



Figure 8. Sediment mixture was manually and consistently added to the influent water over the 30 minute test period.

TEST METHODOLOGY FOR CONTROLLED SEDIMENT CAPTURE TESTS

The test described below used several known concentrations of particulate solids over a wide range of particle sizes and an influent flow rate that averaged 24 gallon per minute (having a standard deviation of 0.3 gpm). Each experiment was conducted for 30 minutes, during which time measured aliquots of the dry sediment were constantly poured into the pumped influent "river flow" from the Black Warrior River. River water was also collected before any sediment was added to measure the background solids in the test water to determine the background conditions. Effluent samples were collected using a dipper grab sampler every 1 minutes and composited in a churn sample splitter during the 30 minutes test period. The effluent was sampled at a completely mixed cascading flow exiting the filter in a specially constructed sampling chamber. Using the churn splitter, two samples of 1000 mL each were placed in sample bottles for duplicate laboratory analyses for each test.

In preparation for the tests, test sediment portions were pre-weighted in many 50 mL polyethylene bottles. The sediment was manually feed into the influent water over the whole period of each experiment, according to the desired particulate solids concentration for the specific flow rate for each test (Figure 8). This method ensured that all of the sediment and all particle sizes entered the test chamber. Depth readings of the water levels were also taken during each experiment to determine the head loss during the Up-Flo^{TM} Filter operation. Also, after completion of each experiment, additional multiple flow and depth readings were taken to determine the final flow rate and available head to detect any change in filtration rate during the test.

During these tests, four different influent sediment concentrations were tested: 50mg/L, 100mg/L, 250mg/L, and 500mg/L.

INITIAL CONTROLLED TEST RESULT OF FILTER

Controlled tests can measure the filter behavior under known conditions. Mixtures of ground silica available from U.S.Silica Co. were used for these initial tests, reflecting filter performance for a variety of particle sizes. Figure 9 shows the influent and effluent concentrations during tests using 50 to 500 mg/L influent conditions. Further controlled tests are being conducted, along with measurements conducted during actual rain conditions.

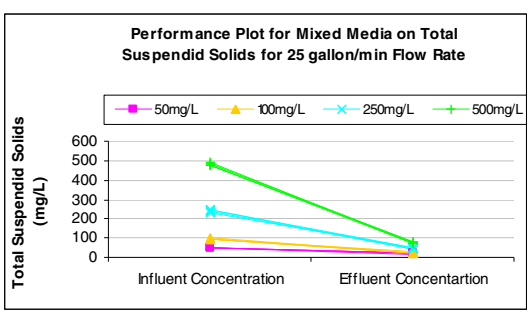

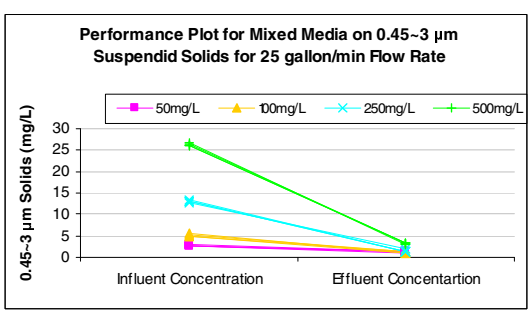

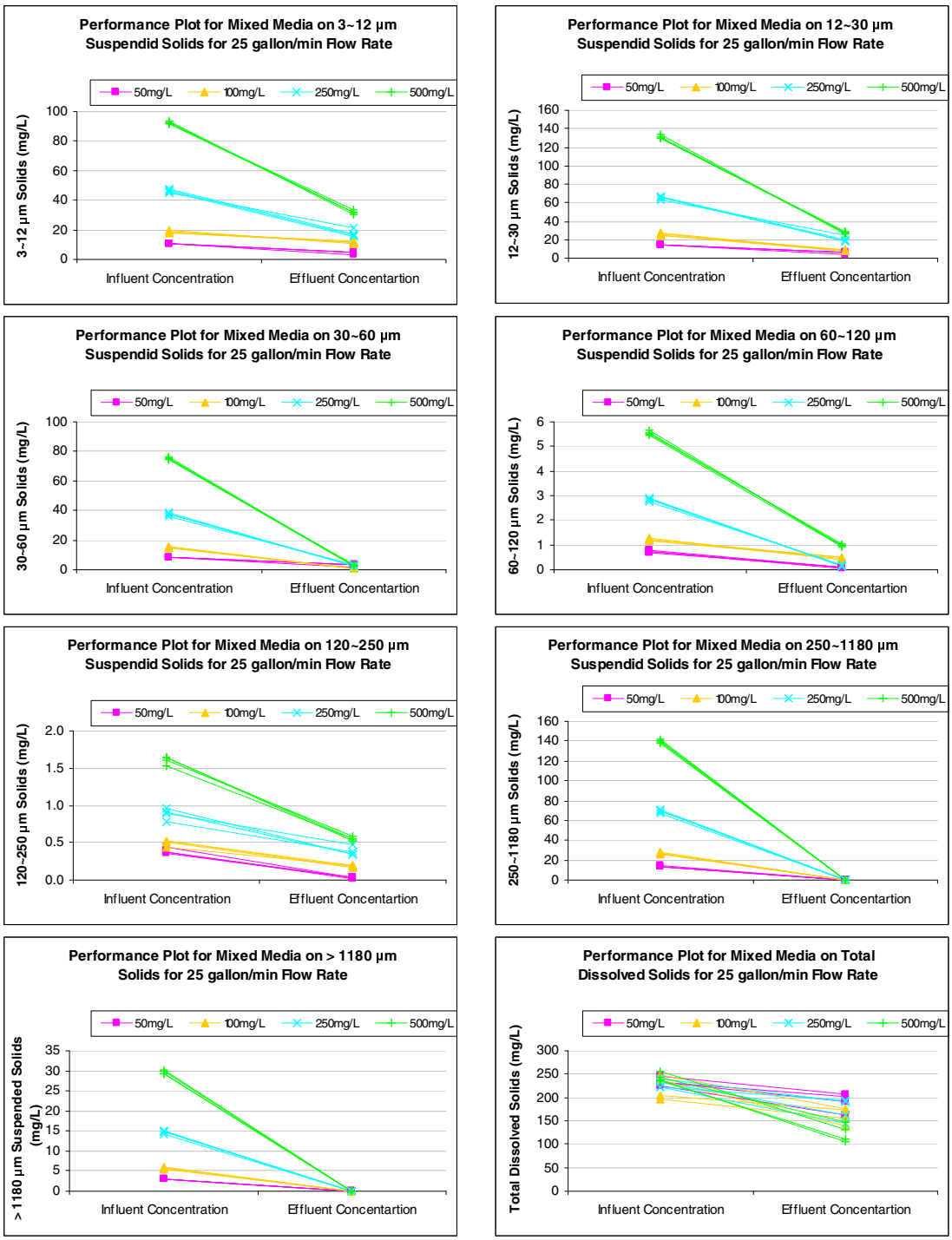

Figure 9. Controlled test results for different particle sizes.

Table 2 summarizes the average influent and effluent concentrations, along with the percentage reductions for 100 and 500 mg/L influent conditions (including river water additions). Table 3 shows the average influent and effluent concentration of TDS concentrations.

Table 2. Average Influent and Effluent Concentration

25 gallon/min Flow Rate and 100 mg/L Concentration			
Particle Size (μm)	Average Influent Concentration (mg/L)	Average Effluent Concentration (mg/L)	Average Reduction (%)
< 0.45	220	160	27
0.45 to 3	5.2	1.1	78
3 to 12	19	11	38
12 to 30	26	8.3	68
30 to 120	16	1.3	92
120 to 1180	28	0.18	99
> 1180	5.7	0	100
sum >0.45 μm	99	21.9	78

25 gallon/min Flow Rate and 500 mg/L Concentration			
Particle Size (μm)	Average Influent Concentration (mg/L)	Average Effluent Concentration (mg/L)	Average Reduction (%)
< 0.45	240	120	49
0.45 to 3	26	3.2	88
3 to 12	92	32	65
12 to 30	130	28	79
30 to 120	81	3.9	95
120 to 1180	142	0.55	100
> 1180	30	0	100
sum >0.45 μm	500	67.7	86

Table 3. Average Influent and Effluent Concentration for TDS

25 gallon/min Flow Rate and TDS Concentration					
Concentration (mg/L)	Average Influent Concentration (mg/L)	Average Effluent Concentration (mg/L)	Average Reduction (%)	Maximum Reduction (%)	Minimum Reduction (%)
50	230	190	19	28	13
100	220	160	27	42	15
250	230	170	25	35	13
500	240	120	49	55	39

REFERENCES

Pitt, R. and Khambhammettu, U. (2006). *Field Verification Report for the Up-Flo™ Filter. Small Business Innovative Research, Phase 2 (SBIR2) Report*. U.S. Environmental Protection Agency, Edison, NJ. 275 pages. March 2006.

Pitt, R. and Clark, S. (2006). *Stormwater Treatment Filtration As A Stormwater Control.*

Clark, S. and R. Pitt. *Stormwater Treatment at Critical Areas, Vol. 3: Evaluation of Filtration Media for Stormwater Treatment*. U.S. Environmental Protection Agency, Water Supply and Water Resources Division, National Risk Management Research Laboratory. EPA/600/R-00/016, Cincinnati, Ohio. 442 pgs. October 1999.

Urbonas, B. (1999). *Design of a Sand Filter for Stormwater Quality Enhancement. Water Environment Research, 71(1), 102-113.*

The Observed Effects of Stormwater Infiltration on Groundwater

M. D. Machusick[1] and R. G. Traver[2]

[1] Environmental Engineer/Geologist, Science Applications International Corporation (SAIC), Exton, PA 19341; PH (484) 343-1697; email: Matthew.D.Machusick@saic.com
[2] Professor, Dept of Civil & Environmental Engineering, Villanova University, Villanova, 19085; PH (610)519-6754; email: Robert.Traver@Villanova.edu

ABSTRACT

This research presents a case study of the impacts of stormwater infiltration on a shallow unconfined aquifer at a bioinfiltration BMP on the campus of Villanova University. The study site is a vegetated basin that with a 0.53 hectares drainage area consisting of parking areas and recreational fields with 35% directly connected impervious area. The study utilizes continuous monitoring of groundwater elevation, temperature and conductivity in conjunction with surface water hydrologic monitoring to assess the transport of conductivity and to examine the extent of groundwater mounding. Results indicate a direct impact on groundwater conductivity near the BMP, but also show significant attenuation compared to influent surface water. Following storms less than approximately 1.9 cm the upgradient control well presents larger increases in groundwater elevation, but for larger storms the well adjacent to the site displays increased mounding. Groundwater elevation monitoring indicates that the extent of groundwater mounding is related to infiltration rate and groundwater temperature. This study demonstrates the utility of groundwater monitoring for the purpose of BMP performance assessment. It is suggested that groundwater monitoring be considered for site monitoring plans and as a tool for BMP site selection.

INTRODUCTION:

Infiltration BMP have become essential tools of urban stormwater management (Mikkelsen *et al.* 1996; USEPA 2000; Hsieh and Davis 2005; Schuster *et al.* 2007). Research has examined many parameters related to the design, construction and evaluation of infiltration BMP, but less emphasis has been placed on the impact to groundwater and subsurface contaminant transport (Mikkelsen *et al.* 1997; Strecker *et al.* 2001; Akan 2002; Winogradoff 2002; Fischer *et al.* 2003; Birch *et al.* 2005; Dietz and Clausen 2005; M. Clar *et al.* 2007). On an annual basis, baseflow, which is derived from groundwater, typically comprises a major component of total stream flow (Leopold 1974; Bouwer 1978; Viessman and Lewis 2003). Since groundwater flow is the link between infiltration and base-flow; it is essential to consider the fate of water at infiltration BMP to ensure the protection of streams and water resources (Winter *et al.* 1998; Barraud *et al.* 1999; Pitt *et al.* 1999).

The primary concerns of stormwater infiltration related to groundwater include the contamination of soil and groundwater and the subsurface impacts of

groundwater mounding. Infiltration BMP are primarily designed to provide volume and contaminant reduction to protect surface water. Infiltration BMP typically have little or no pretreatment devices, therefore contaminants in stormwater are conveyed directly to the BMP and the potential exists for subsurface contamination. BMP rely on the physical and biological processes involved with infiltration to remove contaminants from influent water (Muthukrishnan *et al.* 2004; PADEP 2006; Mikula *et al.* 2007). Concerning groundwater mounding, the potential exists for subsurface damage to utilities, basements and building structures. Groundwater mounding may also result in detrimental changes in the groundwater flow regime, therefore it is important to understand the impacts of mounding (Rai *et al.* 1998; Guo 2001; Park *et al.* 2006; Schreffler *et al.* 2006).

To assess the impacts of stormwater infiltration on groundwater, this study examines the following questions:

- What is the extent of groundwater mounding that occurs in response to focused recharge?
- Do the physical, chemical and biological processes involved with infiltration and groundwater flow attenuate the impacts related to total dissolved solids as measured by conductivity?
- What pertinent information can be gathered from groundwater monitoring of infiltration BMP?

Specifically, the study focuses on groundwater mounding, temperature and the transport of conductivity through a bioinfiltration basin. Continuous groundwater monitoring is coupled with hydrologic modeling and storm sampling to assess the hydrologic and chemical impact of infiltration on the shallow aquifer.

SITE DESCRIPTION

Research for this study was conducted at the Villanova Bio-Infiltration Traffic Island. The site is on the campus of Villanova University in Southeastern Pennsylvania; a suburban area about 17.7 km miles west of center-city Philadelphia. The site is located in a parking area with a total drainage area of approximately 0.53 hectares including 35% directly connected impervious area (Emerson 2008). Villanova is located in PADOT region 5 precipitation area and receives an average annual precipitation of 114 cm (Aron et al. 1986). Furthermore, between 80 to 90% of the average annual precipitation occurs in storms with less than 2.5 cm of precipitation (Traver 2002).

The BMP was constructed as a retrofit of an existing parking lot traffic island and was designed to retain and infiltrate the runoff produced by a 2.5 cm storm. The BMP was constructed by excavating the existing traffic island to a depth of approximately 1.8 meters. The excavated soil was mixed with sand at a 1:1 ratio and replaced into the excavation to a depth of 1.2 meters. The area was then formed into a basin, mulched and planted with appropriate vegetation. The site is equipped with a variety of hydrologic monitoring equipment and has is used as a research and demonstration site. Additional information pertaining to site history, performance,

construction and research is presented by Prokop (2003), Ermilio (2005), Heasom et al. (2006), Traver (2002), Traver et al. (2007), and Emerson (2008).

METHODOLOGY

This study consists of continuous monitoring conducted between November 2007 and August 2008. Four monitor wells are located around the site; MW1 is located upgradient, MW3 is located downgradient and both MW2 and MW4 are located adjacent to the site. Wells MW1, MW2 and MW3 are equipped with In-Situ Aqua Troll 200 multi-meters that are programmed to measure and record groundwater elevation, temperature and conductivity. MW4 is equipped with an Instrumentation Northwest (INW) PT2X pressure transducer that logs groundwater elevation. Precipitation at the site is measured with a Sigma tipping bucket rain gauge. Basin water level is measured by a Sigma ultra-sonic sensor and outflow from the basin is measured by an INW PT2X located behind a v-notch weir near the outlet structure. Data from these gauges are logged by a Sigma 950 flow meter. The site hydrology, including total runoff and hydrologic timing is estimated using rainfall and basin water level data in conjunction with the HEC-HMS model developed for the site by Heasom et al (2006). The predicted inflow volume is compared to the resulting changes in groundwater elevation and is used to examine the hydrologic impacts of stormwater infiltration on groundwater. Continuous

RESULTS

Approximately 79.2 centimeters of precipitation was recorded during the study period. The majority of this precipitation occurred in storms less than 2.5 centimeters and the great majority of the runoff was infiltrated by the site. Significant fluctuations in groundwater elevation were observed at each well. The groundwater elevation at MW1 responds to precipitation within about two hours, whereas MW2 and MW4 generally required over 30 hours and MW3 typically required over 35 hours. The range between the maximum and minimum water level was 1.32 m at MW1, 2.22 m at MW2, 1.08 m at MW3 and 1.76 m at MW4. The largest fluctuation in groundwater elevation occurred after the storms on 3/4/08 and 3/7/08, which produced a total rainfall of 7.8 centimeters and an estimated inflow volume of 185.6 m^3. During this period, the groundwater elevation at MW1 rose 0.56m, 1.04m at MW2, 0.28 m at MW3 and 0.87 m at MW4.

In general the groundwater elevation was highest at MW4 followed by MW1 then MW2. At times MW1 had the highest elevation and for several brief periods the elevation at MW2 exceeds MW1. Groundwater elevation at MW3 remained the lowest over the entire period and in general showed only gradual longer-term fluctuations. The resulting hydraulic gradient is relatively flat in the vicinity of the MW1, 2 and 4, with a fairly steep gradient towards MW3. Over the study period, the water table was highest from mid-January to mid-May and lowest towards the end of summer and beginning of winter. Figure 1, below presents the groundwater elevation during the study period.

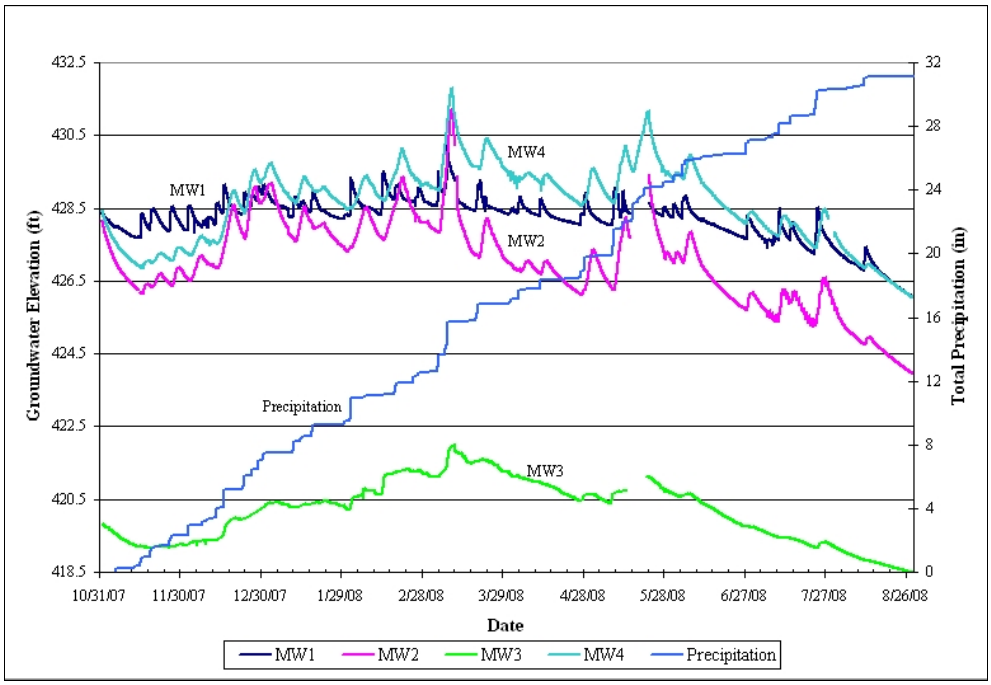

Figure 1. Groundwater Elevation

During the study period, MW2 displayed a wide range in conductivity, while MW3 displayed a narrower range and MW1 had a moderate range. The minimum and maximum values were 68 to 465 µS/cm at MW1, 90 to 815 µS/cm at MW2 and 291 to 353 µS/cm at MW3. The conductivity at MW1 was generally stable except after large storm events when the conductivity displays a rapid decline followed by a rapid return to previous conditions. The conductivity at MW2 fluctuated between 75 and 275 µS/cm for most of the period, except for an extended period in the early spring following the storm events in early March 2008. During this period the conductivity generally remained above 675 µS/cm. The conductivity at MW3 remained within a narrow range during the study period, but was observed to display a general decline between November 2007 and April 2008, after which the conductivity followed a general incline. Overall, MW2 displayed the widest range, with the highest and lowest values, while MW1 and MW3 followed similar trends with MW1 typically higher than MW3. Figure 2, below presents the groundwater conductivity and temperature during the study period. It should be noted that the monitoring record was interrupted for a brief period in May 2008.

The groundwater temperature at MW1 and MW3 remained very stable and followed a similar gradual trend with an average temperature difference of about 0.2 ^{o}C over the study period. In contrast, MW2 had a highly variable temperature and followed a very different trend. While MW1 and MW3 had a range of less than 1 ^{o}C, MW2 had a range of over 6.2 ^{o}C. The temperature curves at MW1 and MW3 were smooth and gradual, while MW2 had a variable curve with many fluctuations. In November 2007, MW1 and MW3 had temperatures of 13.35 and 13.16 ^{o}C, respectively. The temperatures rose gradually to 13.76 and 13.56 ^{o}C, respectively, by early March and then proceeded to gradually decline to 13.20 and 12.98 ^{o}C by August 2008. MW1 had two large temperature decreases in March 2008, both occurring

immediately after large storm events. In November 2007, MW2 had a temperature of 14.41 °C and increased to 15.05 °C by the end of December 2007. From January 2008 until late May 2008, the temperature at MW2 decreased from 15.05 °C to 8.77 °C and then from 5/22/08 until the end of the study period in 8/28/08, the temperature rose steadily to 11.68 °C with only minor variations.

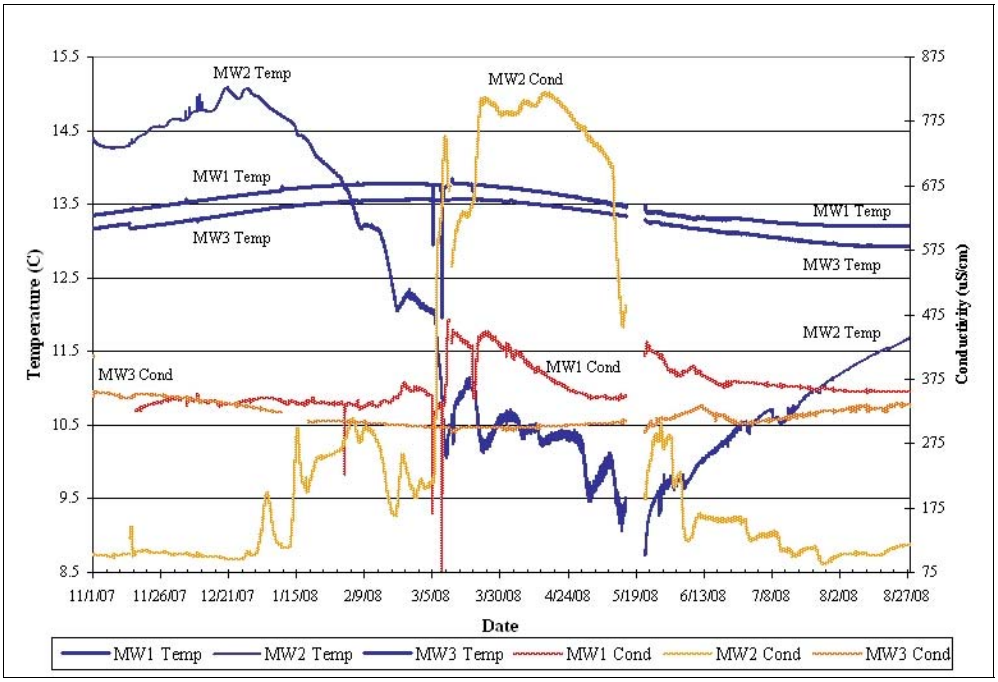

Figure 2. Groundwater Conductivity and Temperature

DISCUSSION

Groundwater Mounding

Infiltration of water to an unconfined aquifer naturally causes the groundwater elevation to rise, thus the fluctuations observed at the monitor wells are to be expected. Infiltration BMP focus recharge in a specific area rather allowing rainfall to infiltrate over a dispersed area. The question thus arises, how does focused recharge effect the change in groundwater elevation? Groundwater monitoring for this study shows that for storms smaller than approximately 1.9 centimeters the upgradient well (MW1) exhibits a larger change in groundwater elevation than the wells closer to the site (MW2 and MW4). For storms greater than 1.9 centimeters the reverse is generally observed. However, for larger storms, the groundwater elevation at MW3 demonstrates that the increased mounding observed at MW2 is attenuated before reaching MW3. These findings are illustrated in Figure 3, below which plots the change in groundwater elevation versus the total rainfall.

An interesting observation regarding groundwater fluctuations is that the observed rise in groundwater elevation does not correlate well to the amount of precipitation received. Figure 4, presents the R^2 value for the trend-line correlating

the volume of precipitation to the associated rise in groundwater elevation. MW1 has the highest R^2 value and correlation coefficient of 0.863 and 0.929, while MW4 has the lowest values of 0.818 and 0.904. These statistics indicate that the parameters are related, but that there is not a strict correlation. This implies that other factors, such as rainfall intensity, temperature, antecedent moisture content and evapotranspiration play a significant role in the magnitude of groundwater mounding. Along these lines it should be noted that in general, it was observed that for events with similar rainfall, MW2 displayed larger increases in groundwater elevation when the groundwater temperature was lower.

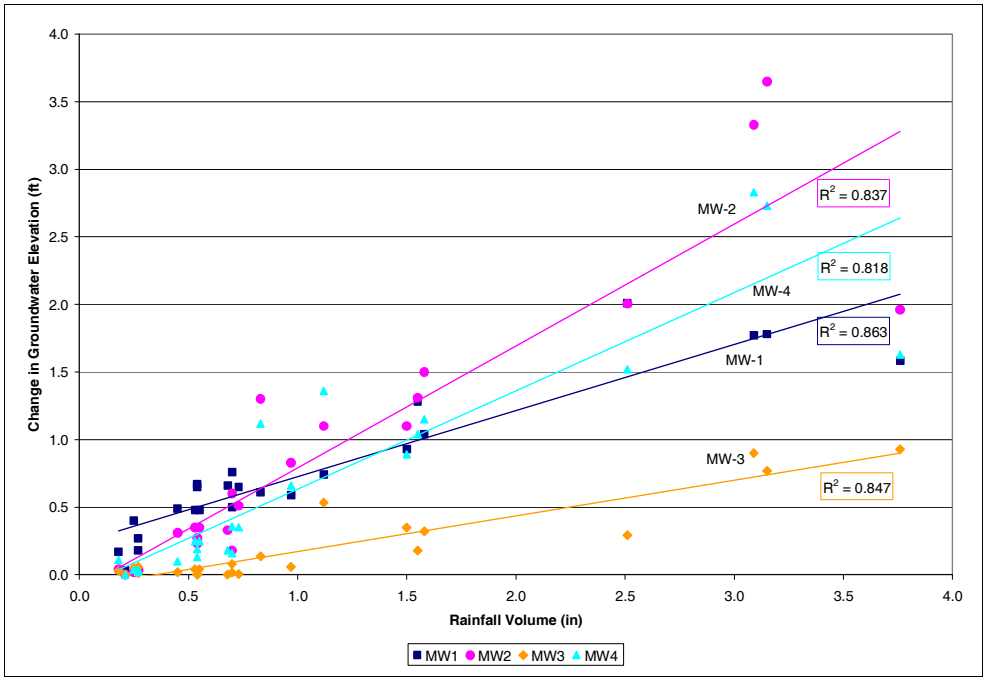

Figure 3 Comparison of Groundwater Mounding and Total Precipitation

Based on the results it is observed that infiltration rate, which is temperature dependent, is a primary factor affecting the extent of groundwater mounding. As an analogy, it is hypothesized that the subsurface below the site is similar to a retention basin and that the infiltration rate is equivalent to an outlet control structure. Expanding upon this analogy, it is observed that the infiltration rate at MW1 is quicker than at MW2 and MW4 as can be seen by the rapid rise in groundwater elevation after a storm. For a given storm less than 1.0 cm centimeters, rain rapidly infiltrates near MW1 causing a quick increase in groundwater level. At MW2, a slower infiltration rate requires a longer duration for water to reach the groundwater. Thus in a given time period, less volume of water is delivered, resulting in a lower rise in groundwater elevation. However, more total volume of water is infiltrated near MW2, because of the basin and this larger volume is conveyed to the groundwater over a longer period of time. Therefore the hydrograph at MW2 has slow gradual changes in elevation that are sustained for a longer duration. Returning to the retention basin analogy, just as a retention basin stores a volume of water and releases it at constant rate, the infiltration rate slowly releases water to the groundwater at a

low rate for a long duration. It appears that for storms smaller than 1.9 cm centimeters the infiltration rate is sufficiently low to allow the water to be stored in the vadose zone without causing a large increase in groundwater elevation. However, for larger storms, infiltration occurs for a sufficient duration to cause larger increases in groundwater elevation. Also for larger more intense storms the basin is maintained at capacity for longer durations and the surface soil of the drainage area may become saturated so that rainfall produces runoff rather than infiltration and this runoff flows into the basin rather than the groundwater near MW1.

Although larger storms lead to a larger groundwater mound at MW2 and MW4, the hydrographs from MW3 indicate that the mounding does not extend very far laterally. In addition, the mounding near the site remains at a significant depth below the site. The maximum elevation observed at MW2 occurred on 3/10/08 in response to 7.8 centimeters and was still 3.66 m below the bottom of the basin. Thus substantial storage space exists in the vadose zone to accommodate larger volumes.

Conductivity

The conductivity at MW2 was observed to be significantly effected by stormwater infiltration. During warm periods when no de-icing salts are applied, the groundwater has low conductivity, but in winter and early spring when road salts are applied the conductivity rises. Precipitation naturally has low conductivity due to the lack of dissolved solids, but as the rainfall travels across the land it picks up dissolved solids and ions, such as the chloride ions derived from de-icing salts. Thus it is intuitive that the conductivity at MW2 is low during warm periods and higher during colder periods, when de-icing salts are applied. Furthermore it follows that the low conductivity water that infiltrates the site will dilute the ambient conductivity level of the groundwater near the basin and down gradient. Although the groundwater at MW2 varies between high and low conductivity, it appears that this fluctuation is sufficiently attenuated by the time it reaches MW3. However, the conductivity at MW3 is generally lower than at MW1 and this may be due to dilution caused by infiltration at the site. Still the difference in conductivity between MW1 and MW3 is relatively small and likely represents an inconsequential impact, if any.

CONCLUSIONS

While the formation of a groundwater mound is a natural occurrence associated recharge to an unconfined aquifer, increased groundwater mounding was observed to occur at the site in response to storms greater than 1.9 centimeters. However the extent of mounding appears to be confined to the area adjacent to the site. This is indicated by a steep gradient between MW2 and MW3 and the minimal groundwater elevation increases observed at MW3. The rate of infiltration was observed to be a primary factor affecting groundwater mounding; additionally temperature was observed to affect the infiltration rate and resulting mound. Despite the observed mounding, the depth of groundwater remained a sufficient depth below the site (12 ft). Given the maximum extent of groundwater mounding, it is believed

the sufficient storage capacity exists in the vadose zone to accommodate larger storms without adversely affecting the local subsurface.

Continuous monitoring of the groundwater temperature and conductivity, indicate that the bioinfiltration best management practice causes significant fluctuations near the site but that these fluctuations are attenuated downgradient. The temperature and conductivity of wells MW1 and MW3 were observed to be similar, indicating that infiltration by the site does not significantly impact the downgradient water. However, at MW2 stormwater infiltration was observed to significantly alter the groundwater temperature for prolonged periods. Decreases in temperature were observed to be related to increased groundwater mounding, thus while the downgradient temperature may not be effected variations in temperature effect the performance of the system.

RECOMMMENDATIONS

A surprising observation of this study is that the upgradient well, MW1 displayed rapid responses to precipitation indicating a rapid infiltration rate. This observation underscores the importance of minimizing site disturbance during construction and further the capability of un-compacted turf areas to infiltrate water. Thus it is recommended that site design seek to minimize site disturbance and maximize pervious surfaces.

Another interesting observation was the prolonged decrease in temperature observed at MW2. While the effects were observed to be very localized, the decreased temperatures also lead to slower infiltration rates, even after surface temperatures may have increased. Thus, it is important to consider the variation in infiltration rate due to temperature during the selection and design of infiltration BMP. Further it is suggested that groundwater monitoring may be a useful tool for BMP design. For instance, continuous monitoring data would provide accurate estimation of infiltration rates and expected mounding, in addition to establishing the groundwater elevation at a site.

Lastly, the effectiveness of infiltration BMP for smaller storms should be noted. As observed in the study, for smaller storms the BMP did not lead to excessive mounding. Additionally it was observed that downgradient conductivity, temperature and groundwater elevation were not significantly effected by the BMP. Therefore it is suggested that similar infiltration BMP be considered to treat similar water quality issues for smaller storms.

REFERENCES

Akan, A. O. (2002). "Sizing Stormwater Infiltration Structures." Journal of Hydraulic Engineering **128**: 534-537.

Aron, G., *et al.* (1986). Field Manual of PA Dept of Transportation Storm Intensity-Duration-Frequency Charts Penn State University**:** 10.

Barraud, S., *et al.* (1999). "The impact of intentional stormwater infiltration on soil and groundwater." Water Science and Technology **39**(2): 185-192.

Birch, G. F., *et al.* (2005). "Efficiency of an infiltration basin in removing contaminants from urban stormwater." Environmental Monitoring and Assessment **101**: 23-38.

Bouwer, H. (1978). Groundwater Hydrology, 480 pp., McGraw-Hill, New York, NY.

Dietz, M. E. and J. C. Clausen (2005). "A Field Evaluation of Rain Garden Flow and Pollutant Treatment." Water, Air and Soil Pollution **167**: 123-138.

Emerson, C. H. (2008). Evaluation of Infiltration Practices as a Means to Control Stormwater Runoff. Civil and Environmental Engineering. Villanova, Villanova. **Doctor of Philosophy:** 331.

Ermilio, J. R. (2005). Characterization Study of a Bio-Infiltration Stormwater BMP. Civil and Environmental Engineering. Villanova, PA, Villanova University. **Master of Civil Engineering:** 238.

Fischer, D., *et al.* (2003). "Effects of Stormwater Infiltration on Quality of Groundwater Beneath Retention and Detention Basins." JOURNAL OF ENVIRONMENTAL ENGINEERING **129**(5): 464-471.

Guo, J. C. Y. (2001). "Design of Circular Infiltration Basin Under Mounding Effects." Journal of Water Resources Planning and Management **127**(1): 58-65.

Heasom, W., *et al.* (2006). "Hydrologic Modeling of a Bioinfiltration Best Management Practice." Journal of the American Water Resources Association **42**(5): 1329-1347.

Hsieh, C.-h. and A. P. Davis (2005). "Evaluation and Optimization of Bioretention Media for Treatment of Urban Storm Water Runoff." JOURNAL OF ENVIRONMENTAL ENGINEERING **131**(11): 1521-1531.

Leopold, L. B. (1974). Water: A Primer, 172 pp., W. H. Freemand and Company, San Francisco.

M. Clar, A. D., R.W. Hunt, R.G. Traver, *et al.* (2007). Bioretention Technology: An Overview of Current Practice and Future Needs. LID Conference 2007, Wilmington, NC.

Mikkelsen, P. S., *et al.* (1997). "Pollution of soil and groundwater from infiltration of highly contaminated stormwater: A Case Study." Water Science and Technology **36**(8-9): 325-330.

Mikkelsen, P. S., *et al.* (1996). "Infiltration practice for control of urban stormwater." Journal of Hydraulic Research **34**(6): 827-840.

Mikula, J. B., *et al.* (2007). Appyling a Vadose Zone Model to Stormwater Infiltration. World Environmental and Water Resources Congress 2007: Restoring Our Natural Habitat, EWRI-ASCE.

Muthukrishnan, S., *et al.* (2004). The Use of Best Management Practices (BMPs) in Urban Watersheds. Washington D.C., USEPA. **EPA 600/R-04/184**.

PADEP (2006). Pennsylvania Stormwater Best Management Practices Manual. B. o. W. Management, PADEP. **363-0300-002**.

Park, H., *et al.* (2006). "Uncertainty Analysis of Mound Monitoring for Recharged Water from Surface Spreading Basins." JOURNAL OF ENVIRONMENTAL ENGINEERING **132**(12): 1572-1579.

Pitt, R.*, et al.* (1999). "Groundwater contamination potential from stormwater infiltration practices." Urban Water **1**: 217-236.

Prokop, M. J. (2003). Determining the Effectiveness of the Villanova Bio-Infiltration Traffic Island in Infiltrating Annual Runoff. Civil and Environmental Engineering. Villanova, PA, Villanova University. **Master of Civil Engineering:** 103.

Rai, S. N.*, et al.* (1998). "On the prediction of Ground-Water Mound Formation in Response to Transient Recharge from a Circular Basin." Water Resources Management **12**: 271-284.

Schreffler, C. L.*, et al.* (2006). Effects of Spray-Irrigated Treatment Effluent on Water Quantity and Quality, and the Fate and Transport of Nitrogen in a Small Watershed, New Gardent Township, Chester County, Pennsylvania. USGS, USGS**:** 1-170.

Schuster, W. D.*, et al.* (2007). "Prospects for enhanced groundwater recharge via infiltration of urban storm water runoff: A case study." Journal of Soil and Water Conservation **62**(3): 129-136.

Strecker, E.*, et al.* (2001). "Determining Urban Storm Water BMP Effectiveness." Journal of Water Resources Planning and Management **127**(3): 144-149.

Traver, D. R. (2002). Villanova Stormwater Bioinfiltration Traffic Island Growing Greener Grant Final Project Report, Villanova University.

Traver, D. R.*, et al.* (2007). "Bioretention and Bioinfiltration BMPs: Three researchers experience." Stormwater **8**(7).

USEPA (2000). Low Impact Development (LID): A Literature Review. USEPA. Washington, D.C. **EPA-841-B-00-005**.

Viessman, W. J. and G. L. Lewis (2003). Introduction to Hydrology, 551 pp., Pearson Education, Inc., Upper Saddle River, NJ.

Winogradoff, D. A. (2002). The Bioretention Manual. Prince George's County Department of Environmental Resources.

Winter, T. C.*, et al.* (1998). Ground Water and Surface: A Single Resource. U. S. D. O. INTERIOR, U.S. Government Printing Office.

Water Quality Assessed by Benthic Macro-Invertebrates: Proposing the WQABI method

J.K. McNett[1] and W.F. Hunt[2]

[1] Department of Biological and Agricultural Engineering, North Carolina State University, 141 Weaver Labs, Box 7625, NCSU Campus, Raleigh, NC 27695
[2] Department of Biological and Agricultural Engineering, North Carolina State University, Weaver Administration Bldg 208, Box 7625, NCSU Campus, Raleigh, NC 27695

ABSTRACT: Stormwater experts agree that the currently used percent removal methodology metric has many flaws, and some have suggested utilizing a BMP effluent concentration metric. This paper examines a new method that establishes effluent target concentrations for BMPs based on the health of macro-invertebrates in the receiving water. 193 ambient water quality monitoring stations in North Carolina were paired with benthic macro-invertebrate health ratings collected in very close proximity. Water quality for the sites ranged from Excellent to Poor and was divided into three distinct eco-regions. Median NO_3 + NO_2, TKN, TN, and TP concentrations all increased with poorer benthic ratings; however, there was no such trend with respect to DO, TSS, and Fecal Coliforms. Overall, the new method was most effective in the Piedmont and Coastal eco-regions; however with more data collection, the Mountain eco-region may also benefit. For example, if regulators were to require "Good" water quality in the Piedmont eco-region, designers would have to limit effluent concentrations of TN and TP would be 0.99 mg/L and 0.11 mg/L, respectively, per the method presented herein.

INTRODUCTION

The USEPA requires that all stormwater pollution is controlled to the maximum extent practicable (MEP) through the use of best management practices (BMPs). Local and state stormwater manuals and handbooks provide guidance on BMP designs, including the assignment of load reductions and/or percent removals of pollutants. For example, The North Carolina Department of Environment and Natural Resources (NCDENR) utilizes a post-development standard of 0.45 kg/ha/yr (0.4 lb/ac/yr) and 4.5 kg/ha/yr (4.0 lb/ac/yr) for total phosphorus (TP) and total nitrogen (TN), respectively, in the Tar-Pamlico River Basin (NCDENR, 2007). BMPs are implemented to meet post-development regulatory standards and are given credit based on percent nutrient removal for that BMP type. For instance, a stormwater wetland is credited with a 35% and 40% pollutant reduction of TP and TN, respectively, in North Carolina (Table 1). The load reduction and percent removal methods do not typically account for variations in BMP designs, eco-region, or background contaminant levels in receiving waters.

As stated by the Center for Watershed Protection, "Stormwater management criteria commonly assign the median removal efficiency, but this often masks the role of certain design factors in reducing or enhancing performance" (Winer, 2007). Other studies show that changes in design, including media composition and depth, ratio of watershed area to BMP surface area, and/or ponding and retention times, heavily influence BMP efficiency (Dietz and Clausen, 2006; Li et al, 2009; Clary et al., 2002; Hunt et al, 2006; Urbonas, 1995; Scholes et al., 2008). Similarly, local hydrology, climate and system age impact BMP performance (Scholes et al., 2008; Urbonas, 1995; Line et al., 2008), creating variations in reported removal rates (Table 1).

Table 1. Assigned total nitrogen (TN) and total phosphorus (TP) BMP removal efficiencies by state.

	BMP type							
	Bioretention		Wetpond		Wetland		Sand Filter	
State	TN	TP	TN	TP	TN	TP	TN	TP
New Jersey [1]	30%	60%	30%	50%	30%	50%	35%	50%
North Carolina [2]	35%	45%	25%	40%	40%	35%	35%	45%
Virginia [3]	46%	5%	31%	52%	24%	48%	32%	59%*

*Sand Filter was not specifically listed in the VA Stormwater Handbook. "Other Infiltration Practices" was used in lieu.

[1] NJDEP (2004.)

[2] NCDENR (2007.)

[3] VDCR (1999.)

The documentation of physical, chemical, climatic, geological, biological, and meteorological parameters are often not required in BMP monitoring (Urbonas, 1995), yet are essential in correlating design characteristics with performance (Clary et al., 2002; Urbonas, 1995). Percent removals and load reductions, as a performance indication, can be misleading. Such metrics do not necessarily coincide with water quality. For example, Lenhart and Hunt (2009) show that influent TN concentrations at a wetland in River Bend, North Carolina, appear to approach irreducible levels.

The wetland demonstrated poor performance, when evaluated through the percent removal metric, even though influent and effluent nutrient concentrations were lower than BMP effluent concentrations measured in other nearby studies (Line et al., 2008). Conversely, (Schaafsma et al., 1998) showed that for a wastewater wetland, even when TN, TP, and total suspended solids (TSS) influent loads were reduced by more than 90%, effluent concentrations remained above regulatory levels.

In some situations, a BMP may produce higher effluent concentrations due to surrounding environmental conditions. For example, a bioretention cell receiving runoff from a well-fertilized area tends to have higher inflow nutrient concentrations than a cell receiving runoff from a lightly used parking lot (Passeport and Hunt, 2009; Sharkey, 2006). Similarly, Emilsson et al. (2007) showed that runoff nutrient concentrations increase when vegetative roof systems are conventionally fertilized, when compared to roofs that receive controlled release fertilizers. Finally, runoff from greyfield developments, brownfield developments, and reclaimed lands are expected to show higher pollutant loads than runoff from greenfield developments (Stehouwer et al., 2006). Hence, background and inflow concentrations impact nutrient removal performance and should be considered when setting regulatory standards.

The ultimate goal of stormwater management is to protect water quality and promote healthy aquatic ecosystems. The percent removal and load reduction methods do not take into account aquatic health when assessing BMPs and do not ensure high quality, healthy waters. The following study introduces a novel methodology of assessing BMPs by relating aquatic health to ambient water quality data, and then selecting BMPs able to meet this ambient water quality.

POSSIBLE SOLUTION: ASSESSING WATER QUALITY USING BENTHIC MACRO-INVERTEBRATES. Biotic indicator species, such as benthic macro-invertebrates (benthos), periphyton, and certain fish populations, are used to assess water quality of streams and rivers across the world (Skoulikidis et al., 2004; Van Duinen, 2006; Gray, 2008). The organisms predict the degree of impairments in streams and can be an evaluation metric to determine the effectiveness of best management practices (Barbour et al., 1999). Forty-three states use biotic protocols in water resource management (NCDENR, 2008) with benthos being the most commonly used indicator species by state agencies in the United States (Southerland and Stribling, 1995). Benthos reside in rivers, streams, and estuaries in the following 5 habitats: cobble (hard substrates common in the mountain and piedmont regions), snags (woody debris including sticks and branches), vegetated banks (submerged lower banks with the presence of plants and roots), submerged macrophytes (seasonal aquatic plants rooted to the stream bottom), and sand/fine sediment (Barbour et al., 1999). A different collection technique is recommended for each habitat (Barbour et al., 1999). Different benthos are used in monitoring, corresponding to the native species of the particular eco-region of interest. For example, common freshwater benthos include mussels (class bivalvia), crayfish (order decpoda), worms (order oligochaeta), and stoneflies (order plecoptera). Benthos range in tolerance and therefore may be predicative of varying water qualities (Table 2).

After collection, the benthos are preserved and identified by family and genus/species type. Depending on the abundance and diversity of benthos collected, a stream health rating is assigned, including: Excellent, (E), Good, (G), Good-Fair, (GF), Fair, (F,) and Poor, (P) (Barbour et al., 1995). Similar ratings and modified collection and assessment techniques are used in other regions of the world (Buffagni et al., 2004; Simboura and Reizopoulou, 2008).

Table 2. Tolerance of Benthos in terms of Water Quality (Barbour et al., 1995)

Rating	Description of Benthos	Sample Organisms by Scientific Name
Excellent	Very sensitive	Ephemera Guttulata (mayfly), Litobrancha recurvata (mayfly)
Good	Sensitive	Drunella allegheniensis (mayfly), Rhyacophila fuscula (caddisfly)
Good-Fair	Semi-tolerant	Amnicola (snail), Elliptio complanata (mussel)
Fair	Tolerant	Cambarus (crayfish), Crangonyx (crustacean)
Poor	Very tolerant	Enchytraeidae (worm), Limnodrilus cervix (worm)

Benthic macro invertebrate health ratings (BMR) are commonly used in European countries to assess water quality, as shown by the **A**ssessment System for the Ecological **Q**uality of Streams and Rivers throughout **E**urope using Benthic **M**acroinvertebrates (AQEM) project. The program uses BMRs to assign a stream health rating from 5 (best) to 1 (worst) and, furthermore, aspires for all rivers and streams across 8 countries in Europe to reach at least a "good" or "4" quality rating by 2015 (Skoulikidis, 2004) .

Trends toward regional specificity have increasingly emerged with regards to BMR collection techniques and analysis. Using BMRs, Skoulikidis (2004) examined the difference in water quality among three eco-regions in Greece with varying geographical and climatic features. A nutrient metric, reflecting ambient water quality (AWQ), exhibited satisfactory correlation with the biotic metric (BMR). Another study expands on the collection techniques of Barbour et al. (1999) by assessing benthos from 53 streams in Illinois. The study determined that high nutrient levels in streams corresponded to degraded aquatic habitat (Heatherly and Whiles, 2007). Contrasting Skoulikidis (2004), Heatherly and Whiles (2007), caution against using an eco-regional approach to stream classification. The study suggests that a certain eco-region may not exhibit the same benthos throughout. However, like Skoulikidis (2004), the study shows an overall correspondence between elevated nutrient levels and degraded habitats of benthos (Heatherly and Whiles, 2007). In addition to regional studies, notable efforts are being made to localize collection techniques. The Mid Atlantic Coastal Streams (MACS) workgroup (including North Carolina) and the Florida Department of Environmental Protection (FLDEP) have developed a scientifically validated sampling procedure for low-gradient coastal streams (Barbour et al., 1999).

Previous North Carolina studies have not yet directly compared ambient water quality nutrient concentrations to BMRs, yet plentiful data collected by NCDENR provides potential to do so. The ambient water quality (AWQ) at 339 stream and river sites throughout North Carolina has been monitored for the past 30 years, including monthly visits and five-year basin wide assessment reports (NCDWQ, 2008). AWQ data include concentrations of dissolved oxygen (DO), total suspended

solids (TSS), nitrogen-ammonia (NH3), Nitrate-Nitrite (NO3 + NO2), Total Kjeldahl Nitrogen, (TKN), TP, and Fecal Coliforms. Simultaneously, the water quality of approximately 200 North Carolina streams has been rated using benthos or fish (NCDWQ, 2008).

PROPOSING THE WQABI METHOD. Similar to the study by Skoulikidis (2004), the following method evaluates regional impact on ambient water quality. This study is different from others because all data are specific to North Carolina, including: BMRs, AWQ data, BMP efficiencies and effluents, and pollutant regulations. Relating pollutant concentrations associated with healthy streams and estuaries to BMP effluent concentrations provides an innovative method for BMP performance evaluation. While these particular findings are regionally specific, the methodology presented has wide application.

To properly design BMPs for a given watershed, target pollutant effluent concentrations need to be established. While excellent water quality conditions are encouraged, it is understood that background local ambient water quality may create exceptions. For example, most greenfield developments have cleaner background water quality, so perhaps they should be held to more stringent ratings such as E or G. A greyfield or infill development, with degraded background water quality, however, may have lower standards such as GF. It is expected that DO concentrations will increase with higher BMRs, while concentrations of TSS, NH3, NO3 + NO2, TKN, TP, and Fecal Coliforms will increase with lower ratings. Additionally, it is hypothesized that some pollutants will show a higher correlation in one eco-region than in another, therefore it is expected that the WQABI method may be better able to be used in one eco-region over another.

This study evaluates a method of assessing BMP performance using water quality assessed by benthic macro-invertebrate health ratings (WQABI), specific to one of three eco-regions. Specifically, in North Carolina, do the mountain, piedmont, and coastal regions require different regulatory standards? This concept is important in determining criteria for development and whether or not a developed land can meet pre-developed, or target, water quality conditions.

METHODS

AWQ, benthos, and fish sampling locations were obtained from the North Carolina Division of Water Quality (NCDWQ) and imported into ArcGIS, version 9.2. (NCDENR, 2008). Each BMR or fish sampling location was located in one of three eco-regions: mountain, piedmont, or coastal.

The mountain eco-region is the smallest of the three and is separated from the piedmont region by the Blue Ridge Mountain range. The piedmont eco-region is located between the mountain region and the coastal region. It consists of a wide variety of streams, with higher levels of urbanization. Lastly, the coastal region is located in eastern North Carolina, and consists of coastal wetlands, sand hills, and swamps (NCDENR, 2008). Numerous states have accepted the eco-region approach in benthos assessment (e.g. Iowa (IADNR, 2008), North Carolina (NCDENR, 2008), and Virginia (VDEQ, 2008)).

AWQ monitoring sites were then paired with BMR and fish collection sites within a 402 m (¼-mile) range. All paired monitoring locations (AWQ with BMR, or AWQ with fish monitoring sites) were located in the same river or estuary. Also, if the monitoring date ranges of AWQ and BMR/fish population data collection did not fall within two years of each other, the pair was omitted from the study due to possible temporal changes in water quality. If multiple benthic ratings were given within the time range of AWQ collection, the lowest rating documented was used. Additionally, if both fish community and BMRs were available, the BMR was used, as the majority of water quality ratings from NCDENR are based on BMR data. Ultimately, each match included one of 5 ratings and one of three eco-regions, yielding a total of 15 possible combinations. Lastly, the significance between BMR and AMS data was analyzed using SAS statistical software package (2004).

RESULTS AND DISCUSSION

There were 193 DWQ stations in which both AWQ data were collected and BMRs were assigned. For accuracy, if a pair contained a station where collected AWQ data were limited (a sample size of 10 or less), the pair was excluded. Also, if the number of pairs in a given eco-region was less than 8 that rating was excluded from the study. Namely, Fair (F) and Poor (P) ratings from both the mountain and coastal eco-regions were omitted (Table 3).

Table 3: The number of paired AWQ and BMR collection sites for each eco-region

Number of Location Matches			
	Eco-Region		
BMR Rating*	Mountain	Piedmont	Coastal
E	8	8 (1)	10
G	19	20	14
GF	10 (1**)	31 (2)	16
F	4	39 (3)	3
P	1	8 (1)	2

* E = excellent, G = good, GF= good-fair, F = fair, and P = poor ratings

** Values in parentheses represent DWQ stations in which both AWQ and fish populations were monitored. The values outside of parenthesis represent stations in which BMR and AWQ were monitored.

The Piedmont region had the most stations in which both AWQ and BMRs were monitored (106), followed by the Coastal (45), and the Mountain (42) (Table 3).

Median pollutant concentrations for the Piedmont eco-region exhibited the most apparent trend with BMR. As expected, median $NO_3 + NO_2$, TKN, TN, and TP concentrations all increased with decreased BMR (Table 4). NH_3 concentrations typically increased with decreased BMR. Median DO concentrations decreased with increased BMR, yet median concentrations of TSS and fecal coliforms did not exhibit a noticeable relationship with BMR.

Table 4. Median Concentrations of Pollutants in the Piedmont Eco-region

	PIEDMONT							
	Constituent concentration (mg/L)							
Rating	DO	TSS	NH3	NO2 + NO3	TKN	TN	TP	Fecal (#/100mL)
E	9.25	4.00	0.02	0.39	0.30	0.69	0.06	229.0
G	8.80	6.40	0.04	0.59	0.40	0.99	0.11	103.1
GF	8.40	5.00	0.06	0.67	0.50	1.17	0.13	93.0
F	7.70	7.00	0.06	1.60	0.56	2.16	0.22	169.2
P	6.80	5.00	0.13	6.34	1.25	7.59	0.63	316.4

The coastal eco-region exhibited similar results (not shown): however, the mountain eco-region did not show an obvious relationship between AMS data and BMRs (not-shown). It is suggested that more data be collected in the fair and poor water-quality classes of both the mountain and coastal eco-regions, to more accurately define the relationship between BMR and AMS data. As of now, the WQABI method could only apply to the Piedmont eco-region *with confidence*.

Stormwater regulators could use the data presented for the Piedmont eco-region to establish target BMP effluent concentrations. For example, suppose a green field development were to take place. Regulators could require that practices be used such that the composite water quality from the development met "Good" water quality standards of 0.99 mg/L and 0.11 mg/L for TN and TP, respectively (Table 4). Perhaps a grey field development could have more relaxed standards placed on it ("Good-Fair").

Overall, macro-invertebrate tolerance to "dirtier" ambient conditions appears to increase with eco-region as follows: mountain, coastal, and piedmont. This suggests that it is more difficult to design a treatment system to achieve comparable benthos protection in the mountain than in the piedmont. Of the three eco-regions, the piedmont exhibited the most apparent trend between AWQ data and BMRs and would therefore benefit most from using the WQABI method. WQABI does not work for all constituents, but it does appear reasonable for some. NH_3, NO_2, TN and TP exhibited significant BMR effects, as they increased with decreased BMR. The mountain eco-region typically exhibited lower median nutrient concentrations than either the coastal or piedmont eco-regions, however there was little to no correlation between BMR and AMS data, and therefore use of WQABI in this eco-region is not recommended without further research.

FUTURE DIRECTIONS OF WQABI. Numerous flaws have been documented in using load reduction and percent removals for assessing BMPs (Lenhart and Hunt, 2009; Schaafsma et al, 1998; Jones et al., 2008), including the false notion that high concentration and load percent removals directly correspond to excellent BMP performance. The WQABI method accounts for errors associated with the conventional BMP assessment methods by relating performance to target ambient water quality concentrations. The purpose of this paper was to introduce this concept; however, many questions about using WQABI persist. For example, do the various types of indicator species (benthos, fish, periphyton) give equivalent water quality

ratings? How much variation lies among species collection techniques? What is the appropriate course of action when no BMP can meet desired water quality effluent concentrations? Further studies are encouraged to ensure consistency in the measurement of biotic health ratings. Likewise, detailed reporting of BMP design parameters, such as those required by the International BMP database (Clary et al., 2005), is encouraged to determine optimal BMP design criterion.

All three eco-regions exhibited a similar tendency: differentiation among AWQ data begins to blur as BMRs improve. For instance, there is a noticeable difference in AWQ data between GF, F, and P, but not much variation among E, G, and GF. It appears there are two distinct categories of AWQ data: those associated with cleaner water and those associated with poorer water quality. It is recommended that this ambiguity between BMRs be studied further by considering the tolerance of different biotic indicators, fish versus benthos for example.

Furthermore, it is important to recognize that the WQABI method only considers water quality and not quantity. Total Maximum Daily Loads (TMDLs) may be surpassed when runoff volume increases with large storm events, negating potential benefits of cleaner effluent concentrations. Volume control must be considered in addition to the WQABI method to prevent flooding, maintain stable stream morphology, and meet target or pre-development hydrology. While the WQABI method can be completed independent of hydrologic data, it is strongly recommended that hydrologic design guidance be provided in addition to the WQABI method. Also, WQABI works when substantial BMP studies reporting effluent concentrations from the region exists or if a reliable, deterministic way of predicting effluent concentrations is employed. It is recognized that for some practices in some parts of the U.S.A, a deficiency exists in data collection and BMP performance prediction.

CONCLUSIONS

Several conclusions were drawn from this study:

(1) AWQ data and BMRs can be combined to set target nutrient concentrations that protect high quality waters. Target concentrations can be used as a baseline for BMP assessment. This study examined NC-specific data, but similar analyses could be conducted elsewhere.
(2) Unlike the percent removal method, the WQABI method accounts for irreducible and background concentrations.
(3) Different eco-regions require different regulatory standards. This study showed that the streams in the mountain eco-region of North Carolina held lower median nutrient levels across all BMRs when compared to streams in the piedmont and coastal eco-regions. The higher background water quality implies a need for more stringent regulations on development. Perhaps development in some pristine parts of the mountain eco-region should be prevented altogether if excellent water quality is to be maintained. A similar trend is evident in the coastal eco-region, where stream nutrient concentrations are generally lower than those in the piedmont eco-region.

(4) The WQABI method allows different target conditions/standards to be chosen depending upon existing in-ground conditions. For example, a greenfield development could be held to a more rigorous standard (an E or G BMRs) than a greyfield, infill development (perhaps a GF BMR).
(5) Some eco-regions respond better to the WQABI method than other eco-regions. This study showed that the piedmont eco-region exhibited the most obvious trend between AWQ-data and BMRs; however, more AQW data and BMRs were monitored in the piedmont compared to the mountain and coastal regions. More paired data (AWQ and BMRs) from the mountain and coastal eco-regions are recommended for further analysis.
(6) Some pollutants responded better to the WQABI method. For example, NH_3, NO_2, TN and TP concentrations exhibited significant BMR effects; whereas, TSS, DO, and fecal coliform concentrations showed little or no relation to BMR.
(7) The WQABI method needs further refinement. Efforts are needed to synchronize benthos collection and identification techniques and more data are needed to differentiate water quality among the five BMRs, particularly among the better water quality ratings. Additionally, hydrologic function, especially reductions in outflow volume should be considered and combined with the WQABI method in order to ensure optimal BMP effectiveness.

ACKNOWLEDGEMENTS

The authors would like to thank The Cooperative Institute for Coastal and Estuarine Environmental Technology (CICEET) for funding this research.

REFERENCES

Barbour, M.T., Gerritsen, J., Snyder, B.D., and Stribling, J.B. (1999). “Rapid Bioassessment Protocols for Use in Streams and Wadeable Rivers: Periphyton, Benthic Macroinvertebrates and Fish, Second Edition.” EPA 841-B-99-002. U.S. Environmental Protection Agency; Office of Water; Washington, D.C. <http://www.bmpdatabase.org/Docs/FAQPercentRemoval.pdf>

Buffagni, A., Erba, S., Cazzola, M., Kemp, J.L. (2004). "The AQEM Multimetric System for the Southern Italian Apennines: Assessing the Impact of Water Quality and Habitat Degradation on Pool Macroinvertebrates in Mediterranean Rivers." Hydrobiologia., 516 (1-3), 313-329.

Clary, J. Urbonas, B., Jones, J., Strecker, E., Quigley, M., O'Brien, J. (2002). "Developing, Evaluating and Maintaining a Standardized Stormwater BMP Effectiveness Database." *Water Science and Technology*, 45(7), 65-73.

Dietz, M.E. and Clausen, J.C. (2006). "Saturation to Improve Pollutant Retention in a Rain Garden." *Environmental science technology.*, 40(4), 1335-1340.

Emilsson, T., Berndtsson, J.C., Mattsson, J.E., and Rolf, K. (2007). “Effect of Using Conventional and Controlled Release Fertiliser on Nutrient Runoff from Various Vegetated Roof Systems”. *Ecological Engineering*, 29(3), 260-271.

Gray, N. F., and Delaney, E. (2008). "Comparison of Benthic Macroinvertebrate Indices for the Assessment of the Impact of Acid Mine Drainage on an Irish River Below an Abandoned Cu–S Mine." Environmental Pollution., 155(1), 31-40.

Heatherly, T., Whiles, M.R., Royer, T.V., David, M.B. (2007). "Relationships between

Water Quality, Habitat Quality, and Macroinvertebrate Assemblages in Illinois Streams." Journal of Environmental Quality., 36(6), 1653-1660.

Hunt, W. F., Jarrett, A. R., Smith, J. T., and Sharkey, L. J. (2006). "Evaluating Bioretention Hydrology and Nutrient Removal at Three Field Sites in North Carolina." *Journal of Irrigation and Drainage Engineering*, 132 (6), 600-608.

IADNR/IGS. 2008. Biological Assessment of Iowa's Streams and Rivers. Watershed Monitoring and Assessment. Iowa City, IA.

Jones, J.E., Clary, J., Strecker, E., Quigley, M.M. 15 reasons you should think twice before using percent removal to assess BMP performance. *Stormwater*. January - February2008, (1/16/2009), undefined (accessed 1/16/2009).

Lenhart, H.A. and Hunt, W.F. (2009). "Evaluating Four Stormwater Performance Metrics with a North Carolina Coastal Plain Stormwater Wetland" *Journal of Environmental Engineering*. (Submitted)

Li, H., Sharkey, L.J., Hunt, W.F., Davis, A.P. (2009). "Mitigation of Impervious Surface Hydrology Using Bioretention in North Carolina and Maryland." *Journal of Hydrologic Engineering*, 14(4), TBD.

Line, D.E., Jennings, G.D., Shaffer, M.B., Calabria, J., Hunt, W.F. (2008). "Evaluating the Effectiveness of Two Stormwater Wetlands in North Carolina." *Transactions of the ASABE*, 51(2), 521-528.

NCDENR. Biological Assessment Unit. Environmental Sciences Section. NC: NC Division of Water Quality. Last updated: 01/23/08. Last accessed: 11/05/2008. <http://h2o.enr.state.nc.us/esb/BAU.html>

NCDENR. 2007. Stormwater Best Management Practices Manual. Raleigh, NC: N.C. Division of Water Quality.

"NC Division of Water Quality: Basin Assessment Reports." 10/3/2008 <http://h2o.enr.state.nc.us.www.lib.ncsu.edu:2048/esb/bar.html>.

"NC Division of Water Quality: Ecosystems Unit, Ambient Monitoring System." 10/3/2008 <http://www.esb.enr.state.nc.us.www.lib.ncsu.edu:2048/ams.html>.

"NC OneMap." Geographic Data Serving a Statewide Community. NCDENR and NC Geographic Information Coordinating Council. June-July 2008 <http://www.nconemap.com/>.

NJDEP. 2004. New Jersey Stormwater Best Management Practices Manual. Division of Watershed Management. Trenton, NJ.

Passeport, E., and W.F. Hunt. 2009. "Asphalt Parking Lot Runoff Nutrient Characterization for Eight Sites in North Carolina, USA." *Journal of Hydrologic Engineering*, 14(4), TBD.

SAS Institute Inc., SAS 9.1.3 Help and Documentation, Cary, NC: SAS Institute Inc., 2000-2004

Sharkey, L.J. (2006). "The Performance of Bioretention Areas in North Carolina: A Study of Water Quality, Water Quantity, and Soil Media". M.S. thesis. Raleigh, NC: North Carolina State University, Biological and Agricultural Engineering.

Schaafsma, J. A., Baldwin, A. H., and Streb, C. A. (1998). "An evaluation of a constructed wetland to treat wastewater from a dairy farm in Maryland, USA". Ecological *Engineering*, 14,199-206.

Scholes, L.,Revitt, M., and Ellis, J.B. (2008). "A systematic approach for the comparative assessment of stormwater pollutant removal potentials." *Journal of Environmental Management*, 88, 467-478.

Simboura, N., and Reizopoulou, S. (2008). "An Intercalibration of Classification Metrics of Benthic Macroinvertebrates in Coastal and Transitional Ecosystems of the Eastern Mediterranean Ecoregion (Greece)." *Marine Pollution Bulletin*., 56(1), 116-126.

Skoulikidis, N. Gritzalis, K.C., Kouvarda, T., and Buffagni, A. (2004)."The Development of an Ecological Quality Assessment and Classification System for Greek Running Waters Based on Benthic Macroinvertebrates." *Hydrobiologia*, 516(1-3), 149-60.

Stehouwer, R., Day, R.L., Macneal, K.E. (2006). "Nutrient and Trace Element Leaching Following Mine Reclamation with Biosolids." *Journal of Environmental Quality*, 35(4), 1118-1126.

Southerland, M.T. and J.B. Stribling. (1995). "Status of biological criteria development and implementation." *Biological assessment and criteria: Tools for water resource planning and decision making*. 81-96.

Urbonas, B.R. (1995). "Recommended Parameters to Report with BMP Monitoring Data." *Journal of Water Resources Planning and Management*, 121(1), 23-24.

Van Duinen, G. A., Timm, T., Smolders, A.J.P., Brock, A.M.T., Verberk, W.C.E.P., and Esselink, H. (2006). "Differential Response of Aquatic Oligochaete Species to Increased Nutrient Availability - A Comparative Study between Estonian and Dutch Raised Bogs." *Hydrobiologia*, 564(1), 143-145.

VDEQ. 2008. Biological Monitoring. Richmond, VA. <Virginia.gov> Virginia Department of Conservation and Recreation. 1999. Virginia Stormwater Management Handbook, First Edition. VA Division of Soil and Water Conservation. Richmond, VA.

Winer, R. (2000). National Pollutant Removal Performance Database for Stormwater Treatment Practices: 2nd edition. Center for Watershed Protection. Ellicott City, MD.

A ROBUST AND FAST MODEL FOR SIMULATING STREET FLOODING

Arturo S. León[1], Leonardo S. Nanía[2], Arthur Schmidt[3], Marcelo H. García[4]

[1] Post-doctoral Research Associate, Dept. of Civil and Environmental Engineering, University of Illinois, Urbana, Illinois 61801, USA. E-mail: asleon@illinois.edu
[2] Associate Professor, Dpto. de Mecánica de Estructuras e Ingeniería Hidráulica, Universidad de Granada, Granada 18071, SPAIN. E-mail: LNania@ugr.es
[3] Research Assistant Professor, Dept. of Civil and Environmental Engineering, University of Illinois, Urbana, IL 61801, USA. E-mail: aschmidt@illinois.edu
[4] Professor and Director of the Ven Te Chow Hydrosystems Lab., Dept. of Civil and Envir. Eng., University of Illinois, Urbana, IL 61801, USA. E-mail: mhgarcia@illinois.edu

Abstract

This work is part of a long term project which aims to simulate (1) the hydrology, (2) street flows, (3) flow interception at inlets and (4) storm-sewer flows in urban areas. The present work describes the application of the model using only the first two modules. The hydrologic model (first module) transforms rainfall to runoff using the kinematic wave approximation and simulating the infiltration process with the Green-Ampt method. The street model (second module) is based on a finite volume-shock capturing scheme that solves the full conservative Saint-Venant equations and can be used to simulate subcritical and supercritical flows. The formulation of boundary conditions at the street crossings in the street model is general and can be used for any number of streets, any combination of inflowing and outflowing streets, and any flow type (e.g., supercritical flows). The model using the first two modules is fast and robust and it has several potential applications. Perhaps the most important one is that it can be used in new urban developments to identify critical zones of urban flooding (e.g., zones with high water depths and flow velocities) in order to take appropriate measures of drainage control (e.g., to increase capacity of inlets). This model can also be used in developed urban areas to locate the critical areas in case of inlet clogging. In order to illustrate the capabilities of the model (first two modules) it was applied to an urban catchment in the village of Dolton, a southern suburb of Chicago. The watershed of this village drains to the dropshaft CDS-51 in the Calumet TARP (Tunel and Reservoir Plan) system which is operated by the Metropolitan Water Reclamation District of Greater Chicago. The fact that this model is fast makes suitable its application to large urban areas.

Introduction

Urban catchments in rainy climates commonly are exposed to flood threats. In upland areas urban flooding is often associated with an inadequate drainage system, in most cases due to inadequate inlet capacity. Urban flooding may cause material losses in the form of public and private property damage. Furthermore, street flooding may interfere with traffic and in some cases, may jeopardize pedestrian safety. To identify the critical zones of urban flooding (e.g., zones with high water depths and flow velocities) so that appropriate

measures of control (e.g., to add inlet grates) can be taken, hydrologic/hydraulic modeling of a large urban catchment is required, especially in flat urban areas. For a flood modeling tool to be practical, the flooding analysis needs to be done in a relatively short time frame.

Street runoff is frequent in cities which have either direct surface or combined or separated storm/sanitary sewer systems. Nanía (1999) presented a model for simulating street runoff in steep urban areas using a finite difference scheme. This model was later improved using laboratory results (Nanía et al. 2004) for a better representation of the flow distribution at the crossings (supercritical flow). In flat urban areas such as in the city of Chicago, most of the street flows are in subcritical regime for which the model of Nanía (1999) can not be used.

As part of a long term project, a new street model that can be used for simulating subcritical and supercritical flows was developed based on previous works of the authors for pipe transient flows (León et al. 2006, León et al. 2009). In the new model, the formulation of boundary conditions at the street crossings are general and can be used for any number of streets, any combination of inflowing and outflowing streets and any flow type.

Model description

This work is part of a long term project which aims to develop an integrated model to simulate the hydrology and hydraulics of urban drainage systems. This integrated model has four modules. The first module is a hydrologic model, which transforms rainfall into effective runoff depending on surface characteristics (e.g., slope, roughness, paved/unpaved surface area). The resulting runoff of each block is distributed over the respective street and it is used as input for the hydraulic street model (second module). The street model routes the flow over the streets. The third module estimates flow interception at inlets, which lead street runoff into the underground storm-sewer system. The intercepted runoff is used as input for the storm-sewer model. For modeling storm-sewers the Illinois Transient Model (ITM) developed by the first author of this paper was adopted. As mentioned before the present work describes the application of our model using only the first two modules. The application of the integrated model (four modules) will be presented in the near future. Following a brief overview of these modules is presented.

First module: hydrologic model

The hydrologic model transforms rainfall to runoff considering both impervious and pervious surfaces and simulating the infiltration process with the Green-Ampt method (Green and Ampt, 1911; Chow et al, 1988). The depression storage (initial abstraction) is also considered to obtain an effective rainfall. The transformation from effective rainfall to runoff is made considering overland flow on two independent equal-length sloping planes, one pervious and one impervious, and using the kinematic wave approximation of the Saint Venant equations.

Second module: street flow routing

The street model solves the one-dimensional open channel flow continuity and momentum equation that for non prismatic channels or rivers may be written in its vector conservative form as follows (e.g., Chaudhry 1987, León et al. 2006):

$$\frac{\partial \mathbf{U}}{\partial t} + \frac{\partial \mathbf{F}}{\partial x} = \mathbf{S} \tag{1}$$

where the vector variable **U**, the flux vector **F** and the source term vector **S** are given respectively by:

$$\mathbf{U} = \begin{bmatrix} A \\ Q \end{bmatrix}, \ \mathbf{F} = \begin{bmatrix} Q \\ \frac{Q^2}{A} + \frac{A\overline{p}}{\rho} \end{bmatrix} \text{ and } \mathbf{S} = \begin{bmatrix} q \\ F_w + (S_0 - S_f)gA \end{bmatrix} \tag{2}$$

where A = cross-sectional area of the channel; Q = flow discharge; $\overline{p}$ = average pressure of the water column over the cross sectional area; ρ = liquid density; g = gravitational acceleration; S_o = slope of the bottom channel; S_f = slope of the energy line, which may be estimated using an empirical formula such as the Manning's equation; q = lateral flow discharge per unit width, and F_w = momentum term arising from the longitudinal variation of the channel width.

The governing equations [Eq. (1)] are solved using a Finite Volume (FV) shock-capturing scheme in an identical way to that presented in León et al. (2006). The FV scheme used is the second-order MUSCL-Hancock method with the MINMOD Total Variation Diminishing (TVD) pre-processing slope limiter. The FV-shock capturing scheme used ensures that mass and momentum are conserved. For the boundary conditions at the street crossings an identical approach to that presented in León et al. (2009) was used. The formulation of boundary conditions presented in León et al. (2009) is general and can be used for any number of streets, any combination of inflowing and outflowing streets, and any flow type (e.g., supercritical flow).

Third and fourth modules: inlets and sewer system

The third module comprises a model for estimating flow interception at inlets. Inlets lead street runoff into the underground storm-sewer system. The inlet module was implemented according to manual HEC-22 (Federal Highway Administration, 2001).

The fourth module is the Illinois Transient Model (ITM) developed by the first author of this paper. In the ITM model, the free surface region is simulated using the 1D Saint-Venant equations, the pressurized region is modeled using the 1D compressible waterhammer equations and open channel-pressurized flow interfaces are modeled by enforcing mass, momentum and energy relations across the interfaces. The ITM model is a finite volume-shock capturing scheme that can simulate transient free surface flows, transient pressurized flows and the simultaneous occurrence of free surface and pressurized flows (mixed flows) in complex pipe networks.

Evaluation of the model

The primary objective of this section is to illustrate potential applications of the model (first two modules). For instance the model can be used to identify critical zones that need more attention in terms of inlet capacity and maintenance when most of the inlets in the urban watershed are clogged.
In this section the first two modules of the model are applied to an urban catchment in the village of Dolton, a southern suburb of Chicago.

Project storm

In the current application the triangular storm proposed by Chow and Yen was used (Chow and Yen, 1976). The storm which is depicted in Figure 1 has a duration of 80 minutes and a maximum intensity of 45.72 mm/h at 30 minutes and it is a simplification of the storm that occurred in Chicago on July 2nd, 1960.

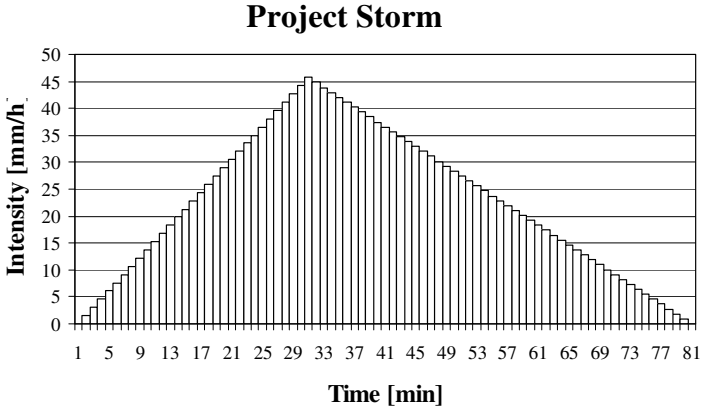

Figure 1: Simplified rainfall hyetograph for Chicago on July 2nd, 1960 (Chow and Yen, 1976).

Characteristics of the watershed

CDS-51 is the name given to the dropshaft that captures the pluvial waters from the sewer system of the village of Dolton. The characteristics of the 3.55 km^2 CDS-51 watershed are presented in the following table:

	Pervious area	Impervious area
Percentage of total area	42.6	57.4
Average slope m/m	0.0133	0.0133
Manning coefficient	0.2	0.015
Depression storage [mm]	1.27	
Hydraulic conductivity [mm/h]	10.7	
Effective saturation	0.418	
Effective porosity	0.412	
Suction head [m]	0.169	

The street network which is depicted in Fig. 2 is composed by 267 blocks (or fraction of blocks), 454 nodes (street crossings) and 637 streets, being the total area modeled of 3.55 km^2 (aprox. 2.22 sq. miles). For the street flow routing the street cross-section shown in Fig. 3 (Nania 1999) was used.

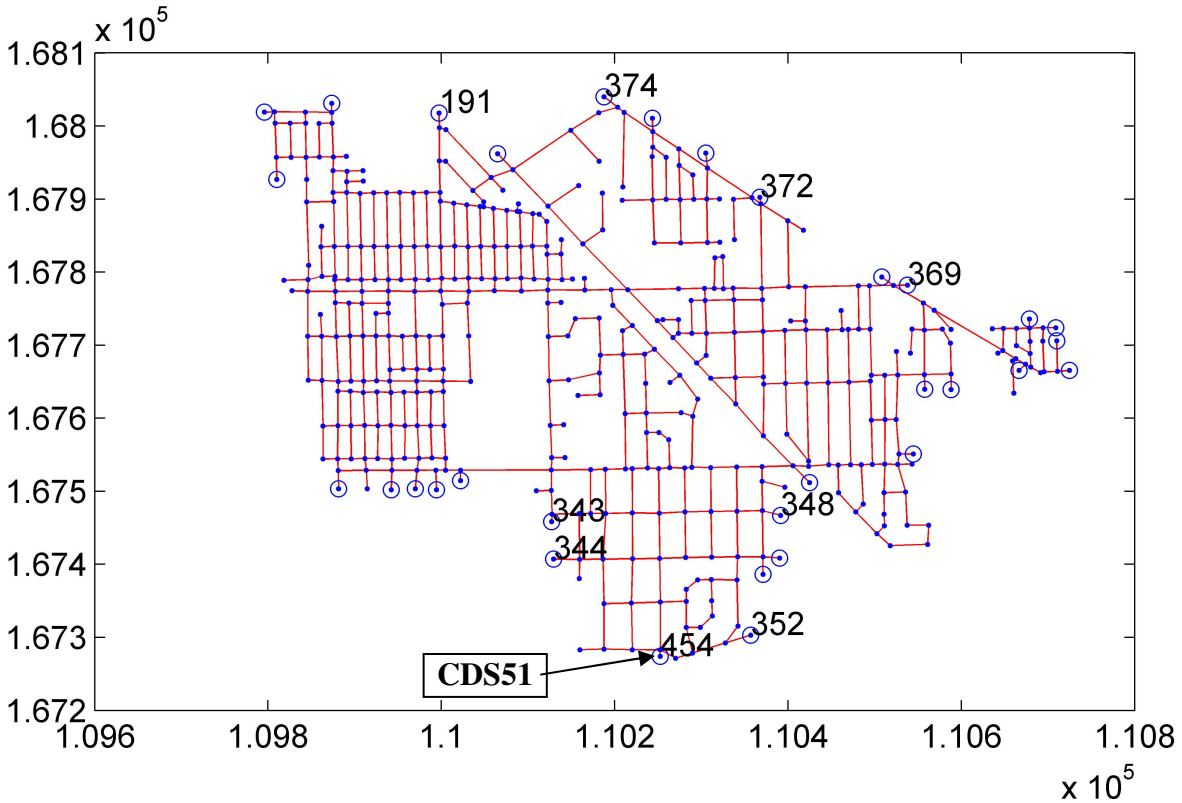

Figure 2: Street network showing the nodes with the largest outflow discharges (*x* and *y* axes on this figure show distances in feet).

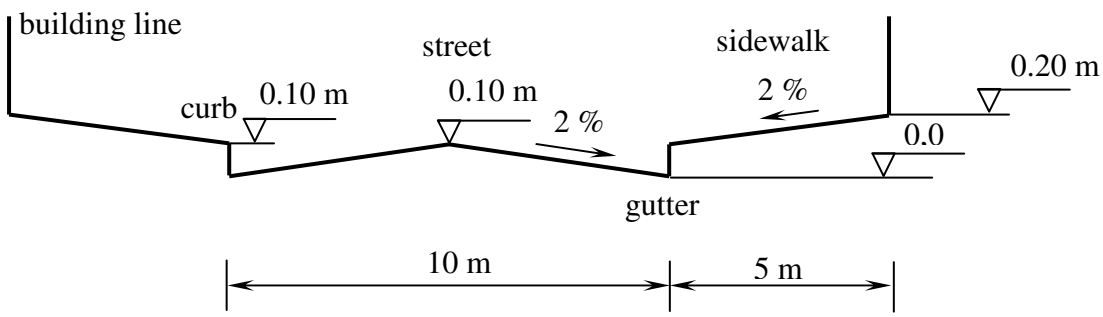

Figure 3: Typical street cross-section (Nania 1999)

Outflow discharge hydrographs

The CDS-51watershed has 32 outflowing streets at the boundaries of the watershed which are represented by blue circles in Figure 2. A street is denoted outflowing if draws water

from the node (street crossing) in normal conditions (e.g., uniform flow) and inflowing otherwise. If the street has zero slope, the street can be treated as either inflowing or outflowing. The numbered outflowing streets presented in Figure 2 (e.g., 454) represent those streets having the largest outflow (flow out of the watershed) discharges. The sum of the hydrographs at these nodes (numbered) represent 90% of the total outflow. The outflow of node 454 coincides with dropshaft CDS-51 and it has the largest outflow of the watershed (23% of total outflow). The outflows from nodes 343, 344 and 348 represent 52% of the total (20, 14 and 18%, respectively). The total outflow hydrograph which is the sum of the hydrographs at the nodes marked by blue circles in Figure 2 is presented in Figure 5 along with the rainfall hyetograph. The reader must notice that the inlets module (module 3, flow interception) is not considered so that the only way the flow can be drained from the watershed is through outflowing streets at the boundary of the watershed.

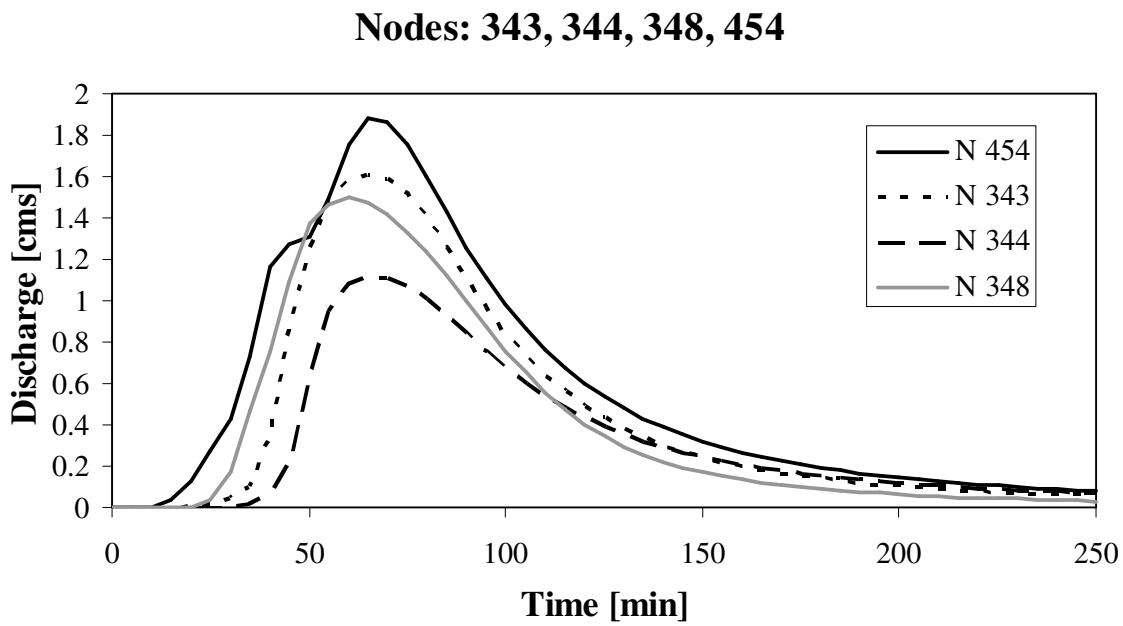

Figure 4: Hydrographs for the four largest outflow discharges in the watershed. The sum of these outflows represent 75% of the total outflow.

Danger analysis of street flows

The water depths and flow velocities in the street network can be used for a danger analysis using some criteria of the literature such as those presented by Nanía et al. (2006 and 2007). These authors suggest a threshold value for maximum flow depth, maximum flow velocity, maximum product between depth and velocity and maximum product between depth and squared velocity. As an example of danger analysis, a map of water depths obtained 65 minutes after the beginning of the storm is presented in Figure 6. As can be observed in this figure, water depths between 10 to 30 cm are the most common in the street network. An area can be denoted as critical when the water depth exceeds for instance a depth of 30 cm. The most critical areas (water depths up to 1.2 m) in Fig. 6 are marked with red circles. Evidently these critical areas are the zones that need more attention in terms of inlet capacity and maintenance. It should be noted that for the

simulations, the curb edge was assumed to be extended vertically, confining the flow to the streets. Figure 7 shows a map of water depths at the end of the simulations (250 minutes). As can be observed in this figure, the water depths in most streets have been depleted except in the critical zones (red circles), where the water is trapped. The latter is expected since the inlet module (flow interception) was not considered in the simulations.

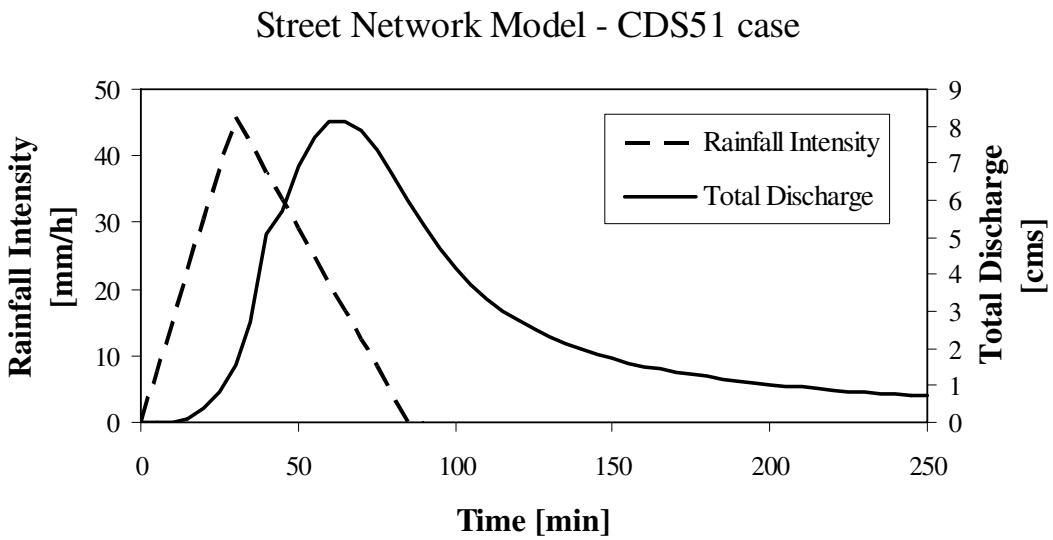

Figure 5: Sum of outflow hydrographs for the 32 outflowing streets at the boundaries of the watershed which are represented by blue circles in Figure 2 along with the rainfall hyetograph.

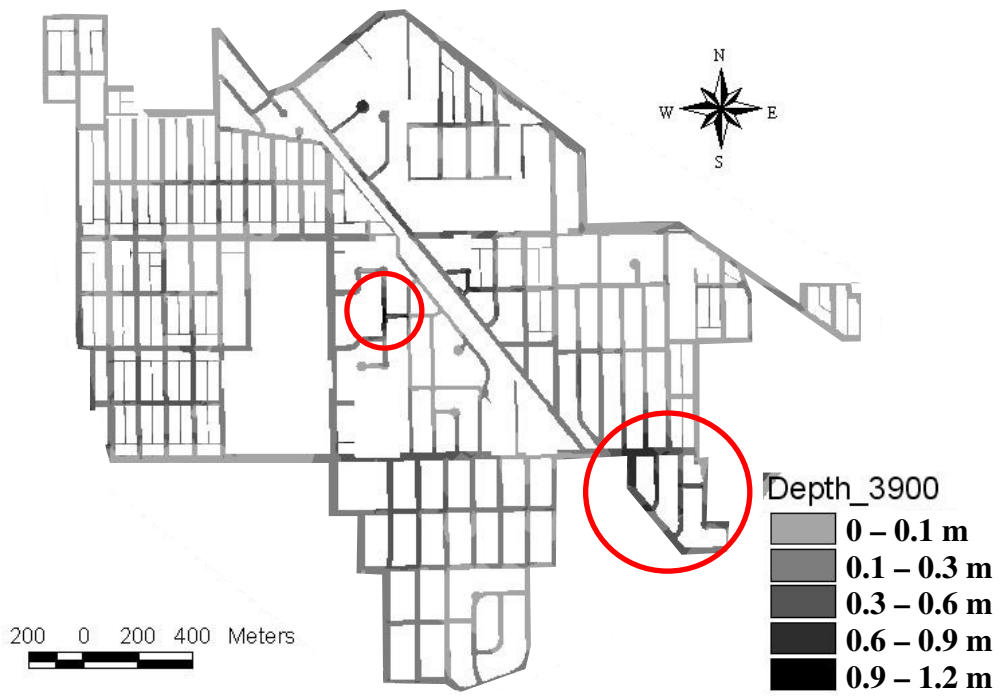

Figure 6: Water depths 65 minutes after the beginning of the project storm.

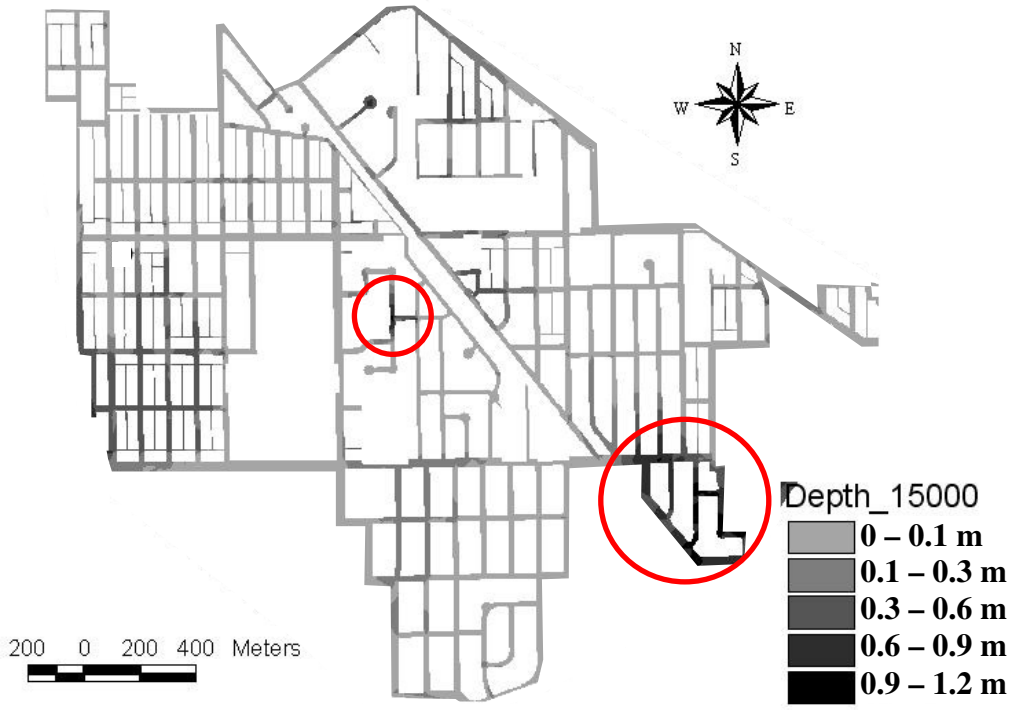

Figure 7: Water depths 250 minutes after the beginning of the project storm.

Conclusions

This work is part of a long term project which aims to simulate (1) the hydrology, (2) street flows, (3) flow interception at inlets and (4) storm-sewer flows in urban areas. The present work describes the application of the model using only the first two modules. The hydrologic model (first module) transforms rainfall to runoff using the kinematic wave approximation and simulating the infiltration process with the Green-Ampt method. The street model (second module) is based on a finite volume-shock capturing scheme that solves the full conservative Saint-Venant equations and can be used to simulate subcritical and supercritical flows. The formulation of boundary conditions at the street crossings in the street model is general and can be used for any number of streets, any combination of inflowing and outflowing streets, and any flow type (e.g., supercritical flows). In order to illustrate the capabilities of the model (first two modules) it was applied to an urban catchment in the village of Dolton, a southern suburb of Chicago. The watershed of this village drains to the dropshaft CDS-51 in the Calumet TARP (Tunel and Reservoir Plan) system which is operated by the Metropolitan Water Reclamation District of Greater Chicago.

The aforementioned application of the model (two first modules) identified two critical zones (maximum water depths) in the CDS-51 watershed. The first zone is located on the

center of the watershed and the second on the SE border. Evidently these critical areas are the zones that need more attention in terms of inlet capacity and maintenance. The results also show that when no inlets are considered (e.g., clogged inlets), most of the total flow generated in the watershed are drained out of the watershed through outflowing streets at the watershed boundary and only 23% of the total flow will reach dropshaft CDS-51.

The CPU time of the model (first two modules) for the present application (~ 600 streets) was about one hour which makes suitable its application to large urban areas.

Acknowledgements

The financial support of the Metropolitan Water Reclamation District of Greater Chicago (MWRDGC) through a research grant to the Ven Te Chow Hydrosystems Laboratory of the Department of Civil and Environmental Engineering at the University of Illinois at Urbana-Champaign is gratefully acknowledged.

References

Chaudhry, M. H. (1987). *Applied hydraulic transients*, Van Nostrand Reinhold, New York.
Chow, V.T.; Maidment, D.R.; Mays, L.W. (1988) *Applied Hydrology*. McGraw-Hill, New York.
Chow, V.T. and Yen, B.C. (1976) "Urban Stormwater Runoff: Determination of Volumes and Flowrates", *Environmental Protection Technology Series*, EPA-600/2-76-116, US EPA Municipal Environmental Research Laboratory, Cincinnati, Ohio.
Federal Highway Administration (2001) *Urban Drainage Design Manual*. Hydraulic Engineering Circular Nº 22 (HEC-22), second edition. U.S. Department of Transportation.
Green, W.H. y Ampt, G.A. (1911) *Studies on soil physics: 1. The flow of air and water through soils*. J. Agric. Sci., Vol. 4, Nº1, pp. 1-24.
León, A.S. (2006) *Improved Modeling of Unsteady Free Surface, Pressurized and Mixed Flows in Storm-sewer Systems*, Ph.D. thesis, University of Illinois at Urbana-Champaign.
León, A.S., Ghidaoui, M.S., Schmidt, A.R., and García, M.H. (2006). *Godunov-type solutions for transient flows in sewers*. J. Hydraul. Engng., 132(8), 800-813.
León, A.S., Liu X., Ghidaoui, M.S., Schmidt, A.R., and García, M.H. (2009). *Boundary conditions for modeling mixed free surface-pressurized transient flows*. Advances in water resources. Submitted for review.
MWRDGC (2009) *Tunnel and Reservoir Plan*, http://www.mwrd.org/plants/tarp.htm, accessed on January, 2009.
Nania-Escobar, L.S. (1999) *Numerical and experimental methodology for danger analysis of urban runoff in a street network*. PhD Thesis. E.T.S.I.C.C.P., Universitat Politècnica de Catalunya. Barcelona, Spain, ISBN: 978-84-690-5623-3 (In spanish).
Nanía, L.; M. Gómez; J. Dolz (2007) *Surface stormwater hazard assessment in steep urban areas. Case of the city of Mendoza, Argentina*. Urban Water Journal, Vol. 4, Nº2, pp. 119-130, ISSN: 1573-062X

Nanía-Escobar, L.S.; M. Gómez-Valentín; J. Dolz-Ripollés (2006) *Análisis de la peligrosidad de la escorrentía pluvial en zona urbana utilizando un enfoque numérico-experimental*. Revista Ingeniería Hidráulica en México, Vol. XXI, Nro. 2. pp. 5-15, Morelos, México. ISSN: 0186-4076

Nanía, L., M. Gómez, J. Dolz (2004) *Experimental Study of the Dividing Flow in Steep Street Crossings*. Journal of Hydraulic Research. Vol. 42, Nº 4, pp. 406-412

Evaluating the Mixing Mechanism of Outfall Discharges from Municipal Separate Storm Sewer Systems

MICHAEL H. WOO, Ph.D., P.E.[1]

[1]Department of Civil and Environmental Engineering, THE CITADEL, 171 Moultrie St., Charleston, SC 29409; PH (843) 953-7679; FAX (843) 953-6328; email: Michael.woo@citadel.edu

Abstract: Under the National Pollutant Discharge Elimination System (NPDES) stormwater program, operators of large, medium, and regulated small municipal separate storm sewer systems (MS4s) require authorization to discharge pollutants under an NPDES permit. MS4s can be linear or complex, open, piped, manmade, natural, or a combination of all of the above. Some carry groundwater or piped streams, are tidally influenced, or have some other constant source of non-stormwater discharge. An MS4 is not always just a system of underground pipes-it can include roads with drainage systems, gutters, and ditches. Typically, an outfall from a MS4 discharges into a creek system and ultimately into a larger receiving water body which might or might not be tidally influenced. In order to evaluate the existing and expected water quality of the ultimate receiving water body, mathematical models are used to conduct flushing modeling and water quality modeling of the ambient waters. A hydrodynamic mixing zone model will be used to simulate steady or unsteady discharge from a single open channel outfall or a system of outfalls from municipal separate storm sewer systems (MS4s). This model is applicable for a wide range of hydrologic situations wherein flow and transport are governed by time-dependent forcing functions. Permit requirements will consist of a Water Quality Monitoring Program to be implemented and samples collected according to permitting agencies' procedures for collection, control and preservation.

INTRODUCTION

The treated effluent from the City of Gainesville, Georgia Linwood Wastewater Treatment Facility is currently discharged through a submerged outfall into Lake Lanier. The effluent is first chlorinated and then dechlorinated before being discharged. The outfall is located just offshore from the City of Gainesville at approximately one mile downstream from the Thompson Bridge. Figure 1 shows the aerial view of the facility. The original outfall is a three-port diffuser. However, according to the report entitled "Development of Linked Watershed and Water Quality Models for Lake Lanier", two of three ports are silted over (Limno-Tech, Inc.). The remaining functional port is a 24-inch diameter pipe and is located at approximately 120 to130 meters (m) (394 to 427 feet (ft)) from the bank. The effluent is discharged vertically from this port. The water depth at the discharge location is about 30 m (98 ft) and the discharge port is approximately 0.5 m (1.64 ft) above the lake bottom. Future improvement plans call for the Linwood Wastewater Treatment Facility be upgraded in stages and expanded to increase the future ultimate peak day treatment capacity.



Figure 1. City of Gainesville, GA Linwood Wastewater Treatment Facility

IMPACT OF STORMWATER DISCHARGE STUDY

The CORMIX 2 model (Gerhard H. Jirka et. al. 1996) is applied to a range of discharge rates to study the impact of stormwater temperature on the ambient water temperature adjacent to the Linwood Wastewater Treatment Facility. This paper documents the results and final recommendation from a CORMIX 2 evaluation of the effect of the higher water temperature of the effluent on the ambient water temperature of the lake.

DESIGN CRITERIA

The Environmental Protection Division (EPD) of the Georgia Department of Natural Resources stipulates that "at a sampling point 3 m (9.8 ft) from the outfall diffuser, the temperature shall not exceed 90 degrees Fahrenheit (F) nor increase the lake ambient temperature more than 5 degrees Fahrenheit." This study was conducted to establish the new outfall discharge location and optimum outfall diffuser configuration to achieve the above stated EPD requirement.

Instead of applying a mixing zone to regulate a point source wastewater discharge to a natural water body, the State of Georgia establishes that any point source effluent parameter must be diluted by a factor of at least two (2.0) at a sampling point 3 m (9.8 ft) from the outfall diffuser. The model will evaluate the dilution level at this location.

Ambient (Lake Lanier) Condition and Modeling Assumption

Ambient conditions were assumed primarily based on the assumptions used in a previous study. The CORMIX 2 model input parameters are listed below.

- The ambient winter water temperature range is between 42.8°F to 46.4°F (6°C to 8°C) and the temperature does not vary over the water depth. An ambient winter water temperature of 42.8°F is used in the model.
- The ambient summer water temperature varies with depth, with a pycnocline at approximately 20 to 60 ft below the water surface. The upper layer temperature varies from 82.4°F to 87.8°F; while the lower layer temperature is about 46.4°F to 50°F**.** An ambient lower layer summer water temperature of 46.4°F is used in the model with a pycnocline height of 30 ft.
- The stormwater discharge temperature is assumed to be 82.4°F.
- The model tested the impact of various discharge rates of 22.6 cubic feet/second (ft^3/s), 33.6 ft^3/s, and 51.7 ft^3/s.
- The ambient current velocity is estimated to be 0.13 ft/s (0.04 m/s).
- The Manning's n for the lake bottom is assumed to be 0.02 (smooth, earth channel, no weeds).
- The wind speed at the water surface is assumed to be 6.6 ft/s (2 m/s) (a breeze condition). CORMIX 2 defines a breeze as a wind speed from 0 ft/s to 9.8 ft/s.

MODEL EVALUATION AND RESULTS

The critical parameter that is evaluated for all the results is the water temperature at a sampling location of 3 m (9.8 ft) from the diffuser port. This study used the CORMIX 2 model to analyze numerous combinations of the following outfall diffuser location and diffuser configuration. Based on the results, the recommended design configuration is detailed in the Table 1 and shown in Figure 2.

- Outfall discharge depth.
- Number of diffuser ports.
- Distance of the diffuser from the shoreline.
- Size of each diffuser port.
- Effluent discharge direction – Against or perpendicular or in the same direction as ambient current direction.
- Orientation of the diffuser to the ambient current direction (Beta angle). Refer to Figure 3.
- Discharge vertical angle (Theta angle). Refer to Figure 3.
- Height of each diffuser port above the lake bottom.

Table 1. Final Design Configuration

(1) Outfall discharge depth	88 ft
(2) Number of diffuser ports	30; spaced evenly at 5 ft apart.
(3a) Distance of the closest diffuser port from the shoreline	500 ft
(3b) Distance of the furthest diffuser port from the shoreline	650 ft
(4) Size of each diffuser port	4-inch diameter
(5) The orientation of the diffuser to the ambient current direction (Beta angle)	90°
(6) Discharge vertical angle (Theta angle)	65°

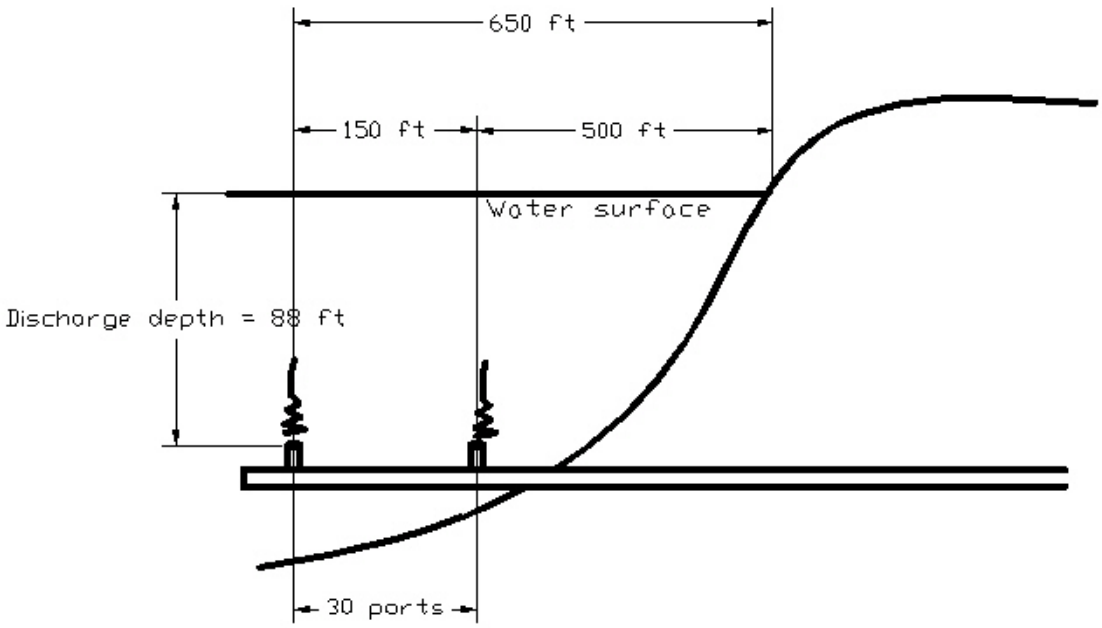

Figure 2. Diffuser Port Design Configuration

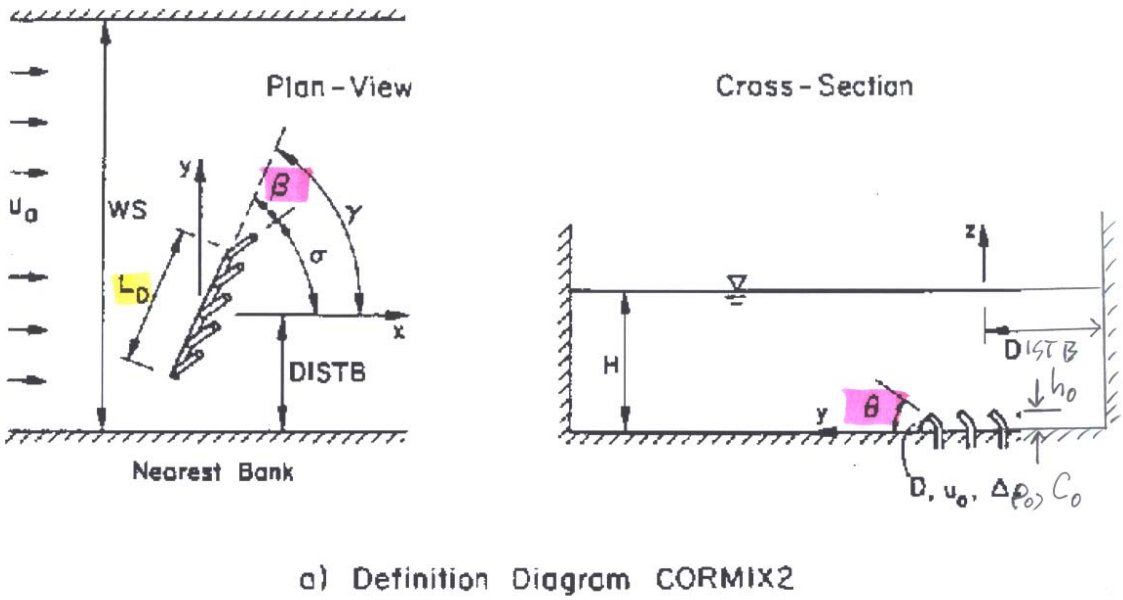

Figure 3. Discharge Vertical Angle (Gerhard H. Jirka et. al. 1996)

Using the recommended outfall diffuser location and diffuser configuration as given in Table 1, the CORMIX 2 results are shown in Table 2. It tabulates the water temperatures at EPD's regulatory critical location of 3 m (9.8 ft) from the discharge port under the various discharge rate scenarios.

Table 2. Ambient Temperature at 3 meters (9.8 feet) from Each Diffuser Port

		Increase in Ambient Temperature and Actual Temperature			
Discharge	Discharge Depth	Temperature Increase	Actual Temperature	Temperature Increase	Actual Temperature
(ft^3/s)	(Ft)	(°F)	(°F)	(°C)	(°C)
		Winter Ambient Temperature is 42.8°F or 6°C			
22.6	88	1.59	44.39	0.881	6.88
33.6	88	2.07	44.87	1.15	7.15
51.7	88	2.57	45.37	1.43	7.43
		Summer Ambient Temperature is 46.4°F or 8°C			
22.6	88	2.38	48.78	1.32	9.32
33.6	88	2.97	49.37	1.65	9.65
51.7	88	3.55	49.95	1.97	9.97

CONCLUSION

As shown in Table 2, none of the evaluated discharge rates cause any increase in the ambient temperature above EPD's regulatory requirement of no greater than 5°F at a sample location of 3 m (9.8 ft) from the discharge point. This holds true for both the winter period as well as the critical summer period. As such, as long as the diffuser configuration and discharge location as established in Table 1 are implemented, the EPD regulation on temperature increase will be met.

REFERENCES

Gerhard H. Jirka, Robert L. Doneker, and Steven W. Hinton (1996). "User's Manual for CORMIX: A Hydrodynamic Mixing Zone Model and Decision Support System for Pollutant Discharges into Surface Waters,"

Limno-Tech, Inc.."Development of Linked Watershed and Water Quality Models for Lake Lanier

Physical Processes Resulting in Geyser Formation In Rapidly Filling Stormwater Tunnels

Steven J. Wright[1], James W. Lewis[2] and Jose G. Vasconcelos[3]

[1] Member ASCE, Professor, Civil and Environmental Engineering, 113 EWRE, University of Michigan, Ann Arbor, MI 48109-2125; PH (734) 764-7148; FAX (734) 763-2275, email: sjwright@umich.edu
[2] PhD student, Civil and Environmental Engineering, The University of Michigan, email: jimlewis@umich.edu
[3] Professor, University of Brasilia, Brazil, email: jvasconcelos@unb.br

ABSTRACT

A significant concern in the design of large, underground conduits for storm or combined sewer systems is the avoidance of geyser formation, a phenomenon which involves the explosive release of water through vertical shafts. Current practice for transient analyses of these systems involves application of numerical models to simulate the rapid filling processes. Since these models do not consider interactions between the inflows and air being displaced during the filling process, it is felt that these models cannot predict geyser formation.

Data from a large diameter stormwater tunnel in Minneapolis, Minnesota has been analyzed to determine the events that led to a series of observed geyser events. Data include pressure and velocity measurements within the tunnel that can be correlated with a videotape of the geyser events themselves. The pressure records are inconsistent with hydrostatic pressure lifting water to the ground surface. Features of the pressure records can be interpreted to indicate the release of large air pockets through the dropshaft. A qualitative comparison of these results with smaller scale laboratory experiments indicates similarities in the pressure responses. These results suggest that the entrapment of large air pockets is an important component to the geysering process and that tunnel design procedures need to properly account for these effects.

INTRODUCTION

The phenomenon commonly referred to as "geysering" that occurs in below grade sewer systems is manifest as an explosive release of water through vertical ventilation shafts or manholes. Figure 1 presents images of two such events, one in Novosibirsk, Siberia and the other in Minneapolis, Minnesota. These clips are parts of larger images and based on other features such as nearby buildings, the geyser rises at least 20 m above the land surface. Such occurrences following the construction of the Chicago Tunnel and Reservoir Project (TARP) in the early 1980s initiated interest in development of analysis methods so that geyser formation



a.) Novosibirsk, Siberia b.) Minneapolis, Minnesota

Figure 1. Images of geysers formed in underground sewer systems.

could be predicted during design and modifications implemented to avoid such problems. Numerical models of transient mixed flow where both free surface and pressurized flow can occur simultaneously in nearly horizontal conduits were developed for this purpose with the model by Cardle and Song (1988) being a notable early contribution to the literature on the topic. Additional investigations in more recent years include Capart, et al (1997), Politano, et al (2007), and Vasconcelos, et al (2006). These represent various approaches to the problem of predicting the simultaneous occurrence of both free surface and pressurized flow with sufficient numerical accuracy to predict the hydraulic bores that may form in a rapidly filling conduit.

In spite of the numerical sophistication associated with the implementation of these models, it is not clear that any of them are relevant to the issue of geyser formation. To date, there is very little discussion in the literature on the physical processes involved in geyser formation. The geyser images in Figure 1 could be interpreted as a mixture of air and water, raising the possibility of air-water interactions. Small scale laboratory experiments reported in Vasconcelos (2005) indicated that the most likely explanation for geyser formation was the escape of discrete air pockets through vertical shafts that were in a pressurized state at the time of air arrival such that water was forced upwards ahead of the rising air pocket. Vasconcelos and Wright (2006) describe a number of different ways in which trapped air pockets can form in a rapidly filling pipeline, even with very simple geometries. Wright, et al (2008) suggest that a common situation for trapping large air pockets involves the reflection of a free surface bore at a conduit transition that results in the filling of the pipe at the transition with air behind the bore becoming pressurized. However, the small scale of the experiments from which these observations were made does not permit generalization to the much larger prototype

scale of large natural systems. Other studies that discuss the phenomenon of geysering are curiously quiet on this issue. For example, Guo (1989) and Guo and Song (1990) discuss geyser formation but then present simple hydraulic analyses that don't consider air interactions. In Guo and Song (1991), the following discussion is presented "…If the water level rises above ground surface, the geyser occurs. It has been ascertained that if the dropshaft is ventilated, as most are, the cover could not be blown off by air pressure alone. That is, most blowoffs are caused by the impact force of the rising water. Therefore, it is sufficient to study the hydrodynamics alone." Although it is true that adequate ventilation will prevent buildup of air pressures sufficient to displace manhole covers, a simple calculation will show that air pressures as small as 3 kPa can be sufficient to lift a typical manhole cover on the order of 0.8 m diameter. The first writer was involved in an application where providing additional ventilation at an appropriate location eliminated a recurring problem with manhole cover displacements in a 1.8 m diameter combined sewer system. However, the above statement does not address the fundamental question of whether geyser formation involves an air-water interaction. This question is of critical importance to design issues since a numerical model that requires the hydraulic grade line to rise to the ground surface in order for a geyser to occur would entirely miss an occurrence that is associated with an air-water interaction. Fortunately, data has been collected on one large scale system that allows this issue to be addressed.

SYSTEM DESCRIPTION

The image of the Minneapolis geyser depicted in Figure 1b was extracted from a video recorded as part of a data collection effort due to a recurrence of geyser formation at two dropshafts in a stormwater collection system that flowed beneath the median of Interstate 35W in Minneapolis, Minnesota. The video recorder was installed at a dropshaft near the 35th Street overpass and was accompanied by the installation of velocity and pressure transducers. Records spanned the time from at least 1997 through 2005 with 13 events captured between 1999 and 2005 (and additional ones prior to 1999). Individual events often involved more than one discrete geyser event. Data is presented below for a rainfall event that occurred on the morning of July 11, 2004 and involved nine individual geyser events that formed and subsided at intervals of approximately two minutes. A video record of two geyser events is provided on the Minneapolis Star Tribune website at www.startribune.com/video/15509842.html/. It is noted that the writers possess other video records from this same installation that depict even stronger geysers.

The general details of the system are as follows:

- Stormwater tunnel diameter of 3.66 m;
- Dropshaft diameter of 2.44 m;
- Tunnel invert located 28.6 m below grade;
- Pressure transducers installed at 0.47 and 2.88 m above the local tunnel invert. The data acquisition system was programmed to record pressures only when

water depths in the tunnel exceeded 1.46 m. Data was collected every five seconds for water depths (as determined by the velocity meter) between 1.46 and 2.93 m and every second for indicated depths greater than 2.93 m;

- Velocities were recorded at five minute intervals with an American Sigma area-velocity meter.

RESULTS

The particular data presented below were collected on July 11, 2004 at approximately 5:30 AM. Nine independent geysers were observed in the video record of the event; there is some variability in strength as some of the geysers were not explosive, each geyser lasted for about 10-25 seconds with about 75-90 seconds between separating the onset of each one. The velocity record indicates that the velocity was relatively constant at about one meter per second between about 5:30 and 8:50 AM with no indication of fluctuations that might be indicative of inertial oscillations in the pipeline. Figures 2 and 3 present the pressure and velocity records, respectively, for a time period spanning the occurrence of the geyser events. The pressure record is from the lower pressure transducer and converted to a pressure head relative to the tunnel invert. Superimposed on the figures are the visual observations of the geyser occurrences indicated in the video record. This is indicated by the vertical rise and fall in the line; the height of the line has no relationship to the pressures indicated on the vertical axis.

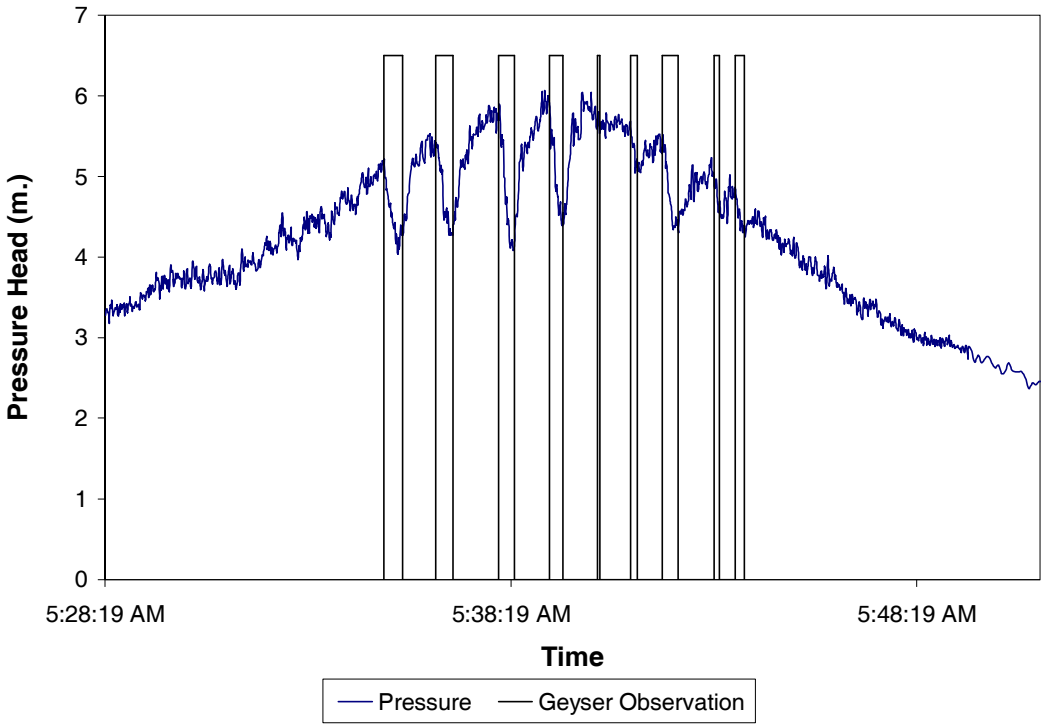

Figure 2. Pressure head relative to tunnel invert in tunnel recorded during geyser events.

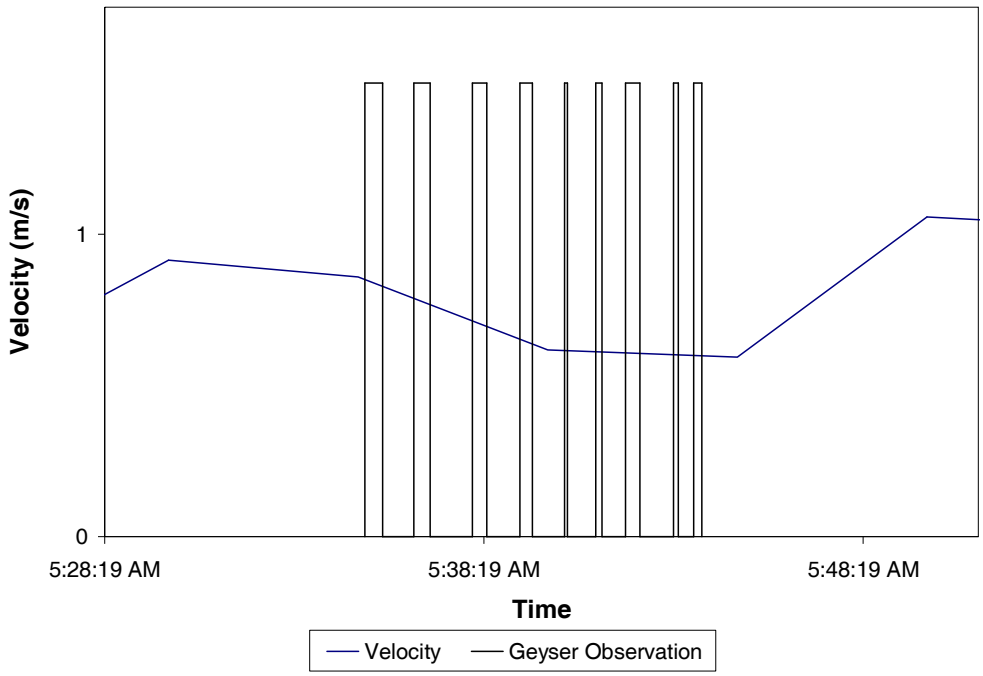

Figure 3 Velocity recorded during geyser events.

A number of observations can be made from the results presented in Figures 2 and 3. First of all, the pressure head never went above about 6 m during the entire event which is only nominally greater than the tunnel diameter of 3.66 m. Since the tunnel invert is 28.6 m below grade, the discussion in Guo and Song (1991) discussed in the Introduction would exclude the possibility of geyser formation as the hydraulic grade line never approaches the land surface. This clearly indicates that some other mechanism must be invoked to explain the observed geysers. Another interesting observation is related to the observed geyser height. If it is assumed that the geyser height is approximately 20 m from the video record, the exit velocity of a water jet can be estimated by the simple conversion of velocity to elevation head as $V^2/(2g) = h$ with h the rise height of the water jet. Using h = 20 m would result in an exit velocity of 19.8 m/s, suggesting an upward discharge in the dropshaft of 93 m^3/s. This compares to a tunnel discharge of approximately 9 m^3/s during the geyser events according to the velocities presented in Figure 3. Thus, there is an insufficient source of water to produce a water jet rising that high in the air. Finally neither the pressure nor the velocity records in Figures 2 or 3 suggest any indication of inertial oscillations that would be necessary to produce the discrete geyser events according to the explanation suggested by Guo and Song (1990). Although there does appear to be a velocity oscillation in Figure 3 during the time that the geyser events occur, a careful inspection of the timing indicates that the velocity is continuously declining during the geysering interval and then increases again once the events cease. This is more indicative of additional flow resistance during that time period such as partial flow blockage due to air pocket

migration upstream against the water flow. Therefore, there is a total lack of evidence to support the concept that geysers are created by water column rise in a vertical shaft to above grade. A different explanation must be invoked to explain the geyser formation in these particular events. While the data is only applicable to the particular physical setting and the particular event, it is felt that the observations can be more generally applied to understand geyser formation.

A more careful inspection of the pressure records provides additional insight. Assuming that the tunnel becomes pressurized when the pressure height exceeds the diameter, this occurs about six minutes prior to the commencement of the first geyser event. The last geyser event finished about two minutes before the system transferred back to a free surface state. Figure 4 is an expansion of the pressure record to examine the pressure variation during the sequence of geyser events. It is seen that each geyser lasted for about 10-25 seconds with about 75-90 seconds separating the onset of the next one. The pressure tends to rise gradually between geyser events and then drop abruptly at the onset of the geyser. This behavior is inconsistent with a "hydraulic" or water flow only explanation of geyser formation but would be consistent with the arrival of discrete air pockets at the dropshaft with a pressure drop as the air releases into the vertical shaft. Although this is not conclusive proof, the data are far more consistent with an air-water interaction, specifically with the expulsion of discrete air pockets through vertical shafts than other explanations considered. It is also noted that the apparent regularity of the geyser events displayed in Figure 4 is not necessarily consistent with observations during other events and the time intervals between individual occurrences is also inconsistent between events. The writers believe that the geometry of the particular system results in the propagation of discrete air pockets from the downstream direction, but are awaiting further investigation to confirm this hypothesis.

LABORATORY OBSERVATIONS

An adaptation of the experimental setup described by Vasconcelos (2005) was used to measure pressures during laboratory events that were interpreted as geysers. Figure 5 indicates the experimental setup. A 0.038 m diameter, 2.5 m tall ventilation shaft was installed on the top of the horizontal pipeline at about its midpoint. Experiments were performed with the pipe initially partially full of stagnant water. The two-way valve indicated in Figure 5 was opened in two steps. The first step produced a free surface hydraulic bore that propagated to the downstream end and reflected off the closed end of the pipe, with a higher free surface bore propagating back towards the inlet. An additional partial valve opening increased the upstream flow rate and produced a pressurized condition with a significant amount of air trapped between the two fronts. The timing of the second inflow increase was selected to result in the two bores interacting near the ventilation shaft so that water rose a few cm into the shaft prior to the arrival of the discrete entrapped air pockets. The flow was switched off once the water level began to rise in the inflow shaft so that the pressure head within the pipeline never exceeded about 1.2 m. Regardless of this, water was expelled out the top of the 2.5 m high ventilation shaft at a height far above the hydrostatic pressure level. Each arriving air pocket lifted the water successively higher in the shaft. Although there

was no attempt to reproduce the unknown inflow conditions associated with the field event described above, the height of the laboratory ventilation shaft, when scaled by the pipe diameter, is greater than the 28.6 m for the Minneapolis stormwater tunnel and it appears reasonable to conclude that air can indeed lift water to the heights observed in the video.

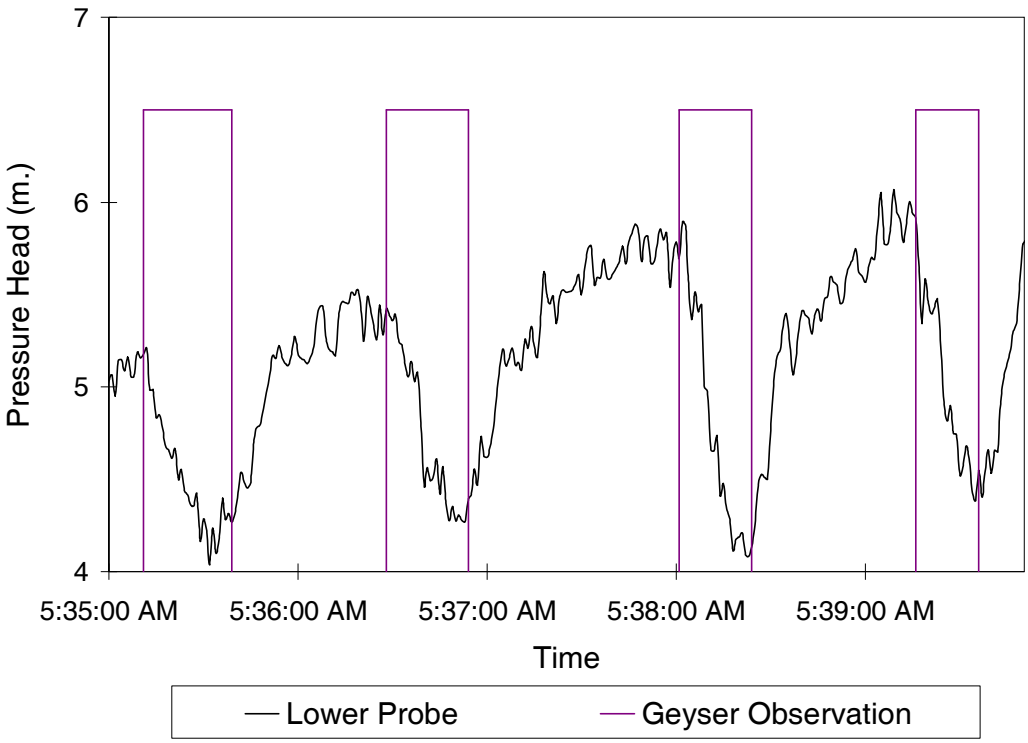

Figure 4. Output from lower pressure probe during geyser events.

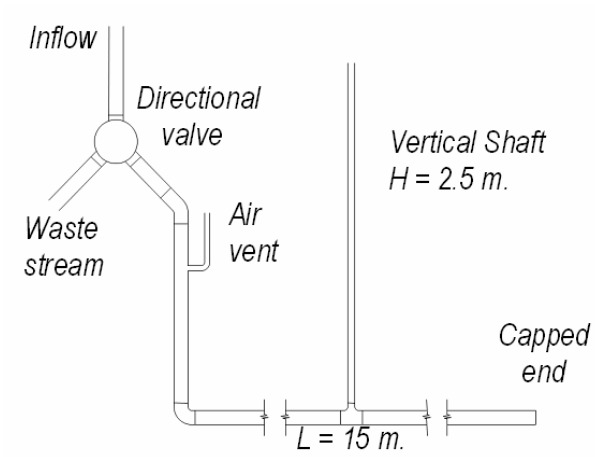

Figure 5. Schematic of laboratory apparatus.

Two piezo-resistive pressure transducers (Endevco model 8510B-1) were connected at the bottom of the pipe at distances of 6.45 m and 11.70 m downstream of the center of the inflow pipe. Outputs from these transducers were sent to a data acquisition system (National Instruments DAQPad MIO-16XE-50) at a frequency of 10 Hz. A typical pressure record from the transducer located upstream of the ventilation shaft is presented in Figure 6. The effect of the air pockets rising in the shaft is seen as sudden drops in the overall trend of the pressure variation. This feature is similar to the behavior indicated in Figure 4.

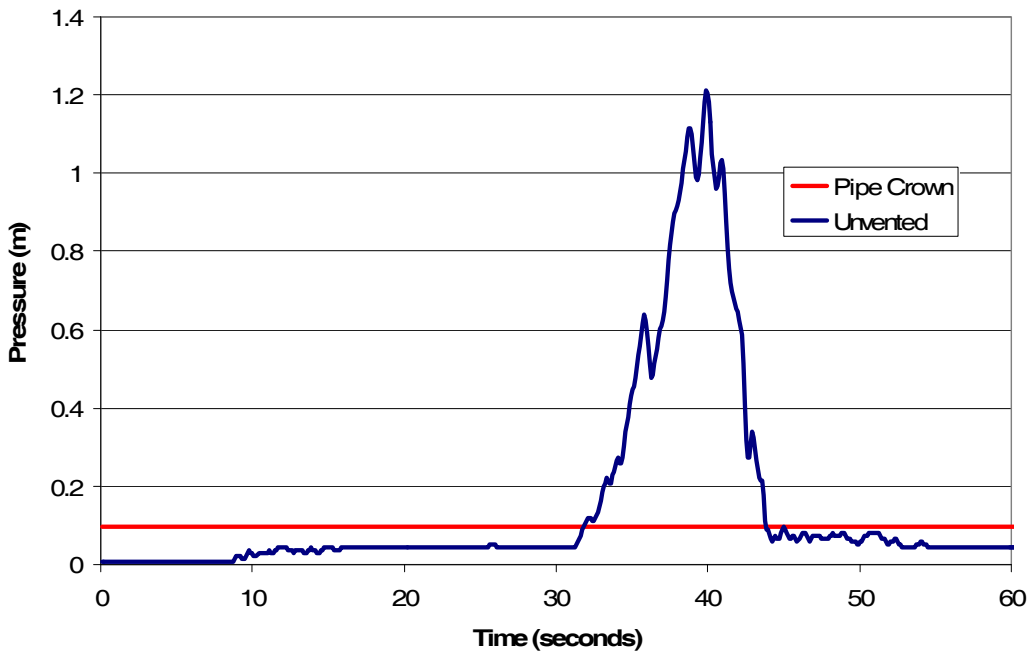

Figure 6. Pressure in pipeline upstream from ventilation shaft during expulsion of entrapped air pockets.

DISCUSSION AND CONCLUSIONS

The field measurements collected during a rainfall event in Minneapolis, Minnesota in 2004 included visual observations of the dropshaft at the ground level along with velocity and pressure measurements within the stormwater tunnel immediately upstream from the dropshaft. The most plausible explanation for the observed geyser formation is the interaction of trapped air with water initially standing in the drop shaft due to the existence of surcharge conditions. The measured pressures within the pipeline were incapable of lifting that water even close to the ground surface, let alone eject it 20 m into the air. Converting the estimated rise height of the geyser into a vertical velocity in the dropshaft requires a discharge an order of magnitude than actually measured to be flowing within the tunnel at the time of geyser formation. Furthermore, the measured pressures and

velocities do not support the presence of large scale inertial oscillations within the tunnel such as might be required to lift the water to the ground surface in a series of short duration events. The patterns of water pressure drop during air expulsion through the ventilation shaft are similar in the field and laboratory measurements, suggesting that in spite of possible limitations due to the small laboratory scale, there are similarities between the mechanisms for water rise in the vertical shaft in both situations.

There are several implications associated with these findings. The process of geyser formation is apparently not directly connected with surging in the tunnel system as suggested by the previous literature on the subject. Numerical models that are currently applied to simulate transients in rapidly filling tunnel systems do not account for the air phase. The predicted results of these models should be interpreted with caution with respect to the issue of geyser formation. Predictions that transient hydraulic grade lines remain below grade should not be interpreted to suggest that geyser formation will not occur. Model capability to predict the location of air entrapment within a system is useful, even if the subsequent motion of the air cannot be predicted with a single phase flow model. This information can be used judiciously to make design decisions about the location and capacity of air ventilation required in a system.

ACKNOWLEDGEMENTS

The authors would like to acknowledge the cooperation of Dr. Christopher Ellis (originally with the St. Anthony Falls Hydraulics Laboratory) and Bruce Irish of the Minnesota Department of Transportation in providing the field data used in this manuscript.

REFERENCES

Capart, H., Sillen, X., and Zech, Y. 1997. Numerical and Experimental Water Transients in Sewer Pipes. J. Hydr. Res. 35 (5), 659-670.

Cardle, J.A. and Song, C.S.S. 1988. Mathematical Modeling of Unsteady Flow in Storm Sewers. Int. J. Eng. Fluid Mechanics, 1(4), 495-518.

Guo, Q. 1989. Geysering in Urban Storm Drainage Systems. Proc. XXIII IAHR Cong. Ottawa, Canada S75-S81.

Guo, Q., and Song, C.S.S. 1990. Surging in Urban Storm Drainage Systems. J. Hydraulic Engineering, V. 116(12), 1523-1537.

Guo, Q., and Song, C.S.S. 1991. Dropshaft Hydrodynamics Under Transient Conditions. J. Hydraulic Engineering, V. 117(8), 1042-1055.

Politano, M., Odgaard, A.J., and Klecan, W. 2007. Case Study: Numerical Evaluation of Hydraulic Transients in a Combined Sewer Overflow Tunnel System. J. Hyd. Eng. 133 (10) 1103-1110.

Vasconcelos, J.G. 2005. Dynamic Approach to the Description of Flow Regime Transition in Stormwater Systems. PhD dissertation, Environmental Engineering, The University of Michigan, Ann Arbor, Michigan.

Vasconcelos, J.G., Wright, S.J. and Roe, P.L. 2006. Improved Simulation of Flow Regime Transition in Sewers: Two-component pressure approach. J. Hydraulic Engineering, 132(6), 553-562.

Vasconcelos J.G. and Wright, S.J. 2006. Mechanisms for Air Pocket Entrapment in Stormwater Storage Yunnels. Proceedings of World Water and Environmental Resources Congress, Omaha, Nebraska, Paper 40856-14275.

S.J. Wright, C.T. Creech, J.M. Lewis and J. G. Vasconcelos, "Mechanisms of Flow Regime Transition in Rapidly Filling Stormwater Storage Tunnels," Journal of Environmental Fluid Mechanics, 2008, 8, 605-616.

THE "SILVER BULLET": PROPRIETARY BMPS AND METROPOLITAN ST. LOUIS SEWER DISTRICT'S STORMWATER PROGRAM

J.S. Hoskins[1] and M.T. Buechter[2]

[1] Metropolitan St. Louis Sewer District, 2350 Market Street, St. Louis, MO 63103-2555; PH (314) 768-6272; FAX (314) 768-6302; e-mail: jshosk@stlmsd.com
[2] Metropolitan St. Louis Sewer District, 2350 Market Street, St. Louis, MO 63103-2555; PH (314) 768-6272; FAX (314) 768-6302; e-mail: mtbuec@stlmsd.com

ABSTRACT

In February 2006, as part of its Phase II Stormwater Quality Management Program, the Metropolitan St. Louis Sewer District (MSD) implemented rules that require post-construction stormwater best management practices (BMPs) at development and redevelopment sites. MSD references the Maryland Department of the Environment's *Stormwater Design Manual* as a BMP design guide. However, this document does not specifically address proprietary BMP devices and currently there is not a national or Missouri state standard by which to evaluate them.

For a proprietary BMP to be approved for use within MSD boundaries, the device's manufacturer must present it to MSD and request approval for one or more use levels. Possible use levels include General Use Level, Redevelopment Use Level, Highway Use Level, and/or Provisional Use Level. Submittal requirements and use level descriptions are provided in *Proprietary Water Quality Products and the MSD's Stormwater Management Program* (rev. Jan 2009), which can be downloaded from the MSD web site (www.stlmsd.com). Devices are approved for a particular use level based on (1) the treatment performance requirement for that use level and (2) the certified performance of the device. Performance certification testing must comply with the Technology Acceptance and Reciprocity Protocol (TARP) or the Technology Assessment Protocol-Ecology (TAPE). When approved for use by MSD, each device is issued an approval letter that is posted on the MSD web site. Advantages of the process include (1) MSD recognition that the device is effective for its use, (2) manufacturers quickly ascertain whether their product can be approved, and (3) BMPs that meet requirements are approved in a reasonable time period.

INTRODUCTION

History of MSD. The St. Louis Metropolitan Statistical Area covers 16,555 square kilometers, and has a population of 2,603,607. This area includes the City of St. Louis, St. Louis County and ten (10) other surrounding counties located in both Missouri and Illinois. The bulk of the metropolitan area's population and infrastructure lies within the City of St. Louis and St. Louis County, with the outlying counties being developed at a much lower density. St. Louis County and the City of

St. Louis are two distinct entities, with the City of St. Louis being a county unto itself. St. Louis County includes not only its own incorporated areas but also 91 separate municipalities (East West Gateway, 2002).

As shown in Figure 1, St. Louis stormwater drains into three major watersheds: the Mississippi River, Meramec River and Missouri River. All stormwater runoff ultimately enters the Mississippi River. All three rivers serve as sources for public drinking water, while both the Mississippi and Missouri serve as a commercial barge transportation corridor. The Meramec is a major recreational asset for the region.



Figure 1. Major Watersheds and Municipalities within MSD [source: MSD]

Prior to the formation of MSD the City of St. Louis, St. Louis County, and the various municipalities handled sanitary and stormwater drainage issues independently. This fragmented approach was complicated by the fact that the area is drained by the Mississippi, Missouri, Meramec Rivers, contains many sinkholes and floodplains, and

the City of St. Louis is drained by combined sewers. In 1954 increasing frustration with the status quo, ongoing problems, and an increased appreciation for water quality issues in general lead to the formation of Metropolitan St. Louis Sewer District (MSD) by state constitutional amendment (Moore, 2003). Today, MSD is the fourth largest sewer district (based on miles of pipe) in the U.S., and roughly forty percent of the regulated MS4s in Missouri are located within its boundaries.

The St. Louis region's form continues to change as the population sprawls outward from the urban core. The vast majority of MSD has been developed; only outer portions of west and north St. Louis County remain undeveloped. It is anticipated that much of the future construction activity within MSD boundaries will be redevelopment.

Stormwater Quality Regulations. With the passage of the Water Quality Act of 1987 and the establishment of the national stormwater program, most large metropolitan areas were forced to address stormwater quality issues under the 1990 Phase I regulations. However, given that combined sewers serve the City of St. Louis, and St. Louis County is made up of a patchwork of small municipalities, each less than 100,000 in population, the St. Louis region escaped regulation under the Phase I requirements. The St. Louis area may have been the largest "donut hole" (exempted area) under Phase I of the National Pollutant Discharge Elimination System (NPDES) storm water program.

The 1999 Phase II regulations specifically required many of the political subdivisions within St. Louis County to obtain a Phase II NPDES permit. Given that MSD has been given authority for providing adequate sewer and drainage facilities within its boundaries, it was the obvious choice to coordinate compliance activities associated with Phase II. Sixty additional co-permittees were also named under the small MS4 permit. While MSD is the coordinating authority and regulates post-construction stormwater management, either the individual municipalities or St. Louis County are responsible for construction site stormwater control.

MSD PROPRIETARY BMP APPROVAL PROCESS

MSD Regulations. MSD has adopted regulations (*Rules and Regulations and Engineering Design Requirements for Sanitary Sewer and Stormwater Drainage Facilities*, February 2006) that represent a more comprehensive approach to stormwater management, and include water quality standards that must be met at development and redevelopment sites. These standards apply to any construction activity disturbing, individually or in aggregate, one (1) acre or more. While providing incentives and preference for nonstructural practices, these standards also address the design of structural BMP's to mitigate water quality and channel stability impacts.

For specific guidance regarding the design of structural BMPs, MSD references the Maryland Department of the Environment's (MDE), April 2000, *Stormwater Design*

Manual, Vol. I and Vol. II (herein referred to as the Maryland Manual). The Maryland Manual outlines the selection, design and construction of various "generic" structural BMPs (ponds, wetlands, infiltration basins/trenches, filtering systems, and open channel systems), but the Maryland Manual does not address proprietary BMPs. This was a problem because, in some redevelopment and/or highway projects, space availability and utility conflicts make construction of generic BMPs impractical. Also, experience indicates generic BMPs are not cost effective on some 1-2 acre redevelopment projects (i.e., a gas station or drugstore redevelopment).

Proprietary BMPs were proposed as potential solutions for redevelopment and highway projects. A proprietary BMP (also referred to as mechanical BMPs or manufactured BMPs) is a pre-fabricated stormwater treatment structure utilizing settling, filtration, absorptive/adsorptive materials, vortex separation, vegetative components, and/or other appropriate technology to remove pollutants from storm runoff. Proprietary BMPs are intended to capture sediments, metals, hydrocarbons, floatables, and/or other pollutants in stormwater runoff before being conveyed to a storm sewer system, or water body.

Different types of sites produce different pollutant and runoff characteristics, and it is reasonable that different sites may necessitate the use of different types of BMPs and that what is suited for one site may not be suited for another. MSD researched the literature for the types and particle sizes of contaminants in runoff from small drainage areas with a predominance of impervious cover (e.g., small parking lots, gas stations, and roadways), and compared this information with available testing data on proprietary devices (such as hydrodynamic separator devices). Based on this comparison, it appears that some proprietary BMPs provide effective treatment at these sites. The challenge is to develop a regulatory framework for (1) focusing these devices on the types of sites where they can be effective and (2) approving BMPs that have been appropriately tested.

Use Level Designations. All MSD approved proprietary BMPs are given a Use Level Designation that describes the types of site where a proprietary BMP can be applied. The four Use Level Designations that MSD considers are provided in Table 1.

Table 1: Proprietary BMP Use Level Designations

USE LEVEL DESIGNATIONS	DEFINITION / USES
General Use Level (GUL)	BMPs approved at this level may be used at all types of sites.
Redevelopment Use Level (RUL)	BMPs approved at this level may be used at non-residential redevelopment sites (i.e., total property area) less than five (5) acres in size.
Highway Use Level (HUL)	BMPs approved at this level may be used on public highway and public road projects.
Provisional Use Level (PUL)	BMPs approved at this level may be used only according to specific "provisions" outlined in the approval. This designation is intended only for use in certain and specific instances.

Additionally, underground BMPs are not allowed on residential projects. A site (i.e., total property area) is considered a redevelopment site if at least 20% of the existing site was impervious coverage as of January 15, 2000.

Performance Certification. New stormwater BMP products keep appearing in the marketplace, yet the availability of good testing data and standards on some of these technologies is scarce. To address this problem, MSD requires specific performance for each Use Level Designation and certification of that performance claim. Performance requirements and certifications required are outlined on the next page in Table 2.

A cornerstone of the MSD program is that all performance claims must be supported by test data and third party certification. The performance certification may be provided by the New Jersey Department of Environmental Protection (NJDEP) or by the Washington State Department of Ecology. (While neither agency has authority in Missouri, these protocols are largely consistent with MSD's goals, and their certification programs are the most thorough ones available.) The NJDEP certification utilizes the New Jersey Center for Advanced Technology (NJCAT) verification as conducted according to the Technology Acceptance and Reciprocity Partnership (TARP) Protocol. Washington State Department of Ecology utilizes the Technology Assessment Protocol - Ecology (TAPE).

In January 2009, MSD began to allow use of some RUL approved BMPs at redevelopment sites larger than five (5) acres, and these BMPs would be provided the PUL designation in addition to the RUL designation. The additional PUL designation is limited to proprietary devices, such as proprietary filters, that have conditional interim certification of proprietary BMP performance claims by the NJDEP in accordance with NJCAT performance verification program. These devices must also be actively pursuing field testing in accordance with NJCAT Tier II protocol and final certification by the NJDEP.

Table 2: Proprietary BMP Performance Requirements and Certifications

USE LEVEL DESIGNATION	PERFORMANCE REQUIREMENT	CERTIFICATION REQUIREMENT
General Use Level (GUL)	The BMP must be able to achieve a removal rate of 80% Total Suspended Solids (TSS) from stormwater runoff generated by the stormwater quality design storm.	Final certification of proprietary BMP performance claims by the NJDEP in accordance with TARP Tier II protocol, or General Use Level Designation for Basic Treatment by the Washington Department of Ecology.
Redevelopment Use Level (RUL)	BMP must sequester all non-aqueous phase hydrocarbon, scum, and floating debris and achieve an instantaneous removal rate of 80% TSS for the storm water quality design storm. TSS removal efficiency shall be based on an influent concentration of <300 mg/L and OK-110 particle size distribution.	Interim certification of proprietary BMP performance claims by the NJDEP in accordance with a NJCAT technology performance verification, or General Use Level Designation for Pretreatment by the Washington Department of Ecology.
Highway Use Level (HUL)	BMP must sequester all non-aqueous phase hydrocarbon, scum, and floating debris and achieve an instantaneous removal rate of 80% TSS for the storm water quality design storm. TSS removal efficiency shall be based on an influent concentration of <450 mg/L and OK-110 particle size distribution.	Interim certification of proprietary BMP performance claims by the NJDEP in accordance with a NJCAT technology performance verification, or General Use Level Designation for Pretreatment by the Washington Department of Ecology.
Provisional Use Level (PUL)	A specific Total Suspended Solids (TSS) removal rate applicable to the use requested is required.	Third party documentation from a public agency or testing agency confirming removal efficiency is required.

Key provisions of the PUL approval include a firm due date for obtaining the final certification and some form of annual reporting during the testing period. The manufacturer sets the due date, but in no case is the PUL due date allowed to extend beyond the expiration date of the region's current MS4 permit (June 2013). Annual reporting includes results from the TARP monitoring or a letter from NJCAT/NJDEP stating the results of the quarterly performance monitoring reports. Annual reporting allows the manufacturer and MSD to identify any performance or operational issues during TARP testing. Also, given the uncertainty of design flow rates tested in the laboratory versus actual flow rates encountered in the field, MSD may require for devices not holding Tier II certification a reduced allowable flow rate in the design of the BMP.

For larger site development projects, MSD does not believe the sole use of a BMP filter device is sufficient to addresses a site's obligation to manage site stormwater to the maximum extent practicable (MEP). These devices do not minimize stormwater pollutant loading at the point of generation nor do they mimic a site's natural runoff condition (i.e., these devices accept whatever loading and pollutants are created). For these larger sites, the overall stormwater management plan should also include practices that minimize directly connected impervious areas, stormwater pollution, and stormwater runoff. While MEP is not a required percentage or amount, the goal is that proprietary devices will be treated as a supplementary (rather than a primary) means of meeting the region's MS4 permit.

Proprietary BMP Application. Each BMP manufacturer submits an application packet and provides a presentation on their product to the MSD Proprietary BMP Committee. The Proprietary BMP committee is composed of MSD development review engineers and an outside consultant. The committee typically meets monthly or bi-monthly, depending on the number of applications under consideration.

The application packet and presentation discuss many topics, but are primarily focused on:

- A detailed description of the operation of the device, including a depiction of the flow path of water through the BMP.
- Construction specifications or installation instructions, engineering drawings or catalog sheets, and details on how BMP construction should be phased during site development.
- Product performance claim and certification, including data that support the manufacturer's claim of TSS removal, the appropriate verification/certification documents, and a summary table of BMP models and their peak water quality volume or flowrate (appropriate for the use level's performance requirement).
- Product design criteria, including sample proprietary BMP sizing calculations that indicate how to size and select the device as well as how to size and select any special components. A sample site layout plan (including pretreatment methods) for a typical site should also be included.
- Device, installation, and shipping costs, as well typical annual maintenance costs.
- One of advantages of proprietary BMPs is that the maintenance activities may be uniform from site to site. Manufacturers are required to provide a generic maintenance plan that includes a description of specific preventative and corrective maintenance tasks, a schedule of regular inspections and tasks, tools and supplies necessary to perform the maintenance tasks, and maintenance and replacement instructions for special components.

Approval Letter. Each approved device is issued an approval letter that specifies the device's use level designation; treatment rates, volumes, special equipment, and/or dimensions; and what reporting requirements apply. A hard copy of the approval

letter is provided to the applicant, and an electronic copy is posted on the MSD website. Posting the approval letters to the web works well because it allows vendors, designers, and developers convenient access to this information.

CONCLUSION

As of January 15, 2009, fourteen proprietary BMP devices have been approved for some level of use by MSD. The majority of manufacturers have requested RUL and/or or HUL approval. MSD has only approved one proprietary device for GUL. However, where space is available and utility conflicts are manageable, most designers prefer the generic BMP because these typically cost less to construct. The number of sites implementing generic BMPs is greater than the number using proprietary BMPs. Proprietary devices are mostly filling a niche for smaller redevelopment and public highway projects.

Feedback from manufacturers is that the approval process is "straight-forward" – manufacturers know where they stand when their application is submitted, and applications are typically processed within a few weeks. Some manufacturers have voiced concern about a lack of product competition at GUL eligible sites because at present only one device has met the GUL performance verification requirements (specifically, the field testing component). However, to efficiently and knowledgeably evaluate these BMPs, MSD feels third party field verification is very important. The TARP Tier II and TAPE verification protocols are compatible with our program. When available, consideration will be made for the protocol and certification recommendations of the ASCE/EWRI Task Committee on Guidelines for Certification of Manufactured BMPs.

In June 2008, the Missouri Department of Natural Resources renewed the regions MS4 permit. The permit has new language that states "*The permittee's program shall ensure that controls are in place that have been designed and implemented to prevent or minimize water quality impacts by reasonably mimicking pre-construction runoff conditions on all affected new development property and by effectively utilizing water quality strategies and technologies on all affected redevelopment projects, to the maximum extent practicable*" (emphasis added). This statement is significant because, inherently, the agency is expressing preference for low-impact development (LID), as opposed to structural techniques. Regulatory trends nationwide indicate a greater emphasis on LID techniques is coming. If requirements for mimicking a site's natural hydrology are applied to redevelopment projects, then MSD's proprietary BMP program will likely be revised and proprietary BMP use further restricted.

Also in 2008, several urban streams within the MSD were proposed for addition to Missouri's 303(d) list of impaired waters. Pollutants include bacteria, heavy metals, mercury, and chloride. The agency is attributing these pollutants to urban non-point sources. How this is addressed remains to be seen, but BMP design could be affected.

As such, the MSD proprietary BMP approval program will be somewhat fluid in the near term as the regulations, science, accepted standards, and industry mature.

REFERENCES

East-West Gateway Coordinating Council (2002). *Where We Stand: The Strategic Assessment of the St. Louis Region, 4th Ed.*, St. Louis, MO.

Center for Watershed Protection and Maryland Department of the Environment Water Management Administration (2000). *2000 Maryland Department of the Environment Stormwater Design Manual, Volumes I & II*, Baltimore, MD. http://www.mde.state.md.us/Programs/WaterPrograms/SedimentandStormwater/stormwater_design/index.asp

Metropolitan St. Louis Sewer District (MSD) (2006). *Rules and Regulations and Engineering Design Requirements for Sanitary Sewer and Stormwater Drainage Facilities*, St. Louis, MO.

Metropolitan St. Louis Sewer District (MSD) (2009). *Proprietary Water Quality Products and the MSD's Stormwater Management Program*, St. Louis, MO. http://mkasmtp1.stlmsd.com/MSD/PgmsProjs/planreview/StormwaterBMPs

Moore, G. T. (2003). "Water Quality and Watershed Initiatives at the Metropolitan St. Louis Sewer District." *At the Confluence: Rivers, Floods, and Water Quality in the St. Louis Region*, Missouri Botanical Garden Press, St. Louis, MO.

The St. Louis Municipalities Phase II Storm Water Planning Committee (Fall 2002). *St. Louis County Phase II Stormwater Management Plan* (First Permit Term, 2003-2008), Metropolitan St. Louis Sewer District (MSD), St. Louis, MO.

The St. Louis Municipalities Phase II Storm Water Planning Committee (Summer 2007). *St. Louis County Phase II Stormwater Management Plan* (Second Permit Term, 2008-2013), Metropolitan St. Louis Sewer District (MSD), St. Louis, MO.

St. Louis Metropolitan Small MS4 Storm Water Permit, MO-R04005, issued by the Missouri Department of Natural Resources (MDNR) Water Pollution Control Program.

The Technology Acceptance Reciprocity Partnership (Final Protocol 8/01, Updated: 7/03). *Final Protocol for Stormwater Best Management Practice Demonstrations*. http://www.state.nj.us/dep/dsr/bscit/Stormwater%20Protocol.pdf

Washington State Department of Ecology Water Quality Program (January 2008 Revision). *Guidance for Evaluating Emerging Stormwater Treatment Technologies: Technology Assessment Protocol – Ecology (TAPE)*, Publication Number 02-10-037, Olympia, WA. http://www.ecy.wa.gov/pubs/0210037.pdf

Survey of Water and Wastewater Utility Security Standards

Dale Gabel, PE[1], Yakir J. Hasit, PhD, PE[2], and Yaron Ben Ari[3]

[1]Vice President, CH2M HILL, Inc., 9193 S. Jamaica Street, Englewood, CO 80112; PH: 720-286-5880; FAX: 720-286-9594; email: dale.gabel@ch2m.com
[2]Principal Technologist, CH2M HILL, Inc., 1717 Arch Street, Suite 4400, Philadelphia, PA 19103; PH: 215-640-9027; FAX: 215-640-9227; email: yakir.hasit@ch2m.com
[3]Water Technology Program Manager, Standardization Division, SII-The Standards Institution of Israel, 42 Chaim Levanon St, Tel Aviv 69977, Israel; PH: 972-3-6465315; FAX: 972-3-6412762; email: yaronbenari@sii.org.il

ABSTRACT

A primary responsibility of water utilities is the protection of their water and wastewater infrastructure from significant threats created by natural disasters, malicious actions, and accidents. Following the events of September 11, 2001, water utilities placed additional emphasis on protecting their infrastructure from malicious threats, and security standards and guidelines were developed by various organizations across the world. A noteworthy set of guidelines was developed through the U.S. Environmental Protection Agency's (USEPA's) Water Infrastructure Security Enhancements (WISE) project, which was cooperatively executed by the American Society of Civil Engineers (ASCE), the American Water Works Association (AWWA), and the Water Environment Federation (WEF). In this project, both guidance documents that cover all aspects of water security (design, management, operations) and voluntary standards that cover physical security were developed. During the execution of this project a very thorough review of national and international guidances and standards was conducted. It was found that efforts by various organizations were at different stages of development and few, if any, had reached the stage of the WISE documents.

The International Organization for Standardization (ISO) has recently published a limited consensus document, the International Workshop Agreement (IWA) 6, for managing drinking water supplies during crisis conditions, and related efforts are currently being undertaken by ISO Technical Committee 224, Working Group 7 convened jointly by Germany and Israel (ISO TC 224/WG7) to develop a guideline standard for water and wastewater utilities to design, implement, operate, maintain, and improve a crisis management system to protect a utility's infrastructure from all threats. Similarly, the European Committee for Standardization or "Comite European de Normalisation" (CEN) has also started the preparation of a water security document.

It is important to note that water security is a sensitive issue among many countries due to significant differences of opinion on what constitutes threats. Some countries are reluctant to implement advanced security technologies and methods that may cause unease among their populations as well as controversy at the political level. Recognizing the sensitivity of security approaches to individuals and organizations, neither the WISE documents nor the ISO documents were developed to serve as regulatory requirements. Rather they were developed to provide best practice guidance to utility managers and policy makers.

INTRODUCTION

Protection of water and wastewater infrastructure from natural disasters and man-made accidents has been and continues to be a key focus for water and wastewater utilities (hereinafter referred to as water utilities) as part of their overall missions to protect the public health and provide affordable and reliable service to its customers. Following the terrorist attacks of September 11, 2001 in the United States (US) and similar incidents throughout the world, water utilities have significantly increased efforts to protect their infrastructure from malicious actions.

In the international arena, water system security has a slightly different connotation than in the US. Internationally it usually refers to the sustainable use of water and sustainable development of water resources, the protection of systems from drought and floods, and the safeguarding of access to water utility services. As a result, international efforts in the development of water security guidances and standards have covered a wider range of topics than in the US. International efforts that resemble the US definition of water security have thus focused on "crises management" which is equivalent to emergency response, remediation, and recovery (or consequence management).

Guidance documents and standards have been prepared in the US to assist utilities in the development and implementation of effective security systems. Notable guidance documents among these have been prepared under the USEPA's WISE project. The first water security focused document backed by international consensus was recently released by the International Standards Organization (ISO). Similarly, the European Committee for Standardization or "Comite European de Normalisation" (CEN) has also started the preparation of a water security document. Most of the ISO and CEN standards and other approved documents are drawn up in Technical Committees (TC). If a faster track of document development is required, then workshops are convened to deliver formal documents. Highlights of the documents prepared, including key aspects of emergency response planning, and each organization's objectives and structural make-up are presented below.

UNITED STATES WISE DOCUMENTS

A cooperative effort of the ASCE, AWWA, and WEF under the general direction WISE Standards Committee was funded by the USEPA to prepare a set of consensus documents. The majority of the documents were prepared by CH2M HILL under the guidance of the appropriate WISE Subcommittees: i.e. Water Supply, Wastewater/Stormwater, and Methodology and Characteristics, and reviewed by members of the WISE Standards Committee, members of various technical and standards committees from the three professional organizations, representatives from the USEPA, and other stakeholders who volunteered to provide input.

Under the WISE project, six guidance documents were prepared to assist water utilities in implementing infrastructure security systems and approaches. The first three documents were Interim Voluntary Security Guidance documents (ASCE 2004, AWWA 2004, and WEF 2004) prepared as Phase 1 of the project. These documents provided a centralized starting point for utilities to integrate modern security practices into the management, operation, and construction/retrofit of their infrastructure systems. The documents also provided guidance on integrating security related activities in a utility's emergency response plans. Training materials on these documents were developed as Phase 2 of the project to facilitate dissemination of the guidance information to US utilities.

Phase 3 documents (ASCE 2006a and ASCE 2006b) focused only on the physical security of water utility infrastructure and presented best engineering guidelines for physical protection approaches and measures of individual facilities or assets.

The Recovery Practices Primer for Natural Disasters (ASCE 2008) was also prepared under the WISE project. Its focus is to document recent successful actions and responses by utilities to mitigate natural disaster impacts and quickly restore service operations. The document is intended to be used by utilities to improve their emergency response plans and supplement existing guidance on emergency preparedness planning and response.

In addition to the above documents and to support the WISE overview and awareness initiative, three webcasts were presented in 2007 on the importance of security, security design considerations, and operational and maintenance changes to improve security. Two supporting videos were produced in 2008, one for public officials on the importance of water utility security and one for utility managers and operators on the principles of water security.

The primary purpose of the WISE documents is to provide water utilities guidance on the design of new facilities or the retrofit of existing facilities to reduce the risks posed by malevolent threats. Management and operational practices that can reduce risk are presented along with guidance on the development of emergency response plans that include malevolent threats as well as natural disasters and accidents.

Two of the WISE Phase 1 documents, "Interim Voluntary Security Guidance for Water Utilities" (AWWA 2004) and "Interim Voluntary Security Guidance for Wastewater/Stormwater Utilities" (WEF 2004) present concepts for effective emergency response planning for water and wastewater utilities, respectively. The purpose of an Emergency Response Plan (ERP) is to provide a utility with a standardized response and recovery protocol to prevent, minimize, and mitigate injury and damage resulting from emergencies or disasters of human-caused or natural origin. Emergency response is divided into four types of actions: planning, response, recovery, and termination.

The WISE Phase 3 documents, *Guidelines for the Physical Security of Water Utilities (2006) and Guidelines for the Physical Security of Wastewater/Stormwater Utilities* only focused on the physical security of utilities. These two documents covered physical security measures for perimeter, site, facility, water quality, SCADA security, etc. for various design basis threats (vandal, criminal, saboteur, etc).

ISO DOCUMENTS

ISO is a network of the national standards institutes and similar organizations from 160 countries and its technical work is normally carried out through ISO technical committees in which each ISO member has the right to be represented. For urgent market requirements, ISO has established a procedure to prepare documents through a workshop mechanism, external to the normal committee processes. These documents are published by ISO as International Workshop Agreements (IWAs).

The Standards Institution of Israel (SII) identified water security as critical and crucial for communities, countries, and society in general and proposed to develop an IWA on water security. Thus, the first international consensus document on water security was prepared by under the leadership of SII through the ISO process as the IWA 6 "Guidelines for the management of drinking water utilities under crisis conditions" (ISO 2008). IWA 6 was drafted at a workshop held in Tel Aviv, Israel in October 2007 and sponsored jointly by Israel's Water Authority and the SII.

This document provides a framework for management of a water crisis using an approach similar to emergency response plans, and was developed to be consistent with three established ISO standards on management of water and wastewater utilities (ISO 24510, ISO 24511, and ISO 24512). Unlike the WISE documents that focus primarily on malicious

incidents by individuals intending to damage or destroy the utility infrastructure or threaten the health of customers, IWA 6 focuses equally on all potential threats, whether natural or man-made, intentional or non-intentional. The document summarizes the framework for effective crisis management in Figure 1. This is similar to the framework presented in the WISE documents.

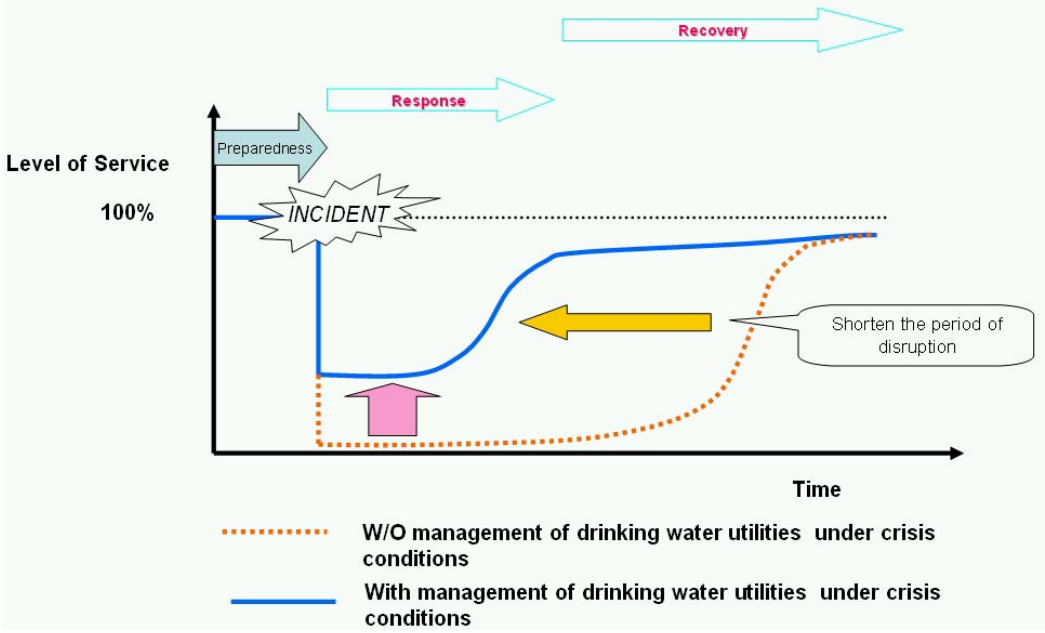

Figure 1. Effectiveness of crisis management (*Source – ISO/TC 223 - ISO/PAS 22399*)

The IWA 6 document identifies four stages for responding to a water crisis that parallel the four actions presented in the WISE documents: preparedness, response, recovery, and lessons learned. These stages are based on the Plan-Do-Check-Act (PDCA) model, which is also referred to as the Assess-Protect-Confirm-Improve (APCI) model. Figure 2 adapts the PDCA model to water security. The IWA 6's crisis management elements are similar to the ones identified in the WISE documents with the exception of an Incident Command System. Furthermore, the WISE documents provided significantly more information on each element.

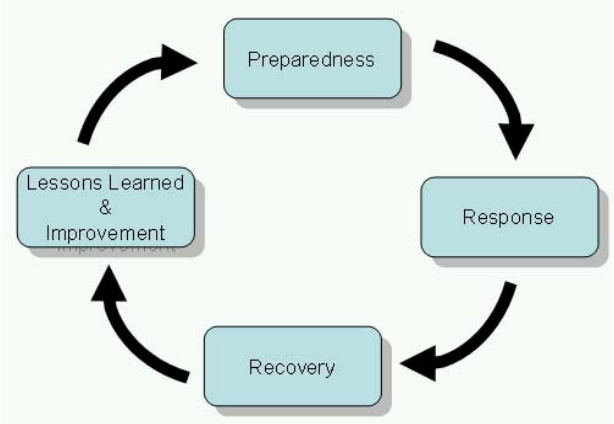

Figure 2. The water crisis management cycle (*Source – ISO/TC 223 - ISO/PAS 22399*)

The document also recommends a number of areas for the development of ISO standards including crisis management, on-line monitoring instrumentation, and hydraulic

network models to identify the locations and number of monitoring instruments and to predict the area of contamination. This recommendation covered many elements included in the WISE online contaminant monitoring systems (ASCE 2004) guidance. To assist in the development and installation of these warning systems, IWA 6 recommended the development of future standards for on-line monitoring instrumentation, models for establishing the number and location of monitoring instruments, models for defining the contaminated area within a water distribution system, and distribution system hydraulic models. The online monitoring systems were identified as a secondary tier of the security tier. Development of standards for the primary security tier, physical protection approaches, was also recommended.

Based on a proposal by SII to TC 224, a separate ISO/TC 224 working group (WG7) under the joint leadership of Israel and Germany was created to prepare a guideline standard for "crisis management in water utilities" that will include both water and wastewater utilities. The guideline, which currently is in a draft stage, will focus on establishing an incident preparedness and operational continuity management system for water utilities, similar to the emergency response plans used in the United States. Current plans are to complete a draft document by the end of 2010 and initiate the ISO process for achieving international consensus of the standard.

EUROPEAN DOCUMENTS

The European Committee for Standardization (CEN) develops European Standards and other technical specifications for its 30 nation members. These standards also constitute the national standards for each of its 30 member countries. With one common standard in all these countries, and every conflicting national standard withdrawn, a product can reach a far wider market with much lower development and testing costs. The European standards are developed by Technical Committees, approved by the CEN members and go through a public comment period. On the other hand, CEN Workshop Agreements (CWAs) are standardization documents open to the direct participation of any interested party. CWAs are fast and flexible, usually completed in 12-18 months. There is no requirement to adopt them as national standards in the CEN member countries, but they can be used as an alternative route towards a formal voluntary standard or taken up at international level within ISO.

One relevant guideline is *Security of Drinking Water Supply - Guidelines for risk and crisis management,* currently being prepared by the Working Group 15 "Security of Drinking Water" of the CEN/TC 164 "Water Supply". This guideline describes the fundamentals of crisis management, including relevant recommendations for water utilities, and offers abundant examples about the disaster and crisis management organization of the relevant national authorities. The objective of this Guideline is to enable the water supplier to take action in the event of a crisis in order to ensure the continued supply of water to the greatest possible extent and to restore normal operating conditions as quickly as possible.

SUMMARY

A survey of the international standards on water and wastewater system security shows that most of the available documentation in use has been prepared under the WISE project. These documents have covered the design, operational and management aspects of utility security, including emergency response, remediation and recovery (or crisis management). Other standardization efforts include those by ISO and CEN, but to date their efforts have focused primarily on crisis management. Efforts on other aspects of water security have also commenced.

REFERENCES

ASCE (2004), *Interim Voluntary Security Guidelines for Designing an Online Contaminant Monitoring System,* Reston, VA (Publication No. 817R08007)

ASCE/AWWA (2006a), *Guidelines for Physical Security of Water Utilities,* Reston, VA (Publication No. 817R08009)

ASCE/WEF (2006b), *Guidelines for Physical Security of Wastewater/Stormwater Utilities,* Reston, VA (Publication No. 817R08008)

ASCE (2008), *Recovery Practices Primer for Natural Disasters,* Reston, VA

AWWA (2004), *Interim Voluntary Guidance for Water Utilities,* Denver, CO (Publication No. 817R08010)

CEN/TC 164/WG 15 (2008), Security of Drinking Water Supply - Guidelines for risk and crisis management, Part 1: Crisis management (Draft Version 2): November 19, 2008

ISO (2008), International Workshop Agreement IWA 6 - *Guidelines for the management of drinking water utilities under crisis conditions* (Reference number IWA 6:2008(E))

Sack Rener,J. Ben-Ari, Y., and Akerman, I. D. (2009). "Avoiding the worst – Safe drinking water during crises (IWA 6)", *ISO Focus*.

WEF (2004), *Interim Voluntary Guidance for Wastewater/Stormwater Utilities,* Alexandria, VA (Publication No. 817R08006)

Advances in Data Validation, Event Detection, and Communications Structures for a CWS: Case Study – Glendale, Arizona

Kenneth A. Thompson[1]; Rick Scott[2]; Dr. Raja Kadiyala[3];
Andreas Weingartner[4]; and Dr. Joep van den Broeke[5]

[1]CH2M HILL, 9193 S. Jamaica St., Englewood, CO, 80112-5313; PH 720-286-5407; email: ken.thompson@ch2m.com

[2]City of Glendale, Arizona Utilities Department, Oasis Water Campus, 7070 W. Northern, Glendale, AZ 85303-1306; PH 623-930-4101; email: rscott@glendaleaz.com

[3]CH2M HILL, 155 Grand Avenue, Suite 1000, Oakland, CA 94612; PH 510-587-7676; email: raja.kadiyala@ch2m.com

[4]scan Messtechnik GmbH, Brigittagasse 22-24, A-1200 Wien, Vienna, Austria; PH 43-1-219-73-93-0; email: aweingartner@s-can.at

[5]s::can Measuring Systems, LLC, P.O. Box 36402, Cincinnati, OH 45236-4204; PH 513-275-1360 ext 8631; email: jvandenbroeke@s-can.at

ABSTRACT

The City of Glendale, Arizona has been developing and implementing the various elements of a Contamination Warning System (CWS) since 2005. The purpose of the CWS is to provide multiple benefits to the utility through early identification of unusual water quality events, including those due to operational changes, occurring in the distribution system.

The key to a successful CWS is the rapid analysis and evaluation of data from multiple sources to extract the relatively small amount of information related to the unusual occurrences in the distribution system. To effectively accomplish this, Event Detection System (EDS) software needs to have robust processes in place for both data validation and data analysis to enable accurate event detection.

s::can and CH2M HILL are developing an EDS for the City of Glendale with the following attributes:

- Unique sensor station management system that captures sensor failure, maintenance, and repair activities
- Enhanced Data Validation: Minimum/maximum boundaries, drift analysis, step change analysis, and outlier analysis
- Data Analysis: Capability of evaluating both single and multi-dimensional data
- Advanced Event Detection: Both single-point and spatial recognition within the distribution system

This paper provides an overview of the Glendale EDS and its capabilities for data validation and event detection.

Background

The City of Glendale has partnered with CH2M HILL to create a state-of-the-art Contamination Warning System (CWS) to detect, assess, and respond to potential water contamination events through the use of strategically placed water quality monitoring (WQM) stations. The monitoring stations constantly feed water quality data into a data warehousing application that analyzes this data and other critical data streams (e.g., customer complaint information and field operations activities) that can indicate possible contamination in the system. CH2M HILL and s::can have collaboratively developed an event detection system (EDS) for the Glendale CWS to streamline the collection of data from several sources, enable rapid understanding of water quality events in the distribution system, quickly identify areas for operational improvement, and enhance response capabilities to reduce the potential for public health/aesthetic impacts. Glendale is one of just two cities in the nation to implement a full-scale CWS program, which takes a cutting-edge, holistic approach to safeguarding public water systems from terrorist attacks, accidental events, and operational malfunctions. The EDS utilized by Glendale's CWS is the first of its kind to be implemented in the United States.

The main objective of the Glendale CWS is to enhance the ability to detect, assess, and respond to water quality changes in the water distribution system, thus minimizing the potential impact on public health, economic loss to business customers and the City, liability to the City, and loss of confidence by the public. To meet these objectives, the CWS monitoring stations are designed to continuously monitor traditional water quality parameters, including pH, conductivity, residual chlorine, turbidity, total organic carbon (TOC), dissolved organic compounds (DOC), and nitrate (NO_3), as well as spectral fingerprinting. Different water quality monitoring technologies are deployed at the water quality monitoring stations within Glendale's system, including instrumentation from Hach, ATI, and s::can, and Sandia's unattended water sensor (UWS) prototype. The water quality monitoring instruments, along with EDS equipment, are deployed locally at eight CWS monitoring stations. These stations are all linked to the central CWS.

The central part of the CWS, the EDS integrates all of the data sources, analyzes the data, identifies water quality trends, and develops contamination event alarms, essentially tying together the individual pieces of the CWS. Without a properly functioning EDS, the data and databases would be of limited usefulness because the system would generate a high number of false alarms, resulting in an unreliable contamination warning system.

Online water quality monitoring data are an integral part of the system, but are not the only data utilized to identify a potential contamination event. Several other sources of data and databases, as depicted in Figure 1, have been considered in the implementation of this system-wide CWS, including customer complaints, health care information, laboratory and field data, security alarms, and operations and maintenance information.

Local Data Validation, Storage, and Event Detection

The s::can - CH2M HILL EDS comprises both local components (installed at the WQM stations) and centralized components. The individual WQM stations are interfaced via diverse protocols to a central database. Though this interfacing structure of the EDS is not absolutely necessary, it greatly enhances the system security and multi-station management. More importantly, performance is improved because additional information may be obtained by comparing station data and adding in supervisory control and data acquisition (SCADA) information (pressure and flow), thus allowing additional events to be generated based on the aggregated data.

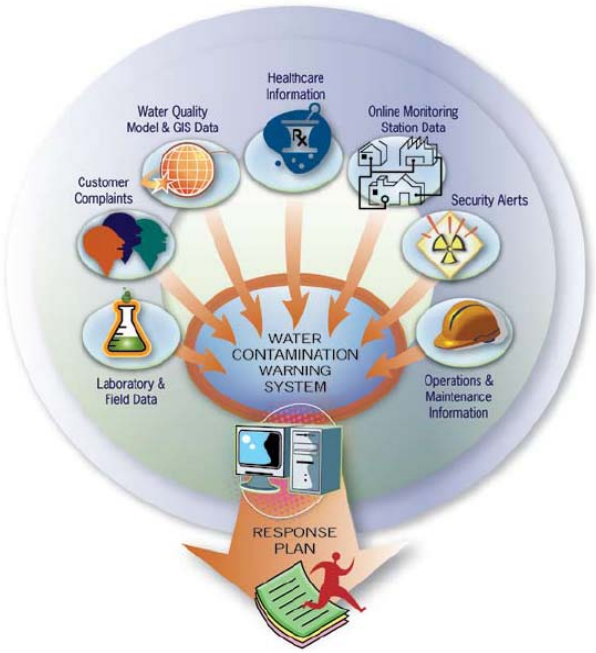

Figure 1: Data from numerous sources are captured in one central data warehouse

In addition, an EDS without prior state-of-the-art sensor/station management and real-time data validation has been shown to yield countless false alarms. Such a system will, under real-world conditions, fail to meet desired system-level performance and lead to low operator acceptance and confidence in the long term.

The station-level EDS software package minimizes the generation of non-interpretable data by combining local station management with an enhanced data validation component to keep full control of sensors and parameters. Figure 2 is a picture of an industrial PC, which is used as part of the local EDS, installed at a local WQM station. The local station software package consists of three tools:

- (Sensor/Station) Control and Management Tool (moni::tool)
- Data Validation Tool (vali::tool)
- Event Detection Tool (ana::tool)

The **(Sensor/Station) Control and Management Tool (moni::tool)** provides a web-based graphical user interface for easy and transparent station and sensor configuration. All configuration data are stored in a local database which is synchronized with the central database. The database not only stores the current configuration, but also stores previous configuration information as a timeline, allowing proper metadata information to be presented with the results. The moni::tool also monitors the “health” of instruments by querying instrument diagnostics.

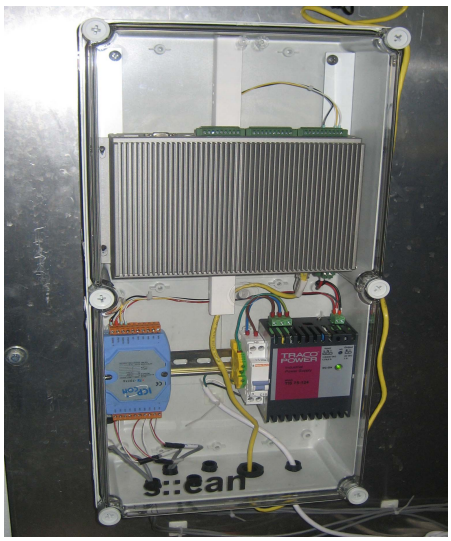

Figure 2: Industrial PC provides local event detection

Clear and transparent management of all sensors and stations by dedicated software is the indispensable backbone of any complex monitoring system. When systems exceed a certain level of complexity and are used for critical applications and real-time control (i.e., for alarm and protection purposes), traditional data management and SCADA software is no longer adequate for system management. The moni::tool provides unique sensor identification management and tracks any *activities* and *status information updates* (e.g., any changes in inputs, configurations, settings, exchange of sensors or components, calibration or service activities), in addition to all other sensor messages or functional checks. All of this information is locally communicated, collected, managed, utilized, and documented, then synchronized with the central database. This station metadata is essential for the later qualification and interpretation of any generated data. This management information also allows statistical evaluation of operational parameters such as "operational availability of sensor X," and "total service time/yr." All of these parameters are important in defining proper maintenance procedures and ensuring that the WQM stations are providing the best data possible.

The **Data Validation Tool (vali::tool)** provides dynamic analysis of incoming data from any sensor or analyzer. By comparing the incoming data to locally stored historical data and reference values, the system can determine if values are:

- Within expected ranges
- Outliers
- Exhibiting noise or scatter
- Drifting
- Exhibiting step jumps
- Non-plausible (as compared to other related parameters)

Incoming data, regardless of the source (SCADA, monitoring stations, or single sensors) or the interface by which the data are communicated, are validated in real-time by comparing them to their reference data sets, considering statistical parameters and time-dependent behavior. Data validation is performed using innovative statistical tools in a fully automated fashion. Once adjusted during system initialization to account for the dynamic behavior of the system, the only parameter that needs to be adjusted afterwards is "sensitivity." Automatic data validation ensures that only unmarked, "clean" data are used for further analysis, training, and alarms. Any non-event related, deviating data are identified and marked before being fed into the EDS module to avoid the system being trained on invalidated data.

The **Event Detection Tool (ana::tool)** allows the EDS to integrate the output of the spectral ana::larm too, and combinesit with all other collected parameters into a single stationlevel EDS. It typically runs on the local station level, but also can be integrated into the central database. The proven spectral EDS ana::larm software is a standard package used by many water utilities worldwide. It "learns" the shape and features of the "normal" spectrum of the water body within a defined range. The initial definition of the reference (i.e., baseline) spectra for later identification of extraordinary composition is done automatically, and can be continuously improved and re-trained. The spectral baseline training is simple and reliable and has adjustable false alarm levels.

The spectral alarms also detect a high percentage of "organic" events. A key advantage with this algorithm is that ana::larm is able to distinguish between changes of background/natural organics and "abnormal" organics. Thus the system will not react to normal changes of TOC and DOC, but will distinctively react to any organics in the water that are not part of the natural composition.

The spectral absorption values provide an extremely rich source of data to perform event detection. This data provides more complete EDS functionality than would be found by relying on just the traditional surrogates of conductivity, pH, chlorine, turbidity, and so on. All collected and validated parameters from all provided sensors and tools are fed into a module for baseline definition and event detection. A baseline of normality versus the typical pattern for all parameters relative to each other is established during a training period.

Central EDS Database

The EDS is applied both on a local (monitoring station) level and at a central database. The same local data validation and algorithms are applied to all data entering the central database (i.e., from the SCADA system and multiple WQM stations). Spatially and hydraulically resolved data analysis in the central database allows for additional information to be generated from spatial differences between sampling points in the distribution network. This unique method allows for the nearly complete elimination of any baseline noise of "normal" water composition, and with this method, the lowest limits for detection of events can be achieved. By performing spectral data differencing on time-shifted spectrum from upstream and downstream sampling points, additional events can be resolved. This spatial differencing also yields potential contamination locations and provides more insight on the possible contaminant.

Advantages of Glendale's EDS Approach

The station and sensor management tool eliminates the risk of sensor misuse, malfunction, or mismanagement, and allows sensors and stations to be operated by non-expert, entry-level staff. The data validation step before event detection eliminates non-interpretable data and thus reduces false alarms dramatically. The s::can - CH2M HILL approach used by the City of Glendale provides an EDS with high sensitivity: the sensors and algorithms offer the lowest detection limits for most contaminants (organic and inorganic), lower than any system on the market (e.g., as low as a part-per-billion (ppb) level for some solvents and pesticides). The Glendale

EDS approach also provides high selectivity; the EDS can distinguish between changes of organic background matrix (i.e., natural organics) and organic contaminants, thus greatly reducing false alarms.

Implementing a Contamination Warning System at a Department of Defense Facility: Case Study – Port Hueneme, California

Kenneth A. Thompson[1]; Steve Fann[2]; Dr. Raja Kadiyala[3];
Dr. Yakir J. Hasit, PE[4]; and Gary Jacobson, PE[5]

[1]CH2M HILL, 9193 S. Jamaica St., Englewood, CO, 80112-5313; PH 720-286-5407; email: ken.thompson@ch2m.com

[2]NAVFAC Engineering Service Center, 1100 23rd Avenue, OP421, Port Hueneme, CA 93043; PH 805-982-1016; email: steve.fann@navy.mil

[3]CH2M HILL, 155 Grand Avenue, Suite 1000, Oakland, CA 94612; PH 510-587-7676; email: raja.kadiyala@ch2m.com

[4]CH2M HILL, 1717 Arch St, Suite 4400, Philadelphia, PA 19103; PH 215-640-9027; email: yakir.hasit@ch2m.com

[5]CH2M HILL, 25 New Chardon St., Suite 300, Boston, MA 02114-4770; PH 617-626-7033; email: gary.jacobson@ch2m.com

Abstract

The Naval Facilities Engineering Command, Engineering Service Center (NAVFAC ESC) in Port Hueneme, California is in the final stage of the development and implementation of a Contamination Warning System (CWS) Pilot Program, culminating a 3-year effort. The purpose of the pilot program is to demonstrate the multiple benefits associated with a CWS, and it will serve as a model for other Department of Defense facilities.

The CWS will include real-time online water quality monitoring (OWQM) stations at multiple locations in the water distribution system. The OWQM stations will provide continuous data for pH, chlorine residual, turbidity, conductivity, total organic carbon, dissolved organic carbon, and ultraviolet/visual spectral imagery (200 to 700 nm). OWQM technologies that will be evaluated as part of the pilot program include the s::can spectro::lyzer™, s::can ammo::lyzer™, the Analytical Technologies (ATI) Water Quality Panel (for pH, free chlorine residual, conductivity, and turbidity), ATI mono-chloramine analyzer, the Hach Q45WQ Water Quality Panel (also for pH, free chlorine residual, conductivity, and turbidity), and the Intelletect Intellisonde™ (pH, free chlorine, mono chlorine, turbidity, conductivity, color, pressure, temperature, and flow).

The event detection system (EDS) being developed by s::can and CH2M HILL for the Port Hueneme will have the attributes listed below:

- Enhanced Data Validation: Minimum/maximum boundaries, drift analysis, step change analysis, and outlier analysis
- Data Analysis: Capability of evaluating both single- and multi-dimensional data
- Advanced Event Detection: Both single-point and spatial recognition within the distribution system

Introduction

Naval Base Ventura County (NBVC) is a major aviation shore command, and its Port Hueneme (PH), California facility provides logistical support to construction battalions worldwide. The NAVFAC ESC executes this demonstration project funded by the Navy's Environmental Sustainability Development to Integration (NESDI) program. The project is in the design and construction stage of the development and implementation of a Contamination Warning System (CWS) Pilot Program. The purpose of the pilot program is to demonstrate the multiple benefits associated with a CWS (which are contamination warning, regulatory compliance, and operational support) and to serve as a model for other Department of Defense (DoD) facilities.

Overall, this project has three primary tasks:

1. Design of the CWS
2. Installation and testing of the CWS
3. CWS data analysis and lessons learned

This paper presents the basic structure of the CWS design process used at a Department of Defense Naval base. While the information to consider when making the design decisions was essentially the same as that used for municipal water distribution systems, the system characteristics of size, water usage, and monitoring station location at Port Hueneme makes the ultimate design more applicable to water distribution systems at other military bases and very small systems instead of typical municipal systems.

System Design

To successfully design a CWS, information about a number of elements is required:

- Utility characteristics
- CWS characteristics
- Available online monitoring technologies
- Data handling and transfer options

Utility Characteristics

When designing a CWS for either a DoD or municipal system, it is critical that the infrastructure, water quality, and operations and maintenance (O&M) practices of the utility are clearly understood prior to the start of the project.

Infrastructure

Water distributed to the more than 10,000 residents at Port Hueneme comes primarily from a single source, the Port Hueneme Water Agency. Two secondary sources exist, but are rarely used. The daily quantity provided by Port Hueneme Water Agency averages 768,000 gallons.

The water distribution system infrastructure includes typical facilities such as turnouts (some with chlorine booster stations), a source well, a small treatment plant, storage

tanks, pump stations, pressure-reducing valves, piping, and appurtenances. Detailed information about the facilities and their characteristics and locations was gathered.

The water system was originally designed for firefighting and warehouse use, thus an extensive system comprising large pipes was put in place. Today, the system is used primarily to supply potable water to Base housing and the Engineering Center. The demand and usage patterns from these geographically separated areas is too low for the size of the system, resulting in non-moving water.

Water Quality

Water quality at Port Hueneme is monitored through samples collected to meet regulatory requirements and for operational reasons. Data regarding existing sample stations (such as age, location, and types of parameters monitored), sample collection, regulatory and operational sampling parameters, and laboratory analysis were compiled to create a complete picture of existing water quality. Regulatory and operational sampling parameters included total and fecal coliform, heterotrophic plate counts (HPC), and Total Trihalomethanes (TTHMs)/Haloacetic Acids (HAA5), total and free chlorine residual, total and free ammonia, pH, temperature, and nitrite.

The primary water quality issues at the base were determined to be nitrification and low residual chlorine. These system operations problems were used as part of the criteria for selecting a suite of water quality monitoring technologies (ammonia, nitrate, free chlorine and mono-chloramines).

Operations and Maintenance

Use of chloramines as a disinfectant creates nitrification issues for Port Hueneme. The ratio of chlorine to ammonia-N in the system is lower than what would be required to prevent the formation of nitrites. Short- and long-term prevention strategies to maintain an acceptable chlorine residual throughout the distribution system while preventing the formation of nitrites are employed. Short-term strategies include flushing, an annual period of free chlorine use, creation of additional demand and closing of redundant mains to decrease detention times, and increased monitoring at turnouts. Long-term strategies include the construction of an additional turnout to reduce detention time and investigation of other potential disinfectants.

The CWS demonstration project will collect real-time water quality data that can be directly related to retail water quality entering into the water system and the effectiveness of operational activities in the distribution system.

Contamination Warning System Characteristics

To develop a CWS for a distribution system, detailed information about the following elements needs to be collected and considered:

- Contaminant classes to be monitored
- Water quality instruments and analyzers that respond to the selected contaminant classes
- Contaminant fate and transport models that are applicable under the utility's existing hydraulic and water chemistry conditions

- Potential monitoring locations
- Communications links and protocols for collection, transfer, and analysis of data
- Integration with the existing supervisory control and data acquisition (SCADA) system
- Tools and guidance for data interpretation

The CWS must also include the features specified by the U.S. Environmental Protection Agency (USEPA) in its draft documents, *WaterSentinel System Architecture*:

- **Capability** to sense changes to water quality parameters that can indicate potential contamination
- **Contaminant coverage** that has a high-to-medium detection potential for most classes of contaminants evaluated by USEPA
- **Spatial coverage** that provides adequate detection capability, including location, number, and density of monitoring stations
- **Timeliness** of detection, including hydraulic travel time from the contamination source and the concentration of the contaminant
- **Reliability,** including the expected rate of false positive and negative results
- **Sustainability** to provide a better understanding of water quality variability throughout the distribution system

Information about contaminants that may potentially be found within the distribution system and the surrogate parameters that can indicate the presence of these contaminants is also essential to the design of a CWS. This information is relevant to instrument selection and the understanding of the dynamic nature of distribution systems, which can be affected by operational changes or source water blending.

All of the CWS characteristics identified above were evaluated to determine how they should be applied to Port Hueneme and its specific requirements. For example, the CWS must assist in the monitoring and prevention of nitrites in the distribution system. As a result of the Port Hueneme-specific evaluation, the following parameters were selected for monitoring by the CWS:

- Chlorine residual
- Conductivity
- Turbidity
- pH
- Total organic carbon
- Nitrate
- Dissolved organic compounds
- Temperature
- Pressure
- Ammonia
- Continuous spectral data

The next consideration was the location of the monitoring stations. Because of the extent of water distribution systems and the large number of potential contaminant insertion points, a large number of monitoring stations may be recommended. The costs associated with monitoring stations can be substantial, so the number and location of the stations must be optimized to be both financially and functionally effective. Criteria to be considered when locating monitoring stations include the following:

- Pressure zones
- Employee access
- Available utilities (sewer, power, communications)
- Physical security
- Turbulent hydraulic conditions
- Existing sampling sites
- Potential entry for contamination
- Vulnerable populations
- Instrument performance in the installed conditions

Two monitoring station locations were ultimately selected. The criteria that most affected the selection process were available utilities, physical security, and existing sampling sites. In addition, because this is a pilot program, the minimum number of stations was used.

Available Online Monitoring Technologies

Prior to the start of this pilot project, NAVFAC ESC performed an extensive evaluation of the wide range of instruments currently available. Based on experience, parameters to be monitored, and site constraints, the following instruments were selected:

- HACH Water Distribution Monitoring Panel sc (purchased prior to project)
- ATI Q45WQ Water Quality Panel
- s::can spectro::lyser™
- s::can ammo::lyser™

The Intelletect Intellisonde™ (a multi-parameter probe for pH, free chlorine, mono chlorine, turbidity, conductivity, color, pressure, temperature, and flow) will be tested at Port Hueneme.

The selection of technology was driven by the triple bottom line of sustainability at Port Hueneme:

- Economics
  - Capital costs
  - Operations costs
    - Labor
    - Expendables
    - Replacement costs

- Societal
  - Security
  - Regulatory
  - Consumer aesthetics
- Environmental
  - Landfill impacts
  - Water quality discharge impacts (reagents)
  - Air impacts (greenhouse gases)

Data Handling and Transfer Options

When identifying data handling and transfer options, the following items are typically considered:

- Data collection
- Sample collection
- Operator interaction
- Centralized SCADA system data archiving
- Sensor monitoring
- Data storage
- Monitoring station and sensor definition
- Data analysis
- Data communication protocols
- Digital communication

Port Hueneme will use secure/encrypted communication over a cellular link to relay the water quality data to a centralized database. Local data validation and event detection is provided by an industrial personal computer prior to the data being transferred to the central database using the Transducer Markup Language (TML), a standards-based data transfer method for communicating real-time sensor data. This methodology avoided the complexities of setting up radio telemetry on an operating base and the time delay of obtaining a Certificate To Operate (CTO). Communication will be provisioned in a matter of minutes instead of months. In addition, this choice allows the project team to have direct access to the data to provide real-time assistance in data evaluation and management.

Data Analysis

The event detection system (EDS) being developed by s::can and CH2M HILL for the Port Hueneme will have the attributes listed below:

- Enhanced Data Validation: Minimum/maximum boundaries, drift analysis, step change analysis, and outlier analysis
- Data Analysis: Capability of evaluating both single- and multi-dimensional data
- Advanced Event Detection: Both single-point and spatial recognition within the distribution system

Current Status

With the information gathered, CH2M HILL is providing NAVFAC ESC with strategies to identify potential water quality monitoring station locations, a conceptual system design for the monitoring stations, development of an operational test plan for the installed systems, and technical support to collect and analyze data collected from the system.

Conclusion

The information considered when making the CWS design decisions was essentially the same as that used for municipal water distribution systems. However, the system characteristics of size, water usage, and monitoring station location at Port Hueneme makes the ultimate design more applicable to water distribution systems at other military bases and very small systems instead of typical municipal systems.

Concentrate Management and Disposal Practices in Australia

James H Jensen, PG

Member, Zero Liquid Discharge Concentrate Disposal Systems Subcommittee,
Committee on Concentrate Management in Desalination, EWRI of ASCE
Parsons Brinckerhoff Australia Pty Ltd. GPO 398, Adelaide SA 5001, Australia;
email: Jensen@pbworld.com

Potable water supplies are a limited resource in an arid continent like Australia where many areas have experienced extended droughts further limiting available water supplies. However, Australia has built comparatively few desalination plants until recently. Isolated mining towns and small communities as well as industrial processes such as power stations that require high quality water have been the main users of desalination technologies in Australia. Now, a number of the coastal located capital cities like Sydney, Brisbane, Melbourne, Adelaide and Perth are among cities that are either investigating or developing seawater desalination facilities as a means to ensure that water demands can be met successfully and supplies are sustainable.

This paper summarises the concentrate management and disposal methods currently used and proposed in studies in Australia based on publically available information. Concentrate disposal considerations for desalination facilities in Australia include the potential environmental impacts and regulatory permitting requirements, including concentrate water quality, receiving water quality, stakeholder perception and issues, costs of the disposal system and other site specific issues. The operating 143,000 m^3/day Perth seawater desalination facility and the coastal facilities under development use ocean outfalls with diffuser systems for mixing the concentrate with the receiving waters for disposal. However, the inland desalination plants have limited options for concentrate disposal. The disposal methods are often further limited by locally endangered and/or fragile habitat. The most common methods of concentrate disposal for inland facilities include surface water discharge, mixing with process or wastewater and concentration/evaporation. There may be other disposal methods that are unique to a particular facility and situation.

Although Australia is depending for the most part on research being conducted elsewhere concerning the disposal options for desalination concentrate, the Commonwealth Scientific and Industrial Research Organisation (CSIRO) is assessing brine chemical composition as a source for mineral recovery and salt extraction.

BACKGROUND

Australia is often described as the driest inhabited continent. In an arid continent like Australia, potable water supplies are a limited in many areas. Recent studies have

indicated further decline in the quality of water supplies over the next fifty years arising from the impacts of salinity on groundwater and surface water resources.

Australia has had comparatively few desalination plants until recently. Isolated mining towns and small communities as well as industrial processes such as power stations that require high quality water have been the main users of desalination technologies in Australia (AFF 2002). Desalination is now being evaluated or developed as potable water supplies in a number of both small and large communities in Australia to supplement other water sources so that current and future demands can be met and are sustainable.

The coastal seawater desalination facilities in Australia use ocean outfalls with diffuser systems for mixing the concentrate with the receiving waters as the disposal method. However, the inland desalination plants have limited options for concentrate disposal. The disposal methods are often further limited by endangered and/or fragile habitat in the area. The most common methods of concentrate disposal for inland facilities include surface water discharge, mixing with process or wastewater and concentration/evaporation. The following sections cover concentrate management and disposal practices of representative desalination facilities in Australia based on publically available information. The facilities were selected in part because of the level and perceived reliability of the information. However, the projects underwent rigorous environmental and design studies over a period of several years and any changes overlooked should not take away from the overall value of the review.

ENVIRONMENTAL PROTECTION

The National Environment Protection Council (NEPC) which is comprised of the environment ministers from the Australian Government, each state and territory is tasked with ensuring that major environment protection initiatives are established and are similar in each member government. The NEPC establishes National Environment Protection Measures (NEPMs) which are broad framework-setting statutory instruments that outline agreed national objectives for protecting or managing particular aspects of the environment. NEPMs are similar to environmental protection policies. (AGDEWHA, 2008)

Each member government has established an independent Environmental Protection Agency or similar named entity which is in charge of environmental matters including protecting air, water and soil quality, managing waste, preventing or controlling pollution, managing the state's coastline, and promoting environmentally sustainable industry. There are stringent requirements for project development including environmental assessment and documentation, compliance monitoring and mitigation measures. The responsibilities for managing the assessment procedures, monitoring compliance and the enforcement of environmental matters vary among the member governments.

The environmental assessment, permitting and compliance requirements for desalination projects in Australia are similar to those in the United States. Environmental considerations for desalination facilities in Australia include the potential environmental impacts of the concentrate effluent (temperature and quality), receiving water quality and site specific issues. The major environmental concern for concentrate discharge relate to the effectiveness of concentrate plume dispersion in the mixing zone.

PERTH KWINANA SWRO PLANT

The greatest amount public information is available for the Perth Seawater Desalination Plant, the first large capacity seawater desalination plant in Australia. The facility is located at Kwinana, south of Perth, Western Australia. The Perth Desalination Plant commenced delivering up to 144 ML/day of much needed drinking water in November 2006.

Intake screening at the intake structure for the Kwinana facility consists of course barred screens offshore and automatically cleaned travelling band screens onshore. Ferric sulphate and an organic coagulant are added to the seawater influent to the multimedia pressure filters to coagulate particulate and colloidal material. The backwash materials (solids) from the pretreatment system are disposed to landfill due concerns about possible discolouration of the white sandy beaches if the backwash was discharged at sea (Crisp, 2008).

The partial two pass RO system produces a permeate of less than 100 mg/L Total Dissolved Solids (TDS) from a feedwater salinity of ~37,500 mg/L. The facility incorporates isobaric energy recovery devices (PX) from ®ERI resulting in a specific energy consumption of less than 3.9 kWh/m3. At a 43% recovery, the facility discharges up to 200 ML/d of concentrate at an average TDS of 66,000 mg/l (Crisp 2008, Ludetina and Christie, 2008).

During the environmental approval process, disposal of the concentrate in Cockburn Sound was raised as an area of concern by the Department of Environment and Conservation (DEC). The hypothesis was that it could exacerbate the naturally occurring stratification, particularly during the autumn when long periods of calm occur, and cause oxygen depletion in the deep basin of the Sound (Ludetina and Christie, 2008).

To ensure that the environment is protected, a series of marine monitoring studies were commissioned prior to and as part of the environmental approvals, including in the discharge area. These studies included Whole Effluent Toxicity testing on simulated brine and actual seawater concentrate at commissioning and 12 months later, sediment oxygen demand tests, international literature review of dissolved oxygen levels, ecological investigations, cause effect models, and an intensive baseline investigation commissioned to document water quality and macrobenthic fauna present prior to operations (Crisp, 2008).

Western Australia's Environmental Protection Authority (EPA) set strict criteria for the concentrate discharge, requiring the salinity within 50 meters of the discharge point to be within 1.2 ppt of background levels and at one kilometre offshore within 0.8 ppt of background levels. Computer modelling of the diffuser system, a scale physical model testing study and a rhodamine die dispersion test indicate that the seawater concentrate is effectively mixed within the mixing zone of less than 2.5 hectares (Crisp, 2008).

The concentrate is fully oxygenated by a drop structure before being discharged. The seawater concentrate is delivered via an underground 1.6 m diameter pipeline to the eastern shelf of Cockburn Sound in a depth of about 10 m of water (Craig 2005). The pipeline terminates about 270 metres offshore in Cockburn Sound at a 200 metre long diffuser system with the 40 discharge nozzles about 0.5 m from the seabed surface at a 60 degree angle and spaced at five metre intervals. The diffuser system is designed to ensure 45 times dilution of the effluent within 50 m on each side of the diffuser system. A real time monitoring system within Cockburn Sound feeds water quality data back to the plant to confirm the effectiveness of the diffuser system. Temperature and conductivity is recorded at 1-2 m intervals through the water column, and dissolved oxygen is recorded at the bottom of each monitoring buoy and at mid-depth (Crisp, 2008).

After a year of operation, the diffusers were found to be heavily populated by marine growth, mussels and surrounded by feeding fish. Nevertheless, in its first year of operation the plant was shutdown or capacity reduced by the DEC as a precautionary basis for two, two-week periods during extended calm periods in the autumn (Luketina and Christie, 2008).

GOLD COAST SWRO FACILITY

In order to meet the tight deadline to complete the Gold Coast project before the end of 2008, construction had to get underway whilst the approvals process was still in progress. This meant that the design team had to be able to amend the design of systems, if required, to achieve improved environmental outcomes (SKM, 2008)

The process consists of initial coarse screening followed by pretreatment by coagulation and gravity sand filtration, cartridge filtration and desalination by a two-pass reverse osmosis system to ensure that treated water meets the required water quality limits. A dedicated filter backwash water treatment system is being constructed. Backwash solids will be transported off site (SKM, 2008).

Concentrate effluent from the RO process is discharged back to the ocean via the discharge tunnel and a seabed diffuser system. The plant will initially discharge up to 125 ML/day of effluent. The effluent will be 1.8-1.9 times the salinity of the intake seawater, an elevated temperature of 1-2º C and may possess a reduced concentration of dissolved oxygen (1.5-2.0 mg/L) (Tripodi and Ramsay, 2008).

Intake and outfall concrete-lined tunnels were constructed about 70 m below the surface extending about 1.5 km offshore (water depth about 20 m) to riser shafts for the intake and outfall systems. (SKM, 2008). Extensive computer modelling, supported by physical modelling, was used to design the diffuser system. The diffuser design was modified during the design period to 397 m in length with a 20-port diffuser based on the State Government desire to facilitate increased clear water production without changes to the diffuser if the effluent discharge is increased to a maximum of 170 ML/day (Tripodi and Ramsay, 2008).

The investigations indicate that under worst case mixing conditions, defined as the highest salinity concentration (100% plant duty) and lowest observed receiving water oceanic currents, a 40-fold dilution is predicted at the edge of the near-field mixing zone (bounded at 60 m from any point of the diffuser – total area 120 m x 404 m) and a 25-fold dilution at the point where the brine plume impacts with the sediment (16 m from the diffuser). These dilution figures and supporting evidence from concentrate dispersion at the Perth Desalination Plant indicate that minimal adverse environmental impact is expected from elevated salinity concentration in the near-field mixing zone. These model-predicted dilution values will be validated in the field during plant operations through a Diffuser Performance Monitoring Plan (DPMP) (Tripodi and Ramsay, 2008).

BURRUP MVC DESALINATION FACILITY

In the Burrup Peninsula in Western Australia, the capacity of the potable water supply was determined to be insufficient to meet requirements of industrial development in the region (EPA, 2001). As a result, Water Corporation built the Burrup Desalination Plant as part of the Burrup Peninsula Industrial Water Supply Project. The pipeline supplies up to 380 ML/day of seawater including 3.6 ML/day of desalinated water. The desalination plant is now operational and supplying water to their first customer, Burrup Fertilisers, the world's largest Ammonia plant. (Water Corp, 2006)

The 3.6 ML/day of desalinated water is produced by three mechanical vapour compression (MVC) units. A cooling tower was installed designed to cool the concentrate from the thermal desalination process. The concentrate is returned to the Indian Ocean via a control tank, a four-kilometre pipeline and a 1.3 km ocean outfall (GWA, 2003).

The seawater temperature in the vicinity of the proposed outfall was found to vary due to natural causes by as much as 2° C over a tidal cycle and by up to 5° C in a month. The temperature variation is caused by the large area of shallow water in King Bay and the large tides in the region. Near-field modelling (CORMIX v.3.2) of the saline plume (approximately 55,000 mg/L) predicted that the environmental quality criteria for increase in salinity (<5% variation) would be met, apart from within a 40 m mixing zone at the outfall. Near-field modelling for thermal dispersion

was based on a high, worst case discharge temperature of 5° C above ambient seawater temperature. The model predicted that within distances of 7 m and 110 m of the outfall the temperature elevation would be less than 2° C and 0.25° C above ambient, respectively. Far field modelling predicted the temperature increase to be less than 0.1° C above ambient within a few hundred metres of the discharge. The EPA considers the predicted temperature increase to be acceptable, given that the nearest coral communities are approximately 500 m away. Operations will be managed to ensure that the effluent discharge (end of pipe) temperature is less than 2° C above ambient seawater temperature for 80% of the time; and does not exceed 5° C above ambient seawater temperature. (EPA 2001)

OTHER DESALINATION PROJECTS

A number of other coastal located capital cities are among cities that are either investigating or developing seawater desalination facilities as a means to ensure that water demands can be met successfully and supplies are sustainable. Each facility has undergone or is undergoing a number of specified environmental assessment studies and the process of establishing operating conditions and compliance monitoring.

Southern Seawater Desalination Plant. The Water Corporation has selected a consortium to build by 2011 a new seawater desalination plant at a coastal site near Binningup, south of Perth. The plant, powered by renewable energy, will have a production capacity of 140 ML/day in Phase I, with a possible extension up to 280 ML/day in Phase 2. The approximately 42 hectare site owned by Water Corporation is located within the coastal dunes. The site includes a small wastewater treatment plant (Worley Parsons, 2007).

To minimise both dune disturbance and beach closure, tunnelling will be used to construct 2, 2.4m diameter intake pipes and a 2 metre diameter outlet pipe. The intake structures will be about 500 m offshore. A dredged trench will be used from the end of the outfall pipe to the end of diffuser at 950 m offshore in ~12 m of water. The bathymetry of the site slopes relatively uniformly down to the west, with little north-south variation (Water Corp, 2008).

The site is located in a high energy environment, exposed to ocean swell and wind. To evaluate concentrate dispersion, a Rhodamine WT dye plume study was conducted over four hours by keeping track of the same parcel of water using a combination of drogues, dye measurements and vertical profiling. Analysis of the measurements indicates horizontal mixing is dominated by the prevailing wind, with shear dispersion dominating over horizontal diffusion.

Adelaide Desalination Project. SA Water is currently in the process of selecting a consortium to build and operate a 150 ML/day SWRO project. The SWRO facility will be located at Port Stanvac, south of Adelaide. Pilot plant testing is underway to

monitor seawater quality and assess the pre-treatment process and at a later stage reverse osmosis membrane testing will be conducted.

Siting investigations identified that seawater depth significantly decreases north of Port Stanvac along the Gulf St Vincent, which has ramifications for concentrate dispersion. A nominal water depth of at least 10 m was identified as preferred for seawater concentrate dispersion. The sensitivity of marine habitats and water quality considerations were also identified as additional constraints for sites further north of Port Stanvac due to their proximity to seagrass meadows and sensitive marine nursery areas (SA Water, 2008a).

Marine investigations and modelling work for the project include sea dispersion patterns, seawater quality, seasonal effects, diffuser options/locations and methods, and potential impact on marine organisms. At the outfall, a minimum initial dilution of 50:1, sufficient to avoid any effects on marine species has been specified (SA Water, 2008b).

Sydney Desalination Plant. Sydney Water is building a desalination plant to be completed in late 2009 in the Kurnell industrial estate area, in Sydney's southern suburbs. The plant will be able to generate 250 ML/day of potable water, with the possibility of scaling up to 500 ML/day in the future if needed. Both the intake and outfall tunnels and the pipeline to the water supply will be built to the ultimate capacity of 500 ML/day (Wikipedia, 2008).

The seawater intake and discharge outlet will be tunnelled at a depth of 50 to 70 m under the Kurnell Headland and approximately 30 m under the seabed. There are four drill shafts connecting each of the tunnels to the intake and outfall systems. The Four intake and four outlet structures are being built on the seabed about 300 m offshore in the Tasman Sea in water approximately 20 to 25 m deep. The diffuser system is designed disperse the 65,000 mg/l salinity and temperature of the seawater concentrate return to the background level of 34-36,000 mg/l within 50-75 m from the discharge point (GHD Fichtner, 2008).

Agnes Water Desalination Plant. The desalination plant will be located on the coast north of Brisbane between Bundaberg and Gladstone immediately adjacent to the existing Spring Road water treatment plant. The plant will supply 12 ML/day of potable water by 2026; with first-stage output estimated at 1.5 ML/day.

The offshore seawater intake is planned at a depth of some 8m to 10m sea level by constructing an intake pipeline some 600 m from shore. From an underground break tank, concentrate can discharge under gravity to the pipeline diffuser. Directional drilling is proposed for construction of the ~280 mm diameter concentrate discharge pipeline to terminate about 800 m off shore with a diffuser system (Cardno 2006).

Lake Beach Desalination Plant. The Wyong Shire Council in New South Wales is planning the construction and operation of a 20 ML/day SWRO plant adjacent to the

Toukley sewage treatment plant. Saline concentrate water will be discharge through the existing Norah Head Outfall after mixing with effluent from the Tourley Sewage treatment Plant.

Dalby Coal Seam Methane Water (CSM) Reverse Osmosis Plant. Dalby Town Council is designing a .3.75ML/day RO plant to augment drinking water supplies to the Dalby water distribution system. The new RO plant is to be constructed at the same facility as a conventional water filtration plant and brackish water RO plant.

The new desalination plant will be supplied by CSM sourced water from approximately extraction 100 bores with an approximately TDS of about 6,000 mg/l. The CSM sourced water will be blended with a varying proportion of water from other groundwater sources

The CSM-sourced groundwater is to be treated through two parallel treatment trains of equal capacity. The water treatment process will be comprised of pre-treatment including membrane filtration, two-stage reverse osmosis, aeration, and post-treatment. The overall recovery goal for the CSM-sourced water is approximately 72%. The particulate matter removed during the pretreatment stage will be blended with the brine from the RO units and transferred to existing evaporation ponds.

RESEARCH ON CONCENTRATE DISPOSAL IN AUSTRALIA

Although Australia is dependent for the most part on research being conducted elsewhere for disposal options for desalination concentrate, the Commonwealth Scientific and Industrial Research Organisation (CSIRO) may play a significant role including in the characterisation of water quality proposed for desalination, concentrate disposal issues and options and in salinity management projects.

CISRO is involved in the identification of the areas where desalination may contribute to the salinity management program as a part of salinity control measures. In particular, the salt interception works coordinated through the Murray-Darling Basin Commission have been implemented to control salinity levels in the River Murray through disposal of saline waters in specifically designed basins or lakes. Some of these basins have been constructed as controlled leakage basins permitting ultimate disposal to the deep aquifers whilst others are constructed to minimise leakage and rely solely on evaporation to dispose of water drawn from the salt interception works. A major programme emphasis has been given to improving solar evaporation techniques (Barron, 2006).

There is limited data available on the ionic composition of the waters in the disposal basins and therefore the nature of the salts, besides sodium chloride, that may be recovered. It can be expected that solar evaporation of waters in the disposal basins will yield halite, probably gypsum, and magnesium salts (sulphate and chloride) (Barron, 2006).

Initially it was thought that some commercial use could be found for the salt components of the concentrate, for example, chemical feedstock, which might cover the costs of dewatering. However, the composition of the salts present and the contamination with soluble organics mean that the salt is of limited commercial value. It is recognised that there still may be some value in the salt for remediation or other purposes and that this could become the ultimate disposal route for the dry product. The beneficial reuse avoids the estimated $500/t cost for ultimate disposal to landfill (ACTEW Corp Ltd, 2007).

REFERENCES

ACTEW Corporation Ltd. (2007). "Water Purification Scheme for the ACT, Document No: 313952. (July 2007)

Australian Government Department of the Environment, Water, Heritage and the Arts (AGDEWHA). (2008). "National Environment Protection Council", http://www.environment.gov.au/about/councils/nepc/index.html (22-Dec-2008)

Barron, O. (2006). *Desalination Options and their possible implementation in Western Australia: Potential Role for CSIRO Land and Water*. CSIRO: Water for a Healthy Country, National Research Flagship, Canberra.

Cardno. (2006). "Agnes Water & Town of 1770 water supply desalination planning report, Miriam Vale Shire Council"

Crisp, G. (2008). "Seawater desalination in Australia and the Perth experience—a sustainable solution", 2nd International Salinity Forum, Salinity, Water and Society–Global Issues, local action, Perth.

Craig, P., and Wild-Allen, K. (2005). "Peer review of studies for desalination plant discharge, Cockburn Sound", CSIRO Marine Research.

Environmental Protection Authority (EPA). (May, 2001). "Desalination and Seawater Supplies Project, Burrup Peninsula, Water Corporation; Report and Recommendations of the Environmental Protection Authority". Perth, Western Australia.

GHD Fichtner. (2008). "Assessment of Seawater Intake and Concentrate Outlet Project Components." Prepared for Sydney Water, http://www.planning.nsw.gov.au/asp/pdf/chapter7.pdf

Government of Western Australia (GWA). "Media Statement - Jim McGinty on 17/1/2003"; http://www.nativetitle.wa.gov.au/uploadedFiles/Agreements/Burrup_and_Maitland/Media_Releases/19012003%20mcginty.pdf

Luketina, D., Christie, S. December 2008. "Monitoring of the Perth SWRO brine outfall". *Water*.

Maunsell. (2008). "Burrup Water Projects, Pilbara Region, Western Australia". http://www.maunsell.com/MarketsAndServices/39/76/index.html, (January 27, 2009).

Marti, C., Okely, P., Antenucci, J., and Imberger, J. (2007). Horizontal mixing and dispersion at the proposed outfall site for the Southern Seawater Desalination

Plant, Binningup Centre for Water Research, The University of Western Australia.
SA Water. (2008). "Proposed Adelaide Desalination Plant Environmental Impact Statement, Chapter 2 – Need for Proposed Desalination Plant." Adelaide SA.
SA Water. (2008). "Proposed Adelaide Desalination Plant, Environmental Impact Statement -- Executive Summary." Adelaide SA.
Sinclair Knight Merz (SKM). (2008). *Delivering sustainable desalination*. From the Sinclair Knight Merz magazine; http://www.skmconsulting.com/publications/AM4_sustainable+desalination.htm
Sydney Water (2008) "Desalination"; http://www.sydneywater.com.au/ensuringthefuture/desalination/
Tripodi, N. and Ramsay, I. (2008) "Managing Increasing Brine Concentrate Discharges in Drought Conditions". Freshwater & Marine Sciences Unit, Environmental Sciences, Queensland Environmental Protection Agency, Brisbane, Australia.
Water Corp. (2006). "Water for life report 2006"; http://www.watercorporation.com.au/_files/PublicationsRegister/6/WCReport2006.pdf, Perth WA.
Water Corporation. (2008). "Southern Seawater Desalination Project". http://www.watercorporation.com.au/D/desalination_plant2.cfm, Perth WA.
Wikipedia (2008) Sydney Desal, Kurnell Desalination Plant, http://en.wikipedia.org/wiki/Kurnell_Desalination_Plant#Infrastructure_and_capacity
Worley Parsons. (2007). "Southern seawater desalination plant comparison of sites in the Kemerton Industrial Park for the Water Corporation of WA". (8 August 2007).

Desalination of Brackish Groundwater and Deep Well Injection of Concentrate in El Paso, Texas

William R. Hutchison, Ph.D., P.E., P.G.[1]

[1]Water Resources Manager, El Paso Water Utilities, 1154 Hawkins Blvd., El Paso, TX 79925, 915-594-5516, bhutchison@epwu.org

ABSTRACT

El Paso has relied on the Hueco Bolson as a major water supply source since 1903. As a result of high pumping, groundwater levels in the Hueco have declined and brackish groundwater has intruded into areas that historically yielded fresh groundwater. El Paso Water Utilities (EPWU) began reducing its Hueco pumping in 1989 as a result of a variety of water management initiatives. The reduction in pumping resulted in stabilized groundwater levels in many areas. However, brackish groundwater intrusion remains an issue. A 27.5 mgd desalination plant has recently been completed that will result in reductions in brackish groundwater intrusion, and allow EPWU to better utilize its fresh groundwater wells during droughts. The location of the pumping wells will provide an opportunity to intercept the brackish groundwater before it intrudes into historically fresh groundwater areas. This approach is a component of EPWU's overall groundwater management of the Hueco Bolson.

OVERVIEW OF DESALINATION PROJECT

Since 1903, fresh groundwater from the Hueco Bolson has constituted a significant portion of the water supply for the greater El Paso area (Figure 1). Prior to 1989, pumping from the Hueco Bolson to supply El Paso Water Utilities (EPWU) customers was increasing each year. Since 1989, EPWU pumping from the Hueco Bolson has been decreasing due to concerns regarding decreasing groundwater levels and brackish groundwater intrusion. Increases in surface water diversions, aggressive and innovative water conservation programs, and increased reclaimed water use have allowed EPWU to reduce pumping in the Hueco Bolson. As a result of the decreased pumping in the Hueco Bolson, groundwater levels have stabilized in many areas.

The Hueco Bolson has a large volume of brackish groundwater that can be used as a potable supply after desalination. Brackish groundwater lies to the east and beneath a relatively small lens of fresh groundwater. Groundwater pumping of the fresh groundwater has caused brackish groundwater to intrude into areas where wells had historically pumped fresh groundwater. Figure 2 shows a simplified representation of where fresh groundwater and brackish groundwater occur at depths normally associated with production wells in El Paso. The interface has been moving east to west and northeast to southwest in response to cones of depression caused by pumping in El Paso and Ciudad Juarez.

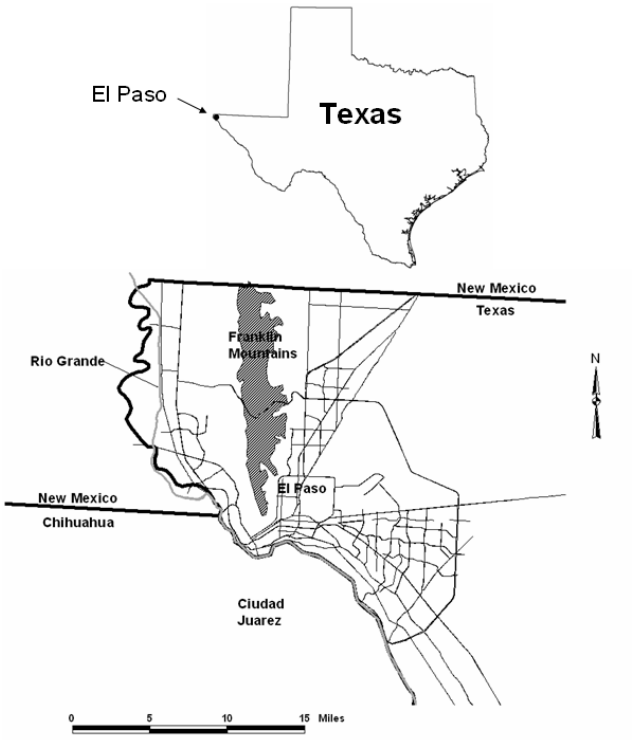

Figure 1. Location of El Paso, Texas

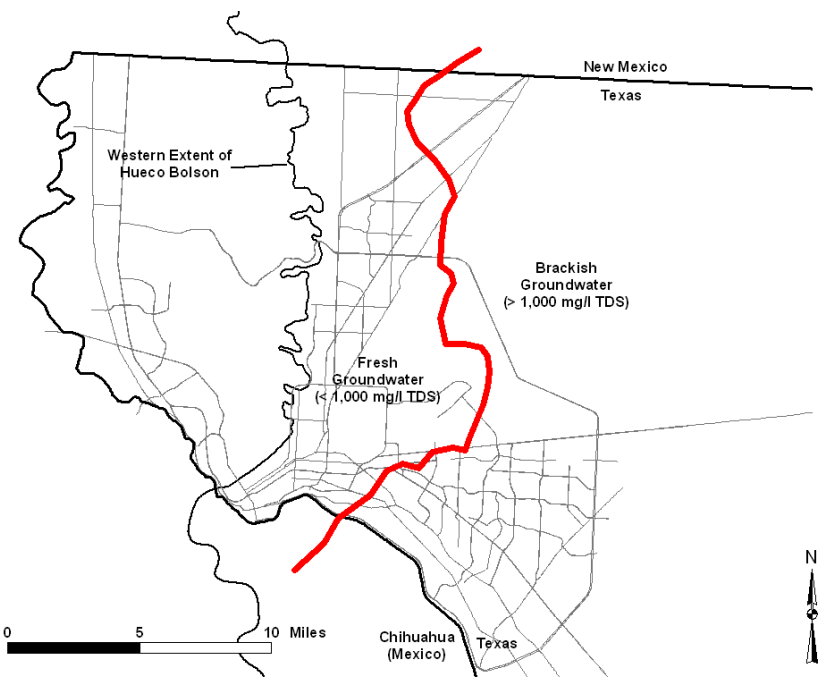

Figure 2. Location of Approximate Interface between Fresh Groundwater and Brackish Groundwater

Technological advances in the last decade have made desalination a more economically viable water source. Integrating desalinated brackish groundwater resources into the overall EPWU water supply portfolio presents certain opportunities to manage the brackish groundwater intrusion, which has caused wells that had historically pumped fresh groundwater to exceed secondary water quality standards for chloride and total dissolved solids.

A critical issue in the development and treatment of brackish groundwater is the disposal of the concentrate that is produced by the desalination process. After completion of various studies and a test drilling program, EPWU selected deep well disposal of the concentrate in the northeast corner of the South Training Area of Ft Bliss (Figure 3). Also shown on Figure 3 are the locations of existing and new EPWU wells in the Hueco Bolson that supply the desalination plant.

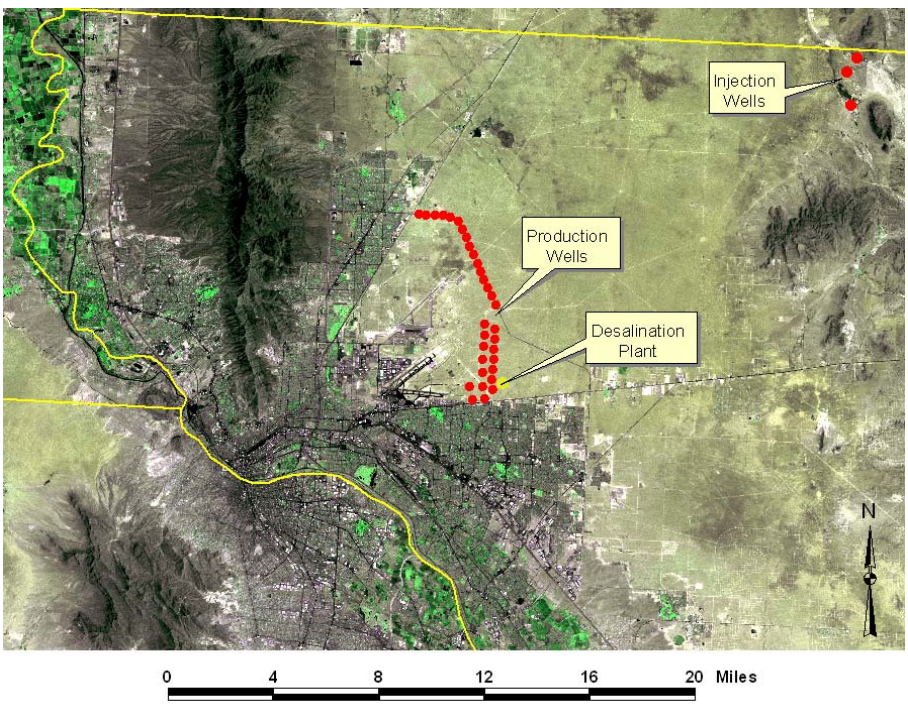

Figure 3. Location of Desalination Plant, Production Wells, and Injection Wells

Figure 4 presents a schematic of the desalination plant project at design capacity. 30.5 mgd of brackish groundwater from the Hueco Bolson is pumped. 18.5 mgd of this brackish water is processed in the plant, which yields 15.5 mgd of permeate and 3 mgd of concentrate. The remaining 12 mgd of brackish groundwater is blended with the 15.5 mgd of permeate to yield 27.5 mgd of finished water with a TDS of between 600 and 700 mg/l. The concentrate is sent 22 miles to the injection wells for disposal.

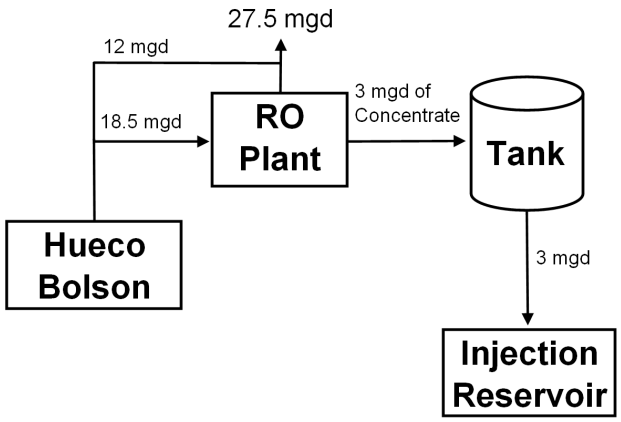

Figure 4. Schematic of Desalination Plant Process

COMPONENTS OF DESALINATION PROJECT

The major components of the desalination project are:

- Production wells and collector lines
- Reverse osmosis and near-plant pipelines
- Concentrate disposal wells and pipeline

As shown previously in Figure 3, there are 36 production wells that are connected to the desalination plant. These wells are a combination of existing wells (4), rehabilitated wells (3), and new wells (29), and are connected to the plant by 88,700 ft of new collector lines. The location of the wells is designed to intercept brackish groundwater. The drawdown trough that will be created will prevent further migration of brackish groundwater into areas that have historically pumped fresh groundwater. The production wells and collector lines were constructed under 12 separate contracts from March 2005 to June 2007.

The reverse osmosis plant has five skids of membranes manufactured by Hydranautics. Each skid is capable of flow rates between 1.70 and 3.64 mgd. Expected water recovery is between 70% and 82.5%, and expected salt rejection is up to 93%. The plant inflow is pre-treated with an antiscalant to control mineral precipitation (notably silica) and hydrochloric acid to adjust pH. The finished water is treated with caustic soda to raise the pH, a corrosion inhibitor, and disinfected with sodium hypochlorite. The concentrate can be treated with hydrochloric acid to adjust the pH prior to disposal, if needed. The near-plant pipelines include the completion of the two well collector lines, the initial part of the concentrate disposal line, and the finished water pipeline. The plant and pipe projects were constructed under two separate contracts (one for the plant and one for the pipe) from July 2005 to June 2007.

The concentrate disposal portion of the project consists of the remainder of the concentrate pipeline, three injection wells, and above-ground facilities associated with the injection wells (Surface Injection Facilities). The three injection wells are between 3,700 and 4,000 ft deep, and are completed in the Silurian Fusselman Formation, a fractured dolomite, and the underlying Montoya Formation, a fractured limestone. The Surface Injection Facilities consist of yard piping, a 300,000 gallon storage tank at each site, a solar power system (with generator backup), and various instrumentation and controls to manage the injection and collect performance data. The work associated with concentrate disposal was completed under seven separate contracts, including a test-hole contract by the US Army Corps of Engineers that represented the initial characterization of the area. The work was completed from April 2003 to June 2007.

CONCENTRATE DISPOSAL VIA DEEP WELL INJECTION

The investigations and analyses that culminated in the construction and operation of the three injection wells began in 2001. Initially, three methods of concentrate disposal were considered: passive evaporation, enhanced evaporation and deep well injection. Passive evaporation for 3 mgd of concentrate would have required a 700-acre double-lined pond. Enhanced evaporation would have required a smaller pond and mechanical sprayers to enhance the evaporation rate. An economic analysis of the three alternatives completed in 2002 showed that deep well injection would be significantly less expensive than either of the evaporation alternatives, if a suitable site was located. Because of the attractive costs, a detailed investigation of the deep well disposal option was completed from 2002 to 2004, and consisted of geologic investigations, test drilling, geophysical studies, preliminary modeling, and culminated in the construction and testing of a pilot well in 2004.

The results of the studies and the testing of the pilot well were used in 2004 and 2005 to prepare an application to the Texas Commission on Environmental Quality (TCEQ) for a Class V Authorization to inject concentrate into the Fusselman and Montoya formations of Silurian and Ordovician age. The authorization was obtained on July 13, 2005, and included a provision that the injectate had to meet primary drinking water standards.

During the development of the TCEQ application and after the authorization was obtained, several studies were completed related to the potential for mineral precipitation in the well and formation. Of notable concern were calcite, barite and silica. Mitigation strategies were identified (e.g. lowering the pH of the concentrate), and a plan for initial operation was developed to further test the potential for mineral precipitation during initial operation.

The second and third injection wells were constructed in 2006 and the beginning of 2007. These wells were also completed to Class I standards. The wells are completed with open holes in the injection zone (below 2,900 ft). A key aspect of the

injection wells is that no pumps are needed. The wells are capable of accepting water by gravity at rates that approach 2,000 gpm.

Initial testing of the wells began in May 2007 and initially involved injecting fresh water in order to develop well performance data without concern of mineral precipitation. At the beginning of plant operations, the concentrate was diluted, thus continuing baseline data collection. After sufficient baseline data were collected, the dilution of the concentrate was reduced and finally eliminated, with no observable change in well performance (i.e. injection rate and groundwater level build-up).

INITIAL OPERATION OF INJECTION WELLS

As of the submission of this paper (late January 2009) data have been collected from the beginning of operation of the plant after initial testing (September 2007) through the end of December 2008. A summary of operations is presented in Table 1.

Table 1. Summary of Operations – September 2007 to December 2008

Component	***Total Flow***
Airport Well Pumping	5,100 AF
Ft. Bliss Well Pumping	1,000 AF
Total Pumping	6,100 AF
Finished Water to Distribution System	5,100 AF
Concentrate from Reverse Osmosis Units	1,000 AF
Dilution Water from Ft Bliss Wells	1,400 AF
Total Concentrate Flow to Injection Wells	2,400 AF

Note that dilution water from Ft Bliss wells has been added to the concentrate from the reverse osmosis units in an attempt to comply with the requirement that the injectate meet primary drinking water standards. Several of the monthly samples of the concentrate, however, slightly exceed the primary standard for arsenic and selenium despite using different combinations of wells for dilution. TDS of the injectate during this initial operating period ranges from 2,500 mg/l to about 5,100 mg/l, which is considerably below the receiving formation TDS of about 8,800 mg/l.

In response to the difficulties in meeting the primary standard requirement, EPWU initiated discussions with Texas Commission on Environmental quality (TCEQ) and EPA in December 2007 to obtain an aquifer exemption status under 40 CFR Parts 144-146 and 30 TAC Chapter 331 for the injection zone. Because the receiving formation has a TDS below 10,000 mg/l, it is considered an Underground Source of Drinking Water (USDW). Under the regulations, exemptions can be sought if:

- The aquifer does not currently serve as a source of drinking water
- The aquifer cannot now and will not in the future serve as a source of drinking water based on certain criteria
- The TDS of the ground water is more than 3,000 and less than 10,000 mg/L and it is not reasonably expected to supply a public water system

An Aquifer Exemption application was submitted to TCEQ in August of 2008. It was also submitted to the New Mexico Environment Department (NMED) because the plume of injectate will eventually extend slightly north into New Mexico. If approved by TCEQ and NMED, it will then be submitted to EPA for concurrence and final action. Highlights of the application include:

- The wells are located in a remote area with no other production or injection wells
- The receiving formation meets TDS guidelines of the regulations (less than 10,000 mg/l and more than 3,000 mg/l)
- The receiving formation water does not meet primary drinking water standards
- Treatment would be required to meet primary drinking water standards and reduce TDS
- Introduction of the injectate would not necessitate further or more expensive treatment

Well performance during the initial operating period is summarized in Figures 5, 6 and 7, which show the minimum and maximum depth to water from September 2007 to December 2009 for each of the three wells. Note that the maximum depth to water each month is coincident with the highest injection rate, and the minimum is coincident with periods of non-operation.

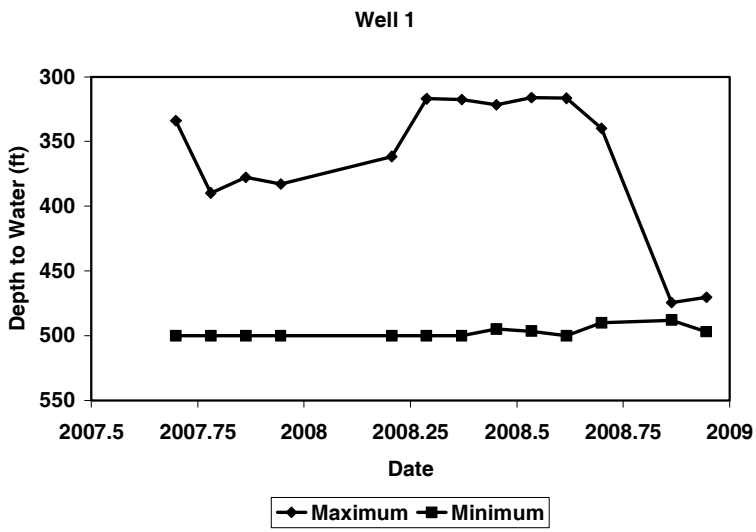

Figure 5. Monthly Minimum and Maximum Depth to Water in Injection Well 1

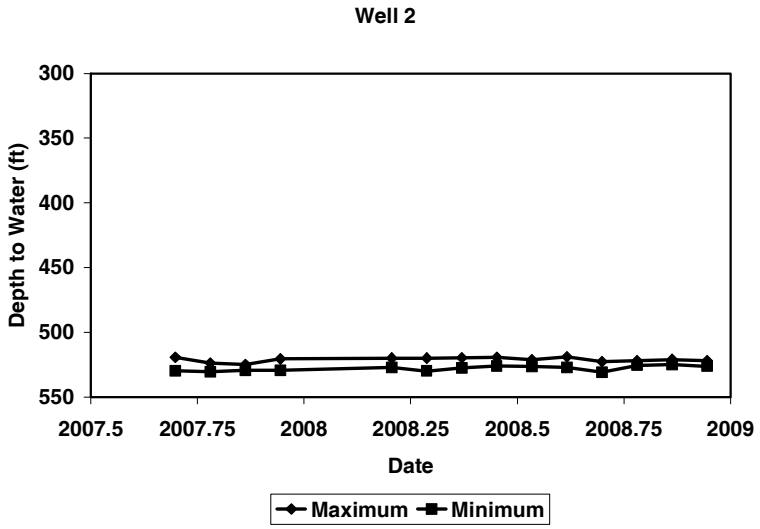

Figure 6. Monthly Minimum and Maximum Depth to Water in Injection Well 2

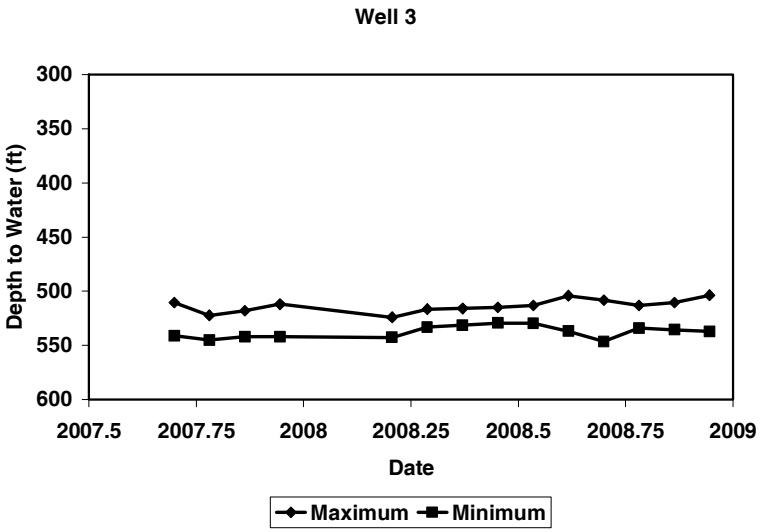

Figure 7. Monthly Minimum and Maximum Depth to Water in Injection Well 3

Note that during operation of Well 1, depth to water rises from a static level of about 500 ft below ground surface to as high as about 320 ft below ground surface (rise of about 180 feet). Injection rates have been as high as about 1,800 gallons per minute (gpm).

Well 2 is not operational due to issues with the annular space monitoring system. The depth to water ranges from about 520 feet below ground surface to about 530

feet below ground surface. Response to the injection in Wells 1 and 3 has been about 4 or 5 feet.
The injection rate in Well 3 has been as high as approximately 1,800 gpm, and depth to groundwater has risen 25 to 30 ft in response to the injection. Minimum depth to water (during non-operation) is about 530 ft below ground surface, and maximum depth to water during injection has been as high as about 500 feet below ground surface.

It is also important to note that all three wells exhibit no upward trend in minimum depth to water during the initial 16-month operational period. An upward trend would suggest limitations to the injection reservoir. Based on this initial operational period, well performance is considered acceptable, and monitoring continues.

PROJECT COSTS

Total capital cost of the project was about $91 million as follows:

- Production wells and collector lines: $32 million
- Plant and near-plant pipelines: $40 million
- Concentrate disposal: $19 million

Funding for the capital costs was as follows:

- Congressional appropriations: $26.0 million
- Texas Water Development Board interest-free loan: $1.0 million
- EPWU Bonds and cash: $60.7 million
- US Army contribution: $3.3 million

Annual operating costs (assuming a electrical cost of $0.07/kwh and 80% operation) are estimated to be $4.8 million. Amortized capital and operations costs (assuming a 5% discount rate) are estimated to be about $534/AF. The cost of the project (in terms of $/AF) are reasonable when compared to other EPWU sources ($163/AF for groundwater, $300/AF for surface water, and $706/AF for reclaimed water), and are far more attractive than importation from other parts of Far West Texas ($1,400/AF).

Membrane Treatment of Rio Grande Water for Municipal Water Production During the Non-Irrigation Season

Anthony J. Tarquin[1], Michael P. Fahy[2], and John E. Balliew[3]

[1]Department of Civil Engineering, University of Texas at El Paso, 500 W University, El Paso, TX 79968; PH (915) 747-6915; FAX (915) 747-8037; email: atarquin@utep.edu
[2]El Paso Water Utilities, P.O. Box 511, El Paso, TX 79961-0001; PH (915) 594-5681; FAX (915) 594-5699; email: mpfahy@EPWU.org
[3]El Paso Water Utilities, P.O. Box 511, El Paso, TX 79961-0001; PH (915) 594-5595; FAX (915) 594-5699; email: jeballiew@EPWU.org

ABSTRACT

Using impaired waters to meet increasing municipal demands has become nearly mandatory in many locations. This pilot scale project was undertaken to determine the feasibility of using brackish irrigation return flows (that also contain a small percentage of treated wastewater) to satisfy part of El Paso's municipal water demand during the non-irrigation season.

The first step was to determine if a sufficient quantity of water is available during the non-irrigation season to provide 10 MGD of potable water. Historical data obtained from the United States Geological Survey for the years 1936 through 2004 revealed that a flow of at least 20 MGD is available 89% of the time.

A simple microfiltration system (MF) was installed ahead of the reverse osmosis (RO) and nanofiltration (NF) membranes for suspended solids removal. The desalting results showed that both the RO and NF systems performed very well, with salt rejections in the 98% range. The lowest cost blended water was $0.76 per thousand gallons, produced in the NF unit when operating at 170 psi with a flux of 25 gallons per square foot per day. This cost includes disposal of concentrate through re-blending with available irrigation return flows for possible irrigation of onions, the major winter crop in El Paso County, Texas.

INTRODUCTION

The El Paso Water Utilities (EWPU) receives as much as 85% of its potable water supply from the Rio Grande during the irrigation season of the U. S. Bureau of Reclamation's Rio Grande Project. The irrigation season normally runs from March through September during a typical water supply year. The raw water quality is acceptable for treatment to potable water standards using conventional treatment methods during this period. However, when raw water releases from Elephant Butte and Caballo Reservoirs are curtailed at the end of the regular, irrigated growing season, the river water consists primarily of return flows from agricultural drains. These simple, incised drains were excavated to remove water from the root zone, thereby relieving the soil of excess water and improving crop production.

EPWU must curtail diversions from the river during the non-irrigation season (approximately October through February) because the total dissolved solids (TDS) content of Rio Grande water during that time generally exceeds 1000 mg/L. This represents a considerable portion of the year during which surface water is essentially unusable as a potable supply due to high TDS. This project was undertaken to determine the feasibility of treating river water after

the irrigation season ends (i.e. irrigation return flows) to meet potable water quality standards using membrane technology, thereby utilizing an available water resource that is currently not put to full beneficial use.

METHODOLOGY

The first step in the project involved assessing the availability, reliability, and quantity of winter return flows in the Rio Grande. If the water available during the non-irrigation season is insufficient from a quantitative standpoint, any qualitative evaluation would be irrelevant. Therefore, historical data were obtained from the United States Geological Survey (USGS) for the years 1936 through 2004 at the Courchesne Bridge and analyzed for average, median, and low flows during the non-irrigation season. Once the quantity of water available was determined to be adequate, the same database was used to obtain water quality parameters as a function of flow. Treatability studies were then conducted using pilot plants containing different types of membranes as discussed below. This part of the study also generated design and cost information for possible full-scale implementation of the project.

Three different pilot units were set up at EPWU's Canal Street surface water treatment plant site to collect data for this study. The MF unit, which was used for suspended solids removal, consisted of four, 4-inch (10 cm) diameter microfiltration membrane housings 40" (100 cm) long connected in parallel and mounted horizontally on a stand, one above the other. The other two pilot units were single-membrane GE-Osmonics units, one equipped with a nanofiltration membrane and the other with an RO desal membrane. Ball valves at the end of each housing allowed for any of the membranes to be isolated for cleaning or other servicing. The antiscalant Pretreat Plus Y2K from King Lee Technologies was added at 2 ppm during all testing.

In addition to the treatment units themselves, there were two storage tanks included in the treatment system. All pilot equipment (i.e. everything except the two storage tanks) was housed in a 12'x 24' (3.7 x 7.3 m) building located close to the American Canal. A schematic of the pilot treatment system is shown in Figure 1. For a full-production scale plant, permeate water would be blended back with river return flows treated in the conventional treatment plant and pumped into the potable water distribution system.

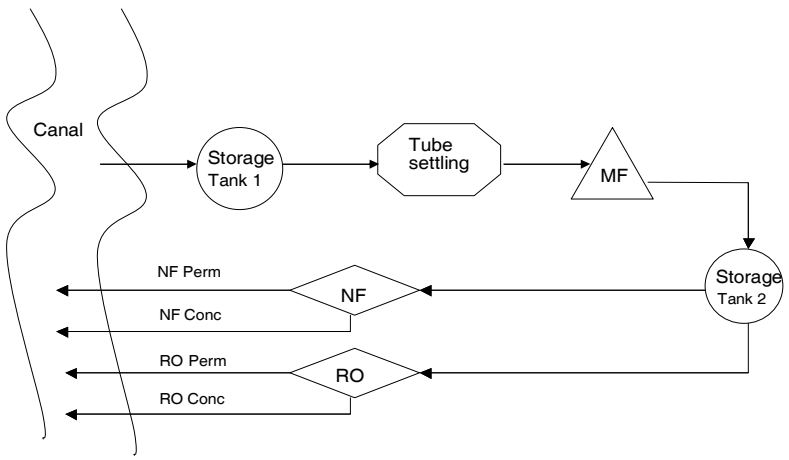

Figure 1. Pilot Plant Schematic

DATA COLLECTION PROCEDURES

Data collection activities for this project spanned parts of the 2006 thru 2008 irrigation and non-irrigation seasons. The pilot plants were operated on an intermittent basis, ranging from a few hours at a time to several weeks continuously, depending on the task at hand. The water quality parameters that were measured also varied according to what was being investigated at the time. Some of the water quality parameters were measured at the site, but most were measured in the lab. Besides the operating parameters that obviously had to be recorded at the site (such as temperatures, pressures, flows, etc.), some of the conductivity, pH, and turbidity readings were also made at the site. Conductivity and temperature readings were made with an Oakton model Con 110 combination pH, conductivity, TDS meter. Turbidity readings were made with a HACH model 2100N Turbidimeter. The more routine analyses such as alkalinity, chlorides, hardness, etc. were done at The University of Texas at El Paso using HACH standard procedures. The more robust sample analyses were done at the International Water Quality Laboratory of EPWU, including analyses for anions and cations, total organic carbon, silica, etc.

QUANTITY AND QUALITY OF IRRIGATION RETURN FLOWS

As stated previously, USGS data spanning a 65-year period were used for determining the quantity and quality of the river water during the non-irrigation season. The summarized flows for October thru February are shown in Table 1, and the data show that the lowest average and median monthly values occur during January, at 91.5 MGD and 63.7 MGD, respectively.

Table 1. Average and Median Flows

	Years of Record	Avg, MGD	Median, MGD
Oct	68	197.1	184.8
Nov	68	111	96
Dec	68	105.6	76.2
Jan	68	91.5	63.7
Feb	68	119	84.1

Source: Riley, R. T., “Treatment of Non-Irrigation Water at the Canal Street Water Treatment Plant”, Master of Science Thesis, Department of Civil Engineering, August 2005, University of Texas at El Paso.

The October median flow at 185 MGD is almost three times greater than the January median, showing that the flows decrease considerably in a fairly short period of time. On the other hand, these results also show that relatively large volumes of water are available in the non-irrigation season winter months.

Table 2 shows that flows below 40 MGD occur about 20% of the time, and flows below 20 MGD occur about 11% of the time. Review of Table 2 also indicates that a plant designed to treat 10 MGD would be able to operate at full capacity 92% of the time, based on flow. If the plant were operated only when the river flow exceeded 20 MGD, it would be able to provide water during the non-irrigation season 89% of the time.

Table 2. Winter Flows in the 10 – 40 MGD Range

Month	Years of Record	No. Flows > 40	% Flows > 40	No. Flows > 20	% Flows > 20	No. Flows > 10	% Flows > 10
Oct	68	59	87%	64	94%	66	97%
Nov	68	56	82%	60	88%	62	91%
Dec	68	54	79%	59	87%	61	90%
Jan	68	53	78%	60	88%	62	91%
Feb	68	49	72%	58	85%	61	90%
		Avg =	**80%**		**89%**		**92%**

Source: Riley, R. T., "Treatment of Non-Irrigation Water at the Canal Street Water Treatment Plant", Master of Science Thesis, Department of Civil Engineering, August 2005, University of Texas at El Paso.

Given that the *quantity* of water available is adequate for winter operation, the next most important consideration is water quality, since that determines the type of treatment system that will be required. The primary parameters of interest for this project were total dissolved solids (TDS), sulfates, and chlorides, since one or more of them is usually what dictates when the Canal Street plants terminate their normal seasonal operations. Figure 2 is a plot of TDS, sulfates and chlorides for flows less than 100 MGD and, as the figure shows, all concentrations increase significantly as the flow decreases to less than 20 MGD.

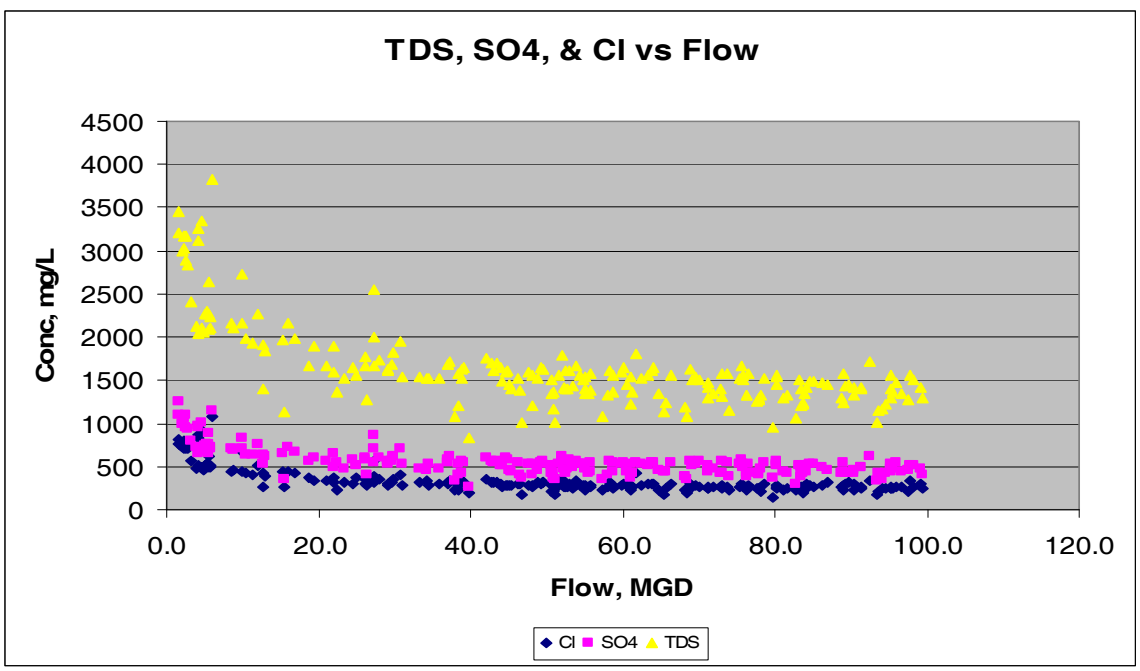

Figure 2. TDS, Sulfate, and Chloride Concentrations for Flows Below 100 MGD

The approximate concentrations associated with each parameter at flows of 10, 20, and 40 MGD are shown in Table 3. These data show the significant deterioration in water quality that occurs at flows below 20 MGD.

Table 3. TDS, Sulfate, and Chloride Concentrations vs. Flow

	10 MGD	20 MGD	40 MGD
Cl	512	335	287
SO4	726	586	453
TDS	2292	1780	1407

Source: Riley, R. T., "Treatment of Non-Irrigation Water at the Canal Street Water Treatment Plant", Master of Science Thesis, Department of Civil Engineering, August 2005, University of Texas at El Paso.

PERFORMANCE OF RO AND NANO MEMBRANES

The RO membrane was a GE - RO desal membrane and the nano membrane was a Filmtec nano NF90-4040 membrane. Table 4 shows some of the chemical parameters for the permeate and concentrate from each membrane. As the data show, both membranes performed very well from the standpoint of salt rejection, with the nano membrane performing as well as the RO membrane. (There is a wide spectrum of the performance in nanofiltration membranes).

Table 4. Permeate & Concentrate Quality from RO and Nano Membranes

Parameter	Tank 2 (Feed)	RO Perm	RO Conc	Nano Perm	NanoConc
Calcium	95.1	<10	364	<10	380
Magnesium	25.8	<0.5	97	<0.5	102
Potassium	12.3	<2	44.1	<2	46.5
Sodium	396	25.9	1480	16.1	1560
Bromide	<0.05	<0.05	<0.50	<0.05	<0.50
Chloride	341	30.7	1250	16.89	1360
Fluoride	0.76	<0.1	2.33	<0.1	2.43
Nitrate-N	2.68	0.97	6.16	0.66	6.94
Nitrite-N	0.25	0.07	0.56	<0.05	0.62
Ortho-P	0.3	<0.05	0.82	<0.05	0.94
Sulfate	427	4.8	1640	1.26	1760
Alkalinity	226.8	11.7	771	<5	880.3
Conductivity	2360	150	7500	79.5	8000
TDS	1450	62	5410	58	5790
pH	8.2	7.1	8.2	6.9	8.2
Silica	20.3	<5.0	77.4	<5.0	83.9

Note: All units mg/L except Cond (µS/cm) and pH

Source: Data from "Membrane Treatment of Impaired Irrigation Return and Other Flows for Creating New Sources of High Quality Water." Copyright 2008. Awwa Research Foundation. ALL RIGHTS RESERVED.

The flux in the RO unit was 12.7 gallons per square foot per day (gfd) at a recovery rate of 73%, with the values in the nano unit at 23.5 gfd and 75%, respectively. The results are for treatment that occurred in the month of February during a period of prolonged, multiple-year, regional drought. The raw water conductivity of 2440 µS/cm is approximately the 93rd percentile of non-irrigation season conductivities, so these results can be considered as nearly worst-case conditions. Even so, the TDS of both permeates is so low that a considerable amount of blending can be done. The silica concentration of 84 mg/L in the nano concentrate is well below the concentration that would be of concern with respect to membrane fouling, even if an antiscalant weren't used. Thus, in general, these results appear to be very favorable from the standpoint of system performance.

FINANCIAL ANALYSIS

Since both the RO and nano systems performed well from the standpoint of salt rejection, an economic analysis was conducted to determine the optimum operating conditions for each system based on the cost of the produced water. Data were collected over a full range of permeate flows and pressures for both systems by changing the variable frequency drive (VFD) settings from 25% to 75% and adjusting the recoveries from 35% to 90%. The data were collected in three different time periods: November, 2006, and January and February of 2007. These data were then used to project the capital and operating costs of a full scale system so that the unit cost of water could be determined for each condition.

The values used in the cost calculations are shown in Table 5. Note that the costs are based on a permeate water volume of 5 MGD and a final product water quality of 750 mg/L TDS. Blending would be approximately 1:1, using pretreated river water, so the total net river water removal volume would be about 10 MGD. Membrane concentrate is assumed to be discharged back into the raw water canal for winter crop irrigation, or for eventual return to the river. Personnel costs for the 5-month operating season are estimated at $100,000. Contingency costs of $100,000 per season are also included in the calculations. The unit costs are plotted as a function of pressure in Figures 3 and 4 for the RO and nanofiltration units, respectively.

Table 5. Values Used in Financial Calculations

Item	Value
Permeate volume, MGD	5
River TDS, mg/L	1400
Final product water TDS	750
Raw water cost, $/acre-ft	$16.00
Pretreatment cost (Canal plant), $/1000 gal	$0.15
Interest rate, %	5%
Equipment life, yrs	20
Recovery of pretreated water,%	96%
RO capital cost, $/ft^2 membrane	$8.64
Power cost, $/kw-hr	$0.07
Pump & Motor efficiency, %	75%
Building Cost, $	$500,000
Building Life, yrs	30
Membrane cost, $/80 sq ft	$300
Membrane life , yrs	3
Antiscalant, $/9 lb gal	$11.00
Antiscalant dosage, mg/L	2.0
Personnel, $/yr	$100,000
Contingencies, $/yr	$100,000

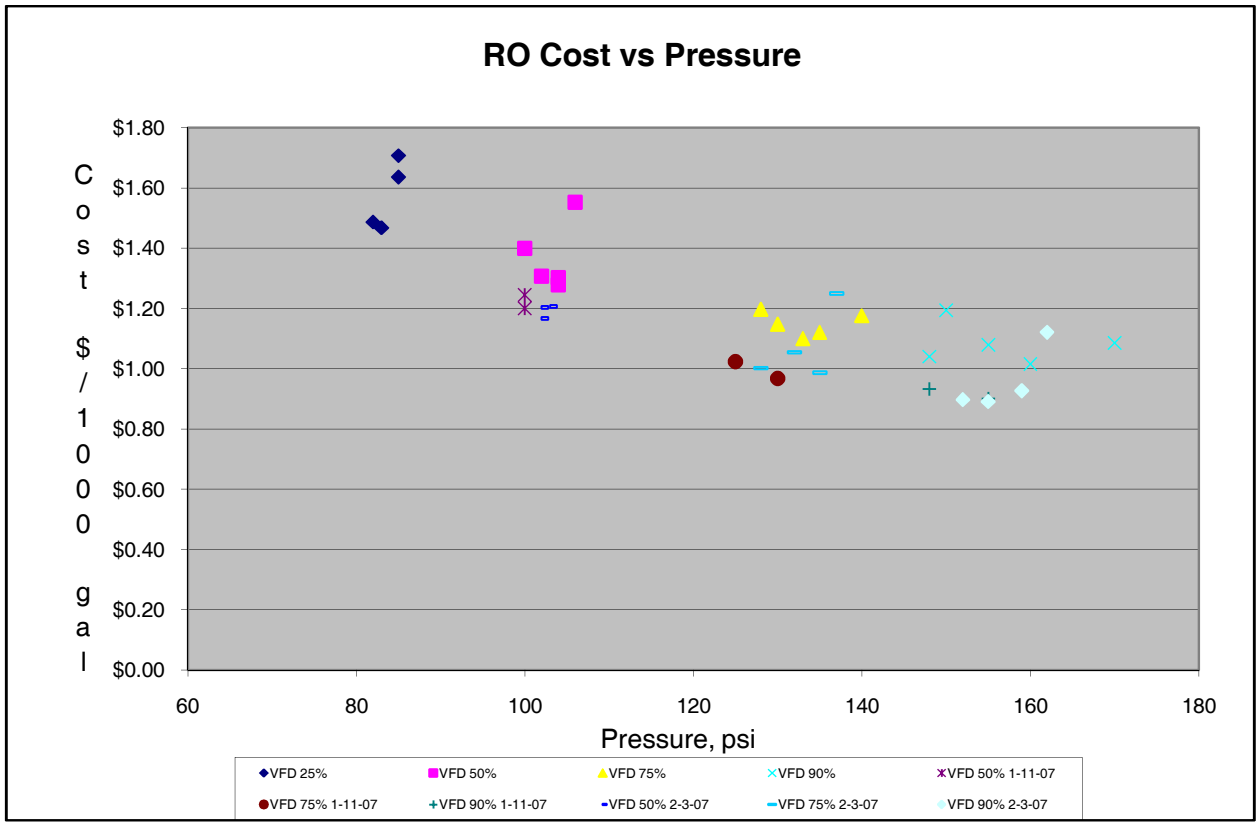

Figure 3. RO Unit Water Costs versus Pressure

Source: Data from "Membrane Treatment of Impaired Irrigation Return and Other Flows for Creating New Sources of High Quality Water." Copyright 2008. Awwa Research Foundation. ALL RIGHTS RESERVED.

The results show that the unit cost of the final product water (i.e. blended water) generally decreases as the pressure and recovery increase in both the RO and nano units. The pressure effect is more pronounced for the RO unit than for the nano. For the RO unit, the lowest costs are generally associated with recoveries around 75% and pressures in area of 150 psi. The lowest costs are in the $0.89 to $0.96 per thousand gallon range for the 2007 data, which were collected under conditions that were more normal than in 2006. The 2006 data gave higher unit costs because the water was a little saltier at that time. Even so, the cost for desalting Rio Grande irrigation return flows in a reverse osmosis system would still be about the same as water produced in the conventional surface water treatment plants during the normal irrigation season (because of the much lower cost of the raw water).

For the nano unit, the costs are lower than for RO over a rather broad pressure range, but the lowest unit costs are generally associated with pressures above 170 psi and recoveries in the 60% to 80% range. Since the fluxes above 200 psi tended to exceed 30 gfd, a pressure of around 170 psi would probably be preferable for the final design. The unit water costs are in the $0.70 - $0.80 range for the 2007 data.

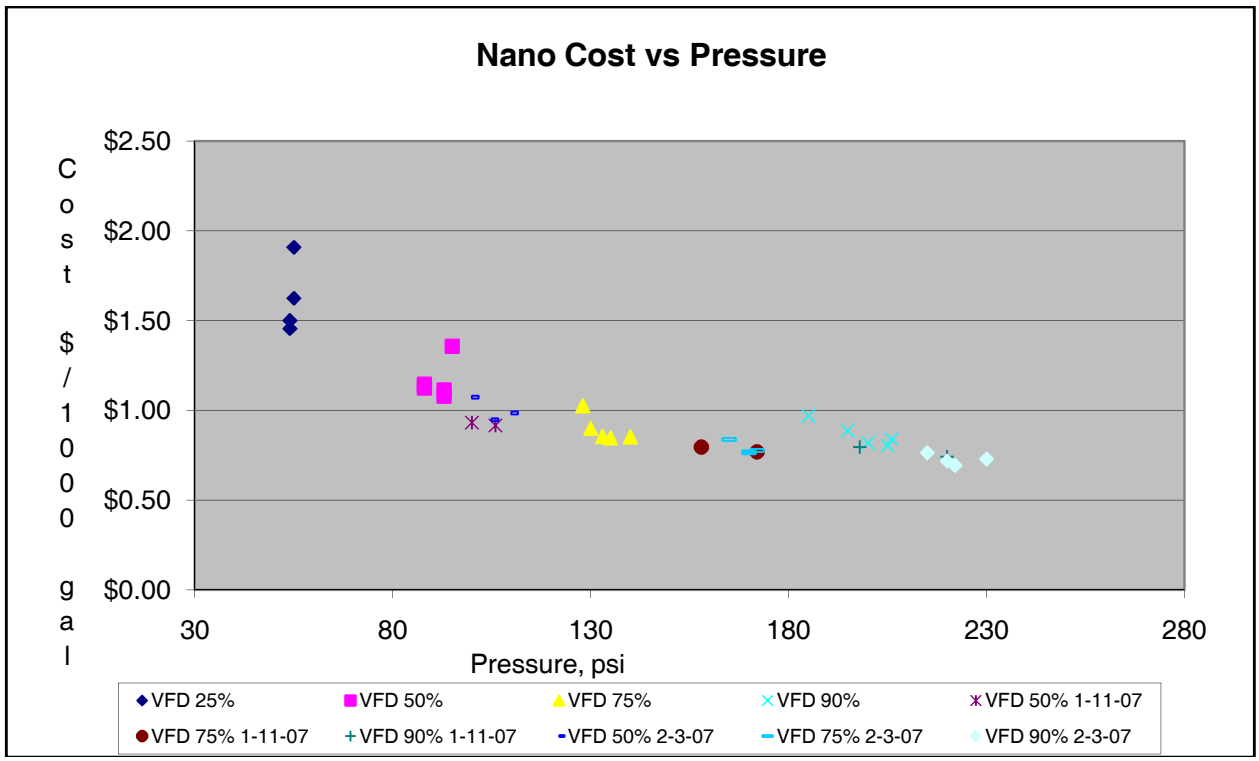

Figure 4. Nano Unit Water Costs versus Pressure

Source: Data from "Membrane Treatment of Impaired Irrigation Return and Other Flows for Creating New Sources of High Quality Water." Copyright 2008. Awwa Research Foundation. ALL RIGHTS RESERVED.

Research nursery testing of the RO and Nano concentrates for irrigation of commercial onions indicates that the concentrate may be successfully blended back with raw winter return flow waters and used for irrigation. Since the concentrate can easily be discharged back into the raw water source canal at this plant location, and thereby blended back with additional raw winter return flow waters for downstream winter irrigation, there should theoretically be no additional cost for concentrate disposal.

CONCLUSIONS

Based on the results of this investigation, the following conclusions can be made with reasonable certainty:

1. From a technical point of view, desalting of Rio Grande irrigation return flows during the non-irrigation season appears to be quite feasible for producing at least 10 MGD of drinking water for EPWU customers.

2. A nanofiltration system using a Filmtec nano NF90-4040 nanofiltration membrane will produce drinking water having a slightly lower cost than a reverse osmosis system. The unit cost of water produced in such a system is projected to be about $0.76 per thousand gallons.

3. Several nanofiltration full-scale system designs would produce water in the $0.76 - $0.79 per thousand gallon range. The one that would seem to produce the least amount of stress in the system would operate at 170 psi with a recovery of about 75% and a flux of 25 gfd.

4. Both of the membranes tested in this study (RO and nano) produced very high quality water (TDS concentrations generally less than 100 mg/L). This will allow for a high blend ratio of 1:1, which results in low-cost product water, rendering the project very attractive from an economic point of view.

5. Winter irrigation of commercial onion crops is possible using RO or Nano concentrate during periods when an adequate supply of raw winter return flows is available for blending prior to application. Careful management would be required for germination and crop establishment.

Acknowledgements

Funding and support for this project was provided by the following organizations: American Water Works Association Research Foundation, U.S. Bureau of Reclamation, El Paso Water Utilities, the U.S. EPA through the Southwest Center for Environmental Research and Policy, Texas A&M AgriLife Research Center at El Paso, U.S.D.A.-CSREES Rio Grande Basin Initiative, and the University of Texas at El Paso.

Reference

Riley, R. T., “Treatment of Non-Irrigation Water at the Canal Street Water Treatment Plant”, Master of Science Thesis, Department of Civil Engineering, August 2005, University of Texas at El Paso.

Synopsis of National Research Council's Report on Desalination

Sandeep Sethi, Ph.D., P.E.
Carollo Engineers, 401 N. Cattlemen Road, Suite 306, Sarasota, FL 34232; PH. 941-371-9832; FAX 941-371-9873; email: ssethi@carollo.com

ABSTRACT

The National Academies' National Research Council (NRC) formed a committee on desalination that was tasked with performing a critical analysis of the desalination technology, barriers to its widespread implementation, and the development of a national strategic research agenda. A synopsis of the final committee report including the major conclusions and recommendations are presented in this paper.

Desalination is an established technology and has advanced significantly over the past five decades, making it a realistic option for increasing water supplies in some parts of the U.S. Desalination, using both brackish and seawater sources is likely to have a niche in the nation's future water management portfolio. However, while the required source water resources and inherent technology capabilities are themselves not constraining, the potential of desalination is somewhat constrained by associated financial, social, and environmental factors. Potential environmental impacts of desalination are characterized with uncertainty, which leads to costly delays in permitting.

The committee concluded that resolving these uncertainties and developing methods to mitigate the impacts is the highest priority for future research. Other priorities include research and development to continue current trends in reducing the process costs of desalination and developing cost-effective, environmentally sustainable approaches for concentrate management. The committee recommended that a coordinated, strategic research effort with steady funding is needed to better understand and minimize desalination's environmental impacts and to find ways to further lower its costs and energy use. Thus, implementing the proposed research agenda will require federal leadership and a coordinated, strategic plan among multiple agencies, with successful implementation depending on participation by federal, state, local agencies, nongovernmental entities, and the private sector.

INTRODUCTION

The National Academies' National Research Council (NRC) formed a Committee on Advancing Desalination Technology in 2006, with the support of the U.S Bureau of Reclamation and the U.S Environmental Protection Agency. The committee was tasked with performing a critical analysis of current desalination technologies and the barriers to widespread implementation, as well as addressing the development of a national strategic research agenda for desalination. The project's findings and analysis were recently published in the report entitled "Desalination: A National Perspective." (NRC, 2008). A synopsis of the report, focusing on the major topics and findings, as well as key aspects of the research agenda, is presented and discussed in this paper. This report builds on a 2004 NRC report (NRC, 2004) that provided a scientific assessment of the Bureau of Reclamation's and Sandia National Laboratories' Desalination and Water

Purification Technology Roadmap, which was intended to serve as a strategic pathway for future desalination and water purification research (USBR and Sandia National Laboratories, 2003).

The author of this paper served as a member of the committee, and the complete list of team and committee members who contributed to the report is acknowledged at the end of this paper.

BACKGROUND

Only 2.5 percent of the water on earth is freshwater and much of even that small percentage is bound up in glaciers and snowpack, leaving only a small fraction available to meet the world's freshwater demands. Climate change, population growth, and local water scarcity are driving factors for desalination of brackish water and seawater. Desalination can provide a safe, reliable, and sustainable water supply to communities. However, while the required source water resources and inherent technology capabilities are themselves not constraining, the potential of desalination is somewhat constrained by associated financial, social, and environmental factors. Potential environmental impacts of desalination are characterized with uncertainty, which leads to costly delays in permitting.

Since the 1960, desalination capacity has seen an exponential increase both globally and nationally. This increase was fueled in part by the growing concern for local water scarcity and was made possible to a great extent by a major federal investment for desalination research and development in the late 1950s to the early 1980s. Desalination technology offers the potential to substantially reduce water scarcity by converting the almost inexhaustible supply of seawater and the apparently vast quantities of brackish groundwater into new sources of freshwater. Although total water use in the United States has remained steady over recent decades, interest in brackish water and seawater desalination will likely continue, particularly in water-scarce regions, in localities experiencing rapid population growth, or where users are able and willing to pay for a high-quality, reliable new supply.

Recent advances in technology, especially improvements in membranes, have made desalination a realistic water supply option. The cost of desalinating seawater in the United States is now competitive with other alternatives in some locations and for some high-valued uses, and there is considerable interest in hastening the time when costs of desalination are routinely competitive with the costs of alternatives. Through this NRC project, priority research areas and goals were identified to help make desalination a competitive option among water supply alternatives.

STATUS-QUO OF INVESTMENT IN DESALINATION R&D

The committee performed a survey of investment in desalination research and development. This included gathering data on federal investments and estimates of state, nongovernmental organizations, and private-sector funding. Based on the survey data and corresponding analysis, the committee reached the following conclusions that emphasize the need for the development of a national strategic research agenda for desalination:

- There is no integrated and strategic direction to the federal desalination research and development efforts.

- Some states, especially California, have also made sizeable recent investments in desalination research and development.

- The private sector appears to fund the majority of desalination research, with total annual spending estimated to be more than twice that of all other surveyed sources of such funding.

STATE-OF-SCIENCE OF DESALINATION TECHNOLOGY

The committee assessed the state-of-science of desalination technology for its five major components including intakes, pretreatment, desalination processes, post-treatment, and concentrate management. Significant improvements have been made in the reduction of energy use for RO with the improvements in membrane technology and commercialization of high-efficiency energy recovery devices. Although RO and thermal desalination technologies are relatively mature, there are opportunities to further reduce energy and costs. For RO, and current energy use is within a factor of 2 of the theoretical thermodynamic minimum value for separating solutes from water; practical constraints are likely to limit the further decrease in energy use to approximately 15 percent. Thus, the committee concluded that opportunities exist to further reduce cost and energy use of current technologies by small but economically significant amounts:

- In RO desalination, the costs and energy requirements of water production can be further reduced by mitigating fouling through pretreatment; developing high-permeability, fouling-resistant, high-rejection, oxidant-resistant membranes; and optimizing membrane module and membrane system design.

- Seawater desalination using thermal processes can be cost effective when waste heat is utilized effectively.

- Few, if any, cost-effective environmentally sustainable concentrate management options exist for inland desalination facilities.

MITIGATION OF POTENTIAL ENVIRONMENTAL IMPACTS

Desalination has been used worldwide for municipal applications for several decades, however, since the potential environmental impacts have not been fully quantified, it is considered a “new” water supply option by many entities. In order to change this, it is essential to systematically assemble knowledge of the potential environmental impacts of desalination processes so that is easily available to water supply planners for consideration of desalination as an alternative water supply. The key environmental considerations can be categorized as:

- Impacts from the acquisition of source water.

- Impacts from the management of concentrate and other waste products (e.g. cleaning chemicals) from the desalination process.

- Impacts of greenhouse gas emissions due to energy intensive nature of desalination processes.

- Considerations with product water quality in terms of specific challenges (e.g. boron rejection).

Ideally, these considerations should be compared against equally rigorous environmental impact analyses of water supply alternatives, so that decisions can be made based on comparisons of the full economic costs and benefits, including environmental and social costs and benefits, among the various water supply alternatives.

The committee concluded that there is a considerable amount of uncertainty about the environmental impacts of desalination and, consequently, concern over its potential effects. However, desalination efforts do not need to be halted until this research is done and uncertainties are removed, but research investments should be made to help reduce potential risks. Therefore, the following research is recommended:

- Site-specific assessments of the impacts of source water withdrawals and concentrate management should be conducted and the results synthesized in a national assessment of potential impacts.

- Monitoring and assessment protocols should be developed for evaluating the potential ecological impacts of surface water concentrate discharge.

- Longer-term, laboratory-based assays on the sublethal effects of concentrate discharge should be conducted to understand the range of environmental impacts from desalination plants.

- Water quality guidance, based on an analysis of the human health effects of boron in drinking water and considering other sources of exposure, is needed to support decisions for desalination process design.

- Further research and applications of technology should be carried out on how to mitigate environmental impacts of desalination and reduce potential risks relative to other water supply alternatives.

COSTS AND BENEFITS OF DESALINATION

In the past, the relatively high financial costs of desalination has limited the application of desalination technologies in most areas. However, the costs and relative economic scenario of desalination application are both changing in a number of important ways, largely due to the following key factors:

- Improved membrane technologies are less expensive.
- The desalination process is becoming more energy efficient.

- Cost of desalination is becoming relatively more competitive due to increasing costs of alternatives for augmenting water supplies.

When two of the noteworthy benefits of desalination, including provision of a drought resistant supply and a means to diversify a community's water supply portfolio are considered in the analysis, the current costs of desalination costs can generally be low enough to make it an attractive option for some communities. However, this is subject to several key factors that can play an important role in determining the costs of desalination. First, like the costs of other water supply alternatives, the costs of desalination are locally variable and are influenced by factors such as site conditions. Secondly, the availability and final selection of the concentrate disposal options can influence the overall costs of desalination in a significant fashion. Thirdly, the increasing awareness of potential environmental impacts is raising the costs of permitting and intake and out fall configurations in the United States. Finally, the future costs of energy are uncertain. Conservation and water transfers will usually be less costly than desalination, and conservation of water often comes with associated benefits, such as reduced energy costs.

The committee made the following key conclusions with respect to the cost and benefits of desalination:

- Substantial reductions in the financial cost of producing desalinated water will require substantial reductions in either energy costs or capital costs.

- For brackish water desalination, the costs of concentrate management can vary enormously from project to project and may rival energy and capital costs as the largest single component of cost.

- Conservation and transfers from low- to high-valued uses will usually be less costly than supply augmentation schemes, including desalination.

- There are small but significant efficiencies that can be made in membrane technologies that will reduce the energy needed to desalinate water and, therefore, offer potentially important process cost reductions.

- To make the true costs of desalination transparent, the economic costs should be accounted for and reported accurately.

STRATEGIC AGENDA FOR FUTURE DESALINATION R&D

Although desalination technology has advanced significantly over the past five decades, concerns remain about its potential environmental impacts and costs. The committee identified two overarching long-term research goals that need to be met for desalination to become a more attractive option for municipal application.

1. Understand the environmental impacts of desalination and develop approaches to minimize these impacts relative to other water supply alternatives, and

2. Develop approaches to lower the financial costs of desalination so that it is an attractive option relative to other alternatives in locations where traditional sources of water are inadequate.

The committee concluded that a coordinated, strategic research effort with steady funding is needed to better understand and minimize desalination's environmental impacts - and to find ways to further lower its costs and energy use. Thus, the committee also developed a strategic research agenda in support of these two overarching goals. Broad based objectives are identified as part of the research agenda that can be funded and conducted in either the public or the private sector. Several recommendations for implementing the proposed research agenda follow:

- A coordinated, strategic plan should be developed to ensure that future federal investments in desalination are integrated and prioritized and address the two major goals identified above.

- Environmental research should be emphasized up front when implementing the research agenda.

- Research funding in support of reducing the costs of desalination should be directed strategically toward research topics that are likely to make improvements against benchmarks set by the best current technologies for desalination.

Besides research, other practical implementation issues also require consideration to address the barriers to increased application of desalination technology. Some issues identified in the report include building trust and educating the public on desalination project planning, anticipating the sometimes cumbersome regulatory and permitting process, and utilizing pilot testing to optimize the process design.

The committee identified priority research areas to help make desalination a competitive option among water supply alternatives for communities facing water shortages. Some of this research may be most appropriately supported by the private sector. The research topics for which the federal government should have an interest - where the benefits are widespread and where no private-sector entities are willing to make the investments and assume the risk - are marked with asterisks.

Priority Research Areas:

GOAL 1. Understand the environmental impacts of desalination and develop approaches to minimize these impacts relative to other water supply alternatives.

1. Assess environmental impacts of desalination intake and concentrate management approaches**
   a. Conduct field studies to assess environmental impacts of seawater intakes**
   b. Conduct field studies to assess environmental impacts of brackish groundwater development**

c. Develop protocols and conduct field studies to assess the impacts of concentrate management approaches in inland and coastal settings**
d. Develop laboratory protocols for long-term toxicity testing of whole effluent to assess long-term impacts of concentrate on aquatic life**
e. Assess the environmental fate and bioaccumulation potential of desalination-related contaminants**

2. Develop improved intake methods at coastal facilities to minimize impingement of larger organisms and entrainment of smaller ones**

3. Assess the quantity and distribution of brackish water resources nationwide**

4. Analyze the human health impacts of boron, considering other sources of boron exposure, to expedite water-quality guidance for desalination process design**

GOAL 2. Develop approaches to lower the financial costs of desalination so that it is an attractive option relative to other alternatives in locations where traditional sources of water are inadequate.

5. Improve pretreatment for membrane desalination
   a. Develop more robust, cost-effective pretreatment processes
   b. Reduce chemical requirements for pretreatment

6. Improve membrane system performance
   a. Develop high-permeability, fouling-resistant, high-rejection, oxidant-resistant membranes
   b. Optimize membrane system design
   c. Develop lower-cost, corrosion-resistant materials of construction
   d. Develop ion-selective processes for brackish water
   e. Develop hybrid desalination processes to increase recovery

7. Improve existing desalination approaches to reduce primary energy use
   a. Develop improved energy recovery technologies and techniques for desalination
   b. Research configurations and applications for desalination to utilize waste heat**
   c. Understand the impact of energy pricing on desalination technology over time**
   d. Investigate approaches for integrating renewable energy with desalination**

8. Develop novel approaches and/or processes to desalinate water in a way that reduces primary energy use**

GOAL 1 and 2 Cross Cuts.

9. Develop cost-effective approaches for concentrate management that minimize potential environmental impacts**

ACKNOWLEDGEMENTS

This paper is based on the report entitled "Desalination: A National Perspective" published by the National Research Council (NRC, 2008), which was developed as part of the NRC committee formed in 2006 on "Advancing Desalination Technology." The author of this paper served as a member of the committee; and the complete list of team and committee members who contributed to the report includes: Amy K. Zander (Chair), Clarkson University; Menachem Elimelech, Yale University; David H. Furukawa, Separation Consultants Inc.; Peter Gleick, Pacific Institute for Studies in Development, Environment, and Security; Kenneth Herd, Southwest Florida Water Management District; Kimberly L. Jones, Howard University; Philip Rolchigo, Pentair, Inc.; Sandeep Sethi, Carollo Engineers; John Tonner, Water Consultants International; Henry J. Vaux, University of California, Berkeley; Judith S. Weis, Rutgers University; Warren W. Wood, Michigan State University; Stephanie E. Johnson (Study Director), Laura J. Ehlers (Interim Study Director (October 2006 to January 2007)), and Michael Stoever (Sr. Project Assistant), National Research Council.

REFERENCES

NRC, 2008. Desalination: A National Perspective. Washington D.C.: National Academy Press.

NRC, 2004. Review of the Desalination and Water Purification Technology Roadmap. National Academies Press, Washington, D.C.

USBR and Sandia National Laboratories, 2003. Desalination and Water Purification Technology Roadmap: A Report of the Executive Committee. Desalination & Water Purification Research & Development Report #95. Denver, CO: United States Department of the Interior, Bureau of Reclamation, Water Treatment and Engineering Group.

Cost Comparison of Membrane Treatment and Concentrate Management Practices at Drinking Water Treatment Plants in Florida

Berrin Tansel[1] and Irina Sosnikhina[2]

[1]Civil and Environmental Engineering Department, Florida International University
10555 West Flagler Street, Engineering Center Miami, FL, 33174;
Ph (305)348 2928; e-mail:tanselb@fiu.edu
[2]Miami-Dade Water and Sewer Department, 3071 SW 38 Avenue Miami, Florida 33146;
Ph (786) 552 8226; e-mail:irinas@miamidade.gov

Abstract

Design improvements, operational simplicity, advancements in new membrane materials, and competition in membrane industry have reduced both capital and operating costs of nano filtration (NF) and reverse osmosis (RO) systems for drinking water treatment applications. In Florida, the use of membrane technologies has increased to about 200 MGD today in comparison to 60 MGD in 1994. Currently, there are 125 membrane treatment systems in Florida with design capacities ranging from 800 gallons per day (gpd) to 25 MGD. A survey of economics of membrane treatment (NF and RO) facilities for drinking water treatment and concentrate management options were conducted for facilities located in Florida. Cost comparisons were based on data from different planning documents and plant surveys (Bergman, 1995; LEC, 2000; and budget data provided by the facilities). Since the capital costs depend on land cost, loan interests, consulting fees, design cost, pilot tests, costs of permits and other site specific factors; for accuracy of comparison, only the construction costs were considered for capital costs.

Introduction

Once considered as an expensive technology to be economically attractive in comparison to conventional water treatment processes; membrane technology has become a widely used water treatment process option. In the US, the installed desalination capacity using membrane technologies has increased to over 3.8 million cubic meters (one billion gallons) per day, accounting for about 91 percent of desalination capacity (RosTek Associates, Inc., 2003). Only in Florida, the use of membrane technologies has increased to about 200 MGD today in comparison to 60 MGD in 1994. Currently, there are 125 membrane treatment systems in Florida with design capacities ranging from 800 gallons per day (gpd) to 25 MGD. A survey of economics of membrane treatment (NF and RO) facilities for drinking water treatment and concentrate management options were conducted for facilities located in Florida.

Construction Costs

The construction cost data for membrane treatment facilities were obtained from planning documents and plant surveys (Bergman, 2005; LEC 2000, facility budget data). These costs include all facilities including installed membrane process equipment, buildings, degasifiers, clearwells, and transfer pumps (if applicable), ground storage and high-service pumping, bulk chemical storage, emergency power, yard piping, and site development. Supply wells and raw water piping are not included. However, where applicable, concentrate treatment and disposal facilities are included. Table 1 lists the plants and their capacities that are included in this study. Figure 1 presents the construction costs for membrane treatment plants in Florida. As shown in Figure 2, the constructions costs in terms of product water quantity vary from about $3/gpd for 1 MGD facilities to $1.2 to $1.8/gpd for 20 MGD plants.

Table 1. Construction costs of some of membrane treatment (NF, RO) plants in Florida.

Plant name	Capacity (MGD)	Construction cost (million $)(a)
Plantation	12.0	16.23
Ft. Myers (Bergman,1995)	12.0	18.89 (b)
Collier Co.(Bergman,1995)	12.0	22.34
Indian River Co. (Bergman, 1995)	6.0	15.16 (b)
Dunedin (Bergman, 1995)	4.8	13.97 (b)
Boynton Beach (Bergman, 1995)	4.0	16.23
Village Palm Beach (Bergman, 1995)	1.5	5.05 (b)
St. Lucie West Dev.(Bergman, 1995)	1.0	9.31 (b)
Hollywood	14.0	23.14 (b)
Miramar	4.5	16.36
North Miami Beach	15.0	29.9 (d)
South Miami Heights	25.0	39.0 (d)

(a) Does not include raw water supply.
(b) Does not include concentrate disposal well costs.
(c) Actual budgeted O&M costs, the other data are estimates are based on 1994 costs.
(d) In construction

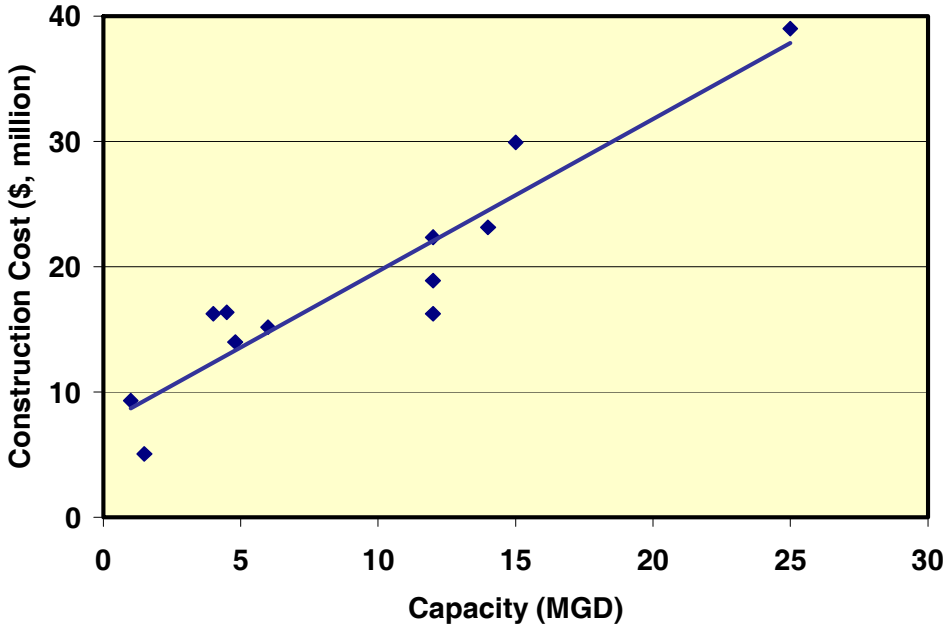

Figure 1. Construction costs of membrane treatment plants in Florida.

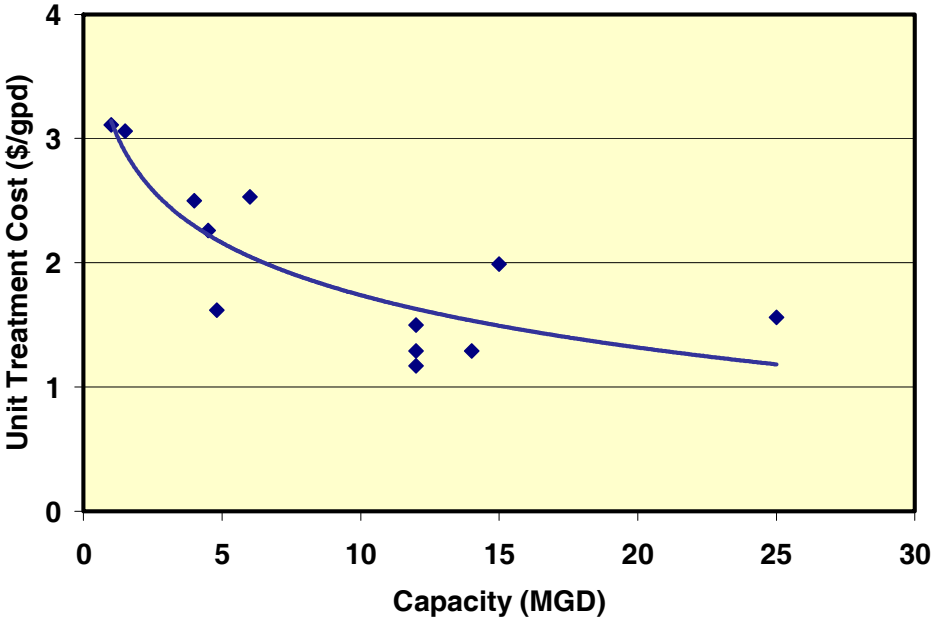

Figure 2. Constructions costs expressed as unit product water treatment cost of membrane treatment plants in Florida.

O&M Costs

Membrane replacement has become a less significant cost concern in the recent years as the average membrane life has increased from about 5 years to 10 or more years. When estimating the construction, operating and maintenance (O&M), and unit costs for treated water, membrane bypass/blending and plant operating factor must be considered. In O&M cost calculations, costs are usually lowered in proportion to the amount of water that is bypassed around the membrane system. The water flow rate that is bypassed the membranes and blended with permeate to produce the overall finished water is controlled by the membrane feed and permeate water qualities and the product water goals. At most plant, all of the water must be treated by the membranes (i.e. no bypass/blend is acceptable). However, in seawater or high brackish water supply systems this may be an option. For low brackish or softening applications, there is also an option that involve treating the raw water to a high level of purity, enabling blending of permeate with raw water to reduce the quantity of water that must be treated by the membrane system. Blending the filtered water with raw water is an effective way to provide alkalinity and pH control, thus reducing the amount of post-treatment chemicals. This scenario is projected for North Miami Beach membrane treatment plant which is in construction. There are advantages and disadvantages to each approach and a cost analysis should be performed to weigh the cost impacts. The amount of chemicals required can vary site-specifically. Typically a high level RO treatment process will require higher pre-treatment chemical dosages as a result of rejecting more ions and producing a more scale-forming concentrate.

O&M costs include labor salaries, fringe benefits, chemicals, power, membrane replacements, repair and maintenance. The ratio of actual production to plant capacity is called the plant utilization factor. Because all the plants have different utilization factor, a utilization factor of 0.9 was used for calculation of O&M costs per 1,000 gallons of permeate.

The average breakdown of O&M costs is as follows:

Labor costs (salaries and fringe benefits)	30%
Power	30%
Chemicals	15%
Membrane replacement	10%
Other (filter replacement, repairs and maintenance)	15%

About 5% up to 10% of the time operational time is generally adequate for membrane cleaning and other facility maintenance requiring full or partial plant shutdown. As shown in the Figure 3, the average annual O&M costs vary from $2.7 per 1,000 gallons for 1 MGD plant to about $0.5 to $0.7 per 1,000 gallons for 20 MGD facilities.

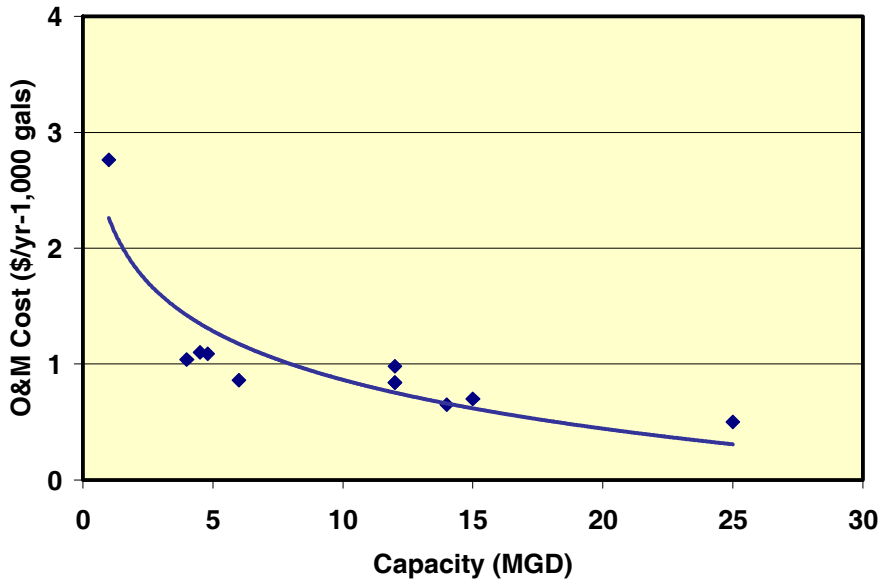

Figure 3. Annual O&M costs of membrane treatment plants in Florida.

Concentrate Management Options

Membrane filtration systems may generate different types of waste streams such as the effluent from backwash and chemical cleaning as well as the concentrate stream. The term "concentrate" is usually associated with the continuous waste stream of concentrated dissolved solids produced by NF and RO processes. Concentrate is typically 4 to 10 times more concentrated than the feed with respect to suspended and dissolved constituents and represents about 15 to 25 percent of the total feed flow. As a result, concentrate management is a significant operational and regulatory concern for utilities and is often a critical factor in the planning and design of NF or RO facilities. There are a variety of chemicals that may be used for membrane cleaning to minimize rate of fouling as shown Table 2. Chemical cleaning residuals are generally treated on-site and discharged to either a suitable surface water body or sanitary sewer, subject to state and/or local regulations. Some pretreatment may be necessary (i.e., quenching for for oxidants such as chlorine, and neutralization for acids and bases). The rinse water used the cleaning process also represents a chemical waste and must be treated prior to discharge.

Typical concentrate management options include:

- Surface water discharge
- Sanitary sewer discharge
- Land application / irrigation
- Deep well injection
- Evaporation

Because there are site specific factors associated with each of these options, no single option is ideal for every application. In the U.S., about 55% of the facilities use surface discharge, 25% discharge to sanitary sewer, 18% deep well injection, and 1% other methods for concentrate management (Mickley, 2001). Zero liquid discharge which involves sufficiently concentrating the residual stream through the use of such technologies as crystallizers and evaporators to allow remaining solids to be landfilled. In many cases surface water discharge is the least expensive option, although the permitting process may be difficult, since there are potential environmental impacts if the salinity of the concentrate is significantly higher than that of the receiving body. Discharge to the sanitary sewer may have similar issues, since the wastewater treatment process does not typically affect dissolved solids concentrations, and the treatment plant effluent may ultimately be discharged to surface water receiving body.

Table 2. Chemical used to reduce membrane fouling.

Chemical type	Chemical	Control Target
Acid	Citric acid Hydrochloric acid Sulfuric acid	Inorganic scale
Base	Caustic	Organics
Disinfectant	Sodium hypochlorite Chlorine gas Hydrogen peroxide	Biofilm
Surfactant	Various	Organics Inorganics Inert

Table 3 presents examples of the concentrate disposal practices for the water treatment plants in Florida. Only the State of Florida practices deep well injection for concentrate disposal (RosTek Associates, Inc., 2003). Deep disposal wells are defined as wells that inject fluids beneath the lowest geologic formation. The wells must be at least 0.4 kilometer (km) (0.25 mile) from an underground drinking water source. Many States do not permit deep well injection at all. Feasibility of deep well injection is highly dependent on regional geology. Evaporation ponds are extremely land intensive and are, therefore, only applicable in areas with low land value. Ponds are most appropriate for smaller desalination facilities located in arid climates such as the Southwestern U.S.

Table 3. Examples of concentrate disposal methods at some of Florida's membrane treatment facilities.

Plant	Concentrate management practice
Miramar	injection wells
Plantation Central	injection wells
Plantation East	injection wells
Jupiter	injection wells
North Miami Beach (projected)	injection wells
Cape Coral	to WWTP
Dunedin	to WWTP
Hollywood	to WWTP
South Miami Heights (projected)	to WWTP
Marco Island	ocean discharge
Sanibel	ocean discharge
Tampa Bay	ocean discharge
Melbourne	lagoon
North Collier County	lagoon
Melbourne	lagoon
North Collier County	lagoon

References

Bergman, R.A., 1995, Membrane Softening versus Lime Softening in Florida: A Cost Comparison Update, Desalination, 102 (1): 11-24.

LEC 2000, Lower East Coast Regional Water Supply Plan, May 2000.

Mickley, M., 2001, "Membrane Concentrate Disposal: Practices and Regulations," U.S. Bureau of Reclamation Desalination and Purification Research Development Program, Report No. 69, Denver, Colorado, USA.

RosTek Associates, Inc., 2003, Desalting Handbook for Planners, Desalination Research and Development Program Report No. 72.

U.S. EPA, 2003, United State Environmental Protection Agency, membrane Filtration Guidance Manual. EPA 815-D-03-008.

Desalination Concentrate: Bay vs. Ocean

Patrick Treanor[1], P.E. and Val S. Frenkel[2], Ph.D., P.E.

[1] Kennedy/Jenks Consultants, 303 Second St., Suite 300 S, San Francisco, CA 94107; PH(415) 243-2435; FAX (415) 896-0999; email: PatrickTreanor@KennedyJenks.com
[2] Kennedy/Jenks Consultants, 303 Second St., Suite 300 S, San Francisco, CA 94107; PH (415) 243-2435; FAX (415) 896-0999; email: ValFrenkel@KennedyJenks.com

ABSTRACT

Sea and ocean Reverse Osmosis (RO) desalination plants are often designed to remove more than 90% of dissolved ingredients (organic and inorganic) from feed water, thus creating a permeate water that is potable. Typically 40-60% of the feed water is recovered as permeate water. The water not recovered as permeate becomes concentrated into a stream of RO concentrate (brine) because the salts rejected by RO remain in the unrecovered water. The RO concentrate is usually about 1.67 to 2.5 times the salt concentration of the source water, but can be as high as four times.

RO concentrate discharged into a source water body is a major environmental consideration during the planning and design of bay or ocean desalination plants. Co-location of desalination plants with wastewater treatment plants or power plants allows using a shared outfall to dilute the high salt concentration of RO concentrate. Diluting the RO concentrate in a shared effluent outfall mitigates the issue of high salinity around the outfall.

This paper compares side by side two main classes of water bodies that receive concentrated brine discharge from Reverse Osmosis (RO) Desalination Plants: oceans (or open seas) and estuarine bays (under the influence of fresh water). These two classes of water bodies have inherent properties which drive not only the operation of RO plants, but also the physical and chemical reactions of outfall discharge. Major differences between oceans and estuarine bays are evident when comparing salinity levels, variability of salinity, and variability of the overall water quality. Furthermore, there are differences in terms of flora and fauna. Using a nuanced approach of comparing and contrasting oceans and estuarine bays as receiving waters for desalination plant concentrate, this paper brings to light the natural processes occurring offshore of potential desalination plant sites, and distinguishes what natural processes may be affected by brine entering the ecosystem.

Indeed the receiving waters for different regional RO desalination plants will be unique in many ways. The prevailing currents, type of aquatic habitat, water quality, and seasonal weather patterns must be evaluated for each individual site in order to accurately model the effects that RO plant outfall plumes will have on the environment. Yet, understanding the differences between ocean outfalls and estuarine bay outfalls brings to light many factors that should be addressed in planning and design.

INTRODUCTION

The major commercial seawater desalination technologies are: Thermal Desalination, and Membrane Desalination. Membrane desalination will be the focus of this paper because this technology has gained more attention and popularity lately due to lower costs, lower energy demand and flexibility of operation. All desalination processes separate the feed water into two major streams:

- product water (i.e. permeate), and
- concentrate (i.e. brine).

One of the reasons Desalination Plants are becoming more attractive is that, in certain geographical locations, human, industrial and agricultural consumptive use of fresh water is growing past the point where natural surface water flows necessary for a healthy environment can concurrently be maintained. The dramatic drop in salmon populations along the North Pacific coast of the U.S. exemplifies how fresh water ecosystems are impacted when natural flows are pumped and diverted. Desalination of the vast water resources in ocean and brackish waters can directly address the growing water imbalance between fresh water ecosystems and human consumptive use. By moving from strictly fresh water sources to a combination of water sources, which includes brackish and salt water sources, some of the burden that now falls heavily on fresh water ecosystems can be shared by oceans and bays.

In shifting some of the demand for potable water from fresh water sources to salt water sources it must be clear that increasing the number of desalination plants in the U.S. does not necessarily result in environmental or other consequences. To understand potential environmental impacts of desalination plant concentrate on the receiving waters of oceans and bays several key factors need to be discussed:

- Desalination Plant – Seawater Reverse Osmosis (SWRO) Operation (Bays vs. Oceans)
- Salinity and Water Quality Variations (Bays vs. Oceans)
- Desalination Plant (SWRO) Power Requirements (Bays vs. Oceans)
- Temperature (Bays vs. Oceans)
- The Salt Wedge (Estuarine Bays)
- Discharge Plume Dispersion/Mixing (Bays vs. Oceans)
- Ecology (Bays vs. Oceans)
- Co-Location and Shared Outfalls (Bays vs. Oceans)

Estuarine Bays in Brief

In general, estuarine bays on the Pacific Ocean under the influence of fresh water have lower salinity levels ranging from 0.5-32 psu (500-32,000 mg/l), because of the influence of fresh water from rivers, run-off, and municipal and industrial discharges. Due to seasonal variations in flows from rivers, estuarine bays have seasonal fluctuations in water quality and salinity. Tidal activities can contribute to

daily fluctuations of water quality, and tidal influences are major drivers of mixing in bays. The introduction of autochthonous (organic detritus) material from a river into a bay brings nutrients into the bay water. The most nutrient rich part of estuarine bays is in the zone where salty ocean water mixes with fresh water, causing nutrients that were suspended to drop out due to the difference in density between salt and fresh water. The high nutrients in estuarine bays and the shallower waters make estuarine bays "nurseries" for many aquatic species.

Oceans in Brief

In general, the Pacific Ocean has salinity averaging 35 psu (35,000 mg/l) which is higher than the salinity of bays. The water quality and salinity of ocean water fluctuate fractionally compared to that of estuarine bay water. In other words, ocean water quality and salinity is relatively unchanging on a daily basis and does not change drastically over the year. Currents and upwelling in the ocean dominate mixing. Nutrients in the ocean are much less concentrated and thus productivity (per unit area) in oceans is less than in bays. Although ocean species are much more diverse than in estuaries, the species are also generally more spread out and less concentrated compared to estuarine bays.

DISCUSSION

Desalination Plant (SWRO) Operation (Bays vs. Ocean)

Osmosis is the natural phenomenon that occurs when two solutions with different concentrations exist side by side, separated by a semi-permeable barrier (membrane). The solution of lesser concentration will flow through the membrane into the solution of greater concentration until equilibrium is reached. Osmotic pressure is the static pressure when the system is balanced and no flow occurs. The pressure required to desalinate water through a reverse osmosis desalination membrane is equal to the osmotic pressure plus hydraulic head loss across the membranes. The pressure required to desalinate salt water is exponentially proportional to the salinity due to the increase of the concentration gradient between two solutions. The pumping pressure required to desalinate estuarine bay water can often be around 300 psi or higher depending on the water salinity, system recovery, and temperature while the pressure required to desalinate ocean water reaches 900 psi and greater depending on the same major parameters. The exact pressure required, however, is a function of the salinity, the percentage of permeate water that is produced from the feed (system recovery), water temperature, type of membranes, system configuration, and other factors.

Bay and ocean SWRO desalination plants are often designed to remove more than 90% of dissolved ingredients (organic and inorganic) from feed water, thus creating a permeate water that is potable. Typically 40-60% of the feed water is recovered as permeate water by SWRO desalination plants. The water that is not recovered as permeate becomes concentrated into a stream of SWRO concentrate (brine), because the salts rejected by SWRO remain in the unrecovered water.

The percent of water that is recovered is an operational consideration which can affect the concentration of brine discharge. At 40% recovery the concentration of the brine is about 1.7 times that of the source water. At 60% recovery the concentration of the brine is about 2.5 times that of the source water. For salinity less than about 7 psu (7,000 mg/l) the recovery can be increased to the high end of 75%. ***Operating at 75% recovery results in a concentrated brine with close to 4 times the salinity of the source water.*** In order to optimize the efficiency of a particular plant, adjustments must be made to the percentage of recovery in a RO desalination facility. For instance, increasing the percentage of recovery results in lower costs for intake pumping power and pretreatment, but increases the cost for pumping at higher pressure through the RO membranes, and also increases maintenance intervals on RO membranes. Higher recovery would be feasible at facilities with higher intake pumping costs as it would reduce volume of the pumped water and cost accordingly. At higher recovery the product quality suffers because more leakage through the membranes is achieved. The inverse of this is true for plants operating at a lower percentage of recovery.

Ocean SWRO plants usually run at a lower percentage of recovery than do estuarine bay SWRO plants due to higher salinity levels in ocean water. Ocean and sea water around the globe ranges from as low as TDS 18 psu (18,000 mg/l) in the Baltic Sea up to 50 psu (50,000 mg/l) in the Red Sea and higher in the Middle East regions. While these mentioned ocean and sea salinities are varied between geographic regions they remain relatively consistent locally. In the Pacific Ocean along the California coast, water salinity ranges from 32 psu (32,000 mg/l) up to 37 psu (37,000 mg/l). This high salinity (32 and 37 psu) requires pressure for SWRO treatment in the range of 900 psi up to 1,200 psi, depending on the major design and operational factors described above. Maintaining lower energy requirements is the driving force for optimizing the percentage of recovery for ocean RO desalination.

Flows coming from rivers into bays fluctuate seasonally and even daily. This directly affects the salinity of the water because the mixture of fresh water and salt water varies with river flows. Snow melts, rainy seasons and droughts all influence the amount of fresh water flowing into an estuarine bay.

The lower salinities of water in estuarine bays directly correlates to lower power costs required for the operation of SWRO desalination equipment compared to ocean water desalination. This translates into an overall lower demand for power, reducing the associated effects of power generation on the environment. The reduced energy requirements for the SWRO treatment of estuarine bay water allows a higher percentage of recovery. Therefore, for higher recovery discharges in estuarine bays, there is a resulting greater difference in the salinity of the concentrated brine discharge relative to the source.

Salinity and Water Quality Variations (Bays vs. Oceans)

While salinity in the Pacific Ocean is relatively consistent, averaging 35 psu (35,000 mg/l), estuarine bays vary widely depending on the geography. San Francisco Bay can range from 5 psu – 30 psu (5,000 mg/l – 30,000 mg/l) because fresh water influences can be high during the wet weather season. San Diego Bay, on the other hand, does not have a wide salinity range because there is less influence of fresh water than in the San Francisco Bay.

Turbidity fluctuations are more drastic in bays than oceans because of the shallower water and silty benthos. Oceans do see fluctuations in turbidity; however, this occurs nearer to shore and depends on how shallow the water is and on proximity to rivers and creeks. Site specific pollutant point sources can be of equal concern for both oceans and bays. Algal blooms (red tides) are also of concern for SWRO desalination and can occur in both ocean waters and bay waters, while historically red tides are more intensive in ocean waters.

For example, Figure 1 shows data from the San Francisco Bay which illustrates the seasonal variations of salinity (measured as conductivity), as well as turbidity and TOC that can occur in estuarine bays. Turbidity was higher in December through April, when storms and winds were prevalent, making the shallow waters turn up the settled benthos material into a suspended state. The increase in turbidity during these months increases the stress placed on the SWRO pretreatment equipment.

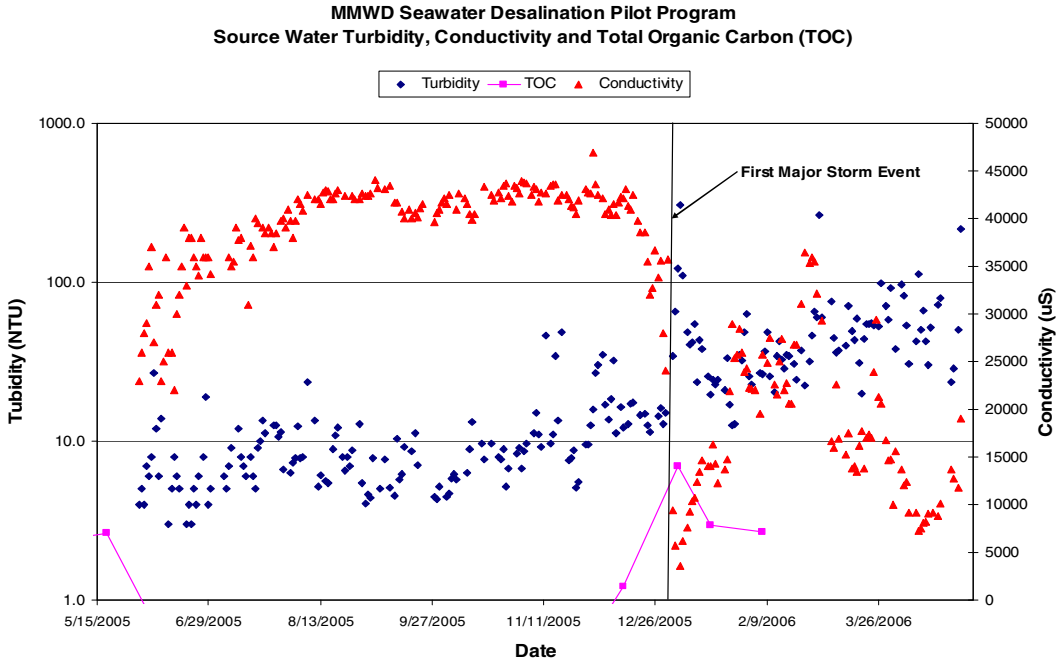

Figure 1. Source Water Conductivity (Salinity) and Turbidity in San Francisco Bay. (Frenkel et al, 2007)

Desalination Plant (SWRO) Power Requirements (Bays vs. Oceans)

Although this discussion is primarily about concentrate discharge, it is important to recognize that the power requirements for SWRO equipment can contribute to the overall environmental impacts of a desalination facility. Simply stated, the lower salinity of estuarine bays can result in much lower power requirements for SWRO treatment than for ocean SWRO.

Temperature (Bays vs. Ocean)

The temperature of water being treated by SWRO membranes affects the pressure required for desalting. Lower temperature water requires higher pressure for SWRO and more energy as a result. Source water temperatures can vary seasonally with shallower estuarine waters showing greater fluctuations in seasonal temperatures than oceans. In addition to fluctuations in source water temperature, an outfall plume can have a temperature that is slightly higher than the ambient temperature, because of heat transferred to the water during pumping. Generally, the heat transferred from pumping equipment into the process water is about 1° to 2° Celsius for desalination plants.

The Salt Wedge (Estuarine Bays)

At the interface between a fresh water river and a bay there is an area called the salt wedge. The salt wedge occurs as a result of the difference in density between salt water and fresh water. Salt water is denser than fresh water and, therefore, can form a salt water wedge underneath the advancing fresh water flow at the interface between fresh water and salt water. Flocculation of nutrients transported within the river system occurs at this interface. Autochthonous material, silts, dissolved organic matter and organic compounds such as phosphates can flocculate and fall out of suspension in the salt wedge. The nutrients that fall to the bay floor provide food for young larvae, such as crabs and oysters that are carried upstream by the salt water counter flow.

The density-salinity variation in the salt wedge illustrates how concentrated brine interacts with receiving waters as it is discharged. The denser concentrated brine discharge will tend to stay lower in the water column and thus can slow vertical mixing. It is not a surprise, then, that mixing and plume dispersion will be primarily driven horizontally by currents and tidal action.

Discharge Plume Dispersion/Mixing (Bays vs. Oceans)

Plume dispersion and mixing are driven primarily by changing tides and by prevailing currents. In general, bays are influenced more significantly by bi-modal tidal mixing currents than are ocean locations. Ocean outfall locations are more subject to prevailing currents that are caused by weather patterns over the ocean.

Currents are not the only factor that affects brine plume dispersion. As discussed previously, there is a bigger difference in salinity between brine and receiving water in estuarine bays because these plants can run at a higher recovery. The more pronounced difference in salinity reduces mixing because of the salinity-density effect. The density difference inhibits vertical mixing. Mixing can also be inhibited in bays because they are often shallower than offshore ocean outfall locations.

Because bay SWRO plants are usually designed with higher recovery than ocean SWRO plants, the difference in the feed water and concentrate is higher for bay SWRO plants than for ocean SWRO plants. At lower source water salinity levels, the recovery can be run at 75% to increase efficiency. ***At 75% recovery the brine concentration will be almost 4 times that of the source water. This drives the requirements to design much more intensive and sophisticated brine mixing for bay projects than for ocean projects.***

Ecology (Bays vs. Ocean)

The ecology of bays differs greatly from the ecology of oceans. Benthic species live in the sediment of bay floors and are the basis of the food chain in estuarine bays. The nutrient rich benthos of estuarine bays is what makes them such thriving environments. Interestingly, while the amount of biological production is high in estuarine bays, the species diversity is low when compared to that of the ocean. The species that do exist in estuarine bays are either salt water (marine) species or euryhaline species, such as salmon or eels, which can live in fresh water and salt water environments. Marine species that migrate to estuaries can tolerate lower salinities, but have been shown to sometimes prefer salinities that are closer to ocean levels. A study conducted by the Marin Municipal Water District and Weston Solutions, Inc (Bodensteiner et al, 2008) tested the impacts of desalination brine mixed with treated wastewater effluent and found that "the sublethal effects observed on kelp spore growth and bivalve embryo development were substantially less significant among organisms exposed to High Brine blend than those observed with Average Brine blend exposures."

Co-Location and Shared Outfalls (Bays vs. Oceans)

Power plants and wastewater plants are both attractive options when it comes to co-locating potential RO desalination plant sites. Co-locating RO desalination facilities with power or wastewater treatment plants allows for outfall blending which can reduce the concentration of the brine discharge to levels that are more similar to the receiving water. For instance, if the % recovery of a RO facility is 50% and the brine is mixed 50/50 with outfall water from a power plant or wastewater plant, the result is a salt concentration that is similar to that of the receiving water.

Power plants are located on many ocean shores and can prove to be beneficial because the proximity of a power plant to a RO desalination plant with high electricity demands can reduce the actual power generation requirements as

transmission inefficiencies are reduced. Furthermore, desalinating the power plant cooling water (which carries higher temperatures and needs less energy for the RO process) can be beneficial. On the other hand, higher temperature water can have higher biological productivity and therefore a greater potential for RO membrane bio-fouling.

Wastewater treatment plant outfalls can also be used for blending brine discharge. However, in certain cases there can be precipitation of solids in the outfall pipe when wastewater is mixed with concentrated brine. This can be mitigated by periodic cleaning of the outfall pipe.

SUMMARY

Table 1 summarizes the factors that are useful for consideration in assessing possible environmental impacts for new desalination plants for either estuarine bays or the open ocean. At this time the environmental impacts of desalination to marine life can be mitigated through proper diffusion design and mixing analysis. The environmental impact of energy generation remains a concern for the future of desalination. However, with a coordinated effort to reduce power usage by residential, commercial and industrial buildings and processes, the power required for desalination can be completely offset.

Table 1. Outfall Considerations: Estuarine Bays vs. Oceans

Outfall Considerations	In Estuarine Bays	In Oceans
% Recovery	• Recovery generally higher than in oceans • Seasonal changes in salinity require adjustments be made to maintain optimization	• Recovery generally lower than in bays • Operating parameters are relatively constant
Salinity	• For bays on Pacific Ocean waters, salinity has very wide variations ranging from 5 psu to 32 psu (5,000 mg/l up to 32,000 mg/l)	• Salinity is relatively stable from 32 psu to 37 psu (32,000 mg/l – 37,000 mg/l) with insignificant variation affecting control operation of the SWRO
Water Quality	• Turbidity can be quite high during wet and windy weather due to shallow water and silty benthos	• Water quality is relatively stable with some wet weather related increases in turbidity due to runoff • Depends on proximity to the shore and depths of the water

Outfall Considerations	In Estuarine Bays	In Oceans
Power Requirements	• In general, lower salinities equate to lower power costs for desalination	• In general, higher salinities equate to higher power costs for desalination
Salt Wedge	• Nutrient rich flocculation area at the salt wedge	• Very little salt wedge; driven by thermocline
Temperature	• Seasonal temperature changes are site specific and variations can be relatively high	• Seasonal temperature changes are site specific and variations are relatively low
Mixing	• Stronger bimodal currents created by tidal influences • Mixing reduced by shallower water depth • Bigger difference in salinity between brine and receiving water reduces mixing because of salinity-density effect	• Some weaker bimodal currents • Generally deeper water • Smaller difference in salinity between brine and receiving water
Ecology	• Benthic micro-algae dominate	• Planktonic processes dominate
Production	• High organic production	• Lower organic production than in estuaries
Types of Species	• Low species diversity • Mostly marine and euryhaline species (i.e. not freshwater species)	• High diversity among marine species
Co-location Options	• Generally more wastewater plants, some power plants	• Generally a wide range of choices of wastewater and power plants
Co-location and Shared Outfalls (*Wastewater Treatment Plants vs. Power Plants*)	***Wastewater Treatment Plants*:** • Blending SWRO brine in a shared outfall with wastewater treatment effluent mitigates high brine concentration • Precipitation of solids in wastewater may occur in outfall	***Power Plants:*** • Benefit of blending brine in shared outfall. • Added benefit to power transmission efficiency • Can reduce energy costs by desalinating higher temperature cooling water • Less precipitates in outfall

REFERENCES

Frenkel, V., Reynolds, T., Lozier, J., Castle B., Macpherson, L., 2007. *Results of Seawater Desalination in the San Francisco Bay*. 2007 World Congress on Desalination and Water Reuse International Desalination Association, October 21-26, 2007, Maspalomas, Gran Canaria, Spain.

Scott Bodensteiner, Matt Zinkl, Jenner McCloskey, Susanne Brander, Larry Grabow, Paul Sellier (2008), "Effects of Desalination Brine Waste Blended with Treated Wastewater in the Aquatic Environment of San Francisco Bay", Water Practice Vol. 2 No. 3, Water Environment Federation.

Future Water Supply Desalination Technology: Forward Osmosis Co-Located With Power Generation

Tina Coop[1] and Dr. Les Lampe, P.E.[2]

[1]The University of Kansas, School of Chemical Engineering, Chemical and Petroleum Engineering, Room 4132, Learned Hall, 1530 W. 15th Street, Lawrence, KS 66045; PH (913) 269-2690; email: Tina.Coop@gmail.com

[2]Black & Veatch Corporation, 8400 Ward Parkway, Kansas City, MO 64114; PH (913) 458-3363; FAX (913) 458-3518; email: LampeLK@bv.com

ABSTRACT

Desalination - processes that remove excess salt and other minerals from water - is a critical technology in today's age of shrinking freshwater supplies. Currently Reverse Osmosis (RO) and thermal technologies, such as Multi-Effect Distillation (MED) and Multi-Stage Flash (MSF), dominate the desalination market. However, rising energy costs and government regulations on carbon emissions are likely to change the future of desalinating water.

Seeking to identify and validate market attractiveness of emerging technologies to power and treat non-freshwater sources, the authors evaluated whether the cutting-edge membrane technology known as Forward Osmosis (FO) was a viable desalination method. Forward Osmosis (FO) uses highly concentrated carbon dioxide (CO_2) and ammonia (NH_3) to separate the freshwater from the brine. A thermal process is used to remove the CO_2 and NH_3 from the freshwater; the CO_2 and NH_3 are then recycled to be used again.

The study concluded that even with its increased efficiency, FO alone will not resolve all of the world's desalination challenges. The study concluded that with its increased efficiency, FO can be successful under the proper circumstances.

FORWARD OSMOSIS: THE TECHNOLOGY OF THE FUTURE

Forward Osmosis is a cutting-edge membrane technology using age-old principles to solve a modern day problem. Unlike Reverse Osmosis (RO), which uses high pressure pumping, Forward Osmosis (FO) uses natural osmotic pressure to separate seawater into freshwater and brine. It does so by using a draw solution of highly concentrated carbon dioxide (CO_2) and ammonia (NH_3) to pull freshwater across a membrane. See Figure 1 for schematic representation. The residual of the FO process is the salt, which dilutes the draw solution.

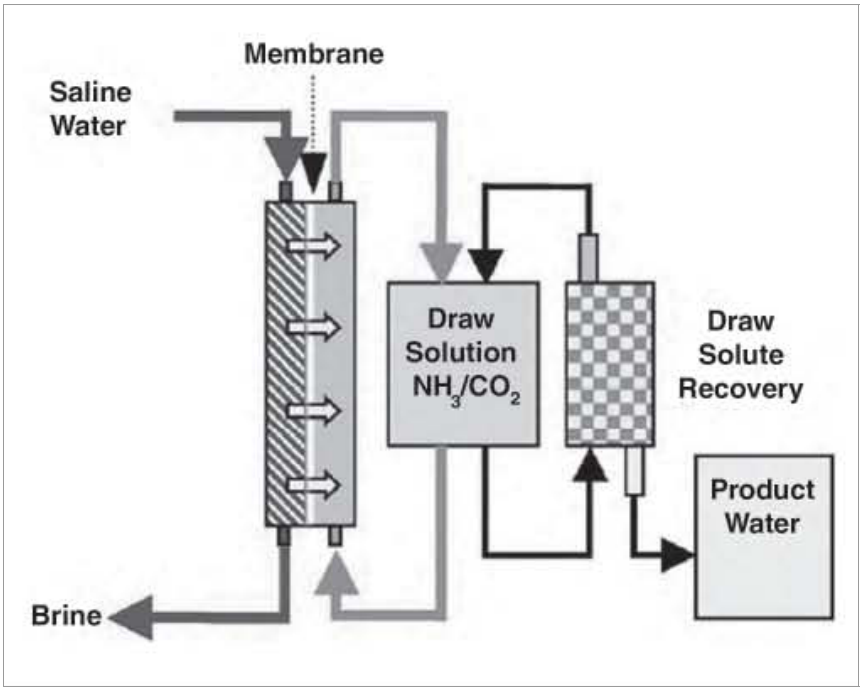

Figure 1. Schematic of Forward Osmosis Desalination Process

Once freshwater has been pulled across the membrane, a thermal process is used to remove the CO_2 and NH_3 from the freshwater. The CO_2 and NH_3 are then recycled to be used in the draw solution once again. The energy required for the chemical removal process is much less than would be used for a complete thermal desalination processes such as Multi-Effect Distillation (MED) and Multi-Stage Flash (MSF). As indicated in Figure 2, a comparison of desalination technologies based on equivalent work shows that FO requires significantly less (one-sixth) energy use. (McGinnis, 2007).

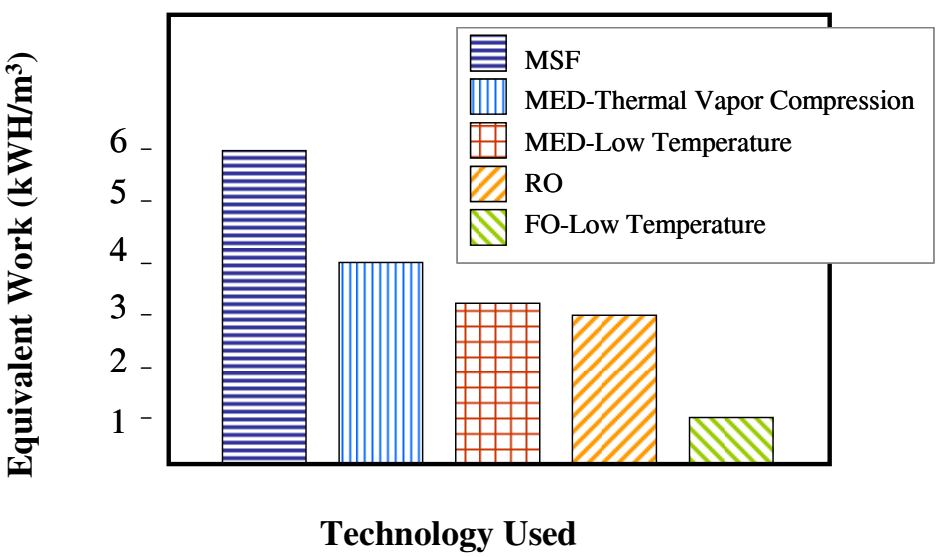

Figure 2. Power Consumption of Desalination Technologies

FO exhibits many sustainability principles not present in any other current desalination technology. First, the energy savings translates into environmental and economic benefits. Another benefit is FO's ability to recover more fresh water (up to 85 percent) than RO, which typically runs at 50 to 80 percent. Over the years, RO membranes have improved greatly, but they now are reaching their theoretical limit of efficiency. Once this occurs the next logical solution may be the FO technology.

CO-LOCATION OF DESALINATION AND POWER GENERATION FACILITIES

Even with its increased efficiency, FO alone is not the solution to all of the world's desalination challenges. Utilizing alternative sources of power can help make the desalination processes more environmentally and economically friendly. For example, currently steam emitted following the end of the power generation process is wasted. By using that steam from the power plant in the desalination facility, it would thereby use less electrical power than is currently being pulled off the grid. In addition, use of currently existing – or shared – ocean intakes and outfalls in the form of simplifying permitting and construction, helps make a case for coupling the desalination and power facilities.

Currently existing desalination processes could benefit from utilizing waste heat from power generation. For RO, heat will increase the efficiency of the process, and for thermal processes this waste heat can be used for a portion of the heating needed. For FO, however, these benefits are much greater, as removing the chemicals from the draw solution requires heat of about 60 degrees Celsius, whereas the waste steam from a low pressure turbine is usually 48 to 60 degrees Celsius. Professor Menachem Elimelech and Robert McGinnis demonstrated (see Figure 3) this theory in their study of energy requirements of ammonia-carbon dioxide forward osmosis (Elimelech, 2007).

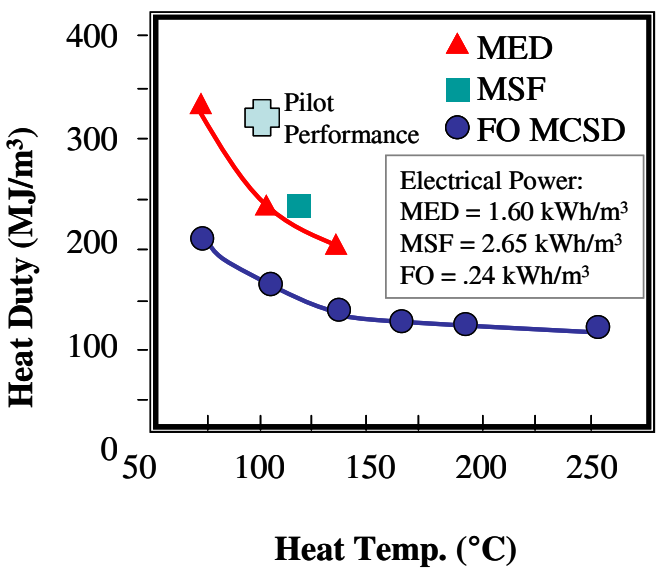

Figure 3. Heat Duty versus Temperature of Heat

Most desalination plants today use electricity derived from fossil fuels. In addition to being costly, this is also less environmentally friendly than a renewable resource. One option that has been tried largely in Kazakhstan, India and Japan is the integration of a nuclear power generator with a desalination plant (WNA, 2008). The general schematic of how it would be configured is shown in Figure 4.

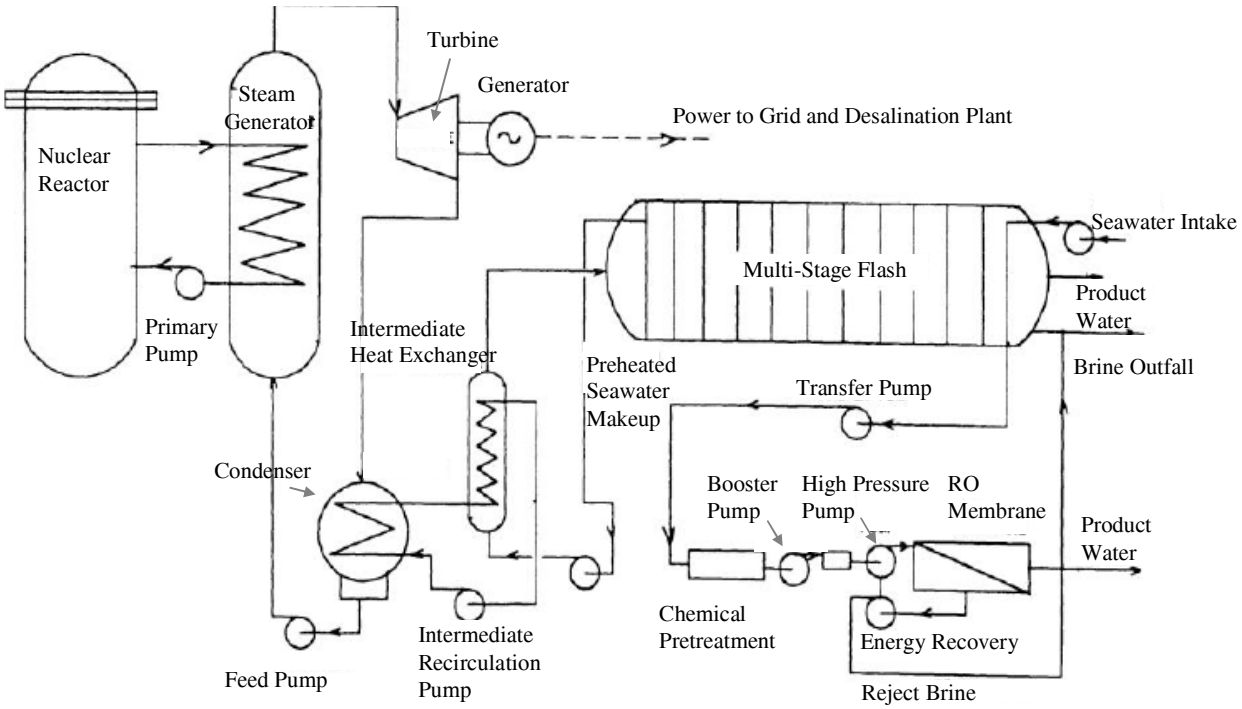

Figure 4. Schematic diagram of nuclear reactor coupled with an MSF-RO plant.

Powering desalination through nuclear power would provide freshwater in a way that emits less carbon dioxide compared to relying on power generated with fossil fuels. Nuclear power is economically compatible with current desalination techniques. For example, Figure 5 (NEI) provides an economic comparison of costs per kilowatt-hour for electricity generated by various methods. Also, Figure 6 (Churchman, 2005) illustrates the comparison of carbon dioxide emissions for a variety of power options.

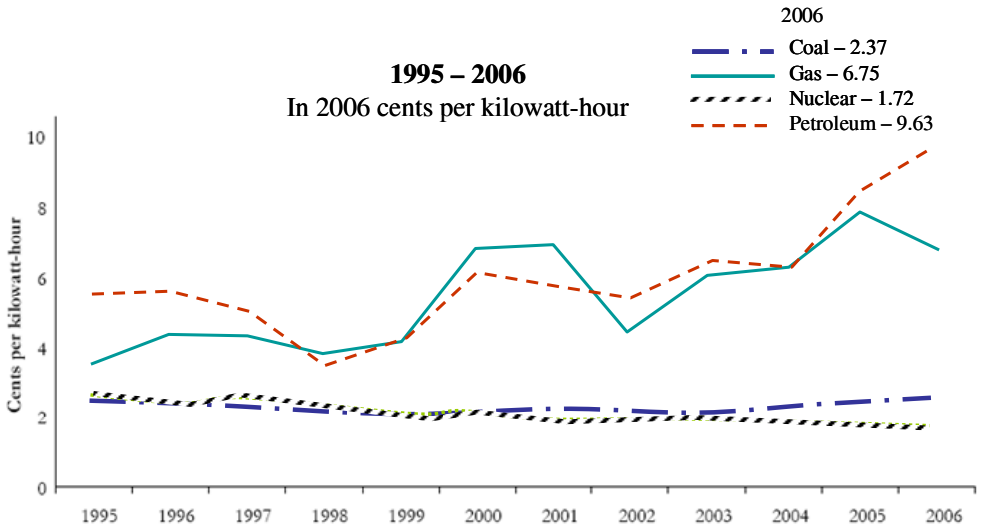

Figure 5. Economic Cost (in 2006 dollars) Comparison of Power Options

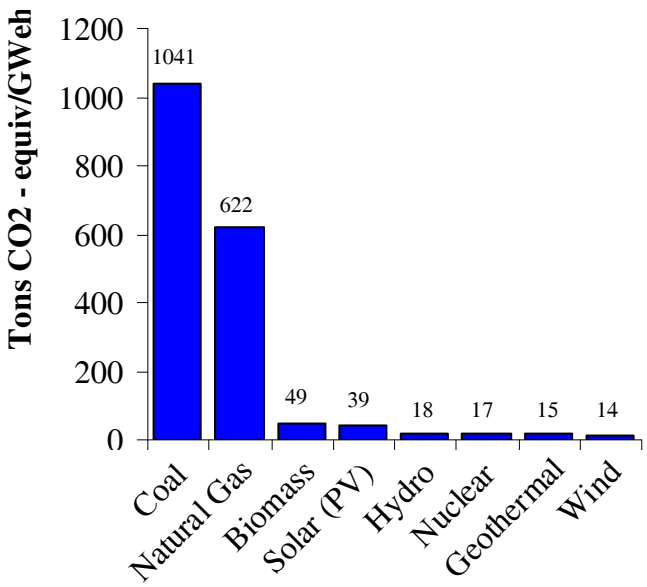

Figure 6. Comparison of Carbon Dioxide Emissions

CONCLUSIONS

Forward Osmosis, because it operates at low or no hydraulic pressure, is very simple to use and requires less energy to operate. FO also has the benefit of needing lower temperature water (60 degrees C), which can be readily supplied through the recycling of power plants' waste steam. This synergy between power plants and desalination is a natural coupling and does not depend on whether this energy source is a fossil fuel or renewable resource such as nuclear. Large-scale deployment of nuclear desalination on a commercial basis would depend primarily on economic factors. The authors believe that neither FO nor a reemergence of reliance on nuclear power alone will be sufficient to solve the emerging problem of drinking water scarcity. They conclude, however, that future testing for FO is warranted to determine its long term viability as an energy efficient desalination solution.

REFERENCES

Churchman, D. (2005) "The Myths and Truths of Nuclear Energy," Internal Presentation to Black & Veatch Nuclear Division, November 2005.

Elimelech, M. (2007) "Yale constructs forward osmosis desalination pilot plant." *Membrane Technology*, January 2007, 6-7.

McGinnis, R.L., and Elimelech, M. (2007) "Energy requirements of ammonia-carbon dioxide forward osmosis desalination," *Desalination* 207, (2007), 370-382.

Nuclear Energy Institute, (Date unknown) "U.S. Electricity Production Costs, 1995-2006, In 2006 cents per kilowatt-hour."

World Nuclear Association, (2008) "Desalination," http://www.world-nuclear.org/info/inf71.html, November 2008, Retrieved on 26 January 2009.

New Strategies for Managing Desalination Concentrate with Zero Liquid Discharge from Two WRF Research Projects

Rick Bond and Srinivas Veerapaneni
Black & Veatch

ABSTRACT

The need for affordable inland desalination in the U.S. is urgent. Many utilities are struggling to meet growing water demands and manage increasing salinity levels in their fresh water sources. The greatest challenge faced by utilities wishing to desalinate inland water sources is concentrate management. Discharge of concentrate to surface waters or deep well injection raise environmental concerns and these alternatives are increasingly difficult to permit. Discharge to a wastewater treatment plant simply recycles salinity or passes it on to a downstream user. The alternative is zero liquid discharge (ZLD) treatment. In ZLD, concentrate is treated so that the water is recovered for beneficial use and there is no discharge of liquid waste from treatment.

Desalination with zero liquid discharge is the subject of two recent AwwaRF research projects. The technical approach in both projects involves treating RO concentrate to reduce its membrane fouling potential prior to a second desalination step. The report for the first project, *Zero Liquid Discharge for Inland Desalination,* was published in 2007. The research involved computer modeling, bench-scale testing and pilot-scale testing. The research results were used to estimate cost and energy requirements for the proposed approach and compare them to those for the established ZLD approach using thermal desalination and evaporation ponds. It was estimated that treatment costs and energy consumption could be reduced by 50 to 70 percent with the proposed treatment approach.

The second project, *Zero Liquid Discharge Desalination for Waters with High Organic Content*, is underway. The focus of this research is the unique challenge posed by water sources that have high concentrations of natural organic matter (NOM) in addition to salinity. NOM inhibits chemical precipitation by the same mechanism as the antiscalants that are added in RO pretreatment for this purpose. Inhibition of chemical precipitation by NOM may have a significant impact on the processes selected for removal of calcium and barium during concentrate treatment. NOM also causes organic fouling of RO membranes, and interactions between NOM and calcium have been shown to increase the potential and severity of organic fouling. Consequently, concentrate treatment in this project will address NOM removal to prevent organic membrane fouling as well as calcium, barium, and silica removal to prevent inorganic membrane fouling.

INTRODUCTION

Increasing population, changing weather patterns, and pollution of renewable water resources have exerted unprecedented demands on water supplies around the world. In 2008, the two largest manmade reservoirs in the US, Lakes Powell and Mead on the Colorado River, were at their lowest levels ever. In Florida, Lake Okeechobee was

at its lowest recorded level, and significant portions of the state were classified as priority water resource caution areas, defined as areas where existing and reasonably expected sources of water and water conservation are not expected to be adequate to meet future needs.

Whether caused by natural or human induced climate change, or some combination of these factors, the current drought has illuminated an urgent need for development of drought proof water supplies. There is consensus in the water industry that increased use of desalination will be needed to meet the world's need for drinking water. The greatest challenge for implementing inland desalination is concentrate management. The options for handling concentrate are as follows:

- Direct discharge.
- Deep well injection.
- Discharge to POTW.
- Zero liquid discharge.

The need to protect receiving streams and groundwater sources from increased salinity may preclude concentrate disposal by the first three methods. The alternative is zero liquid discharge (ZLD). In ZLD, concentrate is treated to produce desalinated water and essentially dry salts. Hence, there is no discharge of liquid waste from the process.

Most ZLD applications in operation today treat industrial waste streams using thermal desalination, evaporation ponds, or both. Thermal desalination is a mature technology that has been practiced for over 30 years, particularly in the Middle East, but it is energy-intensive and expensive. Evaporation ponds require large land areas, even in arid climates, and they are expensive to construct due to the lining and laek protection systems typically required.

New ZLD approaches are being investigated that involve treatment of RO concentrate to reduce its precipitation potential followed by a second application of RO to recover more water and reduce concentrate volume. Secondary desalination can reduce the volume of concentrate sent to evaporation ponds or thermal desalination by two to five times, significantly reducing cost and energy requirements for ZLD.

This ZLD approach is the subject of two recent AwwaRF research projects. The first, *Zero Liquid Discharge for Inland Desalination*, focused on treatment of concentrate in which the precipitation of inorganic salts was the primary concern. This report was published in 2007. The second project, *Zero Liquid Discharge of Waters with High Organic Content*, is ongoing, and its focus is examination of this ZLD approach for brackish waters with high concentrations of natural organic matter (NOM).

PROCESS DESCRIPTION

A general version of this ZLD approach is illustrated by the process schematic in Figure 1. The schematic shows a primary RO system followed by an intermediate concentrate treatment step, secondary RO system, brine concentrator, and evaporation pond. The key step is treatment of primary RO concentrate to reduce its membrane fouling potential in preparation for desalination in the secondary RO system.

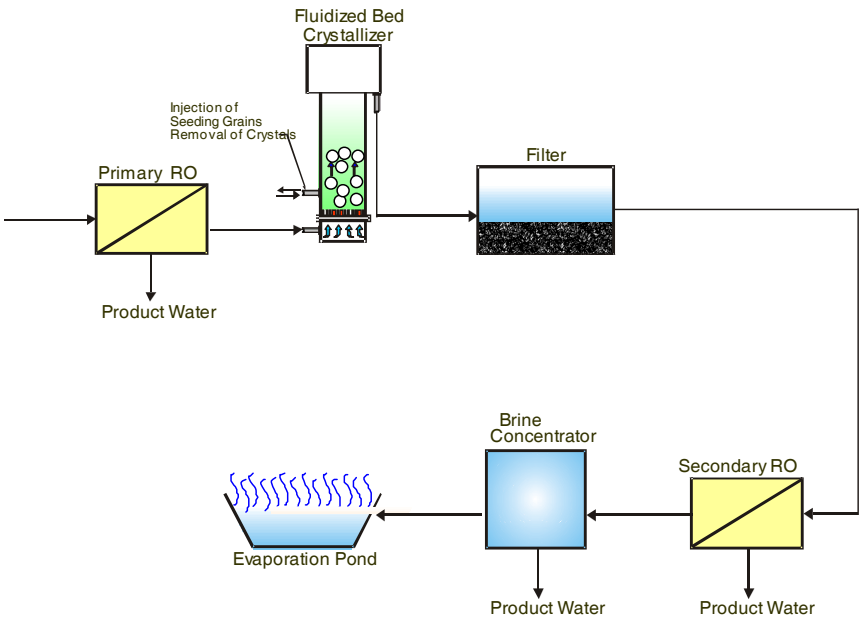

Figure 1 – ZLD Process Schematic

After recovery of as much of the concentrate as possible in the secondary RO, a small percentage of the feed water is discharged as concentrate from the secondary RO to the brine concentrator, a thermal desalination process. Brine concentrators typically recover about 95 percent of RO concentrate from brackish water desalination as a distillate with very low TDS. The remaining volume of concentrate not recovered by the brine concentrator is discharged to an evaporation pond. Consequently, no liquid waste is discharged from the site.

INORGANIC FOULING

RO membranes are designed to reject a high percentage of dissolved salts while allowing water to pass through the membrane. Water that passes through the membrane is recovered as product water, and the ratio of product water flow to feed flow is defined as RO recovery. As RO recovery is pushed to its sustainable limit, water on the feed side of the membrane becomes increasingly concentrated and supersaturated with respect to sparingly soluble salts such as calcium carbonate ($CaCO_3$), calcium sulfate ($CaSO_4$), and barium sulfate ($BaSO_4$). If the feed solution becomes sufficiently supersaturated, these salts precipitate and deposit on the membrane surface. Deposition of inorganic precipitates on the membrane surface, reduces the permeability of the membrane, and

consequently, recovery in RO systems is limited by the precipitation potential of sparingly soluble salts.

RESULTS FROM "ZERO LIQUID DISCHARGE FOR INLAND DESALINATION"

Bench-scale and pilot-scale tests were conducted to evaluate treatment of concentrate to reduce the inorganic membrane fouling potential of RO concentrate. Tests were conducted with five source waters in the Southwestern United States. The test waters included three groundwaters, one surface water, and one reclaimed water.

An understanding of how, when, and why precipitation occurs was essential to this ZLD approach. Precipitation of salts from solution occurs in the following sequential steps, however, in a supersaturated solution containing crystalline solids of the precipitate, precipitation can occur directly by crystal growth:

1. Solution supersaturation
2. Nucleation
3. Crystal growth

RO systems are operated to avoid precipitation of sparingly soluble salts that would foul the membranes, and chemicals designed to inhibit precipitation, commonly referred to as antiscalants, are applied to the feed stream of the RO system. Antiscalants act to retard crystal growth, an integral step in the precipitation. Conversely, a goal of concentrate treatment is to precipitate the salts antiscalants are designed to keep in solution.

The key to this ZLD approach was discovery of a concentrate treatment process that maximizes efficiency of the precipitation process, is not adversely affected by the antiscalant used in RO pretreatment, minimizes the volume of solids generated, and generates solids that are managed easily.

The potential for precipitation exists when a solution is supersaturated, but precipitation is influenced by kinetics, hydrodynamics, and the presence of impurities. Hence, two waters with the same supersaturation ratio can exhibit different propensities for scaling. The time required for precipitation to begin is referred to as induction time, which is defined as the period from start of supersaturation until the appearance of a new crystalline phase. As crystals form and grow, they precipitate from solution, and dissolved concentrations of the constituent ions of the precipitate decrease. Induction time is inversely related to rate of nucleation, and the nucleation rate is dependent on a number of factors including supersaturation, temperature, water chemistry, and the presence of foreign particles.

Foreign particles can reduce induction time by making precipitation more energetically favorable. Induction time decreases as the fit between the foreign particle and the crystal to be formed increases. The best fit between the two solid phases occurs when the particle is a seed crystal of the same salt. A fluidized bed crystallizer was tested in this research to take advantage of the effect of crystals to enhance the rate of precipitation. The fluidized bed crystallizer contains a bed of calcium carbonate pellets, and calcium and carbonate are removed from solution by crystal growth of the pellets.

A preliminary process analysis was conducted to evaluate the salts with the greatest precipitation potential. This analysis indicated that for each water source secondary RO recovery would be limited by the scaling potential of silica (SiO_2), calcium sulfate ($CaSO_4$), and barium sulfate ($BaSO_4$), and in each case, two or all three of these salts would limit recovery. Consequently, calcium, barium, and silica were identified as the treatment targets for the concentrate treatment step.

Figure 2 shows an example of bench-scale test results that were conducted to evaluate presence of calcium carbonate pellets on precipitation of calcium, barium, and silica. Two sets of jars were dosed with sodium hydroxide. One set of jars contained calcium carbonate pellets to simulate fluidized bed crystallization and the other did not to simulate chemical precipitation. Calcium and barium remaining are plotted against pH. The results show that comparable removals of calcium and barium occurred at lower pH in the presence of calcium carbonate crystals. This means calcium and barium can be removed with smaller doses of caustic or lime to increase pH and lower doses of post-treatment acid to bring pH back down.

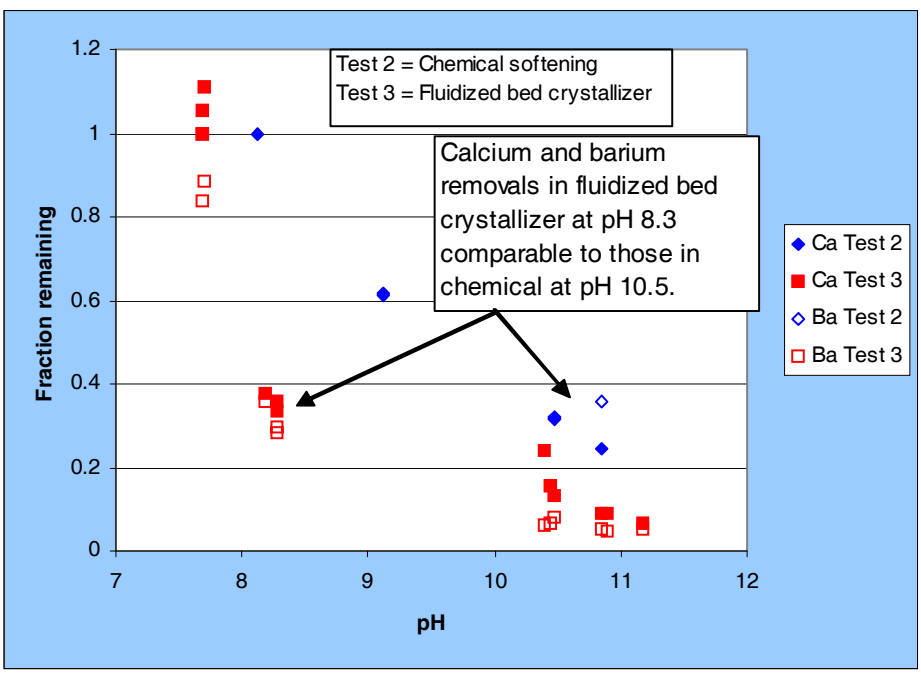

Figure 2 – Removal of calcium and barium by fluidized bed crystallization and chemical precipitation

As illustrated by Figure 3, it was found that barium removal was proportional to calcium removal. This likely occurs due to substitution of barium ions for calcium ions in the calcium carbonate lattice structure. This result was consistent in all tests of fluidized bed crystallization and chemical precipitation. This result indicates that one process, fluidized bed crystallization or chemical precipitation, can be used to remove calcium and barium.

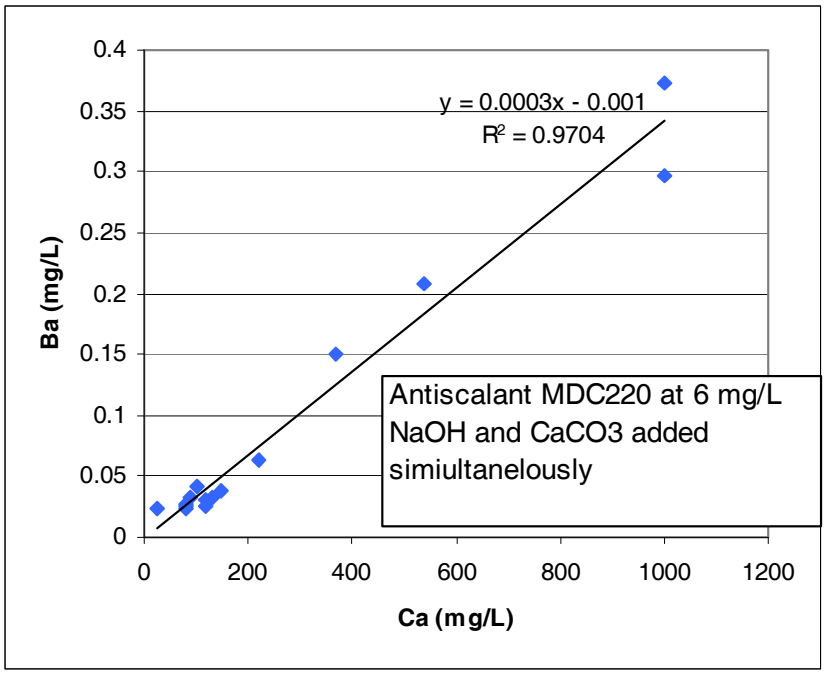

Figure 3 – Correlation between calcium and barium removal in jar tests of fluidized bed crystallization

Silica, however, was not effectively removed below pH 10 as illustrated by Figure 4. Silica concentrations remained relatively unchanged until pH exceeded 10 for fluidized bed crystallization and chemical precipitation tests of all water sources. Calcium carbonate precipitates are not a particularly good adsorbent media for silica but magnesium hydroxide is. Magnesium hydroxide precipitation is pH dependent and typically occurs above pH 10.

Figure 5 shows the silica and magnesium concentrations remaining from one of the fluidized bed crystallization tests. Silica concentration decreased in proportion to the decrease in magnesium concentration, indicating silica removal occurred by sorption to magnesium hydroxide precipitates. Alum and sodium aluminate were tested for silica removal in the fluidized bed crystallization tests, and the aluminum salts were effective for removing silica at pH 8 and higher.

Treatment costs and energy requirements for the ZLD process were compared to traditional ZLD treatment with thermal desalination followed by an evaporation pond. Treatment costs were projected to be reduced by 50 to 70 percent less and energy requirements by 60 to 70 percent compared to the traditional ZLD approach.

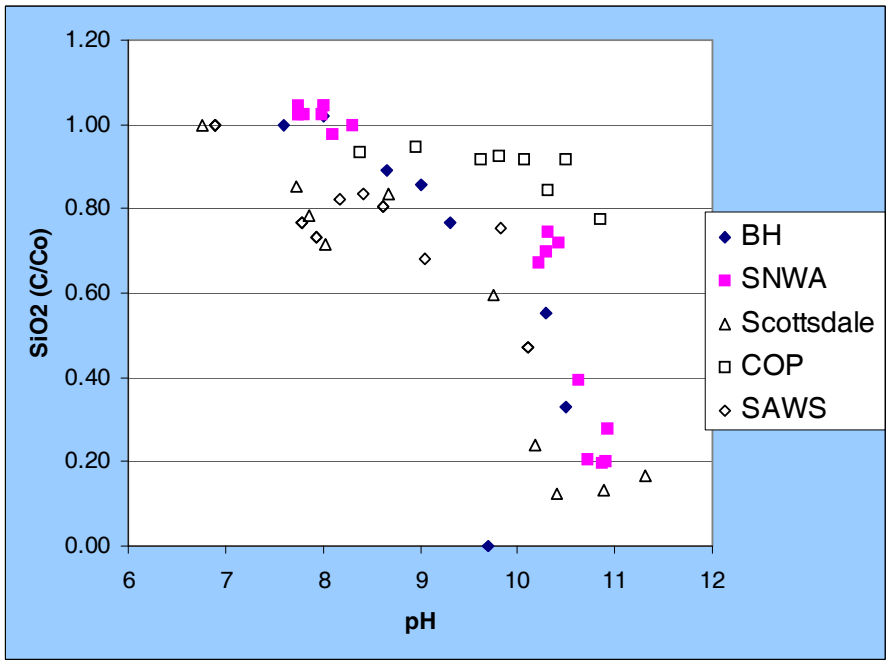

Figure 4 – Silica removal in fluidized bed crystallization tests was not effective below pH 10

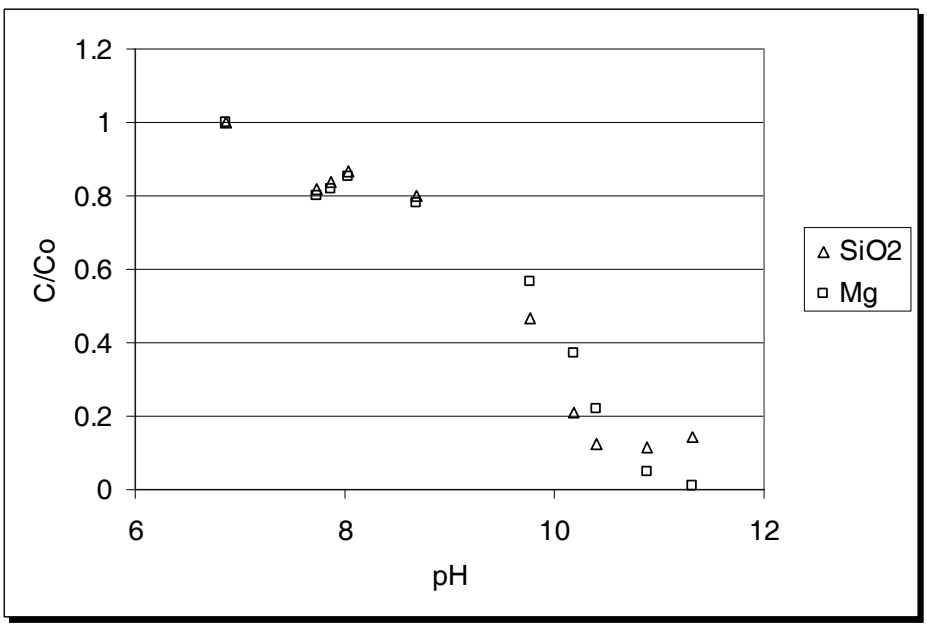

Figure 5 – Silica and magnesium fractions remaining in fluidized bed crystallization test

ORGANIC FOULING

NOM can have a detrimental effect on the ZLD process during: 1) membrane desalination using RO or nanofiltration (NF) membranes, and 2) treatment of concentrate to allow further recovery with membrane desalination. The major fraction of NOM in natural waters is composed of humic substances that are negatively charged in the pH range of natural aquatic systems (Aiken *et al.* 1985). Consequently, NOM molecules readily react with divalent metal cations such as calcium and magnesium (Stumm and Morgan 1996). These reactions produce negative effects on the precipitation processes (chemical precipitation with lime, NaOH, alum, or sodium aluminate and fluidized bed crystallization. Low concentrations of NOM are known to inhibit the kinetics of precipitation and the morphology of crystals formed in precipitation (Stumm and Morgan 1996, Boerlage *et al*. 2000). Conventional theory is that NOM molecules are adsorbed to the surface of precipitate nuclei and block the integration of lattice ions. Adsorption of NOM disrupts crystal growth and changes the shape of the highly ordered crystal lattice structure.

NOM is also the cause of an important type of membrane fouling referred to as organic fouling. Organic fouling of membranes is influenced by the characteristics of the NOM and membrane, the chemical composition of the feed water, and hydrodynamic conditions in the membrane system (Hong and Elimelech 1997). The potential for and severity of organic fouling increases significantly in the presence of calcium (Li and Elimelech 2004), which makes NOM in concentrate an even greater membrane fouling threat.

Jucker and Clark (1994) compared the adsorbability of fulvic and humic acids onto ultrafiltration membranes. The membranes tested had less adsorption capacity for fulvic than for humic acid. The influences of inorganic water chemistry and of membrane charge on NOM adsorption were also studied. Adsorption increased with high calcium concentrations, low pH, and high membrane pore zeta potential. Nilson and DiGiano (1996) also examined the influence of NOM composition on fouling of nanofiltration membranes. The hydrophobic NOM fraction was rejected to a greater extent than the hydrophilic fraction and was responsible for membrane fouling. Hong and Elimelech (1997) examined the chemical and physical interactions that affected NOM fouling of NF membranes. Using three humic acids, they found membrane fouling increased with increased solution ionic strength, decreased pH, and increased divalent cation concentration. Of these factors, the greatest fouling effect was caused by divalent cations.

Li and Elimelech (2004) examined the mechanisms of organic fouling under different solution conditions of pH, total ionic strength, and divalent cation concentration by measuring the attraction and adhesion forces between an organic foulant and the membrane surface. Bench-scale fouling experiments were conducted to evaluate the effect of divalent cations on organic fouling. The test solution had a humic acid concentration of 20 mg/L and a total ionic strength of 10 mM. Three samples were tested, one with Na^+ as the only cation, one with 1 mM of Ca^{2+}, and one with 1 mM of Mg^{2+}. Over a period of 300 minutes, flux declined 11 percent for the solution without cations, 16 percent for the solution with Mg^{2+}, and 49 percent in the solution with Ca^{2+}. Hence, organic fouling was more severe for the solution with calcium than for the solutions with magnesium or sodium ions. These researchers found that attraction forces between the

clean membrane surface and humic acid were comparable for the three solutions, but there were significant differences in adhesion forces. There was no adhesion force for the monovalent solution, slight adhesion for the Mg^{2+} solution, and a significantly greater adhesion force for the solution with Ca^{2+}. This result indicated a much stronger interaction between humic acid and the clean membrane surface when calcium was present. The test was repeated with a fouled membrane with the same result. There was a much stronger interaction between humic acid and the fouled membrane surface in the presence of calcium.

It was concluded that organic fouling was not observed with the monovalent solution because electrostatic repulsion between the negatively charged membrane surface and the negatively charged humic acid prevented deposition of humic acid on the membrane. In contrast, divalent cations form complexes with humic acids, thereby reducing the charge of humic acid and reducing the electrostatic repulsion between it and the membrane surface. The researchers concluded that calcium caused more severe fouling than magnesium because the adhesion force between calcium and the membrane surface was significantly stronger.

NEW CHALLENGES IN "ZERO LIQUID DISCHARGE DESALINATION OF WATERS WITH HIGH ORGANIC CONTENT"

A similar ZLD concept will be applied to the new AwwaRF research project, but the waters tested will pose new challenges as illustrated in Figure 6. High NOM concentrations can affect precipitation kinetics in the concentrate treatment step and the performance of RO membranes. Furthermore, the risk of organic membrane fouling increases in the presence of calcium. The primary RO concentrate in this research will contain high concentrations of ions (including calcium) that can cause inorganic fouling as well as high concentrations of NOM. Consequently, the concentrate treatment step must address the potential for inorganic and organic fouling.

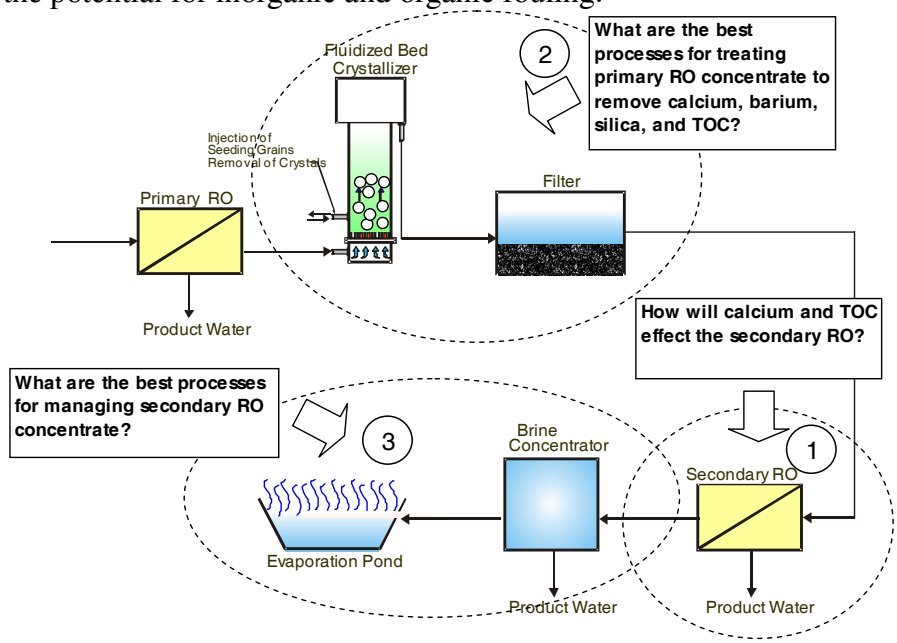

Figure 6 – New challenges posed by waters with high NOM concentrations

The test waters will come from the state of Florida. A second major challenge will be posed by Florida's wet climate. Evaporation ponds will not be an option for concentrate management because average rainfall exceeds the rate of evaporation. Consequently, new technologies will be needed to manage concentrate from the secondary RO.

The high concentrations of NOM and ineffectiveness of evaporation ponds lead to the following three new test objectives:

1. Identify the levels of calcium and NOM removal required in the concentrate treatment step to prevent organic fouling in the secondary RO.
2. Identify the most efficient processes for the concentrate treatment step that meet all treatment goals for reducing the inorganic and organic fouling potential of the concentrate.
3. Identify processes for managing the concentrate from the secondary RO.

The goals for the concentrate treatment step will include removal of calcium, silica, barium, and NOM. Processes that will be considered for evaluation, either individually or in combination, include:

- Chemical precipitation
- Fluidized bed crystallization
- Ion exchange processes such as magnetic ion exchange (MIEX)
- Adsorption processes such as activated alumina and GAC
- Electrodialysis with ion selective membranes

REFERENCES

Aiken, G.R., D. M. McKnight, R.L. Wershaw, and P. MacCarthy. 1985. *Humic Substances in Soil, Sediment, and Water*. Wiley, New York.

Hong, S. and M. Elimelech. 1997. Chemical and physical aspects of natural organic matter (NOM) fouling of nanofiltration membranes. *Journal of Membrane Science*. 132: 159-181.

Hoch, A., M. Reddy, and G. Aiken. 2000. "Calcite Crystal Growth Inhibition by Humic Substances with Emphasis on Hydrophobic Acids from the Florida Everglades". *Geochimica et Cosmochimica Acta*. 64(1), 61-72.

Jucker, C. and M. Clark. 1994. Adsorption of Aquatic Humic Substances on Hydrophobic Ultrafiltration Membranes. *Journal of Membrane Science*. 97: 37-52.

Lebron, I. and D.L. Suarez, 1998. Kinetics and Mechanisms of Precipitation of Calcite as Affected by P_{CO2} and Organic Ligands at 25 ºC. *Geochimica et Cosmochimica Acta.* 62(3), 405-416.

Stumm, Werner and James J. Morgan, 1996. *Aquatic Chemistry. Chemistry Equilibria and Rates in Natural Waters.* New York, NY. John Wiley & Sons, Inc.

A Mobile Emergency Drinking Water System Powered by Renewable Energy

Matthew Vitello[1], Andrew Curtis Elmore[2], Mariesa Crow[3]

[1]Department of Geological Engineering, Missouri S&T, 125 McNutt Hall, Rolla, MO 65409;
PH (417) 766-0391; e-mail: mcvd58@mst.edu
[2] Associate Professor of Geological Engineering, Missouri S&T, 125 McNutt Hall, Rolla, MO 65409; PH (573) 341-6784; e-mail: elmoreac@mst.edu
[3]Director, Energy Research and Development Center, F. Finley Distinguished Professor of Electrical Engineering, Missouri S&T, 305 McNutt Hall, Rolla, MO 65409;
PH (573)-341-6305; email: crow@mst.edu

To increase the mobility and wellbeing of U.S. Army units a relatively light-weight, portable source of clean drinking water is needed to replace current practices of obtaining potable water. In addition to the need expressed by the Army, it has become apparent that delivering a reliable source of clean drinking water to municipalities during the aftermath of natural disasters such as Hurricane's Katrina and Ike is essential. Water supply and the associated transportation of potable water is a considerable burden on recovery efforts following a natural disaster. A low cost trailer mounted system, which uses an ultraviolet (UV) disinfection unit in conjunction with cartridge filters, can provide potable water from local surface water bodies until the infrastructure is renewed. The system is powered by a hybrid photovoltaic array and wind turbine system, which allows for the capability to pump and treat surface water when grid power is unavailable. In an effort to maintain low maintenance and increased storability associated with the system, relatively high-maintenance lead acid batteries have been eliminated, which also helps to reduce the system weight. Tests have been conducted to assess the ease of use, effectiveness and feasibility of the system.

INTRODUCTION

Drinking water infrastructure may be damaged or destroyed during natural or man-made disasters. Even if a water treatment plant is not directly damaged, related systems such as the power supply or water distribution system may be disrupted. The transportation of bottled water from unaffected areas may not be desirable because roads and highways may be damaged, the time required for shipment may be unacceptably long, the shipping costs may be too high and/or the shipment of water may displace the shipment of other critical supplies.

The primary objective of this project is the development of a prototype mobile water disinfection system that can provide drinking water to human populations in

areas where the infrastructure has been damaged due to natural or man-made disasters or for deploying troops in areas where a safe water supply does not exist. However, this is a broad and generalized objective and more specific objectives were developed for the system and include:

- Is mobile and which can be relocated to water sources such as surface water bodies
- Is self powered using a hybrid wind turbine/solar cell energy source
- Can be powered through a supplemental power source such as a gasoline generator
- Is relatively lightweight and trailer mounted, so it can be towed by a standard pickup truck
- Can be deployed with small individual military units, set up and functioning with nominal training
- Can be placed in storage for extended periods of time without degradation, without requiring special materials storage, or without requiring periodic maintenance
- Is relatively low-maintenance while in operation and does not require significant consumable supplies
- Has the potential to be produced at a cost that would be affordable for municipal and regional civic entities that are tasked with addressing civil emergencies
- Has on-board test equipment to validate sterilization function

The primary components of the system included an array of photovoltaic panels and a wind turbine to generate energy, an ultracapacitor (UCAP) to provide energy storage, an ultraviolet light system to provide disinfection, and an inverter to manage generated power.

SYSTEM COMPONENTS

To generate the energy needed to operate the system, a hybrid renewable energy system of a photovoltaic array and wind turbine was used. The array of photovoltaic panels was composed of eight Sharp ND216U2 PV panels, with each panel having a maximum power output of 216 W. The array was mounted to the side of the trailer in a fixed position using six 1 inch steel tubes with a piece of angle iron welded at a 53° angle. A piece of UniRac Solar Mount was then bolted to this angle iron to allow for the PV panels to be positioned at 37° to the horizontal. However, due to the size of the solar panels and trailer, this rack only accommodated five PV panels. For the remaining three panels wooden ground racks were constructed, also allowing for the panels to be positioned at 37°.

The wind turbine selected for the project was a Skystream 3.7 manufactured by Southwest Windpower, Inc. with a maximum rated output of 2.4 kW at a wind speed of 13 m/s. The turbine was mounted on a 30 ft guyed tower composed of two 15 ft sections of 5 in Schedule 40 steel pipe. The two tower sections were connected using a coupler composed of three 20.5 in steel sections connected with 9 bolts on each side. Note that the standard 30 ft Skystream tower is composed of one 21 ft section and one 9 ft section. The 21 ft section was too long to be carried on the trailer

and was too heavy to be carried by 3 or 4 people on a routine basis such as would be expected with a mobile system. To raise the turbine tower a third 15 ft section of pipe was used as a gin pole. The tower was anchored into the ground through guy wires composed of 7/16 in wire rope tied into dual anchors. Included with each guy wire was a turnbuckle to allow for adjustments to bring the tower plumb. The anchors used were 30 in dual helix mobile home anchors, with a stabilizer plate to inhibit lateral movement.

To store the energy generated from the renewable energy systems a 48 VDC (nominal) UCAP was used. The use of the UCAP, which replaced a bank of batteries, allowed for a significant reduction in weight of the total system, in addition to an increased robustness of the energy storage system. In addition to the weight reduction achieved by using a UCAP, other benefits over the use of a bank of batteries are attained. A UCAP is a double-layer capacitor incorporating a metal/carbon electrode and a non-aqueous electrolyte solution. Unlike a battery, there are no chemical bonds made or broken in the process. The maximum voltage of the UCAP is not temperature dependent and the UCAP can be fully discharged up to a million times. Due to the low equivalent series resistance, the UCAP can obtain much higher power density than similarly rated lead-acid batteries. Due to its long shelf life and low maintenance, the UCAP provides a simple, reliable solution to buffer short-term mismatches between the power available and the power required by the pump and disinfection system.

In order to convert the alternating current generated by the wind turbine to direct current that could be used to charge the UCAP an Outback inverter was used. The inverter also converted direct current generated by the PV array to alternating current in order to power the disinfection unit. An Outback charge controller managed the direct current charging of the UCAP from either of the renewable energy systems. In addition to these systems a DC/DC converter was used to provide the appropriate level of direct current voltage necessary to power the pumping system.

A pumping and water storage system was also included in the prototype. This was comprised of a 12 VDC submersible pump which delivered water into an elevated 55 gallon HDPE tank. The tank housed level switches which controlled the operation of the pump. The level controls were programmed and operated through a Campbell Scientific CR1000 datalogger. The control logic is described below:

- If both low and high switches are closed, pump will turn on
- Pump will remain on until high switch is open
- Once high switch is open, pump will turn off
- Pump will remain off when the high switch is closed until low switch is closed

A secondary 55 gallon HDPE tank was used to store water post-disinfection.

Disinfection of water was achieved through the use of an ultraviolet disinfection unit. The disinfection unit used was a TrojanUVMax Pro10, which is rated to 10 gallons per minute. The TrojanUVMax unit is certified according to the National Sanitation Foundation (NSF)/American National Standards Institute (ANSI) Standard 55-2007 for Ultraviolet Microbiological Water Treatment Units for Class A systems designed to disinfect and/or remove microorganisms from contaminated

water, including bacteria and viruses, to a safe level using a UV dose of at least 40,000 uw-sec/cm^2 (NSF/ANSI, 2007). The unit is also Underwriter Laboratory (UL) certified. The unit included a solenoid valve which controlled the flow of water through the system based on the UV dosage received by a sensor in the unit's reactor. UV disinfection is a physical process which eliminates the need to generate, handle, transport, or store hazardous, toxic, or corrosive chemicals (USEPA, 1999). With this lack of chemical storage, the UV system enhances the storability and decreases the maintenance associated with the system.

The U.S Environmental Protection Agency promulgated the Surface Water Treatment Rule (SWTR) in 1989 for public water systems using surface water or ground water under the direct influence of surface water. Although the emergency water supply system developed in this project is not technically classified as a public water supply, the SWTR provides appropriate water treatment goals for the project. An important aspect of the SWTR is that solids which naturally occur in surface water must be reduced to concentrations which typically do not interfere with disinfection (USEPA, 2006). To achieve this reduction in solids, a pre-filter system was incorporated into the prototype. This pre-filter system was composed of a dual header system which housed pleated paper filters and activated carbon filters, which removed sediment and discoloration in the water making the water more aesthetically acceptable. A secondary pumping system using a 12 VDC UCAP was also developed and analyzed for the pre-filter system. Detailed information about the water disinfection components can be seen in Table 1.

Table 1 Water Treatment Assembly Components

Description	**Manufacturer**	**Model**	**Serial No.**	**Quantity**
12 VDC Submersible Pump	Proactive Environmental Products	Typhoon	17126	1
12 VDC UCAP	Maxwell Technologies	BMOD0058	4407-K-00130	1
Voltage Control Switch	Solar Converters, Inc.	VCS-1AL	49626	1
Pleated Filter	Pentair Filtration, Inc.	S1-20	N/A	2
Carbon/Fiber Block Filter	Pentair Filtration, Inc.	CFB-20	N/A	2
Filter Housing	Pentair Filtration, Inc.	3G #20	N/A	4
UV Disinfection Unit	TrojanUV	Pro10	000029	1

The prototype system was mounted on a 16 ft tandem axle utility trailer, which was modified to accommodate the needs of raising the wind turbine and mounting of the solar panels. The modifications included; the addition of four mechanical jacks to support and level the trailer, mounting a 4 ft x 3 ft steel plate to

act as a base for and distribute the load of the wind turbine more evenly across the trailer, and the alteration of the front rail to accommodate the gin pole for raising the wind turbine.

PERFORMANCE CHARACTERIZATION

The majority of the prototype testing was conducted in the field, however prior to completion of the prototype, small field and laboratory tests were conducted to characterize the energy generation and consumption of the various components. The prototype system was deployed in the field at Fort Leonard Wood in Missouri for testing. Field testing occurred between the months of August to November 2007 and included; operation of the system under varying weather conditions and periods of time, as well as water sampling and analysis.

During system operation voltage sensors manufactured by Ohio Semitronics, Inc. were used to monitor and log energy generated and consumed of major components including; the wind turbine, the PV array, the UCAP, the UV disinfection unit and the 12 VDC pump. Detailed information about these sensors can be seen in Table 2.

Table 2 Energy Monitoring Components

Description	Manufacturer	Model	Serial Number	Quantity
Datalogger	Campbell Scientific, Inc.	CR1000	13575	1
Solar Panel	BP Solar	SP20	5448153	1
Voltage Sensor	Ohio Semitronics	PC5-001X5	08050717	1
Voltage Sensor	Ohio Semitronics	PC5-020X5	08050740	1
Voltage Sensor	Ohio Semitronics	PC8-001-01X5	08050592	1
Voltage Sensor	Ohio Semitronics	PC8-002-01X5	08050768	1
Voltage Sensor	Ohio Semitronics	PC8-003-01X5	08050591	1

Water sampling and analysis was conducted in four separate events. The water samples came from various surface water bodies located near the field deployment site on Fort Leonard Wood, these included a pond and a lake that were each sampled once, as well as a river that was sampled twice. A small amount of activated sludge from a wastewater treatment plant was added to the second river sample in order to increase the number of coliform bacteria present in the sample prior to disinfection. All water samples were processed in the field or in a lab at Missouri S&T, and were not sent to off-site laboratories.

Water disinfection was characterized by analyzing water samples for the presence of coliforms, including E. coli, which are organisms that indicate the

presence of or potential for fecal pathogen contamination. The U.S Environmental; Protection Agency Total Coliform Rule (TCR) provides a quantitative means for measuring disinfection effectiveness (USEPA, 2001). As with the SWTR, the TCR is only applicable to public water systems. However, by following the TCR during this project, the resulting emergency water supply will provide a safe product to the consumers.

Two methods were used during the project to evaluate the presence of coliforms; IDEXX Colilert and Micrology Labs Coliscan MF (membrane filtration). The Coliscan MF kits were used to quantify total coliform and E. coli concentrations, while the Colilert kits indicate a presence/absence of coliforms. Although removal of coliform bacteria was the primary goal for the disinfection unit, several other water quality parameters were monitored during testing. These include pH, TDS, Turbidity, Phosphate, Dissolved Oxygen and Nitrate. Detailed information about the equipment used for water quality testing is shown in Table 3.

Table 3 Water Quality Monitoring and Test Kits

Description	**Manufacturer**	**Model**	**Serial Number**
Water Quality Kit	Lamotte	Low Cost Water Monitoring Kit	3-5886
Coliform Testing	Micrology Labs	Coliscan MF	N/A
Coliform Testing	IDEXX	Colilert	N/A
Turbidimeter	Hach	2100P Portable Turbidimeter	06120C020542
pH Tester	Hach	pH Pocket Pal	N/A
TDS Tester	Hach	Pocket Pal TDS Tester	N/A
Incubator	Boekel	133000	0815 02185

RESULTS AND DISCUSSION

The prototype successfully pumped and disinfected water using the UV system powered by renewable energy. The use of the UCAP instead of batteries was successful, and the PV array supplied sufficient power for system operation. The wind turbine was redundant and was not used to a significant extent to generate power for the system.

The water quality testing results can be seen in Table 4. Throughout each sampling event samples were taken in triplicates of pre- and post-treated water. The membrane filtration tests were not conducted to quantify total coliforms during the pond sampling event. The numbers of total coliform colonies were too great to count in every pre-treatment sample so only E. coli counts are reported in Table 4. The membrane filtration testing indicated that there were no coliform (including E. coli) colonies present in the post-treatment samples. The Colilert testing did not provide colony counts, but the presence/absence results were consistent with the membrane filtration testing. The remaining water quality parameters tested were all in acceptable ranges as outlined by the Code of Federal Regulations Title 40 Part 141

National Primary Drinking Water Regulations and Part 143 National Secondary Drinking Water Regulations.

Table 4 Water Quality Testing Results

Parameter	Al Kut Pre-Treatment	Al Kut Post Treatment	Bloodland Lake Pre-Treatment	Bloodland Lake Post Treatment	Big Piney Pre-Treatment	Big Piney Post Treatment	Big Piney (spiked) Pre-Treatment	Big Piney (spiked) Post-Treatment
Sampling Date	10/9/2008		10/13/2008		10/20/2008		10/28/2008	
E. coli (colonies/100 mL)	N/A	N/A	0	0	15	0	37	0
	N/A	N/A	2	0	28	0	42	0
	N/A	N/A	1	0	33	0	31	0
Coliforms (**P**resence/**A**bsence)	P	A	P	A	P	A	P	A
	A	A	A	A	P	A	P	A
	A	A	A	A	P	A	P	A
DO (ppm)	8	8	8	8	8	8	8	8
	8	8	8	8	8	8	8	8
	8	8	8	8	8	8	8	8
Nitrate (ppm)	<1	<1	<1	<1	<1	<1	<1	<1
	<1	<1	<1	<1	<1	<1	<1	<1
	<1	<1	<1	<1	<1	<1	<1	<1
pH	7.0	7.0	6.5	7.3	8.1	8.9	8.3	8.5
	7.0	7.0	7.0	7.3	8.8	9.0	7.8	8.3
	7.0	7.0	6.8	7.2	8.6	8.8	8.1	8.7
Phosphate (ppm)	<1	2	<1	1	2	< 1	<1	1
	<1	1	1	1	<1	1	2	1
	<1	1	1	1	1	< 1	<1	< 1
TDS (ppm)	16	66	54	55	168	165	175	179
	14	65	52	56	146	171	182	194
	18	66	55	55	154	168	164	170
Temperature (^{o}C)	16	26	22	24	16	20	18	21
Turbidity (NTU)	25	20	15	5	1.72	1.73	1.49	1.62
	30	25	20	0	1.16	1.77	1.37	1.54
	25	25	20	5	1.35	1.74	1.23	1.71

During testing of the prototype it became apparent that the wind turbine was unnecessary and proved to be problematic. The alteration of the tower from a 21 ft and 9 ft sections to two 15 sections, as well as the trailer-mounted base made keeping the tower plumb difficult. The increased moment created by the upper 15 ft section used in place of the 9 ft section could not be adequately controlled by the relatively small coupler used, which caused a slight deflection from vertical affecting the turbine's ability to rotate downwind. In addition to the problems created by the tower alteration, the erection of the turbine was labor and time intensive, as well as inherently dangerous to personnel and other system components during erection. The wind turbine was primarily designed to operate in grid inter-tie mode and the manufacturer-supplied control modification hardware and software necessary to

operate the wind turbine system in off-grid (UCAP charging) mode did not function well.

The limiting factor of the system was the water treatment capacity. This factor was limited by the hydraulic capacity of the elevated holding tank and tubing carrying the water, as well as the energy consumption of the pump. To characterize the system's ability to operate without energy being generated, the renewable energy system was disabled and energy consumption of the disinfection unit and pumping system were monitored. The disinfection unit operated for 19 minutes beginning on a full 48 VDC UCAP charge and continuing until the UCAP reached 36 VDC at which point the inverter automatically shuts itself off, which allowed for the treatment of 45 gallons of water. If the solar panels were charging the UCAP, the disinfection unit would operate as long as there was sufficient water supply. The typical flow through the disinfection unit was 2.4 gpm. If the flow through the system were increased to the UV system's operational maximum of 10 gpm, approximately 200 gallons of water could be treated on a single UCAP charge. One hour of continuous operation would result in the disinfection of 600 gallons of water. Assuming an average daily per capita drinking water consumption of 2.0 L (0.53 gal), a single UCAP charge has the potential to treat enough drinking water for 360 people for one day, while 1 hr of continuous operation would provide enough drinking water for more than 1,100 people.

The water pump operated at a flow rate of 3.6 gpm for four minutes on a full UCAP charge. This short pumping time only allows for 14 gallons of water to be pumped into the holding tank. It can be seen that the water pump operation was a significant limiting factor in the quantity of water to be treated. If the solar panels were charging the UCAP, the pumping system consumed energy at a faster rate than energy was generated resulting in varying inverter shutdown times dependent upon the available solar radiation. The typical recharge time for the UCAP ranged between 2 and 16 min depending on the available solar radiation. Therefore, an estimated 340 gallons of water could be pumped in a typical day (assuming 3 cycles/hr) if not other loads were imposed on the system.

The water treatment capacity time constraints presented previously provides the primary findings regarding the impact of the energy balance. Therefore, the utility of the actual energy balance using data collected from the OSI voltage sensors is of somewhat diminished importance. Typical data received from the voltage sensors is shown in Table 5. It can be seen in the data that there is some variability in the energy generated by the PV array which reflects the varying amount of available solar radiation, the wind turbine energy generated remains essentially constant because the wind turbine was not in operation, the UCAP data show variability as the voltage varies with PV input from the charge controller, and the pump and UV system loads remain essentially constant over the operational period.

Table 5 Typical Voltage Sensor Data

Time	Sensor Output (mV)				
	PV Array (Generate)	Wind Turbine (Generate)	UCAP (Store)	Pump (Consume)	UV System (Consume)
2:00:00 PM	19.64	8.81	31.84	37.94	14.23
3:00:00 PM	14.9	8.8	0.677	37.93	13.55
4:00:00 PM	16.26	8.13	10.84	38.6	13.55
5:00:00 PM	9.49	8.13	9.49	38.62	14.23
6:00:00 PM	5.42	8.81	32.52	36.59	2.71

CONCLUSIONS AND RECOMMENDATIONS

The prototype system met or exceeded all objectives outlined in the scope of the project and demonstrated the proof of the concept that renewable energy systems could be used to operate the UV disinfection unit. However, several technical recommendations became apparent during testing of the prototype system. These recommendations include; abandoning the wind turbine, increasing the quantity of water treated, and an evaluation of issues specific to potential use by the military.

By abandoning the wind turbine, the potential for energy generation is decreased, however it could be seen during testing that the system did not require the increased energy generation potential provided by the wind turbine. If the need for increased energy generation is required it could be achieved through an increased number of panels in the PV array. In addition to the diminished need for the wind turbine to generate energy, other benefits achieved through its removal include; complexity of the system will decrease, overall system weight will decrease, visibility of the system will decrease, overall cost of the system will decrease, potential for lightning damage is decreased, mobility and ease of set-up of the system will be increased, and the area of deployment for the system will increase because wind obstructions and acceptable soil conditions required for anchoring the turbine will not be siting factors.

An increase in the quantity of water treated could be achieved through the alteration of the water storage and piping system and by identifying an inverter that functions throughout a wider voltage range. To achieve the rated 10 gpm of the disinfection unit, the system would need to be replumbed with larger piping and/or an increased elevation of the holding tank. Identifying an inverter that will function at lower DC voltages would take advantage of the UCAP's ability to be discharged to lower levels without damage relative to a battery, allowing the disinfection unit to run longer than 19 min on a single UCAP charge.

Further recommendations for evaluating issues specific to military use are focused on making the unit more troop friendly and increasing the ease of deployment by creating a system housed in a container more readily handled by military equipment.

ACKNOWLEDGEMENTS

The project described was funded by a grant from the Leonard Wood Institute (LWI). Additional support was provided by Filter-Tek Inc. of Rolla, Missouri and Missouri University of Science and Technology.

REFERENCES

U.S Environmental Protection Agency (USEPA). (2006). "Ultraviolet disinfection guidance manual for the final long term 2 enhanced surface water treatment rule", EPA 815-R-06-007, Washington, D.C.

U.S Environmental Protection Agency (USEPA). (2001). "Total coliform rule: a quick reference guide", EPA 816-F-01-035, Washington, D.C.

U.S Environmental Protection Agency (USEPA). (1999). "Wastewater technology fact sheet – ultraviolet disinfection", EPA 832-F-99-064, Washington, D.C.

National Sanitation Foundation/American Standards Institute (NSF/ANSI). (2007). "Ultraviolet microbiological water treatment units", NSF/ANSI 55-2007, Washington, D.C.

Adding Value to Sanitary Sewers – An Important Asset of Municipalities

V. Firat Sever[1] and Barton Bradshaw[2]

[1] Corresponding author. BOYLE | AECOM 4415 Metro Parkway Suite 404, Fort Myers, Florida 33916. PH (239) 278-7996; FAX (239) 278-0913; E-MAIL firat.sever@aecom.com

[2] City of Marco Island, 50 Bald Eagle Drive, Marco Island, Florida 34145. PH (239) 389-5000; FAX (239) 389-4359; E-MAIL bbradshaw@cityofmarcoisland.com

Keywords: sanitary sewer, rehabilitation, asset management

Abstract

Sanitary sewer rehabilitation programs are generally triggered by the need for reducing infiltration and inflow and restoring structural integrity of a collection system. On the other hand, improving the condition of the components (essentially pipes and manholes) of a wastewater collection system may turn sanitary sewer rehabilitation into a financially beneficial practice in addition to maintaining desired level of service and regulatory compliance. This study discusses a sanitary sewer rehabilitation program being applied on Marco Island, Florida as a case study of proactive wastewater collection system management. The existing system was evaluated using closed-circuit-TV inspection of pipelines and visual inspection of manholes. Accordingly, a rehabilitation program was developed which is based on using trenchless technologies to maximum extent. Depreciation of the system was analyzed for the next 70 years without rehabilitation to estimate the rate of return of rehabilitation. The results indicated the rehabilitation cost is approximately 16 percent of the depreciation that would occur in 70 years in today's dollars.

Introduction

Wastewater collection systems are valuable capital assets of municipalities, which turns operation and maintenance of these assets into an important matter. The majority of the underground infrastructure in the developed nations were built in the nineteenth or early twentieth century, and have reached far beyond their design life. Wastewater collection systems are comprised of pipelines (main lines, force mains, and service laterals), manholes, and lift stations, where main pipes comprise the highest portion of the cost (approximately 70 percent). Like any structure, sewer systems are subject to degradation over time. Nature and extent of damage to sewer systems is dependent on site conditions, which include loads on the pipelines, groundwater table, wastewater characteristics, materials used for the pipes and other components, and installation quality. To date, there have been several studies on sanitary sewer asset management, with various aspects in defining wastewater collection system needs and how to address them. A formal definition is provided in

the International Infrastructure Management Manual (INGENIUM, 2002): "The combination of management, financial, economic, and engineering practices applied to physical assets with the objective of providing required level of service in the most cost-effective manner."

La Gauffre et al. developed a comprehensive study on identifying sewer system defects, their consequences, and impacts on the overall system. In other terms, discrete (along a pipe segment or particular point) defects were combined into an impact function, which was then used as a tool for a decision matrix to determine whether a particular defect should be addressed by spot repairs, rehabilitation (lining, chemical grouting, etc.) or replacement. The methodology is composed of six principles, which includes system inspection and evaluation criteria, defect identification/classification, a nomenclature to define system discrepancies and actual/potential effects, decision criteria on whether to employ spot repairs, rehabilitate or replace a pipe segment, and a numerical method to make a decision on rehabilitation strategy, into which the decision criteria are incorporated. This study identifies performance indicators in three levels as defects, dysfunctions, and impacts. Where, defect is a deviation from design/initial conditions such as cracks on pipes; dysfunctions are the consequences of defect; e.g., infiltration due to a crack, and impacts are the negative effects of these consequences to the environment, operation conditions and costs.

A similar approach for decision making on rehabilitation of an infrastructure asset was discussed in Guide to Water and Wastewater Asset Management (Underground Infrastructure Management, 2008). A wastewater collection system may be functioning in compliance with the regulations in action, despite of apparent defect that may impact the operation. For instance, a cracked pipe, unless causing significant exfiltration, will not be a problem from regulatory standpoint; however, depending on location, soil conditions, and severity of the cracking, this defect may lead to a structural failure of that pipe segment, which will in return interrupt operation, result in soil or groundwater contamination and social costs due to road closures associated with excavation for fixing it or possible damage to the road. The UIM publication outlines a cost comparison between fixing a problem or leaving it as is. For the cracked pipe example, the cost of not fixing it is the cost of failure, possibility of which can be predicted versus time; i.e., if the failure appears to be imminent in 15 years, then the cost of leaving as is will be at minimum the cost of replacement and social cost per year. On the other hand, the proactive approach would be rehabilitating the crack (e.g., by inserting a liner into the pipe). The capital cost of rehabilitation (note the social cost is trivial with rehabilitation, since it is applied trenchless) can be calculated as annual cost over 15 years so that it can be compared to the annual cost of replacement and social cost as the other option. If the annualized rehabilitation cost per year is less than replacement after failure, then it is justified. This analysis should take the life cycle of each option as well. There will be a design life for the rehabilitated pipe to be compared to the remaining life of the cracked pipe, which is predicted as 15 years.

In their overview of asset management practices of underground infrastructure in the USA, UK, and Australia, Aikman and Doherty (2006) listed the following as the components of asset management programs in the USA: Desired level of service,

performance goals, information systems, asset identification and valuation, consequences of failure analysis and risk management planning, condition assessment, capacity analysis and assurance, maintenance analysis and planning, financial management, and capital improvements and expansion of system. The need for asset management is primarily driven by Government Accounting Standards Board (GASB) Statement 34 (GASB-34), which requires governmental entities to provide an inventory of their long-term assets such as underground infrastructure (water and wastewater pipelines, pump stations and other components of collection and distribution systems) and EPA's Capacity, Management, Operation and Maintenance (CMOM) initiative.

This study discusses the sanitary sewer rehabilitation program being applied on Marco, Island, Florida as an example of proactive wastewater collection system management. The program consists of three phases: Condition assessment, rehabilitation design, and implementation. Based on the condition assessment, depreciation of the existing sanitary sewer system was predicted in long-term. This analysis was used to determine the financial benefits of sanitary sewer rehabilitation in addition to preventing failures, reducing infiltration and inflow (I&I); thereby maintaining the desired level of service.

City of Marco Island, Existing Sewers Assessment and Rehabilitation

Scope of Work: Marco Island, Florida Sanitary Sewer Rehabilitation Project was analyzed as an example of proactive asset management practice. The City of Marco Island purchased the water and wastewater utility from a private company in November of 2003 and was named Marco Island Utilities. As the management became familiar with the utility's capital needs, the projects were prioritized from the most critical to the least critical. At the beginning of the fourth year of ownership, the Utility Director set aside funds to begin an assessment of the wastewater gravity system that was built between early and late 1960s. The existing central wastewater collection system consists of vitrified clay (VCP), built in early 60s, and polyvinyl chloride (PVC) pipes, built in late 60s clay. Only 40 percent of the Island was served by centralized wastewater collection system at the time.

In coordination with BOYLE | AECOM the City started an assessment / rehabilitation program for its sanitary sewers. The goals of this program were to assess the structural integrity of the pipelines; identify sources of infiltration and inflow into the system, and develop a capital improvement plan to prioritize and correct defects that are discovered. Methods used for inspecting the existing system are cleaning the pipelines using a water jet, surveying pipe condition using closed-circuit television (CCTV), and smoke testing of lateral sewers and selected manholes. Defects noted during the CCTV inspection were identified using the Pipeline Assessment and Certification Program (PACP) coding system. The video records were reviewed by BOYLE | AECOM to verify and evaluate the reported defects.

Existing System Inventory: Sanitary sewers on Marco Island consist of polyvinyl chloride (PVC) and vitrified clay pipe (VCP), with clay pipes being older than the PVC pipes. PVC pipes did not demonstrate any notable damage except a few discrete holes and cracks due to rock or miscellaneous object penetration. The

majority of the inspected VCP is in sound or moderate condition requiring spot repairs or no repair at all in the foreseeable future. Approximately 16 percent of the existing clay pipes demonstrated extensive damage such as cracks, fractures, and loose/offset joints. These defects require complete rehabilitation using a structural liner such as cured-in-place-pipe (CIPP).

Approximately 40 percent of the existing pipes are made of clay and the remaining 60 percent are PVC pipes. Vitrified clay is known for its inertness against chemical attack. However, it is more brittle than PVC and tends to generate longitudinal or circumferential cracks due to external loads. In addition, VCP is less flexible than PVC and tends to separate at joints. Marco Island is a barrier island located on the eastern section of the Gulf of Mexico in southwest Florida. Marco Island's groundwater table is on the average of 3 ft (0.9 m) to 3.5 ft (1.1 m) below the surface and is affected by tidal action. Because of the fluctuating water table and the constant movement of the sandy soil the nonflexible clays pipes have sustained most of the damage. Additionally, traffic loads and installation deficiencies (e.g., poor bedding and backfill) may have played a significant role on service life of sanitary sewer pipes.

Extensive defects such as cracks, fractures, holes, loose joints on the pipelines and manholes will potentially allow I&I. Infiltration and inflow will increase the total flow rate and cost of wastewater treatment. In addition, I&I may cause overburdening of the WWTP, which could negatively affect the treatment processes and risk the quality of the effluent. Moreover, infiltration is a result of defects in the pipelines as well as manholes, which may be indicative of premature failure of the sewer lines that may have costly consequences such as sanitary sewer backups and damage to the road above the collapsed pipe segment. Sanitary sewer failures also pose environmental hazard by wastewater leaks out of the pipeline (exfiltration).

The cleaning and televising program included the existing sewers, which are distributed over the Island on the northeast, northwest, and southwest. These areas were divided into phases to prioritize and coordinate the project. The overall project included approximately 190,000 linear ft (58,000 linear m) of sanitary sewer pipes ranging from 8-inch (200 mm) to 12-inch (300 mm) in diameter and 833 manhole, which serves the 34 percent of the island. Approximately 6 percent of the existing sewers were excluded from the rehabilitation program due to pipes/manholes being new or recent rehabilitation.

Sanitary Sewer Pipes

Based on the review of the CCTV records BOYLE | AECOM evaluated condition of the pipelines, which was indicated using color coded plans (Figure 2). Three levels of deterioration; i.e., sound, moderate, and poor, were indicated by green, yellow, and red, as defined below.

Green: Pipe segments that have few or no observed damage. No rehabilitation is recommended for green pipes.

Yellow: pipe segments that have moderate amount of defects such as fractures and cracks. While the yellow pipes, in general, appear to be sound, immediate rehabilitation of some of them may be advisable due to localized severe damages (e.g., a hole or a broken pipe).

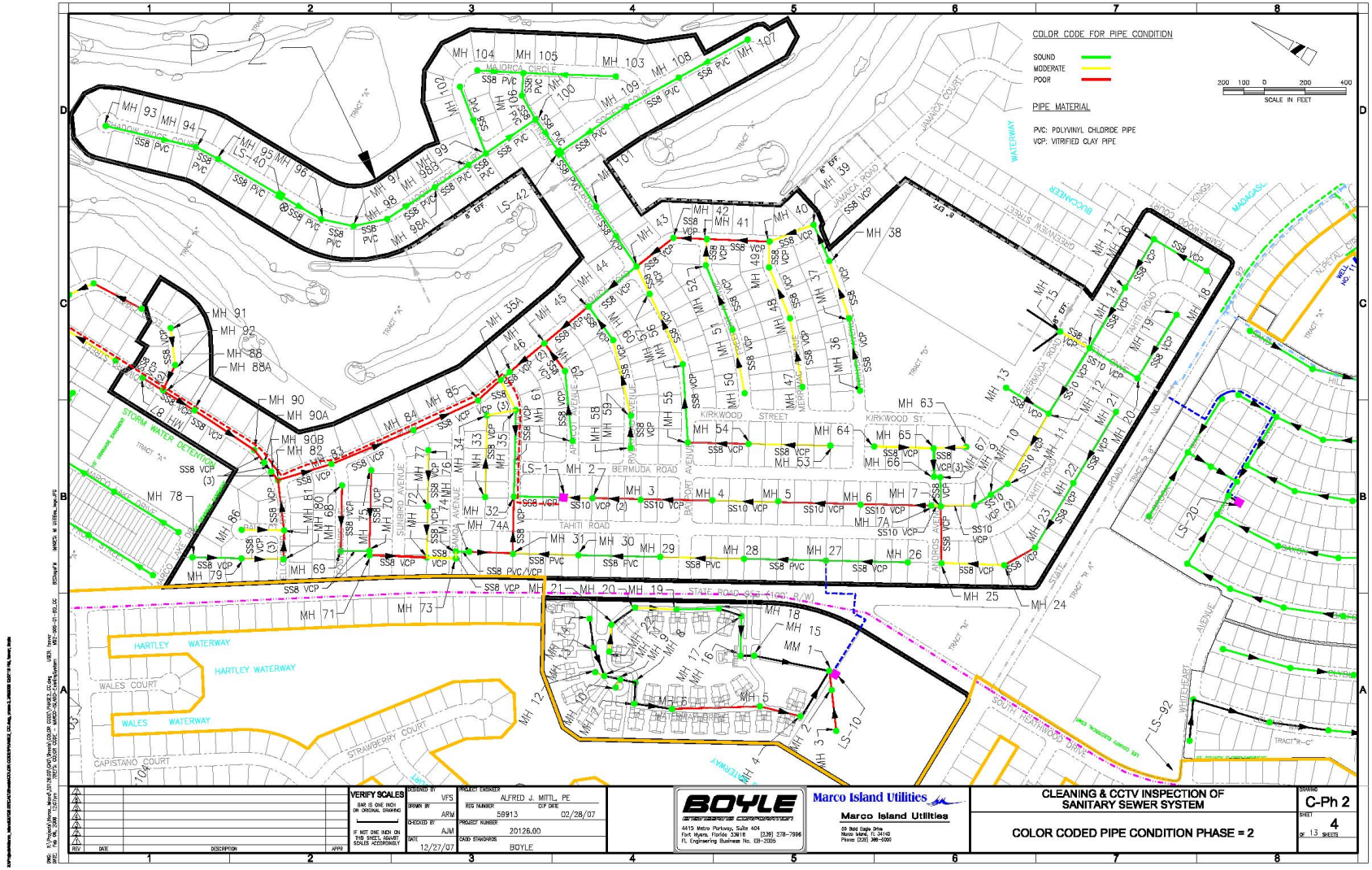

Figure 1. A sample color coded map indicating condition of the inspected pipes in one lift station area.

Red : Pipe segments with frequent cracks and fractures were coded red. Red pipes are not structurally sound; they are prone to failure and source of infiltration. Figure 2 shows a breakdown of inspected sanitary sewer pipes based on their condition.

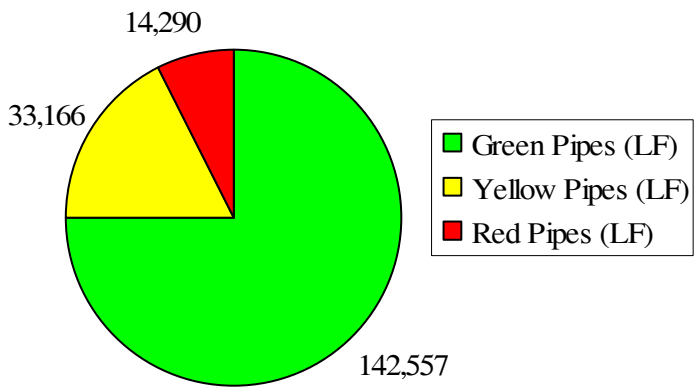

Figure 2. Quantities of inspected of sanitary sewers with respect to their condition indicated by color code.

The condition of the pipelines was highly dependent on the location and material. Accordingly, minor or no damage was noted to the PVC sewers; whereas, the magnitude of damage to the VCP sewers ranged from no damage to extensive (Figure 3). The most common types of defect were cracking, fracture, and root intrusion (at joints) in VCP and sagging in PVC pipes. Pipe segments that have frequent fractures and cracks will allow infiltration or exfiltration depending on the water table and the location of the pipe. In addition, structurally unsound pipe segments are prone to a collapse, which may cause sanitary sewer backups and damage to the road above the pipeline.



Figure 3. A view from a fractured clay pipe.

Based on the condition of the pipelines and flow rates into the system, upsizing any pipe segments was not deemed necessary by the project team; and therefore, pipe replacement was not one of the methods included in the project. Available relining methods include cured-in-place-pipe (CIPP) liner and sliplining (fold and form or deform/reform). CIPP is the method chosen for relining, which is an established method of structural pipeline rehabilitation in North America (ASCE, 1994). A well installed CIPP with adequate resin will minimize, if not eliminate, the annular space between the host pipe and liner (Bakeer and Sever, 2008); thus the risk of annular flow that may enter into the system through service lateral connections (after the liner is cut out at service laterals) and crack/holes on the host pipe.

CCTV records indicated non-structural, localized damages and leaks in some of the sanitary sewers that are otherwise in sound condition. A complete relining of these pipe segments would not be economical; therefore the suggested method for fixing loose joints and circumferential cracks in the pipe segments that are otherwise in sound condition was chemical grout (acryl amide) injection.

Manholes

CCTV inspection survey records did not provide a clear view of the manholes; and therefore, manholes were visually inspected by the project team. Forty six percent of the manholes included in the assessment program were included in the inspection (386 of 833). This selection was based on age and location as manholes in low lying areas (i.e. swales and areas at low elevations). Wet weather flow rates to the Marco Island Wastewater Treatment Plant are significantly higher than dry weather; whereas, based on the CCTV records review, it was understood that infiltration into the collection system is not substantial. Hence, manhole inspection and assessment was aimed at reducing inflow through manholes and enhancing structural integrity of the deteriorated ones. Inspection was conducted using a standard form developed by the project team.

Majority of the manholes had defects on the upper section; i.e., cover, frame, and chimney; whereas, some of them underwent corrosion due to hydrogen sulfide release, which damaged cone and wall. Damage to the bench or trough was observed in only a few manholes, and this was mainly due to root intrusion. Like the sanitary sewer pipes, condition of each manhole is depicted using a color code. Color coding identifies a manhole's condition at three levels as sound (green), moderate (yellow), and poor (red).

Green Manholes are the ones with minimal or no apparent corrosion on the interior or top (frame and lid). Green manholes do not require any rehabilitation or frame/lid replacement. However, some of them require lid sealing to prevent inflow.

Yellow Manholes are the ones with moderate damage. They are structurally sound; i.e., minor or no corrosion to the bench, wall, and cone. Yellow manholes typically require replacement of the frame and sealing of the lid, and partial lining (chimney and/or joints) or grouting.

Red Manholes are the ones with extensive corrosion throughout the interior and significant inflow (and infiltration for some). Lining the interior of red manholes would prevent further corrosion thus a failure or extensive I&I. Red manholes

comprise only 12 percent of the inspected manholes. Figure 4 shows a breakdown of inspected manholes based on their condition.

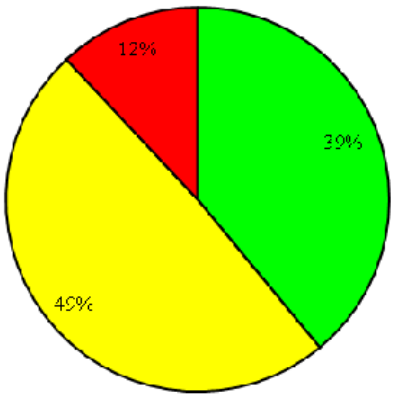

Figure 4. Percentage of green, yellow, and red manholes.

Smoke Testing – Service Laterals: Lateral sewers along with manholes were surveyed by smoke testing before visual inspection on manholes. Smoke testing verified inflow through manholes and revealed apparent defects on service laterals such as missing clean-out caps, illegal connections, and leaks. Rehabilitation of lateral sewers is not included in the current rehabilitation program, as they appear to be in better condition, hence have less priority in comparison with main sewers and manholes.

Anticipated Benefits of Rehabilitation

The rehabilitation program is primarily based on the defects noted and their consequences. For instance, a crack is identified as a defect to be fixed only if there is infiltration through it or imposes a risk of further propagation; hence failure in the long run. Likewise a loose joint was noted and included in the list of joints to be grouted only if there is apparent infiltration through it. The rehabilitation program is aimed at addressing all of the defects that has or will have an impact in the operation of the system in the desired level of service, which is essentially minimized infiltration and inflow and risk of failure. On the other hand, all of the yellow and red sanitary sewer pipes and manholes will be upgraded to green. In addition to minimized operational problems, this will increase the overall value of the wastewater collection system, an important capital asset of the City.

Conditions of the sanitary sewer pipes and manholes were predicted in long-term if a rehabilitation program was not implemented. This prediction is based on a linear correlation between degradation observed in 40 years to date and the degradation that would occur without rehabilitation in 70 years. Condition of the pipelines after 40 years (average age of the inspected pipes and manholes, which vary from 35 to 45 years) was broken down in accordance with the material (clay or PVC). Then it was assumed that the pipe degraded from green to yellow or red over this period in constant increments (i.e. linear degradation), which is a much greater value for clay pipes. To illustrate, the rate at which clay pipes turned yellow from green was 40 percent; whereas, this rate was 3 percent for PVC pipes. Figures 5 and 6 depict

predicted degradation of sanitary sewer pipes and manholes, respectively for the next 70-year term based on degradation in 40 years. It is more than likely that degradation of a sanitary sewer pipe or manhole is not linear over time as deterioration would be expected to occur at an accelerated pace when the pipes and manholes reach their design life. However, there isn't sufficient data to create a model for the deterioration of the pipes and manholes in long-term in the case of Marco Island, as the pipes were inspected once after 40 years. The nonlinearity in the condition of pipelines versus time plot is a result of different rate of degradation between PVC and clay pipes. All of the clay pipes are expected to sustain, at minimum, minor damage, and degrade to yellow in 40 years. In other words, there would be no green clay pipes in the system after forty years without rehabilitation. This results in a decline in yellow pipe quantity as yellow clay pipes proceed to degrade and turn red; whereas, available green PVC pipes turn yellow at a lower rate than transition to red pipes of clay pipes.

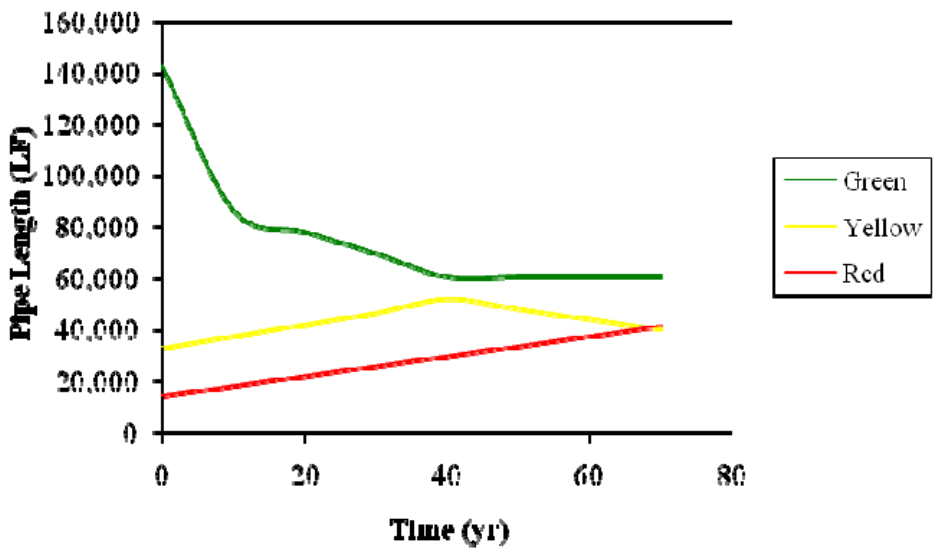

Figure 5. Anticipated change of condition of the sanitary sewer pipes without rehabilitation.

Anticipated benefits of rehabilitation in monetary terms were analyzed in long-term (70 years). Value of a green pipe segment was taken equal to a new sanitary sewer pipe, which is based on new construction ongoing on the other parts of the island. The average unit price ($/linear ft for sanitary sewer pipes) for new construction was amplified by 25 percent to account for relatively low quantity and additional cost of replacing the existing pipes (which would include flow bypassing and extra labor). On the other hand, there is a social cost associated with traffic interruption and nuisance to the public for new construction or open-trench replacement, which is very complex to define in mathematical terms and excluded from the value of a green pipe.

A yellow or red pipe segment is the cost of a green pipe segment (per linear ft) less the cost of rehabilitation required to bring these pipes' conditions to green. The cost difference between green and red pipes would be much greater if any of the red pipes required replacement.

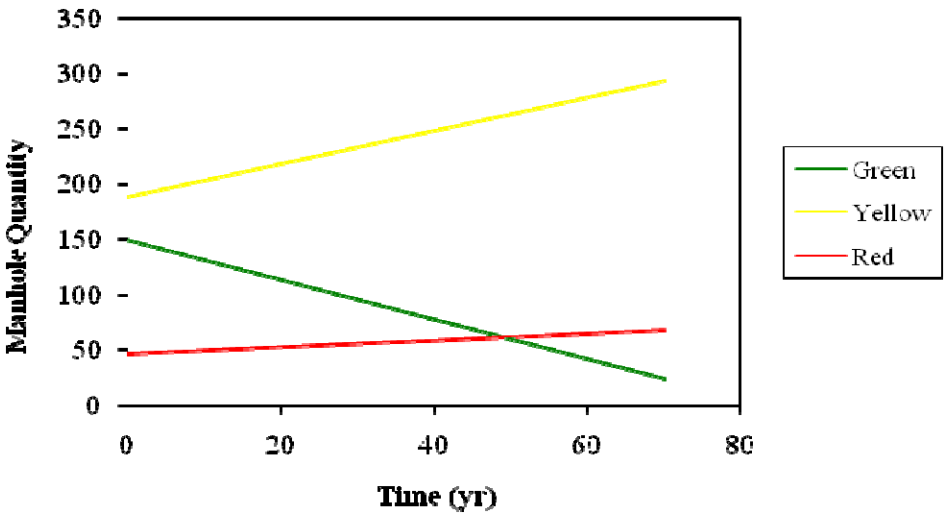

Figure 6. Anticipated change of condition of the sanitary sewer manholes without rehabilitation.

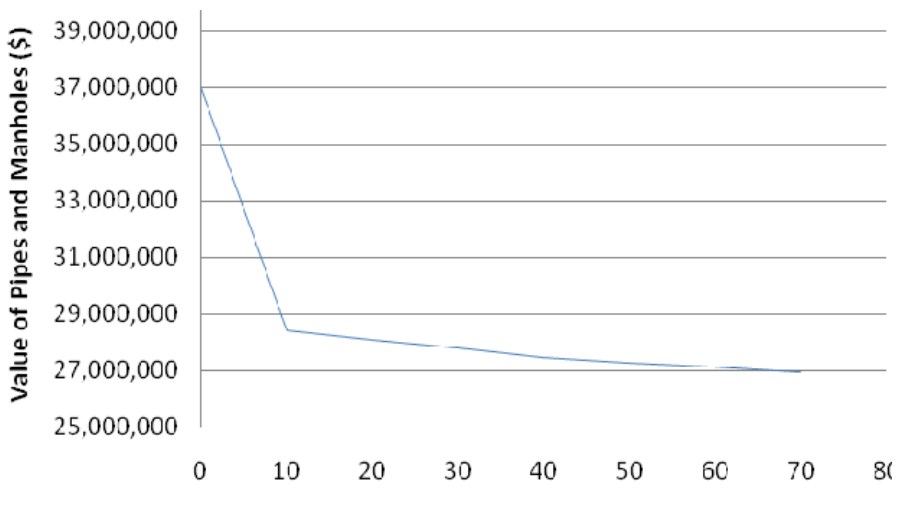

Figure 7. Anticipated depreciation in value of the sanitary sewer pipes and manholes without rehabilitation.

This would more than likely be the case in the future if rehabilitation was not implemented, as a significant portion of the red/yellow pipes would further deteriorate and require replacement. Long-term depreciation of sanitary sewer mains and manholes is shown in Figure 7. The dramatic slope change after ten years is a result of clay pipes being deteriorated and the trend is controlled by PVC pipes after this point, which deteriorate at a much slower rate than the clay pipes (as discussed).

Conclusions

The ongoing sanitary sewer rehabilitation program of Marco Island, Florida was evaluated as a proactive asset management practice. The rehabilitation program

for sanitary sewer mains and manholes consists of three phases: Condition assessment, rehabilitation design, and implementation. Currently, the program is at final phase of the design. Condition assessment for the pipelines is based on review of closed-circuit-TV (CCTV) survey conducted by an inspection company. Vitrified clay (VCP) and PVC pipes were used for the existing sewer system of the Island. Generally, older clay pipes had more damage than the PVC pipes. The most common damages noted were cracks, fractures, sags, and loose joints on the VCP pipes. Damage observed to PVC pipes included minor sagging and occasional holes due to penetration of a rock or another object. None of the inspected pipes were completely blocked or collapsed due to extensive damage. CCTV inspection did not provide a clear view of the manholes, and therefore, manholes in selected areas were visually inspected. The most of the defects were noted at the top part of the manholes. These defects include corrosion of frames and lids, damage to brick chimneys, and gaps between frames and chimneys/cones.

It is anticipated that by implementing this program, the City will eliminate the risk of failure of its sanitary sewers, reduce I&I, and increase the value of an important capital asset. It is also expected that by reducing I&I rehabilitation of defective sewer pipes will lower the cost of wastewater conveyance and treatment. The estimated cost of rehabilitation is approximately $1,600,000, which is approximately 16 percent of the anticipated depreciation without rehabilitation as present value.

The next steps are implementing the rehabilitation program and incorporating pre/post rehabilitation condition of the sanitary sewer system into the GIS database of the City. A continuous asset management with inspections/assessments and rehabilitation on a periodic base will maintain the level of service that will be achieved after rehabilitation and result in savings in economic and social cost by preventing a possible failure and avoiding pipe replacement.

References

Aikman, I, and Doherty, D.J. (2006). Overview of infrastructure asset management a view from both sides of the Atlantic Ocean, *Proceedings WEFTEC'06*, Water Environment Federation, Alexandria, VA.

Bakeer, R.M., and Sever, V.F. 2008. Quantification of annular flow in lined pipelines, *Tunnelling and Underground Space Technology*, 23 (6), 723-727.

ASCE Manuals and Reports on Engineering Practice No. 62. 1994. Existing Sewer Evaluation and Rehabilitation, American Society of Civil Engineers, New York, NY.

Underground Infrastructure Management (UIM, 2008). *Guide to Water and Wastewater Asset Management*, Benjamin, Peninsula, OH.

NAMS (2002). *International Infrastructure Management Manual*, Thames, New Zealand.

Le Gauffre, P., C. Joannis, E. Vascocelos, D. Breysse, C. Gibello, and J.J. Desmulliez (2007). Performance indicators and multicriteria decision support for asset management., *Journal of Infrastructure Systems*, 13 (2), 105-114.

Ecosystem Services Approach to Public Facility Planning

A.Yap[1], G. Honan[2], M. Kealy[3]

[1] City of Damascus, Oregon, Community Development Department, 19920 SE Highway 212, Damascus, Oregon, 97089; PH (503) 353-4500; FAX (503) 658-5786; email: ayap@ci.damascus.or.us.
[2] CH2M HILL, 2020 SW 4th Ave. Portland, Oregon, 97201; PH (503) 736-4258; FAX (503) 777-6667; email: ghonan@ch2m.com.
[3] CH2M HILL, 1717 Arch Street Suite 4400, Philadelphia, PA, 19103, PH (302) 478-1521; FAX (215) 640-9236; email: mary.kealy@ch2m.com.

Abstract

For the City of Damascus, Oregon incorporated in 2004, achieving sustainability includes balancing the preservation of natural capital and ecological services with provision of public facilities and services to support new development. This rural, forested and agricultural rich City is set among volcanic buttes and a network of perennial and ephemeral streams and riparian corridors tributary to the Clackamas River. Current residents value the diversity of the natural landscape for its scenic beauty as well as for its contributions to biodiversity, clean water, clean air, and the rural character of the area, as well as for the opportunities for income from use of their lands from timber sales and agricultural endeavors. These agricultural endeavors range from organic vegetable farms to Christmas tree lots. Inclusion of this area into the Urban Growth Boundary (UGB) in 2002 dramatically changed the land use regulations that had previously protected the forest and agricultural uses and opened the door to more intensive residential and commercial development.

The City, recognizes that the existing natural and modified ecosystems within and outside of their boundaries are providing benefits, that if lost would result in costs to the citizens of Damascus. This recognition of the services provided by natural resources has led the City to focus on identifying and quantifying these services so that decisions about there preservation, mitigation or restoration can be incorporated into their plans and implementation mechanisms. In initiating planning for provision of necessary public facilities such as water, waster water treatment, stormwater management and transportation, the City proposed an approach that explicitly accounts for changes in natural capital and its ability to provide valued ecosystem services for people.

The focus of this paper is on the conceptual approach to identifying, assessing, and valuing ecosystem services; and on the development of approaches for managing natural capital to provide valued ecological services.

What Are Ecosystem Services?

Ecosystem services are those flows of services from natural resources that are valued directly or indirectly by humans or contribute toward supporting the natural resource

base. Such ecological services can include capture of sunlight for food, shelter, nutrient recycling, capture of pollutants from runoff, nursery area for fish/shellfish, flood protection, recreational fishing, commercial fishing, etc. Researchers have found that as population, income, and consumption levels increase, humans put more and more pressure on the natural environment to deliver benefits. Sixty percent of ecosystem services assessed globally are either degraded or are being used unsustainably (Cowling, 2008).

Climate change, pollution, over-exploitation, and land-use change are some of the drivers of ecosystem loss, as well as resource challenges associated with urbanization. Often the benefit derived from altering the ecosystem is immediate and accrues to one individual, entity, or group, as in money made from the sale of clear-cut timber; whereas the cost, (erosion of soil, sedimentation of streams leading to loss of a fishery) is experienced by others and may not be realized for years or even decades. This unequal distribution of benefit obtained from use of an ecological good and the cost borne by its loss is evidence of the growing need for mechanisms for balancing use and loss of natural resources with maximizing the value of ecosystem services conserved.

Many of these goods and services are traditionally viewed as "public goods," that is free benefits to society. Without a formal market their important and even critical contributions are often overlooked in decision-making (USFS, 2009). When the ecosystem services provided by our natural and open space lands are not valued, or are undervalued, the areas supporting them are susceptible to development pressures and ultimately conversion to another use. When municipalities view their ecosystems as natural assets with economic and social value, these values can be brought into the overall balance sheet leading to more responsible decision-making (USFS, 2009).

Ecosystem Services: City Perspective

Damascus is the first new city in Oregon in over 22 years. The city was formed under regulatory circumstances, stemming from the expansion of the Portland metropolitan area's urban growth boundary in 2002. The Damascus area, which is predominately developed as rural residential, currently contains 9,775 people and is expected to accommodate 50,000 to 60,000 people in the future.

Oregon's land use planning framework was considered cutting edge for growth management in the late 1970s. Each City or metropolitan area must draw an urban growth boundary to contain urban development and provide urban services, such as sewer, water, stormwater, parks and transportation systems. The state mandated planning framework still exists today and has undergone many legal battles and refinement over the last 30 years. The incorporation of Damascus will challenge the regulatory, financial and technical standards that have been used over the last 30 years to build cities.

Damascus is currently 10,333 acres (16.15 square miles). Approximately 10% of the city is served by a sanitary sewer system. In addition, the community is rural in nature, where most properties are served by either wells, or small private water systems and on-site septic systems. No municipal stormwater system exists in

Damascus. Most of the roads are rural in nature, which contain two auto lanes, drainage ditches, no shoulders or curbs or sidewalks. It is estimated that it will take approximate $3 to 4 billion to provide needed infrastructure. (Metro, 2008).

Faced with limited financing from typical federal sources for wastewater, stormwater and transportation systems, the city is seeking creative alternatives to infrastructure development. Ecosystem Services approach will provide a way for the city to quantify natural resources contribution to the public facility system and, in the end reduce the cost of providing built infrastructure for the community. It is essential for the city to develop an analysis and system to provide developers and property owners certainty in the expectations and requirements for property development. The approach needs to be clear and understandable for a single property owner, in addition to staff, with limited scientific background to apply to situations on the ground.

Ecosystem Services – Identification, Assessment and Valuation

What is Net Environmental Benefit Analysis (NEBA)?

The net environmental benefit analysis framework shares the same theoretical foundation as benefit-cost analysis. The NEBA approach identifies and values the primary environmental services that an area or portfolio of holdings may provide given different land uses and actions (for example, wildlife management, building roads and infrastructure, siting facilities, discharging effluent, restoring stream habitat). The NEBA approach uses the recent emphasis in the ecological sciences to consider environmental services within a landscape context. Proposed actions will affect the valued quality and quantity of ecological services produced at the site or parcel differently depending upon the broader ecological and human landscapes. Some services may be improved, some may not be affected, and some may be harmed. A systematic evaluation of these service flows is needed to establish the existing condition, to make consistent comparisons across alternative actions affecting the City's natural resources, to evaluate trade-offs, to determine mitigation for offsetting losses, and to optimize the achievement of environmental objectives at least cost.

Even with advances in measurement, the services of nature are sufficiently varied, abundant, and specific to the human and ecological landscape, that it is not practical to attempt to assign a monetary value to every ecological service provided by every parcel. Fortunately, the quality and quantity of ecological services can be measured using ecological units. This can be accomplished at a high level using metrics that are intended to capture the aggregation of ecosystem service flows from each broad class of ecosystem/habitat types. This is the approach taken for incorporating natural resources and ecological services into the City's Public Facilities Planning Process. The basic economic principles guiding quantification of ecological services are straightforward.

1. Choose ecological metrics that capture the valued functions and services of the natural resources. A higher score on the quality scale and a larger number of units corresponds to an increase in value.

2. Ensure that these metrics are sensitive to the actions or changes to be evaluated. The application of the metric facilitates a credible and defensible priority ranking of different quality parcels of similar type ecosystems.
3. Finally, establish that the ecological metrics are understandable to decision-makers and other stakeholders.

When properly planned and implemented, the NEBA approach provides a systematic, consistent, and defensible process that can significantly enhance stakeholder support for selected environmental and land use planning decisions.

Ecological Service Value Quantification

The methodology adopted for the high level quantification of valued ecological services is the habitat equivalency analysis (HEA) methodology, which is used to quantify the ecological service value associated with selected parcels of similar functionality and ecosystem type. The HEA methodology is supported by many Federal Agencies (NOAA, DOI, USFWS, and NRCS) and in Federal Court Rulings (USA vs. M. Fisher et al. 1997) as a valid approach for quantifying impacts and benefits of ecological services associated with various actions, including preservation. The origin of this approach is presented in the 1991 USEPA commissioned paper entitled "*Scientifically Defensible Compensation Ratios for Wetland Mitigation*," (King and Adler, 1991). The HEA methodology has also been used with multiple state regulatory agencies across the United States (California, Texas, New Jersey, South Carolina, Virginia, Indiana, Louisiana, Florida, Oregon, Idaho, Alabama, plus others). Several peer reviewed articles have been published discussing the merits and limitations of this approach (King and Adler, 1991; Mazzotta, et al., 1993; Unsworth and Bishop, 1994; NOAA, 1995; NOAA, 1997; NOAA, 1998; Fonseca, et al., 2000; Nicolette et al., 2001; Efroymson et al., 2004).

The HEA methodology values natural resource assets in terms of the discounted sum of valued ecological service flows over time. Specifically, to quantify ecological service flows it uses indicators to measure the functionality of the ecosystem as a percentage of maximum functionality per acre (or an alternate spatial measure). An acre of wetland that is fully functioning for one year receives a score of 100% and provides one service-acre-year (SAY) of wetland services. However, an acre of wetland that is functioning at 80% of maximum potential provides only 0.8 service-acre-years of wetland services. Looking to the future, in the baseline condition, these wetland acres will continue providing a flow of ecological services, which are similarly measured in terms of their anticipated level of functionality. However, just as with valuing any asset based upon the stream of benefits that it "pays" over time, the future "payments" are discounted to reflect the preference for receiving the benefits sooner rather than later. Thus the total ecological service value of a natural resource asset is found by taking the discounted sum of service acre years or DSAYs. In the case of the City, it is assumed that the planning horizon extends for 100 years. If the wetland were to be developed in the future, the subsequent flow of ecological services (i.e., the future discounted SAYs) would be diminished.

Ecosystem Services Evaluation for City of Damascus, Oregon

The scale and complexity of evaluation is a key component in the cost and practicality of an approach to quantifying ecosystem services. The Natural Capital Project undertaken by a consortium of academics has laid out a 3-tiered approach to ecosystem services evaluation, moving from landscape level to detailed and site specific, that is a helpful starting place in determining the scale or level of detail appropriate for a given purpose or situation (Natural Capital Project, 2009) Using the concept of a three-tiered approach the definitions used for the City of Damascus evaluation are:

- **Tier 1** is fundamentally simple, provides a relative sense of the level of services provided across the landscape, and uses readily available data from standard municipal planning efforts.
- **Tier 2** provides a level of certainty based on more site specific data on current and future expected habitat characteristics.
- **Tier 3** is more in-depth with inclusion of parcel level data on habitat type and specific characteristics of the ecosystem dynamics and plant community characteristics linked to measurement of a specific ecosystem service. It is time, data, and cost intensive.

The Public Facilities Plan is a vehicle for a Tier 1 assessment that will introduce the concept of ecosystem services and allow discussion and action to incorporate these values as part of City policy and procedure. More in-depth analyses of ecosystem services at the Tier 2 and Tier 3 level can then be undertaken in partnership with landowners, developers and agencies when the need for these increasingly higher levels of resolution arise. For example, in the future, this high level assessment can be augmented with detailed evaluations of specific ecosystem services that stakeholders target for active management. The City of Damascus is specifically concerned about the thermal quality of their streams to meet temperature total maximum daily load requirements. In order to reach and maintain water temperature targets, metrics and measurement methods specific to this goal must be developed. Accounting for such individual services on an as needed basis is considerably more manageable then attempting to comprehensively identify and measure all of the ecosystem services provided by each land parcel, stream mile, and lake area.

The Tier 1 evaluation used existing natural features inventory mapping and habitat quality assessment to identify the location of the City's natural resources by ecosystem type and to assess their relative function. Habitat quality assessments were based on collection of field data related to provision of specific ecosystem services. Table 1 lists the habitat types and the ecosystem services evaluated in the functional assessment and Table 2 shows how the assigned alpha designators for function (e.g. A for high; B for moderate, and C for low) were translated to numeric scores of a measurement of how well each habitat type is providing its ecosystem services. Where data were not available, an assessment based on ecological principals was made using various geographic information system (GIS) tools.

Each ecosystem parcel in the GIS database was then identified by type of ecosystem and assigned the functionality score to estimate the ecological services per acre per

year that are supported by that ecosystem parcel. These DSAYs were computed for each ecosystem parcel and included in the inventory. For this purpose, it was assumed that the parcel would remain in its existing condition into perpetuity, if undisturbed. For example, an evergreen forest rated as 'A' quality by the City's assessment team was assumed to be providing the ecosystem services of an evergreen forest at 75% to 100%; 'B" at 50% to 74% and "C' at 25% -49% into the future.

Table 1. Ecosystem Services by Habitat Type

Habitat Type	Associated Ecosystem Services
Evergreen Forest	Wildlife habitat Erosion control Hydrologic control Water quality
Deciduous and Mixed Deciduous Forest	Wildlife habitat Erosion control Hydrologic control Water quality
Wetlands	Wildlife habitat Fish habitat Water quality Hydrologic control
Riparian Corridors/Streams	Wildlife habitat Fish habitat Water quality Streamflow moderation/water storage (Hydrologic control) Biodiversity support
Non-built/Non-native Lands (pasture and agricultural lands primarily)	Wildlife habitat Water quality

Table 2. Habitat Functional Rankings from City of Damascus, Oregon Natural Features Inventory Translated to Measure of Ecosystem Service Function

Habitat Functional Rating	Percent Ecosystem Service Function
A	75 % to 100% (mid-point 87.5%)
B	50%-74% (mid-point 62%)
C	25% - 49% (mid-point 37%)

Table 3 shows a portion of the results of the HEA value quantification for the evergreen forest habitat type. In this example there are 164.2 acres of 'A' quality

evergreen forest. For year 1 the 164.2 acres is multiplied by the percent function for an 'A' quality habitat shown in Table 2, or 87.5%. This yields the service acre years (SAYS) value of 143.68. This is discounted by 3% annually yielding the discounted service acre years (DSAYS) of 139.5 for year 1. The sum of the DSAYS for the 100-year model run yields the net present value (NPV) of the DSAYS for evergreen forest of 'A' quality, of 4, 540 DSAYS. Dividing this by the number of acres (164.2) yields the value of 27.65 DSAYS per acre when valued for 100-years. Discounting the SAYS out into perpetuity yields a NPV of 4,789. Dividing this by the number of acres (164.2) yields the value of 29.17 DSAYS when valued on into perpetuity. As seen in Table 3 the DSAYS for all 164.2 acres at year 100 is only 7.5 as compared with 139.5 in year 1. At some point after 100 years the DSAYS will approach zero. The Perpetuity NPV column accounts for the sum of DSAYS beyond 100 years until they approach zero.

Table 3. Sample Discounted Service Acre Years Calculations for 100 Years and for Perpetuity for Evergreen Forest 'A' Quality Habitat

Evergreen Forest									
Calendar Year	**Year**	**Discount Rate**	**Acres A**	**Quality**	**SAYS[1,2]**	**DSAYS[1,3]**	**Cumulative DSAYS[4]**	**NPV DSAYS/ acre[1,5]**	**Perpetuity NPV DSAYS/ acre[1,6]**
2008	0	0.03	164.2	0.875				27.65	29.17
2009	1		164.2	0.875	143.7	139.5	139.5		
2010	2		164.2	0.875	143.7	135.4	274.9		
2011	3		164.2	0.875	143.7	131.5	406.4		
Etc.	*	*	*	*	*	*	*	*	*
2108	100		164.2	0.875	143.7	7.5	4,540		
NPV[1]					4,540				
Perpetuity NPV					4,789.2	Perpetuity NPV			

Notes:
[1] SAY = service acre years; DSAYS = discounted service acre years; NPV = net present value
[2] *Acres* X *% function* = SAYS
[3] $SAYS/(1 + discount\ rate)^{year}$ = DSAYS
[4] Sum of annual DSAYS (i.e. year 1 DSAYS + year 2 DSAYS = year 2 cumulative DSAYS etc.)
[5] Cumulative NPV DSAYS for year 100/ total number of acres = net present value of discounted service acre years per acre
[6] Perpetuity cumulative NPV/ total number of acres = net present value of discounted service acre years per acre

Preservation of Ecosystem Services

Regulations or flexible ordinances, land acquisitions, conservation easements, and tax incentives are some of the tools that the City of Damascus can use to protect and conserve the public goods provided by their natural resources while providing for growth and development. Traditional conservation programs are not likely sufficient to safeguard the natural landscapes and traditional markets may not provide landowners with a sufficient economic incentive to own and sustainably manage their privately held lands for public benefits. To prevent the indiscriminate loss or degradation of ecosystem services, the City has the opportunity to incorporate into any decision-making the value of ecosystem services and to provide economic and financial motivations for conservation of high valued services (Cowling, 2008).

Mechanisms are being explored by which private landowners can seek returns on their land *in addition* to or in place of those commonly associated with urban uses. The ability to capture the financial value of ecosystem services may help landowners who currently do not benefit from the true value of their land and all of the goods and services their natural resources provide. Because ecosystem services are not traded and do not have a "price," landowners are not typically compensated for the critical benefits their land naturally deliver to the public. New natural revenue streams might help owners cover the costs of owning natural lands and provide them with incentives to hold onto their land in lieu of selling or developing. Valuing ecosystem services will encourage preservation and restoration and may provide a new means to finance these activities.

The Tier 1 ecosystem service assessment provides a screening level valuation that can form the basis for a scaled assessment fee for all City lands or to value lands for purchase of their ecosystem service value. Developers would be charged a fee for loss of the NPV DSAYS of their given property or required to purchase equivalent NPV DSAYS to compensate for loss of services. If a fee were assessed the City could use this revenue to purchase the development rights or conservation easements of high ecosystem service values lands, or to fund restoration efforts. Using the evaluation of NPV DSAYS completed for the City, the per acre NPV DSAYS of 29.17, shown in Table 3, can be used to quantify the lost ecosystem service value of developing anywhere from 1 to 164.2 acres of 'A' quality evergreen forest or to establish the acres of 'B' or 'C' evergreen forest necessary for restoration to an 'A' level as compensation for lost 'A' quality evergreen forest ecosystem service values.

Conclusion

The City Planners of Damascus, Oregon are charting new territory in their attempt to include the services that the region's natural assets provide their citizens into their Public Facilities Planning. Implementing a fair and equitable system for regulation of these areas or development of effective incentive based programs is challenging and as yet, untested. The goal is a practical integration of ecosystem services into decision-making, in a way that is credible, replicable, scalable, and useable. There remain many challenges to understand how human actions affect ecosystems, the provision of ecosystem services, and the value of those services, but the Tier 1 assessment provides a screening level valuation that can form the basis for

preservation of ecosystem service values. The City still faces the challenges associated with incorporating this understanding into effective policy that accurately reflect the social values of ecosystem services to its citizens (Daily, 2008)

References

Cowling, R.M., B. Egoh, A.T. Knight, P.J. O'Farrell, B. Reyers, M. Rouget, D.J. Roux, A. Welz, and A Wilhelm-Rechman. 2008. An Operational Model for Mainstreaming Ecosystem Services for Implementation. *Proceedings of the National Academy of Sciences*. Vol. 105, No. 28, pp 9483-9488. July 15, 2008.

Daily, G.C. and P.A. Matson. 2008. Ecosystem Services: From Theory to Implementation. *Proceedings of the National Academy of Sciences*. Vol. 105, No. 28, pp 9483-9488. July 15, 2008.

Department of Commerce. 1996. Oil Pollution Act Regulations. Part 990. Natural Resource Damage Assessments. 15 CFR Part 990. http://www.epa.gov/superfund/programs/nrd/15cfr990.pdf

DOI (U.S. Department of the Interior). 1995. 43 CFR Subtitle A, Part 11. Natural Resource Damage Assessments.

DOI (U. S. Department of the Interior), Virginia Department of Environmental Quality, and District of Columbia Department of Health. 1999. Colonial Pipeline Oil Spill, Reston, Virginia. Final Restoration Plan and Environmental Assessment. National Park Service, U.S. Department of the Interior, Washington, D.C.

Efroymson, R.A., J.P. Nicolette, and G.W. Suter II. 2004. "A Framework for Net Environmental Benefit Analysis for Remediation or Restoration of Contaminated Sites," *Environmental Management*. Vol. 34, No. 4, pp. 315-331. 2004.

Fonseca, M. S., B. E. Julius, and W. J. Kenworthy. 2000. Integrating biology and economics in seagrass restoration: How much is enough and why? *Ecol. Eng.* 15:227–237.

King, D. M., and K. J. Adler. 1991. Scientifically defensible compensation ratios for wetland mitigation. U.S. Environmental Protection Agency Office of Policy, Planning and Evaluation. Washington, D.C.

Metro, July 9, 2008, Comparative infrastructure costs: local case studies. Regional Infrastructure Analysis Discussion, Draft

National Research Council. 2001. *Operational Guidelines for Creating or Restoring Self-Sustaining Wetlands*, from 'Compensating for Wetland Losses Under The Clean Water Act,' June 2001 (Chapter 7, pp. 123-128).

Natural Capital Project. 2009. InVEST: Integrated Valuation of Ecosystem Services and Tradeoffs. http://www.naturalcapitalproject.org/InVEST.html

Nicolette, J. P., M. Rockel, and M. J. Kealy. September 2001. Quantifying ecological changes helps determine best mitigation. *Pipe Line Gas Ind.* 52–57.

NOAA Damage Assessment and Restoration Program. 1995. Habitat equivalency analysis: an overview. National Oceanic and Atmospheric Administration. Silver Spring, Md.

NOAA Damage Assessment and Restoration Program. 1997. Scaling compensatory restoration actions, guidance document for Natural Resource Damage Assessment. National Oceanic and Atmospheric Administration. Silver Spring, Md.

NOAA Hazardous Materials Response Branch. 1990. Excavation and rock washing treatment technology: Net environmental benefit analysis. National Oceanic and Atmospheric Administration. Seattle, Wash.

United States Environmental Protection Agency (USEPA). 2000. Guidelines for Performing Regulatory Impact Analysis. EPA-240-R00-003. Office of the Administrator, Washington, D.C. 20460. September, 2000. http://epa.gov/osa/spc/eaeb.htm.

United States Environmental Protection Agency (USEPA). 2006. Ecological Benefits Assessment Strategic Plan. EPA-240-R06-001, National Center for Environmental Economics (1809T) Office of the Administrator, USEPA, 1200 Pennsylvania Ave., N.W., Washington, D.C. 20460. October, 2006. http://www.epa.gov/economics/

Unsworth, R. E., and R. C. Bishop. 1994. Assessing natural resource damages using environmental annuities. *Ecol. Econ.* 11:35–41.

USFS (United States Forest Service). 2009. Ecosystem Services. www.fs.fed.us/ecosystemservices/; www.fs.fed.us/ecosystemservices/About_ES/index.shtml

An Evaluation of Graywater Reuse Utilizing a Constructed Wetland Treatment System

A.W. Jokerst[1], L. A. Roesner[2], and S.E. Sharvelle[3]

[1]Department of Civil and Environmental Engineering, Colorado State University, Fort Collins, CO 80523-1372; PH (970)491-2838; email: adam.jokerst@colostate.edu

[2]Department of Civil and Environmental Engineering, Colorado State University, Fort Collins, CO 80523; PH (970) 491-7430; email: larry.roesner@colostate.edu

[3]Department of Civil and Environmental Engineering, Colorado State University, Fort Collins, CO 80523; PH (970) 491-6081; email: sybil.sharvelle@colostate.edu

ABSTRACT

Increasing demand for conservation of water resources has prompted the notion that the separation of graywater (all wastewater not including toilet and kitchen sources) from sewer effluents through the use of dual-plumbed systems may enable graywater to be reused. Constructed wetland systems for conditioning combined wastewater effluents are widely used, and offer an efficient solution for onsite wastewater treatment of a variety of pollutants. However, limited long-term research has been conducted to determine the effectiveness of such systems specifically on graywater. This paper aims to determine the viability and efficiency of constructed wetlands for graywater treatment, and assess the water quality produced from such systems. The experimental method involves monitoring of specific water quality constituents under varying operating conditions in a prototype constructed graywater wetland. Preliminary findings show the wetland significantly reduces many graywater contaminants including pathogens, biochemical oxygen demands, solids, and nitrogen and phosphorus species.

INTRODUCTION

Conventional wastewater management practices collect all used indoor water into a single pipe leading to the sewer and treat it at a wastewater treatment plant. Mounting pressure to conserve water supplies, however, has lead to the suggestion that the separation of wastewater at its source may enable graywater to be reused for such non-potable uses as landscape irrigation and toilet flushing.

Graywater Quantity and Quality Characterization

A general definition of graywater is any residential wastewater which has not come in contact with toilet water. This definition is restricted in the United States where graywater is defined as wastewater not originating from toilets, kitchen sinks, or dishwashers, and that is produced in showers, bathtubs, sinks, and cloths washers (Roesner et al., 2006).

An American Water Works Association (AWWA) sponsored study of water usage in 14 North American cities found that on average over 50% of all residential indoor water demands generate graywater (Mayer et al., 1999). This same study showed that outdoor irrigation constituted the largest of all total residential potable water demands, and that while highly variable depending on geographical location, on average over 50% of all residential potable water is used for landscape irrigation. Considering this large demand and the fact that the source water for outdoor irrigation water need not be of the same quality as indoor potable water, reusing graywater for outdoor irrigation offers a substantial and attractive water savings. In addition to landscape irrigation, recycled graywater is a potential source for other demands not requiring potable source water such as toilet flushing.

Graywater recycling in Europe and Australia is gaining in popularity; however, in the U.S. the practice is not yet commonplace. The degree to which graywater reuse can reduce household potable water demand is variable depending on geographical location, landscaping preferences, and personal water use habits. Rose, 1991; Karpiscak, 1990; and the City of Los Angeles, 1992 among others have estimated that reusing graywater for outdoor irrigation and toilet flushing could reduce household water demand by 25 – 50%.

The chemical, physical, and microbial qualities of graywater are highly variable depending on the source, and are influenced by many factors including the number of household occupants, types of cleaners and personal care products used, grooming and hygiene habits, and sink waste disposal practices (Eriksson et al., 2002). Concentration ranges for common water quality constituents and pathogen indicators compiled from three studies are listed in Table 1.

Constructed Wetlands

Constructed wetlands are treatment systems that replicate natural wetlands to improve water quality through physical, chemical, and biological treatment mechanisms (Kadlec and Knight, 1996), and are commonly employed to treat municipal wastewater (Metcalf and Eddy, 2003; U.S. Environmental Protection Agency (USEPA), 1999; Hammer, 1989). Not only can constructed wetlands provide important water quality improvements with low energy and maintenance requirements, they can also offer pleasing aesthetics, ecological benefits, and wildlife habitat (USEPA, 1999).

While treatment wetlands have been shown to effectively treat whole wastewater, their effectiveness in treating graywater has had limited research, especially in the United States. However, past studies involving graywater wetland treatment have shown promising pollution removal efficiencies (Dallas, 2004; Gross, 2007; Frazer-Williams, 2005).

Constructed wetlands can take on various designs, with two of the most common being the free water surface (FWS) and the subsurface flow (SF) wetland. FWS wetlands closely resemble natural wetlands in both appearance and function, and

feature elements typical of a natural wetland such as emerging vegetation and open-water areas (USEPA, 1999). SF wetlands, on the other hand, resemble natural wetlands very little, but instead contain a bed of media such as gravel or sand in which aquatic plants are rooted. Water passes through the media and root zone, but is not exposed to the surface, and is therefore not visible or accessible by humans or wildlife.

Table 1: Graywater quality characterization

Reference	Eriksson et al., 2003	Rose et al., 1991	Casanova et al., 2001
Source	Composite, Range	Composite, Mean	Composite, Mean
pH	7.6 - 8.6	6.54	7.47
BOD_5, mg/L	26 -130		64.85
Total Suspended Solids, mg/L	4 - 207		35.09
Turbidity, NTU		76.3	43
Ammonia, mg/L	0.02 - 0.42	0.74	
Nitrate, mg/L	<0.02 - 0.26	0.98	
Total Nitrogen, mg/L	3.6 - 6.4	1.7	
Orthophosphate, mg/L		9.3	
Total Phosphorus, mg/L	0.28 - 0.779		
Sulfate, mg/L		22.9	59.59
Chloride, mg/L		9	20.54
Alkalinity, mg/L		158	
Total Coliform, CFU/100mL	6.0×10^3 - 3.2×10^5	2.8×10^7	8.03×10^7
Fecal Coliform, CFU/100mL		1.82×10^4- 7.94×10^6	5.63×10^5
E.Coli, CFU/100mL	<100 - 2800		

MATERIALS AND METHODS

Wetland Design

To evaluate the potential of graywater wetland treatment, a prototype graywater wetland and two dual-plumbed facilities were constructed at Colorado State University. The graywater wetland is a tandem wetland system consisting of a FWS wetland cell followed SF wetland cell. The combination of both a FWS and a SF wetland type was designed to enhance water contaminant removal, and to allow for each wetland type to be evaluated individually. Out of initial public safety concerns, effluent from the prototype system is currently routed to a sanitary sewer; however, future plans call for the effluent to be reused for non-potable demands.

FWS and SF wetland cells are arranged in series with the FWS being upstream of the SF (Figure 1) so that the FWS provides the bulk area for sediment settling and prevents clogging of the gravel matrix in the SF. Also, since the FWS is exposed to the atmosphere and the SF is not, having the FWS upstream of the SF also allows an aerobic/anerobic flow progression. The wetland includes flow distributing and collection headers to prevent flow short circuiting, diversion berms to prevent surface water runoff intrusion, and impermeable liners to restrict groundwater flux.

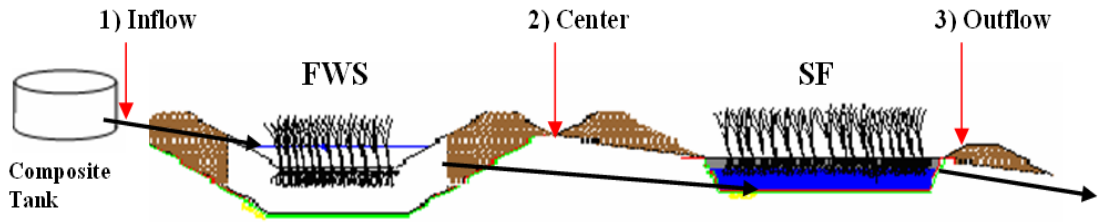

Figure 1: Graywater wetland schematic and sampling locations.

Graywater is provided to the wetland system from several of sources: lavatory sink water from a dual-plumbed office/laboratory facility, lavatory sink and shower water from a residential dormitory, and whole graywater (all wastewater except toilet and kitchen sources) from a single-family residence. Graywater from the office/laboratory facility is piped directly to the wetland. Graywater from the dormitory and residence is collected in batches onsite and hauled to the wetland where it is dispensed via metering pump. Hauling graywater proved necessary since the office/laboratory facility is not yet fully occupied and does not produce the flow rate of graywater desired. Hauled graywater is mixed with the graywater stream from the office/laboratory building before flowing to the wetland. A storage tank is provided just upstream of the wetland inlet, which is sized to collect approximately one day's flow volume, and it thus used to collect a daily composite of inflow.

Common Cattails (*Typha latafolia*) are planted in the FWS cell, and have been established since September, 2007. The SF is planted with Hardstem Bulrush (*Scirpus acutus*), which have been established since June, 2008.

Flow and Water Quality Monitoring

Flow and water quality measurements are made at three locations (Figure 1): the inflow to the FWS at the composite tank (Site 1; raw graywater influent), between the FWS and SF (Site 2; center; FWS effluent/SF influent), and the outflow of the SF (Site 3; system effluent). Site 1 is taken from the composite tank, and represents a daily composite. Sites 2 and 3 are located in manholes and are not composited.

Flow meters are located at each sampling site. The flow metering system features a dosing vessel that collects inflowing water until it is full, at which time a pump is activated which pumps the water through an inline, turbine flow meter. This design is necessary to accommodate the low flows produced by the office/laboratory building (down to 19 L/day), while being capable of handling large flow events (as in the case of heavy precipitation entering the wetland) with high solids concentrations. No data

recording hardware is used; instead, readings of the cumulative flow at each location are collected manually, and the flow computed as the difference in cumulative flows from two sequential readings divided by the time between readings. A counter switch is provided to count the number of times the dosing vessel fills and empties, which can be used in redundancy to compute flow.

Sampling was conducted starting in September, 2008. Sampling commenced weekly for four weeks, after which samples were collected every three weeks. Water quality measurements evaluated the physical, chemical, and biological composition of the raw and treated graywater (Table 2), and included measurements of the solids, carbon, nitrogen, phosphorus, and pathogen indicator content of the water. These measurements were chosen to evaluate the wetlands' treatment efficiency in removing such constituents, as well as determine the quality of the effluent produced from the system. In addition to the measurements listed in Table 2 other water quality measurements have been commenced to test for different pathogenic indicator species and trace organics. Standard analytical methods (Eaton et al., 1998) were used for all analyses, and quality assurance samples (blanks, duplicate analyses, and standards) were analyzed at a rate of 10%.

Table 2: Water quality measurements and analytical methods used to determine the treatment performance of the graywater wetland system.

Parameter	Analytical Method	Standard Method #
Ammonia	Ion Selective Electrode	4500-NH_3 D
5-day Biochemical Oxygen Demand (BOD_5)	5-day; Dissolved Oxygen Probe	5210 B
Dissolved Oxygen (DO)	Membrane Electrode	4500-O G
E. Coli	Enzyme Substrate	9223 B
Nitrate	Ion Chromatography	4110 B
Orthophosphate	Ion Chromatography	4110 B
pH	Potentiometric Probe	4500-H^+ B
Specific Conductivity	Electrical Conductivity	2510 B
Temperature	Thermometer	2550 B
Total Dissolved Solids (TDS)	Gravimetric, Dried at 103-105 C	2540 C
Total Nitrogen (TN)	UV Persulfate Digestion and Oxidation w/ Flow Injection	4500-N B
Total Organic Carbon (TOC)	Heater-Persulfate Oxidation	5310 C
Total Phosphorus (TP)	Colorimetric; Persulfate Digestion	4500-P H
Total Suspended Solids (TSS)	Gravimetric, Dried at 103-105 C	2540 D
Turbidity	Nephelometric	2130 B

RESULTS

Flow Monitoring

During the sampling period, graywater inflow to the wetland system averaged 318 L/day (Site 1, Figure 2). This inflow rate is averaged over two distinct periods. Prior to December 11, 2008 hauled graywater was collected from the dormitory and the average flow rate of inflow was 346 L/day. After December 11, the dormitory was unoccupied, graywater was collected from the single family residence, and the inflow averaged 154 L/day. For the entire monitoring period, flow between the FWS and SF wetlands (Site 2) averaged 282 L/day, and the system outflow (Site 3) averaged 245 L/day. Differences in flow rates between monitoring stations result from precipitation additions and losses attributed to seepage over the wetlands' liners and evapotranspiration. Losses diminished as weather cooled and the vegetation became dormant.

Wetland volumes were used to compute the hydraulic residence times (HRTs) in each wetland cell. The FWS volume was estimated at 2.0 m^3, assuming a porosity of 0.8 for the established cattails. SF volume was 2.9 m^3 assuming a porosity of 0.3 for the gravel and plant root matrix. Using these volumes and the average flows previously given, an average HRT of 6.3 days and 10.3 days were computed for the FWS and SF cells respectively over the entire monitoring period.

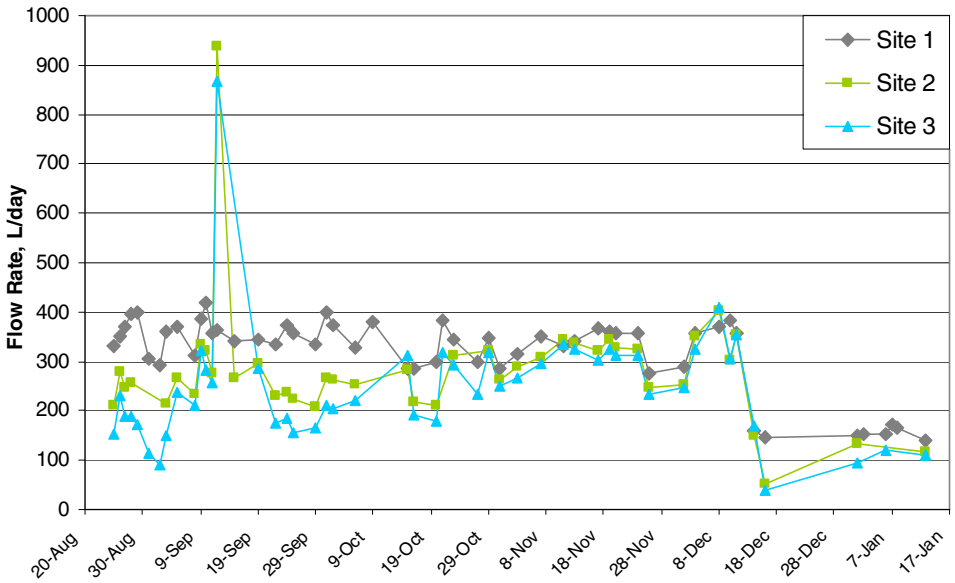

Figure 2: Flow rates measured at the graywater wetland system. The large flow rate increase at Sites 2 and 3 on 9/12/08 results from a precipitation event.

Water Quality Monitoring

Nine water quality sampling events were conducted over the monitoring period. All sampling sites were monitored during each sampling events except the first two; to allow for steady state conditions, Sites 2 and 3 were omitted from the first sampling event and Site 3 was omitted from the second event. Selected water quality measurements are presented subsequently (Figure 3 and 4; Table 3).

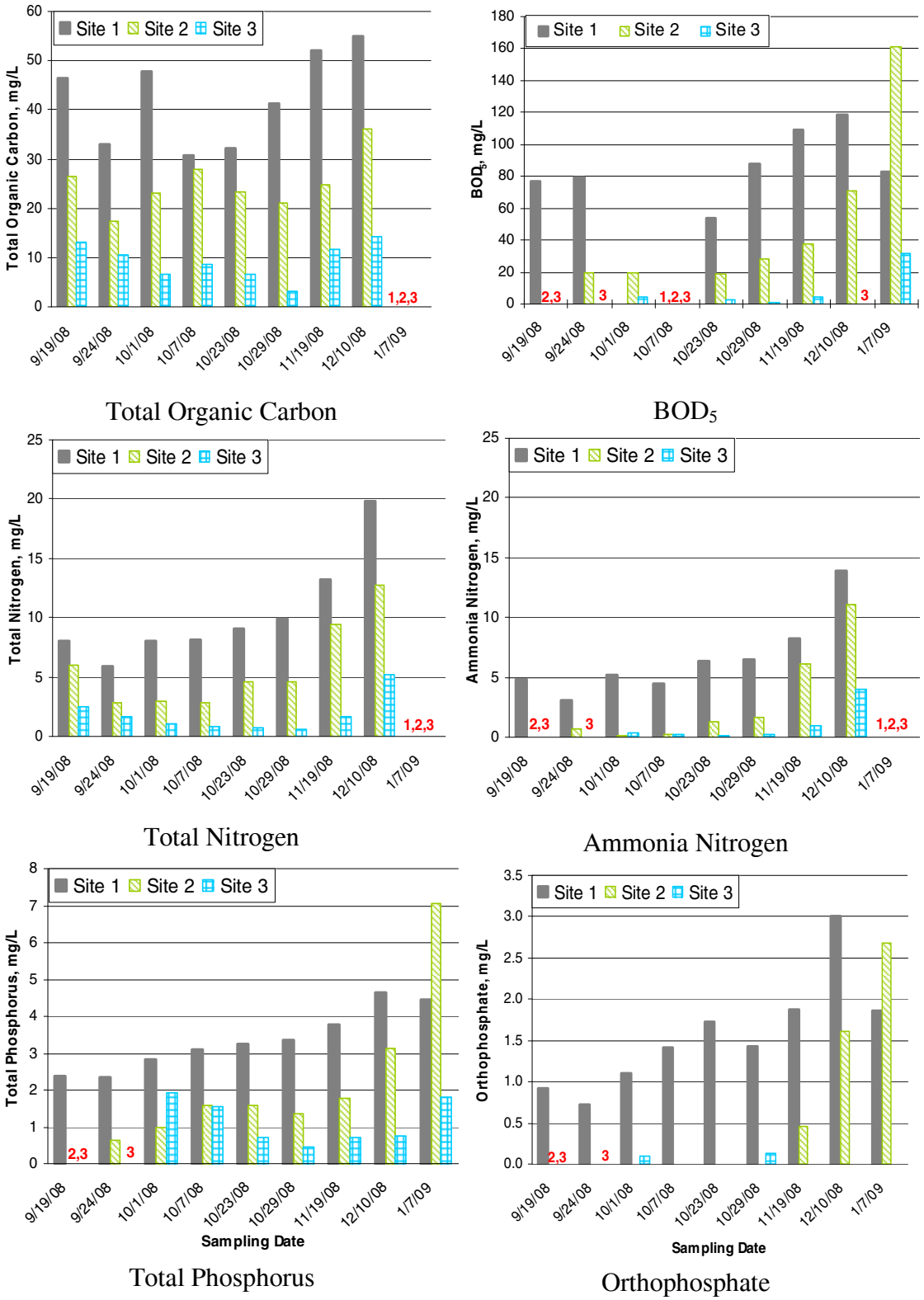

Figure 3: Average concentrations of carbon, nitrogen, and phosphorus water quality constituents at three sampling locations in the graywater wetland taken over nine sampling events. Numbers in red represent erred or omitted measurements.

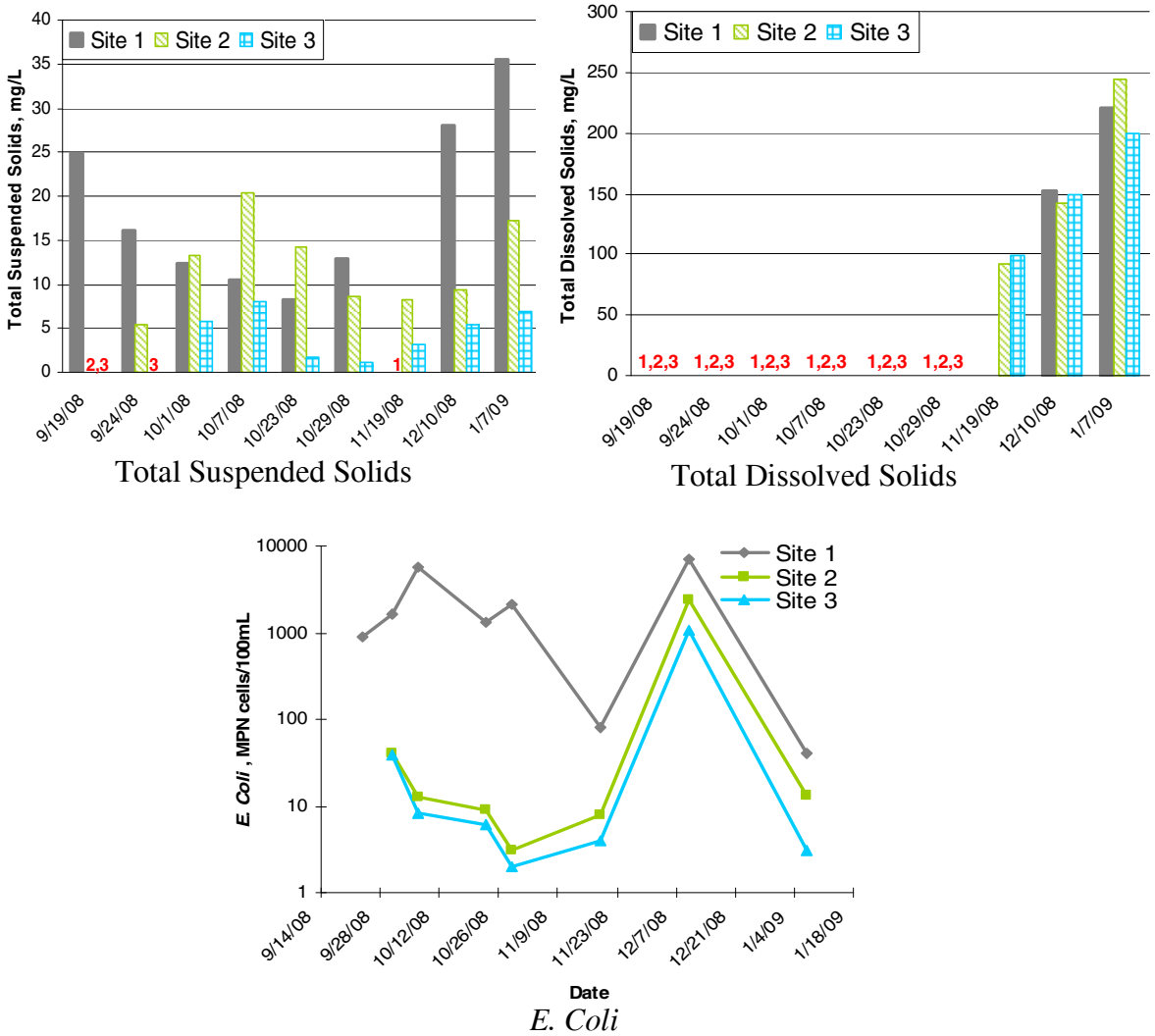

Figure 4: Average values of solids and pathogen indicator measurements at three monitoring locations in the graywater wetland. Red numbers represent erred or omitted measurements.

Table 3: Field measurements taken at graywater wetland.

		Site 1	Site 2	Site 3
Dissolved Oxygen, mg/L	Range	0.02 - 0.17	0.89 - 5.46	0.82 - 2.96
	Mean	0.11	2.65	2.18
pH	Range	6.0 - 6.7	6.3 - 6.9	6.3 - 6.8
	Mean	6.3	6.7	6.5
Specific Conductivity, uS/cm	Range	197 - 348	235 - 409	256 - 404
	Mean	232	276	299
Turbidity, NTU	Range	8.1 - 58.2	5.6 - 46.0	1.5 - 18.5
	Mean	27.4	17.7	7.9

Removal efficiencies were computed for each wetland cell and for the total system (Table 4), and were calculated from the average concentration values for all sampling events. Pathogen levels were shown to decrease approximately 0.8 and 0.4 orders of magnitude on average through the FWS and SF wetlands respectively. Removal efficiencies for all constituents were generally greatest in the FWS.

Table 4: Average removal efficiencies of various constituents in the graywater wetland. Values presented exclude the January 7, 2009 sampling event.

	FWS	SF	Total
BOD_5	63%	33%	96%
TOC	41%	37%	78%
TN	44%	39%	83%
TP	50%	18%	68%
Turbidity	42%	31%	73%
TSS	30%	44%	74%
E. coli	85%	9%	93%

DISCUSSION

As determined from repeat water quality analysis in the prototype wetland, treatment of graywater via constructed wetlands demonstrates great potential. Effluent water has shown to be of the quality suitable for reuse, as in the case of *E. coli* levels, which were shown to be below recommended single-sample levels for primary contact waters according to USEPA, 1986 for all but one sample. It should be noted that the one sample out of compliance was taken while significant ice had formed on the wetlands, greatly reducing the wetland's HRT. This problem is only expected in the winter when graywater reuse for irrigation is not needed.

Water quality monitoring is expected to continue through 2009, which should shed light on the long-term performance of the graywater wetland. Expanded water quality analysis, including those of additional pathogenic indicators and trace organics will further evaluate the graywater wetland's treatment potential.

REFERENCES

Casanova, L.M., V.Little, R.J.Frye, and C.P.Gerba 2001. A survey of the microbial quality of recycled household graywater. *Journal of the American Water Resources Association (JAWRA)* 37(5)

City of Los Angeles. 1992. Graywater pilot project, final report. Office of Reclamation at the City of Los Angeles.

Dallas, S., Scheffe, B. and Ho, G. 2004. Reedbeds for greywater treatment—case study in Santa Elena-Monteverde, Costa Rica, Central America. *Ecological Engineering*, 23, No. 1.

Eaton, A.D., L. S. Clesceri, and A. E. Greenburg, 1998. *Standard Methods for the Examination of Water and Wastewater, 20th Edition*. American Public Health Association, AWWA, and Water Environment Federation.

Eriksson, E., K. Auffarth, A.A.Eilersen, M Jenze, and A. Ledin, 2003. Household chemicals and personal care products as sources for xenibiotic organic compounds in grey wastewater*, Water SA*. 29

Eriksson, E.; Auffarth, K.; Henze, M., Ledin, A. 2002. Characteristics of grey wastewater. *Urban Water* 4

Frazer-Williams R., Avery, L. and et al. 2005. Constructed wetlands for urban greywater recycling. *Proceedings of the First Conference on Sustainable Urban Wastewater Treatment and Reuse*, Nicosia, Cyprus

Gross, A., Shmueli, O., Ronen, Z. and Raveh E. 2007. Recycled vertical flow constructed wetland (RVFCW)—a novel method of recycling greywater for irrigation in small communities and households. *Chemosphere*, 66, No. 5.

Hammer, D.A. 1989. *Constructed Wetlands for Wastewater Treatment*, Lewis Publisher Inc., Chelesea, MI (1989).

Kadlec, R. H., and Knight, R. L. 1996. *Treatment wetlands*, CRC, Boca Raton, FL

Karpiscak, M., Foster, K, E., and Schmidt, N. 1990. Residential water conservation: Casa Del Agua. *Water Research* **26**(6)

Mayer, P.W., De Orea W.B., and et al. 1999. Residential end uses of water. American Water Works Association sponsored report

Metcalf and Eddy, Inc., (2003). *Wastewater Engineering, Treatment and Reuse, 4th Edition*, McGraw-Hill, Boston Burr Ridge, IL, USA.

Roesner, L. A., Qian, Y., and et al. 2006, Long-term effects of landscape irrigation using household graywater – literature review and synthesis. Water Environment Research Federation sponsored report

Rose, J. B.; Sun, G.; Gerba, C. P.; and Sinclair, N. A. 1991. Microbial quality and persistence of enteric pathogens in graywater from various household sources. *Wat. Res.* **25**(1)

U.S. Environmental Protection Agency (USEPA), 1986. Ambient water quality for bacteria – 1986. EPA440/5-84-002. Washinton, DC

U.S. Environmental Protection Agency (USEPA), 1999. Constructed wetlands treatment of municipal wastewaters. EPA/625/R-99/010. Cincinnati, OH

Application of Enhanced Methods of Phosphorus and Nitrogen Removal from Wastewater

Mohammad Reza Fallahpour[1] and Mojtaba Fazeli[2] and Seyed Ahmad Mirbagheri[3]

1. Power and Water University of Technology (PWUT), MSc student, Tehran, Iran
mrfallahpour@gmail.com
2. PWUT member of the water and wastewater engineering board, Tehran, Iran
fazeli_m@hotmail.com
3. Khaje Nasir Toosi head of the environmental engineering board, Tehran, Iran
mirbagheri@knut.ac.ir

Abstract

Compounds of nitrogen and phosphor in wastewater treatment plant effluents have caused serious and even dangerous problems including incidence of methemoglobinemia in new born babies as a result of consumption of water contaminated with nitrate and also nitrification in surface water. Various processes and methods at different scales have been used with the aim to remove effectively such compounds so as to prevent the potential of harmful and dangerous incidences mentioned above at its lowest level. One of these processes is the use of A^2/O (Anaerobic, Anoxic, Oxic) in activated sludge process. The purpose of this process undertaken in a pilot system is removal of carbon and phosphor over 90 percent and also reduction of nitrogen density in effluent in MLSS.

Keywords: Nitrification, Denitrification, A^2/O process, activated sludge, nitrogen and phosphor removal

1. Preface

Urban wastewater treatment plants were established in the past mainly with a view to remove organic pollutants, suspended materials and microbic contaminants. As the effects of nitrogen and phosphor compounds in water (mainly ammoniac poisoning, high growth of water plants and formation of nitrification, contamination of underground water by nitrate) and also incidence of methemoglobinemia disease in new born babies all of these have resulted in restricting density of such compounds in effluents flowing in the environment and also flowing into water streams. The main example of the effect of such pollutants entering the environment are the nitrification phenomena in the Caspian sea (fig. 1) and incidence of methemoglobinemia disease (fig. 2)



Figure 1. Formation of nitrification phenomena in the Caspian sea (green areas)



Figure 2. Child afflicted with methemoglobinemia disease or blue baby.

Consumption of water containing more than 50 mg/l nitrate ion, specially in children, causes methemoglobinemia due to compound of this ion with blood hemoglobin. This compound prevents oxygen reaching the tissues resulting in local suffocation and ultimately in death. On the other hand due to low bowel acidity of children (normally bowel acidity of children is more than 4.9) the bacteria transforming nitrate to nitrite have high activity and nitrite compounds with hemoglobin to form methemoglobinemia causing death. It is essential therefore that, in designing urban wastewater treatment plants (WWTP) to take into consideration the amount of such compounds and to eliminate compounds of nitrogen and phosphor in designing WWTP up to the standard level. To reach the standard level it is necessary to remove both nitrogen and phosphor. The biological process for removal of these pollutants easily compound with activated sludge. In all such processes the basic components are similar and include anaerobic, anoxic and aeration, their difference being in the number of components, their order and places of flow return [1]. One of these processes is A^2/O which is used when it is necessary to remove ammoniac alone (nitrification), or to remove nitrogen (nitrification-denitrification). In this process and

anoxic area locates between anaerobic and aerobic zones causing removal of ammoniac and reduction of nitrate charge present in sludge returned to anaerobic chamber. Because due to this area some of the nitrogen is eliminated under removal of nitrate this process improves phosphor elimination. Because presence of nitrate in returned sludge incoming to the anaerobic chamber causes slow down of phosphor removal process. By return of the solution mixed nitrified from aeration chamber, the oxygen present in the chemical compound is added to it in the form of nitrate or nitrite. The expected concentration of phosphor without being filtered is less than 2 mg/l. By filtering the outlet effluent, phosphor concentration could be less than 1.5 mg/l. The most important advantage of the A^2/O process can be described briefly as follows:

- Useful in high loading
- Sludge fertilizer value with high phosphor content (3-5%)

The only disadvantage of this process is its unreliability in cold weather where the anoxic/oxic A/O removal of phosphor only is more complex [3]. The schematic diagram of the process is shown in the following figure. The primary principle of the process in given below, and the pilot system used together with the results obtained is discussed below.

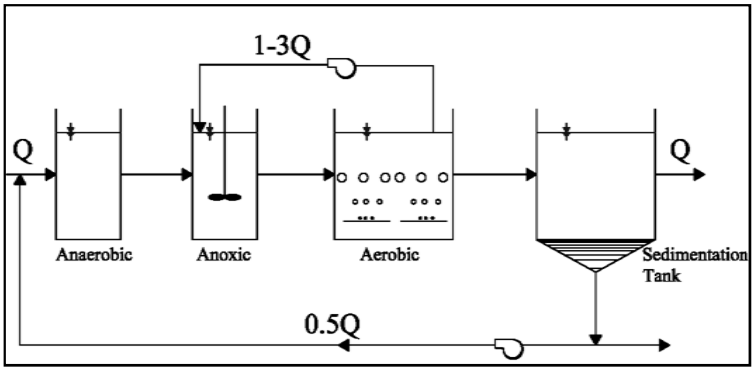

Figure 3. A^2/O process scheme [1]

2. Acquaintance with the primary principle used in A^2/O process compared with the usual activated sludge

Phosphor in wastewater is seem as orthophosphate (PO_4^{-3}) polyphosphate (P_2O_7) and phosphor organic compound, the last two compounds comprise up to 70% of the input phosphor. The microbes during cell synthesis and energy transformation consume phosphor. As a result 10-30 % of the inlet phosphor is separated in secondary biological treatment. But the main reason for success in biological phosphor separation is rendering microorganism alternatively in anaerobic an aerobic conditions. When the microorganisms are put alternatively in anaerobic and aerobic conditions, they are more agitated thus their consumption of phosphor is more than

normal. Phosphor is consumed not only for cell protection, synthesis and energy transformation but it is also reserved for later consumption of the microorganisms.

In urban wastewater, mainly of the residential type, nitrogen is found in the form of or organic and ammonia. This compound is the waste as a result of protein metabolism in human body. In fresh wastewater about 60% of nitrogen is in organic and 40% in ammonia forms. As a result of bacterial break-up (analysis) of the protein and urea hydrolyze compound, the organic nitrogen is converted to ammonia nitrogen. Normally, in fresh wastewater small quantity (less than one percent) nitrogen is found in the form of oxidized nitrate or nitrite.

Organic nitrogen present in untreated wastewater is changed to ammoniac by way of bacterial analysis of protein and ureas hydrolyze. In any biological treatment system, some bacteria growth take place, because 12-13% of the cell dry mass is composed of nitrogen, some ammoniac nitrogen is absorbed by the new cells. Also, self-oxidization and the cells becoming slippery would depend on the treatment process and the loading conditions. Thus, a protein of the ammoniac used for the cell synthesis is returned back again to the wastewater by way of becoming slippery and self-oxidization. The remaining absorbed nitrogen can be removed as pure growth or disposable biological sludge.

The main point in removal of both phosphor and nitrogen compound is the amount of dissolved oxygen in the wastewater. As can be seen in figure 4, in the (a) condition, the low dissolved oxygen concentration and F/M ratio, all the flocs are aerobic and the nitrification process continues by maximum speed. In the (b) condition, due to high F/M ratio, the oxygen consumption is higher, therefore nitrification process is halted. In (c) condition, by increasing the dissolved oxygen concentration together with higher F/M ratio, oxygen penetration is higher resulting in increased nitrification process rate.

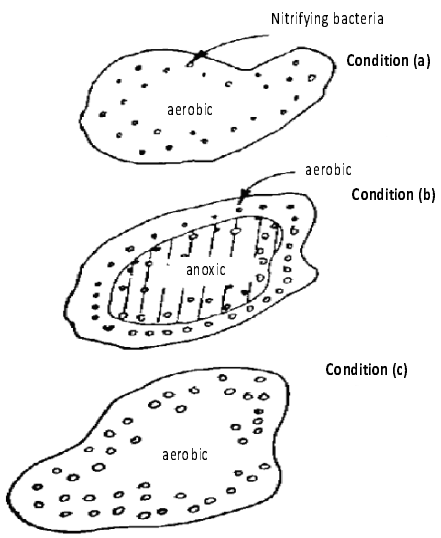

Figure 4. the effect of F/M ratio on nitrification process

Biological transformation of nitrate in more deoxidized forms, such as NO, N_2O, N_2 is called denitrification. This process is conducted by various facultative heterotrophic organisms (contrary to nitrification process microorganisms which are autotrophic), which can use nitrate instead of oxygen as final electron recipients. Analysis of carbon containing organic compounds in the denitrification process is similar to what takes place in aerobic process, the only difference being in the final stage of electron transformation. Consequently the term denitrification without oxygen is more suitable than anaerobic. This shows that in denitrification system a complete anoxic condition (DO concentration between 0.1-1 mg/l) is necessary.

3. The pilot system used in this experiment

With a view to study comparatively the presented data and more fully the A^2/O process and its effective role in elimination of pollutants a pilot system was set up on batch basis as shown in figures 5 and 6.

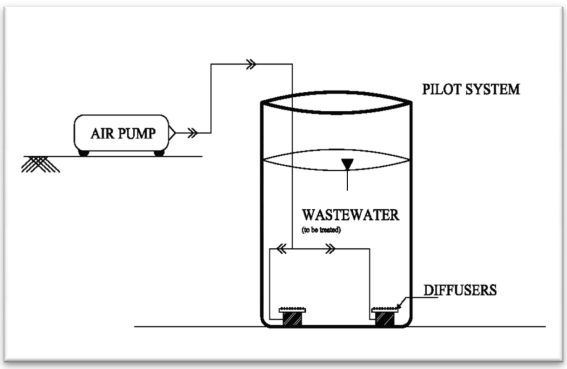

Figure 5. scheme of the pilot system

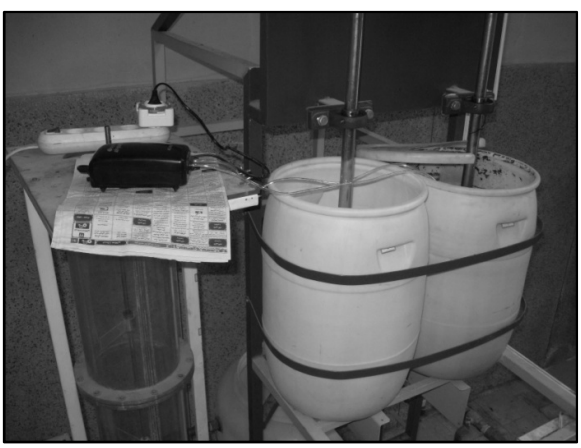

Figure 6. pilot system

The pilot specification is as follows:

Treatment pond with a capacity of 30 lit, aquarium air pump with a capacity of blowing max. 4.5 lit/min, mechanical timer. Aquarium hose and aeration stones as diffusers for air blowing.

In this study, the Tehran Ghaytarieh wastewater treatment plant returned sludge and also the raw wastewater after the screen bars has been used as raw wastewater. By adding phosphate and nitrate fertilizers and vinegar in the pilot pond, the concentration of the pollutants is increased, up to the desired level. As per the schedule anaerobic, anoxic and aerobic phases were set up. Then BOD, COD, PO_4, MLSS factors and also the nitrate were analyzed.

4. Findings

During the experiment, at various inflow concentration and retention time, results were obtained, according to the following tables. The various retention times and the influent and effluent of the treated wastewater are shown.

Table 1. experiment #1, (time left to right)

Phase	Anaerobic& anoxic	Oxic	anoxic	Oxic	anoxic	Oxic	Settling
Time (hr)	2	3	3	3	3	3	1

Table 2. experiment #1 results

Parameter	BOD	COD	PO4	NO3
Influent	89	111	14.8	0.78
Effluent	22	30	1	5.92

Table 3. experiment #2, (time left to right)

Phase	Anaerobic	anoxic	Oxic	anoxic	Oxic	anoxic	Oxic	anoxic	Oxic	Settling
Time (hr)	2	0.5	5	1	4	1	3	1	2	1

Table 4. experiment #2 results

Parameter	BOD	COD	PO4	NO3
Influent	250	300	30	2.67
Effluent	22	30	10	4.4

Table 5. experiment #3, (time left to right)

Phase	Anaerobic	anoxic	Oxic	anoxic	Oxic	anoxic	Oxic	Settling
Time (hr)	2	0.5	5	1	4	1	3	1

Table 6. experiment #3 results

Parameter	BOD	COD	PO4	NO3
Influent	240	300	25	3.12
Effluent	22	30	10	4.24

Table 7. experiment #4, (time left to right)

Phase	Anaerobic	anoxic	Oxic	anoxic	Oxic	Settling
Time (hr)	2		1	0.5	1	2

Table 8. experiment #4 results

Parameter	BOD	COD	PO4
Influent	133	167	4
Effluent	44	58	2

Table 9. experiment #5, (time left to right)

Phase	Anaerobic	anoxic	Oxic	anoxic	Oxic	Settling
Time (hr)	2		2	0.5	2	2

Table 10. experiment #5 results

Parameter	BOD	COD	PO4
Influent	200	240	4
Effluent	44	58	2

The first experiment indicates the effects of A^2/O process in removing the said pollutants. The amount of BOD and COD in the inflow proves low level pollution. As a matter of fact, the amount of carbonic source required to the removal pollutants was at an acceptable level. In the second and third experiments, the aeration is reduced gradually. In other words, the duration of aeration in further steps is reduced. This reminds us of the oxidization streams by tapered aeration. The amount of removal phosphate in the second experiment with a total aeration time more than two hours than the third experiment (14 hours against 12 hours) was a difference of seven percent. It may be noted that the effluent phosphate concentration in both

experiments was at the standard level recommended by the environmental department. The efficiency of this process in phosphate removal can be seen. As regards BOD and COD elimination, the same result is obtained and the difference in the two experiments is negligible. As a result the experiment shows that in longer aeration period, the removal of pollutants takes place more slowly, which means in case it is necessary to remove pollutants at a high level the cost should be high. As regards the amount of nitrate at nitrification stage which takes place at the aeration phase, an increased amount of nitrate is seen. The same case holds true in Tehran Zargandeh WWTP comparing the inflow and outflow whether at contact and stabilization and whether at extended aeration.

In experiment four and five, the main reason for selecting low period aeration was to experience the special condition of treatment. For example, in critical situation such as sudden electricity failure or a change in the inflow volume to the treatment plant (in most treatment plants there are bypass canals, but the canals may not be usable due to any reason), complete aeration of wastewater may not be possible. Moreover, it was required to determine the lower level of treatment so that by comparing it with the results of the other experiments the optimum aeration period and the number of aeration replication could be determined in a defined condition.

The dissolved oxygen concentration in all the experiments in the aeration period was about 2.5 to 3 mg/l and in anoxic period it was less than 1.5 mg/l.

Increase in nitrate concentration means oxidization of ammonia nitrogen. In case the effluent is in a situation lacking oxygen, denitrification process would occur, freeing nitrogen gas thus reducing the danger of nitrate in the effluent to surface water. the amount of MLSS in all experiments was about 2500 mg/l which is acceptable in normal WWTPs.

5. Conclusion

Considering that all the samples were analyzed in the Power and Water University of Technology laboratory, the function of A^2/O process in removal of phosphate and conversion of ammonia nitrogen to nitrite and then to nitrate can be seen.

With two hours aeration in the fourth experiment the amount of BOD was reduced from 133 to 44 mg/l. (67% removal) by doubling the aeration period that is by exposing wastewater to aeration for four hours, amount of BOD is reduced from 200 to 44 (78% removal). In other words, elimination of 70 to about 80 percent BOD can be attained fast and with rather low energy consumption. Should it be required to remove over 90 percent BOD, the aeration period would be approximately ten to fourteen hours. Elimination of phosphate to 90% has been experienced, one of the reasons being lack of nitrogen compound in the returned sludge (as the process here was not continuous). As described in the beginning, presence of nitrate in returned sludge is the reason for reducing the phosphate removal rate.

As regards other factors, the amount of microorganisms or MLSS can be mentioned. In case the amount of MLSS is increased and supposing the amount of BOD is stable during the same period of time, the amount of F/M is reduced, indicating increase of microorganisms compared to organic materials (food). Consequently, there would be more possibly of tread bacteria overtaking the round bacteria, causing the bulking of the sludge.

6. References

[1] Sedlak, Richard,"*Phosphorous and Nitrogen Removal from municipal Watewater",* translated ISBN 964-3834-62-0, 2002, Fardabeh, Tehran, Iran

[2] Walsh, T.K., B.W. Behrman, G. W. Weil, and E.R. Jones: *"A Review of Biological Phosphorus Removal Technology"* presented at the Water Pollution Control Federation Annual conference, October 1983.

[3] Metcalf and Eddy, Inc. *"Wastewater Engineering: Treatment, Disposal, Reuse"* McGraw Hill Book Company, New York, 1979

[4]Christensen, M. H. *"Denitrification of Sewage by Alternating Process Operation. Progress in Water Technology"* Pergamon Press, 7,2,339, 1975

[5] Mirbagheri.Seyed Ahmad, Jaberinasab.Behnam, *"Activated Sludge Contact and Stabilization Application in capacity building for Zargandeh WWTP, Tehran",* Abo Mohit Zist Journal, issue69, summer 2008

[6] Documents and Recordings of Zargandeh WWTP, Operational Administration of Tehran Sewage Company

Bench-Scale Ozonation of Raw Industrial and Municipal Wastewater

Richard O. Mines, Jr.[1], Cary M. Oglesby[2], and Laura W. Lackey[3]

[1]Mercer University, Department of Environmental Engineering, 1400 Coleman Avenue, Macon, GA 31207; PH (478) 301-2347; FAX (478) 301-5433; email: mines_ro@mercer.edu
[2]Pangean-CMD Associates, 9874 Main Street, Suite 100, Woodstock, GA 30188; PH (770) 926-8883; FAX (770) 925-5383; email: coglesby@pangean-cmd.com
[3]Mercer University, Department of Environmental Engineering, 1400 Coleman Avenue, Macon, GA 31207; PH (478) 301-4106; FAX (478) 301-2331; email: lackey_l@mercer.edu

ABSTRACT

This project involved the design, operation, and testing of a bench-scale ozonation wastewater treatment system. Untreated municipal and industrial wastewater was collected from the influent chamber to the Rocky Creek Wastewater Treatment Plant (WWTP) in Macon, Georgia. The industrial wastewater consisted of paper mill effluent from the Graphic Packaging Plant adjacent to the Rocky Creek WWTP. The Rocky Creek WWTP treats wastewater in an extended aeration activated sludge process. To accomplish this research, a 10-liter clear PVC, semi-batch, bubble column was used to disperse ozone bubbles through a porous diffuser near the bottom of the column. Three 24-hour runs were conducted on each type of wastewater. The ozone was administered at loading rates of 0.60, 4.70, and 9.92 mg O_3/min, respectively, to 6 liters of either raw municipal or industrial wastewater. The following parameters were measured frequently during each 24-hour run: pH, chemical oxygen demand (COD), ammonia, nitrite, nitrate, phosphorus, conductivity, turbidity, total suspended solids (TSS), volatile suspended solids (VSS), total dissolved solids (TDS), and total volatile solids (TVS). Overall COD removal for the municipal and industrial wastewater averaged 82% and 84%, respectively, whereas, overall TSS removal averaged 83% and 81%, respectively. The ozonation degradation rate constant (K_D) based on TSS destruction ranged from 0.054 hr^{-1} to 0.072 hr^{-1} for the municipal wastewater and from 0.017 hr^{-1} to 0.066 hr^{-1} for the industrial wastewater.

BACKGROUND

Ozone is a powerful oxidizing agent that has been primarily used for disinfecting drinking water. In recent years, its use has been expanded and several applications for the treatment of municipal and industrial wastewater have been studied. Much of the research has focused on minimizing the quantity of sludge or biosolids produced at wastewater treatment plants (WWTPs). More recently, the pre-

treatment of wastewater and waste activated sludge (WAS) with ozone to enhance biological degradation in follow-up processes has been of much interest. Gonzalez et al. (2003) evaluated the combined sequential ozonation, activated carbon treatment, and aerobic biological treatment of a pulp bleaching effluent containing aromatic contaminants. Ozonating raw pulp effluent for 5 minutes at a rate of 2 mmol of ozone per minute decreased the average chemical oxygen demand (COD), five day biochemical oxygen demand (BOD_5), and total organic carbon (TOC) by 21%, 3%, and 18%, respectively. The BOD_5/COD ratio increased from 0.36 to 0.44 making the industrial wastewater more biodegradable. Pre-treatment of a textile finishing wastewater for 30 minutes at an ozone dosage of 18.5 mg/L resulted in overall removals of 64%, 39%, and 86% in total COD (TCOD), filtered COD, and color (Eremektar et al., 2007). Alvarez et al. (2005) indicated that pre-treating cherry stillage (high-strength organic wastewater generated from the manufacture of alcoholic products) at an ozone dose of 25 mg O_3 per gram of initial COD resulted in over 75% of raw polyphenols being removed and less than 5% overall COD removal. Dogruel et al. (2003) reported that complete color removal and a 21% reduction in TCOD were achieved by ozonating a textile wastewater at a rate of 62 mg O_3/min for 15 minutes. However, they also indicated that increasing the ozone contact time to 30 minutes only increased the COD removal to 32%.

Experimental results presented by Park et al. (2003) showed that an overall mass reduction of 70% and volume reduction of 85% was achieved by ozonating waste activated sludge at a dose of 0.5 gram of ozone per gram of dried solids (DS). Two main mechanisms were discussed in regard to biomass degradation: disintegration due to cell destruction of suspended solids in the sludge and subsequent oxidation of soluble organic matter into carbon dioxide. At an ozone dose of 0.5 g O_3 per g of DS, the mineralized, disintegrated solids, and residual biosolids fractions were 20%, 46%, and 34%, respectively. Pre-treatment of WAS at ozone dosages of 0.10 and 0.16 g O_3 per g of total solids (TS) was evaluated by Bougrier et al. (2006). Between 20% and 25% of the particulate fraction of the sludge solids was converted to a soluble fraction at these dosages.

MATERIAL AND METHODS

A 10-L, clear PVC, semi-batch bubble column was used for treating raw municipal wastewater and raw industrial wastewater with ozone. A peristaltic pump (Master Flex, Cole Parmer) operating at 290 ml per min provided a continuous recycle around the column to keep the contents of the bubble column well mixed and to suppress foaming. Untreated domestic and industrial wastewater samples were obtained from the influent structure to the Macon Water Authority's Rocky Creek WWTP, Macon, Georgia. The Rocky Creek WWTP uses an extended aeration activated sludge process for treating municipal wastewater. The influent structure is constructed such that the industrial wastewater does not mix with municipal wastewater and is treated in a separate train at the facility. Ozone was supplied by an Ozotech, Incorporated ozone generator (Model OZ1BTUSL). Table 1 provides a summary of the ozone application rates used during each run. Three different ozone

application rates were achieved by adjusting the rheostat setting on the ozonator to 40%, 70%, and 100%, respectively, resulting in application rates of 0.60, 4.70, and 9.92 mg O_3/min. The initial volume of wastewater added to the bubble column was 6.0 liters. The operating temperature of the bubble column reactor was maintained between 18 and 20°C.

During the 24-hour ozonation period, samples were withdrawn from the column at each of the following times: 0, 5, 10, 30, 60, 120, and 1,440 minutes. For each sample, the following analyses were performed: chemical oxygen demand (COD), soluble chemical oxygen demand (SCOD), total suspended solids (TSS), total volatile solids (TVS), total dissolved solids (TDS), volatile suspended solids (VSS), and pH. Also, the final concentrations of ammonia, nitrite, nitrate, and phosphate were determined at the end of the 24-hour run.

The ozone generated by the Oztech generator was quantified according to Standard Methods 2350 E, a titration method utilizing a 0.005N sodium thiosulfate solution. COD was quantified colorimetrically by HACH method 8000 utilizing the HACH DR/2000 spectrophotometer. Solids analyses were conducted in accordance with Standard Methods Sections 2540 B, D and E.

Table 1. O_3 Application Rates and Contact Time.

Semi-batch Bubble Column	Ozone Application Rate Used (mg O_3/min)	Contact Time (days)
Run #1	0.60	24
Run #2	4.70	24
Run #3	9.92	24

RESULTS AND DISCUSSION

pH. Figure 1 is a plot of pH versus ozonation time for the municipal wastewater runs. The initial pH of the municipal wastewater was approximately 7.0 at the start of each run and increased during the first 30 minutes of ozonation to between 7.5 and 7.8. At the lowest ozone application rate of 0.60 mg O_3/min, the pH increased to 7.9 at 120 minutes before decreasing to around 6.9 at the end of 1,440 minutes (24 hr). For the higher ozonation application rates of 4.7 and 9.92 mg O_3/min, the pH of the wastewater decreased after 30 minutes of ozonation, ending around a pH of 2.7 to 2.9. The drop in pH may be attributed to the increased presence of nitrate ions in solution (forming nitric acid) and the lowering of the buffering capacity of the wastewater due to air stripping (Metcalf and Eddy, 2003).

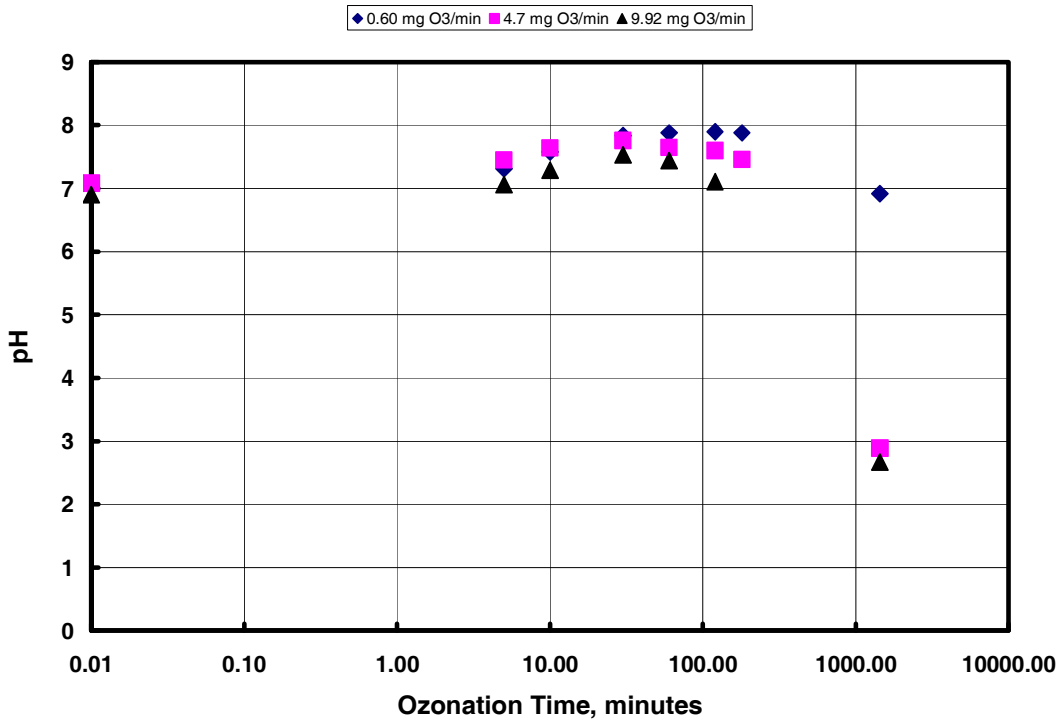

Figure 1. Plot of pH versus ozonation time for municipal wastewater runs.

Figure 2 is a plot of pH versus ozonation time for the industrial wastewater runs. For these runs, the initial pH was approximately 7.5 and generally increased to between 7.7 and 8.1 within the first hour of ozonation. Continued ozonation at the lowest application rate of 0.60 mg O_3/min caused the pH to remain near 8.0. At the higher ozone application rates of 4.7 and 9.92 mg O_3/min, the pH decreased with further ozonation resulting in pH values between 2.5 and 3.0 at the end of 24 hours. As previously stated, the drop in pH may be attributed to reduced buffering capacity and the presence of nitrate ions that are more prevalent due to the oxidation of ammonia.

Solids Removal. The total suspended solids removal levels achieved during the ozonation runs with municipal wastewater were slightly higher averaging 83% versus 81% for the runs performed on the industrial wastewater. Recognize that the average influent TSS concentration of the untreated municipal wastewater was 118 mg/L which is much different from the average TSS concentration of the industrial wastewater which averaged 298 mg/L.

The degradation rate constant (K_D) was determined for each run by plotting the natural logarithm of the TSS concentration remaining versus ozonation time. Figures 3 and 4 show the plots used to determine K_D for the municipal and industrial wastewater runs.

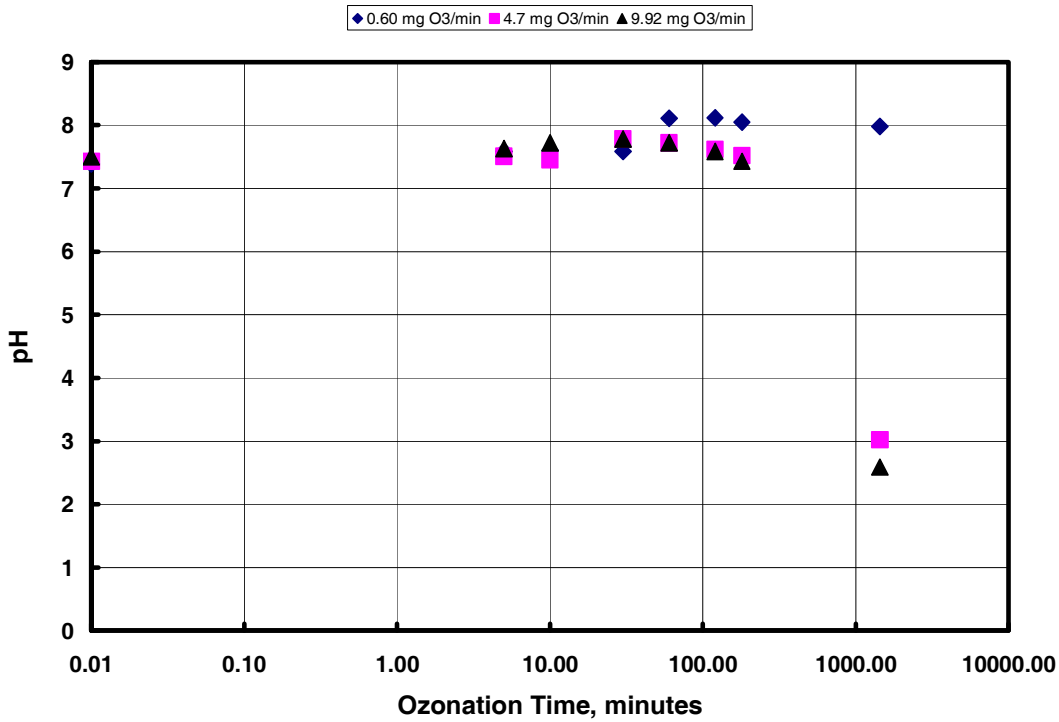

Figure 2. Plot of pH versus ozonation time for industrial wastewater runs.

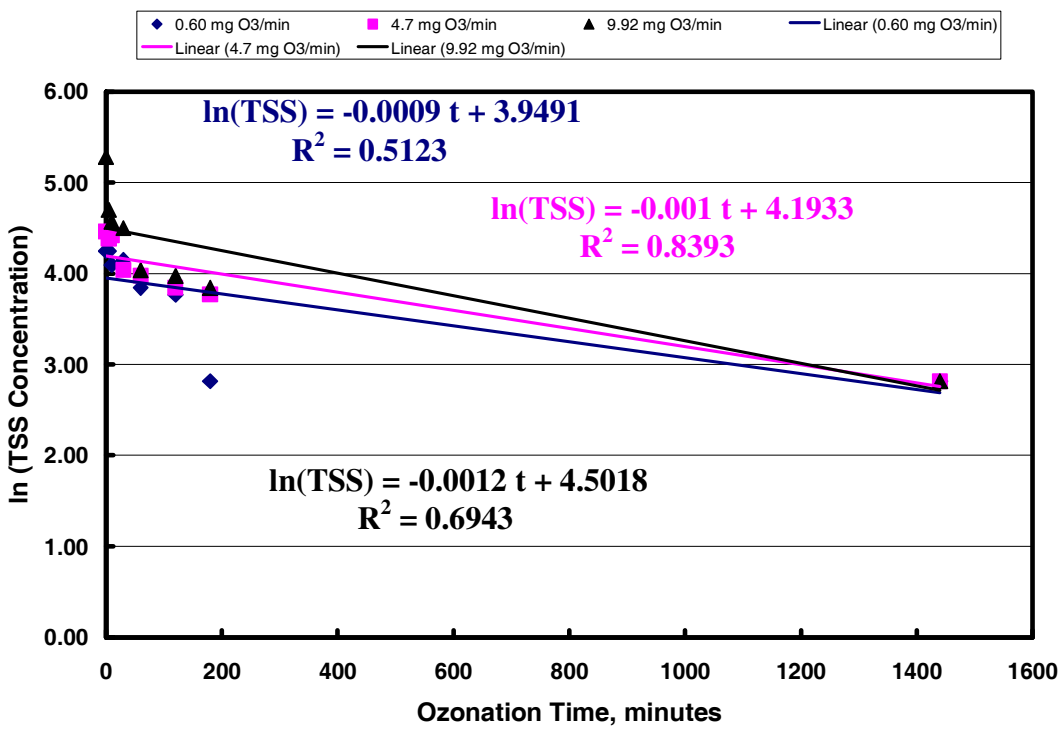

Figure 3. Plot of ln(TSS) versus ozonation time for municipal wastewater runs.

The degradation rate constants for the municipal wastewater runs and their associated R^2 values (square of the correlation coefficient) were: 0.054 hr^{-1} (0.0009 $min^{-1}\times$ 60min/hr) and 0.51, 0.06 hr^{-1} and 0.84, and 0.072 hr^{-1} and 0.69, respectively, for ozone application rates of 0.60, and 4.70, and 9.92 mg O_3/min. Overall, the ozone was more effective at degrading the municipal wastewater solids versus the suspended solids in the paper mill wastewater which contain cellulose and lignin particles which are difficult to oxidize. The degradation rate constants for the industrial wastewater runs and their associated R^2 values were: 0.066 hr^{-1} and 0.47, 0.042 hr^{-1} and 0.18, and 0.042 hr^{-1} and 0.18, respectively, for ozone application rates of 0.60, and 4.70, and 9.92 mg O_3/min. The pseudo-first order equation did not fit the data as well at the higher ozone application rates.

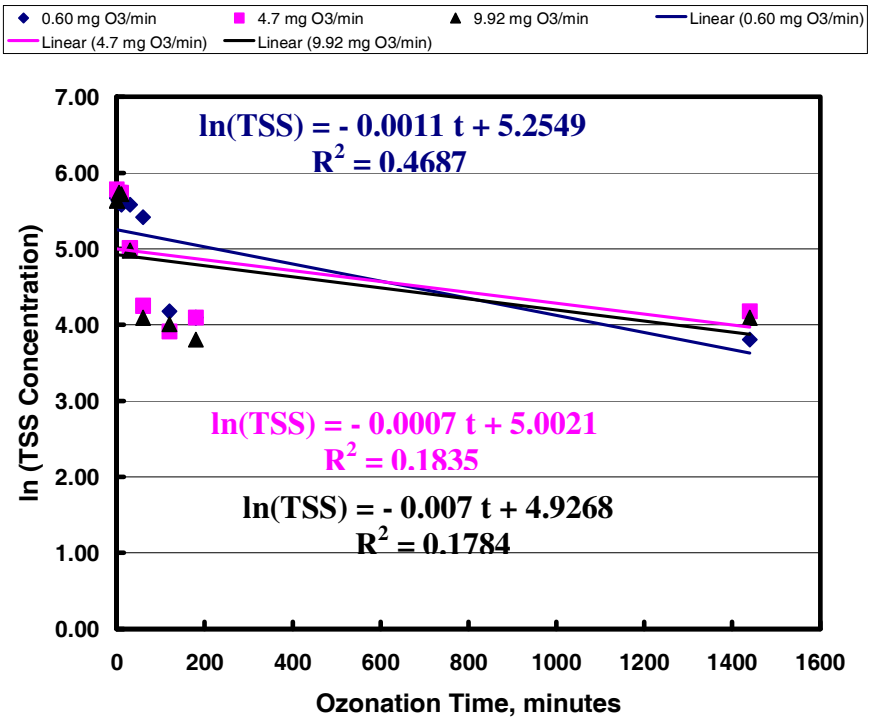

Figure 4. Plot of ln(TSS) versus ozonation time for industrial wastewater runs.

Degradation rates of volatile solids in aerobic digesters vary with temperature and have been reported to vary from 0.002 hr^{-1} at 15˚C to 0.007 hr^{-1} at 30˚C (EPA, 1979; Metcalf & Eddy, 2003) corresponding with our K_D values.

COD Concentration. Figures 5 and 6 are plots of COD concentration versus ozonation time for each run performed on the municipal and industrial wastewaters. The COD concentration decreased during both runs. Overall COD removal averaged 82% and 84% respectively, for the municipal and industrial wastewater runs. Although overall removals were essentially the same, the average COD concentration of the untreated municipal wastewater was 300 mg/L compared to 745 mg/L for the industrial wastewater.

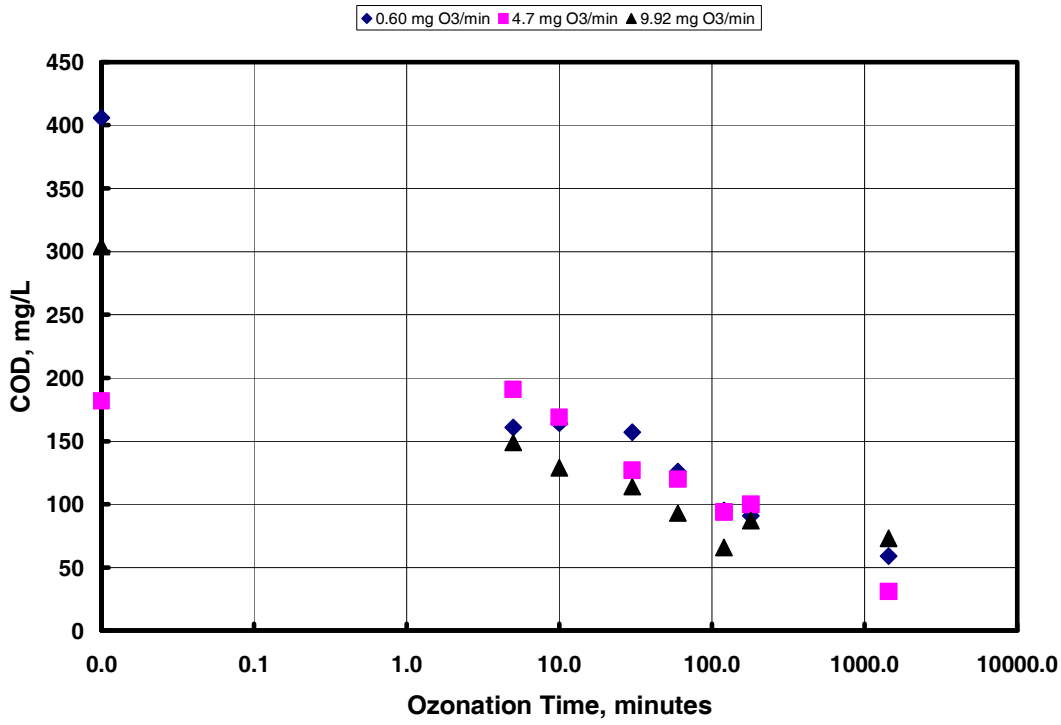

Figure 5. COD versus ozonation time for municipal wastewater runs.

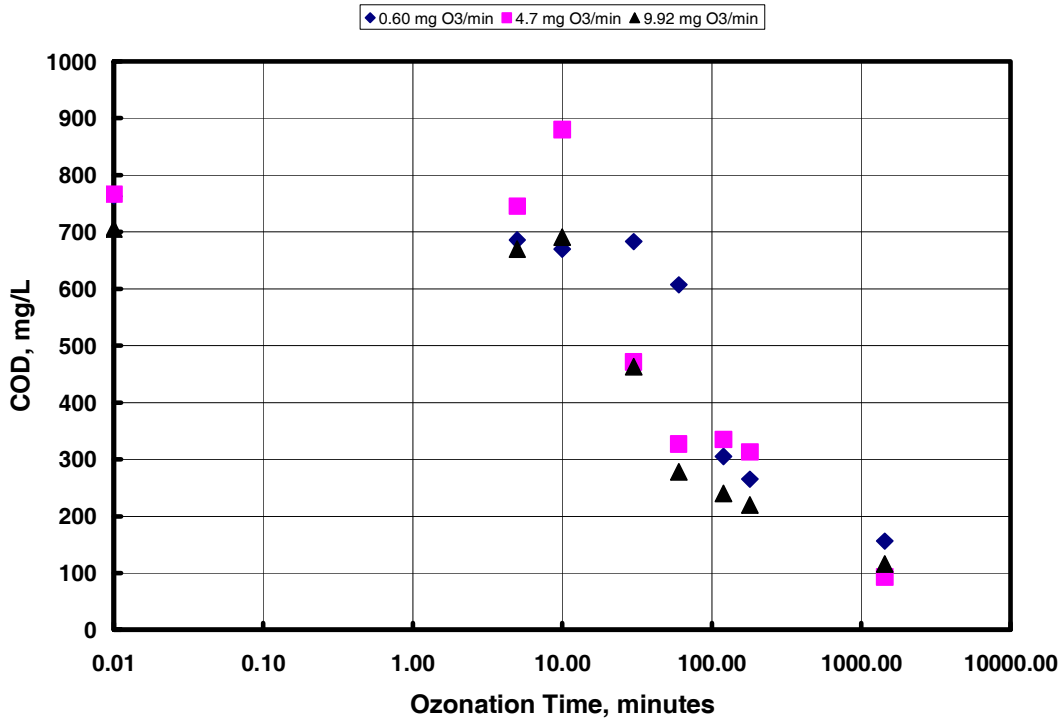

Figure 6. COD versus ozonation time for industrial wastewater runs.

Soluble COD Concentration (SCOD). Figures 7 and 8 are plots showing how the SCOD concentration varied as a function of ozonation time during the experimental runs with the municipal and industrial wastewater. Ozone was effective at solubilizing the suspended solids resulting in an increase in the soluble COD. In Figure 7, soluble COD concentrations increased as ozonation contact time increased until 10 to 20 minutes before decreasing for the ozone application rates of 4.7 and 9.92 mg O_3/min, whereas, for the lowest application rate, soluble COD concentrations generally decreased as ozonation time increased.

The SCOD concentrations for the industrial wastewater decreased as ozonation time increased for each ozone application rate (Figure 8). The average initial SCOD concentration in the industrial wastewater was 241 mg/L and at the end of the 24-hour ozonation period, the average SCOD concentration was 67 mg/L.

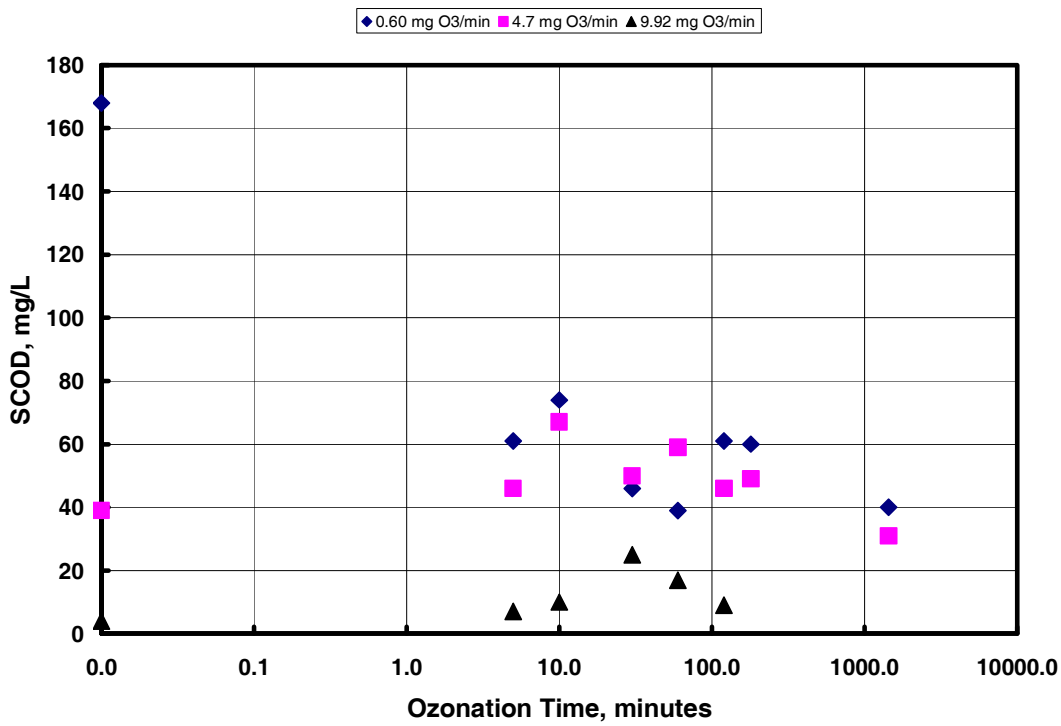

Figure 7. Soluble COD versus ozonation time for municipal wastewater runs.

Ozone Dosages. Tables 2 and 3 show the average ozone dosages used per mg of COD and TSS removed for the municipal and industrial wastewater runs. In general, the ozone dosages utilized increased as the quantity of ozone applied to the wastewater was increased from Run#1 to Run#3. The ozone dosages utilized were lower for the industrial wastewater runs since the initial concentrations of COD and TSS were higher.

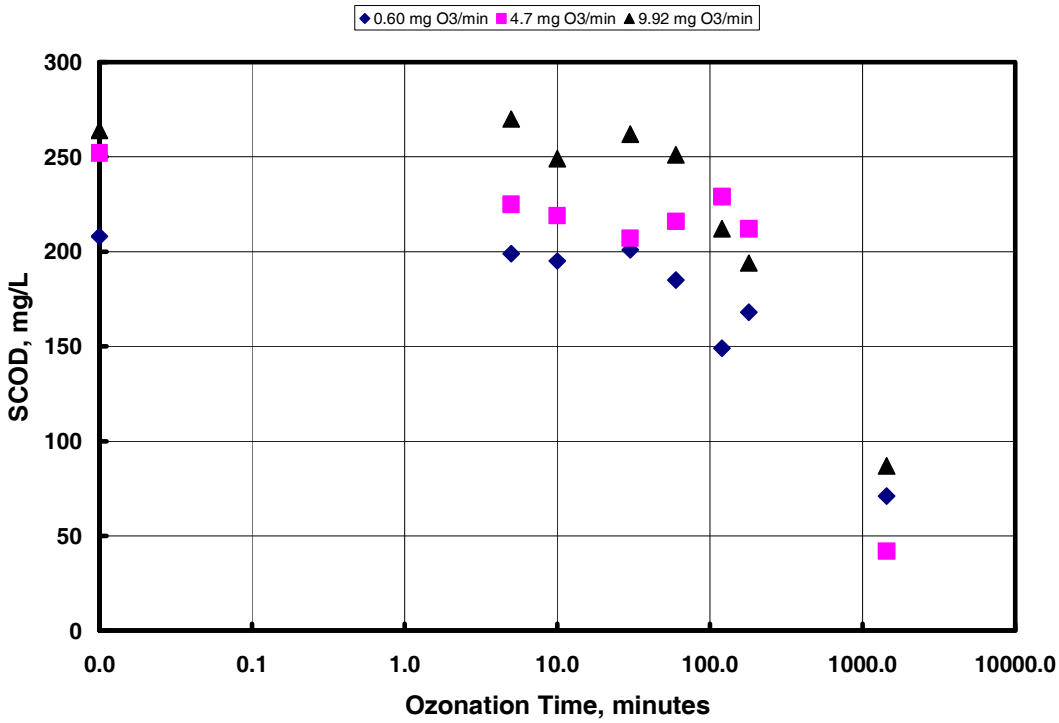

Figure 8. Soluble COD versus ozonation time for industrial wastewater runs.

Table 2. Average Ozone Dosage Utilized during Runs #1, #2, and #3 for Municipal Wastewater.

O_3 Dosage or Utilization	Run #1	Run #2	Run #3
mg O_3 /mg COD removed	0.41	7.47	10.3
mg O_3 /mg TSS removed	2.70	16.1	13.2

Table 3. Average Ozone Dosage Utilized during Runs #1, #2, and #3 for Industrial Wastewater.

O_3 Dosage or Utilization	Run #1	Run #2	Run #3
mg O_3 /mg COD removed	0.24	1.68	4.04
mg O_3 /mg TSS removed	0.59	4.34	10.8

Nutrient Concentrations. Figures 9 and 10 show the final nutrient concentrations in the wastewater for the municipal and industrial runs. The final ammonia and nitrite concentrations were low for both the municipal and industrial wastewaters. Effluent nitrate concentrations increased due to the oxidation of ammonia and organic nitrogen present in the wastewater. The phosphate concentration increased during ozonation and was more pronounced for the industrial wastewater.

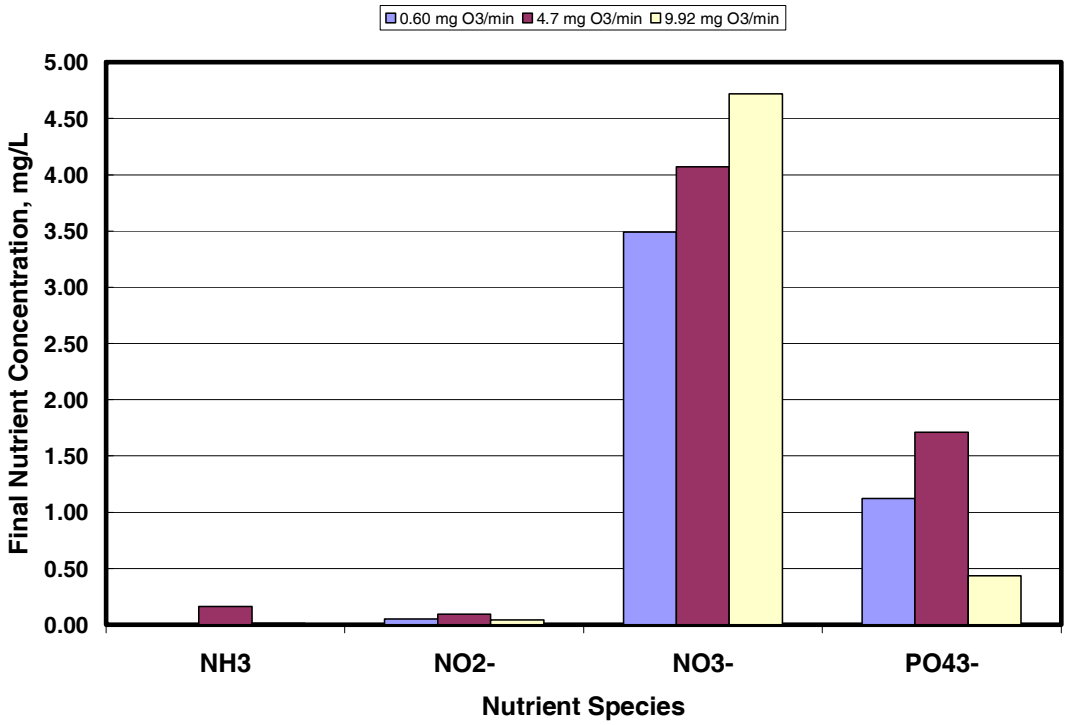

Figure 9. Final nutrient concentrations for municipal wastewater runs.

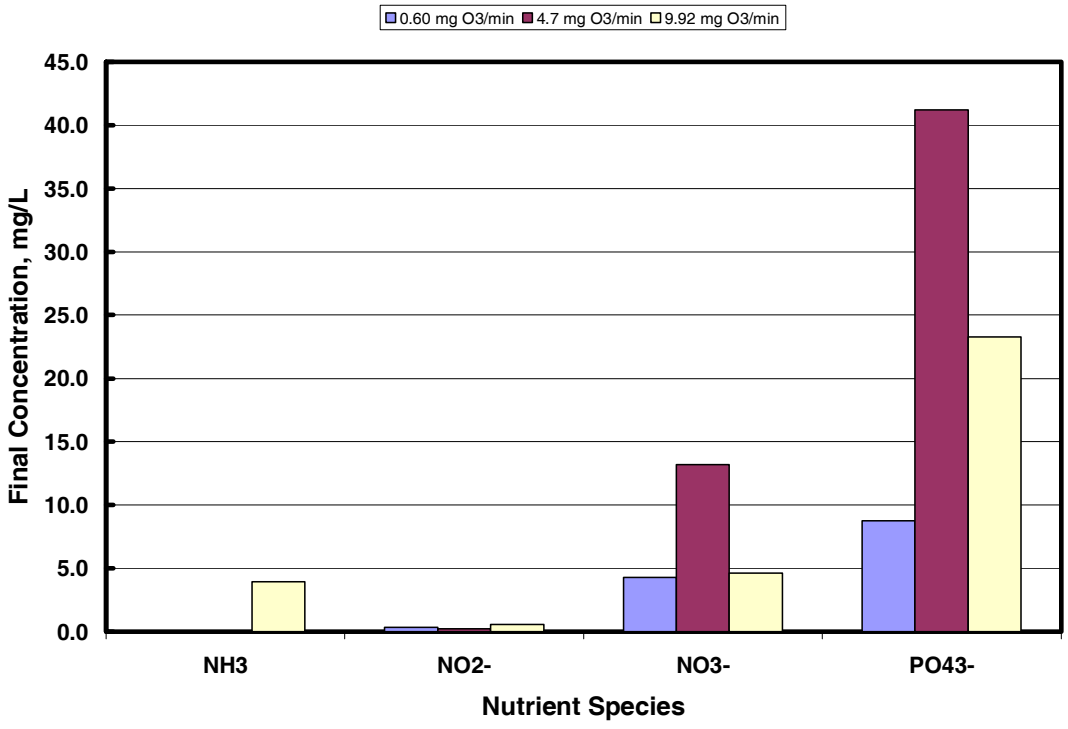

Figure 10. Final nutrient concentrations for industrial wastewater runs.

SUMMARY AND CONCLUSIONS

Ozone was applied to 6-liters of municipal and industrial wastewater for a 24-hour period. Three runs were made on each type of wastewater at ozone loading rates of 0.60, 4.70, and 9.92 mg O_3/min. A 10-L, semi-batch, bubble column reactor was used in the experimental study.

Major conclusions from the study are listed below:

1. Ozonation of both wastewaters caused the pH to decrease as a function of time. The final pH of the ozonated wastewater was approximately 2.6.
2. Overall COD removal averaged 82% for the municipal wastewater resulting in residual COD concentrations ranging from 31 to 73 mg/L. The average overall COD removal for the industrial wastewater was 84% with residual COD concentrations ranging from 93 to 156 mg/L.
3. Overall TSS removal averaged 83% for the municipal wastewater with an average TSS concentration of 17 mg/L remaining, whereas, for the industrial wastewater, overall TSS removal averaged 81% resulting in an average TSS concentration of 57 mg/L of TSS remaining.
4. The concentration of ammonia and nitrite after ozonating for 24 hours was negligible in the runs conducted on both the municipal and industrial wastewaters. The nitrate concentration remaining after 24 hours of ozonation averaged 4.1 mg/L for the municipal wastewater and 7.4 mg/L for the industrial wastewater.
5. The average residual phosphate concentration remaining after 24 hours of ozonating the municipal and industrial wastewater was 1.09 mg/L and 24.4 mg/L, respectively.
6. The ozonation degradation rate constant (K_D) based on TSS destruction ranged from 0.054 hr^{-1} to 0.072 hr^{-1} for the municipal and 0.042 hr^{-1} to 0.066 hr^{-1} for the industrial wastewater.

ACKNOWLEDGEMENTS

We extend our appreciation to Jeremiah Johnson and Stevie Odom for their assistance in the collection and analysis of the wastewater samples.

REFERENCES

Alvarez, P.M., Beltran, F.J., Rodriguez, E.M., (2005). “Integration of ozonation and an anaerobic sequencing batch reactor (AnSBR) for the treatment of cherry stillage.” *Biotechnol. Prog*. 21 (5), 1543-1551.

Bougrier, C., Albasi, C., Delgenes, J.P., Carrere, H. (2006). "Effect of ultrasonic, thermal and ozone pre-treatments on waste activated sludge solubilisation and anaerobic biodegradability." *Chemical Engineering and Processing*, 45(8), 711-718.

Dogruel, S., Germirli-Babuna, F., Kabdasli, I., Insel, G., Orhon, D. (2003). "Effect of stream segregation on ozonation for the removal of significant COD fractions from textile wastewater." *Journal of Chemical Technology and Biotechnology*, 78(1), 6-14.

Eremektar, G. Selcuk, H., and Meric, S. (2007). "Investigation of the relation between COD fractions and the toxicity in a textile finishing industry wastewater: Effect of preozonation." *Desalination*, 211(1-3), 314-320.

Gonzalez, P., Zaror, C., Carrasco, V., Mondaca, M.A., and Mansilla, H. (2003). "Combined physical-chemical and biological treatment of poorly biodegradable industrial effluents." *Journal of Environmental Science and Health Part A*, A38 (10), 2201-2208.

Metcalf & Eddy (2003). *Wastewater Engineering Treatment and Reuse*, McGraw-Hill, New York.

Park, K.Y., Ahn, K., Maeng, S.K., Hwang, J.H. and Kwon, J.H. (2003). "Feasibility of sludge ozonation for stabilization and conditioning." Ozone Science and Engineering, 25, 73-80.

Standard Methods for the Examination of Water and Wastewater (1992). 20th Edition. American Public Health Association, Washington, DC.

U. S. Environmental Protection Agency (1979). *Process Design Manual for Sludge Treatment and Disposal*, EPA/625/1-79/011, Office of Research and Development, Cincinnati, OH 45268.

Biological nutrient removal from on-site wastewater treatment systems using a membrane aerated bioreactor

Zhihua Liang, Zhiqiang Hu
Department of Civil and Environmental Engineering,
University of Missouri-Columbia

Abstract

This study aimed to develop a low cost bioreactor process to efficiently remove organic compounds and nutrients from on-site wastewater treatment systems. A laboratory-scale anaerobic membrane-aerated biofilm bioreactor (ANMABR) using a gas-permeable silicone tubing covered with non-woven fabrics was constructed to evaluate the efficiency of chemical oxygen demand (COD) and nitrogen removal in the system.

After 250 days of continuous reactor operation, the experiment results showed consistent COD and NH_4-N removal efficiencies at 89±6 and 82±5%, respectively. The total nitrogen (TN) removal efficiency was 64±8% with an effluent average total nitrogen concentration of 11 mg/L. From day 89 to day 120 the biofilm reactor experienced a shock load running with C/N ratio of 2:1 with influent NH_4-N increased to 150 mg/L. The COD removal efficiency was not affected after the shock load, but NH_4-N and TN removal efficiencies were decreased down to 44 and 22%, respectively.This study demonstrated that gas-permeable tubing/membrane could be used to treat wastewater containing low organic and nitrogen loadings from on-site wastewater treatment systems. Improvement is still needed under the shock loading conditions for on-site wastewater treatment systems.

1. Introduction

Onsite wastewater systems are widely used in the United States because of its relatively simple components and low cost of operation and maintenance. It is estimated that 23 percent of 115 million occupied homes nationally use onsite wastewater systems for wastewater treatment. Because of the limitedremoval efficiency in onsite wastewater systems, effluent from onsite wastewater system still contains high concentrations of organic matters (BOD_5 > 100 mg/L), nitrogen (TN>30 mg/L) and phosphorus (TP>10 mg/L). These high level pollutants make onsite wastewater system a significant contamination source of nutrients to the receiving surface and ground waters. There are 4,773 water bodies around the states that are reported impaired by nutrients (USEPA 2002). It is needed to find a cost-effective and efficient treatment technology to remove nutrients and organics from onsite wastewater systems.

Recent research efforts proposed a novel membrane aerated biofilm reactor (MABR) to achieve nitrification and denitrification simultaneously. Walter et al. (Walter 2005) investigated a membrane tube module reactor with oxygen supplied on the inside of a membrane tube. The membrane module system used synthetic wastewater at which the COD level is around 900 mg/L and ammonium concentration 1000 mg/L to test the biological degradation capacity. Under the convective mass transport condition, combined nitrification and denitrification was proved on the heterotrophic and autotrophic biofilm which were developed at the membrane module surface. In their study of simultaneous COD removal, the nitrification and denitrification achieved in the membrane aerated biofilm reactor, Satoh et al. (Satoh 2004) constructed the membrane module which consisted of gas permeable, polyurethane hollow fiber membranes to treat synthetic wastewater at a COD loading rate of 1.0 g-COD/m^2/day and an ammonium loading rate of 0.5 g-N/m^2/day. Their results showed simultaneous COD removal, nitrification and denitrification achieved with 95% of nitrification and 90% COD removal efficiencies respectively, at low COD loading rate. At a high COD loading rate, to achieve stable nitrification, the MABR had to be supplied with high intra-membrane air pressure. In a similar study, Semmens et al. (Semmens 2003) constructed membrane module with polyethylene hollow fiber membrane to investigate COD and nitrogen removal of synthetic wastewater. After the start-up period, their experimental data showed effectiveness of MABR in removing COD and nitrogen as over 90% removal rate of COD and 90% total nitrogen removal. But with the thickness of biofilm increased, the performance of the bioreactor was diminished until the COD and nitrogen removal had no effect. Liu et al. (Liu 2007) selected microporous carbon tubes to construct the MABR for treatment of synthetic wastewater. Because carbon membrane have high ability of bacterial adhesion and good permeability, removal rate of ammonium and COD reached 35.6 g-COD/m^2/day and 9.3 g-N/m^2/day, respectively. But they reported excessive biofilm accumulation abated the mass diffusion rate and oxygen aeration impaired the performance of MABR treatment.

For MABR using microporous hollow fiber membrane to provide oxygen aeration there is a drawback of pore clogging make them unsuitable applied to the on-site wastewater treatment system which contains high contents of suspended solids and organics. To avoid this problem silicone membrane was used in membrane aeration for their high resistance to chemical and mechanical stress in the development of cost-effective and efficient environmental technologies to remove nutrients from onsite wastewater systems. The objective of this study was to evaluate the effectiveness of a silicone membrane aerated biofilm reactor system for COD and nitrogen from domestic wastewater.

2. Materials and methods

A 7.2L membrane-aerated biofilm reactor (MABR) was constructed with two identical vertical cross stands (6 cm x 16 cm), made of bamboo, evenly in the central chamber of reactor. The reactor consisted of three compartments: an anaerobic fermentation basin followed by an anoxic basin, and further followed by an internal clarifier. In the anoxic basin, a gas-permeable membrane aerated module covered was submerged (Figure 1).

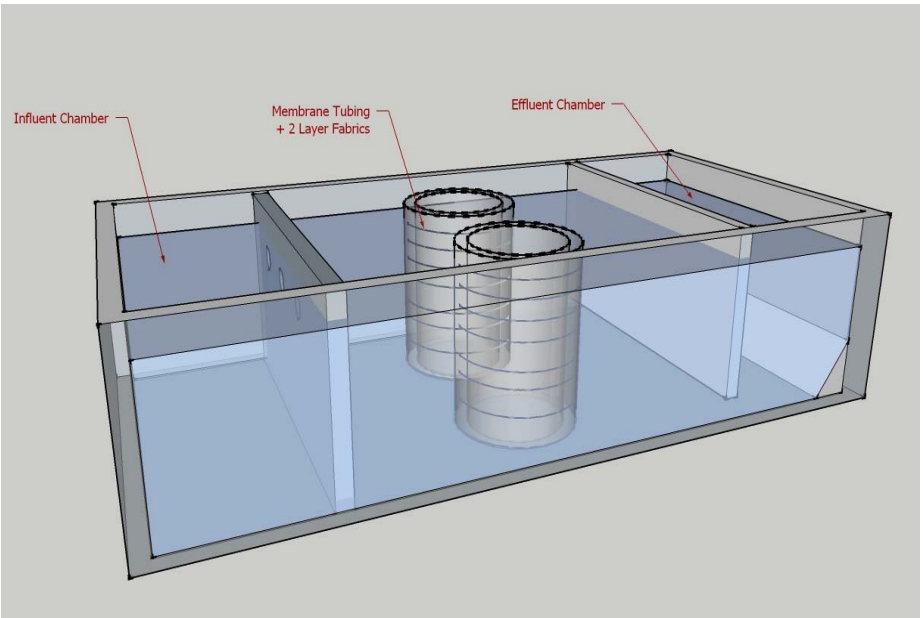

Figure 1. Scheme of membrane aerated biofilm reactor

The gas-permeable membrane tubings (Silastic® medical grade tubing, outer diameter = 2.0 mm and inner diameter =1.5 mm, Dow Corning, active length = 7 m) were arranged in a coiled form around inner layer of fibrous non-woven fabrics (diameter = 10μm, Kunin Group Inc., Hampton, NH) wrapped with cross stands. At the outside of the coiled gas-permeable tubing another layer of fibrous non-woven fabrics was wrapped. Oxygen was delivered to the inside of the membrane tube at an airflow rate of <1 ml/min. at atmospheric pressure throughout the experiment.

Reactor operation

The synthetic wastewater was fed into the reactor by a peristaltic pump (Cole Parmer, Chicago, IL) at a rate of 2.0 L/day. The synthetic wastewater components contained 300mg/L COD as sodium acetate, 30mg/L ammonium-nitrogen as ammonium chloride, 6mg/L phosphorous with a micro nutrient solution. The MABR was operated at 26°C with a dilution rate of 0.29 day^{-1}. The biofilm was initially cultured in the fed-cycle mode for seven days with inoculation of 1 L nitrifying biomass from the active nitrifying reactor and 150mL secondary tank activated sludge taken from the Columbia Regional Wastewater Treatment Plant, Columbia, Missouri.

Analytical methods

The NH_4^+ concentration was determined by standard electrode method. The NO_2 and NO_3 concentrations were determined colorimetrically. The COD sample was analyzed using colorimetric digestion method. The DO in the reactor was measured by a YSI 550A Dissolved Oxygen and Temperature System (YSI Inc., Yellow Springs, OH).

3. Results and discussion

COD concentrations measured from the influent and effluent of the MABR reactor are shown in Figure 2. Similarly, the ammonium concentration of influent and effluent of the MABR reactors are shown in Figure 4. In Figure 5, the effluent concentrations of nitrogen species from the MABR are shown. After a short start-up period of 15 days, the MABR reactor reached 90% removal of organic matter. Simultaneously, nitrification was indicated because nitrate was observed in the effluents. Ammonium removal of MABR reached over 90% while the nitrate concentration of MABR effluent was low. This demonstrated that almost complete denitrification was achieved shortly after the start-up period.

During the period of nitrogen shock loading the behavior of COD removal for the MABR was not changed. When receiving much higher influent ammonium concentrations (>100 mg/L of NH_4-N), significant ammonia accumnulation was observed in the MABR reactor, indicating low shock buffering capacity of the MABR. Although effluent nitrate concentration of MABR increased with increase loading of influent ammonium, it only accounts for less than 50% nitrification for influent ammonium concentration.

After the shock loading period, the organic and ammonium nitrogen loading were switched back to a normal level of 300 mg/L and 30 mg/L respectively. The experimental data illustrated that the MABR reactor had stable performance on COD and ammonium removals for over 250 days. COD removal efficiency and ammonium removal efficiency of of the MABR reactor were 89% and 82%, respectively. The total nitrogen removal in the MABR reactor was about 65%.

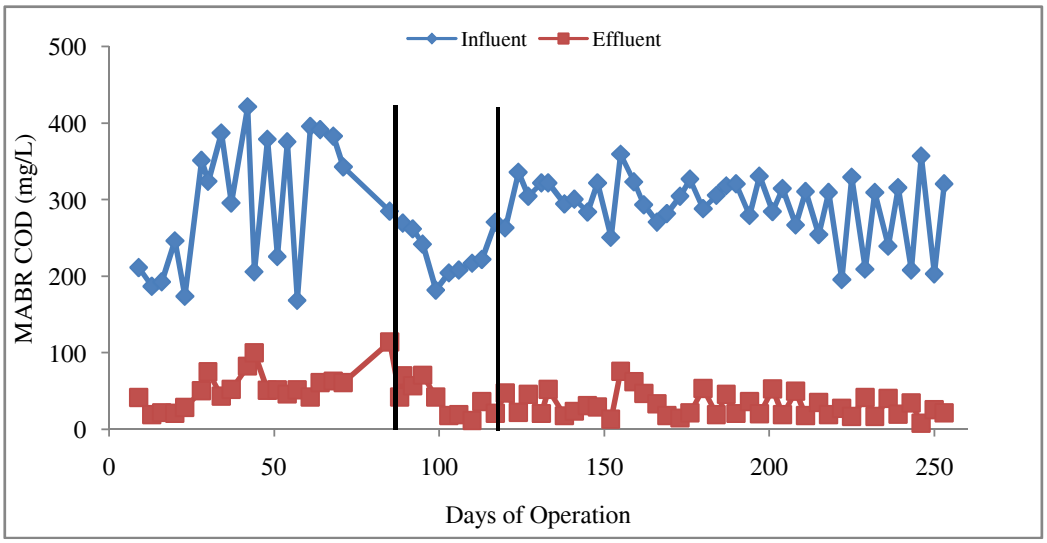

Figure 2. Influent and effluent COD concentration of the MABR over the whole period. Vertical lines indicate the nitrogen shock loading period.

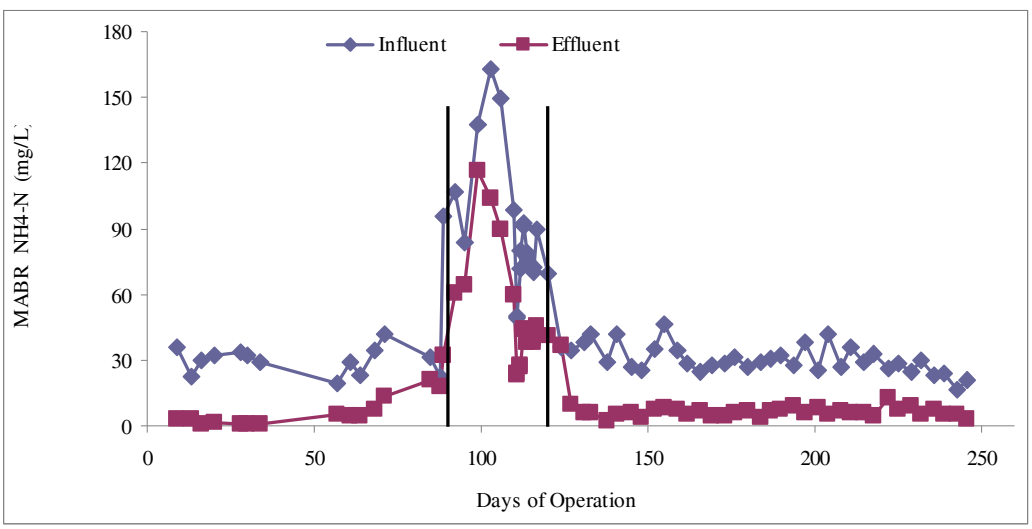

Figure 3. Influent and effluent ammonium-N concentration of MABR over the whole period. Vertical lines indicate the nitrogen shock loading period.

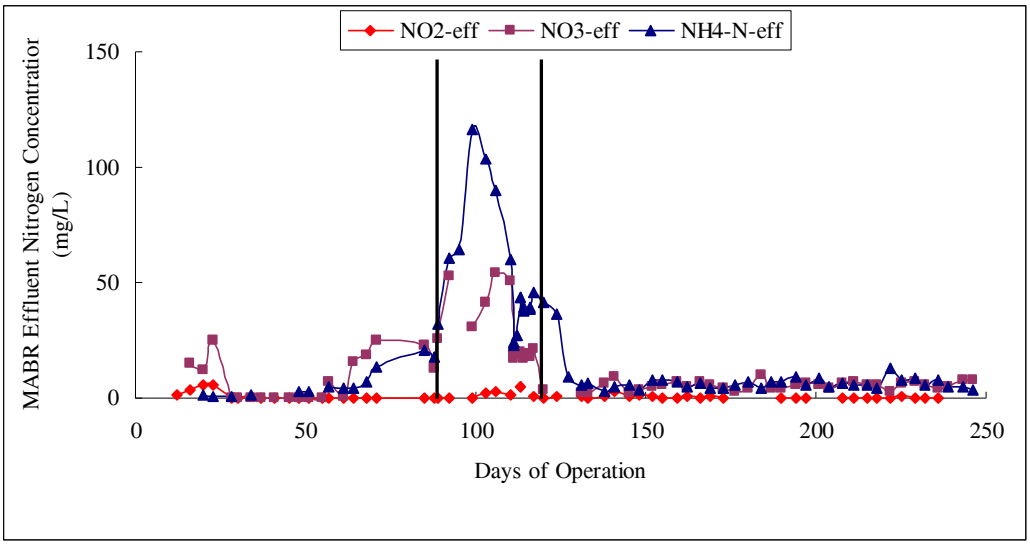

Figure 4. Effluent nitrogen species concentration of the MABR over the whole period. Vertical lines indicate the nitrogen shock loading period.

The configuration of gas-permeable membrane with non-woven fibrous fabric of MABR reactor makes it possible to develop a local nitrifying layer at the bottom of biofilm. These nitrifying bacteria existed in the favorable conditions of high oxygen concentration and low organic carbon concentration. Although no autotrophic activities of sedimentary biomass was inferred from the microbial activity measurements, the existing nitrifying bacteria layer contributed a significant extent of the nitrification to achieve ammonium removal from influent of MABR. Even the non-woven fibrous fabric can provide large surface area for bacteria adhesion thick biofilm formation after sufficient time increased the oxygen diffusive resistance and limited mass diffusive transport. This can explain after the shock loading period by the fact that the average effluent ammonium concentration was a little bit higher than that before the shock loading period. This thick biofilm resistance also limited the mass transport rate of nitrate produced in the deeper parts of biofilm to the outer layer of denitrification zone to be utilized as electron acceptor and cause the uncompleted denitrificaiton to achieve non-total nitrogen removal with some nitrate concentration in the effluent. Because the totally anaerobic conditions maintained at the outside layer of membrane module and in bulk liquid solution, the simultaneous sludge digestion was accomplished. In the whole operation period of the MABR reactor there was no wasted sludge produced except the sedimentary sludge taken out for microbial activity measurements. This characteristic makes ANMABR an attractive advantage with a minimum need of maintenance for actual application.

4. Conclusions

This study investigated the MABR system for simultaneous COD and nitrogen

removal by constructing a gas-permeable membrane aerated biofilm reactor with non-woven fibrous support. The configuration of the reactor was capable of forming different environmental zones in a single membrane module to achieve simultaneous nitrification, denitrification and COD removal. The long term operation of the MABR reactor showed the effective COD removal and nitrification rate of 89% and 82%, respectively at regular COD and nitrogen loading conditions. Improvements are needed under the shock loading conditions for keeping the efficient organic and nitrogen..

References

Hu, Z. (2002). "Effect of nickel and cadmium speciation on nitrification inhibition." *Environmental Science and Technology*, 36(14), 3074-3078.

Liu, H. (2007). "Carbon membrane-aerated biofilm reactor for synthetic wastewater treatment." *Bioprocess and Biosystems Engineering*, 30(4), 217-224.

Satoh, H. (2004). "Macroscale and microscale analyses of nitrification and denitrification in biofilms attached on membrane aerated biofilm reactors." *Water Research*, 38(6), 1633-1641.

Semmens, M. J. (2003). "COD and nitrogen removal by biofilms growing on gas permeable membranes." *Water Research*, 37(18), 4343-4350.

USEPA. (2002). "Onsite Wastewater Treatment Systems Manual. EPA-625-R-00-008."

Walter, B. (2005). "Combined nitrification/denitrification in a membrane reactor." *Water Research*, 39(13), 2781-2788.

BOUNDARY CONDITIONS FOR SIMULATING COMPLEX STORM-SEWER SYSTEMS IN FREE SURFACE, PRESSURIZED AND MIXED FLOW CONDITIONS

Arturo S. León
Post-doctoral Research Associate, V. T. Chow Hydrosystems Lab., Dept. of Civil and Envir. Engng., Univ. of Illinois at Urbana-Champaign, 2519 Hydrosystems Lab., MC-250. 205 North Mathews Av., Urbana, IL 61801. E-mail: asleon@illinois.edu (corresponding author).

Xiaofeng Liu
Post-doctoral Research Associate, V. T. Chow Hydrosystems Lab., Dept. of Civil and Envir. Engng., Univ. of Illinois at Urbana-Champaign, 2519 Hydrosystems Lab., MC-250. 205 North Mathews Av., Urbana, IL 61801. E-mail: liu19@illinois.edu.

Mohamed S. Ghidaoui
Professor, Dept. of Civil Engineering, The Hong Kong University of Science and Technology, Room 3569, Clear Water Bay, Kowloon, Hong Kong. E-mail: ghidaoui@ust.hk.

Arthur R. Schmidt
Research Assistant Professor, V. T. Chow Hydrosystems Lab., Dept. of Civil and Envir. Engng., Univ. of Illinois at Urbana-Champaign, 2535a Hydrosystems Lab., MC-250. 205 North Mathews Av., Urbana, IL 61801. E-mail: aschmidt@illinois.edu.

Marcelo H. García
Chester and Helen Siess Professor and Director, V. T. Chow Hydrosystems Lab., Dept. of Civil and Envir. Engng., Univ. of Illinois at Urbana-Champaign, 2535b Hydro Lab., MC-250. 205 North Mathews Av., Urbana, IL 61801. E-mail: mhgarcia@illinois.edu.

Abstract

This paper describes part of the work presented in León et al. (2009), which presents integrated boundary conditions (BCs) for simulating free surface, pressurized, and the simultaneous occurrence of free surface and pressurized flows (mixed flows) when the free surface region is modeled using the 1D Saint-Venant equations and the pressurized region is modeled using the 1D compressible waterhammer equations. The present paper describes the results of the application of the integrated boundary conditions for modeling free surface, pressurized, and mixed transient flow conditions in two test cases. The first test case is a hypothetical test and the second is an experimental work in an oscillation tube performed by the authors of this paper. Computational Fluid Dynamics (CFD) modeling results were used as frame of comparison for the first test case and experimental results besides CFD results were used for the second one. The results show that the integrated boundary conditions can be used with good accuracy for simulating complex storm-sewer systems in free surface, pressurized and mixed flow conditions. The integrated boundary conditions are general and they can be used to simulate point and storage junctions with any number of inflowing and outflowing pipes. The integrated boundary conditions were implemented in the Illinois Transient Model (ITM), which has been used to study hydraulic transients

in the Calumet system of the Metropolitan Water Reclamation District of Greater Chicago (MWRDGC). The results of the latter study are not presented in this paper.
Keywords: Boundary conditions; Mixed flow; Open channel flow; Pressurized flow; Sewer; Transient flow; Unsteady flow.

1. Introduction

The simultaneous occurrence of free surface and pressurized flows (mixed flows) can be modeled using either a single set of governing equations or separate equations for free surface and pressurized flows (e.g., León et al. 2008b). With either approach, the Method of Characteristics (MOC) with space-line interpolation usually is used to connect the boundaries and the adjacent internal cells (e.g., Sjöberg 1976, Politano et al. 2007). Naturally, when using a single governing equation (1D Saint-Venant equations), the well-known Preissmann slot approach is used for simulating pressurized flows. In this case the boundary conditions (BCs) for mixed flows are equivalent to those used in free surface flows. When a different governing equation is used for free surface and pressurized flows (e.g., 1D Saint-Venant equations are used for free surface flows and 1D compressible waterhammer equations are used for pressurized flows), different MOC boundary conditions are specified for free surface and pressurized flows. The MOC approach is suitable for pure pressurized flows (e.g., Karney and Ghidaoui 1997, León et al. 2008a) and for free surface smooth flows (e.g., León et al. 2006, León et al. 2008b). However, for free surface flows in the presence of shocks, the MOC approach results in smoothing (damping) of waves (e.g., León et al. 2006). Naturally this restriction is extended to the boundaries. Furthermore in mixed flow conditions at the boundary, it is uncertain what equations should be used when the mixed flow interface is positive or negative. An open channel-pressurized flow interface is defined as negative or retreating if it is moving towards the pressurized flow region, and positive otherwise (e.g., Song et al. 1983). Current models based on the MOC approach cannot simulate open channel-pressurized flow negative interfaces at internal nodes in the pipe when the flow in the open channel region is supercritical (e.g., Cardle 1984). This limitation is also extended to the boundaries. Thus, when separate equations are used for free surface and pressurized flows, it is necessary an integrated approach at the boundaries for simulating free surface flows, pressurized flows and mixed flows (positive and negative interfaces).

Guo and Song (1991) suggested three equations for solving the flow variables at a drop shaft boundary. The aim of these authors was to simulate pressurized flows in a drop shaft (vertical shaft) under rapid variation with time of its water surface level. The equations suggested by these authors were the energy equation, a combined mass and y-momentum equation and an equation based on the Method of Characteristics (MOC) that connected the drop shaft boundary with an adjacent internal node of an horizontal tunnel. This model was tested by the authors of the present paper and it was found that it leads to numerical instabilities and to an inaccurate prediction of frequency and amplitude of water surface levels. Our reasoning about the source of these numerical instabilities are explained in the drop shaft boundary section. Because a drop shaft boundary is very common in storm-sewer systems, a robust approach for the treatment of this type of boundary is necessary.

This paper describes part of the work presented in León et al. (2009), which presents boundary conditions (BCs) for simulating free surface, pressurized, and the simultaneous occurrence of free surface and pressurized flows (mixed flows) when the free surface region is modeled using the 1D Saint-Venant equations and the pressurized region is modeled using the 1D compressible waterhammer equations. The present paper describes the results of the application of the integrated boundary conditions for modeling free surface, pressurized, and mixed transient flow conditions in two test cases. The first test case is a hypothetical test and the second is an experimental work in an oscillation tube performed by the authors of this paper. The CFD package FLOW-3D was used as frame of comparison for the first test case and the open source code OpenFOAM besides experimental results

was used for the second one. The integrated boundary conditions were implemented in the Illinois Transient Model (ITM) developed by the first author of this paper, which has been used to study hydraulic transients in the Calumet system of the Metropolitan Water Reclamation District of Greater Chicago (MWRDGC). The results of the latter study are not presented in this paper.

2. Formulation of Boundary Conditions

In a typical storm-sewer system, various types of boundaries are present. These may include drop shafts, reservoirs, junctions, dead ends, control gates, pumping stations, etc. Following, a brief overview of the integrated boundary conditions for two types of boundaries is outlined.

2.1. *N-way junction boundary*

A N-way junction boundary (N pipes) is depicted schematically in Fig. 1 and consists of "p" inflowing pipes and "q" outflowing pipes, with $N = p + q$. A pipe is denoted as inflowing pipe when it conveys flow to the boundary in normal flow conditions (e.g., uniform flow). Likewise, a pipe is denoted as outflowing pipe when it draws flow from the boundary in normal flow conditions. If a pipe has zero longitudinal slope, the pipe can be treated as either inflowing or outflowing. In a N-way junction boundary, $2N+1$ variables are unknown, namely, the water depth and the flow discharge at each pipe boundary, and the flow depth at the junction pond (y_d). Thus, $2N+1$ equations are needed in order to determine the unknown variables. To fulfill the number of equations ($2N+1$), two equations are required for each pipe and an additional equation is needed at the junction pond. The reader is referred to León et al. (2009) for these equations.

2.2. *Drop shaft boundary*

As depicted in Fig. 2, a drop shaft consists of one vertical shaft connected to a drift tube, which in turn is connected to a main tunnel system. For a drop shaft boundary, three variables are unknown, namely, the water depth at the drop shaft (H), and the water depth (y_b) and flow discharge (Q_b) at the outlet pipe boundary. Thus, three equations are needed in order to determine the unknown variables. The reader is referred to León et al. (2009) for these equations.

As mentioned in the introduction, the approach used by Guo and Song (1991) for simulating pressurized flows in drop shafts under rapid variation of their water surface levels leads to numerical instabilities. We speculate that the reason for these instabilities may be due to coupling the energy and momentum equations. Notice that between sections 0 and 1 in Fig. 2, the head loss can not be quantified using the classical relation for a local head loss $[ku|u|/(2g)]$ because if k is constant the head loss between these sections is only a function of the flow velocity at the boundary. However in the actual case, the head loss depends not only on the velocity but also on the highly variable length of the water column in the vertical pipe (H). Under these conditions, the head loss between 0 and 1 (Fig. 2) is mainly due to frictional losses, which in turn are a direct function of the water column length in the vertical pipe. Clearly, variation of the frictional losses due to rapid variation of the water column length can not be taken into account by the classical local head loss relation. The incongruence described above for representing the head losses in the drop shaft is not critical when coupling the conservation of energy and mass equations. The reason is that in the latter case the flow dynamics in the vertical pipe are neglected. However this approach leads to inaccuracies on the frequency of oscillation of water surface levels in the vertical pipe as will be shown later. For the accurate prediction of frequency and amplitude of rapid variation of water surface levels in drop shafts the momentum equation and not the energy equation must be used. The equations presented by Guo and Song (1991) were

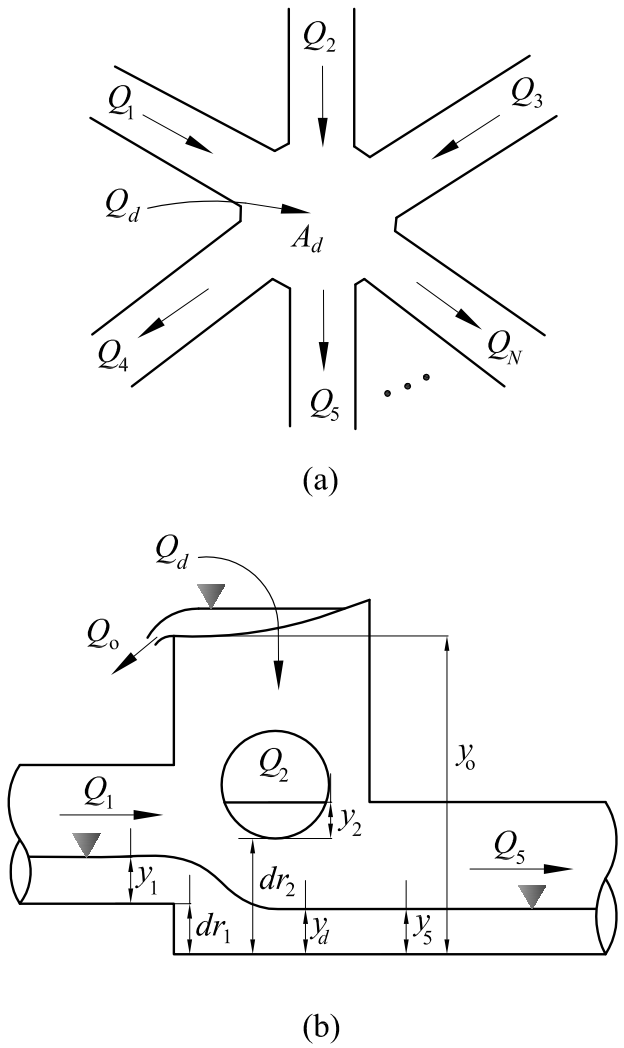

Fig. 1. Schematic of a N-way junction boundary (a) plan view, (b) side view [To avoid cluttering the side view only pipes 1, 2 and 5 were drawn]

modified/replaced by the authors of this paper to overcome the aforementioned problems. The reader is referred to León et al. (2009) for the modified/replaced equations.

3. Evaluation of the model

The purpose of this section is to evaluate the accuracy and robustness of the integrated boundary conditions for simulating free surface, pressurized, and mixed transient flows. Because of the lack of experimental data for the flows of interest in complex boundaries, the first test case presented herein considers a hypothetical test case, namely a three-way merging flow system. The second test case is an experimental work in an oscillation tube performed by the authors of this paper. In the first test case, the length of the pipes is intentionally chosen to be short so that the boundaries have a clear effect on the results. With the aim of evaluating the integrated boundary conditions, Computational Fluid Dynamics (CFD) modeling results were used as frame of comparison. The CFD package FLOW-3D (Flow Science Inc. 2005) is used as frame of comparison for the first test case and OpenFOAM (OpenCFD Ltd. 2007) besides experimental results is used for the second test case. The results of these two models can be trusted as they have been tested extensively with

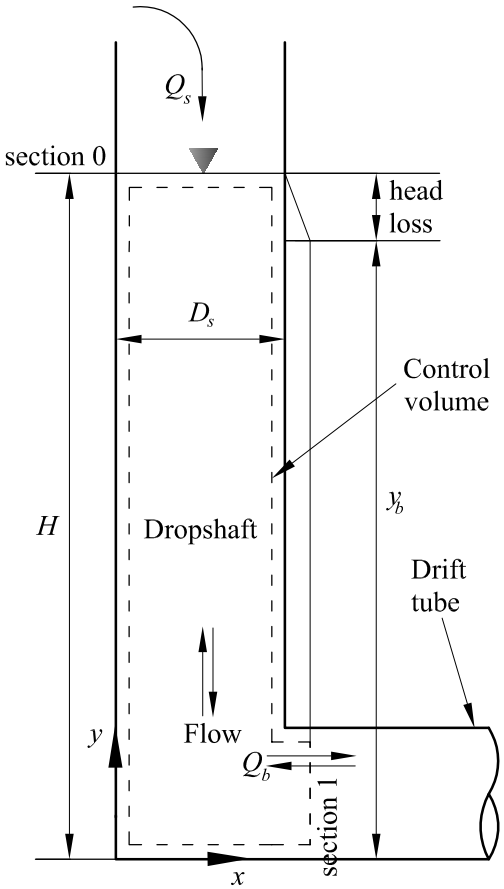

Fig. 2. Schematic of a drop shaft boundary

good success. Unlike OpenFOAM, FLOW-3D has a module that allows modeling acoustic waves in pressurized flow conditions. The propagation of acoustic waves is associated with the compressibility of the flow; however not all CFD compressible models can simulate acoustic waves. In the first test case pressure heads inside horizontal pipes are of interest, for which modeling of acoustic waves is important if pressurized flows are present. In the second test case, even when fully pressurized flows are simulated, modeling of acoustic waves is not important because in this test the interest is water level oscillations at drop shafts (vertical pipes) and not pressure heads inside the horizontal pipe. The main reason for using OpenFOAM in the second test case is that the unstructured mesh used by OpenFOAM allows a better representation of the pipe geometry (e.g., cross-sectional area) than the cartesian mesh used by FLOW-3D.

3.1. *Three-way merging flow*

The hypothetical test presented in this section considers a three-way merging flow system that is depicted in Fig. 3(a). As shown in Fig. 3(a), all pipes have a length of 5 m, the junction pond has a diameter of 1 m, the inflowing pipes (pipes 1 and 2) have both a diameter of 0.5 m and the outflowing pipe (pipe 3) has a diameter of 0.8 m. The Manning's roughness coefficient used in the 1D simulation is n_m = 0.015 $m^{1/6}$, the waterhammer wave speed considered is 100 m/s and the initial flow velocity in all pipes is 0 m/s. A waterhammer wave speed of 100 m/s was used because of PC hard disk storage limitations (200 GB) when running FLOW-3D. For instance when using a mesh of 6,000,000 cells,

a pressure wave celerity of 100 m/s, an output time of 0.001 s (to be able to capture the pressure head traces associated with a pressure wave celerity of 100 m/s) and a simulation time of 0.2 seconds, the storage required in the PC was about 150 GB. Given the PC hard disk storage limitations, it was decided to use a maximum pressure wave celerity of 100 m/s in this and the next test case. It is pointed out that the pressure wave celerity is not a limitation for the 1D integrated model. To ensure that the CFD results for this and the next test case are mesh independent a mesh convergence study was performed (not presented herein due to space limitations).

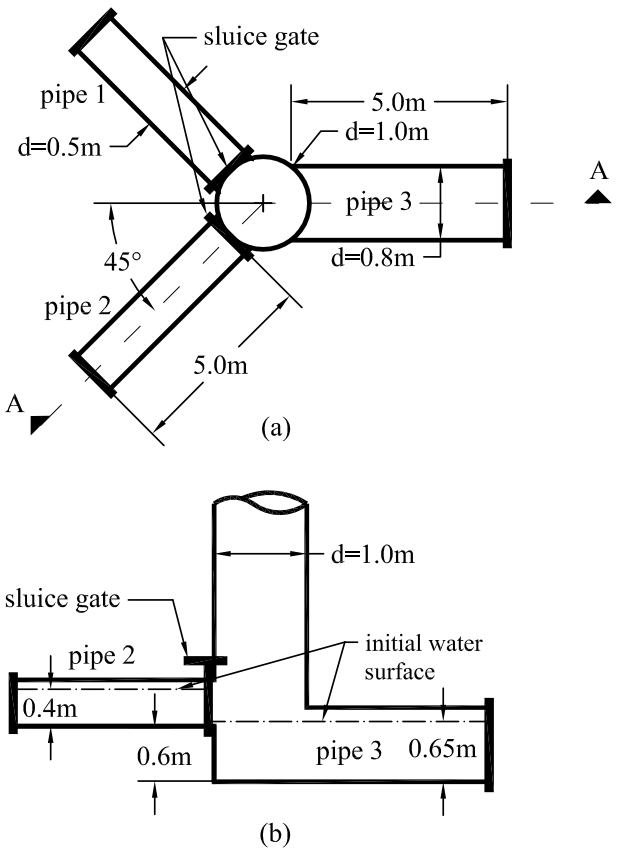

Fig. 3. (a) Plan and (b) section A-A view for three-way merging flow hypothetical case

The initial water surface levels for this test are presented in Fig. 3(b). As can be observed in Figs. 3(a) and 3(b), the initial zero-velocity water pools in each pipe are separated by two sluice gates located at the downstream end of each inflowing pipe. The boundary conditions at the upstream end of the inflowing pipes (pipes 1 and 2) and at the downstream end of the outflowing pipe (pipe 3) were assumed to be zero-flux boundaries, which represent a dead-end pipe. The transient flow is obtained after an instantaneous and simultaneous opening of the sluice gates at time $t = 0$.

The opening of the sluice gates generated a free surface flow surge at the upstream end of pipe 3 that moved in the downstream direction. The continuous supply from the inflowing pipes into the outflowing pipe (pipe 3) pressurized the upstream end of pipe 3 making the free surface flow surge become an open channel-pressurized flow positive interface that moved in the downstream direction. Once this positive interface reached the downstream end (dead-end) the whole pipe 3 was pressurized and remained that way during the entire simulation. At the inflowing pipes (pipes 1 and 2), the flow remained fully free surface

during the entire simulation, although some wave reflections originated at their boundaries (dead-end and junction pond) were observed during the visualization of the simulations. The simulated pressure head traces mid-way of pipes 2 (results for pipe 1 are the same as pipe 2 because of symmetry) and 3 are presented in Figs. 4 and 5, respectively. The simulation time for this test case was 12 seconds, however for pipe 3 (Fig. 5) that involves pressurized flows (high frequency of oscillations) the results are shown only for the first 2.8 seconds for better visualization. The simulated results using the proposed approach were obtained using 200 cells in each pipe and a maximum Courant number of Cr = 0.8.

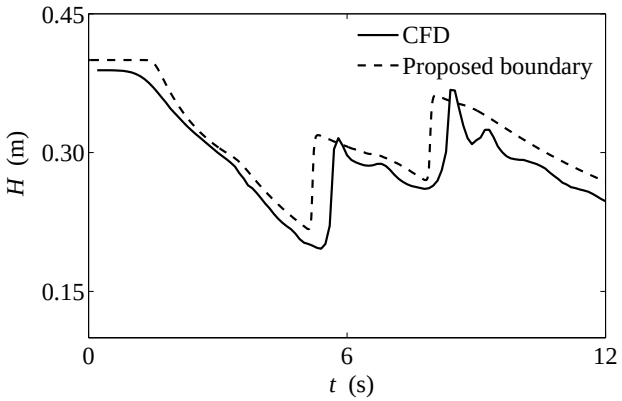

Fig. 4. Pressure head trace at mid-way of pipe 2

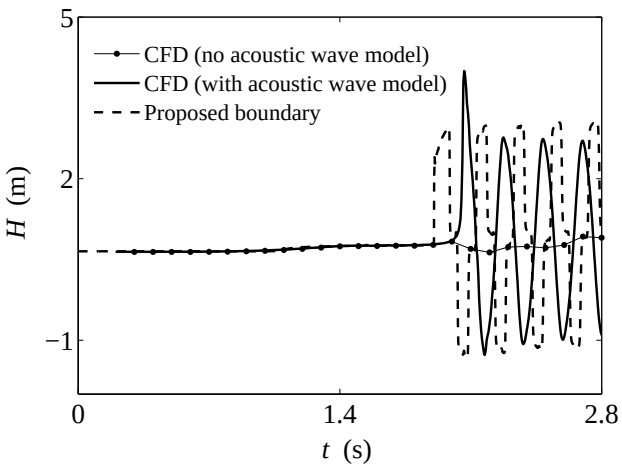

Fig. 5. Pressure head trace at mid-way of pipe 3

The results of pressure head traces for pipe 2 (Fig. 4) obtained using the proposed approach agree well with the results obtained using the FLOW-3D model, although the slightly earlier pressurization of the upstream end of pipe 3 when using the proposed model made the free surface flow surge generated at the junction pond arrive earlier at mid way of pipe 2. Fully free surface flow was achieved in pipes 1 and 2 during the entire simulation. The results for pipe 3 (Fig. 5), which undergoes a flow type change from free surface flow to mixed flow to pressurized flow, also show good agreement between the proposed approach and FLOW-3D (using the acoustic wave model), although this pipe is fully pressurized earlier when using the proposed model. Fig. 5 also shows the results of FLOW-3D without

using the acoustic wave model. These results show that for pressurized transient flows, the pressure heads obtained without using the acoustic wave model are much smaller than when using this model. The latter results show that the compressibility of the flow (associated with the propagation of acoustic waves) is very important when simulating pressurized transient flows. For simulating free surface flows, considering compressibility of the flow is not important as they produce identical results.

3.2. *Oscillation tube*

The purpose of this section is to test the ability of the proposed model in simulating pressurized flows in vertical pipes in which water surface level varies rapidly with time. With the aim of evaluating the proposed approach besides CFD modeling, laboratory results were used as frame of comparison. The experimental setup which layout is depicted in Fig. 6 (a) was built in the Ven Te Chow Hydrosystems Laboratory of the University of Illinois at Urbana-Champaign. As shown in Fig. 6, the experimental setup consisted of a 4.98 m long horizontal plexiglass pipe connected at its upstream and downstream ends by a 2.2 m long vertical pipe of the same material as the horizontal pipe. The inside diameter of all pipes was 50.8 mm (2"). At the center of the horizontal pipe, a quarter-turn ball valve was installed, which as shown in Fig. 6 (b), separated the initial water levels upstream and downstream of the valve. The length of the vertical pipes are intentionally chosen to be of the same scale as of the horizontal pipe so that the vertical flow has a clear effect on the results. The water levels in the upstream vertical pipe (left vertical pipe in Fig. 6) were recorded using a Canon GL2 color video camera. For a better visualization of the water levels, the water in the oscillation tube was previously dyed. The acquired images were post-processed using the Image Processing Toolbox of MATLAB. For the MATLAB analysis, the video images were converted first to gray-scale images that in turn were converted to black and white images (binary system: 1 = black and 0 = white). The water level for each image was determined by computing the maximum row that has a pixel with a value of 1.

The transient flow in the experiments was obtained by a rapid opening of the valve, which created periodic oscillations of water surface levels in the vertical pipes. The measured and simulated water level traces at the upstream vertical pipe (left vertical pipe in Fig. 7) are presented in Fig. 7. The simulated results using the proposed approach were obtained using 400 cells, a pressure wave celerity of 1000 m/s, a Manning roughness coefficient of 0.010 $m^{1/6}$ (typical for a plexiglass pipe), and a Courant number of Cr = 0.8. The results show a good agreement between the proposed approach, CFD, and measured results for the frequency and amplitude of water level oscillations. The results in Fig. 7 labelled "mass/energy" are obtained with the 1D FV model using the mass and energy equation instead of the mass and momentum equation (proposed boundary). As can be observed in Fig. 7, the former approach leads to inaccuracies on the frequency of oscillation of the water surface level. For the accurate prediction of frequency and amplitude of rapid variation of water surface levels in drop shafts the momentum equation and not the energy equation must be used.

4. Conclusions

This paper describes part of the work presented in León et al. (2009), which presents boundary conditions (BCs) for simulating free surface, pressurized, and the simultaneous occurrence of free surface and pressurized flows (mixed flows) when the free surface region is modeled using the 1D Saint-Venant equations and the pressurized region is modeled using the 1D compressible waterhammer equations. The key results are as follows:

(1) The integrated boundary conditions was used for modeling free surface, pressurized, and mixed transient flow conditions in two test cases, namely, a three-way

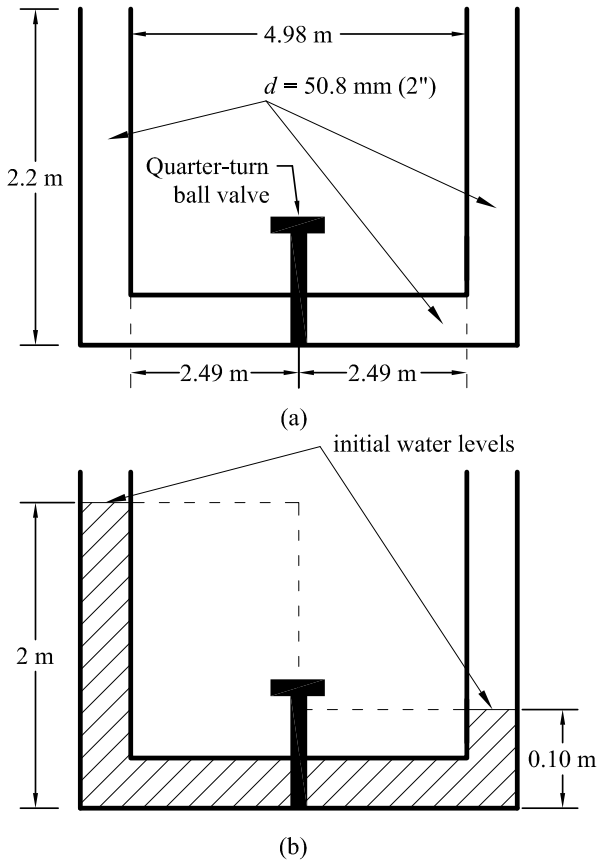

Fig. 6. Experimental setup (not to scale) (a) dimensions and (b) initial water levels

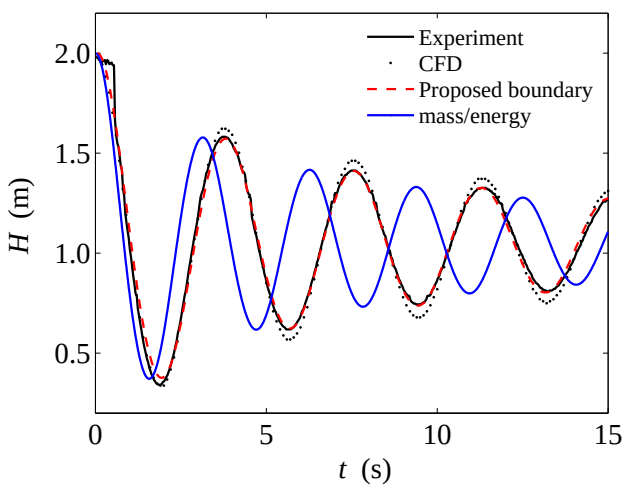

Fig. 7. Water level elevation at upstream drop shaft

merging flow boundary and a drop shaft boundary. The first test case considered a hypothetical test and the second test case is an experimental work in an oscillation tube performed by the authors of this paper. The CFD package FLOW-3D was used as frame of comparison for the first test case and the open source code OpenFOAM

besides experimental results was used for the second test case. The results showed that the integrated boundary conditions can be used for modeling free surface, pressurized, and mixed transient flow conditions at these complex boundaries with good accuracy.

(2) For the accurate prediction of frequency and amplitude of rapid variation of water surface levels in drop shafts the momentum equation and not the energy equation must be used.

(3) Overall, the integrated boundary conditions can be used to simulate any flow regime (free surface, pressurized and mixed flow) at complex boundaries such as drop shafts, reservoirs and junctions with any number of inflowing and outflowing pipes. The integrated boundary conditions were implemented in the Illinois Transient Model (ITM), which has been used to study hydraulic transients in the Calumet system of the Metropolitan Water Reclamation District of Greater Chicago (MWRDGC). The results of the latter study are not presented in this paper.

5. Acknowledgments

The authors gratefully acknowledge the Metropolitan Water Reclamation District of Greater Chicago for their financial support. Special thanks to MSc. Andrew Waratuke and Ph.D. candidate Octavio Sequeiros for their assistance on the experimental work and to Engineer Nils Oberg for his assistance on the video image processing analysis.

References

Cardle, J.A. (1984). An investigation of hydraulic transients in combination free surface and pressurized flows. *Ph.D. thesis*, Dept. of Civil and Mineral Engng., Univ. of Minnesota, Twin Cities, MN.

Cardle, J.A., and Song, C.C.S. (1988). Mathematical modeling of unsteady flow in storm sewers. *Int. J. of Engng. Fluid Mechanics*, 1(4), 495-518.

Flow Science, Inc. (2005). FLOW-3D v. 9.0 user's manual, Flow Science, Inc., Santa Fe, N.M.

Guo, Q., and Song, C.S. (1991). Dropshaft hydrodynamics under transient conditions. *J. Hydraul. Engng.*, 117(8), 1042–1055.

Karney, B.W., and Ghidaoui, M.S. (1997). Flexible discretization algorithm for fixed-grid MOC in pipelines. *J. Hydraul. Engng.*, 123(11), 1004–1011.

León, A.S., Ghidaoui, M.S., Schmidt, A.R., and García, M.H. (2006). Godunov-type solutions for transient flows in sewers. *J. Hydraul. Engng.*, 132(8), 800-813.

León, A.S., Ghidaoui, M.S., Schmidt, A.R., and García, M.H. (2008a). An efficient second-order accurate shock capturing scheme for modeling one and two-phase waterhammer flows. *J. Hydraul. Engng.*, 134(7), 970-983.

León, A.S., Ghidaoui, M.S., Schmidt, A.R., and García, M.H. (2008b). A finite volume approach for modeling the simultaneous occurrence of free surface and pressurized flows. *J. Hydraul. Research*. Tentatively accepted.

León, A.S., Liu X., Ghidaoui, M.S., Schmidt, A.R., and García, M.H. (2009). Boundary conditions for modeling free surface, pressurized, and mixed free surface-pressurized transient flows in complex storm-sewer systems. *Advances in water resources*. Submitted for review.

OpenCFD, Ltd. (2007). OpenFOAM User Guide, OpenCFD, Ltd., Berkshire, United Kingdom.

Politano, M., Odgaard, A.J. and Klecan, W. (2007). Case study: Numerical evaluation of hydraulic transients in a combined sewer overflow tunnel system. *J. Hydraul. Engng.*, 133(10), 1103–1110.

Sjöberg, A.(1976). Calculation of unsteady flows in regulated rivers and storm sewer systems, Tech. Rep. Division of Hydraulics, Chalmers Univ. of Technology, Goteborg, Swe-

den.
Song, C.C.S., Cardle, J.A. and Leung, K.S. (1983). Transient mixed-flow models for storm sewers. *J. Hydraul. Engng.*, 109(11), 1487-1503.

City of St. Louis Permeable Pavement Alley Pilot Study

By: Dave Yates, PE Author[1] and Marjorie Melton, PE C.O. Author[2]

[1] CH2M HILL, 1034 South Brentwood Blvd, Suite 2300, Saint Louis, MO 63117; PH (314) 421-0900; FAX (314) 454-8720; email: dave.yates@ch2m.com

[2] President, Board of Public Service, City of Saint Louis, MO, 1200 Market Street, Room 301, Saint Louis, MO 63103; PH (314) 622-4143; FAX (314) 613-7365; email: meltonm@stlouiscity.com

1. Abstract

The City of St. Louis Board of Public Service (BPS) formed a partnership with the Missouri Department of Conservation (MDC), CH2M Hill, the Metropolitan St. Louis Sewer District (MSD), Southern Illinois University – Edwardsville (SIUE), and East-West Gateway Council of Governments (EWG) in mid-2007 to find ways to incorporate low impact development (LID) techniques into City of St. Louis projects. The team identified pervious paving as the first best management practice (BMP) to investigate due to the multiple benefits it provides and the ample opportunity to utilize the practice in City-owned projects. This project is one of many initiatives in the City of St. Louis Climate Change Plan.

Impervious surfaces, such as roads, rooftops and sidewalks within the City of St. Louis contribute to water quality and quantity problems as well as the urban heat island. Converting impervious surfaces to pervious paving, an Environmental Protection Agency (EPA) recognized best management practice (BMP), reduces stormwater runoff, captures peak flows, replenishes water tables and aquifers, minimizes flash flooding and standing water, prevents warm and polluted water from entering the streams, mitigates surface pollutants and reduces heat island effect.

Pilot study data will be used to support a change in City of St. Louis policy to potentially require pervious paving in its alleys citywide. The data will also be used to promote change in private developments and other City paving projects where appropriate. The results will be used by MSD to determine if permeable pavements can be used as BMP either in junction with other BMPs or as a stand-alone BMP.

2. Background

The City of St. Louis has approximately 485 miles of alleys, and is seeking to develop an alley replacement program to provide for pervious pavements to be constructed in lieu of the more traditional and conventional asphalt pavements that are now common to many alleys in the City.

This study aimed to evaluate the effectiveness of porous pavement on flow reduction and water quality improvement in combined sewers. The flows and water quality of samples taken from combined sewers at three alleys in the City of St. Louis are

compared between before and after porous pavements are implemented. The project consists of three phases: Phase I was to monitor and characterize the flows and water quality under existing conditions; Phase II is design and construction of the porous pavement; and Phase III is to monitor and characterize the flows and water quality under improved conditions where LID has been implemented. This report describes findings from Phase I study that was conducted from May to July 2008.

In order to generate needed data to determine the effectiveness of the practice in reducing stormwater quantity and improving stormwater quality in City of St. Louis conditions, justify the increased cost over conventional asphalt paving, and to select the best materials, the team chose to conduct a pilot project. Representatives investigated other projects and met with Chicago Department of Transportation (CDOT) staff to build on knowledge they had gained from internal sources as well as research. From visiting with CDOT it was determined the most feasible porous pavement design appeared to contain traditional concrete aprons with a porous center running the length of the alley. This design incorporated a reverse crown to direct runoff to the porous pavement section.

The three pilot alleys were identified and equipment was installed to measure stormwater quantity and quality along with rainfall. Results are currently being processed by SIUE. Phase II construction began with the permeable asphalt alley, which was completed in October 2008. Funding for the pervious concrete alley is being provided by the Ward 6 Alderwoman, Kacie Starr-Triplett. Funding is still being secured for construction of the permeable paver alley.

3. Methodology

Automatic samplers and flow meters were installed at three sites by the staff of Metropolitan St. Louis Sewer District (MSD), who also collected the samples and flow data and provided rainfall data. The alley sites are shown in Fig. 1 through 3. The manholes where automatic samplers and flow meters were installed are summarized in Table 1.

Composite samples from four storm events (May 7, 25, June 20, July 8) were collected. The sampler for the Cardinal site did not trigger during Phase I study, subsequently no data were available for this site. The sampler for the Eads site was not triggered during the June 20 storm event. The collected samples were split into subsets and preserved following the Standard Methods Table 1060:I (APHA 1998) and relevant MSD protocols. The staff of SIUE picked up the samples from MSD and delivered to the Madison County Environmental Laboratory in Edwardsville, IL. The following parameters were analyzed for each sample.

- Total Suspended Solids (TSS), Standard Methods 2540D (APHA 1998)
- Total Phosphorous (TP), USEPA Method 365.3 (USEPA 1979)
- Total Nitrogen (TN): TN was determined by summing the measured TKN and nitrate. Standard Methods 4500-Norg B for TKN (APHA 1998). Standard Methods 4500-NO_3^- D for nitrate (APHA 1998)

- Metal (Total Zinc), Standard Methods 3500-Zn and 3111B (APHA 1998)
- Metal (Total Copper), Standard Methods 3500-Cu and 3111B (APHA 1998)



Fig. 1 Eads Ave. Site in City of St. Louis


Fig. 2 Geyer Ave. Site in City of St. Louis



Fig. 3 Cardinal Ave. Site in City of St. Louis

Table 1. Sites of Phase I Study

Site	Current Pavement	Location	Sampler MH	Flow-meter MH	Composite Period
3127 Eads Ave.	Asphalt	Parallel to Compton, between Eads and Henrietta	21F2-278C	21F2-284C	May 7, 6:55 May 25, 13:21-13:46 June 20, no data July 8, 19:04-19:23
3217 Geyer Ave.	Brick	Parallel to Compton Hill, between Geyer and I-44	21F2-147C	21F2-147C	May 7, 5:59 May 25, 13:20-13:56 June 20, 01:20-02:02 July 8, 19:06-19:32
1412 Cardinal Ave.	Brick	Parallel to Park and Caroline, between Montrose and Cardinal	21E1-383C	21E1-385C	No data

The MSD reports of flow monitoring show flow rates that were calculated using the measured depths and velocities. The depth and velocity data were recorded mostly in 15-minute interval or in one-minute interval during rain events. The flow reports show negative flows in a number of instances, due to negative velocities and were likely due to the malfunctioning of the flow meters. When the flow hydrographs were prepared, the negative flow rates were corrected zero values.

The rainfall data for the Eads and Geyer sites were based on data from MSD's rain gauge stations of C-24 and C-13, respectively. The rainfall data, although collected in

5-minute interval, were reported in hourly interval for clarity (i.e. cumulative rainfalls in each hourly interval were plotted).

The water qualities from samples taken at the studied sites are summarized in Table 2 and are illustrated in Fig. 4 through 8. Results indicate that pollutants in the samples from the Eads site are in lower concentrations than those from the Geyer site. For facilities that discharge to MSD sewers, the MSD Pretreatment Ordinance sets the daily average discharge limit of total Zinc and total Copper to be 3.0 mg/L and 2.7 mg/L, respectively; but doesn't set limits for TSS, TP and TN. TSS from a facility to MSD sewers is monitored for billing purpose and MSD wastewater treatment plants monitor TP and TN for operation information. For the flows in MSD sewers, currently, there are no target pollutant limits or desirable pollutant concentrations.

Table 2. Water Quality – Phase I Study

	Sampling Date	TSS	mg/L	TP	mg/L	TN	mg/L	Zn	mg/L	Cu	mg/L
3127 Eads	7-May-08	E_TSS1	293	E_TP1	0.63	E_TN1	12.0	E_Zn1	0.161	E_Cu1	0.041
Ave.	25-May-08	E_TSS2	519	E_TP2	0.59	E_TN2	17.8	E_Zn2	0.236	E_Cu2	0.045
	20-Jun-08	E_TSS3		E_TP3		E_TN3		E_Zn3		E_Cu3	
	8-Jul-08	E_TSS4	185	E_TP4	0.46	E_TN4	9.1	E_Zn4	0.123	E_Cu4	0.026
3217 Geyer	7-May-08	G_TSS1	472	G_TP1	1.34	G_TN1	16.0	G_Zn1	0.534	G_Cu1	0.105
Ave.	25-May-08	G_TSS2	528	G_TP2	1.16	G_TN2	31.6	G_Zn2	0.573	G_Cu2	0.094
	20-Jun-08	G_TSS3	1230	G_TP3	3.22	G_TN3	37.4	G_Zn3	0.687	G_Cu3	0.342
	8-Jul-08	G_TSS4	476	G_TP4	1.37	G_TN4	21.4	G_Zn4	0.367	G_Cu4	0.159

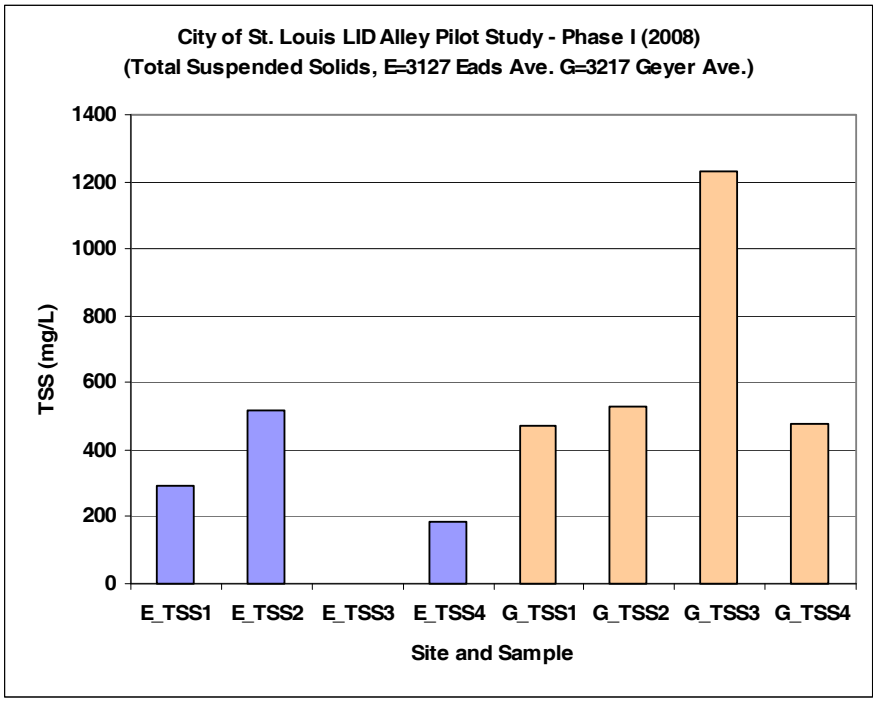

Fig. 4 Total Suspended Solids (TSS)

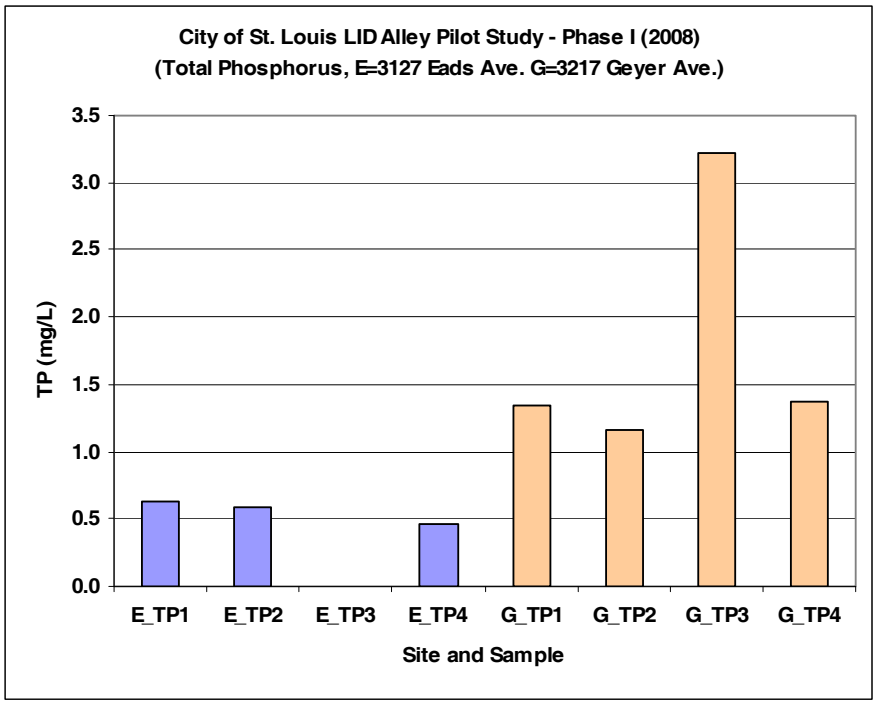

Fig. 5 Total Phosphorous (TP)

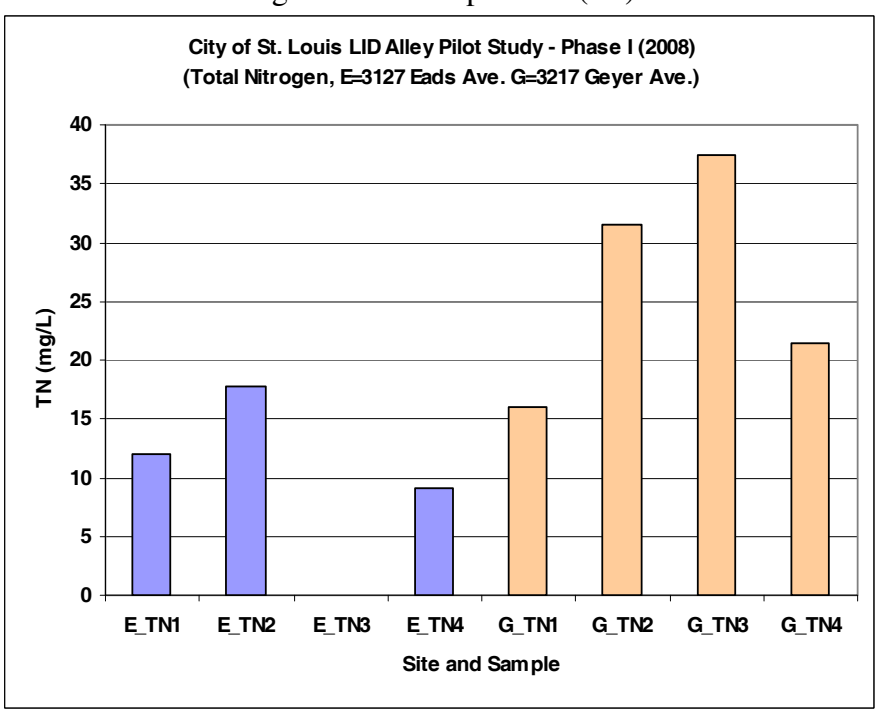

Fig. 6 Total Nitrogen (TN)

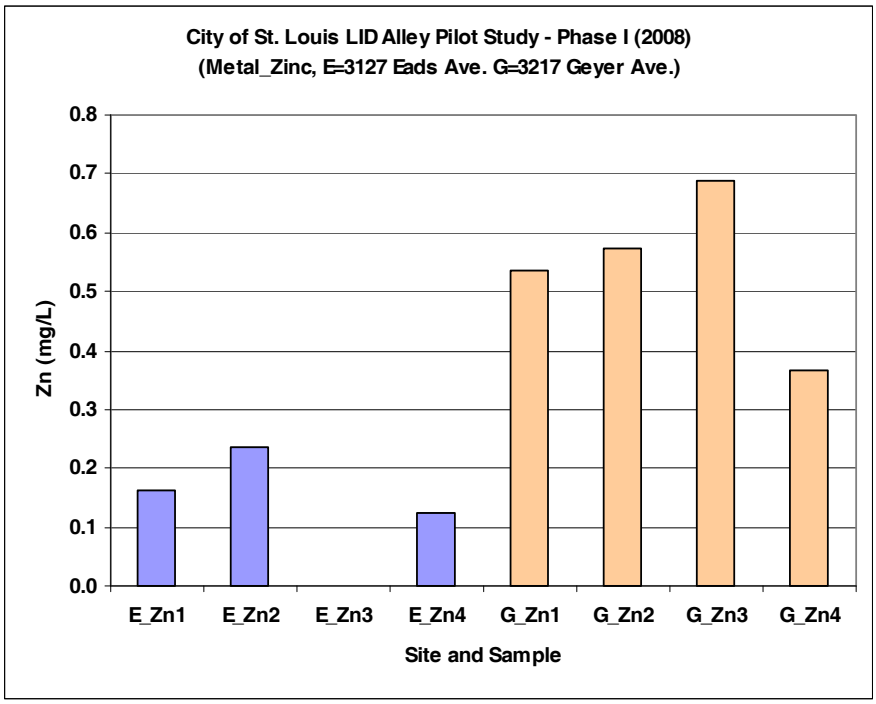

Fig. 7 Metal – Total Zinc (Zn)

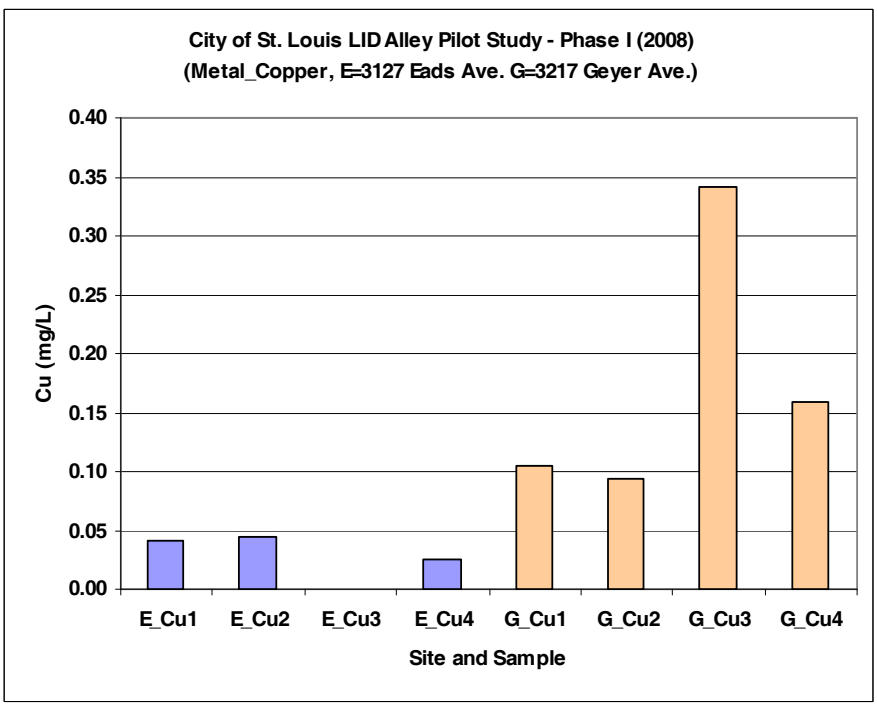

Fig. 8 Metal – Total Copper (Cu)

The flow and rainfall data for each site and each rainfall event were prepared. A sample graph is shown in Fig. 9 for the May 7 storm at the Eads alley, which shows the correlation between rainfall and metered flow in the combined sewer as expected. The peak flows and rainfalls are summarized in Table 3. It was found that flow rates

at the Eads site (up to 800 gpm) were much higher than those at the Geyer site (up to 35 gpm). For the Eads site, the two peak flows found on May 25 (564 gpm at 13.6 hr and 748 gpm at 22.3 hr) resulted from the two peak rainfalls (0.40 in/hr at 13 hr and 0.53 in/hr at 22 hr). When water quality and water quantity are correlated, it was found that the composite samples taken on May 25 at the Eads site also contained higher levels of pollutants when compared to other samples, suggesting the higher amount of stormwater runoff resulted in decreased water quality in the combined sewers. For the Geyer site, although some correlation was found between peak flows and peak rainfalls (e.g. 8.9 gpm at 14.3 hr vs. 1.20 in/hr at 13 hr on May 25), peak flows did not correlate well to peak rainfalls in many instances.

Table 3. Peak Flows and Rainfalls – Phase I Study

Site	Sampling Date	Peak Flows (gpm)	Hourly Rainfall (in/hr)
3127 Eads Ave.	7-May-08	111 at 14:00 hr	0.20 from 12:00 to 13:00 hr 0.17 from 13:00 to 14:00 hr
	25-May-08	564 at 13:38 hr 748 at 22:15 hr	0.40 from 12:00 to 13:00 hr 0.53 from 21:00 to 22:00 hr
	20-Jun-08	114 at 1:45 hr	0.11 from 0:00 to 1:00 hr
	8-Jul-08	613 at 19:19 hr	0.49 from 18:00 to 19:00 hr
3217 Geyer Ave.	7-May-08	8.1 at 13:45 hr 8.8 at 15:00 hr	0.20 from 12:00 to 13:00 hr 0.17 from 13:00 to 14:00 hr 0.09 from 14:00 to 15:00 hr
	25-May-08	8.9 at 14:15 hr 11.7 at 23:15 hr	1.20 from 12:00 to 13:00 hr 0.24 from 21:00 to 22:00 hr
	20-Jun-08	26.0 at 8:00 hr 31.7 at 9:00 hr 35.3 at 10:15 hr	0.27 from 0:00 to 1:00 hr 0.08 from 6:00 to 7:00 hr
	8-Jul-08	24.3 at 22:30 hr	0.75 from 18:00 to 19:00 hr

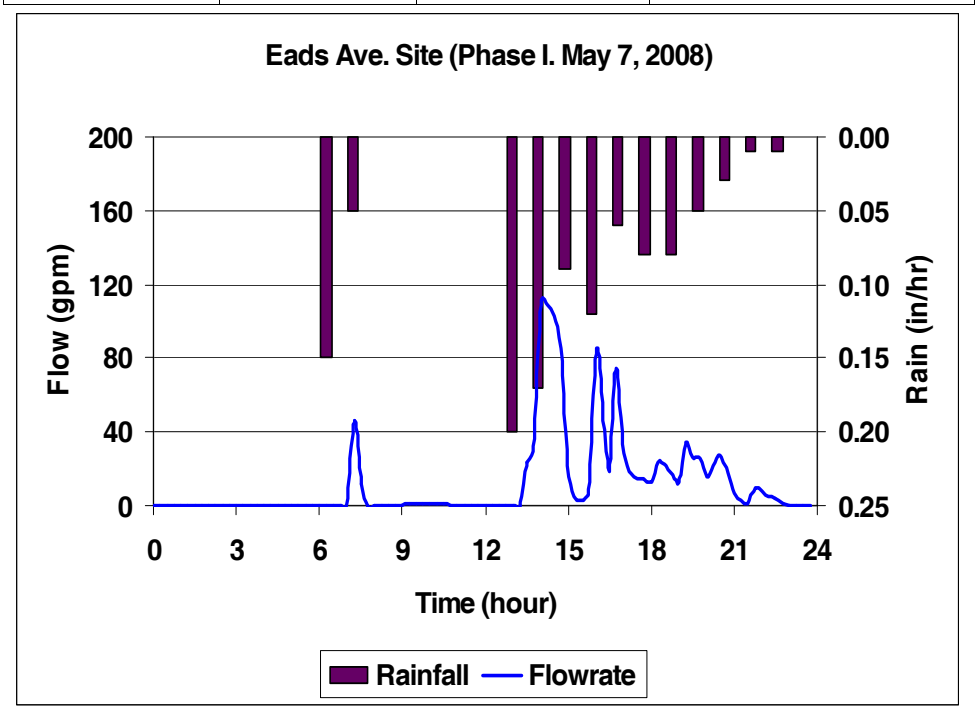

Fig. 9 Eads Ave. Site (May 7)

4. Results

This report describes findings from City of St. Louis low impact development alley pilot study - Phase I, which monitored and characterized the flows and water quality under existing conditions. Composite samples from the Eads and Geyer sites were obtained during four storm events in 2008. Studied water quality parameters included total suspended solids, total phosphorous, total nitrogen, total zinc and total copper. The study found that the flow rates at the Eads site were much higher than those at the Geyer site; pollutants in the samples from the Eads site are in lower concentrations than those from the Geyer site. For the Eads site, peak flows correlated well to peak rainfalls and higher amount of stormwater runoff resulted in worse water quality in the combined sewers. For the Geyer site, peak flows didn't correlate well to peak rainfalls in many instances, likely due to malfunctioned instruments. It is recommended that flow meters and automatic samplers are further verified and calibrated before they are used in Phase III study.

5. References

Attarian, Janet L., 2007, *Chicago Department of Transportation Sustainable Infrastructure Initiatives*.

Zhou, Jianpang, PhD, PE, DEE, Southern Illinois University – Edwardsville, 2008. *Combined Sewer Overflows and Water Quality Analysis, City of St. Louis Low Impact Development Alley Pilot Study – Phase 1.*

APHA, AWWA, WEF (APHA 1998) *Standard Methods of the Examination of Water and Wastewater*. American Public Health Association, Washington, D.C., 20th Ed.

USEPA (1979) *Methods for Chemical Analysis of Water and Wastes*, USEPA/600/4-79/020

Competing risks and the development of adaptive management plans for water resources: Field reconnaissance investigation of risks to fishes and other aquatic biota exposed to endocrine disrupting chemicals (EDCs) in Lake Mead, Nevada USA

Greg Linder[1] and Edward E. Little[2]

[1]US Geological Survey, Columbia Environmental Research Center (USGS/BRD/CERC), HeronWorks Field Office, Brooks OR 97305; linder2@usgs.gov
[2]US Geological Survey, USGS/BRD/CERC, 4200 New Haven Road, Columbia MO 65201; elittle@usgs.gov

ABSTRACT

The analysis and characterization of competing risks for water resources rely on a wide spectrum of tools to evaluate hazards and risks associated with their management. For example, waters of the lower Colorado River stored in reservoirs such as Lake Mead present a wide range of competing risks related to water quantity and water quality. These risks are often interdependent and complicated by competing uses of source waters for sustaining biological resources and for supporting a range of agricultural, municipal, recreational, and industrial uses. USGS is currently conducting a series of interdisciplinary case-studies on water quality of Lake Mead and its source waters. In this case-study we examine selected constituents potentially entering the Lake Mead system, particularly endocrine disrupting chemicals (EDCs). Worldwide, a number of environmental EDCs have been identified that affect reproduction, development, and adaptive behaviors in a wide range of organisms. Many EDCs are minimally affected by current treatment technologies and occur in treated sewage effluents. Several EDCs have been detected in Lake Mead, and several substances have been identified that are of concern because of potential impacts to the aquatic biota, including the sport fishery of Lake Mead and endangered razorback suckers (*Xyrauchen texanus*) that occur in the Colorado River system. For example, altered biomarkers relevant to reproduction and thyroid function in fishes have been observed and may be predictive of impaired metabolism and development. Few studies, however, have addressed whether such EDC-induced responses observed in the field have an ecologically significant effect on the reproductive success of fishes. To identify potential linkages between EDCs and species of management concern, the risk analysis and characterization in this reconnaissance study focused on effects (and attendant uncertainties) that might be expressed by exposed populations. In addition, risk reduction measures that may be of interest to resource managers are considered relative to emerging contaminants in

treated effluents, interdependencies among biological resources at risk, and uses of reservoir waters derived from multiple inflows of widely varying qualities.

INTRODUCTION AND PROBLEM IDENTIFICATION

Lake Mead is located on the lower Colorado River on the border of Nevada and Arizona (Figure 1). The metropolitan Las Vegas area and growing urban development downstream of the reservoir in Arizona, Nevada, and California are highly dependent

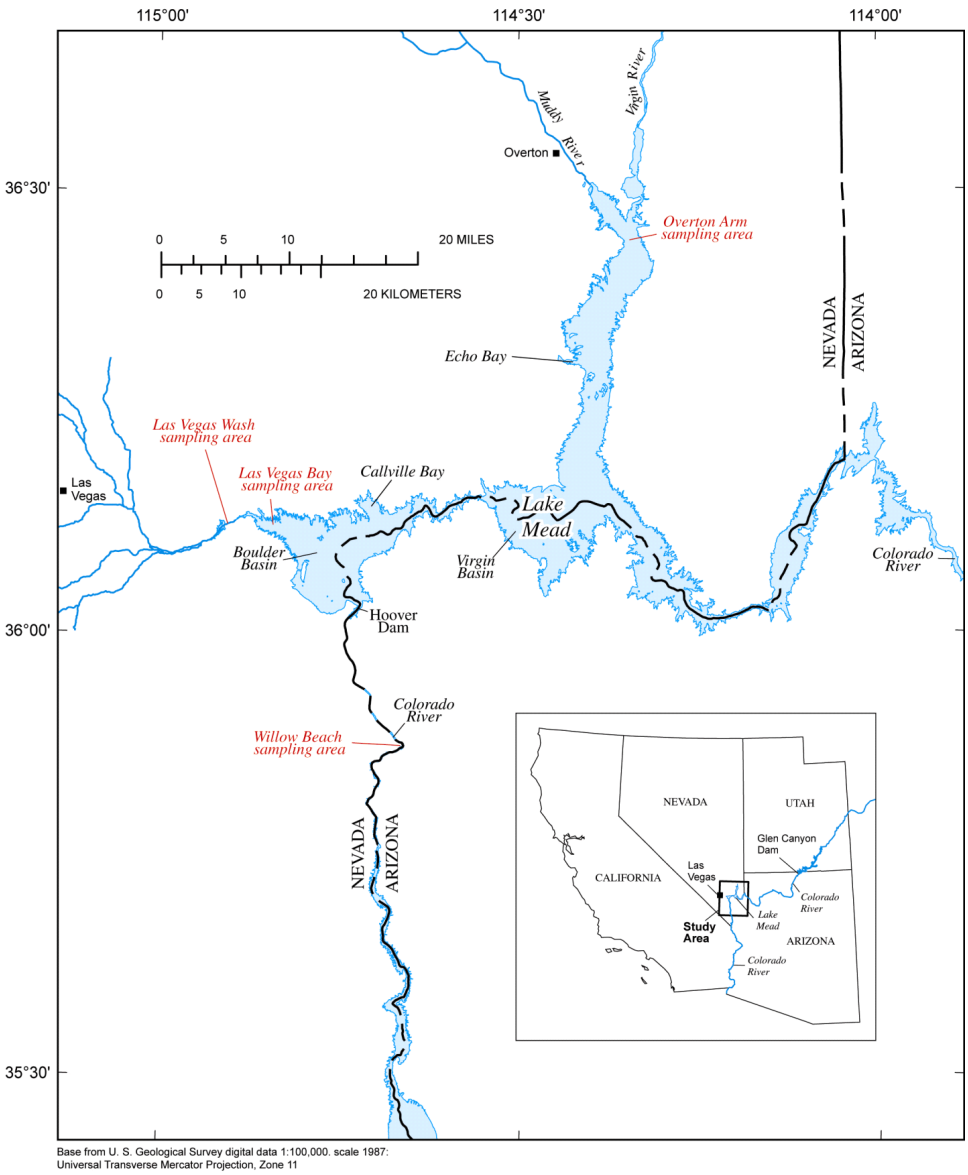

Figure 1. Lake Mead on the Nevada-Arizona border (map courtesy M. Rosen, USGS, Nevada Water Resources Center).

on water resources from the Colorado River system. Reduced water quantity associated with seasonal and decadal trends in precipitation have yielded drought conditions; degraded water quality associated with point source and non-point source inflows have also degraded water quality that may affect fish and wildlife dependent on the reservoir. Various federal and state agencies are involved in managing the Lake Mead National Recreation Area (LMNRA) including the National Park Service (NPS) which served 7.6 million visitors in 2007, and other state and federal agencies which manage the fish and wildlife resources. The states of Nevada and Arizona manage the recreational fisheries in LMNRA that are based on striped bass (*Morone saxatilis*), largemouth bass (*Micropterus salmoides*) and others sport fishes, and U.S. Fish and Wildlife Service (FWS) administers the Endangered Species Act (ESA) within LMNRA, given the occurrence of endangered species such as razorback sucker (*Xyrauchen texanus*) throughout the Colorado River system.

Chemical contaminants are among the multiple stressors that may affect the water resources of Lake Mead. EDCs have been identified in aquatic environments throughout the world including Lake Mead. Complex chemical mixtures released to surface waters in river-reservoir systems such as that at LMNRA may adversely affect endocrine systems of fishes, if effects thresholds are attained. Consequent effects on reproduction, development, and behavior of exposed fishes may occur. Many EDCs occur as constituents of sewage treatment effluents released to aquatic habitats, and some synthetic organic chemicals (SOCs) in these chemical mixtures may be unaffected by current treatment technologies. Several chemicals may be of concern relative to adverse impacts to the sport fishery and the endangered razorback sucker populations of Lake Mead that require characterization and mitigation. From existing ecotoxicological studies on contaminant-altered endocrine function, various aquatic organisms have displayed reproductive impairments, as well as altered thyroid function that may foreshadow impaired metabolism and development. Few studies, however, have addressed the wider question of whether these responses to EDC exposures in the field have ecologically significant effects on the biochemical and physiological processes and their associated reproductive behaviors critical to long-term reproductive success and maintenance of sustainable populations. The present reconnaissance-level analysis of risk and attendant uncertainties relies on existing literature and data, as well as study-specific data to estimate effect threshold concentrations for chemicals potentially affecting target species. A preliminary evaluation of bioaccumulation and food-chain partitioning of EDCs based on existing data and literature for EDCs will also be presented. This reconnaissance-level analysis will provide a preliminary assessment of EDC impacts occurring in Lake Mead and help inform NPS in developing their adaptive management plans..

BACKGROUND STUDIES

Prior studies of Lake Mead indicate the presence of numerous SOCs in water, bottom sediments, and fish, including chemicals capable of disrupting endocrine function in fishes (see, e.g., Bevans et al. 1996; Goodbred et al. 2007). Resource management issues associated with exposures of fish and wildlife to complex

chemical mixtures characteristic of surface waters and sediments in Las Vegas Wash (LVW) and Lake Mead were identified by USGS and FWS (Tuttle, et al. 2002). Presumptive links between EDCs and common carp (*Cyprinus carpio*) inhabiting waters of Lake Mead via treated wastewater discharges released to Las Vegas Bay (LVW) have been characterized (see, e.g., Goodbred et al. 1997; Patiño et al. 2003). Treated effluents include polycyclic aromatic hydrocarbons (PAHs), polychlorinated biphenyls (PCBs), chlorinated pesticides, and pharmaceuticals and personal care products (PPCPs). In addition to point sources such as treated wastewater discharges from municipal wastewater treatment plants in the Las Vegas Valley, non-point source inputs also contribute water inflows to LVW and include urban runoff from lawns, gardens, and golf courses, as well as storm-water runoff and subsurface inflow. Chemical constituents linked to point-source and non-point source inputs into Lake Mead are listed in Table 1. These constituents are similar to treated wastewater discharges from other urban systems (Koplin et al. 2002). Based on the literature the compounds included in Table 1 have environmental risks associated with chronic or acute exposures that may be linked to adverse effects observed in aquatic biota of Lake Mead. Many of these chemicals have different biochemical modes of toxic action, including endocrine disruption, that may cause or contribute to expression of adverse affects observed in aquatic biota of Lake Mead.

BOUNDING THE ANALYSIS OF RISK IN THE RECONNAISSANCE STUDY

To facilitate this reconnaissance investigation, a short list of chemicals of concern with known or presumptive modes of action through endocrine disruption was selected for our investigation (Table 1). The short list of chemicals was primarily focused on EDCs previously identified in the waters and sediments of Lake Mead, as well as tissue-residues of EDCs or metabolites of EDCs identified in fishes collected at various times and locations in Lake Mead in previous studies. In part, the short list of chemicals considered in the risk analysis reflected point-source and non-point source inputs observed in other systems experiencing chemical inputs and associated stresses.

Within the context of exposure risk, the Lake Mead system includes a number of aquatic biota that are representative of other species commonly encountered in riverine and reservoir habitats of the southwest U.S. and of endangered or threatened status under the Endangered Species Act. The conceptual model for this reconnaissance analysis of risk is illustrated in Figure 2, which highlights the primary focus on fishes and aquatic invertebrates dependent on habitats characteristic of Lake Mead and water inflows such as that illustrated by LVW. Here, our focus on fishes centered on striped bass and largemouth bass as representative sport fishes, and razorback sucker as a special status species. Because common carp inhabit a wide range of aquatic habitats within Lake Mead, this abundant species served as a surrogate species. Despite the initial emphasis on fish and aquatic invertebrates, past and ongoing studies have identified a wide range of aquatic receptors that should bring an ecological scale to future investigations.

Fragrances
- tonalide (AHTN)
- galaxolide (HHCB)
- indole
- benzophenone
- oxybenzone

Household chemicals
- caffeine
- butylated hydroxyanisole (BHA)
- triclosan

PAHs and Heterocyclic Aromatics
- naphthalene
- benzo[a]pyrene
- 2-methyl naphthalene
- acetophenone
- phenanthrene
- indole
- pyrene
- d-limonene
- 1-methyl naphthalene
- 2,6-dimethyl naphthalene
- p-cresol
- isoquinoline

Pesticides, Herbicides, & Commercial Biocides
- chlorpyrifos
- o,p-DDE
- triazine herbicides including atrazine and its metabolites
- acetochlor
- alachlor
- diazinon
- dichlorvos
- diuron
- isoproturon
- metolachlor
- DDT
- endosulfan
- methoxychlor
- cis/trans-chlordane
- HCB
- dacthal
- trifluralin

Other Chemicals Associated with Wastewater Treatment
- urobilin

Natural Products, Pharmaceuticals & Illicit Drugs
- methyl salicylate
- acetaminophen
- carbamazepine
- azithromycin
- erythromycin
- sulfa drugs and other antibiotics
- tetracycline antibiotics
- DEET
- 17-beta-estradiol, 17-beta-ethynylestradiol and their metabolites: estrone and estriol
- methamphetamine (MDMA)

Surfactants
- 4-tert-octylphenol
- alkyl phenols such as nonylphenol and octylphenol

Other Priority Pollutants Chemicals of Concerns
- PCB Congeners
- chlorinated dibenzodiox & dibenzofurans (2,3,7,8-TCDD; 2,3,7,8-TCDF)
- perfluorinated compoun (PFOS, telomer alcohol
- flame retardants (PBDE including PBDE 47, 99, 100, 138, 146, 160)
- tributyl tin
- diethylphthalate
- diethylhexylphthalate
- bisphenol A
- isophorone
- tris(2-chloroethyl) phosphate
- tris(2-buthoxyethyl) phosphate
- 5-methyl-1H-benzotriaz
- 3,4-dichlorophenyl isocyanate
- tributylphosphate
- triphenylphosphate

Table 1. Chemicals identified in surface water, sediment, and tissues collected during recent studies at Lake Mead. (List compiled from various sources, including Bevans et al. 1996; Covay et al. 1998, 2001; Goodbred et al. 1997, 2007.)

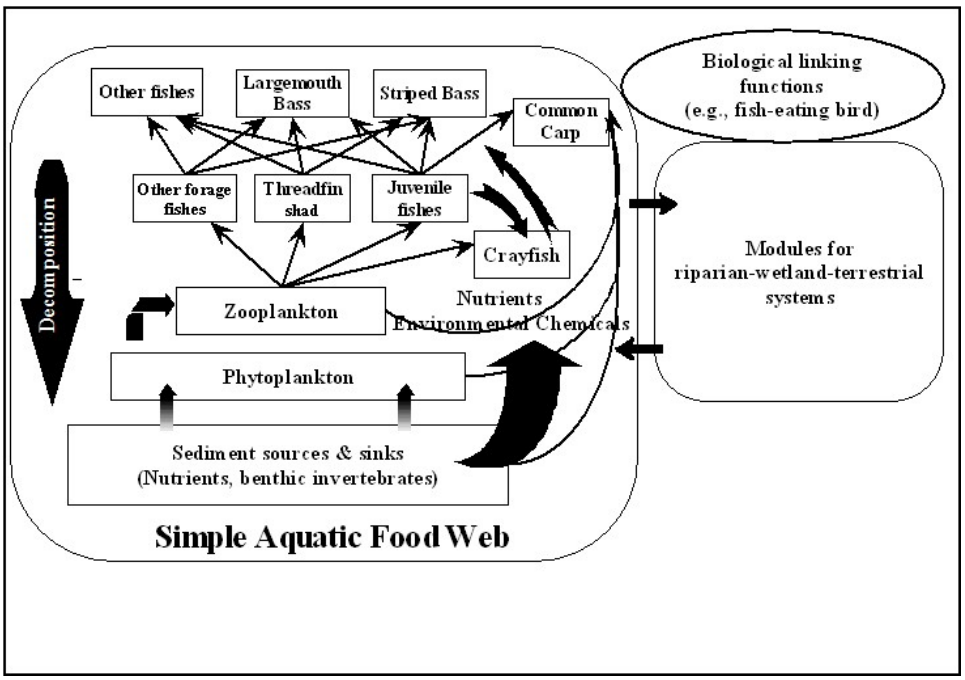

Figure 2. Conceptual model guiding reconnaissance level of analysis of risks associated with exposures of aquatic biota of Lake Mead to EDCs in surface waters and sediments.

The reconnaissance analysis of contaminant risks was focused on fishes and aquatic invertebrates (Table 2), because of their impairment as a result of exposure and their role in food-web transfer of contamination as depicted in the conceptual model in Figure 2. In addition to these representatives of the sport fishery at Lake Mead, razorback sucker was a key species in the analysis of risks, because of its endangered status.

Receptor	Scientific name
Largemouth bass	*Micropterus salmoides*
Carp	*Cyprinus carpio*
Striped bass	*Morone saxatilis*
Rainbow trout	*Oncorhynchus mykiss*
Threadfin shad	*Dorosoma petenense*
Razorback sucker	*Xyrauchen texanus*
Crayfish	*Pacifastacus gambelii*
	Pacifastacus leniusculus leniusculus
	Pacifastacus leniusculus trowbridgii
	Procambarus clarkii

Table 2. Species of concern in the reconnaissance level analysis of risks associated with the presence and inflow of EDCs in Lake Mead.

The conceptual model (Figure 2) guiding this reconnaissance analysis also includes microbial biodegradation studies (see, e.g., Kudłak and Namieśnik 2008) linked to the environmental fate of EDCs occurring in inflows to Lake Mead, and aquatic food-web studies that examined potential interactions among environmental chemicals characteristic of the point-source and non-point source inputs released to the Lake Mead system (see, e.g., Belgrano et al. 2005). When these ongoing studies are completed, a comprehensive analysis of ecological risks based on study-specific empirical data should follow this reconnaissance analysis and characterization of risks to fishes and other aquatic biota.

METHODS AND MATERIALS

Reconnaissance level risk analysis of EDC exposures to fishes and other aquatic biota inhabiting Lake Mead relied on study-specific investigations and data-mining tools.

Study-specific investigations

Project-specific field sampling events occurred during 2006 and were focused on potential effects of chemical stressors on fishes in LMNRA. Bottom sediments and fish tissue were sampled from LMNRA, Las Vegas Wash (LVW), Las Vegas Bay (LVB), Overton Arm (OA), and Willow Beach (WB) and were characterized for EDCs and other SOCs (Rosen et al. 2006a,b). For this initial report of findings derived from these reconnaissance investigations, fish, bottom sediments, and samples from semi-permeable membranes devices (SPMDs; Huckins et al. 2006) and polar organic chemical integrative samplers (POCISs; Alvarez et al. 2007) were evaluated for chemicals of concern. Samples were collected at LVB, OA, LVW, and WB and were analyzed for a variety of SOCs, including pesticides, PAHs, PCBs, BDEs, and emerging contaminants, including EDCs represented by pharmaceuticals and PPCPs and other constituents of treated wastewater discharges. The SPMDs/POCISs were deployed at various locations on Lake Mead, including venues close to locations where fish were collected. Fish were collected at sample locations four times during the year to cover a full reproductive cycle (March, July, and November 2007 and March 2008). Biomarkers for analysis included sex steroids (11-ketotestosterone, estradiol-17β), thyroid hormones (triiodothyronine, thyroxine), vitellogenin, gonadosomatic index and parameters of sperm quality (viability, mitochondrial function, motility by computer and unaided eye, DNA integrity and percent spermatogenic stage, sperm count). Whole fish were analyzed for a suite of pesticides, PAHs, PCBs, and for emerging contaminants including BDEs, musks, fragrances, and PPCPs.

Complementing these sampling efforts, food-web biota characteristic of Lake Mead were also used in developing models for food-web energetics and predator-prey dynamics. The SOCs accumulating in tissue of animals at each trophic level were measured for comparison to food-web models to determine biological pathways for organic contaminants in Lake Mead. Similarly, microbial sampling was

completed in parallel with sampling for fishes; microbial sampling was focused on species isolation and DNA sequencing to evaluate the biodegradation potential of microbial communities in sediments and the sediment-water interface. Isolated microbes that degrade SOCs may effectively reduce risk by mediating degradation and transport of EDCs such as ethinylestradiol (EE2).

Literature search and data mining

Review of existing toxicity data was accomplished through data mining of existing sources and through literature searches of primary data published in peer-reviewed literature and searchable public domain sources. Data mining and literature searches are complementary activities which may include redundancies that act as data quality measures. For example, existing databases may reflect a collection of original literature and original data/metadata supporting data compiled from publications encountered as part of the literature search. Analytical tools applied to the compiled data included traditional methods of environmental informatics (Avouris and Page 1995; Huang and Chang 2003), as well as supplemental tools applied as part of a comparative analysis. Databases queried in data mining included assembled data packages such as ECOTOXicology database (ECOTOX; http://cfpub.epa.gov/ecotox/ index.html last accessed November 8, 2008). ECOTOX integrates AQUIRE, TERRETOX, and PHYTOTOX which include toxicity data derived predominately from the peer-reviewed literature for aquatic life, terrestrial wildlife, and terrestrial plants, respectively. As noted in supporting documentation for ECOTOX, the database presents limitations related to data retrieval and requirements of the online implementation of search, as well as data gaps reflected by technically reviewed data published by research agencies such as USGS but not captured in ECOTOX. Such data gaps are most often offset by recently published literature that includes relevant toxicity data that has yet to be incorporated into ECOTOX. As recommended, original scientific papers were reviewed, as needed, to ensure an understanding of the context of the data retrieved from ECOTOX. Data collected outside EPA's efforts with ECOTOX revealed data sources previously published in technical reports by USGS and NOAA/NMFS that do not appear in ECOTOX.

In addition to assembled data packages such as ECOTOX, ongoing collections of existing data and information were also used as supplemental data sources for evaluation of toxicity thresholds for EDCs pertinent to exposures at Lake Mead. Nested literature search and acquisition of existing peer-reviewed data and literature were completed through:

- Focused search using on USGS/CERC data mining resources
- Open literature search using on PubMed-NLM
- Open literature search using on Synergy and ScienceDirect
- Focused manual search based on networked citations derived from data and literature sources encountered in directed computer-aided data mining searches

Literature searches relied on USGS/CERC resources and were initiated and completed using primary database providers Cambridge Scientific Abstracts (CSA) and OCLC FirstSearch. Databases searched in CSA included Aquatic Sciences and Fisheries Abstracts, Biological Sciences, Environmental Sciences and Pollution Management; and to a lesser extent, AquaLine, Water Resources Abstracts, GeoRef, Biology Digest, Conference Papers Index, Medline and Toxline. Databases in OCLC FirstSearch included Agricola, ArticleFirst, BasicBiosis, Dissertations, GeoBase, WorldCat, BioAgIndex, Electronic Collections Online, PapersFirst, and Proceedings. Ingenta database provider was also used for some searches.

Other than chemical name, searches for species of concern used the scientific name (at genus or species level), and common names, if applicable. Depending on the number of citations found, additional search terms were added. Terms also included keywords related, e.g., to distribution of the species, its life history and habitat, and its interaction with other species.

Independent literature searches relied on existing numeric ecotoxicological data that had not been captured in historic data collections from USGS sources, as well as recent data found in recent literature not included in ECOTOX (e.g., literature published after 2000, and more frequently, after 2006). Updated open literature searches were completed using available online search engines from PubMed-NLM, Synergy, and ScienceDirect. These searches focused on journal-specific peer-reviewed literature and provided limited redundancies relative to primary search accomplished using USGS/CERC sources. Focused manual searches of existing data and literature were initiated using networked citations discovered during the computer-aided searches. Once assembled, sufficient data were combined with toxicity data from ECOTOX and from supplemental literature and data searches. These compiled data provided a basis for evaluating presumptive threshold values for EDCs. In general, data analysis and application of empirically-based derived values were consistent with "Guidelines for Deriving Numerical National Water Quality Criteria for the Protection of Aquatic Organisms and Their Uses" (Stephan et al. 1985). Available data on chemicals of concern were reviewed with respect to their toxicity to and bioaccumulation by aquatic biota, including consideration of endpoints other than survival, growth, and reproduction which conforms to the "best available science" qualification implicit to Stephan et al. (1985) and posited by NAS (2000). For EDCs included in Table 1, data were frequently not sufficient to satisfy data specifications for each chemical concern; hence, three specifications for data were also considered within the reconnaissance level analysis for this investigation (modified from Stephan et al. 1985):

(i) Are "effects-no effects" ratio estimators (e.g., Acute-chronic ratios; ACRs) calculable for at least two different families of aquatic species?
(ii) Are toxicity data available for at least one freshwater plant (either algal or a vascular plant)?
(iii) Are bioconcentration or bioaccumulation data available?

Each of these data specifications was considered within the context of the exploratory data analysis for this reconnaissance investigation. Ideally, freshwater species toxicity data presented median lethal concentration (LC50) data and chronic (no-observed-effect-concentration) NOEC data of appropriate duration. In practice, most chemicals with water quality criteria have sufficient LC50 data to permit derivation of an acute water quality criterion from measured LC50 data, but do not have sufficient measured chronic NOEC to calculate reconnaissance level thresholds. Hence, ratio estimators reliant on "effect-no effect" empirical data provide measures analogous to the typical ACR values commonly encountered in regulatory applications.

Exploratory data analysis of encountered data compiled from the search of existing data and literature. For evaluating threshold effect levels for chemicals of concern, extrapolation methods were required for evaluating toxicity data for surrogate species regardless of whether the surrogate is a listed or non-ESA-listed species. Interspecies Correlation Estimation (ICE) models and species sensitivity distributions (SSDs) are commonly used in evaluating risks associated with chemical exposures to a wide range of species and can be used with toxicity data from multiple taxa levels. The SSDs, ICE, and development of ACRs (Mayer et al. 1999) for representative species and for threatened and endangered species served as the primary tools for extrapolations of toxicity data from traditional aquatic toxicity test species to other species presumptively protected by these surrogates.

The SSDs are based on the assumption that available toxicity data for a group of taxonomically related species are representative of the responses of other species for which toxicity data are not available. A statistical description of the toxicity data can then be generated which permits calculation of the proportion of all species that would be adversely affected by exposure to a chemical at a given concentration. As long as the toxicological endpoint for each species is the same (e.g. LC50s, NOECs), an SSD can be generated for any toxicological endpoint and mix of species. This feature of SSDs is one of their great advantages relative to other endpoint estimation methodologies, in that they explicitly consider the results of all available toxicological information for a given assemblage of species (Dyer et al. 2006; Awkerman et al. 2008; Raimondo et al. 2008; Posthuma et al. 2002). Although no one estimation method is universally used, the most commonly used distributions to estimate 5th percentiles from SSDs are the log-logistic and lognormal distributions. As such, cumulative probability distributions of toxicity values for multiple species were applied to this reconnaissance level analysis (Dyer et al. 2006), and SSDs were assembled based on single-species toxicity data to predict hazardous concentrations (HCps) affecting a certain percentage (p) of species in a community. The fit of the lognormal model and required number of individual species values were evaluated with published data sets. For this reconnaissance level investigation, tools of exploratory data analysis (e.g., percentile-based ratio estimators) were opted for rather than the common assumption that a lognormal model best fit the data assemblage (see Newman et al. 2000, 2003 for alternative methods).

The ICE models were also considered in extrapolation from literature-acquired toxicity data to representative species considered in this investigation. It is impractical for toxicologists to perform laboratory toxicity studies on all aquatic species present in North America with all chemicals to which they are exposed in the environment, and even more so for ESA listed species whose rarity or limited distribution in the environment generally precludes their use as test organisms in aquatic toxicology. The ICE models are statistical regressions that estimate LC50s for a species or higher taxa (genus, family) having no measured acute toxicity information from a species for which five or more LC50s have been measured. The detailed description of how ICE models were developed and their use to estimate LC50s for taxa for which no toxicity information is given in Asfaw et al. (2003). Toxicity of a chemical to one species can be predicted from toxicity to another species with a known certainty, which is expressed as the 95% upper and lower confidence intervals around the predicted LC50. Asfaw et al. (2003) recommend performing ICE model evaluations on species taxonomically no further apart than the family level. For higher taxonomic ICE models (e.g. genus or family), data from two surrogate species from the genus or family being estimated should be available before using ICE models for higher taxonomic groupings to ensure that the ICE models do not significantly over or under estimate the data. If evaluation of a chronic criterion was being performed, the lower 95% confidence interval of the predicted LC50 was divided by the acute-chronic ratio (ACR) to estimate a lower 95% confidence interval of the NOEC for the chemical and species under evaluation.

The ACRs are typically applied to acute toxicity data to estimate chronic values, yet for EDCs with modes of actions that do not typically yield diminished survival at environmentally relevant concentrations, reconnaissance level analysis relied on ratio estimators based on lowest-observed-effect-concentrations (LOECs)-to-NOECs for surrogate species, especially when special-status species were considered. In such a reconnaissance level analysis ratio estimators based on percentiles were applied to evaluation of effect *v.* no effect levels. In contrast to regulatory guidance wherein water quality criteria are not designed to protect all aquatic species from exposure to chemical concentrations, the reconnaissance level analysis of risk was intended to conservatively posit such levels, or in the absence of data sufficient to such an interpretation, provide a numeric estimate with statements regarding uncertainty about these estimates. For national water quality criteria, many are presumptively protective of more than 95% of aquatic genera from adverse effects, including ESA-listed species known to occur within discrete geographical areas. ESA-listed aquatic species as a group have not been consistently characterized as being more sensitive to chemicals than aquatic species as a whole (Dwyer et al. 2005, Sappington et al. 2001, Dwyer et al. 1995, 1999).

Exploratory analysis of data derived from study-specific investigations.

All data compiled from the data mining (principally through ECOTOX) and data compiled as outcomes of open literature searches were included in this analysis. As a preliminary data reduction effort, study-specific data were tabulated and

evaluated relative to biological effects data recorded from fishes collected in sampling areas at various locations at Lake Mead. Correlation analysis was completed using a binary rank-sums approach wherein estimates of location-specific concentrations of waterborne EDCs were compared to biological measures determined in co-located fish samples (Dietz 1985; Hollander and Wolfe 1999).

RESULTS AND CHARACTERIZATION OF RISKS AND UNCERTAINTIES

In this initial report of outcomes from the reconnaissance level analysis of risks, project-specific studies were considered in parallel with outcomes of the data mining efforts focused on characterizing existing toxicity data and supporting literature, with a particular focus on exploratory analysis for characterizing threshold effect levels for selected EDCs.

Preliminary findings of project-specific studies

Preliminary reports of technical findings from chemical and biological investigations were initially reported at the Lake Mead Science Symposium convened in early 2009 (http://www.lakemeadsymposium.org/ last accessed February 9, 2009). SPMD and POCIS estimates of concentrations of chemicals in surface waters collected during early sampling events are summarized in Table 3. Comprehensive data reduction and interpretation of results remains ongoing, yet preliminary results of the biological assessments based on fishes indicated the existence of location-specific environmental influences on indices of reproductive condition in male common carp from the LMNRA. From highest to lowest values, reproductive condition in common carp by site showed that OA > LVB > LVW > WB (see Patiño, et al. 2009 available at http://www.lakemeadsymposium.org/ program_e.htm last accessed February 10, 2009). These outcomes based on condition were consistent with results from exploratory correlation analysis wherein biological effects indicated by reproductive condition were correlated with rank-sum EDC scores (see Table 3). Although SPMDs and POCIS devices were not deployed in LVW, binary rank-scores for selected analytes were negatively correlated with biological effects and consistent with those trends noted immediately above, i.e., highest binary rank-sums for chemicals sampled via SPMDs occurred at locations near LVB which were characterized by lowest values for reproductive condition in male carp. In these preliminary findings of the reconnaissance investigation, low reproductive condition at WB is not uniquely linked to chemical exposures, as suggested by the low rank-sum score for selected chemicals at that location. Given the wide range of stressors potentially affecting biological organisms, clearly characterized linkages between chemicals and biological effects must be deferred until ongoing chemical and biological analyses are complete.

Table 3a. SPMD Target Analytes (Electron Ionization)	MQL	Las Vegas Valley	Overton Arm	LVB1-4m	LVB1-8m	LVB1-12m	LVB1-18m	LVB2-8m	LVB2-12m	LVB2-18m	Boulder Basin	Willow Beach
	Pg/L	pg/L	pg/L	pg/L	pg/L	pg/L	pg/L	pg/L	Pg/L	pg/L	pg/L	pg/L
Tonalide (AHTN)	200	< 200	< 200	2000	2100	4500	7300	5800	1900	9500	< 200	< 200
Galoxolide (HHCB)	490	< 490	< 490	45000	35000	62000	90000	75000	22000	95000	1300	< 490
4-Tert-octylphenol	< 45	< 45	< 45	*33*	45	74	< 45	< 45	< 45	< 45	< 45	< 45
Pyrene	45	< 45	< 45	230	190	240	< 45	320	87	< 45	< 45	< 45
Naphthalene	850	< 850	< 850	1600	1400	*700*	< 850	*820*	*230*	*380*	< 850	*188*
2-Methylnaphthalene	290	1400	< 290	2400	2000	1300	< 290	2000	780	620	< 290	130
1-Methylnaphthalene	290	1100	< 290	1200	970	780	< 290	1100	450	530	86	*188*
2,6-Dimethylnaphthalene	100	860	< 100	330	250	220	< 100	330	110	180	< 100	< 100
Phenanthrene	90	1300	< 90	270	280	300	< 90	410	82	240	< 90	< 90
Table 3b. Rank-sum binary scores for selected chemicals measured at various locations at Lake Mead												
Tonalide (AHTN)	200	0	0	1	1	1	1	1	1	1	0	0
Galoxolide (HHCB)	490	0	0	1	1	1	1	1	1	1	1	0
4-Tert-octylphenol	< 45	0	0	0	1	1	0	0	0	0	0	0
Pyrene	45	0	0	1	1	1	0	1	1	0	0	0
Naphthalene	850	0	0	1	1	0	0	1	0	0	0	*0*
2-Methylnaphthalene	290	1	0	1	1	1	0	1	1	1	0	0
1-Methylnaphthalene	290	1	0	1	1	1	0	1	1	1	0	*0*
2,6-Dimethylnaphthalene	100	1	0	1	1	1	0	1	1	1	0	0
Phenanthrene	90	1	0	1	1	1	0	1	0	1	0	0
Rank-sum binary scores (total)		4	0	8	9	9	2	8	6	6	1	0

Table 3. Top panel (Table 3a) presents summary of concentrations of chemicals (in pg/L) estimated via SPMDs. Bottom panel (Table 3b) presents rank-sum binary scores (values < MQL (minimum quantitation limit) received score of 0, values ≥ MQL received score of 1.

Exploratory data analysis and preliminary characterization of threshold effects concentrations

Exploratory data analysis was completed on toxicity data mined from available databases such as ECOTOX and compiled public domain data compilations and updated from existing literature sources. When these existing toxicity data

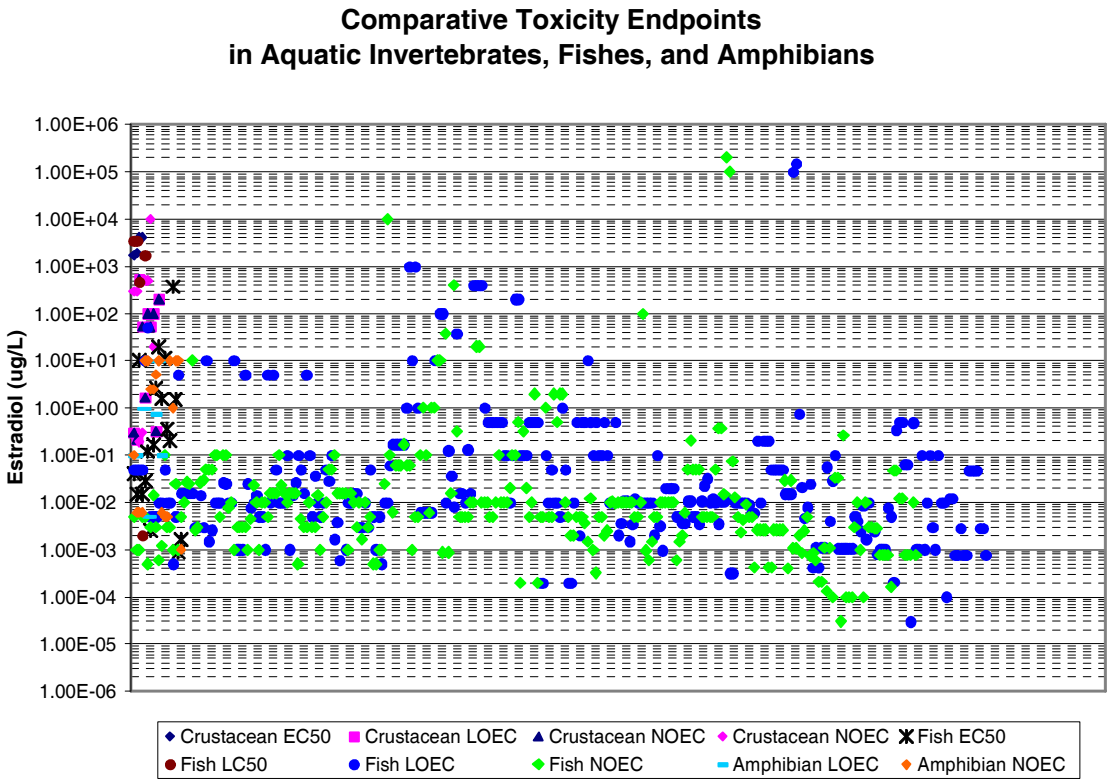

Figure 3. Differential data display for toxicity values of various types compiled as outcomes of data mining for estradiol.

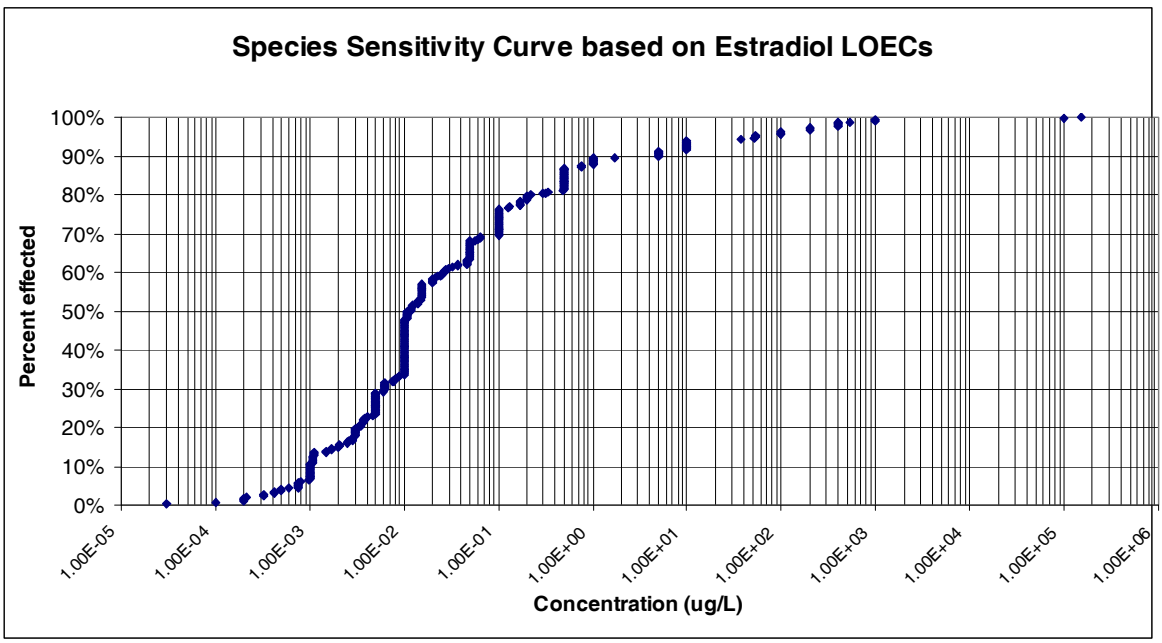

Figure 4. Species sensitivity curve for estradiol based on LOECs.

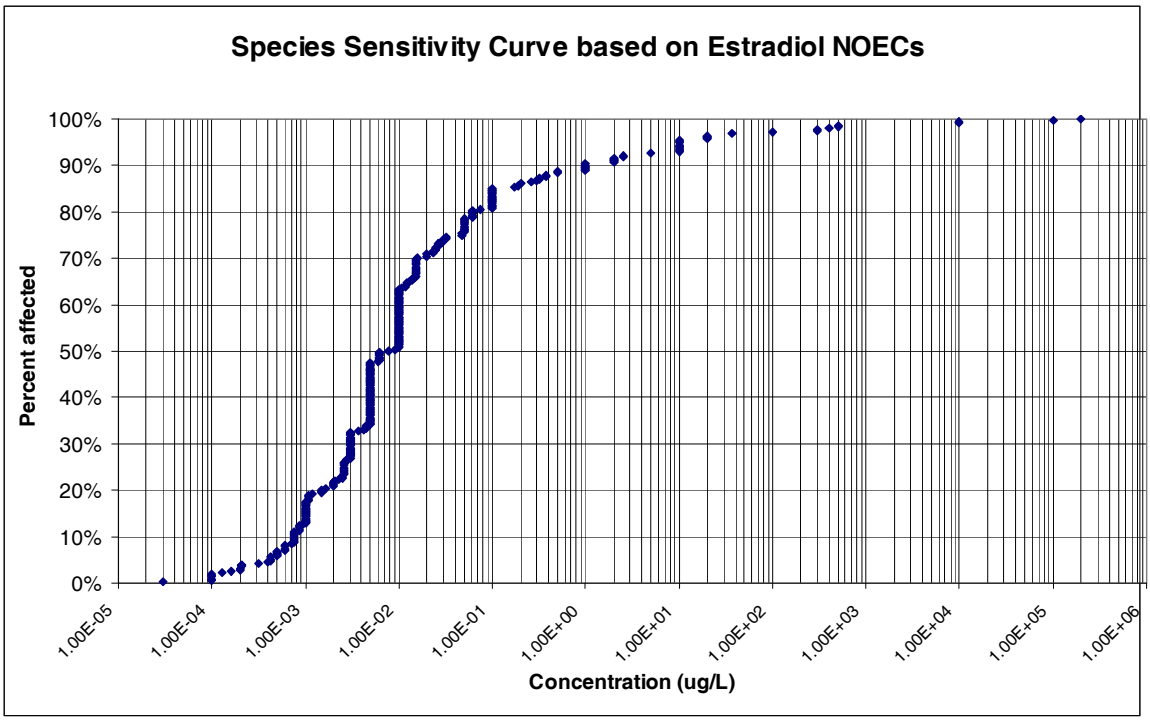

Figure 5. Species sensitivity curve for estradiol based on NOECs.

Percentile	LOEC percentiles	NOEC percentiles	LOEC:NOEC estimator
	Value (ug/L)	Value (ug/L)	
5%-tile	0.00076	0.00042	1.81
25%-tile	0.005	0.00262	1.91
50%-tile	0.0113	0.0084	1.35
75%-tile	0.1	0.047	2.14
95%-tile	53.5	10.0	5.35

Table 4. Reconnaissance estimators of effects v. no effects estimators for estradiol (based on percentiles for LOECs and NOECs as presumptive estimators of toxicity-based ratio estimators).

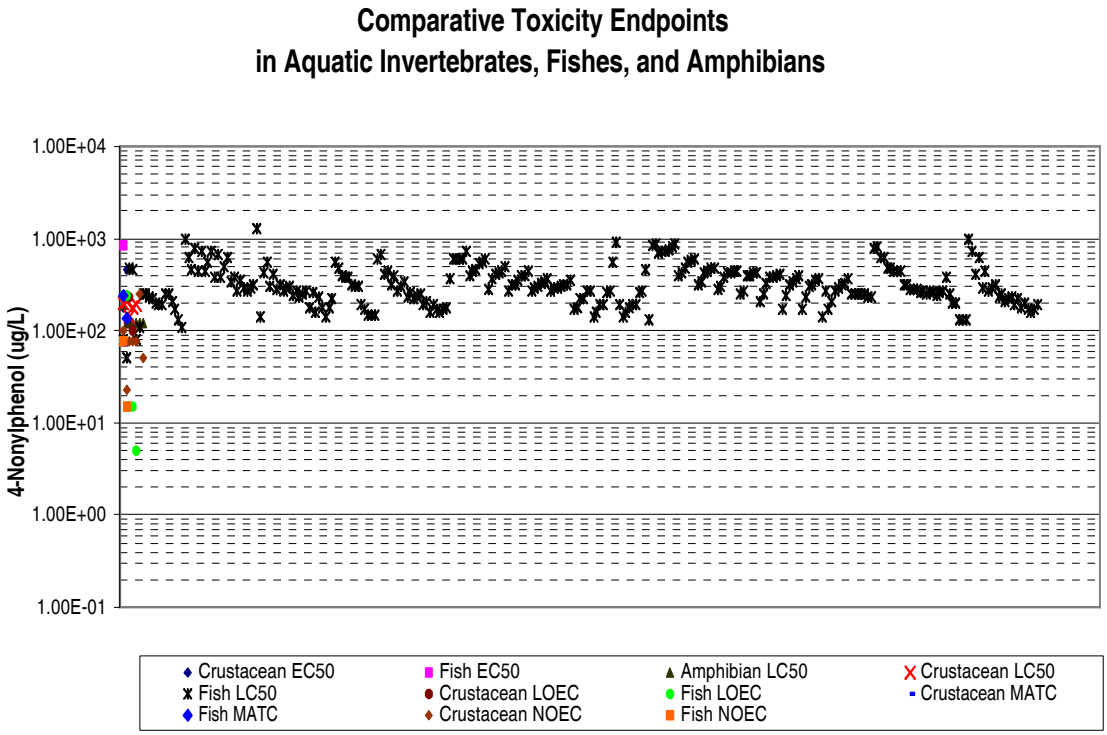

Figure 6. Differential data display for toxicity values of various types compiled as outcomes of data mining for 4-nonylphenol.

Reconnaissance effects v. no effects ratios for 4-Nonylphenol		
Based on Acute and Chronic Means		
Geometric	**Arithmetic**	
4.41	4.23	
Based on Percentiles from Species Sensitivity Distribution		
1%-tile	**5%-tile**	**10%-tile**
7.0	7.1	7.5

Table 5. Reconnaissance estimators of effects v. no effects estimators (based on LC50s as traditional acute values and NOECs as traditional chronic values) for 4-nonylphenol.

were sufficient, graphic summaries and exploratory data reductions for chemicals of concern listed in Table 1 were characterized as illustrated in Figures 3-6 and Tables 4-5 for estradiol and 4-nonylphenol. Graphic and tabular data summaries varied as a function of data availability; for many EDCs identified as chemicals of concern, toxicity data required for reconnaissance analysis of risks were highly limited, and in some cases insufficient for exploratory data analysis. For example, Figure 3 summarizes the available toxicity data for estradiol that includes predominately chronic data with relatively few high-quality data available from acute studies. In part, the paucity of acute data (e.g., LC50s) reflects a common attribute for EDCs that are similar to steroid hormones commonly measured in fishes. As a consequence, conventional guidance (Stephen et al. 1985) may not be sufficient to reliabily forecast threshold effects concentrations for selected EDCs (Table 1). Hence, alternative tools were employed within an exploratory data analysis completed for this reconnaissance investigation.

For example, in the absence of data sufficient to apply ICE models or to characterize ACRs, exploratory tools considered "effect *v.* no effect" estimators, in part, to characterize spreads between empirical distributions of traditional chronic toxicity endpoints (LOECs and NOECs) that might contribute to characterizations of risk. Given the mode of action of EDCs, it is not unlikely that spreads between effect and no-effect levels may reflect marked inflections in dose-response curves where upper critical points sharply delineate between nominal endocrine function and dysfunctional states linked to exceedance of threshold levels in field exposures.

In a similar manner, preliminary evaluations of bioaccumulation potential of EDCs have been included in this reconnaissance level analysis of risks. For example, early rounds in the reconnaissance studies focused on this aspect of the analysis of risks and uncertainties. Leiker et al. (2008) analyzed SOCs in tissues from common carp collected from LVB and SPMDs deployed in LVW and found methyl triclosan, which is likely a methylated product of the antibacterial agent triclosan (2, 4, 4'-trichloro-4-hydroxydiphenyl ether). The methylated product is presumptively a product of microbial activity in sediments and surface waters and was detected in all 29 male common carp from LVB with a mean concentration of 596 ug/kg wet weight (ww). These tissue levels are more than an order of magnitude higher than previously reported concentrations in the literature. Halogenated analogs of the methylated product were detected less frequently (21%–76%) and at much lower concentrations (< 51 ug/kg ww). None of these compounds was detected in common carp from a Lake Mead reference site in Overton Arm, Nevada.

In aquatic environments, triclosan is expected to adsorb to suspended solids and sediments, reducing its bioconcentration potential in water-only exposures. However, given the chemical's physicochemical properties, Leiker et al. (2008) confirmed that triclosan (K_{ow} 4.76) accumulates in fish tissues, although the relative contributions of dietary or water-borne sources remains unclear. Bioaccumulation of triclosan or its metabolites may be problematic for aquatic organisms and biota dependent on aquatic organisms as food sources. In surface waters hydrolysis is not expected to be an important environmental fate process, given the chemical's stability under environmental conditions commonly encountered in Lake Mead

surface waters. However, triclosan is susceptible to degradation via aqueous photolysis, having a half-life in lakes of between < 1 hour to 10 days under abiotic conditions. As suggested by Leiker et al. (2008), triclosan is susceptible to biodegradation based on the presence of methyl-triclosan following wastewater treatment.

As model EDCs from the short-list of chemicals of concern in this reconnaissance analysis of risks (Table 1), estradiol and 4-nonylphenol illustrate technical issues common to EDCs and the evaluation of their effects on aquatic biota and adverse expression of these effects at higher levels of biological organization. For example, Figure 3 clearly indicates a wide dispersion of toxicity data for estradiol, which is dominated by chronic toxicity endpoints such as NOECs and LOECs and a paucity of acute endpoints. As noted previously, this trend will be common, given the mode of action of most EDCs in receptors most likely exposed to these chemicals in the field and will require risk analysis tools beyond application of ACRs. If data are sufficient, ICE models may be applicable, yet in the absence of relational data linking acute effects and chronic effects, forecasts of threshold effects levels should be advanced with caution. For example, based on SSD for chronic LOECs and NOECs for estradiol (Figures 4 and 5), an HC5 would be about 0.0004 ug/L (see Table 4). Regulatory guidance indicates an HC5 is not intended to protect all species; hence, special status species such as razorback sucker may not occur in the 95 percentile protected category. From a conservative view opted for in this reconnaissance analysis of risks, an estimated HC1 based on the SSD for estradiol would be 0.0001 ug/L. Such thresholds are poorly supported by existing literature and region-specific empirical studies, and regulatory guidance values are lacking. Therefore, the value may be practically limited as an effects threshold. If viewed as a point of departure for future studies, however, these threshold goals may be applicable to the risk tolerance of resource managers facing decisions in the presence of uncertainty.

In contrast to estradiol, the available toxicity data for 4-nonylphenol is dominated by acute LC50s, e.g., for fishes (Figure 6). The ACRs based on the limited chronic data (as NOECs) would range from 4.2 to 7.5, depending on distribution assumptions framing the ratio analysis (Table 5). Although limited, available chronic toxicity data for 4-nonylphenol indicate that 15.6 ug/L and 18.2 ug/L would be forecast as HC1 and HC5 values, respectively. These threshold effects values are consistent with estimates based on LC50s modified by ACRs. In this instance, forecasts of NOECs for special status species such as razorback sucker is estimated at 54 ug/L based on fathead minnow (*Pimephales promelas*) acute and chronic data and their derivative ACRs. NOEC forecasts reflect inputs of empirical acute values for razorback sucker and an ACR equivalent to 5.1. Caution is recommended when interpreting either of these forecast threshold values, given the uncertainties linked to their derivation in this reconnaissance level analysis of risks.

CONCLUSIONS AND FUTURE STUDIES

Results of the reconnaissance studies, particularly those focused on field biomarker studies for fishes, indicate that reproductive condition of fish in the Lake Mead ecosystem was spatially variable, with markedly reduced fish condition at LVB relative to OA. Preliminary characterization of chemical constituents through SPMDs deployed in surface waters at various locations in Lake Mead indicated that exposure linked to altered endocrine function is possible. Reduced reproductive condition in fishes collected at locations spatially related to those where surface waters were sampled using SPMDs also indicated that other stressors may be acting independently or in concert with chemical stressors as indicated by fishes collected at Willow Beach that presented reduced condition, but at a low incidence of EDCs in SPMD samplers. Technical findings to date suggest that additional work could reduce uncertainties related to exposure, especially as those uncertainties serve as confounding factors in cause-effect analysis. These additional studies could be addressed through integrated field and laboratory studies if adaptive management plans are going to be developed within a multiple stressors context.

Prior studies at Lake Mead indicate the presence of numerous SOCs in water, bottom sediments, and fish, including identification of EDCs in waters and sediments capable of inducing biological responses in fishes and other aquatic biota. For example, altered gonad development and diminished reproductive capacity in fishes have provided evidence of endocrine disruption in common carp (Covay et al. 1998, 2001; Goodbred et al. 1997, 2007; Jenkins and Goodbred 2005, Patiño et al. 2003). These earlier studies determined that SOCs released to LVW entered Lake Mead via LVB, and included PAHs, PCBs, chlorinated pesticides, and PPCPs. Exposure to these compounds may be linked to altered system structure and function through diminished reproduction of aquatic life and expression of adverse effects at population levels of organization. The sources of SOCs include urban runoff from lawns, gardens, and golf courses, storm-water runoff, subsurface inflow, and sewage effluent from three municipal wastewater treatment plants (see, e.g., Covay et al. 1998, 2001; Goodbred et al. 1997, 2007; Jenkins and Goodbred 2005, Patiño et al. 2003).

Despite these earlier studies of Covay et al. 1998, 2001; Goodbred et al. 1997, 2007; Jenkins and Goodbred 2005, Patiño et al. 2003, few subsequent studies have considered the ecological significance of exposures to EDCs in the field. For example, population-level responses in fishes that are linked to their diminished reproductive success associated with the disruption in their normal biochemical and physiological processes have not been observed. Given that the reconnaissance level analysis of risks cannot answer questions related to the ecological significance of EDC exposures, this suggests that future studies be focused on the effects of exposure to EDCs on the reproductive potential of fish. Furthermore, outcomes of these reconnaissance investigations should contribute to design and implementation of future studies focused on toxicity assessment, including early life-stage and multiple generation toxicity tests or toxicity identification evaluations (TIEs) that contribute to risk reduction measures (US EPA 2005, 2002a,b,c).

Alternative water treatment regimens may be considered in parallel with TIE determinations. Combined water treatment technologies are currently being evaluated

with respect to their capacity to reduce risks associated with EDCs and may be applicable within a TIE experimental design targeted on changes to biological treatment, changes to wastewater treatment process (e.g., addition of ozone and biologically active carbon or addition of advanced membrane treatment and advanced oxidation; see, e.g., Westerhoff et al. 2005; WERF 2007; Linden and Kullman 2008; Snyder et al. 2008), infrastructure development intended to reduce risk (NPS 2008), or upfront planning for implementation of natural treatment options. In parallel with trophic transfer and biodegradation studies, outcomes of future investigations developed as outgrowths of reconnaissance analysis of risks and uncertainties will contribute to informed adaptive management plans for Lake Mead and the Colorado River below Hoover Dam. In contrast to initial discovery, future studies can build upon previous findings and outcomes of the reconnaissance level analysis of risk to address resource management queries that would benefit development of adaptive management plans for Lake Mead, Nevada based on countermeasures identified as part of risk trade-offs captured by ongoing risk reduction strategies (e.g., NPS 2008).

Acknowledgements. Much of the existing literature and existing data for Lake Mead and environs yields a long list of researchers and resource managers doing work as a result of past, ongoing, and future studies. Currently, research on environmental quality issues related to fish and wildlife, and complex chemical mixtures entering Lake Mead is being conducted by government and academic scientists working under the auspices of many funding mechanisms. Special thanks go to Erik Orsak, Dave Alvarez, Kathy Echols, Reynaldo Patiño, and Jill Jenkins for updates on their ongoing field and laboratory research.

Disclaimer: Use of trade names does not imply U.S. government endorsement

REFERENCES

Alvarez, D.A., J.N. Huckins, J.D. Petty, T.L. Jones-Lepp, F. Stuer-Lauridsen, D.T. Getting, J.P. Goddard, and A. Gravell. 2007. Tool for monitoring hydrophilic contaminants in water: Polar organic chemical integrative sampler (POCIS). p. 171–198. In R. Greenwood et al (ed.) Passive sampling techniques. Comprehensive analytical chemistry. Vol. 48. Elsevier, Amsterdam.

Asfaw, A., Ellersieck, M.R., Mayer, F.L. 2003. Interspecies correlation estimation (ICE) for acute toxicity to aquatic organisms and wildlife. II. User manual and software. EPA/600/R-03/106. U.S. Environmental Protection Agency, National Health and Environmental Effects Research Laboratory, Gulf Ecology Division, Gulf Breeze, FL. 2003. 14 p.

Avouris, N.M., Page, B. (editors), 1995, Environmental Informatics: Methodology and Applications of Environmental Information Processing, Springer, New York, 472 pp.

Awkerman, Jill, Sandy Raimondo and Mace Barron. 2008. Development of Species Sensitivity Distributions for Wildlife Using Interspecies Toxicity Correlation Models. Environ. Sci. Technol. 42(9):3447-3452.

Belgrano A., Scharler U. M., Dunne J. and Ulanowicz R. E., 2005, Aquatic Food Webs: An Ecosystem Approach. Oxford University Press, Oxford, 272 pp.

Bevans, H.E., Goodbred, S.L., Miesner, J.F., Watkins, S.A., Gross, T.S., Denslow, N.D., and Schoeb, T. 1996. Synthetic organic compounds and carp endocrinology and histology in Las Vegas Wash and Las Vegas and Callville Bays of Lake Mead, Nevada, 1992 and 1995: U.S. Geological Survey, Water-Resources Investigations Report 96–4266, 12 p

Covay, K.J., and Beck, D.A., 2001. Sediment-deposition rates and organic compounds in bottom sediment at four sites in Lake Mead, Nevada, May 1998: U.S. Geological Survey Open-File Report 01–282, 34 p.

Covay, K.J. and Leiker, T.J., 1998, Synthetic organic compounds in water and bottom sediment from streams, detention basins, and sewage-treatment plant outfalls in Las Vegas Valley, Nevada, 1997: U.S. Geological Survey Open-File Report 98-633, 15p.

Dietz, E.J. 1985. The rank sum test in the linear logistic model. The American Statistician 39(4): 322-325.

Dwyer, F.J., Mayer, F.L., Buckler, D.R., Bridges, C.M., Greer, I.E., Hardesty, D.K., Henke, C.E., Ingersoll, C.G., Kunz, J.L., Sappington, L.C., Whites, D.W., Augspurger, T., Mount, D.R., Hattala, K., Gary Neuderfer, G. 2005. Assessing contaminant sensitivity of endangered and threatened aquatic species: Part I. acute toxicity of five chemicals. Arch. Environ. Contam. Toxicol. 48(2):143-154.

Dwyer, F.J., Hardesty, D.K., Henke, C.E., Ingersoll, C.G., Whites, D.W., Mount, D.R., Bridges, C.M. 1999. Assessing contaminant sensitivity of endangered and threatened species: toxicant classes. EPA/600/R-99/098. U.S. Environmental Protection Agency, National Health and Environmental Effects Research Laboratory, Gulf Ecology Division, Gulf Breeze, FL. 15 p.

Dwyer, F.J., Sappington, L.C., Buckler, D.R., Jones, S.B. 1995. Use of surrogate species in assessing contaminant risk to endangered and threatened fishes. EPA/600/R-96/029. U.S. Environmental Protection Agency, Environmental Research Laboratory, Gulf Breeze, FL. 78 p. (EPA/600/X-92/139, Environmental Research Laboratory, Gulf Breeze, FL).

Dyer, S.C., Versteeg, D.J., Belanger S.E., Chaney J.G., Mayer, F.L. 2006.

Interspecies correlation estimates predict protective environmental concentrations. Environ Sci Technol. 2006 May 1;40(9):3102-3011.

Goodbred, S.L., Leiker, T.J., Patino, Reynaldo, Jenkins, J.A., Denslow, N.D., Orsak, Erik, and Rosen, M.R., 2007, Organic chemical concentrations and reproductive biomarkers in common carp (*Cyprinus carpio*) collected from two areas in Lake Mead, Nevada, May 1999-May 2000: U.S. Geological Survey Data Series 286, 19 p.

Goodbred, S.L., Gilliom, R.J., Gross, T.S., Denslow, N.P., Bryant, W.L., and Schoeb, T.R., 1997, Reconnaissance of 17-β-estradiol, 11-ketotestosterone, vitellogenin, and gonad histopathology in common carp of United States streams: Potential for contaminant-induced endocrine disruption: U.S. Geological Survey Open-file Report 96-627, 47p.

Hollander, M., Wolfe, D.A., 1999, Nonparametric Statistical Methods, 2nd Edition. Wiley, New York, 816 p.

Huang, G.H., Chang, N.B., Perspectives of Environmental Informatics and Systems Analysis, 2003. Journal of Environmental Informatics 1 (1) 1-6. doi:10.3808/jei.200300001

Huckins, J.N., Petty, J.D., and Booij, K., 2006, Monitors of organic chemicals in the environment: semipermeable membrane devices. Springer, New York, 223 p.

Jenkins, J.A. and Goodbred, S.L., 2005, Viability of male gametes in common carp (Cyprinus carpio) along the Lower Colorado River from the Cibola National Wildlife Refuge (NWR),
Havasu NWR, and Lake Mohave of Lake Mead National Recreation Area, USGS, OF 2006-1007, 25 pages. http://www.nwrc.usgs.gov/wdb/pub/others/05-298.pdf

Kolpin, D.W., Furlong, E.T., Meyer, M.T., et al. 2002. Pharmaceuticals, Hormones, and Other Organic Wastewater Contaminants in U.S. Streams, 1999-2000: A National Reconnaissance. Environmental Science and Technology. 36(6): 1202-11.

Kudłak B., Namiełnik J. 2008. Environmental Fate of Endocrine Disrupting Compounds-Analytical Problems and Challenges, Critical Reviews in Analytical Chemistry 38(4): 242 - 258.

Leiker, T.J., Abney S.R, Goodbred, S.L., Rosen M. 2008. Identification of methyl triclosan and halogenated analogues in male common carp (*Cyprinus carpio*) from Las Vegas Bay and semipermeable membrane devices from Las Vegas Wash, Nevada. Science of the Total Environment: In Press. Available online doi:10.1016/j.scitotenv.2008.11.009

Linden, K., Kullman, S., 2008, Impact of UV and UV/H2O2 AOP on EDC Activity

in Water, AwwaRF Report 91175, American Water Works Association Research Foundation, Denver, Colorado, 109pp.

Mayer, F.L., Jr., Sun, K., Lee, G., Ellersieck, M.R., Krause, G.F. 1999. User Guide: Acute to chronic estimation. EPA/600/R-98/152. U.S. Environmental Protection Agency, National Health and Environmental Effects Research Laboratory, Gulf Ecology Division, Gulf Breeze, FL. 18 p.

National Park Service (NPS), 2008, Systems Conveyance and Operations Program (SCOP), Environmental Assessment for Activities within the National Park Service Lake Mead National Recreation Area, National Park Service, 83pp plus appendices.

National Academy of Science (NAS). 2000. Strengthening Science at the U.S. Environmental Protection Agency: Research-Management and Peer-Review Practices, Committee on Research and Peer Review in EPA, Board on Environmental Studies in Toxicology, National Research Council, National Academy Press, Washington, D.C. 178pp.

Newman, M. C., Ownby, D. R., Mézin, L. C. A., Powell, D. C., Christensen, T. R. L., Lerberg, S. B., Anderson, B.-A., and Padma, T. V. 2002. Species sensitivity distributions in ecological risk assessment: Distributional assumptions, Alternate bootstrap techniques, and Estimation of adequate number of species. Pages 119-132 in Posthuma, L., Traas, T. P., and Suter, G. W., II, editors. Species Sensitivity Distributions in Ecotoxicology. Lewis Publishers, Boca Raton, FL, USA.

Newman, M. C., Ownby, D. R., Mézin, L. C. A., Powell, D. C., Christensen, T. R. L., Lerberg, S. B., and Anderson, B.-A. 2000. Applying species-sensitivity distributions in ecological risk assessment: Assumptions of distribution type and sufficient numbers of species. Environmental Toxicology and Chemistry 19:508-515.

Posthuma, L., Suter II, G.W., Traas, T.P. (editors). 2002. Species sensitivity distributions in ecotoxicology, CRC Press, Boca Raton, Florida. 616pp.

Patiño R., Goodbred, S.L., Draugelis-Dale, R., Barry, C.E., Foott, J.S., Wainscott, M.R., Gross, T.S., and Covay, K.J., 2003, Morphometric and histopathological parameters of gonadal development in adult common carp from contaminated and reference sites in Lake Mead, Nevada, Journal Aquatic Animal Health 15:55-68.

Raimondo, S., Vivian, D.N., Delos, C., Barron, M.G., 2008, Protectiveness of species sensitivity distribution hazard concentrations for acute toxicity used in endangered species risk assessment, Environmental Toxicology and Chemistry 27: 2599-2607.

Rosen, M.R., Leiker, T.J., and Goodbred, S.L. 2006a. Use of passive samplers for detecting vertical gradients and potential sources of organic contaminants to Lake

Mead, Nevada, U.S.A.: Geological Society of America Abstracts with Programs, v. 38, no. 7, p. 160

Rosen, M.R., Goodbred, S.L., Patino, R., Leiker, T.J., Orsak, E. 2006b. Investigations of the effects of synthetic chemicals on the endocrine system of common carp in Lake Mead, Nevada and Arizona: U.S. Geological Survey Fact Sheet 2006-3131, 4 p.

Sappington, L.C., Mayer F.L, Dwyer F.J., Buckler D.R., Jones J.R., Ellersieck M.R. 2001. Contaminant sensitivity of threatened and endangered fishes to standard surrogate species. Environ. Toxicol. Chem. 20(12):2869-2876.

Snyder, S., Wert, E., Lei, H., Westerhoff, P., Yoon, Y., 2008, Removal of EDCs and Pharmaceuticals in Drinking Water, AwwaRF Report 91175, American Water Works Association Research Foundation, Denver, Colorado, 331pp.

Stephen, C.E., Mount, D.I., Hansen D.J., Gentile, J.R., Chapman, G.A., Brungs, W.A., 1985, Guidelines for deriving numerical national water quality criteria for the protection of aquatic organisms md their uses, U.S. Environmental Protection Agency, PB85-227049, 105pp.

Tuttle, P., Orsak, E.L., and Williams, R.D., 2002, Las Vegas Wash Water Quality and Implications to Fish and Wildlife, U.S. Fish and Wildlife Service and Nevada Fish and Wildlife, FFS Numbers: 1F27 and 1F31, DEC IDs: 199810009 and 200010001, 57pp.

USEPA 2005. Multi-chemical evaluation of the short-term reproduction assay with the fathead minnow. EPA Contract Number 68-W-01-023 Work Assignment 5-5, U.S. Environmental Protection Agency, Washington, D.C., Draft Final Report, 165 pp.

USEPA 2002a. A Short-Term Method for Assessing the Reproductive Toxicity of Endocrine Disrupting Chemicals Using the Fathead Minnow (Pimephales promelas). EPA/600/R-01/067. U.S. Environmental Protection Agency, National Health and Environmental Effects Research Laboratory, Mid-Continent Ecology Division, Duluth, Minnesota.

USEPA 2002b. A fish two-generation toxicity test. EPA Contract Number 68-W-01-023 Work Assignment 2-13, U.S. Environmental Protection Agency, Washington, D.C., Draft Detailed Review Paper 133 pp.

USEPA. 2002c. Draft detailed review paper A fish two-generation toxicity test. EPA Contract number 68-W-01-023, Work Assignment 2-13 (http://www.epa.gov/scipoly/oscpendo/pubs/edmvs/fishlifecycledrp.pdf)

Water Environment Research Foundation (WERF), 2007, Fate of Pharmaceuticals and Personal Care Products through Wastewater Treatment Processes, Water Environment Research Foundation, Alexandria, Virgina, 116pp.

Westerhoff, P., Yoon, Y., Snyder, S., Wert E., 2005, Fate of endocrine-disuptor, pharmaceutical, and personal care product chemicals during simulated drinking water treatment process. Environmental Science and Technology 39: 6649-6663.

CONSTRUCTION OF A LOW-FLOW CHANNEL IN BARBER CREEK: CASE STUDY IN THE POWDER RIVER BASIN, WYOMING

Robert W. Thoman, P.E.[1] and J. J. Brown[1]

[1]Lowham Engineering LLC, 205 South Third Street, Lander, Wyoming 82520, PH (307)335-8466; FAX (307)335-7343; email: bthoman@low-water.com, jjbrown@low-water.com

Abstract

Design and construction of low-flow channels to convey coalbed natural gas-produced (CBNG-produced) waters to higher-order streams is a relatively new water management option being employed in the Powder River Basin (PRB) of northeast Wyoming. In this case study, a low-flow channel was designed, constructed, and maintained on Barber Creek and South Prong Barber Creek in the PRB near Gillette, Wyoming. Engineering design challenges include large ephemeral flows, steep slopes, and cohesive soils. Initial design was based on aerial photography analysis, low-level reconnaissance flights, and field exploration. Existing channels were surveyed to establish representative channel sinuosity, depth, slope, and stability of streams in close proximity to the study area. The final design includes approximately 1,370 m (4,500 ft) of channel reconstruction on South Prong Barber Creek and 1,800 m (5,900 ft) of channel reconstruction on Barber Creek. Clay soils hardened by severe drought conditions presented an unexpected challenge during construction, as did several significant rainfall events which occurred immediately following initial construction, damaging design elements already in place. Automatic streamflow gages located upstream and downstream of the study area recorded the subsequent flood events. Post construction design considerations include stabilization of the existing channel and installation of erosion mitigation measures. This study provides a full range of design criteria, construction procedures, and mitigation efforts for consideration in the design of stable low-flow conveyance channels for CBNG-produced waters.

Introduction

Coalbed natural gas (CBNG) development has occurred in the Powder River Basin (PRB) of northeast Wyoming since the early 1990s. To extract CBNG, large quantities of water are pumped from coal seams to reduce pressure and allow the gas to disassociate. Produced water is often managed through storage in reservoirs, surface application (irrigation), reinjection, and/or direct discharge to ephemeral and perennial streams. Direct discharge in ephemeral headwater tributaries close to production wells is a preferred management tool for CBNG-produced water due to

low capital costs (Bank and Kuuskraa, 2006). This can be problematic in areas where a channel is discontinuous, contains erosional features, or produced water discharges exceed the carrying capacity of the channel.

Construction of a low-flow channel to convey produced water is a relatively new management technique. Many of the first channel construction projects were "field-fit" by contractors with little oversight and no engineering analysis. Successful projects were often short lived due to neglected maintenance following construction. Designing and constructing a low-flow channel involves many variables that are difficult to quantify and may result in increased mitigation costs if not addressed. An engineered design prepared by a qualified engineering firm will significantly reduce cost and construction time.

Due to the complex nature of stable channel design and construction, many stakeholders have expressed a need for methodology specific to the PRB. The objective of this study was to design, construct, and maintain a low-flow channel to convey CBNG-produced water and natural runoff specific to typical conditions encountered in the PRB. This study presents design criteria, construction procedures, and maintenance and mitigation efforts of a successful low-flow channel project in the Barber Creek drainage.

Background

Thoman and Niezgoda (2008) developed a method of estimating critical shear stress from cohesive soil properties in an effort to simplify the evaluation of stable channel capacity. In their analysis, Thoman and Niezgoda (2008) balanced the critical shear stress, τ_c, of the soil, determined by a submerged jet device, against the effective shear stress, τ_e, of the flowing water (also termed the tractive force). Erosion, ε_r, is assumed to occur when τ_e exceeds τ_c of the bounding soils

$$\varepsilon_r = k_d (\tau_e - \tau_c) \quad (1)$$

This equation is commonly referred to as the excess stress equation where, ε_r = erosion rate (m/s), k_d = erodibility coefficient ($m^3/N \cdot s$), τ_e = effective shear stress (Pa), and τ_c = critical shear stress (Pa). For channel stability analysis, the erosion rate is set to zero, which simplifies the equation to

$$\tau_e = \tau_c \quad (2)$$

In cohesive soils, τ_c is most commonly determined through laboratory or *in-situ* testing. One proven method of *in-situ* testing to determine τ_c is to use a submerged jet device developed by Hanson (1991) and improved by Hanson et al. (2002). Hanson and Cook (2004) provide detailed procedures for operation of the device.

Evaluation of τ_e requires channel geometry information. The effective shear stress under bare soils conditions is given as

$$\tau_e = \gamma d S (n_s/n)^2 \quad (3)$$

where, γ = unit weight of water, d = flow depth, S = friction slope (approximated by the channel bed slope for uniform flow), n_s = Manning's coefficient for soil grain roughness (equal to 0.0156) (Temple, 1980; Hanson, 1989) and n = Manning's coefficient for channel roughness. Temple (1980) modified the equation to account for vegetation by introducing an empirical vegetal cover factor

$$\tau_e = \gamma dS(1-C_F)(n_s/n_v)^2 \quad (4)$$

where, C_F = vegetal cover factor (common range is 0.5-0.9, values approaching 1 indicate increased vegetation density and uniformity) and n_v = Manning's roughness coefficient for vegetated channel roughness. A check of the vegetal stress must be made to ensure the vegetation remains intact

$$\tau_{va} = 35.91 C_I \quad (5)$$

where, τ_{va} = maximum allowable vegetal stress (Pa), C_I = dimensionless retardance curve index ($C_I = 2.5(h\sqrt{M})^{1/3}$; h = stem length, and M = stem density) (Temple et al. 1987).

Data Collection

A watershed study was performed by Lowham Engineering LLC (LELLC) to collect and compile data in the drainage of Barber Creek. The results of the watershed study are presented in the report, "The Hydrology of Barber Creek – A Tributary to the Powder River in Wyoming" (LELLC, 2005). The Barber Creek drainage is located 32 km (20 mi) west of Gillette, Wyoming, and covers approximately 192 km^2 (74 mi^2) (Figure 1). Barber Creek is an ephemeral channel with streamflow occurring in response to runoff events. Step-backwater surveys were completed at ten locations to indirectly evaluate bankfull channel capacity near the study area shown in Figure 2. Channel depth, slope, and sinuosity were established from the survey data. Bankfull estimates ranged from 1.05 m^3/s (37 ft^3/s) to 3.51 m^3/s (124 ft^3/s), corresponding to a return interval of 1.5 to 2 years. Return interval runoff was modeled using regional regression equations developed by Lowham (1988).

Data collected from aerial photography and low-level reconnaissance flights indicated locations where the natural channel was discontinuous and provided initial indications of erosion features. Field reconnaissance verified erosion features and locations of channel discontinuity. On South Prong Barber Creek, construction of two spreader dikes in the 1950's resulted in aggradation of the valley floor, obscuring channel characteristics. Aggradation of the channel in the study reach on Barber Creek was thought to be due to excessive sediment loading upstream (LELLC, 2005).

A related study was completed in 2006 to analyze natural streamflow data including quantity, quality, and relationships between the two (LELLC, 2006). Data were collected at six stream flow gages (2 automatic gages and 4 staff gages) located 11.2 stream km (7 mi) downstream of the study area. An additional automatic streamflow gage was installed 4.1 stream km (2.6 mi) upstream of the study area to

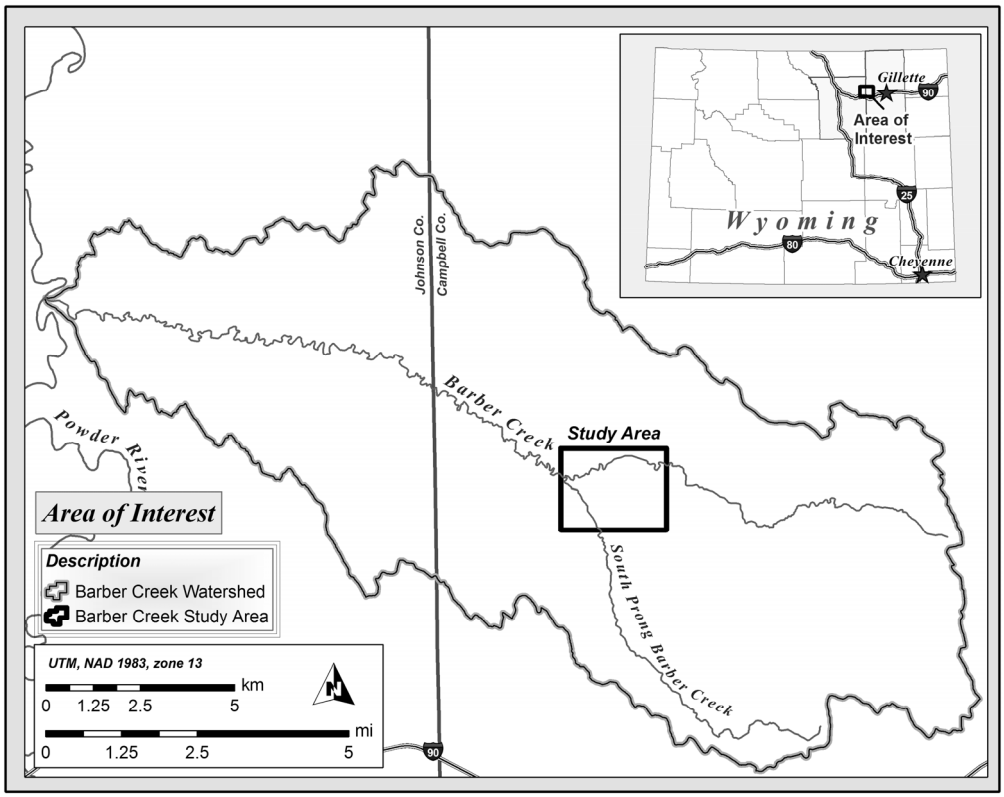

Figure 1. Overview of the Barber Creek drainage in the Powder River Basin of Wyoming

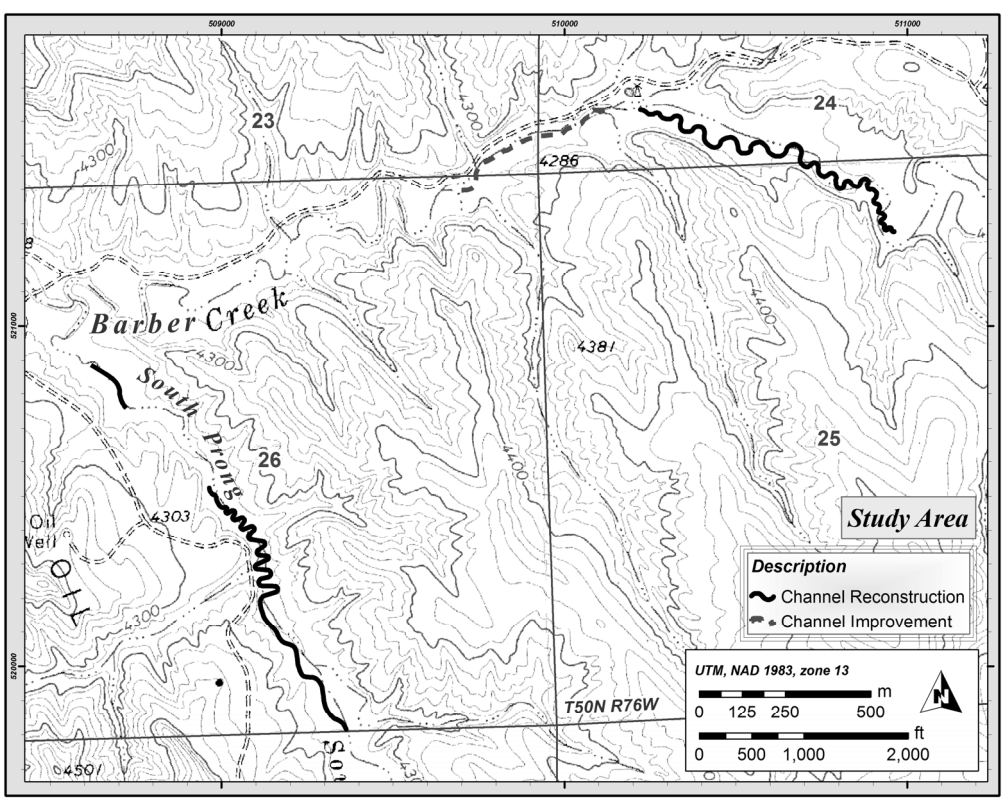

Figure 2. Channel design locations in the study area along Barber Creek and South Prong Barber Creek in Wyoming

characterize ephemeral stream flows upstream of the study area.

Critical shear stress estimates were needed to perform the stability analysis. A subset of the critical shear stress values collected by Thoman and Niezgoda (2008) was used to estimate a design value for the study area. Fifteen data points located within a 15.8 km (9.8 mi) radius of the study area were averaged to estimate a design critical shear stress that would account for local variability in soil conditions throughout the study area.

Channel Design

Design channel capacity was based on estimated planned development, well production, and dilution. Maximum well production was predicted to be less than 0.28 m^3/s (10 ft^3/s). Additional channel capacity of 0.28 m^3/s (10 ft^3/s) was required to ensure adequate dilution of CBNG-produced water with natural runoff prior to bank overflow, resulting in a design discharge of 0.57 m^3/s (20 ft^3/s).

Natural channel geometry, sinuosity, slope, and stability were evaluated near the study area to develop design parameters. Channel geometry needed to be conducive to establishing vegetation while also preventing ice sheeting and limiting total disturbance. Channel sinuosity is a controlling factor for promotion of conveyance losses by increasing channel length and decreasing channel slope. Proper channel slope is imperative to controlling erosion and plays a significant role in channel stability. Additional design considerations include soil type, livestock traffic and grazing, channel construction methods, and storm water runoff.

The valley slope in the study area was too steep to support a stable earthen channel. A slope of 0.5% achieved the goals of the design by providing stability and increasing sinuosity. Exceptions include the upstream, straightened section of the reach on South Prong Barber Creek and the channel improvement reach along Barber Creek (Figure 2). The reach on South Prong Barber Creek was designed with a channel slope slightly less than the valley slope of 1% due to landowner agreements. The channel improvement reach on Barber Creek consisted of cleaning an existing channel with slopes ranging from 0.6-1.2%. Final channel design lengths include 1,370 m (4,500 ft) on South Prong Barber Creek and 1,800 m (5,900 ft) on main stem Barber Creek (Figure 2).

Channel design geometry included a trapezoidal channel with a bottom width of 0.23 m (0.75 ft), depth of 0.64 m (2.1 ft), and 1:1 side slopes. Channel side slope steepness was of concern for establishment of new vegetation, but was weighed against the threat of ice sheeting that may develop with flatter slopes.

Shear stress and velocity profiles were used to evaluate stability of the channel design (Figure 3). Soil types in the study area ranged from clay loam on South Prong to silt clay loam on Barber Creek. A critical shear stress analysis of the soil and vegetation stability using Equations (2), (3), (4), and (5) is presented in Figure 4. Average critical shear stress for the study reach was 4.5 Pa, determined from data provided in Thoman and Niezgoda (2008). Figure 4 shows that for the design capacity, the unvegetated channel is not stable. However, the addition of minimal vegetation cover ($C_F = 0.6$) results in a factor of safety (FS) of 1.8. The unvegetated channel is stable (FS = 1) at a depth of 0.34 m (1.1 ft) for a discharge of 0.14 m^3/s (4.8 ft^3/s). Vegetation cover is

DEPTH m (ft)	DISCHARGE m^3/s (ft^3/s)	VELOCITY m/s (ft/s)	EFFECTIVE SHEAR STRESS, τ_e, Pa (lbs/ft^2)
0.15 (0.5)	0.027 (1.0)	0.46 (1.5)	2.0 (0.042)
0.30 (1.0)	0.10 (3.8)	0.67 (2.2)	4.0 (0.084)
0.46 (1.5)	0.26 (9.1)	0.82 (2.7)	6.1 (0.13)
0.65 (2.1)	0.57 (20)	1.0 (3.3)	8.5 (0.18)
0.76 (2.5)	0.83 (29)	1.1 (3.6)	10.1 (0.21)

Manning's roughness (n) = 0.030 Channel slope = 0.005

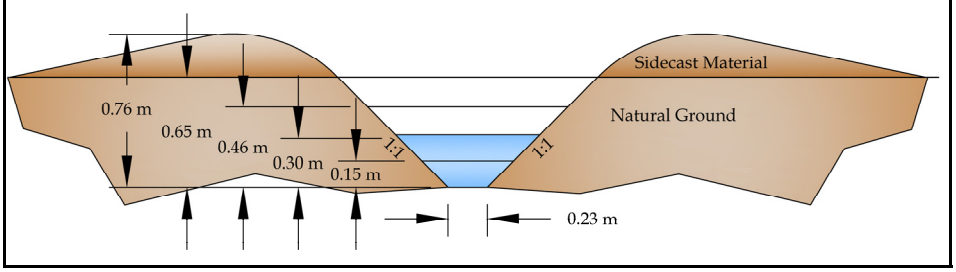

Figure 3. Channel geometric design parameters and computations for Barber Creek channel reconstruction in the Powder River Basin of Wyoming

SHEAR STRESS ANALYSIS					(Pa)	(lbs/ft^2)
Effective Shear Stress (bare soils), $\tau_e = \gamma dS(n_s/n)^2$ =					**8.6**	**0.18**
(shear stress applied by flowing water)						
γ	*9810*	(N/m^3)	*62.4*	(lbs/ft^3)	unit weight of water	
d	*0.65*	(m)	*2.1*	(ft)	flow depth	
S	*0.005*	channel slope				
n_s	0.0156	Manning's coefficient for soil grain roughness				
n	*0.030*	Manning's coefficient for unvegetated channel roughness				
Vegetated Effective Shear Stress, $\tau_{ev} = \gamma dS(1-C_F)(n_s/n_v)^2$ =					**2.5**	**0.05**
(resultant shear stress acting on the soil surface below the vegetation)						
C_F	*0.6*	Cover Factor - vegetation uniformity and density				
n_v	*0.035*	Manning's coefficient for vegetated channel roughness				
Vegetal Shear Stress (psf), $\tau_v = \tau_e - \tau_{ev}$ =					**6.0**	**0.13**
(resultant shear stress that acts on the vegetation)						
Max Allowable Vegetal Shear Stress, $\tau_{va} = 35.91C_I$ =					**92**	**1.9**
(shear stress that will damage/remove the vegetated layer)						
C_I	2.55	Retardance Curve Index = $2.5(h\sqrt{M})^{1/3}$				
h	*0.046*	(m)	*0.15*	(ft)	stem height	
M	*538*	($\#/m^2$)	*50*	($\#/ft^2$)	stem density	
Critical Shear Stress (psf), τ_c =					**4.5**	**0.10**
(shear stress required to initiate incipient motion, i.e. erosion)						
Bare channel:	$\tau_c - \tau_e$ =	-4.1	=>	**UNSTABLE**	**0.5 FS**	
Vegetated channel:	$\tau_c - \tau_{ev}$ =	2.0	=>	**STABLE**	**1.8 FS**	
Vegetation:	$\tau_{va} - \tau_v$ =	86	=>	**STABLE**	**15 FS**	

Figure 4. Shear stress analysis for Barber Creek channel design in the Powder River Basin of Wyoming

critical to ensure channel stability for the design discharge. Short growing seasons, drought conditions, and cohesive soils presented unanticipated challenges to constructing a stable, vegetated channel.

Channel Construction

Channel construction began on South Prong Barber Creek and Barber Creek in August of 2006. A 'V'-type ditcher (Figure 5) was used for channel construction to limit disturbance and reduce construction time. Hard soil conditions from years of drought necessitated the use of a ripper to loosen the soil. Tight meander radi had to be pre-cut with a road grader. The effective radius for channel construction with the ditcher was about 10 m (33 ft). Repeated passes with the ditcher were required to achieve the design depth. Hardened soil conditions required field modifications to repair and reinforce the ditcher. Constructed channel geometry is shown in Figure 6.

Eight culverts were installed at specific locations along the constructed channel to serve as livestock and access crossings and to provide locations for storm water overflow. The culverts were sized to only allow conveyance of the design flow. Drop pipes were installed through two spreader dikes on South Prong Barber Creek with erosion protect at the outlets. Following construction, the channels were hydroseeded and the banks and disturbed areas were drill seeded.



Figure 5. View of channel construction using a ditcher on South Prong Barber Creek in the Powder River Basin of Wyoming (August 2006)



Figure 6. View of completed channel construction on South Prong Barber Creek prior to hydroseeding (August 2006)

Channel Maintenance and Mitigation

Shortly after construction, a rainstorm and runoff event was recorded at the streamflow gage located upstream of the channel reach. Additional snowmelt and rainfall runoff events were recorded throughout the winter and spring of the following year. A site visit was conducted in May 2007 to evaluate channel conditions. Observations indicated that overbank flow had occurred from natural runoff events, as produced-water discharge had not begun. The South Prong channel was in excellent condition with emerging vegetation growth. The main channel of Barber Creek suffered from the formation of a headcut and channel erosion at the beginning of the construction reach shown in Figure 7. Vegetation had not established in the

channel bed or on the side slopes as hoped, likely due to the hard soil conditions. Sand and silt lenses that were not apparent during construction were noted in the channel bed. A mitigation plan was developed and implemented in August 2007. Approximately 190 m (620 ft) of channel was lined with turf reinforcement mat (TRM) to stabilize the reach and support revegetation efforts (Figure 8). The TRM used in this project is a propylene fiber matrix designed to protect bare soils up to shear stress levels of 98 Pa. Once vegetation has established in areas lined with TRM, allowable shear stress values increase to 384 Pa. Additional maintenance work performed in 2007 included placement of TRM below the culvert crossing outlets to prevent scouring, cleaning deposited sediments from the channel, and reseeding.



Figure 7. Downstream view of eroded channel on Barber Creek following a large runoff event on May 30, 2007



Figure 8. Downstream view of Barber Creek following channel lining with turf reinforcement mat (TRM) on August 28, 2007

The 10-year drought appeared to break in 2008 as evidenced by increased rainfall and associated runoff (Water Resource Data System, 2008). An increased number of runoff events were recorded at the upper streamflow gage during the spring and summer months. A project visit in June 2008 revealed channel conditions during the recession of a runoff event. Overland flow entering the channel on South Prong Barber Creek resulted in the formation of rills in the channel banks. The upper section of Barber Creek was unaffected by the flows, but the lower channel improvement reach experienced some minor erosion. Similar to the previous year, a maintenance and mitigation plan was developed. Implementation of the mitigation plan began in August 2008.

South Prong Barber Creek and the Barber Creek channel improvement reach were the focus of the mitigation efforts in 2008. Channel banks were ripped, reshaped, seeded, and lined with TRM (Figure 9). Approximately 122 m (400 ft) of channel on South Prong Barber Creek and 365 m (1200 ft) of channel in the improvement reach on Barber Creek were mitigated using TRM.

Maintenance was also required to repair erosion protection below the spreader dike outlet pipes and to clean channel sediment caused by debris jams at the culvert crossings. The erosion protection was repaired by placing another layer of TRM over the structure, and plywood checks were removed from the culverts to alleviate debris jamming and subsequent sedimentation.



Figure 9. Upstream view of sequence of channel mitigation measures (clockwise from top left) taken to repair rills in the bank from tributary flow entering the channel on South Prong Barber Creek in the Powder River Basin of Wyoming (August 20-22, 2008)

Summary and Conclusions

A low-flow conveyance channel was designed and constructed on Barber Creek and South Prong Barber Creek in August 2006. The channel was designed for conveyance of 0.57 m^3/s (20 ft^3/s) of CBNG-produced water and natural runoff. Channel geometry and bed slope were designed to remain stable with minor revegetation. To date, discharge of produced water has not occurred. However, numerous natural runoff events have been documented since construction, impacting the channel. Tributary flow entering the channel was responsible for the majority of the impact. Erosion mitigation plans were implemented following site inspections in the summer of 2007 and 2008. Channel banks were ripped, reshaped, seeded, and lined with TRM to mitigate destabilized locations along the study reaches. Annual maintenance was performed to remove debris from the channel and reinforce erosion protection below culvert outlets.

The results of this study provide design criteria, construction procedures, and maintenance and mitigation efforts for a successful low-flow channel project in Barber Creek in the Powder River Basin of Wyoming. The methodology presented in this study is intended to help stakeholders as they look to utilizing direct discharge to manage CBNG-produced water.

References

Bank, G. C., and Kuuskraa, V. A. (2006). *The economics of Powder River coalbed methane development.* Advanced Resources International, Inc., Washington, D.C.

Hanson, G. J. (1989). "Channel erosion of two compacted soils." *Transactions of the ASAE,* 32(2), 485-490.

Hanson, G. J. (1991). "Development of a jet index to characterize erosion resistance of soils in earthen spillways." *Transactions of the ASAE,* 34(1), 132-137.

Hanson, G. J., and Cook, K. R. (2004). "Apparatus, test procedures, and analytical methods to measure soil erodibility in-situ." *Transactions of the ASAE,* 20(4), 455-462.

Hanson, G. J., Robinson, K. M., and Cook, K. R. (2002). "Scour below an overfall. Part II: Prediction." *Transactions of the ASAE,* 45(4), 957-964.

Lowham Engineering LLC (2005). *The hydrology of Barber Creek – a tributary of the Powder River in Wyoming.* Lander, Wyoming.

Lowham Engineering LLC (2006). *Streamflow data for Barber Creek – a tributary of the Powder River in Wyoming.* Lander, Wyoming.

Lowham, H. W. (1988). *Streamflows in Wyoming.* Report No. 88-4045, U.S. Geological Survey, Cheyenne, Wyoming.

Temple, D. M. (1980). "Tractive force design of vegetated channels." *Transactions of the ASAE,* 23(4), 884-890.

Thoman, R. W., and Niezgoda S. L. (2008). "Determining erodibility, critical shear stress, and allowable discharge estimates for cohesive channels: case study in the Powder River Basin or Wyoming." *J. Hydraulic Engineering*, 134(12), 1677-1687.

Water Resource Data System (2008). Water and Climate Data for the State of Wyoming (http://www.wrds.uwyo.edu/SCD/climate-office.html).

Decentralized Anaerobic Treatment of Blackwater:
A Sustainable Development Technology Concept for Urban Water Management

Gallagher, NT[1] and Sharvelle, S[2]

[1]Department of Civil and Environmental Engineering, Colorado State University, 1372 Campus Delivery, Fort Collins, Colorado 80523-1372; PH (970) 491-8288; FAX (970) 491.7727; email: neal.gallagher@colostate.edu

[2]Department of Civil and Environmental Engineering, Colorado State University, 1372 Campus Delivery, Fort Collins, Colorado 80523-1372; PH (970) 491-6081; FAX (970) 491.7727; email: sybil.sharvelle@colostate.edu

ABSTRACT

As populations continue to increase, the demand for limited water resources has increased. Sustainable water technologies and management methods are critical to our meeting future water quantity and quality demands. Decentralized treatment of blackwater under anaerobic conditions is a wastewater treatment technology being explored for application in new developments. Decentralized anaerobic treatment of blackwater stands out in its ability to conserve available green water and energy resources and promote reuse of these resources at a local level.

A pilot scale anaerobic reactor is under construction at the Colorado State University Foothills Campus to treat blackwater (toilet and kitchen sink wastewater) from a building occupied by laboratory and office space. This project is a demonstration study on the economic and technical feasibility of using anaerobic digestion for treatment of blackwater. Eventually, it is anticipated that biogas produced in digesters will be used as a green energy alternative to current energy sources and treated effluent water will be evaluated for reuse onsite for irrigation or other non-potable uses. Treatment efficiencies of the anaerobic process under varying loading and environmental conditions will be monitored in addition to methane production. A decision analysis tool for cluster decentralized wastewater treatment (DWWT) will be developed to assist decision making entities in determining the applicability of DWWT.

It is anticipated that the data provided by this study will also provide important data for basis of legislation related to the effectiveness and safety of DWWT and reuse of resources contained within wastewater. Such data is vital to encourage incorporation of sustainable treatment technologies, e.g. DWWT, as aging and failing infrastructure is rapidly becoming in need of replacement and new developments are constructed. This research is in line with recent study efforts put forth by the USEPA attempting to develop technologies and methods for new and existing developments to achieve both water and energy independence from typical centralized grid systems.

INTRODUCTION

In a 1997 report to congress, the United States Environmental Protection Agency (US EPA) noted that well managed decentralized wastewater treatment (DWWT) systems, including onsite (septic) and small community cluster treatment systems, were an economical and long-term option to meet both public health and water quality goals (US EPA 2009).

Decentralized wastewater treatment technologies have been used previously as some of the very first methods of primitive human waste disposal into the environment. In recent times, developed countries have drifted away from use of decentralized systems because of the federal money made available to research and implement centralized wastewater treatment plants. In the past 25-30 years, a progressive change in thought and the cost effective availability of advanced technologies has permitted DWWT to compete with centralized wastewater treatment.

Unfortunately, a minimal number of full scale DWWT systems have been put into practice and little data is available on their effectiveness, as well as their technical and economical feasibility. Further study and demonstration scale implementation is crucial to provide data as well as ensure public acceptance of DWWT technologies. DWWT systems are emerging as a potential challenger to supplement and replace commonly used centralized systems. In order to justify implementation of DWWT systems, it is necessary to gain both public support and legislative permission to construct and implement these systems on a larger scale.

Efforts are being made by Colorado State University (CSU) to implement DWWT technologies on their Foothills Campus. Currently, demonstration projects for treatment of blackwater and graywater are underway. In addition, a decision making tool is under development to determine the technical and economical feasibility of DWWT for specific applications. The purpose of this decision making tool is to assist decision making entities in finding the best wastewater treatment system layout for their chosen service area.

DECENTRALIZED WASTEWATER TREATMENT (DWWT)

Decentralized wastewater treatment provides a rational concept for wastewater treatment which resonates with the push for more sustainable development within the US and abroad. DWWT systems serve smaller footprints than their centralized counterparts.

In DWWT, wastewater streams can be separated by the relative amount of treatment and care in handling required. For example, graywater produced in showers, hand sinks, and laundry machines contains a relatively clean, low pathogen wastewater which can be easily treated for use in toilet flushing or directly reused for landscape irrigation. Blackwater, from toilets and garbage disposals contains high organic and high pathogen loadings and must be carefully handled and requires high levels of treatment.

More localized treatment and separated wastewater streams encourage extraction and reuse of valuable wastewater constituents by facilitating end user access e.g. methane biogas and nutrient rich effluent for irrigation. Capture and reuse of wastewater constituents reduces the amount of nutrient and organic rich effluent deposited into natural waterways by centralized treatment systems.

Figure 1 presents a comparison of (a) DWWT and (b) centralized wastewater treatment servicing identical development. As shown in the figure, DWWT encourages treatment for localized clusters of development. Because development often occurs in relatively dense clusters, DWWT concepts can drastically reduce both the diameter and length of required conveyance infrastructure. Smaller service areas require smaller infrastructure footprints and smaller piping, resulting in lower environmental impact from construction and reduced waterway crossings.

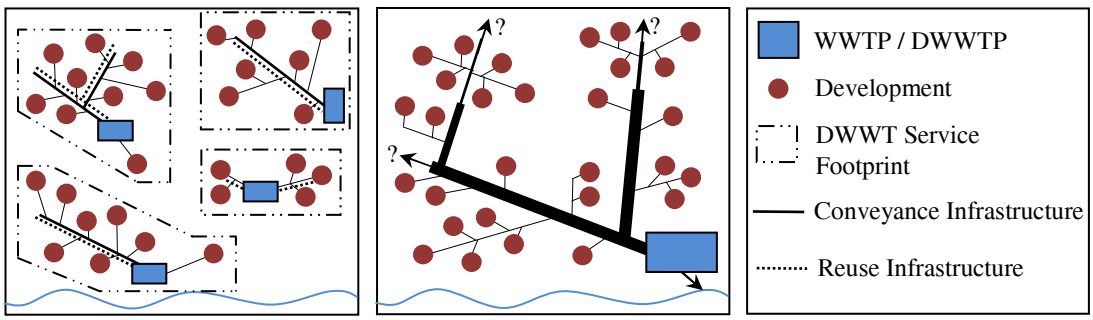

Figure 1: Comparison of (a) DWWT and (b) centralized treatment

Smaller service areas with generally known maximum wastewater demands facilitate conveyance infrastructure planning. Arrows at the ends of conveyance infrastructure in Figure 1(b) represent future development direction predictions often encountered during centralized infrastructure capacity planning. Centralized treatment requires infrastructure capacity planning to occur decades before capacity is required in directions of predicted development.

Two major roadblocks encountered in centralized planning include (1) conveyance infrastructure can flow at fractions of capacity for years, encouraging infiltration and requiring high capital investment long before capacity is needed and (2) predicted development directions change, resulting in unused infrastructure capacity and misspent capital.

DWWT systems can offer many benefits over centralized systems. However, typically these two systems must be compared on a case by case basis to effectively determine which is more feasible for specific applications. Higher costs associated with DWWT tend to surround economies of scale which benefit centralized treatment in dense service areas. However, DWWT has potential to reduce infrastructure costs by making more efficient planning possible, provide cost savings by increased capabilities for water reuse, as well as reduce the environmental impacts associated with centralized wastewater collection and treatment systems.

Decentralized wastewater treatment has global applications. According to the EPA, approximately one in four households in the United States relies on an onsite treatment system (US EPA 2009). DWWT is able to replace failing septic systems, providing higher levels of treatment and preventing nutrients and contaminants from leaching into natural waterways. New developments and small communities can capture and treat wastewater locally. Clusters of development, e.g. residential neighborhoods or commercial business parks, where centralized treatment is uneconomical or plant/conveyance capacity is not available are candidates for DWWT.

Developing communities in less affluent regions of the world also benefit from decentralized wastewater treatment. Many areas of the world do not have or have very minimal centralized wastewater infrastructure supporting communities. In these areas, creation of a centralized wastewater treatment network from scratch can be unaffordable. DWWT technologies present opportunity to provide treatment, greatly increasing sanitation and public health in regions which could otherwise not afford treatment. DWWT also has potential to provide these areas with useable biogas, as well as nutrients and irrigation water for non-consumptive agricultural uses.

CSU BLACKWATER DEMONSTRATION PROJECT

Colorado State University (CSU) department of Facilities Management has provided funding for a DWWT demonstration project to treat blackwater on the CSU Foothills Campus. Over the next 30 years, CSU plans to expand development within their Foothills Campus adding classrooms, offices and laboratories. With the expansion of the Foothills Campus, CSU intends to embody a demonstration of environmental sensitivity and sustainability (RNL Design 2003).

The blackwater DWWT demonstration project is among several studies underway to determine the best way to maximize sustainability in wastewater treatment on the CSU Foothills Campus including a wetland graywater treatment study and a wastewater planning study for the entire CSU Foothills Campus. This study will provide important data on the technical and economic feasibility of separated blackwater treatment as well as decision making for DWWT systems.

Currently, a process review is underway to determine the most appropriate available technology for demonstration process design. Both aerobic and anaerobic processes are being considered. However, because biogas from anaerobic digestion can be used to produce heat for the reactor, to heat buildings and provide steam to autoclaves in laboratories, it is somewhat favorable for application. Also, production of biogas and capture of valuable nutrients which can be used to replace synthetic fertilizers contribute to the sustainability of wastewater treatment and therefore it is likely an anaerobic process will be studied.

The source of blackwater being studied is a building located on the Foothills Campus with plumbing separated into three streams: blackwater, labwater and sinkwater. Toilets, emergency showers and kitchen sinks contribute to the blackwater line although toilets supply the majority of wastewater.

During blackwater sampling, efforts were made to capture composite samples. One 6" PVC sewer line leaves the study building containing blackwater. A valve was installed on this line and an access point was placed upstream of the valve. Sampling was performed by temporarily shutting the valve and routing blackwater through the access point into a 30 gallon drum. Once filled, the 30 gallon drum was disconnected from the blackwater line. Wastewater within the drum was composited by placing a laboratory bench mixer fitted with a 4 foot metal rod with two propellers into one of two access ports at the top of the drum. One propeller was oriented at the bottom of the drum to kick up settled solids and the second propeller was oriented midway in the barrel to assist in mixing. While the mixer was operating, a hand operated 1" drum pump was inserted into the second drum access port and approximately three gallons of sample was withdrawn for analysis.

Blackwater composition was analyzed for total suspended solids (TSS), volatile suspended solids (VSS), chemical oxygen demand (COD), dissolved COD (dCOD), dissolved organic carbon (DOC), dissolved total nitrogen (dTN) and dissolved ammonia (dNH_3). TSS, VSS, dCOD, COD and dNH_3 were measured according to Standard Methods for The Examination of Water and Wastewater (APHA 1998) methods SM2540-D (TSS & VSS), SM5220-D (dCOD & COD) and SM4500-NH_3-F (NH_3). DOC and dTN were measured using a Shimadzu TOC-V combustion analyzer with TNM-1 total nitrogen module.

Table 1 provides a comparison of CSU blackwater to typical household blackwater and untreated domestic wastewater. Total suspended solids composition of the blackwater is approximately 0.3%. These values have been determined from three sets of sampling data except for TSS, VSS, and dissolved ammonia which have been determined from two sampling periods.

Table 1: Blackwater Characteristics

	Units	CSU Blackwater	Untreated Blackwater[1]	Untreated Domestic Wastewater[2]	Notes:
TSS	mg/L	3,248	920 - 4,320	120 - 400	[1] Palmquist & Hanæus (2005)
VSS	mg/L	2,931	420 - 3,660	95 - 315	[2] Tchobanoglous et al. (2003)
dCOD[3]	mg/L	598	--	--	[3] 0.45μm filter
COD	mg/L	3,530	806 - 3,138	250 - 800	[4] 0.45μm filter
DOC[3]	mg/L	126	--	80 - 260	
dTN[3]	mg/L	128	130 - 180	20 - 70	
dNH_3[4]	mg/L	127	--	12 - 45	

Characterization of CSU blackwater shows values within the range of previous blackwater studies. As seen in Table 1, most blackwater constituents are higher in concentration than those found in untreated domestic wastewater due to the lack of dilution from a typical collection system as well as separated blackwater and graywater plumbing.

Initial characterization of CSU blackwater has been supplemented by two additional studies to determine the biochemical methane production potential and to determine the biodegradation potential of the stream. Results from these tests provide insight into the treatability of the waste subject to both anaerobic and aerobic processes. Potential for biogas production from the waste is also realized, giving an indication of the contact times necessary to reach optimal conditions and what those conditions may be in an operational reactor.

Biochemical Methane Potential

Biochemical methane production potential (BCMP) testing was performed on blackwater samples to determine the volume of CH_4 produced per liter of blackwater substrate. Tests were performed as 200 ml batch anaerobic reactors modeled after the bioassay method for testing biodegradation outlined in (Owen, Stuckey et al. 1979). Tests were performed at a constant temperature of 35°C. Gas samples were analyzed for methane concentration on a HP5980II Gas Chromatograph using a packed column and thermal conductivity detector.

Figure 2 provides a cumulative volume of methane gas produced by BCMP batch tests per liter of blackwater substrate. The final cumulative value shows that 0.34 liters of methane ware produced per liter of blackwater over the duration of testing. This value was used to determine a methane production of 100 liters CH_4 per day. Using a methane lower heating value of 35,800 kJ/m^3 (Tchobanoglous et al. 2003), at 100% efficiency this provides 3,600 kJ/day or 1 kilowatt hour of energy. This is enough energy to run a 100 watt light bulb for 10 hours.

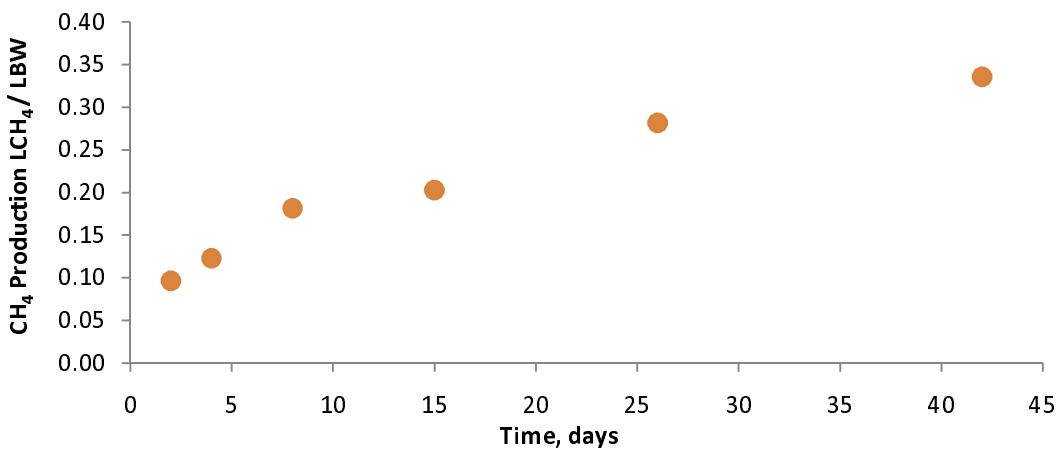

Figure 2: Cumulative CH_4 Production from CSU Blackwater

A study by (Luostarinen and Rintala 2005) of synthetic blackwater showed methane production of 2.5 and 0.81 liters CH_4 per liter anaerobic sludge in two respective reactors. Assays in this study were performed combining sludge, blackwater and distilled water to reach a volume of 60 ml. The methane production values provided included the entire assay and therefore can be expected to be somewhat higher than those provided in Figure 2 due to additional production from sludge.

It is expected that the process selected to treat backwater in the CSU demonstration project will be a high-rate flow-through reactor. BCMP tests are configured as batch reactors for convenience of study and therefore do not show the full potential methane production. Optimization and adjustment of environmental conditions within the flow through demonstration reactor provide for higher expected methane yields.

Aerobic & Anaerobic Biodegradation

Aerobic and anaerobic biodegradation tests were performed on CSU blackwater to gage both aerobic and anaerobic treatment potential. These tests were configured as simple batch reactors consisting of inoculum, nutrient solution (Owen, Stuckey et al. 1979) and blackwater substrate for a combined total assay of 1000 ml. Inoculum was taken from either the aerobic or anaerobic waste sludge

A total of six anaerobic tests were setup, three containing blackwater substrate and three controls. Each anaerobic biodegradation assay contained 500 ml blackwater and 500 ml anaerobic defined media (inoculum & nutrient solution) for a total average DOC of 392.9 mg/l and total average dTN of 154.8 mg/l. Anaerobic controls contained 500 ml DI water and 500 ml anaerobic defined media nutrient solution for a total average DOC of 34.7 mg/l and total average dTN of 108.23 mg/l.

Each aerobic biodegradation assay contained 500 ml blackwater, and 500 ml aerobic defined media (inoculum & nutrient solution) for a total average DOC of 74.9 mg/l and total average dTN of 110.5 mg/l. Aerobic controls contained 500 ml DI water and 500 ml aerobic defined media with a total average DOC of 15.2 mg/l and total average dTN of 48.1 mg/l.

DOC and dTN were measured using a Shimadzu TOC-V combustion analyzer with TNM-1 total nitrogen module. For aerobic tests, 15 ml samples were taken from assays by removing foam stopper and pouring composite sample into a 15 ml sample vial. Anaerobic tests were sampled by inserting a 16 gauge syringe through the rubber stopper located in the mouth of the test bottle and extracting 15 ml of sample. Extracted sample was then placed in a 15 ml sample vial for transport. Sample analysis was performed the day of sampling. Prior to analysis, samples were filtered through 0.45μm filter cartridges.

As seen in Figure 3 and Figure 4 below, identical trends in dTN were experienced in both assays over the first nine days of experimentation. On the second sampling date, 5.0% and 6.3% dTN increases were experienced in anaerobic and aerobic assays respectively. dTN is the sum of all dissolved species of nitrogen including nitrite, nitrate, organic nitrogen and ammonia. Nitrogen speciation was not performed. However, it is possible that this increase is caused by nitrogen fixing bacteria during the initial growth phase. An increase in dTN is also experienced at the end of testing in anaerobic tests which may be contributed to release via dying cell mass.

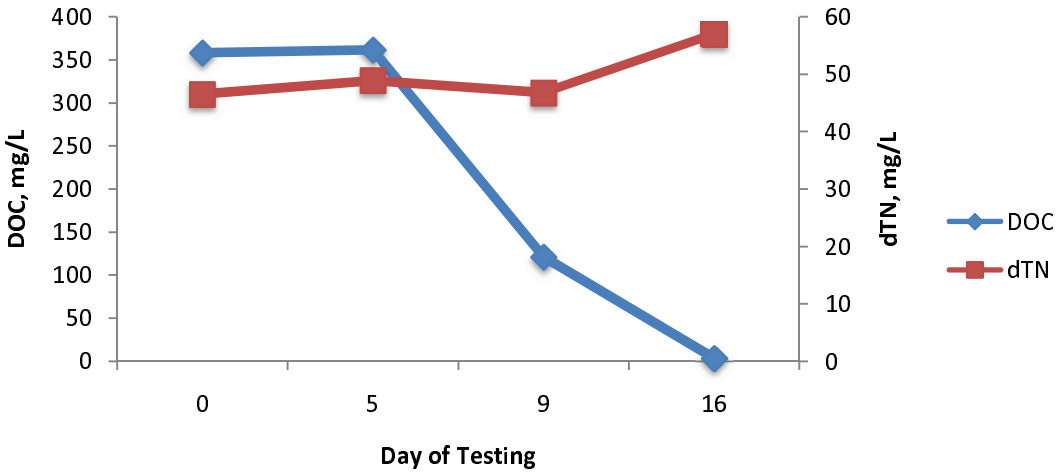

Figure 3: Anaerobic Biodegradation Results

DOC concentration did not change substantially between the first two sampling periods in anaerobic tests. Anaerobic assays were not prepared in an anaerobic environment and therefore this trend could represent a biomass startup phase caused by remnant oxygen in the headspace of the anaerobic bottles. However, effective DOC reduction was experienced between days 5 and 16.

Aerobic testing shown in Figure 4 experienced an increase in DOC at the end of testing. This increase may be contributed by DOC release from dying cell mass. Decreasing dTN in the final days of testing is noticed which may be due to biological uptake of nitrogen by nitrifying bacteria.

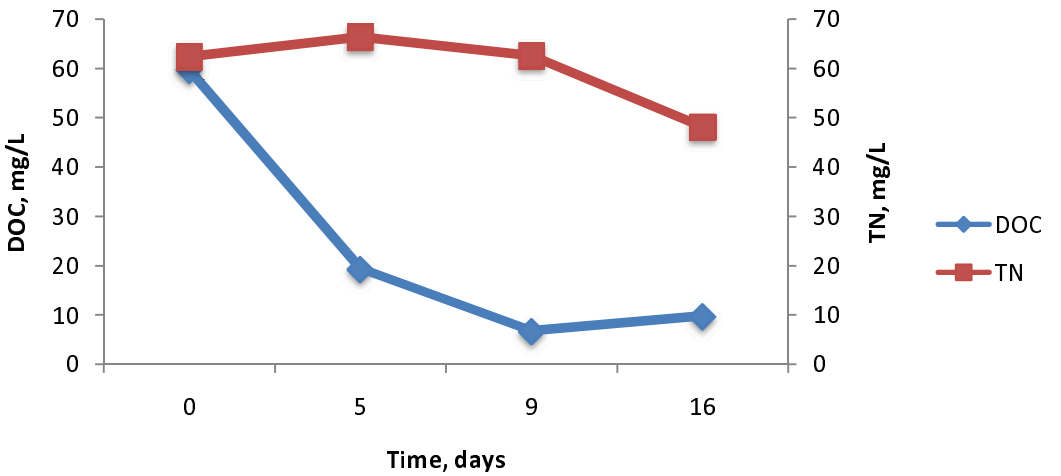

Figure 4: Aerobic Biodegradation Results

Percent reductions from initial DOC concentration during each sampling date are presented in Figure 5 below for both anaerobic and aerobic tests. As expected, substrates were degraded at a higher rate in an aerobic environment compared to an

anaerobic environment. However, it is anticipated that anaerobic tests most likely had some initial startup period due to residual oxygen present in the headspace of each assay. For this reason it can be expected anaerobic processes would degrade waste somewhat quicker in an acclimated reactor than what the results of these tests provide.

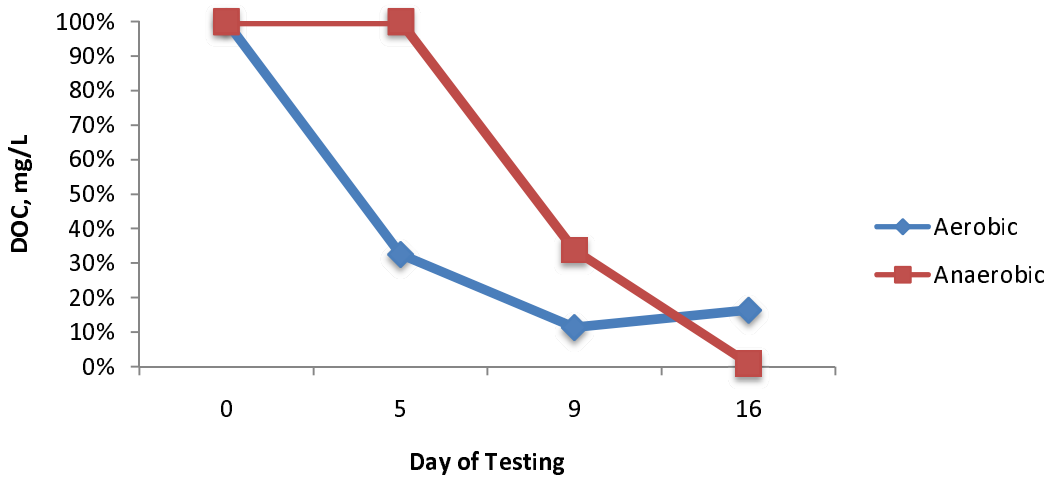

Figure 5: DOC Degradation during Experimentation

DECISION ANALYSIS TOOL

Decentralized treatment systems development clusters such as neighborhoods, business parks and small communities have potential to be more economically and environmentally favorable than routing these developments to centralized treatment systems. One major setback in current planning capacity is the absence of tools which provide technical and economical feasibility of DWWT by specific application to decision making entities. Access to such a tool would allow more effective comparison of DWWT with centralized treatment. One goal of the CSU blackwater demonstration project is development of a tool to facilitate wastewater infrastructure planning decisions.

Analysis for CSU Blackwater Demonstration Project

To facilitate decision making for the CSU blackwater demonstration project, basic economic analysis has been performed to provide a comparison between aerobic and anaerobic treatment processes. Table 2 provides examples of parameters used for comparison of processes. Currently all costs for treatment are lumped into one parameter, which represents the total cost for treatment processes including O&M, heating, aeration, lifetime capital and any other related costs. Valuable outputs include reusable water from both processes and biogas from anaerobic digestion.

Table 2: Example Economic Analysis Parameters

	Inputs	Unit	Value	Type	Description
Water	P^w	$/m^3	0.53	Input	Price of Water
	q^w_a	m^3/day	2500	Input	Quantity of Wastewater Treated Anaerobically
	q^w_b	m^3/day	2500	Input	Quantity of Wastewater Treated Aerobically
	Θ_a	%	97%	Calculated	Quantity of Water Produced Per unit of WW Treated Anaerobically
	Θ_b	%	89%	Calculated	Quantity of Water Produced Per unit of WW Treated Aerobically
	C^w_a	$/m^3	0.1	Calculated	Cost to Treat Water Anaerobically per Unit
	C^w_b	$/m^3	0.08	Calculated	Cost to Treat Water Aerobically per Unit
Energy	P^e	$/KWH	3.5	Input	Price of Energy
	Φ_a	KWH/$m^3	0.001	Calculated	Quantity of Energy Produced Per unit of WW Treated Anaerobically

These input parameters were analyzed under varying prices for water and energy to determine the breaking point at which either process became favorable. Analysis results showed that anaerobic digestion is far more economical mainly because biogas produced during treatment was valued at its ability to supplement natural gas usage BTU for BTU. The value of biogas produced in anaerobic treatment far outweighed the additional reusable water produced in aerobic treatment.

In addition to economical analysis of treatment alternatives, a criteria based decision making tool will be used to compare different treatment technologies for use in the demonstration project. Some of the criteria which processes will be compared based on include reliability, complexity of operations and maintenance, treatment quality, as well as resource extraction and reuse potential.

Future Improvements to Decision Analysis Tool

Eventually, economic feasibility modeling and criteria based technical applicability modeling will be combined into one tool to assist with wastewater planning. This tool will be tailored to provide insight into the feasibility of different types of treatment to treat wastewater on the CSU foothills campus.

The purpose of this tool is to provide a useful comparison of treatment options, including process selection, treatment area sizing and reuse scenarios such that reliable decisions can be made for application of the most suitable wastewater treatment system for specific sites. Additional parameters for comparison include: wastewater flow, wastewater quality, wastewater source, available sources of heat and energy, maximum footprint, operation and maintenance capacity, and regional development density.

CONCLUSIONS

Decentralized wastewater treatment provides an opportunity for cost effective advanced treatment in small communities and rural areas where centralized treatment is not feasible. Traditionally the majority of these communities have relied on septic systems. These septic systems are often in serious disrepair or not operated properly, contributing greatly to degradation of local ground and surface water quality.

Decentralized wastewater treatment systems have potential to offer many benefits and costs as compared to centralized systems. However, typically these systems have to be compared on a case by case basis to effectively determine which is more feasible for specific applications. Facilitated planning, potential for local reuse of valuable constituents of wastewater, prospect for graywater reuse, and ability to feasibly focus on a specific pollution type (e.g. household, industrial, or blackwater, graywater) allows for more efficient treatment.

Studies are underway at Colorado State University to show the effectiveness and applicability of DWWT technologies. The current blackwater demonstration project on the CSU Foothills Campus will provide a continuously operating DWWT process providing treatment quality data. Insight into the quantity and quality of nutrients and effluent water as well as biogas available for reuse within the Foothills Campus will also be made available. The availability of such data will allow improvements to be made to legislation and public perception of water reuse and land application of treated effluents for non-consumptive purposes e.g. landscape irrigation.

In addition to technical data, development of a decision analysis tool will assist decision making entities in providing the best treatment options to their service areas. Because DWWT systems are not largely implemented in full-scale treatment operations, it is necessary to provide decision makers with a tool to effectively compare the applicability of DWWT systems to the expansion or construction of centralized systems.

REFERENCES

APHA, AWWA, WEF (1998). Standard Methods for The Examination of Water and Wastewater. Washington, DC, American Public Health Association (APHA), American Water Works Association (AWWA), Water Environment Federation (WEF).

Luostarinen, S. A. and Rintala, J. A. (2005). "Anaerobic On-site Treatment of Blackwater and Dairy Parlour Wastewater in UASB-Septic Tanks at Low Temperatures." Water Research **39**(2-3): 436-448.

Owen, W. F. and Stuckey D. C., et al. (1979). "Bioassay for Monitoring Biochemical Methane Potential and Anaerobic Toxicity." Water Research **13**(6): 485-492.

Palmquist, H. and Hanæus, J. (2005). "Hazardous Substances in Separately Collected Grey- and Blackwater from Ordinary Swedish Households." Science of the Total Environment 348: 151-163.

RNL Design (2003). Colorado State University - Foothills Research Campus Master Plan.

Tchobanoglous, G., Burton F. L. and Stensel, D. H. (2003). Wastewater Engineering Treatment, Disposal, and Reuse. 4th Edition. New York, McGraw-Hill, Inc.

US EPA. (2009). "Septic (Onsite) Systems." Retrieved January 25, 2009, 2009, from http://cfpub.epa.gov/owm/septic/index.cfm.

Development of a National GIS Database for Municipal Water and Wastewater Pipe Infrastructure System

Sunil Sinha[1], Randy Dymond[2], Rahul Vemulapally[3], Thomas Dickerson[4], Seth Perry[5]

ABSTRACT

The problems posed by aging infrastructure are receiving increased attention in the United States, thanks to critical reports by the American Society of Civil Engineers, and in some cases, due to public outcry in the wake of infrastructure failures. The U.S. Environmental Protection Agency (EPA) has a special interest in the operations and management of public drinking water and sanitary sewer systems. Infrastructure utilities are facing increasing pressure to implement advanced asset management plans in order to improve the efficiency with which their systems are operated and maintained. As a result, most utility operators are actively working to develop GIS mapping and databases of their pipe networks. However, there is no standard data model for water or sewer systems, thus each utility has developed its own method for storing data; this has created complex problems associated with multi-jurisdictional planning activities, research, and oversight.

The U.S. EPA, through the Buried Asset Management Institute – International, funded Virginia Tech researchers to investigate municipal water and sewer infrastructure databases, with an emphasis on the condition assessment aspect of asset management. A partnership of at least 17 major U.S. cities expressed an interest in advancing this research, and five municipal utility operators donated sewer and/or water infrastructure GIS data for this pilot project. First, researchers worked to define those data elements required for condition assessment of buried assets. With these data elements defined, the researchers developed a standardized data model to organize the previously identified data elements. This data model was tested against the real-world municipal utility datasets, documenting the methods and issues associated with transforming the disparate datasets to conform to the data model. Finally, data from multiple utility operators was loaded into a common, secured enterprise-class, web-accessible geo-database to demonstrate the future potential for cross-utility planning and analysis. The results of this investigation illustrated the challenges inherent in any effort to conflate disparate municipal utility datasets into a common data model, and demonstrated the scarcity of data relevant to water and sewer infrastructure condition assessment. By incorporating additional attributes related to condition assessment in publicly-promoted data models, municipal utilities will be better able to manage their infrastructure internally, and share their utility data with neighbors, researchers, and regulators.

[1,2] Associate Professor, Department of Civil and Environmental Engineering, Virginia Tech, Room No.121, Patton Hall, Blacksburg, VA 24061,
Phone: 540-2431-9420; Fax: 540-231-7532; e-mail: ssinha@vt.edu
[3,4,5]Research Assistant, Department of Civil and Environmental Engineering, Virginia Tech, Room No.118C, Patton Hall, Blacksburg, 24061.

INTRODUCTION

This paper presents a research project to create Center of Excellence for Municipal Asset Management (CEMAM), is a collaboration between the Buried Asset Management Institute – International (BAMI-I), participating municipal utilities, and researchers at academic institutions. The Virginia Tech team's research on this project includes defining data elements required for condition assessment of buried assets, and developing a standardized data structure to serve as a common foundation for future analysis and research. In addition to researching current literature, much of this work relies on relationships with participating utilities who have agreed to provide geospatial and asset management data to the researchers. After establishing standards for asset management data, Virginia Tech examined the implications of the standards on municipal utility programs, and created an example database that conflates the varied municipal data into a common data framework. Development and testing of related technologies, such as a web-based mapping application, is also pursued as appropriate. In summary, the utility data is collected, analyzed and transformed into the common data framework. The data has been collected from a majority of the participating utilities who agreed to provide data. The Virginia Tech team analyzed this data, by comparing the structure and content of the utilities' data to a desired list of attributes, to each of the other utilities. This center of Excellence will reap the following benefits:

- Will help in creating linkage to all utilities across the nation irrespective of utility size
- provide timely access to asset management information and resources that will lead to more efficient programs
- promote and provide training, education, research, and outreach programs
- provided the public with a convenient tool to learn about municipal water and wastewater infrastructure system
- develop a National database that will help in developing tools, techniques, models (Prediction and optimal performance) for data analysis

The initial work in this project consisted of forming relationships with municipal utilities and reviewing literature related to the development of a standard database model. This review of literature addresses current and proposed research related to the development of sanitary sewer database models, computer applications, and infrastructure management practices in other localities, states, and countries.

Autodesk Homeland Security Initiative Data Model

The Autodesk Homeland Security (HLS) Data Model is a collection of several individual data models that share the stated objective of supporting homeland security and promoting interoperability. The data models are intended to serve as the core of day-to-day utility management, although most users will need to extend the proposed data models with additional data relevant for utility management applications.

Atlanta Track – Paper Three: Clean Water Atlanta Enterprise GIS

The city's new management system uses an enterprise GIS with web-based user interface applications. The system is built on an Oracle database, with ESRI's ArcSDE providing a geographic interface to the database.

IBM Maximo Asset Management Software

At its core, Maximo is a database-driven application focused on tracking assets throughout their lifecycle, including the tracking of contracts and inventories, work order generation and tracking, and maintenance operations and planning. The system is generally installed on a central server, with editing of data distributed to a number of individuals through a web interface. Systems such as Maximo are intended to be implemented at the enterprise level, and provide structure and standardization for asset management record-keeping. Recently, Maximo has expanded into the geospatial sector by integrating their asset management system with the ESRI ArcGIS Server system. Termed "Maximo Spatial Asset Management," this system adds spatial context to the Maximo asset management system.

Shamsi: GIS Tools for Water, Wastewater, and Storm water Systems

U.M. Shamsi's book, GIS Tools for Water, Wastewater, and Storm water Systems, neatly condenses the concepts necessary for a civil engineer to begin implementing a GIS system to manage water, sewer, and/or storm water assets. In general, infrastructure data is divided into two categories: assets data and applications data. Assets data describe the composition, geometry, and physical properties of the infrastructure. Assets data is typically the core of the GIS data model. Applications data is that which extends the assets database into fields such as maintenance operations, business and accounting, planning, and modeling.

PROPOSED PIPE DATA PARAMETERS

In the recent months at Virginia Tech, about 100 parameters which may affect the pipe infrastructure have been identified each for the wastewater and water systems. This project is funded by Water Environmental Research Foundation (WERF) under SAM challenge program. The goal is to eventually create a national standard data model for the pipe infrastructure. This national standard data model was developed to aid the decision making process in asset management program. The data model can be used in developing of condition index, prediction model, prioritizing repair and rehabilitation, prioritizing inspection, planning operation and maintenance, developing capital improvement program and making high level decision etc. The parameters which may affect the pipe performance were divided into five classes based on their characteristics: Physical/Structural, Operational/Functional, Environmental, Financial, and Others. These classes are presented in Figure 1.

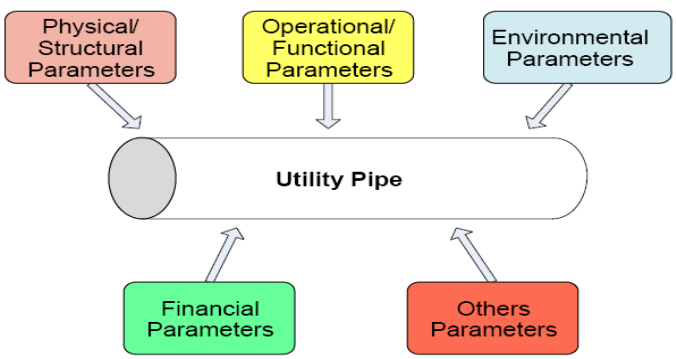

Figure 1: Parameter classes that effect pipe performance

The physical parameters include pipe related attributes like age, thickness, length, diameter etc while operational include general operational attributes of the utility such as capacity, connection density, population, sewershed and more . Attributes classified as environmental include soil parameters, climate, loads etc. Financial parameters are more into costs of operations, maintenance and some related attributes.

DATA MODELS

In this study, the research team has considered data from major cities as well as smaller towns within the U.S. The data model was broken into four separate models: **Wood, Bronze, Silver, and Gold**. Also, due to the utilities lack of readily available number of parameters, the wastewater pipe data model was broken into essential and preferable/desirable data.

The wood data model is for utilities which are very small and do not have resources to collect enough data. This model represents most important 6 essential and 5 preferable parameters for a wastewater pipe based on the research teams' knowledge of pipe infrastructure. The bronze data model is for utilities which are small and do not have a lot of man-hours due to a smaller workforce. This model represents most important 11 essential and 12 preferable parameters for a wastewater pipe. The silver data model is for utilities which are larger than bronze utilities; however, still may not have a special team designed to devote all their time to developing wastewater pipe data parameters within a system. This model represents most important 23 essential and 28 preferable parameters for a wastewater pipe. The gold data model is for the utilities which represent some of the largest cities within the U.S. and have a special team devoted to the continuation of updates to the wastewater data parameters. This model entails all 51 essential and 47 preferable parameters which affect the wastewater pipe.

GEOSPATIAL DATA STORAGE

After receiving the Utilities' GIS and tabular data, the Virginia Tech researchers are storing it at the San Diego Supercomputing facility, using an ArcSDE connection to Oracle tablespace at San Diego. The ArcSDE connection is being hosted by Virginia Tech's E-Corridors program. Once loaded through ArcSDE, the geospatial and tabular data may be viewed directly in GIS software (with appropriate access permissions). The access permissions have been given to Virginia Tech research people only as of now. The data from Seattle has been uploaded as a test trial to check for efficiency and speed of transfer. This trial proved to be a good test, with tabular data of around 30,000 pipes transferring in 2 hrs. Once the data is uploaded to the server, subsequent retrieval and viewing is very quick, almost as though it were hosted locally. The proposed effective structure to store data is to create a feature dataset for each city on its name and then create individual feature classes for manholes, pipelines etc in each dataset. The main advantage of this structure is that the data from each city is stored separately and can be retrieved also in a similar fashion. The illustration in Figure 2 gives a better understanding of the structured storage. The table names (manholes, pipelines, laterals, hydrants, valves etc) may change accordingly to the final proposed data model.

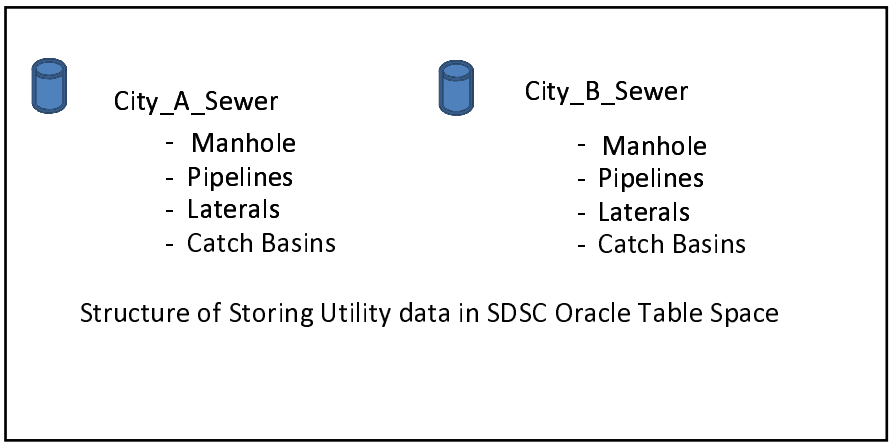

Figure 2: Storage of Utility Data in Standard Format

The data received from utilities would be reviewed and initial analysis would be done to familiarize with their fields and attributes. This data will be then loaded to the standard data model template, this would further be transferred to SDSC oracle table space. The schematic in Figure 3 gives a better understanding of the data transfer.

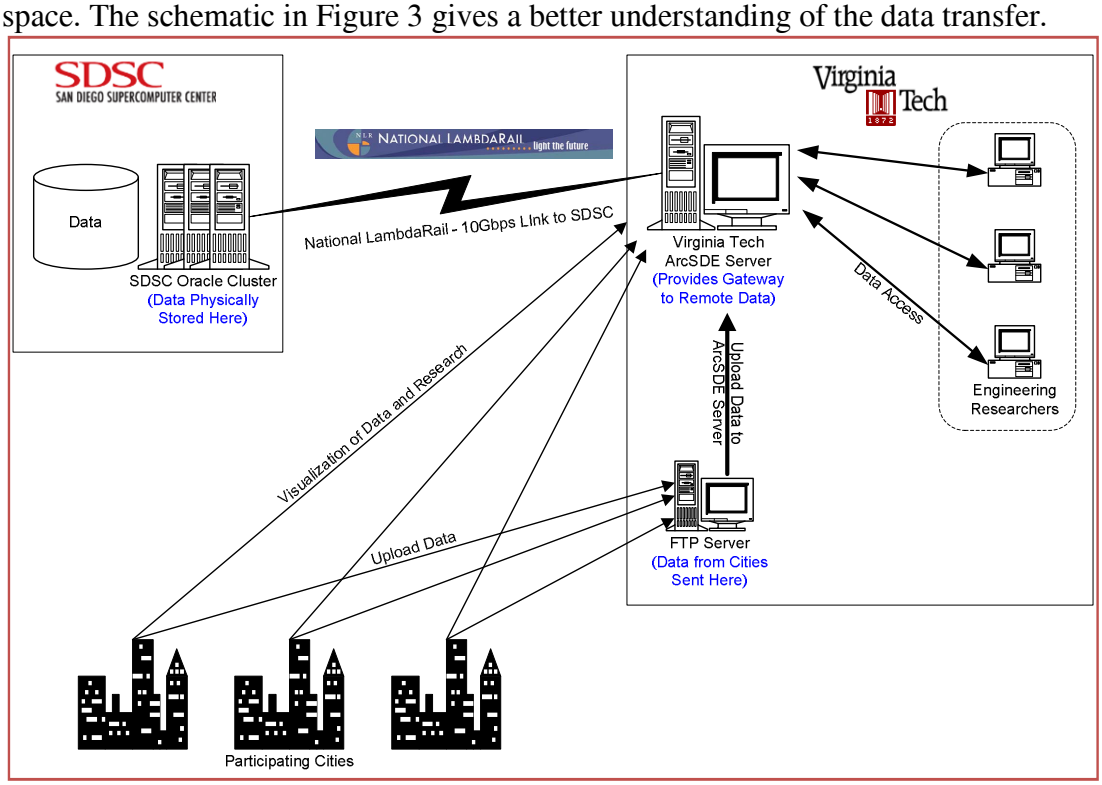

Figure 3: Data Transfer, Analysis, and Visualization Protocol

Virginia Tech team will construct an example geospatial database of aggregated wastewater pipe infrastructure data. As illustrated in Figure 4, a common data framework to support condition assessment have been defined and populated by conflating disparate datasets from several partner utilities.

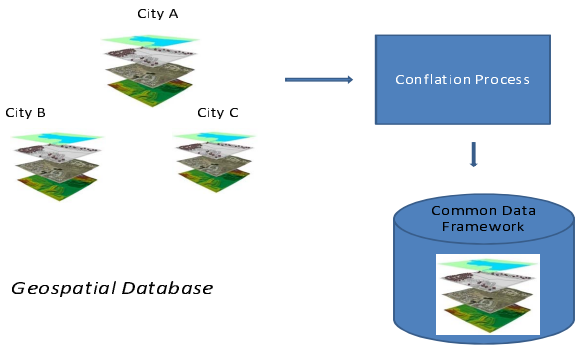

Figure 4: Conflation Process between Multiple Utilities

Existing Geo-Database - A Priori Data

There are several existing geo-databases relevant to pipe infrastructure which are available online or published. Some of these features included soil, geology, land cover, river, forcing, DEM, and stream flow. These geo-databases will help the research team in comparing the data provided from the utilities as well as filling in missing data parameters of the utility databases. For example, if the utility does not know the soil type within the area, the utility or the research team can visit online to the CONUS, Soil Survey Geographic (SSURGO) Database, or State Soil Geographic (STATSGO) Database websites to determine the type of soil. A sample of existing geo-databases relevant to pipe infrastructure can be seen in Figure 5.

GeoDataBase – A Priori Data

Feature	Property	Source
Soil	Porosity; Sand, Silt, Clay Fractions; Bulk Density	CONUS, SSURGO and STATSGO http://www.soilinfo.psu.edu/index.cgi?soil_data&conus http://datagateway.nrcs.usda.gov/NextPage.asp http://www.ncgc.nrcs.usda.gov/products/datasets/statsgo/
Geology	Bed Rock Depth; Kx/Kz	http://www.dcnr.state.pa.us/topogeo/, http://www.lias.psu.edu/emsl/guides/X.html
Land Cover	LAI	http://glcf.umiacs.umd.edu/data/landcover/data.shtml, http://ldas.gsfc.nasa.gov/LDAS8th/MAPPED.VEG/LDASmapveg.shtml;
	Manning's Roughtness	Hernandez et. al., 2000
River	Topology:	Derived using pihmGIS (Kumar et. al., 2007a)
	Manning's Roughness;	Dingman (2002)
	Coefficient of Discharge	ModHms Manual
	Shape and Dimensions;	Derived from regression using depth, width and discharge data from http://nwis.waterdata.usgs.gov/usa/nwis/measurements
Forcing	Precip Temp	Gauge data from MARFC. 6 hourly point data was spatially gridded conforming to the monthly precipitation distribution obtained from parameter-elevation regressions on independent slopes model (PRISM) (Daly et. al., 1994, 1997)
DEM		http://seamless.usgs.gov/
Streamflow		http://nwis.waterdata.usgs.gov/nwis/sw

Figure 5: Existing Geo-database

Security and Confidentiality of Participating Utilities Database

Utility Wastewater Infrastructure Data/Information is fully protected by MOU and at multiple points in our Cyber-Infrastructure System, as described in the following steps below.

1. Data is initially uploaded to the secure FTP server web.cgit.vt.edu
    a. Only the participating cities are provided with login credentials.
    b. The data only resides on this server as a staging area, until it can be uploaded to its permanent storage location, after which time it is deleted from the FTP server.

2. The data permanently resides on an Oracle Real Applications Clusters server at the San Diego Supercomputing Center.
    a. The data is owned by a single Oracle schema, and the only other user accounts that exist in this database instance are assigned to approved researchers at Virginia Tech.
    b. The owners of these accounts must request access to each individual GIS feature layer they need.
    c. Access is only granted on a "need to know" basis, and no user receives anything but read-only permissions.
    d. All IP addresses are blocked at the firewall at SDSC, with one exception: the ArcSDE middleware server we use as a gateway to access the data from ArcGIS.

3. The ArcSDE server functions as our gateway to the data.
    a. ArcSDE adheres to Oracle's authentication and authorization controls; any access that is prohibited in the database itself is likewise prohibited in ArcSDE.
    b. All IP addresses are blocked at the firewall on the ArcSDE server, with the exception of valid Virginia Tech IP addresses.

4. The Fiber-Optic Communication Link between VT & SDSC.
    a. The fiber-optic communications link between Virginia Tech and the San Diego Supercomputing Center is a dedicated point-to-point pathway.
    b. It is NOT part of the public Internet; rather, it is a link in the National Lambda Rail research network that is only used by major universities and institutions.

5. San Diego Super Computer Center.
    a. The primary goal of computer and network security activities at the San Diego Supercomputer Center is to protect the confidentiality, integrity, and availability of computing resources. As an Organized Research Unit at UCSD, SDSC Security Policies are consistent with UC and UCSD policies. The SDSC Security Manager and authorized designees have the authority to take actions necessary to prevent, detect, and respond to security policy violations involving SDSC

computing resources. These actions will be consistent with SDSC, UCSD, and UC policies, and applicable laws.

b. The Data Intensive Computing Environments (DICE) group at the San Diego Supercomputer Center (SDSC) has implemented software to make use of a variety of authentication/data-security systems in the SDSC Storage Resource Broker (SRB) and other distributed applications. These include the SSL(X.509 Certificate)-based Grid Security Infrastructure (GSI) developed by Globus with assistance from NCSA and others , Kerberos, DCE Security, and SDSC Encryption/Authentication system (SEA).

DATA QUERY & VISUALIZATION

A prototype web application has been developed to demonstrate how this aggregated data in the example geospatial database can be published, queried, and visualized in a map-based browser application (Figure 6). The application will deliver rich, interactive maps, data exploration tools.

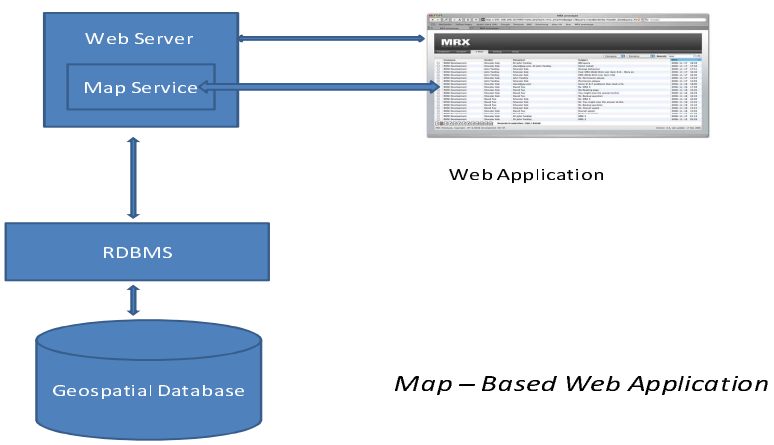

Figure 6: Map Based Web Application and Supporting Components

Data Visualization is one another important aspect which helps in making decisions for the utility officials. The main goal of data visualization is its ability to visualize data, communicating information clearly and effectively. Arc GIS can be very efficiently used to over lay shapefiles corresponding to soil, roads, land cover, elevation and many other types of data which are available in open source or collected by the utilities. The illustration in Figure 7 gives a better idea of data visualization system for City of Blacksburg, Virginia.

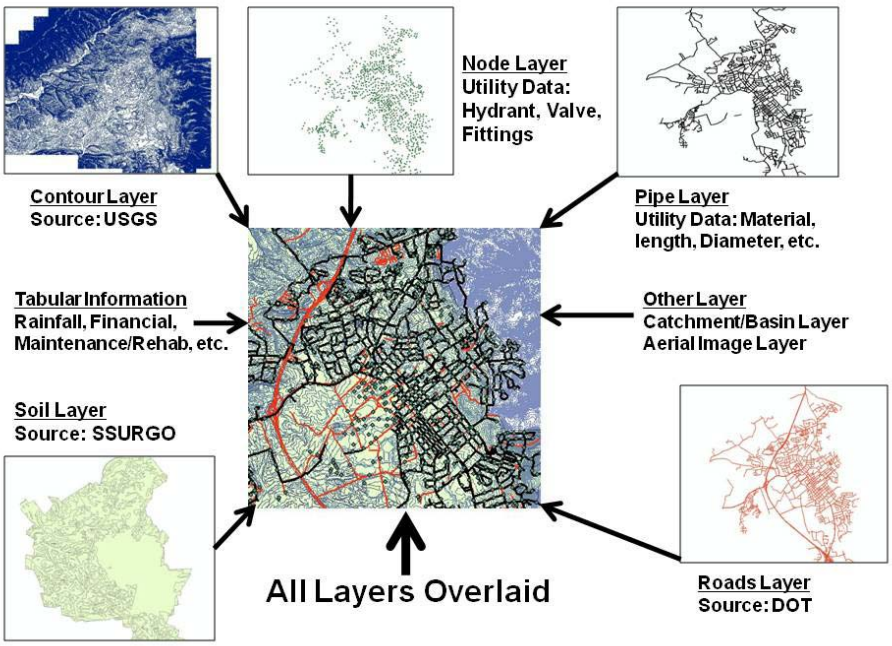

CONCLUSIONS

The existence of this data model can act as a standard database storage model for various utilities. Also, organized storage of data can be very crucial to take high level decisions for a utility. These models with stored data (with acceptable accuracy) can generate reports which can be vital for taking strategic level decisions. This can be a very useful tool for any utility (small, medium, and/or big) in managing their pipes strategically and cost effectively.

FUTURE WORK

With the existence of a standard database with utilities data stored, condition index of a pipe or predictive index of pipe condition can be developed. Also, dynamic data querying and extraction of data can be done with restricted privileges depending on the level of importance of data. Web applications can be developed to demonstrate such querying and map based visualization techniques. Alternatively, some of the pipeline data can be converted to KML file format and can be imported to Google Earth for an ultimate 3D visualization experience of the buried pipes.

The future of these geo-databases will ultimately lead to a realistic three dimensional (3-D) models and simulation, which can demonstrate the pipe infrastructure and its surroundings at the watershed scale. Presently, only air and water quality 3-D models are available for simulation at the watershed scale. Since a pipe database does not exist, this pipe infrastructure cannot be modeled and simulated. Once the pipe infrastructure database is created a simulated 3-D pipe infrastructure model can be produced. These models will benefit the utilities in simulating their actual environment and wastewater pipes.

ACKNOWLEDGEMENT
The authors would like to acknowledge various utilities across the country for their valuable comments and feedback related to this research project.

REFERENCES

Shamsi, U.M. (2002). "GIS Tools for Water, Wastewater, and Stormwater Systems." Reston, Virginia: American Society of Civil Engineers (ASCE) Press.
"Autodesk Homeland Security Initiative: Storm and Sanitary System Data Model." Autodesk, Inc., May 2004.

Ross & Associates Environmental Consulting, Ltd., "Managing for Excellence: Analysis of Water and Wastewater utility Management Systems,"EP-W-04-023, The United States Environmental Protection Agency (USEPA), August 2005.

Brown and Caldwell, "Seattle Public Utilities 2006 Wastewater Systems Plan," March 2006

Pittsburgh Water and Sewer Authority (PWSA), "Monitoring & Sampling Plan", PWSA CSO Long-Term Control Plan Development Project, https://courses.worldcampus.psu.edu/public /buried_assets/resources/pittsburgh.pdf.

More information on FME and related products is available at: http://www.safe.com

Engineering Natural Filtration Systems to Remove Selenium, Nitrate, and Bacteria from Impaired Surface Waters – Foundational Studies

Ken Susilo[1], PE, CPSWQ, Eric Strecker[2], PE, Randy Sundberg[3], PE,

[1]Geosyntec Consultants, 2566 Overland Ave., Suite 670, Los Angeles, CA 90064; PH (310) 839-6040; FAX (310) 839-6041; email: ksusilo@geosyntec.com
[2]Geosyntec Consultants, 55 SW Yamhill St., Suite 200, Portland, OR 97204; PH (503) 222-9518; FAX (503) 242-1416; email: estrecker@geosyntec.com
[3]Irvine Ranch Water District, 15600 Sand Canyon Ave., Irvine, CA 92618; PH (949) 453-5300; email: sundberg@irwd.com

ABSTRACT

Selenium is among the pollutants of concern in a growing number of areas within California. TMDLs proposed by USEPA (USEPA, 2002) for the San Diego Creek watershed in Orange County, California (and in Ballona Creek and Los Angeles River in Los Angeles County) calls for an in-stream standard of 5 ppb total selenium. Selenium sources and treatment methods, however, are significantly different than those typically utilized as stormwater BMPs for metals such as copper, lead and zinc.

Studies on the sources of selenium in the San Diego Creek Watershed indicated that a major potential source is groundwater seepage, particularly in areas where the groundwater table is shallow. Thus dry-weather concentrations and loads are of the most interest. Within the San Diego Creek Watershed, flows appear to correspond to a location where historically, naturally occurring selenium became sequestered under anaerobic conditions in the peat soils within a swamp. Urbanization and draining of the swamp appears to have created aerobic conditions, releasing selenium from these sediments into groundwater in a soluble phase. Selenium concentrations in the surface water discharge have been observed in the 50 ppb range, and local groundwater selenium concentrations commonly exceed 100 ppb.

Several technologies potentially reduce selenium (Se) concentrations to low levels (<10 ug/L). Many of these technologies involve physical, chemical, and biological processes developed as part of the wastewater, agricultural and mining industries. Siting, sizing, and engineering constraints related to the volumes of water potentially requiring treatment, however, limit the applications of many of these technologies for storm water.

Foundational studies supporting IRWD's Cienega Filtration Demonstration Project supported a program to proactively reduce dry-weather Selenium loads in the San Diego Creek Watershed. The technology is an engineered and controlled system intended to mimic subsbsurface wetland processes that were in existence prior to urbanization. This effort included batch laboratory testing and mesocosm-scale tests, which confirmed the efficacy of the technology given conditions requiring treatment of significant flows. Pre-design optimization studies and a field demonstration have

an ultimate objective of developing a permanent, maintainable, and fully operative, subsurface treatment system that utilizes natural reduction processes to sequester and remove selenium from the creeks. Results from these studies provide engineers valuable design and process guidelines that should be considered before similar types of facilities are contemplated.

BACKGROUND: LOCAL AND SCIENTIFIC CHALLENGES

The focus of this paper is work done in the San Diego Creek Watershed. Selenium concentrations in the main stem of San Diego Creek as well as its tributaries have routinely been detected at levels well above the EPA's chronic criteria of 5 µg/L for surface waters. The US Fish and Wildlife service has suggested a TMDL of 2 µg/L should be adopted to ensure the protection of aquatic species and wildlife (RWQCB, 2001), as it is believed that concentrations as low as 3 µg/L may lead to detrimental bioaccumulation in some waterfowl and shorebirds.

Hibbs and Lee (2000) indicated that the selenium source is the historic "Swamp of the Frogs" and groundwater seeps distributed throughout the watershed. Selenium-laden sediments in the Swamp release soluble selenium (primarily in the form of selenate) as the historically anoxic soils oxygenate due to draining of the Swamp, applied irrigation waters and seasonal fluctuation of the groundwater table.

Many historical applications for selenium treatment originate from the wastewater, agricultural and mining industries. A review of selenium removal technologies that highlights potentially successful treatment mechanisms but also potential limitations with respect to storm water and urban runoff treatment – most notably the need for extened residence times. In the aforementioned San Diego Creek Watershed, it was desired focus on summer and winter dry- weather flows that have a groundwater origin. The highest selenium concentrations in the watershed are found in dry-weather flows that originate from a major tributary is on the order of 4 cubic feet per second. Preliminary results of this study indicate a treatment residence time as short as one-day can provide the desired level of treatment (below 5 ppb). Even at this low residence time, approximate land requirements to provide treatment of these flows are on the order of about 3.5 acres. Lastly, long term, sustainable hydraulic conductivity of treatment systems must be maintainable for the aforementioned flow rates. The following summary is presented in more detail in Susilo et.al (2005).

Selenium treatment objectives. Frankenberger (1999) noted that treatment for removal of selenium in subsurface agricultural drainage water has several regulatory considerations, that include (a) reducing constituents below hazardous levels (1000 µg/l), (b) meeting agricultural water quality goals, (c) meet water quality objectives in surface waters (5 µg/l), and (d) reduce constituents below the lowest risk levels for wildlife (2 µg/l). Most of the treatment approaches he described did not have selenium removal data. Of those that did provide data removal rates or treated effluent quality, percentage removals were high. Most systems, however, could not meet the latter two effluent target levels. (For example, Algal-Bacterial Selenium Removal systems and the recommended biological precipitation methods had effluent

concentrations of approximately 30 µg/l). In addition, agricultural influent selenium concentrations were generally significantly higher than the San Diego Creek concentrations (Kovac, 2005). Recent studies of low cost methods of treatment (Scheidlinger, 2005) confirm the ability to treat significant percentages of influent with high selenium concentrations, but these methods still do not meet water quality objectives for the effluent. These methods include the utilization of bio-barriers and straw-filled conveyance facilities.

Selenium speciation. In natural waters, selenium can exist in four primary oxidation states and as a variety of different inorganic and organic compounds. Inorganic selenium can exist as selenide, Se(-II); elemental selenium, Se(0); selenite, Se(IV); and selenate, Se(VI). Organic selenium species include selenoamino acids, seleno-amino acid derivatives, methyl selenides, methyl selenic esters, methyl selenones, and methylselenonium ions.

The volatile methyl selenide, dimethyl selenide (DMSe), is the product of selenium biomethylation; a natural process that detoxifies and removes inorganic selenium from soil/water environment. Selenate is the most soluble and, therefore the most mobile form of selenium in the aquatic environment. Selenite is less soluble than selenate and will often exist as a sorbed ion. Toxicity studies conducted by Yu et. al. (1997) found selenite to be the most toxic form of inorganic selenium in the aquatic environment. The oxidation of selenite to selenate is believed to be a slow process, so selenite is still common in oxygenated waters (Cooke and Bruland, 2000). Reduction of selenate to selenite is also a slow process and occurs within the nitrate-reducing zone of wetland soils, characterized by sub-oxic conditions having a redox potential of approximately +200 to +300 mV (Masscheleyn and Patrick, 1993).

Selenite has been reported to be reduced to elemental selenium and/or selenide species at a redox potential of 0 to -50 mV, which is well below normally oxidized surface soil conditions (+500 mV). Furthermore, the same species of bacteria that reduce nitrate also reduce selenium. Nitrate, however, is consumed preferentially so selenium reduction generally requires greater residence time than nitrate reduction (Reinsel and Botz, 1999). Under anoxic conditions, the dominant forms of selenium are elemental selenium and insoluble metal selenides (Cooke and Bruland, 1987). A selenium speciation study conducted at the Kesterson Reservoir in Merced County, California by Weres et. al. (1989) found that, in permanently wet areas, the highest selenium concentrations were found in the top organic/peat layers of the wetland soils, indicating that selenium would be reduced and immobilized in anoxic soils.

Methylation and volatilization. Selenium removal through volatilization received attention after high levels led to waterfowl deformities in the Kesterson Reservoir in Merced County, California during the 1980's. Several studies have been conducted to determine the optimal plant species and conditions to remove selenium from the soil and water through biomethylated volatilization (Zhang and Moore, 1997; Allen, 1991; Hansen et. al., 1998; Azaizeh et. al., 1997; Thompson-Eagle and Frankenberger, 1990a and 1990b; Frankenberger et. al., 1999; Zayed and Terry, 1994; Bañuelos et. al., 1997; Pilon-Smits et. al., 1999; Stork et. al., 1999).

Selenium volatilization through methylation is a biogeochemical process responsible for detoxifying and removing selenium from aquatic environments. Microbial and phyto methylation convert organically bound selenium into volatile forms (i.e. dimethyselenide (DMSe) and dimethyldiselenide (DMDSe)). Inorganic selenium species (particularly selenate and selenite) need to first assimilate to organic selenium before methylation can occur (Zhang and Moore, 1997). This intermediate reduction pathway is not well understood, however dimethyl selenone has been proposed as the primary organic chemical involved (Yu et. al., 1997). There are many conditions that affect the rates of methylation including: pH, temperature, redox potential, microbial activity, soil moisture, and trace element addition (Stork et. al., 1999).

Flooding and drying also may affect rates of selenium volatilization. An experiment conducted by Zhang and Moore (1997) showed that the rate of selenium volatilization from selenium-laden soils increased by 1-2 times during drying as compared to flooding. The theory behind this observation is based on the high solubility of DMSe in water determined by Karlson et. al. (1994). Periodic dewatering of anaerobic or anoxic sediments promotes the atmospheric release of dissolved DMSe as well as the decomposition of solid organic materials and oxidation of selenium in surface sediments to forms that are readily converted to DMSe (Zhang and Moore, 1997).

Adsorption and phytoaccumulation. Phytoaccumulation is a method of selenium removal from water and soil that is often coupled with volatilization. Plant uptake of toxic chemicals can lead to bioaccumulation in higher trophic levels if the plants are a significant food source. Horne (2001) believes the winter accumulation of resident birds at the Kesterson reservoir was due to the high selenium concentration in the seeds of widgeon grass. If phytoaccumulation is to be used as a selenium removal strategy, the plants selected should not be a significant food source and the remediation area should be designed to not attract wildlife. Of twenty different wetland plants studied, Pilon-Smits et. al. found that *Typha latfolia* L. (cattail) and *Scripus acutus* Muhl. (hardstem bulrush) accumulated the greatest amount of selenate and selenite, respectively, per square area. However, the seeds of bulrushes are significant food sources of waterfowl and terrestrial birds (NRCS, 2002). Cattail is not a primary food source for many wild animals, particularly most waterfowl.

The presence of trace elements may affect the rate of selenium uptake by plants. The chemical similarities between sulfur and selenium may promote competition for electron providers and therefore high sulfate concentrations can significantly reduce the rates of selenate reduction.

Sequestering selenium in the soils by promoting anoxic conditions is another method to remove toxic selenium from surface waters. Bacteria have been shown to reduce selenite to elemental selenium at a much faster rate under anoxic conditions than under oxic conditions (Kessi et. al., 1999). Significant selenate concentrations have been found in the soils of the anoxic waters of Drammenfjord, Norway, indicating that selenium is not always reduced under anoxic conditions (Abdullah et. al., 1995). However, the majority of the literature reviewed indicates that selenium will be

reduced to elemental selenium or metal selenides under oxygen deficient conditions.

Best demonstrated available technology. Ferric oxyhydroxide adsorption of selenium has been chosen as the EPA's Best Demonstrated Available Technology (BDAT) for the removal of selenium from wastewater, and shows the most potential (out of the other adsorption technologies). However, this method requires significant chemical additions and produces a highly concentrated sludge that must be dewatered and disposed of in a municipal landfill. Furthermore, adsorption processes are generally not very effective on selenate (Twidwell et al., 2000) and are designed for higher influent (wastewaterlevel) concentrations (MSE, 2001).

PRECEDENTS AND LIMITATIONS: SUCCESSFUL SELENIUM REMOVAL FIELDAPPLICATIONS

Chevron Richmond. A 36-ha constructed wetland was built at Chevron's oil refinery in Richmond, California to reduce selenium concentrations prior to discharging into the San Francisco Bay. A 16-week study conducted by Hansen et. al. (1998) showed that the wetland achieved significant selenium removal through volatilization, plant uptake and soil adsorption. Inlet selenium concentrations were consistently between 20 and 30 µg/L. Effluent concentrations were maintained below 5 µg/L. Flow rates varied between 1.2 and 4.1 cfs and the residency time over the entire wetland was 7-10 days. Therefore, while the treatment levels were adequate for meeting water quality goals for San Diego Creek, the required residence time exceeds engineering constraints for the urban runoff applications of interest as the residence time would require a land area 7 to 10 times larger than a 1 day residence time.

Corcoran-DWR, EPRI, UC Berkeley. A wetland study in Corcoran, California was initiated in 1996 on land donated by J. G. Boswell and Company (Warnert, 1998). Ten quarter-acre wetland cells were built to study selenium removal. With funding from the UC Salinity/Drainage Taskforce, the California Department of Water Resources and the Electric Power Research Institute, UC Berkeley plant biologist Norman Terry and his staff planted the cells with different combinations of wetland species to compare their effectiveness in reducing selenium. In the 1998 season, the average selenium concentration in the drainage water influent to the cells was 22 µg/L. With a 7-day residence time, selenium removal ranged from less than 30% in the unplanted cell and cells planted with cordgrass, salt grass, and a combination of bulrush and tule, to as much as 60% in the combination cell planted with cattail and widgeon grass. As with the Chevron example, the 7-day residence time makes direct application infeasible for large flows or in urban areas.

Stillwater Mine, Montana. Anoxic treatment of selenium at much higher concentrations was achieved at the Stillwater Mine in Montana. Hydrometrics, Inc. designed an Anoxic Biotreatment Cell (ABC) to treat nitrate, selenium, and perchlorate in the mining effluent discharge. The ABC is a "semi-passive" bioreactor, which utilizes pressurized flow and nutrient addition (Reinsel, 1999). Influent selenium concentrations to the ABC were between 1.2 and 0.30 mg/L (e.g.,

300 to 1200 ppb). These concentrations were reduced to 0.03-0.2 mg/L (30 to 200 ppb) prior to discharge. Flow rates varied between 0.2 and 1.0 cfs and the residency time in the reactor was 6-24 hours. No studies were found where the ABC was used to remove low selenium concentration from water, however the proprietors of the technology (Hydrometrics, Inc.) claim that the ABC can be designed for a variety of flow rates and concentrations. However, increased residence time and additional amendments would likely be necessary. For this example application, the effluent concentrations would not satisfy the San Diego Creek regulatory requirements.

Garfield Wetlands Kessler Springs, Utah. The EPA's Mine Waste Technology Program tested three technologies for the Kennecott Utah Copper Corporation's Garfield Wetlands Kessler Springs site. These three technologies were: 1) ferrihydrite adsorption (wastewater BDAT), 2) catalyzed cementation process, 3) and proprietary biologicial selenium reduction processes. For these studies the target effluent concentration was 50 ug/l, however, the proprietary biological system was able to reduce effluent concentrations to near detection limits for significant flow rates (300 gpm) with residence times less than 24 hours (MSE 2001).

IRWD Wetland Mesocosm Pilot Study, Irvine, California. This study was conducted by Geosyntec Consultants for the Irvine Ranch Water District in two phases. Phase one was a bench-scale study in which several media were examined for their potential effectiveness at reducing selenium from the source water using static column tests. Phase two of the study was a mesocosm-scale study that examined how well the selected media performed under dynamic conditions similar to what would be expected in a full-scale subsurface wetland like environment. The purpose of the mesocosm experiment was to estimate reduction rate, effluent quality, and effectiveness of the media at reducing selenium, as well as establish the design parameters for constructing a full-scale wetland. Study results indicated that subsurface treatment wetlands can achieve selenium reductions to water quality standards (5 ppb) with residence times of approximately 3 days or less. A full-scale project in the San Diego Creek watershed constructed with a similar soil depth and hydraulic characteristics, would require approximately 20 acres to treat a design flow of about 5 cfs, however additional testing for engineering parameters was required (GeoSyntec, 2003).

IRVINE RANCH WATER DISTRICT'S CIENEGA FILTRATION PROJECT

The Irvine Ranch Water District completed Pre-Design Optimization Studies (PDOS) and constructed a Field Demonstration to test and develop the next generation of selenium treatment best management practices. The project, named the *Cienega Filtration Project* was developed to recreate natural treatment processes found in the historic Swamp of the Frogs which naturally sequestered soluble selenium in native soils, removing it from the water column.

The underlying concept for these activities is that optimizing of bacteria populations, electron donors, and residence times will create anoxic, reducing conditions to reduce soluble selenium to its particulate form, so that it is removed from the water column

to be collected and disposed of. It is also recognized, however, that redox potential, as shown below in Figure 1, should not drop below -200 mV as below this level there is the potential for selenium gas formation.

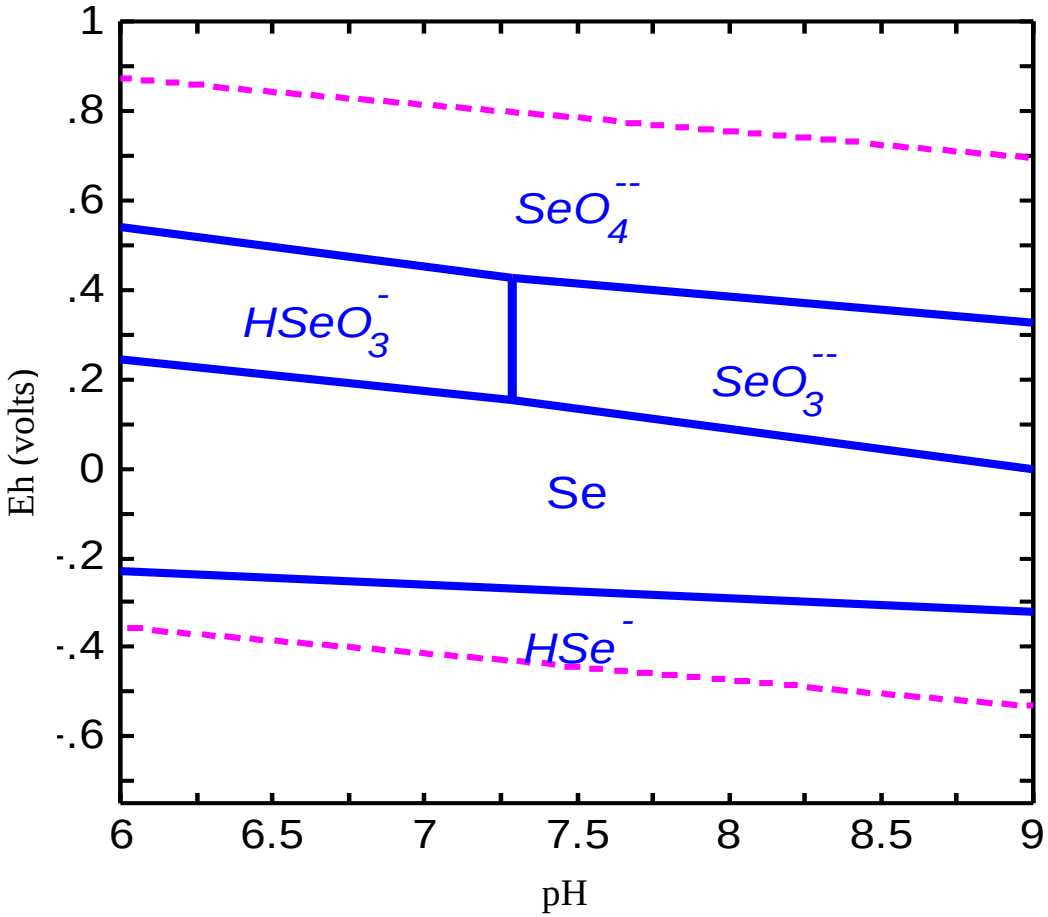

Figure 1. Optimal redox conditions for removal of soluble selenium.

PDOS Test apparatus. Seven continuous flow columns were designed to test the effectiveness and sensitivity to various levels of inoculation, electron donor, media matrix as part of the PDOS. Inoculation was tested by adding: a) native mud extracted from the source creek and b) chopped and mixed cattails. Electon donors included food grade citric acid and sodium benzoate at up to 2.5 times stoichometric-required levels. Media matrix materials included sand, 3/8" crushed rock, and ¾" crushed rock. A schematic of the testing apparatus is shown below in Figure 2.

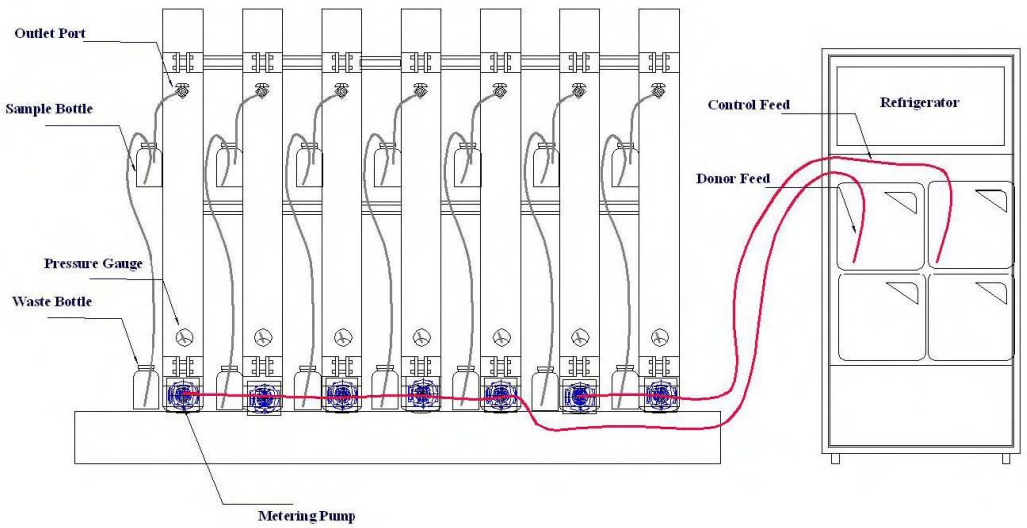

Figure 2. Pre-Design Optimization Study Apparatus.

CONCLUSIONS

At the conclusion of the PDOS, a number of preliminary conclusions were made to support the development of a Field Demonstration and future applications on a full scale. These conclusions are as follows:

Performance. The PDOS confirmed the efficacy of a Cienega Filtration Project type of system in reliably reducing soluble selenium below targeted levels of 5 ug/l, and that this can be achieved with a residence time of approximately 24 hours, with the precise addition of organic material to promote sufficient bacterial growth to achieve moderately reducing conditions.

Matrix materials. The PDOS concluded that the coarsest media – ¾" crushed rock, performed as well or better than sand. Thus for the Field Demonstration (and if confirmed) for full project implementation, it is recommended to utilize coarser-grained materials to allow for residence times to be controlled via inlet and outlet hydraulic controls rather than limited the hydraulic conductivity of the matrix. This also adds structural stability (reduces total and differential settlement).

Bacteria inoculation. It was established that the combination of naturally-occuring native bacteria found in the existing creek bed provides adequate inoculation of selenium-reducing bacteria. It was further found that without inoculation, appropriate redox conditions would eventually be reached. A significantly longer equilibrating start-up time, however, appeared to be required to begin selenium removal. It was also found that the inclusion of chopped cattails accelerated the selenium reducing process, but posed other engineering control issues and created less than ideal ancillary conditions (discussed below).

Electron donor. The need of an appropriate electron donor was confirmed, and various types of donors were considered. It is desired that a food grade supplement be introduced, and while both citric acid and sodium benzoate were tested, the sodium benzoate performed more satisfactorily. It was estimated that application levels should be 2.25 to 2.5 times the calculated stoichiometric nitrate levels. Figure 3 illustrates the drop in effluent selenium levels once electron donor addition was increased. Reducing conditions were more quickly and reliably established using citric acid, rather than sodium benzoate, as the electron donor; however twice the mass of citric acid was required for similar results.

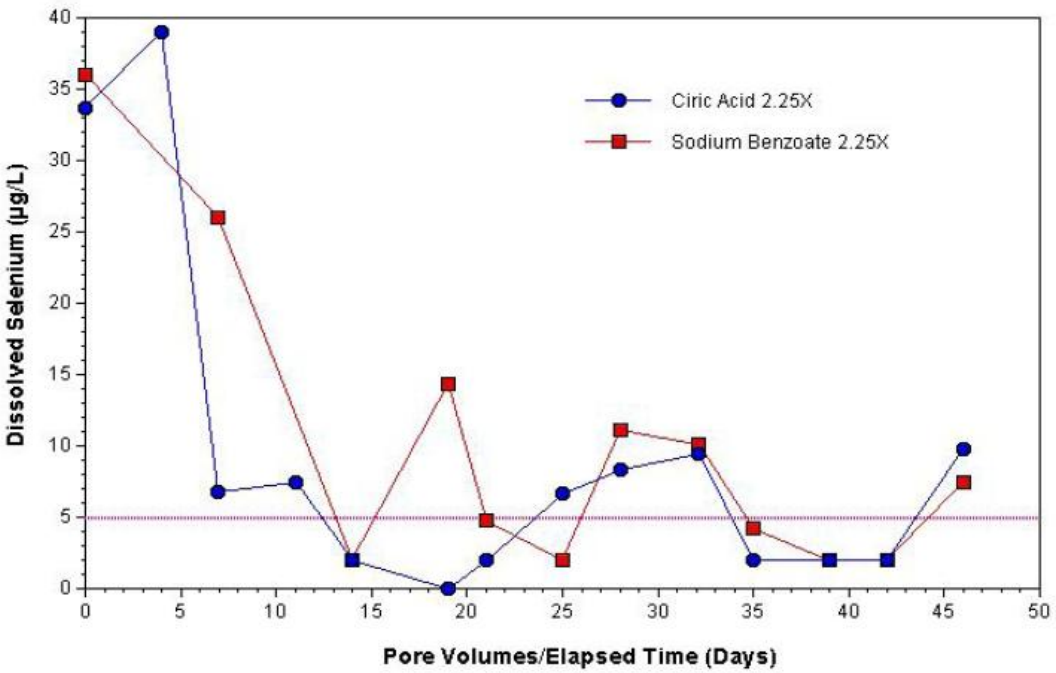

Figure 3. Dissolved Selenium with varying electron donor contributions.

Nitrate removal. The PDOS showed extremely efficient removal of nitrates. This is expected as at the target redox levels, nitrates are preferentially removed. Effluent nitrate concentrations were below detection limits.

Bacteria. While not a primary objective of this study periodic sampling for fecal indictor bacteria was conducted in the system effluent, yielding concentrations below detection limits.

Dissolved metals in effluent. The reductive dissolution of iron and manganese oxides present in the crushed rock media under selenium reducing conditions results not only in an increase in levels of these metals in the effluent, but the liberation other trace constituents metals and metalloids that are associated with these oxides. In the PDOS, the onset of iron and manganese reducing conditions occurs at 27 pore volumes. The magnitude of the release of these metals, however, was dependent on the media. As the supply of reducible iron and manganese become exhausted the levels of dissolved iron and manganese decline to the source water concentration so

the media is neither a source nor a sink. Although the potential for arsenic precipitation in the media had been identified as a potential limiting factor for long-term operations, secondary iron oxides generally control the mobility of arsenic when it is present in trace quantities. In an oxidizing environment arsenic is readily adsorbed by iron oxides, while the reductive dissolution of iron oxides released selenium. This pattern was also observed in the column study, where arsenic was adsorbed by the media until the liberation of iron and manganese. The release of arsenic ceased after the available arsenic in the media was exhausted, after which the source water arsenic concentration was unaffected by passage through the columns.

OTHER ISSUES AND CONSIDERATIONS

The PDOS revealed that there are a number of other issues that are directly relevant in the consideration of selenium treatment in urban areas for storm water and urban runoff. These must be carefully considered in conjunction with siting and design studies. These issues include:

- **Biofouling.** Maintenance of long term hydraulic conductivity is critical for system operations. Preliminary results indicate that after 8 weeks of operation, hydraulic conductivity remains sufficiently high to meet design requirements.
- **Accumulation and disposal.** For full scale implementation of the Cienega Filtration Project, decommissioning and disposal of a full scale project would be extremely expensive and cost-prohibitive. Refreshing could be accomplished by periodic aeration and flushing of the media with proper disposal.
- **Hydrogen Sulfide.** The conditions and bacteria required to reduce selenium to a solid form potentially causes the release of hydrogen sulfide gas. Various measures will tested in the Field Demonstration for implementation.

FIELD DEMONSTRATION

Prior to full scale implementation, a Field Demonstration (Geosyntec 2006b) was designed, built and is currently in operation by IRWD. The primary objective of this Field Demonstration is to test critical elements (such as large scale geometries, efficiencies of electron donor dosing, operations and maintenance considerations, etc.) prior to consideration of full scale implementation.

CONCLUSIONS

Treatment of selenium in dry-weather urban runoff can be achieved, by adopting technologies and concepts established in the wastewater, agricultural, and mining industries. This paper presents information from flow-through column testing that confirms the ability to achieve significant selenium reduction through a wetland-like treatment process with residence times as short as 24 hours and using food-grade carbon sources.

The challenges in the urban environment include the cost of land, public perception and environmental issues, the volume of water treated, and the standards for effluent quality. The work reported here and currently underway is believed to substantially advance the state of the practice in cost-effectively removing selenium in dry-weather flows.

REFERENCES

Abdullah, M.I., Z. Shiyu and K. Mosgren, 1995. "Arsenic and Selenium Species in the Oxic and Anoxic Waters of Oslofjord, Norway." Marine Pollution Bulletin 31(1-3):115-126.

Allen, K.N., 1991. "Seasonal Variation of Selenium in Outdoor Experimental Stream-Wetland System." J. Environ. Qual. 20: 865-868.

Azaizeh, H.A., S. Gowthaman, and N. Terry, 1997. "Microbial Selenium Volatilization in Rhizosphere and Bulk Soils from a Constructed Wetland." J. Environ. Qual. 26: 666-672.

Bailey, F.C., A.W. Knight, R.S. Ogle, and S.J. Klaine, 1994. "Effects of Sulfate Level on Selenium Uptake by Ruppia Maritima." Chemosphere 30(3): 579-591.

Bañuelos, G.S., H.A. Ajwa, B. Mackey, L. Wu, C. Cook, S. Akohoue, and S. Zambruzuski, 1997. "Evaluation of Different Plant Species Used For Phytoremediation of High Soil Selenium." J. Environ. Qual. 26: 639-646.

Besser, J.M., J.N. Huckins, and R.C. Clark, 1994. "Separation of Selenium Species Released From Se-Exposed Algae." Chemosphere 29(4): 771-780.

Cooke, T.D. and K.W. Bruland, 1987. "Aquatic Chemistry of Selenium: Evidence of Biomethylation." Eviron. Sci. Technol. 21: 1214-1219.

Frankenberger, W. T., C. Amrhein, T. W. M. Fan, D. Flaschi, J. Glater, E. Kartinen, Jr., K. Kovac, E. Lee, H. M. Ohlendorf, L. P. Owens, N. Terry, and A. Toto. 1999. "Advanced Treatment Technologies in the Remediation of Seleniferous Drainage Waters and Sediments."

Drainage Water Treatment Final Report. Drainage Water Treatment Technical Committee. The San Joaquin Valley Drainage Implementation Program and The University of California Salinity/Drainage Program. February.

Frankenberger, W.T., L. Guo, and W.A. Jury, 1999. "Adsorption and Degradation of Dimethyl Selenide in Soil." Environ. Sci. Technol. 33: 2934-2938.

GeoSyntec Consultants. 2003. "Wetland Selenium Mesocosm Pilot Study" Prepared for the Irvine Ranch Water District.

Geosyntec Consultants. 2006. "Results of the Pre-Design Optimization Study Supporting the Cienega Filtration Project." Prepared for the Irvine Ranch Water District. January.

Geosyntec Consultants. 2006. "Cienega Filtration Project Field Demonstration Project Design Report." Prepared for the Irvine Ranch Water District. October.

Hansen, D., P.J. Duda, A. M. Zayed, and N. Terry, 1998. "Selenium Removal by Constructed Wetlands: Role of Biological Volatilization." Environ. Sci. Technol. 32:591-597.

Hibbs, B.J. and M.M. Lee, 2000. "Sources of Selenium in the San Diego Creek Watershed." Prepared for Defend the Bay & California Urban Environmental Research & Education Center. June 27, 2000.

Horne, Alex, 2001. Personal Communication: Memo to Eric Strecker, GeoSyntec Consultants. Selenium Removal in the San Diego Creek Drainage. Nov. 2, 2001.

Kadlec, R.H. and R.L. Knight, 1996. Treatment Wetlands. CRC Press LLC, Boca Raton, Florida.

Karlson, U., W.T. Frankenberger, and W.F. Spencer, 1994. "Physiochemical Properties of Dimethyl Selenide and Dimethyl Diselenide." J. Chem. Eng. Data 39:608-610.

Kessi, J., M. Ramuz, E. Wehrli, M. Spycher and R. Bachofen, 1999. "Reduction of Selenite and Detoxification of Elemental Selenium by the Phototrophic Bacterium Rhodospirillum rubrum." Appl. Environ. Microbiol. 65(11): 4734-4740.

Kovac, K. 2005. "Selenium Removal Selenium Removal at Adams Avenue Agricultural Adams Avenue", Agricultural Drainage Research Center, California Department of Water Resources, San Joaquin District.

Masscheleyn, P.H. and W.H. Patrick, 1993. "Biogeochemical Processes Affecting Selenium Cycling in Wetlands." Environ. Tox. Chem. 12: 2235-2243.

Masscheleyn, P.H., R.D Delaune, and W.H. Patrick Jr., 1991. "Biogeochemical Behavior of Selenium in Anoxic Soils and Sediments: An Equilibrium Thermodynamics Approach." Envirn. Sci. Health A26(4): 555-573.

MSE Technology Applications, Inc. (MSE) 2001. "Selenium Treatment/Removal Alternatives Demonstration Project" Mine Waste Technology Program Activity III, Project 20. EPA/600/R01/077 June 2001. http://www.epa.gov/ORD/NRMRL/pubs/600r01077/600r01077.pdf

NRCS, Natural Resource Conservation Service, 2002. Plant Guide [Online] Available http://plants.usda.gov, Feb. 26, 2002.

Pilon-Smits, E.A.H., M.P. de Souza, G. Hong, A. Amini, R.C. Bravo, S.T. Payabyab, and N. Terry, 1999. "Wetlands and Aquatic Processes: Selenium Volatilization and Accumulation by Twenty Aquatic Plant Species." J. Environ. Qual. 28: 1011-1018.

Reinsel, M.A. and M.K. Botz, 1999. "Anoxic Biotreatment Cell (ABC) for Removal of Nitrate & Selenium from Mining Effluent Waters." American Society for Surface Mining and Reclamation; Annual meeting; Mining and reclamation for the next millenium - 16th, Aug. 1999. pp. 556-560.

RWQCB, Santa Ana Regional Water Quality Control Board, 2001. "Draft Selenium (Se) Total Maximum Daily Load (TMDL) for Newport Bay and San Diego Creek Watershed. Oct. 2001.

Scheidlinger, 2005. "Biobarriers for Removal of Selenium from Agricultural Drain Water" Selenium Treatment Technology Symposium, Sacramento, CA, March 23.

Stork, A., W.A. Jury, and W.T. Frankenberger, 1999. "Accelerated Volatilization Rates of Selenium from Different Soils." Biol. Trace Elem. Research 69:217-234.

Susilo, Strecker, Brandt, Sundberg, Howell, and Leisenring. 2005. Selenium Treatment and Management Approaches. California Stormwater Quality Association Conference. Ontario, CA. March.

Thompson-Eagle, E.T. and W.T. Frankenberger, Jr., 1990a. "Volatilization of Selenium from Agricultural Evaporation Pond Water." J. Environ. Qual. 19:125-131.

Thompson-Eagle, E.T. and W.T. Frankenberger, Jr., 1990b. "Protein-Mediated Selenium Biomethylation in Evaporation Pond Water." J. Environ. Qual. 9:1453-1462.

Twidwell, L., J. McCloskey, P. Miranda, and M. Gale, 2000. "Potential Technologies for Removing Selenium from Process and Mine Wastewater." *Proc. Minor Elements*, SME, Salt Lake City, UT, Feb. 2000 pp53-66.

Twidwell, L.G., J. Mccloskey, P. Miranda, M. Gale "Technologies And Potential Technologies For Removing Selenium From Process And Mine Wastewater" Montana Tech Of The University Of Montana Butte, Montana, USA 59701. http://www.mtech.edu/metallurgy/Faculty%20Info/Twidwell/Selenium/Microsoft%20Word%20 -%20REWASSE%20for%20proceedings99%20word.pdf

Warnert, Jeannette, 1998. "UC Scientists Try Nature's Own Selenium Cleanup Strategy." Press Release: Public Info. Ag & Natural Resources. [Online] Available http://www.uckac.edu/press/pressreleases98/wetlands.htm

Weres, O., A.R. Jaouni and L. Tsao, 1989. "The Distribution, Speciation and Geochemical Cycling of Selenium in a Sedimentary Environment, Kesterson Reservoir, California." Appl. Geochem. 4: 543-563.

Yu, R., J.P. Coffman, V. Van Fleet-Stalder, and T.G. Chasteen, 1997. "Toxicity of Oxyanions of Selenium and of a Proposed Bioremediation Intermediate, Dimethyl Selenone." Environ. Tox. Chem. 16(2): 140-145.

Zayed, A.M. and N. Terry, 1994. "Selenium Volatilization in Roots and Shoots: Effects of Shoot Removal and Sulfate Level." J. Plant Physiol. 143: 8-14.

Zhang, Y. and J.N. Moore, 1997. "Environmental Conditions Controlling Selenium Volatilization from a Wetland System." Environ. Sci. Technol. 31: 511-517.

Extension of an LA-QUAL model for evaluating a proposed wastewater discharge to realistic receiving water temperature and flow conditions

Chris Herrington[1], PE

1. City of Austin, Watershed Protection and Development Review Department, PO Box 1088, Austin, TX 78767. PH (512) 974-2840; email: chris.herrington@ci.austin.tx.us

ABSTRACT

Multiple steady-state LA-QUAL(version 8.0) models for varying temperature and flow conditions were evaluated and used to generate a time-series prediction of water quality impacts from a proposed wastewater discharge to Bear Creek (Hays County, Texas) at the upstream boundary of the Barton Springs portion of the Edwards Aquifer Recharge Zone. LA-QUAL predicted output is sensitive to dilution (amount of natural creek flow present) and temperature (removal rates are temperature-dependent) (Herrington 2008) . Although LA-QUAL (or QUAL-TX) models are commonly used by Texas Commission on Environmental Quality staff to evaluate potential dissolved oxygen degradation for new discharges (TCEQ 2003), typically only a single critical condition (low flow, high temperature) is considered. The use of multiple models is a more accurate representation of the temporal variability in flow and temperature. Using this approach, the proposed discharge is predicted to degrade the water quality of Bear Creek and the Edwards Aquifer. However, this analysis is still only a conservative approximation of the actual degradation potential and does not simulate more dynamic ecological responses such as nutrient spiraling or storm event driven sediment re-suspension.

INTRODUCTION

A residential development has applied to the Texas Commission on Environmental Quality (TCEQ) for a permit (Table 1) to discharge up to 500,000 gal/day (1,893 m^3/day) of treated wastewater directly to the headwaters of Bear Creek, Hays County, Texas. If approved, the discharge would be the first in the surface water contributing zone of the Barton Springs segment of the Edwards Aquifer. The aquifer provides drinking water for many central Texas residents and it's primary discharge point, Barton Springs, is the sole habitat for the federally endangered Barton Springs salamander (*Eurycea sosorum*). Bear Creek is an oligotrophic (Herrington and Scoggins 2006), intermittent, stream with many small perennial impoundments and primarily limestone bedrock substrate. The 62 km^2 watershed is bisected by the recharge zone of the aquifer. The discharge point is 12.5 km upstream of the recharge zone boundary.

The water quality of Bear Creek with the proposed discharge was previously predicted at the upstream recharge zone boundary of the Barton Springs segment of

the Edwards Aquifer using the steady-state one-dimensional LA-QUAL (version 8.0) model (Miertschin and Obenour 2006, COA 2006, Herrington 2008) for several varying temperature and flow scenarios. However, the temporal distribution of the varying temperature and flow scenarios has not been previously assessed against measured creek flow and ambient temperature. Thus, the increase in long-term average concentrations and mass loading from the proposed discharge to the Edwards Aquifer has not been accurately represented. By developing LA-QUAL models for multiple sets of temperature and flow conditions and then applying model output to measured daily time-series creek flow and temperature measurements, a more realistic assessment of the long-term impacts of the proposed discharge may be conducted. Utilizing these distributions of results allows toxicologists, aquatic scientists, and risk assessors a more familiar probability basis to evaluate impacts to aquatic ecology in the discharge route and the Edwards Aquifer.

Table 1. Final phase draft permit limitations for the proposed discharge (WQ0014293-001).

Effluent Characteristic	Daily Average	7-day Average	Daily Maximum	Single Grab Maximum
Flow, MGD	500,000	n/a	n/a	n/a
Carbonaceous BOD (5-day), mg/L	5	10	20	30
Ammonia Nitrogen, mg/L	2	5	10	15
Total Phosphorus, mg/L	0.15*	0.3	0.6	0.9

*expressed as a daily median

Previous LA-QUAL model results of the impacts of proposed discharge (Miertschin and Obenour 2006, COA 2006, Herrington 2008) have demonstrated that model predictions are highly sensitive to selected ambient temperatures and Bear Creek flow rates. TCEQ assessed the potential impacts of the discharge using the steady-state QUAL-TX model (version 3.5, updated November 1999) in a single condition with warm water temperature (29.7 ºC) and no ambient Bear Creek headwater or tributary flow additions. The low flow, hot temperature condition represents a system with maximum hydraulic residence time and maximum nutrient removal in the QUAL-TX or LA-QUAL models. Although this may be appropriate for assessing critical dissolved oxygen (DO) conditions, it may not represent time periods when biochemical oxygen demand (BOD) or nutrient loadings to the aquifer are higher. Therefore, it is only a local extreme of critical conditions whereas the low temperature and low dilution rates may yield a worse condition for the aquifer.

METHODS

Bear Creek daily average flow and average Austin air temperature are variable across the year (Figure 1). Bear Creek daily average flow may be represented by the United States Geological Survey (USGS) gage 08158810 upstream of the upper recharge

zone boundary from 1978 to present. Long-term records of daily Bear Creek water temperature are not available. Air temperature data at the Austin Mueller municipal airport station were obtained from the National Climatic Data Center of the National Weather Service from 1930 to 2007. Daily maximum and minimum air temperature values were averaged to yield daily average temperature. Daily average air temperature data were converted to daily average water temperatures by linear regression ($T_{water} = 0.8139*T_{air} + 3.3732$, $r^2=0.85$) of 99 ambient instantaneous water temperature readings recorded by the USGS and City of Austin (COA) at the Bear Creek gage 08158810 site and concurrent average Austin air temperature (Figure 2).

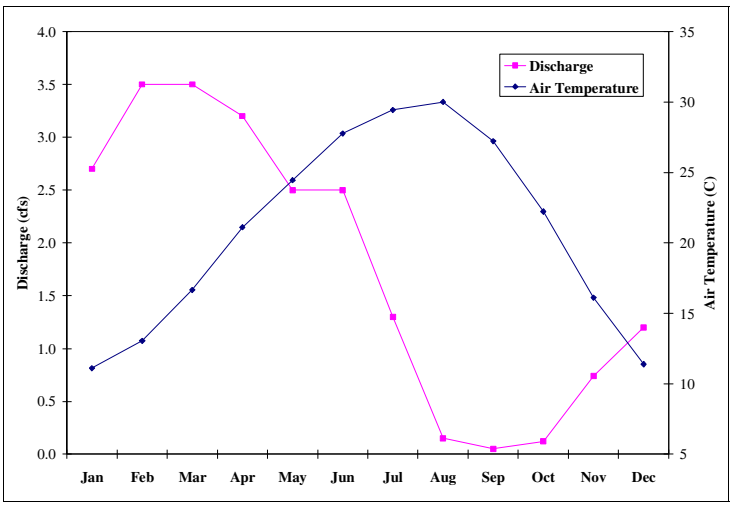

Figure 1. Monthly average Bear Creek flow at 08158810 (1978-2007) with monthly average Austin air temperature (1930-2007).

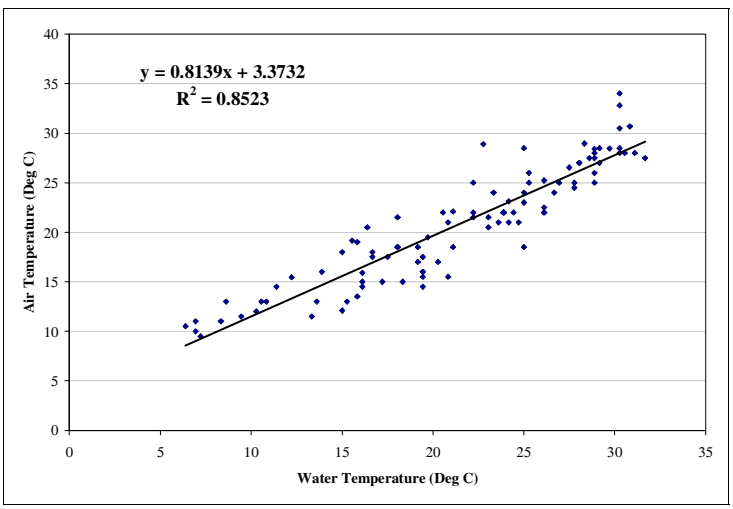

Figure 2. Scatter plot of daily average air temperature from NCDC Austin Mueller gage and instantaneous water temperature at Bear Creek USGS gage 08158810 with linear regression.

LA-QUAL reach identifications, program constants, temperature correction constants, reaeration coefficients and advective hydraulic characteristics were

identical to the original TCEQ model and previous COA model (Herrington 2008). Nutrient removal rates were also identical to the TCEQ and previous COA model (Herrington 2008) (Table 2). Effluent discharge concentrations were set to daily average permit limits (Table 1) except for total phosphorus, which was modeled at a concentration of 0.3 mg/L. Because the 0.15 mg/L daily limit for total phosphorus is calculated as a daily median, it is possible in any given month to meet the 7-day average, daily maximum and daily median permit requirements but maintain a daily average 0.3 mg/L total phosphorus concentration. The draft permit indicates that the 0.15 mg/L total phosphorus daily median limit is based on a long-term average of 0.10 mg/L but there is no description of how the long-term average should be calculated or any compliance restriction to insure that the 0.10 mg/L long-term average is achieved. From the TCEQ implementation manual for permitting, it is evident that this median permit limit is unique and does not follow the assumed distributions for effluent quality determined from statewide variability in discharge and stream water quality modeling. Additionally, a conservative material was modeled in LA-QUAL with a discharge concentration of 1.0, so that predicted output concentrations reflect the fraction of any conservative material remaining after dilution. Note that if dilution reduces the percentage of the conservative material to less than 1%, LA-QUAL output reports the percent remaining as 0.00.

Table 2. Nutrient removal rates.

Parameter	**Removal Rate (day^{-1})**
Organic Nitrogen	0.03
Ammonia (NH_3)	0.30
Nitrate (NO_3)	0.14
Total Phosphorus	0.08

Bear Creek ambient (background) concentrations were calculated using all available USGS and COA data at the USGS gage 08158810 (1978-2006), with mean values for parameters with censored observations (i.e., values less than detection limits) estimated by non-parametric Kaplan-Meier methods (Kaplan and Meier 1958, Allison 1995, Helsel 2005) (Table 3). Average ambient concentrations were estimated separately for storm and non-storm flow conditions. Current day mean daily flow was compared to previous day mean daily flow to determine if storm or base flow ambient concentrations should be used, following the procedures of Barrett and Charbeneau (1996). If the ratio of current day to previous day mean daily flow was greater than 1.5, the current day was considered a storm-influenced sampling event.

Table 3. Bear Creek ambient concentrations calculated from USGS and COA data, used for all natural incremental inflows in the model.

Parameter (mg/L)	Base Flow	Storm Flow
BOD_5	0.529	1.577
Organic Nitrogen-N	0.307	0.594
NH_3-N	0.034	0.038
NO_3+NO_2-N	0.117	0.233
Total Phosphorus	0.015	0.041
Total Nitrogen	0.458	0.865

Three water temperature ranges were evaluated (Table 4) using predicted water temperatures from NCDC average daily air temperatures. Five Bear Creek flow scenarios (not including the proposed discharge) were evaluated based on target flow as measured at the USGS gage 08158810 (Table 5). Flow ranges were selected based on ratios of wastewater effluent to ambient (natural) Bear Creek discharge at gage 08158810. Concurrent daily average Bear Creek flow and predicted water temperature (assuming water was present) were determined for the matched period of record of the USGS gage and NCDC climate data (07/07/1979 – 07/31/2007).

Table 4. Bear Creek ambient water temperature ranges (1979-2007) as represented in model scenarios.

Scenario Name	Range of Water Temp (ºC)	Water Temp Used in Model (º C)	% of Time
Cold	<15	10	23.6
Moderate	15-25	20	45.6
Hot	>25	30	30.8

Table 5. Bear Creek mean daily discharge ranges at 08158810 as represented in model scenarios (1979-2007). Percentile of all mean daily discharge measurements shown for target discharge value.

Scenario Name	Range of Daily Average Discharge (ft^3/s)	Target Discharge at 08158810 used in Model (ft^3/s)	Target Discharge as Percentile	Ratio of wastewater to natural flow (Qww/Qnat)	% of Time from period of record
No	0	0	16th	∞	16.1
Low	0.01 – 0.5	0.10	28th	∞ – 1.5	22.4
Median	0.5 – 1.5	1.1	50th	1.5 – 0.5	16.9
High	1.5 – 15	10	85th	0.5 – 0.05	35.4
Flood	>15	22	95th	<0.05	9.0

Incremental ambient inflows were added at tributaries junctions to achieve the target discharge at the 08158810 gage. Bear Creek flow was apportioned based on fraction of drainage area relative to drainage area at the gauge 08158810 (Table 6).

Table 6. Incremental inflows in model for varying flow scenarios. Area fraction represents fraction of drainage area for reach relative to USGS gage 08158810 drainage area. Area fractions were multiplied by target flow at USGS gage to determine total flow in each reach. Incremental inflows were then determined by subtraction.

Reach ID	Name	Drainage Area (acres)	Area Fraction	Incremental Inflow in Model (m3/s)				
				No	Low	Median	High	Flood
1	headwaters	0	0.000	0.0	0.0000	0.0000	0.0000	0.0000
9	unknown trib	1021.3	0.130	0.0	0.0004	0.0041	0.0368	0.0809
24	spring creek	6479.1	0.824	0.0	0.0019	0.0216	0.1965	0.4324
30	friday mtn	6981.8	0.888	0.0	0.0002	0.0019	0.0181	0.0398
36	north fork	11483.2	1.460	0.0	0.0016	0.0178	0.1621	0.3566

Previous models have used ambient DO concentrations of 6.0 mg/L. In this evaluation, ambient DO was allowed to vary with temperature scenario (Table 7). Average DO concentrations were estimated from all available ambient instantaneous USGS and COA field measurements for the 3 temperature ranges (Table 4).

Table 7. Bear Creek ambient DO concentration (mg/L) by temperature scenario.

Temperature Scenario	Background DO (mg/L)
Cold	10.012
Moderate	8.157
Hot	7.091

Combining the flow, temperature and base/storm conditions yields 30 model scenarios (Table 8). LA-QUAL was used to determine predicted concentrations at the upper recharge zone boundary for each scenario. Predicted output were then applied to reported daily average discharge (without HCWID#1), water temperature and flow condition (storm/base) for the discharge data period of record to provide a daily estimate of Bear Creek concentrations at the recharge zone boundary. Essentially, the steady-state concentrations output from multiple LA-QUAL models were combined to generate a time-series record of predicted concentrations.

Table 8. LA-QUAL model scenarios evaluated, and fraction of time each scenario occurred from 1979-2007.

Scenario Name	Bear Creek Flow	Water Temperature	Storm Condition	Fraction of Time
Flood - Cold - Base	Flood	Cold	Base	0.0271
Flood - Cold - Storm	Flood	Cold	Storm	0.0034
Flood - Hot - Base	Flood	Hot	Base	0.0116
Flood - Hot - Storm	Flood	Hot	Storm	0.0010
Flood - Moderate - Base	Flood	Moderate	Base	0.0367
Flood - Moderate - Storm	Flood	Moderate	Storm	0.0102
High Flow - Cold - Base	High Flow	Cold	Base	0.0946
High Flow - Cold - Storm	High Flow	Cold	Storm	0.0029
High Flow - Hot - Base	High Flow	Hot	Base	0.0801
High Flow - Hot - Storm	High Flow	Hot	Storm	0.0020
High Flow - Moderate - Base	High Flow	Moderate	Base	0.1649
High Flow - Moderate - Storm	High Flow	Moderate	Storm	0.0097
Low Flow - Cold - Base	Low Flow	Cold	Base	0.0386
Low Flow - Cold - Storm	Low Flow	Cold	Storm	0.0021
Low Flow - Hot - Base	Low Flow	Hot	Base	0.0838
Low Flow - Hot - Storm	Low Flow	Hot	Storm	0.0041
Low Flow - Moderate - Base	Low Flow	Moderate	Base	0.0876
Low Flow - Moderate - Storm	Low Flow	Moderate	Storm	0.0073
Median Flow - Cold - Base	Median Flow	Cold	Base	0.0375
Median Flow - Cold - Storm	Median Flow	Cold	Storm	0.0014
Median Flow - Hot - Base	Median Flow	Hot	Base	0.0548
Median Flow - Hot - Storm	Median Flow	Hot	Storm	0.0013
Median Flow - Moderate - Base	Median Flow	Moderate	Base	0.0732
Median Flow - Moderate - Storm	Median Flow	Moderate	Storm	0.0030
No Flow - Cold - Base	No Flow	Cold	Base	0.0285
No Flow - Cold - Storm	No Flow	Cold	Storm	0.0000
No Flow - Hot - Base	No Flow	Hot	Base	0.0690
No Flow - Hot - Storm	No Flow	Hot	Storm	0.0000
No Flow - Moderate - Base	No Flow	Moderate	Base	0.0636
No Flow - Moderate - Storm	No Flow	Moderate	Storm	0.0000

Models were evaluated with and without the proposed discharge. Model output without the proposed discharge was used to represent adjusted background concentrations to determine the magnitude of the water quality impact of the proposed discharge. Using LA-QUAL to adjust background concentrations is a more

equivalent comparison than simply comparing predicted output to measured concentrations since some nutrient removal beyond what is observed is predicted to occur in Bear Creek in LA-QUAL even without the proposed discharge.

RESULTS

Predicted concentrations at the recharge zone boundary with and without the proposed discharge by model scenario are presented in Appendix A and B, respectively. Long-term averages were calculated for the period of record (1979-2007), and indicate that the proposed discharge will degrade Bear Creek concentrations of DO, BOD, nitrogen and phosphorus at the upper recharge zone boundary (Table 9). Phosphorus concentrations are predicted to increase 300% based on change in long-term average at the upper recharge zone boundary. Total nitrogen concentrations are predicted to increase 270% based on the change in long-term average concentrations at the upper recharge zone boundary. Additionally, on average 39.1% of any conservative materials in the proposed discharge such as chloride or any personal care and pharmaceutical products will be recharged to the aquifer.

Table 9. Long-term average (1979-2007) predicted concentrations at the upper recharge zone boundary from LA-QUAL output with and without the proposed discharge. CM = conservative material fraction remaining.

Parameter	Unit	With HCWID#1	Without HCWID#1
CM	*	0.391	0.000
DO	mg/L	8.316	8.409
BOD	mg/L	0.515	0.384
ORG-N	mg/L	0.370	0.252
NH3-N	mg/L	0.052	0.028
NO3-N	mg/L	0.583	0.091
TOTN	mg/L	1.007	0.372
TOTP	mg/L	0.028	0.009

Bear Creek concentrations at the upper recharge zone boundary with the proposed discharge are predicted to be degraded relative to predicted background concentrations for all modeled constituents for the majority of the time (Table 10). Relative to actual estimated long-term average concentrations input to the models, the proposed discharge is predicted to degrade the water quality of Bear Creek at the upper recharge zone boundary at least 30% of the time for all constituents and as much as 99% of the time for nitrate-nitrogen.

Table 10. Percent of period of record (1979-2007) proposed discharge is predicted to degrade Bear Creek water quality at the upper recharge zone boundary versus predicted and measured ambient (background) concentrations.

Parameter	% of Time Proposed Discharge Degrades Bear Creek Recharge	
	vs. predicted	vs. measured
CM-I	55.57	55.57
DO	78.29	30.76
BOD1	99.87	42.79
ORG-N	99.90	79.60
NH3-N	84.92	69.24
NO3-N	100.00	99.59
TOTN	100.00	99.46
TOTP	97.37	33.53

Daily loadings at the upper recharge zone boundary for each constituent were calculated using Bear Creek mean daily flow and predicted concentrations with and without the proposed wastewater discharge. The proposed discharge is predicted to increase loads to the recharge zone from Bear Creek for all constituents based on averages over the period of record (1979-2007) (Table 11). Expression of the average increase in daily loads with the proposed discharge as a percentage of the daily load discharged from the treatment plant based on permit limits is a representation of the average fraction of material in wastewater effluent that will recharge the aquifer.

Table 11. Wastewater discharge daily load from permit limits at point of discharge, average increase in daily load with discharge over the period of record at upper recharge zone boundary (1979-2007), and expression of the average increase in daily load as a percentage of daily load discharged by wastewater treatment plant.

Parameter	Daily Load from HCWID#1 at permit limits at point of discharge (kg/d)	Avg. Increase in Daily Load with HCWID#1 at recharge zone boundary (kg/d)	Avg. Increase at recharge zone boundary as % of HCWID#1 Discharge (%)
CM	1884	928	49.3
BOD1	9419	1848	19.6
ORG-N	1884	994	52.8
NH3-N	3768	285	7.6
NO3-N	32026	4503	14.1
TOTN	37677	5710	15.2
TOTP	565	178	31.5

CONCLUSIONS

The combination of multiple steady-state LA-QUAL models varying water temperature and creek flow with daily records of actual temperature and creek flow provide a unique opportunity to use LA-QUAL output to generate a time-series dataset. This method provides a more complete representation of the potential impacts of a proposed wastewater discharge using the LA-QUAL model as it more accurately represents the temporal scale of effluent dilution in ambient flow and sensitivity of removal rates to temperature. While this approximation is useful, a model capable of simulating natural processes occurring in the discharge route, particularly algal growth and nutrient re-release, would necessarily be dynamic in construction and necessary to accurately evaluate the full range of potential impacts.

Based on model output, the proposed discharge will increase the loads for all constituents from Bear Creek to the Barton Springs portion of the Edwards Aquifer, and will increase or degrade long-term average concentrations of all affected constituents in Bear Creek. These impacts are not predicted when using the LA-QUAL model in only a single discharge and flow condition.

References

Allison, P.D. 1995. Survival Analysis Using the SAS System: A Practical Guide. SAS Institute, North Carolina.

Barrett, M., and R. Charbeneau. 1996. A parsimonious model for simulation of flow and transport in a karst aquifer. The University of Texas at Austin Center for Research in Water Resources. Technical Report 269.

City of Austin (COA). 2006. Predicted impacts from the proposed Hays County Water Control and Improvement District #1 Discharge in Bear Creek and Barton Springs. City of Austin Environmental Resource Management Division, Watershed Protection and Development Review Department. SR-06-07.

Helsel, D.R. 2005. Nondetects and Data Analysis: Statistics for Censored Environmental Data. John Wiley & Sons, New Jersey.

Herrington, C. 2008. LA-QUAL (version 8.0) modeling of potential water quality impacts to Bear Creek from proposed HCWID#1 wastewater discharge. City of Austin Environmental Resource Management Division, Watershed Protection and Development Review Department. SR-08-03.

Herrington, C., and M. Scoggins. 2006. Potential impacts of Hays County WCID No. 1 proposed wastewater discharge on the algae communities of Bear Creek and Barton Springs. City of Austin Environmental Resource Management Division, Watershed Protection and Development Review Department. SR-06-08.

Kaplan, E.L. and P. Meier. 1958. Nonparametric Estimation from Incomplete Observations. Journal of the American Statistical Association 53: 457-481.

Mierstschin, J., and D. Obenour. 2006. Technical Memorandum-Proposed Contributing Zone Wastewater Discharge Evaluation, Austin, Texas. James Miertschin and Associates, Inc., prepared for the Barton Springs/Edwards Aquifer Conservation District. March 4, 2006.

Texas Commission on Environmental Quality (TCEQ). 2003. Procedures to implement the Texas surface water quality standards. Prepared by the Water Quality Division. RG-194 (Revised).

Turner, M. 2006. Predicting phosphorus with the parsimonious model. City of Austin Environmental Resource Management Division, Watershed Protection and Development Review Department. SR-06-08 (Draft).

Appendix A. Predicted Bear concentrations at upper recharge zone boundary with HCWID#1.

Code	Temp deg C	CM *	DO mg/L	BOD mg/L	Org-N mg/L	NH3-N mg/L	NO3-N mg/L	TOT N mg/L	T P m
Flood - Cold - Base	10	<0.01	10.3	0.57	0.31	0.05	0.33	0.69	
Flood - Cold - Storm	10	<0.01	10.26	1.55	0.59	0.06	0.43	1.08	
Flood - Hot - Base	30	<0.01	6.87	0.51	0.31	0.03	0.21	0.55	
Flood - Hot - Storm	30	<0.01	6.79	1.45	0.58	0.04	0.31	0.93	
Flood - Moderate - Base	20	<0.01	8.27	0.54	0.31	0.04	0.27	0.62	
Flood - Moderate - Storm	20	<0.01	8.21	1.5	0.59	0.05	0.38	1.01	
High Flow - Cold - Base	10	<0.01	10.42	0.6	0.32	0.07	0.48	0.87	
High Flow - Cold - Storm	10	<0.01	10.37	1.53	0.59	0.07	0.59	1.25	
High Flow - Hot - Base	30	<0.01	6.78	0.49	0.31	0.03	0.23	0.57	
High Flow - Hot - Storm	30	<0.01	6.68	1.36	0.57	0.04	0.33	0.94	
High Flow - Moderate - Base	20	<0.01	8.31	0.54	0.32	0.04	0.35	0.71	
High Flow - Moderate - Storm	20	<0.01	8.24	1.45	0.58	0.05	0.45	1.08	
Low Flow - Cold - Base	10	0.8	10.69	0.93	0.48	0.17	2.16	2.81	
Low Flow - Cold - Storm	10	0.8	10.68	1.05	0.52	0.17	2.17	2.87	
Low Flow - Hot - Base	30	0.8	6.51	0.16	0.36	0.02	0.22	0.6	
Low Flow - Hot - Storm	30	0.8	6.5	0.24	0.4	0.02	0.23	0.65	
Low Flow - Moderate - Base	20	0.8	8.36	0.43	0.42	0.05	0.79	1.27	
Low Flow - Moderate - Storm	20	0.8	8.34	0.53	0.46	0.05	0.81	1.32	
Median Flow - Cold - Base	10	0.3	10.66	0.76	0.38	0.12	1.3	1.8	
Median Flow - Cold - Storm	10	0.3	10.61	1.34	0.56	0.13	1.37	2.06	
Median Flow - Hot - Base	30	0.3	6.57	0.33	0.34	0.02	0.24	0.6	

Median Flow - Hot - Storm	30	0.3	6.48	0.8	0.51	0.03	0.29	0.83	
Median Flow - Moderate - Base	20	0.3	8.36	0.51	0.36	0.04	0.62	1.02	
Median Flow - Moderate - Storm	20	0.3	8.29	1.04	0.54	0.05	0.68	1.27	
No Flow - Cold - Base	10	1	10.69	0.96	0.51	0.18	2.35	3.04	
No Flow - Cold - Storm	10	1	10.69	0.97	0.51	0.18	2.36	3.04	
No Flow - Hot - Base	30	1	6.51	0.12	0.37	0.02	0.21	0.6	
No Flow - Hot - Storm	30	1	6.51	0.12	0.37	0.02	0.21	0.61	
No Flow - Moderate - Base	20	1	8.36	0.41	0.44	0.05	0.82	1.32	
No Flow - Moderate - Storm	20	1	8.36	0.41	0.44	0.05	0.83	1.32	

CM = fraction of conservative material remaining

Appendix B. Predicted Bear concentrations at upper recharge zone boundary without HCWID#1.

Code	Temp degC	CM *	DO mg/L	BOD mg/L	ORG-N mg/L	NH3-N mg/L	NO3-N mg/L	TOT N mg/L	T P m
Flood - Cold - Base	10	0	10.31	0.51	0.3	0.04	0.11	0.45	
Flood - Cold - Storm	10	0	10.27	1.51	0.58	0.04	0.22	0.85	
Flood - Hot - Base	30	0	6.89	0.48	0.3	0.03	0.11	0.44	
Flood - Hot - Storm	30	0	6.8	1.43	0.58	0.04	0.22	0.83	
Flood - Moderate - Base	20	0	8.28	0.5	0.3	0.03	0.11	0.45	
Flood - Moderate - Storm	20	0	8.22	1.48	0.58	0.04	0.22	0.84	
High Flow - Cold - Base	10	0	10.44	0.49	0.3	0.04	0.11	0.44	
High Flow - Cold - Storm	10	0	10.39	1.46	0.57	0.05	0.22	0.84	
High Flow - Hot - Base	30	0	6.79	0.45	0.29	0.03	0.11	0.43	
High Flow - Hot - Storm	30	0	6.69	1.35	0.56	0.04	0.21	0.81	
High Flow - Moderate - Base	20	0	8.33	0.47	0.29	0.03	0.11	0.44	
High Flow - Moderate - Storm	20	0	8.25	1.41	0.57	0.04	0.21	0.83	
Low Flow - Cold - Base	10	0	10.83	0.13	0.14	0.03	0.05	0.22	
Low Flow - Cold - Storm	10	0	10.8	0.38	0.27	0.05	0.1	0.41	
Low Flow - Hot - Base	30	0	6.53	0.06	0.11	0.01	0.03	0.14	
Low Flow - Hot - Storm	30	0	6.5	0.17	0.21	0.01	0.05	0.28	
Low Flow - Moderate - Base	20	0	8.42	0.09	0.12	0.01	0.04	0.18	
Low Flow - Moderate - Storm	20	0	8.39	0.27	0.24	0.03	0.08	0.34	
Median Flow - Cold - Base	10	0	10.72	0.39	0.26	0.04	0.1	0.39	
Median Flow - Cold - Storm	10	0	10.64	1.15	0.5	0.06	0.18	0.74	
Median Flow - Hot - Base	30	0	6.56	0.29	0.25	0.02	0.08	0.35	
Median Flow - Hot - Storm	30	0	6.45	0.86	0.48	0.03	0.15	0.66	
Median Flow - Moderate - Base	20	0	8.38	0.34	0.25	0.03	0.09	0.37	
Median Flow - Moderate - Storm	20	0	8.29	1.02	0.49	0.04	0.17	0.7	
No Flow - Cold - Base	10	0	0	0	0	0	0	0	
No Flow - Cold - Storm	10	0	0	0	0	0	0	0	

No Flow - Hot - Base	30	0	0	0	0	0	0	0	
No Flow - Hot - Storm	30	0	0	0	0	0	0	0	
No Flow - Moderate - Base	20	0	0	0	0	0	0	0	
No Flow - Moderate - Storm	20	0	0	0	0	0	0	0	

CM = fraction of conservative material remaining

Note: Concentrations of 0.00 mg/L for no-flow scenario represent time periods when creek is dry/not flowing.

Gray Water and Treated Effluent Reuse

Steven Roznowski[1], Kristofer Bruun[2] and Larry Roesner, Ph.D., P.E.[3]

[1] Graduate Research Assistant, Department of Civil and Environmental Engineering, Colorado State University, Fort Collins, CO 80523; email: Steve.Roznowski@colostate.edu
[2] Graduate Research Assistant, Department of Civil and Environmental Engineering, Colorado State University, Fort Collins, CO 80523; email: Kris.Bruun@colostate.edu
[3] Professor, Department of Civil and Environmental Engineering, Colorado State University, Fort Collins, CO 80523; email: Larry.Roesner@colostate.edu

Abstract

Graywater and treated effluent reuse is a concept that has been gaining favor in recent years. For reuse to be implemented, issues with water usage rights, health risks, and environmental impacts will need to be resolved. Even with the resolution of these issues, graywater reuse will not become prevalent until it has been shown to be cost effective. Cities looking to implement a city-wide or community graywater or treated effluent reuse system would be particularly interested in knowing the cost savings created by water reuse.

The reuse of graywater and treated effluent impacts demand for potable water supply as well as the loads placed on wastewater treatment facilities, therefore a fully integrated urban water system must be considered in any cost analysis. This report outlines a computer program developed to grapple with the problems of creating a fully-integrated urban water model. This program is capable of calculating the cost of a wide array of scenarios ranging from no urban water reuse to complete reuse of graywater and/or wastewater effluent. It considers factors such as rainfall volumes, population data, residential water demand, industrial water demand, and of course water supply and redistribution costs.

Furthermore, the program can perform analyses on a seasonal or annual basis to account for varying residential irrigation demands. Average household lawn area and lawn irrigation requirements can be changed and calculations are automatically updated based on mean temperature and rainfall frequency.

Several different combinations of reuse options are discussed in this report and the potential cost savings are analyzed for each. For the purposes of this report, the model was set to consider data from Fort Collins, CO. The potential cost savings are compared and the feasibility of each option is considered in detail. This report coupled with the program it describes, is a valuable tool in the process of considering graywater and treated effluent reuse.

1 Introduction

Graywater reuse has become a topic of concern particularly in areas where water supply is scarce. There have been several papers and publications regarding graywater research however there are still several areas that have not been adequately addressed. A report by the Water Environment Research Foundation (WERF) titled Long-term Effects of Landscape Irrigation Using Household Graywater – Literature Review and Synthesis was published in 2006. This report compiled the findings of previous graywater tests and studies and identified those areas requiring further research.

Graywater can be broadly defined as any household water that does not come from toilets. Most regulations in the United States also exclude water that has come into contact with food, such as water from kitchen sinks or dishwashers, from their definition of graywater (WERF 2006). For graywater reuse to become widely practiced and accepted, several obstacles will need to be overcome. The WERF report primarily focused on the environmental and health concerns associated with graywater reuse and only briefly touched upon the problems associated with graywater distribution. For graywater reuse to be implemented on a large scale, methods would need to be developed to make the use of graywater simple for the average homeowner and cost effective for communities.

1.1 Graywater Model

As a first step in a city or community graywater system, an integrated urban water model must be created to show the cost effectiveness of such a system. This report outlines such a model that has been designed to analyze various scenarios to determine cost-effectiveness of graywater reuse. The model has been designed on a community-wide basis. The reason for this, as mentioned previously was the variability and difficulty of implementing graywater reuse on a household basis. Additionally, a city-wide system would introduce such wide ranges of capital expenditures that its cost would have to be quantified on a city-by-city basis. For instance, a sprawling city such as Fort Collins, CO would require a vast network of pipes while a more centralized urban setting such as Denver would require graywater to be pumped a shorter distance but to higher elevations.

1.1.1 Capabilities

The Gray-Water and Treated Effluent Reuse program (G-WATER) was developed with the purpose of analyzing the cost for a city to implement community graywater reuse. As the name implies, G-WATER was designed to analyze the reuse of graywater and treated waste for use primarily in irrigation and toilet flushing. The program allows the user to do a variety of cost analyses by varying water consumption, reuse levels, and water use sources.

The program uses background average rainfall criteria to analyze irrigation demand and is capable of adjusting the daily irrigation requirement on a seasonal basis. Rain barrels can also be added to further reduce the lawn irrigation demand. By varying

vegetation types and areas, complex analyses can be completed based on average irrigation demands for a typical yard configuration.

Costs assigned to graywater supply, blackwater treatment, effluent reuse, and raw water treatment for potable use are applied to the water consumption data tabulated in G-WATER. The program provides the user a daily operation cost. The analysis can be run under a variety of scenarios to observe differences in cost.

2 Model Development

Development of the G-WATER model was based on the notion of an all-inclusive water balance from source water to receiving body. The model needed to be flexible so as to be capable of analyzing a variety of water usage and conservation techniques.

A raw water scenario exists only for collected rainwater from residential roof runoff. This is due to the complex nature of supplying industrial processes and residential landscape irrigation with stored or diverted raw water. The complicated interrelated combination of evaporation, evapotranspiration, seepage, inflow, and consumptive use are site-specific and therefore would need to be evaluated on a site-by-site basis.

Recorded values from NCDC rain gages in Fort Collins for the 2007 rainfall year were subtracted from required irrigation demand over the irrigation season. The exact calculation of demand is a function of temporally varied precipitation, maximum daily temperature, on-site temporary storage capacity, and vegetation type(s). Specific calculations are based on equivalent bluegrass demands, which vary depending on daily maximum temperature. Alternative vegetation such as xeriscaping and bedding plants can be selected by defining the area of coverage per household and average irrigation demands. Estimated demands found in the WERF report were used to calculate equivalent areas of bluegrass coverage. Residual irrigation demands were satisfied by graywater, wastewater effluent, and/or potable water, depending on the preferred source according to user inputs. The calculated data was divided into seasons (Spring, Summer, Autumn, and Winter) at the dates of bi-annual equinoxes and solstices. Daily average demands and irrigation volumes were then calculated for each season.

The residential demands were based on suggested uses published by the City of Fort Collins. These consist of irrigation, sinks, drinking, dish washing, clothes washing, toilets, showers, and baths. Each demand type was described on a per capita basis by number of uses per day. These were then multiplied by the determined volume (in gallons) per use.

The only remaining variables to be set were the costs associated with treatment and distribution of potable water, blackwater, and graywater, and the percentage of wastewater effluent being reused. The values gathered from the City were utilized throughout the modeling process without change. These can be seen in Table 1 of the Results section. Treated effluent reuse was permanently set as a secondary source to graywater. Additionally, the program combined any treated effluent with available

graywater therefore source inputs must be set to "graywater" to allow for effluent reuse.

3 Results

Several scenarios were analyzed using G-WATER to show the cost effectiveness of various water usage and output combinations. The results of these analyses can be found below.

Values outlined in Table 1 are the initial and unchanging inputs for the G-WATER model analyses performed hereafter. The following scenarios utilize variables that are described in more detail when applicable.

Table 1: Unchanging Inputs

Population	150,000
Households	43,857
Wastewater Treatment Cost	$2.40/1000 gals
Potable Water Base Cost	$13.86/month
Potable Water Treatment Cost	$1.24/1000 gals
Distribution Cost	$0.50/1000 gals

G-WATER was used to analyze a variety of scenarios. The first of these was a baseline estimate for water demand and cost to provide potable and wastewater treatment. Using standard water usage criteria shown in Table 2, from the City of Fort Collins, Table 3 was developed which shows base water demand and cost.

Table 2: Base Demands

Use	Uses/Day	Vol/Use (gal)
Industrial Processes	1	2000
Drinking	3	1
Sink	1	21
Dish Washing	0.15	16
Clothes Washing	0.3	50
Toilets	4	3.5
Shower	1	32
Bath	1	40

Table 3: Base Water Demand and Cost Analysis

Criterion	Daily Average	Annual Total
Volume Potable (gal)	32,200,000	11,750,000,000
Potable Treatment	$61,000	$22,300,000
Volume Waste (gal)	17,400,000	6,350,000,000
Waste Treatment	$42,000	$15,200,000
Total Cost	$103,000	$37,500,000

A second analysis was conducted for a conservative water demand pattern, set forth in Table 4 by the City of Fort Collins. This city-wide conservation also assumed an industrial usage reduction of ten percent. Table 5 shows the annual data from the G-WATER analysis given the conservative usage scenario. A comparative study is

presented in Table 6 showing the water and cost savings created as a result of implementing conservative usage demands.

Table 4: Conservative Water Demands

Use	Uses/Day	Vol/Use (gal)
Industrial Processes	1	1800
Drinking	3	0.1
Sink	1	2
Dish Washing	0.15	7
Clothes Washing	0.3	27
Toilets	4	1.6
Shower	1	8
Bath	1	15

Table 5: Water Conservation Demand and Cost Analysis

Criterion	Daily Average	Annual Total
Volume Potable (gal)	19,200,000	7,000,000,000
Potable Treatment	$45,000	$16,400,000
Volume Waste (gal)	5,700,000	2,080,000,000
Waste Treatment	$14,000	$5,000,000
Total Cost	$59,000	$21,400,000

Table 6: Conservative Use Savings

Potable Water (gal)	4,750,000,000
Treatment Costs	$16,100,000

Cost and water usage data for a scenario involving effluent reuse for landscape irrigation purposes is outlined below in Table 7. An additional cost of $0.50 per 1000 gallons of treated effluent delivered was applied to the total volume reused to represent the cost of pumping and distribution. Table 8 is a compilation of the annual wastewater reuse volume and cost savings as compared to the base values presented in Table 3.

Table 7: Wastewater Effluent Irrigation Reuse

Criterion	Daily Average	Annual Total
Volume Potable (gal)	19,300,000	7,050,000,000
Potable Treatment	$45,000	$16,500,000
Volume Waste (gal)	17,400,000	6,350,000,000
Waste Treatment	$42,000	$15,200,000
Effluent Reuse	$6,000	$2,300,000
Total Cost	$93,000	$34,000,000

Table 8: Wastewater Effluent Reuse Savings

Potable Water (gal)	4,700,000,000
Costs	$3,500,000

The effects of roof rainwater catchments on a residential level were also determined. This analysis assumed an average of two rain barrels at 50 gallons each, with no

additional cost to the city. The annual water volumes and respective costs are shown below in Table 9. The associated volume and cost savings are shown in Table 10.

Table 9: Rain Barrel Catchments

Criterion	Daily Average	Annual Total
Volume Potable (gal)	32,000,000	11,690,000,000
Potable Treatment	$61,000	$22,200,000
Volume Waste (gal)	17,400,000	6,350,000,000
Waste Treatment	$42,000	$15,200,000
Total Cost	$103,000	$37,400,000

Table 10: Annual Rain Catchment Savings

Potable Water (gal)	60,000,000
Costs	$75,000

Implementation of graywater reuse for residential landscape irrigation was analyzed for varying areas of bluegrass lawn. These areas represent the maximum and minimum values selected for analysis. The average daily and annual volumes and costs are shown in Table 11.

Table 11: Graywater Irrigation

	Bluegrass 5000sft		Bluegrass 1500sft	
Criterion	**Daily Ave.**	**Annual Total**	**Daily Ave.**	**Annual Total**
Volume Potable (gal)	24,900,000	9,090,000,000	19,300,000	7,050,000,000
Potable Treatment	$52,000	$19,000,000	$45,000	$16,500,000
Volume Blackwater (gal)	10,100,000	3,690,000,000	10,100,000	3,690,000,000
Waste Treatment	$24,000	$8,800,000	$33,000	$11,900,000
Graywater Reuse	$4,000	$1,300,000	$2,000	$700,000
Total Cost	$80,000	$29,200,000	$80,000	$29,100,000
Savings	Potable (gal)	2,660,000,000	Potable (gal)	4,700,000,000
	Costs	$8,300,000	Costs	$8,400,000

Under the assumption that 50 percent of non-consumptive residential indoor water use could be recycled for graywater reuse purposes, graywater was applied toward toilet flushing. The results of this analysis can be seen below in Tables 12 and 13.

Table 12: Indoor Graywater Reuse

Criterion	Daily Average	Annual Total
Volume Potable (gal)	30,000,000	10,980,000,000
Potable Treatment	$58,000	$21,300,000
Volume Waste (gal)	10,100,000	3,690,000,000
Waste Treatment	$37,000	$13,400,000
Graywater Reuse	$1,000	380,000
Total Cost	$96,000	$35,100,000

Table 13: Annual Graywater Reuse Savings

Potable Water (gal)	770,000,000
Costs	$2,400,000

The final scenario evaluated by the G-WATER model was a compilation of all the aforementioned water-saving scenarios. It was intended to generate the maximum water volume and cost savings for the City of Fort Collins. The results from this extreme analysis are described below in Table 14. Yearly totals for volume and cost savings can be seen in Table 15.

Table 14: Composite Water Savings Scenario

Criterion	Daily Average	Annual Total
Volume Potable (gal)	5,300,000	1,950,000,000
Potable Treatment	$28,000	$10,200,000
Volume Waste (gal)	3,500,000	1,260,000,000
Waste Treatment	$8,000	$3,000,000
Graywater Reuse	$1,000	408,000
Effluent Reuse	$0	$0
Total Cost	$37,000	$13,600,000

Table 15: Optimal Scenario Savings

Potable Water (gal)	9,800,000,000
Costs	$23,900,000

4 Discussion

This analysis considers existing centralized systems as compared to individual household treatment systems, and the cost differences associated with the treatment and distribution of effluent reuse only. The cost associated with distribution is based solely on operational pumping costs. This was therefore assumed to be the same for graywater distribution.

The following parameters were held constant throughout the analysis: Population, number of residences and industries, negligible industrial irrigation demand, and typical residential and industrial consumptive water use. The number of residences was compared to the US Census Bureau data from 2000. The average number of persons per household was calculated based on these findings. Consumptive use is defined for the purpose of this analysis as the amount of water that leaves the urban water system through any number of immeasurable means.

4.1 Base Costs

Initial modeling efforts were conducted using standard water usage rates collected from the City of Fort Collins. The total volumes and costs associated with the treatment of raw and wastewater were evaluated on a seasonal basis. As expected, more water was required over summer months due to the higher temperatures, which correlated to an increased need for irrigation. This scenario represents typical water usage currently employed by the average citizens of Fort Collins, and thus represents the baseline for comparison.

When compared to other published data, these baseline values seemed accurate. Tables published in “Water Conservation In and Around the Home” by R. Waskom

and M. Neibauer (2006) and The Home Water Supply by Stu Campbell (1983) correlate well to data provided by the City of Fort Collins.

4.2 Water Conservation

Water conservation data, also from the City of Fort Collins, was analyzed in a similar fashion as the base data. These rates produced a 40 percent decrease in potable water demand, resulting in an overall treatment cost savings of more than $16 million annually.

It should be noted that these values push the limits of water conservation, and it would be difficult to implement and ensure continued practice of such rigorous expectations. Many people who lease their homes do not pay for water. In such instances, there is not financial incentive to practice water conservation.

4.3 Effluent Reuse

Using base conditions, treated wastewater effluent was reused for landscape irrigation purposes. This assumed that pathogen removal was sufficient such that the applied graywater did not represent a risk to public health. Due to the nature of the irrigation season, this condition incurred the most significant cost savings over the summer months. While the volume of wastewater treatment did not change, the amount of potable water demand was decreased by the less costly treated effluent. Hence, an annual savings of only $3.5 million was seen through this analysis. Again, 40 percent savings of treated potable water was seen, compared to the base values. The volume of treated effluent capable of being supplied was sufficient to meet the requirements of irrigation for all seasons except summer.

4.4 Rainwater Catchments

Under this scenario, rain barrels were used to collect runoff from residential roofs. The total household collection area was assumed constant at 2,750 square feet. This allowed for the capture of 100 gallons of rainwater based on an assumed average of two 50 gallon barrels per household. The initial runoff was used as raw water irrigation to supplement potable water use. Only during those rainfall events that exceeded the irrigation demand for a 5,000 square foot bluegrass yard, did the rain barrels begin to store water for future irrigation use. Data from an entire irrigation season was obtained from NCDC rain gauges located in the City of Fort Collins. The average seasonal daily demand was calculated to obtain a daily average of water applied for irrigation. The supplemental raw water collection was able to decrease annual potable water demand by 0.5 percent leading to a total annual cost savings of $75,000.

4.5 Graywater Reuse

Graywater reuse for residential irrigation was analyzed under the assumption that 50 percent of all non-consumptive indoor water use, excluding dishwashing and toilet flushing, could be converted to graywater. Initially, the analysis was performed with an average residential landscape area of 5,000 square feet of bluegrass. Under this scenario, an annual cost savings of approximately $8.3 million was realized. By

reducing the average landscape area to 1,500 square feet, annual cost savings were less than $100,000 greater than with 5,000 square feet. The reason for this was that the reduced area of landscaping did not require as much graywater and therefore, unused graywater had to be treated as blackwater. This additional treatment cost essentially negated the reduction in potable demand.

To fully utilize the potential for graywater reuse savings, the lawn area had to be optimized such that it required exactly as much graywater as was produced. This meant that no potable water was required for irrigation nor was any graywater being sent to waste treatment. Under these conditions, the optimal area was found to be 2,874 square feet of bluegrass at which point the annual cost was minimized. Furthermore, if water conservation was in effect, this optimal area was reduced to 908 square feet of bluegrass as the graywater available decreased.

Graywater reuse was next analyzed for use in residential toilets. Industrial toilet flows were not included due to the variability inherent in industrial graywater effluent. For this analysis, no graywater was used for outdoor irrigation. Again, 50 percent of non-consumptive indoor water use was applied toward available graywater volumes. Savings of $2.4 million and 766 million gallons of potable water annually were calculated.

This final scenario was unrealistic as it would be unlikely that graywater would be used indoors and not outdoors. If, however, the analysis were run with both indoor and outdoor graywater reuse, the entire graywater volume produced would be utilized and therefore would require potable water supplementation regardless of the application. This would make the cost and potable water use equivalent to the scenario applying graywater for irrigation only. The exception to this would be during the winter months when no irrigation is required.

4.6 Composite Water Savings Scenario

With this scenario, the total annual cost was minimized by combining all of the most useful scenarios mentioned above. Because water uses were conservative, the optimum landscape area was reduced as mentioned before. To get the optimum net irrigation demand and maintain a total yard area of 5,000 square feet, xeriscape and bedding plants were used instead of bluegrass, with the areas of 4,318 and 682 square feet, respectively. For these criteria, an annual cost savings of $23.9 million and potable water savings of 9.8 billion gallons would be realized.

It should be noted that this optimization of cost resulted in no reuse of effluent. This was because cost was saved by using graywater which was diverted from wastewater treatment. Conversely, effluent reuse requires wastewater treatment costs plus an additional charge for redistribution. This need for redistribution was eliminated by reducing the lawn area to an optimal value. However, if the lawn area were kept at 5,000 square feet of bluegrass, effluent reuse would be preferable to potable water for irrigation due to its lower cost.

5 Conclusion

Cyclic processes define water reuse practices. This is verified by either direct or indirect reuse, both of which can represent a "zero sum" water balance within a defined system. Typically, urban treated wastewater and collected stormwater are discharged to receiving bodies which inevitably supply populations downstream with a potable water source. The delaying of this discharge process or bypassing of raw water volume, in exchange for reused water, results in higher quality water sources downstream while providing necessary non-potable water for residential and industrial uses. Whatever the reuse technique, the importance of water reuse is growing due to increasing population densities around the world.

Rain catchments for individual households were found to produce negligible profits. A net gain of $75,000 per year was calculated assuming no cost for the implementation of rain barrels. For this scenario, over 80,000 barrels would be required. This would imply that residential capture of stormwater runoff would not be significant in reducing city potable water supply costs.

Graywater for toilet use was also determined to be inconsequential. Graywater could be completely consumed by irrigation, therefore requiring potable water. This potable volume would be the same irrespective of the use to which it was applied.

Considering the analysis of all scenarios calculated with G-WATER, it can be concluded that the most cost effective case is the final scenario which incorporates all possible water-saving techniques. However, due to the extremely strict nature of this scenario, prolonged application on a residential level would not be feasible. Therefore, the best reasonable scenario would be some combination of all of these cost reduction techniques. Though they may not be implemented to their theoretical potential, they still could contribute to significant savings.

6 References

Campbell, Stu. The Home Water Supply: How to Find, Filter, Store, and Conserve It. North Adams, MA: Storey Publishing, LLC, 1983.

Monthly Indoor Water Use. Table. Fort Collins, CO: City of Fort Collins, 2001.

National Climatic Data Center. NCDC.NOAA.gov. 18 September 2008. Fort Collins, CO. <http://www4.ncdc.noaa.gov/cgi-win/wwcgi.dll?wwDI~StnSrch~COOPID~053005>.

Waskom, R., and M. Neibauer. "Water Conservation In and Around the Home." Consumer Series: Housing 9.952 (2006) <http://www.ext.colostate.edu/pubs/consumer/09952.pdf>.

Water Environment Research Foundation. "Long-term Effects of Landscape Irrigation Using Household Graywater – Literature Review and Synthesis." 2006.

Water-Wise Lawn Care. Pamphlet. Fort Collins, CO: Fort Collins Utilities.

Green Alternatives to Channel Stabilization

Richard E. Besancon, P.E.[1]

1. Burns & McDonnell Engineering; 9400 Ward Parkway, Kansas City, MO 64114; PH 816-822-3950; FAX 816-822-3514; email: rbesanc@burnsmcd.com

ABSTRACT

The purpose of the project was to improve water quality, repair and stabilize eroding banks, and add wetlands to the project site.

As mitigation for channel and wetland disturbance on a commercial and residential development in eastern Illinois, Burns & McDonnell performed channel restoration/stabilization using a combination of traditional and green techniques to repair severely eroded bank and construct additional wetlands adjacent to the creek.

Canteen Creek is a highly eroded and degraded due to uncontrolled stormwater discharges into the creek upstream of the site. The existing stream has degraded and left vertical banks in many locations.

The solution was a combination of traditional channel protection using a longitudinal peak stone toe protection and non traditional using root wad protection. Longitudinal peak stone toe protection is a windrow of rock at the toe of slope, while root wad protection is a method of channel stabilization where existing trees and roots are used to stabilize the bank in combination with large rock. Both stabilization plans incorporated live willow plantings and revegetation with native wetland and upland seed mixes.

The engineer and contractor worked together on site to install the toe protection. The interaction between the two parties worked to improve the design and increase the ease of construction. This worked to increase the speed of construction and improve the integrity of the protection.

After three years in operation, the longitudinal peak stone toe protection and root wad mitigation areas are performing exactly as hoped. Both applications are preventing additional erosion while providing an environment to grow willows and other native species. The root wad mitigation in particular allows sediment to settle out and collect, thereby rebuilding the stream channels and restoring previously destroyed habitat.

Green Alternatives to Channel Stabilization

Burns & McDonnell Engineering performed a design build project for a commercial and residential development. The development size totaled approximately one square mile. The area of western Illinois where the project is located consists of heavily treed loess hills with steep slopes. The overall project included providing infrastructure for the entire development. The roads on site required multiple stream crossings, impacts to wetlands and riparian areas. Based on the impacts to the streams, the U.S. Army Corps of Engineers required mitigation contiguous to the site. The mitigation included two thousand feet of stream bank stabilization and the creation of lowland wetlands along Canteen Creek, a creek which forms the north boundary of the site.

Canteen Creek has been degraded by increased storm flows due to development upstream. The flood events on Canteen Creek are characterized by short duration high peak events. The creek is incised due to the high flows and velocities and the loess soils that make up its banks. The loess complicates grading and mitigation practices due to the high potential for erosion. Erosion will occur in loess with velocities as low as two feet per second (fps).

To stabilize the banks of Canteen Creek a number of options were reviewed. An adjacent property had large quantities of broken bridge abutments, held over from a previous bridge replacement. The bridge material consisted of large chunks of concrete without any exposed rebar. The concrete piles had been in place for many years, however there was concern about using rubblized concrete as stream bank stabilization with the potential for leaching of the lime and chemicals from the concrete degrading the water quality in the creek. Corps, EPA, and county personnel examined the concrete, evaluated the time it had been in place and determined that the concrete posed no danger to water quality.

In addition of the recycled concrete, another resource was available on site to use to stabilize the banks. The project site was heavily treed and many acres of trees were cleared for the residential lots and roads. Based on these materials on site and readily available, Burns & McDonnell decided to use a combination of longitudinal peak stone toe protection (LPSTP) and root wad mitigation to stabilize the banks. Longitudinal peak stone toe protection is basically a windrow of stone at the toe of an eroded slope. The purpose is to keep the erosive forces of the water away from the toe of the slope. LPSTP is easily placed from the top of the slope, which was required due to the permitting restrictions not allowing any equipment in the channel. Root wad mitigation uses felled trees to prevent scour at the toe of slope. The trees are laid in the channel longitudinally with the root wad facing upstream. The trees prevent the erosion at the toe and the root wads accumulate silt and sediment, thereby aggrading the eroded banks. The typical installation includes trees placed longitudinally along the channel with other trees dug into the back with their root wads holding the longitudinal trees in place. Additionally, duckbills and cables are anchored into the banks and wrapped around the trees to hold the trees in place.

Both the LPSTP and root was mitigation incorporate willow plantings within the construction to develop a root system to add additional holding power into the bank and provide long term stabilization.

Burns & McDonnell was self performing the project as a design build, therefore the contractor worked hand in hand with the engineer to accomplish the stream bank stabilization. The only plans produced for the contractor were sketches of each method of stabilization and the locations each were to be installed. Due to the contractor's unfamiliarity with the techniques, the engineer traveled to the site to work with the contractor to get the project constructed.

The first item the contractor suggested was not to dig the trees into the bank because that introduces a point for erosion to work at the bank in high flow conditions. Especially considering the loess soil, any disturbance of the in situ material could lead to catastrophic erosion. Instead, the contractor used the trackhoe to push the trees in normal to the stream. He was able to use the trackhoe to shove the trees into the bank and anchor the longitudinal trees without digging into the slope.



Picture looking upsteam of the root wad mitigation; notice the longitudinal trees anchored by the trees pushed into the bank and large concrete chunks.



The root wad mitigation was installed in the flowline of the creek, thereby allowing bank aggradation and habitat creation.



Same location two years after construction; notice deposition on right.

After two years, the channel stabilization is working effectively and is producing deposition along the banks where the root wad mitigation was installed.



Outer end in Canteen Creek where root wad mitigation was installed. The bank has re-vegetated and stabilized.

The LPSTP has also performed well by preventing scour at the toe of slope and provide area for siltation to occur.



The overall keys to the success of these methods of channel stabilization in challenging soils were the anchoring of the trees into the banks and the upstream protection to prevent the water from getting a foot hold for erosion to begin. At the upstream ends of each root wad location LPSTP was used to provide a hard armoring to prevent scour and failure. The use of design build contract allowed for open and honest collaboration between the contractor and engineer and producing a higher quality project.

The site U.S. Army Corps of Engineers and the Illinois EPA continue to monitor the site to be sure the site continues to meet the permitting agreement.

Hydraulic Modeling and Engineering Evaluation of Fort Myers Beach's Water Distribution System

Jinsheng Huo, PhD, PE, BCEE[1], Robert Garland, PE[1], Doug Eckmann, PE, BCEE[1], Jack Green[2], Cathie Lewis[2]

[1] AECOM Technology Corporation, 4415 Metro Parkway, Suite 404, Fort Myers, FL 33916, Phone: (239) 278-7996, E-mail: Jinsheng.Huo@AECOM.com
[2] Town of Fort Myers Beach, 2523 Estero Boulevard, Fort Myers Beach, FL 33931, Phone: 239-765-0202, E-mail: jack@fortmyersbeachfl.gov

Abstract

This paper applies hydraulic modeling to evaluate the water distribution system of the Town of Fort Myers Beach, Florida. Fort Myers Beach is a small island town located in Southwest Florida. The Town does not have its own water treatment plant. Instead, the finished water is provided by Lee County. To meet fire protection and other emergency uses, the Town has two ground storages and three booster pumping stations to provide adequate water flow and residual pressure. Like other coastal communities in Florida, the number of residence and water demand patterns in the Town vary significantly by two seasons (wet and dry). Therefore, it is a challenging task to design and evaluate a water supply system to meet two dramatically different demand characteristics. In this paper, engineers evaluate flow and pressure in the water distribution system under both PDD + FF (Peak Day Demand + Fire Flow) and PHD (Peak Hour Demand) scenarios, and the existing storage and pumping capacities as compared to the national standards and local ordinances. Based on the simulation results, critical areas with potential low pressures, especially when fire flow is needed, are identified and recommendations of system upgrading are also provided. The feasibility study of building the Town's own water treatment plant is also recommended due to increasing water demand at the south end of the island and raising water fees per the annual and monthly water bill reports. Furthermore, the additional ground storage tank capacity is suggested to meet fire protections and other emergencies (for example, hurricane events).

Keywords: Hydraulic Modeling, Evaluation, Water Distribution System, Pumping Stations, Ground Storage Tank, Simulation

I. Introduction

The Fort Myers Beach Water Distribution System (FMB Water System) includes two water supply lines from Lee County Utilities (LCU); three booster pumping stations (Marina, North, and South); two ground storage tanks (North and South); transmission piping, distribution piping; and fire hydrants.

Water Supply Lines from Lee County Utilities (LCU)

Potable water for the Town of Fort Myers Beach is provided by Lee County Utilities through 16-inch and 12-inch water supply lines. The master flow meter is located on the LCU side (mainland) and records the total water delivered. Both water supply lines operate at 50 psi and initial chlorine concentration of 2.0 mg/L.

Marina, North, South Booster Pumping Stations

The system has three booster pumping stations: Marina, North, and South. When discharge pressures at a pump station are below 40 psi, the booster pumps shall activate to maintain the discharge pressure at 50 psi or above.

Marina In-line Booster Pumping Station is located at Moss Marina, downstream of the 16-inch water supply line from LCU. As the water approaches the island, if the water pressures are below 40 psi, the booster pumps will activate to maintain pressure at or above 50 psi. As water passes through the initial booster pumps at Moss Marina, it has two functions: one function is to fill the two ground storage tanks (North and South); the other function is to serve water demands in the water system. This station is outdoors but protected with a chain link fence. This station has several components including two vertical turbine pumps (U.S. Electric 20-hp 1775-rpm Layne pumps), and one 200 KW portable backup power generator. Each has suction and discharge gauges. Flow rates and pressures are monitored at the Green Meadows WTF through a SCADA system. Controls for each unit are also at the WTF. Figure 1 shows the Moss Marina Pumping Station.

North Booster Pumping Station is located at 815 Lagoon Street, to the north of San Carlos Boulevard. If water pressures are below 40 psi, the booster pumps will activate to maintain pressure at or above 50 psi. This station has several components including one 0.50 MG Storage Tank (1973 Horton Tank Co.), one 10-inch Clay Fill Valve, three 75-hp 1750-rpm booster pumps (2 Aurora, 1 Goulds, one Aurora is out of service), online chlorine analyzer CL17, Tank Level Transmitter, Flow Transmitter, and one 200 KW portable backup power generator. Figure 2 shows the North Booster Pumping Station and 0.5-MG Ground Storage Tank.



Figure 1. Moss Marina In-line Booster Pumping Station.



Figure 2. The North Booster Pumping Station and 0.5-MG Ground Storage Tank.

South Booster Pumping Station: is located at 131 Lenell Road, on the south end of the island. If water pressures are below 40 psi, the booster pumps will activate to maintain pressure at or above 50 psi. This station was built in the mid-to-late 1980's. The South end of the island is more populated and houses the majority of the high rise hotels as well as permanent housing (condominiums). It also contains a golf course and a marina. Due to these dynamics, water is at a greater demand when compared to the North end of the island. This booster system also operates on system pressure. When called for, the water enters the tank via an altitude valve or fill valve and exits the tank via pumping. This station is enclosed with the exterior modeled to blend into the neighborhood. It includes one 1.0 MG Storage Tank (1987 Crom Corp.), one 10-inch Altitude Fill Valve, one Flow Meter (out of service), Tank Level Indicator (Monitored thru Green Meadows), 175 KVA CAT Diesel Generator, and three Gould pumps (30 hp, 50 hp, and 75hp). Figure 3 shows South Booster Pumping Station and 1.0-MG Ground Storage Tank.



Figure 3. The South Booster Pumping Station and 1.5-MG Ground Storage Tank.

North and South Ground Storage Tanks.

The North Ground Storage Tank is located at the North Booster Pumping Station and has a capacity of 0.5 MG, and the South Ground Storage Tank is located at the South Booster Pumping Station and has a capacity of 1.0 MG. This provides a total storage capacity of 1.5 MG for the Town.

II. Hydraulic Modeling and Discussions

2.1 Basis of Design

Based on the FMBPWSI Operations Manual, Lee County Utilities Operations Manual (2000) and AWWA M-31 (1998), AECOM established the following design criteria to be used for preparing the hydraulic model for the project:

Table 1. Design Criteria.

1	Pipe Material & C-Factor	• Ductile Iron Pipe or PVC Pipe for diameters larger than 12-inch (C= 100 for existing and 120 for new pipes) • PVC Pipe for diameters no larger than 12-inch (C= 100 for existing and 120 for new pipes) • HDPE Pipe for diameters no larger than 12-inch (C= 100 for existing and 120 for new pipes)
2	Water Usage per Capita	• 110 gpcd
3	Occupancy per ERU	• 2.5
4	Flow Peaking Factor	• Peak Day Factor = 2.5 • Peak Hour Factor = 3.5
5	Fire Suppression	• Fire Flow Demand = 1000 gpm [1]
6	Assumed conditions at two water supply lines from LCU	• Design Feeding Pressure = 50 psi (PHD Scenarios) • Design Feeding Pressure = 50 psi (PDD + FF Scenarios) • Working Pressure Range = 35 – 80 psi • Feeding Chlorine Concentration = 2.0 mg/L • Chlorine Decay Rate = 0.012/hr (Global Bulk = -0.288, and Global Wall = 0)
7	Proposed System Minimum Performance	• Minimum Residual Pressure = 20 psi (PDD+FF Scenarios) • Minimum Residual Pressure = 35 psi (PHD Scenarios) • Minimum Residual Chlorine Level = 0.6 ppm

[1] Fire flow estimation uses Insurance Service Office (ISO) procedure and was confirmed with the Fort Myers Beach Fire Control District.

Fire Flow Estimation Using Insurance Service Office (ISO) Procedure

Step 1: Needed Fire Flow (NFF)

For one- and two-family residences, the needed fire flow is determined based on the distance between structures, as shown in Table 2.

Table 2. Needed Fire Flow for Residences Two Stories and Less.

Distance Between Buildings (ft)	**Needed Fire Flow (gpm)**
More than 100	500
31-100	750
11-30	1,000
Less than 11	1,500

For commercial and industrial buildings, the NFF is based on building area, construction class, occupancy, exposure, and communication. The formula can be summarized as:

$$NFF = 18FA^{0.5}O(X + P)$$

Where NFF = needed fire flow (gpm)
F = class of construction coefficient
A = effective area (ft^2)
O = occupancy factor
X = exposure factor
P = communication factor

As shown the NFF for commercial and industrial buildings is estimated case by case. Therefore, in this paper, a NFF of 1000 gpm is selected to run fire flow scenarios after discussions with the Town and Fire Control District's representatives.

The Town of Fort Myers Beach Land Development Code requires buildings to be at least 7 feet away from the property lines, which provides at least 14 feet between two neighboring buildings (the code requires a minimum 5 feet for the side setback of non-waterfront SANTOS lots). Based on this code and Table 2, the needed fire flow is 1000 gpm. However, some areas of the Town were constructed prior to the adoption of the codes and might not meet the new development requirements. In these areas, distances between two buildings might be less than 11 feet, which could lead to a larger fire flow of 1,500 gpm. Figure 4 shows a residential neighborhood near the Fort Myers Beach Fire Control District. As discussed with the Town Staff and Fire Control District, AECOM recommends using a fire flow of 1,000 gpm.

Step 2: Fire Flow Duration Time

The duration of the fire is related to the fire flow, as shown on Table 3. With selected fire flow of 1,000 gpm, the duration of fire should be 2 hours.



Figure 4. Examples of the Close Distance between Two Buildings.

Table 3. Duration of Fire.

NFF (gpm)	Required Duration (hrs)	Class
More than 3,500	4	Individual Property Fire Suppression
3,000 to 3,500	3	Public Fire Suppression
2,500 and less	2	Public Fire Suppression

Other Parameters:

Based on the FMBPWSI Operations Manual and discussions with the Town's representatives, AECOM recommends the following parameters:

- The average population: The seasonal peak population is 25,000, which lasts about 3 months (February to April). Per 2006 census, the permanent population is 6,559. Therefore, the weighted average population shall be 25,000 * 3/12 + 6559 * 9/12 = 11,169 (11,100 is recommended).

- Average daily demand: From January 2007 to August 2007, the total water usage volume is 287,400,000 gallons for a period of total 242 days, based on the Monthly reports to FDEP (Florida Department of Environmental Protection). Therefore, the average daily flow is 287,400,000 gallons / 242 days = 1,187,603 gpd.

- Average daily demand per capita: 1,187,603 gpd / 11,100 persons = 107 gpd per capita (110 gpd per capita), as compared to the ratio of 100 gpd per capita as stated on FMBPWSI Operations Manual.

- Average daily demand per ERU: assume 2.5 person per ERU, the average daily demand per ERU = 110 gpd per capita * 2.5 persons per ERU = 275 gpd/ERU, as compared to the FMBPWSI and LCU's ratio of 250 gpd / ERU.

- The peak day factor (PDF) shall be 2.5 per FMBPWSI Operations Manual. The peak hour factor (PHF) shall be 3.5.

2.2 Water Demand

By applying the parameters previously stated in the Basis of Design, AECOM estimated the ERU-based water demand for the proposed water distribution network for four scenarios: AADD (Annual Average Daily Demand), PDD (Peak Day Demand), PDD+FF (Peak Day Demand + Fire Flow), and PHD (Peak Hour Demand). They are summarized on Table 4.

Table 4. Summary of Water Demands.

Scenario	**AADD**	**PDD**	**PDD+FF**	**PHD**
Total ERU[1]	9,589	9,589	9,589	9,589
Demand (gpm)	1,831	4,578	5,578	6,409
Demand (gpd)	2,636,975	6,592,438	8,032,438	9,229,412

Note: 1. The total ERU is counted from the water system plans and the GIS condominium data, provided by the Town.

The reported average daily demand and peak day demand are 1,187,603 gpd and 2,190,000 gpd, respectively, based on the monthly reports to FDEP. The actual reported average daily demand is approximately 45 percent of ERU-based calculated average daily water demand, while the actual peak day demand is approximately 33 percent of ERU-based calculated peak day demand. This is because the reported demands are based on the real water usage while the calculated demands are based on the design assumption that all residences are occupied. The ERU-based calculated flows are used in the hydraulic modeling.

2.3 Hydraulic Modeling

By applying the parameters previously stated in the Design Criteria (Table 1) and the estimated water demand (Table 4), AECOM developed a hydraulic model of the proposed water distribution network and evaluated it for two different modeling scenarios using H2OMAP: PDD+FF (Peak Day Demand + Fire Flow) and PHD (Peak Hour Demand).

PDD + FF (Peak Day Demand + Fire Flow)

The fire flow condition is simulated by adding a fire flow of 1,000 gpm to one of the nodes where a fire hydrant is located. The fire is assumed to last 2 hours As shown on Table 4, the total estimated flow at the PDD condition is 4,578 gpm, thus the total combined of water demand at PDD + FF is 5,578 gpm. The total water demand under this condition is the controlling factor that is used to size the water mains to maintain a minimum residual pressure of 20 psi. As stated in the Basis of Design, under this scenario the assumed feeding pressure and chlorine concentration at the entry point to the system is 50 psi and 2.0 mg/L. The fire flow condition is simulated separately at two different nodes: Fire Hydrant 731 (FH-731) located on Bay Beach Lane, Fire Hydrant 755 (FH-755) located at

the corner of Lagoon Road and Buccaneer Drive, Fire Hydrant 765 (FH-765) located on the south end of Estero Boulevard, and Fire Hydrant 200 (FH-200) located at the north end of Estero Boulevard. The selection of these fire hydrants is based on the Peak Day Demand condition simulations, which show the lowest pressures at the south end of the island. Therefore, the most sensitive fire hydrants were determined to be Fire Hydrants 731, 755, and 765. Fire Hydrant FH-200 is the farthest one at the north end of the island, which can serve as one pressure monitoring point of the system. Table 5 shows that the residual pressures at various critical nodes under these three fire flow conditions. All nodes on Table 5 meet the pressure requirements except for Node 600, and Fire Hydrants FH-731 and FH-755. The pressures at Node 600, FH-731 and FH-755 are 2.89, 2.26 psi and -2.96 psi, respectively. All three are below required residual pressure of 20 psi. Therefore, improvements are recommended to upgrade the hydraulic conditions along the Bay Beach Lane community and Buccaneer Lagoon community. The photos of four fire hydrants are shown below.



Figure 5. Critical Fire Hydrants (FH-731, FH-755, FH-765, and FH-200).

PHD (Peak Hour Demand)

The second condition evaluates the existing water distribution system and its capacity to perform under the Peak Hour Demand condition. As shown on Table 4, the total estimated

water demand under this condition is 6,409 gpm. Similar to PDD+FF, the assumed feeding pressure and chorine concentration are 50 psi and 2.0 mg/L, respectively. Table 5 shows that the residual pressures at various critical nodes under PHD scenario. All nodes on Table 5 meet the pressure requirements except Node 600. The pressure at Node 600 under the PHD scenario is 28.26 psi, which is less than 35 psi. Therefore, improvements are needed to upgrade the hydraulic conditions along the Bay Beach Lane community.

Based on the hydraulic analyses above, apparently, the Bay Beach Lane community where Node 600 is located is a potential problem area under both PHD and PDD+FF at FH-731 or FH-755 scenarios. This is because there is only one 10-inch water main to feed a heavy population dense area (high rise condominiums). Also, another potential problem area is Buccaneer Lagoon community, which cannot deliver required residual pressure of minimum 20 psi at the fire hydrant FH-755. The hydraulic modeling results match the reported low pressure complains received at FMBPWSI.

The FMBPWSI Operations Manual states: all water mains shall be sufficiently looped and in no case shall water mains be less than 8-inch in diameter unless specifically approved by FMBPWSI. Therefore, the minimum 8-inch pipe will be recommended to update the water system. For water mains at the dead end of side streets, a minimum 6-inch might be used based on case by case hydraulic modeling results. For water mains connected to fire hydrants, a minimum 8-inch pipe should be used to meet a fire flow of 1,000 gpm, based on the hydraulic modeling. However, about 30 years ago, most of the pipes along side streets from the Estero Boulevard to where fire hydrants are connected to were upgraded to minimum 6-inch PVC pipes. Based on the modeling results, 6-inch pipes can meet a fire flow of 750 gpm but cannot provide adequate fire flow of 1,000 gpm at minimum 20 psi residual pressure.

Based on the hydraulic modeling results, recommendations are:

- Bay Beach Lane community: the existing 10-inch pipe should be replaced with a minimum 12-inch pipe. The existing 10-inch PVC pipe is approximately 3,200 feet from the corner Estero Boulevard and Bay Beach Lane to the fire hydrant FH-731 on Bay Beach Lane. This pipe is still in operating condition but is already more than 30 years old. Therefore, AECOM recommends adding one 3,200 feet 12-inch PVC water main parallel to the exiting 10-inch water main instead of replacing the existing 10-inch PVC pipe. This can provide needed redundancy and add a loop to exiting water mains, which is important to the high-dense high-rise community.
- Buccaneer Lagoon community: the 4-inch and smaller pipes should be replaced with minimum 8-inch PVC pipes per FMBPWSI Operations Manual. As shown on the hydraulic model, approximate 6,000 feet 8-inch PVC pipes are needed to replace existing pipes.

III. Conclusions and Recommendations

The results of hydraulic modeling identified two areas with low pressure: Bay Beach Lane community and Buccaneer Lagoon community. Low pressure complains received at Beach Water Bay Beach Lane community and fire hydrant test data provided by the Fire Control District confirm AECOM's findings. Based on the hydraulic modeling, Recommended Standards for Water Works, and current updating FMBPWSI Operations Manual, AECOM recommends the following improvements:

- Bay Beach Lane community: the existing 10-inch pipe should be replaced with a minimum 12-inch pipe. The existing 10-inch pipe is approximately 3,200 feet from the corner Estero Boulevard and Bay Beach Lane to the fire hydrant FH-731 on Bay Beach Lane. This pipe is still in operating condition. Therefore, AECOM recommends adding one 3,200 feet 12-inch PVC pipe parallel to the exiting pipe. This can provide needed redundancy and add a loop to exiting water mains, which is important to the high-dense high-rise community.
- Buccaneer Lagoon community: the 4-inch and smaller pipes should be replaced by minimum 8-inch PVC pipes per FMBPWSI Operations Manual. As shown on the hydraulic model, approximate 6,000 feet 8-inch PVC pipes are needed to replace existing pipes.

References

American Water Works Association (2005), Computer Modeling of Water Distribution Systems, Second Edition, 2005

American Water Works Association (1998), Distribution System Requirements for Fire Protection, AWWA Manual M-31, Denver, Colorado

Huo, J., Eckmann, D.H., and Hoskins, K.P. (2007) Hydraulic Simulation and Variable Speed Pump Selection of a Dual-function Pumping Station: Pumping Treated Water to a Reclaimed Water System or Deep Injection Well System, Proceeding of ASCE/EWRI'07 World Water & Environmental Resources Congress, Tampa, Florida

Huo, J., Garland, R.H., and Shimokubo, R. (2008) Hydraulic Modeling and Engineering Design of the Big Coppitt Wastewater Collection System, Proceeding of ASCE/EWRI '08, World Water & Environmental Resources Congress, Honolulu, Hawaii

Insurance Services Office (ISO), Fire Protection Rating System (1998)

Recommended Standards for Water Works, Great Lakes – Upper Mississippi River Board of State and Provincial Public Health and Environmental Managers, 2003 Edition

Walski, T.M.; Chase, D.V.; Savic, D.A. (2001) Water Distribution Modeling, First Edition, Haestad Methods, Inc., Waterbury, CT, USA

Abstract

Innovative strategies alleviate water stress in South East Queensland, Australia

Brisbane, located in South East Queensland, Australia, is one of the fastest growing major metropolitan areas in Australia and Queensland's state capital. In the past seven years, rapid population growth and unprecedented drought has placed tremendous pressure on Brisbane's drinking water supply. As a result, in July 2007, the combined dam levels fell to a historical low of 17 percent, or less than 16 months supply. Recycled water is one of several strategies that the Queensland Government has adopted as part of its efforts to secure the region's drinking water supplies and to support sustainable economic growth. The Bundamba Advanced Water Treatment Plant (BAWTP) is part of the AU$2.5 billion Western Corridor Recycled Water Project that will produce up to 232 megaliters of purified recycled water each day for use in power stations, industry, agriculture and, should the regional water storages fall below 40 percent, to supplement the Wivenhoe Dam.

Black & Veatch entered a joint venture with Thiess to design, build, and commission the BAWTP. The BAWTP consists of two stages – Stages 1A and 1B – with a combined capacity of 66 million liters per day (ML/d) (17.4 mgd). The plant purifies secondary treated wastewater from four municipal wastewater treatment plants. Treatment trains feature pretreatment by coagulation/flocculation, followed by microfiltration, reverse osmosis, UV/hydrogen peroxide, and post-treatment/stabilization in series. Water that meets Australian Drinking Water Guidelines is produced and pumped to three power stations located at Swanbank, Tarong and Tarong north. These plants had previously sourced water from the Wivenhoe Dam - the main water supply for Brisbane and surrounding area. This paper will focus on the commissioning, startup and performance testing of the BAWTP Stage 1B. It will discuss individual treatment processes, waste treatment processes and their performance and optimization. This paper also discusses the plant's capability to manage contaminants, in particular endocrine disrupting chemicals.

Innovative strategies alleviate water stress in South East Queensland, Australia

Hua Jiang[1], Scott Freeman[2] and Jonathan Bates[3]

1. Black & Veatch, 8400 Ward Parkway, Kansas City, MO 64114; PH (913) 458-3067; FAX (913) 458-3626; email: JiangH@bv.com (to whom correspondence should be addressed)
2. Black & Veatch, 8400 Ward Parkway, Kansas City, MO 64114; PH (913) 458-3421; FAX (913) 458-3626; email: FreemanSD@bv.com
3. Black & Veatch, Brisbane, Queensland, Australia; PH +61 (7) 3816-8910; email: BatesJM@bv.com

Introduction

Brisbane is the state capital of Queensland, Australia. It is situated on South East Queensland's Brisbane River, on a low-lying floodplain between Moreton Bay and the Great Dividing Range. With a population of 1.8 million, it is Australian's third-most populous city and one of its fastest-growing metropolitan areas. From 2001 to 2008, Brisbane experienced the worst drought in more than 100 years (Queensland Water Commission, 2008). The drought, combined with the rapid population growth, generated tremendous pressure on the area's drinking water supply. As a result, the combined dam levels which provide Brisbane's drinking water supply fell to 17 percent in July 2007 (Queensland Water Commission, 2008). To cope with the water shortage and to support the region's sustainable development, the Queensland Government initiated the following strategies (Wallis-Lage et al. 2007 and Freeman et al., 2008):

1. Evaluation of new groundwater sources.
2. Seawater desalination.
3. Pipeline-interconnection projects.
4. Modifications to the elevation of the Mt. Crosby Water Treatment Plant (Brisbane's primary water treatment plant) weir.
5. System-pressure reduction to reduce leakage.
6. Water-saving initiatives.
7. Two new dams.
8. Water reuse.

The Western Corridor Recycled Water Project (WCRW) is an AU$2.5 billion water supply network designed to diversify South East Queensland's drinking water sources. The project involves treating wastewater to the highest standard – resulting in purified recycled water that is supplied to power stations, industry, agricultural customers and, should regional water storages fall below 40 percent, the Wivenhoe Dam. When completed, the project will have the capacity to deliver up to 232 megaliters (ML) of purified recycled water a day to end users. The Queensland Government is contributing $2.1 billion to the project and the Australian Government has contributed $408 million through the Water Smart Australia Program (WCRW, 2007a). This cost reflects the scale and aggressive schedule for this project. The project comprises three advanced water

treatment plants located at Bundamba, Luggage Point and Gibson Island, more than 200 kilometres of large diameter pipelines, as well as associated water storage tanks and pump stations. The plants treat wastewater from the region's six municipal wastewater treatment plants.

BAWTP was the first plant to be built and consists of two stages – Stage 1A and Stage 1B. Stage 1A was successfully designed, built, and commissioned in 17 months and has been in production since August of 2007 as scheduled (WCRW, 2007b). Stage 1B was commissioned in May 2008. This paper will focus on Bundamba Stage 1B and will discuss the performance test results.

Liquid Treatment Processes

Stage 1A of the BAWTP purifies treated wastewater from the nearby Bundamba Wastewater Treatment Plant (WWTP), and Stage 1B purifies treated wastewater from Bundamba, Oxley, Goodna, and Wacol WWTPs. The BAWTP has a rated plant capacity of 66 ML/d (17.4 mgd), which consists of 30 ML/d (7.9 mgd) for Stage 1A and 36 ML/d (9.5 mgd) for Stage 1B. The Stages 1A and 1B treatment trains consist of pretreatment by coagulation/flocculation/sedimentation, microfiltration (MF), reverse osmosis (RO), advanced oxidation with UV and hydrogen peroxide, and stabilization with lime and carbon dioxide. A schematic of the main liquid treatment processes is presented at Figure 1. The Stage 1A contract was awarded to a joint venture by Thiess (Brisbane, Queensland, Australia) and Black & Veatch (Kansas City, MO, USA) on March 30, 2006. The design was completed in October 2006, and construction began in November 2006. Stage 1A produced "first water" in August 2007. Construction of Stage 1B started concurrently with Stage 1A in November 2006; the facility was commissioned in May 2008. It has been pumping purified recycled water to Swanbank, Tarong, and Tarong north power stations ever since.

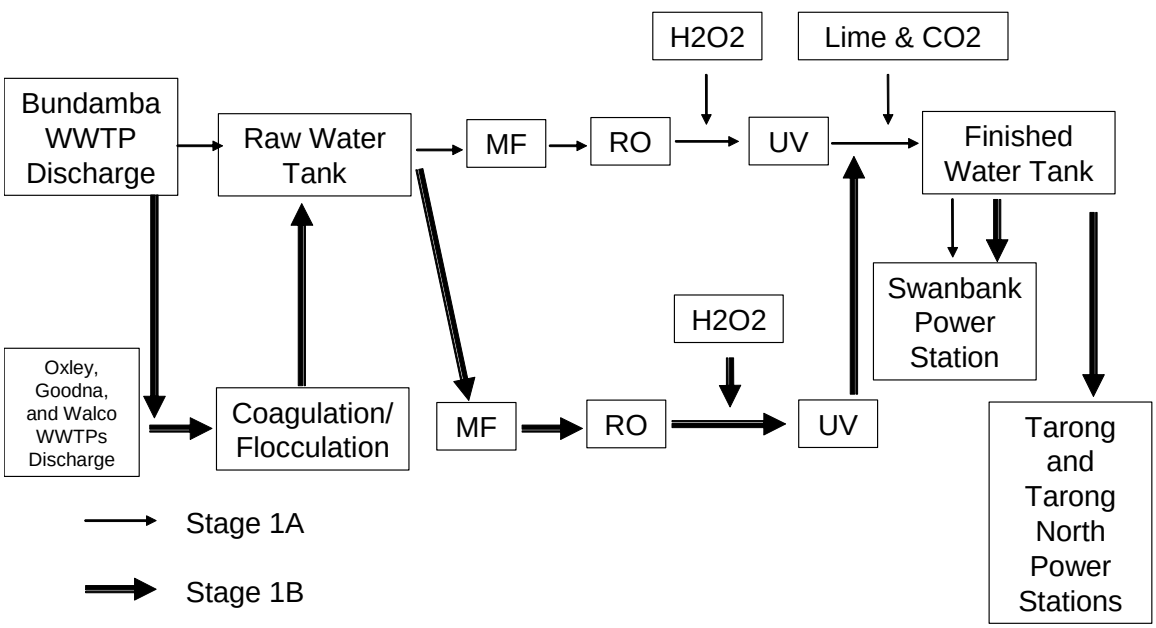

Figure 1. BAWTP main plant liquid treatment process schematic

Pretreatment. Pretreatment is provided for the influent to BAWTP to remove phosphorus. Ferric chloride is used as coagulant. Ferric ion reacts with phosphorus in the water to form phosphate precipitate. The basic overall reaction is shown below (Metcalf & Eddy, Inc, 2003):

$$Fe^{3+} + H_nPO_4^{3-n} \leftrightarrow FePO_4 + nH^+$$

The phosphate precipitates are then settled at the plate settler and removed as sludge. Pretreatment was not provided for the influent to Stage 1A as phosphorus in the Bundamba WWTP effluent is removed to insignificant levels before it enters BAWTP. Feedwater to Stage 1B includes effluent from additional WWTPs with elevated phosphorus levels, so the pretreatment process was incorporated with Stage 1B.

Pre-disinfection is provided to control membrane biofouling in the microfiltration (MF) and reverse osmosis (RO) downstream. Ammonia sulfate and sodium hypochlorite are added in series at a chlorine to ammonia ratio of 3.5 : 1 before the water enters the coagulation basin. The hypochlorite reacts with ammonia instantaneously to form chloramine. Hypochlorite is dosed at a dosage to produce and maintain a set level of combined chlorine residual in the RO feed water.

The pretreatment process at BAWTP includes two trains, each of which consists of two stages of rapid mixing/flocculation and a plate settler. Each rapid mixing/flocculation basin is sized 14 m X 5 m X 9 m and provides hydraulic detention time of about 12 minutes at a peak flow rate of 150 ML/d. The plate settler is manufactured by MRI (Golden, CO, USA). Each plate settler unit consists of eight plate pack rows and each row has three plate packs. The hydraulic loading is 0.60 m/h (0.24 gpm/ft^2).

Microfiltration. MF is used at the BAWTP Stage 1B facility to treat settled water and serve as a pretreatment step for the RO membrane downstream. The MF membrane is manufactured by Siemens/Memcor (South Windsor, New South Wales, Australia) and the treatment train consists of five MF units. Each unit has a capacity of 8.8 ML/d and the average net flux is 30.78 liters per square meter per hour (lmh) (18.13 gfd).

Reverse osmosis. The RO unit is at the heart of BAWTP treatment process. It removes most of the impurities from the influent water and produces a high-quality permeate. The RO process consists of five trains in parallel. Each train contains 11 pressure vessels and is configured in three stages (7 x 4 x 2) in series. Each pressure vessel houses five membrane elements. The RO membrane is 18 inch Koch MegaMagnum manufactured by Koch Membrane Systems (Willington, MA, USA). It is the largest commercial application of large diameter RO membrane by plant capacity. The RO train operates at a recovery of 85 percent. The feed water pressure is about 31 bar (450 psi). Conductivity of the feed water is about 1200 to 1400 μs/cm and combined permeate conductivity is about 50 μs/cm.

UV Advanced Oxidation. The RO permeate is further treated by a UV-hydrogen peroxide unit. Hydrogen peroxide is added to the permeate before it enters the UV unit. The UV unit consists of two trains, and each of which includes two reactors in series. The UV reactors are provided by Trojan Technologies, Inc. (London, Ontario, Canada) and are equipped with high-intensity low pressure amalgam UV lamps. Each reactor contains 72 UV lamps. The UV intensity of each reactor is in the range of 12 – 15 mW/cm^2. This process is designed to remove remaining micro-contaminants that may have passed through the previous treatment processes. Contaminants of particular focus are endocrine disrupting chemicals (EDC) and chloramine disinfection byproducts, such as n-nitrosodimethylamine (NDMA). The UV dosage applied is chosen to achieve 1-log removal of NDMA and 0.5-log removal of 1, 4-dioxane. These parameters were established as design basis factors during the projects' planning, even though the compounds and concentrations had not been quantified.

Stabilization and post-treatment. RO permeate is highly unstable and aggressive. Lime and carbon dioxide are added to the UV treated permeate before it enters the finished water storage tank. Quicklime is used at BAWTP and hydrated lime is generated onsite. Carbon dioxide is fed in gas form. Dosages of lime and carbon dioxide are determined to achieve a pre-set range of calcium carbonate precipitation potential (CCPP) of -5 to 0 at the inlet of the finished water storage tank.

Waste Treatment Processes

Sludge generated in the pretreatment process is thickened by a gravity thickener and dewatered by centrifuges. The centrifuge centrate is combined with RO brine and are treated further by nitrification and de-nitrification units before being discharged into the Brisbane River. The dewatered sludge is hauled off-site for disposal. The waste treatment process schematic is presented in Figure 2.

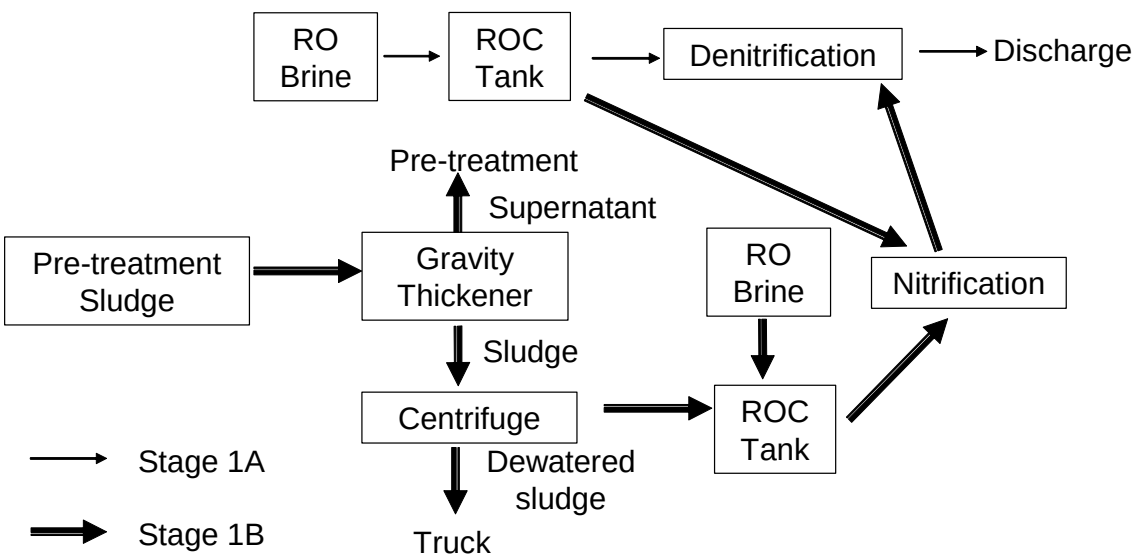

Figure 2. BAWTP waste treatment process schematic

Gravity thickener. Settled sludge is withdrawn periodically from the pretreatment basin and pumped to a gravity thickener. The gravity thickener at BAWTP is an above-ground, pre-manufactured circular structure by Outotec Pty Ltd (Frenchs Forest, New South Wales, Australia). It has an inside diameter of 10.5 m (34.4 ft). The thickened sludge is pumped to a holding tank for further processing. A polymer feed system is provided with the gravity thickener. To date, the polymer has not been required for the gravity thickener.

Centrifuge. Two centrifuges are provided at BAWTP. The centrifuges are manufactured by Alfa Laval. Polymer is fed to the sludge before it enters centrifuge. The dewatered sludge cake is trucked off-site. The centrate is pumped to a holding basin, mixed with RO brine, and then sent to the nitrification and denitrification units for further treatment before being discharged into to the river.

Nitrification. Nitrification followed by de-nitrification downstream is used to convert ammonia in the mixed centrate and RO brine to nitrate (nitrification) and then nitrogen gas (de-nitrification). The nitrification system at BAWTP consists of three identical basins. The first two basins are in parallel and the third basin is in series for effluent polishing. Each basin has a volume of 250 m^3 (8829 ft^3) and a working volume of 200 m^3 (7063 ft^3). The basin is filled with polyethylene discs that provide the surface area for nitrifying bacteria to grow with compressed air constantly introduced at the bottom of the basin. The ammonia concentration at the basin inlet and outlet is monitored online.

Denitrification. The denitrification unit is manufactured by Severn Trent Services (Pittsburgh, PA, USA). The unit consists of 4 basins that are loaded with high-grade silica sand media. Methanol is fed at the unit inlet to provide nutrients for the growth of denitrifying bacteria. The concentration of nitrate at the inlet and outlet of the unit is monitored by online analyzers.

Plant Performance

BAWTP Stage 1B performance testing commenced in April 2008 and lasted for 30 days. The performance goal was to meet contractual agreements relating to water quality and production capacity. The finished water was required to meet Australian Drinking Water Guidelines (Australian Government, 2004). One of the concerns regarding recycled wastewater is the presence of EDCs. The specific limits for the concentration of EDCs in finished water were included in the contractual agreement. Table 1 lists finished water quality goals and sampling frequency for the BWAT Stage 1B performance test. The finished water is defined as a 24-hour composite sample at the inlet of the finished water tank.

Table 1. BAWTP Finished Water Quality Goals

Parameters	Units	Specification Requirement		Sampling Frequency
Alkalinity	mg/L	>	40	Daily
Calcium Carbonate Precipitation Potential (CCPP)	-		0 to -5	Daily

Clostridium perfringens, 95%ile	cfu/100mL	<	10	Weekly
Clostridium perfringens, median	cfu/100mL	<	1	Weekly
EDC Estrone (E1)	nano-g/L	<	3	Daily
EDC 17-beta Estradiol (E2)	nano-g/L	<	1	Daily
EDC Ethinylestradiol (EE2)	nano-g/L	<	0.1	Daily
EDC Total PNEC	nano-g/L	<	1	Daily
EDC Nonlyphenol (NP)	nano-g/L	<	7	Daily
Hardness, as CaCO3, 21 Day average	mg/L	>	50	Daily
Nitrogen (Total), 50th Percentile	mg/L	<	0.8	Daily
Nitrosodimethylamine (NDMA)	nano-g/L	<	10	Daily
Phosphorus Total, 50th Percentile	mg/L	<	0.13	Daily
Total Organic Carbon (TOC)	mg/L	<	1	Daily
Acrylamide	mg/L	<	0.0002	Weekly
Antimony	mg/L	<	0.003	Weekly
Benzene	mg/L	<	0.001	Weekly
Bromate	mg/L	<	0.02	Weekly
Carbon Tetrachloride	mg/L	<	0.003	Weekly
Chlorine	mg/L	<	5	Weekly
Chlorine Dioxide	mg/L	<	1	Weekly
Chlorite	mg/L	<	0.3	Weekly
Chlorobenzene	mg/L	<	0.33	Weekly
Chromium as Cr (VI)	mg/L	<	0.05	Weekly
Cyanide	mg/L	<	0.08	Weekly
Cyanogen chloride	mg/L	<	0.08	Weekly
Dichlorobenzene (1,2-Dichlorobenzene)	mg/L	<	1.5	Weekly
Dichlorobenzene (1,4-Dichlorobenzene)	mg/L	<	0.04	Weekly
Dichloroethanes (1,2-Dichloroethane)	mg/L	<	0.003	Weekly
Dichloroethenes (1,1-Dichloroethene)	mg/L	<	0.03	Weekly
Dichloroethenes (1,2-Dichloroethene)	mg/L	<	0.06	Weekly
Dichloromethane	mg/L	<	0.004	Weekly
Epichlorohydrin	mg/L	<	0.0005	Weekly
Ethylbenzene	mg/L	<	0.3	Weekly
Ethylenediamine tetraacetic acid (EDTA)	mg/L	<	0.25	Weekly
Formaldehyde	mg/L	<	0.5	Weekly
Hexachlorobutadiene	mg/L	<	0.0007	Weekly
Iodide	mg/L	<	0.1	Weekly
Lead	mg/L	<	0.01	Weekly
Mercury	µg/L	<	1	Weekly
Molybdenum	mg/L	<	0.05	Weekly
Monochloramine	mg/L	<	3	Weekly
Nickel	mg/L	<	0.02	Weekly
Nitrilotriacetic acid	mg/L	<	0.2	Weekly
Organotins (Tributylin Oxide)	mg/L	<	0.001	Weekly
PAHs (Benzo(a)pyrene)	nano-g/L	<	10	Weekly
Plasticisers (Di(2-ethylhexyl)adipate)	mg/L	<	0.01	Weekly
Styrene	mg/L	<	0.03	Weekly
Sulfate	mg/L	<	500	Weekly
Tetrachloroethene	mg/L	<	0.05	Weekly

Toluene	mg/L	<	0.8	Weekly
Trichloroacetaldehyde	mg/L	<	0.02	Weekly
Total Trichlorobenzenes	mg/L	<	0.03	Weekly
Total Trihalomethanes	mg/L	<	0.25	Weekly
Uranium	mg/L	<	0.02	Weekly
Vinyl Chloride	mg/L	<	0.0003	Weekly
Xylenes	mg/L	<	0.6	Weekly
2-4-D	mg/L	<	0.03	Weekly

The following section was intended to cover plant performance test results. However, these data can not be published before the pending release of the water quality report by the Queensland Water Commission (Queensland Water Commission, 2009), therefore these will be not presented here. The test results will be ready to be presented at the conference. In the mean time, the reader can refer for detailed information to the pending water quality report which is due to be issued soon. Although not shown here, the performance test results indicate that the finished water meets the water quality goals outlined in the contractual agreements, and the finished water meets the Australian Drinking Water Guidelines.

Conclusion and Discussion

The 66 ML/d BAWTP, which incorporates innovative treatment processes such as MF, RO and UV-H_2O_2 to produce purified recycled water, has been successfully commissioned. The BAWTP has been providing up to 40 ML/day of high-quality treated water to three power stations located at Swanbank, Tarong and Tarong north since June 2008. Water produced at the BAWTP will also be used for industry, agriculture and, should regional water storages fall below 40 percent, the Wivenhoe Dam. The treatment process used at BAWTP produce water that has been verified to satisfy Australian Drinking Water Guidelines. The plant plays a significant role in alleviating water stress and supporting sustainable social and economical development in the region. Brisbane was able to lift extreme stringent Level 6 (Target 140) water restriction on July 31, 2008. The Queensland Government anticipates its new water infrastructure initiatives will remove the need to implement such tight restrictions in the future.

Acknowledgment

The authors thank WaterSecure of Brisbane, Australia for supporting this article. WaterSecure is a sustainable water business the develops new water sources for South East Queensland and manages the Western Corridor Recycled Water Project and Gold Coast Desalination Project on behalf of the Queensland Government. Special thanks are extended to Dr. Cedric Robillot and Paul Rees of the WaterSecure for reviewing this manuscript and for providing constructive comments.

References

Australia Government. (2004). "National Water Quality Management Strategy: Australian Drinking Water Guidelines 6." National Health and Medical Research Council, Natural Resource Management Ministerial Council, Canberra, Australia

Freeman, S., Bates, J. Wallis-Lage, C. and McEvoy, J. (2008). "Drought Relief in South East Queensland, Australia, Provided by Membrane-Reclaimed Water." *J. AWWA*, 100(2), 40-52

Metcalf & Eddy, Inc. (2003). "Chapter 6 - Chemical Unit Processes in *Wastewater Engineering Treatment and Reuse*." fourth edition, Tata McGraw Hill Publishing Company Limited, New Delhi, India

Queensland Water Commission. (2008). "Purified Recycled Water for Drinking: The Technical Issues." Brisbane, Australia

Queensland Water Commission. (2009). "The Interim Water Quality Report for the Western Corridor Recycled Water Project." Brisbane, Australia

Schock, M. (1999). "Chapter 17 – Internal Corrosion and Deposition Control in *Water Quality & Treatment*" fifth edition, American Water Works Association, McGraw Hill, Inc

Wallis-Lage, C. Freeman, S., Steichen, M. Bates, J., Pressdee, J., Peries, I. and McEvoy, J. (2007). "No Rain, No water, Big Problem: Water Reuse Should Ease Water Supply Strain in Brisbane, Australia." Water Environment & Technology Magazine, August Issue, 60-63

Western Corridor Recycled Water Project. (2007a). "Press Release – Site Guide: Bundamba Advanced Water Treatment Plant." Brisbane, Australia

Western Corridor Recycled Water Project. (2007b). "Press Release – Stage 1A First Water." Brisbane, Australia

Multi-objective Design of Transient Network Models

Bong Seog Jung[1], Misgana Muleta[2], and Paul F. Boulos[3]

[1]Engineering Director, MWH Soft, 618 Michillinda Avenue, Suite 200, Arcadia, CA 91007; PH 626-568-6822; email: bongseog.jung@mwhsoft.com
[2]Assistant Professor, California Polytechnic State University, San Luis Obispo, CA 93407; PH 805-756-1337; email: mmuleta@calpoly.edu
[3]President and COO, MWH Soft, 380 Interlocken Crescent, Suite 200, Broomfield, CO 80021; PH 303-533-1933; email: paul.boulos@mwhsoft.com

ABSTRACT

The optimal design of a water distribution system under transient conditions is formulated as a two-objective optimization problem. The objectives are minimization of the total pipe costs and maximization of the hydraulic reliability for the transient network design model. Unlike most optimization models in which demands are set to their end-of-life levels, this approach assumes that the demand loadings vary throughout the design life of the system. Evolutionary algorithms are applied to support efficient search for Pareto optimal solutions to the dual-objective optimization problem. An example application is presented and relevant conclusions are stated.

INTRODUCTION

A water distribution system is a complex network of pipes, pumps, valves, reservoirs, and storage tanks that is used to transport water from source to consumer. It is designed and operated to consistently deliver water in sufficient quantity, of acceptable quality, at appropriate pressure, as economically as possible. Traditionally, after choosing critical loading conditions in distribution system design, the greater of peak-hour demand or peak-day demand and a chosen fire flow, optimization methods are applied to select the most economical set of pipe sizes that will produce the desired range of pressures in the network. The rationale underlying the economical design is that, by selecting the smallest possible diameter set to minimize cost, pressures are marginally above an acceptable level for the specified design loading conditions. However, because the design problem is posed as a static one (i.e., the design loads are not treated as dynamic variables), the conventional design could well be suboptimal under transient pressures, or even seriously inadequate for other design events.

The optimization of a water distribution system under hydraulic transient conditions is difficult due to the complexity of the transient flow problem. Although a transient analysis is essential to estimate the worst-case events in the system, its inherent complexities have induced hydraulic design engineers to focus perhaps too much on steady state conditions. However, transient regimes in water distribution systems are both inevitable and naturally occurring (Boulos et al., 2005). Recent water quality studies have emphasized the need for transient analysis of large pipe

networks to properly assess the potential level of intrusion associated with negative pressure events and the resulting impact on disinfectant residual effectiveness (Besner, 2007; Boulos et al., 2006; NRC, 2006; Fleming et al., 2006; Friedman et al., 2004; LeChevallier et al., 2002-2003; Kirmeyer et al., 2001). In reality, since all pipeline systems leak and hydraulic transients will occur continuously in a water distribution system, it is not surprising that low-pressure transient events offer considerable potential to draw untreated and possibly hazardous water into the piping system.

Numerous hydraulic transient approaches have been developed to identify system weak points, to predict the potentially destructive effects of hydraulic transients under various worst-case scenarios, and to evaluate how they may possibly be eliminated or controlled (e.g., Wylie and Streeter, 1993; Chaudhry, 1987; Thorley, 2004; Boulos et al., 2005; Wood et al., 2005; Ghidaoui et al., 2005; Jung et al., 2007). In particular, Boulos et al. (2005) provided a detailed transient analysis flow chart for the selection of components for surge control and suppression in water distribution systems, and concluded that a transient analysis should always be carried out to determine the impact of each proposed strategy on the resulting system performance. Jung et al. (2007) argued that only a systematic transient analysis can be expected to resolve complex transient characterizations and adequately protect water distribution systems.

In addition, optimization methods have been widely applied to many problems associated with water distribution system design, management and operation. Alperovits and Shamir (1977) applied linear programming and Lansey and Mays (1989) suggested using nonlinear programming to optimize component sizing and the operational decisions arising in water distribution systems. Simpson et al. (1994) and Dandy et al. (1996) compared a Genetic Algorithm (GA) approach to both complete enumeration and nonlinear programming in the context of pipeline optimization. Much of the pipeline optimization literature has been concerned with systems under steady or near steady flow conditions; however, a few optimization approaches dealt with operating conditions pertaining to system integrity, safety and performance. Laine and Karney (1997) applied optimization to a simple pipeline connecting a pump and a storage reservoir. A complete enumeration scheme as well as a probabilistic selection procedure were incorporated with both transient and steady state analysis. Lingireddy et al. (2000) described a surge tank design model based on a bi-level genetic optimization framework that produces optimal tank sizes while satisfying a specified set of pressure constraints. Jung and Karney (2004) considered the impact of transients on the choice of optimal diameter in a network considering both steady and transient criteria. More recently, Jung and Karney (2006) presented an optimum selection approach of hydraulic devices for water hammer control in a water distribution system. GA and Particle Swarm Optimization (PSO) were used to optimize the preliminary selection, sizing and placement of surge protection devices.

In this paper, the optimal design of a water distribution system under transient conditions is formulated as a two-objective optimization problem. The objectives are

minimization of the total pipe costs and maximization of the hydraulic reliability for the transient network design model. Unlike most optimization models in which demands are set to their end-of-life levels, this approach assumes that the demand loadings vary throughout the design life of the system. Evolutionary algorithms are applied to support efficient search for Pareto optimal solutions to the dual-objective (pipe costs and hydraulic reliability) optimization problem. The model is tested (by simulation) on the classical New York tunnel system and relevant conclusions are stated.

MATHEMATICAL FORMULATION

Whether designing a water distribution system (WDS) using trial-and-error enumeration methods or with formal optimization tools, a broad range of concerns must be considered. Cost is likely to be the primary emphasis and includes the costs for construction, operation and maintenance. The initial capital investment for the system includes pipes, pumps, tanks, and valves. Energy consumption occurs over time as the system is operated. The main constraints are that the nodal demands are supplied at a minimum pressure. In addition, the network flows and pressure heads must satisfy the governing equilibrium laws of conservation of energy and mass.

In this paper, the optimal design of a water distribution system under transient conditions is formulated as a two-objective optimization problem. The first objective is formulated in Equation (1) as a least-cost optimization problem with the selection of pipe diameters as the decision variables. The second objective is to maximize hydraulic reliability for the transient network design model. This objective given in Equation (2) is formulated to minimize the integration of the transient pressures that are lower than the minimum required level (e.g., datum) or higher than the maximum allowable transient pressure level (e.g., pipe ratings). In contract with traditional optimization models in which demands are set to their end-of-life levels, this approach assumes that the demand loadings vary throughout the design life of the system. The pipe network layout, nodal demands, and minimum head requirements are assumed known. The optimal design of water distribution networks can be stated mathematically as:

$$\text{minimize} \sum_{k \in N_{pipe}} C_k(D_k, L_k) \tag{1}$$

$$\text{minimize} \sum_{i \in N_{node}} \int^{\forall Time} |H_i(t)| dt \text{, where } H < H^*_{\min} \text{ or } H > H^*_{\max} \tag{2}$$

Subject to the governing transient equations

$$\frac{1}{gA_p}\frac{\partial Q}{\partial t} + \frac{\partial H}{\partial x} + \frac{R}{\Delta x} Q|Q|^{n-1} = 0 \tag{3}$$

$$\frac{\partial H}{\partial t}+\frac{a^2}{gA_p}\frac{\partial Q}{\partial x}=0 \tag{4}$$

and a set of algebraic constraints:

$$H_i(t)=C_1,\ \ Q_i(t)=C_2, \text{ where } t=0,\ \ \forall i\in N_{node} \tag{5}$$

$$f(H_i(t),Q_i(t))=C_3, \text{ where } t>0,\ \ i=\text{boundary nodes} \tag{6}$$

$$H_i(t)\geq H_{\min i}, \text{where}\ \ t=0,\ \ \forall i\in N_{node} \tag{7}$$

$$D_k\in\{D\},\ \ \forall k\in N_{pipe} \tag{8}$$

where D_k = discrete pipe diameters selected from the set of commercially available pipe sizes $\{D\}$[Equation (8)]; $C_k(D_k\ L_k)$ = cost of pipe k with diameter D_k and the length L_k; H = piezometric head; and $H^*_{\max}$ and $H^*_{\min}$ are the maximum and minimum permissible heads (say representing pipe ratings or health concerns for negative pressures), respectively. Equations (3) and (4) represent the momentum equation and mass conservation for transient flow in closed conduits (Wylie and Streeter, 1993). Here, x is distance long the centerline of the conduit; t is time; Q = volumetric flow rate; a = celerity of the shock wave; A_p = cross-sectional area of the pipe; and g = acceleration due to gravity. The friction term R in the Equation (3) can be represented by

Darcy-Weisbach: $R=\ f_p\Delta x/2gD_pA_p^2,\ n=2$ (9)

or

Hazen Williams: $R=\ \Delta x/(0.278CD_p^{\ 2.63})^{1/0.54},\ n=1/0.54$ (10)

in which f_p = Darcy-Weisbach friction factor; and C = Hazen-Williams roughness coefficient. The two hyperbolic partial differential equations in (3) and (4) are subject to the initial conditions of Equation (5) and boundary conditions of Equation (6), where C_1, C_2 and C_3 are constants. Initial conditions are typically taken as steady. Simple boundary conditions of constant reservoir level and fixed demand are assumed, but combined relationships between H and Q are typical for most boundaries. Equation (7) requires that the nodal pressure H for any node i (where total number of nodes is N_{node}) is equal to or greater than a specified minimum pressure $H_{\min}$ for steady state condition.

The remaining and challenging question is how to apply an optimization method to the suggested problem of water distribution optimization. Gradient-based mathematical optimization methods (Alperovits and Shamir, 1977; Bhave, 1985) have been widely applied and have provided efficient computational procedures for

achieving a lower cost solution but the methods suffered from some disadvantages, such as: (1) being ineffective at reaching the least cost solution due to zero-gradient optimality criteria, which easily trapped a search process at a local optimal solution; (2) the lack of flexibility in handling discrete design variables and optimizing a partial network that is often required for many practical engineering designs; (3) the complexity of implementing and using the techniques (Wu and Simpson, 2001); and (4) the requirement to compute either first or second derivative information in order to generate improvements in the objective function. Recently, several researchers have used genetic algorithm (GA) optimization for solving such complex WDS optimization (Simpson et al., 1994; Dandy et al., 1996). Ant Colony Optimization (Maier et al., 2003) and Shuffled Frog Leaping Algorithm (Eusuff and Lansey, 2003) have also been applied for obtaining specific optimal designs of WDSs. These methods offers significant advantages over gradient-based optimization approaches in that they do not require any gradient information and search for the optimal solution by continuing to evaluate multiple solution vectors simultaneously.

For the given dual-objective (pipe costs and hydraulic reliability for the transient network design model) problem, genetic optimization is used to circumvent subjective decision making and to generate Pareto optimal solutions for the multi-objective optimization problem. In this study, Nondominated Sorting GA (NSGA), developed by Srinivas and Deb (1994), is employed to find the Pareto optimal solutions. Figure 1 depicts a flowchart of the framework for optimizing the pipeline system considering the dual-objective problem. First, an optimization program initializes the pipe sizes as decision variables, and the pipe cost is calculated. The hydraulic model then analyzes the given system and uses the optimization program to check if the solution satisfies the required constraints given by Equations (3) to (8) and then computes the second objective function shown in Equation (2). With the dual objective function values, the optimization model then evaluates the system and creates a new set of system alternatives for the next iteration. The iterations continue until the optimal solution is reached. This allows rapid solutions to be obtained with a minimal computational overhead.

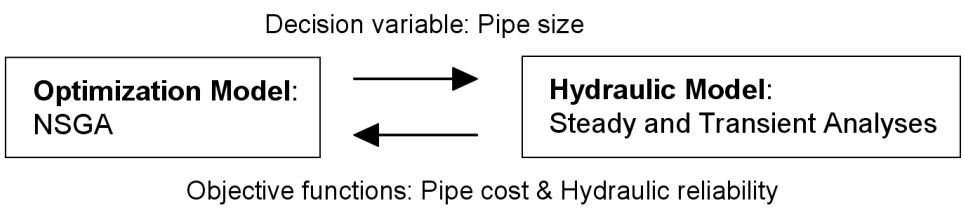

Figure 1. Flowchart of pipeline optimization

CASE STUDY

The proposed method is illustrated using the classical New York tunnel system (Schaake and Lai, 1969). The network, which is shown in Figure 2, has been extensively studied for steady state conditions. It comprises 22 nodes (20 demand

nodes), 21 pipes, and one source node. The system is gravity driven and draws water from the Hillview reservoir to the downstream network. The objective of the optimization problem is to add new pipes parallel to the existing ones. The new pipe diameters need to be selected from 15 available sizes. A single demand pattern (57,130 L/s) was considered and a minimum allowable hydraulic grade was specified for each node. The network and cost data are given in Dandy et al. (1996).

Since the system was first examined in 1969 by Schaake and Lai, numerous subsequent researchers have used it to test the numerical effectiveness, efficacy and performance of their respective techniques (Dandy et al., 1996; Savic and Walters, 1997; Wu et al., 2001; Eusuff and Lansey, 2003; Maier et al., 2003). However, all these approaches were based on steady state optimization only. In this paper, not only the steady state problem is considered, but also the transient analysis is included in the optimization process. By doing so, it is shown that different design decisions would be required, and the restrictive search based on limited operating conditions is likely suboptimal for a broader range of demand loadings.

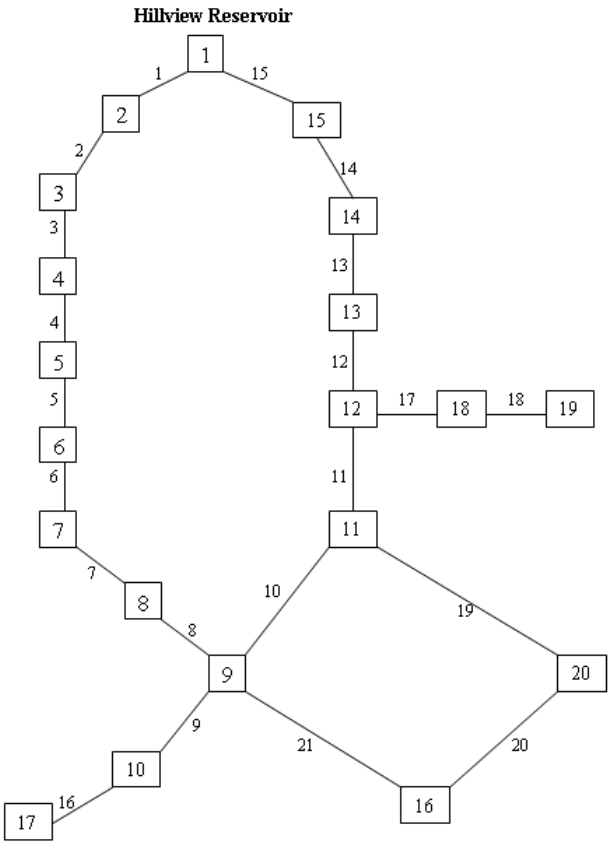

Figure 2. New York tunnel system schematic

To introduce transient conditions into this case study, a variety of possible causes could be selected. For convenience, a valve opening that increases the demand at node 10 from 28 L/s to 4814 L/s for a 1 second period is chosen to characterize the transient performance of the system. This increased demand may represent a fire

flow, a pipe burst, an operator error or a temporary increased in water consumption. The maximum permissible heads $H^*_{\max}$ and $H^*_{\min}$ in Equation (2) are assumed to be 304.8 m and 54.9 m, respectively, for the whole system. Due to the rapid demand increase at node 10, a reduced pressure wave moves through the system. This wave is reflected from the upstream reservoir and then propagates back and forth in the system, being tracked numerically using the method of characteristics (Wylie and Streeter, 1993). The different pipe lengths and sizes in the system create uneven computational lengths in the characteristic grids. The smallest Courant number in the system is 0.019 and it can be adjusted to unity by dividing the pipes into smaller computational units. The process of discretization is repeated until the smallest Courant number exceeds 0.75. After discretization, the smallest Courant number and the computational time step are 0.755 and 1.11s, respectively. For the uneven computational units, a linear timeline interpolation is used to obtain head and flow at a grid point in the characteristic mesh.

The multi-objective method, NSGA, is considered to satisfy Equations (1) to (8). For this problem, the probability of mutation is set to 0.025, the probability of (single-point) crossover is set to 0.9, the population size is set to 400, the length of each chromosome is set to 84, and the simulations are run for 100 generations. For this problem, 16 decision variables including the "do nothing" option make up a solution space of 16^{21} or 1.93 x 10^{25} possible pipe combinations. The NSGA initializes the population of pipe diameters, and then calculates the cost of pipelines and the hydraulic reliability of transient network design model satisfying the given constraints, and then create a new population for the next generation. After 100 generations, the resulting Pareto optimal solutions are shown in Figure 3 and Table 1. The hydraulic reliability results indicate that the previous approaches that considered only steady state design are inadequate for coping with water hammer events. The results also suggest that the proper sizing of pipe diameters is crucially important to prevent water hammer as well as to decrease cost.

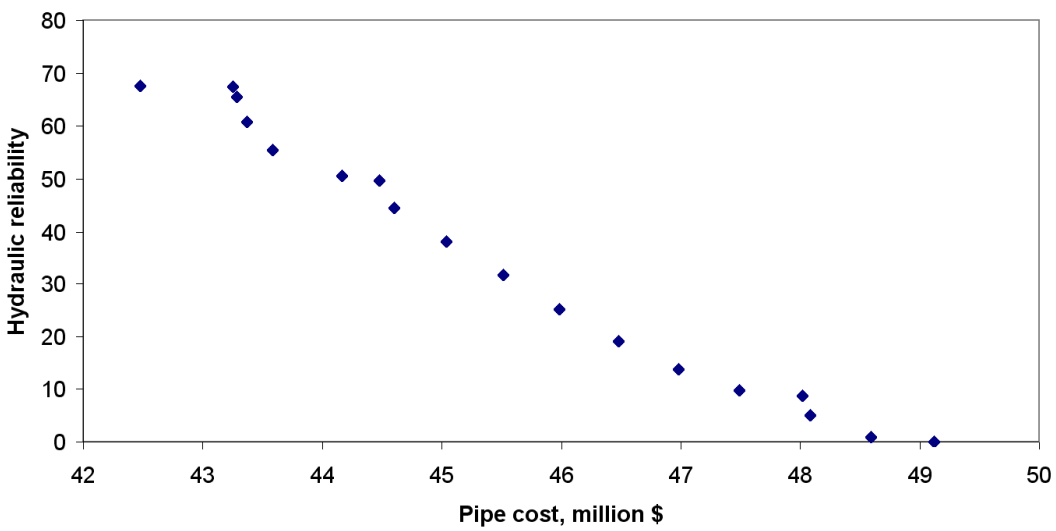

Figure 3. Pareto optimal solutions of pipe cost and hydraulic reliability

Table 1. Pareto optimal solutions for pipe sizes

Pipe	Pipe size (mm)		
1 – 8	-	-	-
9	3900	2700	-
11 – 15	-	-	-
16	3000	3000	3000
17	2100	2100	2100
18	3000	3000	3000
19	2100	1800	1800
20	3000	3000	3000
21	-	-	-
22	1500	1500	1500
Pipe Cost, $ million	49.12108	45.98196	42.47795
Hydraulic Reliability	0	25.21	67.51

CONCLUSION

Transient analysis, despite its significant concern for water distribution system design, is a complicated problem and so is the optimization of a transient control strategy for water distribution systems. The purpose of this paper is to obtain the optimal design of a pipe network by considering simultaneously steady and transient states. The objectives are minimization of the total pipe costs and maximization of the hydraulic reliability for the transient network design model. Unlike most optimization models in which demands are set to their end-of-life levels, this approach assumes that the demand loadings vary throughout the design life of the system. To achieve the dual-objectives, evolutionary algorithms based multi-objective optimization is used to circumvent subjective decision making and generate Pareto optimal solutions.

The case study using the New York tunnel system indicates that the previous approaches that considered steady state design only are inadequate for coping with water hammer events. In addition, the study suggests that proper sizing of pipe diameters is crucially important to prevent water hammer as well as to decrease cost. Although this paper considers the optimal selection of pipe diameters for a surge protection strategy, a more global and comprehensive approach is ultimately needed. Water distribution system optimization should also consider, in addition to pipe size, the transient properties (e.g., operation speed), system characteristics (e.g., system topography, pipe material and thickness) and transient protection devices. This comprehensive design framework will offer a more complete range of systematic surge protection strategies resulting in more reliable cost optimization solutions.

REFERENCES

Alperovits, E., and Shamir, U. (1977). "Design of optimal water distribution systems." *Water Resources Research,* 13(6), 885-900.

Besner, M. C. (2007). *Risk evaluation of drinking water distribution system contamination due to operation and maintenance activities*. Ph.D Dissertation, Universite of Montreal, Quebec, Canada.

Bhave, P. R. (1985). "Optimal expansion of water distribution systems." *Journal of Environmental Engineering*, ASCE, 111(2), 177-197.

Boulos, P. F., Karney, B. W., Wood, D. J., and Lingireddy, S. (2005). "Hydraulic transient guidelines for protecting water distribution systems." *Journal of the American Water Works Association*, 97(5), 111-124.

Boulos, P. F., Lansey, K. E., and Karney, B. W. (2006). *Comprehensive water distribution systems analysis handbook for engineers and planners*. 2nd Edition, MWH Soft, Inc. Publ., Pasadena, CA.

Chaudhry, M. H. (1987). Applied hydraulic transients. 2d ed., *Van Nostrand Reinhold*, NY.

Dandy, G. C., Simpson, A. R., and Murphy, L. J. (1996). "An improved genetic algorithm for pipe network optimization." *Water Resources Research*, 32(2), 449-458.

Eusuff, M. M., and Lansey, K. E. (2003). "Optimization of water distribution network design using the shuffled frog leaping algorithm." *Journal of Water Resources Planning and Management*, ASCE, 129(3), 210-225.

Fleming, K. K., Gullick, R. W., Dugandzic, J. P., and LeChevallier, M. W. (2006). *Susceptibility of distribution systems to negative pressure transients*. AWWARF, Denver, CO.

Friedman, M., Radder, L., Harrison, S., Howie, D., Britton, M., Boyd, G., Wang, H., Gullick, R., LeChevallier, M., Wood, D, and Funk, J. (2004). *Verification and control of pressure transients and intrusion in distribution systems*. AWWARF, Denver, CO.

Ghidaoui, M. S., Zhao, M., McInnis, D. A., and Axworthy, D. H. (2005). "A Review of water hammer theory and practice." *Applied Mechanics Reviews*, 58, 49-76.

Jung, B. S., and Karney, B. W. (2004). "Fluid transients and pipeline optimization using GA and PSO: the diameter connection." *Urban Water Journal*, 1(2), 167-176.

Jung, B. S., and Karney, B. W. (2006). "Optimization of transient protection devices using GA and PSO approaches." *Journal of Water Resources Planning and Management*, ASCE, 132(1), 44-52.

Jung, B. S., Karney, B. W., Boulos, P. F., and Wood, D. J. (2007). "The Need for comprehensive transient analysis of distribution systems." *Journal of the American Water Works Association*, 99(1), 112-123.

Kirmeyer, G. J., Friedman, M., Martel, K., Howie, D., LeChevallier, M., Abbaszadegan, M., Karim, M., Funk, J., and Harbour, J. (2001). *Pathogen intrusion into the distribution system*. AWWARF, Denver, CO.

Laine, D. A., and Karney, B. W. (1997). "Transient analysis and optimization in pipeline - a numerical exploration." *3rd International Conference on Water Pipeline Systems*, Hague, Netherlands, 281-296.

Lansey, K. E., and Mays, L. W. (1989). "Optimization model for water distribution system design." *Journal of Hydraulic Engineering*, ASCE, 115(10), 1401-1418.

LeChevallier, M. W., Gullick, R. W., and Karim, M. R. (2002). *The potential for health risks from intrusion of contaminants into the distribution system from pressure transients*. American Water Works Service Company, Inc., Voorhees, NJ: Distribution System White Paper prepared for the USEPA (http://www.epa.gov/safewater/tcr/pdf/intrusion.pdf).

LeChevallier, M. W., Gullick, R. W., Karim, M. R., Friedman, M., and Funk, J. E. (2003). "The potential for health risks from intrusion of contaminants into the distribution system from pressure transients." *Journal of Water and Health*, 1(1), 3-14.

Lingireddy, S., Funk, J. E., and Wang, H. (2000). "Genetic algorithms in optimizing transient suppression devices." *Proc. ASCE 2000 Joint Conference on Water Resources Engineering and Water Resources Planning and Management*, Minneapolis, MN.

Maier, H. R., Simpson, A. R., Zecchin, A. C., Foong, W. K., Phang, K. Y., Seah, H. Y., and Tan, C. L. (2003). "Ant colony optimization for design of water distribution systems." *Journal of Water Resources Planning and Management*, ASCE, 129(3), 200-209.

NRC (National Research Council/National Academies) (2006). *Drinking water distribution systems: assessing and reducing risks*. The National Academies Press, Washington DC.

Savic, D. A., and Walters, G. A. (1997). "Genetic algorithms for least-cost design of water distribution network." *Journal of Water Resources Planning and Management,* ASCE, 123(2), 67-77.

Schaake, J., and Lai, D. (1969). "Linear programming and dynamic programming applications to water distribution network design." Rep. 116, Dept. of Civ. Engrg., Massachusetts Inst. of Technol., Cambridge, MA.

Simpson, A. R., Dandy, G. C., and Murphy, L. J. (1994). "Genetic algorithms compared to other techniques for pipe optimization." *Journal of Water Resources Planning and Management*, ASCE, 120(4), 423-443.

Srinivas, N., and Deb, K. (1994). "Multi-objective function optimization using non-dominated sorting genetic algorithms." *Evol. Comput*., 2(3), 221-248.

Thorley, A. R. D. (2004). *Fluid transients in pipeline systems, 2nd edition*. D&L George Ltd., Herts, England.

Wood, D. J., Lingireddy, S., Boulos, P. F., Karney, B. W., and McPherson, D. L. (2005). "Numerical methods for modeling transient flow in distribution systems." *Journal of the American Water Works Association*, 97(7), 104-115.

Wu, Z. Y., and Simpson, A. R. (2001). "Competent genetic-evolutionary optimization of water distribution systems." *Journal of Computing in Civil Engineering*, ASCE, 15(2), 89-101.

Wu, Z. Y., Boulos, P. F., Orr, C. H., and Ro, J. J. (2001). "Using genetic algorithms to rehabilitate water distribution systems." *Journal of the American Water Works Association*, 93(11), 74-85.

Wylie, E. B., and Streeter, V. L. (1993). *Fluid transients in systems*. Prentice Hall, Englewood Cliffs, NJ.

MUNICIPAL WATER SYSTEMS IN THE COLUMBIA RIVER BASIN: A PORTFOLIO MANAGEMENT APPROACH FOR MULTIPLE BENEFITS

Mark A. Anderson[1]

[1]CH2M HILL, Inc., 2020 SW 4th Avenue, 3rd Floor, Portland, Oregon, 97201; PH (503) 872-4700; e-mail: Mark.Anderson@ch2m.com

ABSTRACT

The City of Gresham, Oregon has a population of 100,000 people. On the eastern edge of the Portland metropolitan area, Gresham is located on the south shore of the Columbia River. Gresham's water supply is anticipated to be adequate until at least 2050 from surface and groundwater sources.

Wastewater is collected for secondary treatment. Treated effluent is discharged directly to the Columbia River. This reach of the Columbia River is designated as a temperature-limited stream under Section 303(d) of the Clean Water Act. A number of other potential nutrient and pollutant limits may affect permitted effluent discharge in the future. A draft Total Maximum Daily Load (TMDL) for temperature assigns a heat load allocation to Gresham that is projected to be exceeded by as early as 2020.

A water reuse evaluation was performed to address the City's goals of meeting water quality requirements for the Columbia River and providing a sustainable water supply, including preservation of aquifer integrity. The study evaluated the feasibility of non-potable blended use and re-use, utilizing treated effluent, industrial water, stormwater runoff, and agricultural wells. Potential applications included landscape irrigation, multi-family domestic and commercial/industrial non-contact flushing water, industrial process use, and aquifer recharge. Recycling of a fraction of non-consumptive use was expected. Seasonal storage evaluated included aquifer storage and recovery, wetlands, and surface storage options.

A dynamic, object-oriented system model was built to evaluate feasibility of alternatives. The model evaluated water balance and storage characteristics for combinations of source, treatment, storage, and demand options. Cost functions were applied to relate conceptual capital and operating costs for a preferred alternative to expected benefits in source water supply preservation and reduced effluent discharge to receiving waters. Non-financial elements were assessed with multi-criteria analysis.

Results of the study indicate that reuse within Gresham alone does not provide sufficient financial advantage. However, regional or watershed-scale solutions, wherein adjacent single-purpose utilities and neighboring municipalities join to share resources across jurisdictional boundaries, indicate promise for solutions that are cost effective and meet sustainability goals, including efficient use of resources, protection of surface water quality, and prudent management of limited groundwater resources.

Keywords: Watershed planning, Integrated water supply, Reuse, Systems modeling

INTRODUCTION

The City of Gresham, Oregon has a population of 100,000 people. On the eastern edge of the Portland metropolitan area, Gresham is located on the south shore of the Columbia River. The area within the City corporate limits includes 23.44 square miles (Metro Regional Land Information System, 2008).

The City is composed of four watersheds: Fairview Creek, Johnson Creek, Kelly Creek, and the Columbia Slough. The planning area comprises a variety of different land covers, including significant amounts of forest, agricultural lands, and rural residential areas.

The City climate is marked by cool, rainy winters and warm, dry summers. As a result, little or no supplemental water is required for landscape purposes from October through April.

Water Portfolio Services

The City owns and operates water facilities serving a majority of City residents. Approximately one-third of City residents are served by the Rockwood Water People's Utility District (RWPUD). Gresham purchases water through metered connections with the Portland Water Bureau (PWB) Bull Run watershed surface supply, as well as a connection to the RWPUD groundwater system. Recent average day water demands are about 8 million gallons per day (mgd). These supplies are anticipated to be adequate to 2050.

In the coming years, Gresham's water system area will be expanded to include large portions of two urban reserve areas (URA) that are included in the study area: Pleasant Valley and Springwater. These two areas will add approximately 20,000 people to the City's water service population.

The Gresham wastewater treatment plant (WWTP) is located near the Columbia River. The WWTP receives domestic, commercial, and industrial wastewater from incorporated areas of Gresham and nearby communities and treats the wastewater using a suspended media-activated sludge process.

The Gresham WWTP currently discharges oxidized and disinfected effluent to the Columbia River at river mile (RM) 117.5 under a National Pollutant Discharge Elimination System (NPDES), as issued by the State of Oregon. The current permit expired in May 2007 and stipulates limits that vary seasonally for BOD_5 and TSS as well as E. coli, residual chlorine, and total silver. The draft permit expires in April 2012.

The discharge permit for the Gresham WWTP does not currently include limits for thermal mass load, ammonia, phosphorus, or mercury.

The U.S Environmental Protection Agency (EPA) has issued a draft temperature TMDL for the Columbia River that includes a total heat load allocation of 106.7 megawatt (MW) (8,740 MBtu/day) for the City. Figure 1 illustrates the total heat load for the City's discharge based on a range of four effluent temperatures. This plot illustrates the rate and point at which the City's discharge would approach such

a total heat load limit. Using the projected worst-case conditions, the City will exceed its current total heat load allocation in Year 2020, with a projected flow of 23.8 mgd and temperature of 24.5°C.

FIGURE 1
Projected Gresham Discharge Total Heat Loads for Range of Effluent Flows and Temperatures

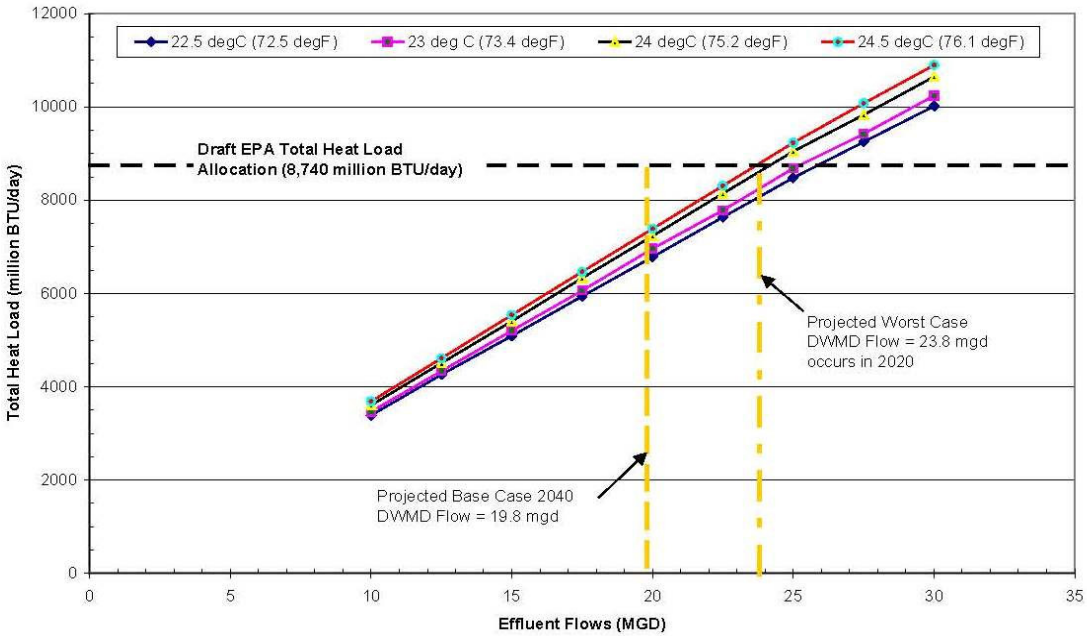

A reuse project could reduce the amount of water discharged to the river and, therefore, reduce or delay potential temperature compliance issues.

Several sources of nonpotable water could be included in a reuse program for the City. These include WWTP effluent, industrial effluent, a decentralized membrane bioreactor wastewater treatment facility, stormwater runoff, agricultural well water, and harvested rainwater. Each of these sources has unique water quality characteristics, use applications, and treatment requirements.

In Oregon, reuse of treated municipal wastewater is regulated by Oregon Department of Environmental Quality (DEQ). The reuse of industrial wastewater is also regulated by Oregon DEQ.

The reuse of gray water has been approved in Oregon on a case-by-case basis. The reuse of gray water for systems discharging to public wastewater systems would require plumbing code approval and treatment specific to a particular use.

Rainwater harvesting is currently permitted in Oregon for a variety of indoor uses including toilet flushing and landscape irrigation. A rainwater harvesting system will usually collect water from rooftops and store the collected rainwater in catchment areas.

METHODS

A water reuse evaluation was performed for the Springwater development area (as part of a larger study) to address the City's goals of meeting water quality

requirements for the Columbia River and providing a sustainable water supply, including preservation of aquifer integrity. The study evaluated the feasibility of non-potable blended use and re-use, utilizing treated effluent, industrial water, stormwater runoff, and agricultural wells. Potential applications included landscape irrigation, multi-family domestic and commercial/industrial non-contact flushing water, industrial process use, and aquifer recharge. Recycling of a fraction of non-consumptive use was expected. Seasonal storage evaluated included aquifer storage and recovery, wetlands, and surface storage options.

The study evaluated direct non-potable reuse. Potable (direct or indirect) reuse has not been considered in this evaluation.

Monthly precipitation data for the Portland International Airport were obtained from the National Oceanic and Atmospheric Administration (NOAA) for water years starting October 2000 and ending September 2007.

Monthly evapotranspiration data were obtained from the Pacific Northwest Cooperative Agricultural Weather Network (AgriMet) for an evapotranspiration station in Aurora, Oregon. The evapotranspiration rates tabulated for the Aurora station are for alfalfa, bluegrass, and established poplar trees, which should be representative of the water needs of landscaping materials in Gresham.

A water balance approach was used to evaluate supply and demand options to serve Springwater, a 1,272-acre area to be developed immediately south and east of the City.

The evaluation included 19 criteria covering cost, environmental, societal, and management impacts of the water resources alternatives.

Cost estimates presented are screening level (Class 5) estimates. They are suitable for comparing alternatives. The cost estimates would be updated as the level of project definition increases, the scope of each project is better established, and the timing of construction is determined.

Databases maintained by the State of Oregon Water Resources Department show existing agricultural wells in Springwater with a total capacity of 1.4 mgd.

Combinations of the alternative sources were evaluated for their ability to deliver the 4.6 mgd of peak water use anticipated in Springwater.

A dynamic, object-oriented model, Voyage™, was used to provide the quantitative analysis needed to evaluate reuse alternatives. The model evaluates alternative supply options based on the specific characteristics of each demand needed to meet cost or non-financial criteria.

Alternatives would supply the water use projected for Springwater, including water for indoor, landscape, industrial, and firefighting. The peak total water supply use in Springwater was estimated as being 4.6 mgd based on analysis of land uses and evapotranspiration. For this analysis, landscape water needs were estimated at evapotranspiration less rainfall. Indoor water use was estimated at 80 gallons per resident per day for residential land uses and 15 gallons per employee per day for

industrial and commercial land uses. The water supply alternatives included the following:

- Base Case—Supplying all potable water use in Springwater from the City's potable water system
- Alternative 1—Supplying 1.4 mgd of landscape water use with a raw water system drawing from agricultural wells and supplying the remaining water use from the City's potable water system
- Alternative 2—Supplying 0.3 mgd of reuse from industrial sources and supplying the remaining water use from the City's potable water system
- Alternative 3—Supplying 2.6 mgd of reuse from stormwater detention basins and supplying the remaining water use from the City's potable water system
- Alternative 4—Supplying 0.63 mgd of reuse from a satellite WWTP and supplying the remaining water use from the City's potable water system
- Alternative 5—Supplying 0.63 mgd of use from rainwater harvesting and supplying the remaining water use
- Alternative 6—Onsite/distributed system using membrane bioreactors as in a distributed ISDS system operated by a district, municipality, or similar regional entity

The qualitative scoring was based on comparison of each alternative to supplying water use in Springwater from the City's potable water system. An alternative that offered no advantage compared with supplying use from the City's potable water system scored zero. An alternative offering an advantage compared with supplying water use from the City's potable water system scored positively. An alternative that was not as favorable as supplying water use from the City's potable water system scored negatively. These scores are shown in Table 1.

RESULTS AND DISCUSSION

Based on the evaluation of water supply alternatives for Springwater, water use in Springwater could be supplied cost effectively using a combination of potable water from the Gresham potable water system, agricultural well water, and industrial reuse. A dual distribution (purple pipe) system would be needed to distribute reuse water provided by agricultural wells and industrial reuse. The cost of such a system was not included in this analysis and was assumed to be borne by private development.

Reuse could become more cost effective if discharge requirements for the Gresham WWTP become more restrictive in the future. In particular, Gresham should monitor phosphorus limits and mixing zone requirements.

Table 2 indicates the result of financial and non-financial evaluation of the alternatives.

TABLE 1
Reuse Scoring Table
City of Gresham Reuse Study

	Springwater Evaluation Factors															
	Investment		Environmental							Societal		Management				Sum of Qualitative Rankings
Description of Alternative	Reduces Capital Cost	Reduces O&M Cost	Impact on Ambient Water Quality (Augmentation of Johnson Creek)	Reduces Peak Potable Water System Demands	Reduces Greenhouse Gas (Carbon Dioxide and Nitrogen Oxide Emissions)	Less Groundwater Impact	Better WW Discharge Quality	Improves Long-term Reliability of Water Supply	Less WW Discharge/Productive Use of WW	Enhances Public Trust	Beneficial Land Use Impact—Reduces Footprint	Ease of Management	Implementability	Skilled Workforce Availability	Compatible with Codes	
All PWB water/SGA groundwater, 4.6 mgd total peak day demand for Springwater	0	0	0	0	0	0	0	0	0	0	0	0	0	0	0	0
Agricultural wells @ 1.4 mgd plus 3.2 mgd peak day demand PWB water and SGA groundwater	1	-1	0	1	0	0	0	0	0	0	0	-1	-1	0	0	-1
Industrial effluent reuse @ 0.3 mgd plus 4.3 mgd peak day demand PWB water and SGA groundwater	1	-1	0	1	1	1	1	1	1	0	0	-1	-1	-1	-1	2
Storm water collection @ 2.6 mgd plus agricultural wells at 1.4 mgd plus 0.63 mgd peak day demand PWB water and SGA groundwater	-1	-1	1	1	0	1	0	1	0	0	-1	-1	-1	0	-1	-2
Satellite WWTP reuse @ 0.63 mgd plus 0.3 mgd industrial reuse plus 3.7 mgd PWB water and SGA groundwater	-1	-1	0	1	-1	1	0	1	1	-1	-1	-1	-1	-1	-1	-5
Rainwater harvesting @ 0.63 mgd plus 4 mgd peak day demand PWB water and SGA groundwater	-1	-1	1	1	1	1	0	0	0	-1	1	-1	-1	0	-1	-1
Regional ISDS system using membrane bioreactors operated by regional entity	-1	-1	1	1	-1	1	0	0	0	-1	-1	-1	-1	-1	-1	-6

TABLE 2
Springwater Water Supply Alternatives

Description of Springwater Water Supply Alternative	Capital Cost Factors		Estimated Sales Price		Sum of Qualitative Factors*	Notes
	Capital Cost	Ranking	Sales Price per HCF	Ranking		
All potable, 4.6 mgd total peak day demand for Springwater	$6,730,000	1	$1.88 to $2.84	3	0	Purchase price of $0.54 per thousand gallons
Agricultural wells at 1.4 mgd plus 3.2 mgd potable	$6,400,000	2	$0.85 for wells	2	-1	0.9 mgd available in Springwater
Industrial effluent reuse at 0.3 mgd plus 4.3 mgd potable	$6,624,000	3	$0.45 for 0.3 mgd of Water from Industrial	1	2	Assumes water quality similar to current industrial users
Storm water collection at 2.6 mgd, ASR 1.6 mgd, agricultural wells at 1.4 mgd, 0.63 mgd potable	$8,220,000	4	$3.80 for Stormwater Recovery Including Surface and ASR	4	-2	1 mgd capacity, 30 acres of impoundments 15 feet deep, pumps, self-backwashing strainer, no land costs, piping required;
Satellite reuse at 0.63 mgd plus 0.3 mgd industrial reuse plus 3.7 mgd potable	$14,400,000	5	$7.40 per for Satellite Reuse	5	-5	Membrane bioreactor with disinfection, Seasonal operation, Solids discharged to sewer and treated at Gresham WWTP, Does not include land or permitting costs, piping
Membrane bioreactors operated by regional entity	$21,000,000	6	$19.40 for ISDS Systems	6	-6	4,000 distributed units
Rainwater harvesting at 0.63 mgd plus 4 mgd potable	$35,800,000	7	$21.00 for Rainwater Harvesting	7	-1	100 gpd systems, 2,100 square-foot catchment area, roof washer,10,000-gallon tank, pump, and disinfection

* Sum of Qualitative Evaluation Factors: Zero is based on maximizing use of existing potable water supplies, +1 indicates better -1 indicated not as good

Notes:

(1) Estimated sales price based on 20-year present worth analysis of capital and operating costs discounted at 3.5 percent.

(2) Cost estimates are Class 5, suitable for comparison of alternatives in a planning study.

(3) Cost estimates include contingencies at 30 percent, engineering and legal costs at 25 percent, and City administrative costs at 14 percent.

mgd = million gallons per day

The following three alternative water supplies for Springwater had substantially similar costs and high qualitative evaluation scores:

- Reusing water produced by industrial operations and supplying the remainder of water demand from the Gresham potable water system scored the highest qualitatively and was similar in cost to supplying all water use from the Gresham potable system. This alternative had an evaluation cost of $14.3 million and qualitative evaluation scores with a total value of 2. In addition to constructing the potable water system, a reuse supply pipe system would be needed to convey industrial reuse water to point of use.
- Constructing a reuse system supplied from converted agricultural wells coupled with supplying the remainder water demand from the Gresham potable water system had the lowest evaluation cost of $13.8 million and qualitative evaluation scores of -1. In addition to constructing a reuse supply system to convey water from the wells to points of use, existing agricultural wells would need to be converted to supply the system.
- Supplying all water demand in Springwater from the Gresham potable water system had the second lowest evaluation cost at $14.1 million and qualitative evaluation scores totaling 0 because it was the alternative all other alternatives were compared against.

Based on current conditions and assumptions (e.g., potable water quality, quantity, and costs to further develop), the other alternatives should not be considered further at this time.

CONCLUSION

Water reuse in the Pacific Northwest is driven primarily by increasingly strict wastewater discharge limits. However, the global focus on water supply and climate change impacts on water supply reliability are other key factors driving wastewater reuse. The recommendations of this study are based on conditions that may change over time, possibly making reuse a more cost-competitive water resource.

Results of the study indicate that reuse within Gresham alone does not provide sufficient financial advantage. However, regional or watershed-scale solutions, wherein adjacent single-purpose utilities and neighboring municipalities join to share resources across jurisdictional boundaries, indicate promise for solutions that are cost effective and meet sustainability goals, including efficient use of resources, protection of surface water quality, and prudent management of limited groundwater resources.

The City should continue to consider the possibility of constructing a large, regional reuse system supplied from the Gresham WWTP over the next 5 to 10 years. A 4-mgd or larger regional system would achieve economies of scale that would start to make the cost of reuse water competitive with potable water from existing sources. Estimated sale price of such a source is $3.95/hundred cubic feet supplied. A regional reuse system would be cost competitive only if the Gresham WWTP needs to be modified to remove phosphorus seasonally in the future.

Reuse would add a water resource to the City's water supply. The reliability or cost of either existing source may change in the future as a result of regulatory changes, climate change, overdrafting of the aquifer, and other causes. If the reliability of sources of supply changes, the City should re-evaluate reuse as a source of supply.

If the City needs to construct significant conveyance infrastructure to transport wastewater from new development in Springwater to the Gresham WWTP, distributed or satellite reuse may be used to postpone investment in additional pump stations and pipeline.

Meaningful public involvement is critical to the success of reuse programs. The public often supports nonpotable reuse programs. Where concerns emerge, they generally include environmental safety, bacteria, and health risks to children. The acceptance of reuse projects is enhanced when the project is perceived as being part of a total water resources management program, the public has confidence in government's ability to protect public health, benefits of the project are quantified, and personal exposure is limited.

ACKNOWLEDGEMENTS

Michael Nacrelli, Project Manager, Wastewater Services Division, Department of Environmental Services, City of Gresham

Joseph Broberg, Consultant Principal Investigator, CH2M HILL

Portions of this paper and figures are reproduced from *Water Reuse Evaluation – Final Report* (CH2M HILL 2008) with permission of CH2M HILL, Inc.

REFERENCES

American Water Works Association (1992). *Guideline for Distribution of Nonpotable Water*.

Metro Regional Land Information System. (2008). Population Inside Metro 1980 – 2004.

Portland State University (2007). *Oregon Population Report*.

Springwater (2008). *Springwater Community Plan and Five Initiatives*. http://www.ci.gresham.or.us/fiveInitiatives/springwater/. Accessed March 26, 2008.

Springwater (2005). *Springwater Community Plan*. November 1.

CH2M HILL (2008). *Water Reuse Evaluation – Final Report*. Prepared for Gresham, Oregon.

Reliability based design of water distribution network (WDN) considering the reliability of nodal pressures

N. Ghajarnia[1], O. Bozorg Haddad[1], and M. A. Mariño[2]

[1] Department of Irrigation & Reclamation Engineering, Faculty of Soil & Water Engineering, College of Agriculture & Natural Resources, University of Tehran, Karaj, Tehran, Iran. PH (FAX) +98-261-2241119;
E-mail: ghajarnia@ut.ac.ir, obhaddad@ut.ac.ir

[2] Departments of Land, Air & Water Resources, Civil & Environmental Engineering, and Biological & Agricultural Engineering, 139 Veihmeyer Hall, University of California, Davis, CA 95616-8628, USA. Ph (530) 752-0684; Fax (530) 752-5262;
E-mail: MAMarino@ucdavis.edu

Abstract

Optimization of water distribution networks (WDN) has been one of the main challenges of researchers for many years. By paying one-dimensional attention to the minimization of WDN costs, one would ignore efficiency factors such as the reliability in delivering nodal demands with desired pressure. By considering the nodal pressure satisfaction as a rigid constraint, the maximum reliability will occur not reflecting the influence of a minor reliability reduction in the system cost. Hence, there is a need for designers and decision makers to have a landscape of the system performance, considering the flexible permissible nodal pressure and its effect on the system cost. In this paper, honey-bee mating optimization (HBMO) is applied in a benchmark WDN (two-loop) problem. The objective is minimization of cost with respect to different levels of reliability in the system during the operational period. Because in WDNs the decision variables are in a discrete domain, a minor decrease in the reliability of nodal pressure can yield a major cost reduction. Furthermore, by, considering different nodal pressure reliabilities, critical nodes of the network can be determined.

Keywords: WDN, Optimization, Reliability, HBMO.

Introduction

In the design of water distribution networks in spite of considering the system robustness in supplying nodal demands, reduction of the network capital cost should be taken into consideration. This necessity has prompted investigators to develop different methods and models to optimize the design of WDNs. Walski (2001) noted that "over the past decade and a half, distribution system optimization has not become the tool of the practicing engineer and, with good reasons, in spite of the several hundred research papers written on the subject." In his opinion, too much concentration on minimizing the cost of WDN without enough attention to the WDNs efficiency had been the main reason these methods had not become applicable. Thus, in the optimal design of WDNs, achieving the minimum cost in

addition to the analysis of network reliability should be considered as the basis of the optimization process.

Stanic et al. (1998) showed that if the objective function of the design problem is only minimizing pipe costs, the optimization model will definitely result in a tree-shaped network. On the other hand, the main reason of preferring a loop WDN to a tree-shaped one is having a more reliable network or, in other words, ensuring the supply of water with desired pressure especially under pipe failure conditions. This simple example showed that design of a WDN relying upon the minimization of its capital cost, regardless of analyzing the reliability factors in the system is not sufficient for designing a reliable network.

According to Mays (1996), there are two types of pipe failures in WDN; mechanical and hydraulic failures. Considering these two types of failures, many investigators have tried to introduce a well-defined reliability factor by combining both types (Todini, 2000). Nevertheless, reliability consideration in the water distribution network's design is really a complicated issue (Goulter & Bouchart, 1990). Moreover, existence of a large number of investigations on finding a unique definition for reliability and risk in WDNs indicates the lack of a universally accepted definition for this important issue in the networks (Todini, 2000). In this regard, Walski (1987) mentioned that a reliability factor should be able to reflect the condition of consumers during different failures in the network. Mainly, reliability in a water distribution network is the probability of meeting a desirable operation in the system, as it had been expected in the designing period (Farmani et al., 2005).

In what follows, the HBMO method is used to minimize the capital cost of a well-known two-loop network. With the aid of developing a simple definition of pressure reliability in the network nodes, a reliability measure is implemented in the optimization model by adding a penalty function. The results are assessed based on the final curve for network expenditure against different levels of reliability in the system. Identification of the network behavior during the years of operation for different levels of reliability and cost is the main objective of this study. Finally a simple approach for the recognition of critical nodes in the network is presented.

Honey-Bee Mating Optimization (HBMO) Algorithm

The Honey-Bee Mating Optimization (HBMO) algorithm is mainly inspired from the special manner of honey-bees living and mating in the beehive. In each hive there is a queen which is in fact the best bee of the colony. In the mating season the queen flies to a proper place and attracts the attention of the drones with a special dance. Afterwards with a fast sudden move, it flies towards the sky, which is known as mating flight, and in this manner only some of the best drones will be able to mate with the queen. After the mating flight the queen returns to the hive and starts laying eggs. Then the workers breed the broods and the best broods will be selected for becoming a new queen. Selected broods are fed by a special nutrient called royal jelly. After growing up, the best nurtured brood will replace the present queen provided that it is better than the queen. Hereby successive generations of honey-bees in the hive will move toward evolution.

Inspiring this natural process, Bozorg Haddad et al. (2006) developed a new heuristic approach named HBMO for engineering optimizations. In this algorithm, firstly a random set of decision variables is generated and is assumed as the queen. Then some other random answers will be generated and best ones will be combined

with the queen (queen generation). Afterwards, the new answers (broods) are improved by some predefined functions, and then the best answer is replaced by the queen if it is better. For a more comprehensive definition of the HBMO algorithm as a generalized metaheuristic, the reader is referred to Bozorg Haddad et al. (2006).

The HBMO algorithm was also applied on some mathematical optimization problems as well as a reservoir optimum operation. Since the results were promising, the HBMO algorithm has been selected as the optimization algorithm in this study.

Problem Formulation

With the aid of the HBMO algorithm, the optimization of pipe diameters in order to find the least-cost solution is performed. Thus, the objective function is minimizing pipe costs and the decision variables are pipe diameters. Furthermore, the problem consists of two integrated stages: optimization and simulation. In the optimization stage, the optimum diameters for all of the pipes are searched and in the simulation stage, for each set of decision variables the system performance is evaluated during the operational period. The optimum network cost for different levels of reliability is obtained by the optimization model, and in this way, comparison of different designs is possible. The following are the objective function and subjected constrains in the optimization model.

$$Minimize \quad OF = \sum_{i=1}^{NI} Cost_i + PF \tag{1}$$

$$Cost_i = C(D_i) \times L_i \tag{2}$$

$$PF = K \times (NF - \alpha)^2 \quad , \quad IF \quad NF > \alpha \tag{3}$$

$$NF = \sum_{t=1}^{T} \sum_{j=1}^{Nj} F_{j,t} \tag{4}$$

$$F_{j,t} = \begin{cases} 0 & , \quad If \quad h_{j,t} \geq h_{\min} \\ 1 & , \quad If \quad h_{j,t} < h_{\min} \end{cases} \tag{5}$$

$$h_{j,t} = \varphi(De_{j,t}, C_{(H-W)i}, D_i, L_i, H_R, Z_1, Z_2, ..., Z_j) \quad \begin{cases} \forall\ j = 1 \ \ to\, Nj \\ \forall\ i = 1 \ \ to\ NI \\ \forall\ t = 1 \ \ to\ T \end{cases} \tag{6}$$

$$De_{j,t} = EXP(Ln(De_{j,T}) - K_g \times t) \tag{7}$$

where: $Cost_i$ = cost of pipe i; $C(D_i)$ = unit cost of pipe i with diameter D; L_i = length of pipe i; PF = penalty factor; NF = number of failure conditions occurred in the simulation period; $F_{j,t}$ = failure condition in junction j and year t, which is zero if the pressure head in that junction is equal to or greater than the minimum permissible pressure head and is equal to one if the pressure head of the abovementioned node is less than the minimum head; α = allowable number of observing a pressure head less than h_{min} in network nodes during the operational period; h_{min} = minimum permissible pressure head in the network; $h_{j,t}$ = pressure head of junction j in year t; $De_{j,t}$ = demand discharge in junction j in year t; $C(H\text{-}W)_i$ = Hazen-Williams roughness coefficient for pipe i; H_R = reservoir head; Z_j = elevation of junction j on the ground; $De_{j,T}$ = demand of junction j in the final year of operational period; Nj = number of junctions in the network; T = number of years in the operational period;

K_g = coefficient of geometrical progression in equation (7); and K = a constant value dependant on the problem condition.

Network hydraulic analysis is performed using EPANET 2.0 hydraulic solver. Meanwhile the demand pattern during the operational period is considered as a geometrical progression.

In this study, according to the number of times that the pressure head in different nodes during the operation period is less than minimum permissible head (NF), I_{pr}[1] index is defined as

$$I_{pr} = 1 - \frac{NF}{T \times Nj} \tag{8}$$

Theoretically, the value of the pressure reliability index (I_{pr}) may vary between zero and one. If the summation of failures occurred in the operational period (NF) is equal to the denominator of the above fraction, the reliability of the network is zero and it means that in all junction nodes of the network, and in each year of operational period, it can not find any desirable condition in securing the minimum allowable pressure head. Subsequently, if the system is able to deliver water with at least the minimum desirable pressure head in all nodes during the operational period, numerical quantity of NF will be zero and therefore I_{pr} will be equal to one. It means that the reliability of the network is 100%.

Case Study

In this study, the benchmark problem developed by Alperovits and Shamir (1977) is used for testing the proposed approach. The two-loop network is a simple gravity-fed WDN, consisting of eight pipes (each 1000 m long with Hazen-Williams C value of 130), seven nodes and a single reservoir (Figure 1). The minimum pressure head requirements are 30-m for each node. Table 1 contains the commercially available pipe sizes and corresponding cost per unit length while the information of the network nodes is given in Table 2.

Furthermore the operational period is considered to be 30 years and the K_g coefficient is equal to one. Using the concept of the simple reliability index developed in this study, design of the two-loop network is performed in different levels of pressure reliability or for different quantities of α equal to 0, 3, 5, 8, 10, 13, 25, 62 and 124 which will correspondingly lead to the reliability values (I_{pr}) equal to 100%, 98.39%, 97.31%, 95.7%, 94.62%, 93.01%, 86.56%, 66.67%, 33.33%.

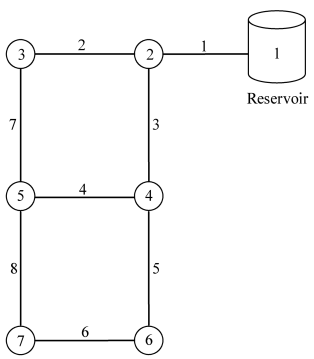

Figure 1. Two-loop network (Alperovits & Shamir, 1977)

[1] Pressure Reliability Index

Table 1. Cost data for the two-loop network

Diameter (inches)	Cost (unit)
1	2
2	5
3	8
4	11
6	16
8	23
10	32
12	50
14	60
16	90
18	130
20	170
22	300
24	550

Table 2. Node data for the two-loop network

Node	Demand (m^3/hr)	Ground Elevation (m)
1(Reservoir)	-1120	210
2	100	150
3	100	160
4	120	155
5	270	150
6	330	165
7	200	160

Results and Discussion

The results obtained using the HBMO for minimization of the network cost under different levels of reliability are shown in Table 3. In this study, for each level of reliability, six different runs of the HBMO algorithm were conducted. The average and the least costs obtained out of these six runs are also reported in Table 3 and the diameters mentioned in this table are relevant to the best runs (minimum cost). As it can be seen in this table, for the reliability measure of 100% (NF = 0) the network cost obtained is 419,000, which has been reported by other investigators (Savic and Walters 1997; Cunha and Sousa 1999; Zong Woo Geem 2006). The succeeding columns are relevant to the higher values of NF or in other words lower levels of I_{pr}, which have resulted in lower expenditures for the two-loop network. Clearly, by decreasing the level of I_{pr} or increasing the value of NF applied in the optimization model, the HBMO is able to consider lower diameters for the network pipes and consequently the network capital cost will be decreased. In Table 3, optimum commercial diameters for the two-loop network under different levels of reliability are also shown.

Table 3. Optimum diameters (inch) for designs under different levels of reliability and their costs

I_{pr}	100	98/38	97/31	95/69	94/62	93/01	86/56	66/67	33/33
NF / Pipe No.	0	3	5	8	10	13	25	62	124
1	18	18	16	16	16	16	14	12	10
2	10	10	12	12	10	10	8	6	4
3	16	14	14	14	14	14	14	10	8
4	4	4	1	1	1	10	10	6	4
5	16	14	14	12	14	10	10	8	1
6	10	12	12	8	8	1	3	6	1
7	10	10	10	10	10	6	1	1	1
8	1	1	1	4	1	8	6	1	1
Mimimum Cost	419000	377000	346000	318000	301000	287000	233000	157000	85000
Average Cost	419000	387250	350000	319000	309167	292833	241333	159333	89666

The changing manner of I_{pr} against network cost can be seen in Figure 2. The first noticeable point in this figure is the close proximity of the average cost graph to the minimum cost graph which shows the appropriate convergence of the HBMO algorithm in different runs. Second point is the low gradient of both graphs within the area of I_{pr} changing between 90% to 100%. This indicates that a slight decrease in the system reliability will result in a large decrease in the cost of the network. As shown in Table 3, if the network design is done based on the reliability level of 98.38%, the network cost will be 377,000 which is 10 percent less than the design with reliability of 100% and associated cost of 419,000. In this case, in the total 30 years of operation, only in two nodes; one during two years and the other during one year, a minor pressure deficit will occur (Table 4). Thus, for reliability levels of I_{pr} equal to 97.31%, 95.7%, 94.62% and 93.01%, we observe a cost decrease of 17.42%, 24.1%, 28.16% and 31.5%, respectively.

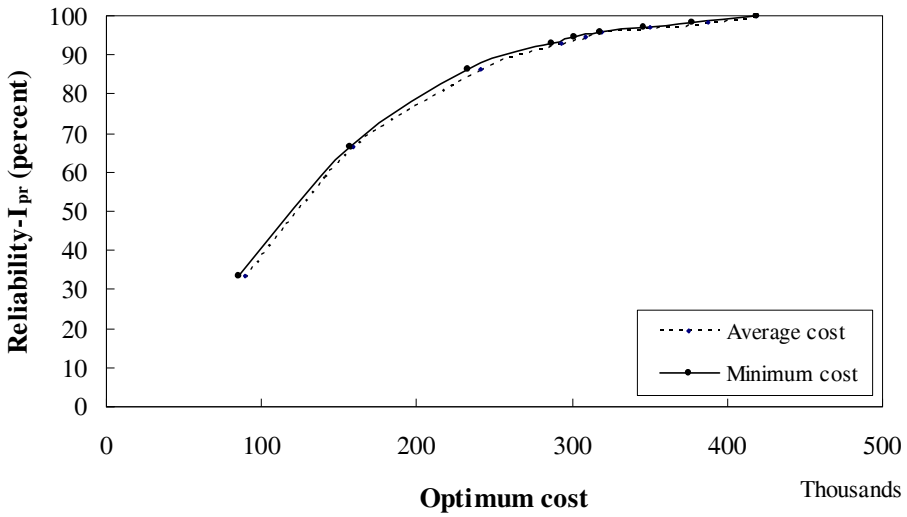

Figure 2. Changing manner of reliability against optimum cost

In contrast, by taking an overall look on the pressure matrix of six network nodes during the 30 years of operation, we can evaluate the performance of the system in supplying consumer's requirements. Nodal pressures for networks with reliabilities of 98.38% and 95.69% are shown in Tables 4 and 5 and Figures 3 and 4. As it can be seen in these tables and figures, nodal pressures in the first years of operation are much more than 30 m (minimum permissible pressure), and in the following years, because of the increase in the nodal demands, the pressure heads get nearer to 30 m. However, if the reliability of the network (I_{pr}) is equal to 98.38%, the maximum allowable number of pressure deficit is three, and for the reliability of 95.69% eight deficits are acceptable. As it can be seen, pressure deficits only occurred in nodes 6 and 7. Thus, these two junctions can be reported as the critical nodes of the two-loop network. Hence, if failure conditions occur because of the aging of the pipes and also due to the increasing of the network demands, the failures can be explored in these two nodes with acceptable probability. In the renewal and rehabilitation periods, finding the most impressive pipes and making decision about the kind of activities; such as changing, relining or adding pipes, are the most important challenging issues for the decision makers (Luong and Nagarur, 2005). Thus in these cases, having prior

information about the critical nodes can be a very good guide for engineers and water distribution network's decision makers.

Table 4. Nodal pressures for reliability level of 98.38%

Year / Node	1	2	3	…	27	28	29	30
2	59.97	59.97	59.96	…	56.13	55.34	54.39	53.25
3	49.92	49.91	49.89	…	38.60	36.28	33.48	30.12
4	54.94	54.93	54.91	…	45.92	44.07	41.85	39.17
5	59.90	59.88	59.85	…	44.64	41.51	37.74	33.20
6	44.92	44.90	44.88	…	32.61	30.09	27.07	23.42
7	49.91	49.89	49.87	…	36.46	33.71	30.40	26.41

Table 5. Nodal pressures for reliability level of 95.69%

Year / Node	1	2	3	…	27	28	29	30
2	59.95	…	57.32	56.78	56.13	55.34	54.39	53.25
3	49.93	…	42.13	40.52	38.60	36.28	33.48	30.12
4	54.92	…	48.73	47.45	45.92	44.07	41.85	39.17
5	59.89	…	49.39	47.23	44.64	41.51	37.74	33.20
6	44.87	…	36.45	34.71	32.61	30.10	27.07	23.42
7	49.87	…	40.65	38.75	36.46	33.71	30.40	26.41

Finally, Tables 4 and 5 (especially Table 4) indicate that by accepting a minor decrease in the reliability of the network; which will not lead to a major failure in its performance, we can reach a noticeable decrease in its capital costs. This can be valuable in developing countries facing severe cost limitations, and can be suggested to decision makers as a logical and economical option.

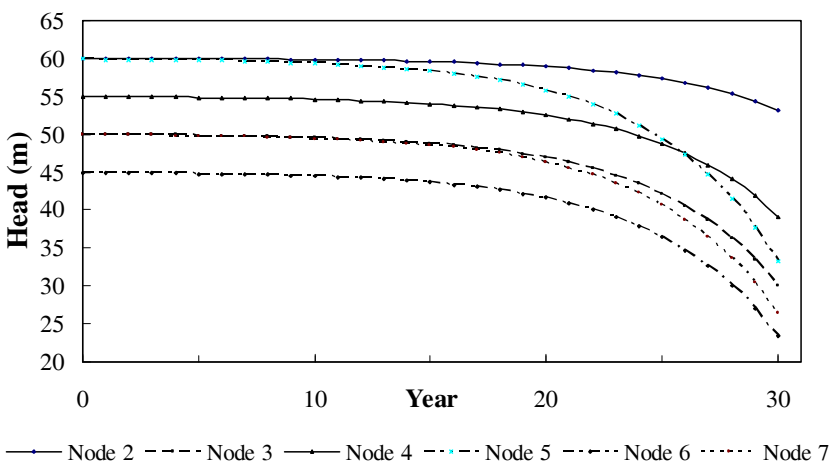

Figure 3. Changing manner of nodal pressures for I_{pr} = 98.38%

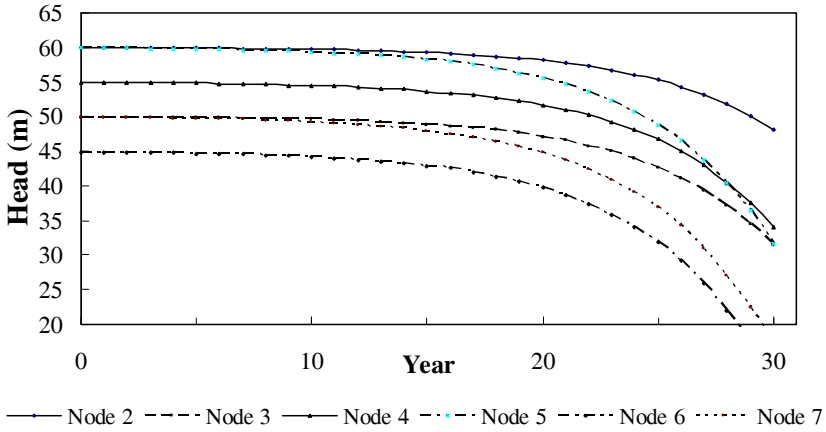

Figure 4. Changing manner of nodal pressures for I_{pr} = 95.69%

Concluding Remarks

This paper presented the optimization of a water distribution network under different levels of reliability. A constrained, single-objective HBMO is used as the optimization algorithm and by developing a simple definition for pressure reliability in network nodes, the proposed reliability index is placed in the constraint of the optimization model. Based on the results of this study, acceptance of a minor decrease in the network reliability yields noticeable cost savings. In fact, provided that it is possible to tolerate minor failures in the network in final years of operation or even if it is acceptable to renew the system in final years, one can decrease the network's capital costs by a small decrease in the system's reliability. Furthermore, by decreasing the reliability of the system during the optimization process, one can find critical nodes in the network. Since a decrease in the pressure reliability in a WDN is due to the reduction of its nodal pressures, by imposing a minor decrease in the reliability of a constrained optimization model one can easily find the critical junctions in the network.

Reference

Alperovits, E. and Shamir, U. (1977). "Design of optimal water distribution systems." *Water Resour. Res.,* 1977, 13(6), 885-900.

Bozorg Haddad, O., Afshar, A. and M. A. Mariño. (2006). "Honey-bee mating optimization (HBMO) algorithm: A new heuristic approach for water resources optimization" *Water Resour. Manage.,* 20, 661- 680.

Cunha, M. C. and Sousa, J. (1999) "Water distribution network design optimization: simulated annealing approach." *J. Water Resour. Plan. Manage,* 125(4), 215-221.

Farmani, R., Walters, G. A., and Savic, D. (2005). "Trade-off between total cost and reliability for anytown water distribution network." *J. Water Resour. Plan. Manage.,* 131(3), 161-171.

Geem, Z. W. (2006). "Optimal cost design of water distribution networks using harmony search." *J. Eng. Optimiz.* 38(3). 259-280.

Goulter, I. C., & Bouchart, F. (1990). "Reliability constrained pipe networks model." *J. Hydraulic Engineering ASCE*, 116(2), 221-229.

H. T. Luong and N. N. Nagarur. (2005). "Optimal maintenance policy and fund allocation in water distribution Networks." *J. Water Resour. Plan. Manage.,* 131 (4), 299-306.

Mays, L. W., (1996). "Review of reliability analysis of water distribution systems. In Tikle, Goulter, Xu, Wasimi, & Bouchart (Eds.)," *Stochastic hydraulics,* (96), 53-62.

Savic, D. A. and Walters, G. A. (1997) "Genetic algorithms for least-cost design of water distribution networks." *J. Water Resour. Plan. Manage.,* 123(2), 67-77.

Stanic, M., Avakumovic, D., & Kapelan, Z., (1998). "Evolutionary algorithm for determining optimal layout of water distribution networks." *Hydroinformatics* 98, 901-908.

Todini, E. (2000). "Looped water distribution networks design using a resilience index based heuristic Approach." *Urban Water,* 2(3), 115–122.

Walski, T. M. (2001). "The wrong paradigm-Why water distribution optimization doesn't work." *J. Water Resour. Plan. Manage.,* 127(4), 203-205.

Removal of Selenium and Nitrate from Surface Waters Using a Subsurface Microbial Filter

Stephen Lyon, Scott Lynch, Imad Feghali, CH2M HILL, 6 Hutton Centre Drive Santa Ana, CA 92707, tel 714 435 6207, fax 714 429 2050.

Randy Sundberg, Irvine Ranch Water District, 15600 Sand Canyon Ave., Irvine, CA 92618, tel 949 453 5300

Abstract

Many surface waters throughout the United States exceed one or more common forms of regulated contaminants. This study describes a pilot-scale facility that was designed to remove nitrate and selenium (selenate) from surface waters by microbial processes. In an oxygen-free environment, nitrate is reduced to nitrogen gas and selenate is reduced to an insoluble salt that precipitates onto the biofilm. Based on the results from bench-scale tests, a demonstration facility was designed and constructed adjacent to a creek in Irvine, CA. This paper describes the design, construction and lessons learned in the development of a gravel-filled filter whose effluent will meet the current standards for nitrate and selenium in surface waters. The facility treated in approximately 194,000 gallons per day and was designed to run in a contaminant removal, recycling and back-flush mode. The benefits of this system are the consistent removal of nitrate and selenium throughout the year with a low O&M cost and the possibility of multiple uses of the land that could include both the below-grade filter and a parking lot or recreational area at the surface. This project is an example of a local water district assuming the role of environmental steward whose projects provides multiple benefits to the community and wildlife within the watershed.

Introduction

This is a companion paper to the presentation and paper entitled “Engineering Natural Filtration Systems to Remove Selenium, Nitrate, and Bacteria from Impaired Surface Waters - Foundational Studies” by Ken Susilo, Eric Strecker, and Randy Sundberg. This first paper deals with initial bench-scale studies to determine the feasibility of removing nitrate and selenium from surface waters using a bacteria-based filter. The use of bacterial filters for contaminant removal is in-part is based on the earlier studies of gravel-based subsurface flow constructed wetlands such as the works by Gersberg et al. (1989, 1986 and 1985). There is a substantial body of scientific literature that characterized the microbial processing of contaminants such as selenium and nitrate (Rege et al., 1999 and Takada et al., 2008). The complex microbial communities that form on gravel have the abilities to remove a broad spectrum of dissolved pollutants. By understanding the principals of

oxidation/reduction potential (ORP) and microbial ecology, systems can be designed to treat contaminated water on a scale of gallons to millions of gallons per day. By developing a slight gradient in ORP within the facility, it is possible to remove both the nitrate at the ppm level and selenium at the ppb level.

There is always a certain level of difficulty in making the transition from bench-scale studies to full-scale operations. This report describes the design and construction of a field-scale project entitled the "Cienaga Filtration Project Field Demonstration Facility". The source water comes from Peters Canyon Wash in Irvine, CA. The companion paper to this report describes the basic biogeochemistry that is involved in the simultaneous removal of nitrate and selenium from surface waters and the optimal conditions needed to consistently perform this task on a continuous basis. Figures 1 and 2 below show the various oxidation states of selenium and how it can be reduced from its most oxidized form of selenate (SeO_4^-) to elemental selenium or an insoluble selenium salt.

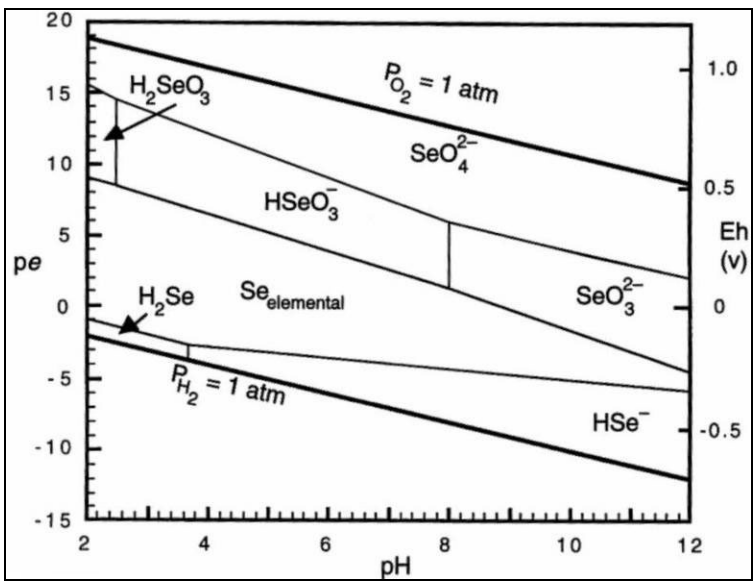

Figure 1. A plot with the ORP shown on the Y axes expressed at p*e* or Eh and the X axis as the pH showing the different oxidation states of selenium.

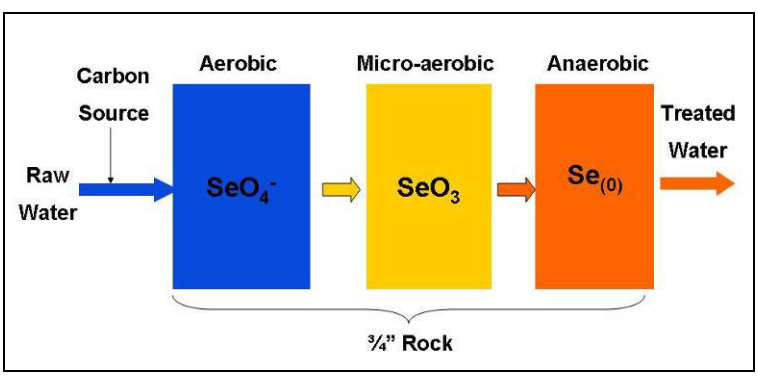

Figure 2. A simplified flow diagram showing the reduction of selenate to elemental selenium.

Background
The Irvine Ranch Water District (IRWD) service area encompasses a large part of San Diego Creek watershed. IRWD voluntarily proposed the Cienega Filtration Project (Project), included in the Natural Treatment System (NTS) Master Plan as Site No. 67, for the removal of nitrogen and selenium from Peters Canyon Channel, a tributary of the watershed. The environmental impacts of the Project were evaluated in accordance with the requirements of the California Environmental Quality Act (CEQA) in the NTS Environmental Impact Report, which was adopted on April 24, 2004.

Project Location
The Project is located on Irvine Unified School District (IUSD) property, at the site of the IUSD new Creekside Continuation School in the City of Irvine in Orange County, California. The Project is constructed within a 3.75-acre utility easement on the eastern, down gradient, end of the IUSD property.

Project Description
The proposed Project will intercept surface flow from Peters Canyon Channel and pump it through a subsurface filter, consisting of an aggregate matrix encased within a geomembrane cell, to remove nitrogen and selenium through a microbial reduction process. Treated water will be adjusted for minor hydrogen sulfide levels and restored to a proper dissolved oxygen level prior to being reintroduced to Peter Canyon Channel. The proposed Project will be implemented in two phases: Field Demonstration Phase and Full Size Phase.

Field Demonstration Phase
The Field Demonstration Phase will process approximately 0.3 cfs of diverted flow from Peters Canyon Channel. Once constructed in June 2008, this phase will operate for approximately two years during which data will be collected in order to set the design criteria for the Full Size Phase.

The Demonstration Phase consists of the following elements:
Intake System - The Intake System includes collection piping, wet well structure, and pump to intercept surface flow from Peters Canyon Channel. Water from the channel will be directed to an intake wet well from where it will be pumped to the subsurface filter through the Pretreatment System.
Pretreatment System - Pretreatment includes filter units and electron donor injection. The filters are intended to remove particles from water while the electron donor is intended to encourage bacterial growth in the subsurface filter bed.
Subsurface Filtration - Subsurface filtration consists of a below grade 200'x40'x10' (Length x Width x Depth) media matrix cell. This media matrix will be below finished grade by at least 3 feet and will be sealed using geomembrane fabric.
Post-treatment System - Post-treatment includes an oxygenation cascade structure and an off-gas collection and polishing system. The oxygenation cascade structure will be

located west of the proposed process area pad and will be few feet above finished grade. It will also house the finished water pump needed to return the treated flow back into the creek. The gas polishing system will consist of carbon filters.
Full Size Phase - The Full Size Phase will adopt the same operational methodology as the Field Demonstration Phase. The design criteria for this phase will be refined per the information that will be learned during the operation of the Field Demonstration Phase. The overall subsurface filtration will include 10 individual below grade cells, which are expected to treat up to 3.0 cfs of creek diverted flow.

The challenge in designing this demonstration facility was to create an environment that maintains a constant oxygen-free (anaerobic) condition that allows for the removal of nitrate and selenium. The addition of an electron donor in the form of a carbon source that is easily assimilated by the bacteria helps to create necessary reducing conditions. The processes in the demonstration facility are given in the summary below.

- A temporary diversion structure will be installed in Peters Canyon Wash to channel water to a wet-well.
- Within the wet-well, a pump station will provide the necessary lift to feed the treatment system.
- A self-cleaning pressure filter will be installed on the discharge side of the pump to remove solids from the influent water prior to introduction to the treatment wetland.
- The influent will be amended with an electron donor in the form of a soluble carbon-containing compound to encourage bacterial growth in the media bed.
- A distribution network will introduce water uniformly along the upstream cross-section of the underground media bed that is enclosed by a watertight barrier. The media matrix is an inert mass of coarse aggregate that provides attachment sites for bacteria.
- The amended water will flow by gravity through the media bed where it will come in contact with nitrate and selenium reducing bacteria. As the amended creek water passes though the media matrix, bacteria utilize the food and oxygen for respiration establishing complex community of organisms called a bio-film. After all of the available oxygen in the water has been consumed, some bacteria will begin to use other substances (electron donors) to fuel their respiratory cycle. Under these anoxic conditions, soluble selenium (selenate and selenite) lose electrons and become reduced to insoluble elemental selenium or combine with other elements to form selenides which are also insoluble. The insoluble forms of selenium become trapped in the bio-film as long as the reduced oxidation state is maintained.
- If the system becomes too reduced, sulfate could be reduced liberating hydrogen sulfide gas (H_2S) which, if present in high enough concentration, can be an odor nuisance or even create a public health risk. In the pre-design optimization study (PDOS), appropriate conditions for selenium removal were achieved without generating noticeable amounts hydrogen sulfide gas. However, the PDOS was conducted under laboratory conditions and was monitored frequently for chemical

constituents, (ORP), and mechanical conditions. The Field Demonstration will not receive the same frequency of attention and a number of factors could result in the system becoming too reduced and H_2S being generated. Therefore, a gas monitoring, collection, and treatment system will be included as a contingency.

- A collection network will convey the treated water to a discharge wet-well.
- Within the discharge wet-well, a pump will provide the lift required to discharge the treated water.
- A pressure filter on the discharge line will remove biosolids entrained in the effluent stream. Similar to the influent stream, the amount of solids collected from the effluent stream is anticipated to be small, and will not reach hazardous levels of metals of interest or legacy pesticides. This will be confirmed during the Field Demonstration by laboratory testing. Solids will be handled, stored, and disposed of in accordance with all applicable regulatory requirements.
- A system will be provided to re-oxygenate the effluent prior to discharge to the Peters Canyon Wash.
- An energy dissipater will be installed where the treated water is reintroduced to Peters Canyon Wash to prevent erosion and scour when treated flows and untreated flows are mixed. (GeoSyntec, 2005)

Having tested a variety of substrates, the research team from GeoSyntec developed a set-criteria for the gravel substrate in the demonstration facility as shown in Table 1.

Table 1. Specification for Filter Media

$C_u=D_{60}/D_{10}$ =	<2.5
$C_c=D^2_{30}/(D_{10}\ D_{60})$ =	1.0<Cc<3.0
Specific Gravity, Bulk S.S.D.	NA
Absorption, %	<4%
Cleanness Value	>70
Abrasion Loss, C 131	<35%
Sodium Soundness, C 88	<15%

Figure 3 below shows a schematic of the demonstration facility where the water can be distributed from the side and collected in the middle or distributed at one side and can be collected at on the opposite side. The system was designed to be 40'W X 200'L X 10'D and have a one day residence time. The was designed to treat 0.3 CFS (194,000 gallons/day) which is one tenth the flow needed to be treated in Peters Canyon Wash. Figure 4 is a schematic diagram of the flow from Peters Canyon Wash through the system and back to the wash.

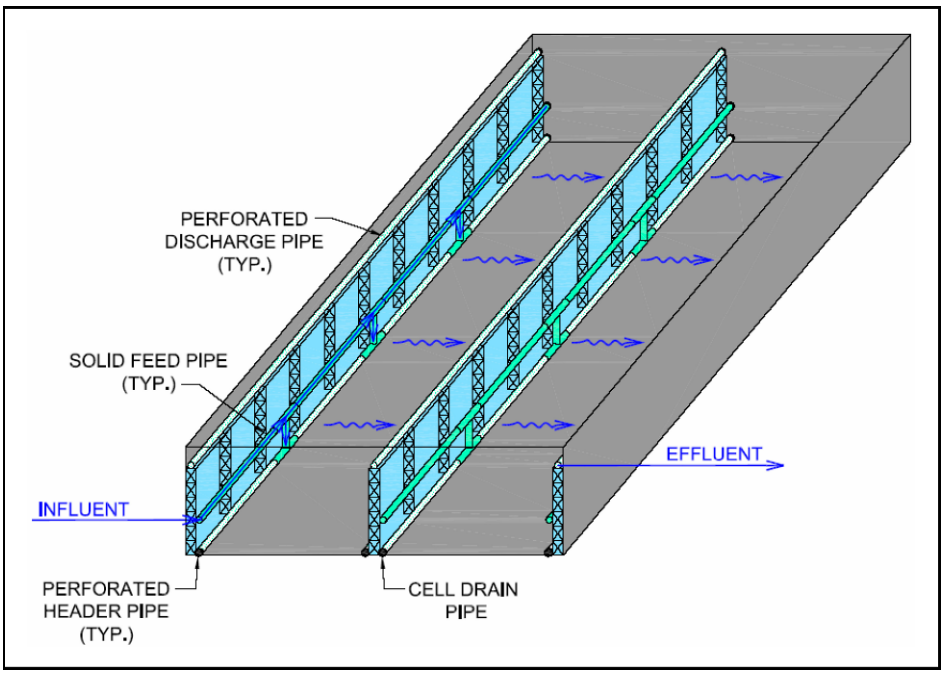

Figure 3. Schematic diagram of the water distribution system within the demonstration facility.

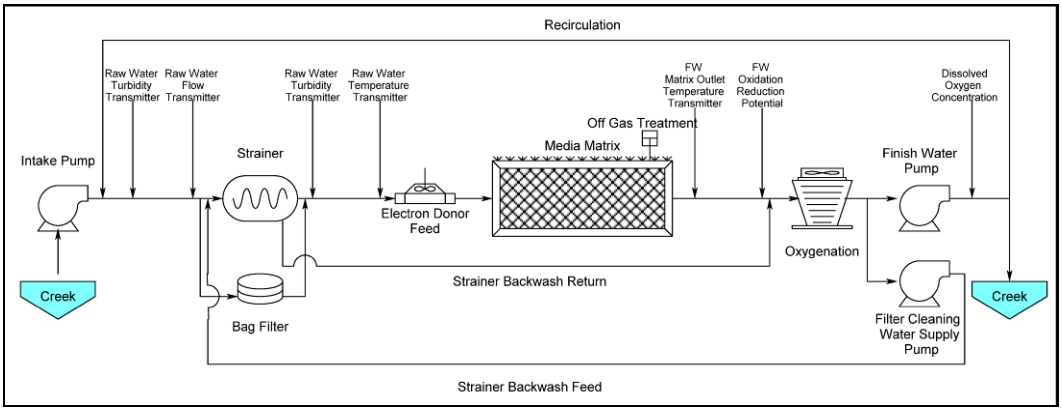

Figure 4. Flow diagram of the demonstration facility in its normal operation mode.

The demonstration facility was designed to operate in three modes. In the normal operating conditions the water goes from highly aerobic conditions to anaerobic, the selenium and nitrate are removed, the water is filtered, oxygenated and returned to the wash. During storm events the flow in the wash can increase by one to two orders of magnitude and can carry a high solids load. During these times the facility goes into a recycle mode where the effluent is fed back to beginning of the system and no new water is brought into the system until the storm has passed and the solids load in the wash has decreased. Over time, there will be an accumulation of biosolids within the facility. A full-scale version of this facility will also have a back-wash mode that will allow the excess biomass to be removed from the gravel matrix and sent to a waste treatment plant. This aspect of treatment was not incorporated in the demonstration phase of the project.

In order to build the demonstration facility it was necessary to obtain permits from several agencies. These agencies included; USACE - Nationwide Permit (404 compliance), The Santa Ana River Regional Water Quality Control Board - 401 Water Quality Certification, The California Department of Fish and Game - Streambed Alteration Agreement (Section 1602), The Orange County Flood Control District - Encroachment Permit, The Orange County Sanitation District - Special Purpose Discharge Permit (periodic back flush water) and The South Coast AQMD - Air/Odor Control Permit. Construction of the facility began in July 2007 and took one year to complete. The approximate cost of construction was $ 2.2 million and the facility was to be operated for two years.

The facility was designed to operate with a minimum of maintenance or oversight. All the electrical components and sensors were linked into a SCADA system and connected to the IRWD Michelson Treatment Plant. During normal operations a field worker would visit the site once each day for approximately one hour. The authors of the companion report will discuss the results from the first year of operations of this facility with regards to water quality and optimization of operating conditions.



Figure 5. Different Stages of Construction beginning in July 2007.

References

Geosyntec. 2005. Cienaga Filtration Project Field Demonstration 30% Preliminary Design Report, Prepared for the Irvine Ranch Water District.

Gersberg, R.M., Lyon, S.R., Brenner, R., and Elkins, B.V. (1989) Integrated wastewater treatment by artificial wetlands: A gravel marsh case study. In Constructed Wetlands for Wastewater Treatment. Chelsea, Michigan: Lewis Publishers, Inc, 145-152.

Gersberg, R.M., Elkins, B.V., and Goldman, C.R. (1986) Role of aquatic plants in wastewater treatment by artificial wetlands. Water Res. 20: 363-368.

Gersberg, R.M., Lyon, S.R., Elkins, B.V., and Goldman, C.R. 1985. The removal of heavy metals by artificial wetlands. Proceedings of Water Reuse Symposium III. AWWA Research Foundation, August 26-31, 1984. San Diego, California.

Rege, M.A., Yonge, D.R., Mendoza, D.P., Petersen, J.N., Bereded-Samuel, Y, Johnstone, D.L., Apel, W.A., and Barnes, J.M. 1999. Selenium Reduction by a Denitrifying Consortium. Biotechnology and Bioengineering. 62(4):479-484.

Takadaa, T., Hirataa, M., Kokubua, S., Toorisakaa, E., Ozakib, M. and Hano, T. 2008. Kinetic study on biological reduction of selenium compounds. Process Biochemistry 43:1304–1307.

Research and Application of Activated Sludge Models

Jinsheng Huo, Ph.D., P.E., BCEE[1], Min Ji[2], Yan Jiang[3]

[1] AECOM Technology Corporation, 4415 Metro Parkway, Suite 404, Fort Myers, FL 33916, Phone: (239) 278-7996, E-mail: Jinsheng.Huo@AECOM.com
[2] School of Environmental Engineering, Tianjin University, Tianjin, China, Phone: 86-22-2740-6057, E-mail: jimin@tju.edu.cn
[3] School of Business and Entrepreneurship, Nova Southeastern University, Fort Lauderdale-Davie, FL 33314, Phone: (561) 635-7100, E-mail: jyan@nova.edu

Abstract

With the growing demands on better effluent quality and higher cost-effectiveness wastewater treatment systems, the traditional methods to design and manage the Wastewater Treatment Plant (WWTP) by experiences and current standards could not meet rapidly developing wastewater industry. As a result, it is an inevitable trend to develop mathematical models and corresponding simulating software for wastewater treatment processes to improve the performance and cost-effectiveness of critical environmental protections. Based on International Water Association (IWA)'s activated sludge models (ASMs), an Activated Sludge Process Simulator – Carbon Oxidation (ASPS-CO) program is developed to simulate and optimize the design, operation, and management of WWTPs. With the focus on the carbon oxidation only, the ASPS-CO program models three typical biological processes: aerobic growth of heterotrophs, death and lysis of heterotrophs, and "hydrolysis" of particulate organics. This ASPS-CO program also develops its own sub-modules to calibrate model parameters, convert traditional measured data, and replace commonly missing data, etc. Therefore, it can simulate not only the water quality of influent and effluent in WWTPs, but also the operating conditions of series continuous stirred-tank reactors (CSTRs): for example, concentration and composition of biomass, and quality and composition of the wastewater, etc. The simulations of the Tianjin Ji-zhuang-zi WWTP using the ASPS-CO program indicate that the results closely match the measured data, which proves to be a reliable method to simulation other WWTPs. In conclusion, this method can provide a reliable theoretical foundation for engineers and researchers to design, operation, and management of wastewater treatment processes. Furthermore, it provides confidences in decision-makers to use this method as an important reference to make critical decisions.

Keywords: ASM (Activated Sludge Model), Activated Sludge Process, Mathematical Model, Wastewater Treatment Plant (WWTP), Simulation, Calibration, ASPS-CO

1. Introduction

With the growing demands on better effluent quality and higher cost-effectiveness wastewater treatment systems, the traditional methods to design and manage the Wastewater Treatment Plant (WWTP) by experiences and current standards could not meet rapidly developing wastewater industry. As a result, it is an inevitable trend to develop mathematical models and corresponding simulating software for wastewater treatment processes to improve the performance and cost-effectiveness of critical environmental protections. There are several mathematical models available for activated sludge wastewater treatment processes, of which the most widely used ones are Activated Sludge Model (ASM) series by International Water Association (IWA). However, current design, operation, and water quality measurement of wastewater treatment make it difficult to apply the complicated ASM models. Therefore, based on experience on ASM models and process design, the ASM No.1 model is simplified to be applied specifically to conventional carbon-oxidation plug-flow activated sludge process. The simplified activated sludge process simulator – carbon oxidation (ASPS-CO) model is developed on MATLAB platform and includes 8 components, 3 biochemical processes. Related parameter optimization and conversion module between conventional measured and new modeling data are also developed to be applied to simulate the real operation in Tianjin Ji-zhuang-zi wastewater treatment plant (WWTP).

2. Mathematical Modeling

2.1 Model Assumptions

The mathematical model is specifically for conventional plug flow activated sludge process. The simplified model only considers the carbon-oxidation and lysis of particulate organic matters by heterotrophs under aerobic condition. This model includes three key biochemical processes: aerobic growth of heterotrophs, death and lysis of heterotrophs, and "hydrolysis" of particulate organics. Therefore, the simplified model is called Activated Sludge Process Simulator – Carbon Oxidation (ASPS-CO). The model assumptions are:

- System is operated under constant temperature.
- Constant pH and close to neutral.
- Reaction rates are constant and not affected by wastewater characteristics.
- Do not consider the effect of N, P and other inorganic nutrients on the organic matter removal and cell growth.
- Assume secondary clarifier has only physical sedimentation and no biochemical reactions.

2.2 Biochemical Process and Component Matrix

Table 1 shows the 8 components and three biochemical processes in ASPS-CO system. Table 2 shows the symbols and definitions of components and parameters on Table 1.

Table 1. ASPS-CO system matrix of components and biochemical processes.

i–Components / j-Biochemical process		1 X_S	2 X_{BH}	3 X_D	4 S_S	5 S_O	6 S_{ALK}	7 X_I	8 S_I	Biochemical reaction rate r_j
1	Aerobic growth of heterotrophs		1		$-\frac{1}{Y_H}$	$\frac{1-Y_H}{Y_H}$	$-\frac{i_{N/XB}}{14}$			$\hat{\mu}_H(\frac{S_S}{K_S+S_S})(\frac{S_O}{K_{OH}+S_O})X_{BH}$
2	Death and lysis of heterotrophs	$1-f$	-1	f'_D						$b_{LH}X_{BH}$
3	"Hydrolysis" of particulate organics	-1			1					$k_h\frac{X_S/X_{BH}}{K_X+X_S/X_{BH}}(\frac{S_O}{K_{OH}+S_O}$
	Observed convention rates	$r_i=\sum_{i=1}^{3}\psi_{ij}r_j$								

Table 2. Symbols and definitions of the ASPS-CO system components and parameters.

Component No.	Component symbol	Definition
1	X_S	Slowly biodegradable substrate, mg/L as COD
2	X_{BH}	Active heterotrophic biomass, mg/L as COD
3	X_D	Debris from biomass death and lysis, mg/L as COD
4	S_S	Readily biodegradable substrate, mg/L as COD
5	S_O	Oxygen, mg/L as COD
6	S_{ALK}	Alkalinity
7	X_I	Inert particulate organic matter, mg/L as COD
8	S_I	Inert soluble organic matter, mg/L as COD
9	Y_H	Heterotroph yield rate, mg biomass/mg COD removed
10	f'_D	Debris to active biomass ratio, dimensionless
11	$i_{N/XB}$	Nitrogen content rate of biomass, mg N / mg biomass
12	$\hat{\mu}_H$	Heterotroph growth rate, hr^{-1}
13	K_S , K_X	Half saturation coefficient, mg COD / mg biomass COD
14	K_{OH}	Soluble oxygen switch coefficient, mg/L as O_2
15	b_{LH}	Heterotroph decay rate, hr^{-1}
16	k_h	Hydrolysis rate, mg COD / (mg biomass COD·hr)

2.3 Simulation System with 5-CSTR Model

Conventional activated sludge processes commonly use rectangular plug-flow aerobic reactor, where the influent and recycled biomass are met at the front end of the reactor. For simulation purposes, the reactor is usually assumed to be 3-5 continuous stirred tank reactors (CSTR) in series. In this paper, 5-CSTR in series is used and its schematic diagram is shown below on Figure 1.

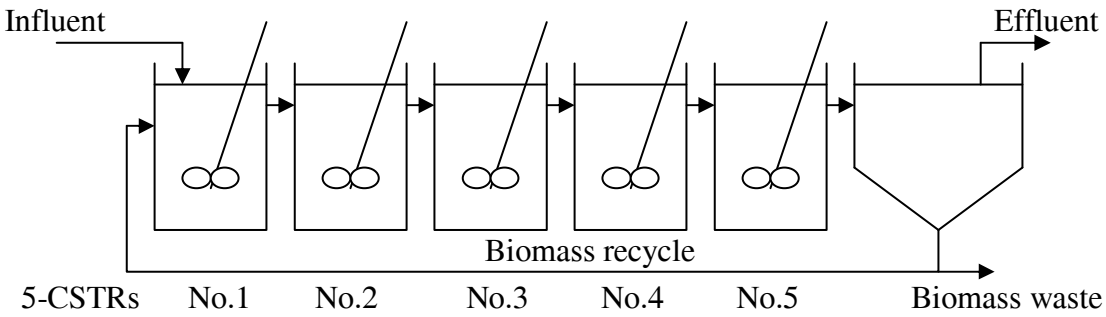

Figure 1. Schematic diagram of five CSTRs in series with all influent and all biomass recycle to the first reactor.

3. Data Conversion Methods

The traditional measurement only includes COD, BOD, SS, which are different from what are used in the ASM model. Therefore, a proper conversion method is required to convert between the traditional data and modeling data. The ASPS-CO divides the total COD (COD_{TO}) into four parts: (1) particulate slowly biodegradable COD (X_{SO}), (2) soluble readily biodegradable COD (S_{SO}), (3) inert particulate COD (X_{IO}), and (4) inert soluble COD (S_{IO}). The influent and effluent conversion methods are shown below.

Influent conversion method:

$$COD_{TO} \approx (2.1)(BOD_5) \quad (1)$$

$$COD_{BO} \approx (1.14)(BOD_u) \approx (1.71)(BOD_5) \quad (2)$$

$$COD_{IO} = COD_{TO} - COD_{BO} \quad (3)$$

$$X_{IO} \approx (0.375)(1.50)(VSS) = (0.56)(VSS) \quad (4)$$

$$S_{IO} = COD_{IO} - X_{IO} \quad (5)$$

$$X_{SO} \approx (0.375) \times (COD_{BO}) \quad (6)$$

$$S_{SO} = COD_{BO} - X_{SO} \quad (7)$$

Effluent conversion method:

$$BOD_5 \approx X_S + S_S \quad (8)$$

$$COD_{Cr} \approx (X_S + S_S + X_I + S_I)(0.9) \quad (9)$$

$$SS = X_I / 0.56 / 0.75 \quad (10)$$

4. Simulation of Tianjin Ji-zhuang-zi Wastewater Treatment Plant

Tianjin Ji-zhuang-zi wastewater treatment plant was constructed in 1980s, which adopts the conventional activated sludge process. In order to consider the temperature effect, the simulation is divided into four "seasons": Winter, Spring, Summer and Fall. The simulation results as compared to the real measured data for Winter and Summer are shown below.

Winter:

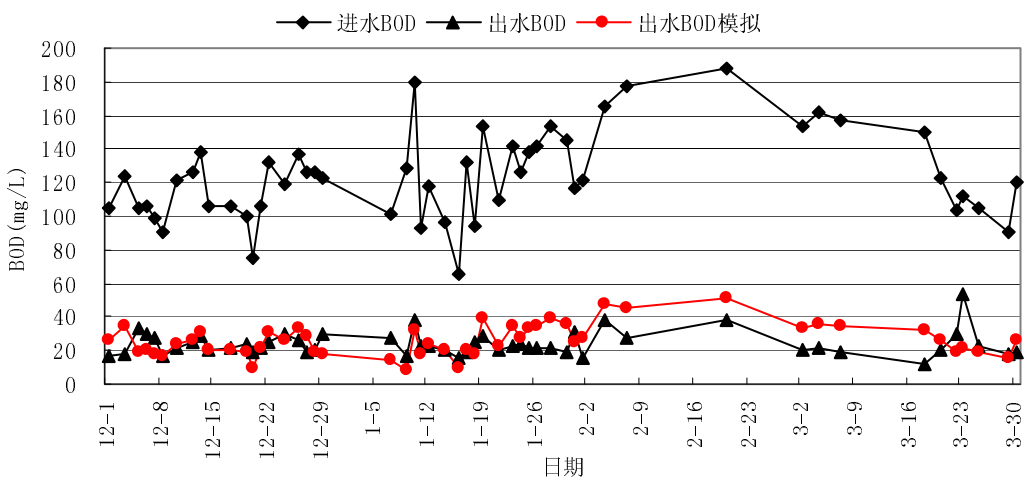

Figure 2. BOD_5 of influent measured (diamond), effluent measured (triangle), and effluent simulated (circle) at Tianjin Ji-zhuang-zi WWTP in Winter.

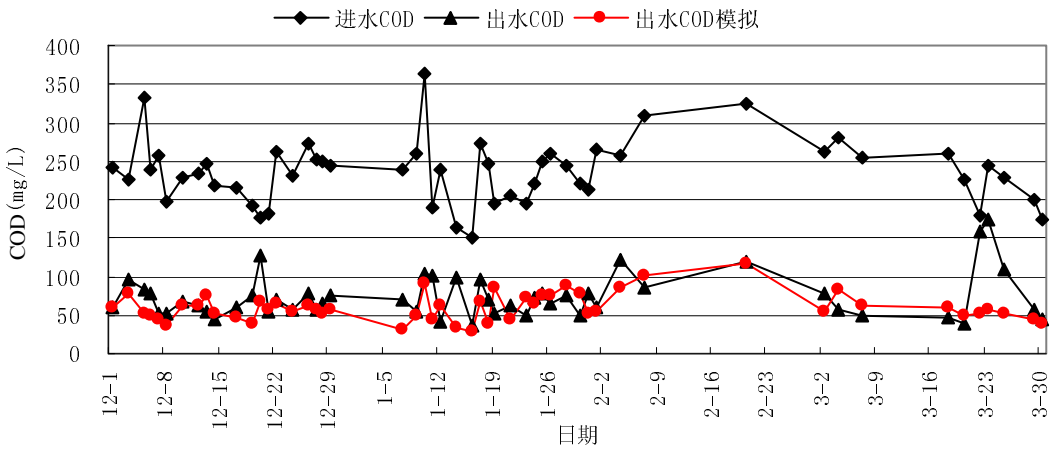

Figure 3. COD_{Cr} of influent measured (diamond), effluent measured (triangle), and effluent simulated (circle) at Tianjin Ji-zhuang-zi WWTP in Winter.

Summer:

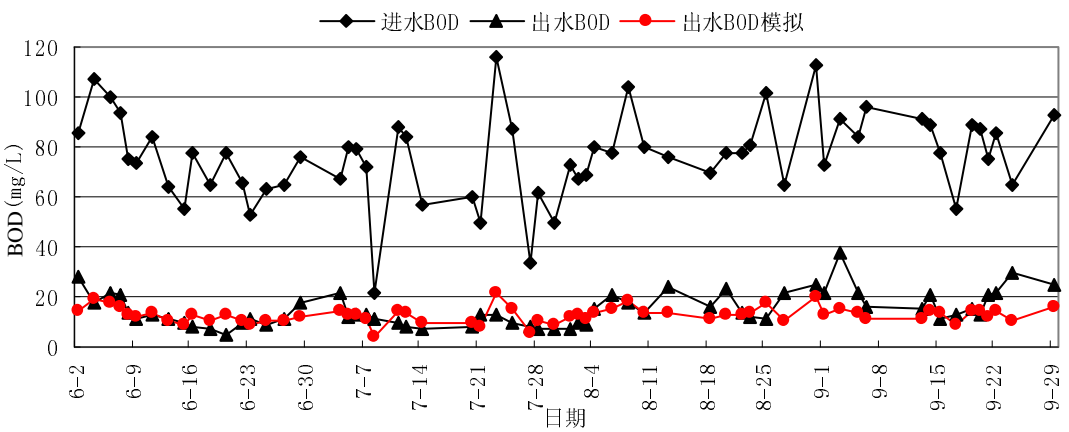

Figure 4 BOD_5 of influent measured (diamond), effluent measured (triangle), and effluent simulated (circle) at Tianjin Ji-zhuang-zi WWTP in Summer.

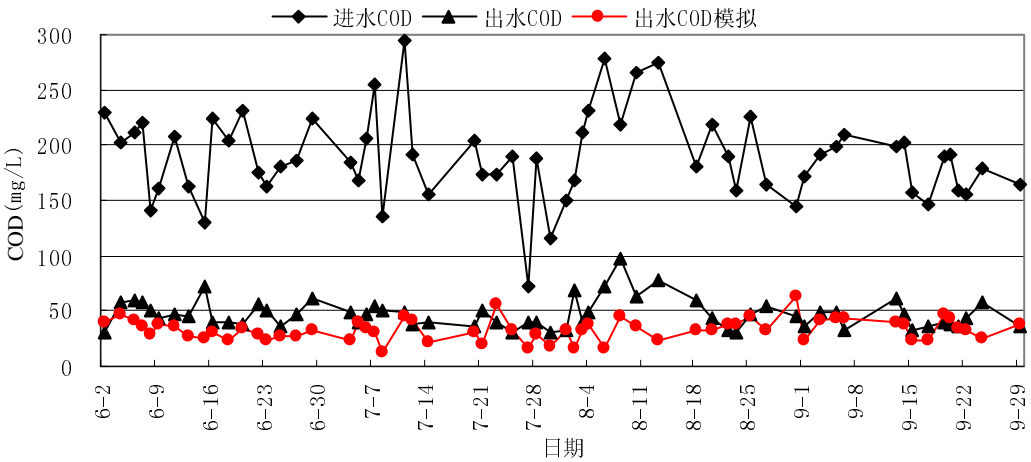

Figure 5. COD_{Cr} of influent measured (diamond), effluent measured (triangle), and effluent simulated (circle) at Tianjin Ji-zhuang-zi WWTP in Summer.

As shown on Figures 2-5, the modeling results match the measured effluent data very well, which reflects the influent wastewater characteristics and changing trends. It should be noted that the simulated results are finalized after several rounds of systemic calibrations. At the beginning, the default parameter values are used. Then the measured effluent data are used to calibrate corresponding model parameters. This calibration step will be repeated until the simulation results are satisfied to a preset standard.

5. Conclusions

The practical application of the ASPS-CO program to Tianjin Ji-zhuang-zi WWTP indicates the simulation results are very close to the real measured data, which proves that the ASPS-CO can be applied to activated sludge processes. The ASPS-CO simulation can reflect the effect of parameters and operation conditions on the treatment performance, which can assist in optimizing the treatment facility during the design and operation phases. In other words, this method can provide a reliable theoretical foundation for engineers and researchers to design, operation, and management of wastewater treatment processes. Furthermore, it provides confidences in decision-makers to use this method as an important reference to make critical decisions.

It should be noted that the ASPS-CO model is only one model module of the whole simulation system. The whole simulation system will be a powerful application program that includes different programming modules and various treatment process models. Therefore, continuous development of computing technologies and wastewater treatment process models will significantly affect the improvement and widely applications of the modeling and simulation system.

Reference

Henze, M.; Grady, C.P.L., Jr; Gujer, W.; Marais, G.v.R.; and Matsuo, T. (1986) *Activated Sludge Model No. 1.* International Association on Water Pollution Research and Control, London, England.

Huo, J.; Robinson, R.B.; and Cox, C.D. (2004) *Uncertainty and Sensitivity Analysis of Activated Sludge Model No.1 by Monte-Carlo Simulation for Single CSTR with Universal Distribution Parameters*, Proceeding of EWRI'04 World Water & Environmental Resources Congress, Salt Lake City, Utah.

Risk Assessment to the Environment Due to Anionic Surfactants in Treated Sewages and Dried Sludges

Arvind Kumar Mungray[1*] and Pradeep Kumar [2]

[1]Department of Chemical Engineering, S. V. National Institute of Technology, Surat - 395007, INDIA, PH (+91-261-2201642); email: akm@ched.svnit.ac.in
[2]Department of Civil Engineering, Indian Institute of Technology Roorkee, Roorkee - 247667, INDIA, PH (+91-1332-285446); email: pkumafce@iitr.ernet.in

ABSTRACT

Paper presents the outcome of a 21 month monitoring study on the anionic surfactants (AS) at the 70 ML/d UASB-PP (up-flow anaerobic sludge blanket - polishing ponds) based sewage treatment plant (STP). The average removal of AS was only around 30%. Appreciable concentration of AS was being discharged to the watercourse (average 3.60 mg/L; range 1.69 – 4.94 mg/L). Compare to this >92% removal was found in an 18 ML/d activated sludge process (ASP) based STP with an average 0.13 mg/L of AS is discharged to the surface waters. AS concentrations averaged 5909 and 810 mg/kg dry wt. in wet UASB and dried sludges respectively.

Treated sewage from UASB-PP based STP when discharged to aquatic ecosystems are likely to generate substantial risk. Post-treatment using 1 day detention, anaerobic, non-algal polishing ponds was found ineffective. Need of utilizing an aerobic method of post-treatment of UASB effluent in place of an anaerobic one has been emphasized. Natural drying of UASB sludge on sludge drying beds (SDBs) under aerobic conditions results in reduction of adsorbed AS by around 86%. Application of UASB sludges on SDBs was found simple, economical and effective. While disposal of treated UASB-PP effluent may cause risk to aquatic ecosystems, use of dried UASB sludges is not likely to cause risk to terrestrial ecosystems.

Key words: Anionic surfactants; up-flow anaerobic sludge blanket process; sand drying beds; risk assessment; aquatic risk; terrestrial risk.

---

*Corresponding author. Tel: +91-9904173019,

E-mail address: akm@ched.svnit.ac.in , amungray@yahoo.com (Arvind Kumar Mungray)

INTRODUCTION

Advantages of anaerobic technology over aerobic in terms of production of biogas, less sludge production, less land requirement, etc., up flow anaerobic sludge blanket (UASB) based sewage treatment plants (STPs) are more preferred than activated sludge process (ASP) based STPs (Mahmoud, 2002). Anionic surfactants (AS) specially deserve special interest since they (i) show a pronounced ecotoxicological effect on aquatic/terrestrial organisms and (ii) are used in large quantities in consumer products like laundry detergents, cleaning and dish washing agents and personal care products, which are discharged into wastewater after use. Largest group of anionic surfactants (AS) is linear alkylbenzene sulfonate (LAS) and it may enter the aquatic environment when raw or partially treated sewage is discharged. Venhuis and Mehrvar (2004) has reported that 0.02 to 1.0 mg/L LAS in aquatic environment can damage fish gills, cause excess mucus secretion, decrease respiration in the common goby, and damage swimming patterns in blue mussel larva. van de Plaasche et al. (1999), Belanger (2002), HERA (2007) reported no-effect concentration of 0.27 mg/L for LAS to aquatic organisms. The key for protecting the environment from the negative impact of down-the-drain-chemicals (surfactants) is the treatment of the sewage in a (biological) wastewater treatment plant (WWTP).

In the last 20 years, over 150 UASB reactor units have been built in the world for treating high BOD industrial wastes. More than 900 UASB reactor units are currently operating all over the world (Alves et al., 2000). Nearly 35 plants already exist in India, which treat wastewaters from widely varying sources like distilleries, dairies, pulp mills, pharmaceutical units, starch maize units, textile units, tanneries and sewage (Arceivala, 1999).

Anaerobic sewage treatment technology has been successfully used in India as a large number of UASB based STPs (over 25 in number with total installed capacity more than a million m^3/d) are currently working. However, in spite of the full-scale application of UASB since over fifteen years, fate of AS in UASB based STPs is not known. Limited information available is based on research carried out in laboratories and reported results are varying in nature as the experiments and scenarios investigated by the authors were different (Denger and Cook, 1999; Angelidaki et al., 2000; Mogensen and Ahring, 2002; Sanz et al., 2003). Risk generated by UASB effluents and sludges to both aquatic and terrestrial environments is not assessed. This paper presents results of an extensive risk assessment study carried out over a period of 21 months using European Union Technical Guidance Document (EU-TGD).

MATERIALS AND METHODS

UASB and ASP based STPs located in Ghaziabad (28^0 40′ N, 77^0 28′ E) and in Haridwar (29^0 58′ N, 78^0 13′ E) were selected for the study. Their installed capacities are 70 and 18 ML/d respectively. Ghaziabad is situated along river Hindon and Haridwar is

situated along river Ganga respectively. A general schematic flow diagram of the combined upflow anaerobic sludge blanket-polishing pond (UASB-PP) system along with sampling locations is shown in Fig. 1. Study was carried over a period of twenty one months covering different seasons. One conventional ASP based STP of 18 ML/d capacity situated at Haridwar was selected for the study.

At the STP, sewage reaches after multistage pumping. It is primarily because of flat topography of the city and presence of number of water channels. At every stage, sewage is detained for a short time and gets mixed up in the sewage sump. It is finally collected at the main pumping station (MPS) just ahead of each STP. From MPS, it is pumped round the clock more or less at a uniform rate. It flows through the STP by gravity. Based on this, it was decided to collect only grab samples during the present study. Grab samples of wet UASB reactor and dried SDB sludges were also collected in polyethylene containers. All samples were collected, preserved, and transported as per methods listed in Standard Methods (APHA, 1998, 2005).

AS were measured in samples of sewage as methylene blue active substances (MBAS) as prescribed in Standard Methods (APHA, 2005). LAS (Hach, USA) was taken as a reference. AS in sludge samples were extracted by soxhlet extraction technique using methanol (Marcomini and Giger, 1987) and than analyzed using MBAS method. All AS concentrations are reported in this paper as "mg/L for sewage and mg/kg dry wt. for sludge samples (calculated as LAS, mol. wt., 318)". A spectrophotometer (DR 4000, Hach, USA,) was used for colorimetric measurements.

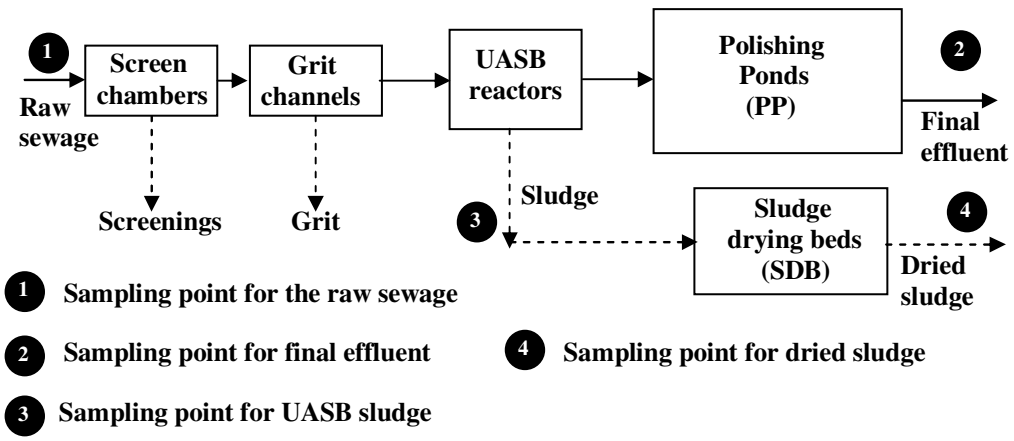

Fig. 1 Typical flow diagram of UASB based STPs studied along with sampling locations.

RESULTS AND DISCUSSION

UASB-PP based STP

Wide variations in influent characteristics were noticed. Over the period of study, total AS averaged 5.16 mg/L. Table 1 presents the influent and effluent concentrations of AS with standard deviations. The average removal of AS was only around 30%. Appreciable concentration of AS was being discharged to the watercourse (average 3.60 mg/L; range 1.69 – 4.94 mg/L). On the contrary, average BOD removal was 81%. In a UASB-PP system aerobic conditions do not develop at any stage. The polishing ponds that receive effluent from UASB reactors are different than conventional waste stabilization ponds that treat raw sewage. PPs were designed for a significantly shorted hydraulic retention time (HRT) of 1 days compared to oxidation ponds (20-30 days). Algal growth is not expected at HRT < multiplication rate of algal cells at 20^0 C i.e. 2 to 2.5 days. PPs could be defined as non-algal, anaerobic, and having short HRT of 1 days. Use of such PPs for post-treatment of UASB effluents is a widely accepted practice especially in India. It can be attributed mainly to low initial cost and their easy design, operation, and maintenance. Accordingly, effluents were found to be devoid of oxygen at all the STPs throughout the study period. This was perhaps the main factor which contributed towards limited reduction 30% of AS. AS is strongly sorbed to sludge due to its hydrophobic character. Prats et al. (1997) have also suggested that a large amount of the load of AS into sewage treatment plant is associated with suspended material. It is subsequently withdrawn from UASBR as sludge is removed. Part of it is also removed in PP as biosolids escaping from UASB settle. It is presumed that aerobic post-treatment of UASB effluent can substantially reduce AS concentration rather than an anaerobic option like PP. Many aerobic post-treatments have been tried including ASP, trickling filter (TF), aerated lagoon (AL), and down-flow hanging sponge (DHS) etc. However, MBAS has been measured as a parameter only by Gasi et al. (1991) while using ozonation as post-treatment of UASB effluent. The effluent from UASB reactor contained 4.63 to 5.30 mg/L of AS. Application of ozone for 30 and 50 minutes resulted in effluent AS concentrations of 1.52 and 0.53 mg/L respectively. Ozone oxidized AS effectively.

Average concentrations of AS in wet UASB and finally dried SDB sludges over a period of twenty one months are given in Table 2. UASB wet sludges contained considerable amount of AS concentration. Average values ranged from 5909 mg/kg dry wt. (70 ML/d STP, Ghaziabad). Municipal sludges in India have not been analyzed for AS concentrations earlier. The AS concentrations in dried-stabilized sludges were also found to be averaged 810 mg/kg dry wt. for the five STPs. Drying on SDB on an average resulted in an overall AS reduction of around 86% Application of anaerobic wet UASB sludge on SDBs not only resulted in drying and volume reduction but also in considerable elimination of AS.

ASP based STP

Final effluent contained on an average 0.13 mg/L AS with a removal of around 94%. Removal of AS was found to be much higher compared to that found in UASB-PP system.

Removal efficiencies of AS in different treatment systems: A comparison

Average AS concentration in the treated effluents and percentage removals for different STPs are summarized in Table 1. Concentrations of LAS (or AS) in treated sewage from previous studies and present work are compiled in Fig. 1. Low effluent LAS (or AS) concentrations (<0.2 mg/L) in case of ASP are quite clear. Compared to this UASB-PP effluents contain very high concentrations of AS (>3.5 mg/L). LAS (or AS) removals >99% have been reported by several researchers for ASP while in case of UASB it was found to be ≤30%.

Risk assessment: Aquatic environment

The risk assessment to aquatic environment due to the presence of AS in treated sewage was evaluated according to the procedure laid down in European Union Technical Guidance Document (EU-TGD, 1996, 2002). Risk is assessed depending on (a) predicted environmental concentration (PEC) of AS, and (b) predicted no effect concentration (PNEC) i.e. the concentration below which unacceptable effects on organisms are not likely to occur. Risk assessment is based on the risk quotient (RQ) which can be calculated by using Eq. 1.

$$RQ = PEC/PNEC \quad (1)$$

RQ>1 indicates a risk of adverse effect to the environment.

PEC_{Water} **:** The measured average concentrations of anionic surfactants in final effluents from different STPs are summarized in Table 1 (column 4). EU-TGD has suggested a dilution factor of 10 (TGD default dilution coefficient) which was used to calculate predicted environmental concentration in receiving water (PEC_{water}, Table 1, column 7).

$PNEC_{Water}$ **:** No observed effect concentrations (NOEC) of LAS worked out by Peterson et al. (2003) based on long-term laboratory screening tests for aquatic plants/organisms at three trophic levels (algae, crustaceans, and fish) are 18, 0.27, and 0.90 mg/L respectively. SIDS (2005) has also mentioned several references in which NOEC of 0.27 mg/L has been utilized for assessment of risk to aquatic environment. Values reported are for LAS while in the present work AS were determined. However, since LAS predominate among AS, NOEC values reported for LAS were used to calculate PNEC. An assessment factor of 10 has been suggested (EU- TGD, 2002) for the estimation of PNEC for LAS. An assessment factor of 10 is normally applied when long-term toxicity NOECs are available for at least three species across three trophic levels. This yields lowest value of predicted no effect concentration in receiving water ($PNEC_{water}$) of 0.027 mg/L.

Calculated values of RQ for different STPs are also given in Table 1. Values of RQ were also calculated using LAS or AS concentrations in treated effluents as reported

by several research workers (Fig. 2). These values are much greater than 1. Even ozonation of UASB effluent as tried by Gasi et al. (1991) did not reduce RQ to <1 (Fig. 3). Treated effluents from UASB based STPs when discharged to aquatic ecosystems are likely to generate substantial risk. There is a need to provide effective aerobic post-treatment to UASB effluents. The RQ values in case of ASP reported by various research workers and also found in the present work were <1. Compared to UASB based STPs, RQ for ASP is quite low.

It could be concluded that present method of post-treatment of UASB effluent is not effective as far as removal of AS is concerned. Use of any of the aerobic methods e.g. ASP, DHS, AL, TF, OP etc. may yield better removal of AS. Recently, at some of the STPs in India, aerated lagoons have been installed for post-treatment in place of PPs. At one of STPs in Karnal (India) of treatment capacity of 40 ML/d, a 1 ML/d DHS post-treatment experimental unit is being operated since last 4 years. However, since AS is not a monitoring parameter in India, no data regarding concentrations of AS in influent and effluent is available for ALs or DHS system.

Table 1: UASB and ASP based STPs: Effluent Concentrations and Estimated PEC, and RQ Values (aquatic ecosystem).

STP	Capacity (ML/d)	Average AS conc. (mg/L)		Average % Removal		PEC_{water} (mg/L)	RQ
		Influent(±SD)	Effluent(±SD)	AS	BOD		
UASB	70	5.16 (± 0.78)	3.60 (±0.81)	30	81	0.360	13.3
ASP	18	2.05	0.13	94	92	0.013	0.48

$PNEC_{water}$= 0.027 mg/L (Petersen et al., 2003; HERA, 2004)

Risk assessment: Terrestrial environment

The PEC is used for characterization of risk to (a) terrestrial organisms: direct exposure and (b) to humans via crops and /or cattle product: indirect exposure. A value of PNEC of 4.6 mg/kg dry wt. has been as suggested by Gejlsbierg et al. (2001), Jensen et al. (2001), and HERA (2004) with an idea to protect all terrestrial microbial processes and functions.

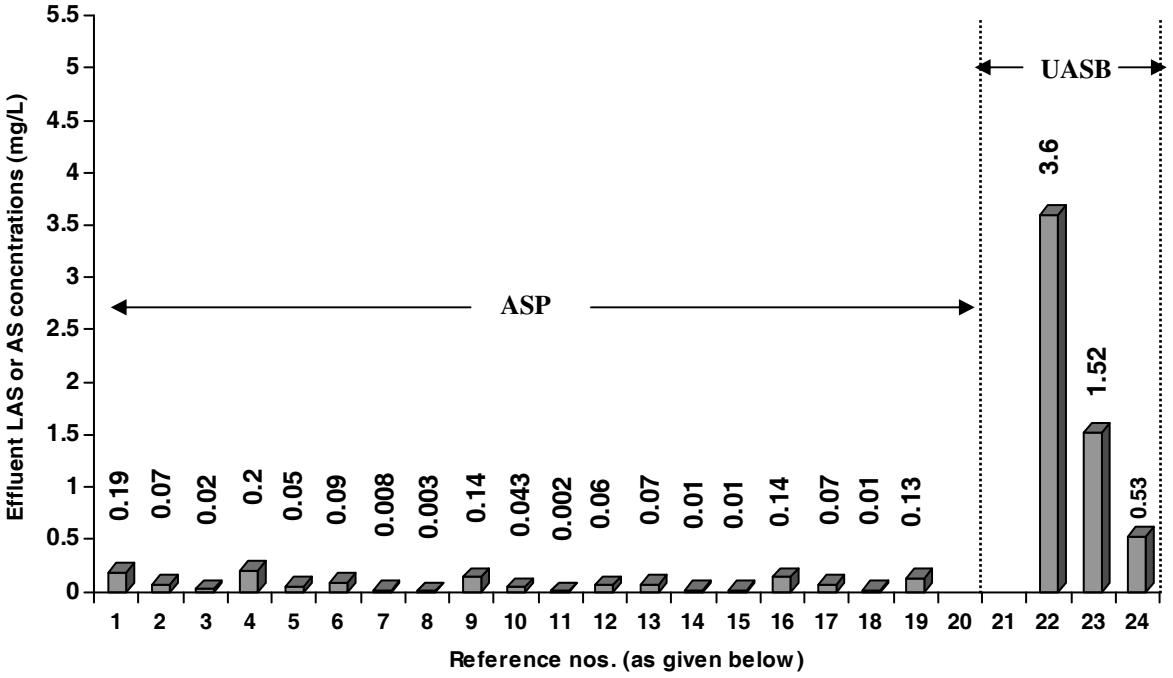

1-2 Matthijs and DeHenau 1987	8 Field et al. 1995	13-18 Feijtel et al. 1995
3 Paul et al. 1988	9 Prats et al. 1997	19 Present study, 18 ML/d
4 Berna et al. 1989	10 Matthijs et al. 1999	22 Present study, 70 ML/d
5-6 Rapaport and Eckhoff 1990	11 Holt et al. 2003	23-24 Gasi et al. 1991
7 Feijtel et al. 1995	12 SIDS 2005	

Fig.2. ASP and UASB based STPs: Concentration of LAS or AS in treated effluent.

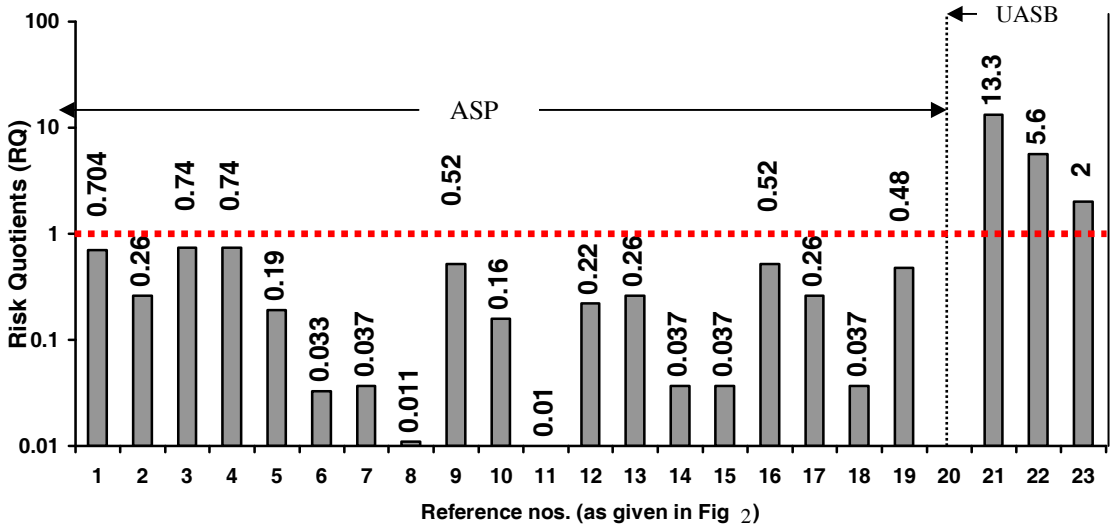

Fig. 3. Values of risk quotients to aquatic environment due to discharge of ASP, OP, and UASB effluents.

The starting concentration at time t = 0 in soil ($C_{o\ soil}$) due to one sludge application in the year can be calculated using Eq. 2 as suggested by EU-TGD (1996).

$$C_{o\ soil} = C_{sludge}\ APPL_{sludge} / DEPTH_{soil}\ RHO_{soil} \quad (2)$$

Where:

C_{sludge} = average concentration of AS in dry sewage sludge (mg /kg dry wt.) (Table 2, column 2)

$APPL_{sludge}$ = dry sludge application rate (kg/m^2 yr)
Soil and agricultural soil: 0.5 kg/m^2 yr (EU-TGD 1996)
Grassland: 0.1 kg/m^2 yr (EU-TGD 1996)

$DEPTH_{soil}$ = mixing depth of soil (m)
Soil and agricultural soil: 0.20 m (EU-TGD 1996)
Grassland: 0.10 m (EU-TGD 1996)

RHO_{soil} = bulk density of wet soil (1500 kg/m^3)

The concentration of AS will be high just after sludge application (in the beginning of the growing season), and much lower at the end of the year due to removal processes. Therefore, the concentration of AS in soil needs to be averaged over a certain time period. Different averaging times are considered (EU-TGD 1996) for different end uses of sewage sludge. For the soil based ecosystems a period of 30 days after application of sludge is suggested. In order to determine biomagnification effects and indirect exposure to man, extended period of 180 days has been recommended.

The average concentration of AS over a certain period of time can be calculated considering the first order biodegradation rate in the top soil. Summation of all concentrations over a certain period (30 or 180 days) and dividing by the corresponding days gives the average daily concentration. This is achieved by integrating the equation given in the EU-TGD (1996), which simplifies to the following expression (Eq. 3) if one neglects the contribution of aerial deposition.

$$PEC_{local} \text{ or } C_{avg.\ soil} = C_{o\ soil}\ \{ (1- e^{-kt}) / k\ t\} \quad (3)$$

Where:

k = first order rate constant in top soil (d^{-1})

t = averaging time (d)

AS monitoring studies in sludge amended soil (Holt et al., 1992) have indicated a biodegradation rate corresponding to a half-life of 10 days, namely $k = \ln 2 / t_{0.5} = 0.0693\ d^{-1}$. Taking $k = 0.0693\ d^{-1}$, values of $C_{avg.\ soil}$ (PEC local) were calculated for the three different end uses two STPs (Table 2).

Taking values of PEC and PNEC, RQ were calculated for different applications and STPs (Table 2). RQ values were found <1 It could be concluded that (a) aerobic digestion or (b) natural drying on SDBs of aerobic and anaerobic sludges result in biodegradation of AS in sludges to such a level that there subsequent application on land for any end use is not likely to pose any risk.

Table 2: Estimated PEC and RQ values for three different applications of dried sludges

STP: capacity (ML/d)	Dried-stabilized sludge: average AS concentration (mg/kg dry wt.)	Soil		Agriculture soil		Grassland	
		PEC local (mg/kg dry wt.)	RQ	PEC local (mg/kg dry wt.)	RQ	PEC local (mg/kg dry wt.)	RQ
UASB: 70	810	0.57	0.12	0.11	0.02	0.04	0.01
ASP:18	760	0.53	0.12	0.10	0.02	0.04	0.01

PNEC = 4.6 mg/ kg dry wt. (Jensen et al., 2001; Gejlsbierg et al., 2001; HERA, 2004)

CONCLUSIONS

1. In a UASB-PP system, removal of anionic surfactants were found only 30%. Removal of AS were found much less compared to ASP based STPs.
2. UASB-PP effluents were found to have very high concentrations of AS (>3.5 mg/L) compared to low concentrations of AS in ASP (<0.2 mg/L) effluents.
3. AS concentrations averaged 5909 and 810 mg/kg dry wt. in wet UASB and dried-stabilized sludges from sludge drying beds respectively.
4. Post-treatment using 1 d detention, anaerobic, non-algal polishing ponds was found ineffective in reducing risk generated by UASB effluents to aquatic ecosystems. Need of utilizing an aerobic method of post-treatment of UASB in place of anaerobic one has been emphasized.
5. Natural drying of UASB sludges on sludge drying beds (SDBs) under aerobic conditions results in reduction of adsorbed AS by around 86%. Use of dried UASB sludges is not likely to cause risk to terrestrial ecosystems.

REFERENCES

Alves, M., Cavaleiro, A.J., Ferreira, E.C., Amaral, A.L., Mota, M., daMotta, M., Vivier, H., Pons, M.N. (2000). "Characterization by image analysis of anaerobic sludge under shock conditions." *Water Science and Technology*, 41 (12), 207-214.

Angelidaki, I., Mogensen, A.S., Ahring, B.K. (2000). "Degradation of organic contaminants found in organic waste." *Biodegradation,* 11, 377-383.

APHA (1998, 2005). *Standard methods for the examination of water and wastewater, 21st edition,* American Public Health Association, Washington, DC.

Arceivala, S.J. (1999). *Wastewater treatment for pollution control. Second edition,* Tata McGraw-Hill, publishing company limited, N. Delhi.

Belanger, S.E., Bowling, J.W, Lee, D.M., LeBlanc, E.M., Kerr, K.M., McAvoy, D.C., Christman, S.C., Davidson, D.H. (2002). "Integration of aquatic fate and

ecological responses to linear alkyl benzene sulfonates (LAS) in model stream eco systems." *Ecotoxicology and environmental Safety,* 52, 150-171.

Berna, J.L., Ferrer, J., Moreno, A., Prats, D., Ruiz, B.F. (1989). " The fate of LAS in the environment." *Tenside Surfactant detergent,* 26,101-107.

Denger, K., Cook, A.M. (1999). "Note: Linear Alkylbenzene sulphonate (LAS) bioavailable to anaerobic bacteria as a source of sulphur." *Journal of Applied Microbiology*, 86, 165-68.

EU-TGD (1996). Technical Guidance Document in support of the Commission directive 93/67/EEC on risk assessment for new notified substances and the Commission regulation (EC) 1488/94 on risk assessment for existing chemicals.

EU-TGD (2002). Technical Guidance Document in support of the Commission directive 93/67/EEC on risk assessment for new notified substances and the Commission regulation (EC) 1488/94 on risk assessment for existing substances. (Revision of the 1996 version, Office for official publications of the European Communities. Brussels).

Feijtel, T.C.J., Matthijs, E., Rottiers, A., Rijs, G.B.J., Kiewiet, A., de Nijs, A. (1995). "AIS/CESIO environmental surfactant monitoring programme. Part 1: LAS monitoring study in "de Meer'' sewage treatment plant and receiving river, "Leidsche Rijn"." *Chemosphere,* 30(6),1053-1066.

Field, J.A., Field, M.A., Poiger, T., Siegrist, H., Giger, W. (1995). "Fate of secondary alkane sulfonate surfactants during municipal wastewater treatment." *Water Research,* 29,1301-7.

Gasi, T.M.T., Amaral, L.A.V., Pacheco, C.E.M., Filho, A.G., Garcia, A.D., Vieira, S.M.M., Francisco, R., Orth, P.D., Scoparo, M., Dias, M.S.R.D., Magri, M.L. (1991). "Ozone application for the improvement of UASB reactor effluent. 1: Physical-Chemical and Biological appraisal." *Ozone Science and Engineering*, 13(2), 179-193.

Gejlsbierg, B., Klinge, C., Samsoe-Petersen, L., Madsen, T. (2001). "Toxicity of linear alkylbenzene sulfonates and nonylphenol in sludge amended soil." *Environmental Toxicology and Chemistry*, 20, 2709-2716.

HERA (2007). "HERA-LAS Human and Environmental Risk Assessment: Linear Alkylbenzene Sulphonates," LAS. CAS No. 68411-30-3, Version 3.0.

HERA, 2004. "HERA-LAS Human and Environmental Risk Assessment: Linear Alkylbenzene Sulphonates, LAS. CAS No. 68411-30-3, Version 2.0, June 2004. http://www.heraproject.com/RiskAssessment.cfm

Holt, M.S., Fox, K.K., Daniel, M., Buckland, H. (2003). "LAS and Boron monitoring in four catchments in the UK contribution to GREAT-ER." *The Science of the Total Environment*, 314-316, 271-288.

Jensen, J., Lokke, H., Holmstrup, M., Krogh, P.H., Elsgaard, L. (2001). "Effect and risk assessment of Linear Alkylbenzene Sulphonates (LAS) in agricultural soils. V. Risk Assessment of LAS in sludge amended soils." *Environmental Toxicology and Chemistry,* 20 (8), 1690-1697.

Marcomini, A., Giger, W. (1987). "Simultaneous determination of LAS, alkylphenol polyethoxylates, and nonylphenol by high performance liquid chromatography." *Analytical Chemistry*, 59, 1709-1715.

Matthijs, E., DeHenau, H. (1987)." Determination of LAS." *Tenside Surfactant Detergent,* 24(4), 193-198.

Matthijs, E., Holt, M.S., Kiewiet, A., Rijs, G.B.J. (1999). "Environmental monitoring for linear alkylbenzene sulfonate, alcohol ethoxylate, alcohol ethoxy sulfate, alcohol sulfate, and soap." *Environ. Toxicol. Chem*,.18, 2634-2644.

Mogensen, A.S., Ahring, B.K. (2002)." Formation of metabolites during biodegradation of linear alkylbenzene sulfonate in an up-flow anaerobic sludge bed reactor under thermophilic conditions." *Biotechnology and Bioengineering,* 77, 483-488.

Paul, H., Brunner, Capri, S., Marcomini, A., Giger, W. (1988)." Occurrence and beheviour of linear alkylbenzenesulfonate, nonyphenol, nonyphenol mono- and nonyphenol diethoxylates in sewage and sewage sludge treatment." *Water research,* 22(12), 1465-1472.

Petersen, G., Rasmussen, D., Maenpaa, K., Kallqvist, T., Madsen, T., Kukkonen, J.V.K. (2003). "Transport and fate of surfactants in the aquatic environment." http://www.nordtest.org/register/techn/tlibrary/tec 524. pdf,.

Prats, D., Ruiz, F., Vazquez, B., Rodriguez-Pastor, M. (1997). "Removal of anionic and nonionic surfactants in a wastewater treatment plant with anaerobic digestion: a comparative study." *Water Research*, 31(8), 1925-30.

Rapaport, R.A., Eckhoff, W.S. (1990). "{Monitoring linear alkyl benzene sulfonate in the environment: 1973-1986." *Environ. Toxicol. Chem*., 9(10), 1245-1257.

Sanz, J.L., Culubret, E., deferrer, J., Moreno, A., Berna, J.L. (2003). "Anaerobic biodegradation of linear alkylbenzene sulfonate (LAS) in upflow anaerobic sludge blanket (UASB) reactors." *Biodegradation,* 14, 57-64.

SIDS (2005). Sponsor country: USA, Dossier on LAS (draft).

van de Plaasche, E. J., de Bruijn, J. H. M., Stephenson, R. R., Marshall, S.J., Feijtel, T. C. J., and Belanger, S. E. (1999). "Predicted no-effect concentrations and risk characterization of four surfactants: Linear alkyl benzene sulfonate, alcohol ethoxylates, alcohol ethoxylated sulfates, and soap." *Environmental Toxicology Chemistry,* 18, 2653-2663.

Venhuis, S.H., Mehrvar, M. (2004). "Health effects, environmental impacts, and photochemical degradation of selected surfactants in water." *International journal of Photoenergy,* 6, 115-125.

Riverbank Filtration for Water Supply: Indian Experience

Pradeep Kumar[1] and Indu Mehrotra[2]

[1]Professor, Department of Civil Engineering, Indian Institute of Technology Roorkee, Roorkee – 247 667 (Uttarakhand), India; PH: 91-1332-285446 and 91-1332-274009; FAX 91-1332-273560; email: pkumafce@iitr.ernet.in
[2]Professor, Department of Civil Engineering, Indian Institute of Technology Roorkee, Roorkee – 247 667 (Uttarakhand), India; PH: 91-1332-285451 and 91-1332-274009; FAX 91-1332-273560; email: indumfce@iitr.ernet.in

ABSTRACT

The efficiency of three RBF systems has been presented. At Haridwar dug wells are water abstraction devices and the source water is the River Ganga which is relatively less polluted. In non-monsoon months, RBF reduced turbidity and coliform by 1 and 3 logs respectively. Removal in monsoon increased to more than 2 and 4 logs for turbidity and coliform respectively. Vertical tube-wells in the vicinity of the Lake Nainital pump lakebank-filtrate at Nainital. The well water when compared with lake water showed 5.2 log removal of total coliform, 4.2 log removal of fecal coliform, 1.4 log removal of turbidity and 1.6 log removal of COD. At Mathura, water is collected by a radial collector well placed in the bed of the River Yamuna, a polluted river. Reduction in DOC and UV absorbance was 0.3 log. Colour decreased by 0.4 log. Total and fecal coliform removals were 2.6 and1.3 logs respectively.

INTRODUCTION

In India, in almost all major cities, raw waters exhibiting wide range of temporal variations are drawn from surface sources and treated to provide safe drinking water for human consumption. Natural purification of polluted river water through riverbank/riverbed filtration (RBF) could be one of the alternatives to attenuate organic, microbial and other pollutants. RBF is a process in which surface water is subjected to ground passage before being collected, treated and used as drinking-water. During infiltration and travel through aquifer, surface water contaminants are attenuated as water is subjected to a combination of processes such as filtration, microbial degradation, attachment to aquifer grains, and dilution with background groundwater to name a few (Kuehn and Mueller, 2000; Ray et al., 2002; Worch et al., 2002, Partinoudi and Collins, 2007). Bank-filtration facilities constructed in favorable hydro-geological settings yield high-quality waters that need little further treatment.

In many countries of the world, alluvial aquifers hydraulically connected to a watercourse are preferred sites for drinking water production given the relative ease of shallow groundwater exploitation, the generally high production capacity and the proximity to demand areas (Doussan et al., 1997). In Europe, river and lake-bank filtration sites are in operation over a century to provide safe drinking water to cities

like Dusseldorf, Berlin, Dresden, Amsterdam, Zurich, Bratislava, Budapest, Belgrade etc. The success of such schemes is dependent on the microbial activity and chemical transformations that are commonly enhanced in the colmation layer within the riverbed compared to those that take place in the surface or ground waters. It has been found to effectively remove pollutants like particulate matter, man made or natural organic compounds, bacteria, protozoa, algae, viruses, disinfectant byproduct precursors and a large number of chemical micro pollutants (Kühn and Müller, 2000). The process is also in use in many communities in the USA like Louisville, Jacksonville, Sonoma County, Lincoln, Cedar Rapids etc. However, designs of RBF facilities vary. Grischek et al. (2002) have summarized data from some RBF sites in United States and Europe. They have found that the most sites are located in alluvial sand and gravel aquifers having hydraulic conductivities more than 1×10^{-4} m/s (more than 9 m/d). The thickness of exploited aquifers ranges from 5 to 60 m. At most sites in Europe, the distance between river bank and production wells is more than 50 m and travel times are more than 50 days.

In India, riverbank filtration is in practice for more than 25 years. However, scientific background and documentation is lacking. RBF sites have a wide range of variation in (a) nature of the abstraction devices (b) quality of the source water and (c) hydro-geological characteristics of the aquifer. Efficiency of three RBF systems, in terms of quantum of removal of river-borne pollutants through the geological material has been presented in this paper. These systems are widely different from each other. At one of the sites dug wells are water abstraction devices and the source water is the River Ganga which is relatively less polluted. Vertical tube-wells in the vicinity of the Lake Nainital pump lakebank-filtrate at the second site. At the third site, water is collected by a radial/horizontal collector well placed in the bed of the River Yamuna, a polluted river. RBF has special relevance for India where most of the rivers receive domestic, industrial and agricultural wastes. A few rivers in certain stretches are quite polluted. Despite pollution, these rivers continue to be used as the source of water for the water supply schemes. This article presents the results of field monitoring from 2005 to 2006 (Haridwar), 1997 to 2006 (Nainital), and 2006 to 2008 (Mathura) covering non-monsoon and monsoon months.

STUDY SITES

At Haridwar (29° 58' N, 78° 13' E; State-Uttarakhand; Northern part of India), sixteen dug wells abstract nearly 22 ML of bank-filtrate every day. Study was carried out at one of the dug wells (partially penetrating, large diameter, bottom entry, lined well; diameter = 10 m, depth = 8.7 m) located on an island. The well is made-up of bricks. The bottom is open and packed with gravel and course sand to allow the water to enter. In the east River Ganga flows at a distance of 320 m while Upper Ganga Canal (UGC) and New Supply Channel (NSC) flows at distances of 252 and 90 m respectively. River Ganga is polluted by municipal wastewater from small communities and non point urban and agriculture surface runoff. Water is filtered through 17 m thick unconfined sand-gravel aquifer which is in direct hydraulic contact with the river and its two canals. Over a period of 25 years, production capacity has reduced by around 83% (3.28 to 0.55 ML/d) due to aquifer clogging.

At Nainital (29° 23' N, 79° 27' E; State-Uttarakhand; Northern part of India), between 1990 and 2005, five tube-wells were installed adjacent to the Nainital Lake. The depths of these tube-wells range from 22.6 to 33.4 m. The sixth and seventh tube-wells of 36.7 and 35.9 m depths respectively were commissioned in 2006. At present, 24.1 ML/d of water is drawn from the tube-wells located at a distance of less than 100 m from the lake. They abstract (a) lake water after passage through the bank/bed (b) subsurface water flowing towards the lake and (c) groundwater during non-monsoon. However, as the wells are located in unconsolidated landslide debris very close to the lake, a substantial portion of the pumped water is replenished by the sub-surface out flow from the Lake Nainital as seepage. The proportion of lake water in the water delivered by wells located near the lake was estimated to vary from 25% to 80% in the non-monsoon and monsoon seasons respectively (Nachiappan et al., 2002).

Mathura (27° 28' N, 77° 41' E; State-Uttar Pradesh; Northern part of India) was selected for the investigations based on the two reasons. The first reason concerns the characteristics of the Yamuna water exploited for the water production. At Mathura, river water is polluted, coloured and unacceptable. According to Central Pollution Control Board (CPCB, 2006) about 85% of the total pollution in the river is caused by the domestic sewage, mainly from the urban centers. The second reason was the placement of the well in the centre of the river which is quite different than the well established practice in Europe and USA (Hunt et al., 2003). Sub-surface water is collected from a radial well having thirteen radials (total length of 522 m) laid at 15.5 to 18 m below the bed of the river. The detailed water quality studies for such a centrally placed well have not been reported.

MATERIALS AND METHODS

At the first site i.e. Haridwar, water samples from production well, River Ganga (3 locations), NSC (3 locations) and UGC (3 locations) were collected nine times during non-monsoon and monsoon periods starting from November 2005 (beginning of the winter) to September 2006 (end of the monsoon) at regular intervals. At the second site i.e. Nainital, water samples from tube-wells (1-5) and Nainital Lake (12 locations) were collected six times during non-monsoon and monsoon periods from 1997 to 2006. At the third site i.e. Mathura water samples from the Yamuna at several locations and riverbank filtrate were collected 7 times starting from the month of November, 2006 to May, 2008. Temperature, pH, conductivity, and dissolved oxygen (DO) were measured on-site by Thermo Orion 4 Star pH and conductivity meter, and DO meter (Hach HQ10). Samples were transported to the Environmental Engineering Laboratory, IIT Roorkee and analyzed for turbidity, major ions, residues, DOC, colour, UV-absorbance, ammonium nitrogen, and most probable number (MPN) of coliform bacteria in accordance with the procedures laid down in the Standard Methods (2005). DOC concentrations of water samples were determined using a TOC-V CSN Total Organic Carbon Analyzer (Shimadzu). UV-absorbance at 254 nm was measured using Hach DR/4000U Spectrophotometer. Hach 2100AN turbidity meter was used to measure turbidity. Colour on Pt-Co scale (expressed in colour units, CU) was determined using Hach DR/890 colorimeter with 25 mm cell.

RESULTS AND DISCUSSIONS

Site 1: Haridwar. The range of values of water quality parameters are compiled in Table 1. Water from river and canals was 50-100 times more turbid in monsoon than non-monsoon. The increased bacterial count by around 10 times and decreased conductivity by around 0.6 times were also noticed in the monsoon samples as compared to non-monsoon period. The quality of water from the production well, however, was not found to vary significantly in monsoon and non-monsoon periods. Water from canal and/or river becomes rich in minerals as it flows through the aquifer to the production well. The extent of mineralization depends on the rate of water flow, extent of groundwater mixing, duration for which water is held up in the aquifer, chemical nature of the aquifer material, and the nature of water flowing through the aquifer. Cumulative effect of these processes was judged by measuring and comparing the conductivity and total dissolved solids (TDS) in water from river/canal and production well.

As the river water passes through the aquifer, the water also gets filtered and most of the turbidity and organics are removed. This is quite clear from the results compiled in Table 1. Reduction in turbidity, total coliform, fecal coliform and organics in the water samples collected from the production well are quite noticeable (Fig. 1). The water from production well when compared with the source water showed 2.5 log removal of total coliform, 3.5 log removal of fecal coliform, 0.7 log removal of turbidity in non-monsoon period and 4.7 log removal of total coliform, 4.4 log removal of fecal coliform and 2.5 log removal of turbidity in monsoon period. A removal of 1.0 log is also observed for organics (in terms of UV absorbance) during the monsoon period. The removal can be attributed to physical filtration and straining of particles.

Site 2: Nainital. Water samples from the tube-wells (1-5) and from the lake at different depths were analyzed separately during monsoon and non-monsoon periods. The detailed observations regarding water quality parameters are compiled in Table 2. Tests for total coliform in all the tube-well samples yielded negative results indicating that water is free from any fecal contamination and is fit for drinking purpose as per Indian Standard (IS 10500, 1991).

The lake is fed by surface, sub-surface and groundwater. The water from tube-wells is the groundwater under the direct influence of (i) surface water from Lake Nainital and (ii) seepage water flowing through faults and fractures from Sukhatal sub-catchment. The water drawn from the tube-wells is expected to be different from the lake water depending upon the mixing of the bank filtrate and groundwater during different months in a year. Following were the main points of difference:

- TDS, electrical conductivity : Tube-well water > Lake water
- Organic matter : Lake water > Tube-well water
- Total coliform : Lake water > Tube-well water

Lake water of widely varying characteristics e.g. temperature, TDS, oxidation reduction potential (ORP) etc. (due to seasonal variations, depth stratification,

Table 1. Water Quality Comparison: River/Canal Water vs. Production Well Water.

Parameter	River and canals		Production well	
	Non-monsoon	Monsoon	Non-monsoon	Monsoon
pH	7.9–8.5 (8.3)	6.9–8.1 (7.5)	7.3–7.9 (7.6)	7.5–7.7 (7.6)
Turbidity (NTU)	1.0–3.1 (1.4)	100–200 (149)	0.2–0.4 (0.3)	0.4–0.6 (0.5)
Conductivity (µS/cm at 25 ^{O}C)	218–262 (251)	140–184 (155)	415–466 (440)	425–440 (432)
TDS (mg/L)	108–172 (136)	92–114 (101)	194–332 (256)	287–294 (290)
UV absorbance at 254 nm (cm^{-1})	NA	0.156–0.217 (0.190)	NA	0.006–0.039 (0.017)
TOC (mg/L)	NA	0.72–20 (8.56)	NA	ND
Total coliform (MPN/100 mL)	4300 –9300 (6420)	23000–93000 (51670)	<2–93 (20)	<2
Fecal coliform (MPN/100 mL)	2100–6400 (3030)	1500–43000 (22500)	<2	<2

NA not available; ND not detectable; values in parenthesis are average values.

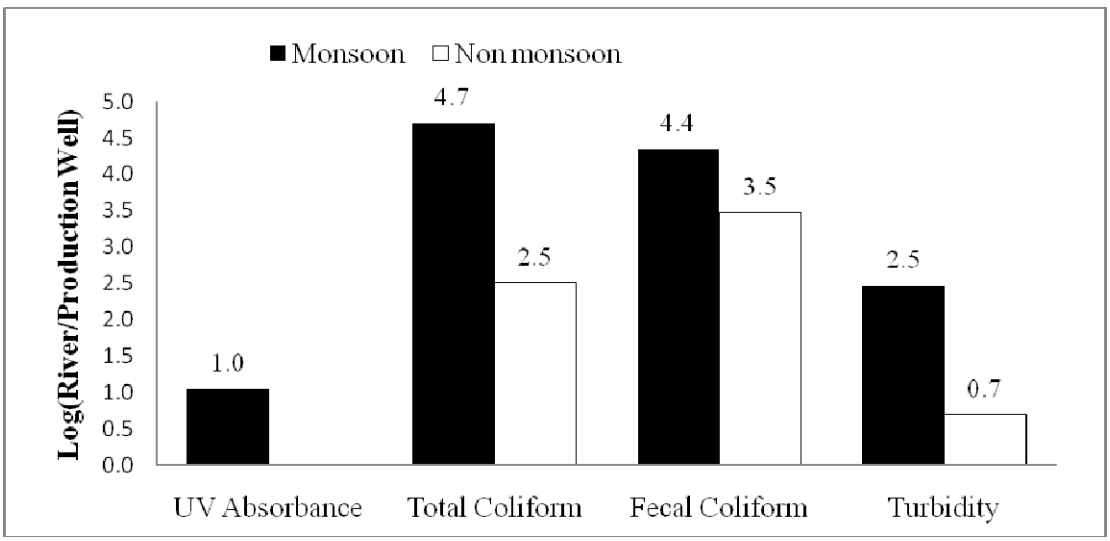

Figure 1. UV absorbance, turbidity and coliform counts of production well relative to river/canal water.

seasonal overturn, and yearly changes) enters into slotted pipes of tube-wells at different levels after traveling through the aquifer formed by natural deposits around the lakebank. During bank filtration the water from the lake presumably causes weathering and/or leaching of materials from the deposits. Average electrical

conductivity of lake water increases from 577 μS/cm in monsoon period to 640 μS/cm in non-monsoon period. It therefore, seems that processes operating in monsoon and non-monsoon seasons are somewhat different. It has been shown that during monsoon, more water flows (80% lake water + 20% groundwater probably from fault and fractures, Nachiappan et al., 2002) through the deposited aquifer material, causing weathering and/or leaching of material. During non-monsoon, however, the flow of lake water through deposits is reduced considerably resulting in reduced level of leaching. The proportion of mixing of groundwater predominates and most probably leads to significant increase in minerals.

Table 2. Water Quality Comparison: Lake Water vs. Tube-Well Water.

Parameters	**Monsoon**		**Non-monsoon**	
	Lake water	**Tube-well water (Nos.1-5)**	**Lake water**	**Tube-well water (Nos.1-4)**
Temperature (^{0}C)	18-24 (21)	16.5-17 (17)	NA	NA
Turbidity (NTU)	6.7-7.3 (7.1)	0.1-0.4(0.25)	3.7-6.1 (4.9)	0.1-0.3 (0.2)
Conductivity (μS/cm)	544-605 (577)	821-954 (869)	631-653 (640)	573-708 (655)
Total dissolve solids (mg/L)	361-398 (376)	542-639 (580)	324-472 (407)	471-528 (501)
Suspended solids (mg/L)	24-31 (28)	ND	18-31 (25)	ND
pH	8.4-8.8 (8.64)	8.1-8.24(8.16)	7.6-8.1(7.9)	7.6-7.7(7.68)
Chlorophyll-a (μg/L)	NA	NA	11.4-102 (35)	ND
COD (mg/L)	19-42 (31)	ND	20-80 (57)	ND
UV absorbance at 254 nm (cm^{-1})	0.056 – 0.061 (0.059)	0.002-0.009 (0.007)	NA	NA
Total coliform (MPN/100 mL)	$0.5x10^2$-$50x10^4$ ($17x\ 10^4$)	<2	$4.6x10^4$-$24x10^4$ ($14.3\ x\ 10^4$)	<2
Fecal coliform (MPN/100 mL)	$0.5x10^2$-$50x10^3$ ($19x\ 10^3$)	<2	$5x10^3$-$24x10^3$ ($14.5\ x\ 10^3$)	<2

NA not available; ND not detectable .Values in parenthesis are average values

The impact of catchment activities on the quality viz. chemical oxygen demand (COD), coliform, nutrients of lake-water is quite evident. Nevertheless, during lake bank filtration all the suspended solids, COD, chlorophyll-a and bacteria are reduced to less than the detection limit of the method(s). The tube-well water when compared with lake water showed 5.2 log removal of total coliform, 4.2 log removal of fecal coliform, 1.4 log removal of turbidity and 1.6 log removal of organics (in terms of COD) (Fig. 2). The removal can be attributed to physical filtration and straining of particles.

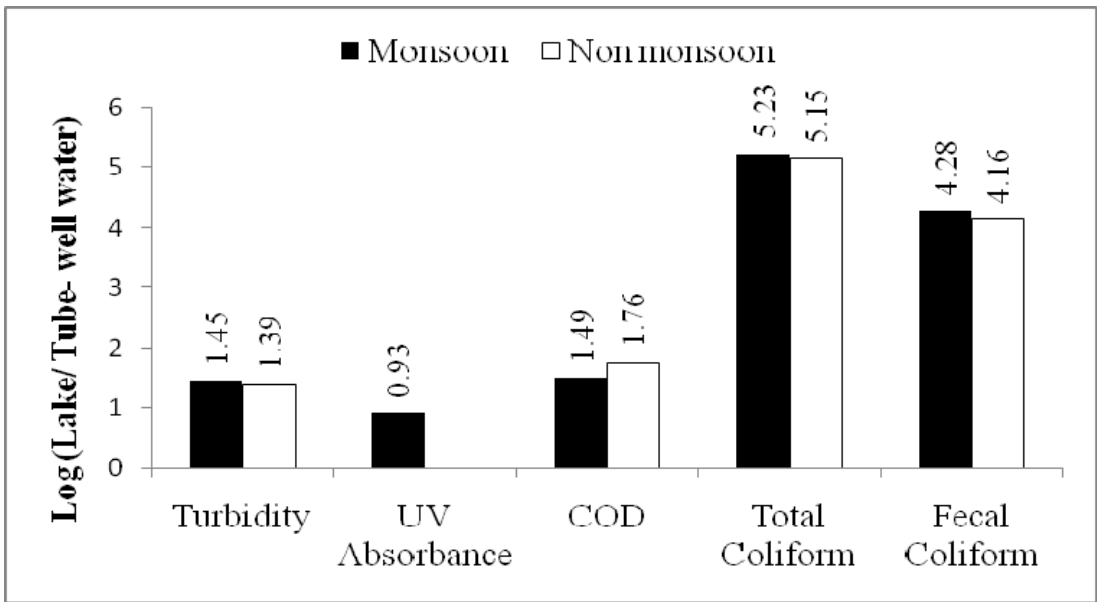

Figure 2. Turbidity, UV absorbance, COD and coliform counts of tube-well water relative to lake water.

Site 3: Mathura. The water bearing strata at the RBF site at Mathura was estimated to be up to around 26 m below the bed of the river. The horizontal collector well at Mathura which was constructed about 25 years back is placed in the centre of the river. All the laterals are completely beneath the river bed. Indian practice of using the horizontal collector wells in general, is different than the practice in Europe and USA. In India, it is a common practice to place the caisson in the river bed so that all the laterals remain completely below the river bed. Water supply scheme of Ahmedabad, India where seven radial wells are placed in the centre of the River Sabarmati is another example. Although exact comparison has not been attempted, Indian practice is quite successful where groundwater is saline. The aquifers in and around Mathura are characterized by varying hydro-geological conditions, even within short lateral distances. Placement of the well in the centre of the river in such a situation yields filtered river water with little or no mixing with groundwater. One of the major disadvantages is that the travel time is relatively short and accordingly limited purification is expected particularly in terms of organics and microorganisms.

Range of the values of some selected water quality parameters for the River Yamuna and riverbed filtrate are presented in Table 3. Perusal of the data indicates variation of turbidity of the river water only up to around 14 NTU. This was due to the reason that samples were collected in pre- and post-monsoon periods only. Turbidity of the Yamuna water during monsoon ranged from 70 to 180 NTU (CPCB, 2006). pH of the river water varied from 7.4 to 8.2. River water on an average contained dissolved salts of around 800 mg/L which is more than the desirable limit of 500 mg/L. Average conductivity (~1390 μS/cm at 25°C) and alkalinity (~320 mg/L as $CaCO_3$) were also high. Average values of dissolved organic carbon (DOC) (~7 mg/L), UV-absorbance (~21 m^{-1} at 254 nm) and colour (~63 colour unit, CU) indicated the presence of organic compounds in the Yamuna water. The colour due to inorganic metal ions at pH 7.4 to 8.2 is unlikely. River water as well as filtrate was

found to be contaminated with coliform bacteria having MPN in the range from 23 x 10^2 to 15 x 10^5 per 100 mL.

Larger values/fluctuations of conductivity indicate substantial feeding of the river by ground water/effluents particularly during the non-monsoon months. Bed filtration effectively reduced UV-absorbance and DOC by 0.3 log and colour by 0.4 log. Accordingly, radial well water was found to have an average UV-absorbance of around 10 m^{-1} at 254 nm, DOC of 3.2 mg/L and colour of 23 CU. Total coliform of the river water (23 x 10^2 to 15 x 10^5 MPN/100 mL) were reduced to 43 to 75 x 10^3 MPN/100 mL, a reduction of around two logs.

Table 3. Water Quality Parameters: River Water vs. Radial Well Water.

Water Quality parameter	River water (n=17)	River bed filtrate (n=13)
Temperature (ºC)	19.8 - 21.6 (20.8)	21.4 - 24.7(22.2)
Conductivity (µS/cm at 25ºC)	1170 – 1527 (1390)	1292 – 1483 (1404)
Total dissolved solids (mg/L)	690 – 902 (804)	622 – 934 (817)
Turbidity (NTU)	3.83 - 13.6 (7.3)	0.67 - 4.29 (1.3)
pH	7.43 - 8.2 (7.9)	7.18 - 8.23 (7.8)
Colour (CU)	40 – 166 (62.8)	18 – 29 (23.3)
UV absorbance (cm^{-1} at 254 nm)	0.11 – 0.28 (0.21)	0.07 – 0.13 (0.1)
DOC (mg/L)	4.04 - 29.1 (7.0)	1.65 - 6.3 (3.2)
DO (mg/L)	5.14 - 7.17	0.22 - 0.97
TC (MPN/100 mL)	23×10^2 - 15×10^5	43 - 75×10^3
FC (MPN/ 100 mL)	150 -23×10^4	43 - 93×10^2

n is number of observations**.** Values in parenthesis are average values.

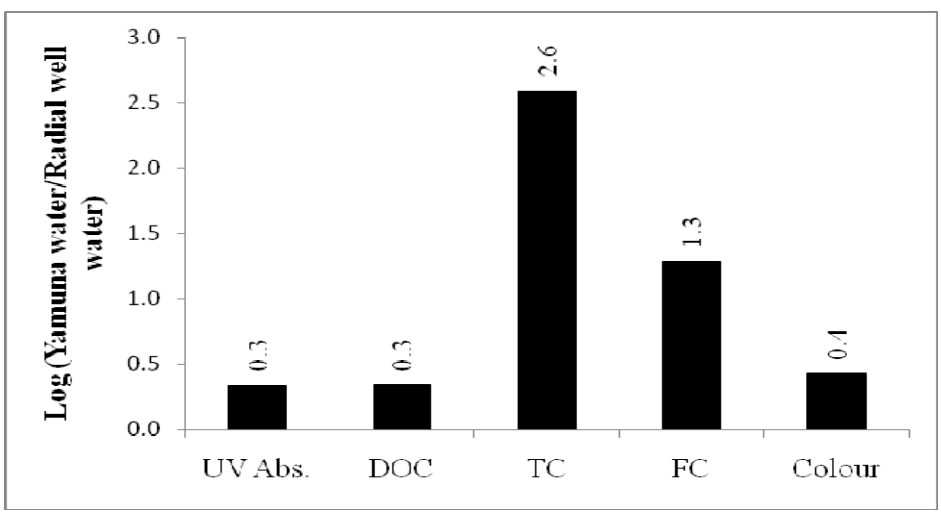

Figure 3. UV Absorbance, DOC, Coliform counts and colour of radial well water relative to river Yamuna water.

CONCLUSIONS

This study clearly illustrates the benefits of riverbank filtration as an alternative to direct surface water abstraction.

REFERENCES

Central Pollution Control Board, New Delhi. (2006). "Water quality status of Yamuna River (1999-2005)."

Doussan, C., Poitevin, G., Ledoux, E., Detay, M. (1997). "River bank filtration: modeling of the changes in water chemistry with emphasis on nitrogen species." *J. Contam. Hydrol.,* 25:129–156.

Grischek , T., Schoeheinz D. and Ray C. (2002). "Siting design issues for river bank filtration schemes." River bank filtration: Improving source water quality, C . Ray, G. Melin, and R. B. Linky. eds., *Kluwer Academic Publishers.,* Dordrecht, Netherlands.

Hunt, H., Schubert, J. and Ray, C. (2003). "Conceptual design of riverbank filtration systems. In Riverbank Filtration: Improving Source-Water Quality," C. Ray et al. (eds.). *Kluwer Academic Publishers.*, Dordrecht, 19-27.

IS 10500, (1991). "Indian Standard: Drinking Water-Specification." *Bureau of Indian Standards*., New Delhi, India.

Kuehn, W. and Mueller, U. (2000). "Riverbank filtration: an overview." *J. Am. Water Works Assoc.,* **92** (12), 60-69.

Nachiappan, R.P., Kumar, B., Manickavasagam, R. (2002). "Estimation of sub-surface components in the water balance of Lake Nainital (Kumaun Himalaya, India) using environmental isotopes". *Hydrol. Sci. J.,* 47:41–54.

Partinoudi, V., and Collins, M.R. (2007). "Assessing RBF Reduction/removal mechanisms for microbial and organic DBP precursors." *American Water Works Association*., 99(12), 61-71.

Ray, C., Grischek, T., Schubert, J., Wang, J.W., and Speth, T.F. (2002). " A perspective of riverbank filtration." *J. Am. Water Works Assoc.,* **94** (4), 149-160.

Standard Methods for the Examination of Water and Wastewater 21st edition, (2005). *American Public Health Association/American Water Works Association/Water Pollution Control Federation, Washington D.C.*

Worch. E., Grischek, T., Bornick, H., and Eppinger, P. (2002). "Laboratory tests for simulating attenuation processes of aromatic amines in riverbank filtration." *Journal of Hydrology*., 266, 259-268.

Sustainable Design and Construction of Earthen-dam Reservoirs for Water Produced in Association with Coalbed Natural Gas in the Powder River Basin, Wyoming

J. J. Brown[1] and Robert W. Thoman[1]

[1]Lowham Engineering LLC, 205 South Third Street, Lander, Wyoming 82520, PH (307) 335-8466, FAX (307) 335-7343, jjbrown@low-water.com, bthoman@low-water.com

ABSTRACT

Surface impoundment of produced water from coalbed natural gas (CBNG) development is a water management option routinely employed by operators in Wyoming's Powder River Basin (PRB). A substantial increase in CBNG development in recent years has resulted in the need for documented guidance and standards regarding the sustainable design and construction of impoundment structures; specifically earthen-dam reservoirs. Earthen-dam reservoirs are a cost effective, relatively low-impact management alternative for produced water, which also allows for a variety of secondary water management options such as evaporation, infiltration, local aquifer recharge, irrigation, and livestock and wildlife watering. Earthen dams are also high-risk structures with the potential for extensive property damage and possible threat to public safety upon failure. A guidance document is beneficial to all stakeholders, from regulators and local governments to land and resource management agencies, ranchers, and landowners. Design elements and construction procedures presented in the guidance document are based on data collected during the design and construction of nearly 1,000 large reservoirs and more than 4,000 smaller stock reservoirs in the PRB over the past eight years. Soil conditions, subsurface and surface hydrology, topography, and geology specific to the PRB are considered, as are the regulatory requirements of the Wyoming State Engineer's Office and the Wyoming Oil and Gas Conservation Commission. While design considerations vary depending on intended beneficial use, landowner requirements, and pertinent regulations, sustainability and minimal disturbance are the governing objectives in all circumstances. Remediation and mitigation procedures for potential short and long-term concerns such as differential settlement, piping, excess surface erosion, and seepage are derived from field trial observations. Design aspects specific to on- and off-channel impoundments, planned long term use, and reclamation following short term use are provided.

INTRODUCTION

The Powder River Basin (PRB) in northeastern Wyoming is a strategically important gas producing area that has seen a dramatic increase in coalbed natural gas (CBNG) development over the last decade. The development of CBNG reserves in the PRB

produces relatively high volumes of fresh to very brackish waters. Water is pumped from coal seams in order to release methane gas trapped in solution by groundwater pressure and to cause migration of the gas toward the recovery wellbore. The water produced from CBNG wells varies in quality from high quality (meeting state and federal drinking water standards) to having very high total dissolved solids (TDS) concentration (ALL Consulting, 2003). Landowners and livestock have come to rely on CBNG-produced water during the drought conditions that have persisted over the last ten years, and natural flood flow chemistry has not been affected by discharge of produced water to major drainages (Sanders et al., 2007).

While there are a number of management options for CBNG-produced waters, construction of earthen-dam reservoirs for surface impoundment is the most cost effective, low-impact storage option preferred by operators and landowners. Hundreds of new earthen-dam reservoirs were constructed and existing reservoirs were upgraded during the initial rush of CBNG development in the PRB, with very little engineering design or construction oversight. As regulatory agencies caught up with the flurry of development, inspection revealed numerous concerns regarding dam safety, location, construction methods and landscape disturbance. Regulators, operators and landowners called for design standards and procedural guidance specific to earthen-dam construction in the PRB.

The design elements and construction procedures presented here represent a sample of the specifications developed in response to the construction challenges and conditions routinely encountered in the PRB. Each design is based on numerous field trial observations, with sustainability and minimal disturbance as the governing principles in all cases. This guidance is based on data collected during the design and construction of nearly 1,000 large reservoirs and 4,000 smaller stock reservoirs in the PRB over the past eight years. Additional information and input was provided by regulatory agencies and industry members directly involved with CBNG development in the PRB.

REGULATORY AGENCIES

The primary agencies responsible for regulating impoundment of CBNG-produced waters in the state of Wyoming are the State Engineer's Office (WSEO) and Wyoming Oil and Gas Conservation Commission (WOGCC). Regulatory authority is dependent on the type of impoundment and proposed beneficial use(s) of the water. On-channel reservoirs are created to hold coalbed methane water in existing ephemeral drainages where water normally flows only in response to precipitation events or snowmelt. Off-channel reservoirs are essentially pits which have associated beneficial uses, and are constructed outside of an existing drainage course. Off-channel reservoirs with no other beneficial use than storage of produced water are regulated by the WOGCC. On-channel and off-channel reservoirs with additional beneficial use are regulated by the WSEO.

Reservoirs permitted by the WSEO fall into two general categories. Reservoirs greater than 2.5 ha (20 ac-ft) in capacity require a detailed design completed by a professional engineer or land surveyor licensed to practice in Wyoming. Smaller reservoirs that are designated for stock use and have a dam fill height of 6.1 m (20 ft) or less do not require detailed designs and permit applications can be completed by the landowner or appointed agent.

If water from oil and gas related operations is discharged to an off-channel site and construction will occur on fee, patented, or state leases, a permit from the WOGCC must be submitted and approved prior to construction. If these facilities have a beneficial use (stock, wildlife, irrigation, etc.) then they must also be permitted by the WSEO (2000). If not permitted for beneficial use, off-channel reservoirs must be fenced to prevent access. The Bureau of Land Management (BLM) will approve, bond, inspect, and enforce compliance on all off-channel pits receiving discharge from federally leased CBNG wells. The BLM also requires an on-site review for all reservoirs located on federal surface, over federal mineral interest, or on fee or state surface if it contains water produced in association with the extraction of federal minerals.

RESERVOIR SITING

The Powder River Basin lies within the Great Plains physiographic province described by Fenneman (1931) and Keefer (1974). It is both a topographic drainage and a geologic structural basin, generally bounded by mountainous terrain to the south, east and west and by the Missouri Plateau to the north. The landscape is characterized by rolling to fairly steep, grass and sage covered plains dissected by incised tributaries. Topographic relief is typically moderate, except where steep-sided, flat-topped buttes rise sharply above the surrounding plains, and where rugged badlands exist near major rivers.

Siting an earthen-dam reservoir in the PRB can be tricky due in part to the local climate, and more so due to soil conditions specific to the region. Climate in the PRB is semi-arid to cold continental, with dry winters and warm summers (McNab and Avers, 1994). Annual precipitation ranges from 25 to 51 cm (10 to 20 in), most of which falls as spring and fall rain (Lowham, 1988). Local drainage is typically ephemeral, and streamflow occurs in direct response to storm events and snowmelt. These ephemeral streams are especially vulnerable to gullying and destruction of vegetation.

Surficial deposits are composed of Quaternary colluvial and alluvial clay-rich soils over interbedded coal, shale, siltstone and sandstone of the Tertiary Fort Union and Wasatch Formations (Ellis et al., 1999). In places, a relatively thick mantle of collapsible windblown silt is present above the bedrock. Soils in the PRB tend to be very fine grained and highly erodible, and shallow, transmissive seams of coal (lignite) and associated organic soils are common (Figure 1). These seams tend to pinch and swell over short distances, making it difficult to define the areal extent of a

particular deposit. Fractured clinker and scoria deposits are often associated with larger coal beds; large, shallow head basins underlain by coal or scoria are regional water collection areas (McNab and Avers, 1994). Subsurface deposits of these materials are difficult to identify based on topography alone.



Figure 1. Shallow coal seam and associated organic soil typical of the PRB

An acceptable reservoir site contains a sufficient amount of soils suitable for use as construction material and a minimal amount of deleterious materials that might promote seepage, erosion or excessive settlement. Mild topography with relatively small contributing drainage area is preferred in order to maximize storage for CBNG-produced water. These ideal conditions are not often readily available, however, and mitigative measures must be incorporated into the reservoir design. Mitigative measures may include the addition of a chimney drain, toe drain and sand blanket, intercept trench, and/or a sump and pump-back system.

DESIGN ELEMENTS

Embankment

In order to facilitate the safe operation of heavy equipment, the top width of the dam should be a minimum of 3.7 m (12 ft), though WSEO (2000) regulations specify a 2.4-m (8-ft) minimum. The upstream slope should be no steeper than 3:1 and the downstream slope no steeper than 2:1. In all cases, a 3:1 downstream slope is easier to seed and maintain than a 2:1, and provides improved stability. If significant wave action is anticipated, the upstream slope may be flattened to 4:1 or designed with a wave shelf. For long term protection, turf reinforcement mat (TRM) or rip rap may be required on the upstream face of the dam along the high water line. Rip rap should consist of dense, competent rock such as granite or limestone.

Spillway

The emergency spillway is designed to accommodate flood flows and prevent overtopping of the earthen dam. A natural spillway across a flat area, away from the embankment, leading to a stable side drainage or a low-gradient bench is ideal. If a natural spillway does not exist, a stable spillway must be constructed around at least one end of the dam with a dike to prevent erosion at the groin. Earthen spillways will not sustain continuous flows and will eventually erode. Where continuous flows are expected, install a separate pipe structure (trickle tube) to protect the spillway from erosion. For spillways with higher velocity flows, the contact area between the spillway and embankment will need protection to at least the design flow depth. Required spillway width will vary based on site-specific conditions including dam height, high water line area, and contributing drainage area.

Outlet Works

If continuous low flow through the reservoir is expected, a trickle tube is useful to prevent erosion of the earthen emergency spillway (Figure 2). The invert of the pipe in the upstream face of the dam is installed at the elevation of the desired high water line, typically 0.3 to 0.6 m (1 to 2 ft) below the elevation of the spillway. High-density polyethylene (HDPE) storm drain pipe with watertight fittings works well for the trickle tube, as it is durable, easy to install, and has excellent hydraulic characteristics. A 46-cm (18-inch) diameter pipe is recommended for most reservoir sites. A pipe of this size can carry as much as 0.4 m^3/s(15 ft^3/s) during occasional flood events and is large enough to pass debris. A 30-cm (12-in) diameter pipe is acceptable for small drainages of less than 16 ha (40 ac). Corrugated metal pipe (CMP) is not recommended because it is susceptible to corrosion and the formation of anchor ice during the winter months. High-density polyethylene pipe (ASTM D3350 Cell Classification 335420C) or HDPE heat-welded pipe (minimum SDR-17, 689 kPa, 100 psi) are suitable alternatives.

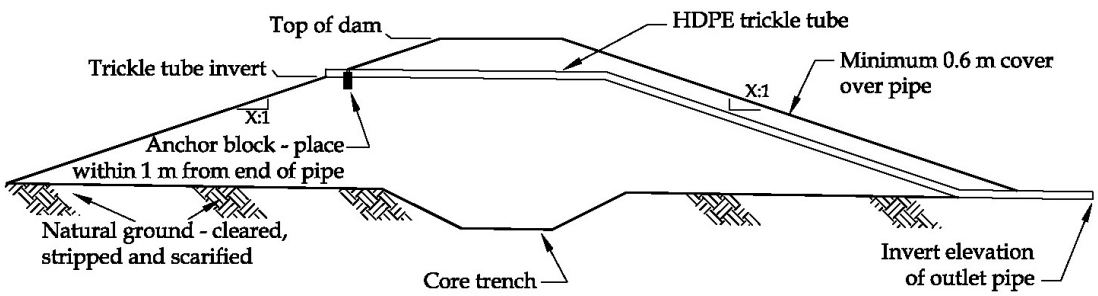

Figure 2. Dam cross-section with trickle tube design detail

The WSEO specifies that all new, on-channel reservoirs built to store CBNG-produced water must be equipped with a controllable, low-level outlet (Figure 3). The minimum diameter for the low-level outlet pipe is 30 cm (12 in). This requirement was expanded in scope to include existing, unpermitted reservoirs that contain CBNG-produced water. High-density polyethylene pipe (minimum SDR-17, 689 kPa, 100 psi) with heat-welded joints and a resilient wedge gate valve with mechanical

joint adapters (AWWA C509) have proven effective for this use. Locating the valve in the downstream face of the dam allows safe, easy access for maintenance and operation. Installing the valve on the downstream side of the dam results in a pressurized pipe beneath the embankment. Regulators were initially resistant to this design modification due to the potential for leakage at the valve or other pipe seams. However, careful pipe installation using bentonite slurry bedding has proven effective to prevent piping, and this configuration is now an accepted standard.

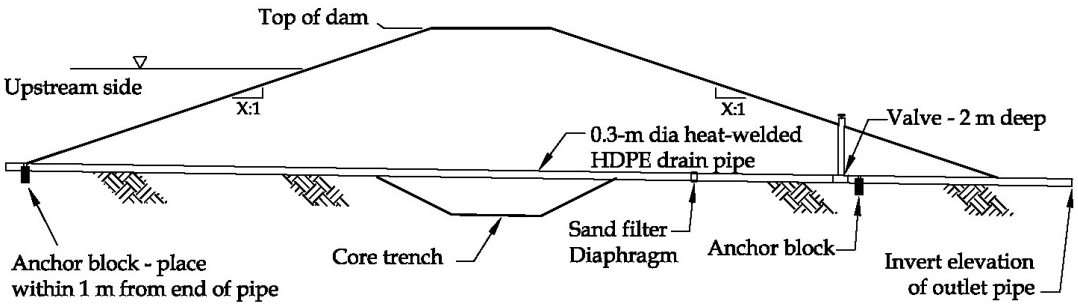

Figure 3. Dam cross-section with low-level outlet design detail

A valve riser is required to operate the gate valve from the ground surface. The riser typically consists of a 30-cm (12-in) diameter polyethylene pipe and cap. The pipe is centered over the top nut of the gate valve. Fill is compacted around the pipe using hand-operated mechanical compaction equipment, and a minimum of 0.6 m (2 ft) of the riser is left exposed above the finish grade. A rebar livestock guard can be installed over the top of the riser to prevent damage from livestock and to aid in locating the valve.

Installing a traditional low-level outlet in an existing dam requires draining the reservoir and excavating to the base of the existing embankment. This is a costly procedure that can compromise the integrity of the dam, and landowners and operators called for an alternative design. The siphon-style outlet design has proven to be a safe and effective option that greatly reduces the cost and construction effort (Figure 4). The siphon consists of a 30-cm (12-in) diameter heat-welded HDPE (minimum SDR-17) pipe. A saddle tee with riser pipe and ball valve are set at the highest point of the siphon tube, near the upstream face. A valve at the downstream toe of the dam enables the siphon tube to be primed when closed.

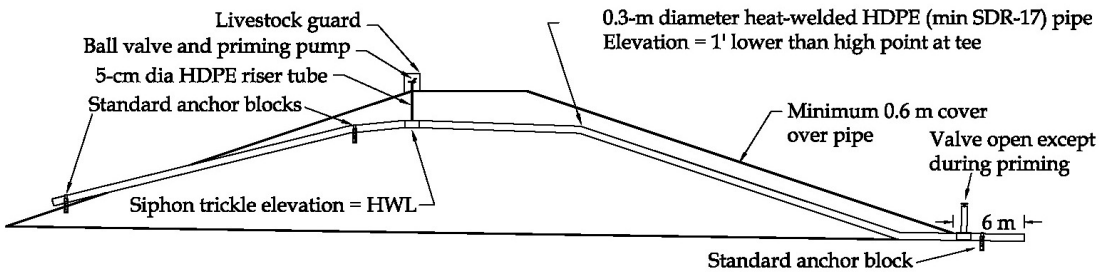

Figure 4. Dam cross-section with siphon-style outlet design detail

A mechanical or hand operated pump is required to prime the siphon pipe and drain the reservoir whenever the water level is below the level of the pipe. The priming pump is attached to the priming tube at the completion of construction. The primer pipe should extend 0.9 m (3 ft) from the ground for ease in operating the priming pump. A livestock guard can be installed to protect the pump and priming tube. The ball and downstream valves must be carefully attended to limit the potential for self-priming by floodwaters. If the siphon is installed near high water line and the downstream valve is left open while the ball valve is closed, floodwaters could potentially prime the siphon and evacuate the entire reservoir.

WATER RIGHTS AND DESIGN FOR COMPLIANCE

WSEO (2004) requires that new reservoirs located above permitted irrigation with catchments larger than 16 ha (40 ac) have a self-regulating bypass structure installed. This can be waived through submittal of a signed waiver by the downstream irrigator. The self-regulating bypass is intended to convey runoff around the impoundment so that irrigation rights downstream are not compromised. The type of self-regulating bypass is depends on the drainage, the amount of the downstream water right, water quality of the discharged water and local topography.

Water Level Control Structure

Water level control structures enable the water surface elevation to be preset and controlled during a runoff event. The structure has a low-level outlet pipe and a riser conduit with stop logs that are set to the desired water level (Figure 5). For some drainages in the PRB, including the Belle Fourche River, Cheyenne River, Horse Creek, Wild Horse Creek and Wildcat Creek, water level control structures meet the WSEO requirement for a bypass structure to provide natural runoff to downstream users with senior irrigation rights. The level of the CBNG-produced water is maintained within approximately six inches from the top stop log of the riser structure so that runoff pass through the reservoir. This requires close monitoring by the operator as storage in the reservoir fluctuates.

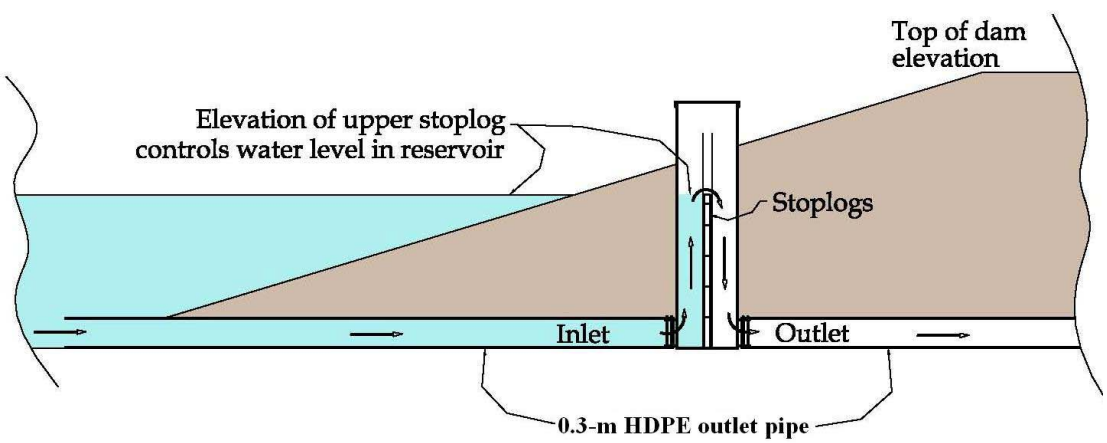

Figure 5. Conceptual design of a water level control structure

Water level control structures using stop logs work best for reservoirs less than about 4.3 m (14 ft) in water height. The increased water pressure in deeper reservoirs can cause leakage around the stop logs.

Flow Bypass

While a water level control structure will serve as an adequate bypass system in some drainages, other drainages, such as SA, LX Bar, Dead Horse, and Spotted Horse Creeks require bypass of natural runoff around the reservoir. The type of bypass depends on the amount of water diverted and the type of terrain. Designs using either a ditch or a pipe have proven effective.

The ditch bypass design includes a diversion dike, a ditch around the reservoir and erosion protection (Figure 6). The ditch is designed with a cross-sectional area and



Figure 6. Ditch flow bypass system to convey runoff around a CBNG reservoir

slope to accommodate the necessary discharge and is seeded to establish vegetative cover for erosion protection. The ditch system can bypass relatively large flows, but requires periodic maintenance and may be subject to erosion, particularly at the point where the bypass channel merges with the original channel downstream of the impoundment.

The pipe system (Figure 7) is an effective alternative to the ditch system when topography or soil conditions are not conducive to ditch construction. Maintenance is minimal after installation, but includes keeping the pipe full of water. Relatively high water velocity during flood events prevents suspended sediment from settling out in the pipe.

HDPE pipe with heat-welded joints (minimum SDR-17), sized to pass the required flow, can be used to construct the bypass. Polyethylene has a lower specific gravity

than water and unless the pipe is anchored, it will float, even when filled. The pipe will require concrete anchor blocks at intervals along the alignment.



Figure 7. Downstream view of a pipe flow bypass and diversion dike

The pipe and anchors can be buried, if desired. From the diversion dike, the pipe is placed on the ground surface or buried up to the face of the dam. The pipe is then buried over the upstream face, through the dam (at trickle tube elevation), and down the downstream face to the drain pipe outlet. An eccentric reducer is required at the beginning of the bypass pipe in the diversion dike. Fitting a vent tube in the pipe will prevent siphoning of the pipe following a runoff event. The vent tube is placed on the upstream face of the dam before the highest point of elevation so that it can be used to fill the upstream portion of the bypass pipe with water.

Both bypass systems require placement of a diversion dike upstream of the high water line. The size of the diversion dike depends on the flow to be bypassed while allowing excess runoff to overflow into the reservoir. The diversion dike is the controlling device for the pipe bypass system as it will encase the pipe, create a pool, and direct flow into the pipe. A dike constructed with a minimum top width of 2.4 m (8 ft) and a minimum height of 0.9 m (3 ft) will allow a pool to form and create minimal head for full pipe flow.

SUMMARY AND CONCLUSIONS

Large numbers of hastily constructed earthen-dam reservoirs built to accomodate increased CBNG production in the PRB over the past decade precipitate the need for engineering oversight and procedural guidance. Standard design specifications based on regulatory requirements and proven construction techniques promote sustainable development with minimal environmental impact.

Additional design elements and construction procedures specific to earthen-dam construction in the PRB can be found in the guidance document *Procedures for Permitting and Constructing Reservoirs* (Lowham, 2008).

REFERENCES

ALL Consulting (2003). *Handbook on coal bed methane produced water: management and beneficial use alternatives: Coal bed methane resources and produced water management*, U.S. Department of Energy, Office of Fossil Energy, National Energy Technology Laboratory, CD. (http://www.all-llc.com/CBM/BU/index.htm)

Ellis, M. S., Gunther , G. L., Ochs, A. M., Roberts, S. B., Wilde, E.M., Schuenemeyer, J. H., Power, H. C., Stricker, G. D., and Blake, D. (1999). "Coal Resources, Powder River Basin", *1999 Resource assessment of selected Tertiary coal beds and zones in the Northern Rocky Mountains and Great Plains region,* U.S.Geological Survey Professional Paper 1625A.

Fenneman, N. M. (1931). *Physiography of the Western United States*, McGraw-Hill, New York.

Keefer, W. R. (1974). *Regional Topography, Physiography, and Geology of the Northern Great Plains*, U.S.Geological Survey Open File Report 74-50.

Lowham Engineering LLC. (2008). *Procedures for Permitting and Constructing Reservoirs*, Lander, Wyoming.

Lowham, H. W. (1988) *Streamflows in Wyoming*, U.S. Geological Survey Water Resources Investigations Report No. 88-4045, Cheyenne, Wyoming.

McNab, W. H. and Avers, P.E. (1994). *Ecological Subregions of the United States*, U.S.Forest Service Report WO-WSA-5, 41-331G.

Sanders, F. S., Carlson, G., Boram, L., Lowham, H. W., and Druse, S. A. (2007). *Water Resource Monitoring of Streams in the Coal Bed Methane Production Area of the Powder River Basin, Wyoming, 2003 to 2006 Water Years,* Laramie, Wyoming.

Wyoming State Engineer's Office. (2000). *Instructions for filing applications for stock reservoir,* Cheyenne, Wyoming.

Wyoming State Engineer's Office. (2004). *Revised interim policy Memo-State Engineer's Office permitting requirements for water produced during the recovery of coal-bed methane (CBNG)*, Cheyenne, Wyoming.

SUSTAINABLE DEVELOPMENT OF AGRICULTURE: URBAN WASTE WATER A VIABLE MEAN FOR IRRIGATION

Dr. CHHEDI LAL[1] and VAIBHAV GUPTA[2]

[1] Senior Scientist, Irrigation and Drainage Engineering, Central Soil Salinity Research Institute, Regional Research Station, Lucknow-226016 (UP) INDIA, email lalc_verma@yahoo.com

[2] Final year undergraduate student, Agricultural Engineering, College of Technology, G. B. Pant University of Agriculture and Technology,Pantnagar-263145, Distt. Udham Singh Nagar (Uttarakhand),India, email vbhv.gupta@gmail.com

ABSTRACT

World Commission on Environment and Development in "Our Common Future" (**Brundtland, 1987**) defines the sustainable development as "a strategy that meets the needs of the present without compromising the ability of future generation to achieve their own requirements". Developing countries have to face double challenge for sustainable agriculture, firstly to increase food production and secondly to maintain if not to improve resource and environmental quality. **EI Bassam** (1998) reported that per capita land required for food, oxygen and water security are 15-20 m^2, 6-10 m^2 and 3-6 m^2, respectively under controlled conditions. This could be achieved if innovative technical means and efficient material recycling systems are implemented.

One of the biggest problems that agriculture will face in the years to come will be of availability of good quality water for irrigation purpose. The water available and the ultimate irrigation potential do not level up. Under ground water contributes to more than 70% of the total ultimate potential through minor irrigation. To cater to the depletion of good quality water alternate sources are being looked into.

Domestic effluent or waste water generated from urban areas is generally being disposed off into the existing natural streams or water bodies. Rivers passing from the big cities have become heavily polluted and need immediate attention. Huge quantity of waste water is being generated in cities every day. Domestic waste water may be used as an alternate resource for irrigation. Only a fraction of this is being treated at present and reused for various purposes. Waste water reuse may have one or combination of several objectives such as: 1. Use of a reliable water source for irrigation, 2. Fertilization of infertile lands; 3. Re-use of scarce water resources; 4. Safe disposal of waste water to avoid contamination; and 5. Ground water recharge.

The population of the countries and size of the cities are growing rapidly. According to a survey, more than 50% of the population will be in urban areas by 2050 against present level of 30%. Domestic and industrial sectors use 15% of the present water resources which will grow to 30% by the year 2050. Waste water generated from concentrated population will increase in similar proportion. Waste water may be used as water resource for agriculture and aquaculture. Domestic waste water need to be diverted for irrigation purposes. Typical waste water is composed of 99.5% to 99.9% of water and remaining percentage is composed of inorganic and organic solids,

colloids and dissolved solids, which contain major nutrients and trace elements. Average annual application of waste water may correspond to about 300 kg/ha.N and 50 kg/ha P. Waste water irrigation in over-exploited ground water areas may arrest the decline of ground water table. Growing pressure on available fresh quality irrigation water resources and increasing awareness to environmental issues among human masses will force researchers and planners to design waste water disposal system in such a way that it could be safely made available to its users. This is the right time to give a rational thought in this direction to make the waste water a safe water resource for irrigation and make agriculture sustainable for the future.

INTRODUCTION

Domestic effluent in most developing nations, are being discharged into the inland water bodies or streams without any pretreatment deteriorating water quality. This has created a matter of great concern in developing countries. Streams and rivers passing from the large cities in India have become a sewage disposal channel deteriorating environmental quality as overall impact and interest killing of down stream users as specific impact.

The demand for good quality water by the industry and domestic sectors are continuously growing. Available share of good quality water for irrigation is being diverted to these sectors making less and less good quality water available for irrigation making horizontal expansion of irrigated area almost impossible with conventional irrigation methods. To increase total agricultural productivity, cropping intensity needs to be increased (it has already increased in many regions and continuously increasing in other pockets) demanding more and more water with decreasing share of good quality irrigation water. With diminishing share of good quality water for irrigated agriculture is left with no option other than to utilize poor quality water (saline, high RSC water, domestic and industrial effluents) for crop irrigation. Industrial effluents needs special attention and treatment before it can be used for irrigation purposes. Domestic effluents have great potential to be used as irrigation source. Conventional irrigation methods offer little flexibility to utilize such a poor quality water.

Conventional water management techniques have spelled disaster in the past. A vast area has gone out of cultivation due to excessive water logging and salt build up in the root zone and the problem is still increasing. More than 8.2 million hectares of land has become salt affected and about 12 million hectares of land is suffering due to water logging in the country.
Ground water was used as assured source of irrigation water and also for domestic and industrial uses. Excessive utilization of ground water has resulted in steep decline in ground water table failing thousands of shallow tube wells in country like India. Conventional irrigation methods have become incapable to avoid such problems.

Increasing threat to environment be it water logging, Stalinization, problems associated with large scale water storage and diversion structures, deteriorating surface and subsurface water quality and disposal of sewage water and associated problems or decreasing flow of water in rivers have become a matter of great

concerns to the common people with increasing awareness of deteriorating environmental health. More and more advanced technologies are required to avert the impending problems with past interventions of technologies and management strategies.

INCREASING DEMAND FOR WATER WITH INCREASING POPULATION

The population of the world and India in rural as well as in urban areas are growing and consequently the demand of water is also growing. **Table 1** shows the population distribution of the world content wise. **Table 2** shows the growth in urban and rural areas. Population is a direct index for water demand and hence the rising demand and crises may be looked accordingly. As table shows more than 70% population of the country lives in rural areas. Agriculture is the main occupation of rural mass. Major share of fresh water supply is being used by the agriculture sector. More and more water is being extracted from ground water reserves for crop irrigation. The excessive pumping for intensive cropping and high water demanding crops are main reasons for water table decline in rural areas.

Table 1. Continent wise population distribution.

	population estimate/projected			
continent	**1950**	**1975**	**2000**	**2030**
Northern America	172,000,000	243,000,000	314,000,000	396,000,000
Latin America & the Caribbean	167,000,000	322,000,000	519,000,000	723,000,000
Oceania	13,000,000	21,000,000	31,000,000	42,000,000
Europe	548,000,000	676,000,000	727,000,000	670,000,000
Asia	1,399,000,000	2,397,000,000	3,672,000,000	4,950,000,000
Africa	221,000,000	406,000,000	794,000,000	1,489,000,000
World	2,520,000,000	4,065,000,000	6,057,000,000	8,270,000,000

Table 2. Population growth in rural and urban areas in India.

Census Year	**Number of UAs/Towns**	**Total Population**	**Rural Population**	**Urban Population**	
				Number	**% of total**
1901	1830	238396327	212544454	25851873	10.8
1911	1815	252093390	226151757	25941633	10.3
1921	1944	251321213	223235046	28086167	11.2
1931	2066	278977238	245521249	33455989	12.0
1941	2253	318660580	274507283	44153297	13.9
1951	2522	361088090	298644156	62443934	17.3
1961	2334	439234771	360298168	78936603	18.0
1971	2567	548159652	439045675	109113977	19.9
1981	3347	683329097	523866550	159462547	23.3
1991	3769	846387888	628836076	217551812	25.7
2001	4378	1027015247	741660293	285354954	27.8

GLOBAL WATER RESOURCES

The distribution of global water resources are given in **Table 3**. Major share of fresh water is in form of polar ice (77.2%). Ground water reserves have a share of 22.4% and need to be wisely planned and utilized. Water available in rivers and lakes are too less and all the countries are not blessed with good perennial streams and rivers. The river water supplies are going to be critical in many developing countries due to diversion for different users and further pollution of streams in lack of strict regulation to dispose pollutants.

Table 3 Distribution of global water resources.

Water Resources	Share
Total Water Resources	1460 Million BCM
Saline water	97.3%
Fresh Water	2.7%
o Polar Ice Caps	77.2%
o Ground Water & Soil Moisture	22.4%
o Lakes, Swamp & Reservoirs	0.35%
o Atmosphere	0.04%
o Rivers & Streams	0.01%

WATER RESOUCES OF INDIA

The water resources of the India are presented in **Table 4.** It may be seen from **Table 4** that out of total precipitation of 400 million ha-m, 115 million ha-m goes as surface runoff, 215 million ha-m as percolation and 70 million ha-m as immediate evaporation. Total ground water available in the country is 85 million ha-m and total surface runoff to the tune of 180 million ha-m. The usage of ground water on full development will be 42.3 million ha-m.

Table 4. Water Resources of India.

	Hydrologic units	Amount of water million ha-m
Total precipitation		400
1.	Percolation	215
1.1	Percolation of rainfall to soil moisture	165
1.1A	Percolation of irrigation to soil moisture	+ 5
	Total evapotranspiration	**170**
1.2	Percolation of rainfall to ground water	50
1.2A	Percolation from rivers, streams, seepage	+35
	Total ground water	**85**

2.	Immediate evaporation	70
3.	Surface runoff	115
3.A	Regenerated flow from ground water	+45
3.B	Flow brought from outside India through streams and rivers	+20
	Total surface water	**180**

GLOBAL WATER USE

Global water withdrawal and use for selected categories are presented in **Table 5.** It may be seen from the table that agriculture is the major water user on the globe and demand is growing continuously with increasing population. Industries are the second largest user and the domestic supplies come at the last. Irrigated areas of the world had continuously increased from 47.3 million ha in year 1900 to 264 million ha in year 2000.

Table 5. Global water withdrawal and use for selected categories (1900-2025)

Category	**1900**	**1950**	**1980**	**2000**	**2025**
Population (million)	-	2542	4410	6181	7877
Irrigated area (million, ha)	47.3	101	198	264	329
Agricultural use (km^3/year)					
Withdrawal	525	1122	2179	2560	3097
Use	406	849	1688	1970	2331
Industrial use (km^3/year)					
Withdrawal	37.8	181	699	768	1121
Use	3.4	14.4	59	85	133
Municipal use (km^3/year)					
Withdrawal	16	53	207	389	649
Use	4.2	14	42	64	84

The total water demand for agriculture, domestic and industrial sectors of India in 1995 was estimated to be about 650 km^3, of this about 90% is withdrawn for agriculture sector alone. Government of India had given great emphasis from time to time to create more and more water potential for bringing more and more agricultural area under irrigation in order to increase total food grain production in the country. Coming section will be discussing about the irrigation status in the country.
Table 6 presents the estimates of future water demands in India

Table 6. Estimates of future water demands (billion cubic meter) in India.

Category	Year 2010			Year 2025			Year 2050		
	Low	Medium	High	Low	Medium	High	Low	Medium	High
Irrigation	489.0	536.0	556	619	688	734	830	1008	1191
Domestic	39.4	41.6	61	47	52	78	59	67	104
Industrial	37.0	37.0	37	61	67	79	69	81	116
Total	555.4	614.6	654	727	807	881	958	1156	1411

IRRIGATION POTENTIAL CREATED AND UTILIZED THROUGH GROUND WATER

The use of ground water for irrigation purposes had increased continuously after the independence. Ground water may be used as 100% source for irrigation or as a source for assured irrigation. Government of India and various State Governments have continuously worked for creating more and more irrigation potential through ground water utilization. The present potential created at the end IX Plan was 44.98 million ha and potential utilized is 37.09 million ha(**Table 7).** Sources of irrigation water are mainly tanks, canals, tube wells and different type of wells. Out of total irrigated areas in the country about 48% is through wells and 38% through canals and 8% through tanks and 6% from other sources.

. **Table 7. Irrigation potential created and utilized through ground water.**

Plan	**Potential Created (in m. ha)**	**Potential Utilized (in m. ha)**
Pre Plan upto 1951	6.50	6.50
I Plan (1951-56)	7.63	7.63
II Plan (1956-61)	8.30	8.30
III Plan (1961-66)	10.52	10.52
Annual Plan 1966-69	12.50	12.50
IV Plan (1964-69)	16.50	16.50
V Plan (1974-78)	19.80	19.80
Annual Plan (1978-80)	22.00	22.00
VI Plan (1980-85)	27.82	26.24
VII Plan (1985-90)	35.62	33.15
Annual Plan (1990-92)	38.89	36.25
IX Plan (1997 -2002)	44.98	37.09

The numbers of ground structures have increased significantly after the independence. **Table 8** shows the growth of ground water structures after the independence of India. Shallow tube wells are cheap and easy to construct if the site is favorable. The continuous increase in ground water structures in lack of strict ground water legislation is one of the reasons for ground water decline

Table 8. Growth in number of ground water structures.

Years	**Dugwells**	**Shallow**	**Tube wells**	**Pumsets**	
				Electric	**Diesel**
1950-51	3860000	3000	2400	21000	66000
1973-74	6700000	1140000	22000	2460000	175000
1979-80	7786000	2132000	33300	3265000	265000
1989-90	9407000	4754000	63600	8766000	446700
1991-92	10120000	5379000	67600	9336000	458500

MAJOR ASSOCIATED PROBLEMS WITH AGRICULTURE

1. WATER LOGGING

Water logging is the major problems in canal irrigated areas. Excessive seepage from the canals and field channels, high rainfall, field losses, insufficient drainage facilities and blockage of natural drainage systems are the main reasons for water logging. Introduction of high water demanding crops such as paddy, sugarcane and mentha resulting higher losses from the fields further aggravates the problems. Now a days in many parts of the country such as Punjab and Haryana double crops of paddy is being taken resulting more losses. **Table 9** shows the extent of water logging in different states of the country. There are various estimates presented in this table showing the seriousness of the problems. Area under water logging is increasing continuously.

Table 9. Extent of Water logging areas in million hectare estimated by various agencies.

State	National Commission on Agriculture (1970)	National Commission on Agriculture (1972)	Ministry of Agriculture (1990)	CSSRI, Karnal	Wasteland Board &
Andhra Pradesh	0.339	NR	0.339	0.339	0.1035
Bihar	0.117	NR	0.707	0.312	0.1198
Gujarat	0.484	NR	0.484	0.484	0.2656
Haryana	0.620	0.650	0.620	0.275	0.0238
Karnataka	0.01	0.007	0.010	0.036	0.0032
Kerala	0.061	NR	0.061	0.012	0.0136
Madhya Pradesh	0.057	0.057	0.057	0.057	0.0051
Maharashtra	0.111	0.028	0.111	0.111	0.0527
Punjab	1.009	1.009	1.009	0.198	0.0352
Rajasthan	0.348	0.348	0.348	0.348	0.0289
Tamilnadu	0.018	NR	0.018	0.128	0.0415
Uttar Pradesh	0.810	0.810	1.980	1.980	0.4981

Source: DES.1995.Directorate of Economics and Statistics, Government of India.

2. SALINITY PROBLEMS

Rising water table due to increased recharge of ground water (excessive seepage from canals, field channels and deep percolation losses from agricultural fields) dissolves salts from deeper profiles and brings it near to the ground surface. Because of solar radiation water gets evaporated leaving salts behind. The water received through rainfall dissolves these salts and moves them down to deeper soil layer. If the annual evaporation is higher than the annual precipitation the salt deposition is more pronounced and area becomes salt affected. Salinization is generally coupled with the water logging. There are various estimates for salt affected lands in the country. More than 8 million ha of land is salt affected in the country causing a huge loss to the nations and suffering to the farmers.

National Remote Sensing Agency has given an estimate of salt affected soils in different state (**Table 10**).

Table 10. State-wise extent of salt affected soils in India (based on 1986/87 satellite data with adequate field checks)

S.N.	State (ha)	Saline soils (ha)	Sodic soils (ha)	Total (ha)	Total in million ha
1.	Andhra Pradehs	77598	196609	274207	0.274
2.	Andaman & Nicobar Island	77000	0	77000	0.077
3.	Bihar	47301	105852	153153	0.153
4.	Gujarat	1680570	541430	2222000	2.222
5.	Haryana	49157	183399	232556	0.232
6.	Karnataka	1893	148136	150029	0.150
7.	Kerala	20000	0	20000	0.020
8.	Madhya Pradesh	0	139720	139720	0.140
9.	Maharastra	184089	422670	606759	0.607
10.	Orissa	147138	0	147138	0.147
12.	Punjab	0	151717	151717	0.152
13.	Rajasthan	195571	179371	374942	0.375
14.	Tamil Nadu	13231	354784	368015	0.368
15.	Uttar Pradesh	21989	1346971	1368960	1.369
16.	West Bengal	441272	0	441272	0.441
	Total	2956809	3770659	6727468	6.727

Source: National Remote Sensing Agency and Associates, 1996
Total salt affected land in the country is 8.57 million ha out of which 2.07 million ha is costal salinity, 3.47 million ha is salinity in canal command and 3.027 million ha is salinity outside the canal.

3. GROUND WATER DEPLETION

Total area irrigated using ground water reserves is higher than canal irrigated areas. Shallow tube wells have becomes quite common to be used by the farmers due to low cost, subsidy and lack of legislation for ground water utilization. The numbers of ground water structures have increased several folds after the independence of the country. **Table 8** shows the increase of ground water structures in the country from 19950-51 to 1991-92.

Ground and surface water constitute an integral part of the hydrologic cycle and form the available resource of water supply on earth. In the event of failure of monsoon ground water becomes more assured water supply. This has brought about rapid acceleration of well construction in the country. Old water lifting devices are becoming obsolete and being replaced by tube wells.

Ground water development in different parts/regions of the country is not uniform and influenced by hydrological parameters as well as agricultural and socio-economic activities of the regions. Over exploitation of ground water has become a well known fact in the state of Haryana, Punjab, Western UP and Tamil Nadu etc. As per the

National Water Policy ground water development is limited to annual replenishable ground water resource. Guidelines for status of ground water utilization are presented in **Table 12**. **Table 13** shows the stage of ground water utilizations in different states of the country The problem of over exploitation of ground water is becoming increasingly worse and requires immediate attentions of planners and researchers. The irrigated agriculture is going to face severe water shortage in years to come in many parts of the country.

Table 12. Guidelines for classifications

Category	State of GW Development
1. Over-exploited	>100%
2. Dark Areas	>85% to 100%
3. Grey Areas	>65% to 85%
4. White Areas	<65%

Table 13. State-wise categorization as per the NABARD

SN	State	Unit	Total Unit	White (No.)	Grey (No.)	Dark	Data base
1.	Andhra Pradesh	M	1104	966	36	102	March,1994
2.	Bihar	B	588	533	55	-	January 1989
3.	Gujarat	T	183*	101	35	45	April 1994
4.	Haryana	B	108	62	14	32	September 1993
5.	Karnataka	T	175	132	22	21	December 1994
6.	Kerala	B	151	145	4	2	March 1996
7.	Madhya Pradesh	B	459	442	14	3	December 1990
8.	Maharashtra	W	1503	1408	59	36	June 1995
9.	Punjab	B	118	33	13	72	September 1993
10.	Rajasthan	B	237	120	34	83	July 1996
11.	Tamil Nadu	B	384	196	90	98	January 1993
12.	Uttar Pradesh	B	895	639	184	72	February 1996

B- block, M- Mandal T = Taluka W= Watershed
* 2 taluka unassessed (saline area) $ 57 unassessed

4. WASTE WATER GENERATION, DISPOSAL AND IRRIGATION

Demographic growth, increasing urbanization, industrialization, improving living standard and changing life style triggering greater use of detergents, domestic sprays, medical wastes, etc. expected to produce large quantities of anthropogenic wastewaters with different compositions. Population growth rate in rural and cities are indicative of future trends of liquid/solid wastes. Untreated domestic and industrial effluents are being disposed in natural streams and water bodies posing a great threat to environment. Domestic and industrial effluents if used for irrigation without treatment, proper selection of crops and irrigation methods it may affect the health of end users of agricultural produce, irrigation water handler and field workers. A large numbers of associated health hazards have been published in the literature with waste water irrigation without proper planning and selection of crops. **Table 14**

presents the basin wise waste water generation and **Table 15** presents disposal modes of waste water in class I cities.

Table 14. Basin-wise wastewater generation, collection and treatment in class-I cities.

Name of river basin	No. of class-I cities	Volume of waste water (MLD)		Treatment capacity (MLD)
		Produced	Collected	
Brahmani	1	17.3	13.0 (75)[1]	NA
Brahamputra	7	178.9	91.9 (51)	NA
Cavery	16	726.9	471.5 (65)	396.1 (51)[2]
Ganga	103	5812.4	4341.1 (69)	1618.9 (28)
Indus	15	624.3	330.5 (53)	93.8 (10)
Godvari	25	634.8	467.8 (74)	65.4 (10)
Krishna	27	1313.8	1055.5 (80)	489.0 (37)
Mahanadi	9	412.9	321.9 (78)	86.0 (21)
Non-major	37	908.7	525.2 (58)	639.0 (70)

On an average about 72% of domestic effluents are collected from class I cities, and only 24% is being treated.

Table 15. Basin-wise disposal modes of wastewater in class-I cities.

Name of river basin	No. of class-I cities	No of cities with mode of disposal				Other (Sea/Land/ drain etc)
		Agriculture	River	Both Agric. & River	Agric. & Others	
Brahmani	1	-	-	1	-	-
Brahamputra	4	-	3	-	-	4
Cavery	16	3	3	-	1	7
Ganga	103	29	16	23	8	25
Indus	15	6	2	-	1	6
Godvari	25	3	1	4	4	13
Krishna	27	4	3	2	3	15
Mahanadi	9	-	1	2	2	4
Coastal	29	6	3	2	1	17
Non-major	37	11	1	4	7	14

Water quality deterioration is matter of great concern due to increased withdrawal of river water for agriculture and domestic supplies and increased flow of untreated domestic effluents.

Disposal of untreated industrial effluents is further worsening the water quality of river.

The domestic waste water need to be treated reused, and discharged in the streams to preserve water ecosystems

Table 16 shows the effect of long term effect of sewage irrigation on physical properties of the soil. Table shows that after long term sewage irrigation will reduce the bulk density but the aggregate stability, stability index, water holding capacity, hydraulic conductivity, total porosity and organic carbon will increase.

Table 16. Effect of long term sewage irrigation on physical properties of the soil.

Properties	**Fresh water**	**Sewage water after**	
		15 years	**25 years**
Bulk density (g/cm^3)	1.53	1.53	1.06
Aggregate stability (%)	72.4	84.4	83.5
Stability index (%)	62.3	65.8	71.1
Water holding capacity (%)	33.2	49.7	59.8
Hydraulic conductivity (cm/hr)	19.1	23.6	26.6
Total porosity (%)	36.2	49.7	59.8
Organic carbon (%)	1.42	2.56	4.63

Table 17 shows the health status of sewage farm workers. The table shows the risks of health hazards to farm workers. Sewage irrigation too need special attention for management to avoid associated health hazards to field workers and end users of the agricultural produce.

Table 17. Health status of sewage farm workers.

Study area	Test group		Control group	
	Number	Per cent	Number	Per cent
Nagpur sewage farm				
Total examination	360	306		
Total positive	303	84	179	59
Positive for hookworms	231	64	123	40
Positive for roundworms	245	68	159	52
Infected with two or more parasites	156	43	44	14
Madurai sewage farm				
Total examinations	663	2644		
Total positive	520	78	512	19

Source: Shende et al. (1987)

5. BUILD-UP OF DISEASES AND PESTS

There is a great risk of occurrence and build up of some obnoxious pests and diseases in the area of crop intensification under high input use. This factor hinders the vertical growth and questions are obvious about the sustainability of the environment under intensive input use which is unavoidable for maximizing crop yields. Heavy infestation of Phelaris minor in continuous rice-wheat cropping system in north-western plains, increasing occurrence of sheath blight in rice and the incidence of

Altenaria and Helminthosporium leaf blight are eye catching example. Under extreme situations further strong repulsive response of nature is yet to come.

6. LOW INPUT USE EFFICIENCY

Water application and water use efficiency are quite low (30-40%) in developing countries like India. Cropping intensity in the country is only about 135%. The Indian agriculture is running a net negative balance of 8-10 million tones per year. In addition, about 8 million tones of nutrients is lost annually due to soil erosion. The present efficiency of nutrient use is about 30-40%. The long-term experiments have shown a decline in organic carbon, nitrogen and phosphorus in cereal-cereal intensive cropping.

7. SLOW GROWTH IN RAIN-FED AREAS

About 70% of the agriculture in India is under rain-fed conditions and contributing about 40% of the national food grain production. The productivity of the rain-fed agriculture is quite low (0.8 tonne/ha) against the productivity of irrigated agriculture (2.0 tonne/ha). Erratic behaviour of monsoon has started precipitating and changing climatic conditions may further worsen situation of rain-fed agriculture in years to come due too global worming and deforestation. Natural resources will be over burdened in these areas and their trafficking will become essential making the ecosystems more fragile and unsustainable.

8. INCREASING POPULATION AND SHRINKING RESOURCE BASE

Growing population of the country is reducing the per capita natural resources share. Country's population has already reached a level of one billion. The per capita land availability for cultivable land will reduce to about 0.14 ha in 2025 A.D. compared to about 0.17 ha at present level. Livestock population has increased from 292 to 416 million and is still increasing with a rate of 2% per annum mounting a tremendous pressure on land, water and forest resources. The availability of drinking water per capita per annum is 2001 m^3 at present which will reduce to a level of 1700 m^3 in the next 2-3 decades. Below this threshold, water availability will be considered a severe constraint to socio-economic development and environmental quality. This is mere a statistic. At present, water supply in the cities are not in good shape at all. If we apply quality constraints of the country or WHO and international norms the availability will go further down. Ground water and surface water is subjected to great risks of pollution. Almost all the rivers passing from a big city are highly polluted and have become a sewage disposal channels. They are not suitable for human use. Lack of supervision and strict regulation allows people to discharge highly polluted industrial effluent into the natural streams and rivers. Presently agriculture sector is utilizing 85% of total developed potential and is likely to be reduced by 10-15% to meet the growing demand for drinking and industrial usage. Shrinking natural resources will force fast recycling of many natural resources such as water and forest making system more fragile than ever. Near 30% population in the country is residing in the

cities against about 11% during the year 1901. Demands for natural resources have risen steeply with increasing population and will grow further not only to match increasing population but also to match the living standards of the people with growing economy. More efforts and huge money will be needed to tackle on this front for reaching sustainable level. For developing countries like India, with the growing population and rapid urbanisation, the demand for fresh water is growing up from all the competing sectors - agriculture (demands about 80-90% of fresh water), domestic (about 5-7%), industry (about 10-15%), environment & ecosystem, etc. Inter and intra sectoral conflicts are growing up, almost all the surface flows are consumptively utilised, and there is no left over for environmental flows, as a result less groundwater recharge and more wells failure. Apart from that surface water (river water) based drinking water schemes are also get very much affected during dry seasons, as only municipal sewage (mostly untreated or partially treated) feeds the rivers. Since there is no groundwater recharge from surface water, only options for groundwater recharge is rainfall. However, rising variability in rainfall along with the encroachments of traditional water harvesting structures resulted in less recharge. So, only recharge is possible from agricultural return flow laced with deadly pesticides and fertilizers. Recently, there is an increasing trend for all the sectors to go for groundwater to meet the demand, as a result groundwater quantitatively depleted and qualitatively degraded in many basins. In this scenario, both the regulators and so-called experts are suggesting for waste water (untreated or partially treated sewage water) based irrigation activities, and there are provisions for industries to discharge their effluents on land. Since the land disposal is less stringent, hence most of the industries are going for that. As a result, groundwater water is getting polluted and application of polluted groundwater for irrigation is degrading the soils.

WASTE WATER: A WATER RESOURCE FOR AGRICULTURE

Demographic growth, increasing urbanization, industrialization, improving living standard and changing life style triggering greater use of detergents, domestic sprays, medical wastes, etc. expected to produce large quantities of anthropogenic wastewaters with different compositions. Population growth rate in rural and cities are indicative of future trends of liquid/solid wastes. Untreated domestic and industrial effluents are being disposed in natural streams and water bodies posing a great threat to environment. Domestic and industrial effluents if used for irrigation without treatment, proper selection of crops and irrigation methods it may affect the health of end users of agricultural produce, irrigation water handler and field workers. A large numbers of associated health hazards have been published in the literature with waste water irrigation without proper planning and selection of crops.

Table 18 presents the details of sewage farming in class I cities in India. The cities where more than 1000 ha under sewage irrigation are Chandigarh, Hyderabad, Rajkot, Vadodara and Varanasi. Charges for sewage irrigation ranges from Rs. 30.60 to Rs. 400.00 per hectare per annum. **Table 19** presents effect of sewage irrigation on

alkalinity and salinity of the soil. There is not much problems with the salinity but the alkalinity may become prominent in several cases if proper attentions is not paid.

Table 18. Details of sewage farming in class-I cities.

SN.	City	Waste Water Collected (mld)	Supplies to sewage farms (mld)	Percentage of WW supplied to sewage farm	Land used for sewage farming (ha)	Application rate
1.	Ahemedabad	445.0	NA	-	NA	
2.	Bangalore	300.0	NA	-	NA	
3.	Bhopal	95.0	13.6	14	44.5	306.0
4.	Bombay	2210.0	20.0	0.9	NA	
5.	Calcutta	1075.0	817.0	76	NA	
6.	Chandigarh	209.8	136.2	65	1000.0	136.0
7.	Delhi	1270.0	NA	-	NA	
8.	Hyderabad	288.0	40.0	14.0	1085.0	37.0
9.	Jaipur	165.0	22.7	14.0	200.0	114.0
10.	Kanpur	150.0	NA		NA	
11.	Lucknow	80.0	NA		NA	
12.	Madras	257.0	10.0	4	8.0	91250
13.	Patna	184.0	NA		NA	
14.	Pune	367.0	80.0	22.0	NA	
15.	Tirenvelli	44.8	18.0	40	184.0	98.0
16.	Visakhapatnam	55.0	NA		NA	

Table 19. Effect of sewage irrigation on soil salinity, alkalinity and contents on major nutrients.

Site/years of sewage use	Treatment	pH (1:2)	EC (1:2) dS/m	O.C. (%)	Total N (%)	Total P (%)	Total K (%)	Source
Nagpur (8 years)	SI 2SI:1NSI 1:1 1:2 NSI	8.50 8.87 8.93 8.88 9.00	0.23 0.24 0.13 0.04 0.48	1.00 0.70 0.65 0.62 0.57	0.41 0.26 0.12 0.04 0.05	0.05 0.25 0.11 0.04 0.43	0.50 0.27 0.09 0.03 0.04	Juwarkar et al (1987)
Calcutta (50-60 years)	SI NSI	7.7 7.2	0.34 0.13	0.37 0.19	0.10 0.056	0.10 0.05	0.13 0.073	Gupta and Mitra (2002)

Delhi (21 years)	Nilothi SI	8.3	0.51	0.45	-	38.1	92	Rattan et al. (2002)
	NSI	8.64	0.47	0.25	-	16.0	219	
	Ranhola SI	7.86	0.64	0.66	-	22.1	49	
	NSI	8.54	0.39	0.39	-	13.8	92	
	Mundka SI	8.13	0.82	0.51	-	30.6	138	
	NSI	7.99	0.24	0.37	-	18.5	83	
Jaipur	SI	8.9	0.12	0.55	-	-	-	Sharma et al. (2001)
	NSI	8.8	0.21	0.21	-	-	-	
Hyderabad	SI	5.8	4.66	0.54	570	26.2	784	Anonymous (2002)
	NSI	7.4	0.38	0.26	210	8.4	208	

SI=Sewage Irrigation, NSI = Non sewage Irrigation, * Average

Table 20 and table 21 tell about the inorganic constituents and the chemical characteristics added to the waste water through domestic use.

Table 20. Inorganic constituents added to effluents through domestic use

Constituent	**Range of increment mg/l**
Total dissolved solids	150 – 400
Sodium	40 – 70
Potassium	7 – 15
Calcium	15 – 40
Magnesium	15 – 40
Chloride	20 – 50
Carbonate	0 – 10
Bicarbonate	50 – 100
Sulfate	15 – 30
Silica	2 – 10
Alkalinity (as calcium carbonate)	100 – 150
Boron	0.1 – 0.4
Phosphate	5 – 15
Ammonium	15 - 40

Source: feign et al. 1991

Table 21. Physical and chemical characteristics of domestic wastewater

Major constituents	**Concentration (in mg/l)**

	Strong	Medium	Weak
Total solids	1200	700	350
Dissolved solids	850	500	250
Suspended solids	350	200	100
Nitrogen (as N)	85	40	20
Phosphorus (as P)	20	10	6
Chlorides*	100	50	30
Alkalinity (as $CaCO_3$)	200	100	50
Grease	150	100	50
BOD_5+	300	200	100

Source: These data are adapted from Metcalf and Eddy Inc. (1972). P. 231
* This amount should be increased by the concentration of these constituents in the carriage , Water: the table shows major constituents only.
+ BOD_5 is the 5-day biochemical oxygen demand at 20oC. It is a measure of the biodegradable organic content of wastewater.

Source: in Pescod/arar ed. 1988

POTENTIAL OF DOMESTIC WASTE WATER

Potential for wastewater irrigation still exist in many countries and with growing populations in urban centers, the availability of domestic wastewaters will rapidly increase. Nevertheless, it is estimated (early 1980s) that in 80% of the situations where wastewater is collected and water is an agricultural development constraint, wastewater, either raw or treated, is already used for permanent or seasonal irrigation (Wright/Quick in: Shovel et al. 1986). The use may be direct via immediate use of the effluent or indirect by using groundwater or surface water resources with effluent additions further upstream.

Waste water reuse may have one or a combination of the following objectives.

1. Use of waste water for reliable irrigation.
2. Fertilization of marginal lands having poor fertility or specially inert medium.
3. Reuse of scarce water available in the arid and semi-arid areas.
4. Safe disposal of waste water in order to avoid ground water or surface water pollution by direct mixing.
5. Ground water recharge.
6. Safe disposal of waste water containing toxic concentration of inorganic or organic chemicals.

GENERAL PRINCIPLE FOR CONVENTIONAL WASTE WATER IRRIGATION

General principle for waste water irrigation to reduce potential negative health and environmental impacts are,

1. Soil should not be contaminated with persistent toxic organic solids.
2. Waste water should not be contaminated with excessive concentrations of pathogens which may cause an outbreak of infectious diseases.

3. Water application rate should be moderate to avoid ponding conditions like in paddy crops. Actually application rate should match the intake rate of the soils.
4. Waste water should not contain sodium, trace element, heavy metals in excess that the required by crops and buffering capacity of the soils.

Waste water utilization may be beneficial in one way or ht more as given below.

1. Reuse of waste water will create additional water resource for irrigation.
2. Cost pr unit sewage water volume may be much lesser than the fresh water and hence cost of irrigation may go lower.
3. Extra investment in normal sewage water treatment or special treatment for its safe disposal or reuse for domestic supply could be minimized to a greater extent.
4. Associated health hazards and environmental problems due to raw sewage disposal in to natural streams of water bodies could be checked.
5. Waste water irrigation has potential to decrease the net demand of chemical fertilizer like N and P and also trace elements as these nutrients are present in waste water.
6. Excessive pumping can be minimized by utilizing waste water for irrigation.
7. Salt intrusion in costal and arid areas could be prevented.
8. Overall a healthy atmosphere could be given to the city people.
9. Natural streams and rivers could be brought back to live conditions just by checking or minimizing raw sewage disposal into them.

Sources: WHO 1989; Mara/Cairncross (WHO) 1989; Pescod/Arar ed. 1988; Biswas/Arar ed. 1988, shuval et al. (WB) 1986

PROBLEMS ASSOCIATED WITH WASTE WATER DISPOSAL

Volume of waste water generation from house hold is increasing due to increasing population and urbanization in developing countries and problems associated with its safe disposal is becoming threat to environment. In country like India where large cities are generally situated over a river bank is facing real problem of surface and ground water pollution. Urban population is direct measure of waste water generation and growth rate of cities indicates associated problems to be faced in future. The rivers passing from large cities have become a sewer drain due to indiscriminate disposal of domestic effluent without any treatment. **Table 22** presents disposal modes of waste water in class I cities. The problem of water quality deterioration is increasingly becoming a matter of great concern due to increased withdrawal of river water for agriculture and domestic supplies and increased flow of untreated domestic effluents. Disposal of untreated industrial effluents is further worsening the water quality of river. The domestic waste water need to be treated and then discharged in the streams to preserve water ecosystems and overall environmental quality for coming generation. Reuse of domestic waste water for irrigation of agricultural crops will reduce the pollution load of streams and rivers and also the treatment cost of the effluent. For diverting domestic effluent for agricultural use sewage disposal system need to be designed separately carrying water directly to the fields or to some common conveyance system optimizing cost of the system

Table 22. Basin-wise disposal modes of wastewater in class-I cities.

Name of river basin	No. of class-I cities	No of cities with mode of disposal				Other (Sea/Land/ drain etc)
		Agriculture	River	Both Agric. & River	Agric. & Others	
Brahamputra	4	-	3	-	-	4
Cavery	16	3	3	-	1	7
Ganga	103	29	16	23	8	25
Indus	15	6	2	-	1	6
Godvari	25	3	1	4	4	13
Krishna	27	4	3	2	3	15
Mahanadi	9	-	1	2	2	4
Coastal	29	6	3	2	1	17
Non-major	37	11	1	4	7	14
Total	**299**	**63**	**41**	**44**	**33**	**118**

HEALTH HAZARDS ASSOCIATED WITH WASTE WATER

A wide variety of bacteria, viruses, protozoan, helminthes, worms are found in waste water. Pathogens in waste water are high and can survive in extreme conditions. There is a great risk of infection to the people exposed to the soil and the crops irrigated with waste water. Cereal crops irrigated with waste water are safe for human consumption but the field losses in long run may pollute ground water of the area. Vegetables have risk for spreading epidemic among people. Cholera outbreak in Jerusalem during year 1970 was due to unauthorized irrigation of salad crops with untreated waste water (**Cohen et al. 1971, and Fattal et al. 1986b**). In India and other developing countries there are several cases reported for out break of various diseases due to leakage in water supply lines and sewage disposal systems. **Gunnerson et al. (1985)** reported that the full spectrum of excreted human pathogens endemic in the community is present in sewage. **Table 23** presents list of such pathogens.

Table 23. Pathogens present and excreted in faeces and associated disease.

Pathogens		Disease	Can symptomless infection occur	Reservoir
1. Virus				
a)	Adenoviruses	Numerous conditions	Yes	Man
b)	Enteroviruses	Poliomyelitis,	Yes	Man

	Polioviruses Echoviruses	paralysis Numerous conditions	Yes Yes	Man Man
c)	Hepatitis A	Infectious hepatitis	Yes	Man & Mammals
d)	Rivo virus	Numerous conditions	Yes	Probably man
e)	Rotoviruses	Diarrhea	Yes	
2. Bacteria				
a)	Salmonella			
	S. typhi	Typhoid fever	Yes	Man
	S. paratyphi	Paratyphoid fever	Yes	Man
b)	Shgella spp. Vibrio	Cholera	Yes	Man
3. Protozoa				
a)	Balentidium coli	Diarrhea, dysentery and colonic ulceration	Yes	Man & Mammal
b)	Entamoeba coli Entamoeba histolytica	Colonic ulceration, amoebic dysentery and liver abscess	Yes	Man & Mammal
c)	Giardia lamblia	Diarrhea and malabsorption	Yes	Man & Mammal

Table 24. Health status of sewage farm workers.

Study area	Test group		Control group	
	Number	Per cent	Number	Per cent
Nagpur sewage farm				
Total examination	360			
Total positive	303	84	179	59
Positive for hookworms	231	64	123	40
Positive for roundworms	245	68	159	52
Infected with two or more parasites	156	43	44	14
Madurai sewage farm				
Total examinations	663	2644		
Total positive	520	78	512	19

ASSOCIATED BENEFITS OF WASTE WATER IRRIGATION

Wastewater reuse may have several benefits, among which are the following;
- Reuse of water can be considered as an additional source of water for irrigation,
- The marginal cost of providing the same volume of good quality water is generally higher than the cost of producing wastewater under conditions of water shortage; wastewater will be produced irrespective of whether or not it is used since sewage treatment works are essential to prevent groundwater pollution, and hence, it makes sense to use it beneficially,
- Properly planned use of wastewaters can reduce environmental and health impacts which have been observed with traditional wastewaters can reduce environmental and health impacts which have been observed with traditional wastewater disposal practices in developing countries,
- Wastewater reuse can prevent or reduce environmental of water bookies, especially closed ones such as lakes, where uncontrolled disposal can contribute to nutrient overloading,
- Wastewater can provide nutrients to soil and plants, especially N and P but also trace elements, and thus may reduce the need for fertilization, which may increase the total economic return to farmers,
- Salt water intrusion in coastal areas can be prevented by recharge of groundwater with treated wastewater.

Constraints to Development

1. Site Suitability

Suitability of locations depends on technical aspects;
- Irrigation areas should be close to the treatment plant (effluent source) to avoid transportation costs, risks of exposure, unfavorable changes in water quality during transport (especially in pipelines) and maintenance problems in conveyance canals or pipelines,
- Irrigation areas should be at a safe distance from settlements, usually >1 km to avoid odor nuisance and aerosol pollution of nearby settlements,
- Irrigated areas should be close to markets to minimize transportation of goods,
- There should be non irrigated areas in the vicinity which can be used outside the cropping season for safe disposal (rapid infiltration fields) or groundwater recharge, if no groundwater induced salinity problems exist; this applies also in emergencies for example in the case of treatment plant failure, if polluted water is released from the plant which does not meet quality standards for use in irrigation.
- Size of irrigated areas must be adapted to the quantity of available water (or vise versa) to avoid over irrigation and the consequent contamination of soils,
- If effluent quality does not meet standards, the ability of mix it with freshwater (ground or surface water) must be ensured at the site; this mixing may be required necessary temporarily or routinely,
- For deep percolating water (unavoidable groundwater recharge) the quality standards of maximum permissible concentrations of chemical constituents (e.g. toxic heavy metals) must be met; if soil filtering capacity is too low, e.g. in sandy soils, then other sites must be selected if groundwater pollution would cause problems (e.g. if groundwater is used for domestic supply to the local population),
- Water quality standards must also be observed for surface drainage outflow.

Site specific criteria are;
- Suitability of the terrain for a specific irrigation method (topography, micro relief, general slope),

- Climatic water balance and temperature, e.g. evaporation rates will affect the salt balance, and temperature and soil moisture regulate the transformation of constituents in the soil,
- Soil properties regarding the in-suitability to filter, buffer and transform inorganic and organic constituent s of wastewaters (precondition to avoid pollution of groundwater),
- Infiltration and permeability properties (precondition to avoid water logging in the root-one and allow the movement of wastewater constituents; precondition for well aerated soils),
- Adequate land drainage (precondition for sustainable irrigation to avoid water logging and salinity build up; either natural or artificial, or both),
- Nutrient status (determines the acceptable level of additional nutrient supply),
- Risk of solidity and alkalinity (affects structure and mobility of elements).

If follows that most soils are suitable for wastewater applications but not all wastewaters are suitable for all soils if the above objectives are to be met.

2. Socio-Cultural Aspects

It is essential that the acceptance of excreta or wastewater reuse by farmers, farm-workers, consumers and people living in the vicinity is ensured before it is considered for irrigation. Socio cultural studies or other information is required to ensure that there are no objections. Suitably designed information programmes may contribute to increased acceptance.

The introduction of human/animal excreta or wastewater use and the adoption of health safeguards related to wastewater irrigation may require changes in behavioral pattern. Human societies have evolved very different responses to the use of excreta, e.g. in many African communities it is regarded with disaffection whereas the use of excreta (or derivates) for fertilization of soils and its use in aquaculture has been common in Asian communities for thousands of years .Often, no distinction is drawn between products irrigated or fertilized with excreta or wastewater; the reuse of wastewater is not often hampered by socio-cultural disgust, although the possibility should be given serious attention.

3. Crop Selection

Crop selection should be based on the following criteria:

- Suitability to general agronomic and economic criteria (e.g. climate, soils, markets),
- Suitability to salinity and specific toxicity criteria
- Constraints to marketing imposed by public health concerns or regulations related to pathogens and toxic chemicals.

The most obvious problem related to health constraints is the contamination by wastewater of plants destined for human consumption without further processing, within a short time after contamination. The most effective precaution would be to irrigate only wood and fiber crops (e.g. cotton). Safety rules for the cultivation of food crops should observe:

- Minimal contact between effluent and edible crop part, e.g. tall growing fruit crops and trees,

- Preference for crops which are normally washed or treated before consumption, e.g. olives, citrus, avocados,
- Crops which are exposed for some days (or weeks) to desiccation and ultraviolet radiation before being marketed, e.g. crops which are not irrigated for several weeks before harvest,
- Low growing but erect crops if grown in furrows, ridge and furrow or drip irrigation systems.

Toxic chemicals in the form of heavy metals may occur in soils or in irrigation waters; some of them are taken up and accumulate in plants. Toxic concentrations must be avoided in both fresh water and wastewater. Similar regulations are applicable for both waters.
Guidelines for restrictions on types of crops irrigated with wastewater can be an effective remedial strategy. Crops can be grouped into three broad categories in increasing order of public health risk involved. Regulations exist for example in the USA (1977).Guidelines for crop categories have been established by WHO (1973). They have been effective in some countries with efficient means of control.
Careful cleaning and disinfection of contaminated crops at the point of use (i.e. consumer) may be effective in industrialized countries where public health standards are high and high quality freshwater is available. It is not applicable on a larger scale for developing countries. Market disinfection stations (e.g. at vegetable markets) may be theoretically considered, especially for large scale, centralized irrigation schemes.

Survival and retention of pathogens in the soil is of great interest. Moisture content, water holding capacity, pH, solar radiation, salinity and alkalinity, organic matter content and mineral composition etc are the deciding factors for survival and retention of these pathogens in the soil. It has been observed that bacterial pathogens survive only for a limited time compared to protozoa and helminthes. Survival time of pathogens in soil is longer than the plants. Enteric virus diseases are least effectively transmitted by waste water irrigation where as helminthes diseases are prone to be transmitted by waste water irrigation. Helminth like ascaris, hook worm and teniasis have high risk, protozoan infection like amoebiasis, and giardiasis have low risk and viral infection like viral gastro-entritis and infectous hepatitis have least associated risk. Generally sewage farm workers (87%) have been found seriously infected with more than one parasite. Epidemiological studies from developed and developing countries showed evidence of transmission of certain diseases associated with the use of raw or partially treated waste water. People consuming salad and other raw vegetables irrigated with waste water have great risk to hook worms. In developing countries in lack of proper legislation raw domestic effluent being used for irrigation and agricultural produce are being marketed without knowing much about associated health hazards.

WASTEWATER TREATMENT FOR IRRIGATION

Wastewater treatment is the most effective remedial measure in reducing health effects and soil contamination due to wastewater irrigation. The primary objectives in the following order of priority are:
- Maximum removal of helminthes (close to 100%),
- Effective reduction in bacterial and viral pathogens (minimum 99 to 99.9 %)
- Effective reduction of suspended load (site and irrigation type specific criteria),
- Maintain aerobic conditions,
- Production of nuisance and odor free effluent which is attractive to users.

These criteria are different that the traditional waste water treatment. Well designed and well operated stabilization ponds can meet all four criteria in warm climate like India.

A typical sewage treatment plant in tropical regions may have the following layout:
(i) Anaerobic ponds, at least two in parallel, with a minimum of 2 days total retention time: effects on helminthes; BOD,
(ii) Facultative pond(s),usually 5-10-15 days total detention time (temperature dependant) to reduce BOD, to remove bacteria by one or two orders of magnitude, and to serve as a security factor for Delmont eggs carried over from anaerobic ponds,
(iii) Maturation ponds(s) in series to achieve reasonably high bacterial removal; a standard unit for each location is recommended ideally, a retention time of 5 days each.

There are a number of options to consider in the final selection of initial and final treatment systems
The removal of heavy metals as well as removal of synthetic organic trace compounds (eg carbohydrates, organic acids, organic bases, poly-nuclear hydrocarbons (HC), halogenated HC, phenols, aliphatic and aromatic materials) are not primary objectives in developing countries, since waters contaminated with these industrial chemicals or metals should not even be considered as a source of irrigation water in developing countries. Removal of metals requires more sophisticated secondary biological treatment stages, e.g. activated sludge, bio-filters or algal ponds. These are complicated in design, difficult to operated and expensive in comparison with the pond system.

The advantages of ponds are: low costs for design, construction, operation and maintenance; no expenditures of energy (run by solar energy); high ability to absorb organic and inorganic shock loads; extreme simplicity of operations (fool proof) and ability to treat a wide variety of different domestic wastewaters (Mara/Cairn-gross 1989). The main disadvantage of pond systems is the large area of land they cover. However, recent research has shown that increasing pond depth (from 1-2 m to 2-3 m) may be successful in metropolitan areas with limited land resources.

An efficient reduction of COD and BOD, aimed at minimizing the potential eutrophication of surface or groundwater by effluents, is not a primary objective for wastewater treatment because the water is used on fields where biodegradation of organic materials (mainly C and N) takes place in the soil and many organic compounds and minerals are considered as useful agents to improve soil fertility and the aggregation of soils.
Disinfection, usually chlorination of raw sewage can reduce the number of bacteria but it is, unlike chlorination of fresh water, a vastly more compiled and unpredictable operation for wastewaters. Except when high levels of operation and maintenance are guaranteed it cannot be recommended as a general treatment, because irregular or inadequate disinfection is of little use for health protection. Effluent chlorination may have, in addition to its costs, a number of detrimental effects: treated effluents, rich in nutrients but low in microbiological activity, are ideal for the growth of some surviving bacteria; secondly it may contribute to proliferation of simple or complex chlorinated organics (chloramines) that may be toxic to fish or carcinogenic and mutagenic (Pescod/Arar 1988); further, some solutions will react with emulsifiers, fertilizers and pesticides and reduce their effectiveness. Occasionally chlorination may be used to reduce clogging hazards in drip irrigation systems or if bacterial

slimes and algae within the water transfer system pose serious problems. Dosages are in the range of 0.5 to 1 mg/l to control algae, iron bacteria and slimes

Table 25. Suggested treatment processes to meet the given health criteria for wastewater reuse

	Irrigation			**Recreation**		**Industrial reuse**	**Municipal reuse**	
	Crops not for direct human consumption	**Crops eaten cooked: fish culture**	**Crops eaten raw**	**No contact**	**Contact**		**Non potable**	**Potable**
Health criteria (see helow for explanation of symbols)	A + F	B + F OR D + F	D + F	B	D + G	C or D	C	E
Primary treatment	●●●	●●●	●●●	●●●	●●●	●●●	●●●	●●●
Secondary treatment		●●●	●●●	●●●	●●●	●●●	●●●	●●●
Sand filtration or equivalent polishing methods		●	●		●●●	●	●●●	●●
Nitrification						●		●●●
Denitrification								●●
Chemical clarification						●		●●
Carbon adsorption								●●
Ion exchange or other means of removing ions						●		●●
Disinfection		●	●●●	●	●●●	●	●●●	●●●

Health criteria:
A freedom from gross solids: significant removal of parasite eggs.
B as A. plus a significant removal of bacteria.
C as A. plus more effective removal of bacteria. Plus some removal of viruses.
D not more than 100 coli-form organisms/ 100 ml in 80 % of samples.
E no facial coli-form organisms in 100 ml. plus no virus particles in 1000 ml. plus no toxic effects on man. And other drinking water criteria.

F no chemicals that lead to undesirable residues in crops or fish.
G no chemicals that lead to irrigation of mucous membranes and skin.

In order to meet the given health criteria. Processes marked ●●● will be essential. In addition, one or more processes marked ●● will also be essential, and further processes marked ●may sometimes be required.
· Free chlorine after 1 h.

SUITABILITY OF METHODS

Waste water irrigation does not require additional factors to be considered in designing the irrigation system however special attention is required to minimize direct contact and contamination of field workers working with waste water in fields. Water should be applied to achieve higher distribution efficiency of waste water in order to avoid or minimize the deep percolation losses.

1. Wild flooding is most simple method of irrigation in generally leveled fields for wide varieties of crops. The method is not suitable for waste water irrigation because of low irrigation efficiency (30%-40%) and irrigators have to stand in waste water or the mud while working in the fields. Field may get inundated and depth of application may vary significantly in the field.

2. Check basin irrigation are most commonly use irrigation methods in India and other developing countries with small stream size for most of the crops. It is suitable for fairly leveled fields. The method offers better control over the amount of water to be applied and possible most suitable surface irrigation method which can handle waste water safely. The method is labour intensive and there is risk for labourers for exposure to waste water and produce contamination.

3. Furrow irrigation is suitable for row crops grown over ridges. Actually ridges are well above the water surface and hence have least risk for contamination of agricultural crops from erect crops. It is most flexible among all methods in terms of length, slope limitation and stream size. Accumulation of salts on the top of the ridges due to peculiar wetting pattern may impair the crop growth and may need leaching. There remains the risk of contamination of agricultural produce specially for the vegetable crops.

Table 26. Factors affecting choice of irrigation method, and special measures required when wastewater is used

Irrigation method	Factors affecting choice	Special measures for wastewater
Border (flooding) irrigation	Lowest cost, exact leveling not required	Thorough protection for field workers, crop-handlers and consumers
Furrow irrigation	Low cost, leveling may be needed	Protection for field warders, possibly for crop-handlers and consumers
Sprinkler irrigation	Medium waster use	Some Category B crops,

	efficiency, leveling not required	especially tree fruit, should not be grown. Minimum distance 50-100 m from houses and roads.
		Anaerobic wasters should not be used because of odour nuisance
Subsurface and localized irrigation	High cost, high water use efficiency, higher yields	Filtration to prevent clogging of emitters.

REDUCING HUMAN EXPOSURE

Four groups of people can be identified as being at potential risk from irrigation use of wastewaters: farmers and agricultural field workers, crop handlers, consumers, and those living near affected fields.
Regarding on farm risks, exposure to many parasites can be reduced by adoption of certain health safeguards, e.g. use of footwear. Rigorous health education programmes are needed to propagate meticulous personal hygiene.
Immunization is not possible against helminthes infections ad control of other infections (e.g. typhoid and hepatitis) is not feasible on a large scale. Additional protection may be provided by the availability of medical facilities to treat diarrhoeal disease and by chemotherapeutic control of nematode infections.
Many risks can be reduced by strict personal, kitchen and food hygiene, e.g. by thorough cooking of vegetables, meat, milk, etc. regular health education campaigns are required to improve standards, especially in societies with poor education.
Local residents should be kept fully informed about the location of irrigated fields, so that they may avoid entering them and also prevent children from doing so. Warning notices may be posted and fences may be erected.

MONITORING AND EVALUATION

Without regular and effective surveillance during project implementation, the anticipated benefits from the project will be endangered and there may be real possibilities that the project may contribute to the development or serious health and environmental hazards. Thus, a monitoring system should be implemented which focused on targeted outputs in terms of water quantity and quality, delivery of water to the irrigated area, quantity and quality of agricultural products, and compliance with health standards on the part of farmers, treatment plant workers, traders or consumers of irrigated crops. Since the aim of monitoring and evaluation is to achieve successful project performance, it should be an integral part of an effective management information system in orders that:

- Timely corrective actions can be taken to reduce the probability of occurrence of any environmental or health hazard,
- Project assumptions are seen to be value and can be verified,
- Achievement of project objectives and impacts can be determined,

Lessons for other projects can be learnt for more effective planning and operation in future

CONCLUSION

The unchecked and uncontrollable population of the world has increased the stress on the recourses available to mankind. Agriculture being the primary need of, the biggest problem faced is the decline good quality ground water. Major problems arising with the conventional irrigation methods followed like, water logging, salinity problem, ground water depletion and waste water disposal add to the stress on the global water recourses.

Major problems arising with the conventional irrigation methods followed like, water logging, salinity problem, ground water depletion and waste water disposal add to the current issues. More over the irrigation potential of India and the actual irrigation are two distant neighbors.

As the population in the urban areas increase so does the effluent domestic water. Due to this increase the amount of waste water being disposed into the rivers and other water bodies add to the unavailability of good quality water. This is a direct impact on the environment and affects the ecosystem. The waste water having high nitrogen and nutrient content can best be seen as a source for Eutrophication. Using waste water as a medium of irrigation fulfills many objectives such as ground water recharge, fertilization of land and safe disposal of toxic concentrations of organic and inorganic chemicals. But using waste water can lead to numerous health hazards as well. Proper selection of site and selection of crop is required where domestic effluent is to be used. As the waster water contains numerous pathogens and bacteria the farmers working in close contact with it should take proper safety measures. Moreover the waste water used should be treated first and then applied to the fields. This can be done effectively and economically by the use of stabilization ponds.

Growing pressure on available fresh quality irrigation water resources and increasing awareness to environmental issues among human masses should force researchers and planners to design waste water disposal system in such a way that it could be safely made available to its users. This is the right time to give a rational thought in this direction to make the waste water a safe water resource for irrigation

REFERENCES

Adhikari, S.; Mitra, A. and Gupta, S.K. 1994. Proc. Indian National Science Acad. B(60). 541-546.

Arora, B.R.; Azad, A.S.; Singh, B. and Sekhon, G.S. 1985. Indian Journal of Ecology. 12:1-7 (1985).

Anonymous.2004. Annual Progress Report 2000-03. NATP-MM projects on “Use of Urban and Industrial Effluent in Agriculture”, CSSRI, Karnal.

Bhupal-Raj, G.1997. Proceedings Acad. Environmental Biol.. 6(2):177-82.

Sharma, R.C.; Rao, B.R.M.; and Saxena, R.K.2004. Salt affected soils in India-Current Assessment. Advances in Sodic Land Reclamation, International Conference on Sustainable Management of Sodic Lands, Feb. 9-14, Lucknow, pp.1-26.

2. NRSA and Associates.1996. Mapping salt affected soils of India, 1:250000, Legend, NRSA Hyderabad.

Minhas, P.S.; Sharma, D.R. and Chauhan, C.P.S.2004. Management of saline and alkali waters for irrigation. Advances in Sodic Land Reclamation, International Conference on Sustainable Management of Sodic Lands, Feb. 9-14, Lucknow, pp.121-162.

Gupta, R.K.; Singh, N.T. and Sethi, M. 1994. Ground water quality for irrigation in India. (Map 1:6 million scale). Technical Bulletin 19, CSSRI, Karnal, pp. 16.

Gupta, S.K.; Phanish Kumar Sinha and Chhedi Lal.2004. Hydro-techniques for sodic land reclamation: issues and options. Paper presented at International Conference on Sustainable Management of Sodic Lands held at Lucknow from February 9-14, 2004.

CBIP.1998. Reading Material for Seminar on Agricultural Pumping- Emerging Dimensions and Empact on Power Sector held at Bangalore from 27-28 August 1998.

Kaul, S.N.; Juwarkar, A.S.; Kulkarni, V.S.; Nandy, T.; Szpyrkowicz, L. and Trivedi, R.K.2002. Uitlization of waste water in agriculture and aquaculture. Science Publications, Jodhpur, p. 675.

Gupta, S.K. and Mitra, A. 2002. In. Advances in Land Resource Management for 21st Century, Soil Conservation Society of India, New Delhi, pp. 446-460.

Treatment Performance of Wastewater Lagoons in South Yungas Province of Bolivia

Helen E. Muga[1], James R. Mihelcic[2], Nathan W. Reents[3], Santiago Morales[4], Gabriela Gemio[5], Meredith Ballard[6], Valerie J. Fuchs[6], Cara M. Hanson[6], Esther M. Johnson[6], Alison M. Hoyt[7]

[1] Department of Civil and Environmental Engineering, University of South Florida, 4202 East Fowler Avenue, ENG 303, Tampa, Florida, 33620. Email: hmuga@eng.usf.edu; Ph: (813) 396-9316; Fax: (813) 974-2957
[2] Department of Civil and Environmental Engineering, University of South Florida, 4202 East Fowler Avenue, ENB 118, Tampa, Florida, 33620. Email: jm41@eng.usf.edu; Ph: (813) 974-9896; Fax: (813) 974-2957.
[3] ACDI/VOCA, Oficiana: Caranavi, Calle Calama #15, Complejo Hotelero Landivar, Casilla 574, Bolivia. Email: nreents@gmail.com
[4] Universidad Technologica de Bolivia, Calle Colombia 154, Casilla 5819, La Paz, Bolivia.
[5] Universidad Technologica de Bolivia, Calle Colombia 154, Casilla 5819, La Paz, Bolivia. Email: exoticagabicha@gmail.com
[6] Michigan Technological University, 1400 Townsend Drive, Houghton, Michigan 49931. Email: mmballar@mtu.edu
[6] Michigan Technological University, 1400 Townsend Drive, Houghton, Michigan 49931. Email: vjfuchs@mtu.edu
[6] Michigan Technological University, 1400 Townsend Drive, Houghton, Michigan 49931. Email: cmhanson@mtu.edu
[6] Michigan Technological University, 1400 Townsend Drive, Houghton, Michigan 49931. Email: esjohnso@mtu.edu
[7] Yale University, New Haven, Connecticut, Ohio. Email: aahoyt@gmail.com

Abstract

The operation of wastewater lagoons systems located in the South Yungas Province of Bolivia has been analyzed over a 2-year period. Facultative and maturation lagoons were evaluated for their performance in removing total suspended solids (TSS), biochemical oxygen demand (BOD), chemical oxygen demand (COD), nitrogen, phosphorus, and coliforms. Facultative lagoons operating in San Antonio were found to remove approximately 74% total suspended solids, 70-89% BOD, 62-85% COD, 53% nitrogen, 52% phosphorus and 97.8-99.9% coliforms. Maturation ponds were found to remove 74-93% total suspended solids, 22-62% BOD, 10-95% COD, 3% nitrogen, 20-95% phosphorus and 77.4-99.96% coliforms. Results from the 2-year study indicate that these wastewater treatment systems are currently performing as expected; however regular maintenance, specifically removing algae every (2 weeks) is required. The removal percentages of the treatment systems (comparing influent to effluent) ranged from 74-97% TSS, 78-98% BOD, 70-99.7% COD, 58-77% nitrogen, 62-99.9% phosphorus, and 99.99% coliforms.

Introduction

Improved water sources, sanitation, and hygiene are key factors in improving health and reducing deaths in developing countries. With 900,000 people lacking access to improved water sources (WHO, 2008), and 2.5 billion having no access to improved sanitation (WHO, 2008), the need for appropriate, cost-effective technologies in addressing some of these issues is becoming increasingly important. In addition, the maintenance and operation of these technologies is critical to the systems performance in achieving the desired objectives related to protecting public health and water quality, as measured by the presence of pathogens and physical-chemical parameters (e.g., biochemical oxygen demand, nitrogen, phosphorus).

Implementation of alternative wastewater technologies such as lagoons in addressing sanitation issues has been reported in countries such as Mexico and Honduras. There is however, minimal research on evaluating the performance of these lagoons in most developing countries. The performance of lagoons (serving population sizes – 800; 7,280; 11,000) in Mexico in terms of sludge accumulation/removal and inactivation of fecal coliforms and *Ascaris* eggs has been studied by Nelson et al., (2004). The performance of lagoons in removing *Escherichia* coli, fecal coliforms, suspended solids (SS), five-day biochemical oxygen demand (BOD_5) in Honduras has also been studied (Oakley, 2005). However, the performance of lagoon systems in South America, for example in countries such as Bolivia, remains largely un-evaluated.

Accordingly, the objective of this study is to evaluate the performance and effectiveness of lagoon systems operating in the South Yungas Province of Bolivia in removing total suspended solids, BOD, chemical oxygen demand (COD), nitrogen, phosphorus, and coliforms. The lagoons are used in two small communities: San Antonio (950 inhabitants) and Sapecho (1,030 inhabitants).

Bolivia is particularly unique because it the most indigenous country in South America, with almost 40% of the country's population representing indigenous people. It is the poorest country in South America and the 3rd poorest country in the Americas with per capita GDP of less than US$1,000 per year and 64 percent of its population living below the poverty line. The mean income per capita in indigenous households was approximately US$46 per month in 2001 compared with US$74 for non-indigenous households (World Bank, 2008). STATcompiler (2008) reports that La Paz has the highest percentage of untreated diarrhea cases (28.2% compared to 18.6% average of Bolivian departments). Further, lack of access to sanitation and unhygienic practices has lead to diarrhea diseases that cause 6% of all deaths in Bolivia. It is estimated that in Bolivia, only 22% of the rural population has access to improved sanitation (WHOSIS, 2006). Thus, understanding how existing community-based systems operate is important if sanitation technologies are to be implemented successfully on a wide basis.

Background

Demographics, location, and costs

The South Yungas region is characterized as the transition zone between the Andes Mountains and the Amazon River basin: smaller mountain ranges paralleling the Andes are divided by rivers which generally flow north to the Amazon (Fuchs et al., 2008). Income of people in the South Yungas is derived from agriculture, primarily

from coffee, cacao, citrus and bananas. These are the main exports that contribute to the economic activity of the area (Palos Blancos Municipal Report, 2007). A majority of the people living in communities such as San Antonio, Sapecho and Palos Blancos are immigrants from the higher elevation Alto Plano region near La Paz. The population growth is estimated to be greater than 3% per year, as migrants move to this agriculturally productive area and the communities urbanize (Fuchs et al., 2008).

The community of San Antonio is located in the South Yungas Province, northeast of La Paz city, and at 1,500 feet above sea level. There are 950 habitants of this community. The community is served by a wastewater treatment/collection system. There are reported to be 130 connections to the sewage systems. This serves "almost all" of the urban population of San Antonio. However, several outlying agricultural regions which are served by San Antonio's water supply are not connected to the sewage system. The neighborhood of Nueva Esperansa is not connected because it lies to low for sewer connections, and instead utilizes composting latrines.

The total capital cost of the wastewater treatment and collection system of San Antonio was US$231,748. US$62,790 of the total was covered by the habitants of San Antonio. This local cost includes home installations of bathrooms and household sewer connections. The remainder of the cost included items such as the preliminary investigation, land costs, infrastructure for the sewer system, transmission of potable water, and hygiene education. The costs were financed by the U.S. Agency for International Development (USAID) through ACDI/VOCA (Meredith et al., 2007). ACDI/VOCA is a non-governmental organization that implements sanitation measures in rural communities in eastern La Paz department, in the province of South Yungas.

The community of Sapecho is also located in the South Yungas Province at 1,500 feet above sea level. There are 1,039 habitants of this community. During the research period, the number of sewage connections ranged from 150-180 as more residents connected to the system. The system was designed for 201 connections. The water distribution system serves approximately 300 connections, including several in rural areas outside of the town center. Due to the rapid rate of connections that was taking place during the first year of our research project, it was difficult to estimate what percentage of the population was served by the sewage system (Meredith et al., 2007).

The total cost of construction and installation of the Sapecho wastewater treatment and sewer system was US$321,655, paid for by contributions from ACDI/VOCA and the community. US$134,372 of the total was paid by the community and included the cost of home installations. The remainder of the cost included items such as the preliminary investigation, land costs, the infrastructure for the sewer system, transmission of potable water, and the reactor for wastewater treatment (Meredith et al., 2007).

Wastewater Treatment System

San Antonio: The town treats its wastewater with a lagoon system. One facultative lagoon is followed by two maturation lagoons in series (Figure 1). The facultative

lagoon is 28 m × 55 m and approximately 1.5-m deep. A facultative lagoon consists of three layers. The upper-most layer is oxygenated by photosynthesis and wind-induced mixing. In this aerobic zone, bacterial action provides biological treatment. This is followed by a facultative layer which can have varying oxygen concentrations. The deepest layer is anaerobic. Large biological solids (solids in influent, algae, etc.) settle on the lagoon bottom. These settled biological solids create a sludge which is estimated to require removal every ten years. San Antonio's lagoons were implemented in 2006, therefore no sludge has been removed from the lagoons as of June 2008. After leaving the facultative lagoon (point B in Figure 1) wastewater flows through two maturation lagoons which continue the process of treating the wastewater. The other two lagoons (maturation) are smaller than the facultative lagoon, at 13 × 39 m. These lagoons are also half as deep as the facultative lagoon. While they also provide some suspended solids removal, their primary function is pathogen and nutrient removal.

Sapecho: The Sapecho wastewater treatment system (Figure 2) has the following processes: i) grit removal - 6.15 m × 1.45 m × 0.95 m; ii) upflow sludge blanket reactor (UASB) - 9.84 m × 6.35 m (length × height)(extending tube for biogas collection and release: 3.50 m (height)); iii) sludge drying beds (two beds of 10.30m × 12.45m (designed for 30 cm gravel, 10 cm of sand, and 25 cm of sludge); and iv) two maturation Lagoons (two lagoons)- total dimensions 74.40m × 61.35m (1st: 51.50m × 12.50m and (2nd: 49.50m × 12.50m).

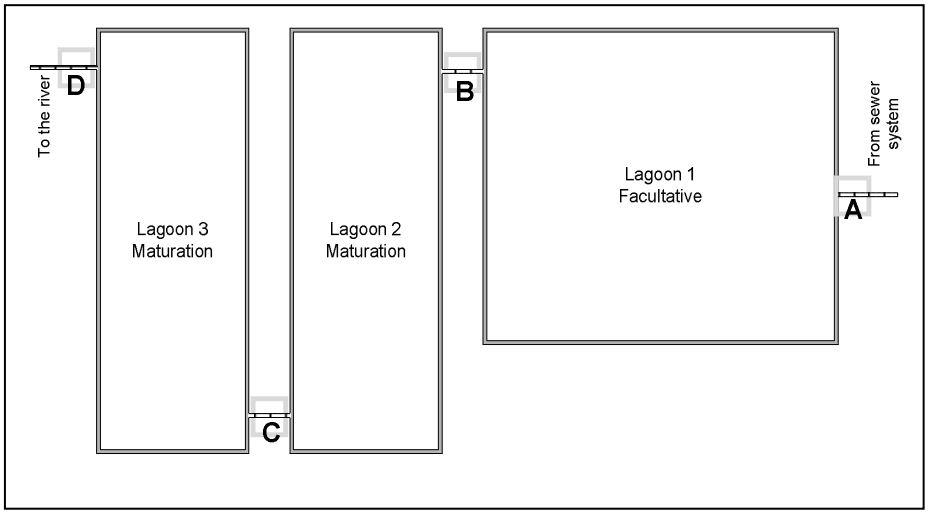

Figure 1 San Antonio System Diagram with Sampling Points (A, B, C, D). Wastewater flow is from right to left.

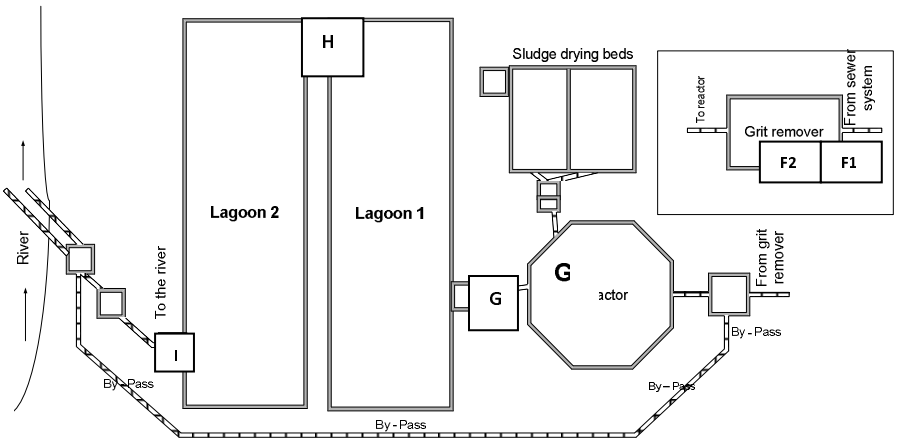

Figure 2 Wastewater treatment systems in Sapecho, Bolivia, with sampling locations from the plant and receiving water body labeled F,G, I. Flow of wastewater is right to left.

Methodology

Measurements have been made over a 2-year period (June/July 2007, and June/July 2008) by undergraduate and graduate students participating in an NSF Research Project. For both years, samples were collected and tested for TSS, BOD, COD, nitrogen, phosphorus, and coliforms. The results from 2008 were compared with the results from 2007 to monitor changes in the lagoon's removal efficiencies.

San Antonio. The first wastewater samples in San Antonio were collected at four different locations sites A, B, C, D (Figure 1). These sites are accessed through inspection boxes where wastewater is entering or exiting a particular lagoon.

Using a 2.5-L plastic container a grab sample was collected in the morning from these four separate inspection boxes. Grab samples at each site were then poured into 2-L and 300-mL sample bottles and sent to an approved laboratory. The 2-L sample bottles were tested for several chemical and physical properties: e.g., TSS, BOD, COD, nitrogen, and phosphorus. The 300-mL samples were tested for total fecal coliforms, an indicator of the presence of *E. Coli*. All samples were immediately transported by boat and taxi to Palos Blancos, Bolivia where they were immediately packed in ice and shipped overnight to La Paz, Bolivia by bus to the Instituto de Ingeniería Sanitaria y Ambiental (IIS) laboratory.

Additional measurements were performed on the facultative lagoon. These measurements compared the difference in dissolved oxygen and pH to provide information on how the facultative lagoon is functioning over the day. Using a reach pole with a 2-L attachment, grab samples were collected throughout the day to monitor changes in the lagoon biochemistry. Grab samples were taken from the surface of the lagoon with minimal disturbance and mixing with the atmosphere. Each grab sample was tested two to three times. In this sampling dissolved oxygen was measured with a handheld Hach® DR/820 Colorimeter and *Dissolved Oxygen Reagent High Rand Cat. 25150-25.* A pH reading was taken using *AquaCheck* litmus

paper, and results were interpreted by color differential of the paper and the scale provided on the bottle. The pH and DO readings were taken over a 16-hour period.

Sapecho. Similar sampling procedures employed in San Antonio were also administered in Sapecho. Using a 2-L plastic water bottle, a grab sample of wastewater was collected from sites F1, F2, G, and I, Figure 2. A 300-mL sample bottle was filled at sites F2, G, and I. These sites are accessed through inspection boxes where waste is entering or exiting a specific part of the system. Samples were immediately transferred to Palos Blancos by taxi where they were immediately packed in ice with the 2-L plastic water bottle samples and shipped overnight to La Paz by bus.

The 2-L sample bottles were tested for the following chemical and physical properties: BOD, COD, nitrogen, phosphorus, total coliforms, total solids, and volatile, fixed, and total suspended solids. The 300-mL samples were tested for total fecal coliforms which is an indicator of the presence of *E. Coli*.

The research conducted in Sapecho also involved determining the composition of methane gas that was produced by the upflow sludge blanket reactor. For methane determination, a sample of the biogas exiting the reactor was collected on June 29, 2008 in a 20-mL syringe. The attachment on the top of the gas tube was removed and replaced in order to read the pressure of the gas. The attachment had a small opening to allow the release of gas. This small opening was covered with rubber to ensure only biogas entered the syringe at the time the sample was retrieved. A test was first performed to make sure biogas was entering the syringe. After gas was collected by directly inserting the syringe through the rubber and into the small opening, it was exerted over a lit match. The match held flame, and it was concluded that the gas did enter the syringe. Next, two real samples were obtained. Immediately after the syringe was filled, it was capped with a small piece of rubber. A masking tape was then used to seal shut the syringe. The next morning another flame test was performed successfully. The first sample was collected and sent to the Facultad de Ingeniería Química laboratory in La Paz to determine the composition of the biogas. A second sample was collected on July 3, 2008 and sent to the lab for similar analysis.

Results

San Antonio-Facultative Lagoons: Results of removal efficiency in facultative lagoons operating in San Antonio are shown in Table 1. The results obtained in 2008 are compared 2007 results. Total suspended solids in the influent from 2007 to 2008 rose significantly. Influent biochemical and chemical oxygen demand have also risen to a large extent from 2007 to 2008.

All measurements suggest the wastewater has gotten stronger over the 2-year sampling period. The BOD/COD ratio of the samples has remained relatively similar over the sampling period (0.56 and 0.63) which suggests the organic and solid loadings to the treatment plant are municipal sewage. No water conservation measures were implemented over the course of the year that might explain the higher influent concentrations; however, the community uses significant less water than North American communities which will result in a higher strength wastewater. The high values for the wastewater constituents along with the large differences between

the two years point to a difficulty in designing and operating treatment plants in these settings; that is, the strength of the wastewater and variability in wastewater characterization and subsequent plant loadings.

Important to these communities, coliform removal has been in the 98-99% removal range for the two years of sampling (the expected removal in these types of systems is 92-99.8%) (Crites and Tchobanoglous, 1998).

Even with the increase in concentration, Table 1 shows that the facultative lagoon has been able to function as designed as indicated by the percent removal of BOD, COD, TSS, nitrogen, and phosphorus. The removal for TSS and BOD for both years is slightly lower than typically expected for TSS and BOD removal in a facultative lagoon system (the expected removal in a facultative lagoon is 90-95% TSS and 75-95% BOD) (Crites and Tchobanoglous, 1998). However, measurements we made for turbidity indicate that it decreased by approximately 66% across the facultative lagoon (Point A and Point B) and 77% (Point A and Point D) across the whole lagoon system. The turbidity results are comparable to TSS removal which is in the range of 74% (2007) and 55% (2008).

Table 1 Removal efficiency results (2007/2008) of facultative lagoon operating in San Antonio, Bolivia. Results are from Sampling Points A and B, Figure 1.

Parameters	**Infl.**2007**	**Infl.** 2008**	**Effl.^ 2007**	**Effl.^ 2008**	**% Rem.* 2007**	**% Rem.* 2008**
Total Suspended Solids (mg/L)	215.0	850.0	56.0	384.0	74.0	54.8
Biochemical Oxygen Demand (mg O_2/L)	190.0	340	58.0	38	69.5	88.8
Chemical Oxygen Demand (mg O_2/L)	444.0	700	168.0	102	62.2	85.4
Total Nitrogen (mg Nt/(Kt)-N/L))	53.0	202.2	25.2	20.4	52.6	90
Total Phosphorus mg P/L	8.4	11.84	4.0	6.08	52.1	48.6
Coliforms (U.F.C. per 100 mL)	9.2×10^8	6.4×10^7	1.1×10^6	1.4×10^6	99.9	97.8

Infl.**=influent; Effl.^=effluent; Rem.*=removal

The measured nitrogen removal of 53% in the single facultative lagoon was found to be in the expected range of 43-82% (Crites and Tchobanoglous, 1998). Nitrogen removal in the lagoons is dependent on mechanisms of volatilization, for example of ammonia which is pH-dependent, algal uptake, nitrification and denitrification, sludge deposition, and adsorption onto bottoms soils. A higher number of facultative ponds in series, increased number of detention time, water temperature and pH all play a significant role in nitrogen reduction (Crites and Tchobanoglous, 1998). Phosphorus removal was determined to be 52%, which is within the expected removal range for lagoon systems (expected removal is 10-50%) (Muga and Mihelcic, 2008).

Overall, the system in San Antonio appears to be operating well. It is believed that if the community continues to use the system appropriately and the water committee ensures the maintenance of the lagoons the wastewater system will be a sustainable and functioning asset to the community.

Dissolved oxygen and pH were also measured in this study and used as an indicator of photosynthetic processes occurring in the facultative lagoon. Over the 16-hour period, the DO concentrations increased steadily throughout the period from 0.5 mg/l to 7 mg/l. However, temperature and pH remained stable (temperature over the day ranged from 22-27°C). The ambient temperature ranged from 25-28°C. The pH remained stable in the range of 7.5-8.0.

Dissolved oxygen and pH were also measured at San Antonio in 2008 and used as an indicator of photosynthetic processes occurring in the facultative lagoon. Over the 16-hour period, the DO concentrations increased steadily throughout the period from 0.5 mg/l to 7 mg/l (data not shown). However, temperature and pH remained stable. The lagoon temperature ranged from 22-27°C over the sampling period while the ambient temperature ranged from 25-28°C. The pH remained stable over the sampling period in the range of 7.5-8.0.

An explanation for the low concentrations of DO observed early in the morning could be because microscopic, aquatic animals and plant life present in the lagoon have utilized any oxygen present in the water. The low level of DO usually begins late in the afternoon and at night when photosynthesis ceases, but animal/plant respiration continues. A lower DO level could also indicate decomposition, whereby bacteria utilize oxygen to breakdown dead material. An increase in DO during the day indicates photosynthetic activity from the plants.

However, in contradiction of the DO data that suggests that photosynthesis was taking place, stable pH values were also observed. This suggests that aeration was not due to photosynthetic algae as they would contribute DO to the system (unless the alkalinity was so high to buffer any pH change; however, we did some screening alkalinity measurements which suggested the alkalinity was not abnormally high). Instead, the increase in DO concentrations may be attributed to wind-driven mixing. On the days the lagoons were monitored, wind was sufficient to move surface flocs across the lagoon to the down-wind side of the lagoon.

It should also be noted that in a stratified lagoon, the DO should decrease with depth, with lower DO expected at the bottom of the lagoon near the decomposing sludge, then on the surface. Temperature, pH and alkalinity also change with depth and may influence how physical-chemical parameters such as nitrogen, phosphorus and coliforms are removed. Future studies should consider collecting samples at different depths and analyzing for the different physical-chemical characteristics.

Dark brown-black flocs on the surface of the facultative lagoon were also observed. These flocs were identified as a build-up of floating solids, fats, grease and scum. Regular maintenance is required to remove the solids from the lagoon surface about every three days (Oakley, 2005).

San Antonio Maturation Lagoons: These lagoons are smaller than the facultative lagoon; specifically 13 × 39 m. They are also half as deep as the facultative lagoon. While they also provide some suspended solids removal, their primary function is pathogen and nutrient removal.

As shown in Table 2, the percent removal changed significantly in the maturation lagoons from 2007 to 2008. In 2007 the maturation lagoon removed 20% of phosphorus and 95% of coliforms. Phosphorus removal in ponds is usually limited and application of chemicals such as ferric chloride may be utilized for high strength loadings (phosphorus concentrations of 15 mg/L) (Crites and Tchobanoglous, 1998). The effluent concentration of phosphorus of 3.2 mg/L in 2007, was still higher than effluent target of 1 mg/L in the U.S (Crites et al., 2000).

There appears to be minimal removal of nitrogen, about 1% in 2008. Nitrogen removal in maturation and facultative ponds may occur through several processes, for example, nitrification, denitrification, uptake by pond algae, and accumulation in the pond sediments associated with dead algae. The lack of reduction in nitrogen removal, as observed from the 2007 data may be due to organic nitrogen associated with dead algae. Hence, as previously suggested, regular cleaning and removal of the algal biomass is required to enable proper functioning of the maturation pond.

Coliform removal was found to be 95% in 2007 and 77.4% in 2008. These removal values especially for 2008, is below the expected removal of 1-2 orders of magnitude (Crites and Tchobanoglous, 1998). Removal of bacteria and viruses in maturation and facultative ponds is highly dependent on temperature and detention time (Crites et al., 2000). High temperatures and longer detention times are conducive to bacteria and virus inactivation.

When compared to the facultative pond, the maturation pond has comparable removal of TSS, but lower removal of BOD, COD, nitrogen, phosphorus and coliforms. The results show that a majority of these physical-chemical parameters are removed in the facultative lagoon.

Table 2 Removal efficiency results (2007/2008) of maturation ponds operating in San Antonio, Bolivia. Results are for Points C and D, Figure 1.

Parameters	Influent 2007	Influent 2008	Effluent 2007	Effluent 2008	Percent Removal 2007 (%)	Percent Removal 2008 (%)
Total Suspended Solids (mg/L)	215.0	265	56.0	260	74.0	2.0
Biochemical Oxygen Demand (mg O_2/L)	54.0	22	42.0	14	22.2	36.4
Chemical Oxygen Demand (mg O_2/L)	166.0	76	134.0	68	19.3	10.5
Total Nitrogen (mg Nt/(Kt)-N/L))	19.6	31.5	22.4	31.15	Increase	1.0
Total Phosphorus mg P/L	4.0	5.74	3.2	5.24	20.5	9
Coliforms (U.F.C. per 1000mL)	1.0×10^5	2.7×10^5	5.0×10^3	6.1×10^4	95	77.4

Overall Removal in Santonio: When looking at removal of pollutants across the whole facultative-maturation lagoon treatment process, overall the system removed 74% TSS, 78% BOD, 70% COD, 58% nitrogen, 62% phosphorus, and 99.99% coliforms. The system is performing well in removing TSS, BOD, COD, nitrogen, phosphorus and coliform.

Sapecho - Anaerobic Reactor: Table 3 shows data from the 2007 sampling period. It shows that BOD, COD, nitrogen, phosphorus and coliforms were decreased by 75%, 80%, 76%, 85%, 97%, respectively in the anaerobic reactor (between Points F and G, Figure 2). The anaerobic reactor significantly reduces the BOD and COD concentrations from 972 mg/L to 252 mg/L and 1,914 mg/L to 394 mg/L, respectively. It also reduces nitrogen from 26.6 mg/L-N to 6.4 mg/L-N, phosphorus from 64 mg/L-P to 9.07 mg/L-P, and coliforms from $9.0x10^8$ UFC/100 mL to $2.7x10^7$ mL.

The first gas sample collected from the reactor had the following gas composition: 77% methane, 15% carbon dioxide, and 8% other gases. The second sample had the following gas composition: 56% methane, 11% carbon dioxide, and 33% other gases. According to the EPA if the recovered gas is between 60-80 percent methane, the gas can be used to produce electricity or it may be directly combusted as a cooking fuel. It was concluded however that it was not feasible at this time to collect and utilize the gas because no users were identified physically close by to the reactor.

Sapecho - Maturation Lagoons: Data obtained between Points G and I as shown in Figure 2, are used to calculate the removal efficiency in the maturation lagoons. Data collected for these two points in 2007 are shown in Table 3. Data collected for these two points in 2008 are shown in Table 4.

Removal efficiency calculations between Points G and I in 2007 show there is 93% removal of TSS, 98% removal of BOD, 98.6% COD, 3% nitrogen, 99.8% phosphorus, and 99.96% coliforms. The lagoon is functioning well, with high removal percentages in TSS, BOD, COD, phosphorus, and coliforms.

Removal efficiency calculations between Points G and I in 2008 show there is 71% removal of TSS, 80% removal of BOD, 48% COD, 36.5% nitrogen, 16.7% phosphorus, and 98.8% coliforms. The lagoon is functioning well, with high removal percentages in TSS, BOD, COD, phosphorus, and coliforms. These results indicate a properly functioning lagoon.

Overall Removal in Sapecho: When the overall removal efficiency of the system is considered, the data obtained from influent (Point F of Figure 2) to the effluent discharge point (Point I of Figure 2), we see that there is a 98% reduction in BOD, 99.7% reduction in COD, 77% reduction in nitrogen, 99.9% reduction in phosphorus and 99.99% reduction in coliforms (2007 data). These values are shown in Table 3.

When 2008 data are considered for Points F and I (Table 4), we see 97% reduction in TSS, 97% reduction in BOD, 91% reduction in COD, 61% reduction in nitrogen, 7% reduction in phosphorus, and 99.90 reduction in coliforms.

When maturation ponds operating in San Antonio and Sapecho are compared, we find that the maturation ponds in Sapecho are performing more efficiently than

the maturation ponds in San Antonio. Regular maintenance is important in proper functioning of lagoon. The use of an appropriate technology net device for regular cleaning (for example a net to skim algae of lagoon surface) and the introduction of ducks to eat surface vegetation were proposed to operators as needed for proper lagoon functioning.

Table 3 Comparison of influent, reactor effluent, and system effluent characteristics in Sapecho, Bolivia (Points F, G and I of Figure 2, 2007)

Parameters	**Units**	**Point F** (influent)	**Point G** (exiting anaerobic reactor)	**Point I** (effluent	**% Removal** (between influent and effluent)
Total suspended solids	mg/L	NA	63	5.0	-
Biochemical Oxygen Demand	mg O_2/L	972	252	4.0	98
Chemical Oxygen Demand	mg O_2/L	1,914	394	6.0	99.7
Total Nitrogen	mg $N_t(K_j)$-N/L	26.6	6.4	6.2	77
Total Phosphorus	mg P/L	64	9.07	< 0.01	99.9
Coliforms	U.F.C./100 mL	9.0×10^8	2.7×10^7	8.9×10^3	99.99

Table 4 Comparison of Influent and effluent characteristics in Sapecho, Bolivia (Points F, G and I of Figure 2, 2008)

Parameters	**Units**	**Point F** (influent)	**Point G** (exiting anaerobic reactor)	**Point I** (effluent)	**% Removal** (between influent and effluent)
Total suspended solids	mg/L	520.0	52	15.0	97.0
Biochemical Oxygen Demand	mg O_2/L	420.0	60	12.0	97
Chemical Oxygen Demand	mg O_2/L	766.0	130	68.0	91
Total Nitrogen	mg $N_t(K_j)$-N/L	106.4	65.1	41.3	61
Total Phosphorus	mg P/L	9.73	10.9	9.07	7
Coliforms	U.F.C./100 mL	6.8×10^7	6.8×10^6	8.0×10^4	99.9

Conclusions

Results from the 2-year study indicate that the wastewater treatment systems in the South Yungas, Bolivia are currently performing as they should, and the overall wastewater treatment systems are not having a large impact on the receiving stream. However, regular maintenance, for example manually cleaning/removing algae from the lagoons is needed in order to ensure their proper operation. Frequent cleaning/removal of sludge from the exit/entrance pipes are needed to enable smooth flow of the wastewater. The energy content and gas composition evaluation from a

wastewater reactor in Bolivia is an initial star to determining the feasibility of using methane as an energy source. More experiments/tests are however needed to determine the composition of gases over a continuous period of time. Also of interest is the volume of methane gas that is produced during a day and whether that can be used by a local domestic or industrial user.

Acknowledgements

The authors wish to acknowledge the NSF for support of the Sustainable Development Research Experience in Bolivia under Grant No. 0623558.

References

Crites, R.W. and Tchobanoglous, G. *Small and Decentralized Wastewater Management Systems.* McGraw Hill; United States,1998.

Crites, R.W., Reed, S.C, Bastian, R.K. 2000. *Land Treatment Systems for Municipal and Industrial Wastes*. McGraw-Hill, New York.

Fuchs, V.J., Fry, L.M. Mihelcic, J.R. "Delivering Sustainable Waste Infrastructure in an Urbanizing World," *Proceedings of the Third International Conference on Sustainability Engineering and Science*, Auckland, New Zealand, December 9-12, 2008.

Ballard, M. A.Clarke, R. Feldpausch, A. Manty, S. Pereira, E. Quinley, A. Sather-Knutsen, M. Aliaga, J. Chino, G. Gemio, S. Quevedo, M. José Quezada, M. Romero, S. Morales. 2007. *International Sustainable Development Engineering Research Experiences Program*, Final Report.

Muga, H.E., Mihelcic, J.R., "Sustainability of wastewater treatment technologies," *Journal of Environmental Management*, 88: 437-447, 2008.

Nelson, K., Cisneros, B.J., Tchobanoglous, G., Darby, J.L. "Sludge accumulation, characteristics, and pathogen inactivation in four primary waste stabilization ponds in central Mexico," *Water Research*, 38; 111-127, 2004.

Oakley, Stewart M. "The need for wastewater treatment in Latin America: A case study of the use of wastewater stabilization ponds in Honduras," *Small Flows Quarterly*, 6(2): 36-51, 2005.

Palos Blancos Municipal Report, (Plan de Desarrollo Municipal Palos Blancos, 2008-2012), Municipality of Palos Blancos, La Paz Department, Bolivia, 2007.

STATcompiler Custom Table, http://www.statcompiler.com/tablebuilderController.cfm?userid=243115&usertabid=264167. Measure Demographic and Health Surveys, table built and accessed March, 2008.

World Health Organization Statistical Information System (WHOSIS). *Mortality Country Fact Sheet 2006,* http://www.who.int/whosis/mort/profiles/mort_amro_bol_bolivia.pdf, 2006.

World Bank, 2008. *Economic Opportunities for Indigenous People in Latin America-Bolivia*, February 2007. http://siteresources.worldbank.org/EDUCATION/Resources/278200-1169235401815/Bolivia.pdf, Accessed January, 2008.

World Health Organization (WHO) *UN-Water Global Annual Assessment of Sanitation and Drinking Water. 2008 Pilot Report. Testing a New Reporting Approach*, Geneva, 2008.

Understanding and Controlling Fouling in Membrane Bioreactors

Roger Babcock Jr.

University of Hawaii, Civil and Environmental Engineering Department, 2540 Dole Street, Honolulu, Hawaii 96822; PH (808) 956-7298; FAX (808) 956-5014; email: rbabcock@hawaii.edu

ABSTRACT

Membrane bioreactors (MBRs) are an activated sludge process in which the conventional secondary clarifier is replaced by a membrane separation process (either microfiltration or ultrafiltration). As with other membrane systems, the most important characteristics are the membrane flux and the membrane permeability both of which are highly dependent upon temperature and degree of fouling. Like other membrane systems but to a greater degree, MBRs are susceptible to biofouling. Biofouling is not well understood but does increase operating pressure, reduce maximum flux, increase recovery cleaning requirements, and possibly reduce total membrane life. All of these effects of biofouling have adverse effects on either initial capital cost or ongoing operation and maintenance costs for MBRs. The overall goal of this research is to obtain a better understanding of biofouling in MBRs and methods to control said fouling in order to improve the economics of water recycling. The conclusions thus far from the pilot and bench-scale studies are that SMP and EPS are very important relative to biofouling in MBRs and that several tools are useful to examine biofouling trends. These tools include the critical flux test, resistance in series component analysis, and measurement of different fractions of EPS and SMP.

INTRODUCTION

Membrane bioreactors (MBRs) are a relatively new wastewater treatment technology which is nearly ideal for water recycling operations including satellite reclamation (sewer mining) due to exceptional processed water quality and minimal footprint compared to conventional treatment process trains. MBRs are quite simply an activated sludge process in which the conventional secondary clarifier is replaced by a membrane separation process (either microfiltration or ultrafiltration). The MBR can be operated either with or without primary clarification, but always requires fine screening (3 mm or smaller) to protect the membranes from abrasive and stringy waste components (hair in particular). Due to the presence of an absolute barrier for suspended solids, MBRs are able to maintain very high solids concentrations (8,000 to 20,000 mg/L) and solids retention times which allows for smaller aeration basins and high BOD removals. Since MBR effluent is micro- or ultra-filtration permeate, effluent suspended solids are typically near the detection limit and turbidities are typically less than 0.2 NTU. As with other membrane systems, the most important characteristics are the membrane flux and the membrane permeability both of which are highly dependent upon temperature and degree of fouling. Flux is often expressed as gallons permeated per day per square foot of membrane area (GFD) and permeability is usually the water flux per unit transmembrane pressure (TMP). Like other membrane systems but to a greater degree, MBRs are susceptible to biofouling. Biofouling is not well understood but does increase operating pressure, reduce maximum flux, increase recovery cleaning requirements, and possibly reduce total membrane life. All of these effects of biofouling have adverse effects on either initial capital cost or ongoing operation and maintenance costs for MBRs. Because MBRs are quickly becoming the process of choice for water recycling, there is a need to improve cost efficiency by controlling biofouling.

METHODS

The overall goal of this research is to obtain a better understanding of biofouling in MBRs and methods to control said fouling in order to improve the economics of water recycling. Membrane flux (J) is directly proportional to transmembrane pressure drop (TMP) and inversely proportional to viscosity (η) and a "resistance" factor (R_T).

$$J = \frac{TMP}{\eta R_T}$$

The resistance to passage of water through a membrane submerged in activated sludge mixed liquor has been modeled as consisting of at least three components including the inherent membrane resistance (R_m), the resistance of the cake layer (R_c) and the resistance of the foulants (R_f) (Chang et al, 1998). It may also be possible to separately quantify the biofilm resistance (R_b) as a portion of the foulants. Thus,

$$R_T = R_m + R_c + R_f + R_b$$

Experimental methods have been developed to estimate each of these individual resistances. The foulants may consist of fine colloidal particles that can block pores, macromolecules that coat and narrow or block pores, or even complex biofilm communities consisting of organisms engaged in community sensing, voids, extracellular polymers, and cellular debris. We are attempting to catalog the types and quantities of microorganisms present in MBRs. Comparisons are being made between MBRs operated under different conditions such as flux rate, hydraulic retention time, solids retention time, and organic/nutrient loading rate. In addition, we are quantifying various parameters such and transmembrane pressure (TMP), biofilm thickness, soluble microbial products (SMP), extracellular polymeric substances (EPS), viscosity, particle size distribution (PSD), soluble COD, and filterability and looking for correlations with microorganisms/biofouling. One goal is to correlate microorganism population dynamics with biofouling conditions and system operating conditions. This presentation will describe relationships between biofouling (expressed as increased transmembrane pressure (TMP)), operating conditions, predominance of certain bacteria types, and measured water quality parameters observed in bench and pilot MBRs.

RESULTS AND DISCUSSION

Six different brands of MBRs have been pilot tested side-by-side in Honolulu, Hawaii. The pilot testing began in September 2003 and is on-going. Pilot MBR units from Zenon Environmental (vertical hollow fiber UF), US Filter (vertical hollow fiber MF), Ionics Inc (horizontal hollow fiber MF), Enviroquip (vertical flat panel MF), Huber Inc (rotating flat panel UF), and Koch (vertical hollow fiber MF) have been tested. The Enviroquip MBR was converted to a membrane thickener/aerobic digester (PAD-K) for a period of time. In addition to the pilot MBRs, two bench-scale MBRs; one employing Enviroquip membrane panels and one using Ionics horizontal hollow fiber membranes were started-up in November 2005 for additional studies on membrane fouling due to SMP, EPS and the specific bacteria that produce them.

The Koch pilot MBR, was operated at an average flux of approximately 10 GFD, an average TMP of -1.0 psi, and the MLSS increased in the first 30 days from an initial seed value of 3,000 mg/L and then

was maintained at a steady value of 11,000 mg/L. The carbohydrate fraction of EPS appears to have initially increased and then reached a semi-stable value of 50 to 60 mg/g VSS. The protein fraction, was lower in magnitude (15-25 mg/g). The average values for the SMP fractions are 5.9 and 6.3 mg/L for carbohydrates and proteins, respectively. In contrast to this are the observations in relation to experiments on sludge thickening using the Enviroquip PAD-K thickener/digester system. The PAD-K conducted thickening/digestion of TF/SC waste sludge. With the intentional creation of high-fouling conditions, the carbohydrate SMP increased dramatically (from approximately 20 mg/L to approximately 200 mg/L), while the carbohydrate EPS also went up a lot (from 36 to 160 mg/L), the protein SMP also went up a lot (from < 1 to 10 mg/L), and the protein EPS did not change very much (from 25 to 30 mg/L). The most important is the SMP which can foul the membranes by blocking membrane pores. These data indicate that carbohydrate microbial products and to a slightly lesser extent, protein products, were elevated when the membranes approached a fouled state. In addition, it appears that the production of excessive extracellular products could be a biological response to the presence of excess ammonia.

The bench-scale reactors (one flat-plate type and one hollow fiber type) are operated via PLCs and SCADA. Table 1 shows average SMP values and reductions across the membranes which are 40-50% for Enviroquip and 5 to 40% for Ionics. The reductions across the membrane indicate the potential for fouling. Monitoring total filtration resistance and critical flux periodically can be useful for determining fouling rates. The first values for critical fluxes were estimated to be 26 and 32 GFD for the Enviroquip and Ionics MBRs, respectively (Figures 1 and 2). These values are interpreted to indicate the maximum flux that can be sustainably utilized. If the membranes become fouled during operation, the critical flux values (and therefore the maximum sustainable flux) are expected to decline. Values of total resistance were also monitored in the bench reactors. The slope of the total resistance verse time is the fouling rate. Figures 3 and 4 give the fouling rate as a function of various operating conditions. Tests were conducted to estimate the components of the membrane resistance to flux at the beginning of bench tests and after the membranes were quite well fouled. The resulting data are presented in Table 2. These data indicate that resistances due to both foulants and the cake layer increased significantly during the 65 day operating period. Many bulk sludge and several cake/biofilm samples have been collected from the pilot and bench reactors for PCR/DGGE genetic fingerprinting analyses. A general description of the findings are that the microbial diversity within each type of MBR are somewhat different, that as MBRs enter fouling conditions there are shifts in bacterial speciation, and that the organisms in the cake/biofilm are dissimilar to those in the bulk sludge.

CONCLUSIONS

The conclusions thus far from the pilot study are that SMP and EPS are very important relative to biofouling in MBRs and that several tools are useful to examine biofouling trends. These tools include the critical flux test, total resistance slope, resistance in series component analysis, and measurement of different fractions of EPS and SMP. Future results collected under different operating conditions will allow correlations between fouling rates, bacterial species, and environmental/growth conditions.

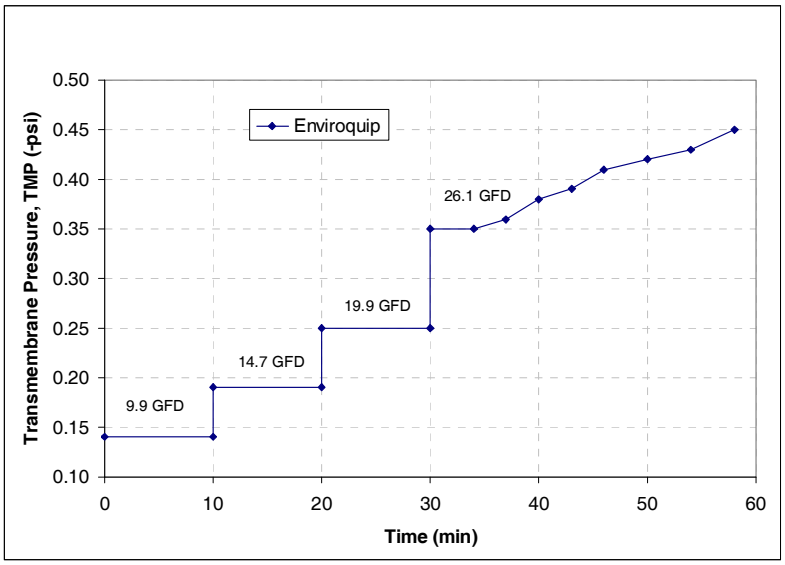

Figure 1 – Critical flux test data for bench-scale Enviroquip MBR.

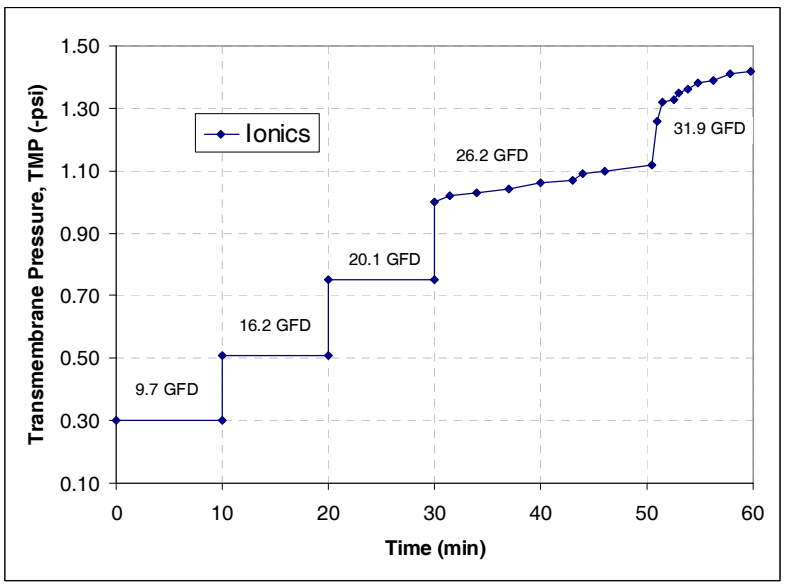

Figure 2 – Critical flux test data for bench-scale Ionics MBR.

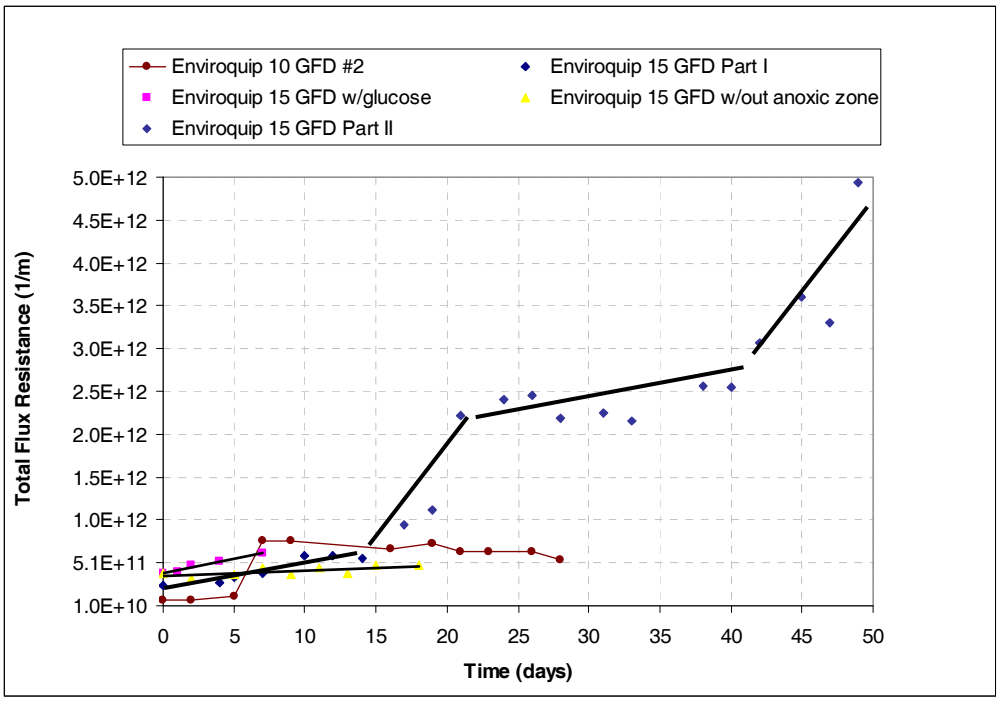

Figure 3 – Total resistance data for bench-scale Enviroquip MBR

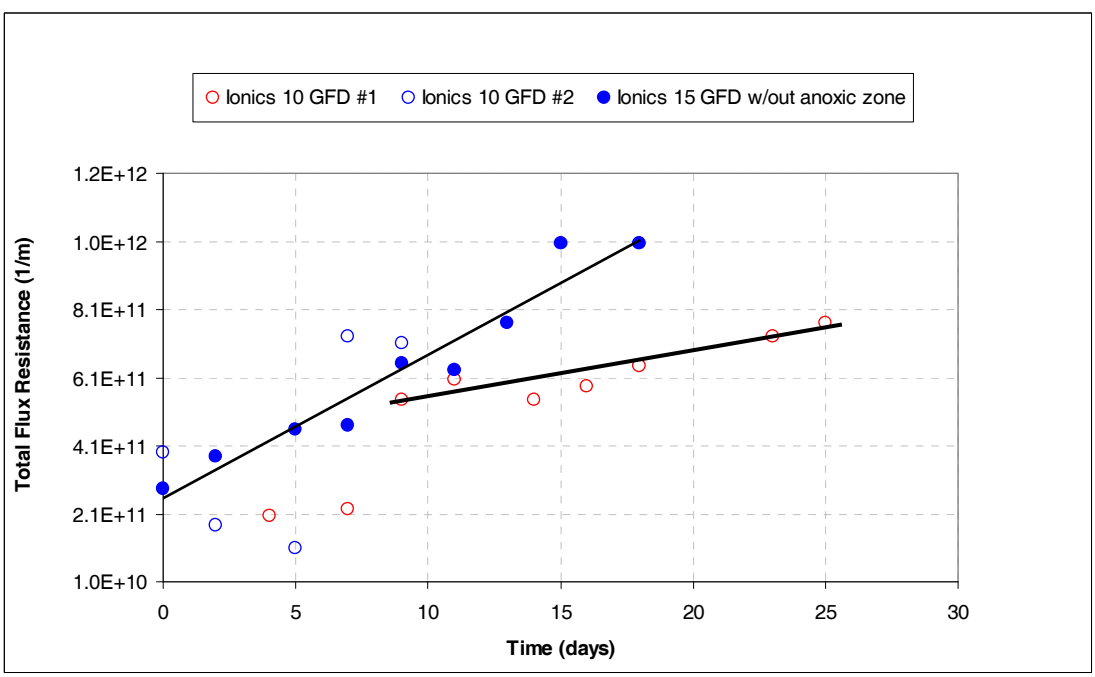

Figure 4 – Total resistance data for bench-scale Ionics MBR

Table 1 – Average SMP and EPS concentrations for bench-scale MBRs and SMP removal rates across the membranes (in parentheses).

Analyte	Influent	Enviroquip Permeate	Ionics Permeate	Enviroquip Liquor	Ionics Liquor
Carbohydrate SMP (mg/L)	9.5	3.6 (40%)	4.9 (5%)	6.0	5.2
Protein SMP (mg/L)	15.4	2.2 (49%)	3.1 (39%)	4.4	5.0
Carbohydrate EPS (mg/gVSS)	NA	NA	NA	34.3	32.4
Protein EPS (mg/gVSS)	NA	NA	NA	18.8	18.0

Table 2 – Calculated resistance values for bench-scale MBRs and the percentage of non-membrane related resistance (in parentheses).

Bench-Scale MBR	R_T (m^{-1})	R_m (m^{-1})	R_c (m^{-1})	R_f (m^{-1})
Enviroquip 3/7/2006	3.9×10^{11}	3.2×10^{11}	6.8×10^{10} (100%)	0 (0%)
Enviroquip 5/12/2006	6.4×10^{12}	3.2×10^{11}	1.7×10^{12} (28%)	4.4×10^{12} (72%)
Ionics 3/7/2006	2.20×10^{11}	6.06×10^{10}	7.94×10^{10} (100%)	0 (0%)

Using Media Filters in a Distributed Wastewater System Serving an Ecotourism-Oriented Development

Kevin M. Sherman[1]

[1]Quanics, Inc., PO Box 1520, Crestwood, KY 40014; PH (502)751-7258; FAX (502) 992-8249; email: ksherman@quanics.net

ABSTRACT

Ecotourism developments are becoming popular worldwide. The term is being used by those who may not fully understand its implications, yet still wish to exploit the concept's popularity. One of the ways an ecotourism operator's true intent is revealed is through their choice of wastewater treatment. A historically important and ecologically unique island is being developed in Northwest Florida using ecotourism principles. Distributed wastewater clusters are being installed with fixed film treatment and drip irrigation. Central to these decisions was the preservation of the numerous palm trees found throughout the island. A pretreatment system using the recycled husks of coconuts was chosen to treat wastewater from 26 single-family cottages, a restaurant, and bar. This paper provides information on the design concept and treatment train of this fixed film treatment system. The paper concludes with an update of the longevity of media from the longest continually operating coir fiber system in the United States.

INTRODUCTION

In recent years, various locations around the world have labeled themselves as ecological tourism (or ecotourism), responsible tourism or sustainable tourism destinations. The concept of ecotourism is widely misunderstood and, in practice, is often simply used as a marketing tool to promote tourism that is related to nature. Most definitions of ecotourism boil down to a form of tourism that provides for environmental conservation, includes community participation, and is profitable and environmentally, economically and socio-culturally sustainable in the long-term.

Critics of ecotourism claim that ecotourism as practiced and abused often consists of placing a resort in a splendid landscape, to the detriment of the surrounding ecosystem. According to them, ecotourism must above all sensitize people with the beauty and the fragility of nature. They condemn some operators as "green-washing" their operations — that is, using the label of "ecotourism" and "green-friendly", while behaving in environmentally irresponsible ways.

One of the ways ecotourism operators distinguish their true intent is in their choice of wastewater treatment. In many developing countries, wastewater regulations are virtually nonexistent. Developers are often left to their own consciences in dealing with the wastewater to be generated by their operations. In order to live up to the ideals of ecotourism, the wastewater system selected will far exceed local regulations and integrate with the nearby environment to better protect the special places they inhabit.

Historical Background of Study Area

In Florida, one ecotourism destination is Black's Island. Located in Port St. Joe Bay in Northwest Florida (Figure 1) this nearly seven-acre island holds an important place in Florida's history. Archeological investigations of the island (Mayo, 2003) show extensive temporary use of the island as fishing and hunt camps by Native American peoples. The French explorer Jean Beranger was the first European to survey and name the island in 1718. He chose the name Ile de la Tortue (Island of the Turtle) to highlight the sea turtles who nested on the shores of the island every summer.



Figure 1. Black's Island within the context of Port St. Joe Bay, Cape San Blas, and Florida.

The town of Port St. Joe sprang up the in the 1820's and by 1835 was one of the largest seaports in Florida, along with St. Augustine, Pensacola and Key West. During the mid 1830's, Captain Black, an English sea captain, arrived in St. Joe Bay to carry on his trade. Captain Black is the first recorded owner of the island and is the person for whom the island is still named. The date of platting of the island preceded Florida's statehood by ten years.

In 1970, the island became a camp for young men. This camp was destroyed by a hurricane in 1975. It was reestablished as Camp Nautilus by one of the current owners, William Koran, in 1976. After several unsuccessful attempts to interest the State of Florida in purchasing the property for preservation or as an adjunct to nearby Cape San Blas State Park, Mr. Koran and Mr. Grimsley the current owners set upon the current path for developing an ecotourism-related property.

The island and its surrounding waters boast several unique ecological resources. The bay scallop *Argopecten irradians* is plentiful in the shallow turtle grass beds offshore of the island (Sherman, 1985). A relic population of Black mangroves is found on the island. Their nearest living relatives exist more than 100 miles south of the island on the Florida mainland.

The current development consists of 26 single-family cottages, connected to each other and to a community center, restaurant, and bar (not open to the public) by an elevated, 10 ft wide boardwalk. Cottages are either one-story 2 bedroom units (floor plan 1,156 square feet) or two-story 3 bedroom units (floor plan 1,350 square feet). All are built on elevated pilings ten to twelve feet above the ground. The colors of the vertical wood surfaces and the greenish color of the roofs closely match those of healthy palm trees. This means that a visitor must get relatively close to the island before they recognize that development has occurred (Figures 2 & 3).



Figure 2. Black's Island from the water. Camera is approximately 500 m from island.

One of the hallmarks of a visit to Black's Island is isolation and the corresponding tranquility it brings. Central to this concept is the large number of palm trees throughout the island. There are over 700 palm trees on the island. The primary species are Cabbage Palm *Copernicia cowellii* and Palmetto *Sabal palmetto*.



Figure 3. Black's Island from the water. Camera is approximately 50 m from island.

The wastewater system selected for this island had to mesh with the presence and continued health of these palm trees. Because palm trees have a compact root ball (Figure 4) and are resistant to soil burial, drip irrigation was chosen to preserve as many palm trees as possible. An advanced treatment fixed film system was selected to pretreat the wastewater prior to drip irrigation. Per State of Florida Rules, the systems have to meet an effluent standard of 30 mg/L $CBOD_5$ and TSS (64E-6, FAC).

Systems serve either three to four cottage clusters (distributed system) or the community center and food service operation. Tanks are whenever possible placed below the 12 to 15 foot elevated walkway or under adjacent walks toward the shore, thereby eliminating the need to remove or relocate trees to set tanks. All tanks will be accessible for service through hinged access lids where necessary. Graded service paths from the dock to each tank have been designed onto the property. Some trees were relocated because their existing location placed them in danger of being damaged inadvertently during construction. They are surviving quite satisfactorily, only occasionally needing hand watering.

Typical Treatment Train – Residential Cluster Systems

All clusters on the island were designed based on a 1000 gpd cluster of two 3-bedroom plus two 2-bedroom cottages flowing to one system. Only two of the eight clusters achieve this flow. The most common estimated sewage flow from a cluster was 700 gpd (Table 1).

Under Florida's code (64E-6, FAC) the minimum size of the septic tank would be 2200 gallons for the 1000 gpd flow from a 4-home cluster. The minimum size of the dose tank would be 1050 gallons.



Figure 4. A trio of cabbage palms await replanting. The entire root ball is directly below the trunk.

Design Concept for BioCoir Fixed-Film Wastewater Systems

Fixed-film wastewater systems share several design considerations (Jantrania and Gross, 2006). The first is the effective loading rate. In other words, how much media will be needed to treat a known volume of wastewater? With regard to recycled coconut fibers (trade name BioCoir™), the effective loading rate is set by the manufacturer at 12.5 gpd per cubic foot of media. This loading rate is similar to the loading rate suggested for open cell foam media (Jowett, 1997). This loading rate was nearly cut in half with the restaurant and lounge system, anticipating a higher strength wastewater. The anticipated BOD loading for the high strength waste system is 0.032 pounds per cubic foot per day. Oversized grease interceptors and servicing on a 3 to 6 month basis in season is anticipated.

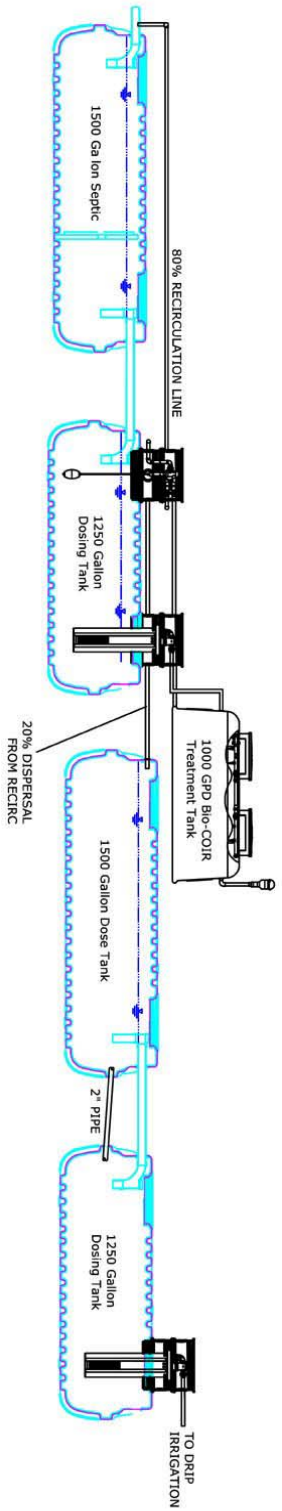

Figure 5 – Typical Tank configurations for residential clusters.

Table 1. System data for Black's Island

Serves	GPD	Septic volume	Treatment capac.	Dose tank vol	Linear feet Drip tubing	2nd drip**
Units 1, 3,5, & 26	1000	2750	1000	2750	418	0
Units 2,4 & 6	600	2750	1000	2750	350	0
Units 7, 8 & 10	600	2750	1000	2750	556	0
Units 9, 12 & 14	700	2750	1000	2750	208	198
Units 11, 13 & 16	700	2750	1000	2750	323	0
Units 18, 20 &15	900	2750	1000	2750	472	0
Units 22,17,24,19	1000	2750	1000	2750	293	204
Units 21, 23 & 25	700	2750	1000	2750	327	0
Restaurant & Bar*	1700	6000	3000	2000	610	556

* also includes 2 – 1250 gallon grease interceptors in series

** if not 0, a second area of drip irrigation was used, supplied by a sequencing valve if a single area was not large enough by itself

The second design consideration is uniform surface coverage with wastewater without channeling. The BioCoir system achieves this through use of pumps connected to helical spray nozzles pointed down. The uniformity of surface coverage is improved even more when the pumps serving the modules use time dosing. The septic/recirculation tank volume is larger than required (2,750 gallons actual versus 2,200 gallons) and allows for storage of dose volume until called for by the time dose control panel.

The third design consideration is biological nutrient reduction. The critical influence of nitrogen on the health of turtle grass *Thalassia testudinum* beds and the scallops that rely on them for settlement of juveniles has been elucidated over the past two decades by the Tampa Bay National Estuary Program (Johansson and Greening, 2000). Nitrogen reduction will be accomplished in this project, although such treatment was not required for system permitting. The anticipated effluent standard for these systems is 5 mg/L $CBOD_5$ and TSS, 10 mg/L TN and TP, and fecal coliform 200 colonies per 100 ml. Effluent sampling will be accomplished by the certified maintenance entity annually.

Recirculation of nitrified effluent is accomplished using a variable splitting device. Because occupancy and therefore sewage flow will be peaked throughout the year, this sort of device is ideal. Once again, tank volumes in the dosing tanks 2,750 gallons versus 1,050 gallons far exceed code requirements. The pump will be set to activate below 2/3 of the total tank volume. The rest of the volume is surge volume

to be used only during peak holiday weekends. The 2" line connecting the tanks below the mid-seam ensures that the tanks will act in unison as a single surge tank.

During periods of normal usage, the float inside the first 1,250 gallon tank will allow 80% of the treated effluent to return to the head works of the septic/recirculation tank. This is the theoretical optimum recirculation value for denitrification. The remaining 20% will flow into the 1,500 gallon dose tank, to be pumped out to drip irrigation, once again using a time dosed control panel. If the majority of homes on the cluster are unoccupied, or the flow is below normal for other reasons, the effluent level in the first 1,250 gallon tank will be below normal. Now the float in the dose tank closes off the 20% outlet and 100% of the flow is routed to recirculation. Use of this relatively simple device ensures the media will be moistened (and fed) regularly regardless of whether the homes in the cluster are occupied.

Other considerations with biological nutrient reduction are effluent temperature at or above 10°C, alkalinity at or above 200 mg/L as $CaCO_3$, and keeping acetone and other nitrification inhibitors out of the system (Oakley et al., 1996).

The final design consideration for these kinds of systems is they must be designed for maintainability. If these systems are difficult to maintain, they simply will not be properly maintained, with disastrous consequences. Specific to this design, nozzles in the coir modules are attached with a simple snap. This allows easy removal and cleaning of nozzles during every six-month maintenance visit. . Tank locations are accessible to pumping. A ground-level pathway to each cluster's tanks avoids driving over drip irrigation areas. Extra grease interceptor volume will allow grease trap cleaning to occur when other service visits occur.

During biannual service visits, the certified maintenance entity will examine the coir media, sludge judge tanks, check nozzles for plugging, service filters and clean pump chambers filter plates. Data will be retrieved from the control panels, such as the number of alarm conditions since the last visit.

Coir Longevity- an update

An important consideration in natural media is longevity. In other words, how long will it take before the media will need to be replaced? Over time, peat materials degrade to a muck material. The time required to degrade varies from peat source to peat source, but ranges from 4.5-16 years. Coir material will also degrade to a muck-like material over time. When its treatment ability is exhausted, it can then be pumped out of its container with a liquid vacuum pump truck. The spoil material will be taken to a septage processing plants and can be land applied.

The coir system with the longest continuous use in the country was installed on July 1, 2004 as a single pass addition to an existing system in Oldham County, Kentucky. In Sherman, 2006 media sampled from the surface of the unit on July 2006 was contrasted with fresh media from the warehouse (reprinted as Figure 6). Continuing in that vein, photos of coir fiber sampled from the surface of this system on January 29, 2007 showed a lightening of the original coir characteristics from the

July sample (Figure 7). In other words, this sample looked more like virgin material than a sample taken 1.5 years earlier. Based on these early results, longevity of about one decade remains a reasonable
estimate



Figure 7. Coir media after 1 year, 11 months of continuous use (left) versus virgin material (right).



Figure 7. Virgin material (left) versus material collected January 26, 2009 (4.5 yrs continuous use).

References

Florida Administrative Code (2007). "Chapter 64E-6 Standards for Onsite Sewage Treatment and Disposal Systems", Tallahassee, Florida.

Jantrania, A. R., and Gross, M.A. (2006) *Advanced Onsite Wastewater Systems Technologies*, CRC Press, Boca Raton, Florida.

Johansson, J.O.R. and Greening, H.S. (2000). "Seagrass restoration in Tampa Bay: a resource-based approach to estuarine management". pp. 279-293. In Bortone, S.A. (ed.), Seagrasses: Monitoring, Ecology, Physiology, and Management. CRC Press, New York.

Jowett, E.C. (1997) Sewage and leachate wastewater treatment using the absorbent Waterloo Biofilter®. Pp 261-282. In Bedinger, M.S., J.S. Fleming and A.I. Johnson (eds.), Site characterization and design of on-site septic systems, ASTM STP 1324. American Society for Testing and Materials, West Conshohoken, Pennsylvania.

Mayo, K. L. (2003). Archaeological and Historical Investigations of Black's Island, Gulf County, Florida. Master's Thesis, University of South Florida, Tampa, Florida.

Oakley, S., Greenwood, W.P. and Lee, M. (1996). Recirculating trickling filter systems for onsite nitrogen removal. Final Report to Butte County. CSUC Environmental Laboratory, Department of Civil Engineering, California State University, Chico, California.

Sherman, K. M., (1985). Ecological investigations of the epifauna and flora of Bay scallops, with special reference to free-living marine nematodes. Ph.D. Dissertation, Florida State University, Department of Oceanography. Tallahassee, Florida.

Sherman, K. M. (2006). Introducing a new media for Fixed Film Treatment in Decentralized wastewater systems. IN: National Onsite Wastewater Recycling Association CD rom.

Water Supply Industry Course Correction Required

John A. Kliem, PE

Commander, Civil Engineer Corps, U.S. Navy, Graduate, Industrial College of the Armed Forces, National Defense University, Fort McNair, Washington D.C. 20340. PH (703) 571-9780; email john.kliem@js.pentagon.mil. CDR Kliem is currently serving at the Pentagon on the Joint Staff. The information contained in this paper is solely the opinion of the author and in no way reflect the policy of the United States Department of Defense or any other agency of the U.S. Government.

Abstract

Water is an essential ingredient for life. Our current pricing system does not reflect the value of water nor account for its scarcity. Current water rates are inefficient and subject to government subsidies resulting in wasteful water usage practices. Additionally, the inefficiencies in the market place act to discourage competition and improved water practices. Policies to internalize the externalities inherent in our water rates would help make the market more efficient as well as changes to the tax code to allow for tax exempt status for private debt for domestic firms engaging in water supply projects. This improvement would improve domestic competition in the marketplace.

Introduction

Water is essential for life and critical for security. In fact, the United Nations has gone so far as to declare access to clean water as a human right (Brundtland, 2003). Publically owned treatment works dominates the water supply industry in the United States. This trend is prevalent throughout the globe but not a universal constant. The water industry is supported by subsidies and regulations distorting the supply and demand relationship. This paper will describe the water market and the industry that supplies water along with outlining the peculiarities that exist with in the market. Finally recommendations will be made to reform the market pricing and competition for this vital resource.

Water Market

The U.S. consumes 408 billion gallons of water per day generating $30 billion in revenues for the industry (Hutson, 2004) (Environmental Business International, 2005). Thermoelectric plants use 48 percent of this water or 195 billion gallons per day mostly for cooling at power plants (Hutson, 2004). The next biggest consumer is the agricultural sector using about 137 billion gallons (Hutson, 2004). Public supplied and self supplied industrial consumption complete the spectrum at 43 and 20 billion gallons per day respectively (Hutson, 2004).

The world's water market generates about $73 billion dollars in revenue if water used for agricultural purposes is included gross revenues could reach $7 trillion according to industry estimates (Buisnessline, 2002). Globally the demand for safe drinking water in some cases is not being met. According to the United Nations Environmental Program report *Our Planet,* the uneven distribution and increasing demand creates regions of water stress. Currently 40 percent of the world's population, about one billion people, is under water stress and will increase to 67 percent by 2025 (U.N. Environmental Program, 2003). Another billion people live in regions with adequate water supply but cannot afford water (Economist, 2006). The largest user of water

is the agricultural sector using 3,000 liters of water to grow food per person per day. Domestic and industrial water use is very small when compared to agricultural use (Economist, 2006).

Consumers have very little choice in their water service provider. Large capital investments are required to construct and operate treatment works. Usually the government determines the water supplier and regulates operation. Governmental control over the market acts to distort the industry and limit competition. In the case of water subsidies and marginal costing strategies have acted improperly value water causing wasteful practices and making technological conservation practices uneconomical (Clark, 2007).

Water Industry Infrastructure

The infrastructure that delivers the water to the market consists of a wide variety of size and span of various systems that deliver water to the market. The U.S. has about 58,000 water distribution networks serving 80 percent of the population (Environmental Business International, 2005). These organized systems can be further subdivided into 311 large networks serving 43 percent of the population (Environmental Business International, 2005). This leaves the remainder 36,000 systems serving populations that are fewer than 500 people. The variety of sizes in distribution systems causes inefficiencies in the market place. There are small community water systems located next to larger water systems not taking advantages of the economies of scale that declines with the size of the system (Renzetti, 1999)(USA Today 2007).

The water industry must make a substantial capital investment to ensure the presence of an infrastructure and water supply to meet demands. In some regions of the U.S. water demand has exceeded the ground water supply and according to the National Research Council resulted in over pumping of aquifers leading to the saltwater contamination of 300,000 wells. The cost to clean up these sites could reach one trillion dollars over the next 30 years (Howard, 2003). Deterioration of existing infrastructure will impact the industry. The American Water Works Association estimated that $250 Billion over the next 30 years to ensure a reliable source of water (National Academy of Sciences, 2002).

Water Supply Industry

Most people connected to a water distribution network get their water from a government owned and or operated utility (Barlow, 2004). A few companies are in the small privately owned or operated water supply market. The top three industry leaders are Veolia and Suez, both French companies, followed by RWE a German company (Barlow, 2004) (Economist, 2003). There are a few American owned firms in the market such as Bechtel Utilities and CH2MHill. Few companies are working water supply projects in developing countries. Pricing policies and governance seems to be preventing most companies from entering the world market (Economist, 2003). One notable exception is another French company Saur a 1.45 billion euro company who is supplying water to Abjijion, Cote' D'Ivore (Economist, 2003). Absent additional world regulations, we can expect more firms to enter this market as climate change drives regional water scarcity increasing the value of water.

The water supply industry in the U.S. is dominated by publically owned treatment works supplying 84 percent of the water. Private sources control the remaining 16 percent of the market (Environmental Business International, 2005). The two largest private water suppliers in the U.S. are the American Water Company and U.S. Filter and are owned by RWE (German) and Veolia respectively (Economist, 2003). There is a pronounced absence of domestic firms providing water. Market segmentation and government regulations are acting to keep private companies from entering into the U.S. market (National Academy of Sciences, 2002).

Factors Effecting Market Performance: Marginal Cost and Subsidies

Existing water rates are adversely affecting the U.S. water supply system and to some extent the world. A study published by the *Canadian Journal of Economics* concluded that existing water rates are inefficient. They stressed the importance of a marginal costing system that would account for all costs and capital expenditures including accounting for distance and time costs associated with providing water service (Renzetti, 1999). Costs should include externalities like watershed conservation expenses. Current marginal costing in the U.S. does not include many pieces like infrastructure maintenance and aquifer development. The study showed that residential and non residential demands for water demonstrated elasticity and that a marginal cost system would impact demand (Renzetti, 1999). Another significant pricing error occurs when moving to a marginal cost system by failing recapitalization expenditures (Renzetti, 1999).

Water subsidies affect the market by not reflecting the true cost of water. Subsidies are also applied unequally across the market benefitting specific groups. In developing countries, water infrastructure is present in wealthy neighborhoods where water subsidies are good. However, poorer areas lack water infrastructure and people get water from truck vendors paying from $1 dollar per cubic meter (Clark, 2004). Agricultural water subsidies also impact the water market. According to the Earth Policy Institute, California farmers use 20 percent of the region's water and pay only one cent per cubic meter, about two percent of what residents of Los Angles pay for their water (Clark, 2004).

Water Market Reforms

Publically owned treatment work's in the U.S. need to establish a comprehensive marginal cost system for water based on volume used. The price must include production, pumping, and infrastructure costs and all other externalities like aquifer development and watershed protection. The marginal cost system cannot include subsidies. Complete marginal costs for water will cause consumers to realize increased water costs but this will drive innovation in water conservation especially in the agricultural sector. Perhaps if consumers were actually charged the value of the water it would become more economical to expand water distribution systems to poorer regions. Additionally, a marginal cost system will encourage competition in the industry as firms see the potential for profit they will enter the market. As city budgets become more and more constrained the tax base will no longer be able to support subsidies and must institute marginal costs. Additionally, charging water for what its worth will discourage wasteful use of the resource such as water intensive agricultural practices.

The U.S. needs to encourage the development of domestic water supply industries. Domestically we have firms that could be competitive in this industry like Bechtel, CH2MHill, and URS to name a few. Domestic firms could be encouraged to enter the market by changing the Federal tax code to allow private debt for municipal infrastructure to be tax exempt as currently done for municipal debt. This would encourage private investment in the water infrastructure and allow private firms to compete with the existing publically owned treatment works allowing municipalities to make better financial decisions. At the very least the policy would push publically owned treatment works to become more efficient.

Conclusion

Water is a basic ingredient in any civilization and is required for economic development. In most cases in the U.S. and in parts of the world water is treated as if it were in infinite supply. Unfortunately, this is not the case; requiring our country and the globe to institute price reform to properly incorporate all the marginal costs and externalities into a volumetric water charge.

Instituting comprehensive marginal costs along with allowing for tax exempt status for private debt for domestic firms engaging in water supply projects would encourage the creation of domestic water supply companies. This would improve the country's water supply system and would be in the best interest of our national security.

Bibliography

"Saur." Saur S.A. http://www.saur.com/en/index.html (accessed April 14, 2008, 2008).

"Water Prices Rising Worldwide." *USA Today* 135, no. 2743 (Apr, 2007): 16.

"Water, Water Everywhere?" *Economist.Com / Global Agenda* (Aug 21, 2006): 1.

The U.S. Environmental Industry Overview. San Diego: Environmental Business International, Inc., 2005.

Our Planet. Nairobi, Kenya: United Nations Environment Programme, 2003, www.ourplanet.org.

"Survey: Savoir Faire." *The Economist* 368, no. 8333 (Jul 19, 2003): 7.

*Privatization of Water Services in the United States: an Assessment of Issues and Experience*National Academy of Sciences, 2002, http://www.nap.edu/catalog/10135.html (accessed April 5, 2008).

"Water Markets Exclude the Poor." *Businessline* (Aug 23, 2002): 1.

Barlow, Maude and Tony Clarke. "Water Privatization: The World Bank's Latest Market Fantasy." *Global Policy Forum* (January 2004, 2004): 1-3, Global Policy Forum (accessed April 16, 2008).

Brundtland, Dr. Harlem Gro and Sergio Mello. *The Right to Water*. France: World Health Organization, 2003, http://www.who.int/water_sanitation_health/rightowater/en/ (accessed April 14, 2008).

Clark, Edwin H. "Water Prices Rising Worldwide." *Eco-Economy Updates* 2, (2007, 2007): 1-4, http://www.earth-policy.org/Updates/2007/Update64.htm (accessed April 11, 2008).

Howard, Brian. "The World's Water Crisis." *E : The Environmental Magazine* 14, no. 5 (Sep/Oct, 2003): 32.

Hutson, Susan S., Nancy L. Barber, Joan F. Kenny, and et al. *Estimated use of Water in the United States in 2000*. Washington D.C.: United States Geologic Survey, 2000, http://pubs.usgs.gov/circ/2004/circ1268/ (accessed April 14, 2008).

Renzetti, Steven. "Municipal Water Supply and Sewage Treatment: Costs, Prices, and Distortions." *The Canadian Journal of Economics* 32, no. 3 (May, 1999): 688.

ASSOCIATED DISASTERS TO THE DEBRIS FLOWS

Guillermo Cardoso-Landa[1]

[1]Land Sciences Department, Instituto Tecnológico de Chilpancingo, Av. J. F. Ruiz Massieu # 5, Col. Villa Moderna, C. P. 39000, Chilpancingo, Gro., México; PH (747)4725899; e-mail: gclanda@prodigy.net.mx

ABSTRACT

In this article some of the disasters associated to the presence of the debris flows are described briefly happened in some countries of the world in recent years, which have been observed and, in some occasions, measures its fundamental characteristics, for example: The United States, China, Japan, Italy, Taiwan, Central Asia, Germany, Switzerland, Russia, the Philippines, the Ukraine, Canada, Brazil, Ecuador and Venezuela. In the country of Mexico have appeared great amount of debris flows in the recent years, many of them in the Mexican trans-volcanic axis and coastal mountain ranges, such as the happened ones in Popocatepetl volcano, the volcano Pico de Orizaba, the volcano Nevado de Toluca, mountains of Puebla, in Acapulco, Gro., in the city of Tijuana, B.C. and in the coastal mountain range of Chiapas and Oaxaca, to only mention those that have produced important disasters in recent times. In the article the characteristics of the disasters produced in different regions from Mexico are also described.

To identify the mechanisms that they involve to the solid material within a liquid flow, it is necessary to analyze the roles played by the several operating forces in the genesis of the movement in a debris flow. The developed approaches to date are the following ones: model of stability of infinite slope, approach of Shields, approach of Takahashi and recent developments.

In order to be able to apply the previous models it is necessary to have very great information of diverse points on the land, with which a calculation mesh forms, therefore is essential to develop a GIS in the analysis site. A model appears in the complete article to determine the characteristics in the zone of beginning of a debris flow, which includes the development of a SIG.

INTRODUCTION

A disaster associated to a natural phenomenon is defined as a serious upheaval triggered by a phenomenon of the nature that causes human losses, material, economic and environmental, that exceeds the capacity the affected ones to fight with them.

The associated disasters to natural phenomena constitute a serious obstacle for the human development and the fulfillment of the Objectives of as important Development of the Millennium as the reduction of the extreme poverty to half before year 2015. Not in vain the natural disasters caused annual economic losses that go from the 75.500 million American dollars in years 60, 138.400 million in

years 70, 213.900 million in 80 and 659.900 million in the 90, most of them in the developed world. However, the economic estimations suitably do not catch the impact of the disasters in the poorest countries, where the costs in terms of human lives, of means of subsistence and destroyed infrastructure reconstruction more are elevated. At the moment, the 85 percent of those who is exposed to earthquakes, tropical revolving storms, floods and droughts, lives in countries whose human development is average or low. In absolute terms, it has been demonstrated that the economic cost of the disasters has increased in the course of the last decades.

The data base EMDAT offers a very precise panorama of the total losses by disasters with a suitable level of national detail. The period of chosen time it is sufficient to represent the fluctuations whereupon they are pronounced most of the natural threats and also it agrees with the more trustworthy period of data of the EMDAT. In figure 1 the total number of disasters registered by the EMDAT appears entre 1900 and 2000.

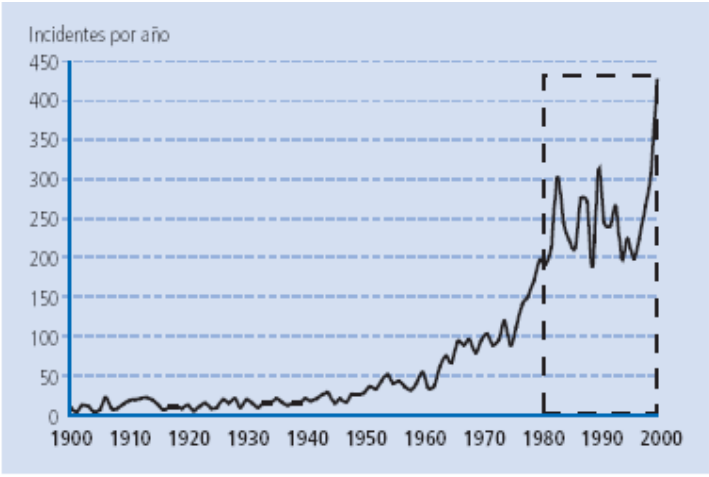

Figure 1 Disasters registered by the EMDAT

The tendency in increase suggests, first, an exponential increase of the frequency of the disasters, although the factor that contributes more is the improvement in the elaboration of information on disasters. Although the one cannot be discarded that it has increased the number of hydrometeor logics catastrophes, that the denounced disasters tend to probably increase has more to do with the advances in the technology of the telecommunications and the cover of the different alert networks that every time arrive at more corners of the world. Therefore, nowadays there are more possibilities of denouncing and of registering the casualties inflicted by the disasters.

DISASTERS ASSOCIATED TO THE DEBRIS FLOWS

The debris flows are the fast landslide earth movements, caused by hyper concentrated flows of water and sediments, which happen in a great variety of environment throughout everybody. They are particularly dangerous for the life and the properties due to its high speeds and great destructive force, lowering natural

houses, ways, bridges, trees and cultures, currents and ecosystems throughout its trajectory. The debris flows are generally associate with periods of high precipitation and intensities of snow-covered very strong rains or with intense that tends to appear as reconciled of mixtures sediment-water with catastrophic results for the zone in where they appear.

Next some of the disasters associated to this phenomenon in some countries of the world in recent years are described briefly, which have been observed and, in some occasions, measures its fundamental characteristics.

UNITED STATES

Utah received national attention and his first presidential declaration of zone of disaster in the spring of the year 1983 due to the floods, earth sliding and debris flow caused by severe snow storms in the region (Wieczorek et al, 1983). The worse damages caused by the debris flows appeared in the County Davis, in the opening of the Rudd stream. Some debris flows happened in at least 600 tributary ones of the Colorado River in Great the Canon, between Less Ferry and Surprise Canyon, Arizona (Melis et al., 1994; Griffiths et al., 1996). Most of the flows they appeared during convective storms of the summer with intensities of rain of the order of 40 mm/h.

More than 1.000 debris flows they happened in wooded slopes of the County of Madison, Central Virginia, during an intense happened storm the 27 of June of 1995 (Wieczorek et al., 1996).

Numerous observations of the occurrence of debris flows have been made in the mountainous areas of the Southeastern of British Columbia in the last decade. In November of 1995 two debris flows appeared in Pierce Creek in Valle Chilliwack and Hope Creek, with 50.000 m^3 of rubbish carried during two hours, closely together of the city of Hope (Jacob et al., 1997).

A series of debris flows appeared in several canyons to 35 miles to the east of Portland, Oregon, days 7 and 8 of February of 1996, near the small localities of Dodson and Warren dale, destroying 84 interstate highway as well as the railroad and having to be evacuated the residents from the area the being destroyed their houses (Powell et al., 1996).

CHINA

The Liaoning province is located in the south of the northeast region of China between 118°53' and 125°46' of length and from 38°43' N to 43°26' N of latitude, divided in four regions.

The 28 of 1981 July an intense extreme precipitation produced avalanches, rock sliding and debris flows in more than 100 ravines and slopes of the Laomao mountain in this province, having themselves like result 115 villas affected in 6 counties affecting to 556.000 people, destroying 38.517 houses, 60.000 hectares of cultures and 4, 9 kilometers of the line of the Changchun-Dalian railroad were destroyed. The Chinese economy losses ascended to 547' 000.000 of yeans (Zhao Huanchen et al., 1992).

In the presented/displayed relation next, table 1, some places affected by this type of phenomena in recent years in China are appraised.

Table 1 Affectations produced by debris flows in China

LOCATION	PROVINCE	DATES
Pingwu, Songpan, Disable,	Sichuan	16-08-76 to 24-08-76
Songpan, Wenchuan,	Sichuan	16-07-77 to 17-07-77
From Baoji to Tianshui,	Shanxi	12-07-78
Dongchuan,	Yunnan	22-10-80 to 25-10-80
Zhaojue	Sichuan	22-10-80 to 25-10-80
Shanxi, Gansu, the Sichan northeast,	Sichuan	19-08-81 to 22-08-81
Rangtang, Jinchuan, Heishui	Sichuan	20-07-83 to 29-07-83
Hanzhong,	Shanxi	12-07-84 to 18-07-84
Wenchuan, Nanping,	Sichuan	12-07-84 to 18-07-84
Dongchuan,	Yunnan	26-07-85
Dandong, Fuxian,	Liaoning	14-08-87 to 20-08-87
Dangchang, Zhuoni, Jingxi,	Gansu	06-07-88 to 14-07-88
Miduogou, Midui	Sicuani, Xizhang	85 to 88

JAPAN

In Japan during twenty years, between 1967 and 1987, 4598 people were killed by natural disasters, of who 1257 passed away due to the debris flows, which corresponds to the 27,3% (Takahashi, 1991). This high percentage must to that every time most frequently the people tend to live in zones on high risk on the foot of mountains where they appear this type of draining.

In 1990 volcano Mount Unzen, in Japan, made eruption and they appeared but of 114 debris flows (lahars) that deposited near 8' 000.000 of m^3 of debris that destroyed 1123 buildings. The number of refuges required by this event was greater to the 11.000 in August of 1991 (Suwa & Yamakoshi, 1997).

ITALY

Day 19 of 1985 July the fault of two dams in the Valley of the Stava River, to the northeast of Italy caused a catastrophic debris flow, which destroyed 2 villas and killed 270 people (Berti et al., 1997).

A debris flow happened day 18 of October of 1990 in Pomonte Creek, with flows towards waters underneath Monte Capanne in the Elbe Island, of the Archipelago of Toscana, Italy, with approximately 34.000 ms^3 of debris, (Iotti & Simoni, 1997).

TAIWAN

During the last decade, hundreds of deaths, hurt losses and people, as well as damages in houses, schools, ways, bridges and other public and deprived properties happened several disasters produced by debris flows in Taiwan, causing (Cheng et al.). In table 2 the characteristics of 6 disasters produced by debris flows appear in recent years in this region.

Table 2 Zones affected by debris flows in Taiwan

LOCATION	DATE	IMPACTS
Tug-Men, Hualien, Taiwan	23-06-90	29 deads, 6 lost, 7 wounded, 24 destroyed houses, 68 victims and important damages to ways.
Chun-Keng Kuo, Nantou, Taiwan	31-07-96 a 01-08-96	4 deads, important damages to houses, ways and other properties.
Er-Bu-Keng, Taiwan	31-07-96	5 deads, 10 houses and 3, 78 hectares of fruit destroyed, important stream damages.
Feng-Chiu, Nantou, Taiwan	31-07-96 a 01-08-96	2 deads, 10 houses and 14 hectares of cultures destroyed, serious damages in 18 ways, prey and rivers.
Tung-Fu, Nantou, Taiwán	31-07-96	2 deads, 18 destroyed or damaged houses.
Shen-Mu Village, Nantou, Taiwan	31-07-96 a 01-08-96	5 deads, 6 wounded, 8 destroyed houses and bridges, important damages to 3 hectares of cultures.

SWITZERLAND

The debris flows are a phenomenon common in the Swiss Alps, as well as in other mountainous zones of the world. A tool important to understand the mechanics of this type of flows is the installation of observation stations that allow collecting data in real times. They settled this type of stations in 3 river basins of Switzerland, equipped with ultrasonic video cameras, devices, radars, geophones and instruments for measurement of the precipitation. In figure 2 appears the location of these stations.



Figure 2 Location of the 3 stations of observation of debris flows in Switzerland

They appear in graph 3 the number of events of debris flow per year that has been registered in two of these hydrological river basins of Switzerland.

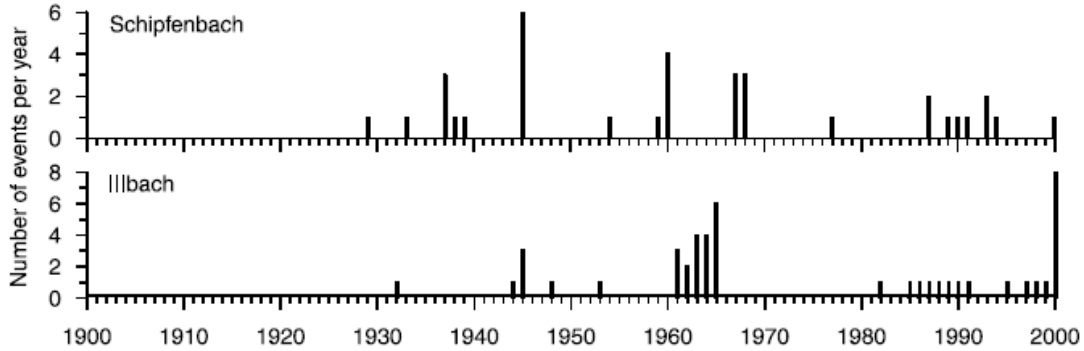

Figure 3 historical Registries of debris flows during century XX in Schipfenbach and Illbach, Switzerland. (Hurlimann et al., 2003)

In year 2000 four important debris flows were observed in this zone of Switzerland, being moderate their more outstanding characteristics, varying the volume of material deposited from 5.000 m^3 up to 35.000 m^3; the rank of average speeds was of 2,0 m/s up to 5,0 m/s and the maximum expenses of flow appeared between 20 m^3/s to 125 m^3/s.

CENTRAL ASIA

Central Asia is an area with a high degree of risk by debris flows, being the most important hills of Valle Fergana, Valle Zerafshan, the Issyk-Kul river basin, the central and south part of Tdjikistan and also the hills of Kopetdag. In all these areas the destructive flows happen during the period of the spring-summer in small rivers and ephemeral channels (Salikhova & Liahovskaya, 1992).

GERMANY

The villa of Tramin in the south of Tyrolia was affected by a sudden debris flow which day 23 appeared during a severe storm of June of 1986, that it completely destroyed the new local rest center and damaged a wine cooperative seriously, being considered the total damage in 6 million dollars (Strunk, 1990).

RUSSIA

The areas in where greater amount of debris flows has appeared in this country are three regions: to the east of the Sayan mountains, the mountain to the Southeastern of Baikal Lake and the northeast of the Baikal region, with registries from 1871 to 1971, (Makarov and Agafonov, 1977).

The PHILIPPINES

The eruption of Monte Pinatubo in June of 1991 deposited of 7 to 8 km^3 of pyroclastic material in slopes of the volcano. These pyroclastics deposits formed the sediment sources for the rubbish flows of volcano (lahars) frequent and great scale, that appear each season of rains causing great morphologic changes and massive devastation in the zone. To the date more than 400.000 people they have been moved

and around 350 km^2 with territories of agricultural culture they are covered with material of lahars.

The number of died in a series of debris flows happened in the Philippines after six days of intense rains can surpass the hundred, said the authorities of the country, after 35 corpses were recovered and tens of people followed disappear, in December of 2003, 300 people were evacuated towards safer zones after the soldiers got at the zone of disaster to rescue to victims cached under mud and the rubbish come off hills of the environs, said the authorities.

The UKRAINE

The combination of natural conditions in the mountains Carpathian, Crimean and the defiles along the rivers Dnieper and Dniester is favorable for the formation of the debris flows, (Yablonskiy et al, 1992).

CANADA

Howe Sound is a region prone to the presence of debris flows, which extends from the Horseshoe bay (20 km to the northwest of Vancouver) to Squamish, in Canada, where they have appeared a great number of these events due to the type of ground, slopes in his valleys as well as the deforestation and fires in the zone.

B*RASIL*

At the beginning of August of 2000 great debris flows took place caused by five days of torrential rains in the northeast of Brazil, causing 28 died and 90.000 abandoned. Bad weather caused the most serious damages in the states of Pernambuco and Halagaos, affecting to 46 localities.

ECUADOR

At least 36 died people, 11 disappeared and 212 families damaged were the balance who left to the debris flows happened in Ecuador day 13 of June of 2001, affecting the provinces of Papallacta, Amazonia, Tungurahua and Zamora Chinchipe.

MÉXICO

In our country great amount of debris flows has appeared in the recent years, many of them in the Mexican trans-volcanic axis and coastal mountain ranges, such as the happened ones in Popocatepetl volcano, the volcano Pico of Orizaba, the Nevado de Toluca volcano, in the mountains of Puebla, in Acapulco, Gro., in the city of Tijuana, B.C. and in the coastal mountain range of Chiapas and Oaxaca, to only mention those that have produced important disasters in recent times.

VENEZUELA

Probably one of the disasters produced by the combination of diverse processes of removal in mass, including the debris flows, greater dimensions in recent years, is due to the storm from the 14 to the 16 of December of 1999 in the coasts of Venezuela, particularly in slopes of the Mountain range of Avila, to the north of Caracas, Venezuela.

The severe storm from the 14 to the 16 of December of 1999 caused to catastrophic sliding of earth and floods with debris flow throughout 40 kilometers on the coast of Caracas, between the Guaira and Naiguita, located in the coastal state of Vargas, Venezuela. The damages to the communications and the infrastructure of this zone were very ample. In Vargas more than 8.000 individual residences and 700 buildings of departments completely they were destroyed (Salcedo, 2000). In photography 4 some damages in this zone are observed.



Photography 4 some damages in buildings and located houses in the main trajectory of the debris flows in Vargas, Venezuela.

The ways, the telephone services, of electricity, water and sewage system severely were damaged. Total the economic losses calculate in $ 1,79 trillions and preliminary estimations established that between 5.000 and 50.000 people they passed away (Brandes, 2000; Sancio and Districts, 2000; Salcedo 2000; and USAID; 2000). The handled present number of people died by this catastrophe is of approximately 30.000 (USAID, 2001), although has been difficult to need the exact number of victims, due to the zone of disaster which the city of Vargas and to the drag bodies towards the sea was turned, being obtained to recover around 1.000 bodies. The estimation of the number of inhabitants of Vargas was of 300.000 inhabitants before the catastrophe, which means that approximately 10% or passed away more by this event.

MODELS FOR THE DETERMINATION OF THE BEGINNING OF THE DEBRIS FLOWS

The analysis of the main leading mechanisms of the beginning of the movement in a debris flow emphasizes that the factors causes of this phase of the process are the location of the leading area and the leading main mechanism (actions geotechnical hydrodynamics, causes and mechanical balance). In a prognosis level it is difficult to identify which of these mechanisms is most probable or makes the greater contribution; in any case, some of these types of mechanisms can include

others, or rather, within he himself event different leading mechanisms can happen in different areas from the river basin.

In some studies relative to the conditions of outbreak of followed noncohesivos debris flows of a superficial water flow, the analysis is concentrated in the study of the instability of the accumulation of materials that takes place after the saturation. A superficial flow that slips throughout a slope, originating of an intense rain, firstly saturates the alluvium layers; next it mobilizes, causing them in this way the dispersion of solid particles of the accumulation throughout the complete depth of the superficial draining, which becomes a debris flow finally.

In order to identify the mechanisms that they involve to the solid material within a liquid flow, it is necessary to analyze the roles played by the several operating forces in the genesis of the movement. The developed approaches to date are the following ones, (Lorenzini et al., 2004):

a. Model of stability of infinity slope.
b. Approach of Shields.
c. Approach of Takahashi.
d. Recent developments.

The process of beginning of the debris flows is influenced by great amount of factors, emphasizing: geologic and morphologic, hydrologic, vegetal cover, topographic and atrophic; being necessary to establish a methodology that takes in consideration these aspects most of. Some investigations have tried to understand the relation between the geomorphologic processes and the climatic ones that trigger the debris flows. In these works they have been analyzed physical properties of the failed slopes, the effects of the rake and the pore pressure in grounds, the mechanics of the movement of the debris flows and the properties of the resulting deposits, (Scott 1972, Williams and Guy 1973, Hollingsworth and Kovacs 1981, Istok and Harward 1983, Pierson and Costa 1987, Montgomery and Dietrich, 1994; Wu and Sidle, 1995; Pack, 1995; Morgan et al. 1997, Reid et al. 1997, Griffiths et al. 1997, Wieczorek et al. 1997, Tognacca & Bezzola 1997, Gregoretti 2000, Iverson 2000, Chen & Jan 2003, Reid et al. 2003, Savage & Baum 2003).

In most of these works of investigation the necessity is observed to carry out a series of determinations and calculations on a great land extension affected by the presence of an debris flow , which originates the necessity to develop a GIS , that it allows to carry out the calculations of way ordered in the propose mesh of calculation.

GEOGRAPHIC INFORMATION SYSTEMS

According to the necessary requirements for the determination of the zones of beginning produced by the debris flows in a mountainous region, it is possible to be selected the use of the software developed by ESRI for a GIS, call 3,3 Arc View GIS or some more recent other, had to its versatility and characteristics.

Throughout the decade of the 1990, the packages for designed professional GIS for heavy productive work were of not-friendly use for accidental users of a GIS. For example, older versions of Arc Info and MGE were systems of complex software that required a special training and technical abilities. Most of the users of

application of a GIS, such as the civil engineers and the environmental engineers, do not have the technical experience to develop, to run and to maintain a GIS complicated.

On the other hand, Arc View 3.x is software for mapped with friendly atmosphere and a tool for SIG that can be learned by most of the people without extensive training or experience in a GIS. Arc View 3.x is sophisticated software for mapped and a package for GIS that brings the power of a usury GIS to the average of PC (Personal Computer). With more than 500.000 users, Arc View can be considered like the package for a more popular GIS in everybody.

CONCLUSIONS

The increase of the presence of the disasters associated to the natural phenomena in the territories at world-wide level and Mexico has been increased of significant way in the last decades, as it is the case of the disasters associated to the debris flows. Reason why it is necessary to implement models, studies and developments that allow to know the genesis this type of natural phenomena, which allow to implement systems of early alert in the different territories, that allow to reduce the magnitude of the losses of human and economic lives that are associate to these phenomena of the nature.

The four developed approaches were analyzed to date to identify the mechanisms that they involve to the solid material within a liquid flow, also analyzed the roles played by the several operating forces in the genesis of the movement of an debris flow and it selected to the use of the model of stability of infinite slope and the development of a GIS in the zone of the debris flow.

The calculation of the factor of safety (FS) is based on the form for infinite slope of the law of fault of Mohr-Coulomb, expressed by means of the stabilizing force ratio with respect to the destabilizing forces in a parallel plane of fault to the surface of the ground, (Hammond et al., 1992, Montgomery and Dietrich, 1994) that compares the no equilibrants components due to the action of the gravity and the resistive components of friction and cohesion on a parallel plane of fault to the surface of the land with despicable effects of edge. The pore pressure due to the ground mixture reduces the effective normal effort, which thanks to the angle of internal friction is related to the sharp effort. The hydraulic pore pressure is calculated supposing a hydrologic properly dressed be with the depth of the saturated ground sufficiently calculated to maintain proportional a lateral unloading to the area of specific pick up (the area slope arrives by unit of contour length). These relations are expressed through the general equation of stability of infinite slope, that it displays the following form:

$$FS = \frac{C_r + C_s + \cos^2\theta\left[\rho_s g(D - D_w) + (\rho_s g - \rho_w g)D_w\right]\tan\phi}{D\rho_s g \sin\theta\cos\theta}$$

In this expression the variables immediately have the meaning shown in figure 5,

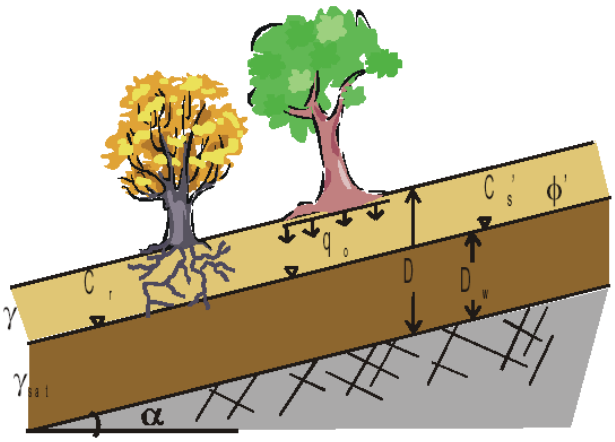

Figure 5 Variables used in the equation of
Model of stability of infinite slope

Taking care of the leading factors of the process of beginning in the debris flows the subjects enlisted to continuation like integral part of the analysis of a debris flow set out by means of a GIS:

Layer 1 Topography of the zone of study.
Layer 2 Superficial hydraulic data.
Layer 3 Angle of internal friction of the ground.
Layer 4 Density of the ground.
Layer 5 Cohesion of the ground.
Layer 6 Vegetal cover (force by the root of the trees).
Layer 7 Underground hydraulic data.

In the scheme displayed in figure 6 the subjects or layers proposed for the development of a SIG used in the study of a debris flow are observed:

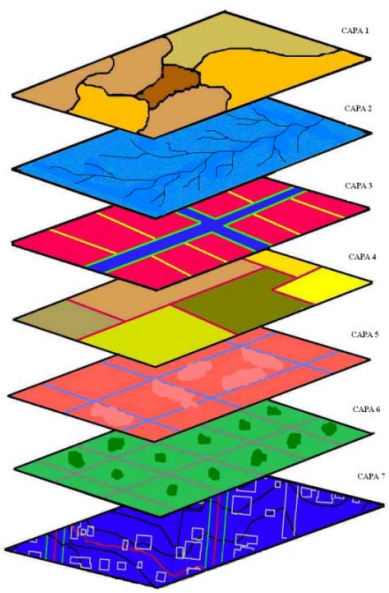

Figure 6 Subjects or propose layers in the selected model
in order to carry out the analysis of a debris flow.

FUTURE WORKS

It is required to apply to the model of stability of infinite slope and the propose layers for a GIS to an debris flow happened somewhere with real measurements in field of its characteristics, which will allow to carry out the validation of the model proposed in this article, with which it is working in the present, hoping to be able to present the numerical results in the future next.

REFERENCIAS

Cheng, K., Lin, L., Chang, S. (1997). "The field investigation and GIS application in a potential hazardous area of debris flow". *Proceedings of the First International Conference on Debris-Flow Hazards Mitigation,* ASCE,83-92.

Cho, S. E., and Lee, S. R. (2002). "Evaluation of surficial stability for homogeneous slopes considering rainfall characteristics". *Journal of Geotechnical and Geoenvironmental Engineering,* ASCE, 128(9), 756-763.

Hamilton, R. M. (2000). "Science and technology for natural disaster reduction". *Natural Hazards Review*, ASCE, 1(1), 56-60.

Highland, L. M., Ellen, S. D., Christian, S. B., y Brown III, W. M. (1997). *Debris-flow hazards in the United States.* USGS, Fact Sheet 176-97.

Honda, N., Egashira, S. (1997). "Prediction of debris flow characteristics in mountain torrents". *Proceedings of the First International Conference on Debris-Flow Hazards Mitigation,* ASCE, 707-716.

Lanfear, K. J. (2000). "The future of GIS and water resources". *Water Resources Impact,* AWWA, Vol. 2, and number 5, September 2000, 9-11.

López, J. L., García, R. (2002). "Análisis y mapeo de inundaciones torrenciales en abanicos aluviales" (Parte I y Parte II). *XX Congreso Latinoamericano de Hidráulica*, Cuba, IAHR.

Makarov, S., Agafonov, B. (1997). "Activity of debris-flow process in the Baikal region during the recent centuries". *Proceedings of the First International Conference on Debris-Flow Hazards Mitigation*, ASCE, 64-73.

Sakellariou, M. G., y Ferentinou, M. D. (2001). "GIS-based estimation of slope stability". *Natural Hazards Review,* ASCE, 2(1), 12-21.

Shamsi, U. M. (2002). *Gis tools for water, wastewater, and stormwater systems.* First Edition, ASCE Press, 375 pages.

Vasconcelos, M., Goncalves, A., Catry, F. (2002). "A working prototype of a dynamic geographical information system". *International Journal of Geographical Information Science,* Pubs. Taylor & Francis, 16(1), 69-91.

Experimental analyses of sedimentation in the slit dam Reservoir

Mohammad Ebrahim Banihabib [1] and Ehsan Bahram[2]
[1] Assistant professor, Department of Irrigation and Drainage Engineering, University of Tehran, Iran Department of Irrigation and Drainage Engineering, College of Aburaihan, University of Tehran, Pakdasht, Tehran, Iran, E-mail: banihabib@ut.ac.ir
[2] Graduated student of M.Sc. Water Structure Engineering, Islamic Azad University, Science and research Campus, Iran PH. (0098912) 714-5928 E-mail: ehsanbahram@yahoo.com

Abstract
Debris flow is a very destructive flood. These floods mostly occur in high steep mountain areas, and cause lots of economic damages and live claims. The flood contains very dense mixtures of different grain size sediment.
In recent years, open-check dams, specially slit dams, are widely used to control debris flows.
Slit dams are one of the open check dams presenting one or several vertical openings, going from the dam's base up to the weir. The slit has decreased the dam sedimentation.
Analyzing the results in this study shows because of the slit in these dams, sediment evacuation has been increased and Trap Efficiency (TE) has been reduced significantly.
In this study, to indicate the sedimentation in the dam reservoir 25 experiment had been set up in a steep tilting flume (22 degree) for 5 width of slit and 5 different particle size, sedimentation is function of volume of the flood in the dam's reservoir, slit width and the particle size. After analyzing the sedimentation profile a dimensionless equations is proposed for the sediment distribution in these dam's reservoir.

Keywords: Debris flow, Trap Efficiency, Slit dams, Slit width, Particle size, Sediment distribution in the dam reservoir.

1. Introduction

Debris flows are floods with a large volume sediment and water with viscid mud. These floods mostly occur in very steep mountainous rivers [1]. To control these heavy floods check dams are usually proposed. They were not very successful; hence they are filled up with sediments before debris flow happen. Usually the factors listed below are effective in the debris flow phenomenon:

a) enough rain
b) presence of enough initial soil moisture
c) enough sediments

To defeat these destructive floods, check dams that are built in series are proposed, but they weren't very successful. Because usually these dams are filled up with sediments and boulders before debris flow happens and so open check dams are used in Austria, Japan Taiwan and Italy [2]. In recent years very good researches were down in the field of slit dam.

The researches that were done in this filled can be categorized as follow:

- equations that estimates sediment deposition in the dams reservoir
- relations that estimate the height of the sediment behind the slit dam
- design of slit dam, slit width and the spacing between posts
- the criteria that's denotes the requirement of the slit dam

These equations are mostly experimental and are the results of modeling the slit dam in an elevated flume. The particle size was not considered in any of the equations, so 25 experiments had been set up with 5 different particle sizes of sediments and 5 different slit width.

2. Methods and Material

2.1. Experiments

Experimental set up is built up from five major parts which are: high slope tilting flume, slit dam, ultrasonic point gage, and digital point gages.

Slit dam was modeled in a high slope tilting flume with 7.6m length, 0.3m width and 0.25m depth. This flume has been made up of plexiglass with the body of iron. The slope maximum is 22 degrees. To know the slope of the flume in any time a slope meter was used. Figure 1 shows the flume general shape. Different parts of the flume are shown in this figure.

Main reservoir is the reservoir with dimension of 0.6*0.6*0.6 m that would make a 0.256 m^3 volume. This reservoir has an inlet of 2" from the pump with an evaluation valve in the bottom. Sediment reservoir is just after the main reservoir with a 0.4*0.3*0.2m dimension and a volume of 0.024m^3. It is also used as a energy dissipater.

Slit dams are made up of plexiglass and it is placed 137.5 cm from the flume end.

The average thickness of these dams is 6 mm and slits are 1,2,3,4 and 5 cm in the middle of the dam. Fig 2 shows a picture of the flume and the slit dam in the 22^0 slope.

Ultrasonic energy is an electromagnetic sound wave that is above the human ability of hearing. This part of electromagnetic waves has the characteristic that when they face an object that is denser than air they reflect to the source that they are spread from. This border between air and water is called an interface. This interface shows the water level using this rule we can obtain the fluid depth. To have precise measurement of the

sediment thickness deposited in the dam reservoir a digital point gage is used. This point gage is placed vertical to the flume and it can measure three points in a section. These three points are in the middle, right and left axis. The right and the left axis are 8 cm away in the left and right side of the middle axis.

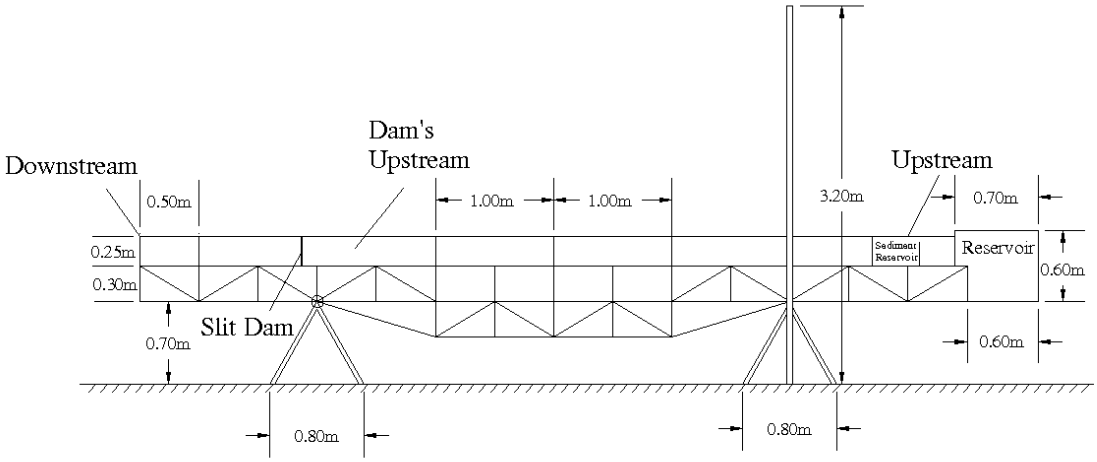

Fig. 1 high slope tilting flume general shape

The experiments were done for five different slit widths and five different particle size of sediment that makes 25 exterminates overall. In theses experiments the slope was constant at 22^0. To begin the experiment first we place the sediment with a known weight in the sediment reservoir, and then we slowly saturate the sediment with water the amount of water is written down. A known water volume also is added to our saturated soil as apart of flood volume. The sediment that is used in the experiment is five different particle sizes as we can see in table (1).

Table 1. Sediment characteristic used in the experiments

Sediment	characteristics	Mean particle diameter(d_{50})mm
First Size	Finer than no. 4 sieve remains on no. 10 sieve	3.55
Second size	Finer than no. 10 sieve remains on no. 16 sieve	1.59
Third size	Finer than no. 16 sieve remains on no. 30 sieve	0.89
Fourth size	Finer than no. 30 sieve remains on no. 40 sieve	0.5125
Fifth size	Finer than no. 40 sieve remains on no. 100 sieve	0.2875

In the next step flume is moved upward to a specific height until the 22 degrees angle is gained. Now the sediment reservoir gate is opened suddenly and the flood moves toward the slit dam and debris flow occurs. Some of the sediments deposit at the dam reservoir or they are trapped indeed, some of them would escape to the downstream. The ultrasonic

sensors have recorded the data i.e. the water depth in three different positions of the flume with the precision of ±0.1mm. The temperature is also recorded. After the experiment is done the water and sediment volumes are measures in the downstream. The profile is gained using digital point gages. The sediment deposited in the dam reservoir, upstream, downstream and between the ways, is dried and weighted.
To investigate the flood concentration we have used the equation below:

$$C = \frac{V_{sed}}{V_{total}} \tag{3}$$

In this equation C is the mean volumes concentration, V_{sed} is the sediment volume, V_{Total} is the total volume of the flood. To calculate the trap efficiency equation (4) is used:

$$T_e = \frac{W_{sediment}}{W_{flood}} \tag{4}$$

Where $W_{sediment}$ is the dry weight of the sediment in the dam's reservoir and W_{flood} is the weight of the sediment of the flood.
Trap efficiency in different experiments are shown in table 2. In the first five experiments the slit width 1 one centimeters. Investigating these data shows that the smallest slit has bigger trap efficiency and as the particle size decreases the trap efficiency decreases too. In the sixth experiment that the slit width is changed, the biggest particle size is used again. So the trap efficiency increases and the procedure is repeated for the other slit width and particle size. For example sediment profile for the first experiment in the right, left and middle axis is shown in figure 2.3D view of the sediment in the dam's reservoir is also shown in figure 3.

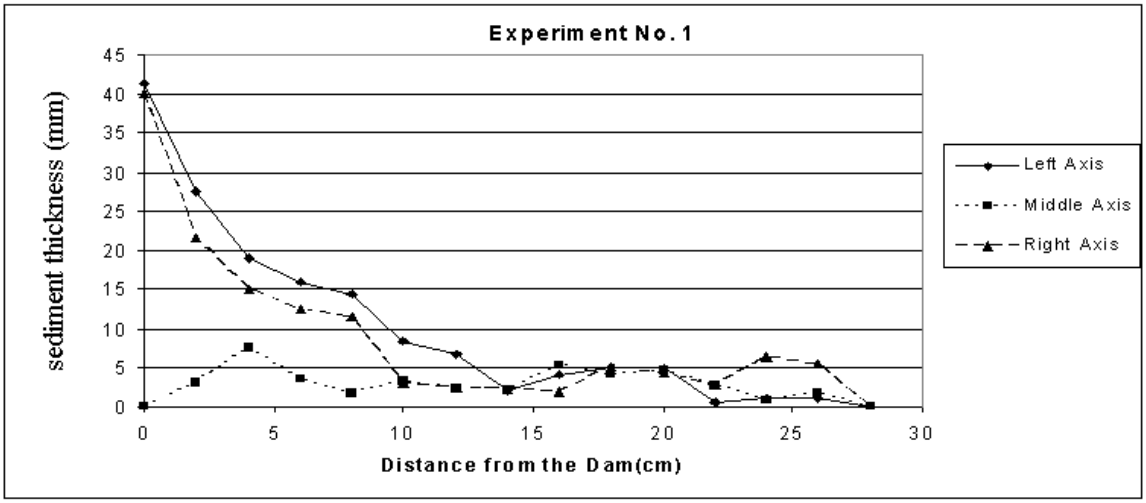

Fig. 2 profile of sediments in the right, left and middle axis in the first experiment

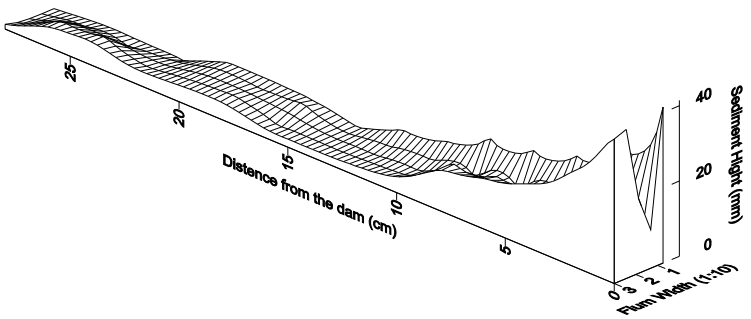

Fig 3. 3D view of sediment in the dam s reservoir

2.2. Dimensional analyses

Effective factors on the deposition in the slit dam reservoir in the experiments are defined as:

$$V_s, V_T, B, b, d_{50}, C, T_{s\max}, L_{s\max}, D_{\max}, L_{w\max}, x, y \quad (1)$$

Where V_s is the slit dam reservoir maximum volume, V_T Total flood volume, B canal width, b slit width, d_{50} mean grain diameters, C volumetric concentration, T_{smax} maximum deposition thickness, L_{smax} maximum deposition length, L_{wmax} and D_{max} maximum length and maximum water level in the reservoir when flood occurs, x distance point from the dam, y is the sediment thickness on that point. According to Π dimentional analysis method we have:

$$\Pi_1 = V_s / V_T \quad (1) \qquad \Pi_5 = x / L_{s\max} \quad (5)$$

$$\Pi_2 = B / b \quad (2) \qquad \Pi_6 = y / T_{s\max} \quad (6)$$

$$\Pi_3 = d_{50} / b \quad (3) \qquad \Pi_7 = T_{s\max} / D_{\max} \quad (7)$$

$$\Pi_4 = C \quad (4) \qquad \Pi_8 = L_{s\max} / L_{w\max} \quad (8)$$

Dimensionless parameters Π_5 and Π_6 denotes the dimensionless profile factors, so the equation (9) is used to define the dimentionless profile in this research:

$$y / T_{s\max} = f_1(x / L_{s\max}) \quad (9)$$

To specify the length and the thickness of the maximum deposition equations (10) and (11) are used:

$$T_{\max}/D_{\max} = f_2(V_s/V_T, B/b, d_{50}/b, C) \quad (10)$$

$$L_{s\max}/L_{w\max} = f_3(V_s/V_T, B/b, d_{50}/b, C) \quad (11)$$

To evaluate different linear and exponential equations, correlation coefficient and mean average relative error:

$$MARE = \frac{\sum_{i=1}^{n} \frac{|X_{0i} - X_{ci}|}{X_{0i}}}{n} \quad (12)$$

In that equation X_{0i} is the observed quantity, X_{ci} is the calculated quantity and n is the observed data.

3. Results and Conclusion

To find the mean longitude profile of the deposition in the slit dam's reservoir we use the right, left and middle axis average. Then the thickness of the sediments and distance of the point from the dam is obtained by dividing to the maximum thickness(T_{smax}) and the maximum length(L_{smax}) to have the dimensionless relation. Obtained points are the dimensionless profiles and they are shown in fig. 5. Data procedure of the profile shows that a 3-variant power curve can be trended with a square correlation coefficient of R^2=0.94. This equation is also shown in Fig.5. to define the thickness and the length of the maximum deposition sediment multi variant exponential and linear equations are discussed.

Determining the equation to gain the maximum sediment deposition relation
Investigating the proper relation to define the maximum deposition thickness are like relations (12) and (13) as a function of the dimensionless factors Π_1 to Π_4:

$$T_{s\max}/D_{\max} = \alpha_1 + \beta_1\left(\frac{V_s}{V_T}\right) + \gamma_1\left(\frac{B}{b}\right) + \theta_1\left(\frac{d_{50}}{b}\right) + \eta_1(C) \quad (12)$$

$$T_{s\max}/D_{\max} = \alpha_2 . \left(\frac{V_s}{V_T}\right)^{\beta_2} . \left(\frac{B}{b}\right)^{\gamma_2} . \left(\frac{d_{50}}{b}\right)^{\theta_2} . (C)^{\eta_2} \quad (13)$$

Table 2 and 3 shows the linear and exponential multi variant equations to define the dimensionless equations. R^2 and MARE indexes are shown in the last column for comparison. Investigating the linear equation in table (2) shows that A1 has the largest R^2

and A4 has the smallest MARE. Investigating the exponential equation in Table 3 shows that B1 has the largest R^2 and also has the smallest MARE. Comparison between R^2 and MARE in the equations A7,A4 and B1 shows that B1 has the largest R^2 and the smallest MARE. Investigating the indexes in the one and two variant exponential equation factors in table 1, shows that the factors V_s/V_T and B/b has the most correlation with T_{smax}/D_{max}. This investigation also shows that the important factors in defining the dimensionless factors in the maximum deposition are V_s/V_T and B/b.

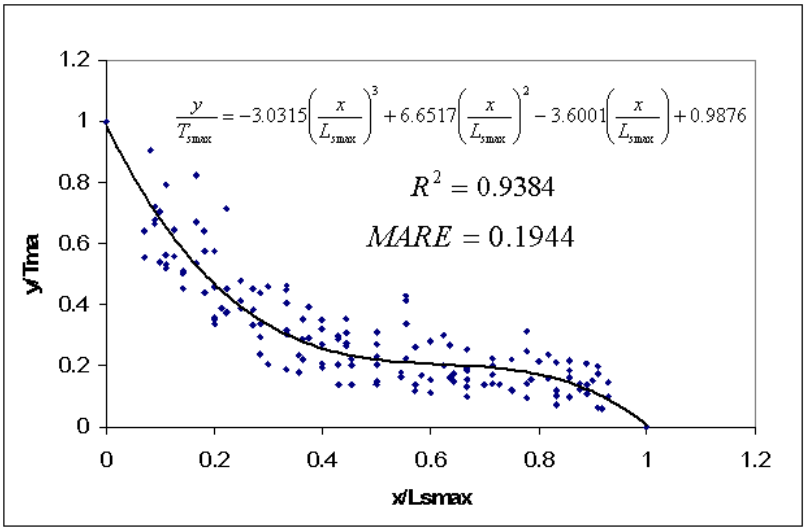

Fig 5. dimensionless deposition profile

Investigating the three-variant equation in that table shows adding dimensionless factors d_{50}/b has increased the correlation more than the factors C. so the third effective factor in determining maximum deposition thickness is d_{50}/b and the proper equation is the A2 relation. Comparison between equation and four variant equation A1 shows that although we have added C, there is no significant change in R^2 and MARE indexes. So the proper relation for the maximum deposition thickness is:

$$T_{s\max}/D_{\max} = 1.775\left(\frac{V_s}{V_T}\right)^{5.2271}\left(\frac{B}{b}\right)^{0.2403}\left(\frac{d_{50}}{b}\right)^{0.4720} \quad (14)$$

Table 2: Dimensionless factors and the coefficient in the linear equation of Tsmax

Number of equation	Number of independent variants	Dimensionless factors in the equation				coefficient of dimensionless factors					R^2	MARE
		$\frac{V_s}{V_t}$	$\frac{B}{b}$	$\frac{d_{50}}{b}$	C	α_1	β_1	γ_1	θ_1	η_1		
A1	4	√	√	√	√	-2.7959	6.6039	0.0431	3.1730	-2.5399	0.6211	0.6380
A2	3	√	√	√		-4.3796	6.7826	0.0455	3.2949	--------	0.6137	0.6673
A3		√	√		√	-1.9053	5.8135	0.0560	--------	-3.1189	0.5775	0.6189
A4		√		√	√	-1.2163	6.7226	---------	5.6933	-4.7461	0.5060	0.5619
A5			√	√	√	3.6355	---------	0.0453	0.3037	-5.6179	0.2916	1.2601
A6	2	√	√			-3.8248	5.9971	0.0596	--------	--------	0.5663	0.6628
A7		√		√		-4.1534	7.0862	---------	6.2073	--------	0.4790	0.5836
A8		√			√	2.0050	4.9428	---------	--------	-7.6771	0.3215	0.8078
A9			√	√		0.4117	---------	0.0509	0.4051	--------	0.2544	1.3255
A10			√		√	3.6485	---------	0.0467	--------	-5.6405	0.2911	1.2698
A11				√	√	5.4195	---------	---------	2.9018	-7.9978	0.1642	1.3054
A12	1	√				-2.5283	5.2904	---------	--------	--------	0.2467	0.8690
A13			√			0.4117	---------	0.0527	--------	--------	0.2536	1.3386
A14				√		0.9077	---------	---------	3.5371	--------	0.0847	1.3653
A15					√	6.2773	---------	---------	--------	-9.2103	0.1091	1.4266

Table 3. Dimensionless factors and the coefficient in the exponential equation of Tsmax

Number of equation	Number of independent variants	Dimensionless factors in the equation				coefficient of dimensionless factors					R^2	MARE
		$\frac{V_s}{V_t}$	$\frac{B}{b}$	$\frac{d_{50}}{b}$	C	a	b	c	d	e		
B1	4	√	√	√	√	0.2791	0.5771	0.8460	0.8351	0.7106	0.9942	0.074
B2	3	√	√	√		0.1882	0.5277	0.8294	0.8347	-----	0.9931	0.079
B3		√	√		√	0.0021	0.5453	1.6777	-----	0.5984	0.6210	0.700
B4		√		√	√	1.8477	0.1096	-----	1.0737	-0.6354	0.8858	0.684
B5			√	√	√	0.2114	-----	0.8232	0.8347	0.5157	0.9906	0.095
B6	2	√	√			0.0015	0.5037	1.6633	-----	-----	0.6202	0.700
B7		√		√		2.7570	0.1469	-----	1.0784	-----	0.8848	0.318
B8		√			√	0.0083	-0.7688	-----	-----	-3.2010	0.0282	0.713
B9			√	√		0.1606	-----	0.8123	0.8344	-----	0.9900	0.090
B10			√		√	0.0016	-----	1.6557	-----	0.4143	0.6178	0.717
B11				√	√	1.7335	-----	-----	1.0724	-0.6662	0.8856	0.314
B12	1	√				0.0575	-0.5971	-----	-----	-----	0.0040	1.389
B13			√			0.0013	-----	1.6468	-----	-----	0.6174	0.715
B14				√		2.5951	-----	-----	1.0769	-----	0.8846	0.840
B15					√	0.0125	-----	-----	-----	-3.0054	0.0216	1.360

Linear and exponential multi variant relations for estimating the maximum deposition length are similar to equations (15) and (16) and they are a function of dimensionless factors Π_1 to Π_4 . the result of investigation are shown in table 4 and 5.

$$L_{s\max}/L_{w\max} = \alpha_3 + \beta_3\left(\frac{V_s}{V_T}\right) + \gamma_3\left(\frac{B}{b}\right) + \theta_3\left(\frac{d_{50}}{b}\right) + \eta_3(C) \quad (15)$$

$$L_{s\max}/L_{w\max} = \alpha_4 \cdot \left(\frac{V_s}{V_T}\right)^{\beta_4} \cdot \left(\frac{B}{b}\right)^{\gamma_4} \cdot \left(\frac{d_{50}}{b}\right)^{\theta_4} \cdot (C)^{\eta_4} \quad (16)$$

Investigating these tables shows that the exponential equations have more correlation and less MARE. So the exponential relation are investigated similar to the discussion we had in determining the maximum deposition thickness different relation indexes are investigated and the effective factors defined as B/b,d_{50}/b and V_s/V_T in order. Comparison between the three variant relation D2 and 4 variant relation D1 shows that the D2 indexes does not have a significant different with D1. So D2 is the proper relation for estimating maximum deposition length:

$$L_{s\max}/L_{w\max} = -0.7608\left(\frac{V_s}{V_T}\right)^{0.7325} \cdot \left(\frac{B}{b}\right)^{0.3358} \cdot \left(\frac{d_{50}}{b}\right)^{0.349} \quad (17)$$

4.Conclusion

In the present paper, the results of 25 experiments in a in high steep tilting flume for modeling slit dam is analyzed. The effective factors on deposition profile in the slit dam reservoir are discussed and according to the multi variant correlation analyses the following results are gained:

- deposition profile can be expressed as a 3-variant power equation
- the effective dimensionless factors in determining the maximum deposition thickness are V_s/V_T, B/b and d_{50}/b respectively.
- the effective dimensionless factors in determining the maximum deposition length are B/b, d_{50}/b and V_s/V_T respectively.

References:

[1] Takahashi T. (1978) Mechanical characteristics of debris flow.Journal of Hydraulics Division, ASCE, 104(8), 1153–1169.

[2] Lien, H.P. 2003, DESIGN OF SLIT DAMS FOR CONTROLLING STONY DEBRIS FLOWS. international Journal of Sediment Research, Vol. 18, No. 1, 2003, pp. 74-87.

Table 4. Dimensionless factors and the coefficient in the linear equation of L_{smax}

Number of equation	Number of independent variants	Dimensionless factors in the equation				coefficient of dimensionless factors					R^2	MARE
		$\frac{V_s}{V_t}$	$\frac{B}{b}$	$\frac{d_{50}}{b}$	C	α_3	β_3	γ_3	θ_3	η_3		
C1	4	√	√	√	√	-0.0860	0.1386	0.0025	0.4805	0.0578	0.8624	0/1885
C2	3	√	√	√		-0.0500	0.1345	0.0024	0.4777	---------	0.8612	0.1937
C3		√	√		√	0.0488	0.0189	0.0045	---------	-0.0299	0.5575	0.3467
C4		√		√	√	0.0056	0.1454	---------	0.6267	-0.0703	0.7442	0.2685
C5			√	√	√	0.0489	0.0025	---------	0.4203	-0.0068	0.7922	0.2499
C6	2	√	√			0.0304	0.0206	0.0045	---------	---------	0.5572	0.3467
C7		√		√		-0.0379	0.1508	---------	0.6344	---------	0.7424	0.2664
C8		√			√	0.3602	-0.0505	---------	---------	-0.3929	0.0626	0.5461
C9			√	√		0.0450	---------	0.0026	0.4204		0.8182	0.2496
C10			√		√	0.0668	---------	0.0044	---------	-0.0381	0.5566	0.3543
C11				√	√	0.1492	---------	---------	0.5664	-0.1406	0.6955	0.3075
C12	1	√				0.1282	-0.0327	---------	---------	---------	0.0029	0.5398
C13			√			0.0450	---------	0.0045	---------	---------	0.5561	0.3552
C14				√		0.0699	---------	---------	0.5775	---------	0.6880	0.3001
C15					√	0.3166	---------	---------	---------	-0.3773	0.0558	0.5369

Table 5. Dimensionless factors and the coefficient in the exponential equation of L_{smax}

Number of equation	Number of independent variants	Dimensionless factors in the equation				coefficient of dimensionless factors					R^2	MARE
		$\frac{V_s}{V_t}$	$\frac{B}{b}$	$\frac{d_{50}}{b}$	C	α_4	β_4	γ_4	θ_4	η_4		
D1	4	√	√	√	√	-0.7023	0.7494	0.3415	0.3491	0.2431	0.9059	0.1399
D2	3	√	√	√		-0.7608	0.7325	0.3358	0.3490	---------	0.9052	0.1381
D3		√	√		√	-1.5882	0.7361	0.6891	---------	0.1962	0.5593	0.2961
D4		√		√	√	-0.3710	0.5607	---------	0.4454	-0.3001	0.8120	0.1978
D5			√	√	√	-0.8589	---------	0.3119	0.3485	-0.0099	0.8736	0.1585
D6	2	√	√			-1.6352	0.7224	0.6844	---------	---------	0.5589	0.2967
D7		√		√		-0.2889	0.5783	---------	0.4476	---------	0.8109	0.2016
D8		√			√	-1.3441	0.1963	---------	---------	-1.3643	0.0277	0.4646
D9			√	√		-0.8566	---------	0.3121	0.3485	---------	0.8736	0.1584
D10			√		√	-1.7406	---------	0.6595	---------	-0.0522	0.5282	0.3197
D11				√	√	-0.5127	---------	---------	0.4386	-0.4577	0.7935	0.2059
D12	1	√				-0.9867	0.2695	---------	---------	---------	0.0044	0.4554
D13			√			-1.7285	---------	0.6606	---------	---------	0.5281	0.3198
D14				√		-0.3923	---------	---------	0.4417	---------	0.7909	0.2078
D15					√	-1.3889	---------	---------	---------	-1.4143	0.0254	0.4679

Geochemistry of Yukon and Copper River Tributaries, Alaska

Melissa Carney[1*], Andre Ellis[1], Thomas Bullen[2] and Jeff Langman[1]

[1*]Department of Geological Sciences, University of Texas at El Paso, 500 W. University Ave, El Paso, TX 79968; PH (915)747-5503 email: mccarney@miners.utep.edu

[2]Water Resources Unit, US Geological Survey, 345 Middlefield Rd., MS 420 Menlo Park, CA 94025; PH (650) 329-4577; email: tdbullen@usgs.gov

ABSTRACT

Alaska is already beginning to be affected by changes in global climate which make it a good location to study the feedback effects between climate, the water cycle and the carbon cycle. Using river dissolved elements and Sr isotopes we examine changes and/or differences in chemical weathering between watersheds in predominantly permafrost areas and glacial watersheds. Tributaries of the Tanana, Yukon, Nenana and Copper rivers were sampled during the early snow melt in late May and the late permafrost/glacial melt period in September of 2007. Waters are predominantly Ca–HCO_3^-/SO_4 which is typical of glaciated terrains. $^{87}Sr/^{86}Sr$ isotopes indicate three potential end-members, young basalts, radiogenic silicates and marine carbonates. The results are consistent with weathering observed in glaciated regions with trace calcites and salts dominating the dissolved load; however we have evidence for silicate weathering. Results also indicate that permafrost watersheds experience more progressive silicate weathering than glacial watersheds.

MOTIVATION, BACKGROUND AND SCOPE

Geochemistry and isotope geochemistry of rivers are often used to understand hydrogeological processes in watersheds. For example, we can get a better understanding of the interaction between the carbon and hydrogeological cycles. An important issue that has recently received attention, and is partially motivating the proposed study, is calculating atmospheric CO_2 drawdown as a function of the type of silicate mineral being weathered. Weathering of certain types of silicates, especially calcium and magnesium silicates, are of interest because it removes atmospheric CO_2 through transport of bicarbonate to the ocean (Berner et al. 2003). The long-term carbon cycle is an important component of climate on a geologic time scale.

Weathering of silicate and carbonate material is shown through the following reactions (Dupré et al. 2003);

$$CaCO_3 + H_2O + CO_2 = Ca^{2+} + 2HCO_3 \quad (1)$$

$$CaSiO_3 + 3H_2O + 2CO_2 \rightarrow Ca^{2+} + 2HCO_3^- + H_4SiO_4 \quad (2)$$

$$Ca^{2+} + 2HCO3 = CaCO_3 + H_2O + CO_2 \quad (3)$$

The carbonate dissolution reaction (1) requires one mole of CO_2 which is taken up from the atmosphere and then released with precipitation of calcites (3) while during silicate weathering (2) two molecules are taken up and only one is released via calcite precipitation on geological timescales. Therefore, carbonate dissolution or weathering is not expected to contribute to changing climate. This reaction applies not only to Ca but Mg silicates as well. According to several studies, lithology is the major control on river dissolved chemistry (Miller 1961; Garrels and Mackenzie 1971; Drever 1988). Therefore, river dissolved chemistry is often used to determine contributing lithology and estimate atmospheric CO_2 drawdown. One of the challenges with this fluvial method is that water entering the rivers has traversed over several different types of lithology so discriminating sources and climate variables is not trivial. Traditional methods of calculating weathering rates of different lithologies have included using major elements in combination with strontium (Sr) isotopes in river dissolved loads where, $^{87}Sr/^{86}Sr$ ratios were used to distinguish radiogenic and non-radiogenic silicates (Brantley et al. 2006).

The overall goal of the larger study is to determine if CO_2 drawdown will increase along with silicate weathering as climate changes. However, while weathering of most silicates is a CO_2 sink, weathering of carbon rich lithologies such as shale is a net source for CO_2. Quantifying net CO_2 drawdown by taking weathering of shales into account is still elusive and is one of the main goals of the larger study. Before net CO_2 fluxes can be determined we need to examine the contributions from different lithologies especially silicates and shales. In addition, weathering reactions are more likely to have progressed to a greater extent in permafrost watersheds as opposed to glacial watersheds; the river dissolved load chemistry will reflect this control. We use major ions and isotopes to distinguish sources and relative contributions from lithology and with the help of isotopes look for variations caused by greater chemical weathering. Using trace elements requires that watersheds be pristine, free from anthropogenic effects.

Rivers in Alaska (see Figure 1) were chosen for this study for several reasons. Briefly, Alaska is relatively pristine, at a latitude which is currently seeing effects of climatic change, we can study both permafrost and glacial fed watersheds, and the geology is very diverse. Permafrost cover is decreasing in the study area and is predicted to be gone in 25 years. In addition, in the future we can examine the effects of tectonic activity and exhumation on weathering. The rapid exhumation and increase in elevation apparently controls the weather and climate patterns in the area.

A number of tributaries on the Tenana, Nenana and Copper were sampled during the early snow-melt period (May) and again later in the summer (September) of 2007. It should be noted that not all of the rivers sampled in May were also sampled in September. Since permafrost has a very low flow rate the increased contact time between the water and minerals will result in a higher relative proportion of chemical weathering than the glacial areas. The glacial areas will more than likely see an increase in physical weathering due to more rainfall and more melt water runoff but the relative proportion of chemical weathering will still be small because there is less time for the water to remain in contact with the lithology. We will also examine any differences between the early and late melt seasons probably caused by the extended duration of water-rock interaction and increasing temperature.

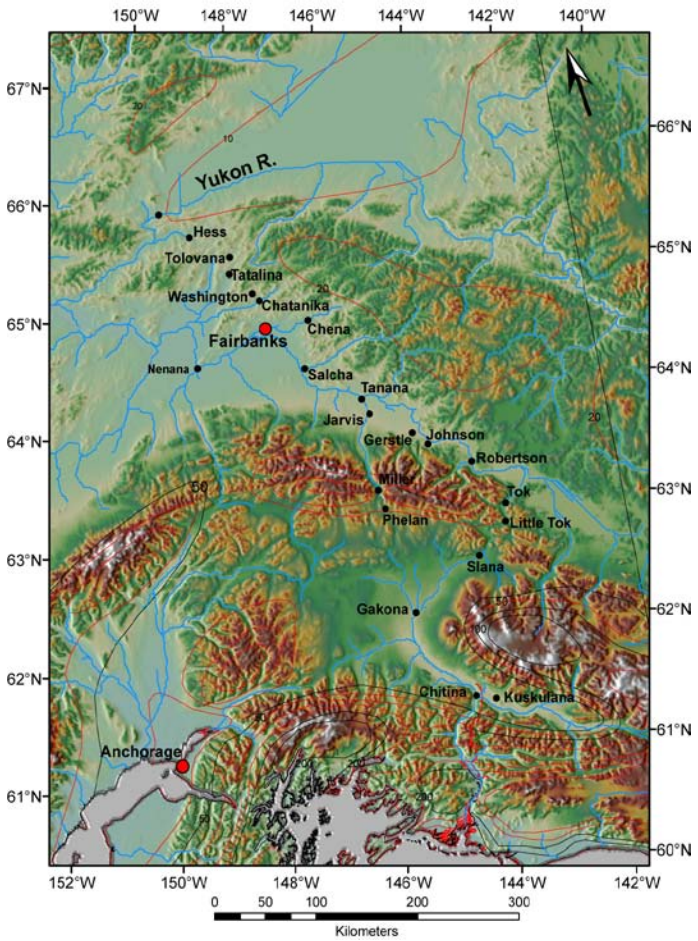

Figure 1. Study area and rivers sampled. Precipitation contours show variation consistent with topography and circulation patterns.

METHODOLOGY

Sample Collection:

Water samples were collected at the locations shown in Figure 1. All sites were sampled near the road and unless otherwise noted, all rivers were sampled upstream of the bridges. Field parameters measured on site include temperature, pH, dissolved oxygen and redox potential. All samples were filtered in the field using 0.4μm filter, half of the filtered samples were acidified with nitric acid to a pH~2.0.

Analytical Methods:

Major Ions and Trace Elements

Ion Chromatography was used to measure the anions (Cl^-, SO_4^{2-}, NO_3^-). Samples for cations and trace element analyses were sent to Activation Laboratories in Canada

and measured on an Inductively Coupled Plasma-Mass Spectrometer (ICP-MS). For quality control purposes as well as to obtain data not acquired by Activation Laboratories the same samples were run on an Inductively Coupled Plasma-Optical Emission Spectroscopy (ICP-OES) in the Geology Department at the University of Texas at El Paso.

Sr Isotope Purification and Analysis

Strontium was enriched and separated from interfering ions by using ion exchange chemistry. $^{87}Sr/^{86}Sr$ ratios were measured on a Nu Plasma multi-collector ICPMS at the University of Illinois at Urbana-Champaign, Urbana, IL. $^{87}Sr/^{86}Sr$ ratios are normalized to the $^{86}Sr/^{88}Sr$ ratio of 0.1194.

RESULTS AND DISCUSSION

Major ions and River Geochemistry:

The major ion geochemistry of these rivers essentially shows a Ca-Mg/HCO_3-SO_4 type water (Figure 2). Most of the rivers appear to be dominated by carbonate

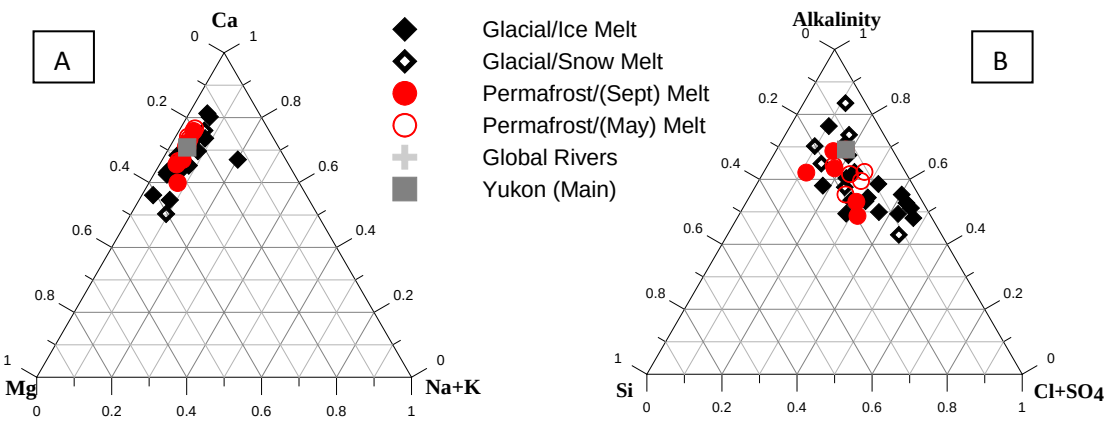

Figure 2. (A) Cation Ternary. (B) Anion Ternary. All the following figures use the same symbols.

weathering with varying degrees of contribution from silicates and salts. Although carbonate weathering appears to be dominant, the data does not completely lie on the alkalinity - ($Cl+SO_4$) tie line but shows up to 30% silica indicating substantial contributions from silicate weathering. On the cation ternary diagram (Figure 2A) the Alaskan rivers plot in the carbonate fields typical of most global rivers. Ca ranges from 50-80% though Mg can be as high 40%. The "excess" Mg could from silicate weathering but is more likely from Mg-sulfates (see below). The exception to the above is Chitina which has Na+K value as high as 20%. The glacial fed rivers sampled late in the season appear to be influenced more by evaporite dissolution than the other groups. Except for the above, there appears to be no significant difference in major ion chemistry between the four sampling groups (late season, early season, permafrost and glacial). The contribution from carbonate weathering is clearly evident from plots of Alkalinity vs Mg/Na (Figure 3). The river samples are generally clustered near the carbonate end-members and appear to fall along the typical mixing

line of carbonate and silicate/evaporite end members. For comparison, data from a number of global rivers (taken from Gaillardet et al. (1999)) are plotted in the background. It should be noted that the global rivers are averages and measurements are from the main channels.

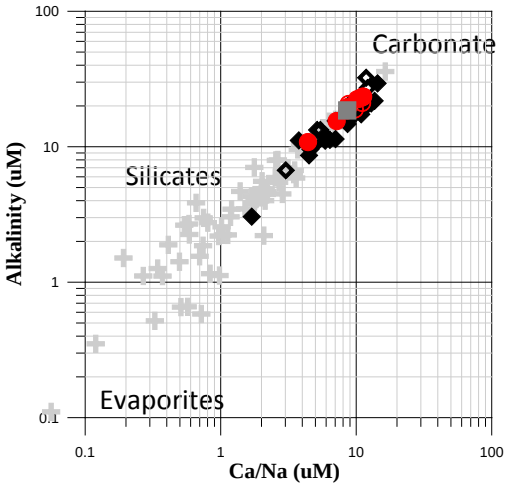

Figure 3. Alkalinity/Na vs Ca/Na. Generalized fields are adapted from Gaillardet (1999).

Sources contributing Na can be examined using a Na vs Cl plot (Figure 4A). Rivers that plot below the 1:1 line show excess Na that cannot be associated with halite dissolution. The excess Na is likely from the weathering of silicate minerals. There are rivers sampled from the late melt for both permafrost and glacial areas where the Na appears to be in excess and independent of Cl which may indicate a relative increase in silicate weathering. Further examination of the progression of weathering is done by plotting Si versus Na*+K which shows silicate weathering without the influence of carbonate or evaporite weathering (Figure 4B). Na* is Na without any Na associated with Cl removed (Na* = Na-Cl). As weathering progresses with silicates, the resulting sequence of clay formation is beidellite->kaolinite (for a more detailed description refer to Huh et al. (1998)). All of the rivers show that aluminosilicate weathering has gone through limited progression. It appears that the aluminosilicate weathering occurring in the permafrost regions has progressed farther than the glacial watersheds; this is significant because the information implies that there may be more silicate weathering in the permafrost regions. At this point it is unclear what is causing the excess Cl but local anthropogenic contamination cannot be ruled out. Sr isotope ratios increasing with Na*+K concentrations typically indicates weathering of aluminosilicates containing radiogenic strontium (Moon et al. 2007). Some of these

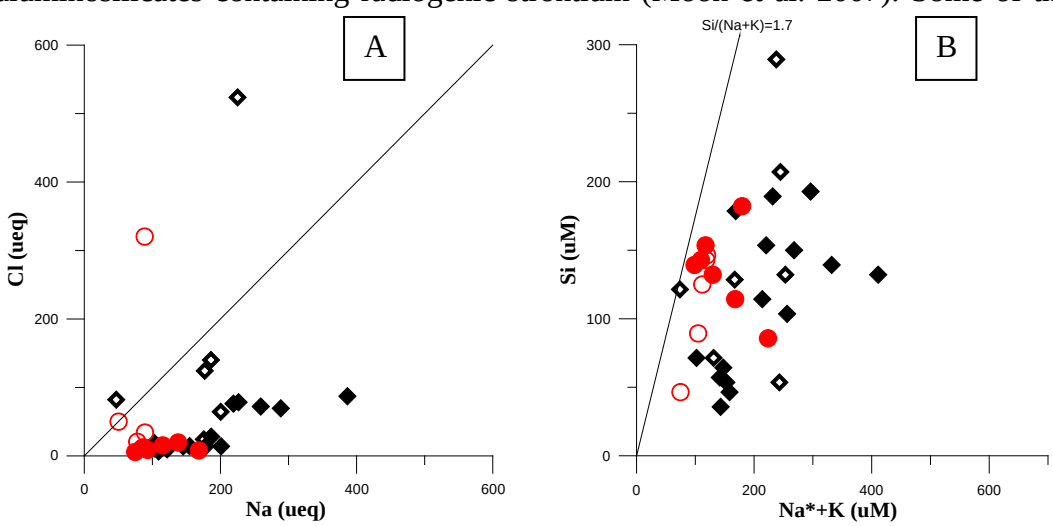

Figure 4. (A) Cl vs Na (B) Si vs Na*+K

watersheds clearly show weathering of depleted Sr isotope minerals are associated with ultramafic silicates (Figure 5). The permafrost and glacial snow melt rivers show that the Sr isotope ratios increase independently of the Na*+K concentrations. Glacial (ice melt) rivers show a decrease in Sr isotopes occurring with an increase in Na*+K concentrations. This is opposite of the trend usually seen for silicate weathering. This result indicates that weathering of trace calcites is contributing radiogenic Sr.

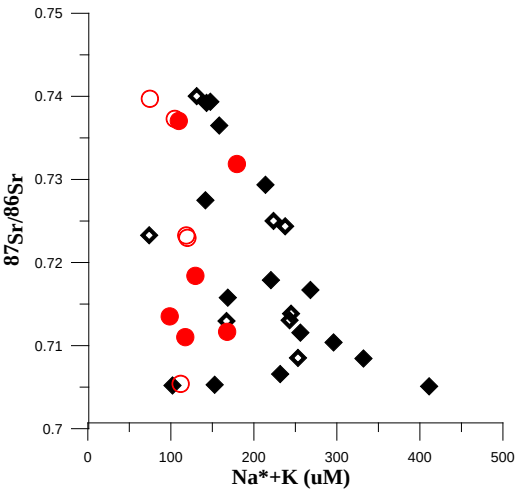

Figure 5. $^{87}Sr/^{86}Sr$ vs Na*+K

Evaporite minerals are the most easily dissolvable minerals and therefore even though they may not be the dominant lithology, they may still have significant influence on the river water chemistry. Gypsum ($CaSO_4$) is an evaporite mineral which may be contributing to the dissolved chemistry of the rivers sampled. It is clear from Figure 6 that SO_4 in glacial (ice melt) is well correlated with both Ca and Mg indicating the presence of Mg-sulfates associated. But that does not appear to be the case for the glacial (snow melt) or the permafrost samples. The Mg/Na vs SO_4/Na graph shows a mixing line between a

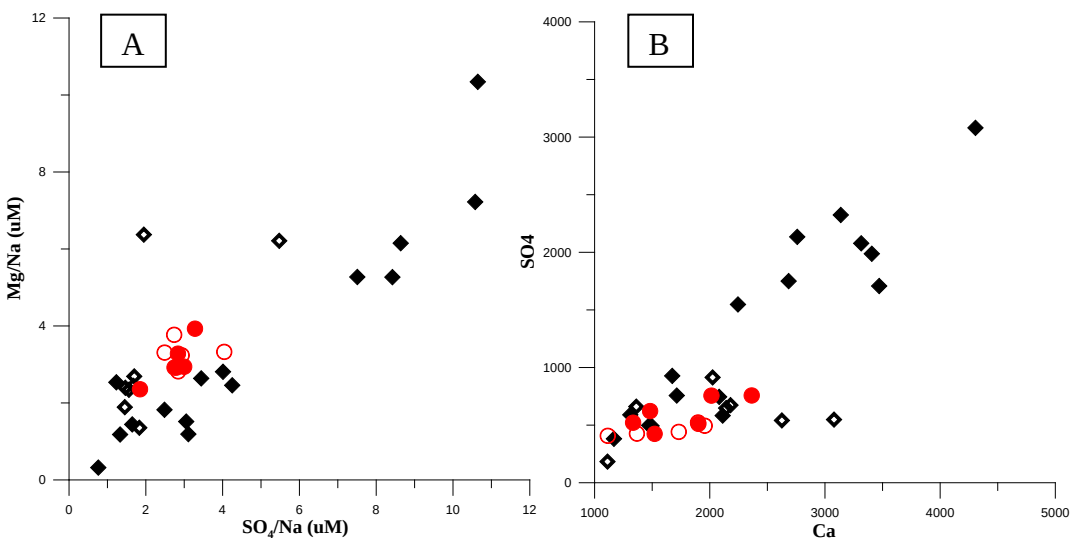

Figure 6. (A) Mg/Na vs SO_4/Na (B) SO_4 vs Ca

silicate end member and a possible $MgSO_4$ end member.

CONCLUSION

Major ions in the rivers of the central Alaskan region show dominance of carbonate weathering with evidence of silicate weathering. This is expected because carbonates

weather more easily than silicates. There also appears to be evidence in the glacial ice melt samples that dissolution of evaporites is a major contributor. Sr isotope ratios indicate two potential silicate end members, one radiogenic and the other depleted. There is some evidence that the permafrost regions are experiencing more intensive aluminosilicate weathering than the glacial regions. Through previous work it has been found that radiogenic Sr isotopes can be consistent with trace calcite weathering but further evaluation is needed to verify that it is the case in this area.

REFERENCES

Berner, E.K., Berner, R.A., Moulton, K.L., Heinrich, D.H. and Karl, K.T., 2003. Plants and Mineral Weathering: Present and Past. In: J.I. Drever (Editor), Surface and Groundwater, Weathering and Soils. Treatise on Geochemistry. Pergamon, Oxford, pp. 169-188.

Brantley, S. L., Fletcher, R. C., Buss, H., Moore, J., Hausrath, E., Navarre, A., Lebedeva, M., and White, A. F. (2006). "Weathering from the soil profile to the watershed: what controls the weathering advance rate?" *Geochim. Cosmochim. Acta*, 70(18, Supplement 1), A64.

Drever, J.I., 1994. The effect of land plants on weathering rates of silicate minerals. *Geochim. Cosmochim. Acta,* 58(10): 2325-2332.

Dupré, B., Dessert, C., Oliva, P., Goddéris, Y., Viers, J., François, L., Millot, R., and Gaillardet, J. (2003). "Rivers, chemical weathering and Earth's climate." *Comptes Rendus Geosciences*, 335(16), 1141-1160.

Gaillardet, J., Dupre, B., Louvat, P., and Allegre, C. J. (1999). "Global silicate weathering and CO (sub 2) consumption rates deduced from the chemistry of large rivers." Global carbon cycle., J. L. Probst, H. Faure, and J. Veizer, eds., *Chem. Geol.*, Elsevier, Amsterdam, Netherlands, 3-30.

Garrels, R. M. and Mackenzie, F.T., 1971. The Evolution of Sedimentary Rocks. W. W. Norton, New York

Huh, Y., Tsoi, M. Y., Zaitsev, A., and Edmond, J. M. (1998). "The fluvial geochemistry of the rivers of eastern Siberia; I, Tributaries of the Lena River draining the sedimentary platform of the Siberian Craton." *Geochim. Cosmochim. Acta*, 62(10), 1657-1676.

Miller, J. P., 1961. Solutes in small streams draining single rock types, Sangre de Cristo Range, New Mexico. US Geol. Surv., Water Supply Pap., 1535-F.

Moon, S., Huh, Y., Qin, J., and van Pho, N. (2007). "Chemical weathering in the Hong (Red) River basin: Rates of silicate weathering and their controlling factors." *Geochim. Cosmochim. Acta*, 71(6), 1411-1430.

THE HYDROLOGY OF THE CONGO RIVER BASIN: A GIS-BASED HYDROLOGICAL WATER BALANCE MODEL

J. Bahati Chishugi [1] and B.F. Alemaw [2]

[1]Department of Geology, University of Botswana, and Département de Géologie et Minéralogie, Université Officielle de Bukavu, Bukavu, D.R.Congo, Email : josuebc2002@yahoo.fr
[2]Department of Geology, University of Botswana, Gaborone, Botswana, email: alemaw@mopipi.ub.bw

Abstract

A GIS-based hydrological model, namely HATWAB - Hybrid Atmospheric and Terrestrial Water Balance (Alemaw, 2006), was developed to compute water resource availability, simulating its spatial and temporal distribution over the CRB. HATWAB model simulates the Integrated Moisture Convergence (C), soil moisture (SM), Actual Evapotranspiration (AET) and Runoff (ROF). The spatial distribution of the simulated parameters shows a strong correlation with the rainfall pattern, especially in the high rain fed region (Effective Rainfall >1100 mm/year), corresponding to the heart of the equatorial forest which extend between 5 and -5 degrees of latitude; whereas some disturbances are observed in the lowest rain fed (Effective Rainfall <1000 mm/year) regions of the basin located the south-eastern and the up-north part of the CRB. The Evapotranspiration Ratio (ETR) defines two main climatic regions, ETR close to 1 for region 1 and ETR < 7, with an intermediate zone between (07 < ETR < 0.8). The Annual average SM varies between 0 and 400 mm while the AET varies between 400 and 1700 mm/year with highest values on the water bodies. The total annual grid ROF varies between 0 and 1400 mm. Swamps are characterised by 0 to 40 mm values while highest runoff (> 900mm) are computed on the rivers and lakes. The inland grid ROF varies between 50 and 900 mm per year with an average of 324 mm/year. The accumulated ROF computed final outlet reaches 44700m^3/second which is within an error margin of 5 % compared to the observed discharge. The HATWAB model still proved its ability of simulating water balance for large scale basins such as the CRB if input data are available and well prepared at acceptable resolution.

Author Keywords: Water balance model; GIS; hydrological modelling; Central Africa; Congo River Basin; Runoff; Soil moisture; Evapo-transpiration; Convergence

1. INTRODUCTION

During the last decade African continent has been characterised by a shortage of water, electricity and food. This situation seems to endure and requires serious attention. The evaluation of spatial and temporal distribution of water resources of the Congo River basin is of great importance as the basin and its equatorial forest play an important role in the sustenance of the global climate equilibrium and the ecosystem stability. The fifth-longest river in the world and the second longest in Africa, Congo River basin (CRB) contains the second largest forest in the world, after the Amazon. Its watershed measures over 4.1 million sq. km with 4375 km of length and 0.8 to 16 km of width. In order to understand and evaluate the spatial and temporal

[1] Corresponding author : Email: josuebc2002@yahoo.fr , Tel: 00243994086126

distribution of the CRB water balance, a distributed GIS-based hydrological model, namely Hybrid Atmospheric and Terrestrial Water Balance (HATWAB) (Alemaw, 2006) was developed and parameterised for the Congo basin using GIS and computational hydrology techniques. The HATWAB model is based on consideration of surface and subsurface processes (Fig. 1). In the subsurface zone, soil moisture accounting technique of Thornthwaite and Mather (1957), modified as part of this study, is used to compute the water balance components known as actual soil moisture (SM), evapotranspiration (AET) and runoff (TRO). The surface abstractions in terms of overland runoff, interception and integrated vertical convergence are accounted for by HATWAB model (Alemaw 2006) which is a soil water balance method.

The model leads to the creation of high-resolution data sets of SM, AET and TRO over the several catchments in the Central African region, which are represented by geographically referenced grids of 12x12 degree resolution.

2. DATA PROCESSING AND METHOD

Developed in MS FORTRAN studio and supported by GIS packages, the HATWAB model estimates the SM, AET and ROF based on the equations listed below.

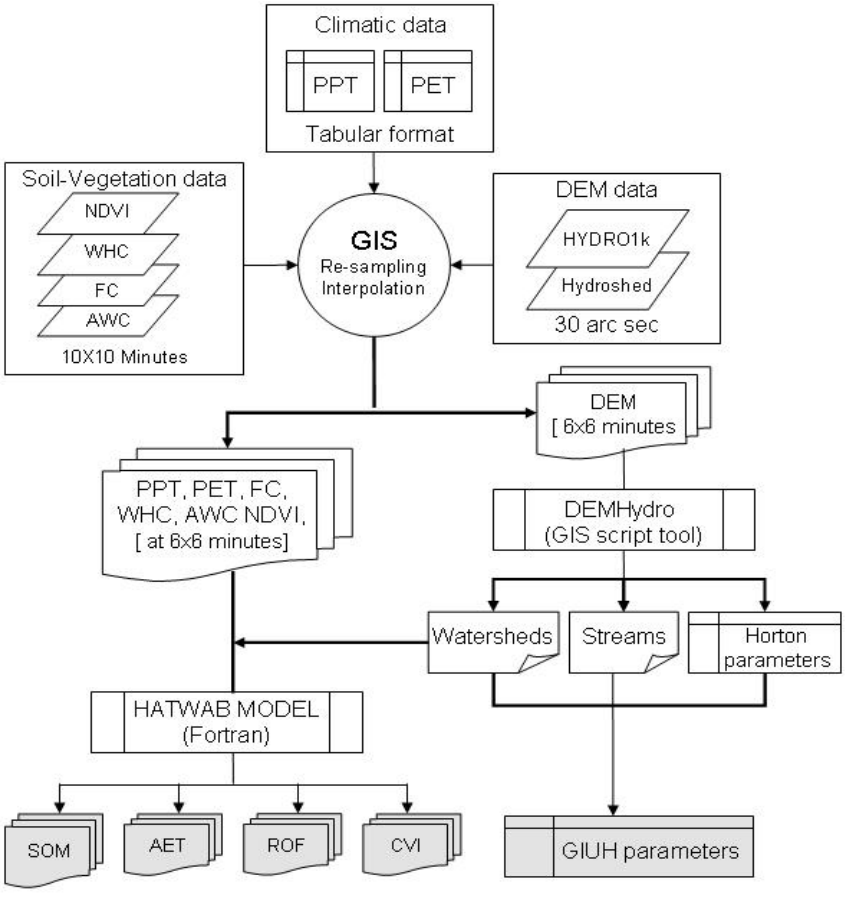

Figure 1 General terrestrial Water Balance model structure

2.1. Water Balance Model Development

Supposing the principle of continuity in hydrologic system, Chow (1998) assumes that the time rate change of storage is equal to the difference between the input and the output of the hydrologic model (equation 1).

$$\frac{ds_t}{dt} = I_t - O_t \tag{1}$$

where, S_t is the time-variant storage in a grid cell, I_t , the summation of input coming into the cell from upstream cells and the runoff generated in the cell, and O_t , the outflow from the cell which is calculated by various methods such as the linear reservoir method.

2.1.1. Atmospheric water balance

The atmospheric component of the water balance model is expressed as

$$\frac{dW}{dt} = -P + E + C \tag{2}$$

$$C = -\nabla \times Q \tag{3}$$

Where dW/dt is the amospheric storage change, C is the vertical integrated moisture convergence and was expressed as a function of the water vapour flux (Q) in Equation (3).

$\nabla \times Q$ is the divergence or net outflow of water vapour across the sides of the atmospheric column, Q is the vapour flux, E is evaporation, and P is precipitation.

The quantity W is also referred to as the precipitable water and may be expressed in units of mass per unit surface area or converted to an equivalent depth of liquid water by dividing by the density of liquid water (1000 kg m^{-3}).

In mean water balance computation like the HATWAB model which is a monthly water balance model, the atmospheric storage change is often assumed to be negligible (Reed et al, 1998 and Marengo, 2005); thus equation (3) is reduced to

$$P - E = C \quad or \quad P - E = -\nabla \vec{Q} \tag{4}$$

From Equation (4), it is seen that if the divergence ($\nabla \vec{Q}$) in a region is positive, then evaporation is greater than precipitation (P-E < 0), while a negative divergence or "convergence" indicates that precipitation is greater than evaporation (P-E > 0).

2.1.2. Terrestrial water balance

At monthly time scale a terrestrial water balance model is written as follow:

$$\frac{ds}{dt} = P - E - R \tag{5}$$

Where *S* is soil moisture storage; *P* is precipitation; *E,* actual Evapotranspiration; and *R*, the observed runoff.

Linearising Equation (4), the terrestrial water balance has the following form,

$$SM_1 = SM_{t-1} + P_t - E_t - R_t \tag{6}$$

Where t is the time period, which is a single month is this model, P is precipitation, E is the Evapotranspiration, and RO is the runoff.

Once the initial soil moisture (S_{t-1}) and the actual soil moisture (S_t) are determined, the monthly Actual Evapotranspiration E_t and the Runoff R_t can be calculated.

2.1.3. Imbalance estimation

Combining Equations (5) and (6), the vertical integrated moisture convergence (C) is computed as follows

$$C - \frac{dS}{dt} = R \tag{7}$$

In a steady state $P - AET = R$. Changes in storage could however lead to $P - E$ being different from R. These could also be due to certain errors in representing rainfall within the Congo River Basin. These lead to the expression of an *imbalance equation*

$$I_{mb} = \frac{C - (ds/dt + R)}{R} \tag{8}$$

The imbalance in I_{mb} is calculated using equation 9:

$$I_{mb} = \frac{C}{R} - \frac{ds/dt}{R} + 1 \tag{9}$$

Contrary to the formulation adopted in this study based on (9), Marengo (2005) assumes that *dS/dt* is negligible for monthly time scales and applied it in the Amazon basin, which reported unaccounted residuals in his water budgets. Whereas in the proposed model in this study, the soil moisture variation *dS/dt* is varying from season to season as a function of the prevailing *PET* and *PPT* at a given location according to Equation (5), in which the imbalance should also cater for this variability according to Equation (9). One of the contributions of this study is that, once the imbalance is kept to a minimum in the water balance computation at each grid, then the simulated variables and water balances, *PPT*, *ET*, *RO*, *RO/PPT*, *ET-PPT*, *ET/PET, S* and *C* can then be used to investigate the seasonal and temporal variability of water budget of the Congo basin.

The amount of precipitation and potential evapotranspiration determines soil moisture availability, which in turn is controlled by the water holding capacity of the soils.

2.1.4. Rainfall-Actual, Evapotranspiration-Soil moisture-Runoff modelling

2.1.4.1.Effective Precipitation (EPPT) and overland runoff (Direct runoff DRO)

One of the main inputs required in the proposed water balance model is the effective precipitation (EPPT). At a monthly time scale, the effective precipitation is calculated as per the formula of the USDA soil conservation available from FAO (1990) as follows:

$$EPPT = PPT(\frac{125-0.2PPR}{125}) \quad for\ PPT < 250 \tag{10}$$

$$EPPT = 125 + 0.1\ PPT \quad for\ PPT \geq 250 \tag{11}$$

Where $EPPT$ is effective precipitation and PPT is the total precipitation

The direct runoff (DRO) is the difference between the precipitation (PPT) and the Effective precipitation (EPPT).

2.1.4.2.Soil moisture estimation (SM)

Soil moisture is determined from the interaction between effective PPT and PET. During wet months (when effective PPT in excess of PET), soil moisture can increase up to a maximum of field capacity determined by soil texture and rooting depth.

$$\frac{dSM}{dt} = PPT - PET \quad when\ PPT > PET\ \ and\ SM < FC \tag{12}$$

$$\frac{dSM}{dt} = 0 \quad when \quad SM = FC \tag{13}$$

$$\frac{dSM}{dt} = a\,SM\,(PET - EPPT) \quad when \quad EPPT < PET \tag{14}$$

Where, FC is the soil moisture at field capacity of the soil millimetres, PPT is precipitation in mm/month; PET is potential evapo-transpiration in mm/month.

During the dry periods where the EPPT < PET, the soil becomes increasingly dry, soil moisture becomes a function of potential soil loss. Thus, different authors assumed different relationship to find the soil moisture during the dry periods (Thornthwaite, 1948; Vorosmarty *et al*., 1989).

For a particular soil, there is a linear relationship between Log (SM) and Σ(EPPT-PPT) summed from the start of the dry season to the current month. Thus, to calculate the rate of change of soil

moisture (ΔSM) through the dry season, the soil moisture is directly estimated from the empirical relation suggested by Vorosmarty *et al*. (1989). To calculate dSM/dt through Equation (14) for intermediate field capacities, the HATWAB model defines a slope a to the retention function as:

$$a = \ln(FC)/(1.1282\ FC)^{1.2756} \tag{15}$$

where the numerator represents the soil moisture (millimetres) with no net drying. The denominator is the accumulated potential water loss or APWL $\left(\sum [PET - PPT]\right)$ in mm at SM=1 mm. With a determined, the model can calculate dSM/dt as a function of soil dryness and update SM. The following Figure 2 shows the relationship between soil moisture and the Evapotranspiration.

Calculations commence at the end of the wet season when it is assumed the soil is at the field capacity. Soil water stocks are then depleted during the dry season in accordance with the moisture retention function. For each wet month, soil moisture is determined by incrementing antecedent values by the excess of the available water over PET. This recharge may or may not be sufficient to bring the soil to field capacity at the end of subsequent wet season.

Analysis of the ratio PPT/PET at the various grids in Central Africa has shown that the region can not be represented by one homogeneous climatic zone; rather it is a combination of climate influenced by the diversified hydro-climatic conditions in the region. In this analysis, it has been observed that the long-term monthly rainfall distribution varies greatly in the region.

It is assumed that the ratio PPT/PET could be a good indicator of the seasonal distribution of monthly rainfall, and accordingly the wet season ends when the ratio PPT/PET just starts to fall below unity. In line with this, therefore, the soil moisture can be assumed to be at its field capacity. Consequently, HATWAB fixes a starting month of any grid across the region according to the aforementioned criterion. The solution of the basic mass balance equation for the subsequent months can determined once the initial soil moisture state is obtained.

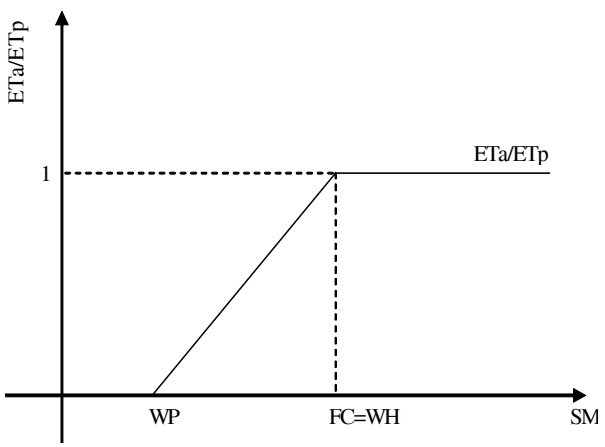

Figure 2 Functional relationship between soil moisture and Evapotranspiration (ETa is the actual Evapotranspiration, ETp is the potential Evapotranspiration, SM is the soil moisture, FC is the field capacity and WP, the Wilting point

2.1.4.3.Actual Evapotranspiration (AET)

Once the actual soil moisture is determined, the corresponding actual evapotranspiration (AET) is calculated for the month. Following the Thornthwaite and Mather (1957) approach, AET is set equal to PET in wet months, when EPPT > PET. During this time it is assumed that EPPT is in sufficient abundance to satisfy all the potential water demands of the resident vegetation. During dry season when EPPT < PET, the monthly average AET is modified down wards from its potential value as shown below.

$$AET = PET \quad when \quad EPPT > PET \tag{16}$$

$$ET = PPT - \frac{dSM}{dt} \quad when\ PPT < PET \tag{17}$$

Where the soil moisture drops below the wilting point, the AET is equal to the EPPT but if there is no EPPT at all time, AET becomes zero.

2.1.4.4.Total runoff (TRO) generated at a grid spatial scale

Most of the water does not leave the basin as soon as it becomes available as surplus. The portion that constitutes overland flow is assumed to flow out of the watershed within the month it occurs but the portion that infiltrates may take a number of months to move slowly through upper layer of the soil column to emerge in the surface water courses as base flow. The lag or delay factor depends not only the size of the basin but also on the vegetation cover and the soil type, degree of slope, characteristics of the soil layers, etc. over and added to the surplus of the next month. This factor is set according to Thornthwaite & Mather (1957) which is equal to 0.5.

$$RO = 0.5*(D + (EPPT - PET)); \quad when\ \ SM = FC\ \ \&\ \ EPPT > PET \tag{18}$$

$$RO = 0.5 * D, \quad when\ SM < FC\ \ \&\ EPPT < PET \tag{19}$$

Where, RO is rainfall-driven runoff or surplus runoff (mm/month) and D is the amount of detention storage in millimetres that is assumed to leave each grid cell next month.

Thornwaite suggests that 50% of the water surplus could be assumed to runoff each month from large basins with the remainder being held.

2.2. Study region and Data used

The Congo drainage basin is situated in Central Africa. Its hydrological system straddles several countries; Congo and the Democratic Republic of Congo for the most part, but also Angola, Cameroon, the Central African Republic, Zambia and Tanzania, stretching through Lake Tanganyika. The fifth-longest river in the world and the second longest in Africa, Congo River

contains the second largest forest in the world, after the Amazon. Its watershed measures over 4.1 million sq. km with 4375 km of length and 0.8 to 16 km of width

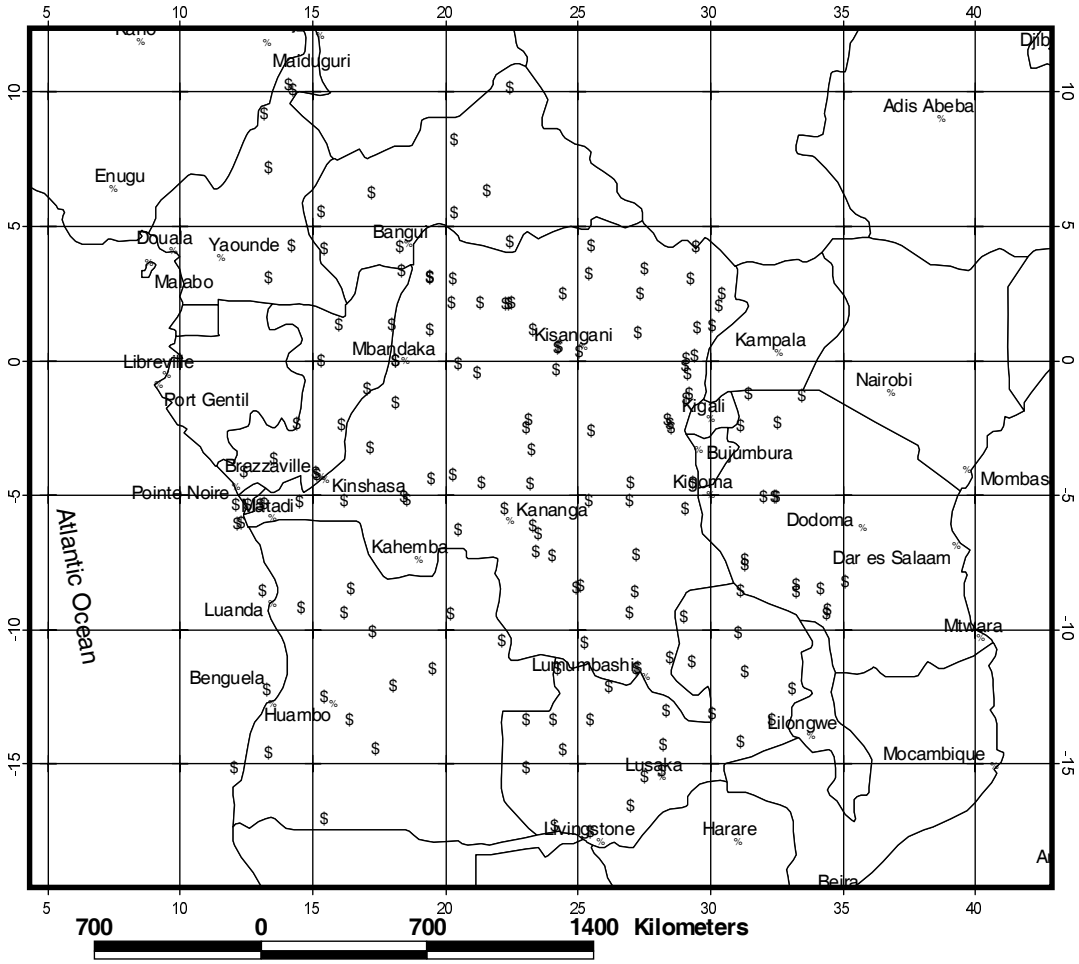

Figure 3: Distribution of Climatic stations in the study area. The study area covers more than 145 stations:

2.2.1. Meteorological data sets

Free meteorological data for 3262 global climatic stations are available at FAO-UNESCO /CLIMWAT, with a record time of 30 years (1961 -1990) at a monthly scale; where 145 climatologic stations covering the study area (Figure 3 and Appandix B) were extracted to compile the meteorologic database for the model. These climatologic data sets include monthly averages of maximum and minimum of temperatures, mean relative humidity, wind speed, sunshine hours, radiation data as well as rainfall and Reference Crop Evapotranspiration (ETo) calculated with the Penman-Monteith method (Allen et al, 1998). Below, Figures 4 and 5 show the Potential Evapotranspiration and Rainfall distribution in the basin, respectively.

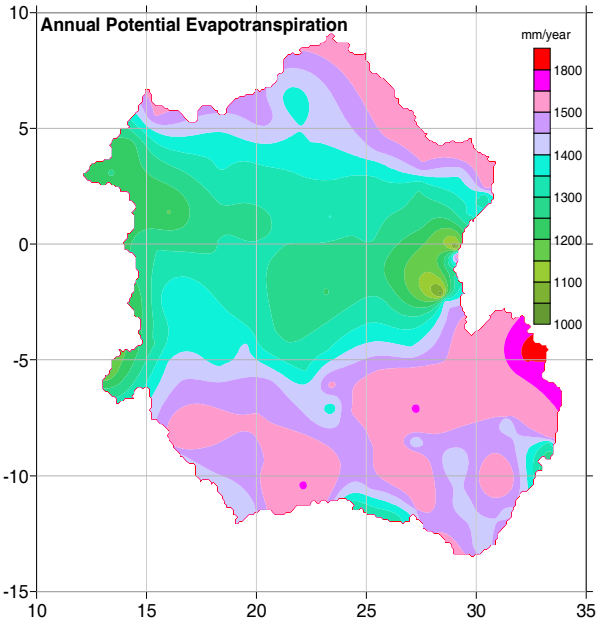

Figure 4 Mean Annual Potential Evapo-transpiration (1961-1990) map

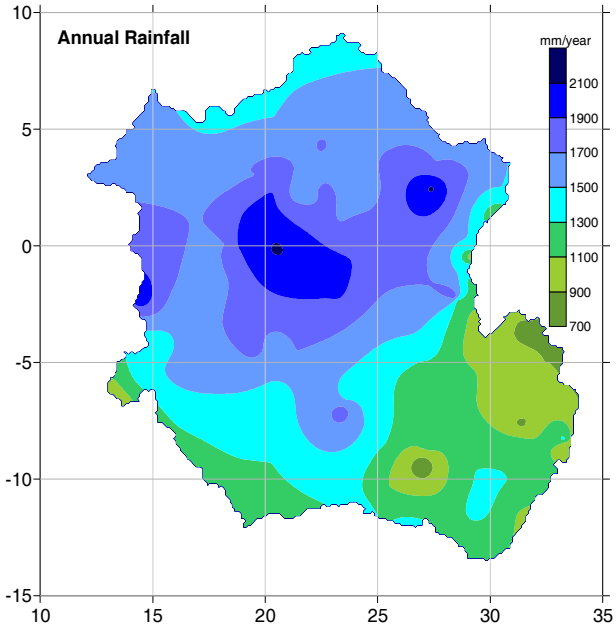

Figure 5 Rainfall averaged (1961-190) data from 145 stations. 1. Rainfall,

2.2.2. Discharge data

There is a lack of discharge data in the Congo Basin. The availability of recharge data is limited to a few numbers of rivers gauges. At the basin final outlet, discharge has been amounted to an average of 45000 m^3/sec (Asante, 2000). Discharge data indicates a series of four distinct phases in the Congo and the Oubangui since the beginning of the 20th century. During the 1960s they increased, overtaking their average over a century. The Congo discharge then fells, returning in 1970 to what had been the normal level, whereas the Oubangui entered a drought phase. This trend accentuated from 1980 and, until 1996, the Congo discharge weakened by 10% (37 400 m3/s in 1992 compared with an average of 40 600 m3 /s over that period as a whole), which was the most dramatic decrease of the century. This fall is much stronger in the Oubangui (- 29%), yet negligible (- 0.2 %) in the Kouyou sub-basin.

2.2.3. NDVI and vegetation database

The monthly NDVI images for each basin were acquired from the Global Land Cover Characteristics database. Satellite data have been used extensively for mapping the land use and for monitoring the seasonal change of vegetation of river basins (Nemani & Running, 1989).

The Normalized Difference Vegetation Index (NDVI) is commonly applied to derive the leaf area index (LAI) from channels 1 and 2 of NOAA-AVHRR data at 1-km^2 resolutions. Monthly twelve NDVI images, expressed in percentage, for 1987 are acquired from USGS database. Based on NDVI values the LAI for different land use groups can be estimated by empirical formulae. Table 13 presents rooting depth assigned for various soil textures and SCS soil groups.

2.2.4. Soil properties

A global Soil map at 10x10 minutes resolution is freely available at FAO/UNESO database (FAO, 1984). This map is used to extract the submap of the study area and later re-sampled to a spatial resolution of 6x6 minutes so that it can overlay onto the model.

Table 1 Rooting depth assigned for various soil textures and SCS soil groupings

Veg. Group	NDVI	Assigned Root Depth (M) For Different Soil Types					
		Sand	Sandy Loam	Silty Loam	Clay Loam	Clay	Lithosol
VEG2	>50%	2.5	2	2	1.6	1.2	0.1
VEG1	≤50%	1	1	1.3	1	0.7	0.1
SCS soil group (Singh, 1992)		A	B	D	C	C	B

Table 2 Soil texture distribution in the Congo River basin

Class ID	1	2	3	4	5	6	0	
Soil type	Sand	Sandy Loam	Silty Loam	Clay loam	Clay	Lithosol	Water body	Total
No grids	4847	0	58	21867	989	2374	513	30640
% gris	15.8	0	0.2	71.3	3.2	7.7	1.7	100

Since the Soil Water available to plants depends on soil water content, soil texture, and consequently, the rooting depth of vegetations, the 133 agronomic groups of FAO agronomical soil map were therefore used to derive and reclassify textural soil classes which are required as input data for the model. For this matter a FORTRAN algorithm was developed and six hydrological textural classes of soil (Table 1) were identified in the study area.

The reclassified textural soil and vegetation maps are used to derive the soil retention parameters such as Field Capacity (FC), Wilting Point (WP) which determine the soil moisture capacity known as Available Water Content (AWC) for each soil group. Based on field measurements, Saxton *et al.* (1986) have developed a technique to estimate the matrix potential of different soils by using multiple regression techniques. Therefore, at a matrix potential equivalent to field capacity (33 KPa) and wilting point (1500 KPa) for a unit meter depth of soil, approximate values of FC and WP for the various soil textures have been extracted. Accordingly, the FC and WP values as per the rooting depth are then derived for the whole region.

Available water content (AWC) of a soil of given texture is defined as the difference between the field capacity and wilting point. The depth of soil water which can be used by the crop, the Total Available Water (AWC), depending on the root depth of the crop and on the soil moisture holding properties of the soil (Eilers et al, 2007), Equations (20 and 21) bellow shows the relationship between these soil parameters:

$$AWC = (UFC - UWP)R \tag{20}$$

$$\text{With} \quad \begin{aligned} FC &= UFC \times R \\ WP &= UWP \times R \end{aligned} \tag{21}$$

Where AWC is the available water content per root depth; *FC* and *WP* are the field capacity and wilting point, respectively; R is the current depth of the roots; UFC and UWP are the field capacity and the wilting point per unit volume of the soil, respectively.

3. RESULTS

3.1. Soil Moisture

Figure 8 shows the Annual average Soil moisture. The mean annual soil moisture for the entire basin ranges between 0.7 and 431.4 mm, with highest mean monthly soil moisture of 546.2 mm during November and lowest, in July (146.2mm). A general trend is observed in the spatial distribution of the moisture: the regions around the equator are characterised by high soil moisture and this is reduced as the distance to equator is increased (Figure 9).

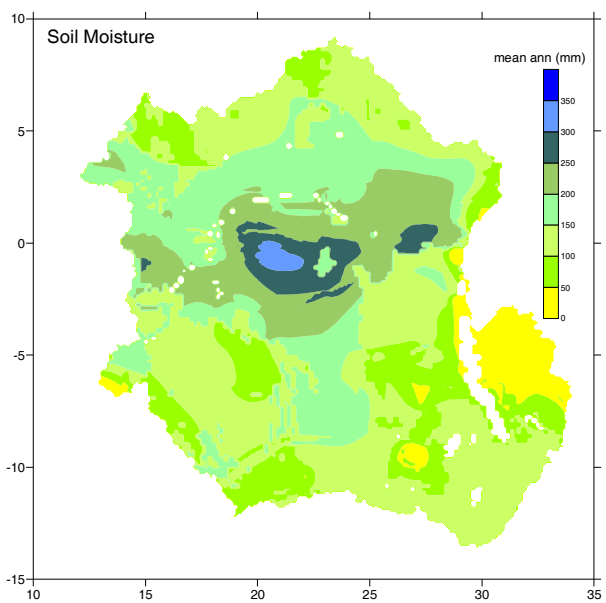

Figure 6 Mean annual moisture (in mm) over the Congo basin.

Spatially, the highest values are located in the centre of the basin which coincides with the core of the dense equatorial forest. These values range between 200 and 432 mm (mean annual). The lowest value ranging between 0 and 50 mm are located in the western part on Tanzania (eastern part of Tanganyika Lake). This region is also characterised by the small amount of annual rainfall (< 800) compared to other region inside the basin. Statistically, the soil moisture distribution over the basin correlates strongly with the hydrological soil group and the climatic parameters such as rainfall and Evapotranspiration. “Lithosol” is the type of soil Available Water content (<120 mm/root depth). The computed soil moisture values would be better interpreted as indexes of relative wetness rather than absolute estimates because none are calibrated against measured values in the field.

3.2. Actual Evapotranspiration (AET)

The simulated Actual Evapotranspiration (AET) over the basin is shown is Figure 10. The mean annual AET ranges between 564.13 and 1576.8 mm/year with a mean of 1098 mm/year. It is well observed that the AET trends similarly with the Rainfall and the existing land cover map of the basin. Consequently, the area with lowest AET is located in the south-eastern region of the basin which coincides with low rain feed region of the area.

High annual averaged AET values are sequentially observed over the water bodies such as the Tanganyika with a maximum of 1576.8 mm/year, followed by Upemba, Rukwa, Mweru, Delcommune, Bangwelungu Lakes (1300 - 1531 mm/year) and Kivu, Mai-Ndombe Lakes (>1250 mm/year). Some portions of the Congo River inside the heart of the Tropical forest present also high annual values of AET. Excluding the water bodies, the density of the equatorial forest varies positively with AET distribution.

The seasonal distributions of AET are characterised by alternation of high values in the northern hemisphere during the two seasons of December-February and March-May and low values in the southern hemisphere; inversely during the other 2 seasons (June-August and September-November

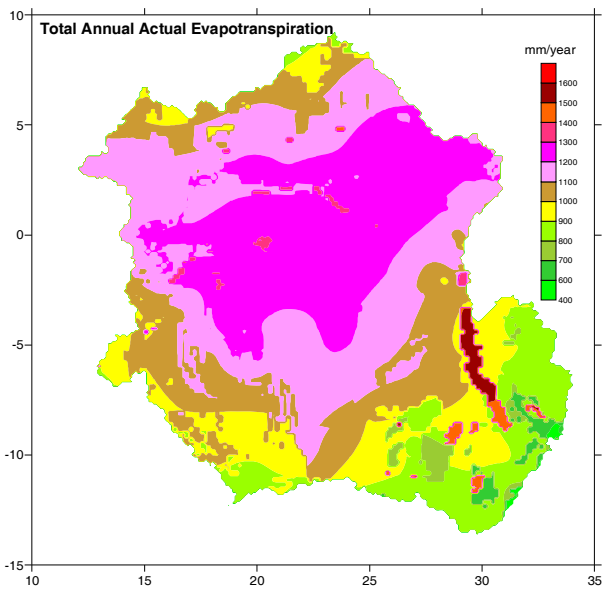

Figure 7 Mean Annual Actual Evapo-transpiration over the Congo River basin

3.3. Runoff

The simulated Annual Total runoff is shown in Figure 11. The mean annual Runoff for the Congo Basin varies between O and 1945 mm with a mean annual runoff of 342 mm. The highest values are concentrated in the heart of the equatorial forest along the Middle Congo river branch. This area records higher rainfalls in the whole basin. The lowest value is simulated in the southern hemisphere around the grid of coordinate 31^0E and 6.73^0S (western part of Tanzania). A part the lakes, the highest values of runoff are simulated in the heart of the equatorial forest across the equator, and decrease

progressively towards the tropics. This trend is relatively disturbed with the soil types especially in the south-eastern, the extreme north region and along the main Congo River.

The annual simulated runoff show a general trend strongly influenced by the distribution pattern of precipitation (Figure 12) in the basin, while seasonal and monthly runoff correlate strongly with both rainfall and soil type during dryer seasons. The area with zero runoff values corresponds to swamps and some inland lakes where there is negligible flow to the river system.

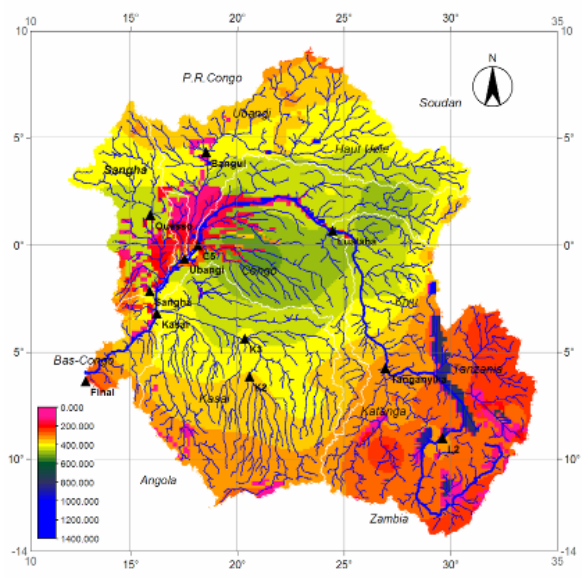

Figure 9 Mean annual runoff over Congo basin (mm/year)

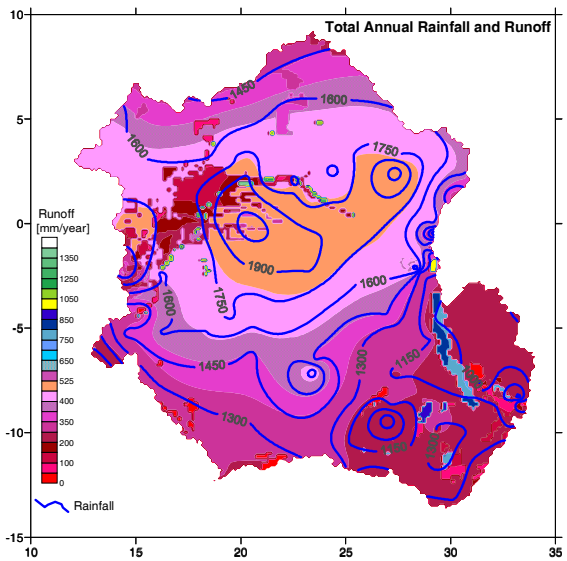

Figure 8 The relationship between precipitation and gridv- simulated runoff in the CRB

Seasonally, the September-November period records the highest amount (658432 mm. /season) of runoff whereas the lowest (358223 mm/season) is generated during June-August. This shows again the influence of rainfall on the generated runoff pattern in the Congo basin where , in general, the period June-July season records the lowest rainfall in the southern hemisphere which occupies more than 55% of the basin area. Two picks runoff are observed in March-May and September-November (658432 mm.) seasons which record higher rainfall during the year in the southern region.

3.3.1. Simulated sub-watershed and basin-wide runoff

Table 3 Subwatershed runoff averages

Area name	ROF Mean Ann	ROF Simulated (m3/sec)	ROF Observed (m3/sec)	Error (%)
Sangha	335.5	3,565	No data	-
Ubangi	348.6	8,274	No data	-
Kasai	344.7	11,545	No data	-
Lualaba	297.3	12,314	No data	-
Congo	385.5	12,177	No data	-
CRB	342	47,418	45,000	5.1

The runoff averages for each subwateshed are given in table 18 below. The Lualaba subcatchement knows the highest runoff than others. The higher amount accumulated runoff was expected in the Congo but this is not the case due to the presence of swamps in the subcachements where are simulated small values averaged to 0 mm per year. At the basin scale, the total annual runoff is about 47,418 m^3/sec. This amount is comparable to those reported in literature (45,000 m^3/sec; Asante, 2000) with a marginal error of 5.1%.

3.3.2. Local water balance over the Congo river basin

Appendix 1 shows the local water balance graphs for 11 grid cells around some meteorologic stations used in the model. The hydrological behavior correlates strongly with the rainfall betwenn -5 and 5 degree latitude zone. In the South-eastern region (Lubumbashi, Urambo, South-westen) and the Up-North station, runoff starts to increase in the mid-year as well as the soil moisture. An inverse situation is observed in the high rain fed region.

CONCLUSION

The HATWAB model permits to establish the hydrologic regimes of the Congo River Basin. Spatial and temporal distribution of the major components of water balance (Soil moisture, Actual Evapotranspiration and Runoff) were estimated.

This work is the first comprehensive distributed hydrological model that utilises the hydroclimatic, soil texture and Vegetation information, using the state of the art GIS technique to compute the water balance for the whole Congo River basin.

This model approach provides an operational hydrological tool to deal with national, or regional planning and developing decision support systems, with possible linkage with the inter-related multi-sectoral nature of the natural resources, socio-economic and climatic dynamics of the region and beyond.

REFERENCES

Alemaw, B.F. 2006, A Hybrid Atmospheric and Terrestrial Water Balance Model. A GIS based approach for large drainage basins. Unpublished Research Report. University of Botswana.

Alemaw, B.F. and T.R. Chaoka, 2003 A continental scale water balance model: a GIS-approach for the Southern Africa. Physical and Chemistry of the Earth, **28**: 957-966

Allen R. G., L.S. Pereira, D. Raes and M. Smith, Crop evapotranspiration - Guidelines for computing crop water requirements - FAO Irrigation and drainage. Paper 56. FAO, Rome, 1998

Chow V.T., D.R. Maidment, L.W. Mays, 1988. Applied hydrology, MacGraw-Hill. pp. 572.

Eilers, V.H.M., Carter, R.C. and Rushton, K.R. (2007). A single layer soil water balance model for estimating deep drainage (potential recharge): An Application to cropped land in semi-arid North-east Nigeria. *Geoderma,* **140**:119-131

FAO (1984). FAO-UNESO soils map of the world revised legend, world soils resources report, series No. 60 Rome

ILWIS, The integrated Land and Water Information System.

Maathuis, B., 2006, DEM based Hydro-Processing-Introduction to the tools developed, tutorial with exercises (Version 1). International Institute for Geo-information Sciences and Earth Observation (ITC), Enschede, 71 pp

Marengo, J.A., 2005, Characteristics and spatio-temporal variability of the Amazon River Basin Water Budget Climate. Dynamics, vol. 24, pp. 11 –22

Nemani & Running, 1989)

Saxton,K.E., Rawls, W.J., Romberger, J.S. and Papendick, R.I. (1986). Estimating generalized Soil-Water Characterstics from Texture. Soil SCI. SOC. AM. J., Vol. 50

Thornthwaite, C.W. and Mather, J.R. (1955), *The Water Balance*. Drexel Inst. Techno. Laboratory of Climatology, USA.

Vorosmarty, C.J., Fekete, B.M. and Tucker, B.A. (1998). Global River Discharge Database (RivDis). V. 1.1. http://www-eosdis.ornl.gov (Accessed: June 2007)

ACKNOWLEDGEMENTS

I wish to express my thankful words to the German Academic Exchange (DAAD) for the fellowship which enabled us to complete this study at the University of Botswana, leading to a M.Sc. degree in Hydrogeology. The HATWAB model was originally developed by B.F. Alemaw. He is also the supervisor of this research.

APPENDIX A. LOCAL WATER BALANCE FOR SELECTED GRID CELLS IN THE CONGO RIVER BASIN (GRAPHS)

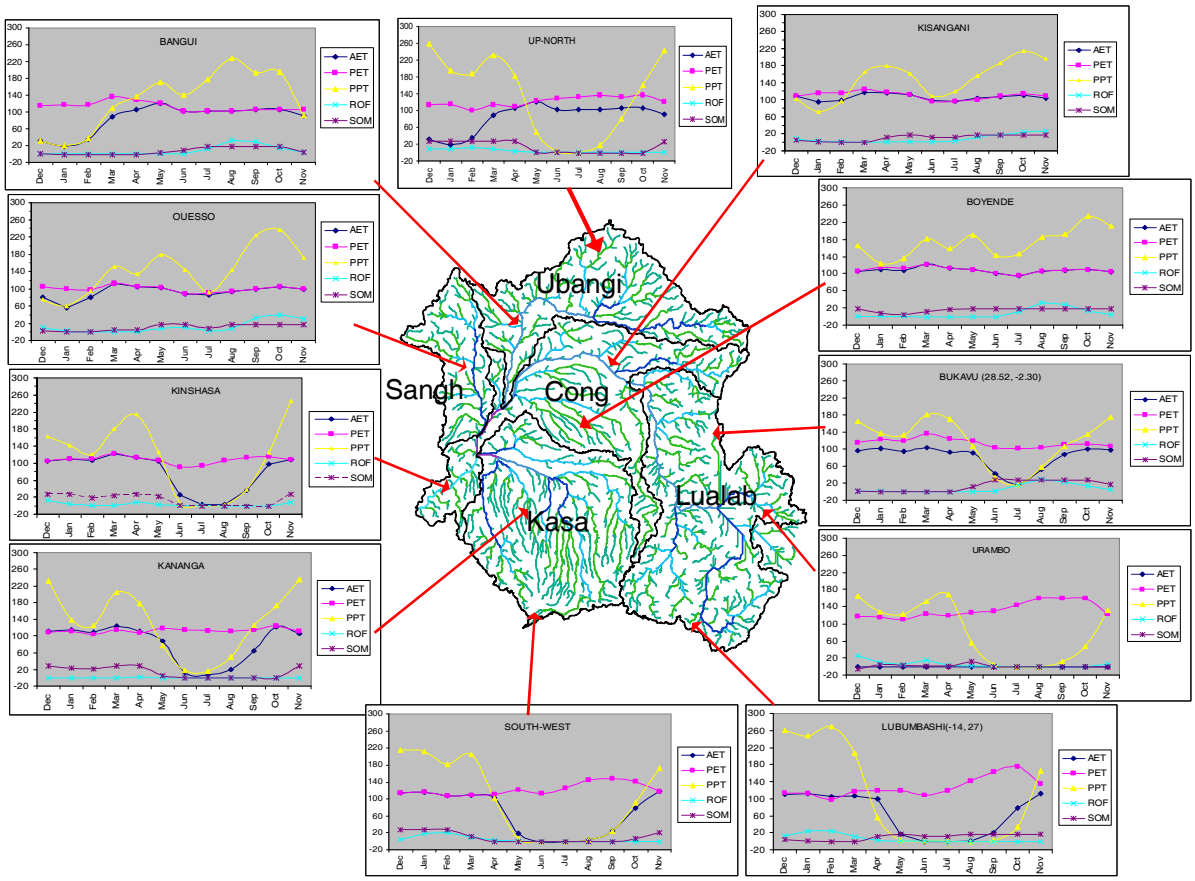

Preliminary assessment of planform change at low flows with vegetation expansion: Platte River, Nebraska

Lisa M. Fotherby[1]

[1] River Engineer, Sedimentation and River Hydraulics Group, Technical Service Center, Bureau of Reclamation, Denver, Colorado; email: lfotherby@do.usbr.gov

ABSTRACT

A central reach of the Platte River in Nebraska has braided, anastomosed, meandering, and wandering channel form. Proliferation of phragmites (*Phragmites australis*) and other in-channel vegetation during eight years of low flow may be altering channel shape. Deterioration of braided reaches, as represented by decreases in width-to-depth ratios (W/D), could reduce habitat for three endangered and threatened bird species. In this preliminary assessment, W/D values for ten cross sections at five study sites surveyed in 2008, are compared to W/D values from surveys at the same locations in 2005, 1998-2001, and 1985. All ten cross sections are on managed lands where vegetation is controlled and removed. ANOVA and paired t-tests showed no significant difference in primary indicator W/D_{ave} between 1985, 2000 and 2005 data sets, but some indication of planform change between 2005 and 2008 (P=0.052). No change between 1985, 2000, and 2005, and significant change between years 2005 and 2008 (P=0.01) are confirmed using a second indicator W/D_{max}. Finding is not the result of vegetation stabilized banks at the sites, or hydrologic regime, but may be due to sediment-short flows. Recommendations are made to extend this study with surveys on unmanaged lands and at sites of meander planform. Future studies may determine if vegetation is altering planform through bank stabilization, and assess if sediment trapping by vegetation and phragmites in overbank areas is reducing sediment transport during high flows.

Key words: low flow, vegetation, invasive species, phragmites, Platte River, planform, braided, width-to-depth ratio, sediment

INTRODUCTION

The study area is a 150-km reach of the Platte River between the cities of Lexington and Chapman in central Nebraska. Although river alignment in this reach forms a large bend to the south, flow is generally west-to-east and discharges to the Missouri River near Omaha, 265 river km downstream of the study area on the eastern border of Nebraska. With no large tributary convergence within the central Platte River study area, flow is relatively consistent from Overton, NE to Chapman, NE. Exceptions are variations at low flow due to small tributaries and groundwater losses and gains, and variations at high flows due to temporary bank storage.

Historically, the river is a sand bed, braided system with a wide shallow channel and multiple instream sand bars. In conjunction with large water resource development in the twentieth century, river planform evolved from predominantly fully-braided to a blend that includes island-braided, anastomosed, wandering, and meandering river

(Fotherby, 2008). The endangered whooping crane (*Grus americana*) uses the river during spring and fall migrations, and the endangered interior least tern (*Sternula antillarum*) and threatened piping plover (*Charadrius melodus*) nest on bare sand areas from May to August (USDOI, 2006). Beginning operation in 2007, the Platte River Recovery Implementation Program (Program) seeks to improve tern and plover productivity and whooping crane migration survival through implementation of adaptive management actions including Program land and water resources (AMP, 2006).

Low Flow and In-Channel Vegetation

Beginning in year 2000 and continuing to year 2008, only one flow approaching 140 m^3/s (Figure 1) was recorded on the Platte River near Kearney (river km 346). Vegetation expanded into the former active channel area while low flows remained concentrated in main channels. In 2005 a rainfall-driven high flow event centered downstream of Kearney, caused a peak flow of 210 m^3/s at Grand Island (river km 265) but less than 85 m^3/s at Kearney. In 2008, a 370 m^3/s high flow at Kearney inundated overbank areas and interrupted an extended period of low flows.

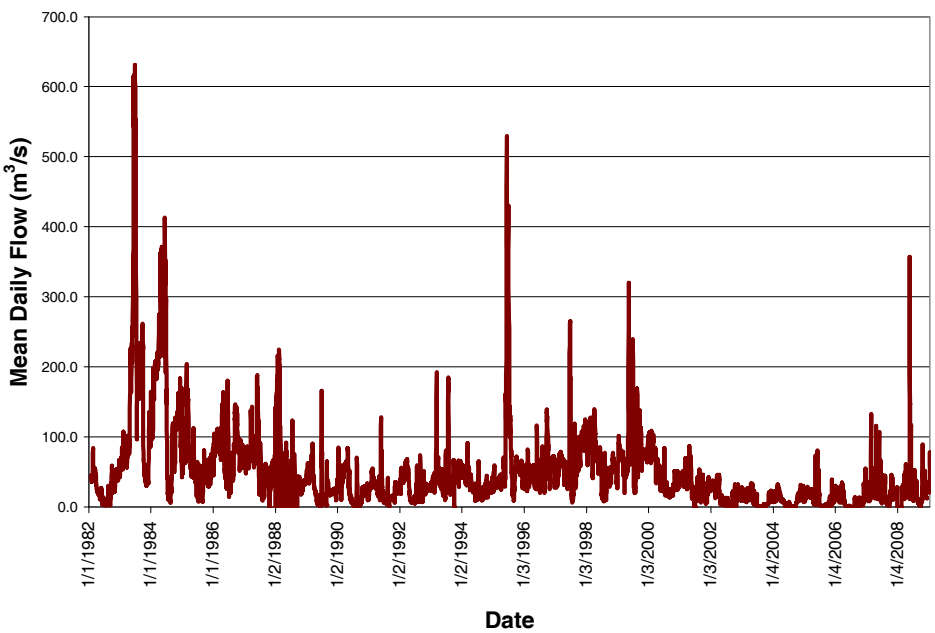

Figure 1. USGS mean daily flows for Platte River nr. Kearney, Nebraska (USGS Site 06770200). Kearney is located at river km 346.

Prior to the low-flow years of 2000-2008, Eastern cottonwood (*Populus deltoides*) and willow species were often the first vascular plants to colonize new sandbars with annual herbaceous also a component of this early succession community (Johnson, 2000). Cottonwood and willow were the plant species believed to have the largest influence on geomorphic processes through bank stabilization. Phragmites (*Phragmites australis*), an invasive plant that has become prevalent during the low-flow years, is now suspect for having a greater affect than cottonwood or willow on physical river processes. In 2005, phragmites was identified as a cause of reduction in floodplain

capacity at North Platte, 100 river km upstream of Lexington (J.F. Sato and Associates, 2005). A 2005 GIS vegetation data base, jointly developed by the Program and the Platte River Whooping Crane Maintenance Trust, shows intermittent phragmites infestations throughout the study area from Lexington to Chapman.

This pervasive species spreads through seeds, rhizomes, and stolons. Stolons can extend thirty feet across the dry bed of a channel and plants can establish on bare sand or in areas of less dense vegetation that are not shaded. There is also a relatively wide elevation band for phragmites to establish since the roots appear tolerant of some submergence, and the stands can establish high on the banks and still reach surface or groundwater through root extension.



Figure 2a and 2b. Figure 2a (left) shows a phragmites thicket on a stabilized bar with a stolen, held aloft by photographer, extending from the thicket. Figure 2b (right) shows flow debris and stolons from 2008 high flow, protecting undercut bank vegetated by young phragmites.

Proliferation of this species produces a great deal of biomass. During higher flows, stolons lay across the submerged banks creating a protective mat, while floating detritus, often broken pieces of upstream phragmites, also catch on the banks adding to the protective cover. As the plant forms impenetrable stands contributing to a protective mat of coverage, bank and bar resistance values for the channel increase. Sediment can also be trapped amongst the plants in bar or overbank areas during high flows. Based on field observations, thickets of phragmites are resistant to erosion in the central Platte River in most locations, but are occasionally susceptible to undercutting due to a shallow root system (0.3 – 0.4 m estimated). Plants and roots on high, steep banks or bars can be undermined by flow directed towards a bank, or undermined by erosive shear forces from secondary currents. Bed incision can also promote failure.

Vegetation and River Planform

Stabilizing effects of vegetation on banks have been reported in foundation papers on river planform by Friedkin, 1945, Lane, 1957, and Brice, 1964. Papers by Murray and Paola (2003), Tal et al., (2003), Tal and Paola (2007), Griffin and Smith (2004) further demonstrate planform transitions between braided and single channel with the expansion or reduction of riparian vegetation. Width-to-depth ratio, W/D, can be used as an indicator of planform change (Fergusson, 1987). As vegetation stabilizes banks and bars, and stores sediment in overbank areas, erosion resistant banks concentrate

flow in the channel. Gran and Paola (2001) report an order of magnitude difference in W/D between channels with vegetated and unvegetated banks in laboratory studies. Trimble (2004) provides field examples where streams with grassed banks have smaller W/D than streams with forested banks, and store more silts and fine sands.

Purpose

Field observations of more prevalent steep banks and fine to coarse gravels in the bed of many sub channels, in addition to the pervasiveness of phragmites and other vegetation in the channel floodplain, suggest a relatively rapid change in channel conditions. An opportunistic survey in the summer of 2008, following a high flow event, provides data for preliminary analyses to assess changes in river form. However 2008 cross sections are only available from managed sites where vegetation was periodically removed to improve bird habitat. In future studies, cross sections from unmanaged sites can be used to extend findings from this study.

River changes that decrease braided channel and increase meander channel are believed to reduce the occurrence of desirable habitat for target species in this study area. Program management actions were developed prior to the period of low flows and the advance of phragmites and other vegetation. Proposed management actions can be modified under adaptive management to accommodate identified changed conditions. In addition to aiding Platte River management efforts, conclusions from this paper contribute to improved understanding of vegetation impacts on river form.

Purpose of this paper is to assess river planform change coincident to the recent period of low flows, rapid spread of phragmites, and general expansion of vegetation into former areas of active channel in the Platte River study area. Change in planform is assessed using indicators of W/D computed from four sets of cross sections in different years, with two sets surveyed during the period of low flows.

METHODS

Between 1983 and 1988, 85 transects at 16 local areas of the river were surveyed two to nine times (USDOI, 1989: Farmer et al., 2000). Surveys were for whooping crane habitat studies and the sites were primarily selected at locations of fully braided river. Reclamation resurveyed some sites between 1998 and 2001, and again in 2005. Three transects from six sites were selected in the 2005 survey based on the presence of active sand bars at transect locations. Transect data, a description of surveys, and description of data reduction from repeat surveys in July 1985, the 1998 to 2001 period (described here as year 2000), and in 2005 are reported in Holburn et al., 2006. A fourth survey in June 2008 of two transects at five sand bar/habitat sites was conducted by the Executive Director's Office of the Program. Habitat transects are also referred to here as cross sections.

Transect data from each survey year are entered as sets of cross sections in a HECRAS 4.0 Beta program to compute water surface and flow area of the main channel. Cross sections are assigned a spacing of 305 m at a thalweg invert slope of 0.0012. A steady reference flow of 57 m^3/s is input for computing flow area, wetted width of the main channel, maximum flow depth, and hydraulic depth of the transect (Table 1). As an indicator of planform change, W/D is normally defined by an average value of depth (Lane, 1957; Brice, 1964; Gran and Paola, 2002; Kiss and Sipos, 2006). Main indicator

W/D_{ave} is computed as wetted main channel width divided by hydraulic depth (D_{ave}) of the main channel at every transect (Table 2).

Table 1. Hydraulic parameters at 57 m^3/s and slope of 0.0012

	Hydraulic depth (m)				Maximum channel depth (m)				Top width wetted channel (m)			
River Sta	1985	2000*	2005	2008	1985	2000*	2005	2008	1985	2000*	2005	2008
4A-TR3	0.70	0.37	0.51	0.53	1.02	0.84	1.05	1.18	200.1	191.1	196.1	142.9
4A-TR2	0.43	0.61	0.48	0.48	1.07	0.90	0.97	0.98	155.3	233.1	188.7	194.0
6 -TR4	0.33	0.36	0.39	0.41	0.84	1.04	1.00	1.05	393.0	361.8	385.9	382.3
6 -TR3	0.38	0.41	0.32	0.37	0.80	1.11	0.96	1.12	309.4	360.5	313.0	310.4
8B-TR3	0.44	0.34	0.43	0.35	0.87	1.08	0.97	0.93	324.9	285.7	346.9	272.3
8B-TR2	0.37	0.53	0.41	0.49	0.86	1.16	1.03	0.91	256.3	280.7	261.6	253.1
9BW-TR4	0.60	0.28	0.42	0.59	0.89	1.07	0.87	1.05	206.6	212.2	213.5	214.6
9BW-TR2	0.47	0.47	0.49	0.33	1.01	0.82	0.87	0.98	253.8	262.6	262.1	226.9
9BE-TR7	0.33	0.57	0.41	0.70	0.86	0.98	0.89	1.19	246.8	261.6	241.7	276.4
9BE-TR2	0.44	0.44	0.44	0.45	0.67	1.12	0.82	1.42	263.0	254.0	256.3	243.9
Average	0.45	0.44	0.43	0.47	0.89	1.01	0.94	1.08	260.9	270.3	266.6	251.7

2000* data from 1998 to 2001

Table 2. W/D_{ave} and W/D_{max} at 57 m^3/s for1985, 2000, 2005, and 2008 transects.

		W/D_{ave} 0.0012 slope				W/D_{max} 0.0012 slope			
Transects	RM	1985	2000*	2005	2008	1985	2000*	2005	2008
4A-TR3	227.4	285	518	383	271	195	227	186	121
4A-TR2	227.25	359	382	397	408	145	259	194	198
6-TR4	206.4	1183	1015	997	929	466	348	387	364
6-TR3	206.2	819	883	969	835	389	325	327	277
8B-TR3	191.1	735	845	807	777	374	266	357	293
8B-TR2	190	695	526	631	513	297	243	253	280
9BW-TR4	178.32	346	749	508	365	231	199	244	205
9BW-TR2	178.23	541	563	537	683	250	319	300	230
9BE-TR7	177.4	743	459	587	393	286	266	272	231
9BE-TR2	177.15	604	571	580	537	392	226	313	172
Mean		631	651	640	571	303	268	283	237
Variance		72356	43264	47024	49802	10189	2351	4358	4769

2000* data from 1998 to 2001 Average Variance W/D_{ave} = 53,112 Average Variance W/D_{max} = 5,417

Kiss and Sipos (2006) used D_{max} values to assess the variability in the channel bed. Disparity between mean depth (D_{ave}) and maximum depth (D_{max}) can represent a more expressed thalweg and less homogeneity of the channel bed although there may be little variation in bed shape outside the limits of concentrated low flow. Wetted width and depth values are listed for comparison in Table 1. W/D (Table 2) is also computed as wetted main channel width divided by maximum depth of the main channel (D_{max}) to provide a second indicator of planform change.

Assessment of W/D is aided by a statistical examination (Excel Analysis ToolPak) using paired t-tests and ANOVA evaluations of variance. Statistical assessments of the primary indicator W/D_{ave}, a second indicator W/D_{max}, and review of plotted results are

used to determine if there is a significant difference in river planform at study cross sections between survey years.

RESULTS

Information from Table 2 is presented in a series of figures. Plotted in figures 3 and 4 are W/D_{ave} and W/D_{max} with respect to time for each transect surveyed. There are two lines in Figure 5, the W/D_{ave} mean for all transects and the W/D_{max} mean for all transects. In Figure 6, all study W/D_{ave} and W/D_{max} values are plotted by river km.

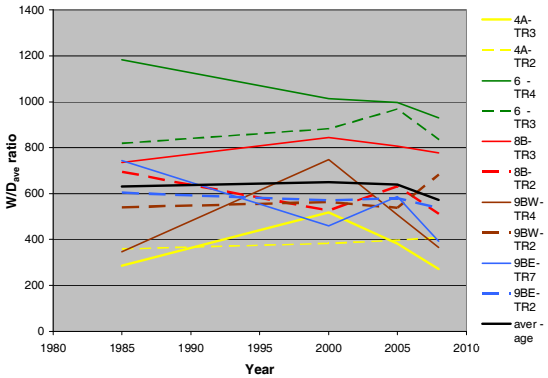

Figure 3. W/D_{ave} for each transect.

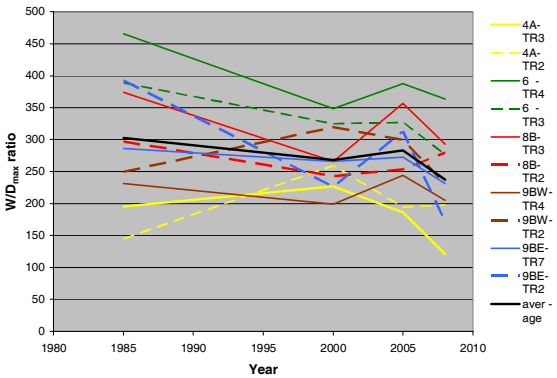

Figure 4. W/D_{max} for each transect.

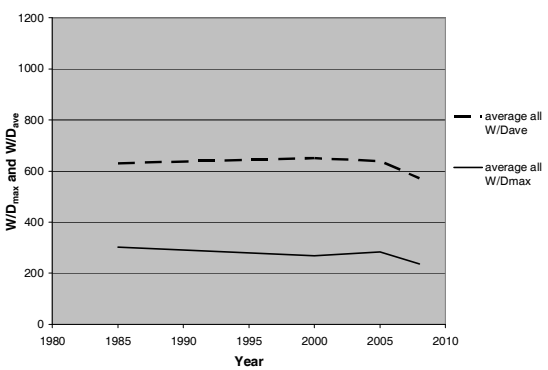

Figure 5. Average W/D_{ave} (dashed line) and W/D_{max} (solid lines).

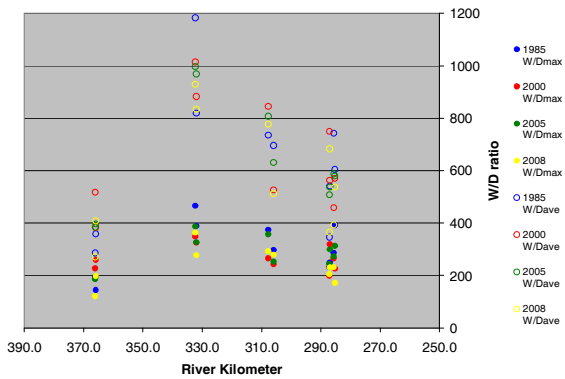

Figure 6. W/D_{ave} and W/D_{max} by river kilometer.

W/D_{ave} Results

There is no consistent trend in W/D_{ave} between 1985 and 2000, and between 2000 and 2005 in Figure 3; however seven of ten transects had a decline in W/D_{ave} between 2005 and 2008. Average values in Figure 5 are consistent from year 1985 to 2000, and from year 2000 to year 2005, but between year 2005 and year 2008 there is a decrease in W/D_{ave}. Statistical assessments using ANOVA Single Factor and ANOVA Two Factor with Replication indicate there is no significant difference in mean W/D_{ave} between all four years of transects (Table 3). An exception is site data: ANOVA with Replication testing confirms significant differences in means for transects at each site.

Based on ANOVA testing, the average decline (Table 3) in W/D_{ave} between 2005 and 2008 is not significant and could be the result of random occurrence of values. Paired

t-tests (Table 4) provide specific information between years, with some indication that the average decline in W/D_{ave} between year 2005 and 2008 is significant. To be a significant change, probability from the paired t-test for 2005 and 2008 should be 0.05 or less. Computed probability from this paired t-test was slightly higher at 0.052.

W/D_{max} Results

Planform comparison is based on W/D_{ave}, but W/D_{ave} results are ambiguous in comparisons of 2005 and 2008 data. To resolve the question of significant differences, a second indicator, W/D_{max}, is also examined. Values of W/D_{max} in Figure 4 are more consistent than W/D_{ave} values in Figure 3, and have smaller variance within the data set for each year (Table 2). Data from six out of 10 transects have a decline in W/D_{max} between years 1985 and 2000, and 8 out of 10 transects have a decline in W/D_{max} from year 2005 to year 2008. Consistent with W/D_{ave} results, there is no clear pattern of change for W/D_{max} between years 2000 and 2005.

Results of the second indicator W/D_{max} appear to be more sensitive to changes in the channel bed. Both ANOVA tests (Table 3) indicate the difference in means between years is significant and probably not the result of random chance. Paired t-tests (Table 5) provide specific information confirming a significant difference between channel planform in years 2005 and 2008 (P=0.010), and also indicate significant difference between years 1985 and 2008 (P=0.019). Wetted top width is the same value in both W/D indicators so increased sensitivity is a function of maximum depth.

Table 3. ANOVA statistical results for W/D_{ave} and W/D_{max}

W/D_{ave}				W/D_{max}			
Variation between	F	P-value	F crit	Variation between	F	P-value	F crit
ANOVA: Single Factor				*ANOVA: Single Factor*			
Years	0.241	0.867	2.866	Years	1.417	0.254	2.866
ANOVA: Two-Factor With Replication				*ANOVA: Two-Factor With Replication*			
Sites	**23.571**	**0.000**	**2.866**	Sites	**15.378**	**0.000**	**2.866**
Years	0.806	0.505	3.098	Years	**3.792**	**0.027**	**3.098**

Table 4. Results of paired t-tests for W/D_{ave}

t-Test: Paired Two Sample for Means

W/D_{ave}	1985	2000	1985	2005	1985	2008	2000	2005	2000	2008	2005	2008
Mean	631	651	631	640	631	571	651	640	651	571	640	571
t Stat	-0.315		-0.232		1.229		0.322		1.794		**2.243**	
P(T<=t) two-tail	0.760		0.821		0.250		0.755		0.106		**0.052**	
t Critical two-tail	2.262		2.262		2.262		2.262		2.262		**2.262**	

Table 5. Results of paired t-tests for W/D_{max}

t-Test: Paired Two Sample for Means

W/D_{max}	1985	2000	1985	2005	1985	2008	2000	2005	2000	2008	2005	2008
Mean	303	268	303	283	303	237	268	283	268	237	283	237
t Stat	1.260		1.285		**2.840**		-0.961		1.958		**3.231**	
P(T<=t) two-tail	0.239		0.231		**0.019**		0.362		0.082		**0.010**	
t Critical two-tail	2.262		2.262		**2.262**		2.262		2.262		**2.262**	

DISCUSSION

As presented in Holburn et al., 2006, habitat sites were originally selected by searching for the widest reaches of river and the locations with highest use by sandhill cranes. Sites in 2005 and 2008 were also selected because of relatively easy access provided by the owners who were in most cases non-government organizations (NGO's). NGO's actively manage their lands for bird use by periodically removing vegetation from the banks and within the active channel. In effect, this study looks for phragmites and in-channel vegetation impacts to W/D ratios, with cross sections from lands where vegetation is mechanically removed by discing (tractors pulling agricultural discs turn over the upper soil layer and chop vegetation).

If the cross section sites were successfully managed to restrain vegetation, the expectation for these sites is that there should be no change in planform as represented by the indicator W/D_{ave}. ANOVA tests detect no significant difference between W/D_{ave} values for each year when all years are considered. Paired t-tests support this conclusion between W/D_{ave} values from 1985, 2000, and 2005, but there is a near-significant finding (P=0.052 instead of 0.050 or smaller) when 2005 data is paired with 2008 data. Because this result is not conclusive, a second indicator is considered.

Secondary Indicator, W/D_{max}

W/D_{max} is based on thalweg geometry and was selected because of the significance of thalweg slope to hydraulic computations and to planform determination. W/D_{max} values prove more consistent than W/D_{ave} values, having an average variance one-tenth (Table 2) the magnitude of the average variance for the W/D_{ave} values. This second indicator is also more sensitive to differences between years of data. Paired t-tests confirm W/D_{ave} results of no significant differences between 1985, 2000, and 2005 planform; confirm there is a difference between 2005 and 2008 planform; and also detect a difference between 2000 and 2008 planform.

A finding of significant difference in 2008 planform sites managed to restrain vegetation, prompts consideration of factors beyond the presence or absence of vegetation at the site.

Hydrologic Regime

Timing and occurrence of high and low flow events can affect channel shape, but with one exception, the data sets represent similar hydrologic conditions: surveys occurred within two years of a high flow event that had a recurrence interval greater than 1.5 years. Data from July 1985 represent a wet period with high flows occurring in 1983 and 1984, less than one year prior to the survey. The 2000 data set was surveyed, depending on location, from 1998 to 2001 and there was no more than two years of low flow succeeding a high flow event. A 510 m^3/s peak flow in 1995 at Kearney (Figure 1) was followed by a 255 m^3/s peak flow in 1997 and a 340 m^3/s peak flow in 1999. Sites 4A and 6 in 2005 are the one exception where the survey was preceded by five years of low flow. Although sites 8B, 9BW, and 9BE were surveyed at the same time as sites 4A and 6 in 2005, a rainfall event downstream of Kearney generated high flows at sites 8B, 9BW and 9BE four months previous to the survey.

Results from paired t-tests of both the primary and secondary indicators indicate no difference in planform between the 1985, 2000, and 2005 data sets, measured from

four months to two years after a high flow event. Surveys in 2008 represent channel conditions immediately following a high flow event and there is less than four months of low flows preceding the measurements.

Sediment Transport

Sediment regime in conjunction with flow regime can also affect channel bed shape. Kiss and Sipos (2006) describe a braided river in South Hungary that aggrades in wide braided channel during the falling limb of a high flow event, but narrows and deepens channel when flow is concentrated during low flow periods with less sediment transport. In Colorado River studies, high flow events cause greater aggradation when sediment is delivered by tributaries and stored in the channel previous to the high flow event. Platte River 1985, 2000, and 2005 cross sections were used to compute area changes in the channel bed in Holburn et al., 2006. Cross sections at sites 4A and 6 have more aggradation (increases in area at the transect) in 2005 succeeding five years of low flow, than measured in previous surveys. Downstream cross sections at Sites 8B, 9BW, and 9BE conveyed high flows from a rainfall event in 2005. At these locations there was no measured aggradation, and the channel bed area was similar to previous years.

A shortage of transported sediment during the 2008 high flow event could account for the narrowing and deepening of the channel at the study sites. Sediment-short flows were computed to extend as far downstream as site 4A under conditions existing previous to 2002, and to cause some erosion (Holburn et al., 2006, Murphy et al., 2006). Downstream limits of this erosion process may have been extended by increased presence of instream vegetation and phragmites. Phragmites are observed to trap sediment and 2008 planform change at the managed study sites could be due to sediment trapping in extensive phragmites thickets and other instream vegetation at unmanaged sites upstream.

Future Directions

With this preliminary study, we begin to assess impacts of an eight-year low flow period on river morphology in the central Platte River. Results indicate planform change has occurred between 2005 and 2008 at fully braided and managed sites, and change may be a result of upstream sediment shortage. It is surmised that in channel vegetation upstream of study sites could be a contributing factor to the sediment shortage. Future studies should include surveys at 2008 cross sections, surveys at unmanaged sites, and surveys at sites with meander form to continue an investigation of geomorphic change; specifically to measure impacts of phragmites and other in channel vegetation on bank stabilization and on river sediment storage.

ACKNOWLEDGEMENTS

My thanks go to reviewers Jason Farnsworth and Chad Smith, from the Executive Directors office of the Program, for their constructive comments during preparation of this paper; and to the Executive Directors Office of the Platte River Recovery Implementation Program for use of the 2008 survey data.

REFERENCES

Adaptive Management Plan (AMP) (2006). "Final Platte River Recovery Implementation Program." U.S. Department of the Interior, State of Wyoming, State of Nebraska, State of Colorado.

Brice, J.C. (1964). "Channel patterns and terraces of the Loup River in Nebraska." *U.S. Geological Survey Professional Paper, 422-D*.

Farmer, A.H., Cade, B.S., Terrell, J.W., Henriksen, J.H., Schneider, D.M., and T.S. Fancher (2000). "Evaluation of a suitability model and associated procedures utilized for assessment of Whooping Crane (Grus Americana) habitat in the Platte River, Nebraska." Final report to U.S. Fish and Wildlife Service, Region 6. Contract #1448-60181-99-N292. Midcontinent Ecological Science Center, Fort Collins, Colorado, 198p.

Fergusson, R.I. (1987). "Hydraulic and sedimentary control of channel pattern." In: Richards, K.S. (Ed.), *River Channels: Environment and Process*, Blackwell, Oxford, 129-158.

Fotherby, L.M. (2008). "Valley confinement as a factor of braided river pattern for the Platte River." *Geomorphology*. doi:10.1016/j.geomorph.2008.08.0011

Friedkin, J.F. (1945). "A laboratory study of the meandering of alluvial rivers." U.S. Waterways Experiment. Station, Vicksburg, Mississippi, 40p.

Gran, K., and Paola, C. (2001). "Riparian vegetation controls on braided stream dynamics." *Water Resources Research*, 37(12), 3275-3283. doi:10.1029/2000WR000203.

Griffin, E.R. and Smith, J.D. (2004). "Floodplain stabilization by woody riparian vegetation during an extreme flood." In. Bennet, S.J., and A. Simon, (Eds.), *Riparian Vegetation and Fluvial Geomorphology*, Water Science and Application 8, Washington D.C., AGU, 221-236.

Holburn, E.R., Fotherby, L.M., Randle, T.J., Carlson, D.E. (2006). "Trends of aggradation and degradation along the central Platte River: 1985 to 2005." U.S. Department of Interior, Bureau of Reclamation, Denver, Colorado, 180p. Avail. online at: http://www.usbr.gov/pmts/sediment/projects/ index.html

J.F. Sato and Associates, (2005). "Final report North Platte channel capacity study." Littleton, Colorado: Lowrey.

Johnson, W.C. (2000). "Tree recruitment and survival in rivers: influence of hydrological processes." *Hydrological Processes*, 14, 3051-3074.

Kiss, T., and Sipos, G. (2006). "Braid-scale channel geometry changes in a sand-bedded river: Significance of low stages." *Geomorphology* 84 (2007), 209-221.

Lane, E.W. (1957). "A study of the shape of channels formed by natural streams flowing in erodible material." U.S. Army Engineer Division, Missouri River Corps of Engineers, Omaha, Nebraska, M.R.D. Sediment Series. No. 9, 106 p.

Murphy, P.J., Fotherby, L.M., Randle, T.J., Simon, R. (2006). "Platte River Sediment Transport and Riparian vegetation Model." U.S. Department of Interior, Bureau of Reclamation, Denver, Colorado, 136p. Avail. online at: http://www.usbr.gov/pmts/sediment/projects/index.html.

Murray, A.B., and Paola, C. (2003). "Modeling the effects of vegetation on channel pattern in bedload rivers." *Earth Processes and Landforms*, 28, 131-143. doi: 10.1002/esp.428.

Tal, M., Gran, K., Murray, A.B., Paola, C., Hicks, D.M. (2004). "Riparian vegetation as a primary control on channel characteristics in multi-thread rivers." In. Bennet, S.J., and Simon, A. (Eds.), *Riparian Vegetation and Fluvial Geomorphology*, Water Science and Application 8, Washington D.C., American Geophysical Union, 43-58.

Tal, M. and Paola, C. (2007). "Dynamic single-thread channels maintained by the interaction of flow and vegetation." *Geology*, 35(4), 347-350. doi: 10.1130/G23260A

Trimble, S.W. (2004). "Effects of Riparian Vegetation on Stream Channel Stability and Sediment Budgets." In: S.J. Bennet and A. Simon (Eds.). *Riparian Vegetation and Fluvial Geomorphology*, Water Science and Application 8, Washington, D.C., American Geophysical Union, 153-169.

U.S. Department of the Interior (USDOI) (1989). "Prairie Bend Unit, P-S MBP, Nebraska. Regional Directors Planning report/Draft Environmental Statement." Hydrology Appendix Volume 1 of 3. Bureau of Reclamation.

U.S. Department of the Interior (USDOI) (2006). "Platte River Recovery Implementation Program Final Environmental Impact Statement." Bureau of Reclamation and U.S. Fish and Wildlife Service, Platte River EIS Office, Denver, Colorado.

Sediment Management for Shallow Water Habitat Creation on the Missouri River

Michael Gossenauer, PE[1]

[1]River Engineering & Restoration Section, U.S. Army Corps of Engineers, Kansas City District, 700 Federal Building, 601 East 12th Street, Kansas City, Missouri 64106; PH (816) 389-3162; FAX (816) 389-2011;
email: michael.b.gossenauer@usace.army.mil

ABSTRACT

For the last several years the Corps of Engineers has engaged in a major effort to restore Shallow Water Habitat (SWH) on the Lower Missouri River to prevent continued jeopardy of the federally-endangered Pallid Sturgeon. Much of the SWH has been restored through the mechanical creation of side channel chutes, river top-width widening, and backwater excavation. Almost all methods require the removal of previously deposited alluvial sediments existing adjacent to the river as well as in the floodplain. The number and size of these projects have created new challenges in the management of this sediment. Issues with the reintroduction of sediment into the active river system, such as nutrient loads, contaminants, impacts on downstream interests, and public perceptions, illustrate the wide variety of topics that complicate the management of those sediments. Some of the issues are not well understood and the process of sediment reintroduction can appear to be at odds with current national priorities to keep sediments out of rivers. To help clarify the issues related to sediment management associated with SWH creation and to provide guidance for future projects, the Corps of Engineers (Corps) has initiated an independent review of its practices by the Water Science and Technology Board of the National Research Council (NRC). Description of sediment displacement activities on SWH projects and details of the NRC review will be discussed.

BACKGROUND

Prior to 1900, the Missouri River existed in its natural state and meandered across the river valley eroding approximately 9,100 acres per year in the meander belt (USACE, 1981). Subsequently, the habitat in and around the river was varied and dynamic as the erosion and related deposition reshaped the river and floodplain. However, from 1912 to 1945, seven Congressional Acts set in motion the Corps' Bank Stabilization and Navigation Project (BSNP), which was completed in 1981 and reshaped the face of the river by the construction of revetments, dikes, and side-channel closures that effectively locked the river in place and created a reliable navigation channel.

A less desirable effect of the BSNP was the loss of 100,200 acres of aquatic habitat and over 421,800 acres of terrestrial habitat (USACE, 1981). With various acts between 1986 and the present, Congress authorized the Corps' Missouri River Mitigation project to acquire land for habitat development to replace 32 percent of that which was lost due to construction of the BSNP (USACE, 2003).

The U.S. Fish and Wildlife Service completed a Biological Opinion (BiOp) in 2000, amended in 2003, in regard to Corps operation and maintenance of the BSNP, the six Corps dams on the Missouri River, and the Kansas River Reservoir system. The BiOp offered measures and alternatives to avoid continued jeopardy of three threatened and endangered species on the Missouri River, including the pallid sturgeon. As outlined in the BiOp, a component of the reasonable and prudent alternative for recovery of the pallid sturgeon was to restore 20 percent of the shallow water habitat (SWH) that historically existed on the river. For the lower 752 miles of river below Gavin's Point Dam, a target was set to restore 19,565 acres of SWH, or approximately 20-30 acres per mile of river, by the year 2020 (USFWS, 2000).



Figure 1. Typical Chute Project on the Missouri River

The BiOp provided for restoration of SWH by either mechanical manipulation of the river itself and/or modification of the flow regime by Corps operated upstream dams (USFWS, 2000). Since altering the flow regime could negatively impact other users of the river, the Corps of Engineers focused on reaching the target acreage through mechanical manipulation of the river itself. This entails the modification of the Corp's river training structures to increase top-width and the creation of side channel chutes. The mechanical excavation of chutes (Figure 1), and top-width widening

(Figure 2) involve the removal of large quantities of alluvial sediments from the bank or floodplain adjacent to the river.



Figure 2. Typical Bank Notches for Increasing Top Width

ISSUES

Overview. The Corps' management of the displaced sediments from SWH projects has been questioned by the Missouri Clean Water Commission (MCWC) and has given rise to ongoing discussions on Missouri River sediment management that highlight the numerous related issues that complicate the decision making process including nutrient loads, contaminants, impacts on downstream interests, and public perceptions. While much has been done in an attempt to resolve issues through communication between the Corps, the MCWC, and various other state and federal agencies, questions still remain as to an appropriate path forward. To assist in evaluating these issues, the Water Science and Technology Board of the National Research Council (NRC) was engaged to perform an independent review of the Corps' sediment management on the Missouri River.

SWH Construction. The Corps has designed projects that include multiple methods of addressing the sediments that must be displaced to restore SWH. The most common methods fall into three categories: side-casting the material directly adjacent to the chute or bank work, mechanical placement of the material in the river channel to be gradually removed by natural river flows, and dredging of the material and discharging directly into the river channel to mix with the existing bed sediment load.

In nearly all cases, the designs also involve construction of a narrow pilot channel, then allowing natural river processes to redistribute the adjacent sediments over time and enlarge the projects to the designed size but with controls to prevent unchecked expansion beyond the design limits. After development, the projects would continue to meander and promote natural riverine processes, but without significant changes in channel width.

Per the BiOp, the Lower Missouri River is impacted by reduced sediment inputs that are important to creating and maintaining the diversity of habitats important for pallid sturgeon reproduction and survival. In addition, the reduction of turbidity has highly altered the river environment, impacting pallid sturgeon capability to forage successfully, increasing competition with other species and making the species more susceptible to predation (USFWS, 2000). Due to these reasons, the Corps viewed placement of the excavated or dredged sediments into the river as not only an economical alternative, but as potentially beneficial to the river. However, the MCWC raised questions as to the potential water quality impacts of placing the sediments in the water. In particular, they expressed concern that there could be agricultural chemicals present in the sediments since some of the sites had been farmed in the past, prior to being used for SWH construction.

To address the MCWC concerns, the Corps implemented a coordinated soil and water testing program to evaluate both the sediments that would be removed for the SWH projects as well as the impacts those sediments would have on water quality if reintroduced into the river. The water quality variables that were analyzed are shown in Table 1. The Corps began this program in 2007 with five SWH chute sites in Missouri that were either under construction or scheduled to be constructed. The testing and analysis showed that there was no reason to believe the placement of the sediments in the river would cause the violation of any water quality standards for the sampled variables (CDM, 2007a,b,c,d,e; CDM, 2008).

Table 1. Water and Soil Quality Variables Analyzed at SWH Chutes

Ammonia	Metals – Total and Dissolved
Biological Oxygen Demand (BOD)	Cadmium
Chemical Oxygen Demand (COD)	Chromium
Nitrogen – Total	Copper
Nitrogen – Total Kjeldahl Nitrogen	Lead
Kjeldahl Nitrogen	Nickel
Nitrogen – Total Nitrate/Nitrite as N	Zinc
Phosphorus – Total	
Phosphorus - Soluble Reactive	Pesticides
Total Organic Carbon	Chlordane
PCBs – Total	Dieldrin
TPH -DRO	DDT and metabolites
BTEX	

Despite the results of the soil and water testing, the MCWC continued to express concern with the implications of allowing the sediments to be placed back into the river for several reasons. Among these concerns were the perceived contradiction

with Missouri's soil conservation efforts, questions as to whether sediment itself is a pollutant, and the concern that *any* increase in nutrient load, even if not violating water quality standards, could be increasing the Missouri River's contribution to Gulf of Mexico hypoxia.

While the Corps and cooperating agencies continued communications with the MCWC, a fundamental difference of interpretation of the role of sediment in a river system, with regards to soil conservation efforts and the Clean Water Act led to significant impasses for State of Missouri permitting of the SWH projects. As a result, nearly all SWH projects that were either underway or planned in Missouri were suspended and/or terminated during 2007 and 2008.

PATH FORWARD

With support of a joint federal position between the Corps, the U.S. Fish and Wildlife Service, and the U.S. Environmental Protection Agency, the Corps requested the National Academies to provide an unbiased, independent look at the issues, suggest a path forward, and evaluate the Corps sediment management on the Missouri River. In mid 2008, the NRC assembled a committee to conduct a two year review to answer the following questions regarding sediment issues on the Missouri River:

1) How and why is sediment a significant variable in the environmental restoration of a river system like the Missouri River?
2) What is the significance of the Missouri River sediments to the Gulf of Mexico Hypoxia problem?
3) What is the significance of the Missouri River sediments to the restoration of Louisiana coastal wetlands?
4) What are the key environmental and economic considerations regarding nutrient loads and/or contaminants in Missouri River sediment? To what extent can such issues be addressed with management strategies?
5) Are there long-term consequences to the lack of sediment in the system to the human environment, either environmentally or economically?
6) Are there alternatives for reintroducing sediment into the system? What are they and what are the key constraints surrounding these alternatives?
7) Are current Corps' management strategies, restoration tools (e.g., channel widening, creation of chutes, shallow water habitat, etc.), and other activities adequate and comprehensive enough to address issues associated with sediment and nutrients in the system? If not, how might such strategies and activities be improved?

While constraints on SWH construction in Missouri have indefinitely suspended many projects and reduced options for others, the Corps plans to use the NRC report to gain clarification on the controversial issues and suggestions for a path forward that will enable the Corps to continue the restoration of SWH on the Missouri River in an environmentally conscious, and socially acceptable manner.

REFERENCES

CDM Federal Programs Corporation. 2007a. *Missouri River Fish and Wildlife Mitigation Project for the Baltimore Bend Site*. September.

CDM Federal Programs Corporation. 2007b. *Missouri River Fish and Wildlife Mitigation Project for the Barney Bend Site*. September.

CDM Federal Programs Corporation. 2007c. *Missouri River Fish and Wildlife Mitigation Project for the Jameson Island Site*. September.

CDM Federal Programs Corporation. 2007d. *Missouri River Fish and Wildlife Mitigation Project for the Rush Bottom Bend Site*. September.

CDM Federal Programs Corporation. 2007e. *Missouri River Fish and Wildlife Mitigation Project for the Tarkio River Fish and Wildlife Mitigation Project Site*. September

CDM Federal Programs Corporation. 2008. *Missouri River Fish and Wildlife Mitigation Project for the Jameson Island Site, Addendum Report*. January.

USACE (U.S. Army Corps of Engineers). 1981. *Missouri River bank stabilization and navigation project final EIS for the fish and wildlife mitigation plan.* Omaha District, Omaha, Nebraska.

USACE. 2003. *Final Supplemental Environmental Impact Statement for the Missouri River Fish and Wildlife Mitigation Project.* March.

USFWS (U.S. Fish and Wildlife Service). 2000. *Biological opinion on the operation and maintenance of the Missouri River Main Stem Reservoir System, operation and maintenance of the Missouri River Bank Stabilization and Navigation Project, and operation of the Kansas River Reservoir System.*

Design of Solar Radiation Sensor Network Using Geo-statistical Methods

Chandra S. Pathak[1], John R. Mecikalski[2], Ramesh S. Teegavarapu[3], and Jayanthi Srikishen[2]

[1] Operations and Hydro Data Management Division, South Florida Water Management District, West Palm Beach, FL 33416; PH (561) 682-2567; email: cpathak@sfwmd.gov

[2] University of Alabama in Huntsville, Atmospheric Sciences Department, Huntsville, Alabama 35805; PH (256)961-7046; e-mail: johnm@nsstc.uah.edu

[3] Department of Civil Engineering, Florida Atlantic University, Boca Raton, FL 33431; PH (561) 297-3444; e-mail: ramesh@civil.fau.edu

Abstract

Accurate measurement of solar radiation via optimal number of ground sensors and their respective location is important to estimate evapotranspiration (ET). One way of estimating ET on regional scales at high spatial resolution (~2 km) on daily time scales is through the use of GOES Satellite solar radiation data. The goal of this study is to perform analysis that helps determine the design of a ground-based solar radiation sensor network that can accurately estimate solar radiation spatially. This paper developed several optimal sensor network designs considering different levels of accuracy characterizing the spatial and temporal variability of solar insolation data. GOES Satellite-estimated solar insolation and ground sensor network based data were used for this purpose. A regular array analysis blocks with two different sizes (20 and 40 km) were used to account for the spatial variability of solar insolation data. Geo-spatial along with geo-statistical analyses were used to assess the spatial variability of the solar insolation within each analysis block. The methods and analysis were performed for the solar radiation sensor network of the South Florida Water Management District (District). Through use of ArcGIS geostatistical processing, the spatial statistical analysis, sensor network design was formed. The existing ground sensor network of the District was evaluated. A proposed sensor network that is expected to provide a standard error of 5.0 MJ $day^{-1}m^{-2}$ was recommended. Recommendations for an enhanced sensor network design across the District were made.

Introduction

Acquisition of hydrologic and hydraulic data is the key component of water resources management in south Florida. The Operations and Hydro data Management Division of the Supervisory Control and Data Acquisition (SCADA) system and Hydro Data Management Department at South Florida Water Management District (District), shown in Figure 1, is responsible for the collection, validation, and archiving of the District's hydrologic data. The types of data include rainfall, evaporation, water levels (stage), water control structure (gate and pump) operations, and flow. In addition, several meteorological parameters (such as barometric pressure, solar radiation, air temperature, relative humidity, and wind speed) are measured at the weather stations that form the District meteorological monitoring network. The District requires accurate data collection, processing and archiving of these data for the purposes mentioned above. There is a constant need for adding new sites with instrumentation for hydrologic data collection within the

District, and this need will be growing at a faster pace as more Comprehensive Everglades Restoration Plan (CERP) projects are implemented. The District's broad objective is to optimize the regional hydro-meteorological monitoring network of the District. This study is Part I of the ET network design study. In this study, the solar radiation network design is considered as the spatial optimization of the network. The proposed design and optimization studies are a prerequisite to expanding and refining the District's hydrologic network to meet the needs of CERP projects.

Evapotranspiration (ET) is a major component of the hydrologic cycle. This hydro-meteorological parameter is needed for various water budgeting purposes, which accounts for surface and groundwater. Potential ET (PET), and reference ET (RET), are the hydrologic parameters needed to estimate ET which is the rate at which water loss to the atmosphere occurs from well-watered soil and plant surfaces. Methods available for PET estimation are generally classified into three groups: energy balance methods, mass balance methods, and combination methods The District developed historical and current daily PET data sets for wetlands using Simple Method (Abtew et al., 2002).

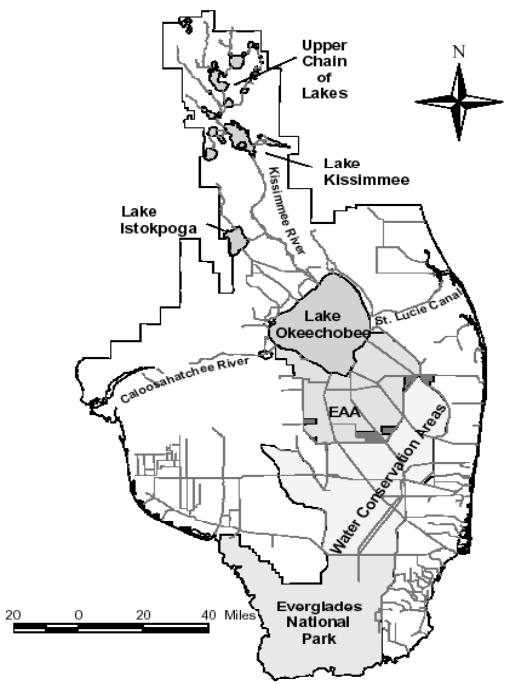

Figure 1: Project Study Area: South Florida Water Management District.

The most desirable ET datasets for these purposes are spatially continuous, rather than point values derived from the traditional field weather station networks. These datasets (enhanced estimates) of ET across Florida are needed. An important parameter for estimating ET (Potential ET and Reference ET) is net radiation (R_{net}). A main component of R_{net} is incoming (downwelling) solar radiation, which can be estimated as solar insolation from geostationary satellite data. Figure 2 illustrates this via a simple energy balance model.

Solar radiation amounts vary geographically within central and south Florida. For example, radiation characteristics and patterns on land surrounding Lake Okeechobee and ocean are different from that of central overland mass. In addition, spatial variation in radiation amounts for shorter durations, such as one-day, is significantly greater than monthly, seasonal and annual radiation. Therefore, in this study, it was recommended that spatially varying sensor density should be considered based on varying solar radiation conditions during dry and wet periods. In addition, solar radiation estimates of local patterns should be used for determining optimum sensor placement as opposed to laying out the sensor in an evenly spaced grid.

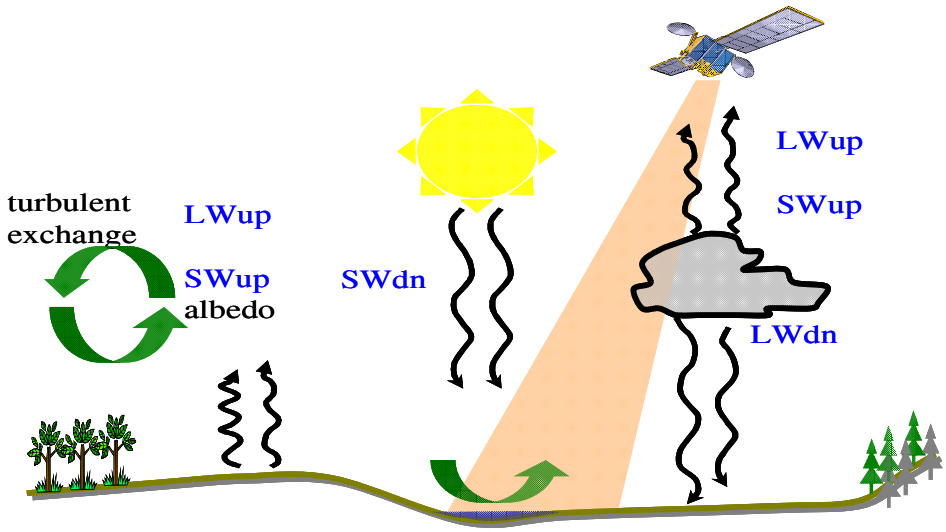

Figure 2: Simplified energy balance model. Here, "up" and "dn" pertain to the upward and downward components, respectively. "SW" is shortwave radiation, and "LW" is longwave radiation.

The goal of this study is to understand the spatial and temporal variability of Geostationary Operational Environmental Satellite (GOES)–estimated solar insolation at a resolution of 2 x 2 km using geo-spatial analysis. The results from spatial analysis are used in a geo-statistical framework to assess the spatial variability of the solar insolation across the District, and for determining optimal sensor location so to properly capture the spatial variations. The goal is to design network that recommends: (i) total number of ground sensors; (ii) location of sensors and (iii) frequency of data sampling that provide equivalent or better data quality (or data accuracy/data representability) with same or less number of sensors. A properly sized and optimized network can result in significant increased efficiencies of the monitoring network in terms of extensive spatial and temporal coverage of parameters of interest.

Methodology

The available solar radiation data from GOES satellite based daily solar radiation data from 1995 to 2004 available from University of Alabama in Huntsville (UAH) was used to evaluate the District's solar radiation ground sensor network. In addition, daily solar radiation data from 29 ground-based sensors known as Pyranometers are available in DBHYDRO database and was used for this study. Pathak (2008) provide details of pyranometers (i.e. the ground sensors) used in the current study. For this study, the existing data and the network of sensors was evaluated, and a review of the existing location for suitability was performed (SFWMD, 2008).

Insolation data were processed from the 2 x 2 km resolution onto a 20 x 20 km analysis block covering the District. A total of 119 non-intersecting blocks for the District region were used. Each 20 x 20 km analysis block contains approximately 100 insolation pixels at 2-km resolution. Due to spatial projection limitations, this number varies from 81 to 100 2 x 2 km pixels. These insolation data were mapped and processed, with use of the ArcGIS package. A sensitivity analysis between the block size and correlation lengths was performed. As a result, block sizes of 40 x 40 km and 80 x 80 km were used in this sensitivity analysis. The computed correlation lengths (i.e. "range parameters from semi-variograms") defined the optimal distances between the ground sensors for the network design, which were determined as a function of location across the District.

The insolation data were divided by seasons that exist across south Florida. The climatology of South Florida demands that the data set be sub-divided into a "cool" and "warm" seasons, as well as a "transitional." After initial analysis, the datasets were divided into the following time periods: (a) dry season – November-March, (b) wet season – April-October, (c) a set of completely (100% cloud cover) cloudy days, and (d) a set of completely clear days. Transitional time periods were not considered to add significance to these analyses. For sets (c) and (d), considerable effort was needed to identify days with these characteristics, given the relative rarity of clear and cloudy days across the entire District, especially during the wet season. Using 2 x 2 km gridded insolation data, polygons of homogeneous areas were developed. This used mean, standard deviation, and coefficients of variation. The covariance structure of insolation was formulated across the District. This required formation of analysis blocks large enough to encompass the range of existing spatial correlation but sufficiently small to capture climatological gradients near coastal areas and inland water features such as Lake Okeechobee. This is very important given the driving force for cumulus convection across South Florida. In particular, time-dependent changes in cumulus due to land, lake and sea breeze circulations were considered. **Figures 3a and 3b** present the homogeneity analysis across the District, for mean insolation (**Figure 3a**), standard deviation (**Figure3b**) for the wet season. These values are derived from measures of temporal variability at each 2 km pixel, based on daily values. **Figures 3a and 3b** also shows layers of 20 x 20 km analysis blocks over the District. There are 119 intersecting blocks for the District.

Figure 3a shows that the mean values *decrease* slightly from north to south, reaching maximum values in the east (and over approximately Lake Okeechobee). Values are mainly from 18.6-19.6 $MJm^{-2}day^{-1}$ in the north and west, yet locally decrease to near 18 $MJm^{-2}day^{-1}$ in the far southeast. Note that these values are ~8 $MJm^{-2}day^{-1}$ below the maximum values that would be expected under clear-sky conditions, yet this is not unexpected given the high-frequency of convective and other clouds across this portion of Florida during the wet season. Values over the ocean and Lake Okeechobee are much higher, ≥20 $MJm^{-2}day^{-1}$. Standard deviations (**Figure 3b**) show several features. First, values are lowest over land ~5.2-5.8 $MJm^{-2}day^{-1}$. Second, higher values to near 6 $MJm^{-2}day^{-1}$ are found near the coasts. This could be caused by a high variability in convective clouds (varying largely from day to day, specifically either mostly clear or mostly cloudy), which is especially exemplified near lakes and the ocean. The analysis of coefficient of variance indicated that the gradients in insolation along the east coast, with values exceeding 0.3 in these areas (SFWMD, 2008).

The variability in the entire wet-season of daily solar insolation dataset and the histogram for all approximately 10,186 days (April-October, 1995-2004) were determined. Here, the data are binned about the mean (19.13 $MJm^{-2}day^{-1}$). The highest frequency of days with a given values occur at ~1.0 $MJm^{-2}day^{-1}$ above and below 19.3, which suggests a delineation between cloudier and clearer days, and land versus water regions, across the District. From a mesoscale weather perspective, this would denote days with either a low or high coverage of convective storms, which is not atypical of tropical (or subtropical) weather). The analysis of insolation data over the District was performed to compute the statistical variation of these data (SFWMD, 2008).

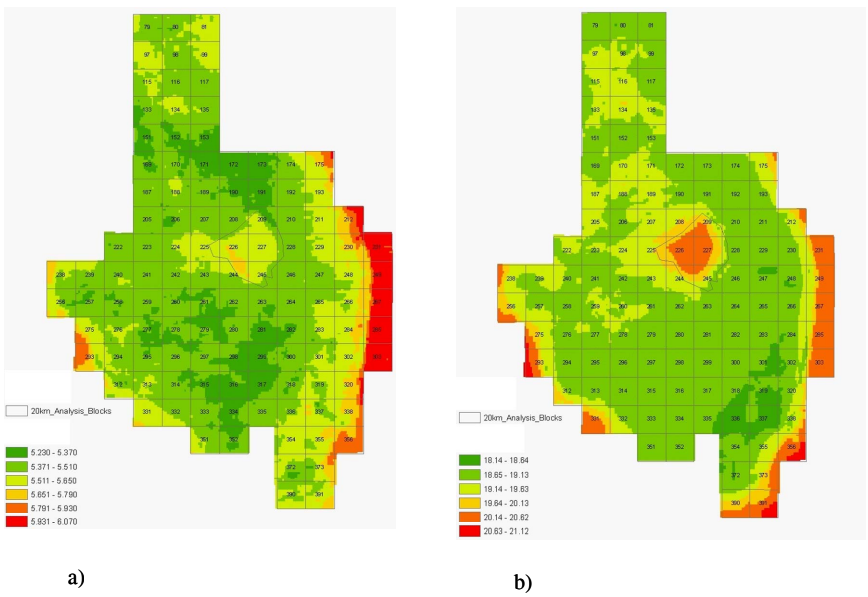

a) b)

Figure 3: Mean solar insolation and Standard deviation map for 2 km pixels and overlay of 20 km blocks for the wet season (April-October) from years 1995- 2004 in $MJm^{-2}day^{-1}$.

Detrending of the insolation data sets were performed for purposes of identification of spatial correlation through a (semi-)variogram analysis approach. Detrending specifically will remove the means of the data, and any trend in insolation not yet addressed in the calibration work of Paech et al. (2008) so to better isolate the true variability within the data. The "parametric" form of detrending in each analysis block was intended to remove non-stationarity. Without detrending, correlation length of the insolation magnitudes can become spuriously large (Wilks, 2006). This processing resulted in the eventual subtraction of the mean structure from the insolation. The detrended data were then be used to compute empirical semivariograms within ArcGIS, as well as for the covariance analysis (Pathak and Vieux, 2007). The semivariogram analysis is applied to the daily insolation data, by the breakdown over the 10-year period. As stated above, the detrended data were used to compute the empirical semivariograms. For each analysis block, the semivariogram analysis was applied to the daily insolation, over subsets of the 10-year long data set (e.g., wet and dry seasons, cloudy days). Because there should be relatively weak correlation in space for insolation, especially when the small-scale (2-25 km) convective clouds dominate the cloud climatology (and hence the insolation variability), the mean empirical semivariogram ordinates were selected. Subsequently, an "exponential" semivariogram model was fitted to empirical semivariograms of mean detrended pixel values in

each block. The "upper quartile" pixel values were used, but did not provide useful results because it changed the data's distribution away from "normal." A robust nonlinear estimator was used to obtain the optimal range and sill parameters of the two-parameter model. The nugget variance of insolation was often zero.

In summary, the following items were concluded from these efforts:1) Wet season insolation had lower range values than those from the dry season. Therefore, wet season insolation data were used for the network design analysis. This is due to the higher frequency of occurrence of small cumulus clouds; 2) Upper quartile and mean detrended insolation data, which were derived from daily insolation values for the wet season over the ten-year period, were evaluated; 3)Mean detrended data provide reasonable and more stable (i.e. consistent across years) range values, and were used in the following analysis; 4) Range values were highly variable in time. Therefore, annual mean insolation data for the wet season, and for each year, were used for the following analysis; 5) Range values were highly variable in space for 20-km, 40-km, and 80-km block sizes. Therefore, based on preliminary results, a mix of 20 and 40 km blocks across the District were chosen for the detailed semivariogram analysis.

Ground Sensor Data Analysis

Ground sensors measuring solar radiation are shown in **Figure 4**. Solar insolation data collected from 29 ground sensors in the District were analyzed. Details of the ground sensors, data collection methods and frequency are discussed by Pathak (2008). The satellite based solar insolation data were obtained from the study that produced daily solar radiation data for the entire State of Florida over ten years from 1995 to 2004. An initial assessment of available solar insolation data from the District revealed several limitations of ground sensors due to observational and systematic errors. The suspicious data, flagged by the District, were removed prior to the subsequent outlier identification analyses. Outlier tests using standard statistical methods were performed for identification and removal of outliers from the data. A variant of the standard normal test for outlier detection was used. The satellite data were used for this outlier test. The standard deviations for the satellite data, at each of sensor locations, were calculated. Sensor observations that lie outside the range of "satellite data $\pm$ standard deviation" were identified as outliers. The satellite-sensor paired observations were eliminated if the sensor data on any given day was identified as an outlier.

The analysis of point data from ground sensors was performed. The point variance and mean values were obtained from 29 ground sensors for the wet periods in each of the years from 1995 to 2004. In order to spatially characterize the solar insolation data, the variance of the point measurements needed detailed analysis. Spatial interpolation methods were used to obtain a surface from the point variances of solar insolation values. Two different interpolation methods: 1) *Inverse Distance Weighting Method* (IDWM) and 2) *Ordinary Kriging Method* were used (SFWMD, 2008). The two interpolation methods performed well in estimating the values at validation sensor locations. The inverse distance weighting methods performed better than the ordinary Kriging method. The overall error was higher for the Kriging method. Based on error statistics, inverse distance weighting method was recommended for the analysis.

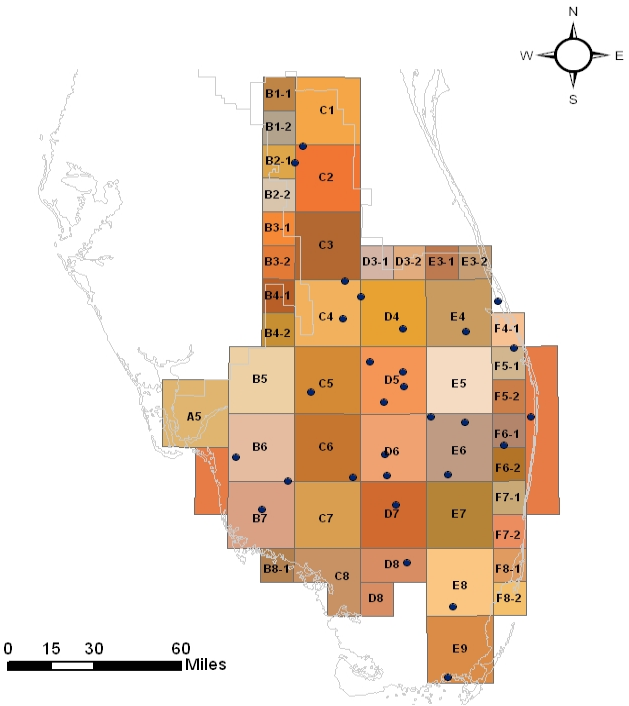

Figure 4: Existing active solar radiation sensor stations in the District.

Effective Sensor Network Design

The design of sensor network is aimed at capturing and characterizing the spatial variability of the solar radiation across the District. The standard error of mean was used, as a metric, to identify the optimal number of ground sensors in the study (SFWMD, 2008). The required number of sensors in a specific analysis block can be obtained by improving the accuracy of the mean solar insolation measurement (SFWMD, 2008). An exponential semivariogram, used to model the covariance structure of the solar insolation from satellite data, provided the decorrelation lengths as range parameters of the model. The effective number of sensors was obtained from the correlation distance from satellite data and point variance from sensor data for each analysis block. Matalas and Langbein (1962) described the information contained in a number of correlated stations. The information contained in data from n stations in a region having a correlation of ρ is equivalent to the information contained in n' uncorrelated stations (sensors) in the region, where n' is given by Equation 1:

$$n' = \frac{n}{1 + \rho_{ave}(n-1)} \qquad (1)$$

where, n' is effective number of stations, n is the total number of stations, and ρ_{ave} is the average correlation coefficient among n stations. Equation 1 suggests that as n increases, n' approaches $1/\rho_{ave}$. The effective number of sensors n' was related to separation distance "h." The covariance structure defined by spatial correlation coefficient was modeled by exponential semivariogram in each analysis block. The standard error of the mean (*SE*) was calculated for all the blocks. The standard error is calculated based on effective number of sensors (n'). Depending on the value of

the average correlation coefficient, range parameter and inter-sensor distance, the values of n' have an increasing trend up to a threshold value and then they decrease as the number of sensors increases. The variations in standard errors in relation to number of sensors are evident from plots shown in **Figure 5.** The exponential decay curves between *SE*, and number of sensors in all the 40-km analysis blocks are also shown in the same figure. This information is used to estimate the number of sensors needed per block, which is identified as the location on the graph where the lines begin to become level, which is between about 2 and 4 sensors per block (SFWMD, 2008).

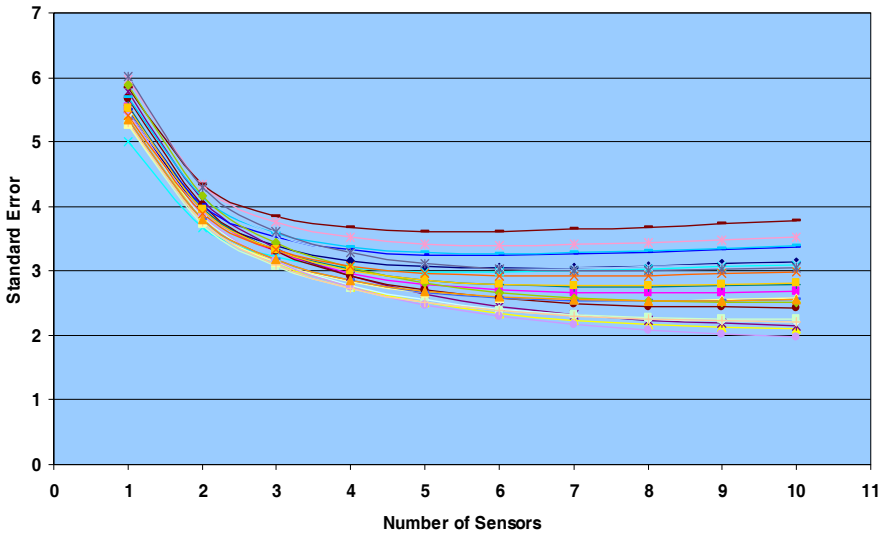

Figure 5: Exponential decay curves between standard error and number of sensors in all the 40-km analysis blocks.

Optimal Network Design

The optimum network design was based on the standard error and the number of gauges in each block. Based on the covariance structure of the solar insolation data, it is evident that there is no uniform analysis block size that is identifiable for the region under consideration. Two analysis size blocks, 40 km x 40 km and 20 km x 20 km, were identified for the use of optimum design of sensor network. SFWMD (2006) outlined two methods of optimum network design in a study related to rain gauge network optimization. The network designed is optimal considering the stipulations imposed on the block size and other constraints. The detailed analysis was conducted based on the historical data available from the network of 29 sensors for wet season. However, recently changes to the sensor network have occurred. The existing sensor network in the District is shown in the **Figure 4** (SFWMD, 2008). In this study, the approach with uniform standard error was adopted to obtain the optimum number of sensors for each block. Once the optimum number was obtained for each block, this number was compared with existing number of sensors in each analysis block. If the existing number of sensors in a block was higher than the optimum number, then a recommendation was made to remove the additional number of sensors. When the existing number of sensors was less than the optimum, additional sensors were recommended for that block.

Proposed Ground Sensor Network Recommendation

For recommending an optimal sensor network to the District, three standard errors of 4.5, 5.0 and 5.5 MJday^{-1}m^{-2}, and a total umber of required new sensors of 50, 19 and 16 respectively, were considered. Based on discussion and consultation with District staff, the proposed ground sensor network with standard error of 5.0 MJday^{-1}m^{-2} would require 19 additional new sensors was recommended. The selection of this network was based on two facts: (a) the standard deviation of satellite solar insolation data from wet seasons over ten years varied between 5.23 and 6.07 MJday^{-1}m^{-2} (**Figure 3b**), which is in the range of the selected standard error (5.5 MJday^{-1}m^{-2}) of the proposed network; and (b) the selected proposed network required three additional sensors (19 minus 16 sensors) compared to 16 new required sensors for the proposed network with the standard error of 5.5 MJday^{-1}m^{-2} that was considered to base optimal network. Therefore, the recommended optimal ground sensor network would need a total of 19 new sensors with the standard error of 5.0 MJday^{-1}m^{-2}. **Figure 6a** shows insufficient sensor distribution and **Figure 6b** shows excess sensor distribution of the District.

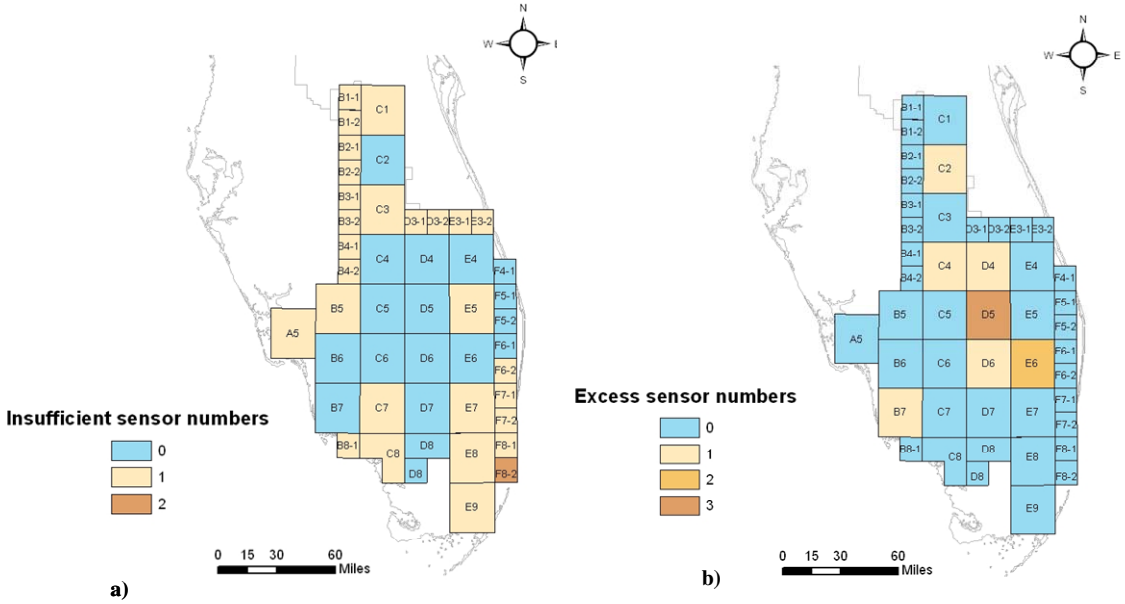

Figure 6: Insufficient and excess ground sensor numbers to achieve a 5.0 MJday^{-1}m^{-2} standard error across the District.

Conclusions

Accurate measurement of solar radiation via optimal number of ground sensors and their respective location is important to the District. This report developed several optimal sensor network designs considering different levels of accuracy characterizing the spatial and temporal variability of solar insolation data. Satellite and ground sensor network based data were used for this purpose. A regular array analysis blocks with two different sizes were used to account for the spatial variability of solar insolation data. Geo-spatial along with geo-statistical analyses were used to assess the spatial variability of the solar insolation within each analysis block. In

addition, the existing ground sensor network was evaluated. A proposed sensor network that is expected to provide a standard error of 5.0 $MJday^{-1}m^{-2}$ was recommended. The standard error used in the currently study is based on time-averaged solar insolation. Recommendations based on two procedures for both sensor assignments and placements were also provided.

References

Abtew, A., M.Irizarry-Ortiz, D. Lyon and J. Obeysekera. 2002. Historical Potential Evapotranspiration Estimation for Sites in South Florida. Technical Notes. South Florida Water Management District, West Palm Beach, Florida.

Matalas, N. C. and W. B. Langbein, Information Content of the Mean, J. Geophys. Res., 67(9): 3441-3448.

Paech, S. J., J. R. Mecikalski, D. M. Sumner, C. S. Pathak, Q. Wu, S. Islam, and T. Sangoyomi, 2008: Satellite-based solar insolation estimates in support of a long-term climatology of potential and reference evapotranspiration estimates over Florida. Submitted, J. Amer. Water Res. Assoc.

Pathak, C. S., and B. E. Vieux, 2007: Geo-spatial analysis of NEXRAD rainfall data for central and south Florida. American Society of Civil Engineers /Environmental and Water Resources Institute, World Water & Environmental Congress 2007, May 15-19, 2007. Tampa, Florida, USA. 15 pp.

Pathak, C.S. (Ed.). 2008. Hydrologic Monitoring Network of South Florida Water Management District –Technical Report, South Florida Water Management District, West Palm Beach, Florida

SFWMD. 2006: Rain Gauge Network Optimization Study. Prepared by Vieux & Associates, Inc., Final Report, South Florida Water Management District. West Palm Beach, Florida.

SFWMD. 2008. Evapotranspiration (ET) Network Design Study- Part I - Solar Radiation Ground Sensor Network Design, Final Draft Report, South Florida Water Management District, West Palm Beach, Florida

Wilks, D. S., 2006: Statistical Methods in the Atmospheric Sciences, 2nd Ed. Academic Press, St Louis, MO, USA.

EPM Approach for Erosion Modeling by Using RS and GIS

Fazel Amiri [1] and T. Tabatabaie [2]

[1] Faculty Member of Scientific Board of Islamic Azad University Bushehr Branch, Iran. *Email:* amiri_fazel@yahoo.com , famiri@na.iut.ac.ir

[2] Forme MS.c. Student of Environmental Pollution, Islamic Azad University Branch Science and Research, Ahwaze, Iran.

Abstract

Lack of information to prepare erosion maps for quantitative and qualitative sediment evaluation is a major need in watershed management in Iran. The goal of this study was to use EPM model and apply GIS to minimize the probable errors in evaluation of soil erosion and sedimentation in Ghareh Aghach watershed in central part of Iran. To achieve this goal, in the first step a topographic map in 1:25000 scale of the study area was digitalized by ILWISE program to provide a contour map. Using the contour map, the slope and aspect maps as well as the digital evaluation model (DEM) of the site were prepared. In the second step the satellite images, aerial photos of 1:40000 scale and data obtained from the field visits were used to provide with geological, geomorphologic, vegetation cover, peddological and land use maps of the study area. By integration of geological, geomorphology facieses and slope maps and classifying them in 5 categories (0-10%, 10-20%, 20-30%, 30-40% and >40%), 21 homogenous uniform sampling units were identified to apply EPM model. Model information layers comprised of nine effective factors in erosion and sedimentation in the watershed site were obtained by digitalizing and classifying the basic information data in GIS program. In frequent field visits all the necessary data for EPM model were collected, checked and improved in 21 homogenous and uniform sampling units. Following of finalizing the information layers, all of them were integrated to create the final erosion map. The results of EPM model for homogenous and uniform sampling units indicated that 0.19% (16.69 ha) of the total watershed area was classified at class I of erosion category with very low sedimentation and 15.1% (1352.64 ha) was classified at class II of erosion category with low sedimentation and 41.3% (3698.8 ha) was classified at class III of erosion category with medium sedimentation and 13.2% (1175.3 ha) was classified at class IV of erosion category with high sedimentation and finally 30.2% (2711.41 ha) was classified at class V of erosion category with very high sedimentation, respectively. The result of comparing erosion and sediment values by EPM model with measured values showed that no significant difference between estimated and measured values ($P<0.05$).

Keywords: EPM model, GIS, sedimentation, erosion, watershed

Introduction

The over population in the world have lead to an increased demand for food and other necessities of human beings (Lu. et. al., 2001). The gradual soil salinization along with deterioration of rangelands vegetation covers have caused accelerating soil erosion and sedimentation in water reservoirs (Meijering, A., 1995). United Nation in its development plan has reported that at present the soil erosion in Iran is about 20 ton/he , which has in creased by 10 ton/he compared to the last decade (UNDP, 1999). There is not enough sediment measurement stations in most watersheds in the country which makes it more difficult to provide with a specific models based on local watershed characteristics. One of the most important problems with empirical models of soil

erosion is its lack of accuracy in processing the huge number of data which should be digitalized by GIS system and analyzed by mathematical models. EPM is an empirical model to estimate the quantity and quality of sediment. In fact quantifying and digitalizing the sediment data is an important break through in sediment assessment models development (Nearing et. al., 1999). This problem could be partially solved by estimating models (Lufafa et.al., 2003). Since soil erosion is a product of few different interacting factors, there is not a simple model to assess all the contributing elements in the same time (Daroussin and King, 2001).

The goal of this research was to apply EPM model and GIS system (to reduce the error level to the minimum) to have the most possible accurate assessment of the soil erosion and sedimentation in the study area and make the best applicable suggestions to control it.

Material and Methods

1. The Experimental site

The area of Ghareh Aghach watershed is about 8954. 8 hectares which is located between 51º 45' 53" and 51º 34' 54" eastern latitudes and 31º30' 28" and 31º26' 19" northern altitudes. The maximum and minimum heights of the area are 3810 and 2630m from the sea level. The mean altitude of the watershed is 2936 meters from the sea level. The watershed area is divided in five major hydrologic sections according to its topographic feature. Long term mean annual precipitation and temperature are 358 and 10.5 degrees Celsius which classifies the site in semi-arid climatic conditions according to Ambergie (Q= 40.7) and Demartin (Ia= 17.4) categories. There are about 17 different vegetation types and four major landscapes of mountainous lands, hilly lands, plateau and gravel lands consisting of nine minor land units (Isfahan Regional Water Organization, 2006).

2. EPM Model

EMP model is the other package which has been used to estimate soil erosion in Iran. However, since fewer environmental factors are considered in this model, its accuracy in sediment estimation is less them the other models (Ahmadi, 2006, Rafahi, 1994). This model was created based on erosion measurements during 40 years in previous Yugoslavia and for the first time was introduced in River Stream International Conference (Gaverlovic, 1988). Sediment estimation in this model is based on four factors consisting:

Ψ : Erosion coefficient of watershed, X: Land use Coefficient, Y: susceptibility of rock and soil to erosion, I: mean watershed slope each one of these factors will receive a proper value according to its contribution to erosion process (Table 1).

Table1. The contributing factors in EPM model to estimate the soil erosion

Factor	necessary information	results
1	Slope map	I: mean watershed slope
2	aspect map	Ψ : value for different erosions
3	land use	Xa: value for different land uses
4	rock and soil susceptibility to erosion	Y: value for rock and soil susceptibility

3. The relationship between erosion and sedimentation in EMP model

This model is able to measure erosion, sediment carrying capacity as well as a primary as estimation of sediments behind the reservoirs.

The coefficient of erosion intensity (Z) is calculated by the following equation in this model:

$$Z = Y. Xa (\Psi + I\ 0. 5) \quad (l)$$

Were:

Y: susceptibility of rock and soil to erosion, Xa: land use coefficient, Ψ : Erosion coefficient of watershed , I: mean watershed slope

The volume of soil erosion is calculated by the following equation in this method.

$$WSP = T. H. \pi. Z^{1. 5} \quad (2)$$

Were:

H: mean annual rainfall (mm), π: 3. 14, WSP: the volume of soil erosion (m3/km2/yr)

T: coefficient of temperature which is calculated by equation No. 3 :

$$T = (t/10 + 0. 1)^{0. 5} \quad (3)$$

Were: t: mean annual temperature

The sediment production rate in this model is calculated based on the ratio of eroded materials in each section of the stream to the total erosion in the whole watershed area (Equation No. 4)

$$Ru= 4 (P. D) 0. 5 /L+10 \quad (4)$$

Were:

P: circumference of the watershed, L: watershed length (km), D: height difference in watershed area (km), After calculation of Ru value the special sediment rate is estimated by equations No. 5 and 6 (9).

$$GSP = WSP. Ru \quad (5)$$

$$GS = GSP. F \quad (6)$$

Were:

GSP: special sediment rate, WSP: volume of special erosion, Ru: coefficient of sedimentation

GS: total sediment rate (m^3/yr) , F: total watershed area (Km^2) (Ahmadi, 2006, Rafai, 2004).

Results

When the proper maps are prepared in EPM model, different contributing factors in erosion and sedimentation will receive their values in GIS system.

1. EPM model

Using the EPM model to estimate the erosion, the boundary of units and subunits of the watershed were identified based on proper maps (land use, soil map and etc.) (Figure1). The maps were matched by GIS and then the mean coefficient values for each homogenous and uniform sampling units and subunit were calculated. The calculated values of four contributing factors for Ghareh Aghach watershed in EPM model is presented in Table 2 and 3. The maps of susceptibility values for each contributing factor created by ILWIS3.3 system are presented in figures 2 to 5. After the information layers were valuated to produce the erosion map, the map of erosion intensity (Z) was prepared and the susceptible sites to erosion were identified. The volume of erosion (WSP) was then calculated by equation No. 2 (Table 4) Figure No. 4 shows the erosion in the watershed area. The sedimentation yield in the Ghareh Aghach

watershed was classified in four categories eroded (low, medium, high and very high) using EPM model.

Table 2. Coefficients of four contributing factors in erosion and Erosion intensity by EPM model

Uniform unit	Ψ	Y	Xa	I	Z	Erosion class
1_FS_d	0.35	0.15	0.4	2.236	0.155	Low
1_FS_Ekk	0.35	0.54	0.4	2.236	0.559	Medium
1_FS_omk2	0.35	0.66	0.38	2.236	0.649	Medium
1_FS_PL(b,c)	0.35	0.48	0.38	2.236	0.427	Medium
1_FS_Q	0.35	0.3	0.38	2.236	0.295	Low
2_FS_d	0.35	0.15	0.38	3.873	0.241	Low
2_FS_Ekk	0.35	0.54	0.39	3.873	0.889	High
2_FS_omk2	0.35	0.66	0.38	3.873	1.059	Very High
2_FS_PL(b,c)	0.35	0.48	0.27	3.873	0.547	Medium
2_FS_Q	0.35	0.3	0.38	3.873	0.481	Medium
4_FS_Ekk	0.35	0.54	0.38	5.916	1.286	Very High
4_FS_omk2	0.35	0.66	0.4	5.916	1.654	Very High
5_DM_Ekk	0.07	0.54	0.4	7.746	1.688	Very High
5_FAk_omk2	0.49	0.66	0.4	7.746	2.174	Very High
5_FAm_omk2	0.56	0.66	0.4	7.746	2.193	Very High
5_FS_d	0.35	0.15	0.4	7.746	0.486	Medium
5_FS_Ekk	0.35	0.54	0.4	7.746	1.749	Very High
5_FS_omk2	0.35	0.66	0.4	7.746	2.137	Very High
5_FS_Q	0.35	0.3	0.38	7.746	0.923	High
F	0.14	0.3	0.16	3.873	0.193	Low
Rock	0.21	0.54	0.24	6.325	0.847	High

Table 3. Coefficients of four contributing factors in erosion by EPM model

Subunits of watershed	C1	C2	C3	C4	C5
Y	0. 59	0. 53	0. 46	0. 47	0. 50
Ψ	0. 34	0. 32	0. 30	0. 33	0. 33
Xa	0. 35	0. 34	0. 33	0. 36	0. 37
I	6.87	6.22	3. 03	3.78	3. 35

2. The efficiency of EPM model to estimate erosion and sedimentation in Ghareh Aghach watershed

GIS system minimizes the personal effects in integrating the different information layers to identify the working units and detects and classifies the different erosion sites in the watershed. t student test was employed to compare the estimated erosion and sediment values by EPM model with measured values using SPSS statistical package (Isfahan Regional Water Organization. 2006.). the results in Table 5 showed that there

were no significant differences (P < 0. 05) between the estimated and measured values. These results support the pervious achievements by the other researchers (Gaverlovic 1988, Shakeri,*et al*., 1996. and Shahbazi kia, *et al*., 2006).

Table 4. The calculated erosion and sediment for Gharehach watershed by EPM model

Subunits of watershed	C1	C2	C3	C4	C5
Coefficient of erosion intensity	2. 1	1. 7	0.427	0.42	0.42
Erosion class	V	V	III	III	III
Erosion intensity	Very high	Very high	Medium	Medium	Medium
WSP (m^3 /km^2/yr)	1534.1	1285.6	638.7	844.1	895.4
Area (km^2)	18. 39	16. 71	29. 08	13. 57	11. 79
Special erosion (ton/km^2/yr)	1903.9	1595.4	792.7	1047.5	1111.2
Annual erosion (ton)	14069.4	12145.7	10111.1	5565.4	11923.2
Observed erosion (ton)	31992. 5	17016. 9	124. 97	19584. 7	15901. 98
Coefficient of sedimentation (Ru)	0.1139	0.1083	0.1084	0.1332	0.1309
Special sediment (ton/km^2/yr)	281.3	233.8	114.8	151.7	162.8
Annual sedimentation (ton)	2073.4	1783.1	1465.4	809.1	1738.3
Observed sedimentation	12828. 99	7147. 1	5498. 7	7794. 7	6599. 32

Table 5. The statistical analysis and mean comparisons in EPM model

Statistical Characters	Erosion statistical Analysis					Sedimentation statistical Analysis				
	C5	C4	C3	C2	C1	C5	C4	C3	C2	C1
d_i	10574.8	-4427.3	108628	124.4	10234.2	4027.1	-1788.2	-461.5	4716.7	4114.9
$\overline{d}$			27484.736					14803.207		
S_{n-1}			45861.896					33429.46		
$S_{\overline{d}}$			20510.0637					14950.1		
Calculated **t**			1.34*					0.991*		

t: from table of P<0.05 for df=5 equal to 2.776

di: The difference between erosion and sediment (measured and estimated) (ton/ha/yr)

*: no significant difference between calculated t and t from table (P< 0.05)

Reference

1. Ahmadi. H., (2006). Application Geomorphology, Vol.1 (*Water Erosion*), Publish by Tehran University.
2. Daroussin, J. and D. King, (2001). Mapping erosion risk for cultivated soil in France, *Catena,* 46: 207-220.
3. Gaverlovic, Z., (1988). The use of an empirical method (Erosion Potential Method) for calculating sediment production and transportation on in unstudied or torrential streams. *Proc. Int. Conf. on River Regime* : 411-422.
4. Isfahan Regional Water Organization. (2006). Study of Physiology, Climatic, Hydrology, and Geomorphology in Ghareh Aghach watershed. Isfahan University of Technology.
5. Lufafa, A., M. M. Tenywa, M. Isabirye, M. J. G. Majaliwa and P. L. woomer, (2003). Prediction of soil erosion in alake victoria basin catchment using a GIS- based *universal soil loss model, Agri. Systems.,* 76:883-894.

6. Lu, H., J., Geollant prosser, L. Moran and G. Priestly. (2001). Prediction of sheet and rill erosion over the Australian continent: Incorporating monthly soil loss distribution. *National Land and water Resource. Technical Report.* No. 31, Australia.
7. Meijering, A. M. J., (1995). Erosion and sediment yield in catchments , *ITC, Iecture notes.* The Netherlands.
8. Nearing, M. A., G. Govers, and L.D. Norton, (1999). Variability in soil erosion data from replicated plots, soil. *Sci. Soc. Am. J*: 1829-1835.
9. Rafahi, H. Gh., 2004. Water Erosion and Conservation, Vol. 1. Publish by Tehran University.
10. Rafahi, H., and M. Namati. (1994). Using EPM for study erodibility and sediment yield in Alamout watershed. *Iranian Journal of Agriculture Science.* Vol. 26(2): pp: 32-45.
11. Shakeri, Sh., and F. Blalipour, (1996). Comparing MPSIAC and EPM model for estimating erosion and sediment yield in Dou Abe watershed. *Conference of water resource management, Isfahan University of Technology*, pp: 272-281.
12. Shahbazi kia, S., and S. Restami, (2006). Comparing MPSIAC and EPM model for estimate erosion and sedimentation in in Azarbayejan Province. *International Conference of erosion and sedimentation,* pp: 598-602.
13. UNDP. (1999). Human Development Report of the Islamic Republic of IRAN. Chapter 8, pp: 109-121.

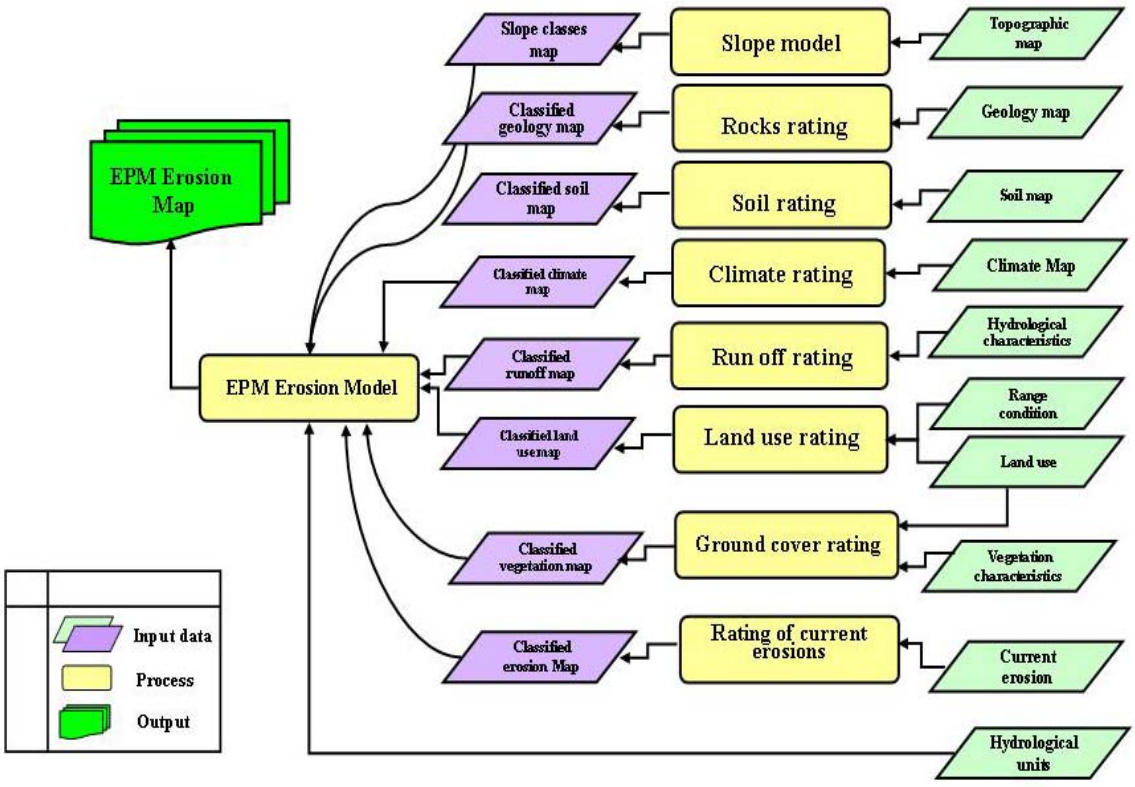

Figure 1. EPM Model for Soil Erosion

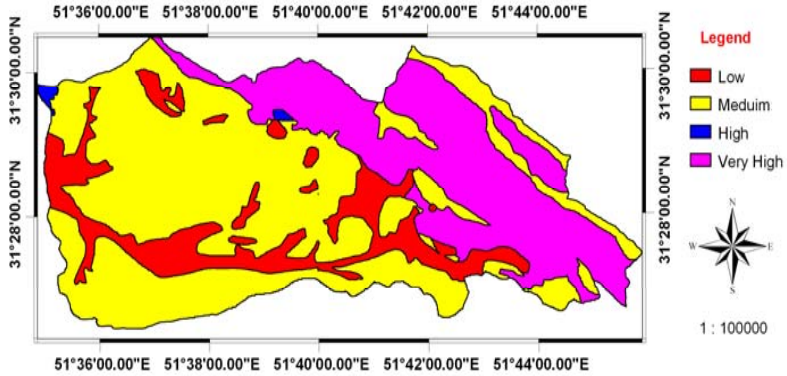

Fig. 4. The Intensity Erosion map (WSP) of Ghareh Aghach watershed

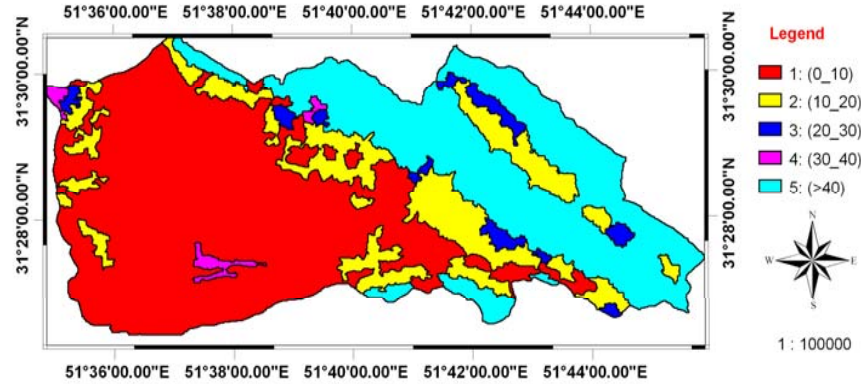

Fig 2. The Slope map of Ghareh Aghach watershed

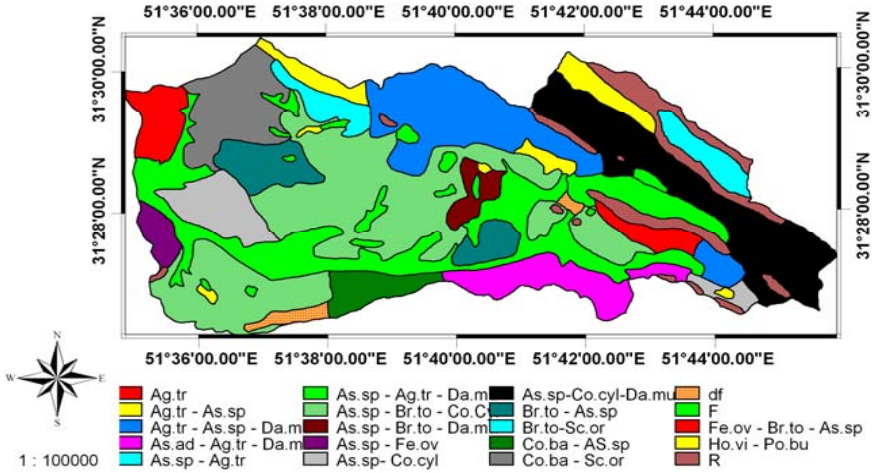

Fig. 5. The Vegetation map of Ghareh Aghach watershed

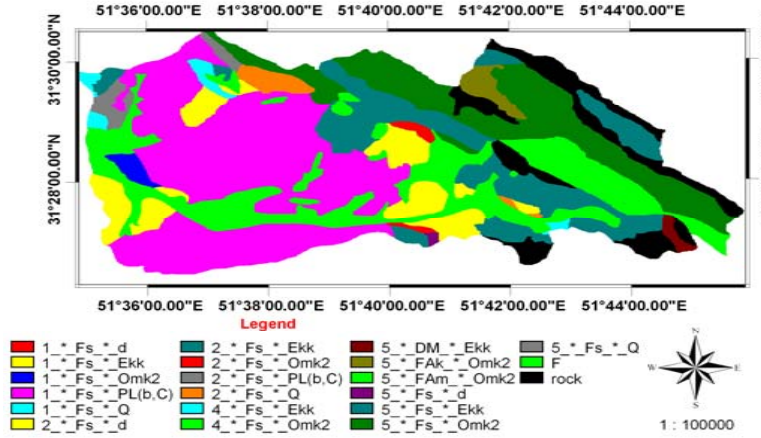

Fig. 3. Uniform Sampling Units map of Ghareh Aghach watershed

Evaluation of Improvised Spatial Interpolation Methods for Infilling Missing Precipitation Records

Alaa Aly[1] , Chandra Pathak[2], Ramesh S. V. Teegavarapu[3], Jon Ahlquist[4], Henry Fuelberg[5]

[1]INTERA, Inc., Niwot, CO, 80544, PH (303)-652-8899, Fax. 303-652-8811, aaly@intera.com

[2] Operations and Hydro Data Management Division, SCADA and Hydro Data Management Department, South Florida Water Management District, 3301 Gun Club Road, West Palm Beach, FL 33416-4680; PH (561) 681-2567; FAX (561) 681-6265; email: cpathak@sfwmd.gov

[3] Department of Civil Engineering, Florida Atlantic University, Boca Raton, FL 33431; PH (561) 297-3444; FAX (561) 297-0493; e-mail: ramesh@civil.fau.edu

[4] Department of Meteorology, Florida State University, 1017 Academic Way, Tallahassee, FL 32306-4520, PH (850) 556-0859 , FAX (850) 644-9642, email: jon.ahlquist@gmail.com

[5] Department of Meteorology, Florida State University, 1017 Academic Way, Tallahassee, FL 32306-4520, PH (850) 644-6466, FAX (850) 644-9642, email: fuelberg@met.fsu.edu

Abstract

Historical rainfall records are of extreme importance to most hydrologic analyses, including water resources evaluation, impact of land use changes, urban runoff volumes and durations, hydro periods, flood analyses, climate variability, among many others. However, daily precipitation records are rarely complete and suffer from occasional and extended periods of missing values. This study involves evaluation of deterministic and stochastic interpolations methods to fill the gaps in daily precipitation records. Evaluated methods include four improvised methods as well as three benchmark methods, with implementation variations for all methods. Benchmark methods are selected to provide a basis against which the evaluated methods performance can be quantified and compared. Evaluated methods include variations of Inverse Distance Weighting Method (IDWM), Correlation Coefficient Weighting Method (CCWM), Linear Weight Optimization Method (LWOM) and Artificial Neural Networks (ANNs). Benchmark methods are variations of the Single Best Estimate (SBE) method and spatial and climatological mean estimators (SME and CME). In addition, two classification methods were evaluated in combination with the estimation methods in an attempt to separate zero and non-zero precipitation estimates. The evaluated classifiers are Support Vector Machine (SVM) and variations of a Single Best Classifier (SBC). The methods are tested for application at 53 NOAA rain gauges that cover areas of interest to the Southwest and South Florida Water Management District regions in South Florida.

Introduction

Availability of continuous precipitation data at different spatial and temporal scales is essential for hydrologic simulation models that use precipitation as input for accurate prediction of watershed response to different precipitation events. Often hydrologists encounter the problem of

missing data due to a variety of reasons. Also, measurement of hydrologic variables (e.g., rainfall, stream flows, etc) is prone to systematic and random errors (Larson and Peck, 1974; Vieux, 2001). The task of estimating missing precipitation data is generally achieved by traditional weighting and data-driven methods (Smith, 1993), distance based weighting methods (Simanton and Osborn, 1980; Wei and McGuiness, 1973), non-linear deterministic and stochastic interpolation methods (e.g. kriging) and regression and time series analysis methods (Salas, 1993). The handbook of hydrology (ASCE, 1996) recommends two methods for estimation, namely 1) normal-ratio method, and 2) inverse distance weighting method. Comparative study of rainfall estimation using some of these methods can be found in Singh and Chowdhury (1986) and Tung (1983). Inverse distance weighting method (IDWM) is most commonly used method for estimating missing data in hydrology and geographical sciences. Recent studies of Ahrens (2006), Teegavarapu and Chandramouli (2005), and Teegavarapu (2007) provided several variants of IDWM. Global interpolation methods that use trend surface analysis with polynomial equations of spatial coordinates (Chang, 2004) and regression are also applicable for spatial interpolation. All these traditional and more recent variants still have several limitations. The main motivating factors to re-visit the inverse distance weighting method and develop a new variant of this method are described in the arguments here. The success of inverse distance weighting method depends primarily on the existence of positive spatial autocorrelation. The existence of negative autocorrelation may be become a major limitation as distance alone is not the measure of strength of spatial autocorrelation. Distance, a surrogate for strength of correlation, often works well when all the rain gaging stations are located in one meteorologically homogeneous and topographic region. In the current study four improvised methods or variants of traditional methods to estimate missing precipitation data are proposed and investigated. The performance of these methods is compared with three benchmark methods using several error and performance measures.

Improvised Estimation Methods

Four methods ranging from simple distance and correlation based weighting techniques to an artificial intelligence (AI) paradigm support were selected. The brief description of each method in the following sections is summarized in SFWMD (2007) with additional implementation details.

Method I: Inverse Distance Weighting Method (IDWM)

The inverse distance (reciprocal-distance) weighting method (Simanton and Osborn, 1980) is the first recommend procedures for estimating missing data. The missing value α_m at base gauge m, based on observed values at other gauges is given by

$$\alpha_m = \frac{\sum_{i=1}^{n} \theta_i d_{mi}^{-k}}{\sum_{i=1}^{n} d_{mi}^{-k}} \qquad (1)$$

where n is the number of gauges with recorded daily rainfall values on the estimation day, θ_i is the recorded observation at gauge i, d_{mi} is the distance from the location of rain gauge i to the gauge m, and k is denoted friction distance (Vieux, 2001). Values from 0.1 to 10.0 were evaluated for parameter k using direct search until an optimal value was found to minimize the method's RMSE.

Method II: Coefficient of Correlation Weighting Method (CCWM)

The success of the inverse distance weighting method (IDWM) depends on the existence of large positive spatial correlations between the observations being used for infilling. One way to determine this needed correlation is to obtain the coefficient of correlation (CC) between any two data sets at different locations. Since CC is one way of quantifying the spatial correlation, it is reasonable to replace the weighting factor by CC. In case of CCWM, the weighting factors are replaced by the correlation coefficients, with the resulting estimation method given by:

$$\alpha_m = \frac{\sum_{i=1}^{n} \theta_i R_{mi}^k}{\sum_{i=1}^{n} R_{mi}^k} \qquad (2)$$

where R_{mi} is the coefficient of correlation, i.e., the ratio of covariance of the two data sets at stations m and i to the product of their standard deviations. Coefficient R_{mi} is obtained using the data at station m and any other station i. The correlation coefficient is calculated using the entire data set, including zero and non-zero values of precipitation. That is, the available historical data are used tor derive R_{mi}. This method was used by Teegavarapu and Chandramouli (2005) for estimating missing daily precipitation data. Preliminary evaluations of this method indicated that superior performance could be obtained if an exponent value is used. As in Method I, a direct search algorithm is used to obtain the optimal value of k (in the range 0.1 to 10) that minimizes the RMSE.

Method III: Ordinary Kriging (OK) and Linear Weight Optimization Method (LWOM)

Ordinary kriging (Journel and Huijbregts, 1978; Webster and Oliver, 2001) is widely recognized as an optimal estimation method based on scalar measurements at different locations based on spatially dependent variance. The degree of spatial dependence in the kriging approach generally is expressed using a semi-variogram. The expression generally used to estimate the semi-variogram is given by

$$\gamma(d) = \frac{1}{2n(d)} \sum_{d_{ij}=d} (\theta_i - \theta_j)^2 \qquad (3)$$

where $\gamma(d)$ is the semi-variogram which is defined over observations θ_i and θ_j lagged successively by distance d. Surface estimation using kriging depends on the semi-variogram model that is selected which must be fitted with a theoretical form that can be used to estimate the semi-variogram values at arbitrary separation distance values. Depending on the shape of the

semi-variogram, several models are possible, including linear, spherical, circular, exponential, and Guassian forms. A typical spherical semi-variogram is shown in Figure 1.

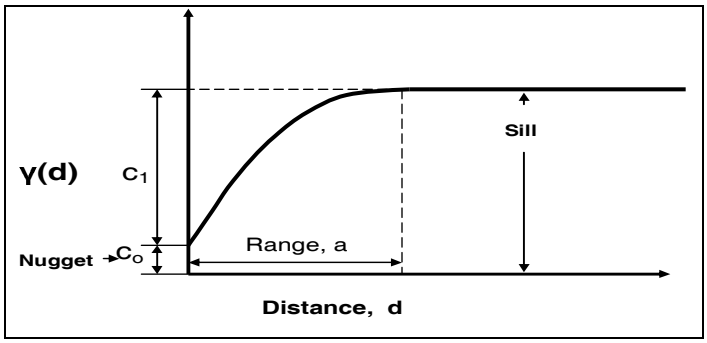

Figure1. Typical parameters of a semi-variogram.

The parameters C_o, d, and a are referred to as nugget, distance, and range, as shown in Figure 24. The sum of C_o and C_1 is referred to as sill, and the semi-variogram at range, a, nearly equals the sill value. The values of C_o and C_1 are obtained using either trial and error or an optimization formulation. Weights in the kriging approach are based not only on the distance between the measured points and the prediction location, but also on the overall spatial arrangement among the measured points and their values. The weights mainly depend on the fitted model (i.e., the semi-variogram) to the measured points. The general equation for estimating missing value, α_m, is given by

$$\alpha_m = \sum_{i=1}^{N} \lambda_i \theta_i \qquad (4)$$

where λ_i is the weight obtained from the fitted semi-variogram through the solutions of a system of linear equations (Journel and Huijbregts, 1978), and θ_i is the value of the observation at location i. The observed data are used twice, once to estimate the semi-variogram and then to interpolate the values. In kriging application, adequate number of semi-variogram forms are evaluated to provide the best possible fit for the spatial correlation structure obtained from the data set. It is important to note that the kriging estimate shown in equation 4 is in the form of a linear estimator, with the weights, λ_i, determined from the spatial correlation structure. Other linear methods can be easily applied with the weights assigned based on some optimization criterion. A variation of the ordinary kriging is to start with alternative initial values for λ_i in equation 2 then use an optimization algorithm to find the optimal values for the linear weights, λ_i, to minimize the estimation RMSE. This method will be referred to as a Linear Weight Optimization Method (LWOM). This LWOM approach is equivalent to multiple linear regression. A common implementation of the multiple linear regression model uses a stepwise procedure to ensure that each rain gauges appearing in the final linear model contributes to the estimation accuracy without degrading the estimation's standard error.

Method IV: Artificial Neural Networks Estimation Method

Artificial neural networks (ANN) have been used extensively during the past decade to estimate and forecast hydrologic variables (Govindaraju and Rao, 2000). A wealth of literature on the architecture of neural networks, including their training and testing can be found elsewhere (e.g., Freeman and Skapura, 1991). The architecture (Figure 2) used in the current study for infilling purposes is a feed-forward network, consisting of one or two hidden layer neurons. The number of hidden layer neurons is typically selected using trial and error and professional judgment. The input neurons use values selected from all gauges except the gauge of interest. The output neuron provides the missing value at the gauge of interest. The input to ANN is the daily observed precipitation values at pre-selected rain gauges. The input gauges are selected based on a pre-assigned threshold value of correlation coefficient calculated from the historical data. The number of inputs selected will depend on the computational resources available for executing the ANN models and any other issues related to training and testing. During the ANN evaluation, preliminary data analysis can be used to identify the stations and finalize the number of inputs.

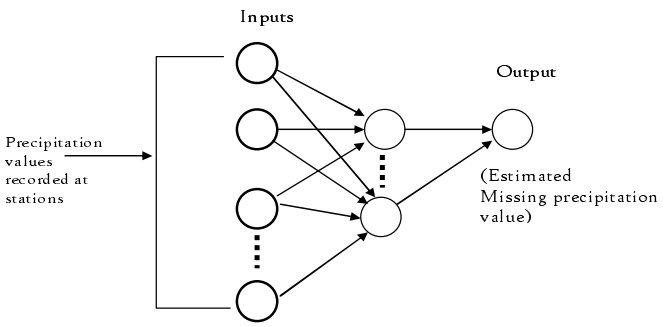

Figure 2. Architecture of ANN method

Benchmark Methods

Three conceptually simple benchmark methods to evaluate the methods are recommended. These methods are described in the SFWMD (2007) and are discussed briefly below.

Benchmark Method 1: Single Best Estimator (SBE)

The Single Best Estimator (SBE) procedure is one of the simplest methods for estimating missing data. Data from the gauge "closest" to the gauge with missing data are used for in-filling. This closest station is not selected by Euclidean separation but by using information about the strongest positive correlation. The availability of historical data again is essential to use this estimator. Eischeid et al. (2000) has described the use of the SBE method for estimating time series of temperature and precipitation.

Benchmark Method 2: Gauge Mean Estimator (GME)

Estimating missing precipitation values by this method is an arithmetic average of all the gauges reporting observed rainfall. The method is a special case of inverse distance weighting and

correlation coefficient weighting where all the weights are raised to an exponent of zero. It is similar to the average precipitation method recommended by McCuen (1998).

Benchmark Method 3: Climatological Mean Estimator (CME)

This Climatological Mean Estimator method is similar to GME but the estimate is an average based on the climatological mean for the day based on the available historical record at the gauge. This method requires at least one available measurement for each day of the year.

Application to Case Study

The four missing data estimation methods are tested for application at 53 NOAA rain gauges that cover areas of interest to the Southwest and South Florida Water Management District regions in South Florida. Rainfall rates across Florida are known to exhibit strong seasonality is known to exist in the rainfall values across Florida. In this study the definition of wet and dry seasons follows that of (SFWMD, 2007), with the dry (winter) season lasting between November and April when precipitation is dominated by frontally-induced widespread storms. The wet (summer) season accounts for approximately 70% of the annual rainfall and has a greater frequency of convective storms whose size is relatively small. Further, the evaluation data set is broken into two sets, before and after January 1, 1950. The rain gauges have considerably more gaps in the record before 1950. Results from all methods are rounded to the nearest 0.01 inch to match the precision of the daily rainfall values obtained from the National Climatic Data Center (NCDC). Further, the two evaluated methods (linear weights, ANNs) can produce negative estimates for daily precipitation. To ensure that the results are physically meaningful, a lower limit of zero was imposed on results from these methods. That is, any negative estimate was replaced with a zero value. All evaluation results are based on these rounded non-negative estimated values. It must be noted that the ANN method uses a training (calibration) and a verification data set to terminate the training algorithm. Therefore, the verification data set was extracted from the available training data in order to maintain the same evaluation data set for all methods.

Several quantitative and qualitative measures were developed to evaluate the benchmark and estimation methods. The quantitative measures included: 1) Root Mean Square Error (RMSE, inches); 2). Mean Absolute Error (MAE, inches); 3). Mean Error (ME, inches); 4. Correlation Coefficient (*CC*); 5). Percent of Correct State for Wet Days (P_w); 6) Percent of Correct State for Dry Days (P_d) and 7) Percent of Correct State for All Days (P_A).

Evaluation of Benchmark Methods

Three benchmark methods (single best estimator method, gauge mean estimator and climatological mean estimator) are initially evaluated. The two mean estimator methods are straightforward and were applied as described above. However, the SBE method was applied using several definitions of the "best" estimator. In the first variation, distance was used to define the best estimator. That is, the best estimator ($\alpha_{m,i}$) for rainfall at gauge m on day i is taken as the same rainfall value recorded at the nearest gauge k ($\theta_{k,i}$) with observed daily rainfall on the same day as the missing datum; $\alpha_{m,i} = \theta_{k,i}$. Other variations of the SBE method used correlation or

seasonal correlation instead of distance. When correlation was used, the best estimator ($\alpha_{m,i}$) for rainfall at gauge m on day i was taken as the same rainfall value recorded at gauge k ($\theta_{k,i}$) having the highest correlation and with observed daily rainfall on the day in question, regardless of season. When seasonality was considered, two sets of correlation coefficients were calculated; one each for the wet and dry seasons. Then the selection proceeded in the same way, with possibly different gauges selected for different seasons based on the different correlation coefficients.

Table 1 summarizes the evaluation metrics for all three benchmark methods. The results lead to several important conclusions. Results of the various benchmark methods were very similar for the time periods before and after 1950. This suggests that the methods do not depend on the number of available measurements on a given day. All benchmark methods appear to be unbiased, i.e., with very small values of mean error (ME). The accuracy of all benchmark methods is similar (as measured by the RMSE and MAE), with the GME method exhibiting the smallest value of RMSE. However, SBE is superior to the GME and CME methods, as measured by the small ME, similar CC and highest percentage of correct state identification, albeit with larger RMSE than the GME method. The large differences between the RMSE and MAE suggest that the error statistics may be dominated by a few large values. This will be explored later using graphical techniques. The SBE methods show significantly better success for determining the rain state at a given gauge (rain/no rain), with a correct classification rate of about 79%, compared to 56% and 31% for the GME and CME methods, respectively. This suggests that that SBE can be used as a classifier. That is, using the SBE method to determine whether zero or non-zero rainfall value should be predicted at a given gauge on a given day. Variations in the SBE method yielded similar results, with slightly better results for the version based on daily seasonal correlation values (as seen in Table 1). However, the accuracy of state determination is not improved by considering the seasonality. The SBE is the best benchmark method and will be the method against which the other methods will be evaluated. Daily Rainfall Estimation Methods Evaluation

The results from the four evaluation methods selected for this Table 2 are the ones that showed the best overall performance or are different enough from other methods to warrant comparison. In this table, the best value for each statistic is highlighted in yellow and the second best value is highlighted in green. As can be seen from this table, the LWOM or ANNs show the best overall performance with an RMSE value of 0.33 and an MAE value of 0.13, which is very close to the minimum MAE value of 0.12. The ME value for the LWOM is fairly close to the minimum value and is order of magnitude lower than the ANN ME value. Finally, the correlation coefficient values obtained for the LWOM are the highest across all evaluated methods, with the ANNs showing very close values. The results show a virtual tie between the LWOM and ANNs, with both methods providing much improvement over the best benchmark method (SBE) as indicated by the smaller RMSE (0.33 vs 0.45), smaller MAE (0.13 vs 0.17), and higher correlation coefficient (0.66 vs 0.45). Simplicity of the LWOM led us to the recommendation of the LWOM over ANNs. Finally, the cumulative errors calculated for the LWOM results show that very small cumulative errors are exhibited by the LWOM-predicted daily precipitation values.

The LWOM has the additional advantage of providing standard error values for the predicted daily rainfall. It must be stated that standard errors (or variance values) can be calculated for the ANN predictions but this requires more complex procedures to be applied. The LWOM standard error values were found to be fairly large, ranging between 0.43 and 0.66. This shows that each predicted daily value has a large variance associated with it making the method not suitable for providing a single prediction. That is, the evaluated methods should only be used for long-term filling of gaps where some gaps exist in the middle of a fairly long record.

Table 1. Evaluation of Benchmark Methods

	Method	Benchmark Methods				
		Single Best Estimator (SBE) (Distance)	Single Best Estimator (SBE) (Correlation)	Single Best Estimator (SBE) (Seasonal Correlation)	Gauge Mean Estimator (GME)	Climatological Mean Estimator (CME)
All Data	RMSE (in)	0.46	0.45	0.45	0.38	0.43
	MAE (in)	0.17	0.17	0.17	0.17	0.21
	ME (in)	-7.82E-04	-8.58E-04	-1.92E-04	2.12E-04	3.32E-05
	CC (all data)	0.45	0.47	0.48	0.48	0.16
	CC (wet season)	0.40	0.42	0.42	0.42	0.10
	CC (dry season)	0.54	0.59	0.59	0.56	0.03
	% of Correct State (rain)	64%	66%	65%	97%	100%
	% of Correct State (no rain)	84%	84%	84%	38%	0%
	% of Correct State (rain or no rain)	78%	79%	79%	56%	31%
1/1/1900 - 12/31/1949	RMSE (in)	0.46	0.45	0.45	0.38	0.44
	MAE (in)	0.17	0.17	0.17	0.17	0.21
	ME (in)	-2.13E-04	-1.94E-03	-2.20E-03	-2.81E-04	1.12E-03
	CC (all data)	0.45	0.48	0.47	0.49	0.16
	CC (wet season)	0.42	0.43	0.43	0.44	0.10
	CC (dry season)	0.51	0.57	0.55	0.55	0.02
	% of Correct State (rain)	63%	65%	64%	97%	100%
	% of Correct State (no rain)	83%	84%	84%	38%	0%
	% of Correct State (rain or no rain)	77%	78%	78%	56%	30%
1/1/1950 - 12/31/2006	RMSE (in)	0.46	0.45	0.44	0.38	0.43
	MAE (in)	0.17	0.16	0.16	0.17	0.21
	ME (in)	-1.10E-03	-2.61E-04	9.17E-04	4.83E-04	-5.66E-04
	CC (all data)	0.45	0.47	0.48	0.48	0.16
	CC (wet season)	0.40	0.41	0.41	0.41	0.11
	CC (dry season)	0.55	0.60	0.61	0.57	0.03
	% of Correct State (rain)	65%	66%	66%	97%	100%
	% of Correct State (no rain)	84%	85%	85%	38%	0%
	% of Correct State (rain or no rain)	78%	79%	79%	56%	31%

Table 2. Evaluation of Benchmark Methods

	Method	Daily Rainfall Estimation Methods					
		Single Best Estimator (SBE) (Seasonal Correlation)	Inverse Distance Weighting Method (IDWM) Optimum k=0.9	Coefficient of Correlation Weighting Method (CCWM) Optimum Weight = 4.5	LWOM	Weight Optimization with SBE	Artificial Neural Network (ANN)
All Data	RMSE(in)	0.46	0.37	0.35	0.33	0.34	0.33
	MAE(in)	0.17	0.16	0.15	0.13	0.12	0.13
	ME(in)	-1.92E-04	7.86E-04	-2.15E-04	-8.74E-04	3.30E-02	2.68E-03
	CC(all data)	0.48	0.53	0.59	0.66	0.63	0.66
	CC(wet season)	0.42	0.47	0.54	0.62	0.59	0.62
	CC(dryseason)	0.59	0.62	0.68	0.75	0.71	0.74
	%of Correct State (rain)	65%	97%	96%	99%	66%	98%
	%of Correct State (no rain)	84%	42%	49%	22%	84%	32%
	%of Correct State (rain or no rain)	79%	59%	64%	46%	79%	53%

The implemented evaluation method is based on the comparison between omitted values and the predicted values by each of the methods. This highlights another limitation and potential misuse of the evaluated methods. All methods should only be used to fill gaps in available records. No extrapolation should be used to estimate daily rainfall before or after the record exists at any

gauge. The evaluation data set did not include any data to allow the evaluation of interpolation methods outside the limits of the available record.

In summary, the results underline the selected method as a two-step methodology. In the first step the CCWM is used to estimate daily rainfall at all gauges on the missing days. It must be noted that the optimal value of 4.5 for the exponent k in equation 2 is an empirically obtained value for the evaluated data set. The theoretical basis for this particular value is thoroughly evaluated. For different applications, this value should be determined for the available data whenever possible. In the second step, the LWOM is implemented using stepwise regression, with the CCWM-predicted values used to fill any gap in the explanatory variable matrix. Again, the number of gauges used as input should be evaluated for different applications. The presented results clearly show that the LWOM-predicted daily precipitation values can be used for water resources evaluation purposes where accurate water budgets are required. The use of interpolated rainfall values is not recommended for event-based hydrologic simulation modeling. For these applications, the modeler is encouraged to search the record for the longest possible windows of time where no data gaps exist. However, if no such windows exist, the LWOM can be used to fill only a small number of gaps, relative to the size of the utilized data sets. Results must still be interpreted with careful reference to the underlying precipitation values. The use of a classification method can greatly improve the accuracy of the modeling state (rain vs. no rain). Results show that the SBC (with a small search radius) is preferred to the SVM classifier for its superior performance as well as its simplicity. However, application of this classifier is not recommended for water budget applications as it introduces some bias into the estimated values.

Conclusions

The study reported in this paper has evaluated four improvised interpolation methods to fill gaps in the daily precipitation records at 53 rain gauges in areas of interest to the Southwest and South Florida Water Management Districts. The evaluated methods include four methods and three benchmark methods, with implementation variations for each. Benchmark methods were selected to provide a basis against which the evaluated methods performance could be quantified and compared. The four evaluated methods include variations of the Inverse Distance Weighting Method (IDWM), Correlation Coefficient Weighting Method (CCWM), Linear Weight Optimization Method (LWOM), and Artificial Neural Networks (ANNs). The benchmark methods are variations of the Single Best Estimate (SBE) method and gauge and climatological mean estimators (GME and CME). In addition, two classification methods were evaluated in combination with the estimation methods in an attempt to separate zero and non-zero precipitation estimates. The evaluated classifiers are Support Vector Machine (SVM) and variations of a Single Best Classifier (SBC). Results showed that a reasonable performance can be achieved using a two step procedure which implements stepwise regression to provide the final estimates. Two classifiers were evaluated in conjunction with the interpolation methods, the Single Best Classifier (SBC) and Support Vector Machines (SVM). Results showed that the SBC, with a search radius set to 2 gauges, provides the most accurate determination of state (rain Vs no rain). However, this introduces additional bias into the estimated daily precipitation values. Results in this study show enough support for the LWOM for the evaluated data sets and is recommended for infilling precipitation records.

References

Ahrens, B., 2006, Distance in spatial interpolation of daily rain gauge data, Hydrology and Earth System Sciences, 10, 197-208.

Chang, K-T., 2004. Introduction to Geographic Information Systems, McGraw Hill, New York.

Eischeid, J. K., P. A. Pasteris, H. F. Diaz, M. S. Plantico and N. J. Lott, 2000. Creating a serially complete, national daily time series of temperature and precipitation for the western United States, Journal of Applied Meteorology, 39, 1580-1591.

Freeman, J. A. and Skapura, D. M., 1991. *Neural Networks: Algorithms, Applications and Programming Techniques*, Addison-Wesley Inc., USA, 1991.

Govindaraju, R. S., and A. R. Rao., 2000. *Neural Networks in Hydrology*, Kluwer Academic Publishers, Netherlands.

Journel, A. G. and C. J. Huijbregts, 1978. *Mining Geostatistics*, Academic Press, New York.

Larson, L. W., and E. L. Peck., 1974. Accuracy of Precipitation Measurements for Hydrologic Forecasting*, Water Resources Research*, 156, 1687 - 1696.

McCuen, R. H., 1998. *Hydrologic Analysis and Design*, Prentice-Hall, NJ

Osborn, H. B., K.G. Renard, and J. R. Simanton., 1979. Dense Networks to Measure Convective Rainfall in the Southwestern United States, *Water Resources Research*, 156 : 1701-1709.

Salas, J. D.-J., 1993. Analysis and Modeling of Hydrological Time Series, *Handbook of Hydrology*, D. R. Maidment, ed, Mc-Graw-Hill, NY

Simanton, J. R., and H. B. Osborn, 1980. Reciprocal-Distance Estimate of Point Rainfall, *Journal of Hydraulic Engineering Division*, 106HY7

SFWMD, 2007. South Florida Water Management District Technical Advisory Group Report: An Assessment of In-filling Methods for Estimating Missing Precipitation Records.35 pages.

Singh, V. P., and K. Chowdhury., 1986. Comparing Some Methods of Estimating Mean Areal Rainfall, *Water Resources Bulletin*, 222, 275-282.

Smith, J. A., 1993. Precipitation, chapter 3, *Handbook of Hydrology*, D. R. Maidment ed.. McGraw Hill, New York.

SFWMD (2007)

Teegavarapu, R. S. V., Chandramouli, V., 2005. Improved weighting methods, deterministic and stochastic data-driven models for estimation of missing precipitation records, Journal of Hydrology, 312, 191-206.

Teegavarapu, R. S. V., 2007. Use of universal function approximation in variance dependent surface interpolation technique: An application in Hydrology. Journal of Hydrology, 332, 16-29.

Tung, Y. K., 1983. Point Rainfall Estimation for a Mountainous Region, *Journal of Hydraulic Engineering, American Society of Civil Engineering ASCE*, 10910:1386 -1,393.

Vieux, B. E., 2001. *Distributed Hydrologic Modeling using GIS*, Water Science and Technology Library, Kluwer Academic Publishers.

Webster, R. A., and M. A. Oliver., 2001. *Geostatistics for Environmental Scientists*, John Wiley and Sons, Chichester, UK.

Wei, T. C., and J. L. McGuinness., 1973. Reciprocal Distance Squared Method, a Computer Technique for Estimating Area Precipitation, *Technical Report ARS-Nc-8., U.S. Agricultural Research Service*, North Central Region, Ohio.

Quantifying Uncertainty in Discharge Measurements: A New Approach

J.E. Kiang[1], T.A. Cohn[2], and R.R. Mason, Jr.[3]

[1] U.S. Geological Survey, Office of Surface Water, 12201 Sunrise Valley Drive MS415, Reston, VA 20192 ; PH 703-648-5364; FAX 703-648-6693 ; email: jkiang@usgs.gov

[2] U.S. Geological Survey, Office of Surface Water, U.S. Geological Survey, 12201 Sunrise Valley Drive MS415, Reston, VA 20192 ; PH 703-648-5711; FAX 703-648-6693 ; email: tacohn@usgs.gov,

[3] U.S. Geological Survey, Office of Surface Water, 12201 Sunrise Valley Drive MS415, Reston, VA 20192 ; PH 703-648-5305; FAX 703-648-6693 ; email: rrmason@usgs.gov

ABSTRACT

The accuracy of discharge measurements using velocity meters and the velocity-area method is typically assessed based on empirical studies that may not correspond to conditions encountered in practice. In this paper, a statistical approach for assessing uncertainty based on interpolated variance estimation (IVE) is introduced. The IVE method quantifies all sources of random uncertainty in the measured data. This paper presents results employing data from sites where substantial over-sampling allowed for the comparison of IVE-estimated uncertainty and observed variability among repeated measurements. These results suggest that the IVE approach can provide approximate estimates of measurement uncertainty. The use of IVE to estimate the uncertainty of a discharge measurement would provide the hydrographer an immediate determination of uncertainty and help determine whether there is a need for additional sampling in problematic river cross sections.

INTRODUCTION

Tens of thousands of discharge measurements are made annually by the U.S. Geological Survey (USGS), other government agencies, and private entities to quantify the flow in rivers and streams. These measurements are used for design of hydraulic infrastructure, water supply management and planning, or other water resources needs and the ability to assess the uncertainty of the measured flow is useful for many purposes. This paper presents uncertainty estimates using the Interpolated Variance Estimator (IVE), a newly developed method for estimating uncertainty in discharge measurements made using the traditional velocity-area measurement technique.

The discharge of a channel is equal to the flux integral of the flow velocity over the flow area. The conventional USGS velocity-area method of discharge measurement approximates this calculation by measuring the width, depth, and velocity at a minimum of 24 discrete points along the channel cross section. The total discharge in a channel is estimated by summing the discharge estimated for *m* vertical subsections, which together span the width of the channel:

$$Q = \sum_{i=1}^{m} b_i d_i v_i \tag{1}$$

where Q is the discharge, b_i is the width, d_i is the depth, and v_i is the velocity in vertical subsection i.

Within the velocity-area method, the USGS uses the mid-section method to define discharge in the vertical subsections. The subsection associated with each depth and velocity measurement extends half the distance to the location of the preceding and following measurements. The measured depth and velocity are assumed to represent the average depth and average velocity throughout the vertical subsection. This assumption is valid only if an adequate number of subsections are used, such that the measured depth and velocity profiles vary approximately linearly.

To estimate the average velocity in each vertical subsection, velocity is typically measured at 1, 2, or 3 points in each vertical column, depending on the total depth and the apparent velocity profile for the vertical. The average velocity at these points is used to estimate the mean velocity of the entire vertical subsection. In the USGS, the flow velocity is measured either by using mechanical flow meter or by acoustic velocity meter. Additional details on discharge measurement techniques used by USGS are described by Rantz and others (1982).

Traditional methods of estimating the uncertainty in discharge measurements include hydrographer estimates (Rantz and others, 1982) and statistical error propagation techniques (International Standards Organization, 2007; Sauer and Meyer, 1992; Herschy 1971). The statistical error propagation techniques estimate the total uncertainty in a discharge measurement as a function of the uncertainty in individual components of the discharge measurement:

$$u(Q) = \pm\sqrt{u_m^2 + u_s^2 + \frac{\sum_{i=1}^{m}[(b_i d_i v_i)^2 (u_{bi}^2 + u_{di}^2 + u_{vi}^2)]}{(\sum_{i=1}^{m} b_i d_i v_i)^2}} \tag{2}$$

where

$u(Q)$ = Relative uncertainty in discharge (fraction)
u_b = Relative uncertainty in width of a vertical subsection(fraction)
u_d = Relative uncertainty in average depth of a vertical subsection (fraction)
u_v = Relative uncertainty in average velocity of a vertical subsection (fraction)
u_m = Relative uncertainty in discharge measurement due to approximation of integral using limited verticals (fraction)
u_s = Relative uncertainty in discharge measurement due to calibration errors and other systematic errors (fraction)

Estimates of the various components of the total uncertainty are derived from empirical and laboratory studies and are generally insensitive to the site-specific measurement and flow conditions. Pelletier (1988) provided an overview of these studies. The uncertainty in velocity is attributed to various causes such as uncertainty due to pulsation in the flow, uncertainty due to the accuracy of the instrument, and uncertainty due to approximation of average velocity using only 1 to 3 points in the vertical (Pelletier, 1988; Herschy 1975; Carter and Anderson 1963).

Estimation of uncertainty using these methods is most likely to yield accurate estimates of discharge measurement uncertainty if the measurement conditions are similar to those experienced in the empirical or laboratory studies. The IVE method applies the same statistical error propagation techniques, but also takes advantage of the many measurements of depth and velocity in a cross section so that the estimated uncertainty of these components reflects the site-specific measurement and flow conditions.

INTERPOLATED VARIANCE ESTIMATOR (IVE): METHOD

As applied using the mid-section method, the discharge measurement equation (equation 1) is an approximation that assumes that the depth or velocity measured at the midpoint of each vertical subsection adequately represents the true *average* depth or velocity for the entire subsection. In reality, the midpoint measurement is imperfect as a measure of the average, and using depth as an example, this can be expressed as:

$d_i = D_i + \varepsilon_i$	(3)

where D is the true average depth and ε represents random error. These random errors may arise from measurement error or because the midpoint value, even if measured perfectly, is just an approximation of the average value. The midpoint is only a good approximation if depth and velocity vary linearly. With an adequate number of verticals, the depth and velocity profiles will vary approximately linearly.

The IVE method uses adjacent vertical subsections to interpolate a second estimate of the mean depth (or velocity) for each vertical. This estimate is compared to the measured depth or velocity. The difference between these two estimates is treated as a random variable, Δ (see Figure 1):

$$\Delta_{i,d} = d_i - d_{i,est} \tag{4}$$

where $d_{i,est}$ is the depth interpolated from the adjacent verticals. If depth and velocity vary linearly (as assumed by the mid-section method), the expected value of Δ is zero. Δ is assumed to have the same distribution for all verticals. For equally spaced verticals, the expression for Δ can also be expanded to:

$$\Delta_{i,d} = D_i + \epsilon_i - \frac{1}{2}(D_{i-1} + \epsilon_{i-1}) - \frac{1}{2}(D_{i+1} + \epsilon_{i+1}) \tag{5}$$

To employ IVE, it is also necessary to assume that the errors, ε, in estimating the average depth or velocity are independent and random and that the distribution of the errors is the same at each vertical, with variance u_d^2 or u_v^2. Then, for equally spaced verticals, the variance of Δ can be expressed analytically as:

$$\begin{aligned} Var[\Delta_{i,d}] &= Var\left[D(x_i) + \epsilon_i - \frac{1}{2}(D(x_{i-1}) + \epsilon_{i-1}) + \frac{1}{2}(D(x_{i+1}) + \epsilon_{i+1})\right] \\ &= Var\left[\epsilon_i - \frac{1}{2}\epsilon_{i-1} + \frac{1}{2}\epsilon_{i+1}\right] \\ &= Var[\epsilon_i] + \frac{1}{2}^2 Var[\epsilon_{i-1}] + \frac{1}{2}^2 Var[\epsilon_{i+1}] \\ &= u_d^2 + \frac{1}{2}^2 u_d^2 + \frac{1}{2}^2 u_d^2 \\ &= (1 + \frac{1}{4} + \frac{1}{4})u_d^2 \\ &= \frac{3}{2}u_d^2 \end{aligned} \quad (6)$$

The variance of Δ can also be estimated as the sample variance:

$$Var[\Delta_{i,d}] = \frac{1}{(m-4)-1}\sum_{i=3}^{m-2}(\Delta_{i,d} - E[\Delta_{i,d}])^2 \quad (7)$$

Note that verticals at the edges of the measurement are omitted from this calculation. Using the two expressions for the variance in Δ(equations 6 and 7), and assuming that the expected value of Δ equals zero, the variance of the depth measurement can be derived as:

$$\hat{u}_d^2 = \left(\frac{1}{m-5}\right)\sum_{i=3}^{m-2}\frac{2}{3}(\Delta_{i,d})^2 \quad (8)$$

An analogous calculation can be used to estimate the velocity uncertainty as:

$$\hat{u}_v^2 = \left(\frac{1}{m-5}\right)\sum_{i=3}^{m-2}\frac{2}{3}(\Delta_{i,v})^2 \quad (9)$$

These equations can be generalized for the case of non-equally spaced verticals. All of the random sources of uncertainty are accounted for using IVE, eliminating the need to enumerate, quantify, and sum the many possible sources of random error.

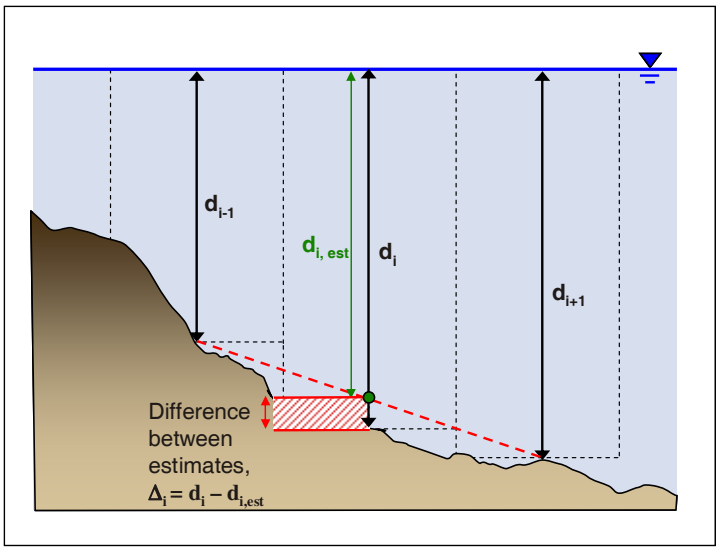

Figure 1. Illustration of Δ, the difference between two estimates of flow depth. The first estimate, d_i, is the measured depth at a vertical. The second estimate, $d_{i,est}$, is the depth estimated by linear interpolation between two adjacent verticals.

Measurement error will tend to increase Δ as well as the estimate of u_d and u_v. In addition, if the depth or velocity profiles do not vary linearly from subsection to subsection, Δ (u_d and u_v) will tend to be large, as the linear interpolation will not provide a good estimate of the variable.

The u_d and u_v estimated using IVE are substituted into equation 2 to calculate total uncertainty in the discharge measurement. The uncertainty due to the limited number of verticals is considered part of the random uncertainty estimated by u_d and u_v and so is not included as a separate term. It is important to note that the IVE method cannot account for systematic uncertainty due to instrument miscalibration, improper use of the streamgaging equipment, or other factors. The systematic uncertainty, u_s, as well as uncertainty in the width measurement, u_w, must still be estimated using other means, such as empirical or laboratory studies.

INTERPOLATED VARIANCE ESTIMATOR (IVE): RESULTS

The IVE method was tested at 11 locations in which multiple discharge measurements were made during steady flow conditions (Table 1). For example, 21 discharge measurements were made on the Watauga River at Sugar Grove, NC (USGS Station ID 03479000) on October 22, 1991. Assuming that each discharge measurement had the same uncertainty and that discharge remained relatively constant, the "true" uncertainty of an individual discharge measurement was estimated as the standard deviation of this set of measurements. As shown in Table 1, the Watauga dataset is unusual for the large number of measurements available. In all other cases, 10 or fewer measurements were available, and particularly for the very small sets, the sample estimate of the standard deviation may not be as reliable as for the Watauga dataset. In addition, these sets of measurements were taken for

different reasons, including for training purposes or comparison of different types of current meters. Thus, a mix of experienced and inexperienced hydrographers and a mix of different instruments were often used to collect the measurements.

For estimates of uncertainty using the IVE method, the width uncertainty was assumed to be 0.5 percent, and the systematic uncertainty was assumed to be 1 percent, consistent with suggestions by the International Standards Organization (2007). Figure 2 plots the "true" uncertainty versus the IVE-estimated uncertainty. As can be seen, the IVE method does seem to give a reasonable indication of measurement quality. There is a significant positive correlation between the two estimates of uncertainty, with an R^2 (coefficient of determination) value of 0.6. Although the IVE estimates appear to be biased somewhat low in these examples, this could be due to mis-specification of the systematic uncertainty of these measurements. Additional testing will provide more information to better evaluate the suitability of the IVE method for routine use.

Table 1. Discharge measurement datasets

Station ID	Site name	Date	Mean flow, ft^3/s	# of meas.
06187950	Soda Butte Creek near Lamar Ranger Station, WY	8-13-93	155	10
06190540	Hot (Boiling) River near Mammoth, WY	8-15-93	29	8
06232600	Popo Agie river at Hudson Siding near Lander, WY	8-16-93	205	4
06037000	Gibbon River near West Yellowstone, WY	8-14-93	136	10
06721500	St Vrain Creek near Allenspark, CO (set A)	8-17-93	67	8
06721500	St Vrain Creek near Allenspark, CO (set B)	8-18-93	65	7
n/a - special study	Little Bushkill Bushkill at Route 115, PA	3-29-06	10	4
03479000	Watauga River at Sugar Grove, NC	10-22-91	33	21
01479000	White Clay Creek near Newark, DE	8-23-06	109	5
n/a - special study	Reese Creek near Corwin Springs, MT	7-17-06	5	4
12331800	Clark Fork near Drummond, MT	10-11-95	706	5

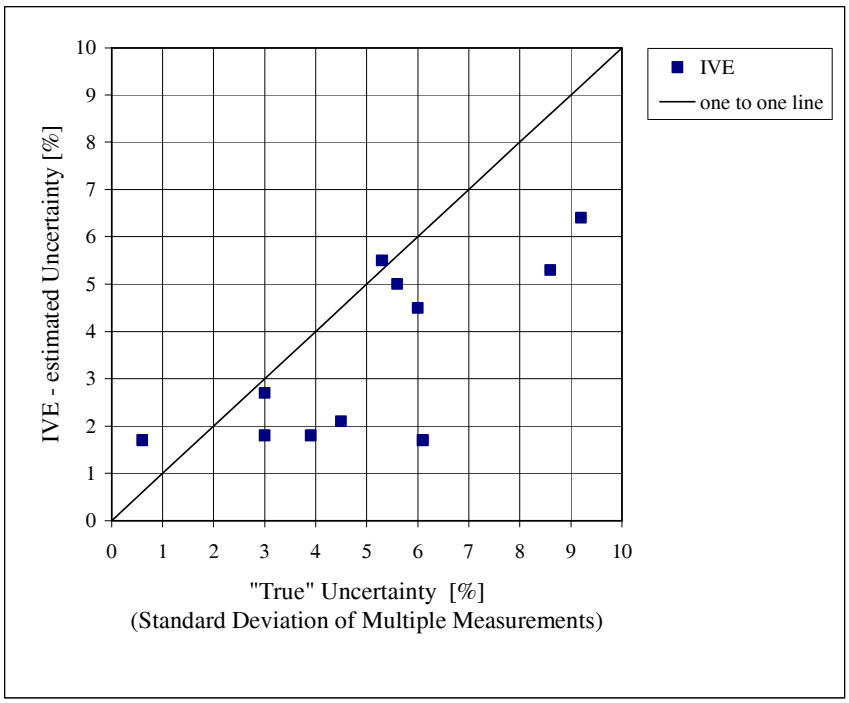

Figure 2. Uncertainty of discharge measurements. "True" measurement uncertainty, calculated as the standard deviation of multiple measurements during steady flow conditions, is compared to estimated uncertainty derived from the IVE method.

CONCLUSIONS

The analysis of measurement datasets with repeat observations suggests that the IVE method has promise as a method for quantifying the uncertainty that arises from random errors in a discharge measurement. The IVE method has the advantage of being an objective measure of uncertainty that is based on the actual channel and flow conditions experienced during the discharge measurement. It can easily be programmed into a computer, providing the hydrographer with immediate assessment of the measurement uncertainty. A large uncertainty may indicate the need for additional measurements, or the need to find a more suitable cross section.

The IVE method is also being tested using Monte Carlo simulations of discharge measurements. Preliminary results indicate that the method provides a good assessment of measurement uncertainty. Further testing of the IVE method will include additional field measurements.

ACKNOWLEDGEMENTS

Data for this study were provided by USGS hydrologists Janice Fulford, Dennis Risser, Ron Shields, Anthony Tallman, and Ron Shields (retired). Greg Schwarz and Phil Turnipseed, also of USGS, provided helpful reviews of an early manuscript.

REFERENCES

Carter, R.W. and Anderson, I.E. (1963) Accuracy of current meter measurements, Journal of the Hydraulics Division, Proceedings of the American Society of Civil Engineers, 89(HY4), 105-115.

Herschy, R. (1971) The magnitude of errors at flow measurement stations, Technical report, Water Resources Boad, Reading, UK.

Herschy, R. (1975) The accuracy of existing and new methods of river gauging, Technical report, Department of Geography, University of Reading, Reading, UK.

International Standards Organization (2007) Hydrometry – velocity-area method using current-meters – collection and processing of data for determination of uncertainties in flow measurement, International Standard 748.

Pelletier, P.M. (1988) Uncertainties in the single determination of river discharge: a literature review, Canadian Journal of Civil Engineering, 15, 834-850.

Rantz, S. and others (1982) Measurement and computation of streamflow: Volume 1. Measurement of stage and discharge, Water-Supply Paper 2175, U.S. Geological Survey, Washington, D.C., USA.

Sauer, V. and Meyer, R. (1992) Determination of error in individual discharge measurements, Open-File Report 92-144, U.S. Geological Survey.

Assessment of Lumped, Quasi-Distributed and Distributed Hydrologic Models of the US Army Corps of Engineers

Murari Paudel[1], Dr. E. James Nelson[2], and Charles W. Downer[3]

[1]Graduate Student, Brigham Young University, mpaudel@et.byu.edu

[2]Professor, Brigham Young University, jimn@byu.edu

[3]Senior Researcher, U.S. Army Corps of Engineers, Charles.W.Downer@usace.army.mil

1 Introduction

The conceptual or computational procedure for numerically simulating a process(s) which occur in a watershed is generally called hydrologic modeling. Modeling is commonly used to estimate runoff from a watershed, which is one of the most important aspects of any hydraulic and hydrologic design project. One of the widely used applications of these estimates is to determine the design or flood discharge of a watershed. While useful, any simulation model is a simplification of the real world processes and parameters. Because of these simplifications, there is a range of suitable problems for which models can be applied.

Traditionally, hydrologic simulation modeling systems have been classified as 1) Lumped parameters, 2) Quasi-distributed parameter or 3) Distributed systems. In terms of spatial discretization/ resolution, we can organize these hydrologic model categories on an ascending scale of sophistication beginning with lumped models to the physically based distributed model. The lumped models treat the complete basin as a single homogeneous element and develop a single outflow hydrograph (Jones, 1997). The quasi-distributed models discretize the watershed into homogeneous sub-areas or sub-basins based on the topography or drainage area. The infiltration or rainfall parameters are treated as homogeneous within each sub-basin and the flow is determined (Gan, 2001). The physically based fully distributed models divide the entire basin into elementary unit areas such as grid cells and flows are passed/routed from one grid cell to another as water drains through the basin (Jones, 1997). These three model categories are presented graphically in Figure 1. This allows the heterogeneity of the watershed to be incorporated on the scale of a grid cell. Grid resolution is generally chosen so that each grid cell will be fine enough to represent the spatial variation of all the input parameters such as rainfall, infiltration/loss parameters etc (Vazquez, 2002).

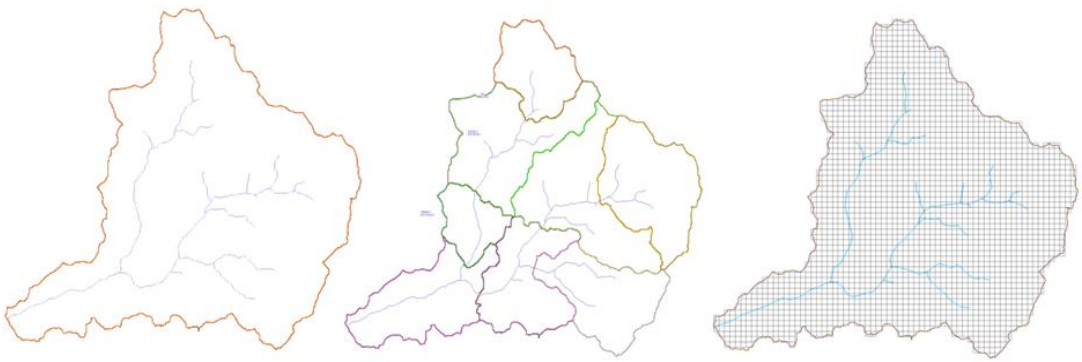

Figure 1: Graphic representation of lumped, quasi-distributed and distributed models

The majority of the modeling systems used in practice today are the simple lumped parameter models (Butts, 2004). This can be attributed to the fact that these models require a fewer number of parameters or data to be defined/calibrated for their operation (Butts, 2004). Despite many significant simplifications in these models, many of them have proven to be quite successful in simulating an observed flow hydrograph. The major benefit of using such simplified models is the ease in their calibration as smaller number of control parameters is used and it is easy to establish some pattern in their variation to produce desired watershed response.

An important shortcoming of simple lumped parameter models is that their parameters are not directly related to the physical characteristics of the catchment (Zhang et al, 2004). In general, their applicability is limited to gauged watersheds where the expected conditions are within the historic data used for calibration and no significant change in catchment conditions has occurred (Zhang et al, 2004).

The relationship between rainfall and runoff is a complicated process which is defined by numerous parameters each with inherent uncertainties. If these uncertainties are modeled using a stochastic, or even a statistical deterministic approach, it results in significant computational requirements (Jones, 1997). To better incorporate the variations and uncertainties involved in defining a watershed response to the rainfall, a physically based distributed model is always preferable (Kalin & Hantush, 2006). Distributed models can simulate both spatial and temporal variability of the watershed characteristics. These models, because of the larger computational requirements, add a massive computational burden. Historically, these computational resources were not available to general practitioners. With the advent of powerful computers, numerous quasi-distributed and distributed hydrologic models are emerging and many claim to be the best model, or at least capable of solving a wide variety of problems (Sui & Maggio, 1999). Because each model intrinsically has various limitations and assumptions, it can be concluded that model selection has always been a difficult problem for practicing engineers. Selection is not only limited by the accuracy of simulated results, but also includes the ability, knowledge and efforts to correctly develop a model from available data sources.

2 Models and tool selection

The USACE has played a vital role in the development and application of hydrologic models in the Unites States. It is the agency which establishes the modeling standards and guidelines and has developed a series of hydrologic, hydraulic and environmental models since the early 1960's. USACE models are extensively used throughout the world and they included such pioneering models as HEC-1, HEC-2, HEC-HMS, HEC-RAS, and GSSHA. Two of their models HEC-HMS and GSSHA will be used as the tools for this research. As a straightforward and well established standard model, HEC-HMS is widely used in the US and worldwide. GSSHA is a more sophisticated physically-based research model that the USACE is promoting as a model capable of simulating more complicated hydrologic/hydraulic situations such as the levee

failures in New Orleans and sediment and nutrient transport within a watershed (reference). Both models are commonly used and are promising, with many applications in peer-reviewed literature. GSSHA is supported by the US Army Engineer Research and Development Center and is embedded into the Watershed Modeling System (WMS) (Nelson, 2006). Moreover, this research is promoted and funded by the USACE to test and establish the reliability of their models so that the broader engineering community can take advantage of such models.

HEC-HMS, GSSHA, and WMS are the hydrologic models and tools used in this research. The following sections talk in brief about these tools and Models.

2.1 HEC-HMS

The USACE model, Hydrologic Modeling System (HEC-HMS) is designed to simulate the precipitation-runoff processes of dendritic watershed systems (HEC-HMS, 2000). HMS is widely used in a broad range of hydrologic problems varying from the analysis of large river basin water supply and flood hydrology to the study of small urban or natural watershed runoff. HEC-HMS has been used for studies of water availability, urban drainage, flow forecasting, future urbanization impact, reservoir spillway design, flood damage reduction, floodplain regulation, and systems operation (HEC-HMS, 2000).

HEC-HMS is popular for its simple and relatively easy approach, and it has been shown to perform excellently for certain problems, but the general perception (largely because of familiarity) is that it can be applied for almost all problems, even for complex scenarios. The capability of HEC-HMS to analyze the watershed hydrology in both lumped and quasi-distributed (HEC-HMS ModClark Method) fashion is its strength.

2.2 GSSHA

The Gridded Surface Subsurface Hydrologic Analysis (GSSHA) model is a reformulation and enhancement of the distributed runoff model CASC2D (Ogden, 2000). GSSHA is a physically based, two-dimensional model in which the watershed is discretized into uniform raster grids of any size. It is capable of both long-term and single event simulation, sediment and nutrient transport, ground water surface interaction, wet land simulation, lumped and distributed rainfall etc. by solving the finite difference equations. The model solves transport equations using finite difference and finite volume techniques and includes 2-D diffusive-wave overland flow routing and 1-D diffusive-wave channel routing (Downer, 2006). GSSHA is a process-based model with an option to select the specific processes to be modeled for a particular application. Among the processes that can be simulated are precipitation distribution, snowfall accumulation and melting, precipitation interception by vegetation, surface water retention, infiltration, overland flow runoff, overland erosion and deposition, channel routing of water, channel routing of sediments, channel routing of conservative contaminants, unsaturated groundwater flow (Vadose

zone modeling), saturated groundwater flow, stream recharge/discharge to groundwater, exfiltration of groundwater to land surface, and evapo-transpiration (ET) (S. Hunter et al, **19xx)**.

2.3 WMS 8.2

The interface for developing the input files from the geo-spatial information using the GIS based platform are available in Watershed Modeling System (WMS 8.1) for both GSSHA and HEC-HMS (Nelson, 2006). WMS has GIS based user interface and is capable of both pre and post processing the data necessary for hydrologic modeling.

3 Methodology

The discretization of watershed is done to consider the spatial variations in the watershed. The discretization might be in the form of sub basins or in the form of grids. Most of the times, the watershed boundaries within the watershed are taken as the sub basin boundaries and the hydrologic parameters are assumed to be same over such sub basins. This helps in incorporating the distinct variation in the watershed parameters during hydrologic modeling. Another approach is to divide the watershed into grid cells of uniform size and allocate the watershed properties to each such cell. This will help consider the spatial variability of the parameters in greater detail and with higher resolution. Each grid cell in some way is a small sub basin where all the computations are done to determine the abstractions and losses.

3.1 Lumped Vs Quasi-distributed models in HEC-HMS:

In the lumped model, the entire basin is assumed as a single unit and the hydrologic computations are done. As seen in Figure 2, the watershed is not further divided into sub basins or grids. For the quasi–distributed approach, three different cases were analyzed, one with 2, next with 4 and the last with 8 sub basins. This comparison was done to see how these different discretizatins affect the watershed response. SCS curve number method was used for loss methods and SCS equation was used to determine the lag time for Clark transformation methods. A uniform precipitation of 2.5 inches with SCS type-II 24 hour distribution resulted in the following (see **Figure 4**) outflow hydrograph.

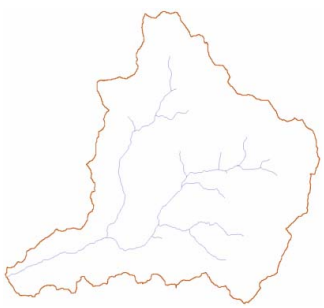



Figure 2: Lumped Model

Figure 3: Quasi-distributed Model (2 sub basins)

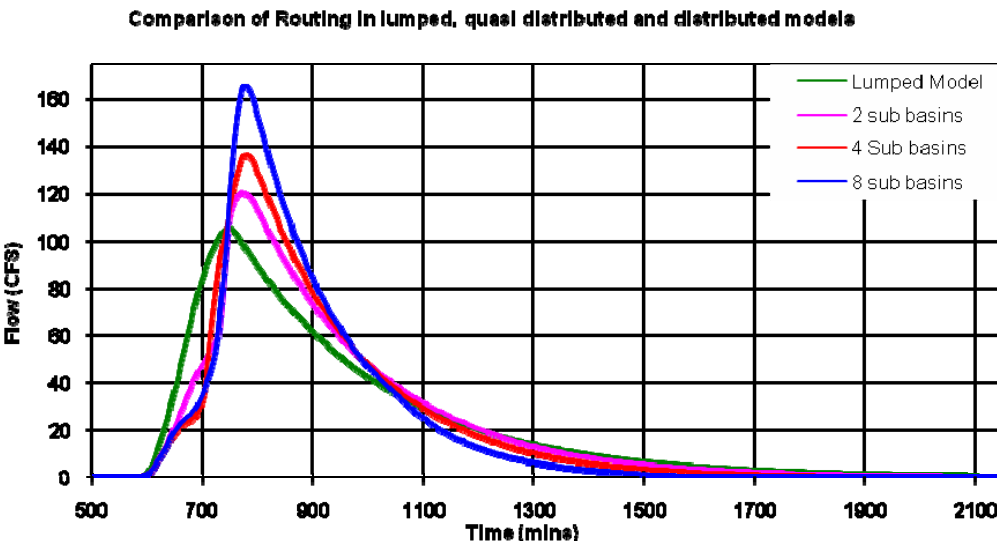

Figure 4: Results from Lumped and Quasi-distributed models

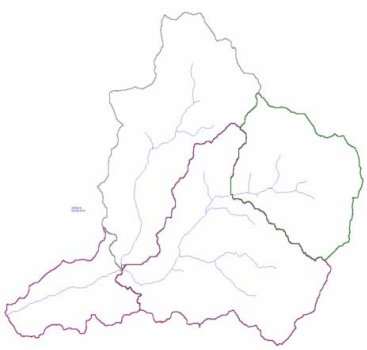

Figure 5: Quasi-distributed Model (4 sub basins)

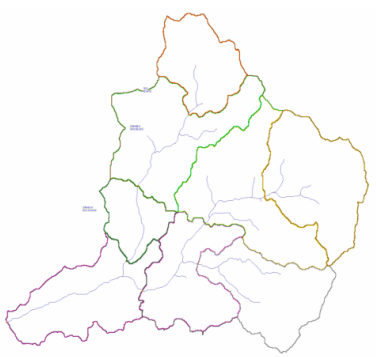

Figure 6: Quasi-distributed Model (8 sub basins)

Muskingum routing method was used to transfer the outflow hydrograph from intermediate outlet points in the quasi-distributed models to the final basin outlet. The parameters required for routing were extracted using WMS. The results show (Figure 4) that the lumped model gives smaller peak under the same conditions as compared to the quasi-distributed models. The increasing number of sub basins shows the increase in the peak flow.

This leads us to believe that the quasi-distributed models give conservative results as compared to the lumped models and the higher the resolution of discretization the sub basins; the more conservative is the result.

3.2 Lumped Vs distributed models in HEC-HMS:

In another part of this research, a comparison was made between lumped and distributed HEC-HMS models. Two test watersheds were studied and the comparison of the two methods is done.

The lumped model uses SCS CN loss method with Clark transformation method. Similarly, the distributed model uses gridded CN method with ModClark transformation method. A uniform rainfall of 2.5inches with SCS type-II 24 hour distribution resulted in the following outflow hydrograph (Figure 7).

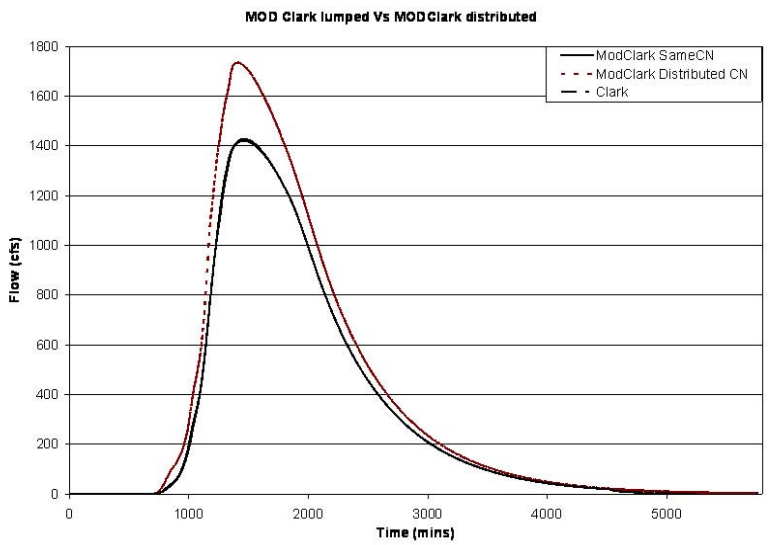

Figure 7: Hydrograph Comparison from Clark and ModClark methods

The hydrograph from the Clark method results in a smaller peak as compared to that from the ModClark method. This means that further distributing the watershed parameters such as the curve number results in a higher and thus more conservative response.

3.3 Distributed models in GSSHA

Although the ModClark method in HEC-HMS is distributed as compared to the lumped and the quasi-distributed models, it is not a physically based model. It uses unit hydrograph approach for the transformation. Because of this there are several problems which cannot be solved by the

ModClark method. To deal with such issues, the USACE has developed GSSHA which is a fully distributed physically based hydrologic model.

GSSHA is capable of solving a wide range of hydrologic problems varying from simple problems that can be modeled using a lumped model to much complex scenarios. Further, it is capable of handling other important ecological processes such as wetland simulation, sediment and nutrient transport etc. (Downer, 2006).

GSSHA itself is not a standalone program because it does not have the graphical user interface (GUI) but it has been developed in WMS. Advanced pre and post processing tools for analyzing the geospatial data are developed in WMS to facilitate the distributed modeling with GSSHA. WMS also provides the post processer which is very useful in result visualization as well as calibration of the GSSHA models.

3.4 Analysis of land use change scenario in GSSHA

Because of rapid change in the human needs, the engineering practice is also facing new problems and design requirements. Change of land usage and its effects on the watershed response has been studied for a long time and it is one of very important aspect of land development studies. GSSHA is capable of simulating the effects of the land use changes.

A research has been carried out with an experimental watershed (See

Figure 8) to see how well GSSHA can simulate the land use change scenario. Such a generic watershed is used for this study instead of using a real world watershed because the parameters can be controlled easily and there are smaller numbers of factors that affect the outflow.

The land use is changed at various locations of the watershed such as near and away from the stream, near and away from the outlet, on steep and mild slope etc. The main goal of this study is establish the fact that GSSHA can simulate the scenarios as intuitively such changes are expected to act.

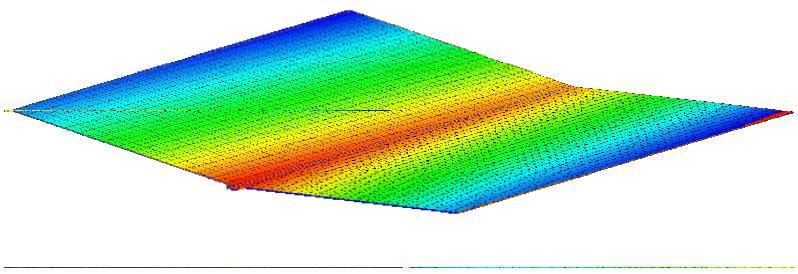

Figure 8: Experimental watershed to analyze land use change scenario

Nine different locations of the changed land use and its effect on the outflow hydrograph are studied. Similarly, a lumped model is created in HEC-HMS and the same scenarios are analyzed. But in case of the lumped model, the location of changed land use does not matter significantly because it is represented by the percentage of the watershed area that is impervious. The following figure (see Figure 9) shows some of the preliminary results of this research.

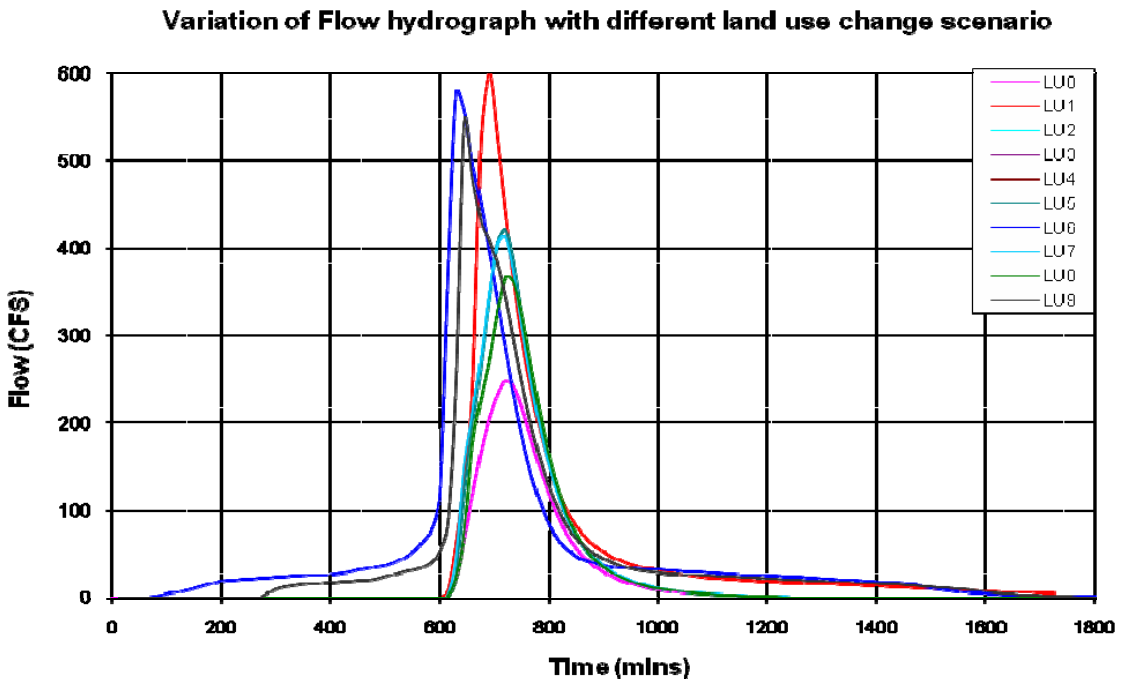

Figure 9: Results from land use change scenario simulation

In the figure (see Figure 9), the smallest hydrograph represents the outflow from the watershed when there is no land use change and all other cases are under different location of the changed land use. This research is still ongoing and a lot of other facts are yet to be analyzed. The results from this research will be validated with the real world watershed to establish that GSHSA is usable in solving such problems.

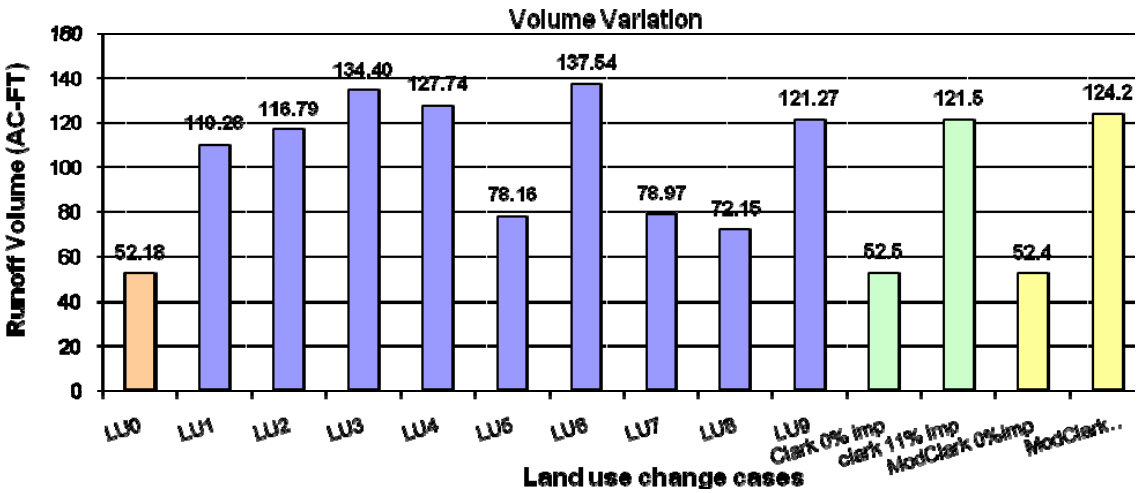

Figure 10: Runoff volumes in land use change scenario analysis

As seen in the above figure (see Figure 10), the results from a lumped model (HEC-HMS simulations) are the same for all different land use locations and it does not represent the actual responses of such changes. From this observation, it can be inferred that it is not always safe to use the lumped models and there are very good models like GSSHA for such cases.

4 Discussion and conclusion

Various research components discussed above are a part of bigger project in which the assessment of the distributed models in terms of the usability, accuracy and necessity has been done. As already been stated, this project is funded by the USACE to see how well their models perform for all these different hydrologic problems and scenarios.

The use of distributed hydrologic models by the engineering community is still limited. Different literatures discuss about the reasons behind the problems and complications in using such models. This study is mainly focused on finding such hurdles and suggesting the solutions to overcome them. It is evident that the physically based distributed models are data hungry and a lot of high resolution spatial data is necessary. The tools to process such data is another concern because it consumes a lot of time and resources and at the same time it is the vital part of modeling as the parameters for the model are derived from them.

At present, the GIS data are available for majority of areas and are easily accessible. There are tools like WMS which facilitate the pre and post processing of the data. In this study, we are evaluating the ease of modeling GSSHA and HEC-HMS models using WMS interface. This evaluation includes all different aspects from data collection, processing, parameterization,

visualization to calibration of the models. It has been a continuous process and a lot of improvement has been made in WMS interface for GSSHA and HEC-HMS.

With such effective tools, the distributed models are now as easy as the lumped models to develop and they can be applied to solve a wider of range of problems than that can be done with the lumped models. The only problem that such models are facing is the prevailing perception that these are difficult to develop and calibrate. We expect that the outcomes of this research help changing such perception and encourage people to start using these tools. Summary and conclusion

5 References

1. Ajami, N. K., Gupta, H., Wagener, T., and Sorooshian, S. (2004). *"Calibration of a semi-distributed hydrologic model for streamflow estimation along a river system."* Journal of Hydrology, 298, 112-135.
2. Biftu, G., and Gan, T., 2001, *"Semi-distributed, physically based, hydrologic modeling of the Paddle River Basin, Alberta, using remotely sensed data"*, Journal of Hydrology, 244, 137-156.
3. Butts, Michael B., Jeffrey T. Payne, Michael Kristensen, and Henrik Madsen (2004). *"An Evaluation of the Impact of Model Structure on Hydrological Modelling Uncertainty for Streamflow Simulation."* Journal of Hydrology, 298, pp. 242-266.
4. Charley, W., Pabst, A., and Peters, J. (1995). *"The Hydrologic Modeling System (HEC-HMS): Design and Development Issues."* Technical Paper 149.
5. Davis, D. W. (1993). *"The HEC NEXGEN Software Development Project, Technical Paper 138."* Rep. No. TP-138, US Army Corps of Engineers, Hydrologic Engineering Center.
6. Downer, C. W., and Ogden, F. L., 2006, *"GSSHA User's Manual, Gridded Surface Subsurface Hydrologic Analysis Version 1.43 for WMS 6.1"*, ERDC Technical Report, Engineer Research and Development Center, Vicksburg, Mississippi
7. Downer, Charles W. and Fred L. Ogden (2004). *"GSSHA: Model to Simulate Diverse Stream Flow Producing Processes."* Journal of Hydrologic Engineering
8. Feldman, Arlen, Editor. (2000). *"Hydrologic Modeling System - HEC-HMS - Technical Reference Manual"*, Davis, California
9. Hartman, B. R., and Nelson, E. J. *"A Central Method for GeoSpatial Data Acquisition (GSDA)."* Proceedings of the World Water & Environmental Resources Congress, American Society of Civil Engineers (ASCE) and the Environmental Water Resources Institute (EWRI), Orlando.
10. Hayakawa, Kiroshi, Kunihide Uchijima, and Mutsuhiro Fujita (1995). *"A Study on Subcatchment Scale for a Distributed Runoff Model."* Environment Internation, Vol. 21, No. 3., pp. 491-496.

11. Hunter, S., J. Jorgeson, S. Meyer, and B.E. Vieux, (2002). *"A Test Of Two Distributed Hydrologic Models with WSR-88D Radar Precipitation Data Input"*. 2nd Federal Interagency Hydrologic Modeling Conference, July 28-August 1, 2002, Las Vegas, Nevada.
12. Jones, J.A.A., 1997. *"Global Hydrology"*, Pearson Education Limited, Edinburgh Gate, Harlow, England.
13. Kalin, L., M.M. Hantush (2006), *"Comparative Assessment of two distributed watershed models with application to a small watershed"*, Hydrological Processes, 20(11):2285-2307.
14. Koren, V.I., B.D. Finnerty, J.C. Schaake, M.B. Smith, D.-J. Seo, and Q.-Y. Duan (1999). *"Scale Dependencies of Hydrologic Models to Spatial Variability of Precipitation."* Journal of hydrology, 217, pp. 285-302.
15. Kull, D. W., and Feldman, A. D. (1998). *"Evolution of Clark's Unit Hydrograph Method to spatially distributed runoff."* Journal of Hydrologic Engineering, 3(1), 9-19.
16. Nelson, E. J. (2006). *"Watershed Modeling System (WMS), User's Manual."*, Environmental Modeling Research lab, Brigham Young University.
17. Ogden, F. L., H. O. Sharif, S. U. S. Senarath, J. A. Smith, M. L. Baeck, and J. R. Richardson (2000). *"Hydrologic Analysis of the Fort Collins, Colorado, Flash Flood of 1997."* Journal of Hydrology, 228, pp. 82-100.
18. Ogden, Fred L. and Pierre Y. Julien (1994). *"Runoff Model Sensitivity to Radar Rainfall Resolution."* Journal of Hydrology, 158, pp. 1-18.
19. Peters, J. C. (1995). *"The Hydrologic Modeling System (HEC-HMS)."* Technical Paper 150.
20. Peters, J. C., and Easton, D. J. (1996). *"Runoff Simulation Using Radar Rainfall Data."* Water Resources Bulletin, 32, 753-760.
21. Reed, Seann, Victor Koren, Michael Smith, Ziya Zhang, Fekadu Moreda, Dong-Jun Seo, and DMIP Participants (2004). *"Overall Distributed Model Intercomparison Project Results."* Journal of Hydrology, 298, pp. 27-60. 388
22. Refsgaard, Jens Christian and Jesper Knudsen (1996). *"Operational Validation and Intercomparison of Different Types of Hydrological Models."* Water Resources Research, Volume 32, No. 7, pp. 2189-2202
23. Smith, Michael B. (1993). *"A GIS-Based Distributed Parameter Hydrologic Model for Urban Areas."* Hydrologic Processes, Volume 7, pp. 45-61.
24. Sui, D. Z., and Maggio, R. C. *"Integrating GIS with hydrological modeling: practices, problems, and prospects."* Computers, Environment and Urban Systems, 23(1), 33-.
25. US Army Corps of Engineers, Hydrologic Engineering Center. (1996). *"MODClark Model Development for the Muskingum River Bain, OH."* Rep. No. PR-33, US Army Corps of Engineers Hydrologic Engineering Center.
26. Vazquez, R. F., L. Feyen, J. Feyen, and J.C. Refsgaard (2002). *"Effect of Grid Size on Effective Parameters and Model Performance of the MIKE-SHE Code."* Hydrological Processes, Volume 16, pp. 355-372.

CHANGE IN SURFACE HYDROLOGY DUE TO LAND USE CHANGE IN A MIDWESTERN WATERSHED

A. Spencer[1], B. Walker[2], M. Arabi[3], J. Frankenburger[4], and R.S. Govindaraju[2]

[1]Department of Civil and Environmental Engineering, Colorado State University, Campus Delivery 1372, Fort Collins, CO 80523-1372; email: Anthony.Spencer@colostate.edu
[2]School of Civil Engineering, Purdue University, 550 Stadium Mall Drive, West Lafayette, IN 47907-2051
[3]Department of Civil and Environmental Engineering, Colorado State University, Campus Delivery 1372, Fort Collins, CO 80523-1372
[4]Department of Agricultural and Biological Engineering, Purdue University, 225 S. University Street, West Lafayette, IN 47907-2051

Abstract

Land use change and urbanization can have significant impacts on hydrologic processes within watershed systems. Monitoring data, however, are rarely sufficient to fully understand the spatial and temporal factors that contribute to the change in streamflows. This paper presents a modeling framework to evaluate changes in flow regimes at various spatial scales as a result of rapid urbanization in the Eagle Creek watershed in the Midwestern United States. We also aim to determine which components of land use change and preexisting conditions (previous land use and hydrologic soil group) have greater impacts on changes in the flow regime. The Soil and Water Assessment Tool (SWAT) model was used to simulate 50 years of streamflows for the 273 km^2 watershed under the land use conditions of the years 2000 and 2004, as defined by the National Agricultural Statistics Service (NASS) and National Land Cover Data (NLCD) geospatial datasets. Flow duration curves (FDCs) were constructed for 230 subbasins within the watershed under the 2000 and 2004 land use conditions. A two sample Kolmogorov-Smirnov test (KS test) was used to quantify the significance of the difference between the FDCs corresponding to the year 2000 versus 2004 land use scenarios for each subbasin. A multivariate regression analysis indicated that change in urban area, change in forest area, and coverage by hydrologic soil group A have the greatest impact on the change in streamflows associated with land use change.

Introduction

The significance of the impact of urbanization upon the nation's surface waters has long been recognized by several monitoring programs. As early as the 1960's, the United States Geographical Survey (USGS; Leopold, 1968) began alerting planners to the increased dangers of flooding and lost groundwater storage that may occur as the area occupied by roads, parking areas, and other impervious structures expanded. Recent studies have brought to light that the intensity and spatial distribution of urban development are key factors in the generation and timing of surplus runoff (Burges, 1998). It is well understood that with urbanization comes increasing imperviousness and disruption of the natural hydrologic cycle. But, the role of other watershed characteristics in conjunction with land use change has not been fully investigated. For example, will urbanizing pastureland have the same hydrologic impact as urbanizing cropland or forest areas? Will land use/land cover change in areas with predominantly permeable soils have similar impacts on runoff generation and streamflows as areas with poorly drained soils?

Past efforts to understand the impacts of urbanization have typically involved monitoring and/or hydrologic modeling at the watershed outlet. At the watershed scale, it would be rare to find geospatial homogeneity. If a watershed contains clustered areas of urban, crop, and forest, for example, an analysis based on the watershed outlet will provide results which are an amalgamation of effects due to the varying land uses throughout the watershed. This averages or 'washes out' the effects of individual components within the watershed. It seems that monitoring solely at the watershed outlet is inadequate to understand the impacts of urbanization and land use change on hydrologic regimes within the watershed.

A portion of the Upper White River Watershed located in the Midwestern United States has been selected for a study of the impacts of urbanization, prior land use conditions, and soil characteristics on a changing streamflow regime. The watershed was selected due to two of the receiving streams within the watershed, Eagle Creek and Fishback Creek, having witnessed rapid expansion of surrounding urban areas during the previous decade. The availability of long records of precipitation data, flow measurements and yearly land use data over the period of rapid urbanization make this watershed an ideal candidate for the analysis.

There are two main objectives of this study. The first objective is to determine the long-term change in streamflow regimes under observed conditions at various spatial scales within the watershed. The second objective is to determine other important factors that may have an impact on changes in the flow regime.

The Study Watershed

The 368.5 km^2 Eagle Creek Watershed spreads across Boone, Hamilton, Hendricks, and Marion Counties in central Indiana, as seen in Figure 1. The area is composed of the catchments draining into Fishback and Eagle Creek before they empty into the Eagle Creek Reservoir, a large recreational lake that also provides direct intake for the T.W. Moses water treatment plant (Tedesco et al., 2003). For a fuller description of the watershed characteristics, including the results of several water quality studies, refer to Tedesco et al. (2003) and Tedesco et al. (2005).

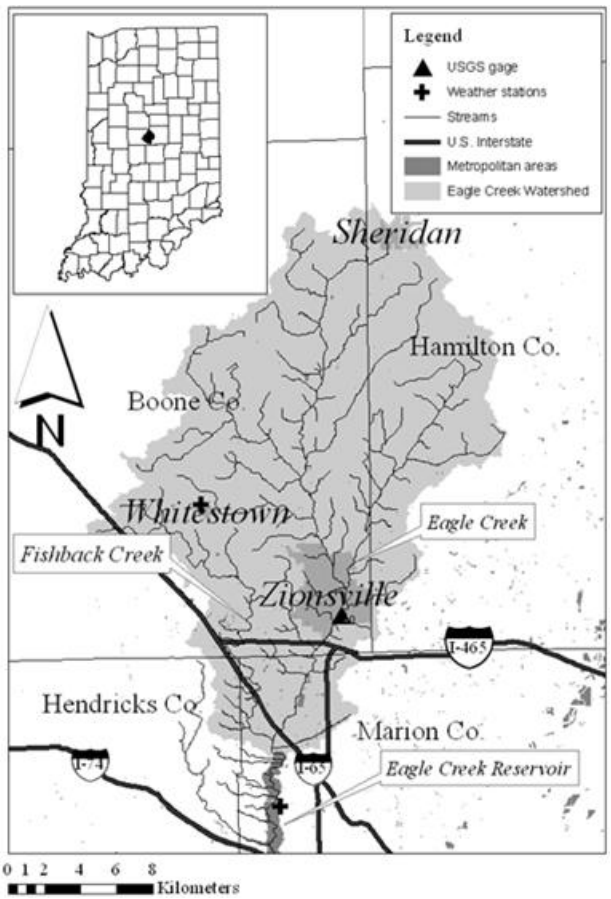

Figure 1. The Eagle Creek Watershed and its location in central Indiana (inset)

The watershed has traditionally been under extensive agricultural production. Land use data from the USDA's National Agricultural Statistics Survey (NASS) documenting the years 2000 and 2004 (Table 1) shows row crops (corn and soybeans) occupying 50.1 and 51.3% of the total area. Over the same period, urban area increased from 4.2% in 2000 to 12.7% in 2004. The increase of urban space led to a significant loss of pasture, as over 60% of the newly developed areas had been pasture in 2000, while another 13% had been under agricultural production.

Table 1. Land use of Eagle Creek Watershed in years 2000 and 2004

Year	% Corn	% Soybeans	% Pasture	% Forest	% Urban	% Water
2000	23.2	26.9	38.9	6.2	4.2	0.6
2004	27.8	23.6	27.4	8.1	12.7	0.4

The SWAT Model

The Soil and Water Assessment Tool (SWAT; Neitsch et al., 2001a,b) was chosen to investigate the long-term effects of land use change under observed conditions based on the insights it has provided into the hydrology of predominantly agricultural watersheds (Borah and Bera, 2003). SWAT is a process-based, semi-distributed model specifically designed with the intent of simulating the effects of land management decisions for continuous, multi-year periods at a daily time-step (Arnold

et al., 1998). Previous studies utilized the model for assessment of watersheds throughout the Midwest, including Illinois (Arnold and Allen, 1996), Kentucky (Spruill et al., 2000), and Indiana (Smithers and Engel, 1996; Arabi et al., 2006). Like Eagle Creek Watershed, the watersheds modeled in those studies were predominantly under row crop production. Fohrer et al. (2001) suggest that the semi-spatially distributed approach taken by SWAT is invaluable for studying relatively small (< 20% of total watershed area) shifts in land use.

SWAT employs a process-based model to simulate watershed hydrology. A two-stage procedure routes runoff from precipitation first overland and then through the stream network. Runoff generation begins at the hydrological response unit (HRU), a unique combination of soil type, land use, and management procedure within a subbasin. For each HRU, SWAT determines a curve number value based on the land cover, the hydraulic properties of the soil, and the antecedent moisture condition. The total generated runoff is summed for the subwatershed and is routed overland using a kinematic model and a modified Manning's equation to determine the time required for the entire subbasin to be contributing runoff (Neitsch, et al., 2001b). The total volume is then routed downstream through the channel network.

Methods

SWAT required three basic inputs to represent the physical characteristics of Eagle Creek Watershed: a digital elevation map (USGS 30 m resolution digital elevation map), a land use dataset (NASS 2000, 2004), and a soil dataset (Soil Survey Geographic Database, SSURGO). In the hopes to make the representation of land management more realistic, default crop schedules were replaced with observed management practices, and tile drains were added to poorly drained soils. Recorded precipitation and temperature data from National Climate Data Center station ID# 129557 and #124249 were used for each simulation. The watershed was divided into 230 subbasins and 4177 HRUs. This detailed watershed subdivision scheme provided the basis for examination of long-term (50-year) changes in flow regimes at various spatial scales.

Calibration & Validation

Three indices were used to evaluate model performance during calibration and validation: the coefficient of determination (R^2), the Nash-Sutcliffe model efficiency coefficient (E_{NS}), and the relative error (percent total difference). The study area for model calibration and validation was determined by the drainage area contributing into the USGS gage (#03533200) at Zionsville (see figure 1). The corresponding drainage area is contained within the Eagle Creek Watershed and has an area of 273 km^2, or roughly 75% of the Eagle Creek Watershed. Calibration of SWAT was accomplished by using both a genetic algorithm-based automatic calibration program and a manual calibration procedure (Arabi, 2005). SWAT was calibrated for the years 1995-1999 using the 2000 NASS dataset. Validation of the calibrated model was performed with the observed flow data for 2000-2004 using NASS datasets corresponding to the respective years.

Flow duration curves

The calibrated SWAT model was used to simulate 50-year periods of daily streamflows in the Eagle Creek Watershed under two land use scenarios. The two scenarios included the observed land use conditions of the years 2000 and 2004, during which the watershed underwent change in land uses. All other factors such as soil type and climatic inputs were left unchanged between the two scenarios.

Flow duration curves (FDCs) were constructed for each of the 230 subbasins from the simulation data. To understand the changes in flow regime at a given outlet, several comparisons were made between the FDCs from land use conditions of 2000 and 2004. The overall average flow change and the flow change over selected exceedance intervals (0-10%, 10-90%, and 90-100% flows) were calculated as flow change indices. In order to assess the significance of the flow regime change, a two-sample Kolmogorov–Smirnov test (KS tests) was implemented on each of the flow change indices. Two-sided tests were used to assess if there was significant increase or decrease in the flow regime. One-sided tests assessed if there was significant increases in the flow regime.

Multiple regression models

It was desired to understand if land use change alone was the primary factor which caused a change in the flow regime or if there were other factors which might predispose an area to more significant change in the flow regime. Regression models were used to understand which factors had the greatest impact on flow regime change.

The regression models were broken up into groups by the response variables to be predicted. Each group of models predicted average flow change over the aforementioned flow change indices. The first group of models predicted average flow change (i.e., =[change in streamflows]). The second group predicted the absolute value of average flow change (i.e., =|[change in streamflows]|). The models used various combinations of land use change, soil type, and interactions thereof as predictors. The coefficient of determination, adjusted for number of predictors (R_a^2), was used as the measure of goodness of fit and a t-test was used to assess the significance of each predictor.

Results & Discussion

Performance indices for the SWAT model were sufficient for the entire calibration period (E_{NS} = 0.67, R^2 = 0.70) and validation period (E_{NS} =0.59, R^2=0.63). The KS test results yielded that 2004-FDCs corresponding to 178 out of the 230 subbasins were significantly different from 2000-FDCs at a 0.05 significance level.

A comparison of FDCs for numerous subbasins suggested that changes in the flow regimes at the subbasin level were not solely a product of urbanization. Table 2, below, compares the land use and flow regime change experienced by subbasins 166 and 209. From the table, it can be seen that the subbasins are similar in size (0.89 and

1.23 sq km) and experience similar amount of average flow change (23.42% and 23.01% increase in flows). However, the land use change experienced by the two subbasins is different. Subbasin 166 experiences 18.26% urban area increase and a 19.82% decrease in pasture area. The flow increase is likely attributed to the urbanization of pasture area. Subbasin 209 experiences a 13.65% increase in crop area and a 12.01% decrease in forest area. The increased flows in subbasin 209 are likely caused by forest area being converted to croplands.

Table 2. Land use change, soil group, and flow change for subbasins 166 and 209

Subbasin	Area	Flow change	Land use change (%)				Soil group (%)		
(#)	(km^2)	(%)	Urban	Crop	Pasture	Forest	Soil A	Soil B	Soil C
166	0.89	23.42	18.26	2.64	-19.82	-2.64	0.00	100.00	0.00
209	1.23	23.01	-1.10	13.65	2.81	-12.01	26.69	64.67	8.64

Figure 2 shows the FDCs for subbasins 166 and 209. Although the average flow rates from the subbasins experienced a similar increase, it can be seen that different parts of the flow duration curves are affected. Subbasin 166 has a greater increase in the larger magnitude, lower probability flows. Subbasin 209 experienced a greater increase in the mid range of exceedance probabilities and mid range of flows.

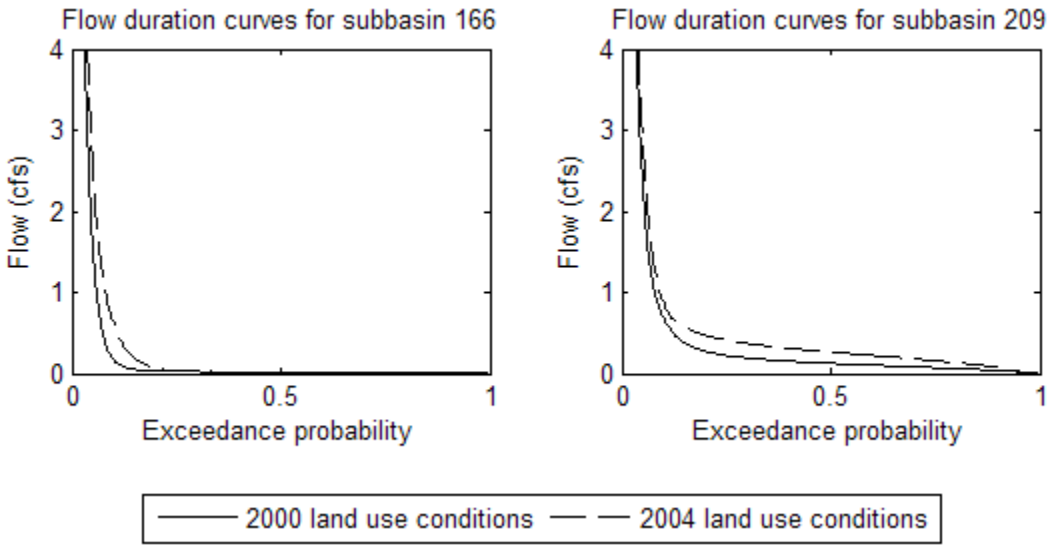

Figure 2. Flow duration curves for subbasins 166 and 209 for land use conditions 2000 and 2004

Table 3 compares the land use and flow regime change experienced by subbasins 166 and 72. The two subbasins are similar in size and experience nearly identical land use changes. Subbasins 166 and 72 both experience a reduction of pasture areas and an increase in urban areas. Yet, subbasin 166 experiences a much larger flow increase of 23.42% whereas the flows in subbasin 72 increase by only 7.33%.

Table 3. Land use change, soil group, and flow change for subbasins 166 and 72

Subbasin	Area	Flow change	Land use change (%)				Soil group (%)		
(#)	(km^2)	(%)	Urban	Crop	Pasture	Forest	Soil A	Soil B	Soil C
166	0.89	23.42	18.26	2.64	-19.82	-2.64	0.00	100.00	0.00
72	0.62	7.33	16.35	1.85	-16.85	-1.70	0.00	48.57	51.43

The primary difference between the two subbasins is the hydrologic soil group composition. Subbasin 166 is completely covered by NRCS hydrologic soil group B, which is a soil with a moderate infiltration rate. The majority of subbasin 72 is covered by soil group C, which has a lower infiltration rate and a higher runoff potential than soil group B.

One of the main ways urbanization increases runoff is by increasing imperviousness which reduces infiltration. Covered by a soil with a lower inflation rate, subbasin 72 would be predisposed to producing more runoff even before urbanization, as compared to subbasin 166. So, the increased imperviousness associated with urbanization may not have as drastic an impact on runoff and streamflows, which is supported by Table 3. A much more drastic change in the FDCs of subbasin 166 than the change in FDCs of subbasin 72 can be seen in Figure 3, below. These results suggest that soil type is an important factor in predicting flow changes with changing land use.

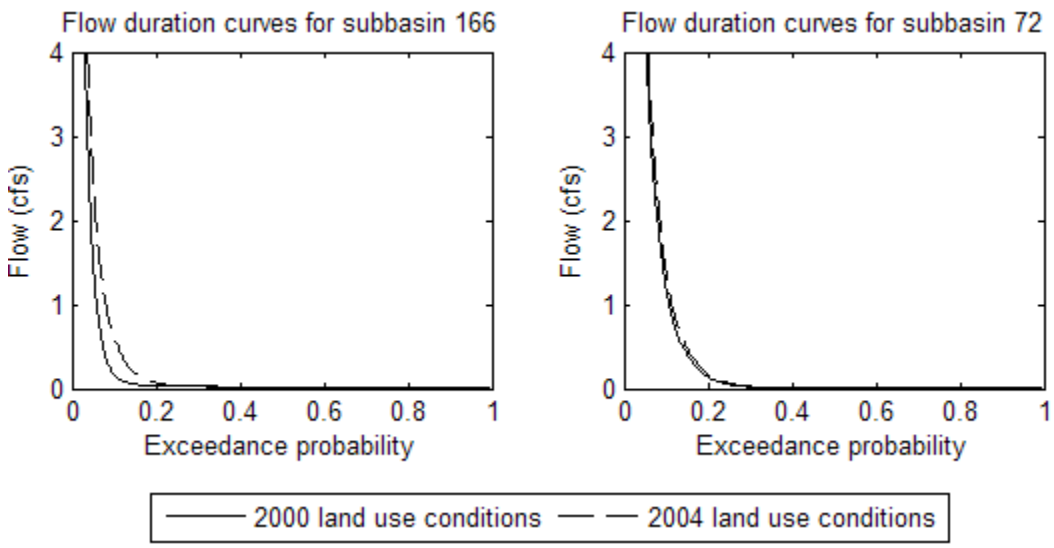

Figure 3. Flow duration curves for subbasins 166 and 72 for land use conditions 2000 and 2004

Multiple regression models

The regression models varied greatly in their ability to predict the change in flows associated with the changing land use conditions of 2000 and 2004. The R_a^2 of the models ranged from as high as 0.91 to as low as 0.14, as seen in Table 4, below. The models with the best fit were consistently the models which predicted the low exceedance probability (0-10%) high level flows and the models which predicted the overall average flow change. Further, it was the models which included all predictors that were found to have the greatest R_a^2.

Table 4. Goodness of fit of regression models prediction of flow change

	Absolute value models				Actual value models			
Flows predicted	**0-100%**	**0-10%**	**10-90%**	**90-100%**	**0-100%**	**0-10%**	**10-90%**	**90-100%**
Lowest Ra^2	0.216	0.258	0.160	0.175	0.216	0.203	0.141	0.162
Highest Ra^2	0.761	0.846	0.591	0.595	0.839	0.913	0.597	0.594

Although many combinations of predictors were explored, a model was chosen for further analysis which has a reasonable fit (R_a^2 = 0.77), a manageable number of predictors and several notable features. The chosen model defined in Table 5, below. Since each predictor is in terms of percent land use change or percent coverage by hydrologic soil group, the coefficients are able to be compared to one another. This comparison allows for determination of which predictor has greater impact on flow change by which coefficient is larger in magnitude.

Table 5. Selected regression model which predicts average flow change

Predictor	Estimate of Coefficient	Std. Error	t value	Pr(>|t|)
(Intercept)	-3.971	1.888	-2.103	0.037
Urban change (%)	0.352	0.778	0.452	0.652
Crop change (%)	0.206	0.727	0.283	0.777
Pasture change (%)	-0.195	0.725	-0.269	0.788
Forest change (%)	-0.533	0.745	-0.715	0.475
Soil A (%)	0.408	0.043	9.425	< 2e-16
Soil B (%)	0.061	0.035	1.760	0.080
(Urban change)(Soil A)	0.004	0.009	0.458	0.647
(Urban change)(Soil B)	0.016	0.015	1.103	0.271
(Crop change)(Soil A)	0.016	0.009	1.704	0.090
(Crop change)(Soil B)	0.019	0.014	1.355	0.177
(Pasture change)(Soil A)	0.024	0.008	2.861	0.005
(Pasture change)(Soil B)	0.015	0.014	1.067	0.287
(Forest change)(Soil A)	0.025	0.009	2.849	0.005
(Forest change)(Soil B)	0.010	0.014	0.731	0.465

From Table 5, it can be seen that the predictors with the greatest impact on flow change are forest area change, coverage by soil group A, urban area change, crop area

change, and pasture area change, ordered from largest impact to smallest impact. All other predictors have coefficients of nearly one order of magnitude less than the aforementioned factors. The direction of impact is also important for these predictors; increased urban and crop areas, decreased pasture and forest areas, as well as coverage by soil group A are all predicted to increase flows. Coverage by soil group A is also the most significant predictor in the model, as determined by the high t-value. Additionally, the coefficient of percent cover by soil group A is roughly an order of magnitude greater than the coefficient of coverage by soil group B. This supports the earlier suggestion that more permeable soils could predispose land use change to increasing flows since soil group A is more permeable than soil group B.

There are also a number of disagreements in the model. All of the interaction terms have positive coefficients. Although this agrees with the predictions of urban and crop area change and coverage by soil groups A and B, it predicts an opposite flow change as a result of forest and pasture area change. It is worth noting that the interaction terms also have a much lesser impact on flow change than the other predictors in the model since their coefficients are an order of magnitude lesser in most cases.

Conclusions

The goals of this study were to determine the influence of land use change on streamflow regimes within the watershed and to determine the other important factors that may have an impact on changes in the flow regimes. The KS test showed there was significant change in the 50-year daily flow simulations under observed land use conditions 2000 and 2004 in the majority of the subbasins. An examination of the FDCs showed that similar flow regime change is not solely a product of urbanization. In fact, similar amounts of land use change and urbanization resulted in different amounts of flow regime change. It was found that preexisting conditions (i.e., prior land use and soil type) can influence flow regime change in conjunction with land use change and urbanization. Further, when lands covered by more permeable soils (soil groups A and B) are urbanized, they are prone to more drastic changes in flow regime than urbanizing an area covered by less permeable soils. Finally, multivariate regression analyses suggested that the amount of urban change, amount of forest change, and coverage by hydrologic soil group A have the greatest impact on flow regime changes associated with land use change.

References

Arabi, M., Govindaraju, G.S., Hantush, M.M., Engel, B.A., 2006. Role of watershed subdivision on modeling the effectiveness of best management practices with SWAT. Journal of the American Water Resources Association, 42(2): 573-528.

Arnold, J.G., Allen, P.M., 1996. Estimating hydrologic budgets for three Illinois watersheds. Journal of Hydrology, 176(1996): 57-77.

Arnold, J.G., Srinivasan, R., Muttiah, R.S., Williams, J.R., 1998. Large area hydrologic modeling and assessment part I: model development. Journal of the American Water Resources Association, 34(1): 73-89.

Borah, D.K. and M. Bera. 2003. Watershed-scale hydrologic and nonpoint-source pollution models: Review of mathematical Bases. *Trans. ASAE* 46(6): 1553-1566.

Burges, S.J., Wigmosta, M.S., Meena, J.M., 1998. Hydrological effects of land-use change in a zero-order catchment. Journal of Hydrologic Engineering, 1998: 86-97.

Fohrer, N., Eckhardt, K., Haverkamp, S., and Frede, H.-G., 2001. Applying the SWAT model as a decision support tool for land use concepts in peripheral regions in Germany. In: Sustaining the Global Farm. Selected papers from the 10th International soil Conservation Organization Meeting. Stott, D.E., Mohtar, R.H, and Steinhardt, G.C., (eds): 994-999.

Leopold, L.B. 1968. Hydrology for urban land planning: A guidebook on the hydrologic effects of urban land use. *U.S. Geological Survey Circular 554*, 18p.

Neitsch, S.L., Arnold, J.G., Kiniry, J.R., King, K.W., 2001a. Soil and Water Assessment Tool theoretical documentation, version 2000, Grassland, Soil and Water Research Laboratory, Agricultural Research Service, Temple, TX.

Neitsch, S.L., Arnold, J.G., Kiniry, J.R., King, K.W., 2001b. Soil and Water Assessment Tool user's manual, version 2000, Grassland, Soil and Water Research Laboratory, Agricultural Research Service, Temple, TX.

Smithers, J.C., and Engel, B.A., 1996. An initial assessment of SWAT as a hydrological modeling tool for the Midwest USA. ASAE Paper No. 96-2065. St. Joseph, MI: ASAE.

Spruill, C.A., Workman, S.R., Taraba, J.L., 2000. Simulation of daily and monthly stream discharge from small watersheds using the SWAT model. Transactions of the ASAE, 43(6): 1431-1439.

Tedesco, L.P., Atekwana, E.A., Filippelli, G., Licht, K., Shrake, L.K., Hall, B.E., Pascual, D.L., Latimar, J., Raftis, R., Sapp, D., Lindsey, G., Manness, R., Pershing, D., Peterson, D., Ozekin, K., Mysore, C., Prevost, M., 2003. Water Quality and Nutrient Cycling in Three Indiana Waterhseds and Their Resevoirs: Eagle Creek/Eagle Creek Reservoir, Fall Creek/Geist Reservoir and Cicero Creek/Morse Reservoir. Central Indiana Water Resources Parntership, CEES Publication 2003-01, IUPUI, Indianapolis, IN, 163 p.

Tedesco, L.P., Pascual, D.L., Shrake, L.K., Hall, R.E., Casey, L.R., Vidon, P.G.F., Hernly, F.V., Salazar, K.A., Barr, R.C., Ulmer, J., Pershing, D., 2005. Eagle Creek Watershed Management Plan: An Integrated Approach to Improved Water Quality. Eagle Creek Watershed Alliance, CEES Publication 2005-07, IUPUI, Indianapolis, 182p.

Do Upland Soil Conservation Measures Reduce Watershed Sediment Yield?

Jurgen D. Garbrecht[1] and Patrick J. Starks[2]

[1]USDA, Agricultural Research Service, Grazinglands Research Laboratory
7027 West Cheyenne Str., El Reno, Oklahoma, OK 73036; PH (405) 262-5291; FAX (405) 262-0133; e-mail: jurgen.garbrecht@ars.usda.gov

[2]USDA, Agricultural Research Service, Grazinglands Research Laboratory
7027 West Cheyenne Str., El Reno, Oklahoma, OK 73036; PH (405) 262-5291; FAX (405) 262-0133; e-mail: patrick.starks@ars.usda.gov

ABSTRACT

Implementation of conservation measures do not always result in an immediate and measurable sediment yield reduction at the outlet of large watersheds. In this study, instantaneous suspended sediment and discharge measurements, taken in 1943-1948 and again in 2004-2008, in the Fort Cobb Reservoir watershed were used to estimate the downstream cumulative effects of 60 years of conservation practices on sediment yield. The analysis showed a substantial reduction in mean annual sediment yield between 1943-1948 and 2004-2008. This reduction was attributed to the gradual implementation of land use conversion and broad range of conservation measures over a 60- year time span.

INTRODUCTION

Soil and water conservation measures are highly effective at reducing overland soil erosion and sediment delivery from hillside to adjacent channels (Berg et al., 1988; McGregor et al., 1990). However, in large watersheds, the effectiveness of upland conservation measures, as well as channel stabilization efforts, does not necessarily lead to an immediate measurable sediment yield reduction at the watershed outlet (Trimble, 1999; Shields, 2008). The apparent disconnect or lag in response between upstream conservation measures and downstream sediment yield reduction, can be attributed to a variety of confounding factors, such as protracted implementation of conservation measures; spatial and seasonal variability of soil erodibility (especially in agricultural settings); timing of runoff producing storms in relation to agronomic activities; highly variable rainfall (amount, intensity) and resulting runoff with storm event; and potential shifting of sediment sources resulting from changing land use and management over time. Furthermore, in large watersheds, a lag in sediment yield response to upstream

conservation measures can be anticipated due to the slower propagation of sediments through the channel network and effects of sediment storage and subsequent remobilization. These factors and their complex interactions contribute to the notoriously large variability of watershed runoff and sediment yield, and frustrate efforts to identify the timing and magnitude of impacts of upstream conservation measures on sediment yield at the outlet of large watersheds (Pearson et al., 2006; Walling, 1999; Vente et al., 2007).

In this study, the effectiveness of upstream conservation measures to reduce sediment yield at the outlet of a watershed is determined by comparing historic and recent discharge and suspended sediment observations on a mixed agricultural watershed in west central Oklahoma. Discharge and suspended sediment were measured in the 1940s and again in 2004-2008 at several U.S. Geological Survey (USGS) gauging stations within the watershed which offered the opportunity to estimate changes in watershed sediment yield as a result of extensive conservation effort over the span of 60 years between the two measurement periods. Findings are interpreted in terms of land use conversion, conservation practices, urban development, and variations in climate.

WATERSHED DESCRIPTION

The Fort Cobb Reservoir watershed is a 787 km^2 agricultural watershed consisting primarily of crop and range/pasture land. Thirty event-based suspended-sediment and discharge measurements were taken by the USGS at the Cobb Creek gauging station near Fort Cobb during 1943-1948 (Figure 1; Table 1). In 1959 the Fort Cobb Dam was constructed. Subsequently, in 2004-2008 a total of 133 suspended-sediment and discharge measurements were taken at four gauging stations on the three major streams discharging into the reservoir (Figure 1; Table 1). The gauging station names were: Lake Creek near Sickles; Lake Creek near Eakly; Willow Creek near Albert; and Cobb Creek near Eakly (Figure 1).

LAND USE AND CONSERVATION PRACTICES

1943-1948. Historical crop data and land use distribution information were used to estimate land use for the 1940-1957 period (Storm et al., 2007). About 72% of the watershed area was in production agriculture, about 25% in pasture and range, and the remaining 3% in forest, roads, and urban areas. For the purposes of this study, these land use estimates were assumed to adequately represent the 1943-1948 time period. The extent of implemented conservation practices in the watershed during the 1940s was very limited and assumed to be of little practical relevance.

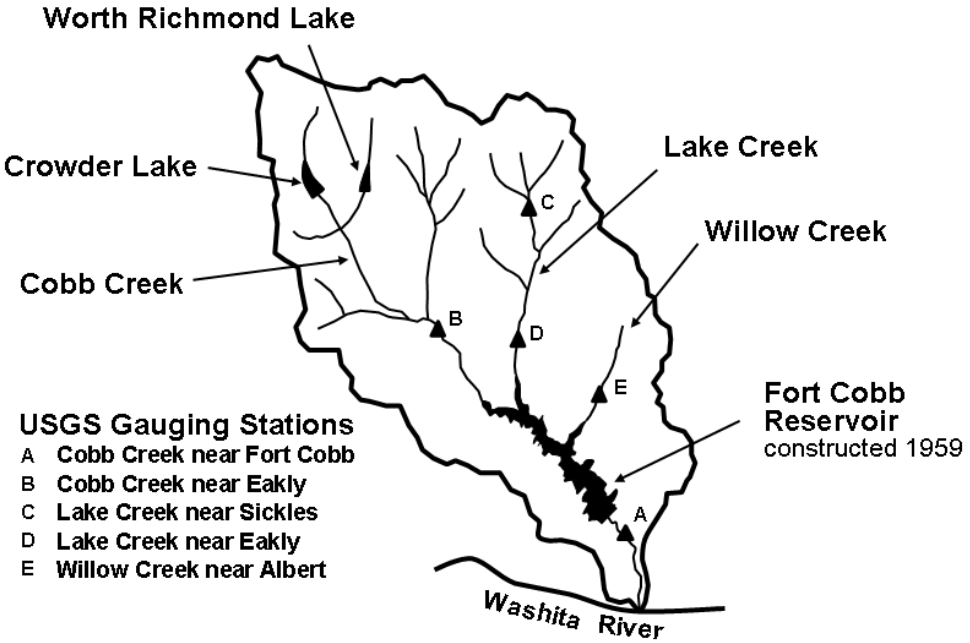

Figure 1. Fort Cobb Reservoir watershed and locations of U.S. Geological Survey discharge and suspended sediment gauging sites.

Table 1. U.S. Geological Survey discharge and suspended-sediment gauging stations.

Gauge Name	USGS Gauge Number	Drainage Area [km^2]	Period of Observations	Number of Data Points	Data Source
Cobb Creek nr Eakly	07325800	342	Nov 2004 – Apr 2008	46	USGS
Lake Creek nr Sickles	07325840	49	Jun 2006	1*	USGS
Lake Creek nr Eakly	07325850	154	Nov 2004 – Apr 2008	41	USGS
Willow Creek nr Albert	07325860	75	Nov 2004 – Apr 2008	45	USGS
Cobb Creek nr Fort Cobb	07326000**	826	May 1943 – Dec 1948	30	USGS

* Not a permanent suspended-sediment collection site; only one measurement available.
** After 1959, discharge below the dam is gate controlled.

2004-2008. Land use for the 2004-2008 period was estimated based on three separate remote sensing studies conducted in 2003, 2005 and 2006. The average land use from these three studies was assumed to adequately represent the land use conditions for the 2004-2008 timeframe. About 52% of the watershed was in production agriculture, 36% in grass/pasture lands, and the remaining area in forest (9%), water (2%) and roads/urban (1%). Soils in the central and eastern portion of the watershed (about 70% of the watershed area) are sandy, fertile, extensively cultivated and vulnerable to erosion, whereas soils in the far western portion of the watershed are more stable and not as extensively cultivated.

Over the last 50 years, about 80% to 90% of cropland that needs terraces has been terraced, and over the last 10 years about 50% of the cropland was in conservation tillage, minimum disturbance tillage, or no-till. Cost-sharing conservation programs supported some reshaping of gullies and installation of grade stabilization structures, and further conservation treatments were installed without cost-sharing assistance. In addition, small impoundments and flood retarding structures were constructed in the late 1950s and early 1960s, and more recently selected unstable stream bank sections were stabilized. Despite these efforts, a geomorphic assessment in 2007 identified several long unstable channel reaches (Simon and Klimetz, 2008), and controlling soil erosion continues to be a priority to protect fragile and erosion prone soils the watershed.

SEDIMENT RATING CURVES

1943-1948. Thirty instantaneous suspended-sediment and discharge measurements were taken by the USGS at the Cobb Creek gauge near Fort Cobb during 1943-1948 (Table 1; station A in Figure 1). To facilitate subsequent data comparison between gauging stations and across time periods, the sediment and discharge data were reformulated on a unit area basis, and a second-order regression was fitted to the data (Figure 2). The resulting sediment-discharge rating curve represent land use and management conditions that prevailed during the 1940s and 1950s and is referred to as the pre-conservation rating curve.

2004-2008. Another 133 sediment and discharge measurements were taken at four USGS gauging stations during 2004-2008 (Table 1; stations B, C, D and E in Figure 1). Again, the data were expressed on a unit area basis and displayed in a scatter diagram (Figure 3). The high degree of similarity and overlap in the data from the four gauging stations led to the assumption that a single second-order regression curve would adequately represent the sediment and discharge relationships at the four gauging stations. This rating curve represented the land use and management conditions that prevailed in 2004-2008 (post-conservation conditions) and embodied the broad range of conservation practices that were implemented in the second half of the 20th century.

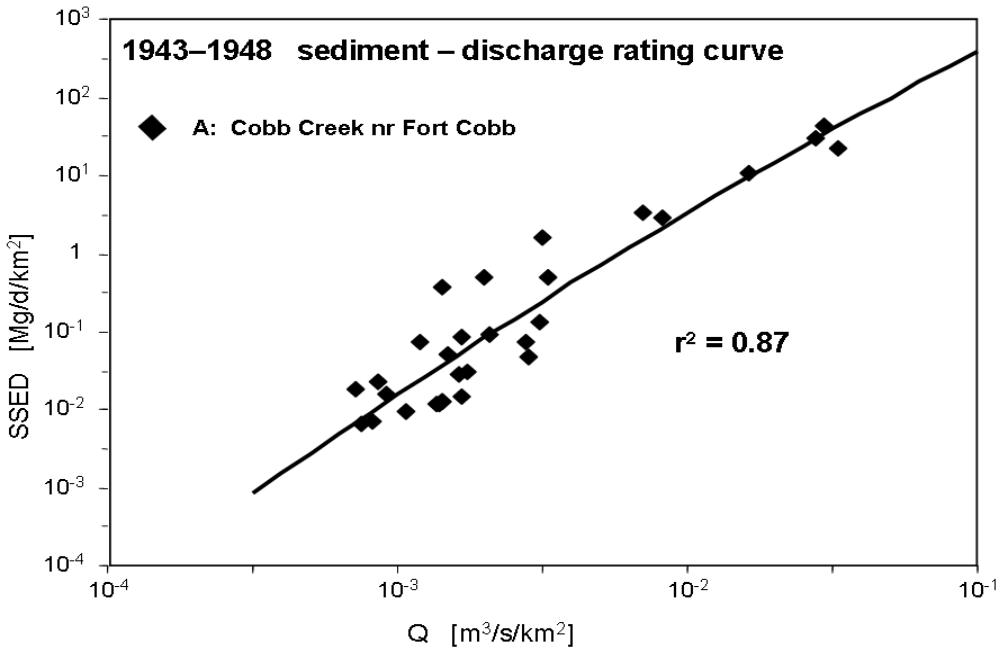

Figure 2. Instantaneous suspended sediment (SSED) – discharge (Q) rating curve at Cobb Creek near Fort Cobb, representing the 1943-1948 land use and management conditions.

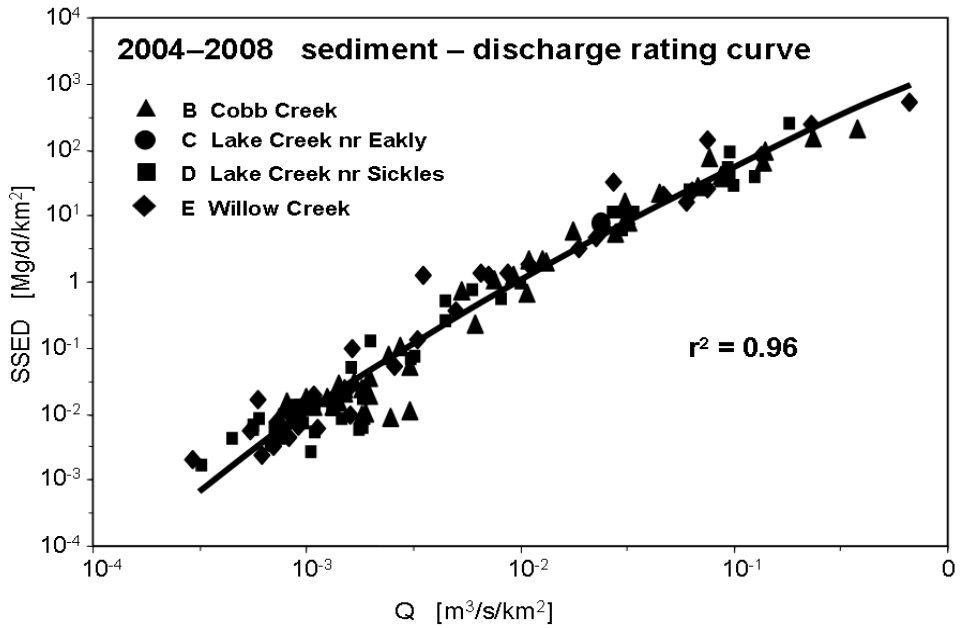

Figure 3. Instantaneous suspended sediment (SSED) – discharge (Q) rating curve at Cobb Creek near Fort Cobb, representing the land use, management and conservation conditions that were in place during 2004-2008.

The implication that a single sediment-discharge rating curve applied for gauging stations with upstream drainage area ranging from 49 to 342 km^2, suggested that the rating curve was to a large extent independent of drainage area and applicable throughout the watershed for drainage areas within the range defined by the gauging stations. It was also noted that topographic, soil and land use characteristics immediately below the four gauging stations was very similar to those above the stations. Thus, the absence of any change in physiographic watershed characteristics and the independence of the rating curves on drainage area, led to the assumption that the rating curve for the 2004-2008 land use and management conditions for the four stations (representing 70% of the watershed area) was also representative of the one that would have existed at the Cobb Creek gauging station near Fort Cobb, provided the reservoir had not been constructed in 1959. This sediment-discharge rating curve was referred to is the post-conservation rating curve.

SEDIMENT YIELD

Annual suspended sediment yield at the Cobb Creek gauging station near Fort Cobb was calculated by summing daily sediment yield obtained from the sediment rating curve for given daily discharge values. Sediment yield for the pre-conservation time period was estimated by evaluating the pre-conservation rating curve with 18 years of observed daily discharge values at the Cobb Creek gauging station near Fort Cobb. The average annual sediment yield for pre-conservation land use and management conditions was estimated to be 740 [$Mg/yr/km^2$]. Sediment yield for post-conservation time period was estimated for the same 18 years of observed daily discharge, except that the post-conservation rating curve was used. The average annual sediment yield for post-conservation land use and management conditions was estimated to be 115 [$Mg/yr/km^2$]. This represented an 85% reduction from the pre-conservation sediment yield and was attributed primarily to conversion of cropland to grassland and implementation of a broad range of conservation practices during the second half of the 20th century.

DISCUSSION

Urbanization was not a leading factor affecting watershed sediment yield, because the two small rural communities in the watershed have not grown very much over time. Influences of climate variations were largely avoided by using the same 18-year daily discharge record for estimating sediment yield. And, effects of climate variability on the sediment-discharge rating curves were also minimal because instantaneous sediment and discharge measurements were taken at various times and seasons during the year, and for high and low flow conditions, irrespective of any variations in climatic conditions.

Land use conversion and conservation measures implemented in the second half of the 20th century were the most likely reason for the identified sediment yield reduction. While conversion of cropland to grassland greatly reduced sediment delivery to the channel, terraces and conservation tillage were also important contributors to the sediment yield reduction from cropland. Further impediments to sediment movement towards the

watershed outlet were provided by small flood control reservoirs which effectively trap sediments. However, many existing gullies, long incised channels, unstable banks and head cuts provide for an ample source of sediments. Incised channel are difficult to remediate because the damage is rarely reversible and comprehensive solutions along the entire channel length are difficult, costly and involve agreement and cooperation of all land owners along the water course.

SUMMARY AND CONCLUSIONS

Efforts to measure a reduction in sediment yield at the outlet of large watersheds as a result of upstream conservation measures are often frustrated by the high variability of discharge and sediment load and lag in watershed response that result from complex interactions between rainfall, runoff, soil erosion, sediment transport, sediment storage and subsequently remobilization, and gradual implementation of conservation measures. In this study, effects of conservation practices on watershed sediment yield were investigated for the Fort Cobb Reservoir watershed. Instantaneous suspended sediment and discharge data were obtained from the USGS and watershed sediment yield was estimated based on sediment-discharge rating curves and daily discharge records. The rating curve based on sediment and discharge data from 1943-1948 reflected land use and management conditions prevailing in that era (i.e. no conservation practices). The rating curve based on 2004-2008 data reflected land use and conservation conditions prevailing during these years and embodied the cumulative and integrated effects of extensive conservation practices implemented in the second half of the 20th century. Average annual sediment yield was estimated to be 740 [Mg/yr/km^2] for the 1943-1948 pre-conservation period, and 115 [Mg/yr/km^2] for the 2004-2008 land use and conservation conditions.

The substantial reduction in annual sediment yield between 1943-1948 and 2004-2008 was related to conversion of land use and implementation of conservation practices. The gradual implementation and cumulative effects of land use conversion and broad range of conservation measures over a 60- to 70-year time span was likely the cause of the reduction in today's watershed sediment yield over that from the 1940s. While it may be difficult to identify beneficial impacts of conservation practices on sediment yield at the watershed outlet during the short time span of a conservation project (up to 5 years), this study demonstrated that targeted, widespread and sustained conservation efforts can lead, with some delay, to sizable reduction in sediment yield at the watershed outlet, as was the case for the Fort Cobb reservoir watershed.

REFERENCES

Berg W.A., Smith S.J., and Coleman G.A. 1988. Management effects on runoff, soil, and nutrient losses from highly erodible soils in the Southern Plains. *Journal of Soil and Water Conservation*, 43(5):407-410.

McGregor K.C., Mutchler C.K., and Roemkens M.J.M. 1990. Effects of tillage with different crop residues on runoff and soil loss. *Transactions of ASAE*,33(5):1551-1556.

Pearson A.J., Wainwright J., Brazier R.E., and Powell D.M. 2006. Is sediment delivery a fallacy? *Earth Surface Processes and Landforms*, 31:1325-1328.

Shields F.D. Jr. 2008. Long-term evaluation of regional erosion control. *Journal of Soil and Water Conservation*, 63(2):50A.

Simon A., and Klimetz L. 2008. Relative magnitudes and sources of sediment in benchmark watersheds of the conservation effects assessment program (CEAP). *Journal of Soil and Water Conservation*, 63(6):504-522.

Storm D.E., Busteed P.R., and White M.J. 2007. Hydrologic modeling of the Fort Cobb Basin, Oklahoma, using SWAT 2005. Final Report to USDA, ARS, Grazinglands Research Laboratory, April 2, 2008. Biosystems and Agricultural Dept., Div. of Agricultural Sciences and Natural Resources, Oklahoma State University.

Trimble S.W. 1999. Decreased rates of alluvial sediment storage in the Coon Creek Basin, Wisconsin, 1975-1993. *Science*, 285(5431):1244-1246.

Walling D.E. 1999. Linking land use, erosion and sediment yield in river basins. *Hydrobiologia*, 410:223-240.

Vente J., Poesen J., Arabkhedri M., and Verstraeten G. 2007. The sediment delivery problem revisited. *Progress in Physical Geography*, 31(2):155-178.

Human impact on the mobilization of a naturally-occurring source of selenium in an urbanizing catchment

Rachel Andrus[1], Barry Hibbs[2] and Andre Ellis[3]

[1] California State University-Los Angeles, Department of Geological Sciences, 5151 State University Drive PS 216, Los Angeles, CA 91801; PH (217)-333-1769; FAX (217)-244-3219; email: andrus1@illinois.edu
[2] California State University-Los Angeles, Department of Geological Sciences, 5151 State University Drive PS 216, Los Angeles, CA 91801; PH (323)-343-2414; FAX (323)-343-2435; email: bhibbs@exchange.calstatela.edu
[3] University of Texas-El Paso, Department of Geological Sciences, 500 West University Boulevard , Geology 201, El Paso, TX 79968; PH (915) 747-5503; FAX (915) 747-5073; email: aellis@utep.edu

ABSTRACT

The central part of the San Diego Creek Watershed was historically occupied by an extensive swamp that was drained in the late 19th century to accommodate the expansion of ranching and agriculture. Stable isotopes (δ^{34}S-SO_4, δ^{15}N-NO_3, δ^{18}O-NO_3, and $\delta^{82/76}$Se) are used to examine the link between denitrification of fertilizer-derived nitrate and sulfide/selenide oxidation along three discrete groundwater flowpaths that begin at the inferred outer boundary of the historic marsh and terminate at or near a surface water boundary. Isotopes along one flowpath strongly suggest a link between denitrification and sulfide oxidation: both δ^{15}N-NO_3 and δ^{18}O-NO_3 increase from upgradient values of 6.8‰ and 6.8‰ to downgradient values of 19‰ and 14.3‰ respectively while δ^{34}S-SO_4 becomes more negative from an upgradient value of 0.1‰ to a downgradient value of -12.7‰. The other two flowpaths show little to no isotopic evidence of denitrification and δ^{34}S-SO_4 signatures do not change dramatically, suggesting that, in the vicinity of these flowpaths, oxidation may not be the primary mechanism mobilizing sulfate and selenium from more reduced forms. Selenium isotopes do not directly demonstrate a link between denitrification and oxidation of reduced forms of selenium, but rather preserve information about the redox gradient in the historic marsh. The data do not rule out the possibility of nitrate acting as an electron acceptor in the oxidation of reduced forms of selenium. This hypothesis is further supported by results from soil slurry experiments where nitrate-rich water was more effective than oxygenated artificial rainwater in mobilizing selenium in select soil samples.

INTRODUCTION

The San Diego Creek Watershed covers approximately 291 square kilometers in Orange County, California. Historically, a wetland known as the "Swamp of the Frogs" marsh occupied the central, low-lying part of the watershed. This marsh was drained in the late 1800s to make way for the expansion of ranching and agriculture. Today the area is undergoing rapid urbanization. The water table in the wetland

system existed at land surface, creating a reducing environment in which redox sensitive elements such as sulfur and selenium were sequestered in marsh sediments (Hibbs and Lee, 2000). After channels were dredged to drain the marsh, the water table was permanently lowered to a few feet below land surface. This change in hydrology induced a geochemical shift from a reducing environment to an oxidizing environment that now acts as a source of sulfur and selenium by permitting the oxidation and remobilization of the reduced forms that had been sequestered in the marsh. Fertilizer associated with historic agriculture supplies nitrate to the shallow aquifer, which can oxidize sulfides and selenides. Groundwaters, enriched in nitrate and selenium, feed surface streams. This scenario could potentially have adverse impacts on wildlife that depend on these streams and the receiving water body, Upper Newport Bay, which is an ecological preserve.

METHODS

Three groundwater flowpaths were investigated to understand the evolution of groundwater chemistry within the boundaries of the historic "Swamp of the Frogs" Marsh (Figure 1). Historical soil maps were consulted to characterize matrix properties and water table maps were used to estimate the direction of groundwater flow along the three flowpaths. Fifteen groundwater seeps were sampled: four along the El Modena flowpath (EM), five along the Valencia flowpath (V) and six along the Edinger flowpath (E). All seeps span marginal and interior reaches of the historic swamp. Water samples were analyzed for nitrate, dissolved selenium, selenium speciation and a suite of stable isotopes (δ^{34}S-SO_4, δ^{15}N-NO_3, δ^{18}O-NO_3, and $\delta^{82/76}$Se). The EM flowpath was also sampled for δ^{13}C-DIC. Selenium speciation data were used in the Nernst equation to compute redox potentials. Two of the three flowpaths were also sampled for dissolved iron and manganese to further aid in the characterization of redox potential.

Four soil samples were collected for soil leaching experiments. Two clays were collected from a fresh trench *within the boundary of the historic swamp*. The "upper" clay was collected approximately three meters below land surface from the unsaturated zone. De-watering associated with local construction permitted the collection of the "blue" clay, which normally resides below stream head in the saturated zone, from approximately six meters below land surface. Two soil samples were also collected from the dry streambeds of upland basins (HC and RC), *well outside the boundary of the historic swamp*. Soils collected from both within and outside the boundaries of the historic swamp were subjected to leaching experiments in order to quantify the amount of leachable selenium contained therein (modified from Black et al., 1965). Soils were subjected to leaching by two types of water: artificial rainwater, which was made to mimic the composition of rainwater native to southern California; and nitrate-rich water, which was mixed to approximate the average nitrate concentration found in the shallow aquifer (11 mg/L NO_3-N). Two soil-water slurries were prepared for each soil by mixing 250 mL of one of the leaching agents with 125 g of dried soil in a 1000 mL HDPE bottle, which were shaken via wrist-action shaker for one hour. Leachate was immediately filtered after shaking and aliquots were set aside for dissolved selenium and anion analysis. The

clay soils were too viscous to filter directly and were "diluted" with an additional 250 mL of ultra-pure water following the period of shaking. They were then centrifuged at 5000 rpm for 10 minutes and the supernatant filtered for analysis. Several complementary analyses were run on these soils to support the leaching experiment including total selenium and selenium speciation.

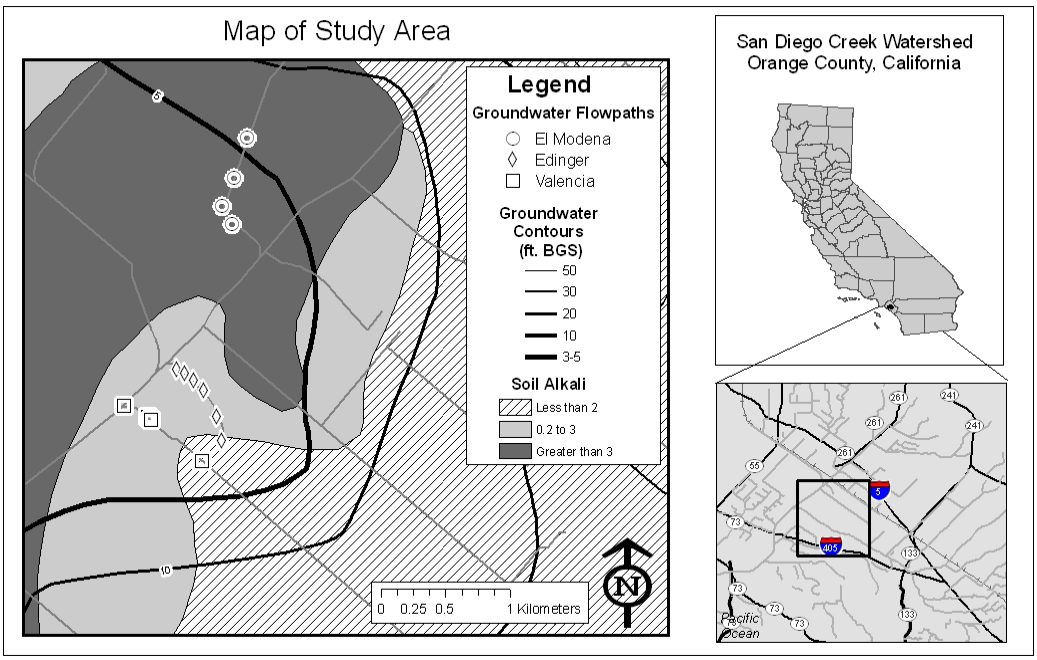

Figure 1. Map showing three groundwater flowpaths, depth to groundwater contours in feet below ground surface, and soil alkali contours.

RESULTS AND DISCUSSION

Soils in the study area have properties that are consistent with deposition in a shallow marsh environment. They are composed of fine-grained material with moderate to high alkali (Figure 1 and Table 1). Finer-grained material and higher soils alkali (> 3%) comprise the matrix through which the EM waters flow, while the matrix for the V and E flowpaths are comprised of a greater proportion of sand with only moderate alkali (0.2 to 0.4%; USDA, 1901).

Background concentrations of *total* selenium in typical soils (i.e. those that are not impacted by selenium) are on the order of 0.4 mg/kg, while soils derived from Cretaceous rocks have higher *total* selenium content on the order of 5 mg/kg (Thomas et al., 1998). Selenium data show that total selenium levels in the upland soils as well as in the "upper" clay are comparable to those found in unimpacted soils (Table 2). Speciation data show that selenium oxyanions (Se^{6+} and Se^{4+}) comprise about 40% of total selenium in the soils collected from within the boundary of the historic swamp. The dominant form of selenium in the "upper" clay is selenate (Se^{6+}), whereas there is more than twice as much selenite (Se^{4+}) as selenate (Se^{6+}) in the

"blue" clay. This indicates that selenium in these soils exists in readily leachable forms.

Results of the leaching experiments are shown in Table 2. As expected, the clay soils from within the boundary of the historic swamp contain more leachable selenium than the soils collected from the upstream basins. Leachable selenium in the upstream soils as well as the "upper" clay is less than typical background concentrations of *total* selenium. The "blue" clay contains elevated levels of leachable selenium on the order of 7 mg/kg, which agrees reasonably well with the total selenium in these soils. The artificial rainwater and nitrate-rich water were equally effective at leaching selenium from all soils except the "blue" clay. The nitrate-rich water leached 21.6% more selenium from the "blue" clay than artificial rainwater did. This result suggests that nitrate may have acted to oxidize the more reduced selenite (Se^{4+}) in the "blue" clay to selenate (Se^{6+}).

Selenium speciation data show that groundwaters are oxic to suboxic, with redox potentials ranging from 0.44 to 0.51 mV with respect to the Se^{4+}/Se^{6+} redox couple (Table 1). Negligible concentrations of dissolved iron and manganese support calculations of positive redox potentials. The down-gradient seeps along two of the three flowpaths (EM and E) show some evidence of more suboxic conditions, which may affect the mobility of contaminants like nitrate and selenium in the shallow aquifer.

Selenium is positioned just below sulfur in the periodic table of the elements and behaves in similar ways. It is proposed that sulfides (FeS_2), metal selenides (Se^{2-}), elemental selenium (Se^0), and adsorbed selenite (Se^{4+}) distributed in soils of the historic marsh are being oxidized by nitrate to sulfate and selenate (Se^{6+}), the most mobile species, by a process similar to the reactions in Equations 1 and 2 below, which describe processes that prevail in systems with positive redox potentials (Steinberg et al., 1992; Masscheleyn, 1990). Soil leaching experiments support these conclusions.

$$5FeS_2 + 14NO_3^- + 4H^+ \rightarrow 7N_2 + SO_4^{2-} + 5Fe^{2+} + 2H_2O \qquad \text{Equation 1}$$

$$5FeSe_2 + 14NO_3^- + 4H^+ \rightarrow 7N_2 + SeO_4^{2-} + 5Fe^{2+} + 2H_2O \qquad \text{Equation 2}$$

Stable isotopes of the redox sensitive elements sulfur and nitrogen have been used to track oxidation-reduction processes in a variety of natural settings (Bohlke and Denver, 1995; Bottcher et al., 1990). This is possible because of microbial and/or kinetic fractionation processes that tend to segregate the "lighter" isotopes in the products. Research has shown that as denitrification proceeds in the presence of reduced forms of sulfur (such as pyrite), that the sulfide will be oxidized and that stable isotopes could be used as viable tracers of this process (Bottcher et al., 1992 *in Matthess*).

Stable isotopes of sulfur ($\delta^{34}S\text{-}SO_4$) provide evidence of sulfide oxidation along the EM flowpath, with signatures becoming progressively lighter in the down-gradient direction. Lighter values of $\delta^{34}S\text{-}SO_4$ are consistent with the biologically-mediated oxidation of reduced forms of sulfur (Clark and Fritz, 1997). A concomitant

Table 1. Matrix Properties and Hydrochemical Parameters along Three Groundwater Flowpaths
----------Groundwater Flow Direction for each Flowpath ----------→

	EM-B2	EM-B3	EM-B4	EM-2	V-13	V-5	V-2	V-1	V-O	E-1	E-10	E-13	E-13.5	E-14	E-15
Soil Alkali (%)	3	3	3	3	< 0.2	0.2 to 0.4	0.2 to 0.4	0.2 to 0.4	0.2 to 0.4	< 0.2	< 0.2	0.2 to 0.4	0.2 to 0.4	0.2 to 0.4	0.2 to 0.4
Soil Type*	SJBA	SJBA	SJBA	SJBA	FSA	SJBA	SJBA	SJBA	SJBA	FSA	FSA	SJBA	SJBA	SJBA	SJBA
Diss. Fe (mg/L)	< 0.02	<0.02	< 0.02	< 0.02	na	na	na	na	na	< 0.02	< 0.02	< 0.02	< 0.02	< 0.02	< 0.02
Diss. Mn (µg/L)	< 2	< 2	93	200	na	na	na	na	na	< 2	< 2	<2	7	30	70
NO_3-N (mg/L)	19.84	28.71	26.61	16.56	18.41	16.53	15.35	15.04	13.01	14.65	13.75	13.41	2.73	2.72	2.72
Diss. Se (µg/L)	12.01	80.09	52.65	76.79	42.89	53.34	107.42	123.14	141.08	50.43	92.94	228.51	70.89	68.79	72.63
Se-IV (µg/L)	0.763	0.827	1.313	1.307	0.767	0.69	0.85	0.82	1.12	0.86	1.08	1.83	7.70	7.47	7.32
Se-VI (µg/L)	11.25	79.26	51.34	75.48	42.12	52.64	106.57	122.31	139.95	49.57	91.86	226.68	63.19	61.32	65.31
Redox potential (mV)	0.49	0.49	0.48	0.47	0.50	0.50	0.51	0.50	0.50	0.50	0.50	0.51	0.44	0.44	0.44
$\delta^{18}O$-H_2O (‰)	-6.8	-7.6	-6.6	-6.8	-6.5	-6.6	-6.6	-6.6	-6.6	-6.9	-6.9	-6.8	-6.5	-6.4	-6.6
$\delta^{2}H$-H_2O (‰)	-51	-48	-48	-47	-46	-48	-47	-48	-47	-49	-51	-48	-48	-49	-48
$\delta^{15}N$-NO_3 (‰)	6.8	11.4	14.4	19	9.9	9.6	9.9	10.3	10.6	10	10.9	12.5	14.2	13.3	14.9
$\delta^{18}O$-NO_3 (‰)	6.8	10	14	14.3	6.6	11.3	3.9	8.6	11	8.5	9.2	10.7	20.4	18.5	20.7
$\delta^{34}S$-SO_4 (‰)	0.1	-3.2	-17.2	-12.7	2.5	2.9	2.4	2.1	2.1	2	1.5	0.9	-2.4	-2.4	-2.2
$\delta^{82/76}S$-SeO_4 (‰)	0.971	-0.968	2.05	2.306	0.59	-	0.560	0.65	0.635	0.91	0.5	0.27	1.75	1.7	1.61

**SJBA: San Joaquin Black Adobe, FSA: Fullerton Sandy Adobe (USDA, 1901)*

increase in the isotopic signature of nitrate (δ^{15}N-NO_3 and δ^{18}O-NO_3) is observed along this flowpath, indicating a trend of denitrification as water flows down the hydraulic gradient (Figure 2). Denitrification often proceeds via the oxidation of organic carbon. Data from these springs show a minimal enrichment of δ^{13}C-[DIC] along the flowpath (from an upgradient value of -14‰ to a down-gradient value of -11‰), which is inconsistent with denitrification via the oxidation of organic carbon as the dominant electron donor. The isotopic signature of DIC suggests it originated from atmospheric CO_2 with possibly some contribution from carbonate cement disseminated in soils. Isotopic data strongly support a model of sulfur oxidation by nitrate along the EM flowpath. Nitrate associated with historic fertilizer application in upgradient orchards acts as an electron acceptor for metal sulfides (such as pyrite) disseminated in soils. Ferrous iron (Fe^{2+}) released in this way may be subsequently removed from solution via oxidation by nitrate and/or oxygen (Clark and Fritz, 1997).

Table 2. Soil Selenium Content with Speciation and Leaching Data

	Se-speciation (mg/kg)		Total Se (mg/kg)	Leachable Se (mg/kg)	
	Se (IV)	Se(VI)		Artificial Rainwater	Nitrate-rich water
Blue clay	2.98	1.27	10.4	6.54	7.95
Upper clay	< 0.02	0.155	0.383	0.088	0.087
RC streambed	ND (< 0.02)	ND (< 0.046)	0.360	0.003	0.004
HC Streambed	ND (< 0.02)	ND (< 0.046)	0.198	0.01	0.009

Along the EM flowpath, the isotopic signature of selenium ($\delta^{82/76}$Se) varied from an observed upgradient value of about 1.0‰ at the outer boundary of the historic marsh, decreasing to approximately -1.0‰ as groundwater moves slightly inside the marsh interior. From there, $\delta^{82/76}$Se increases to nearly 3‰ toward the end of the flowpath, well inside of the interior of the historic marsh. A discernable fractionation has been shown to accompany reduction of selenate (Se^{6+}) to selenite (Se^{4+}) and in the reduction of these oxyanions to less mobile forms (Johnson et al., 1999). This is similar to the isotope fractionation that accompanies the reduction of sulfur species. Minimal isotope fractionation observed in the oxidation of elemental and organically-bound selenium (Johnson et al., 1999) and the fact that selenium is a trace element may explain the observed evolution of selenium isotopes and the differences of the patterns observed for δ^{34}S-SO_4.

Because of the chemical similarities between sulfur and selenium, it was expected that, like sulfur, selenium would grow isotopically lighter. However, two factors contribute to a different pattern emerging from the selenium isotope data. First, recent research suggests that, contrary to the fractionation observed in redox transformations of sulfur, selenium undergoes significant fractionation only during reduction, but not upon re-oxidation (Johnson et al., 1999). Therefore, its historic isotopic signature is preserved as it is re-oxidized to a mobile, aqueous phase. Second, because selenium is a trace element it is not as abundant as sulfur and therefore cannot be expected to show a similar isotopic pattern. As a trace element, selenium has the potential to be completely removed and immobilized in the reducing sediments of the historic marsh, whereas sulfur is much more abundant, which limits

its potential for complete removal from the aqueous system. Regional patterns of selenium concentrations support this interpretation where higher levels of selenium are observed in the outer fringes of the historic marsh and much lower concentrations deep within its interior.

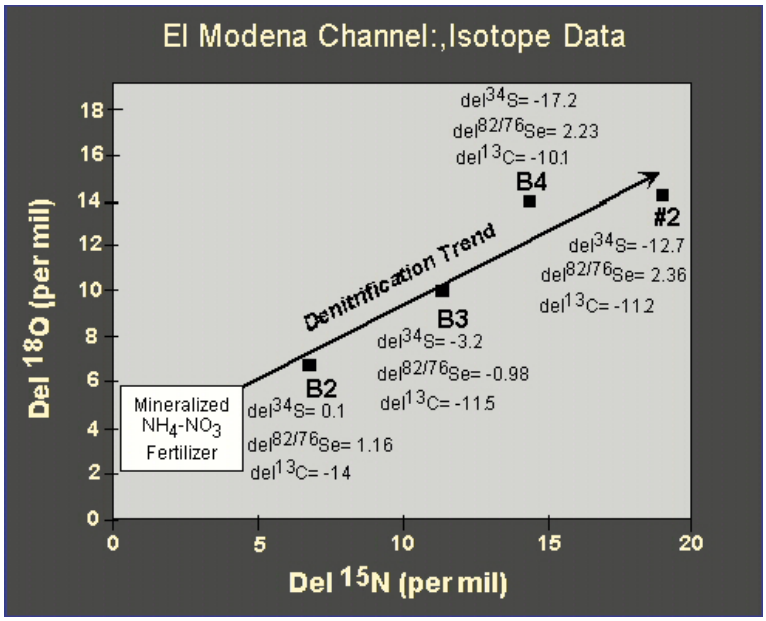

Figure 2. Denitrification trend along the El Modena flowpath with complementary stable isotope values supporting sulfide/selenium oxidation.

A scenario based on a closed system Rayleigh fractionation model may explain the observed isotopic pattern for selenium along the EM flowpath. Selenium enters the marsh with a natural "above marsh" isotopic signature of approximately 1.0‰. As it flows into the reducing waters of the marsh, it undergoes partial (~50%) reduction and isotopic fractionation, which imparts a "lighter" (-1.0‰) signature to the reduced fraction, leaving the mobile phase with an isotopically enriched signature (~3‰). This "heavy" signature is found toward the interior of the historic swamp where strong reducing conditions would have prevailed, resulting in complete removal of the residual dissolved selenium. These signatures are retained upon re-oxidation of the reduced forms of selenium from the marsh sediments after drainage of the marsh. Upstream surface water samples collected from upland tributaries reveal the source end-member isotopic signature of selenium to be ~1.6‰, which is consistent with these interpretations.

Along the V flowpath, stable isotopes of redox sensitive elements show minimal variation: δ^{34}S-SO_4 varies less than one per mille; δ^{15}N-NO_3 varies from 9.6‰ to 10.6‰; δ^{18}O-NO_3 varies from 3.9‰ to 11.3‰; and $\delta^{82/76}$Se varies less than 0.1 ‰. These variations are small enough to discount the role of redox processes that would mobilize reduced forms of sulfur and selenium in the subsurface, such as those observed along the EM flowpath. Another mechanism is proposed to explain the observed data along this flowpath. Previous work has shown that this flowpath coincides with high silica concentrations, which may indicate excess phytoplankton

activity in the shallow waters of the fringes of the "Swamp of the Frogs" (Meixner et al., 2004). It is possible that, due to abundant organic matter, a more homogenized reducing environment existed in the vicinity of the V flowpath, which would have prevented sulfate and selenium in these waters from migrating further into the marsh interior. Thus, uniform isotopic signatures of $\delta^{34}S\text{-}SO_4^{2-}$ and $\delta^{82/76}Se$ are preserved along this flowpath.

Stable isotopes of sulfur and selenium along the E flowpath, exhibit a similar trend to that observed along the EM flowpath. Stable isotopes of sulfur decreases steadily as water flows down the hydraulic gradient from 2.0‰ to -2.3‰. This increasingly negative isotopic signature is consistent with sulfide oxidation. Selenium isotopes exhibit an up-gradient $\delta^{82/76}Se$ signature of 0.91‰, becomes marginally depleted as waters move down-gradient, then, toward the end of the flowpath, $\delta^{82/76}Se$ becomes isotopically heavier (~1.7‰). This pattern is not as dramatic along the E flowpath as it is along the EM flowpath. It is difficult to say whether this pattern is indicative of the historic redox gradient in the historic marsh (as described along the EM flowpath) or if it instead is a reflection of present-day redox patterns. A substantial fractionation (3 to 12‰) of selenium isotopes has been observed during the reduction of Se^{6+} to Se^{4+} (Johnson et.al., 1999). Trace element data for the redox sensitive species iron and manganese suggest intermediate redox conditions presently exist along the down-gradient portion of the flowpath (Table 1). Thus the conversion of selenate to selenite in these down-gradient waters may explain the observed isotopic enrichment of selenium toward the end of the flowpath.

Analysis of $\delta^{15}N\text{-}NO_3$ and $\delta^{18}O\text{-}NO_3$ along the E flowpath was complicated by excess concentration of sulfate in these waters. Therefore $\delta^{18}O\text{-}NO_3$ values must be interpreted with caution (Jack Liu, Isotech Labs, personal communication). Generally $\delta^{15}N\text{-}NO_3$ and $\delta^{18}O\text{-}NO_3$ both grow isotopically enriched as waters flow down-gradient, suggesting an overall trend of denitrification, which may be linked to sulfide and selenium oxidation. Upgradient waters have concentrations of ~14 mg/L NO_3-N while down-gradient waters have concentrations of ~2.7 mg/L NO_3-N. This represents an 86% reduction in the concentration of NO_3-N. If denitrification alone explained the reduced concentration of NO_3-N observed in down-gradient waters, we would expect $\delta^{15}N\text{-}NO_3$ to show enrichment in excess of approximately 10‰ along the flowpath (Bottcher et.al., 1990). However, a maximum enrichment of only 5‰ in $\delta^{15}N\text{-}NO_3$ is observed along the flowpath. When plotting $\delta^{18}O\text{-}NO_3$ versus $\delta^{15}N\text{-}NO_3$, these waters cluster in two distinct groups (Figure 2). The upgradient sites exhibit a slight enrichment of both $\delta^{15}N\text{-}NO_3$ and $\delta^{18}O\text{-}NO_3$, suggesting that denitrification is occurring in these waters to a small extent. The upgradient waters possess a relatively lighter isotopic signature with little evidence of denitrification along this portion of the flowpath, suggesting that there may be a combination of factors operating to produce the observed results (i.e. mixing of multiple sources of nitrate along this flowpath, dilution by waters with low nitrate concentrations). Based on the available data, denitrification alone is insufficient to explain the decrease in nitrate concentration observed in downgradient waters.

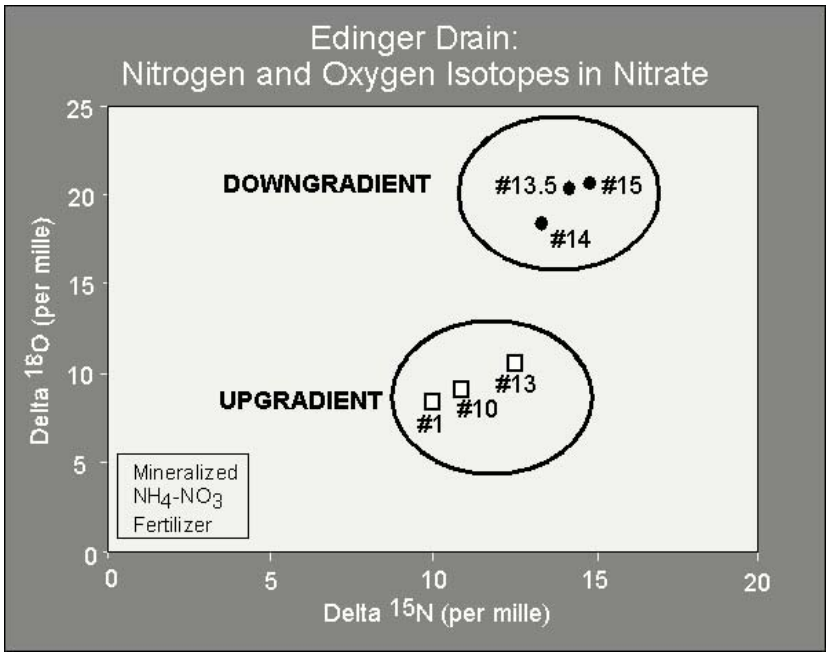

Figure 3. Stable isotopes of nitrate along the Edinger flowpath.

CONCLUSIONS

Groundwaters of the shallow aquifer can be largely characterized as oxidizing, though areas exhibiting intermediate redox conditions have been identified. Isotopic data support a model of sulfur oxidation by nitrate along the EM and E flowpaths. Along the V flowpath, stable isotopes show no evidence for groundwater evolution via the redox processes that appear to operate along the other two, but may be explained by more homogeneous redox conditions that prevailed in the historic marsh due to abundant organic matter.

The observed pattern of selenium isotopes along the EM and E flowpaths may be explained by two possible scenarios. It may reflect the reduction of selenium along the historic redox gradient that existed locally in the fringe of the historic swamp, whereby selenium becomes progressively lighter along the upgradient part of the flowpath (along the margin of the historic marsh) and then becomes markedly heavier toward the end of the flowpath (within the interior of the marsh). Alternatively, along the E flowpath, it may reflect the present-day redox gradient that controls the mobility of selenium along these flowpaths, where selenium concentrations are reduced and partially removed via sorption and/or precipitation in the more suboxic waters toward the end of these flowpaths. Nevertheless, isotopic data do not rule out the possibility that nitrate acts to oxidize reduced forms of selenium from the soil matrix within the boundary of the historic swamp.

REFERENCES

Black, C.A. (Ed). 1965. *Methods of Soil Analysis, Part 2, Chemical and Microbiological Properties*. American Society of Agronomy, Madison, Wisconsin.

Bohlke, J.K., J.M. Denver. 1995. Combined use of groundwater dating, chemical and isotopic analyses to resolve the history and fate of nitrate contamination in two agricultural watersheds, Atlantic coastal plain, Maryland. *Water Resources Research*. Vol. 31: 2319- 2339.

Bottcher, J., O. Strebel, S. Voerkelius, H.L. Schmidt. 1990. Using Isotope Fractionation of Nitrate-Nitrogen and Nitrate-Oxygen for Evaluation of Microbial Denitrification in a Sandy Aquifer. *Journal of Hydrology*. Vol. 114: 413-424.

Clark, I., P. Fritz. 1997. *Environmental Isotopes in Hydrogeology*. Lewis Publishers, New York.

Hibbs, B.J. and M.M. Lee. 2000. *Sources of Selenium in the San Diego Creek Watershed, Orange County, California.* Prepared for Defend the Bay & California Urban Environmental Research and Education Center. Department of Geological Sciences, California State University, Los Angeles.

Johnson, T.M., M.J. Herbel, T.D. Bullen, P.T. Zawislanski. 1999. Selenium Isotope ratios as indicators of selenium sources and oxyanion reduction. *Geochimica et Cosmochimica*, Acta 63(18): 2275-2783.

Masscheleyn, P.H. and R.D. Delaune, W.H. Patrick, Jr. 1990. Transformations of selenium as affected by sediment oxidation-reduction potential. *Environmental Science and Technology*, Vol. 24: 91-96.

Matthess, G., F. Frimmel, P. Hirsch, H.D. Schulz, H.E. Usdowski (Eds.) 1992. *Progress in Hydrogeochemistry*. Verlag, Springer.

Steinberg, N.A., J.S. Blum, L. Hochstein, R.S. Oremland. 1992. Nitrate is preferred electron acceptor for growth of freshwater Selenate-Respiring Bacteria. *Applied Environmental Microbiology*, Vol. 58(1):426-428.

USDA. 1901. Soil Survey for Orange County and Western Part of Riverside County, California. Department of Agriculture, Soil Conservation Service. U.S. Government Printing Office. pp. 158.

Long Term Effect of a Stream Restoration Plan on Water Quality

Yuan Cheng[1], Ph.D., P.E.

[1]Senior Civil Engineer, Benatec, a Division of Century Engineering, Inc., 200 Airport Road, New Cumberland, PA 17070; PH (717)-901-7055; FAX (717)-901-7059; email ycheng@centuryeng.com

ABSTRACT

A stream restoration plan near the headwaters of the Swatara Creek was implemented to reduce the acidity and dissolved metals associated with coal mine drainage. The plan has been in effect since 1995, though various components of the plan have been phased in over several years, the last of which was installed in 2002. Specific stream restoration components included limestone channels and diversion wells, anoxic and oxic limestone drains and constructed wetlands. The stream data selected for the analysis includes: daily mean flow, daily pH value, daily specific conductance, and daily water temperature. Low flow and high flow are predicted to have significant effects on acidity reduction. An autoregressive model is used to study trends associated with daily specific conductance and daily pH values. The prediction model, based on current effectiveness derived from available data, can provide future benefit to those responsible for the development or refinement of similar restoration plans.

INTRODUCTION

This study evaluates the long term effect on stream water quality after the stream restoration plan has been installed. Daily data can be converted into a time series model containing water quality characteristics such as pH value, specific conductance measured at 25°C, and water temperature. Stream flow is the driving force that carries the elevated acidity and high level metals downstream. Thus, the correlation between stream flow and pH value, as well as the other water quality parameters such as specific conductance and stream water temperature, are developed. In using the correlated values, the daily data (stream flow, pH value, specific conductance, and temperature) are not treated as independent and random. Therefore, an autoregressive model is applied to work with the correlated values. Since the restoration plan was implemented in phases over several years, the time-series record has been affected by plan maturation. Thus, the recorded daily data should become a non-stationary time-series. For this non-stationary time series, an unsteady term is included in the autoregressive model.

STUDY SITE

Northern Swatara Creek is a perennial stream and one of the headwaters for the Swatara Creek in eastern central Pennsylvania. The Northern Swatara Creek watershed has a contributory area of 43 square miles. The land use in the Northern Swatara Creek watershed is comprised of large forest, small townships, some spread farms, and extensive areas of abandoned coal mining. In the watershed, coal mine drainage from abandoned mines was the primary cause of stream pollution. From 1995 to 2002, a stream restoration project (PADEP, 2002) has been implemented in phases. At that time, USGS gauge stations were installed and monitored to record stream flow and stream water quality data. Some data records were discontinued after 2003, but some records continued until 2007. The data from two USGS gauge stations was used in this study. One USGS gauge station is at Site C3, which is gauge USGS 0157155014 (USGS web site, 2008) in Newtown, Schuylkill County. The other gauge station is at Ravine (USGS web site, 2008), which is gauge USGS 01571820 in Ravine, Schuylkill County. Site C3 is approximately 6 miles upstream from Ravine.

The Northern Swatara Creek has been contaminated with high levels of metals and elevated acidity due to coal mine drainage. Since 1995, several components of the stream restoration plan, including limestone channels, limestone diversion wells, anoxic limestone drains, oxic limestone drains, and constructed wetlands, have been implemented within the watershed. The project was completed in 2002.

GRAPHICAL VIEW ON THE SELECTED DATA FOR THE STUDY

The selected records, shown on Figure 1 and Figure 2 for Site C3, as well as Figure 3 and Figure 4 for Ravine, are used to study the change in stream water quality. The maximum time span represented by the available data through the implemented phases is about 10 years. The 1996-1997 dataset is the earliest result available. The 2002-2003 dataset represents implementation of the final phase for the plan and a point when some water quality data collection at Site C3 was discontinued. The 2006-2007 dataset represents the last available records for the gauge station at Ravine.

By visual inspection of Figure 1, the record shows that the pH value at the troughs is synchronous with the stream flow at the peaks. This relationship means the acidity is elevated when the flow increases. Also according to Figure 1, the specific conductance increases when the stream flow decreases but is synchronous with the increased pH value. The stream water temperature cycles with the seasonal weather, but it does not rhythmically change with the stream flow. A similar phenomenon occurs with the datasets from 2002-2003 and 2006-2007 (see Figures 2, 3, and 4 in the next pages).

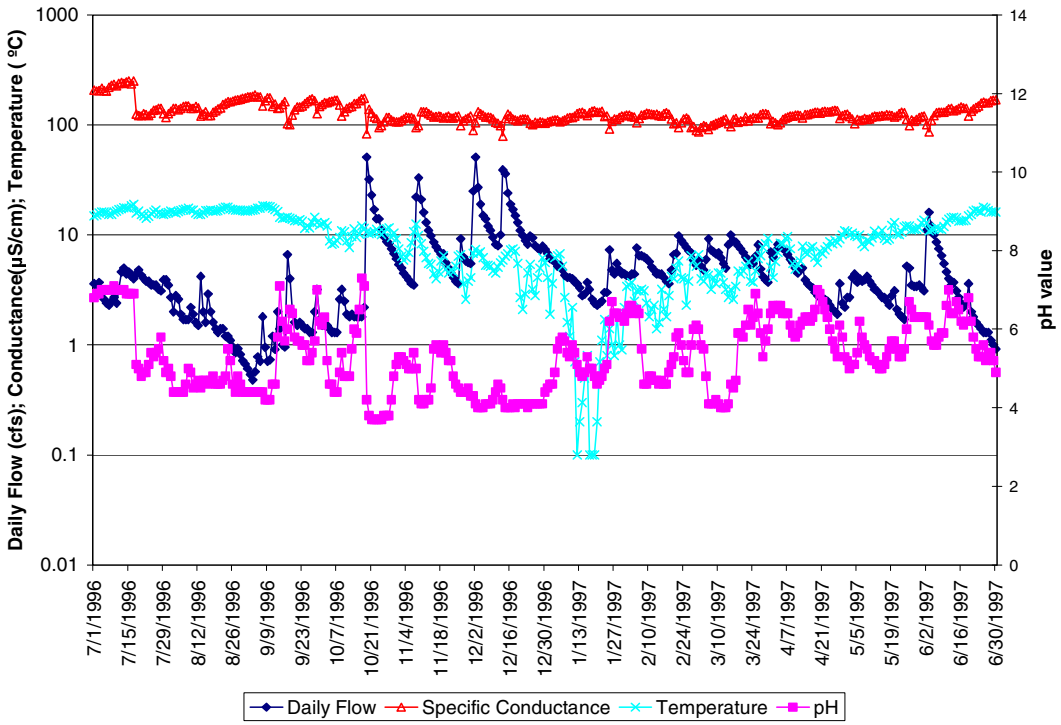

Figure 1 Daily data of Site C3 from July 1, 1996 to June 30, 1997

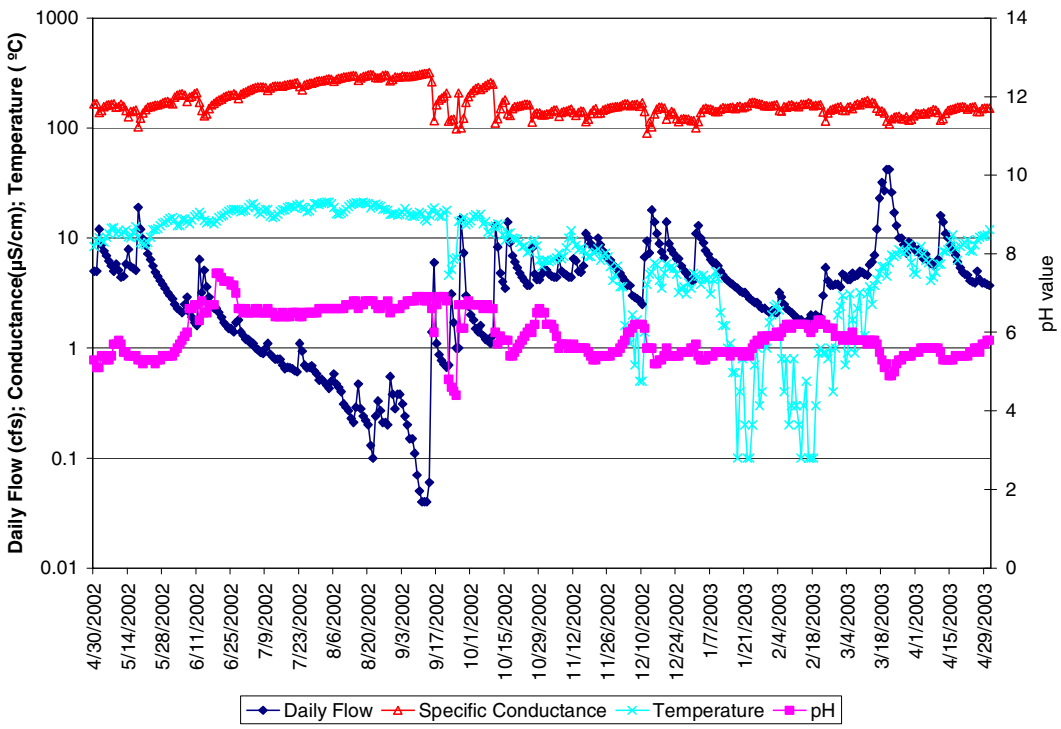

Figure 2 Daily data of Site C3 from April 30, 2002 to May 1, 2003

For Site C3, it is graphically indicated that the variation in pH values for 2002-2003 shown in Figure 2 are less than the variation for 1996-1997 shown in Figure 1. That means the plan has been working well to stabilize the pH value in the

stream although the stream flow exhibited greater fluctuation in 2002-2003. The draught season in the summer of 2002 sustained a long period of low flow, so the pH values only varied within a small range from 6.5 to 6.8 (see Figure 2).

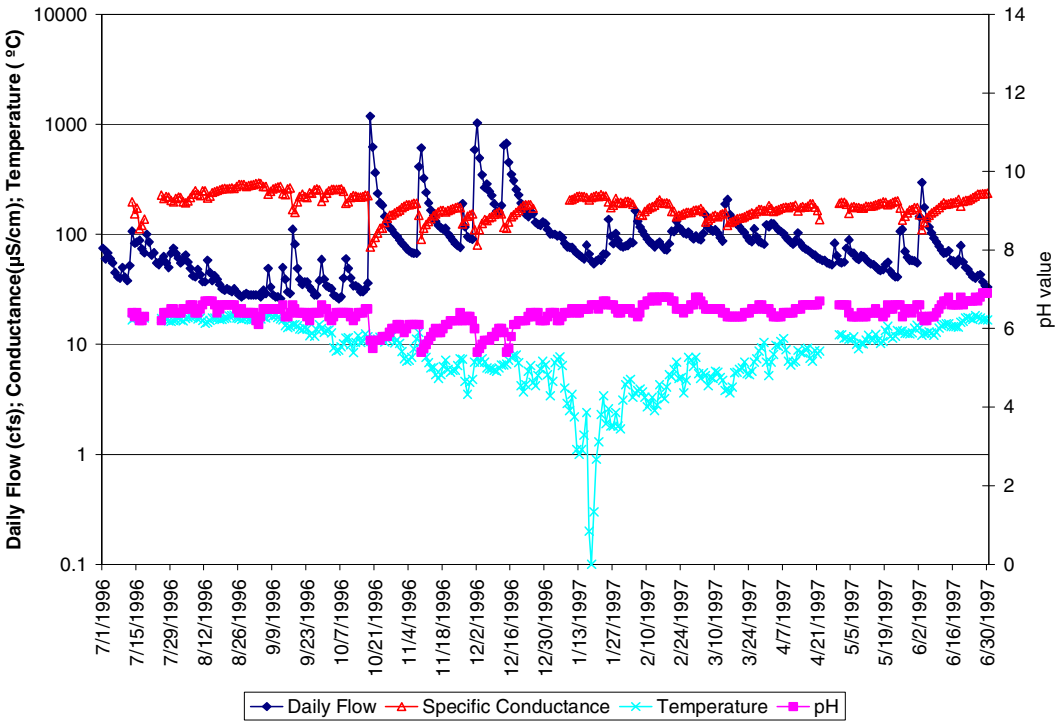

Figure 3 Daily data of Ravine from July 1, 1996 to June 30, 1997

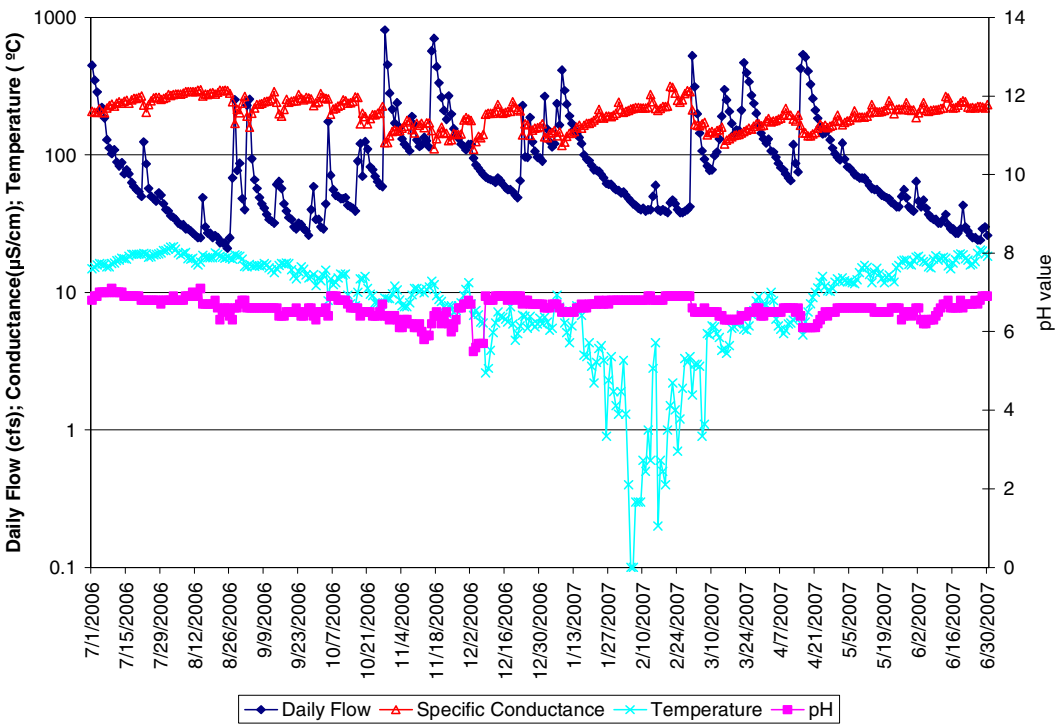

Figure 4 Daily data of Ravine from July 1, 2006 to June 30, 2007

For the site at Ravine, it is graphically indicated that the pH values shown on Figure 4 exhibit less variation when compared with the pH values shown on Figure 3. This observation regarding pH value is similar to what is seen at Site C3. However, the specific conductance shown on Figure 4 is larger than the one shown on Figure 3, which is a similar observation for the specific conductance shown on Figures 1 and Figure 2.

CROSS-CORRELATION COEFFICIENTS

The cross-correlation coefficient is used to assess if two time-series models are correlated to some extent which describes the dependence of one set of data on the other. In this study, the cross-correlation coefficient is defined as

$$R_{xy} = \frac{C_{xy}}{S_x S_y} \quad \text{(EQ.1)}$$

In EQ.1 S_x and S_y are the estimated standard deviations of the X_t and Y_t time-series, respectively. The cross-covariance is $C_{xy} = \frac{1}{N}\sum_{t=1}^{N}(X_t - \overline{X})(Y_t - \overline{Y})$. The variable X_t is the daily flow and the variable Y_t is one of the water quality parameters, such as pH value or specific conductance (SC). The mean value for each time-series X_t and Y_t is $\overline{X}$ and $\overline{Y}$, respectively. Based on EQ.1, the cross-correlation coefficients are computed and summarized in Table 1.

Table 1. Cross-correlation Coefficients for Flow and pH, as well as for Flow and SC

Gauge Name	Site C3		Ravine		
Period	1996-1997	2002-2003	1996-1997	2002-2003	2006-2007
$R_{\text{Flow pH}}$	-0.19	-0.75	-0.82	-0.65	-0.37
$R_{\text{Flow SC}}$	-0.57	-0.92	-0.93	-0.88	-0.79

The negative cross-correlation coefficients shown in Table 1 indicate that an increased daily flow will have both decreased pH value and specific conductance on the same day. The negative cross-correlations also verify the flow peaks and the pH troughs occurred at the same time.

TIME-SERIES AND STOCHASTIC ANALYSIS

The set of stream gauge records consists of a series of observations for the stream quality after stream restoration plan components were implemented. The observed data was modeled and the study results were successful in quantifying the improvement of the stream quality. Also, the developed stochastic model based on

actual data can be used to predict improvement or impairment of the stream water quality.

The daily data was not treated as independently random but rather as auto-correlated. Thus, a time-series analysis was appropriately applied in this study in order to consider the autocorrelation between the individual daily data. To predict the change in water quality due to the plan, an autoregressive model with a non-stationary term *kt* was introduced as follows.

$$X_t = m + kt + \{\ [\sum_{i=1}^{p} a_i X_{t-i}] + e_t\ \}\ \text{(EQ.2)}$$

In EQ.2, X_t is the observed data at the time t, X_{t-i} is the observed data at the previous time t-i, m is a constant, k is the time rate change, a_i are autoregression coefficients of AR (p), and e_t is the random error with zero mean and constant variance. For this study, the order p of the autoregressive model AR (p) is limited to 2 although a higher order p can be used. The e_t in EQ.2 represents randomness and uncertainty as a part of the series data.

Three different sets of the coefficients of EQ.2 are determined by the Least Squares Method to fit the USGS daily record within 1996-1997, 2002-2003, and 2006-2007, respectively.

COMPUTED COEFFICIENTS OF THE MODEL

The stream restoration plan is expected to have effectively changed the stream water quality. The changes can be detected if the coefficients in EQ.2 are significantly changed during the years. Using the stochastic model, EQ.2, the validated coefficient changes can be used to quantify the improvement of the water quality. Then the EQ.2 with the fitted coefficients is used as a stochastic model to predict the trend of water quality in the stream channel. The computed coefficients are summarized in Table 2 for the pH time-series and in Table 3 for the specific conductance (SC) time-series in different years.

Table 2. Computed Coefficients Based on Time-Series Data of the pH

Gauge Name	Site C3				Ravine			
Coefficients	m	k	a_1	a_2	m	k	a_1	a_2
1996-1997	0.55	2.7E-4	1.14	-0.25	0.63	9.7E-5	1.01	-0.11
2002-2003	0.56	-2.4E-4	0.892	0.02	0.71	-4.0E-5	0.86	0.04
2006-2007	No data	No data	No data	No data	0.95	-4.9E-5	0.88	-0.03

For $AR(2)$ coefficients, a_1 and a_2 are constrained so that $-1 < a_2 < 1$, $a_1 + a_2 < 1$, and $a_2 - a_1 < 1$.

Table 3. Computed Coefficients Based on Time-Series Data of the SC

Gauge Name	Site C3				Ravine			
Coefficients	m	k	a_1	a_2	m	k	a_1	a_2
1996-1997	15.1	-8.2E-3	0.80	0.09	23.6	-0.019	0.97	-0.08
2002-2003	15.3	-0.018	0.87	0.06	16.6	-0.015	1.02	-0.09
2006-2007	No Data	No Data	No Data	No Data	23.6	-0.014	0.90	5.6E-4

For $AR(2)$ coefficients, a_1 and a_2 are constrained so that $-1< a_2<1$, $a_1+ a_2 <1$, and $a_2- a_1<1$.

As an example, the coefficients of m, k, and AR (2) of Site C3 shown in Table 3 are used to simulate the daily specific conductance. The results are shown in Figure 5 and Figure 6, respectively and compared to the 1996-1997 and 2002-2003 records of Site C3.

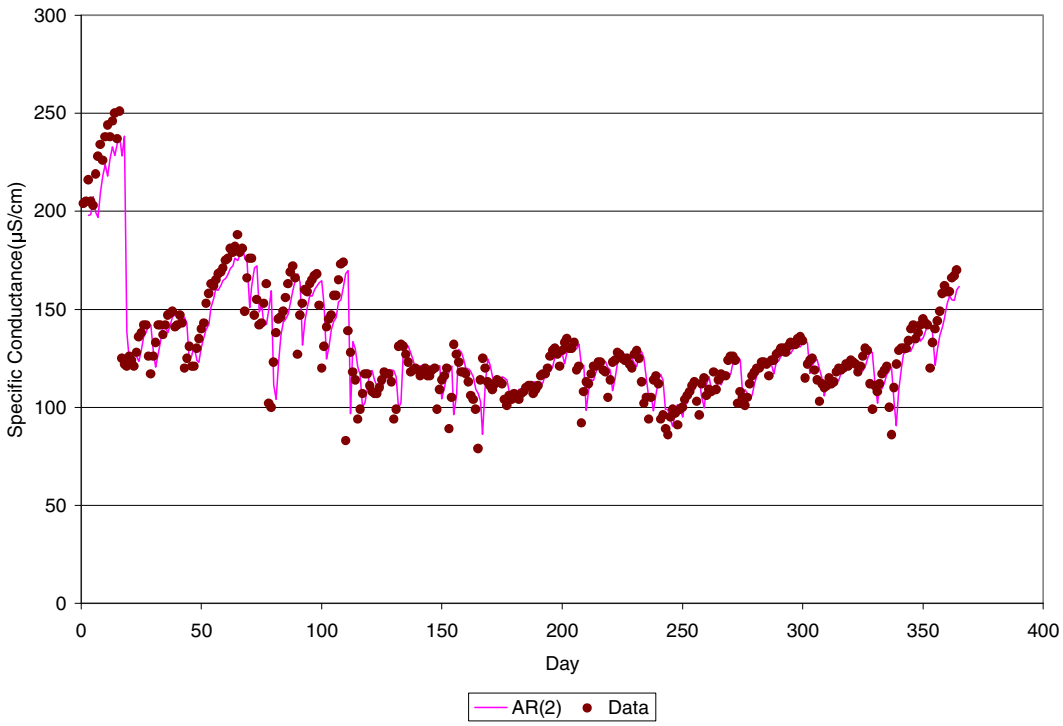

Figure 5 Simulation Result of the Daily Specific Conductance at Site C3 for 1996-1997

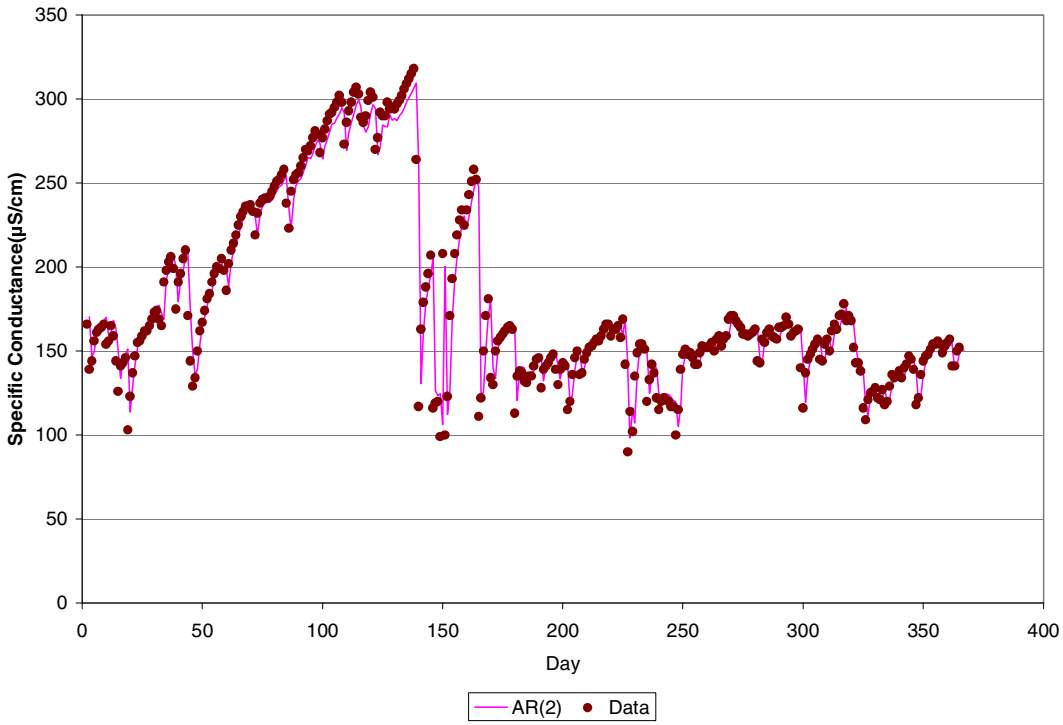

Figure 6 Simulation Result of the Daily Specific Conductance at Site C3 for 2002-2003

Based on the results shown on Figure 5 and Figure 6, it is concluded that the model coefficients in the simulation represent the stream specific conductance very well.

THE EXPECTED TREND OF THE WATER QUALITY IMPROVEMENT

A further mathematical operation on EQ.2 is shown as follows to compute the steady state *K* values, which are statistically expected trend coefficients. Let

$$E[X_t] = M + Kt \text{ , EQ.3,}$$

where *M* is the expected initial constant at the time *t*=0 for a specific year, and E [ ] stands for "Expected Value of [ ]". Then, apply the operator E[ ] on EQ.2 to get EQ.4.

$$E[X_t] = m + kt + \sum a_i E[X_{t-i}] = m + kt + \sum a_i (M + K(t-i)) \quad \text{EQ.4}$$

Rearranging the coefficients for 1 and *t* in EQ.4 and equating EQ.3 to EQ.4, the coefficients of *M* and *K* are solved as follows:

$$M = \frac{m - K\left(\sum i a_i\right)}{1 - \sum a_i} \qquad K = \frac{k}{1 - \sum a_i} \quad \text{EQ.5}$$

Using EQ.5 and the values shown in Table 2 and Table 3, the expected trend coefficient *K* for different years and different gauges are computed and shown in Table 4 and Table 5.

Table 4. The Expected Constant *M* and Trend *K* for pH

Gauge Name	Site C3		Ravine	
Expected Coefficient	*M* for pH	*K* (1/day)for pH	*M* for pH	*K* (1/day)for pH
1996-1997	4.81	2.4E-3	6.23	9.6E-4
2002-2003	6.54	-2.8E-3	7.05	-4.0E-4
2006-2007	No data	No data	6.65	-3.4E-4

Table 5. The Expected Constant *M* and Trend *K* for SC

Gauge Name	Site C3		Ravine	
Expected Coefficient	*M* (μS/cm) for SC	*K* (μS/cm-day)for SC	*M* (μS/cm) for SC	*K*(μS/cm-day) for SC
1996-1997	144	-0.078	219	-0.171
2002-2003	231	-0.267	269	-0.235
2006-2007	No data	No data	231	-0.138

For Site C3 and Ravine, the expected trend coefficient *K* of the time-series in different years is presented in the third and last column of Table 4 and Table 5. A negative value for *K* indicates that the expected trend is downward. A trend showing a decreasing pH value is indicated by the negative *K* values in 2002-2003 and 2006-2007 (see the third and last column of Table 4), but it has a positive trend in 1996-1997. The decreased pH value means that acidity will be elevated in the coming years. Thus, the cause for this prediction can be investigated by inspecting the installed components of the restoration plan. The non-functioning components may need to be replaced; for example, a new limestone channel may need to be installed, or the constructed wetlands and ponds may need to be cleaned out by removing the build up of sediment.

CONCLUSIONS

The negative cross-correlation coefficients show that an increase in daily flow can elevate the acidity of the stream. Conversely, a decrease in daily flow can reduce the stream's acidity.

The expected trend *K* provides one piece of information to predict the long term effectiveness of the plan. In the 1996-1997 dataset, the expected trend *K* of pH is positive for both gauges (see Table 4). This indicates the pH value was expected to increase although the plan was only partially implemented. However, in the 2002-2003 and 2006-2007 datasets, the expected trend *K* is negative. This indicates the pH value was expected to decrease thus increasing the acidity over the next few years.

The deterioration of long term effectiveness is predicted provided that the current trends are sustained. Thus, it is recommended that the installed components of the restoration plan should be inspected and restored.

The expected *M* represents the expected initial mean value of the evaluated time-series for a specific year. As shown in Table 4, the expected *M* of pH value is significantly increased at Site C3 when comparing the 1996-1997 and 2002-2003 datasets. After 2003, all the expected *M* for the pH values at Ravine are between 6 and 7, which indicates a sustained improvement within the acceptable range from 6 to 9 according to the Pennsylvania State stream water quality regulations.

All the values of the expected trend *K* for specific conductance (SC) are negative although some expected *M* did not decrease (see table 5). This indicates the plan has been successful in reducing the specific conductance in succeeding datasets for years 1996-1997, 2002-2003, and 2006-2007. The trend, however, was not sufficient to keep the similar mean value for the specific conductance in the following years.

REFERENCES

PADEP (Pennsylvania Department of Environmental Protection, 2002). "Pennsylvania, Swatara Creek, Section 319, National Monitoring Program Project." Harrisburg, Pennsylvania.

USGS web site (2008). "USGS 0157155014 Swatara Creek, Site C3, at Newtown, Pennsylvania", http://waterdata.usgs.gov/pa/nwis

USGS web site (2008). "USGS 01571820 Swatara Creek, Ravine, at Ravine, Pennsylvania", http://waterdata.usgs.gov/pa/nwis

Measurement of Velocity and Discharge of a Stream using a New Floating Rod Equipped with a GPS Receiver

W. Kim[1] and C. Lee[2]

[1]River and Coast Research Division, Korea Institute of Construction Technology, 1190 Simindaero, Ilsanseo-gu, Goyang-si, Gyeonggi-do, Republic of Korea; PH +82-31-910-0265; email: wonkim@kict.re.kr
[2]River and Coast Research Division, Korea Institute of Construction Technology, 1190 Simindaero, Ilsanseo-gu, Goyang-si, Gyeonggi-do, Republic of Korea; PH +82-31-910-0657; email: c0gnitum@kict.re.kr

ABSTRACT

It is quite difficult and risk-taking to directly measure velocity and discharge of the streams during rapidly changing floods under nasty weather. Traditionally, floating rod method as well as indirect method is used in this situation. Though safe, floating rod method is regarded as relatively less accurate. We developed a new floating rod equipped with an integrated module composed of a GPS receiver and a RF transceiver on the head, which can measure flood velocity by tracking its position. Furthermore, simultaneous deployment of up to fifteen floats provides longitudinal velocity of streamlines along which they pass. Discharge is instantaneously calculated by combination of measured velocities and pre-surveyed cross-section area data for every deployment of floating rods. Some application examples show measured velocity and a 2D flow vector plot, and discharges calculated with this floating rods system indicate fairly good agreement with reference discharges like dam release and rated discharge.

INTRODUCTION

Recently, large flood events occur more frequently either by intense and severe rainstorms which are caused by tropical storms like typhoon and hurricane, or by serious summer snow-melt related with global warming. In order to control these floods and prevent damages brought about by them, it is necessary to make accurate measurement of flood discharge.

It is quite difficult and sometimes highly risk-taking to make direct measurement on flood velocity and discharge since water level and flow are rapidly changing with nasty weather accompanied. In addition, in order to secure accuracy of flood discharge measurement, quick measurement is also necessary. For this condition, rod float method is widely used (WMO, 1994). In some countries, indirect slope-area computation is utilized to measure flood discharge.

Simple, safe and easy to measure, traditional rod float method have been widely used in some countries. However, since it assumes that rod floats move downstream along the straight-lines, inaccuracy may occur if the paths of flowing rod floats are not straight.

In the context, we developed a new floating rod system equipped with a GPS

receiver and a RF transceiver and named as Electronic float. It doesn't need assumption on straight-line flow path as is a shortcoming of traditional rod float method. In this paper, some application examples for measurement of velocity and discharge using this new method are presented with basic concepts and equipments introduced.

BASIC CONCEPTS AND EQUIPMENTS

Traditional rod-float method. Generally, a straight reach located downstream of either a bridge or a float throwing equipment is selected. Along the reach at least two cross-sections are surveyed before and after flood season. Up- and downstream cross-sections are divided into 10~15 subsections according to mid-section method. Spacing between each section is set to either 50 or 100 m considering flowing time of a rod float. When a measurement is made, a rod-float will be thrown at each sub-section and flowing time of it will be checked to compute water velocity. Here, a rod-float is assumed to move along the straight-line and velocity is equal to distance divided by time of travel between two sections. Finally, discharge is calculated by summing up of sub-section discharges which are computed by multiplying water velocity of each rod-float by mean of corresponding up- and downstream sub-section area. Concept of the rod-float method is summarized in Figure 1.

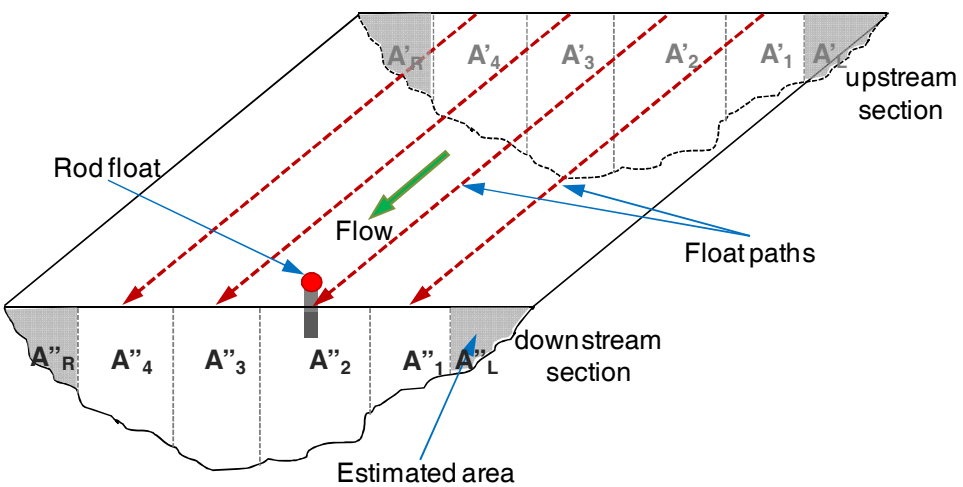

Figure 1. Basic concept of rod-float method (modified from ISO(1997))

The electronic float (EF). In the traditional rod-float method, position of a rod-float cannot be known. While, the electronic float receives GPS signal to determine its absolute position and is capable of tracking its path along the stream. Essentially, it does not need assumption on straight-line flow path and make velocity measurement more accurately.

The EF can also transmit its position information real-time to the hydrographic technician by radio-frequency (RF) communication. Three bands of low power RF are used: 424, 433, 447MHz. This system are provides up to 500 m

communication distance (may be increased by increasing power) and characterized as generality, low power consumption, relative communicative freedom from nasty weather and swell, and suitable to velocity and discharge measurement in streams. Consequently, once the EF is thrown to a river, its flowing path can be traced regardless of recollection of it. It is different from the previously developed GPS-based drogues (Hopping & Smith, 2002) in that they are not capable of real-time wireless communication so that they cannot be used for flood measurement condition in which it is unable to be recollected.

The system can use three frequencies mentioned above and five EFs can be supported in each frequency, so that maximum fifteen EFs can be operated simultaneously. The EF only picks out and transmits &GPRMC string among all the received GPS position information. Five EFs controlled in the same band conduct correspondence with one another and the base station collects their position information by time-sharing technique.

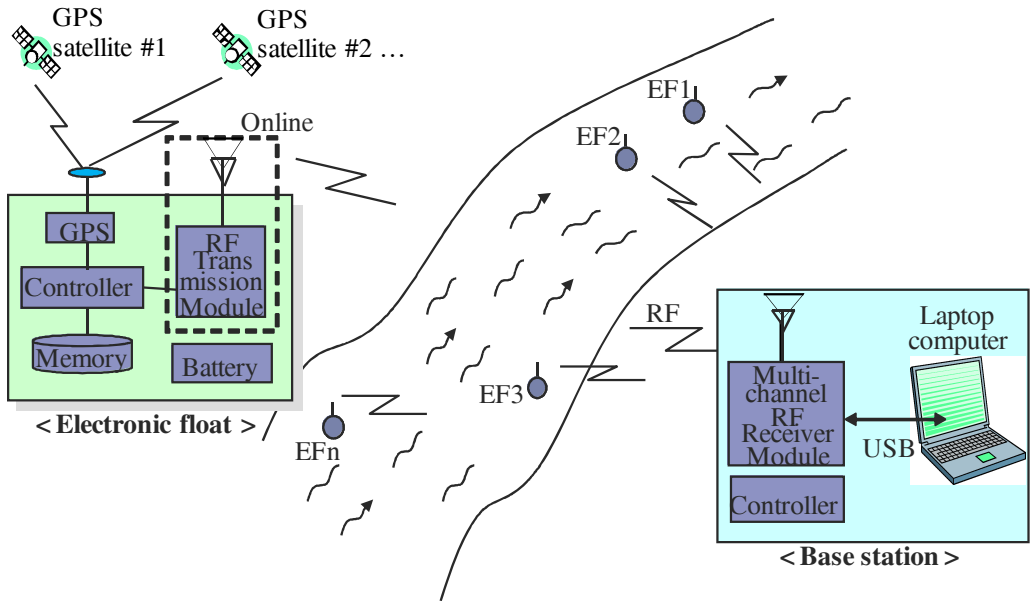

Figure 2. Concept of the electronic float system for flow measurement

FIELD APPLICATION

In order to test performance of the EF for measurement of velocity and discharge, field campaigns were made at five sites near official gauging stations in South Korea. Test sites are listed in Table 1. They are located at roughly straight river reaches. Three of them are located downstream of dams. Field campaigns at the Gumangyo and the Gangchon sites were made when the dam released for hydroelectric power generation in low flow season. At the other three sites, flood measurements were made. For each site, four cross-sections were surveyed for area calculation before either field campaign or flood season.

Table 1. General information on field campaigns

River	Site	Location	Date (yyyy.mm.dd)	Flow	Reference discharge
Dalcheon	Goesan	127-50-40, 36-45-51	2007.08.31	flood	dam release
North Han	Gangchon	127-38-08, 37-48-53	2008.04.15	flood	dam release
	Gumangyo	127-47-00, 38-07-00	2008.05.02 2008.05.16	low flow	dam release
South Han	Yeoju	127-38-58, 37-17-33	2008.07.24	flood	rated discharge
Imjin	Jeoksung	126-55-15, 37-58-56	2008.07.21	low flow	rated discharge

Figure 3 shows site locations with observed float tracks (left) and cross-sections (right). The EFs were thrown at the upstream bridge of each site. Four to ten EFs were used simultaneously at each site according to its measurement condition. For most sites, all the EFs moved straightly downstream. Cross-sections of the three sites (Goesan, Gumangyo, Jeoksung) are roughly symmetric and uniform, while the Gangchon site has rocky and rugged boundary and the Yeoju asymmetric cross-sections.

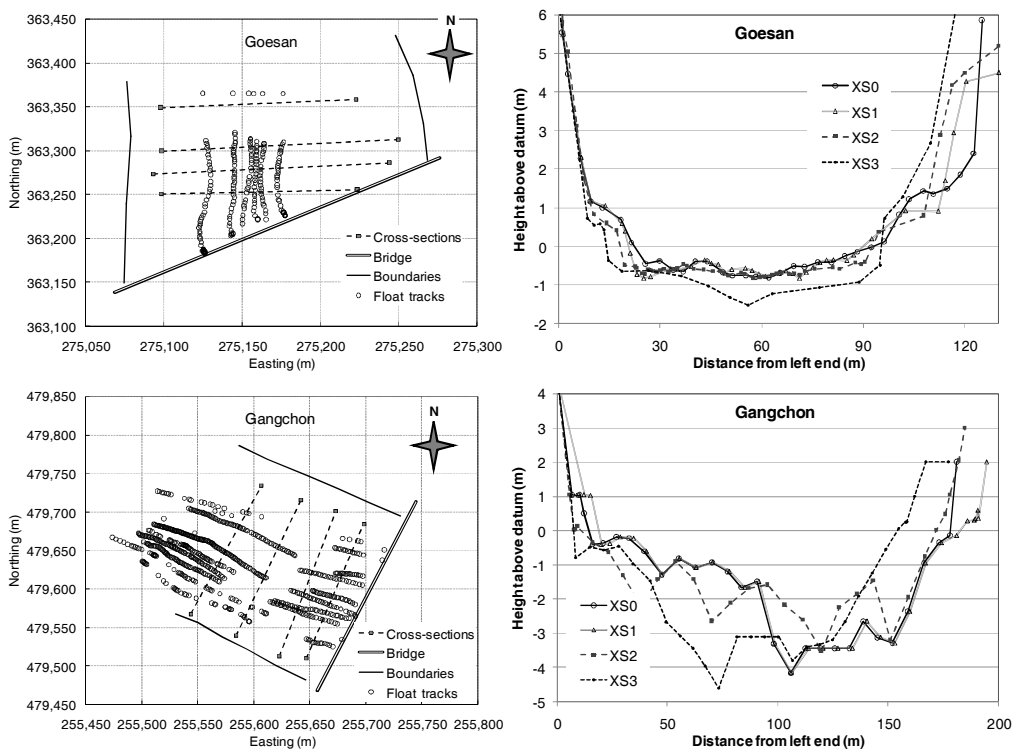

Figure 3. Site location with observed float tracks (left) and cross-sections (right)

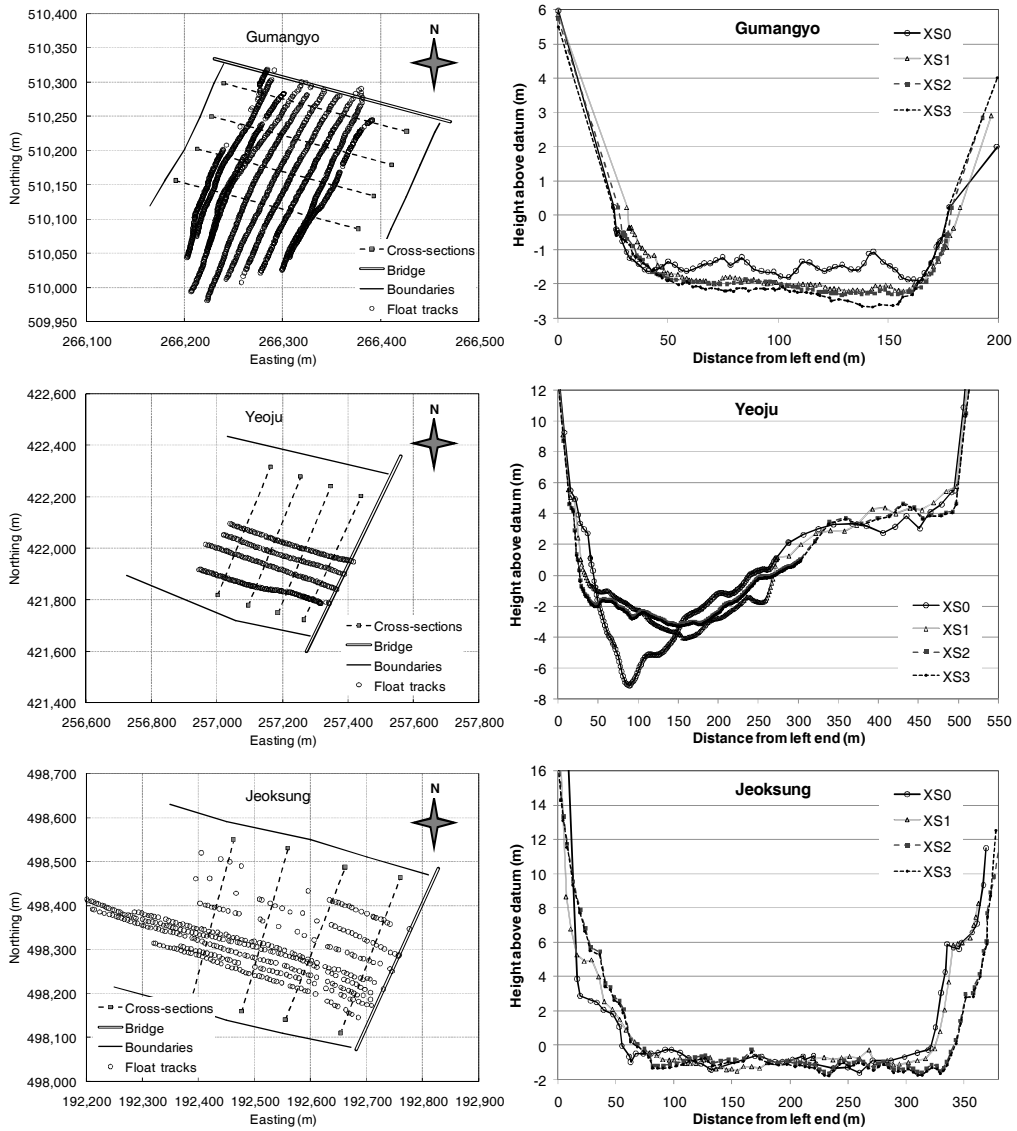

Figure 3. (continued)

VELOCITY CALCULATION

Calculation of flow velocity. Generally, in the rod-float method, depth-averaged flow velocity in a vertical can be expressed as follows:

$$v = k\frac{l}{t}$$

where, v is depth-averaged flow velocity, k calibration factor concerning the draft of the rod-float, l length of the path, and t travel time. The EF calculates l and t using GPS position information. For calculation of instantaneous velocity at every point during the travel, the EF uses following equation:

$$v_i = k\frac{l_i}{\Delta t} = k\frac{\sqrt{(x_i - x_{i-1})^2 + (y_i - y_{i-1})^2}}{t_i - t_{i-1}}$$

where, v_i is instantaneous velocity at time i, l_i is displacement from a point (x_{i-1}, y_{i-1}) to another point (x_i, y_i), Δt is time span, and x and y are positions in the earth coordinates. For calculation of discharge, velocity for travel time of a rod-float passing through two successive cross-sections is to be considered with angle calibration as expressed in the following equation.

$$v_{j,j+1} = k\cos\theta\frac{L_{j,j+1}}{\Sigma\Delta t}$$

where, $v_{j,j+1}$ is velocity for travel between successive cross-sections j and $j+1$, θ is angle difference between real direction and perpendicular direction to cross-section, $L_{j,j+1}$ is line distance between up- and downstream intersection points.

Results. Figure 4 shows velocity vectors of the Gumangyo site. Though calculated velocity using the EFs were not yet directly verified with velocity obtained by other instruments like conventional current meters, it displays well flow patterns in the straight reach of a stream which cannot be easily measured with other methods.

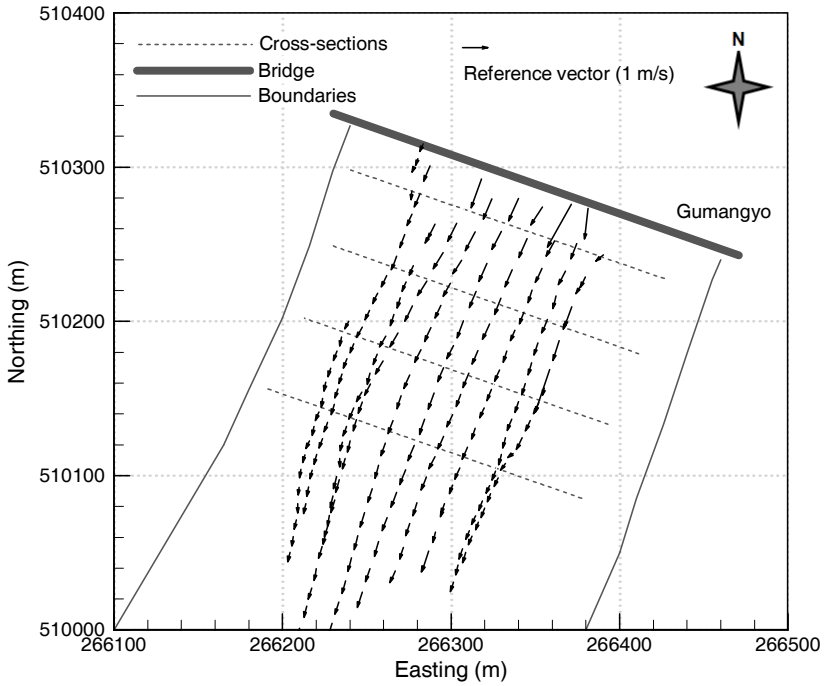

Figure 4. Velocity vectors calculated using the EFs for the Gumangyo site

Figure 5 indicates lateral velocity distributions of selected sections at four sites. Though measured velocity by the EFs is not compared with velocity by other

methods, lateral velocity distributions except the Gangchon data represent similarity with generally accepted forms.

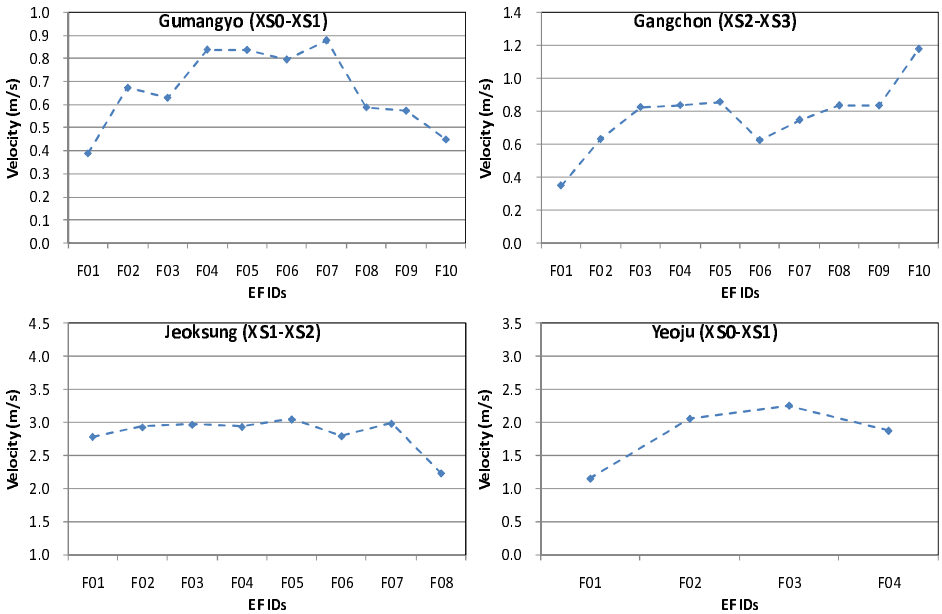

Figure 5. Lateral velocity distributions of the four sites

DISCHARGE CALCULATION

Cross-section area measurement. In order to compute discharge, cross-section areas should be calculated. In the rod-float method, a sub-section area for each rod-float is calculated averaging corresponding up- and downstream sub-sections areas based on the cross-section survey data using mid-section method (Figure 1). Since each EF has position information where it intersects with pre-established cross-sections, a sub-section area for computation of sub-section discharge is delineated by two neighboring EFs. Finally, remnant sub-section areas near both banks are delineated by the position of either the first or the last EF (Figure 6).

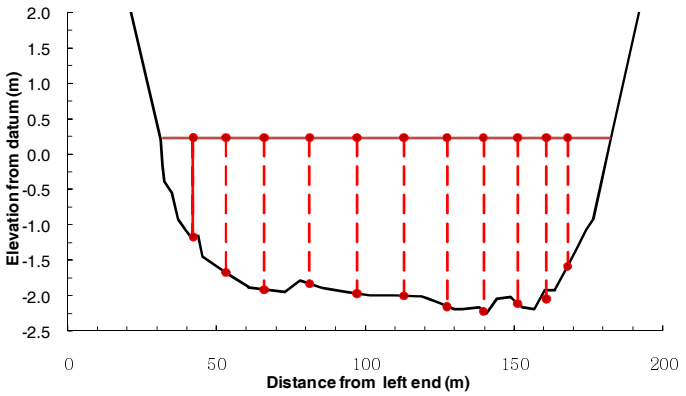

Figure 6. Sub-section delineation by the EFs

Discharge calculation. Discharge for each site is calculated by summing up of all sub-section discharge which is a product of flow velocity and sub-section area (Table 2). The Yeoju site is excluded because entire channel width of it cannot be sufficiently covered with only four EFs. Discharge for near-bank zone is calculated according to following equation presented by Simpson (2001).

$$Q_{L(R)} = 0.707 V_{1(n)} \frac{A'_{L(R)} + A''_{L(R)}}{2}$$

For three sites which have roughly symmetric and homogeneous cross-sections in the straight reach, measured discharge is very close to reference discharge. Measured discharge of the Gangchon site shows rather large difference with reference discharge. It seems related to irregular cross-section characteristics. Though the tests are preliminary and application is to be made for various sites, this result indicates that the EF system can be used as a good method for discharge measurement as well as velocity. Especially, it will be very useful for hazardous flow condition.

Table 2. Measured discharge values compared with reference ones

Date (yyyy-mm-dd)	Site	Measured discharge (m^3/s)	Reference discharge (m^3/s)	Difference (%)	Remarks
2007.08.31.	Goesan	64.8	63.0	2.86	Dam release
2008.04.15.	Gangchon	317.8	276.1	15.10	Dam release
2008.05.03.	Gumangyo	155.1	154.0	0.71	Dam release
2008.07.21.	Jeoksung	2,702.6	2,656.0	1.76	Rated discharge

CONCLUSION

In this study, the electronic float (EF) system which is developed based on GPS and RF technology, is briefly introduced and field application results of the EF system are presented. Velocity and discharge are well measured with the EF. Though it is necessary to test the EF for various sites, it is expected to be a useful tool for measurement of velocity and discharge for risky flow condition.

ACKNOWLEDGEMENT

This research was supported by a grant from Sustainable Water Resources Research Center (2-1-3) of 21st Century Frontier Research Program of Republic of Korea.

REFERENCES

Hopping, P. N., and Smith, B. T. (2002) "Measurement of flow patterns using GPS Drogues," *Proceedings of Hydraulic measurement and experimental method 2002* (CD-ROM)

International Organization for Standardization (ISO). (1997) *Measurement of liquid flow in open channels-Velocity-area methods* (ISO 748)

Simpson, M. R. (2001). *Discharge measurements using a broad-band acoustic Doppler current profiler*, US Geological Survey Open-File Report 01-1

World Meteorological Organization (WMO). (1994) *Guide to hydrological practices*, WMO-No. 168

Prediction of Nitrate Concentration in Stream Water Based on Watershed Land Use and Stream Flow Rate

Jingjie Teng[1], Mira Olson[1], Patrick Gurian[1], Anna Sofranko[2], Janet Herman[2], Aaron Mills[2]

[1]Department of Civil, Architectural, and Environmental Engineering, Drexel University, 3141 Chestnut Street, Philadelphia, PA 19104; PH (215)-895-2987; FAX (215)-895-1363; email:tj62@drexel.edu
[2]Department of Environmental Sciences, University of Virginia, 291 McCormick Rd., Charlottesville, VA 22904

Abstract

Non-point source nitrate loading to stream water can be affected by land use, soil type, slope of discharging watershed, water flow rate, and storm events. This study considers the effects of land use type, water flow rate and seasonal and regional variation in order to understand and predict transport of nitrate in stream water discharging from watersheds along Virginia's Eastern Shore. A simple regression analysis was performed to check the relationship between nitrate concentration and land use type. Fertilized land was found to be the strongest contributor to nitrate concentration in stream water. Developed land was also a contributor but with a lower weighting factor. Forested land acted as a significant inhibitor. A predictive model was generated using multiple regression analysis. Besides land use type, nitrate concentration was also significantly influenced by stream flow rate. Other variables, including sampled area, seasonal and regional variation, may be treated as background information, in which they may have some effect on nitrate concentration, but not significantly enough to be included in the predictive model. Therefore, stream nitrate concentration levels can be predicted along the Eastern Shore of Virginia based on land use type and stream flow rate. Predictions may be improved by incorporating other geomorphic or hydrologic information.

1. Introduction

Nitrogen inputs to stream water have increased considerably over the past several decades. Human activities and products, including agricultural fertilizers, livestock ranch runoff, sewage discharge and fossil fuel combustion elevate natural nitrogen concentrations (Monti 2003). Approximately one third of the net anthropogenic input of nitrogen is discharged to streams and rivers (Jordan 1997a).

Stream water quality is influenced by a variety of parameters and mechanisms. The effects of these parameters during biogeochemical processes are confounded in the natural environment. Land use plays a very important role in determining the nitrogen loading level in stream water. Other factors, including stream flow rate, and seasonal and regional variation, which may indicate different levels of water-rock, microbial, and dilution processes, may influence base flow biogeochemistry, the pathways of water, and nutrient transformation.

Recent studies indicate a strong relationship between agricultural activities and nitrogen concentration in streams and rivers (Judith 2004; Monaghan 2007; Pieterse 2005). Low-end values of nutrient loading are based on estimated nutrient exports from forested watersheds, which can intercept and store precipitation-borne nutrients and are treated as one possible nitrogen sink (Jordan 1997a). Developed areas have the potential to generate large amounts of wastewater or sewage, which is associated with high concentrations of nitrogen (Jordan 1996; Monti 2003). Urbanization has a great impact on stream flow and ground water. Other specific indicators that warrant further consideration include housing, road and population densities, and the presence or absence of wastewater treatment facilities (Wayland 2003).

Base flow rate also has a strong influence on stream water quality, especially nitrate concentration. Greater infiltration and ground water flows are likely to promote discharge of nitrate, since nitrate has a high solubility in water and is more prone to leaching from soil (Jordan 1997c).

Other factors contributing to varying nitrate concentration levels include seasonal and regional variation. The highest stream flows generally occur in the winter and spring, when the water table is high, groundwater discharge to streams is greatest, and evaporation is lowest, compared to summer and fall (Judith 2004). Lower chemical reactions and biological activity further this difference (Monti 2003). Another seasonal factor is that agricultural applications of fertilizer generally occur in the spring. There is also a relationship between nitrate loading and hydrogeomorphic region. It is seen that there is more serious groundwater nitrate contamination in areas with well-drained soils compared to areas with poorly drained soils(Bachman 1998; Jordan 1997c). One possible explanation for this phenomenon is that anoxic conditions associated with saturated soils may favor denitrification, which decreases the nitrogen concentration in groundwater (Groffman 1993).

In this study, the effects of land use, water flow rate, and seasonal and regional variation are analyzed in order to understand and predict the fate and transport of nitrate in stream water discharging from watersheds along the Eastern Shore of Virginia. It was

expected that nitrate discharge to streams increases as the anthropogenic input of nitrogen to the watersheds increases. Factor analysis was conducted to determine significant variables impacting nitrate concentration. Next, multiple regression analysis was used to generate a predictive model of nitrate concentration in stream water using the selected variables. As a result of this model, nutrient concentrations can be predicted based on land use type and a regional dummy variable. Other geomorphic or hydrologic information may add to the accuracy of the model.

2. Methods

2.1 Description of study site

Virginia's Eastern Shore, bounded by the Atlantic Ocean to the east and the Chesapeake Bay to the west, contains most of Delaware and parts of Maryland and Virginia. The eastern shore area is a rural region with agriculture and forest as the dominant land use types, with scattered industrial and developed areas around the existing towns. The catchment area of this study site is located between latitude 37°10'-37°46'N and longitude 75°36'-75°58'W. The study area was a mixed land-use site, with 54.08% fertilized land (including crop land and fertilized grassland), 39.18% forested land (including deciduous forest, evergreen forest, mixed forest, and palustrine forest), 3.49% developed land (including high intensity and low intensity), and 3.22% mixed shrub.

There are many studies on the water quality of streams in the Chesapeake drainage basin (Jordan 1997a; Jordan 1997b; Jordan 1997c; Lindsey 1998; Miller 1997; Puckett 1992), most of which are based on large watersheds, which have a complex combination of different land cover and geomorphic, hydrologic, and biological processes. The watersheds in this study are mostly small (from 36.25 ha to 712.35, with a median area of 197.7 ha). There is relatively little climate variation or point-source input. Because of this, it is easier to test the impacts of land cover and other factors, which would be confounded in larger watersheds.

2.2 Sample collection

Thirteen watersheds were selected for nutrient sampling and discharge measurements, ranging in size from 36 ha to 712 ha. Individual sampled watersheds varied in size and land-use distribution, and are characterized in Table 1.

Eight synoptic surveys were performed, between April, 2005 and October, 2006, measuring $N0_3^-$ concentration and discharge at stream locations downgradient in the watershed but uninfluenced by tidal effects. Stream 1 is on the southern-most part of the study site, and stream 13 is furthest north. Grab samples were analyzed for nitrate concentration using ion chromatography.

2.3 Sample analyses

2.3.1 Stream discharge measurements

Stream velocity measurements were made using a Marsh-McBirney, Inc. Model 2000 Flow-Mate portable flowmeter. Cross-sectional reaches of the sampled streams were divided into several segments and an average velocity for each segment was recorded

Table 1 Percentage of land use types for study watersheds

Sample ID	Creek name	Total area (ha)	Land-use Type (%)			Mean NO_3^- (mg/L)
			Forest	Developed	Fertilized	
1	Tommy's Ditch	97.92	16.14	8.85	74.47	5.42
2	Mill Creek S	201.40	25.14	3.90	70.32	4.79
3	Pt Rocks	173.40	21.24	4.17	71.50	6.69
4	Narrow	223.20	28.68	0.08	68.52	2.95
5	Taylor	135.86	20.19	3.28	75.67	2.86
6	Mill Creek N	225.25	59.98	2.39	36.11	0.57
7	Red Bank	36.25	15.09	0.50	84.16	5.93
8	Green's	231.13	62.61	4.02	25.89	1.69
9	Coal Kiln	197.70	42.35	1.89	52.39	1.92
10	Frogstool Branch	712.35	49.52	4.67	41.14	1.21
11	Ross Branch	211.78	40.98	1.04	53.93	2.43
12	Parker's	146.31	21.74	2.23	74.16	1.47
13	Bundick	115.14	22.45	7.57	68.67	2.67

using the portable flowmeter. Stream discharge was calculated by determining the cross-sectional area of each segment, and adding the contributing water flow from all segments.

2.3.2 Chemical analysis

Triplicate stream-water samples were collected at each sampling site using 150-mL sampling bottles, and stored in a cooler. Upon returning to the laboratory, samples were refrigerated and filtered through 0.2-m disposable filters. Stream-water samples were analyzed for nitrate, chloride and sulfate using a Dionex® ion chromatograph equipped with a Gilson® 234 autoinjector and a Dionex IonPac AS4A® 4 x 250 mm analytical column.

2.4 Statistical analyses

2.4.1 Single factor analysis: One-way ANOVA

SPSS for Windows (SPSS Inc. 2007) was used to perform one-way ANOVA analysis to observe the effects of seven factors (stream flow rate, sampled area, percentages of agricultural, developed and forested land, seasonal variation and regional variation) on nitrate concentration in stream water. The null hypothesis (H_0) assumes that all mean nitrate concentrations are equal:

$$H_0 : \mu_1 = \mu_2 = \mu_3 = ... = \mu_C \quad (1)$$

All mean nitrate concentrations are equal

$$H_1 : \mu_1 \neq \mu_2 \neq \mu_3 ... \neq \mu_C \quad (2)$$

At least one mean nitrate is different: the null hypothesis is not true

The F statistic, which is the ratio of the among estimate of variance and the within estimate of variance (F=MSA/MSW), was used to interpret the results of the one-way

ANOVA. The decision rule is to reject H_0 if $F>F_U$ (F_U is the critical F-value at the level of significance at 0.05), otherwise not to reject H_0.

2.4.2 Simple regression analysis

Microsoft Office Excel 2007 (Microsoft Corporation) and its add-in software PHStat (Prentice Hall, Inc.) were used to perform a simple regression analysis, in order to check the relationship between nitrate concentrations and land use.

2.4.3 Multiple regression analysis

Microsoft Office Excel 2007 (Microsoft Corporation) and its add-in software PHStat (Prentice Hall, Inc.) were used to perform multiple regression analyses in order to predict stream nitrate concentration based on the land use type or other known geomorphic or hydrologic information.

The hypotheses are:

$$H_0 : \beta_1 = \beta_2 = \beta_3 = ... = \beta_k = 0 \quad (3)$$

No linear relationship between X_j and Y

$$H_1 : At\_least\_one\_\beta_i \neq 0 \quad (4)$$

Linear relationship does exist between X_j and Y

The F-test statistic mentioned before was used to test for overall significance of the multiple regression models. Then residual analysis was performed to check the regression assumptions: independence of errors, normality of error, and equal variance. The heteroscedasticity-consistent standard errors (HCSEs) procedure was used to check if unequal variances in different observations existed. A stepwise regression was performed to check if there was a better model to complete the prediction.

A full model was constructed (Equation 5) including seven factors: log (flow rate), log (sampled area), fraction of forested land, fraction of developed land, fraction of fertilized land, and dummy variables for seasonal and regional variation.

$$Y = \beta_0 + \beta_1 X_1 + \beta_2 X_2 + \beta_3 X_3 + \beta_4 X_4 + \beta_5 X_5 + \beta_6 X_6 + \beta_7 X_7 \quad (5)$$

where Y - log (nitrate concentration); X_1 - log (sampled area); X_2 - log (flow rate); X_3 - fraction of forested land; X_4 - fraction of developed land; X_5 - fraction of fertilized land; X_6 - seasonal dummy variable, 1 for data between Dec and May, and 0 otherwise; X_7 - regional dummy variable, 1 for southern group (sample ID 1-7), and 0 otherwise.

A reduced model (Equation 6) was assumed, dependent only on flow rate and land-use characteristics.

$$Y = \beta_0 + \beta_1 X_1 + \beta_2 X_2 \quad (6)$$

where Y-log (nitrate concentration); X_1-log (flow rate); X_2-fraction of forested land.

3. Results

3.1 Relationships between nitrate concentration and individual variables

Effects of individual variables, including regional and seasonal variation, sampled area and land use, on nitrate stream concentration were tested and are presented below. Table 2 shows results of one-way ANOVA data analysis.

It was observed that northern streams had lower nitrate concentrations than southern streams. Averaged nitrate concentrations over the entire sampling period for the southern and northern stream groups were 4.08 mg/L and 1.85 mg/L, respectively. This regional difference may be due to the different levels of forested land and fertilized land, so it was not treated as an independent variable in our model. Forested land accounts for less than half of the total area of the southern and northern groups (30.67% and 44.95%, respectively). Fertilized land accounts for 64.59% of the total area for the southern group, compared with 46.97% for the northern group. Stream 7, with the highest fraction of fertilized land (84.16%) and the lowest fraction of forested land (15.09%) had a stream nitrate concentration much higher than the overall trend. It most likely receives the largest quantity of fertilizer or net imports of nitrogen-fixing crops (Charmbers 2005; Jain 2007; Jordan 1996), and there is only minimal forested land to intercept and store these nitrogen nutrients (Jordan 1997a; Jordan 1997c).

Nitrate concentrations in stream water samples displayed seasonal fluctuations during the sampling period, although there was no statistically significant correlation between nitrate concentration and season. The lowest nitrate values were observed during summer and highest values during winter. The two lowest mean values of nitrate concentration were 2.10 mg/L (August 28th, 2005) and 2.08 mg/L (May 12th, 2006), and the highest was 3.65 mg/L (January 28th, 2006). This effect can be explained by low groundwater discharge to streams, and high chemical reactions and biological activity during the summer time (Judith 2004; Monti 2003). However, there were two high nitrate concentrations measured on April 12th, 2005 (3.98 mg/L) and May 8th, 2005 (3.72 mg/L), which made the pattern of nitrate concentration less clear.

Sampled area size was a statistically significant factor for nitrate concentration in stream water, but it was not included in the final model because the effect of sampled area was accounted for by flow rate, which was significantly correlated with sampled area.

Strong correlations were observed between nitrate concentration and both fertilized and forested land fractions (Figures 1, Table 3). The fraction of developed land also affected stream nitrate concentration, although the effect was not as strong as the other two land-use types (Figure 1, Table 3).

Stream water from primarily forested watersheds (with a forested land fraction larger than 50%) had lower average nitrate concentrations (0.57 mg/L in stream 6, 1.69 mg/L in stream 8, and 2.43 mg/L in stream 11) than the mean value of 3.12 mg/L. Stream 6, with 59.98% forested land, had the lowest average nitrate concentration during the sampling period (0.57 mg/L) of all 13 streams. Nitrate concentrations decreased with larger fractions of forested land, possibly because forested land can intercept and store

Table 2 One-way ANOVA for each individual variable

variables	F value	Critical F value	Decision made from F-test	Included in model or not
Regional variation	28.79	3.94	Significant	No
Seasonal variation	1.47	3.94	Not significant	No
Sampled area	10.60	3.94	Significant	No
Land use	5.40	4.84	Significant	Yes

Table 3 Regression equations for exponential relationship between average nitrate concentration and fraction of fertilized land, forested land, and developed land

	Nitrate concentration and fertilized land fraction	Nitrate concentration and forest land fraction	Nitrate concentration and developed land fraction
R-squared values (R^2)	0.542	0.548	0.031
C_1 constant	0.420	7.037	2.148
C_2 constant	0.029	-0.03	0.049

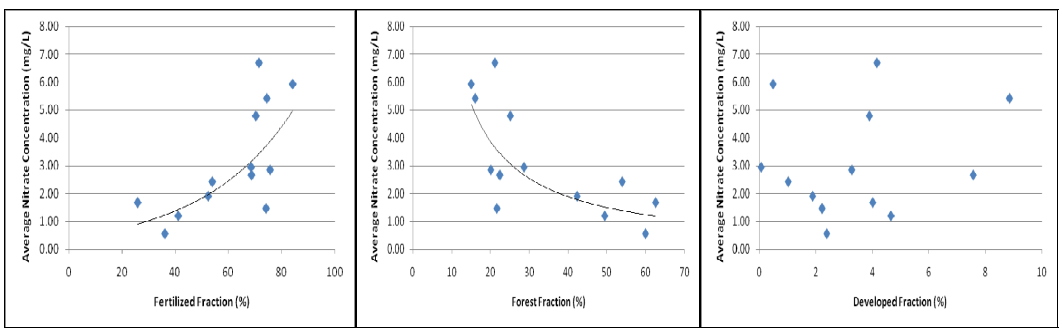

Figure 1 Nitrate concentrations in stream water averaged over the sampling period varied with fertilized, forested and developed fraction of watershed

nutrients, resulting in effective nitrate removal (Jordan 1997a; Jordan 1997c). It is attributed not only to plant uptake, but also to soil type in the forested area, which is suitable for removal of nitrate through denitrification (Speiran 1996).

The fraction of fertilized land had an inverse impact on nitrate concentration. Streams discharging from highly fertilized land areas produced high nitrate concentrations. The nitrate concentrations for stream 7 with 84.16% fertilized land, and stream 1 with fertilized land fraction of 74.47 % were 5.93 mg/L and 5.42 mg/L, respectively, approximately twice as high as the mean nitrate concentration for all streams. The reason would be higher fertilizer application and cultivation of nitrogen-fixing crops (Charmbers 2005; Jain 2007; Jordan 1997a; Jordan 1996).

It was found that the fraction of developed land also affected stream nitrate concentration, although the effect was not as strong as the other two land-use types.

Stream 1 discharging from land with the highest fraction of developed area (8.85%) had nitrate concentrations as high as 5.42 mg/L. The same level of nitrate was also found in stream 7 (5.93 mg/L), although only 0.5 % of the drainage area was developed land. Developed land may be affected by human activity, which produces larger volumes of runoff from storm-sewer systems (Scorca 2001). It may be associated with deteriorated water quality, and with subtle impacts on stream nitrate concentrations.

Based on the scatter plots of nitrate concentration versus land use, we checked the fitness of both exponential and power relationships between stream nitrate concentrations and fertilized, forested and developed land fraction through simple regression analysis (Table 3). Exponential relationship fit data better, but still near 0 between nitrate concentration and developed land fraction. Nitrate concentration predictions based solely on individual land-use type were very poor. Therefore a multiple regression, including all land-use type components and other factors, was assumed to describe the trend of nitrate concentration.

3.2 Multiple regression analysis

According to the multiple regression analysis, there was overall significance for the full model, with an F-value of 20.62 and R^2 of 0.6266 (Table 4). The variables for sampled area, fraction of developed land, seasonal and regional variation did not contribute as much as the other three variables of flow rate, fractions of forested land, and fertilized land to nitrate concentration. Since fraction of fertilized land was highly correlated with fraction of forested land (with R square of 0.9729), forested land was treated as the representative land-use variable in the reduced model (Equation 6). Flow rate is another significant variable. The overall significance of this reduced model increased to an F-value of 49.1, with a slightly decreased R^2 of 0.5190 (Table 5). Both of the two variables in the reduced model had significant effects on nitrate concentration (all p-values less than 1E-5), so the reduced model had advantages in describing nitrate concentration over the original full model. It was also verified from the stepwise regression that there was no significant relationship between the predicted nitrate concentration and the deleted variables (i.e. stream flow rate, sample area, fraction of developed land, seasonal and regional dummy-variable).

4. Conclusions

This study has shown that fertilized land was the strongest contributor to elevated nitrate concentrations in stream water. Developed land was also a contributor but with a lower weighting factor. Forested land acted as a significant inhibitor. Nitrate concentrations were also influenced by increased stream flow rate, which confirms that the major source of non-point pollution in stream water is from discharged ground water and surface runoff from watersheds. Other variables, including sampled area, and regional and seasonal variation, may be treated as background information. A predictive model correlating land use type and stream flow rate with stream nitrate concentration was constructed.

Table 4 Multiple regression results for full model

	Parameters	Coefficients	Standard Error	Significance
Full model:	intercept	24.04	5.039	7.443E-06
	log (flow rate)	0.2141	0.05463	1.778 E-04
F=20.62	log (sampled area)	-0.2278	0.1227	6.675 E-02
R^2=0.6266	% forested	-25.30	5.291	7.135E-06
Adjusted	% developed	-16.09	5.318	3.273 E-03
R^2=0.5962	% fertilized	-20.65	4.987	8.068E-05
	seasonal variable	0.0660	0.1398	0.6380
	regional variable	0.5714	0.1472	2.024 E-04

Table 5 Multiple regression results for reduced model

Reduced model:	Parameters	Coefficients	Standard Error	Significance
F=49.10	intercept	3.202	0.3314	1.294E-15
R^2=0.5190	log (flow rate)	0.2361	0.05734	8.403E-05
Adjusted R^2=0.5084	% forested	-4.215	0.4254	3.963E-16

The statistical approach applied in this work can help us to determine the relative impact of different land use types on nitrate pollution in stream water. This approach is based on the assumption that nitrate in stream water is contributed by non-point pollution from discharging watersheds, and nitrate concentration can be predicted based solely on land use type and stream water flow rate. Regional and seasonal variation did have some impact on nitrate concentration in stream water, but the relation was not clear enough due to the lack of data for watershed soil type, slope, and precipitation. More hydrological and geomorphic parameters may be incorporated into the model for future study.

List of References

Bachman, L. J., Lindsey, B., Brakebill, J., and Powars, D.S. (1998). "Ground-water discharge and base-flow nitrate loads of nontidal streams, and their relation to a hydrogeomorphic classification of the Chesapeake Bay watershed, middle Atlantic Coast." *U.S. Geological Survey Water-Resources Investigations Report 98-4059*, 71.

Charmbers, D. K., Arruda, J.A., and Jaywardhana, A.A. (2005). "A synoptic water quality survey of the Spring River and its tributaries." *Transactions of the Kansas Academy of Science*, 108(1/2), 47-56.

Groffman, P. M., Zak, D.R., Christensen, S., Mosier, A., and Tiedje, J.M. (1993). "Early spring nitrogen dynamics in a temperate forest landscape." *Ecology*, 74(5), 1579-1585.

Jain, C. K., Singhal, D. C., Sharma, M. K. (2007). "Estimating nutrient loadings using chemical mass balance approach." *Environmental Monitoring and Assessment*, 134(1-3), 385-396.

Jordan, T. E., Correll, D.L., Weller, D.E. (1997a). "Effects of agriculture on discharges of nutrients from coastal plain watersheds of Chesapeake Bay." *Journal of Environmental*

Quality, 26(3), 836-848.

Jordan, T. E., Correll, D.L., Weller, D.E. (1997b). "Nonpoint source discharges of nutrients from Piedmont watersheds of Chesapeake Bay." *Journal of the American Water Resources Association*, 33(3), 631-645.

Jordan, T. E., Correll, D.L., Weller, D.E. . (1997c). "Relating nutrient discharges from watersheds to land use and streamflow variability." *Water Resources Research*, 33(11), 2579-2590.

Jordan, T. E., Weller, D.E. . (1996). "Human contributions to terrestrial nitrogen flux." *Bioscience*, 46(9), 655-664.

Judith, M. D., Scott, W.A, Linda M.D., Matthew, J.F., Jeffrey, R.B., Tracy, C.H., Michael, J.B., and Mark, R.N. (2004). "Water quality in the Delmarva Peninsula, Delaware, Maryland, and Virginia, 1999-2001." *U.S. Geological Survey Circular 1228*.

Lindsey, B. D., Breen, K.J., Bilger, M.D., Brightbill, R.A. (1998). "Water quality in the Lower Susquehanna River Basin, Pennsylvania and Maryland, 1992-95." *USGS Circular 1168, U.S Geological Survey, Lemoyne, Pennsylvania*, 38 pp.

Miller, C. V., Denis, J.M., Ator, S.W., Brakebill, J.W. . (1997). "Nutrients in streams during baseflow in selected environmental settings of the Potomac River Basin." *Journal of the American Water Resources Association*, 33(6), 1155-1171.

Monaghan, R. M., Wilcock, R. J., Smith, L. C., Tikkisetty, B., Thorrold, B. S., Costall, D. (2007). "Linkages between land management activities and water quality in an intensively farmed catchment in southern New Zealand." *Agriculture Ecosystems & Environment*, 118(1-4), 211-222.

Monti, J., Jr., and Scorca, M.P. (2003). "Trends in nitrogen concentration and nitrogen loads entering the South Shore Estuary Reserve from streams and ground-water discharge in Nassau and Suffolk Counties, Long Island, New York, 1952-97." *U.S. Geological Survey*.

Pieterse, N. M., de Venterink, H., Schot, P.P., Verkroost, A.W.M. . (2005). "Is nutrient contamination of groundwater causing eutrophication of groundwater-fed meadows?" *Landscape Ecology*, 20(6), 743-753.

Puckett, L. J., Bricker, O.P. (1992). "Factors controlling the major ion chemistry of streams in the Blue Ridge and Valley and Ridge Physiographic Provinces of Virginia and Maryland." *Hydrological Processes*, 6(1), 79-97.

Scorca, M. P., Monti, Jack, Jr. (2001). "Estimates of nitrogen loads entering Long Island Sound from ground water and streams on Long Island, New York, 1985-96." *U.S. Geological Survey Water-Resources Investigations Report 00-4196*, 29p.

Speiran, G. K. (1996). "Geohydrology and geochemistry near coastal ground-water-discharge areas of the Eastern Shore, Virginia." *U.S.Geological Survey Water-Supply Paper 2479*, 73.

Wayland, K. G., Long, D.T., Hyndman, D.W., Pijanowski, B.C., Woodhams, S.M., Haack, S.K. . (2003). "Identifying relationships between baseflow geochemistry and land use with synoptic sampling and R-mode factor analysis." *Journal of Environmental Quality*, 32(1), 180-190.

STUDYING THE IMPACT OF LAND USE/COVER CHANGES ON THE WATER QUALITY OF WEEKS BAY, AL: MODEL vs. REGRESSION

Harsh Vardhan Singh, Latif Kalin, and Graeme Lockaby

M.S. Student, Assistant Professor, and Professor, respectively
School of Forestry and Wildlife Sciences, Auburn University, Auburn, AL 36830
(Correspondence: latif@auburn.edu)

ABSTRACT

This study focuses on Weeks Bay, a small sub-estuary of the Mobile Bay and one of only three designated Outstanding National Resource Waters in the state of Alabama. We assess the impact of LULC changes in its watershed through watershed modeling and regression equations. The watershed model is calibrated using USGS flow measurements on the main river. Water quality data collected between 1992 and 1996 is used in developing regression equations between TSS, NO_3, P and various LULC types. The 1992 NLCD has been used and assumed to represent the LULC conditions of the period from 1992 to 1996. Comparison of model simulations with observed data for the period [1990-2003] showed that urbanization caused increase in streamflows. The 2002 NLCD has been fed into Regression model and TSS, NO3, and TP concentrations are estimated. The similarities and differences in predictions with each method are investigated.

INTRODUCTION

Coastal areas all around the world are experiencing population increase. One of the consequences of population growth is urbanization and urban sprawl, which often have adverse impacts on the environment. Increased percentages of imperviousness may lead to rise in sediment and nutrients loading in the streams (Arnold and Gibbons 1996 and Nelson and Booth 2002). Urbanization has also shown to increase heavy metal (Callender and Rice 2000), and bacteria loadings (Gregory and Frick 2000). This study focuses on the rapidly urbanizing Weeks Bay watershed in Southwest Coastal Alabama. Weeks Bay is one of only three designated Outstanding National Resource Waters in the state of Alabama, which is the highest standard for water bodies with no point-discharges allowed. The 513 km^2 watershed is in Baldwin County, which has the 2nd fastest population growth rate in the state of Alabama. Land use and cover of the watershed has seen significant changes during the past decade. It is therefore anticipated that these human induced land use changes will impact the quality and quantity of the waters draining into the bay. This paper focuses on studying the relationship between LULC changes and water quality in the

Fish River Watershed (Fish River supplies about 75% of the fresh water of the bay) with the help of regression analysis and watershed modeling. Three separate groups have collected water quality data in the past at different times in the tributaries of the Fish River from 1994 to 2001 (Basnyat 1998, Lehrter 2003, and Geological Survey of Alabama, GSA 2003). Arial photos and on-site visits revealed that there has been a significant increase in urban areas in the watershed lately. Hence, we found a unique opportunity in this watershed for assessing LULC change impacts on water quality.

STUDY AREA

Weeks Bay Watershed (Figure 1) is located in Baldwin County, Alabama. It is a small sub-estuary of the Mobile Bay receiving freshwater from the Magnolia (~25%) and Fish Rivers (~75%). The total drainage is about 513 km^2. It consists of southern Pine Hills and coastal lowlands. Figure 1 shows the sampling sites used for data collection by Basnyat (1998) and GSA (2003); out of these we have chosen 10 sites for our project. Selection of sites was based on the amount of available data and LULC variability between 1992 and 2002 (Table 1). Major LULC types in the watershed are pasture, agriculture, evergreen forest and urban areas. Large fraction of the watershed was covered by pasture in early 1990's, which shrunk almost by half by early 2000's due to built out and conversion to sod farming (Table 1).

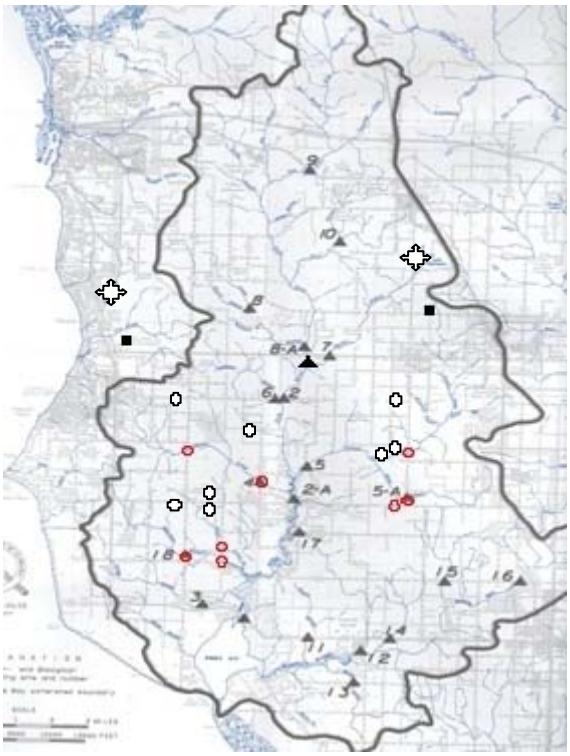

Figure 1. Weeks Bay watershed. (✣ : weather stations; ⬡,▲: Sampling sites)

WATERSHED MODEL

The watershed model selected in this study is the Soil Water Assessment Tool (SWAT). SWAT applications can be found all around the globe; e.g. Jha et al.2007 (Raccoon River, USA), Karim et al.2006 (Thur River basin located in the north east of Switzerland), Kang et al. 2005 (watershed containing rice paddy fields in the Republic of Korea). SWAT has been used in the past for evaluating the changes in water quality due to varying land use practices (Kalin and Hantush 2008).

The SWAT model requires specific information about elevation, soil, slope, weather, and land management practices within the watershed (Arnold & Allen, 1996). Spatial data used in the study for SWAT include a digital elevation model (DEM), LULC, soil data, climatic and stream flow records. National Elevation

dataset with a 1/3 arc second resolution (10 m pixels) was used for delineating the Fish River watershed and the drainage areas of the sampling sites. State Soil Geographic (STATSGO) and Soil Survey Geographic (SSURGO) data are the two types of spatially different digital soil data sets created by NRCS. Both were used in the model to check the differences in the model simulations with respect to each.

Table 1. Summary statistics of LULC types in the drainage areas of sampling sites.

LULC Type (%)	Minimum 1992 / 2001	Maximum 1992 / 2001	Average 1992 / 2001
AGR	9.5 / 9.0	39.9 / 39.1	24.6 / 30.7
PAST	16.0 / 8.6	64.6 / 42.5	48.9 / 26.3
FRSE	1.6 /1.5	41.5 / 44.4	10.6 / 10.7
URLD	0 / 5.4	2.1 / 16.6	0.5 / 11.4
URMD	0 / 0	0 / 3.9	0 / 0.9
URHD	0 / 0	0 / 1.3	0 / 0.2
URBAN	0 / 5.4	2.7 / 29.1	0.5 / 12.9
IMPERVIOUS	0 / 5.3	0.9 / 18.8	0.2 / 10.4
Urban Vegetation	0 / .1	1.8 / 11.01	0.5 / 2.5
Other *	8.2 / 3.9	32.7 / 36.8	15.3 / 19.4

* Wetland, Deciduous Forest, Mixed Forest, Water etc.

National Land Cover Data (NLCD) for 1992 was used as an input for LULC data. The choice of NLCD'92 was motivated by the fact that the period of previous data collections started in 1994, and 1992 NLCD is the closest LULC data available. The watershed in 1992 was dominantly pasture, forest, row crops, and urban.

Rainfall data for this project was available from two climate stations, one situated slightly outside one barely inside the watershed. 30 years of climate data was available. Temperature data was available only from one station. However this was not a concern as temperature does not show big spatial variations in Southern Alabama. Streamflow prediction, especially at early stages in model simulations, is highly dependent on the soil antecedent moisture condition. Thus, a warm up period of about a decade was used to minimize uncertainties due to antecedent moisture.

Flow calibration and validation for weeks bay watershed was completed by using the stream flow data from USGS gauge 02378500 (Fish River near Silver Hill, AL) (Same as Site 8A in Figure 1). The period of calibration was from 1990 to 1994 and validation period was from 1995 to 1998. We are currently calibrating SWAT for sediment and nutrients at subwatershed level by utilizing the past data reported in Basnyat (1998) and GSA (2003). These studies were conducted from 1994 to 1998 with major focus on TSS and NO_3 along with some other water quality parameters. P and PO_4 concentrations were also reported for some days, though at significantly low levels. The challenge is that they did not collect flow data; only concentrations of TSS and nutrient from grab samples were reported. At this stage we are unsure about model performance in simulating flow at subwatershed level. We recently installed

pressure transducers at those sites and are taking flow measurements to develop stage-discharge curves. Once we get flow data at those sites we will fine tune the model by further calibrating model parameters at subwatershed level. We also performed simulations for the period 2001-2003 to assess differences between streamflow for the periods with differing LULC. Performance of model was evaluated using mass balance error (MBE = Simulated / Observed - 1), coefficient of determination (R^2) and Nash-Sutcliffe efficiency (E_{NS}) (Kalin and Hantush, 2006).

REGRESSION MODEL

Multiple Linear Regression was performed to develop relationships between various LULC types and water quality parameters TSS, NO_3 and P. The data collected by Basnyat (1998) and GSA (2003) from 1994 to 1998 is utilized in development of these regression equations. Water quality parameters were treated as dependent variables and percentage area of different LULC as independent variables. Three different categories were considered for representing urban areas based on the 1992 NLCD. Below are LULC categories for which regression was carried out:

(i) Agriculture (AGR), Pasture (PAST), Evergreen Forest (FRSE), Urban(URB)
(ii) Agriculture (AGR), Pasture (PAST), Evergreen forest (FRSE), Urban High Density Residential (URHD), Urban Medium Density Residential (URMD), Urban Low Density Residential (URLD).
(iii) Agriculture (AGR), Pasture (PAST), Evergreen Forest (FRSE), IMPERVIOUS (Impervious), Urban Vegetation (Urban_Veget).

The percent imperviousness in category (iii) was estimated using the method described by ASCE/ESRI Impervious Surface Task Committee. The average imperviousness corresponding to low density, medium density and high density residential areas are given given as 25, 38 and 65%, respectively. We categorized urban areas not classified impervious as urban vegetation.

Regression equations were developed between percent LULC and concentration of sediment and nutrients using forward selection method of Statistical Analysis Software (SAS). Normality of data was tested using Shapiro-Wilk test. It was found from the test that the null hypothesis could not be rejected. In forward selection method SAS first calculates the fixation indices for each variable which is the measure of the contribution of that variable if it is included in the model. Probability (p- value) for these indices is compared to 0.5. If the value is less than 0.5 then the variable is included in the model. For choosing the next dependent variable SAS again calculates fixation indices for rest of the variables and it goes until there is no variable with p- value less than 0.5.

RESULTS AND DISCUSSIONS

SWAT Model Results

Figure 2 and 3 compare observed flow at the USGS station on the Fish River with SWAT simulated flow for the calibration and validation periods, respectively. It is clearly seen that SWAT was able reproduce observed flow. Table 2 shows SWAT model performance. Surprisingly the validation period shows slightly better performance, especially in MBE. We also run the model from 2001 to 2003 in prediction mode with the same model set up, which covers Lehrter's (2003) data collection period. Note that 1992 NLCD was used during model setup and 2001 NLCD show some substantial changes in LULC in some areas. Figure 4 compares models results with observed flow. Model performance is also reported in the last column of Table 2. SWAT overestimates streamflow on average by 16% in this period. From Figure 4 it is clearly seen that most of the increased flow is due to increase in high flows, a typical consequence of urbanization. As a matter of fact although SWAT underestimated flow by almost 8% during the calibration period, this underestimation diminished during the validation period and it turned into overestimation during the prediction period.

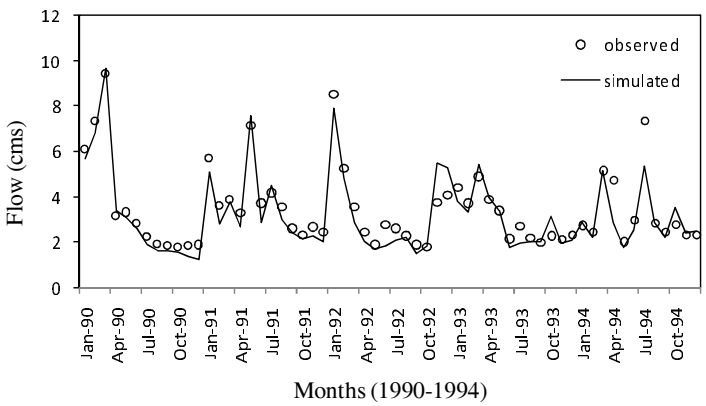

Figure 2. Comparisons of SWAT simulations with the observed data during calibration period (1990-1994).

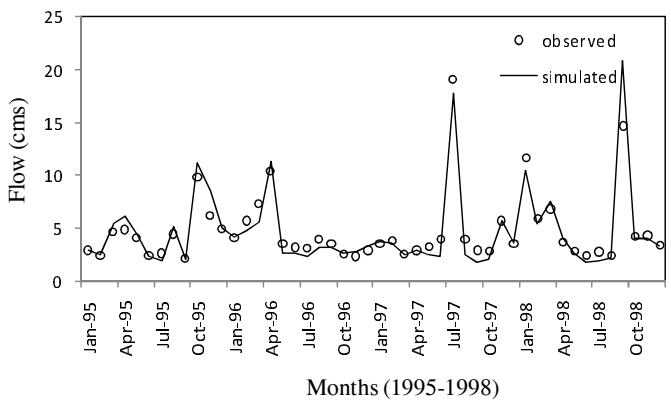

Figure 3. Comparisons of SWAT simulations with the observed data during validation period (1995-1998).

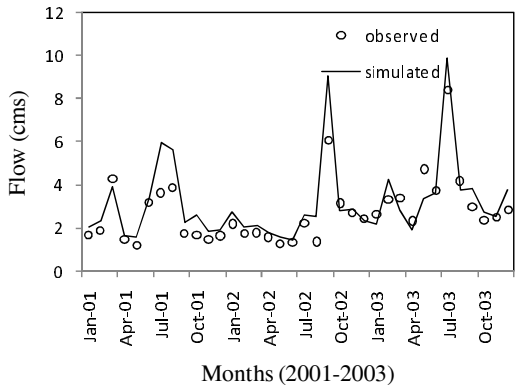

Figure 4. Comparisons of SWAT simulations with the observed data during prediction period (2001-2003).

Table 2. Model performance parameters for flow.

	Calibration (1990 – 1994)	Validation (1995 -1998)	Prediction (2001-2003)
R^2	0.89	0.91	0.82
E_{NS}	0.87	0.87	0.61
MBE	-7.7%	0.21%	15.91%

Regression of LULC vs. Water Quality

Regressing LULC percentages against average concentrations of TSS, NO_3 and P (all in mg/L) from various sites resulted in following equations.

$$TSS = -0.00081*AGR + 0.00038*PAST + 0.0129*URB + 0.028 \quad (R^2 = 0.56)$$
$$NO_3 = 0.169*AGR + 1.954*URB - 0.6649 \quad (R^2 = 0.45)$$
$$P = -0.00079*AGR + 0.04848 \quad (R^2 = 0.2)$$

Agriculture, pasture and urban percentages explain 56% of the variability in TSS concentrations; agriculture and urban areas explain 45% of the variability in Nitrate concentrations. The only significant factor in P was agriculture which barely explains 20% of the variation in Phosphorus concentrations. TSS showed the highest correlation against LULC percentages. P had almost no correlation. This was expected as measured P values were too small to get a meaningful relationship. A big surprise was having AGGR negatively correlated to TSS. There could be several reasons for this. It could be due to the nature of the agricultural activities. Sod and Orchard tree farming are widespread in the watershed, which are not known to produce heavy TSS loadings. Further, best management practices (BMP) around agricultural fields could be filtering out TSS extremely well. In fact, there are well established riparian buffers around most streams and creek in the watershed. Having high contribution from urban areas is not surprising at all due to two reasons. One is that the study watershed started urbanizing by early 1990's meaning there could be

many ongoing construction activities during that time span. Secondly, as urbanization results in flashier flows, one can expect higher streambed and stream bank erosion in urban areas. Nitrate results are not surprising at all with agricultural and urban areas being the major role players. Note that the reason for higher coefficients with urban areas is that urban percentage during this period was still relatively small.

Since LULC types don't cover a wide range in 1990's (see Table 1) we don't consider these regression equations reliable enough to be used in predictions. Still we fed 2001 LULC percentages into these equations and compared to data collected by Lehrter (2003) from 2000 to 2001. Figures (5-7) compares Lehrter's data with those predicted through regression equations. Box plots were first developed for 5 sampling sites to see the spread of data collected by Lehrter (2003). It is clear that there are no outliers for any of the parameters. The concentration values for three sites for NO_3 are higher than the other 2 sites (Figure 5). These higher concentrations can be attributed to the higher percentage of Agricultural areas in sub watersheds of these sites. For P (Figure 6) and TSS (Figure 7) spread was similar for all the sampling sites. Regression based NO_3 predictions significantly overestimate observed NO_3 values of Lehrter at all sites. On the contrary TSS and P values are within observed data ranges. This is quite interesting as NO_3 had the highest R^2 with P having the lowest. This once again shows the danger of using regression equations in predicting water quality parameters without having full LULC coverage.

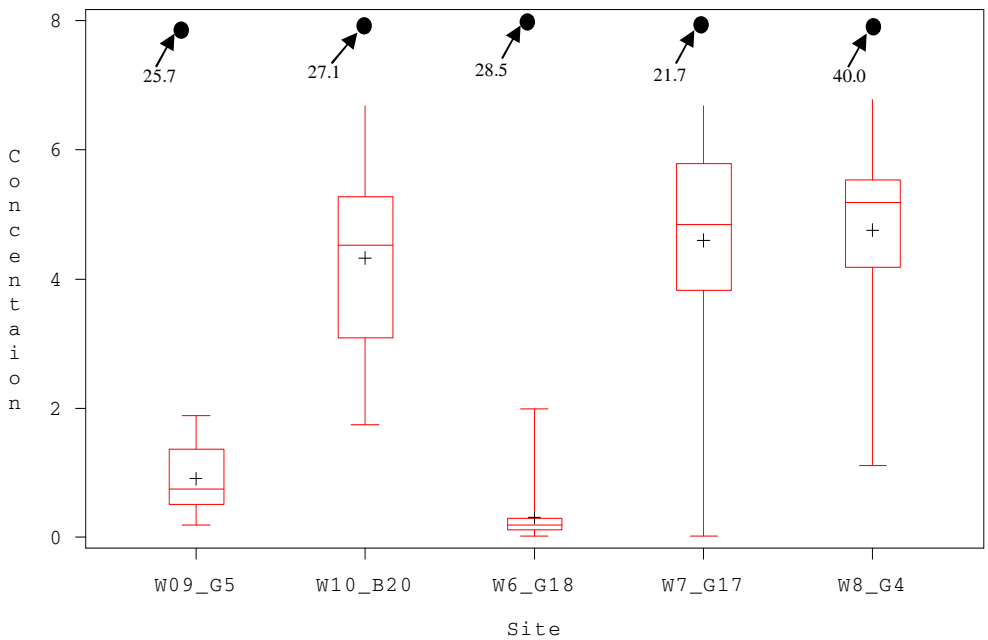

Figure 5. Box Plot for NO_3 concentrations for Lehrter (2003) data and its comparison with data developed from the Regression equations shown with (●).

It would be interesting to perform the same type of analysis using Lehrter's data and 2001 NLCD and then feed 1992 NLCD to those regression equations to see whether it can predict the 1994-1998 conditions. We expect that will have a higher predictive power as various LULC types in 2001 NLCD show more variability than

LULC of 1992 NLCD. Since we recently obtained Lehrter's data we did not have the chance to explore this facet yet.

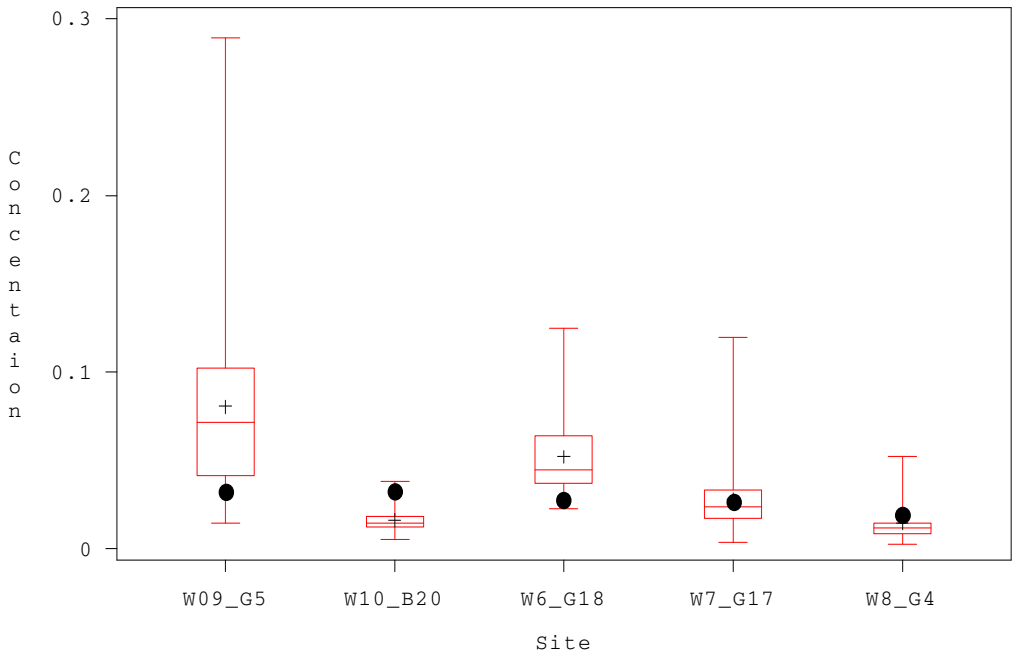

Figure 6. Box Plot for P concentrations for Lehrter (2003) data and its comparison with data developed from the Regression equations shown with (●).

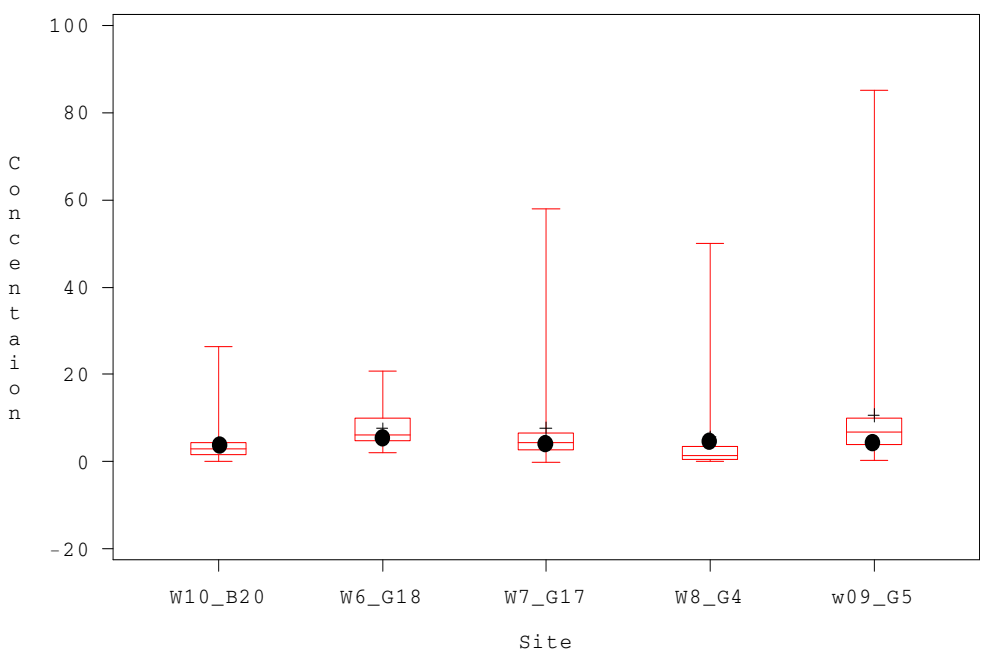

Figure 7. Box Plot for TSS concentrations for Lehrter (2003) data and its comparison with data developed from the Regression equations shown with (●)

SUMMARY AND CONCLUSIONS

In this paper we assessed the urbanization impacts in the Weeks Bay Watershed through regression and watershed modeling based approaches. Watershed model simulations revealed that urbanization has led to increased stream flow. Developed regression equations between land use/cover (LULC) and water quality data collected from 1994 to 1998 showed the limitations and the danger of using regression equations in such studies. It is suggested that in order to perform dependable regression based predictions, the data must come from several watersheds whose LULC should form a nice gradient, i.e. most LULCs should be represented and their percentages should cover a wide range, comparable to the range of the future expected LULC.

Empirical models usually work well within a particular range of dependent and independent values. Due to the fact that Weeks Bay Watershed is under constant stress of population growth and urbanization, regression based analysis is still a promising option as urban areas will keep growing. However, mechanistic hydrology and water quality models are still more efficient and effective means for assessing impacts of land use/cover (LULC) changes on water quality/quantity. Process based models like SWAT are effective in modeling natural process like hydrology of watershed. Their performance for the most part depends on the reliability of input data for the sensitive parameters.

REFERENCES

Arnold, C. & Gibbons, J. (1996).Impervious Surface Coverage: The Emergence of a Key Environmental Indicator. Journal of the American Planning Association, 62(2):243-258.

Arnold, J. G., & Allen, P. M. (1996). Estimating Hydrologic budgets for three Illinois Watershed. Journal of hydrology (176), 57-77.

Basnayat, P. (1998). Valuation of Forested Buffers. Ph. D. Dissertation, Auburn University, Alabama .

Callender, E. & Rice, K. C. (2000). The Urban Environmental Gradient: Anthropogenic Influences on the Spatial and Temporal Distributions of Lead and Zinc in Sediments. Environmental Science & Technology, 34(2), 232-238.

Gregory, M. B. & Frick, E. A. (2001). Indicator-Bacteria Concentrations In Streams Of The Chattahoochee River National Recreation Area, March 1999–April 2000. Proceedings of the 2001 Georgia Water Resources Conference, 2001.

Hantush, M. M. & Kalin, L. (2008), "Stochastic residual-error analysis for estimating hydrologic model predictive uncertainty", Journal of Hydrologic Engineering, 13(7):585-596.

Jha, M. K., Gassman, P. W., & Arnold, J. G. (2007). Water quality modeling for the Raccoon River Watershed using SWAT. Transaction of the ASABE , 50 (2), 479-493.

Kalin, L., & Hantush, M. H. (2006). Hydrologic Modeling of an Eastern Pennsylvania Watershed with NEXRAD and rain gauge data. journal of hydrologic engineering , 555-569.

Kalin, L. & Hantush, M. M. (2009), An Auxiliary Method to Reduce Potential Adverse Impacts of Projected Land Developments: Subwatershed Prioritization. Environmental Management, 43, 311-325

Kang, M., Park, S., Lee, J., & and Yoo, K. H. (2005). Applying SWAT for TMDL programs to small watershed containing rice paddy fields. Agricultural Water Management , 79 (1), 72-92.

Lehrter, J. C. (2003). Estuarine Ecosystem Metabolism and Retention of Allochthonous Nutrient Loads in Three Tidal River Easturine Systems. Ph.D. Dissertation, University of Alabama, Tuscaloosa.

Lehrter, J. C. (2006). Effects of Land Use and Land Cover, Stream Discharge, and Interannual Climate on the Magnitude and Timing of Nitrogen, Phosphorus, and Organic carbon Concentrations in Three Coastal Plain Watersheds. Water Environment Research , 78, 2356-2368.

Loveland TR and DM Shaw. 1996, 'Multiresolution land characterization: building collaborative partnerships', in Gap Analysis: A Landscape Approach to Biodiversity Planning (eds. J.M. Scott, T. Tear, and F. Davis), Proceedings of the ASPRS/GAP Symposium, Charlotte, NC, (National Biological Service, Moscow, ID), pp. 83-89.

Moglen, G. E. The ASCE/EWRI Impervios Surface Task Committee.

Neil, P., & Chandler, V. R. (2003). Water Quality and Biological Monitoring in Weeks Bay Watershed, Alabama 1994-1998. Geological Survey of Alabama, Bulletin 173, Tuscaloosa, Alabama.

Neitsch, S., Arnold, J. G., Kiniry, J. S., & Williams, J. (2005). Soil and Water Assessment Tool User's manual Version 2005. Agricultural Research Service and the Texas Agricultural Experiment Station.

Nelson, E., & Booth, D. B. (2002). Sediment sources in an urbanizing mixed land-use watershed. Journal of Hydrology, 264 (1-4), 51-68.

Soil Conservation Service,(1986). Urban Hydrology for Small Watersheds, Technical Release 55, Washington, DC.

Modeling the Hydrology and Hydraulics of the Cache River System

Misganaw Demissie, PhD., P.E. [1], Laura Keefer[2],
Yanqing Lian[3], Feng Yue[4] and Elias Bekele[5]

[1]Principal Scientist and Center Head, Center for Watershed Science, Illinois State Water Survey, 2204 Griffith Drive, Champaign, IL 61820, USA; PH (217) 333-4753; email: demissie@uiuc.edu.
[2]Fluvial Geomorphologist, Center for Watershed Science, Illinois State Water Survey, 2204 Griffith Drive, Champaign, IL 61820.
[3]Professional Scientist, Center for Watershed Science, Illinois State Water Survey, 2204 Griffith Drive, Champaign, IL 61820.
[4]Graduate Research Assistant, Center for Watershed Science, Illinois State Water Survey, 2204 Griffith Drive, Champaign, IL 61820.
[4]Assistant Professional Scientist, Center for Watershed Science, Illinois State Water Survey, 2204 Griffith Drive, Champaign, IL 61820.

ABSTRACT

The Cache River is located in the extreme southern part of Illinois, just north of the confluence of the Ohio and Mississippi Rivers. Major floods in both of the two rivers have significant impact on the hydrology and hydraulics of the Cache River. In 1915, a cutoff to the Ohio River was constructed east of Karnak that resulted in sub-dividing the Cache River watershed into the Upper and Lower Cache River watersheds. The Upper Cache River watershed consists of the eastern part of the watershed draining directly to the Ohio River through the Post Creek Cutoff. The Lower Cache River watershed consists of the western part of the watershed draining to the Mississippi River through a diversion channel at the outlet. However, part of the Lower Cache River can at times reverse flow, draining to the Upper Cache River and Post Creek Cutoff.

Hydrologic and hydraulic models have been developed to simulate the hydrology and hydraulics of the Cache River system to evaluate flow and water level conditions along the river under different alternative scenarios that can be implemented as part of a restoration effort for the Cache River. The hydrologic model that simulates the rainfall-runoff process for tributary watersheds is based on the HEC-HMS model. The model is used to compute runoff from tributary watersheds for selected storm events. Outputs from the HEC-HMS model are then used as inputs to the hydraulic model, UNET. The UNET model, a one-dimensional unsteady-flow dynamic wave routing model, is capable of modeling the complex hydraulics of the Cache River System that experiences flow reversals during flood events in the Lower Cache River.

ACKNOWLEDGMENTS

The work upon which this report is based was supported in part by funds provided by the Cache River Joint Venture Partnership (JVP), which includes the Illinois Department of Natural Resources (IDNR), The Nature Conservancy, the U.S. Fish and Wildlife Service, Ducks Unlimited, and the Natural Resources Conservation Service.

BACKGROUND

The Cache River is located in extreme southern Illinois, just north of the confluence of the Ohio and Mississippi Rivers (Figure 1). The total drainage area of the basin was 737 square miles (sq mi), or 1,909 sq km, until the construction of Post Creek Cutoff in 1915, which divided the Cache River basin into the Upper and Lower Cache River watersheds with 368 and 358 sq mi (953 and 927 sq km) of drainage, respectively. Karnak Levee (also known as Cache River Levee), along the western bank of Post Creek Cutoff near Karnak, separates the Upper and Lower Cache River watersheds. This levee was built in 1952 across the old Cache River channel and forces drainage from the Upper Cache River to flow directly to the

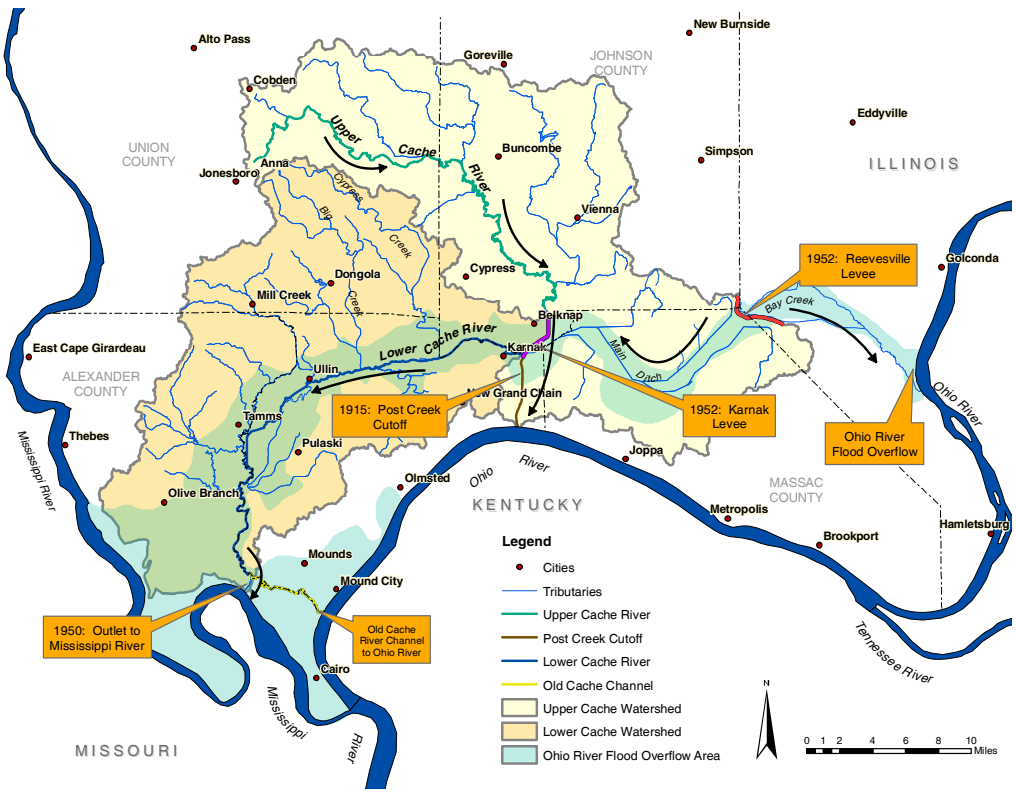

Figure 1. Historical major drainage alterations and current drainage pattern of Lower and Upper Cache River watersheds (Demissie et al., 1990a,b).

Ohio River through the Post Creek Cutoff. It also was designed to prevent any flood from the Upper Cache and Ohio Rivers from backing into the Lower Cache River. Karnak Levee was designed with two 48-inch (1.22 m) gated culverts to allow local drainage along the west side of the levee to flow to Post Creek Cutoff. Drainage from the Lower Cache River watershed was assumed to flow west into the Mississippi River. However, during flood events, some drainage from the Lower Cache River flowed east to Post Creek Cutoff through the culverts in Karnak Levee. Since 2002, however, Karnak Levee has been breached and the culverts washed away. It is now possible for major floods from the Upper Cache and Ohio Rivers to back into and flood the Lower Cache River floodplain and for flood waters from the Lower Cache River to flow to Post Creek Cutoff without any control.

Because of these alterations and the influence of the Ohio and Mississippi Rivers, the hydraulics of the Lower Cache River are very complex. Since the division of the Cache River basin into two watersheds, the Lower Cache River does not receive flow from the Upper Cache River to maintain a sustained flow in the downstream direction. Local tributaries are now the headwaters and the source of water for the upper portion of the Lower Cache River where the Cache River wetlands are located.

Big Creek, Cypress Creek, and Mill Creek are the three major tributaries that drain the upper portion (headwaters) of the Lower Cache River watershed. Big Creek has a drainage area of 51.7 sq mi (133.9 sq km) and flows into the Cache River at River Mile (RM) 24.1. Cypress Creek has a drainage area of 46.3 sq mi (120 sq km) and flows into the east side of the wetland at RM 29.4. Mill Creek has a drainage area of 53 sq mi (137 sq km) and flows into the Lower Cache River at RM 15.0. However, low to moderate flows from the upper third of the Mill Creek watershed are diverted to Indian Camp Creek (approximately 1 mile (1.6 km) northwest of the town of Ullin), which enters the Lower Cache River south of Ullin (RM 20.5). Several smaller tributaries also flow into the Lower Cache River. The most significant of these smaller tributaries, Limekiln Slough, has a drainage area of 22.1 sq mi (57 sq km) and flows into the west end of the Cache River Wetlands Area at RM 25.2.

Big Creek, Limekiln Slough, and Cypress Creek flow into the Lower Cache River where the channel bed elevation is the highest. East of the Cypress Creek confluence, the Lower Cache River has a downward slope to the east toward Karnak Levee. During low and moderate flows, the Cache River Wetlands Area is normally the divide between the two portions of the Lower Cache River that flow east towards Karnak Levee and west towards the Mississippi River (Allgire, 1991). During flood conditions, all or part of the wetland flows to the west. The location where the flow divides to the east or west is not constant and varies during flood events (IDNR, 1997).

Once water from tributaries enters the Lower Cache River, it can flow in an easterly direction toward culverts in Karnak Levee or flow in a westerly direction

toward the Lower Cache River outlet on the Mississippi River. If the flows are high enough to overtop streambanks, which is the case during most flood events, then water flows into the wetland areas, which have large water storage capacity. A combination of several factors determines which way water flows in upper parts of the Lower Cache River. Some of the factors are magnitude of the floods, channel capacity and slope, flood heights, floodplain storage, outlet capacity at bridge openings, and resistance to flow.

Demissie et al. (1990a, 2001, 2008) and IDNR (1997) provide more complete descriptions of the hydrology, land use, and climate of the Cache River, and the reader is referred to these publications for additional information.

The objective of the research that this paper is based on was to develop hydrologic and hydraulic models that can simulate the hydrology of the tributary watersheds and the hydraulics of the Lower Cache River. The models then were used to evaluate current conditions under different flooding possibilities and future conditions under different management scenarios, including a managed reconnection with the Upper Cache River.

HYDROLOGIC AND HYDRAULIC MODELING

The hydrology and hydraulics of the Lower Cache River were investigated intensively by updating models previously developed by the Illinois State Water Survey (ISWS) and the U.S. Army Corps of Engineers (USACE), St. Louis District. Two models, one for hydrology and the other for hydraulic simulation, were updated and used to evaluate different scenarios that represent reference conditions, current conditions, and future alternatives.

The hydrologic modeling system (HEC-HMS) developed by the Hydrologic Engineering Center of the USACE simulates rainfall-runoff processes for the tributary watershed to the Lower Cache River. The HEC-HMS model for the Lower Cache River watershed was prepared based on an earlier HEC-1 model developed by the ISWS. The present model was updated by calibrating and validating the model with recently collected ISWS hydrologic data. The model was used to compute runoff from tributary watersheds for 1- to 100-year storm events. Outputs from the HEC-HMS model for the different storm events then are used as inputs to the One-Dimensional Unsteady Flow through a Full Network of Open Channels (UNET) model. The UNET model for the Lower Cache River initially was developed by the St. Louis District and previously had been used by the ISWS for a research project on Big Creek. The UNET model is capable of modeling the complex hydraulics of the Lower Cache River where flow directions change over time. The UNET model was used to route flows through the Lower Cache River under different storm events and boundary conditions at the east and west outlets. Development of the current version of both models and their applications are discussed in this paper.

CALIBRATION AND VALIDATION OF HEC-HMS MODEL FOR BIG CREEK WATERSHED

The ISWS operates two raingages and two streamgages in the Big Creek watershed . Hourly precipitation and streamflow data since 2001 are available for calibration and validation of the Big Creek watershed HEC-HMS model using the SCS method for runoff simulation in this study. A storm event in September 2001 was selected for calibration purposes, and calibration results are shown in Figure 2 where the simulated runoff is compared to the observed streamflow at gaging station 502 on Big Creek. The simulation matches the observed data very well with less than 1 percent error on the peakflow and less than 5 percent error on the total runoff.

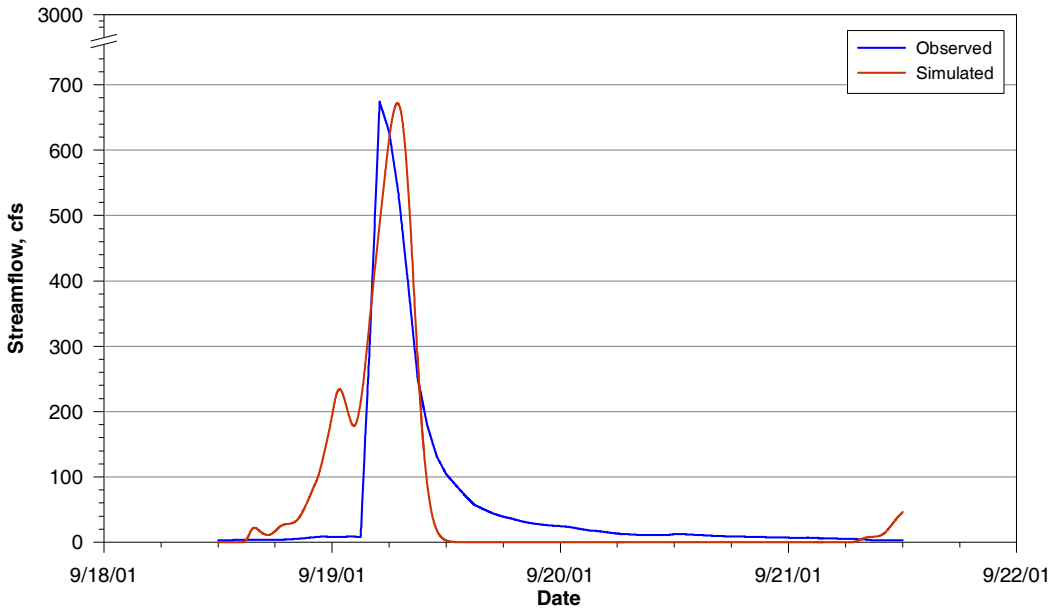

Figure 2. Comparison of simulated and observed flows at gaging station 502 of Big Creek for storm event in September 2001 for calibration of HEC-HMS model.

Calibrated model parameter values including the Curve Numbers then were validated by comparing simulated runoff and observed streamflow for a rainstorm event in January 2003 (Figure 3). As shown in Figure 3, the model reproduces the observed flows with less than 5 percent error on the peakflow and less than 10 percent error on the total runoff. The calibrated and validated HEC-HMS model then was used to generate runoff hydrographs for storm events of different frequencies and durations generated based on the third quartile of the Huff rainfall distribution (Huff and Angel, 1989). Runoff hydrographs for the tributary watersheds for storms with 1- to 100-year return periods were generated using the HEC-HMS model. These results then are used as input to the UNET model.

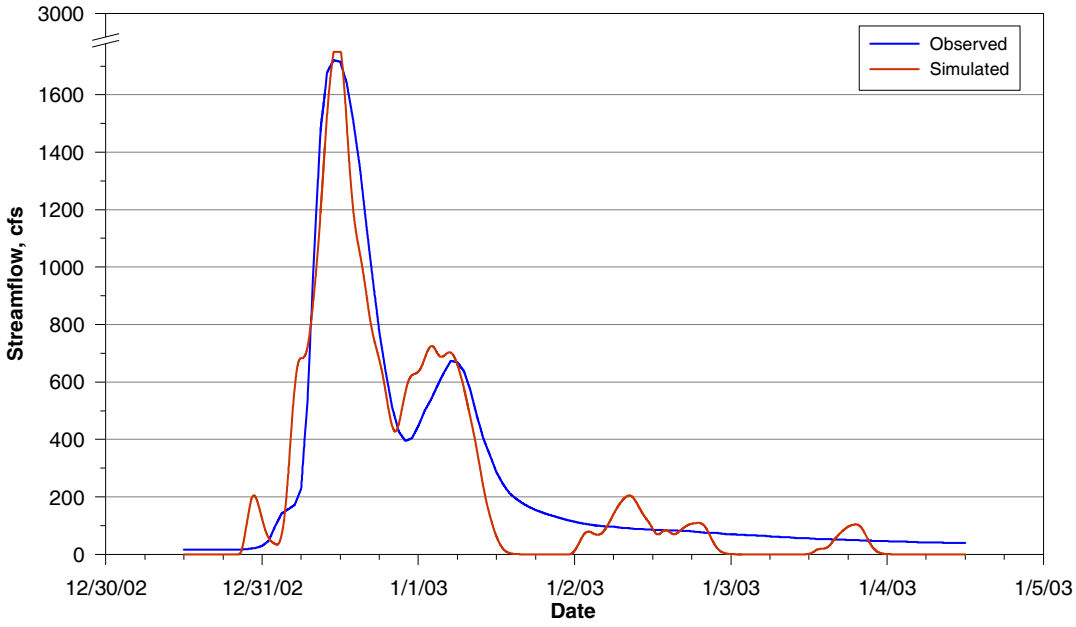

Figure 3. Comparison of simulated and observed flows at gaging station 502 of Big Creek for storm event in January 2003 for validation of HEC-HMS model.

HYDRAULIC MODEL DEVELOPMENT AND APPLICATION

In situations where the flow hydraulics are complex, resulting in reverse flows, and where the channel slopes are very low, analyses of hydraulics of flow use an unsteady flow, dynamic wave routing model. The UNET model (USACE, 1997), developed and maintained by the USACE, was chosen as the tool to analyze flow dynamics in the Lower Cache River. The USACE, St. Louis District developed several sets of data for use in UNET modeling of the Lower Cache River, including cross-sectional data of the channel and floodplain geometry (USACE, personal communication, 2000). For this study, the UNET data files from the St. Louis District were updated with new input hydrographs generated from the new HEC-HMS model. Even though no additional surveying was conducted outside the dredged segment of the river, some channel and floodplain cross sections have been extended based on DEM data to contain the 100-year flood elevations. New channel cross sections were used for the segment of the river dredged in 2005 based on survey data provided by Shawnee Survey and Consulting, Inc., which was contracted by the IDNR.

A schematic of the whole Lower Cache River as represented in the UNET model is shown in Figure 4 and includes the important features in the UNET model. Flood stages in the five reaches identified in Figure 4 are affected by different control structures and flow inputs.

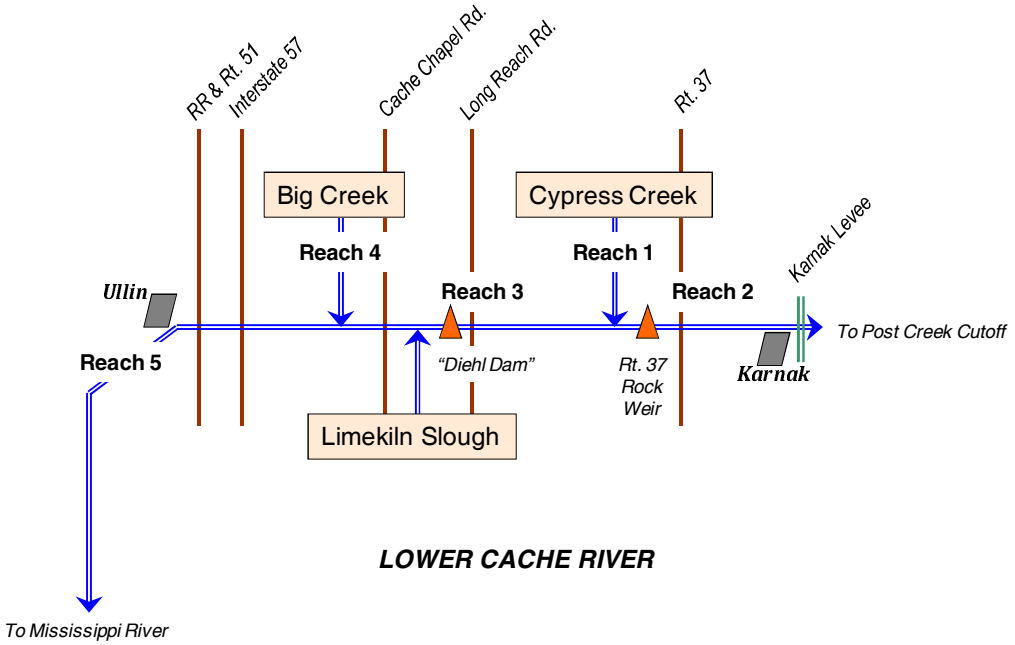

Figure 4. Schematic of UNET model for Lower Cache River.

Boundary Conditions for UNET Model

Boundary conditions for the Lower Cache River UNET model have to be defined for the confluence of Lower Cache River with the Mississippi River and the junction of the Lower Cache River with the Upper Cache River at Karnak Levee. Table 1 gives water surface elevations for 2-, 10-, and 100-year floods for the Mississippi River from the USACE Upper Mississippi River flood frequency study (USACE, 2004). In order to obtain the water surface elevations for different frequency floods at the junction of the Upper and Lower Cache River, flood frequency analysis was conducted for the Upper Cache River. The water surface elevations for the 2-, 10-, and 100-year floods at the junctions of the Lower Cache River with the Upper Cache River at Karnak Levee outlet/breach based on the frequency analysis are given in Table 1.

Table 1. Boundary Conditions for UNET Model.

Return period	*Mississippi River elevation at confluence with Lower Cache River*	*Upper Cache River elevation at Karnak Levee outlet/breach (ft-msl)*
2-year	318.20	319.00
10-year	325.20	334.05
100-year	331.40	341.51

SUMMARY OF RESULTS AND CONCLUSIONS

Hydrology and hydraulics of the Lower Cache River were investigated intensively by updating hydrologic and hydraulic models previously developed by the ISWS and the USACE, St. Louis District.

The two models then were used to evaluate selected scenarios in four categories: 1) reference/base condition (prior to levee breach); 2) current condition (with levee breach); 3) future alternatives; and 4) future alternatives with reconnection. The reference/base condition refers to the condition when the hydrology of the Lower Cache River was controlled on the east end by Karnak Levee with two 48-inch (1.22 m) gated culverts that prevented flow from Post Creek Cutoff into the Lower Cache River and by in-channel structures at Route 37 and "Diehl Dam" west of Long Reach Road. Because this condition was in existence for many years and had been agreed to by the drainage district and State of Illinois as acceptable drainage and water level management in the Lower Cache River, it was used as a reference for all other conditions and alternatives.

The current condition refers to conditions as they are now where a major change from the reference/base condition is the breach at Karnak Levee and the absence of the two 48-inch (1.22 m) culverts. The current condition will allow floodwaters from Post Creek Cutoff to flow back into the Lower Cache River. Both "Diehl Dam" and Route 37 Rock Weir are assumed to be in place.

Future alternatives refer to management alternatives under consideration by the JVP. The two main features include moving "Diehl Dam" 2,800 feet (853 m) west of its current location and installing an East Outlet Structure with stop logs in front of three 72-inch (1.83 m) gated culverts through Karnak Levee. This outlet structure will maintain low water elevations at desirable levels, allow increased outflow to Post Creek Cutoff during flood events, and prevent flow from Post Creek Cutoff into the Lower Cache River. Partial reconnection alternatives refer to future alternatives that re-establish the connection between the Upper and Lower Cache Rivers by diverting some flow from the Upper Cache River into the Lower Cache River. Under each of these four major categories, several different scenarios with different combinations of flood events and boundary conditions were evaluated.

For the reference/base condition, 100-year flood profiles were computed and mapped for eight different combinations of flood events and boundary conditions. For current conditions, seven different combinations of flood events and boundary conditions were evaluated and compared to the reference/base condition. Reconnection alternatives evaluated diverting water from the Upper Cache River under the reference, current, and future alternatives. Diversion of 200, 400, and 800 cubic feet per second or cfs (5.7, 11.3, 22.7 cu m/sec) was considered, and a combination of elevations for the East Outlet Structure and West Rock Weir were evaluated. All these alternatives are discussed in detail in the report by Demissie et al. (2008).

Based on analysis of all of these scenarios with different combinations of flooding, structural changes, and boundary conditions, the findings can be summarized as follows:

1) The current condition exposes the Lower Cache River corridor, especially the eastern portion, including the community of Karnak, to more flooding during major floods, such as 100-year or greater floods from the Upper Cache and Ohio Rivers. However, the current condition improves flood drainage for some parts of the area during more frequent 1-, 2-, and 5-year floods.

2) Installing the East Outlet Structure with stop logs and three or more 72-inch (1.83 m) culverts will lower flood elevations from the reference condition for the portion of the river east of Karnak Road Bridge, including the community of Karnak, because of increased outlet capacity of the larger culverts.

3) Moving "Diehl Dam" 2,800 feet (853 m) from its current location under current conditions will increase the area flooded by the 100-year flood by only 8 acres (3.2 ha). The additional acres flooded are distributed in small increments throughout the Lower Cache River floodplain. Water levels in the stream channel between current and proposed locations will be higher than the current condition during low- and moderate-flow conditions.

4) Partially reconnecting the Lower Cache River with the Upper Cache River by diverting some flow from the Upper Cache to the Lower Cache River will not increase flood elevations during major floods such as a 100-year flood but will raise flood elevations during more frequent 1- and 2-year floods. During low- and moderate-flow conditions, reconnection will not cause flooding, but will create slow-moving westerly flow in the Lower Cache River that does not exist under the current condition. More detailed cross-sectional surveys will be necessary to model low- and moderate-flow conditions more accurately, and the reconnection option should use an adaptive management approach that allows adjustments based on observations.

REFERENCES

Allgire, R. 1991. *Comparison of 1987 and 1989 Bed Profile Surveys of the Lower Cache River*. Illinois State Water Survey Contract Report 508.

Demissie, M., L. Keefer, Y. Lian, F. Yue, B. Larson. 2008. *Hydrologic and Hydraulic Modeling and Analyses for the Cache River for the Purposes of Evaluating Current Conditions and Alternative Restoration Measures*. Illinois State Water Survey Contract Report 2008-01, Champaign, IL.

Demissie, M., H.V. Knapp, P. Parmar, and D.J. Kriesant. 2001. *Hydrology of the Big Creek Watershed and Its Influence on the Lower Cache River*. Illinois State Water Survey Contract Report 2001-06.

Demissie, M., T.W. Soong, R. Allgire, L. Keefer, and P. Makowski. 1990(a). *Cache River Basin: Hydrology, Hydraulics, and Sediment Transport. Volume 1: Background, Data Collection, and Analysis*. Illinois State Water Survey Contract Report 484.

Demissie, M., T.W. Soong, and R. Camacho. 1990(b). *Cache River Basin: Hydrology, Hydraulics, and Sediment Transport. Volume 2: Mathematical Modeling*. Illinois State Water Survey Contract Report 485.

Huff, F.A., and J.R. Angel. 1989. *Frequency Distributions and Hydroclimatic Characteristics of Heavy Rainstorms in Illinois*. Illinois State Water Survey Bulletin 70.

Illinois Department of Natural Resources (IDNR). 1997. *Cache River Area Assessment. Volume 1, Part 1: Hydrology, Air Quality, and Climate*. IDNR, Office of Scientific Research and Analysis, Springfield, IL.

U.S. Army Corps of Engineers. 2004. *Upper Mississippi River System Flow Frequency Study.* Final Report, USACE Rock Island District, Rock Island, IL.

U.S. Army Corps of Engineers. 1997. *UNET, One-Dimensional Unsteady Flow Through a Full Network of Open Channels, User's Manual*. USACE, Hydrologic Engineering Center, CPD-66, Version 3.2, Davis, CA.

The Mississippi River: A National Resource

Nani G. Bhowmik, Ph. D. P.E., F. ASCE, D. WRE
Principal Scientist Emeritus, Illinois State Water Survey
Institute of Natural Resource Sustainability
University of Illinois, Urbana-Champaign, IL.

Abstract: The Mississippi River with its tributaries is the third largest river of the world. The river drains about 40% of the continental Unites States. The main stem of the river is about 3,500 km long travelling from Minnesota in the north to the Gulf of Mexico in the south. During this travel the river crosses also through 10 states. The present day river was formed during the last glacial melt, consequently the present day size and shape is too large for the flow and the sediment load. Thus the river valley has been filling up with sediments. For identification and management purposes the river has been divided into two segments, Upper Mississippi River and the Lower Mississippi river. The Upper Mississippi River extends from its headwater to its confluence with the Ohio River near Cairo, Illinois. Upper Mississippi River does not include Missouri River for management purposes even though the Missouri river do come and join the main stem of the river upstream of St. Louis. The river is also the main inland transportation artery of the United States. Over the year the river and its watershed has altered significantly. Currently, the Mississippi River States, the Federal Government and many no-governmental entities are working together to enhance the ecosystem of this great river.

The Basin

The drainage basin of the Mississippi River is shown in Figure 1. The total drainage area of the basin is about 3 million sq km. The Mississippi river was not always the major river in North America, Dobney (Undated). The river assumed its present form after the ice age. Before the ice age, the river probably followed a different path than one it occupies today. During the movement of ice sheet, the Missouri and Ohio rivers became ice marginal streams flowing along the leading edge of the glaciers. Subsequently these two ice marginal rivers came to a halt at the leading edge of the ice and thus were permanently absorbed by the Mississippi River. In Geologic times, the river has been filling the lower part of the country. As a matter of fact, the Mississippi River valley below its confluence with the Ohio River is called the Mississippi River delta. The deltaic region covers about 90,000 sq km areas extending over 219 counties of the Middle America.

For management purposes, the River is divided into two parts, The Upper Mississippi River from the headwaters to its confluence with the Ohio river and the Lower Mississippi river from Ohio river confluence to the Gulf of Mexico. Below its confluence with the Ohio river, it is sometimes called ‘poised’ stream, that is it has not shown much aggradation or degradation.. The river is flowing on the lowest valley slope, which it has attained over the last 2,000 years or more.

The Mississippi river is the third largest river of the world behind Congo and Amazon and its basin covers as area fourteen times that of Rhine. The river has more than 50 navigable tributaries with about 24,000 km of navigable streams and thousands of un-navigable stream km. The river either traverses or borders 31 states, making it truly a national resource. Figure 2 shows a photograph of the headwater of the Mississippi River at lake Itasca in Minnesota.

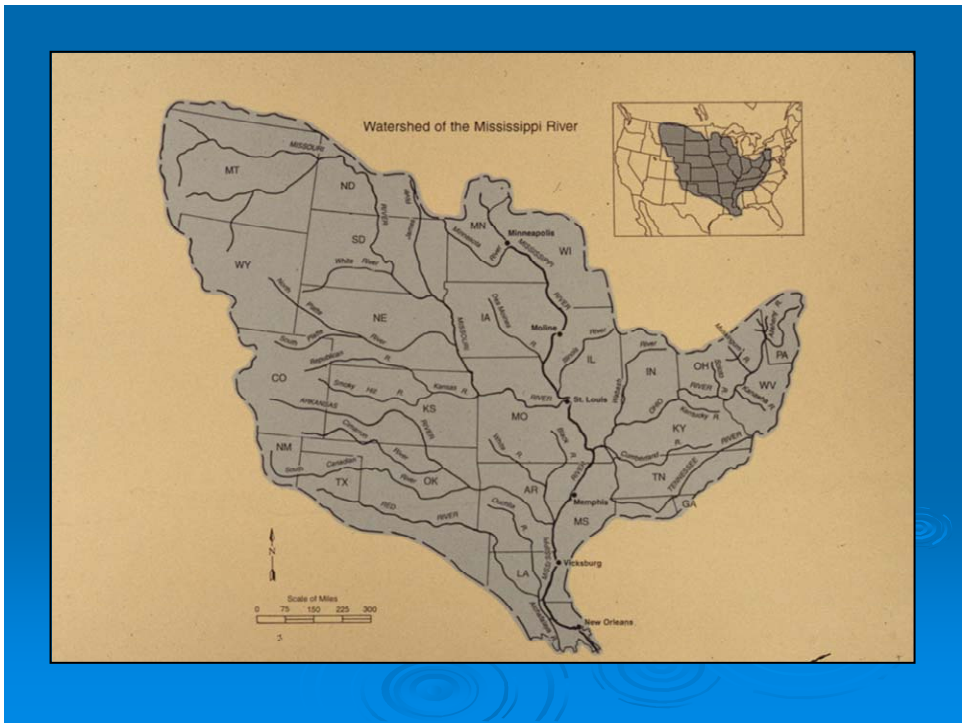

Figure1. Drainage Basin of the Mississippi River

Climate

These materials after Wendland (See Bhowmik et al, 1995). The Mississippi River flows from Minnesota to Louisiana, from a northern region with wet summers to a southern region that is wet all year without snow. In the northern region, winter daytime temperature occasionally rises above the freezing point, whereas in the south, winter nighttime temperatures only occasionally drop below freezing point. The frost free season in Minnesota is limited to about 150 days, varying form 120 to about 180 days, whereas at the mouth of the river at the Gulf of Mexico the frost free season is 290 days, varying from 230 to 345 days.

As might be expected, precipitation is substantially greater in the southern reaches than in the north. Average precipitation near the mouth is about 1,600 mm, whereas in the middle reaches it is about 1,000 mm and in the north is about 760 mm.

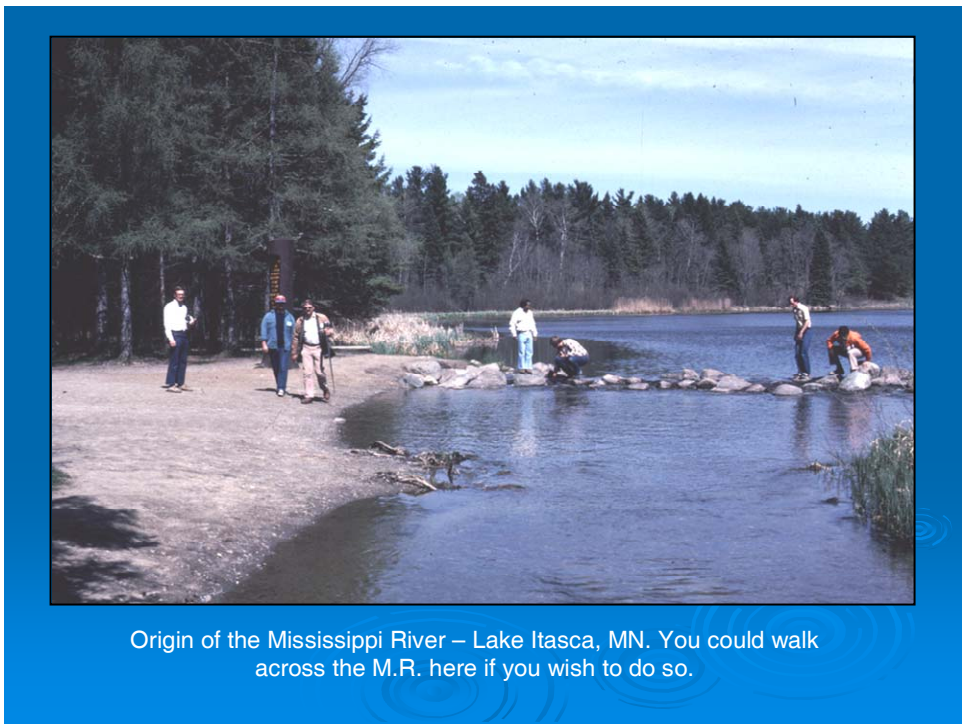

Figure 2. Origin of the Mississippi River in Lake Itasca, Minnesota

Agricultural Land

The Mississippi River with its major tributaries also contains most of the prime farmland in the country. Many wetlands on and along the basin has been drained to make them suitable for farming. Figure 3 shows the percent of farmland at locations throughout the United States. A close examination of this figure will show that this river valley and most of its tributaries essentially contain most of the prime farmland of the United states.

Similarly, as mentioned earlier most of the wetland along this river basin was drained for farming. This is quite predictable since the highly productive Mississippi River valley contains most of the 'hydric' soils, a major characteristic of wetlands that had to be drained for agricultural purposes. For example, in Iowa about 11% of the land that used to be wetland in 1780, has now about 1% wetland in 1980, Knapp (see Bhowmik et al, 1995).

Population

Within the main corridor of the Mississippi River, roughly 12 plus million people live and work producing more than $7 billion worth of agricultural and forest products and approximately $29 or more billion worth of manufactured goods. About 5% of the US population lives within this river corridor not including the drainage basin.

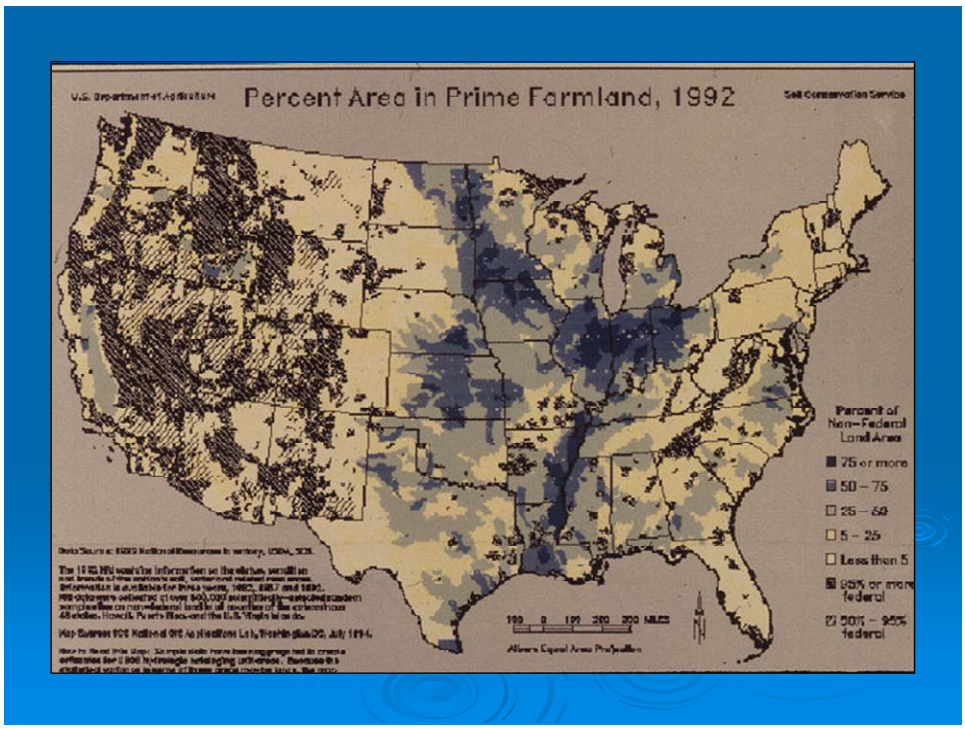

Figure 3. Percent of Prime Farmland in the USA

Navigation

The entire main length of the Mississippi River and its major tributaries such as, the Illinois, Missouri, Ohio, White, Yazoo, Ouchita, and Red Rivers is used extensively for commercial navigation. Significant amount of recreation navigation also takes place on all of these major rivers and many of its tributaries. The navigation system on the Upper Mississippi, Illinois, Ohio and few other tributaries is accomplished with a system of Locks and Dams. The Lock and dam system on the Upper Mississippi River is depicted in Figure 4.

Most of the Lock and dams on the Upper Mississippi River, Illinois River were constructed in late 1930s. The goals of these Locks were to maintain a low water depth of 2.75 m. The majority of the Locks and Dams are kept wide open during the flood periods thus the river behaves as an open waterway during those periods of time. Commercial traffic on the main stem of the Upper Mississippi River and Illinois River normally consist of a flotilla of Barges three wide and five long pushed by a tow boat. When fully loaded this flotilla could occupy an area 32 m wide, 335 m long with a draft of 2.75 m.

These Barge flotilla could move about 18 m/sec in the downstream direction and about 10 m/sec in the upstream direction. Movement of such a huge body within the Upper Mississippi and especially the narrower and shallower Illinois River is associated with significant amount of hydraulic and sediment related effects.

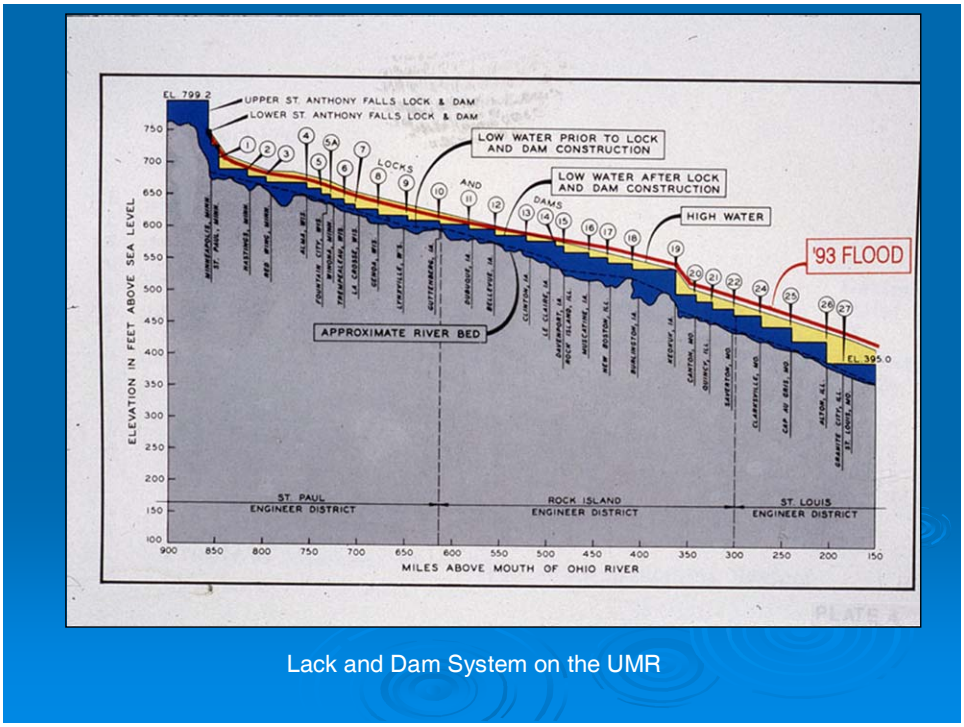

Figure 4. Lock and dam System on the Upper Mississippi River with the 1993 Flood Levels

The movement of barges generally will create waves, re-suspend sediments, create drawdown, make lateral change in the velocity distributions and sometimes generate lateral flows near the shorelines. Depending upon the size, speed, draft and direction of the barges, sometimes the return flows could be in the upstream direction when a heavily loaded barge flotilla moves at a high speed in the downstream direction. The Author with several associates have done tremendous amount of research in this topic and some of those results are being utilized now for the formulation of ecosystem restoration and navigation sustainability on the Upper Mississippi River and Illinois River.

Within the main stem of the Mississippi River below St. Louis, The Missouri River, and at few other river segments, the navigation is accomplished through the construction of river closing structures, wing dams and river training structures. All of these areas are designated as open river system.

In late 1990s, the river provided significant amount of U.S. grain export to other countries. With its multitude of tributaries, the river also provides facilities for thousands of miles of recreational boating, canoeing, fishing, camping and other outdoor activities. It is estimated that visitors spend more than $10 billion on the main corridor for various recreational activities.

Flows and Floods

A companion paper will go into details of flows and floods especially on the Upper Mississippi, Illinois and Missouri Rivers. Some mention is made here on the Great flood of 1993 on the Mississippi, Illinois and Missouri Rivers. The midsection of the Mississippi River especially that portion bordering the State of Illinois also was subjected to flooding during the spring of 2008. The 1993 flood was by far the largest measured flood on the Upper Mississippi River. During this flood extending more than 5 months near St Louis did impart a loss of $12 billion. However, flood control measures implemented over the years also save damages to the tune of $19 billion.

River Morphology

The Great floods such as the one that occurred in 1993 is also associated with some morphological changes within the main stem of the river. The Mississippi River attempted to shorten its length near the confluence with the Ohio River. This area is called the Dog Tooth Bend area. During the height of the flood a levee called, Len Small Levee was breached and in the ensuing days water started to flow through the breach. Finally the breach was as much as 1,600 m wide and some areas as much as 33 m deep. At the height of the flood about 20% of the Mississippi River flow was passing through this breach. This amounted to about 5,600 cms.



Figure 5. Areal View of the Levee Breach Near the Miller City at the Height of the 1993 Flood on the Mississippi River

Figure 5 shows an areal view of the levee breach at the height of the flood near the Dog Tooth Bend on the Mississippi River. This breach is located near the Miller City in Illinois close to the Ohio River. Fortunately the river was not successful to recreate a new channel at this location since the flow started to decrease. If the River was successful to recreate this new channel, it would have shortened the river from about 32 km to 10 km increasing the gradient accordingly. With this increased gradient, the velocity would have increased substantially making normal navigation much more difficult.

Erosion

As mentioned previously, the Mississippi River valley contains some of the important prime farmland in the USA. A plot of the sheet and rill erosion of the USA, will show that the so called "bread basket" of USA, i.e., the Central USA, is also subjected to highest erosion rates. In many instances the soil erosion rates exceeds the so called 'soil tolerance values'. However, since 1930's Best management Practices have been implemented on agricultural lands with a goal to reduce the erosion rates to soil tolerance values.

It is also a known fact that severe erosion will take place during extreme flooding events. The Great Flood of 1993 was no exception to this concept. For example, in Iowa, about 20% of the State lost more than 5.7 tons /hectares of top soil compared to a soil tolerance value of 1.9 tons/hectares. Most of the erosion occurred on the agricultural land as sheet and rill erosion and within rivers as bank erosion or cutting off of old meander loops or creation of new meanders.

Summary

The Mississippi River with all of its tributaries is the third largest river in the world. The river also drains about 40% of the continental USA with a small portion of Canada. The River is about 3,500 km long and traverses or borders 31 States. The present day Mississippi River resulted from the ice melt after the last glacier melted.. The river is divided into two Segments, Upper Mississippi River and Lower Mississippi River. This river basin also contains most of the prime farmland of the USA. The river is also a major navigation artery of the USA. Most of the grains that are transported for export do also pass through this river. The navigation traffic which is important for the economic well being of the country do also have some hydraulic and ecological impacts on the river.

The River, covering about 40% of the continental USA play an important role in the national scene. The river is also used extensively for recreational purposes. The river is also subjected to extreme natural variations from floods to droughts. The great Flood of 1993 on the Upper Mississippi, Missouri and Illinois River covered substantial portion of the mid-west. This flood was also associated with some morphological changes and surface and river erosion. Sediment deposition was also a major impact of the great flood.

With its numerous tributaries, the Mississippi River is a significant lifeline of the USA. The river also played an important role in the migration of population, music, art, transport of goods, cross cultural exchanges and an integrating force of the country. The river played and will play a significant role in the well being of the USA. The river is a true National Resource of the Country.

References Cited

Dobney, F. J. (Undated). River Engineers on the Middle Mississippi. Superintendent of Documents, U. S. Government Printing Office, Washington, DC.

Bhowmik, N. G., A. G. Buck, S. A. Changnon, S. A. Dalton, R. H. Durgunoglu, S. M. Demissie, A. R. Juhl, h. V. Knapp, K. E. Kunkel, S. A. McConkey, R. W. Scott, K. P. Singh, Ta-Wei D. Soong, R. E. Sparks, A. P. Visocky, D. R. Vonnahme, and W. M. Wendland. (1995). The Great Flood on the Mississippi River in Illinois. Illinois State Water Survey Miscellaneous Publication 151, 165 p, 2nd Printing.

The Nature Conservancy's Mississippi River Program: Sustainable Conservation of a Working River that Works

C. Stephen Haase[1] and K. Douglas Blodgett[2]

[1]Sr. Biohydrologist, Lower Mississippi River Program, The Nature Conservancy (shaase@tnc.org; 865-809-4719)
[2]Illinois River Program Director, Upper Mississippi River Program, The Nature Conservancy (dblodgett@tnc.org; 309-357-2732)

ABSTRACT

The Mississippi River is one of the world's truly great working rivers (Upper Mississippi River Conservation Committee, 2000), not only in terms of the essential services it provides to the nation (transportation, water resources, and hydroelectric power) but also in terms of its biological diversity and richness, and the ecosystem services (recreation, fisheries, carbon sequestration, water quality improvement, and sediment management) it provides to citizens throughout its watershed. Despite more than two centuries of intensive management and control, the Mississippi and its floodplains and tributaries still support diverse, globally-significant populations of aquatic and terrestrial species, many of which are threatened or endangered, and some of which are unique to the Mississippi River basin.

The Nature Conservancy is working with diverse partners from industry, government, and the natural resource community to develop an integrated "source to sea" conservation program based on ecologically sustainable management principles. This paper will discuss key aspects of Conservancy work with floodplain restoration and reconnection, hydrologic restoration, sediment and nutrient reduction, stream channel restoration, sustainable agriculture, and the USACE's Navigation and Ecosystem Sustainability Program at diverse sites including Boone River IA; Pecatonica River WI; Mackinaw River, Emiquon, and Spunky Bottoms IL; Big Woods and Cache River AR; and Mollicy Farms and Atchafalaya Basin LA

INTRODUCTION

At 2,320 miles, the Mississippi River ranks among the largest of the world's rivers, draining all or parts of 31 states and two Canadian provinces. It is a vital migration corridor for 60 percent of North America's bird species and provides critical habitat for a high diversity of fish and mussels as well as rare creatures like the Louisiana black bear and the elusive ivory-billed woodpecker. The river's delta—an area of land and water that links the river to the Gulf of Mexico—is one of the most ecologically rich places on Earth. The Mississippi has nurtured human life for more than 12,000 years. Native Americans and European settlers alike were drawn to

its shores by fish, game, fertile soils and dense forests. Today the river continues to play a vital role in the well-being of human communities who depend on it for water, food, jobs, transportation and recreation. It provides drinking water to 18 million people, links agricultural producers to markets around the world and provides hunters, anglers, boaters and other outdoor enthusiasts with exceptional recreational opportunities.

THREATS

Over time, the Mississippi has been altered in ways that are endangering its health and vitality. Once a vibrant body of water in harmony with its surroundings, the river has been extensively modified during the last century by locks, dams and levees. In most places, the river no longer inundates its floodplains during high water periods, contributing to a decline in the abundance and diversity of plant and animal life. With fewer flooded wetlands to filter the river's flows, increased run-off of excess nutrients and sediment has reduced water quality. Conversely, because of altered water flows into the Gulf of Mexico, coastal estuaries are being starved of needed sediment and a dead zone in the Gulf, where little plant and animal life survives, is increasing. The Mississippi River's delta loses 25 square miles every year, making it the fastest disappearing habitat in the world. Marshes, wetlands and islands protect coastal communities like New Orleans from flooding and storm events. If not conserved, scientists estimate that 20 percent of Louisiana's remaining wetlands will disappear completely in the next few decades. Coastal cities will be more at risk of catastrophic natural events, plants and animals will be lost and people's livelihoods will be impacted. The economic repercussions of lost fisheries alone are estimated at $500 million per year.

STRATEGIES

Working at local, state, regional and national levels with public agencies, private landowners, corporations and non-government agencies, the Lower Mississippi River Program is implementing diverse conservation strategies throughout the Mississippi Basin that include:

- *Water Quality Improvement* by promoting best management practices that reduce water-polluting runoff and sedimentation, through the use of expanded incentives and targeted education;
- *Ecologically Sustainable and Compatible Forestry* through reforestation of private lands and developing carbon sequestration projects throughout the region;
- *Restoration of Altered Hydrology* by working with the U.S. Army Corps of Engineers and other natural resource managers to stabilize river channels and reestablish the natural flow and function of key Mississippi River tributaries;
- *Reconnection and Restoration of Floodplains* through bottomland hardwood forest and wetland Restoration to reconnect blocks and corridors of forested land large enough to sustain native species and the natural ecological processes that keep them alive, by supporting federal incentive programs. for

forest and wetland protection, acquiring and restoring land and providing technical assistance to public and private land managers; and

- *Application of Natural Channel Design and Ecologically Compatible River Restoration and Stabilization* to soften the ecological impact of channel engineering and stabilization projects and to increase the diversity of in-channel and riparian habitats created during river stabilization and restoration activities.

CONSERVATION THAT WORKS FOR ALL

The Nature Conservancy has 50 years of conservation experience in the Mississippi River basin. Today, teams in 10 states are working in more than 30 priority project areas to address some of the river's most critical threats including habitat loss and incompatible land use. Application of conservation strategies such as reconnecting the river with its floodplain at places along the Mississippi and Illinois rivers, reforesting bottomland hardwood forests along rivers in Arkansas and Louisiana, and collaborating with partners on restoration of the Mississippi River delta and working with farmers to identify sustainable approaches to land use are paying economic and ecological dividends. Acquisition of land and conservation easements, working with private landowners on voluntary land management practices, partnering with state and federal governments and programs, and building support for the river—at both the highest levels of government and the community level—remain key components of the Conservancy's lasting conservation work. The Conservancy is also exploring market-driven approaches to habitat protection and restoration. Forests, wetlands and other habitats provide valuable services to humanity, including storing flood waters, keeping pollutants and sediment out of rivers and removing carbon dioxide from the atmosphere. Conservancy staff are analyzing the potential financial returns to landowners of adopting land uses aimed at the production of ecosystem services such as sustainable timber, recreation and nutrient retention rather than marginal agricultural activity. Issues impacting the Mississippi River—including habitat loss due to expanding crop production and urban development, impacts of hydropower, potential for carbon storage, restoration of water quality and conservation of biodiversity— link it to other great rivers around the world. Through the Great Rivers Partnership, an effort to advance conservation of large rivers, the Conservancy is collaborating with universities, government agencies, private businesses, landowners and other non-profit entities to share its science expertise and knowledge about the Mississippi River to accelerate progress on a local, regional and global scale.

TOWARD A SUSTAINABLE FUTURE

For centuries, the Mississippi River has pulsed through America's heartland, supporting an abundance of plants and animals and enriching human lives and livelihoods. Competing interests for use of the river and its lands have altered the river's seasonal flows, diminished water quality and caused species and habitat declines. But, with human interest, resources and ingenuity invested in conserving the

river, the wildlands that remain can still be conserved and hundreds of thousands of acres can be restored. The Conservancy's Mississippi River project is bringing people together to restore the health and vitality of this mighty waterway, a river that is so much a part of who we are as a nation and who we can become.

ACKNOWLEDGMENTS

Much of this paper is drawn from summary and planning documents prepared in conjunction with the Conservancy's Upper and Lower Mississippi River programs (The Nature Conservancy, 2006; 2007)

REFERENCES

The Nature Conservancy (2006). The Lower Mississippi River Program – Working to Save a Critically Endangered Landscape.

The Nature Conservancy (2007). The Mississippi River – Conserving and Restoring an American Icon.

Upper Mississippi River Conservation Committee (2000). A River that Works and a Working River. 36p.

Historical Reconstruction of Hydroclimatic Data Based on the Control Runs of GCMs over Sabah and Sarawak, Malaysia

Noriaki Ohara[1], M. Levent Kavvas[1], ZhiQiang Chen[1], Ahmad Jamalluddin bin Shaaban[2]
[1]Dept. Civil and Env. Engineering, University of California, Davis, CA
[2]National Hydraulic Res. Inst. of Malaysia

Abstract
The historical reconstruction of hydroclimate conditions over Sabah and Sarawak states of Malaysia was performed as a first step for the assessment study of climate change impact on water resources. The outputs of ECHAM5 GCM simulation from Max Planck Institute for Meteorology of Germany were downscaled to fine grid resolution data by means of a Regional Hydroclimate Model (RegHCM). The RegHCM, which is a coupled non-hydrostatic atmospheric and upscaled land surface process model, has been customized for Sabah and Sarawak region. A sequence of three model domains, respectively at 81km, 27km, and 9km grid resolutions, was used. The GCM output datasets in the 200-300 km spatial resolution during the historical period of 1970-2000 were downscaled into the 9 km grid resolution that is required for water resources analysis at the watershed scale. The detailed soil and land cover maps provided by Malaysian government have been processed for preparation of required model parameters: such as, roughness height, emissivity, albedo, leaf area index (LAI), soil hydraulic conductivity, and soil rooting depth. Sea surface temperature data in the GCMs was used in the downscaling exercise in order that the historical simulations are consistent with corresponding future simulations.

INTRODUCTION

A Regional Hydroclimate Model for Sabah and Sarawak (RegHCM-SS) has been developed and is being applied to the region of Sabah and Sarawak in order to downscale the available global historical atmospheric databases and global climate change databases (ECHAM5 GCM simulations data from the Max Planck Institute for Meteorology of Germany at a grid resolution of 1.85 degree by 1.85 degree) that are at very coarse resolution, to Sabah and Sarawak at fine spatial resolution of 9km by 9km.

The main objective of this study is to carry out a detailed study on the expected changes in the hydrologic regime and water resources at Sabah and Sarawak region of Malaysia that result from the global change of climate and also due to local landuse change. Development of a regional hydrologic/atmospheric hydroclimate model of Sabah and Sarawak (RegHCM-SS), and the preliminary hydrometeorological results from the downscaling of the historical control runs' results from the ECHAM5 Global Climate Model to the Sabah and Sarawak region by the RegHCM-SS are described in this paper.

The RegHCM-SS consists of two major model components: 1) a mesoscale atmospheric model component, and 2) a regional land surface hydrology model component (Chen et. al. 1996; Kavvas et. al. 1998). The atmospheric model component

of the RegHCM-SS is MM5 (the Fifth Generation Mesoscale Model) from NCAR (US National Center for Atmospheric Research). MM5 is a nonhydrostatic model which can be downscaled even to 0.5km spatial resolution, which makes it very desirable for downscaling climate study results to the scale of watersheds. As such, it is then possible to capture the effect of steep topography of Sabah and Sarawak at watershed scale (spatial resolutions <10km) on the local climatic conditions. In the RegHCM-SS, the land hydrology model is based on upscaled hydrologic conservation equations (Chen et. al. 1993; Chen et. al., 1994a,b). The land hydrologic processes in RegHCM-SS are linked to the atmospheric processes through a landsurface-atmospheric boundary layer module.

Regional Hydroclimate Model (RegHCM) of Sabah and Sarawak is run first with its initial and boundary conditions provided from the ECHAM5 GCM historical control runs' atmospheric data at an outer domain, covering the whole Sabah and Sarawak region and the surrounding areas, to be called "outer domain". Then, RegHCM is run over the inner domain with its initial conditions coming from ECHAM5 GCM control runs' atmospheric data, interpolated at 9 km, while its boundary conditions are provided from the simulation results of the outer domain RegHCM simulations during the historical period. The simulations of the inner domain RegHCM with these initial and boundary conditions provide comprehensive atmospheric data (precipitation, air temperature, radiation, wind, relative humidity, evapotranspiration) at 9 km spatial grid resolution at 1 hr time intervals.

The model parameters for the regional land surface hydrology model component of the RegHCM-SS are being updated by the newly-obtained datasets from the National Hydraulic Research Institute of Malaysia (NAHRIM). The new datasets include most recent vegetation cover and land use information of Sabah and Sarawak, soil survey data of Sabah and Sarawak, and grid based DEM at 3-arc-second spatial grid resolution (approximately 90 meters) derived from the SRTM datasets.

Reconstructed historical hydrometeorological conditions, simulated by the RegHCM-SS are discussed in this paper.

MODEL CONFIGURATION

MM5, as the atmospheric component of RegHCM-SS, is used to downscale global scale atmospheric data to the region of Sabah and Sarawak through several nesting procedures. The model configuration of RegHCM-SS is discussed in this section.

Mercator map projection is used in the updated RegHCM-SS. Horizontally, a nest of three model domains, respectively at 81km, 27km, and 9km grid resolutions, were used. Inner domain has 136 x 91 grids with a grid size of 9 km x 9 km. The inner domain of the updated RegHCM-SS encompasses the entire Sabah and Sarawak region and a portion of the northern section of the Borneo Island. In the vertical direction, the MM5 model for Sabah and Sarawak region has 23 sigma layers for both outer domain and inner domain. The top pressure level was chosen to be 20 mb.

The time interval for the output from the MM5 model can be chosen according to the needs of the RegHCM's hydrologic model component. In this project, we chose one-hour as the precipitation input time interval for the RegHCM-SS. Therefore, the MM5 model outputs were also in one-hour intervals.

MODEL INITIAL AND BOUNDARY CONDITIONS

RegHCM-SS requires atmospheric boundary conditions and initial conditions in order to simulate atmospheric processes and hydrologic processes in a geographical region. In this study, the ECHAM5 GCM historical control runs' atmospheric data sets provide the outer domain RegHCM-SS (MM5) with its initial and boundary conditions during its simulation of the historical atmospheric conditions over the Sabah and Sarawak region during the January 1993- December 1999 period.

A program has been developed to compile ECHAM5 GCM control runs' atmospheric data files and to retrieve the gridded data that cover the Sabah and Sarawak region. MM5 receives its boundary conditions from the ECHAM5 data set that has a grid resolution of 1.85 degrees. The atmospheric 3-D data set and the 2-D data set that the MM5 model requires for its boundary and initial conditions were retrieved from the ECHAM5 data sets. The ECHAM5 data sets provide 3-D temperatures, 3-D wind vectors, 3-D relative humidity, 3-D geopotential heights, 2-D surface pressures, etc. at every 6 hours. The MM5 model's boundary data on its outermost row of points were obtained by direct interpolation from the ECHAM5 data sets at 6-hour intervals. The initial conditions of MM5 were also obtained by direct interpolation from the ECHAM5 data sets.

MODEL PARAMETERS

Like many other physically based atmospheric-hydrologic models, RegHCM relies heavily on GIS data, such as soils, vegetation, land use/land cover, and topography in order to estimate its parameters. The following local data sets have been used in this study:

i) Malaysia Department of Agriculture (DOA) data on the region's vegetation and land use covers in a vector coverage format;
ii) Malaysia Department of Agriculture (DOA) data on the region's soils in a vector coverage format.

The roughness length and albedo parameter maps for RegHCM's inner domain at 9km resolution were constructed using both Malaysia DOA land cover dataset and USGS land cover dataset. The soil hydraulic parameter maps of saturation soil water content (porosity), residual water content, bubbling pressure head, pore size distribution index, mean saturated hydraulic conductivity, variance of saturated hydraulic conductivity, and soil depth were developed based on the Malaysia DOA soil dataset and the FAO soil dataset, USDA soil texture classification, and Brooks and Corey's hydraulic parameter relationships. The LAI values and monthly green fractions for RegHCM's inner domain grid mesh were generated from MODIS and NCAR datasets.

MODELING RESULTS AND VALIDATION

In this project phase on the historical simulations with RegHCM-SS, we have reconstructed the historical hydroclimate conditions during the period of January 1993 – December 1999 at hourly intervals at 9-km grid resolution over the whole Sabah and Sarawak region with the newly updated model configuration and model parameters. RegHCM-SS transformed the coarse time-space resolution ECHAM5 GCM historical control runs' atmospheric data during the period of January 1993 – December 1999 to 1-

hour-increment hydroclimate information at 9-km spatial resolution over Sabah and Sarawak region. Due to the limitation of space availability, the output variables of the hydroclimate conditions from the RegHCM of Sabah and Sarawak (RegHCM-SS) include precipitation and air temperature are presented here.

Figure 1 (left) shows the representative simulated distributions of monthly precipitation during January 1999. The black lines that are overlaid on each plot delineate the boundaries of the Sabah and Sarawak region. Figure 1 (right) shows the representative simulated monthly average air temperature. It can be seen that the downscaled model outputs reflect the topographic effect both in precipitation and air temperature distributions.

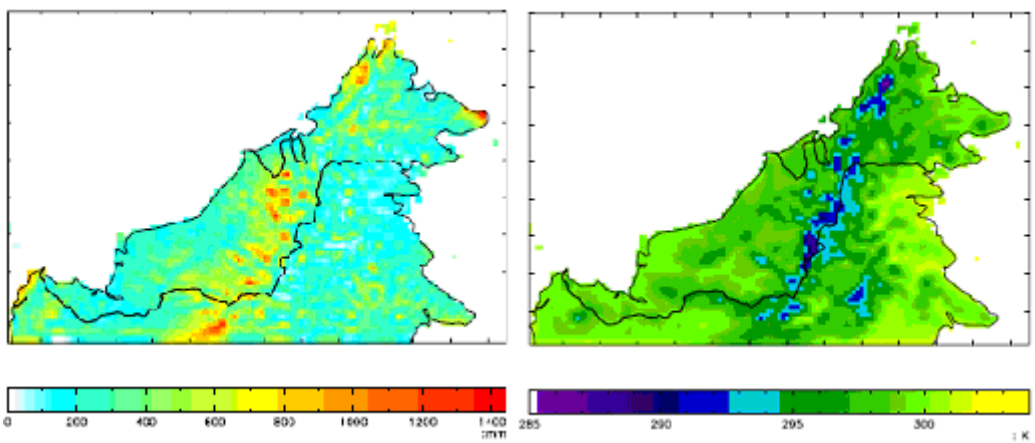

Figure 1 Representative computed total precipitation (left) and mean air tempeature (right) fields over Sabah and Sarawak region during January of 1999.

The computational results of RegHCM-SS during a historical period over the Sabah and Sarawak region were evaluated by comparing them against the observations in terms of rainfall. Although the GCM output of the historical control run was downscaled to the 9 km resolution, the simulated precipitation still is the average over a 9km X 9km grid area which is a much larger control volume than the corresponding observation at the point scale of a ground station. The precipitation field is known to be highly heterogeneous.

Therefore, the direct comparisons between the RegHCM-SS downscaled area-average precipitation over an 81 square kilometer grid area and the observed point location-scale rainfall may not be a good measure of the model performance. Additional two global precipitation databases, GPCP (Global Precipitation Climatology Project) (Huffman et al. 2001) and Willmott data (Terrestrial Precipitation:1900-2006 Gridded Monthly Time Series) (Willmott et al. 1985) were retrieved in order to obtain more appropriate comparisons.

The Global Precipitation Climatology Project (GPCP) quantifies the distribution of precipitation around the globe by merging the data from over 6,000 rain gauge stations, and satellite geostationary and low-orbit infrared, passive microwave, and sounding observations. The advantage of this dataset is the spatial coverage over the ocean because it relies not only on the ground observations but also on remotely sensed

precipitation data. However, the spatial resolution of 1 degree is still very large, and the time coverage of the data is very limited.

The other dataset that was retrieved is Terrestrial Precipitation:1900-2006 Gridded Monthly Time Series. This dataset is called "Willmott data" in this paper. The monthly total precipitation fields were developed by compiling several updated data sources and interpolating to a 0.5 degree by 0.5 degree of latitude/longitude grid. These data are available from 1900 to the present. Figure 2 shows the data points of Willmott data over the Sabah and Sarawak region. In this figure there is no data over the ocean since the dataset is based on the ground observation records.

The three datasets: ground observations, GPCP 1DD, and Willmott data, are compared, and it is found that the data, based upon observations at different spatial scales, result in quite different values. The authors believe that the data that represent averages over a finite-size grid area, such as the Willmott data, are more appropriate for comparisons to the model simulation results that themselves are area-averages, than the point-location-scale data of the ground stations. Consequently, in this study the Willmott data set was used for the evaluation of the performance of RegHCM-SS in reconstructing the historical rain fields over the Sabah and Sarawak region.

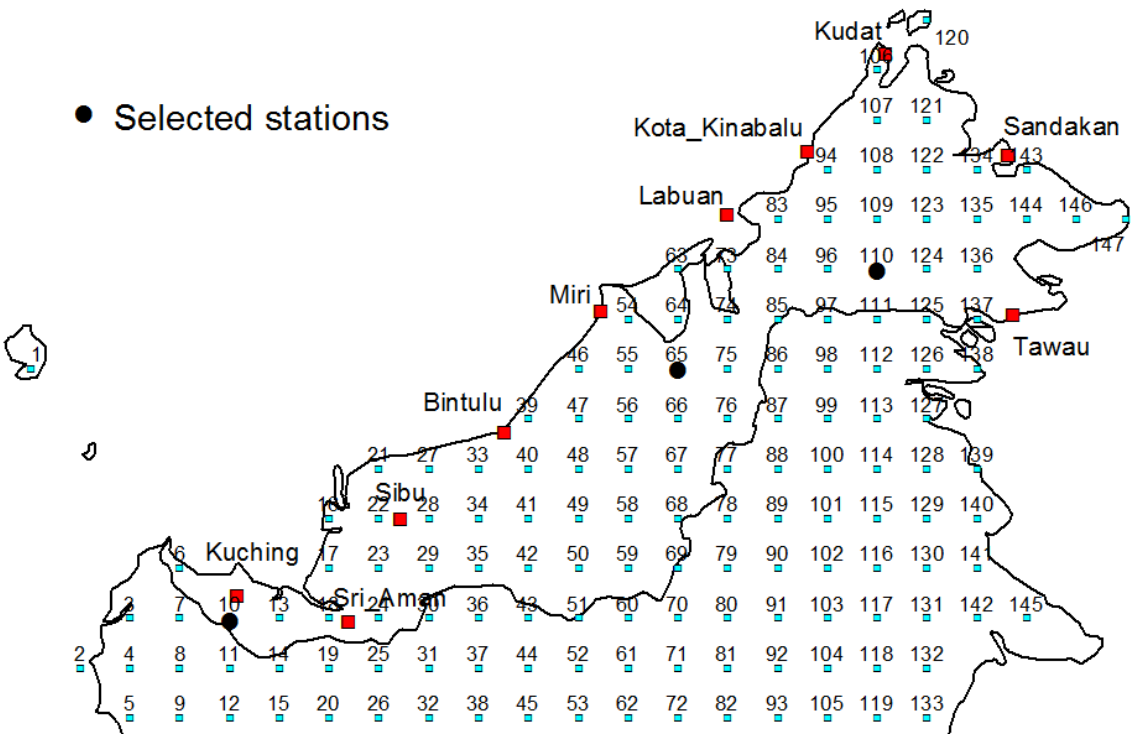

Figure 2 - Data points of the Willmott data network (shown by blue squares), and the ground observation network (shown by red squares). The 3 black data points were selected for demonstrative comparisons.

Figure 3 shows the comparisons of the monthly precipitation that were downscaled by RegHCM-SS from the coarse-resolution ECHAM5 historical control run data, against the Willmott data at 3 selected locations. At each of the graphs in this figure the Willmott precipitation data are compared against the area averages of the

RegHCM-SS downscaled precipitation for each grid area of the Willmott data. The location number of the data point that corresponds to the numbers in Figure 2 is indicated at the upper left corner of each graph. The selected stations are highlighted in Figure 2 with black dots. The RegHCM-SS simulated area average values are in the same value range as in the Willmott data at all 3 locations without any calibration or data assimilation.

SUMMARY AND DISCUSSION

In this study, the historical hydroclimate conditions were reconstructed by RegHCM-SS during the period of January 1993 – December 1999 at hourly intervals at 9-km grid resolution over the whole Sabah and Sarawak region with the newly updated model configuration and model parameters. RegHCM-SS transformed the coarse time-space resolution ECHAM5 GCM historical control runs' atmospheric data during the period of January 1993 – December 1999 to 1-hour-increment hydroclimate information at 9-km spatial resolution over Sabah and Sarawak region. ECHAM5 GCM historical control runs' data provided the initial and boundary conditions for the nested simulations of RegHCM-SS at 3 nestings centered over the Sabah and Sarawak region. At this stage of the model simulations, the output variables of the hydroclimate conditions from the RegHCM of Sabah and Sarawak (RegHCM-SS) include precipitation and surface air temperature.

In order to evaluate the RegHCM-SS performance in the reconstruction of the historical precipitation, its simulation results were compared against the spatially-averaged Willmott data at 0.5 degree grid resolution, over Sabah and Sarawak region. Since the atmospheric data that are reconstructed by RegHCM-SS are also areally-averaged (at 9km grid resolution), the comparison of RegHCM-SS simulations against the Willmott data make more sense than comparison against point location station observations. The comparisons of monthly precipitation, simulated by RegHCM, against corresponding observations of the Willmott data resulted in quite satisfactory results.

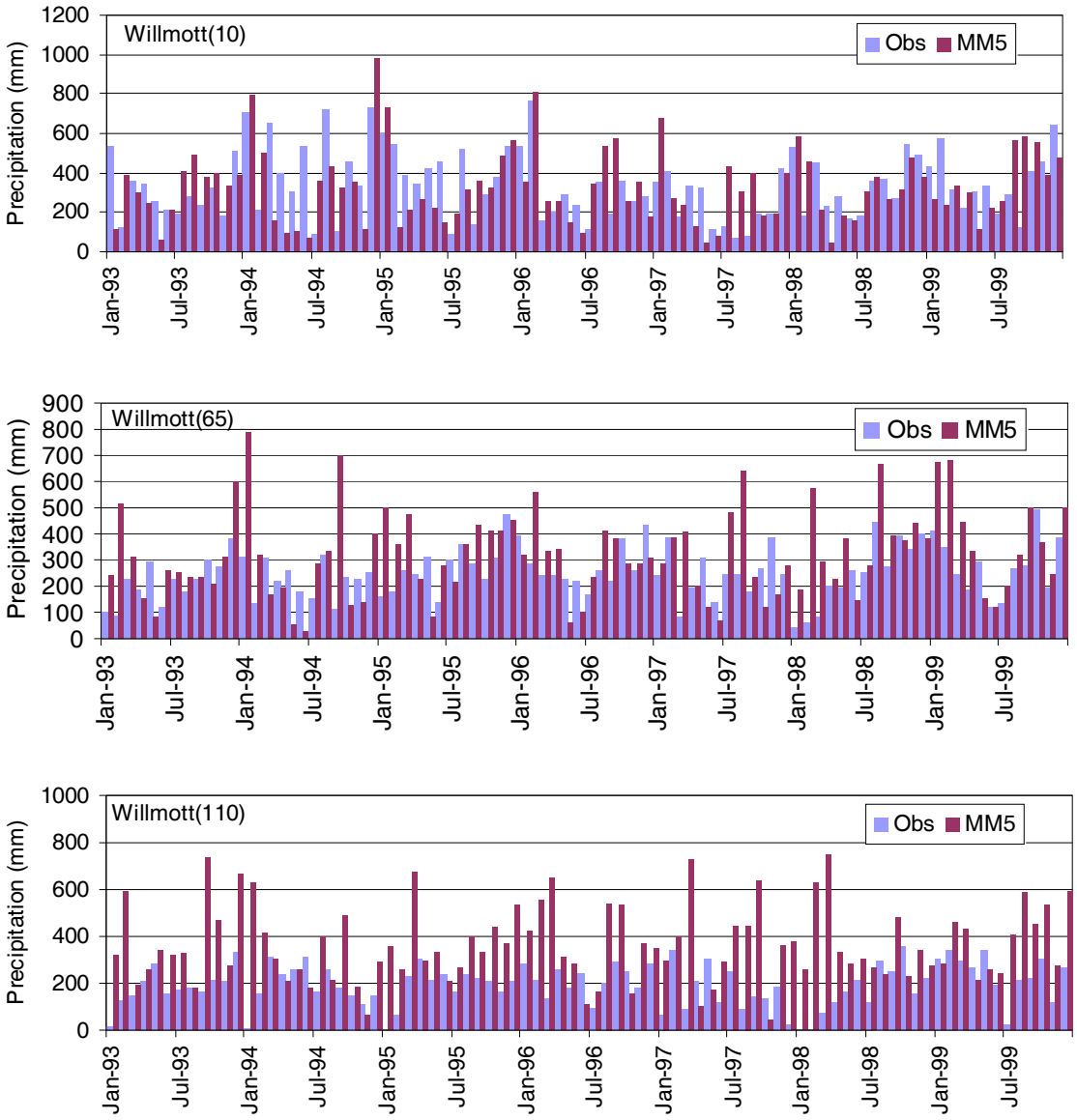

Figure 3 – Comparisons of the monthly precipitation that were downscaled by RegHCM-SS from the coarse-resolution ECHAM5 historical control run data, against the Willmott data at 3 selected locations

REFERENCES

Chen, Z.Q., M.L.Kavvas, L.Tan and S-T.Soong (1996) "Development of a regional atmospheric-hydrologic model for the study of climate change in California." Proceedings of ASCE North American Water and Environment Congress & Destructive Water, ed. by. Chenchayya Bathala, Conf. in Anaheim, California, pp. 1093-1098, June, 1996.

Chen, Z.-Q., R.S.Govindaraju, M.L.Kavvas. (1994a). "Spatial averaging of unsaturated flow equations under infiltration conditions over areally heterogeneous fields: 2. Numerical simulations". Water Resources Research,Vol.30,No.2, pp.535-548, February,1994.

Chen, Z.-Q., R.S.Govindaraju, M.L.Kavvas. (1994b). "Spatial averaging of unsaturated flow equations under infiltration conditions over areally heterogeneous fields: 1. Development of models". Water Resources Research, Vol.30,No.2, pp.523-533, February,1994.

Chen, Z.-Q., M.L. Kavvas and R.S. Govindaraju (1993). "Upscaling of Richards equation for soil moisture dynamics to be utilized in mesoscale atmospheric models." In Exchange Processes at the Land Surface for a Range of Space and Time Scales (Proceedings of the Yokohama Symposium, July 1993). IAHS Publ. no. 212. pages 125-132.

Kavvas, M.Levent, Richard Z.Q. Chen, Michael L. Anderson, Noriaki Ohara, Jaeyoung Yoon (2006). A Regional Hydroclimate Model for Tigris-Euphrates Watershed, RegHCM-TE: Reconstruction of Historical Hydroclimatic Data over the Watershed, BALWOIS 2006 - Ohrid, 23-26 May 2006

Kavvas, M.L., Z.Q. Chen, L.Tan, S.-T.Soong, A.Terakawa, J.Yoshitani, K.Fukami (1998). "A regional-scale land surface parameterization based on areally-averaged hydrologic conservation equations". Hydrological Sciences Journal, 43(4), 611-631, 1998.

Huffman, G.J., R.F. Adler, M. Morrissey, D.T. Bolvin, S. Curtis, R. Joyce, B McGavock, J. Susskind, 2001: Global Precipitation at One-Degree Daily Resolution from Multi-Satellite Observations. J. Hydrometeor., 2, 36-50.

Willmott, C. J., C. M. Rowe and W. D. Philpot (1985). Small-scale climate maps: a sensitivity analysis of some common assumptions associated with grid-point interpolation and contouring. American Cartographer, 12, 5-16.

Statistical Characteristics of Land Surface Properties for the Regional Hydroclimate Model

S. Kure[1], S. Jang[2], N. Ohara[3], and M.L. Kavvas[4]

[1234] Department of Civil & Environmental Engineering, University of California Davis, CA95616, USA; PH (530) 752-2469; FAX (530) 754-9278

[1]e-mail; krso@ucdavis.edu, [2]e-mail; shjang@ucdavis.edu

[3]e-mail; nohara@ucdavis.edu, [4]e-mail; leventkavvas@sbcglobal.net

ABSTRACT

In order to obtain good regional hydroclimate simulation results, land surface properties such as leaf area index (LAI), albedo, emissivity, and roughness height are important for land surface hydrology modeling. A number of models have been proposed to describe the interaction between land surface and atmosphere during the last decade. The problem of these models is not taking account of spatial and temporal variability of the land surface properties within a computational grid. In an actual watershed, spatial distribution of vegetation is inhomogeneous, and its canopy varies seasonally. As such, it is necessary to consider the seasonal change of land surface properties in the land surface parameterization that is required for a regional hydroclimate model. The objective of this study is to understand the statistical characteristics of land surface properties. The satellite driven data from MODIS combined with local vegetation survey have been analyzed at a few selected watersheds in California in this study. The monthly spatial distributions of the land surface parameters have been computed. It was found that spatial distributions of the land surface parameters vary significantly in space and with seasons. This result indicates that non-stationarity as well as spatial variability of land surface parameters needs to be considered in land surface parameterization.

INTRODUCTION

The interface between the atmosphere and the land surface plays an important roll for the both of the atmospheric dynamics and land surface condition. The land surface processes such as infiltration, evapotranspiration and sensible heat exchange significantly affect on the simulation results of climate models of large scale models as well as in regional atmospheric models. The importance of the land surface parameterization is recognized to improve the climate model simulation results. During the last decade, a number of refined models have been proposed to describe the interaction between land surface and atmosphere. The problem of these models is not taking account of spatial and temporal variability of the land surface properties within a computational grid.

Kavvas *et al.* (1998) developed a regional-scale land surface parameterization based on areally-averaged hydrological conservation equations. Ensenble mean value of the land surface fluxes over a regional model grid cell were obtained by numerical algorithm for the arealy averaged equations with a mosaic scheme in this model in order to account for subgrid-scale spatial variability of land surface characteristics. Another stochastic upscaling technique to predict the dynamic probability density function for nonlinear hydrologic processes was developed by Kavvas (2003), and have been applied to the many hydrologic processes (For example, Ohara *et al*., 2008). This approach enables us to obtain not only the mean behavior but also the probability distribution of the state random variables of hydrologic process. This kind of stochastic upscaling approach may be applicable for the land surface processes. However in order to upscale the land surface processes using this approach, statistical characteristics of the processes need to be known because of the Gaussian assumption for the processes and the evaluation of time-space-dependent covariance terms in the Fokker Planck Equation of the upscaled processes.

The objective of this study is to understand the statistical characteristics of land surface properties. In order to improve the land surface parameterization and obtain the upscaled equations of land surface processes to account for the spatial variability in the computational grids, the characteristics of spatial distribution and seasonal change of the land surface properties, such as Leaf Area Index (LAI), albedo and emissivity are investigated and discussed in this paper. These parameters have been only crudely represented in the models due to limited observations. In this study, the derived parameters by MODIS (MODerate resolution Imaging Spectroradiometer) data is used in 1km spatial resolution.

DESCRIPTION OF THE LAND SURFACE PARAMETERIZATION

Two-way coupling scheme and areally averaged conservation equations (Kavvas *et al*., 1989) are employed in the land surface model, named Integrated Regional Scale Hydrologic/Atmospheric Model (IRSHAM). This made long-term realistic simulation possible at regional scale.

In order to calculate the latent heat flux from land surface it is necessary to calculate evapotranspiration (ET). The evapotranspiration rate can be estimated according to the moisture availability and the atmospheric conditions and the evapotranspiration rate from bare-ground and vegetated ground are estimated separately. When the water availability parameter h over bare soil, the water availability parameters for evaporation from the plant leaves, h_{vd}, and for transpiration, h_{vt}, (Noilhan & Planton, 1989) and the bulk transfer coefficient, C_H (Stull, 1988), are available by the Monin-Obukhov surface similarity theory, the aerodynamic formulas can be used to estimate the bare-ground evaporation (E_g) , the direct evaporation from canopy (E_{vd}), and the vegetation transpiration from canopy (E_{tr}).

Importantly, land surface temperature is determined from the heat budget of the land surface and therefore is also dependent upon evaporation. It means the

land/atmosphere is a nonlinear system with strong feedback and these are solved in a coupled way in this parameterization.

Areal averaging was applied to the land surface equations and areally-averaged hydrological conservation equations have been obtained (Kavvas, *et al.*, 1998). The areally averaged Green-Ampt models (Chen *et al.*, 1994a,b) for the infiltration and exfiltration process from/into the ground was incorporated in the land surface model and this physically based model provided the basis for the land surface hydrologic model in the IRSHAM. This areally averaged Green-Ampt models accounts for the heterogeneity of soils with in a computational grid by assuming a lognormal distribution of saturated hydraulic conductivity.

The characteristics of spatial and temporal variability of land surface parameters such as surface albedo, Leaf Area Index (LAI) and emissivity will be investigated in this paper. These land surface parameters significantly affect on the simulation results of the land surface model. Possibility for more reliable stochastic upscaling for the evapotranspiration and sensible heat exchange will be examined by computing the spatial autocorrelation function.

Following section, in order to obtain the statistical characteristics of land surface properties, the satellite driven data from MODIS will be analyzed at the foothills region in the northern California.

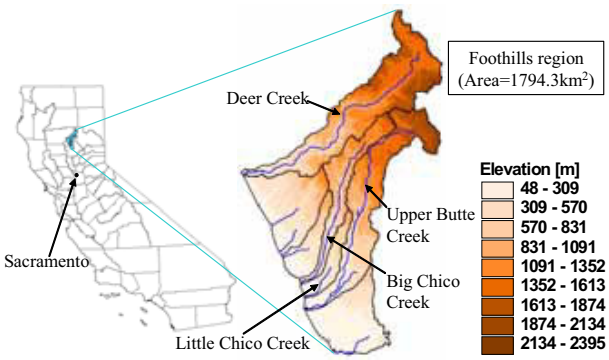

Figure 1. Map of the foothills region , California

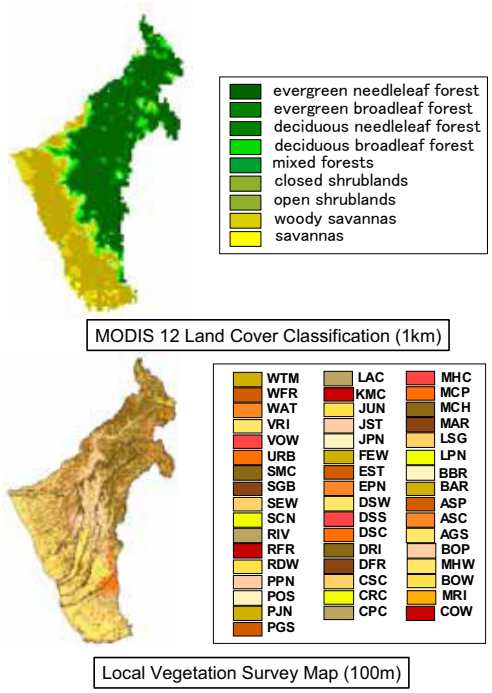

Figure 2. Vegetation map over the foothills region

STUDY AREA

The foothills region, encompassing Big Chico Creek, Little Chico Creek, Upper Butte Creek and Deer Creek watersheds, in the northern California was selected in this paper as shown in Figure 1. Infiltration of these watersheds into the groundwater aquifer

systems of Northern Sacramento Valley is very important for the water resources in this area.

Figure 2 shows MODIS12 land cover type map (upper) and Multi-source Land Cover Data (v02_1) published by CDFF (lower) in the foothills region. The local vegetation survey has the finest spatial resolution available (100m) and it provides the land surface cover types and vegetation type information. However, the satellite driven LAI, albedo and emissivity data is combined with MODIS 12 land cover classification data to obtain the seasonal change of the parameters for each land cover types in this paper.

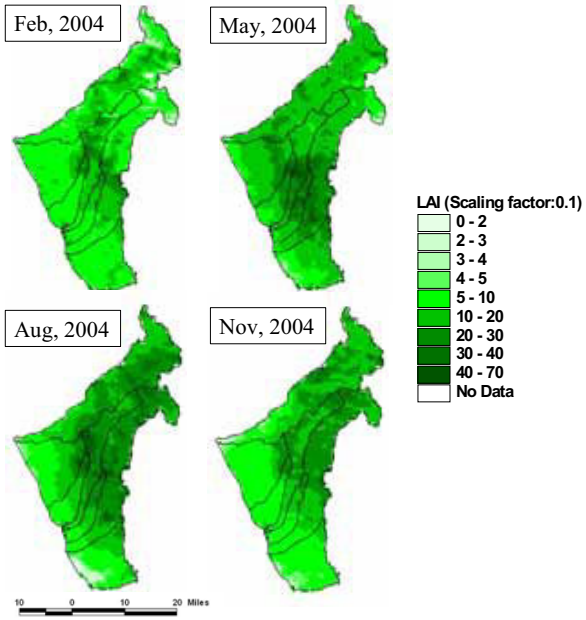

Figure 3. LAI distribution derived from MODIS observations over the foothills region

MODIS Leaf Area Index (LAI)

Leaf Area Index (LAI), defined as the area of leaves that covers a given unit of ground area. This property is essential to evaluate transpiration from the canopy in the land surface model.

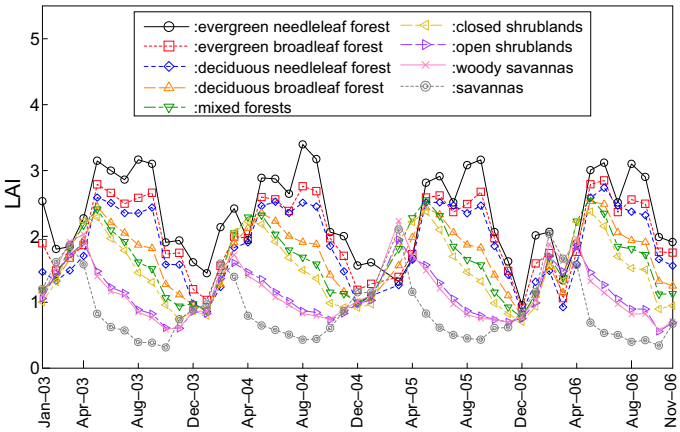

Figure 4. Monthly change of LAI based on MODIS observation (MYD15+MOD12)

Figure 3 shows the seasonal example plots of LAI derived from MODIS observations (MYD15). The LAI in MODIS is derived by comparing the observed and modeled surface reflectances for a suite of canopy structures and soil patterns. Spatial resolution of MODIS LAI is 1km. In order to establish relationships between the vegetation class and the estimated LAI, the land cover data derived from MODIS data (MOD12) are adopted in this study. Figure 4 shows the seasonal variation of LAI for each vegetation type. Seasonal change of LAI is clearly seen in Figure 4. From Figure 3 and 4, it is found that LAI values significantly change in spatially and temporally. It is because the vegetation canopies change seasonally. Figure 5 shows seasonal change of histogram (Relative frequency) of LAI. It seems that relative

frequency of LAI may be treated as the log normal distribution function. However, the histograms in some months do not seem to be the log normal distribution. Figure 6 shows the spatial autocorrelation coefficients of LAI and Albedo (discussed in later section). The spatial autocorrelation coefficients are calculated using the following equation.

$$g[LAI(\mathbf{x}), LAI(\mathbf{x}-r)](r) = \frac{\sum_{i=1}^{n}\left(LAI(\mathbf{x})-\overline{LAI}\right)\left(LAI(\mathbf{x}-r)-\overline{LAI}\right)}{\sqrt{\sum_{i=1}^{n}\left(LAI(\mathbf{x})-\overline{LAI}\right)^2\sum_{i=1}^{n}\left(LAI(\mathbf{x}-r)-\overline{LAI}\right)^2}} \quad (1)$$

Fig. 6 shows that the strong spatial correlation of LAI more than 0.5 values can be found , but it doesn't have a "long memory" in space. This exponential behaviour which autocorrelation coefficient approaches to zero sufficiently rapidly implies the process can be treated as the Gaussian process. Which means stochastic upscaling proposed by Kavvas (2003) can be applicable for this process. Ohara *et al.* (2008) focused on the spatial correlation function of the daily shortwave radiation in the upper Upper Cosumnes River watershed. They found the spatial correlation function of the daily shortwave has a "long memory" in space. However, after subtracting the local mean from the original radiation data, the obtained spatial correlation function appears to be a white noise and the delta correlation assumption was applied for the spatial distribution of daily shortwave radiation. This type of operation may be useful to approximate spatial correlation of LAI with the delta correlation assumption to evaluate the time-space-dependent covariance

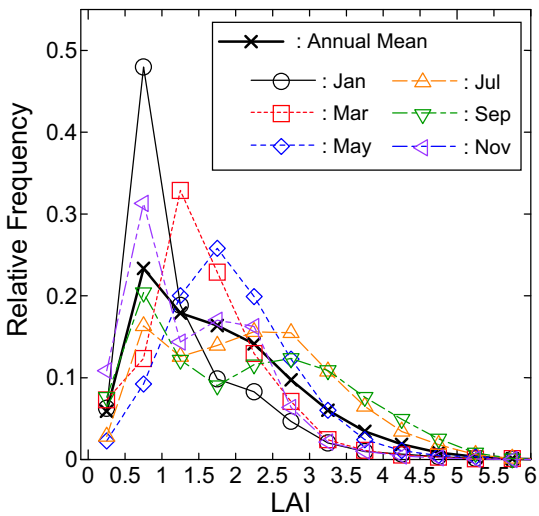

Figure 5. Monthly histogram (relative frequency) of LAI

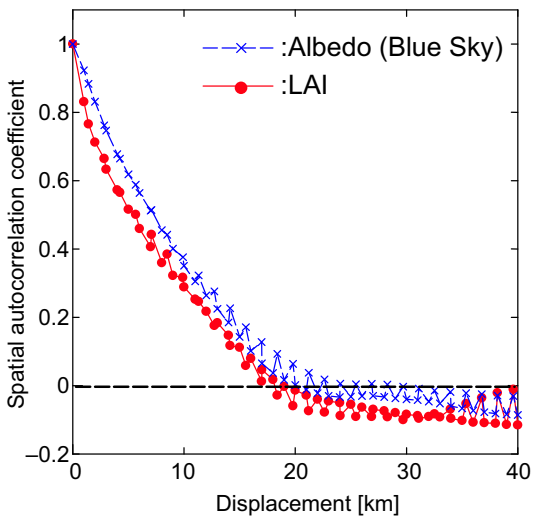

Figure 6. Spatial Correlation of LAI and Albedo over the foothills region

in the stochastic modeling approach.

MODIS Albedo

Seasonal change and spatial variability of surface Albedo are examined in this section. Albedo is defined as the ratio of upward to downward radiative flux on the land surface. This property is essential to evaluate the net shortwave radiation on the land surface in the energy budged equation of the land surface model. The MOD43 Albedo product provides both the white-sky albedos and the black-sky albedos (at local solar noon) for MODIS bands 1-7 as well as for three broad bands. Actual albedo (blue sky) of short wave band was estimated using the following equation.

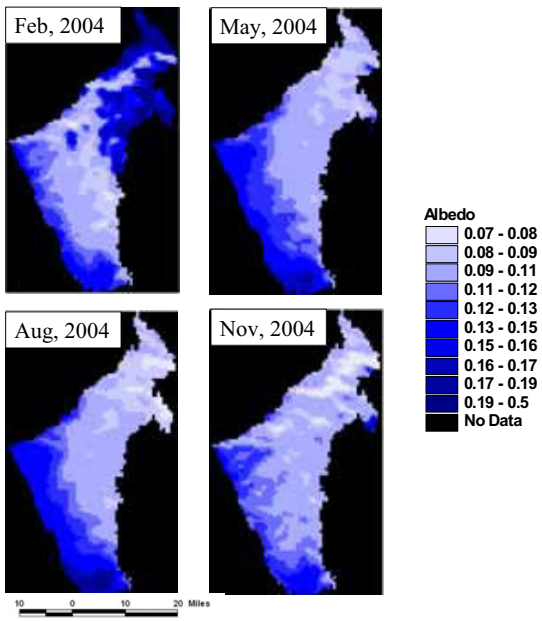

Figure 7. Albedo distribution derived from MODIS observations over the foothills region

$$ActualAlbedo = (1 - S(\theta, \tau(\lambda)))BSA + S(\theta, \tau(\lambda))WSA \quad (2)$$

where $S(\theta,\tau(\lambda))$ denotes a fraction of diffuse skylight, θ is the solar zenith angle, λ is the wavelength and $\tau(\lambda)$ is the atmospheric optical depth. It means the actual albedo values were determined based upon the solar zenith angle, wavelength and the atmospheric optical depth. The value of 0.5 as the fraction of diffuse skylight was used in this paper.

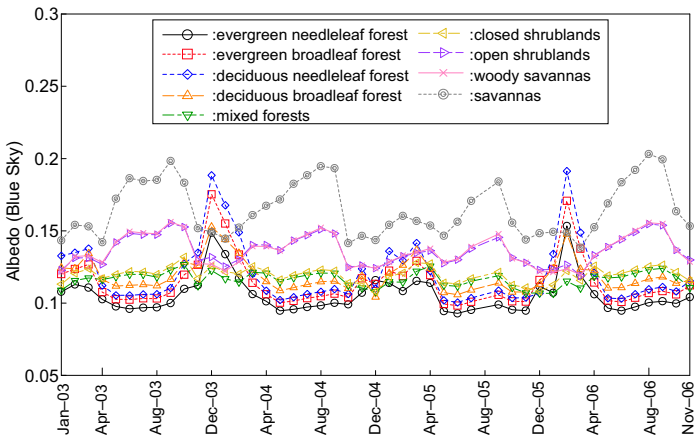

Figure 8. Monthly change of albedo based on MODIS observation (MOD43+MOD12)

Figure 7 shows the seasonal representative plots of Actual Albedo and Figure 8 shows the seasonal variation of Albedo for each vegetation type. Surface albedo

values for each vegetation type are increased during the dry periods and then decreased in the wet periods. The increase of albedo value in deciduous needleleaf forest and evergreen broadleaf forest during the wet periods is influenced by snow cover. From Figure 7 and 8, albedo significantly change in spatially and seasonally and these behaviors are similar to the LAI because the both of LAI and albedo values in this foothills region are based on the vegetation types. Figure 9 shows seasonal change of histogram (Relative frequency) of albedo. The annual and monthly mean distribution of albedo may be treated as the log normal distribution function. The spatial autocorrelation coefficient of albedo is shown in Figure 6 with LAI plots. The spatial autocorrelation coefficients are calculated using the same equation of LAI case written in Eq.(1). The spatial autocorrelation functions of albedo almost same as the spatial correlation coefficients of LAI. This is because of these 2 parameters depends on the vegetation types.

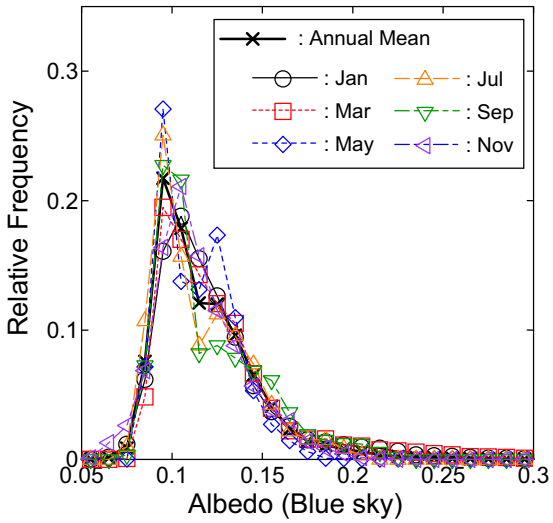

Figure 9. Monthly histogram (relative frequency) of albedo

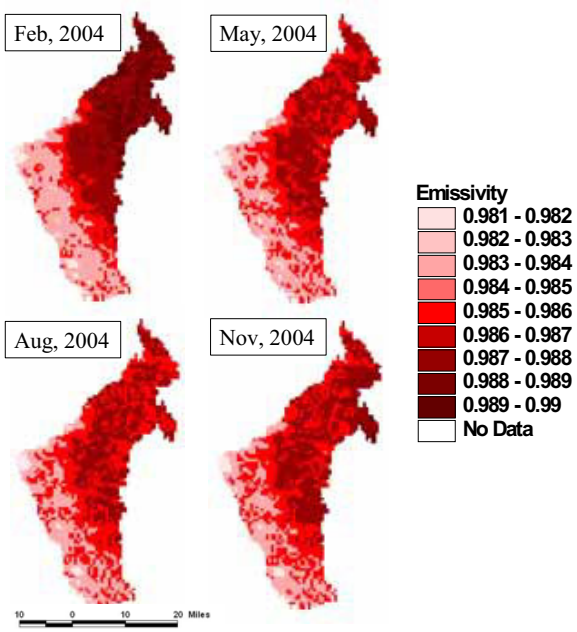

Figure 10. Emissivity distribution derived from MODIS observations over the foothills region

MODIS Emissivity

Finally, seasonal change and spatial variability of emissivity are focused in this section. Emissivity is defined as the ratio of thermal radiation emitted by a surface to that of a blackbody. This property is necessary to evaluate the net longwave radiation at the land surface. The MOD11 (1km resolution) emissivity values are estimated from land surface temperature and land cover types.

Figure 10 shows the seasonal example plots of emissivity and Figure 11 shows the seasonal variation of emissibity for each vegetation type. From Figure 10 and 11, emissivity values are spatially and seasonally changed, but the variability of the emissivity is apparently smaller than that of Albedo and LAI. It may be concluded that emissivity values of land surface can be treated as the constant value in seasonally.

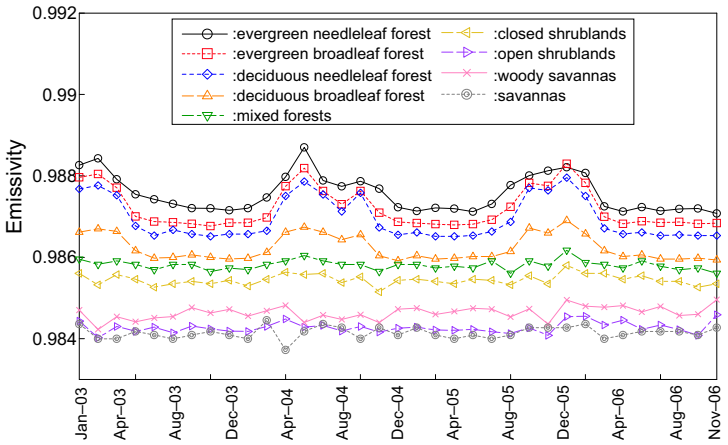

Figure 11. Monthly change of emissivity based on MODIS observation (MOD11+MOD12)

DISCUSSION

Spatial distribution of vegetation is inhomogeneous, and its canopy varies seasonally in an actual watershed. It is necessary to consider the seasonal change of land surface properties in the land surface parameterization that is required for a regional hydroclimate model. The seasonal change and spatial variability of Leaf Area Index, albedo and emissivity at foothills region in northern California are estimated from MODIS data in this paper. Also, monthly averaged histogram and spatial autocorrelation coefficient of Albedo and LAI were obtained. These results indicate that albedo and LAI values were significantly changed in seasonally and spatially. As such, it is necessary to consider the non-stationarity as well as spatial variability of land surface parameters in land surface parameterization.

Furthermore, strong spatial correlation coefficients of LAI and Albedo of more than 0.5 values were found but they don't have a "long memory" in space. This exponential behaviour which autocorrelation coefficient approaches to zero sufficiently rapidly implies the process can be treated as the Gaussian process. Which means stochastic upscaling proposed by Kavvas (2003) can be applicable for the land surface processes. And it was also found that provability distribution function of annual and monthly mean albedo and annual mean LAI can be treated as the lognormal distribution.

This exercise on the spatial and temporal variability of land surface parameters presented in this paper is important to examine the applicability of the stochastic upscaling approach for the land surface parameterization.

REFERENCES

Chen, Z. Q., R. S. Govindaraju, and M. L. Kavvas (1994a). "Spatial averaging of unsaturated flow equations under infiltration conditions over areally heterogeneous fields. 1. Development of models", *Wat. Resour. Res.*, 30(2), 523-533.

Chen, Z. Q., R. S. Govindaraju, and M. L. Kavvas (1994b). "Spatial averaging of unsaturated flow equations under infiltration conditions over areally heterogeneous fields. 2. Numerical solutions", *Wat. Resour. Res.*, 30(2), 535-548.

Kavvas, M. L., Z. Q. Chen, L. Tan, S. –T. Soong, A. Terakawa, J. Yoshitani, and K. Fukami (1998). "A regional-scale land surface parameterization based on areally-averaged hydrological conservation equations" *Hydrological Sciences Journal*, 43(4), 611-631.

Kavvas, M. L. (2003). "Nonlinear Hydrologic Processes: Conservation Equations for Determining Their Means and Probability Distributions", ASCE *Journal of Hydrologic Engineering.* Vol.8, No.2, 44-53.

Nolihan, J. and Planton, S. (1989). "A simple parameterization of land surface processes for meteorological models" *Mon. Weath. Rev*. 117, 536-549.

Ohara, N., M. L. Kavvas, Z. Q. Chen, M. Anderson, L. Liang, J. Wilcox and L. Mink (2007). "Estimation of ET based on reconstructed atmospheric conditions and remotely sensed information over Last Chance Creek watershed, Feather River basin, California", ASCE, World Environmental & Water Resources Congress 2007 in Tampa.

Ohara, N., M. L. Kavvas, Z. Q. Chen. (2008). "Stochastic Upscaling for Snow Accumulation and Melt Processes with PDF Approach", ASCE *Journal of Hydrologic Engineering.* Vol.13, No.12, 1103-1118.

Stull, R.B. (1988). "An Introduction to Boundary Layer Meteorology", Kluwer Academic, London.

Modeling the kinematic wave parameters with regression methods

I. Haltas[1] (Assoc. Member ASCE)

[1] Northwest Hydraulic Consultants, 3950 Industrial Blvd Suite 100C, West Sacramento, 95691. email: ihaltas@gmail.com

Abstract

The momentum equation in the kinematic wave model is a power law equation and involves two kinematic wave parameters. It is a common practice to use Manning's equation to calculate the kinematic wave parameters. One can obtain a kinematic wave equation by inserting the momentum equation into the continuity equation. The kinematic wave equation becomes a partial differential equation with kinematic wave parameters that depend on the flow depth. However, working with a partial differential equation comprised of kinematic wave parameters that are independent of the flow depth is a lot more convenient. Here, regression methods were used to calculate the kinematic wave parameters that are independent of the flow depth for a trapezoidal channel cross-section, which is a common cross-section shape. The developed expressions for the kinematic wave parameters provided very good approximation for the momentum equation of the kinematic wave model.

Keywords: kinematic wave parameters; trapezoidal channel; least squares fitting; power law.

Introduction

The kinematic wave model is a simplified form of the St. Venant equations under the assumption that the bed slope is approximately equal to the friction slope (Lighthill and Whitham, 1955). Kinematic wave routing is frequently used for modeling both the overland and open channel flows due to its simplicity and accuracy. The kinematic wave model is defined by the following two equations:

Equation of continuity: $$\frac{\partial A}{\partial t}+\frac{\partial Q}{\partial x}-q=0 \qquad [1]$$

Equation of momentum: $$Q=\alpha \cdot A^{\beta} \qquad [2]$$

The parameters α and β in Eq. [2] are called as kinematic wave parameters and are commonly derived using Manning's equation,

$$Q = \frac{S^{1/2}}{n}\left(\frac{A^{5/3}}{P^{2/3}}\right) \quad [3]$$

In Equations [1]-[3]; A is flow area (m^2), Q is flow discharge (m^3/s), q is lateral inflow (m^2/s), S is bedslope of the channel (m/m), n is Manning's roughness coefficient ($s/m^{1/3}$), and P is wetted perimeter (m).
Let Eq. [3] be expressed in the power law form given in Eq. [2].

$$\frac{S^{1/2}}{n}\left(\frac{A^{5/3}}{P^{2/3}}\right) = \alpha \cdot A^{\beta} \quad [4]$$

Since both the flow cross-sectional area A and the wetted perimeter P depend on the cross-section geometry and the flow depth, it is not possible to find α and β parameters as independent of the flow depth except for some special cross-section geometries.

When Eq. [2] is inserted into Eq. [1] one can obtain a combined kinematic wave equation as follows,

$$\frac{\partial A}{\partial t} + \frac{\partial(\alpha \cdot A^{\beta})}{\partial x} - q = 0 \quad [5]$$

In Eq. [5] the kinematic wave parameters α and β depend on the flow depth. However, working with a partial differential equation comprised of kinematic wave parameters that are independent of the flow depth, is a lot more convenient than working with a partial differential equation comprised of kinematic wave parameters that depend on the flow depth. In a recent work of Haltas and Kavvas (2008) the technique they used for developing an ensemble averaged kinematic wave equation required a combined kinematic wave equation with kinematic wave parameters that are independent of the flow depth.

Overland Flow

In the case of the overland flow, flow is assumed to have a wide rectangular cross-sectional area where flow width is much greater than flow depth. Then, the flow area and the wetted perimeter can be written as:

$$A = w \cdot y \quad [6]$$
$$P = w + 2 \cdot y \quad [7]$$
$$y / w \approx 0 \quad [8]$$

Where w is the overland flow width (m) and y is the overland flow depth (m).
When Equations [6] and [7] are plugged into Eq. [3] one obtains:

$$Q = \frac{S^{1/2}}{n}\left(\frac{(w \cdot y)^{5/3}}{(w + 2 \cdot y)^{2/3}}\right) \qquad [9]$$

Rearranging the terms in Eq. [9] yields:

$$Q = \frac{S^{1/2}}{n}\left(\frac{y}{1 + 2 \cdot y / w}\right)^{2/3}(w \cdot y) \qquad [10]$$

By applying the approximation given in Eq. [8], to Eq. [10] one obtains:

$$Q / w = \frac{S^{1/2}}{n} y^{5/3} \qquad \text{or} \qquad q = \frac{S^{1/2}}{n} y^{5/3} \qquad [11]$$

In Eq. [11]; $q = Q / w$ is the flow per unit width (m^2 / s), the corresponding kinematic wave parameters are obtained as $\alpha = S^{1/2} / n$, $\beta = 5/3$. As such, the kinematic wave parameters for overland flow are independent of the flow depth.

Open Channel Flow

In practical applications circle, triangle, rectangle, and trapezoid are the most commonly used shapes for describing the channel flow cross-sections. In a study by MacArthur and DeVries (1993), the expressions for kinematic wave parameters were provided for circular, triangular, rectangular and trapezoidal channel flow cross-sections. In that study the kinematic wave parameters were calculated as independent of the flow depth for the triangular cross-sections. For the case of circular and rectangular channel cross-sections some assumptions were necessary to obtain the kinematic wave parameters as independent of the flow depth. However for the trapezoidal cross sections the calculated kinematic wave parameters were dependent on the flow depth. Here an attempt is made to derive expressions for the kinematic wave parameters that are independent of the flow depth for trapezoidal channel cross-sections. The triangular and rectangular cross-sections are special cases of the trapezoidal cross-sections. Figure 1 depicts a typical trapezoidal channel flow cross-section.

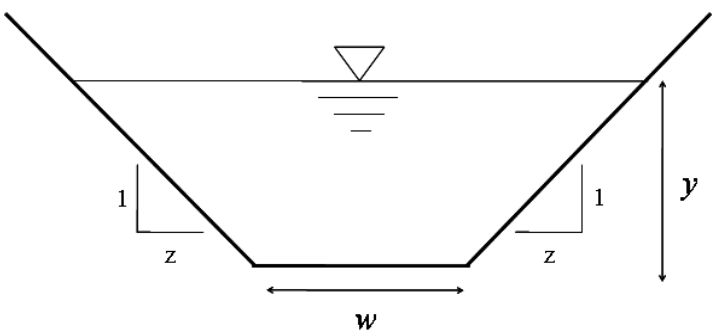

Figure 1: Trapezoidal Cross Section

From Figure 1, it follows that

$$A = y \cdot (w + z \cdot y) \quad [12]$$

$$P = w + 2 \cdot y \cdot \sqrt{(1 + z^2)} \quad [13]$$

$$Q = \frac{S^{1/2}}{n} \frac{(y \cdot (w + z \cdot y))^{5/3}}{(w + 2 \cdot y \cdot \sqrt{(1 + z^2)})^{2/3}} \quad [14]$$

In Eq. [14], the channel slope S, the roughness coefficient n, the channel side slope z, and the channel bottom width w are independent of the flow depth, yet the flow discharge Q is a function of the flow depth. As such, the equation form of Q, as given in Eq. [14], does not allow Q to be expressed in the power law form in terms of A and flow depth-independent kinematic wave parameters. However, regression methods can be used to derive the kinematic wave parameters as independent of the flow depth for some set of A and Q values.

Let's re-write Eq. [14] as follows:

$$Q = \frac{S^{1/2}}{n} \cdot \theta(z, w, y) \quad [15]$$

where

$$\theta(z, w, y) = \frac{A^{5/3}}{P^{2/3}} = \frac{(y \cdot (w + z \cdot y))^{5/3}}{(w + 2 \cdot y \cdot \sqrt{(1 + z^2)})^{2/3}} \quad . \quad [16]$$

Let

$$\theta(z, w, y) = c(z, w) \cdot A^{m(z,w)} \quad [17]$$

The functions $c(z, w)$ and $m(z, w)$ can be calculated by least squares fitting for some set of A and θ values as follows.

Power law-least squares fitting method

For the sequences $\{x_i\}_{i=1}^n$ and $\{y_i\}_{i=1}^n$ and for a function of the form $y = c \cdot x^m$ the least squares fitting gives the coefficients as (Weisstein, 2008):

$$b = \frac{n \cdot \sum_{i=1}^{n} (\ln x_i \cdot \ln y_i) - \sum_{i=1}^{n} (\ln x_i) \cdot \sum_{i=1}^{n} (\ln y_i)}{n \cdot \sum_{i=1}^{n} (\ln x_i)^2 - \left(\sum_{i=1}^{n} (\ln x_i) \right)^2} \quad [18]$$

$$a = \frac{\sum_{i=1}^{n} (\ln y_i) - b \cdot \sum_{i=1}^{n} (\ln x_i)}{n} \qquad [19]$$

where $m \equiv b$ and $c \equiv e^a$

Case study

Let a trapezoidal cross section as shown in Figure 1 has the bottom width $w_0 = 50$ meter and side slope $z_0 = 1$. Table 1 lists a range of flow depths y and the calculated A and θ values.

Table 1: A and θ calculated for a range of flow depths y

y_i	0.60	1.20	1.80	2.40	3.00	3.60	4.20	4.80	5.40	6.00
A_i	30.36	61.44	93.24	125.76	159.00	192.96	227.64	263.04	299.16	336.00
θ_i	21.29	67.47	132.42	213.66	309.72	419.57	542.48	677.91	825.43	984.71

For the sequences $\{A_i\}_{i=1}^{10}$ and $\{\theta_i\}_{i=1}^{10}$ listed in Table 1 the functions c and m are estimated as $c(z_0 = 1, w_0 = 50) = 0.095$ and $m(z_0 = 1, w_0 = 50) = 1.593$ by the least squares fitting method. Then the approximate momentum equation for this specific trapezoidal channel cross-section can be written as:

$$Q = 0.095 \cdot \frac{S^{1/2}}{n} \cdot A^{1.593} \qquad [20]$$

Note that, the momentum equation given in Eq. [20] is valid only for the trapezoidal channels with the specified dimensions. The calculated least squares fitting equation has a coefficient of determination $R^2 = 0.9998$. Although Eq. [20] is estimated for a specific range of flow depths as given in Table 1, it is still valid for flow depths outside of the specified range with poorer accuracy.

The above regression method can be repeated for sequences of channel side slope z_i, and the channel bottom width w_j to estimate the approximate numerical values of the functions $c(z, w)$ and $m(z, w)$. Table 2 and Table 3 list these estimated numerical values.

Table 2: Numerical values of $c(z_i, w_j)$ estimated with regression methods

z_i / w_j	0	0.5	1	1.5	2	2.5	3	3.5	4	4.5
5	0.322	0.320	0.316	0.311	0.305	0.300	0.295	0.290	0.285	0.281
10	0.237	0.238	0.240	0.244	0.246	0.248	0.249	0.249	0.249	0.249
20	0.163	0.165	0.170	0.176	0.182	0.188	0.192	0.196	0.199	0.201
50	0.090	0.091	0.095	0.100	0.105	0.110	0.115	0.119	0.123	0.127
75	0.067	0.068	0.071	0.075	0.079	0.083	0.087	0.090	0.094	0.097
100	0.055	0.055	0.058	0.061	0.064	0.067	0.070	0.073	0.076	0.079
150	0.041	0.041	0.043	0.045	0.047	0.049	0.051	0.053	0.056	0.058
200	0.033	0.033	0.035	0.036	0.038	0.039	0.041	0.042	0.044	0.046
300	0.025	0.025	0.026	0.026	0.027	0.028	0.030	0.031	0.032	0.033
400	0.020	0.020	0.021	0.021	0.022	0.023	0.024	0.024	0.025	0.026

Table 3: Numerical values of $m(z_i, w_j)$ estimated with regression methods

z_i / w_j	0	0.5	1	1.5	2	2.5	3	3.5	4	4.5
5	1.587	1.582	1.566	1.548	1.531	1.515	1.500	1.488	1.476	1.466
10	1.563	1.558	1.541	1.521	1.502	1.486	1.471	1.459	1.448	1.439
20	1.579	1.574	1.558	1.539	1.521	1.505	1.490	1.477	1.466	1.456
50	1.610	1.605	1.593	1.578	1.563	1.548	1.535	1.523	1.512	1.502
75	1.622	1.618	1.608	1.595	1.582	1.569	1.557	1.546	1.536	1.526
100	1.630	1.626	1.617	1.606	1.594	1.583	1.572	1.562	1.552	1.543
150	1.639	1.636	1.629	1.619	1.610	1.600	1.591	1.582	1.574	1.566
200	1.644	1.641	1.635	1.628	1.619	1.611	1.603	1.596	1.588	1.581
300	1.650	1.648	1.643	1.637	1.631	1.624	1.618	1.612	1.606	1.600
400	1.653	1.652	1.648	1.643	1.638	1.632	1.627	1.622	1.616	1.611

Eq. [20] can be generalized so that it will be valid not only for a specified bottom width w_0 but for a variable bottom width w. Then Eq. [17] will take the form given as follows:

$$\theta(z_0, w, y) = c(z_0, w) \cdot A^{m(z_0, w)} \qquad [21]$$

Similar to θ, the functions $c(z_0, w)$ and $m(z_0, w)$ in Eq. [21] can also be formulated in a power law form by using the power law-least squares fitting method.
Let

$$c(z_0, w) = cc(z_0) \cdot w^{cm(z_0)} \qquad [22]$$

$$m(z_0, w) = mc(z_0) \cdot w^{mm(z_0)} \qquad [23]$$

Equations [22] and [23] are estimated for the sequence of channel bottom widths w_j and the corresponding $c(z_0, w_j)$ and $m(z_0, w_j)$ given in Table 2 and Table 3, as follows,

$$c(z_0, w) = 1.515 \cdot w^{-0.722} \qquad (R^2 = 0.997) \qquad [24]$$

$$m(z_0, w) = 1.340 \cdot w^{0.039} \qquad (R^2 = 0.929) \qquad [25]$$

Furthermore, the parameters $cc(z_0)$, $cm(z_0)$, $mc(z_0)$, and $mm(z_0)$ in Equations [22] and [23] can also be expressed as functions of the channel side slope z by using the regression methods, as follows,

$$cc(z) = -0.006 \cdot z^2 + 1.0431 \qquad (R^2 = 0.998) \qquad [26]$$

$$cm(z) = 0.0016 \cdot z^2 + 0.0131 \cdot z - 0.6505 \qquad (R^2 = 0.997) \qquad [27]$$

$$mc(z) = 0.0021 \cdot z^2 + 0.0489 \cdot z + 1.5438 \qquad (R^2 = 0.992) \qquad [28]$$

$$mm(z) = -0.0003 \cdot z^2 + 0.0046 \cdot z + 0.0117 \qquad (R^2 = 0.990) \qquad [29]$$

The actual values of $\theta(z, w, y)$, calculated using Eq. [16], are compared with those calculated using regression model Eq. [17] and the regression parameters given in Tables 2 and 3. The percent relative differences among the Eq. [16]-calculated and Eq. [17]-calculated $\theta(z, w, y)$ are shown in Figures 2-6 for different channel bottom widths w.

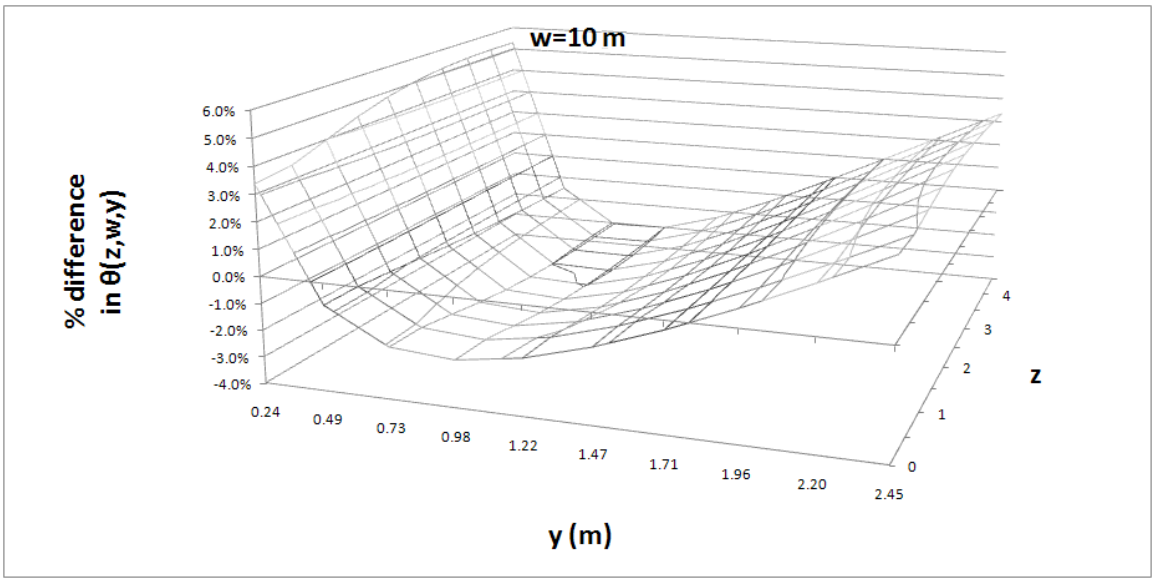

Figure 2: Percent relative differences among the Eq. [16]-calculated and Eq. [17]-calculated $\theta(z, w, y)$ for channel bottom width $w = 10$ m

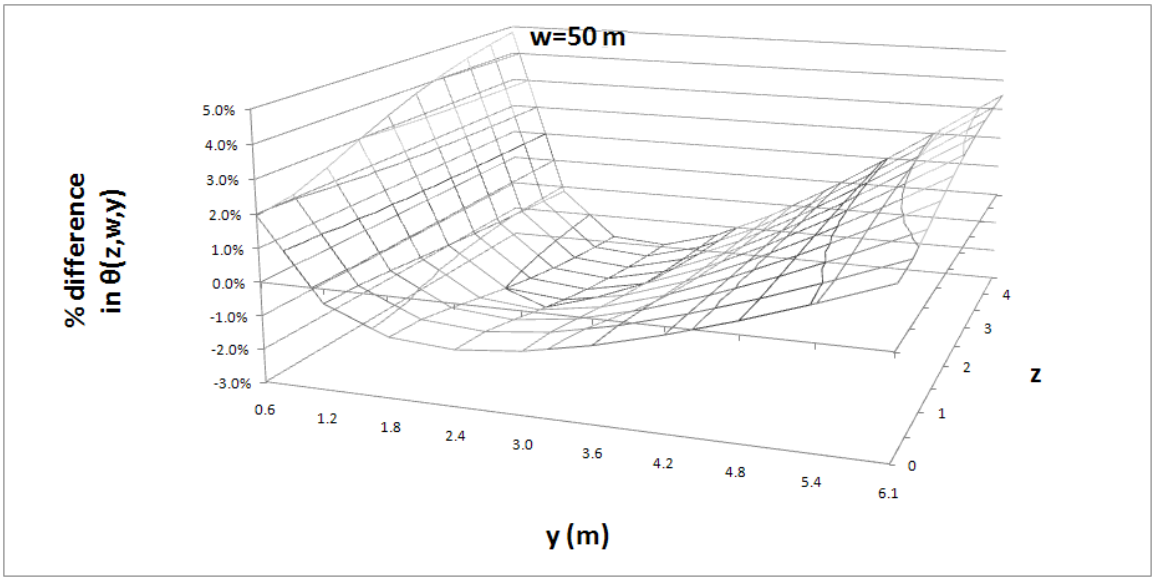

Figure 3: Percent relative differences among the Eq. [16]-calculated and Eq. [17]-calculated $\theta(z,w,y)$ for channel bottom width $w = 50$ m

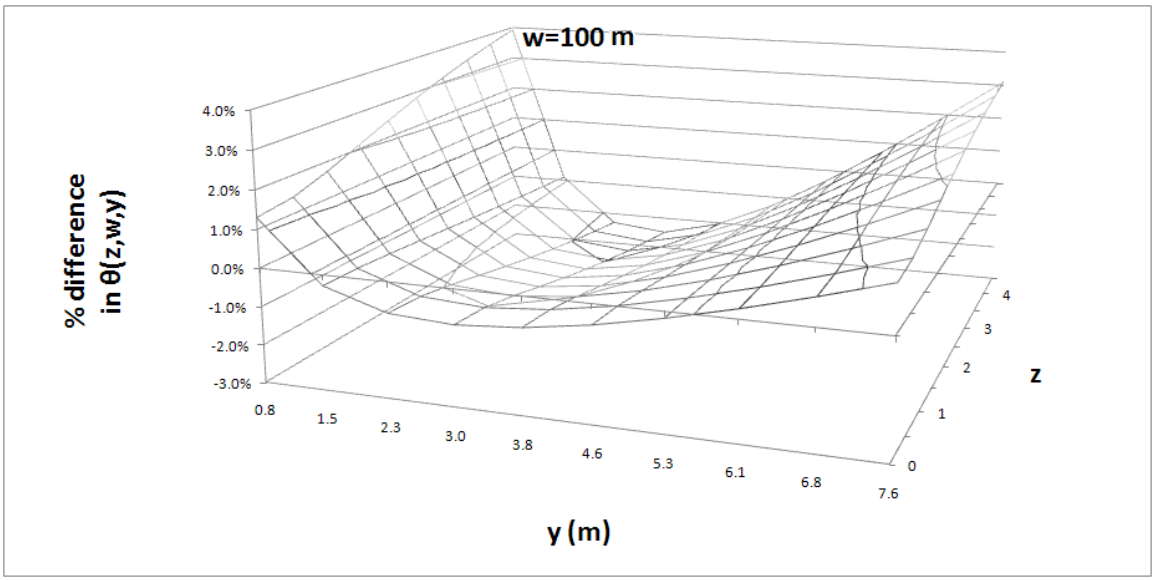

Figure 4: Percent relative differences among the Eq. [16]-calculated and Eq. [17]-calculated $\theta(z,w,y)$ for channel bottom width $w = 100$ m

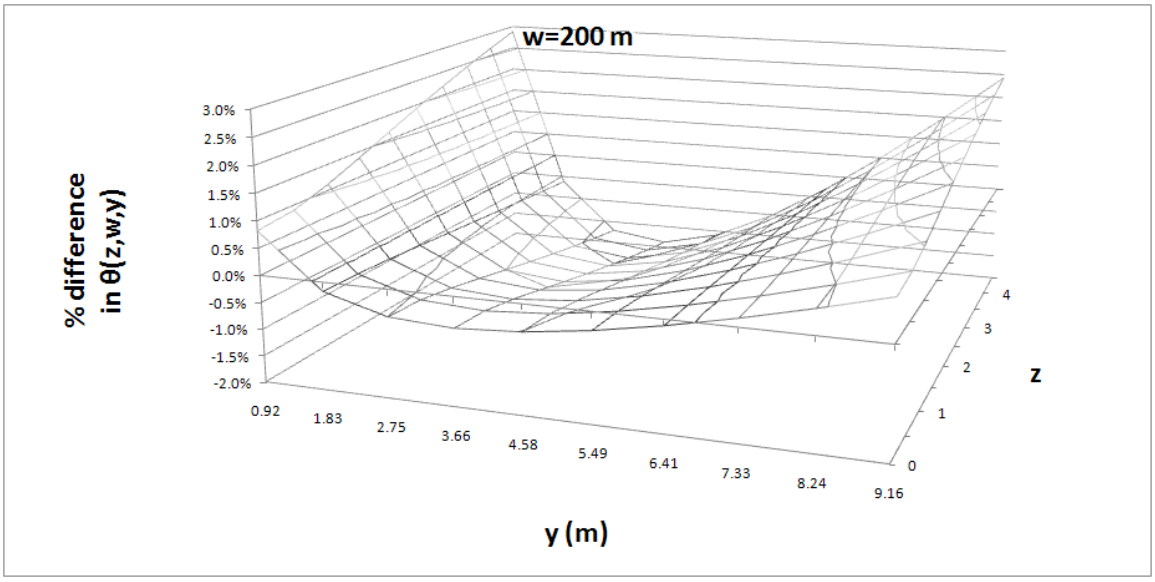

Figure 5: Percent relative differences among the Eq. [16]-calculated and Eq. [17]-calculated $\theta(z,w,y)$ for channel bottom width $w = 200$ m

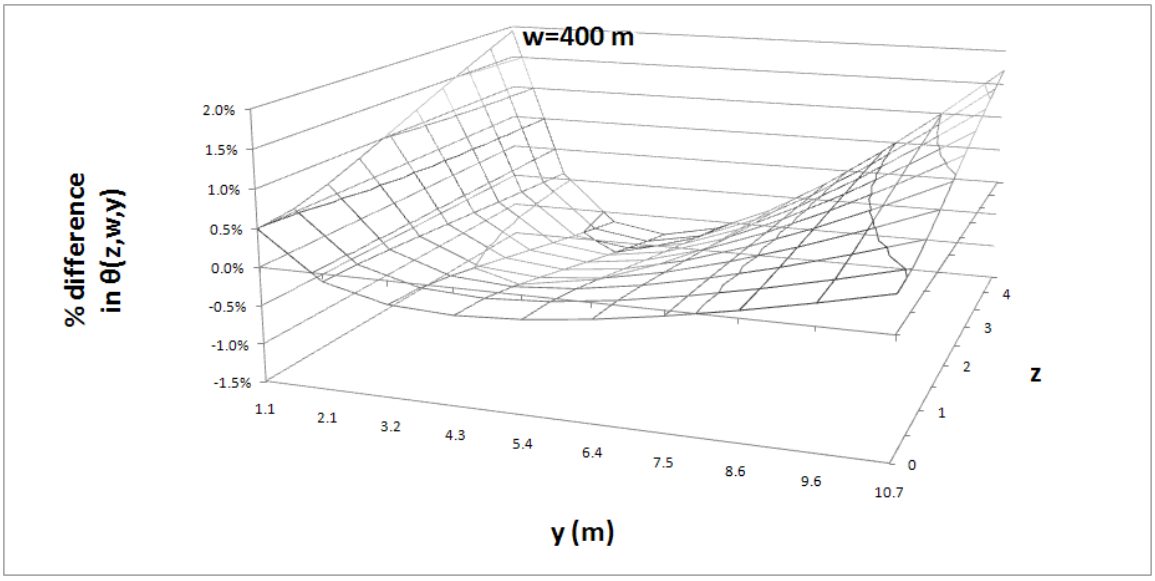

Figure 6: Percent relative differences among the Eq. [16]-calculated and Eq. [17]-calculated $\theta(z,w,y)$ for channel bottom width $w = 400$ m

As shown in Figures 2-6 the modeled $\theta(z,w,y)$ values are within %6 of the actual values of $\theta(z,w,y)$.

Finally, the two kinematic wave equations Eq. [1] and Eq. [2] are reduced into a partial differential equation with a state variable A and parameters, z, w, S, n, $c(z,w)$ and $c(z,w)$ that are independent of the flow depth, as follows,

$$\frac{\partial A}{\partial t} + \frac{\partial}{\partial x}\left(\frac{S^{1/2}}{n} \cdot c(z,w) \cdot A^{m(z,w)}\right) - q = 0 \qquad [30]$$

Discussion and Conclusion

When the Manning's equation is used for the momentum equation in the kinematic wave model, the kinematic wave parameters emerge as variables dependent on the flow depth except for some special cross-sections. In this study the kinematic wave parameters were modeled by using the power law-least squares fitting method in order to obtain these parameters independent of the flow depth. The estimated numerical values of the kinematic wave parameters for varying channel bottom width and channel side slope were also tabulated as a reference for future studies. Here the kinematic wave parameters were modeled only for trapezoidal channel cross-sections, yet they also cover the rectangular and triangular cross-sections. The power law-least squares fitting method was introduced as a tool and evaluated for its potential for modeling kinematic wave parameters. The modeled kinematic wave parameters provided very good approximation for the momentum equation of the kinematic wave model. Since the kinematic wave parameters were modeled as variables independent of the flow depth, the resulting kinematic wave equation is much easier to work with than the conventional kinematic wave equations.

References

Haltas, I. and Kavvas, M.L. (2008), "Ensemble averaged flow routing in channel networks: Kinematic wave equation", J. of Hydrological Engineering (accepted, October 2008)

Lighthill, M. J. and C. B. Whitham, (1955), "On Kinematic Waves: Flood Movement in Long Rivers.", Proc. Royal Society (London), Series A, 229, pp. 281-316.

MacArthur, R. C. and DeVries, J. J. (1993), "Introduction and Application of Kinematic Wave Routing Techniques Using HEC-1.", Training Document 10, US Army Corps of Engineers.

Weisstein, E. W. (2008) "Least Squares Fitting--Power Law.", From MathWorld--A Wolfram Web Resource.
http://mathworld.wolfram.com/LeastSquaresFittingPowerLaw.html

On the Use of Data Uncertainty in Hydro-climatic Modeling: a Bayesian Approach

Shivam Tripathi and Rao S Govindaraju

School of Civil Engineering, Purdue University, West Lafayette, IN 47907, USA
PH (765) 496-3402; FAX (765) 496-1988; email govind@ecn.purdue.edu

Abstract

Sea surface temperature (SST) is an important link between global climate and regional hydrology, and consequently its use is ubiquitous in statistical and physical models for hydrologic prediction. Historical observations of SST are based on in situ measurements from ships and buoys. These measurements have large associated uncertainties that have been archived with the data, but are vastly ignored in the literature either because of lack of appropriate tools or because the benefits of engaging uncertainties are not well understood. In this study, a Bayesian framework is developed to incorporate data uncertainty when performing supervised (regression analysis) and unsupervised (principal component analysis) learning. The developed methods are applied to predict all Indian summer monsoon rainfall (AISMR) using SST as inputs. The benefits of engaging data uncertainties, which include better assessment of predictions skills, are discussed.

Keywords: Hydrologic prediction, data uncertainty, sea surface temperature, Bayesian learning, Indian monsoon

Introduction

A recent trend in hydrologic prediction models is to derive predictability from variables governing atmospheric and oceanic circulations that are measured using *in situ* and\or remote-sensing observations and have various sources of uncertainties. The magnitude of measurement uncertainties, which are now often quantified, differ from variable to variable and for a given variable vary substantially in space and time. This information, though available, is mostly ignored in traditional models because methods for engaging uncertainty are subjective, difficult, and the associated benefits are not well established.

In statistical hydrologic models, measurement uncertainties in data can influence various stages of model development including selection of predictors, estimation of model parameters, and quantification of prediction uncertainties. This

study develops a methodology to engage data uncertainty in principal component analysis and regression using Bayesian framework.

Principal component analysis (PCA) is arguably the most popular method to extract predictors in hydrologic prediction models. However, standard PCA (SPCA) ignores data uncertainty information in deriving principal components (PCs). Tripathi and Govindaraju (2008) developed Bayesian noisy PCA (BaNPCA) to overcome this problem and demonstrated that BaNPCA improves the performance of PCA by extracting PCs that have low data reconstruction error. However, BaNPCA algorithm is based on type-II maximum likelihood using local Gaussian approximation for the posterior distribution of the model parameters, an assumption that is likely to be violated if the sample size is small. This study develops an alternative algorithm for BaNPCA using *variational inference* or *variational Bayes* method (Jordan et al., 1999) that avoids local approximations thus making it more suitable for typical hydrologic data sets. The algorithm is termed as variational Bayes noisy PCA (VBaNPCA).

The predictors identified after PCA are mapped to the predictand by a functional relationship that takes form of a *regression* model if the predictand is a continuous variable, or *classification* model if the predictand is a categorical variable. This study considers the former case and employs relevance vector machine (RVM ; Tipping, 2001) as a regression model. Standard RVM does not account for measurement uncertainites in independent variabels. Quiñonero Candela et al. (2003) modified the RVM algorithm to engage that information during prediction phase and demonstrated its advantages for multi-step forecast. However, their method ignores uncertainty during RVM training phase, a limitation that, to our knowledge, has not been addressed in the literature. In this study, a methodology is proposed to utilize information of measurement errors in predictors during both training and prediction phases of RVM algorithm. The algorithm is based on variational principles and is termed as variational noisy RVM (VNRVM).

The following objectives have been set for this study: (i) to develop a fully Bayesian method (VBaNPCA) for deriving PCs by engaging data uncertainty information, (ii) to propose variational noisy RVM (VNRVM) that learns regression relationship when dependent variables have uncertainties, and (iii) to explore the benefits of proposed algorithms in predicting all India summer monsoon rainfall.

The remainder of this paper is structured as follows. Mathematical details of VBaNPCA and VNRVM are given in the next section. Following this, data used in the study are described and the methodology is presented. Results obtained are presented and discussed in the last section.

Mathematical formulation

The following notation are used: N samples of independent variables in p dimensional real space are denoted by $\boldsymbol{X} = [\boldsymbol{x}_n]^{\mathrm{T}}$ ($n = 1, \ldots, N$; $\boldsymbol{x}_n \in \Re^p$), and the corresponding dependent variable is given $\boldsymbol{y} = [y_n]^{\mathrm{T}}$ ($y_n \in \Re$). The independent variables are observed with known measurement errors given by

$$\tilde{\boldsymbol{x}}_n = \boldsymbol{x}_n + \boldsymbol{\zeta}_n \tag{1}$$

where $\tilde{\boldsymbol{x}}_n$ are the observed values of the nth sample, and $\boldsymbol{\zeta}_n$ is associated measurement error following Gaussian distribution with mean zero and variance $\boldsymbol{B}_n^{-1}$.

Matrices are represented by upper case bold italic letters. All vectors are column vectors and are represented by lower case bold italic letters. Normal font italic letters represent scalars, $m \times m$ identity matrix is shown as $\boldsymbol{I}_m$, symbol $\langle x \rangle$ denotes expected value of a random variable x, and diag($\boldsymbol{x}$) represents a diagonal matrix with diagonal elements $\boldsymbol{x}$.

Variational Bayes noisy principal component analysis

The goal of PCA is to linearly map $\boldsymbol{x}_n$ from p dimensional real to q dimensional real space so that the transformed data $\boldsymbol{z}_n$ ($\boldsymbol{z}_n \in \Re^q$; $q < p$), for a given q, preserves maximum variance in $\boldsymbol{x}_n$. In probabilistic formulation of PCA, $\boldsymbol{x}_n$ is defined as linear transformation of $\boldsymbol{z}_n$ using following linear Gaussian latent variable model

$$\boldsymbol{x}_n = \boldsymbol{W}\boldsymbol{z}_n + \boldsymbol{\mu} + \boldsymbol{\varepsilon}_n \tag{2}$$

where $\boldsymbol{z}_n$ are the latent variables, $\boldsymbol{\varepsilon}_n$ is isotropic Gaussian noise $\boldsymbol{\varepsilon}_n \sim \mathcal{N}(\boldsymbol{\varepsilon}_n|0, \sigma^2\boldsymbol{I}_p)$, $\boldsymbol{\mu}$ is a p dimensional vector, and $\boldsymbol{W}$ is a $p \times q$ matrix. For notational simplicity, variance of the error term (σ^2) will be represented by τ, where $\tau = \sigma^{-2}$. Tipping and Bishop (1999) proved that if the prior distribution over $\boldsymbol{z}_n$ is zero mean Gaussian distribution, $p(\boldsymbol{z}_n) \sim \mathcal{N}(\boldsymbol{z}_n|0, \boldsymbol{I}_q)$, then the maximum likelihood solution of $\boldsymbol{W}$ contains principal directions of data matrix $\boldsymbol{X}$ in its column.

Tripathi and Govindaraju (2008) extended probabilistic PCA to engage measurement uncertainties of observed data in the analysis and developed a Bayesian framework for estimating model parameter $\boldsymbol{W}$. However, the algorithm was not fully Bayesian because apart from $\boldsymbol{W}$ other model parameters and hyper-parameters were estimated either by using Expectation-Maximization (EM) algorithm or maximum a posteriori (MAP) method that approximates a posterior distribution by a delta function at its mode. This approximation is justified when $N >> p$, a case seldom satisfied by hydro-climatic datasets including SST data. In this study, a complete Bayesian treatment of BaNPCA algorithm is proposed; the new algorithm is referred to as variational BaNPCA (VBaNPCA). Mathematically, the algorithm is given by Eqs.1 and 2. An important difference between BaNPCA and VBaNPCA is the introduction of true data $\boldsymbol{x}_n$ as a latent variable in VBaNPCA, which substantially reduces the mathematical complexity in estimating noise variance σ^2, a computational bottleneck in the earlier BaNPCA algorithm.

In VBaNPCA, the following hierarchical priors are assigned to model parameters and hyper-parameters

$$p(\boldsymbol{W}|\boldsymbol{\alpha}) = \prod_{j=1}^{p} \mathcal{N}(\boldsymbol{w}_j|0, \alpha_j); \quad \text{where} \quad \boldsymbol{\alpha} = [\alpha_1, \ldots, \alpha_q]^{\mathrm{T}} \tag{3}$$

$$p(\alpha_j) = \text{Gamma}(\alpha_j|a_0, b_0); \quad j = 1, \ldots, p \tag{4}$$

$$p(\boldsymbol{\mu}) = \mathcal{N}(\boldsymbol{\mu}|0, \beta_0^{-1}\boldsymbol{I}_p) \tag{5}$$

$$p(\tau) = \text{Gamma}(\tau|c_0, d_0) \tag{6}$$

where the column vector $\boldsymbol{w}_j$ denotes j^{th} column of $\boldsymbol{W}$. The priors are made broad or non-informative by setting $a_0 = b_0 = c_0 = d_0 = \beta_0 = 10^{-3}$. The posterior distribution for the model parameters and latent variables, $p(\Theta|\tilde{\boldsymbol{X}})$, where $\Theta = [\boldsymbol{X}, \boldsymbol{Z}, \boldsymbol{W}, \boldsymbol{\mu}, \boldsymbol{\alpha}, \tau]$, does not have a closed form and is therefore approximated. Herein, variational principles are employed to deterministically approximate $p(\Theta|\tilde{\boldsymbol{X}})$ by $Q(\Theta|\tilde{\boldsymbol{X}})$ such that $Q(\Theta|\tilde{\boldsymbol{X}})$ is similar to $p(\Theta|\tilde{\boldsymbol{X}})$ and at the same time has a closed form. The variational method used in this study has its origin in *mean field theory* (Parisi, 1988) where it was developed to approximate lowest-energy state in quantum mechanical calculations. It assumes that the approximating distribution $Q(\Theta|\mathcal{D})$ factorize as

$$Q(\Theta) = Q(\boldsymbol{X}, \boldsymbol{Z}, \boldsymbol{W}, \boldsymbol{\mu}, \boldsymbol{\alpha}, \tau) = q(\boldsymbol{X})q(\boldsymbol{Z})q(\boldsymbol{W})q(\boldsymbol{\alpha})q(\boldsymbol{\mu})q(\tau). \tag{7}$$

where to make the notation uncluttered, explicit dependence of approximating distribution on data $\tilde{\boldsymbol{X}}$ is dropped. The optimal solution for the individual components in the factorized distribution are obtained by minimizing the Kullback-Leibler (KL) divergence (Kullback and Leibler, 1951) between $Q(\Theta)$ and $p(\Theta|\tilde{\boldsymbol{X}})$ with respect to those components. The optimal solution for the components of factorized distribution takes the following closed form

$$\begin{aligned}
q^\star(\boldsymbol{X}) &= \prod_{n=1}^{N} \mathcal{N}(\boldsymbol{x}_n|\boldsymbol{m}_{x_n}, \boldsymbol{P}_{x_n}^{-1}) \\
q^\star(\boldsymbol{Z}) &= \prod_{n=1}^{N} \mathcal{N}(\boldsymbol{z}_n|\boldsymbol{m}_{z_n}, \boldsymbol{P}_{z_n}^{-1}) \\
q^\star(\boldsymbol{W}) &= \prod_{i=1}^{p} \mathcal{N}(\acute{\boldsymbol{w}}_i|\boldsymbol{m}_{\acute{w}_i}, \boldsymbol{P}_{w}^{-1}) \\
q^\star(\boldsymbol{\alpha}) &= \prod_{j=1}^{q} \text{Gamma}(\alpha_j|a_\alpha, b_{\alpha_j}) \\
q^\star(\boldsymbol{\mu}) &= \mathcal{N}(\boldsymbol{\mu}|\boldsymbol{m}_\mu, \beta^{-1}\boldsymbol{I}_p) \\
q^\star(\tau) &= \text{Gamma}(\tau|c, d)
\end{aligned}$$

where column vector $\acute{\boldsymbol{w}}_i$ denotes i^{th} row of $\boldsymbol{W}$, and

$$\begin{aligned}
\boldsymbol{P}_{x_n} &= \boldsymbol{B}_n + \langle\tau\rangle\boldsymbol{I}_p \\
\boldsymbol{m}_{x_n} &= \boldsymbol{P}_{x_n}^{-1}[\langle\tau\rangle(\langle\boldsymbol{W}\rangle\langle\boldsymbol{z}_n\rangle + \langle\boldsymbol{\mu}\rangle) + \boldsymbol{B}_n\tilde{\boldsymbol{x}}_n] \\
\boldsymbol{P}_{z_n} &= \langle\tau\rangle\left\langle\boldsymbol{W}^{\text{T}}\boldsymbol{W}\right\rangle + \boldsymbol{I}_q \\
\boldsymbol{m}_{z_n} &= \langle\tau\rangle\,\boldsymbol{P}_{z_n}^{-1}[\langle\boldsymbol{W}\rangle^{\text{T}}(\langle\boldsymbol{x}_n\rangle - \langle\boldsymbol{\mu}\rangle)] \\
\boldsymbol{P}_{w} &= diag(\langle\boldsymbol{\alpha}\rangle) + \langle\tau\rangle\textstyle\sum_{n=1}^{N}\left\langle\boldsymbol{z}_n\boldsymbol{z}_n^{\text{T}}\right\rangle \\
\boldsymbol{m}_{\acute{w}_i} &= \langle\tau\rangle\,\boldsymbol{P}_{w}^{-1}\left[\textstyle\sum_{n=1}^{N}\langle\boldsymbol{z}_n\rangle(\langle x_{ni}\rangle - \langle\mu_i\rangle)\right] \\
a_\alpha &= a_0 + p/2 \\
b_{\alpha_j} &= b_0 + \left\langle\boldsymbol{w}_j^{\text{T}}\boldsymbol{w}_j\right\rangle/2
\end{aligned}$$

$$
\begin{aligned}
\beta &= \beta_0 + N\langle\tau\rangle \\
\boldsymbol{m}_\mu &= \langle\tau\rangle \beta^{-1} \boldsymbol{I}_p \textstyle\sum_{n=1}^{N} (\langle\boldsymbol{x}_n\rangle - \langle\boldsymbol{W}\rangle\langle\boldsymbol{z}_n\rangle) \\
c &= c_0 + N/2 \\
d &= d_0 + \frac{1}{2}\textstyle\sum_{n=1}^{N} [\langle\boldsymbol{x}_n^{\mathrm{T}}\boldsymbol{x}_n\rangle + \mathrm{trace}\left(\langle\boldsymbol{W}^{\mathrm{T}}\boldsymbol{W}\rangle\langle\boldsymbol{z}_n\boldsymbol{z}_n^{\mathrm{T}}\rangle\right) + \langle\boldsymbol{\mu}^{\mathrm{T}}\boldsymbol{\mu}\rangle \\
&\quad +2\langle\boldsymbol{\mu}\rangle^{\mathrm{T}}\langle\boldsymbol{W}\rangle\langle\boldsymbol{z}_n\rangle - 2\langle\boldsymbol{x}_n\rangle^{\mathrm{T}}(\langle\boldsymbol{W}\rangle\langle\boldsymbol{z}_n\rangle + \langle\boldsymbol{\mu}\rangle)].
\end{aligned}
$$

The expected values required in the equations were evaluated using following properties. For a Gaussian distribution, $p(\boldsymbol{x}) \sim \mathcal{N}(\boldsymbol{x}|\boldsymbol{\mu}, \boldsymbol{P}^{-1})$,

$$\langle\boldsymbol{x}\rangle = \boldsymbol{\mu}, \quad \langle\boldsymbol{x}\boldsymbol{x}^{\mathrm{T}}\rangle = \boldsymbol{\mu}\boldsymbol{\mu}^{\mathrm{T}} + \boldsymbol{P}^{-1}, \text{ and } \quad \langle\boldsymbol{x}^{\mathrm{T}}\boldsymbol{x}\rangle = \boldsymbol{\mu}^{\mathrm{T}}\boldsymbol{\mu} + \mathrm{trace}(\boldsymbol{P}^{-1}); \tag{8}$$

and for a Gamma distribution, $p(x) \sim \mathrm{Gamma}(x|a, b)$,

$$\langle x\rangle = \frac{a}{b}, \text{ and } \quad \langle x^2\rangle - \langle x\rangle^2 = \frac{a}{b^2}. \tag{9}$$

Variational noisy relevance vector machine (VNRVM)

Let the regression relationship between between independent variable $\boldsymbol{x}_n$ and dependent variable y_n be given by

$$y_n = f(\boldsymbol{x}_n, \boldsymbol{X}; w_0, \boldsymbol{w}) + \varepsilon = w_0 + \boldsymbol{w}^{\mathrm{T}}\boldsymbol{\phi}_n + \varepsilon \tag{10}$$

where parameter w_0 that allows for a fixed offset in the data is termed as 'bias'; $\boldsymbol{w} = [w_1, \ldots, w_M]^{\mathrm{T}}$ is weight vector; ε is noise term assumed to have zero mean Gaussian distribution with variance σ_ε^2 (precision $\tau_\varepsilon = \sigma_\varepsilon^{-2}$), i.e. $\varepsilon \sim \mathcal{N}(\varepsilon|0, \sigma_\varepsilon^2)$; and $\boldsymbol{\phi}_n = [\phi(\boldsymbol{x}_1, \boldsymbol{x}_n), \ldots, \phi(\boldsymbol{x}_M, \boldsymbol{x}_n)]^{\mathrm{T}}$ is a vector of basis functions. In RVM, basis functions are functions with one kernel associated with each data point in the training data, i.e. $M = N$. In standard RVM the complexity of the regression model is governed by assigning following hierarchical priors over bias and weight vectors

$$p(w_j|\alpha_j) = \mathcal{N}(w_j|0, \alpha_j^{-1}); \qquad j = 0, \ldots, M. \tag{11}$$

where α_j is a hyper-parameter with a non-informative uniform prior over log space as with σ_ε^2. Ideally, model parameters should be estimated by determining their posterior distribution using Bayes rule. Since this is analytically intractable, posterior distribution is estimated only for bias and weight vectors whereas point estimates are obtained for other parameters using type-II maximum likelihood approach that approximates posterior distributions by a delta function at their modes. This assumption is justified when number of data points (N) is very large because in that case posterior distribution is tightly concentrated around its mean. However, in typical hydrologic applications, N tends to be small and this approximation is rarely justified.

A complete Bayesian treatment of RVM through variational inference was proposed by Bishop and Tipping (2000). In this study, their method is extended to incorporate measurement uncertainties of input data into RVM learning.

As in VBaNPCA, the true input $\boldsymbol{x}_n$ is treated as a latent variable in VNRVM. The following prior distributions were assigned to model hyper-parameters and noise variance

$$p(\alpha_j) = \text{Gamma}(\alpha_j|a_0, b_0); \quad j = 0, \ldots, M \tag{12}$$
$$p(\tau_\varepsilon) = \text{Gamma}(\tau_\varepsilon|c_0, d_0). \tag{13}$$

The priors were made flat or non-informative by setting $a_0 = b_0 = c_0 = d_0 = 10^{-3}$. For this choice of prior distribution, the posterior distribution does not have analytical solution and is approximated using variational method described in the previous section. The approximation to the posterior distribution of model parameters and latent variables is given by

$$Q(\boldsymbol{X}, \boldsymbol{w}, w_0, \boldsymbol{\alpha}, \alpha_0, \tau_\varepsilon) = q(\boldsymbol{X})q(\boldsymbol{w})q(w_0)q(\boldsymbol{\alpha})q(\alpha_0)q(\tau_\varepsilon).$$

The optimal solution for $q(\boldsymbol{X})$ depends on the choice of kernel function and will be discussed shortly. Optimal solution for other components of Q were analytically estimated as

$$q^\star(\boldsymbol{w}) = \mathcal{N}(\boldsymbol{w}|\boldsymbol{m}_w, \boldsymbol{P}_w) \tag{14}$$
$$q^\star(w_0) = \mathcal{N}(w_0|m_{w_0}, p_{w_0}) \tag{15}$$
$$q^\star(\boldsymbol{\alpha}) = \prod_{j=1}^{M} \text{Gamma}(\alpha_j|a_\alpha, b_{\alpha_j}) \tag{16}$$
$$q^\star(\alpha_0) = \text{Gamma}(\alpha_0|a_\alpha, b_{\alpha_0}) \tag{17}$$
$$q^\star(\tau_\varepsilon) = \text{Gamma}(\tau_\varepsilon|c, d) \tag{18}$$

where

$$\boldsymbol{P}_w = \text{diag}(\langle\boldsymbol{\alpha}\rangle) + \langle\tau_\varepsilon\rangle \sum_{n=1}^{N} \left\langle \boldsymbol{\phi}_n^{\mathrm{T}}\boldsymbol{\phi}_n \right\rangle$$
$$\boldsymbol{m}_w = \langle\tau_\varepsilon\rangle \boldsymbol{P}_w^{-1} \sum_{n=1}^{N} \langle\boldsymbol{\phi}_n\rangle (y_n - \langle w_0\rangle)$$
$$p_{w_0} = \langle\alpha_0\rangle + N \langle\tau_\varepsilon\rangle$$
$$m_{w_0} = \langle\tau_\varepsilon\rangle p_{w_0}^{-1} \sum_{n=1}^{N} (y_n - \langle\boldsymbol{w}\rangle^{\mathrm{T}} \langle\boldsymbol{\phi}_n\rangle)$$
$$a_\alpha = a_0 + 1/2$$
$$b_{\alpha_j} = b_0 + \left\langle w_j^2 \right\rangle; \quad j = 0, \ldots, M$$
$$c = c_0 + N/2$$
$$d = d_0 + \frac{1}{2} \sum_{n=1}^{N} [y_n^2 + \text{trace}(\left\langle \boldsymbol{w}\boldsymbol{w}^{\mathrm{T}} \right\rangle \left\langle \boldsymbol{\phi}_n\boldsymbol{\phi}_n^{\mathrm{T}} \right\rangle) + N \left\langle w_0^2 \right\rangle$$
$$+ 2 \langle w_0\rangle \langle\boldsymbol{w}\rangle^{\mathrm{T}} \langle\boldsymbol{\phi}_n\rangle - 2y_n(\langle\boldsymbol{w}\rangle^{\mathrm{T}} \langle\boldsymbol{\phi}_n\rangle + \langle w_0\rangle)]$$

and the required moments are estimated using Eqs. 8 and 9. For linear VNRVM, i.e. $\boldsymbol{\phi}_n = \boldsymbol{x}_n$, the optimal solution for $q(\boldsymbol{X})$ has a closed form given by

$$q^{\star}(\boldsymbol{X}) = \prod_{n=1}^{N} \mathcal{N}(\boldsymbol{x}_n | \boldsymbol{m}_{x_n}, \boldsymbol{P}_{x_n}^{-1}) \tag{19}$$

where

$$\begin{aligned} \boldsymbol{P}_{x_n} &= \boldsymbol{B}_n + \langle \tau_\varepsilon \rangle \langle \boldsymbol{w}\boldsymbol{w}^{\mathrm{T}} \rangle \\ \boldsymbol{m}_{x_n} &= \boldsymbol{P}_{x_n}^{-1} [\langle \tau_\varepsilon \rangle \langle \boldsymbol{w} \rangle (y_n - \langle w_0 \rangle) + \boldsymbol{B}_n \tilde{\boldsymbol{x}}_n]. \end{aligned}$$

For nonlinear regression, the distribution $q^{\star}(\boldsymbol{X})$ does not have closed from and was approximated using Metropolis-Hasting algorithm (Bishop, 2006).

Data used in the study

Sea surface temperature

Gridded sea surface temperature data available at monthly time step from HadSST2 (Rayner et al., 2006) prepared at the Hadley Centre for Climate Prediction and Research, UK, website `http://hadobs.metoffice.com/hadsst2/` were used in the study. HadSST2 is an un-interpolated sea surface temperature data set based on *in-situ* measurements of SST obtained mainly from ships and buoys. The climatological values were subtracted from the SST measurements to estimate anomalies. The resulting anomalies were gridded onto a 5^0 latitude by 5^0 longitude monthly grid by taking *winsorized mean*. Bias correction was applied on the gridded anomalies to remove spurious trends caused by changes in SST measuring practices, following the procedure of Folland and Parker (1995).

HadSST2 accounts for uncertainty arising from - (i) measurement and sampling errors (M&SE). Measurement errors are related to precision of the instruments used for measuring SST, while sampling errors are caused by estimating an area-averaged quantity from a finite number of noisy observations; (ii) bias due to different measurement practices over the observation period. The combined uncertainty was obtained by adding M&SE and errors due to bias correction, in quadrature, i.e. by taking square root of the sum of the squares of errors.

All India summer monsoon rainfall

The area weighted rainfall data for India (Parthasarathy et al., 1994) was extracted from Indian Institute of Tropical Meteorology, Pune, web site `http://www.tropmet.res.in`. The data extends from January 1871 to December 2006. Primary source of the data is India Meteorological Department. The time series of summer monsoon rainfall was derived by adding monthly rainfall values for monsoon months (JJAS).

Methodology, Results, and Discussion

HadSST2 dataset is available from 1850 onwards, but data from January 1901 to December 2006 were used in this study. The grid points with more than 50% of missing records were not considered in the analysis. The data were partitioned

into five non-overlapping sectors - (i) Tropical Pacific sector (30^0S – 30^0N), (ii) North Pacific sector (north of 30^0N), (iii) Tropical Atlantic sector (30^0S – 30^0N), (iv) North Atlantic sector (north of 30^0N), (v) and Indian Ocean sector (north of 30^0S) to reduce the influence of strong ENSO signals on variability of SST data outside of the tropical Pacific Ocean. The monthly SST anomalies were averaged to get seasonal anomalies for four seasons (DJF, MAM, JJA, and SON). Since the measurement errors in monthly anomalies were independent, the error variance in the seasonal anomaly was estimated by taking the average of error variance in monthly anomalies. Seasonal SST tendencies, defined as a change in SST anomalies from the previous season, were estimated and the associated error variances were calculated by adding variances in the anomalies of current and previous season. In the following, the term 'SST data' will refer to both SST anomalies and SST tendencies. The predictors for mean monsoon rainfall were identified from the SST data, one season lag to three years lag from the monsoon season. The data were partitioned into a training set (1901 to 1985) and a test set (1986 to 2006), only the former set was used for identifying predictors.

The models were developed following two approaches. In the first approach, SST data for each season in an oceanic sector were processed using PCA, the PCs obtained were correlated with AISMR to select predictors, which were then used by a regression model to learn a functional relationship between them and AISMR. The approach is referred to as *PCR*, which reflects the order in which the algorithms were applied, i.e. PCA, followed by correlation, and regression. In the second approach, termed *CPR*, AISMR data were first correlated with SST data at each grid points to select useful features. The selected features were subsequently processed by PCA to yield PCs, which in turn form input to the regression model. The advantages of the two approaches are complementary. On the one hand, in PCR, dimensionality of potential predictors is reduced by PCA that removes noise in the data but in the process may also remove important information resulting in poor performance. On the other hand, in CPR, all the information is retained and the predictors are searched in a much larger space of potential predictors leading to good results but possibly poor generalization performance.

Table 1 shows correlation and relative root mean square error (RRMSE) between observed and predicted values during training and testing periods using PCR approach by a set different algorithms. The following steps were taken to facilitate comparison among different algorithms

1. PCA: Only first three PCs of SST data from SPCA and VBaNPCA were used in the analysis;

2. Correlation: A feature was selected as a potential predictor if its Pearson product moment correlation with AISMR was greater or smaller than zero at 10% significance level.

3. Regression: The regression relation was learned using linear versions of RVM and VNRM algorithms.

PCA	Regression	Training		Testing	
		r	RRMSE	r	RRMSE
SPCA	RVM	0.80	5.52	0.33	6.97
VBaNPCA	RVM	0.88	3.09	0.52	1.57
	VNRVM	0.89	2.99	0.51	1.70

Table 1: Prediction of all India summer monsoon rainfall using PCR approach. The symbols r and RRMSE correspond to the correlation and relative root mean square error between observed and predicted rainfall values after normalization

The results indicate that the models engaging data uncertainty information perform better than the models that do not use it. VBaNPCA algorithm appears to significantly affect the prediction performance while other two methods, BaNCorr and VNRVM, only marginally alter the prediction performance.

Table 2 summarizes the results obtained form algorithms following CPR approach. For the results reported, the first step in CPR approach was performed using Pearson product moment correlation. The step involves selecting grid points in SST data for which the null hypothesis of no correlation with AISMR was rejected at 1% significance level. The selected feature were processed using SPCA and VBaNPCA to obtain predictors for the regression model. In VBaNPA, the number of predictors was automatically selected to be 11; for consistency, the same number of predictors were used in SPCA. The results in Table 2 corroborate the previous conclusion that the models engaging input uncertainty information improves prediction performance. Comparison of PCR and CPR approaches show that for training period the performance of CPR is not statistically different form PCR model, however, during testing it performs poorly, suggesting that including too many potential predictors may actually degrade the generalization performance of the model.

Correlation	PCA	Regression	Training		Testing	
			r	RRMSE	r	RRMSE
Pearson	SPCA	RVM	0.85	2.68	0.27	43.31
	VBaNPCA	RVM	0.84	4.42	0.35	7.42
		VNRVM	0.85	4.45	0.36	8.44

Table 2: Prediction of all India summer monsoon rainfall using CPR approach. The symbols r and RRMSE correspond to the correlation and relative root mean square error between observed and predicted rainfall values after normalization

The results obtained in this study suggest that incorporating measurement errors in hydrologic models improves their prediction performance and provides better assessment of their predictive capabilities.

REFERENCES

Bishop, C. M. (2006). *Pattern Recognition and Machine Learning*. Information Science and Statistics. Springer, New York, USA, first edition.

Bishop, C. M. and Tipping, M. E. (2000). "Variational relevance vector machines." *Proceedings of the sixteenth conference on uncertainty in artificial intelligence*, C. Boutilier and M. Goldszmidt, eds., San Francisco, CA, USA. Morgan Kaufmann Publishers Inc., 46–53.

Folland, C. K. and Parker, D. E. (1995). "Correction of instrumental biases in historical sea surface temperature data." *Quarterly Journal of The Royal Meteorological Society*, 121(522), 319–367.

Jordan, M. I., Ghahramani, Z., Jaakkola, T. S., and Saul, L. K. (1999). "An introduction to variational methods for graphical models." *Machine Learning*, 37(2), 183–233.

Kullback, S. and Leibler, R. A. (1951). "On information and sufficiency." *The Annals of Mathematical Statistics*, 22(1), 79–86.

Parisi, G. (1988). *Statistical Field Theory*. Addison-Wesley, New York.

Parthasarathy, B., Munot, A. A., and Kothawale, D. R. (1994). "All-India monthly and seasonal rainfall series: 1871-1993." *Theoretical and Applied Climatology*, 49(4), 217–224.

Quiñonero Candela, J., Girard, A., Larsen, J., and Rasmussen, C. E. (2003). "Propagation of uncertainty in Bayesian kernel models - Application to multiple-step ahead forecasting." *IEEE International Conference on Acoustics, Speech and Signal Processing*, Vol. 2, IEEE, Hong Kong. 701–704.

Rayner, N. A., Brohan, P., Parker, D. E., Folland, C. K., Kennedy, J. J., Vanicek, M., Ansell, T. J., and Tett, S. F. B. (2006). "Improved analyses of changes and uncertainties in sea surface temperature measured in situ since the mid-nineteenth century: The HadSST2 dataset." *Journal of Climate*, 19(3), 446–469.

Tipping, M. E. (2001). "Sparse Bayesian learning and the Relevance vector machine." *Journal of Machine Learning Research*, 1(3), 211–244.

Tipping, M. E. and Bishop, C. M. (1999). "Mixtures of probabilistic principal component analyzers." *Neural Computation*, 11(2), 443–482.

Tripathi, S. and Govindaraju, R. S. (2008). "Engaging uncertainty in hydrologic data sets using principal component analysis: BaNPCA algorithm." *Water Resources Research*, 44(W10409), doi:10.1029/2007WR006692.

Adjustment of the Z-R Relationship in Real-time for Use in South Florida

Amy Henschke[1], Emad Habib[1], Chandra S. Pathak[2]

[1] Department of Civil Engineering, University of Louisiana at Lafayette, P.O. Box 42291, Lafayette, LA 70504-2291; Ph (337) 482-0638; Fax (337) 482-0631

[2] Operations and Hydro Data Management Division, SCADA and Hydro Data Management Department, South Florida Water Management District, 3301 Gun Club Road, West Palm Beach, FL 33416-4680; PH (561) 682-2567; FAX (561) 682-2028; email: cpathak@sfwmd.gov

Abstract

Due to the limitations of rain gauges in representing spatial rainfall variability, radar estimates are of particular importance, especially in areas subject to variable rainfall from convective storms. This study explores the use of a real-time adjustment of the reflectivity-rainfall (Z-R) relationship in determining radar rainfall estimates throughout the South Florida Water Management District (SFWMD). Level II reflectivity data from the Melbourne (KMLB) NEXRAD radar site, operated by the National Weather Service (NWS), was used in conjunction with 15-minute precipitation data from real-time gauges operated by the SFWMD. The coefficients A and b of the Z-R relationship were adjusted at each time step of the study period, based on gauge and reflectivity pairs obtained from the preceding 24 hours, allowing for variability within the Z-R relationship as the rainfall event progressed. Verification of the radar estimates was conducted with a separate set of rain gauges, not included in the estimation of A and b, using various graphical and statistical methods. To further explore the applicability of this study to the SFWMD, radar estimates currently being supplied to the District by means of a different algorithm were also verified with the same methods for comparison to the real-time adjusted estimates.

Introduction

Accurate prediction of rainfall events through the use of radar is becoming increasingly important for water management and planning activities, particularly in areas where the representativeness of rain gauge readings is limited by highly variable rainfall from convective storms. Inherent errors within the radar estimation process itself, such as the calibration of the relationship between reflectivity (Z) and surface rainfall rates (R), however, lead to uncertainties in the radar rainfall estimates. The complexities of the estimation process are increased due to the variation of the Z-R relationship with rainfall type and location, which has been represented by many different power-law equations (Battan, 1973). This variation is attributed in part to changes in the rainfall drop size distribution (DSD) which can exhibit inter-storm and intra-storm variability. Through the use of DSD measurements, Steiner and Smith (2000) showed that the multiplicative coefficient, A, is particularly sensitive to variation on a storm-by-storm basis. Variation within a single storm was also proven to be a significant source of uncertainty in radar estimates by Uijlenhoet et al. (2003)

in the evaluation of a squall line rainstorm. Lee and Zawadzki (2005) in an analysis of the scale dependence of DSD variability showed that most of the DSD variability occurred within storms or between storms within a day. Habib et al., (2008) showed that variability in Z-R relationships can have a significant effect on the simulation of streamflow. This variable nature of the Z-R relationship therefore justifies the exploration of real-time calibration of the Z-R relationship to account for changing rainfall characteristics. Legates (2000) showed that calibrating the Z-R relationship in real-time using a sample of gauge and reflectivity pairs from the preceding month, while including a correction to account for overshooting of the radar beam, demonstrated marked improvement over fixed Z-R relationships for an area of the Southern Great Plains. In a further study on real-time Z-R adjustment, Alfieri et al. (2008) analyzed the optimal length of time to be considered in calibration, which was determined to be between 8-24 hours, based upon calculated bias and random error of trial calibration windows ranging from 1 hour to 1 day.

In this study, we evaluated the performance of real-time estimation of the Z-R relationship for use in the South Florida Water Management District as an alternative to the radar estimates currently supplied to the District. Estimation is conducted for October 2007 using 32 real-time rain gauges in the proximity of the Melbourne NEXRAD radar site and the results are verified using 21 additional gauges. Statistical comparisons are made between the two sets of radar estimates for a quantitative analysis of the results.

Study Site and Data Sets

The South Florida Water Management District (SFWMD) is located in the southern part of the Florida peninsula, covering approximately 17,930 square miles and 16 counties from Orlando to the Keys. Highly variable rainfall events produced by convective storms are common in this area during the wet season from June to October. The task of the SFWMD to monitor the quality and supply of water in this area of Florida includes the maintenance and operation of 287 rain gauge stations throughout the district, of which, approximately 151 are operated on a real time basis. Also included in the domain of the SFWMD are four NEXRAD WSR-88D radar stations operated by the National Weather Service (NWS), which include KBYX in Key West, KAMX in Miami, KMLB in Melbourne, and KBTW in Tampa.

The focus of this study was the area of the SFWMD located within the coverage of the KMLB site over a period of one month (October 2007). Data from this radar was obtained as a Level II reflectivity product which is released in approximately 5-minute intervals on a radial grid of 1° x 1 km. This data was then converted to a 2 km x 2 km grid and averaged over a 15 minute interval to match the time scale of the gauges.

Of the real-time gauges operated by the SFWMD, 32 were chosen for use in the calibration of the Z-R relationship based on their proximity (120 km or less) to the KMLB radar (Figure 1). These tipping-bucket gauges use a supervisory control and data acquisition (SCADA) system to transmit data by way of microwave, telemetry, or telephone lines, which allows them to be used for real-time evaluation of rainfall events. An additional 18 gauges (referred to here as CR-10), which do not

operate in real-time, were chosen as an independent reference for the validation of the radar estimates.

Methodology

The benefit of a real-time adjustment of the Z-R relationship for use in constructing radar rainfall estimates was evaluated using pairs of corresponding real-time rain gauge and reflectivity data. The calibration of the Z-R relationship was based upon the standard power-law form of

$$Z = AR^b .$$

The coefficients A and b in the above equation were determined at each 15-minute time step of the study period. For each time step, the sample consisted of Z and R pairs corresponding to all of the selected real-time gauges for the 24 hours preceding the interval, which allowed for a continuous assimilation of new rainfall information into the estimation of the coefficients. After preliminary work was conducted using calibration windows of 1-24 hours, the length of 24 hours was chosen in an effort to eliminate complications due to insufficient sample size associated with shorter windows of time. Only the estimation of A and b for time intervals occurring within the first day of the study period was determined based upon time windows of less than 24 hours, depending on the available length of time preceding each.

The sample used in the calibration at each time step was restricted to data pairs during rainy intervals in which the R values were greater than the gauge minimum hourly detectable rain rate of 1.016 mm and in which the Z values were between 20 and 50 dBZ to account for ground clutter and bright banding. For time intervals where the specified restrictions led to a sample size of less than 30 (i.e. at the onset of a rain event), default values of 300 and 1.4 were used for the coefficients A and b, respectively, due to an insufficient number of data pairs with which to generate reliable A and b values. In all other instances, the values of A and b were determined from the Z-R sample using three regression analysis techniques. The first method is a commonly used procedure based on a least-square-fit regression technique, which showed less positive results than the other two methods and has not been included in this paper. The second estimation method (BIAS-RMSE) is based on bias removal and minimizing root-mean-square errors. The parameter A is determined in such a way that the total rainfall accumulations estimated by the Z–R relationship (i.e., summation of $(Z_i /A)^{1/b}$; i=time step) is set equal to the accumulation of reference rainfall ($R_{ref,i}$) as observed by the gauge, whereas b is sought by minimizing the summation of squared residuals between measured reference rainfall rates, $R_{ref,i}$ and the corresponding estimates of the Z–R relationship, $(Z_i /A)^{1/b}$. Values of A that fell outside of the range of 10-700, as well as b values that were < 1 or > 3, were considered to be unreasonable based upon currently accepted Z-R relationships. For time steps where the regression yielded an unreasonable value for either coefficient, the parameters were recalculated by fixing the exponent b at 1.4 and determining *A* in a similar manner to the BIAS-RMSE method.

In order to assess the performance of the real-time Z-R estimation method, the set of 18 CR-10 gauges, which were independent of the estimation of A and b, were

used for verification. Using the A and b coefficients that had been established for each time step with the real-time gauges, the Z-R relationship was applied with reflectivity data corresponding to the location of the CR-10 gauges for the time period of October 1 – 19, 2007. The rainfall estimates produced by this application of the Z-R relationship were then compared to the corresponding CR-10 gauges based on several graphical and statistical methods. To further demonstrate the specific applicability of the real-time adjustment of the Z-R relationship to the SFWMD, the radar estimates produced by the algorithm currently provided to the District (SFWMD-NRT) were also compared to the CR-10 gauges using the same methods of comparison. These methods include time series plots of rainfall events throughout the 19-day period, the correlation coefficient, standard deviation of errors, histograms of estimation errors, and the distribution of the probability of exceedance of the estimation errors.

Results

The values of the A and b coefficients that were obtained during the study from the BIAS-RMSE method are shown in the Figure 2. These histograms illustrate the variation of the A and b values from the standard values of 300 and 1.4, which are currently used by the SFWMD for estimating radar rainfall data. Figure 2 also shows the correlation coefficient between log (Z) and log (R) of the calibration sample at each time step, which gives an indication of the linearity that would be obtained using the least-square-fit regression technique.

Time series plots of rainfall were produced for various rainy increments throughout the study period (Figure 3). As can be seen from the plots, the real-time (RT) radar estimates follow the pattern of the rainfall fairly well, in both intensity and temporal location, with some underestimation observed in cases of high intensity rainfall. The SFWMD-NRT estimates show similar results in general, however, it is observed on several occasions that instances of extreme overestimation in the SFWMD-NRT is significantly reduced in the RT estimates. Similarly, the timing of the peak rainfall intensity is seen to be more closely captured by the RT estimates at several points throughout the study period. The correlation of both the RT and SFWMD-NRT estimates to each of the CR-10 gauges was measured using the Pearson's correlation coefficient, a measure of linear association. These results, which are shown in Figure 4, show that the correlation of the RT estimates falls mainly in the range of 0.5 to 0.7, while the SFWMD-NRT shows a wider range of values, with some as low as 0.1 and the majority in the 0.4 to 0.6 range. From this figure, it is observed that the RT estimates demonstrate an improved correlation to the recorded gauge rainfall intensity, as compared to the SFWMD-NRT estimates, in almost all of the gauges that were used, with some gauge sites (i.e. 1, 12, and 16) showing very large improvement.

Similarly, the standard deviation of the RT and SFWMD-NRT estimation error was also calculated at each gauge site (Figure 5), where the standard deviations of the error were defined as:

$$\sigma(R_{RT} - R_G) \text{ and } \sigma(R_{SFWMD-NRT} - R_G),$$

respectively. The standard deviation of the RT estimates ranged from approximately 2 to 7, which again showed positive improvement over the SFWMD-NRT at most gauge locations, particularly in the case of more extreme values (> 10) that were observed in some instances with the SFWMD-NRT estimates. The characteristics of the error of both sets of radar estimates were further analyzed by plotting frequency histograms of the error magnitudes (Figure 6). The error distribution for the RT estimates is approximately symmetrical about the zero mark with most occurrences of error falling within ± 2 mm/h. The frequency of zeros for RT is nearly double that of the SFWMD-NRT, while the wider tails of the SFWMD-NRT histogram reflect a higher frequency of error beyond the ± 2 mm/h range. In addition, the distribution of the SFWMD-NRT error is slightly skewed to the right, illustrating the higher frequency of positive errors which was observed previously in the time series plots.

Finally, the error distribution was characterized by its probability of exceedance, which was calculated as the probability that the error exceeded a certain rainfall threshold value. For all values of the rainfall threshold, the probability of exceedance was smaller for the RT estimates when compared to the SFWMD-NRT estimates (Figure 7). These distributions were further decomposed into separate plots of the positive and negative components of the error (Figure 8 and Figure 9). When comparing the positive errors of the two sets of radar estimates, the probability of exceedance for the RT is consistently less than the SFWMD-NRT, with the difference between the two becoming increasingly larger after the 20 mm/h threshold. After this point, the probability drops off steadily for the RT, while the decrease in the probability for the SFWMD-NRT is slower due to the presence of the several very large rainfall intensity values noted earlier. The probability of exceedance for the negative component of the error, however, shows more similarity between the two radar estimates. For error thresholds below 30 mm/h, the RT and SFWMD-NRT show comparable results, while at threshold values above 30 mm/h, the RT again shows smaller exceedance probabilities.

Summary and Conclusions

This study evaluated the performance of a real-time adjustment of the Z-R relationship for use in estimating rainfall from reflectivity at the SFWMD in southern Florida. The objective was to provide an alternative to the radar estimates currently provided to the District that would offer improved results through the incorporation of real-time variability of the Z-R relationship in the estimation procedure. The coefficients, A and b, were estimated at each 15-minute time step for a 19 day period in October, 2007, using real-time gauge and reflectivity data from the 24 hours preceding each time step. Comparison of the radar estimates based on these applied real-time Z-R relationships was conducted using an independent set of gauges excluded from the estimation process. An identical verification was conducted with the radar estimates (SFWMD-NRT) currently used by the District for comparison between the performances of the two radar data sets. Based on the results of the study, the following conclusions can be made:

- The overall performance of the RT estimates showed visual improvements over the SFWMD-NRT estimates in terms of matching the recorded rainfall on a quantitative and temporal scale.

- Further signs of positive improvement of the RT were observed with the correlation coefficient of the RT estimates being significantly higher than the SFWMD-NRT estimates for nearly all of the reference gauges and the standard deviation of the error being lower.
- The distribution of error for the RT estimates was shown to be narrower with a higher frequency of zero error, indicating that the tendency towards overestimation in the SFWMD-NRT estimation was not present to as great an extent in the RT estimates.
- Based on this study, it was recommended that the District consider developing Z-R relationship specifically for the District use to improve the radar rainfall estimation.

References

Alfieri, L., Claps, P., and L. Francesco (2009) "Radar rainfall estimation by means of continuous-time readjustment of the Z-R relationship" *Journal of Hydrology* (in review).

Battan, L. J. (1973). *Radar Observation of the Atmosphere,* The University of Chicago Press.

Habib E., Malakpet C. G., Tokay A., and P. A. Kucera (2008) "Sensitivity of streamflow simulations to temporal variability and estimation of Z-R relationships", ASCE Journal of Hydrologic Engineering, Vol. 13(12), 1177-1186.

Lee, G. W., and Zawadzki, I. (2005). "Variability of drop size distributions: Noise and noise filtering in disdrometric data." *J. Appl. Meteorol.*, 44 (5), 634–652.

Legates, D.R. (2000). "Real-time calibration of radar precipitation estimates." *Professional Geographer*, 52 (2), 235-246.

Steiner, M., and Smith, J.A. (2000). "Reflectivity, Rain Rate, and Kinetic Energy Flux Relationships Based on Raindrop Spectra." *Journal of Applied Meteorology*, 39 (11), 1923-1940.

Uijlenhoet, R., Steiner, M., and Smith, J.A. (2003). "Variability of Raindrop Size Distributions in a Squall Line and Implications for Radar Rainfall Estimation." *J. Hydrometeor.*, 4 (1), 43–61.

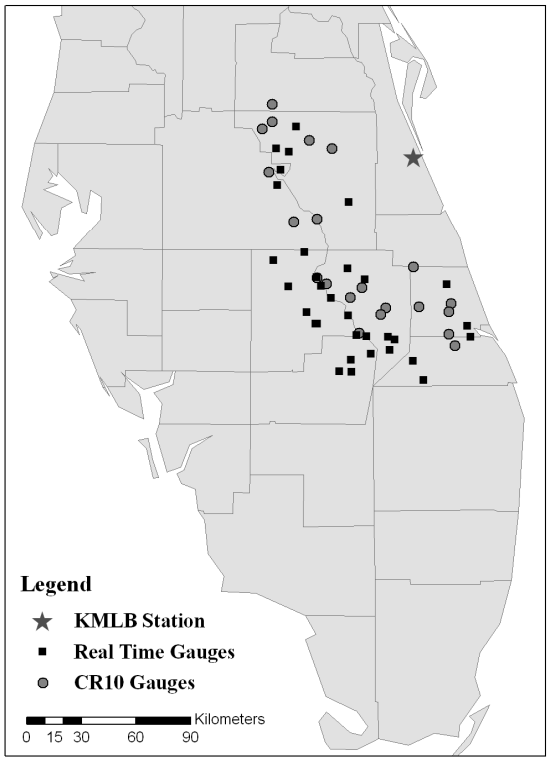

Figure 1 Real-Time and CR-10 gauge locations in the SFWMD.

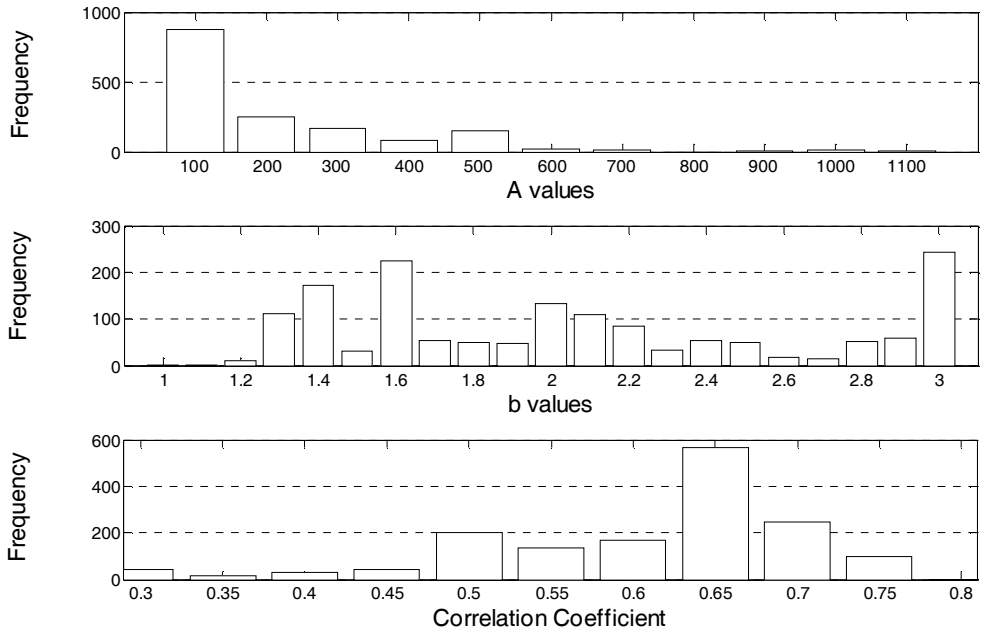

Figure 2 Histograms of the values of the coefficients A and b for each time step in October 2007 (top and middle) and the correlation coefficient of the log (Z) and log (R) at each time step (bottom).

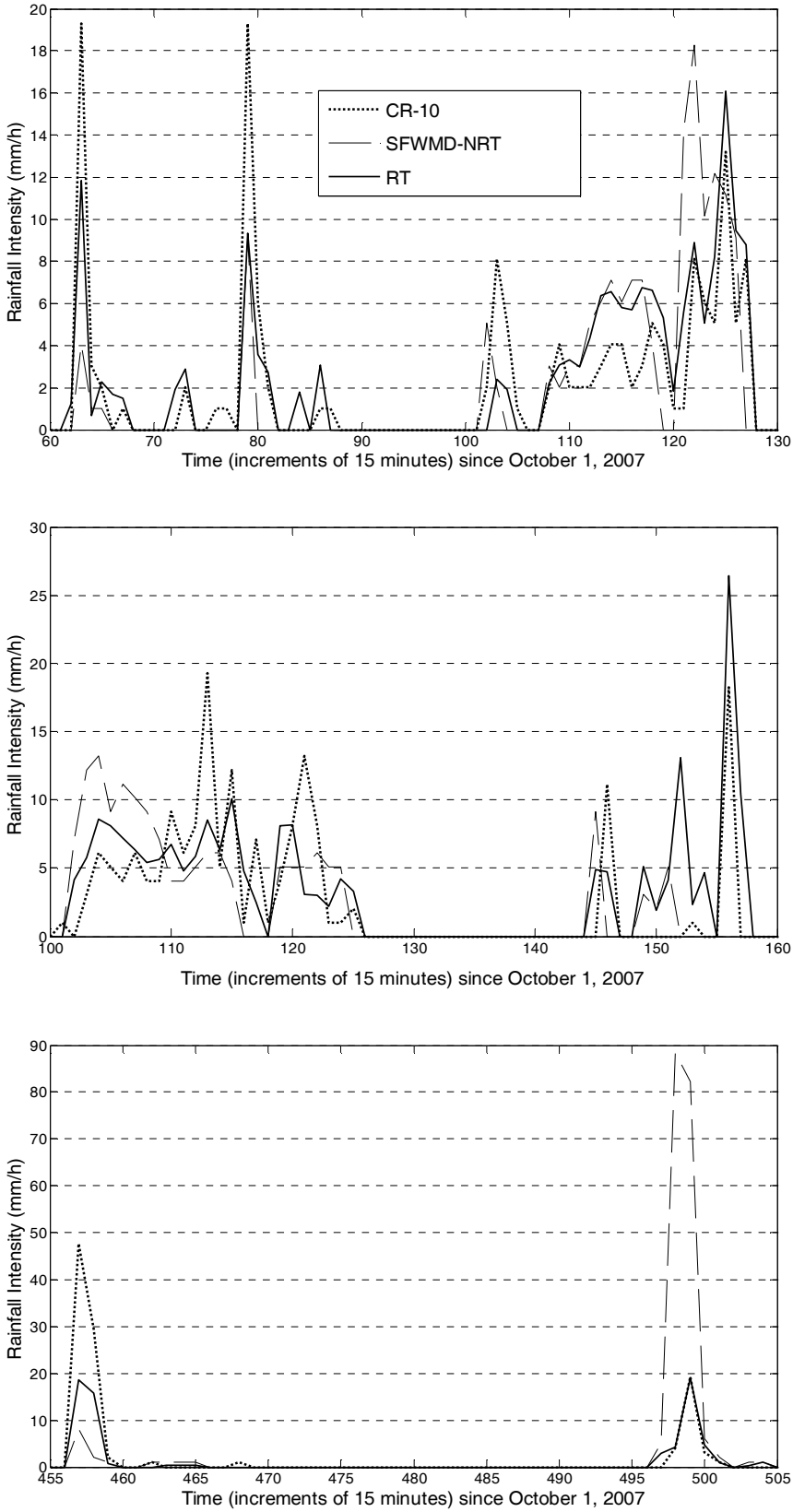

Figure 3 Time series plots for selected rain gauge locations during October 2007.

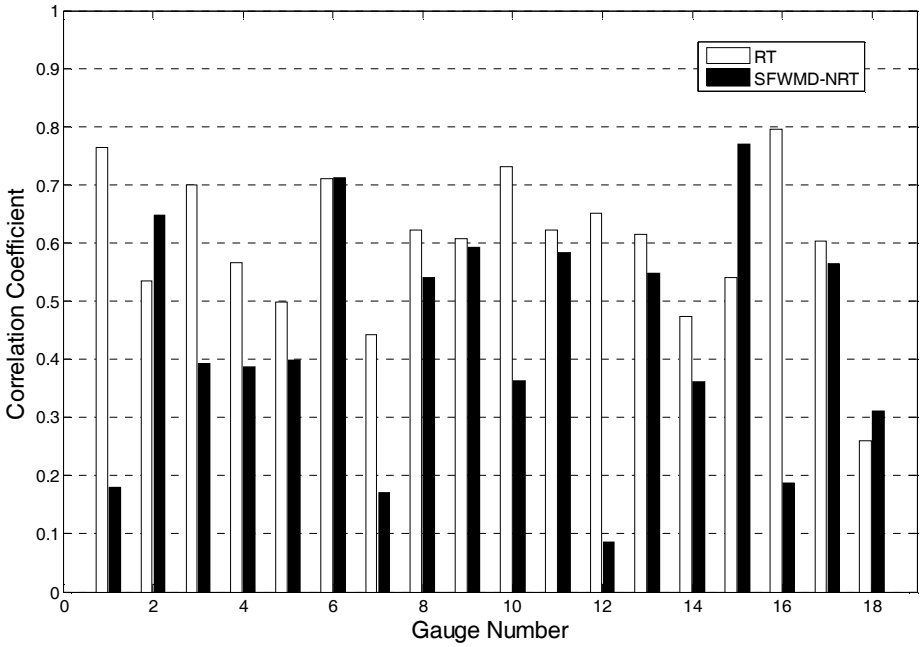

Figure 4 Correlation coefficients of RT and SFWMD-NRT radar estimates versus CR-10 gauge measurements.

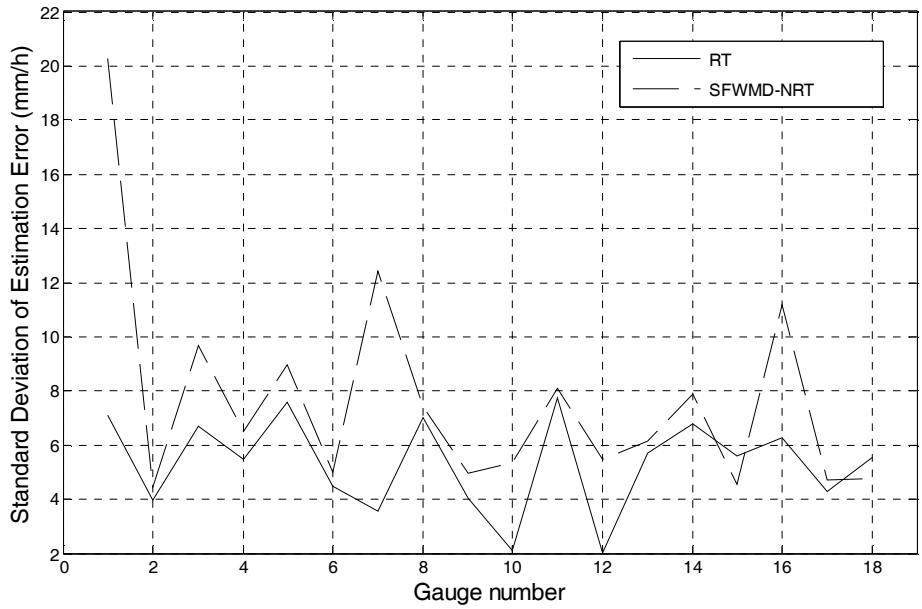

Figure 5 Standard deviation of the error of RT and SFWMD-NRT estimates.

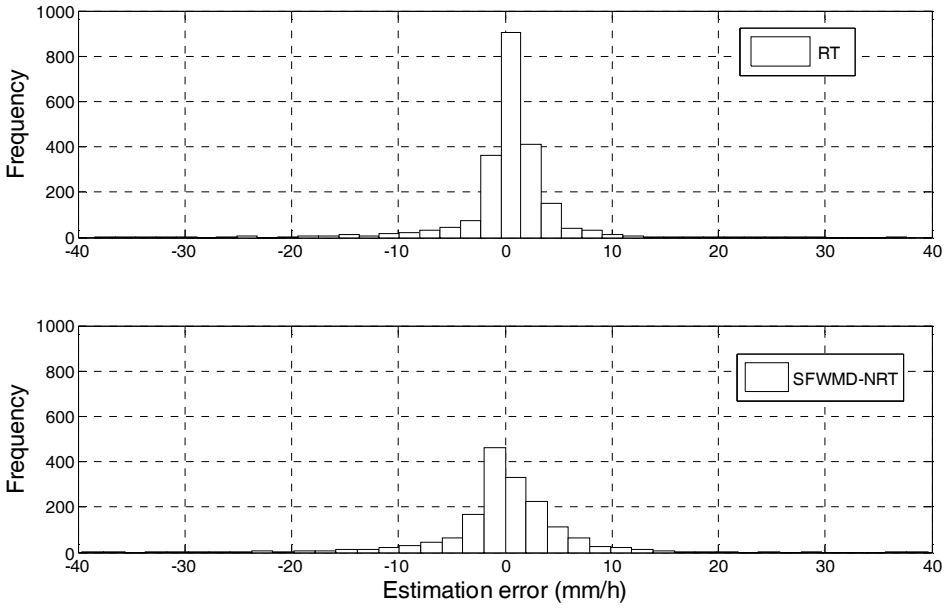

Figure 6 Error histograms showing the frequency of error for the RT and SFWMD-NRT rainfall estimates.

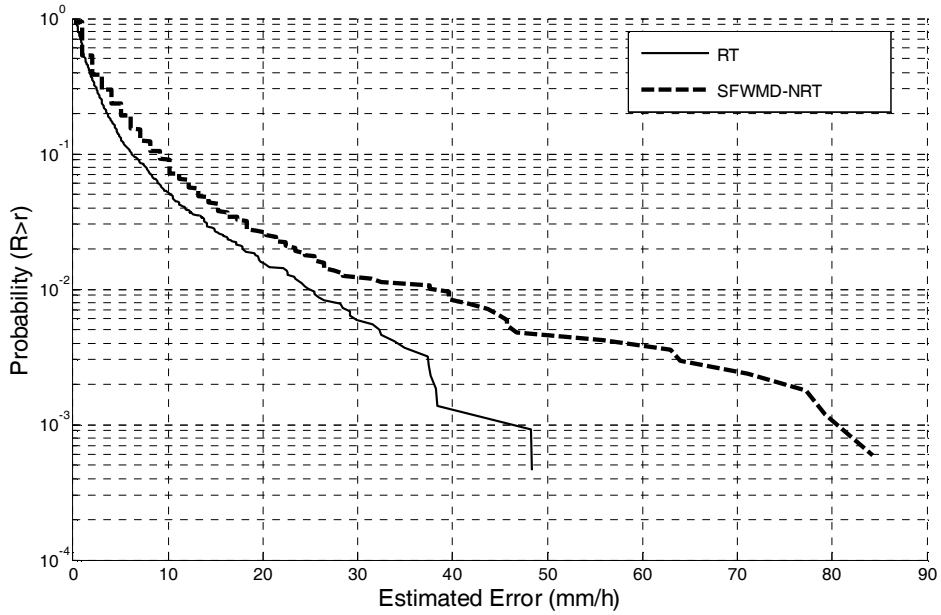

Figure 7 Probability of exceedance for the error of the RT and SFWMD-NRT estimates.

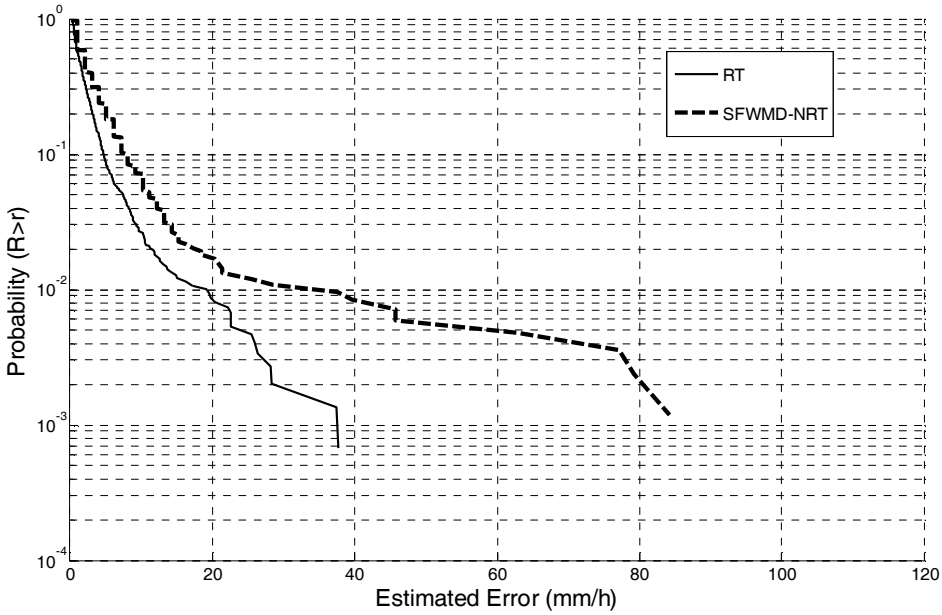

Figure 8 Probability of exceedance for the positive component of the error for the RT and SFWMD-NRT estimates.

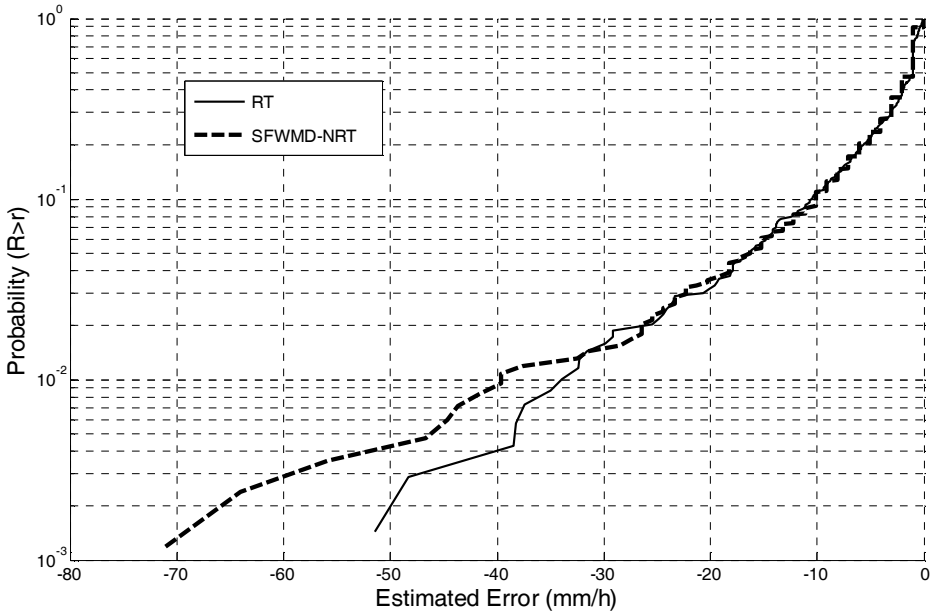

Figure 9 Probability of exceedance for the negative component of the error for the RT and SFWMD-NRT estimates.

Radar-Rainfall Analysis for Extreme August Storm in Sacramento

By

David C. Curtis, Ph.D.

Carlton Engineering, 3883 Ponderosa Road, Shingle Springs, CA, 95682.
PH 530-677-5515; email: dcurtis@carlton-engineering.com

Abstract

The climate in California's central valley is distinctly divided into two seasons: wet and dry. Sacramento's six-month wet season runs roughly from mid-October through mid-April, while the dry season runs through the remaining six months from mid-April to mid-October.

While rainfall during Sacramento's "dry" season is not unheard of, it is relatively rare, especially in August. At one long-term climatological observing station in Sacramento from 1877 to 2006, there were 4024 non-missing daily August rainfall observations. Of those 4024 rainfall observation days, only 41 days (1.02%) recorded more than a "trace" and daily observations of more than 0.30 inches were reported just two times. The maximum August daily rainfall in Sacramento from 1877-2006 was 0.66 inches.

That is why the events of August 21-22, 2003 were remarkable. A series of unusually strong thunderstorms rolled through region during the late afternoon on August 21st and continued sporadically through the early morning hours of August 22nd. Rainfall totals in excess of 1.4 inches were recorded in 24 hours, more than double the maximum daily August rainfall observed in the 130 year record.

High resolution radar rainfall estimates were calibrated using gage observations from the local flood ALERT system. The gage-adjusted radar rainfall estimates were used to track the intense storm cells through the city of Sacramento and to the localized flooding that occurred.

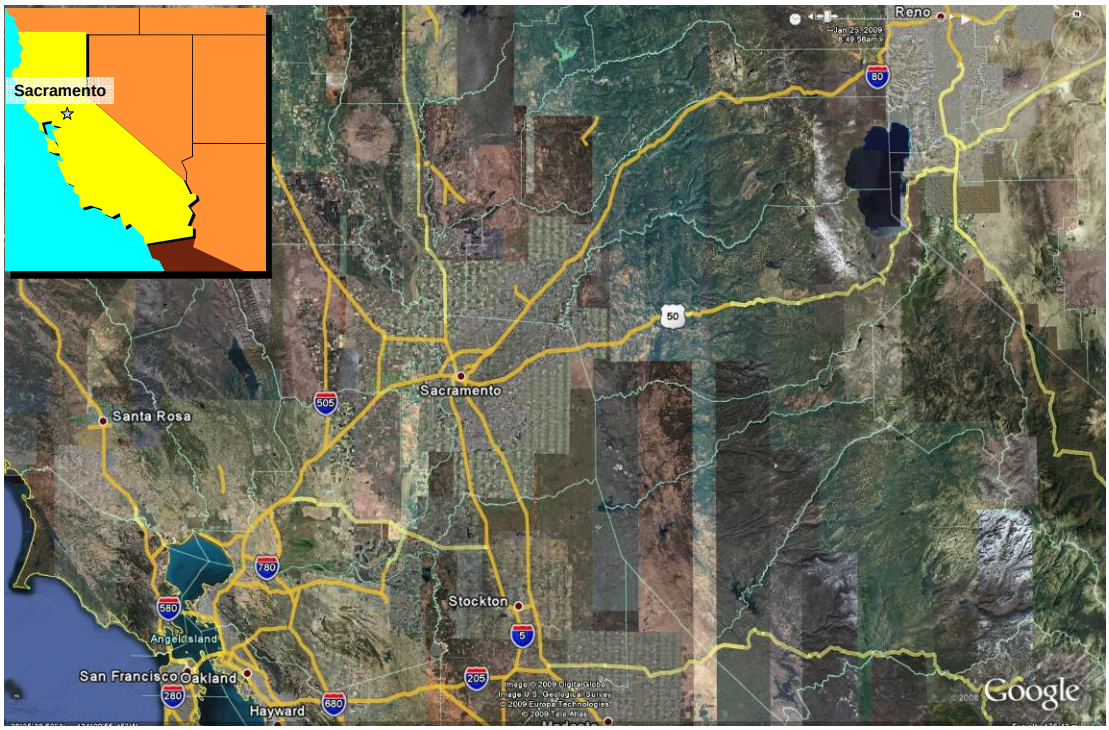

Figure 1: Map of Sacramento Region

Background

Located in northern California, roughly midway between San Francisco and Lake Tahoe, Sacramento enjoys a Mediterranean climate with typically hot dry summers and mild winters. The period October-April receives nearly 90% of Sacramento's 19.87 inches of annual rainfall, based on the latest climate figures for1971-2000. As noted in Figure 2, January is typically the wettest month with 4.18 inches of rainfall, on average, while July and August are the driest at 0.05 inches.

August in Sacramento is typically so dry that the maximum daily rainfall observed on seven August days from 1877-2006 was 0.00 inches and 0.01 inches on four others. The official maximum daily rainfall observed in August is 0.66 inches, which occurred on August 29, 1953 (Cline and Garcia, 2007).

From 1877 to 2006 there were 4024 non-missing daily August rainfall observations. Of those 4024 rainfall observation days, only 41 days (1.02%) recorded more than a trace and daily observations of more than 0.30 inches were reported just two times. Over the 130 year record, measureable August rainfall occurred about once every three years, on average, although the more recent experience (i.e. 1971-2000) is closer to once every year.

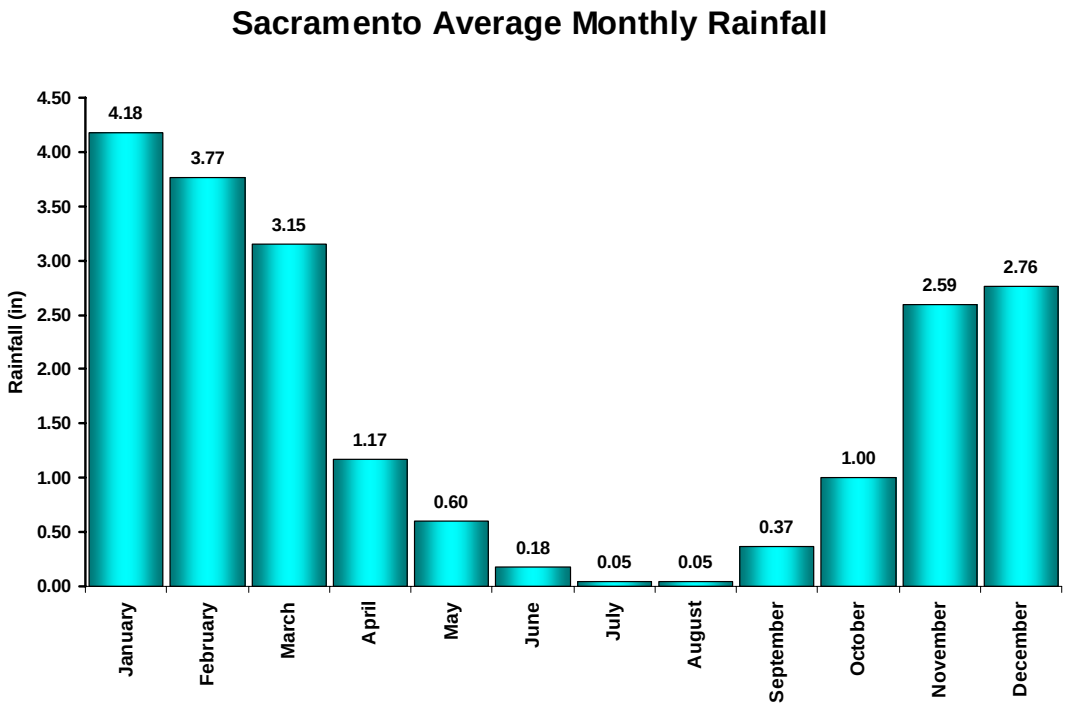

Figure 2: Sacramento Average Monthly Rainfall

August 2003

Despite the climatologically dry August conditions in Sacramento, occasionally enough moisture moves into the area, creating conditions for isolated thunderstorms and locally heavy downpours. Such was the case on August 21-22, 2003.

On August 20th, the Sacramento office of the National Weather Service (NWS) observed a significant surge of subtropical moisture headed to northern California on a collision course with an area of low pressure forecast to move onshore from the eastern Pacific on August 21-22. This mix of air masses was ripe for thunderstorm development and locally heavy rainfall as indicated by the 9:30 PM August 20, 2003 NWS Special Weather Statement shown in Table 1.

By mid-afternoon on August 21st, the first of a series of thunderstorm complexes with locally heavy downpours moved into Sacramento and lasted until about 10 AM on August 22nd. Table 2 presents the NWS Hazardous Weather Outlook issued at 3 PM on August 21st. In the end, the storms knocked out power to 22,000 homes and businesses, flooded city streets, and inundated approximately 100 vehicles to a depth of 6-7 feet in a temporary parking area at the California State Fair.

The magnitude of flooding at the California State Fair seemed surprising to observers at the site. While downpours on the afternoon of August 21st were briefly intense, the rainfall volumes didn't seem large enough to cause the deep flooding observed. An analysis of local rain gage observations and radar rainfall estimates was conducted to determine what caused the flooding.

Table 1: National Weather Service Special Weather Statement.

WWUS86 KSTO 210439
SPSSTO
CAZ013>019-063-064-066>069-220000-
SPECIAL WEATHER STATEMENT
NATIONAL WEATHER SERVICE SACRAMENTO CA
930 PM PDT WED AUG 20 2003

...SHOWERS AND THUNDERSTORMS EXPECTED TO AFFECT NORTHERN CALIFORNIA THURSDAY AND FRIDAY...WITH LOCALLY HEAVY RAIN...

THE WEATHER PATTERN HAS TRANSITIONED INTO ALLOWING A SIGNIFICANT SURGE OF SUBTROPICAL MOISTURE INTO NORTHERN CALIFORNIA. SHOWERS AND THUNDERSTORMS ARE EXPECTED TO AFFECT THE SIERRA NEVADA OVERNIGHT. ADDITIONAL SHOWERS AND THUNDERSTORMS WILL DEVELOP AND MOVE ACROSS THE LOWER ELEVATIONS OF THE SIERRA NEVADA LATE TONIGHT. SOME OF THIS MAY AFFECT PARTS OF THE CENTRAL VALLEY LATE TONIGHT AND EARLY THURSDAY MORNING.

SHOWERS AND THUNDERSTORMS ARE EXPECTED TO BECOME MORE WIDESPREAD ON THURSDAY ...INCLUDING AREAS FROM THE COASTAL RANGE TO THE CENTRAL VALLEY AND EASTWARD TO THE SIERRA NEVADA. THE ACTIVITY WILL MOVE FROM SOUTH TO NORTH ACROSS THE STATE. THE PRECIPITATION WILL AFFECT THE CENTRAL VALLEY AND THE HIGHER TERRAIN. THEN ADDITIONAL WIDESPREAD SHOWERS AND THUNDERSTORMS WILL DEVELOP AND CONTINUE THURSDAY NIGHT INTO FRIDAY. DURING THIS PERIOD THE RAIN WILL BE LOCALLY HEAVY IN THE STRONGER SHOWERS AND THUNDERSTORMS. THIS WILL BE THE RESULT OF AN UPPER LEVEL LOW PRESSURE AREA IN THE EASTERN PACIFIC THAT MOVES INLAND THURSDAY NIGHT AND INTERACTS WITH THE DEEP UNSTABLE SUBTROPICAL MOISTURE THAT WAS CARRIED INTO THE REGION. PRECIPITATION WILL TAPER OFF FROM SOUTHWEST TO NORTHEAST ON FRIDAY.

THE HEAVIEST RAIN FRIDAY AFTERNOON WILL OCCUR OVER THE WEST SLOPE OF THE SIERRA NEVADA AND THE SHASTA COUNTY MOUNTAINS. NORTHERN CALIFORNIA EXPERIENCED A SIMILAR OUTBREAK OF SHOWERS AND THUNDERSTORMS EARLIER THIS MONTH. RAINFALL TOTALS ARE EXPECTED TO BE SIGNIFICANT FROM THURSDAY INTO FRIDAY.

IF YOU ARE PLANNING ANY OUTDOOR ACTIVITIES BE AWARE OF RAPIDLY CHANGING WEATHER CONDITIONS. THUNDERSTORMS CAN PRODUCE DEADLY CLOUD TO GROUND LIGHTNING...EVEN A FEW MILES AWAY FROM THE MAIN STORM CENTER. LOCALIZED AREAS OF HEAVY RAIN WILL CAUSE SMALL STREAMS TO RISE RAPIDLY.
$$
TARDY

Table 2: National Weather Service Hazardous Weather Outlook

HAZARDOUS WEATHER OUTLOOK
SPECIAL WEATHER STATEMENT
URBAN AND SMALL STREAM FLOOD ADVISORY
SOUTHERN SACRAMENTO VALLEY-
NATIONAL WEATHER SERVICE SACRAMENTO CA
300 PM PDT THU AUG 21 2003

NOW... AT 300 PM...DOPPLER RADAR INDICATED A THUNDERSTORM WITH HEAVY RAIN IN CENTRAL SACRAMENTO. THE THUNDERSTORM IS MOVING NORTHEAST AT 20 MPH AND IS PRODUCING LIGHTNING AND GUSTY WINDS. CALIFORNIA RESIDENTS AT THE STATE FAIR SHOULD TAKE COVER FOR AT LEAST THE NEXT HOUR THROUGH 4PM. MINOR URBAN FLOODING IS POSSIBLE IN MANY LOCATIONS THIS AFTERNOON. IF YOU ARE OUTDOORS...MOVE TO A PLACE OF SHELTER IMMEDIATELY IF A STORM APPROACHES. MOTORISTS SHOULD REMAIN ALERT FOR REDUCED VISIBILITIES DURING DOWNPOURS OF RAIN. POWELL

Rainfall Analysis

Sacramento County and nearby agencies, Placer County and the cities of Roseville and Folsom, collectively operate an automated rainfall and stream level information system known as ALERT (Automated Local Evaluation in Real-Time, http://www.sacflood.org/). The network of rain, stream, weather, and status sensors includes nearly 60 automatically reporting tipping bucket rain gages. Rain gage locations are shown on Figure 3. Recorded rain gage data including the date and time of each bucket tip were obtained from Sacramento County's Department of Water Resources.

These rainfall data were used by OneRain, Inc. (www.onerain.com) to calibrate 5-minute, 1 km resolution radar rainfall estimates for the storm event. The resulting gage-adjusted radar rainfall estimates of storm totals are shown on Figure 3. Also shown are the location of the California State Fair Grounds (CalExpo) and the contributing watershed to the flooded parking area, Chicken Ranch Slough.

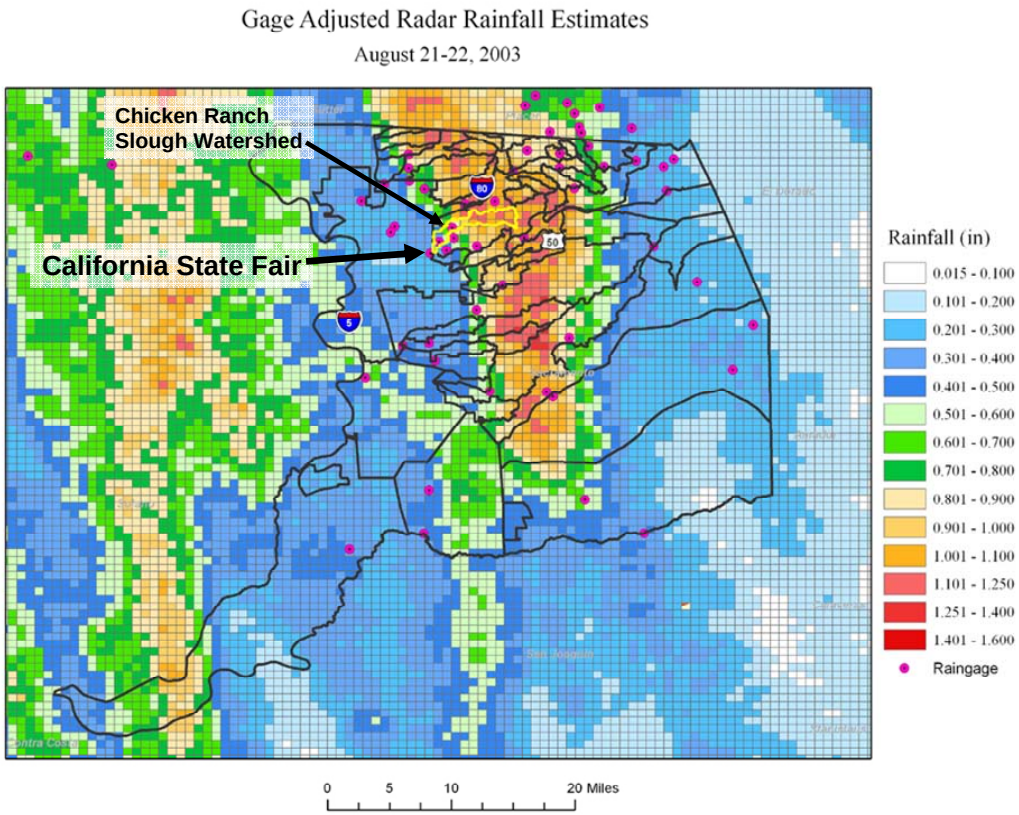

Figure 3: Sacramento County Watershed Map with Rain Gage Locations. Each rectangular grid cell or pixel represents 1 km^2 or 100 hectares (247 acres).

Chicken Ranch Slough includes approximately 20 km^2 (7.7 mi^2) of generally flat residential/commercial area gently sloping east to west/southwest. Total radar-estimated rainfall for the event exceeded 36 mm (1.4 in) at several locations along a north-south band of heavy rain in eastern Sacramento County.

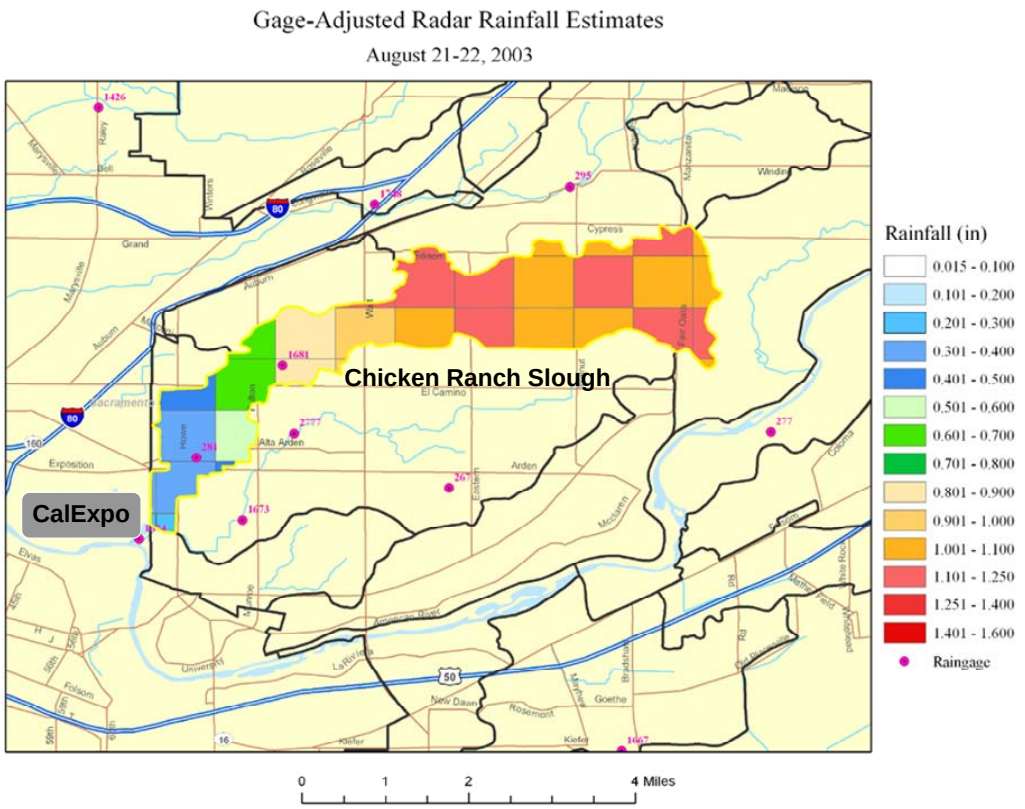

Figure 4: Isolated Close-up View of the Chicken Ranch Slough Watershed and Surrounding Area.

An isolated view of the Chicken Ranch Slough Watershed is shown in Figure 4. Rain gages in the vicinity of Chicken Ranch Slough are also shown. Radar rainfall estimates show a strong rainfall gradient from east to west with storm totals ranging from approximately 36 mm (1.41 in) to 6 mm (0.24 in) within Chicken Ranch Slough. The strong east-west gradient was caused by the northerly storm movement with heavier cells repeatedly tracking over the eastern half of the watershed. An example of the south to north movement of storm cells is shown in Figure 5A-C covering the period from 0215 to 0300 August 22, 2003.

Although there were a number of rain gages in the immediate vicinity of Chicken Ranch Slough, only two gages were located within the watershed. Both of those gages were located in the western half of the watershed, which received much less rain than the eastern section. More than five times as much rain fell in upper portions of Chicken Ranch Slough than at the flooded parking area at CalExpo. The distance between the maximum and minimum storm totals in Chicken Ranch Slough was about 5 km (3.1 mi).

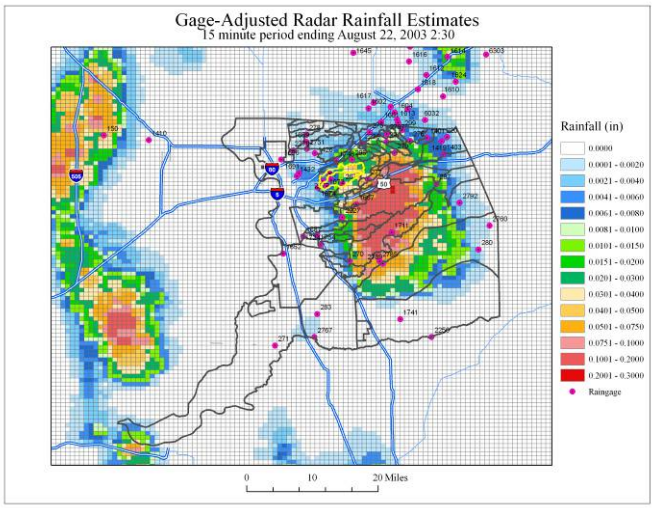

(A)

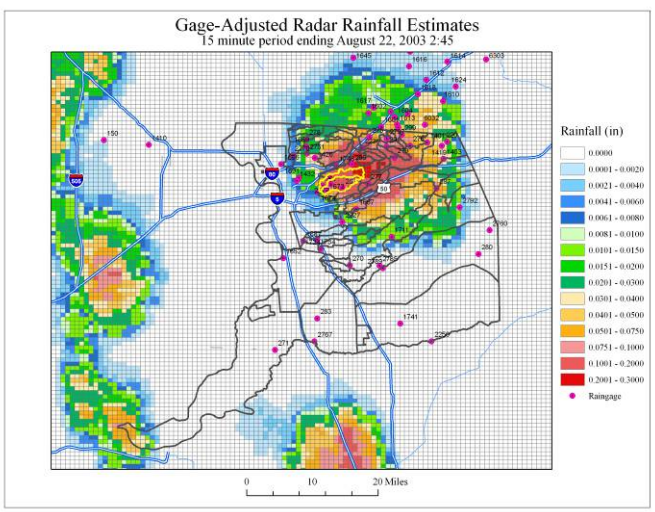

(B)

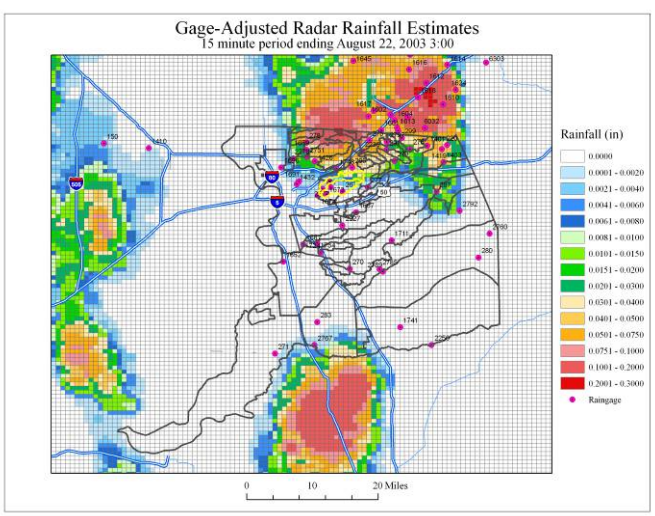

(C)

Figure 5: Storm Sequence - 0215 to 0300 on August 22

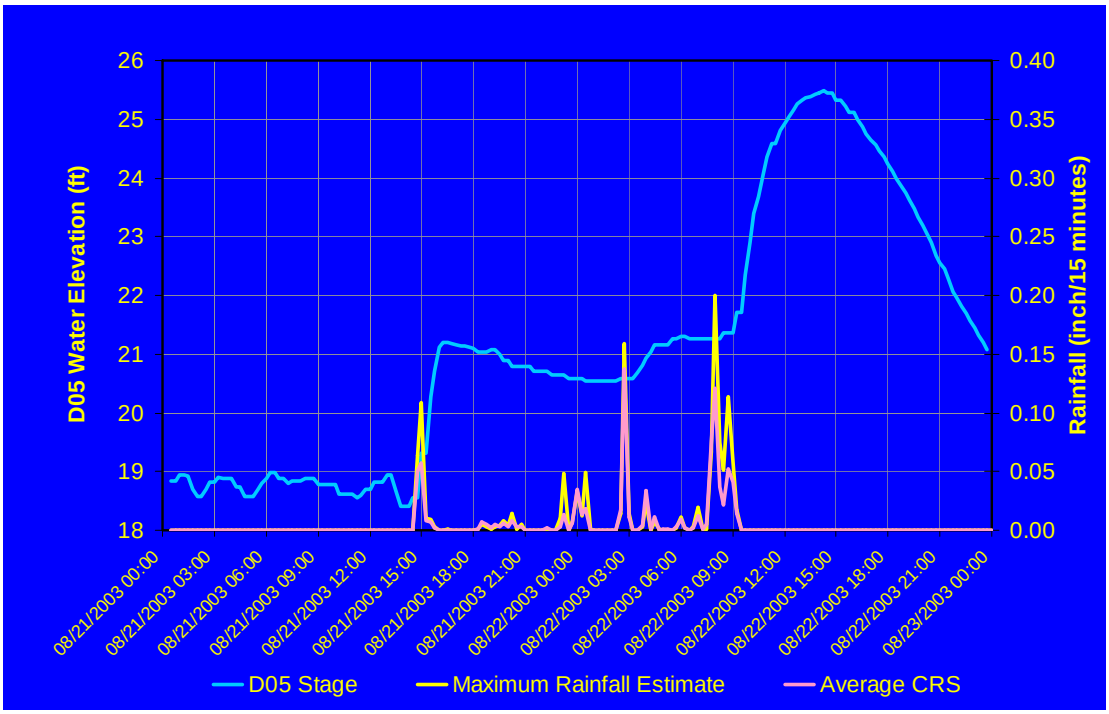

Figure 6: Chicken Ranch Slough Rainfall Response

Chicken Ranch Slough's response to the series of storm cells on August 21-22 is shown in Figure 6 and compared to the watershed average radar estimated rainfall and the maximum radar estimated rainfall in the watershed. The water elevation indicated is the DO5 detention facility at the outlet of Chicken Ranch Slough.

Three main pulses of heavy rainfall are apparent. The first intense pulse occurred between 1400 and 1530 on August 21st, triggering an almost immediate response at the watershed outlet. The quick response suggests that the heavier rain was relatively close to the basin outlet. A second pulse occurred between 0200 and 0300 on August 22nd, which reversed the recession from the first pulse then contributed to a small increase in stage.

The largest pulse fell between 0715 and 0915 on the 22nd, producing an additional four-foot rise in water surface elevation. However, response to the third pulse took significantly longer, suggesting that the rain fell in the upper watershed. A time-step by time-step analysis of the radar rainfall estimates verified that heavier rain fell in the upper reaches of the watershed throughout this period. Figures 7A-C clearly show the heavier rainfall over the upper portions of Chicken Ranch Slough and the adjacent Strong Ranch Slough.

It is also interesting to note that the heavier rain occurred in the portion of Chicken Ranch Slough with no rain gages. Radar provided the information needed to determine the rainfall distribution throughout the watershed. Even the relatively dense network of Sacramento County rain gages could not adequately resolve the spatial distribution of rain falling on this small urban watershed.

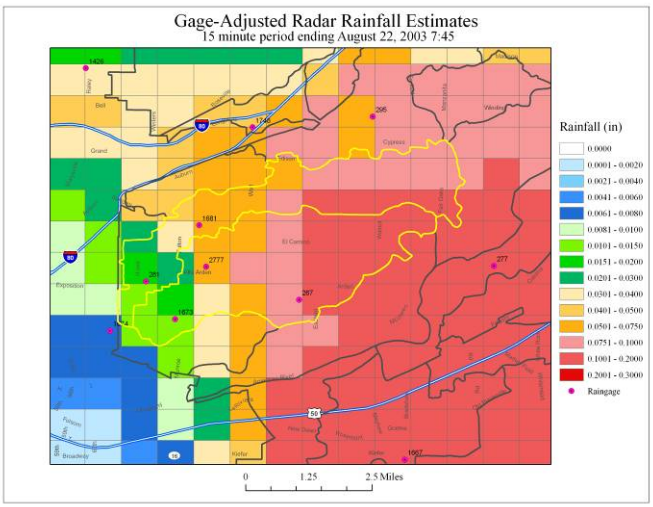

(A)

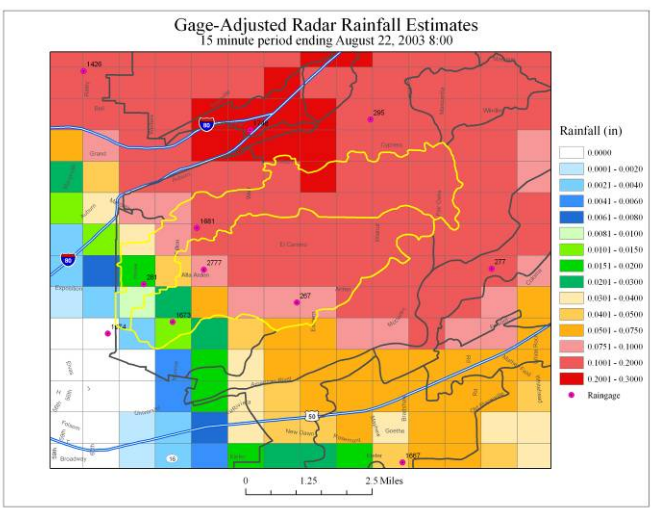

(B)

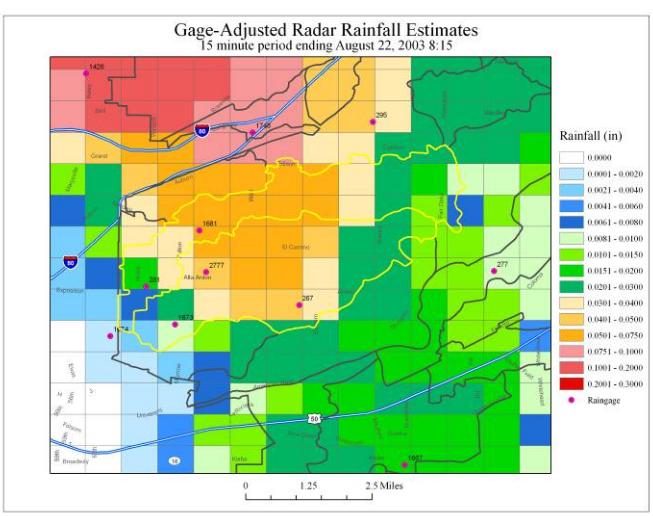

(C)

Figure 7: Gage Adjusted Radar Rainfall Estimates Showing Heavier Rain in Upper Watershed

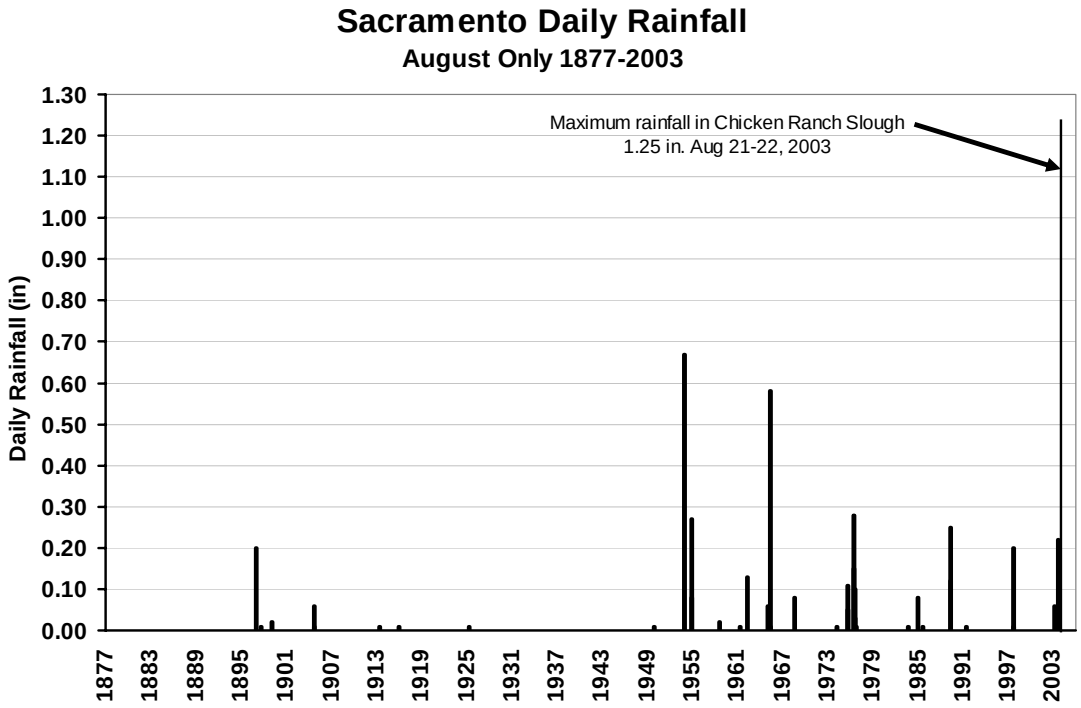

Figure 8: August Daily Rainfall from 1877 to 2003

Historical Context

To put the 24-hr rainfall of Aug 21-22 in historical context, Figure 8 shows the daily rainfall in each August from 1877 to 2003. While August rainfall in Sacramento does occur, significant amounts are rare. No more than a trace of rainfall occurred on 99% of the days since 1877. Only two days recorded more than 7.6 mm (0.3 in). The maximum August daily rainfall in the Sacramento record was 16.8 mm (0.66 in), which was also the greatest 2-day August total on record.

The maximum 24-hr radar estimated rainfall in Chicken Ranch Slough for the August 21-22, 2003 storm was 31.75 mm (1.25 in) or almost double the highest August daily rain gage reading since 1877. Perhaps more impressively, the *watershed average* radar rainfall estimate was 22.4 mm (0.88 in) for Chicken Ranch Slough or 33% higher than the daily August maximum rain gage measurement in Sacramento since 1877.

Another interesting observation that surfaced during this investigation is the apparent stark difference in the frequency of August rainfall in Sacramento between the pre-1950 record and the post-1950 record. From 1887-1950, just one day of rainfall greater than 0.10 inches was observed. Since 1950, at least ten such days were observed. While the cause of this apparent shift is not clear, it is consistent with a general change in weather volatility between the pre/post 1950 years. Since 1950, weather conditions in the Sacramento region have been generally been more volatile compared to pre-1950 conditions.

Summary
On August 21-22, 2003, an extreme rainfall event occurred in Sacramento, CA, during what is normally the driest part of the year. Average monthly rainfall for August in Sacramento is just 0.05 inches or about 0.25% of its annual total. However, on this date, a large plume of subtropical moisture moved into northern California colliding with an area of low pressure from the eastern Pacific. The result created conditions for rare August thunderstorms in Sacramento.

Local rainfall data from a network of automatically reporting tipping bucket rain gages were used to calibrate 5-minute, 1 km x 1 km resolution radar rainfall estimates. The resulting gage-adjusted radar rainfall data were used to assess the storm event and, specifically, the response of 20 km^2 Chicken Ranch Slough, whose discharge flooded nearly 100 vehicles parked near the California State Fair.

The radar data clearly indicated nearly 5 times more rainfall occurred in the upper reaches of Chicken Ranch Slough than occurred at the site of the flooded vehicles. Radar provided the ability to "see" between the rain gages in a relatively dense rain/stream monitoring network and accurately represent the highly variable rainfall topology associated with this event. Maximum 24-hr radar rainfall estimates during the event were double the highest observed August daily rainfall in Sacramento's 130 year historical record.

References
Cline, George and Felix Garcia, *Climate of Sacramento, California,* National Weather Service, Sacramento, CA, September 2007.
Hume, Elizabeth, "Outages, Flooding, Follow Big Storm," *Sacramento Bee Metro Section*, August 23, 2003.

Use of Lightning and Storms Life Cycle Information in Radar Rainfall Estimation

Emmanouil N. Anagnostou[1], Chandra S. Pathak[2] and C.A. Morales[3]

[1] University of Connecticut, Civil and Environmental Engineering, Connecticut, USA
[2] South Florida Water Management District, West Palm Beach, Florida, USA
[3] University of Sao Paolo, Department of Meteorology, Sao Paolo, Brazil

Abstract

Radar rainfall estimates derived from conversion of reflectivity are known to contain systematic and random errors (bias) that limit the quantitative use of radar rainfall in various applications. Enhancement of radar rainfall estimates is normally accomplished through gauge-adjustment procedures; however, those procedures require long integration periods to moderate sampling differences between the two sensors. To improve the efficiency of radar-gauge based adjustment techniques, classification based on storm microphysical information is needed. In this study, use of two auxiliary data derived from cloud-to-ground (CG) lightning measurements and a storm tracking algorithm was performed. This information was used to classify storms into thunderstorms (storms associated with CGs) vs. showers (storms without lightning) and according to the storm's maturity stage (i.e., growing, mature or decay stage). The radar rainfall data from South Florida Water Management District and for a period of twenty months were used. The radar rainfall estimates at 2-km resolution and 15-min time intervals, and corresponding rain gauge measurements from 120 gauges, and CG occurrences from the National Lightning Detection Network were used. Tracking was applied to the radar rainfall data to identify the storm families used in this analysis. The radar error analysis for different storm types and storm stages indicates that precipitation microphysical information is critical for improving radar rainfall estimation. It has shown that radar rain estimates tend to give stronger biases in storms of strong convective nature (both in terms of lightning occurrences and in terms of the growing stage of the storm), while showers and storms at mature stage tend to be better represented by the fixed climatological Z-R relation. Results from this study demonstrated that CG lightning and storm's maturity stage information could help reduce the variability in the Z-R conversion. Such classification may have a consequential effect on improving the efficiency of a mean-field bias-adjustment algorithm applied at higher temporal scales of aggregation (hourly, daily, etc.) for the radar rainfall estimate.

Introduction

The South Florida Water Management District (District) is responsible for managing and protecting water resources in a 46,439-square kilometer (17,930 square-mile) region. The area extends from Orlando to Key West and from the Gulf Coast to the Atlantic Ocean and contains the Lake Okeechobee. The area is also the site of an environmental restoration program based on the Comprehensive Everglades Restoration Plan. The District operates 2,898 kilometers (1,800 miles) of canals and more than 420 water

control structures. The District encompasses 16 counties and serves a population of over six million people. The District operates an extensive network of 279 active rain gauges in order to obtain rainfall data necessary for use in operations, planning, and regulatory aspects of water management. The rainfall data from 233 stations are available on a breakpoint basis. The breakpoint data can be obtained in a format of 15-minute, hourly, and daily intervals from the District's hydro-meteorological database, DBHYDRO. The rainfall data from the remaining 46 stations are available as daily rainfall (from non-recording rain gauges) in DBHYDRO database. Additionally, historical rainfall time series data from the District and other external government agencies are also available in DBHYDRO to both internal and external users (Pathak, 2008).

Next Generation Radar (NEXRAD) or Weather Surveillance Radar 88 Doppler (WSR-88D) data provide complete spatial coverage of rainfall amounts unobtrusively using a predetermined grid resolution (2 x 2 km). The NEXRAD rainfall dataset is limited due to its reliance on the measurement of raindrop reflectivity, which can be affected by factors such as raindrop size and signal reflection by other objects. Because the reflected signal measured by the radar is proportional to the sum of the sixth power of the diameter of the raindrops in a given volume of atmosphere, small changes in the size of raindrops can have a dramatic effect on the radar's estimate of the rainfall. For this reason, the radar is generally scaled to match the volume measured at the rain gauges in the region. The best of both measurement techniques is realized by using rain gauge data to adjust NEXRAD rainfall values (Pathak, 2006).

Four NEXRAD sites operated by the National Weather Service (NWS) cover the District: KBYX in Key West, KAMX in Miami, KMLB in Melbourne, and KBTW in Tampa. The District uses weather data acquired from NEXRAD in making operational decisions. The District has been acquiring NEXRAD data coverage from OneRain, Inc. since July 2002 (Huebner et al., 2003). In that time, the District has worked in conjunction with three of the other four Florida water management districts to develop a corporate database and methods for data access based on NEXRAD data coverage. The use of rain gauge-adjusted NEXRAD 15-minute data (i.e., taken at 15-minute intervals) by the District's Operations Control Center (OCC) is a major objective of the acquisition. The District is receiving the NEXRAD rainfall data as two types of datasets -- near-real time (NRT) and end-of-month (EOM). The District developed ArcIMS-based application for NEXRAD data retrieval. The application provides varied spatially and temporally aggregated datasets in tabular and image formats (Pathak, 2008). Since October 1, 2007, the District and other water management districts have been acquiring NEXRAD rainfall data from Vieux and Associates, Inc. (VAI) (Pathak, 2008). The use of 15-minute data (i.e., taken at 15-minute interval), rain gauge-adjusted NEXRAD data by the District's Operations Control Center (OCC) was a major objective of the acquisition for the District. VAI provides near real-time (NRT), 15-minute rainfall amounts by using the following process:

- Acquires 15-minute radar reflectivity volume scans from the NWS and uses an appropriate Z-R relationship to convert reflectivity values to rainfall intensities.

- Concurrently, 15-minute rainfall accumulation data from approximately 180 District telemetry rain gauge sites are sent to VAI via File Transfer Protocol (FTP)
- Gauges are compared to radar rainfall estimates to adjust radar rainfall amounts
- Adjusted radar rainfall depths are placed in a flat file and sent via FTP to the District
- The District checks the flat file for completeness and loads the data into the Oracle® database.

Prior to gauge adjustment of radar data, the radar data is normalized to minimize discontinuity in the data from various radar sites that may run hot or cold. Currently, the near-real-time data uses a uniform adjustment technique, such that a single (averaged) gage-radar (G-R) ratio is applied for the entire domain. Further, there is currently no quality control on the incoming rain gage data for the near-real-time processing. Although the effect of a single bad gage is tempered somewhat in the G-R ratio averaging process, a quality control algorithm is desirable. The advantages of uniform adjustment technique are that the adjusted radar volume is guaranteed to match the gage volume (averaged across the domain) and the process is relatively insensitive to erroneous gage data. The main drawback to this technique is that it assumes a constant G-R ratio, an assumption that becomes less appropriate as the size of the domain increases. Accuracy can decrease for large domains because the process allows storm structure and rainfall characteristics from isolated areas to impact the solution for the entire domain.

Near real-time data are verified each month and an end-of-month (EOM) verified set of 15-minute files is produced. The EOM files use 60 additional rain gauge measurements that were not available in real-time and a proprietary algorithm based on the modified Barnes Objective Analysis method to adjust radar rainfall values. An expert from VAI reviews the results to identify and correct any anomalies or apparent errors. When the EOM files are received by the District, the near real-time data are archived, primarily to preserve the information upon which operational decisions may have been made, and are replaced with the EOM verified data set.

The spatial gauge adjustment method uses a G-R ratio field that is not constant. Instead, each radar pixel has its own G-R value. This is achieved by calculating a G-R ratio at each pixel utilizing a Kriging-based distance weighting scheme that considers data from several nearby gauges. The Kriging method allows the geometry of the gage data to be considered in the interpolation and maximizes the use of the available data. G-R ratios at pixels that are coincident with gauge locations are used, but this calculated value is not forced on the pixel that is covered by a three dimensional rainfall field surface which covers a larger area. This provides consideration for intra-pixel variation and does not create artifacts in the resulting rainfall field surface.

The goal of this study was to develop and investigate an algorithm and methodology aiming at improving the accuracy of NEXRAD rainfall estimates on the basis of auxiliary datasets and advanced tracking techniques. Specifically, the study investigated NEXRAD radar rainfall versus rain gauge rainfall differences for a variety of storm life durations, types, locations/time of formation and maturity stages so that improvements to the accuracy of NEXRAD rainfall data could be achieved. The information and data for this

study were obtained from the District's NRDP database, GIS coverage maps and variety of other sources. The study developed a methodology that would be used to improve the NEXRAD rainfall data. The proposed method could be applied to the existing available data and its performance would be evaluated and assessed. Upon successful development and verification of the model, the model will be used in near-real time and QA/QC datasets.

The physical background of the study relies on the fact that Z-R variability depends on the microphysical properties of rainfall and specifically on the distribution of raindrop sizes per unit volume. A characteristic example of this Z-R variability is shown in one of the figures of Atlas et al. (1999) publication in the Journal of Geophysical Research-Atmospheres (copy of the Figure is shown below; see Figure 1) where they demonstrate separate regions of A and B coefficients for convective, stratiform and transition (from convective to stratiform) regimes. A point to note from Figure 1 is the distinct differences of the A & B coefficients in the convective vs. stratiform regimes (for the same B coefficient we note up to two times lower A value in convective regime relative to stratiform). Also note the difference between convective and transition convective regimes. The above indicate that a mean Z-R relationship could introduce up to 100% error in radar rainfall estimates of the individual storm types, which is an issue that needs to be moderated prior to any radar-gauge adjustment in real-time radar rainfall estimation. The study investigated ways to identify those distinct precipitation types based on auxiliary data such as lightning and storm maturity stage derived from tracking analysis and determines the impact of those regimes in radar rainfall estimation error.

Data Preparation and Study Area

The study area for tracking of convective systems for this work is South Florida and surrounding waters. The data used are ½-hourly IR images from the global-IR composite (Janowiak et al. 2001), 15-min NEXRAD radar rainfall fields and gauges provided by the district and Cloud-to-Ground lightning flashes (CG lightning flashes) from the National Lightning Detection Network (Cummins et al. 1998; Orville and Huffines 2001). The period of the data analysis is October 2007 to August 2008 for the VAI product. The gauges, CG flashes and IR data were acquired for the same period.

For storm tracking we applied an algorithm presented by Machado et al. (1998) to the IR and radar images to track the life cycle of convective systems in the above period. The first step in tracking storms is to identify and delineate convective systems (CS) in an IR array using a brightness temperature threshold value. The threshold brightness temperature selection is based on the following criteria: it represents levels in the atmosphere that must be crossed by the top of a cloud for lightning to take place, i.e. above the -15 to -20°C level (Houze 1993), while being warm enough to pick up warm convective systems. The chosen threshold temperature values in this study are 258K for clouds and rain greater than zero for the radar estimates. A match for each of the CS delineated in the IR & radar images based on the selected thresholds is searched for in subsequent images until no match is found, or the end of the period for which the CS tracking is reached. The properties to be looked at to match CSs are presented in

Machado et al. (1998). The maximum speed at which a CS would travel is approximated to 60m/s (Machado et al. 1998), based on which we can deduce that a CS system can travel a maximum distance of 54 km between 15-min radar images (for this purpose the ½ hourly IR images are interpolated on the radar 15- minute intervals). This distance (0.5 deg radius around the center of mass of a CS area) is used here to restrict the search domain for a matching CS in consecutive IR/radar images. There can be some convective systems traveling with higher speed than this, however, such systems are expected to be very few and will be neglected to maximize computation efficiency. In summary, the first step in the tracking is to determine the locations of the pixels in a window of 0.5-by-0.5 deg domain about the center of mass of each convective system at time t0. The image at time t0+15min is then searched for all possible candidates within the domain. All convective systems have equal probability of being the continuation of the convective system at time t0, however, the system that has the highest number of matching parameters (listed in Machado et al. 1998) is selected. If a match is found properties of the convective systems such as the area, area expansion (the change in area), time rate of area expansion, direction of movement, shape (eccentricity), minimum temperature, modal temperature, and other relevant information is documented. If no match is found then the search will be conducted for the next cluster of convective systems (adjacent pixels of convective system). If the search is completed for all clusters of convective systems in the image under consideration, the search will then take place for new systems in the next IR image and the process repeats for all images for the period.

Systems tracked based on IR gave very few families as they were mostly generating or decaying outside the radar domain. Our alternative solution was to use the tracks from the radar rainfall fields using as threshold the 0.2 mm/h value and identify convective cells. An example of a tracking analysis based on radar data is reported in Figure 1 where we show the locations and life cycle of the storms in terms of rainfall volume, area, mean rainfall, and radar/gauge differences. A point to note is the distinct differences between radar-gauge errors in the growing stage vs. mature and decay stages. From the VAI tracking analysis of convective systems in the period Oct 07-Aug 08 we identified 4500 convective systems in Florida.

The convective systems have different life durations and analyzing their properties on a statistical basis requires grouping them on the same time scale. Hence, the life time of each tracked storm was normalized by its life duration, according to Eq 1, so that all systems can have developmental stages between 0 and 1. The normalization equation is:

$$t_n = \frac{(t - t_i)}{(t_d - t_i)} \tag{1}$$

where tn is normalized time, ti and td, are the times of initiation and dissipation, respectively, while t is the running time of the convective system's life evolution. Normalized times were divided into 10 equal intervals (i.e., 0.1 normalized time step) for which, the mean area expansion of the CSs, divergence, and other parameters from the different convective systems were grouped to compute statistics.

Summary of the convective system characteristics used in the herein analysis is shown in Figures 2 for the VAI product. Mean size of the tracked convective clusters is around

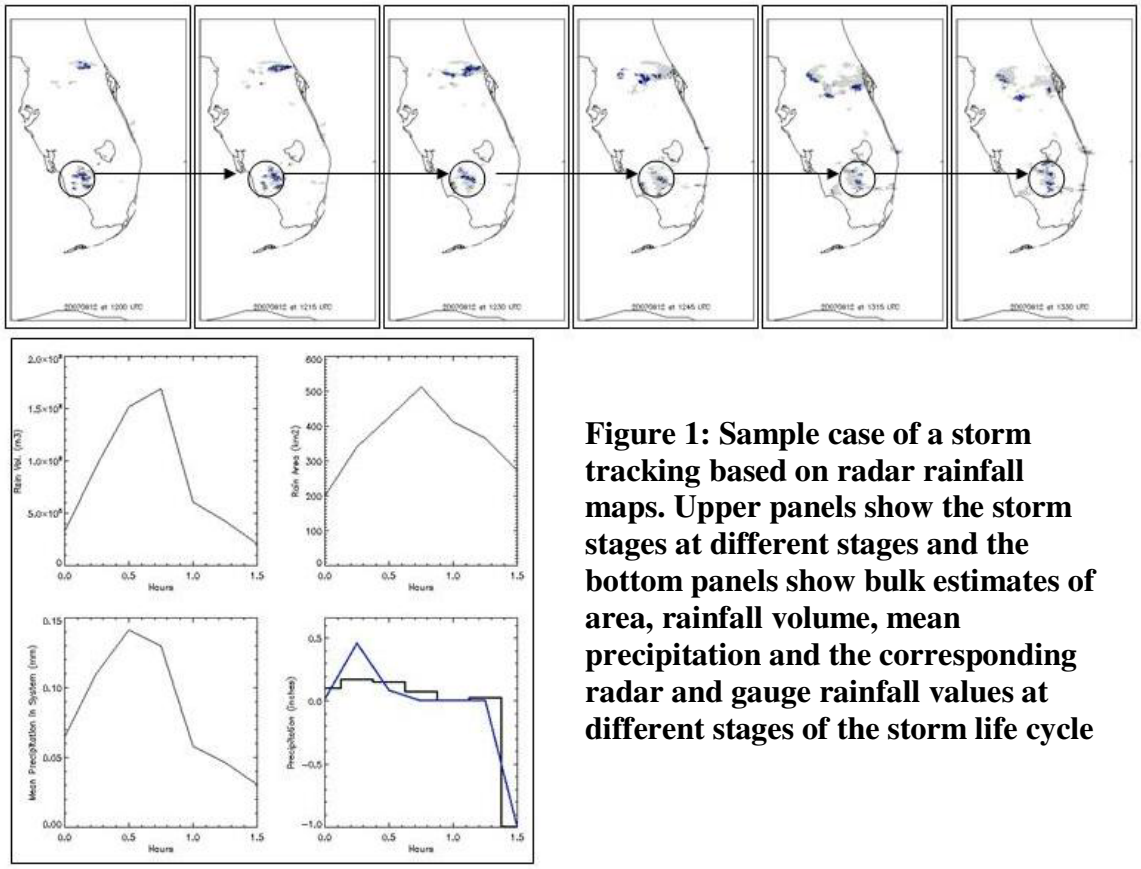

Figure 1: Sample case of a storm tracking based on radar rainfall maps. Upper panels show the storm stages at different stages and the bottom panels show bulk estimates of area, rainfall volume, mean precipitation and the corresponding radar and gauge rainfall values at different stages of the storm life cycle

10km in diameter of an equivalent circle, while in life duration most system lived between 1 and 3 hrs. A point to note is that the herein analysis does not include cases where families of convective systems merge or separate, so that we can establish a direct physical connection of the radar rainfall error (bias) on the maturity stage of a convective system.

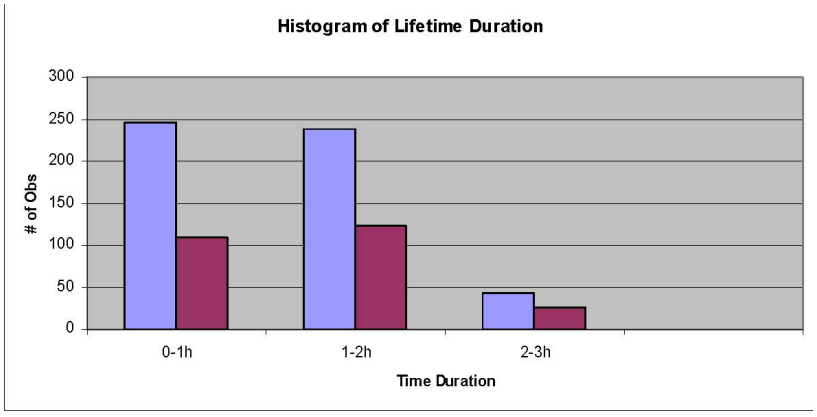

Figure 2: Life duration (in hrs) of the tracked convective systems (shaded bars correspond to clusters with available gauge data)

Data analysis and Results

The error statistics between radar rainfall and gauges are determined in two ways:

- using a Eulerian framework applied on each gauge location and using the lightning information from NLDN as a proxy of the convective nature of the estimated storm
- using a Lagrangian framework based on the storm tracking analysis and using the storm stage maturity as proxy of the convective nature of the storm

The two error analysis frameworks are presented in the figure shown below (Figure 3)

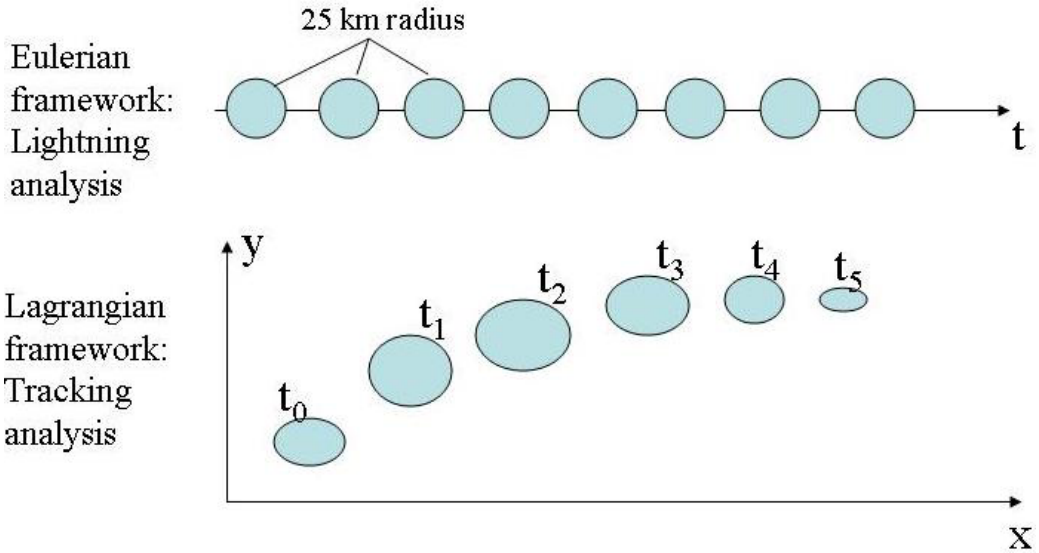

Figure 3: Two error analysis frameworks devised for the radar-gauge error statistics.

The top panel of Figure 3 shows the error analysis performed at each individual gauge location using radar-gauge pairs separated by storm type (i.e. T-storms vs. showers) classified using lightning information within a 25-km radius of the gauge location. The bottom panel shows the error analysis performed for each family of convective cells tracked based on the radar rainfall fields. The objective of this combined analysis is to demonstrate that microphysical related information for a storm can be used to minimize the systematic error in the radar reflectivity to rainfall conversion. Both the storm maturity stage and lightning occurrence are indicators that can be used to classify convective systems into thunderstorms vs. rain showers and into further growing mature and decay stages. In this analysis we consider T-storm origin rain associated with at least one CG lightning occurrence within 5 km radius and within the 15-min time interval of the radar estimate at a particular location.

The growth, mature and decay stages of the storms' life have been identified based on the convective systems area expansion defined through cloud top divergence. Specifically, the divergence values increase rapidly at normalized times below 0.3, while moderate values are noted between 0.3-0.7 and close to zero beyond 0.7. Repeated experiments of this nature for storms of different duration confirms that there are distinct stages in the

life of convective systems, which we herein classify in an ad hoc way by normalized times 0.3 and 0.7. Namely, normalized times below 0.3, 0.3-0.7 and greater than 0.7 are considered to group the majority of growing, mature and decay stages of the convective systems that were tracked in this study. In the following we present the radar vs. gauge error analysis based on the two error analysis frameworks.

Storm type dependence of radar rainfall error

In the following figures we present the frequency distribution of the gauge-to-radar ratios (i.e. error=gauge/radar) for the VAI product available at 15-minute intervals and classified by season (warm—wet season, cold—dry season, and transition period—north/south migration) and by storm type (T-storm—lightning occurrence vs. rain shower—no lightning occurrence). The warm/cold/transition periods are defined as following: warm—June to September; cold—November to April; transition periods—May and October. The histograms are presented below.

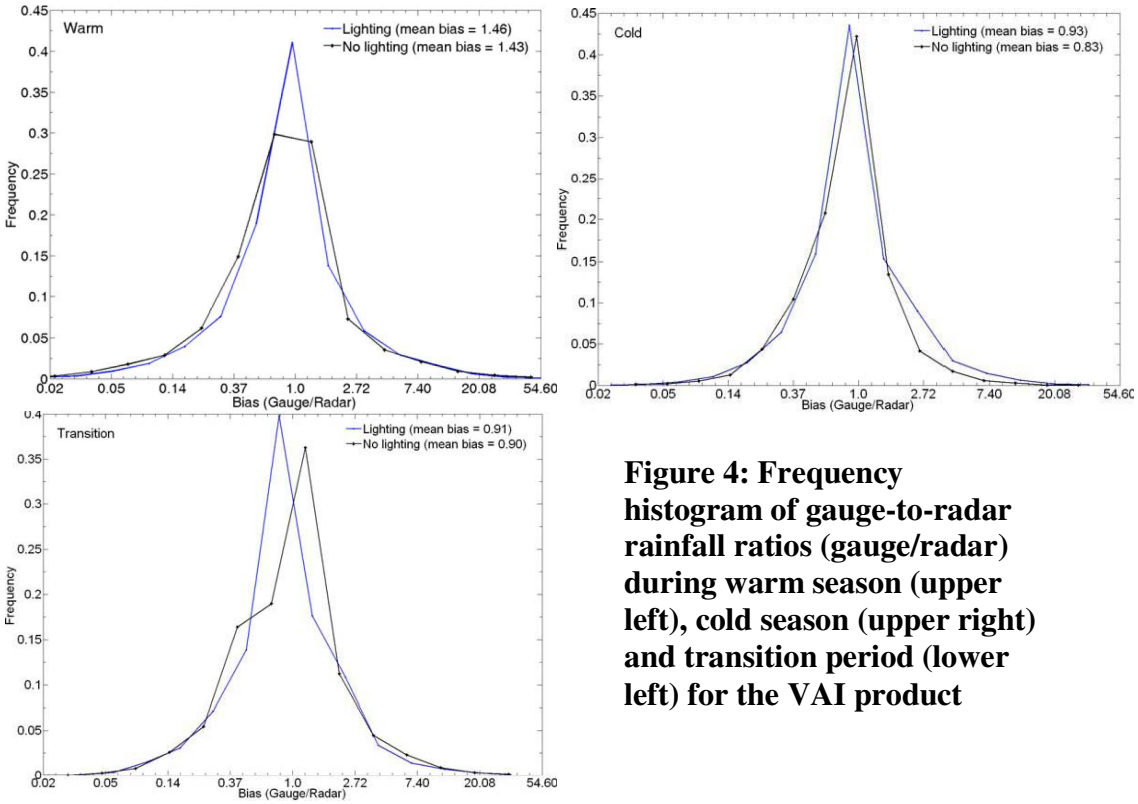

Figure 4: Frequency histogram of gauge-to-radar rainfall ratios (gauge/radar) during warm season (upper left), cold season (upper right) and transition period (lower left) for the VAI product

Several points are noted from the above radar/gauge bias histograms, but, most importantly that there is a distinct shift of radar-gauge ratios (named here Bias) towards radar overestimation in T-storms versus showers and less convective storm types during the transition period. A physical explanation is that in the transition period we expect mixture of storm case exhibiting differences between rain microphysics of the two storm types that reflect in the Z-R relationship parameters, which are commonly used over the whole radar domain. Since the existing radar algorithm does not differentiate the Z-R parameters between the two storm types the mean Z-R will exhibit different biases for

each storm type, as it is apparent in the above histograms of radar-gauge ratios. This issue has been discussed and demonstrated in the past by Anagnostou and Krajewski (1999a,b) who have shown that applying a precipitation classification prior to rain estimation moderates the variability in the Z-R transformation error. Another point to note is that the the data exhibits significant shift in the radar bias in the cold and warm months: 0.95 and 0.99 mean bias (radar/gauge ratio) for the T-storms vs. 0.89 and 0.95 for the non T-storms in the warm and cold seasons, respectively. Overall, we note a tendency for radar overestimation during rain showers, which is moderated or turns to weak underestimation during T-storms (SFWMD, 2008). The presented stats indicate that there is moderate difference in correlation between the different categories of storms, but, in relative RMS the errors tend to increase in most cases from non-lightning storm types (rain shower or less convective storm type) to T-storms associated with higher intensity CG flashes. A cause to this can be an increase in the systematic component of the error in the Z-R conversion. Collective evidence from the above statistics (histograms and Table) indicates that calibrating separately the Z-R relationship for T-storms vs. rain showers and using lightning data from NLDN in real-time in the algorithm of VAI could improve the consistency of the radar-rainfall conversion, which would consequently improve the efficiency of the overall bias adjustment of the rainfall products at the mean-field level. The new Z-R conversions would need to be implemented at the initial stage of the VAI conversion algorithm by ingesting in real-time lightning occurrence data from NLDN. Such lightning data can be available in real-time by the National Weather Service (SFWMD, 2008).

Storm maturity stage dependence of radar rainfall error

As explained in a previous section of this report the storms were tracked and classified according to their life stage (growing, mature and decay). The life stage dependence is depicted in the histograms of gauge to radar ratios presented for the three maturity stages of the storms (i.e., growing, mature and decay) as defined earlier in this paper. Figure 5 shows the histograms for the VAI product. The histograms of the two products show a common pattern of gauge to radar ratio values. For the VAI product the mode of the growing stage distribution (~1.6) is significantly larger than the mode of the decay stage distribution (~0.65), while the mature stage mode is between the two (~1.1). If we combine the information provided by the shape of the histograms with the mean values of the bias ratios shown on the figure one can note that the tendency is for the radar algorithm to underestimate during the growing stage, while overestimate in the mature and more significantly during the decay stage of the storms.

Specifically, the mean of the gauge-to-radar ratios for the different maturity stages of the VAI product are: growth (1.07), mature (0.90) and decay (1.00). growth (0.69), mature (0.67) and decay (0.73). The presented statistics indicate dependence of radar bias on storm maturity stage in the radar rain product. Specifically, we note an increased rain estimation bias in the growth stage relative to the mature and decay, which is consistent to the results of the comparison between T-storms and showers. Combination of storm tracking with the radar rainfall conversion algorithm could potentially provide a radar

algorithm superior to what currently is achieved based on a single Z-R conversion (SFWMD, 2008).

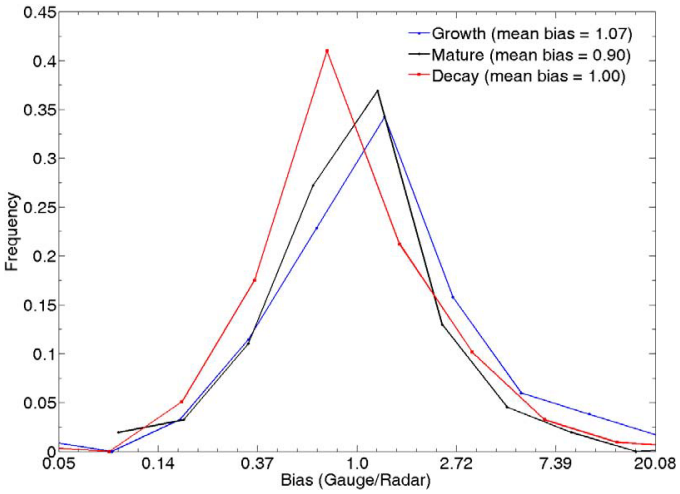

Figure 5: Frequency histograms of gauge-to-radar ratios (bias) for radar-gauge pairs of VAI product (period B) associated with the three storm maturity stages (growth, mature, decay)

Conclusions & Recommendations

The primary conclusion of the herein radar error analysis for different storm types and storm stages is that precipitation microphysical information is critical for improving radar rainfall estimation. Specifically, we showed that

- VAI rainfall product tends to give stronger biases in storms of stronger convective nature (i.e. growth stage and lightning occurrence)
- Rain showers and storms at mature & decay stage tend to be better represented by the existing Z-R conversion (VAI product)

Results from this study indicate that CG lightning information as well as information on the storm's maturity stage could help reduce the variability in the Z-R conversion (at least in the mean sense). Such classification would have a consequential effect on improving the efficiency of a mean-field bias-adjustment algorithm applied at higher temporal scales of aggregation (hourly, daily, etc.).

The results were based on limited radar rainfall data values from VAI products (one year). Future work should concentrate on acquiring larger datasets of the new radar rainfall products (i.e. VAI) to investigate improvements in the Z-R conversion. Based on the results of this report on radar rainfall error statistics we would recommend that the storm tracking and lightning frequency estimation procedures be further investigated for potential use in the operational radar rainfall algorithm to determine characteristic Z-R relationships for different storm types (T-storms vs. rain showers) and storm maturity stages. Such act would potentially lead to a reduction of the estimation uncertainty of the radar rainfall algorithm particularly in the real-time product, which can only include limited gauge information for the on-line radar bias adjustment (SFWMD, 2008). Future directions of this work should include:

- Quantitative estimation of climatological Z-R relationships for the different storm types based on a minimum of 2 years of radar, rain gauge, storm tracking and lightning data analysis
- Integration of the storm tracking and lightning procedures along with the newly determined Z-R relationships in the VAI system and verification of the system performance versus the current approach on the basis of a longer term (2+ years) radar-gauge validation record.

References

Anagnostou, E.N., and W.F. Krajewski, 1999a: Real-Time Radar Rainfall Estimation: 1. Algorithm Formulation, Journal of Atmospheric and Oceanic Technology, 16(2), 189-197.

Anagnostou, E.N., and W.F. Krajewski, 1999b: Real-Time Radar Rainfall Estimation: 2. Case Study, Journal of Atmospheric and Oceanic Technology, 16(2), 198-205.

Atlas, D., C.W. Ulbrich, F.D. Marks, E. Amitai, and C. Williams, 1999: Systematic variation of drop size and radar-rainfall relations, Journal of Geophysical Research, Vol. 104, pp. 6155-6169

Cummins, K. L., M. J. Murphy, E. A. Bardo, W. L. Hiscox, R. B. Pyle, and A. E. Pifer, 1998:A combined TOA/MDF technology upgrade of the U. S. National Lightning Detection Network. J. Geophys. Res., 103, D8, 9035-9044

Janowiak, J. E., R. I. Joyce, and Y. Yarosh, 2001: A real-time global half-hourly pixel resolution infrared dataset and its applications. Bull. Amer. Meteor. Soc., 82(2), 205-217

Lopez, R.E., R. Ortiz, W.D. Otto, and R.L. Holle, 1991: The lightning activity and precipitation yield of convective cloud systems in central Florida. Preprints, 25th Intern. conf. on radar meteor., AMS, 907-10.

Machado, L. A. T., W. B. Rossow, R. L. Guedes, and A.W. Walker, 1998: Life cycle variations of mesoscale convective systems over the Americas. Mon. Wea Rev., 126, 1630–1654

Orville, R. E., and G. R. Huffines, 2001: Cloud-to-ground lightning in the United States: NLDN results in the first decade, 1989-1998. Mon. Wea. Rev., 129, 1179 – 1193

Pathak, C.S. (Ed.). 2008. Hydrologic Monitoring Network of South Florida Water Management District – Appendix 2-1, 2008 South Florida Environment Report, South Florida Water Management District, West Palm Beach, Florida. Available online at: https://my.sfwmd.gov/pls/portal/docs/PAGE/PG_GRP_SFWMD_SFER/PORTLET_SFER/TAB2236041/VOLUME1/appendices/v1_app_2-1.pdf

SFWMD. 2008. A Pilot Study on NEXRAD Data Quality Improvement. Draft Final Report, Prepared by Emmanouil N. Anagnostou, South Florida Water Management District, West Palm Beach, Florida.

Use of NEXRAD Rainfall Data to Develop Climatologically Homogenous Rain Areas for Central and South Florida

Chandra S. Pathak[1], Matthew Onderlinde[2], Henry E. Fuelberg[2]

[1] Operations and Hydro Data Management Division, South Florida Water Management District, 3301 Gun Club Road, West Palm Beach, FL 33416-4680; PH (561) 682-2567; FAX (561) 682-2028; email: cpathak@sfwmd.gov

[2] Department of Meteorology, Florida State University, Tallahassee, FL 32306-4166; PH (860)644-6466; FAX (860)644-4968; e-mail: fuelberg@met.fsu.edu

Abstract

Climatologically homogeneous rainfall regions were developed for the South Florida Water Management District (District) using statistical techniques in conjunction with physical meteorological processes. Rain gauge adjusted NEXRAD (radar) derived rainfall datasets were prepared and stored in the Florida State University (FSU) MPE database. The variability in these data then were analyzed both spatially and temporally to determine rainfall processes and local rainfall patterns. Spatial averages and correlation maps were developed to identify regions that vary similarly in the amount and timing of rainfall. The spatial variability of the multi-sensor rainfall data was identified using daily data. The climatologically homogenous rain areas were derived for four seasons, namely, wet, dry and two transitional seasons. Homogenous rainfall regions were also developed for the annual scale.

This paper will describe methodologies in detail and will present examples of the homogeneous areas, showing their locations and presenting their rainfall characteristics. It is believed that similar techniques could be used in other parts of Florida to identify areas having similar rainfall behavior. These approaches can be very useful in various hydrologic designs.

Introduction

The South Florida Water Management District (District) is responsible for managing and protecting water resources in a 46,439-square kilometer (17,930 square-mile) region. The area extends from Orlando to Key West and from the Gulf Coast to the Atlantic Ocean and contains the Lake Okeechobee. The area is also the site of an environmental restoration program based on the Comprehensive Everglades Restoration Plan. The District operates 2,898 kilometers (1,800 miles) of canals and more than 420 water control structures. The District encompasses 16 counties and serves a population of over six million people.

The District operates an extensive network of 279 active rain gauges in order to obtain rainfall data necessary for use in operations, planning, and regulatory aspects of water management. The rainfall data from 241 stations are available on a breakpoint basis. The breakpoint data can be obtained in a format of 15-minute, hourly, and daily intervals from the District's hydro-meteorological database, DBHYDRO. The rainfall data from the remaining 46 stations are available as daily rainfall (from non-recording rain gauges) in DBHYDRO database.

Additionally, historical rainfall time series data from the District and other external government agencies are also available in DBHYDRO to both internal and external users (Pathak, 2008).

The District operates a network of rain gauging stations to provide precipitation data for use in water management operations, modeling, and planning (Huebner et al., 2003). Several limitations have been shown to exist with sole reliance on point rain gauge measurements, including the introduction of error through the spatial extrapolation of such data. Accounting for spatial rainfall distributions is of particular concern in South Florida, where intense, highly variable convective rain events predominate in the wet season that starts in June and ends in October. Because of the tropical nature of summer rainfall in South Florida, the gauges give only representative rainfall measurements for long averaging periods, and can often miss or erroneously assess the magnitude of significant rainfall events (Pathak, 2008).

Next Generation Radar (NEXRAD) or Weather Surveillance Radar 88 Doppler (WSR-88D) data provide complete spatial coverage of rainfall amounts unobtrusively using a predetermined grid resolution (usually 2 x 2 km or 4 x 4 km). The NEXRAD rainfall dataset is limited due to its reliance on the measurement of raindrop reflectivity, which can be affected by factors such as raindrop size and signal reflection by other objects. Because the reflected signal measured by the radar is proportional to the sum of the sixth power of the diameter of the raindrops in a given volume of atmosphere, small changes in the size of raindrops can have a dramatic effect on the radar's estimate of the rainfall. For this reason, the radar is generally scaled to match the volume measured at the rain gauges in the region. The best of both measurement techniques is realized by using rain gauge data to adjust NEXRAD rainfall values (Pathak, 2008). Four NEXRAD sites operated by the National Weather Service (NWS) cover the District: KBYX in Key West, KAMX in Miami, KMLB in Melbourne, and KBTW in Tampa. The District uses weather data acquired from NEXRAD in making operational decisions. The District has been acquiring NEXRAD data coverage since January 2002 (Huebner et al., 2003).

Temporal and Spatial Variation of Rainfall in Central and South Florida

South Florida is a high-rainfall area, with frontal, convective, and tropical system-driven rainfall events. The heaviest rains in South Florida are produced by mesoscale convective systems – extra-tropical in the dry season and tropical in the rainy season. In Central and South Florida, 57 percent of total summer rainfall occurs on undisturbed sea breeze days, 39 percent on disturbed days, and 4 percent on highly disturbed days. Average Annual Rainfall varies across the District, with 1,118 mm (44 inches) in the Lower Kissimmee to over 1,600 mm (63 inches) in the Palm Beach rain areas. The annual average rainfall on the entire area managed by the District is 1,341 mm (52.8 inches). Ali and Abtew (1999) showed that the spatial structure and distribution of monthly rainfall differ in wet and dry seasons. In the study (Ali and Abtew, 1999), exponential semivariograms were fitted to each month of the year. The sill/nugget and range characteristics in the wet season exhibited weak stationarity with large correlation lengths, while the dry season exhibited strong stationarity with shorter correlation length. Average rainfall over 145 stations was used to evaluate the estimation error variance for the dataset (SFWMD, 2006). Based on the long period of record, the climatological setting of the District is summarized below.

- Dry season (November-April) monthly rainfall values are generally below 102 mm (4.0 inches).

- October rainfall values are below 102 mm (4 inches) in the western part and above 102 mm (4 inches) in the eastern part of the District.
- Average rainfall is higher along the east coast in the dry season and higher along the west coast in the wet season. The spatial range of average rainfall is 25 mm (1.0 inch) or less in the dry season and 51 mm (2.0 inches) or less in the wet season.
- October shows a significant break in rainfall, with higher east coast rainfall than west coast rainfall. In this month, a steep inland gradient 1.9 mm drop/km (3-inch drop/25 miles) is present.
- Wet season variograms exhibit higher nugget effects than those for the dry season indicating that the existing rain gauge network is less capable of resolving rainfall variation in the wet season than in the dry season.
- Rainfall maps show a change in pattern between seasons, with average rainfall that is higher along the east coast in the dry season and higher along the west coast during the wet season.

Many of the factors that determine rainfall over the Florida peninsula are mesoscale features including sea-breeze circulations and daytime heating. To adequately identify locations where these phenomena are most likely, a higher resolution analysis was desired. While larger-scale features such as fronts and tropical systems occasionally do provide large amounts of rainfall within the District, the rainfall statistics are dominated by mesoscale features. Seasonal analysis of rainfall supports this idea, with the exception of the drier winter months when frontally induced precipitation becomes a significant factor, particularly in the northern portion of the district. The goal of the study was to use multi-sensor-derived rainfall data on a 4 × 4 km grid to define homogeneous rainfall regions in the District in which rainfall varies similarly in space and time.

Methodology

In this study, the multi-sensor rainfall data within the District were statistically analyzed. The Florida State University (FSU) multi-sensor data set includes rainfall estimates for the period January 1996 through December 2005 that were prepared. The multi-sensor procedure optimally combines hourly rain gauge data with hourly radar-derived estimates from National Weather Service (NWS) radars. The FSU procedure is a variation of the Multi-Sensor Precipitation Estimator (MPE) that was developed by the NWS Office of Hydrology and is used by the NWS at its River Forecast Centers and Weather Forecast Offices. Details about the original NWS MPE procedure can be found in Fulton et al. (1998) and Dyer and Garza (2004), while FSU's modifications and use of the procedure are described in Marzen and Fuelberg (2005) and VanCleve and Fuelberg (2006). MPE combines the "ground truth" of the gauge-derived amounts with the spatial details provided by the radars. The output is available on a 4 × 4 grid at hourly intervals. For this study, the hourly data were added to produce daily rainfall amounts, and then they were analyzed in both space and time.

The first task of the study was to generate rainfall maps of the District on various time scales. The daily rainfall totals on the 4 × 4 km multi-sensor grid were summed on monthly, seasonal, annual, and multi-annual time scales. A 20 mile buffer surrounding the District boundaries was created and used to define our area of interest. All subsequent data processing was performed interior of this buffer. **Figure 1** shows summed rainfall over the District for the full 10 year period during which MPE data are available. Sea breeze regions along the east and west coasts

are easily identified, with maximum rainfall occurring in regions of irregular coastlines. Conversely, a region of anomalously lighter rainfall is located over and around Lake Okeechobee. A region of somewhat lighter precipitation extends north and south of the Lake to the borders of the computational area. Relatively light precipitation also is located at the southern tip of Florida where swampy conditions limit the development of strong land-sea temperature gradients that lead to sea breezes. **Figure 1** clearly reveals that rainfall is not uniform over the District.

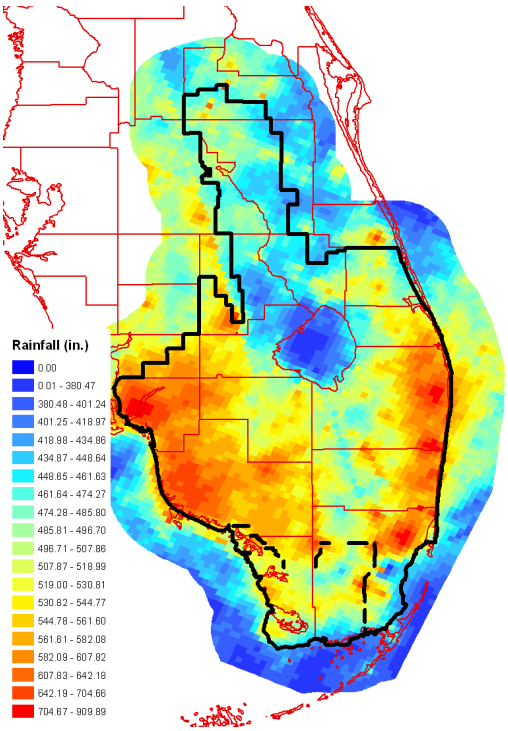

Figure 1: Total accumulated rainfall (in.) for the District based on MPE data between January 1996 and May 2006.

The second task was to complete a temporal analysis of rainfall. A time series of daily mean areal precipitation for the entire District was plotted in **Figure 2**. This time series was generated to gain insight into the regularity of seasonal transitions. It was hypothesized that the transitions were fairly irregular in time, and this indeed was confirmed by the time series. A moving filter to reduce noise was applied to the daily rainfall data to examine the periodicity of the rainfall signal. Specifically, for each day during the 10 year period, the filter calculated an average of the seven surrounding days and returned that average value. Thus, a running average was generated using the technique, with 365 seven day averages plotted each year. If strong seasonality were occurring, one should see a sine shaped curve each year, with one maximum and minimum at approximately the same times each year. **Figure 2** shows the absence of a clear seasonal transition since many minima and maxima occur independent of a one year signal. Because of this lack of a clear seasonal signal in the rainfall, the seasons were defined as follows.

i) Wet Season: June – October

ii) Dry Season: December – April

iii) Transition Spring Season: May

iv) Transition Fall Season: November

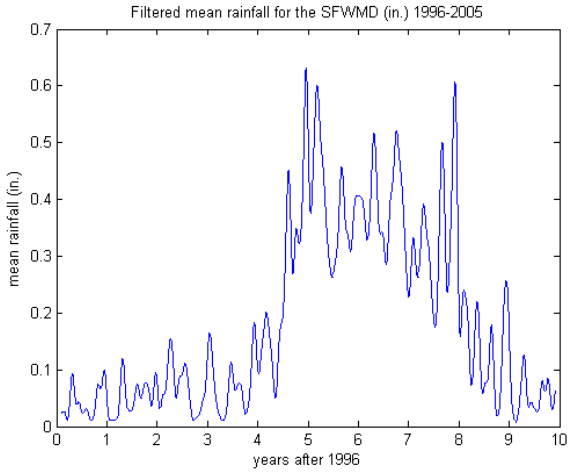

Figure 2: Time series of filtered mean areal precipitation (in.) for the entire District during the period January 1996 to May 2006.

The next task was to use correlation mapping to identify and define regions having homogeneous rainfall in space and time. An average rainfall accumulation were calculated for nine adjacent grid cells (denoted a "seed area") within the District for each day between 1 January 1996 to 31 December 2005. Seasonal versions (wet, dry, etc.) also were generated. The seeds created a quantity with which to correlate values over the remainder of the District. In this case, the "seed areas" were selected from the rainfall maps shown in **Figure 1**.

Specifically, regions that had similar rainfall accumulation and that corresponded spatially to known meteorological phenomenon like the sea breeze were used to define the "seed areas". The 9 point seed values then were correlated in time to every other 4 × 4 grid cell within the District. At the end of the process, the correlation was calculated for each grid cell and plotted in ArcGIS. A minimum correlation criterion was defined for each season, and all correlations greater than or equal to the criterion were plotted. The criterion was selected so that the sizes of individual correlation regions would be similar to the regions of relatively uniform rainfall accumulation.

The final task was to perform a sensitivity analysis of the aforementioned correlation procedure. It was hypothesized that the correlation regions would be highly sensitive to the selected seed areas. To identify such sensitivity, correlations outside of the correlation region were compared with those inside the region to show that the individual regions were, in fact, homogenous. Finally, statistics (mean, standard deviation, variance, and coefficient of variance) for each homogenous region were calculated to show the variability between different regions. By determining whether each region had unique statistics, the degree of homogeneity was determined. Although some differences occasionally were small between several rainfall regions, the correlation mapping technique allowed us to identify regional discontinuities in the time variability of rainfall in the District.

Results

As described above, the identification of correlation regions in combination with the mean rainfall for the different seasons allowed homogeneous regions in the District to be determined. This procedure was followed to define homogeneous regions during the spring, fall, and dry seasons, as well as for the annual time scale. Interestingly, during the fall season only two regions of correlation are required to define homogenous regions. Conversely, the maximum number of homogeneous regions was twelve during the wet season. The corresponding maps for

all seasons were developed and shown in the study report (FSU, 2008). As an example, **Figure 4** shows these homogeneous regions during the wet season.

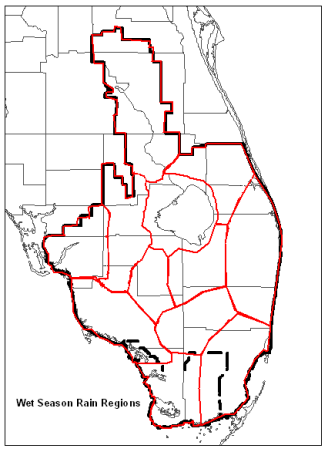

Figure 4: Twelve homogeneous rainfall regions during the wet season in the District.

Figures 5a shows the 10-year mean rainfall during the wet season (June – October) along with one example of a correlation region. In this example, strong correlations occur along the east coast of South Florida, in agreement with the sea breeze circulation that occurs in this area of convex coastline. Both rainfall accumulation and variability are fairly consistent within the region of correlation ≥ 0.6 (the value at which the colors begin).

Although some non-contiguous correlation regions also exist (e.g., northwest of Lake Okeechobee), they are not considered homogeneous since they are due to meteorological factors other than the sea breeze. **Figure 5b** demonstrates how the correlated area mimics the shape of the predominant meteorological forcing; in this case the sea breeze.

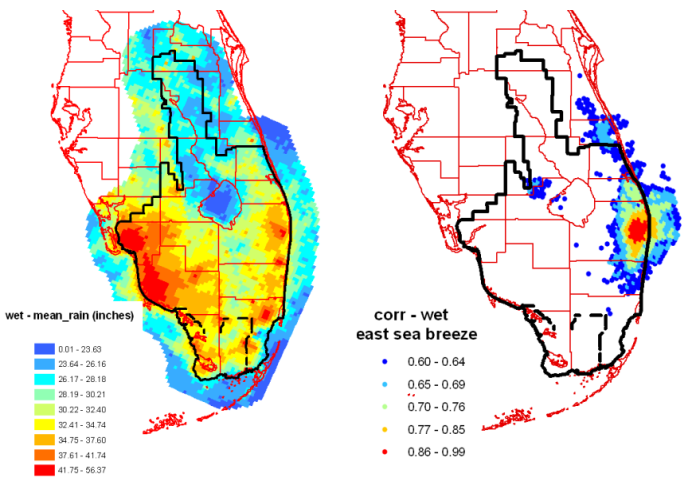

Figure 5a (left): Mean rainfall (in.) during the wet season (June – October) for the District. Figure 5b (right): Homogeneous correlation region containing the East Coast sea breeze. The minimum correlation criterion is 0.6.

Another example that demonstrates homogeneity is the correlation region over Lake Okeechobee which approximately follows the shape of the Lake. While the region of correlation ≥ 0.6 extends beyond the Lake itself, the greatest correlations (correlation > 0.75) are located almost exclusively over the Lake. Clearly the divergence generated by cool outflow in all directions away from the Lake's center creates subsidence over this region, thus limiting convective potential during the spring and summer months. **Figure 6a** and **b** compare mean rainfall with correlation over Lake Okeechobee during the wet season. The rainfall totals are significantly less over and around the Lake, and the correlation region ≥ 0.6 agrees closely with the area of diminished rainfall. This spatial consistency lends credence to the idea that rainfall is homogeneous within this region, being consistent in both space and time.

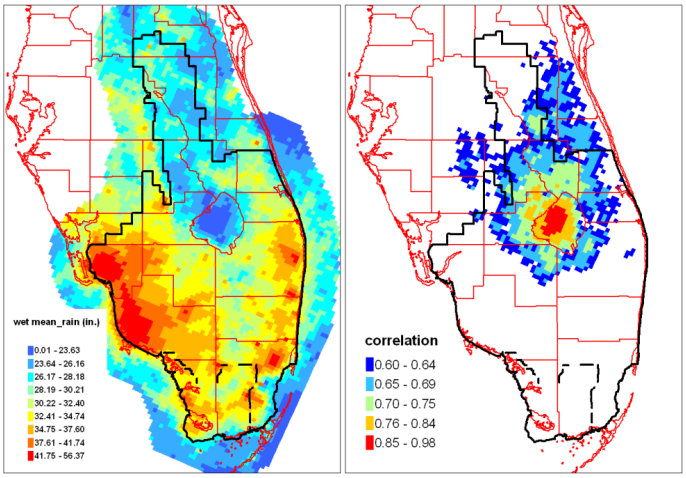

Figure 6a (left): Mean rainfall (in.) during the wet season (June – October) for the District. Figure 6b (right): Correlation region for the Lake Okeechobee region. The minimum correlation criterion is 0.6.

In the previous two examples, the rainfall anomalies associated with the sea breeze and Lake Okeechobee were easily identifiable sites for seed areas from which to calculate correlation with the remainder of the District. That is, by considering the meteorology of the region and by viewing the mean rainfall maps (**Figures. 5a** and **6a**), these seed areas were chosen. On the other hand, a few seed regions were identified because they were located between areas of obvious meteorological forcing. These areas most often were located in the center of the southern Florida peninsula where neither the East nor West Coast sea breezes or Lake Okeechobee contributes directly to their rainfall. Instead, the scenario that occurs most often during the wet season is that their convection results either from simple daytime heating or from the collision of thunderstorm outflow boundaries propagating away from storms associated with the various sea and lake (Okeechobee) breezes. Although these regions are not as easily defined by the mean rainfall maps in Figs. 5a and 6a, they become more apparent through correlation mapping.

Figure 7a and **b** show an example of such a case in the middle to western regions of the Florida peninsula between Lake Okeechobee and the Gulf Coast. The area is well defined by correlation, but not as clearly defined by a qualitative visual analysis of rainfall patterns. This technique also defined regions south of Lake Okeechobee toward the south coast (see **Figure 4**) where daytime instability and colliding outflow boundaries drive most of the wet season convection.

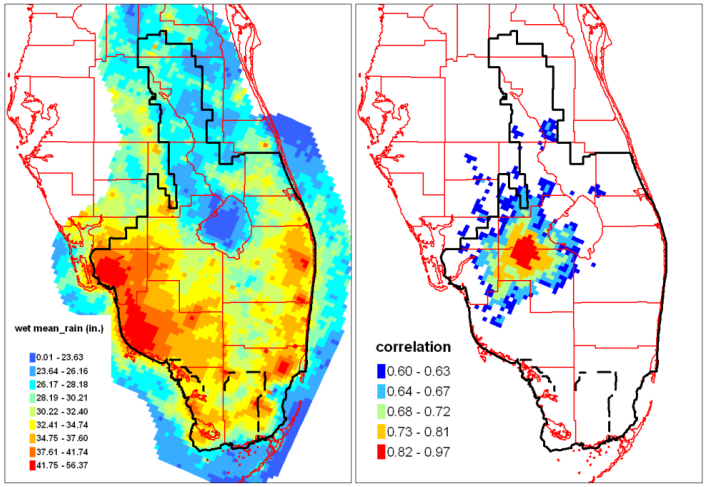

Figure 7a (left): Mean rainfall (in.) for the wet season (June – October) for the District. Figure 7b (right): Correlation region for the Northwest-Mid region. The minimum correlation criterion is 0.6.

After selecting a sufficient number of correlation seed points, the homogeneous regions were defined based on both the summed rainfall accumulation and the correlation regions. That is, those 4 × 4 km grid cells that were within the minimum correlation criterion, lay within similar characteristic accumulation areas, as shown in **Figure 1**, and generally were contiguous were considered to be homogeneous. Once the various homogeneous regions were defined, statistics for each region were calculated to ensure that each area truly was homogeneous and distinct from adjacent areas. The mean, standard deviation, variance, and coefficient of variance were calculated for all regions, for each season. **Figure 9** shows an example of the standard deviation of daily rainfall in the District and a histogram representation of each homogeneous region during the wet season. Statistical maps for all seasons were developed and shown in the report (FSU, 2008). **Table 1** below shows the statistics for each homogeneous region during each season.

In this example rainfall varies the most in the coastal areas where sea breezes are the prominent forcing mechanisms. These sea breezes vary somewhat from day to day due to the background synoptic patterns that determine their strength and inland penetration. Conversely, rainfall is more consistent in inland areas where daily rainfall depends more on daytime heating.

Table 1: Statistics - mean, standard deviation (std), variance (var), and coefficient of variance (coef_var) for each homogeneous region in the District for each season.

Homogeneous regional statistics for all seasons				
WET SEASON				
Region	**Mean**	**Std**	**Var**	**Coef_var**
East Sea Breeze	0.2235	0.0183	0.0515	0.0820
Everglades	0.2147	0.0188	0.0543	0.0878
Lake Okeechobee	0.1776	0.0222	0.0753	0.1249
Miami	0.2194	0.0292	0.1308	0.1332
NE Lake Okeechobee	0.1932	0.0127	0.0248	0.0658
North	0.1777	0.0112	0.0191	0.0629
NW Mid	0.2218	0.0155	0.0368	0.0699
South Lake Okeechobee	0.2038	0.0105	0.0169	0.0515
South Mid	0.2098	0.0106	0.0173	0.0507
SW Mid	0.2240	0.0144	0.0317	0.0642
SW Sea Breeze	0.2526	0.0216	0.0717	0.0857
West Sea Breeze	0.2508	0.0267	0.1087	0.1063
DRY SEASON				
Region	**Mean**	**Std**	**Var**	**Coef_var**
North	0.0730	0.0071	0.0001	0.0972
southwest	0.0573	0.0097	0.0001	0.1689
East Southeast	0.0769	0.0115	0.0001	0.1498
Southwest	0.0610	0.0052	0.0000	0.0850
SPRING SEASON				
Region	**Mean**	**Std**	**Var**	**Coef_var**
North	0.0955	0.0130	0.0002	0.1362
North Lake Okeechobee	0.1160	0.0138	0.0002	0.1194
Everglades	0.1323	0.0231	0.0005	0.1746
Lake Okeechobee	0.1015	0.0106	0.0001	0.1041
Northeast	0.1236	0.0191	0.0004	0.1547
South Lake Okeechobee	0.1368	0.0136	0.0002	0.0991
Southeast	0.1456	0.0203	0.0004	0.1395
Southwest	0.1356	0.0220	0.0005	0.1624
FALL SEASON				
Region	**Mean**	**Std**	**Var**	**Coef_var**
Northwest	0.0673	0.0121	0.0001	0.1796
Southeast	0.0877	0.0299	0.0009	0.3407

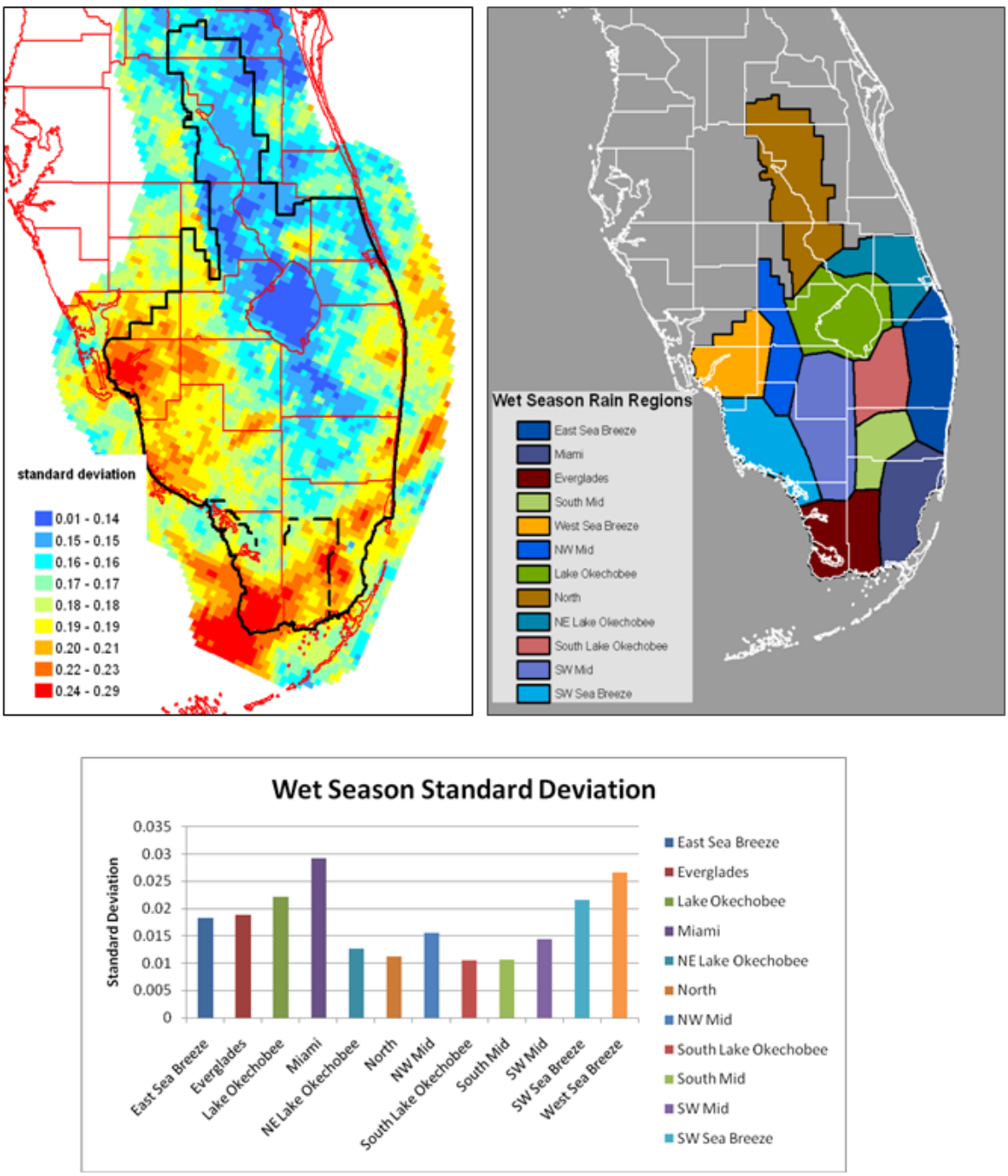

Figure 9: Wet season standard deviation (in.), map showing the wet season homogeneous regions, and the standard deviation (in.) within each region.

The final analysis was to verify that the regions developed in this study were homogeneous when compared to previously developed rain areas within the District. As an example, **Figure 10** shows the correlation of the Lake Okeechobee region with the remainder of the District during the wet season. **Figure 10** shows correlation between the Lake Okeechobee region and the rest of the District, with the new correlation criterion being correlation < 0.6. It is clear that the correlation decreases quickly away from the Lake, particularly in directions toward the sea breeze regions on the east and west coasts of the southern Florida peninsula. It is also important to note that there are no significant discontinuous regions of large correlation away from the original region defined by the Lake. These statistical differences between homogeneous regions also were noted in the histogram shown in **Figure 8**. The standard deviation in the Miami region is nearly 3 times greater than the deviation in the South Lake Okeechobee and South-Mid regions. Another way to test the homogeneity was to move correlation seed areas slightly and note any observed changes in the correlation region. The results showed that the scheme is sensitive to the choice of seed areas which emphasizes the importance of choosing regions of meteorological significance (regions defined by a specific meteorological phenomenon like a sea breeze). When perturbing the initial seed area location slightly within a sea breeze area, for example, little change is observed in the correlation region. The combination of these statistically observed (**Figure 9**) and spatially observed (**Figure 10**) differences lend merit to the homogeneity of the regions.

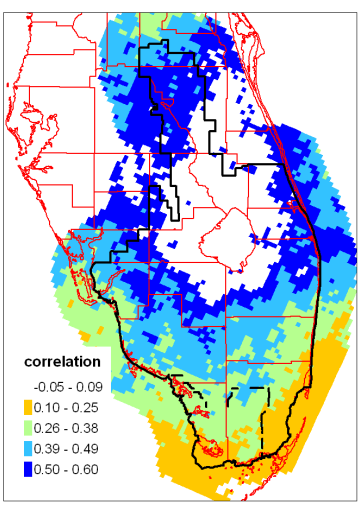

Figure 10: Correlations of the Lake Okeechobee region with the remainder of the District during the wet season.

Discussion and Conclusion

Homogeneous rainfall regions have been identified within the District by combining statistical information derived from multi-sensor precipitation data with known meteorological trends. The two predominant tools used in this procedure were mean rainfall and the spatial correlation of rainfall. By combining these two products, we could qualitatively determine the boundaries of the homogeneous regions. A spatial variability product also identified regions where less trust should be placed on the multi-sensor product when analyzing mean rainfall. The resolution of our rainfall data (4×4-km) is considerably better than in previous studies. Therefore, more detailed features could be identified in the mean rainfall maps. This higher spatial data

resolution provided added confidence in the significance of the results and the homogeneity of the defined regions. Although previous studies had defined as many as fourteen homogenous regions within the District, we believe that the meteorological and statistical information supports only as many as twelve truly homogeneous regions (during the wet season). During the other seasons, only 2-9 homogeneous regions could be identified (2 in the fall, 4 in the dry season, and 9 in the spring). These climatologically homogeneous rainfall regions will help water managers in making improved water management decisions.

References

Ali, A. and W. Abtew, 1999: Regional rainfall frequency analysis of central and south Florida. Technical publication WRE #380, South Florida Water Management District, West Palm Beach, Florida.

Dyer, J. L. and R.C. Garza, 2004: A comparison of precipitation estimation techniques over Lake Okeechobee, Florida. Weather Forecasting. 19(6), 1029-1043.

FSU. 2008. Using NEXRAD Rainfall Data to Develop Climatologically Homogenous Rain Areas for Central and South Florida, Final Draft Report, Prepared by Florida State University, South Florida Water Management District. West Palm Beach, Florida.

Fulton, R. A. 1999: Sensitivity of WSR-88D rainfall estimates to the rain-rate threshold and rain gauge adjustment: A flash flood case study. Weather Forecasting, 14(5), 604-624.

Huebner, R.S., C. Pathak, and B.C. Hoblit, 2003. Development and Use of a NEXRAD Database for Water Management in South Florida. American Society of Civil Engineers /Environmental and Water Resources Institute, World Water & Environmental Congress, June 23-26, 2003. Philadelphia, Pennsylvania, USA

Martinaitis, S. M., 2008: personal communication, Florida State University.

Marzen, J. L. and H.E. Fuelberg, 2005: Developing a high-resolution precipitation dataset for Florida hydrological studies. 19th Conf. on Hydrology, Amer. Meteor. Soc. San Diego, CA, paper J9.2. Available online at: http://ams.confex.com/ams/Annual2005/techprogram/paper_83718.htm

Pathak, C.S. (Ed.). 2008. Hydrologic Monitoring Network of South Florida Water Management District – Appendix 2-1, 2008 South Florida Environment Report, South Florida Water Management District, West Palm Beach, Florida. Available online at: https://my.sfwmd.gov/pls/portal/docs/PAGE/PG_GRP_SFWMD_SFER/PORTLET_SFER/TAB2236041/VOLUME1/appendices/v1_app_2-1.pdf

SFWMD. 2006: Rain Gauge Network Optimization Study. Vieux & Associates, Inc Final Report, South Florida Water Management District. West Palm Beach, Florida.

VanCleve, D. D., and H.E. Fuelberg. 2006: An intercomparison between mean areal precipitation from gauges and a multisensor procedure. 21st Conf. on Hydrology, San Antonio, TX, Amer. Meteor. Soc. 2007. Available online at: http://ams.confex.com/ams/87ANNUAL/techprogram/paper_120249.htm

Impacts of Different Rainfall Estimates on Hydrological Simulation and Satellite Rainfall Retrieval Error Propagation

Tadesse Meskele[1] and Hamid Moradkhani, PhD, PE, MASCE[2]

[1]PhD student, tadesse@pdx.edu, [2]Assistant Professor, hamidm@cecs.pdx.edu

Portland State University, Department of Civil and Environmental Engineering, Portland, Oregon, USA 97201

Abstract

Accurate estimation of rainfall magnitudes and their spatial distribution plays an important role in hydrological applications such as flood risk analysis and river flow forecasts. In addition knowing the forcing data error structure is crucial part of hydrologic data assimilation system. Recent advances in radar and satellite based measurements have provided alternative methods for precipitation estimation. In this study, gauge, radar and satellite precipitation estimates are used to explore the impacts of different precipitation data sources on the accuracy of hydrological simulation over the Leaf River basin in Mississippi. The NEXRAD stage IV, 3B42 gridded TRMM, PERSIANN-CCS and rain-gauge data over the watershed are aggregated to similar resolution in time and forced to a conceptual hydrological model, SAC-SMA. The model performance with each of the rainfall estimates input has been assessed by statistical comparison of the simulated and measured streamflow at the watershed outlet. In this study, the standard error of satellite-based PERSIANN-CCS rainfall estimates conditioning on the assumed true field (i.e. radar rainfall) is obtained according to a multivariate function considering the spatial and temporal scales. Accepting the multiplicative nature of precipitation error, the Monte Carlo simulation based on log-normal distribution of error is conducted to generate the ensemble of precipitation and propagate them into a conceptual hydrologic model to investigate the impact of input error on streamflow simulation.

Introduction

Precipitation is the key hydrologic variable linking the atmosphere with land surface processes, and playing a dominant role in the climate system. Accurate measurements of precipitation on a variety of space and time scales are important not only to weather forecasters and climate scientists, but also to a wide range of decision makers, including hydrologists, agriculturalists, and industrialists (Ebert et al., 2007). In the past the assessment of water resources of a watershed used to be a complicated task due to limited data availability. However, nowadays an increasing number of radar and satellite-based rainfall products are available in near–real time over the Internet. Thus due to ease of accessibility and high-speed communications it is possible to download rainfall maps and digital data provided by national meteorological centers, government institutions, and university research groups in a matter of seconds. Thus owing to such wide spread availability and easy accessibility of satellite–based precipitation estimate has enhanced the hydrological modeling and forecasting at the watershed scale. However it is very crucial to assess the impact of the rainfall estimate from various sources on hydrologic simulations. In addition, quantification of associated errors of these products and evaluating their impacts on hydrologic response is essential in the usage of satellite products in high resolution hydrologic applications. In this study, the rainfall estimates from 3B42V6 gridded TRMM (Tropical Rainfall Measuring Mission) data, PERSSIANN-CCS (Precipitation Estimation from Remotely Sensed Information using Artificial Neural Networks-Cloud Classification System) and NEXRAD Stage IV data have been forced to conceptual hydrologic model and the resulting hydrologic response has been analyzed. Besides, the impact of input error on streamflow simulation has been investigated by generating the ensemble of precipitation to characterize the standard error of satellite-based PERSIANN-CCS

rainfall estimate and propagating them into a conceptual hydrologic model. This study builds upon the detailed analysis conducted by Moradkhani et al. [2006] and more recent study by Moradkhani and Meskele [2009].

Study basin and datasets

The study area selected is the Leaf River Basin (1944 Km^2) located north of Collins, Mississippi, United states which has been widely used in various studies (see [Moradkhani and Sorooshian, 2008] for list of references).

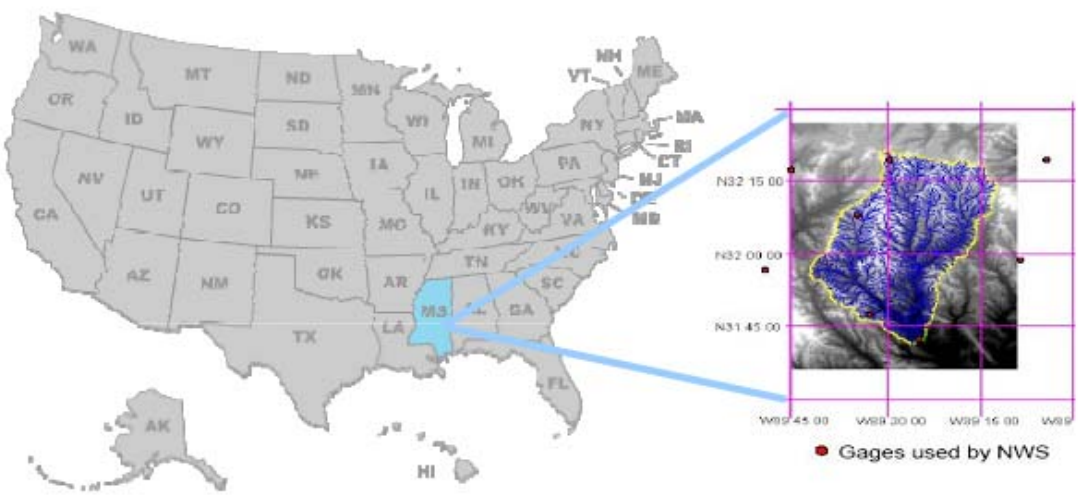

Figure 1. The location of Leaf River basin

The satellite-based precipitation data used was based on the 3B42V6 TRMM (Tropical Rainfall Measuring Mission) data and PERSIANN-CCS (Precipitation Estimation from Remotely Sensed Information Using Artificial Neural Networks- Cloud Classification System) product [Hong et al., 2004]. The TRMM Multisatellite Precipitation Analysis (TMPA) provides a calibration-based sequential scheme for combining precipitation estimates from multiple satellites, as well as gauge

analyses where feasible, at fine scales (0.25° x 0.25° and 3 hourly). The dataset covers the latitude band 50°N–S for the period from 1998 to the delayed present (Huffman et.al, 2006). The PERSIANN-CCS is a satellite infrared-based algorithm that produces global estimates of rainfall based on infrared brightness temperature image provided by geostationary satellites. These data covers 50°S to 50°N globally and an improved version of PERSIANN-CCS algorithm estimates rainfall at spatial 0.04° x 0.04° and temporal resolution of 30 minutes respectively. The other rainfall product used to estimate the error associated with the satellite product, is the National Weather Service WSR-88D Stage IV radar rainfall data. The Next generation weather radar (NEXRAD, formally known as the Weather Surveillance Radar-1988 Doppler -WSR- 88D) of the United States provides precipitation data are obtained from 158 Weather radar deployed by the Weather Service Agency across the country. The data was acquired from NCEP (National Center for Environmental prediction) for the same period and the spatial domain as that of PERSIANN-CCS which was used here as reference (true) rainfall field. The other hydrologic data sets used for the study were the rainfall from rain gages and temperature data extracted from National Climate Data Center (NCDC) and streamflow data from USGS for the period of 1948-2005. These data were utilized for calibrating and validating the hydrologic model.

Methodology

In the study the satellite based precipitation estimates were aggregated over the Leaf watershed and altered to same scale of daily accumulations before forcing them to the conceptual hydrologic model. The Sacramento Soil Moisture Accounting Model (SAC-SMA) is an operational conceptual model originally developed at the California-Nevada River Forecast Center located in

Sacramento, California as a "Generalized Stream flow Simulation System", [Burnash et al., 1973; Burnash, 1995] to ameliorate the region's operational capability of stream flow prediction. The model passed through extensive development and testing on the other catchments in United States before its streamflow determination capability got adopted as major component of the National Weather Service River Forecast System (NWSRFS).

The model consists of six sate variables that represent the soil water content of the upper and lower soil mantels in the form of free and tension water [Burnash, 1995]. The soil moisture storages in both zones vary due to the non linear dynamics of precipitation, percolation, evaporation and lateral drainage. The working principle of the model designates that the precipitation which falls on the impervious area of the catchment produces immediately a direct runoff while the part that falls over pervious area of the catchment infiltrates to the upper zone of the soil mantel. If there is water deficiency in the upper zone of the soil, it gets absorbed till the tension water requirement is met and then starts to flow as free water that percolates to meet the demand of the lower zone. The model has seventeen parameters of which four are considered fixed and the rest are to be calibrated using the Shuffled complex Evolution (SCE-UA) optimization algorithm developed at University of Arizona [Duan et al., 1992].

The model was run using rainfall estimates from TRMM, PERSIANN-CCS and NEXRAD IV for year 2004-2005 and the resulting output of stream flows were compared.

Regarding the satellite rainfall estimates uncertainty, in this study we consider the standard error of satellite-based PERSIANN-CCS rainfall estimates conditioning on the assumed true field (i.e. radar rainfall) which is obtained according to a multivariate function explained briefly by Hong, 2006. The error model illustrated on the paper as:

$$\sigma_e = f(\frac{1}{L}, \frac{\Delta t}{T}, P) = a.\left(\frac{1}{L}\right)^b.\left(\frac{\Delta t}{T}\right)^c (\hat{P})^d \quad (1)$$

Where, $\Delta t = T/N$ is the satellite sampling frequency assuming that the satellite makes N visits over area A during the period of T. This error model was calibrated for various spatial and temporal scales and also precipitation magnitudes which yield the parameters *a, b, c,* and *d* [Hong et al., 2006]. Based on the assumption of multiplicative nature of this error, the Monte Carlo simulation is used to generate the ensemble of precipitation and propagate them into a SAC-SMA model to investigate the impact of input error on streamflow simulation.

Results and discussion

The satellite-based rainfall estimate from the PERSIANN-CCS and TRMM are translated to stream flow hydrograph at the outlet of the Leaf River Basin and compared to the synthetic hydrograph from the NEXRAD Stage IV which is considered as a reference. The plot on Figure 2 shows that even though the hydrograph simulated by the TRMM captures the pattern of the synthetic hydrograph, it is distinctly underestimates the streamflow at the outlet of the catchment while the streamflow simulation from PERSIANN-CSS product comparatively yields better performance. The bias plot on Figure 3 also further strengthen the facts discussed above showing almost a bias of zero throughout for PERSIANN-CCS.

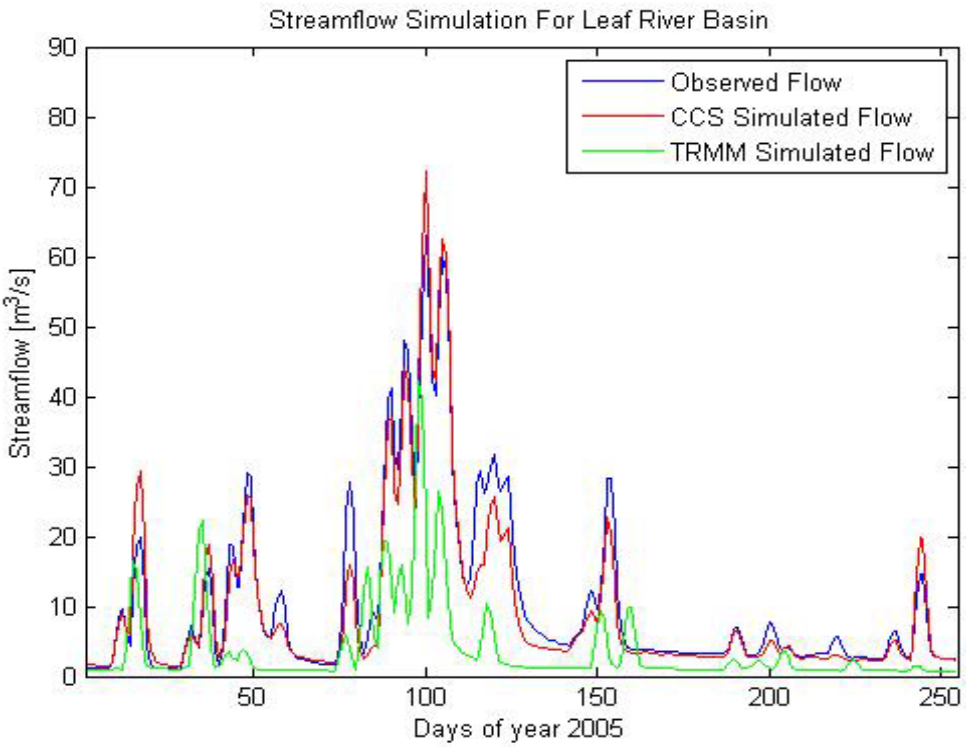

Figure 2 Streamflow simulations for Leaf River basin

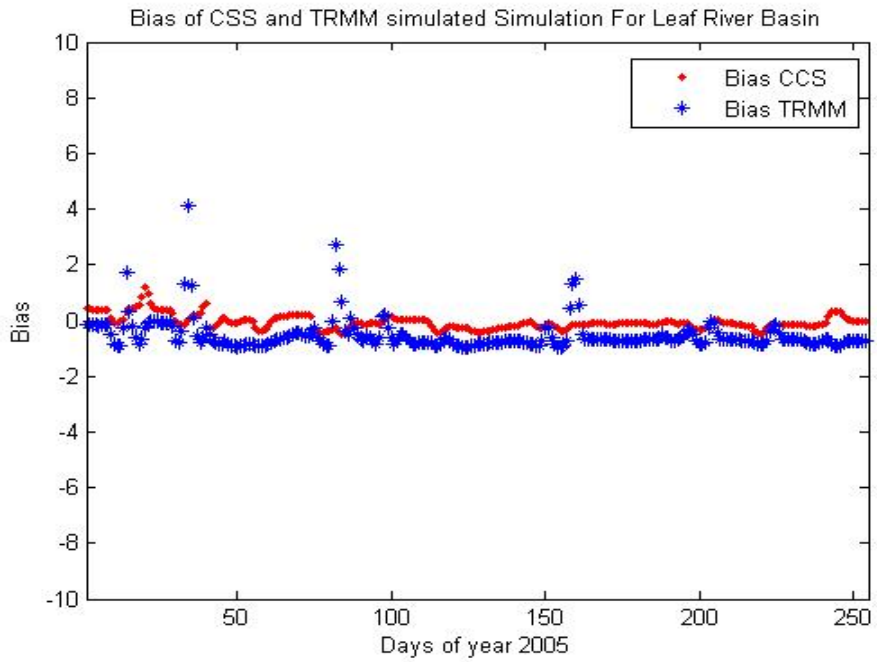

Figure 3 Bias plots for TRMM and PERSIANN-CCS simulated streamflow

The ensemble of satellite-based precipitation for PERSIANN-CCS data is also generated over the catchment and the hydrologic model is derived with this ensemble for the period of 2001 to 2005. For clarity the ensemble streamflow generation for the portion of year 2005 of analysis is displayed in figure 4. Then the model performance in hydrologic predictions is evaluated probabilistically through Normalized Root Mean Square Error Ratio (NRR) since it is a simpler procedure to investigate the quality of ensemble. Moradkhani et al., [2006] and Moradkhani et al., [2005a] used NRR according to [Anderson, 2001] to measure the ensemble dispersion for indicating how confidently the ensemble mean could be extracted from the ensemble spread. According to this method, the ratio of the time-averaged RMSE of the ensemble mean, R_1 to the mean RMSE of the ensemble members, R_2 is calculated and then the ratio is normalized by $E[R_a] = \sqrt{\frac{(n+1)}{2n}}$. This factor shows if the observation is statistically indistinguishable from n ensemble members [Anderson, 2001].

$$R_1 = \sqrt{\frac{1}{T}\sum_{t=1}^{T}[(\frac{1}{n}\sum_{i=1}^{n} y_t^i) - O_t]^2} \quad (2)$$

$$R_2 = \frac{1}{n}\sum_{i=1}^{n}\sqrt{\frac{1}{T}\sum_{t=1}^{T}[y_t^i - O_t]^2} \quad (3)$$

$$Ra = \frac{R_1}{R_2} \quad (4)$$

$$NRR = \frac{Ra}{E[Ra]} \quad (5)$$

Where, n and T are the ensemble size and length of analysis respectively.

It is desired that the ensemble yields *NRR=1*. However, *NRR>1* indicates that the ensemble has too little spread, and *NRR<1* is an indication of an ensemble with too much spread. *NRR* of the streamflow ensemble was obtained annually for the 5 years of simulation from 2001 to 2005. As seen in figure 5 the *NRRs* for all years are above 1 meaning that the streamflow ensemble is under dispersed. This could be explained in part as a result of a large number of ensemble members having zero precipitation creating very narrow ensemble of precipitation resulting in narrow streamflow ensemble. A detail analysis for a wide range of the probabilistic model performance measure is discussed in Moradkhani and Meskele, [2009].

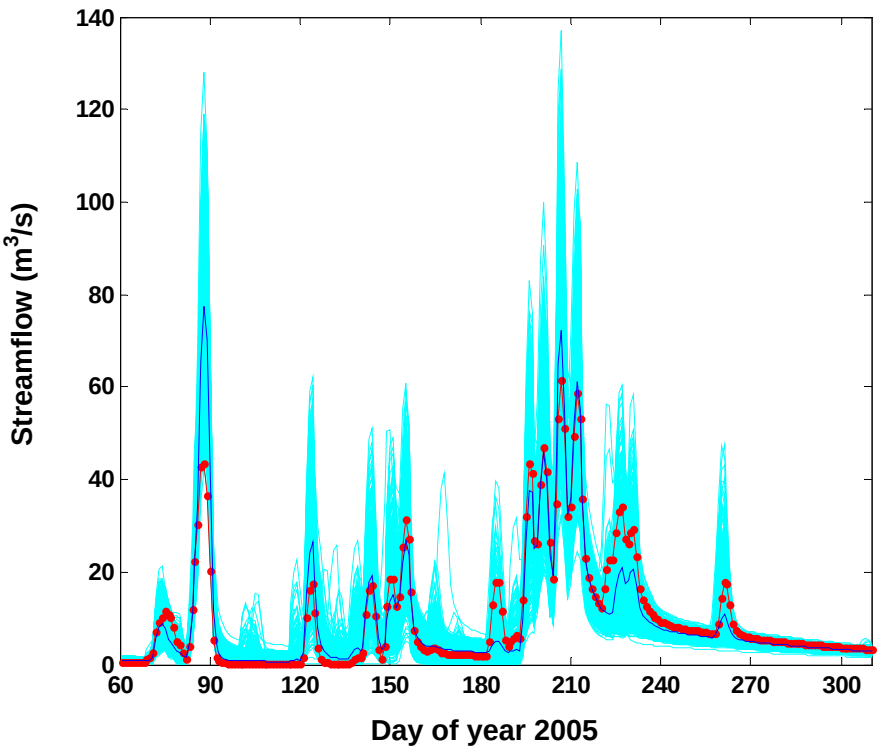

Figure 4. Streamflow ensemble generated by propagating the ensemble of erroneous CCS-PERSIANN rainfall product. The solid dotted line displays the synthetic truth by deriving the SAC-SMA model with radar rainfall data. The shaded area and solid line show the streamflow ensemble and the ensemble mean respectively.

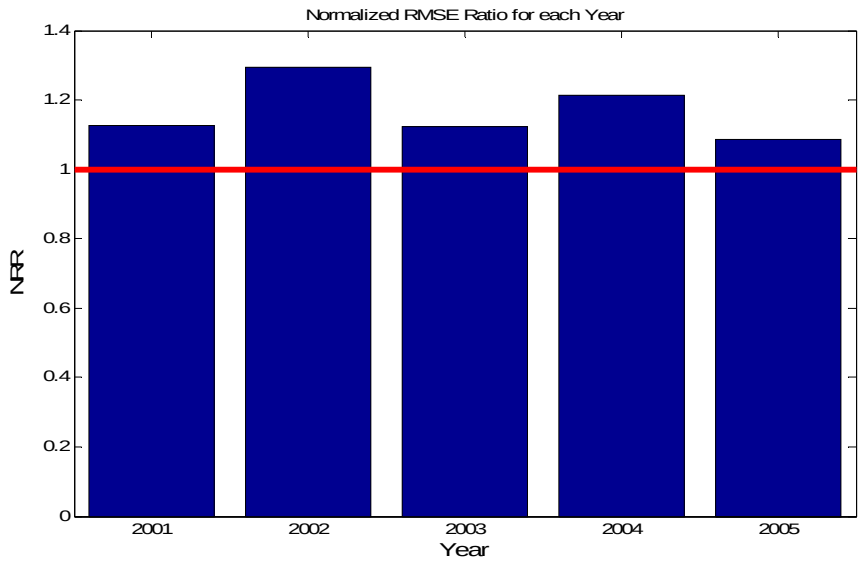

Figure 5. Annual Normalized Root Mean Square Error Ratio (NRR) for the streamflow ensemble generated by CCS-PERSSIAN Satellite precipitation ensemble. The solid line shows the ideal NRR=1.

Summary and Conclusion

In this study, we briefly attempted to evaluate the impact of different satellite based rainfall estimate on a streamflow generation using a conceptual hydrologic model and we performed a Monte Carlos simulation for ensemble generation and propagation of precipitation. It is obvious that an adjustment should be made to TRMM Rainfall estimate before driving the streamflow at an out let of a catchment to remove the systematic underestimation obtained.

An ensemble of streamflow simulation generated by PERSIANN-CCS was also probabilistically evaluated to assess the translation of precipitation uncertainty to a hydrologic simulation.

References

Anderson, J. L. (2001), An Ensemble Adjustment Kalman Filter for Data Assimilation, *Monthly Weather Review, 129*(12), 2884-2903.

Burnash, R. J. C. (1995), The NWS river forecast system- catchment model, in *Computer Models of Watershed Hydrology*, edited by V. P. Singh, pp. 311-365, Water Resources Publications.

Burnash, R. J. C., R. L. Ferral, and R. A. McGuire (1973), A generalized streamflow simulation system: Conceptual models for digital comouters.

Duan, Q. S., S. Sorooshian, and V. K. Gupta (1992), Effective and efficient global optimization for conceptual rainfall- runoff models, *Water Resour. Res., 28*(4), 1015-1031.

Ebert E., Janowiak J., Kidd C. Comparison of Near-Real-Time Precipitation Estimates from Satellite Observations and Numerical Models, 2007. American Meteorological Society.

Hong, Y., H. K., M. H., and S. S. (2006), Uncertainty Quantification of Satellite Precipitation Estimation and Monte Carlo Assessment of the Error Propagation into Hydrologic Response, *Water Resources Research, 42*.Resources, 28(2), 135-147.

Huffman G., Adler R., Bolvin D., Gu G., Nelkin E., Bowman K., Hong Y., Stocker E., Wolff D., 2006. The TRMM Multisatellite Precipitation Analysis (TMPA): Quasi-Global, Multiyear, Combined-Sensor Precipitation Estimates at Fine Scales. Journal of Hydrometeorology.

Moradkhani, H. and S. Sorooshian (2008), General review of rainfall-runoff modeling: Model calibration, data assimilation, and uncertainty analysis, in Hydrological Modeling and

Water Cycle, Coupling of the Atmospheric and Hydrological Models, vol. 63Anonymous , pp. 1-23, Springer, Water Science and Technology Library.

Moradkhani, H., and Meskele, T., 2009. "Probabilistic Assessment of the Satellite Rainfall Retrieval Error Translation to Hydrologic Response", in Satellite Applications for Surface Hydrology, *Springer, Water Science and Technology Library*, in review.

Moradkhani, H., K. Hsu, Y. Hong, and S. Sorooshian (2006), Investigating the impact of remotely sensed precipitation and hydrologic model uncertainties on the ensemble streamflow forecasting, Geophys. Res. Lett., 33, L12401.

Moradkhani, H., K. L. Hsu, H. Gupta, and S. Sorooshian (2005b), Uncertainty assessment of hydrologic model states and parameters: Sequential data assimilation using the particle filter., Water Resour. Res., 41(5), W05012, doi: doi:10.1029/2004WR003604.

Moradkhani, H., S. Sorooshian, H. V. Gupta, and P. R. Houser (2005a), Dual state–parameter estimation of hydrological models using ensemble Kalman filter, Advances in Water Hong, Y., K. Hsu, X. Gao, and S. Sorooshian (2004), Precipitation estimation from remotely sensed imagery using Artificial Neural Network-Cloud Classification System*, 43*, 1834– *J. Appl.Meteorol*., 1853.

Application of NEXRAD for Freshwater Inflow Estimates to Texas Bays and Estuaries

Ruben S. Solis, Ph.D., P.E.[1], Qingguang Lu, P.E.[2]
[1]Texas Water Development Board, Austin, TX 78711-3231;
email:rsolis@twdb.state.tx.us
[2]Texas Water Development Board, Austin, TX 78711-3231;
email:qingguang.lu@twdb.state.tx.us

Abstract
National Weather Service (NWS) rain gauge data has been applied in rainfall-runoff models to estimate inflows to Texas' bays and estuaries for decades by the Texas Water Development Board (TWDB). In an effort to improve the spatial and temporal resolution of rainfall data, TWDB recently launched a pilot project to study the applicability of NEXRAD data for this purpose. Rainfall along the Texas coast is highly variable both spatially and temporally, especially during summer time, making NEXRAD data advantageous over the rather sparsely distributed rain gauge network. Comparisons of rainfall and of modeled runoff using NEXRAD and NWS raingage data are presented at the basin and watershed scale. Advantages and issues with the conversion to use of NEXRAD are presented. Future study will focus on use of distributed rainfall/runoff models to take advantage of the readily available digital data.

Introduction
Estimation of the timing and volume of fresh water that flows into Texas' bays and estuaries is an essential component of virtually all ecological analyses conducted on these systems. The Texas Water Development Board (TWDB) is responsible for estimating these inflows and has compiled this important information for over two decades. Although the majority of the flow reaching the coast is monitored by United States Geological Survey (USGS) stream gages, significant fractions of some contributing drainage basins lie below the gages (Figure 1). In total, 87 % of the entire drainage area is monitored by USGS gages, while the remaining 13 % is ungaged. Rainfall/runoff models have been used for this purpose for several decades (Longley, 1994).

National Weather Service (NWS) raingage data has historically been the primary source of rainfall data used to drive the rainfall/runoff models that were applied in the lower coastal watersheds shown in Figure 1. Both First-Order (FO) weather stations and Cooperative rain gages (Coop) have been used. FO data is generally considered to be of higher quality because these stations generally have better equipment and are maintained by trained professionals (Narasimhan et al. 2006). Nonetheless, Coop data is considered acceptable, and has been an important source of data for less populated areas where FO stations are sparse. FO and Coop raingages for the Galveston Bay and Matagorda Bay lower coastal watersheds are presented in Figure

2. While many of the watersheds contain one or more raingages within their boundaries, many also have none and suffer the possibility of being poorly represented by distant gages.

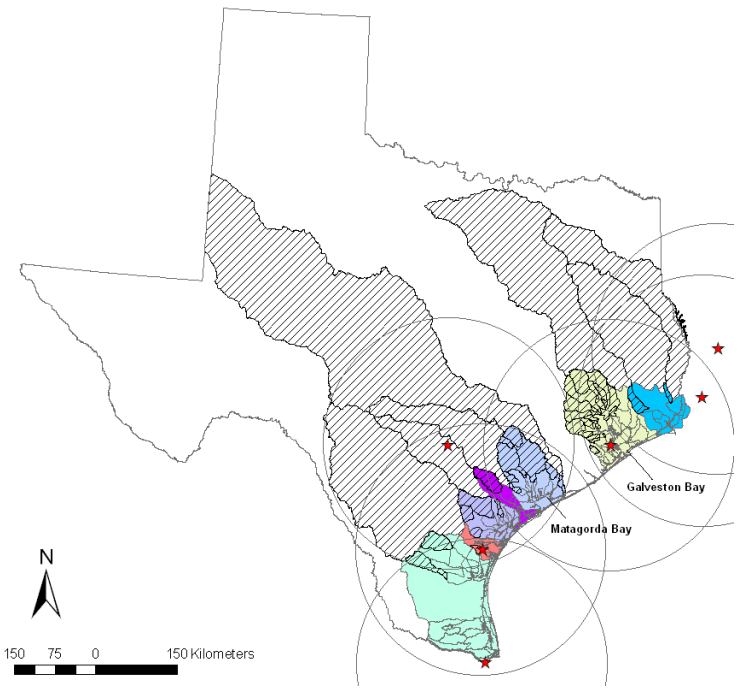

Figure 1. Major river basins in Texas with coastal WSRD-88 NEXRAD radar sites, indicated by star symbols, on the Texas gulf coast. Cross-hatched and shaded areas drain into Texas seven major bays and estuaries. Cross-hatched areas indicate areas monitored by USGS streamflow gages. Shaded areas represent the lower coastal watersheds for Texas' major estuaries where rainfall/runoff models were applied. Matagorda Bay and Galveston Bay watersheds are the focus of this paper. (NEXRAD sites from http://www.roc.noaa.gov/interactive/defaultIE.asp)

Perhaps the greatest limitation to improving the accuracy of runoff estimates to the coast has been the sparse distribution of the raingages in some areas of the coast. The wide spacing of gages in the network leads to the potential for spatial errors, the most extreme example coming from storms being completely missed by the raingages. Studies in Texas now focusing on the minor estuaries and smaller bays on the Texas coast require improved rainfall resolution to allow more accurate estimates of inflow to these systems.

With the improved availability and accuracy of Weather Surveillance Doppler Radar-88D (NEXRAD) data during the last decade, TWDB has embarked on a mission to improve it's estimates of coastal runoff through use of this higher resolution information. This paper describes TWDB's efforts to convert to NEXRAD and some of the issues relevant to that conversion. We provide comparisons between NEXRAD and raingage based estimates of areal rainfall, and results from a rainfall/runoff model that favorably support the improved quality of NEXRAD data in recent years.

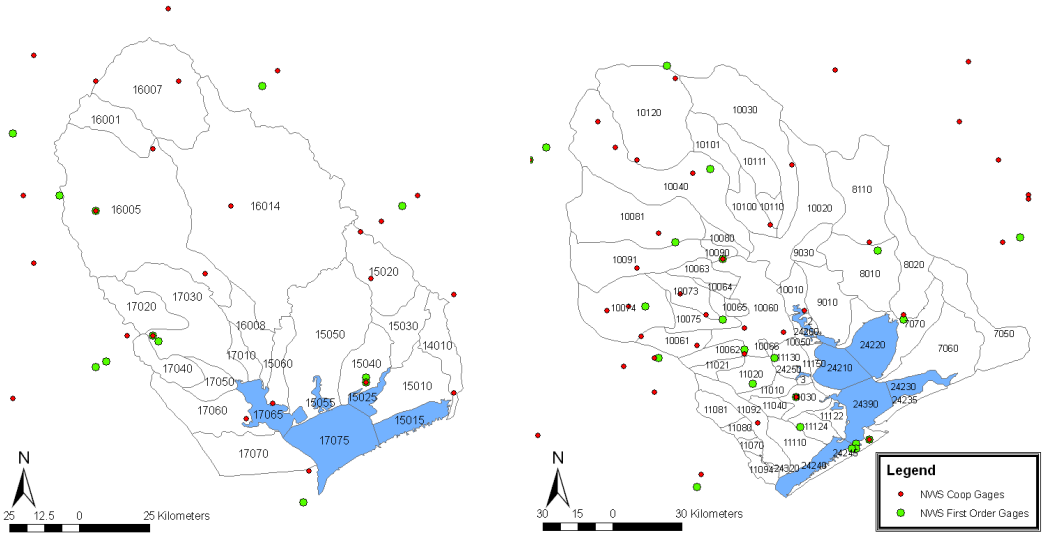

Figure 2. First Order and COOP raingages in the Matagorda Bay and Galveston Bay lower coastal watersheds Texas that are the focus of this study.

Spatial Characteristics of Rainfall on the Texas Coast

Rainfall varies significantly across Texas, averaging less that 11 inches (279 mm) annually in far west Texas and over 59 inches (1499 mm) per year near the Texas-Louisiana border (Narasimhan et al., 2007, Figure 3). From north to south along the gulf coast, annual average rainfall decreases from nearly 59 inches (1499 mm) to less than 27 inches (686 mm). Rainfall generated during spring and fall frontal passages is typically widespread and more spatially uniform, while summer rainfall is less organized spatially, with heavy convection-driven rainfall falling over smaller spatial scales. Spatial variability is more pronounced in coastal watersheds than in inland watersheds, as shown by Narasimhan and Srinivasan (2006) using spatial autocorrelation analyses of NEXRAD data for six study areas in Texas, including three along the coast.

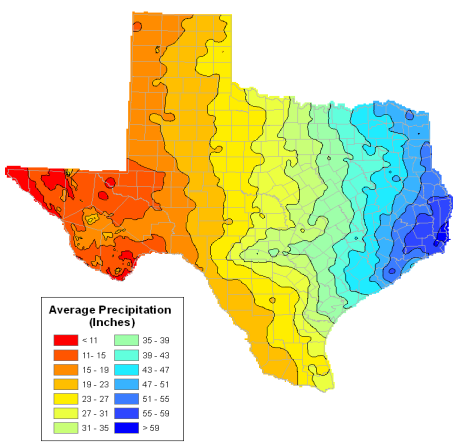

Figure 3. Mean annual rainfall in Texas, showing the spatial variation of rainfall across the state and along the Texas gulf coast (from Narasimhan, et al. 2007).

NEXRAD Rainfall Bias

NEXRAD data prior to 2000 has been shown to be biased relative to raingage data (Jayakrishnan, et al. 2004). Sources of bias, including spatial representation of the measurements, radar overshooting, topographical interference, issues with the Z-R relationship, distance from the radar, and so on are well documented (Breidenbach and Bradberry, 2001; National Weather Service 2002). Over time and with the goal of removing bias, algorithms have been proposed and developed to adjust the raw radar signal to FO raingage data, leading to NEXRAD Stage III (Seo and Breidenbach, 2002). Since about 2002, there have been no significant calibrations or adjustments to the correction algorithms (R. Srinivasan, personal communication). Comparison of NEXRAD Stage III rainfall data with raingage data using data from 1995-1999 (Jayakrishnan, 2004), from 2000-2004 (Narasimhan et al., 2006), and from 2000-2007 in the current study show that bias correction has improved.

Data and Methods

NEXRAD data for this study was obtained from the West-Gulf River Forecast Center (WGRFC), which covers the entire Texas gulf coast region. Raingage data was obtained from the National Climatic Data Center (NCDC). Daily accumulated data from both sources from 2000-2007 was used in this study to generate monthly and annual rainfall totals.

Some studies have compared NEXRAD rainfall to raingage data at the scale of the raingage (Young and Brunsell, 2008), while other that have compared spatially aggregated rainfall at larger scales using different means to distribute raingage data (National Weather Service, 2009). This paper takes the second approach and compares the spatially aggregated rainfall on the subwatershed and basin-wide scale. Area-weighted rainfall for each subwatershed in the lower drainage basins was prepared using Thiessen polygons for the raingage data, and by intersection of the HRAP grids with the watersheds for the NEXRAD data. Daily rainfall volumes were then accumulated to monthly and annual rainfall for comparison on a watershed-scale basis. Rainfall for the individual watersheds was also accumulated to allow basin-wide monthly and annual comparisons of NEXRAD- and raingage-based rainfall.

NEXRAD/Raingage Rainfall Comparison

Comparisons in this study were conducted for the two basins on the Texas coast that drain into Galveston Bay and Matagorda Bay (Figure 4). The Galveston Bay drainage basin includes drainage from the Trinity and San Jacinto River basins and intervening coastal basins. Approximately 86 % of the entire drainage is monitored by USGS streamgages, the majority of that coming from the Trinity River. Runoff from the remaining 14 % must be modeled. The Matagorda Bay basin includes drainage from the Colorado and Lavaca River basins. The majority of flow into Matagorda Bay is also gaged (96%), with the greatest portion of that coming from the Colorado River.

The lower basins draining into each bay are subdivided into sub-watershed units for which rainfall estimates were made using both NEXRAD and raingage data. Rainfall

estimates were made for both gaged and ungaged watersheds – in practice, a rainfall/runoff model was calibrated to USGS gaged flows in the gaged watersheds, and parameters from the gaged watersheds were then extrapolated to the ungaged watersheds to estimate runoff from the ungaged watersheds.

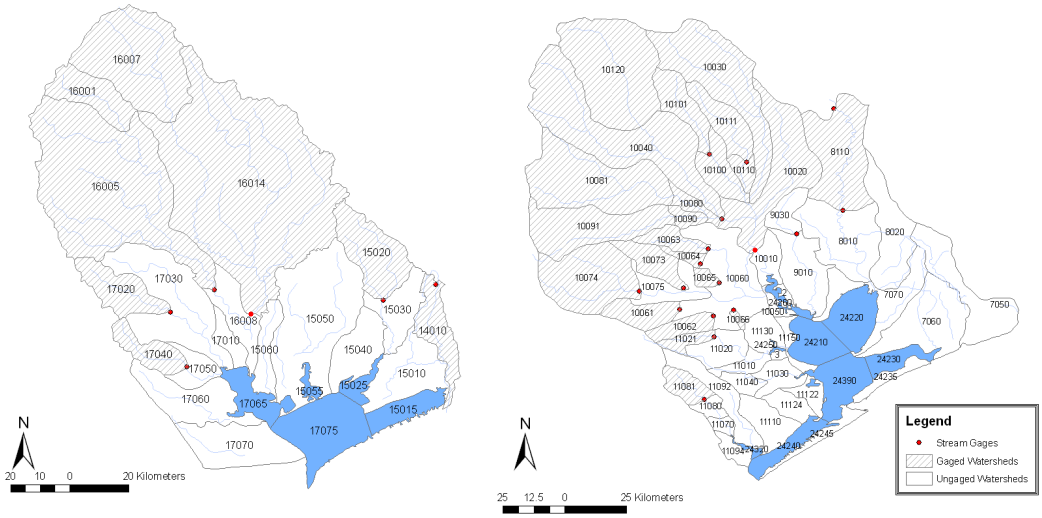

Figure 4. Lower coastal drainage basins for Matagorda Bay (left) and Galveston Bay (right) used in this study. Areas monitored by USGS streamgages indicated by shading.

Temporal Change in Bias

Comparisons between monthly basin-wide NEXRAD and raingage rainfall are presented in Figure 5. Variation of annual basin-wide NEXRAD bias from 2000-2007 is presented in Table 1. Here, bias is calculated as:

$$Bias_i = (PNEXRAD_i - PRaingage_i)/PRaingage_i * 100,$$

where $PNEXRAD_i$ is the mean annual NEXRAD rainfall for watershed i, and $PRaingage_i$ is the mean annual raingage rainfall for watershed i. The maximum annual bias for Galveston Bay watersheds was -15.1% in 2001, and for Matagorda Bay watersheds was +27.6% in 2002.

Bias during the first year (2000) of both records was small (Figure 5), where the cumulative rainfall for NEXRAD and raingage records track closely. However, the NEXRAD data for both basins experienced significant drift relative to the raingage data between 2001 and 2002, indicating large biases during those periods. Following 2003, the cumulative records increase in parallel, indicating that NEXRAD and raingage data are tracking relatively well again, suggesting a reduced bias. The short increase in bias shown in both records between 2001 and 2002 could be due to extreme events, storms not captured by the raingages, or other causes, but this was also a time during which changes to the bias algorithms were being modified (Srinivasan, pers. comm. 2009). Inspection of just the period between 2003 and 2007 suggests that while there are still differences between the NEXRAD and raingage

data on a monthly and annual basis (Table 1, Figure 5), the cumulative differences tend average out (Figure 6). For Matagorda Bay watersheds from 2003 to 2007, cumulative raingage rainfall was 5825 mm, while NEXRAD rainfall was 5905 mm, yielding a +1.4% bias. For Galveston Bay watersheds, the cumulatives were 6715 mm for raingage rainfall and 6538 mm for NEXRAD, or a -2.6% bias. There are clear differences in some months and years, some in which rainfall events might have been missed by the raingages as appears to be the case late in 2006 for Galveston Bay. In other cases events were clearly picked up by both NEXRAD and raingages, but the totals are different as appears to be the case late in 2007 for Matagorda Bay (Figure 5). However, the cumulative differences are small enough to suggest that after 2002 basin-wide rainfall estimates using NEXRAD match raingage estimates to the accuracy needed for our inflow estimates.

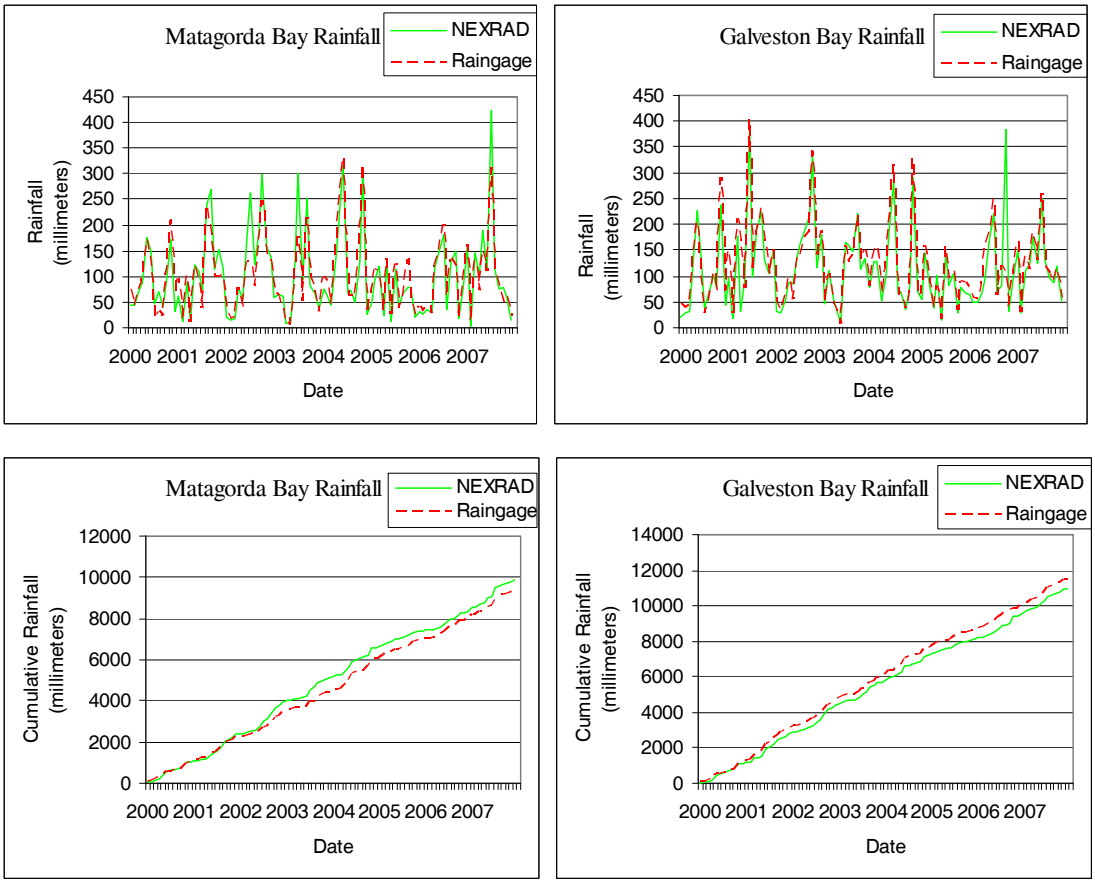

Figure 5. Monthly (top) and cumulative (bottom) basin-wide rainfall for Matagorda Bay and Galveston Bay watersheds, 2000-2007.

Areal Rainfall Comparison by Watershed

Based on the above findings, only 2003-2007 data is used in subsequent comparisons. Mean annual rainfall from 2003-2007 for 24 watersheds in the Matagorda Bay basin and 57 Galveston Bay watersheds are presented Table 2 and Table 3, respectively.

Table 1. Annual basin-wide rainfall for Matagorda Bay and Galveston Bay watersheds, 2000-2007.

Matagorda Bay				Galveston Bay			
Year	Raingage Rainfall (millimeters)	NEXRAD Rainfall (millimeters)	Bias (%)	Year	Raingage Rainfall (millimeters)	NEXRAD Rainfall (millimeters)	Bias (%)
2000	1037.34	1020.57	-1.62	2000	1154.94	1104.39	-4.38
2001	1204.21	1368.04	13.60	2001	2004.31	1701.04	-15.13
2002	1204.98	1536.95	27.55	2002	1612.14	1634.74	1.40
2003	928.62	1158.24	24.73	2003	1258.32	1274.57	1.29
2004	1650.75	1482.34	-10.20	2004	1630.68	1480.57	-9.21
2005	936.75	823.98	-12.04	2005	1023.37	946.15	-7.55
2006	1029.46	967.99	-5.97	2006	1285.75	1391.16	8.20
2007	1279.65	1472.69	15.09	2007	1516.89	1445.26	-4.72

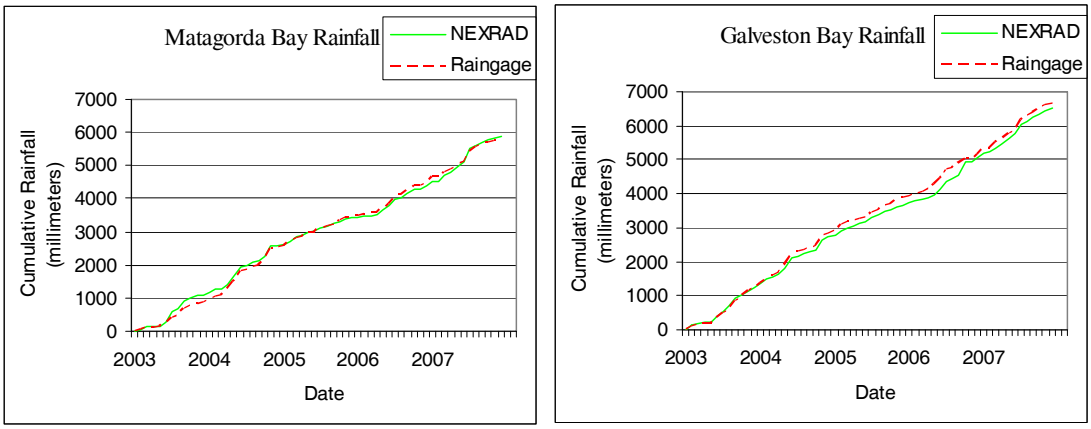

Figure 6. Cumulative basin-wide rainfall for Matagorda Bay (left) and Galveston Bay (right) watersheds, 2003-2007.

Mean annual raingage-based rainfall for Matagorda Bay watersheds, where the rainfall was spatially distributed using Thiessen polygons, varied from 976 mm to 1320 mm. Mean rainfall varied from 949 mm to 1395 mm for NEXRAD data. NEXRAD bias was positive for 16 of the 24 Matagorda Bay watershed for this period and ranged from -6.2% to +8.7%. The area-weighted mean annual rainfall for all of the Matagorda Bay watersheds was 1165 mm using raingage data, and 1181 mm using NEXRAD data, or a +1.4% bias.

Mean annual rainfall for the Galveston Bay watersheds varied from 1172 mm to 1627 mm for raingage data, and from 1165 mm to 1506 mm for NEXRAD data (Table 2). In contrast with the Matagorda Bay watersheds, NEXRAD bias was negative for 44 of the 57 Galveston Bay watersheds. The NEXRAD bias for the Galveston Bay watersheds varied from -16.5% to +5.6%. The area-weighted mean annual rainfall for all of the Galveston Bay watersheds was 1343 mm for raingaged data, and 1307 mm for NEXRAD data, or a -2.6% bias.

Table 2. Comparison of mean annual NEXRAD and raingage rainfall for Matagorda Bay watersheds, 2003-2007.

Watershed ID	Raingage Rainfall (millimeters)	NEXRAD Rainfall (millimeters)	Bias (%)	Watershed ID	Raingage Rainfall (millimeters)	NEXRAD Rainfall (millimeters)	Bias (%)
14010	1320.04	1327.66	0.58	16007	975.87	949.45	-2.71
15010	1295.40	1367.79	5.59	16008	1209.80	1135.13	-6.17
15015	1295.65	1331.21	2.74	16014	1182.12	1227.07	3.80
15020	1237.74	1262.38	1.99	17010	1203.71	1170.18	-2.79
15025	1286.51	1351.79	5.07	17020	1147.57	1178.31	2.68
15030	1272.03	1359.66	6.89	17030	1244.09	1258.82	1.18
15040	1284.22	1395.98	8.70	17040	1271.52	1281.68	0.80
15050	1232.92	1246.38	1.09	17050	1114.81	1159.76	4.03
15055	1233.68	1185.16	-3.93	17060	1102.61	1165.35	5.69
15060	1186.94	1138.68	-4.07	17065	1160.53	1168.91	0.72
16001	1001.78	949.45	-5.22	17070	1141.73	1180.08	3.36
16005	1055.12	1030.99	-2.29	17075	1246.38	1228.34	-1.45
				BASIN AVERAGE	1165.10	1181.10	1.37

Table 3. Comparison of mean annual raingage and NEXRAD rainfall for Galveston Bay watershed.

Watershed ID	Raingage Rainfall (millimeters)	NEXRAD Rainfall (millimeters)	Bias (%)	Watershed ID	Raingage Rainfall (millimeters)	NEXRAD Rainfall (millimeters)	Bias (%)
7050	1459.99	1449.83	-0.69	10110	1409.45	1304.29	-7.46
7060	1476.25	1410.72	-4.43	10111	1281.68	1275.33	-0.49
7070	1474.98	1379.22	-6.49	10120	1208.79	1165.61	-3.57
8010	1468.63	1425.45	-2.94	11010	1445.26	1447.04	0.12
8020	1471.17	1469.64	-0.10	11020	1280.67	1352.80	5.63
8110	1386.33	1405.13	1.35	11021	1348.99	1286.00	-4.66
9010	1458.47	1408.94	-3.39	11030	1485.90	1256.28	-15.45
9030	1424.43	1437.64	0.92	11040	1379.47	1375.41	-0.29
10010	1457.96	1505.97	3.29	11070	1286.00	1227.84	-4.52
10020	1361.44	1349.76	-0.85	11080	1294.64	1185.67	-8.41
10030	1289.30	1278.13	-0.86	11081	1286.00	1186.43	-7.74
10040	1201.42	1180.59	-1.73	11092	1309.12	1235.46	-5.62
10050	1382.27	1364.74	-1.26	11094	1281.94	1241.04	-3.19
10060	1368.81	1429.00	4.39	11110	1317.75	1239.52	-5.93
10061	1397.76	1297.69	-7.15	11122	1401.83	1392.94	-0.63
10062	1367.03	1289.30	-5.68	11124	1408.18	1390.14	-1.28
10063	1376.93	1411.73	2.52	11130	1401.57	1369.06	-2.31
10064	1492.25	1438.15	-3.62	11150	1445.51	1296.16	-10.33
10065	1517.65	1490.98	-1.75	24210	1466.34	1223.77	-16.54
10066	1308.86	1359.41	3.86	24220	1483.36	1248.66	-15.82
10073	1501.39	1445.26	-3.73	24230	1420.37	1350.01	-4.95
10074	1281.94	1244.09	-2.95	24235	1354.58	1362.71	0.60
10075	1627.38	1437.13	-11.69	24240	1297.69	1190.75	-8.24
10080	1335.28	1316.74	-1.38	24245	1283.72	1178.31	-8.21
10081	1172.46	1200.15	2.36	24250	1487.68	1395.98	-6.16
10090	1342.64	1343.66	0.07	24260	1448.56	1385.06	-4.38
10091	1201.93	1215.14	1.09	24320	1313.43	1220.47	-7.07
10100	1381.00	1291.59	-6.47	24390	1362.46	1279.40	-6.09
				BASIN			
10101	1228.34	1240.79	1.01	AVERAGE	1342.90	1307.59	-2.62

NEXRAD bias in both the Matagorda Bay and Galveston Bay watersheds are presented in Figure 7. The largest negative biases, shown in the darkest shade, appear towards the center and near the coast of both basins. A band of negative bias appears to run longitudinally through the Matagorda Bay basin. Positive biases, shown in light shades, are weak in the Galveston Bay basin, and lie on the eastern and western edges of the Matagorda Bay basin. While there may be some structure to the bias distribution, it is weak and balanced enough to not be of great significance in the big picture. Nonetheless, at this spatial scale of the watersheds shown, there remain clear biases between NEXRAD and raingage rainfall.

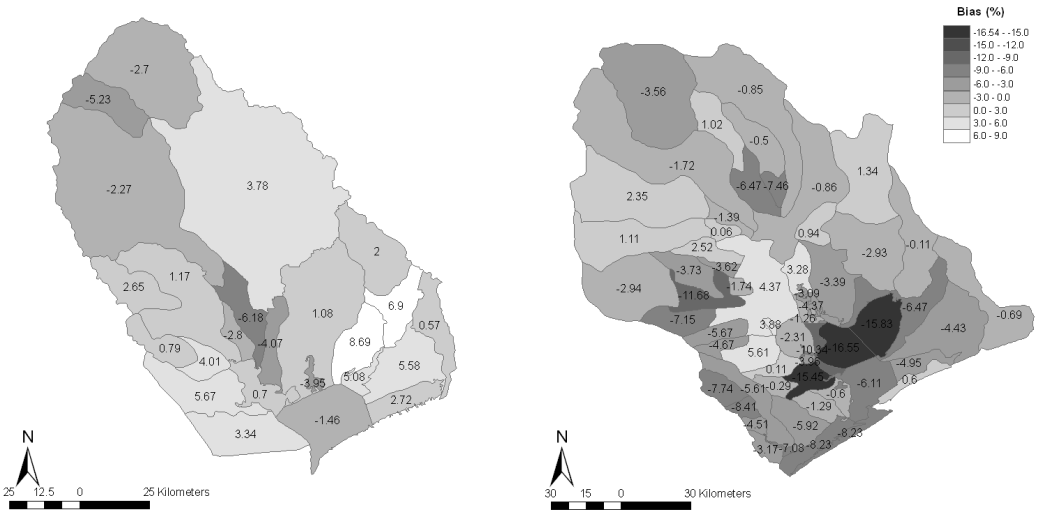

Figure 7. Spatial variation in NEXRAD bias relative to raingage rainfall for Matagorda Bay (left) and Galveston Bay (right) watersheds. Light shades indicate positive bias, and dark shades indicate negative bias.

Application of Rainfall/Runoff Models

Estimates for ungaged watersheds of freshwater inflows to Texas' estuaries made in the late 1970's were based on application of the Soil Conservation Service (SCS) TR55 Model (TWDB, 1983). This lumped-parameter model applies a watershed's Curve Number (CN) and a soil moisture parameter to estimate a monthly runoff from rainfall. Studies over the next two decades led to the development and application of the Texas Rainfall-Runoff Model (TXRR) at TWDB. TXRR is also a lumped parameter model and uses an approach similar to the SCS model to estimate total runoff from a rainfall event. It tracks subsurface soil moisture continuously, and provides a daily runoff output, an improvement to the TR55 model. In both cases, raingage-based rainfall data was used to drive the models. Thiessen polygons created based on the raingage network and overlain on the coastal watersheds were used to estimate the rainfall on each watershed.

Transition from raingage-based inputs to NEXRAD for our modeling purposes has

become feasible as NEXRAD data has become readily available and has improved in quality. However, prior to a full transition to NEXRAD, a clear understanding of the temporal and spatial differences between raingage and NEXRAD is needed. Based on the analyses presented above, at the scale of individual watersheds, there remain clear differences between raingage- and NEXRAD-based rainfall estimates at even monthly and annual time scales. In aggregate over the entire lower coastal basin watersheds, however, the differences between raingage and NEXRAD rainfall totals are lowered to the a few percent, which is acceptable for our purpose.

A further test of the applicability of NEXRAD data is to compare runoff estimates computed using raingage and NEXRAD data with the TXRR Rainfall/Runoff model. These comparisons are presented in Table 4 and Table 5 for the Matagorda Bay and Galveston Bay watersheds, respectively. TXRR model parameters for each watershed were identical between raingage and NEXRAD model runs.

The combined mean annual runoff for Matagorda Bay watersheds was 3484 million m^3 using raingage data, and 3913 million m^3 using NEXRAD data, a bias of +12.3% (Table 6). The bias in runoff varied from -20.8% to +31.9% for individual watersheds. Mean annual runoff for the Galveston Bay watersheds was 8658 million m^3 using raingage data, and 8366 million m^3 using NEXRAD data, a bias of -3.4%. Biases ranged from -31.2% to +16.6% for individual watersheds. For both the Matagorda Bay and Galveston Bay basins, runoff biases are amplified relative the biases observed in rainfall estimates.

Table 4. Comparison of TXRR runoff based on mean annual raingage and NEXRAD rainfall for Matagorda Bay watersheds, 2003-2007.

Watershed ID	Raingage Runoff (million cubic meters/year)	NEXRAD Runoff (million cubic meters/year)	Bias (%)	Watershed ID	Raingage Runoff (million cubic meters/year)	NEXRAD Runoff (million cubic meters/year)	Bias (%)
14010	102.08	101.85	-0.22	16008	107.43	95.78	-10.84
15010	208.15	241.08	15.82	16014	575.09	758.75	31.94
15020	181.91	193.44	6.34	17010	40.66	39.05	-3.96
15030	117.20	146.34	24.87	17020	85.07	98.89	16.24
15040	155.51	180.08	15.80	17030	264.10	296.91	12.42
15050	424.52	474.46	11.77	17040	95.83	96.77	0.98
15060	68.58	57.88	-15.59	17050	37.79	47.44	25.54
16001	70.73	66.56	-5.90	17060	208.64	165.24	-20.80
16005	392.06	475.83	21.37	17070	177.45	187.58	5.71
16007	171.84	189.51	10.28	TOTAL	3,484.63	3,913.46	12.31

Table 5. Comparison of TXRR runoff based on mean annual raingage and NEXRAD rainfall for Galveston Bay watersheds, 2003-2007.

Watershed ID	Raingage Runoff (million cubic meters/year)	NEXRAD Runoff (million cubic meters/year)	Bias (%)	Watershed ID	Raingage Runoff (million cubic meters/year)	NEXRAD Runoff (million cubic meters/year)	Bias (%)
7050	414.08	400.81	-3.20	10080	47.17	43.31	-8.19
7060	518.40	453.67	-12.49	10081	288.02	291.06	1.06
7070	333.29	283.88	-14.82	10090	41.67	39.57	-5.03
8010	449.30	409.96	-8.76	10091	262.93	273.18	3.90
8110	407.18	413.80	1.63	10100	127.36	108.09	-15.13
9010	329.37	297.07	-9.81	10101	94.30	97.82	3.73
9030	110.53	112.47	1.75	10110	53.17	42.21	-20.61
10010	109.92	113.49	3.25	10111	85.24	87.36	2.49
10020	387.99	388.77	0.20	10120	376.97	373.53	-0.91
10030	365.90	361.20	-1.29	11010	77.57	77.42	-0.19
10040	406.80	435.96	7.17	11020	129.08	143.22	10.96
10050	52.86	49.25	-6.82	11021	55.00	51.83	-5.77
10060	444.21	510.60	14.95	11030	132.08	90.86	-31.21
10060	415.19	483.92	16.55	11040	59.85	59.29	-0.94
10061	146.48	125.08	-14.61	11070	30.86	26.93	-12.73
10062	90.95	82.64	-9.14	11080	43.63	33.76	-22.63
10063	90.79	100.21	10.38	11081	86.83	72.85	-16.10
10064	38.76	37.52	-3.21	11092	216.63	198.01	-8.60
10065	42.41	40.43	-4.66	11110	147.43	130.72	-11.34
10066	10.98	12.44	13.23	11122	68.98	66.81	-3.15
10073	171.52	154.06	-10.18	11124	95.25	89.61	-5.93
10074	378.41	346.14	-8.53	11130	134.27	129.68	-3.42
10075	231.88	181.34	-21.80	11150	56.17	44.42	-20.92
				TOTAL	8,657.65	8,366.24	-3.37

Table 6. Annual basin-wide TXRR runoff for Matagorda Bay and Galveston Bay watersheds, 2003-2007.

Matagorda Bay				Galveston Bay			
Year	Raingage Runoff (million cubic meters)	NEXRAD Runoff (million cubic meters)	Bias (%)	Year	Raingage Runoff (million cubic meters)	NEXRAD Runoff (million cubic meters)	Bias (%)
2003	1,732	4,142	139.19	2003	7,245	7,752	6.99
2004	6,928	5,768	-16.75	2004	13,095	10,584	-19.18
2005	2,014	1,455	-27.79	2005	4,966	3,917	-21.13
2006	2,122	1,932	-8.92	2006	7,006	8,907	27.14
2007	4,627	6,271	35.53	2007	10,976	10,672	-2.78
AVERAGE	3,485	3,913	12.31	AVERAGE	8,658	8,366	-3.37

The level of amplification of bias by the rainfall/runoff model when using NEXRAD data, particularly for Matagorda Bay, suggests that raingage-driven models previously calibrated against USGS streamflow will need to be recalibrated when driven with NEXRAD data.

Future Use of NEXRAD Rainfall Data

TWDB has developed hydrological inflow records for Texas bays and estuaries for the period 1941 to the present (TWDB 2008). Rainfall data used for this purpose was based on the NWS raingage network in Texas. The temporal continuity of the raingage network minimized concern for the introduction of artificial trends in calculated runoff using this data. This is significant given an interest for water planning and environmental purposes to identify the real changes in inflow patterns attributed to changing water demands due to population growth, urbanization, changes in agricultural patterns, and other factors. With the continued adjustments in the past of NEXRAD bias correction algorithms, older NEXRAD data may (prior to 2003) not be suited for use for our applications without additional post-processing to correct for evident biases. Although bias correction algorithms appear to have stabilized, TWDB will continue in the immediate future to rely on raingage data in parallel with NEXRAD data. This will allow continuity of the raingage-based hydrological record and the advantages offered by longer data sets. In the meantime, NEXRAD data will also continue to be applied to allow continued comparison to the raingage data. Based on comparisons of model outputs, use of NEXRAD will require recalibration of the rainfall/runoff models. Eventually, we hope to make a full transition to the use of NEXRAD data to reap the benefits of the high degree spatial resolution it offers. Additional plans by TWDB include the transition from the lumped-parameter TXRR rainfall/runoff model to models, such as the Soil and Water Assessment Tool (SWAT) that can more fully take advantage of the spatial resolution offered by NEXRAD and newly developed digital land classification data and curve numbers (Stukey et al. 2008).

Conclusions

Based on analysis of NEXRAD data, bias adjustments to NEXRAD data after 2002 appear to have reduced bias relative to raingage data at the basin-wide scale sufficient to make it suitable for use in determining total volumes of freshwater inflows from ungaged areas adjacent to Texas coastal estuaries. However, comparisons of model outputs indicate that rainfall/runoff models using NEXRAD data will need to be calibrated for use with that data. At the scale of smaller watersheds, significant differences remain between raingage and NEXRAD data. Given the superior spatial resolution of NEXRAD, it is likely that the NEXRAD data better reflects runoff for individual watersheds, and will improve our ability to estimate inflows to the small minor bays on the Texas coast. While our experience with NEXRAD grows, TWDB will continue using raingage data in the near future for continuity with historic records with the expectation of a more complete transition to NEXRAD in the future.

References

Breidenbach, J. P., and Bradberry, J. S. (2001). "Multisensor precipitation estimates produced by National Weather Service river forecast centers for hydrologic applications". *Proc. of the 2001 Georgia Water Res. Conf.*, March 26-27, 2001. Georgia Water Resources Institute.

Jayakrishnan, R., Srinivasan, R., Arnold, J. G. (2004). "Comparison of raingage and WSR-88D State III precipitation data over the Texas-Gulf basin." *J. Hydrology* (292), 135-152.

Longley, W.L. ed. (1994). *Freshwater inflows to Texas bays and estuaries*. Texas Water Development Board and Texas Parks and Wildlife Department., Austin, TX.

Narasimhan, B., and Srinivasan, R. (2006). "Evaluation of NEXRAD rainfall data for hydrologic modeling along Texas coast and inland watersheds." Texas Water Development Board, Austin, TX. 119 pp.

Narasimhan, B., Srinivasan, R., Quiring, S., and Nielsen-Gammon, J.W. (2007). *Digital climatic atlas of Texas*. Texas Water Development Board, Austin, TX.

National Weather Service (2002). "About the Stage III data". *National Weather Service*, < http://www.weather.gov/ohd/hrl/dmip/stageiii_info.htm> (1/27/2009)

National Weather Service (2009). "A comparison of operational precipitation processing methodologies." *National Weather Service*, <http://www.srh.noaa.gov/abrfc/p1vol.html> (1/27/2009)

Seo, D.-J., and Breidenbach, J. P. (2002). "Real-time correction of spatially nonuniform bias in radar rainfall data using rain gage measurements". *J. Hydrometeoro.*, 3(2), 93-111.

Stukey, J., Narasimhan, B., Srinivasan, R. (2008). "Galveston and Lavaca watershed multi-year land use and land cover classifications and curve numbers." Texas Water Development Board, Austin, TX.

Texas Water Development Board (1980). *Lavaca-Tres Palacios Estuary: A Study of the Influence of Freshwater Inflows*. Texas Department of Water Resources. LP-106.

Texas Water Development Board (2008). "Hydrology". *Texas Water Development Board*, < http://midgewater.twdb.state.tx.us/bays_estuaries/hydrologypage.html> (1/27/2009).

Young, C. B., and Brunsell, N. A. 2008. "Evaluating NEXRAD estimates for the Missouri river basin: analysis using daily raingauge data." *J. Hydrol. Eng.*, 13(7), 549-553.

Distributed Hydrologic Modeling: From Research to Operational Forecasting

Michael Smith[1], Victor Koren[1], Ziya Zhang[1,2], and Zhengtao Cui[1,3]

[1]NOAA National Weather Service, Office of Hydrologic Development, 1325 East-West Highway, Silver Spring, MD 20910; phone: 301-713-0640 x154,
email: michael.smith@noaa.gov
[2]UCAR
[3]Lentech, Inc.

ABSTRACT

The NOAA National Weather Service (NWS) is actively conducting research toward operational distributed hydrologic models to improve its products and services to the Nation. Such models attempt to account for the spatial variability of basin features and meteorological forcings at high resolutions. Distributed models are viewed by the NWS as a pathway to provide high space and time resolution information for forecasting hydrologic conditions from flash floods to drought, including water resources forecasting. NWS field offices have been prototyping an operational distributed model since the beginning of 2007.

The purpose of this paper is to provide the engineering community an overview of some of the major issues and approaches developed as the NWS moves forward with distributed models using NEXRAD data for operational forecasting.

INTRODUCTION

Largely as the result of radar-derived precipitation estimates, ever-increasing computer power, spatial data analysis techniques, and the plethora of digital data sets of terrain, soils, vegetation, land use and other data, distributed hydrological models are routinely used for scientific studies, operational river forecasting, and engineering applications. The application of distributed models for operational river and flash flood forecasting requires careful analysis of models and data in order to achieve meaningful results. One basic question is: which model features should be chosen for a specific application? Another key question is: are high-quality precipitation and temperature data available to support distributed models? For over a decade, NWS NEXRAD and other radar-based precipitation estimates have been available for use in the operational, research and engineering communities. However, one must take proper account of the processing and quality of these estimates. For example, errors in such data may be magnified rather than smoothed by the many computational elements in a distributed model. Currently, these are areas of very active research in many institutions.

NWS DISTRIBUTED HYDROLOGIC MODELING

Distributed models are viewed by the NWS as a pathway to provide high space and time resolution information to meet an ever-expanding set of needs from flash floods

to drought, including water resources forecasting. One question faced by the NWS is common to any application or study: given a large number of models to choose from, which one is the most applicable? In addition, how will distributed models compare to the existing lumped model used by the NWS for current operational river forecasting? To address these questions, the NWS conducted the first phase of the Distributed Model Intercomparison Project (DMIP 1), focusing on basins in Oklahoma as test areas. Over a dozen government, private, and academic institutions participated in DMIP 1. Details of the rationale and design of DMIP 1 can be found in Smith et al. (2004), while Reed et al. (2004) present the overall results. One of the interesting results found by Reed et al. (2004) is that calibrated lumped models tended to outperform calibrated distributed models for basin outlet forecasts. However, some calibrated distributed models performed at a level comparable to, or better than, a calibrated lumped model (the current NWS operational standard).

The NWS is currently conducting the second phase of DMIP (hereafter called DMIP 2; Smith et al., 2009a) in order to investigate the use of distributed models in areas with mountainous terrain, orographic precipitation enhancement, snow accumulation and melt, and sparse data collection networks. The questions that arise here include: can existing data collection networks in mountainous areas support the use of distributed models? Or, are higher density data collection networks required? DMIP 2 experiments will leverage the enhanced data collection activities of the Hydromet Test Bed (HMT; www.hmt.noaa.gov). The purpose of the HMT is to expedite the delivery of research into operational weather and streamflow forecasting. As part of HMT, a suite of data collection platforms including 'gap-filling' radars, additional in-situ precipitation gauges, vertically-pointing radars, and other instruments are being used to provide enhanced observations of winter precipitation events in the North Fork of the American River. Another key question is: can distributed modeling more effectively capture the rain/snow elevation? NWS forecasters have stated that perhaps the greatest benefit can result from a better definition of the rain/snow elevation (Arthur Henkle, NWS, personal communication). The DMIP 2 experiments in the western basins will also provide an opportunity to test the performance of snow accumulation and melt models of various levels of complexity. Another key question relates to the ability to calibrate distributed models for use in mountainous areas.

DMIP 2 also includes additional modeling tests in the Oklahoma basins studied in DMIP 1, such as the ability of distributed models to compute soil moisture estimates. The goal here is to test the ability of distributed models to generate basin interior predictions when they are calibrated using only basin outlet streamflow observations.

Initial results from the DMIP 2 experiments in Oklahoma corroborate the DMIP 1 findings. Figure 1 shows the performance of all the eighteen participating DMIP 2 models for each of the test basins (Smith et al., 2009b). The statistic in this case is a modified correlation coefficient R_{mod} (McCuen and Snyder, 1975). Values of R_{mod} close to one are desirable. The results in Figure 1 are from calibrated models run over the calibration and verification periods. The results from two lumped models are shown as solid magenta squares and open black circles, respectively. All other plotting symbols represent the results of various distributed models. As seen in Figure 1, one distributed model (black open square) is one of the top two models for 10 out of 16 cases and is above the median of calibrated models in all but one case. Interestingly, the two lumped

models consistently perform better than the majority of distributed models for basin outlet simulations. As in DMIP 1, all models benefited from some type of parameter calibration, albeit to different degrees. Good initial values of model parameters seemed to enhance the calibration process.

Errors in the radar-derived precipitation data may contribute to this counter-intuitive finding regarding the good performance of the lumped models (see discussion below). Another factor may be that the spatial variability of precipitation may not be great enough to overcome the smoothing and damping of the rainfall signal as the precipitation moves over and through the soil to the outlet. While distributed models need to be applied wherever basin interior information is needed, such basins may not always benefit from distributed modeling compared to lumped models for basin outlet simulations. Interested readers are referred to Smith et al., (2004) and references therein for more discussion of this concept. Given these results, the NWS recommends the use of lumped and distributed models in operational river forecasting (Jones et al., 2009). Figure 2 shows an actual NWS forecast for a basin in Mississippi. In this case, both a lumped and a distributed model are run at an hourly time step. Jones et al. (2009) document several other NWS operational river forecast cases that benefit from distributed modeling.

The DMIP 2 soil moisture experiments in the Oklahoma basins also produced meaningful results (Smith et al., 2009b). Two models participated in this specific experiment and produced soil moisture estimates covering the state of Oklahoma: a modified version of the conceptual NWS Sacramento Soil Moisture Accounting model (SAC-SMA) and the Noah land surface model used in several NWS numerical weather prediction models. Analysis of these results indicates that both models produced good estimates of basin-average soil moisture.

Preliminary analysis of the results of the DMIP 2 western basin experiments yielded interesting results (Smith et al., 2009c). Six organizations participated in these experiments. One finding is that the gauge density in the two basins appears to support the use of distributed models based on point rain gage observations alone. As in the Oklahoma basin experiments, calibrated lumped models produced simulations that were as good as those from distributed models in an overall sense. However, in certain events, calibrated distributed models produced superior streamflow simulations compared to the lumped model. Ongoing analyses are aimed at understanding the source of the simulation improvements in these events. Some distributed models were able to replicate the diurnal snowmelt patterns that result in diurnal streamflow variations. This phenomenon is important to NWS forecasters when the diurnal snow melt patterns cause the river to fluctuate above and below flood stage.

USE OF RADAR-DERIVED AND OTHER GRIDDED PRECIPITATION ESTIMATES FOR DISTRIBUTED MODELING

The NWS Next Generation Radar (NEXRAD) and other weather radar platforms have provided the hydrologic modeling community with high-resolution precipitation estimates for well over a decade. A large volume of research has been conducted on the derivation and use of these radar-based precipitation estimates (e.g., Young et al., 2000; Stellman et al., 2001). As with other data forcings for hydrologic models, the impacts of

errors in the data must be understood. One area of investigation is the interaction between data error and modeling resolution. Koren et al. (2001) performed a numerical experiment to highlight this interaction. Figure 3 shows the hypothetical watershed used by Koren et al. (2001). The size of this basin is 10 by 10 NEXRAD precipitation grid boxes. The precipitation data was taken from the NWS Arkansas-Red Basin River Forecast Center (ABRFC) archive. Rainfall was transformed into runoff in each computational element using the Sacramento Soil Moisture Accounting model (SAC-SMA). The original precipitation data from ABRFC was modified by adding three levels of error, generated from white noise. The basin was modeled at several levels of resolution using the same precipitation data. In Figure 3a, the basin was modeled as a lumped area, with all 100 NEXRAD grid boxes averaged each hour. In Figures 3b and 3c, the basin was subdivided into 4 and 16 cells respectively. Lastly, the hypothetical basin was disaggregated into 100 cells, with each cell matching the nominal 4km x 4km sized of a NEXRAD precipitation grid box. The 'truth' scale and simulation in this experiment were taken as the finest resolution and resultant simulation, respectively. Simulations at each level of disaggregation were run over a multi-month period at an hourly time step.

Figure 4 shows the results of the experiment by Koren et al. (2001). The Y axis denotes an error statistic, in this case the peak volume error from the simulation at any scale compared to the 'truth' simulation. The X axis denotes the level of basin disaggregation. The errors from each level of disaggregation are shown for each precipitation forcing.

Looking first at the zero noise case, the simulation at the lumped scale has the largest error compared to the 'truth' simulation. As the basin is disaggregated further, the error decreases until it finally disappears at the finest resolution. Interestingly, disaggregation of the basin into finer computational elements using 'noisy' data does not follow this expected pattern. For example, basin disaggregation in the 25% noise case (green line) does not reduce the error to zero. Furthermore, basin disaggregation in the 50% and 75% noise level cases actually result in worse simulation errors compared to the lumped, zero noise level case. In this case, there appears to be a 'break point' at a disaggregation scale of between 20 and 30. Koren et al. (2001) believed that the errors in the precipitation data are multiplied rather than smoothed by the non-linearities of the rainfall-runoff model.

Another type of error in the NEXRAD precipitation estimates is shown in Figure 5. This basin is one of the study basins in the DMIP 1 and 2 experiments (Smith et al., 2004). In this case, use of the radar precipitation estimates in modeling the Elk River basin above the USGS gauge at Tiff City, Missouri. resulted in a large over-prediction of the observed hourly streamflow. Analysis of the NEXRAD precipitation estimates revealed the presence of 'bright band' contamination, caused by the radar beam encountering frozen precipitation and generating anomalously high signal returns. Trying to calibrate a hydrologic model in DMIP using this event would be very difficult. The NWS recommends that such events are ignored in model calibration. In manual calibration, the user simply ignores such events. In automatic calibration, the NWS sets the observed streamflow values in the time series to 'missing' so that any statistical procedure ignores such events. Islam et al. (2009) and Looper et al. (2009) discuss

similar analyses of radar-based precipitation. In both cases, bias correction of the radar-based precipitation estimates was found to be justified.

Yet another aspect of using NEXRAD precipitation estimates for distributed modeling concerns the quality of the data over time. Changes in processing algorithms and different levels of forecaster experience can result in time-varying biases in the precipitation data (Young et al., 2000). Such inconsistent data can complicate the process of model calibration (e.g., Reed et al., 2004). This aspect also arose in the DMIP 2 experiments in the western mountainous basins. The algorithm used by the NWS to generate gridded 4km gauge-only precipitation grids for distributed modeling was found to incorrectly handle gauge networks with time-varying densities. (Mizukami and Koren, 2009). Several strategies exist for dealing with this problem. Given a long archive of data, the most recent period may be of sufficient quality for model calibration. Such a strategy was used in DMIP 2 for the Oklahoma basins (Smith et al., 2009a). Other strategies include a simple bias correction performed on a monthly basis (Zhang et al., 2009). A comprehensive and ongoing effort to generate a consistent radar-based multisensor precipitation data set via reanalysis is being conducted at the National Climatic Data Center (NCDC; Nelson et al., 2006). For DMIP 2, and effort is underway to develop a new algorithm to generate gridded precipitation estimates from in-situ gauge networks.

Care must be taken in those cases in which NEXRAD or other radar-based precipitation data sets are used for river or flash flood forecasting and rain gauge data are used for model calibration. Analyses must be performed to compare the two forcings to avoid simulation and forecast biases due to the model parameters being calibrated with data having different statistical properties than the data used for forecasting (e.g., Johnson et al., 1999; Stellman et al., 2001; Bradley and Kruger, 1998; Westcott et al., 2008).

CONCLUSIONS

Operational use of distributed models for river and flash flood forecasting is continuing in the NWS. Comprehensive studies and operational experience have shown that distributed and lumped models can provide valuable information in the forecasting process. Both approaches should continue to be used. However, care must be taken to understand the precipitation data used in the model for calibration and forecasting. Many studies have provided useful guidance and procedures for data analysis. Good initial values of model parameters enhance the calibration of distributed models.

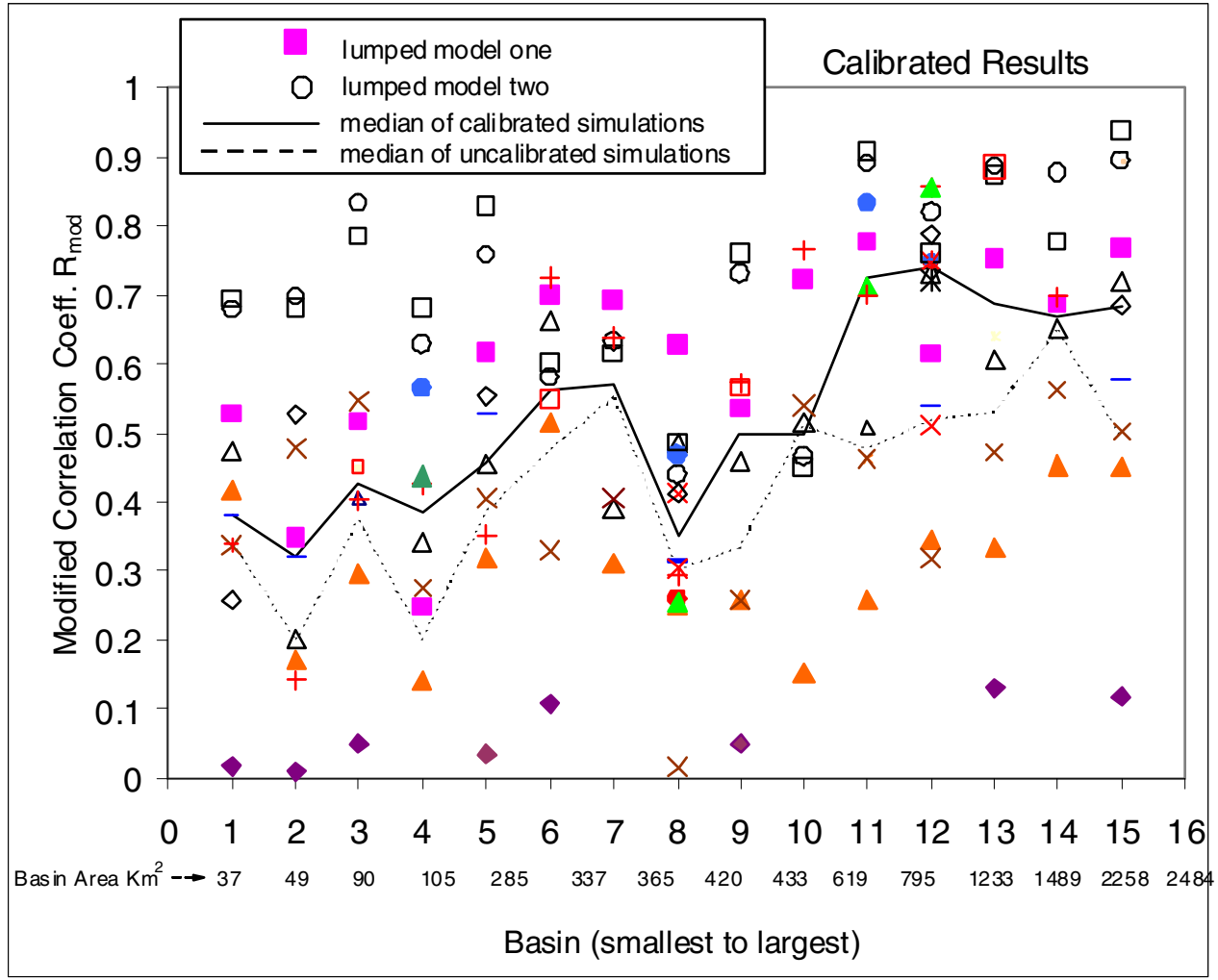

Figure 1. Results from the DMIP 2 experiments in the Oklahoma region. Each plotting symbol represents the overall calibrated Rmod statistic for the test basin. The two lumped models are denoted as a black open circle and a solid magenta square. All other symbols represent the results of distributed models.

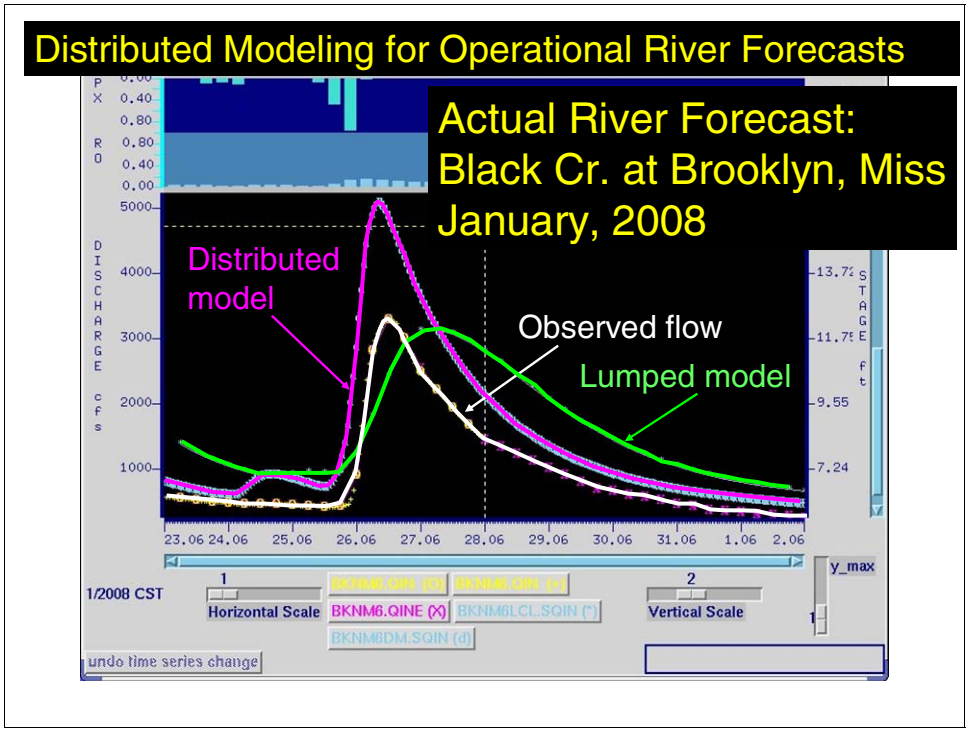

Figure 2. Lumped and distributed model river forecasts for Black Creek, Mississippi.

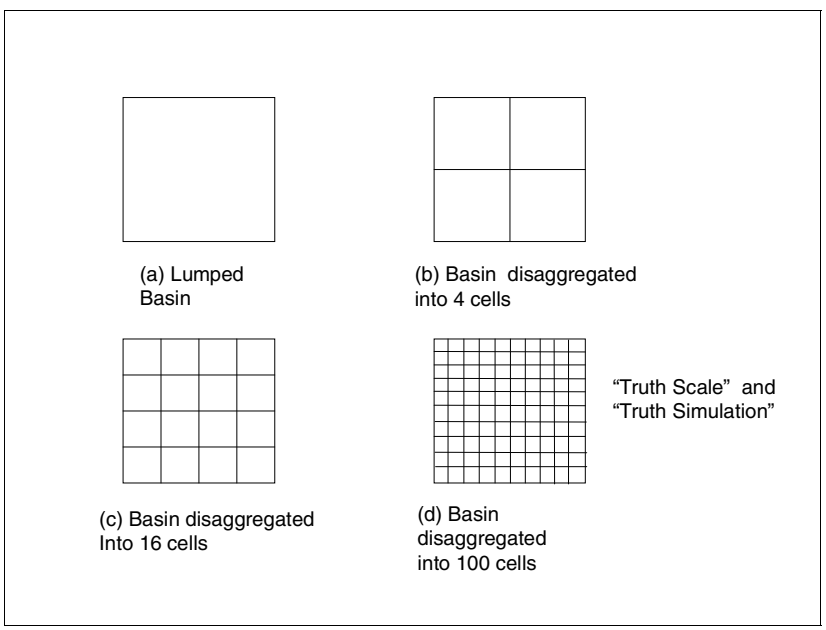

Figure 3. Hypothetical square basin used in the analysis of Koren et al. (2001). Note that the simulation from the finest level of basin disaggregation is considered the 'truth'. Simulations from other levels of disaggregation are compared to this 'truth' simulation.

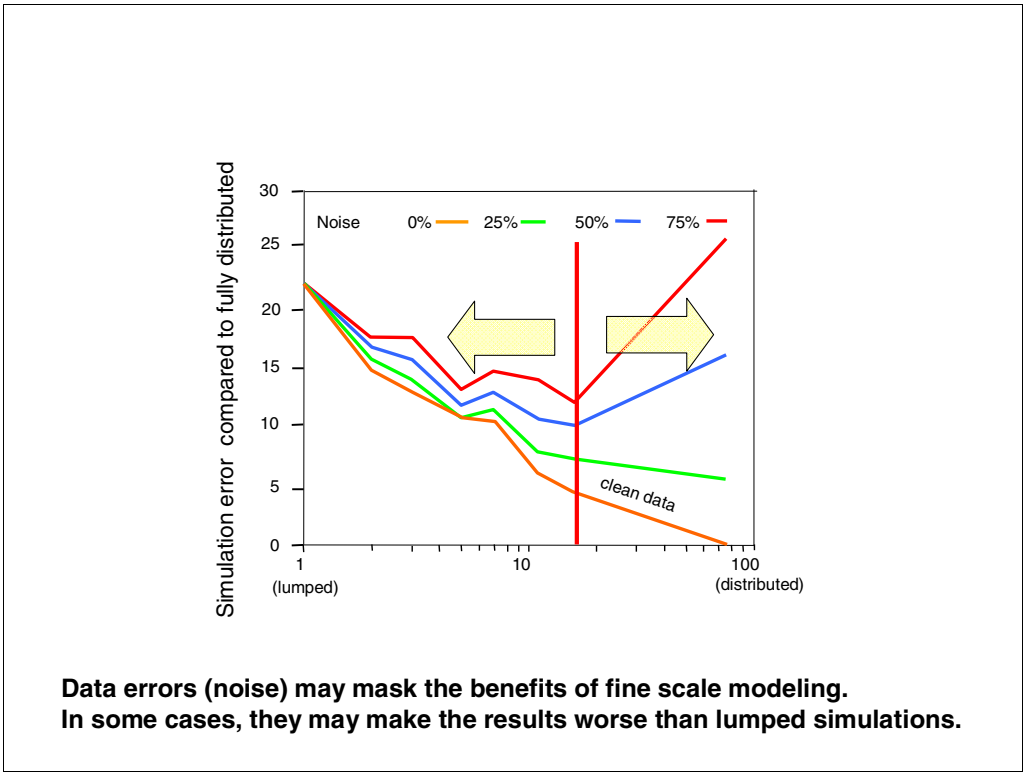

Figure 4. Results of simulations using the hypothetical basin shown in Figure 3. The broad yellow arrows indicate the 'break point' in basin disaggregation, beyond which further improvement in simulation accuracy can be achieved due to data errors.

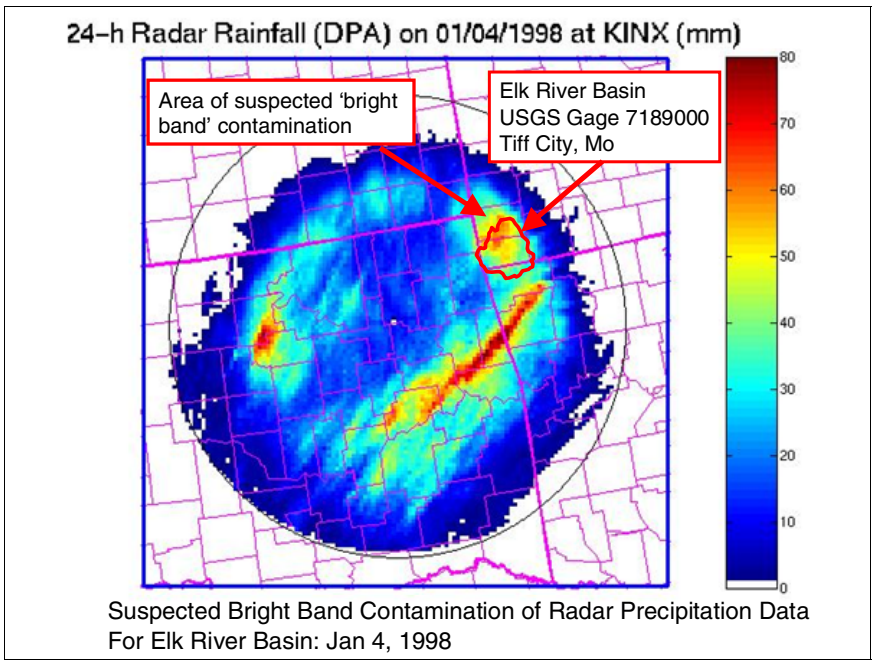

Figure 5. Example of 'bright band' contamination in the NEXRAD multi-sensor precipitation data for Jan. 4, 1998.

REFERENCES

Bradley, A.A., and Kruger, A. (1998). "Recalibration of Hydrologic Models for Use with WSR-88D Precipitation Estimates." Preprints, Special Symposium on Hydrology, American Meteorological Society, 11-16 January, Phoenix, Arizona. Paper 2.16

Islam, M.Z., and Gan, T.Y. (2009). "Effects of Biases in NEXRAD Precipitation Estimates and Sub-basin Resolution in the Hydrologic Modeling of Blue River Basin Using a Semi-distributed Hydrologic Model." 23rd Conference on Hydrology, American Meteorological Society 2009 Annual Meeting, Paper 4.4, Phoenix, Arizona, Jan 11-16.

Johnson, D., Smith, M., Koren, V., and Finnerty, B. (1999). "Comparing mean areal precipitation estimates from NEXRAD and rain gauge networks." *Journal of Hydrologic Engineering*, ASCE, 4(2), 117-124.

Jones, E., Roth, K., and Costanza, K. (2009). "A Comparison of the NWS Distributed versus Lumped Hydrologic Model." 23rd Conference on Hydrology, American Meteorological Society 2009 Annual Meeting, Paper 4.3, Phoenix, Arizona, Jan 11-16.

Koren, V.I., Finnerty, B.D., Schaake, J.C., Smith, M.B., Seo, D.-J., and Duan, Q.-Y. 1999). "Scale Dependencies of Hydrologic Models to Spatial Variability of Precipitation." *Journal of Hydrology*, Vol. 217, 285-302.

Koren, V., Smith, M., Reed, S., and Zhang, Z. (2001). "Use of NEXRAD Precipitation Estimates in Distributed Modeling: Parameterization, Aggregation Scale, and Data Uncertainties." Paper H11A-0210, Spring Meeting of the American Geophysical Union, Boston, MA.

Looper, J., Vieux, B., and Moreno, M.A. (2009). "Evaluating precipitation uncertainties using the Vflo hydrologic model." 23rd Conference on Hydrology, American Meteorological Society 2009 Annual Meeting, Paper 4.5, Phoenix, Arizona, Jan 11-16.

Mizukami, N., and Koren, V., (2009) Significance of precipitation data consistency to streamflow simulation with conceptual rainfall-runoff model. In preparation.

McCuen, R.H., and Snyder, W.M. (1975). "A Proposed Index for Comparing Hydrographs." *Water Resources Research*. Vol. 11, No. 2, 1021-1024.

Nelson, B.R, DJ Seo, D Kim,J.J. Bates (2006). "Multisensor Precipation Reanalysis." American Meteorological Society 2006 Annual Meeting, Paper 4.6, Atlanta, GA, January 29 - February 2, 2006

Reed, S., Koren, V., Smith, M., Zhang, Z., Moreda, F., Seo, D.-J., and DMIP Participants. (2004). "Overall distributed model intercomparison project results." *Journal of Hydrology*, Vol. 298, Nos. 1-4, 27-60.

Smith, M.B., Seo, D. -J., Koren, V. I., Reed, S., Zhang, Z., Duan, Q.-Y., Moreda, F., and Cong, S. (2004). "The distributed model intercomparison project (DMIP): motivation and experiment design." *Journal of Hydrology*, Vol. 298, Nos. 1-4, 4-26.

Smith, M.B., Koren,V., Reed, S., Zhang, Z, Zhang, Y., Moreda, F., Cui, Z., Mizukami, N., and Sheldon, S., (2009). "The distributed model intercomparison project

(DMIP): Phase 2 motivation and experiment design." *Journal of Hydrology*, in preparation.

Smith, M.B., Koren, V., Zhang, Z., Zhang, Y., Cui, Z., Cosgrove, B., Mizukami, N., Sheldon, S., and DMIP 2 participants, (2009). "Overall Results of the DMIP 2 Oklahoma Experiments." *Journal of Hydrology*, in preparation.

Smith, M.B., Koren, V., Reed, S., Zhang, Z., Cui, Z., Mizukami, N., Moreda, F., and Sheldon, S. (2009). Preliminary Results of Phase 2 of the Distributed Model Intercomparison Project. 23rd Conference on Hydrology, American Meteorological Society 2009 Annual Meeting, Phoenix, Arizona, Jan 11-16.

Stellman, K.M., Fuelberg, H.E., Garza, R., and Mullusky, M. (2001). "An Examination of Radar and Rain Gauge-Derived Mean Areal Precipitation over Georgia Watersheds." *Weather and Forecasting*, Vol. 16, 133-144.

Westcott, N.E., Knapp, H.V., and Hilbert, S.D. (2008). Comparison of Gauge and Multi-Sensor Preciptiation Estimates over a Range of Spatial and Temporal Scales in the Midwestern United States. *Journal of Hydrology*, Vol. 351, 1-12.

Young, C. B., Bradley, A.A., Krajewski, W.F., and Kruger, A. (2000). "Evaluating NEXRAD Multisensor Precipitation Estimates for Operational Hydrologic Forecasting." *Journal of Hydrometeorology*, 1, 241-254.

Zhang, Y., Reed, S., Kitzmiller, D., and Brewer, D., (2009). Gauge-based Adjustment of Historical Multi-Sensor Quantitative Precipitation Fields and Resulting Effects on Hydrologic Simulations. Proceedings of EWRI Conference, Kansas City, Mo.

Flash flood forecasting for ungauged locations with NEXRAD precipitation data, threshold frequencies, and a distributed hydrologic model

Brian A. Cosgrove[1], Seann Reed[1], Feng Ding[1,2], Yu Zhang[1], Zhengtao Cui[1,3], Ziya Zhang[1,4]

[1]NOAA, National Weather Service, Office of Hydrologic Development, 1325 East-West Highway, Silver Spring, MD 20910; phone: 301-713-0640 x 226; email: Brian.Cosgrove@noaa.gov
[2]Wyle Information Systems, [3]Lentech Incorporated, [4]UCAR

ABSTRACT

A flash flood forecasting system has been developed which combines distributed modeling and statistical analyses to produce gridded forecasts of return periods. A distributed hydrologic model (DHM) coupled to a threshold frequency (TF) post-processor, DHM-TF, is currently being tested over a Maryland-centered domain, and has verified well against National Weather Service (NWS) flash flood warning areas and verification points. The prototype system is currently running in real-time at the NWS Office of Hydrologic Development (OHD), and efforts are underway to test DHM-TF at several NWS field offices.

INTRODUCTION

Flash floods are a devastating natural disaster, causing millions of dollars of damage each year and putting many lives in danger. With the exception of excessive heat, flooding leads to more weather-related fatalities than any other cause. In 2007, the last year for which statistics were available, flash flooding caused 70 fatalities, 51 injuries, and 1.2 billion dollars in damage (NWS, 2009a). Half of flood-related deaths were caused when victims were caught in vehicles and swept away. Given these statistics, accurate predictions of flash floods are essential for the protection of life and property. Unfortunately, the nature of these events makes them quite difficult to monitor and predict. Flash floods feature a fast onset—less than 6 hours from the causative event (NWS, 2002)—are local in scope, and depend greatly on fine scale weather and land surface conditions.

Monitoring efforts are valuable but do not provide enough lead time for affected parties to take the action needed to prevent loss of life and property. Forecasts, which have the potential to increase warning lead time, can be produced by standard lumped hydrological modeling. However, these models are handicapped by the fact that they only provide information at basin outlets and cannot accurately represent the highly variable land surface and meteorological conditions that impact flash flooding. A promising alternative to lumped modeling is distributed modeling. Gridded distributed models more effectively represent the variable nature of meteorological forcing and land surface parameters and provide flood information at any grid point within the model domain. With this in mind, a method to use a distributed hydrologic model (DHM) in conjunction with a threshold frequency (TF) post processor (Reed et al., 2007) and NEXRAD precipitation data has been developed at NOAA's Office of Hydrologic Development (OHD). Forced by

Multisensor Precipitation Estimator (MPE) and High Resolution Precipitation Estimator (HPE) precipitation observations, and High Resolution Precipitation Nowcaster (HPN) precipitation forecasts, this modeling approach is focused on improving flash flood prediction capabilities by increasing forecast accuracy and usability (Kitzmiller et al., 2008). It also seeks to improve upon the current NWS flash flood warning lead time goal of 49 minutes through leveraging the two available hours of HPN precipitation forecasts (NWS, 2009b). Flash flood warning lead times have improved over the past several years (Figure 1), and DHM-TF forced by HPN output has the potential to lengthen lead times even more.

DHM-TF OVERVIEW

Operating on the Hydrologic Rainfall Analysis Project (HRAP) grid at a 4km resolution and hourly time step, DHM-TF produces gridded flow forecasts, from which gridded frequency forecasts are derived using historical simulations. These frequency forecasts are then compared against threshold frequency grids derived from local information for flash flood determination. DHM-TF relies on several hydrological modeling components to generate the required flow forecasts. These components, which include a gridded Sacramento hydrologic model, overland and channel routing algorithms, and a statistical post processor, are part of the research version of OHD's distributed model (Koren et al., 2004).

Hydrologic Modeling Components

The Sacramento hydrologic model (Burnash et al., 1973) represents spatially heterogeneous runoff processes over river basins ranging from tens to a few thousand square kilometers. It accounts for processes in which the freeze and thaw of soil moisture can have significant effects on water balance and soil moisture dynamics (Koren et al., 1999). Runoff from Sacramento is routed via a kinematic wave channel router (Koren et al., 2004). Routing is a key component of the DHM-TF flash flood forecast approach. Flash floods may occur near the causative rain event, or may occur downstream from the rainfall. The latter case is especially dangerous, as the lack of heavy rain in a particular area may provide residents or forecasters with a false sense of security. With routing enabled, DHM-TF is able to transport water from channels in areas of heavy rainfall to downstream points, providing an accurate simulation of the potential for flash floods along an entire river network.

Statistical Processing

Distributed hydrologic models have the potential to provide valuable gridded flow information, and yet, as with other models, may be subject to biases which limit their applicability without calibration or post processing. To solve this problem, DHM-TF utilizes a threshold frequency post processing approach. Rather than assuming that the exact magnitudes of the simulated flows are correct, DHM-TF relies on the concept that the relative ranking of the flows are accurate. That is, even if the flows are persistently biased, they will be internally consistent and thus can be correctly ranked against each other. It is this assumption which allows for the reliable conversion of flow values to return period values without need for accompanying observations. Reed et al. (2007) demonstrated the effectiveness of this inherent bias

correction for a simulation in the Dutch Mills basin of Arkansas. In particular, they showed that although raw model flow values may be biased, the probabilities of these model flows are accurate and able to support the calculation of return periods.

The statistical package which accomplishes this task depends on a high-quality long-term simulation of flow, which in turn requires high-quality hourly precipitation data as input. Flow values from this long term simulation are first passed through a routine which generates a grid of annual maximum peak flow values. A second routine fits the peaks to a log Pearson Type III distribution, and calculates a corresponding set of summary statistics which describe the distribution. Once the historical baseline simulation and associated computation of summary log Pearson Type III statistics are complete, real-time hourly simulations of discharge can then be ingested into a final DHM-TF routine. This routine utilizes the summary statistics to convert discharge into frequency and then return period for final display. Forecasters can compare these grids to locally derived threshold frequencies (and associated return periods) to aid in warning decisions. Local threshold frequencies may be derived from several sources of information such as known flood frequencies at selected river locations or frequencies associated with culvert designs. An in-depth discussion on this process can be found in Reed et al. (2007)

Taken together, the various components of the DHM-TF modeling approach produce flash flood forecasts which feature many advantages over traditional flash flood guidance. These include the ability to predict flash flooding at ungauged locations, a high resolution 4 km product (versus basin scale for standard flash flood guidance), a rapid update ability (every 15 minutes), and the production of verifiable small basin flow estimates.

NEXRAD PRECIPITATION DATA

Three NEXRAD-based precipitation products are used as input to DHM-TF: MPE, HPE, and HPN. The MPE uses a combination of radar and gauge input data and is produced hourly within the AWIPS environment by each RFC on a 4 km grid (Kitzmiller et al., 2007). Rainfall estimates from Doppler radar, gauges, and satellites are automatically ingested, and bias correction factors are developed from a comparison of radar and gauge data. After automatic derivation of a gauge-only field, and a bias-corrected radar field, a blended radar/gauge product is produced through an automatic merging of the two fields. Since manual adjustments of input fields may occur repeatedly over several hours as additional gauge reports are received, the final MPE field may not be available for several hours (Kitzmiller et al., 2008). Thus, although the high quality of the MPE product makes it ideal for the long term baseline DHM-TF runs, the long lag times and slow updating characteristics of the product makes real-time use in flash flood forecasting impractical.

Although not offering the rigorous manual quality control that defines MPE, HPE features a lower latency time (less than 1 hour), a more rapid update (every 15 minutes), and a higher resolution (1 km), and is thus better suited than MPE for real-time, flash flood operations. HPE leverages recent MPE gauge/radar bias information to automatically generate rainfall and rainrate products statistically corrected for bias. The process also ingests a user-defined radar mask which determines how

overlapping radars will be blended for each pixel within the domain of interest. HPE is slated for implementation within AWIPS during 2009 (Kitzmiller et al., 2008).

While MPE and HPE can be used by DHM-TF to bring model states up to the present, the most important aspect of the DHM-TF approach is its forecast capability which is powered by HPN data. Based on an updated extension of the Flash Flood Potential algorithm (Walton et al., 1985), the HPN process begins with the calculation of local motion vectors. These vectors are derived through a comparison of radar rain rates spaced 15 minutes apart, and are used to project current radar echoes forward in time out to two hours. Rain rates are then variably smoothed by a method based on the observed changes in echo structure over the past 15 minutes, as well as the current observed rain rate field (Walton et al., 1985; Kitzmiller et al., 2008).

CASE STUDY

Both the NWS Mid Atlantic River Forecast Center (MARFC) and the NWS Sterling Weather Forecast Office (WFO) have expressed interest in implementing DHM-TF. As such, DHM-TF developmental work and case study research is currently occurring over a 14,000 km^2 Maryland-centered domain which lies within both the MARFC and Sterling WFO areas of responsibility (Figure 2). Uncalibrated parameters for the gridded Sacramento model were taken from an *a priori* set of land surface parameters derived by Koren et al. (2000) using the National Resource Conservation Service State Soil Geographic Database. These parameters were complemented by a percent impervious area data set derived by Elvidge et al. (2004). Flow measurement data (cross sectional area and flow) at downstream gauges within the test domain were used to derive channel routing parameters. Values at upstream cells were derived using geomorphological relationships (Koren et al., 2004).

Even with automatic and manual error correction procedures in place, a time-changing bias was found in the MPE fields used to force DHM-TF over the Maryland domain prior to 2004. This bias stemmed from a truncation error within the NEXRAD precipitation processing scheme. Given the need for an accurate and internally consistent long-term flow simulation, a bias correction procedure was developed to account for this issue (Figure 3). In this procedure, monthly accumulations of Parameter-elevation Regressions on Independent Slopes Model (Daly et al., 1994) observation-based precipitation data are divided by monthly sums of MARFC MPE data. The resulting monthly ratios form monthly correction factors that are applied to all hourly MPE data within each particular month. Application of this procedure to the MPE fields greatly reduces the inconsistency in the bias of resulting distributed model flow fields (Zhang et al., 2009).

Simulations conducted over the Maryland test area with MPE, HPE, and HPN data fall into two categories: 1) retrospective, and 2) real-time.

Retrospective Simulations

A long-term retrospective flow simulation serves as the baseline for conducting both specific retrospective case studies as well as real-time operations. This simulation provides the annual maximum peak data which is used to construct the Log Pearson Type III distribution needed to convert flow values to return periods, and allows forecasted flows to be put into proper historical context. Currently 10

years in length, this simulation is forced by bias-corrected MPE data, and only needs to be updated once per year to generate new annual maximum peak data.

Leveraging the long-term Sacramento simulation, a case study was performed centering on Tropical Storm Hanna, which brought heavy rain to the Maryland region September 6th-7th, 2008 (Figure 4). The intensity and duration of the rain gave rise to eight flash flood warnings issued by the Sterling WFO for areas within Maryland and Virginia. Several local roads and large parkways were shut down due to flash flooding and several rescues and evacuations were necessary. Five of the warnings were outside the Maryland DHM-TF domain, and were not included in the case study. The remaining three were issued at 16:20Z, 17:58Z, and 19:12Z on September 6th, and collectively covered the period of time from 16:20Z on September 6th through 01:15Z on September 7th.

Flow return periods calculated by DHM-TF were plotted in Google Earth and are displayed in Figure 5 alongside the warning polygons defining the three flash flood warning areas mentioned above. In order to match the multi-hour time period covered by these flash flood warnings, the DHM-TF data displayed is the maximum return period generated by the model during the valid time of the three warnings. As can be seen, DHM-TF generates gridded return values above 2 years (approximately bankfull) in each of the three warning areas. In particular, where available, the DHM-TF output matches the coverage of the southernmost warning polygon over Washington DC very well. As DHM-TF is implemented in field offices, its use may allow forecasters to draw smaller warning polygons and reduce false alarms.

Further focusing on this warning area, Figure 6 depicts a large grouping of 4 km grid boxes where DHM-TF generates flash flood conditions. Two verification points where flash flooding was observed by ground spotters are also depicted, and align well with the DHM-TF output. One of the challenges of flash flood forecasting is verification. In many instances, no ground truth is available to corroborate a flash flood warning. Multiple factors can contribute to the lack of observations including population density, adverse weather conditions, and a lack of verification spotters. Recognizing the importance of ground truth, NOAA NWS is currently in the process of upgrading the warning and verification process. This effort, combined with focused, intense validation efforts such as the Severe Hazards Analysis and Verification Experiment (SHAVE, Ortega et al., 2009), will greatly improve the flash flood forecasting process, and will allow for improved validation of DHM-TF output.

Real-time Simulations

Although a valuable tool for research exploration, DHM-TF is ultimately aimed at expanding the operational flash flood forecasting abilities of NWS WFO and RFC offices. As such, much emphasis has been placed on the development of a robust real-time system of data archiving, model execution, and output visualization scripts. Figure 7 shows that two hydrologic model runs are required each time real-time execution is initiated: a state update phase, and a forecast phase.

In Phase 1, which begins 16 hours before present, Sacramento model states and river channel states are updated using MPE and HPE forcing data. The model makes use of a restart file which is saved by the previous state update run, and which contains soil as well as channel state information. MPE data is used for the first 12

hours, while HPE data is used for the remaining 4 hours. Once the model reaches the present time, HPN data is used to force the model 2 hours into the future. To allow water to flow through the channel system and further highlight downstream impacts, the model is run for an additional 4 hours, albeit without any precipitation data.

Once model execution is complete, the statistical processing routines convert flow output into gridded return periods. Automated scripts then produce plots of these return periods using the freely available GRASS GIS and Google Earth programs (no NWS product endorsement implied). Each program has its own strengths and weaknesses and the use of both ensures that the data will be accessible by a broad range of operational and research stakeholders. Google Earth excels at intuitive visualization, while GRASS is able to perform sophisticated geospatial analyses. Both still image and movie-type views of the data are produced each hour.

Currently, the real-time production cycle is executed once per hour. However, given the 15 minute updating of HPE data, the system could be configured to update as often as every 15 minutes by using more HPE data and less HPN data. In addition, as future upgrades to the HPN product extend forecast length past 2 hours, the DHM-TF system will be reconfigured to use all available forecast data.

FUTURE PLANS

The portability of DHM-TF will be increased through inclusion of the Snow17 snow model (Anderson, 1973) and through the derivation of a nationwide routing parameter dataset. The impact of increasing model resolution to 2km will be examined, and a study of the length of flow record needed to support DHM-TF operations will also be undertaken. Concurrent with the research outlined above, collaborative efforts with several National Weather Service WFOs and RFCs will seek to bring DHM-TF into operational forecasting environments. It is in these locations where DHM-TF will have the largest impact, providing increased flash flood warning time and forecast accuracy, potentially saving lives and property.

REFERENCES

Anderson, E.A. (1973). "NWS River Forecast System-Snow Accumulation and Ablation Model". Technical Memo. NOAA, Silver Spring, MD, pp. 217.

Burnash, R. J. C., Ferral, R. L., and McGuire, R. A. (1973) "A generalized streamflow simulation system - Conceptual modeling for digital computers", Tech. Rep., Joint Federal and State River Forecast Center, U.S. NWS and California State Department of Water Resources, Sacramento, California, 204.

Daly, C., Neilson, R. P., and Phillips, D. L. (1994). "A Statistical-Topographic Model for Mapping Climatological Precipitation over Mountainous Terrain". J. Appl. Meteor., 33, 140-158.

Elvidge, C. D., Milesi, C., Dietz, J. B., Tuttle, B. T., Sutton, P. C., Nemani, R., and Vogelmann, J. E. (2004). "U.S. Constructed Area Approaches the Size of Ohio", Eos Trans. AGU, 85(24), doi:10.1029/2004EO240001.

Kitzmiller, D., Ding, F., Guan, S., Kondragunta, C. (2007). "Sources of NEXRAD and multisensor precipitation estimates and their functional characteristics". In: World Environmental and Water Resources Congress 2007. Restoring our Natural Habitat. Amer. Soc. Civil Engineers, 10pp, (Preprint).

Kitzmiller, D., Ding, F., Guan, S., Riley, D., Fresch, M., Miller, D., Zhang, Y., Zhou, G. (2008). "Multisensor Precipitation Estimation in the NOAA National Weather Service: Recent Advances". In: World Environmental and Water Resources Congress 2008. Amer. Soc. Civil Engineers, 10pp, (Preprint).

Koren, V., Schaake, J., Mitchell, K., Duan, Q.-Y., Chen, F., and Baker, J. M. (1999). "A parameterization of snowpack and frozen ground intended for NCEP weather and climate models", JGR, vol. 104, No. D16, pp. 19,569-19,585.

Koren, V.I., Smith, M., Wang, D., and Zhang, Z. (2000). "Use of Soil Property Data in the Derivation of Conceptual Rainfall–runoff Model Parameters", American Met. Soc. 15th Conference on Hydrology, Long Beach, CA, pp. 103–106.

Koren, V.I., Reed, S., Smith, M., Zhang, Z., and Seo, D.J. (2004). "Hydrology laboratory research modeling system (HL-RMS) of the US national weather service". Journal of Hydrology 291, 297–318.

National Weather Service (2002). "NWS Manual 10-950". [Available from http://www.nws.noaa.gov/directives/010/pd01009050a.pdf]

National Weather Service (2009a) "Summary of Natural Hazard Statistics for 2007 in the United States". [Available from http://www.weather.gov/os/hazstats.shtml]

National Weather Service (2009b). "NOAA's National Weather Service Performance Measures, FY 2006 - FY 2012". [Available at: http://www.weather.gov/cfo/program_planning/doc/All_GPRA2006.pdf]

Ortega, K. L., Smith, M., Manross, K. L., Scharfenberg, K. A., Witt, A., Kolodziej, A. G., and Gourley, J. J. (2009). "Severe hazards analysis and verification experiment". Submitted to Bull. Amer. Meteor. Soc.

Reed, S., Schaake, J., and Zhang, Z. (2007). "A distributed hydrologic model and threshold frequency-besed method for flash flood forecasting at ungauged locations", J. Hydrology, 337, 402–420.

Walton, M., E. Johnson, P. Ahnert, and Hudlow, M. (1985). "Proposed on-site Flash-Flood Potential system for NEXRAD". Preprints, 6th Conf. Hydrometeorology, Amer. Meteor. Soc., 122-129.

Zhang, Y., Reed, S., Kitzmiller, D., and Brewer, D. (2009). "Gauge-based Adjustment of Historical Multi-Sensor Quantitative Precipitation Fields and Resulting Effects on Hydrologic Simulations". In: World Environmental and Water Resources Congress 2009. Amer. Soc. Civil Engineers, 10pp, (Preprint).

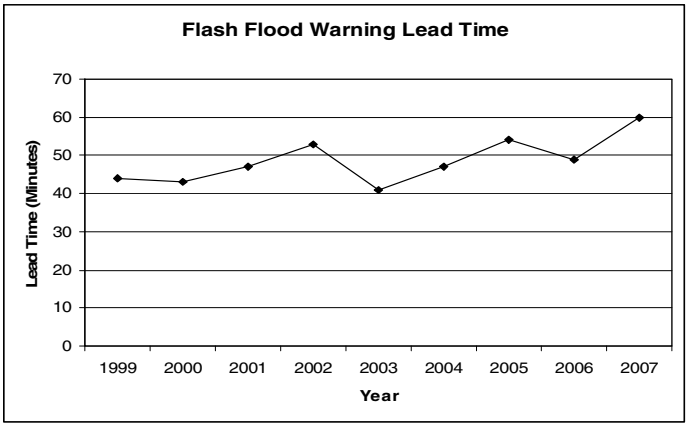

Figure 1. Average yearly National Weather Service flash flood warning lead time from 1999 through 2007.

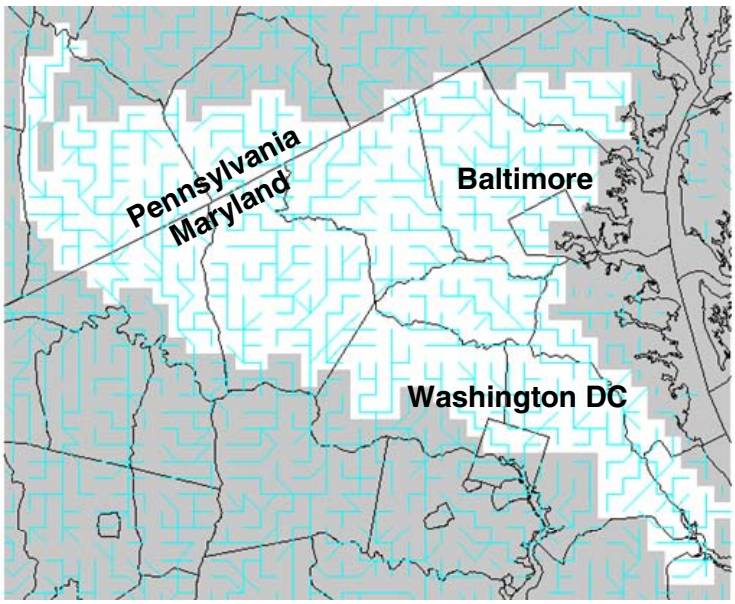

Figure 2. DHM-TF Case study domain centered on Maryland, and featuring a 4km^2 grid resolution.

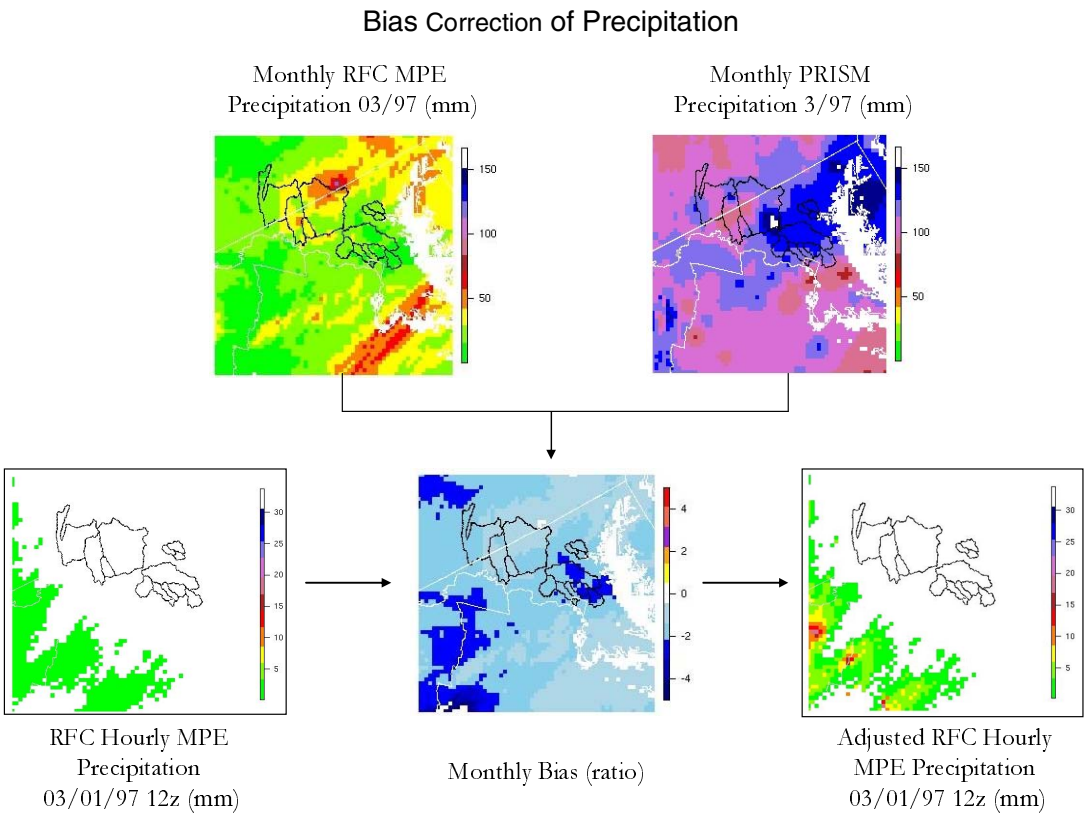

Figure 3. Overview of the bias correction procedure used to reduce the bias present in the MARFC MPE precipitation record prior to 2004.

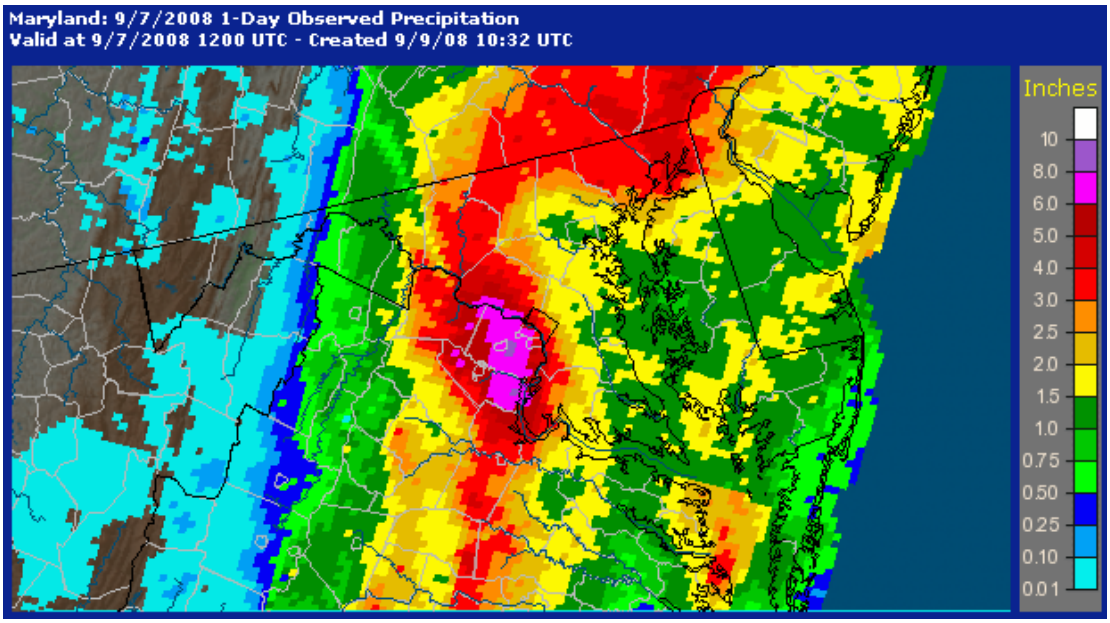

Figure 4. Precipitation (inches) associated with Tropical Storm Hanna from 12Z September 6th, 2008 through 12Z September 7th, 2008.

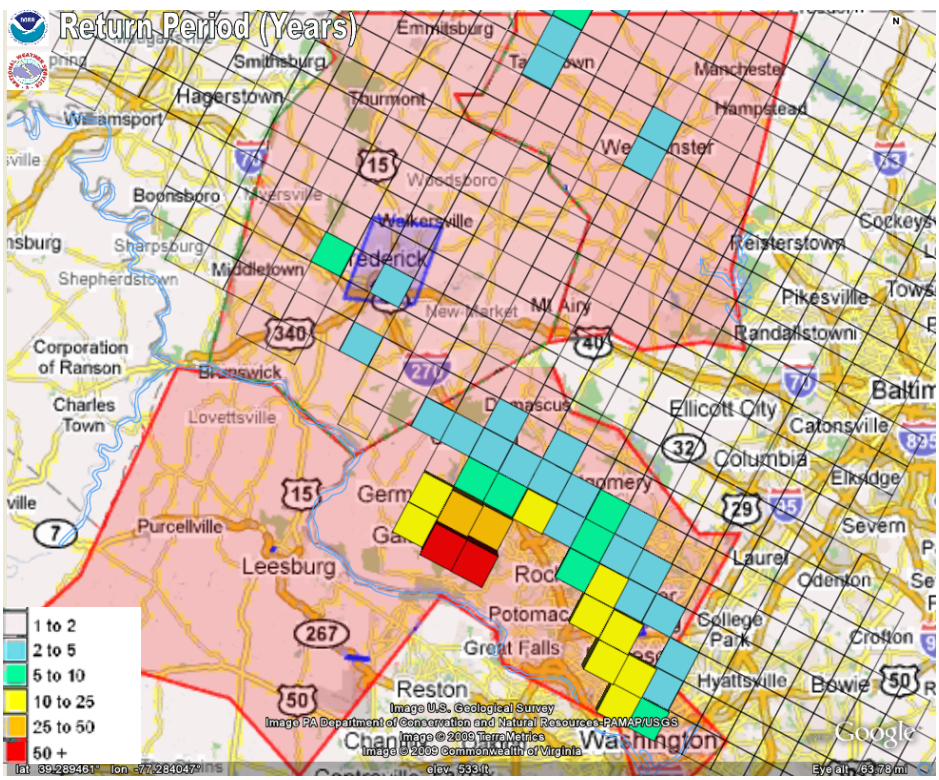

Figure 5. Depiction of the areas covered by the three Tropical Storm Hanna flash flood warnings (outlined in Red) issued by the Sterling WFO that lie within the Maryland DHM-TF case study domain. Figure also depicts maximum return period values from DHM-TF covering a similar time period.

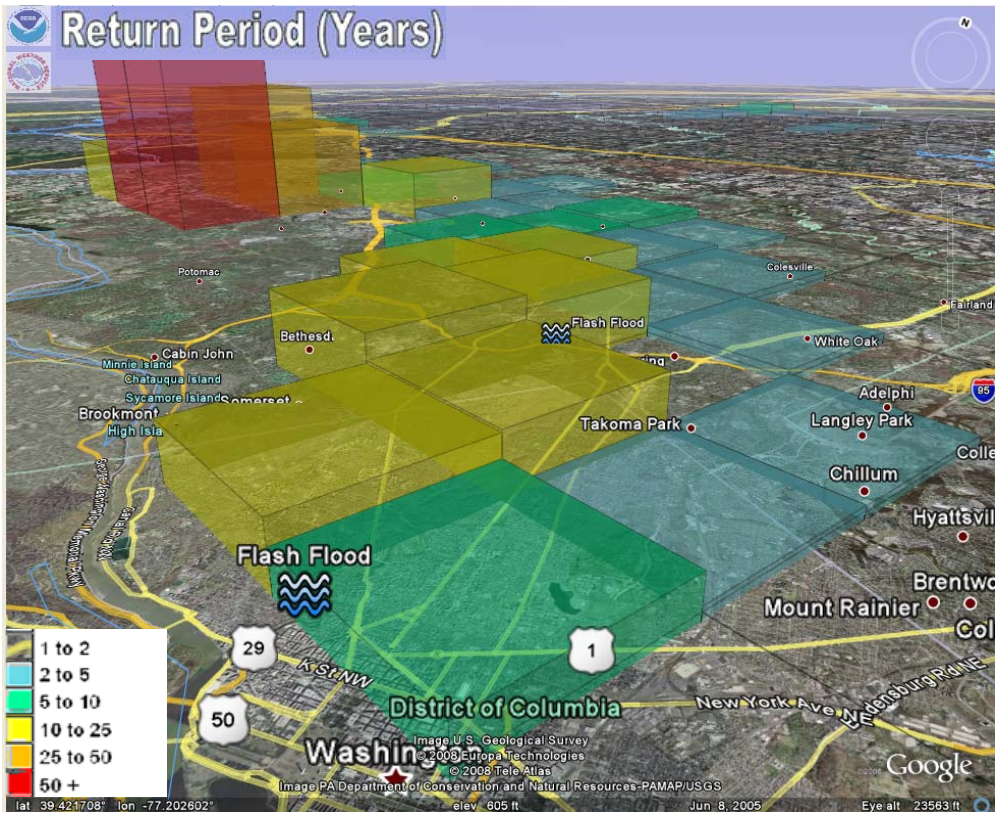

Figure 6. Maximum return period values from DHM-TF simulated during the period of time from 16Z on September 6th through 02Z on September 7th 2008. Spotter-confirmed flash flood events are indicated by the Blue wave symbols.

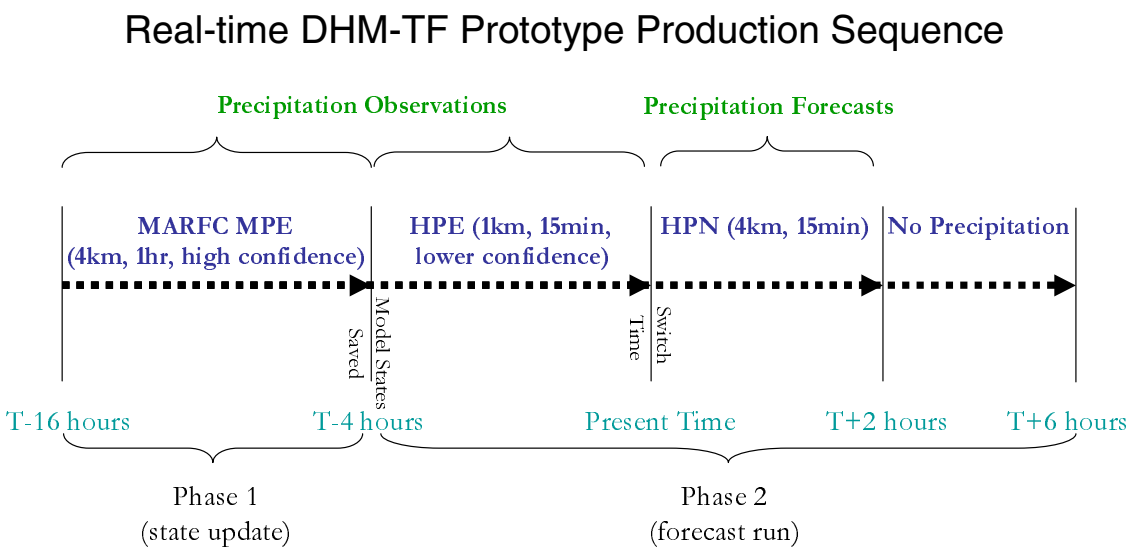

Figure 7. Illustration of the production sequence used in ongoing prototype DHM-TF forecasting prototype.

Gauge-based Adjustment of Historical Multi-Sensor Quantitative Precipitation Fields and Resulting Effects on Hydrologic Simulations

Yu Zhang[1], Seann Reed[1], David Kitzmiller[1], and Daniel Brewer[1]

[1] NOAA, National Weather Service, Office of Hydrologic Development, 1325 East-West Highway, Silver Spring, MD 20910; phone: 301-713-0640 x100; e-mail: yu.zhang@noaa.gov

Abstract

This study presents two rain gauge-based re-adjustment schemes aimed at mitigating the biases in archival Multisensor Quantitative Precipitation Estimates (MQPEs) produced by the National Weather Service (NWS). The first and the second schemes re-adjust the MQPEs on monthly and daily scales to match two gridded gauge-only analyses at the respective time scale. These schemes were applied to archival MQPEs from the Mid-Atlantic River Forecasting Center (MARFC) for 1997-2006 and their effects were examined through streamflow simulations for twelve catchments in the state of Maryland. The results were compared with observed streamflow for two periods divided along November 2003, when a software error that contributed to earlier low bias was corrected. The results indicate that either scheme improved the temporal consistency of MQPE bias, though the monthly scheme was slightly more effective. Between the two periods, the adjustment schemes were generally more effective in the earlier one than the latter one.

Introduction

The National Oceanic and Atmospheric Administration's (NOAA) National Weather Service (NWS) routinely produces hourly Multisensor Quantitative Precipitation Estimates (MQPEs) based on radar and rain gauge observations. These MQPEs serve as forcing in its flash flood and river forecasting operations (Reed et al., 2007; Cosgrove et al., 2009), and their high spatio-temporal resolution (nominal 4 km) facilitates the calibration and the deployment of the NWS distributed hydrologic model (NWS-DHM, Koren et al. 2004). However, historical studies have found that archival MQPEs were subject to biases, and that the biases varied greatly over time (e.g., Hardegree et al. 2003). One of the factors that contributed to the historical biases is the truncation error (TE), a software error in the NEXRAD Precipitation Processing System (PPS) that led to erroneous rounding off of scan-to-scan precipitation accumulation less than 0.1 mm and therefore resulted in underestimation in earlier MQPEs prior to its fix around 2002-3 (Fulton et al. 2003).

The presence of the aforementioned biases, and more importantly their temporal inconsistency, greatly complicates model calibration. In order to mitigate these biases and reduce their historical inconsistencies, an attempt was made to post-process the MQPE's through rain gauge-based re-adjustment at monthly and daily scales. Chosen as references for the monthly and daily re-adjustment schemes are 2.5-minute, monthly Parameter-elevation Regressions on Independent Slopes Model (PRISM) outputs, and a 1/8th degree, daily gauge-only analysis produced by National Centers for Environmental

Prediction (NCEP) Climate Prediction Center (CPC), respectively. MQPEs from River Forecast Centers (RFCs) are adjusted such that the monthly or daily areal-average totals match those of the reference dataset at each grid cell. While MQPEs were created using mostly hourly gauge reports, the reference gauge-only analyses were based on a broader set of gauge records at hourly and coarser resolutions. The integration of the latter data is therefore expected to improve the quality of MQPEs.

In order to evaluate the effectiveness of the re-adjustment methods, a set of streamflow simulation experiments were performed for twelve catchments in the domain of the NWS Mid-Atlantic River Forecast Center (MARFC) for the period of 1997-2006. In these experiments, the MARFC MQPEs, and their re-adjusted versions based on the monthly and daily gauge are comparatively applied as forcings to the NWS-DHM (using the component models described below). The simulated streamflow time series over 1998-2006 are then evaluated against observed values obtained from the United States Geological Survey (USGS). To investigate the impacts of the TE and its correction on MQPE bias and the effectiveness of the re-adjustments, the observed and model simulated streamflow were stratified over two periods divided along November 2003 when the software update correcting TE took effect for the regional radar.

Radar and Multisensor Precipitation Estimation

The NWS precipitation estimation algorithms consist of radar-only and multisensor components. The major radar-only component is the Precipitation Processing System (PPS; Fulton et al. 1998), which produces real-time estimates of liquid ground precipitation. The PPS outputs are disseminated as Digital Precipitation Array (DPA, also referred to as Stage I products). In the legacy multisensor algorithms, the Stage I products underwent bias correction in the Stage II processing, and the results were quality-assured and mosaicked on a regional basis to produce Stage III data. The common map projection for all three stages is the polar stereographic Hydrologic Rainfall Analysis Project (HRAP) grids (nominal 4 km resolution in the central US; Greene and Hudlow (1982)). The legacy Stage II and III algorithms have since been replaced by the Multisensor Precipitation Estimator (MPE). MPE incorporates several algorithmic additions and enhancements, including mean-field and local correction (Seo et al. 1999, 2000; Seo and Breidenbach 2002), as well as methods for creating gauge-only and gauge-radar merged products (Seo 1998a and b). Stage III and the later MPE-based products are both referred to as the multi-sensor quantitative precipitation estimates (MQPEs).

Around 2000, analyses of PPS products revealed that scan-to-scan accumulation of amounts less than 0.1 mm was erroneously rounded off (Fulton et al. 2003). This "truncation error" (TE), as shown by Fulton et al. (2003), is most pronounced during prolonged light rain events, and could lead to considerable underestimation of the cumulative rainfall in the historical MQPEs. TE was corrected in three successive software releases during 2002-3 (Fulton et al. 2003).

At present, forecasters at NWS River Forecast Centers (RFCs) are responsible for running the MPE to create the MQPEs. Normally, a forecaster would quality assure hourly gauge records before ingesting them. Note that the current MPE framework only

allows the use of hourly gauge records. Nevertheless, forecasters at times disaggregate gauge reports at coarser resolutions (e.g., daily scale) to create artificial hourly records that would be ingested in creating the archival MQPEs.

Re-adjustment Methodologies

The monthly scheme uses the monthly Parameter-elevation Regressions on Independent Slopes Model (PRISM; Daly et al. 1994) as the reference. The monthly re-adjustment involves the following steps:

1) 2.4 arc-minute PRISM data are re-projected onto the HRAP grids;
2) Monthly cumulative precipitation from MQPEs is computed;
3) For each HRAP cell, the ratio of PRISM to MQPE monthly accumulation is computed.
4) Each hourly MQPE within that month is multiplied by the ratio grid computed in step 3 for every hour.

The daily scheme proceeds in an analogous manner, except using the CPC 1/8 degree gauge only analysis as reference. To ensure comparability between the PRISM and the CPC data sets, the latter was also adjusted so that the monthly total at each HRAP cell matches the former prior to serving as reference.

Study Sites and Experimental Design

Twelve catchments in the state of Maryland were selected to evaluate the hydrologic impacts of bias-adjustment. The size of catchments range from 84 to 1200 km^2 (Fig. 1; Table 1). The study catchments are under the umbrella of WSR-88D located in Sterling, VA (KLWX, at 38º58'31"N, 77º28'41"W), and each has been gauged continuously at its outlet by the USGS.

The NWS DHM (See description in Koren et al. (2004)) was implemented for each of the catchments. The model represents the landscape on the HRAP grid. The implementation for this study involves three model components. The first one is a snow module that relies on temperature to distinguish snow versus rain and computes snow accumulation and ablation (Anderson 1973). The second is the Sacramento Soil Moisture Accounting (SAC-SMA) module that computes runoff at each HRAP cell (Burnash et al. 1973; Koren et al. 2004). The third is a kinematic wave routing method (Koren et al. 2004). Model calibration was avoided to isolate the impacts of MQPE re-adjustments. Instead, a priori parameter values based on physiographic information (for SAC-SMA and routing) and values commonly used in RFC operations (as for snow model parameters) were used. The SAC-SMA a priori parameters were derived from soil texture and land cover. The cell-to-cell connectivity required for the kinematic routing model was determined from digital elevation model (Reed, 2003). Routing parameters were computed on the basis of site-specific flow measurement data provided by the USGS (Koren et al., 2004).

Hourly MQPEs for the period of 1997-2006 were acquired from the Mid-Atlantic River Forecast Center. The first five years of MQPEs (1997-2001) were produced using

the Stage III algorithm and the rest via the MPE. As indicated earlier, these MQPEs were re-adjusted via the monthly PRISM and the daily CPC schemes (note that the two schemes were applied independently from each other). Both the original and the adjusted MQPEs were then used to drive the model. Additional forcing data obtained include 6-hourly, 2.5 degree NCEP gridded temperature re-analysis (needed for the snow model), and monthly climatological potential evapotranspiration (PET) values. In assigning the initial conditions, it was assumed that upper and lower zone free water storages were each at half capacity, and the channels were dry. Under these assumptions, continuous simulations were performed at hourly time step for each catchment over the ten-year period. The hourly streamflow simulations were subsequently compared against hourly USGS discharge measurements for 1998-2007 (1997 was treated as the warm-up period for the model and the associated results were excluded in the comparison). The results were further stratified into the pre-TE correction (Jan. 1998 – Nov. 2003) and the post-TE correction (Dec. 2003 – Dec. 2006) periods to illuminate the impacts of TE on MQPE biases and on the effectiveness of the re-adjustments.

Simulation Results

The mean areal precipitation for each basin, along with the validation statistics of hourly simulation results, including percentage bias (PB) and correlation coefficients (CC) are shown for the pre and post-TE correction periods separately in Figure 2. The following features are evident for the earlier period:

1) Stream simulations based on unadjusted MQPEs show appreciable low bias;
2) Either monthly or daily re-adjustment scheme substantially increased the precipitation amounts and improved the low bias in streamflow;
3) For most basins, either scheme led to higher CC values;
4) The monthly scheme is more effective than the daily scheme in mitigating the low bias.

The period after TE correction is characterized by the following:

1) Streamflow simulations based on unadjusted MQPEs show low, but less conspicuous bias;
2) Either re-adjustment scheme reduced the precipitation amounts and induced a consistent low bias in the simulated streamflow;
3) For most basins each scheme also yielded improvements in CC, though the amounts of improvements are much less conspicuous relative to the earlier period.
4) Monthly and daily schemes performed comparably judged by PB and CC.

The results are further analyzed separately for the warm (April – October) and cool season (November to March). The validation statistics for streamflow are show in Figures 3 and 4. The following features are notable for the earlier period:

1) Streamflow based on re-adjusted MQPEs were still biased low for the warm season despite substantial improvements, whereas those for cool seasons are nearly bias-neutral.

2) The improvements in CC are more conspicuous for the cool rather than the warm season.

For the later period, notable observations include

1) Simulated streamflow based on unadjusted MQPEs shows considerable low bias for the warm season and high bias for the cool season;
2) For the warm season, each re-adjustment scheme reduced the precipitation amounts and thereby worsened the low bias ;
3) For the cool season, each scheme improved the high bias.

The bias for each set of simulations was computed for each year and the range in values was compared in Figure 5. It is evident that both re-adjustment schemes considerably improved the temporal consistency in the bias values.

Summary and Conclusions

This study presents monthly and daily-based re-adjustment schemes for mitigating the biases in historical MQPEs. Hydrologic simulations for twelve catchments in the domain of MARFC were carried out via a distributed hydrologic model to evaluate the efficacy of these schemes. Comparisons of original MQPE-based results with observations pointed to severe underestimation of streamflow in the period prior to TE correction (1998-Nov. 2003), and a lack of such a feature after TE correction. These observations suggest that a) MQPEs prior to TE correction were biased low, most likely as a consequence of TE, and b) the low MQPE biases were considerably improved with TE correction.

The simulation results further suggest that the re-adjustment schemes were highly effective in mitigating the low MQPE biases before the TE correction, and were less so thereafter. In addition, the two schemes yielded more conspicuous improvements in correlation coefficients in the earlier rather than the later period. Furthermore, the re-adjustment schemes were shown to be more effective during the cool season and less so during the warm season, as judged by PB and CC for streamflow simulations. Between the monthly and daily schemes, the former yielded more pronounced improvements in PB and CC on an overall basis. For the 9-year period studied here, each re-adjustment scheme was shown to improve the historical consistency in the bias of streamflow. These results suggest that applying these re-adjustment schemes may offer substantial benefits for hydrologic model calibration. These re-adjustment schemes are in the process of being evaluated in other RFC domains to determine their effectiveness under broader climate and hydrologic conditions.

Acknowledgements

We wish to thank the staff at NCEP-CPC for providing the daily gauge analysis.

References

Anderson, E. A., 1973: National weather service river forecast system - snow accumulation and ablation model. Technical Report, US Dept. of Commerce, Silver Spring, MD, NOAA Technical Memorandum NWS HYDRO-17.

Burnash, R. J. C., R. L. Ferral, and R. A. McGuire, 1973: A generalized streamflow simulation system - conceptual modeling for digital computers. Technical report, United States Department of Commerce, National Weather Service and State of California, Department of Water Resources.

Cosgrove, B., S. Reed, F. Ding, Y. Zhang, Z. Cui, and Z. Zhang: Flash flood forecasting for ungauged locations with NEXRAD precipitation data, threshold frequencies, and a distributed hydrologic model. In: World Environmental and Water Resources Congress 2009. Amer. Soc. Civil Engineers, 10pp, (Preprint).

Daly, C., R. P. Neilson, and D. L. Phillips, 1994: A statistical-topographic model for mapping climatological precipitation over mountanious terrain. *J. Clim. Appl. Meteorol.*, **33**, 140-158.

Fulton, R. A., J. P. Breidenbach, D. J. Seo, D. A. Miller, and T. O'Bannon, 1998: The WSR-88D rainfall algorithm. *Weather and Forecasting*, **13**, 377-395.

Fulton, R. A., F. Ding, and D. Miller, 2003: Truncation errors in historical WSR-88D rainfall products. 31th Conference on Radar Meteorology, Amer. Meteor. Soc., Seattle, WA.

Greene, D. and M. Hudlow, 1982: Hydrometeorologic grid mapping procedures. Int. Symp. on Hydrometeorology, AWRA, Denver, CO.

Hardegree, S., S. V. Vactor, K. Healy, C. Alonso, J. Bonta, D. Bosch, D. Fisher, D. Goodrich, D. Harmel, J. Steiner, and M. V. Liew, 2003: Multi-watershed evaluation of WSR-88D (NEXRAD) radar-precipitation products. First Interagency Conference on Research in the Watersheds, Benson, AZ., 486–492.

Koren, V., S. M. Reed, M. Smith, Z. Zhang, and D.-J. Seo, 2004: Hydrology Laboratory Research Modeling System (HL-RMS) of the US National Weather Service. *J. Hydrology*, **291**, 297-318.

Reed, S., 2003: Deriving flow directions for coarse-resolution (1-4 km) gridded hydrologic modeling. *Water Resources Research*, **39**, SWC 4-1, CiteID 1238, DOI 10.1029/2003WR001989

Reed, S., J. Schaake, and Z. Zhang, 2007: A distributed hydrologic model and threshold frequency-based method for flash flood forecasting at ungauged locations. *J. Hydrol.,* **337**, 402-420.

Seo, D.-J.,| 1998a: Real-time estimation of rainfall elds using rain gage data under fractional coverage conditions. *J. Hydrology*, **208**, 25-36.

Seo, D.-J., 1998b: Real-time estimation of rainfall elds using radar rainfall and rain gage data. *J. Hydrology*, **208**, 37-52.

Seo, D.-J. and J. Breidenbach, 2002: Real-time correction of spatially nonuniform bias in radar rainfall data using rain gauge measurements. *J. Hydromet*., **3**, 93-111.

Table 1: Study Catchments

Station	USGS ID	Latitude (º)	Longitude (º)	Area (km^2)
canoc	1614500	39.7164	77.8248	1279
antie	1619500	39.4498	77.7302	728
catoc	1637500	39.4273	77.5562	173
monoc	1643000	39.4028	77.3661	2116
senec	1645000	39.1281	77.3358	262
rocks	1648000	38.9725	77.0400	161
nwanac	1651000	38.9523	76.9661	128
neanac	1649500	38.9603	76.9260	189
wbranh	1594526	38.8142	76.7487	232
patuxb	1594440	38.9559	76.6937	901
vnova	1589300	39.3459	76.7332	84
washb	1589352	39.2715	76.6486	171

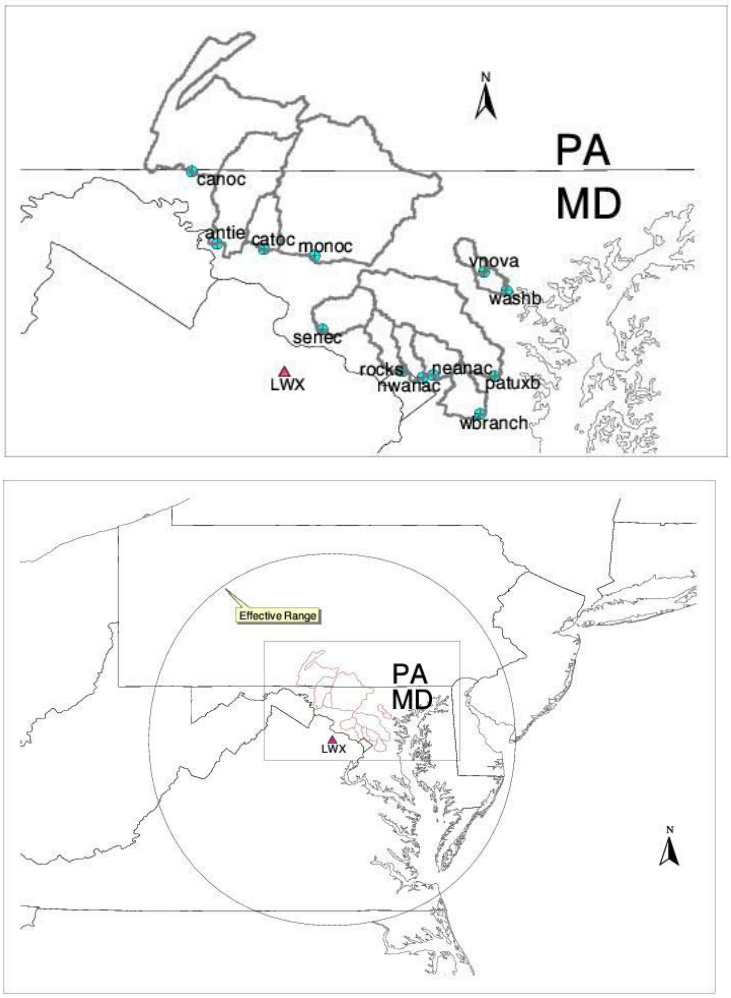

Figure 1. Study catchments in Maryland and their locations relative to the WSR-88D at Sterling,VA (KLWX).

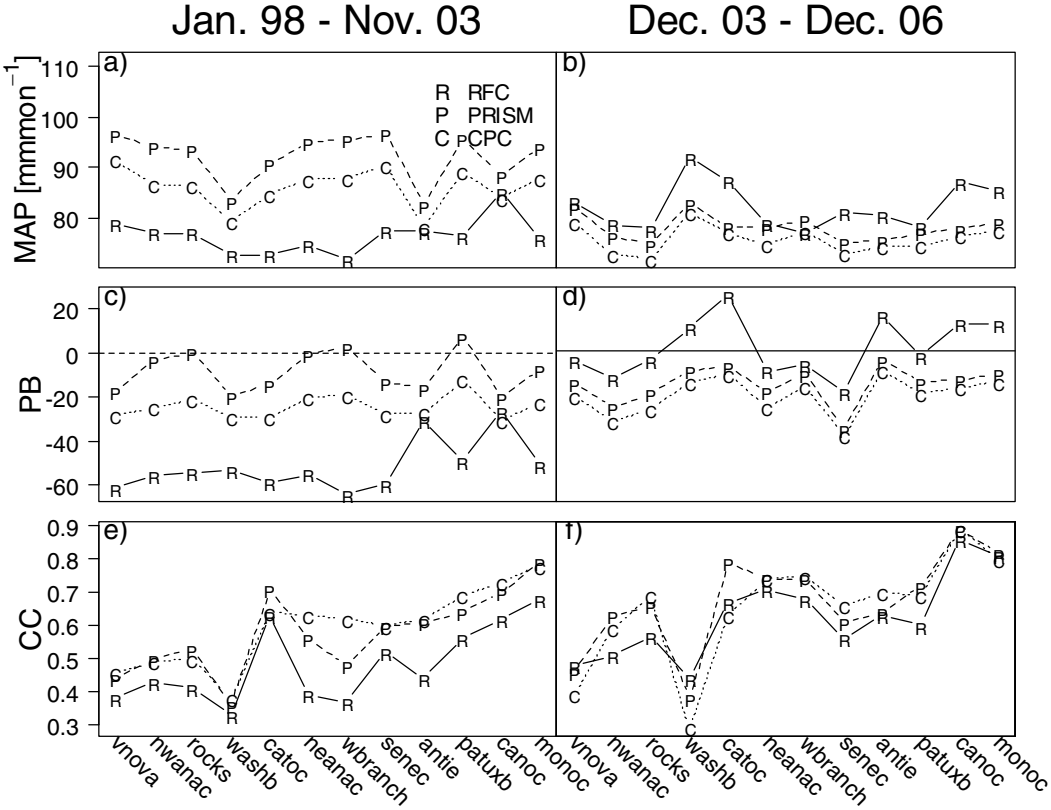

Figure 2. Hourly streamflow validation statistics prior to and after correction (Jan. 1998 - Nov. 2003, and Dec. 2003 - Dec. 2006, respectively), in terms of mean areal precipitation (MAP; a and b), percentage bias (PB; c and d) and correlation coefficients (CC; e and f).

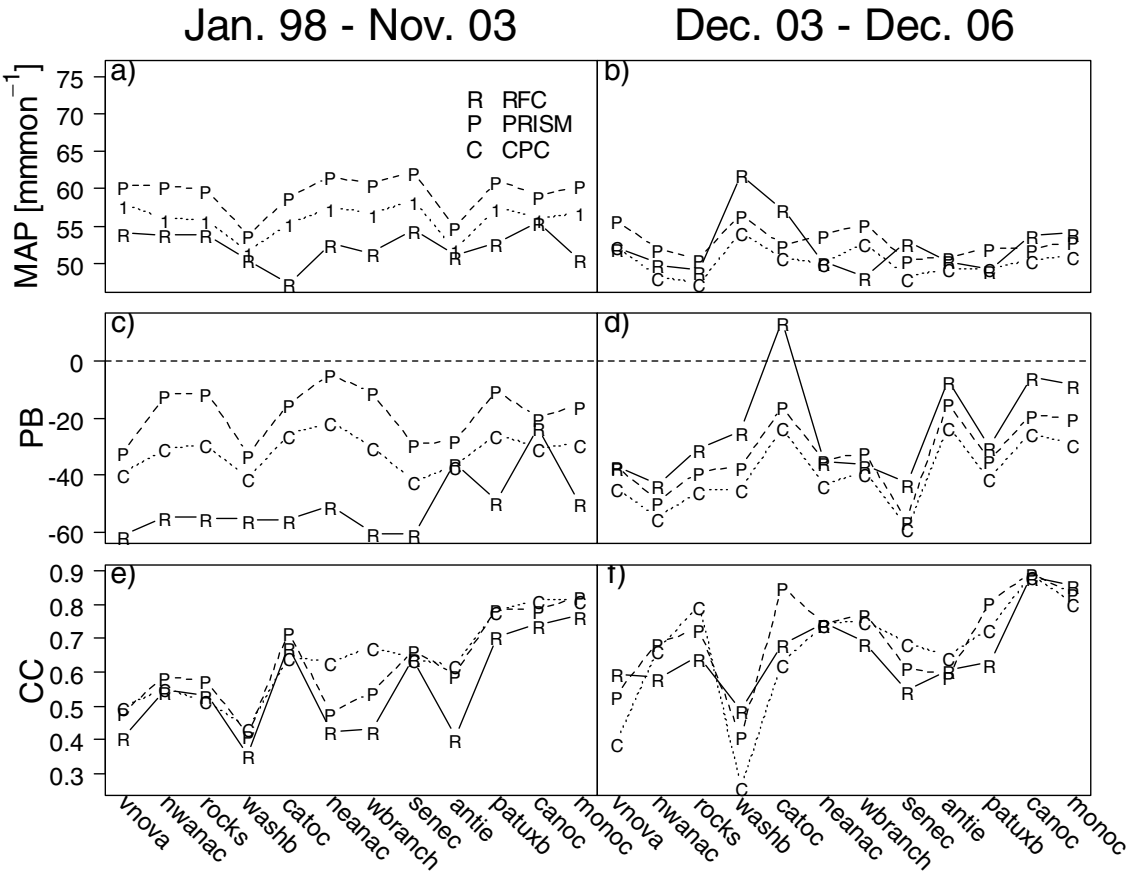

Figure 3: Warm season hourly streamflow validation statistics prior to and after correction (Jan. 1998 - Nov. 2003, and Dec. 2003 - Dec. 2006, respectively), in terms of mean areal precipitation (MAP; a and b), percentage bias (PB; c and d) and correlation coefficients (CC; e and f).

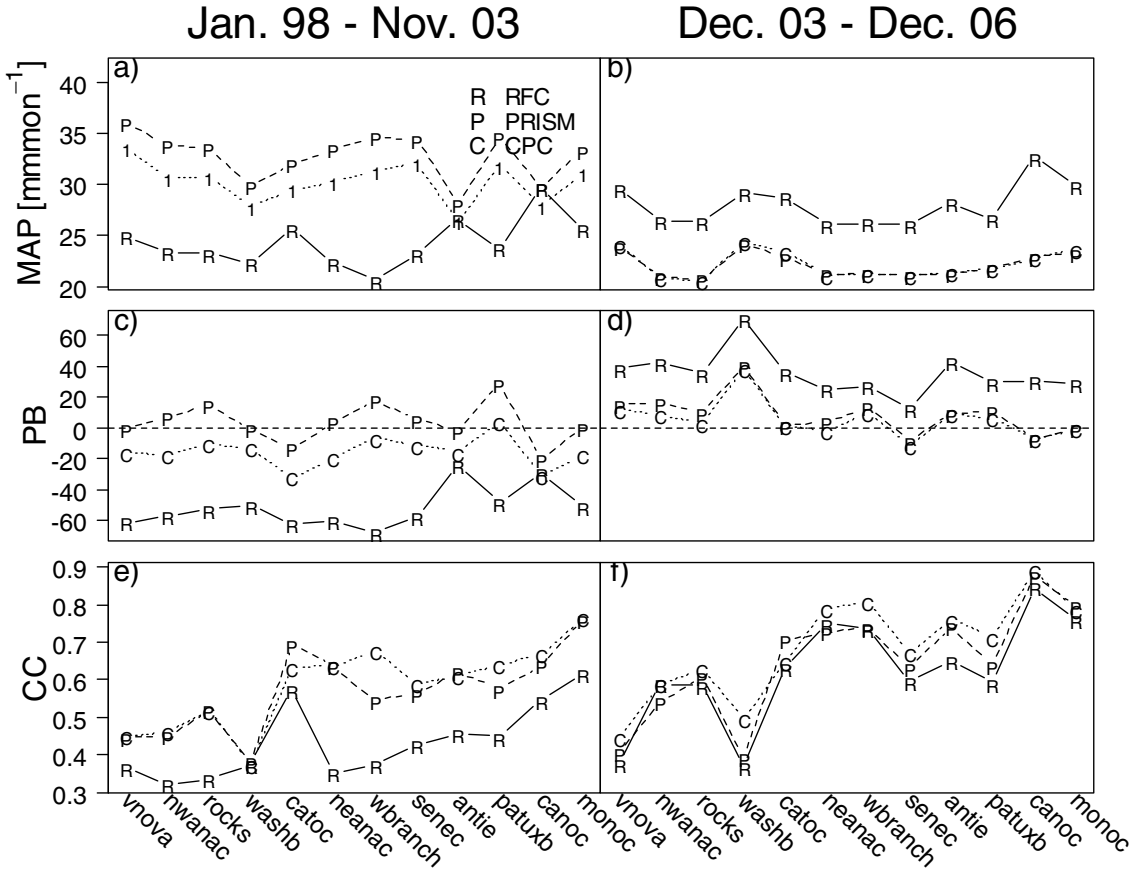

Figure 4: Cool season hourly streamflow validation statistics prior to and after correction (Jan. 1998 - Nov. 2003, and Dec. 2003 - Dec. 2006, respectively), in terms of mean areal precipitation (MAP; a and b), percentage bias (PB; c and d) and correlation coefficients (CC; e and f).

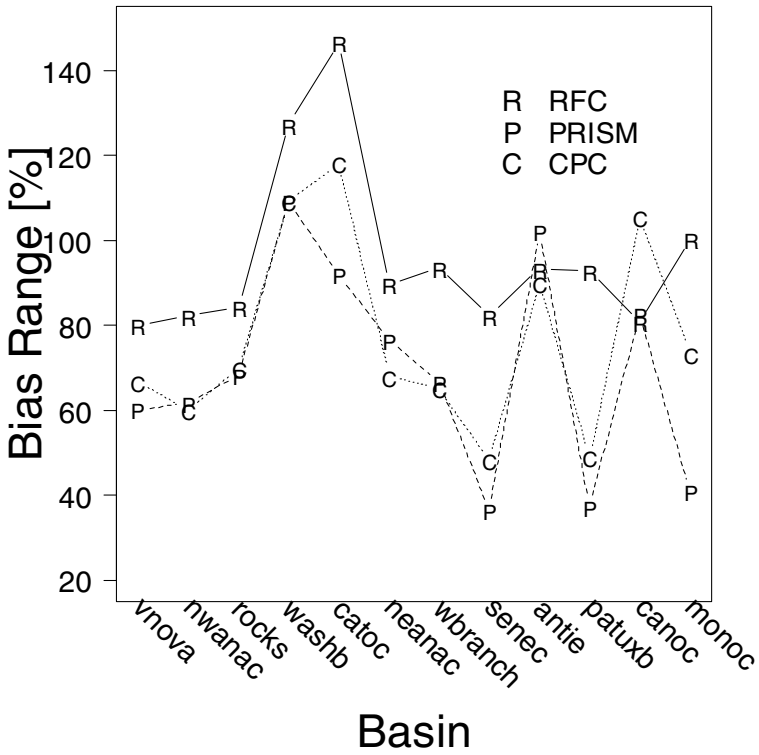

Figure 5: Interannual range of PB for each basin between 1998 and 2006.

Estimating Probability of Extreme Events

By
Jeff Harris[1], Gary Brunner[2], D. Michael Gee, Ph.D.[3]

[1]Chief, H&H Technology Division, Hydrologic Engineering Center, US Army Corps of Engineers, 609 2nd Street, Davis, CA 95616; PH (530) 756-1104; FAX (530) 756-8250; email: david.j.harris@usace.army.mil

[2] Senior Technical Hydraulic Engineer, H&H Technology Division, Hydrologic Engineering Center, U.S. Army Corps of Engineers, Davis, California; email: gary.w.brunner@usace.army.mil

[3] Hydraulic Engineer, H&H Technology Division, Hydrologic Engineering Center, U.S. Army Corps of Engineers, Davis, California; email: micheal.gee@usace.army.mil

Abstract

The Corps of Engineers is currently evaluating its portfolio of dams with regard to risk and related maintenance. A draft Engineer Technical Letter "Risk Analysis and Assessment for Dam Safety" is under review. This ETL describes processes that will be used for screening projects for planning of corrective actions. One of the contributing factors that must be uniformly evaluated across all projects is the development of inflow frequency curves (peak flow and volume frequency) that define the frequency curve in the mid-range events (1 in 500 to 1 in 3000) and then extend out to the probable maximum flood level. Currently, no extension method is uniformly accepted. Multiple methods exist to facilitate extension. The current effort being undertaken by the Hydrologic Engineering Center is to present the variety of methods and provide general guidance for curve extension that can be applied. A consistent method of curve extension allows for a uniform comparison of dams. This paper will provide an overview of the current status of the extension methodology.

Introduction

Currently there is no credible scientific approach to assign a single probability to a flood of the magnitude of the PMF. Additionally, no single method exists for extending gaged frequency curves out to the PMF level. Development of credible estimates of infrequent annual exceedance probabilities will rely on the use of data from multiple sources and a regional approach. The USBR has evaluated the limits of credible extrapolation that can be made from various data sources as shown below (USBR, 2004).

Type of data used for flood frequency analysis	Limit of credible extrapolation for annual exceedance probability	
	Typical	Optimal
At-site streamflow data	1 in 100	1 in 200
Regional streamflow data	1 in 500	1 in 1,000
At-site streamflow and at-site paleoflood data	1 in 4,000	1 in 10,000
Regional precipitation data	1 in 2,000	1 in 10,000
Regional streamflow and regional paleoflood data	1 in 15,000	1 in 40,000
Combinations of regional data sets and extrapolation	1 in 40,000	1 in 100,000

Clearly, none of these methods will produce a single estimate of the annual exceedance probability for rare events of the magnitude of the PMF.

Proposed Techniques

Several techniques have been used recently to assign an exceedance value to rare floods in the range of the PMF. Each of these methodologies are generally used in conjunction with gaged frequency analysis as a way of extending the gaged frequency curves out to events more rare than gaged data analysis would normally warrant. The following is a list of methods that have been selected for evaluation for inclusion in the Portfolio Risk Assessment for Corps dams:

1. Extension of Gaged Frequency Curves with Historic/Paleoflood information
2. Hydrologic Modeling using frequency based storm events
3. The GRADEX Method
4. Stochastic Event Flood Model (SEFM)
5. Regional Probability of the PMF

The following is a short description of each of the techniques:

Extension of Gaged Frequency Curves with Regional Historic/Paleoflood Information

This methodology is used to extend gaged frequency curves to a flood magnitude of the PMF. Historic floods and a range of possible probabilities can be estimated from both regional studies and paleoflood studies. The flood estimates and their probability ranges are plotted, and the gaged frequency curve could be extended out to the PMF by graphically fitting the curve to the mean estimates of the regional historic and paleoflood data.

Hydrologic Modeling Using Frequency Based Storm Events

Hydrologic rainfall runoff models (e.g. HEC-HMS) can be used to develop frequency curves or extend gaged frequency curves. Generally, at projects such as Corps dams, gaged inflow records of reasonable length are available for performing statistical frequency analysis using Log Pearson III techniques. The hydrologic model can be calibrated to historic storm events and the gaged frequency curve for the frequency range in which the gaged data are deemed most appropriate. The curve can then be extended by running storm events for frequencies outside the gaged data range (i.e. 100-, 200-, 500- and 1000-yr events).

Frequency based precipitation data can be obtained from the National Weather Service. Currently, for many states, the NWS has frequency based storm estimates out to the 1000- yr return period (NOAA Atlas 14). For those states that are not covered by NOAA Atlas 14, frequency precipitation estimates are only available up to the 100 yr event from NOAA. For more rare precipitation events, the user would need to look for local studies that have been performed on regional precipitation data within the region of interest, or a regional precipitation-frequency study would need to be performed.

In areas where gaged data are very limited (i.e. less than 20 years of record), then the use of a hydrologic model with regionally based precipitation estimates (NWS, Precipitation Frequency Data) is a viable method for developing frequency curves out to the 1000-yr event range. A general procedure is to develop the hydrologic model by estimating parameters based on physical information; calibrate the model to any significant events that are available in the short gaged record history; then apply frequency based rainfall events from the 2- to 1000-yr frequency to the model. The model parameters should be adjusted to get best estimates of peak flows and runoff volumes, but not to produce estimates that would be upper bounds.

The more typical case in the Corps of engineers is to utilize hydrologic models for extending gaged frequency curves out to the 1000-yr event. When a gaged frequency curve exists, and there is generally high confidence in that curve for the more frequent events, then a hydrologic model can still be developed as described in the previous paragraph. However, after the model is calibrated to all of the relevant historical events, and the frequency based rainfall events are applied, the model should be further calibrated to match the gaged frequency curve over the range of frequencies in which the gaged data are assumed to be the most appropriate.

GRADEX

The GRADEX technique is a method for extending volume frequency curves from the 200 to 500 yr range out to values in the range of the PMF. The methodology was first introduced by Guillot and Duband (1967, 1993), and later refined by Mauro Da Chunha Naghettini (1994) for his Ph.D. degree at the University of Colorado. In simple terms, the GRADEX methodology is based on computing a slope (Grade X) of the regional

precipitation frequency data, then applying that same slope to the runoff volume frequency curve for extending it out into the future. The basic concept is that the runoff volume frequency curve should be parallel to the rainfall volume frequency curve once you get up to the rare events in the 200 to 500 year range and larger. This assumes that during large events, the ground is saturated, and runoff properties are reaching an upper limit, such that any increased volume of precipitation will produce a corresponding increase in flood runoff volume. Figure 1 is a plot depicting the GRADEX technique. This plot was take from the USBR report "Hydrologic Hazard Curve Estimating Procedures (June, 2004).

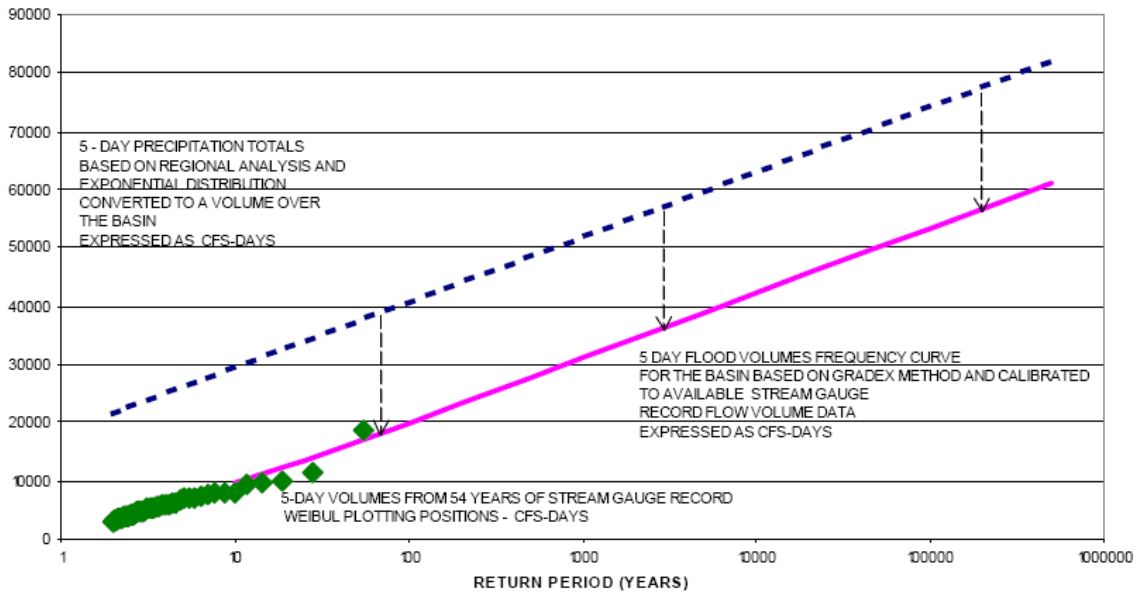

Figure 1. GRADEX Method of Volume Frequency Curve Calculation.

The user must gather daily precipitation records for all of the relevant gages in the region of interest. Records must be gathered for the full period of record of the gages, and the gaged record must be continuous. The user is required to first estimate a critical duration for the watershed above the dam (i.e. 1day, 2day, 3day, etc…). The critical duration is a function of the size of the watershed, the meteorology, runoff characteristics, and available flood storage volume of the reservoir. Each gaged record is analyzed individually and the top annual events for the critical duration are defined. The threshold precipitation value, statistics, and the top 10 percent of the events are then used as input data into the GRADEX computer program. Additional input required for the GRADEX program is mean annual precipitation for each gage, elevation of the gage, drainage area of the basin, critical runoff duration, mean basin elevation, mean annual precipitation for the watershed, and statistics about the flow duration frequency curve computed for the observed runoff data (Qmean, Qref, return period of the reference flow). The GRADEX computer program will then compute a slope for the regional precipitation and apply that to the volume frequency data provided. The output is a volume–duration frequency curve

that starts at the reference flow and reference return period entered (ex. 100 yr), and goes out to the 1,000,000 year return period.

Stochastic Modeling of Extreme Floods (SEFM Model)

SEFM is a stochastic event model that is generally used to extend a frequency curve out to the 200 to 500 year return interval range. However, one could also use it as a way to make an estimate all the way to a PMF level event.

The concept employed with this technique is the simulation of several thousands of years of annual flood maxima. This is accomplished using a deterministic, single event, flood runoff model. Hydro meteorological parameters are treated as variable. Monte Carlo sampling procedures are used to allow climatic and storm descriptive parameters to vary in accordance with season and historical observations. The simulation of any annual flood contains a set of climatic and storm parameters selected via the Monte Carlo technique that collectively preserve any dependencies between the parameters that are contained in the historical record.

The hydro meteorological inputs and their dependencies represent the detailed mechanics of flood generation. The table below, prepared for an SEFM application to Folsom Dam in California, indicates the complexity of the system parameters that are recognized by this method.

HYDROMETEOROLOGICAL INPUTS FOR STOCHASTIC MODEL			
MODEL INPUT		DEPENDENCIES	COMMENTS
1	Seasonality of Storm Occurrence	Independent	End-of-month storm occurrences
2	72-Hour Storm Magnitude	Independent	
3	Temporal and Spatial Distribution of Storms	Independent	24 Prototype Storms, 4-Day to 8-Day Patterns
4	Temperature Temporal Pattern	Varies by Prototype Storm	10-Day Pattern Indexed to Sea-Level Temperature and Freezing Level
5	Sea-Level Temperature	Storm Magnitude	For Day of Maximum Precipitation in storm
6	Freezing-Level	Sea-Level Temperature and Storm Magnitude	For Day of Maximum Precipitation in storm
7	Antecedent Precipitation	Independent	Precipitation Oct 1st to Date of Storm Occurrence Varies with Zones of Mean Annual Precipitation
8	Antecedent Snowpack	Antecedent Precipitation	Varies by Zones of Mean Annual Precipitation and Elevation
9	Antecedent Soil Moisture	Antecedent Precipitation Antecedent Snowpack	Varies by Zones of Mean Annual Precipitation, Elevation and Soil Type
10	Storage in Upstream Reservoirs	Antecedent Precipitation	Preserves Cross-Correlation of Storage in 5 Upstream Reservoirs
11	Initial Streamflow	Independent	Mean Monthly Inflow to Folsom Reservoir
12	Storage in Folsom Lake	Antecedent Precipitation	Utilizes Folsom Rule Curves and Storage in 5 Upstream Reservoirs

.

A summary of the steps that are performed by the simulation model are:

1. Select date (end-of-month) of occurrence of extreme storm.
2. Select all parameters associated with the occurrence of the extreme storm event.

3. Establish antecedent watershed and reservoir conditions at the onset of the extreme storm.
4. Conduct watershed modeling
5. Conduct reservoir routing of inflow flood.

On application of this procedure, various measures of project inflow can be assigned recurrence intervals. Figure 2 shows the SEFM computed relationship for Peak inflow discharge stochastically extended to an annual exceedance probability of 10^{-6}.

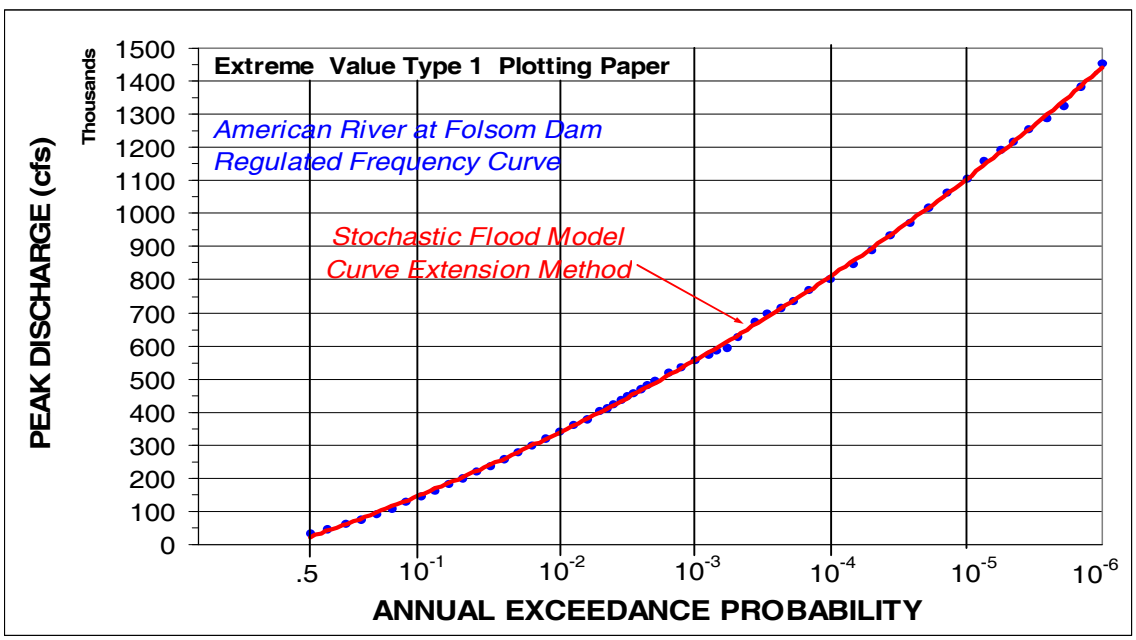

Figure 2. SEFM Model Results Extended to Probability of 10^{-6}

Regionalized Probability of PMF

The regional probability method is a way of estimating a probability of the PMF using regional precipitation data. The method outlined below is based on scaling the probability of the PMF by comparing regional historical precipitation data to that of the PMP, computing a historical to PMP precipitation ratio, then using that ratio to estimate a probability of the PMF within the established institutional range of probabilities. By utilizing regional precipitation data, this procedure would inherently include the effects of regional weather patterns, distance from moisture sources, orographic effects, etc. The method is easy to apply and would be a consistent procedure. In regions where historical precipitation has come close to the PMP, the method would yield a probability towards the more frequent end of the range. Likewise, in areas where historical precipitation is much lower than estimates of the PMP, the probability of the PMF would tend towards the less frequent end of the range.

The steps are:

1. An institutionally assigned range of probabilities for the PMF must be decided upon. A possible suggestion for the range is 10^{-3} to 10^{-7}.

2. Determine the storm duration that is most critical to the watershed of interest (24-hr, 48-hr, or 72-hr). Also determine the storm area size critical to the watershed. This should be the same storm area size that was used in the determination of the basin average PMP for developing the PMF for the watershed.

3. Determine the historically maximum observed precipitation volume that has occurred within the region of interest, for the storm area size and duration of interest. The region of interest would most likely extend into neighboring basins of similar hydrologic and meteorological characteristics. The idea is to find the largest storm that has occurred within the region, not limiting specifically to the basin of interest. One way to compute the maximum observed historical precipitation volume is to acquire maximum observed precipitation at all gages in the region of interest for the largest storms of record. Compute the area averaged (based on the selected storm area in step 2) maximum storm volume for the duration of interest (24, 48, or 72 hr). Other methods for obtaining maximum historical rainfall may be more appropriate depending on the area of the country you are in (such as using radar rainfall data, etc…).

4. Use standard NWS procedures for computing your basin average PMP (HMR reports).

5. Compute the maximum historical precipitation to PMP ratio within the region of interest for the Dam being studied.

6. Calculate the probability of the PMF using the following equation:

$$AEP = 10^{-[(1-Ratio)\times Range + Min.Value]}$$

Where:

Ratio =	Max historic storm precipitation divided by PMP for region of interest.
Range =	Corps institutional range for probability of the PMF (10^{-3} to 10^{-7})
Min Val =	Minimum value of Corps institutional range.

This equation will yield values close to 10^{-3} for areas that have experienced precipitation close to PMP values. Likewise, those areas that the historic precipitation is very low in comparison to the computed PMP values would have a PMF probability near the 10^{-7} value.

Method Blending

When multiple methods are applied it will be necessary to perform a graphical fit of all of the methods. This should be done by weighting the values of each of the methods for

each of the frequencies used to define the final curve. In other words, at higher frequencies, such as the 2 through 100 yr events, the gaged points and resulting LP III curve would be given a very high weight and the other methods would be given either low weights or zero. As you go out to less frequent probabilities, the weighting will change between the methods based on the perceived reliability of the estimates at that specific frequency. Obviously, this will require engineering judgment on the part of the team performing the study. An example plot of what this might look like is shown below in Figure 3. The newly developed Statistical Software Package, HEC-SSP, will have methods added to it to help facilitate the blending of the curves. It will take into account uncertainty data from each of the curves, or values, to generate the blended curve.

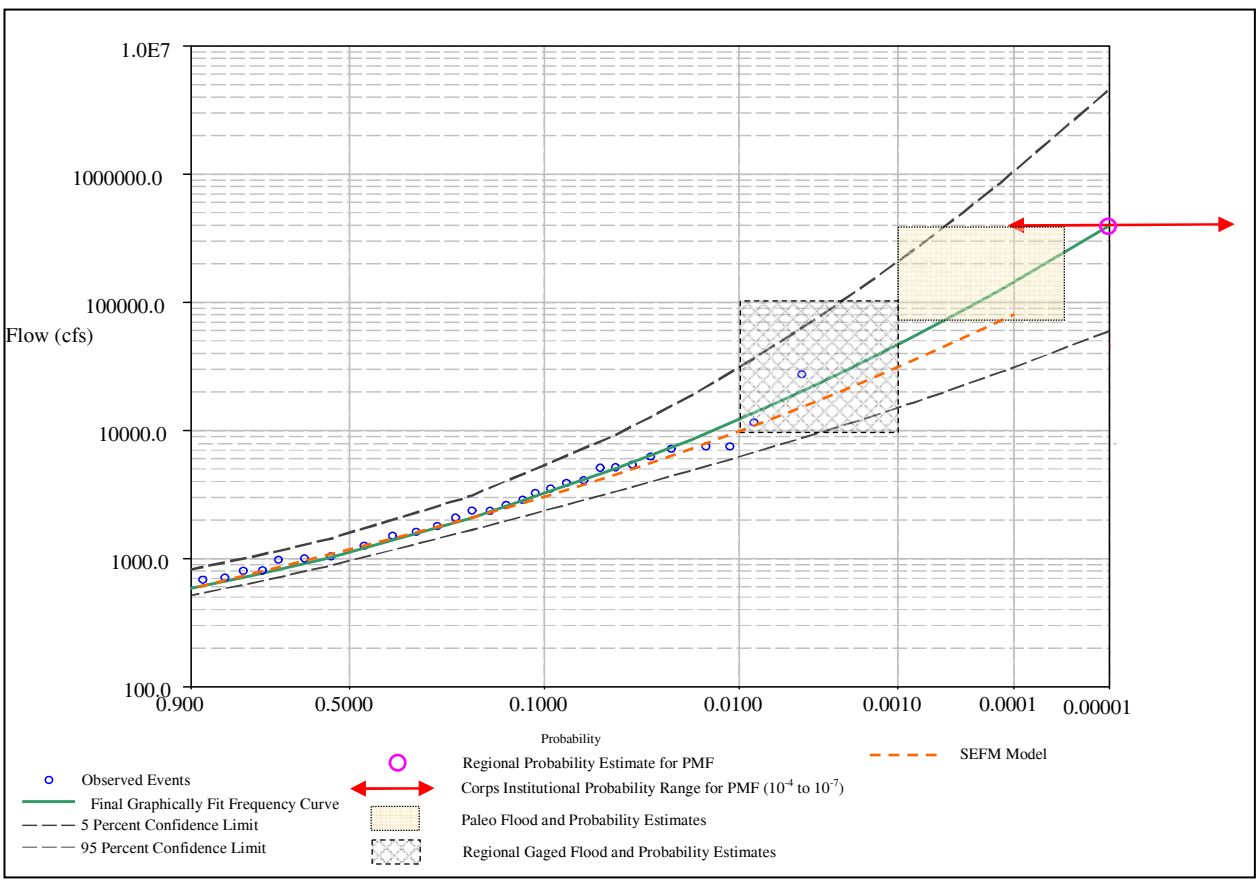

Figure 3. Example Flow Frequency Curve by Combined Methods

Conclusion

All the methods listed above have inherent shortcomings. There may be a very short gaged record, paleo flood is generally applicable in the western US, hydrologic models are usually based on the premise that the frequency of the runoff equals the frequency of the rainfall, GRADEX involves extrapolation, SEFM can be data and cost prohibitive and the regional PMF range requires an institutionally agreed upon range. All of these are challenges. Based on this, HEC's proposal is that no single method should be used for extending frequency curves out to the magnitude of the PMF. Rather, all of the methods described above, or appropriate combinations of the methods, should be used to extend

the gaged data frequency curve out to the PMF. This will require plotting results from all of the methods used, then extending the gaged frequency curve out to the PMF graphically.

If a dam is classified as a high hazard dam (i.e. large damage potential downstream and possible loss of life), then most likely all of the methods should be used together to make an estimate of the inflow frequency curve. However, if a dam is not classified as a high hazard dam, then maybe the appropriate combination of the methods could be used. At a minimum, the frequency curve could be developed by using the gaged data, hydrologic modeling with regional precipitation data, and the regional method for estimating the probability of the PMF. This level of analysis would probably be appropriate for the initial PRA studies. More detailed analysis could include the SEFM modeling method and/or the GRADEX method when deemed appropriate, and financially viable. Paleoflood estimates should only be used in areas where they are considered to be viable (such as in the western states).

References:

Gulliot, P. and D. Duband. 1967. La methode du GRADEX pour le calcul de la probabilite des crues a partir des pluies. In "Floods and their computation – proceedings of the Leningrad symposium". IASH Publication, 84, 560-569.

Gulliot, P. 1993. The arguments of the GRADEX method: a logical support to assess extreme floods. In "Extreme Hydrologic Events: Precipitation, floods, and droughts proceedings of Yokohama Symposium" I.A.S.H. Publication 213, 287-298.

HEC, "Hydrologic Research Needs for Dam Safety," SP-29, (http://www.hec.usace.army.mil/publications/SeminarProceedings/SP-29.pdf), Nov. 2001.

HEC, "Stochastic Modeling of Extreme Floods on the American River at Folsom Dam – Flood-Frequency Curve Extension," RD-48, Sept. 2005.

Naghettini, M.D.C. 1994. Methodology for Estimating the Upper Tail of Flood-Peak Frequency Distributions using Hydrometeorological Information. Ph.D. Dissertation at the University of Colorado, Department of Civil, Environmental, and Architectural Engineering.

USBR, "Hydrologic Hazard Curve Estimating Procedures," Research Report DSO-04-08, June 2004.

Prediction of Changes in Soil Moisture Due to Rainfall, Infiltration, and Evapotranspiration Using a Physically-Based Model

Zhiguo He[1], Weiming Wu[2], and Sam S.Y. Wang[3]

[1] Post-doctoral Research Associate, National Center for Computational Hydroscience and Engineering, University of Mississippi, University, MS 38677; PH: (662) 915-6559; email: zhe@olemiss.edu
[2] Research Associate Professor, National Center for Computational Hydroscience and Engineering, University of Mississippi, University, MS 38677; PH: (662) 915-6561; email: wuwm@ncche.olemiss.edu
[3] F.A.P. Barnard Distinguished Professor and Director, National Center for Computational Hydroscience and Engineering, University of Mississippi, University, MS 38677; PH: (662) 915-7788; email: wang@ncche.olemiss.edu

ABSTRACT

Soil water content changes with time due to rainfall, infiltration, evaporation, and transpiration. This paper presents a physically-based coupled surface and variably saturated subsurface flow model to simulate the distribution of soil moisture in three dimensions. The flow in variably saturated soil is described by the 3D Richards equation in the mixed form, which is discretized using the finite volume method and solved implicitly using the modified Picard iteration. In the present model, the actual evaporation from bare soil is calculated using the physically-based relationship of VS2D method, which takes into account both constant and falling rate stages. The actual transpiration by plants is modeled using the root water uptake module with water stress compensation, which considers soil water pressure head and soil resistance to water flow. The model has been tested using published data.

INTRODUCTION

Temporal and spatial variations of soil moisture are receiving increased attention in climate studies because soil moisture is an essential element in processes that drive land surface water and energy fluxes, which affect ecosystem dynamics and biogeochemical cycles in the land-atmosphere system. To predict the hydrological processes at a watershed scale, especially in a long-term simulation, a hydrologic watershed model should be able to simulate rainfall-runoff, infiltration, evaporation, and transpiration.

Evaporation is the process whereby liquid water is converted to water vapor (vaporization) and removed from the evaporating surface (vapor removal). Theoretical consideration and laboratory and field observations have shown that evaporation following wetting is a variable process (Hillel, 1980; Jalota and Prihar,

1998) and it depends on both climatological parameters, such as solar radiation, air temperature, humidity, and wind speed (Ritchie, 1972; Parlange and Katul, 1992), and soil properties (Ritchie, 1972; Hillel, 1980; Wallace et al., 1999). Many equations exist in the literature to describe the evaporation rate (Lappala et al., 1987; Brisson et al., 1998; Wallace et al., 1999; Allen et al., 2005; Romano and Giudici, 2007). In numerical modeling, evaporation is often considered as an upper boundary condition in the flow equation.

Transpiration consists of the vaporization of liquid water contained in plant tissues and the vapor removal to the atmosphere. Transpiration depends on climatological parameters and soil properties, as well as the ability of the soil to conduct water to the roots. Numerical models simulating changes in soil water content with time rely on accurate estimation of transpiration due to root water uptake. Two approaches – microscopic and macroscopic – have been developed to simulate water uptake by plant roots.

The microscopic approach (Gardner, 1964) simulates the radial flow movement of soil water toward and into individual roots (e.g. Doussan et al., 1998; Personne et al., 2003). This approach is physically based, which requires the detailed geometry of the growing root system. Since those information are difficult and time-consuming to measure (Vrugt et al., 2001), this type of model is currently not practical in a watershed scale simulation.

The macroscopic approach treats the root system as an abstract object whose vertical distribution is described throughout the soil profile (Feddes et al., 1978; Molz, 1981; Li et al., 2001; etc.). The macroscopic water extraction is represented by a depth-dependent sink term that can be incorporated into the Richards soil water flow equation, which has been greatly used in many application-oriented hydrological models (e.g. Braud et al., 2005; Li et al., 2001 and 2006). Based on the concept of Feddes et al. (1978), macroscopic root-water-uptake modules are different in the way that the potential transpiration is distributed and/or potential transpiration is reduced by water stress. The distribution of potential transpiration has been based either on root distribution only (e.g., Feddes et al., 1978; Simunek et al., 1998; Li et al., 1999) or on both root distribution and soil water availability (Li et al., 2001). Various linear (e.g. Hoogland et al., 1981; Prasad, 1988) and nonlinear (e.g. Jarvis, 1989; Li et al., 2001) root distribution functions have been used in the root-water-uptake models.

Recent research shows that the macroscopic models can achieve a good compromise between physical realism, data requirement and facility of implementation for the solution of the Richards equation (Varado et al., 2006). Braud et al., (2005) and Varado et al. (2006) compared two root water uptake models with compensation mechanisms, proposed by Lai and Katul (2000) and Li et al. (2001), against the existing data set of various soil types. Li et al.'s module was recommended for inclusion as a physically-based infiltration-evapotranspiration module into a larger scale hydrological model due to its robustness (Braud et al., 2005; Varado et al., 2006).

He et al. (2008) developed an integrated surface-subsurface flow model. However, evapotranspiration was not taken into account since only single storm events were simulated. In the present study, for the purpose of long-term simulation, a module of simulating evapotranspiration has been implemented in the variably

saturated 3D subsurface flow model of He et al. The module has been verified by reproducing the results of problems involving a 1D infiltration and transpiration in layered soils and a 2D response to rainfall, evaporation and transpiration.

GOVERNING EQUATIONS

The water flow in variably saturated soil zone can be described by the Richards equation. Evaporation and plant transpiration are considered using sink functions. For 3D variably saturated soil, the mixed form of Richard equation can be written as

$$\Theta s_s \frac{\partial H}{\partial t} + \frac{\partial \theta}{\partial t} = \frac{\partial}{\partial x_i}\left[K_{x_i}(\psi)\frac{\partial H}{\partial x_i}\right] - Q_b^T - Q_b^E + Q_b^s \qquad (1)$$

where θ is the volumetric soil water content; Θ is the saturation of the soil; S_s is the specific storage; H is the total head for subsurface flow, which is equal to the sum of the soil water pressure head ψ and the elevation head z; K_x, K_y, and K_z are the hydraulic properties for unsaturated/saturated soil, usually defined as the product of the saturated hydraulic conductivity k_s and the relative permeability k_r, i.e., $K_i(\psi) = k_{si}k_{ri}(\psi)$ ($i = x, y, z$); Q_b^T and Q_b^E represent the actual transpiration and evaporation sinks, and Q_b^s represents other volumetric source and/or sink fluxes. The above parabolic equation is highly nonlinear, due to the nature of the hydraulic properties of soil layer $K_i(\psi)$ and soil water content $\theta(\psi)$, and can be applied for both saturated and unsaturated soil water flows. Here, the relationships suggested by van Genuchten (1980) or Brooks and Corey (1964) are used to describe the relative saturation and permeability functions.

In the present model, the net inflow of precipitation, infiltration, and evaporation is applied as a boundary condition at the ground surface, and Q_b^T is calculated as a point sink term distributed vertically over cells in the root zone. The treatment of rainfall and infiltration follows the way described in He et al. (2008), and only evaporation and transpiration are discussed herein.

Potential Evapotranspiration. Potential evapotranspiration (*PET*) is often used to determine the evaporation and transpiration rates. Generally, two different options can be used to calculate *PET*. The first option is the pan evaporation technique, which requires daily measured pan evaporation values and pan coefficients (Fares, 1996). The second method for calculating *PET* is based physically on the energy conservation method. There are a number of equations to calculate *PET*, such as Penman (1948), Monteith (1965), Priestley and Taylor (1972), and FAO Penman-Monteith equation (FAO, 1998). In most cases, *PET* is often calculated as an input reference at first, and then it is separated into potential evaporation (E_P) and potential transpiration (T_P). The partition can be performed using the Beer-Lambert law based on the leaf area index *LAI* (Huygen et al., 1971). In the present model, the FAO Penman-Monteith equation (FAO, 1998) is implemented to calculate *PET*.

Evaporation. Evaporation is a variable process, which depends on the atmospheric conditions and soil properties. A two-stage evaporation process is considered in this study. At first, evaporation is at a constant rate as long as the soil can conduct water to the soil surface at a rate equal to E_P. As the soil near the surface becomes drier, evaporation is reduced to below the potential value, which is mainly determined by the hydraulic properties of the soil and could be controlled both by atmosphere and/or by soil water content.

E_P can be calculated as a fraction of *PET* using the *LAI* of the soil surface as

$$E_P = \psi(LAI) \cdot PET \tag{2}$$

$$\psi(LAI) = \exp(-f_{sr} LAI) \tag{3}$$

where $\psi(LAI)$ is a function of the leaf area index *LAI*, and f_{sr} is the extinction coefficient for solar radiation (dimensionless). The value of f_{sr} varies from 0.4 to 0.5. Here, a physically based relationship used in the VS2D model (Lappala et al., 1987) is applied to predict the actual evaporation as

$$Q_b^E = Min\{k_{sz} k_{rz} SRES(h_{atm} - h_{top}), E_P\} \tag{4}$$

where h_{atm} is the pressure potential of the atmosphere; h_{top} is the pressure head at the first node on the land surface; and *SRES* is the surface resistance.

The atmospheric pressure potential can be determined as (Lappala et al., 1987)

$$h_{atm} = (RT / M_w g) \ln(h_r) \tag{5}$$

where R is the ideal gas constant; T is the absolute temperature; M_w is the mass of water per molecular weight; h_r is the relative humidity; and g is the gravitational acceleration.

Assuming that the pressure at the land surface is atmospheric and the pressure at the top cell is applied to the node of the first cell, *SRES* is calculated as

$$SRES = (2.0 / DZ_{top}) / (K_c / k_{sz,top}) \tag{6}$$

where DZ_{top} is the thickness of the top cell; K_c is the saturated hydraulic conductivity of the land surface material; and $k_{sz,top}$ is the saturated hydraulic conductivity of the first cell on the land surface.

Transpiration. The present study applies the macroscopic approach of the root water uptake concept to predict the actual transpiration rate, which considers the integrated properties of the entire root system. The actual amount of water taken up by a root system can be calculated using the following general relation:

$$Q_b^T = \beta_T T_P \tag{7}$$

where T_P is the potential transpiration rate, and β_T is the dimensionless empirical function depending, for example, upon the distribution of roots with depth, the type of plant, the availability of liquid water, and the minimum permissible pressure head. T_P is part of the *PET* and can be calculated as

$$T_P = PET - E_P = [1 - \psi(LAI)] \cdot PET \tag{8}$$

β_T can be expressed as

$$\beta_T = \alpha \cdot g(z) \tag{9}$$

where α is a water response function accounting for restriction to transpiration caused by soil moisture limitations, and $g(z)$ is a root density distribution function.

The present model implements four different water uptake models based on the different water response function and root density distribution function, which are the constant model (Feddes et al., 1978), linear model (Prasad, 1988), exponential model (Li et al., 1999), and exponential model with the water stress compensation (Li et al., 2001).

The constant model determines the root density distribution function as (Feddes et al., 1978)

$$g(z) = 1/z_r \tag{10}$$

where z_r is the bottom of the root zone depth. The water stress response function α ($0 \le \alpha \le 1$) is a prescribed dimensionless function of the soil water pressure head around the root zone, first introduced by Feddes et al. (1978). α can be calculated using the following expression of $\alpha_1(h)$:

$$\alpha_1(h) = \begin{cases} 0 & h \ge h_1 \text{ or } h \le h_4 \\ (h_1 - h)/(h_1 - h_2) & h_2 < h < h_1 \end{cases} \text{and} \begin{cases} 1 & h_3 \le h \le h_2 \\ (h - h_4)/(h_3 - h_4) & h_4 < h < h_3 \end{cases} \tag{11}$$

In Eq. (11), the water uptake function is set to zero if the soil water pressure is greater than h_1 (oxygen deficiency) or less than h_4 (the wilting point). If the soil water pressure is between h_2 and h_3, the water uptake function reaches its maximum value. The value of h_3 varies with the potential transpiration rate T_P (T_P=5 mm/day or 1 mm/day) (see Feddes et al., 1978).

The linear model expresses the root density distribution function as (Prasad, 1988)

$$g(z) = (2/z_r)(1 - z/z_r) \tag{12}$$

where z is the current depth and z_r is the bottom of the root zone depth. The water stress response function α is calculated using $\alpha_1(h)$.

The exponential model expresses the root density distribution function as (Li et al., 1999)

$$g(z) = g_0 \frac{\exp(-bz)\left[1.5 + 0.5\exp(-bz)\right]}{1 + \exp(-bz)} \tag{13}$$

$$b = 24.66 F_{10}^{1.59} / z_r \tag{14}$$

where F_{10} is the fraction of the root length density in the top 10% of the root zone and g_0 is the root density at the soil surface. The water stress response function α is calculated using $\alpha_1(h)$.

In the exponential model considering the water stress compensation, the root density distribution function is determined using Eqs. (13) and (14) of the exponential model (Li et al., 1999). The water stress response function α uses the following expression to consider the water stress compensation mechanism (Li et al., 2001):

$$\alpha = \alpha_1(h) \cdot \alpha_2(\theta, z) \tag{15}$$

$$\alpha_2(\theta, z) = \frac{\alpha_1(h) G(z)^{\lambda - 1}}{\sum_{z=0}^{z_r} \alpha_1(h) G(z)^{\lambda}} \tag{16}$$

where λ is the empirical parameter and $G(z)$ is the fraction of the total root length in a layer of thickness Δz at depth z.

The method used in VS2D (Lappala et al., 1987) is also implemented in the present model as an option to calculate the actual transpiration. This method is relatively easy to use and the expressions are not repeated here.

NUMERICAL SOLUTION

The 3D mixed form of the modified Richards equation is discretized using the finite volume method in space and an implicit scheme in time. To handle the nonlinearity of the system, the Picard procedure with under-relaxation is used to linearize the surface and subsurface flow equations. The subsurface flow model uses a rectangular hexahedral mesh (see He et al., 2008). The time derivative term for the volumetric soil water content in Eq. (1) is discretized using the Taylor series expansion presented by Celia et al. (1990). The diffusion terms are discretized by a central scheme, and the time derivative terms are discretized by the first-order backward implicit scheme. The discretized equations are solved by the Strongly Implicit Procedure (SIP) of Stone (1968). Accurate numerical solution and mass balance are reached when the convergence criteria of both the Picard iteration and SIP solution loops are satisfied at each time step. There are numerous methods suggested in the literature for computing the intercell average of the relative permeabilities between grid cells in the discretized equation (Desbarats, 1995; Dogan and Moltz, 2005; etc.). In general, the mean hydraulic conductivity between grid cells can be estimated using the distance-weighted arithmetic mean for unsaturated zone and the weighted harmonic mean for saturated zone, if the relatively fine space-time meshes used.

MODEL TESTING

1D Water Flow in a Field Soil Profile under Grass. This example uses the data set of 1D water flow in a field profile of the Hupselse Beek watershed in the Netherlands, obtained from the research report of SWMS3D (Simunek et al., 1995). The soil profile consisted of two layers, as shown in Figure 1. The soil layers A and B were 40 and 190 cm thick, respectively. The depth of the root zone was 30 cm. The hydraulic properties of the two soil layers were represented by the van Genuchten functions (1980). The saturated hydraulic conductivities k_s were 29.75 cm/day and 45.34 cm/day; the saturated moisture content values θ_s were 0.399 and 0.339; the residual moisture content values θ_r were 0.001 and 0.001; and the van Genuchten (1980) parameters (α, n) were (0.0174 cm, 1.3757) and (0.0139 cm, 1.6024) for layers A and B, respectively. The model simulates the period of April 1 to September 30 of the relatively dry year 1982. The soil surface boundary conditions involved actual precipitation and potential transpiration rates for a grass cover, as shown in Figure 2. The bottom condition consisted of a prescribed drainage flux (Simunek et al., 1995). The initial groundwater level was set at 55 cm below the soil surface and the initial moisture profile was taken to be in equilibrium with the ground water level. Figures 3 and 4 give the simulated cumulative actual transpiration and bottom discharge

amounts as obtained with the present model and SWMS3D, respectively. Figure 5 shows the simulated groundwater table with time. As can be seen from the figures, the results obtained with the present model agree well with those calculated with SWMS3D.

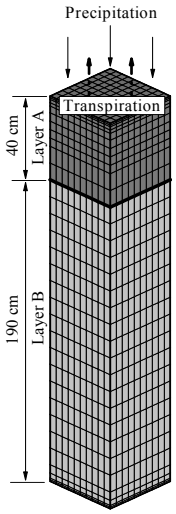

Figure 1. Sketch of 1D Example

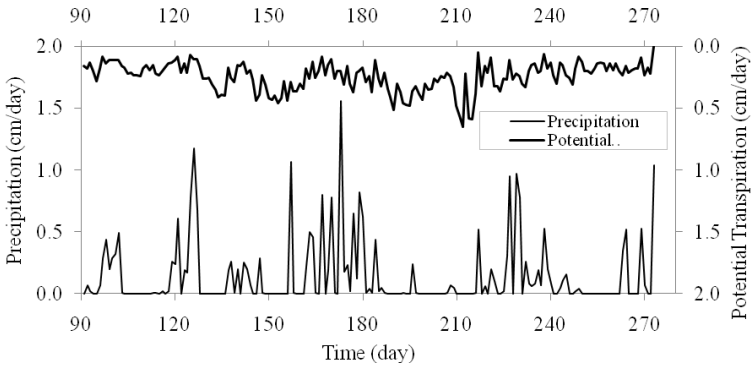

Figure 2. Actual precipitation and potential transpiration rate for Ex. 1

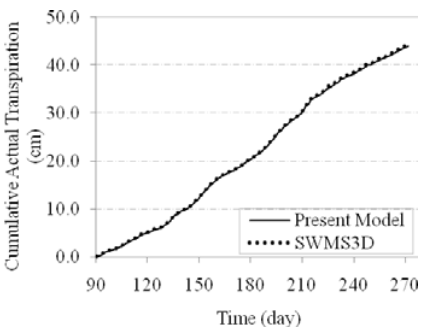

Figure 3. Cumulative values for actual transpiration

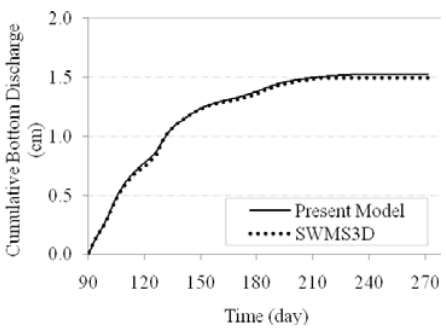

Figure 4. Cumulative values for bottom discharge

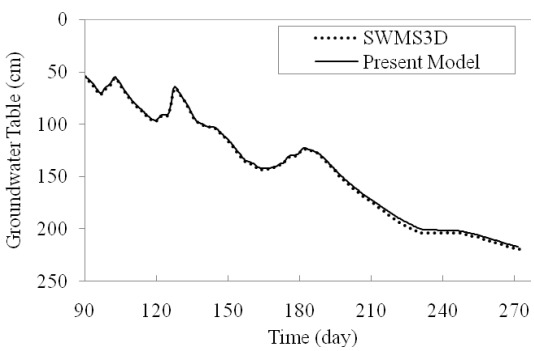

Figure 5. Simulated groundwater table versus time

2D Problem Involving Rainfall, Infiltration, and Evapotranspiration. The present model is used to simulate a relatively complex 2D problem involving rainfall, infiltration, evaporation, and transpiration obtained from the technical report of VS2D model (Lappala et al., 1987). The computational domain consists of a clay layer with 1.5 m in depth and 3.0 m in width which overlies a 0.6 m thick gravel layer. A discontinuous sand layer with a thickness of 0.3 m and a length of 1.5 m is embedded in the clay at a depth of 0.4 m, as shown in Figure 6. Four recharge periods totaling 77 days were simulated. The first period was a 1 day rainfall event at a rate of 7.5 cm/day; the second period was a 30 days with a bare-soil potential evaporation of 0.2 cm/day; the third period was a 1 day rainfall event at a rate of 7.5 cm/day. The last period was a 45 days that consists of both evaporation and transpiration. The root depth was 35 cm. The user-defined variables that control evaporation and transpiration were assumed to remain constant throughout the simulation, with the exception of *PET*, root depth, and root pressure (Lappala et al., 1987). The other parameters used in the simulation can be found in Lappala et al. Initial conditions consist of an equilibrium head profile specified above a fixed water table at a depth of 2.0 m. The minimum pressure head is set at -1.00m. The hydraulic properties of the three different layers are represented by the Brook-Corey function. The saturated hydraulic conductivities were 5, 100, and 300 cm/day; the saturated moisture content values were 0.45, 0.40, and 0.42; the residual moisture content values were 0.15, 0.08, and 0.05; and the Brooks and Corey parameters (bubbling pressure head, pore-size distribution index) were (-50 cm, 0.6), (-15 cm, 1.0), and (-8 cm, 1.2) for the clay, sand, and gravel layers, respectively.

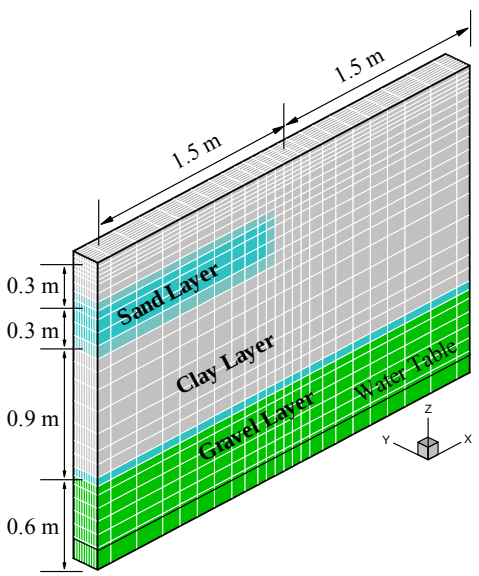

Figure 6. Computational domain of the 2D example

Figure 7 shows the pressure head versus time at four locations at the same depth of 0.33 m. The first two are in the sand lens and the last two are in the clay layer. The

results from the present model agree well with the pressure heads obtained from the VS2D model. There are some differences between the pressured heads in clay layer simulated by the two models, which may be due to the hydraulic properties of the clay soil. The present model solves the mixed form of the Richards equation, which is more mass conservative and more sensitive to the moisture content gradients, since a small moisture content change in the clay layer may require substantial pressure gradient.

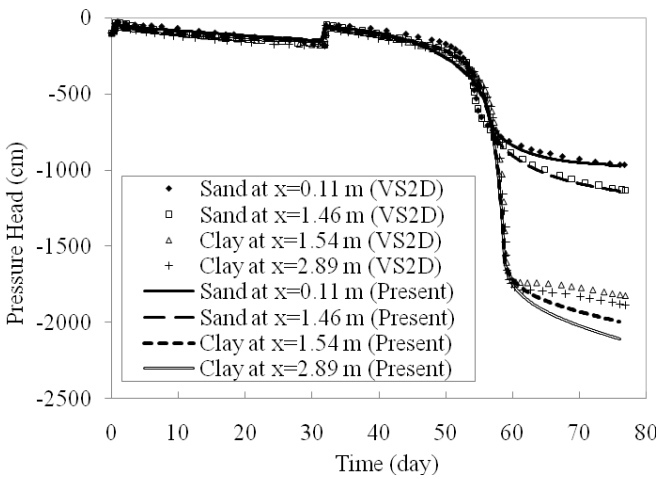

Figure 7. Simulated pressure head profiles at four locations for Ex. 2

CONCLUSION

This paper presents an evapotranspiration model that has been implemented into an integrated surface-subsurface flow model. The mixed form of the 3D Richards equation is discretized by the finite volume method and solved using the modified Picard iteration scheme based on Celia et al. (1990). Evaporation is applied as the upper boundary condition at the ground surface, while transpiration is calculated as a point sink term distributed vertically over cells in the root zone. The model has been tested against two sets of data in the literature and will be further verified and applied to field studies.

ACKNOWLEDGEMENT

This study is part of the research project sponsored by the USDA-ARS Specific Research Agreement No. 58-6408-7-236 (monitored by the USDA-ARS National Sedimentation Laboratory) and the University of Mississippi.

REFERENCES

Allen, R.G., Pruitt, W.O., Raes, D., Smith, M., and Pereira, L.S. (2005). "Estimating Evaporation from Bare Soil and the Crop Coefficient for the Initial Period Using Common Soils Information", *J. Irrigation and Drainage Engineering*, 131, 14–23.

Braud, I., Varado, N., and Olioso, A. (2005). "Comparison of root-water-uptake modules using either the surface energy balance or potential transpiration." *J. Hydrol.*, 301, 267–286.

Brisson, N., Itier, B., L'Hotel, J.C., and Lorendeau, J.Y. (1998). "Parameterisation of Shuttleworth–Wallace model to estimate daily maximum transpiration for use in crop models." *Ecol. Model*. 107, 159–169.

Brooks, R.H. and Corey, A.T. (1964). *Hydraulic Properties of Porous Media*, Colorado State University, Fort Collins.

Celia, M. A., Bouloutas, E. T., and Zarba, R. L. (1990). "A general mass-conservative numerical solution for the unsaturated flow equation." *Water Resour. Res.*, 26(7), 1483–1496.

Desbarats, A. J. (1995). "An interblock conductivity scheme for finite difference models of steady unsaturated flow in heterogeneous media." *Water Resour. Res.*, 31(11), 2883–2889.

Dogan, A., and Motz, L.H. (2005). "Saturated-unsaturated 3D (SU3D) groundwater model, I: Development." *J. Hydrologic Eng.*, 10(6), 492–504.

Doussan, C., Pagès, L., and Vercambre, G. (1998). Modelling the hydraulic architecture of root systems: An integrated approach to water absorption—Model description." *Ann. Bot. London*, 81, 213–223.

Fares, A. (1996). *Environmental impact of unharvested forest buffer zones upon cypress-pond system in coastal plains regions: modeling analyses*, PhD dissertation, Univ. of Florida, Gainesville, Fla.

FAO (1998). Crop evaporation—guidelines for computing crop water requirements. *Irrigation and Drainage Paper*, 56, Rome.

Feddes, R.A., Kowalik, P.J., Malinka, K.K., and Zaradny, H. (1978). *Simulation of Field Water Use and Crop Yield*, John Wiley and Sons, Pudoc, Wageningen, Netherlands, 189 pp.

Gardner, W.R. (1964). "Relation of root distribution to water uptake and availability." *Agron. J.*, 56, 41–45.

He, Z., Wu, W., and Wang, S. S. Y. (2008). "A coupled finite-volume model for 2D surface and 3D subsurface flows." *J. Hydrol. Eng.*, ASCE, 13(9): 835–845.

Hillel, D. (1980). *Applications of Soil Physics*, Academic Press, New York, London, p. 385.

Hoogland, J.C., Feddes, R.A., and Belmans, C.. (1981). "Root water uptake model depending on soil water pressure head and maximum extraction rate." *Acta Hortic.*, 119, 123–131.

Huygen, J., Van Dam, J.C., Kroess, J.G., and Wesseling, J.G. (1997). *SWAP 2.0: Input and Output Manual*, Wageningen Agricultural University DLO-Staring Centrum, Wageningen.

Jalota, S.K., and Prihar, S.S. (1998). *Reducing Soil–Water Evaporation with Tillage and Straw Mulching*, Iowa State University Press, Ames (ISBN 0-8138-2857-0), 142.

Jarvis, N.J. (1989). "A simple empirical model of root water uptake." *J. Hydrol.*, 107, 57–72.

Lai, C.T. and Katul, G. (2000). "The dynamic role of root-water uptake in coupling potential to actual transpiration." *Adv. Water Resour.*, 23, 427–439.

Lappala, E.G., Healy, R.W., and Weeks, E.P. (1987). "Documentation of Computer Program VS2D to Solve the Equations of Fluid Flow in Variably Saturated Porous Media." *U.S. Geological Survey Water Resources Investigations Rep. 83-4099*, Washington, D.C.

Li, K.Y., Boisvert, J B., and De Jong, R. (1999). "An exponential root-water-uptake model." *Can. J. Soil Sci.,* 79, 333–343.

Li, K.Y., De Jong, R., and Boisvert, J.B. (2001). "An exponential root-water-uptake model with water stress compensation." *J. Hydrol.*, 252, 189–204.

Li, K.Y., De Jong, R., Coe, M.T., and Ramankutty, N. (2006). "Root-water uptake based upon a new water stress reduction and an asymptotic root distribution function." *Earth Interactions*, 10, 1-22.

Molz, F.J. (1981). "Models of water transport in the soil-plant system: A review." *Water Resour. Res.*, 17(5), 1245–1260.

Monteith, J.L. (1965). *Evaporation and Environment, 19th Symposia of the Society for Experimental Biology*, University Press, Cambridge, 19:205-234.

Parlange, M.B. and Katul, G.G. (1992). "Estimation of the diurnal variation of potential evaporation from a wet bare soil surface." *J. Hydrol.*, 132, 71–89.

Penman, H.L. (1948). "Natural evaporation from open water, bare soil and grass." *Proc. Roy. Soc. London,* A193, 120-146.

Personne, E., Perrier, A., and Tuzet, A. (2003). "Simulating water uptake in the root zone with a microscopic-scale model of root extraction." *Agronomie,* 23, 153–168.

Prasad, R. (1988). "A linear root water uptake model." *J. Hydrol.*, 99, 297–306.

Ritchie, J.T. (1972). "Model for predicting evaporation from a row crop with incomplete cover." *Water Resour. Res.*, 8, 1204–1213.

Priestly, C.H.B. and Taylor, R.J. (1972). "On the assessment of surface heat flux and evaporation using large-scale parameters." *Mon. Weather Rev.*, 100, 81–92.

Romano, E. and Giudici, M. (2007). "Experimental and modeling study of the soil-atmosphere interaction and unsaturated water flow to estimate the recharge of a phreatic aquifer." *J. Hydrologic Engineering*, 12, 573–584.

Simunek, J., Huang, K., and Van Genuchten, M.Th. (1995). *The SWMS_3D Code for Simulating Water Flow and Solute Transport in Three-Dimensional Variably-Saturated Media, Version 1.0*, U.S. Salinity Laboratory, ARS-USDA, Riverside, CA.

Simunek, J., Sejna, M., and Van Genuchten, M.Th. (1998). *The HYDRUS-1D Software Package for Simulating the One-Dimensional Movement of Water, Heat, and Multiple Solutes in Variably Saturated Media, Version 2.0*, U.S. Salinity Laboratory, ARS-USDA, Riverside, CA.

Stone, H. L. (1968). "Iterative solution of implicit approximation of multidimensional partial differential equations." SIAM *J. on Numerical Analysis*, 5, 530–558.

Van Genuchten, M.Th. (1980). "A closed-form equation for predicting the hydraulic conductivity of unsaturated soils." *Soil Sci. Soc. Am. J.*, 44, 892–898.

Varado, N., Braud, I., and Ross, P.J. (2006). "Development and assessment of an efficient vadose zone module solving the 1D Richards' equation and including root extraction by plants." *J. Hydrology*, 323, 258–275.

Versteeg, H.K. and Malalasekera, W. (1998). *An Introduction to Computational Fluid Dynamics - The Finite Volume Method*, Longman Group Ltd, England.

Vrugt, J.A., Van Wijk, M.T., Hopmans, J.W., and Simunek, J. (2001). "One-, two-, and three-dimensional root water uptake functions for transient modeling." *Water Resour. Res.*, 37, 2457–2470.

Wallace, J.S., Jackson, N.A., and Ong, C.K. (1999). "Modelling soil evaporation in an agroforestry system in Kenya." *Agric. For. Meteorol.*, 94, 189–202.

Reining in Log-Pearson Type III Flow-Frequency Estimates - Applying a Reasonable Bound through the Skew Parameter

By Ben Tustison PE & Joseph D. Countryman PE; D. WRE

Contact at 2450 Alhambra Boulevard. Sacramento, CA, USA, 95817;
Email: tustison@mbkengineers.com or countryman@mbkengineers.com

ABSTRACT

In the United States, the flow-frequency distribution established for use by federal agencies is the log-Pearson Type III (LP3). Fitting an LP3 requires the estimation of three log-space parameters: mean, standard deviation, and coefficient of skewness (skew). The resulting flow-frequency estimates for extreme floods are very sensitive to the value of the skew parameter. Many researchers and practitioners have made attempts to better estimate the skew, e.g., through regional skew maps and relating skew to physical watershed characteristics. These attempts have been mainly unsuccessful. In practice, using unfiltered LP3 fitted parameters to estimate project design flows and their associated confidence limits for floods greater than those recorded has lead to extreme flow estimates, which often exceed perceived physical basin limits.

In order to improve the LP3 extrapolations, a simple procedure was developed by which the skew parameter was adjusted such that the resulting flow-frequency estimates respected the physical basin limits. This procedure was applied to several major watersheds of the Sacramento and San Joaquin River system in California. In this application, the skew was adjusted such that the probable maximum flood had an annual exceedance probability (AEP) of 1-in-10,000 or less. Monte Carlo simulations were performed with an assumed underlying test flood-frequency distribution. The distribution was sampled with representative flood record lengths (50 and 100 years). Estimates and confidence limits of commonly used design frequencies (1-in-10 to 1-in-500 AEP) and the risk of flooding in the next 50 years were computed using both the standard (Bulletin 17B) procedure and the procedure with the described skew adjustment. The design flood estimates were compared for reasonableness and consistency with the expected, underlying test distribution values.

BACKGROUND

The principal challenging aspect of performing flood frequency estimation in the United States is the lack of available flow data to form the basis of the estimate. Since a primary interest in utilizing flow-frequency data is to estimate floods whose return intervals are beyond the coverage of the data, extrapolations must be made. As

federal procedures outline (IACWD, 1982), this extrapolation is based on a statistical procedure using the Log-Pearson Type III (LP3) distribution. For watersheds in California, Countryman and Tustison (2008) have recognized that due to the lack of sufficient data and the characteristics of the statistical estimation procedure, these extrapolated estimates often produce results which exceed, sometimes greatly, perceived physical basin limits, such as the probable maximum flood (PMF). This is not a desired product of the estimation procedure, and overestimates at these extreme frequencies may be indicative of overestimation at more frequent, design frequencies (1-in-10 through 1-in-500 AEP).

The authors of Bulletin 17B recognized that to extrapolate flow-frequency curves to exceedance probabilities less than those represented by the range of data for which the statistics were calculated was problematic and thus recommended physical hydrologic and/or meteorologic methodologies be considered when making such extrapolations (IACWD 1982). This paper proposes a simple technique which follows the standard federal Bulletin 17B procedure but adjusts the calculated skew value such that the resulting extrapolated estimates recognize physical hydrologic limits.

BASIC DATA

For this analysis, fifteen California Central Valley watersheds were chosen. The basins lie along the western slope of the Sierra Nevada mountain range. The geographic scope and elevation ranges for the watersheds varied considerably. Watershed data for the basins studied are shown in Table 1.

The 3-day annual maximum flow data was chosen as the basis for this analysis. This flow duration has the advantage of containing peak flood flows in California without having portions of the peak existing in two different time intervals. Additionally, the 3-day duration is the critical duration for the analysis of reservoir flood operations. That is, the reservoir volume set aside for flood control storage is based on a 3-day duration. Therefore, use of the 3-day flow volume is critical to the analysis of a flood system controlled by reservoirs in California. The statistical analysis presented in this paper would be equally applicable in a flood analysis based on peak flows or other durations.

Table 1. Watershed data (USACE, 2002).

Basin	Years of Record	Drainage Area (sq. mi.)	Maximum 3-Day Flow Rate (cfs)	Maximum Elevation (ft, msl)
American R.	100	1,888	166,000	10,400
Bear R.	93	292	32,000	6,000
Calaveras R.	53	363	18,000	6,000
Chowchilla R.	71	235	10,000	6,100
Cottonwood Cr.	58	927	38,000	8,000
Feather R.	96	3,624	244,000	9,100
Fresno R.	58	234	7,000	7,800
Merced R.	96	1,037	44,000	13,000
Mokelumne R.	93	677	39,000	10,000
San Joaquin R.	94	1,676	53,000	13,900
Shasta R.	67	6,421	168,000	14,100
Stanislaus R.	82	904	50,000	11,500
Stony Cr.	98	740	31,000	6,500
Tuolumne R.	100	1,533	92,000	13,000
Yuba R.	100	1,339	124,000	8,200

FREQUENCY CURVES

Graphically-derived frequency curves were developed for each watershed following the procedure outlined in Countryman and Tustison (2008). These curves were based on a combination of recorded data and expert opinion as to the exceedance probability of the PMF, and "standard project flood", SPF, (USACE 1965) for each of the basins. These frequency curves were assumed to be the underlying ("real") probability distribution of flood flows for each basin.

ESTIMATION (STANDARD)

Each of the "real" frequency curves was sampled in independent sets of 50 and 100 years of data for each watershed. This sampling was done 10,000 times in each case to form the basis for characterizing the resulting estimates. These sets of data were then used to estimate flow values at exceedance probabilities commonly used for design purposes (1-in-10 through 1-in-500 AEP) and compared with the underlying "real" frequency curve values. The mean, standard deviation, and skew were computed for each of the sample data sets. In addition, the 95% upper confidence bound (results not presented herein but available) was estimated for each of the data sets at the same frequencies as the estimates. The techniques outlined in Bulletin 17B were explicitly followed in this procedure. This estimation procedure is hereby referred to as the "standard" procedure.

ESTIMATION (BOUNDED)

As the authors have previously shown in Countryman and Tustison (2008), extrapolations made using the "standard" procedure often result in values which are significantly greater than the SPF and PMF values at the extreme frequencies. In order to improve the LP3 extrapolations, a simple procedure was developed by which the skew parameter was adjusted such that the resulting flow-frequency estimates respected the physical basin limits. The skew, as opposed to the other statistical parameters, was chosen for adjustment because the upper tail (extreme estimates) of the probability distribution is of primary interest, and, of the three LP3 fitting parameters, the extreme frequency estimates are generally most sensitive to the skew.

In this application, the skew was adjusted such that the resulting estimates reproduced the 1-in-10,000 AEP value from the underlying "real" frequency curve. This technique was intended to simulate knowledge of a physical bound, e.g. the PMF. Specifically, this estimation was done as follows: (1) estimate the statistical parameters (mean, standard deviation, skew) of the underlying distribution; (2) adjust the skew parameter until the frequency estimate at 1-in-10,000 AEP matches the 1-in-10,000 AEP value from the underlying "real" frequency curve; (3) form estimates and confidence bounds following Bulletin 17B procedures with the originally calculated mean and standard deviation and the new, adjusted skew value. This estimation procedure is hereby referred to as the "bounded" procedure. For comparison, the same quantities calculated using the "standard" procedure were computed with the "bounded" procedure.

RESULTS

Tables 2a and 2b show the skew values estimated from the historical record and mean and standard deviation of those using the standard and bounded procedures with the randomly generated data for record lengths of 50 and 100 years, respectively. In every basin for both 50 and 100 year record lengths, the mean skew value was reduced using the bounded procedure. This indicates the originally calculated (standard procedure) skew values were overestimates. An overestimated skew will result in the tail of the statistical distribution being too "fat", i.e., excess probability. This will lead to overestimation of the extreme values. As an example, Figure 1 shows histograms for the standard and bounded skew estimates resulting from the 10,000 sample data sets on the Stanislaus River. The mean calculated standard and bounded skew values and the skew calculated from the historical record are also shown for comparison. As this figure shows, the bounded skew values have less variation than those using the standard calculation. It is interesting to note that the mean skew value is considerably different using the two methods, with the bounded mean skew value being much less than the standard. Additionally, there is very little overlap of the two histograms.

Table 2a. Skew values estimated from historical record and mean and standard deviation of skew values using standard and bounded procedures for record length = 50 yr.

Watershed	Historical Record	Standard		Bounded	
		Mean	Std. Dev.	Mean	Std. Dev.
American R.	-0.05	-0.43	0.28	-0.50	0.17
Bear R.	-0.73	-0.42	0.24	-0.66	0.14
Calaveras R.	-1.15	-0.34	0.24	-0.55	0.14
Chowchilla R.	-0.76	-0.36	0.25	-0.62	0.15
Cottonwood Cr.	-0.89	-0.24	0.24	-0.39	0.15
Feather R.	-0.23	-0.11	0.24	-0.28	0.16
Fresno R.	-0.38	-0.14	0.25	-0.26	0.16
Merced R.	-0.25	0.02	0.25	-0.22	0.18
Mokelumne R.	0.07	0.06	0.26	-0.23	0.18
San Joaquin R.	0.21	0.05	0.24	-0.31	0.17
Shasta R.	-0.48	-0.12	0.24	-0.33	0.16
Stanislaus R.	0.04	0.00	0.24	-0.40	0.16
Stony Cr.	-0.59	-0.23	0.24	-0.47	0.15
Tuolumne R.	-0.12	0.00	0.25	-0.16	0.18
Yuba R.	-0.31	-0.44	0.28	-0.56	0.16

Table 2b. Skew values estimated from historical record and mean and standard deviation of skew values using standard and bounded procedures for record length = 100 yr.

Watershed	Historical Record	Standard		Bounded	
		Mean	Std. Dev.	Mean	Std. Dev.
American R.	-0.05	-0.50	0.21	-0.53	0.12
Bear R.	-0.73	-0.44	0.17	-0.67	0.09
Calaveras R.	-1.15	-0.36	0.17	-0.56	0.10
Chowchilla R.	-0.76	-0.40	0.18	-0.63	0.10
Cottonwood Cr.	-0.89	-0.25	0.17	-0.40	0.10
Feather R.	-0.23	-0.10	0.17	-0.29	0.11
Fresno R.	-0.38	-0.14	0.18	-0.27	0.11
Merced R.	-0.25	0.04	0.18	-0.23	0.12
Mokelumne R.	0.07	0.06	0.20	-0.25	0.13
San Joaquin R.	0.21	0.07	0.18	-0.32	0.12
Shasta R.	-0.48	-0.12	0.17	-0.33	0.11
Stanislaus R.	0.04	0.01	0.17	-0.40	0.11
Stony Cr.	-0.59	-0.23	0.17	-0.47	0.10
Tuolumne R.	-0.12	0.01	0.19	-0.18	0.13
Yuba R.	-0.31	-0.51	0.21	-0.59	0.12

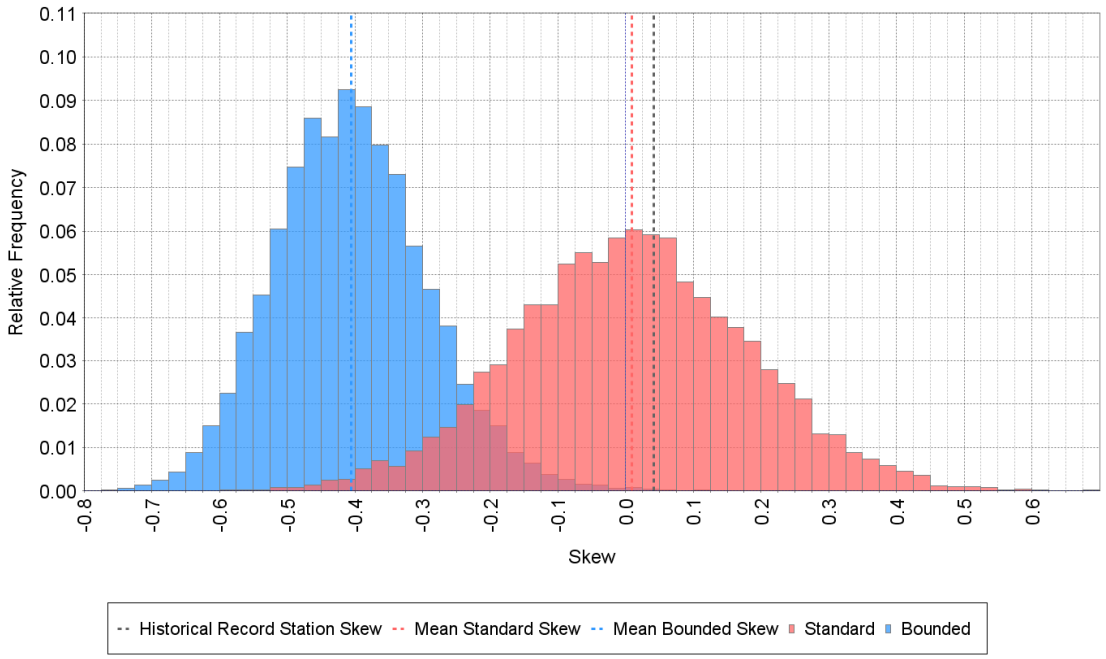

Figure 1. Stanislaus River: Comparison of standard and bounded skew values for 10,000 simulations of 100 year record length.

Figure 2 shows two histograms for the 1-in-100 AEP estimates: one using the standard method and another utilizing the bounded method. As this figure shows, there is much less variation in the bounded case versus the standard case. This was typical of the watersheds studied. Also, Figure 2 shows the bounded methodology underestimated while the standard methodology overestimated the "real" 1-in-100 AEP value.

Tables 3a and 3b show the normalized (by the underlying "real" value at each frequency) root mean square error (RMSE) of the flow estimates at the frequencies 1-in-10, 1-in-100, and 1-in-500 AEP, using the standard and bounded procedures with the randomly generated data for record lengths of 50 and 100 years, respectively. In every basin, for both 50 and 100 year record lengths, the RMSE value was reduced in the bounded case. However, the difference in RMSE between the standard and bounded cases was less for the more frequent estimates. The 1-in-10 AEP estimates showed little RMSE difference between the two estimation techniques, while the 1-in-500 AEP estimates fared much better for the bounded technique, as exhibited by RMSE values considerably less than their counterparts estimated with the standard procedure. The RMSE also decreased in the 100 year record length trials as compared with the 50 year record length trials for both the standard and bounded cases, as would be expected since the additional 50 years of data provided additional support to the estimation procedure.

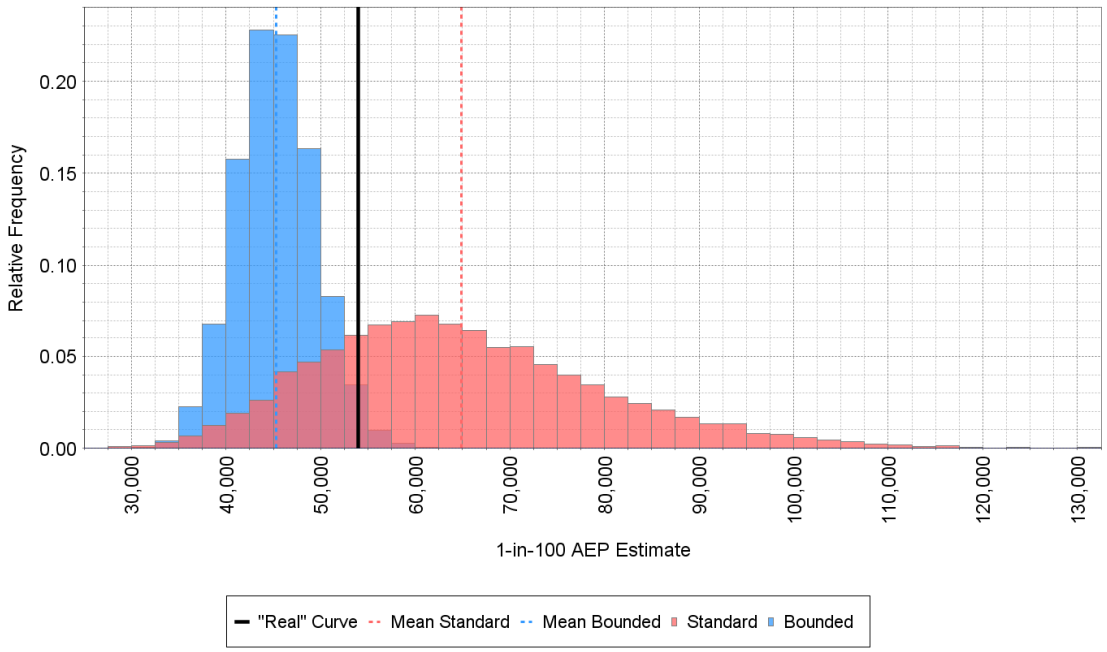

Figure 2. Stanislaus River: Comparison of standard and bounded 1-in-100 AEP estimates for 10,000 simulations of 100 year record length.

Table 3a. Normalized root mean square error (RMSE) using standard and bounded procedures for record length = 50 yr.

Watershed	1-in-10 AEP		1-in-100 AEP		1-in-500 AEP	
	Std.	Bnd.	Std.	Bnd.	Std.	Bnd.
American R.	0.18	0.16	0.34	0.12	0.50	0.08
Bear R.	0.13	0.11	0.30	0.08	0.48	0.05
Calaveras R.	0.16	0.14	0.36	0.10	0.59	0.07
Chowchilla R.	0.19	0.16	0.45	0.11	0.78	0.08
Cottonwood Cr.	0.13	0.12	0.27	0.08	0.41	0.06
Feather R.	0.16	0.14	0.31	0.11	0.56	0.07
Fresno R.	0.23	0.19	0.47	0.14	0.78	0.10
Merced R.	0.20	0.17	0.38	0.18	0.69	0.16
Mokelumne R.	0.22	0.18	0.45	0.18	0.85	0.16
San Joaquin R.	0.20	0.16	0.35	0.26	0.76	0.21
Shasta R.	0.11	0.10	0.23	0.07	0.37	0.05
Stanislaus R.	0.21	0.17	0.46	0.19	0.77	0.26
Stony Cr.	0.16	0.13	0.33	0.11	0.52	0.11
Tuolumne R.	0.20	0.17	0.38	0.15	0.60	0.16
Yuba R.	0.16	0.14	0.32	0.10	0.48	0.07
Mean	**0.18**	**0.15**	**0.36**	**0.13**	**0.61**	**0.11**

Table 3b. Normalized root mean square error (RMSE) using standard and bounded procedures for record length = 100 yr.

Watershed	1-in-10 AEP		1-in-100 AEP		1-in-500 AEP	
	Std.	Bnd.	Std.	Bnd.	Std.	Bnd.
American R.	0.13	0.12	0.23	0.09	0.31	0.06
Bear R.	0.10	0.08	0.23	0.06	0.37	0.04
Calaveras R.	0.12	0.10	0.27	0.07	0.44	0.05
Chowchilla R.	0.14	0.12	0.34	0.08	0.57	0.06
Cottonwood Cr.	0.10	0.08	0.20	0.06	0.31	0.04
Feather R.	0.12	0.10	0.23	0.09	0.41	0.05
Fresno R.	0.17	0.14	0.34	0.10	0.54	0.07
Merced R.	0.15	0.12	0.27	0.16	0.49	0.15
Mokelumne R.	0.16	0.13	0.32	0.16	0.62	0.14
San Joaquin R.	0.14	0.12	0.25	0.25	0.57	0.20
Shasta R.	0.08	0.07	0.18	0.05	0.28	0.04
Stanislaus R.	0.15	0.12	0.34	0.18	0.56	0.25
Stony Cr.	0.12	0.10	0.24	0.09	0.38	0.10
Tuolumne R.	0.14	0.12	0.27	0.12	0.42	0.14
Yuba R.	0.11	0.10	0.22	0.08	0.31	0.05
Mean	**0.13**	**0.11**	**0.26**	**0.11**	**0.44**	**0.10**

In addition to the RMSE, the mean bias of the standard and bounded estimates was calculated. The bias is defined as the difference between the estimate and the "real" value. Tables 4a and 4b show the calculated mean estimation bias values for record lengths of 50 and 100 years, respectively. As these tables show, the standard estimation method tends to lead to overestimation (positive bias values), while the bounded methodology tends to lead to slight underestimation (negative bias values). The bounded methodology did lead to considerably smaller biases, especially for the 1-in-500 AEP flow estimates. The degree of bias generally increased with the extremity of the flow being estimated. Record length had minimal effect on this bias magnitude, with a slight decrease in the overall bias magnitude with the increase in record length from 50 to 100 years. The tendency for the bounded methodology to slightly underestimate should be better understood before applying this method in practice, as the underestimation of a hydrologic design event could lead to severe repercussions, including underestimating threats to public safety.

Table 4a. Mean estimation bias (estimate minus "real") of common design frequencies using standard and bounded procedures for record length = 50 yr.

Watershed	1-in-10 AEP		1-in-100 AEP		1-in-500 AEP	
	Std.	Bnd.	Std.	Bnd.	Std.	Bnd.
American R.	0.05	0.04	0.13	0.03	0.19	0.00
Bear R.	0.04	0.00	0.18	-0.01	0.31	-0.01
Calaveras R.	0.05	0.01	0.20	-0.01	0.36	-0.01
Chowchilla R.	0.06	0.00	0.28	-0.02	0.51	-0.02
Cottonwood Cr.	0.03	0.02	0.12	0.01	0.21	0.00
Feather R.	0.04	0.01	0.11	-0.05	0.28	-0.01
Fresno R.	0.06	0.04	0.19	0.00	0.35	-0.01
Merced R.	0.04	0.01	0.08	-0.14	0.28	-0.14
Mokelumne R.	0.04	0.00	0.15	-0.14	0.43	-0.13
San Joaquin R.	0.02	-0.02	0.05	-0.24	0.39	-0.20
Shasta R.	0.00	-0.01	0.11	-0.01	0.21	-0.01
Stanislaus R.	0.03	-0.03	0.22	-0.16	0.40	-0.25
Stony Cr.	0.04	0.01	0.15	-0.05	0.26	-0.09
Tuolumne R.	0.03	0.00	0.09	-0.09	0.17	-0.13
Yuba R.	0.03	0.01	0.15	0.02	0.24	0.01
Mean	**0.04**	**0.01**	**0.15**	**-0.06**	**0.31**	**-0.07**

Table 4b. Mean estimation bias (estimate minus "real") of common design frequencies using standard and bounded procedures for record length = 100 yr.

Watershed	1-in-10 AEP		1-in-100 AEP		1-in-500 AEP	
	Std.	Bnd.	Std.	Bnd.	Std.	Bnd.
American R.	0.05	0.04	0.08	0.04	0.09	0.01
Bear R.	0.04	0.00	0.16	0.00	0.27	0.00
Calaveras R.	0.04	0.01	0.18	0.00	0.30	-0.01
Chowchilla R.	0.05	0.00	0.23	-0.02	0.42	-0.02
Cottonwood Cr.	0.03	0.01	0.11	0.01	0.19	0.00
Feather R.	0.04	0.01	0.10	-0.05	0.25	-0.01
Fresno R.	0.06	0.03	0.17	0.00	0.28	-0.01
Merced R.	0.04	0.01	0.08	-0.14	0.26	-0.14
Mokelumne R.	0.04	0.00	0.14	-0.13	0.38	-0.13
San Joaquin R.	0.02	-0.03	0.04	-0.24	0.36	-0.19
Shasta R.	0.00	-0.02	0.10	-0.01	0.19	0.00
Stanislaus R.	0.03	-0.03	0.20	-0.16	0.35	-0.25
Stony Cr.	0.04	0.01	0.14	-0.05	0.23	-0.09
Tuolumne R.	0.03	0.00	0.08	-0.08	0.15	-0.13
Yuba R.	0.03	0.02	0.10	0.02	0.15	0.01
Mean	**0.04**	**0.01**	**0.13**	**-0.05**	**0.26**	**-0.06**

Tables 5a and 5b show the mean calculated risk of the estimated flow at the specified frequency being exceeded in the next 50 years for the design frequencies of 1-in-100, 1-in-200, and 1-in-500 AEP for record lengths of 50 and 100 years, respectively. The tabulated values should be compared with the theoretical risk of exceeding these respective frequency events of 0.39 (1-in-100 AEP), 0.22 (1-in-200 AEP), and 0.10 (1-in-500 AEP). When these comparisons are made, these tables show the standard procedure generally produced design event estimates with less risk of failure than would be expected at those frequencies. This means that designs using this procedure would tend to be overly conservative and perhaps more costly than necessary. The bounded procedure, on average, produced estimates which underestimated the risk of failure in the next 50 years. While this would potentially produce less costly designs for a given frequency, these designs would also underestimate the flood risk of the design, and potentially compromise public safety if left unchecked. Using both procedures, the mean calculated risk was decreased by adding the additional information in going from a 50 year to a 100 year record. The tendencies of these estimators to overestimate and underestimate the flooding risk of a design should be carefully considered when applying either of these techniques to a potential project.

Table 5a. Mean risk of common design frequency estimates using standard and bounded procedures for record length = 50 years.

Watershed	1-in-100 AEP		1-in-200 AEP		1-in-500 AEP	
	Std.	Bnd.	Std.	Bnd.	Std.	Bnd.
American R.	0.35	0.38	0.23	0.22	0.13	0.10
Bear R.	0.25	0.42	0.14	0.25	0.07	0.11
Calaveras R.	0.28	0.42	0.16	0.25	0.08	0.11
Chowchilla R.	0.25	0.44	0.14	0.27	0.06	0.12
Cottonwood Cr.	0.33	0.40	0.20	0.24	0.10	0.10
Feather R.	0.36	0.46	0.21	0.27	0.11	0.11
Fresno R.	0.36	0.41	0.22	0.25	0.12	0.11
Merced R.	0.41	0.54	0.25	0.37	0.13	0.19
Mokelumne R.	0.39	0.58	0.23	0.38	0.12	0.19
San Joaquin R.	0.37	0.55	0.22	0.44	0.11	0.26
Shasta R.	0.33	0.45	0.19	0.28	0.09	0.11
Stanislaus R.	0.32	0.57	0.18	0.39	0.09	0.22
Stony Cr.	0.33	0.48	0.20	0.31	0.10	0.16
Tuolumne R.	0.41	0.50	0.27	0.32	0.15	0.16
Yuba R.	0.32	0.39	0.19	0.22	0.11	0.10
Mean	**0.34**	**0.47**	**0.20**	**0.30**	**0.10**	**0.15**

Table 5b. Mean risk of common design frequency estimates using standard and bounded procedures for record length = 100 years.

Watershed	1-in-100 AEP		1-in-200 AEP		1-in-500 AEP	
	Std.	Bnd.	Std.	Bnd.	Std.	Bnd.
American R.	0.36	0.37	0.22	0.21	0.12	0.10
Bear R.	0.23	0.42	0.11	0.24	0.04	0.11
Calaveras R.	0.26	0.41	0.13	0.24	0.06	0.11
Chowchilla R.	0.24	0.43	0.12	0.26	0.05	0.12
Cottonwood Cr.	0.30	0.40	0.17	0.23	0.08	0.10
Feather R.	0.33	0.45	0.17	0.26	0.07	0.11
Fresno R.	0.34	0.41	0.19	0.24	0.09	0.11
Merced R.	0.38	0.54	0.21	0.36	0.09	0.19
Mokelumne R.	0.36	0.57	0.19	0.37	0.08	0.19
San Joaquin R.	0.35	0.54	0.18	0.44	0.07	0.25
Shasta R.	0.31	0.44	0.16	0.27	0.06	0.11
Stanislaus R.	0.29	0.56	0.15	0.38	0.05	0.21
Stony Cr.	0.31	0.47	0.17	0.31	0.07	0.16
Tuolumne R.	0.38	0.49	0.23	0.31	0.11	0.16
Yuba R.	0.32	0.38	0.19	0.21	0.09	0.10
Mean	**0.32**	**0.46**	**0.17**	**0.29**	**0.08**	**0.14**

CONCLUSION

Countryman and Tustison (2008) concluded by stating that the development of graphical frequency curves which incorporate design flood information such as PMF and SPF should be investigated as a replacement for the Bulletin 17B procedure. This paper presents a technique by which this objective is met. However, unlike a purely graphical technique, this procedure largely falls within the Bulletin 17B framework, only deviating where necessary to overcome the limitations of Bulletin 17B.

Although a purely graphical technique, by which the resulting frequency curve remains true to the observed data within its limited frequency range, is still preferred by the authors, the procedure recommended in this paper provides an alternative which: (1) remains within the guidelines of Bulletin 17B as closely as possible; (2) corrects the overestimation of flow estimates produced using the Bulletin 17B procedure at extreme frequencies; (3) provides more accurate estimates of the underlying flow-frequency relationship at the frequencies commonly used in water resources design (1-in-10 to 1-in-500 AEP).

FURTHER INVESTIGATION

Past attempts of the authors to relate the standard skew to physical basin parameters in the California (and others throughout the United States) have been largely unproductive. Perhaps, some of the difficulty can be related to the inherent variability in estimating the standard skew from the limited historical record. The authors would like to further explore the technique of skew adjustment. Of particular interest is to determine if the adjusted skew can be closely related to physical basin parameters. If so, this would potentially have significant implications to regional skew analysis.

REFERENCES

Countryman, J., Tustison, B. (2008) "Flood Frequency Confidence Bounds- Art, Science or Guess!!" Proceedings of the World Environmental and Water Resources Congress 2008: Sustainability from the Mountains to the Sea, ASCE, Reston, VA.

Interagency Advisory Committee on Water Data, Hydrology Subcommittee (IACWD) (1982). *Guidelines for Determining Flood Flow Frequency*, Bulletin #17B.

USACE, (1965). Engineer Manual 1140-2-1411.

USACE Sacramento District (2002). "Sacramento and San Joaquin River Basins, Comprehensive Study, California." Sacramento, CA.

Understanding Water Quality Responses to Long-term Acidic Deposition in a High-elevation Southern Appalachian Watershed: A Focus on Soil Watershed Processes

Meijun Cai[1,3], John S. Schwartz[1], R. Bruce Robinson[1], Steve E. Moore[2], and Matt A. Kulp[2]

[1]Department of Civil and Environmental Engineering, University of Tennessee, Knoxville, Tennessee, 37966-2010; [3]PH (865) 974-8678; Email: mcai@utk.edu.

[2] U.S. Department of Interior, National Park Service, Great Smoky Mountains National Park; Gatlinburg, Tennessee 37738.

Abstract

Noland Divide Watershed (NDW), locating in the Great Smoky Mountains National Park, is characterized as one of the watersheds to receive some of the highest acidic deposition in the US. It has been continuously monitored for deposition, soil water and stream water chemistry weekly and biweekly, since 1991. The long-term trend analysis over past 17 years (1991-2007) found that decreasing sulfate and proton in the precipitation, however stream sulfate concentration, pH and ANC did not show the same significant trends. In contrast, atmospheric deposition of nitrogen was found to be increasing over time, but stream nitrate concentration was observed to be declining, apparently due to increasing overstory vegetation uptake. This long-term study has found mean annual detention of sulfate, nitrate and ammonium of 60%, 3% and 95% respectively in the watershed. Sulfate is accumulated in soil matrix by soil adsorption. Ammonium was mainly converted to nitrate by soil mineralization and nitrification at surface soil layer, and combined with deposited nitrate to be uptaken by plant. Despite the decreasing nitrate concentration and stable sulfate concentration, stream recovery from acidification is not observed in the NDW, due to the depletion of base cations with decreasing stream base cation concentrations.

Introduction

The Noland Divide Watershed (35°34'N, 83°29'W), located in the Great Smoky Mountains National Park on the North Carolina and Tennessee border, is a small (17.4 ha), high-elevated (1700~1900 m) watershed (Figure 1). Two perennial first-order streams (NE and SW streams) drain the study area headwaters, and merge downstream as Noland Creek.

As part of the Integrated Forest study (IFS) program, stream acidification in the NDW was initially observed in the 1980's by Johnson and Lindberg (1992) and Cook et al. (1994). This watershed was characterized as one of the watersheds to receive the highest atmospheric deposition in US. After the IFS, GRSM resource managers initiated a long-term study utilizing the NDW site to further investigate impacts of acidic deposition on high-elevation forested watersheds and stream acidification. In 1991, the NDW was equipped with wet deposition, throughfall, soil lysimeters, and stream monitoring stations, designed to characterize and assess deposition, soil, and stream water chemistries, over time. In this article, analysis focused on estimating ion

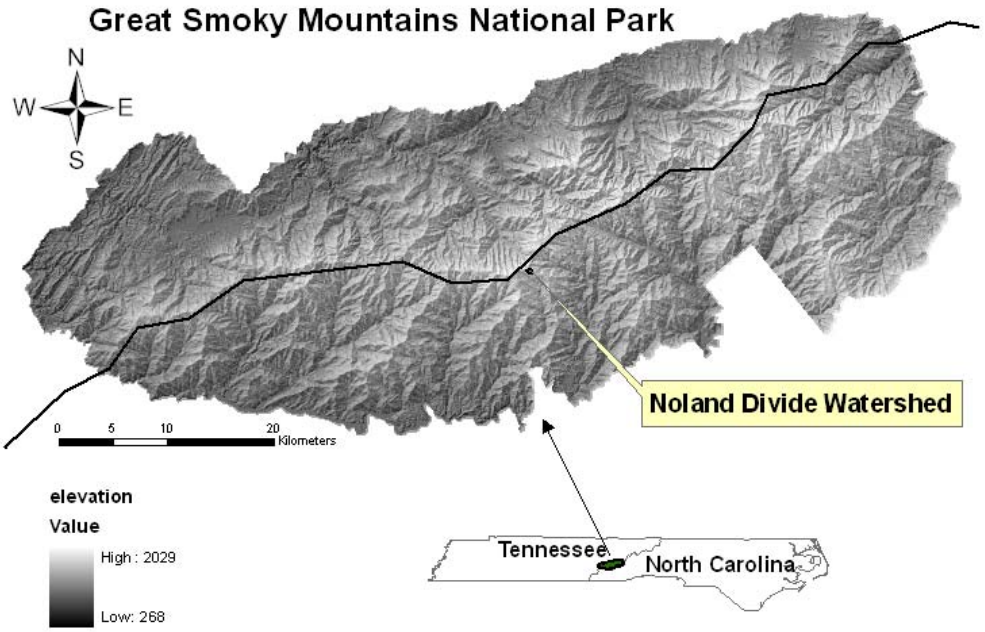

Figure 1. Location of Noland Divide Watershed (NDW) in the Great Smoky Mountain National Park (GRSM) at the border of Tennessee and North Carolina.

mass fluxes for long-term trend and annual input-output budgets using the NDW monitoring data from 1991 through 2007.

Methods

Study Area

The NDW is a fully forested basin, and its overstory vegetation was dominated by red spruce fir (*Pices rubens* Sarg, 77%) and interspersed patches of yellow birch (*Betula alleghaniensis,*19%) as well as Fraser fir (*Abies fraseri* (pursh.) Poir, 2.5%) (Baker et al. 2002). The invasion of balsam woolly adelgid (BWA, *Adelges piceae*, Ratzeburg) on spruce-fir forests (Nicholas et al. 1992) in 1970s resulted in a heavy mortality of the forest (Jenkins 2007). The BWA feeds in the bark fissures of *A. fraseri* trees over 4 cm dbh (Eagar 1984), resulting in the death of most mature fir. Recently, the forest has shown signs of recovery, indicated by increasing standing live biomass and growth (Van Meigroet et al. 2007).

The soils in the NDW are generally shallow with total depth below 1 meter throughout the NDW (Johnson and Lindberg, 1992). The soils are inceptisols with spodic characteristic classified as Dystrochrepts or Haplumbrepts (McCracken et al. 1962; Van Miegroet et al. 1993), with a silt loam to sandy loam texture. Soil layers were consisted of 4-cm thick Oi + Oe horizon of needles and leaves; 4-cm thick Oa horizon of mucky humus; 8-cm thick A horizon of dark, reddish-brown, mucky loam; 27-cm thick Bw horizon of dark brown, sandy loam; 35-cm thick Cb horizon of dark, yellowish-brown loam; and 20-cm thick C horizon of olive-brown, loamy sand

(Johnson and Lindberg 1992). Underneath the soil lies the Thunderhead Sandstone formation, thick-bedded, low porosity bedrock composed principally of quartz and potassic feldspar (King et al. 1968; Silsbee and Larson 1982).

Field data collection and laboratory analysis

Atmospheric deposition was collected by wet deposition and throughfall deposition. Wet deposition was collected at an open site (without forest cover) using a rainfall collector with a precipitation-triggered cover. Throughfall was collected during frost-free periods by covered collector buckets mounted with 90-mm diameter funnels minimizing evaporation, and during the frost season two open 5-gal collector buckets were used. Deposition water was collected and weighed biweekly to obtain a precipitation volume biweekly, computed by use of the water specific weight.

Soil water was collected monthly by ceramic suction lysimeters at three different soil depths. The shallowest lysimeter was placed in the A horizon, the intermediate lysimeter depth was placed in the Bw horizon, and the deepest lysimeter was placed in the Cb horizon. Lysimeters were installed in the same location as the throughfall collectors.

Grab samples were routinely collected from the SW and NE streams weekly from 1991-2000 and biweekly since 2001. Most samples were collected during baseflow conditions; however no effort was made to collect baseflow samples only. Each stream was also equipped with water quality sondes recording pH, conductivity and temperature. Float-type stage recorders were installed in stilling wells on 3.0-ft H flumes, in which discharge was calculated from flow depth according to standard H-flume tables in USDA-ARS (1979) and periodically verified. Water quality and stage data were recorded every 15 minutes on a Campbell CR10 data logger.

The collected water samples were transported to the University of Tennessee Water Quality Laboratory within 4 hours and, and analyzed for pH, conductivity, and ANC utilizing an autotitrator within 24 hours. Samples in holding were kept cooled at 4°C. Samples were filtered by a 0.4-μm membrane and separated into two bottles for analysis of SO_4^{2-}, NO_3^-, Cl^-, and NH_4^+ by ion chromatography; and Ca^{2+}, Mg^{2+}, K^+, Na^+ by atomic absorption spectrometry (1991-1993, 1998-2003) and inductively-coupled plasma spectrometry (2003-2006). From 1993 to 1998, Na^+ and K^+ were measured by ion chromatography, but Ca^+ and Mg^+ were not measured. Measurement of ANC for wet deposition, throughfall, and soil water began in 2005. All samples met quality criteria set forth in a quality assurance/quality control (QA/QC) program, which included sample spikes, replicates, blanks and U.S. Geological Survey known samples; in addition to adherence to analytical equipment maintenance.

Water and chemical mass balance calculations

Annual throughfall and wet precipitations were computed by converting each volume collected biweekly to a depth (cm) based on the total surface area of the collection funnels/buckets, and summing each biweekly measurement to equate to an annual total. Water export from NDW was equal to the total flow from both SW and NE streams. Annual volume for total flow was computed by summing measured volumetric discharges (m^3 s^{-1}) per 15-minute increments for both SW and NE streams, combining these individual stream annual volumes (m^3), dividing total annual volume

by total watershed area (17.4 ha), and converting units to obtain estimates in cm yr^{-1}.

An annual chemical mass balance was estimated as the difference between total mass deposition (TD) and mass stream export, reported in flux units of eq ha^{-1} yr^{-1}. Per chemical, TD was calculated by the sum of wet deposition and dry deposition representing the entire atmospheric input to NDW. Wet deposition represents that portion captured from the open site. Dry deposition generally represents that portion computed by the difference between throughfall and wet deposition; however for Ca^{2+}, Mg^{2+}, K^+, H^+, and NH_4^+ dry deposition was calculated by using canopy uptake and leaching model (Ulrich 1983; Van der Maas et al. 1991; Cai et al. 2009). Total stream mass flux export was computed by summing eq yr^{-1} for both SW and NE streams, divided by the total NDW drainage area of 17.4 ha. Chemical mass balances for NDW in eq ha^{-1} yr^{-1} were computed as follow:

$$\text{Retention/depletion} = \text{TD} - \text{Total Stream Export} \quad (1)$$

where, retention is the chemical mass remaining in the watershed if positive, and depletion is the chemical mass removed beyond that amount entered through atmospheric deposition if negative.

Statistical analysis of chemistry among deposition, soil, and stream waters

Statistical analysis of water chemistry includes: 1) long-term trend analysis for chemical flux and concentration from 1991 to 2007; 2) multiple analysis of variance (MANOVA) among watershed hydrologic system compartments (i.e., atmospheric deposition, soil, and stream) to compare mean annual concentrations among compartments from 1991 to 2006. Mean annual concentrations were computed for the 16-year (1991-2006) monitoring period and hydrologic system compartments, specifically wet deposition, throughfall, soil water (A, Bw, and Cb horizons), and SW and NE streams. Compartments were compared using a MANOVA Tukey's HSD mean separation procedure (Hayter 1984). Significance groupings of mean concentration differences were indicated by superscript letters, e.g., A, B, C, etc. If the data did not share the same letter, it indicates there was a significant difference between those compartments. Statistical analysis was preformed with JMP® v.6.0.2 (JMP, 2005). Significant trend and differences were noted at $p < 0.05$. For analysis of temporal trend, only SW stream is selected since water chemistries between the NE and SW streams were found to be statistically similar (Cai et al. 2009).

Results and Discussions

Long-term trend of annual flux

From 1991 to 2007, wet precipitation and throughfall precipitation declined, from above 250 cm yr^{-1} in early 1990s to around or below 200 cm yr^{-1} in recent years, a decrease of approximately 20%. Precipitation was particularly low in 2007, because that year is the most severe drought year in US southeastern region since 1989 (Hampson 2008; Logan 2008). In response to the declining precipitation amount, the averaged annual stream outflow through SW stream was reducing from above 100 cm yr^{-1} to around 70 cm yr^{-1} during this study period. The hydrological temporal trend

can affect the chemistry fate through dilution effect and by changing the dominant biogeochemical processes due to varied flow pathway (Mulholland 1993).

Deposition flux and SW stream export of sulfate had similar decreasing trend, just like water precipitation and discharge. The significant downward trend of deposited sulfate flux was consistent to many other watersheds (Stoddard et al. 1999; Forsius et al. 2003). Greater decline of sulfate flux in throughfall than in wet deposition implied a proportionally greater reduction in dry deposition than wet deposition (Ukonmaanaho et al. 1998). This provided evidence that the reduction of emission of SO_2 was actually reducing the acidic deposition of sulfur, especially through dry deposition. Due to simultaneously decreasing trend of water volume and sulfate flux, sulfate concentration in SW stream did not show a trend over 17 years, indicating the NDW streams have not recovered from excessive sulfate deposition. This is consistent with the regression models by Robinson et al (2004; 2008) finding that there was little temporal variation of sulfate for streams at elevation above 1,067 m in the GRSM. Positive retention values in all 17 monitoring years indicated that the NDW was working as sink for sulfate. Although the retention amount varied from 1500 eq ha^{-1} yr^{-1} in some years to 500 eq ha^{-1} yr^{-1} in other years, the variation did not give significant temporal trend. The positive retention provided the evidence that this watershed was not saturated with sulfate yet and could accumulate more sulfate.

Wet and throughfall depositions for nitrate and ammonium, except ammonium flux in throughfall, did not have significant time trend. In contrast, retention of nitrate and ammonium in the NDW gave increasing trend from 1991 to 2007. Consequently, stream export of nitrogen, mainly in the form of nitrate, was decreasing over time. This is primarily because the spruce-fir forest in the NDW was recovering from the BWA by showing increased standing live biomass and uptake of nitrogen in 2000s than that in 1990s (Jenkins 2007; Van Miegroet et al. 2007). The nitrogen uptake by the overstory during 1993 to 1998 was observed to be 8 kg ha^{-1} yr^{-1} (Barker et al. 2002), which was increased to 11-15 kg ha^{-1} yr^{-1} in the following 5 years after 1998 (Moore et al. 2007). As a result, more nitrogen was assimilated by vegetation, leading to increasing retention and decreasing export of nitrogen from the NDW.

Throughfall deposition pH averaged 0.5 pH unit lower than that from wet deposition during the study period, and increased from 4 in 1991 to 4.2 in 2007. Wet and throughfall deposition pH increased at the rate of about 3.6×10^{-5} pH unit per day, leading to the declining trend of deposition H^+ flux, in which cloud be also partially attributed to declining precipitation. Sulfate and nitrate are the main acidifying anions in the NDW. Because of decreasing nitrate concentration and stable sulfate concentration, stream recovery from acidification (reflecting increasing pH and ANC) was expected. However, stream pH and ANC did not reflect the deposition pattern. SW stream pH remained around 5.8, while ANC fluctuated year to year without significant temporal trend. Some studies attributed the delay of stream recovery to the decrease in soil pools of base cations (Stoddard et al. 1999; Fölster et al. 2003). This could be evidenced by the declining total base cations concentration (slope = -0.0017 $\mu eq\ L^{-1}$, $p = 0.0211$, $n = 270$), despite of the relatively constant base cation deposition. The decreasing rate of total base cation was big enough to account for the declining nitrate concentration. As a result, the stream recovery of pH and ANC was delayed, leading to very small or no recovery at all. This indicates that watershed acidification

will continue for a long time until the soil cations are improved and the deposition of S and N is further reduced.

Ion input-output budget

Deposition water chemistry was dominated by SO_4^{2-} and NO_3^- inputs averaging annually 1,946 and 892 eq ha^{-1} yr^{-1}, respectively (Figure 2). Throughfall concentrations of 115.87 μeq L^{-1} SO_4^{2-} and 58.08 μeq L^{-1} NO_3^- were among the highest of the ion concentrations measured (Table 1). The influence of these two acid anions on proton equilibrium can be observed by the mean annual pH of 4.65 for wet deposition and 4.17 for throughfall. Also, mean annual ANC was –10.31 μeq L^{-1} for wet deposition and –56.79 μeq L^{-1} for throughfall. This indicated that acidification in this watershed was mainly caused by deposition of sulfate and nitrate. Less dominant, total annual deposition of Cl^- averaged 601.84 eq ha^{-1} yr^{-1} and NH_4^+ averaged 297.65 eq ha^{-1} yr^{-1}. Total deposition of base cations ranged from 144.31 to 451.66 eq ha^{-1} yr^{-1}. In general, annual wet deposition of ions were approximately 26 to 34% of total deposition, except for NH_4^+ at 82%. Wet deposition and throughfall NH_4^+ concentrations were similar at 14.08 and 18.01 μeq L^{-1}, respectively.

Stream export chemistry was dominated by Ca^{2+}, NO_3^-, and SO_4^{2-} averaging 49.30, 41.46, and 29.40 μeq L^{-1} in SW stream, respectively (Table 1). The data showed stream anions were dominated by NO_3^- although SO_4^{2-} dominated deposition anions. Annual SO_4^{2-} mass output and concentration were lower in the SW stream than the NE stream. These results provide some explanation to the higher pH and ANC found in the SW stream than in the NE stream. Annual pH averaged 5.83 and 5.59, and ANC averaged 11.75 μeq L^{-1} and 4.20 μeq L^{-1} for the SW and NE streams, respectively. Mean annual NH_4^+ concentrations of 0.72 μeq L^{-1} in the SW stream and 1.07 μeq L^{-1} in the NE stream, were small compared to other ions. Measurable stream ions also included: Na^+, Mg^{2+}, Cl^-, and K^+ with mass outputs averaging 497.35, 334.51, 331.47, and 200.62 eq ha^{-1} yr^{-1}, respectively.

Over this 16-year period in NDW, acid anions were retained. Retention of SO_4^{2-} was greatest among the anions estimated at 60.16%, whereas Cl^- was estimated at 44.92% and NO_3^- at 3.58% (Figure 2). Although NO_3^- retention appeared small, total inorganic nitrogen consisting of both NH_4^+ and NO_3^- was retained at 26.63%, presumably due to vegetative uptake. Johnson and Lindberg (1992) found that vegetation uptake to be approximately 15% of the NO_3^- inputs. Barker et al. (2002) found that the annual N sequestering in aboveground biomass was 8 kg ha^{-1} yr^{-1} in a NDW study. In addition, NH_4^+ retention was estimated at 95.69%, which represents conversion to NO_3^- in the soil rather than adsorption. This percentage is not uncommon in forested watersheds (Peterjohn et al. 1996; Willard et al. 1997). Consistent with the mass flux estimates for acid anions, concentrations of SO_4^{2-}, NO_3^-, and Cl^- were greater in the throughfall than the stream water.

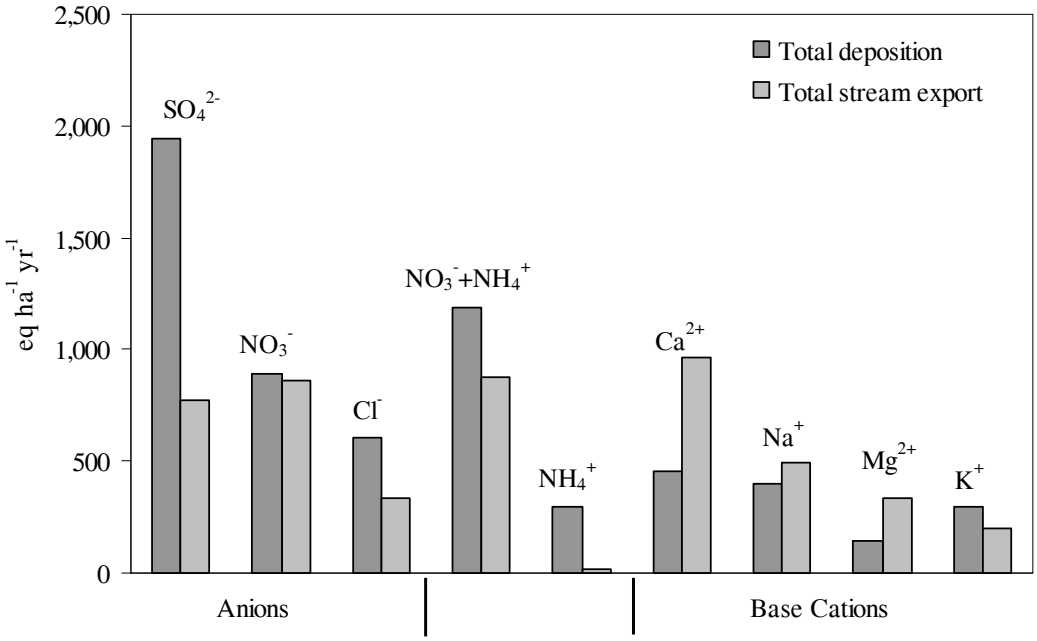

Figure 2. Mean annual fluxes in eq ha^{-1} yr^{-1} for total deposition and total stream export by SW and NE streams in NDW from 1991 to 2006 for major anions and cations.

In contrast to acid anions, base cations, except for K^+, were mostly exported with Ca^{2+} and Mg^{2+} mass export of 510.99 eq ha^{-1} yr^{-1} and 190.20 eq ha^{-1} yr^{-1}, respectively. (Figure 2). Loss of watershed base cations has been attributed to prolonged acidic deposition (Fernandez et al. 2003; Lawrence 2002; Tomlinson 2003). In NDW, the only cation retained was K^+, in which 31% was assumed assimilated annually into forest biomass. Castro and Morgan (2000) also found K^+ retention in a Maryland watershed, however K^+ export appears more typical among ion input-output budgets in northeastern US (Watmough et al. 2005). The export of cations from watersheds is of concern to the GRSM since mass export of base cations may impact the long-term health of forests (Tomlinson 2003; Holzmueller et al. 2007).

Concentration variation and biogeochemical processes among soil layers

Water chemistry changes were observed between throughfall and soil horizon A, which in most instances ion concentrations were significantly less in soil water than throughfall (Table 1). These ions included SO_4^{2-}, Cl^-, NH_4^+, Ca^{2+}, and K^+. Mean SO_4^{2-} decreased from 115.87 μeq L^{-1} in the throughfall to 91.39 μeq L^{-1} in soil horizon A, and Ca^{2+} decreased from 66.66 to 51.07 μeq L^{-1}. Mean annual NH_4^+ greatly decreased from 18.01 μeq L^{-1} in the throughfall to 2.87 μeq L^{-1} in the soil horizon A. Cations Mg^{2+} and Na^+ were found to be similar between throughfall and soil horizon A. The only ion to increase significantly in mean annual concentration from throughfall to soil horizon A was NO_3^-, increasing from 58.08 to 142.07 μeq L^{-1} indicating the occurrence of nitrification. Evidence suggests most of NH_4^+ deposition is converted to NO_3^- in the upper soil layer because the A horizon NH_4^+ concentration

Table 1. Mean chemical concentrations from late 1991 to 2006 for hydrologic system compartments. Stream ANC was measured for the 16-year period, but deposition and soil water ANC was only measured for two years (2005 and 2006). For one chemical, data sharing same letter are not significantly different among hydrologic system compartments.

	Hydrologic System Compartments (Chemical ion concentrations in μeq L^{-1}; pH in standard pH units)						
	WD	TF	A	Bw	Cb	SW	NE
Cl^-	10.89^{E}	34.38^{A}	26.64^{B}	25.57^{B}	23.29^{BC}	15.92^{D}	18.41^{CD}
SO_4^{2-}	31.57^{D}	115.87^{A}	91.39^{B}	95.01^{B}	89.40^{B}	29.40^{D}	40.75^{C}
$NO_3^- + NH_4^+$	27.06^{D}	76.09^{B}	145.60^{A}	78.50^{B}	87.39^{B}	42.18^{C}	47.43^{C}
NO_3^-	13.09^{E}	58.08^{C}	142.07^{A}	78.24^{B}	85.60^{B}	41.46^{D}	46.60^{D}
NH_4^+	14.08^{B}	18.014^{A}	2.87^{C}	1.74^{C}	1.43^{C}	0.72^{C}	1.07^{C}
pH	4.65^{C}	4.17^{E}	4.01^{F}	4.41^{D}	4.47^{D}	5.83^{A}	5.59^{B}
ANC	-10.31^{C}	-56.79^{E}	-148.58^{F}	-72.09^{E}	-35.18^{D}	11.75^{A}	4.20^{B}
Ca^{2+}	10.46^{D}	66.66^{A}	51.07^{B}	31.04^{C}	35.93^{C}	49.30^{B}	54.05^{B}
Mg^{2+}	2.57^{D}	21.82^{AB}	24.79^{A}	20.02^{ABC}	24.12^{A}	18.89^{C}	20.98^{AB}
K^+	9.73^{C}	45.80^{A}	23.19^{B}	9.57^{C}	9.85^{C}	8.61^{C}	11.60^{C}
Na^+	7.30^{C}	21.19^{B}	23.51^{AB}	22.84^{AB}	20.04^{B}	25.99^{A}	25.64^{A}

WD = wet deposition; TF = throughfall; A, Bw, and Cb = soil horizons; SW = southwest stream; and NE = northeast stream.

decreased, and NO_3^- and H^+ concentration increased (Table 1). For NO_3^-, nitrification and vegetation uptake are the dominant processes within NDW. Nitrification was observed by the abrupt increase of NO_3^- concentration and reduction of NH_4^+ concentration from throughfall to soil horizon A. Nitrification and mineralization of organic N both have a strong acidifying effect on the soil because of the net proton release during this oxidation process. Both these N processes may be involved in generating the NDW mean pH of 4.01 in the upper soil horizon water, which was significantly lower than pHs measured in throughfall and deeper soil horizons. Concurrently observed with the NO_3^- increase were decreases in mean ANC (–56.79 to –148.58 μeq L^{-1}) from throughfall to soil, observed as –56.79 to –148.58 μeq L^{-1}.

Within the soil column (A, Bw, and Cb horizons), mean annual concentration of several ions remained relatively uniform, including SO_4^{2-}, Cl^-, NH_4^+, Mg^{2+}, and Na^+ (Fig. 4). NO_3^- significantly decreased from 142.60 μeq L^{-1} in the A horizon to 78.24 and 85.60 μeq L^{-1} in the Bw and Cb horizons, presumably due to root uptake in soil (Table 1). Cation concentrations for Ca^{2+} and K^+ were also found to significantly decrease from the A horizon to the Bw and Cb horizons. Ca^{2+} concentrations in the A horizon decreased from 51.07 μeq L^{-1} to 31.04 and 35.93 μeq L^{-1} in the Bw and Cb horizons, respectively; and K^+ concentrations decreased from 23.19 μeq L^{-1} to 9.57 and 9.85 μeq L^{-1}. Mean annual pH of the soil water increased from 4.01 in horizon A to 4.41, and 4.47 in horizons Bw and Cb. Mean annual ANC also increased through

the soil horizons, as well from -148.58 μeq L^{-1} in the A horizon to –72.09 μeq L^{-1} in Bw horizon, and and further to –35.18 μeq L^{-1} in the Cb horizon. Other than ANC, pH and ion concentrations were similar between the Bw and Cb horizons.

Conclusions

Studies of long-term chemistry data from 1991 to 2007 showed that the control of sulfur emission was actually working in the NDW by reducing sulfate deposition. However, stream sulfate concentration remained constant during this study period, because of soil retention of more than 50% sulfate by adsorption. The relatively stable retention percentage of sulfate indicated the NDW was not saturated with sulfate and could accumulate more sulfate in future. In contrast to sulfate, stream nitrate was decreasing over time, even though deposition of inorganic nitrogen was increasing or relatively stable. This is primarily due to increasing plant uptake of nitrogen, which retain around 26.63% of total deposited inorganic nitrogen. Among them, more than 95% of deposited NH_4^+ was converted to NO_3^- in the shallow soil layer. The decreasing trend of nitrate concentration was compensated by decreasing trend of base cations, resulting in relatively stable stream pHs and ANC. Base cations, except K^+, was depleted from this watershed. Those results imply that the NDW streams are not recovered from acidification yet, and the depletion of base cations was prolonging watershed recovery from acidification. Findings from this NDW study provide essential information to understand the biogeochemical processes inside and predict future water chemistry in high-elevation GRSM watersheds.

Acknowledgements

Research for this project was funded by the U.S. Department of Interior, National Park Service Cooperative Agreement Grant No. 1443-CA-5460-98-006 (Amendment 10), and the US Environmental Protection Agency through the University of Tennessee Natural Research Policy Center, USEPA Grant No. EM-83298901-1. Because of the 17-year monitoring effort, the individuals who have helped in sample collection, laboratory analysis, and data management over the years are too numerous to list. In recent years, we are thankful for the support of Keil Neff, Tom Zimmerman, and Lee Mauney.

References

Barker, M., Van Miegroet, H., Nicholas, N. S., and Creed, I. F. (2002). "Variation in overstory nitrogen uptake in a small, high-elevation southern Appalachian spruce-fir watershed." *Can. J. For. Res.*, 32(10): 1741-1752

Cai, M., Schwartz, J.S., Robinson, B., Moore, S.E., and Kulp, M.A. (2009). "Long-term effects of acidic deposition on water quality in a high-elevation Great Smoky Mountains National Park Watershed: use of an ion input-output budget." In review.

Castro, M.S., and Morgan II, R.P. (2000). "Input-output budget of major ions for a forested watershed in Western Maryland." *Water Air Soil Poll.,* 119: 121-137.

Cook, R.B., Elwood, J.W., Turner, R.R., Bogle, M.A., Mulholland, P.J., and Palumbo, A.V. (1994). "Acid-base chemistry of high-elevation streams in the Great Smoky Mountains." *Water Air Soil Poll.,* 72: 331-356.

Eagar, C. (1984). "Review of the biology and ecology of the balsam woolly aphid in southern Appalachian spruce-fir forests." In P.S. White (Ed.). *The Southern Appalachian Spruce-fir Ecosystem: Its Biology and Threats. Research/ Resource Management Report SER-71.* USDI, National Park Service, Southeast Regional Office, Atlanta, GA.

Fernandez, I.J., Rustad, L.E., Norton, S.A., Kahl, J.S., and Cosby, B.J. (2003). "Experimental acidification causes soil base cation depletion at the Bear Brook Watershed in Maine." *Soil Sci. Soc. Am. J.,* 67: 1909–1919.

Forsius, M., Vuorenmaa, J., Mannio, J., and Syri, S. (2003). "Recovery from acidification of Finnish lakes: regional patterns and relations to emission reduction policy." *Sci. Total Environ.,* 310: 121-132

Fölster, J., Bishop, K., Krám, P., Kvarnäs, H., and Wilander, A. (2003). "Time series of long-term annual fluxes in the streamwater of nine forest catchments from the Swedish environmental monitoring program (PMK 5)." *Sci. Total Environ.,* 310: 113-120

Hampson, P.S. (2008). "The hydrologic drought of 2007: a historical perspective." In *the Eighteenth Tennessee Water Research Symposium*, A-1.

Hayter, A.J. (1984). "A Proof of the Conjecture That the Tukey-Kramer Multiple Comparisons Procedure Is Conservative." *Ann. Stat.,* 12(1): 61-75.

Holzmueller, E.J., Jose, S., and Jenkins, M.A. (2007). "Influence of calcium, potassium, and magnesium on Cornus florida L. density and resistance to dogwood anthracnose." *Plant Soil,* 290: 189-199.

Jenkins, M.A. (2007). "Vegetation communities of Great Smoky Mountains National Park." *Southeast. Nat.,* Special Issue 1: 35-56

JMP. (2005). *JMP 6 documentation set English,* SAS Institute Inc, North Carolina.

Johnson, D.W., and Lindberg, S.E. (*eds*). (1992). *Atmospheric deposition and nutrient cycling in forest ecosystems: a synthesis of the Integrated Forest Study.* Springer-Verlag, New York.

King, P.B., Neuman, R.B., and Hadley, J.B. (1968). *Geological Survey Professional Paper #587*, Washington D.C.

Lawrence, G.B. (2002). "Persistent episodic acidification of streams linked to acid rain effects on soil." *Atmos. Environ.,* 36: 1589–1598.

Logan, J. (2008). "Trends in Tennessee droughts." In *the Eighteenth Tennessee Water*

Research Symposium, A-2.

McCracken, R.J., Shanks, R.E., and Clebsch, E.E.C. (1962). "Soil morphology and genesis at higher elevations of the Great Smoky Mountains." *Soil Sci. Soc. Am.* Pro., 26: 384-388.

Moore, P.T., Van Miegroet, H., and Nicholas, N.S. (2007). "Relative role of understory and overstory in carbon and nitrogen cycling in a southern Appalachian spruce-fir forest." *Can. J. For. Res.*, 37: 2689-2700.

Mulholland, P.J. (1993). "Hydrometric and stream chemistry evidence of three storm flowpaths in Walker Branch Watershed." *J. Hydrol.,* 151: 291-316.

Nicholas, N.S., Zedaker, S.M., and Eagar, C. (1992). "A comparison of overstory community structure in three southern Appalachian spruce-fir forests." *B. Torrey Bot. Club,* 199: 316-322.

Peterjohn, W.T., Adams, M.B., and Gilliam, F.S. (1996). "Symptoms of nitrogen saturation in two central Appalachian hardwood forest ecosystems." *Biogeochemistry,* 35(3): 507-522.

Robinson, R.B., Barnett, T.W., Harwell, G.R., Moore, S.E., Kulp, M., and Schwartz, J.S. (2008). "pH and acid anion time trends in different elevation ranges in the Great Smoky Mountains National Park." *J. Environ. Eng.,* 134(9): 800-808.

Robinson, R.B., Wood, M.S., Smoot, J.L., and Moore, S.E. (2004). "Parametric modeling of water quality and sampling strategy in a high-altitude Appalachian stream." *J. Hydrol.,* 287: 62-73

Silsbee, D.G., and Larson, G.L. (1982). "Water quality of streams in the Great Smoky Mountains National Park." *Hydrobiologia,* 89: 97-115.

Stoddard, J.L., Jeffries, D.S., Lükewille, A., Clair, T.A., Dillon, P.J., Driscoll, C.T., et al. (1999). "Regional trends in aquatic recovery from acidification in North America and Europe." *Nature,* 401(6753): 575-578.

Tomlinson, G.H. (2003). "Acidic deposition, nutrient leaching and forest growth." *Biogeochemistry,* 65: 51-81.

Ulrich, B. (1983). *Interaction of forest canopies with atmospheric constituents: SO_2, alkali and earth alkali cations and chloride*. In Effects of Accumulation of Air Pollutants in Forest Ecosystems Ulrich B, Pankrath J (eds). Dordrecht Reidel Publication, Holland, 33-45.

USDA-ARS. (1979). *Field manual for research in agricultural hydrology.* In: Agricultural Handbook 224. US Department of Agriculture, Washington DC.

Ukonmaanaho, L., Starr, M., Ruoho-Airola, T. (1998). "Trends in sulfate, base cations and H^+ concentrations in bulk precipitation and throughfall at integrated monitoring sites in Finland 1989-1995." *Water Air Soil Poll.,* 105: 353-363

Van der Maas, M.P., Van Breemen, N., and Van Langenvelde, I. (1991). *Estimation of atmospheric deposition and canopy exchange in two Douglas fir stands in the Netherlands,* Internal publication, Department of Soil Science and Geology, Agricultural University of Wageningen, The Netherlands.

Van Miegroet, H., Johnson, D.W., and Todd, D.E. (1993). "Foliar response of red spruce saplings to fertilization with Ca and Mg in the Great Smoky Mountains National Park." *Can. J. For. Res.*, 23: 89-95.

Van Miegroet, H., Moore, P.T., Tewksburg, C.E., and Nicholas, N.S. (2007). "Carbon sources and sinks in high-elevation spruce-fir forests of the Southeastern US."

Forest Ecol. Manag., 238: 249-260.

Watmough, S.A., Aherne, J., Alewell, C., Arp, P., Bailey, S., Clari, T., et al. (2005). "Sulfate, nitrogen and base cation budgets at 21 forested catchments in Canada, the United States and Europe." *Environ. Monitor. Assess.,* 109: 1-36.

Estimation of TMDLs and Margin of Safety Under Conditions of Uncertainty

Mohamed M. Hantush[1]

[1] National Risk Management Research Laboratory, U.S. EPA, Cincinnati, OH, 45268; PH (513) 569-7089; FAX (513) 569-7105; email: hantush.mohamed@epa.gov

ABSTRACT

In TMDL development, an adequate margin of safety (MOS) is required in the calculation process to provide a cushion needed because of uncertainties in the data and analysis. Current practices, however, rarely factor analysis' uncertainty in TMDL development and the MOS is largely arbitrarily selected. This paper presents a formal methodology for the estimation of TMDL and MOS as a function of analysis uncertainty, degree of protection provided, and fuzziness in water-quality standards. The probabilistic methodology is demonstrated through a hypothetical lake-sediment phosphorus model and eutrophication problem. Impacts of parametric uncertainty on the TMDL distribution and MOS are discussed. The performance of the widely used first-order approximation (FOA), with Gaussian and log-normal assumptions, is tested against the Monte Carlo (MC) method. The dependence of the MOS on the degree of protection provided against violating water quality standard is computed.

INTRODUCTION

Section 303(d) of the Clean Water Act (CWA) requires all states to develop and implement Total Maximum Daily Loadings (TMDLs) for their impaired water bodies and water bodies threatened to become impaired. Estimating the maximum load of pollutants that will not exceed water quality standards is part of the TMDL process and implies a known cause-and-effect relationship; once impaired water bodies are identified through assessment of water quality data collected by a variety of monitoring techniques, computer modeling is typically then used to estimate required reduction in pollutant loadings such that water quality standards are met within MOS. The MOS is intended to account for uncertainty about the relationship between pollutant loads and receiving water quality, and to provide a given degree of assurance that water quality standards will be met. Explicit and implicit approaches have been used for the estimation or selection of MOS (Dilks and Freedman, 2004; and Shirmohammadi et al., 2006). However, these approaches are subjective and, with a few exceptions (Borsuk et. al. 2002; Zhang and Yu, 2004; and Shirmohammadi et al., 2006), rarely have reflected model uncertainty in the MOS. Further, the relationship between the MOS and the degree of protection provided is opaque, if not existing, in most of the currently practiced TMDLs (Dilks and Freedman, 2004). In a comprehensive report, NRC (2001) cautioned against the practice of arbitrary selection of the MOS and instead recommended uncertainty analysis as the base for MOS determination.

While in current TMDLs development, fixed water quality numeric targets are often imposed, it is likely that these criteria are themselves subject to uncertainty. That is, the adequacy of the criterion as a measure (surrogate) for the designated use is not clear cut. For example, in TMDL analyses discrete impaired and unimpaired cutoffs do not exist in natural systems (U.S. EPA, 1999) and a degree of uncertainty might be associated with the designated-use water quality target value; in which case it is no longer known with certainty. Further, methods for selecting target values for designated use indicators invariably vary among experts and states. A TMDL based on a single, predefined criterion, therefore, might lead to a false sense of reliability in maintaining the designated use of a water body even when model uncertainty is factored into the analysis.

This paper outlines a probabilistic methodology for the estimation of TMDLs under conditions uncertainty. A formal methodology for the estimation of MOS on the basis of analysis' uncertainty as well as uncertainty in water quality standards is presented. The methodology, which is suitable for measurable water quality standards, relates calculated TMDLs and associated MOS to a prescribed degree of protection provided.

TMDLs

TMDL is the maximum pollutant load a water body can receive without violating water quality standards within margin of safety (MOS). This total load includes point sources (waste load discharge), nonpoint sources (stormwater runoff and groundwater flow), as well as MOS, which provides a cushion needed because of uncertainty naturally associated with estimates. A TMDL therefore can be expressed as

$$\text{TMDL} = \Sigma \text{WLA} + \Sigma \text{LA} + \text{MOS} \quad (1)$$

where TMDL is the system loading capacity or maximum pollutant load; WLA is point sources (wasteload) allocation; LA is nonpoint source load allocation including natural background; and MOS is margin of safety intended to account for uncertainty embedded in the analysis.

The most common approach for the estimation of MOS is the explicit selection of MOS as a percentage of the TMDL, a concept that is equivalent to a safety factor. The implicit approach is another widely adopted approach in which the margin of safety is introduced implicitly through the use of conservative assumptions in calculating the allowable load. In the implicit approach, neither the degree of protection nor the magnitude of the resulting MOS is known (Dilks and Freedman, 2004). In the explicit approach, model uncertainty is neither calculated nor reflected in the selection of MOS, and the TMDL calculation becomes independent of the level of uncertainty in the analysis or modeling exercise.

A formal methodology is presented below for TMDL estimation under conditions of uncertainty and from which MOS can be computed as a function of reliability (or degree of protection provided) and fuzziness in the water quality standard.

PROBABILISTIC RISK-BASED APPROACH

By definition (Eq. 1), a TMDL is a conservative estimate of the total point source and nonpoint source load that a water body can assimilate without violating water quality standards. Rather than relying on arbitrarily selected MOS, a more transparent

approach is to fully utilize the uncertainty in model predicted water quality indicator to insure compliance with designated-use criterion, but with a desired level of confidence. Such an approach makes explicit use of both uncertain estimate of water quality indicator and fuzzy designated-use criterion in TMDL estimation. Mathematically, the problem can be posed probabilistically as limiting the risk of violating water quality standards:

$$P\{Y \geq Z\} \leq \beta \tag{2}$$

where Y is a water quality indicator (e.g., pollutant concentration [ML^{-3}]) describing the condition of the water body, measured or predicted by empirical or mathematical models; Z is water quality numeric target selected for designated-use attainment of the water body; and β is the acceptable risk or probability of failure whose choice is a matter of policy. Y is random due to combinations of model inadequacies, parametric uncertainty, and measurement errors. If Y is purely based on observations, its uncertainty stems from natural (spatiotemporal) variability and measurement errors. Z is a random variable if viewed as a fuzzy, measurable surrogate for designated-use attainment.

By treating Z as a fuzzy measure, but known with confidence to fall in some range [a, b], a mathematical expression for the probability of noncompliance $P\{Y > Z\}$ can be obtained by integrating the joint probability density function $f_{Y,Z}(y,z)$ over the domain of criterion violation and assuming statistically independent Y and Z

$$\begin{aligned} P\{Y > Z\} &= \int_a^b \int_z^\infty f_{Y,Z}(y,z)\, dy\, dz \\ &= 1 - \int_a^b F_Y(z)\, f_Z(z)\, dz \end{aligned} \tag{3}$$

Certain water quality problems require the exceedance of a minimum threshold (e.g., oxygen levels), in which case, none compliance risk is $P\{Y \leq Z\} = 1 - P\{Y > Z\}$.

Equation 3 is useful if the analysis permits any of the known family of parametric distributions for both water-quality variable and the regulatory criterion. For example, a parametric PDF may be fit to measurements of Y using the method of moments or maximum-likelihood estimates. A suitable distribution for Z is the triangular distribution, $f_Z(z) \sim T(a,z_m,b)$, especially when available information reveals a most likely value in addition to minimum and maximum values of the variable

The noncompliance probability, $P\{Y > Z\}$, can be computed with MC simulation or by evaluating the integral in Eq. 3, analytically or numerically, for specific CDFs and PDFs of Y and Z, respectively.

In the following section, we demonstrate application of the theory to a hypothetical eutrophication TMDL problem. The selected water quality indicator for designated-use criterion is chlorophyll *a* concentration.

LAKE-PHOSPHORUS TMDL APPLICATION

Figure 1 depicts the conceptual lake-sediment-phosphorus model. The lake is divided into two completely-mixed compartments, water body and bottom sediments. Flow and sediment transport within lake are assumed at steady-state. Sediments enter and leave the lake by advection, subject to deposition to the lake bottom, resuspension back to the water column, and burial. The bottom sediment layer receives

depositional flux, releases some of the sediments back to the water column, and is buried by sedimentation. Phosphorus is usually highly sorbed to sediment particles and the dissolved component is assumed to be at equilibrium with the adsorbed phase in both the lake water and the bottom sediment. Mass transfer of dissolved phosphorus is assumed to occur across the sediment-water column interface by diffusion, and sediment-bound phosphorus is subject to resuspension.

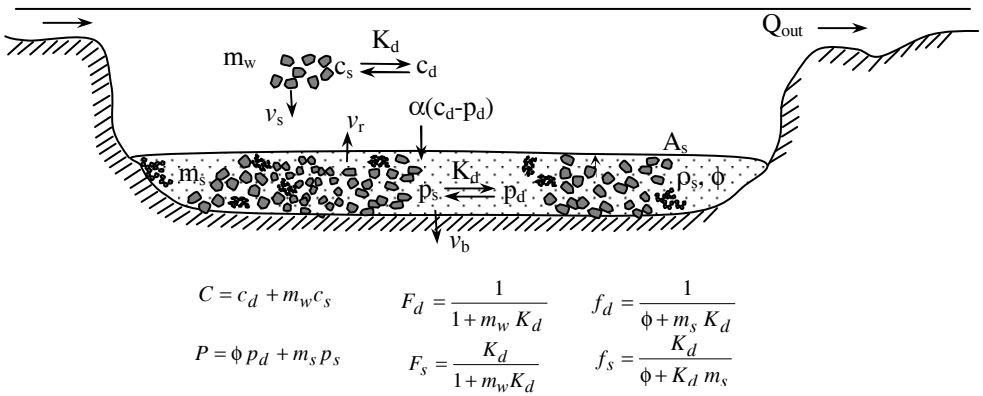

Figure 1. Schematics of lake-sediment phosphorus processes

Mass balance of sediment in lake can be described by the following ordinary differential equation (e.g., Chapra, 1997)

$$V\frac{dm_w}{dt} = Q_{in}\, m_{w,in} - v_s A_s\, m_w + v_r\, A_s\, m_s - Q_{out}\, m_w \tag{4}$$

Mass balance of lake-bottom sediment is

$$V_s\frac{dm_s}{dt} = v_s\, A_s\, m_w - v_r\, A_s\, m_s - v_b\, A_s\, m_s \tag{5}$$

Mass balance of total phosphorus in lake water

$$V\frac{dC}{dt} = Q_{in}\, C_{in} - v_s\, A_s F_s C + \alpha A_s (f_d P - F_d C) + v_r A_s\, f_s P - Q_{out}\, C \tag{6}$$

Mass balance of dissolved phosphorus in sediment

$$V_s\frac{dP}{dt} = v_s\, A_s F_s C - \alpha A_s (f_d P - F_d C) - v_r A_s f_s P - v_b A_s P \tag{7}$$

where m_w is sediment concentration in lake water [ML^{-3}]; $m_{w,in}$ is inflow sediment concentration [ML^{-3}]; m_s is lake-bottom sediment concentration [ML^{-3}]; C is total phosphorus concentration in lake water [ML^{-3}]; P is total phosphorus concentration in sediment layer [ML^{-3}]; V is lake water volume [L^3]; Q_{in} is lake inflow rate [L^3T^{-1}]; Q_{out} is lake outflow rate [L^3T^{-1}]; A_s is lake bottom surface area [L^2]; V_s is volume of sediment layer [L^{-3}]; v_s is settling velocity [LT^{-1}]; v_r is resuspension/recycling velocity [LT^{-1}]; v_b is burial velocity [LT^{-1}]; α is effective mass-transfer velocity coefficient at the sediment-water interface [T^{-1}]; f_d, f_s [L^3M^{-1}], F_d, and F_s [L^3M^{-1}] are partition coefficients relating dissolved and sorbed-phase phosphorus concentration to total phosphor concentration (equations shown in Fig. 1, where p_d is pore-water phosphorus concentration in bottom sediments [ML^{-3}]; p_s is sorbed phosphorus

concentration in bottom sediments [MM^{-1}]; K_d is phosphorus sorption coefficient [L^3M^{-1}]); ϕ is sediment layer porosity [L^3L^{-3}]; and ρ_s is sediment particle density [ML^{-3}]. For illustrative purposes, we assume $\alpha = D^*/\delta$, where D^* is free-water phosphorus diffusion coefficient [L^2T^{-1}]; and δ is thickness of sediment-water interface diffusion boundary layer [L].

The total phosphorus concentration and load input to the lake, respectively, are given by

$$C = c_d + m_w c_s \tag{8}$$

$$W = Q_{in} c_{d,in} + Q_{in} m_{w,in} c_{s,in} \tag{9}$$

where W is total phosphorus loading rate [MT^{-1}]; c_d is dissolved phosphorus concentration in lake water [ML^{-3}]; c_s is sediment-bound phosphorus concentration in lake water [MM^{-1}]; $c_{d,in}$ is inflow dissolved phosphorus concentration [ML^{-3}]; and $c_{s,in}$ is inflow sediment-bound phosphorus concentration [MM^{-1}].

Chlorophyll a, *Chl a*, which reflects the nuisance conditions caused by excessive algal blooms, is a more direct measure of eutrophication than total phosphorus concentration. For example, Schnoor (1996) report this Chl a-Total Phosphorus relationship

$$Y = 0.081\, C^{1.46}\ , \qquad R = 0.95 \tag{10}$$

where Y denotes *Chl a* concentration; both Y and C have the units of μg/L (mg/m^3).

Table 1 lists all model parameters, their units, and assumed probability distributions and related parameters selected from typical values and ranges reported in the literature. A hypothetical bottom lake surface area, A_s, of 5×10^6 m^2 is assumed. Dissolved phosphorus is assumed to be 5% of the sorbed phosphorus in (g/m^3): $c_{d,in} = 0.05\, m_{w,in}\, c_{s,in}$. Z is *Chl a* enforced water quality target concentration; it is assumed to be a random variable and follows a triangular distribution with minimum, most probable (mode), and maximum values of 2.7, 10, and 14 μg/L, respectively. $P\{Y>Z\} > 0.1$ implies a eutrophic condition at greater than 10% level of confidence, in which case, for the TMDL to be achieved with 90 % compliance, total phosphorus loading rate, W, should be reduced such that $P\{Y>Z\}\leq 0.1$.

Vollenwieder and Kerekes (1980) reported *Chl a* concentration between 2.7 and 78 μg/L as the range for eutrophication and 3 to 11 μg/L for mesotrophic status. The overlap is among the reasons for treating Z as a random variable whose probability distribution expresses the degree in one's belief that compliance based on particular Z values would restore or prevent the degradation of the water body.

Equations 4-7 are solved at steady state for C as a function of W and other related flow, hydrodynamic, and geochemical parameters. For simplicity, and without loss of generality, it is assumed that $Q_{out} = Q_{in} = Q$.

For each MC simulation 100,000 independent parameter sets were sampled by randomly generating parameter values from their respective PDFs in Table 1. An ensemble of model outputs was generated with 100,000 evaluations of the steady-state solution for C, and a similar size ensemble of Z was generated from its corresponding PDF in Table 1. The MC simulation and the sampled Z yielded $P\{Y \geq Z\} = 0.73$. A reduction in total phosphorus loading rate, W, was therefore needed to reduce $P\{Y \geq Z\}$ to 0.1 and achieve the TMDL at 90% compliance. From Eq. 9, it is

evident that either or both of the two variables $m_{w,in}$ and $c_{s,in}$ can be manipulated to achieve this target (recall, $c_{d,in}$ is assumed to be a fixed fraction of $c_{s,in}$).

Table 1. Lake-sediment phosphorus model parameters and assumed probability distributions

Parameter	Unit	Distribution	Parameter	Unit	Distribution
Q	m^3/yr	~N(2×10^8,2×10^6) [a]	D^*	m^2/yr	~U(1.5,2.32) [d]
$m_{w,in}$	g/m^3	~N(35,5)	δ	mm	~log-N(1.0,1.0)
$c_{s,in}$	g/g	~log-N(10^{-3},4×10^{-4})[b]	ϕ	m^3m^{-3}	~T(0.4,0.7,0.95)
v_s	m/yr	~log-N(37,20)	ρ_s	g/cm^3	~T(1,2.6,2.7)
K_d	m^3/g	~log-N(4.87×10^{-4}, 2.59×10^{-5})	Z	mg/m^3	~T(2.7,10,14)
v_b	m/yr	~T(8×10^{-4},0.005,0.01) [c]			

[a] N(λ, σ) denotes normally-distributed random variable with mean λ and standard deviation σ.
[b] log-N(λ, σ) denoted log-normally distributed random variable with mean λ and standard deviation σ.
[c] T(a,b,c) denotes triangular distribution of random variable with minimum value a, mode c, and maximum value c.
[d] U(a,b) denotes a uniformly distributed random variable in the interval [a,b].

Figure 2 depicts the results of two selected TMDL strategies; the first seeks the reduction of sediment loading concentration, $m_{w,in}$, and the second involves the reduction of sediment-bound phosphorus concentration, $c_{s,in}$. MC simulation and a nonlinear-based root's finding technique were implemented to identify the mean $m_{w,in}$, or mean $c_{s,in}$ such that $P\{Y \geq Z^*\} = 0.1$. The variance of both management-control variables was held constant during the search procedure. The search procedure was programmed and executed using MATLAB software.

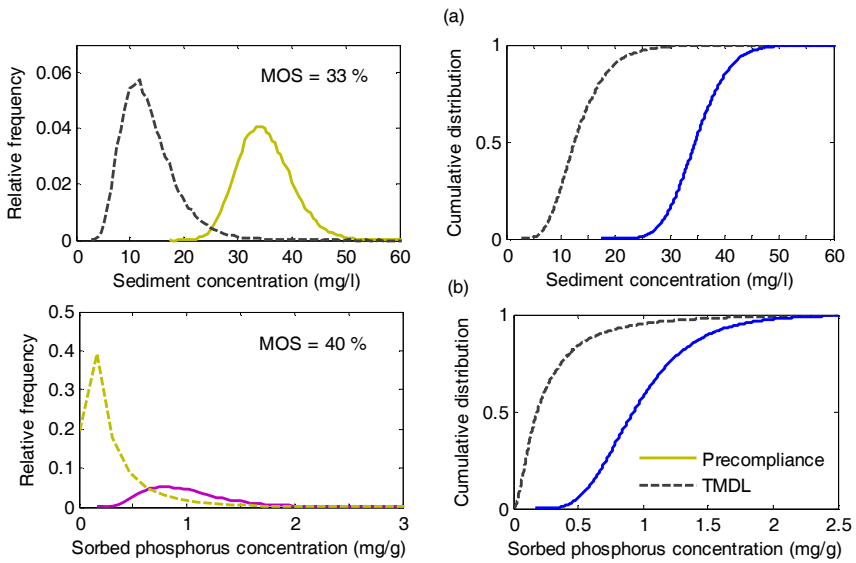

Figure 2. Monte Carlo simulated pre-compliance (solid-line) and 90% compliance (β =0.1) (dashed-line) relative frequencies and cumulative distributions: (a) Loading sediment concentration, $m_{w,in}$; and (b) loading sorbed phosphorus concentration, $c_{s,in}$. Results are based on MC simulation with 100,000 model runs.

The upper panel (a) in Fig. 2 shows relative frequency (100 bins) and cumulative distribution functions of pre-compliance sediment loading, $m_{w,in}$, and those required to achieve the phosphorus TMDL at 90% confidence (i.e., $\beta = 10\%$). The lower panel (b) shows similar output for the input sediment-bound phosphorus concentration, $c_{s,in}$. For the first strategy, an estimated 62% reduction in mean total phosphorus loading rate, W, was needed to meet the 10% requirement; whereas the second strategy yielded a higher 69% reduction in W.

The increased required load reduction in the second strategy compared to the first highlights the importance of parametric uncertainty on model estimated TMDL. Inspection of data in Table 1 shows higher uncertainty in $c_{s,in}$ than $m_{w,in}$: the coefficient of variation associated with the former is almost three times higher than the latter. Although not shown in a figure, the relative frequency of the computed total phosphorus TMDL was relatively more skewed to the left for the second strategy, in favor of higher probability densities for lower phosphorus loading rate values, than for the first strategy; again, this is attributed to higher uncertainty in $c_{s,in}$.

MARGIN OF SAFETY ((MOS)

Note that a TMDL has been computed taking into consideration uncertainty in the analysis and for a given risk of violating the water quality standard, but without an explicit reference to (or even the need for) the margin of safety (MOS). For completeness, however, MOS may be computed as a function of the desired degree of protection, but in a more rigorous and formal way than the aforementioned implicit and explicit approaches.

The MOS can be computed as the difference between required load reduction neglecting analysis uncertainty and the required load reduction taking into consideration the uncertainty. In a normalized form, MOS may be estimated as follows:

$$MOS = \frac{LR2 - LR1}{L_p} \times 100\,, \quad LR1 = L_p - L_c, \quad \text{LR2} = L_p^{*} - L_c^{*} \tag{11}$$

where L_p is pre-compliance load computed with expected parameter values (i.e., deterministic); L_c is compliance load computed with expected parameter values and expected Z; L_p^{*} is mean pre-compliance load based on random parameters and Z; and L_c^{*} is mean compliance load based on random parameters and Z. Noting that L_p is a first-order approximation of L_p^{*}, and for this particular example, $L_p \approx L_p^{*}$, we have

$$MOS \approx \frac{L_C - L_C^{*}}{L_p} \tag{12}$$

Note that the reduction in the required mean phosphorus load is expressed relative to the deterministic pre-compliance load. For the data in Table 1, MC simulation yielded MOS = 33% for the TMDL strategy involving $m_{w,in}$ as the management-control variable, whereas the strategy based on $c_{s,in}$ control produced MOS = 40%; these results are consistent with the estimated larger mean load reduction required for the second strategy, as discussed above.

Figure 3 plots MOS for the two management scenarios based on MC simulation of steady-state total phosphorus concentration, C, and normal and log-normal

approximation of *C*. For Gaussian and log-normal *C*, the mean and variance are estimated using First-Order Approximation (FOA) of steady-state *C* and evaluating the integral in Eq. 3 analytically for normal or log-normal *C*. MOS values computed on the basis of 100,000 MC model runs are deemed sufficiently accurate.

As the standard deviation of both $m_{w,in}$ or $c_{s,in}$ increases, the assumption of normality deviates and considerably overestimates the MOS values; this is evident when the coefficient of variation of both parameters exceeds one. The deviations are much less conspicuous for log-normal approximation of *C*; however, the computed MOS values underestimated the MC-based values.

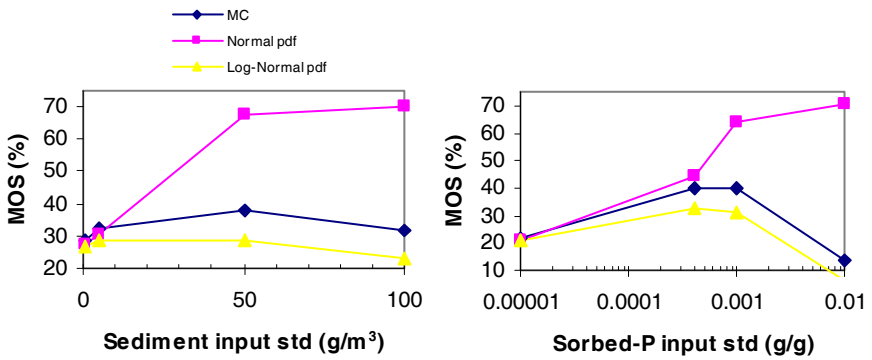

Figure 3. Comparison of MC method with FOA and normal and log-normal approximation of total phosphorus concentration, *C*.

The variation of MOS with β is shown in Fig. 4. The larger the value of β, the smaller the level of protection against violating the water quality standard, the smaller the MOS. Smaller β is associated with larger MOS, consequently, greater load reduction and costlier management actions.

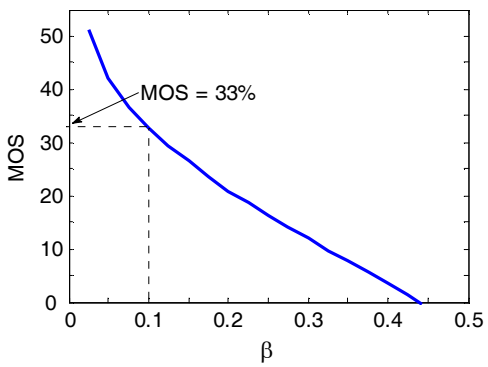

Figure 4. MOS versus β.

A NOTE ON BAYESIAN UPDATE

It's worth noting that as new monitoring data become available and more knowledge about the dynamics of total phosphorus are gained or better relationship between *Chl a* and *P* is identified, the computed TMDL distribution and associated MOS can be updated using Bayesian inferences and associated uncertainties might be reduced. With the knowledge gained and conditioning of prior TMDL and parameters'

distributions on new data, the initial TMDL forecast can be revised and improved. Consequently, reduction of the MOS can potentially lead to significant reduction in TMDL implementation cost. In this regard, Bayesian techniques that integrate model calibration with uncertainty estimation hold promise for adaptive TMDLs. Such techniques include the Generalized Likelihood Uncertainty Estimation method (GLUE) (Beven, 2006), classical Bayesian Analysis (e.g., Thiemann et al., 2001), and Ensemble Kalman Filtering (Kim et al., 2007). These methods are best positioned to address a TMDL within an adaptive implementation framework, because they combine the value of empirical evidence and modeling.

CONCLUSIONS

The margin of safety (MOS) in TMDL development is intended to account for the uncertainty embedded in the modeling exercise. Current practices, however, seldom consider model or analysis uncertainty as a basis for MOS estimation; instead, MOS is subjectively selected. Consequently, the relationship between calculated TMDL and MOS and the degree of protection provided is also left unknown in most of currently established TMDLs. This paper outlined a formal methodology for the estimation of TMDLs and required MOS under conditions of uncertainty.

A hypothetical lake-sediment phosphorus model illustrated the methodology; however, it can be extended to solve real TMDL problems through the use of system analysis and optimization. The PDF and CDF of the total phosphorus TMDL were derived using Monte Carlo (MC) simulation, and the associated MOS was computed on the basis of model uncertainty and as a function of the degree of protection provided (i.e., compliance probability).

The results showed that parametric uncertainty influences required mean total phosphorus load reduction, the probability distribution of required TMDL and associated MOS. Further, results illustrated that under relatively high parametric uncertainty the widely used first-order approximation and Gaussian or log-nomality assumption could lead to significant overestimation or underestimation of the MOS and exaggeration or underestimation of required load reductions to achieve the TMDL.

The value of monitoring and processes knowledge update on reducing uncertainty and revising TMDL estimation by means of Bayesian deductions has yet to be demonstrated and certainly constitutes an endeavor worthy of future research.

REFERENCES

Beven, K. (2006). “A manifesto for the equifinality thesis”. *J. Hydrol*., 320, 18-36.

Beven, K. and Binley, A. (1992). “The future of distributed models: Model calibration and uncertainty prediction”. *Hydrol. Process*., 6: 279-298.

Borsuk, M. E., Stow, C. A., and Reckhow, K. H. (2002). “Predicting the frequency of water quality standard violations: A probabilistic approach for TMDL development”. *Environ. Sci. & Technol*., 36(10), 2109-2115.

Chapra, S. C. (1997). *Surface water-quality modeling*, McGraw-Hill, NY.

Dilks, D. W., and Freedman, P. L. (2004). “Improved consideration of the margin of safety in Total Maximum Daily Load development”. *J. Environ. Engrng*., 130 (6), 690-694.

Kim, S., Tachikawa, Y., and Takara, K. (2007). "Applying a recursive update algorithm to a distributed hydrologic model". *J. Hydrol. Engrng*., 12(3), 336-344.

NRC. (2001). *Assessing the TMDL approach to water quality management*, National Research Council, National Academy Press, Washington, D.C.

Schnoor, J. L. (1996). *Environmental modeling: Fate and transport of pollutants in water, air, and soil*, John Wiley & Sons, NY.

Shirmohammadi, A., Chaubey, I., Harmel, R. D., Bosch, D. D., Muñoz-Carpena, R., Dharmasri, C., Sexton, A., Arabi, M., Wolfe, M. L., Frankenberger, J., Graff, C., and Shorabi, T. M. (2006). "Uncertainty in TMDL models". *Trans. ASABE*, 49(4): 1033-1049.

Thiemann, M., Trosset, M., Gupta, H., and Sorooshian, S. (2001). "Bayesian recursive parameter estimation for hydrologic models". *Water resour. Res*., 37(10), 2521-2535.

U.S. Environmental Protection Agency. (1999). "Protocols for developing nutrient TMDLs", *Rep*., EPA-841-B-99-007, Office of Water, Washington, D.C.

Vollenweider, R. A., and Kerekes, J. J. (1980). "Background and summary results of the OECD cooperative program on eutrophication". In *International Symposium on lnland Waters and Lake Restoration*. EPA 440/5-81-010. U.S. Environmental Protection Agency, Washington, DC.

Zhang, H. R., and Yu, S. L. (2004). "Applying the first-order error analysis in determining the margin of safety for Total Maximum Daily Load computations". *J. Environ. Engrng*., 130(6), 664-673.

Probable maximum precipitation for 24 h duration over four central provinces in Iran

M. Naseri Moghaddam[1]
S. Ghazanfari [2]
B. Ghahraman [3]
K. Davari[4]

1- MSc. student of Irrigation and Drainage engineering, water engineering department, Ferdowsi university of Mashhad, P.O. Box: 9177948978 Iran. Email: mahyar.nm@gmail.com, phone: +98-9155173267.
2- Ph.D. student of water science and engineering, water engineering department, Ferdowsi University of Mashhad, Iran.
3- Associate professor, water engineering department, Ferdowsi University of Mashhad, Iran, email: bijangh@ferdowsi.um.ac.ir.
4- Assistant professor, water engineering department, Ferdowsi University of Mashhad, Iran.

ABSTRACT

Probable maximum precipitation (PMP) is a common way to synthesize corresponding probable maximum floods (PMF) to design large hydraulic structures in short-data cases. The PMP for many stations in Iran and other places using the Hershfield formula is routinely estimated as the mean plus 15 standard deviations processed from one-day yearly maximum rainfall values. However, the value of 15 may not be suitable for all stations with different climatic specifications. In this paper, yearly maximum one day rainfall data of 23 synoptic and climatology stations in the four central provinces of Iran were analyzed in an attempt to estimate PMP for a one day duration based on an appropriate frequency factor. Based on the actual maximum daily rainfall data of these stations the highest value of frequency factors was found to be 7.63 for one day duration. The frequency factor obtained for each station was subsequently used to estimate one-day point PMP values. The mean ratio of one-day PMP values to the highest observed one-day rainfall was about 1.3 over the study area. The PMP maps are considered important tools to determine reliable and consistent estimates for any location in the area for large hydraulic structure designs. Using these PMP estimates a generalized pattern for the spatial distribution of one day PMP could be demonstrated.

Key words: PMP, precipitation, Iran, frequency.

INTRODUCTION

The need for the development of water resources has become of considerable importance with a view to ensuring sufficient potable and industrial water supplies, providing irrigation for food production, flood control and power generation. As a result, great amounts of money are invested each year for the construction of different water resources projects such as large dams, diversion dams, storage reservoirs, etc. Probable maximum precipitation (PMP) is a common way to synthesize corresponding probable maximum floods (PMF) in short-data cases.

The PMP is defined as the greatest depth of precipitation for a given duration that is meteorologically possible over a given station or a particular area and geographical location at a certain time of year (WMO, 1986). This definition has remained largely unchanged since first being introduced by United States meteorologists in the middle 1930's, and makes no allowance for the effects of climate change.

There are two main methods for calculating PMP including hydro-meteorological approaches and statistical analyses of extreme rainfalls. Due to the shortage of data for applying the first method, there is a great tendency to adopt the second one. In statistical approaches the estimates of PMP rainfall at a particular location or area are determined from the frequency distribution fitted to the annual maximum rainfall data. Therefore, the method requires a series of maximum annual daily rainfall at an observation point, yet the partial duration series may also be an alternative (Ghahraman, 2004).

Hershfield (1961, 1965) was a pioneer who developed a statistical method for estimating PMP values for small areas around the world. The use of the Hershfield method has shown that the PMP estimates obtained by this method are closely comparable to those obtained by the elaborate physical method. Having this in mind, several researches in Iran have employed Hershfield's statistical techniques extensively for estimating PMP for stations having a long period of rainfall records (Ghahraman, 1994; Khalaji, 2002). The purpose of this study is to carryout a study on the estimation of PMP for a 24-h duration using the Hershfield technique for 23 synoptic and climatology stations in four central provinces of Iran with sufficient daily rainfall data.

Table 1- List of stations within study area

Station Name	Latitude	Longitude	Elevation	Data length (year)
Tafresh	34 41	50 02	1930	36
Khondab	34 24	49 12	1742	21
Dozaj	35 24	49 49	2100	16
Shah-Zand	33 56	49 25	1918	28
Shamsabad-Arak	33 49	49 44	2400	30
Milajerd	34 38	49 13	1675	13
Arak	34 06	49 46	1708	47
Aminabad	35 35	51 28	1000	25
Hamand-Absard	3539	52 05	1800	35
Abali	35 45	51 53	2465	21
Shomale Tehran	35 47	51 37	1548	13
Tehran Mehrabad	35 41	51 19	1191	50
Doushan Tappeh	35 42	51 20	1209	31
Karaj	35 55	50 54	1313	16
Ghom	34 42	50 51	877	17
Torood	35 28	55 07	781	13
Chehel-Dokhtar	36 42	55 18	1520	17
Hosseinan	35 13	54 34	895	14
Kouhan-Shahroud	36 37	55 53	1004	13
Biarjamand	36 03	55 50	1106	12
Shahroud	36 25	54 57	1345	52
Semnan	35 33	53 23	1171	39
Garmsar	35 12	52 16	825	17

STUDY AREA AND DATA USED

Maximum annual daily rainfall data series of 23 synoptic and climatology stations in four central provinces of Iran (Tehran, Qum, Markazi and Semnan provinces) were used for PMP estimations. The provinces are located in arid and semi-arid parts of Iran.

The data were obtained from Iran meteorological organization archive. The stations with the data length less than 12 years were not considered in obtaining the estimates of the point PMP values. The names of the stations with record lengths larger than 12 years are given in table 1. The data lengths ranged from 12 to 52 years with a mean of 25 years.

METHODOLOGY

The Hershfield technique for estimating PMP is an adopted version of Chow (1951) technique of frequency analysis of rainfall. Hershfield (1961, 1965) considered that for PMP estimation, there is a value of frequency factor which will not be exceeded, say K_m. He then modified chow's equation as:

$$X_{PMP} = \overline{X}_n + K_m \sigma_n \tag{1}$$

Where X_{PMP} is PMP for a given set of data, $\overline{X}_n$ and σ_n are the mean and standard deviation of annual maximum, respectively. The K_m factor is simply calculated using the fallowing equation:

$$K_m = \left(X_1 - \overline{X}_{n-1}\right) / \sigma_{n-1} \tag{2}$$

Where X_1 is the highest observed annual maximum rainfall in the series, and $\overline{X}_{n-1}$ and σ_{n-1} are the mean and standard deviation of the annual maximum, respectively, when the highest value is excluded in calculating the parameters.

Rainfall data were thoroughly checked and any doubtful observations were discarded. For each station, the annual maximum series of a one day maximum amount of rainfall was selected and an array of annual maximum values of rainfall was formed.

HOMOGENITY OF THE DATA SERIES

The use of longer series in the estimation of PMP is only valid if they show no long-term changes in their behavior.

The homogeneity of all 23 series was checked bye a non-parametric Mann-Kendall rank test (WMO, 1966). The Mann-Kendall rank method has been suggested as a powerful test by Kendall and Stuart (1961). The statistic τ is computed by using the formula:

$$\tau = \frac{4\sum n_i}{N(N-1)} - 1 \tag{3}$$

Where: n_i is the number of values larger than the ith value in the series subsequent to its position in the time series of N values. The expected value of τ in a random series is 0 and its standard deviation (σ_τ) is given by:

$$\sigma_\tau = \sqrt{\{(4N+10)/[9N(N-1)]\}} \quad (4)$$

The ratio of τ to σ_τ, is considered as an indication of a possible trend in the data. For no trend in the data series this value lies within the limits of ± 1.96 at the 5% level significance. Afterwards K_m value and the corresponding one day PMP value were determined using Eqs. (2) and (1), respectively, for all 23 stations.

An average factor of 1.13 (e.g. Tomlinson, 1980) was used to convert one day PMP estimates into 24-h PMP.

STATISTICAL ESTIMATES OF PMP

One day annual maximum rainfall values of 23 stations were analyzed to extract the station-based PMP estimates. The values of $\overline{X}_n$, $\overline{X}_{n-1}$, σ_n, σ_{n-1} and a coefficient of variability ($CV = \frac{\sigma_n}{\overline{X}_n}$) were also calculated. The frequency factor (K_m) was determined for each station using Eq. (2). The results are summarized in table 2. As indicated, the values are mostly less than 4. Only four values were found between 4 and 7.63, with the latter being the upper limit of the estimated K_m. As PMP deals with unusual rainfall values, the corresponding frequency factor must also be chosen from the extremely high values. One support for the K_m value 7.63 could be found in Desa et al (2001). These authors derived $K_m = 8.7$ as an upper limit for a humid region of Malaysia. Desa et al (2001) used 33 stations with 30-60 years of data each. Ghahraman (2008) in his studies on 30 stations in a watershed located at north-east of Iran derived a value of $K_m = 9.63$ and applied this value for PMP estimations. Yet it may be acknowledged that K_m is highly dependent on the climatic conditions of the study area. Hershfield (1965) showed that empirically derived coefficient K_m varies directly with rainfall duration and inversely with the mean of the series.

This result implies that $K_m = 15$, (Hershfield, 1961) gives an overestimated value for PMP in the study area.

Using K_m values, the mean and standard deviation for each station, one day point PMP values for all the stations were computed using Eq. (1). An average factor of 1.13 (e.g. Tomlinson, 1980) was used to convert one day PMP estimates into 24-h PMP. The values of the mean, the standard deviation and the corresponding PMP for all the 23 stations are given in table 2. The observed one day highest rainfalls, as well as the ratio of estimated PMP to these rainfall values, are shown to facilitate comparisons. For different stations this ratio varies between 1.18 and 1.53 with a mean of 1.3. Desa et al (2001) reported similar values ranging from 1.5 to 2.7 which are higher than those obtained in this study. Such variation may originate from: (a) stations with different microclimates, and (b) a different record length of stations. One possible reason may also be due to the dryness of the study area which may produce more severe rainfall and also more variability of rainfall among different years (it also

is supported by higher K_m values of Attrak watershed (Ghahraman, 2004) as compared with Malaysia.

CONCLUSION

The main purpose of this study was to introduce a simple standardized method of PMP computation. Statistical estimates of 24-h PMP for 23 stations in four central provinces in Iran were made using an appropriate frequency factor for each station.

Based on these PMP estimates, a generalized map could be prepared showing the spatial distribution of 24-h PMP. The PMP ranges from 44.1mm over Hosseinan station to 101.2 mm on the Shamsabad-Arak station. The ratio of 24-h PMP to the highest observation ranges from 1.18 to 1.53 with an average of 1.3. The mean ratio of 24-h PMP to the mean one day maximum rainfall was 2.62. The point PMP rainfall estimates can be converted into areal PMP estimates using a depth-area relationship. This method could be recommended for other regions; however, future records may be needed to verify the ensuing results of PMP and the corresponding resulted PMF values.

Table 2- Frequency factors and 24-h PMP estimates for stations in the study area

Station Name	Mean (mm)	Coefficient of Variation	K_m	24-h PMP (mm)	24h PMP/Mean	24-h PMP/ highest observation
Tafresh	31,2	0,47	3,74	97,3	3,12	1,26
Khondab	34,1	0,41	2,74	82,3	2,41	1,28
Dozaj	25	0,49	2,93	70,4	2,82	1,41
Shah-Zand	43,1	0,33	2,9	95,6	2,22	1,24
Shamsabad-Arak	40,2	0,3	4,1	101,2	2,52	1,26
Milajerd	26,4	0,38	1,57	49,2	1,86	1,29
Arak	38,2	0,38	3,16	95,2	2,49	1,19
Aminabad	24,9	0,35	2,21	50,5	2,03	1,23
Hamand-Absard	29,4	0,31	2,73	61,5	2,09	1,21
Abali	39,6	0,24	1,9	67,6	1,71	1,25
Shomale Tehran	36,7	0,33	1,83	68,6	1,87	1,27
Tehran Mehrabad	25,7	0,37	2,79	60,4	2,35	1,21
Doushan Tappeh	25,9	0,29	2,26	49,1	1,9	1,23
Karaj	26,8	0,45	3,45	77,7	2,9	1,36
Ghom	18,9	0,43	2,9	49,7	2,63	1,42
Torood	17,7	0,58	2,56	49,4	2,79	1,35
Chehel-Dokhtar	17,9	0,42	7,63	83,6	4,67	1,39
Hosseinan	13,4	0,54	3,56	44,1	3,29	1,38
Kouhan-Shahroud	20,1	0,49	4,51	71,7	3,57	1,37
Biarjamand	23,2	0,62	4,37	95,8	4,13	1,53
Shahroud	21,7	0,44	2,37	49,7	2,29	1,18
Semnan	19,9	0,42	2,91	49,7	2,5	1,21
Garmsar	19,3	0,45	3,15	53,2	2,76	1,4

REFERENCES

Chow, V.T., (1951). A general formula for hydrologic frequency analysis. Transactions, American Geophysical Union, 32: 231–237.

Desa M.N.M, Noriah A.B. and Rakhecha P.R., (2001). Probable maximum precipitation for 24-hr duration over Southeast Asian monsoon region-Selangor, Malaysia. Atmos. Res., Vol. 58, pp. 41- 54.

Ghahraman, B. and Kalili, D., (2004). A re-visit to partial duration series of short duration rainfalls. Iranian Journal of Science and Technology, Volume 28, Transaction B, Number B5: 547-558.

Hershfield, D. M. (1961a). Estimating the probable maximum precipitation.J. Hydraul. Div. ASCE 87 (HY5), 99-116.

Hershfield, D.M. (1965). Method for estimating probable maximum precipitation, J. Am. Water Works Assoc. 57 (1965), pp. 965–972.

Kendall, M. G. and Stuart, A. (1961). The advanced theory of statistics, volume 2: Hafner publishing Co. New York, USA.

Tomlinson, A.I. (1980). The frequency of high intensity rainfalls in New Zealand. Water. and Soil Technical Publication No. 19, National Water and Soil Conservation, Wellington, New-Zealand, 63p.

World Meteorological Organization (1986). Manual for Estimation of Probable Maximum Precipitation, 2nd edition, Operational Hydrology Report No. 1, WMO - No. 332, Geneva, ISBN 92 - 63 - 11332 – 2.

World Meteorological Organization, (1996). Climate change. WMO tech. Note No.79, P. 80.

Regional Regression Analysis and the Rational Method

By C. B. Young[1], B. M. McEnroe[2], and A. C. Rome[3]

[1]Dept. of Civil, Environmental, and Architectural Engineering, University of Kansas, 1530 W. 15th St. Rm. 2150, Lawrence, KS 66045; PH (785) 864-2999; FAX (785) 864-5631; e-mail: cbyoung@ku.edu
[2]Dept. of Civil, Environmental, and Architectural Engineering, University of Kansas, 1530 W. 15th St. Rm. 2150, Lawrence, KS 66045; PH (785) 864-2925, FAX (785) 864-5631; e-mail: mcenroe@ku.edu
[3]Wilson & Company, Inc., 8735 Rosehill Road, Suite 200, Lenexa, KS 66215

ABSTRACT

The Rational equation is often thought of as being less sophisticated and less accurate than regional flood frequency equations. As such, the application of the Rational equation is typically limited to small watersheds. This paper compares the Rational equation with regional flood frequency equations for 72 gaged rural watersheds in Kansas. The Rational equation is found to perform better than the regional flood frequency equations, as long as appropriate values of the Rational C are selected.

INTRODUCTION

Engineers have several options for estimating flood quantiles, or peak flood discharges for given return periods. These options include flood frequency analysis, regional flood frequency analysis, watershed modeling, and the Rational equation ($Q_T = C\ i_T\ A$). Although the Rational equation is widely used, it is often dismissed by engineers as a rule-of-thumb method. In most cases, the application of the Rational equation is limited to very small watersheds. The definition of 'small' varies, but typical upper limits for the equation range from 200 acres to one square mile. Due to these limitations, the Rational method is commonly used only for sizing storm sewer components and small culverts.

When designing large culverts and bridges, engineers generally use regional flood frequency equations or watershed modeling. Regional flood frequency equations are constructed via multiple linear regression analysis of flood quantiles and watershed characteristics. These equations are often thought to be more sophisticated and more accurate than the Rational equation.

The purpose of this paper is to compare the Rational equation with regional flood frequency equations. The comparison uses data for 72 gaged, rural watersheds in Kansas.

DATA

The watersheds selected for this study are smaller than 30 mi^2 and have USGS streamflow gaging records that are twenty years or longer. All watersheds used for this analysis are rural and are not significantly regulated by flood control structures. The 72 watersheds range in size from 0.17 to 29.6 mi^2, with an average size of 7.76 mi^2. The average watershed land cover is 62% (+/- 20%) grassland or pasture, 33% (+/- 20%) cropland, and generally less than 5% forest, urban, or other uses. Figure 1 shows the locations of the 72 gages across the State of Kansas, along with contours of mean annual precipitation.

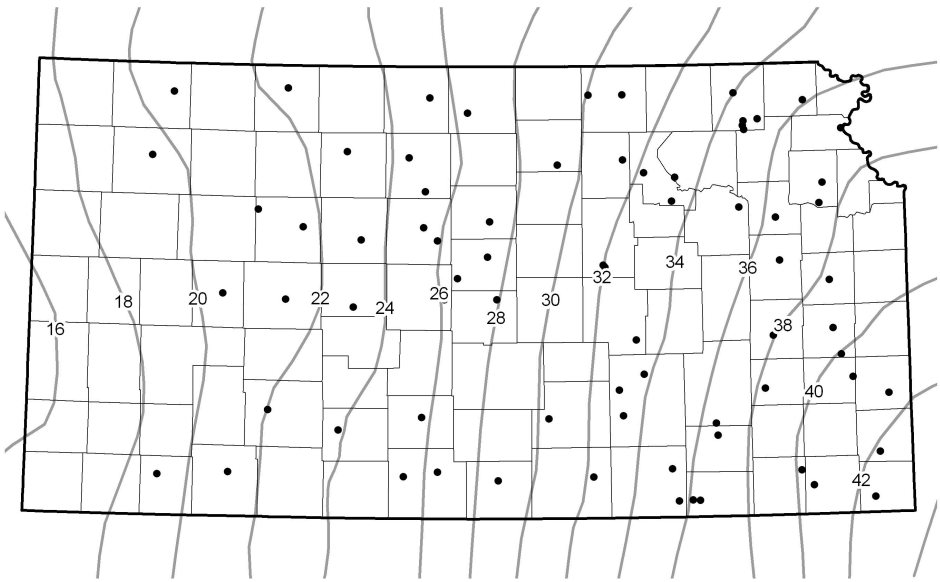

Figure 1. Locations of 72 Gaged Watersheds and MAP Contours

Six flood quantiles (the Q_2, Q_5, Q_{10}, Q_{25}, Q_{50}, and Q_{100}) were estimated for each watershed in accordance with Bulletin 17B methods using the software package PEAKFQ (Flynn et al. 1992). Watershed characteristics were assembled for all gaged locations; these characteristics are listed in Table 1. A brief description of how each variable was determined follows.

Drainage areas were delineated and measured in ArcGIS 9.2, using scanned and georectified USGS 7.5-minute topographic maps, also called Digital Raster Graphics (DRGs). The watershed shape factor was computed as:

$$Sh = \frac{L^2}{A} \tag{1}$$

where L is the main channel length (in miles) and A is the drainage area (in mi^2). The average main channel slope was determined as:

$$Sl = \frac{El_{85} - El_{10}}{0.75 \cdot L} \quad (2)$$

where El_{85} and El_{10} are the elevations (in feet) 85% and 10% of the way up the channel from the watershed outlet to the basin divide.

Table 1. Watershed Characteristics Used in Analysis

Symbol	Watershed Characteristic	Units
A	Drainage Area	mi^2
Sh	Basin Shape Factor	--
Sl	Average Slope of Main Channel	ft/mi
SP	Generalized Soil Permeability	in/hr
CN	NRCS Runoff Curve Number	--
i_T	Rainfall Intensity, $i(T,t_c)$	in/hr
MAP	Mean Annual Precipitation	in
MAE	Mean Annual Lake Evaporation	in
MAD	Mean Annual Precipitation Deficit	in

Generalized soil permeability (SP) was determined using the STATSGO soils database (USDA 1994) produced by the Natural Resources Conservation Service (NRCS). The NRCS runoff curve number (CN) was estimated using the hydrologic soil group of the watershed obtained from the STATSGO soils map of Kansas and the landcover as designated by the USGS National Landcover Dataset (NLCD) of 1992. The rainfall intensities for duration = t_c and recurrence interval T were obtained from the KDOT rainfall intensity-duration-frequency tables, which were in turn compiled from HYDRO-35 (Frederick et al. 1977) for durations less than or equal to one hour and from TP-40 (Hershfield 1961) for durations in excess of one hour. The mean annual precipitation was obtained from 1960-1990 climate normals (Rasmussen and Perry 2000). The mean annual lake evaporation was obtained from a National Weather Service (NWS) evaporation atlas (Farnsworth et al. 1982). The mean annual precipitaton deficit was computed as:

$$MAD = MAE - MAP \quad (3)$$

METHODOLOGY

Regional flood frequency relations are typically constructed using multiple linear regression of the $\log_{10}$ of peak discharge (Q_T) against the log-transforms of a variety of predictor variables. The basic form of such regional flood frequency equations is:

$$Q_T = 10^{\alpha} \cdot X_1^{\beta_1} \cdot X_2^{\beta_2} \cdots \quad (4)$$

where X_1, X_2, etc. are the predictor variables and α, β_1, β_2, etc. are coefficients determined using least-squares regression on the $\log_{10}$-transforms of the variables.

Regional flood frequency analysis was performed using the $\log_{10}$-transforms of the variables listed in Table 1. Forward stepwise linear regression was used to find equations for the flood discharges (Q_T). Regression relationships were compared on the basis of the coefficient of determination, R^2; the adjusted R^2; and the standard error of the estimate, S_e. Equations were evaluated for statistical significance using an F-test (H_0: regression not significant, H_A: regression is significant) with a confidence level equal to 95%. The statistical significance of each regression parameter was determined using a t-test (H_0: parameter coefficient equal to zero, H_A: parameter coefficient not equal to zero) also using a confidence level equal to 95%.

The data assembled for each location were also used to compute Rational C values for the six recurrence intervals (2-year through 100-year) by solving the Rational equation for C:

$$C = \frac{Q_T}{i \cdot A} \quad (5)$$

Multiple linear regression analysis was used to develop predictive equations for the Rational C as a function of the watershed characteristics listed in Table 1. The Rational equation was then compared against the regional flood frequency equations.

RESULTS AND ANALYSIS

Tables 2 and 3 give the best two- and three-parameter regression equations determined for the flood quantiles. The best two-parameter equations all include the drainage area and either the MAP or rainfall intensity as predictors. This is consistent with the standard USGS regression equations for Kansas for watershed areas less than 30 mi^2, which are of the form:

$$Q_T = a \cdot MAP^{\beta_1} \cdot A^{\beta_2} \quad (6)$$

The standard error (in $\log_{10}$ terms) for the two-parameter equations ranges from 0.199 to 0.260.

The best three-parameter equations all include the drainage area, MAP, and rainfall intensity as predictors – except for the equation for Q_2. The standard error (in $\log_{10}$ terms) for the three-parameter equations ranges from 0.178 to 0.245. For all but one flood quantile, the three-parameter equations shown in Table 3 were the best overall equations (in one case a four-parameter equation was slightly better).

It is interesting to note that the exponents on i and A in the three-parameter equations (Table 3) are all very near one. Young et al. (2009) demonstrate that the exponents for i and A are in fact statistically indistinguishable from one, and that the equations in Table 3 can be re-written in the form of the Rational equation, with C being a function of the mean annual precipitation.

Table 2. Two-Parameter Regional Flood Frequency Equations

Equation	Adj. R^2	S_e
$Q_2 = 0.00372\ A^{0.591}\ MAP^{3.155}$	0.804	0.210
$Q_5 = 0.0723\ A^{0.607}\ MAP^{2.529}$	0.795	0.199
$Q_{10} = 0.278\ A^{0.617}\ MAP^{2.253}$	0.766	0.211
$Q_{25} = 1.01\ A^{0.630}\ MAP^{1.996}$	0.723	0.232
$Q_{50} = 172.2\ A^{1.424}\ i_{50}^{1.916}$	0.691	0.248
$Q_{100} = 185.4\ A^{1.412}\ i_{100}^{1.871}$	0.673	0.260

Table 3. Three-Parameter Regional Flood Frequency Equations

Equation	Adj. R^2	S_e
$Q_2 = 0.0416\ A^{0.696}\ MAP^{2.654}\ Sh^{-0.550}$	0.844	0.187
$Q_5 = 0.324\ A^{1.088}\ MAP^{1.896}\ i_5^{1.143}$	0.837	0.178
$Q_{10} = 1.01\ A^{1.113}\ MAP^{1.624}\ i_{10}^{1.188}$	0.813	0.189
$Q_{25} = 2.858\ A^{1.146}\ MAP^{1.365}\ i_{25}^{1.245}$	0.773	0.210
$Q_{50} = 5.012\ A^{1.164}\ MAP^{1.226}\ i_{50}^{1.271}$	0.741	0.227
$Q_{100} = 8.072\ A^{1.180}\ MAP^{1.106}\ i_{100}^{1.294}$	0.711	0.245

Once the regression equations for Tables 2 and 3 were established, another analysis was performed to develop a predictive equation for the Rational C as a function of watershed characteristics. The Rational C was computed for each watershed for each recurrence interval using Eq. 5. Young et al. (2009) discuss the Rational C values established for the 72 watersheds in Kansas. This paper focuses on the development of a predictive equation for C. Forward stepwise linear regression showed that only one-predictor equations were statistically significant for the Rational C for all recurrence intervals. In each case, the best predictor of Rational C was the mean annual precipitation. Table 4 shows the correlations between the $\log_{10}(C_{25})$ and the $\log_{10}$s of the various watershed characteristics.

Table 4. Correlations Coefficients for $\log_{10}(C_{25})$ vs. $\log_{10}$(Predictor)

Predictor	Correlation Coeff.
A	0.07
Sh	-0.23
Sl	-0.02
SP	-0.42
CN	0.37
i_{25}	0.08
MAP	0.57
MAE	-0.47
MAD	-0.55

As shown in Table 4, the best predictor for the C_{25} was the mean annual precipitation. Interestingly, the MAP is a much better predictor of C than the NRCS runoff curve number (CN). This held true for all six recurrence intervals. Table 5 shows the regression equations for the Rational C for all six recurrence intervals, along with the standard errors for the Rational equation.

Table 6 lists the standard errors for the 2- and 3-parameter regional regression equations, along with the standard errors for the Rational equation. For all but the 2-year recurrence interval, the Rational equation yields lower standard errors than the regional regression equations.

Table 5. Regression Equations for Rational C with S_e for the Estimate of Q_T in Log Units

Equation		S_e (log units)
$Q_2 = C\ i_2\ A$,	$C = 0.0000366\ MAP^{2.53}$	0.192
$Q_5 = C\ i_5\ A$,	$C = 0.000440\ MAP^{1.97}$	0.176
$Q_{10} = C\ i_{10}\ A$,	$C = 0.00137\ MAP^{1.72}$	0.187
$Q_{25} = C\ i_{25}\ A$,	$C = 0.00397\ MAP^{1.48}$	0.209
$Q_{50} = C\ i_{50}\ A$,	$C = 0.000724\ MAP^{1.35}$	0.227
$Q_{100} = C\ i_{100}\ A$,	$C = 0.0121\ MAP^{1.24}$	0.224

Table 6. Comparison of Standard Errors (in log units) for the Regression and Rational Equations

Flood Quantile	S_e for 2-Param.	S_e for 3-Param.	S_e for Rational
Q_2	0.210	0.187	0.192
Q_5	0.199	0.178	0.176
Q_{10}	0.211	0.189	0.187
Q_{25}	0.232	0.210	0.209
Q_{50}	0.248	0.227	0.227
Q_{100}	0.260	0.245	0.224

DISCUSSION AND CONCLUSION

The findings of this study show that the Rational equation can outperform traditional regional regression equations, as long as appropriate values of the runoff coefficient are used. This contradicts conventional wisdom, which holds that the Rational equation is less sophisticated and less accurate than regression equations. The research for this study also indicates that the form of the rational equation is appropriate for watersheds larger than typically assumed. The correlation analysis presented in Table 4 shows that the Rational C is independent of drainage area.

One reason that the Rational equation may outperform regression equations is the Rational equation actually considers more predictive variables. At first glance, the Rational equation appears to include only three predictors: the C value, rainfall intensity, and drainage area. However, the rainfall intensity is a function of both watershed location (the local extreme rainfall climatology) and the watershed time of concentration. The time of concentration, in turn, is a function of the length and slope of the watershed main channel. As such, the Rational equation assimilates more information about the watershed than do most regional flood frequency equations.

The Rational method has been in widespread use for decades and has been used to design billions of dollars of drainage infrastructure. Many engineers assume that the Rational method is a rule-of-thumb technique, or that it is inferior to regional flood frequency equations. This paper demonstrates that the Rational method can actually work better than regional regression equations, as long as the Rational C values are properly determined for the area of interest.

The equations in this report were developed for watersheds in the State of Kansas and should not be used elsewhere.

ACKNOWLEDGEMENTS

This work was funded by the Kansas Department of Transportation under K-TRAN grant KU-06-4. James Richardson, P.E., of KDOT served as project monitor. This support is gratefully acknowledged.

REFERENCES

Farnsworth, R. K., E. S. Thompson, and E. L. Peck (1982). *Evaporation Atlas for the Contiguous 48 United States*, NOAA Technical Report NWS 33.

Flynn, K. M., Kirby, W. H., and Hummel, P. R. (2006). *User's Manual for Program PeakFQ, Annual Flood-Frequency Analysis using Bulleting 17B Guidelines,* U. S. Geological Survey.

Frederick, R. H., Myers, V. A., and Auciello, E. P. (1977). *Five- to 60-Minute Precipitation Frequency for the Eastern and Central United States,* NOAA Technical Memorandum NWS HYDRO-35, National Weather Service, U.S. Dept. of Commerce, Washington, D.C.

Hershfield, D. M. (1961). *Rainfall Frequency Atlas of the United States for Durations from 30 Minutes to 24 Hours and Return Periods from 1 to 100 Years*, Technical Paper No. 40, Weather Bureau, U.S. Dept. of Commerce, Washington, D.C.

McEnroe, B. M., Young, C. B., and Rome, A. C (2007). *Flood Frequency Relationships for Small Watersheds in Kansas*, Kansas Department of Transportation Report No. K-TRAN: KU-06-4.

Rasmussen, P. P., and C. A. Perry (2000). *Estimation of Peak Streamflows for Unregulated Rural Streams in Kansas*, Water-Resources Investigations Report 00-4079, U.S. Geological Survey.

USDA (1994). *State Soil Geographic (STATSGO) Data Base, Data Use Information,* U.S. Department of Agriculture Miscellaneous Publication Number 1492, Fort Worth, Texas.

Young, C. B., McEnroe, B. M., and Rome, A. C. (2009). "Empirical Support for the Rational Method." *TRB 88th Annual Meeting: Compendium of Papers DVD*, Transportation Research Board of the National Academies, Washington, D.C.

STOCHASTIC NON-EQUILIBRIUM BEDLOAD TRANSPORT MODEL

Ken Z. Kuai[1] and Christina W. Tsai[2]

[1] Research Assistant, 207 Jarvis Hall, Department of Civil, Structural, and Environmental Engineering, State University of New York at Buffalo, Buffalo, NY 14260, USA (Email: kzheng@buffalo.edu)
[2] Associate Professor, 233 Jarvis Hall, Department of Civil, Structural, and Environmental Engineering, State University of New York at Buffalo, Buffalo, NY 14260, USA (Email: ctsai4@eng.buffalo.edu)

ABSTRACT

Sediment particle transport can be viewed as a Markov chain. In a nonequilibrium condition, the interchange of sediment particles occurs not only between the bedload layer and the bed surface, but also across the interface between bedload and suspended load. The bedload transport rate is the product of the total particle volume in saltation and the average saltating velocity. We can quantify the number of saltating particles by modeling the occupancy probabilities vector of particles staying in three states (i.e., bed surface, bedload layer, and the interchange layer between the bedload and the suspended load.). The new stochastic bedload relation is validated against existing bedload model (Soong and Graf 1997). The influence of sudden changes in flow-sediment properties on the bedload transport rate is investigated in this preliminary study.

INTRODUCTION

Most of bedload transport formulas in literature were based on the empirical or semi-empirical flow-transport relations that are only valid for equilibrium conditions. Traditional stochastic bed load models aimed to solve for the equilibrium bedload transport rate by matching the rate of bed erosion with the rate of deposition (Einstein, 1950; Wu and Yang, 2004). Bedload transport can be in nonequilibrium even under the steady flow condition, as the quantity of moving particles in the bedload layer may vary. In the nonequilibrium condition, the interchange of sediment particles happens not only between bedload layer and the bed surface, but also across the interface between bedload and suspended load. Current stochastic approaches in the bedload transport mostly consider only the particle interchange between the bed surface and the bedload layer, and are restricted to equilibrium conditions. The proposed stochastic approach attempts to circumvent this deficiency by adding a bedload-suspended load interchange layer to model particle movement under nonequilibrium conditions.

Particle interchange across the bedload layer can be viewed as a Markov process. A Markov process is a stochastic process where the future development of the process only depends on the present value, not on the past ones. Markov process is simple to use and has broad applications to engineering systems. The number of instantaneous moving particle in the bedload layer can be quantified based on the master equations of the

Markov process. At each time step, a sediment particle may change its state from the current state to the adjacent state, or remain in the same state, in conformity with respective transition probabilities. These transition probabilities are functions of flow conditions and sediment characteristics, and their relations were frequently discussed in literature. The bedload transport rate may reach a constant value (i.e., equilibrium condition) given fixed transition probabilities in a long run. Once the values of transition probabilities vary due to sudden changes of flow and/or sediment conditions, the bedload rate would change correspondingly and deviate from its equilibrium value. The influence of suddenly changed flow-sediment properties on the bedload transport rate has not been fully explored in literature.

MODEL DEVELOPMENT

The bedload transport rate, q_b, is equal to the total volume of moving particles in the bedload layer multiplied by particle moving velocity ,

$$q_b = N_2 V_p u_s \tag{1}$$

where N_2 denotes the number of sediment particles in saltation (or rolling, sliding, as special cases of saltation.) per unit bed area. V_p is the average single particle volume. We define N_1 and N_3 as the number of bed particles and suspended particles, in an active exchange process with saltating particles, respectively.

$$N_1 = N \Pr_1, \quad N_2 = N \Pr_2, \quad N_3 = N \Pr_3 \tag{2}$$

where $N = N_1 + N_2 + N_3$ is the total number of sediment particles in the exchange process. $\Pr_i$ is the occupancy probability of particles in i state. $i = 1$ is the state of sediment particle resting on the bed surface; $i = 2$ represents the state of sediment particle in saltation in the bedload layer; $i = 3$ is the state of suspended sediment particle in an active exchange process with bedload particles. State 3 is postulated to be confined to a thin layer on the top of the bedload boundary, and it can be viewed as the exchange layer between suspended load and bedload. All bedload particles are entrained into suspension through this layer, and vice verse.

The total number N of exchanging particles is unknown. However, the number of active exchanging suspended particles N_3 can be taken as constant, which can be deduced from the equilibrium near bed suspended sediment concentration c_a. Here, the following relations derived by van Rijn (1984b) are followed:

$$c_a = 0.015\frac{d_{50}T^{1.5}}{aD_*^{0.3}},\quad T = \frac{(u_*')^2 - (u_{*c})^2}{(u_{*c})^2},\quad D_* = d_{50}\left[\frac{(s_s - 1)g}{v^2}\right]^{1/3} \tag{3}$$

where d_{50} = median diameter of sediment particle ($d_{50} = d$ here for uniform sediment particles); u_{*c} = critical bed-shear velocity obtained from the Shields diagram; $u_*' = g^{0.5}U / C'$ is effective bed shear velocity related to grains; U = mean flow velocity; $C' = 18\log(12R_b / 3d_{90})$ = Chézy-coefficient related to grains; R_b = hydraulic radius related to the bed obtained from Vanoni and Brooks (1957); d_{90} = 90% passing bed particle diameter; $s_s = \rho_s / \rho$ is the specific gravity; v = kinematic viscosity coefficient; a = reference level above bed. van Rijn (1984b) set a equal to half the bed-form height, or the equilibrium roughness height, with a minimum value of $0.01d$. In the present analysis, the reference level a is set equal to an average saltation height, h_s. The exchange layer between suspended load and bedload is hypothesized to have the thickness of one sediment diameter height. Then,

$$N_3 = \frac{c_a d}{V_p} \tag{4}$$

And total number N of exchanging particles can be found as

$$N = N_3 / \Pr_3 \tag{5}$$

The transition probabilities in the exchange process between these three states can be expressed as the following matrix:

$$P_{ij} = \begin{bmatrix} P_{11} & P_{12} & P_{13} \\ P_{21} & P_{22} & P_{23} \\ P_{31} & P_{32} & P_{33} \end{bmatrix} = \begin{bmatrix} 1 - P_{12} & P_{12} & 0 \\ P_{21} & 1 - P_{21} - P_{23} & P_{23} \\ 0 & P_{32} & 1 - P_{32} \end{bmatrix} \tag{6}$$

where P_{12} is the probability of bed erosion into bedload layer and defined as $P_{12} = P(F_L > W)$. Einstein (1950) assumed the lift force F_L acting on bed particle follows a Gaussian distribution. $W = (\rho_s - \rho)gV_P$ is the submerged weight. The formula of F_L is from Cheng and Chiew (1998):

$$F_L = C_L \frac{\pi d^2}{4}\frac{\rho u_b^2}{2} \tag{7}$$

in which u_b = instantaneous flow velocity approaching the bed particle; $C_L = 0.2$ is the

lift coefficient. Cheng and Chiew (1998) assumed that u_b follows the Gaussian distribution instead of F_L, and they derived the formula of P_{12}:

$$P_{12} = 1 - 0.5\frac{B-\overline{u_b}}{\left|B-\overline{u_b}\right|}\sqrt{1-\exp\left[-\frac{2\left(B-\overline{u_b}\right)^2}{\pi\sigma^2}\right]} - 0.5\sqrt{1-\exp\left[-\frac{2\left(B+\overline{u_b}\right)^2}{\pi\sigma^2}\right]} \tag{8}$$

$$B = \sqrt{\frac{4s_s gd}{3C_L}}$$

where $\overline{u_b}$ is the time averaged velocity acting on the bed particle, and $\overline{u_b} = 5.52u_*$ when we assume the bed particle level as $y_b = 0.6d$; $\sigma = \sqrt{\overline{\left(u_b - \overline{u_b}\right)^2}}$ is the longitudinal intensity of turbulence, and $\sigma = 2u_*$ (Cheng and Chiew, 1998).

It is assumed that the channel bed is formed by randomly packed spheres and the relative vertical position of bed particle is also random. A saltating particle may come to rest when it falls into a "hole" in the bed, which can be assumed to be of the Gaussian distribution. The value of P_{21} is related to bed irregularity and needs to be determined from experiment. In this paper, P_{21} is assumed to be proportional to P_{12}, and the ratio α_s has the magnitude of 0.1.

In turbulent flow, bedload is entrained into suspension when the vertical velocity fluctuation v' of the flow exceeds the settling velocity w of the sediment particle. The probability of suspension is $P_{23} = P(v' > w)$, which is also assumed to follow the Gaussian distribution. P_{23} is approximated as follows (Cheng and Chiew, 1999).

$$P_{23} = 0.5 - 0.5\sqrt{1-\exp\left(-\frac{2}{\pi}\frac{w^2}{u_*^2}\right)} \tag{9}$$

It is noted that the probability of the complementary event $P(v' < w) = 1 - P_{23}$ can be viewed as the probability of the termination of suspension (or deposition probability). But this happens throughout the suspended load layer. The deposition probability at the exchange layer between suspended load and bedload should be smaller than $(1 - P_{23})$. Let $P_{32} = \alpha_d(1 - P_{23})$ and α_d is a coefficient less than 1. We propose that α_d is equal to the ratio of N_3 to the total number of suspended sediment. This ratio can be determined from the suspended sediment concentration profile.

The occupancy probabilities of particles at i th step is denoted by

$$\mathrm{Pr}^{(i)} = \begin{bmatrix} \mathrm{Pr}_1^{(i)} \\ \mathrm{Pr}_2^{(i)} \\ \mathrm{Pr}_3^{(i)} \end{bmatrix} \tag{10}$$

After n exchanging steps

$$\mathrm{Pr}^{(n)} = \mathrm{Pr}^{(0)} P_{ij}^{\ n} \tag{11}$$

$\mathrm{Pr}^{(0)}$ is the initial occupancy probabilities. P_{ij} is the transitional probability The new $\mathrm{Pr}_2^{(n)}$ from Eq. (11) would lead to the bedload transport rate q_b after n exchanging steps using Eq. 1 and Eq. 3.

When n is large enough ($n > 500$), $\mathrm{Pr}^{(n)} = \mathrm{Pr}^{(n-1)}$ and q_b will approach a constant. This constant q_b is the bedload transport capacity as shown in Fig. 1. The time step is the exchange time t_e, which is the time necessary for sediment particle to make a single transition from one state to another. The ratio d/w is often used to represent the time scale of particle saltation in literature. Herein, assume $t_e = \alpha_t d/w$ and α_t is between 1-2. It is found that t_e has the magnitude at around 0.05 seconds.

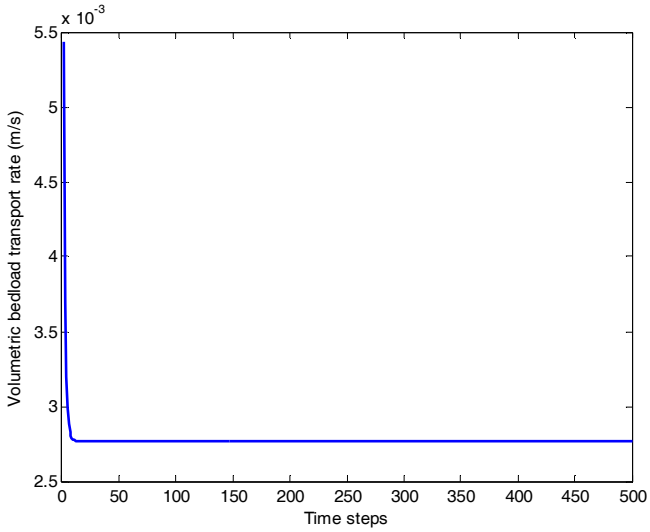

Figure 1. Volumetric bedload transport rate ($v_s = 0.5$ m/s; $h_s = 1.5d$; $d = 5.8$ mm; $U = 1.5$ m/s; averaged flow depth $h = 3$ m; channel width $b = 10$ m; bed slope $S = 0.001$; $s_s = 1.65$; $u_{*c} = 0.02$ m/s; drag coefficient $C_D = 0.5$; $\alpha_d = 0.8$; $\alpha_s = 0.05$).
Asymptotic transitional probabilities $P_{12} = 0.4378$, $P_{23} = 0.0083$, $P_{32} = 0.7934$, $P_{21} = 0.0219$. Note: all the following figures have the same parameter values.

MODEL VALIDATION

Graf's bedload formula

The bedload capacity results can be compared with the bedload transport formula derived under an equilibrium condition. The semi-empirical formula from Song and Graf (1997) is used here for this comparison:

$$\Phi = 10.4\mathrm{K}\Psi^{-1.5} \tag{12a}$$

$$\Phi = \frac{(q_b/q)UR}{\sqrt{(s_s-1)gd^3}} \qquad \Psi = \frac{(s_s-1)d}{RS_f} \tag{12b}$$

$$\mathrm{K} = \begin{cases} \Psi^{-1} & \Psi \le 14.6 \\ (1-0.045\Psi)^{2.5} & 14.6 < \Psi \le 22 \\ 0 & \Psi > 22 \end{cases} \tag{12c}$$

where Φ is the Einstein's dimensionless transport rate, and Ψ is the reciprocal of the dimensionless parameter of flow intensity; q the average flow rate per unit width ($q = UH$). R is the hydraulic radius, and herein $R = R_b$. S_f is the friction slope. Based on the given particle and flow conditions as depicted in Figure 1, it is found that the volumetric bedload transport rate by the proposed model agrees reasonably well with the bed load transport rate predicted by Soong and Graf (1997).

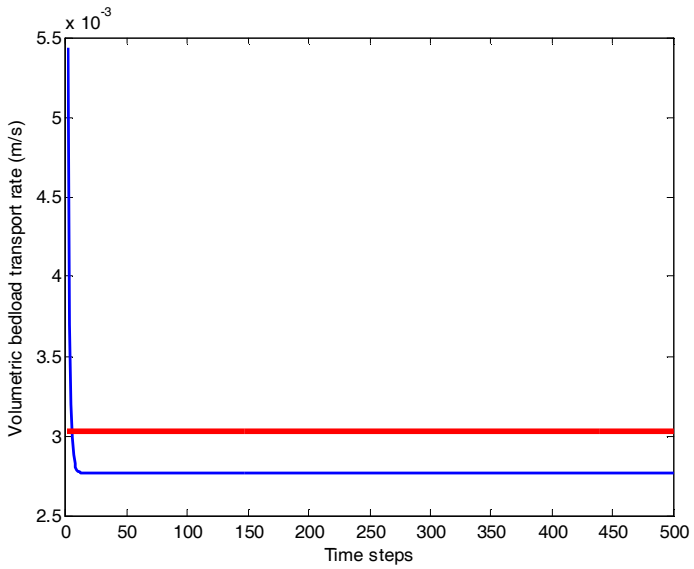

Figure 2. Comparison of the model results and calculated bedload transport rate from Graf's formula, under same input parameters as those used in Fig. 1. (The thick straight horizontal line is the result from Graf's formula).

DISCUSSIONS

Figure 3 shows that the small variations of transition probabilities make the bedload curve wavy. If N_3 is not constant, the q_b curve also becomes wavy as shown in Fig. 4. We can still see the trend of a constant q_b given that the mean value of N_3 is kept the same.

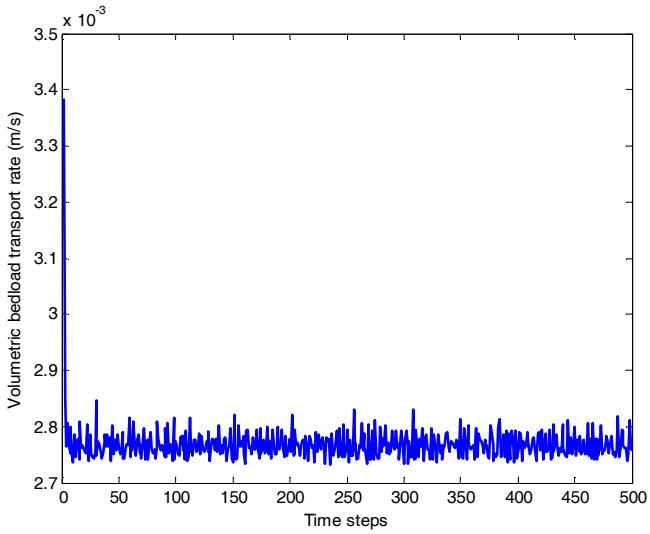

Figure 3. Bedload transport rate with one smaller order of uniform random noises in the erosion probability P_{12}.

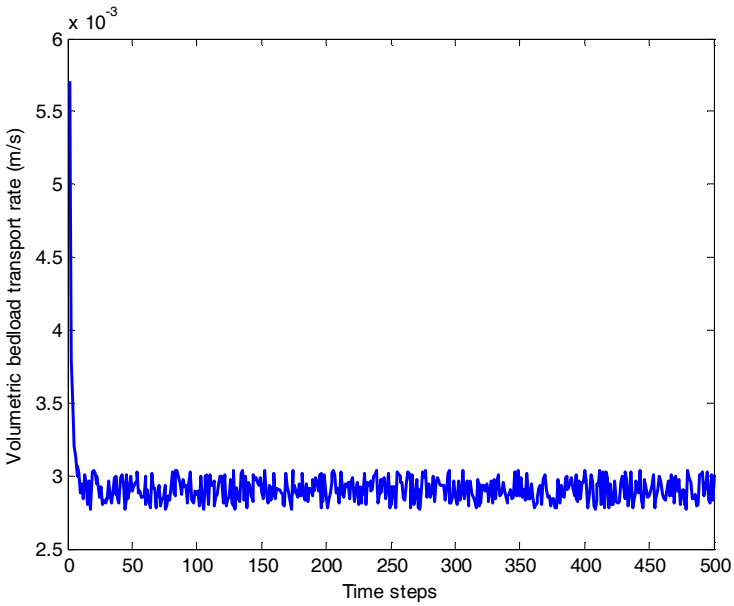

Figure 4. Bedload transport rate with one smaller order of uniform random noises in N_3 (N_3 = 472/m^2)

Below are the examples illustrating the impact of hypothetical abrupt changes to transitional probabilities and the bedload transport rates. The sudden change of flow and/or sediment condition leads to changes in the transition matrix. The instantaneous q_b will deviate from its transport capacity (Fig. 5-6). A sudden increase of entrainment probability (P_{23}) leads to the decrement of particle numbers in the bedload layer (N_2), and therefore q_b is decreased. q_b will increase with the number of sediment particles in the bedload layer when the deposition probability (P_{23}) increases. The theoretical examples herein manifest that the neglecting the exchange process between the bedload layer and the suspended layer may lead to non-negligible errors in bedload calculation when the flow and/or sediment conditions change.

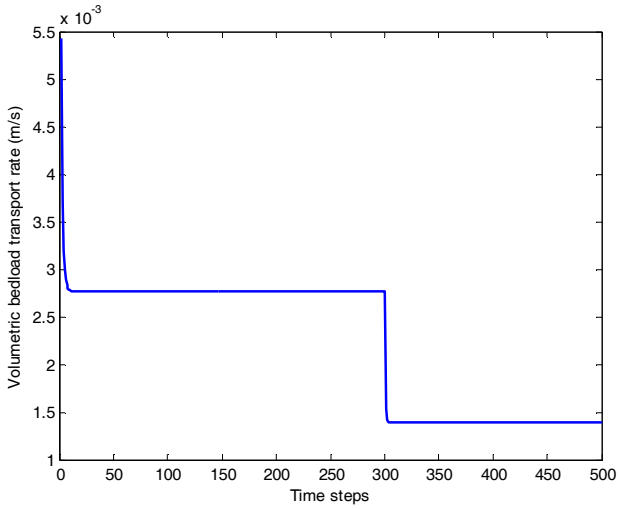

Figure 5. Sudden increase of entrainment probability from P_{23}=0.0083 to P_{23}=0.0166

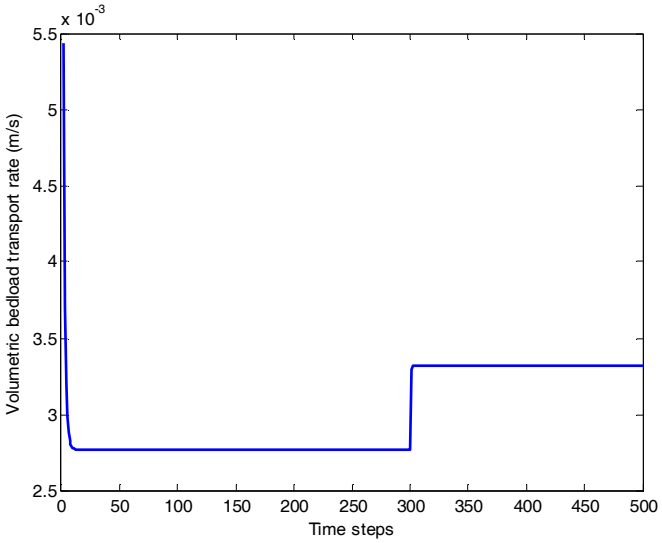

Figure 6. Sudden increase of deposition probability P_{32}=0.7934 to P_{23}=0.952

CONCLUSIONS

In a nonequilibrium condition, the interchange of sediment particles occurs not only between the bedload layer and the bed surface, but also across the interface between bedload and suspended load. A bedload-suspended load interchange layer is added to a stochastic bedload transport model. The proposed nonequilibrium stochastic bedload model can quantify the bedload transport capacity in an equilibrium condition, and also can demonstrated the influence of sudden changes flow-sediment properties on bedload transport rate.

ACKNOWLEDGMENTS

The writers gratefully acknowledge the financial support from the National Science Foundation under grant number #0748787.

REFERENCES

Cheng, N. S., and Chiew, Y. M. (1998). "Pick-up probability for sediment. entrainment." *J. Hydraul. Eng.*, 124(2), 232-235.

Cheng, N. S., and Chiew, Y. M. (1999). "Analysis of initiation of sediment suspension from bed load." *J. Hydraul. Eng.*, 125(8), 855-861.

Einstein, H. A. (1950). "The bed load function for sediment transportation in open channel flow." *Technical bulletin no. 1026*, U.S. Dep. Of Agriculture, Washington, D.C.

Song, T. and Graf, W. H. (1997). "Experimental study of bedload transport in unsteady open-channel flow." *Internat. J. of Sediment Res.,* 12(3), 63-71.

Wu, F.-C., and Yang, K.-H. (2004). "A stochastic partial transport model for mixed-size sediment: Application to assessment of fractional mobility", *Water Resour. Res.*, 40(4), w04501.

van Rijn, L. C. (1984b). "Sediment transport. Part II: Suspended load transport." *J. Hydraul. Eng.*, 110(11), 1613–1641.

Vanoni, V.A., and Brooks, N.H. (1957). "Laboratory studies of the roughness and suspended load of alluvial streams. Sedimentation Laboratory." California Institute of Technology, Report E-68, Pasadena, Calif.

EWRI Congress 2009, Kansas City, Missouri, May 17-21

Parameter Uncertainty Estimation of Hydrologic Models, Using Bootstrap Resampling

Mohammad Ebtehaj [a], Hamid Moradkhani, PhD, PE, MASCE [b]

[a] Department of Civil and Environmental Engineering, University of Minnesota, Saint Antony Falls Laboratory , P.O. Box 55414, Minneapolis, Minnesota, USA, Phone: 612-624-4629, email: ebteh001@umn.edu

[b] Assistant Professor, Department of Civil and Environmental Engineering, Portland State University, P.O. Box 97201, Portland. Oregon USA, Phone: 503-725-2436, Fax: 503-725-5950; email: hamidm@cecs.pdx.edu

Abstract

Hydrologic parameters and state variables estimation for the purpose of forecasting hydrologic system dynamics have been among the most challenging tasks in the filed of hydrologic modeling. Most of the efforts in this area can be categorized broadly into deterministic and stochastic approaches. The former approaches generally adopt the paradigm as an optimization problem and attempt to minimize an error cost function for estimating the optimum parameter set. The latter approach analyzes the problem in the discourse of estimation theory. Because of existing uncertainties associated with model structure, measurement and initial boundary condition, forecasts using the deterministic approaches lack the ability to explicitly address the mentioned uncertainties and so one can not relay only on the results of the first approach. Although several attempts have been made to develop a well scientifically accepted and robust framework to estimate hydrologic parameters in a probabilistic context, several open questions still exist. In this paper we introduce a new approach to employ Block Bootstrap resampling coupled with a global optimization algorithm to quantify probabilistic structure of hydrologic parameter space using nonparametric confidence interval analysis.

Introduction

At the early stage of hydrologic modeling, hydrologic parameters were determined by visual inspection and forecaster consensus of observed streamflow and model simulation of system behavior. In the past two decades several attempts have been made to enhance the accuracy and efficiency of hydrologic prediction via hydrologic model parameters estimation [Sorooshian and Dracup,1980; Duan et al., 1992; Beven et al., 1992; Gupta et al., 1998.; Moradkhani et al., 2005].

Generally, systematic attempts for parameter hydrologic estimation can be categorized into deterministic and probabilistic methods. Commonly, in the deterministic methods, in a batch mode process, the hydrologic parameter estimation is defined as an optimization problem to seek a global minimum and associated optimum parameters set as the mode of the forecast without explicitly addressing the associated uncertainty and error characteristics. In the probabilistic approach, parameters of a hydrologic model are considered as random variables and typically Monte Carlo analysis is employed to estimate the probability distribution or uncertainty around statistics of interest.

The approaches toward hydrologic parameter estimation via solving an optimization problem lead to development of some well known algorithms. Shuffled Complex Evolutionary (SCE-UA) Method [Duan et al., 1992], is one of those algorithms that has been widely used and extensively applied successfully to find global optima points of hydrologic optimization problems. The SCE-UA strategy combines the strengths of the simplex procedure of Nelder and Mead [1965] with the concept of controlled random search, competitive evolution and information shuffling.

In probabilistic approaches, researchers believe that because of hydrologic model structural inefficacy, observation and boundary condition uncertainties; hydrologic parameters shall be treated as variables with random nature and their efforts have been focused on estimating the probabilistic structure of the parameters space. In hydrologic prediction context, the generalized likelihood uncertainty estimation (GLUE) method [Beven et al., 1992] was among the first attempts which brought up this concept into the Hydro-science arena. The GLUE framework might be categorized as belonging to the general field of Monte Carlo rejection sampling techniques which benefits from a Bayesian scheme to update the likelihood associated with behavioral parameter sets. In GLUE method, the rainfall runoff model is run several times and each simulation is assigned a likelihood weight, based on the degree of closeness of the simulation to observation. Then a cut off threshold is employed to accept or reject each simulation and its associated parameter set.

In this study Block Bootstrap technique is employed to estimate the statistical characteristics of hydrologic parameters, using SCE-UA as one of the most robust optimization algorithms in the field of hydrology. In this method, based on a sample with finite length of observation (i.e. streamflow) the empirical bootstrap version of observation time series population is constructed to estimate the hydrologic parameters and their confidence intervals.

This paper is structured as follows. In the next section, a brief background on the non parametric bootstrap resampling for independent and dependent data is presented. A next section provides information about method and the proposed framework of hydrologic bootstrap parameter estimation. Implementation of the proposed method in a case study is also discussed, and at the end some results and subsequent

achievements are presented. Finally, conclusions and potentials for further research in this area are also discussed in section 6.

Review of Bootstrap Methods

Bootstrap method was originally proposed by *Efron 1979*, as a non parametric procedure for population inference from iid samples. Bootstrapping is a method for estimating the sample distribution of a random variable *R(***X**,*F),* which possibly depends on both **X** and an unknown distribution of *F* on the basis of the observed data [Efron, 1979]. Let **X**=(X_1,X_2,...,X_n) and x=(x_1,$x_{2,....}$,x_n) denote the random sample and its observed realization , respectively. For one independent sample problem the bootstrapping idea includes the following steps:

1. Construct of empirical probability distribution $\hat{F}$ (Bootstrap population), which is the nonparametric maximum likelihood estimator of the underlying population distribution function.
2. Draw random sample of size n with replacement from $\hat{F}$, say
   $X_i^* = (x_1^*, x_2^*, ..., x_n^*)$, $X_i^* \sim_{independent} \hat{F}$
   where $x_i^* \quad i = 1,2,...,n$ are bootstrap samples.
3. Estimate the sampling distribution of *R(***X**,*F)* by the resample (or bootstrap) distribution of, $R^* = R(\mathrm{X}^*, \hat{F})$.

More generally, the nonparametric empirical distribution $\hat{F}$ consists of multiple copies of the available random sample from real population. By assuming a large population size (i.e. N/n > 20), sampling without replacement from that large empirical population means sampling with replacement from a single copy of the random sample. Using resampling one could calculate the sampling distribution of interest (or estimator distribution). For dependent processes, the construction of approximate distribution (Bootstrap population) is more complicated and far less obvious than seminal proposal for independent setup by Efron, 1979. Block bootstrap (BB) is a technique to get *iid* samples from weakly dependent (strongly mixed) data structures [Künsch, 1989]. The commonly used block bootstrap method, known as Moving Block Bootstrap (MBB) was presented by *Künsch* [1989]. Let $\zeta_n \equiv \{X_1, ..., X_n\}$ denote an observation segment from a stationary time series $\{X_i\}_{i \in Z}$ and $R_n = r_n(\zeta_n; \theta)$ be a "root" or an approximation pivot, which has some functional dependence on the data. For example R_n might be of the form $R_n = \sqrt{n}(\overline{X}_n - \theta)$ or possibly a studentized version. $\overline{X}_n$ is sample parameter (i.e. mean) and θ denotes the population parameter (i.e. mean). The objective of the method is to estimate sampling distribution of R_n and its functionals. To describe the method in mathematical form, let l be the block size (integer value) and n be the sample size such that as $n \to \infty$ and $l \to \infty$ then $n^{-1}l \to 0$. Consider, $B_i = (X_i, ..., X_{i+l-1})$, $i = 1,...N$, $N = n - l + 1$ stand for all possible overlapping blocks of length l contained in ζ_n. In addition assume

$b = \lceil n/l \rceil$ denote the smallest integer not less than n/l, In this method b blocks are sampled at random with replacement from $\{B_1,....,B_N\}$ to generate pseudo time series by concatenating the elements of the resampled blocks (see figure 1). Let $\zeta_n^* = \{X_1^*,....,X_n^*\}$ be the first generated pseudo time series, then the MBB estimation of R_n is given by:

$$R_n^* = r_n(\zeta_n^*; \hat{t}_n)$$

Methodology and Framework

From statistical standpoint the available measurement of streamflow are samples from large populations which are not available. In fact the purpose of this study is to employ MBB as a nonparametric method in conjunction with optimization techniques to estimate population characteristics of hydrologic model parameters based on the available observation.

The principle of the proposed methodology for block bootstrap estimation of optimal hydrologic parameters is summarized in three main modules (see figure 2). As a consequence of module 1, any functionals of optimal hydrologic parameters marginal distribution (i.e. mean) can be estimated via implementation of the second module, using an independent bootstrapping of sampled hydrologic parameters. In the third module one can smooth the jagged sample distribution to estimate the density of optimal hydrologic parameters which can be used for ensemble prediction.

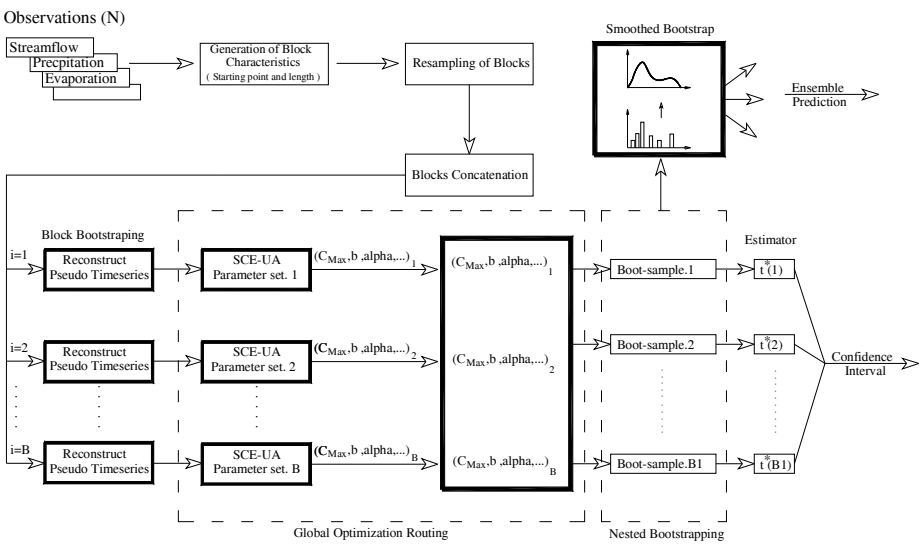

Figure 1: **Flow chart of Moving Block Bootstrap hydrologic parameter estimation using SCE-UA global optimization method.**

Implementation of the Method

The Leaf River as a subbasin of Pascagoula basin totally drains nearly 9200 square kilometers. The headwater of the river originates in west-central Mississippi. The basin has approximately total length of 170 kilometers and maximum width of 90 kilometers. The river falls 55 meters over its length. The basin topography is comprised a low rolling hills and ridges, characteristic of the coastal plain regions. Because of severe flood records, the basin has been a test basin in numerous studies [i.e. Yapo et.al, 1998, Moradkhani et.al, 2005]. We used forty years of reliable data set available in the Collins station (drainage area: 1944 km2) approximately 28 miles northwest of Hattiesburg, Mississippi.

HyMod (HYdrologic MODel [Moore, 1985 & Boyle, 2000]) as a parsimonious conceptual model has been used for the purpose of implementation of the proposed methodology in this study. The model is based on the probabilistic principle of spatial distribution of catchment runoff response to rainfall. HyMod consists of two series of connected linear reservoirs including three identical quick and a single slow tank to simulate catchment runoff response. The model requires the optimization of five parameters based on the observed streamflow data, including, the maximum storage capacity in the catchment (C_{max}), the degree of spatial variability of the soil moisture capacity (b_{exp}), the factor that distributes the flow between the two series of reservoirs (*Alpha*), and the residence time of the linear quick (R_q) and slow reservoirs (R_s). Feasible range of the model parameters are defined in table1.

Table 1: Feasible range of parameters

Parameters	Description	Minimum	Maximum
Cmax	Maximum storage capacity of watershed	1	1000
Bexp	Residence time for quick-flow tanks	0	2
Alpha	Distribution Factor	0	1
Ks	Slow flow tank residence time	0.0002	0.1
Kq	Quick flow tanks residence time	0.1	0.99

As mentioned, we employed SCE-UA to compute optimum hydrologic samples in MBB scheme. In calibration process, we chose root mean square error (RMSE) of the predicted flow and observation as optimization cost function.

$$\min(RMSE(e \mid N,o)) = \min\left\{\sqrt{Bias(e \mid N,o)^2 + Var(e \mid N,o)}\right\}$$

Where, N is sample size, *(e)* is the estimation (i.e mean of simulated flow) and *(o)* is the observation (i.e. mean of observed flow). Therefore it is obvious that by minimizing *RMSE*, the bias and variance of estimation are minimized.

In batch hydrologic calibration methods, it is clear that the estimated parameters have a functional dependence on the calibration length. To raise the major questions that we are going to answer in this study, we did several calibration experiments on Leaf River basin data set with different calibration periods. To resemble the law of large

number, we followed a cumulative calibration approach ranging from 1(1948) to 40 (1988) years (i.e. see figure 2). As the employed optimization algorithm is designed based on a competitive random search, it was also worthwhile to explore the sensitivity of the estimated optimal parameters on random initialization of the algorithm and local minima effects of error surface as well (see Duan et al., 1992). As an example, we repeated the calibration scheme for thirty times and the results for $C_{\max}$ parameter are displayed in figure 2.

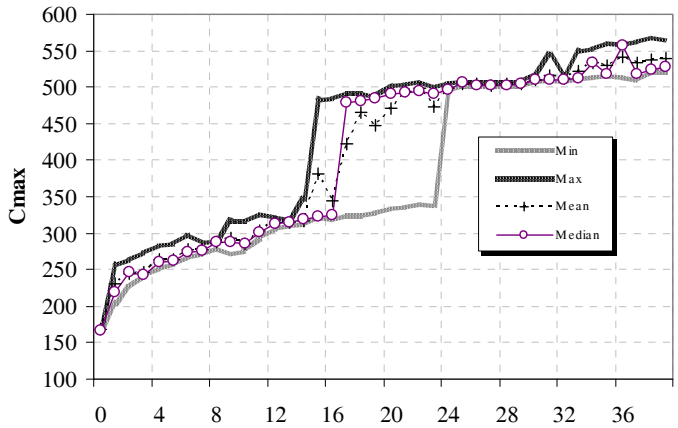

Figure 2 : Cmax ensemble variation and statistics

Accordingly, two questions may arise: (1) Is the available observation time series as large as it is required to ensure that the computed parameters are close to population expected value? (2) What is the degree of accuracy and confidence limits around the estimated hydrologic parameters based on the entire available calibration data set?

Assuming the functional dependence of optimal hydrologic parameters to the observed streamflow, we employed the original idea of moving block bootstrap algorithm for parameter estimation [Künsch, 1989]. To preserve physical and temporal properties of observed time series (i.e. streamflow) we used non-overlapping scheme for construction of pseudo time series. Using overlapped block scheme, means that we may have some pseudo time series for instance with two successive seasonal high flow regimes without any low flow between them. Therefore using overlapping scheme, we may have unrealistic pseudo time series.

Observations from October 1948 to October 1963 were used for block bootstrap calibration scheme. To implement MBB the fifteen years of the data were divided into annual non-overlapping blocks, the blocks were sampled with replacement based on a discrete uniform distribution and then concatenated to form pseudo time series. For each constructed time series an optimal set of hydrologic parameters are calculated using optimization algorithm with the same parameterization. So by implementation of the proposed methodology, we will end up with B (i.e. B=100)

bootstrap samples of optimal hydrologic parameters which can be used for density estimation and confidence interval analysis of hydrologic parameter estimator (i.e. mean, quantiles) as well.

One of the well known bootstrap CI estimation methods, is the so-called bootstrap-*t* is based on the assumption that the sampling distribution of the plug-in estimator in pivotal form can be characterized as a standard normal or student-*t* distribution in case of infinite and finite sample size. Pivotal properties of studentized bootstrap plug-in estimator lead to the assumption that studentized bootstrap sampling distribution $t(t^*) = \left[(t^* - \theta) / SE(t^*)\right]$ provides an unbiased approximation to the real world sampling distribution of $t(t) = \left[(t - \theta) / SE(t)\right]$ [Lunneborg, 2000], where $t, \theta, SE(.)$ are the estimator, population parameter and operator of standard error of estimation respectively. To perform bootstrap-*t* nonsymmetric confidence interval analysis, θ shall be a location parameter, *t* shall be a plug-in estimator of θ and we need to have robust computational method to estimate the standard error of the estimator from the bootstrap samples. It shall be noted that this method can be applied to location parameters include not only for example mean and median but also the quantiles of a distribution. To have the most robust CI analysis and avoid any prior parametric assumptions about population estimator distribution, we used a second level bootstrap estimate method to compute $SE(t^*)$ [Efron and Tibshirani, 1993]. In this method, simply, from each of the first level B bootstrap samples, we resampled *B1* random sequence and then computed the first level bootstrap estimator (t_b^*) standard error as follows:

$$SE(t_b^*) = \sqrt{\frac{\sum_{i=1}^{B1}[t_{bi}^* - \frac{\sum_{i=1}^{B1} t_{bi}^*}{B1}]}{B1 - 1}}$$

For having a satisfactory estimation of CI, as a rule of thumb *B* generally may be taken from 2000 to 5000 in size. On the other hand, the number of second level bootstrap resamples (*B1*) doesn't need to be as large as B, and might be selected perhaps between 50 to 150 [Lunneborg 2000]. It is worthwhile to mention that higher order bootstrap estimation of pivotal statistics provides a powerful and more accurate estimation method than single level bootstrap sampling techniques; however it drastically increases the computational burden of the problem.

The results of Bootstrap-*t* equal tail exclusion CIs analyses of the computed hydrologic parameter sets are presented in table 4. To make our estimation more robust against outliers, we chose 20% percent winsorization scheme to compute the mean and its confidence interval [Wilcox 2005]. As an example, studentized transformation of two bootstrap sampled hydrologic parameters is presented in figure 3. The results of the analyses indicated that in all cases bias and standard error of studentized transformation deviate form the ideal values (0,1) less than 5 percent. Although we don't have any specific information about the population distribution of

hydrologic parameters, based on the estimated bias and standard error of the pivotal distribution it can be concluded that studentized trimmed mean behaves acceptable as a strong pivotal statistics in the sense of possessing mathematical and shape stability. The results of confidence interval analysis of hydrologic parameter estimators are presented in table 2.

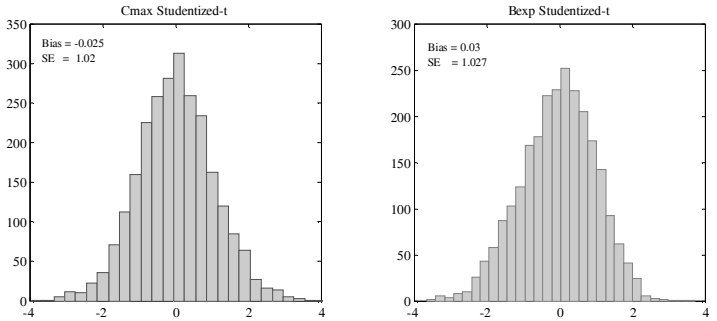

Figure 3: Bootstrap transformed sample distribution for mean of Cmax and Bexp

Parameters		2.5% Quantile	Winsorized Mean	97.5% Quantile
Cmax	*t* [1]	272.4628	406.44	576.3296
	Boot-CI [2]	255.3881 283.4984	389.2 424.8	514.9116 580.8819
Bexp	*t*	0.14081	0.19882	0.30274
	Boot-CI	0.13653 0.1609	0.1912 0.2182	0.26632 0.32224
Alpha	*t*	0.81756	0.96154	1.00
	Boot-CI	0.7925 0.84403	0.94521 0.97606	1.00 1.00
Ks	*t*	0.0002	0.022175	0.091178
	Boot-CI	0.0002 0.0002	0.013219 0.032101	0.081172 0.09493
Kq	*t*	0.45877	0.46739	0.47684
	Boot-CI	0.45499 0.4597	0.46647 0.46833	0.4742 0.48192

1- *t,* represents the bootstrap estimation of the sampled hydrologic parameters using MBB

2- Boot-CI represents bootstrap confidence interval

Table 2: Bootstrap CI analysis of hydrologic optimal parameter statistics

Summary and Conclusion

Hydrologic model calibration and analysis of the uncertainties associated with the forecasts is still a challenging process in hydrologic literature. Batch mode calibration scheme as the most commonly used method for hydrologic parameter estimation is not capable to explicitly address the uncertainty and confidence bound around the forecast. Moving block bootstrap resampling in combination with a robust optimization algorithm such as SCE-UA, can be a bridge to fill the gap between the existing parameter estimation concepts. In this new method, in parallel of using an efficient optimality scheme, the well accepted concept of the non-uniqueness of hydrologic parameters or behavioral parameters [Beven and Binley,1992] is also preserved.

In the MBB hydrologic parameter scheme, we followed the principal that the observation time series (may be corrupted with noise) as a segment of our process, contains the information to assess the system behavior. In general, in the presented method based on the available observations, several bootstrap versions of error surface are constructed as inputs of an optimization algorithm and consequently associated optimal hydrologic parameters can be computed. Then the drawn samples resulted from the MBB scheme, provide a platform for other bootstrap data analysis such as confidence interval and smoothed density estimation which finally can lead to a probabilistic hydrologic forecast.

In the performed real case study, we implemented MBB parameter estimation scheme for fifteen years of total available record (forty years). Computed parameters from that calibration length scale (see table 4), are well conformed to the computed parameters range for forty years of calibration (see figure 2). The computed expected value and associated confidence bounds completely cover the range of the calibrated parameters for the longer and even entire period of observation. It shall be noted that statistically speaking as an implicit results of law of large number, the calibrated parameters for the entire observation are more reliable descriptors of watershed runoff generation mechanism. As a result, it seems that the presented inferential statistical method can play a significant role for parameter estimation in watersheds with short record of observations.

Reference

1- Beven, K. J., (1993), Prophecy, reality and uncertainty in distributed hydrological modeling. *Adv. Water Resour*., *16*, 41–51

2- Beven, K. J., and A. M. Binley, (1992), The future of distributed models: Model calibration and uncertainty prediction, *Hydrol. Process*., *6*, 279–298

3- Blasone R.S., Vrugt J.A., Madsen H., Rosbjerg D., Robinson B.A., and Zyvoloski G.A., (2008), Generalized likelihood uncertainty estimation (GLUE) using adaptive Markov Chain Monte Carlo sampling , *J. Adv. In Water Resour.,* 31, 630-648

4- Burnash, R.J.C., (1995), The NWS River Forecast System – Catchment Modeling. In: Computer Models of Watershed Hydrology, V.P. Singh (Editor). Water Resources Publications, Highlands Ranch, CO, 311-366

5- Carlstein, E. (1986), The use of subseries values for estimating the variance of a general statistic from a stationary sequence. *Ann. Statist*., 14, 1171-1179

6- Duan, Q., S. Sorooshian, and V. Gupta, (1992), Effective and efficient global optimization for conceptual rainfall-runoff models, *Water Resour. Res*., *28*, 1015–1031

7- Efron, B., (1979), Bootstrap Methods: Another look at Jackknife*, Ann. Statist.*, 7, 1-26

8- Efron B., Tibshirani R., (1993), An introduction to the bootstrap, 1st ed., 430 pp., Chapman & Hall/CRC. FL., USA

9- Freer, J., Beven, K., and Ambroise, B., (1996), Bayesian estimation of uncertainty in runoff prediction and the value of data: An application of the GLUE approach. *Water Resour. Res.,* 7, 2161–2173

10- Künsch, H.R., (1989), The Jackknife and the bootstrap for general stationary observations. *The Ann. statist.*, 17(3), 1217-1241

11- Lahiri, S.N., (1995), On the asymptotic behavior of the moving block bootstrap normalized sums of heavy-tailed random variables. *The annals of stat.,* 23(4), 1331-1349

12- Lahiri, S.N., (1999), Theoretical Comparison of block bootstrap methods., *The annals of stat* ., 27(1), 386-404

13- Lunneborg, C.E., (2000), Data analysis by resampling concepts and applications, 1st ed., 561 pp., Duxbury Press, CA., USA

14- Moradkhani, H., Soorooshian S., and Gupta H.V., (2005), Dual state parameter estimation of hydrological models using ensemble Kalman Filter, *Adv. Water Res*.,28, 135-147

15- Nelder, J. A., and R., Mead, (1965) A simplex method for function minimization, *Comput. J.,* 7(4), 308-313

16- Nash, J. E., and J. V. Sutcliffe, (1970), River flow forecasting through conceptual models, 1, A discussion of principles, *J. Hydrol.*, 10, 282–290

17- Politis, D.N., Romano J.P. and Lai T.L., (1992), Bootstrap Confidence Bands for Spectra and Cross-Spectra', *IEEE Trans. Signal Proc.*, 40(5), 1206-1215

18- Politis, D.N., and Romano J.P., (1994), The stationary bootstrap. *J. American Stat. Assoc.,* 89, 1303-1313

19- Sorooshian, S., Dracup J.A., (1980), Stochastic parameter estimation procedures for hydrologic rainfall-runoff models: correlated and heteroscedastic error cases. *Water Resour Res.,* 16(2), 430–42

20- Wilcox, R. R. (2005), Introduction to robust estimation and hypothesis testing. 2st ed., 516 pp. Elsevier Academics Press CA., USA.

21- Zoubir, A.M., Iskander D.R., (2004), Bootstrap techniques for signal processing, 1st ed., 217 pp., Cambridge Univ. Press, UK

American Society of Civil Engineers /Environmental and Water Resources Institute
World Water & Environmental Congress 2009
May 17-21, 2009. Kansas City, Missouri, USA

Optimization of Regional Stormwater Quality Control Systems Using Genetic Algorithms

Pradeep K. Behera[1] and Ramesh S. V. Teegavarapu[2]

[1] Department of Engineering, Architecture & Aerospace Technology, University of the District of Columbia, Building 42, Suite 213H, 4200 Connecticut Avenue NW Washington, DC 20008; PH (202) 274-6186; FAX (202) 274-6232; email: pbehera@udc.edu

[2] Department of Civil Engineering, Florida Atlantic University, Boca Raton, FL 33431; PH (561) 297-3444; FAX (561) 297-0493; e-mail: ramesh@civil.fau.edu

Abstract

Stormwater system management with a set of objectives in urban watersheds is often achieved by effective design and use of detention ponds. These ponds help mitigate impacts of urban drainage from water quantity and quality perspectives. The design, site selection for these ponds, operation and management over time are important aspects of effective stormwater management. This involves costs to land developers and there is always a need for minimizing these costs at that same time fulfilling the objectives of the management with environmental and regulatory compliance. A nonlinear programming formulation and genetic algorithm (GA) based optimization approaches are proposed to design a single stormwater detention pond system in the current study. The optimization methodology is also extended to consider multiple detention systems. The main objective is to minimize the cost constrained on system performance related to pollution control. The optimization techniques employs analytical probabilistic models for urban stormwater management analysis which mathematically closed form are enabling them easily integrated into optimization frame work. The results provide optimal design parameters considering the runoff control and pollutant reduction considering environmental and regulatory issues. Application of the methodology for a case study system is demonstrated with results and the benefits of using GA based optimization approach are illustrated.

Introduction

To minimize the adverse impacts of urban development, storm water detention ponds have been are commonly used in watersheds. These ponds commonly known as stormwater management systems not only provide runoff quantity control such as peak flow attenuation, volume control and erosion but also runoff pollution control. In the era of eco-system based watershed developments, the role of stormwater management ponds have been very significant. They provide a sustainable development by minimizing the impacts of stormwater runoff. These ponds usually occupy valuable land and involve initial construction, as well as operation and maintenance, costs. The developer typically viewed as loss of developable lands which otherwise It is the objective of land developers and/or municipalities to minimize these costs of implementing stormwater management ponds while satisfying regional environmental regulations for runoff quantity and quality control

American Society of Civil Engineers /Environmental and Water Resources Institute
World Water & Environmental Congress 2009
May 17-21, 2009. Kansas City, Missouri, USA

At the planning-level analysis, typically statistical/analytical procedures are preferable for identifying least-cost system design variables that provide required level performance which are based on the regulatory requirements (Nix and Heaney, 1988; Segarra-Garcia and El Basha-rivera, 1996; Adams and Papa, 2000). The objective function for this study consists of minimizing the cost associated with the implementing stormwater management ponds that will comply the environmental regulations. Typical costs of ponds include the cost of land occupied by the ponds and pond construction costs. The cost of the land can be considered as purchase value of the land or opportunity cost of lands occupied by the ponds. The construction cost of the pond can be related the volume of the pond in terms of excavation and grading cost per unit volume. The phrases 'catchment' and 'watershed' are used interchangeably in this paper.

This paper presents a methodology for optimizing pond geometries through minimizing above mentioned costs for a single watershed as well as for a set of parallel watershed. Papa and Adams (1997) provided such formulation using dynamic programming technique however, this paper solves the problem using nonlinear optimization and genetic algorithm (GA) techniques. The regional watershed involves three parallel watersheds as presented in following Figure 1.

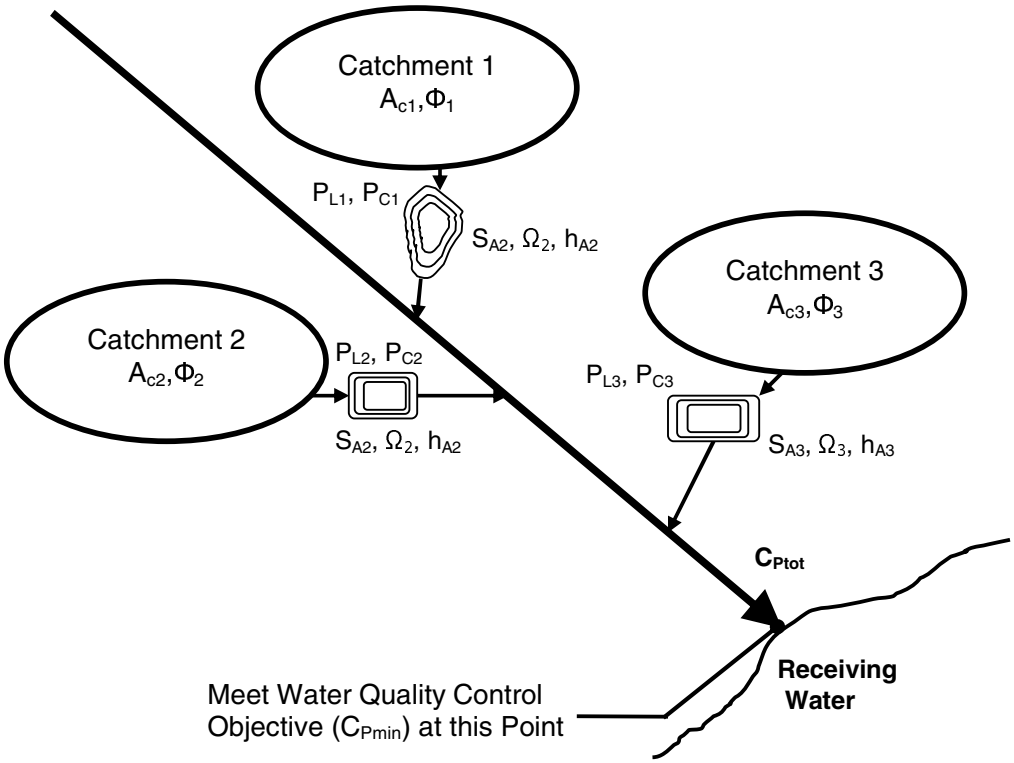

Figure 1: Schematic Representation of the Optimization Problem

American Society of Civil Engineers /Environmental and Water Resources Institute
World Water & Environmental Congress 2009
May 17-21, 2009. Kansas City, Missouri, USA

Optimization Formulation

In order to develop the develop the optimization methodology a system of sub-watersheds, each with a stormwater quality control pond upstream of its outlet, draining into a common collection system (e.g., trunk sewer) which subsequently conveys the stormwater to the local receiving water. This scenario is depicted in Figure 1 for system of three sub-watersheds. Each watershed is characterized by spatially by an area on its local topography, imperviousness and land cost as well as pond construction costs. The discharge from the trunk sewer is required to meet or exceed a defined quality control objective (C_{Pmin}). Based on this formulation, it is conceivable that different levels of water quality control can be provided at the outlet of each sub-watershed such that overall control of runoff quality meets or exceeds the regional environmental regulations for the group of sub-watersheds. Thus, the total cost of implementing stormwater quality ponds for all of the watersheds may be minimized by providing an optimal blend of individual watershed controls in the multiple watershed system, as opposed to providing uniform control in all watersheds.

The water quality control constraints can be expressed mathematically by:

$$C_{Ptot} = \frac{\sum_{i=1}^{n} C_{Pi} A_{Ci}}{\sum_{i=1}^{n} A_{Ci}} \geq C_{P\min} \qquad (1)$$

The objective function of the optimization scheme is to minimize the total cost of implementing the stormwater quality control ponds in each of the watersheds. The cost of implementing a single pond can be estimated by

$$P_{Pond} = P_L A_P + P_C V_P \qquad (2)$$

Where A_P and V_P are the pond surface area (m^2) and volume of the pond (m^3), respectively, P_{Pond} is the total cost of the pond (current \$), P_L is the present land value (\$/m^2) and P_C is the present value of construction and OMR costs (\$/m^3).

The decision variables in this design optimization procedure are the active storage volume of the pond (S_A expressed in mm uniformly distributed over the catchment), the controlled release rate from the pond (Ω expressed in mm uniformly distributed over the catchment per hour) and pond depth (h_A in m). It is therefore required to express the cost function (2) in terms of these decision variables as follows:

$$P_{Pond} = P_L \frac{A_C S_A 10}{h_A} + P_C A_C S_A 10 \qquad (3)$$

Using Equation (3) coupled with the pollution control model presented in the following section, a least-cost combination of above decision variables can be obtained for each of the watersheds

American Society of Civil Engineers /Environmental and Water Resources Institute
World Water & Environmental Congress 2009
May 17-21, 2009. Kansas City, Missouri, USA

based on the level of pollution control (C_P) required from the pond. The least The objective of the optimization scheme is to minimize the total cost of implementing the stormwater quality ponds in each of the sub-watersheds.

$$Minimize\left\{TC = \sum_{i=1}^{n}\left(P_{Pond}\right)_i = \sum_{i=1}^{n}\left(P_{Li}\frac{A_{Ci}S_{Ai}10}{h_{Ai}} + P_{Ci}A_{Ci}S_{Ai}10\right)\right\} \quad (4)$$

Analytical Model for Runoff Quality Control Performance

During planning-level analysis, the long-term runoff quantity and quality control performance of ponds can be easily obtained by employing analytical probabilistic models for urban stormwater management analysis. These models are based on derived distribution theory in which the probability density functions (PDFs) of rainfall characteristics (e.g., event volume, duration, average intensity and inter-event time) are transformed into PDFs of system performance depicting watershed hydrology, control system hydraulics and pollution removal processes. The input parameters include (i) parameters of PDFs of rainfall characteristics (λ, ζ and ψ are the parameters of the exponential PDFs of the meteorological characteristics of rainfall event duration, rainfall event volume and interevent time, respectively), which are obtained from the long-term rainfall records, constitute the input parameters, (ii) watershed parameters such as runoff coefficient (Φ), which can be obtained from the watershed imperviousness, (iii) control system parameters such as pond storage volume (S_A), pond outflow rate (Ω) and pond depth (h_A), (iv) particle size distribution and corresponding settling velocity.

This paper focuses on the use of stormwater quality control ponds, particularly extended detention dry ponds. Adams and Papa (2000) presents following expressions for predicting the total suspended solids (TSS) from the detention basin:

$$C_P = E_d\left[1-\left[\frac{\frac{\lambda}{\Omega}}{\frac{\lambda}{\Omega}+\frac{\zeta}{\phi}}\right]\left[\frac{\frac{\psi}{\Omega}+\frac{\zeta}{\phi}\exp\left\{-\left(\frac{\psi}{\Omega}+\frac{\zeta}{\phi}\right)S_A\right\}}{\frac{\psi}{\Omega}+\frac{\zeta}{\phi}}\right]\right] \quad (5)$$

where the annual fraction of runoff controlled is treated in the pond at an efficiency of E_d given by

$$E_d = \sum_i F_i\left\{1-\left[1+\frac{V_{Si}}{nh_A}\frac{S_A}{2\Omega}\right]^{-n}\right\} \quad (6)$$

American Society of Civil Engineers /Environmental and Water Resources Institute
World Water & Environmental Congress 2009
May 17-21, 2009. Kansas City, Missouri, USA

The overall removal efficiency, E_d is based on settling of suspended solids in turbulent conditions, where n is the turbulence factor expressing the settling characteristics of the pond, V_{Si} and Fi are the average settling velocity and the fraction of total mass of solids contained in the ith size fraction, respectively, of the settling velocity distribution of suspended solids in the stormwater runoff. The terms ζ, λ, and ψ are parameters for the exponential distribution of probability density of the rainfall characteristics of rainfall event volume, event duration and interevent time, respectively. The detail description of the model can be found elsewhere (Adams and Papa, 2000).

Papa et al. (1997) present a comparison of results from the above analytical model with continuous simulation model results for the pollution control performance of extended detention dry ponds and concluded that the results compare favorably.

In the present study, the rainfall characteristics values are taken from the statistical analysis of hourly rainfall data for the period 1960 to 1992 from the Toronto Pearson International Airport based on a 2 hour interevent time definition (Adams and Papa 1997). The corresponding parameter values are: ζ=0.20 mm^{-1} (inverse of mean rainfall event volume), λ=0.282 hr^{-1} (inverse of mean rainfall event duration), and ψ=0.23 hr-1 (inverse of mean rainfall interevent time), respectively. In addition, a commonly used settling velocity distribution of suspended solids in storm water is used for estimation of removal efficiency with a value of n = 3 for the pond settling performance factor.

Optimization of Pond Design for Single and Multiple Watersheds

Papa and Adams (1997) developed an optimization procedure to evaluate the values of decision variables (S_A, Ω, and h_A) of a stormwater quality control pond based on a cost function (3) and the required levels of pollution control performance. They investigated the behavior of pollution control as a function of the decision variable values and suggested a strategy to optimize the geometries of a stormwater quality management pond.

For the multiple watersheds, they employed a dynamic programming procedure for estimating the optimal combination of stormwater management pond decision variables for achieving a prescribed minimum level of pollution control at the common discharge outlet. The objective of the procedure is to minimize the overall cost of implementing ponds by providing varying level of control in each of the watersheds while meeting the required level of control at the common outlet. The Dynamic Programming transforms the multiple watershed (stage) problem into a series of single watershed problems, then combines the solutions of the individual problems to obtain the solution policy of overall (multiple watershed)

In the present study, a similar strategy is adopted for the design of a SWM pond; however, the decision variables are optimized to meet both performance levels of runoff quantity and quality simultaneously at the minimum cost. Papa and Adams (1997)

American Society of Civil Engineers /Environmental and Water Resources Institute
World Water & Environmental Congress 2009
May 17-21, 2009. Kansas City, Missouri, USA

Limitations of DP Solution

Dynamic programming (DP) formulation was adopted in the previous study by Behera et. al., 1999). The catchments were used as stages in the DP formulation along with the level of control as a state variable at each stage. The state variable is discretized into several classes to enable the solution of the problem. Dynamic programming formulations are generally plagued by two limitations: 1) curse of dimensionality and 2) computational intractability. These two limitations are not a concern in the current context as the state variables number is limited to one and the number of finite stages will not introduce any computational intractability problems. However, the discretization level (i.e., the number of classes) of the state variable in case of a discrete DP will affect the optimal solution. Finer discretization schemes will result in more computational time while coarser schemes will result in sub-optimal solution. In order to improve the solution, a non-linear optimization formulation based on traditional optimization solvers or state-of-the-art optimization techniques such as genetic algorithms can be experimented. In the current study, two optimization formulations based on non-linear programming (NLP) and genetic algorithms are investigated.

Genetic Algorithm based Optimization

Genetic Algorithms (Holland, 1975) are well researched and applied optimization techniques in civil engineering and other disciplines. A GA deals with a population of individual solutions which undergo constant changes by means of genetic operations of reproduction, crossover and mutation (Goldberg, 1989). A solution of GA is represented as a string of decision variables (also referred to a chromosome) that evolve through generations to further improve its fitness. In the first step, the GA searches for the optimal decision variables associated with a specific objective function. The objective function used in the current study is same as defined in equation # 3. The method uses the basic structure of GA optimization involving selection, crossover, and mutation processes to obtain an optimal functional form by selecting functions of decision variables (model inputs) and mathematical operators that maximizes or minimizes the fitness of the function. Mutation and crossover parameters are used to select individuals from an initial population size.

Results and Analysis

The optimization formulation developed for the three catchment (i.e., watershed) problem is solved using a conventional dynamic programming model. The basic parameters used for the hypothetical problem are provided in Table 1. In case of DP, the watersheds are regarding as multiple stages and the state variable is discretized for solution of a discrete DP. A spreadsheet based DP is developed and solved for this purpose. Results related to the DP formulation are provided in Table 2. For all the formulations, the pond depth values are restricted to a range of 1 – 3 m. A value of 0.5 (50%) is used for $Cp_{min.}$

American Society of Civil Engineers /Environmental and Water Resources Institute
World Water & Environmental Congress 2009
May 17-21, 2009. Kansas City, Missouri, USA

Table 1: Data for Example Problem:

Description	Watershed 1	Watershed 2	Watershed 3
Area (ha)	100	40	70
Runoff Coefficient, Φ	0.3	0.6	0.7
Cost of Land, P_L ($/m^2)	40	70	90
Cost of Construction , P_C ($/m^2)	20	40	60
Minimum Pond Depth, h_A, (m)	1.0	1.0	1.0
Maximum Pond Depth, h_A (m)	3.0	3.0	3.0

Table 2. Optimal Design Policy using Dynamic Programming (DP)

Design Variables	Watershed 1	Watershed 2	Watershed 3
Pollution Control, C_P^* (%)	63.0	52.5	30.0
Pond Depth, h_A^*, (m)	1.0	1.70	3.00
Storage Volume, S_A^* (mm)	4.74	6.18	2.68
Release Rate, Ω^* (mm/hr)	0.19	0.30	0.22

The hypothetical multi-catchment optimization problem is solved using two optimization methodologies, namely 1) non-linear optimization and 2) genetic algorithms. The non-linear optimization formulation is solved using Microsoft Excel solver which uses a generalized reduced gradient (GRG) nonlinear optimization algorithm for solution. However, there is no restriction on the type of approach or solver used for solution of the mathematical programming formulation. Results related to nonlinear optimization are provided in Table 3. The non-linear optimization resulted in a total cost of $619,728

Table 3. Optimal Design Policy using Non-Linear Programming Formulation

Design Variables	Watershed 1	Watershed 2	Watershed 3
Pollution Control, C_P^* (%)	62.9	52.49	29.99
Pond Depth, h_A^*, (m)	1.095	2.208	2.464
Storage Volume, S_A^* (mm)	0.200	0.255	0.254
Release Rate, Ω^* (mm/hr)	4.290	4.613	3.625

The application of GA is based on the selection of decision variables and the algorithmic parameters. The mutation and crossover parameters are selected as 0.1 and 0.4 respectively. An initial population of 200 is selected for the GA process to continue. Results related to GA optimization are provided in Table 4. The GA optimization resulted in a total cost of $625,625

American Society of Civil Engineers /Environmental and Water Resources Institute
World Water & Environmental Congress 2009
May 17-21, 2009. Kansas City, Missouri, USA

Table 4. Optimal Design Policy using GA

Design Variables	Watershed 1	Watershed 2	Watershed 3
Pollution Control, C_P^* (%)	61.66	43.5	37
Pond Depth, h_A^*, (m)	1.356	2.377	2.429
Storage Volume, S_A^* (mm)	0.183	0.250	0.256
Release Rate, Ω^* (mm/hr)	5.259	4.310	3.615

The non-linear programming formulation and genetic algorithms techniques provide optimal solutions for the hypothetical problem. However, the real values obtained for the pond depth are impractical for application in the field. A formulation that can use only discrete values (pre-fixed values) of pond depth is required. The formulation is identified as mixed integer nonlinear programming (MINLP). A total of 6 discrete pond depths, i.e., 0.25, 0.75, 1.25, 1.75, 2.25 and 3 meters are used for the formulation. All the constraints and the objective function apply for this formulation except additional constraints defined in equations 7 and 8 are included.

$$h_{Ai} = \sum_{m=1}^{6} y_{im} ds_{im} \qquad \forall i \tag{7}$$

$$\sum_{m=1}^{6} y_{im} = 1 \qquad \forall i \tag{8}$$

The variables, y_{im} and ds_{im} are binary variables and discrete pond depths associated with catchment, i. The index variable, m, represents the number of discrete pond heights used in the formulation. The entire formulation can solved using these additional constraints (equations 7 and 8). GA optimization with restrictions on the pond depth limited to 6 possible values is carried out. The decision variables for relate rate and storage volume are fixed based on the previously obtained best solution using nonlinear programming formulation. Results related to this scenario are shown in Table 5. The GA optimization with restrictions on the pond depth sizes resulted in a total cost of $582,643.

Table 5. Optimal Design Policy using GA with restrictions on the Pond Depth

Design Variables	Watershed 1	Watershed 2	Watershed 3
Pollution Control, C_P^* (%)	51.8	42.8	35.5
Pond Depth, h_A^*, (m)	1.250	2.250	3.000
Storage Volume, S_A^* (mm)	0.200	0.255	0.254
Release Rate, Ω^* (mm/hr)	4.290	4.613	3.625

American Society of Civil Engineers /Environmental and Water Resources Institute
World Water & Environmental Congress 2009
May 17-21, 2009. Kansas City, Missouri, USA

Conclusions

A hypothetical regional stormwater system containing multiple catchments (watersheds) with detention ponds is optimized using two optimization methodologies. These methodologies include traditional non-linear optimization and genetic algorithms. The basic nonlinear programming formulation is also modified to adapt discrete values for the pond depth. The formulation with discrete values is referred to as mixed integer non-linear programming (MINLP) with binary variables. The nonlinear programming and genetic algorithm formulations provided improved solutions compared to the traditional DP formulation. These formulations overcome the restrictions and limitations of DP formulation associated with state variable descretization. The formulation using MINLP resulted in lowest objective function value and also provided a mechanism to arrive at practical dimensions for pond depths. The formulations using GA resulted in different levels of pollution control in different watersheds compared to those achieved by traditional DP and nonlinear optimization.

References

Adams, B. J., and Bontje, J. B. (1984). "Microcomputer application of analytical models for urban stormwater management," Proc., Emerging Computer Techniques in Stormwater and Flood Management, W. James, ed., ASCE, New York, 138-162.

Adams, B. J. (1996). "Development of analysis methods for stromwater management with ponds", Report to the Ontario Ministry of Transportation, Toronto, Ontario, Canada.

Adams, B. J., and Papa, F. (1997). "Urban stormwater management planning with analytical probabilistic models", Dept. of Civil Engineering, Univ. of Toronto, Toronto, Canada.

Benjamin, J. R. and Cornell, C. A. (1970). Probability, statistics, and decision for civil engineers, McGraw-Hill, New York.

Garcia, R. S. and Rivera, M. E. B., (1996). " Optimal estimation of storage-release alternatives for stormwater detention systems", J. Water Resour. Plng. and Mgmt., ASCE, 122(6), 428-436.

Goldberg, D. E. (1989). Genetic Algorithms in Search, Optimization and Machine Learing, Addison-Wesley, Reading, MA, USA.

Holland, J. H. (1975). Adaptation in Natural and Artificial Systems, University of Michigan Press, Ann Arbor, USA.

Li, J. Y. (1991). "Comprehensive urban runoff control planning." PhD thesis, Department of Civil Engineering , University of Toronto, Toronto, Ontario, Canada.

Mays, L.W., and Tung, Y.K. (1992). Hydrosystems Engineering and Management, McGraw-Hill Inc., New York, N.Y.

Nix, S. J. and Heaney, J. P. (1988). "Optimization of storm water storage-release strategies." Water Resour. Res., 24(11), 1831-1838.

Papa, F. and Adams, B. J., (1997) "Application of derived probability and dynamic programming techniques to planning regional stormwater management systems", Water Sci. Tech., Pergamon, Oxford, England, 36(5), 227-234.

Papa, F., Adams, B.J., and Bryant, G.J. (1997). "Models for water quality by stormwater ponds," Advances in modeling the managements of stormwater impacts, Vol. 5, W. James, ed., CHI, Guelph, Ontario, Canada, 1997, 1-22

American Society of Civil Engineers /Environmental and Water Resources Institute
World Water & Environmental Congress 2009
May 17-21, 2009. Kansas City, Missouri, USA

Papa, F., and Adams, B.J. (1996). "Quality control optimization of extended detention dry ponds", Advances in Modelling the Management of Stromwater Impacts, W.James, ed., CHI, Guelph, Ontario, Canada. 201-222.

Statistical Seasonal Streamflow Forecasting: An Intercomparison and Evaluation of Current Forecasting Procedures

Matthew Meier[1] and Hamid Moradkhani Ph.D., P.E., MASCE[2]

[1]Graduate student, meierma@cecs.pdx.edu, [2]Assistant Professor, hamidm@cecs.pdx.edu

Portland State University, Department of Civil and Environmental Engineering,
1930 SW 4th Ave. suite 200, Portland, Oregon, USA 97201

Abstract

The primary goal of this research is to compare and analyze the results from three statistical procedures used for producing long-lead streamflow forecasts. The models and techniques covered in this work include principal component analysis, z-score regression, and independent component analysis. These procedures were tested on a three watersheds in the Pacific Northwest while merits and disadvantages of each procedure are explored and recommendations are made useful in providing more accurate, reliable and skillful seasonal forecasts.

Introduction

Water in the western US is an essential part of the physical environment and is needed to sustain the growing communities of the region. An integral tool for successful and efficient management of western water supplies is accurate and reliable forecasts of seasonal streamflow volumes. Seasonal streamflow forecasts represent an estimate of the range of total volumetric flow expected to occur over a particular period at a specific point in a basin. These forecasts are possible in the western US because much of the streamflow in this area is the result of the accumulation of seasonal snowpack over the winter months and the melting of this snowpack over the spring and summer. This pattern of snow accumulation and melt makes it possible for forecaster to provide water supply forecasts with lead-times of several months. This lead-time is essential for the planning of reservoir and flood control management, navigation, hydroelectric generation, fish and wildlife management, and maximizing the efficiency of existing water systems (Palmer 1988). The purpose of this paper is to 1) review the current status of models and techniques utilized for water supply forecasting in the Western US; 2) present a case study from three Pacific Northwest basins using three different statistical forecasting models; 3) compare and analyze the model results.

Operation Streamflow Forecasting in the Western US

The Natural Resource Conservation Service (NRCS), formally the Soil Conservation Service (SCS), was the first agency in the US tasked with collecting snow related data and providing forecasts of future water supplies (Fisher and Portland State University 2000). The NRCS have been generating long-lead seasonal volumetric streamflow forecasts throughout the western US since the 1930's. Traditionally, the primary recipients of the forecasts were agricultural users for irrigation water management. The Division of the NRCS responsible for these forecasts is the National Water and Climate Center (NWCC). Currently, in partnership with the National Weather Service (NWS) and local cooperating agencies, the NRCS-NWCC produces seasonal

volumetric water supply forecasts monthly, January through June (Pagano and Garen 2003). All of the NRCS generated forecasts are for streamflow volumes that would occur naturally without any upstream influences, unless specified otherwise. The forecasts are done on the first of each month and include the forecast location, the forecast period, the long-term historical average streamflow volume, and the forecasted streamflow volume. There are three forecasted streamflow volumes published for each location and forecast period. The three forecasts correspond to each of the 10%, 50%, and 90% exceedance probabilities. The three separate forecasts express the uncertainty in the model and the wider the spread among the forecasted values, the greater the uncertainty in the forecast (Pagano and Garen 2003). Generally, as the season progresses the forecasts become more accurate. The forecast error early in the season is primarily due to unknown future precipitation after the forecast issue date and during the runoff period, but also include uncertainties associated with the prediction methodologies and the spatial coverage of the data network.

Current Operation Streamflow Forecasting Models and Techniques

The NRCS-NWCC relies on a statistical regression-based model for developing seasonal volumetric streamflows in the Western US. Linear regression, in various forms, is the methodology currently used at the NWCC. The NWCC develops linear regression equations for specific locations in a basin, which relates monthly predictor variables, such as snow-water equivalent, precipitation, antecedent streamflow, and climate teleconnection indices, to compute the median value of the seasonal water volume forecast distribution. At locations in a basin where linear relationships do not exist between streamflow volumes and predictor variables, nonlinear equations are used in which transformed streamflow values are predicted by a linear equation (Pagano and Garen 2003). Statistical models have the advantage that they are relatively simple and straightforward to calibrate, maintain and use, and they are usually acceptably accurate (Garen 1992). The disadvantages to using a regression model are that they require long historical records, do not represent all known physical processes that affect streamflow, work only for seasonal volumes, and the equations are typically developed to be run only at the beginning of the month.

Study Area

Three basins in the western US have been used for analysis in this paper, the locations of which are shown in Figure 1. A more detailed analysis of three forecast points within these basins was conducted and a description of these forecast locations and subbasins is provided below.

Yakima River at Cle Elum, Washingtion

The Yakima River is located in central Washington in the Yakima River Basin and is approximately 215 miles in length. The Yakima Basin drains approximately 6,150 square miles of area and has a 30-year mean annual unregulated streamflow of 4.2 million acre-feet at Cle Elum, Washington. The basin is bordered on the west by the Cascade Mountains, on the north by the Wenatchee Mountains, on the east by the Columbia, and on the south by the Simcoe Mountains and the Horse Heaven Hills. The climate in most of the basin is dry, with a mean annual precipitation over the entire basin

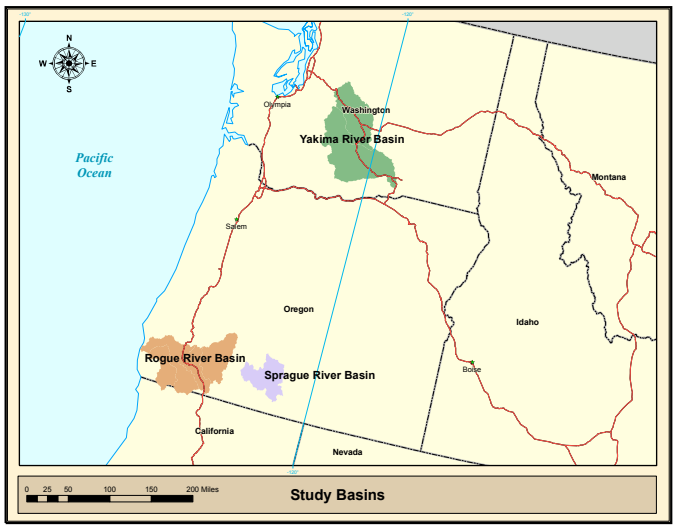

of 27 inches. Most of the precipitation in the basin falls during the winter months as snow in the mountains. The basin is primarily comprised of forest, rangeland, and cropland.

Sprague River near Chiloquin, Oregon

The Sprague River is located in southwestern Oregon in the Upper Klamath River Basin and is approximately 75 miles in length. The Sprague River drains an arid volcanic plateau east of the Cascade Mountains that is approximately 1,600 square miles in area. The basin has a 30-year mean annual unregulated streamflow of 2.3 million acre-feet near Chiloquin, Oregon. The headwaters are located along Winter Ridge and Gearhart Mountain, and flow towards the broad valley of the Sprague River near Bly and Beatty. The climate in most of the basin is much drier than that of western Oregon, and has more extreme temperatures, especially in the winter months. Mean annual precipitation in the headwaters of the basin range from 30 to 40 inches, and 10 to 20 inches in the valley near Chiloquin. Snowfall accounts for 30 percent of the annual precipitation in the valleys and as much as 50 percent in the mountains. The basin is primarily comprised of forest, rangeland, and cropland.

Rogue River at Raygold, Oregon

The Rogue River is located in southwestern Oregon in the Rogue River Basin and is approximately 220 miles in length. The Rogue River drains an area between the Cascade Mountains and the Pacific Ocean that is approximately 5,160 square miles. The basin has a 30-year mean annual unregulated streamflow of 2.5 million acre-feet at Raygold, Oregon. The Rogue headwaters originate in the Cascade Mountains near Crater Lake and the river flows westerly towards the Southern Oregon coastline where it empties into the Pacific Ocean near the city of Gold Beach, Oregon. Much of the western basin is comprised of volcanic tuffs and ash flows, whereas the eastern basin is comprised of layers of basalt flows. The climate of southwestern Oregon is cool and wet in the winter and among the hottest and driest in the western Cascades in the summer. Mean annual precipitation in the headwaters of the basin range from 20 to 30 inches, and 80 to 100 inches near the Oregon coast. The basin is primarily comprised of forest, farmland, and rural communities.

Data Network

Snow-water equivalent, precipitation, teleconnection indices, and streamflow data were used to create both the dependent and independent variables of the models presented in this paper. The data period of record used for the models in the study ranged from 1981 to 2007. A list of the variables is provided in Tables 1-3.

Snow-Water Equivalent and Precipitation

The snow-water equivalent and the majority of the precipitation data were obtained from a network of measurement sites owned and maintained by the NRCS NWCC called SnowTelemetry (SNOTEL) sites. The snow and precipitation data used in this paper are monthly aggregations. In addition, a manual snowcourse site was used in the Yakima Basin and two additional precipitation sites were used in Rogue Basin, Crater Lake National Park and the Medford airport.

Climate Teleconnection Indices

Two large-scale climate teleconnection indices were also selected for predictor variables because of their potential to reduce forecasting uncertainty by providing insight into future climate and weather variability. This paper uses the Southern Oscillation Index (SOI) and a revised Trans-Niño Index (TNI*). SOI is a record of the monthly or seasonal fluctuations in the normalized surface air pressure difference between Tahiti and Darwin, Australia. Much research has been done to understand the relationship between SOI and streamflow in the US (e.g. (Koch and Fisher 2000), (Fisher and Portland State University 2000), (Gutiérrez and Dracup 2001), (Piechota et al. 1997)). TNI is a measure of the standardized sea surface temperature gradient between region Niño 1+2 and Niño 4 (Trenberth and Stepaniak 2001). A revised TNI method is discussed in (Kennedy 2006) and it was shown to have statistically significant correlation with streamflow in the Upper Klamath Basin.

Steamflow

Two of the forecast locations – Cle Elum and Raygold – required adjusted streamflow values be calculated because of reservoir regulation and diversions upstream of the forecast point. The corrected volumetric streamflow for these locations were obtained from NRCS-NWCC. The Sprague River is unregulated and therefore the streamflow data was available directly from the USGS website. All of the streamflow values used in this paper are monthly aggregations of flow volume, in thousand acre-feet.

Statistical Hydrologic Models

Statistical models are based upon information that use observed data to identify relationships in a system. Statistical procedures are useful in highly uncertain systems and when dealing with complex models of physical processes that make it difficult to constrain model parameters. The three statistical models covered in this paper are variations of multiple linear regression models.

Multiple Linear Regression

Much of statistical hydrologic and weather forecasting is based on linear, least-squares regression. Multiple linear regression (MLR) describes the linear relationship between several predictor variables and a dependent variable. The models developed in this study use ordinary least squares (OLS) regression, which chooses the surface that minimizes the sum of the squared errors. The errors are first squared, and then summed, in order to prevent cancellations between positive and negative values. Other error measures are possible, but the statistical procedures discussed here use the OLS

regression. Further OLS regression details should be referred to (Edwards), (Berry 1993), (Younger 1979). When using MLR to summarize the relationship between several predictor variables and volumetric streamflow, one must use caution to ensure that the predictor variables used do not contain redundant information. If the predictor variables have minimal correlation among themselves, then application of the OLS regression methodology works as intended. If, on the other hand, the predictor variables are mutually correlated, then the predictor variables contain redundant information, and this condition leads to parameter estimates that are biased. In the case of using climatic variables for predictor variables, often there are correlations among the predictor variables themselves, which is referred to as multicollinearity. Ideally, when utilizing multiple regression models, it is best to avoid correlations between the predictor variables. However, in observational studies such as streamflow forecasting, it is difficult to break the covariation of the predictor variables used to capture the physical processes of a hydrologic system, and therefore some level of multicollinearity will have to be accepted. Several remediation techniques are available for dealing with datasets that would otherwise give bias parameter estimations. The following section discusses three such strategies.

Principal Component Analysis

PCA is an ordination technique that is used to order multivariate data. PCA is a technique that creates new variables from the original predictor variables that can be scored and ordered. These new variables, called principal components, are composites of many of the original predictor variables and they represent a smaller number of variables that maintain the important patterns in the data (Gotelli and Ellison 2004). The principal components are calculated in such a way that the first principal component accounts for as much of the variability in the data set as possible, and each succeeding component accounts for as much of the remaining variability as possible. In addition, and most importantly, the principal components created from PCA are uncorrelated, which allows them to be used in multiple linear regression. PCA produces the same number of principal components as there are predictor variables and they are generated from linear combinations of the predictor variables. Principal components are calculated by multiplying each predictor variable times a corresponding loading and summing the results. The loadings used in the linear equations are the elements of the eigenvectors, which are calculated from the sample variance-covariance matrix of the standardized predictor variables. The steps used in a PCA for volumetric streamflow forecasting are fully explained in (Garen 1992). One of the strengths of PCA is that it is a non-parametric analysis. As long as the assumptions of the analysis are met, then the calculated principal components are unique and independent of the user. Further PCA details should be referred to (Gotelli and Ellison 2004), (Shlens 2005), (NRCS 2007), (Garen 1992), (HyvMarinen et al. 2001), (Westra S et al. 2007).

Z-Score Regression

The Z-score regression methodology combines individual predictor variables into a composite index that then becomes the independent variable used in a regression. The main objective of the Z-score procedure is to weight those variables that are more highly correlated with the dependent variable and give less emphasis to those variables whose

correlations are lower. The Z-score method is based on correlations between the predictor variable and the dependent variable, and differs from the principal component method in that the loadings used in PCA have no knowledge of the dependent variable. In addition, the Z-score method weightings have no knowledge of the correlations among the predictor variables themselves. The computational steps for Z-score regression are outlined in full detail in (NRCS 2007). One advantage to using the Z-score method for streamflow forecasting purposes is that the method is able to deal with sets of predictor variables that have missing values or have varying periods of record. Other regression methods will generally require that the data for each independent variable be complete for the duration being analyzed. Steps would have to be taken to account for the missing data, such as estimating the values or removing the variables from the regression all-together.

Independent Component Analysis

ICA is a method that separates mutually independent signals, or components, from explanatory variables using higher-ordered statistical characteristics. The standard form of ICA suggests that the observed signals are linear mixtures of unobserved multidimensional independent signals. Typically it is assumed that there is the same number of sources as there are observations. The noise-free linear form of ICA expresses observed variables as the resulting mixture model

$$x = As$$

Where x is the observed data, A is the mixing matrix, and s represents the independent components with zero mean and unit variance. The objective of ICA is to estimate the mixing matrix and the independent components given only the observations. ICA solves the estimation problem by maximizing independence among the independent components by some measure of non-normality (Hyvarinen and Oja 2000). In this paper, a fixed-point algorithm (FastICA) for ICA is applied to a set of predictor variables in order to extract significant components that are statistically independent. The extracted components are then used in a regression analysis, similar to PCA, in order to construct a model for forecasting purposes. A full description of the computational steps used for ICA can be found in (Hyvarinen and Oja 2000), (HyvMarinen and Oja 1997), (HyvMarinen et al. 2001). The major advantage to using ICA, in comparison to other component extraction techniques, is that ICA not only decorrelates the input data, but it also addresses the high-order dependencies. The ICA procedure used in this paper was implemented using Matlab software and the FastICA algorithm for estimation of the independent components.

Application of Statistical Techniques to Three Pacific Northwest Basins

The major objective of this study is to provide an evaluation and comparison of different statistical modeling techniques for producing seasonal streamflow volume forecasts. The three statistical models were developed to forecast the April to September volume. The snow-water equivalent predictor variable used from each site was the April 1st value, because this quantity, when considering the April to September forecast window, gives a good physical indication of the available water in the basin. Following

the same reasoning, this paper used an aggregation of monthly precipitation values from October through March for all of the precipitation predictors. In order to determine statistically significant climate indices a correlation analysis was performed, similar to the methodology in (Opitz-Stapleton et al. 2007), which used 3-month average climate values that were lagged for a period of 12 months and correlated with streamflow. The 3-month season that gave the highest Pearson's correlation coefficient with the Apr-Sept streamflow volume was selected as the predictor variable in the models. A summary of the selected variable time periods is presented in Tables 1-3.

Model Results

A summary of the results from the three models is presented in Tables 4-6. Each regression model was evaluated using the entire period of record and the root mean square error was calculated as a performance measure for each model. Model simulations were performed using different combinations of predictor variables in order to identify statistically significant predictors. In addition, each model was run using a cross-validation procedure to get a sense of the models stability and overall forecasting capabilities. The cross-validation standard error and the cross-validation coefficient of determination were calculated from the model simulations. After every combination of the predictors variables were analyzed, the models were then ranked by the cross-validation standard error in order to gain insight into which predictor variables provide the most predictive power. The top five equations in Tables 4-6 are the optimized solutions for PCA, while the bottom five equations are the optimized equations using ICA. The optimized Z-score equations were consistent with the PCA equations; however, it was found that the ICA model typically selected a slightly different combination of predictors for an optimal solution.

Conclusion

Forecast models used in operation settings are not selected based solely on the lowest standard error, but rather use an optimization algorithm to assist the forecaster in selecting a skillful model that is also physically meaningful. The results of this study show that the three statistical techniques provide a good tool for exploring a set of predictor variables and identifying the statistically significant ones. The three techniques typically identified the same dominant predictor variables, however the models did not converge at the same optimal solution. Additional model simulations, using different forecast windows and lead-times, and further analysis of extracted independent components based on predictor selection is necessary in order to fully understand the performance and forecasting capabilities of ICA. The authors of this paper are planning additional research in these areas.

Table 1 Rogue River Basin streamflow and climate data used as monthly model variables. Period of Record is from 1981-2007 for all data in the table.

Variable ID	Data Description	Data Type	Start	End
	Independent Variables			
R.1	SNOTEL ANNIE SPRINGS	SWE	Apr	Apr
R.2	SNOTEL BIG RED MOUNTAIN	SWE	Apr	Apr
R.3	SNOTEL BILLIE CREEK DIVIDE	SWE	Apr	Apr
R.4	SNOTEL COLD SPRINGS CAMP	SWE	Apr	Apr
R.5	SNOTEL DIAMOND LAKE	SWE	Apr	Apr
R.6	SNOTEL FISH LK.	SWE	Apr	Apr
R.7	SNOTEL FOURMILE LAKE	SWE	Apr	Apr
R.8	SNOTEL SEVENMILE MARSH	SWE	Apr	Apr
R.9	SNOTEL BIG RED MOUNTAIN	PRCP	Oct (-1)	Mar
R.10	SNOTEL BILLIE CREEK DIVIDE	PRCP	Oct (-1)	Mar
R.11	SNOTEL COLD SPRINGS CAMP	PRCP	Oct (-1)	Mar
R.12	SNOTEL DIAMOND LAKE	PRCP	Oct (-1)	Mar
R.13	SNOTEL FISH LK.	PRCP	Oct (-1)	Mar
R.14	SNOTEL FOURMILE LAKE	PRCP	Oct (-1)	Mar
R.15	SNOTEL SEVENMILE MARSH	PRCP	Oct (-1)	Mar
R.16	CRATER LAKE NATIONAL PARK	PRCP	Oct (-1)	Mar
R.17	MEDFORD WSO AIRPORT	PRCP	Oct (-1)	Mar
R.18	ROGUE RIVER AT RAYGOLD, OR	STRM	Mar	Mar
R.19	3-MONTH TNI*	CLMT	Oct (-1)	Dec (-1)
	Dependent Variable			
R.19	ROGUE RIVER AT RAYGOLD, OR	STRM	Apr	Sep

Table 2 Sprague River Basin streamflow and climate data used as monthly model variables. Period of Record is from 1981-2007 for all data in the table.

Variable ID	Data Description	Data Type	Start	End
	Independent Variables			
S.1	SNOTEL TAYLOR BUTTE	SWE	Apr	Apr
S.2	SNOTEL SILVER CREEK	SWE	Apr	Apr
S.3	SNOTEL SUMMER RIM	SWE	Apr	Apr
S.4	SNOTEL QUARTZ MOUNTAIN	SWE	Apr	Apr
S.5	SNOTEL STRAWBERRY	SWE	Apr	Apr
S.6	SNOTEL TAYLOR BUTTE	PRCP	Oct (-1)	Mar
S.7	SNOTEL SILVER CREEK	PRCP	Oct (-1)	Mar
S.8	SNOTEL SUMMER RIM	PRCP	Oct (-1)	Mar
S.9	SNOTEL QUARTZ MOUNTAIN	PRCP	Oct (-1)	Mar
S.10	SNOTEL STRAWBERRY	PRCP	Oct (-1)	Mar
S.11	3-MONTH TNI*	CLMT	Nov (-1)	Jan
S.12	3-MONTH SOI	CLMT	Jan (-1)	Mar (-1)
S.13	SPRAGUE RIVER NEAR CHILOQUIN, OR	STRM	Nov	Dec
	Dependent Variable			
S.13	SPRAGUE RIVER NEAR CHILOQUIN, OR	STRM	Apr	Sep

Table 3 Yakima River Basin streamflow and climate data used as monthly model variables. Period of Record is from 1984-2007 for all data in the table.

Variable ID	Data Description	Data Type	Start	End
	Independent Variables			
Y.1	SNOTEL FISH LAKE	SWE	Apr	Apr
Y.2	SNOTEL OLALLIE MEADOWS	SWE	Apr	Apr
Y.3	SNOTEL SASSE RIDGE	SWE	Apr	Apr
Y.4	SNOTEL STAMPEDE PASS	SWE	Apr	Apr
Y.5	SNOW TUNNEL AVENUE	SWE	Apr	Apr
Y.6	SNOTEL FISH LAKE	PRCP	Oct (-1)	Mar
Y.7	SNOTEL OLALLIE MEADOWS	PRCP	Oct (-1)	Mar
Y.8	SNOTEL SASSE RIDGE	PRCP	Oct (-1)	Mar
Y.9	SNOTEL STAMPEDE PASS	PRCP	Oct (-1)	Mar
Y.10	3-MONTH SOI	CLMT	Dec (-1)	Feb
	Dependent Variable			
Y.11	YAKIMA RIVER AT CLE ELUM, WA	STRM	Apr	Sep

Table 4 Model results for Yakima River at Cle Elum, Washington

Definitions: RMSE, root mean square error; CVSE, cross-validation standard error; CV R2, cross-validation coefficient of determination

Model	RMSE	CVSE	CV R^2	Dependent Variable	Independent Variables									
					Y.1	Y.2	Y.3	Y.4	Y.5	Y.6	Y.7	Y.8	Y.9	Y.10
PCA	88.85	98.06	0.92	Apr-Sep Streamflow				X					X	
Z-SCORE	93.23	100.90	0.91											
ICA	95.14	101.56	0.91											
PCA	88.84	98.32	0.92	Apr-Sep Streamflow				X			X		X	
Z-SCORE	95.49	103.58	0.91											
ICA	88.82	97.89	0.92											
PCA	89.36	98.42	0.92	Apr-Sep Streamflow				X		X	X		X	
Z-SCORE	98.29	106.67	0.90											
ICA	89.44	98.36	0.92											
PCA	89.51	98.50	0.92	Apr-Sep Streamflow				X		X	X	X	X	
Z-SCORE	100.42	108.84	0.90											
ICA	90.36	98.97	0.92											
PCA	88.51	98.59	0.92	Apr-Sep Streamflow				X		X		X	X	
Z-SCORE	100.34	108.61	0.90											
ICA	91.44	100.64	0.92											
PCA	93.90	103.02	0.91	Apr-Sep Streamflow	X			X					X	X
Z-SCORE	97.29	108.35	0.90											
ICA	91.52	98.75	0.91											
PCA	94.49	102.67	0.91	Apr-Sep Streamflow	X			X					X	
Z-SCORE	92.28	101.25	0.91											
ICA	92.15	99.45	0.91											
PCA	95.08	105.38	0.90	Apr-Sep Streamflow	X			X						X
Z-SCORE	89.59	99.34	0.91											
ICA	91.39	99.80	0.91											
PCA	102.72	113.16	0.89	Apr-Sep Streamflow				X	X				X	X
Z-SCORE	102.42	114.56	0.88											
ICA	93.78	100.56	0.91											
PCA	98.45	108.23	0.90	Apr-Sep Streamflow	X			X	X				X	
Z-SCORE	102.96	113.74	0.89											
ICA	92.96	100.65	0.91											
PCA	100.23	109.60	0.89	Apr-Sep Streamflow	X	X	X	X	X				X	
Z-SCORE	106.34	117.04	0.88											
ICA	98.42	106.64	0.90											

Table 5 Model results for Sprague River at Chiloquin, Oregon

Definitions: RMSE, root mean square error; CVSE, cross-validation standard error; CV R^2, cross-validation coefficient of determination

Model	RMSE	CVSE	CV R^2	Dependent Variable	Independent Variables												
					S.1	S.2	S.3	S.4	S.5	S.6	S.7	S.8	S.9	S.10	S.11	S.12	S.13
PCA	29.28	31.66	0.96	Apr-Sep Streamflow	X		X						X	X	X	X	
Z-SCORE	37.71	47.14	0.92														
ICA	35.16	38.44	0.94														
PCA	31.31	33.61	0.96	Apr-Sep Streamflow	X	X	X			X			X	X	X	X	
Z-SCORE	41.49	46.47	0.92														
ICA	35.77	37.96	0.95														
PCA	31.48	33.64	0.96	Apr-Sep Streamflow		X				X				X	X	X	
Z-SCORE	35.87	49.75	0.91														
ICA	38.31	41.24	0.94														
PCA	31.00	33.82	0.96	Apr-Sep Streamflow	X		X		X	X			X	X	X	X	
Z-SCORE	40.72	45.88	0.92														
ICA	37.76	40.67	0.94														
PCA	30.11	33.93	0.96	Apr-Sep Streamflow	X							X	X	X	X	X	
Z-SCORE	33.37	49.82	0.91														
ICA	34.81	42.11	0.94														
PCA	44.63	47.66	0.91	Apr-Sep Streamflow	X				X					X	X	X	
Z-SCORE	37.01	51.19	0.90														
ICA	31.45	34.83	0.96														
PCA	46.92	51.04	0.90	Apr-Sep Streamflow					X					X	X	X	
Z-SCORE	37.13	52.36	0.90														
ICA	31.09	35.57	0.95														
PCA	40.25	45.38	0.93	Apr-Sep Streamflow	X									X	X	X	
Z-SCORE	36.66	52.52	0.89														
ICA	33.39	37.40	0.95														
PCA	43.61	46.33	0.92	Apr-Sep Streamflow	X			X						X	X	X	
Z-SCORE	37.57	50.21	0.90														
ICA	32.53	36.74	0.95														
PCA	35.34	41.20	0.94	Apr-Sep Streamflow	X				X					X	X		
Z-SCORE	36.73	40.80	0.94														
ICA	35.29	40.72	0.94														
PCA	37.59	41.71	0.93	Apr-Sep Streamflow	X		X	X	X	X		X	X	X	X	X	
Z-SCORE	44.44	49.74	0.91														
ICA	43.45	46.09	0.92														

Table 6 Model results for Rogue River at Raygold, Oregon

Definitions: RMSE, root mean square error; CVSE, cross-validation standard error; CV R^2, cross-validation coefficient of determination

Model	RMSE	CVSE	CV R^2	Dependent Variable	Independent Variables																		
					R.1	R.2	R.3	R.4	R.5	R.6	R.7	R.8	R.9	R.10	R.11	R.12	R.13	R.14	R.15	R.16	R.17	R.18	R.19
PCA	103.61	114.20	0.90	Apr-Sep Streamflow		X											X					X	X
Z-SCORE	102.72	117.06	0.90																				
ICA	157.30	173.02	0.75																				
PCA	107.11	115.45	0.90	Apr-Sep Streamflow		X								X							X	X	X
Z-SCORE	102.57	116.24	0.90																				
ICA	156.98	172.69	0.75																				
PCA	106.16	115.69	0.90	Apr-Sep Streamflow		X															X	X	X
Z-SCORE	105.67	119.30	0.89																				
ICA	157.72	173.44	0.75																				
PCA	105.29	115.87	0.90	Apr-Sep Streamflow		X								X								X	X
Z-SCORE	105.19	119.50	0.89																				
ICA	157.12	172.86	0.75																				
PCA	108.08	116.83	0.90	Apr-Sep Streamflow		X											X				X	X	X
Z-SCORE	102.02	115.93	0.90																				
ICA	157.16	172.85	0.75																				
PCA	120.81	132.07	0.86	Apr-Sep Streamflow		X											X						X
Z-SCORE	120.07	135.88	0.86																				
ICA	135.12	144.32	0.84																				
PCA	127.21	136.85	0.85	Apr-Sep Streamflow		X											X				X		X
Z-SCORE	121.32	137.45	0.85																				
ICA	135.68	145.08	0.83																				
PCA	125.44	134.67	0.86	Apr-Sep Streamflow		X					X									X	X		X
Z-SCORE	121.60	134.84	0.86																				
ICA	136.19	145.28	0.83																				
PCA	124.56	134.82	0.86	Apr-Sep Streamflow		X					X									X			X
Z-SCORE	123.51	137.08	0.85																				
ICA	136.47	145.70	0.83																				
PCA	127.73	136.78	0.85	Apr-Sep Streamflow		X					X						X				X		X
Z-SCORE	122.72	136.05	0.86																				
ICA	136.57	146.14	0.83																				
PCA	142.32	153.09	0.81	Apr-Sep Streamflow	X	X	X	X	X	X	X	X	X	X	X	X	X	X	X	X	X	X	X
Z-SCORE	117.92	132.88	0.86																				
ICA	129.97	147.25	0.84																				

References

Berry, W. D. (1993). *Understanding regression assumptions.* Sage Publications, Newbury Park, Calif.

Edwards, A. L. *An introduction to linear regression and correlation.* W.H. Freeman, New York.

Fisher, A. R., and Portland State University. (2000). *Improved regression-based streamflow forecasting considering large-scale climate variability.*

Garen, D. C. (1992). "Improved Techniques in Regression-Based Streamflow Volume Forecasting." *J.Water Resour.Plann.Manage.,* 118(6), 654-670.

Gotelli, N., and Ellison, A. (2004). *A Primer of Ecological Statistics.* Sinauer Associates, Inc., Sunderland, MA.

Gutiérrez, F., and Dracup, J. A. (2001). "An analysis of the feasibility of long-range streamflow forecasting for Colombia using El Niño–Southern Oscillation indicators." *Journal of Hydrology,* 246(1-4), 181-196.

Hyvarinen, A., and Oja, E. (2000). "Independent Component Analysis: Algorithms and Applications."

HyvMarinen, A., Karhunen, J., and Oja, E. (2001). *Independent Component Analysis.* Wiley, New York

HyvMarinen, A., and Oja, E. (1997). "A fast fixed-point algorithm for independent component analysis." *Neural Comput,* 9(7), 1483-1492.

Kennedy, A. (2006). "The Association Between Climate Teleconnection Indices and Upper Klamath Seasonal Streamflow: Trans-Nino Index."

Koch, R. W., and Fisher, A. R. (2000). "Effects of Inter-annual and Decadal-scale Climate Variability on Winter and Spring Streamflow in western Oregon and Washington." *Western Snow Conference.*

NRCS. (2007). "Statistical Techniques Used in the VIPER Water Supply Forecasting Software."

Opitz-Stapleton, S., Gangopadhyay, S., and Rajagopalan, B. (2007). "Generating streamflow forecasts for the Yakima River Basin using large-scale climate predictors." *Journal of Hydrology,* 341(3-4), 131-143.

Pagano, T. C., and Garen, D. C. (2003). "A Poor Man's ESP: Statistical Hydrograph Trace Adjustment." *Western Snow Conference.*

Palmer, P. L. (1988). "The SCS snow survey water supply forecasting program: Current operations and future directions." *Western Snow Conference,* 43.

Piechota, T. C., Dracup, J. A., and Fovell, R. G. (1997). "Western US streamflow and atmospheric circulation patterns during El Niño-Southern Oscillation." *Journal of Hydrology,* 201(1-4), 249-271.

Shlens, J. (2005). "A Tutorial on Principal Component Analysis."

Trenberth, K. E., and Stepaniak, D. P. (2001). "Indices of El Niño evolution." *Journal of Climate,* 14 1697-1701.

Waage, M. D., Baldwin, C. K., Steger, R. G., and Bray, T. J. (2001). "Incorporating Season Streamflow Forecasts into Operational Decision-making." *Western Snow Conference, 2001*.

Westra S, C Brown, U Lall, and A Sharma. (2007). "Modeling multivariable hydrological series: Principal component analysis or independent component analysis?" *Water Resour. Res.,* 43 W06429.

Younger, M. S. (1979). *Handbook for linear regression.* Duxbury Press, North Scituate, Mass.

Analysis of Water Quality Trends and Pollutant Loading for Cypress Creek Watershed

A. Teague [1] , H. Robinson[2], P. Bedient[3]

1. Graduate Student, Department of Civil & Environmental Engineering, Rice University, 6100 Main Street, MS317, Houston TX 77005; PH (713) 348-3798; FAX(713) 348-5239; email: aet1@rice.edu
2. Graduate Student, Department of Civil & Environmental Engineering, Rice University, 6100 Main Street, MS317, Houston TX 77005; PH (713) 348-3798; FAX(713) 348-5239; email: hilaryR@rice.edu
3. Herman Brown Professor of Engineering, Department of Civil & Environmental Engineering, Rice University, 6100 Main Street, MS317, Houston TX 77005; PH (713) 348-4953; FAX(713) 348-5239; email: bedient@rice.edu

Abstract

Lake Houston serves as the primary drinking water source for the City of Houston. Water quality is a problem in Lake Houston due to pollutant loads coming from the influent watersheds, therefore hydrologic models and water quality predictions are key to the operation of the City of Houston drinking water treatment plants. Cypress Creek is one of the watersheds that drains into the lake and has mixed use including urban and agriculture. Rapid urban development is a concern to the water quality of Lake Houston. Water quality issues of potential concern for the lake include nutrient enrichment and aquatic life use. Statistical trend analysis and loading curves have been analyzed using data collected by the USGS at 2 sites in Cypress Creek with corresponding City of Houston water quality data at the sites for the past 10 years to characterize the behavior of the pollutant source and watershed.

Introduction

Lake Houston is the primary source of drinking water for the City of Houston. Over 146 billion gallons are treated annually for 2 million customers (City of Houston, 2008). The lake is impaired for bacteria (TCEQ, 2008) and has concerns for nutrients and Chlorophyll-A (TCEQ, 2008). The watersheds flowing into the lake are also impaired for bacteria and have concerns for nutrients and depressed dissolved oxygen. With rising water treatment costs, the degraded influent has become a key concern for the City of Houston and thus protecting the watersheds is a chief priority. In order to efficiently manage the water quality an understanding of the watersheds and the relationship between pollutant loads and the influent flows is required.

Cypress Creek watershed is located northwest of Houston, Texas in Harris county and drains to Lake Houston (Figure 1). The watershed is primarily undeveloped and encompasses 109,757 Ha. The creek is gauged by the USGS at Grant Road (08068800) and near Westfield (08069000). Water quality samples are analyzed by the City of Houston at 11332 and 11328 stations that correspond to these stations. The land use of the area draining to each station is detailed in Table 1.

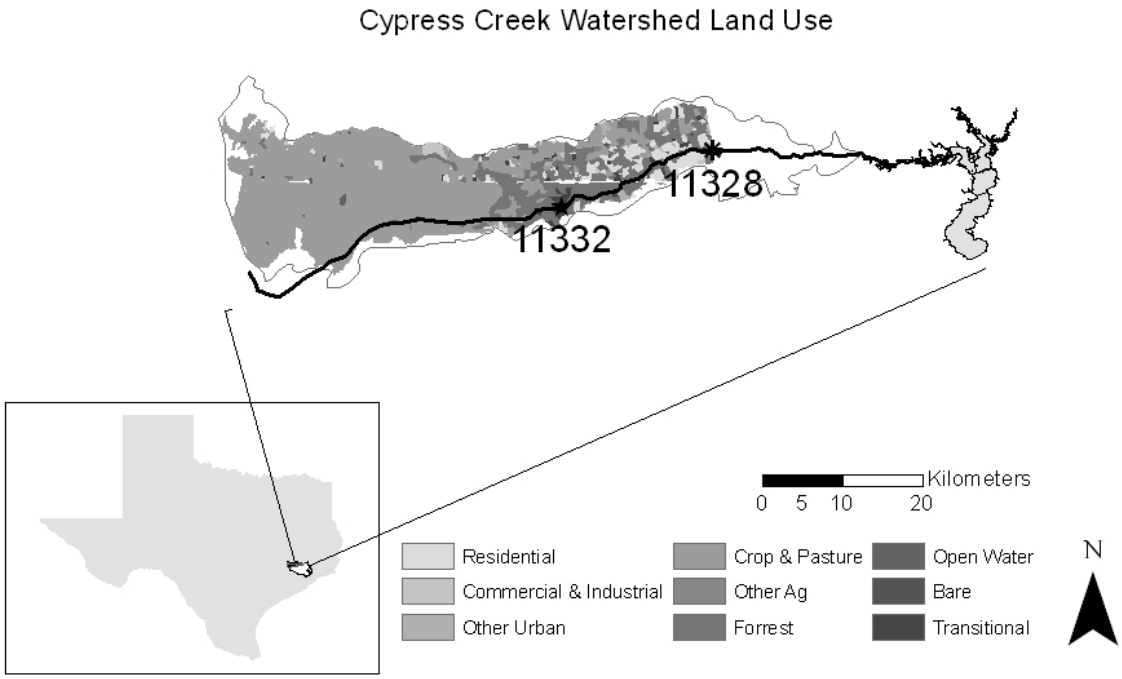

Figure 1: Cypress Creek Watershed

Table 1: Land Use Breakdown by Drainage Area of Water Quality Sampling Station

	Percentage of Drainage Area	
Land Use	**11332**	**11328**
Residential	1.47	6.73
Commercial & Industrial	0.86	0.95
Other Urban	0.14	0.80
Crop & Pasture	87.56	69.64
Other Ag	0.09	0.17
Forrest	8.51	18.68
Open Water	0.52	0.41
Bare	0.00	0.04
Transitional Area	0.83	1.91
Total Area (Hectare)	42,104	58,942

Statistical trend analysis and loading curves are analyzed using data collected by the USGS at 2 sites in Cypress Creek with corresponding City of Houston water quality data at the sites to characterize the behavior of the pollutant source and watershed.

Trend Analysis

Long-term water quality data is commonly used to detect trends in pollutants over time and also to identify, describe, and explain major factors that affect trends in water quality (Yu, 1993). The Mann-Kendall test, also known as Kendall's tau statistic is a nonparametric test for monotonic trends in a time series (Kaha, 2004),

derived from a rank correlation test for two groups of observations (Haan, 2002). This test is tolerant of outliers but requires that data are serially independent (Hamed, 1988). The Mann Kendall test is robust towards missing values, seasonal effect and non-normality (Larsen et al, 1999). Previous research has applied Mann-Kendall test to identify longer term effects of urbanization (Boeder, 2008) and to link stream flow with long term meteorological changes (Burn, 2002).

The Seasonal Kendall test is applied to address situations were data displays seasonality (Hirsch, 1982). By dividing the data into seasonal groups, performing the Mann-Kendall test on each seasonal group, and then summing the results, the effect of seasonality is removed (Hirsch, 1984). In effect the effects of dependence between the seasons is eliminated. This method has been used in various applications including assessment of the effect seasonality has on detecting the effect of acid rain on lake water quality (Taylor, 1989), assessment of spatial-temporal water quality variability (Krusche, 1997), and assessment of the effectiveness of water quality management strategies (Cude, 2001).

Load Duration Curves

A flow duration curve provides information about the percentage of time a particular stream flow was exceeded over some historical period thus providing a hydrologic "signature" of a catchment (Cigizogulo, 2000). This technique has been used in addressing water quality concerns in TMDL (Total Maximum Daily Load) programs (Cleland, 2003).

Load duration curves (LDC) are constructed by plotting the actual load over the allowable pollutant load as calculated by the product of stream flow and either the measured concentration or the water quality standard (Bonta, 2003). Actual loads that fall below the allowable load curve are considered to be in compliance with water quality standards whereas points above the line indicate water quality exceedances. The LDC is then examined to determine the flow conditions where a majority of exceedances occur. Flow conditions are divided into different categories of flow: 0 to 10% exceedance, High Flows; 10-40% exceedance, Moist Conditions; 40-60%, Mid-Range Flows; 60-90% exceedance, Dry Conditions; and 90-100% exceedance, Low Flows (Cleland, 2002).

Exceedances that occur during high flows are associated with rainfall events and pollutant sources characterized as non-point. In contrast, exceedances that occur during low flows are associated with dry weather and pollutant sources characterized as point sources (Bonta, 2002).

Method

Water quality data was collected by the City of Houston Health and Human Services and Water Quality Control departments at three locations within Cypress Creek ranging from 1996 to 2007. Stream flow discharge was measured by the USGS at the

same locations of water quality sampling. Data from 1996 to 2007 was used for both stream flow and water quality parameters.

The USGS trend testing utility (Helsel, 2006) was used to test for trend in stream flow and water quality parameters including dissolved oxygen, pH, total alkalinity, total organic carbon, chloride, sulfate, ammonia, nitrate, nitrates and nitrites, orthophosphate, and total phosphorus and *E. coli*, using Mann-Kendall test at 95% confidence level. Then the same utility was used to test for seasonal trends using a 4 season division of data using the Seasonal Kendall test at 95% confidence.

The *E. coli* dataset is the compilation of fecal coliform and *E. coli* sampling. This is necessary due to the limited time period of *E. coli* measurement, that does not fill the necessary sample size of 10 years required for Mann-Kendall and Seasonal Kendall trend detection. Garcia-Armisen et al. reviewed fecal coliform to *E. coli* ratios for different methods and found that a 1:1 ratio could be used for fecal coliform to *E. coli* ratios when a fecal coliform enumeration technique, MF using TTC Tergitol agar (SM9222D) and IDEXX colilert for *E. coli* were used (2007). These were the techniques used by both the City of Houston Health and Human Services and Water Quality Control (H-GAC, 2005) therefore the fecal coliform and *E. coli* datasets were combined to create the large enough dataset.

Load duration curves were developed for the constituents *E. coli*, orthophosphate, total phosphate, and nitrates at sites 11332 and 11328. Although ammonia measurements were made, the samples never exceeded the concern criteria, therefore load duration curves would not provide useful analysis. For *E. coli*, the water quality standard of 126 cfu/dL was used. The screening levels of 1.95 mg/L, and 0.69 mg/L were used for nitrates and total phosphorus respectively. Load duration curves were not constructed for site 11330 because the data collected by the USGS and the City of Houston did not overlap.

Results

The results of Mann-Kendall test for trend are summarized in Table 2 for station 11328 and Table 3 for station 11332. The tests were assessed at a 95% confidence level, therefore in order to reject the null hypothesis of no trend, Zs must be greater than 1.96 and Kendall's tau greater than 0.4. The p-values, Kendall's tau and magnitude of each test are reported. For station 11328, there were no statistically significant trends for any of the water quality parameters tested for both the Mann-Kendall and Seasonal Kendall tests. At station 11332, only total organic carbon showed statistically significant trends both overall and seasonally. In both cases the trend is decreasing over time.

Table 2: Trend Test results for Station 11328

11328	Overall Trend			Seasonal Trend		
	p	tau	Magnitude	p	tau	Magnitude
Flow	0.0000	0.091	-1.000	0.4290	0.109	1.000
DO	0.2535	0.057	0.081	0.5439	0.113	0.079
pH	0.0966	-0.104	0.036	0.3374	-0.118	0.025
Total Alkalinity	insufficient data					
TOC	0.1219	0.155	0.254	0.3209	0.191	0.278
Chloride	0.5120	-0.043	-0.757	0.4974	-0.118	-1.125
Sulfate	0.0034	-0.139	-0.901	0.4753	-0.127	-0.459
NH3-N	0.2135	0.074	0.120	0.6951	-0.080	-0.733
NO3-N	insufficient data					
Total Phosphorus	0.3558	-0.069	-0.036	0.2667	-0.210	-0.065
Ortho-phosphorus	0.7137	0.038	0.015	-0.0083	-0.016	1.000
E.coli	0.2325	0.060	-25.580	0.7728	-0.050	-15.250

Table 3: Trend Test results for Station 11328

11332	Overall Trend			Seasonal Trend		
	p	tau	Magnitude	p	tau	Magnitude
Flow	0.1817	-0.018	-2.870	0.8000	0.061	0.450
DO	0.8552	0.012	0.000	0.3206	0.086	0.025
pH	0.0650	0.123	0.021	0.1235	0.142	0.015
Total Alkalinity	0.2133	0.131	2.602	0.3485	0.145	2.000
TOC	0.0002	-0.400	-0.338	0.0002	-0.466	-0.400
Chloride	1.0000	0.004	-0.036	0.9745	0.002	0.000
Sulfate	0.0600	-0.122	-0.394	0.2940	-0.149	-0.431
NH3-N	0.0002	-0.251	0.007	0.1978	-0.190	0.003
NO3-N	0.3280	0.098	0.233	0.9035	0.071	0.115
Total Phosphate	0.3953	0.063	0.016	insufficient data		
Ortho-phosphorus	insufficient data					
E.coli	0.0500	0.140	24.880	0.1907	0.189	21.250

The load duration curves are shown in Figures 2 and 3 for *E. coli* and nitrates.

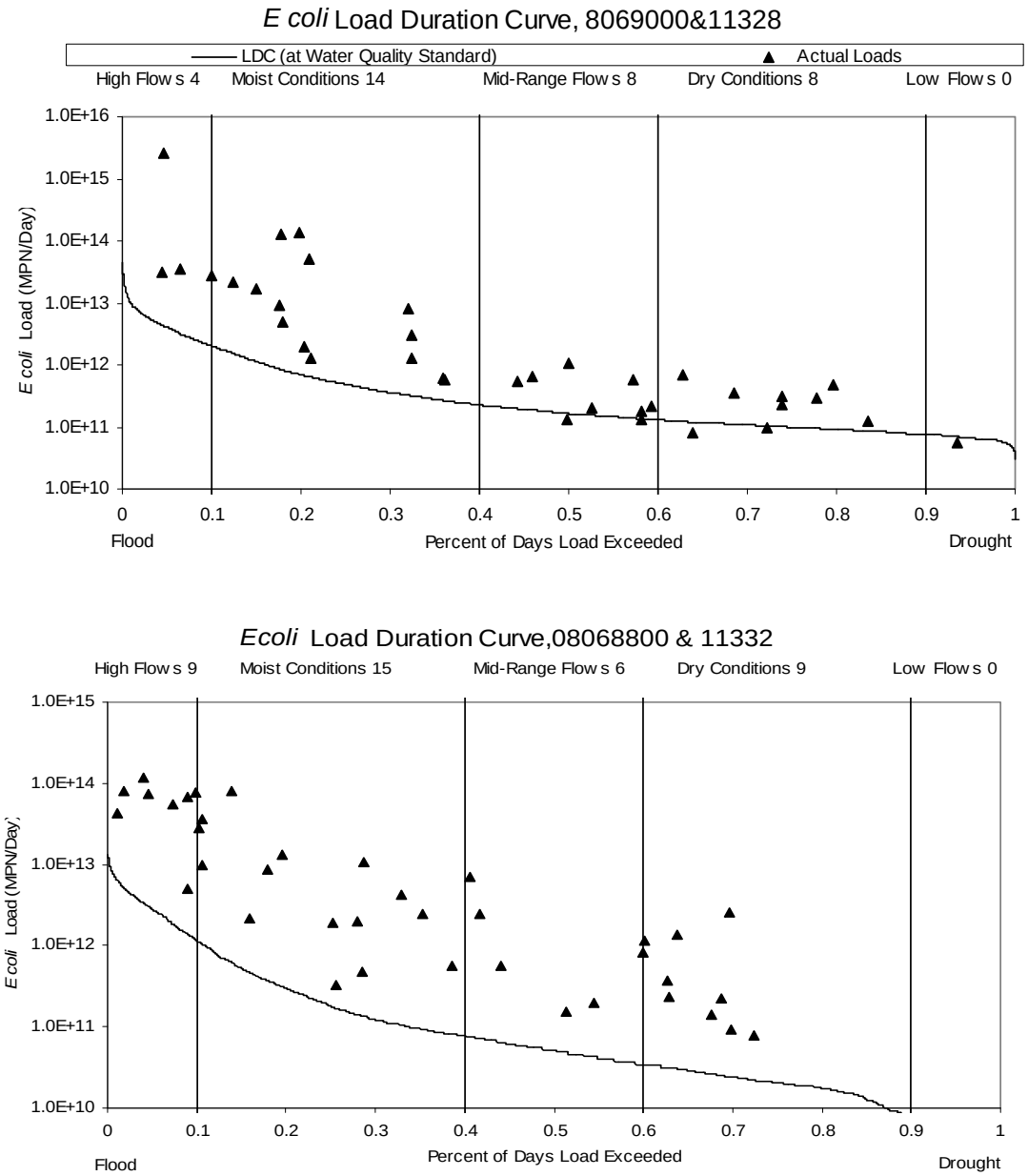

Figure 2: *E. coli* Load Duration Curves for Station 11328 and 11332

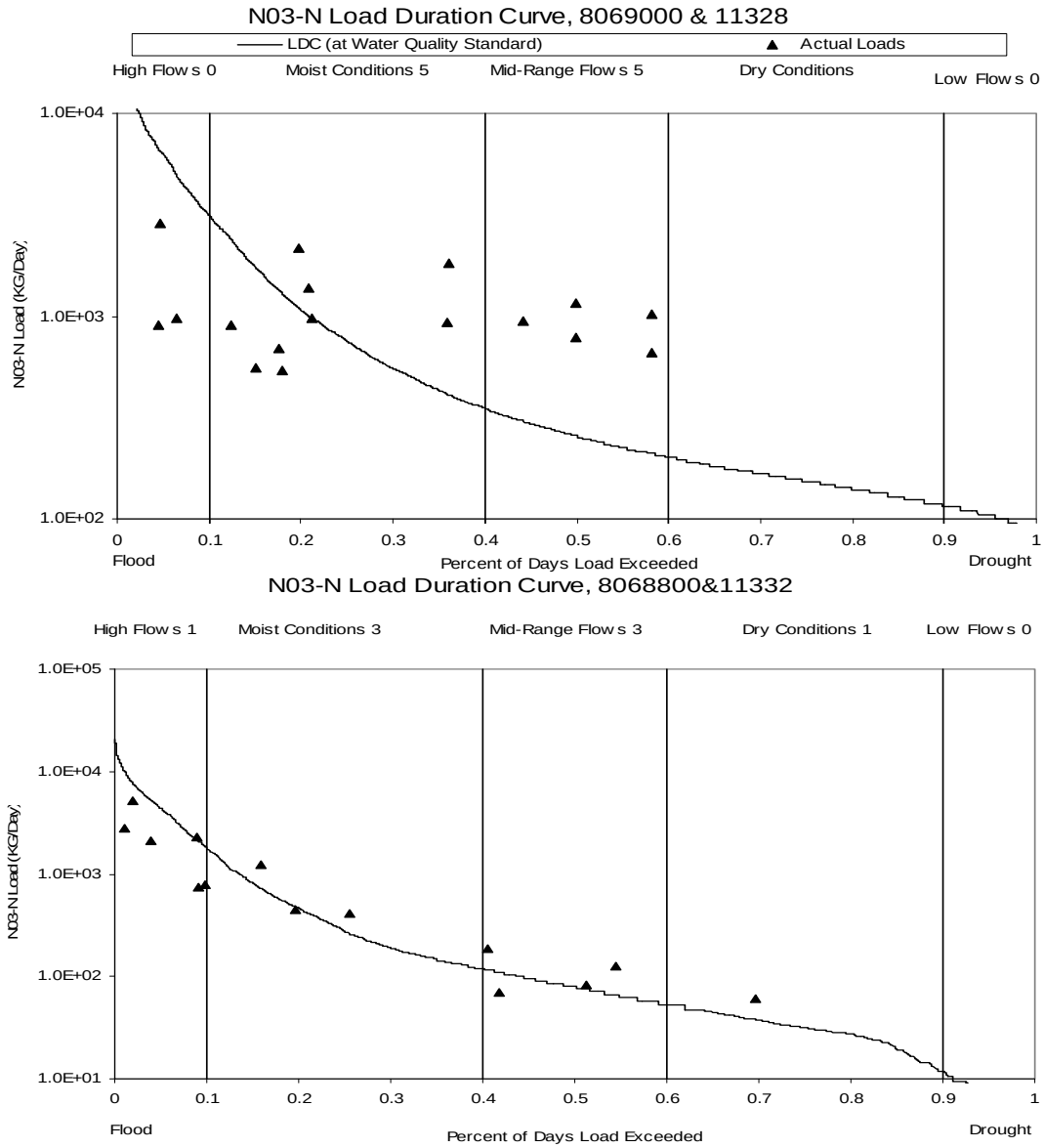

Figure 3: Nitrate Load Duration Curves for Station 11328 and 11332

Discussion

A majority of the water quality parameters showed a lack of trend at both stations within the watershed. Total organic carbon at station 11328 was the only constituent that had statistically significant trend (Table 3) both overall and seasonally. It is hypothesized that the decrease in organic carbon is due to improved land management and best management practices which prevent more organic materials and chemicals from entering the stream than previously practices allowed. The record of water quality data is quite short, encompassing only 11 years. The Mann-Kendall and Seasonal Kendall requires at least 10 years of data. With a longer time period of sampling, testing for trend will have greater statistical strength, with the potential for observing trends not detectable at this point. In addition, the *E.coli* constituent was

the combination of fecal coliform and *E. coli* testing, in order to meet the 10 year requirement. With two more years of *E. coli* testing, the fecal coliform data will not be needed to supplement the dataset, decreasing the uncertainty of the dataset. Unfortunately, trend detection did not provide new analysis for the characterization of the watershed or pollutant sources.

Future trend detection analysis could be improved by customizing the seasonal division of time for Cypress Creek. Multivariate analysis, including temporal cluster analysis should be performed to analyze the variance within the water quality dataset in order to cluster time periods into optimal seasons for Cypress Creek. This would provide a basis for improved seasonal trend detection, and could provide detection of trends obscured by the current seasonal division.

Analysis of the load duration curves for *E. coli* (Figure 2) show that exceedances occurred during all ranges of flows for both stations. This indicates that the sources of *E. coli* within the drainage areas most likely include a combination of point and non-point sources. It should be noted that for station 11332, all samples exceeded the water quality standard. Given this degradation of water quality combined with the eventual use of the water as drinking water, greater sampling frequency for further study would be appropriate. More frequent sampling would provide should be utilized to identify the behavior of stream pollutant loading for spatial and temporal characterization of the pollutant point and non-point sources.

Both stations exhibited exceedances of the nitrate screening level primarily within the moist conditions and mid range flows. As such there is little conclusive evidence for characterizing the source of nitrate. Although the presence of exceedances with the moist conditions suggests a non-point source associated with runoff, the lack of exceedances during high-flows contradicts this. However it should be noted that there are fewer sampling points in the dry conditions and low flows, allowing the potential for sampling bias. Both stations exhibited exceedances of the total phosphorus screening level primarily within the moist conditions and mid range flows in a similar manner to the nitrate loading curves. As such, there is little conclusive evidence for characterizing the source of phosphorus. The sampling bias present should be addressed with further water quality sampling a greater variety of flow conditions. Furthermore sampling throughout a storm event, to analysis of pollutographs would provide greater evidence for characterization of the watershed and pollutant sources.

Conclusions

Trend analysis using Mann-Kendall and Seasonal Kendall at 2 stations within Cypress Creek watershed only detected statistically significant trend for total organic carbon at 1 station. Analysis of load duration curves determined that a combination of point and non-point sources were contributing to pollutant loads that exceeded the water quality standards. The present analysis, with its limited dataset was limited in its utility for characterization of the watershed and its pollutant sources. Given the

severity of water quality violations and the city of Houston's dependence on the water for domestic consumption, it is important that more frequent sampling be performed through a wider range of flow conditions in order to study the nature of water quality violations and characterize the sources and behavior of pollutant sources. With further study of the stream, water quality trends and source characterization will provide valuable information for appropriate watershed management.

References

Boeder, M., and H. Chang. 2008. "Multi-scale Analysis of Oxygen Demand Trends in an Urbanizing Oregon Watershed, USA". Journal of Environmental Management. 87:567-581.

Bonta, J., 2002. Framework for Estimating TMDLs With Minimal Data. Proceedings of the ASAE Conference on Watershed Management to Meet Emerging TMDL Environmental Regulations, Fort Worth, Texas, March 2002, pp. 6-12.

Bonta, J. and C. Cleland. 2003. "Incorporating Natural Variability, Uncertainty and Risk in Water Evaluations Using Duration Curves". Journal of the American Water Resources Association.: 39(6) 1481-1496

Burn, D., and M. Hag Elner. 2002. "Detection of Hydrologic Trends and Variability". Journal of Hydrology. 255:107-122.

Cigizoglu,H. andM. Bayazit. 2000. "A Generalized Seasonal Model for Flow Duration Curve". Hydrological Processes. 14: 1053-1067.

Cleland, B., 2002. TMDL Development From the "Bottom Up" –Part II: Using Duration Curves to Connect the Pieces. ASIWPCA/ WEF National TMDL Science and Policy 2002 SpecialtyConference, Phoenix, Arizona, Session 8, Paper 4.

Cleland. B. 2003. "TMDL Development from the "Bottom Up"—Part III: Duration Curves and Wet-Weather Assessments". America's Clean Water Foundation, Washington, DC. Available online at http://www.tmdls.com/tipstools/docs/TMDLsCleland.pdf accessed on August 13, 2008..

Cude,C. 2001. "Oregon Water Quality Index: A Tool for Evaluation Water Quality Management Effectiveness". Journal of the American Water Resources Association". 37(1):125-137.

Garcia-Armisen, Tamara. J. Prats, and P. Servais. 2007. Canadian Journal of Microbiology. 53:798-801.

Haan, s. 2002. "Statistical Methods in Hydrology". 2nd Edition. Iowa State Press. Ames, Iowa: 340-346.

Hamed, K. and A. Rao. 1998. "A Modified Mann-Kendall Trend Test for Autocorrelated Data". Journal of Hydrology. 204: 182-196.

Helsel, D., D. Mueller, and J. Slack. 2006. "Computer Program for the Kendall Family of Trend Tests". US Geological Survey Scientific Investigations Report 2005-5275.

H-GAC. 2005. "Measurement Performance Specification Tables: A7 Quality Objectives and Criteria". Houston-Galveston Area Council. Acessed online at http://www.h-gac.com/rds/environmental/water/documents/mps_tables_fy04-05.pdf on January 10, 2009.

Hirsch, R.M., Slack, J.R., 1984. A Nonparametric Trend Test for Seasonal Data with Serial Dependence. Water Resources Research 20 (6), 727–732.

Hirsch, R.M., Slack, J.R., Smith, R.A., 1982. Techniques of Trend Analysis for Monthly Water Quality Data. Water Resources Research 18 (1), 107–121.

Kahya, E. and S. Kalayci. 2004. "Trend Analysis of Streamflow in Turkey". Journal of Hydrology. 289:128-144.

Kruesche, A. R. Carvalho, J. Moraes. P. Camargo, M. Ballester, S. Hornink, L. Martinellli, and R. Victoria.1997 "Spatial and Temproal Water Quality Variability in the Piracicaba River Basin, Brazil". Journal of the American Water Resources Association. 33(5):1117-1123.

Larsen, S. B. Kronvang, J. Windolf, and M. Svendsen. 1999. "Trends in Diffuse Nutrient Concentrations and Loading in Denmark: Statistical Trend Analysis of Stream Monitoring Data". Water Science Technology. 39(12):197-205.

Taylor, C., and J. Loftis. 1989. "Testing for Trend in Lake and GroundWater Quality Time Series". Water Resources Bulletin. 25(4):715-726.

Vogel, R. M. and N. M. Fennessey, 1995. Flow-Duration Curves II: A Review of Applications in Water Resources Planning. Water Resources Bulletin 31(6):1029-1039.

Yu, Y., S. Zou and D. Whittemore. 1993. "Non-parametric Trend Analysis of Water Quality Data of Rivers in Kansas". Journal of Hydrology. 150:61-80.

Assessment of the Capability of Hydrologic and Artificial Neural Network Models for Flood Warning System in Land use Change Condition

M.E Banihabib [1] and A. Arabi[2]
[1] Assistant professor, Department of Irrigation and Drainage Engineering, University of Tehran, Iran; Email:Banihabib@ut.ac.ir
[2] M.Sc. Irrigation and Drainage Engineering, University of Tehran, Iran; Email:Azar.Arabi@gmail.com

Abstract
The main purpose of this research is comparing the capability of HEC-HMS model and dynamic artificial neural networks (DANN), forecasting lead time of Golabdare-Darband basin in the north of capital city Tehran. Five scenarios are defined for different land uses, including conditions of 1955, 1988 and 2001, suitable and unsuitable land use of the basin. Floods with different return periods are simulated. The result of HEC-HMS model is used as training and test data of ANN network. The result of artificial neural network showed that the number of rainfall and runoff delays has optimal. Comparison of forecast lead time in two models shows that the lead time increases by decreasing in returned periods. Comparison of forecast lead time of five scenarios shows the scenario of unsuitable management of the watershed has the shortest lead time by using both models. The longest forecast lead time is for the scenario of 1988 land use by using DANN model and the scenario of 1955 land use for HEC-HMS model. The difference comes from instability of simulation by DANN.

Keyword: Artificial neural network, HEC-HMS model, Land use, forecast lead time

1-Introduction

Inundation damage has been estimated several billion pounds in UK in the past five years, while on an international scale, flooding threats lives particularly in tropical and subtropical regions [8]. Although global warming is now recognized as a real threat, there has been little success in establishing protocols for the reduction of greenhouse gases. Therefore, an increase in the occurrence of flooding is likely to continue into the future [8]. For these reasons, flood forecasting is becoming more High-priority for both flood control and watershed management purposes. There are several integrated flood forecasting systems available. These systems generally comprise several interacting components, which usually include a rainfall-runoff forecasting model, a database for the management of historical and real-time data, a dissemination module which issues warnings to hydrologists monitoring the catchment, and a component which continually evaluates and updates the forecasting outputs (Nemec, 1986). Using flood forecasting and flood warning systems accompanied by structural methods would increase flood control plans efficiency. In this case advanced models are needed to increase the accuracy of forecast lead time and to recoginize urbanization affects on lead time.

Some researchers analyzed runoff of basins by different hydrologic models. Kneale, P. et al (2000) compared the results of nine evaluation measures and two forecasting models. The models that they used in the study are artificial neural networks trained with back propagation (BPNNs) and a Time Delay Neural Network (TDNN). Networks were trained to forecast stage on the River Tyne, Northumbria, for lead times ranging from 2 to 6 hours with minimal data. The training data set consisted of continuous data for one winter period and validation was undertaken using data from winter periods for three other years. The results showed that the TDNNs performed better than the BPNNs although the evaluation measures indicate that the performance of these particular models is not yet sufficient for operational purposes [7]. Matreata.,M(2005) compared artificial neural networks and fuzzy logic in hydrological forecasting systems. Their results showed that Both artificial neural networks and fuzzy logic modeling systems offer the potential for a more flexible, less assumption approach to hydrological processes, and they have already been demonstrated as successful substitutes for the classical rainfall – runoff models, and also as tools for real time updating of hydrological forecasting models and especially for the multi model approach [9]. Dawson.,C.W. et al(2002) evaluated two neural networks including the popular multilayer perceptron (MLP), and the radial basis function network (RBF). Using six-hourly rainfall-runoff data for the River Yangtze at Yichang (upstream of the Three Gorges Dam) for the period 1991 to 1993, it was shown that both neural network types can simulate river flows beyond the range of the training set. In addition, they demonstrated that the popular Gaussian function, often used in RBF networks, is not necessarily the ‘best’ function to use in river flow forecasting [3]. Piotrowski., A. et al (2006) compared Multi-Layer Perceptron and Radial-Basis Function Neural Networks, along with the Nearest Neighbor approach and linear regression for flash-flood forecasting in the mountainous Nysa Klodzka river catchment. It turned out that the Radial-Basis Function Neural Network is the best model for 3 and 6 hours lead time prediction and the only reliable one for 9 hours lead time forecasting for the largest flood used as a test case [11]. Vieux, B.,E et al (2002) simulated flash floods and debris floods of a basin in Taiwan by VefloTM model. They could estimate two peaks of hydrograph with the least error [13].

Camorani,G et al (2005) investigated the possible effects of recent land use changes on the frequency regime of floods for reclaimed lands. They modeled the runoff concentration behavior of a reclaimed area located in the Po river plain near city of Bologna (North of Italy), using the combined application of a semi-distributed rainfall-runoff model, and a hydrodynamic stream flow routing model. The results showed significant sensitivity of flood frequency regime of the reclaimed land to land use changes; moreover sensitivity tends to increase as the recurrence interval of the rainfall event decrease [6]. Ad De Roo et al (2003) investigated the causes of the flooding and the influence of land use in the Oder basin in Italy by LISFLOOD model. This study has demonstrated that the proposed measure for flood control by the international Oder commission leads to a significant improvement and reduction in flood risk in the Oder catchment, especially for downstream reaches. Historical land use changes showed an increase in forecasted an urban area between 1780 and 1995, which hydrologically are balancing out each other in terms of discharge. It had been shown that the use of flood forecasting in reservoir management can also reduce downstream flood risk. Finally, it is expected by urbanization growing, flood risk in the next 30 years slightly increases [1, 4]. The examination of last scholarly showed different type of artificial neural networks and hydrologic models were used, predicting and simulating basins flood events, but the effect of land use changing by watershed management was not considered in different periods, accordingly it affected flood hydrograph and forecast lead time. Remarkably, the aim of this paper is evaluating the effects of land use changes on flood forecast lead time for different defined land uses, including land uses of the years 1955, 1988 and 2001, suitable and unsuitable watershed management of the basin in future.

2-Case study

2-1- Study area and data set description

The case study considered in this research is the Golabdare-Darband basin, located in the north of Iran (Tehran). The study areas including subbasins are shown in figure 1. The Golabdare-Darband basin is located in north of capital city Tehran, Iran. It has an area of approximately 739.2 ha. Several watershed management projects have been done in this basin such as mechanical measure (including check dams and detention dams), biological measure and other non-structural methods [2]. The land use of 1955, 1988 and 2001 are defined by using watershed management reports. The land use of 1988 and 2001 are considered the condition of before and after watershed management respectively. Suitable and unsuitable watershed management scenarios are defined on the base of land use of 2001 including following assumptions:

The unsuitable watershed management scenario has two assumptions as follows:

- In sub basins close to the city, the poor vegetation landuse is changed to urbanization land use.
- The pasture land use is changed to poor pasture in all sub basins.

The suitable watershed management scenario has four assumptions as follows:

- In sub basins close to the city, 50% of poor pastures were changed to wooded land use and the other 50% of area of the sub basins are changed to pasture.

- In other sub basins, 50% of the poor pastures landuse were changed to dense pasture.
- In sub basins close to the city, 50% of poor lands are changed to Garden and the remained 50% are changed to poor pasture.
- In other sub basins, 50% of uncovered lands are changed to pasture and the other 50% are changed to poor pasture.

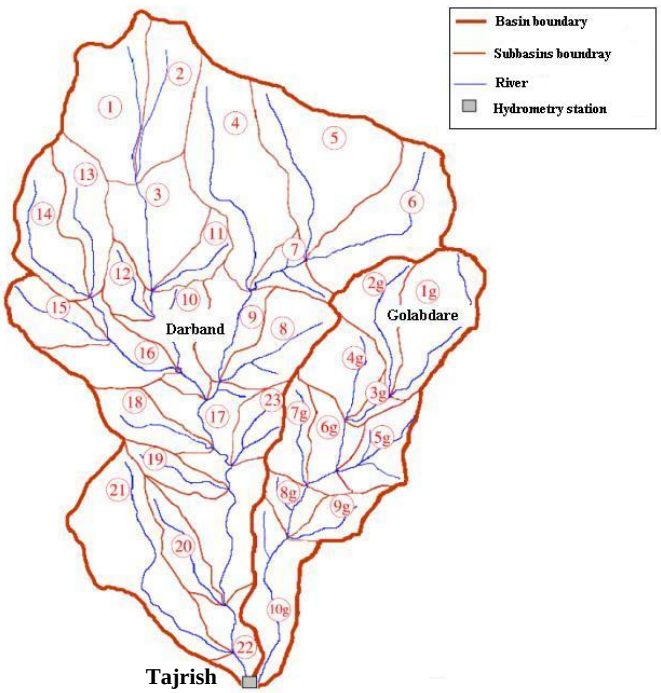

Figure. 1. Golabdare-Darband and sub basins

Stage and rainfall historical data are used for calibration of HEC-HMS model. Then, the floods of are different return periods simulated by calibrated model. Temporal pattern B of Niyavaran station has been recommended for Golabdare-Darband basin that is shown in Table 1. Rainfall intensities of different return periods are shown in Table 2 for duration of one hour [12].

Table. 1. Distribution of rain pattern in Niyavaran station

Time(percentage)	Rainfall(percentage)
25	19.41
25	29.01
25	40.74
25	11.01

Table. 2. One hour rainfall intensity in Niyavaran station

Return Periods(Year)	10000	1000	200	100	50	25
Rain (mm/h)	41.65	33.04	27.5	24.4	21.6	19.1

2-2-1- Rainfall-runoff model

HEC-HMS hydrologic modeling program is used in flood studies throughout the United States. The model was developed by the US Army Corps of Engineers, and it is designed to simulate the precipitation-runoff processes of dendritic watershed systems (USACE, 2005). The physical representation of the watershed is accomplished with a basin model. Various hydrologic elements are connected in a dendritic network to simulate runoff processes. A variety of methods are available for simulating infiltration losses, transforming excess precipitation into surface runoff, computing baseflow contributions to subbasin out flow, flow routing etc. Outflow from a sub-basin is computed from rainfall data by subtracting losses, transforming excess precipitation and adding base flow [2].

2-2-2- Dynamic artificial neural network

One of the ANN models that can deal with the time memory are the dynamic networks. Dynamic networks employ the dynamic feedback mechanism to handle the memory. The dynamic feedback mechanism means that the output of neurons in the hidden layers or the output layer can also be the input of the network itself. In dynamic networks, the memory of the system is embedded implicitly within the network, so the amount of input data is much less than that of the static networks. The Dynamic network also requires the data of the current rainfall, the past rainfall and the past runoff as its input. It can be explained using the following equation:

$$Q = F(pi(t), pi(t-1),...pi(t-k), Q(t-1), Q(t-2),...Q(t-h)) \qquad i = 1,2,...,g \qquad (1)$$

where F is the dynamic network, and pi(t) and Q(t) are defined earlier. The drawbacks of the ANN based rainfall–runoff models arise from the methods to construct memory in the networks and the style of input data. The first drawback results from the evaluation of the memory length. In this paper, output of neurons in the first hidden layers and the output layer are the delay input of the network.

3-2- Expected Lead Time Concept

The forecast lead time varies from storm to storm and location to location. Dotson and Peters (1990) noted that lead time is influenced by spatial and temporal variability of precipitation (the growing and decay of rainfall cells within the storm), rainfall-runoff response characteristics of the watershed, and antecedent soil moisture conditions. The forecasted lead time varies from storm to storm depending on multiple factors. Figure 2 is a hydrograph, showing the flow versus time. Conceptually, Figure 2 illustrates how the warning time is computed for each event. Initially, time is required for system operators to gather, evaluate, and forecast based on available data. This data collection and evaluation time is labeled Tr in the figure (recognition time). The forecast lead time, labeled Tlt in the figure, is the duration of time between threat recognition and threshold limit, that is, the time before the threshold limit when the system operators are first able to forecast an extent. To compute Tlt, we first use the entire rainfall hyetograph to compute a “true” runoff hydrograph, as shown by the solid line in the figure. This is the runoff that will occur when the rainfall event has finished. The time of actual extent, labeled TE, is the time when the flow from the true hydrograph exceeds the threshold. The dotted line represents the forecasted flow hydrograph based upon the precipitation up until the

time of forecasting, TF. As illustrated, as TF is stepped forward in time, additional precipitation will be used in the forecast [10].

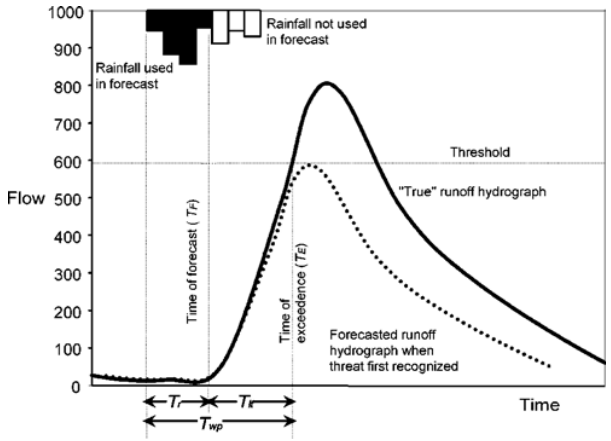

Figure. 2. Warning time components from hydrologic perspective (adapted from USACE 1996a)

3-2-1- Computation Steps

Figure 3 conceptually shows the steps taken to compute TL. As noted, a calibrated rainfall-runoff model, HEC-HMS model, and hypothetical frequency-based events appropriate for the watershed are required to use this procedure. In Step 1 the TL is computed to identify the vulnerable site and the flow threshold for which the value will be computed. The flow threshold is the flow where property is first damaged or lives are put at risk. It can be identified using topographic information, elevation data for vulnerable structures and infrastructure, and simple channel models. The flow threshold is 25-year flood peak in Golabdare-Darband River. In Step 2, the first frequency-based storm is developed. To develop the storm, a time interval, DT, must be selected. Typically, this value is selected based on the time increment from the rainfall-runoff model. For the computations, this same time interval will represent the likely interval between successive forecasts or examination of data for identifying a threat. Therefore, DT is likely to be a relatively short increment, here we used 1 minute. Initially, we set TF equal to 0, the time when the first rain starts falling. In Step 3 we set TF equal to the end of the first DT. Therefore in Step 4, when the first forecast is made, only the precipitation that occurs during that first DT is used for the forecast. Once the forecast is complete, the peak forecasted flow is compared to the flow threshold (25 year peak flood in 1988), Step 5. If the forecasted flow is less than the peak flow, as illustrated in Figure 4(a), the precipitation that has fallen prior to TF is not sufficient to cause a great enough runoff to exceed the downstream threshold. Therefore, TF is advanced by another DT, Step 6, and the runoff is forecasted. This recursive forecasting, illustrated in Figure 4, is repeated until the peak forecasted flow is equal to or greater than the flow threshold. If the flow threshold is exceeded, as illustrated in Figure 4(b), we declare that a warning would be issued and note TF, Step 7. This computation scheme simulates the gradual formation of a storm, observation of the data over time, and attempts detection of the flood event. In Step 8, the entire precipitation event in the forecast model is used to compute the runoff hydrograph from which TE can be computed. This represents the “true” runoff hydrograph. In Step 9, the forecast lead time for that specific precipitation event is then computed as the difference between TE and TF. Note that if the precipitation

event is not large enough to exceed from the threshold, then the value will not exist for that event [10].

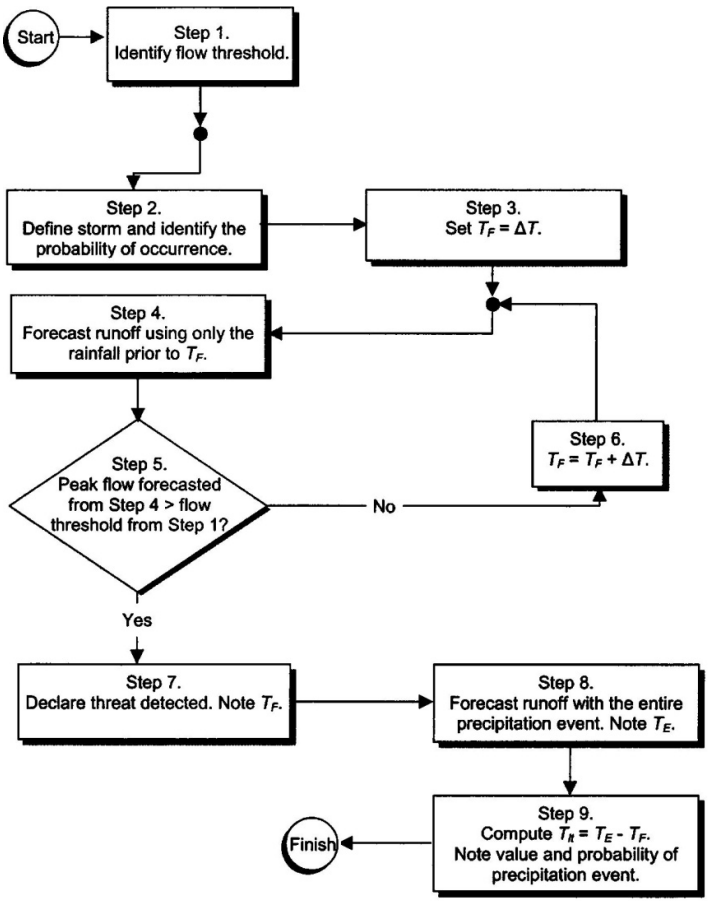

Figure 3. Steps to compute expected forecast lead time

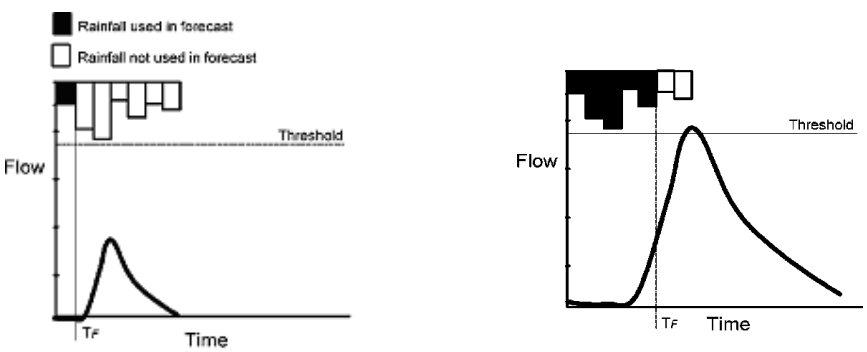

(a) **(b)**

Figure 4. Schematic of forecasted flows with various times of forecast

The Best structure of dynamic artificial neural network is selected by Ka as follows:

$$ka = EQ_{pa} \times RMSE_a \tag{2}$$

(4)

$$RMSE_a = \left(\frac{RMSE_{10000} + RMSE_{1000} + RMSE_{200} + RMSE_{100} + RMSE_{50} + RMSE_{25}}{6}\right) \quad (3)$$

$$EQ_{pa} = \frac{EQ_{p10000} + EQ_{p1000} + EQ_{p200} + EQ_{p100} + EQ_{p50} + EQ_{p25}}{6}$$

$RMSE_a$=Root Mean Square Error
EQ_{pa}= Peak of discharge Error

3-Result

Table 5 shows the result of artificial neural network. Also the lead time of scenarios are shown in figure 5 for different return periods. The results show the forecast lead time of 1988 is longer than 1955, due to better land use in 1955 compare to 1988 scenario. Accordingly, the forecast lead time is decreased by increasing in return periods. The results show 1955, 1988, 2001 and suitable watershed management scenarios do not declare the threat detected for the 25-year flood. The forecast lead time is decreased from 20 min (1988 scenario) to 7 min (unsuitable watershed management) in 10000-year flood. The results clarified the land use of 1988 causes the longest forecast lead time and unsuitable watershed management has the shortest forecast lead time.

Table 5. Forecast lead time and its parameter in different return period(by DANN)

Parameters	Scenarios	25 year	50 year	100 year	200 year	1000 year	10000 year
T_f	1955		49	41	39	35	30
	1988		35	31	28	23	16
	2001		51.63	48.70	46.38	41.23	34.94
	Unsuitable management	53.30	49.10	45.46	41.81	36.74	29.98
	suitable management			54	49	45	37
T_E	1955		60.40	50.8	48.4	44.10	38.4
	1988		58.8	52.50	49	43.6	36.2
	2001		38.52	36	35	30	24
	Unsuitable management	42	39	36	33	28	22
	suitable management			39	36	33	26
T_L	1955		11.40	9.80	9.42	9.06	8.36
	1988		23.8	21.5	20.99	20.6	20.23
	2001		13.11	12.70	11.38	11.23	10.94
	Unsuitable management	11.23	10.10	9.46	8.81	8.74	7.98
	suitable management			15	13.46	12.12	11.2

No need for warning

Table 6 shows the result of HEC-HMS model. The forecast lead time of scenarios in return periods are shown in figure 6. The results show the forecast lead time has decreased from 14min to 3min in different scenarios. Therefore the 1988 scenario has the longest lead time and the unsuitable watershed management scenario has the shortest lead time, due to better land use in 1988 compare to other scenario. The results show the forecast lead time is decreased by increasing in return periods. The 1955, 1988, 2001 and suitable watershed management scenario do not declare the threat detected for the 25-year flood.

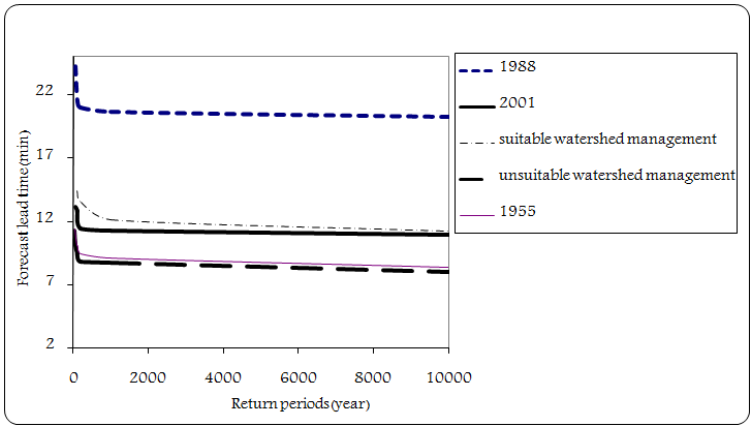

Figure 5 . Forecast lead time in return periods (DANN)

Table 5. Forecast lead time and its parameter in different return periods (by HEC-HMS)

Scenarios	Parameters	25 year	50 year	100 year	200 year	1000 year	10000 year
1955	T_F			43.625	39.919	35.205	30.365
	T_E			55.985	50.122	43.976	37.786
	T_L			12.36	10.204	8.771	7.421
1988	T_F		43.07	39.27	36.1	32.09	26.84
	T_E		56.97	51.18	46.7	41.37	35.71
	T_L		13.9	11.91	10.6	9.28	8.87
2001	T_F		43.9	40.1	36.9	32.7	27.9
	T_E		56.4	49.3	45.1	39.8	34.3
	T_L		12.4	9.2	8.2	7.2	6.4
Unsuitable management	T_F	51.4	42.3	38.7	35.7	31.6	25.9
	T_E	60.4	47.1	43	39.6	34.9	28.9
	T_L	8.9	4.8	4.3	3.9	3.2	3
suitable management	T_F		55.6	42.9	39.3	34.7	30
	T_E		63.1	54.1	48.4	42.6	36.6
	T_L		7.50	11.30	9.10	7.90	6.70

No need for warning

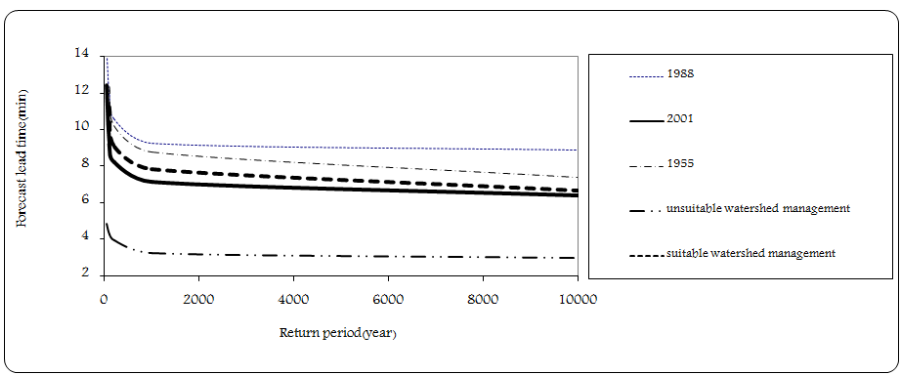

Figure 6 . Forecast lead time in return periods (HEC-HMS)

The results show that land use of 1988 caused the longest forecast lead time in both of models.While unsuitable watershed management has the shortest forecast lead time. However dynamic artificial neural network (DANN) estimated longer forecast lead time for different returns periods than HEC-HMS model but that it caused by the oscillation of simulation of hydrograph. Therefore dynamic artificial neural network estimate less accurancy than HEC-HMS models.

4-Conclusion

In this paper, the effect of land use on forecast lead time has been analyzed with dynamic artificial neural network. To sum up, the most important results can be pointed out as follows:

- The scenario of 1988 causes the longest forecast lead time and the land use of unsuitable watershed management causes the shortest forecast lead time in both models.
- Unsuitable watershed management land use causes shorter lead time.
- Artificial neural network has different results in scenarios for forecast lead time, due to oscillation in simulation hydrograph.
- The result showed that the simulation by HEC-HMS model is more stable than dynamic artificial neural network (DANN).

5. Reference

[1] Ad De Roo, Guido Schmuk, Vanda Perdigao, Jutta Thielen.(2003). "*The influence of historic land use changes and future planned land use scenarios of floods in the Order cathment*". physics and Chemistrv of the Earth 28. 1291-1300.

[2] Banihabib., Mohammad Ebrahim and Azar Arabi.(2007). "*Evaluation of Watershed Management on Flood Forecast Lead Time in Golabdare-Darband Basin*". 4th of watershed engineering and science in Iiran, Watershed management. 2007.

[3] Dawson,C.W.,Harpham, C., Wilby, R.L and Chen, Y.(2002)." *Evaluation of artificial neural network techniques for flow forecasting in the River Yangtze, China*" Hydrology and Earth System Sciences, 6(4), 619-626.

[4] De Roo, A.P.,J.1999. "*LISFLOOD: a rainfall-runoff model for large river basins to assess the influence of land use changes on flood risk"*. In: Balabanis, P., et al.(Eds), Ribamod: River Basin.

[5] Dotson, H. W., and Peters, J. C. ~1990!. "*Hydrologic aspects of flood warning-preparedness programs*." Technical Paper No. 131, U.S. Army Corps of Engineers, Hydrologic Engineering Center, Davis,Calif.

[6] Giorgio Camorani, Attilio Castellarin , Armando Brath.(2005). "*Effects of land-use changes on the hydrologic response of reclamation systems*". Physics and Chemistry of the Earth 30 (2005)
561-574.

[7] Kneale, P.E., See, L., Cameron, D., Kerr, P. and Merrix, R.(2000) "*Using a prototype neural net forecasting model for flood predictions on the Rivers Tyne and Wear*". British Hydrological Society, 7th National Hydrology Symposium.

[8] Kneale, P.E, Linda See; Mr Andrew Smith (2001) " *Towards Defining Evaluation Measures for Neural Network Forecasting Models*". Sixth International hydroinformatic Conference .

[9] Matreata.,M(2005)" *Overview of the artificial neural networks and fuzzy logic applications in operational hydrological forecasting systems*".National Institute of Hydrology and Water Management.
[10] Nathen Pingel,P.E.,M.ASCE; Christy Jones, EIT, A.M.ASCE and David Ford, P.E., M.ASCE, "*Estimating Forecast lead time*", natural hazardsReview, ASCE/MAY 2005.
[11] Piotrowski., A, Napi´orkowski., J. J. and Rowi´nski., P.M. (2006*)" Flash-flood forecasting by means of neural networks and nearest neighbour approach – a comparative study* " . Institute of Geophysics, Polish Academy of Sciences, Warsaw, Poland.
[12] Raziee,T.,(2000)." *Definition of temporal and local short time raining in Tehran*". A thesis for degree of master. Tarbiyat modares university.
[13] Vieux, B.E., and F.G. Moreda. 2002. "*Ordered Physics-Based Parameter Adjustment of a Distributed Model*". Chapter 20 of Advances in Calibration of Watershed Models. Edited by Q. Duan, S., Sorooshian, H.V. Gupta, A.N. Roussean, R. Turcotte, Monograph Series on water Resources, Trans. Amer. Geophys. Union, ISBN 0-87590-355-X, pp. 267-281.

Estimating Groundwater Pumping and Return flow Based On Hydrologic Recession Analysis

Dingbao Wang and Ximing Cai

Ven Te Chow Hydrosystems Laboratory, Department of Civil and Environmental Engineering, University of Illinois at Urbana-Champaign, Urbana, IL 61801; PH (217) 333-2978; FAX (217) 333-0687; email: dwang3@uiuc.edu; xmcai@uiuc.edu

ABSTRACT

Hydrologic processes have been affected by human activities which include both direct and indirect interferences. The indirect human interferences such as land use and land cover change have been studied and modeled in many watersheds around the world. These kinds of human interferences, resulting in land surface changes, usually affect the rising limb and the peak of a hydrograph. The streamflow recession process, are not much affected by the land surface condition and the impacts of indirect human interferences are trivial; however the direct human interferences such as water withdrawals and return flows may affect the recession dynamics significantly. Direct human interferences are difficult to observe and model, and are usually assumed to be known and additive to streamflow. This paper provides a recession analysis involving groundwater pumping and effluent discharge as variables. The analysis is applied to an urban watershed in the Chicago area. Based on the historical streamflow observation during the last half century, the analysis provides results that explain the impact of direct human activities on the streamflow recession process. Moreover, the analytical method allows retrieving human water use data such as groundwater pumping and return flow, which change with socioeconomic development and policy reforms, as long as the streamflow observation is available and long enough. The analysis is verified with the data of the case study watershed and can be applied to other watersheds under intensive human interferences.

Introduction

With the increasing demand of domestic, agricultural, commercial, and industrial uses, humans are increasingly significant components of the global hydrologic cycle and human activities have transformed hydrologic processes crossing the various scales from local to global (NRC, 1992). Human being affects the hydrologic system indirectly by changing the driving forces such as climate and boundary conductions such as vegetation and land use, soils, and topography; human being also directly exerts on water flow or storage by river diversion, groundwater pumping and return flow, which strengthens the connections between the various hydrologic components. For instance, groundwater is a major source of water supply in many areas.

Within a holistic system composed of human and natural sub-systems, the change of human activities propagates within the system and causes changes of other components. It no longer makes sense to study only natural hydrological cycles in watersheds with intensive and extensive human activities (Oki and Kanae, 2006). Indirect human interferences, such as land use change and climate change, have been studied extensively in past decades (e.g., Cörösmarty et al, 2000). We may define land use change and climate change as indirect human interferences to hydrologic systems and define water withdrawal and return flow as direct human interferences. Indirect human interferences usually affect the rising limb and the peak of hydrograph while the direct interferences may have a dominant impact on the declining limb with the flow recession process. Low flows including base flows are usually critical to ecosystem habitats and are important targets of watershed restoration.

However fewer studies have touched the direct human interferences. Recently some studies emphasized the necessity of considering the direct human interferences in hydrologic modeling (Claessens et al. 2006). A number of indicators have been used to measure the degree of direct human interferences to hydrological systems regarding water demand (Vörösmarty et al., 2000), water scarcity (Oki and Kanae, 2006) and water use regime (Weiskel et al., 2007). Some studies used the differences of observed streamflow and the simulated natural flow as an indicator of human interferences (Cong, et al., 2008). However, water uses are still not yet a major focus of scientific studies, the level of integration of water use data with standard

hydrologic data is limited and fundamental understanding of the role of water use in the hydrologic cycle is not clear (NRC, 2002).

Furthermore, natural systems interact with human systems in a dynamic, nonlinear form (Liu et al., 2007) in the so called coupled human and nature systems. However, direct human interferences are difficult to observe and model, and are usually assumed to be known and additive to streamflow. Such simply abstraction or addition of water to the output of mass balance equation may not be a proper way to address the impact of human interferences. It is necessary to simulate human activities and natural processes in a coherent framework. The challenges include data availability and accuracy of human activities and the nonlinear interaction and dynamics of coupled human and natural systems. Data of human interferences, corresponding to the spatial and temporal resolution of physical processes are usually incomplete or even unavailable (Wang and Cai, 2007). Moreover, a consistent, conceptual model that integrates human activities and hydrologic processes and is meaningful with respect to the current data availability is still needed.

The focus of this paper is on the estimation of direct human interferences to hydrologic processes in heavily managed watersheds. We study a specific hydrologic process – the streamflow recession and we argue that direct human interferences at the watershed scale can be reflected by the declining limb of hydrographs, associated with low flows in streams. We extend the recession analysis of natural watersheds to incorporate specific forms of human interferences including groundwater pumping and return flow. An analytical solution is derived under the various natural characteristics and human water use forms. The closed-form equations involved both natural and human system parameters allow retrieving some unknown parameters given the observation of other parameters. The analysis is applied to the Salt Creek Watershed, an urban watershed located in the Chicago area. The changes of the recession pattern of observed hydrographs are simulated by the extended recession analysis model and explained by the water use regime in the study area. Moreover the pumping and effluent discharge rates during the past half century in the Salt Creek Watershed are retrieved using observed streamflows.

Recession analysis of natural watersheds

The storage-discharge relationships, recession curves and recession slope curve have been discussed in the literature since 1900s (e.g., Brutsaert and Nieber, 1977). The conceptual

power-law storage-discharge model has been used to analyze the base flow behavior at the catchment scale (e.g. Wittenberg, 1999):

$$S = aQ_s^{\,b} \tag{1}$$

where Q_s (m^3) is the amount of discharge from groundwater which directly interacts with the stream, and it equals the streamflow under the recession period when quick flow ceases; S (m^3) is the volume of water stored in aquifer; a (m^{3-3b} s^b) and b (m^0) are watershed parameters. Neglecting evapotranspiration, the equation of continuity or the storage equation during recession is

$$Q_s = -\frac{dS}{dt} \tag{2}$$

For a linear model ($b = 1$), the recession of baseflow is described by the exponential function $Q_s(t+\Delta t) = Q_s(t)e^{-\Delta t/a}$. For a nonlinear model, the recession curve can be modeled as (Wittenberg, 1999):

$$Q_s(t+\Delta t) = \left[\frac{(1-b)\Delta t}{ab} + Q_s(t)^{b-1}\right]^{1/(b-1)} \tag{3}$$

The parameters (a and b) of the storage-discharge relationship vary over different basins. For a given watershed, the change of groundwater system parameters in a short time period such as 50 years can be negligible. Although land use change and groundwater pumping may change the compaction of soil and the path way of groundwater flows, it is reasonable to assume the changes of the parameters are small. The values of a and b can be estimated by observed natural flows when human interferences do not exist or are not significant.

Recession analysis with pumping and effluent discharge

The storage-discharge relationship, is still valid under human interferences. If pumping and evapotranspiration are considered during the recession period, Equation 2 can be rewritten as:

$$\frac{dS}{dt} = -Q_s - Q_p - Q_{et} \tag{4}$$

where Q_p (mm d^{-1}) is the pumping rate from the aquifer which interacts with the streamflow; Q_{et} (mm d^{-1}) is the groundwater evapotranspiration rate (but it does not include the irrigation water consumption by crops). In an urban watershed, the total streamflow during the recession stage is the sum of base flow and effluent discharge

$$Q = Q_s + Q_e \tag{5}$$

where Q_e is the return flow.

For the case b=1/2, the base flow is obtained by assuming pumping and evapotranspiration rates are constant during the integration period

$$Q_s(t+\Delta t) = \left(Q_p + Q_{et}\right)\tan^2\left[\arctan\sqrt{\frac{Q_s(t)}{Q_p+Q_{et}}} - \frac{\sqrt{Q_p+Q_{et}}}{a}\Delta t\right] \tag{6}$$

where Δt is the time step such as one day. If $b \neq 1/2$, the integration of Equation (6.7) can be represented by hypergeometric function. Substituting Equation 5 into Equation 6 and eliminating $Q_s(t)$:

$$Q(t+\Delta t) = Q_e + \left(Q_p + Q_{et}\right)\tan^2\left[\arctan\sqrt{\frac{Q(t)-Q_e}{Q_p+Q_{et}}} - \frac{\sqrt{Q_p+Q_{et}}}{a}\Delta t\right] \tag{7}$$

Application to Salt Creek Watershed

The Salt Creek in DuPage and Cook Counties, Illinois, is a tributary to the Des Plaines River in urban Chicago. The Salt Creek watershed covers about 384.6 km^2 of the northeastern Illinois. Residential area occupies 49% of the land use in the watershed. Approximately 23% of the total watershed area is impervious surface. There are 31 point-sources in the watershed, among which there are 11 municipal permits in the watershed, 10 of which are major facilities that have design flows of 0.01 mm d^{-1} or greater (CH2M HILL, 2004). The streamflow is impaired by pollutants such as nutrients, metals, pathogens, etc. associated with effluent discharges.

Figure 1 shows the recession curves during January of 1951 and 2005, respectively. Not only the changing magnitude but also the shapes of the two recession curves are very different.

The recession in 1951 is much steeper than that in 2005. It is reasonable to assume that the human interferences in 1951 were negligible since substantial population increase occurred after 1950s (Spieker, 1970). Thus the watershed could be treated as a natural. In winter (December, January and February), the evapotranspiration loss from groundwater is low and a small value is assumed for Q_{et}. We then test the best parameter value for b in this particular watershed and estimate the value of a. Multiple values of b are chosen, and the best value of a is found under the given value of b by minimizing the RMSE between the observed recession curve and the simulated one. The best value of b is around 0.5.

The estimated pumping rates and return flows are plotted in Figure 2 with observed daily streamflow. The return flow increased significantly in the 1960's, and became stable after the 1980's around the value of 0.36 mm d^{-1}. The number is consistent with the assessment provided by a report sponsored by the Illinois Environmental Protection Agency, in which the effluent discharge is assumed to be constant with the estimated value of 0.35 mm d^{-1} during 1990~1999, and the report projected the change of effluent discharges up to 2020 according to the demographic and socioeconomic development projection in the watershed (CH2M-HILL, 2004).

From Figure 2, the estimated pumping rate increased significantly in the 1960's, which is consistent with the sharp increase of effluent discharge in the same period. In 1965, the estimated pumping rate from the shallow groundwater is estimated as 0.130 mm d^{-1}. According to a USGS report (Spieker, 1970), nearly all the public water supplies in the Salt Creek Watershed depended on groundwater in 1966. Of the total pumpage of 0.355 mm d^{-1}, 0.226 mm d^{-1} was pumped from the deep aquifers, and 0.129 mm d^{-1} was pumped from shallow, unconfined aquifers which directly interact with the streamflow (Spieker, 1970). This then validates the estimation of the water withdrawal from groundwater resulting from the recession analysis. The estimated pumping rates decrease in the 1970's and 1980's; after the 1990's, the pumping rate decreases to 0.01 mm d^{-1}. The reason of decreasing groundwater pumping is the use of water from Lake Michigan. The allocation delivered from Lake Michigan for water supply in the area began with a small amount before 1975. Around 1992-1993, many communities in the Salt Creek watershed obtained water allocation right.

Conclusions

Direct human activities such as groundwater pumping and effluent discharge affect flow recession processes, associated with the alteration of the rising limb and the peak of hydrograph by indirect human interferences such as land use change. The changes of human interferences over years cause the dynamics of low flow regime in heavily managed watersheds. To understand the impact of direct human activities on flow recession, this paper extends recession analysis to incorporate direct human interferences such as groundwater pumping and effluent discharge. The analysis is applied to the Salt Creek Watershed. During the past century groundwater pumping and effluent discharges associated with the socioeconomic development in the area have caused a significant increase of the low flow magnitude, but a decrease of the flow variability. The change of the low flow regime reveals the path and form of water supply in the area through growing groundwater pumping during 1955-1970 (including deep groundwater depletion) and the switch from groundwater pumping to water diversion from Lake Michigan during 1975-1993.

Conventionally direct human interferences such as water withdrawals and return flows are added or distracted from storage or streamflow assuming a linear relationship between the human and natural system. Our study, which integrates water uses as endogenous variables in the recession analysis model, illustrates nonlinear impacts of human interferences on low flows in the case study watershed, which is probably related to dynamics of both water uses and natural processes.

Water withdrawals and return flows are usually difficult to observe and model and they are usually treated as known, deterministic parameters in hydrologic modeling, which can cause biased errors in model parameter estimation and model prediction (Hejazi et al., 2007; Wang and Cai; 2007). Given flow and evapotranspiration observation or assessment, our analytical model can be used to retrieve human interferences, as demonstrated in the case study watershed. Such a procedure is very useful for coupled human - natural system analysis since the data of human systems are usually incomplete or unknown.

The method provided in this paper can be applied to other urban or agricultural watersheds. For some watersheds the physical parameter of b may not be 0.5, then Equation (6.12) will not be applicable and approximation solution will be developed using the same reasoning methods proposed in this paper. In agricultural watersheds, pumping for irrigation

varies seasonally and so does return flow. Moreover, the uncertainties of streamflow observation and the physical parameters of the recession equations need to be considered for sensitivity and uncertainty analysis.

References

National Research Council (NRC) (1992), *Opportunities in the Hydrologic Sciences*, 348 pp., Natl. Acad. of Sci., Washington, D. C..

Oki, T. and S. Kanae (2006), Global hydrological cycles and world water resources, *Science*, 313, 1068-1072.

Cörösmarty, C. J., P. Green, J. Salisbury, and R. B. Lammers (2000), Global Water Resources: Vulnerability from Climate Change and Population Growth, *Science*, 289, 284-288.

Claessens, L., C. Hopkinson, E. Rastetter, and J. Vallino (2006), Effect of historical changes in land use and climate on the water budget of an urbanizing watershed, *Water Resour. Res.*, 42, W03426, doi:10.1029/2005WR004131.

Weiskel, P. K., R. M. Vogel, P. A. Steeves, P. J. Zarriello, L. A. DeSimone, and K. G. Ries (2007), Water use regimes: Characterizing direct human interaction with hydrologic systems, *Water Resour. Res.*, 43, W04402, doi:10.1029/2006WR005062.

Cong, Z., D. Yang, B. Gao, H. Yang, and H. Hu (2008), Hydrological trend analysis in the Yellow River Basin using a distributed hydrological model, *Water Resour. Res.*, doi:10.1029/2008WR006852, in press.

National Research Council, (2002), *Estimating water use in the United States—A new paradigm for the National Water Use Information Program*, Washington, DC, National Academy Press, 176 p.

Liu, J. et al. (2007), Complexity of coupled human and natural systems, *Science*, 317, 1513-1516.

Wang, D. and X. Cai (2007), Optimal estimation of irrigation schedule - An example of quantifying human interferences to hydrologic processes, *Adv. Water Resour.*, 30, 1844-1857. doi:10.1016/j.advwatres.2007.02.006.

Wittenberg, H. (1999), Baseflow recession and recharge as nonlinear storage processes, *Hydrol. Process.*, 13, 715-726.

Brutsaert, W., and J. L. Nieber (1977) Regionalized drought flow hydrographs from a mature glaciated plateau, *Water Resour. Res.*, 13(3), 637-643.

CH2M HILL Inc. (2004), *Total maximum daily loads for Salt Creek, Illinois*, Report for Illinois Environmental Protection Agency.

Spieker, A. M. (1970), *Water in Urban Planning, Salt Creek Basin, Illinois*, U. S. Geol. Survey, Water Supply Paper-2002.

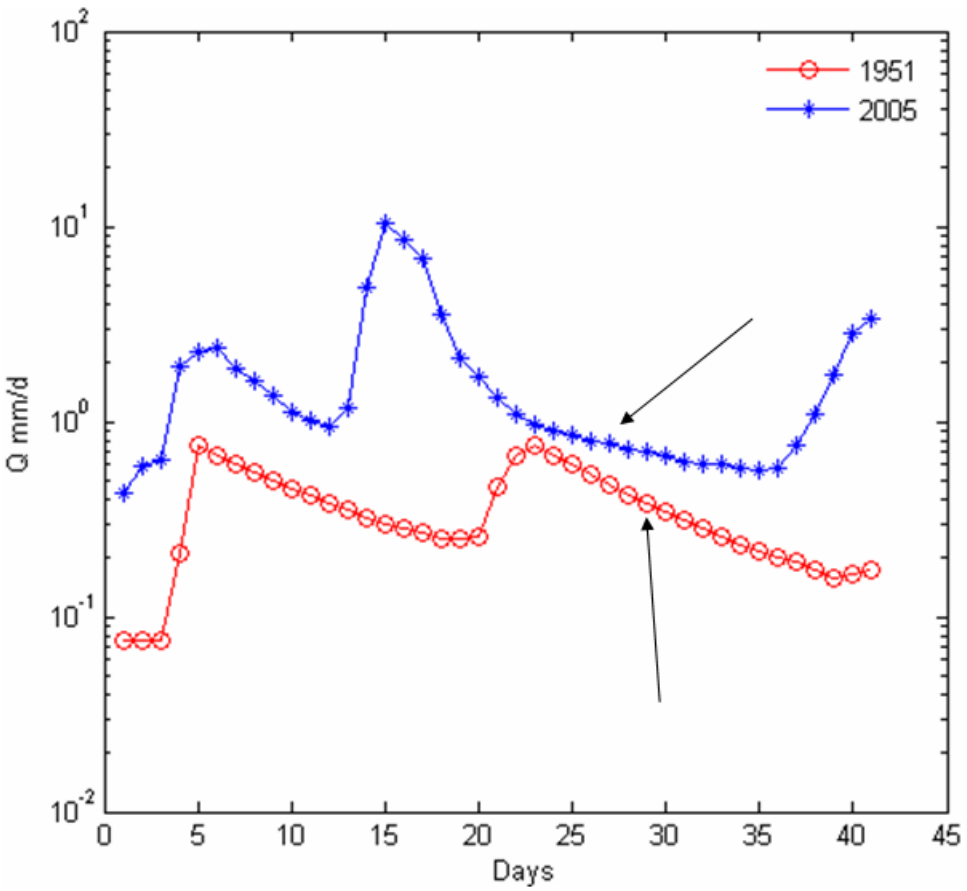

Figure 1. Streamflow recession in January of 1951 and 2005, respectively

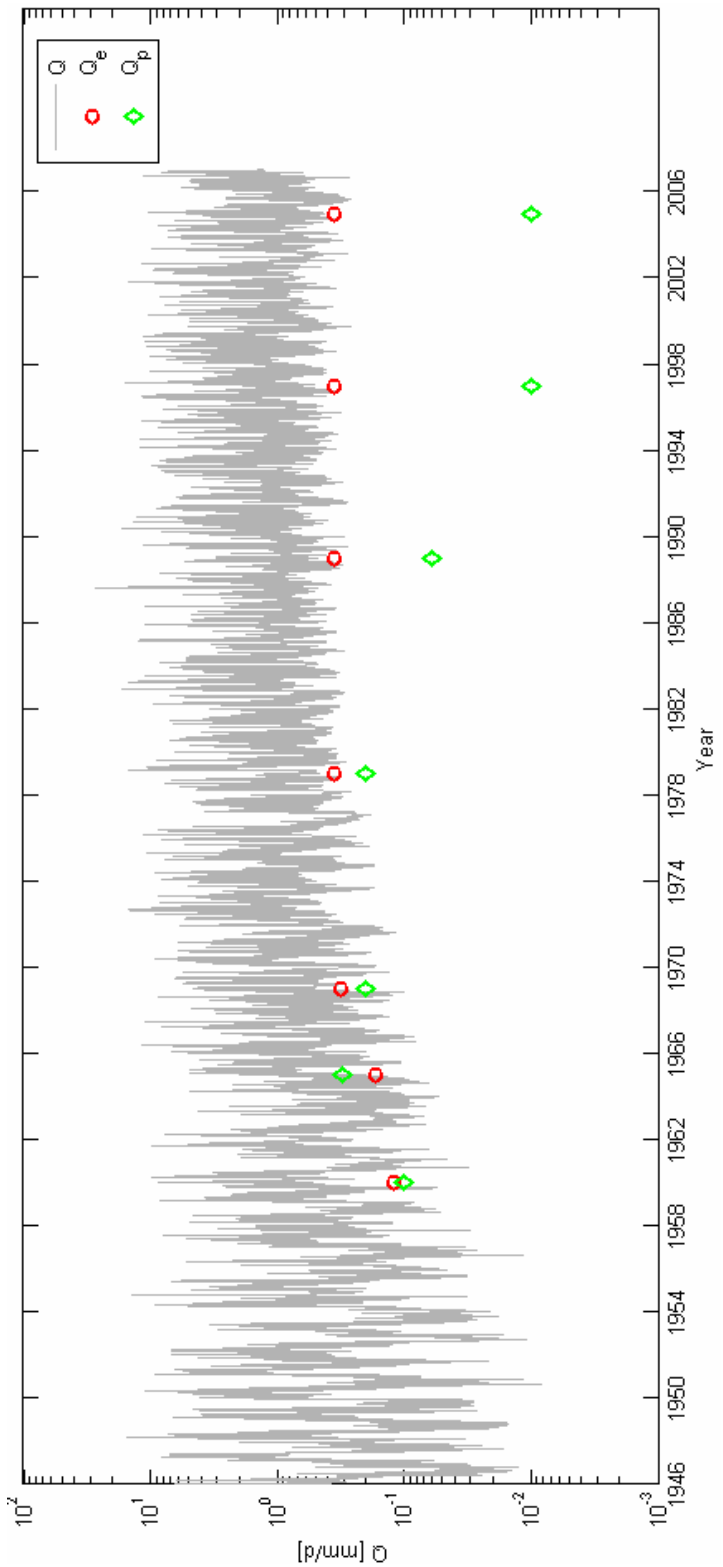

Figure 2. Observed daily streamflow at the outlet of Salt Creek Watershed during Jan-01-1946~Dec-31-2006, and the estimated pumping and effluent discharge based on recession analysis

Historical changes in the streamflow in Kansas streams: variation, causes and implications

Jonathan P. Aguilar[1], James K. Koelliker[2] and Nicole Marie Dick[3]

Abstract

Over the past decades, the streamflow characteristics in the Great Plains streams have changed substantially. These changes have affected the use and allocation of water in the watershed, as well as the lotic ecosystem in the stream network. Changes have affected and will continue to affect the management decisions within the watershed. Our study was undertaken to determine the extent of change in the median and low flows of streams across the state of Kansas and to identify the probable factors affecting these changes, as well as its implications. Several unregulated streams were analyzed by using streams with more than 60 years of daily discharge data. The analysis focused on the median and low flows of the streams. The state of Kansas was divided into four regions, representing roughly the west, central, northeast and southeast sections of the state. Several factors believed to affect the streamflow were identified and their influence was modeled over time. A multi-variate statistical model was run. The results show changes in streamflow pattern have been experienced by Kansas streams. Over the decades, western and central Kansas streams are losing flow, while the eastern streams are gaining flow. Results also show that a climate factor, in terms of water deficit, dictates the regional differences in streamflow. It was apparent that anthropogenic activities of land use, water use and water conservation practices play a significant role in streamflow changes. The role of the physical factors, such as soil type and potential recharge, cannot be downplayed. An interesting result in this study shows that the magnitude and the effects of the factors on the streamflow pattern differed across the regions of the state. There is convincing evidence that the riverine ecosystem has been affected by the changes in the streamflow patterns. Results of this study could be useful to decision makers, water users, watershed stakeholders, and environmental conservation advocates in addressing problems and concerns related to stream and river management.

KEY TERMS: streamflow; instream flow; streamflow changes; streamflow pattern; Kansas streams; unregulated flow; modeling; statistical model; streamflow factors;

---

[1] Graduate Student, Biological and Agricultural Engineering Department, Kansas State University, Manhattan, Kansas. Contact: jaguilar@ksu.edu or 785-532-2941

[2] Professor, Biological and Agricultural Engineering Department, Kansas State University, Manhattan, Kansas, Member ASCE

[3] Graduate Student, Statistics Department, Kansas State University, Manhattan, Kansas

Introduction

Evidence of streamflow changes

Most of Kansas' streams were categorized by some authors as intermittent flashy (Olden and Poff, 2003; Poff, 1996). This is partly due to the fact that most of the precipitation in Kansas is of short duration and high intensity and storms cover a relatively small area. Another controlling factor is the land cover which is generally perennial grass underlain with mostly slowly permeable soil (Sophocleous, 1998), except in the alluvial floodplains and the southeast and south-central regions. Unlike forest trees, grasses tend to hold the surface runoff only for minimal period of time and thus contribute to the flashy characteristic of stream flow. With precipitation ranging from 46 centimeters (18 inches) in the west and a little more than 102 cm (40 inches) in the east, Kansas is considered a semiarid region (Committee on Integrated Observations for Hydrologic and Related Sciences, National Resource Council, 2008).

Today, tributary streams in Kansas might already be categorized as harsh intermittent. In western Kansas, groundwater extraction from aquifers became the most evident human impact in that region. The streams in the area once considered perennial became intermittent as the water table fell below the stream bed and caused the stream to dry up during periods of no rain. The condition is greatly exacerbated in the area considering that the western region receives minimal rainfall, in addition to being theoretically water deficit (i.e. more potential evapotranspiration than precipitation). On the other hand, agriculture, as well as, communities built retention dams along the streams and applied land conservation practices such as terraces and residue management on agricultural fields to conserve water and reduce evaporation and soil erosion. This has a positive effect in terms of water use efficiency and conservation in agriculture, but rather a negative effect on the streams as this reduces runoff from the field. This also has similar effects on the numerous water-harvesting techniques, such as farm ponds and reservoirs that are in operation within the farm lands. It might be argued that these practices also encourage recharge of the aquifers. However, the rate of recharge in western Kansas is so low (~0.6 cm per year) thus, negligible compared to the current rate of groundwater abstraction (Hansen, 1991; Sophocleous, 2005). On the downstream side, the presence of large dams and reservoirs cut the continuity of habitat along the streams and generally control the stream flow discharge further downstream of the structure.

Physical evidence of changes have been documented by photographs at certain stretches of streams across Kansas. For example, a dramatic change in streamflow had happened only in a matter of more than a decade (Figure 1) at a section of Arikaree in extreme northwest Kansas. The base flow of the river is fed by groundwater flow, but because of the agricultural activity in the area, the groundwater level has dropped and is no longer able to sustain the flow in that stretch. In 2006 pioneer species (e.g. wild grasses) had taken over much of the river bed. This is a

typical observation of the streamflows in western Kansas where the once effluent streams, where groundwater supply the base flow, have now become influent streams (Jordan, 1982; Ratzlaff, 1994; Sophocleous, 2000; Szilagyi, 2006).

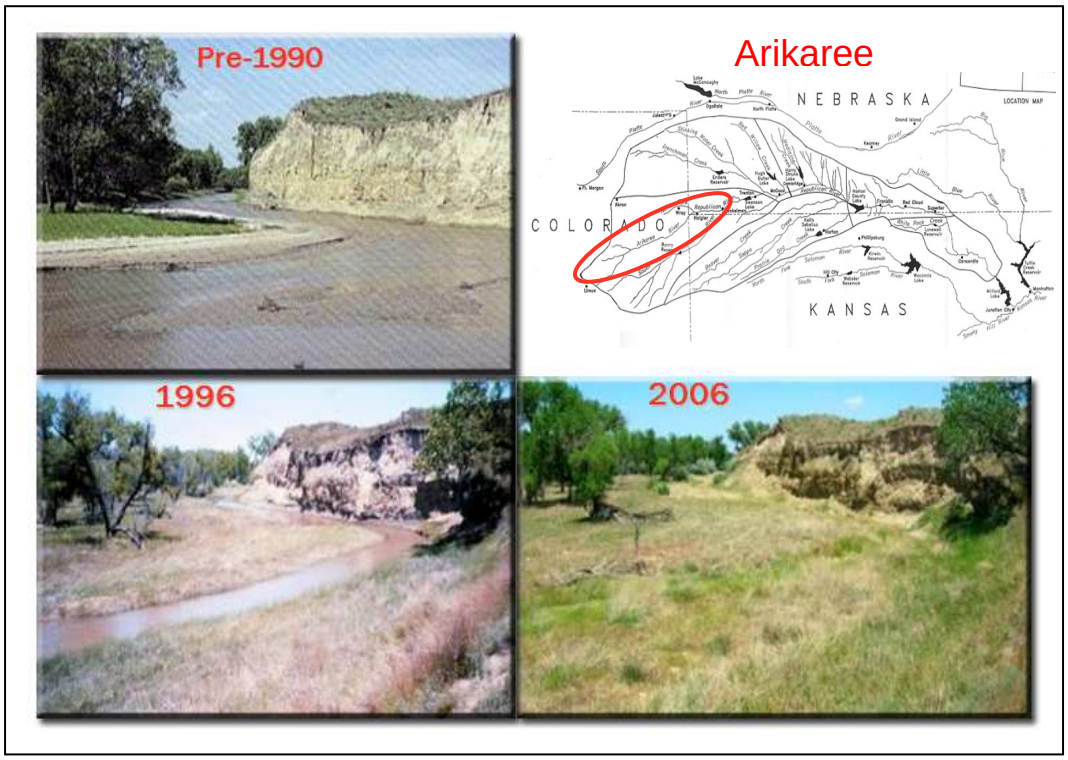

Figure 1. Physical evidence of the condition is depicted by these pictures taken from the Arikaree River in extreme northwest Kansas. Photo source: Kansas Department of Wildlife and Parks.

Changes in the runoff have also been documented in several watersheds of Kansas. Ratzlaff (1994) noted these changes in hydrology at least for the period of 50 years since 1940 in 27 watersheds across Kansas. According to the study, in western Kansas watersheds runoff has declined by as much as 93 percent. These changes were a cumulative effect of changes that was happening in the watershed starting around the 1950s (Ratzlaff, 1994).

Past research

There are now an increasing amount of evidence that the streamflow characteristics of the Great Plains rivers and stream have changed over the past century (Eberle et al., 2002; Perry et al., 2004; Szilagyi, 2006). Attempts to link the streamflow changes to the aquatic ecosystem are also available but limited. In the study that have been reported to the USGS, Perry (2004) made estimates of the median flows of the streams across Kansas using the 1999 surface water register. The study used a median flow of 1.7 cubic meter per minute (1 cfs) as the threshold delineating the sections of the streams with flow. Western Kansas showed not only many streams below the threshold flow, but more alarmingly a long, continuous stretch of the

condition (Figure 2). It should be noted that all the stream segments shown in Figure 2 were considered perennial by the USGS in the 1950s. Another attempt to understand the streamflow patterns was conducted in the Republican River which identified human-induced changes in the basin as the major cause of the declining flow (Szilagyi, 2006). However, there has not been a single research study that focused on Kansas with emphasis or at least in relating the changes to the aquatic ecosystem to other factors.

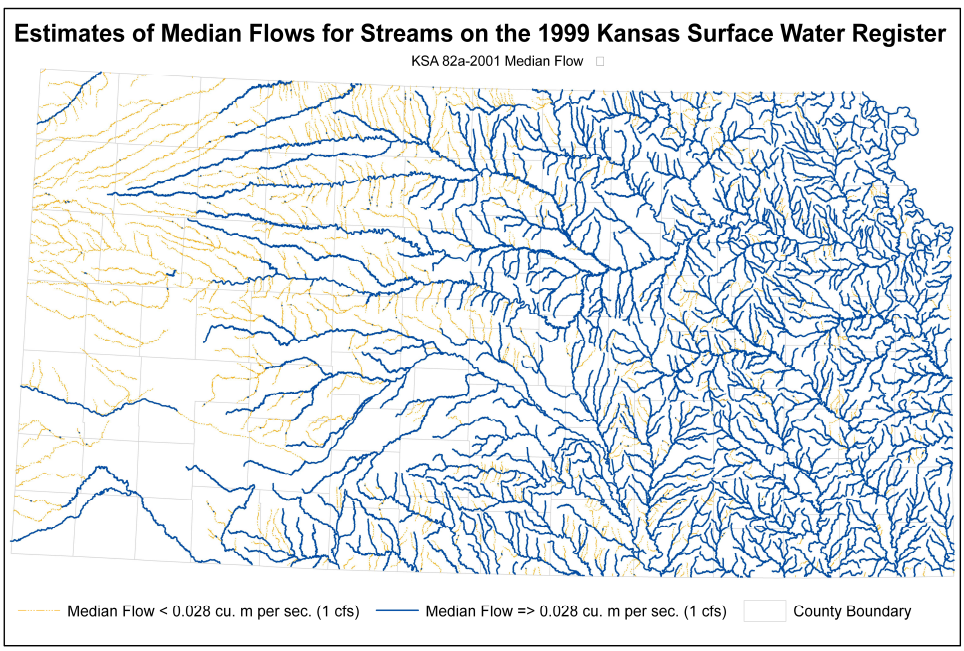

Figure 2. Estimates of median flows for streams on the 1999 Kansas surface water register showing stream reaches below and above a threshold flow of one cubic feet per second. Adapted from Perry et. al (2004).

Methods

Streamflow data

The major emphasis of this study is on streamflow data. USGS gauging station throughout Kansas were considered, but analysis was conducted only on those gauging stations considered unregulated as indicated in the remarks of the USGS Water-Data Reports (Putnam and Schneider, 2003). Another consideration in the selection of gauging stations was on the length of the daily data record. At least 60 years of continuous available data were included in the analysis in order to establish a good historical representation of the period. The records were divided into three 20-year periods. Only streamflow data labeled “approved” by the USGS were included. Kansas is also known to have a wide range of climatic variability across the state (Sophocleous, 1998). Thus, the gauging stations selected for this study where partitioned into four regions, namely west, central, northeast and southeast regions

(Figure 3). Three stations were selected to represent each region. Several flow parameters were computed but for this specific study, much of the focus was on the median to low flows only.

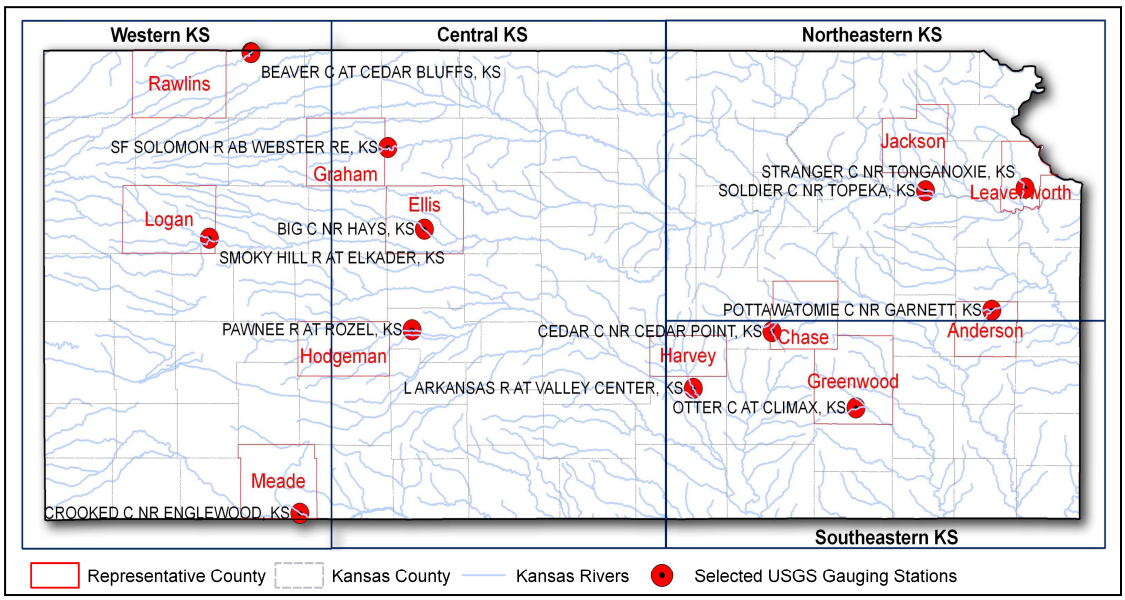

Figure 3. Location of the selected USGS gauging stations in reference to the regional assignment and the representative counties used in the study.

Statistical Model

One of the approaches in determining factors contributing to a certain phenomenon is by running a multi-variate, statistical model. The data was subjected to different statistical analyses. A state-wide analysis was first conducted followed by a regional approach. Several physical and anthropogenic factors were identified as related to the streamflow. The physical factors are recharge rate, soil type and climate, while the anthropogenic factors are water use, land use and soil and water conservation practices. Historical data was sparse and, in most cases, are on per county basis. Thus, representative counties covering most of the watershed area for each given gauging station were considered.

Recharge rate

Recharge is the infiltration of water into the saturated zone or groundwater. The rate at which the water infiltrates after saturating the initial profile is the recharge rate. There are many factors that affect the groundwater recharge rates such as the general soil texture within the soil profile, amount and intensity of precipitation, and land cover and vegetation among others. The groundwater recharge rates were taken from the maps generated by Hansen (1991) and Sophocleous (2005). The values of the recharge rates are actually the potential natural recharge rates for the county.

Soil type

Soil type influence several processes in the soil-water relationship, one of which is surface runoff. Surface runoff refers to the loss of water from an area by flow over the land surface. Surface runoff classes are based on slope, climate, and vegetative cover. The concept indicates relative runoff for very specific conditions. In the US Soil Survey Geographic (SSURGO) database (http://soils.usda.gov/survey /geography/ssurgo) where the data was taken, it is assumed that the surface of the soil is bare and that the retention of surface water resulting from irregularities in the ground surface is minimal. The classes are labeled as negligible, very low, low, medium, high, and very high. These were then assigned numerical values with a scale of 1-10, with 10 as having negligible surface runoff.

Water Use

The water use data was taken from the Kansas Geological Survey's (KGS) Water Information Management and Analysis System (WIMAS) database (http://hercules.kgs.ku.edu/geohydro/wizard/index.html). It contains the information of all the water rights issued in Kansas. The data dates backs in the 1950s when the first water rights were issued. Water rights are the maximum permitted amount of water that can be extracted from water sources such as river and groundwater. Average volume of water use for the county in cubic meter (acre-foot) was used in the analysis.

Land Use

The values used for land use were the average percent cropland of the representative counties. The Kansas State Board of Agriculture, which publishes Kansas Agriculture Annual Report, was the source of data for land use. Part of the publication was the area of land per county that is harvested to specific crops and the aggregated area was used in this study. It is important to note that especially in the western region of Kansas including some counties in the central region, fallowing is being practiced and was included in the cropped area. Fallowing is a farming practice that conserves the water in order to achieve a more dependable wheat production. Fallowing was originally practiced in a 2-year cycle with one crop grown per cycle, but recently the prevailing practice is to have a 3-year cycle with two crops grown per cycle. This generally shortens the fallow period while making the land more productive. It is said that for an inch (2.5 centimeter) of water stored during fallow, it is translated into a certain number of bushels (tons) of grain.

Conservation practices

Conservation practices refer to the adoption of soil and water conservation practices on the farm. The adaption varies over time and extent of area. There are no data available on this aspect for Kansas. Estimation of this factor was based on expert judgment. Dr. Koelliker is one of the leading hydrologist and watershed modeler in Kansas. He was also involved in several water conservation projects across the state and thus is knowledgeable enough to give some figures on the estimated adaption of the practices. A scale of 1-100 was used giving 100 to counties with full adoption of soil and water conservation practices.

Results and Discussion

Frequency analyses of flow were conducted and based on the median and low flows, there is a large difference between the flow pattern in the west and east (Figure 4). To show the trends across the large range of flows and to discount watershed size, trends over time are shown relative to the long-term average for each region. The western and central regions exhibit a general decreasing flow trend and the eastern regions show an increasing flow trend.

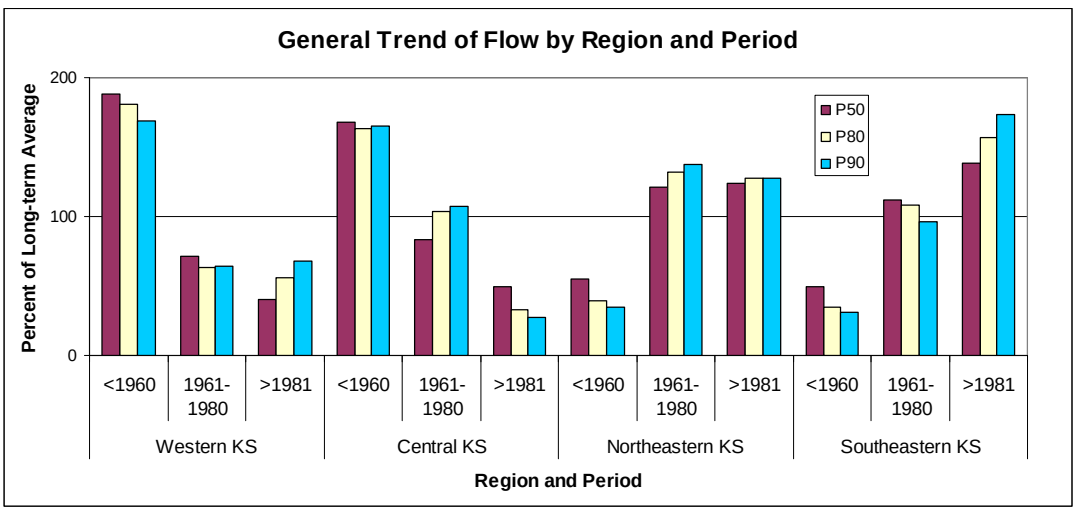

Figure 4. General trend of flow across Kansas by period and regions computed based on the long-term average for each region. P50 represents median flow, P80 is a low flow and P90 is a very low flow.

Correlation between paired parameters was determined using the Pearson correlation method. It showed that climate is highly correlated to the streamflow (Table 1). Thus, high correlation is good in a sense that variation in the streamflow across the state also reflects the variation of climatic factors in the area. However, the large climate effect conceals the probable effect of other variables on the streamflow. It was also observed that analyzing the data on the state-wide basis somehow produces some cancelling effects on the contributions of the individual variables. This reflects the high variation of parameters from east to west across Kansas.

Running the statistical analyses on the regional basis proved to be a better approach. Correlation among the paired parameters was conducted. Surprisingly, based on the tests, climate could be expressed as a function of recharge rate and soil type at each region. When climate was removed from the set of variables, the co-linearity between the variables disappeared except for the southeastern region. But as diagnostic tests are concerned, climate can mask the effect of other variables and thus could be removed in the succeeding analysis.

Using the backward elimination technique in regression, the only significant variable in the model for the whole state is recharge rate at the 90-percent confidence

level. The resulting model has an R-squared value of 0.39 which is high enough considering the varied hydrologic condition of Kansas. A similar exploratory analysis was also done for the data in each region. Climate also has a high correlation with the streamflow and can conceal the probable effect of other variables. The regional analysis generated a summary of statistical results as presented in Table 1.

Table 1. Summary of the model results which used backward elimination regression

Region	Significant Variables (α = 0.1)		R-squared	
	P50 Flow	P90 Flow	P50 Flow	P90 Flow
All	***Climate***	***Climate***	0.52	0.35
	Land Use (-)	Soil (-)		
		Land Use (-)		
Western	***Recharge Rate***	***Water Use***	0.96	0.96
		Recharge Rate		
Central	***Soil***	***Soil***	0.93	0.66
	Practice (-)			
Northeastern	***Land Use*** (-)	***Land Use*** (-)	0.93	0.94
	Practice	Practice		
		Water Use (-)		
Southeastern	***Recharge Rate*** (-)	***Recharge Rate*** (-)	0.74	0.75
	Soil	Practice		
	Practice	Water Use (-)		

Bold – most significant predictor
(-) – negative value in the model (i.e. reduces flow)

In general, there is a higher degree of confidence in doing the regional analyses than the state-wide analysis. The model's R-squared values are at a high of 0.97 to a low of 0.74, which are still relatively acceptable values. This shows that there is a good interaction between the significant variables and the streamflow values.

The result shows that from western region to southeastern region, which could be also interpreted as going from west to east of the state, the recharge rate changes from a positive correlation to negative. Conversely, soil and water conservation practices have a positive influence on the streamflow from the eastern section of the state, then a negative influence on the central section and eventually become insignificant on the western section. Soil type, on the other hand, has a varying response to different regions of the state. It tends to have negative influence on the streamflow in the western region, and a positive influence in central and southeastern regions. In the northeastern region, soil type is insignificant as far as changes in streamflow are concerned. Land use exhibits a negative correlation with streamflow in central and northeastern regions only. The other two regions show insignificant correlation to land use.

CONCLUSIONS

This study has showed changes in streamflow pattern have been experienced by unregulated Kansas streams. These changes differ depending on the location within the state. Western and central Kansas streams are losing flow over the decades, while eastern streams are gaining. Statistical models were used to identify the causes of these changes in streamflow. A good relationship between what is happening in the watershed and the streamflow resulted. The factors identified behave differently between the regions. It was clear though that climate is the overarching factor that dictates the differences among the regions of the state. Between regions, however, there are different factors that dominate. Interestingly, the recharge rate factor was found to have a different effect on the streamflow depending on the region. One thing is definite, anthropogenic factors (i.e. land use and water use) are substantial players on the fate of the stream flow pattern.

There is convincing evidence that the riverine ecosystem has been affected by the changes in the streamflow patterns. An analysis of fish communities in the Little Arkansas River Basin (LARB) by Strong et al. (1998) showed that during the last 100 years, fluctuation in the fish community composition was evident. Agriculture, industry and habitat restrictions are perceived to be playing a role in determining the fish community composition in the area (Strong et al., 1998). Although prairie fish living in upstream tributaries are able to survive the typical drought condition, the intensity and the increasingly harsh conditions (Walks et al., 2007) they are experiencing recently are probably making a toll on them. In a recent article on the status of imperiled North American and diadromous fishes, one of the major threats to at-risk fishes is habitat degradation and introduction of non-indigenous species (Howard L. Jelks et al., 2008). It is apparent that anthropogenic activities are affecting the balance in the aquatic ecosystem through modification in the streamflow patterns.

The results of this study are useful for decision makers and stakeholders in being aware that the factors causing streamflow changes may differ from one region to another. Thus, decisions made in response to the different activities within the watershed may result in different streamflow changes.

There is one caveat in this study; the assignment of the regions is more arbitrary rather than based on scientific delineation or grouping. Care should be practiced in making decisions based on the regional delineation made on this study. It is advisable to use established ecoregions if the application will deal with ecosystems or other environmental groupings and phenomena.

References

Committee on Integrated Observations for Hydrologic and Related Sciences, National Resource Council (2008). Case studies on integrated observatories for

hydrological and related sciences. *Integrating Multiscale Observations of U.S. Waters*, National Academic Press, Washington, DC, pp. 78-142.

Eberle, M. E., Hargett, E. G., Wenke, T. L., & Mandrak, N. E. (2002). Changes in fish assemblages, Solomon River Basin, Kansas: Habitat alterations, extirpations, and introductions. *Transactions of the Kansas Academy of Science*, 105(3), 178-192.

Hansen, C. V. (1991). Estimates of freshwater storage and potential natural recharge for principal aquifers in Kansas. USGS Water Resources Investigations Report, No. 87-4230.

Jelks, Howard L., S.J.Walsh, N.M. Burkhead, S. Contreras-Balderas, E. Diaz-Pardo, D.A. Hendrickson, J. Lyons, N.E. Mandrak, F. McCormick, J.S. Nelson, S.P. Plantania, B.A. Porter, C.B. Renaud, J.J. Schmitter-Soto, E.B. Taylor, & M.L. Warren, Jr. (2008). Conservation status of imperiled North American freshwater and diadromous fishes. *Fisheries*, Vol. 33(8): 372-407.

Jordan, P. (1982). Rainfall-runoff relations and expected streamflow in western Kansas. Kansas Water Office, (Topeka) Bulletin (25).

Olden, J. D., & Poff, N. L. (2003). Redundancy and the choice of hydrologic indices for characterizing streamflow regimes. *River Research and Applications*, 19(2), 101-121.

Perry, C. A., Wolock, D. M., & Artman, J. C. (2004). Estimates of median flows for streams on the 1999 Kansas surface water register. Scientific Investigations Report. United States Geological Survey.

Poff, N. L. R. (1996). A hydrogeography of unregulated streams in the United States and an examination of scale-dependence in some hydrological descriptors. *Freshwater Biology*, 36, 71-91.

Putnam, J.E. & D.R. Schneider (2003). Water Resources Data Kansas Water Year 2002. Water-Data Report KS-02-1. USGS.

Ratzlaff, J. R. (1994). Timing and magnitude of changes in runoff for Kansas watersheds, 1940–1990. *Transactions of the Kansas Academy of Science*, 97(1-2), 26-35.

Sophocleous, M. (2000). From safe yield to sustainable development of water resources- the Kansas experience. *Journal of Hydrology*, 235(1), 27-43.

Sophocleous, M. (2005). Groundwater recharge and sustainability in the high plains aquifer in Kansas, USA. *Hydrogeology journal*, 13(2), 351.

Sophocleous, M. A. (1998). Water resources of Kansas: A comprehensive outline. Perspectives on Sustainable Development of Water Resources in Kansas. Kansas Geological Survey, Bulletin, 239, 1–59.

Strong, A. J., Wilkinson, S. A., & Lydy, M. J. (1998). Fish communities in the little Arkansas River Basin, Kansas 1884-1996. *Transactions of the Kansas Academy of Science* (1903-), 101(1/2), 17-24.

Szilagyi, J. (2006). Identifying cause of declining flows in the Republican River. *Journal of Water Resources Planning and Management*, 127(4), 244-253

Walks, D. J., J.P. Aguilar, W. Dodds, K. Gido, J.K. Koelliker, and K. With (2007). Temporal changes in fish communities of the Central Great Plains, Kansas. In: North American Benthological Society 55th Annual Meeting Proceedings, Anonymous.

Modeling Water Quality Impacts in Delaware's Coastal Bays With AGNPS

William F. Ritter[1], Bret A. Icenogle[2] and Monika N. Meckley[3]

[1]Bioresources Engineering Department, University of Delaware, Newark, DE. 19716; PH (302) 832-2468; FAX (302) 831-2469; e-mail: writer@udel.edu
[2]Former graduate student, Civil and Environmental Engineering Department, University of Delaware, Newark, DE. 19716
[3]Former undergraduate student, Biosystems Engineering Department, Virginia tech University, Blacksburg, VA

ABSTRACT

The AGNPS model was used to model agricultural BMPs for the Delaware Inland Bays . Corn, soybeans and wheat were the crops used in the simulation. Conventional tillage with a winter cover crop along with minimum tillage and no-tillage with and without a winter coverage crop were simulated as BMPs. The model was calibrated with water quality and flow data from Stockely Branch, a 1359 ha watershed. The model was successful in predicting total runoff, but there was some variation in predicted and measured nitrogen and phosphorus loads for the nine storms used to calibrate the model. Nitrogen loads were more accurately predicted then phosphorus loads. For BMP simulations, winter cover crops had a large effect in reducing nitrogen and phosphorus loads regardless of tillage.

INTRODUCTION

One of the major recreational areas in Delaware is the Inland Bays. The Inland Bays are next to the Atlantic Ocean in Southern Delaware. The Bays are estuaries and are inhabited by plants and animals which are typical of the Mid-Atlantic region. Delaware's Inland Bays consist of the three interconnected water bodies, Rehobeth and Indian River Bays. The Assawoman canal connects Little Assawoman and Indian River Bays. The three bays and their tributaries have a surface area of approximately 8300 ha and a drainage area of approximately 77800 ha. The Inland Bays are tidally flushed, with estimates typically converging on 90-100 days for Indian River Bay and 80 days for Rehobeth Bay (Price, 1997). No flushing estimates are available for Little Assawoman Bay. Groundwater is a highly significant component of freshwater flow into the bays. About 70 to 80 percent of total freshwater stream flow is composed of groundwater discharge. Groundwater also flows under the bay shores and discharges directly into the bays (Andres, 1992).

A Comprehensive Conservation and Management Plan (CCMP) was completed in 1995. In the CCMP, two major priorities identified were eutrophication and habitat loss (DNREC, 1995). Overall, the Inland Bays are highly eutrophic. Total nitrogen concentrations are generally in excess of 1.0 mg/L and total phosphorus concentrations generally range from 0.1 to 0.2 mg/L (Price, 1997).

The Total Daily Maximum Load (TMDL) set for the Inland Bays requires nonpoint source phosphorus loads to be reduced from 40 to 65% and nitrogen loads reduced from 40 to 85% in the different tributaries from baseline loads established from monitoring data collected from 1988 to 1990 (DNREC, 1998). The Agricultural Nonpoint Source Pollution model (AGNPS) was used on Stockely Branch one of the sub-watersheds of the Inland Bays to model different agricultural best management practices (BMPs). Water quality data was collected on Stockely Branch from 1976 to 1980 that was used to calibrate the model. Stockely Branch is also a USGS gaging station so long term flow data was available.

AGNEPS PROPERTIES AND PREVIOUS WORK

The Agricultural Research Service in conjunction with the Minnesota Pollution Control Agency and the Soil Conservation Service developed the AGNPS model to analyze and predict runoff water quality from agricultural watersheds. The model is an individual storm event model and not a continuous simulation model. Over the years since its development it has been used worldwide. One of the features of the model is it allows users to pinpoint potential areas of high nutrient loads through a uniform grid cell approach (Comis, 1995). The model routes a single rainfall event through the grid in a step by step manner allowing the user to evaluate any single grid in the watershed. For watersheds > 800 ha, a grid cell size of 16 ha is recommended (Young et al., 1989). For smaller watersheds accuracy can be increased by reducing the size of the cells.

Twenty-one parameters are used to describe each cell of the watershed. The model simulates hydrology, erosion and sediment and chemical transport. For the hydrology component, routines from the CREAMS model are used. Peak runoff and total runoff volume are estimated by the runoff curve number method. The model uses a modified version of the Universal Soil Loss Equation to estimate upland erosion. Using a soil breakdown of five particle sizes, a modified Bagnold stream-power equation determines the amount of soil detached and deposited. Nitrogen, phosphorus and COD are estimated with equations developed for the CREAMS model.

A study on Highland Silver Lake in Illinois found the model could simulate runoff accurately, but underestimated sediment loadings and over estimated nutrient loadings (Lee, 1987). A study on three watersheds near Coshocton, Ohio, agreed with the underestimate of AGNEPS sediment yield. The underestimation occurred especially for heavy rainfall events (Wu et al., 1993). The AGNPS model was used to predict sediment loads on two watersheds in Iowa and Nebraska. Predicted yields compared favorable with the measured values. Agreement between actual and predicted values was also found for runoff and sediment yields for three different types of watersheds in Mississippi (Young, et al., 1989).

MODEL INPUT DATA

AGNPS analyses a set number of equally sized user grid blocks overlaid on the entire watershed. The Stockely Branch watershed was divided into 35 cells based on a 40.5 ha grid cell. By digitizing the topography from the USGS, Georgetown Quadrangle in Sussex County, Delaware and the land uses, soils group and channel characteristics from the aerial photographs found in the 1974 Soil Survey of Sussex County, a composite map of the topography , land use, soils group and chancel characteristics was developed for the Stockely

Branch watershed (Ireland and Matthews, 1974). All physical data input for the cells were derived from this composite map. The land use for the watershed is summarized in Table 1. Most of the soils on the watershed are sandy loam or loamy sand. Slopes on the watershed are generally <0.75%. The average annual rainfall is 1110 mm. It is distributed fairly uniform over the 12 months. The watershed area is 1359 ha.

The current study relied on weather data gathered from weather station 073570 located in Georgetown, Delaware, 16 km northwest of the site. The historic precipitation data from weather station 073570 for the years 1976 through 1980 was available electronically through the state climatologist's web page. All data was entered into an Excel spreadsheet and converted to metric units for use with the watershed model.

Table 1. Land use for the Stockley Branch Watershed

Land Use	Area (ha)
Industrial/Commercial	12
Low Density Housing	21
High Density Housing	14
Cropland	738
Pasture/Grassland	12
Orchard	12
Chicken Houses	3
Forest	544
Wetlands	1
Water	2

Each cell requires 26 inputs. Although most input values remained constant for all storm events, values for the runoff curve number, Manning's overland flow coefficient, cropping factor C and surface conditions constant were changed for some storm events to reflect the conditions at the time of the storm event. To determine how each of these input values changed for the 35 cells, a combined land use and growing stage system was outlined for a specific crop rotation and management practice and values were modified based upon data in Wischmeier and Smith (1978). A common cropping regime was assumed for the entire watershed and each cell's inputs varied based upon land use.

The crops selected to model were chose based on prevalence within the Stockely Branch watershed and the Delmarva Peninsula. Corn, soybeans and winter wheat are the main crops grown in this geographic region and were selected for the BMP simulations. Based on the selected crops, crop specific dates were estimated based on common cropping practices. For calibration of the model for the period 1976 to 1980, a corn/soybean rotation without a cover crop and conventional tillage was used. The cropping and tillage dates and fertilizer application rates and dates for the corn/soybean rotation without a winter cover crop are presented in Table 2.

SENSITIVITY ANALYSIS

The following input variables were chosen for the sensitivity analysis:

- Curve number

- Land slope
- ULSE soil factors K and C
- Field slope length
- Manning's overland flow coefficient
- N and P fertilizer application rates
- N and P availability levels
- N and P nutrient decay

Table 2. Crop Specific Design Dates for a Corn/Soybean Rotation and No Winter Cover Crop

Crop Rotation	Date	Action
Corn/Soybean Rotation Without a Winter Cover Crop	April 15	Apply 75.5 kg/ha Nitrogen Fertilizer and 22.4 kg/ha Phosphorus
	April 30	Moldboard plow (Optional with Management Practice)
	May 21	Apply 140 kg/ha Nitrogen Fertilizer and 22.4 kg/ha Phosphorus
	May 25	Disc (seedbed period)
	May 30	Plant Corn
	June 15	Period 1 (10 percent canopy cover)
	July 1	Period 2 (50 percent canopy cover)
	July 30	Period 3 (75 percent canopy cover)
	October 15	Period 4 (Harvest Crop, Crop Residual)
		Fallow over Winter months
	April 15	Apply 75.5 kg/ha Nitrogen Fertilizer and 22.45 kg/ha Phosphorus
	May 15	Modlboard plow (Optional with Management Practice)
	May 21	Apply 140 kg/ha Nitrogen Fertilizer and 56 kg/ha Phosphorus
	June 25	Disc (seedbed period)
	June 30	Plant Soybeans
	July 15	Period 1 (10 percent canopy cover)
	August 15	Period 2 (50 percent canopy cover)
	September 15	Period 3 (75 percent canopy cover
	October 15	Period 4 (Harvest Crop, Crop Residual)

A single input variable was adjusted to either plus five (5), plus ten (10), plus twenty (20), minus five (5), minus ten (10), or minus twenty (20) percent of the original value. After the adjustment, a simulation was performed and the change in the output variables was noted. The collection data was then manipulated to find the absolute sensitivity for the relationship between a single input and single output variable. Absolute sensitivity was defined as the percent change in output divided by the percent change in input. Some of the sensitivity analysis is summarized in Table 3.

Of the input values evaluated in the sensitivity analysis for AGNPS, the curve number demonstrated the most significant effect of any input variable. The curve number seemed to have an effect on most output variables. Other variables analyzed did not show the same prevalence as the curve number. Other inputs seemed to influence only one or two output variables. For example, changing the Manning coefficient only had a small effect on peak runoff rate. Land slope did not change any of the parameters. The K and C factors affected sediment yield and nitrogen and phosphorus sediment loads.

Table 3. Summary of Sensitivity Analysis for Selected Variables (% change in output for given % change in input)

Input Variable	Change (%)	Total Runoff Volume	Peak Runoff Rate	Sediment Yield	Soluble Total N	Soluble Total P
CN	+20	5.1	6.3	2.0	40	45
	-20	-3.3	-3.7	-1.8	-6.1	-10
Manning's n	+20	0	0.04	0	0	0
	-20	0	0.04	0	0	0
N&P Application	+20	0	0	0	0.82	0
	-20	0	0	0	-0.86	0
N&P Decay	+20	0	0	0	-0.67	-3.0
	-20	0	0	0	0.79	6.0

MODEL CALIBRATION

Water quality data was collected for nitrogen and phosphorus at the watershed outlet from July, 1976 to June, 1980. A total of nine storms were selected for calibrating the model. The storms selected varied in size, duration and season of the year. The model was first calibrated for runoff where the storm simulated runoff volume was compared to the storm total runoff volume measured at the USGS gaging station. An average total flow was computed for x days, where x was the number of days runoff increased due to the storm event. The baseflow proceeding the storm was subtracted from the average daily storm flow to compute the total runoff. The curve number was adjusted for each storm based upon the initial moisture conditions. For calibration purposes it was assumed half of the cropland was in soybeans and half was in corn, no winter cover crop was planted and conventional tillage was used on all of the cropland. The calibration results are summarized in Table 4. For the nine storm events the model under predicted runoff volume for four of them and over predicted the volume for four storms.

Soluble nitrogen and phosphorus concentrations in the runoff were adjusted to fit the actual runoff concentrations by manipulating the levels of the fertilizer applied parameters. Nitrogen and phosphorus decay values were assumed to stay constant for each storm event. In order to obtain a satisfactory calibration between predicted and measured nitrogen and phosphorus concentrations a constant fertilizer application rate could not be used. For example the June 1979 storm required 280.2 kg/ha of nitrogen and 134.4 kg/ha of phosphorus and the March 1980 storm required 123.3 kg/ha of nitrogen and 134.5 kg/ha of phosphorus. The R^2 values for predicated versus measured concentrations for calibration of the nine storms were 0.725 for nitrogen and 0.527 for phosphorus. The model under predicted phosphorus concentrations for most of the storms. One reason for the large under prediction for some

storms could have been the model concentrations are soluble phosphorus and for the measured phosphorus concentration samples were not filtered, so total phosphorus was measured. Sediment concentrations in the Stockley Branch watershed were very low.

Table 4. Calibration Results for AGNPS

Storm	Rainfall (mm)	Moisture Condition	Runoff (mm)	N Conc Mg/L	P conc (mg/L)
Nov 1978			0.76	4.43	0.32
Actual Model	27	II	0.51	4.42	0.33
Dec 1978			1.02	5.70	0.27
Actual Model	29	II	1.02	5.59	0.23
Mar 1979			33.7	4.38	0.16
Actual Model	62	III	23.6	4.27	0.11
June 1979			19.6	6.00	0.18
Actual Model	84	II	19.1	3.59	0.05
Sept 1979			1.27	4.04	0.38
Actual Model	54	I	0.51	3.71	0.11
Dec 1979			2.29	4.77	0.35
Actual Model	24	III	2.79	4.56	0.27
Mar 1980			5.59	3.99	0.41
Actual Model	53	II	6.10	4.04	0.14
April 1980			10.4	2.78	0.16
Actual Model	41	III	12.4	2.85	0.17
April 1980			5.84	3.82	0.17
Actual Model	26	III	4.28	4.28	0.25

BMP SIMULATION

The following BMPs were simulated:

a. Conventional tillage with a winter cover crop (CTW)
b. Minimum tillage without a winter cover crop (MT)
c. Minimum tillage with a winter cover crop (MTW)
d. No-tillage without a winter cover crop (NT)
e. No-tillage with a winter cover crop (NTW)

The BMPs were compared to conventional tillage without a winter cover crop (CT). A corn and soybean rotation was used for all tillage systems without a winter cover crop. For the winter cover crop simulations, a corn-winter wheat-soybean rotation was used. It was assumed the winter wheat was harvested in July a rye winter cover crop was planted in the fall and full season soybeans planted the following spring.

The three tillage operations were associated with a different degree of surface roughness, lending way to establishing curve numbers and surface roughness coefficients. By not removing the surface residue, no-tillage was correlated with the lowest curve numbers and the highest surface roughness coefficients. Conventional tillage by moldboard plowing and disking was associated with the highest curve number and the lower surface roughness coefficient. The curve number and surface roughness coefficients for conservation tillage were established

in the middle of the other two simulated tillage practices. Secondly, the cropping factors were established for the simulations. Modifications resulted in changes to the cropping factor, the tillage practice factor, the maximum leaf area index, the curve number and the planting, fertilizing and harvesting dates. Changes in the curve number were based on the planting and harvest date as well as tillage operations. Lower curve numbers were associated with more ground cover resulting from lower impact cropping practices. Planting and harvest dates were varied only with the addition or subtractions of a winter crop in the BMP simulations. Input values for C, Manning's n, surface conditions constant and curve number were adjusted in each cell based upon land use. Values established at the time of harvest were maintained until the next tillage or planting operation.

The simulated annual runoff and nutrient loads for the different BMPs for 1979 are summarized in Table 5. The weather data and crop rotations were used to simulate BMPs for the period of 1976 to 1979. There was very little difference in the amount of surface runoff for the three tillage systems without a cover crop. There was a reduction in organic N and P nutrient loads with the NT compared to the CT. This would be expected since the sediment load was reduced from 3012 kg/ha for CT to 573 kg/ha for NT. There was very little difference in the amount of soluble nitrate and soluble phosphorus loads for the three tillage systems without cover crops.

Table 5. Annual Runoff, Sediment and Nitrogen and Phosphorus Predictions for Different BMPs

BMP	Runoff (mm)	Sediment (kg/ha)	Org N (kg/ha)	Soluble NO_3-N (kg/ha)	Org P (kg/ha)	Soluble P (kg/ha)
CT	223	3012	8.74	13.38	4.35	0.12
MT	207	1020	3.71	12.55	1.86	0.12
NT	223	573	2.44	13.38	1.20	0.12
CTW	102	1861	5.55	5.81	2.80	0.04
MTW	97	621	2.37	5.02	1.21	0.03
NTW	110	391	1.53	6.62	0.80	0.06

When a winter cover crop is introduced as a BMP, there was a large decrease in the annual nitrogen and phosphorus loads simulated by AGNPS. The CT organic N load was reduced from 8.74 kg/ha to 5.55 kg/ha and the organic P load was reduced from 4.35 kg/ha to 2.60 kg/ha. Both the soluble nitrate and soluble phosphorus loads were reduced for all three tillage systems with the winter cover crop. The CT soluble nitrate load was reduced from 13.38 kg/ha to 5.81 kg/ha and the soluble phosphorus load was reduced from 0.12 kg/ha to 0.04 kg/ha. In general the total phosphorus loads simulated by AGNPS were considerably higher than any measured phosphorus loads in the watershed. In 1979 the measured total phosphorus load was 1.49 kg/ha and the total nitrogen load was 27.8 kg/ha. Measured nitrogen loads were closer to simulated total nitrogen loads for conventional tillage.

Based upon the BMP simulations, it appears introducing a winter cover crop like wheat or rye would have a significant effect on reducing nitrogen and phosphorus loads in southern

Delaware. For no-tillage the annual total nitrogen load was reduced by 48% and the total phosphorus load was reduced by 35 % when a winter cover crop was used.

CONCLUSIONS

The AGNPS model can be used for simulating BMPs for southern Delaware watersheds. The model did a reasonable job of simulating runoff for individual storms when it was calibrated, but there was considerable variation between simulated and measured nitrogen and phosphorus loads for some individual storms Overall, the model was better in simulating nitrogen loads than phosphorus. Introducing winter cover crops has a large effect on reducing nitrogen and phosphorus loads regardless of the tillage operation.

REFERENCES

Andres, A.S. (1992). "Estimate of nitrate flux to Rehobeth and Indian River Bays, through direct discharge of groundwater." Delaware Geological Survey, Newark, DE. Report No. 35.

Comis, D. (1995). "AGNPS tracks nutrients to their source." *Agricultural Research 43(2):22.*

Delaware Department of Natural Resources and Environmental Control. (1995). "Delaware Inland Bays comprehensive conservation and management plan." DNREC, Dover, DE.

Delaware Department of Natural Resources and Environmental Control. (1998). "TMDL for Indian River, Indian River Day and Rehobeth Bay, Delaware." DNREC, Dover, DE.

Lee, M.T. (1987) "Verifications and applications of a nonpoint source pollution model." Engineering Hydrology, *Proceedings of ASAE Symposium*, Aug. 3-7, 1987. pp. 708 – 713. ASAE, St. Joseph, MI.

Price, K.S. (1997) A framework for a Delaware Inland Bays classification. *Proceedings of the Third Environmental Monitoring and Assessment Program Research Symposium*. Albany, NY.

Wischmeier, W.H. and D.D. Smith. (1978). "Predicting rainfall erosion losses; a guide to conservation planning." U.S. Department of Agriculture, Washington, DC. *Agricultural Handbook No. 537.*

Young, R.A., C.A. Onstad, D.D. Bosch and W. P. Anderson. (1989). "A nonpoint source pollution model for evaluating agricultural watersheds." *Journal of Soil and Water Conservation* 44(2):168-173.

Wu, T.H., J.A. Hall and J.V. Bonta. (1993) "Evaluation of runoff and erosion models." *Journal of Irrigation and Drainage Engineering* 119(2):364-382.

Parameterization of Seasonal Freshets for the Study of Effects of Freshwater Inflows on Galveston Bay

Tony L. Smith[1], George H. Ward Jr.[2], William H. Espey, Jr.[3], Richard Browning[4]

[1]Espey Consultants, Inc., Water Resources Department, 3809 S. 2nd St., Austin, TX, 78704; PH (512) 326-5659; FAX (512) 326-5723; email: tsmith@espeyconsultants.com
[2]Center for Research in Water Resources, The University of Texas at Austin, 10100 Burnet Rd, Austin, TX, 78758; PH (512) 417-0114; FAX (512) 471-0072; email: gward@mail.utexas.edu
[3]Espey Consultants, Inc., Water Resources Department, 3809 S. 2nd St., Austin, TX, 78704; PH (512) 326-5659; FAX (512) 326-5723; email: wespey@espeyconsultants.com
[4]Trinity River Authority, 5300 South Collins St., Arlington, TX, 76004; PH (817) 467-4343; FAX (817) 465-0970; email: browningr@trinityra.org

ABSTRACT

The principal freshwater inflows to the Galveston Bay system originate from the Trinity and San Jacinto river basins. It is hypothesized that the magnitude of these inflows to Galveston Bay is an important control on the productivity of the system. There is a distinct seasonality in the historical flows into Galveston Bay, being bimodal with high flows in the spring and fall. Often these inflows appear as intense seasonal pulses of flow (i.e. "seasonal freshets"). Many biologists hypothesize that organisms present in the bay at key lifestages are adapted to these seasonal pulses of inflow. In order to evaluate this hypothesis quantitatively, it is necessary to first characterize these seasonal freshets. An objective technique for identifying these seasonal freshets is derived and applied to the varying watersheds contributing to Galveston Bay. These results have been utilized as a representation of inflows to Galveston Bay in subsequent analyses of organism abundance.

INTRODUCTION

Galveston Bay, the largest estuary on the Texas coast (600 square miles, or 384,000 acres), is a shallow estuary in a drowned river delta (TSHA 2008). Numerous economically and ecologically important organisms utilize habitat areas within this system as a nursery, with various habitat types providing sufficient conditions for survival and development (Minello 1999; Weinstein 1979). Freshwater inflow demonstrates its ecologically important functional roles in several ways: through the transportation of sediments and nutrients; the maintenance of varying salinity gradients; maintenance of wetlands, plant, and animal productivity; and the maintenance of economically important fish and shellfish populations.

The principal freshwater inflows to the Galveston Bay system originate from the Trinity and San Jacinto river basins. The varying hydroclimatology of these watersheds, in which precipitation is almost entirely rainfall derived from deep convection, often results in patterns of freshwater inflows operating as intense seasonal pulses of flow (i.e. "seasonal freshets") to the Galveston Bay ecosystem. Figure 1 displays the occurrence of seasonal monthly rainfall maxima in Texas, wherein it can be seen that the seasonal magnitude of these maximum rainfall amounts vary in space and time (Ward, 2000).

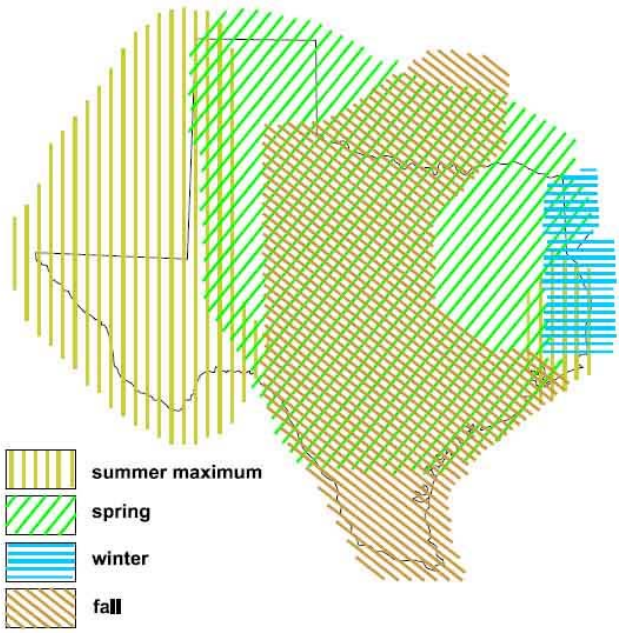

Figure 1. Regions of seasonal rainfall maxima

An objective technique for identifying these freshets has been derived and applied to watersheds contributing to Galveston Bay. The purpose is to improve upon the characterization of the hypothesized characteristics of these pulses of flow believed to determine, among other factors, relative organism abundance in the estuary. Past efforts to search for such a dependency in the Galveston estuary (e.g. Longley, 1994, TPWD, 1998) have utilized calendar monthly flows (or sums thereof) as independent indicators of these seasonal freshets. It is hypothesized that such a practice might not sufficiently depict these events, and by artificially partitioning the freshet into varying time bins, may in fact contribute to the unexplained variance to any dependency upon seasonal freshet events.

It is thus necessary that an objective, quantitative method be developed for identifying seasonal freshet events in a hydrological record for at least three reasons: (1) such freshet determinations would need to be made for a large number of hydrological data extending over many thousands of records (i.e., extended periods of daily-flow data); (2) such a technique would need to be applicable over multiple watersheds with varying hydroclimatologies; and (3) freshet identification must avoid any selection bias of the researchers.

HYPOTHESIS

Taking advantage of the aforementioned fact that Texas hydroclimatology is dominated by deep convection, the quantitative characterization of such seasonal freshet events was developed utilizing what is essentially the characteristics of the impulse-response function of the storm-runoff event. A useful model of this, essentially impulse-response function, is given by:

$$Q(t) = a\, t^n\, exp\{-k\, t^m\} \tag{1}$$

Where m≤1 and n≥1. It is desirable to express the parameters a and k in terms of readily measurable properties of the hydrograph, e.g. the rise time t_r and peak flow Q_p, whereupon:

$$k = (n/m)\, t_r^{-m} \qquad a = t_r^{-n}\, exp\{n/m\}\, Q_p \tag{2}$$

The simpler versions of this model are those with n and m close to 1. An example of (1) with $n = 2$ and $m = 1$ fitted to the data of a runoff event on the Trinity River watershed is shown in Figure 2. A convenient index to the runoff signal is the proportionate response d $logQ/dt$. Both the analytical equation from (1) and the numerical finite-difference approximations from field data are superposed on the plot of Figure 2. (Of course, real hydrographs have the property that d $logQ/dt \rightarrow 0$ quickly after the storm hydrograph, which equation (1) may not.)

The seasonal freshet is created by a sequence of these individual storm events, usually superposed, and the combined hydrographs further distorted by the possible effects of reservoir storage on the watershed. Nonetheless, seasonal freshets have been considered to retain three properties: (1) a long term rise and subsequent recession of flows (usually with multiple extrema); (2) a well-defined onset with a relatively sudden rise in inflow; and (3) a protracted recession.

CONTRIBUTING WATERSHEDS

Assessing the potential relationship between relative organism density and flow requires the development of hydrologic data for the Galveston Bay system drainage, and the formulation of the parameters of flow to serve as variables in subsequent analyses. Watersheds contributing to the Galveston Bay system have been considered and evaluated in these analyses, with a focus upon the Trinity River Watershed (TRNTY), the San Jacinto Watershed (SNJAC), the Coastal Watershed (COSTL), and the Total Galveston Bay Watershed (TGALB). Daily flow amounts have been compiled for the USGS gages contributing to the Galveston Bay system and combined with modeled estimates of daily flows from the ungaged coastal watersheds utilizing the Texas Water Development Board's Texas Rainfall-Runoff Model, TxRR, output (Matsumoto, 1992).

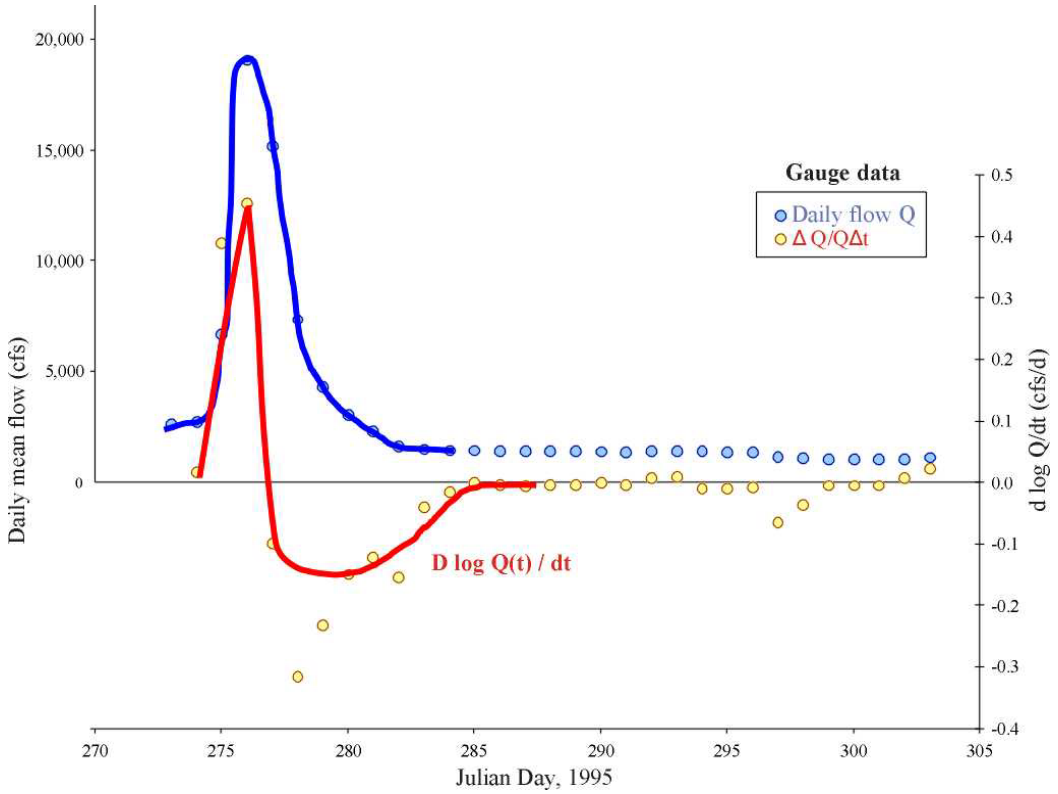

Figure 2. Storm hydrograph October 1995, Trinity River Watershed, with model of equation (1)

METHODOLOGY

In order to first identify the freshet, it is necessary to first apply smoothing to the daily flow data. To take advantage of the aforementioned derivative of the logarithm of flow, this smoothing has been applied to the daily flow data (represented as the light blue line in Figure 3 below) by using a sliding 45-day centered average (the dark blue line in Figure 3, necessary to evaluate both forward and backward in time). The 45-day average has been selected, as it has been deemed to be the appropriate level of sensitivity. A sensitivity analysis was performed utilizing 30-, 45-, and 60-day averages, whereupon results were found to be either too sensitive (for the 30-day average, wherein individual storms were identified) or not sensitive enough (for the 60-day average, where often multi-season freshets were identified). Thus the 45-day average was utilized for identifying a watershed's seasonal pulse from the individual storm events for a given year's hydrology.

The (sliding) slope of the 45-day centered average regression of the 45-day average flow data was calculated and normalized by the maximum of either the POR-median flow or the centered 180-day mean flow, termed m/Qmean. The normalization to the maximum of the period of record (POR) median flow or the centered 180-day mean flow allows for the identification of freshets during wet and dry periods. This identifies a rate of change in flow relative to the magnitude of flow occurring in the surrounding six months (in units of /time), allowing for freshets to be

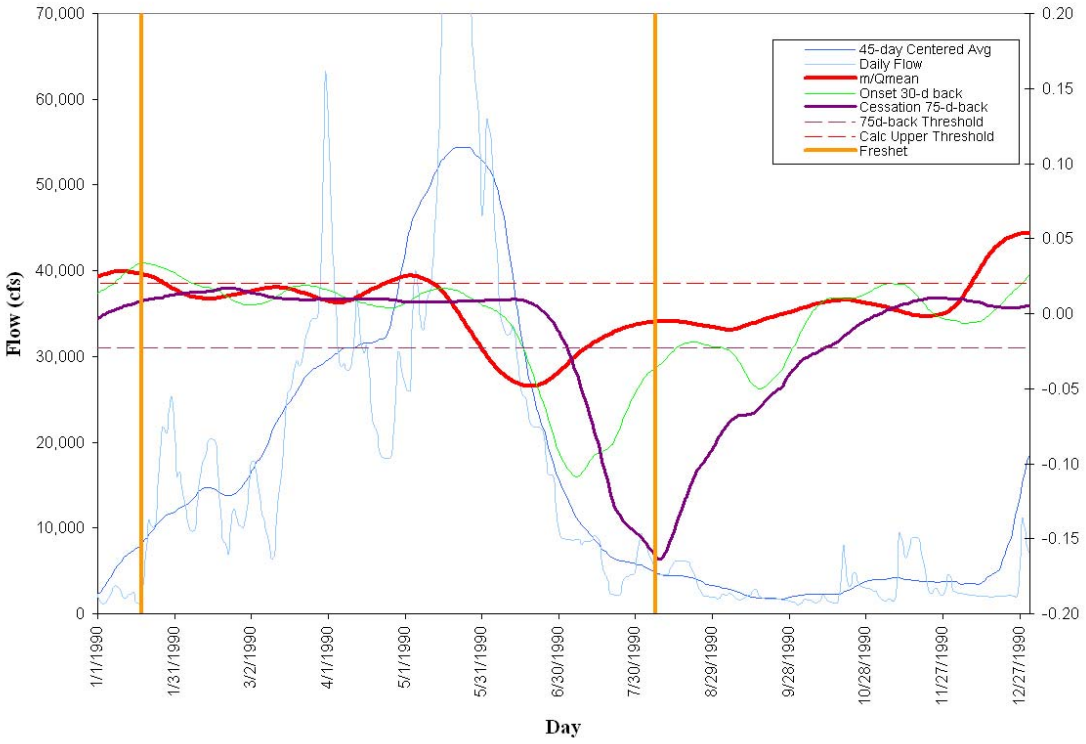

Figure 3. FRESHET Application to 1990 Trinity Watershed Flows

identified with respect to their relative magnitude in a given year (i.e., a small event in a wet year might not be identified as a freshet, but in a dry year would be considered a freshet event). Rather than subjectively culling these data out, the method applied has been developed to objectively capture this information via the method described and let subsequent analyses inform as to whether such events hold any statistical significance. Singular maximum threshold criteria are developed and applied (plotted as the upper horizontal dotted line on Figure 3). These criteria (also in units of /time) identify the *occurrence* of a freshet, and have been developed through the consideration of the distributions of the positive local maxima of the m/Qmeans. While there are many local maxima of m/Qmean (as displayed in Figure 4, depicting a time series plot of local maxima for the Trinity watershed), the focus is on those with the higher values. The question of course is: "where to draw the line (*vis. a vis.* the threshold)?"

As depicted in Figure 4 by the bold red line, the POR average of the positive local maxima of the m/Qmeans does yield an adequate depiction of the magnitude of variability of these local maxima over the entire POR, its mathematical benefit being that it takes into account both extreme values in its calculation, is a depiction of the average long-term characteristics of the system, and neglects those cases where a maximum occurs when the slope of smoothed flows are increasing coming out of a negative slope at the end of a freshet. Thus the POR average of the local maxima for the m/Qmeans is utilized for the *threshold* of identifying that a freshet has occurred. A maximum of the m/Qmean is then calculated (represented as the bold red line in

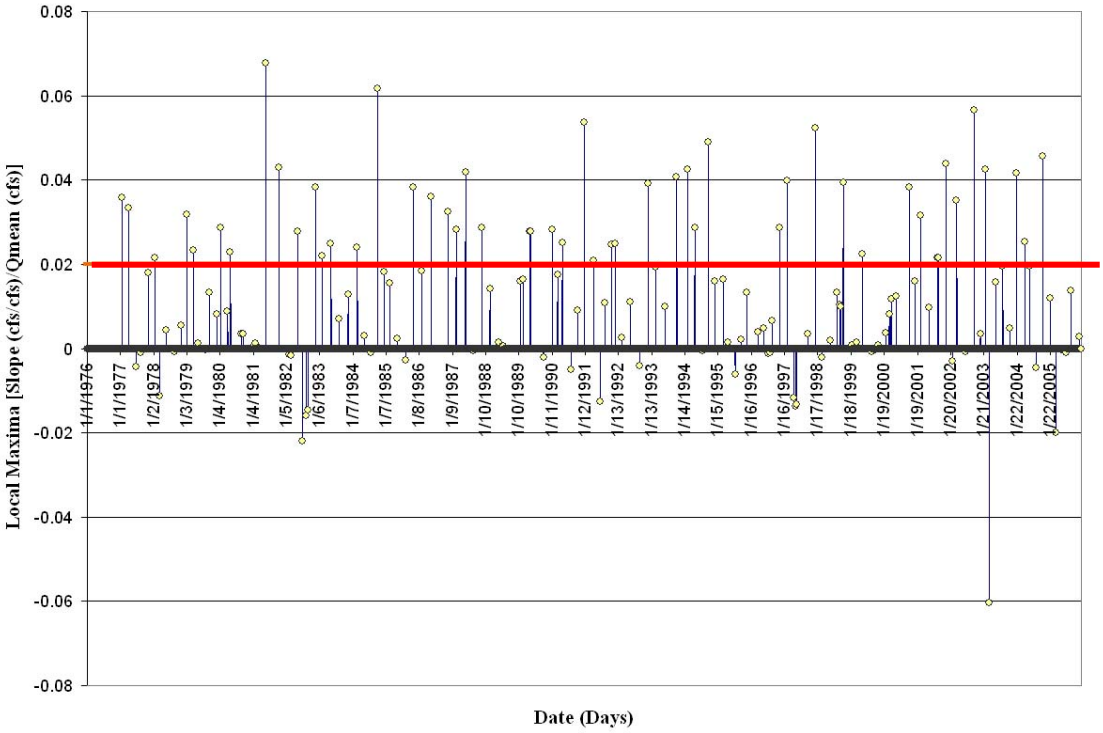

Figure 4. Local Maxima of m/Qmean Time Series for the Trinity Watershed (1977-2005)

Figure 3). When this value achieves a maximum above the threshold, a freshet is identified as *having* occurred.

Upon inspection of the methodology described thus far, due to the fact that a centered average has been utilized, one would note that freshets would typically be identified with onsets slightly earlier than their actual occurrence in the daily flow record. The centered average, by definition, looks 22 days into the future, pulling the average slightly upwards upon the approach of a storm event; hence, the premature identification of the onset when utilizing the centered average. Further calculations are necessary to specifically identify not only the occurrence of a freshet, but the specific timing of the onset and cessation of the freshet event.

To identify the actual timing of the onset of the freshet, a second calculation is performed, this time utilizing a 30-day backwards slope of the 45-day average flows divided by the 45-day average flow, termed the 30-day backwards amount (represented as the thin green line in Figure 3). The date of the first local maximum of the 30-day backwards amount occurring on or after the date a maximum m/Qmean occurs over the threshold identifies the *onset* of the freshet. The utilization of a backwards regression allows for the more precise identification of the onset of the freshet. The first maximum occurring after the identification of the occurrence of a freshet represents the identification of the onset. The onset is calculated as the day number in the year relative to the start of the year.

The identification of the timing of the cessation of a freshet is equally important. Initial evaluations considered a 30-day sliding backwards averages as a viable alternative for utilization in identifying the cessation of a freshet. It is

conceivable that the utilization of the 30-day backwards average as a threshold amount is too sensitive and short a time period, and longer backwards amounts utilizing a POR average of localized minima would be more suitable. The hypothesis herein is that if the bay is truly a slow responder, then the bay should be mathematically allowed more time to note that a freshet has ceased. Indeed, this is reflective of an impulse/response mechanism for salinities found in many bay systems.

While it is acknowledged that this amount might ultimately differ in its final time period, the current estimation is that it would still be greater than 30 days. Table 1 presents comparisons of identified freshets utilizing the POR average m/Qmean threshold for freshet identification and the usage of various 30-, 45-, 75-, and 90-day backwards sliding averages. For the Total Galveston Bay watershed (TGALB), there are approximately 41 freshets over the period from 1977-2005 (although this varies depending upon the backwards average utilized). As depicted by the shaded cells in Table 1, the difference between the usage of a 90-day backwards average and a 75-day backwards average is minor, yielding only 3 freshets whose magnitudes differ by more than 20%. Similarly, there is a minor difference between the usage of the 30-day backwards average and the 45-day backwards average, as again the comparison yields only 3 freshets whose magnitudes differ by more than 20%. The comparison of the 75-day backwards average and the 45-day backwards average shows that 9 out of the 41 freshets (roughly a fifth) have magnitudes that differ by more than 20%.

As there are only slight differences between the 30- and 45-day backwards averages, considering that the objective of this effort was to characterize the seasonal pulses rather than individual events, the 45-day backwards average has been utilized. On the other end of the spectrum, since the 90-day and 75-day backwards averages yield slight differences, the 75-day backwards average has been utilized since the 90-day backwards average occasionally yields extremely long (i.e. multi-year) freshets.

Thus, for subsequent statistical evaluations the 75- and 45-day backwards amounts for the identification of the timing of the cessation of freshets have been utilized as the minimum threshold values (e.g. once the value crosses the threshold, the first minimum beneath the threshold is identified as the cessation of the freshet). Figure 3 above depicts this for the 75-day backwards average. While the m/Qmean for the centered average is similarly utilized in both characterizations, the statistical evaluation of both characterizations of freshets offers a means to evaluate whether organisms are responding to the longer term pulses of flow or more frequent pulses of flow.

RESULTS

Once the onset and cessation of freshet events are identified, calculation of the magnitude and duration of the freshet is easily accomplished. This methodology yields parameters of onset, magnitude, and duration for each identified freshet. These identified seasonal freshets have been found to extend over a duration of just a few weeks to several months, as shown via the time series plot in Figure 5, with the average volume of Galveston Bay depicted in red. As can be seen from this plot, the freshets indeed exhibit an often bimodal pattern, with the intra-annual summer

Table 1. Comparison of Total Galveston Bay Watershed Freshet Magnitudes Utilizing Various Methods of Cessation Identification (1977-2005)

90-Day - 75 Day			45-Day - 30 Day			75-Day - 45 Day		
Difference in			Difference in			Difference in		
Onset [days]	Duration [days]	% Flow [% 75Q]	Onset [days]	Duration [days]	% Flow [% 45Q]	Onset [days]	Duration [days]	% Flow [% 75Q]
0	11	2.4%	0	8	1.1%	0	22	6.5%
0	12	2.7%	0	20	13.4%	0	24	5.6%
0	0	0.0%	0	0	0.0%	0	0	0.0%
0	0	0.0%	0	1	0.1%	0	0	0.0%
0	0	0.0%	0	0	0.0%	0	123	61.7%
0	0	0.0%	0	16	2.4%	0	0	0.0%
0	17	9.8%	0	13	12.5%	0	6	5.5%
0	8	2.3%	0	19	13.3%	0	31	13.0%
0	0	0.0%	0	3	0.4%	0	14	1.1%
0	-1	-0.1%	0	119	69.6%	0	12	0.7%
0	17	5.7%	0	5	4.0%	0	155	71.1%
0	0	n/a	0	21	11.2%	n/a	-60	#DIV/0!
0	17	7.6%	0	1	0.3%	0	7	1.7%
0	1	0.1%	0	4	0.4%	0	10	1.6%
0	98	71.2%	0	0	0.0%	0	6	2.2%
0	18	1.9%	0	1	0.1%	0	1	0.1%
0	106	96.7%	0	-1	-0.3%	0	13	6.0%
0	3	0.3%	0	13	2.1%	0	29	2.5%
0	4	0.3%	0	11	1.8%	0	21	2.2%
0	-16	-1.2%	0	16	16.2%	0	149	55.9%
0	8	1.3%	0	11	4.0%	0	2	0.6%
0	13	0.5%	0	10	0.4%	0	9	0.4%
0	2	0.4%	0	3	0.9%	0	103	38.6%
0	0	n/a	0	9	2.6%	n/a	-60	#DIV/0!
0	14	3.7%	0	1	0.6%	0	248	70.3%
0	5	1.2%	0	6	2.7%	0	29	8.9%
0	1	0.1%	0	25	7.8%	0	1	0.1%
0	0	0.0%	0	18	2.5%	0	19	1.5%
0	9	0.3%	0	188	87.7%	0	6	0.2%
0	0	n/a	-n/a	-54	#DIV/0!	0	0	#DIV/0!
0	21	4.9%	0	13	6.0%	0	4	1.1%
0	1	0.0%	0	83	26.1%	0	11	2.2%
0	1	0.1%	0	16	2.1%	0	11	1.0%
0	15	4.9%	0	7	6.2%	0	22	22.9%
0	2	0.7%	0	5	3.4%	0	18	7.1%
0	-102	-33.7%	0	2	3.1%	0	156	56.8%
n/a	82	n/a	0	11	5.2%	n/a	-57	#DIV/0!
0	0	0.0%	0	6	1.4%	0	166	54.9%
0	0	n/a	0	3	2.5%	n/a	-63	#DIV/0!
0	7	0.9%	0	2	0.6%	0	31	9.3%
0	20	1.8%	0	5	2.0%	0	100	53.4%

*n/a denotes no freshet identified

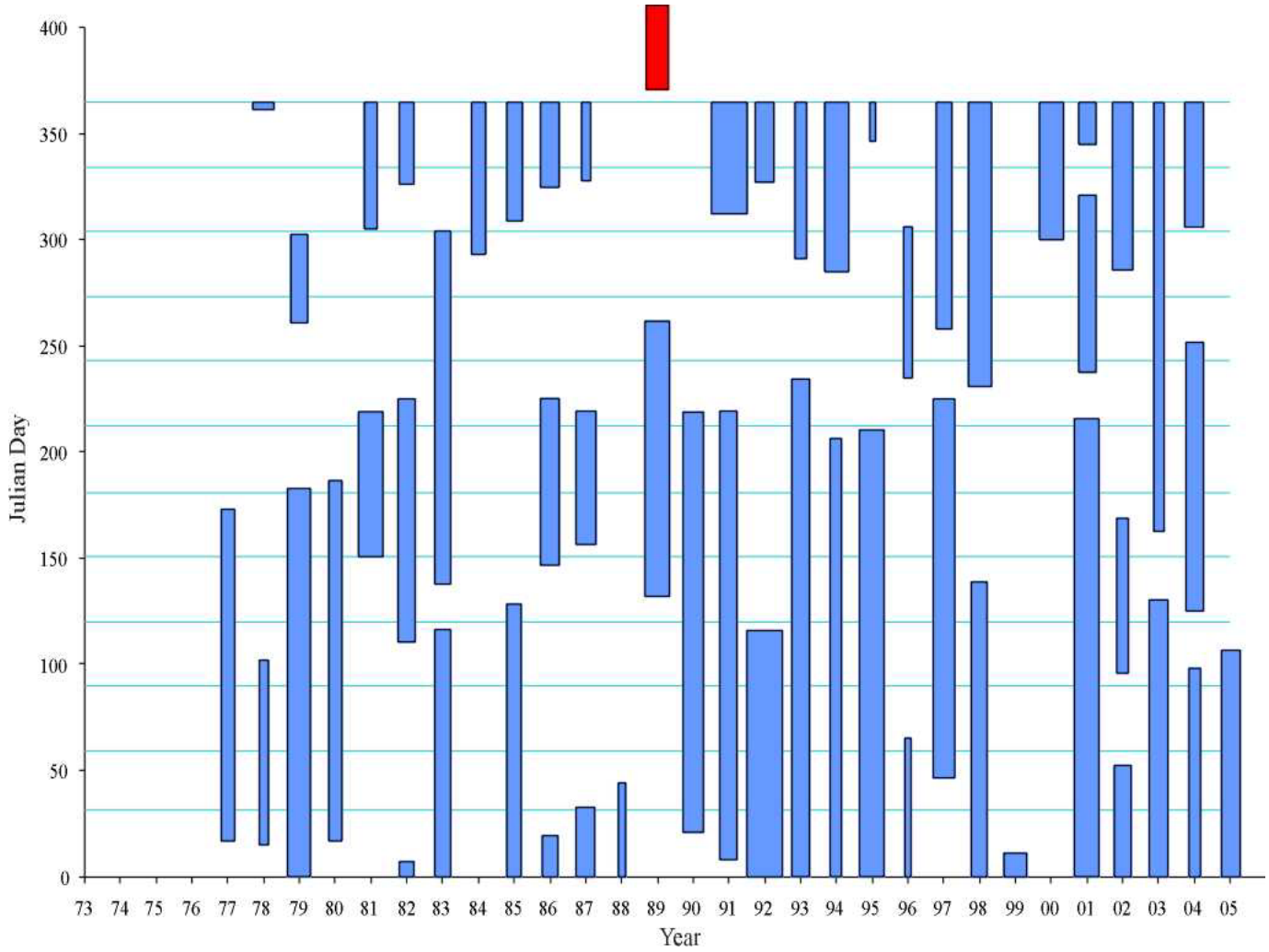

Figure 5. Total Galveston Bay Freshet Time Series utilizing 75-day Backwards Average

drought clearly visible. Also worth noting is that it appears that freshets initiate during the late part of the calendar year, and will span into the next year, suggesting *a priori* decisions to parse hydrologic data into calendar periods might introduce unexplained variance into subsequent analyses.

The results of these hydrologic characterizations have been utilized as representations of inflows for the various watersheds to Galveston Bay in subsequent analyses of relative organism abundance and compared with the more standard representation of annual flow for the same watersheds. As seen in Table 2, of the regressions wherein statistically significant relations were determined, approximately 73% of those regressions utilized hydrologic data wherein the watershed was represented with the parameters of onset, magnitude, and duration of the seasonal freshets. The utilization of this objective methodology for each watershed possibly allows for a level of objectivity to the process that has been previously lacking.

Table 2. Percentage of Regressions wherein Freshet Characterization Yields Greater Explained Variances

Total	Count	%
Freshet	74	73%
Annual	28	27%

REFERENCES

Handbook of Texas Online, "Galveston Bay." http://www.tshaonline.org/handbook/online/articles/GG/rrg1.html>(Jan. 21, 2008).

Longley, W.L., ed. (1994). Freshwater inflows to Texas bays and estuaries: ecological relationships and methods for determination of needs. Texas Water Development Board and Texas Parks and Wildlife Department, Austin, TX. 386 pp.

Matsumoto, J., (1992). *User's Manual for the TWDB's Rainfall-Runoff Model*. Texas Water Development Board, Austin, TX.

Minello, T.J., L. R. Benaka (ed.) (1999). "Nekton densities in shallow estuarine habitats of Texas and Louisiana and the identification of essential fish habitat." *Fish Habitat: Essential Fish Habitat and Rehabilitation,* American Fisheries Society, Symposium 22, Bethesda, Maryland, p. 438–454.

Ward, G. H., (2000). "Texas Water at the Century's turn – perspectives, reflections and a comfort bag." *Water for Texas: 2000 and Beyond*, Texas A&M University, College Station, Sept. 23-25, 2000.

Weinstein, M.P., (1979) Shallow marsh habitats as primary nurseries for fishes and shellfish. Cape Fear River, North Carolina, *Fishery Bulletin,* 77, p. 339-357.

Runoffs of the Xiangride and Qaidum Rivers in the Arid Qaidum Basin, Northwest China

S. Jia[1*], S. Lin[1], Z. Sheng[2,1], R. Li[3], D. Liu[3], H. Yan[4], N. Feng[3]

1. Institute of Geographical Sciences and Natural Resources Research, Chinese Academy of Sciences, Datun Road 11A, Beijing 10010, China. PH 86 10 64856539; email: jiasf@igsnrr.ac.cn.
2. Texas AgriLife Research and Extension Center, Texas A&M University System, USA
3. Water Resources Bureau of Qinghai Province, Xining 810001, China
4. Bureau of Water Resources of Qinghai Province, Xining 810001, China

ABSTRACT

Runoffs collected by the rivers provide water needed to sustain unique ecosystem in an arid basin. Diversion for agricultural application could cause damages to the vulnerable ecosystem. The authors assessed runoffs in the mountainous area, interaction of river water and groundwater, and consumptive uses of water in different geographic units such as desert, manmade oasis, marsh land and terminal lakes in the arid Qaidum Basin in North Qinghai-Tibet Plateau. The Xiangride River collects approximately 510 million m^3 runoffs annually, of which 140 million m^3 is diverted for agricultural irrigation. It then recharges underlying aquifer and provides water for vegetation along the river. The water eventually disappears from the riverbed and reappears as springs, forming the Qaidum River at approximately 20 km downstream. It collects about 90% of seepage water. It is concluded that irrigation diversion has caused groundwater level decline and shift of the spring belt downstream, resulting impacts on ecosystem.

Key words: runoff, interaction of surface water and ground water, oasis irrigation, ecosystem, arid region, Xiangride River, Qaidum River, Qinghai-Tibet Plateau, Qaidum Basin

INTRODUCTION

Human activities (mostly water extraction and diversion) upstream usually reduce water availability in the lower area of the basin, induce lower water table in the lower area, and reduce the vegetation cover, making the arid lands more receptive to wind erosion in arid close basins. In the same time, human activities are modifying the water budget of the terminal lakes, resulting in a local climate change which desiccates the lakes partially or completely into playas (Gill and Cahill, 1992). In those disturbed arid close basins, when terminal lakes undergo anthropogenic desiccation and form playas, the resulting geological process may constitute particulate air pollution, which in turn have major environmental,

economic and health impacts on the human system(Gill, 1996). Probably the most notorious example of the creation of a dust storm resulting from the draining of a saline lake is the Aral Sea in Central Asia. In Aral Sea basin, large scale irrigation along the tributaries Amu Darya and Syr Darya has reduced this inland water body, once the fourth largest in the world, by half it's area and three quarters of it's water volume. The desiccation of Aral Sea results in the collapse of fishing industry and many serious human health problems. And disappearing delta areas cause the extinction of habitats and endemic species (Glantz, 1998).

To understand the situation of disturbed inland river basins and to assess the environmental impacts induced by human activities, researchers have conducted studies on water balance of the inland river basins (Lei et al., 2001; Gao et al., 2004). In this paper, the authors present a case study of Xiangride and Qaidum Rivers located in the southeastern of Qaidum Basin in Northwest China. Water availability, water uses, and impacts of oasis irrigation upon ecosystems within the Xiangride-Qaidum river basin were analyzed using sporadic data.

STUDYING AREA: AN SPARSELY GAUGED ARID BASIN WITH SPECIAL ECOLOGICAL VALUES

The inland Xiangride and Qaidum Rivers are located within the arid Qaidum Basin in North Qinghai-Tibet Plateau, China (Fig.1). Qaidum Basin is an arid basin on the north Tibetan Plateau, located in between 35°00′-39°20′N latitude, 90°16′-99°16′E longitude. With 800 km in length from west to east and 300 km in width from south to north, Qaidum Basin extends from northwest to southeast. The basin is bounded on the south by the towering Kunlun Mountains which have many peaks in the western part exceeding 6,000 meters above sea level, and on the northwest and northeast by Altun and Qilian mountain systems. The elevation in the lowest central area of the basin is 2,675 meters. Qaidum Basin is the highest and the third largest close basin in China. Unlike many other arid zones in the world, the basin exhibits the geomorphologic features of high altitude and low air pressure. The total area of the interior drainage is 0.275 million sq km, of which 54.8 percent (150.8 thousand sq km) is covered by mountains and 45.2 percent (124.2 thousand sq km) by plain area. The plain area in the basin is characterized by low rainfall and high evaporation. The average annual precipitation is approximately 200 mm over the basin, but less than 50 mm in most of the area. The plain area contributes almost no runoff to the river system in the basin. Qaidum Basin is fully dependent on precipitation in mountain range. There are two tributaries for Xiangride River. The eastern tributary flows through a natural regulating lake named Tuosuo Lake, which has a water surface area of 253 km^2, and a catchment area of 3,175 km^2. The western tributary flows through a lake named Ala Lake, which has a water surface area of 73 km^2. The Xiangride and Qaidum Rivers flow through mountain range, piedmont diluvial-alluvial plain, alluvial-lacustrine plain, finally reaches two saline lakes named North Huoluxun

Lake and South Huoluxun Lake respectively.

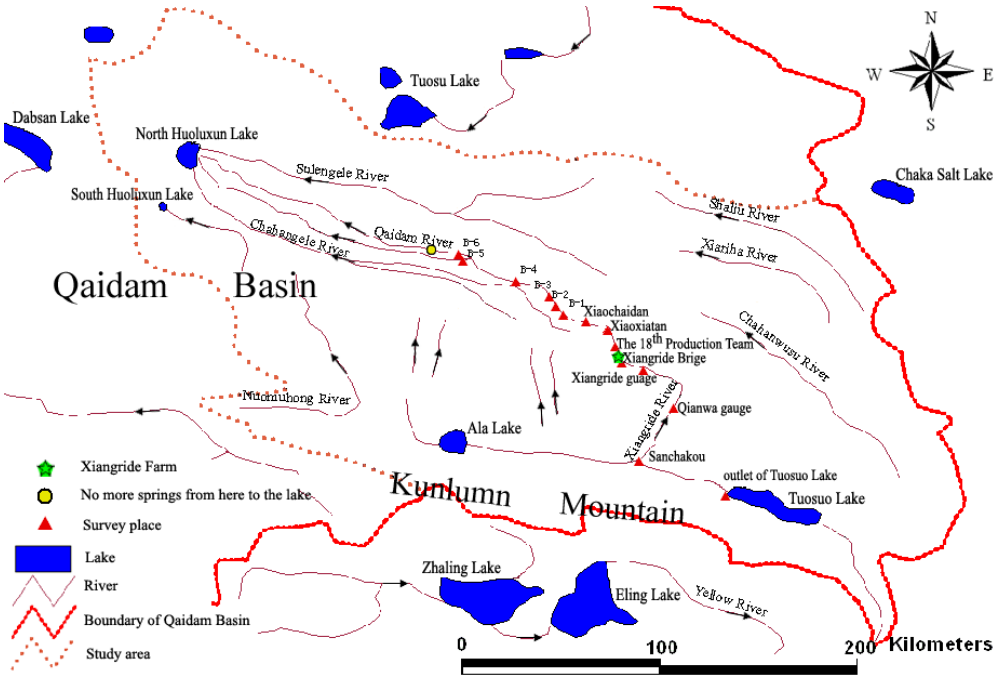

Figure 1 Water system of Xiangride-Qaidum river drainage basin.

The Xiangride River supplies water for agricultural irrigation in Xiangride oasis and ecosystem in the basin, while Qaidum River sustains water supplies for the unique high altitude wetland and desert ecosystem down to the terminal lakes. Between piedmont and spring belt, there is a desert zone. Within and below spring belt, there are marshes, meadow, rivers, lakes, salina and salt shell. These wetland and grass land are the pasturing land, and habitats of many field animals including endangering black neck crane. Xiangride farm is located in the alluvial-diluvial fan outside the mouth of the mountain valleys. Xiangride farm, well-known for its high spring wheat yield record of 15,159kg/ha, is one of the important agricultural irrigational oases in Qaidum Basin. Xiangride Oasis is the major water user in Xiangride-Qaidum Basin as it diverts 140 million cubic meters per year, 30 percent of the Xiangride River flow of 463 million cubic meters. Therefore it is very important to understand runoff formation and its impacts on agricultural irrigation and ecosystem.

METHODOLOGY

Data and Field Survey

All the existing hydrological data for the study area as well as peripheral areas surveyed and kept by different organizations were compiled. Based on assessment of historic data, major data gaps were identified. An integrated catchment investigations involving landform, soil, vegetation, surface water and ground water were carried from the mountain head area to the terminal lake in the bottom within 2003-2006. Additional precipitation, river flows, ground water table,

irrigation water division and drainage data were collected at selected sites. A total of 16 precipitation gauge station and 7 ground water table observation stations, river flow measurements at 10 spring river sections (see Fig.1), monthly flow data for 10 canal sections and 3 drainage sections over 2 years were added as part of this study.

Data Analysis

Time series statistical analysis methods were used to interpolate and extrapolate fragmentary hydrological data. Due to similarity some parameters such as runoff depth were used across the basin. Water balance method was used to assess the seepage of river bed and total water resources quantity from the mountain area.

There were three hydrological gauge stations along the Xiangride River. The two of them, Qianwa gauge and the Xiangride gauge, have over 40 years of recorded hydrological data, which are used to assess the average annual runoff at the two sections. The Tuosuo Lake gauge station only has 7 years of flow data. The recorded data are not enough to calculate the average annual runoff directly. To obtain this average annual runoff, it's assumed that annual runoff in the upper gauge is proportional to that of downstream gauges, and the following equation is used for estimation:

$$AAR1 = AAR2 \times STAAR1 / STAAR2 \quad (1)$$

Where AAR1 is the average annual runoff at section 1, AAR2 is the average annual runoff at section 2, STAAR1 is the short-term average annual runoff at section 1, and STAAR2 is the synchronous short-term average annual runoff at section 2.

RESULTS AND DISCUSSION

Formation of Source Water in Mountain Range

In Xiangride-Qaidum River basin, the water is originated in the mountain range as the river and its tributaries collect runoffs as well as spring discharges. The surface runoff flowing out of the mountain area is almost the sole water source for the middle and lower reaches.

Using the equation 1, the average annual runoff at Tuosuo station and Qianwa station as AAR1 and AAR2, the average annual runoff for the period from 1963 to 1969 at Tuosuo station and Qianwa station as STAAR1 and STAAR2, and obtained the average annual runoff at Tuosuo station. The average annual runoff and the runoff depth of the sub-drainage zone in the mountain area are shown in

the following Table 1.

Table 1 Average annual runoff of sub-drainage units in mountain area

Sub-drainage unit	Drainage area (km^2)	Average annual runoff (10^4 m^3)	Average annual runoff depth (mm)
Headstream-Tuosuo	3175	13130	41.4
Tuosuo-Qianwa	6703	29550	44.1
Qianwa-Xiangride	2461	2617 (8540*)	10.6 (34.7*)
Total	12339	45297 51220* 51030**	36.7 41.5* 41.4**

*Assessment after adjusting the river bed seepage between Qianwa and Xiangride.
** Assessment after further considering the water storage change in Tuosuo Lake.

The average annual runoff depth of Qianwa-Xiangride drainage unit is only 10.6 mm, obviously less than those of the other two drainage units. After comparing with other neighboring drainage basins with similar landform and vegetation, it was concluded that seepage losses account for such low run-ff depth for the reach between Qianwa and Xiangride stations.

After the analysis of the spatial relationships and comparison of the landform and vegetation coverage among the 4 drainage areas, it was estimated that the most possible value of average annual runoff is between 34.7 mm and 44.1 mm for the Qianwa-Xiangride drainage unit. In order to avoid overestimating the water resources amount, the runoff depth of the Qianwa-Xiangride drainage unit was revalued to 34.7 mm, the average annul runoff was adjusted to 85.4 million cubic meters, a total seepage of Qianwa-Xiangride reach of 59.23 million cubic meters was calculated based on water balance.

Another fact about the runoff from mountain area should be noted. After the construction of Xiangride Farm, for guaranteeing water for irrigation while draught, a adjusting gate was constructed in the outlet of Tuosuo Lake and the outlet bottom was cut down for discharging water easier. Now the water level of Tuosuo Lake is about 3 meters lower than that in 1960's. The lake area is 253 km^2. The water storage in the lake decreased about 759 million m^3 over 40 years or 19 million m^3 annually. This means the annual runoff for gauges at Qianwa and Xiangride should be reduced 19 million m^3.

Seepage along Xiangride River in Plain Area

The Xiangride River flows into a piedmont diluvial-alluvial plain after it runs out of the Xiangride hydrological gauge station. The plain area is extremely arid and there is almost no surface runoff discharge into the river. The river water will infiltrate through the river beds, recharging underlying aquifer, and eventually

disappear from the river due to seepage along the river bed made up of cobblestone and sand.

Based on the data collected, the average annual accumulated seepage rate along the Xiangride River was calculated, and shown in Table 2. The accumulated seepage rate varies along the river bed.

$$y = 0.0006x^3 + 0.0774x^2 + 0.0265x \quad (R^2 = 0.9949) \qquad (2)$$

Where y is the accumulated seepage rate, and x is the length of the reach from Xiangride Hydrological Gauge. The equation shows that the accumulated seepage rate increases nonlinearly with the increase in the length of the river reach. The historic records show that the river can't reach the Qaidum River even with a runoff up to 30 cubic meters per second. However it is still not clear how much water is needed to maintain continuous flow from the Xiangride River to the Qaidum River due to lack of data.

Table 2 Seepage along the Xiangride River

Site	Length of the reach form Xiangride Hydrological Gauge(km)	Average annual accumulated seepage rate (%)
Xiangride Hydrological Gauge	0	0
5km below Xiangride Hydrological Gauge	5	5.00
10km below Xiangride Hydrological Gauge	10	9.75
water diverting inlet	12	11.56
Xiangride Bridge	14	14.21
The 8th Production Team Village	20	41.15
Xiaoxiatan Village	32	100.00

Irrigation Division and Consumptive Uses in Xiangride Oasis

On average, Xiangride oasis diverted 140 million m^3 of water annually from the Xiangride River. About 60 million m^3 is consumed by crop evapotranspiration. About 5 million m^3 returned to the Xiangride River at Xiaoxiatan village. About 75 million m^3 recharged the underlying aquifer as deep percolation from the farm field.

Spring Flow Gathering and Consumptive Uses in the Qaidum River

Usually the Qaidum River appears around Xiaochaidan village where

groundwater discharges as springs. The river flow increases continuously as it collects water from springs. The relationship between runoff and the length of the river is shown in Figure 2. In the first 5 km of the river, the river flow increases very slowly because of a small drainage area. From the 5th km to the 25th km, the river flow increases linearly with the river length and reaches a maximum flow of 6 m^3/s. After the 25th km of the river, there is no prominent tributary which drainages into Qaidum River. And below the 34th km of the river, bifurcated channels emergence, and the river flow decreases. The groundwater still feeds the river here, so the river water does not decrease rapidly. Below the 86th km of the river, there is no more groundwater discharge (judged by vegetations and no existence of springs), and the vegetation disappears. Because of the rapid evaporation, the flow decreases rapidly, and the area is covered by playas here.

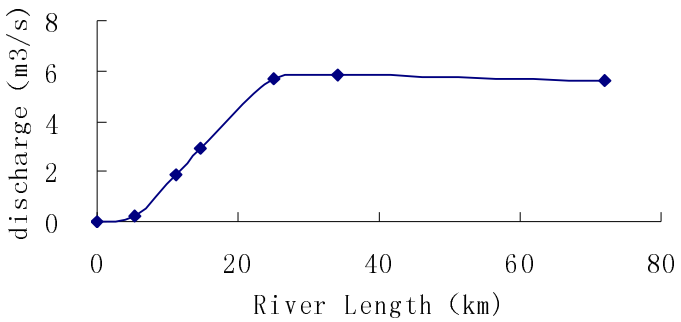

Figure 2 Changes in flow along the Qaidum River

Evaporation from the Terminal Lakes

Parallel to the Qaidum River, there are two other rivers which drainage into North Huoluxun Lake, which named Chahangele River and Sulengele River respectively. In the terminal area of these three rivers, their multiple channels interconnect each other. The average discharge from the Qaidum River is about 5.6 m^3/s, and the summation of discharges from the Chahangele River and Sulengele River is about 6 m^3/s. The average annual water supply of the terminal area is about 0.366 billion cubic meters. The current water surface of the terminal lake, North Huoluxun Lake, is 76.55 km^2. According to data of the evaporation gauge in Qarhan Lake (fresh water, 2,150 mm/year), the annual evaporation of North Huoluxun Lake is less than 2,150 mm, because fresh water is easier to evaporate than saline water. And the annual accumulated evaporation of North Huoluxun Lake is less than 164.58 million cubic meters.

Temporal Variation of Flow of Qaidum River

The historical data shows that the biggest flood in Xiangride-Qaidum River basin was in July 1959 (Fig. 3). The biggest discharge of Zongjia station is 147 m^3/s, while at Xiangride station it is 560 m^3/s. The Qaidum River is fed only by groundwater usually, but it's obvious that there was surface water drainage into

the river in July 1959. From 1956 to 1962, except July 1959 when flood occurred, the discharge of Qaidum River was very stable; the discharge didn't increase even during wet periods.

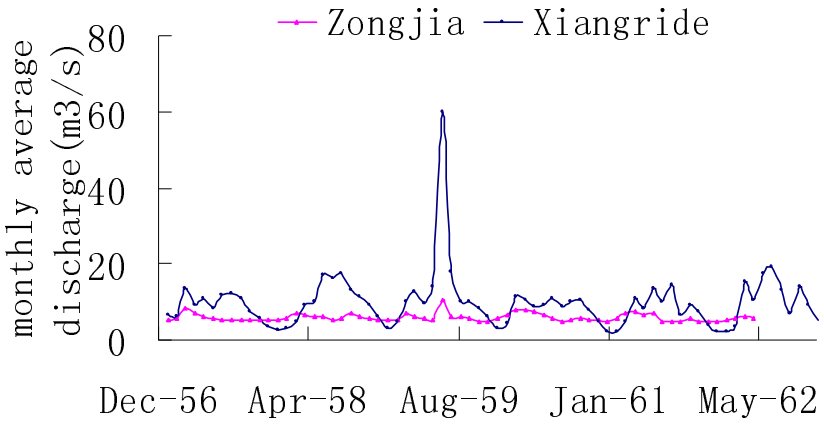

Fig 3 Flow chart of Zongjia and Xiangride gauge station

The comparison of the current discharge with the historical average annual discharge shows no obvious difference in the river discharges as shown in Table 3. There is no evidence to suggest that Qaidum River has changed since the Xiangride Oasis farm was established inn 1958. It seems that decades of water diversion from Xiangride River has not yet change the Qaidum River flow evidently. However the heading of the river (the spring belt) has moved downstream for about 1 km. The land surface gradient there is about 1/1000. If we assume the gradient of ground water table is similar to that of landform, it can be concluded that the ground water table has declined about 1m for last 40 years. As runoffs from the mountain range didn't decrease but increased a little, therefore the possible cause for groundwater level is the irrigation water division and consumptive uses of Xiangride oasis.

Table 3 Comparison of the Historical and Current Runoff in Zongjia Station Section (m^3/s)

Section	Location		Runoff	Note
Zongjia station	Between Section B-5 and Section B-6	1957.1-1962.5	5.905	Average annual runoff
		1965.9-1969.12	5.299	Average annual runoff
Section B-5	97°10′10.1″E 36°25′49.5″N	2005.8.27	5.426	Daily runoff
Section B-6	97°08′47.7″E 36°26′14.3″N	2005.8.27	5.840	Daily runoff

CONCLUSIONS AND DISCUSSIONS

In sum, the Xiangride-Qiadum river basin is a complex system in an arid region. In Xiangride-Qaidum River basin, the source water is originated from the runoffs in the mountain range. The average annual runoff of Tuosuo Lake drainage area is 131.3 million cubic meters. With consideration of the river seepage of 59.23 million cubic meters, the Tuosu-Qianwa drainage unit and Qianwa-Xiangride drainage unit provides 295.5 and 85.4 million cubic meters, respectively.

The average annual accumulated seepage rate along the Xiangride River increases nonlinearly with the length of the river reach. Additional study is recommended to gain a better understanding of surface water and groundwater interaction.

The average annual water discharge into the terminal area is about 0.366 billion cubic meters. And the annual accumulated evaporation of North Huoluxun Lake is less than 164.58 million cubic meters. The exact estimation of evaporation of the entire Xiangride-Qaidum River basin needs further study.

Though the discharge of the Qaidum River does not show significant impacts of irrigation on the river flow, its heading water (spring belt) has moved downstream for about 1 km due to irrigation diversion and consumptive uses of water in the irrigation oasis. Further studies are recommended to assess the impact of the water diversion on the Qaidum River basin including water quality, ground water level and vegetations.

ACKNOWLEDGMENTS

This study is in part supported by the National Natural Science Foundation of China (Grant 90302009), the Institute of Geographical Sciences and Natural Resources Research, Chinese Academy of Sciences and Texas AgriLife Research, Texas A&M University System. The authors are in debt to all the organizations that shared their data. Thanks also go to Mr. Mao Jun, Mr. Fan Guanghui, Ms. Li Tianping, Mr. Dong Xiaobing, Mr. Liu Jiansheng for their help in field surveys.

REFERENCES

Aladin and Plotnikov, 1993. N.V. Aladin and I.S. Plotnikov, Large saline lakes of former USSR: a summary review. In: S.H. Hulbert, Editor, Saline Lakes V. Hydrobiologia 267 (1993), pp. 1–12.

Bortnik, V.N., 1996. Changes in water level and hydrological balance of the Aral Sea. In: Micklin, P.P., Williams, W.D. (Eds.), The Aral Sea Basin. NATO ASI Series, Partnership Sub-Series, 2. Environment, vol. 12. Springer-Verlag, Berlin, pp. 25– 32.

F. Benduhn and P. Renard. A dynamic model of the aral sea water and salt balance. Journal of Marine Systems, 47(1-4) :35–50, 2004.

Gao Qianzhao, Wu Yanqing. 2004. Analysis of water cycle in inland river. Advances in Water Science,15(3):391-396.

Gill, T. E., Eolian sediments generated by anthropogenic disturbances of playas: Human impacts on the geomorphic system and geomorphic impacts on the human system, Geomorphology, 17, 207–228, 1996.

Gill, T.E. and Cahill, T.A., 1992. Drying saline lake beds: a regionally significant PM_{10} source. In: J.C. Chow and D.M. Ono (Editors), PM_{10} Standards and Nontraditional Particulate Source Controls. Air Waste Manage. Assoc. Trans., 22: 440-454.

Glantz, M. H., 1998. Creeping environmental problems in the Aral Sea basin. In: Kobori, I. and Glantz, M. H. (Editors), Central Eurasian water crisis: Caspian, Aral and dead seas, New York, USA, United Nations University Press.

Lei Zhidong, Zhen Baolong, Shang Songhao, et.2003. Formation and utilization of water resources of Tarim River. Science in China (series E), 33(5):473~481.

Liu Yanhua. 2000. Water Resources Rational Utilization and Eco-environmental Protection of Qaidum Basin. Beijing: Science Press.

Small, E.E., Sloan, L.C., Hostetler, S., Giorgi, F., 1999. Simulating the water balance of the Aral Sea with a coupled regional climate-lake model. Journal of Geophysical Research 104 (D6), 6583– 6602.

DESIGN AND IMPLEMENTATION OF OPTIMIZED HYDROLOGIC UNIT WATERSHEDS FOR RAINFALL-RUNOFF MODELING

Ivan Rivas[1], MS, M. ASCE.
Larry A. Roesner[2], PhD, P.E., Fellow, ASCE.

ABSTRACT

The construction of rainfall-runoff models represents one of the most complex and challenging problems in water resources engineering. This is particularly true for urban watersheds in which, the entire watershed is discretized in smaller sub-basins and additional systems need to be modeled such as the drainage network.

This work was aimed at developing a methodology for the development of a rainfall-runoff model that characterizes a complete drainage area using SWMM5. ArcHydro was used to sub-divide the entire basin in sub-watersheds; then, a kinematic wave cascading plane approach was used to convert irregular sub-watersheds to regular shapes. The so-called Hydrologic Unit Watershed (HUW) represents a synthetic sub-watershed, in which their hydrologic parameters are chosen by constrained optimization.

Rather than using individual storms for calibration, the goal was to minimize the difference between the flow duration curves of the model output and observed discharges.

KEYWORDS

Geographic Information Systems (GIS), EPA Storm Water Management Model (SWMM), Rainfall-Runoff modeling, Watershed, Calibration.

[1] Graduate student, Department of Civil and Environmental Engineering
Colorado State University, Fort Collins, CO 80523-1372

[2] Professor, Department of Civil and Environmental Engineering
Colorado State University, Fort Collins, CO 80523-1372

1. INTRODUCTION

The simulation of rainfall-runoff relationships has been a prime focus of hydrological research for several decades and has resulted in an abundance of models having been proposed (Kokkonen, 2001). Accurate and reliable modeling of stormwater runoff and associated phenomena has been in the past and continues today to be a challenge (Urbonas, 2007). Rainfall-runoff models have been under a continuous state of evolution (Hundecha, 2004).

Urbonas (2007) pointed out that for distributed rainfall-runoff models such as SWMM, research and studies are needed to develop guidance in how discretisize a study catchment properly, at least from the end user's perspective. Urbonas (2007) specifies that an issue not solved yet, is how to reduce an irregular shaped catchment with an array of street and development patterns into regular shapes called for in models such as SWMM to get consistent and accurate results.

2. MODEL DESCRIPTION

2.1 Digital Elevation Model (DEM)

DEM was obtained through The USGS National Map Seamless Server (2008a). The website provides The National Elevation Dataset (NED) with a 1/9 Arc Second resolution (approximately 3 meters). One Arc Second is the $1/3600^{th}$ of a degree (1 second) of latitude or longitude. The length of arc subtended is approximately 30 meters.

ArcHydro (2003) was used to discretisize the watershed. Sixty-five (65) sub-watersheds were obtained with an average size of 43 acres. Also, overland slope was computed through the DEM, using the command Slope from Spatial Analysis. For modeling purposes, overland slope was calculated for the whole watershed and then separated to each of its sub-catchments.

2.2 Hydraulic routing

Unlike undeveloped watersheds, urban watersheds present an additional component to be modeled, the drainage network. However, even if there is an existing GIS shapefile with all links and their corresponding geometric features, modeling the complete network may not feasible in large watersheds. Since this task would represent a big engineering effort to model every single storm drainage structure (i.e., gutter flow towards a drop inlet). Therefore, realistic simplifications should be made.

Some attempts have been made to obtain a comparable drainage network. Brink (2004) suggested creating a routing channel with the objective of accounting for in-system storage and attenuation that would occur within a given sub-watershed area (A). Brink (2004) developed empirical relationships for channel length (L_o) and channel width (W_o) of this routing channel as a function of the sub-catchment area. Brink (2004) found good results when: $L_o=\sqrt{A}$ and $W_o=0.50\sqrt{A}$.

Espey et al. (1977) developed a set of generalized equations for the construction of unit hydrographs using a study of 41 watersheds ranging in size from 0.014 to 15 mi^2, and impervious percentage from 2 to 100 percent, nine of the watersheds were located in North Carolina. For this study, using a 24-h SCS Type II storm with an average recurrence interval of 1-Yr, precipitation depth was estimated to be 2.87 in (NOAA, 2008), rainfall excess was estimated and peak discharges were computed using the methodology by Espey (1997) for eight experimental sub-watersheds ranging from 5 to 140 acres.

Then, these sub-watersheds were tested in SWMM5 and the length of the main channel was optimized to match the peak runoff. The best agreement of peak flows were found when the collector channel length was equal to $L_o=A^{0.59}$. The latter result is quite similar with the relationship provided by Brink (2004).

2.3 Characteristic Width Estimation

Huber et al. (1988) suggested combining many sub-catchments into a single lumped or equivalent and calibrate the sub-catchment width. Reducing the width increases the flow length and storage within a subarea, resulting in an effective way to attenuate the runoff hydrograph without modeling in-system storage and pipe networks (Brink et al., 1996), for this reason, the width parameter is often the primary parameter adjusted to obtain desired peak flow rates and hydrograph shapes. Since travel time is larger, this results in more time for infiltration to occur and therefore, infiltration volume might be overestimated. Overall, calibration of the watershed width may lead to unrealistic large runoff lengths.

Another approach is to estimate the runoff length (L), the actual distance that flow typically could be expected to travel before reaching an impervious surface or a natural channel in an urban environment (usually from 100 to 300 feet). Then, compute the Width (W) as W=A/L. Rivas et al. (2007) found the latter procedure successful in large urban watersheds, however, this task requires the estimation of runoff lengths from aerial images.

2.4 Conversion of irregular watersheds to regular watersheds

ArcHydro sub-watersheds present irregular shapes that need to be converted to regular shapes to use in SWMM5. The current state-of-practice recommends the width to be twice the length of the central channel in a symmetric watershed or equal to the length of the side channel along the watershed boundary (Huber et al., 1998).

Guo et al. (2008) developed a methodology to convert an irregular watershed to its equivalent rectangular watershed. A Kinematic Wave (KW) cascading plane is specified by the plane's area, width and slope (Guo et al., 2008); where the continuity and energy principles were interpreted to preserve the watershed area and vertical fall over the receiving waterway's length. After numerous tests Guo (2008) confirmed that the watershed and KW shape factors provide a consistent and stable basis for watershed geometric conversion. In this study, sub-watershed widths were estimated using the KW cascade plane approach.

3. STUDY AREA AND DATA SOURCE

3.1 Watershed Location

The case study is the Pigeon basin located in the metropolitan area of Raleigh, NC. The main properties of this basin are described in Table (1)

Table 1. Watersheds properties (Year 2000)

Watershed Name	Area (mi^2)	TIA[1] (%)	Population density (hab/mi^2)	Housing density ($homes/mi^2$)	UII [2]
Pigeon	4.45	30.62	3,275	239	100.00

[1] *TIA* – Total Impervious Area.
[2] *Urban Infrastructure Index* is a multi-metric parameter that represents the degree of development in the watershed. The UII includes census, socioeconomic, infrastructure, land use and land cover metrics that correlated with population density (McMahon and Cuffney, 2000). However, in this case, UII represents a specific index developed for a set of 30 watersheds in North Carolina, ranging from 0 to 100 (Giddings et al., 2007).

3.2 Channel Routing

Natural streams are an integral part of the drainage system. Preliminary site investigations were performed to identify main conveyance features of the main streams. Field work was done during November 2005 to obtain the cross sections in main channels using level and rod methods as described by Harrelson et al. (1994). Streams cross sections were taken at approximately 2,500-foot intervals along main channels (Pomeroy, 2007). Channel Manning's roughness was estimated during the field work by following the guidelines provided by Chow (1959), Arcement and Schneider (1989). Finally, the geographic coordinates of the cross sections were mapped in GIS with a GPS unit eTrex Legend (Garmin, 2008).

3.3 Hydroclimatology

Precipitation data constitutes the main input to the model, it comes in a spatial distribution of precipitation over time. USGS rain gage (Site No. 0208732885) located at Marsh Creek, New Hope NC, provided 15 min rainfall data (USGS, 2008b). Rain gage was located 10 miles Northeast from the watershed. Evaporation was modeled to account losses, monthly average records were found from 1948 to 1992 (Purvis, 2008). Pan evaporimeter was located at Chapel Hill NC, 25 miles Northwest from the watershed.

3.4 Discharge

USGS streamflow gage No. 0208732610 provided data for calibration. The period of record was from July 4th, 2002 to October 28, 2003 (1.32 years). Flows were registered with a 15 min interval (USGS, 2008c).

3.5 Imperviousness

For modeling purposes, two types of impervious areas have been identified. The first type, effective impervious area, comprises those impervious surfaces that are hydraulically connected to the channel drainage system. Streets with curb and gutter and paved parking lots that drain onto streets are examples of effective impervious surfaces. This area is known as *Directed Connected Impervious Area* (DCIA). The second type, non-effective impervious area, comprises those impervious surfaces that drain to pervious ground such as roof that drains onto a lawn. The sum of both is known as *Total Impervious Area* (TIA). Alley and Veenhuis (1983) developed the following empirical relationship between TIA and DCIA from a highly urbanized portion of Denver, using 14 basins:

$$DCIA = 0.15\ (TIA)^{1.41} \quad \ldots (1)$$

The coefficient of determination (r^2) for the regression equation (1) was 0.98 and the standard error of estimate 7.5%. Since the original parameters proposed correspond to a region in Denver, they were modified to 0.13 and 1.35.

3.6 Infiltration

Initial estimates of a watershed's soil infiltration were obtained through Soil Conservation Society (SCS) maps (USDA, 2008). These maps classify soils into Hydrologic Soil Groups A, B, C, and D. Horton Method was used to model infiltration.

3.7 Groundwater Simulation

Baseflow was removed from the USGS record in a monthly basis. Interflow is the residual groundwater flow that occurs after each storm event; this interflow is not as deep as the baseflow of a watershed and it feeds into stream channels at a slower rate than the flow of runoff produced by the same event. Interflow was modeled through the groundwater component in SWMM5, this allowed to match the USGS monitored records for the frequent, small events. Several soil texture classes were simulated as aquifer material and tested during calibration, the best aquifer material was determined to be Sandy Clay, whose hydraulic properties are shown in Table (2).

Table 2. Soil Textures Used in Aquifer Calibration

Soil Texture Class	Hydraulic Conductivity (in/h)	Porosity (fraction)	Field capacity (fraction)	Wilting Point (fraction)
Sandy Clay	0.02	0.43	0.321	0.221

3.8 Flow Routing

The dynamic wave flow routing method was used in SWMM5. This routing method was selected over the kinematic wave method because it solves the complete one-dimensional Saint Venant flow equations and therefore produces the most theoretically accurate results (SWMM 5.0.013, 2008).

4. MODEL CALIBRATION

Calibration to a single storm is not appropriate for continuous simulation modeling because adjustments of variables to match runoff from one event may over or under adjust variables and inhibit matching of other events (Pomeroy, 2007). Therefore, calibration was done to the 1.32–year record through the flow-duration curves. Table (3) shows the needed input data, where highlighted variables were treated as calibration parameters.

Table 3. Watershed model input data

WATERSHED MODEL INPUT DATA		
Sub-catchment Characteristics	**Channel Conveyance**	**Calibration Data**
Drainage area	Cross sections	Rainfall depth
Width	Bottom slope	Streamflow records
Overland ground slope	Length	
Overland flow slope	Roughness	
Soil Infiltration rates		
DCIA coefficients		
Depresion storage		
Overland flow roughness		
Groundwater parameters		

Parameters chosen by calibration

Model calibration followed the Ordered Physics-Based Parameter Adjustment (OPPA) method after Vieux and Moreda (2003). Finding the best parameters to represent the watershed was done by constrained optimization. That is, setting constraints on the search by establish a range of feasible parameters. The calibrated watershed parameters are listed in Table (4)

Table 4. Calibrated Parameters

IMPERVIOUSNESS		Infiltration				DCIA Parameters		Depression Storage		Manning's Roughness	
GIA	DCIA	fo (in/h)	fc (in/h)	Tw (days)	K (1/h)	K1	K2	Imp	Perv	Imp	Perv
30.62	14.25	4.23	0.70	7.00	3.80	0.13	1.35	0.07	0.25	0.012	0.30

5. RESULTS AND DISCUSION

Even when specific calibration for individual storms was not attempted, the built model showed a good behavior as shown in Figure (1) for different storm sizes.

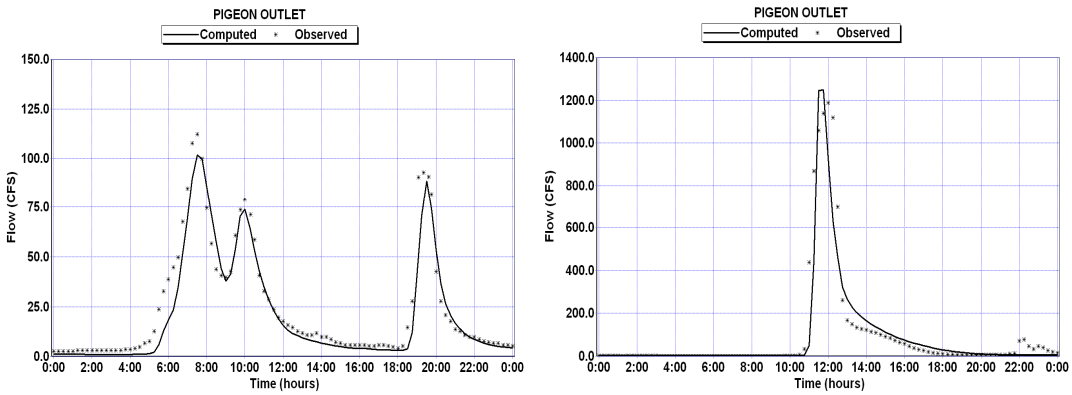

Figure 1. Model output (Storm 1: July 2, 2003 and Storm 2: Aug 08, 2003)

The resulting flow-duration curves are shown in the next Figure (2). The model was able to match the observed flows for the entire flow record.

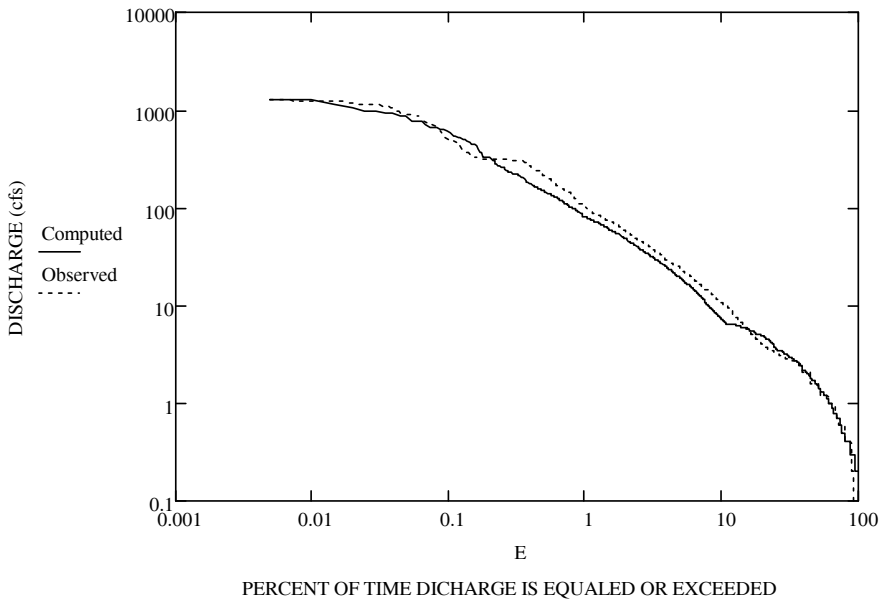

Figure 2. Flow Duration Curves

5.1 Calibration Performance

Measurement of performance allow to assess how reliable are the modeling results and therefore, the predictive power of hydrological models. The agreement between the observed and simulated runoff values may be expressed in terms of a bias or departure. The bias indicates systematic over or under prediction. The departure serves as a measure of the prediction accuracy (Vieux, 2004).

Four indexes were computed:

i) Root Mean Square Error (RMSE)
ii) Product Moment Correlation Coefficient (PMCC)
iii) Nash-Sutcliff Coefficient, NSI (Nash and Sutcliffe, 1970)
iv) Index of Agreement, IOA (Willmott, 1981)

In these indexes, the best condition is when PMC, NSI, IOA yield a value of unity and RMSE to zero. Table (5) shows these indexes for the individual storms and for the obtained flow duration curve. RMSE values depend of the size of the particular storm.

Table 5. Measurement of performance

Event	RMSE (cfs)	PMCC	NSI	IOA
Storm 1	8.44	0.91	0.83	0.95
Storm 2	90.33	0.93	0.87	0.96
Flow duration curve	6.74	0.99	0.97	0.99

6. CONCLUSIONS

The methodology showed to be effective for modeling large urban watersheds. Discretization by limiting the average size to 43 acres was appropriate. The use of DCIA instead of GIA was satisfactory since it represents better the rainfall-runoff process. However, if imperviousness maps are not available, land use covers might be used to estimate imperviousness levels by assigning imperviousness levels to each land use. In this study, field work was performed to identify main cross sections. Nevertheless, cross sections in main channels might be obtained from the DEM.

Routing channel length depends directly of the sub-watershed size, however, the relation found in this paper may not be appropriate to other watersheds, but a similar approach can be used to determine this relationship. The conversion of irregular sub-watersheds to rectangular shapes proposed by Guo (2008) showed to be perform satisfactorily and perhaps this approach may work well for even larger sub-watershed sizes. Groundwater modeling was needed to improve the estimation of low flows. Overall, the proposed hydrologic unit watersheds concept showed an exceptionally good performance.

7. REFERENCES

[1] Alley, W. A., Veenhuis, J. E., (1983). Effective impervious area in urban runoff modeling. Journal of Hydrological Engineering, ASCE, 109(2):313-319.

[2] Arcement, G.J., Schneider, V.R. (1989). Guide for selecting Manning's roughness coefficients for natural channels and floodplains. U.S. Geological Survey.

[3] Arc Hydro Tools (2003). *Tutorial, Version 1.1 Beta 2*. ESRI 380 New York St., Redlands, CA

[4] Brink, P. (2004). Wayne County Rouge Program Office (RPO). Memorandum. March 26, 2004.

[5] Brink, P., Regnemorter, L., TenBroek, M. (1996). Evaluating the City of Detroit's Combined Sewer Overflow Storage/treatment Facilities through Continuous Modeling. Proc. URBAN WET WEATHER POLLUTION: Controlling Sewer Overflows and Stormwater Runoff, Specialty Conf., Quebec City, PQ, Canada, Water Environ. Fed., 2-61.

[6] Chow, V.T. (1959). Open Channel Hydraulics. McGraw-Hill, New York, NY, 680 p.

[7] Espey, W.H., Altman, D.G., Graves, C.B. (1977). Nomographs for Ten-Minute Unit Hydrographs for Small Urban Watersheds. ASCE Urban Water Resources Research Program Technical Memorandum No. 32.7.

[8] Garmin (2008). eTrex Legend ®. http://www8.garmin.com/aboutGarmin/ (Accessed on November 05, 2008).

[9] Giddings, E.M.P., Steuer, J.J. (2007). Hydrologic Variability in Urban Streams of the North Carolina Piedmont.

[10] Guo, James C.Y., Urbonas, B. (2008). Conversion of Natural Watershed to Kinematic Wave Cascading Plane, accepted to ASCE J. of Hydrologic Engineering, (revised in May 2008).

[11] Harrelson, C.C., Rawlins, C.L., Potyondy, J.P. (1994). Stream channel reference sites: an illustrated guide to field technique. General Technical Report RM-245. Fort Collins, CO. US Department of Agriculture, Forest Service, Rocky Mountain Forest and Range Experimental Station. 61 p.

[12] Huber, W. C., Dickinson, R. E. (1988). Storm Water Management Model (SWMM) User's Manual, version 4.0. United States Environmental Protection Agency, Athens, Georgia. 595 pp.

[13] Kokkonen, T., Jakeman, A. (2001). A comparison of metric and conceptual approaches in rainfall-runoff modeling and its implications. Laboratory of Water Resources, Helsinki University of Technology, Helsinki, Finland. Centre for Resource and Environmental Studies, Australian National University, Canberra, ACT, Australia. Water Resources Research, Vol. 37, No. 9, Pages 2345–2352.

[14] McMahon, G., Cuffney, T.F. (2000). Quantifying Urban Intensity in Drainage Basins for Assessing Stream Ecological Conditions. Journal of the American Water Resources Association (JAWRA) 36:1247-1261.

[15] Nash, J.E., Sutcliffe, J.V. (1970). River flow forecasting through conceptual models. Part 1. A discussion of principles. Journal of Hydrology 10, 282–290.

[16] NOAA (2008). Precipitation Frequency Atlas of the United States. Atlas 14, Volume 2, Version 3. Silver Spring MD, 2004. Extracted: Mon Dec 29, 2008.

[17] Pomeroy, Ch.A. (2007). "Evaluating the Impacts of Urbanization and Stormwater Management Practices on Stream Response." PhD Thesis. Department of Civil and Environmental Engineering. Colorado State University. Fort Collins, Colorado.

[18] Purvis, J. (2008). South Carolina Pan Evaporation. South Carolina Department of Natural Resources Water Resources Division. http://www.dnr.sc.gov/climate/sco/Publications/pan_evap_tables.php#4 (Accessed on January 18, 2009)

[19] Rivas, I., Roesner, L. (2007). Spatial Discretization of Large Urban Watersheds ror Rainfall-Runoff Modeling. World Environmental and Water Resources Congress, Tampa, Florida. May 15-19, 2007.

[20] Storm Water Management Model, SWMM. (2008). *Version 5.0.013*. http://www.epa.gov/ednnrmrl/models/swmm/index.htm (Accessed on October 29, 2008).

[21] Urbonas, B. (2007). Stormwater Runoff Modeling; Is it as Accurate as We Think?. Engineering Conferences International Conference on Urban Runoff Modeling: Intelligent Modeling to Improve Stormwater Management, Humboldt State University. Arcata, CA.

[22] USDA (2008). Geospatial Data Gateway, Soil Survey Spatial and Tabular Data. SSURGO 2.2. http://datagateway.nrcs.usda.gov. (Accessed on December 03, 2008).

[23] USGS (2008a). National Map Seamless Server. http://seamless.usgs.gov/index.php (Accessed on October 1, 2008).

[24] USGS (2008b). National Water Information System. Site No. 0208732885 http://waterdata.usgs.gov/nc/nwis/nwisman (Accessed on October 12, 2008).

[25] USGS (2008c). National Water Information System. Site No. 0208732610 http://waterdata.usgs.gov/nwis/nwismap (Accessed on October 18, 2008).

[26] Vieux, B.E., Moreda, F.G. (2003). Ordered Physics-Based Parameter Adjustment of a Distributed Model. Chapter 20 in Calibration of Watersheds Models, Edited by Q. Duan, S. Sorooshian, H.V. Gupta, A.N. Rousseau, R. Turcotte, Water Science and Application Series, 6, American Geophysical Union, ISBN 0-87590-355-X pp. 267-281.

[27] Willmott, C.J. (1981). On the validation of models. Physical Geography 2, 184–194.

Effects of rainfall-runoff on soil surface roughness and erosion processes

D.C. Dermisis[1] and A.N. (Thanos) Papanicolaou[2]

[1]Graduate Research Assistant, IIHR-Hydroscience and Engineering, Dept. of Civil and Environmental Engineering, The University of Iowa, Iowa City, IA 52242; PH (319) 335-5638; email: dimitrios-dermisis@uiowa.edu
[2]Associate Professor, Robert and Virginia Wheeler Faculty Fellow in Engineering, IIHR-Hydroscience and Engineering, Dept. of Civil and Environmental Engineering, The University of Iowa, Iowa City, IA 52242; PH (319) 335-6448; Fax (319) 335-5238; email: apapanic@engineering.uiowa.edu

ABSTRACT

Soil erosion of hills affects the productivity of agriculture lands and threatens our earth environment. There are several factors that trigger and sustain soil erosion. Some of the key mechanisms are believed to be: (i) climate; (ii) soil type; (iii) soil surface roughness; (iv) cropping; and (v) land management practices. This study examines the role of the rainfall-runoff on soil surface roughness and the transport/deposition of the eroded soil. Surface roughness is related to management practices and has been one of the factors that have not received considerable attention. One hindrance of previous studies was the lack of a system and robust methodology for performing adequate acquisition of the soil surface micro-topography. The required resolution in order to adequately describe the soil surface micro-topography is on the scale of a millimeter. Most of the traditional measurement techniques (e.g., roller chain, erosion pins), though, can not provide such a high spatial resolution. Thus, a state-of-the-art laser scanner technique was utilized, providing a resolution of 0.5 mm. Laser scanners use triangulation to measure surface elevation. A laser beam is projected vertically onto the surface and a line camera detects the light spot reflected from the surface. Because of the fixed camera-laser geometry, the surface height is estimated using a simple calibration procedure. The surface heights for the entire soil surface were then imported into the ArcGIS 9.2 software in order to obtain the Digital Elevation Model (DEM), while the built-in Arc Hydro tools were used next to attain the drainage networks, flow direction, flow accumulation, stream definition, and stream segmentation.

INTRODUCTION

Soil erosion on hillslopes is a complex phenomenon that involves two main processes, namely the interrill and rill erosion. Interrill erosion evolves particle detachment due to raindrop impact (splash erosion) and transport by shallow water flow (sheetwash). Rill erosion is defined as the erosion triggered by concentrated flow (surface runoff) within small channels, called rills. Interrills usually supply sediment to rills, whereas rills function as both sediment source areas and sediment conveyors in hillslopes.

Different factors affect soil erosion, such as: (i) climate; (ii) soil type; (iii) soil surface roughness; (iv) cropping; and (v) land management practices. Numerous studies have examined the effects of the aforementioned factors on interrill/rill formation. For example, Bryan (2000) observed a limited flow network development on a sealing soil influenced by subsurface moisture and seepage, while a high-intensity network was developed in a cohesive soil. Berger *et al.* (2008) showed that there is a positive non-linear relationship between soil erosion, rill development, applied rainfall intensity, and slope angle.

One of the parameters that received particular attention is the effect of soil surface roughness in runoff and erosion on hillslopes. There are opposing views concerning the effects of surface roughness and its relationship to hillslope erosion. Some researchers believe that increase roughness leads to an increase in the erosion (e.g., Helming *et al.*, 1998), whereas others think that increase roughness decreases erosion (e.g., Cogo *et al.*, 1984). Römkens *et al.* (2001) showed that the effect of roughness was most significant for high intensity storms and that smooth surfaces yielded a significant larger amount of total soil loss than the rough surface condition. Similar observations were made by Darboux and Huang (2005). Gomez and Nearing (2005) illustrated that soil surface roughness has a significant effect on runoff and sediment yield for moderate slopes, whereas it has little or no effect for steep gradients. Lastly, Helming *et al.* (1998) provided evidence that rough surfaces showed a greater soil loss than smooth surfaces, because flow concentration caused localized increase in erosion.

One hindrance of previous studies on examining soil erosion processes was the lack of technology and a robust methodology for performing adequate acquisition of the soil surface micro-topography. Stroosnijder (2005) provided a critical overview of current measurement techniques for determining the magnitude of erosion at different spatial and temporal scales. Along the same lines, Jester and Klik (2005) provided a summary of different measurement devices -such as roller chain, erosion pins, and laser scanners - which are used for determining the surface roughness. The latest studies have focused exclusively on laser scanners which can provide higher data acquisition rate than other traditional techniques (e.g., Zapp *et al.*, 2001; Darboux and Huang, 2003; Oelze *et al.*, 2003; Schmid *et al.*, 2007).

OBJECTIVES

The overarching objective of this study was to provide a preliminary assessment of the effects of rainfall/runoff in soil surface roughness and how

roughness may, in-turn, affect soil erosion. The sub-objectives of this study included the following:
1) To obtain the topography of the soil surface with a high data-acquisition rate, under different rainfall intensities, using state-of-the-art technology.
2) To use the ArcGIS 9.2 ArcHydro built-in toolset to obtain the drainage networks, flow direction, flow accumulation, stream definition, and stream segmentation.
3) To compare the sediment yield determined under different experimental scenarios (i.e., different rainfall intensity, soil stratification) and provide a quantitative assessment of the effects of surface topology on soil erosion.

METHODOLOGY

To meet the goals of this study, soil erosion laboratory experiments were carried out under simulated rainfall in the IIHR-Hydroscience and Engineering facilities located at the University of Iowa, U.S.A. The two soils used herein were TAMA surface (very dark brown silty clay loam) and TAMA subsurface soil (very dark grayish brown silty clay loam) collected from Iowa County, Iowa. TAMA is a common soil type for the state of Iowa and is considered one of the most productive soils in Iowa that are used for agricultural purposes.

A wooden box (plot) of ~ 1.0x0.3x0.07 m^3 was used for the soil erosion experiments (Figure 1). Holes were drilled at the bottom of the box to allow free drainage and limit the formation of a perched water table (Darboux *et al.*, 2001).

The rainfall simulator used in this study was mounted ~ 2.0 m above the box. Rainfall was applied by an oscillating VeeJet type nozzle. The rainfall intensity was adjusted by the frequency of the oscillating nozzle. Experiments were conducted for two rainfall intensities (60 mm/hr and 75 mm/hr) and for two arrangements of the soil (TAMA) stratification, resulting to four experimental runs. The two arrangements were the following: (1) use only one layer of surface soil ~ 0.075 m thick; and (2) use two layers of soil, a bottom layer of ~ 0.05 m sub-surface soil and a top layer of ~ 0.025 m surface soil. The soil was air dried before placed uniformly in the box. At the beginning of each experiment the soil surface was flattened and smoothed with the aid of a wooden roller (Figure 1).

Preliminary experiments were conducted under the given rainfall intensities to determine the optimal gradient (~ 14 %) to initiate erosion and cause rill development. Thus, in all four experiments the slope of the box was kept constant and equal to ~ 14 %. A funnel located at the downstream end of the plot (Figure 1) was used to quickly convey water and soil at the outlet of the erosion plot. Four moisture probes were installed in the four corners of the box to record frequently the soil moisture content during each experiment.

The micro-topography of the soil surface was determined by using a state-of-the-art instantaneous surface-profile laser scanner (0.5 mm resolution). The laser scanner used triangulation to measure surface elevation. A laser beam was projected vertically onto the surface (Figure 2) and a camera detected the light reflected from the beam. Because of the fixed camera-laser geometry, the surface height was estimated using a simple calibration procedure.

The following process was adopted to perform the individual experiments. Prior to each experiment an inclinometer validated that the surface was leveled in all directions. Next, the flat soil surface was pre-scanned using the laser system. During each experiment, soil moisture was recorded and a bucket was used to collect water and soil exiting the box. Experiments were terminated when steady state conditions were established (i.e., no visual changes in the soil surface). To verify that the experiments were terminated during steady state conditions, subsequent samples of water and sediment were collected at the plot outlet. After the experiment, data points of the bed elevation (~ 1,200,000 points) were transformed from the camera coordinates (CCD) to real (physical) coordinates through a regression-calibration equation (Darboux and Huang, 2003). The calibrated surface heights were then imported into the ArcGIS 9.2 software to obtain the Digital Elevation Model (DEM). DEM's of soil surfaces are used in soil erosion research for a better understanding of the erosion processes. By using the DEM and the Arc Hydro toolset in ArcGIS 9.2 the DEM-based stream network was generated.

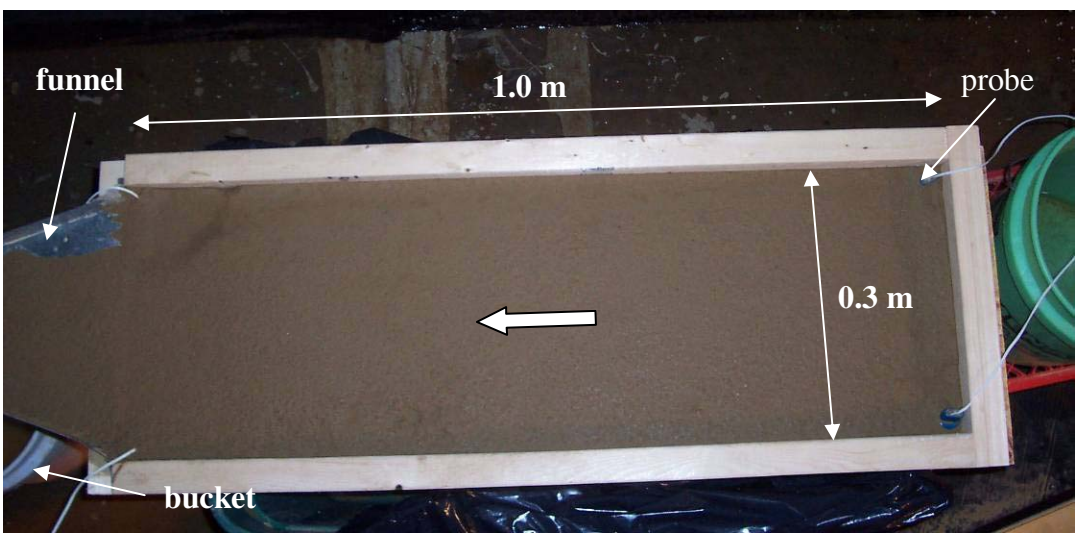

Figure 1. The experimental box used in this study filled with TAMA soil. Arrow illustrates the runoff direction.

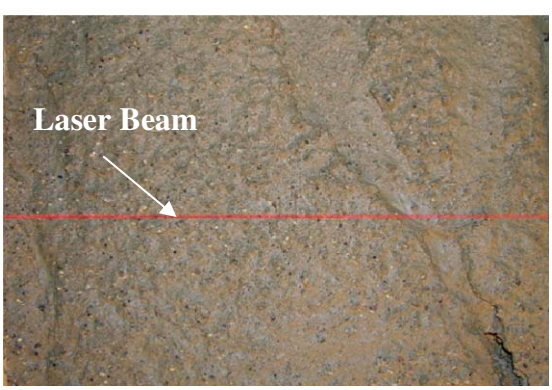

Figure 2. The laser beam over the soil surface.

RESULTS

Table 1 shows the average particle and water flux at the end of the four experimental runs, namely experiments 1-a, 1-b, 2-a, 2-b, when steady state conditions were achieved. The number denotes the soil stratification (1: one layer of soil and 2: two layers of soil, as specified in the ″Methodology″ section) and the letter denotes the applied rainfall intensity (a: 60 mm/hr and b: 75 mm/hr). As expected, higher rainfall intensity produced higher erosion rates.

Figure 3 presents a plan view of the soil surface at the end of experiment 1-b. Dye was used to visualize the eroded soil surface. Three distinct regions (regions I, II, III) were clearly observed. Region I specified the zone of splash detachment and was characterized by the formation of craters (depressions) on the soil surface, due to the impact of the rain drops (splash erosion). Region II illustrated a transition zone where the raindrop impact attenuated and runoff was generated. Additionally, region II was characterized by the initiation of rill formation. Region III depicted the zone where the rills were fully developed (rill erosion). As it can be seen in Figure 3, region I extended approximately 1/3 of the length of the box, while regions II and III together extended approximately 2/3. Similar observations were made for the other experiments.

Figures 4a-d present plan views of the soil surfaces for the four experimental runs at the end of the tests. The average duration of the tests was ~ 1 hr. It is clear that for higher rainfall intensity, more pronounced channel networks/rills were formed. Also, Figure 4b shows that the rills acquired a slightly sinuous shape with irregular width

Figure 5 displays results from the step-by-step data analysis using the ArcGIS software. Surface heights obtained by the laser were transformed from raster to point file (Figure 5a) and then interpolated using the inverse distance weighted technique (Figure 5b). Finally, the catchments and flow networks were defined using ArcHydro tools (Figure 5c).

Figure 6 provides the flow network for the four experiments and verifies the visual observations of the soil surfaces in Figure 4. In all four experiments 2-3 rills were formed (darker lines in Figure 6); distinguished rills, though, were primarily formed in experiments 1-a and 1-b. Formation of rills enhanced erosion and more eroded material was recorded in run 1-b (Table 1). Finally, the flow networks in Figure 6 failed to provide information on the rainfall induced craters formed in region I.

Table 1. The experimental conditions of each run

Experiment	Soil Stratification	Rainfall intensity (mm/hr)	Particle flux (gr/sec)	Water flux (lit/sec)
1-a	One layer	60	0.56	0.0063
1-b	One layer	75	1.23	0.0067
2-a	Two layers	60	0.19	0.0058
2-b	Two layers	75	0.61	0.0080



Figure 3. Characteristic regions formed during the experiments Arrow illustrates the runoff direction.

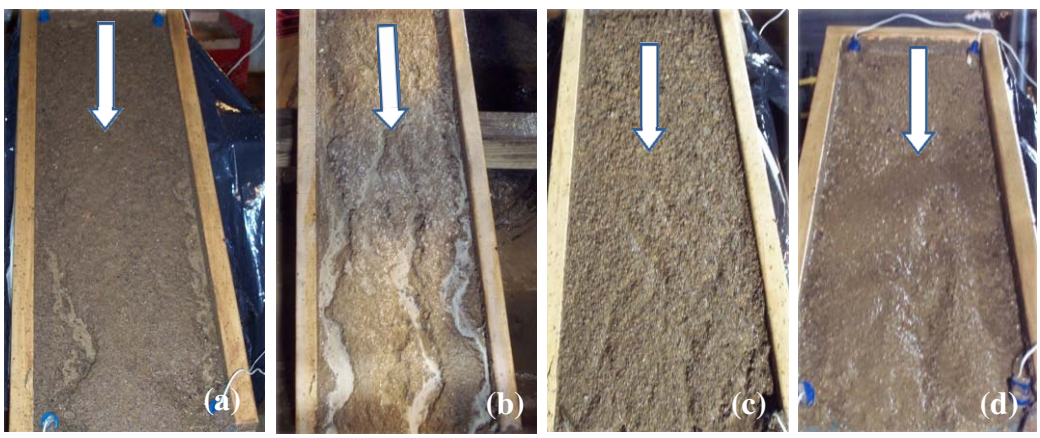

Figure 4. Soil surface at the end of the experiments. From the left to the right: Experiment 1-a, 1-b, 2-a, 2-b. Arrow illustrates the runoff direction.

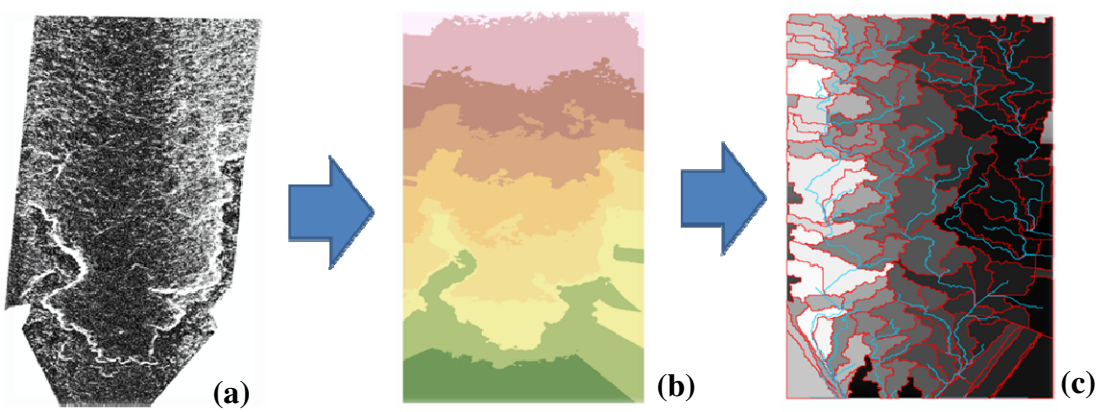

Figure 5. Procedure followed to determine the flow network.

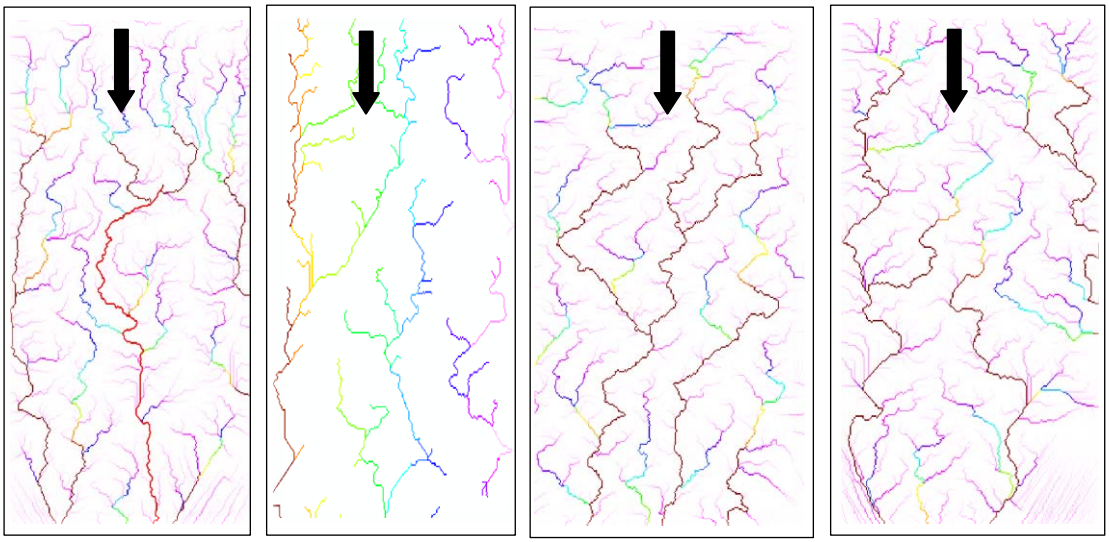

Figure 6. Flow network corresponding to the soil surfaces presented in Figure 4 (from left to right: Experiment 1-a, 1-b, 2-a, 2-b). Arrow illustrates the runoff direction.

CONCLUSIONS

The following can be concluded from this study:

(a) Rainfall and runoff affected flow network. The rainfall impact dominated at the upstream locations of the soil box (crater formation), while downstream the effect of runoff was dictated (rill formation).
(b) More complex flow networks were formed in the case of low rainfall intensity. The soil surfaces under high rainfall intensities were characterized by distinguished rills. In addition, pronounced rills were found to form only when one layer of soil was used (surface soil).
(c) Significant erosion was recorded when distinguished rills were formed. It is believed that rills delivered the material faster to the plot outlet (Bryan *et al.*, 1998).

For future studies the following should be considered:

(a) Time evolution of the bed surface by using the laser scanner multiple times during the experimental run.
(b) Address the temporal changes of the soil surface roughness, which will allow interpreting accurately the temporal variability of water and sediment fluxes.
(c) Determination of the depression storage via the calculation of different roughness indices, i.e., random roughness, tortuosity (Kamphorst *et al.*, 2000), or by using a PCRaster that finds depressions and fills them until they overflow (Van Deursen, 1995).

REFERENCES

Aqid, N., Slak, B., Hasnaoui, D., Touzani, A., Ouazar, D., Macelloni, G. (2002). "Application of remote sensing technology for estimating soil roughness for

hydrological modeling and their interaction into GIS." *Remote Sensing for Agriculture, Ecosystems, and Hydrology III, Proceedings of SPIE*, Vol. 4542.

Berger, C., Schulze, M., Riele-Zapp, D., Schlunegger, F. (2008). "Rill network development and soil erosion: a laboratory study of rainfall intensity and slope angle." Geophys Res Abstracts, Vol. 10.

Bryan, R.B. (2000). "Soil erodibility and processes of water erosion on hillslope." *Geomorhology,* 32, 385-415.

Bryan, R.B., Hawke, R.M., Rockwell, D.L. (1998). "The influence of subsurface moisture on rill system evolution." *Earth Surf. Proc. Land.,* 23, 773-789.

Cogo, N.P., Moldenhauer, W.C., Foster, G.R. (1984). "Soil loss reductions from conservation tillage practices." *Soil Sci. Soc. Am. J.*, 48: 368-373.

Darboux, F., and Huang, C. (2003). "An instantaneous-profile laser scanner to measure soil surface microtopography." *Soil Sci. Soc. Am. J.*, 67, 92-99.

Darboux, F., and Huang, C. (2005). "Does soil surface roughness increase or decrease water and particle transfers." *Soil Sci. Soc. Am. J.*, 69: 748-756.

Darboux, F., Davy, Ph., Gascuel-Odoux, C., Huang, C. (2001). "Evolution of soil surface roughness and flowpath connectivity in overland flow experiments." *Catena*, 46, 125-139.

Gomez, J.A., and Nearing, M.A. (2005). "Runoff and sediment losses from rough and smooth soil surfaces in a laboratory experiment." *Catena*, 59, 253-266.

Helming, K., Römkens, M.J.M., Prasad, S.N. (1998). "Surface roughness related processes of runoff and soil loss: A flume study." *Soil Sci. Soc. Am. J.*, 62, 243-250.

Jester, W., and Klik, A. (2005). "Soil surface roughness measurement- methods, applicability and surface representation." *Catena*, 64, 174-192.

Kamphorst, E.C., Jetten, V., Guerif, J., Pitkanen, J., Iversen, B.V., Douglas, J.T., Paz, A. (2000). "Predicting depressional storage from soil surface roughness." *Soil Sci. Soc. Am. J.*, 64, 1749-1758.

Oelze, M.L., Sabatier, J.M., Raspet, R. (2003). "Roughness measurements of soil surfaces by acoustic backscatter." *Soil Sci. Soc. Am. J.*, 67, 241-250.

Römkens, M.J.M, Helming, K., and Prasad, S.N. (2001). "Soil erosion under different rainfall intensities, surface roughness, and soil water regimes." *Catena*, 46, 103-123.

Schmid, T., Schack-Kirchner, H., Hildebrand, E. (2007). "A case study of terrestrial laser scanning in erosion research." *International Archives of the Photogrammetry, Remote Sensing and Spatial Information Sciences*, vol. XXXVI, part 8 / W2, pp. 114-118.

Stroosnijder, L. (2005). "Measurement of erosion: Is it possible?" *Catena*, 64, 162-173.

Van Deursen, W.P.A. (1995). "Geographical information systems and dynamic models: Development and application of a prototype spatial modeling language." PhD. Diss. Fac. Georg. Sci., Utrecht Univ., NGS 190, the Netherlands.

Zapp, D.R., Wegmann, H., Santel, F., Nearing, M. (2001). "Digital photogrammetry for measuring soil surface roughness." *ASPRS Annual Convention*, St. Louis.

Hydrologic Modeling and Flood Frequency Analysis of the Sonora River Watershed In Sonora, Northwest Mexico

Maureen L. Habarth[1] and Brian D. Barkdoll[2], F. ASCE

[1] Engineer, LimnoTech, 501 Avis Drive, Ann Arbor, MI 48108, PH: 734-332-1200, FAX: 734-332-1212, email: mhabarth@limno.com
[2]Associate Professor, Civil and Environmental Engineering Dept., Michigan Tech Univ., Houghton, MI 49931, PH: (906)487-1981, FAX: (906) 487-2943, email: barkdoll@mtu.edu

ABSTRACT

The state of Sonora is located in northwest Mexico and shares its border with the states of Arizona and New Mexico. Approximately 95% of Sonora is described as arid or semiarid. Precipitation across the state averages 437 mm per year; however, the most arid areas average less than 100 mm of rainfall annually. Sonora's climate is recognized as having a bi-seasonal rainfall pattern, characterized by frequent periods of little or no rainfall followed by periods of heavy rainfall, especially in the summer months of July and September. These periods of drought develop land cover and soil conditions that are conducive to heavy flash flooding during the rainy months, followed by quick recession of flood waters and a return to dry conditions and low streamflows. The high degree of climatic variability has presented serious challenges to water resource planning and management in Sonora. Further, recent drought conditions have led to an almost complete reliance on groundwater sources to meet the needs of the growing population.

The goals of this study are to develop an understanding of how different meteorological events impact streamflow in the study area, how changes in land use and development in the Sonora River basin might impact streamflow, and to better characterize streamflow behavior through various statistical approaches on flood flow data dating from 1942 to 2002. More specifically, a hydrologic model of the area of interest was developed and calibrated using the U.S. Army Corps of Engineers' HEC/HMS version 3.1.0 watershed modeling software, and an array of future development scenarios was simulated in order to predict the impacts to streamflow in the basin as a result of these changes. The work of this study also involved the collection and analysis of an extensive set of geographic data of the region, as well as a detailed flood frequency analysis of 58 years of peak annual flow data in order to select an extreme value distribution to model the river's behavior and predict flood quantiles.

INTRODUCTION

This project's focus is in the state of Sonora, Mexico, a region which is experiencing rapid growth and increasing water scarcity, especially in its capital city, Hermosillo. Sonora is bordered by Baja California to the northwest and the states of Sinaloa and Chihuahua to the south and east, respectively.

The Sonora River basin lies entirely within the central portion of the state and encompasses an area of approximately 26,700 km^2. The river originates in the mountainous north of the basin near the Cananea copper mining region. Historically the river's mouth met the Gulf of California at its outlet, but due to groundwater

overconsumption, the Sonora River runs dry even before it meets the city of Hermosillo. Roughly half of Sonora (260,000 km^2) is covered by the Sonoran Desert, which also includes most of the Baja peninsula, southwest Arizona, and a portion of California. The vegetation in the area of study is predominantly scrub-shrub, with areas of agriculture along stretches of the river, and pastures and forests to the north and along the perimeter of the study region. Soil cover is dominated by very coarse, deep soils with gravel at the surface. In the south of the study area there is a significant region of thin soils described as having average texture. Along the course of the river there exist three distinct regions of deep soils having average texture with areas of gravel and stone.

In examining the topographic data of the area it is noted that the greatest elevations occur in the northernmost portion of the watershed. Elevation data are provided in Figure 1. As stated previously, the lowest elevation encountered in the study area is 221 m asl and occurs at the outlet of the study area (the southwestern-most reach of the main branch of the Sonora River) near the city of Hermosillo. The maximum elevation of 2,610 m asl occurs in the northeastern-most reach of the study area.

Annual water availability in Mexico is estimated to be over 410 billion m^3; however, approximately 68% of available water is concentrated in the southeast and Gulf of Mexico regions, and only 2% in the northern states. Furthermore, approximately 53% of the soils best suited for agriculture are located in the arid and semi-arid regions (Magaña and Conde, 2000).

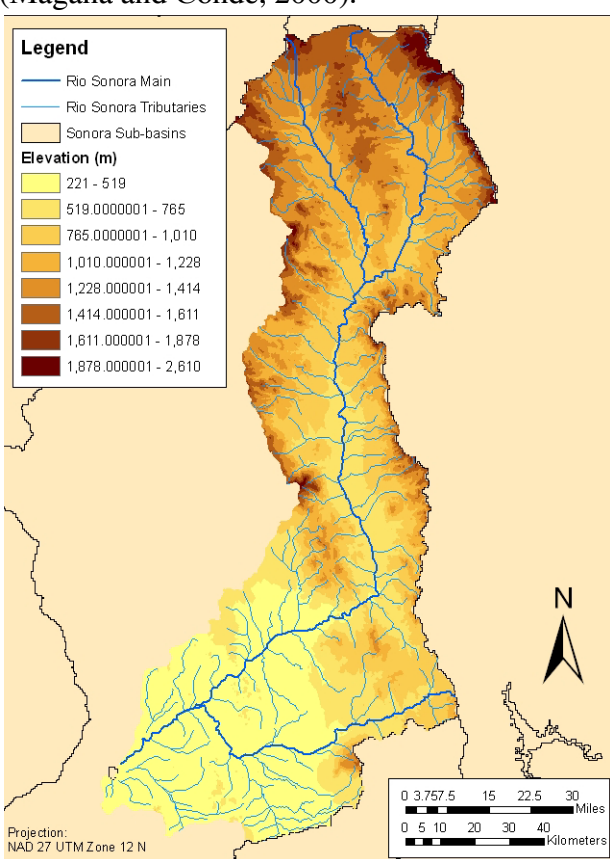

The climate in northwest Sonora is very arid; regular streamflows do not exist here. The main surface water flows in Sonora are in the east and the south and are dammed to provide minimal quantities of water, although they are typically insufficient to meet energy and irrigation demands and must be supplemented with groundwater (Hallack-Alegria, 2005). In the case of Sonora, approximately 95% of the state is characterized as arid or semi-arid, exhibiting year-round high temperatures and low precipitation. The Sierra Madre region of Sonora experiences the greatest rainfall and lowest temperatures. The driest region in the entirety of Mexico, el Desierto de Altar, is located in northwest Sonora (Hallack-Alegria, 2005).

Figure 1: Topographic Map of Sonora Area of Study
Map created by M. Habarth (data from INEGI), 2006

Precipitation in Sonora averages around 437 mm annually, although this is highly variable from year to year. Northwest Sonora, near its border with Baja California, receives an average of only 1 to 100 mm of rainfall each year (Magaña and Conde, 2000). Sonora experiences a bi-seasonal rainfall pattern, with most precipitation occurring during the summer months of July through September. The North American monsoon (NAM) generally determines precipitation in northwestern Mexico, although the large inter-annual variability is influenced by the El Niño/Southern Oscillation (ENSO) (Magaña and Conde, 2000).

The most dominant climate zone in terms of area is Semiseco I ("Semi-dry" I), characterized by warm, rainy summers with a mean annual temperature ranging from 12-18°C. The second most widely-occurring climate zone is Seco II ("Dry" II), characterized as having summer rains, and generally mild temperatures (mean annuals greater than 18°C) throughout the year with cooler winters. In general, the climate shows a pattern of increasing warmth and dryness as one travels from the northeastern-most portion of the study area to the southwestern-most edge near Hermosillo, following the pattern of decreasing elevation.

The study area could be delineated into five distinct sub-watersheds based on geostatistical analyses performed on the digital elevation models. Their names are: Bacanuchi and Arizpe to the north, Banamichi in the center of the study area, and Sonora-Hermosillo and Arroyo La Junta to the south. The mountainous Bacanuchi sub-watershed encompasses an area of approximately 1,600 km^2. Its even more mountainous neighbor, the Arizpe sub-basin, covers an area of roughly 2,300 km^2. To their south lies the largest of the sub-basins, Banamichi, with an area of about 5,500 km^2. In the southeast corner of the study area is Arroyo La Junta with an expanse of 2,000 km^2. Finally Sonora-Hermosillo is reached, geographically the flattest and smallest sub-watershed, covering an area of approximately 1,200 km^2.

Within the study area there exists one dam and reservoir, Rodolfo Félix Valdez, familiarly known as "El Molinito." The dam is located about 23 km upstream of the city of Hermosillo. Located slightly upstream of El Molinito is the streamflow gauging station El Orégano II, currently the only existing flow monitoring station in the area of study. The station is operated by the Mexican National Water Commission, CONAGUA (Comisión Nacional del Agua). The original station, El Orégano I, was located at the dam site and then relocated just upstream during the construction of the dam and its reservoir. Due to the dam's construction and the station's relocation, streamflow was not recorded during the period 1991-1993.

The ultimate goals of this work were to develop an understanding of how different meteorological events impact streamflow in the study area, how changes in land use and development might impact streamflow, and to better characterize streamflow behavior through various statistical approaches on flood flow data dating back to the year 1942. More specifically, the objectives included: (1) the creation of a user-friendly Geodatabase of relevant geographical information pertaining to the study area using Geographic Information Systems (GIS), (2) the development of a specific statistics-based model to adequately represent 58 years of streamflow data and estimate floods at various return intervals, (3) the creation and calibration of a hydrologic model of the study area in HEC-HMS to predict watershed behavior given an array of meteorological events, and

(4) the utilization of this model for the simulation of watershed behavior given specific changes in watershed condition. See Habarth (2008) for additional details.

FLOOD FREQUENCY ANALYSIS

The streamflow data that were utilized for the analyses in this project were obtained from CONAGUA through IMTA (Instituto Mexicano de Tecnología del Agua) via the Instituto de Ingeniería (Institute of Engineering) at UNAM and were available in their 2006 two-part report for CEA (Comisión Estatal del Agua, State Water Commission). Provided were monthly average flows from 1941-2002 (missing 1991-1998) and maximum annual instantaneous flows from 1942-2002 (missing 1991-1993), both at the station El Orégano (UNAM (I), 2006). The data gap between 1991 and 1993 occurred as a result of the construction of the dam El Molinito, during which flow measurements were not taken. Also available in the UNAM report (for CEA, Part I) were annual reported measurements of the maximum flow (m^3/s) that was sustained for 0 (instantaneous), 1, 2, 3, 4, and 5 day durations, for the period 1941-2002 (missing 1991-1993, 1995-1998). The report also published monthly drainage volumes at El Orégano (thousands of cubic meters) for the period of record 1975-2001, with values for missing years estimated by regression. These analyses were also based on the CONAGUA hydrometeorological data.

In their 2006 study, the Institute of Engineering at UNAM (for CEA) provided estimates of flood flows for return periods ranging from two to 10,000 years for durations ranging from instantaneous (maximum) to one to five days sustained.

Probability Plot Correlation Tests, L-Moment Ratio Tests, Kolmogorov-Smirnov bound tests, and other associated hypothesis tests were completed in order to rule out certain flood frequency distributions and to calculate parameters of the various distributions.began. Once the number of feasible distributions was narrowed down, the fitted quantiles for all of these remaining distributions were plotted on the same chart as the empirical cumulative distribution function (CDF) (Figure 2) with the goal of choosing a distribution to best represent the annual maximum instantaneous flow data at El Orégano

It is difficult to select the "best" distribution by only examining the graph. It appears that in the lower tail (discharges less than 250 m^3/s), the Log-normal (using Maximum Likelihood Estimators, MLE) distribution provides the best fit to the empirical data. In the middle of the data, the Gumbel, Pearson Type III (P3), and Generalized Extreme Value (GEV) distributions are closely matched. At discharges between about 650 and 1,000 m^3/s, the data appear to nearly follow a Normal distribution. And the few data points in the upper tail appear to be best represented by the GEV distribution. As one can see based on these observations, assigning a single distribution to reasonably represent a series of true flood data can be challenging. However, it appears that the P3 and Gumbel distributions are the best at following the shape of the empirical CDF, with the P3 distribution perhaps providing a slightly better fit to the data, based on visual observation alone.

Table 1 gives percentiles calculated from the fitted distributions and provides demonstrable proof of the closeness of the fit of the P3 and Gumbel distributions; they are perhaps closer to each other than any of the others, with the single exception of the GEV distribution in the 90th percentile.

Based on the results of the numerous goodness-of-fit tests, hypothesis tests, graphing and diagrams, quantile calculation, and visual examination, the P3 distribution is recommended as the distribution best suited to representing the 58 years of maximum instantaneous streamflow data at El Orégano.

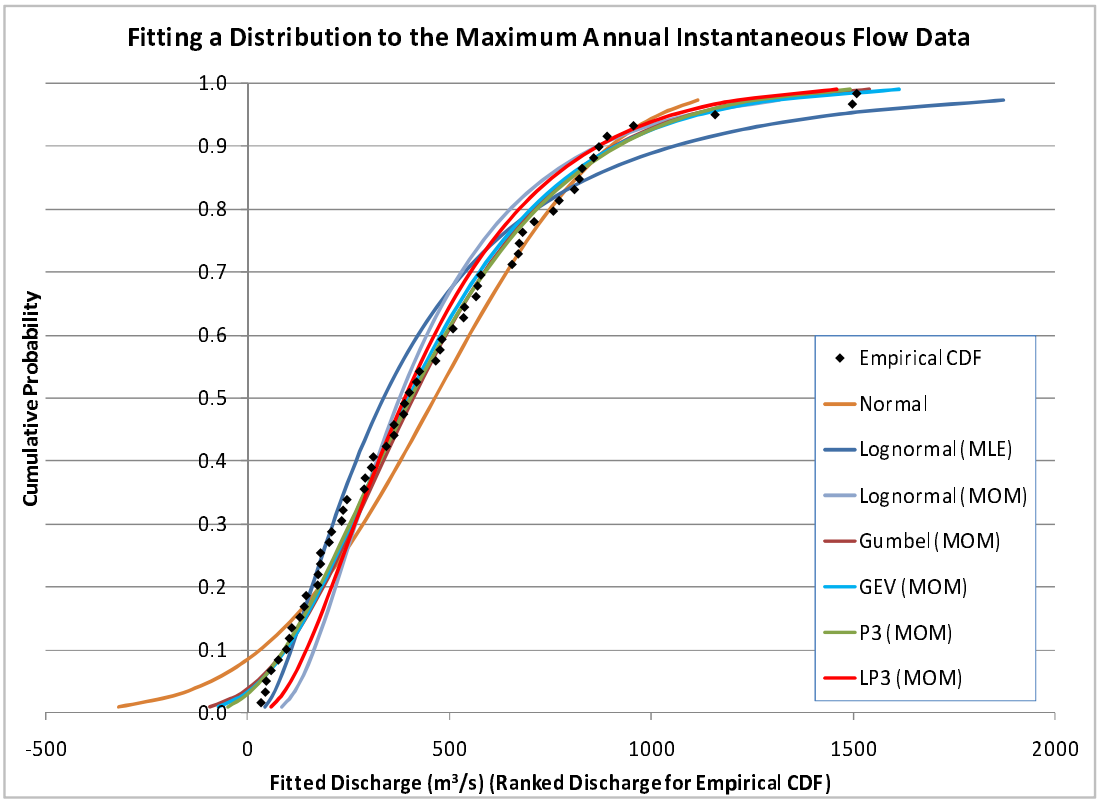

Figure 2. Plot of Fitted Distributions with Empirical CDF (based on CONAGUA data)

Table 1. Percentiles (m^3/s) Calculated (by author) from Fitted Distributions

P3 is in bold, as it was judged most appropriate to represent the data.

Distribution (Method)	10th Percentile	50th Percentile	90th Percentile	99th Percentile
EMPIRICAL	95.0	390.0	870.0	1520.0
Normal	28.8	463.5	898.3	1252.7
Lognormal (MLE)	106.7	335.7	1056.8	2691.2
Lognormal (MOM)	161.6	374.0	865.8	1716.4
Gumbel (MOM)	90.3	407.8	906.1	1527.6
P3 (MOM)	**87.5**	**402.8**	**918.4**	**1509.5**
LP3 (MOM)	143.0	387.0	868.1	1475.6
GEV (L-Moments)	93.6	397.6	911.7	1622.3

HYDROLOGIC MODELING

Figure 3 illustrates the basin model in HEC-HMS 3.1.0 for the Sonora River area of study and an inventory of all of the elements of the model. As the model illustrates, a sub-basin element has been added for each of the five sub-watersheds in the area of

study. A reservoir element indicates the presence of the El Molinito dam. There is an outlet at the watershed boundary near the city of Hermosillo, and two junctions (Arizpe station, Ures station) at the locations where the main branches of the Sonora River meet. It is important to note that the Ures station also indicates the approximate location of the El Orégano streamflow gauge.

For the five sub-basins in the Sonora River area of study, the Muskingum-Cunge Method was implemented as the most appropriate routing method given the available data and knowledge of the system. An optional loss/gain method for consideration of subsurface interactions was not implemented for this study due to the lack of infiltration data, and with the goal of minimizing the number of assumptions made.

Since fairly detailed information was known pertaining to the outlet works of the El Molinito dam and reservoir, the "Specified Release" method was chosen for the reservoir outflow modeling. Since values of the reservoir area at given water elevations were available (2006 UNAM (for CEA) part I report, Chapter 6), the Elevation-Area method was selected to model reservoir storage. Due to limited data, the "Assume None" method was selected for tailwater considerations.

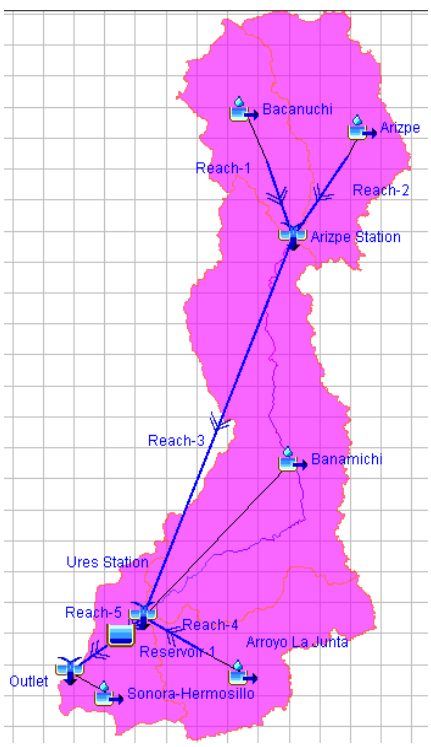

Figure 3. Screenshot of Set-up of Basin Model and Element Inventory in HEC-HMS 3.1.0

The Frequency Storm and Gage Weights methods were both considered for entering precipitation data in the Sonora Meteorologic Model. Although the Frequency Storm method was a feasible option given the available data, the gage weights option was selected to be most appropriate for calibrating the models using actual recorded rainfall data. By default the "Monthly Average" method was selected for this project because these values were available in the 2006 UNAM (for CEA) Part I report (Chapter 8); this included average monthly evaporation values (mm) at the Bacanuchi station (26007) in the north of the basin and at Hermosillo (station 26139) in the south of the basin. These data were measured for the periods 1980-2003 and 1981-2004, respectively, by CLICOM (Mexico Climatological Station Network Data). The standard evaporation pan (Class-A) was developed by the U.S. Weather Bureau, and has an average pan coefficient of 0.7 (American Meteorological Society, 2008).

The model was calibrated by adjusting the runoff curve numbers (CN) to account for dry antecedent soil conditions and resulted in a close agreement between modeled and actual streamflow with notable discrepancies in the latter months of the year. These late-year discrepancies were attributed to initial abstraction being exhausted, resulting in excessive predicted runoff.

HYDROLOGIC MODELING SIMULATION

Urbanization

The first set of scenarios that were investigated for the year 2001 were a 10, 25, 50, and 100% increase in the CN for the Sonora-Hermosillo sub-watershed, where development is occurring and is most likely to occur in the future. The results of the incremental CN increase in the Sonora-Hermosillo sub-watershed alone are shown in Figure 4. Overall, as anticipated, the greatest increase in streamflow was predicted to occur during the months of June through October, or the rainy season, with the greatest overall increase in July and September. When considering urbanization for the year 2001 in only the Sonora-Hermosillo sub-basin, a 10% CN increase resulted in an average streamflow increase of 165%; a 25% CN increase yielded in a 260% average increase, a 50% CN increase resulted in a 417% average streamflow increase, and a 100% increase in CN yielded an average 745% increase.

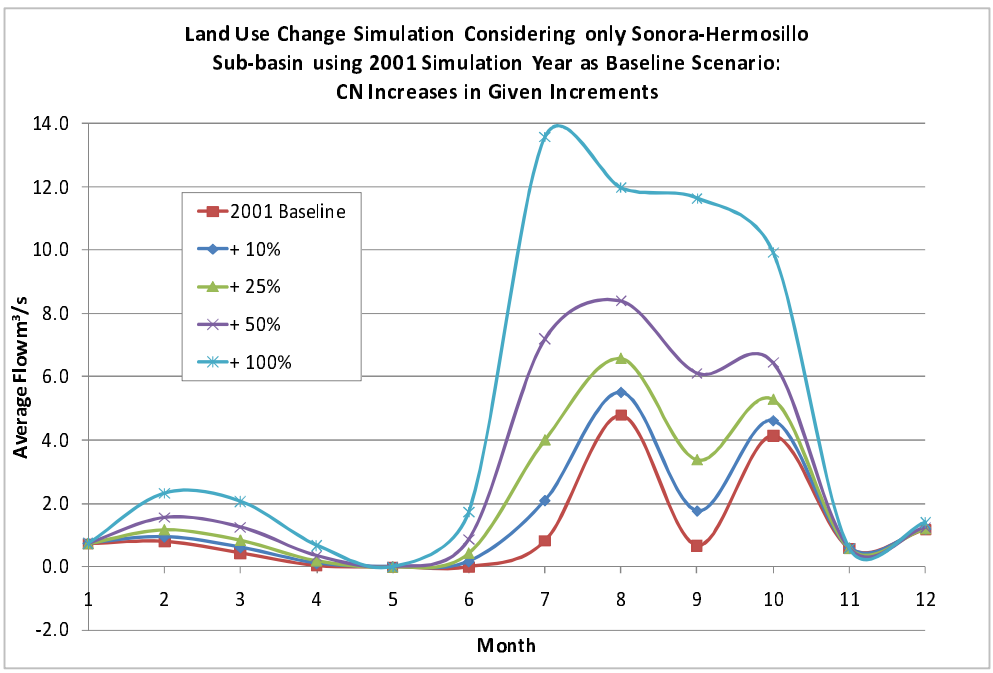

Figure 4. Graphical Results of Land Use Change Simulation, Sonora-Hermosillo
HEC-HMS model output based on year 2001 calibration

The predicted increase in peak streamflows was also examined. The peak streamflow from the 2001 baseline simulation was 15.5 m^3/s. With a 10% CN increase, the peak flow increased to 16.6 m^3/s. At a 25% CN increase, the peak flow was 18.4 m^3/s. At 50%, it was 22.8 m^3/s, and at a 100% increase in the Sonora-Hermosillo CN, the peak flow was 41.6 m^3/s, or approximately 2.7 times the baseline value.

Based on these results, it is likely that even a minimal increase in CN (or impervious surfaces) as a result of urbanization or other land use changes can result in a very significant increase in streamflow. It is important to note that the curve number

increases were applied only to represent hypothetical development scenarios; the exact correlation between population increase, urbanization, and land use change is unknown, therefore these factors should be studied in greater detail before any specific assumptions are to be made regarding increasing streamflows in the basin. Potentially, increased runoff to surface water sources could diminish the availability of groundwater due to reduced infiltration and aquifer recharge. Increased surface runoff could also cause or exacerbate flooding in vulnerable areas.

Stream Channel Modification

The first scenario that was examined for channel modification in 2001 was lining the entirety of Reaches 5 and 6 (upstream and downstream of El Molinito) in concrete, thereby changing Manning's *n* from the original value of 0.04 (for a winding natural channel rated as "fair") to a value of 0.013 for a concrete channel, with a uniform trapezoidal shape having a bottom width of 3 meters and a side slope of 1:1 (H:V). This channel shape and Manning's *n* were then uniformly applied across the entire watershed. Although not a likely scenario anytime in the near future, it is of interest to examine, hypothetically, what may be the possible impacts of heavy human modification of natural channels.

It was expected that a decrease in Manning's *n* and a uniform trapezoidal cross-section would produce, at minimal, a fluctuation in the distribution of streamflow, i.e. an earlier onset of peak flows (decreased travel time through the river reaches) due to a hydraulically smoother, more uniform channel. However, altering these parameters in HEC-HMS 3.1.0 did not produce a significant change. When the channel upstream and downstream (Reaches 5 and 6) of El Molinito (Reservoir-1) was modified, no change in streamflow quantity or shape was observed. When all six reaches in the study area were modified, the result was a nearly negligible 0.1 m^3/s increase in the average monthly flow in January and a 0.2 m^3/s increase in the monthly average flows in July and October.

These results suggest that channel modification in any or all areas of the study area may not result in a significant change in the magnitude of streamflow. However, this will depend on the magnitude of the modification; concrete lined channels with trapezoidal cross-sections were assumed, having a bottom width of 3 meters and a 1:1 side slope. Different materials and cross-sections may produce a different impact.

Additionally, HEC-HMS 3.1.0 does not report flow depth in the model results. It is likely that the depth of flow will be altered due to the change in channel morphology. Altering the flow depth could have significant impacts on flooding and erosion. Furthermore, it is very likely that such channel modification would disrupt the surface-groundwater interaction in the river basin, eliminating the infiltration of water within the streambed. The capability of HEC-HMS 3.1.0 to accurately model and account for hydraulic parameters in a watershed was not examined in detail in this study. It is highly recommended that no stream channel modifications be made without extensive hydraulic modeling in order to predict what the true impacts to streamflow in the study area might be. The effects on streamflow and the magnitude of these effects will be completely dependent on the characteristics of the channel modification.

Dam Removal

To set up the El Molinito dam removal scenario, a duplicate copy of the 2001 simulation year model was produced and the Reservoir-1 element removed. Because the dam El Molinito was located downstream of the flow gauging station (El Orégano, represented by the Ures Station), it was not expected that its removal would have any upstream impacts at the flow station, which was true. However, when the dam was in operation, no streamflow was generated downstream of the structure in any of the simulations. The most important result of the dam removal simulation was that flow occurred downstream of the original dam site after the structure was removed. The streamflow pattern observed at the Outlet is shown in Figure 8.

As El Orégano is currently the only existing flow monitoring station in the area of study (i.e. one that would have monitored flow at or near the outlet prior to the construction of El Molinito), there is no definitive way to confirm these results. However, the shape of this average monthly hydrograph seems to make physical sense. One would expect to see a relatively rapid increase in flow at the onset of the rainy season, then a larger pulse as the streamflow from the upstream elements reaches the outlet following the progression of the wet months.

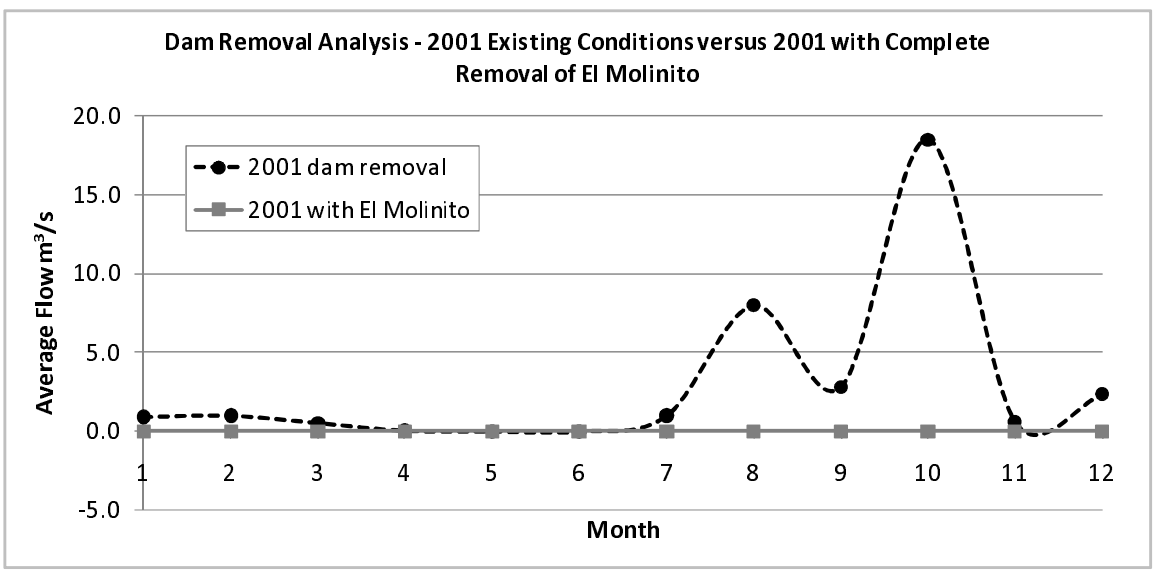

Figure 8. Graphical Results of El Molinito Removal
HEC-HMS model output based on year 2001 calibration

It may be worth considering that the value and function of El Molinito be re-examined; it may better serve the water needs of residents, farmers, businesses and municipalities downstream to remove the dam and restore natural flow to this length of the Sonora River. However, before any drastic measures are taken, the flood protection and water storage/supply benefits of the reservoir should be assessed. The original purpose of the dam's construction was to provide flood protection and water supply to the city of Hermosillo. If the dam is removed, these critical benefits could be permanently lost. If El Molinito is necessary in order to help protect the city of Hermosillo, perhaps the dam's operating procedures should be adjusted accordingly or pumps be installed upstream to assist in delivering flow to downstream users. It is highly recommended that

these many influential factors be examined before any actions involving dam removal or operating procedure modification are executed.

ACKNOWLEDGEMENTS

Agustin Robles Morua is acknowledged for allowing me to play an important role in his extensive work in the Sonora, Mexico region, for his willingness to quickly answer all of my questions and concerns, for his admirable dedication to the project, and for providing me with access to all of the data and resources without which this project could never have been a success. I wish you all the best as you continue your work in Sonora and earn your PhD.

REFERENCES

Habarth, M.L. (2008) *Hydrologic Modeling and Flood Frequency Analysis of the Sonora River Watershed in Sonora, Northwest Mexico,* M.S. Thesis, Michigan Technological University, Houghton, MI.

Instituto Nacional de Estadística Geografía e Informática (INEGI), "ESTADÍSTICAS A PROPÓSITO DEL DÍA MUNDIAL DEL AGUA (Statistics with Regard to World Water Day)". March 22, 2006. http://www.inegi.gob.mx/inegi/contenidos/espanol/prensa/Contenidos/estadisticas/206/agua2006.pdf

Magaña, V. O. and C. Conde, "Climate and Freshwater Resources in Northern Mexico: Sonora, A Case Study." *Environmental Monitoring and Assessment 61*, 2000, pp. 167-185.

Instituto de Ingeniería, UNAM, para Comisión Estatal del Agua de Sonora (CEA), "Estudio Sobre Normas de Operación en las Presas-Acuífero de la Cuenca del Rió Sonora (Primera Parte) en Varias Localidades de Varios Municipios, en el Estado de Sonora", 2006. Used with permission.

Integrated Watershed Protection Plan and Management Strategy for the Calleguas Creek Watershed in Ventura County

Kathleen Higgins P. E.[1], E. Zia Hosseinipour P. E[2], and Jeff Friesen P.E.[3]

[1]CH2M HILL, 6 Hutton Centre Drive, Suite 700, Santa Ana, CA 92707; PH (714) 435-6161; FAX (714) 429-2054; email: khiggins@ch2m.com
[2]Ventura County Watershed Protection District, 800 S, Victoria Ave., Ventura, CA 93009; PH (805) 654-2454; FAX (805) 654-3350; email: Zia.Hosseinipour@ventura.org
[3]CH2M HILL, 1000 Wilshire Blvd., Suite 2100, Los Angeles, CA 900177; PH (213) 228-8216 x35416; FAX (714) 424-2003; email: jfriesen@ch2m.com

Introduction

The Ventura County Watershed Protection District (VCWPD) is preparing the Calleguas Creek IWPP Phase II Management Strategy Study as part of the development of the Calleguas Creek Integrated Watershed Protection Plan.

The 343 square mile Calleguas Creek watershed located in Ventura County, California has developed significantly over the last 50 years including the Cities of Simi Valley, Moorpark, Thousand Oaks, and Camarillo (see Figure 1). The land areas within the city limits are approximately 70 percent developed. Increased development has translated into more impervious ground cover resulting in increases in stormwater runoff volumes and peak flows into Calleguas Creek and its tributaries. These increased flows can (and do) cause erosion, sedimentation, and flooding problems. They also wash more pollutants from paved surfaces or agricultural lands into the waterways. This creates challenges and opportunities within the watershed.

There is a need to increase flood protection and provide for better sediment management in the watershed. While doing this, there is also an opportunity to accommodate or address other multi-use benefits, such as ground water recharge, water quality improvements, recreational enhancement, or habitat restoration.

The goals of the study are to provide multi-purpose conceptual projects for the watershed in order to deal with issues such as flood control, land development, erosion, sedimentation, the environment, parks and recreation, open space, and funding. Cost-effective and environmentally friendly solutions are being developed through a stakeholder driven process.

Alternative Approaches

A number of stakeholder-driven workshops have been held with stakeholders to develop and prioritize the approaches listed below and discussed in the following sections.

1. Land Management Focus
2. Watershed BMPs
3. Regional Basins

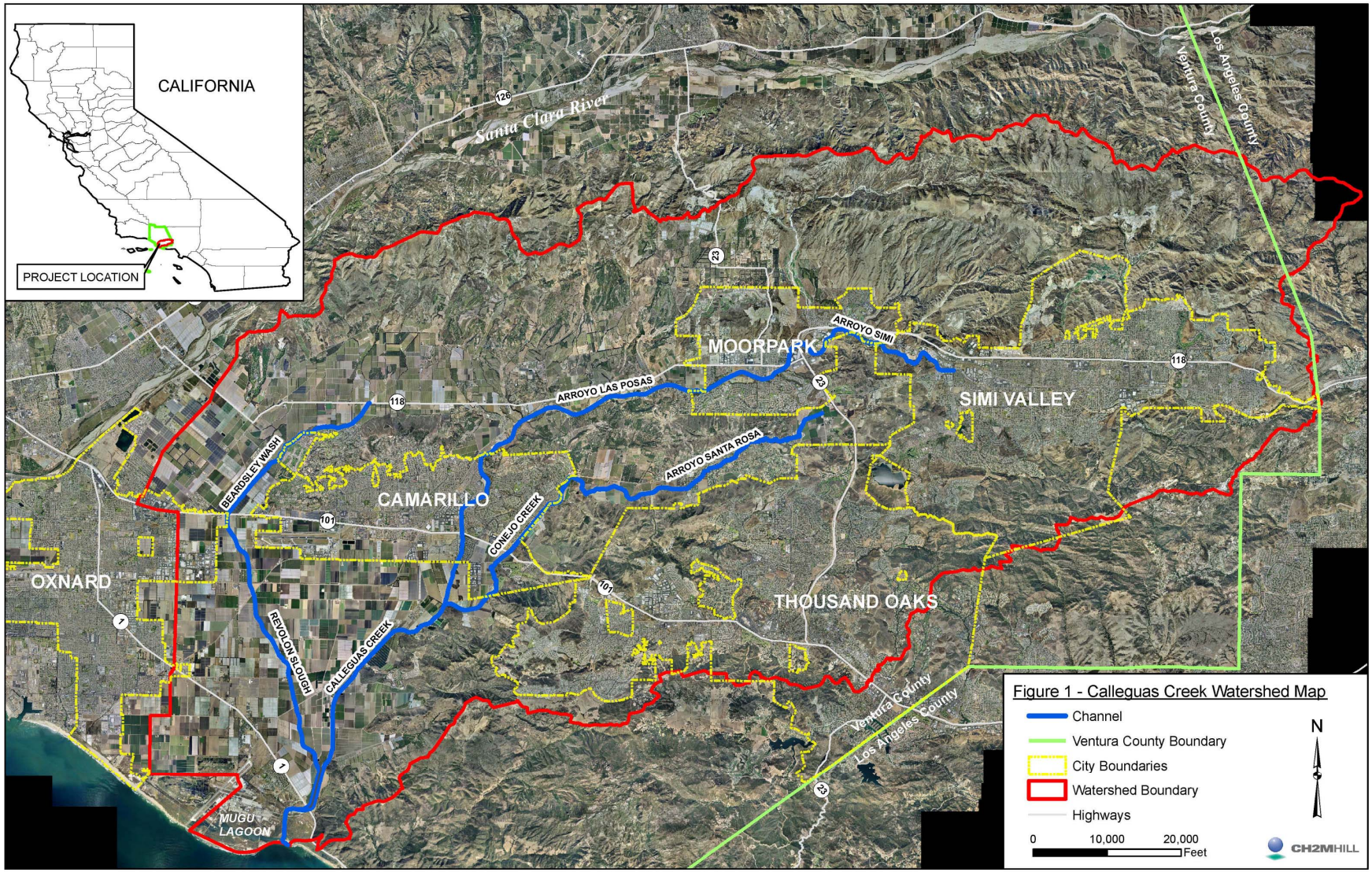
CALIFORNIA
PROJECT LOCATION
Santa Clara River
Ventura County
Los Angeles County
MOORPARK
ARROYO SIMI
SIMI VALLEY
ARROYO LAS POSAS
ARROYO SANTA ROSA
BEARDSLEY WASH
CAMARILLO
CONEJO CREEK
OXNARD
REVOLON SLOUGH
CALLEGUAS CREEK
THOUSAND OAKS
MUGU LAGOON
Figure 1 - Calleguas Creek Watershed Map
Channel
Ventura County Boundary
City Boundaries
Watershed Boundary
Highways
N
0
10,000
20,000
Feet
CH2MHILL

4. Protection-level
5. Channel Improvements

Alternative Approach 1 – Land Management

Land Management refers to the practice of ensuring that undeveloped land remains free of development through regulatory- or policy-based mechanisms. Maintaining land in an undeveloped state may not reduce downstream flows, but it does prevent flow increases. The goals of this approach include:

- Floodplain and agricultural preservation
- Environmental restoration
- Recreation
- Land acquisition through purchase when owners are ready to sell
- Removal of invasive plant species

Current agricultural lands may be incorporated into an Agricultural Preserve which would limit the potential for future development. This would be enacted through an ordinance or other policy mechanism.

Generally, undeveloped land in critical areas (in this case within ¼ mile each side of the main channels) is targeted. However, only 570 acres, or 4% of land use within the established ¼ mile buffer is currently identified in Ventura County's existing land use data as being undeveloped open space. The majority of other land use is agricultural (9,012 acres or 58%), residential (2,388 acres or 15%), and government/public/utilities (2,206 acres or 14%). One option is to purchase land (at market value) from willing property owners in key locations when and if they decided to sell, and then return that land to a reasonably undeveloped state.

Most Significant Issues

- Land Management can contribute to flood or sediment solutions if a significant amount of land previously excluded from the floodplain can be returned to the floodplain.
- Farmers have voiced concerns that recreational use of lands adjacent to farming operations may put recreational users at risk of contact with pesticides or other hazardous chemicals.
- Limited existing open-space undeveloped land exists within the ¼-mile buffer along the main creeks.
- Land availability and cost.
- Regulatory- or policy-based mechanisms that set aside or restrict land use within the established floodplain.

Alternative Approach 2 – Watershed Best Management Practices (BMPs)

This approach would emphasize localized Best Management Practices (BMPs) designed to reduce the volume of stormwater runoff leaving a site, such as a residential or a commercial lot. Ideally, stormwater runoff would be reduced to pre-development levels. Examples of BMPs include rain barrels and surface or underground storage tanks to capture roof runoff; pervious pavements in parking lots

and driveways, landscaping with native plants and other low impact development solutions.

Three possible implementation options are being considered:

1. **Require BMPs in Newly Developed Land –** this would maintain post-development flow rates and volumes at pre-development levels. This strategy has been carried forward for analysis and costing of combined alternative approaches.
2. **Require BMPs in All Newly Developed Land, and to Permitted Improvements –** this would reduce post-development flows to rates and volumes below pre-development levels.
3. **Retrofit BMPs to a Percentage of Existing Land –** this would have the same effect as strategy number 2.

Most Significant Issues

- Long-term effectiveness of watershed BMPs depends greatly upon proper ongoing maintenance.
- The Ventura County draft NPDES permit already incorporates a requirement that future development not increase runoff peaks or volume beyond the undeveloped flow levels for a 2-year return period event.
- Reducing peak flows beyond existing is possible with watershed BMPs, but requires retrofitting BMPs to existing developed land, or a building permit-based system.

Opportunities May Include:

1. Reduced pollutant loading, sedimentation, and erosion of natural water bodies.
2. Enhanced groundwater recharge through infiltration BMPs.
3. Promotion of storm water reuse and decrease in potable water demands.
4. Good potential for multi-use benefits (parks, trails, habitat & wetlands).

Challenges May Include:

1. A Public outreach program would be required for cistern/rain barrel programs for irrigation reuse.
2. Wide-scale implementation needed before significant benefits would be achieved (may take many years – particularly in developed areas).
3. Operation and maintenance requirements typically increase with such solutions, and long-term efficacy depends on proper regular maintenance.
4. Infiltration may not be practical for some areas due to low-permeability soil types.

Alternative Approach 3 – Regional Basins

The Regional Basin approach utilizes larger detention basins at strategic locations to capture and delay storm flow peaks in the main creek channels. Basins are considered *regional* if they are located on one of the main creek channels, or if they

receive flows from multiple significant tributaries. The basins may serve as infiltration basins, but their main purpose is to reduce downstream peak flood flows.

This approach would use regional detention basins on Arroyo Simi, Arroyo Las Posas, Calleguas Creek, at the Conejo Creek confluence with Calleguas Creek, and on Revolon Slough. Risk of flooding would be reduced from Highway 118 to the PCH along Arroyo Simi, Arroyo Las Posas, and Calleguas Creek, and would benefit the Cities of Moorpark and Camarillo, and also agricultural land along lower Calleguas Creek. Projects within creek channels would be minimized with this option.

Stakeholders ranked Regional Basins third out of the five presented approaches. It will be possible to avoid a significant amount of channel improvements downstream of the basins with their implementation.

Most Significant Issues

- Siting and acquisition of land may be a long process.
- Regional basins have a significant effect in reducing the downstream peak flows of large flows.

Opportunities May Include:

1. Significantly reduced need for channel improvements.
2. Removal of some residential and agricultural land from existing floodplain.
3. Potential for multi-use benefits in basin lands (parks, trails, habitat).
4. Reduced channel sedimentation and erosion through reduced flows.
5. Enhanced groundwater recharge.

Challenges May Include:

1. Land acquisition for basin locations (depending on basin size and siting).
2. Environmental permit restrictions.
3. Basins will not provide complete solution – some channel improvements will be required.

Alternative Approach 4 – Protection Level

This approach applies to Calleguas Creek and Revolon slough downstream of Pleasant Valley Road, and is based on channel design objectives: what flows can be contained within the channels. Land within the floodplains would continue to flood, and flood reduction via channel modifications or upstream actions would be undertaken only to restore the channel conveyance design objectives when needed. For example, if a channel was designed to convey 30,000 cfs but sedimentation has reduced the channel's capacity to 20,000 cfs, dredging or other channel modifications would be undertaken to restore the 30,000 cfs capacity of the channel.

Stakeholders ranked Protection Level as fourth out of five presented approaches. This is essentially a "do nothing" approach below Pleasant Valley Road, although a flooding inundation compensation mechanism could be implemented. Other

approaches applied upstream of Pleasant Valley Road would be responsible for reducing peak flows and minimizing the flood potential.

Most Significant Issues

- Channel Improvements were ranked as the second-least desirable approach by stakeholders
- Agricultural land would remain in the 100-year floodplain.
- Agricultural land owners stated that the Protection Level approach was unacceptable if flooding at or below the 100-year level was still possible.
- Some agricultural land owners favor Q_{100} flood protection in lower Calleguas Creek, while others do not want the agricultural land removed from the floodplain because of anticipated development pressure.

Opportunities May Include:

1. Reduced flooding potential in certain areas; accepted and/or compensated flood risk in others.
2. Reduced capital cost of the final selected combined scenario.
3. Creeks remain connected with floodplain in larger flows.
4. Greater opportunity for multi-use benefits.
5. Reduced development opportunity.

Challenges May Include:

1. Flooding risk will continue to exist in agricultural lands.
2. Upper creek reaches still require the application of other approaches to reduce or manage flows.
3. Reduced development opportunity.

Alternative Approach 5 – Channel Improvements

Channel Improvements refer to in-channel projects necessary to provide flood protection and adequate sediment management within the creek channels. Projects typically include widening of channels, raising of levees, removal of sediment, altering the channel grade (slope), adding/repairing bank protection, and constructing or modifying channel grade control and drop structures.

This approach emphasizes primarily channel-based solutions to flooding and sediment issues. The objective is to contain (and to balance the sediment transport for) the 100-year flow on Calleguas Creek (and Arroyo Las Posas and a portion of Arroyo Simi), Revolon Slough and Conejo Creek. Through adjusted channel geometry, slope, and grade control structures, this approach seeks to transport as much sediment as possible to sediment basins to be constructed upstream of Highway 101.

Stakeholders ranked Channel Improvements as the least-preferred of the five presented approaches. It will not be possible to avoid all channel improvements in the final selected combined scenario of approaches, but it will be possible to

minimize the number and extent of these projects with the right mix of other approaches (such as Regional Basins and Watershed BMPs).

Most Significant Issues

- Channel Improvements were ranked as the lowest desirable approach by the stakeholders
- Some channel improvements (both flood and sediment related) will be required regardless of the final combination of approaches selected.

Opportunities May Include:

1. Proposed solutions for all critical main creek systems (Calleguas Creek, Conejo Creek, Revolon Slough).
2. Q_{100} flood protection.

Challenges May Include:

1. Uncertainty of sediment regime within (and through) Mugu Lagoon.
2. Reduced opportunities for multi-use benefits.
3. Extensive in-stream construction required.

Scenarios Being Evaluated

Each of these five approaches is being combined based on stakeholder input for the various reaches within the Calleguas Creek Watershed. One scenario is to combine all five approaches in priority order as discussed below.

Combined Scenario 1 - Regional Basins Plus Channel Improvements

This scenario combines the following Alternative Approaches:

- Land Management*
- Watershed BMPs*
- Regional Basins
- Channel Improvement

** Land Management and Watershed BMP approaches are common to all four Combined Scenarios.*

Combined Scenario 1 utilizes four of the five Alternative Approaches. Land Management will maximize the amount of land that remains in, or is added to, the floodplain over time. The Watershed BMPs will ensure that future flow peaks and volumes do not increase over current flows. The regional detention basins significantly reduce the Q_{100} peak flows in Calleguas Creek and Revolon Slough. Channel improvements will still be required, but significantly fewer will be needed than if regional basins were not implemented. This is because channel capacities have been diminished by sediment deposition over time in Calleguas Creek, and because of ongoing erosion issues in various reaches. Also there are no identified basin locations that would address flows in Conejo Creek or Beardsley Wash.

Regional Basins do not. Therefore, significantly reduce the channel improvements required in these two creeks.

This scenario provides the most significant opportunity to incorporate the multi-benefit opportunities for environmental restoration, recreation, groundwater recharge, water quality and sediment management. Many of the basins could be designed to provide these additional opportunities and trails and other recreational opportunities would be incorporated with the channel improvements where appropriate.

This scenario most closely approaches the priorities voiced by the majority of the stakeholders to date.

Most Significant Issues

- The scenario provides Q_{100} protection to the project study area.
- Significant opportunities for multi-benefit projects are available with this scenario.
- Flood-related channel improvements will be minimized.

Combined Scenario 2 - Regional Basins with Protection Level

This scenario combines the following Alternative Approaches:

- Land Management*
- Watershed BMPs*
- Regional Basins
- Protection Level
- Channel Improvement

** Land Management and Watershed BMP approaches are common to all four Combined Scenarios.*

Combined Scenario 2 applies to all five Alternative Approaches – adding Protection Level to Combined Scenario 1. Land Management will maximize the amount of land that remains in, or is added to, the floodplain over time. The Watershed BMPs will ensure that future flow peaks and volumes do not increase over current flows. The regional detention basins significantly reduce the Q_{100} peak flows in Calleguas Creek and Revolon Slough. Protection Level reduces the required channel improvements below Pleasant Valley Road, and also potentially adds cost implications related to compensation for flooded land were Q_{100} flood protection is not provided.

As in Combined Scenario 1, the Regional Basins significantly reduce the number and extent of channel improvement projects that will be needed. Channel improvements cannot be eliminated because channel capacities have been diminished by sediment deposition over time in Calleguas Creek, and because of ongoing erosion issues in various reaches. Also there are no identified basin locations that would address flows in Conejo Creek or Beardsley Wash. Regional Basins do not therefore significantly reduce the channel improvements required in these two creeks. Many of the same channel improvements noted for Combined Scenario 1 will be required, but a less-than Q_{100} flood protection level would be maintained below Pleasant Valley Road in

Calleguas Creek and Revelon Slough. Flood control projects would be eliminated or reduced (depending on the determined required flood protection level) in this area.

This scenario provides the most significant opportunity to incorporate the multi-benefit opportunities for environmental restoration, recreation, groundwater recharge, water quality and sediment management. Many of the basins could be designed to provide these additional opportunities and trails and other recreational opportunities would be incorporated with the channel improvements where appropriate.

Most Significant Issues

- The scenario provides Q_{100} protection to the project study area, with the exception of the floodplain along Revolon Slough and Calleguas Creek below Pleasant Valley Road.
- The required level of protection (Q_{100} or less) below Pleasant Valley Road has yet to be determined.
- A mechanism for compensation of landowners subject to flooding requires discussion.
- Flood-related channel improvements will be minimized.

Combined Scenario 3 – Channel Improvement Emphasis

This scenario combines the following Alternative Approaches:

- Land Management*
- Watershed BMPs*
- Channel Improvement

* Land Management and Watershed BMP approaches are common to all four Combined Scenarios.

Combined Scenario 3 applies three of the five Alternative Approaches emphasizing channel improvements. Land Management will maximize the amount of land that remains in, or is added to, the floodplain over time. The Watershed BMPs will ensure that future flow peaks and volumes do not increase over current flows. Substantial channel improvements are required to convey the existing Q_{100} flows in all of the main creeks.

Opportunities for multi-benefit improvements are limited with this Scenario. Environmental restoration and recreation opportunities could be provided with the channel improvements. However, there are limited opportunities for groundwater recharge and water quality enhancement with this scenario.

Most Significant Issues

- The scenario provides Q_{100} protection to the project study area.
- The amount of in stream channel construction is maximized with this scenario.
- Opportunities for multi-benefit improvements are limited.
- The emphasis of this Combined Scenario is the least favored approach as determined by stakeholders.

Combined Scenario 4 - Channel Improvements with Protection Level

This scenario combines the following Alternative Approaches:

- Land Management*
- Watershed BMPs*
- Protection Level
- Channel Improvement

** Land Management and Watershed BMP approaches are common to all four Combined Scenarios.*

Combined Scenario 4 applies three of the five Alternative Approaches emphasizing channel improvements, and adding Protection Level to Combined Scenario 3. Land Management will maximize the amount of land that remains in, or is added to, the floodplain over time. The Watershed BMPs will ensure that future flow peaks and volumes do not increase over current flows. Protection Level reduces the amount of required channel improvements below Pleasant Valley Road. Substantial channel improvements are required to convey the existing Q_{100} flows in all of the main creeks. Many of the same channel improvements noted for Combined Scenario 3 will be required, but a less-than Q_{100} flood protection level would be maintained below Pleasant Valley Road in Calleguas Creek and Revelon Slough. Flood control projects would be eliminated or reduced (depending on the determined required flood protection level) in this area.

Opportunities for multi-benefit improvements are limited with this Scenario. Environmental restoration and recreation opportunities could be provided with the channel improvements. However, there are limited opportunities for groundwater recharge and water quality enhancement with this scenario.

Most Significant Issues

- The scenario provides Q_{100} protection to the project study area, with the exception of the floodplain along Revolon Slough and Calleguas Creek below Pleasant Valley Road.
- The required level of protection (Q_{100} or less) below Pleasant Valley Road has yet to be determined.
- Opportunities for multi-benefit improvements are limited.
- The extent of in stream channel construction is the second highest of the four scenarios.
- The Protection Level and Channel Improvement approaches ranked as the least favored by stakeholders

Conclusion

The stakeholder driven process is being used to select a long-term management strategy for the Calleguas Creek Watershed. A combination of the above approaches and scenarios will be selected through the continuation of the stakeholder driven process as the study is completed this year.

McCormick Place West Hall Conference Center Stormwater Reclamation Tunnel and "Green Roof" helps advance Chicago's Clean Water Agenda

W. J. Weaver, PE, D.WRE

[1]AECOM, 750 Corporate Woods Parkway, Vernon Hills, Il, 60061; PH (847) 279-2494; FAX (847) 279-2510; email: bill.weaver@aecom.com

Abstract: The McCormick Place Convention Center in Chicago has undergone a dramatic expansion to remain one of the premier convention venues in this country. The new West Hall designers recognized early on that the City combined sewer system was beyond capacity resulting in periodic flooding and overflow to the Chicago River. The Metropolitan Pier and Exposition Authority (MPEA) initially considered traditional stormwater management alternatives including onsite detention and new gravity sewers to manage runoff from 70 acres of convention center rooftop.

MPEA decided to pursue a "green" approach to stormwater management to complement other environmentally sensitive design features employed at this project. AECOM devised a stormwater conveyance system that would carry clean rain water from the convention center roof to Lake Michigan thereby diverting as much as 55 million gallons of stormwater from the City's combined sewer system each year.

INTRODUCTION AND BACKGROUND

Chicago's McCormick Place Convention Center receives as many as 3 million visitors annually. Convention Center stormwater runoff from nearly 100 acres of rooftops has historically discharged to a combined sewer system. The recent Conference Center expansion for the West Hall employs an innovative stormwater management system that utilizes a "green" approach, and complements a new $1,200,000 3.5-acre green roof and garden at the recently completed West-Hall project.

The project investigated a number of options including detention storage, a traditional cut and cover or shallow tunnel sewer to Lake Michigan, and a rock tunnel to Lake Michigan. The rock tunnel option was considered most feasible. The new stormwater system manages 55 million gallons of runoff each year from 70 acres of the new West Hall and from a portion of the existing North and South Halls. This stormwater is diverted from the City of Chicago combined sewer system, and reduces combined sewer overflows to the Chicago River and Lake Michigan. The new system also reduces the potential for local flooding that has plagued this area in recent years.

The direct discharge of stormwater to Lake Michigan is normally prohibited by regulations in an effort to protect the Lake from pollutants. This policy is targeted to protect Lake water that is the primary drinking water source for the City. In this case, the policy results in rooftop runoff being treated in the City's wastewater treatment system. Rooftop stormwater runoff tests at the Convention Center indicate that the runoff exceeds Lake Michigan water quality standards. This fact and the sustainable design aspects of the proposed stormwater tunnel helped convince the regulatory authorities to allow the diversion of this runoff to Lake Michigan.

AECOM and Atkinson Construction of Broomfield, Colorado formed a design build team that completed constructed of the tunnel system during 2007. The system includes a 3,350 - foot long 12.5 - foot diameter rock tunnel constructed in bedrock approximately 160 feet below ground. The tunnel begins at the West convention center building, extends under Burnham harbor, and terminates at the south end of Northerly Island where an outlet shaft allows water to rise to Lake Michigan. First flush runoff is directed away from the tunnel to the local sewer system. Figure 1 is an aerial photograph of the site.



Figure 1. Location Map

The tunnel project fulfills the project design criteria goal to implement a design solution that supports the City of Chicago Clean Water Agenda and realizes a sustainable design approach.

PROPOSED STORMWATER RECLAMATION TUNNEL

Tunnel Structures

The proposed stormwater reclamation tunnel is a 3,350 foot long 12.5 – foot diameter unlined rock tunnel formed with a tunnel boring machine. The tunnel is 160 feet below the ground surface founded in rock and has a capacity of 500 cfs. Geological studies proved that the tunnel could be constructed without a lining; however, the stability of the tunnel roof needed rock bolts extending six feet into the rock at a horizontal spacing of about six feet and a longitudinal spacing of five feet. Figure 2 is a picture of the completed tunnel. The tunnel boring machine (tbm) cutter head is shown on Figure 3, and the installation of tunnel rock bolts is shown on Figure 4.

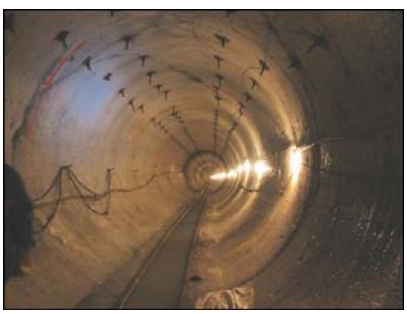

Figure 2:
Tunnel



Figure 3:
TBM cutter head



Figure 4
Rock bolt installation

The unlined tunnel resulted in significant cost savings, and promotes the infiltration of clean stormwater into the water table through rock fractures.

Stormwater from the convention center West Hall roof enters the tunnel through a 7 – foot diameter shaft. The drop shaft was constructed after the horizontal tunnel was completed. The roof downspouts are tied into the down shaft that is shown on Figure 5. The shaft is lined with concrete since it passes through 85 feet of overburden soils before hitting the rock strata that the tunnel is founded in. The tunnel has the capacity to also handle runoff from the North and South Hall roof tops. A separate drop shaft will be constructed in the future to convey runoff from this hall to the lake.



Figure 5:
West Hall Drop Shaft
Lined with Concrete

The nearly two thirds of a mile long tunnel was originally conceived to terminate on the east side of the Convention Center East Hall. AECOM recommended that the tunnel be extended nearly 600 feet under Burnham Harbor to Northerly Island to accomplish the following:

- A tunnel outfall on the east side of the east hall would require the shutdown of the lakefront trail for more than a year. This trail is an important link in the park trail system and alternative pathways would be difficult to create.
- The original outfall location would require the trucking of 20,000 cubic yards of tunnel rock spoil through the streets of Chicago. A Northerly Island outfall location allows for the beneficial reuse of the tunnel rock for the construction of landscape berms and topographic relief on the otherwise flat peninsula.
- The Northerly Island outfall location provides significant construction equipment lay down space when compared to a very restricted space on the west side of Burnham Harbor. The island also provides available nearby office space and electrical hookups for the construction team.
- The outfall location is oriented away from the harbor mouth thereby reducing any possibility of flow currents that could impact harbor operations.

As a result of the above issues, the overall cost of extending the tunnel length by 18 percent was less than the original plan for a shorter tunnel. Figure nos. 6 and 7 are photographs of the south end of Northerly Island after regrading with tunnel rock and planting of the landscape berms.



Figure 6:
Northerly Island south end after tunnel spoil placement, grading and planting.



Figure 7:
Northerly Island south end after tunnel spoil placement, grading and planting.

Tunnel Up Shaft at East End

A 22 – foot diameter vertical shaft was constructed on the east end of the tunnel to connect to the outfall surge chamber located on the south end of Northerly Island. The shaft carries stormwater from the tunnel located 160 – feet below ground back to the surface near Lake Michigan. The shaft was constructed with a reinforced concrete lining to hold back the overburden and fill soils at Northerly Island. Figure

8 shows the tunnel shaft during construction. The tunnel had not yet advanced to the level of 160 feet below grade, and the temporary liner system was still in place.

AECOM developed a grouting program for the rock exit shaft at Northerly Island that included secondary and tertiary stages to resolve leakage and solidify the limestone at the rock/tunnel interface. Groundwater pump tests were used to evaluate the effectiveness of the grouting program. This program allowed for the exit shaft to be constructed with the outside tunnel lining diameter the same dimension as the drill and shoot diameter. Thus, no over-excavation was needed to create rock shelves to accommodate the tunnel lining. This approach significantly minimized the construction cost and accelerated the schedule.



Figure 8: Outlet Shaft

The liability risk associated with the design of the 150-foot-high exit shaft support structures was placed with a specialized construction contractor who was responsible for this construction element. This approach is important since the prime design engineering team is not in a position to direct the transient structural nuances that can occur in the field for this type of construction. This portion of the construction was the most risk intense part of the design effort due to complex conditions and forces that occur during the transient construction progression. Therefore, the risk best resides with the firm responsible for this construction element. As it turned out, any issues that occurred with the shaft perimeter structures during construction that could have resulted in significant settlement of the outfall structure were addressed in real time. The specialty contractor had the appropriate contractual incentives to address these issues in a timely fashion.

Outfall Surge Chamber at Lake Michigan

The tunnel outfall at Lake Michigan includes a 500,000 gallon surge chamber that has a 3,500 square foot footprint located at the south end of Northerly Island. The outfall was located such that the discharge would be directed away from the Burnham Harbor mouth and has the following features:

- Seven 6 – foot diameter outfall orifices between the surge chamber and Lake Michigan. The reinforced concrete wall between the chamber and Lake Michigan is designed to create separation between the tunnel water and Lake Michigan storm surge. Each orifice is outfitted with a steel thimble and sleeve and backflow prevention Tideflex Check Valve by Red Valve; reportedly the largest such application on Lake Michigan. These valves held back Lake Michigan and wave action, with small leakage amounts during construction, and with a still water Lake level that was 13 feet higher than the outfall surge chamber bottom.

- A stop log notch was constructed between the outfall valve structures and the Lake to provide dewatering capability for times when the valve structures need maintenance or replacement.
- The valve structures were placed below the level of anticipated ice action to minimize the potential for ice blockage (Assel, 2004).
- A safety relief is built into the system in the unlikely case where the outfall valves become blocked. A grated opening on top of the surge chamber would allow for the release of tunnel flows on top of the structure. The top of the structure is configured to convey such emergency flows to the lake over ground surfaces that are reinforced with rock filled gabion mattresses and large armor stones. Figure 9 illustrates this structure before final grading and landscaping.
- The existing timber crib seawall was buttressed for a length of 90 feet and an armor stone protection designed to withstand the stress of tunnel flows from upstream and wave attack from downstream was placed at the outfall. The armor stones vary in weight from 1 to 3.3 tons.



Figure 9: Outfall Structure

Figure 10 illustrates a schematic profile of the tunnel outfall works. Figure 11 is a photograph of the outfall chamber and works under construction. Figure 12 is a photograph of the stop log structure downstream of the backflow prevention valves. The stop log support structures are mounted on the inside of a wall that serves as a flow and ice baffle. This wall extends down below the low level of Lake Michigan. The water level in the surge outfall chamber is approximately 13 – feet below the level of Lake Michigan in Figure12. The East Hall of the convention center can be seen in the background.

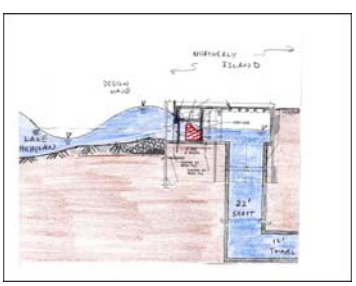

Figure 10:
Tunnel Profile Schematic



Figure 11:
Outfall Chamber



Figure 12:
Outfall Stop Log Structure

The finished outfall structure provides a lake overlook with access to the edge of the lake. This structure serves as a fishing platform and has seating walls that double as flow training works during emergency overflow or extreme wave attack conditions.

TUNNEL HYDRAULIC DESIGN

There is a 5.5 – foot drop between ground surface elevations at street level at the convention center, and the 10 – year Lake Michigan water level at the tunnel outfall. Therefore, the tunnel has to deliver a capacity of 500 cfs with 5.54 – feet of head over a tunnel distance of 3,350 feet. The design condition for the tunnel included a boundary condition that manages the combined occurrence of the following events:

- 10 – year recurrence interval Lake Michigan level (USACE, 1993).
- 100-year recurrence interval rain storm. (Huff, 1989)
- 20 – year recurrence interval Lake Michigan wave event (Hubertz, 1991).

The combined event recurrence interval for a 10 – year Lake level and a 20 – year wave event is approximately a 100 – year event (USACE, 1998). The combined event recurrence interval of the wave, lake, and rain events is estimated to be significantly in excess of a 500 – year event. Therefore, the system is designed to manage an extreme event with a significant factor of safety built in. All parties were in agreement that this design condition was reasonable given the importance of this structure.

The design runoff event for the tunnel included the following parameters:

- Drainage area equals 70 acres of rooftop.
- Rational method runoff coefficient was estimated to be 0.98 (ASCE 1992).
- 100 – year rainfall intensity for a time of concentration is 8.2 inches per hour (Huff, 1989).
- Significant tunnel system headlosses (King & Brater, 1976):
    - Bend losses at bottom of drop shafts and at bottom and top of up shaft.
    - Friction losses in unlined tunnel with Manning's roughness coefficient of 0.0165 (Pennington, 1998), and concrete lined shafts.
    - Assumed restrictions for poor rock areas that could not be determined before construction; assume a 2.5 – foot diameter tunnel reduction for a length of 100 feet of tunnel.
    - Expansion and contraction losses at blasted portion of tunnel at east end and elsewhere.
    - Backflow prevention valve losses of 0.3 – feet.
    - System exit losses.

Figure 13 is a photograph of the unlined tunnel wall and is illustrative of the tunnel roughness characteristics.



Figure 13: Unlined Tunnel

LAKE MICHIGAN STORM SURGE EVALUATION

Lake Michigan wave attack can influence the system in a number of ways. The outfall structure walls had to be designed to address static loads and internal hydraulic loads as well as wave attack loads. Furthermore, wave stresses can influence lake bed erosion potential at the outfall structure as well as stresses produced by tunnel flow conditions. Finally, wave crest attack will shut down the backflow prevention valves on the tunnel system for a portion of the time between wave crests.

A wave climate evaluation was performed to identify the characteristics and loads associated with incident wave conditions attacking from a three directions considered to be reflective of the range of wave conditions that occur at the site. A wave analysis was performed to estimate the wave heights that can attack the outfall structure after transformation from the deepwater environment considering the following effects: refraction, diffraction, shoaling, reflection and surf zone influences that evaluate the largest wave that can be supported in the near shore zone (Goda, 2000). The 5-, 10-, and 20- year wave heights that are incident to the outfall structure are 12.4 feet, 13.0 feet, and 13.6 feet respectively.

The armor stone placed on the lake bed at the outfall is sized to withstand wave attack as well as tunnel discharge currents. This stone has a weight of 1 to 3.3 tons.

LAKE MICHIGAN STORM SURGE EVALUATION

Waves that attack the outfall structure will shut down the backflow prevention valves for a portion of the approximately 8 to 12 seconds that it takes for each wave to pass (Resio and Vincent, 1976). The outfall discharge would effectively drop to zero until the wave trough begins to arrive. During the wave trough, the tunnel tailwater condition would significantly increase and the tunnel discharge would exceed the target design flows. This phenomenon of the push and pull of wave conditions at the outfall would set up a hydraulic transient.

The outfall structure is designed to harness wave action energy to help evacuate water from the tunnel outfall and to manage Lake Michigan storm surge. The seven 6-foot diameter backflow prevention valves are designed to control storm surge from Lake Michigan wave action. This is an important design item since an uncontrolled surge could cause upstream flooding. AECOM performed a hydraulic transient analysis using numerical analysis and the “Hammer” computer program (Bentley, 2005) to optimize the design of the valves and to size the outfall structure. The transient condition can be summarized as follows:

- When the crest of a wave attacks the outfall structure, the valves close automatically due to the wave crest pressure. The outfall structure is designed as a surge chamber with a capacity of 500,000 gallons and continues to accept tunnel flows into storage during periods of valve closure.

- When the wave trough arrives at the outfall structure, the water surface of the Lake drops at the valves which then open automatically. During this period, the available head across the valves allows for a greater outfall chamber discharge than the design flow rate delivered by the tunnel. The system balances the dynamics of wave action to optimize system capacity.
- As summarized by the Hammer fluid transient analysis graphs shown on Figure 14, there is a tendency for the design head in the surge chamber to drop during wave attack due to the fact that the amount of increased discharge during wave trough conditions more than makes up for the lost capacity during wave crest attack. The reality is that wave conditions in nature are anything but uniform; therefore, the analysis conclusions are assumed to indicate that the structure should perform well during the design event. No additional capacity was assumed due to the fluid transient analysis results above conditions associated with the steady flow condition.

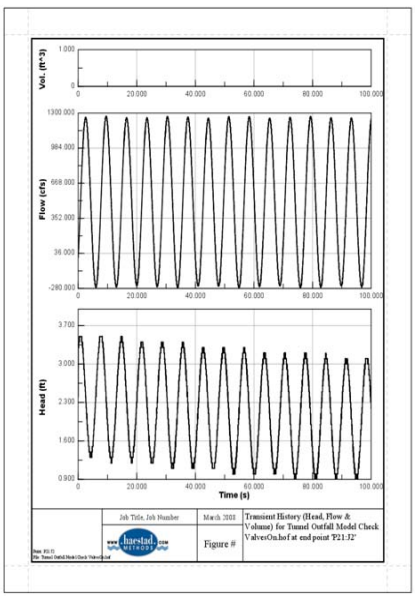

Figure 14: Hammer Analysis

- If for some reason an unusual wave condition were to occur, a safety provision is built into the outfall structure whereby flows can bypass to Lake Michigan through a large diameter grate on top of the structure.

SUMMARY AND CONCLUSIONS

The new McCormick Place convention center stormwater tunnel complements the sustainable design characteristics inherent in the new West Hall designed by Epstein. The building is LEED certified and includes the largest collection of green roof systems in the City of Chicago.

The new stormwater management system manages 55 million gallons of runoff each year from 70 acres of the new West Hall and from South and North Halls. This stormwater is diverted from the City of Chicago combined sewer system, and reduces combined sewer overflows to the Chicago River and Lake Michigan. The rock tunnel is unlined thereby enhancing groundwater infiltration.

The extension of the tunnel outfall under Burnham Harbor to Northerly Island provided tunnel rock fill that was beneficially reused for fill to create landscape berms, topographic relief, and landscaping for the southern Northerly Island edge. The ability to reuse the tunnel fill on the island eliminated the need to truck this material thereby reducing pollution, fuel consumption, and traffic. Relocation of the outfall to Northerly Island also eliminated interruptions of a critical lakefront trail during construction.

REFERENCES

ASCE & Water Environment Federation (1992). "Design and Construction of Urban Stormwater Management Systems", ASCE Manuals and Reports of Engineering Practice No. 77, WEF Manual of Practice FD-20, New York, N.Y.

Assel, R.A., (2004). "Computerized National Weather Service Great Lakes Ice Reports for Winter Seasons 1899-1970": NOAA, Technical Memorandum GLERL-130, NOAA, Great Lakes Environmental Research Laboratory, Ann Arbor, MI, 31 p.

Bentley Systems, Inc. (2005). "Hammer Hydraulic Transient Modeling Software", Watertown, CT

Hubertz, J.A., Driver, D.B., and Reinhard, R.D. (1991). "Hindcast Wave Information for the Great Lakes: Lake Michigan", WIS Report 24, Department of the Army, Corps of Engineers, Washington, DC

Huff, F.A., and Angel, J.R. (1989). "Frequency Distributions and Hydroclmatic Characteristics of Heavy Rainstorms in Illinois", *Illinois State Water Survey*, Champaign, Bulletin 70

King, E.F. and Brater, H.W. (1976). "Handbook of Hydraulics", New York, N.Y.

Pennington, M.S. (1998). "Hydraulic Roughness of Bored Tunnels", IPENZ Transactions, Vol. 25, No. 1/CE

Resio, D.T., and Vincent, C.L. (1976). "Design Wave Information for the Great Lakes", Report 3, U.S. Army Engineer Waterways Experiment Station, Vicksburg, Miss.

USACE (1993). "Design Water Level Determination on The Great Lakes", *Detroit District, U.S. Army Corps of Engineers*, Detroit, MI, 22 p.

USACE (1998). "General Design Memorandum Reach 4 – Interstate 55 to 33re Street", Chicago, Ill, Appendix D, 19 p.

SPATIAL VARIATION OF SEDIMENT OXYGEN DEMAND IN ATHABASCA RIVER: INFLUENCE OF WATER COLUMN POLLUTANTS

KUSUMAKAR SHARMA[1*], PRESTON McEACHERN[2], MARK SPAFFORD[3], DAVID ZHU[1], TONG YU[1],

[1]Department of Civil and Environmental Engineering, University of Alberta, Edmonton, AB, Canada; [2]Alberta Environment, Edmonton, AB, Canada; Alberta Pacific Forest Industry, Boyle, Alberta, Canada

*(*Author of correspondence, e-mail: ksharma@ualberta.ca, Tel. +1-780-4929904)*

ABSTRACT

Sediment samples were collected from fifteen different locations along Athabasca River in an attempt to quantify the sediment contribution to oxygen demand. SOD rates along Athabasca River ranged from 0.09 $g/m^2 \cdot d$ to 0.71 $g/m^2 \bullet d$ near ambient temperature ($<4^0C$). SOD rates generally increased downstream, however, inter-site differences were also influenced by the physical and chemical properties of the sediment. SOD rates were also higher below wastewater discharges and tributary confluences. Variation in SOD rates along the river system were positively correlated with water column concentration of TOC, TDP, Cholorphyll-α. Sediment characteristics such as grain size was a fundamental factor in determining SOD rates. Fine grained sediment in depositional areas tended to have higher SOD. The result also highlighted the importance of inclusion of sediment diagenesis and biochemical reactions inside sediment in water quality models that seek to represent water chemistry and particularly carbon, nitrogen, phosphorus and dissolved oxygen. Results from the Athabasca River suggest that SOD rates are a primary forcing function in large high order rivers that should be determined from the complex physical and chemical factors that control it rather than from water column nutrients.

Keywords River sediment, dissolved oxygen, sediment oxygen demand, water column pollutants

1. INTRODUCTION

Acute depletion in dissolved oxygen (DO) concentration in Athabasca River was observed during record low water flow years of 2002 and 2003 (Chambers et al. 2006; NREI 2004). A one-dimensional stochastic DO model and some two dimensional water quality models were unable to predict the DO level during low flow years (Tian 2005). These models were used to calculate allowable effluent loads from five pulp mills and municipal sewage treatment plants located along the bank of the river. The high concentration of organic matter and nutrients discharged from the mills are a part of water column load that consumes DO in the river to levels that may impact aquatic life. Although improved effluent treatment processes adopted by pulp mills has led to substantial reduction in biochemical oxygen demand (BOD) load. However, nutrient load has remained unchanged or increased (NREI 2004) in part due to activated sludge treatment processes used to reduce BOD. We hypothesized

that this nutrient load may increase sediment oxygen demand (SOD) potentially offsetting the benefits of the reduction in BOD.

Significant SOD rates at different locations, even during ice-cover, were found in previous studies on the Athabasca River (Noton 1996; Moneco 1993; Casey 1990). SOD rates were compared at a site using three techniques: closed chamber, core incubation and use of microsensor; and the closed chamber method used in previous studies was shown to be unreliable (Tian 2005). Yu (2006) developed the core and microsensor method further and investigated the impact of organic carbon and nutrient load on SOD rates. The author concluded that SOD was stimulated by availability of labial carbon. Given this background, water quality management in northern Alberta Rivers required further development of processes and concepts captured in existing models to conclude a better understanding of the factors that control spatial variability and the role of nutrient loads on SOD rates.

This paper summarizes on-going research on the relationship between water column physical-chemical characteristics and SOD rates. Specifically, it examines the relationship between organic carbon, nutrients and SOD rates within the context of spatial variability along the Athabasca River. This research is a component for developing a process-based SOD model for sediment diagenesis in large sand-silt rivers.

2. MATERIALS AND METHODS

The Athabasca River originates from the Rocky Mountains of Alberta and flows in a northeast direction through the province, past the urban centers of Jasper, Hinton, Whitecourt, Athabasca and Fort McMurray prior to emptying into Lake Athabasca. The drainage area of the Athabasca River basin is about 155, 000 square kilometer and contains five pulp mills: Hinton Pulp at Hinton, Alberta News Print Co. (ANC) at Whitecourt, Millar Western Forest Products at Whitecourt, Slave Lake Pulp at Slave Lake, and Alberta Pacific Forest Industries (ALPAC) at the town of Athabasca. The Athabasca River receives discharges from these pulp mills as well as from municipal waste treatment plants situated along its bank. Major tributaries, namely: Berland River, McLeod River, Freeman River, Pembina River, Lesser Slave River, La Biche River and Calling River, drain into Athabasca River above Grand Rapids. Grand Rapids provides substantial reaeration (due to natural cascades) even during winter such that low DO is not an issue below the Rapids.

For this study, fifteen sites along the Athabasca River were selected for sediment and water sampling upstream of Grand Rapids. Fig. 1 depicts the Athabasca River basin that includes tributaries and sampling sites. The sampling sites from upstream (U/S) to downstream (D/S) were: (1) U/S of Hinton Pulp Mill (USHP), (2) Emerson Bridge (EMBG), (3)U/S of Alberta Newsprint Company (UANC), (4) U/S of McLeod River confluence (USML), (5) 2 km D/S of Millar Western Pulp Mill (DSMW), (6)Blue Ridge (BLRG), (7) Fort Assiniboine (FTAS), (8) D/S of Timeau River confluence (DSTR), (9) Chisholm (CHLM), (10) Smith (D/S of Lesser Slave River confluence)

(SMTH), (11) C-Bridge (CBRG), (12) U/S of ALPAC Pulp Mill (USAM), (13) Poacher's Landing (POLG), (14) upstream of Calling River (DSLB), and (15) D/S of Calling River (DSCR). Sediment sampling sites were located upstream and downstream of nutrient sources which either was a tributary or a pulp mill effluent discharge.

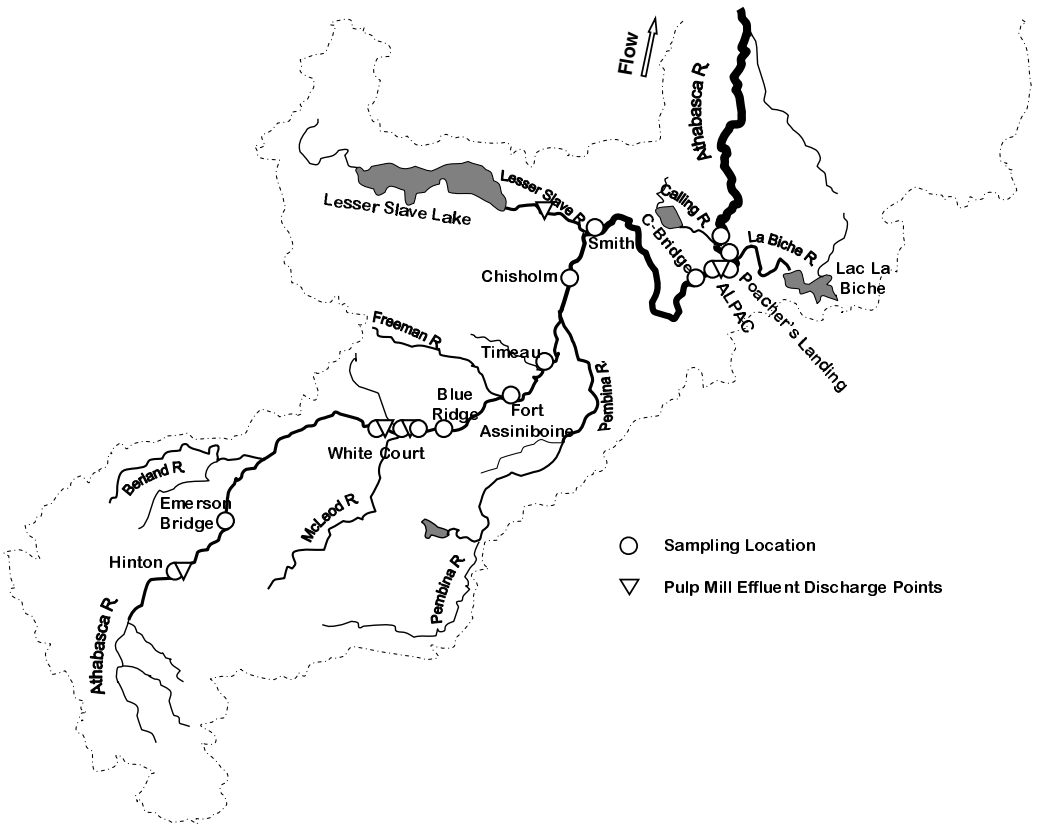

Fig. 1 Athabasca River basin, fifteen sampling sites and five pulp mill locations

Sediment cores and 20 litres of bulk river water were collected at the 15 sites between September 12, 2006 and October 16, 2006 utilizing clear polycarbonate cores to minimize disturbance (Yu 2006). The cores were sealed with no airspace, kept in ice and wrapped with dark plastic, and transported to Environmental Engineering Laboratory at the University of Alberta. SOD rate determinations commenced the following morning within 24 hours of collection. Water in the sediment core was replaced with the bulk river water which had similarly been kept in the dark at near zero condition. A core containing only bulk water served as control, resulting in two sediment cores and one control for each site. The sediment cores and control were equipped with a stirring mechanism consisting of a floating magnetic stir bar inside the core cylinder and an inverted stirrer plate at the top of the corer cylinder. Stirring speed was held constant below the threshold for sediment resuspension. The sediment cores and control were then incubated in the dark for 24 and 48 hours at 4 ± 1^{0}C. Water column DO concentrations at the start and end of the incubation period were measured by Winkler titration (Standard Methods 1998) to determine the decreased

DO concentration in the overlying water column. The replicate SOD rates were averaged for each location.

River water collected immediately after collecting sediment cores was analyzed for water quality parameters, including, total organic carbon (TOC), 5-day carbonaceous biochemical oxygen demand (BOD_5), total suspended solids (TSS), ammonia (NH_4^+), nitrate+nitrite (NO_2^- + NO_3^-), total dissolved phosphorus (TDP), chlorophyll-α (indicator of algal biomass) and iron (Fe), and alkalinity. Total inorganic nitrogen (TIN) was the sum of ammonia and nitrate+nitrite. The DO, temperature, and conductivity were recorded at each site with a polarographic oxygen probe (YSI model 85), while pH was measured in the laboratory by a pH meter.

TOC was analyzed by Shimadzu TOC-5000A carbon analyzer. Phosphorus (TDP) and nitrogen (NH_4^+ and NO_2^-+NO_3^-) were analyzed by colorimetry with Lachat 8500 FIA analyzer following Standard Methods (1998). TDP samples were filtered through pre-washed 0.70 μm Millipore filter. Samples for NH_4^+ and NO_2^-+NO_3^- analysis were treated with sulfuric acid and stored at 4^0C temperature for future analysis to be done within 14 days after sampling (Standard Methods 1998). The iron (Fe) was analyzed by atomic absorption of unfiltered samples. Chlorophyll-α was analyzed by spectroflouoro-photometer. All above parameters were analyzed at the Biogeochemcal Analytical Laboratory of University of Alberta. BOD_5 was determined after 5-days of sample incubation using a polarographic DO meter for DO measurement at Maxxam Analytics Inc., Edmonton.

SOD, or oxygen flux (J_O), is calculated from a linear regression of concentration versus time such that

$$J_0 = m\frac{V_{OLW}}{A_{chamber}} \qquad (1)$$

where $m = \Delta C/\Delta t$ or the slope of the linear regression for change in concentration per unit time, V_{OLW} is the volume of overlying water enclosed within the chamber, and $A_{chamber}$ is the surface area of sediment enclosed by the chamber (Reimer et al. 2001). The surface area of sediment in each core was 25.68 cm^2. The clay/sand composition of the sediment cores made application of a smooth surface area reasonable. With this assumption the SOD (g/m^2•d) was calculated by the following relationship (Murphy and Hicks 1986)

$$SOD = \frac{V_{OLW}}{A_{Chamber}}(O_S - O_W) = h(O_S - O_W) \qquad (2)$$

where, O_s and O_w are the changes in oxygen concentrations in sediment core and control core per unit incubation time (mg/L.h), respectively and h is the height of overlying water (m). For reporting purposes SOD values were transformed to a standard temperature (20^0C) using the following formula:

$$SOD_T = SOD_{20}\theta^{T-20} \quad (3)$$

where, SOD_{20} is the SOD value normalized to 20^0C, SOD_T is the SOD at incubation temperature, T is the incubation temperature in ^{0}C, and θ is the temperature correction coefficient, ranging from 1.04 to 1.13 at temperature range of 2-30^{0}C (Whittemore 1986). The correction coefficient of value 1.04 taken in our study is based on the reduced microbial activity and biochemical reactions at lower temperature (Stefan 1992).

The observed data on water quality parameters and SOD rates represent one point in time and space. Normality tests were conducted for all measured variables using SPSS (2007). The data were also normalized using a weighted normalization method (Bowen 2006, Mazumdar 1996).

$$\text{Normalized value of 'i' variable, } N_i = \frac{Variable_i - Variable_{i_{\min}}}{Variable_{i_{\max}} - Variable_{i_{\min}}} \quad (4)$$

where, $Variable_{imin}$ $Variable_{imax}$ are the minimum and maximum values of variable 'i', respectively.

The normalized data were analyzed by bivariate correlation (Pearson correlation, r) to examine the direction and degree of association among all variables. A principal component analysis (factor analysis) was used to reduce the normalized variables and collinearity in the multivariate analysis. Regression scores generated by SPSS were saved and normalized response variable was regressed against these individual principal components (regression scores). Since the response variable, SOD rate, was also measured as a continuous variable, we used ordinary least square technique to examine the independent effects of each principal components (composite variables) on the response variable. The significance level for these analyses was set at $P<0.05$.

4. RESULTS AND DISCUSSION

4.1 Site Water Column Pollutants

The physical and chemical water quality parameters along Athabasca River varied among the sites (Table 1). The ambient DO ranged from 9.0 mg/L to 11.8 mg/L, the temperature ranged from 3.1 ^{0}C to 11.8 ^{0}C during the field sampling period, pH was stable at 8.1 to 8.2, alkalinity ranged from 93 mg/L to 149 mg/L as $CaCO_3$ and conductivity ranged from 118 μS/cm to 247 μS/cm. In general, total and dissolved constituent concentrations increased moving downstream in the Athabasca River. For example, the lowest and highest concentration of TOC, BOD_5, TDP, Chlorophyll-α, and conductivity were at USHP (upstream site) and at DSCR (downstream site), respectively.

Table 1 Water quality parameters of Athabasca River along its reach

Parameter	USHP	EMBG	UANC	USML	DSMW	BLRG	FTAS	DSTR	CHLM	SMTH	CBRG	USAM	POLG	DSLB	DSCR
Ambient DO, mg/L	10.4	11.1	10.0	9.3	9.7	10.2	9.8	10.1	9.9	9.0	10.3	10.2	10.2	11.6	11.8
Ambient Temp., ^{0}C	5.6	5.7	7.5	13.5	9.5	9.1	8.3	6.6	11.8	11.7	11.4	11.4	11.6	3.1	3.3
Conductivity, µS/cm	210.7	222.7	199.5	270.5	243.7	221.3	206.9	126.2	247.2	238.5	236.0	240.6	239.8	197.9	118.4
pH	8.1	8.2	8.1	8.1	8.2	8.2	8.1	8.1	8.2	8.2	8.2	8.1	8.2	8.1	8.0
Alkalinity, mg/L (as $CaCO_3$)	107.5	109.7	107.3	106.4	147.9	123.9	118.4	117.6	137.5	127.6	131.7	130.3	133.2	126.8	93.3
TOC, mg/L	0.8	2.1	2.2	2.2	3.3	3.6	4.8	5.6	5.6	5.5	6.3	5.1	6.1	5.0	14.7
BOD_5, mg/L	2.0	2.0	2.0	2.0	2.0	2.0	2.4	2.0	2.0	2.0	2.0	2.0	4.5	2.0	2.1
TSS, mg/L	19.0	2.0	3.5	1.0	2.5	1.5	<0.05	5.0	5.0	7.0	7.0	4.0	1.0	<0.05	21.0
TIN, µg/L	81.0	42.0	7.9	7.2	14.5	5.8	12.2	9.7	5.0	5.9	6.1	5.2	7.1	9.4	31.7
TDP, µg/L	1.0	1.4	1.4	2.0	1.8	2.1	2.8	2.1	3.4	4.0	4.7	3.3	3.5	4.1	28.0
Chlorophyll-α, µg/L	0.4	4.7	1.1	1.4	0.7	1.9	2.6	2.2	2.1	2.4	3.3	2.7	3.0	2.9	13.3
Total Fe, mg/L	0.1	0.1	0.02	0.0	0.0	0.1	<0.02	0.06	0.29	0.3	0.3	0.3	0.0	0.2	0.3
SOD, g/m^2.d	0.13	0.38	0.29	0.29	0.25	0.09	0.19	0.21	0.25	0.23	0.30	0.50	0.12	0.25	0.71
SOD_{20}, g/m^{2}d	0.24	0.71	0.54	0.54	0.47	0.17	0.36	0.39	0.47	0.43	0.56	0.94	0.22	0.47	1.33

< denotes data below detection limit

The spatial variations of concentrations of water quality parameters along Athabasca River are shown in Figure 2. The concentrations of TOC revealed clear impact of pollutant discharges in the river. The TOC at EMBG, downstream of Hinton Pulp mill, was about three-fold higher than upstream of the mill. Similarly, TOC was about one and half-fold higher at downstream of DSMW, below discharge points of ANC and Millar Western pulp mills, than UANC, upstream of pulp mills. Similarly TOC

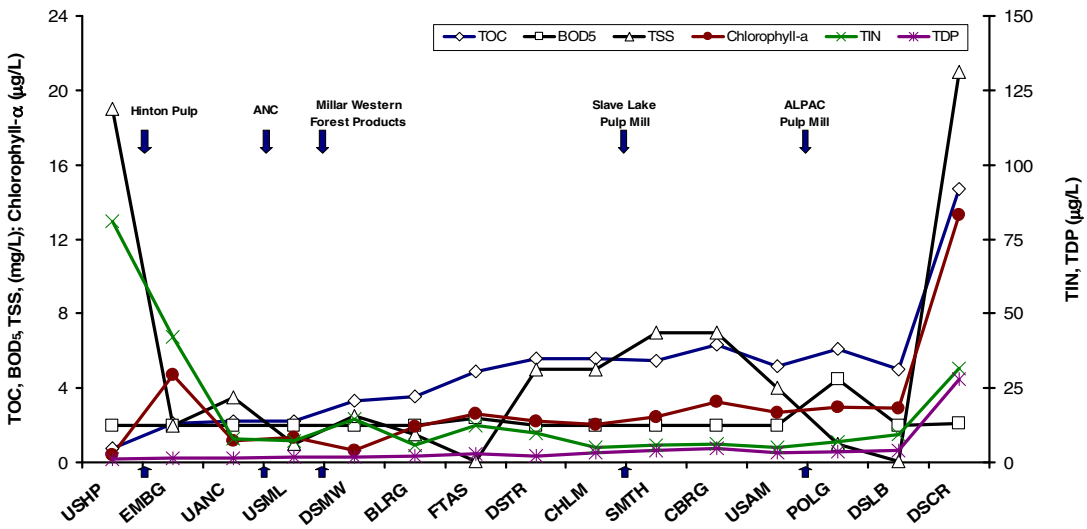

Fig. 2 Spatial variability of water quality parameters along Athabasca River. The arrows represent approximate location of Pulp Mills.

concentration upstream and downstream of the ALPAC pulp mill, at the sites USAM and POLG, was differentiated by a quarter-fold. Tributaries were also large sources of constituent load with clear increases in concentrations of TOC, TDP, and Chlorophyll-α downstream to confluence with Athabasca River. The TOC at FTAS compared to BLRG, indicated organic carbon input from Freeman River to Athabasca

River was considerable. The increase in TOC concentration at CBRG as compared to SMTH was likely due to load from the town of Athabasca wastewater treatment plant, as this is the only large contributor between SMTH and CBRG. The increased TOC concentrations at DSCR were the result of pollutant inputs from La Biche River and Calling River, respectively. The TIN and TSS concentrations were variable but correlated with each other. The TDP and Chlorophyll-α concentrations follow the trend of TOC. The BOD_5 values do not exhibit appreciable variation along the river indicating a relative steady state in oxygen consumption against pollutant load.

4.2 Spatial Variation of SOD Rates along Athabasca River

The spatial variation of SOD rates and TOC concentration are presented in Figure 3 and Table 1. The mean SOD rates determined in this study ranged from 0.09 g/m^2•d at BLRG to 0.71 g/m^2•d at DSCR, when these values are adjusted to SOD rates at 20^0C, the values ranged from 0.17 g/m^2•d to 1.33 g/m^2•d, respectively.

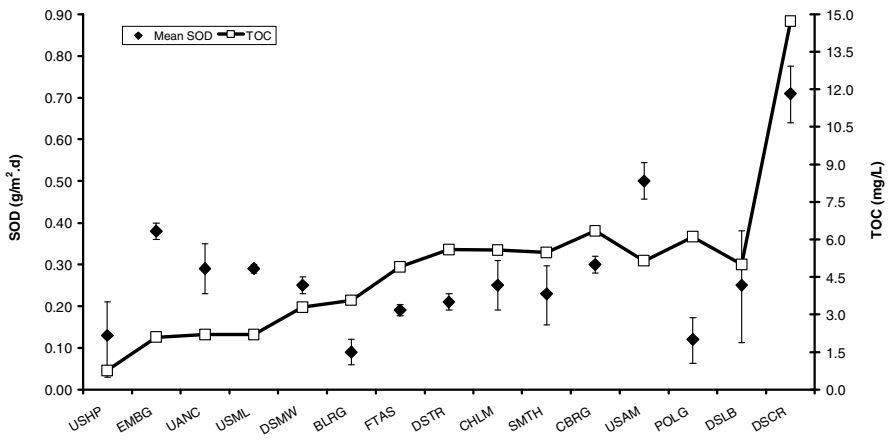

Fig. 3 Spatial variability of SOD rates and TOC concentration along Athabasca River

SOD rates were generally higher at sites downstream of pollutant discharges. The SOD value at EMBG of 0.38 g/m^2•d when compared to the 0.13 g/m^2•d at USHP highlighted the 3-fold effect Hinton Pulp and municipal effluent have on the SOD rates. Similarly, at FTAS, the SOD value of 0.2 g/m^2•d was more than 2-fold higher compared to BLRG of 0.09 g/m^2•d. TOC and SOD rates were positively correlated in the Athabasca River (Figure 3). Other studies have shown that SOD rate is influenced by the availability of organic matter (Doyle and Linch 2005, Yu 2006) and nutrient (Yu 2005). Exceptions were at DSMW and BLRG (Whitecourt area), and POLG (Athabasca) compared to upstream sites. These exceptions were attributed to differences in sediment characteristics. The sediment at USML was fine grained silty, while the sediment at DSMW was course grained silty and sediment at BLRG was sandy. Similarly, the sediment at USAM was fine grained clay/silt, the sediment at POLG was course grained sand/silt. Previous studies indicated that the grain size of sediment influences boundary layer and advective flow at the sediment water interface (SWI) and thus the SOD rate (Grenz et al. 2003).

4.3 Influence of Water Column Pollutants on SOD Rates Along Athabasca River

Historically, the Athabasca River received 5470 kg/day BOD_5, 980 kg/day total nitrogen (TN), and 400 kg/day total phosphorus (TP) load from the effluent discharges of five pulp mills (NREI 2004). In addition to this, 160 kg/day TN and 41 kg/day TP were added by municipal sewage treatment discharges during the period of 1989-1994 (Chambers 2000). Pair-wise correlation revealed strong associations among variables (conductivity, alkalinity, TOC, BOD_5, TSS, TIN, TDP, Chlorophyll–α, and Fe) and the response variable (SOD rate) in normalized dataset pooled for all 15 sites (Table 2). The pH was in very narrow range (8.0 – 8.2) that may not be able to indicate substantial chemical/microbial changes, therefore pH was not included in the correlation. The SOD rate was positively correlated with TOC, TDP and Chlorophyll-α. TOC was negatively correlated with conductivity indicating that groundwater rich water sources were depleted of organic carbon. The BOD_5 and Fe were not correlated with any other variables.

Table 2 Pearson's correlation between SOD rates and water column pollutants for all locations

	SOD	TOC	BOD_5	TSS	TIN	TDP	Chlorophyll-α	Conductivity	Alkalinity
SOD	1.000								
TOC	**0.645****	1.000							
BOD_5	-0.275	0.141	1.000						
TSS	0.436	0.453	-0.196	1.000					
TIN	0.046	-0.188	-0.130	**0.662****	1.000				
TDP	**0.760****	**0.911****	-0.006	**0.645****	0.105	1.000			
Chlorophyll-α	**0.791****	**0.869****	0.032	**0.528***	0.118	**0.948****	1.000		
Conductivity	-0.369	**-0.561***	0.131	-0.483	-0.216	**-0.592***	**-0.595***	1.000	
Alkalinity	-0.405	-0.165	0.199	-0.493	-0.479	-0.448	-0.489	**0.526***	1.000
Fe	0.505	0.465	-0.337	0.373	-0.063	0.384	0.388	0.012	0.149

**. Correlation is significant at the 0.01 level (2-tailed).
*. Correlation is significant at the 0.05 level (2-tailed).

The factor analysis identified three principal components that explained 81.5 % of the variability in SOD rate (Table 3). Principal component 1 was driven by TOC, TDP, Chlorophyll-α, and (negative) conductivity. Principal component 2 was driven by TSS, TIN and (negative) alkalinity. Principal component 3 was driven by (negative) BOD_5 and Fe.

The ANOVA result from the multivariate analysis indicated that the model best fits the data ($F = 5.86$ adjusted $R^2 = 0.61$; $P<0.012$). SOD rate was only significantly related to principal component 1 ($\beta = 0.175$; $P < 0.01$) in regression analysis (Table 4). The result of pair-wise correlation and linear regression confirmed the dependency of SOD rates on TOC, TDP and Chlorophyll-α. But at the same time, there was no strong relationship between SOD rate and TIN, (nitrogen loading). Ammonium oxidation rates may be low and therefore did not consume appreciable amounts of

Table 3 Rotated factor loadings of variables in principal component axes 1-3

	Component		
	1	2	3
TOC	**0.983**	-0.113	0.064
BOD_5	0.163	-0.272	**-0.756**
TSS	0.482	**0.650**	0.370
TIN	-0.104	**0.862**	0.133
TDP	**0.944**	0.216	0.111
Chlorophyll-a	**0.930**	0.210	0.063
Conductivity	**-0.617**	-0.485	0.115
Alkalinity	-0.300	**-0.797**	0.105
Fe	0.408	-0.243	**0.816**
% Variance Explained	46.60	26.20	14.70

Extraction Method: Principal Component Analysis
Rotation Method: Varimax with Kaiser Normalization
Rotation converged in 5 iterations.

DO in water column. Ammonium oxidizing bacteria are slow growing and are severely restricted by low temperature (Metcalf and Eddy 2003). Yu (2006) previously showed that SOD was influenced by organic carbon and nutrients using samples from USAM. In that study increased organic carbon loading caused increased SOD rates. Interestingly BOD_5 was not correlated with TOC or SOD rate. This could be because SOD is created by the microbially mediated degradation of

Table 4 One-way ANOVA - on principal components and SOD rates

Model	Unstandardized Coefficients		Standardized Coefficients Beta	t	Significance
	β	Std. Error			
(Constant)	0.305	0.046		6.662	0.000
Score for Factor 1	0.175	0.047	0.689	3.683	0.004
Score for Factor 2	0.036	0.047	0.141	0.755	0.466
Score for Factor 3	0.088	0.047	0.347	1.856	0.090

Model F = 5.86; P<0.012
Regression degrees of freedom = 3
Error Degrees of freedom = 11
Adjusted R^2 = 0.61
Number of cases = 15

organic matter (labile or refractory) deposited on river bed over a period of time, whereas BOD_5 is only sensitive to easily biodegradable (labile) organic matter in water column. A negative correlation between SOD rate and conductivity as well as the lack of correlation with Fe suggested SOD rate is primarily determined by

carbonaceous degradation and little influenced by the hypertonic input of reduced metals and other species in ground water.

A comparison of SOD results of this study with those undertaken in the past at different time period highlighted spatial and temporal variation, as shown in Table 5. In most sites, the SOD rates found in this study were higher than previous studies. There were variations in SOD rates in the fall of 2006 and fall of 2004, indicating that SOD rates varied with time period as sediment deposition and composition varied. The temporal variations of SOD rates shown in Table 5 could be attributed to climatic condition, quantity of river flow, and to older data, inaccuracy of the chamber method (Tian 2005; Yu 2006). Results from this study suggested that models for predicting SOD rate must incorporate suites of environmental variables, particularly in river

Table 5 Average SOD rates along Athabasca River at different period of times

Site	SOD ($g/m^2.d$)		
	2006 Fall[ξ]	2004 Fall / 2005 Winter[Ŧ]	1990 - 1995*
U/S of Hinton Pulp	0.13	0.16	0.05
Emerson Bridge	0.38	0.12	0.00
U/S of McLeod River	0.29		0.12
2 km D/S of Millar Western Mill	0.29		0.34 (0.23 - 0.57)
Blue Ridge	0.09		
Fort Assiniboine	0.19	0.32	
D/S of Timeu River	0.21		
Chisholm	0.25	0.06	
Smith	0.23		0.13 (0.10 - 0.20)
C-Bridge	0.30		
U/S of ALPAC Mill Intake	0.50		0.18 (0.15 - 0.21)
Poacher's Landing	0.12		
D/S of La Biche River	0.25		
D/S of Calling River	0.71	0.18	0.09

[ξ] This study

[Ŧ] Yu (2006): Averaged SOD rates for 24 hour and 48 hour incubation

* Averaged SOD rates for the period of 1990 to 1995, and ranges are in parantheses (Tian, 2005)

water ecosystems. It is especially difficult to create simple models to predict SOD rates because oxygen demand both depends on and influences the concentration of many chemical parameters. It is shown that SOD can be measured relatively easily. This study was taken in the context of results by Tian (2005) and Yu (2006) that indicated organic carbon and, to a lesser extent, nitrogen and phosphorus influence SOD rates. However, more work is needed on modeling where SOD determined analytically and site specific sediment characteristics, nutrients and physical characteristics (e.g. velocity) are be used to predict temporal and spatial variability.

5. CONCLUSION

The spatial variations of SOD rates at fifteen locations along Athabasca River measured during the fall season of 2006 were presented in this study. SOD rates were

higher downstream from effluent discharges and tributaries. However, other factors such as sediment characteristics were also important. In determining relationship among SOD rates and organic matter or nutrients, it was found that SOD rates are correlated positively with TOC, TDP, and Chlorophyll-α. Observations indicate that SOD rates were also influenced by sediment types revealing that finer sediment grain had higher SOD rates compared to coarser grained sediment. The relationship among SOD rates and water quality parameters show that SOD modeling could be achieved by incorporating several key parameters.

ACKNOWLEDGEMENT

The financial support was provided by Alberta Environment, NSERC, Alberta News Print Co., Alberta Pacific Forest Industries Inc., Hinton Pulp, Millar Western Forest Products Ltd., and Slave Lake Pulp. The assistance of Nathan Findlay in field data collection, and contributions of Joanne Volk of Hinton Pulp, Dan Moore and Boyd Payne of Alberta Newsprint Co, Mark Spafford of ALPAC during site location and sample collection were instrumental. Prem Bhandari of University of Alberta is acknowledged for assistance with statistical analysis.

REFERENCES

Bowen, H. P., Moesen, W., and Sleuwaegen, L. (2006). "A Composite Index of the Creative Economy with Application to Regional Best Practices". *Vlerick Leuven Gent Management School Working Paper Series: 2006-31*, September, Belgium, 1-35.

Casey, R. J. (1990). *Sediment Oxygen Demand during the Winter in the Athabasca River and Wapiti-Smoky River System.* Edmonton, Alberta: Alberta Environment.

Chambers, P. A., Brown, S., Culp, J. M., Lowell, R. B., and Pietroniro, A. (2000). "Dissolved Oxygen Decline in Ice-Covered Rivers of Northern Alberta and its Effects on Aquatic Biota". *Journal of Aquatic Ecosystem Stress and Recovery* 8, 27–38.

Chambers, P. A., Culp, J. M., Glozier, N. E., Cash, K. J., Wrona, F. J., Noton, L. (2006). "Northern Rivers Ecosystem Initiative: Nutrients and Dissolved Oxygen – Issues and Impacts". *Environmental Monitoring and Assessment*, 113, 117–141.

Doyle, M. C. & Lynch, D. D. (2005). "*Sediment Oxygen Demand in Lake Ewauna and the Klamath River, Oregon June 2003*". U. S. Geological Survey, Scientific Investigation Report, 2005-5228.

Grenz, C., Denis, L., Boucher, G., Chauvaud, L., Clavier, J., Fichez, R., Pringault, O. (2003). "Spatial Variability in Sediment Oxygen Consumption under Winter Conditions in a Lagoonal System in New Caledonia (South Pacific)". *Journal of Experimental Marine Biology and Ecology*, 285–286, 33– 47.

Mazumdar, K. (1996). "An Analysis of Causal Flow between Social Development and Economic Growth: The Social Development Index". *American Journal of Economics and Sociology*, 55(3), 361-383.

Metcalf and Eddy (2003). *Wastewater Engineering, Treatment and Reuse*. New York: McGraw Hill.

Monenco Inc. (1993). *Northern River Basin Study Project Report: Sediment Oxygen Demand Investigations Athabasca River January to March 1992*. Northern River Basin Study Project Report No. 3, Edmonton, Alberta.

Murphy, P. J. & Hicks, D. B. (1986). "In-Situ Method for Measuring Sediment Oxygen Demand". *In (K. J. Hatcher Ed.)Sediment Oxygen Demand: Processes, Modeling and Measurement*, INR, University of Georgia, Georgia, pp. 307-322.

Noton, L. R. (1996). *Investigations of Streambed Oxygen Demand, Athabasca River, October, 1994, to March, 1995*. Northern River Basins Study Project; Report No. 94. Edmonton, Alberta.

NREI (2004). *Northern Rivers Ecosystem Initiative 1998-2003: Final Report*. Edmonton, Alberta: Alberta Environment.

Reimers, C. E., Jannke, R. A., & Thomsen, L. (2001). "In Situ Sampling in the Benthic Boundary Layer". (In B. P. Boudreau and B. B. Jorgensen (Eds.), *The Benthic Boundary Layer Transport Processes and Biogeochemistry* (pp. 245). New York: Oxford University Press).

SPSS (Statistical Package for the Social Sciences) version 16.0, (2007), SPSS Inc., Chicago, IL, USA.

Standard Methods for the Examination of Water and Wastewater (1998), 20th Edition, Washington, DC: American Public Health Association.

Stefan, H. G. (1992). "Sediment Oxygen Demand and Its Effect on Winterkill in Lakes". *Proc. US Army of Corps of Engineers Workshop on Sediment Oxygen Demand*, 21-22 August 1990, pp. 137-142.

Tian, Y. (2005). *A Dissolve Oxygen Model and Sediment Oxygen Demand Study in the Athabasca River. Master's Thesis*, Edmonton, Alberta: University of Alberta.

Whittemore, R. C. (1986). "The Significance of Interfacial Water Velocity on the Measurement of Sediment Oxygen Demand". (-In (K. J. Hatcher Ed.). *Sediment Oxygen Demand: Processes, Modeling and Measurement*, INR, University of Georgia, Georgia, pp 63-74).

Yu, M. (2006). *Sediment Oxygen Demand Investigation and CE-QUAL-W2 Model Calibration in the Athabasca River. Master's Thesis*, Edmonton, Alberta: University of Alberta.

A comparison of a SWAT model for the Cannonsville Watershed with and without Variable Source Area Hydrology

Josh Woodbury[1], Christine A. Shoemaker[1], Dillon Cowan[1], and Zach Easton[2]

[1] School of Civil and Environmental Engineering, Cornell University, Ithaca, NY, 14853, USA
[2] Department of Biological and Environmental Engineering, Cornell University, Ithaca, NY, 14853, USA

Abstract:

In this study, two different versions of the Soil and Water Assessment Tool (SWAT) are used to simulate the Cannonsville Watershed. These versions are referred to as SWAT_TS and SWAT_VSA. The SWAT-VSA model distributes overland flow in ways that are consistent with variable source area hydrology, while the SWAT_TS model does not. Since many water quality models, such as SWAT, use some form of the curve number equation to predict storm runoff, these models may fail to accurately describe the effects of variable source areas (VSAs), which are mostly important in rural, humid areas, such as upstate New York. These two models are compared by calibrating each for flow, phosphorous and sediment against measured data.

Introduction:

The Cannonsville Reservoir is a large drinking water reservoir located in Delaware County in upstate New York. The reservoir is one of the largest of New York City's drinking water reservoirs. The Cannonsville Watershed is approximately 1200 km^2 consisting of mostly forested and agricultural lands. Due to agriculture in the area, the reservoir has often experienced water quality problems due to heavy phosphorous loading. The phosphorous has caused concerns as to whether or not New York City can continually use this water without the need for a water filtration plant.

The Soil and Water Assessment Tool (SWAT) has previously been used to accurately model the Cannonsville Watershed (Tolson and Shoemaker, 2007b). The SWAT model is a watershed scale model created to simulate long term runoff and nutrient losses in rural, agriculturally dominated watersheds. The model requires such information as soils data, elevation data and land use information. This data is then lumped together into hydrologic response units (HRUs) to direct flows and sub-basin routing. The model then requires climate data, such as temperature, precipitation and solar data in order to simulate the watershed.

In this study, two different versions of SWAT are used to model the watershed. These versions are called SWAT_TS and SWAT_VSA. The SWAT_VSA version simulates flow using variable source area hydrology, while the SWAT_TS version does not. Variable source area (VSA) hydrology is the concept that runoff generating locations vary both in time and

space, depending on time of year, rainfall, temperature and topography (Easton et al., 2008). In VSA hydrology, surface runoff is not evenly distributed over the land, but is concentrated in specific areas. This concept can have a large impact on nutrient transport, and is therefore an important consideration in management techniques. The SWAT_TS and SWAT_VSA models are calibrated against measured data in order to compare the accuracy of each.

Description:

Both of the models in this study are modified versions of the SWAT 2005 model. The first model, SWAT_TS uses a modified version of the SWAT 2005 source code. Previous work done using the SWAT 2000 model showed that the results improved with certain source code changes (Tolson and Shoemaker, 2007b). These changes include modifications of the daily manure spreading, plant growth, flow in/on frozen soils, monthly subbasin temperatures and the MUSLE equation. These modifications are described in more detail in (Tolson and Shoemaker, 2007b). The source code changes make up the difference between the SWAT_TS model and the SWAT 2005 model.

The second model, SWAT_VSA, includes the modifications in SWAT_TS as well as the variable source area hydrology (VSA). The major difference between the SWAT_VSA and the SWAT_TS models are in the way that the HRUs are created. In SWAT_TS, the HRUs are defined by the coincidence of soil type and land use. In order to incorporate VSA hydrology into SWAT, a topographic wetness index is used together with land use to define the HRUs (Easton). The soil topographic index (STI) is defined as:

$$STI = \ln\left(\frac{a}{T\tan\beta}\right)$$

where a is the upslope contributing area for the cell per unit of contour line (m), tan β is the topographic slope of the cell, and T is the transmissivity (soil depth x saturated soil hydraulic conductivity) of the uppermost layer of soil ($m^2\ d^{-1}$) (Easton et al., 2008). These index classes are then numbered from 1, the driest and least prone to saturate, to m, the most prone to saturate (Easton). For the SWAT_VSA, there are 10 different index classes.

Calibration:

The SWAT_TS and the SWAT_VSA models are calibrated using an algorithm called dynamically dimensioned search, or DDS. DDS is a simple stochastic single-solution based heuristic global search algorithm designed for automatic calibration of watershed models (Tolson and Shoemaker, 2007a). DDS performed better on a Cannonsville subbasin than a variety of other methods (Shoemaker et al., 2007). Although SWAT has many outputs, this study focuses mostly on phosphorous, so calibrations are done for flow, sediment and phosphorous. In order to get the best results, each model is calibrated in steps, with flow calibrated first, sediment second and phosphorous last. When calibrating for each constituent, only parameters that are directly related to the constituent vary, all other parameters remain constant. For example, when calibrating for phosphorous, only phosphorous parameters vary.

For the flow calibrations, the DDS algorithm is used to minimize the sum of squared errors between measured and simulated values over time.

$$SSE = \sum_{t} \left(Measured_t - Simulated_t \right)^2 \quad (1)$$

In equation (1), SSE is the sum of squared errors and t is time. Next, the models are calibrated for sediment, while keeping the optimized flow parameters constant. This is done using the DDS algorithm and a weighted objective function.

$$OF = SSE_{Flow} + \alpha_{Sed} SSE_{Sed} \quad (2)$$

Where:

$$\alpha_{Sed} \approx \frac{SSE_{Flow}}{SSE_{Sed}} \quad (3)$$

Since the SSE values for flow and sediment can vary by orders of magnitude, weighting values, the alphas, are used when calibrating for sediment. The weighting scheme normalizes the SSE values of flow and sediment. It is necessary to include flow when calibrating for sediment because many of the parameters that largely impact sediment output also impact flow output.

The final step involves calibrating for phosphorous. There are two types of phosphorous that are important in this study, total dissolved phosphorous (TDP) and particulate phosphorous (PP), each of which are outputs in the SWAT model. Using the parameters from the flow and sediment calibrations, the phosphorous is calibrated using the following objective function with DDS:

$$OF = SSE_{Flow} + \alpha_{Sed} SSE_{Sed} + \alpha_{TDP} SSE_{TDP} + \alpha_{PP} SSE_{PP} \quad (4)$$

Where:

$$\alpha_{TDP} \approx \frac{SSE_{Flow}}{SSE_{TDP}} \quad (5)$$

$$\alpha_{PP} \approx \frac{SSE_{Flow}}{SSE_{PP}} \quad (6)$$

The weighting values are necessary for the same reasons they are necessary for the sediment calibration. The weighting values normalize the SSE values so that each constituent is equally weighted. The following tables summarize the parameters used for flow, sediment and phosphorous.

Table 1: Parameters used in flow calibration.

Parameters	Description
SFTMP	Snowfall temperature
SMTMP	Snow melt base temperature
SMFMX	Maximum melt rate for snow during year where deg C refers to the air temperature
TIMP	Snow pack temperature lag factor
SURLAG	Surface runoff lag time
GW_DELAY	Groundwater delay time
ALPHA_BF	Alpha factor for groundwater recession curve
GWQMN	Threshold depth of water in shallow aquifer
LAT_TIME	Lateral flow travel time
ESCO	Soil evaporation compensation factor
CN2_f	CN multiplicative factor
DEPTH_f	Depth multiplicative factor
BD_f	Bulk Density multiplicative factor
AWC_f	Available Water Content multiplicative factor
KSAT_f	Saturated hydraulic conductivity multiplicative factor

Note: Multiplicative factors are used to linearly scale the parameters between their minimum and maximum values.

Table 2: Parameters used to calibrate sediment.

Parameters	Description
ADJ_PKR	Peak rate adjustment factor for sediment routing in the subbasin
PRF	Peak rate adjustment factor for sediment routing in the channel
SPCON	Linear parameter for calculating sediment
SPEXP	Exponent parameter for calculating sediment re-entrained in channel routing
LAT_SED	Sediment concentration in lateral flow
SLSUBBSN_f	Sverage slope length multiplicative factor
SLSOIL_f	Slope length for lateral subsurface flow multiplicative factor
CH_EROD	Channel erodibility factor
CLAY_f	Clay content multiplicative factor
ROCK_f	Rock content multiplicative factor

Note: Multiplicative factors are used to linearly scale the parameters between their minimum and maximum values.

Table 3: Parameters used in phosphorus calibration.

Parameters	Description
PPERCO	Phosphorus percolation coefficient
PHOSKD	Phosphorus soil partitioning coefficient
CMN	Rate factor for humus mineralization
P_UPDIS	Phosphorus uptake distribution parameter
ERORGP	Organic P enrichment ratio
PSP	Phosphorus availability index

Acknowledgements:

This research has been supported primarily by a grant from the USDA to Shoemaker and Steenhuis, and supplanted by an NSF grant to Shoemaker. We appreciate the codes and advice provided by Prof. Bryan Tolson, University of Waterloo, Canada.

References:

Easton, Z.M., Fuka, D.R., Walter, M.T., Cowan, D.M., Schneiderman, E.M., Steenhuis, T.S., 2008. "Re-conceptualizing the soil and water assessment tool (SWAT) model to predict runoff from variable source areas". *Journal of Hydrology*, 348 (2008), pp. 279–291

Neitsch, S.L., J.G. Arnold, J.R. Kiniry, and J.R. Williams. 2004a. Soil and Water Assessment Tool Theoretical Documentation Version 2005. US Department of Agriculture – Agricultural Research Service, Temple, Texas.

Neitsch, S.L., J.G. Arnold, J.R. Kiniry, and J.R. Williams. 2004a. Soil and Water Assessment Tool User's Manual Version 2005. US Department of Agriculture – Agricultural Research Service, Temple, Texas.

Shoemaker, C., R. Regis, R. Fleming, 2007. "Watershed calibration using multistart local optimization and evolutionary optimization with radial basis function approximation". *Hydrological Sciences*, 52(3), pp. 450-465 http://www.atypon-link.com/IAHS/doi/abs/10.1623/hysj.52.3.450 (Open Access)

Tolson, B. A., and C.A. Shoemaker, 2007a, "Dynamically dimensioned search algorithm for computationally efficient watershed model calibration". *Water Resour. Res.*, 43, W01413, doi:10.1029/2005WR004723. 2007

Tolson, B. and C.A. Shoemaker, 2007b "Cannonsville Reservoir Watershed SWAT2000 model development, calibration and validation," *Journal of Hydrology*, 337(1-2), pp. 68-89, doi:10.1016/j.jhydrol.2007.01.017, 2007b

Effective management of Natural Resources under dry land farming through watershed basis

Murukannappa[1] and N. Indrakumar[2]

[1] Research Associate. AICRP for Dryland Agriculture, University of Agricultural Sciences, GKVK, Bangalore – 560 065, Karnataka, India

[2] Associate Professor (Agril. Engineering), AICRP for Dryland Agriculture, University of Agricultural Sciences, GKVK, Bangalore – 560 065, Karnataka, India

Abstract

All India Co-ordinated Research Project for Dryland Agriculture, University of Agricultural Sciences, GKVK, Bangalore, conducted an experiment by adopting proven in-situ management of rainwater technologies Vetiver (khus) and Pennisitum (Nase) grass as vegetative live bunds with contour bunds. Runoff water harvesting structure such as farm ponds of 180 cubic meter capacity were dug for runoff collection from about 0.6 to 0.7 hectare area having two per cent land slope with Agro-forestry system has served as crop insurance. Lining materials were used to minimize the seepage loss from the stored water which was used for providing life saving irrigation to highly remunerative vegetable crops like chilli (sambruddi). Results of the study during the period (2000-05) clearly indicated that, the highest runoff of 93.2 mm accounting to 9.7% of the total mean annual rainfall under control plot (no inter terrace management practices) was observed. However, the runoff produced in both the inter-terrace management practices were on par with each other (65.5 to 65.9 mm). The highest mean annual soil loss of 5.66 t/ha/year under control plot and the lowest (3.151 t/ha/yr) was recorded under inter-terrace management with nase live barrier. Organic farming through application of green leaf manure (6 – 8 t/ha) enhanced the productivity of finger millet and an additional income of Rs.50,000/- with agro-forestry.

Introduction

By adopting innovative, low cost and location specific conservation measures may helps in reduced surface runoff, soil erosion and nutrient loss from the fertile top soils. Estimation of such resource degradation is much useful to design and develop suitable location specific conservation measures for different topographic features of that are. Uncertain rainfall with heavy down pour in a single storm is common in dryland situation which may cause surface runoff resulting flooding in down stream area which affect the low laying cropped area. Harvesting and effective recycling of harvested runoff through farm pond in arable lands are very effective harvesting structures increase the cropping intensity by providing life saving irrigations. Keeping this in view, a study was carried out to quantity resources (runoff, soil loss and nutrient loss) degradation under micro-watershed management at the Institute since last two decade. Conservation practices with improved techniques may adopt during the period helps to sustain the productivity of Dryland crops.

Objectives:

1. To promote in-situ soil moisture conservation through inter-terrace management practices.
2. To quantify runoff and soil loss under integrated watershed management with harvesting and recycling.

3. To study the seepage loss from water harvesting structures.
4. To accesses the tree species on the bunds and inter terrace management practices.
5. To workout the economic and sustainability of the system.

Treatments

Khus (vetiver) live barrier.
Nase (Pennisitum) live barrier
No Inter-terrace management practice.
Farm pond lined with 8:1 soil cement lining.
LDPE sheet overlaid with brick lining.
LDPE sheet over lay with brick frame work lining.

Micro-watershed catchments having 2% land slope are delineated into 0.6 to 0.7 hectare each by adopting 0.52 cross sectional contour bunds with open end with a horizontal interval of 30 – 50 mt. Each plot developed with the vegetative barriers (vetiver and penisitum) in between the two bunds and cultivation of crop across the slope. Excess rainwater (runoff) is harvested and stored in a farm pond of 180 m2 capacity which was designed by considering the highest rainfall of 160 mm for the recurring interval of 15 years. Bi-modal distribution of rainfall in the region, uncertain rain produced 6 to 14 runoff events in a year. Water harvesting structures lined with relevant materials to control the seepage loss which is high under red soil regions. Harvested water is effectively utilized through life saving irrigation to second crop may have high remunerative vegetable crops.

Results:

The inter-terrace management practices may help in conserving rainwater and soil which reduced the erosion of these resources. Adoption of inter-terrace management practices like khus and Nase live barriers for the individual land holdings resulted that the maximum mean runoff of 93.2 mm under plot without inter-terrace management practices as compared to khus and Nase live vegetative barriers (65.7 mm). The results clearing indicated that by adopting inter-terrace management practices which may conserve more rain (40 to 46 mm) besides reduce the runoff by 28 per cent compared to control. However, both inter-terrace management practices are on par with each other irrespective of the rainfall amount, intensity and duration and which may helps in enhancing the crop yield as shown below;

Table.1: Inter-Terrace Management Practices produced runoff under Individual Land Holdings

Treatments	Run off (mm)					Mean
	2000	2001	2002	2003	2004	
Khus inter-terrace management	84.1 (6.83)	87.08 (8.7)	29.5 (4.7)	38.1 (5.9)	90.6 (9.1)	65.9 (7.1)
Nase inter-terrace management	88.3 (7.2)	89.2 (8.9)	30.6 (4.9)	36.8 (5.7)	82.8 (8.3)	65.5 (7.0)
Control	129.2 (10.5)	134.0 (12.1)	46.1 (7.4)	51.4 (7.9)	105.3 (10.6)	93.2 (9.7)
Mean	100.5 (8.2)	103.4 (9.9)	35.4 (5.6)	42.1 (6.5)	92.9 (9.3)	74.9 (7.9)

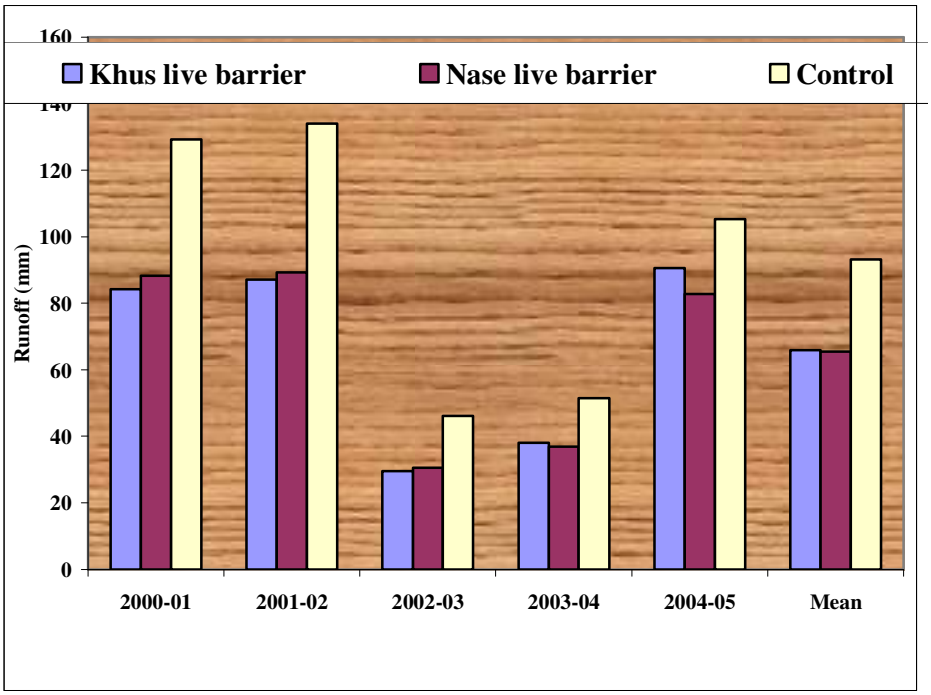

Incorporation of organic (GLM) and inorganic (fertilizers) manures gave highest grain yield of finger millet (2121 kg/ha) under GLM + Nase live barrier followed GLM + khus live barrier (1924 kg/ha) and 1647 kg/ha under with out any GLM and inter-terrace management practices. However, the marginal increase in finger millet grain yield from 1379 kg/ha with 50 % RDF to 1647 kg/ha under 100 % RDF as presented in Table below;

Table.2: Effect of Integrated Micro-Watershed Management Practices and Fertility Management on productivity of Dryland crops

Treatments	**Finger millet grain yield (kg/ha)**		
	100 % RDF	**50 % RDF**	**Mean**
GLM + Khus inter-terrace management	1924	1788	1856
GLM + Nase inter-terrace management	2121	1687	1904
Only GLM	1844	1644	1744
Control (No inter-terrace management)	1647	1379	1513
Mean	1884	1624	-

Horsegram grown as green manure crop for in-situ incorporation gave higher bio-mass yield under khus live barrier plot (8.97 t/ha) followed by nase live barrier plot (8.3 t/ha) compared to control (6.0 t/ha) which influence on grain yield of finger millet under both inter-terrace management practices (2121 kg/ha and 2103 kg/ha) as compared to control (1961 kg/ha) during 2005-06 as presented below;

Table.3: Crop Yield as influence by green manure application Under Dryland condition

Treatments	**In-situ green bio-mass with Horsegram (t/ha)**		**Grain yield (kg/ha)**	
			FB (2004)	**FM (2005)**
Khus inter-terrace management	7.4	8.97	269	2121
Nase inter-terrace management	7.9	8.3	536	2103
Control	5.6	6.0	106	1961

Soil loss of 7.139 t/ha/yr under control plot as compared to 4.036 t/ha/yr and 3.812/ha/year in khus and Nase inter-terrace management practices during 2000-01. However, the mean annual soil loss under both the inter-terrace management practices was on par with each other and which helps in reducing 44 percent (3.15 t/h) and 3.231 t/ha) as compared to 5.6 t/ha under control (without any inter-terrace management practices). More rainfall coupled with higher intensity of rain may cause more soil erosion (ranging from 3.812 to 7.139 t/ha/yr) during the year 2000 and 2001. The result indicate that the amount and intensity of rainfall directly proportional and duration of rainfall indirectly proportional to the soil erosion as presented in table and figure below;

Table.4: Soil Loss as influence by Inter-terrace Management Practices under Individual Land Holding.

Treatments	Soil loss (T/ha)				Mean
	2000-01	2001-02	2002-03	2003-04	
Khus inter-terrace management	4.036	3.971	2.015	2.135	3.210
Nase inter-terrace management	3.812	4.013	1.917	1.986	3.151
Control	7.139	6.981	3.651	3.472	5.6
Mean	4.99	4.98	2.528	2.531	3.99

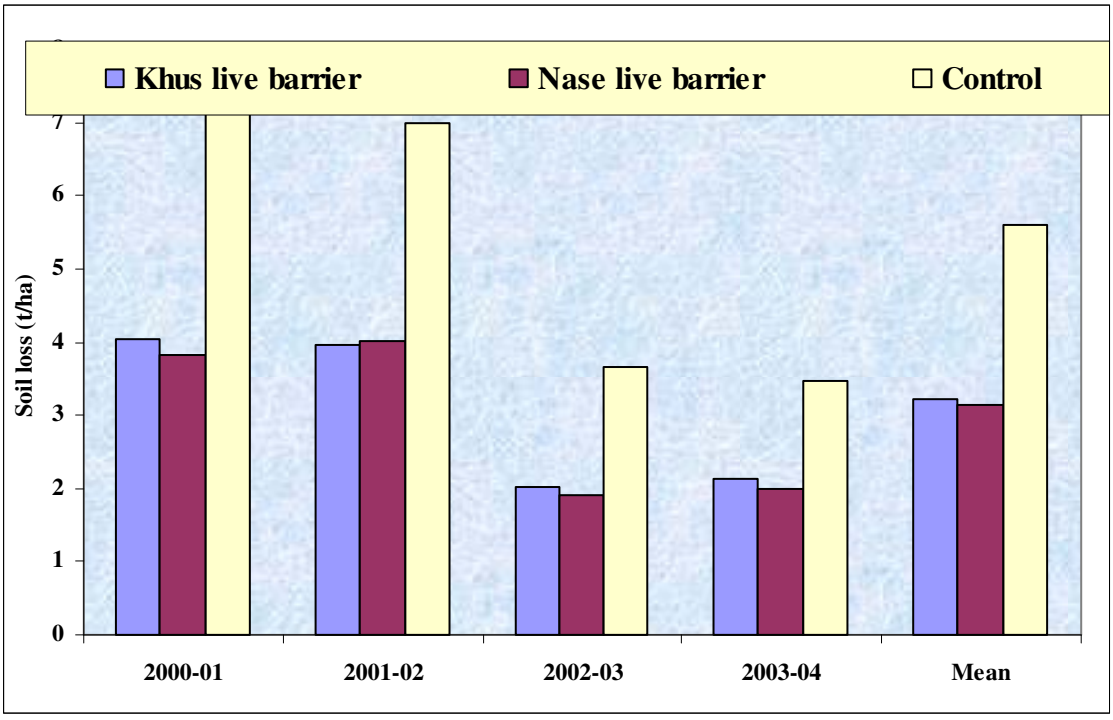

In khus live barrier treatment, Finger millet produced highest yield of 2605 kg/ha as compared to Nase live barrier (2575 kg/ha) and control (2315 kg/ha). By adopting the khus /Nase inter-terrace management practices, the grain yield of finger millet enhanced by 10-15 per cent as compared to the control as presented in table below;

Table-5: Grain Yield of Finger Millet as influence by Inter-terrace Management Practices.

Treatments	Finger millet Grain yield (Kg/ha)				B.C. ratio
	2000	2001	2003	Mean	
Khus inter-terrace management	1924	2892	3480	2605	1.98
Nase inter-terrace management	2121	2815	3260	2575	1.95
Control	1844	2775	2680	2315	1.74
Mean	1963	2827	3140	2498	

Khus and Nase live barriers as inter-terrace management practices for individual land holdings of less than 2 to 3% land slope at an interval of 15 to 30 m horizontal distance are the effective low cost inter-terrace management practices.



References

Anonymous, Land resource management for food and environmental security, soil conservation society of India, New Delhi, 2001, 138-194

Anonymous, 2006, Report for the quinquennial review team, Rain water management, All Indian Co-ordinated Research Project for dryland Agriculture, Bangalore main centre, University of Agricultural Sciences, GKVK., Bangalore-560 065, 78-135

Druvanarayan,V.V.N.,2002, Soil and water conservation Research in India, Directorate of information and publications of agriculture, ICAR, Krishi Anusandhan Bhavan, Pusa, New Delhi.

Murthy,V.V.N., 1998, Land and water management Engineering, A text book published by Kalyani publishers, New Delhi.

Evaluation of uncertainties in the simulation of watershed nutrient load: A case study

M. Karamouz[1], M. Taheriyoun [2], M. Seyedabadi [3], S. Behboodian[3]

[1-]Fellow ASCE , Professor, School of Civil Engineering, University of Tehran; Email: karamouz@ut.ac.ir
[2-] Ph.D. Candidate, Faculty of Environment, University of Tehran; Email: taherion@ut.ac.ir
[3-] M.Sc. student, School of Civil Engineering, University of Tehran,

ABSTRACT

Estimation of watershed nutrient loads into the reservoir through a simulation model is a vital step in eutrophication management of reservoirs. The analysis of uncertainty associated with the utility of simulation models is an important consideration in the development of Total Maximum Daily Load plans in the control of watershed nutrient loading. When using models during the development of the TMDL, either to predict loadings or to simulate water quality, managers should address the inherent uncertainty in the predictions. In this paper, a Monte Carlo based probabilistic approach namely Generalized Likelihood Uncertainty Estimation (GLUE) is utilized to develop a computational procedure for analysis of the model uncertainties on prediction of phosphorous loads of a distributed watershed model, Soil and Water Assessment Tools (SWAT). In the GLUE method a cumulative likelihood for nutrient outputs of the SWAT model is generated. Quantile analysis of the cumulative likelihoods yields expected nutrient loads as well as their corresponding uncertainty limits. Uncertainty bounds could be used to obtain a Margin of Safety (MOS) for such evaluations in the TMDL formula. The analysis is demonstrated for the Aharchai watershed in the North –Western part of Iran.

Keywords: Nutrient load, uncertainty, SWAT model, GLUE method

INTRODUCTION

Eutrophication is the enrichment of waters with plant nutrients which results in an array of symptomatic changes, namely increased production of algae and aquatic macrophytes, deterioration of water quality and other undesirable changes that interfere with water uses. In many regions around the world, eutrophication has been recognized as a priority water quality problem. The main cause of this phenomenon is the excessive nutrient load from the watershed upstream of the reservoir. Thus control and reduction of watershed nutrient loads is a key step in reservoir water quality remediation.

USEPA (1999) has established the Total Maximum Daily Load (TMDL) process for impaired waterbodies especially eutrophied lakes and reservoirs. This process determines the allowable nutrient loading to a reservoir to preserve the water quality standards. In this process, margin of safety should be taken into account to consider the uncertainty about the relationship between pollutant loads and receiving water quality.

When using models during the development of the TMDL, either to predict loadings or to simulate water quality, managers should address the inherent uncertainty in the predictions. Various techniques for doing so include sensitivity analysis, first-order analysis, and Monte Carlo analysis. Implications of uncertainty associated with model predictions have not been widely endorsed in the decision making process mainly as a result of large uncertainty estimates. The magnitude of uncertainty itself is a key factor in the acceptance of the implementation cost of management actions such as the Total Maximum Daily Load (TMDL) program. The larger uncertainty estimates cause a significant increase in the cost.

Arabi 2007, developed a computational framework to investigate the uncertainty in the evaluation of watershed management practices. The Generalized Likelihood Uncertainty Estimation (GLUE) method was employed to generate a cumulative likelihood for sediment and nutrient outputs of the Soil and Water Assessment Tool (SWAT) for two scenarios with and without implementation of BMPs. The analysis focused specifically on the ranges of some model parameters that require site-specific adjustments with available data and the uncertainty associated with estimated effectiveness of BMPs.

Shirmohammadi et al. (2006) described the experience of scientists and engineers in the assessment of uncertainty associated with TMDL models. They reviewed sources and methods of uncertainty including Monte Carlo simulation (MCS), Latin hypercube sampling (LHS), and generalized likelihood uncertainty estimation (GLUE). It also presented strategies for communicating uncertainty in TMDL models to users. Four case studies were presented to highlight uncertainty quantification in TMDL models. It concluded that uncertainty in TMDL models was a real issue and should be taken into consideration during both the TMDL assessment and implementation phases.

Sohrabi et al. (2003) provided appropriate probability distributions for each of the most sensitive input parameters of SWAT2000 and showed the combined effect of such variability on model output in the form of cumulative probability distribution curves. They concluded that variability in model output caused by inaccurate input estimates can be reduced by decreasing the uncertainty in the inputs through increasing the number of measurements of the parameter and improving the methods used to measure the parameter.

Vogel et al. 2008 showed how the choice of a likelihood function in the GLUE methodology is critical and when properly implemented with a statistically valid function can provide credible regions for model prediction.

In this study, GLUE methodology is applied to estimate the uncertainties embedded in the SWAT model for prediction of total phosphorous load input to the Satarkhan dam reservoir at Aharchai river watershed in the north-western part of Iran. In the following sections first the case study is introduced then the methodology and tools

for uncertainty estimation is described and finally the results and conclusion are discussed.

CASE STUDY

The Study area is Aharchai river watershed in north-western Iran in East Azerbaijan province and is one of the sub-basins of the Aras River. The watershed is located between 38° 24' and 38° 41'N and 46° 20' and 46° 55' E as shown in Figure 1. The Satarkhan dam was constructed in 1998 to provide water for drinking, irrigation, mining and industrial use in the region. Therefore, water quality of the reservoir is of great concern which has been deteriorated during recent years due to excessive nutrient loads which have resulted in reservoir eutrophication.
Satarkhan reservoir watershed encompasses 93000 ha with land use distributions of 36.5% dry farming, 1.4% irrigated farming, 5.3% combination of irrigated farming and orchard land use, 12% bared land, 16.6% combination of dry farming and range, 27.3% range, 0.5% urban area, and 0.4% water. The average flow at the outlet of the basin is 2.9m^3/s. The water quality data at Orang station at the intake of the reservoir is available from August 2002 to December 2005 for a 41 month period.

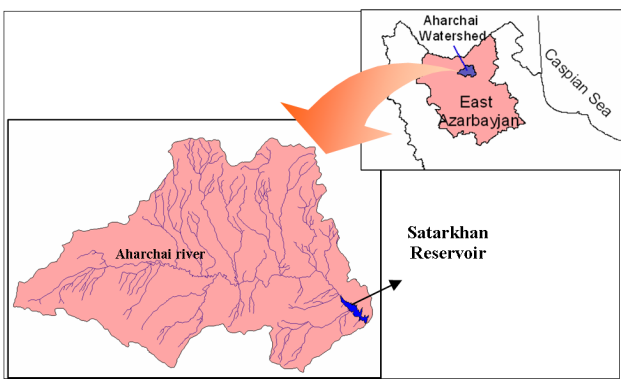

Figure 1 **Aharchai River and Satarkhan reservoir watershed in east Azerbaijan – North-western Iran**

SWAT MODEL

SWAT (Soil and Water assessment Tools) is a physically-based, time continuous simulation model that operates on a daily time step. It is designed to evaluate management effects on water quality, sediment production and yields of agricultural chemicals. The major components of SWAT include hydrology, weather, erosion, pesticide and nutrients. (Neitsch et al. 2000). The SWAT model divides the watershed into sub-basins to represent the large scale spatial heterogeneity of the studied area. Each sub-watershed is parameterized using a series of HRUs (hydrologic response units) which are a particular combination of land cover, soil and management. All model calculations are performed at the HRU level. The EPA currently supports this model for developing TMDLs in agricultural watersheds. SWAT consists of three major components: (1) sub-basin, (2) reservoir routing, and (3) channel routing. GIS interfaces have been developed to facilitate the aggregation

of input data. This interface requires a land cover map, soils map, and DEM. A detailed description of the model can be found at the SWAT website (www.brc.tamus.edu/swat/index.html). In this study the watershed of Aharchai River was subdivided into 20 sub-basins (HRUs) as shown in Figure 2.

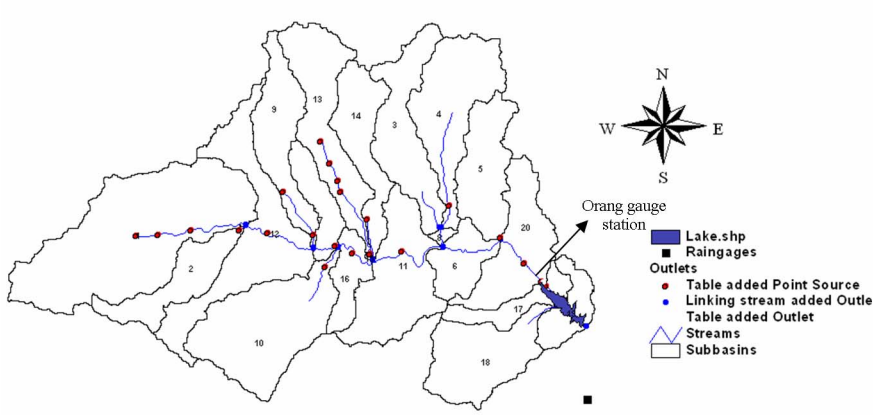

Figure 2 Aharchai Watershed with 20 sub-basins (HRUs)

UNCERTAINTY ANALYSIS TECHNIQUE

Here, the techniques of uncertainty analysis consisting of sensitivity analysis and generalized likelihood uncertainty estimation (GLUE) used in this study will be explained. The total procedure includes a combination of two techniques discussed here.

SENSITIVITY ANALYSIS

Sensitivity analysis is the simplest method in uncertainty analysis and is used to identify the model parameters that have the most influence on predicted outputs. In this process, each model run involves perturbation of only one parameter in turn. Therefore, the variation of model output can be clearly ascribed to the variation of the corresponding input parameter. For each input parameter, local sensitivities are computed at different points of the parameter range, and then the global effect is obtained by calculating their average.

Sensitivity analyses may not be needed when the model contains only a few parameters. However, in a complicated model like SWAT when the number of parameters is large, and as more than one output is affected by the same parameter, sensitivity analysis is needed to identify the model parameters that have the greatest impact on model outputs. A relative sensitivity coefficient can be calculated according to Eq. (1) and used to rank model parameters (Shirmohammadi et al. 2007)

$$S_r = \frac{\partial O}{\partial P} \times \frac{P}{O} \qquad (1)$$

Where *O* is output of interest, and *P* is the input parameter under analysis. The S_r calculated using this method is dimensionless and can be used to compare all parameters. One of the limitations of using S_r to identify the most sensitive model parameters is that it does not account for covariance among parameters. (Shirmohammadi et al. 2007)

GENERALIZED LIKELIHOOD UNCERTAINTY ESTIMATION

The Generalized Likelihood Uncertainty Estimation (GLUE) technique introduced by Beven and Binley (1992) is an innovative uncertainty method that is often employed with environmental simulation models. It is a sampling method that uses the behavior and non-behavior classification concept to distinguish between the fraction of Monte Carlo simulations that matches the system behavior and the complement fraction that does not. The main argument that led to the development of GLUE is that for a selected model structure, several combinations of model parameters (in contrast to a unique optimum) may exist that are equally good for reproducing the system behavior. Beven and Binley (1992) suggested that uncertainties due to errors in model structure and effects of correlation structure in the parameter space are implicitly handled within the GLUE procedure. In the GLUE method, the relative importance of model parameters is not evaluated individually and independently but as a set of parameters. Each set of model parameters within a given model structure is evaluated as a single unit. In other words, it is the parameter set that is important to produce system behavior, not the individual parameters. First, retained behavior-giving Monte Carlo simulations are given weights based on a likelihood function. A likelihood measure based on the Nash-Sutcliffe efficiency criterion with shaping factor *N* is defined as (Freer and Beven, 1996),

$$L(\alpha|y) = (1 - \frac{\sigma_\varepsilon^2}{\sigma_o^2})^N \qquad (2)$$

where $L(\alpha|y)$ is the likelihood of parameter set(α), given the observed data (y); σ_ε^2 refers to the error variance between model simulations and observed data, and σ_o^2 is the variance of the observed data. Beven and Binley (1992) used N=1 but suggested that the shape factor can be chosen by the user. For N = 1, $L(\alpha|y)$ in Eq. (2) is the Nash–Sutcliff efficiency coefficient (E_{N-S}) which is often used as the calibration criteria of hydrologic and water quality models like SWAT.

This coefficient is considered as a qualitative criterion to group the generated model parameters into two sets: (1) *behavioural* sets of model parameters that produced results consistent with the observations, and (2) *nonbehavioural* sets of model parameters that produced results that contradict the observations.

A negative E_{N-S} value indicates that the corresponding model output is unlike the behavior of the system under study, and the likelihood of such simulation in mimicking the system behavior is zero. Therefore, the likelihood function is defined as follows (Arabi,et al, 2007) :

$$L(\alpha|y) = \max\left[(1-\frac{\sigma_\varepsilon^2}{\sigma_o^2}),0\right]; \quad (3)$$

Then, the likelihood estimates associated with model simulations are rescaled such that they sum up to 1.0 and are used as likelihood weights to form a cumulative weighted distribution for the output of interest which can be used for estimation of uncertainty bounds associated with the output by computing its quantiles. The GLUE method is dependent not only on the choice of likelihood function, but also to the cutoff criterion used for classification of Monte Carlo simulations to behavior and non-behavior sets. (Arabi et al. 2007)

METHODOLOGY

The methodology structure utilized in this study consists of the watershed model (SWAT) applied for simulating the fate and transport of phosphorous load input to the reservoir and an uncertainty analysis methodology based on two sampling based methods: sensitivity analysis and Generalized Likelihood Uncertainty Estimation (GLUE; Beven and Binely, 1992).

A computational method was developed to limit the range of input parameters to adjusted ranges corresponding to the observed data, used in the GLUE analysis. The methodology was tested on Aharchai watersheds located in northwest Iran. This shows the usefulness of the developed computational analysis to quantify modeling uncertainties associated with estimated phosphorous load.

A schematic of the uncertainty analysis process used for phosphorous load estimation through SWAT model is presented in Figure 3.

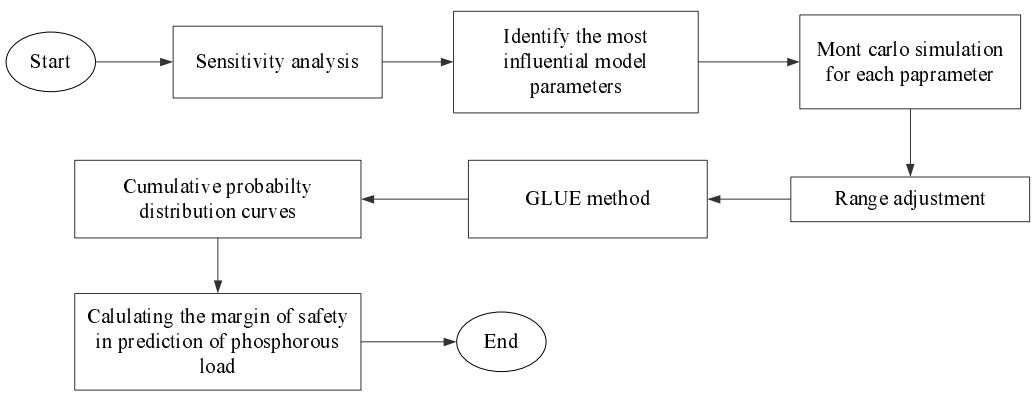

Figure 3. Flowchart of uncertainty estimation process

RESULTS AND DISCUSSION

SENSITIVITY ANALYSIS

Figure 4 presents the results of the sensitivity analysis calculated for the SWAT model parameters. The target output of the SWAT model is the phosphorous load at sub-basin 20 located just upstream of the reservoir.

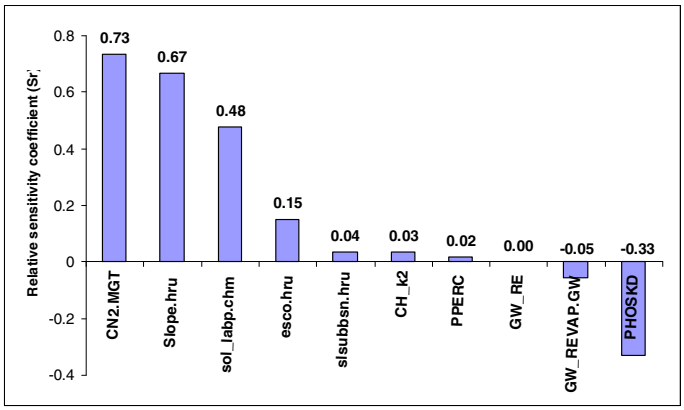

Figure 4. Results of sensitivity analysis

According to results of sensitivity analysis the most sensitive parameters were selected in the GLUE analysis as shown in Table 1.

Table 1 – Top five sensitive SWAT parameters for watershed phosphorous load

No	Parameter	Description	*Sr*
1	CN2.mgt	SCS runoff curve number	0.73
2	Slope.hru	Average slope steepness (m/m).	0.67
3	Sol_labp.chm	Initial soluble P concentration in soil layer	0.48
4	Phoskd.bsn	Phosphorus soil partitioning coefficient (m3/Mg).	-0.33
5	Esco.hru	Soil evaporation compensation factor	0.15

BEHAVIORAL RANGE ADJUSTMENT

Using the entire parameter ranges in the uncertainty analysis may result in a large number of simulations with negative likelihoods ($L(\alpha|y)$) that make the GLUE analysis ineffective and time consuming. Therefore, adjustment of ranges of sensitive input parameters is an essential step before quantifying the uncertainty of model outputs.

To adjust the behavioral range of the parameters for each individual parameter, 60 random value based on the uniform distribution is generated and for each run the phosphorus load and the likelihood measure is calculated. The behavioral range of each parameter is identified according to the positive value of the likelihood function which is depicted in Figure 5 for all 5 sensitive parameters selected in this study. The base case value of the input parameters was selected from a calibrated and validated model for a 41 month data of phosphorous load. The data was measured just upstream of the reservoir at sub-basin 20 from August 2002 to December 2005.

The FORTRAN source code of the SWAT model was developed to derive the probability distribution according to the set of parameter variations.

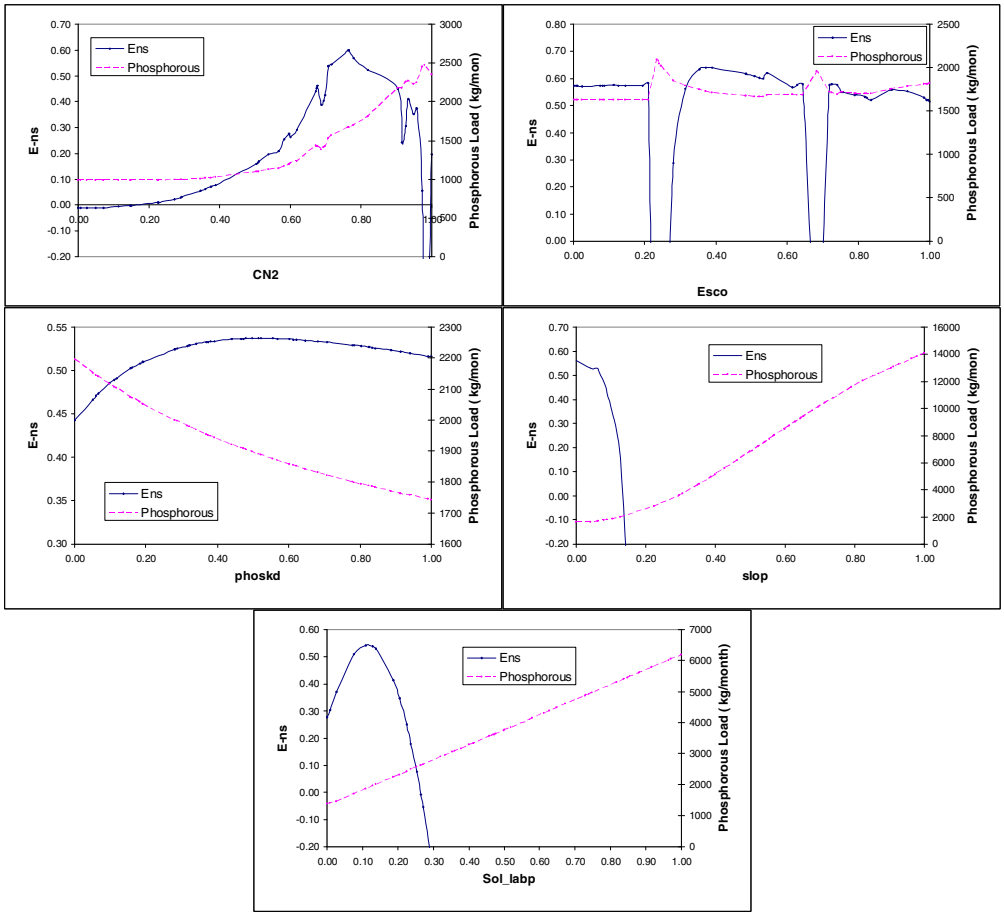

Figure 5- Plots for the top five sensitive SWAT input parameters related to average monthly phosphorous load

Table 2 – Behavioural parameter ranges for the study watersheds

No	Parameter	Suggested range	Behavioral range
1	CN2.mgt	35-96	44-96
2	Slope.hru	0.013- 0.594	0.013-0.09
3	Sol_labp.chm	0.38-94	0.38-25
4	Phoskd.bsn	100- 198	100- 198
5	Esco.hru	0.017-0.971	0-0.22, 0.27-0.65 , 0.68-0.97

THE UNCERTAINTY ANALYSIS

Adjusted parameter ranges from previous step were used to probabilistically determine the margin of safety in the load estimation. In this study, 1000 model simulations using Monte Carlo method were performed for the 2002–2005 period. Five sensitive model parameters in Table 1 were included in the analysis using the behavioral range. For each realization of the parameter space, the uncertainty analysis requires the following steps:

1. Select parameter values from the adjusted ranges randomly.

2. Perform model simulation with the selected values to compute model outputs
3. Compute likelihood of the simulation for monthly output variables based on Nash-Sutcliff equation.
4. Using GLUE-likelihood weights computed at previous step, generate a cumulative density function for phosphorous load

Figure 6 presents the cumulative likelihood distribution of average monthly phosphorous load at inlet of Satarkhan dam reservoir. This figure is very important in determining the margin of safety in total maximum daily load (TMDL) process. Uncertainty bounds could be used to obtain a Margin of Safety (MOS) for such evaluations in the TMDL formula. As shown in Fig. 6, lower and upper bounds are obtained according to 10th and 90th percentiles of the cumulative likelihoods, respectively. Therefore, the uncertainty bounds of phosphorous load simulation model equals to [1140, 1980] kg/month.

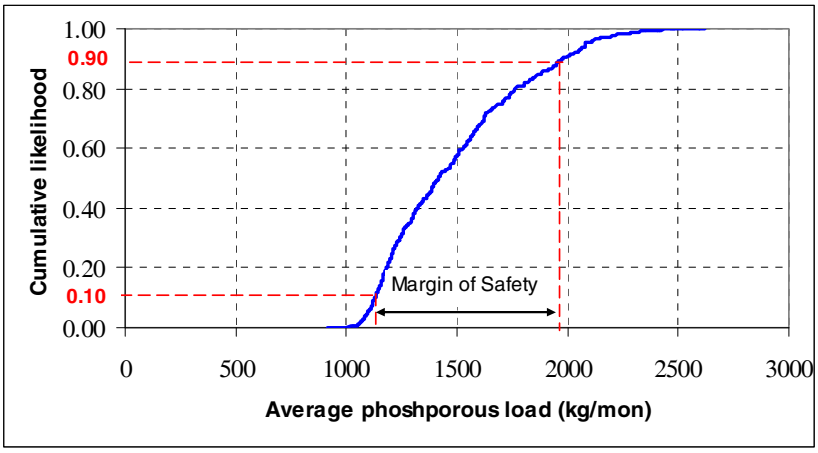

Figure 6. Cumulative GLUE-likelihood for phosphorous load simulated at the Satarkhan reservoir inlet

SUMMARY AND CONCLUSION

An uncertainty analysis process was developed, in which investigation of uncertainty provides complementary quantitative and qualitative information to support management and decision making. The analysis focused specifically on two issues. First, ranges of some model parameters that may require site-specific adjustments with observed data. This was particularly evident for parameters that are not determined from landscape characteristics. The computational procedure for the analysis of uncertainty was performed for Aharchai watershed just upstream of Satarkhan reservoir. It was demonstrated that the computational procedure is able to quantify the uncertainty of phosphorous load of the watershed. The main focus was on investigation of the utility of the developed methodology in the TMDL process. Especially, the means for coping with the margin of safety (MOS) in the TMDL formula.

Once the level of protection is provided by the margin of safety (MOS) by decision makers, the uncertainty analysis presented in this study could be applied to verify the success of a particular management action in achieving its designated goals.

Implementation of the estimated MOS is more feasible in this context, as opposed to the MOS computed from uncertainty analysis of absolute model predictions where the additional cost of implementation may render its consideration impractical. Finally, the methodology can be easily incorporated in other watershed and water quality models that are commonly used for TMDL development.

REFERENCES

Arabi, M., Govindaraju, R., Hantush, M., 2007. A probabilistic approach for analysis of uncertainty in the evaluation of watershed management practices. Journal of Hydrology Elsevier 333, 459– 471

Karamouz M. , Taheriyoun M. Emami F. , Rohanizadeh B. (2008), Assessment of nutrient load input to a reservoir, a case study, World Environmental and Water Resources Congress ASCE 2008 Ahupu a'a

Vogel R. M., Stedinger J. R., Batchelder Rebecca , Lee Seung Uk, (2008), Appraisal of the Generalized Likelihood Uncertainty Estimation (GLUE) Method, World Environmental and Water Resources Congress – ASCE 2008 Ahupua'a

Neitsch, S.L., Arnold, J.G., Kiniry, J.R., Williams, J.R., King, K.W., 2002. Soil and Water Assessment Tool theoretical documentation, version 2000. Grassland, Soil and Water Research Laboratory, Agricultural Research Service, Temple, TX

Beven, K.J., Binely, A.M., 1992. The future of distributed models: model calibration and uncertainty prediction. Hydrological Processes 6, 279–298.

Beven, K.J., Freer, J., 2001. Equifinality, data assimilation, and uncertainty estimation in mechanistic modeling of complex environmental systems using the GLUE methodology. Journal of Hydrology 249 (2001), 11–29.

Spear, R.C., Hornberger, G.M., 1980. Eutrophication in Peel Inlet II: identification of critical uncertainties via generalized sensitivity analysis. Water Research 14, 43–49.

Spear, R.C., Grieb, T.M., Shang, N., 1994. Parameter uncertainty and interaction in complex environmental models. Water Resources Research 30 (11), 3159–3169

Dilks, D.W. and Freedman, P.L. (2004). "Improved consideration of the Margin of Safety in Total Maximum Daily Load development." Journal of Environmental Engineering, ASCE, 130(6):690-694.

Montanari, A. (2005), Large sample behaviours of the generalized likelihood uncertainty estimation (GLUE) in assessing the uncertainty of rainfall-runoff simulations, Water Resour. Res., W08406, doi:10.1029/2004WR003826.

Shirmohammadi, A., Chaubey, I., Harmel, R., Bosch, D., Muñoz-Carpena, R., Dharmasri, D., Sexton, A., Arabi, M., Wolfe, M., Frankenberger, J., Graff, C., Sohrabi, t., 2006. Uncertainty In Tmdl Models. American Society of Agricultural and Biological Engineers Vol. 49(4): 1033−1049

Sohrabi, T. M., A. Shirmohammadi, T. W. Chu, H. Montas, and A. P. Nejadhashemi. 2003. Uncertainty analysis of hydrologic and water quality predictions for small watershed using SWAT2000. Environ. Forensics 4: 229-238.

Modeling Framework for Establishing Water Quality Trading Units near Pacific, Missouri

Yee-Sook Shin and Kathleen M. Trauth, Ph.D., P.E., M.ASCE

[1]Department of Civil and Environmental Engineering, University of Missouri, E2509 Lafferre Hall, Columbia, MO 65211; Ph (573) 882-8015; email: yssvv2@mizzou.edu
[2]Department of Civil and Environmental Engineering, University of Missouri, E2509 Lafferre Hall, Columbia, MO 65211; Ph (573) 882-5843; email: trauthk@missouri.edu

ABSTRACT

The Environmental Protection Agency (EPA) has promulgated a water quality trading policy. (WQT). The discharge of pollutants may be traded within/between locations in a watershed as long as nowhere along the applicable stream are water quality criteria exceeded. The tradable discharges may be of a point or a nonpoint nature. While the trading of point source pollutants has progressed, nonpoint source pollution (NPS) trading has not made as much progress. As the EPA stated in the policy statement, the development of appropriate trading units will be a considerable difficulty for nonpoint trades. The specification of trading units for nonpoint source trading may be difficult because of uncertainty for a number of reasons. The first of these is that trading must be initiated and executed legally in the present in order to trade with/for pollutants generated in the future. Nonpoint source pollutants, by their nature, can be generated by a number of different sources in different locations; the greater the number of sources and locations, the greater the uncertainty in their quantification. In addition, the generation of nonpoint source pollutants is driven, in part, by precipitation. Even as precipitation patterns are understood, there is considerable variability in the precipitation intensity and total volumes at specific locations at specific times. To meet these challenges, a research effort has been undertaken. As a start, a modeling system has been set up/established in a rapidly developing location southwest of St. Louis, Missouri. The test location is the Brush Creek watershed, where the area of the outlet of the watershed intersects the community in and around Pacific, Missouri. Because of its location 30 miles southwest of St. Louis, Missouri, the Pacific region expects to see considerable development that could increase the generation of nonpoint source pollutants. In addition, because Pacific is located in the lower portion of the watershed, nonpoint source pollution expected to be generated in the city could be traded with upstream locations and not cause decreases in water quality anywhere along Brush Creek. Because of the uncertainties associated with NPS trading, it can only be addressed via modeling. For this initial effort, the modeling is being limited to discharges and the generation of sediment. U.S. Geological Survey data for discharges and sediment concentrations in the Meramec River have been used to calibrate EPA's HSPF model for the Brush Creek watershed. Alternative development scenarios have been developed to represent potential conditions in the upstream and downstream locations that may be associated with a trade. Multiple precipitation patterns allow the modeling to represent the variability that may occur in the precipitation that drives the generation of sediment loads. Altogether, the modeling framework is appropriate to investigate and offer insights into the development of NPS trading units. Because Brush Creek is not currently impaired, and is not associated with any regulatory actions, it is an excellent location within which to test the modeling framework.

BACKGROUND

Water Quality Trading

In 2003, the U.S. Environmental Protection Agency (EPA) promulgated a policy regarding water quality trading (WQT). The policy states that WQT could be a means to address water pollution problems in an innovative fashion by trading between various pollutant dischargers that have varying capacities to control pollutant discharges. Those that have excess ability to control pollutant discharges can sell that ability to dischargers that cannot easily control discharges or would like to expand operations that would normally increase discharges. The ultimate goal of the policy is to promote an improvement in water quality.

Trades are theoretically possible two point sources, between a point source and a nonpoint sources, and between two nonpoint sources. Trades involving nonpoint source pollutants would be the most difficult to establish because of the distributed nature of the source and because of the variability associated with nonpoint sources initiated by precipitation rather than irrigation water. This difficulty in characterizing nonpoint source pollutants can be identified as the difficulty in establishing trading units—that is, what exactly is to be traded between pollutant dischargers. With nonpoint source pollutants, one could consider trading actual pollution (e.g., pollutant concentrations or quantities over time). Because nonpoint source pollution is impacted by land use, trading units could theoretically be acres of land with varying characteristics and with varying land uses/land covers. In addition, trading units could be modified based on the implementation best management practices (BMPs) that are intended to improve the quality of storm water runoff. Property owners may have the ability to control nonpoint pollutant discharges from land surfaces either by not developing the land and/or implementing BMPs. Another difficulty with nonpoint sources is that they may simultaneously include multiple pollutants in the runoff water.

Any water quality trades would have to maintain compliance with water quality criteria everywhere along a stream of interest. This means that donating sites (sites that are not developed as might be expected and thus produce less pollution) must always be upstream of receiving sites (sites that might be developed more intensely than might ordinarily be allowed, thus generating additional pollution).

HSPF

There are multiple computation tools available to model water quality associated with nonpoint source pollutants. Once such tool is EPA's HSPF. HSPF simulates water quality incorporating many parameters that arose out of agricultural investigations—land use/land cover, soil type and conditions/performance, as well as the precipitation that provides for the transport of materials from the land surface to a body of water.

OBJECTIVE

The objective of this research effort is to propose and test out a water quality modeling framework that would assist in the establishment of trading units for water quality trades between two nonpoint pollutant sources.

METHODOLOGY

Study Area

The study area is the Brush Creek watershed, as indicated in Figure 1. This watershed is part of the larger Meramec River watershed that has its outlet at the Mississippi River south of St. Louis, Missouri. Brush Creek is located in what is called the Pacific Ring, an area of land within a 7-mile radius of the city of Pacific, MO. Residents of this area are interested in maintaining the environmental quality of their surroundings, even as they are experiencing more and more growth coming from the direction of St. Louis toward their undeveloped agricultural and forested land. The fact that this location contains many undeveloped areas, and is experiencing increasing development pressure, makes this area a perfect one in which to begin to investigate water quality trading. In addition, the lower portions of the Brush Creek watershed coincide with the limits of the City of Pacific. This is shown in Figure 2, where the outline of the City of Pacific is shown in purple. Locations already within the city limits might experience additional pressures to develop where there is already infrastructure and where there is existing economic activity. These lower portions might be considered as receiving sites under a water quality trading proposal. Many upper portions of the watershed are covered in forest or are used for agriculture. If these sites are not developed and/or agricultural areas are taken out of production or operated with conservation practices, they might be considered to function as donating sites.

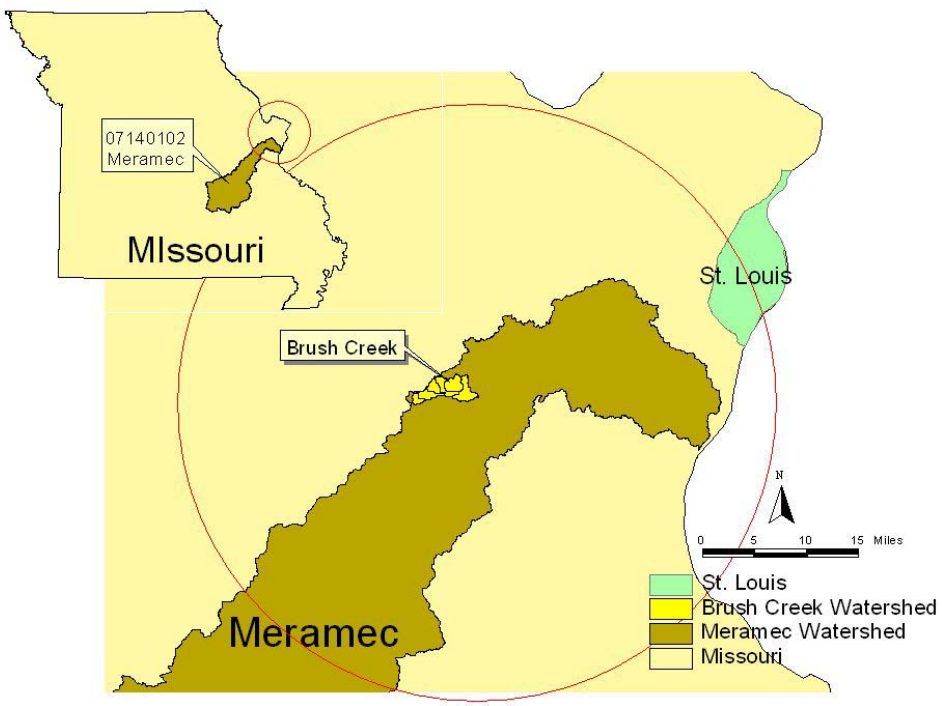

Figure 1. Location of Brush Creek watershed within the Meramec River watershed.

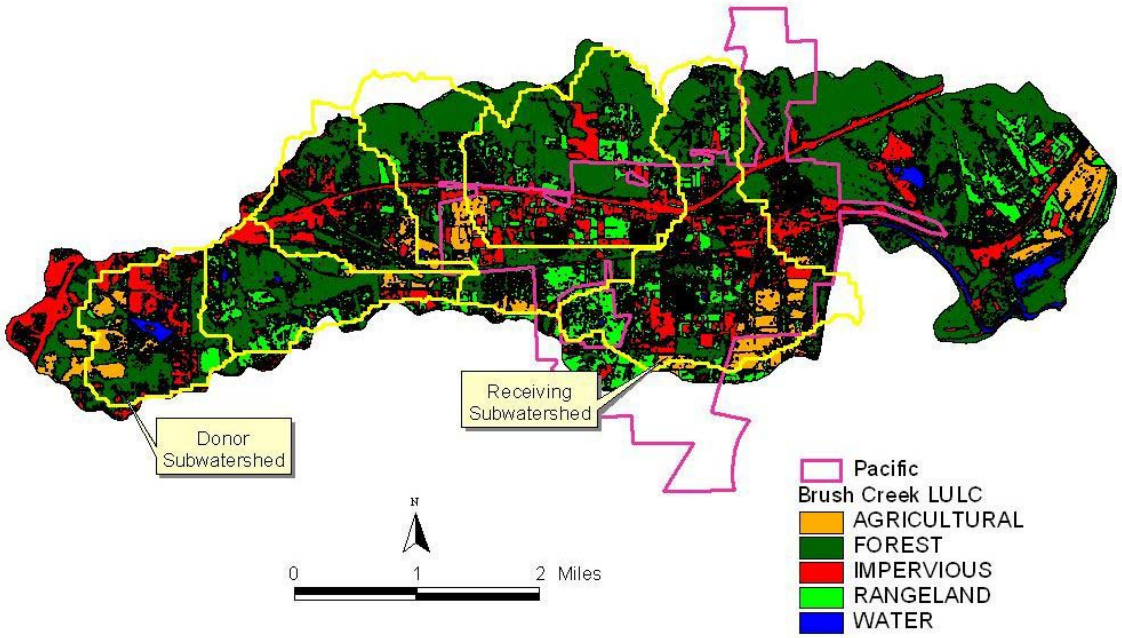

Figure 2. Brush Creek watershed with subbasins superimposed upon a land cover map.

Data Sources

U.S. Geological Survey (USGS) stream flow and sediment concentration data were used to calibrate the HSPF model for the Brush Creek watershed. Data are available for the Meramec River below the confluence with Brush Creek, so it was necessary to calibrate the model for the overall Meramec basin and utilize that model for the trading calculations. The calibration and validation plots for discharge are shown in Figures 3 and 4. The observed and simulated sediment concentrations for the period of USGS data are shown in Figure 5.

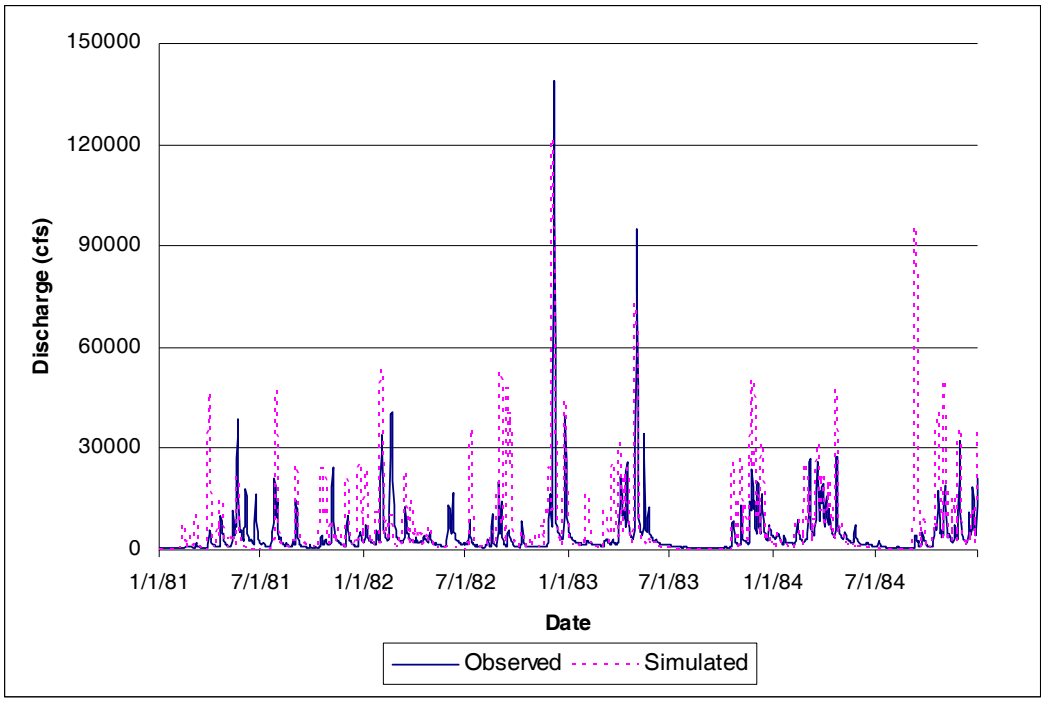

Figure 3.Scatterplot of simulated versus observed runoff for model calibration.

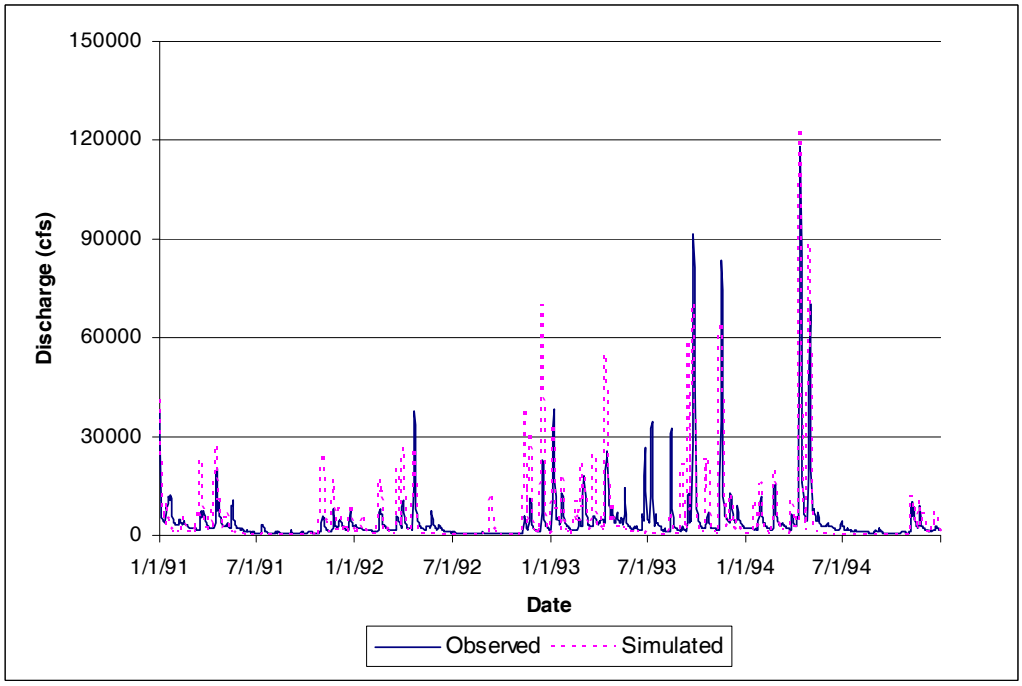

Figure 4. Scatterplot of simulated versus observed runoff for model validation.

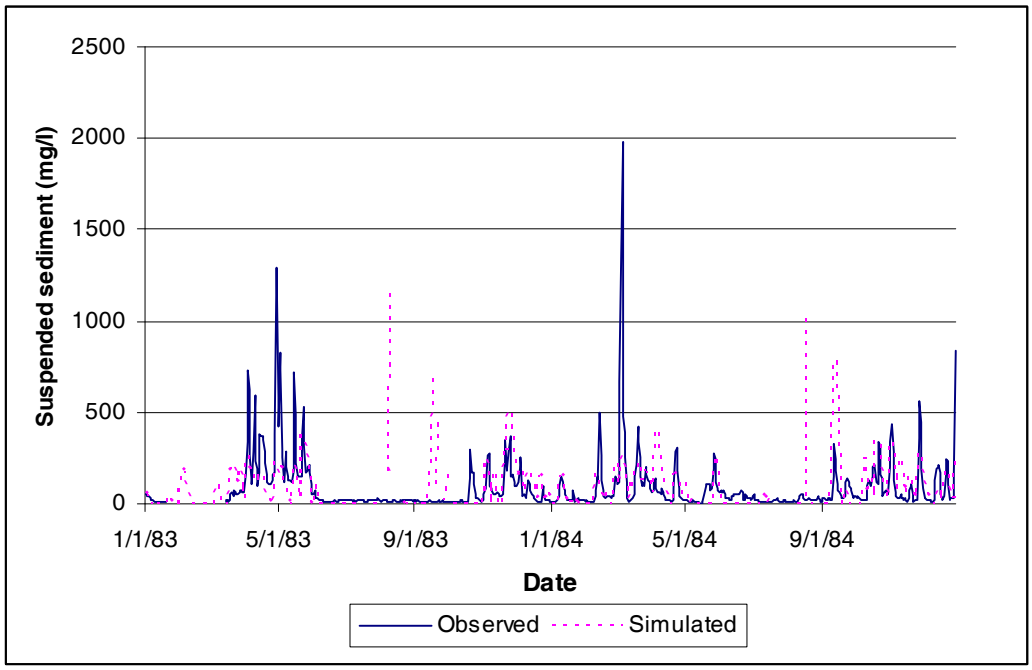

Figure 5. Scatterplot of simulated versus observed suspended sediment concentration.

A land cover classification map was developed for another project within the Pacific Ring. This classification can be seen in Figure 2.

Scenario Development

Nonpoint source water quality trades would be associated with land use patterns that are different than what normally be expected or allowed in a given location. The trade might be implemented through a mechanism such as a transfer of development rights. A trade would be based on understanding how different development scenarios would impact water quality. Such an understanding would allow for the establishment of a trade requirement. Such a requirement could specify how many acres of land at a given level of development and with what, if any BMPs, would be needed to be traded in order to provide a reduction in pollutant discharges equivalent to the increase associated with a more intense development scenario. In the development of this modeling framework, several development scenarios were established. These include the development of agricultural lands and forested lands and range land with varying percents of impervious surface.

RESULTS

Figure 6 shows the average discharges at the Brush Creek watershed outlet associated with Scenario 1, current land cover conditions for both up-watershed donor and down-watershed receiver locations. Scenarios 2-10 have no change to the donor locations, but do incorporate changes to the receiver locations. This graphic shows the trend of increasing discharges with increasing levels of impervious surface, as would be expected. The yellow markers represent changes associated with the development of agricultural land. “Agri 70” indicates that agricultural land was developed to a level of 70% impervious surface. “Agri 50” represents the

discharge associated with development to only 50% impervious surface that is lower than that of "Agri 70." Similar trends are seen for the development of forest land and range land. The exact values are a function of the amount of acreage developed as well as the soil and topographic characteristics of the developed land. The variation in the values shows that the specification of trading units will be site specific in nature.

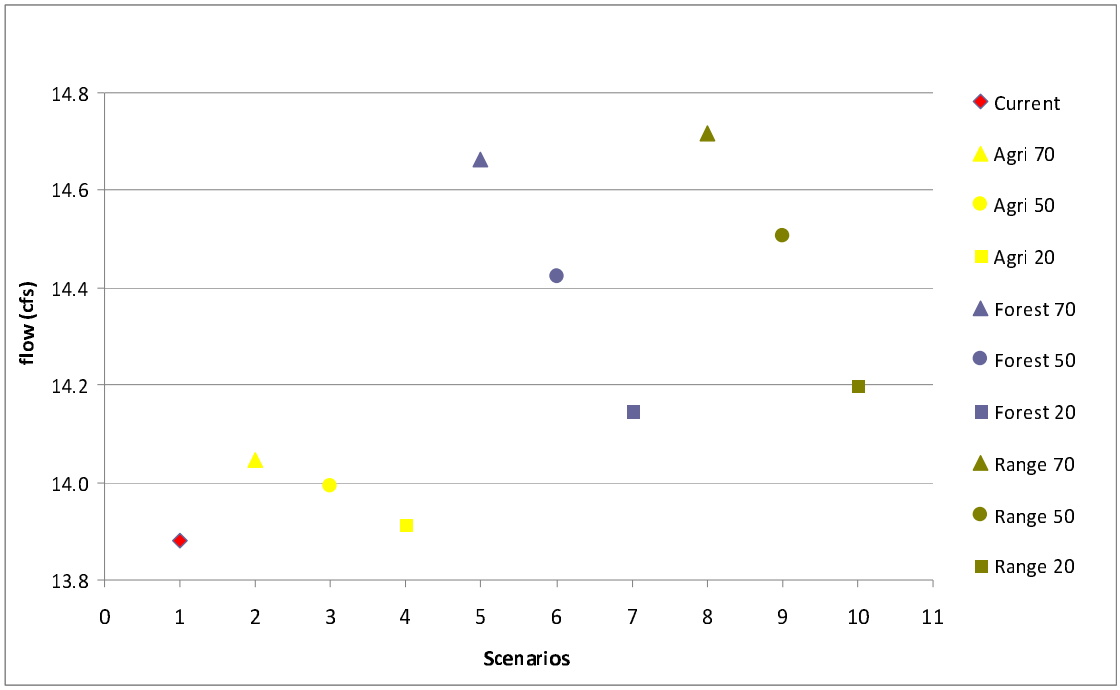

Figure 6. Average annual flow associated with land use changes.

Figure 7 shows the variation in suspended sediment concentration associated with a single storm across the various scenarios. As with Figure 6, comparisons are difficult between agricultural, forest and range lands, but trends within each original land cover are apparent. Within any of the three original land covers, one can see that greater levels of development are associated with a reduction in the sediment concentration when compared to current land cover conditions as represented as Scenario 1. These levels represent some combination of transport of materials from the land surface to the stream and suspension of bed materials. This figure highlights that land covers where there is exposed soil can result in greater sediment concentrations than impervious surface alone. Conditions are complex and the solution is not to cover everything with impervious surface. The results do suggest, however, that serious consideration be given to the specification of land uses in a trade, perhaps including conservation practices.

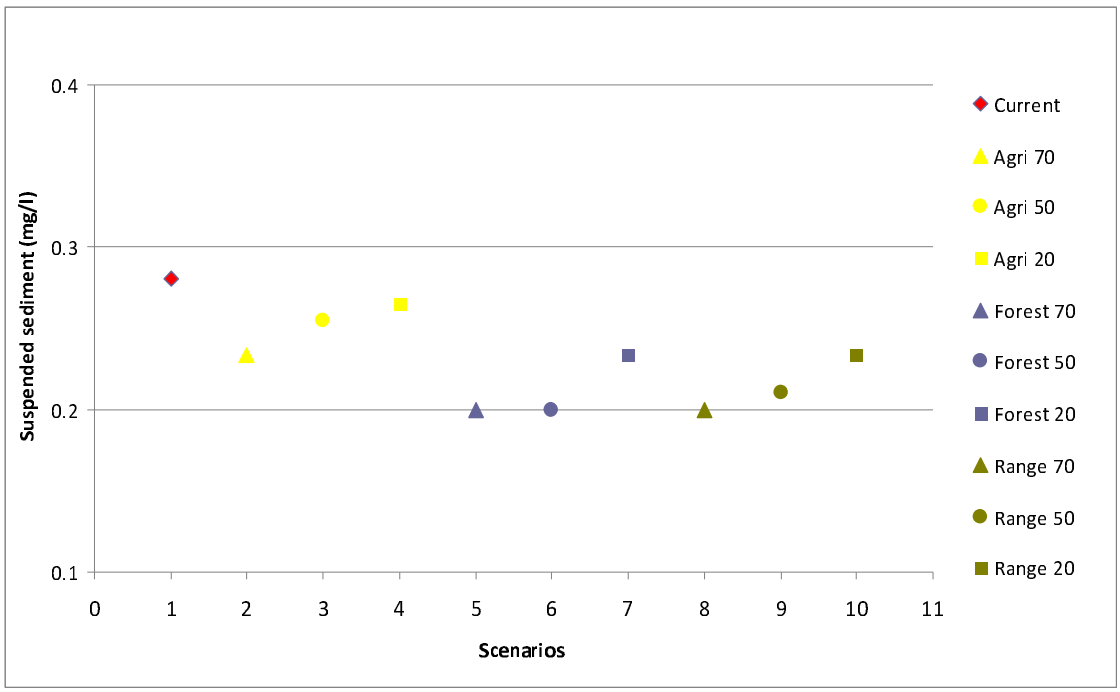

Figure 7. Suspended sediment concentrations (single storm) associated with land use changes.

CONCLUSIONS AND RECOMMENDATIONS

The HSPF model has been calibrated for flow and sediment load. The effort was undertaken with sediment as the only pollutant because the transport mechanisms are well understood and incorporated into freely available software. In addition, an extensive database of measured sediment loads is available from the USGS.

In order for actual trades to take place, they will need to encompass the entire suite of nonpoint source pollutants associated with agricultural, forest and urban land uses. Agricultural land covers may result in sediment loss, but development land covers may be associated with fertilizers, pesticides, heavy metals and petroleum products. A trade must encompass and balance out all of the applicable pollutants.

For complete specification of the water quality impacts of various development scenarios, the calculations must be performed under a full range of precipitation sequences that cover the expected climatic conditions.

The modeling framework has been established within which to evaluate multiple scenarios in order to match donor and receiver locations. Expansion of the precipitation conditions, scenarios, and comparison measures will help to build a robust process upon which to implement nonpoint source water quality trades.

REFERENCES

Bicknell, B. R., J. C. Imhoff, et al. (1997). Hydrological Simulation Program – Fortran, User's Manual for version 11, U.S. Environmental Protection Agency, National Exposure Research Labaratory, Athens, GA.

Donigian, A.S. Jr. 2002. Watershed Model Calibration and Validation: The HSPF Experience. WEF National TMDL Science and Policy 2002, November 13-16, 2002. Phoenix, AZ. WEF Specialty Conference Proceedings on CD-ROM.

Im, S., K. M. Brannan, et al. (2007). Comparison of HSPF and SWAT models performance for runoff and sediment yield prediction. J Environ Sci Health A Tox Hazard Subst Environ Eng 42(11): 1561-70.

Trauth, K. M., and Johnson, T. G., (2006) "GIS Land Cover and Economic Analysis Tool to Promote Water Quality Protection for Sustainable Development" Proposal for EPA-R7WWPD 04-004

Trauth, K. M. and Yee-Sook Shin (2005). "Implementation of EPA's WQT Policy for Storm Water Management and Smart Growth" J. of Urban Plan. & Development., 131 (4), 258-269.

USEPA. (2003) Final WQT Policy http://www.epa.gov/owow/watershed/trading/finalpolicy2003.pdf.

USEPA. (2004a) "Better Assessment Science Integrating point and Nonpoint Sources 3.1 Users' Manual." EPA-823-C-04-004.

USEPA. (2004b) Dartmouth College's WQT and Offset Initiatives in the US: A Comprehensive Survey. http://www.epa.gov/owow/watershed/trading/tradingprojects.html (May 2007)

Statistical Evaluation of BMP Effectiveness in Reducing Nutrient Impairment in Mermentau and Vermilion-Teche River Basins

Z.-Q. Deng[1] and H. Chowdhary[2]

[1] Assistant Professor, Department of Civil and Environmental Engineering, Louisiana State University, Baton Rouge, LA 70803-6405; Email: zdeng@lsu.edu
[2] Graduate Research Assistant, Department of Civil and Environmental Engineering, Louisiana State University, Baton Rouge, LA 70803-6405; Email: hchowd1@lsu.edu

ABSTRACT

The Mermentau and Vermilion-Teche River Basins consisting of 11 watersheds are located in the southwestern part of Louisiana and encompass a drainage area of approximately 17,431 km^2, 52% of which is cropland, primarily rice (34%) and soybeans (17%). Stormwater runoff and rice field discharges from January through May result in high pollutant and nutrient loadings containing nitrogen, phosphorous, and TOC (total organic carbon). As a result, the Louisiana 1998 305(b) Report indicates that 95% of the waterbodies within the basins are not fully supporting their designated uses. Since 1990, a variety of Best Management Practices (BMPs) has been implemented in the Mermentau and Vermilion-Teche River Basins. However, effectiveness of the BMPs in improving water quality and particularly in reducing nutrient impairment is largely unknown due to the lack of source information and to the spatio-temporal variability in hydrological and hydrometeorological parameters controlling nonpoint source pollution. This paper presents a statistical method for evaluating the effectiveness of Best Management Practices (BMPs) in reducing nutrient impairment using water quality data monitored from 1980 – 2006 in the Mermentau and Vermilion-Teche River Basins. The statistical method mainly involves (1) determination of seasonal variations in nutrient (NO_2+NO_3, TKN, total phosphorous, TOC) loading rates in order to identify critical months of nutrient impairment, (2) mapping of mean annual nutrient loads for pre-BMPs and post-BMPs, and (3) evaluation of the effectiveness of BMPs in reducing nutrient impairment based on the trend analysis. Results of the statistical evaluation show that (1) nutrient loading rates vary both seasonally and spatially. Nutrient loading rates become high in winter and spring (January – May) and low in summer and fall. The main impairment in January – March is caused by wet weather runoff. The severe impairment in April and May is related to the releases of muddy rice_field water. High nutrient loading rates are concentrated in the three watersheds: Bayou Queue de Tortue, Bayou Nezpique, and Vermilion River; (2) Since the implementation of BMPs in 1990, water quality in the two river basins has shown an improving trend in terms of nutrient impairment while it was worsening from 1980 – 1990; and (3) BMPs need to be enhanced in the two river basins.

INTRODUCTION

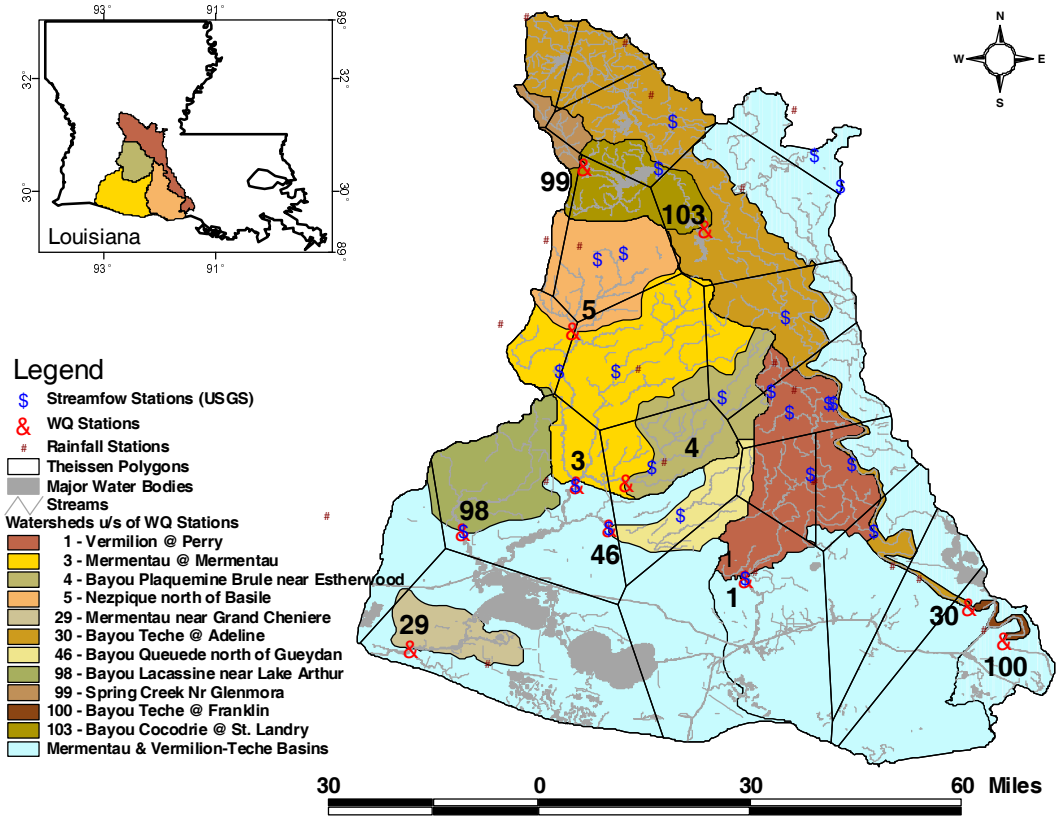

Figure 1. Station network and 11 watersheds in Mermentau and Vermilion-Teche River Basins.

The Mermentau and Vermilion-Teche River Basins are located in the southwestern part of Louisiana and encompasses a drainage area of approximately 17,431 km^2. The Mermentau River Basin has a drainage area of approximately 12,400 km^2. The Mermentau River and its five major tributaries divide the basin into a series of broad, flat areas which are separated by bottomland hardwood riparian corridors, as shown in Figure 1. The Vermilion/Teche Basin on the north and east of the Mermentau basin drains about 5031 km^2 and includes about 1000 km^2 of wetlands. Both river basins are characterized by a dendritic river network, low gradient, and a heavy clay soil. In addition, a dense system of canals for rice irrigation modifies historical overland flow and connects many bayous together such that there may be inter-basin drainage during heavy rainfall events. The two basins are ideal for agriculture and 52% of which was cropland in 2001, primarily rice (34%) and soybeans (17%), as shown in Figure 2. A comparison among the land use maps for the years of 1986, 1991, and 2001 shows that land use change over the period of 1986 – 2001 is less than 3%. Traditional rice-cultivation practices include precision-leveling during water impoundment and releases of rice field water shortly after seeding in the spring months, especially April. The leveling practice increases the erosion of soil. Releases of impounded rice_field water (called “tailwater”) into nearby drainage ditches and bayous can bring large amounts of sediments and agrichemicals (including nutrients) directly into these water bodies. The most significant source of sediment and nutrients in the basins is

suspended solids in wet weather runoff from upland areas. These short pulses of high sediment and nutrient loading in streams can lead to a high biochemical oxygen demand and high turbidity. As a result, the Louisiana 1998 305(b) Report indicates that 95% of the waterbodies within the basins are not fully supporting their designated uses (US EPA 2001, LDEQ 1999). Since 1990, a variety of BMPs, including no-till rice planting, mudding-in with a 15-day setting period, dry cultivation with clear water planting, and mudding-in with a vegetative filter strip, have been implemented in the Mermentau and Vermilion-Teche River Basins through the cost-share assistance provided by various federal, state, and local agencies (Deng et al. 2007). However, the effectiveness of the BMPs in improving water quality has not yet been fully assessed due to the lack of an efficient methodology and significant spatio-temporal variability in hydrological and hydrometeorological parameters controlling water quality.

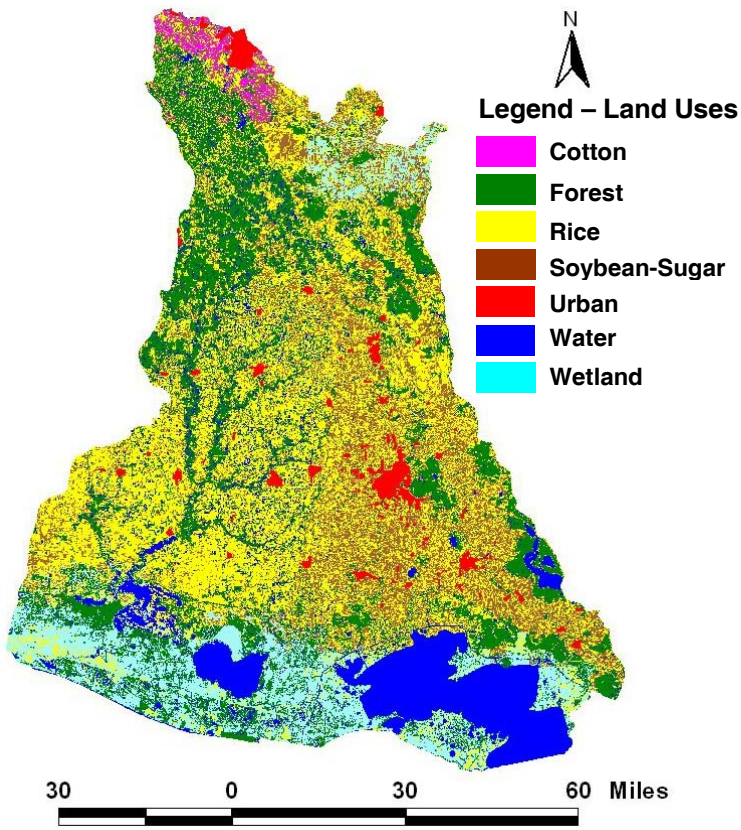

Figure 2. Land use map of Mermentau and Vermilion-Teche River Basins.

The overall goal of this study was to evaluate the effectiveness of BMPs in improving water quality within the Mermentau and Vermilion-Teche River Basins in terms of nutrient impairment. Monthly nutrient data for NO_2+NO_3, TKN, total phosphorous, and TOC) at the outlet of these watersheds, are obtained from Louisiana Department of Environmental Quality for the period of 1980 to 2006. Daily rainfall data for 21 stations for the same period are gathered from the National Climatic Data Center (NCDC). Daily flow data for 22 river gauging stations are available from the National Water Information System (NWIS) of the USGS. Locations of these water quality, rainfall and streamflow stations are shown in Figure 1. Also shown are the Theissen polygons that are used for obtaining daily areal rainfall for each of these watersheds.

Due to the temporal and spatial variability of controlling water quality parameters, a statistical approach is utilized. Nutrient loading rates in the two river basins are computed at various temporal scales including daily, monthly, seasonal, yearly, pre-BMPs, and post-BMPs scales for the nutrient parameters NO_2 + NO_3, TKN, TOC, Phosphorous, and NH_3. Based on results of the loading computations maps showing loading rates in the watersheds of the two river basins are also created for the nutrient parameters on a seasonal basis to see seasonal variations and on the pre-BMP versus post-BMP basis to see the effectiveness of BMPs.

MAPPING OF MEAN SEASONAL NUTRIENT LOADS

Maps for mean seasonal nutrient loading rates are created and shown in Figures 3 and 4. Figure 3 shows that high total phosphorous loading rates mainly occur in the watersheds # 1, 5, and 46, especially in spring and winter. Figure 4 indicates that high TKN loading rates mainly occur in the watersheds # 1, 5, and 46, especially in winter. The TOC loading rate distributions over the river basins are similar to TKN and phosphorous. High TOC loading rates also occur in the watersheds # 1, 5, and 46 in spring and winter. High NO_2NO_3 loading rates mainly occur in the watersheds # 1 and 5, especially in spring. Overall, nutrient loading rates vary seasonally and become high in winter and spring and low in summer and fall. The main impairment in winter (January – March) is caused by wet weather runoff (Deng and Chowdhary 2008). The severe impairment in April and May is related to the releases of muddy rice_field water.

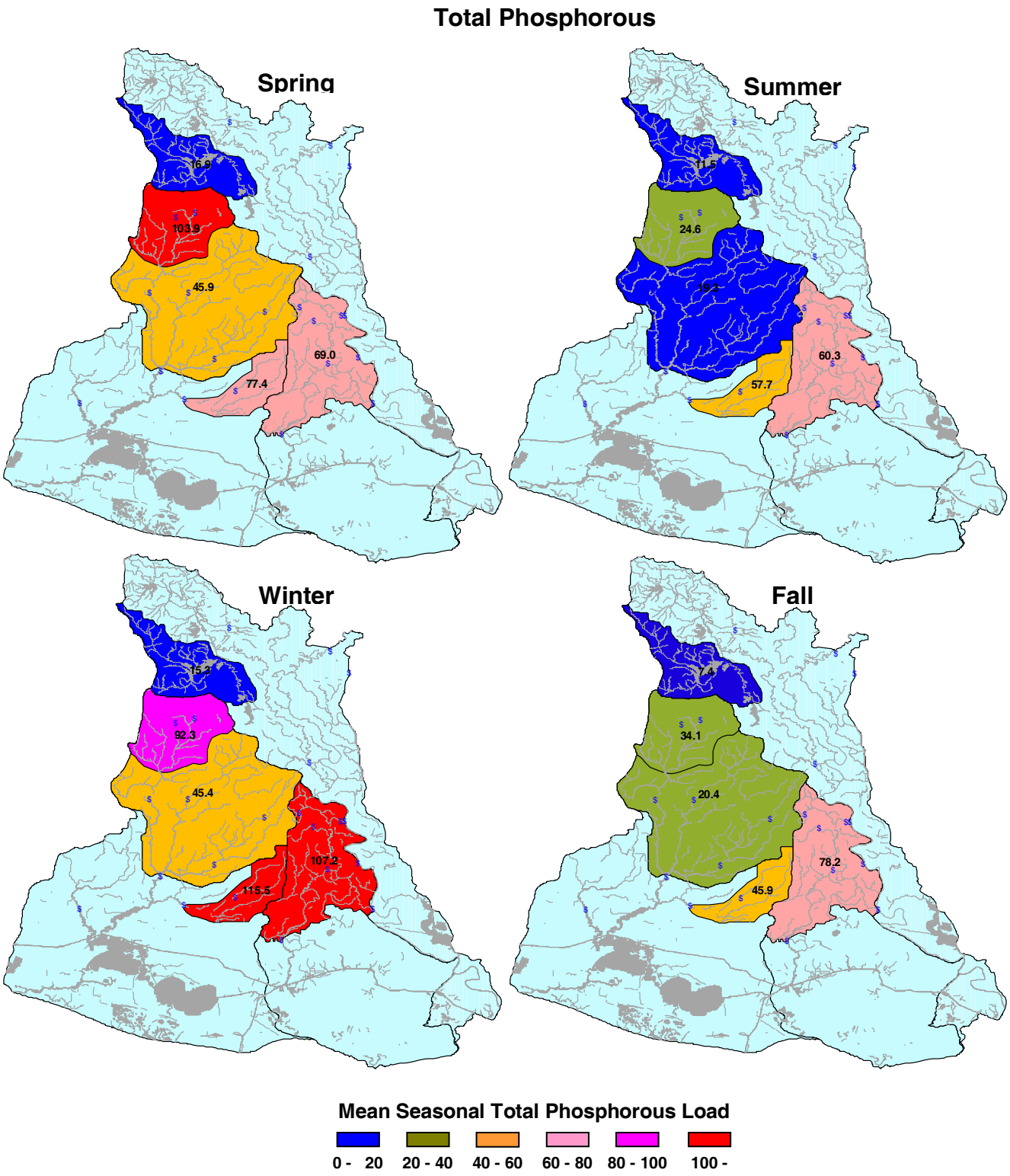

Figure 3. Mean seasonal total phosphorous loading rates (Kg/km^2) in the Mermentau and Vermilion-Teche River Basins.

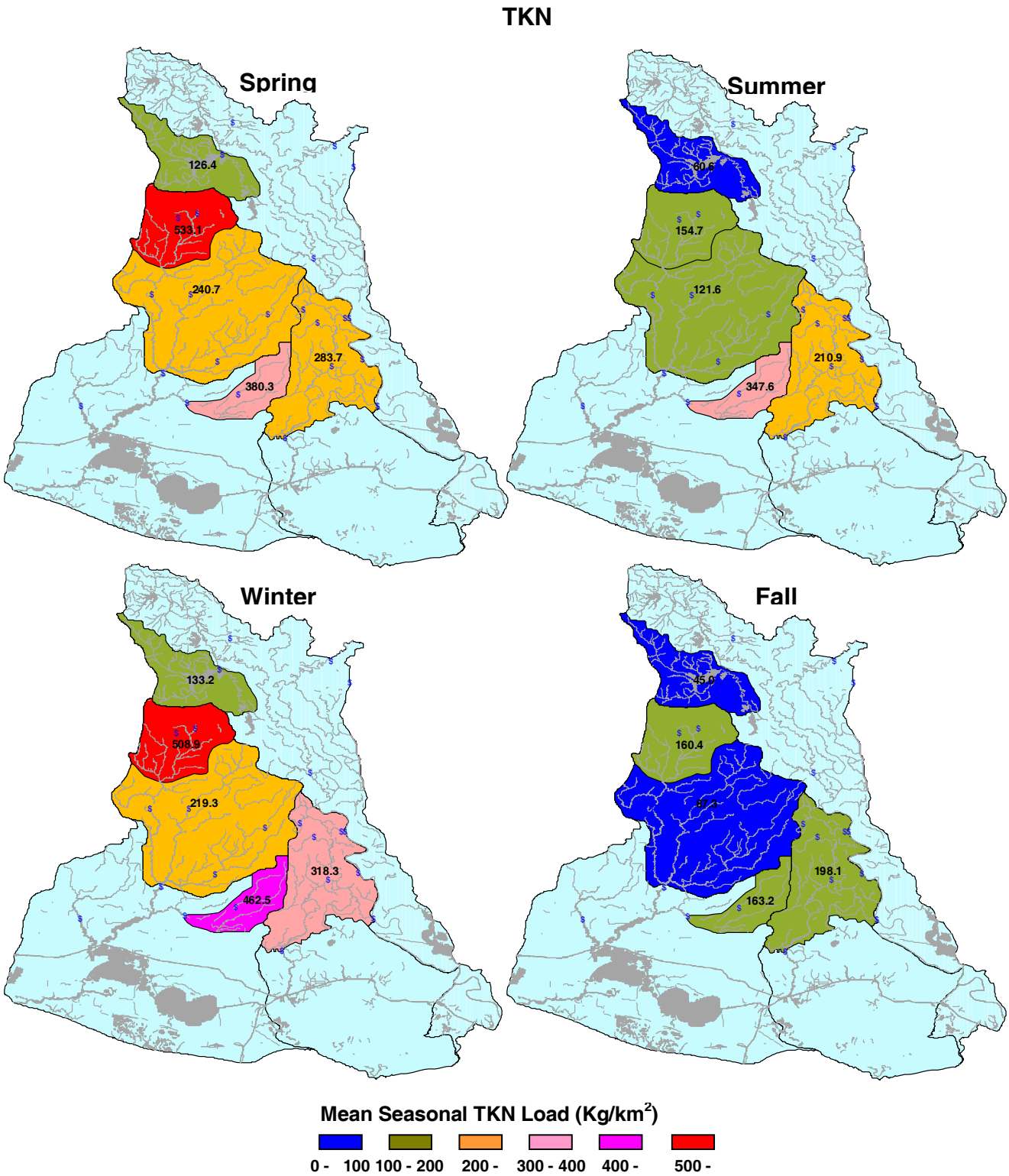

Figure 4. Mean seasonal TKN loading rates in the Mermentau and Vermilion-Teche River Basins.

MAPPING OF MEAN ANNUAL NUTRIENT LOADS FOR PRE-BMP AND POST-BMP

Maps for yearly mean nutrient loading rates are shown in Figures 5 – 7. Figure 5 shows that high TKN loading rates mainly occur in the watersheds # 1, 5, and 46. The TKN loading rate in the watershed #1 has decreased but it increased in the watershed #3 since the implementation of BMPs. The mean yearly loading rates (Kg/km^2) of TKN in the watersheds #1, 3, 5, 46, and 103 are 977.39, 646.79, 1414.65, 1470.12, and 383.04, respectively. Figure 6 shows that high total phosphorous loading rates mainly occur in the watersheds # 1, 5, and 46, especially before the implementation of BMPs. The mean yearly loading rates (Kg/km^2) of total phosphorous in the watersheds #1, 3, 5, 46, and 103 are 296.425, 126.281, 251.072, 317.793, and 52.332, respectively. The TOC loading rate distribution over the river basins is similar to TKN. High TOC loading rates also occur in the watersheds # 1, 5, and 46, as shown in Figure 7. The TOC loading rate in the watershed #1 has decreased but it increased in the watershed #3 since the implementation of BMPs. The mean yearly loading rates (Kg/km^2) of TOC in the watersheds #1, 3, 5, 46, and 103 are 7149.33, 5524.48, 11968.99, 8865.70, and 4633.61, respectively. High NO_2NO_3 loading rates mainly occur in the watersheds # 1 and 5, especially before the implementation of BMPs. The mean yearly loading rates (Kg/km^2) of NO_2+NO_3 in the watersheds #1, 3, 5, 46, and 103 are 302.712, 111.994, 317.757, 141.446, and 22.357, respectively. The mean yearly loading rates (Kg/km^2) of NH_3 in the watersheds #1, 3, 46, and 103 are 138.268, 95.467, 29.174, and 83.794, respectively. Overall, there are no significant variation trends in the nutrient loading rates at the river basin scale although some loading rates decrease but others may increase in some watersheds.

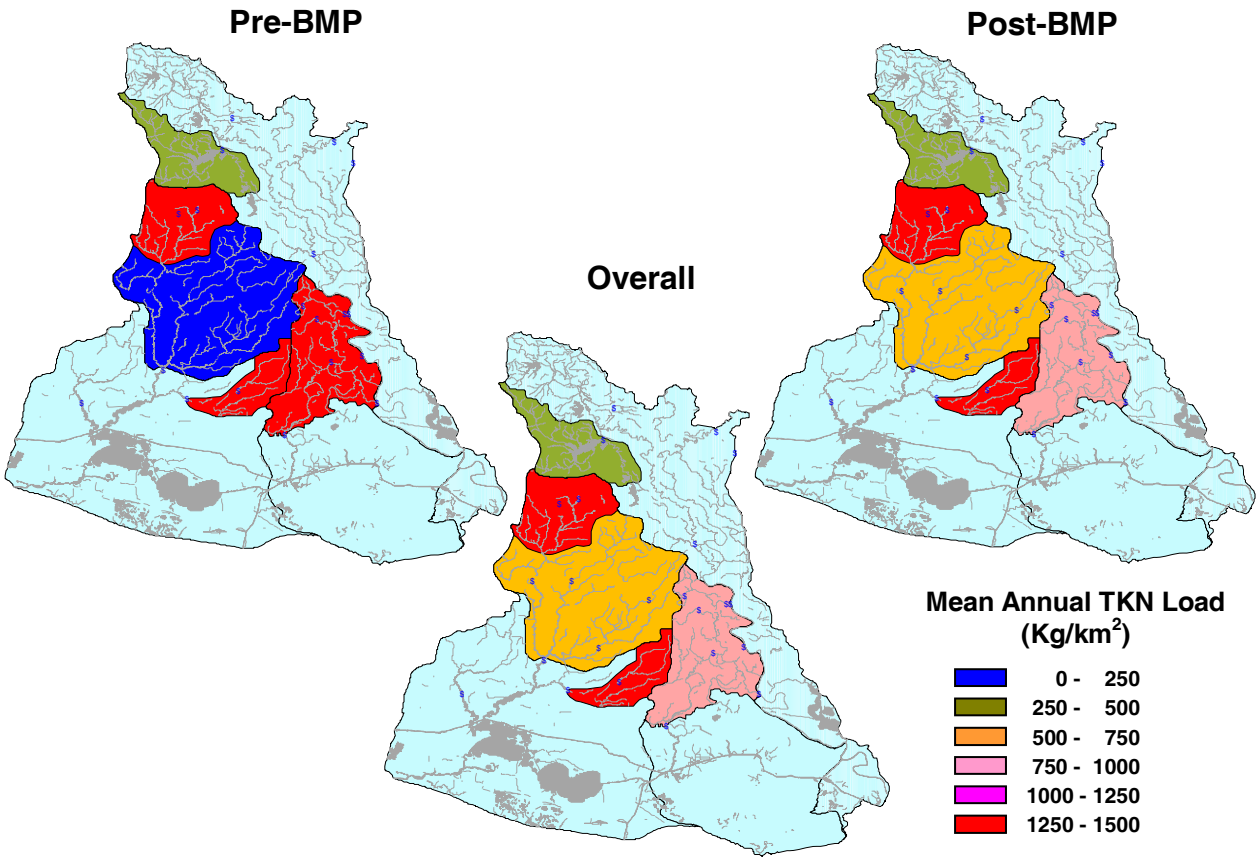

Figure 5. Yearly mean TKN loading rates before and after the implementation of BMPs.

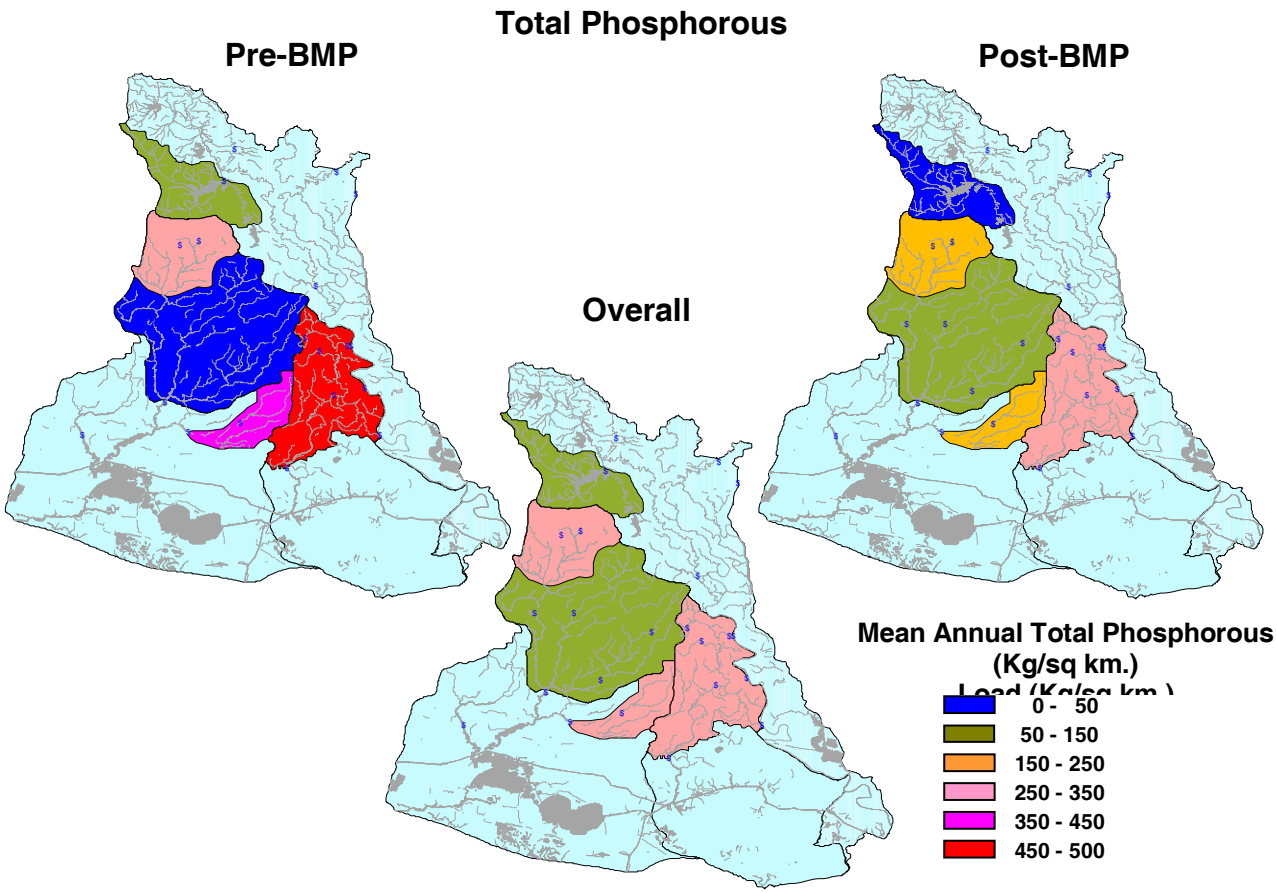

Figure 6. Mean yearly Total Phosphorous loading rates before and after the implementation of BMPs in the Mermentau and Vermilion-Teche River Basins.

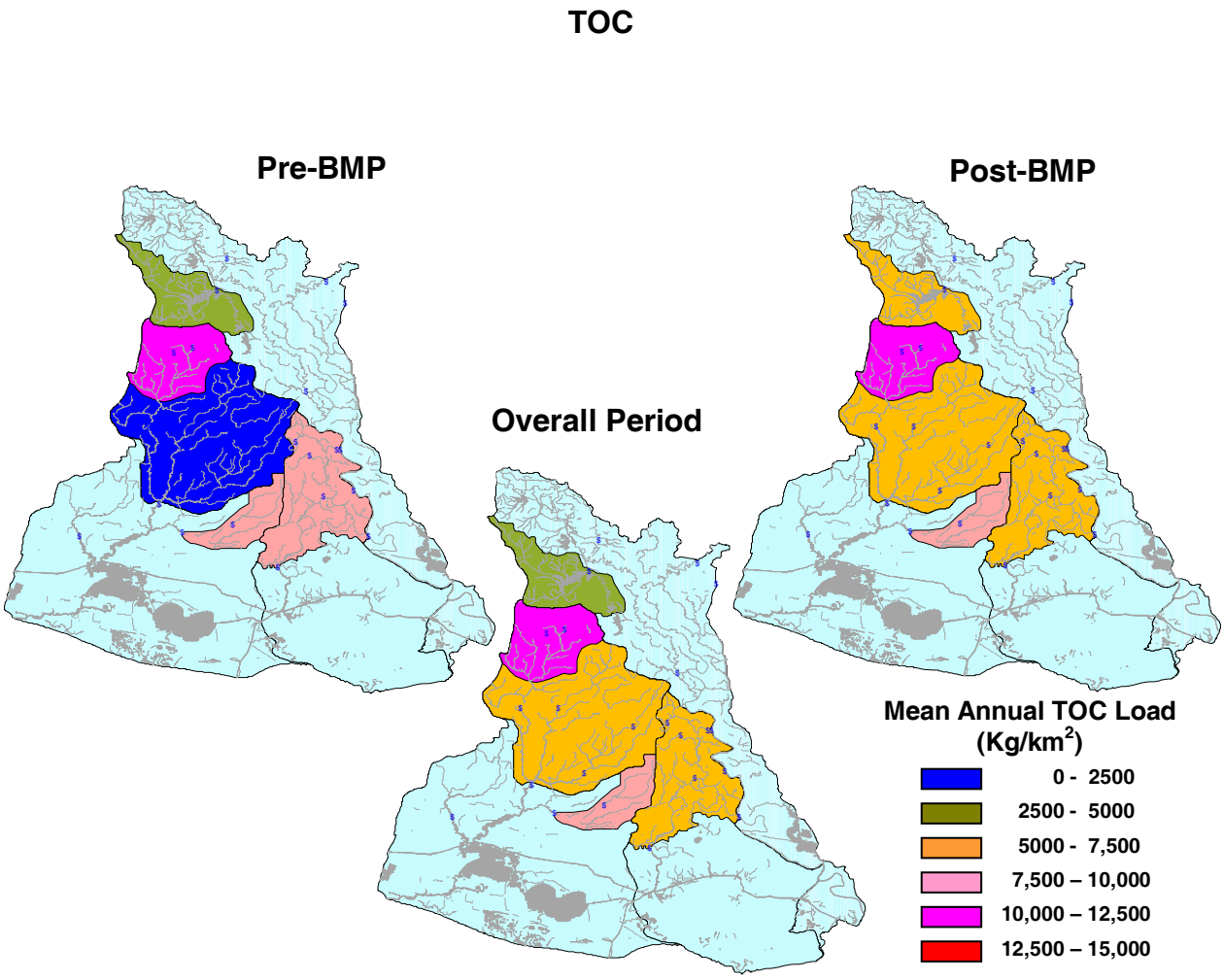

Figure 7. Mean yearly TOC loading rates before and after the implementation of BMPs in the Mermentau and Vermilion-Teche River Basins.

CONCLUSIONS

Based on the results of this study the following conclusions can be drawn:

(1) Nutrient loading rates vary seasonally and become high in winter and spring and low in summer and fall generally.

(2) There are no significant variation trends in the loading rates at the river basin scale although some loading rates decrease but others may increase in some watersheds

(3) The nutrient impairment in winter is primarily caused by wet weather runoff.

(4) The severe pollution in spring is mainly caused by releases of muddy rice_field water, but wet weather runoff makes the water quality even worse.

(5) Since the implementation of BMPs, the water quality in the Mermentau and Vermilion-Teche River Basins has shown some improvements. The most polluted areas in the basin are the two watersheds Bayou Queue de Tortue and Bayou Nezpique, followed by the watersheds Bayou Plaquemine Brule and Bayou Lacassine.

(6) BMPs in the basins need to be enhanced to meet water quality standards.

ACKNOWLEDGMENTS

The authors would like to acknowledge the funding support of the US EPA and the Louisiana Department of Environmental Quality for this research.

REFERENCES

Deng, Z.-Q., Morel, S., and Chowdhary, H. (2007). "Statistical Evaluation of BMP Effectiveness in Reducing Sediment Impairment in Mermentau River Basin." The 2007 EWRI World Water and Environmental Resources Congress, May 15-19, 2007, Tampa, Florida.

Deng, Z.-Q., and Chowdhary, H. (2008). "Statistical Evaluation of BMP Effectiveness in Reducing Fecal Coliform Impairment in Mermentau River Basin." World Environmental & Water Resources Congress 2008, May 12-16, 2008, Honolulu, Hawaii.

Louisiana Department of Environmental Quality (LDEQ). (1999). *Louisiana NPS Management Program 1999 Annual Report*. Baton Rouge, LA.

US EPA. (2001). *Total Maximum Daily Load (TMDL) for TSS, Turbidity, and Siltation for the Mermentau River Basin*. US EPA Region 6.

Using "Big Data" to Optimally Model Hydrology and Water Quality across Expansive Regions

Edwin A. Roehl, Jr.[1], John B. Cook[1], and Paul A. Conrads[2]

[1]Advanced Data Mining International, LLC, 3620 Pelham Rd. PMB 351, Greenville, SC 29615; PH 843.513.2130; FAX 864.848-1262; emails: ed.roehl@advdmi.com, john.cook @advdmi.com
[2]U.S. Geological Survey South Carolina Water Science Center, Stephenson Center. Suite 129, 720 Gracern Rd., Columbia, SC 29210; PH (803) 750-6140; FAX (803) 750-6181; email: pconrads@usgs.gov

ABSTRACT

Data mining has been described as "the search for valuable information in large volumes of data", with its defining characteristic being large datasets, or "big data". In every domain, including the environmental sciences, big data's ubiquitous, massive databases comprise millions and even billions of records, and are the consequence of the powerful, low cost monitoring and computing technology that has evolved over the last three decades. The state-of-the-art models now used for natural resource management and control, such as finite-difference hydrologic and land use models, are time consuming and expensive to develop, and are based on approaches that predate the availability of big data and data-mining technology. The representations of process physics in these types of models can be inherently too simplistic for some applications, which is underscored by their limited ability to incorporate all available data types, including hydrologic, water-quality, and meteorological time series from many sites; and categorical parameters that describe site-to-site differences such as basin characteristics and land uses. Reducing large numbers of parameters to a select subset to accommodate model limitations can lead to model uncertainty, subjective decision-making, and delayed formulation and implementation of management decisions and plans.

This paper describes a new divide and conquer approach that leverages big environmental data, utilizing all available categorical and time-series data without subjectivity, to empirically model hydrologic and water-quality behaviors across expansive regions. The approach decomposes large, intractable problems into smaller ones that are optimally solved; decomposes complex signals into behavioral components that are easier to model with "sub-models"; and employs a sequence of numerically optimizing algorithms that include time-series clustering, nonlinear, multivariate sensitivity analysis and predictive modeling using multi-layer perceptron artificial neural networks, and classification for selecting the best sub-models to make predictions at new sites. This approach has many advantages over traditional modeling approaches, including being faster and less expensive, more comprehensive in its use of available data, and more accurate in representing a system's physical processes. This paper describes the application of the approach to model ground-water levels in Florida, stream temperatures across Western Oregon and Wisconsin, and water depths in the Florida Everglades.

INTRODUCTION

Managers of expansive natural systems often use predictive models to help them make decisions. Models typically are developed from existing or newly collected data. The data used to develop the models should fully represent the diversity of behaviors exhibited across the natural system and may consist of categorical parameters, such as land use or geology, or represent dynamics with time series, also know as signals. The mechanics of integrating multiple data types and reducing large numbers of parameters to a select set often leads to subjective decision-making, which may have important ramifications when applying state-of-the-art multi-step modeling approaches, for example, land-use models driving streamflow models. These models often fail to accurately reproduce observed behaviors because their representations of complex process physics can be too simplistic for some applications, which is underscored by their limited ability to incorporate all available data types, including hydrologic, water-quality, and meteorological time series from many sites; and categorical parameters that describe site-to-site differences such as basin characteristics and land uses.

Weiss and Indurkhya (1998) describe the emerging field of data mining as "the search for valuable information in large volumes of data", with its defining characteristic being large datasets, or "big data". In every field big data's ubiquitous, massive databases comprise millions and even billions of records, and are the consequence of the powerful, low cost monitoring and computing technology that has evolved over the last three decades. While large databases for environmental systems are common, they are usually under interpreted and utilized. Data-mining methods come from different technical fields such as signal processing, statistics, and artificial intelligence (AI), and are used extensively in financial services, banking, advertising, manufacturing, and e-commerce. Data mining employs methods for maximizing the information content of data, determining which parameters have the strongest relations to problems of interest, and developing models that predict future outcomes. This knowledge encompasses both understanding cause-effect relations and predicting the consequences of alternative actions.

This paper describes a new approach for modeling expansive natural systems directly from big data. It employs a number of data-mining algorithms that address the full complexity of these systems in a numerically optimized way. This paper also describes how this powerful technology has been successfully applied to modeling ground-water levels in a Florida aquifer, stream water temperatures in Oregon and Wisconsin, and water depths in the Florida Everglades.

NEW APPROACH

Given that environmental systems can appear intractably complex from the data in hand, a "divide and conquer" approach is needed for developing numerically optimized models by employing multivariate, numerically optimizing methods such as clustering, classification, and nonlinear empirical modeling.

Sub- and Super- Models. At the top level, the new approach uses the concept that a process model of a system is a "super-model" composed of multiple "sub-models". Sub-models are numerically optimized to compute output signals that can be combined to predict complex output behaviors resulting from multiple, interacting physical forces.

Time-Series Clustering. Time-series clustering is used when uncertainty exists about whether a region to be modeled should be sub-divided because of spatial differences in the underlying physical processes. For example, localized pumping can cause gradual or dramatic differences in ground-water behaviors between monitoring sites. Time-series clustering optimally groups (segments) monitoring sites or populations of signals into behavioral classes without subjectivity, allowing different classes to be optimally sub-modeled. The signals that comprise a class are called class "members". To perform time-series clustering, a cross-correlation matrix created for signals of interest is clustered using a clustering algorithm such as the k-means algorithm or others (Goddard and Martinez, 2000). The optimal number of classes "k" to be used is estimated by evaluating the sensitivity of the clustering algorithm's error to k.

Signal Decomposition. Signals can have multiply periodic behavioral components, for example tides are modulated by the attraction between the earth, moon, and sun. Periodicity is by definition highly predictable; however, signals can also display dramatic spatial and temporal variability due to chaotic forcing by humans and weather. Chaotic behaviors are by definition only somewhat predictable, yet it is these behaviors that modelers strive to reproduce. Techniques such as spectral band-pass and moving window average difference filtering can "decompose" a signal to separate the periodic components, leaving behind chaotic components.

Signal decomposition reduces the difficulty of modeling signals with individual sub-models. Subsequently, a super-model combines the outputs from multiple, individually optimized sub-models. This approach can greatly improve the representativeness and accuracy of an empirical process model. Roehl and Conrads (2006) detail the use of "multivariate state space reconstruction" as a method to decompose and model estuary salinity intrusion events using flow and water-level signal component as inputs to artificial neural network sub-models, which were combined into a super-model. For the study area's most inland monitoring site, the determination coefficient R^2, calculated from the Pearson coefficient of the field measurements and super-model predictions for a 6-month drought period, was 0.90 versus an R^2=0.10 for predictions made by a three-dimensional (3D) state-of-the-practice finite-difference hydrodynamic model of the same system (Conrads and Greenfield, 2008).

Spatially Interpolating ANN Models. Environmental systems usually exhibit complexities such as chaotic behaviors and nonlinear relations among parameters, and it is important for modeling methods to accommodate them. The field of Artificial Intelligence offers machine learning algorithms such as artificial neural networks (ANN) for different purposes (Hinton, 1992). An ANN is a flexible mathematical structure based on the biological nervous system. The multi-layer

perceptron (MLP) ANN, as described Jensen (1994) and used here, is "trained" on a database organized into multivariate vectors of input-output data. The training of ANNs synthesizes complex, continuously differentiable, nonlinear functions to near-optimally fit example populations of input-output vectors. In comparison, the ubiquitous ordinary least-squares curve-fitting algorithm only fits prescribed functions, such as planes or hyper-planes, whether the prescribed function describes the actual parameter relations or not.

A study by Conrads and Roehl (1999) found that ANNs offered a number of advantages over finite-difference physics-based models in reproducing the dynamic flow and water-quality behaviors in an estuary. Most importantly, the ANNs gave much better prediction accuracy when using the same input and output parameters and data. Coppola and others (2005) made some of the same observations after applying ANNs to forecast water levels at two monitoring wells in an aquifer affected by climatic parameters and pumping. ANNs can provide near optimal multivariate nonlinear curve fitting for dynamic, nonlinear environmental processes when: the data are well distributed throughout the historical range of conditions of interest; and the input parameters selected by the modeler share significant “mutual information” about the output parameters.

A benefit of finite-difference and finite-element models is their ability to provide spatially semi-continuous predictions from mesh nodes. Similarly, Dowla and Rogers (1996) used a "radial basis function" ANN to provide spatially continuous but temporally static 3D land elevations. This paper's new approach employs ANN models that are configured to simultaneously predict spatial and temporal variability, made possible by using spatial coordinate input parameters with a "stacked" training database. The input coordinates represent the sites where the training output values were measured. For run-time application, the coordinates are for a "new site" where the user wants the model to make a prediction. It is left to the super-model's machinery to "classify" the user's new site coordinates to select the most appropriate sub-model(s) to execute. The outputs of two or more class's sub-models can be averaged for sites that lie on or near class boundaries. A stacked database is used to train ANNs to interpolate between values of spatial coordinates and other categorical parameters. In flat file format, each monitoring site is represented by a block of rows denoting time stamps and columns denoting candidate input and output parameters.

New Site Classification. Some modeling applications must make predictions at new sites where no data of the type being predicted has been collected. A new site can be described by categorical parameters such as spatial coordinates and land uses. For a new site's categorical input values, the super-model application determines which behavioral class's sub-model(s) should make the prediction. This can be handled by programmed logic and/or use of a classification algorithm such as the linear k-nearest neighbor classifier or a nonlinear MLP ANN classifier (Holmstrom and others, 1997).

APPLICATIONS

Four applications of the new approach are provided to illustrate its efficacy on a range of problems having interesting conceptual differences. They predict ground-water

levels in Florida, stream temperatures across Western Oregon and Wisconsin, and water depths in the Florida Everglades.

Upper Floridan Aquifer water levels in the Suwannee River Valley. This model was a development test bed for the new approach, and was first described by Roehl and others (2006). Here, the big data were provided by the study area's (Figure 1) water-resource managers, who were interested in determining how to defensibly reduce the size of their extensive network of approximately 200 wells monitoring the Upper Florida Aquifer.

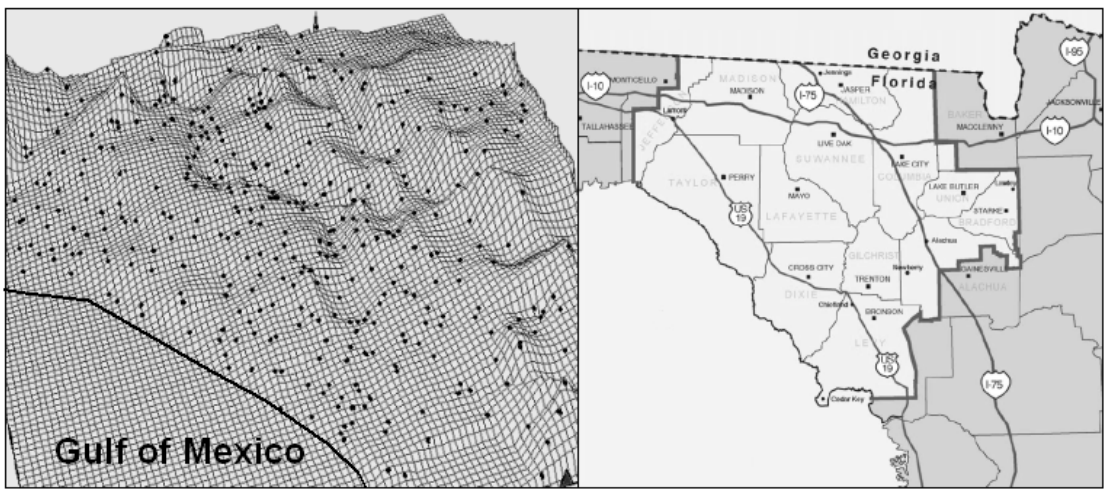

Figure 1. Monitoring well locations on 1x1 km^2 grid (left) on approximate 160x160 km^2 study area (right).

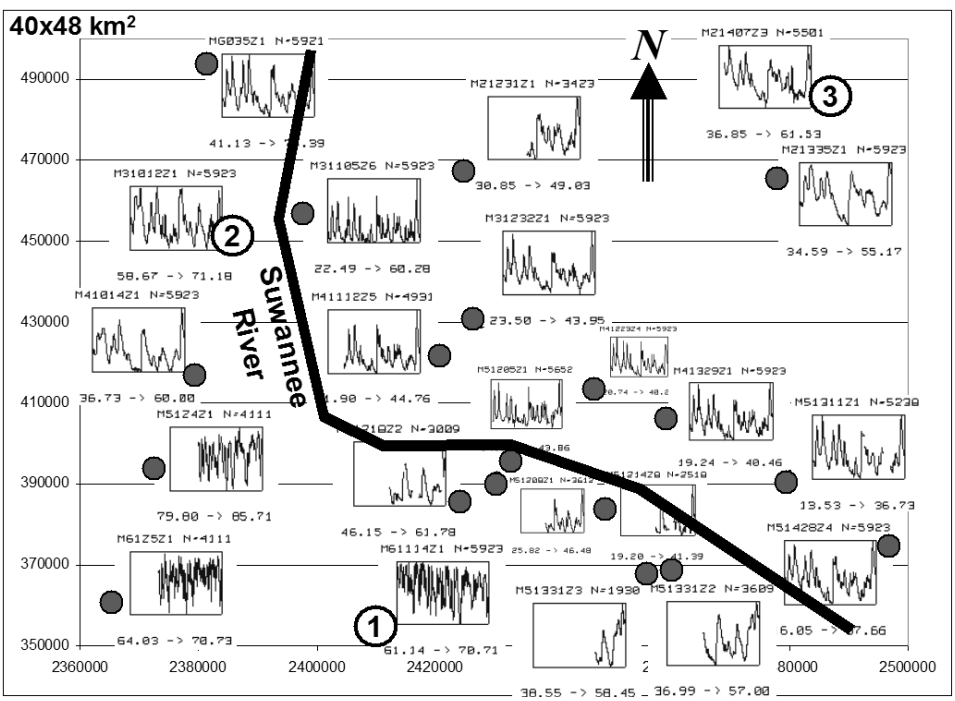

Figure 2. Well locations and daily water levels from 1982 to 1998 in an approximate 40x48 km^2 sub-region of the Suwannee River Valley.

Figure 2 shows an approximate 40x48 km^2 sub-region of the study area with daily measured water-level signals from 1982 to 1998 superimposed next to their well locations. Note that the signals of the three numbered wells are dissimilar, especially well 1, which is completely different from its neighbors to the northeast. This infers a spatial discontinuity in the process physics that would be problematic for both physics-based and empirical model approaches. The new approach segments the signals into different behavioral classes using time-series clustering. Figure 3 shows normalized signals for 2 of 12 classes. It is apparent that the members of each class are similar, and dissimilar to those in the other class.

A side benefit of time-series clustering is that it answers the question, *"Which monitoring site's signals are redundant and possibly unneeded?"* Time-series clustering offers a defensible pathway to optimizing data collection networks with respect to the quality of the information gathered for a given cost.

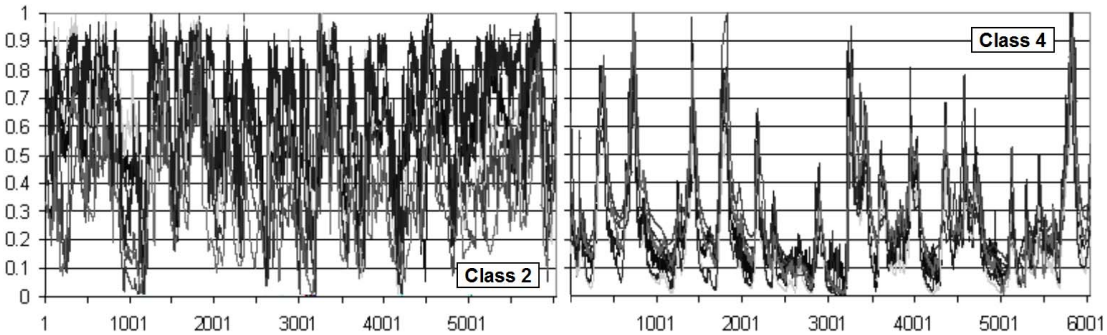

Figure 3. Normalized water-level signals for Classes 2 and 4. The x-axis is in days from April 1982 to October 1998.

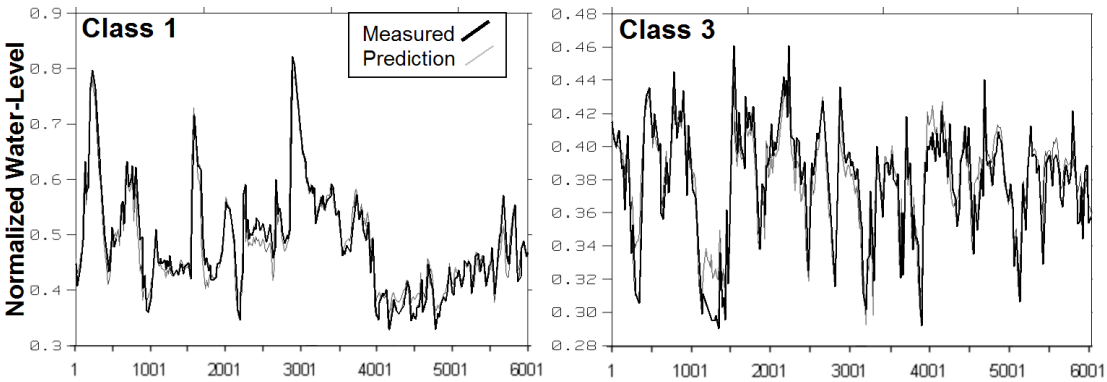

Figure 4. Measured (black) and predicted (gray) normalized water levels for example Class 1 and 3 wells. Here, each signal was normalized using the historical minimum and maximum water levels of all signals in its class.

A divide and conquer approach was also used to model each class's members by cascading sub-models that predict the historical mean and then the dynamic signal components. Sub-models model-1i (i = 1 to k, k=12) were trained for each class to predict the historical mean water levels of its members. These models were quasi-autoregressive, using inputs representing the signals of each class's members plus the spatial coordinates of each output value. A second, autoregressive, sub-model

(model-2i) was trained to predict the dynamic components of the members of each class. The inputs to model-2i were the outputs from model-1i plus the signals of the constituent class members and their spatial coordinates. Figure 4 shows that the sub-model pairs achieved good accuracy in predicting the water levels for typical examples of Class 1 and Class 3 signals.

The next step was to classify regions of the study area so that the most appropriate model class would be applied to a new site. As shown at left in Figure 5, the study area was divided into 1-km^2 cells. All of the cells were assigned to a class by kriging the class assignments of the cells having wells. The kriging method used 12 identical grids, one for each class, on which cells having wells were assigned a 1 or a 0 depending on whether the well was a member of the map's represented class. Each map was kriged and those cells having a value of 0.5 or greater were assigned to the map's class. The kriged maps were then superposed to compile the class assignments. Few cells were found to have been assigned to multiple classes.

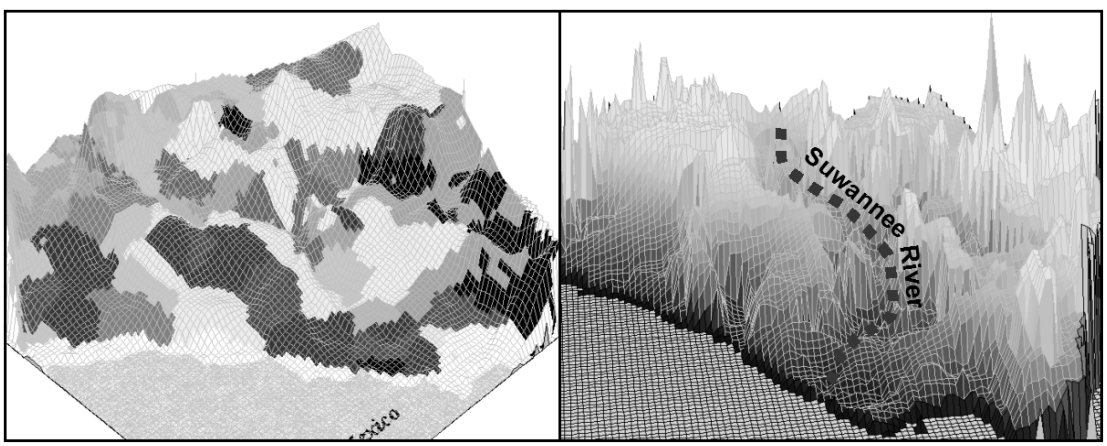

Figure 5. Grid with color-coded class assignments (left) and an aquifer water-level surface (right) predicted by the super-model.

The super-model comprised 12 cascaded sub-model pairs, one pair for each class, for a total of 24 separate ANNs. It was assembled in a spreadsheet program that could run simulations to predict spatially-continuous aquifer surfaces at each time step (Figure 5 right). Long-term simulations revealed highly asynchronous spatial and temporal water-level variability that are caused by rainfall, pumping, and flow.

Western Oregon Stream Temperatures. This model predicts "unimpaired" water temperatures (no anthropogenic influences) in 1st, 2nd, and 3rd order streams in the western third of Oregon, and was first described by Risley and others (2003). Stream temperature is an important parameter for assessing the ecological status of stream segments. The model was developed to support the implementation of the Total Maximum Daily Load requirement under section 303(d) of the Clean Water Act.

Here, the big data was composed of stream temperature, climate, stream habitat, and basin parameters. The stream temperatures were hourly signals collected at 148 unimpaired sites from June to September 1999 (Figure 6). The sites were located on streams that drained basins ranging from 0.3 to over 300 km^2. Site elevations ranged from 7 to 1,445 meters above mean sea level. Six of the 148 sites

were randomly withheld from model development for validating results. The climate parameters were 65 hourly signals of air temperature, dew-point, solar radiation, barometric pressure, snowpack, and precipitation from 25 sites. The stream habitat and basin attributes comprised 34 categorical parameters that included stream bearing, gradient, canopy cover, wetted widths, depth, and bed substrate; and basin topographic and vegetation characteristics such as size and forest cover.

Relative to the Upper Floridan Aquifer model, this problem had a more complex and varied database, and model development was further complicated by a requirement to predict hourly rather than daily output values from which summarizing statistics could be calculated. This indicated a need for three cascaded sub-models for each behavioral class to predict in succession historical mean, daily, and hourly stream temperatures. A second issue was the large list of candidate categorical and dynamic inputs whose interrelations and predictive performance were unknown. Many of the potential input parameters were multicollinear. A third issue was that new site classification could not be based solely on spatial coordinates because of the strong influences of habitat and basin parameters.

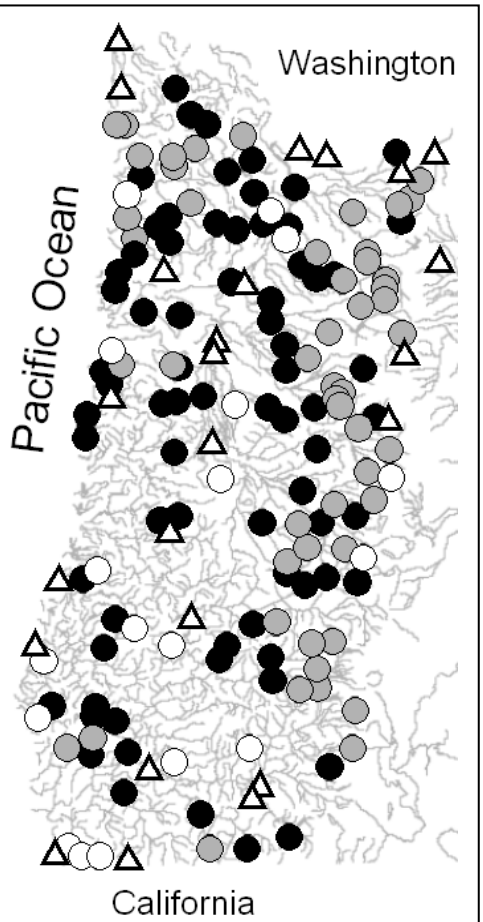

Figure 6. Western Oregon study area. Class 1, 2, and 3 sites are white, gray, and black circles respectively. Triangles mark climatic and snowpack sites.

Signal processing consisted of computing a historical mean and 24-hour (1-day) moving window averages for each hourly signal. The 1-day stream temperatures signals were normalized relative to their individual ranges and time series clustering segmented them into three classes (Figure 6). The Class 1 sites were found to be generally located in warmer sub-regions at lower elevations and in the southern portion of the study area. This includes the Klamath Mountains ecoregion and the Willamette River valley lowlands. The Class 2 sites were more predominant at higher elevations, particularly in the Cascade Mountains. The Class 3 sites were widely distributed at middle elevations. The climatic signals tended to be highly correlated site-to-site, so they were decorrelated by setting one site to be a "standard" for each parameter type and calculating differences from the standard at the other site.

The divide and conquer approach cascaded three sub-models that predict the historical mean, 1-day, and hourly stream temperature signal components. For modeling, the 1-day stream temperature signals were normalized by subtraction from

their means, and the hourly signals were normalized by subtraction from their 24-hour moving window averages. A single ANN sub-model (model-1) was trained to predict the historical mean stream temperatures for all three classes from only categorical input parameters. To predict the normalized 1-day stream temperature components, sub-models model-2i (i = 1 to k, k=3), were trained for each class. Their inputs were selected categorical parameters and 1-day climatic time-series parameters. To predict the normalized hourly components, sub-models model-3i were trained for each class. Their inputs were selected categorical parameters and hourly climatic parameters. The outputs of model-1 and model-2i are summed to predict 1-day stream temperatures, and the outputs of all three sub-models are summed to predict hourly stream temperatures. For each sub-model, the final sets of categorical parameters and climatic time series inputs were arrived at experimentally according to their predictive performance and lack of collinearity. The most important input parameters included air temperature, riparian shade, site elevation, and basin percent forested area.

The new site classifier was developed using ANNs, making it a nonlinear classifier. It was composed of three ANNs, one for each class. Each class's ANN was trained to predict a binary 0 or 1 depending on if a new site's habitat and basin attributes matched those of its member sites. Generally, the class whose classification ANN predicts the highest output indicates the new site's class, with programmed logic being used to resolve ambiguous cases.

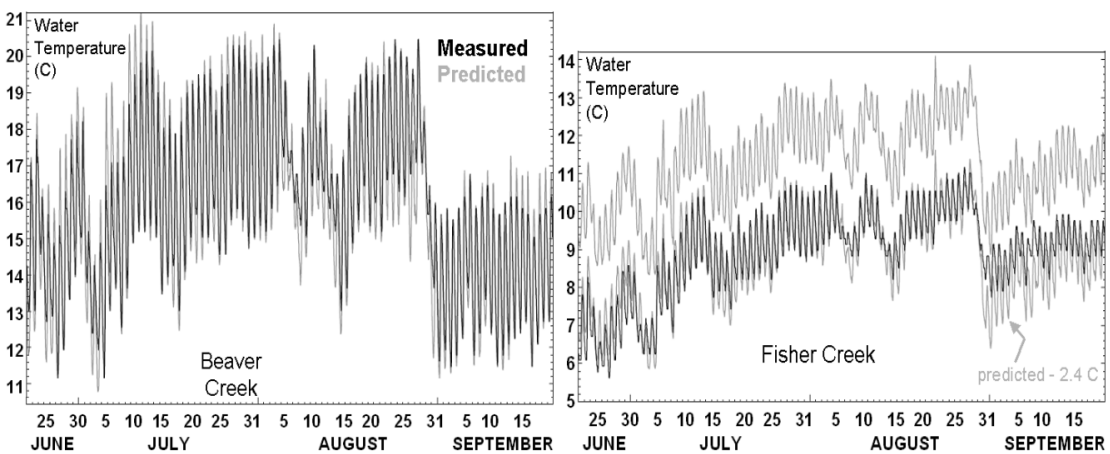

Figure 7. Measured (black) and predicted (gray) hourly stream temperatures at two validation sites.

The super-model is composed of one historical mean sub-model, 1-day and hourly sub-models for each of the three stream temperature classes, and three classification models for a total of 10 separate ANN models. It was assembled in a spreadsheet program that runs simulations using the historical climate input data with categorical input values set for new sites. The simulations predict stream temperature signals that are characterized statistically. Figure 7 shows measured and predicted hourly stream temperatures at the "best" and "worst" of the six validation sites. Both predictions track the climatically-forced dynamic behaviors; however, the Fisher Creek predictions are offset from the measurements by an average of 2.4 C. The offset is

due largely to the error in the predicted historical mean stream temperature caused by the process used to characterize and collect habitat and basin information. A contributing factor is how the validation sites were selected. Here, random selection was used. These results indicate that the Fisher Creek site possesses attributes that are substantively different from the training sites, and unlearned and poorly represented by the empirical model.

Wisconsin Stream Temperatures. This project sought to develop an ANN-based model using landscape and climatic time series data to predict stream temperature signals for stream segments throughout Wisconsin, and was first described by Stewart and others (2006). It was believed that the state-of-the-practice linear modeling approach is not applicable to larger regions where climate factors are heterogeneous. Here, the big data was similar to that used on the Western Oregon model. The stream temperatures were half-hourly signals recorded from June 1 to August 31 in 254 wadeable streams during a 13 year period from 1990 to 2002. No site was measured for more than two years, and most were measured only one year. Daily mean water temperatures were calculated and served as the output parameter of interest. The climate signals were from sites across Wisconsin and consisted of 7 air pressure, 156 air temperature, 13 dew point, 164 precipitation, and 13 solar radiation signals for a total of 353 signals. Forty-two categorical parameters described the basin and stream network characteristics for the watersheds, 60-meter buffers, and the stream network associated with each stream segment. These were culled to 20 parameters using a cross correlation matrix that identified collinear pairs.

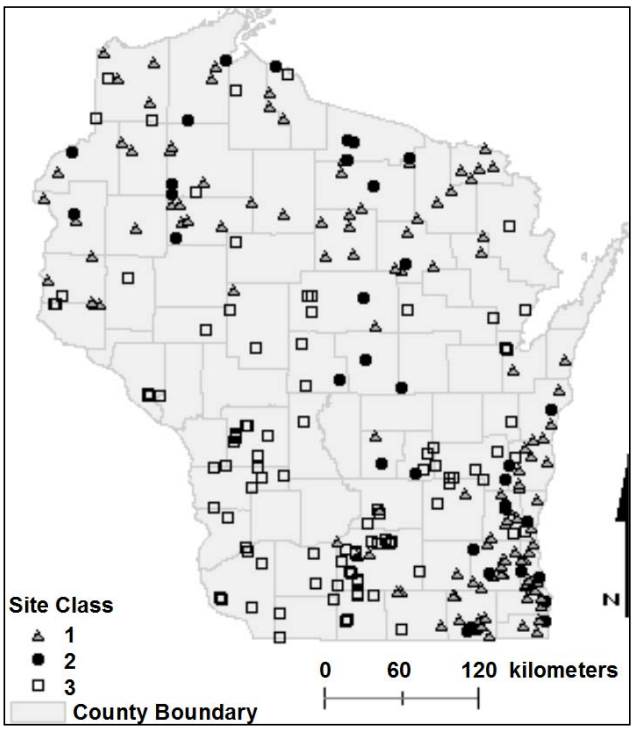

Figure 8. Distribution of 254 stream sample sites identified by class (right).

A few issues made this model more complicated to develop than the Western Oregon model. The large number of climatic signals was too unwieldy to be used directly and required a method for reducing them that would retain potentially important information about stream temperature variability. This was accomplished by clustering the climatic signals using the times-series clustering method. Mean signals for each class were synthesized by computing the daily means of the class members. The mean signals were then decorrelated by assigning one to be a standard signal and calculating differences for the others. This greatly reduced the number of climate parameters to 20 while preserving a semblance of spatial variability.

A second issue is that climate behavior drives stream temperature temporal variability, and daily variability changes greatly year-to-year for any specific calendar period. Here, the population of stream temperature signals were scattered over 13 years, preventing the use of the time-series clustering method and the modeling of the response of all the sites to coincident climatic forcing. An "alternate" time-series clustering algorithm was developed to accommodate the lack of coincident stream temperature signals, consisting of the following steps.

a. Where possible, populations of overlapping signals are compiled.
b. Using time-series clustering, estimate how many classes should be created for each population, then select a single number of classes to be used for all of them.
c. Reapply time-series clustering algorithm to each population using the number of classes determined in (b).
d. Determine which categorical parameters best discriminate between population classes using sensitivities determined from prototype ANN classification models.
e. Use a scoring method to determine which categorical parameters are consistently the best at discriminating between classes for all of the populations.
f. Re-cluster all sites using the important categorical parameters identified in (e).

The alternate algorithm was employed as follows. Streams sampled during the summers of 1998 to 2002 made up 241 of the 254 total sites. They provided five populations in step (a). In step (b) the number of classes was determined by the sensitivity of the mean square error computed by the k-means algorithm. The number chosen was three, which corresponded to low, medium, and high correlations between stream temperatures and climatic forcing. After steps (c) and (d), the scoring method used in (e) was based on how frequently a parameter survived culling in the development of the prototypes classification ANN models, and the sensitivity of the prototype's prediction R^2 to having the parameter included. The top categorical parameters for class discrimination were those that describe land use, upstream drainage area, bedrock depth, and surficial texture. While step (f) produces a linear segmentation of sites, it does so using parameters that were found in step (d) to be the best at discriminating site-to-site behavior by a reliable nonlinear ANN-based method. Site classification results are shown in Figure 8.

Results from the alternate algorithm were used to develop a separate sub-model for each class. Cascaded models were not needed because of the daily time step and the limited dynamic range of the June-August recording periods. Of the 254 sites, 223 were used for training and 31 were set aside for independent validation. The sub-models were trained to predict daily mean stream temperature signals for the June-August periods from 1990–2002. The inputs were selected categorical parameters and mean climate time series parameters. The six decorrelated air temperatures were found to be the best predictor climate parameters, and were included in the models for all three classes. The best categorical parameters, which were also included in all models, were drainage area, Darcy values for watershed and buffer areas, and watershed water and wetland land cover percentages.

A nonlinear classifier for new sites was developed in the same manner as that for the Oregon model. The super-model is composed of one sub-model per class and three classification models for a total of 6 separate ANN models. It was assembled in a spreadsheet program that runs simulations using the historical climate input data and categorical input values set for new sites. The simulations predict June to August stream temperature signals for the years 1990–2002 that are then characterized

statistically. Figure 9 shows measured and predicted hourly stream temperatures at 14 Class 1 validation sites. The sites' signals have been concatenated together. These results are typical of the other models. It is apparent that the prediction tracks the dynamic variability in the measurements, but generally runs either high or low for each site. As was the case for the Western Oregon stream temperature model, this indicates that the primary sources of error are the categorical parameters that predict the mean behavioral component for each site.

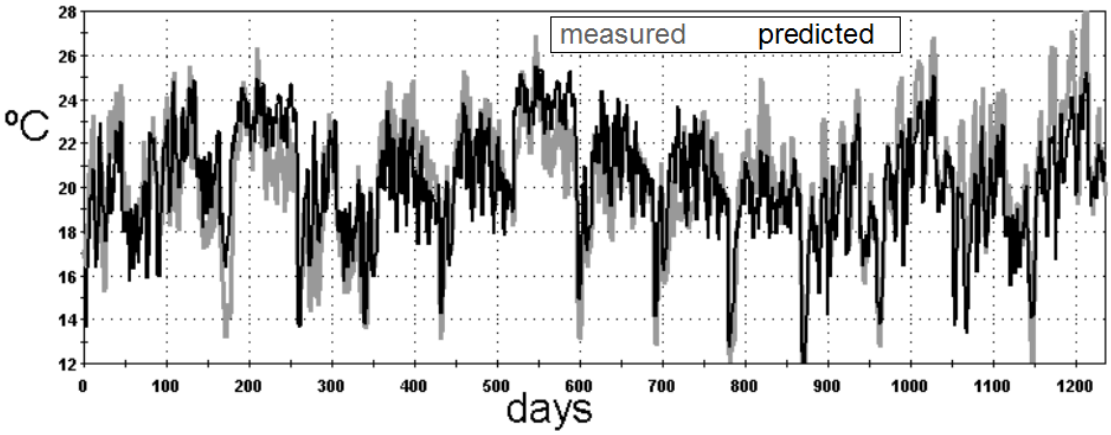

Figure 9. Measured (gray) and predicted (black) Class 1 stream temperatures at 14 validation sites. The 14 time-series are concatenated and show the rise and fall of stream temperature for June–August in the years when they were recorded.

Water Depths in Water Conservation Area 3A in the Florida Everglades. The real-time Everglades Depth Estimation Network (EDEN) supports a variety of scientific and water-management purposes, including the estimation of water depths throughout the greater Everglades from a limited number of reference "gaging" sites. Accurately predicting the water depths at ungaged sites is made difficult by the limited gaging and imperfect knowledge about the complex interactions of topology and vegetation. Linear regression and interpolation techniques are often used to estimate water depths at ungaged locations, however, the dynamic relations between hydrology, topography, and vegetation are nonlinear.

As first reported by Conrads and Roehl (2006), the purpose of this model is to provide better water-depth predictions at ungaged sites in the Water Conservation Area 3A (WCA3A, Figure 10). Note the overlain 400x400 meter^2 grid. This model is similar to the Upper Floridan Aquifer model, but in addition to spatial coordinates, its inputs include categorical parameters that describe each cell's distribution of vegetation types.

Here, the big data comprised water-level and water-depth signals, and categorical parameters representing cell coordinates and vegetation types in percentages of slough, prairie, sawgrass, or upland. The signals were 15-minute time series of water depths from 16 sites (W# in Figure 10) and water levels from 3 sites (Sites 64, 65, and 69 in Figure 10) for the period December 2002 to May 2005. These were reduced to daily values using moving window averages. Note that Figure 10 indicates that 14 of the sites are used for model training - 5 for inputs and 9 for

output. The 5 validation sites were selecting using a filter that identified them to be the least unique according to their categorical parameter values.

A preliminary analysis indicated that good prediction accuracy could be obtained using a single class of water-depth signals. The signals were processed by using the Site 64 water level as a standard and computing the differences between the other water-level and water-depth signals, called the difference-from-the-standard. This effectively set all the water-depth and water-level data to the same datum and decorrelated the signals.

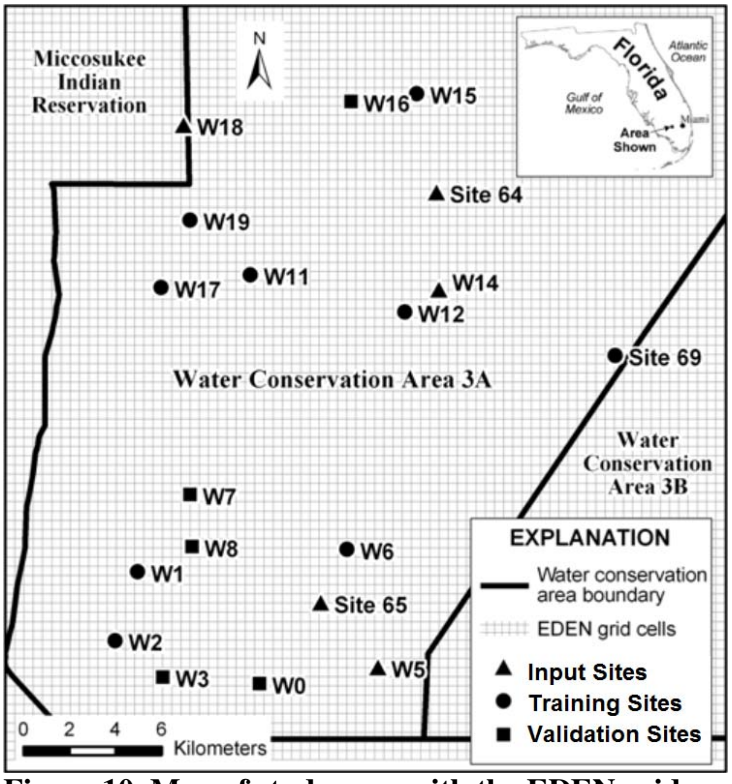

Figure 10. Map of study area with the EDEN grid and input, output, and validation sites.

The divide and conquer approach used two ANN sub-models. Model-1 was trained to predict the difference-from-the-standard signals using only categorical input parameters. Model-2 was trained to predict model-1's prediction error, which exhibits the training site's daily variability, using the categorical inputs, the Site 64 water level, and difference-from-the-standard signals for the input sites. For a given cell, the predicted water depth is the sum of the Site 64 water level and the predictions made by model-1 and model-2.

The super-model is composed of model-1 and model-2, and was assembled in a spreadsheet program that runs simulations to the predict water depth at a specified cell at each time step. Figure 11 shows measured and predicted water depths at the W8 validation site. While the prediction accuracy is good, the model slightly under-predicts the water depths for the majority of the simulation. Like the Western Oregon and Wisconsin stream temperature models, the primary sources of error are the categorical parameter inputs that predict the mean behavioral component for each site.

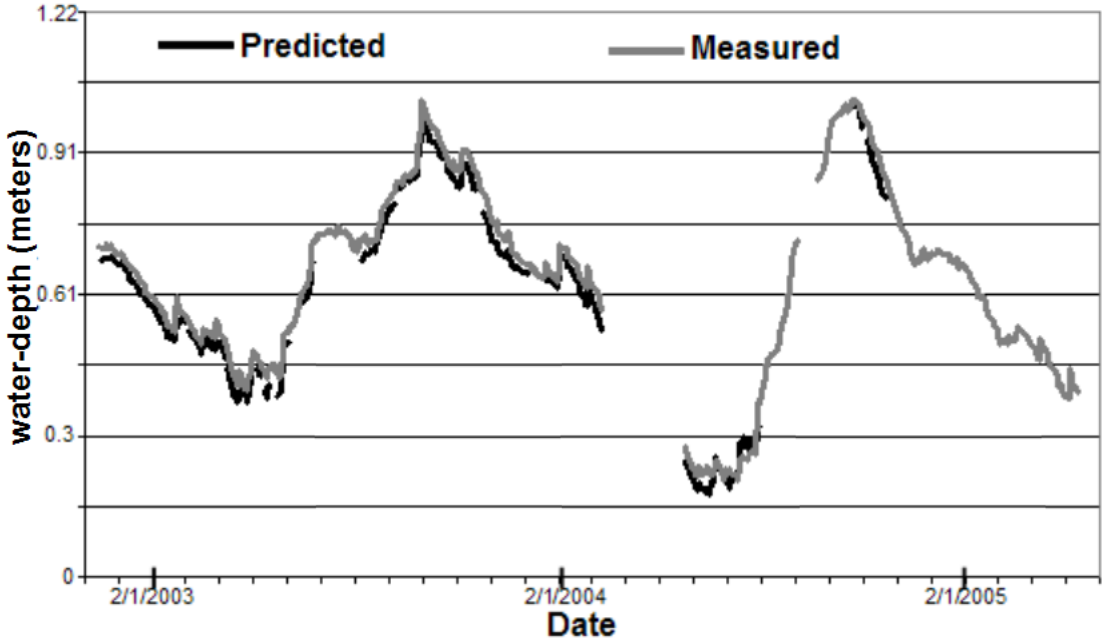

Figure 11. Plot showing measured (gray) and predicted (black) water depths for Site W8. The gaps are caused by periods of missing data.

CONCLUSIONS

This paper describes a new technical approach that leverages big data to provide several advantages over traditional modeling approaches, including being faster and less expensive, more comprehensive in its use of available data, and more accurate in representing complex physical processes. Many problems that confront resource managers and environmental scientists are already described by data that is ready and available. For example, of the four applications described in this paper, only the Western Oregon stream temperature model relied on data that was specifically collected for the problem solved.

The new approach readily solves problems of a scale and complexity that confound other approaches because it employs a divide and conquer approach that breaks large complex problems into smaller, tractable sub-problems, and then solves them using signal processing and numerically optimizing algorithms such as clustering, classification, and nonlinear empirical modeling. For example, the development of the Wisconsin stream temperatures model ensued after state and federal agencies concluded that there was no other way to proceed; and the Everglades water-depth model was developed because of perceived inadequacies of other state-of-the-practice solutions that had already been tried.

REFERENCES

Conrads, P. and Roehl, E. (1999). "Comparing physics-based and neural network models for predicting salinity, water temperature, and dissolved-oxygen

concentration in a complex tidally affected river basin." South Carolina Environmental Conference, Myrtle Beach, SC, March 15-16, 1999.

Conrads, P. and Roehl, E. (2006). "Estimating water depths using artificial neural networks." Hydroinformatics 2006, edited by P. Gourbesville, J. Cunge, V. Guinot, and S. Liong, Vol. 3, p.1643-1650.

Conrads, P. and Greenfield, J. (2008). "Effects of reduced controlled releases from Lake Thurmond on salinity intrusion in the Lower Savannah River Estuary." South Carolina Water Resources Conference, Charleston, S.C, October 2008.

Coppola, E., Rana, A., Poulton, M., Szidarovszky, F., and Uhl, V. (2005). "A neural network model for predicting aquifer water-level elevations." *Ground Water* 43(2), 231-241, 2005.

Dowla, F. and Rogers, L. (1996). *Solving Problems in Environmental Engineering and Geosciences with Artificial Neural Networks*, MIT Press, Cambridge MA, p. 159-172.

Goddard, J., Martinez, A., Martinez, F., and Aljama, T. (2000). "A comparison of different clustering algorithms for speech recognition." Circuits and Systems, 2000. Proceedings of the 43rd IEEE Midwest Symposium on, 3, 1222-1225.

Hinton, G. (1992). "How neural networks learn from experience." *Scientific American,* September 1992, p.145-151.

Holmstrom, L., Koistinen, P., Laaksonen, J., Oja, E. (1997). "Neural and statistical classifiers - taxonomy and two case studies." *Neural Networks, IEEE Transactions on*, 8(1), 5-17.

Jensen, B.A., 1994, "Expert systems - neural networks." *Instrument Engineers' Handbook Third Edition*, Chilton, Radnor PA 2004.

Risley, J., Roehl, E., and Conrads, P. (2003). "Estimating water temperatures in small streams in Western Oregon using neural network models." U.S. Geological Survey Water-Resources Investigations Report 02-4218.

Roehl, E., Risley, J., Stewart, J., and Mitro, M. (2006). "Numerically optimized empirical modeling of highly dynamic, spatially expansive, and behaviorally heterogeneous hydrologic systems – part 1." Proceedings of the Summit on Environmental Modelling and Software. International Environmental Modelling and Software Society, Burlington, VT, July 2006.

Roehl, E. and Conrads, P. (2006). "Hydrologic modeling using multivariate state space reconstruction." Hydroinformatics 2006, edited by P. Gourbesville, J. Cunge, V. Guinot, and S. Liong, Vol. 1, p.765-772.

Stewart, J., Mitro, M., Roehl, E., and Risley, J. (2006). "Numerically optimized empirical modeling of highly dynamic, spatially expansive, and behaviorally heterogeneous hydrologic systems – part 2." Hydroinformatics 2006, edited by P. Gourbesville, J. Cunge, V. Guinot, and S. Liong, Vol. 2, p.831-838.

Weiss, S. and Indurkhya, N. (1998). *Predictive Data Mining - A Practical Guide*. Morgan Kaufmann, San Fancisco, p. 1-2.

Application of Northeast Regional Climate Center Research Results for the Purpose of Evaluating and Updating Intensity-Duration-Frequency (IDF) Curves. Case Study: Rochester, New York

S. B. Wolcott[1], M. Mroz[2], and J. Basile[3]

[1]Scott B. Wolcott, PE, Program Chair, Civil Engineering Technology, Rochester Institute of Technology, 78 Lomb Memorial Drive, Rochester, NY 14623, PH (585) 475-6647; FAX (585) 475-7964; email: sbwite@rit.edu
[2]Matthew Mroz, Undergraduate student, Civil Engineering Technology, Rochester Institute of Technology, 78 Lomb Memorial Drive, Rochester, NY 14623; PH (585) 475-2183; FAX (585) 475-7964; email: mrm1042@rit.edu
[3]James Basile, PE, Senior Civil Engineer, Bergmann Associates, 28 E. Main Street, 200 First Federal Plaza, Rochester, NY 14614; PH (585) 232-5135; FAX (585) 325-8493; email: jbasile@BERGMANNPC.com

ABSTRACT

There has been much discussion regarding global climate change and potential impacts to the environment. One suggested impact of climate change is increasing storm intensity. Changes in rainfall intensity could significantly alter the accuracy of current stormwater management designs.

Civil engineers and community planners use historical precipitation data and statistically generated models to design stormwater management facilities. It is not uncommon for civil engineers to design stormwater management facilities using models that are based on precipitation data published more than 50 years ago.

The design of stormwater facilities is largely based on the amount of runoff generated from a design storm event. Rainfall intensities and depths for various storm frequencies are determined using local Intensity-Duration-Frequency (IDF) curves and isohyetal maps, respectively. The IDF curves currently in use in Rochester, New York were originally published in 1955 and generated using approximately 40 years of data. Approximately 55 years of additional precipitation data is now available.

The purpose of this paper is to: 1) evaluate and report trends in precipitation observed at the Greater Rochester International Airport; and 2) Generate updated Intensity-Duration-Frequency (IDF) curves and compare these to existing IDF curves. This paper will use Rochester, New York as a case study.

Data sources for this paper include daily precipitation depths collected at the Greater Rochester International Airport and published research by the Northeast Regional Climate Center (NRCC) at Cornell.

The methodology used in this study can be applied to any municipality in the United States. However, some comparisons presented herein make use of research limited to the north eastern US.

INTRODUCTION

There has been much discussion regarding global climate change and potential impacts to the environment. Climate models have long predicted that global warming will increase the intensity of extreme precipitation events. Of utmost concern is that heavy rainstorms will become more common and more intense in a warmer climate due to the increased moisture available for condensation. More intense rain events increase the risk of flooding and can have substantial societal and economic impacts (esciencenews, 2008). Changes in rainfall intensity could significantly alter the accuracy of current stormwater management designs.

Stormwater management systems include exceptional projects such the Mississippi River levee system in the US and the Zuiderzee Works in the Netherlands. These are large installations that require consideration of marine weather impacts as well as land based runoff from rainfall. Smaller scale stormwater management devices such as culverts, detention ponds, erosion control methods, and storm sewer networks are common in any community, frequently replaced or constructed and are designed based on rainfall/runoff relationships. This paper will focus on the latter.

The purpose of this paper is to determine if there is significant evidence from precipitation data in the Rochester, New York area to warrant generation of updated stormwater management design tools.

Current Stormwater Management Design Tools

The design of stormwater management devices is largely based on the amount of runoff generated from a design storm event. Rainfall intensities and depths for various storm frequencies are determined using local Intensity-Duration-Frequency (IDF) curves and isohyetal maps, respectively. The rainfall amount is then applied, together with watershed characteristics, to determine the volume or rate of stormwater runoff.

The IDF curves and isohyetal maps are statistically generated and published for use by governmental agencies and engineering firms. In fact, the use of IDF curves and/or isohyetal maps are often required in local regulations. Stormwater management facilities in Rochester, New York are currently designed based on IDF curves (See Figure 1) published in December 1962 (MCPC, 1962).

The 1962 curves were redrawn for engineering application from a 1955 US Weather Bureau publication – Technical Paper No. 25 (TP-25) (USWB, 1955). Precipitation records, tabulated since circa 1910 at the Greater Rochester Area International Airport, provided the basic data from which the TP-25 IDF curves were derived. A Type I Gumbel Distribution was used to generate the recurrence intervals. More recent hydrological research suggests that TP-25 and a later US Weather Bureau publication – TP-40 (USWB, 1961), which also used Gumbel Distribution; underestimate the largest extreme precipitation events (NRCC 1993).

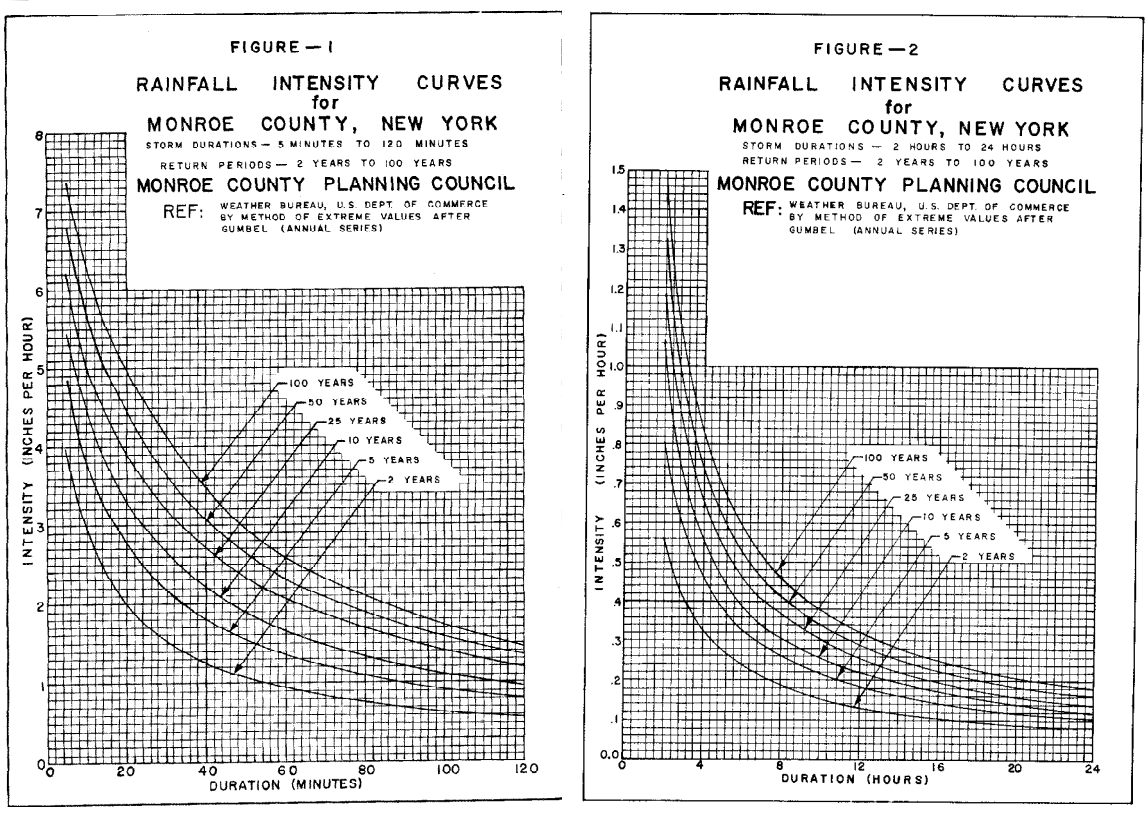

Figure 1. Existing IDF curves for Rochester, New York

Updated isohyetal maps (See Figure 2) have been developed by the Northeast Regional Climate Center (NCRR, 1993). Isohyetal maps describe the expected precipitation over an area based on a given return frequency. Each line represents a line of equal precipitation. By identifying the location on a map and determining the magnitude of the adjacent isohyetal lines, the magnitude of rainfall expected to occur during a specific return frequency can be determined.

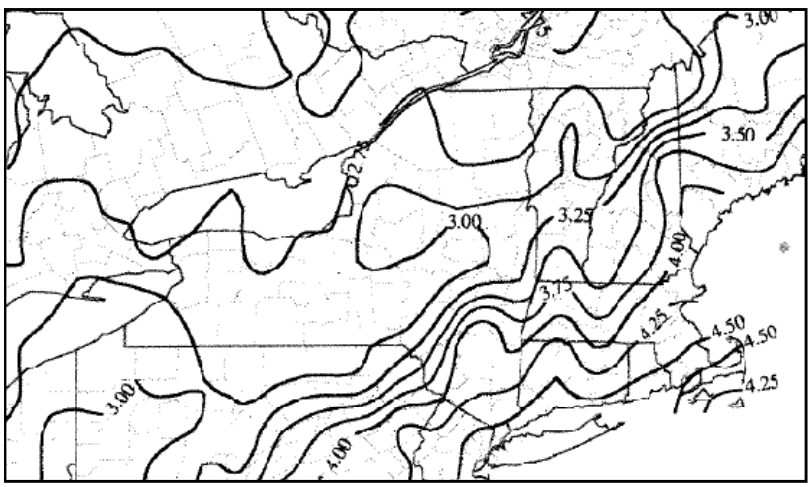

Figure 2. 1-day precipitation, 10-year return period (NCRR 1993)

The *Atlas of Precipitation Extremes for the Northeastern United States and Southeastern Canada* (NCRR 1993) is the most current and comprehensive extreme precipitation study in the region. Isohyetal maps presented in the study will be used to determine one day precipitation depths for 2-year, 5-year, 10-year, 25-year, 50-year, and 100-year return periods for Rochester, New York.

PRECIPITATION TRENDS

Daily precipitation data, collected from the Greater Rochester Area International Airport between 1926 through 2005, has been analyzed to see what trends exist. A simple linear trendline was generated for each parameter evaluated: annual maximum daily precipitation; annual standard deviation; annual precipitation; and the number of days with precipitation.

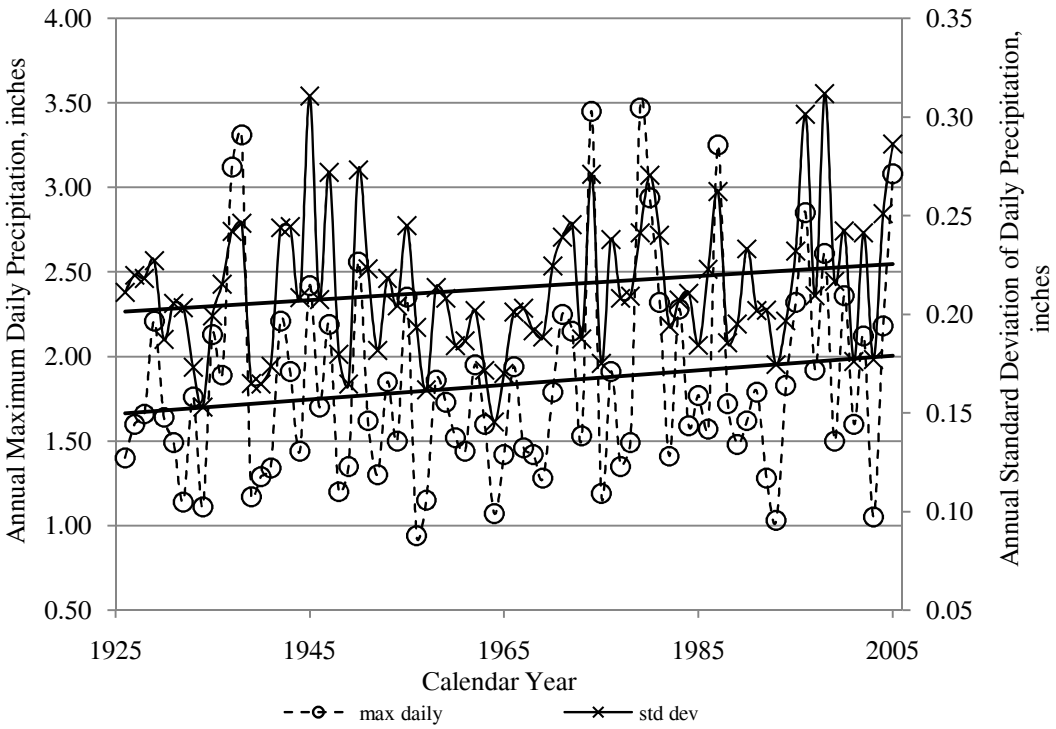

Figure 3. Annual Maximum Daily Precipitation and Standard Deviation

Increasing trends are observed in the four parameters investigated (See Figures 3 and 4). The value of each trend in terms of inches or days per year seems relatively small.

However, if the incremental increase over a 100 year period is divided by the mean of the 80 year period of record the trends seem less trivial (See Table 1). The values of annual maximum daily precipitation, annual standard deviation of daily precipitation and the annual total precipitation increase at least by 14 percent over a 100 year period. However, the number of days of precipitation increases by only 5 percent. This indicates that the intensity, variability and volume of precipitation are increasing at a faster rate than the number of precipitation days. In other words, it won't rain more days in a given year, but it will rain harder (i.e. intensity).

Table 1. Linear Trends of Precipitation Data (1926 – 2005)

Parameter	Mean	Trend	Increase per 100 yrs	% increase
Annual Max Daily Precip.	1.83 in	0.0043 in/yr	0.43 in	+23
Annual Standard Deviation	0.21 in	0.0003 in/yr	0.03 in	+14
Annual Precipitation	32.16 in	0.0532 in/yr	5.3 in	+16
Number of Precip. Days	161.4 days	0.0789 d/yr	8.9 d/yr	+5

The 80 year period of record data supports the hypothesis that storm events are increasing in intensity. IDF curves will be generated and evaluated in this paper because of the following reasons:

1) existing IDF curves were developed using a statistical method (Gumbel distribution) that might underestimate the largest extreme precipitation events (i.e. 100 year storms) (NRCC 1993);
2) existing IDF curves were developed using a relatively short period of data, estimated to be approximately 35 years (~1915 - ~1950); and
3) Analysis of precipitation trends using 80 years of data (1926 – 2005) indicate that precipitation is increasing in intensity.

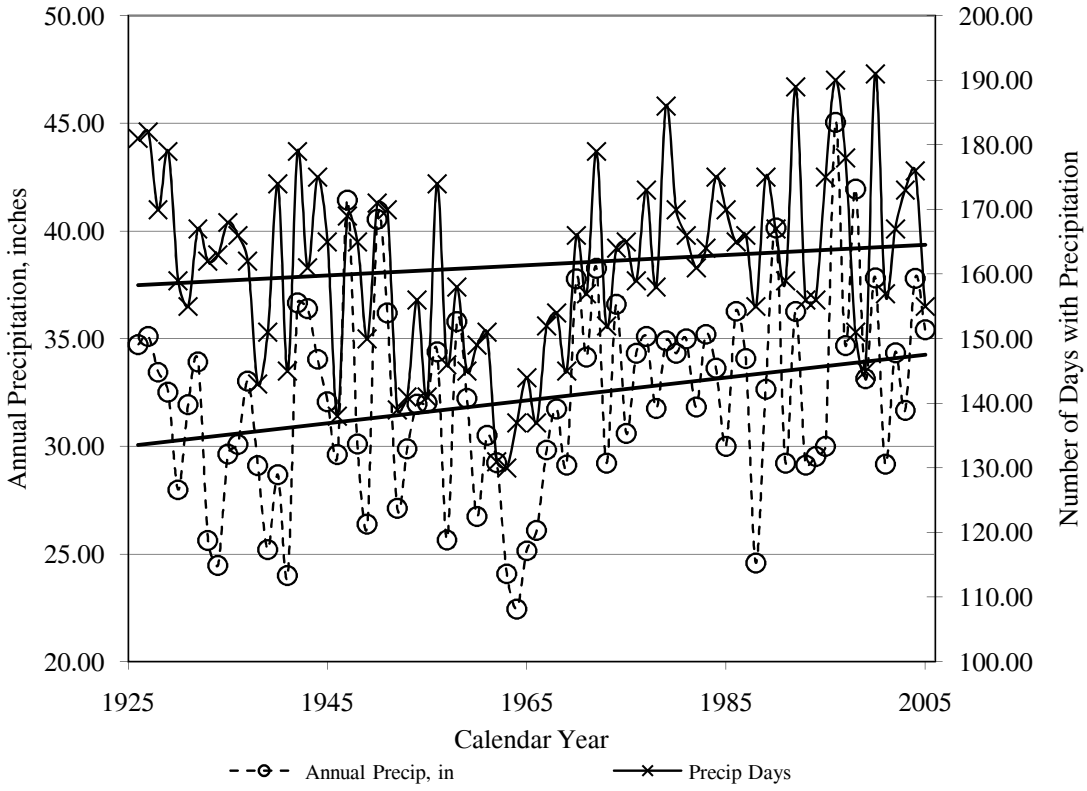

Figure 4. Annual Precipitation and Number of Precipitation Days

GENERATION OF NEW IDF CURVES

The generation of new IDF curves follows a procedure presented by NRCC. One day precipitation depths are selected for the Rochester, New York area from isohyetal maps (NRCC, 1993). One day precipitation depths were selected from maps with return periods (i.e. frequencies) of 2-yr, 5-yr, 10-yr, 25-yr, 50-yr, and 100-yr to correspond with the frequencies on the IDF curves (See Table 2). For comparison purposes, one day precipitation depths from the existing IDF curves and the results of a LOG Person III analysis of the 80 year period of record are also provided. Data selected from the NRCC isohyetal maps are generally higher than the other two sources. Interesting, the return period precipitation depths from existing IDF curves and the Rochester airport are relatively close. The depths generated from data collected from the Rochester airport are within 2% and 6% of the depths estimated from the existing IDF curves. The Rochester data is slightly higher than the return period depths from the existing IDF curves

Table 2. One Day Precipitation Depths, Rochester New York area.

	Precipitation, inches					
	2-yr	5-yr	10-yr	25-yr	50-yr	100-yr
NRCC, 1993	1.90	2.37	2.74	3.45	4.00	4.85
Rochester Precipitation Data	1.71	2.25	2.62	3.10	3.48	3.88
Existing IDF curves*	1.68	2.17	2.53	2.93	3.40	3.80

*24 hour depths estimated from the existing IDF curves were divided by 1.13 (Huff & Angel empirical adjustment factor) to obtain the 1 day depth presented in Table 2.

The one day precipitation depths are multiplied by empirical adjustment factors to modify one day precipitation depths to 24 hour precipitation depths. The one day time frame corresponds to a calendar date and is used during collection of precipitation data. An extreme precipitation event is unlikely to follow a calendar date and can occur over multiple days. Two different multipliers were applied in this analysis (See Table 3) to convert one day depths from isohyetal maps to 24-hour depths used in IDF curves.

Huff & Angel factors were reported in the 1993 NRCC report were based on analysis of data from the Midwestern U.S. NRCC determined that the Huff & Angel factors overestimated precipitation depths for shorter durations. Empirical adjustment factors for the northeast were presented in *Atlas of Short-Duration Precipitation Extremes for the Northeastern United States and Southeastern Canada* (NRCC 1995).

Northeast empirical adjustment factors for durations of less than one hour were not presented. Therefore, short duration values, developed by the World Meteorological Organization (Prodanovic 2007) supplemented the Northeast factors.

Table 3. Empirical Adjustment Factors

	Durations										
	5 min	10 min	15 min	30 min	60 min	2 hr	3 hr	6 hr	12 hr	18 hr	24 hr
Huff & Angel (1992)	0.14	0.24	0.31	0.42	0.53	0.66	0.72	0.85	0.98	1.06	1.13
Northeast & *WMO*	*0.125*	*0.194*	*0.245*	*0.340*	0.43	0.54	0.65	0.79	0.97	1.07	1.13

Several IDF curves have been generated to determine if adopting new IDF curves for the Rochester, New York area are necessary. Only the 10-year return period is presented in these illustrations for clarity.

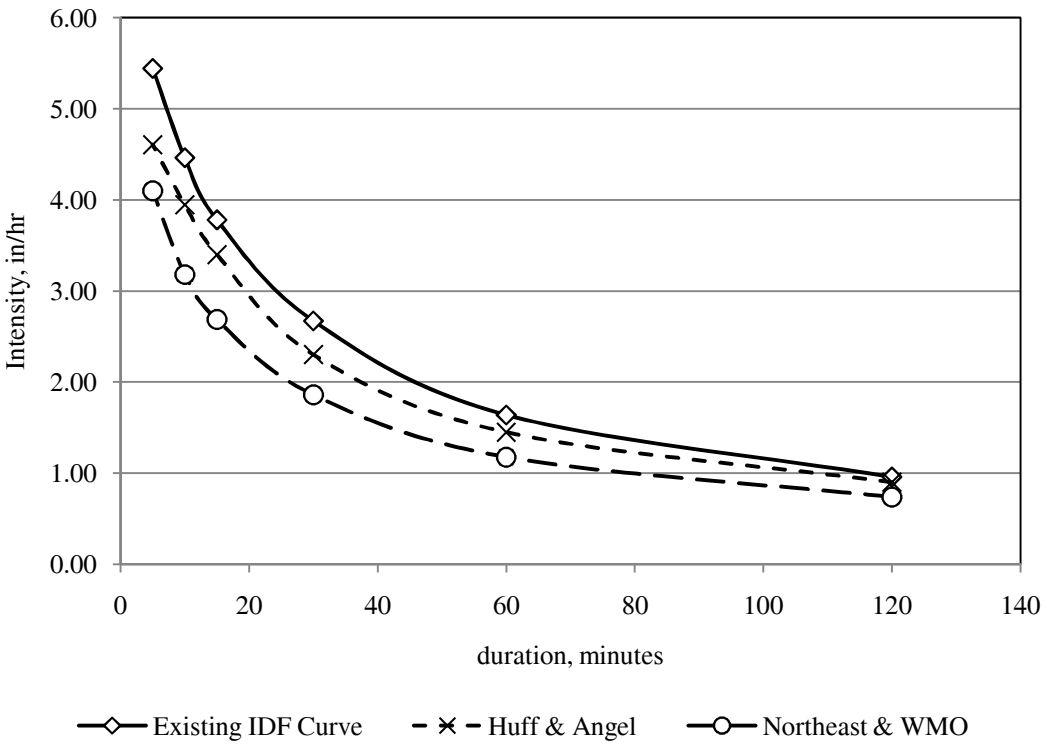

Figure 5. IDF Curve (5 min to 120 min) using NRCC 1993 return period depths

Figures 5 and 6 show that newly generated IDF curves provide lower intensities than the existing IDF curves for a given duration. This is true regardless of which empirical adjustment factor is used. In fact, the Huff & Angel IDF curve is closer to the existing IDF curve than the curve produced using empirical adjustment factors specifically developed for the northeast. The three IDF curves produce nearly identical intensities when the duration is greater than 10 hours (See Figure 6).

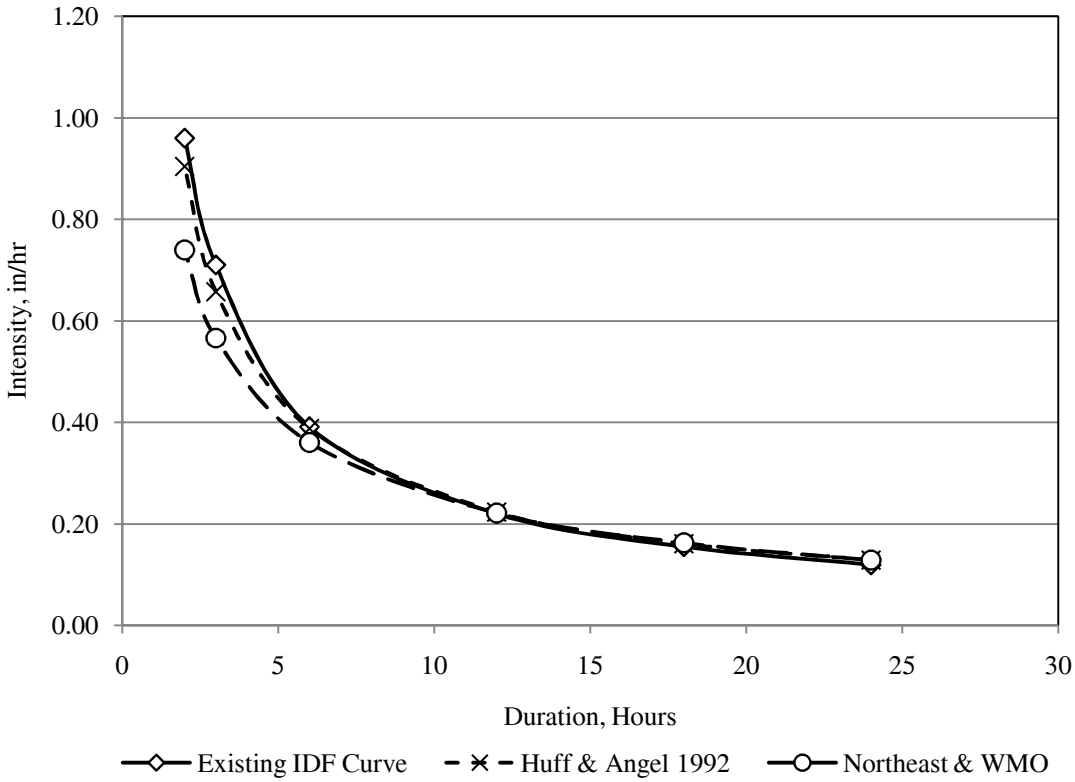

Figure 6. IDF Curve (2 hr to 24 hr) using NRCC 1993 return period depths

Very similar sets of IDF curves are produced if the curves are generated using the return period precipitation depths from the Rochester Airport precipitation data.

CONCLUSIONS

There is no need to replace the existing IDF curves for the Rochester, New York area. Even though precipitation trends indicate increasing intensity of storm events, IDF curves generated with new hydrologic methods and updated precipitation data sets consistently produce lower intensities for a given duration than the existing IDF curves. Stormwater management designs, based on existing IDF curves, will continue to offer some level of conservativeness.

In light of the estimated increasing trends in precipitation intensities, the results of this study were somewhat surprising. It is very possible that the authors of the existing IDF curves purposely used conservative methodologies and assumptions. They may have done so to provide a safety factor comparable to the inherent risk of predicting rainfall depths for 50 or 100 year return periods using a period of record of approximately 35 years.

REFERENCES

Huff, F.A. and J.R. Angel, 1992. Rainfall Frequency Atlas of the Midwest, Illinois State Water Survey, Champaign IL, Bulletin 71, 141 pp.

Monroe County Planning Council (MCPC) (1962), "Drainage Study – Stage I for the Rochester-Monroe County Metropolitan Area," December 1962

U.S. Weather Bureau (USWB) (1955), "Rainfall Intensity-Duration-Frequency Curves for Selected Stations in the United States, Alaska, Hawaiian Islands, and Puerto Rico, Technical Paper No. 25," December 1955

U.S. Weather Bureau (USWB) (1961), "Rainfall Frequency Atlas of the United States, Technical Paper No.40" December 1961

Mroz, M and S. Wolcott, "The Impact of Precipitation Trends on Stormwater Management Practices" (2008), Proceedings of The National Conference on Undergraduate Research (NCUR) 2008, April 2008

Northeast Regional Climate Center (NRCC) (1993), "Atlas of Precipitation Extremes for the Northeastern United States and Southeastern Canada," September 1993

NRCC (1995), "Atlas of Short-Duration Precipitation Extremes for the Northeastern United States and Southeastern Canada," March 1995

Prodanovic, P. and S.P. Simonovic (2007), "Development of Rainfall Intensity Duration Frequency Curves for the City Of London Under the Changing Climate", Report for City of London, Ontario, Canada.

Unknown (2008), "Climate Change: When it Rains it (Really) Pours", e! Science News, http://esciencenews.com/articles/2008/08/07/climate.change.when.it.rains.it.really.pours

Assessment of Flood Risk due to Storm Surge in Costal Bayous Using Dynamic Hydraulic Modeling

T. Ray[1], Z. Feng[2], P.B. Bedient[3]

[1,2,3]Department of Civil and Environmental Engineering, Rice University, 6100 Main St. MS 312, Houston, TX 77005; PH (713) 348-3798; FAX (713) 348-5239; email: jtray41@gmail.com

Abstract

The purpose of this study is to analyze the combined effects of storm surge and inland rainfall on the floodplain of a coastal bayou in the Houston area using dynamic hydraulic modeling.

The hydrologic and hydraulic models that were utilized in the study were created by the Tropical Storm Allison Recovery Project (TSARP). The TSARP HEC-RAS model was run for both the steady and unsteady states. In steady mode, storm surge was introduced by changing the downstream boundary conditions to match that of the measured and predicted peak stage of the surge. HEC-RAS was then used to run a backwater calculation in order to provide a worst case floodplain.

Upon completion of the steady state study, the model was then evaluated in the unsteady state. Running HEC-RAS in the unsteady state allowed both rainfall and storm surge to be introduced dynamically. This allowed for a more accurate representation of the flooding characteristics of this channel, but more work is needed to refine hydrographs.

Introduction

In coastal areas like the Gulf Coast, hurricanes and tropical storms often bring storm surge and inland flooding. The surge threat in these areas is real as was evidenced by Hurricanes Katrina and Ike in 2005 and 2008. The focus area for this study was chosen because of it's proximity to the storm surge impacts of the Texas Gulf Coast.

Clear Lake City is located approximately 25 miles southeast of Houston proper and 5 miles west of Galveston Bay. Because of its proximity to Houston and the industry located in the Galveston Bay area, Clear Lake has been rapidly developing. As it has developed, areas within the city boundary have experienced frequent flooding, primarily in the vicinity of Horsepen Bayou and its tributaries. The Horsepen Bayou watershed is a 2.7 square mile watershed that drains into the downstream portion of Armand Bayou which discharges through Clear Lake and into Galveston Bay. An area map can be seen in Figure 1.

Many of the characteristics of the Horsepen Bayou watershed are typical of a watershed situated on the Texas coast and, in particular, Galveston Bay. There is very little relief in the area and this flat topography results in poor overland drainage

and very low channel slopes. In Horsepen, the overall watershed slope is 0.06 percent, a very low slope. Clay soils are typical in the area and the predominate soil in Horsepen Bayou is Lake Charles clay. This is a somewhat poorly drained soil with very slow permeability and internal drainage. This leads to a very slow surface runoff. It has a high available water capacity and when it is dry its forms deep, wide cracks that will rapidly allow water to enter. During the rainy hurricane season, however, these cracks will disappear, which means that any rainfall will generate large runoff and will do so very slowly. (USDA-SCS, 1976).

In the Houston/Galveston area, there has been a noticeable rise in high intensity rainfall events over the past few decades. There have been two storms larger than the 500 year event and six storms larger than the 100 year event since 1960. This large amount of rainfall coupled with rapid urban development has led to frequent flooding due to an under designed storm water management infrastructure. Horsepen Bayou has risen up to flood Clear Lake City four times in the past 30 years. (Dunbar 2005).

Hurricane Katrina and the damages that it caused have brought a new respect and understanding to the threat that storm surge poses. The National Hurricane Center reported that a 19 ft storm surge was measured in New Orleans during Katrina. In 2008, Hurricane Ike hit the Texas coast and a storm surge that ranged from 12-20 ft leveled the Bolivar Peninsula and caused major damages throughout Galveston Bay. (NHC, 2006) (NWS, 2008).

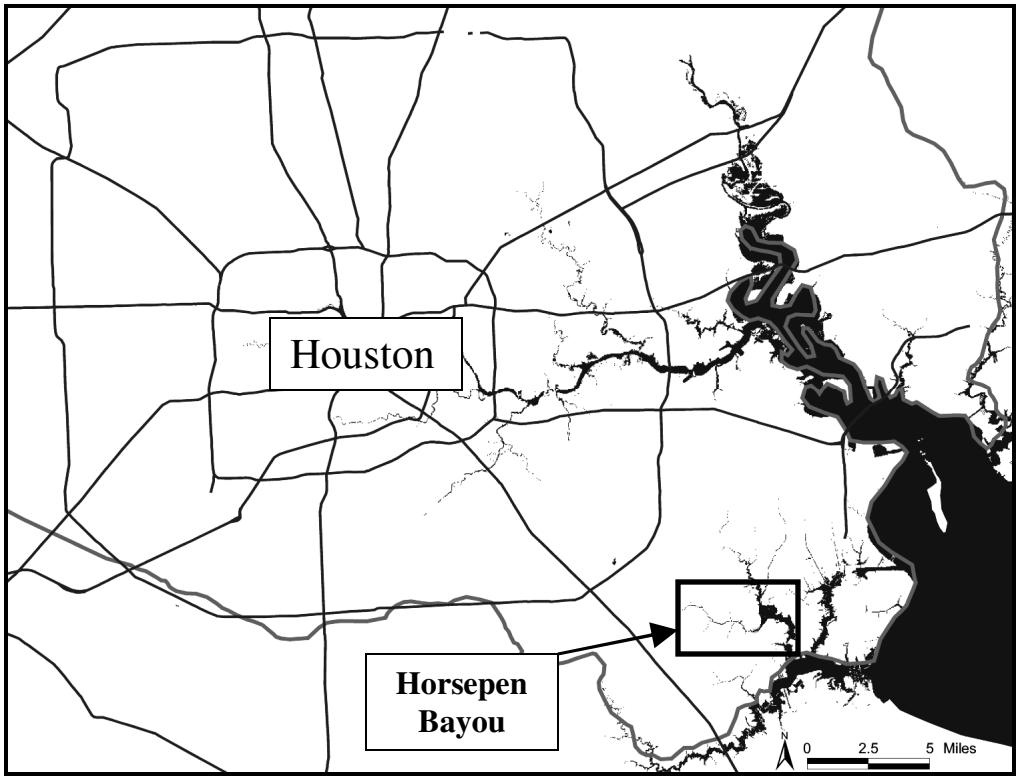

Figure 1: Location Map

Problem Statement

Areas that are frequented by hurricanes and tropical storms are consequentially faced with the threat of storm surge. Because of this, current modeling practices may be insufficient and lead to a false sense of security and safety. For example, when evaluating risk, inland rainfall and coastal storm surge are treated as separate and unrelated events. However, history has shown that this is not practical. The problem with studying these two events separately is that storm surge rarely occurs without inland rainfall. Storm surge is usually associated with tropical storms and hurricanes which are both accompanied by heavy rainfall. Storm surge, when acting alone, presents a problem because it is water moving through a channel and stream network that was only designed to carry the run-off from rainfall. If rainfall and storm surge are combined in the same channel, water flowing in opposite directions meets and any flooding that would normally occur is exacerbated by the combination of the two.

The scope of this study is to determine what affect the convergence of surge and rainfall/runoff will have on the floodplain. Many coastal areas such as Horsepen Bayou are inhabited by residential areas, commercial areas, chemical and power plants, schools, and hospitals. While many of these entities are geographically protected from the direct effects of storm surge, they are not protected by its rarely considered backwater effects. The Clear Lake City Water Authority (CLCWA) has expressed concern regarding the effects of storm surge because of the frequency at which they currently experience flooding without the presence of a storm surge.

With this information, surge-induced floodplains, or scenarios associated with coastal storm surge, could be created to better inform emergency managers, city officials, home owners, and citizens of the potential escalated flood risk. This study will also later investigate the timing of important events such as out of banks flooding, maximum flood depth, maximum floodplain extent, and flood subsidence. Armed with this information, emergency groups will be equipped with the information needed to make informed decisions regarding flooding due to storm surge.

Model Description

A number of models are being utilized in this study and the following is a brief description of each. Hydrologic, hydraulic and shallow water models are all incorporated.

HEC-HMS

This a Hydrologic Modeling Software (HMS) designed by the Hydrologic Engineering Center (HEC) for the Army Corp of Engineers. This software is designed to simulate the precipitation-runoff process of a watershed. Precipitation is entered as a hyetograph (precipitation per time) for each sub-basin in the watershed. By changing parameters such as infiltration, soil type, land use, and overland slope, the model can be calibrated to accurately simulate the amount of runoff that will

occur after a particular storm event. HMS also has basic flood routing abilities. (HEC, 2008)

Vflo

Vflo is a physics-based distributed hydrologic model that allows for spatial variability to be considered within a watershed when calculating runoff. It uses input from a Geographical Information System (GIS) which provides gridded watershed data. Within Vflo, each grid cell can be assigned different properties which allow a watershed with highly diverse characteristics to be modeled more precisely than can be done using HEC-HMS. HMS assigns physical properties to an entire sub-basin whereas Vflo is able to assign it to each individual cell within a sub-basin. Vflo also allows precipitation to vary from cell to cell. Because of this, radar rainfall data that has been calibrated against rain gages can be used in the model. By assigning each grid cell different physical properties and different rainfall amounts, Vflo is able to very precisely model the behavior of a watershed. (Vieux, 2004)

HEC-RAS

Both HMS and Vflo are hydrologic models that predict runoff. HEC-RAS (River Analysis System) is a hydraulic model that aids in channel flow analysis and floodplain delineation. RAS can be directly linked to HMS which makes if very easy to go from a hydrologic model to a hydraulic model. HEC-RAS can be run for steady flow which assumes flow rates are constant, or for unsteady flow which allows flow which assumes that flow rates are dynamic, or vary with time. Cross-sectional data that describe the channel can be imported or user defined and channel properties can then be assigned and modified to make the model an accurate representation of the actual channel. For steady flow, peak flow values are input at each cross-section and HEC- RAS uses the one-dimensional energy equation to make a backwater calculation. From this calculation a floodplain is produced. For unsteady flow, a hydrograph is input at each cross-section and HEC-RAS solves the full, dynamic, Saint-Venant equation using an implicit, finite difference method. As with the steady flow analysis a floodplain is created and a variety of output data is made available. (HEC, 2008) (Bedient et al., 2008)

ADCIRC

This is the Coastal Circulation and Storm Surge Model whose output will be used to provide the storm surge data that will be entered in HEC-RAS. ADCIRC is a system of computer programs for solving time dependent, free surface circulation and transport problems in two and three dimensions (ADCIRC.org). Although this model is capable of providing a variety of outputs, the only data that will be used in this application are simulated stage hydrographs that will act as a downstream boundary condition. This data will be provided by Dr. Clint Dawson at the University of Texas at Austin. Figure 2 is the surge that ADCIRC predicted for Hurricane Ike (Courtesy of Dr. Clint Dawson).

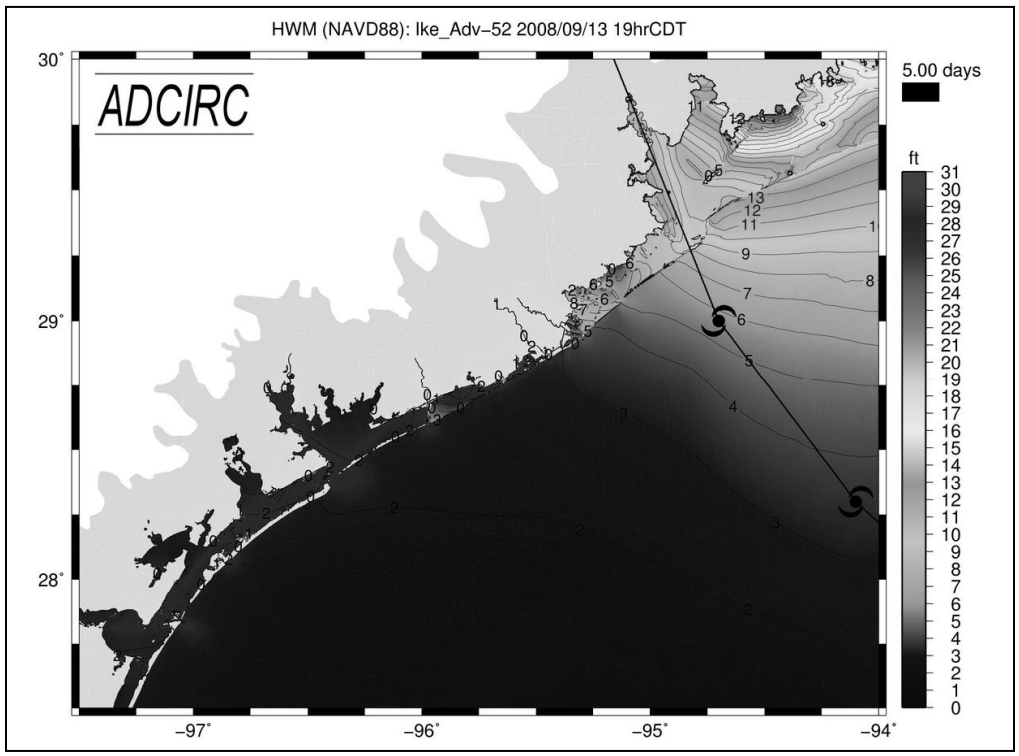

Figure 2: ADCIRC Storm Surge Prediction for Hurricane Ike

Model Application and Setup

Tropical Storm Allison Recovery Project (TSARP) created both hydrologic and hydraulic models. These models were calibrated and used to create new floodplain maps for the Houston-Galveston area. Because these models were available, they were chosen for use in this study. However, to test the accuracy and validity of the TSARP HMS model, a Vflo study was also performed. Model inputs were obtained from a variety of sources. A digital elevation map (DEM) created from the LIDAR data collected by TSARP was input along with soil information (USGS soil survey), land use data (land use classification from remote sensing images), and rainfall data collected during Tropical Storm Allison (June 2001) and a large storm event from October 1994. After running Vflo, the results were compared with TSARP data and observed data and can be seen in Figures 3a and 3b. It can be seen that the TSARP model under predicts on the October storm and over predicts on the Allison storm but the timing on both events is very accurate. The Vflo model almost matches the peak for Allison but the timing is about three hours early. Both models performed similarly in the October 1994 storm. After studying these results it was concluded that, for the purpose of this study, the TSARP model was satisfactory.

The TSARP hydraulic model, which was created using HEC-RAS, was used to obtain preliminary results that will later be compared to unsteady results. However, TSARP only studied the steady state case so an unsteady model did not

exist. The geometry from the steady model was taken and an unsteady model was created from it.

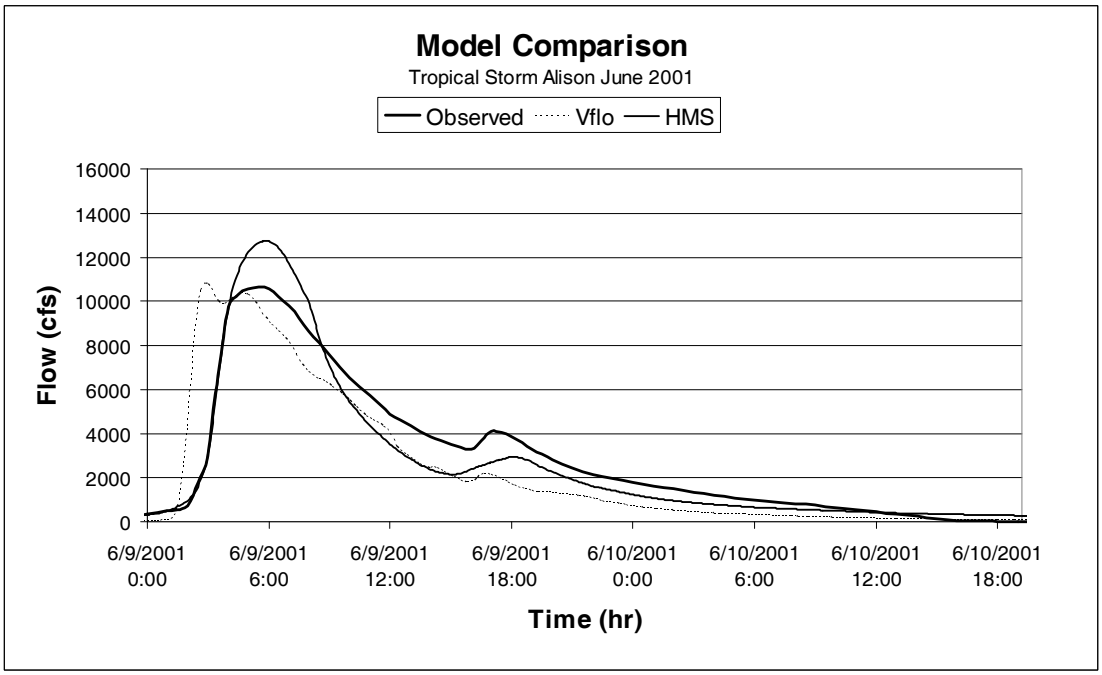

Figure 3a: Model Comparison – June 2001

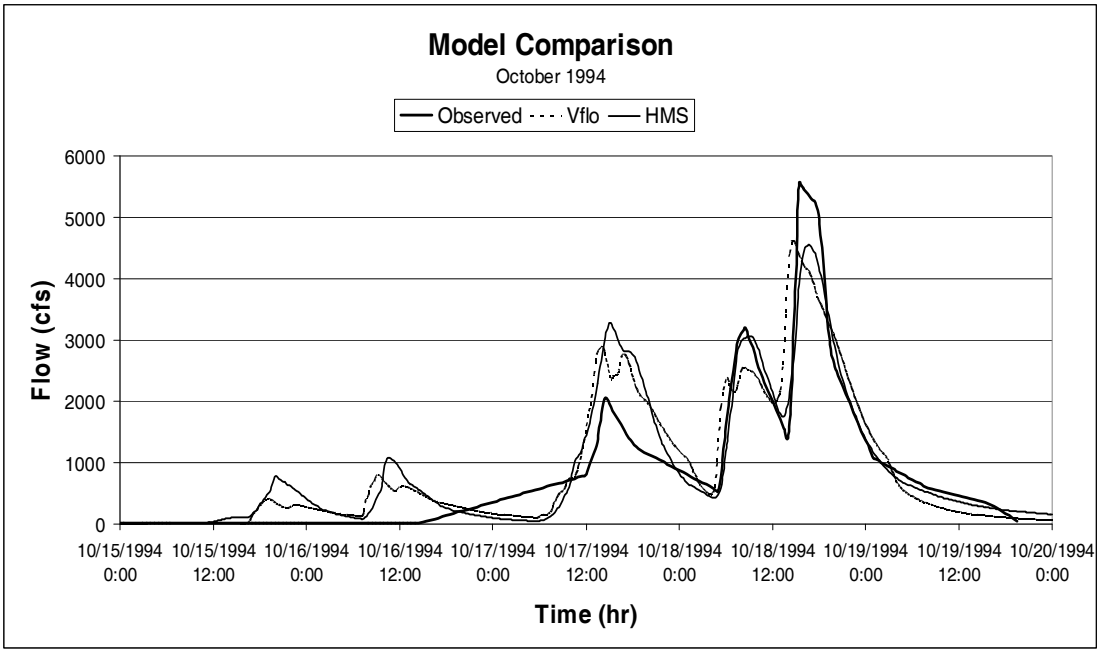

Figure 3b: Model Comparison – October 1994

Results

Initial work began by utilizing the existing steady state model created by TSARP. Storm surge was input in the steady model as a downstream boundary condition. The surge values that were input represent peak stage in Armand Bayou at the outfall of Horsepen Bayou. For the purpose of this study, the 10, 50, 100, and 500-year design storms were selected. Each of these storms was run in HEC-HMS and the data was input into HEC-RAS. All four of these storms were run for each downstream condition (0, 3.5, 6.5, 10, and 15 ft theoretical surge). This was decided to be a reasonable range based on USGS data collected during Hurricane Ike. The information from HEC-RAS was exported to HEC-GeoRAS, a program that works with ArcMap to delineate a floodplain by overlaying the information from HEC-RAS on a digital elevation map. Using these images, the floodplains for different rainfall-surge scenarios were mapped and compared.

Figures 4a and 4b show the floodplains caused by the 10-year and 100-year storm events combined with the effects of no surge and a 15 ft surge. For the 10-year event, storm surge effects can be seen at two locations. At the downstream end there is a significant difference in the two floodplains which is to be expected due to its proximity to the actual surge. In the middle portion of the watershed there is a noticeable difference in the two floodplains which can most likely be attributed to the flat topography in the area. In the case of the 100-year event similar effects can be seen at the downstream end but it is evident that there is a much larger impact throughout the rest of the watershed. The similarities at the downstream end may be attributed to cross-sections that are not wide enough to sufficiently cover the extent of the floodplain. This could be remedied by extending these cross-sections, but, as watershed overflows could result, they were left unchanged. Similar effects can also be seen in other portions of the watershed.

The results from the steady state modeling were produced assuming a peak on peak scenario. In other words, the peak discharge from the Horsepen Bayou happens at the exact same time as the peak stage in Armand Bayou. This is a worst case scenario and one that has a low probability of occurring. To more realistically model the interaction between rainfall-runoff and storm surge, an unsteady model must be employed.

TSARP only looked at the steady state scenario therefore no unsteady model currently exists. The geometry from the steady model was taken and adapted to create an unsteady model. After the unsteady model was created, a few simple runs were made to test the model. For the downstream boundary condition a theoretical surge was introduced. This data is actual surge data collected by the USGS during Hurricane Ike measured at the Clear Lake-Kemah gage. This data was scaled down by 20 percent because Horsepen Bayou is more inland than this gage. With this stage in place, two different scenarios were run.

In the first scenario, a constant 50 cfs (low flow) was input at the upstream most cross-section. This was done to very simply represent the effects of storm surge only. Horsepen Bayou is approximately 5.9 miles long and impacts of this surge were noticeable as far up the channel as 4.9 miles. It caused a 1.4 ft increase in water surface elevation at this point. At the downstream end of the bayou there was

significant out of banks flooding. The bayou got out of banks as far up the channel as 2 miles.

In the second scenario, a constant 1000 cfs (higher flow) was input at the upstream most cross-section. This 1000 cfs was intended to represent a small rainfall event occurring inland. Under this scenario, the surge had an effect the entire way up the bayou with a 1 ft increase in water surface elevation at the upstream most cross-section. Out of banks flooding stopped around the same point but the floodplain was noticeably larger at the downstream end than in the previous scenario.

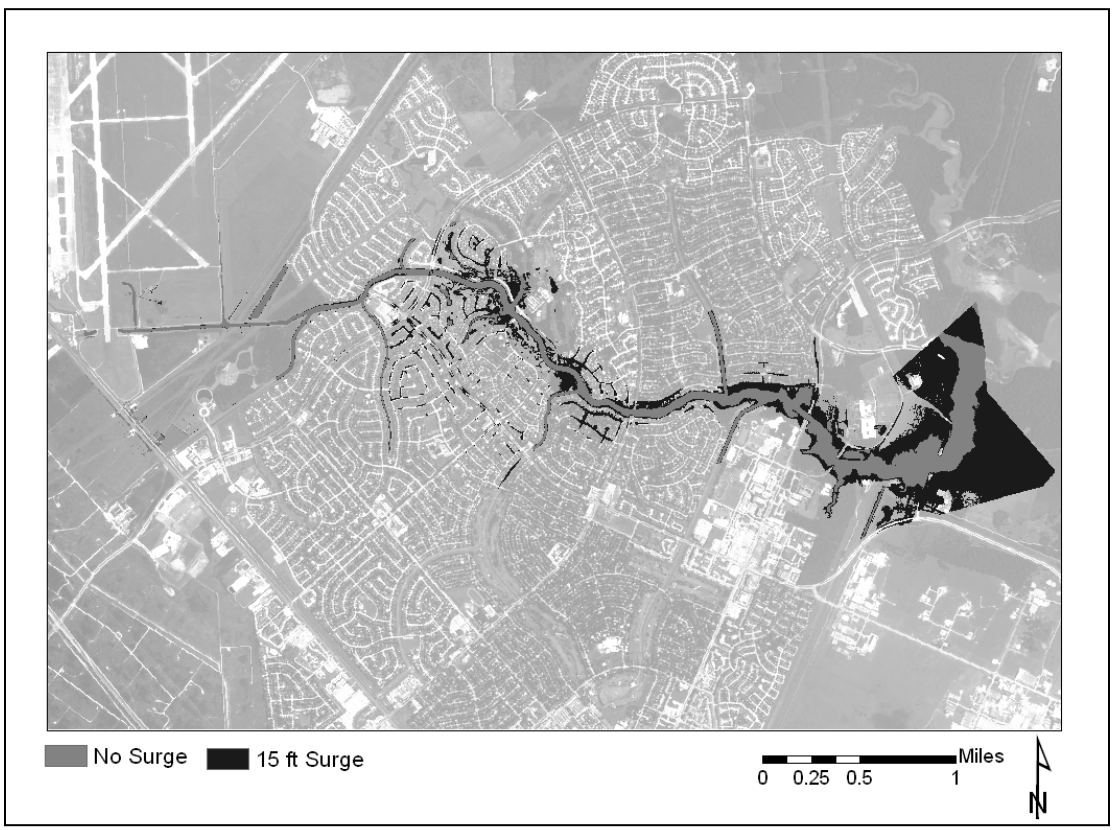

Figure 4a: 10-yr Storm Under Varied Surge Conditions

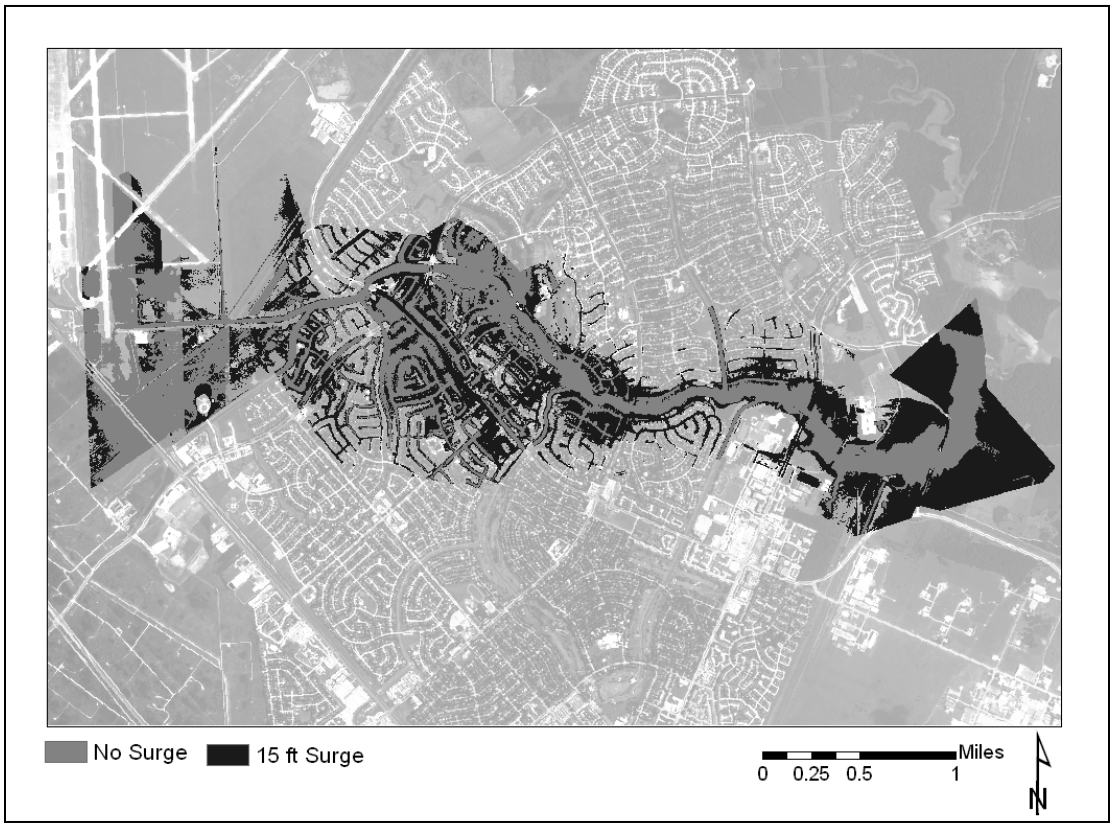

Figure 4b: 100-yr Storm Under Varied Surge Conditions

Future Research

Future research will use the unsteady flow model to model the 100-year design storm event. Flow hydrographs from HEC-HMS will be applied at corresponding cross-sections in HEC-RAS. Running the unsteady model with a varying downstream boundary condition and a varying inflow will allow for the investigation into different timing issues such as out of banks flooding and flood subsidence time. Future work will also vary the beginning times of the surge and rainfall in an attempt to better understand the behavior of this bayou under various scenarios.

References

"ADCIRC Coastal Circulation and Storm Surge Model." (2008). http://adcirc.org/ (Jan. 20, 2009).

Bedient, Philip B., Huber, Wayne C., Vieux, Baxter E., (2008). *Hydrology and Floodplain Analysis,* Prentice Hall, New Jersey.

Dunbar, Lawrence G., (2006). "Evaluation of Existing Drainage and Flooding Problems in Horsepen Bayou Watershed within CLCWA Boundaries." Prepared for: Clear Lake City Water Authority, September 2006, CLCWA 003958.

"HEC-HMS." http://www.hec.usace.army.mil/software/hec-hms/ (Jan. 20, 2009).

"HEC-RAS." http://www.hec.usace.army.mil/software/hec-ras/ (Jan. 20, 2009).

Knabb, Richard D., Rhome, Jamie R., Brown, Daniel P., (2006). "Tropical Cyclone Report: Hurricane Katrina 23-30 August 2005." National Hurricane Center. http://www.nhc.noaa.gov/pdf/TCR-AL122005_Katrina.pdf (Jan. 20, 2009).

National Weather Service Forecast Office, (2008). "Hurricane Ike (September 2008): Storm Surge Estimates from Damage Surveys." http://www.srh.noaa.gov/hgx/projects/ike08/storm_surge_overview.htm (Jan. 20, 2009).

Vieux, Baxter E., (2004). *Distributed Hydrologic Modeling Using GIS*, Kluwer Academic Publishers, Dordrecht.

Wheeler, Frankie. (1976). "Soil Survey of Harris County, Texas." United States Department of Agriculture-Soil Conservation Service. U.S. Government Printing Office: 1976- 216-046/59.

Effects of Freezing and Thawing Processes on Bank Stability

Fabienne Bertrand[1] and A. N. (Thanos) Papanicolaou[2]

[1] Graduate Research Assistant, IIHR-Hydroscience and Engineering, Dept. of Civil and Environmental Engineering, The University of Iowa, Iowa City, IA 52242; Ph (319) 335-5097; email: fabienne-bertrand@uiowa.edu
[2] Robert and Virginia Wheeler Faculty Fellow in Engineering, Associate Professor, IIHR-Hydroscience and Engineering, Dept. of Civil and Environmental Engineering, The University of Iowa, Iowa City, IA 52242; Ph (319) 335-6448; Fax (319) 335-5238; email: apapanic@engineering.uiowa.edu

Abstract

The majority of scour-related studies in rivers and streams in Iowa and the Midwest indicate that bridge pier protection is strongly interrelated to bank stability. Findings from a recent survey conducted as part of a project performed for the IHRB (Iowa Highway Research Board) and HCA (Hungry Canyon Alliance) suggest that accelerated riverbank degradation has resulted in an estimated $1.1 billion in damages to bridge infrastructure and the loss of agriculture lands since the turn of the century in parts of the western United States, including western Iowa.
Yet, a robust technique that systematically quantifies bank erosion on a continuous basis is lacking. This is because conventional, manual, field monitoring methods, typically erosion pins, cross-section resurveys or terrestrial photogrammetry, merely reveal net change in the position of a bank surface since the previous measurement. They do not quantify the precise temporal distribution of that change. This means that erosion event timing, and the precise bank response to individual flow or flow hydrograph changes, is generally uncertain. Because of the limitations of existing measurement methods, little knowledge has yet emerged of the dynamics of bank erosion and deposition events at a time resolution comparable to that available for flow discharges.
Clearly, bank erosion monitoring will be more securely based when (a) the full episodicity of bank change is detected, including event timings and (b) magnitude/timing information for specific erosion and deposition events can be related to continuous information on the temporal fluctuations in the suspected hydraulic forces.

1. Introduction

Relatively few papers (e.g. Raudkivi & Hutchison, 1974; Millar et al., 1998; Julian &Torres, 2005; Papanicolaou et al., 2002, 2007) have investigated erosion of banks comprised of cohesive materials. Thorne (1982) states that erosion of a cohesive river bank is mainly dominated by mass failures and fluvial erosion processes. The former is driven by gravity. This phenomenon occurs as blocks of materials collapse when the critical height and angle of the bank are exceeded. The latter, which is the focus of this paper, occurs when hydraulic shear forces break the bond between particles and provoke the entrainment of aggregates (Millar, 1998; Papanicolaou, 2007).

Previous papers report that fluvial erosion processes occur when the applied side-wall shear stress τ is greater than the critical erosional or simply soil strength τ_c ($\tau > \tau_c$). Hence, accurately predicting the critical shear stress τ_c can lead to a better understanding of fluvial erosion. Unfortunately, this control variable, together with the shear-stress, depends on many factors and it cannot be directly estimated. For instance, to predict the side-wall fluid shear-stress τ, river engineers use a uniform flow approximation to conduct their experiments (Leutheusser, 1963; Simons and Senturk, 1992; Knight et al., 1984; Flintham and Carling, 1988; Millar and Quick, 1998) (as cited in Papanicolaou, 2007). Those studies do not consider the effects of secondary currents which cannot be neglected in natural open-channels. Nevertheless, Guo & Julien (2005) analyze the effect of secondary currents on the side-wall shear stress. By neglecting the secondary currents, observations were made that the near-wall shear stress was underestimated while the bed-shear stress was overestimated. They verified that it was not adequate to make the approximation of the uniform flow for natural rivers.

Another limitation is the little knowledge of the complex electrochemical forces between cohesive particles and the water flow. In 1966, Grissinger found that the erosion rate depends on bulk density and moisture content even though those variables are not correlated to the critical shear stress (as cited in Raudkivi, 1976). Millar (1998) found that vegetation has a significant effect on cohesive river banks that are subject to fluvial erosion. Papanicolaou et al. (2007) developed an experimental method to estimate the critical shear-stress. Although these papers contribute to the overall understanding of hydraulic erosion of cohesive materials, continuous monitoring of bank fluvial erosion for a wide range of discharges is needed. Instruments have been developed to measure erosion and techniques have been created to study bank erosion. Thorne (1981) reviews the methods used to measure the rate of bank erosion and displacement of banks due to erosion. Such techniques require the use of erosion pins for detailed measurements of the site and aerial photography and remote sensing for erosion in a larger scale. The erosion pins allow researchers to measure erosion spatially. This device also permits to measure the degradation of the banks from the last time the measurement was recorded. However, it does not allow automated monitoring of the rate of bank erosion over frequent periods. A consequence of this limitation is a lack of available data for bank change over a period of time, especially during critical flow events, which shape the bank shape. A new technique is needed to address this limitation.

This work is part of a pilot project, and proposes measurement of bank erosion using Photo-Electronic Erosion Pin (PEEP) sensors developed by Lawler (1991, 1994). This will permit researchers to study fluvial erosion on a continuous basis including the effects of flow and of freezing and thawing processes on bank stability. A real analysis of the behavior of the banks under different flow conditions will be possible with the proposed set-up.

2. *Objectives*

The goal of this paper is to demonstrate the use of the PEEP sensors to perform a real-time monitoring system in terms of timing and magnitude of the erosion events. The study will firstly calibrate the PEEPs to automatically monitor fluvial erosion of cohesive banks. The PEEP, together with other instruments, will possibly provide researchers with the opportunity to simulate interactions between the flow peaks and the magnitude of bank erosion. Secondly, this study will demonstrate the PEEP potential to establish more clearly the timing of individual bank erosion events through a pilot study in Clear Creek, Iowa.

3. *Methodology*

3.1. Instrumentation

The PEEP system proposed in this paper is composed mainly of a sensor model 200, a Data Logger, a solar panel, and a computer. The PEEP sensor is designed by Lawler (1991) and consists of an assemblage in series of 20 diodes, so called photovoltaic cells. It is protected by a transparent waterproofed acrylic tube (Lawler 1992). This 20 cm long section constitutes the active length of the sensor; the outer diameter of the acrylic tube is 16 mm. Two reference cells at the beginning and the end of the row of diodes are present. The other 18 diodes will be used to automatically monitor the position of the bank. When the diode is exposed to light, it produces a voltage which is equivalent to the length of tube exposed (Lawler 1992). This means that the more diodes exposed, the higher the voltage. The whole instrument is 66 cm long and is terminated by a cable, which is connected to a Data Logger. This model is a revision of the original sensor and is designed to be more suitable for dynamic erosion sites (Lawler, 2004). A unique feature of this model is that two Thermistors are attached. These Thermistors permit researchers to monitor the soil temperature during an experiment. The first Thermistor is located at the beginning of the sensor and the second one is 68 mm away. This feature allows for the study of soil temperature and

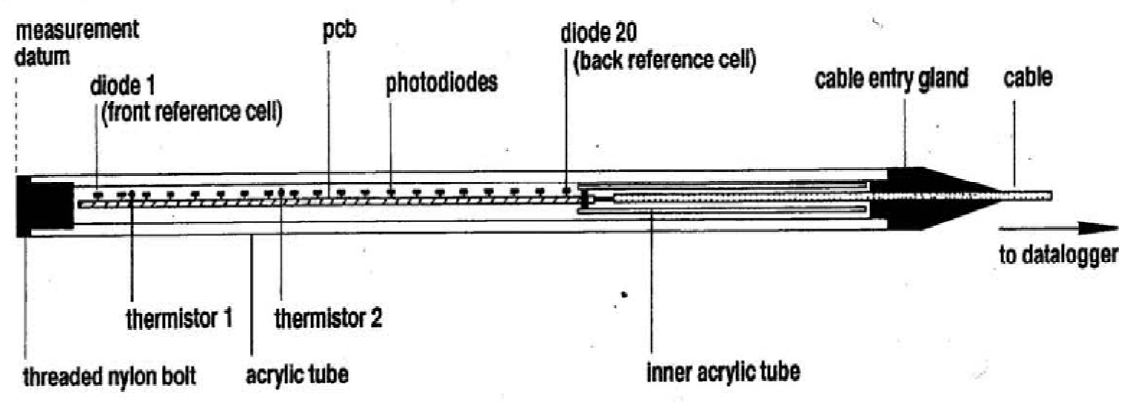

Figure 1. Typical PEEP 200 (PEEP System: User Guide 2004)

soil freeze-thaw processes. Data loggers in the range of 0-225 mV are suitable for the PEEP 200 (Lawler, 2004). For this experiment, a Campbell CR800 Data Logger is used, and with the appropriate computer program, the data is downloaded. As designed by Lawler, the PEEP sensor does not require any power supply. A solar panel is connected to the system and recharges the battery automatically. The system can be easily installed and operated in the field.

3.2. Calibration

The amount of voltage produced can be converted to reveal the amount of exposed active length (Lawler, 1991). The calibration procedure will permit researchers to obtain the relationship between voltage and exposed active length. This step is done outdoors using natural light. To simulate the retreat of the bank, a dark tube is placed around the PEEP sensor to cover all the diodes. The tube represents insertion of the sensor into the bank. Then, the tube is gradually moved to expose the diodes to the sunlight. The interval between the movements is chosen to be three minutes. Once the sensor is completely exposed, the data can be downloaded and analyzed. To calculate the exposed length, the ratio between the voltage output of cell series and reference cell is needed. It is given by the following equation:

$$Rpp = \left(\frac{Vcs}{Vrc} \right) \times 100 \quad (1)$$

where V_{cs} is the voltage output of the cell series in mV and V_{rc} is the voltage output of the reference cell in mV.

Equation (1) allows calculation of the exposed length L using the following relation:

$$L = c + d \times Rpp \quad (2)$$

where L is the exposed length and
c and d are constants (respectively equal to 17.83 and 2.1743)

3.3. Proposed experiment

The calibration of the sensors has been completed in a range of temperatures, ranging from 45°F - 65°F. The purpose is to use the sensors in a pilot project in Clear Creek, a tributary of the Mississippi River, located in Eastern Iowa. The site was chosen because of the cohesiveness of its bank materials and the large amounts of sediment. The Iowa Department of Natural Resources (2006) reports that 239,559 tons of soil were eroded due to a rainfall event in 2004, making this site ideal to study fluvial erosion of cohesive banks.

The PEEP sensors, together with a pressure transducer, are the key instruments. Two cross-sections have been chosen at the site, and four sensors will be installed in each cross section (two on each side of the creek). Eight sensors will be installed in total. One sensor will be as close as possible to the bank toe (See *Figure 2*). Although the installation of the sensors is straightforward, it should be done with extreme caution to avoid breaking of the acrylic tube. The PEEPs will be installed in pre-drilled horizontal holes 16 mm in diameter. It is recommended that the reference cell (1st diode) and that the second diode to be initially exposed. Hence, the first Thermistor

will give the temperature of the air while the second one provides the soil temperature. When the two Thermistors are uncovered they should indicate the same temperature. This feature can be exploited to study the effect of the climate on bank change (e.g., freeze-thaw cycle, flow increase or secondary currents). In order to do so, this paper proposes to exploit the capabilities of the PEEP sensors to create a system which can monitor rate of erosion and permits more secure analysis of the controlling factors (flow peak, weather, and secondary currents).

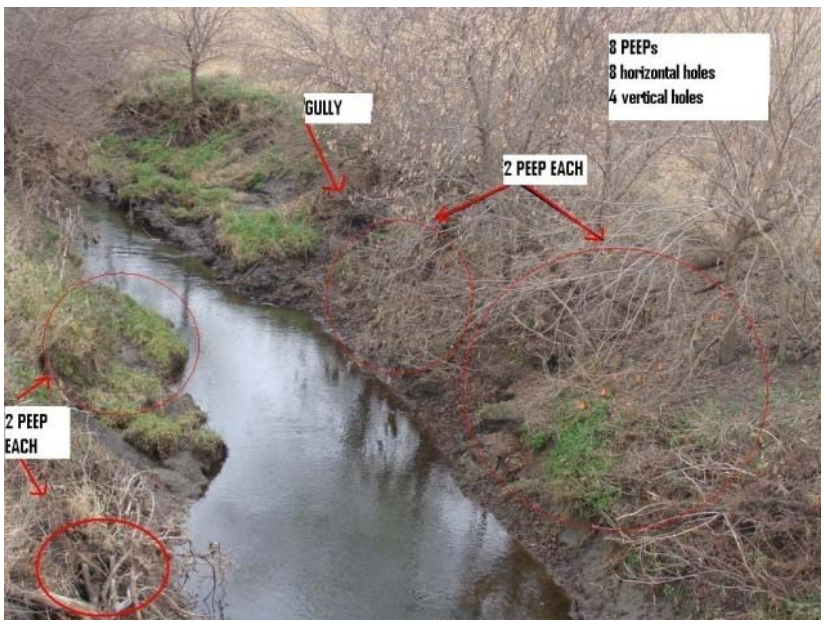

Figure 2: Side view of Clear Creek

The sensors will permit the researchers to monitor temporal changes of the banks. Simultaneously a pressure transducer, model WL400, which is a water level sensor, will be used to measure the stage (H) of the flow. As a consequence, the discharge (Q) can be computed using a log-law relationship between Q and H. The resulted hydrograph and the erosion graph will be plotted together and the data will be analyzed. The correlation of the soil temperature, flow peaks, and real-time erosion will be investigated.

Additionally, to measure the net change of the bank from previous field visits, erosion pins will be used. They can spatially measure the retreat of the bank. A camera may permit a visualization of the phenomenon during the night and show when and if mass failure has occurred. Therefore, it can be distinguished from fluvial erosion when doing the analysis. An Acoustic Doppler Velocity (ADV) will be used to obtain the velocity profile and study the effects of the secondary currents of the flow on the cohesive banks. It is important to state that the PEEP sensors cannot record erosion events during the night. However, more than two Thermistors may be placed and distributed along the sensors. They can be used to monitor the soil erosion during night-time periods along with measuring the soil temperature (Lawler, 2004). Differences between the soil temperature and soil-air interface temperature can indicate whether erosion takes place or not.

4. *Preliminary results*

The calibration procedure has been conducted during the months of September and October 2008. While moving the dark tube around the sensor to simulate erosion, the data logger has been set up to record the data every 15 seconds. At the beginning of the test, the first diode is exposed. Three minutes later, the second diode is exposed, with an additional diode being exposed every three minutes. All 20 diodes are uncovered after 1 hour.

Table 1 gives a summary of the condition of the days when the simulations have been conducted and the number of scans recorded. These tests have been conducted on a bright day using the natural light. The number of scans is for the whole simulation period.

Table 1: Weather Condition of the Simulation

Date	Temp. (°F)	Weather	Number of scans
09/30/2008	54	Sunny	240
10/06/2008	65	Sunny	240
10/14/2008	55	Sunny	240

As indicated in *Table 1*, 240 data points have been recorded for each simulation. The data logger records in mV the voltage of the first diode and the series cells. To make the calibration graph clearer and easily readable for this experiment, the average of the data between two consecutive diodes have been taken. Thus, after applying *equation (1)* to the averaged data, the ratio (in %) is reported in columns 2 and 5 of *Table 2*. The length (in mm) is calculated using *equation (2)* and it is displayed in columns 3 and 6. *Table 2* represents the automated measurements of the active sensor being gradually exposed. For instance, Record Number # 1 (RN 1),means that diode 1 is exposed while all the others are covered and RN 20 means that all the diodes are uncovered which means that the sensor is completely showed.

Table 2: Data for the erosion simulation of a PEEP on September 30th, 2008

RN	Rpp (%)	L (mm)	RN	Rpp (%)	L (mm)
1	24.64451854	71.41	11	78.96284285	189.52
2	56.00633651	139.60	12	81.46560495	194.96
3	55.9436448	139.47	13	85.59561991	203.94
4	59.07246651	146.27	14	86.67546954	206.29
5	62.41851725	153.55	15	89.50065044	212.43
6	66.03480067	161.41	16	92.34980561	218.63
7	68.31858965	166.38	17	94.98888923	224.36
8	70.4561907	171.02	18	97.66384358	230.18
9	73.28275935	177.17	19	99.81462409	234.82
10	75.94637012	182.96	20	101.2659425	238.01

Figure 3 plots a typical calibration graph for the PEEP sensor. For better accuracy in the field, one can measure the distance exposed from the bank and verify the calibration graph.

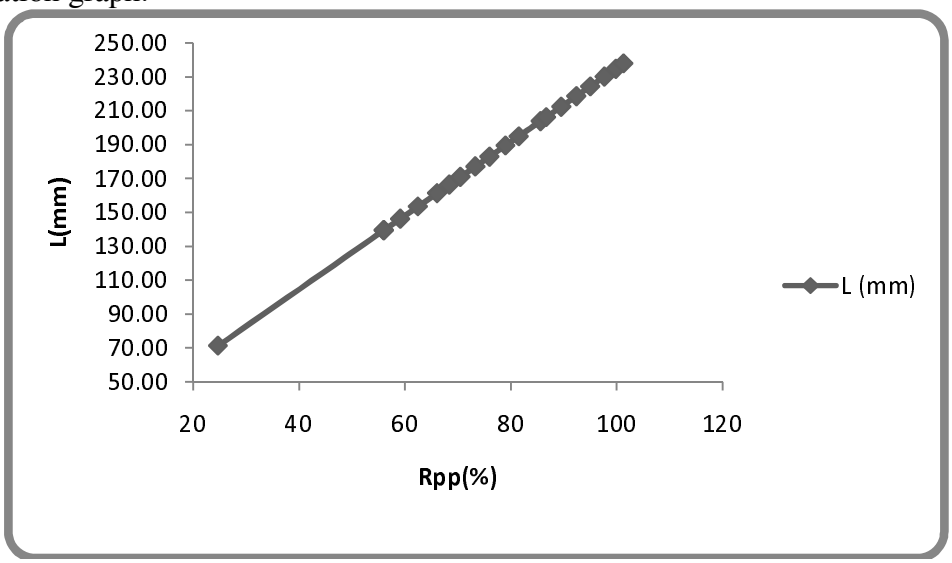

Figure 3: Typical calibration graph for test conducted in 09/30/2008

Another way to present the results is shown in *Figure 4*. Note that a correlation between the exposed cells and the protrude sensor from the bank can be made. As the dark tube is removed, the diodes are exposed to light, simulating erosion.

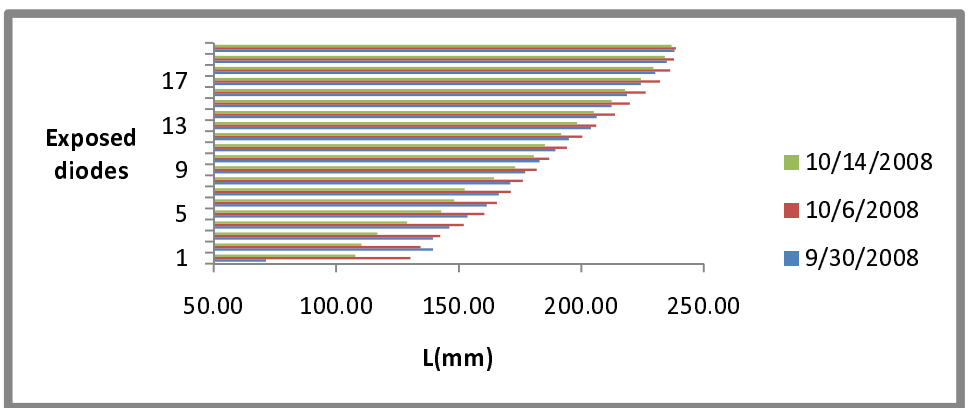

Figure 4: Erosion simulation for the PEEP sensors

The tests conducted September 30th and October 6th have been completed with the PEEP model 200 labeled S-230-30. The calibration graph converged from exposed diodes 2 to diodes 20. The divergence in diode 1 may be explained by a shadow or a cloud in the sky while conducting the experiment. Therefore enough light does not reach the 1st diode to output the necessary voltage. This is one of the apparent weaknesses of the instrument. On October 14th, another PEEP, which is the same model, labeled S-231-30 is utilized. Although a divergence with the data recorded can be observed, the data are close when diode 10 is exposed. Indeed for accuracy of the results, it is required to calibrate each sensor before using it in the field. It is not a

discrepancy because it is required to calibrate each sensor for more accuracy. The calibration graph of each sensor may show some differences.
This system not only will introduce a new technique to automatically monitor bank retreat but also permits a comparison between flow peaks and erosion events. Also, investigation of the effect of the freeze-thaw process on these erosion events is possible.

5. *Conclusion*

This paper demonstrates that the Photo Electronic Erosion Pin is indeed a system which can easily be installed and operated. The capability of the instrument can be exploited to obtain real-time and more secure data in terms of magnitude and frequency. Also, the freeze-thaw induced erosion will be investigated using the features provided by the instrument. Combined with other instruments (e.g.: a pressure transducer), a correlation can be completed comparing flow peaks and erosion events. However, the sensor depends on daylight to output a voltage. It cannot record erosion during the night and when it is submerged in turbid water. This limitation is being considered. The PEEP model 200 gives the soil temperature. Therefore, erosion can be detected by the existing temperature difference and other devices such as a camera, which gives a clear visualization of the event occurring. Although this paper does not study the complex electro-chemical forces existing between particles of cohesive banks, this system, if exploited, can lead to more secure analysis of critical shear stress but most importantly a better analysis of the impact of the freeze-thaw processes on bank stability.

6. *References*

Guo, J., and Julien, P.Y. (2005). "Shear stress in smooth rectangular open-channel." *J. Hydr. Engrg., ASCE*, 131 (1), 30-37

Hydro Scientific Ltd. (2004). "*The Photo Electronic Erosion Pin (PEEP) system: User Guide*."

Iowa Department of Natural Resources (2006). "A return to Clear Creek". http://www.iowadnr.gov/water/nonpoint/files/cleardeer.pdf

Julian, J. P., and Torres, R. (2005). "Hydraulic erosion of cohesive river banks." *Geomorphology*, 76, 193-206

Lawler, D.M., and Leeks, G.J.L. (1992). "River bank erosion events on the Upper Severn detected by the Photo-Electronic Erosion Pin (PEEP) system." *IAHS*, 210, 95-105

Lawler, D.M. (2005). "Advances in the continuous monitoring of erosion and deposition dynamics: Developments and applications of the new PEEP-3T system." *Geomorphology*, 93, 17-39

Millar, R.G., and Quick, M. C. (1998). "Stable width and depth of gravel-bed rivers with cohesive banks." *J. Hydr. Engrg., ASCE*, 124 (10), 1005-1013

Papanicolaou, A.N., Hilldale R. (2002). " Erosion of streams with cohesive banks" *Research & Extension Regional Water Quality Conference 2002*

Papanicolaou, A.N., Elhakeem, M. (2007). "Secondary currents effects on cohesive river bank erosion." *Water Resources Research*, 43

Raudkivi, A.J. (1976). "Chapter 9: Cohesive soils", "Chapter 10: Erosion, deposition, scour." *Loose Boundary Hydraulics, 2nd Edition*, Permagron Press, New York, 262-280, 282-305

Sanders, D.W. (1986). "*Water Erosion Control*". FAO, Rome, Italy

Thorne, C. R. (1981). "Field measurements of rates of bank erosion and bank material strength." *IAHS*, 133, 503-512

Integrated Surface water and Groundwater modeling of Orange River Basin in Southwest Florida for Flood Mitigation/Ecosystem Restoration

E. Zia Hosseinipour
Advance Planning Section, Ventura County Watershed Protection District, 800 S. Victoria Avenue, Ventura, CA 93009; email: Zia.Hosseinipour@Ventura.org

ABSTRACT

MIKE SHE/MIKE 11 water modeling software was applied to develop a comprehensive water resources plan for the East County Water Control District (ECWCD) in southwest Florida. The main objectives of the comprehensive plan were, (1) to reduce the extent, magnitude, and duration of flooding in the upper region of Orange River basin, (2) increase groundwater recharge within the ECWCD to augment water supply, and (3) improve water quality of the waters leaving ECWCD boundaries.

It was envisioned that the comprehensive plan would result in modification of a number of existing structures on canals in the areas covered by the ECWCD jurisdiction. As part of this modeling project, a number of flow diversions and water storage options are being reconsidered. This paper describes calibration of the integrated model and modeling results for a set of potential hydraulic network upgrades and diversion alternatives. The alternatives proposed and fully evaluated were either quick-action projects that can be implemented in the near future or are more long-term projects that have a high potential to meet project objectives and require land acquisition that could be initiated in the near future. Additional alternatives were also evaluated based on the results of the alternatives described here. All of the hydraulic network modifications were evaluated to consider downstream impacts so that problems are not simply transferred from one area to another. The modeling work was performed using the ECWCD version of the Tidal Caloosahatchee River Basin (TCRB) integrated surface-ground water model developed for SFWMD and ECWCD.

INTRODUCTION

The scope of this study included performing integrated modeling in support of hydraulic/hydrologic analysis of existing conditions, and for potential storage and/or diversion of water from the Orange River/Able Canal Basin to a number of other basins during high flows for the purpose of mitigating flooding in the headwaters of Orange River. The initial phase of the work included refinement of the TCRB model to incorporate a more detailed representation of ECWCD canals and water control structures. During the initial phase, the model was used to determine the dimensions of various structures (e.g., S-HC-1 and S-HC-2) on Hickey Creek Canal in support of the re-design of those structures. The model was calibrated using 2004 and 2005 rainfall and landuse data provided by ECWCD. The project's main goal was to provide a basis for better management of runoff during intense storms in ECWCD domain as the area further develops by looking at a number of diversion alternatives that would mitigate flooding while being protective of the fragile ecosystem.

PLANNED LANDUSE AND THE PROJECTED RUNOFF INCREASES

The alternative analyses that provide the foundation for the Comprehensive Water Resources Plan are described below. Undeveloped lands in ECWCD are platted and subdivided into many small ¼-acre parcels. Currently, new development in ECWCD is constructed on a lot-by-lot basis without any stormwater management. Because ECWCD does not provide wastewater collection and seasonal high water tables can be close to the land surface for a portion of the year, all new houses and septic systems are constructed on a pad that is typically 2-4 feet above natural ground. Compaction of the elevated pad and the higher elevation results in lower infiltration and elevated rates of runoff. Figure 1 below shows the domain of the model and conveyance features. Figure 2 presents a comparison of simulated flows at full build-out to existing flows for the 2004 period. Peak flows (summed for all canals that drain ECWCD) in the future will be 50% higher than current flows.

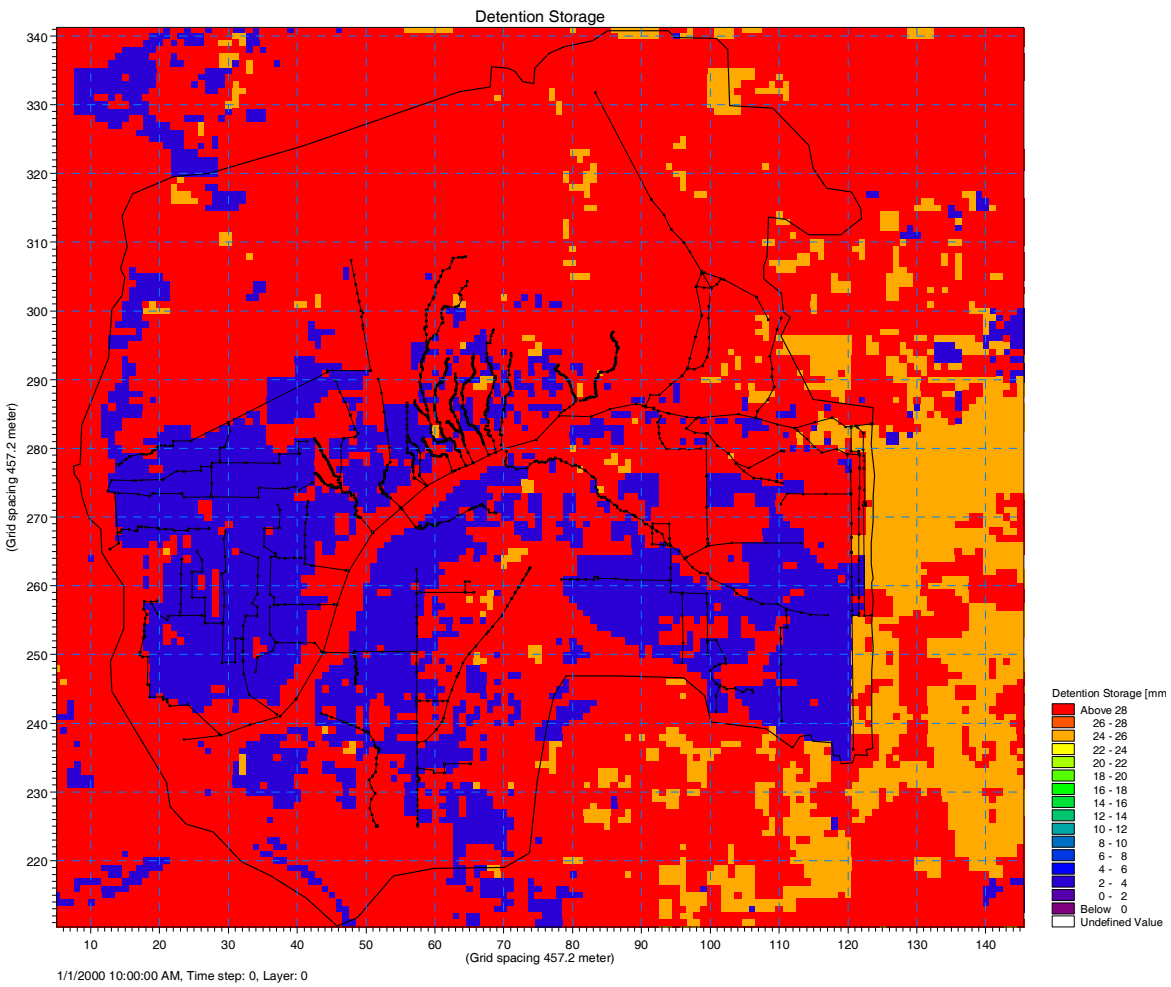

Figure 1- Integrated model domain and major drainage networks

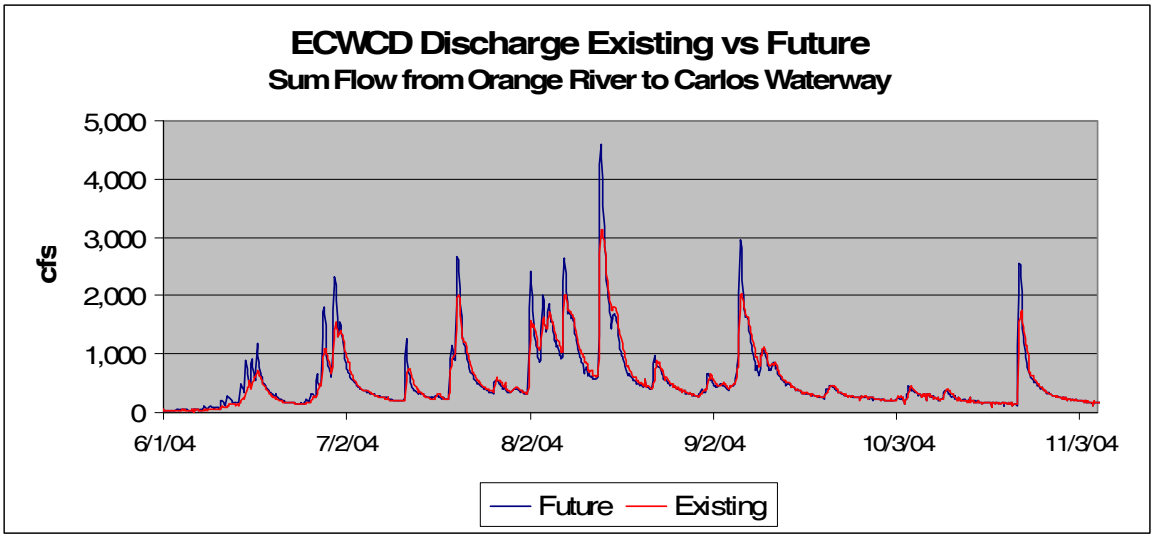

Figure 2 – Total Flow from ECWCD for Existing and Future Conditions

Below we provide initial modeling results for a sub-set of a larger set of possible alternatives. The alternatives considered and simulated using the integrated model is summarized below:

- Modify existing South Harns Marsh hydraulic control structures to provide more storage and detain a larger portion of ECWCD runoff. Increase the area of the marsh system if appropriate.
- Modify weir control elevations to maintain higher canal levels in ECWCD that will reduce peak discharge rates and increase groundwater recharge.
- Divert runoff from the Able Canal/Orange River basin through Charlie Diversion to Hickey Creek to alleviate flooding during high flows in the Orange River catchment. Enlarge Hickey Creek Canal and divert some Hickey Creek Canal flows for water quality treatment.
- Retain runoff from the southeast portion of ECWCD to re-hydrate drained wetlands east of Hendry Canal Extension.
- Route water from Mirror Lakes into the Estero Watershed to alleviate groundwater impacts associated with public water supply well-fields.

The ECWCD canal system has re-distributed runoff from historic watersheds. Figure 3 shows the original and current watershed boundaries. The figure clearly indicates that the current drainage area for Hickey Creek (yellow line polygon) is significantly smaller than the original drainage area (black line polygon).

DESCRIPTION OF ALTERNATIVES

The alternatives that have been evaluated with respect to peak flow reduction, base flow enhancement, and ground water recharge are described here. A simulation of a major storm event was conducted that assumed implementation of a combination of improvements to Hickey Creek, Harns Marsh, and ECWCD groundwater recharge weirs.

The purpose of this combination simulation was to determine if a combination of quick-action features can be implemented to reduce flood impacts in the Orange River basin during the 2006 wet season while maintaining adequate flood protection in Hickey Creek.

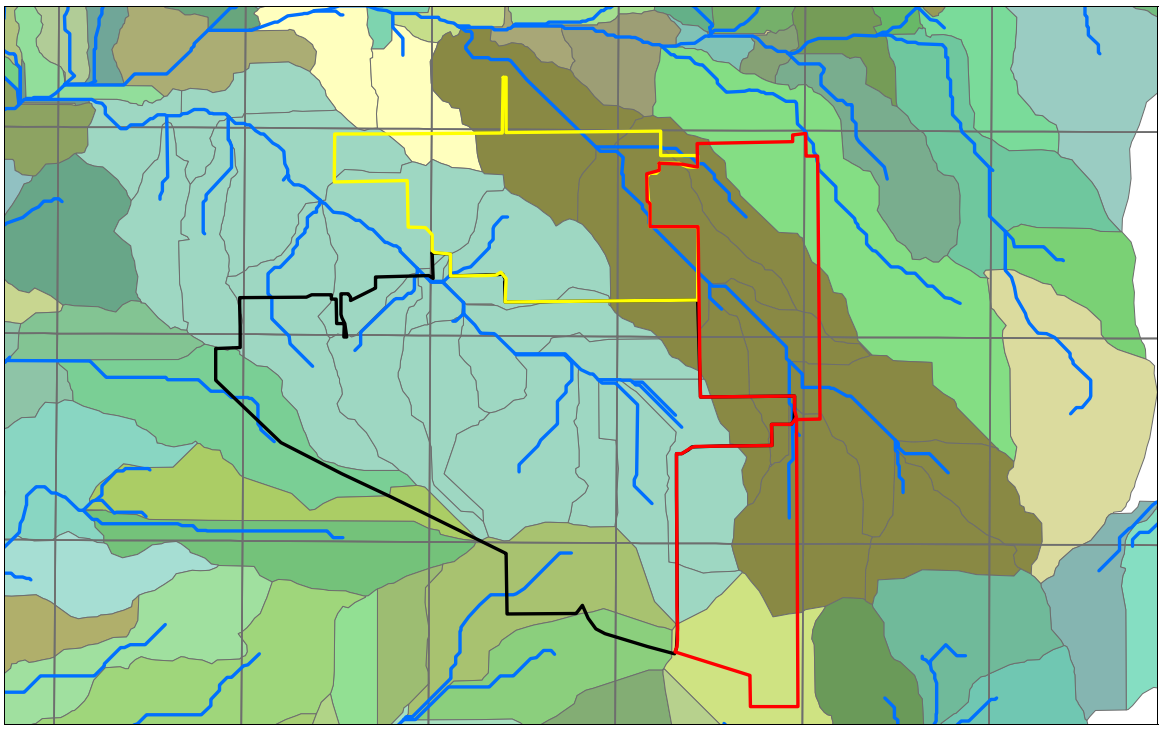

Figure 3 – Historic and Current Drainage Area Boundaries for ECWCD

Harns Marsh Improvements: This alternative, shown in Figure 4, includes improvements to the South Harns Marsh inflow, North and South Harns Marsh outflow gates, and considers the benefits of adding a third treatment cell (referred to as the West Marsh). Simulations were conducted with and without the West Marsh to quantify the benefit of adding additional treatment area. Additional modifications to evaluate in the future may include the realignment of North and South Marsh levees to restore the original Orange River flow pathway.

Groundwater Recharge: The southwest portion of ECWCD has numerous canals that are maintained at relatively low elevations. Figure 4 also shows the layout of typical drainage canals; water levels in these canals are maintained approximately 8 feet below natural ground elevation. Houses and septic systems are typically built on pads approximately 2-3 feet above natural ground elevation. Water levels in these canals are maintained by either S-SF-1 or S-SF-2 weirs. If additional weirs were installed with bleed-down orifices, runoff could be detained in this area to promote more groundwater recharge.

Hickey Creek Improvements: The purpose of this alternative was to restore flows to Hickey Creek that were diverted during initial construction of ECWCD Canals. The diversion of flows will be limited to the conveyance capacity of Hickey Creek so that

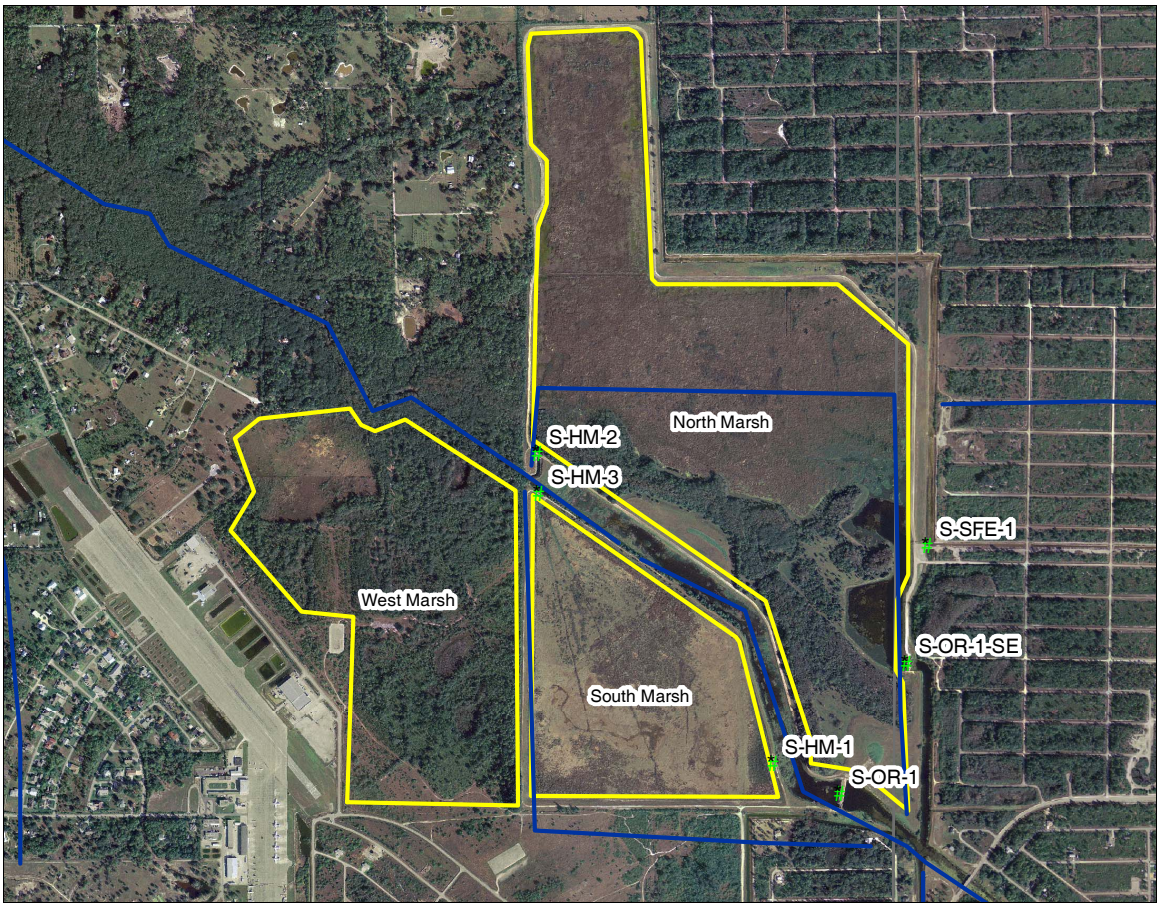

Figure 4 – Features of the Harns Marsh Improvement Alternatives

flooding problems in the Orange River are not transferred to Hickey Creek. The features of this alternative are shown in Figure 5 and are summarized below:

- Widening of Hickey Creek Canal south of S-HC-2 from a 40-foot bottom width to a 200-ft bottom width
- Operation of the gates at S-HC-3, S-HC-2, and S-HC-1 to divert a portion of Orange River flood flows (limited to that amount that can be safely conveyed down Hickey Creek)
- Treatment of a portion of the Hickey Creek Canal flows in a network of canals north of Fox Canal, east of Hickey Creek Canal, and southwest of Greenbriar Swamp
- Drawdown of Greenbriar Swamp prior to storm events so that the Swamp can detain runoff during large events

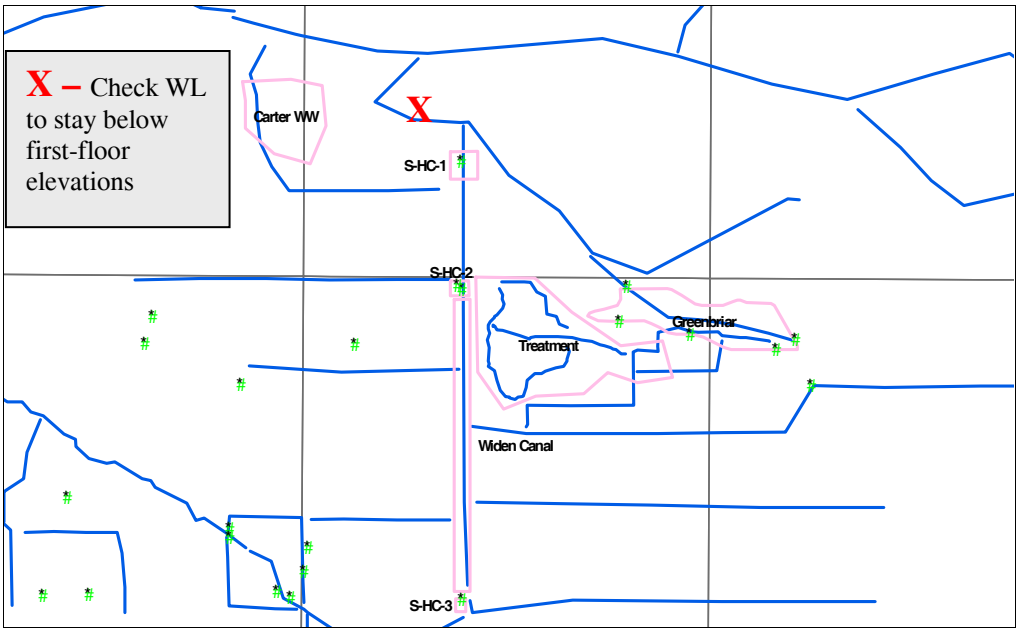

Figure 5 – Features of the Hickey Creek Improvement Alternative

Wetlands Re-hydration East of Hendry Canal Extension: The southeast headwaters of Able Canal and Hendry Canal Extension were part of a broad expanse of wetlands that contributed flows to Hickey Creek and the Orange River to the north, and to the Estero and Imperial Rivers to the south. This alternative involves connection of Nine Mile Canal, Branch 84 (Canal 57-11-3), and Hendry Canal Extension and a pump station to route storm water runoff to drained wetlands east of Hendry Canal Extension. Water would be held in the restored wetlands and then used to augment base flows in the downstream watersheds via hydraulic control structures.

Diversion of Mirror Lakes flow to Re-hydrate Drained Wetlands: Mirror Lakes was originally part of another watershed (Estero River). There are well-fields in the Estero River watershed northeast of the junction of Corkscrew and Alico Roads that have caused lower wetland water elevations in Estero River headwater wetlands north of the well field. This alternative would pump runoff from the Mirror Lakes watershed to a flow-way south of SR 82. Flows would be delivered to these wetlands only during periods when the Estero headwater wetland water levels were below their normal hydro-period elevations. Modeling of Estero headwater wetlands is required to determine an optimum regulation schedule and diversions that would be allowed when these wetlands were below the regulation schedule. This would allow for diversion of Mirror Lakes flow to off-set wetland impacts due to well field operation without causing flooding problems in the Estero River and Imperial River basins.

ALTERNATIVE ANALYSIS

Modeling analysis was conducted for the Harns Marsh expansion, ground water recharge, Hickey Creek Improvements, and Hendry Canal Wetland Re-hydration Alternatives. Analysis of existing conditions was conducted to evaluate the Mirror Lakes

Diversion Alternative. Simulation was also conducted of a merged quick-action alternative to determine the degree of flood control that could have been achieved in the wet season of 2006.

Harns Marsh Alternative: Peak flow reduction was good for small storms, and peak flow reduction can also be significant if the wetland treatment areas can be drained prior to a major storm. Figure 6 presents the results for relatively small storms using rainfall during the early part of the 2004 wet season. Peak flow reduction is improved with the inclusion of west marsh.

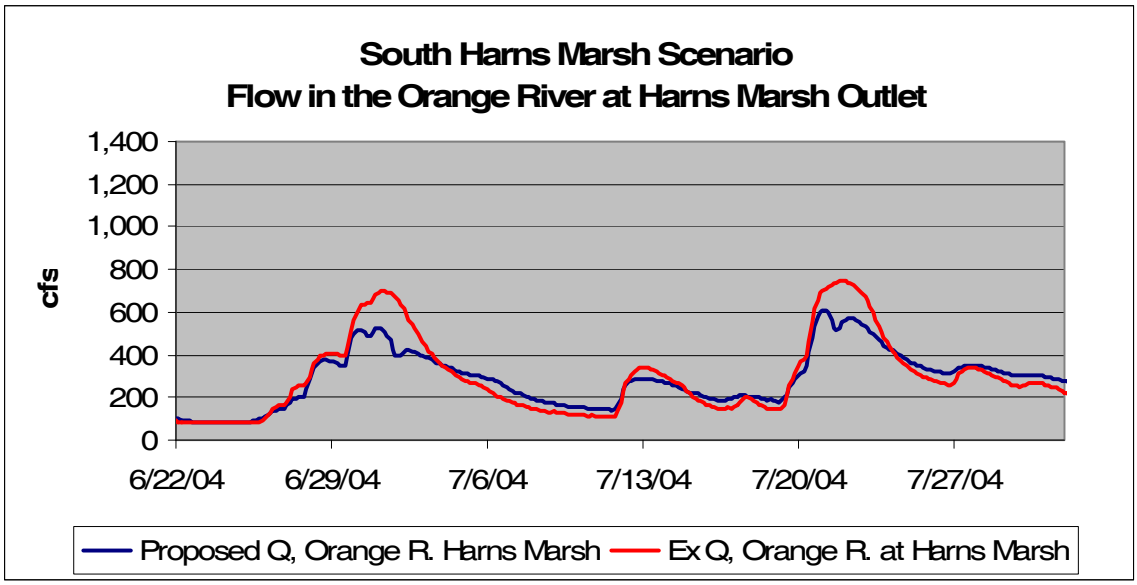

Figure 6 – Peak Flow Reduction for Harns Marsh Improvements Including the West Marsh for the Early Portion of summer 2004

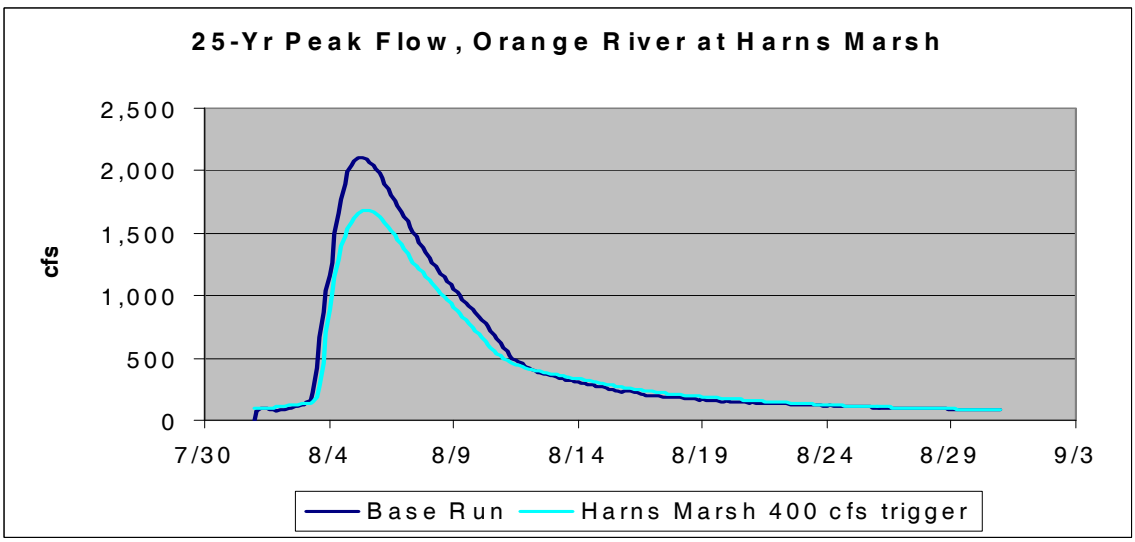

Figure 7 – Peak Flow Reduction for Harns Marsh Improvements Including the West Marsh for a 25-Year Design Storm

Figure 7 above shows results for a 25-year storm when additional capacity is included by expansion of the marsh on the western side (West Marsh addition).

Groundwater Recharge Alternative: Initial runs presented in Figure 8 with high weir elevations do not reduce peak flows for the 25-year storm but are effective in reducing both the peak flow and the volume of runoff for the 10-year storm.

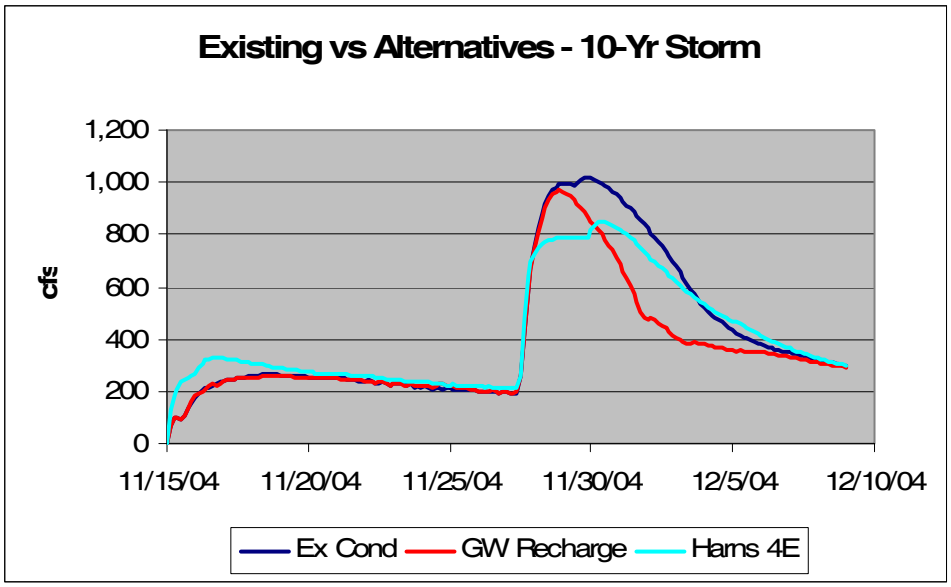

Figure 8 – Orange River at Harns Marsh 2004 Flow with and without Recharge

Hickey Creek Improvements Alternative: The Hickey Creek alternative results presented below do not include improvements to allow flows to enter the canals east of Hickey Creek Canal. The results are presented below in Figures 9 and 10 for design flow and stage.

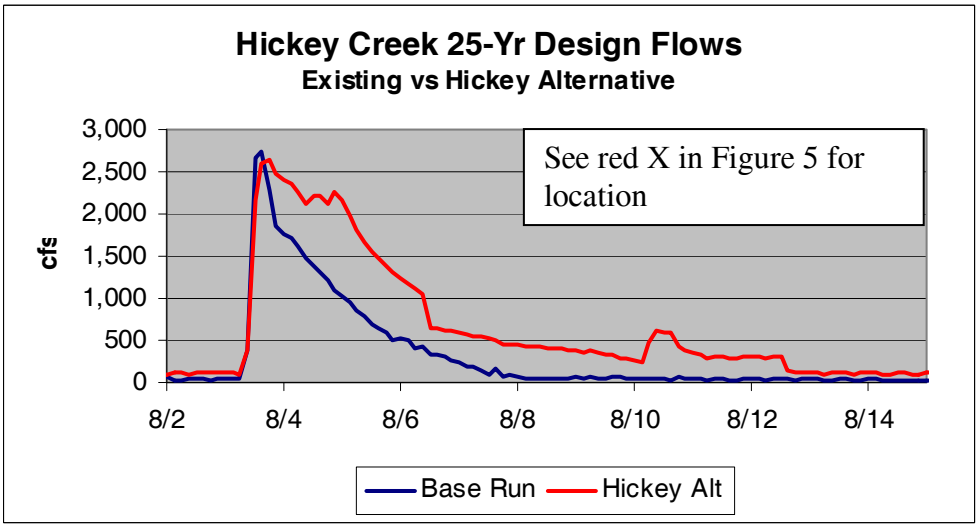

Figure 9– Flow in Hickey Creek with and Without the Diversion

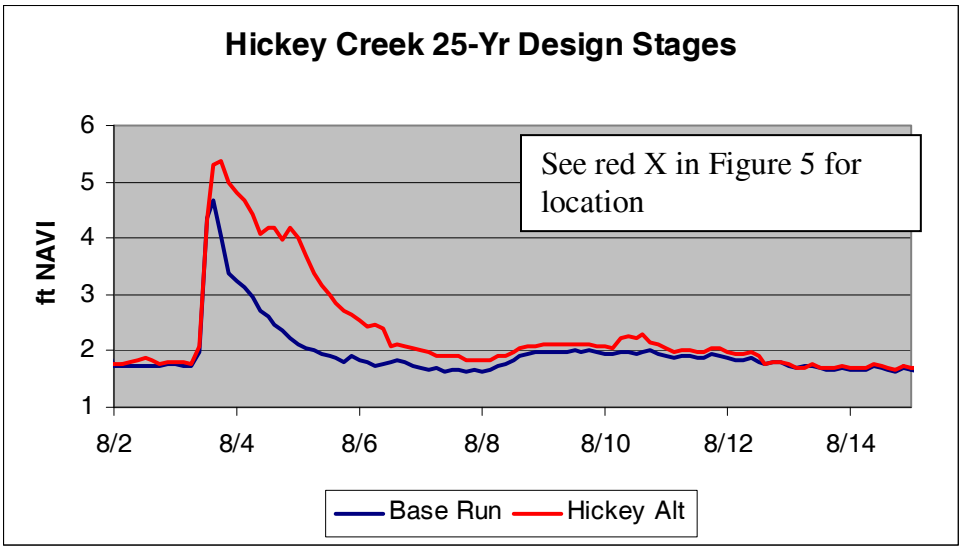

Figure 10 – Stage in Hickey Creek with and Without the Diversion

Hendry Canal Wetland Re-hydration Alternative: This alternative has been tested as a stand-alone alternative and also in combination with South Harns Marsh Improvements. Flow in the Orange River at the Harns Marsh outlet is presented in Figure 11. This wetland re-hydration alternative provides peak flow reductions, however the combination of this alternative and South Harms Marsh Improvements provides increased peak flow reductions. Average dry and wet season ground water elevation difference maps were produced. When the difference values are positive, it indicates higher ground water levels, and the impact of the re-hydration is evident. A number of groundwater difference maps were produced to evaluate the efficacy of rehydration scenarios. Simulation results indicated that if all of the water stored in this wetland area were released to Able Canal during the dry season, the release rate could be as high as 17 cfs over a 180-day period. Thus the wetland alternative provides both ecosystem benefits and groundwater augmentation via enhanced recharge by maintaining optimum wetland hydro-period.

Mirror Lakes Diversion Alternative: An 80 cfs pump station on Canal 57-19-5 could divert approximately 9,200 acre-feet in 2004 and 9,000 acre-feet for June through December (the rainy season) if water levels in Mirror Lakes were maintained above 27 ft-NAVD (28.3 ft-NGVD). Some expansion of canal 57-19-5 would probably be required to accomplish this diversion. There are approximately 6,200 acres of wetland recharge area south of SR 82, therefore it is expected that this diversion would have a negligible effect on water depths within the wetland recharge area.

The diversion rate for this alternative is limited by the small drainage area of Mirror Lakes. This diversion rate is approximately 10% of the 2004 peak flow for the Orange River at Harns Marsh. Accordingly, as shown in Figure 11, this alternative

would not be able to reduce peak flows in the Orange River sufficiently by itself however it could be one component of the comprehensive plan.

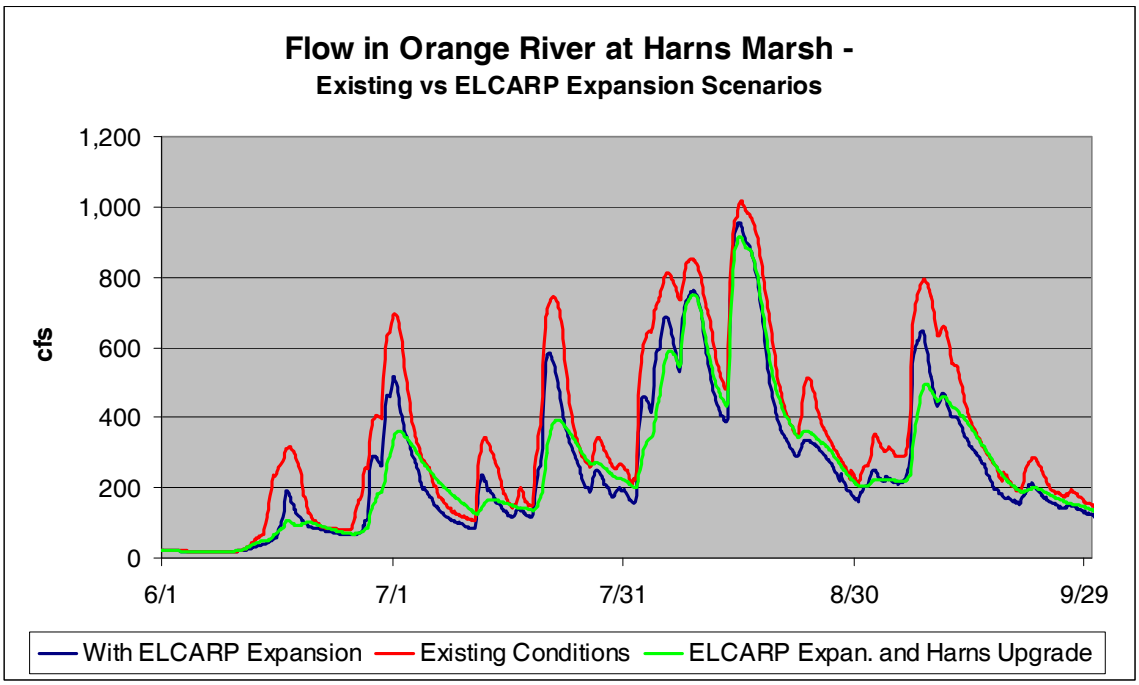

Figure 11 – Flow for the Orange River at Harns Marsh for the Re-hydration Alternative, Re-hydration and Harns Marsh Improvements, and Existing Conditions

CONCLUSIONS

The integrated modeling of the project area using the MIKE SHE/MIKE11 package was very effective because of high ground water table conditions and close interactions of surface and ground waters. Modeling of quick action scenarios as possible components of the comprehensive plan for the ECWCD showed acceptable results and are listed here:

1. Harns Marsh Improvements including addition of the West Marsh
2. Hickey Creek Improvements to divert Orange River flows
3. Ground water recharge in southwest ECWCD
4. Hendry County wetland re-hydration
5. Mirror Lakes Diversion to re-hydrate wetlands near the Corkscrew well field
6. Drawdown of canal water levels prior to major rainfall events

Future modeling is recommended to determine the best mix of effective solutions for: (a) Reducing flooding in the Orange River, (b) Enhancing ground water recharge in ECWCD to reduce Lehigh Estates private residential well failures, (c) Minimizing potential project(s) costs, (d) Augmenting flows in Able Canal and the Orange River during the dry season , and (e) Increasing water levels in drained wetlands near the Corkscrew well-field in the Estero River watershed.

The optimum mix of solutions will likely involve one or more of the scenarios described here along with additional measures based on ecosystem requirements.

Spatially distributed modeling of soil erosion and sediment transport at watershed scale

H. Zeinivand[1&2] and F. De Smedt[1]

[1]Department of Hydrology and Hydraulic Engineering, Vrije Universiteit Brussel, Pleinlaan 2, 1050 Brussels, Belgium; email: Hossein.Zeinivand@vub.ac.be, fdesmedt@vub.ac.be
[2]Lorestan University, P.O. Box 465, Khorram Abad, Lorestan, Iran.

Abstract
A distributed, physical and GIS-based modeling approach is developed to estimate runoff, soil erosion by water and sediment transport within a watershed at a daily time step. The approach relies on the use of GIS data for deriving major model parameters that show distinct spatial variability over the catchment. Surface runoff is calculated by a modified rational method, which depends upon rainfall intensity, soil moisture status, slope, land-use, and soil characteristics. The erosion model simulates soil erosion by raindrop impact and shear erosion in overland and channel flow using equations with a physical basis. A diffusive approximation method is used for routing runoff and sediment transport to the basin outlet. The model uses as few parameters as possible while retaining its physical basics. The model was applied on the Latyan dam catchment in Alborz mountain range in the northern part of Iran. Simulated river discharge and sediment concentration are compared to daily measured data from September 2005 to September 2006. The results indicate that there is a good agreement between simulated and measured discharge and sediment concentration at the basin outlet, though more efforts regarding soil erosion and sediment transport need to be clarified by further research.

Introduction
Soil erosion and transport is a complex process that is influenced by soil type, topography, climate, land use, and antropogenic activities such as tillage systems and soil conservation measures (Kuznetsov et al., 1998). The three main phases of soil erosion are detachment, transport and deposition. Soil detachment and transport by impacting rain drops is an important first step in soil erosion. Physical understanding of the processes causing detachment and transport by falling rain drops has improved considerably over the last two decades, mainly by laboratory experiments (Poesen and Savat, 1981; Ghadiri and Payne 1988; Poesen and Torri, 1988; Sharma and Gupta, 1989; Salles and Poesen, 2000; Van Dijk, et al., 2003). The erosion of soil caused by the raindrop splash and the overland flow is known as sheet erosion or interrill erosion. Models differ in terms of complexity, processes considered, and the data required for model calibration and model use. Sediment transport is sensitive to the flow hydraulics. Therefore, when applying physically based models, detailed and accurate simulation of the velocity and depth of flow is more important than an accurate calibration of rainfall erosion and runoff erosion parameters although, in

some cases, erosion can be sensitive to those parameters (Smith et al., 1999; Aksoy and Kavvas, 2005). In this model water and sediment are routed over the land surface with WetSpa, a GIS-based distributed hydrological model for flood prediction and watershed management on catchment scale. The erosion model simulates soil erosion by raindrop impact and leaf drip impact, shear erosion in overland flow and channel flow, and sediment transport by overland flow and channel flow using physically based equations.

Erosion and sediment transport processes and modeling

Soil detachment by raindrop impact

Modeling soil detachment by raindrop impact is based on relationships between detachment and the kinetic energy of rainfall. In this model, equations for splash detachment by rain drops have been largely taken from the EUROSEM model (Morgan et al., 1998; Koo et al., 2005). Soil particle detachment by raindrop can be predicted as (Morgan et al., 1998; Koo et al., 2005):

$$DR = k\left(KE_r + KE_l\right)\exp\left(-Z_s h\right) \quad (1)$$

where DR is the rate of soil particle detachment by raindrop impact [$gm^{-2}s^{-1}$], k is an index of the detachability of the soil [gJ^{-1}] for which values must be obtained experimentally, KE_r is the kinetic energy rate of direct rainfall [$Jm^{-2}s^{-1}$] which reaches the soil surface, KE_l is the kinetic energy rate of leaf drainage from the canopy [$Jm^{-2}s^{-1}$], and Z_s is a parameter varying between 0.9 and 3.1 [mm^{-1}], depending on soil texture but for which a value of 2.0 [mm^{-1}] can be used for a wide range of conditions (Torri et al., 1987), and h is the mean depth of the surface water layer [mm].

Soil detachment by overland flow

Overland flow detaches soil particles by exerting a shear stress which breaks the inter particle bonds. Soil particle detachment by overland flow [$kgm^{-2}s^{-1}$] is calculated as (Ariathurai and Arulanandan, 1978; Wicks and Bathurst, 1996; Adams and Elliott, 2006):

$$DF = K_f\left(\frac{\tau}{\tau_c} - 1\right) \qquad \text{for } \tau > \tau_c \quad (2)$$

$$DF = 0 \qquad \text{for } \tau \le \tau_c$$

where DF is the rate of soil particle detachment by the flow [$gm^{-2}s^{-1}$], K_f is the overland flow erodibility [$gm^{-2}s^{-1}$], τ is the shear stress [Nm^{-2}], and τ_c is the critical shear stress [Nm^{-2}] which is calculated by the modified Shields diagram (Madsen et al., 1976).

Runoff simulation

A distributed hydrological model WetSpa is applied for simulation of the hydrological processes including precipitation, interception, depression storage, surface runoff, infiltration, evapotranspiration, percolation, interflow, ground water flow, and water balance in each layer. Hydrological processes in each grid cell are set in a cascading way, starting from a precipitation event. Incident rainfall first encounters the plant canopy, which intercepts all or part of the rainfall until the interception storage capacity is reached. Excess water reaches the soil surface and can infiltrate the soil zone, or is diverted as surface runoff. The runoff is subsequently routed through the basin along flow paths determined by the topography using a diffusive wave transfer model that leads to response functions between any start and end point, depending upon slope, flow velocity and dissipation characteristics along the flow lines (De Smedt et al., 2000).

Basic equation for sediment transport

Overland flow is routed prior to implementation of the erosion algorithm, so the depth and velocity of flow are available for sediment calculations. The transport of sediment in a stream commonly can be approximated using the kinematic wave and first-order kinetics for the settling. In one dimension, the partial differential equation describing solute transport in streams is given by:

$$\frac{\partial C}{\partial t} = D(x)\frac{\partial^2 C}{\partial x^2} - v(x)\frac{\partial C}{\partial x} - \lambda(x)C \tag{3}$$

where C is sediment concentration [gm^{-3}], x is the distance along the flow path [m], D(x) is the longitudinal dispersion coefficient at location x [m^2s^{-1}], v(x) is the transport velocity at location x [ms^{-1}], and λ(x) is the settling coefficient at location x [s^{-1}].

For convenience of analysis, the dependent variable of concentration C can be transformed into the rate of transport by multiplying Equation (3) by the rate of water discharge, i.e. (Liu et al., 2005)

$$\frac{\partial q_c}{\partial t} = D(x)\frac{\partial^2 q_c}{\partial x^2} - v(x)\frac{\partial q_c}{\partial x} - \lambda(x)q_c \tag{4}$$

where $q_c = CQ$, denotes the mass rate of sediment transport [gs^{-1}].

The total transport rate at the catchment outlet can be obtained by a convolution integral of the responses from all grid cells, i.e.

$$Q_{sh}(t) = \int_A \int_0^t L(x,t')U(x,t-t')dt'dA \tag{5}$$

where $Q_{sh}(t)$ is the sediment outflow transport rate [gs^{-1}], $L(x,t')$ is the loading rate at a certain location in the catchment [$gm^{-2}s^{-1}$], t' is the delay time [s], U is a unit flow path response function [s^{-1}], and A is the catchment area [m^2]. The loadings can be calculated as:

$$L(x,t) = DF(x,t) + DR_r(x,t) \quad (6)$$

Application

Study area and model simulation

The erosion and sediment module was applied and tested for the Latyan dam watershed located in Alborz mountain range in the northern part of Iran. The drainage area is 435.3 km^2 up to Roodak hydrometric station at the entrance of the Latyan dam reservoir, as shown on the location map in Figure 1. The basin is mountainous with elevations ranging from 1700 to 4212 m. The mean elevation is 2830 m and the mean basin slope is about 45.6%. Land use is composed of 5 different types of land cover: 91% of the basin is covered by deciduous shrubs, 6.2 % by deciduous broad trees, 1.8% by short grass, and about 1.0% by agriculture and impervious areas, mainly villages (Zeinivand and De Smedt, 2008). There are 3 different soil textures in the catchment. The dominant soil texture is clay loam, which covers about 89.4% of the basin, and silt loam and sandy loam about 5.6% and 4.8% respectively (Zeinivand and De Smedt, 2008). Hydrologic data for this study were obtained from Tehran Regional Water Organization and Iranian Water Resources Research Organization (TAMAB Co). The data set include, daily precipitation in 8 stations, temperature and evapotranspiration in 3 stations, and daily discharge and suspended sediment concentration data at Roodak station. All data are available for a one year from September 2005 to September 2006, except for sediment concentrations for which only 13 samples have been collected. The catchment is a mountainous and about 50% of the precipitation is snowfall. The annual precipitation in the study area and for this period is 676 mm; the temperature varies from -11.73 to 23.6 ºC with 8.57 ºC on average.

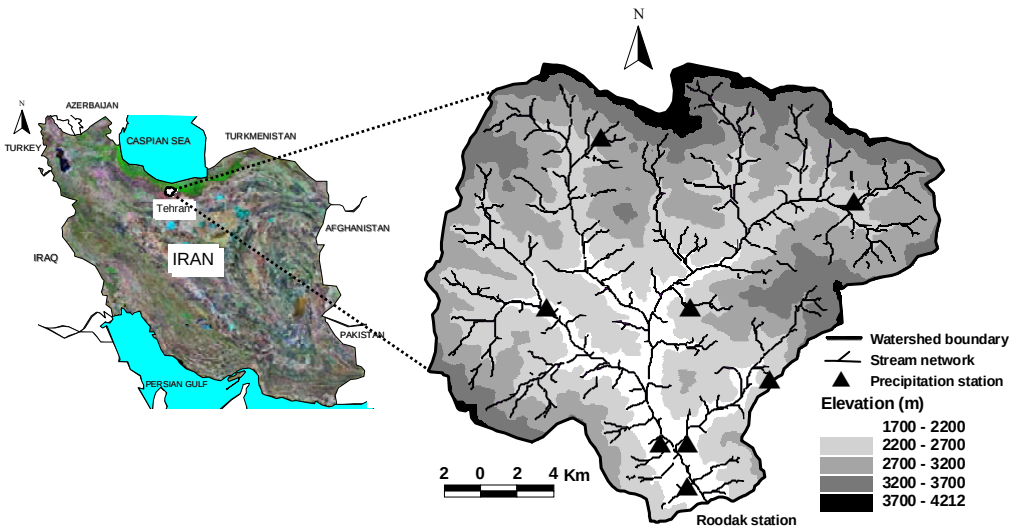

Figure 1. Location of the Latyan dam watershed in Iran and detailed map of the subbasin upstream of Roodak station, showing stream network, topography and location of precipitation stations.

The one year daily discharge data and the 13 sediment concentrations observed at the catchment outlet is used for model simulation and evaluation.
All parameters of the model that are related to the basin are derived from a combination of a digital elevation model, a soil map, and a land use map. For the simulation of hydrographs and suspended sediment concentration at the basin outlet, the catchment was divided into 193 subcatchments. First, model calibration is implemented by comparing the simulated hydrograph with the observed hydrograph graphically and statistically. Then measured suspended sediment concentrations are compared with the simulated sediment concentrations at Roodak station. The calibrated detachability of the soil k is 0.005 gJ^{-1} and the overland flow erodibility K_f is 8.75×10^{-7} $gm^{-2}s^{-1}$ in this catchment. The soil detachability k parameter seems to be lower than in other studies. The reason could be snow cover, because k is the detachability of the soil by raindrops, and when there is a snow cover raindrops no have effect on the soil.

Results and discussion

Three statistical evaluation criteria for the model performance for discharge, suspended sediment concentration, and sediment yield are given in Table 1. The statistical results presented in Table 1 show that the model is able to predict runoff and sediment yield reasonably. The Mean Error (ME) for discharge is -0.33 m^3s^{-1}, which shows that the simulated discharge is a little underestimated compared to the measurements, while for the suspended sediment concentration and sediment yield this is 0.04 gl^{-1} and 1.52 kg s^{-1} respectively, which shows that the suspended sediment concentration and sediment yield are a little overestimated. The Nash-Sutcliffe model efficiency (NS) for discharge is 0.85, which shows that the model can simulate the hydrograph very well. The efficiency for suspended sediment concentration is 0.63 which indicates a reasonable agreement between simulation and observation, which the efficiency for sediment yield is only 0.14 indicating that the model can not simulate sediment yield accurately. The Correlation coefficient (R) for discharge, suspended sediment concentration, and sediment yield is 0.91, 0.93 and 0.95.

Table 1. Evaluation criteria for simulated flow, suspended sediment concentration, and sediment yield.

	Discharge ($m^3 s^{-1}$)	Suspended sediment concentration ($g l^{-1}$)	Sediment yield ($kg s^{-1}$)
ME	-0.33	0.04	1.52
NS	0.85	0.63	0.14
R	0.92	0.90	0.86

ME: Mean Error, NS: Nash-Sutcliffe model efficiency, R: correlation coefficient

The observed precipitation, temperature, and graphical comparison between observed and simulated discharge is shown in Figure 2a. As can be seen, the precipitation occurs mostly in January and February 2006 when temperatures are below zero. Hence, this precipitation falls as snow, and remains in the soil surface.

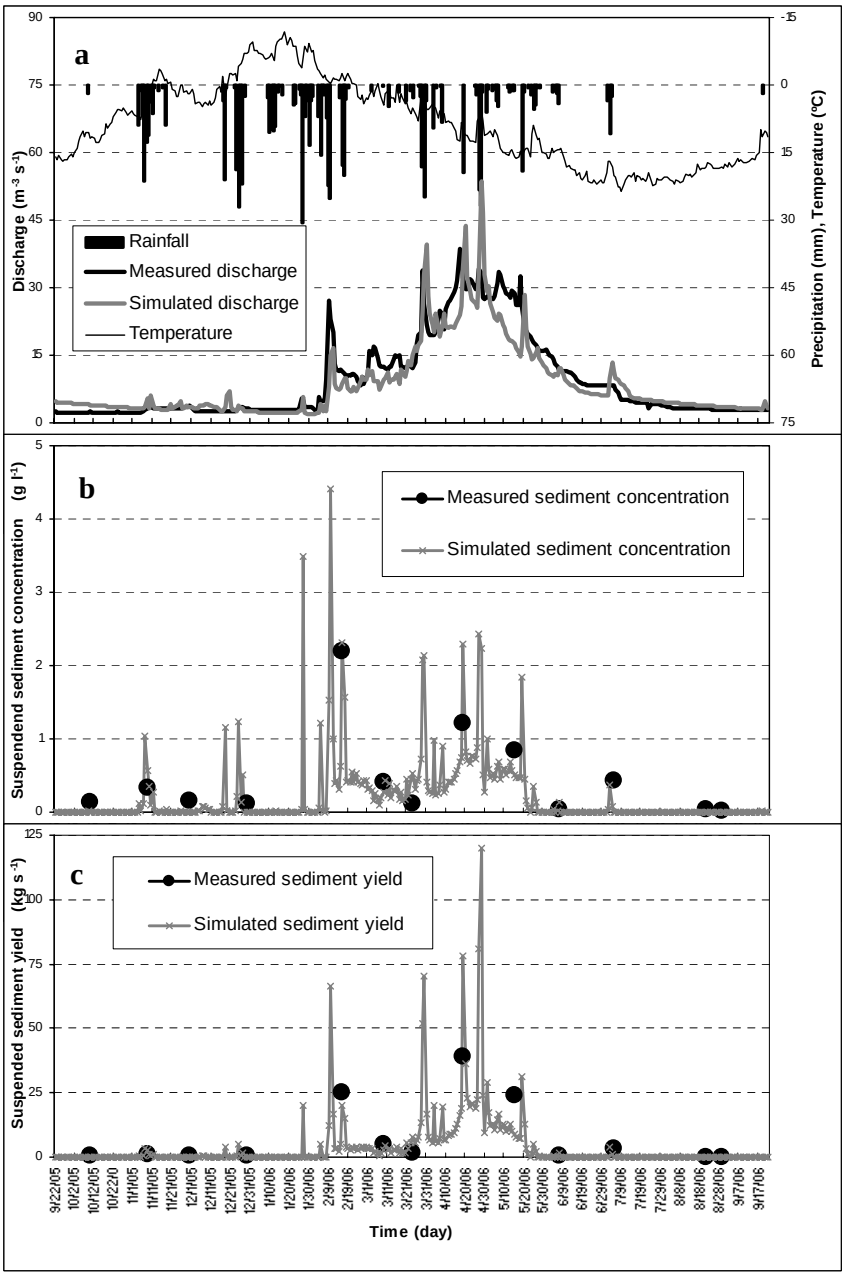

Figure 2. Measured precipitation, temperature, and observed and simulated discharge (a), sediment concentration (b), and suspended sediment yield (c) for September 2005-Septembet 2006 for Latyan dam watershed.

The snow cover melts at the end of April and during May when the weather becomes warmer. The discharge from September '05 till middle of February '06 is very small and almost constant, but from the middle of February increases because of snowmelt and rainfall. The model simulations compare reasonably to the observations. The graphical comparison between measured and simulated suspended sediment

concentration for is shown in Figure 2b. The suspended sediment concentration increases when discharge because of rainfall or snowmelt increases. And there is good agreement between measured and simulated suspended sediment concentration for the days which sediment concentration has been measured. For example measured sediment concentration on 16th of February '06 is 2.19 gl^{-1} which is the highest measured sediment concentration among all measurements and the model simulation is 2.3 gl^{-1}. The graphical comparison between measured and simulated suspended sediment yield for this event is shown in Figure 2c. The general trend of simulated and observed sediment yield is acceptable and model prediction for sediment yield is satisfactory.

For discuss and more details of processes in erosion and sediment transport processes we select 16th February '06 which maximum suspended sediment concentration has been measured among measurements. Figure 3 (left) shows distributed snow water equivalent in the Latyan dam watershed. This figure shows that except small part of catchment in downstream which has no snow, most part of the catchment is covered by snow in this day and snow depth in the upstream of the basin is more than downstream. The reason is obvious and that is because of elevation difference e.g. elevation in the upstream is higher than 4200 m while in the outlet of the basin is around 1700 m.

Snowmelt in mountainous area has a big impact in surface runoff generation. And surface runoff can erode soil and generate and transport sediment. Figure 3 (right) shows distributed snowmelt in the Latyan dam watershed on 16th February '06. This figure shows that snowmelt occurs only in small part of catchment in downstream which has higher temperature than upstream. There is no snowmelt in the upstream of the catchment during that day. The maximum snowmelt is 4.7 mm.

Figure 4 (left) shows distributed surface runoff in the Latyan dam watershed on 16th February '06. This figure shows that there is surface runoff only in the lower part of the basin and compare to snowmelt in Figure 3 (right) it can be concluded that almost all of this runoff is due to snowmelt in this day.

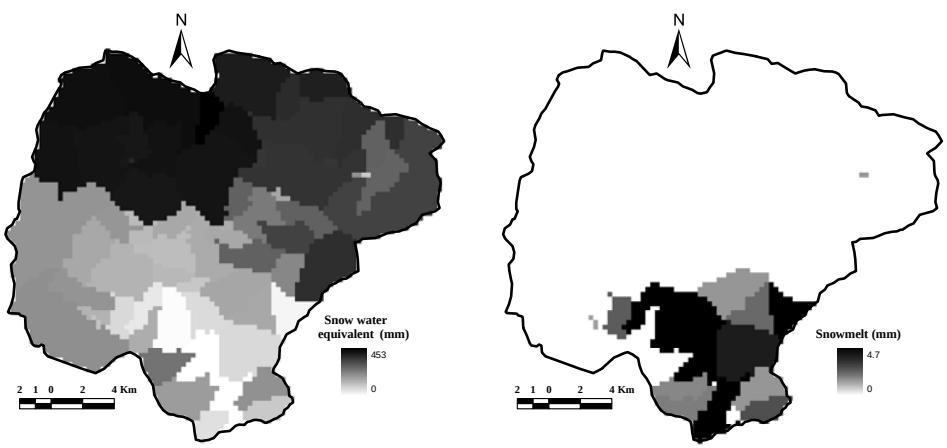

Figure 3. Distributed snow water equivalent (left) and (right) distributed snowmelt in the Latyan dam watershed on 16th February 2006.

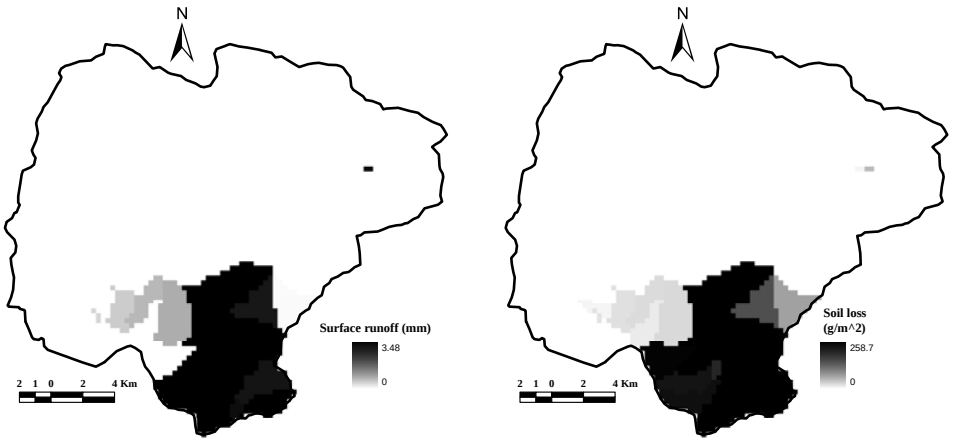

Figure 4. Distributed surface runoff (left) and distributed soil loss (right) in the Latyan dam watershed on 16th February 2006.

Figure 4 (right) shows distributed soil loss in the Latyan dam watershed on 16th February '06. As discussed above there is no snowmelt and surface runoff in upper part of the basin so it can be predicted there is no erosion and sediment in those parts of the catchment. But in lower part of the basin there is snowmelt and surface runoff which resulting erosion and soil loss that has shown in this figure. During this day there are snowmelt and surface runoff only in the area close to the outlet, and there is no long distance to the catchment outlet so there is no high opportunity for deposition, that can be a reason for high sediment concentration measured in this day. Regarding to above explanations it can be concluded that model are able to predict erosion and sediment in the basins with snowfall prominent.

Conclusion

A physically based, spatially distributed model was developed to simulate erosion, sediment transport and deposition, within the framework of the hydrological WetSpa model. Soil detachment by raindrop impact is calculated based on relationships between detachment and the kinetic energy of rainfall. Soil particle detachment by overland flow is calculated based on actual and critical shear stress. Water and sediment are routed over the land surface along topographically determined flow paths with travel times and flow rates determined by the WetSpa model. The applications of this model to the Latyan dam watershed catchment with outlet at Roodak station in Alborz mountain, Iran, shows good overall results for the flow hydrographs and suspended sediment concentration at the catchment outlet.

Further future works and applications are required to demonstrate the usefulness of this model on improve the model's efficiency, validity, and accuracy.

References:

Adams, R., and Elliott, S. (2006). "Physically based modelling of sediment generation and transport under a large rainfall simulator." *Hydrol. Process.,* 20, 2253–2270.

Aksoy, H., and Kavvas, L. (2005). "A review of hillslope and watershed scale erosion and sediment transport models." *Catena.,* 64, 247–271.

Ariathurai, R., and Arulanandan, K. (1978). "Erosion rates of cohesive soils." Proceedings of the American Society of Civil Engineers, *Journal of the Hydraulics Division.,* 104, 279-283.

De Smedt, F., Liu Y. B., and Gebremeskel S. (2000). "Hydrological modeling on a catchment scale using GIS and remote sensed land use information." In: Brebbia CA (ed) *Risk analysis II*. WTI, Boston, pp 295–304

Ghadiri, H., and Payne, D. (1988). "The formation and characteristics of splash following raindrop impact on soil." *Journal of Soil Science.,* 39, 563–575.

Koo, B. K., Dunn, S. M., and Ferrier, R. C. (2005). "A distributed continuous simulation model to identify critical source areas of phosphorus at the catchment scale- model description." *Hydrol. Earth. Sys. Sci.,* Discuss., 2, 1359–1404. www.copernicus.org/EGU/hess/hessd/2/1359/SRef-ID: 1812-2116/hessd/2005-2-1359

Kuznetsov, M. S., Gendugov, V. M., Khalilov, M. S., and Ivanuta, A. A. (1998). "An equation of soil detachment by flow." *Soil & Tillage Research.,* 46, 97–102.

Liu, Y. B., Corluy, J., Bahremand, A., and De Smedt, F. (2005). "Modelling flow and phosphorus transport to the Ruzín reservoir from the Margecany catchment, Hornad, Slovakia." *The Tisza River Project.,* ANNEX 2B: Vrije Universiteit Brussel, Belgium.

Madsen, O. S., and Grant, W. D. (1976). "Sediment transport in the coastal environment." In: Report No. 209, Ralph M. Parsons Laboratory for *Water Resources and Hydrodynamics,* Department of Civil Engineering, M.I.T., p. 105.

Morgan, R. P. C., Quinton, J. N., Smith, R. E., Govers, G., Poesen, J. W. A., Auerswald, K., Chisci, G., Torri, D., and Styczen, M. E. (1998). "The European soil erosion model (Eurosem): A dynamic approach for predicting sediment transport from fields and small catchments." *Earth Surface Processes and Landforms.,* 23, 527–544.

Poesen, J., and Savat, J. (1981). "Detachment and transportation of loose sediments by raindrop splash." Part II. Detachability and transportability measurements. *Catena.,* 8, 19–41.

Poesen, J., and Torri, D. (1988). "The effect of cup size on splash detachment and transport measurements." Part II. Field measurements. *Catena Suppl.,* 12, 113–126.

Smith, R. E., Goodrich, D. C., and Unkrich, C. L. (1999). "Simulation of selected events on the Catsop catchment by KINEROS2." a report for the GCTE conference on catchment scale erosion models. *Catena.,* 37, 457– 475.

Salles, C., and Poesen, J. (2000). "Rain properties controlling soil splash detachment." *Hydrological Processes.,* 14, 271–282.

Sharma, P. P., and Gupta, S. C. (1989). "Sand detachment by single raindrops of varying kinetic energy and momentum." *Soil Science Society of America Journal.,* 53, 1005–1010.

Torri, D., Sfalanga, M., and Del Sette, M. (1987). "Splash detachment: runoff depth and soil cohesion." *Catena.,* 14, 149–155.

Van Dijk, A. I. J. M., Bruijnzeel, L. A., and Eisma, E. H. (2003). "A methodology to study rain splash and wash processes under natural rainfall." *Hydrol. Process.,* 17, 153–167.
Wicks, J. M., and Bathurst, J. C. (1996). "SHESED: a physically based, distributed erosion and sediment yield component for the SHE hydrological modeling system." *Journal of Hydrology.,* 175, 213-238.
Zeinivand, H., and De Smedt, F. (2008). "Hydrological modeling of snow accumulation and melting on river basin scale." *Water Resour Manage Journal.*, DOI 10.1007/s11269-008-9381-2,
< http://www.springerlink.com/content/075r2q8322564051/ >

The Role of the Clast Layer of Desert pavement in Rainfall-Runoff Processes

Li Chen[1] Jun Yin[2] Julianne Miller[3] Michael Young[4]
[1, 3,4] Division of Hydrological Sciences, Desert Research Institute, Las Vegas, NV 89119
Li.Chen@dri.edu; Julie.Miller@dri.edu; Michael.Young@dri.edu
[2] Department of Geosciences, Oregon State University, Corvallis, OR 97331,
jun.yin@geo.oregonstate.edu

Abstract

Desert pavement is a surficial feature widespread throughout arid lands in the world. Whenever found, it can play an important dynamic role in geomorphic, hydrologic, and ecologic processes in desert environments. The hydrological properties, especially the clast layer impact on hydrological processes, are still not clear to the academic community. Anecdotal evidences and empirical observations have reported rapid runoff generation process which implied low permeability of the pavement with the clast layer. Quantitative result, however, has not yet been reported. An experimental study has been carried out in Mojave National Preserve near Providence Mountain to investigate the hydraulic properties of the clast layer. Rainfall simulations were conducted with a pair of portable rainfall simulators. Each group of experiment includes two parallel runs on two adjacent plots, one with intact clast layer and one with clast layer removed. Soil moistures time series were measured with Water Content Reflectometers (WCR). Runoff was collected at the downstream side of each plot. Experimental results of both runoff and soil moisture did not show significant difference between two types of plots, which implied the clast layer at the experiment site is not a restrictive layer for infiltration and rainfall-runoff processes. In addition, the measured soil moisture curves were used to develop an optimization method for Green-Ampt infiltration parameters, which can produce a useful tool of direct estimation of G-A parameters for practical applications.

1. Introduction

Desert Pavement is a common feature of surfaces in arid and semi-arid regions around the world. Evenari et al. (1985) showed that about half of arid land in North America covered by pavement. The structure of desert pavement consists of a clast layer overlying a sand-poor AV horizon. Due to the high occurrence of desert pavement in arid and semi-arid areas, it is expected that the pavement surface plays an important role in the desert hydrological and ecological system. Significant research has been conducted regarding to the mechanism of pavement formation and the geomorphic features. However, the hydrological properties of such surface have not been thoroughly investigated. Among many questions that are not fully understood on desert pavement, the hydrological properties and functions of the clast layer has not been addressed previously. There are anecdotal evidences that tightly packed clast layer reduces the water infiltration rate. Wood et al (2005) showed indirect qualitative evidences for the same trend. This implies that the clast layer can significantly influence the hydrological cycle and ecological processes. Quantitative studies are still void for this topic. It is our purpose to conduct field measurements to quantitatively examine the hydrological properties of the clast layer.

2. Methodology

The method of rainfall simulation was adopted in this study. The rainfall simulation test was conducted on a desert alluvial fan at the Mojave National Preserve, CA (between 115.61 and 115.39ºW and 35.31 and 34.83ºN)) close to the Providence Mountain. The test site is characterized by a layer of desert pavement with the age of ~100 ka (Young et. al., 2004) dated by McDonald, et al. (2003). An early field survey showed that the site is sparsely vegetated by *L. trendentata* and *A. domosa*. In each experimental run, rainfall simulation was simultaneously conducted on two adjacent plots, one intact surface and one surface with clast layer removed, so that we can make comparison directly.

Two portable rainfall simulators (Fig. 1a) were used to conduct rainfall simulation on a selected pavement surface. The rainfall simulator consists of a flat, two-foot-square (61 cm x 61 cm) Plexiglas reservoir for water, with hypodermic needles on the under side (Mutchler and Moldenhauer, 1963; Munn and Huntington, 1976). Water drops were produced on the needles and the rainfall intensity was artificially maintained to a constant rate through a Marriot system. The rainfall intensity was calibrated three times before and after each test to assure that the rainfall intensity was well produced and maintained. At the lower slope of each plot, a trench was dug and a plastic trough was placed into the trench to collect surface runoff. The gap between the trough and the plot was connected by a 900 bend aluminum flashing and sealed using expandable insulating foam to prevent leakage (Fig 1b).

Soil moisture was measured continuously during the rainfall experiment. A Water Content Reflectometry (WCR) was placed under each rainfall simulator to measure the soil moisture of the top 6.5 cm soil at the frequency of 1Hz.

There are several advantages of using the rainfall simulation method. The rainfall simulation approximates the natural rainfall-infiltration process, while most other permeameters test the infiltration at certain constant head. The rainfall simulator can be used for complex surface conditions without intrusion to the soil, whereas application of many other permeameters interfere the surface of soil at various extent. With the direct measurement of the soil moisture, we can observe the whole rainfall-infiltration-runoff process. It may also generate a new parameter estimation approach for infiltration models.



(a) (b)

Fig. 1 (a) rainfall simulator ; (b) Probe of water reflectometer

3. Observation of runoff generation

In total, 7 pairs (14 runs) of rainfall experiment were conducted. Runoff time series at down slope side of each plot were recorded and the results are plotted in Fig.2. Total runoff volumes for different surfaces are compared in Fig.3.

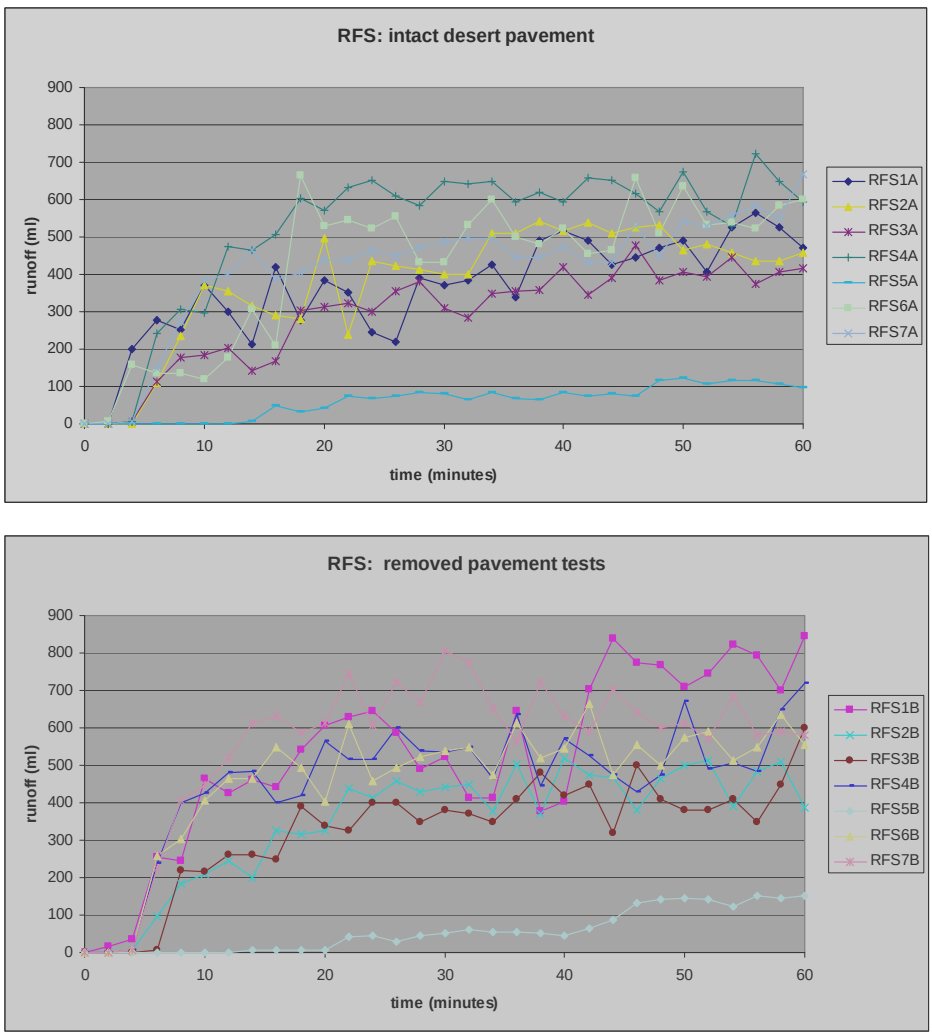

Fig.2 Observed runoff generation processes

Table 1 summarizes the surface runoff characteristics on both paved and unpaved plots. In terms of the averaged timings, observed runoff on clast removed plots (B) is a little delayed than the observed runoff on intact plots (A). However, t-test (for normal distributions) or Mann-Whitney Rank Sum Test (for non-normal distributions) showed that there is not a statistically significant difference between two types of plots in any of the runoff characteristics, showing that statistically desert pavement has very little affect on the runoff generation in the first few minutes after the precipitation started. Fig. 3 shows the comparison of total runoff volumes for the two types of plots. The result indicates that the clast layers generally leads to slightly less runoff or more infiltration,

which may be caused by the micro storage and larger roughness of the clast layer that impede water flowing downstream and thus promote the infiltration process.

Table 1 Characteristic times of runoff generation process

RFS#	Ponding (s)	Initial runoff on surface (s)	Runoff in all quadrants (s)	Flow connection back to front (s)	Flow to trough (s)
2A	68	114	218	340	194
2B	60	90	145	270	225
3A	40	121	252	249	256
3B	60	131	162	224	305
4A	49	130	183	N/A	170
4B	96	179	200	239	233
5A	116	180	300	560	804
5B	96	170	555	N/A	757
6A	38	78	109	128	159
6B	60	130	220	214	192
7A	69	119	138	253	219
7B	80	105	155	192	240
Difference	N (t) (p=0.408)	N (t) (p=0.604)	N (t) (p=0.587)	N/A	N (MW) (p=0.394)
Averaged A	63	124	200	306	300
Averaged B	75	134	240	228	325

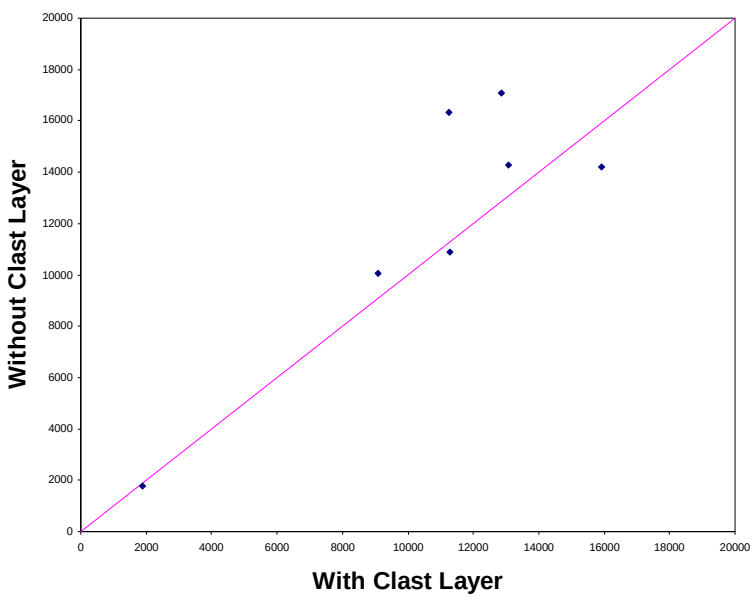

Fig. 3 Total Runoff Volume

4. Green-Ampt Parameters

Green-Ampt (Green and Ampt, 1911) model is the simplest physically based infiltration model. It is widely used in practices for rainfall runoff analyses. We can also use Green-Ampt parameters to examine the physically properties of the clast layer. Previous studies for Green-Ampt parameters (e.g., Rawls et al, 1983) do not determine parameter values directly from the infiltration process. In this study, we propose a method of parameterizing the Green-Ampt model using soil moisture data measured during the infiltration process and apply them to examine the role of the clast layer.

A numerical optimization approach is adopted for the parameterization. The objective function is defined as

$$OF = \sum_{i=1}^{m} \left[y_i - f\left(x_i, \beta\right) \right]^2 = \sum_{i=1}^{m} r_j^2(x) \tag{1}$$

where y_i is the observed value and $f\left(x_i, \beta\right)$ is the optimized function using the optimized parameters β, r is the residual of f. Note that $f\left(x_i, \beta\right)$ in this study is solved implicitly from the Green-Ampt equation. The Levenberg-Marquardt method (Marquardt, 1963) was employed to obtain the minimum of equation (1). The method can be described with the following equations:

$$\min_p \frac{1}{2} \| J_k p + r_k \|_2^2, \text{ s.t. } \| p \| \leq \Delta_k \tag{2}$$

$$\left(J\left(x_k\right)^T J\left(x_k\right) + \mu_k I \right) s = -J\left(x_k\right)^T r\left(x_k\right) \tag{3}$$

where J is Jacobian of r, $p = x\text{-}x_k$ for step k, Δ_k is the trust region radius. For Green-Ampt model, we have the following equations for the objective function and Jacobian J:

$$f(K, MS) = I - MS \ln\left(1 + \frac{I}{MS}\right) - K\left[t - \left(t_p - t_s\right)\right] \tag{4}$$

$$\frac{\partial f}{\partial K} = -(t - (t_p - t_s)) \tag{5}$$

$$\frac{\partial f}{\partial MS} = -(\ln(1 + \frac{I}{MS}) - \frac{I}{(1 + I / MS)MS}) \tag{6}$$

where K is soil hydraulic conductivity, M is moisture deficit, S is suction head, M and S are combined as one parameter, t_p is ponding time and t_s is a virtual time to convert rainfall-infiltration to ponded infiltration. In this study, we only optimize K and MS, and the optimization covers the soil moisture curve after ponding time.

In 6 out of 7 pairs of experimental runs we obtained valid soil moisture curves and optimization was conducted for these 12 cases. Fig.4 shows the results of optimization. It is found that if the actual infiltration curve has a similar shape to the theoretical Green-Ampt curve, the optimized infiltration curve can approximate the real curve fairly well. However, if abnormal curves were observed, for examples, in case 4A and 4B a point of inflection exists which is different from the theory, the optimized curve will not accurately approach the actual curve. The reason for such abnormal curves can be complex. Layered soil, preferential flow, anisotropic soil or vegetation effect may all cause the infiltration deviates from the standard curve. The theory will not be able to well represent highly complex natural conditions.

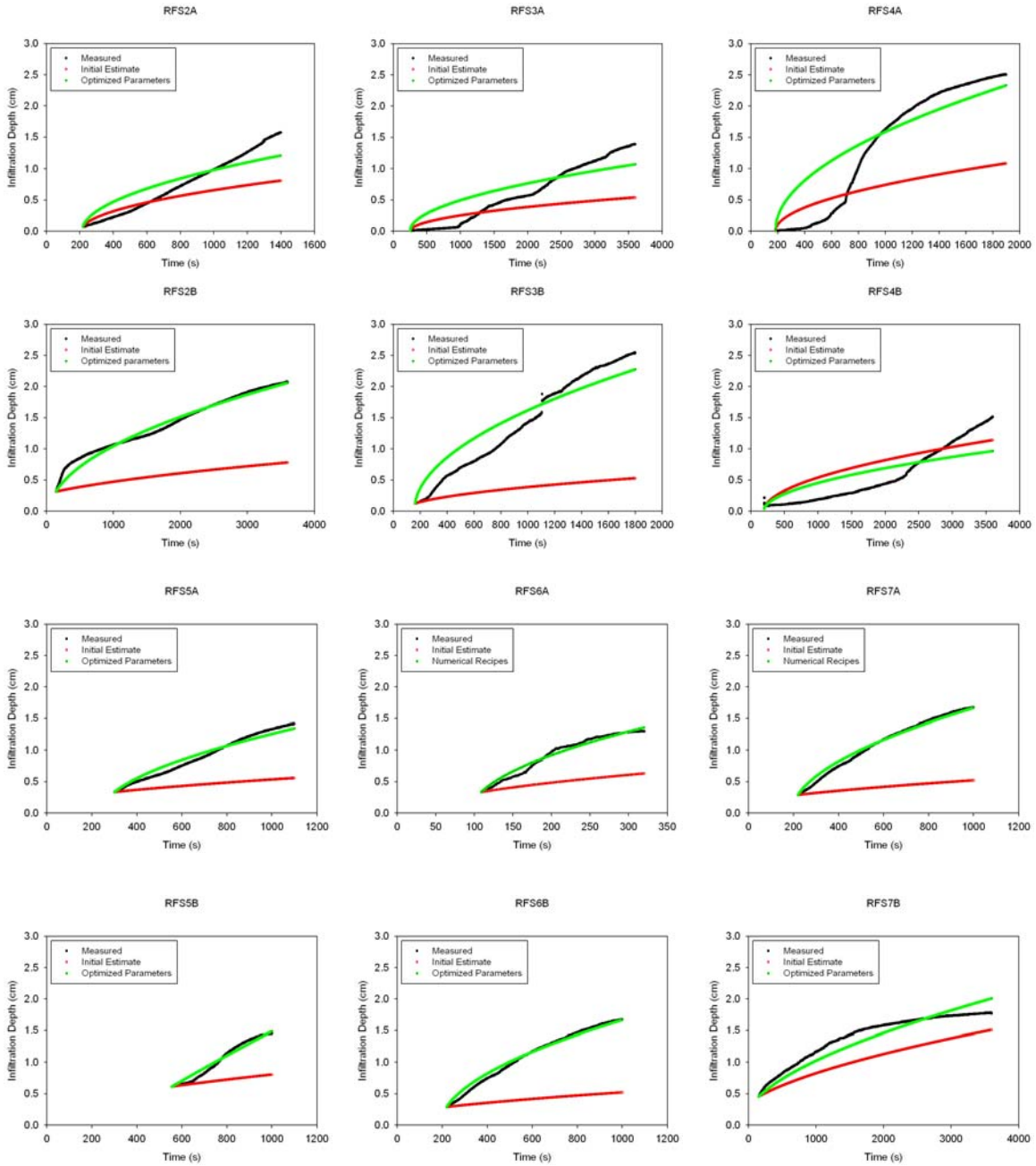

Fig. 4 Optimized Green-Ampt infiltration curves

The results of the optimized Green-Ampt parameters for two types of plots are shown in Fig. 5. Comparison does not show significant difference for the conductivities, whereas it demonstrates the intact surfaces have larger suction head than clast removed surfaces. This implies that the clast layer does not change the soil hydraulic conductivity but may affect the capillary force. Such a trend may be explained by the rain drop influences on the soil. Clast layer may protect the soil structure and prevent the potential surface sealing during rainfall events and thus maintains the capillary effect.

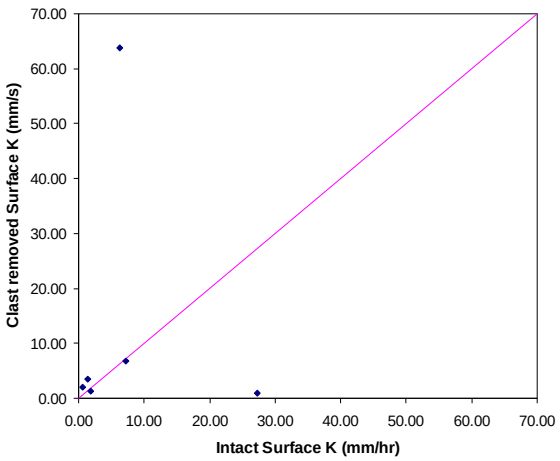

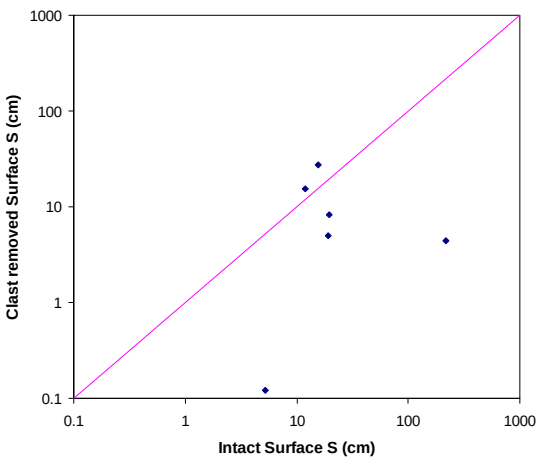

Fig. 5 Comparison of optimized *K* and *S*.

6. Concluding remarks

The role of clast layer within desert pavement in hydrological processes has not been fully understood because quantitative observations on the rainfall-runoff events occurring on such surfaces are largely absent. In this pilot study, we investigated the clast layer function using rainfall simulation method. The rainfall simulation tests described herein provided the in-situ runoff and infiltration measurements. Based on these data the runoff and infiltration characteristics of intact and clast removed plots were analyzed. Although slight differences were observed between two types of plots in terms of total infiltration and timing of surface runoff generation, t-test and Mann-Whitney Rank Sum Test indicated that the difference is not statistically significant. Total runoff volumes on intact surfaces are slightly smaller, implying the clast layer may increase the surface storage and runoff routing time and promote infiltration.

Green-Ampt infiltration parameters were derived from the observed moisture curves through a parameter optimization approach. Results show that the soil hydraulic conductivity values for two types of plots do not have significant difference, but the suction head values for intact surfaces are larger. This may be explained again by the surface storage and the larger roughness of the clast layer. In addition, it implies that the infiltration rate with or without the clast layer will be the same for large time when the gravity dominates the infiltration process. This study also presented a new method to calibrate Green-Ampt or other infiltration model parameters using the observed data and will show application in hydrological analyses.

From this study we found that the clast layer of desert pavement does not act as a restrictive layer for infiltration. Rather, it may provide extra surface storage and increase runoff routing time to allow more infiltration to occur. The results we found in this pilot study may not disclose all truth for the clast layer effect. For some very tightly interlocked clast layer with macro pores fill by fine particles, the clast layer may form a crust for the underneath soil and impede the infiltration process. However, such surface was not observed in our study site.

7. Acknowledgements

This study is supported by USGS/NWRI project 06HQGR0098 and internal IR&D funding of Division of hydrological sciences, Desert Research Institute. The authors are grateful for the help of Scott Campbell in the field work of rainfall simulations.

References

Evenari, M., I. Noy-Meir and D.W. Goodall, (1985), Hot deserts and arid shrublands: Part A. Elsevier, New York.

Green, W. H., and Ampt, G. (1911), Studies of soil physics. Part I, the flow of aur and water through soils, J. of Agricultural Sciences, 4, pp (1-24).

Marquardt, D.W. 1963. An algorithm for least squares estimation of nonlinear parameters. J. Soc. Ind. Appl. Math. 11:431-441.

Rawls, W. J., ASCE, M., Brakensiek, D. L., and Miller, N. (1983), Green-Ampt infiltration parameters from soils data, J. Hydraulic Eng., 109(1), pp62-70.

Wood Y. A., R. C. Graham, S. G. Wells (2005), Surface control of desert pavement pedologic process and landscape function, Cimavolcanic field, Mojave Desert, California, Catena 59:205-230.

Watershed Models for Storm Water Management: Comparing Hydrologic and Hydraulic Procedures

Deva K. Borah, M.ASCE; Jamie H. Weist, M.ASCE; Jack D. Wall, M.ASCE; and
David N. Powell, AM.ASCE
Woolpert, Inc.
415 Port Centre Parkway, Suite 101, Portsmouth, VA 23704-4924

Abstract: Many different watershed models are available today that have various complexities, strengths, and weaknesses. Selecting the most appropriate model to achieve the most accurate and efficient solution possible is a challenging task. Despite the fact that all models are mathematical engines, their basic mathematical foundation is often overlooked due to high demands on model applications such as the ease of the graphical user interfaces and the incorporation of geographic information systems. This often leads to modelers' and managers' making decisions based on model marketers' potentially non-objective pitch. The objective of this investigation is to provide a mathematical-based review of available watershed models used for storm water management and provide insightful facts for the end users, particularly water resource managers, so that an informed decision can be made when selecting a model. Fourteen watershed models simulating storm event runoff were reviewed and evaluated resulting in the development of six summary tables which compile, rank, and compare the models. The dominant hydrologic and hydraulic procedures used in the models are compiled, including rainfall excess or infiltration (most rainfall loss), subbasin or overland (land surface) runoff routing, channel flow routing, and subsurface flow simulation. The rankings are based on the formulations and their relative complexities and accuracies for routing overland runoff and channel flows which provide some base for comparing the models because these procedures are backbones of any watershed simulation model, and ultimate performance of a model depends largely on accuracies and speed of these procedures. The compilations and the rankings would be helpful to managers and modelers in understanding and comparing the models, selecting the most suitable model for a project or an application, and using it to its full potential. The comparison approach and the tools (tables) presented would be useful to conduct objective comparisons of other watershed models as well.

Introduction

Many watershed models are available today most of which were developed during the 1960s-1980s. The most widely used models are the ones having a graphical user interface (GUI). Experiences applying these commonly used models have received mixed results (Borah and Bera, 2004). A question often asked is "was the right model selected?" Selecting the most suitable model to accomplish a project most accurately and efficiently as possible is a challenging task.

The available models are diverse. They are based on a variety of concepts, principles, and equations that mathematically simulate the natural processes of a stormwater drainage system resulting in various complexities, strengths, and weaknesses. Recent reviews of existing watershed models (e.g., Borah and Bera, 2003, 2004; Shoemaker et al., 2005; Muñoz-Carpena et al., 2006; Obropta and Kardos, 2007) acknowledged and addressed some of these modeling issues. However, none are in-depth investigations or compilations of the basic model formulations and relative complexities and accuracies. Without this information, it is almost impossible to select the most suitable model and use it to its fullest potential. Such a detailed investigation is also critical to advancing the fundamental knowledge of model formulations currently being used, most of which are over half-a-century old. It is also vitally important to consider the needs and expectations of the managers who are responsible for the modeling studies. They are simultaneously the user of the results in decision making, and the interpreter of

those results to stakeholders and policy makers. Therefore, managers' understanding of the models is critical as well.

The objective of this paper is to advance the understanding of watershed models among the water resources managers through the summary of available models and providing insightful information, specifically on theoretical (mathematical) basis, sophistication levels (complexities), and relative accuracies. Fourteen models that simulate storm event runoff were reviewed and critically evaluated. Some models were commonly used, and others had applications documented in the literature. Only models having capabilities to simulate single storm events, as opposed to continuous simulation models, were selected.

Review and evaluation of the 14 models resulted in the development of six summary tables compiling, ranking, and comparing the models. The dominant hydrologic and hydraulic procedures used in the models are compiled, including rainfall excess or infiltration, subbasin or overland (land surface) runoff routing, channel flow routing, and subsurface flow simulation. The rankings are based on the formulations and their relative complexities and accuracies for routing the overland runoff and channel flows. These procedures are backbones of any watershed simulation model, and ultimate performance of a model depends largely on accuracies and speed of these procedures. The compilations and rankings would be helpful to managers and modelers, who often rely on model marketers subject to non-objective opinions about other models, to understand and compare the models, select the most suitable model for a project or an application, and use it to its full potential. The comparison approach and the tools (tables) presented would be useful to conduct objective comparisons of other watershed models as well.

Watershed Models

The fourteen watershed models reviewed are listed here in alphabetical order along with their sources, brief backgrounds and key facts are given in a full-length paper (Borah et al., 2009). The models are: (1) ***AGNPS*****:** The Agricultural NonPoint Source pollution model of the U.S. Department of Agriculture – Agricultural Research Service (USDA-ARS) (Young et al., 1987); (2) ***ANSWERS*****:** The Areal Nonpoint Source Watershed Environment Response Simulation model of the Purdue University, West Lafayette, Indiana (Beasley et al., 1980); (3) ***DR3M/DR3M-QUAL*****:** The Distributed Routing Rainfall Runoff Model and water quality extension (DR3M-QUAL) of the United States Geological Survey (USGS) (Alley and Smith, 1982a, 1982b); (4) ***DWSM*****:** The Dynamic Watershed Simulation Model of Woolpert, Inc. (Borah et al., 2002); (5) ***GSSHA*****:** The Gridded Surface/Subsurface Hydrologic Analysis model of the U.S. Army Corps of Engineers' (USACE) (Downer et al., 2006); (6) ***HEC-HMS*****:** The Hydrologic Engineering Center – Hydrologic Modeling System (HEC-HMS) of the USACE (USACE-HEC, 2002); (7) ***HSPF*****:** The Hydrological Simulation Program – Fortran of the U.S. Environmental Protection Agency (USEPA) (Bicknell et al., 2001); (8) ***KINEROS*****:** The Kinematic Runoff and Erosion model of the USDA-ARS (Woolhiser et al., 1990); (9) ***MIKE SHE*****:** MIKE Système Hydrologique Européen of Danish Hydraulic Institute (DHI) (Refsgaard and Storm, 1995); (10) ***MIKE URBAN*****:** MIKE URBAN of DHI (2008); (11) ***PRMS*****:** The Precipitation-Runoff Modeling System of the USGS (Leavesley and Stannard, 1995); (12) ***SEDIMOT III*****:** The Sedimentology by Distributed Modeling Techniques – Version III of Barfield et al. (2006); (13) ***SWMM*****:** The Storm Water Management Model of the USEPA (Rossman, 2007); and (14) ***TR-55*****:** Technical Release 55: Urban Hydrology for Small Watersheds of the USDA-Natural Resources Conservation Service (USDA-SCS, 1986).

Hydrologic and Hydraulic Procedures

Modeling of a watershed involves mainly dividing the watershed into manageable modeling units; computing rainfall excess on each of the units; routing the excess rainfall (runoff)

over the land surfaces and through the stream channels beginning at the uppermost unit and ending at the lowermost (outlet); and parallel computations of subsurface flow contributions to stream flows. The models use various hydrologic and hydraulic methods to compute or simulate rainfall excess, flow routing, and subsurface flow. Each of the models has its unique way of applying the procedures into its source code, sometime through simplification or modification of the original formulation or method. Such details are beyond the scope of this paper. Only the procedure names are listed here, details and mathematical expressions are available in the literature and also in a full-length paper of the authors (Borah et al., 2009).

Rainfall Excess

Computing rainfall excess or runoff volume is the first step in watershed modeling. This involves computing rainfall losses due to interceptions at tree canopy and ground cover, depression storage, and infiltration through the soil layer, then computing the excess rainfall available for runoff. Various procedures are used by the models for computing rainfall excess, directly, or through the above losses, among which infiltration is the major. Below are the rainfall excess or infiltration procedures. Table 1 compiles the models using these procedures.

- SCS Runoff Curve Number
- Richards infiltration equation
- Philip's infiltration equation
- Smith and Parlange infiltration method
- Green and Ampt infiltration equation
- Horton's Infiltration equation
- Modified Holton-Overton infiltration equation
- Initial loss and constant rate

Table 1. Models using different rainfall excess (infiltration) simulation procedures

SCS runoff curve number	*Richard's equation*	*Philip's equation*	*Smith and Parlange procedure*	*Green and Ampt equation*	*Horton's equation*	*Modified Holton-Overton eq.*	*Initial and constant rate loss*
AGNPS	GSSHA (optional)	HSPF	DWSM (optional)	DR3M	SWMM	ANSWERS	HEC-HMS (optional)
DWSM	MIKE SHE		KINEROS	GSSHA	MIKE URBAN (optional)		MIKE URBAN
HEC-HMS				HEC-HMS (optional)			
SEDIMOT III				PRMS			
SWMM (optional)				SWMM (optional)			
TR-55							

The curve number is a rainfall excess procedure, lumps all the factors (soil, land cover, and initial moisture) responsible for rainfall losses and, therefore, is the simplest, most efficient, and more popular method, and has been for more than half a century. Use of infiltration equations

involves estimating losses due to interception at canopy and ground covers and depression storages separately in addition to estimating empirical parameters present in most of these equations.

The initial loss and constant rate infiltration is a rough method of computing rainfall losses, infiltration, and excess rainfall. With the exception of this method, the remaining methods are physically based and practically result in almost the same or similar infiltration and rainfall excess values. For example, Borah et al. (2002) found similar results from SCS runoff curve number and Smith and Parlange procedure on a 100-km^2 watershed in Illinois, and King et al. (1999) found no significantly different results from curve number and Green and Ampt equation on a 21-km^2 watershed in Mississippi.

Flow Routing

Once the rainfall excess is determined, a hydrograph is developed by routing the excess rainfall (runoff) to a common point in the watershed. Flow routing is primarily responsible for accounting the dynamics of a watershed (i.e., the dynamic movement of water) in a model. A model's performance and applicability are largely dependent on speed and accuracy of the flow routing procedure used.

Different levels of flow routing procedures and formulations are used in the models for overland and channel flows, which are all listed below. Table 2 compiles the models with procedures or equations for routing overland runoff and Table 3 ranks those based on relative complexities and accuracies of the equations and/or their solutions. Similarly, Tables 4 and 5, respectively, compile and rank the procedures or equations for channel flow routing.

- Dynamic Wave Equations: Numerical solution
- Diffusive Wave Equations: Numerical solution
- Kinematic Wave Equations: Analytical, shock-fitting, and numerical solutions
- Nonlinear Reservoir Equations
- Muskingum Method
- Unit Hydrograph Method
- Synthetic Unit Hydrograph Methods:
    - Snyder Unit Hydrograph
    - SCS Unit Hydrograph: TR-55 Method
    - Clark's Unit Hydrograph
- Time-Area Histogram
- The Rational Method: Peak Flow Formula

The basic flow-governing equations are the dynamic wave equations, also known as the St. Venant equations, consisting of the continuity and momentum equations for shallow water flows. These are the most physically-based flow routing equations available. However, there is no analytical solution to these equations which require the use of approximate numerical solutions. This requirement causes complexities and challenges with numerical instabilities and errors. Only a few of the models use these equations for routing flows in channels or pipes (Table 4). In order to obtain relief from the solution complexities, approximations are used to eliminate some of the terms and simplify the dynamic wave equations.

Table 2. Models using different overland runoff routing procedures

Diffusive wave equations (numerical solution)	*Kinematic wave equations: numerical solution*	*Kinematic wave equations: analytical solution*	*Nonlinear reservoir equations*	*Unit hydrograph*	*SCS unit hydrograph: TR-55 method (synthetic)*	*Time-area histogram*	*Rational formula or its modifications*
GSSHA	HEC-HMS (optional)	DR3M	ANSWERS	HEC-HMS (optional synthetic: Snyder & Clark)	HEC-HMS (optional)	MIKE URBAN	AGNPS
MIKE SHE	KINEROS	DWSM	HSPF	MIKE URBAN (optional: Snyder)	MIKE URBAN (optional)		
	PRMS		SWMM	SEDIMOT III (synthetic: gamma function)	TR-55		
			MIKE URBAN (optional)				

Table 3. Relative complexity (x-axis) versus accuracy (y-axis) of the overland runoff routing procedures of models

7							**GSSHA MIKE SHE**
6					**DR3M DWSM**		
5						**HEC-HMS KINEROS PRMS**	
4				**ANSWERS HSPF MIKE URBAN SWMM**			
3			**SEDIMOT III**				
2		**TR-55**					
1	**AGNPS**						
	1	2	3	4	5	6	7

Table 4. Models using different channel or pipe flow routing procedures

Dynamic wave equations (numerical solution)	*Diffusive wave equations (numerical solution)*	*Kinematic wave equations: numerical solution*	*Kinematic wave: analytical & shock-fitting*	*Muskingum method*	*Nonlinear reservoir equations*	*Rational formula or its modifications*	*Other methods*
GSSHA (optional for mild channels)	GSSHA	DR3M	DWSM	HEC-HMS	ANSWERS	AGNPS (included in overland cells)	HSPF (outflow is a function of reach volume or demand)
MIKE URBAN	MIKE SHE	HEC-HMS (optional)		SEDIMOT III	HEC-HMS (Modified Puls; optional)		TR-55 (SCS unit hydrograph or TR-55 method)
SWMM	MIKE URBAN (optional)	KINEROS					
		MIKE URBAN (optional)					
		PRMS					
		SWMM (optional)					

Table 5. Relative complexity (x-axis) versus accuracy (y-axis) of the channel or pipe flow routing procedures of models

9									**MIKE URBAN SWMM**
8								**GSSHA MIKE SHE**	
7						**DWSM**			
6							**DR3M HEC-HMS KINEROS PRMS**		
5					**SEDIMOT III**				
4				**HSPF**					
3			**ANSWERS**						
2		**TR-55**							
1	**AGNPS**								
	1	2	3	4	5	6	7	8	9

The next simplified flow governing equations are the diffusive wave equations derived by ignoring the local and convective acceleration terms of the momentum equations. These equations do not have analytical solutions and must be solved using approximate numerical procedures. A few of the models use these equations to route overland and channel flows (Tables 2 and 4).

The most simplified form of the dynamic wave equations are the kinematic wave equations derived by ignoring the pressure term as well from the momentum equation. Quite a few models use these equations (Tables 2 and 4). The kinematic wave equations have the advantage of having an analytical solution by the method of characteristics, although limited by shocks under shock-forming conditions, where the solution is no longer valid. Therefore, some models (Tables 2 and 4) use approximate numerical solution to solve the equations, where the shock is not an issue. These models do not get the benefits of the analytical solution in terms of accuracy and speed. DR3M uses the analytical solution where shocks are not present, generally on overland surfaces, but use approximate numerical solution to other conditions, mostly channels. DWSM is the only model that uses the analytical solution in both overland and channel flow routings by introducing an approximate shock-fitting solution to simulate under shock-forming conditions, which occurs when there is a sudden change of channel grade from steeper to flatter and only during a narrow sharp rising part of the hydrograph.

The next level of physically-based flow routing equations are the nonlinear reservoir equations where the spatial variation is ignored assuming leveled water surface. A number of models use these to route overland flows (Table 2) and a few for channel flows (Table 4). The Muskingum method, used only for channels by a few of the models (Table 4), is also based on mass conservation and uses empirical factors determined from observed flows.

The remaining methods (unit hydrographs, time-area histogram, and the rational formula) are empirical based on historical events. These methods have been traditionally useful for predicting flow hydrographs in rural watersheds with limited data and practically no change in hydrologic or land use characteristics, however, have limited use in modern watersheds undergoing rapid land use changes or urbanization.

Based on the physical basis of the equations and relative complexities and expected accuracies of the solutions or methods used, the models are ranked in two 2-dimensional matrices, one for the overland runoff routing (Table 3) and the other for channel flow routing (Table 5). These two matrices provide comparisons of some basic but critical facts about the models in relative orders (scale of 1-7 for overland and 1-9 for channel) and should be useful to modelers and managers. These show strengths and weaknesses of the models in these two critical operations. For example, watersheds having large-sized overland units, the comparisons in Table 3 would be useful to determine expected performance of a model relative to the others. Similarly, watersheds having long channel units or segments, the comparisons in Table 5 would be useful to determine expected performance of a model relative to the others.

Subsurface Flow

Only half of the models reviewed have a subsurface flow simulation component. The procedures or equations used by the models are listed below. Table 6 compiles the models using these procedures. It also lists the models having no subsurface flow component.

- 3-D Groundwater Flow Equation
- 2-D Groundwater Flow Equation
- Kinematic Storage Equation
- Huggins and Monke Drainage Equation

- Baseflow Recession Curve

Table 6. Models using different subsurface flow simulation procedures

3-D groundwater flow	*2-D groundwater flow*	*Kinematic storage equation*	*Huggins and Monke drainage*	*Baseflow recession curve*	*Other methods*	*None*
MIKE SHE	GSSHA	DWSM	ANSWERS	HEC-HMS	HSPF (empirical relations)	AGNPS
					MIKE URBAN (MOUSE RDI license: linear reservoir)	DR3M
					SWMM (mass balance and empirical fluxes)	KINEROS
						PRMS
						SEDIMOT III
						TR-55

There are vast differences between these procedures from 3-D groundwater flow equation to baseflow recession curve. However, the procedures go along with the respective models and accuracies of their other hydrologic and hydraulic simulation procedures. A model having one of these procedures has a distinct advantage over the models not having one in capturing the subsurface flows or base flows into the total stream flow, which are critical, and also by better representing the hydrologic cycle.

Summary and Conclusions

The rainfall excess (runoff), flow routing, and baseflow components of fourteen watershed models were evaluated resulting in the development of six summary tables which compiled the modeling procedures, and ranked and compared the models based on accuracies and complexities of the model equations and the solution methods used.

With the exception of the approximate initial loss and constant rate infiltration procedure, the remaining methods for determining rainfall excess are physically based. If properly used, they will generate similar results.

The flow routing procedures are the backbones of any watershed simulation model, and ultimate performance of a model depends largely on accuracies and speed of these procedures. Therefore, the models were ranked based on the formulations, their solution procedures, relative complexities, and accuracies used in routing overland runoff and channel flows.

Only half of the models reviewed have a subsurface flow simulation component. There are large differences between procedures used in subsurface flow simulation although a model having one of the procedures has a distinct advantage over any model not having one. Capturing the subsurface or base flows into the total stream flow allows better representation of the hydrologic cycle, a natural process.

The compilations and the rankings shown in the above sections will be helpful to managers and modelers for understanding the models, comparing those, selecting the most suitable model for a project or an application, and using it to its fullest potential.

The model comparison approach and the tools (tables) introduced would be useful to allow objective comparison of other models simply by placing those into the respective tables. Such an approach has been adopted by the Watershed Assessment Model (WAM) peer review panel by adding WAM into Borah and Bera's (2003) comparison table (T. Donigian, personal communication, December 30, 2008).

Acknowledgements

The authors wish to acknowledge the support of Woolpert, Inc. for this investigation and publication. They wish to express their sincere appreciation to Clarence Robbins, Senior Vice President, Woolpert, for his support and encouragement. The views expressed here are solely of the authors and mention of product names does not reflect endorsement.

References

Alley, W.M., and P.E. Smith, 1982a. Distributed Routing Rainfall-Runoff Model: Version II. U.S. Geological Survey Open-File Report 82-344, 201 p.

Alley, W.M. and P.E. Smith, 1982b. Multi-Event Urban Runoff Quality Model. U.S. Geological Survey Open File Report 82-764, 169 p.

Barfield, B. J., J. C. Hayes, E. Stevens, S. L. Harp, and A. Fogle. 2006. SEDIMOT III Model. Chapter 16 in *Watershed Models*, V. P. Singh and D. K. Frevert, eds., CRC Taylor and Francis, Boca Raton, Fla.: 381-398.

Beasley, D. B., L. F. Huggins, and E. J. Monke. 1980. ANSWERS: A model for watershed planning. *Transactions of the ASAE* 23(4): 938-944.

Bicknell, B. R., J. C. Imhoff, J. L. Kittle Jr., T. H. Jobes, and A. S. Donigian, Jr. 2001. *Hydrological Simulation Program - Fortran: HSPF Version 12 User's Manual*. U.S. Environmental Protection Agency, Athens, Ga; Model available at: www.epa.gov/waterscience/basins/bsnsdocs.html#hspf. Accessed 15 December 2008.

Borah, D.K. and M. Bera. 2003. Watershed-scale hydrologic and nonpoint-source pollution models: Review of mathematical Bases. *Transactions of the ASAE* 46(6): 1553-1566.

Borah, D.K. and M. Bera. 2004. Watershed-scale hydrologic and nonpoint-source pollution models: Review of applications. *Transactions of the ASAE* 47(3): 789-803.

Borah, D. K., R. Xia, and M. Bera. 2002. DWSM - A dynamic watershed simulation model. Chapter 5 in *Mathematical Models of Small Watershed Hydrology and Applications*, V. P. Singh and D. K. Frevert, eds., Water Resources Publications, Highlands Ranch, Colo.: 113-166.

Borah, D.K., J.H. Weist, J.D. Wall, and D.N. Powell. 2009. Watershed models for storm water management: Comparing hydrologic and hydraulic procedures. Manuscript under preparation for the *Transactions of the ASABE*.

Danish Hydraulic Institute (DHI). 2008. *MIKE URBAN Introduction to Data Management and Modeling of Urban Drainage and Collections Systems*. MIKE Courses, April 29-30, 2008, Tampa, FL. DHI Water and Environment, Horsholm, Denmark. Model information may be available at: http://www.dhigroup.com/Software/Urban/MIKEURBAN.aspx; accessed 16 December 2008.

Downer, C.W., F.L. Ogden, J. Neidzialek, and S. Liu. 2006. Gridded Surface/Subsurface Hydrologic Analysis (GSSHA) Model: A Model for Simulating Diverse Streamflow-Producing Process. Chapter 6 in *Watershed Models*, V. P. Singh and D. K. Frevert, eds. CRC Taylor and Francis, Boca Raton, Fla.: 131-157.

King, K.W., J.G. Arnold, and R.L. Bingner. 1999. Comparison of Green-Ampt and Curve number methods on Goodwin Creek watershed using SWAT. *Transactions of the ASAE* 42(4): 919-925.

Leavesley, G. H., and L. G. Stannard. 1995. The precipitation-runoff modeling system - PRMS. Chapter 9 in *Computer Models of Watershed Hydrology*, V. P. Singh, ed., Water Resources Publications, Highlands Ranch, Colo.: 281-310. Model information may be available at: http://water.usgs.gov/software/prms.html, accessed December 16, 2008.

Muñoz-Carpena, R., G. Vellidis, A. Shirmohammadi, and W. W. Wallender. 2006. Evaluation of modeling tools for TMDL development and implementation. *Transactions of the ASABE* 49(4): 961-965.

Obropta, C.C. and J.S. Kardos. 2007. Review of urban stormwater quality models: Deterministic, stochastic, and hybrid approaches. *Journal of the American Water Resources Association* 43(6): 1508-1523.

Refsgaard, J. C., and B. Storm. 1995. MIKE SHE. Chapter 23 in *Computer Models of Watershed Hydrology*, V. P. Singh, ed. Water Resources Publication, Highlands Ranch, Colo.: 809-846. Model information may be available at: http://www.dhigroup.com/Software/WaterResources/MIKESHE.aspx; accessed 16 December 2008.

Rossman, L.A. 2007. *Storm Water Management Model User's Manual Version 5.0*. Report No. EPA/600/R-05/040. U.S. EPA National Risk Management Research Laboratory, Cincinnati, OH. Information may be available at http://www.epa.gov/ednnrmrl/models/swmm/index.htm, accessed December 17, 2008.

Shoemaker, L., T. Dai, J. Koenig, and M. Hantush. 2005. TMDL model evaluation and research needs. EPA/600/R-05/149. U.S. EPA, National Risk Management Research Laboratory, Cincinnati, Ohio. Available at: www.epa.gov/ORD/NRMRL/pubs/600r05149/600r05149.pdf. Accessed 11 December 2008.

USACE-HEC. 2002. *Hydrologic Modeling System, HEC-HMS: Applications Guide*. CPD-74C. U.S. Army Corps of Engineers, Hydrologic Engineering Center, Davis, CA. The model may be available at: http://www.hec.usace.army.mil/software/hec-hms/documentation/hms_applications.pdf. Accessed December 11, 2008.

USDA-SCS. 1986. *Urban Hydrology for Small Watersheds*. Technical Release 55, U.S. Department of Agriculture – Soil Conservation Service, Washington, D.C.

Woolhiser, D. A., R. E. Smith, and D. C. Goodrich. 1990. *KINEROS, A Kinematic Runoff and Erosion Model: Documentation and User Manual*. ARS-77. USDA Agricultural Research Service, Fort Collins, Colo.; Model may be available at: www.tucson.ars.ag.gov/kineros/. Accessed December 15, 2008.

Young, R. A., C. A. Onstad, D. D. Bosch, and W. P. Anderson. 1987. AGNPS, Agricultural nonpoint-source pollution model: A watershed analytical tool. Conservation Research Report No. 35. USDA, Washington, D.C..

Water Subdivision for Modeling

Theodore G. Cleveland[1], Thuy Luong[2], , and David B. Thompson[3]

1. ABSTRACT

Rainfall-Runoff models, such as Hydrologic Modeling System (HEC-HMS), Stormwater Management Model (SWMM), etc., are used for predicting the hydrologic response of watersheds. An issue that to be addressed by users of these models is the estimate of an appropriate level of watershed subdivision for simulating runoff. The size and number of subwatersheds can affect a watershed modeling process and subsequent results.

The research reported herein is exploration to evaluate the effect of various levels of watershed subdivision on simulated runoff hydrographs. The HEC-HMS program was applied to five watersheds in Central Texas with drainage areas that varied from 12.3 to 166 square miles. Each of the five watersheds is near one of the following urban areas: Austin, Dallas (the rural watershed studied is close to Dallas), Fort Worth, San Antonio.

In this study, the models were intentionally left uncalibrated, thus the subdivision specification is the result of application of engineering hydrologic modeling practice, as would occur when modeling ungaged watersheds. Watershed subdivision was performed using an iso-area arrpoach where each contributing subdivision contained roughly the same area. The results of the HEC-HMS analysis indicated that the number of subwatersheds had little effect on computed runoff hydrographs.

No consistent pattern emerged as to whether lumped or multiple subbasins produce superior results; thus, the appropriate level of subdividing a watershed is still unanswered by this study.

2. INTRODUCTION

One routine task associated with hydraulic design is the delineation of the watersheds and subsequent computation of the watershed characteristics such as drainage area, main channel length, main channel slope, and etc. After this task is completed, the engineer must decide if the watershed should be further subdivided into smaller components, referred to as subwatershed or sub-basins. The sub-basin parameters are then input into a hydrologic model to develop runoff hydrographs.

[1]Department of Civil and Environmental Engineering, Texas Tech University, Lubbock, Texas 79404. email: theodore.cleveland@ttu.edu (corresponding author)
[2]Texas Department of Transportation, 7600 Washington Avenue, Houston, Texas 77007,email: tluong@dot.state.tx.us
[3]R.O. Anderson Inc., 1603 Esmerelda Blvd., Minden, Nevada 89423. email: dthompson@roanderson.com

The ability of a model to simulate the watershed systems depends on how well the watershed system is described by model input parameters. In a lumped hydrologic model, the watershed is assumed homogeneous with representative parameters. However, the size of the watershed affects the homogeneity assumption, because larger watersheds are more likely to have variable conditions within the watershed. Subdividing a watershed into smaller sub-watersheds would certainly increase the input data preparation effort. In practice, subdividing watershed into smaller components might or might not produce more accurate model results compared to measured, that is observed, streamflow from the watershed. On the other hand, modeling a large watershed as a single lumped model might lead to poor simulation results. Thus, the art of watershed subdivision remains an unsolved problem facing hydrologists wood1988and civil engineers.

Hromadka (1986) developed an application manual for hydrologic design for San Bernardino County. In that manual, mechanics were developed based on the Los Angeles hydrograph method. The manual states:

> Arbitrary subdivision of the watershed into subareas should generally be avoided. The fact is that an increase in watershed subdivision does not necessarily increase the modelling accuracy but rather transfers the models reliability from the valiated unit hydrograph and lag relationships to the unknown reliability of the subsequent flow routing submodels used to link together the divided subareas.

Hromadka (1986) further suggests that subdivisions should be about the same size[4].

Wood et al. (1988) examined the relation between watershed scale and watershed runoff on the 6.5 mi2 Coweeta River experimental watershed located in North Carolina. Their study was to determine the representative elemental area (REA) for the Coweeta River watershed. They divided the Coweeta River watershed into 3, 19, 39, and 87 subwatersheds. They reported that for a drainage area less than 0.4 mi^2, subwatershed response was highly variable. However, at scales greater than about 0.4 mi^2, further aggregation of subwatersheds had little impact of simulated results.

Norris and Haan (1993) studied the impact of watershed subdivision on hydrographs estimated using the Natural Resources Conservation Service (NRCS) unit hydrograph procedure, as implemented in HEC-1. The Little Washita watershed near Chickasha, Oklahoma, was subdivided into 2, 5, 10, and 15 sub-watersheds, as well as treating the watershed as a whole. Results were that watershed subdivision had a pronounced impact on the estimate of peak flow from the watershed. The change from a single watershed to 5 sub-basins resulted in a net increase in peak discharge of about 30 percent. Use of 15 sub-basins increased the difference from a single watershed to about 40 percent. However, the impact of subdivision

[4]The manual states a desirable area ratio of subdivisions — not iso-area, but suggestive of that classification.

diminished with further increase of sub-basins. They concluded that the number of sub-basins for simulating watershed response should not vary through the course of a hydrologic study. Guidance as to how many subdivisions to use was left unanswered.

Michaud and Sorooshian (1994) applied three different model formulations to simulate the rainfall-runoff process for Walnut Creek Gulch in Arizona. They concluded that simpler models[5] appear to perform better than more complex approaches.

Mamillapalli et al. (1996) conducted a study of the impact of watershed scale on hydrologic output. They concluded that, in general, increase of the level of discretization and the number of soil and land use combinations resulted in an increase of the level of accuracy. There is a level of discretization beyond which the accuracy cannot be further improved. Their work suggests that more detailed simulation may not always lead to better results.

Bingner et al. (1997) attempted to determine the degree of watershed subdivision required to achieve reasonable results in predicting watershed runoff and sediment yield of the Goodwin Creek Watershed. A suite of subdivisions was generated with elemental areas that ranged from a maximum of 60 acres to a minimum of 4 acres to model runoff and sediment yield. The authors concluded that model predicted runoff volume was not heavily dependent on the degree of watershed subdivision, however, the model predicted sediment yield did depend on the degree of watershed subdivision.

Fitzhugh and Mackay (2000) conducted a similar study and reported that model predicted watershed runoff was not heavily dependent on the degree of subdivision , but the predicted sediment yield dependened on the degree of subdivision.

Jha et al. (2002) examined the relation between watershed subdivision and water- quality model results. He applied the SWAT model to four Iowa watersheds. Jha (2002) reported that streamflow was not significantly affected by a decrease in sub-watershed scale, where model predicted results stabilized with about ten subdivisions. However, model predicted sediment yields were more dependent on sub-watershed scale, requiring 40-50 divisions to stabilize model predicted sediment yield.

Tripathi et al. (2006) studied the Nagwan watershed in eastern India. The watershed was subdivided into 12 and 22 sub-watersheds, as well as treating the entire watershed as a whole. They found little difference in watershed runoff for different number of sub-watersheds used, however, they did observe variations in other components of the hydrologic cycle.

Nearly all these prior efforts suggests an insensitivity of runoff volume to the level of watershed subdivision. The principal input to the watershed, precipitation, is typically measured at point gages, which measure the rainfall field over an eight-inch diameter (if a standard rain gauge is used) region. In contrast, measurements from a stream gage reflect the integrated

[5]Few subdivisions

response of the watershed to the rainfall field and all of the processes that act as rainfall become runoff. The two phenomena and their measurements are inherently different in magnitude, method, and meaning, so the insensitivity is not completely unanticipated.

Synthesis of these and other references suggests the following approaches to as ways to model watershed subdivision (in the absence of obvious natural features and flow regulation structures):

(1) An iso-characteristic approach, where each sub-basin has about the same physical characteristic (area, length, etc.). Drainage area ratios would fall into this approach. The characteristics may be subtlesome authors have used contiguous areas of similar slope to define watershed subareas. The San Bernardino (1986) manual seems to imply a range of area ratios that are acceptable for preserving sufficient model believability, again a spatial characteristic based concept.

(2) An iso-temporal approach, where each sub-watershed is selected to have about the same characteristic response time, that is, tc. This particular approach may have great value in concurrent flooding (concurrent arrival times of flood waves). A challenge of this conceptualization is that lumped systems will necessarily be replaced by routed systems and any gain in certainty by using smaller sub-basins may be more than offset by increased uncertainty caused by routing.

(3) A scoring approach: Scoring is similar to the above concepts, except a set of characteristicsis assigned a score; similar scores that are geographically connected are selected as watersheds. The scoring approach could admit descriptors not easily quantified numerically.

(4) A gage-defined approach where the locations of existing gages are used to subdivide a watershed not necessarily a modeling tool, but a good comparative tool. An extension would be to locate good gage locations based on measuring requirements and use these locations to divide a watershed.

(5) Stream-order/bifurcation approach. Watersheds are subdivided based on branches in the dendritic drainage network. This approach is arguably a scoring approach.

(6) The ad hoc approach is a research-only approach where basins would be defined at random subareas, perhaps preserving some minimum measure.

3. METHODOLOGY

This research examined an iso-characteristic approach based on sub-basin areas. Area is the principal scale measure common in all hydrologic studies; it is usually always computable. The report by Roussel et al. (2006) illustrated that different analysts, and diferrent methods (manual, automated) compute areas to within 10% of one another; thus, area represents a reasonably consistent metric regardless of analysts involved.

Five sets of watersheds in Central Texas with USGS streamflow-gaging stations were selected for this study: Onion Creek, South Mesquite, Little Fossil, Olmos Creek, and Trinity Basin North. The supporting data include 30-meter DEM information, and a database of incremental cumulative rainfall and runoff values for storms that occurred during the period from 1961 to 1986.

Paper-based USGS quadrangle maps (1:24000 scale) containing the watershed were used for watershed delineation. To subdivide the selected watersheds into 3, 5, and 7 sub-basins, locations of the sub-basin outlets were chosen. The drainage area upstream of the outlet was measured by planimeter. The outlet locations were adjusted until the individual sub-basin areas are about the same[6].

Figure 1 is one example of the subdivision approach applied to the Trinity-North watershed. Similar subdivisions were produced for the other study watersheds. In all the study watersheds, there was an actual configuration where gages were "nested" — this configuration was one of two "validation" configurations used in the study[7].

A discussion of "about the same" is in order. The subdivision process was manual, using paper maps and a mechanical planimeter. Iso-area subdivision is non-trivial and small movements of subdivision outlets on the map, required re-delineation. A particular challenge was the treatment of tributaries to the main channel. In many cases inclusion of a tributary in one sub-basin contributed too much area to that sub-basin and made exact equal area delineation practically impossible. This experience alone suggests that prior works that used stream bifurcation rules encountered similar issues and the author speculates that this division challenge is in-part why these [bifurcation] schemes exist.

Models of the watersheds, with varying degrees of subdivision (lumped, 3, 5, and 7 sub-basin models) were built using HEC-HMS. The runoff generation component used the NRCS CN procedure because CN values were available for these watersheds from prior studies. The routing component, where used, was lag routing chosen for (1) simplicity and (2) because the length of the sub-reaches for the study sub-basins are small enough that routing tends towards pure translation. The routing times were estimated using the Kirpich method reported in Roussel et al. (2006), where the distance is the Euclidean distance from the sub-basin outlet to the next element (into which the flow is routed). The translation method (time redistribution of runoff from the runoff generation procedure) used the Dimensionless Unit Hydrograph (NRCS-DUH) parameterized by the Kerby-Kirpich method reported in Roussel et al. (2006).

[6]The use of manual methods was intentional — automated technology certainly can accelerate the process, however the manual effort teaches the analyst a lot about the watershed in the process of preparing the input data.

[7]Lumped was the other validation configuration.

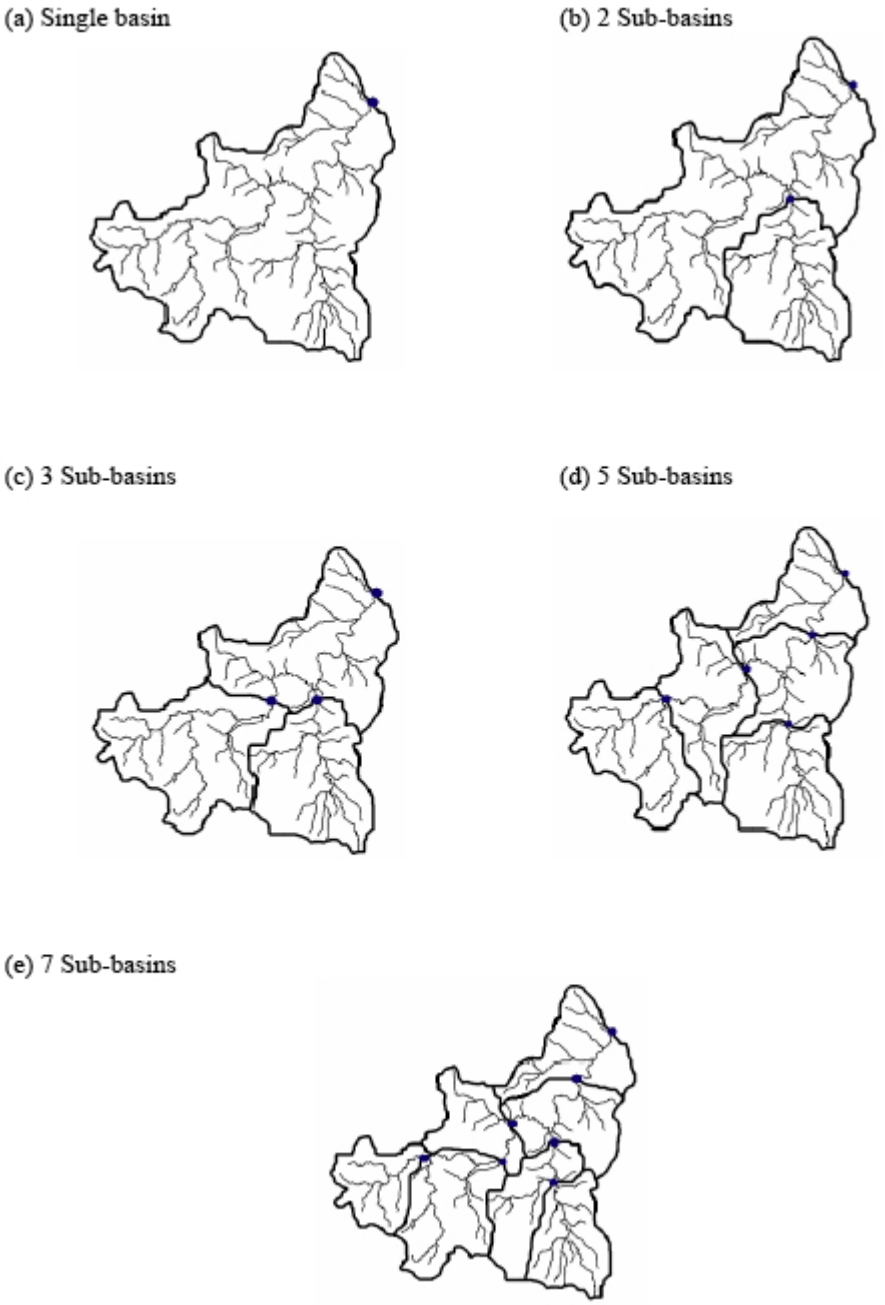

FIGURE 1. Representative basin subdivisions for Trinity-North watershed. The 2-Basin representation is not iso-area; gage locations are "actual" locations for this configuration on the watershed. Remaining subdivisions are approximately iso-area. Adapted from Luong (2008).

4. RESULTS AND INTERPRETATION

The various watershed models were operated and discharges computed by the model were compared to observations and evaluated using selected measures of error. The arithmetic mean relative error, relative root-mean-square error, and an acceptance criteria measure(Cleveland et al., 2006) were used to evaluate the different subdivision scheme performance. Figures 2, 3, and 4 are tabulations of these various metrics as applied to the results from the study watersheds.

Watershed	Peak Discharge	No. Subdivisions					Selected No. Subdivisions
		1	2	3	5	7	
Onion	*AVG (%)*	200.06	285.30	324.68	281.96	331.20	1
	RRMSE (%)	233.08	294.30	366.57	313.13	367.94	1
	MIN_COUNT	2	0	0	0	0	1
South Mesquite	*AVG (%)*	9.67	5.00	16.04	27.63	9.13	2
	RRMSE (%)	16.47	12.09	20.78	32.53	14.50	2
	MIN_COUNT	2	3	1	0	0	2
Little Fossil	*AVG (%)*	78.52	98.97	85.48	123.41	97.63	1
	RRMSE (%)	189.92	214.92	203.43	258.12	224.63	1
	MIN_COUNT	5	2	0	2	0	1
Olmos	*AVG (%)*	244.10	240.92	246.95	149.12	261.98	5
	RRMSE (%)	333.61	331.35	367.80	239.54	382.17	5
	MIN_COUNT	0	0	1	6	0	5
Trinity North	*AVG (%)*	14.42	22.96	17.70	28.83	10.06	7
	RRMSE (%)	72.22	72.90	67.85	74.15	62.77	7
	MIN_COUNT	2	0	0	3	4	7

FIGURE 2. Tabulation of metrics for peak discharge comparisons. Adapted from Luong (2008).

These tabular results of the various measures of model performance indicate that there is no single watershed division scheme that performed well for all observed storms on a particular watershed. The authors interpret this result as typical, and an implication is that there is no consistent pattern on whether lumped or multiple subbasins produce superior results using this quasi-iso area scheme. The models were not calibrated, however even when we calibrated one watershed to observations there was only a marginal change in results.

Watershed	Runoff Volume	No. Subdivisions					Selected No. Subdivisions
		1	2	3	5	7	
Onion	*AVG (%)*	520.10	432.31	465.07	467.38	465.56	2
	RRMSE (%)	662.52	538.34	586.73	589.33	587.29	2
	MIN_COUNT	0	1	1	0	0	2, 3
South Mesquite	*AVG (%)*	3.72	5.63	0.51	0.45	0.43	7
	RRMSE (%)	21.82	18.90	16.52	17.24	16.44	7
	MIN_COUNT	3	1	1	1	0	1
Little Fossil	*AVG (%)*	107.48	104.54	99.59	100.50	105.56	3
	RRMSE (%)	218.30	223.19	223.15	224.10	229.74	1
	MIN_COUNT	4	1	2	0	2	1
Olmos	*AVG (%)*	267.83	263.85	244.71	243.75	231.39	7
	RRMSE (%)	305.66	301.46	288.12	287.03	273.06	7
	MIN_COUNT	0	0	0	0	7	7
Trinity North	*AVG (%)*	33.34	20.22	20.01	17.96	18.29	5
	RRMSE (%)	87.92	72.62	68.93	67.81	68.00	5
	MIN_COUNT	0	1	4	4	0	3, 5

FIGURE 3. Tabulation of metrics for watershed runoff (volume) comparisons. Adapted from Luong (2008).

5. CONCLUSIONS

Runoff hydrographs that were developed for the Onion Creek, South Mesquite, Little Fossil, Olmos Creek, and Trinity Basin-North watersheds were used to determine the affects that number of sub-watersheds had on the runoff hydrographs. It was found that the increase in the number of sub-watersheds does not significantly affect the simulated runoff hydrograph (volume). This study also shows that none of the subdivision schemes were able to accurately simulate peak flows or runoff volumes from all individual events for each watershed.

In general, this study, as performed, indicates that unless the engineer needs internal flows, subdivision simply to gain accuracy does not justify the additional modeling effort.

Continued research is needed to ascertain if the results obtained in this study will change using a runoff generation model that is less sensitive to hyetograph behavior than the CN loss model, and with distributed rainfall observations.

Watershed	Time to Peak	No. Subdivisions					Selected No. Subdivisions
		1	2	3	5	7	
Onion	*AVG (%)*	26.80	22.98	18.74	29.77	25.01	3
	RRMSE (%)	33.45	25.20	23.32	32.40	27.11	3
	MIN_COUNT	0	0	2	0	0	3
South Mesquite	*AVG (%)*	2.76	2.30	0.12	2.77	3.87	3
	RRMSE (%)	9.10	10.09	8.49	11.05	11.96	3
	MIN_COUNT	1	1	1	1	2	7
Little Fossil	*AVG (%)*	6.79	2.03	11.56	12.15	10.18	2
	RRMSE (%)	10.64	13.55	34.91	25.62	23.02	1
	MIN_COUNT	1	5	1	0	2	2
Olmos	*AVG (%)*	15.15	15.87	13.34	8.30	8.49	7
	RRMSE (%)	21.61	23.13	17.27	11.84	10.68	7
	MIN_COUNT	0	0	1	2	4	7
Trinity North	*AVG (%)*	9.20	9.47	13.70	13.95	11.22	1
	RRMSE (%)	31.08	31.36	33.97	34.98	33.22	1
	MIN_COUNT	4	3	1	0	1	1

FIGURE 4. Tabulation of metrics for time of peak discharge comparisons. Adapted from Luong (2008).

6. ACKNOWLEDGEMENTS

The research reported herein was supported by the Texas Department of Transportation. Their financial support is greatly appreciated and acknowledged.

The authors further wish to acknowledge the guidance of their colleagues who contributed to this effort: G. R. Herrmann (Texas Department of Transportation), Matt Wingfield (Texas Department of Transportatin) , W. H. Asquith (U.S. Geologic Survey) , M. S. Roussel (U.S. Geologic Survey), and Xing Fang (Auburn University).

The contents of this report reflect the views of the authors who are responsible for the facts and the accuracy of the data presented herein. The contents do not necessarily reflect the official view of policies of the Texas Department of Transportation or the Federal Highway Administration. This report does not constitute a standard, specification, or regulation.

References

Bingner, R., J. Arnold, and R. Srinivasan (1997). Effect of watershed subdivision on simulation runoff and fine sediment yield. *Transactions of the Am. Soc. of Ag. Engineers 40*(5), 1329–1335.

Cleveland, T. G., X. He, W. H. Asquith, and D. B. Thompson (2006). Instantaneous Unit Hydrograph Evaluation for Rainfall-Runoff Modeling of Small Watersheds in North and South Central Texas. *ASCE J. of Irrigation and Drainage Engineering 132*(5), 479–485.

Fitzhugh, T. and D. S. Mackay (2000). Impacts of input parameter spatial aggregation on an agricultural nonpoint source pollution model. *Journal of Hydrology 236*, 35–53.

Hromadka, T. V. (1986). *San Bernardino county hydrology manual*. San Bernadino County.

Jha, M., P. W. Gassman, S. Secchi, R. Gu, and J. Arnold (2002). Effect of watershed subdivision on SWAT flow, sediment, and nutrient predictions. *Journal of the American Water Resources Association 40*(3), 811–825.

Luong, T. (2008). Subdivision of Watersheds for Modeling. Master's thesis, Civil and Envrionmental Engineering, University of Houston.

Mamillapalli, S., R. Srinivasan, J. Arnold, and B. A. Engel (1996). Effect of spatial variability on basin scale modeling. In *Third International Conference/Workshop on Integrating GIS and Environmental Modeling*, Santa Fe, New Mexico. National Center for Geographic Information and Analysis.

Michaud, J. and S. Sorooshian (1994). Comparison of simple versus complex distributed runoff models on a midsized semiarid watershed. *Water Resources Research 30*(3), 593–605.

Norris, G. and C. T. Haan (1993). Impact of subdividing watersheds on estimated hydrographs. *American Society of Agricultural Engineers ; Soil and Water Division 9*(5), 443–445.

Roussel, M. C., D. B. Thompson, X. Fang, T. G. Cleveland, and C. A. Garcia (2006). Timing-parameter estimation for applicable texas watersheds. Research Report TechMRT Report 0-4696-2, Texas Department of Transportation.

Tripathi, M. P., N. S. Raghuwanshi, and G. P. Rao (2006). Effect of watershed subdivision on simulation of water balance components. *Hydrological processes 20*, 1137–1156.

Wood, E. F., M. Sivapalan, K. Beven, and L. Band (1988). Effects of spatial variability and scale with implications to hydrologic modeling. *Journal of Hydrology 102*, 29–47.

Integrated Watershed Modeling

Gour-Tsyh (George) Yeh[1] (407-823-2317, gyeh@mail.ucf.edu)
Guobiao Huang[2] (561-697-8151, ghuang@sutron.com)
Hsin-Chi (Jerry) Lin[3] (601-634-3023, Hsin-chi.J.Lin@usace.army.mil)

[1]Department of Civil and Environmental Engineering, University of Central Florida, 4000 Central Florida Blvd., Orlando, FL 32816-2450, USA
[2]Sutron Corp., 6903 Vista Parkway, West Palm Beach, FL 33411
[3] Engineering Research and Development Center, US Army Corps of Engineer, 3309 Halls Ferry Road, Vicksburg, MS 39180

Abstract

In the past 30 years, lumped-parameter watershed models have been employed for integrated surface water and groundwater modeling to calculate surface and base runoffs. Physics-based, process-level models that employ consistent sets of governing equations for integrated overland, river, vadose, and groundwater flow have been practically nonexistent until early 1990s. This paper presents the development of an integrated media, physics-based watershed model. Complete coupling simulations among system components of land surfaces, river networks, vadose zones, and groundwater or partial couplings between any two components can be conducted with the model. Various rigorous coupling strategies based on physics and numerics for interactions among these components are described. Two examples were employed to discuss the issues of coupling. One was used to demonstrate differences and implications between continuity and linkage approaches when the surface water and groundwater are in direct connection. Another one, a watershed modeling in Florida, was used to illustrate that complete and partial couplings yield quite different simulations.

1. Introduction

The design of watershed simulators for fluid flows and scalar (e.g., thermal, turbulent energy, dissipation energy, salinity, sediment, water quality, et cetera) transport to analyze response and behavior of a watershed is probably the classic problem in watershed modeling. An extensive review on available simulators and their applications to watershed modeling by practitioners was made in late 1990s (EPA, 1997). These simulators can be classified into two broad groups: parametric-based approaches and physics-based approaches. There are numerous advantages in a physics-based approach. The parameters of the governing equations are the properties of the system media and can be independently determined from physics. As a result, the scaling up or down of a problem is not an issue and extrapolation can be made with confidence as long as the continuum treatment is valid. Repeated calibration of physics-parameters is not necessary although some kinds of

fine-tuning may be required. On the other hand, for the parametric-based approaches, parameters in the working equations are non-physics and they must be repeatedly calibrated for each individual application. The scaling up or down of a problem is problematic and involves numerous types of parameters. The single greatest advantage of parametric-based approaches is their ability to generate numerical results regardless if they are correct or not. This is perhaps the major reason why such approaches, for example HSPF (Bicknell et al., 1993), have dominated watershed modeling in the past four decades since the development of Stanford Watershed Model IV (Crawford and Linsley, 1966).

A watershed includes multiple system-components of river/stream networks, land surface, reservoirs/lakes, and subsurface media of vadose and saturated zones. It encompasses multiple processes of fluid flows and transport of thermal energy, salinity, sediment, and water quality, et cetera. From the EPA compilation (EPA, 1997), only the Hydrologic Smulation Program Fortran (HSPF) or similar parametric-based (lumped parameter) simulators have the design capabilities to deal with the complete system-components in a watershed. Also, only these types of simulators have encompassed the complete suite of fluid flow and scalar transport processes.

There have been tremendous progresses in first principle, physics-based modeling of flow and transport processes in partial system-components. Subsurface flow codes based on Richards' equations have been developed and applied to the prediction of various types of subsurface runoffs. Many overland computer codes based on two-dimensional St Venant equations have been developed for the computation of overland flow and surface runoff. Numerous stream flow codes based on one-dimensional St Venant equations have been developed for the prediction of stage and discharge as functions of time and distance along the stream-river networks.

It is widely recognized that the coupling of system components among subsurface media, overland regime, stream/river networks, and reservoirs/lakes into a complete watershed simulator would be desirable. The development of first principle, physics-based watershed simulators that have the same design capabilities as parametric-based simulators has intensified since the middle of 1990s (Abbott, et al.,1986; Wigmosta and Perkins, 1997; Yeh et al., 1998; VanderKwaak, 1999; Ewen et al., 2000; HydroGeoLogic In., 2001; SFWMD,https://my.sfwmd.gov/portal/page?_pageid=1314,2556300&_dad=portal&_schema=PORTAL&navpage=home; Downer and Ogden, 2002; Swain, Langevin and wolfert, http://sofia.usgs.gov/projects/coupling/comptechnique_03geerab.html; SOBEK: http://delftsoftware.wldelft.nl/; Yeh et al., 2003, 2005, 2006). While these new generation watershed simulators have the potential to further the understanding of the fundamental biological, chemical and physical factors that take place in nature watersheds, and give mechanistic predictions, three key issues remain to be resolved: (1) Coupling among media, (2) applicability of kinematic, diffusive, and fully dynamic wave models, and (3) select of wave directions in multi-dimensional dynamic wave models. This paper focuses on addressing the first issue. From a physical point of view, the surface water and subsurface water can be considered in direct or indirect connection. Form a numerical point of view, the coupling can be conducted with fully coupling, alternatively iterative coupling, or time-lagged decoupling.

The consideration of surface water/subsurface water interactions consists of two parts: stream-aquifer interaction and overland-subsurface interaction. The stream-aquifer interaction has been extensively studied by coupling saturated groundwater flow with

one-dimensional channel flow (for example, Pinder and Sauer 1971; Swain and Wexler 1996; Hunt 1990, among others). The role of unsaturated zone on stream-aquifer interaction is rarely considered. The overland-subsurface interaction is usually studied in the context of runoff generation at the watershed scales (for example, Freeze 1972; Smith and Woolhiser 1971; Akan and Yen 1981; Abbott et al. 1986).

Recently, the physics-based coupling of surface and subsurface flows has been an active research topic. Panday and Huyakorn (2004) discussed the utility of different coupling schemes in a new watershed model and seemed to favor the conductance-type, linkage term approach. Favoring the continuity-of-pressure approach, Morita and Yen (2002) classified coupling approaches, from the numerical point of view, as fully coupled (simultaneous solution), alternating iterative coupling and externally coupling (decoupled). In their model, the concept of infiltrability was introduced. This term refers to the variable boundary conditions in numerical solution of Richards equation; however, a leakage term was used in the coupling process.

2. Coupling among Media

In the core of an integrated, physics-based watershed model is a study of coupling among surface water and subsurface water flows. In this study, we focus on physics-based coupling approaches that utilize partial differential equations both in surface water flow (Saint Venant equations) and variably saturated subsurface flow models (Richards equation). For simpler watershed models, the infiltration term is treated with an empirical algebraic equation; accordingly, the surface water/groundwater interaction computation is straightforward and independent of water flow solutions. Although the numerical solution of the Richards equation is computationally intensive and difficult at watershed scales, it is essential for a complete, physics-based representation of the subsurface flow.

The interaction between the surface water (SW) in river network, overland water (OW) in the land surface, and groundwater (GW) in subsurface media occurs at the interface between these domains. Depending on the mesh resolution and distribution of material properties, there are two types of connections on the SW-GW interface, as schematically displayed by Figure 1. If the distribution of soil property near the SW-GW interface can be fully resolved by the GW mesh, then the interface is termed a direct SW-GW connection. While, an indirect SW-GW connection refers to the situation where the soil property can not be resolved by the mesh, e.g. the GW mesh size is much larger then the thickness of a skin layer of clay/sediment. The direct and indirect connection can also be defined similarly on the OW-GW interface, see also Figure 1.

Mathematically, the continuity of flux and pressure are imposed at the interface for the direct connection. At the SW-GW interface, this condition is mathematically expressed as

$$h^r = h^s \quad and \quad q^r = \int_P \left[-\mathbf{n} \cdot \mathbf{K} \cdot \left(\nabla h^s + \nabla z \right) \right] dP \tag{1}$$

where h^r is the depth of the river [L], h^s is the pressure head of subsurface water [L], q^r is the seepage of groundwater to the river per unit river length [L^2/T], P is the wet perimeter of the river cross-section [L], $\mathbf{n}$ is the outward unit vector of the interface in the direction from groundwater to surface water, and $\mathbf{K}$ is the hydraulic conductivity of the

subsurface media [L/T]. At the OW-GW interface, it is expressed as

$$h^o = h^s \quad and \quad F^o = \mathbf{-n} \cdot \mathbf{K} \cdot \left(\nabla h^s + \nabla z \right) \tag{2}$$

where h^o is the depth of overland water [L] and F^o is the flux from groundwater to overland water [L/T].

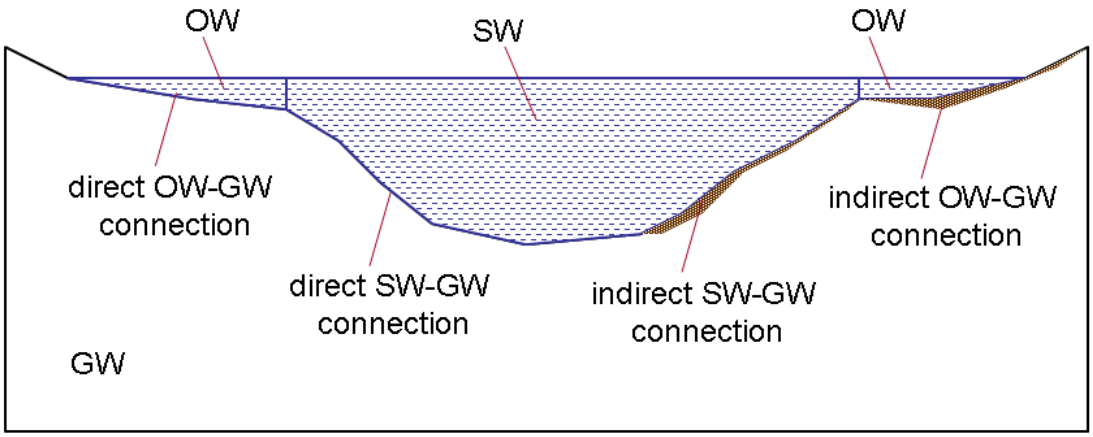

Figure 1 Direct and Indirect Connections on SW-GW and OW-GW interfaces

At the interface of an indirect connection, the mass exchanges between surface water and groundwater and between overland water and groundwater are formulated in terms of the differences of pressure between two media. At the SW-GW interface, the formulation is given as

$$\mathbf{-n} \cdot \mathbf{K} \cdot \left(\nabla h^s + \nabla z \right) = k(h^s - h^r) \quad and \quad q^r = \int_P k(h^s - h^r) dP \tag{3}$$

where k is the exchange coefficient [1/T]. It represents the hydraulic conductivity divided by the thickness of the layer that separate the surface water and groundwater but not included as part of the media. This is the coupling by the linkage term. Even when the media are in direct connection, many models (e.g., Panday and Huyakorn, 2004) still use this linkage approach to coupling. Under such circumstances, k is simply a non-physics fitting parameter. At the OW-GW interface, the formulation is similarly given as

$$\mathbf{-n} \cdot \mathbf{K} \cdot \left(\nabla h^s + \nabla z \right) = k(h^s - h^o) = F^o \tag{4}$$

Even in the case of indirect connection, it is still more rigorous to use the continuity approach than the linkage approach by including thin layer of the material as part of the non-heterogeneous subsurface media. However, computer demands and numerical convergence may be at issues (Huang and Yeh, 2009).

A different classification of coupling strategies is based on numerical schemes rather than physical-connection based mathematical formulation. A simple overland/subsurface flow-coupling example is used to illustrate the classification. As shown in Figure 2, in this simple example, there are 12 overland nodes and six elements in the two-dimensional

overland domain. The three-dimensional subsurface medium consists of 36 subsurface nodes and 12 elements. Finite element discretization of the continuity equation governing the overland flow would result in the following algebraic equations

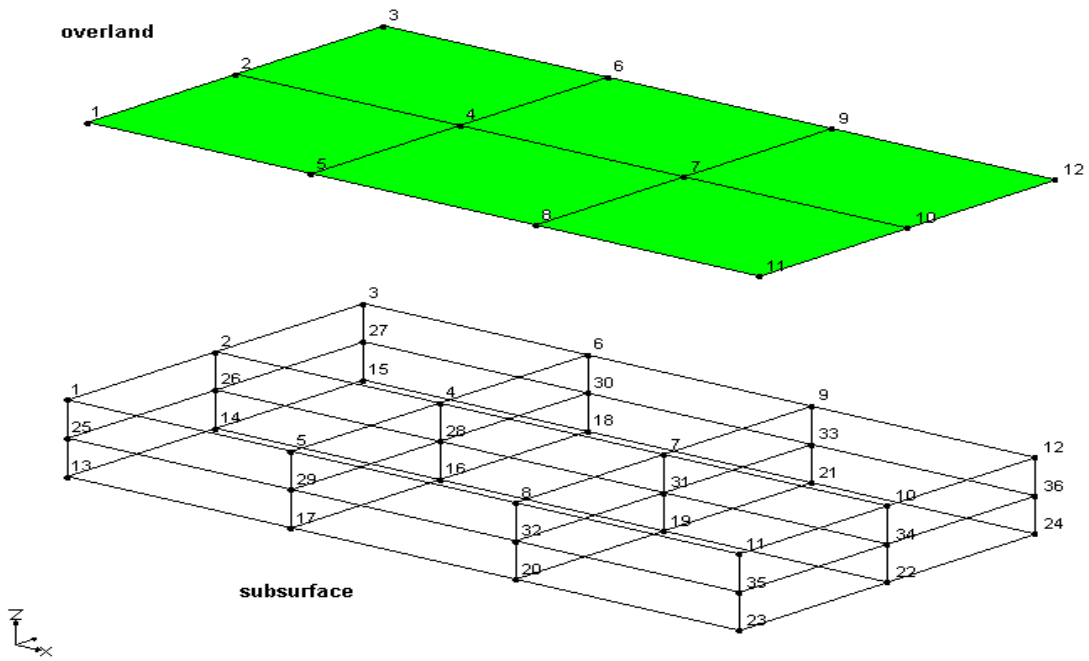

Figure 2: 2D Overland and 3D Subsurface Finite Element Mesh

$$\sum_{j}^{12} a_{ij}^{o} h_{j}^{o} = R_{i}^{o} + Q_{i}^{o},\ i = 1,2,..,12 \tag{5}$$

where a_{ij}^{o} is the coefficient matrix resulting from the discretization of the overland-flow equation; h_{j}^{o} is the water depth at the *j-th* overland node; R_{i}^{o} is the load of the *i-th* overland node resulting from initial condition, external source/sink, and global boundary conditions; and Q_{i}^{o} is the source at *i-th* overland node resulting from groundwater flux. Finite element discretization of Richards equation for subsurface flow would result in the following algebraic equations

$$\sum_{j=1}^{36} a_{ij}^{s} h_{j}^{s} = R_{i}^{s} - B_{i}^{s},\ i = 1,2,..,36 \tag{6}$$

where a_{ij}^{s} is the coefficient matrix resulting from the discretization of the subsurface-flow equation; h_{j}^{s} is the hydraulic head at the *j-th* subsurface node; R_{i}^{s} is the load of the *i-th* subsurface node resulting from initial condition, external source/sink, and global boundary conditions; and B_{i}^{s} is the boundary flux at the *i-th* subsurface node. It should be noted B_{i}^{s}

is zero for node that is not belong to the subsurface-overland overlapping nodes. In other word, the *i-th* nodal flux is zero ($B_i^s = 0$) when *i* is greater than 12 ($i > 12$) in this case.

For decoupled flow simulations, there are 12 overland-flow equations for 12 overland unknowns ($h_j^o,\ j = 1,2,..,12$) with 12 external sources ($Q_i^o,\ i = 1,2,..,12$) considered given; and 36 subsurface-flow equations for 36 subsurface unknowns ($h_j^s,\ j = 1,2,..,36$) with 12 boundary fluxes ($B_i^s,\ \mathrm{i} = 1,2,..,12$) considered prescribed. However, for a coupled flow simulation, the 12 overland external sources and 12 subsurface boundary fluxes, which result from the interaction between overland and subsurface flows, must also be considered unknowns. These 24 unknowns require 24 additional equations to close the system. These 24 equations are obtained from the interface conditions. Obviously, the continuity of interface fluxes provide 12 equations as follows

$$Q_i^o = B_i^s,\ i = 1,2,..,12 \tag{7}$$

The additional 12 equations can be obtained based on the physical condition of the interface. For a direct connection interface, the continuity of pressure at the interface would yield

$$h_i^o = h_i^s,\ i = 1,2,..,12 \tag{8}$$

For an indirect connection, the overland external source or the subsurface boundary fluxes must be formulated in terms of the properties of the material between two flow regimes. Incorporation of the boundary condition given by Equation (4) in the finite element approximation of flow equations would result in

$$Q_i = B_i^s = \mathrm{K}\left(h_i^s - h_i^o\right),\ \ i = 1,2,..,12 \tag{9}$$

In summary, there are 72 equations [12 in Eq. (5), 36 in Eq. (6), 12 in Eq. (7), and 12 in Eq. (8) or in Eq. (9)] for 72 unknowns [12 overland water depths, 36 subsurface pressure heads, and 24 exchange fluxes which compose of 12 overland source/sink terms, Q^o's and 12 subsurface boundary fluxes B^s's].

Nominally, solving the coupled flow problem can be considered as the simultaneous solution of these 72 algebraic equations. Three strategies have been employed in the literature: fully implicit scheme, iteratively implicit scheme, and time-lagged explicit scheme. Take the case of direct connection as an example, the fully implicit scheme solves 72 equations for 72 unknowns simultaneously as

$$\begin{gathered}\sum_j^{12} a_{ij}^o h_j^o = R_i^o + Q_i^o,\ i = 1,2,..,12;\ \ Q_i^o = B_i^s,\ i = 1,2,..,12 \\ h_i^s = h_i^o,\ i = 1,2,..,12;\ \ \sum_{j=1}^{36} a_{ij}^s h_j^s = R_i^s - B_i^s,\ i = 1,2,..,36\end{gathered} \tag{10}$$

The iteratively implicit scheme solves the overland flow unknowns and subsurface unknowns iteratively as

$$\sum_{j}^{12} a_{ij}^{o}(h_j^o)^{(k+1)} = R_i^o + Q_i^o,\ i = 1,2,..,12 \ \text{ with } \ Q_i^o = (B_i^s)^{(k)},\ i = 1,2,..,12 \qquad (11)$$

and

$$(h_i^s)^{(k+1)} = (h_i^o)^{(k+1)},\ i = 1,2,..,12;\ \sum_{j=1}^{36} a_{ij}^{s}(h_j^s)^{(k+1)} = R_i^s - \left(B_i^s\right)^{(k+1)},\ i = 1,2,..,36 \qquad (12)$$

where the superscript $(k+1)$ and (k), respectively, indicate the present iteration and previous iteration, respectively. The time lagged explicit schemes first solve the overland flow equation using subsurface flow information of previous time step, then solve the subsurface flow equations using the newly obtained overland flow water depth as the boundary conditions as

$$\sum_{j}^{12} a_{ij}^{o}(h_j^o)^{(n+1)} = R_i^o + Q_i^o,\ i = 1,2,..,12 \ \text{ with } \ Q_i^o = (B_i^s)^{(n)},\ i = 1,2,..,12 \qquad (13)$$

and

$$(h_i^s)^{(n+1)} = (h_i^o)^{(n+1)},\ i = 1,2,..,12;\ \sum_{j=1}^{36} a_{ij}^{s}(h_j^s)^{(n+1)} = R_i^s - \left(B_i^s\right)^{(n+1)},\ i = 1,2,..,36 \qquad (14)$$

where the superscript $(n+1)$ and (n), respectively, indicate the present time step and previous time step, respectively.

3. Demonstration Examples

Example 1: This example is a simple case of rainfall-runoff process on a horizontal surface of 500 m x 400 m. The closed boundary was applied except a 100 m-outlet is located at the center of a 500 m-side (critical flow) (Figure 3). The Manning's n value is 0.02. A rainfall intensity of 4.0E-5 m/s was applied for 600 minutes. The underlying porous medium has a vertical saturated hydraulic conductivity of 5.5E-5 m/s and an effective porosity of 0.41. There is no physical discontinuity of subsurface media at the interface, that is, the two flow regimes are in direct connection. Initially, the water table is 10 m below the land surface. No flow boundary was applied to subsurface domain except the top boundary, which is the interface between overland and subsurface domains. Constant time steps of 20 s and 180 s were applied for two-dimensional overland flow and three-dimensional subsurface flow, respectively. The 900-minute simulations were performed with the continuity coupling approach and the linkage-term coupling approach. The outflow discharge hydrographs were compared (Figure 4).

The computed outflow discharge hydrograph represents the integrated results of rainfall, surface runoff and infiltration processes. It can be seen from Figure 4 that the linkage-term and continuity coupling approaches resulted in different rising part of the flow hydrograph. After the subsurface domain is fully saturated and the runoff became steady, the simulation results are essentially the same. Since physically, there is no discontinuous interface, the conductance values (k) were tested for three cases (k = 5.5E-6, 5.5E-4 and 3.0E-3). A small k value constrains exchange fluxes; therefore, land surface

saturation leads to surface runoff, at which point the whole unsaturated zone gradually becomes saturated. As for enough big k values, the simulation results are very close to those of continuous coupling.

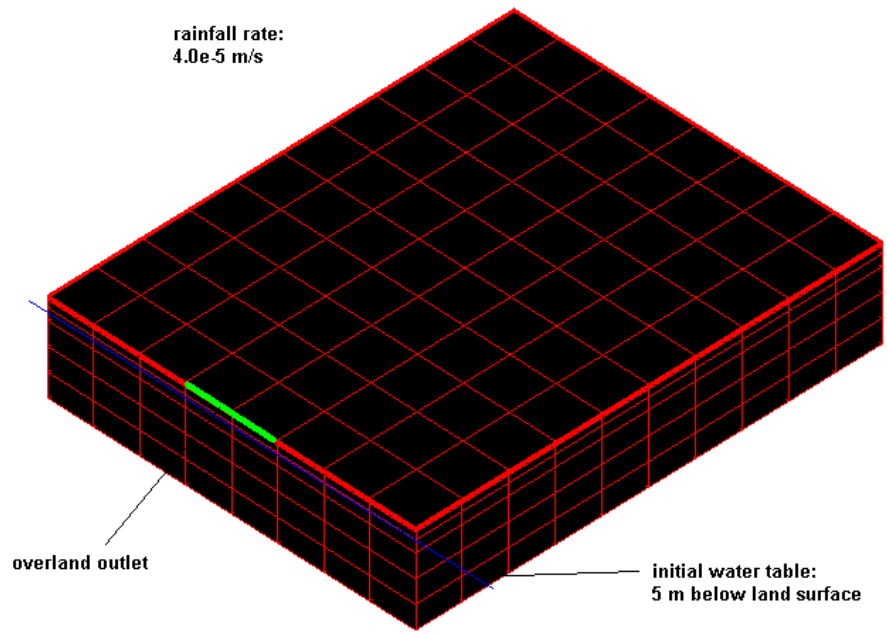

Figure 3: Problem Description and Finite Element Discretization for Example 1

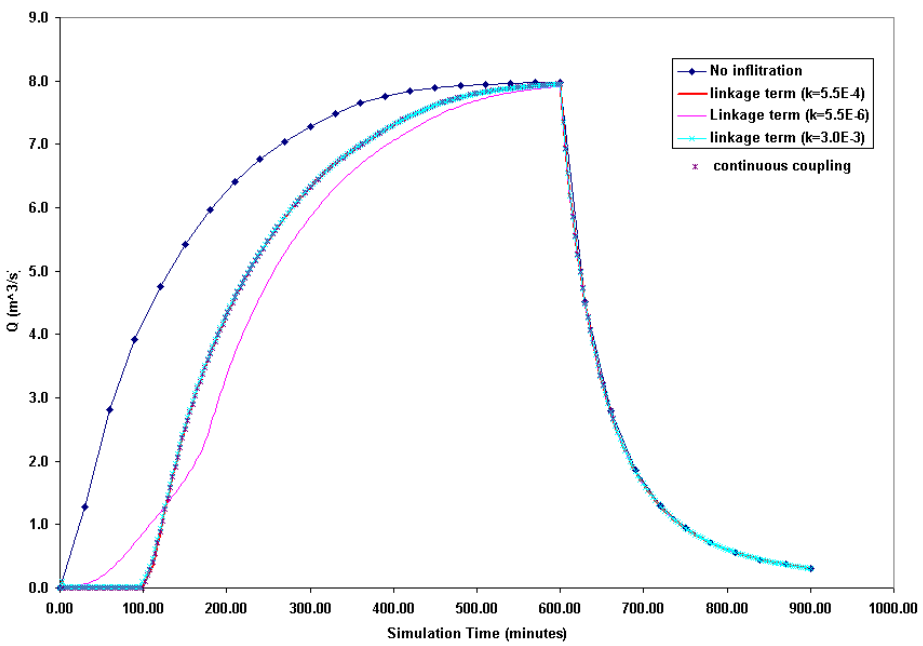

Figure 4: Comparison of Outflow Hydrographs using Continuity and Linkage Approaches

This example demonstrates that the use of linkage-term coupling can produce different results depending on the chosen k values. In Figure 5, the computed time series of total

exchange fluxes were compared for all simulation cases; this is consistent with the pattern shown in the discharge hydrograph.

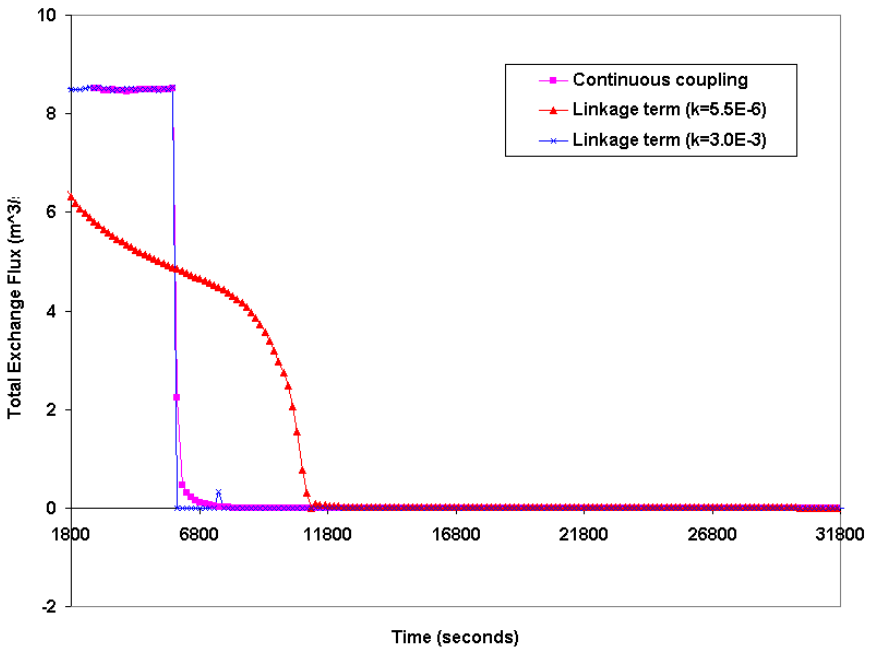

Figure 5 Comparison of Exchange Fluxes using Continuity and Linkage Approaches

Example 2: This is a regional scale modeling effort for the South Florida wetlands. The Dade model domain extends from four miles west of the L-67 Extension dike to the western shore of Biscayne bay and from one mile north of the Tamiami canal south to Florida bay. Vertically, it extends from the land surface to the bottom of the surficial aquifer. Some characteristics of this model are: (1) Strong interaction of overland flow/groundwater flow and canal flow in south Florida; (2) Complex hydraulic structure operations.

The 3-D finite element mesh for subsurface media (as shown in Figure 6) is complex: there are 37,760 global nodes, and 65,429 elements. There are 7 layers in the vertical direction. And levees are incorporated as part of subsurface media. The boundary conditions for subsurface flow were determined from the SFWMM 2x2 model output for the northern boundary, and from structure operation records for the other sides of boundaries. The 2-D overland flow domain consists of 4,720 nodes, and 9,347 triangular elements. Levees are included in the computation domain (Figure 7). Boundary conditions were determined from structure operation records along the boundary. The canal network as simplified in this simulation includes: Canal nodes: 560; Canal elements: 506; River reaches: 55; there are 20 canal junctions, and 11 interior Gates (Figure 8).

Two numerical modeling were conducted. One was a coupled 2-D overland flow and 3-D subsurface flow simulation. A steady state 3-D subsurface flow simulation was run first. The pressure heads from the steady state are then used as the initial pressure heads for the coupled 2-D overland and 3-D subsurface flow. Another one was a coupled 1-D canal flow, 2-D overland flow, and 3-D subsurface flow simulation. Initial conditions were provided from the results of 2D-3D simulations,

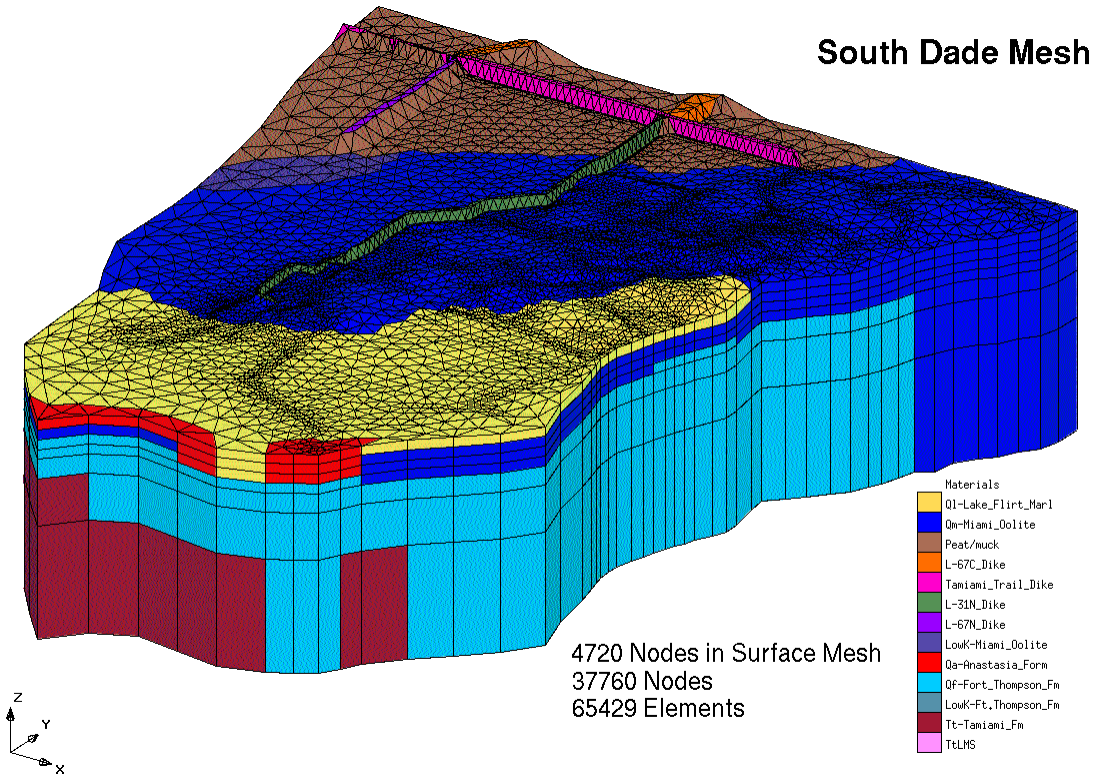

Figure 6 3-D Subsurface Media Finite Element Mesh

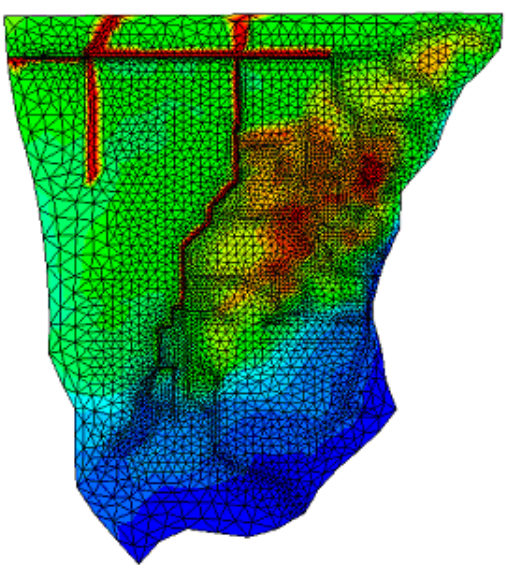

Figure 7 2-D Overland Regime Finite Element Mesh

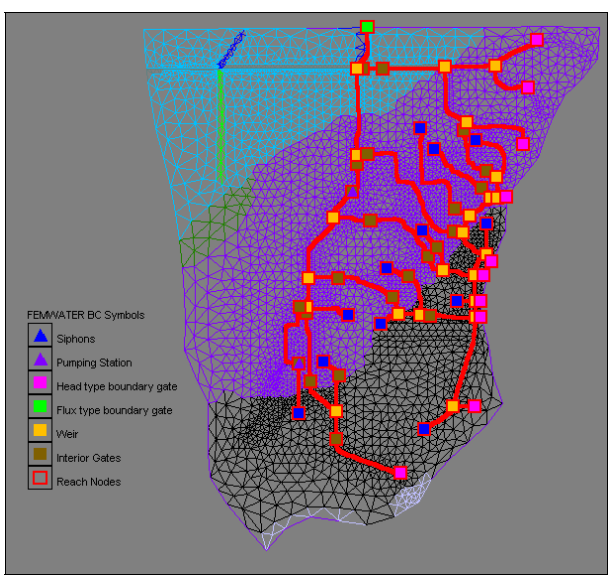

Figure. 8. Canal Network

The combined processes of 1D canals, 2D overland flow, and 3D subsurface flow are complex and require a systematic modeling approach of adding computational complexity until all of the important processes are simulated. This is primarily because the physical processes being simulated cannot all be turned on at the same time due to numerical initial

condition issues. It is important to start with consistent boundary and initial conditions and to run the model first in steady state 3D-only mode followed by 2D/3D overland and groundwater flow, followed by fully coupled 1D/2D/3D mode. In each step of the process, increasingly complicated but accurate initial conditions are provided to the next stage of the simulation until all physical processes are simulated.

Results from the coupled 2D overland flow and 3D subsurface flow simulations are voluminous due to the large mesh and the two-hourly time steps made over the one year time period. Given the temporal and spatial choices for a written paper, only spatial distributions of model output at a discrete time is presented. Figure 9 through Figure 11 show spatial distributions of simulation results for an early point in the yearlong simulation. Figure 9 shows overland flow depths, Figure 10 shows overland flow vectors, and Figure 11 shows coupled 2D/3D total head elevations.

After the model produced reasonable responses based on the coupled 2D overland and 3D subsurface flow simulation, initial conditions were saved and used as input to simulations of coupled 1D canal flow, 2D overland flow, and 3D subsurface flow. These simulations are the most rigorous of the coupled simulations. Figure 12 and Figure 13 show spatial distributions of model output for an early point in the yearlong simulation. Figure 12 shows overland flow depths and Figure 13 shows coupled 1D/2D/3D total head elevations.

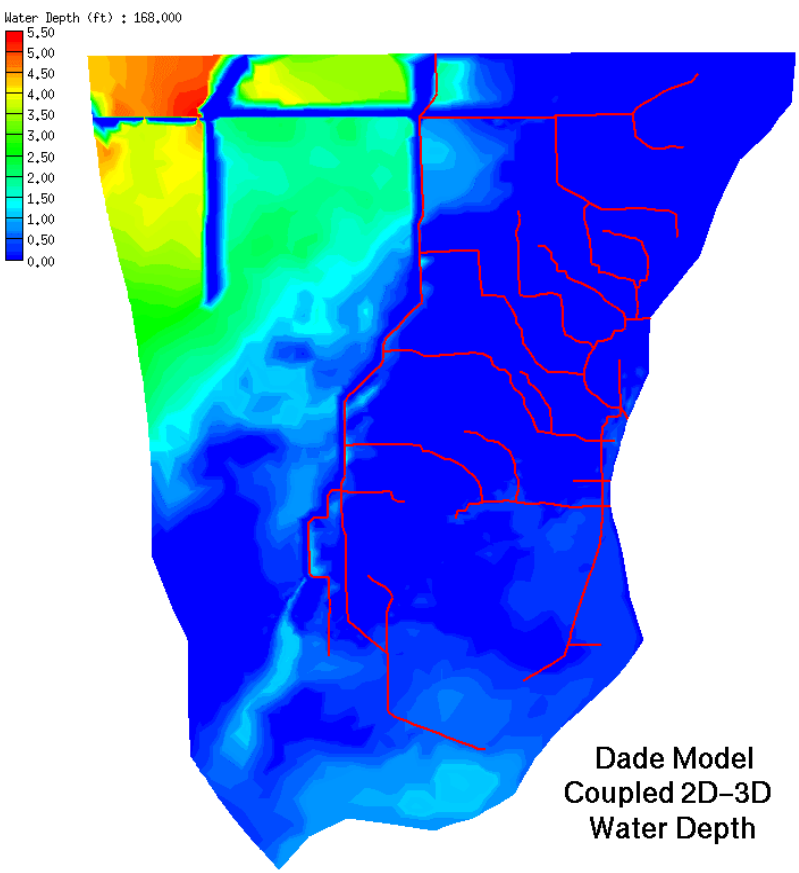

Figure 9 Dade Model Coupled 2D-3D Overland Flow Water Depth Contours

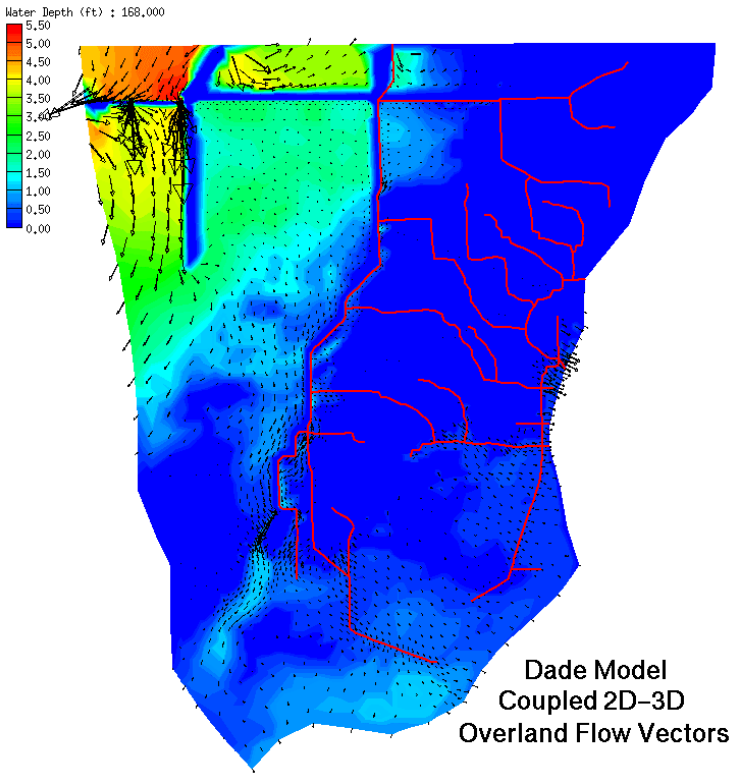

Figure 10 Dade Model Coupled 2D-3D Overland Flow Vectors

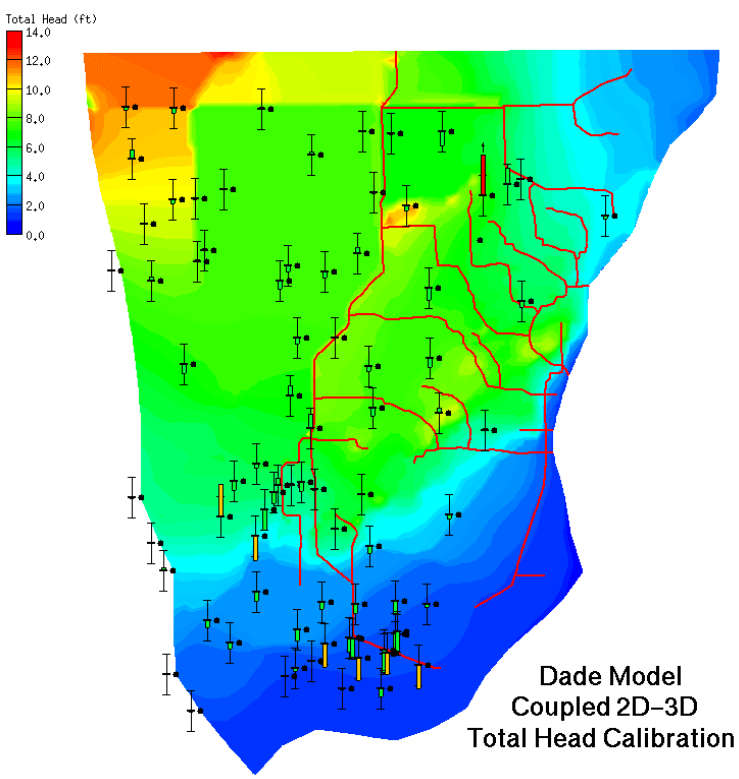

Figure 11 Dade Model Coupled 2D-3D Total Head Calibration

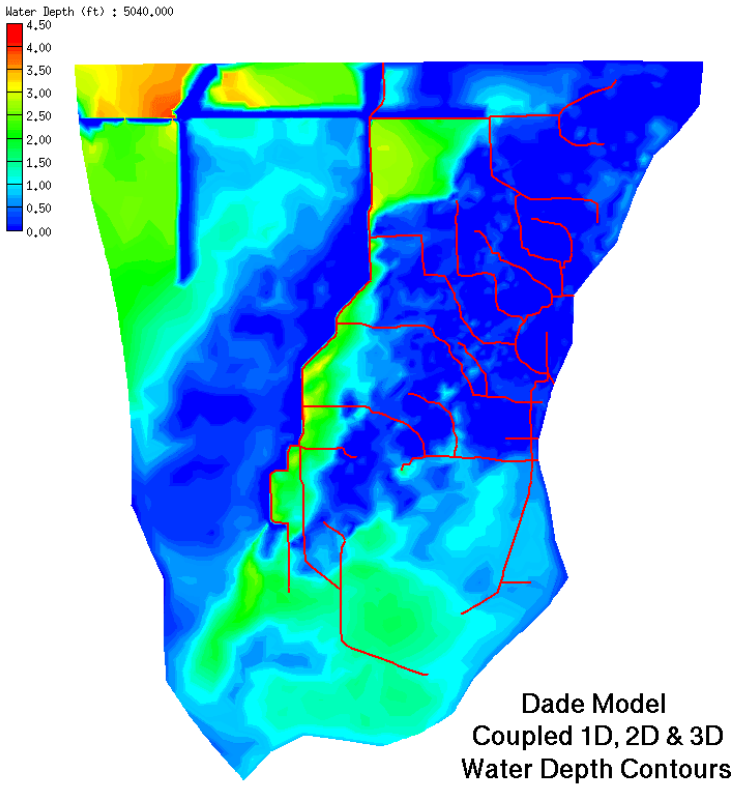

Figure 12 Dade Model Coupled 1D-2D-3D Overland Flow Water Depth Contours

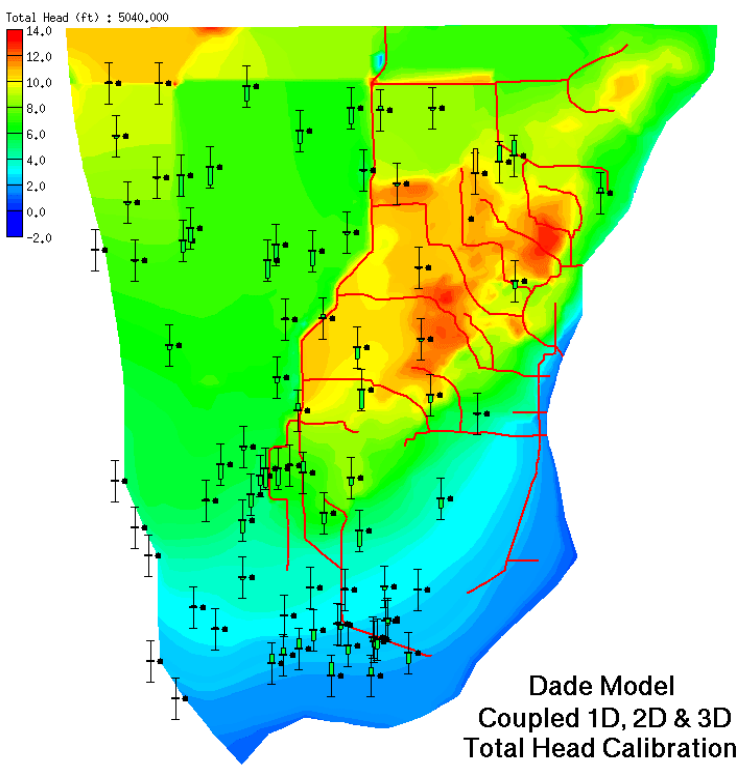

Figure 13 Dade Model Coupled 1D-2D-3D Total Head Calibration

Comparing Figure 9 and Figure 12, it is clearly seen that there is a significant difference between 2D-3D and 1D-2D-3D simulations. It is thus important to consider interactions among all system components.

4. Summary and Conclusion

An integrated media, physics-based watershed model has been developed. Three key issues have to be addressed in a complete watershed model: (1) Coupling among media, (2) applicability of kinematic, diffusive, and fully dynamic wave models, and (3) select of wave directions in multi-dimensional dynamic wave models. The coupling issue is the focus of this paper. From a physical point of view, the surface water and subsurface water can be considered in direct or indirect connection. For the case of direction connection, the continuity of pressure and flux can be mathematically stated. However, many models have used the linkage formulation, which introduces non-physics fitting parameters. For the case of indirect connection, most models have employed the linkage approach. Although the continuity approach can still be taken by including the thin layer separating surface water and groundwater as part of the heterogeneous subsurface media, it may cause numerically convergent problem or demand excessive computational time. Once the mathematical problem is reduced to a set of algebraic equations, there schemes have been widely used to solve the matrix equation: fully implicit scheme, iteratively implicit scheme, and time-lagged explicit scheme. Two examples were employed to discuss the issues of coupling. One was used to demonstrate differences and implications between continuity and linkage approaches in a physically direct connection problem. Another one, a watershed modeling in Florida, was used to illustrate that complete and partial couplings yield quite different simulations.

Acknowledgments

This research was supported, in part, by the U.S. EPA – Science To Achieve Results (STAR) Program under Grant # R-82795602 with the University of Central Florida and, in part, by the U.S. Department of Energy under Grant DE-FG02-04ER63916 with University of Central Florida.

References

Abbott, M., J. Bathurst, J. Cunge, P. OConnell, and R. Rasmussen, 1986. An Introduction to the European Hydrological System, System Hydrologique European, (SHE), 2: History and philosophy of a physically based, distributed modeling system. Journal of Hydrology 87, 45-59.

Bicknell, B. R., J. C. Imhoff, J. L. Kittle, A. S. Donigian, and R. C. Johanson, 1993. Hydrologic Simulation Program - FORTRAN (HSPF): User's Manual for Release 10.0. EPA 600/3-84-066. U.S. Environmental Protection Agency, Environmental Research Laboratory, Athens, GA.

Akan, A. O. and B. C. Yen, 1981, Mathematical model of shallow water flow over porous

media. J. Hydraul. Div. 107 HY4 (1981), pp. 479–494.
Crawford, N. H. and R. K. Linsley, 1966. Digital Simulation in Hydrology: Stanford Watershed Model IV. Technical Report No. 19, Dept. of Civil Engineering, Stanford University, Stanford, CA., 1966. 210 pp.
Downer, C. W. and F. L. Ogden, 2002. GSSHA-User's Manual Gridded Surface Subsurface Hydrologic Analysis. Version 1.43 for WMS 6.1. Coastal and Hydraulic Laboratory, ERDC, US Army Corps., 3990 Halls Ferry Road, Vicksburg, MS 39180.
EPA, 1997. Compendium of Tools for Watershed Assessment and TMDL Development. EPA/841-B-97-006. U.S. Environmental Protection Agency, Office of Water, Washington, DC 20460.
Ewen, J., G. Parkin, and P. E. O'Connell, 2000. SHETRAN: Distributed River Basin Flow and Transport Modeling System. J. Hydrologic Engineering, 5(3):250-258.
Freeze, R. A., 1972.Role of subsurface flow in generating surface runoff. (1972), 1. Base flow contributions to channel flow. Water Resour. Res. 8 (1972), pp. 609–623.
Huang, G. B. and G. T. Yeh, 2009. A Comparative Study of coupling Approaches for Surface water and groundwater interactions. Journal of Hydrologic Engineering, ASCE (in press).
Hunt B., 1990, An approximation for the bank storage effect, Water Resources Research, Vol.26 No.11, Pages 2769-2775.
Hydrologic, Inc., 2001. MOD-HMS: A Comprehensive MODFLOW-based Hydrologic Modeling System. Version 1.1. Document and Users Guide, HydrolGeoLogic Inc., Herndon, Virginia
Morita M, and B C Yen, 2002, Modeling of conjunctive two-dimensional surface–three-dimensional subsurface flows. Journal of Hydraulic Engineering, ASCE 128: 184–200.
Panday S. and P. S. Huyakorn, 2004. A fully coupled physically-based spatially-distributed model for evaluating surface/subsurface flow, Advances in Water Resources, 27 (2004) 361–382
Pinder, G. F. and S.P. Sauer, 1971, Numerical simulation of flow wave modification due to back storage effects. Water Resour. Res. 7 1 (1971), pp. 63–70.
Smith, R. E. and D. A. Woolhiser, 1971. ''Overland flow on an infiltration surface,'' Water Resour. Res., 7(4), 899–913.
SOBEK: http://delftsoftware.wldelft.nl/
Swain E. D. and E. J. Wexler, 1996, A coupled surface-water and groundwater flow model for simulation of stream–aquifer interaction. US geological survey techniques of water-resources investigations, Book 6; 1996. 125 p [chapter A6].
Swain, E., C. Langevin, and M. wolfert. A Model of Flow and Transport in a Linked Overland-Aquifer Density Dependent System (FTLOADDS). http://sofia.usgs.gov/projects/coupling/comptechnique_03geerab.html
SFWMD,https://my.sfwmd.gov/portal/page?_pageid=1314,2556300&_dad=portal&_schema=PORTAL&navpage=home
VanderKwaak, J. E., 1999. Numerical Simulation of Flow and Chemical Transport in Integrated Surface-Subsurface Hydrologic Systems. Ph.D. Thesis, Dept. of Earth Science, University of Waterloo, Waterloo, Ontario, Canada.
Wigmosta, M. S. and Perkins, 1997. A GIS-Based Modeling System for Watershed Analysis. Final Report to the National Council of the Paper Industry for Air and

Stream Improvement. 160 pp.
Yeh, G. T., H. P. Cheng, J. R. Cheng, and Jerry H. Lin. 1998. A Numerical Model to Simulate Water Flow and Contaminant and Sediment Transport in Watershed Systems of 1-D Stream-River Network, 2-D Overland Regime, and 3-D Subsurface Media (WASH123D: Version 1.0). Technical Report CHL-98-19. Waterways Experiment Station, U. S. Army Corps of Engineers, Vicksburg, MS 39180-6199.
Yeh, G. T., G. B. Huang, H. J. Lin, and H. P. Cheng, 2003. A Numerical Model to Simulate Water Flow and Contaminant and Sediment Transport in Watershed Systems of 1-D Stream-River Network, 2-D Overland Regime, and 3-D Subsurface Media (WASH123D: Version 2.0). Technical Report. Department of Civil and Environmental Engineering, University of Central Florida, Orlando, FL 32816-2450.
Yeh, G. T., G. Husng, H. P. Cheng, F. Zhang, H. C. Lin, E. Edris, and D. Richards, 2005. A First principle, Physics based Watershed Model: WASH123D. Chapter 9 in Watershed Models (V. P. Singh and D. K. Frevert, ed.), CRC Press LLC, 6000 Broken Sound Parkway, NW, (Suite 300) Boca Raton, FL 33487, USA. pp. 211-244.
Yeh, G. T., G. B. Huang, F. Zhang, H. P. Cheng, and H. C. Lin, 2006. WASH123D: A Numerical Model of Flow, Thermal Transport, and Salinity, Sediment, and Water Quality Transport in WAterSHed Systems of 1-D Stream-River Network, 2-D Overland Regime, and 3-D Subsurface Media. A Technical Report Submitted To EPA. Dept. of Civil and Environmental Engineering, University of Central Florida, Orlando, FL 32816.

Understanding Uncertainties in Water Budget for Large Constructed Wetlands

R. Scott Huebner[1], Chandra S. Pathak[2] and Ramesh S. Teegavarapu[3]

[1] Water Quality Assessment Division, Environmental Resources Assessment Department, South Florida Water Management District, 3301 Gun Club Road, West Palm Beach, FL 33416-4680; PH (561) 682-2319; FAX (561) 682-6051; email: huebner@sfwmd.gov

[2] Operations and Hydro Data Management Division, SCADA and Hydro Data Management Department, South Florida Water Management District, 3301 Gun Club Road, West Palm Beach, FL 33416-4680; PH (561) 682-2567; FAX (561) 682-2028; email: cpathak@sfwmd.gov

[3] Department of Civil Engineering, Florida Atlantic University, Boca Raton, FL 33431; PH (561) 297-3444; FAX (561) 297-0493; e-mail: ramesh@civil.fau.edu

ABSTRACT

Temporal water budget assessments are necessary for short- and long-term water resources management and operational planning. However, these estimates are subject to a variety of potential sources of error, some of which are not easily quantifiable. Several past water budget studies have focused on quantifying residual errors and improving the water budget balance using statistical methods. In the current study, a weighted mass balance equation, solvable by using mathematical programming models at different time scales, is proposed and investigated. The mathematical programming models employ mixed-integer, non-linear programming formulations and binary variables to estimate weights that can improve the water budget by reducing residual errors. The formulations developed were tested and evaluated for a large constructed wetland operated and managed by the South Florida Water Management District for nutrient control. Hydraulic and hydrologic data from the wetland were used to test the methodology proposed in the current study. Results suggest reduction in residual errors and identify variables that need improvement in measurements and estimation for accurate water budgeting.

INTRODUCTION

Managing water resources and operations requires accurate water budget assessments. These assessments are normally carried out using traditional mass balance equations based on a simple water budget model at different temporal scales. Hydro-meteorological components play a major role in developing accurate water budget assessments, but are subject to systematic and random errors. In addition, various

empirical relationships are used to estimate values for some of these parameters and they have associated uncertainties in their estimation. While some of the errors are easily quantifiable, others are not. In the current study, a weighted mass balance equation, solvable by using mathematical programming models, is proposed and investigated using data from a large constructed wetland in South Florida.

Stormwater Treatment Area 2 (STA-2) is one of six wetland treatment areas operated by the South Florida Water Management District. Its purpose is to reduce water-column phosphorus concentrations in runoff from the Everglades Agricultural Area prior to discharge to Water Conservation Area 2A (WCA-2A), part of the remnant Everglades (**Figure 1**). Nutrient removal is accomplished by sedimentation and uptake by emergent and submerged aquatic vegetation in each treatment cell.

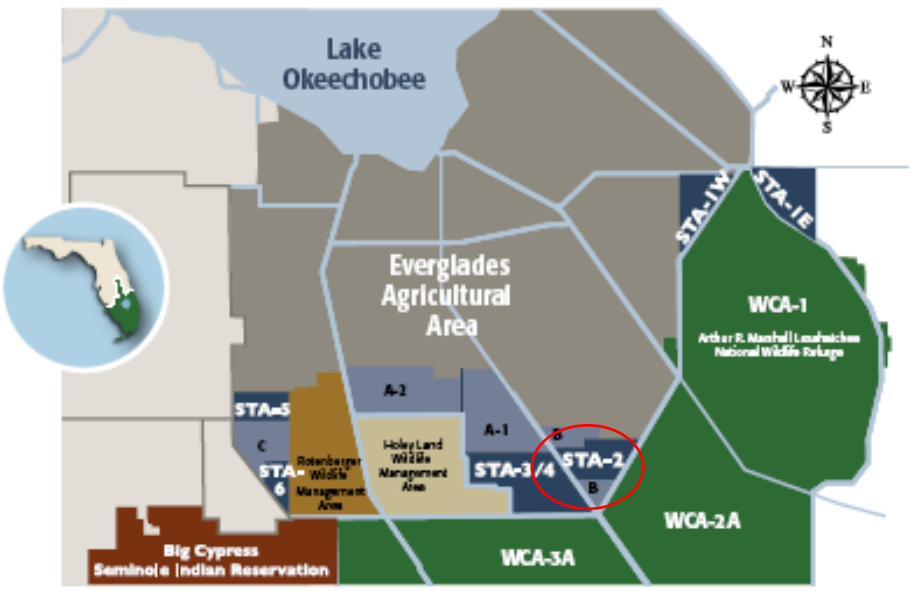

Figure 1. Location of STA-2.

STA-2 has four parallel treatment cells (**Figure 2**) with a total effective treatment area of 3,418 hectares (8,445 acres) (SFWMD, 2008). Cell 4 began operations in 2007 (Hall et al., 2007); the analysis discussed here used data pre-dating flow-through operations in Cell 4.

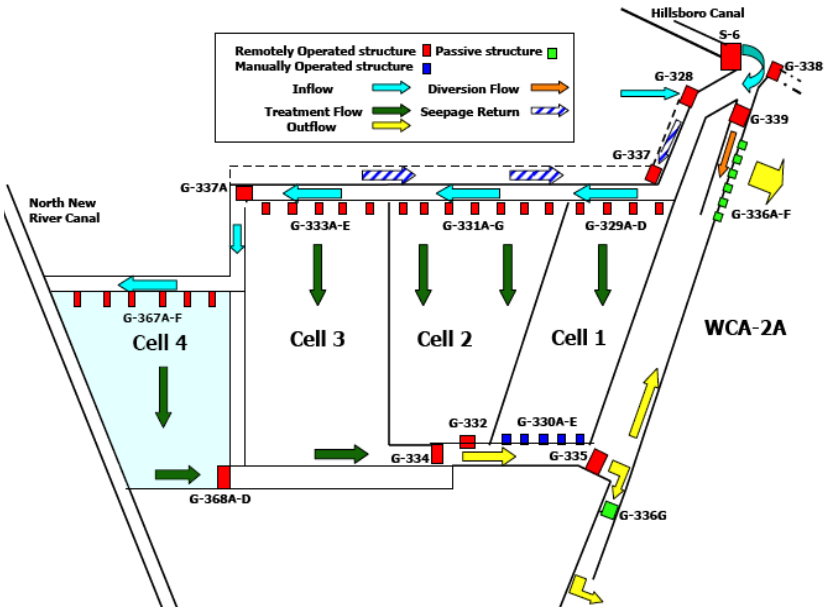

Figure 2. Schematic of STA-2 treatment cells and direction of water flow.

Water budget analysis is critical to understanding and optimizing STA operations. This analysis is mandated and is performed annually. STA-2 water budgets have been produced since the STA began permitted discharges in 2001 and are based on daily mean stages and flows, estimated daily seepage, rainfall, and evapotranspiration (ET). Errors in the water budget can be attributed to uncertainties associated with hydrologic measurements, such as flow and stage, and physical properties of the STA (e.g., ground surface elevation, surface area). A previous study (Huebner et al., 2007) examined the effect of using spatially distributed rainfall data (gauge-adjusted NEXRAD rainfall estimates) versus point data from a raingage network. Although limited in scope, the study indicated that water budget residuals were reduced when using NEXRAD data for larger STAs. Nevertheless, rainfall measurement probably exhibits the least random error with respect to all of the terms used in water budget analysis.

In all STA water budget analyses performed to date (Hall, et al, 2007), daily water budget residuals have demonstrated a trend to increase during significant runoff (flow) and draw-down events (**Figure 3**) suggesting that flows and change of storage responses may be better captured using a time increment smaller than one day. Parrish and Huebner (2004) examined water budget error for another STA, STA-5, using 15-minute increments and found that for the two-week period examined, daily water budget error was reduced on the order of 50 percent.

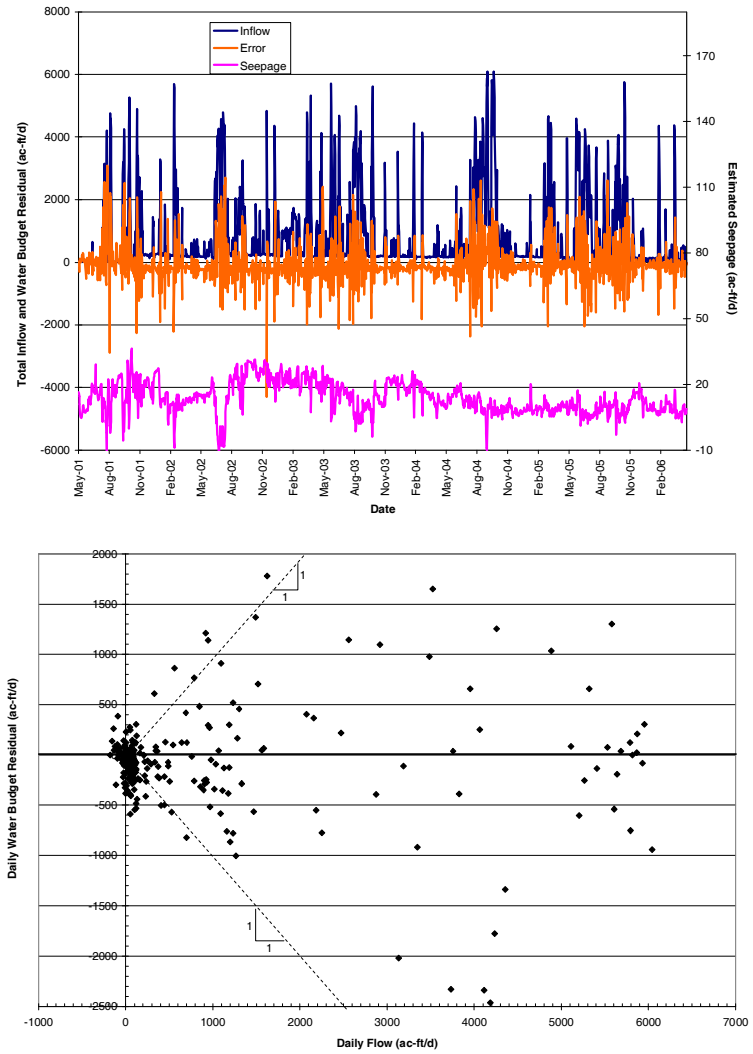

Figure 3. STA-2 water budget residual versus flow.

METHODOLOGY

The main objective was to identify and assess systematic errors in the STA water budget. Methods used by Teegavarapu and Pathak (2009) were repeated in this study to examine the effect of various time-steps on weights applied to independent variables as determined by two models that minimized the mean absolute error (MAE) and the mean squared-error (MSE) in the water budget (**Equation 1**). Time periods used in this study were 15 minutes, 1 hour, 3 hours, 6 hours, and 1 day. The analysis focused on wet season water budgets and results are presented by water year for South Florida (May 1 to April 30). The wet season in this area typically extends from June to October and flow through the STAs is greatest during these months. Similar to the analysis used by Teegavarapu and Pathak (2009), the period of record was divided into calibration and validation sets; the calibration data period was from June 2001 to October 2005 and the validation set contained data from June 2006 to October 2006.

$$\frac{\Delta S}{\Delta t} = I - O + R - ET \pm G + \varepsilon \quad (1)$$

Where, ΔS = change in storage over the time period
Δt = time period
I = average inflow over the time period
O = average outflow over the time period
R = rainfall over the time period
ET = evapotranspiration over the time period
G = levee and deep seepage over the time period
ε = water budget error over the time period

Optimization Formulations

The first model used a "simple" weighting method using the following formulation:

$$Minimize \quad \sum_{i=1}^{N} |\varepsilon_i| \quad (2)$$

$$\varepsilon_i = (\Delta S)_i - (P + w_1 I - w_2 O - w_3 G - w_4 ET)_i \quad (3)$$

$$w_j \geq w_j^l \quad (4)$$

$$w_j \leq w_j^u \quad (5)$$

The weights for inflow, outflow, estimated seepage, and evapotranspiration are w_1, w_2, w_3, and w_4 respectively. Inflow, outflow, seepage, and evapotranspiration are the parameters that tend to have the greatest uncertainty associated with their measurement and therefore were the parameters weighted in the optimization. The upper and lower limits are w_j^l and w_j^u respectively. The optimization used the solver available in Microsoft Excel 2007. The Newton search, tangent estimate, and forward derivation techniques were used in the solver. N is the number of time periods; i and j are indices for time increments and weights.

The second model (binary method) weighted the same variables in the water budget equation as described above and used binary variables (Teegavarapu and Pathak, 2009). **Equations 6** through **12** apply:

$$Minimize \quad \sum_{i=1}^{N} |\varepsilon_i| \quad (6)$$

$$\sum_{i=1}^{4} \lambda_i \leq n_k \quad (7)$$

$$\sum_{i=1}^{4} \lambda_i = n_k \tag{8}$$

$$if\ \lambda_i = 0, then\ \ w_i = 1, else\ w_i = w_i^0 \tag{9}$$

$$\varepsilon_i = (\Delta S)_i - (P + w_1 I - w_2 O - w_3 G - w_4 ET)_i \tag{10}$$

$$w_j^0 \le w_j^u \tag{11}$$

$$w_j^0 \ge w_j^l \tag{12}$$

λ_1, λ_2, λ_3, and λ_4 are binary variables. Only **Equation 7** or **8** is used for the solution of the formulation to constrain the number of binary variables; in this study, **Equation 8** was used to determine the number of binary variables used in the analysis. The term n_k represents the upper limit on the number of binary variables used in the formulation.

RESULTS AND DISCUSSION

This study substantially confirmed the results observed by Parrish and Huebner (2004) concerning 15-minute data and its ability to reduce water budget error during wet season operations as shown in **Table 1**. Water year 2006 is the exception. The results (wet season water budget errors presented by water year) did not use the optimization methods described above. Unfortunately, data for the 1-hour, 3-hour and 6-hour water budgets were aggregated from the 15-minute data so that the water budget tables developed for those time steps simply replicate the water year results for the 15-minute time step. Therefore, they could not be used to verify the results shown in **Table 1**.

Table 1. 15-minute vs. Daily Wet Season Water Budget Residuals (not optimized)

Water Year	Daily Time Step		15-minute Time Step	
	Residual (ac-ft)	Percent Error	Residual (ac-ft)	Percent Error
2002	33,888	18.83%	18,640	10.03%
2003	4,270	2.02%	1,031	0.51%
2004	-16,811	-7.44%	-7,121	-3.23%
2005	2,647	0.90%	-2,153	-0.75%
2006	-1,310	-0.47%	-8,213	-2.93%
2007	-17,403	-7.97%	-16,420	-7.45%
Total	-15,219	-1.10%	6,264	0.45%

The validation data set confirmed the results of optimization using the calibration data for both the MAE and MSE targets although the improvement in the respective targets appears to be insignificant. Results are shown in **Table 2**.

Table 2. Water Year 2007 Wet Season, 15-minute Data Validation Optimization Results

Objective Function	Without Optimization	With Optimization	Percent Improvement
MAE (ac-ft/d)	15.99	15.64	2.21%
MSE (ac^2-ft^2/d^2)	1,585	1,578	0.41%

An unintended result was that using MAE and MSE for objective function targets did not ensure that the total water budget error would be minimized. **Table 3** shows wet season water budget residuals by water year using the 15-minute water budgets and the results of applying method 1 optimization coefficients to the appropriate terms in the water budget. Although counterintuitive, the optimization based on either MAE or MSE relies in minimizing positive measures of error. The un-adjusted water budget residuals for each time step can be either positive or negative and appear to cancel each other when aggregated over a period like a water year wet season. The results shown in **Table 3** show this anomaly. On a wet season, water year basis using the 15-minute data, the MSE target appears to reduce residuals better than the MAE target except for water year 2005 and for the entire period of record. However, since the differences are so small, this may be of little consequence.

Table 3. Effect of Optimization Results on Water Budget Residuals (Wet Season, 15-minute Data)

Wet Season Water Year	Without Optimization		MAE		MSE	
	Residual (ac-ft)	Percent Error	Residual (ac-ft)	Percent Error	Residual (ac-ft)	Percent Error
2002	18,640	10.03%	16,259	12.77%	18,530	11.11%
2003	1,031	0.51%	9,337	6.75%	4,890	2.69%
2004	-7,121	-3.23%	-10,024	-7.07%	-11,793	-6.12%
2005	-2,153	-0.75%	-6,217	-3.35%	-9,551	-3.80%
2006	-8,213	-2.93%	-16,854	-9.48%	-18,891	-7.80%
2007	-16,420	-7.45%	-18,673	-13.19%	-23,854	-12.42%
Total	6,264	0.45%	-26,172	-2.92%	-40,669	-3.36%

The seepage term in the water budget equation (**Equation 1**) was the parameter that was consistently weighted most heavily in the analyses regardless of optimization target, model, or time step. In STA water budgets, the seepage term is typically at least an order of magnitude smaller than the flow terms in the equations for STA-2. The relative magnitude of the weight also suggests that the seepage term has the greatest uncertainty associated with it. **Table 4** shows the weights determined during the optimization runs. In **Table 4**, as the weight approaches 1.00 with increasing time increments the parameter itself appears to became more reliable at reducing water

budget error. Nevertheless, there is no consistent pattern in the data over all time steps and this trend which occurs for several of the parameters is probably caused by the canceling of negative and positive errors as the time increment increases.

Table 4. Parameter Weights from Optimization Runs – Simple Method (Wet Season, 15-minute Data WY2002- WY 2006)

Time Increment	Objective Function	Inflow	Outflow	Seepage	ET
15-minute	MAE	0.63	0.61	8.05	0.06
1-hour	MAE	0.64	0.63	8.46	0.38
3-hour	MAE	0.65	0.64	9.61	0.29
6-hour	MAE	0.69	0.66	9.12	0.47
1-day	MAE	0.59	0.50	5.11	1.67
15-minute	MSE	0.88	0.84	7.82	0.23
1-hour	MSE	0.84	0.84	11.10	0.00
3-hour	MSE	0.80	0.78	11.55	0.00
6-hour	MSE	0.75	0.74	10.08	0.00
1-day	MSE	0.62	0.51	4.82	1.76

The binary optimization scheme (**Equations 6-12**) effectively selects the parameter(s) that most significantly contribute to achieving the optimization goal (minimization of the target, either MAE or MSE). **Table 5** shows the parameter weights resulting from optimization of the 15-minute water budget using the binary method. ET is the first parameter to drop out of the analysis as the number of optimized parameters is reduced from four to three. This is consistent with the results shown in **Table 4** where the weight for the ET term in the water budget equation becomes negligible as the time step increases.

Table 5. Parameter Weights from Optimization Runs – Binary Method (Wet Season, 15-minute Data WY2002- WY 2006)

Number of Weighted Optimized Parameters	Objective Function	Inflow	Outflow	Seepage	ET
4	MAE	0.63	0.61	8.05	0.06
3	MAE	0.61	0.59	8.04	1.00
2	MAE	1.00	0.92	10.29	1.00
1	MAE	1.00	1.00	1.00	0.04
4	MSE	0.88	0.84	7.82	0.23
3	MSE	0.86	0.84	7.82	1.00
2	MSE	0.85	0.84	1.00	1.00
1	MSE	0.99	1.00	1.00	1.00

As the number of variables used to seek the target was reduced, results varied with respect to parameters selected for optimization. The most consistent results resulted from using MSE in the objective function. ET was dropped first, followed by

seepage and then inflow. Using MAE as the optimization target, ET was dropped first. This was consistent with the MSE results. However, inflow was the second parameter dropped from the MAE optimization when only two parameters were used in the optimization. When only one parameter was used in the optimization, outflow was the parameter that is selected using the binary method as the variable that has the greatest effect on achieving the optimization goal of minimizing MAE. ET is brought back into the equation but with a very small coefficient. In both cases when one parameter is selected for optimization, the weight is nearly 1 indicating that the optimization has a minimal effect on the water budget residual values.

Admittedly, the solver in MS Excel 2007 is limited as were the objective functions used (minimizing MAE or MSE). However, the optimization results consistently confirmed that seepage estimation should be an area of focus in reducing the uncertainty associated with STA water budgets. Estimating seepage not only has implications for water budget calculations but also mass balance equations for constituents like soluble phosphorus (Huebner, 2003).

Using MAE or MSE as the optimization target did not result in the water budget with the lowest water budget error (**Table 1**). However, these targets did narrow the range of water budget residuals. Using MSE as an optimization target reduced the variability of the largest errors; using the MAE optimization target results in the reducing the range of all residuals. Again, these are reflected in the optimization function target improvements shown in **Table 2**. However, these improvements are not practically significant and, in fact, imply reductions in parameter uncertainties that may not be necessary. For instance, the MSE result using 15-minute data implies that there may be a 12 percent overestimation of inflow and 16 percent overestimation of outflow. Stream gauging data at those inflow and outflow sites indicate that the error is less than these values.

Some would argue that improving water budget error by half (i.e., from typically less than 10 percent to less than 5 percent) is an exercise without much payoff for STA management and operations. However, few would argue that the cost of resources necessary to perform water budget calculations at time steps smaller than one day has decreased substantially. In addition, water budget computations can be automated so that time step size is effectively inconsequential

CONCLUSIONS

A weighted mass balance equation, optimized using mathematical programming models at different time scales was used to identify independent water budget variables that need improvement in measurement and estimation. The mathematical programming models employed mixed-integer, non-linear programming formulations and binary variables to estimate parameter weights. The formulations were applied to a large constructed wetland operated and managed by the South Florida Water Management District for nutrient control. Results suggested that residual errors could be reduced by improving the measurement of variables associated with estimating seepage. However, there are tradeoffs between cost and benefit that need to be

considered in this context. Further work might include randomizing data over the period of record to develop more robust weights, partitioning flows to examine systematic errors in the parameters and developing a method for quantifying benefits of reduced water budget uncertainty to justify data acquisition expenses.

REFERENCES

Hall, C. A., Pati, S., Huebner, R. S. and Mullen, V. T. (2007). *Water Budget Analysis for Stormwater Treatment Area 2 (Water Year 2002 to 2006)*. Technical Publication ERA #461. South Florida Water Management District, West Palm Beach, FL.

Huebner, R. S. (2003). *Water Budget Analysis for Stormwater Treatment Area 6, Section 1 (Water Years 98-99, 99-00, 00-01 and 01-02 – May 1, 1998 to April 30, 2002)*. Technical Publication EMA #408. South Florida Water Management District, West Palm Beach, FL.

Huebner, R. S., Abtew, W., and Pathak, C. (2007). "Impact of using radar rainfall data in water budgets for South Florida Stormwater Treatment Areas." *Proceedings of the ASCE/EWRI World Water & Environmental Congress, Annual Conference*, May 13-16, 2007. Tampa, FL.

Parrish, D. M. and Huebner, R. S. (2004). *Water Budget Analysis for Stormwater Treatment Area 5 (May 1, 2000 to April 30, 2003)*. Technical Publication EMA #418. South Florida Water Management District, West Palm Beach, FL.

SFWMD. (2008). *2008 South Florida Environmental Report – Volume I*. South Florida Water Management District, West Palm Beach, FL.

Teegavarapu, R. S. and Pathak, C. S. (2009). "Estimation of uncertainties in water budget for large constructed wetlands." *Proceedings of the Conference on an International Perspective on Environmental and Water Resources. Environmental and Water Resources Institute of ASCE and Asian Institute of Technology*. January 5-7, 2009, Bangkok, Thailand.

Author Index

A | B | C | D | E | F | G | H | I | J | K | L | M | N | O | P | Q | R | S | T | U | V | W | X | Y | Z

A

Abad, Jorge D.

Hydraulic Model Study of Canoe Chute and Fish Passage for the Chicago River North Branch Dam

Two-Dimensional BOD and DO Water Quality Model for Engineering Applications: The Case of Bubbly Creek in Chicago, Illinois

AbdelMeguid, H.

Combined Energy and Pressure Management in Water Distribution Systems

Ables, Sean

Implementing Source Water Protection Programs in Texas

A Tale of Two Cities—Source Water Protection Case Studies for Systems in Rural Settings

Selection and Prioritization of Best Management Practices for Potential Sources of Contamination in a Wellhead Protection Area

Abourached, Carole

A Web-Based Advisory Service for Optimum Irrigation Management

Abrishamchi, Ahmad

Detection of Streamflow Trends and Variability in Karun River, Iran as Parts of Climate Change and Climate Variability

Ackerman, Cameron T.

New Floodplain Delineation Capabilities in HEC-RAS

Adams, Bill

Rehabilitation of Mine Impaired Creek in Idaho

Adams, L. M.

Water Supply and Energy Generation

Adeyemo, Josiah

Application of Multi-Objective Differential Evolution Algorithm (MDEA) to Irrigation Planning

Afkhami, M.

The Effect of Sewage Pollutant of Bandar Imam Petrochemical Company on Benthic Macofauna Community Using Biodiversity Indices and Bioindicators

Afshar, Abbas

Optimal Design and Operation of Fuse-Gates Considering Water Loss Due to Gates Tilting

Afshar, M. H.

Industrial Distribution System Simulation for Optimal Water Resource Assignment Using Probabilistic Tabu Search

Afzali, R.

Deriving Rule Curve for Hydropower Reservoirs: Seymareh Experience

Agale, P. K.

Environmental and Water Resources in Developing Countries: Development of Micro Irrigation Facility at Parsoda Village

Aguilar, Jonathan P.

Historical Changes in the Streamflow in Kansas Streams: Variation, Causes, and Implications

Ahlquist, Jon

Evaluation of Improvised Spatial Interpolation Methods for Infilling Missing Precipitation Records

Ahmad, Rasheed

“Let It Rain”—Gage-Adjusted Radar Rainfall (GARR) Data for Peachtree Creek Sewer Basin Modeling

Ahmadi, Azadeh

Optimal Design of Water Diversion System: A Case Study

Long-Lead Forecasting of Monthly Rainfall Using Large Scale Climate Signals and Statistical Disaggregation Models

Ajemian, Greg

Integrating Fluvial Geomorphology and Two-Dimensional Hydraulic and Sediment Transport Modeling to Support Sustainable Design of Large River and Floodplain Improvements: The Trinity River Corridor Project, Dallas, Texas, USA

Al-Hamdan, Osama Z.

Sensitivity Analysis of HEC-HMS Hydrologic Model to the Number of Sub-Basins: Case Study

Al-Raoush, Riyadh I.

Pore-Scale Characterization of Residual Non-Aqueous Phase Liquids (NAPLs) in Fractional Wettability Porous Media

Al-Thamiry, H. A.

Modeling the Evolution of Incised Streams in Hammar Mesopotamian Marsh with Emphasis on the Contribution of Tidal Flow in the Filling Requirements

Alam, W.

Quantifying the Spread of Arsenic Contamination in Groundwater of the Brahmaputra Floodplains, Assam, India: A Threat to Public Health of the Region

Albers, D. P.

Improving the Water Quality of One of the World’s Great Lakes: Tai Lake Case Study of Environmental Responsibility in the Developing World

Alemaw, B. F.

The Hydrology of the Congo River Basin: A GIS-Based Hydrological Water Balance Model

Alexander, James M.

Golden Eagle—Brown County, Kansas: Emergency Streambank Stabilization

Alexander, Matthew T.

Field-Scale Assessment of a Multispecies Water Quality System: A Chloramination Study

Alexander, Mike

ARC Population and Employment Allocation Disaggregator—A Simple GIS-Based Tool for Parcel-Scale Population Projection

Ali, A. A.

Modeling the Evolution of Incised Streams in Hammar Mesopotamian Marsh with Emphasis on the Contribution of Tidal Flow in the Filling Requirements

Alkaabi, A. H.

Modeling the Evolution of Incised Streams in Hammar Mesopotamian Marsh with Emphasis on the Contribution of Tidal Flow in the Filling Requirements

Allen, Mark

A Comparison of Formed Suction Inlets for Flood Control Applications

Allen, R. G.

Evapotranspiration and Net Irrigation Water Requirements for Nevada

Independent Comparisons among Calibration and Output of Energy Balance Components Estimated by the METRIC Procedure

Automated Selection of Anchor Pixels for Landsat Based Evapotranspiration Estimation

Allen, Richard G.

Estimating Crop Coefficients from Fraction of Ground Cover and Height

Adjusting Wind Speed Measured over Variable Height Alfalfa for Use in the ASCE Standardized Penman-Monteith Equation

Estimation of Evaporation and Evapotranspiration during Nongrowing Seasons Using a Dual Crop Coefficient

Allman, Bruce

Hutchinson, KS—4th and Carey Groundwater Remediation and Reverse Osmosis Water Treatment Facility Project

Alp, Emre

Evaluation of Methods to Reduce Backflows from the Chicago Waterway System to Lake Michigan

Flow Augmentation for Dissolved Oxygen Improvement in Chicago Waterways

Altinakar, Mustafa

Representation of Linear Terrain Features in a 2D Flood Model with Regular Cartesian Mesh

Alvi, Khalid

Multiple Watershed Scales Approach for Placement of Best Management Practices in *SUSTAIN*

Aly, Alaa

Evaluation of Improvised Spatial Interpolation Methods for Infilling Missing Precipitation Records

Amiri, Fazel

The Effect of Sewage Pollutant of Bandar Imam Petrochemical Company on Benthic Macofauna Community Using Biodiversity Indices and Bioindicators

EPM Approach for Erosion Modeling by Using RS and GIS

Amsalu, A.

Environmental Impact of Coffee Processing Effluent on the Ecological Integrity of Rivers Found in Gomma Woreda of Jimma Zone, Ethiopia

Anagnostou, Emmanouil N.

Use of Lightning and Storms Life Cycle Information in Radar Rainfall Estimation

Andales, Allan

Alfalfa Reference ET from a Weighing Lysimeter and Estimates from the ASCE Standardized Reference ET Equation in the Arkansas Valley of Colorado

Anderson, Anita

Production of Drinking Water from Lake Water Sources with a Nanofilter Membrane to Prevent the Formation of Disinfection Byproducts

Anderson, Mark A.

Municipal Water Systems in the Columbia River Basin: A Portfolio Management Approach for Multiple Benefits

Anderson, Mark J.

Environmental Aspects of Dredging: What About Air Quality?

Anderson, Paul

Addressing Contaminated Groundwater and Promoting Environmental Stewardship in Wichita, Kansas—The Gilbert and Mosley Project Story

Anderson, Ron

Assessing Potential Implications of Climate Change for Long-Term Water Resources Planning in the Lower Colorado River Basin

Andrus, Rachel

Groundwater Baseflow Sourced from Miocene Rocks and Residuals Carries Elevated Selenium into Southern California

Human Impact on the Mobilization of a Naturally-Occurring Source of Selenium in an Urbanizing Catchment

Annable, William K.

A Monitoring and Assessment Framework to Evaluate Stream Restoration Needs in Urbanizing Watersheds

Arabi, A.

Assessment of the Capability of Hydrologic and Artificial Neural Network Models for Flood Warning System in Land Use Change Condition

Arabi, M.

Change in Surface Hydrology Due to Land Use Change in a Midwestern Watershed

Aral, M. M.

A Critical Realization Identification Method Based on Pareto Dominance Analysis

Aral, Mustafa M.

A Methodology to Reconstruct Groundwater Contamination History with Limited Field Data

Modeling of Chlorinated VOCs Transport under Dual Bioreactions

Arandia-Perez, Ernesto

Preliminary Spatial-Temporal Statistical Analysis of Hourly Water Demand at Household Level

Archfield, Stacey A.

The Implications of Discretizing Continuous Random Variables: An Example Using the U.S. Geological Survey Reporting Standards for Streamflow Data

Arena, C.

Sampling of Residential Water Use for Leak Control via Water Budgets

Ari, Yaron Ben

Survey of Water and Wastewater Utility Security Standards

Armstrong, Daniel J.

Water-Quality Assessment of the Largely Urban Blue River Basin, Metropolitan Kansas City, USA, 1998 to 2007

Artita, K.

Generating Different Scenarios of BMP Designs in a Watershed Scale by Combining NSGA-II with SWAT

Aschwanden, Cecile

Transitioning NWS Operational Hydraulics Models from FLDWAV to HEC-RAS

Aschwanden, Cécile

Inundation Mapping Using Hydraulic Models and GIS: Case Studies of Steady and Unsteady Models on the Tar River, NC

Ashbolt, N.

Simple Model of Attachment and Detachment of Pathogens in Water Distribution System Biofilms

Ashrafzadeh, Afshin

Numerical Modeling of Flushing Process in Dez Dam Reservoir by HR Wallingford Method

Askarinejad, Vahid

Economic Sustainability Evaluation of an Inter-Basin Water Transfer Project Using GWP Statement

Assefa, F.

Environmental Impact of Coffee Processing Effluent on the Ecological Integrity of Rivers Found in

Gomma Woreda of Jimma Zone, Ethiopia

Attari, J.

Water Sustainability Index: Application of CWSI for Ahwaz County

A Comparative Study of Water Quality Indices for Karun River

Austin, R. G.

Multi-Objective Sensor Placements with Improved Water Quality Models in a Network with Multiple Junctions

Avila, Humberto

Physical Experimentation and CFD Modeling to Evaluate Sediment Scour in Catchbasin Sumps

Awata, Isao

Combining Rule-Based Fuzzy Model with GIS to Predict Groundwater Vulnerability to Contamination

Azar, Masoud N.

Graywater Irrigation as a Means to Meet Water Demands in Arid Regions

Aziz, Oubeidillah A.

Paleo Pacific Ocean Sea Surface Temperature Variability and Upper Colorado River Basin Streamflow

B

Return to top

Babcock, Roger Jr.

Understanding and Controlling Fouling in Membrane Bioreactors

Baggett, Christopher C.

Air/Vacuum Valve Breakage Caused by Pressure Surges – Analysis and Solution

Bahadur, Rakesh

Sensor Network Design and Performance in Water Systems Dominated by Multi-Story Buildings

Bahram, Ehsan

Experimental Analyses of Sedimentation in the Slit Dam Reservoir

Baird, Drew C.

Rehabilitation of the Middle Rio Grande near Bernalillo, New Mexico

Bajcsy, Peter

Evaluation of Alternative Geospatial Models Using Image Ranking and Machine Learning: An Application in Shallow Groundwater Recharge and Discharge

Baker, Katherine H.

Codorus Creek Restoration—A Case Study for the Chesapeake Bay

Looking Upstream and into the Watershed for the Big Picture of Stream Health

Pollutant Transport within the Vadose Zone: Interactions of Soil Horizon Chemistry on Water Quality

Bali, K. M.

Mid-Summer Deficit Irrigation of Alfalfa as a Strategy for Saving Water

Ballard, Meredith

Treatment Performance of Wastewater Lagoons in South Yungas Province of Bolivia

Ballestero, Thomas P.

Examination of Pervious Concrete and Porous Asphalt Pavements Performance for Stormwater Management in Northern Climates

LID-SWM Practices as a Means of Resilience to Climate Change and Its Effects on Groundwater Recharge

Sediment Monitoring Bias by Autosampler in Comparison with Whole Volume Sampling for Parking Lot Runoff

Balliew, John E.

Membrane Treatment of Rio Grande Water for Municipal Water Production during the Non-Irrigation Season

Banihabib, M. E.

Empirical Equation for Abrasion of Stilling Basin Caused by Impact of Sediment

Assessment of the Capability of Hydrologic and Artificial Neural Network Models for Flood Warning System in Land Use Change Condition

Banihabib, Mohammad Ebrahim

Experimental Analyses of Sedimentation in the Slit Dam Reservoir

Bannerman, Roger

Laboratory Testing Guidelines for Certification of Manufactured Stormwater BMPs

Barbosa, Paulo S. F.

Climate Flow Forecast Model for the Brazilian Hydropower System

Impacts of the Upstream Storage Reservoirs on Itaipu Hydropower Plant Operation

Barbu, Iulia A.

LID-SWM Practices as a Means of Resilience to Climate Change and Its Effects on Groundwater Recharge

Barfield, David W.

Collaborative Groundwater Model Development

Barfuss, Steven L.

Managing Reservoir Discharge through Accurate Flow Measurement

Barkdoll, Brian D.

Impact of Storage Tanks on Energy Consumption in Municipal Water Distribution Systems

Environmental Aspects of Dredging: What About Air Quality?

A Direct Method for Determining Riprap Size for Erosion Protection in Rivers

Hydrologic Modeling and Flood Frequency Analysis of the Sonora River Watershed in Sonora, Northwest Mexico

Barnas, Cristiana

Hydraulic Model Study of Canoe Chute and Fish Passage for the Chicago River North Branch Dam

Baron, Mary

Pressure vs. Flow Relationship for Pipe Leaks

Barrett, Michael

Water Quality and Hydraulic Properties of the Permeable Friction Course

Barros, Mario T. L.

Climate Flow Forecast Model for the Brazilian Hydropower System

Impacts of the Upstream Storage Reservoirs on Itaipu Hydropower Plant Operation

Barry, William K.

Bedload Composition and Development of 2D Stream Sediment Model for Stream Restoration Design Applications in Urbanizing Watersheds

Basile, J.

Application of Northeast Regional Climate Center Research Results for the Purpose of Evaluating and Updating Intensity-Duration-Frequency (IDF) Curves –Case Study: Rochester, New York

Bastiaanssen, Wim

Comparison of Evapotranspiration Estimates from Remote Sensing (SEBAL), Water Balance, and Crop Coefficient Approaches

Bates, Jonathan

Innovative Strategies Alleviate Water Stress in South East Queensland, Australia

Bathi, Jejal Reddy

Association of PAHs with Size Fractionated Sediment Particles

Bausch, Walter

Water Production Functions for High Plains Crops

Bechara, Alberto

“Let It Rain”—Gage-Adjusted Radar Rainfall (GARR) Data for Peachtree Creek Sewer Basin Modeling

Beckmann, Dennis

Adaptive Long-Term Monitoring at BP Environmental Restoration Sites

Bedekar, Vivek

Managing Salinity in the Upper Santa Clara River System of California

Bedient, P. B.

Distributed Hydrologic Model for Flood Prevention in the Yuna River Water shed, Dominican Republic

Assessment of Flood Risk Due to Storm Surge in Coastal Bayous Using Dynamic Hydraulic Modeling

Bedient, P.

Analysis of Water Quality Trends and Pollutant Loading for Cypress Creek Watershed

Behboodian, S.

Evaluation of Uncertainties in the Simulation of Watershed Nutrient Load: A Case Study

Behera, Pradeep K.

Optimization of Regional Stormwater Quality Control Systems Using Genetic Algorithms

Bekele, Elias

Modeling the Hydrology and Hydraulics of the Cache River System

Belk, Mark

Fish Passage Can Be Improved by Introducing Hydraulic Refuge: Can the Effects Be Quantified?

Bennett, William A.

Challenges of Managing California's Sacramento—San Joaquin Delta

Benty, Jeff

Field Testing Guidelines for Certification of Manufactured Stormwater BMPs: Part II

Berardi, L.

Enhanced Global Gradient Algorithm: A General Formulation

An Operative Approach to Water Distribution System Rehabilitation

Berger, R. Charlie

A Three-Dimensional Numerical Model for Flow in a Lock Filling System

Bernedo, Carmen E.

Some Findings on Effective Discharge Determination for Gravel Bed Rivers

Berrada, Abdel

Alfalfa Reference ET from a Weighing Lysimeter and Estimates from the ASCE Standardized Reference ET Equation in the Arkansas Valley of Colorado

Berthold, Troy

Improving Hydrologic Sustainability of Texas A&M University Campus

Bertrand, Fabienne

Effects of Freezing and Thawing Processes on Bank Stability

Besancon, Richard E.

Green Alternatives to Channel Stabilization

Besner, M.-C.

Comparison of Pressures Simulated Using Transient Analysis with Field Data from a Full-Scale Distribution System

Bhandari, Alok

Peroxidase-Mediated Stabilization of 2,4-Dichlorophenol in a Model Humin-Mineral Geomaterial

Denitrifying Bioreactors for Treatment of Tile Drainage

Bhave, P. B.

Environmental and Water Resources in Developing Countries: Development of Micro Irrigation Facility at

Parsoda Village

Bhowmik, Nancy G.

The Mississippi River: A National Resource

Bhuiyan, Mohammad A.

Simulation of Subsurface Water Flow by Galerkin Finite Element Method in Dhaka City Aquifer

Bicik, J.

Operational Perspective of the Impact of Failures in Water Distribution Systems

bin Shaaban, Ahmad Jamalluddin

Historical Reconstruction of Hydroclimatic Data Based on the Control Runs of GCMs over Sabah and Sarawak, Malaysia

Bitew, Menberu M.

On the Local-Scale Spatial Variability of Daily Rainfall in the Highlands of the Blue Nile: Observational Evidence

Blair, Trenton

Distributed Power Generation at State Facilities: Economic Analysis of Savings and Carbon Credits

Blancett, John

Kansas River Bank Stabilization and Post-Project Conditions

Protecting Infrastructure: Emergency Streambank Stabilization

Blodgett, K. Douglas

The Nature Conservancy's Mississippi River Program: Sustainable Conservation of a Working River that Works

Boccelli, D.

Simple Model of Attachment and Detachment of Pathogens in Water Distribution System Biofilms

Boccelli, Dominic L.

Field-Scale Assessment of a Multispecies Water Quality System: A Chloramination Study

The Impacts of Demand Variability on Distribution System Hydraulics and Transport

Real-Time Implementation of Contamination Source Identification Method for Water Distribution Systems

Preliminary Spatial-Temporal Statistical Analysis of Hourly Water Demand at Household Level

The Development of a Neural-Based Biomarker Forecasting Tool for Classifying Recreational Water Quality

Boccelli, Dominic

Comparing Single- and Multi-Species Water Quality Modeling Approaches for Assessing Contamination Exposure in Drinking Water Distribution Systems

Bochis, Celina

Land Use and Runoff Uncertainty

Boettner, Danita S.

Hutchinson, KS—4th and Carey Groundwater Remediation and Reverse Osmosis Water Treatment Facility Project

Hutchinson, KS—4th and Carey Site Groundwater and Source Control Measures at Two Grain Elevators

Bogardi, Istvan

Multi-Criteria Assessment of Pallid Sturgeon Habitat Restoration for the Missouri River

Bolton, Dale A.

Irrigation Scheduling for Deficit Irrigation

Bond, Rick

New Strategies for Managing Desalination Concentrate with Zero Liquid Discharge from Two WRF Research Projects

Bonner, Andrew J.

Balancing the Budget: A Limited Detail Approach to Flood Studies

Book, Dale E.

Overview of Development and Use of Crop ET Estimates with Hydrological Models for Interstate Compacts

Borah, Deva K.

Watershed Models for Storm Water Management: Comparing Hydrologic and Hydraulic Procedures

Borah, P.

Quantifying the Spread of Arsenic Contamination in Groundwater of the Brahmaputra Floodplains, Assam, India: A Threat to Public Health of the Region

Borovik, I.

Bursts Identification in Water Distribution Systems

Borst, Michael

Enhancing Rain Garden Design to Promote Nitrate Removal

Pervious Pavement System Evaluation

Bosch, Darrell

Case Study: Homeowner's Preference Trade-Offs toward Plumbing Systems in Pipe Failure Prone Area

Boulanger, Bryan

Improving Hydrologic Sustainability of Texas A&M University Campus

Boulos, Paul F.

Multi-Objective Design of Transient Network Models

Bounds, P.

Combined Energy and Pressure Management in Water Distribution Systems

Bourget, L.

Developing Best Practices for Computer Aided Dispute Resolution

Bourne, Stephen F.

A Decision Support System for Water Resources Planning and Management for the North Slope of Alaska

Bourne, Stephen

Clark County Regional Flood Control District Arc Hydro (CCRFCD Arc Hydro): Toward Ongoing Stormwater Master Planning

HCFCD M3 System: Maximizing and Maintaining Local Investments in Floodplain Modeling

ARC Population and Employment Allocation Disaggregator—A Simple GIS-Based Tool for Parcel-Scale Population Projection

How to Build a Broadly Useable GIS Toolset for Estuary Analysis

South Florida Water Control System Tracker: Real-Time Water Budgeting for Pragmatic Water Control Operations

A Pragmatic Cycle for Ongoing Water Resources Research and Management

Bowler, Brian

An Integrated Approach for Distribution System Hydraulic Criticality and Emergency Response

Bradshaw, Barton

Adding Value to Sanitary Sewers—An Important Asset of Municipalities

Brand, Scott R.

Innovative Design at Lake Lenexa

Brengosz, Mary Kay

Interstate Collaboration in the Arkansas River Compact Compliance Process: The “Nuts and Bolts” of Developing PET for Canal Service Areas for Input to the H-I Model

Overview of Development and Use of Crop ET Estimates with Hydrological Models for Interstate Compacts

Brewer, Daniel

Gauge-Based Adjustment of Historical Multi-Sensor Quantitative Precipitation Fields and Resulting Effects on Hydrologic Simulations

Briggs, Joshua F.

Examination of Pervious Concrete and Porous Asphalt Pavements Performance for Stormwater Management in Northern Climates

Bril, Jeremy

Upper Mississippi River Basin Envirohydrologic Observatory

Brill, E. Downey

A Hybrid Heuristic Search Approach for Contaminant Source Characterization

Characterizing Reactive Contaminant Sources in a Water Distribution System

Brown, Darren L.

Hutchinson, KS—4th and Carey Groundwater Remediation and Reverse Osmosis Water Treatment Facility Project

Hutchinson, KS—4th and Carey Site Groundwater and Source Control Measures at Two Grain Elevators

Brown, G. O.

Construction and Performance of Bioretention Cells

Brown, J. J.

Construction of a Low-Flow Channel in Barber Creek: Case Study in the Powder River Basin, Wyoming

Sustainable Design and Construction of Earthen-Dam Reservoirs for Water Produced in Association with Coalbed Natural Gas in the Powder River Basin, Wyoming

Brown, Laurie

Kansas City's Stream Setback Ordinance: A Case Study on the Benefits of Stream Buffers in Urban Areas

Brown, Nathan

Managing Salinity in the Upper Santa Clara River System of California

Brown, R. A.

Bioretention/Bioinfiltration Performance in the Mid-Atlantic

Effects of Media Depth on Bioretention Performance in the Upper Coastal Plain of North Carolina and Bioretention Construction Impacts Study

Browning, Richard

Parameterization of Seasonal Freshets for the Study of Effects of Freshwater Inflows on Galveston Bay

Brumbelow, Kelly

A Multi-Objective Evolutionary Computation Approach to Hazards Mitigation Design for Water Distribution Systems

A Decision Support System for Water Resources Planning and Management for the North Slope of Alaska

Brunner, Gary W.

New Floodplain Delineation Capabilities in HEC-RAS

Brunner, Gary

Estimating Probability of Extreme Events

Brunone, B.

In-Line Partially Closed Valves: How to Detect by Transient Tests

Bruun, Kristofer

Gray Water and Treated Effluent Reuse

Buchberger, S. G.

Axial Dispersion Coefficients for Laminar Flows in Water Distribution Systems

Buchberger, Steven G.

Assessing the Impact of Climate Change on Drinking Water Treatment Plant Design and Operation

Buchberger, Steven

Needs and Trends of the Nation's Water Infrastructure—The Utility Perspective

Buchleiter, Gerald

Water Production Functions for High Plains Crops

Buechter, M. T.

The “Silver Bullet”: Proprietary BMPs and Metropolitan St. Louis Sewer District’s Stormwater Program

Bugarin, R.

Characterizing Water Inputs to Catchments in the Santa Monica Mountains with δ180 and δD

Bulkley, Jonathan W.

Characteristics of Integrated Water Resource Management in the Zambezi River and Great Lakes Basins: A Comparison of Two Approaches

The Memorandum of Understanding (MOU) between the University of Zambia and the University of Michigan: Conception and Subsequent Implementation Goals

Bullen, Thomas

Geochemistry of Yukon and Copper River Tributaries, Alaska

Bullock, Philip

Improving Hydrologic Sustainability of Texas A&M University Campus

Bunn, Simon

Water Distribution Optimization: Taking SCADA One Step Forward

Burchell, M. R. II

Implementation and Performance of Stormwater Best Management Practice Retrofits in Wilmington, NC

Burken, Joel G.

Distributed Power Generation at State Facilities: Economic Analysis of Savings and Carbon Credits

Burken, Joel

Use of In-Planta Solid Phase Sampling Devices to Delineate VOC Plumes

Burrows, R.

A Lattice Boltzmann Model for Dam Break Flows

Busch, Bryan

Evaluation of Magnetic Meters for Irrigation Pipeline Measurement

Busch, John

A Web-Based Advisory Service for Optimum Irrigation Management

Butler, Susan

Assessing Potential Implications of Climate Change for Long-Term Water Resources Planning in the Lower Colorado River Basin

C

Return to top

Cabrera-Bejar, J. A.

Inexpensive Modeling of Intermittent Service Water Distribution Networks

Cadena, Fernando

Evaluation of a UV/Ozone Treatment Process for Removal of MTBE in Groundwater Supplies in New Mexico

Cahill, Thomas

Developing Green Streets Prototypes to Reduce Combined Sewer Overflows for Cincinnati, Ohio

Cai, Meijun

The Effect of Natural Hydrological Disturbances (Defined from HSPF Simulated Hydrographs) on Trout Populations in Ungaged Streams of the Great Smoky Mountains National Park

Understanding Water Quality Responses to Long-Term Acidic Deposition in a High-Elevation Southern Appalachian Watershed: A Focus on Soil Watershed Processes

Cai, X.

Water Quality Effects of Varying Crop, Fertilizer, and Carbon Prices

Cai, Ximing

A Decentralized Optimization Algorithm for Multi-Agent System Based Watershed Management

Spatial Evolutionary Algorithms for Characterizing Large-Scale Spatial Groundwater-Vegetation Dynamics in Arid Region

Estimating Groundwater Pumping and Return Flow Based on Hydrologic Recession Analysis

Cantone, J. P.

An Innovative Approach for Modeling Large Urban Hydrologic Systems

Cantrell, William R.

Bedload Composition and Development of 2D Stream Sediment Model for Stream Restoration Design Applications in Urbanizing Watersheds

Cardenas-Lailhacar, B.

Irrigation Rain Sensors Accuracy

Cardoso-Landa, Guillermo

Associated Disasters to the Debris Flows

Carney, Melissa

Geochemistry of Yukon and Copper River Tributaries, Alaska

Carns, K.

Removal of Waterborne Particles by Electrofiltration

Carpenter, Donald D.

The Lawrence Technological University Greenroof Performance Evaluation Project

A Monitoring and Assessment Framework to Evaluate Stream Restoration Needs in Urbanizing Watersheds

Carrasco, Ernie

Data Reporting Guidelines for Certification of Manufactured Stormwater BMPs: Part II

Field Testing Guidelines for Certification of Manufactured Stormwater BMPs: Part II

Cawlfield, Jeffrey D.

Application of a Mass Balance-Based Subsurface Contaminant Transport Model

Cepero, Keren

Inundation Mapping Using Hydraulic Models and GIS: Case Studies of Steady and Unsteady Models on the Tar River, NC

Cereno, Mervin M.

Assessment of Combined Hydroseeding and Coconet Reinforcement to Control Soil Erosion

Chaichi, Maryam

Estimation of Regional Reference Evapotranspiration from Land Surface Temperature and Co-Kriging Method at Tehran Province, Iran

Chandra, Sudeep

Investigating Aquatic Ecosystems of Small Lakes in Khorezm , Uzbekistan

Chang, Ni-Bin

Comparative Study of Two Standard Septic Tank Drain Fields Using Different Sand with Recirculation for Nutrient Removal

Environmental Impacts on Surface Water and Groundwater for Expanding Urban Water Supply Capacity Using Stone Quarries

Investigating the Temperature Effects on Nutrient Removal in Green Sorption Media

Nutrient and Pathogen Removal with an Innovative Passive Underground Drainfield for On-Site Wastewater Treatment

Chao, Xiaobo

Numerical Simulation of Chemical Spills Using CCHE2D Model and Chemical Property Database

Chapman, Tom

Considering River-Scale Ecological Improvements within Flood Management Planning: The Lower Menomonee River Watercourse Status Report

Charbeneau, Randall

Water Quality and Hydraulic Properties of the Permeable Friction Course

Chasteen, Thomas G.

Deployable Decentralized Biofilm System to Degrade Organic Carbon, Nutrients and Benzene from Wastewater

Chaubey, Indrajeet

Application of Remote Sensing Based Tillage Mapping Technique to Evaluate Water Quality Impacts of Tillage Management Decisions in Upper White River Basin

Chávez, J. L.

Mapping ET at High Resolution in an Advective Semi-Arid Environment with Airborne Multispectral Imagery

Chavez, R. A.

Construction and Performance of Bioretention Cells

Chee, R.

Design of Dual Water Supply Systems

Chen, Dong

Deployable Decentralized Biofilm System to Degrade Organic Carbon, Nutrients and Benzene from Wastewater

One- and Two-Dimensional Modeling of Deep Gravel Mining in the Rio Salado

Chen, Li

The Role of the Clast Layer of Desert Pavement in Rainfall-Runoff Processes

Chen, Luonan

Combining Rule-Based Fuzzy Model with GIS to Predict Groundwater Vulnerability to Contamination

Chen, Xiaolu

Long-Term Effectiveness of a Bioretention System Treating Road Runoff in Northeastern Kansas

Chen, Xuewei

Numerical Simulation of Dissolved Oxygen Concentration in the Downstream of Three Gorges Dam

Chen, Yen-Ju

Composite Analysis of Test-Well and Observation-Well Data during Constant-Head Test

Chen, Yongcan

Numerical Simulation of Dissolved Oxygen Concentration in the Downstream of Three Gorges Dam

Chen, ZhiQiang

Historical Reconstruction of Hydroclimatic Data Based on the Control Runs of GCMs over Sabah and Sarawak, Malaysia

Cheng, Xiangju

Numerical Simulation of Dissolved Oxygen Concentration in the Downstream of Three Gorges Dam

Cheng, Yuan

Data Reporting Guidelines for Certification of Manufactured Stormwater BMPs: Part II

Long Term Effect of a Stream Restoration Plan on Water Quality

Chien, H. Y.

Application of Biopile System for the Remediation of Petroleum-Hydrocarbon Contaminated Soils

Chirnside, Anastasia E. M.

Enzymatic Treatment of a Modified Food Processing Wastewater

Chishugi, J. Bahati

The Hydrology of the Congo River Basin: A GIS-Based Hydrological Water Balance Model

Chitikela, S. Rao

Permitting of Confined Animal Feeding Operations: Issues and Challenges

Choi, C. Y.

Axial Dispersion Coefficients for Laminar Flows in Water Distribution Systems

Multi-Objective Sensor Placements with Improved Water Quality Models in a Network with Multiple Junctions

Design of Dual Water Supply Systems

Choi, Gian

Inflow Forecasting for Real-Time Reservoir Operation Using Artificial Neural Network

Choi, Okkyoung

Nitrification Inhibition by UVA Photocatalytic TiO2 Nanoparticles: The Role of Reactive Oxygen Species on Nanotoxicity

Choi, Y. J.

Seoul (Korea) Online Water Quality Monitoring of Drinking Water

Choudhury, R.

Quantifying the Spread of Arsenic Contamination in Groundwater of the Brahmaputra Floodplains, Assam, India: A Threat to Public Health of the Region

Chowdhary, H.

Statistical Evaluation of BMP Effectiveness in Reducing Nutrient Impairment in Mermentau and Vermilion-Teche River Basins

Chowdhary, Hemant

Copula Approach for Reducing Uncertainty in Design Flood Estimates in Insufficient Data Situations

Christianson, Laura E.

Denitrifying Bioreactors for Treatment of Tile Drainage

Christianson, R.

Impacts of Biota on Bioretention Cell Performance during Establishment in the Midwest

Chu-Agor, M. L.

Predicting Streambank Seepage Flows: Sensitivity to Soil Properties and Layering

A Seepage Erosion Sediment Transport Function and Geometric Headcut Relationships for Predicting Seepage Erosion Undercutting

Chung, Francis I.

Developing Artificial Neural Networks to Represent Salinity Intrusions in the Delta

Water Resources Planning under Non-Stationary Hydroclimate in a Snow Dominant Watershed

Cicogna, Marcelo A.

Multireservoir Simulation Using Multipurpose Constraints and Object-Oriented Software Design

Cicogna, Marcelo Augusto

Computer-Aided System for Managing, Controlling, and Analyzing Data from Hydroelectric Plants

Clark, Byron

Application of SIRMOD to Evaluate Potential Tailwater Reduction from Improved Irrigation Management

Comparison of Evapotranspiration Estimates from Remote Sensing (SEBAL), Water Balance, and Crop Coefficient Approaches

Clark, Robert M.

Assessing the Impact of Climate Change on Drinking Water Treatment Plant Design and Operation

Clark, Robert

Needs and Trends of the Nation's Water Infrastructure—The Utility Perspective

Clark, Shirley E.

Codorus Creek Restoration—A Case Study for the Chesapeake Bay

Looking Upstream and into the Watershed for the Big Picture of Stream Health

Pollutant Transport within the Vadose Zone: Interactions of Soil Horizon Chemistry on Water Quality

Rainwater Harvesting for Non-Potable Use in Gardens: A Comparison of Runoff Water Quality from Green vs. Traditional Roofs

Association of PAHs with Size Fractionated Sediment Particles

Clarke, T. R.

Water Use and Evapotranspiration Coefficients for Camelina Sativa

Clary, Jane

Breaking Down the Barriers to Low Impact Development in Colorado

Challenges in Attaining Recreational Stream Standards for Bacteria: Setting Realistic Expectations for Management Policies and BMPs

Integration of Low Impact Development Studies into the International Stormwater BMP Database

Cleveland, Theodore G.

Use of the Basin Development Factor to Evaluate Urban Watershed Response

Water Subdivision for Modeling

Cohn, T. A.

Quantifying Uncertainty in Discharge Measurements: A New Approach

Cole, James S.

A GIS-Based Decision-Making Methodology for Evaluation of Environmental Justice Impacts of Community Infrastructure Projects

Collins, Kelly A.

The Runoff Reduction Method

Collins, Kent L.

Physical Modeling of River Spanning Rock Structures: Evaluating Interstitial Flow, Local Hydraulics, Downstream Scour Development, and Structure Stability

Conrads, Paul A.

Using "Big Data" to Optimally Model Hydrology and Water Quality across Expansive Regions

Cook, John B.

Using “Big Data” to Optimally Model Hydrology and Water Quality across Expansive Regions

Cook, Mike

Cost-Effective Automated Water Quality Monitoring Systems Providing High-Resolution Data in Near Real-Time

Coop, Tina

Future Water Supply Desalination Technology: Forward Osmosis Co-Located with Power Generation

Copeland, K. S.

Mapping ET at High Resolution in an Advective Semi-Arid Environment with Airborne Multispectral Imagery

Cortés, Oscar J.

Water Distribution Systems Corrective Maintenance Supported by Real-Time Use of Hydraulic Models

Cosgrove, Brian A.

Flash Flood Forecasting for Ungauged Locations with NEXRAD Precipitation Data, Threshold Frequencies, and a Distributed Hydrologic Model

Countryman, Joseph D.

Uncertainty Analysis: You Need to Know What You Don’t Know

Reining in Log-Pearson Type III Flow-Frequency Estimates—Applying a Reasonable Bound through the Skew Parameter

Cowan, Dillon

A Comparison of a SWAT Model for the Cannonsville Watershed with and without Variable Source Area Hydrology

Coyle, E.

Peracetic Acid as an Alternative Disinfection Technology for Wet Weather Sewer Overflows

Creason, Gary W.

Riveside-Quindaro Bend Levee (L-385) on the Missouri River: The Essential Role of O&M and Documentation

Criminisi, A.

Sampling of Residential Water Use for Leak Control via Water Budgets

Crow, Mariesa

Distributed Power Generation at State Facilities: Economic Analysis of Savings and Carbon Credits

A Mobile Emergency Drinking Water System Powered by Renewable Energy

Crowley, Joshua

Comparison of HEC-RAS and InfoWorks RS: A Case Study in Grand Prairie, Texas

Cui, Zhengtao

Distributed Hydrologic Modeling: From Research to Operational Forecasting

Flash Flood Forecasting for Ungauged Locations with NEXRAD Precipitation Data, Threshold Frequencies, and a Distributed Hydrologic Model

Curtis, David C.

Radar-Rainfall Analysis for Extreme August Storm in Sacramento

D

Return to top

Daigger, Glen T.

Urban Water and Wastewater Management in 2050

Damodaram, Chandana

Improving Hydrologic Sustainability of Texas A&M University Campus

Danaei, Erfan

Prediction of Thermal Stratification in Proposed Bakhtyari Reservoir with CE-QUAL-W2

Dandy, Graeme

An Approach for Integrated Optimization of Wastewater, Recycled, and Potable Water Networks

Daranpob, Ammarin

Comparative Study of Two Standard Septic Tank Drain Fields Using Different Sand with Recirculation for Nutrient Removal

Investigating the Temperature Effects on Nutrient Removal in Green Sorption Media

Nutrient and Pathogen Removal with an Innovative Passive Underground Drainfield for On-Site Wastewater Treatment

Davari, K.

Probable Maximum Precipitation for 24 Hour Duration over Four Central Provinces in Iran

Davids, Grant

Application of SIRMOD to Evaluate Potential Tailwater Reduction from Improved Irrigation Management

Davies, Jeffrey W.

Kansas City, MO Overflow Control Program: Line Creek/Rock Creek Sanitary Sewer Study

Davis, A. P.

Bioretention/Bioinfiltration Performance in the Mid-Atlantic

Davis, Allen P.

Analysis of Bioretention Media Specifications and Relationships to Overall Performance

Unit Process Modeling of Stormwater Flow and Pollutant Sorption in a Bioretention Cell

Davis, Jeffery L.

Deployable Decentralized Biofilm System to Degrade Organic Carbon, Nutrients and Benzene from Wastewater

Davis, Meg

Improving Hydrologic Sustainability of Texas A&M University Campus

Davis, Stacia L.

Preliminary Results for Bench Testing of Evapotranspiration-Based Irrigation Controllers in Florida

Dawsey, W. J.

Analysis of Model Sensitivity and Uncertainty for Chlorine Transport and Decay in a Water Distribution System

Day, G. A.

Projecting Future Groundwater Availability for Power Generation Plant Licensing

Assessing Postulated Accidental Releases of Radioactive Liquid Effluents from Nuclear Power Plants

de Bruijn, Hans

Laboratory Testing Guidelines for Certification of Manufactured Stormwater BMPs

De Gilio, Benjamin Bernard

The Impact of Biofilm Development on Pipe Roughness and Velocity Profile

de Ridder, Scott A.

Design Optimization of Hydrodynamic Separators

De Sanctis, Annamaria E.

Real-Time Implementation of Contamination Source Identification Method for Water Distribution Systems

de Santa Olalla, F. Martín

Some Results of Evapotranspiration Measured by Three Weighing Lysimeters in La Mancha, Spain

De Smedt, F.

Multi-Criteria Decision Making under Uncertainty in Rainfall-Runoff Calibration: A Fuzzy Compromise Programming Approach Based on Alpha Level Sets

Spatially Distributed Modeling of Soil Erosion and Sediment Transport at Watershed Scale

Deering, Michael K.

Flood Risk Assessment of Complex Riverine Systems

DeGroot, Gregory P.

Accurate Sampling of Suspended Solids

Demissie, Misganaw

Modeling the Hydrology and Hydraulics of the Cache River System

Deng, Z.-Q.

Statistical Evaluation of BMP Effectiveness in Reducing Nutrient Impairment in Mermentau and Vermilion-Teche River Basins

Denn, Kevin D.

Using Tracers to Derive Sediment Provenance after the Occurrence of a 500-Year Flood in a Midwestern Stream

Dermisis, D. C.

Fish Passage and Abundance around Grade Control Structures on Incised Streams

Effects of Rainfall-Runoff on Soil Surface Roughness and Erosion Processes

Desai, Harshal

Clark County Regional Flood Control District Arc Hydro (CCRFCD Arc Hydro): Toward Ongoing Stormwater Master Planning

Deuerlein, Jochen

Reliability Analysis of Water Distribution Systems Using Graph Decomposition

DeVasher, Michael

Developing Probability of Failure Estimates for Stream Restoration Design Components

Dick, Nicole Marie

Historical Changes in the Streamflow in Kansas Streams: Variation, Causes, and Implications

Dickerson, Thomas

Development of a National GIS Database for Municipal Water and Wastewater Pipe Infrastructure System

Diduch, R.

Application of Optimization Technology to Water Distribution System Master Planning

Dietrich, Andrea M.

Case Study: Homeowner's Preference Trade-Offs toward Plumbing Systems in Pipe Failure Prone Area

Low Pressure Propagation at Service Lines

Ding, Feng

High Resolution Radar Precipitation Evaluation

Flash Flood Forecasting for Ungauged Locations with NEXRAD Precipitation Data, Threshold Frequencies, and a Distributed Hydrologic Model

Ding, Yan

A Process-Based Unsteady Model for Wave-Current-Morphodynamic Changes in Two-Dimensions

Numerical Simulations of Coastal Floods and Morphological Changes Due to Sea Level Rise and Hazardous Storm

Dongell, Beatriz

Integrating Fluvial Geomorphology and Two-Dimensional Hydraulic and Sediment Transport Modeling to Support Sustainable Design of Large River and Floodplain Improvements: The Trinity River Corridor Project, Dallas, Texas, USA

Donnelly, Carolyn

Rehabilitation of the Middle Rio Grande near Bernalillo, New Mexico

Doody, Alexandra

A Tale of Two Cities—Source Water Protection Case Studies for Systems in Rural Settings

Doody, Alexandria

Implementing Source Water Protection Programs in Texas

Selection and Prioritization of Best Management Practices for Potential Sources of Contamination in a Wellhead Protection Area

Doro-on, Anna

Groundwater Baseflow Sourced from Miocene Rocks and Residuals Carries Elevated Selenium into Southern California

Doroudi, Siyamak

Optimal Design of Water Diversion System: A Case Study

dos Santos, Carlos A. C.

Increasing Field Work Productivity in Irrigation Evaluation Processes through the Use of Combined Irrigation Models

Doustdar, Amir Hosein Izad

Prediction of Thermal Stratification in Proposed Bakhtyari Reservoir with CE-QUAL-W2

Dove, E.

The Value of Protecting Ozark Streams: An Economic Evaluation of Stream Bank Stability for Phosphorus Reduction

Downer, Charles W.

Assessment of Lumped, Quasi-Distributed and Distributed Hydrologic Models of the US Army Corps of Engineers

Dremsa, J. J.

South Lake Park Bioretention Gardens

Zona Rosa and Rush Creek Conservation Area—Applied Ecology in a Mixed-Use Development

Duan, Jennifer G.

Comparison of Mean Flow and Turbulence around Experimental Spur Dike

Dukes, M. D.

Irrigation Rain Sensors Accuracy

Dukes, Michael D.

Physiological and Yield Response of Green Bell Pepper to Soil Moisture Sensor Controlled Drip Irrigation

Evaluation of Irrigation Scheduling Efficiency and Adequacy by Various Control Technologies Compared to Theoretical Irrigation Requirement

Preliminary Results for Bench Testing of Evapotranspiration-Based Irrigation Controllers in Florida

Dukes, Michael

The Use of Soil-Water Sensors in Turf Irrigation Control—How Effective Are They?

Dumm, Thomas E.

Planning for Sustainable Growth and Water Resources in the Chesapeake Bay Watershed

Duncker, Alana

An Approach for Integrated Optimization of Wastewater, Recycled, and Potable Water Networks

Dunlap, Patrick J.

Recycling of Multiple Waste Streams for Transportation Fuel Production via Algae Cultivation at Wastewater Treatment Plants

Dunn, Christopher N.

Flood Risk Assessment of Complex Riverine Systems

Dustman, John

Adaptive Long-Term Monitoring at BP Environmental Restoration Sites

Dymond, Randy

Development of a National GIS Database for Municipal Water and Wastewater Pipe Infrastructure System

E

Return to top

Earles, Andrew

Breaking Down the Barriers to Low Impact Development in Colorado

Integration of Low Impact Development Studies into the International Stormwater BMP Database

Easton, Zach

A Comparison of a SWAT Model for the Cannonsville Watershed with and without Variable Source Area Hydrology

Ebacher, G.

Comparison of Pressures Simulated Using Transient Analysis with Field Data from a Full-Scale Distribution System

Eberhardt, Anthony J.

Determining the Causes of Declining Upper Great Lakes Levels—Phase I of the International Upper Great Lakes Study by the St. Clair River Task Team

Ebtehaj, Mohammad

Parameter Uncertainty Estimation of Hydrologic Models Using Bootstrap Resampling

Eck, Brad

Water Quality and Hydraulic Properties of the Permeable Friction Course

Eckhardt, John

Application of SIRMOD to Evaluate Potential Tailwater Reduction from Improved Irrigation Management

Comparison of Evapotranspiration Estimates from Remote Sensing (SEBAL), Water Balance, and Crop Coefficient Approaches

Eckmann, Doug

Hydraulic Modeling and Engineering Evaluation of Fort Myers Beach's Water Distribution System

Edwards, Ryan Wilson John

The Impact of Biofilm Development on Pipe Roughness and Velocity Profile

Eheart, J. W.

Water Quality Effects of Varying Crop, Fertilizer, and Carbon Prices

Ehrhard, R.

Removal of Waterborne Particles by Electrofiltration

Eisenberg, Joseph

A Simplified Model of Combined Sewer Overflows to Estimate Event Driven Enteric Pathogen Concentrations in Drinking Water Sources

El-Didy, Sherif M.

Specific Problems Related to Partially Penetrating Wells in Confined Aquifers

Tool for Estimation of Additional Drawdown Due to Partially Penetrating Wells in Confined and Semi-Confined Aquifers

El-Sheikha, D. M.

Water Use and Evapotranspiration Coefficients for Camelina Sativa

Elahi, M.

Empirical Equation for Abrasion of Stilling Basin Caused by Impact of Sediment

Elgohry, Moustafa

Numerical Simulations of Coastal Floods and Morphological Changes Due to Sea Level Rise and Hazardous Storm

Elhay, Sylvan

A Framework for Alternative Formulations of the Pipe Network Equations

Ellenburg, Walter Lee

Study of Low Dosage Pre-Ozonation on Sand Filtration Efficiency

Ellis, Andre

Geochemistry of Yukon and Copper River Tributaries, Alaska

Human Impact on the Mobilization of a Naturally-Occurring Source of Selenium in an Urbanizing Catchment

Ellis, Philip

The Connectivity of Upland and Instream Processes

Ellison, Rob

Cost-Effective Automated Water Quality Monitoring Systems Providing High-Resolution Data in Near Real-Time

Elmore, A. Curt

Distributed Power Generation at State Facilities: Economic Analysis of Savings and Carbon Credits

Elmore, Andrew Curtis

Application of a Mass Balance-Based Subsurface Contaminant Transport Model

Feasibility Study for Implementing Renewable Energy to Power a Groundwater Pump in Rural Guatemala

Drinking Water Field Analyses for the Detection and Enumeration of Coliform Bacteria in Rural

Guatemalan Highlands

A Mobile Emergency Drinking Water System Powered by Renewable Energy

Elyasi, Asghar

Economic Sustainability Evaluation of an Inter-Basin Water Transfer Project Using GWP Statement

English, Marshall

A Web-Based Advisory Service for Optimum Irrigation Management

Measuring Soil Moisture in a Heterogeneous Field

Ennett, Joe

The Rush Creek Detention Facility: Planning a Permanent BMP in the Real World

Eom, Moosub

Rehabilitation of Mine Impaired Creek in Idaho

Erickson, Andrew J.

Maintenance of Stormwater BMPs

Erickson, Larry

Beyond Compliance and toward Sustainability: Advantages of Systems Environmental Engineering

Ervin, Rhiannon E.

Exploring the Potential of Nonlinear and Non-Equilibrium Alcohol Partitioning for Assessment of DNAPL Source Zone Architecture

Espey, William H. Jr.

Parameterization of Seasonal Freshets for the Study of Effects of Freshwater Inflows on Galveston Bay

Esralew, Rachel A.

Development of Regression Models to Estimate Flow Duration Statistics at Ungaged Streams in Oklahoma Using a Regional Approach

Eubanks, Kevin

Clark County Regional Flood Control District Arc Hydro (CCRFCD Arc Hydro): Toward Ongoing Stormwater Master Planning

F

Return to top

Fahy, Michael P.

Membrane Treatment of Rio Grande Water for Municipal Water Production during the Non-Irrigation Season

Fallah-Mehdipour, E.

MOPSO in Multipurpose Operation of Single-Reservoir System

Fallahpour, Mohammad Reza

Application of Enhanced Methods of Phosphorous and Nitrogen Removal from Wastewater

Falzone, Anthony

Integrating Fluvial Geomorphology and Two-Dimensional Hydraulic and Sediment Transport Modeling to Support Sustainable Design of Large River and Floodplain Improvements: The Trinity River Corridor Project, Dallas, Texas, USA

Fang, Xing

Environmental Impacts on Surface Water and Groundwater for Expanding Urban Water Supply Capacity Using Stone Quarries

Challenges on Three-Dimensional Simulations of Free Surface Flow

Fang, Yilin

Reaction Rates in a Transport System with Both Kinetic and Equilibrium Reactions

Fang, Z.

Distributed Hydrologic Model for Flood Prevention in the Yuna River Water shed, Dominican Republic

Fann, Steve

Implementing a Contamination Warning System at a Department of Defense Facility: Case Study—Port Hueneme, California

Farrokhi, Alireza

Detection of Streamflow Trends and Variability in Karun River, Iran as Parts of Climate Change and Climate Variability

Fayzieva, Dilorom

Investigating Aquatic Ecosystems of Small Lakes in Khorezm , Uzbekistan

Fazeli, M. Sh.

The Effect of Sewage Pollutant of Bandar Imam Petrochemical Company on Benthic Macofauna Community Using Biodiversity Indices and Bioindicators

Fazeli, Mojtaba

Application of Enhanced Methods of Phosphorous and Nitrogen Removal from Wastewater

Feghali, Imad

Removal of Selenium and Nitrate from Surface Waters Using a Subsurface Microbial Filter

Fencl, Luke

Drive for Zero Net Carbon Impact

Feng, N.

Runoffs of the Xiangride and Qaidum Rivers in the Arid Qaidum Basin, Northwest China

Feng, Z.

Assessment of Flood Risk Due to Storm Surge in Coastal Bayous Using Dynamic Hydraulic Modeling

Fernandez-Martinez, Victoria Julia

Water Quality Design Storms for Stormwater Hydrodynamic Separators

Ferrante, M.

In-Line Partially Closed Valves: How to Detect by Transient Tests

Field, Richard

Impact of Wet-Weather Peak Flow Blending on Disinfection Performance

Kansas City—Balancing Green Infrastructure with Traditional Approaches for CSO Control

Filho, Secundino Soares

Computer-Aided System for Managing, Controlling, and Analyzing Data from Hydroelectric Plants

Findikakis, A. N.

Assessing Postulated Accidental Releases of Radioactive Liquid Effluents from Nuclear Power Plants

Fischbeck, Paul S.

Decision Making under Information Constraints

Fleenor, William E.

Challenges of Managing California's Sacramento—San Joaquin Delta

Flowers, Lakin

South Florida Water Control System Tracker: Real-Time Water Budgeting for Pragmatic Water Control Operations

Fontane, Darrell G.

Computer-Aided System for Managing, Controlling, and Analyzing Data from Hydroelectric Plants

Multireservoir Simulation Using Multipurpose Constraints and Object-Oriented Software Design

Foreman, Terry

Managing Salinity in the Upper Santa Clara River System of California

Fortunato, A.

Sampling of Residential Water Use for Leak Control via Water Budgets

Foster, Gene L.

Diversion of S-4 Basin Drainage from Lake Okeechobee: Hydraulic Modeling of Alternatives Using HEC-RAS

Fotherby, Lisa M.

Preliminary Assessment of Planform Change at Low Flows with Vegetation Expansion: Platte River, Nebraska

Fouss, James L.

Agricultural Drainage Management Systems Task Force (ADMSTF)

Fowler, George D.

Sediment Monitoring Bias by Autosampler in Comparison with Whole Volume Sampling for Parking Lot Runoff

Fox, G. A.

Predicting Streambank Seepage Flows: Sensitivity to Soil Properties and Layering

A Seepage Erosion Sediment Transport Function and Geometric Headcut Relationships for Predicting

Seepage Erosion Undercutting

Fox, J. F.

Investigation of Land-Use Change and Hydrologic Forcing upon Streambank Erosion and In-Stream Sediment Processes Using a Watershed Model and Sediment Tracers

Fox, Sandra

How to Build a Broadly Useable GIS Toolset for Estuary Analysis

Francato, Alberto L.

Climate Flow Forecast Model for the Brazilian Hydropower System

Impacts of the Upstream Storage Reservoirs on Itaipu Hydropower Plant Operation

Francis, Tim

Integrated Planning for Dual Distribution Systems

Frank, Paul

Integrating Fluvial Geomorphology and Two-Dimensional Hydraulic and Sediment Transport Modeling to Support Sustainable Design of Large River and Floodplain Improvements: The Trinity River Corridor Project, Dallas, Texas, USA

Frankenburger, J.

Change in Surface Hydrology Due to Land Use Change in a Midwestern Watershed

Freeman, Hunter

The Road to LID Plan Approval in Coastal North Carolina: Development of a Spreadsheet Modeling Tool for LID Based Designs

Freeman, Scott

Innovative Strategies Alleviate Water Stress in South East Queensland, Australia

French, A. N.

Water Use and Evapotranspiration Coefficients for Camelina Sativa

Frenkel, Val S.

Desalination Concentrate: Bay vs. Ocean

Frevert, D.

Developments on Stochastic Analysis, Modeling, and Simulation (SAMS 2009)

Friesen, Jeff

Integrated Watershed Protection Plan and Management Strategy for the Calleguas Creek Watershed in Ventura County

Fringer, O. B.

Simulations of Aquaculture Dissolved Waste Transport and Mixing in Near-Coastal Waters

Fuchs, Valerie J.

Treatment Performance of Wastewater Lagoons in South Yungas Province of Bolivia

Fuelberg, Henry E.

Use of NEXRAD Rainfall Data to Develop Climatologically Homogenous Rain Areas for Central and South Florida

Fuelberg, Henry

Evaluation of Improvised Spatial Interpolation Methods for Infilling Missing Precipitation Records

Fuertes, Vicente S.

Statistical Analysis of Water Distribution Networks Design Using Harmony Search

Funderburk, Katie

Wastewater Utilities: Are You Ready for Kansas' Nutrient Removal Policy?

G

Return to top

Gabel, Dale

Survey of Water and Wastewater Utility Security Standards

Galef, Jefferey K.

Water Resources Planning under Non-Stationary Hydroclimate in a Snow Dominant Watershed

Gallagher, N. T.

Decentralized Anaerobic Treatment of Blackwater: A Sustainable Development Technology Concept for Urban Water Management

Galloway, Gerald

Flood Risk Management circa 2050

Gambucci, Thomas

ADH = Fast and Stable 2D Finite Element Model

Performance Evaluation of Articulated Concrete Matting (ACM) Spillway at Lake Odessa, Iowa

Garbrecht, Jurgen D.

Do Upland Soil Conservation Measures Reduce Watershed Sediment Yield?

Garcia, L. A.

Mapping ET at High Resolution in an Advective Semi-Arid Environment with Airborne Multispectral Imagery

Garcia, M.

Automated Selection of Anchor Pixels for Landsat Based Evapotranspiration Estimation

Garcia, Marcelo H.

Hydraulic Model Study of Canoe Chute and Fish Passage for the Chicago River North Branch Dam

Upstream Intrusion Effect of CSO Event in Bubbly Creek, IL

García, Marcelo H.

Two-Dimensional BOD and DO Water Quality Model for Engineering Applications: The Case of Bubbly Creek in Chicago, Illinois

A Robust and Fast Model for Simulating Street Flooding

Boundary Conditions for Simulating Complex Storm-Sewer Systems in Free Surface, Pressurized, and Mixed Flow Conditions

Garg, Vaibhav

Reservoir Sedimentation Estimation Using Genetic Programming Technique

Garland, Robert

Hydraulic Modeling and Engineering Evaluation of Fort Myers Beach's Water Distribution System

Garrett, Patrick

Protocol Considerations to Improve the Reliability of Data Collection in a Radio Telemetry System

Gaskin, R.

KC-One: Comprehensive City-Wide Management Plan Creates Leading Stormwater Management Program

Gebremichael, M.

A Blueprint for Advancing Hydrologic Predictability in Developing Countries: A Case Study for the Nile River Basin

Gebremichael, M.

On the Local-Scale Spatial Variability of Daily Rainfall in the Highlands of the Blue Nile: Observational Evidence

Gee, D. Michael

Comparison of Dam Breach Parameter Estimators

Estimating Probability of Extreme Events

Geem, Zong Woo

Hydraulic Analysis of Water Distribution Network Using Harmony Search

Gemio, Gabriela

Treatment Performance of Wastewater Lagoons in South Yungas Province of Bolivia

Gerloff, Fred

Pressure vs. Flow Relationship for Pipe Leaks

Ghahraman, B.

Probable Maximum Precipitation for 24 Hour Duration over Four Central Provinces in Iran

Ghajarnia, N.

Reliability Based Design of Water Distribution Network (WDN) Considering the Reliability of Nodal Pressures

Ghassemi, Abbas

Evaluation of a UV/Ozone Treatment Process for Removal of MTBE in Groundwater Supplies in New Mexico

Ghazali, Mirnader

Comparative Evaluation of Two Algorithms for Locating Contaminant Ingress Points

Ghazanfari, S.

Probable Maximum Precipitation for 24 Hour Duration over Four Central Provinces in Iran

Ghidaoui, Mohamed S.

Boundary Conditions for Simulating Complex Storm-Sewer Systems in Free Surface, Pressurized, and Mixed Flow Conditions

Ghimire, Santosh R.

Impact of Storage Tanks on Energy Consumption in Municipal Water Distribution Systems

Giacomoni, M. H.

Hydrologic Footprint Residence: A New Metric to Assess Hydrological Alterations Due to Urbanization

Giacomoni, Marcio

Improving Hydrologic Sustainability of Texas A&M University Campus

Giráldez, J. V.

Integrated Water Management in an Ancestral Water Scheme in a Mountainous Area of Southern Spain

Giridhar, M. V. S. S.

Evaluation of Land Use Land Cover Changes in Palleru (K-11) Sub Basin of River Krishna Using GIS and NDVI

Girma, Y.

On the Local-Scale Spatial Variability of Daily Rainfall in the Highlands of the Blue Nile: Observational Evidence

Gitt, Jennifer

Multi-Criteria Assessment of Pallid Sturgeon Habitat Restoration for the Missouri River

Giustolisi, O.

Enhanced Global Gradient Algorithm: A General Formulation

Enhanced WDN Analysis: Representation of Actual Pipe Connections

An Operative Approach to Water Distribution System Rehabilitation

Glick, R. H.

Linking Environmental Assessment and Solutions

Goel, Arun

Application of SVMs Algorithms for Prediction of Evaporation in Reservoirs

Gómez-Landesa, E.

Integrated Water Management in an Ancestral Water Scheme in a Mountainous Area of Southern Spain

Goo, Robert

Cost Estimating Tools for Low-Impact Development Best Management Practices

Gosselink, L.

Linking Environmental Assessment and Solutions

Gossenauer, Michael

Sediment Management for Shallow Water Habitat Creation on the Missouri River

Govindaraju, R. S.

Change in Surface Hydrology Due to Land Use Change in a Midwestern Watershed

Govindaraju, Rao S.

A Spatio-Temporal Drought Analysis for the Midwestern US

On the Use of Data Uncertainty in Hydro-Climatic Modeling: A Bayesian Approach

Gowda, P. H.

Independent Comparisons among Calibration and Output of Energy Balance Components Estimated by the METRIC Procedure

Mapping ET at High Resolution in an Advective Semi-Arid Environment with Airborne Multispectral Imagery

Gowda, Prasanna H.

Application of Remote Sensing Based Tillage Mapping Technique to Evaluate Water Quality Impacts of Tillage Management Decisions in Upper White River Basin

Gowdish, Leslie

South Florida Water Control System Tracker: Real-Time Water Budgeting for Pragmatic Water Control Operations

Grabow, Garry L.

The Use of Soil-Water Sensors in Turf Irrigation Control—How Effective Are They?

Granich, Will

Distributed Power Generation at State Facilities: Economic Analysis of Savings and Carbon Credits

Feasibility Study for Implementing Renewable Energy to Power a Groundwater Pump in Rural Guatemala

Grayman, Walter M.

Effects of Redesign of Water Systems for Security and Water Quality Factors

Environmental and Developmental Risks and Stressors Impacting a 2050 Vision

Characterization of Water Resources and Environmental Disasters

Grayman, Walter

Sensor Network Design and Performance in Water Systems Dominated by Multi-Story Buildings

Needs and Trends of the Nation's Water Infrastructure—The Utility Perspective

Green, Jack

Hydraulic Modeling and Engineering Evaluation of Fort Myers Beach's Water Distribution System

Green, Ryan

Beyond Compliance and toward Sustainability: Advantages of Systems Environmental Engineering

Greene, A. M.

Impacts of Biota on Bioretention Cell Performance during Establishment in the Midwest

Greimann, Blair P.

Predicting Rock Scour in an Alluvial River with a One-Dimensional Model

Predicting Rock Scour in an Alluvial River with a Two-Dimensional Model

Numerical Model of Channel Meandering in the Middle Sacramento River

Griffin, Mitchell

Selecting Optimal Water Supply Options—A Regional Water Supply Case Study in the Upper Kissimmee Basin, FL

Griffioen, M. L.

Modeling Domestic Water Demand on a Suburb Level

Griffis, Veronica W.

Providing a Physical Basis for Statistical Homogeneity in Regional Frequency Analyses

Grigg, Neil S.

National Mains Failure Database Project

Grimshaw, Frank

Development of a Fuzzy Based Pipe Condition Assessment Model Using PROMETHEE

Grothaus, John

Importance of Levees in the Kansas City Area

Protecting Infrastructure: Emergency Streambank Stabilization

Guan, J.

A Critical Realization Identification Method Based on Pareto Dominance Analysis

Guan, Jiabao

A Methodology to Reconstruct Groundwater Contamination History with Limited Field Data

Guerrero, Felipe M.

Water Retention and Hydraulic Conductivity of Different Media Used for Containerized Agriculture Systems

Guerrero, Frank

Managing Salinity in the Upper Santa Clara River System of California

Guestrin, Carlos

Robust Sensor Placement for Detecting Adversarial Contaminations in Water Distribution Systems

Gulliver, John S.

Accurate Sampling of Suspended Solids

Maintenance of Stormwater BMPs

Proposed Scaling Relations for Manufactured Stormwater BMPs

Gulliver, John

Assessing Hydrodynamic Separators under High Water Flow Conditions

Assessment of Standard Sumps for Stormwater Treatment

Field Testing Guidelines for Certification of Manufactured Stormwater BMPs: Part II

Guo, Qizhong

Proposed Scaling Relations for Manufactured Stormwater BMPs

Sediment Monitoring Bias by Autosampler in Comparison with Whole Volume Sampling for Parking Lot Runoff

Water Quality Design Storms for Stormwater Hydrodynamic Separators

Gupta, Piyush

Multiobjective Differential Evolution and Differential Evolution for Irrigation Planning

Gupta, Vaibhav

Watershed Management in the Indian Himalayan Region: Issues and Challenges

Sustainable Development of Agriculture: Urban Waste Water a Viable Mean for Irrigation

Gurian, Patrick

Prediction of Nitrate Concentration in Stream Water Based on Watershed Land Use and Stream Flow Rate

Gurr, Eric

Non-Point Source Nutrient Loading in an Urban Watershed

Guth, Nicolai

Integrated Hydraulic Analysis and Data Management Tool for Water Supply Systems in Developing Countries

Gutierrez, Angelica

Transitioning NWS Operational Hydraulics Models from FLDWAV to HEC-RAS

H

Return to top

Haase, C. Stephen

The Nature Conservancy's Mississippi River Program: Sustainable Conservation of a Working River that Works

Habarth, Maureen L.

Hydrologic Modeling and Flood Frequency Analysis of the Sonora River Watershed in Sonora, Northwest Mexico

Habib, Emad

Adjustment of the Z-R Relationship in Real-Time for Use in South Florida

Hachett, Sam

Real-Time Implementation of Contamination Source Identification Method for Water Distribution Systems

Haddad, O. Bozorg

MOPSO in Multipurpose Operation of Single-Reservoir System

Reliability Based Design of Water Distribution Network (WDN) Considering the Reliability of Nodal Pressures

Hahn, K. L.

Hydrogeologic Investigation for New Water Supply for Water District No. 1 of Johnson County, Kansas

Hair, Lisa

Cost Estimating Tools for Low-Impact Development Best Management Practices

Hall, Anthony

Brentwood Stream Restoration Project – Lenexa, Kansas

Hall, Brad R.

One-Dimensional Modeling of Sedimentation Processes on the Puyallup River

Hall, Lindsay

Application of SIRMOD to Evaluate Potential Tailwater Reduction from Improved Irrigation Management

Hall, Steve

The Arkansas Irrigation Scheduler

Haltas, I.

Modeling the Kinematic Wave Parameters with Regression Methods

Hamaker, T.

Post Project Appraisal of Riparian, Wetland, and Aquatic Habitat Restoration at Best Slough, Beale Air Force Base, Marysville, CA

Hammack, E. Allen

3D Numerical Modeling of John Day Lock Tainter Valves

Hammouri, Munther

Numerical Simulation of Chemical Spills Using CCHE2D Model and Chemical Property Database

Hampson, Jack

South Florida Water Control System Tracker: Real-Time Water Budgeting for Pragmatic Water Control Operations

A Pragmatic Cycle for Ongoing Water Resources Research and Management

Hampton, Sarah A.

Water-Quality Assessment of the Largely Urban Blue River Basin, Metropolitan Kansas City, USA, 1998 to 2007

Han, Chengwei

The Nitrogen Budget of DRW in Northeastern China

Hanak, Ellen

Challenges of Managing California's Sacramento—San Joaquin Delta

Handy, Jeffrey

A Heuristic Algorithm for Optimal Alignment and Matching of Borehole Stratigraphy

Hanson, B. R.

Mid-Summer Deficit Irrigation of Alfalfa as a Strategy for Saving Water

Hanson, Cara M.

Treatment Performance of Wastewater Lagoons in South Yungas Province of Bolivia

Hanson, Lars S.

Generalized Storage-Reliability-Yield Equations for Rainwater Harvesting Systems

Hanson, Lars

Communicating Drought Severity and Re-Evaluating Firm Yield—Cumberland County, Tennessee As a Case Study

Hantush, Mohamed M.

Estimation of TMDLs and Margin of Safety under Conditions of Uncertainty

Harms, Harold H.

Development of a Community Water Security Filtration System Using Composite Cartridges

Harris, Jeff

Estimating Probability of Extreme Events

Harrison, Kenneth W.

A Markov Chain Monte Carlo Implementation of Bayesian Contaminant Source Characterization in Water Distribution Systems under Stochastic Demands

Hart, David

Trajectory Clustering Approach for Reducing Water Quality Event False Alarms

Hartman, David

Preliminary Spatial-Temporal Statistical Analysis of Hourly Water Demand at Household Level

Hartsig, T. A.

South Lake Park Bioretention Gardens

Hashemi, Seyyed Hosein

Prediction of Thermal Stratification in Proposed Bakhtyari Reservoir with CE-QUAL-W2

Hasit, Yakir J.

Survey of Water and Wastewater Utility Security Standards

Implementing a Contamination Warning System at a Department of Defense Facility: Case Study—Port Hueneme, California

Hatchett, Sam

Comparing Single- and Multi-Species Water Quality Modeling Approaches for Assessing Contamination Exposure in Drinking Water Distribution Systems

Hathaway, J. M.

An Evaluation of Stormwater Wetlands in Series

Field Evaluation of Indicator Bacteria Removal by Stormwater BMPs in North Carolina

Hathaway, Jon

Field Testing Guidelines for Certification of Manufactured Stormwater BMPs: Part II

Haught, Roy C.

Development of a Community Water Security Filtration System Using Composite Cartridges

Hawkes, Trevor P.

Fish Passage Can Be Improved by Introducing Hydraulic Refuge: Can the Effects Be Quantified?

Haxton, Terra Baranowski

Sensor Network Design and Performance in Water Systems Dominated by Multi-Story Buildings

Haxton, Terranna Baranowski

Modeling a Hydraulic Response to a Contamination Event

Hay, C. H.

Recursive and Explicit Combination Methods for Calculating Reference Evapotranspiration

Hays, Matthew D.

Fish Passage Can Be Improved by Introducing Hydraulic Refuge: Can the Effects Be Quantified?

He, Li

Comparison of Mean Flow and Turbulence around Experimental Spur Dike

He, Xin

The Geneva Dam, IL, Hydraulic Roller Problem: Design of a Temporary Steep Riprap Ramp

He, Zhiguo

A Depth-Averaged 2-D Model of Non-Cohesive Dam/Levee Breach Processes

Prediction of Changes in Soil Moisture Due to Rainfall, Infiltration, and Evapotranspiration Using a Physically-Based Model

He, Zhuangxiang

Unit Process Modeling of Stormwater Flow and Pollutant Sorption in a Bioretention Cell

Headley, R. R.

Modeling Stormwater Basins for Potential Retrofit Designs

Heaney, James P.

Urban Stormwater Management in 2050

Heeren, D. M.

Predicting Streambank Seepage Flows: Sensitivity to Soil Properties and Layering

Heineman, Mitchell

State of the Practice of Wet Weather Flow Analysis

Heiner, Bryan J.

Managing Reservoir Discharge through Accurate Flow Measurement

Helbling, D. E.

Propagation of Chlorine Demand Signals Induced by Microbial Contaminants in a Drinking Water Distribution System

Helmers, M. J.

Drainage Main Rehabilitation in Iowa

Helmers, Matthew H.

Denitrifying Bioreactors for Treatment of Tile Drainage

Henderson, Devan

Investigating the Temperature Effects on Nutrient Removal in Green Sorption Media

Henggeler, J. C.

Woodruff Irrigation Charts

Henschke, Amy

Adjustment of the Z-R Relationship in Real-Time for Use in South Florida

Henson, J. W.

KC-One: Comprehensive City-Wide Management Plan Creates Leading Stormwater Management Program

Hydrogeologic Investigation for New Water Supply for Water District No. 1 of Johnson County, Kansas

Heo, Jun-Haeng

Asymptotic Variance of Regional Growth Curve for Generalized Logistic Distribution

Inflow Forecasting for Real-Time Reservoir Operation Using Artificial Neural Network

Herman, Janet

Prediction of Nitrate Concentration in Stream Water Based on Watershed Land Use and Stream Flow Rate

Hernandez Alvarado, Jairo

Sustainability of Rural Water Supply Projects in Nicaragua

Herrington, C.

Linking Environmental Assessment and Solutions

Herrington, Chris

Extension of an LA-QUAL Model for Evaluating a Proposed Wastewater Discharge to Realistic Receiving Water Temperature and Flow Conditions

Hibbs, B.

Characterizing Water Inputs to Catchments in the Santa Monica Mountains with δ180 and δD

Hibbs, Barry

Groundwater Baseflow Sourced from Miocene Rocks and Residuals Carries Elevated Selenium into Southern California

Human Impact on the Mobilization of a Naturally-Occurring Source of Selenium in an Urbanizing Catchment

Hidalgo, Ieda G.

Computer-Aided System for Managing, Controlling, and Analyzing Data from Hydroelectric Plants

Multireservoir Simulation Using Multipurpose Constraints and Object-Oriented Software Design

Higgins, Kathleen

Integrated Watershed Protection Plan and Management Strategy for the Calleguas Creek Watershed in Ventura County

Hill, D. J.

Predicting CSOs for Real Time Decision Support

Hill, David

Evolutionary Optimization of Combined Sewer Overflow Control

Hill, Robert W.

ASCE Standardized Penman-Monteith Alfalfa Reference ET and Crop ET Estimates for Arkansas River Compact Compliance in Colorado

Hillyer, Charles

A Web-Based Advisory Service for Optimum Irrigation Management

Hinkle, Lynn

How the Heart of America is *Goin' Green* to Solve Water and Sewer Issues

Hiratsuka, Akira

Combining Rule-Based Fuzzy Model with GIS to Predict Groundwater Vulnerability to Contamination

Hirpa, F. A.

On the Local-Scale Spatial Variability of Daily Rainfall in the Highlands of the Blue Nile: Observational Evidence

Hirschman, Dave

The Runoff Reduction Method

Hobbs, Benjamin F.

A Bayesian Framework for Cost Effective Management of Sediment Reduction in the Minnesota River Basin

Hoch, Matthew P.

Codorus Creek Restoration—A Case Study for the Chesapeake Bay

Hoffmann, Greg

The Runoff Reduction Method

Holburn, E. R.

Habitat Restoration on the Middle Fork John Day River

Holburn, Elaina

Field Evaluation of Engineered Large Woody Debris for Structure Performance and Habitat Value

Quantitative Evaluation of Rock Weir Field Performance

Holland, Sabin

Deployable Decentralized Biofilm System to Degrade Organic Carbon, Nutrients and Benzene from Wastewater

Hollingsworth, Michelle

Improving Hydrologic Sustainability of Texas A&M University Campus

Holloway, Nathaniel Hanna

Monitoring the Hydrologic Effects of an Extensive Green Roof

Holmes, Hillary

Improving Hydrologic Sustainability of Texas A&M University Campus

Holmquist-Johnson, Christopher L.

Numerical Analysis of the Performance of Rock Weirs: Effects of Structure Configuration on Local Hydraulics

Physical Modeling of River Spanning Rock Structures: Evaluating Interstitial Flow, Local Hydraulics, Downstream Scour Development, and Structure Stability

Honan, G.

Ecosystem Services Approach to Public Facility Planning

Hope, A.

The Effect of Municipal Landfill Leachate on the Characterization of Fluid Flow through Clay

Horn, Patrick F.

Alternatives Study of Willwood Diversion Dam Siltation Removal in Wyoming, USA

Horras, Ashlynn

Drive for Zero Net Carbon Impact

Horsley, M. B.

Hydrogeologic Investigation for New Water Supply for Water District No. 1 of Johnson County, Kansas

Hoskins, J. S.

The “Silver Bullet”: Proprietary BMPs and Metropolitan St. Louis Sewer District’s Stormwater Program

Hosseinipour, E. Zia

Integrated Watershed Protection Plan and Management Strategy for the Calleguas Creek Watershed in Ventura County

Integrated Surface Water and Groundwater Modeling of Orange River Basin in Southwest Florida for Flood Mitigation/Ecosystem Restoration

Hossian, Fahim

Comparative Study of Two Standard Septic Tank Drain Fields Using Different Sand with Recirculation for Nutrient Removal

Nutrient and Pathogen Removal with an Innovative Passive Underground Drainfield for On-Site Wastewater Treatment

Hotchkiss, Rollin H.

Fish Passage Can Be Improved by Introducing Hydraulic Refuge: Can the Effects Be Quantified?

Culvert Retrofit and Fish Passage: An Update

Houdeshel, C. Dasch

Cost Estimating Tools for Low-Impact Development Best Management Practices

Houle, James J.

Examination of Pervious Concrete and Porous Asphalt Pavements Performance for Stormwater Management in Northern Climates

Houle, James

Sediment Monitoring Bias by Autosampler in Comparison with Whole Volume Sampling for Parking Lot Runoff

Houle, Kristopher M.

Examination of Pervious Concrete and Porous Asphalt Pavements Performance for Stormwater Management in Northern Climates

Howard, Adam

Assessment of Standard Sumps for Stormwater Treatment

Howell, T. A.

Independent Comparisons among Calibration and Output of Energy Balance Components Estimated by the METRIC Procedure

Mapping ET at High Resolution in an Advective Semi-Arid Environment with Airborne Multispectral Imagery

Howie, Sean James

The Impact of Biofilm Development on Pipe Roughness and Velocity Profile

Howitt, Richard E.

Challenges of Managing California's Sacramento—San Joaquin Delta

Hoyt, Alison M.

Treatment Performance of Wastewater Lagoons in South Yungas Province of Bolivia

Hu, Gordon

Estimating Groundwater Seepages to St. Lucie Estuary

Hu, W.

Characterizing Water Inputs to Catchments in the Santa Monica Mountains with δ180 and δD

Hu, Wynee

Groundwater Baseflow Sourced from Miocene Rocks and Residuals Carries Elevated Selenium into Southern California

Hu, Zhiqiang

Nitrification Inhibition by UVA Photocatalytic TiO2 Nanoparticles: The Role of Reactive Oxygen Species on Nanotoxicity

Biological Nutrient Removal from On-Site Wastewater Treatment Systems Using a Membrane Aerated Bioreactor

Huang, Guobiao

Integrated Watershed Modeling

Huang, Jianchun

Numerical Model of Channel Meandering in the Middle Sacramento River

Huang, Tinglin

Optimal Distribution of Pressure Measurement Points in Water Distribution Networks

Huebner, R. Scott

Understanding Uncertainties in Water Budget for Large Constructed Wetlands

Hunsaker, D. J.

Water Use and Evapotranspiration Coefficients for Camelina Sativa

Hunt, Bill

Data Reporting Guidelines for Certification of Manufactured Stormwater BMPs: Part II

Field Testing Guidelines for Certification of Manufactured Stormwater BMPs: Part II

Hunt, S. L.

The Effect of Step Height on Energy Dissipation in Stepped Spillways

Hunt, W. F.

An Evaluation of Stormwater Wetlands in Series

Bioretention/Bioinfiltration Performance in the Mid-Atlantic

Effects of Media Depth on Bioretention Performance in the Upper Coastal Plain of North Carolina and Bioretention Construction Impacts Study

Field Evaluation of Indicator Bacteria Removal by Stormwater BMPs in North Carolina

Research of Hydrologic and Water Quality Performance of Four Linear Wetlands in Eastern North Carolina

Implementation and Performance of Stormwater Best Management Practice Retrofits in Wilmington, NC

Water Quality Assessed by Benthic Macro-Invertebrates: Proposing the WQABI Method

Hunt, William F.

A Level Spreader—Vegetated Buffer System for Urban Stormwater Management

Effect of Bioretention on Runoff Temperature in Trout Sensitive Regions

Rainwater Harvesting Experiences in the Humid Southeast USA

Huntington, J. L.

Evapotranspiration and Net Irrigation Water Requirements for Nevada

Huo, Jinsheng

Hydraulic Modeling and Engineering Evaluation of Fort Myers Beach's Water Distribution System

Research and Application of Activated Sludge Models

Hutchinson, Kent

A Web-Based Advisory Service for Optimum Irrigation Management

Hutchinson, S. L.

Impacts of Biota on Bioretention Cell Performance during Establishment in the Midwest

Hutchinson, William R.

Desalination of Brackish Groundwater and Deep Well Injection of Concentrate in El Paso, Texas

I

Return to top

Ibendahl, Elise

Modeling Impacts of Conventional and Low Impact Stormwater Controls on Receiving Streams

Icenogle, Bret A.

Modeling Water Quality Impacts in Delaware's Coastal Bays with AGNPS

Iglesias, Pedro L.

Statistical Analysis of Water Distribution Networks Design Using Harmony Search

Ilorme, Fredline

Providing a Physical Basis for Statistical Homogeneity in Regional Frequency Analyses

Indrakumar, N.

Effective Management of Natural Resources under Dry Land Farming through Watershed Basis

Ingol-Blanco, Eusebio

Hydrologic Modeling for Assessing Climate Change Impacts on the Water Resources of the Rio Conchos Basin

Inthasaro, Podjanee

One-Dimensional Modeling of Water Quality and Aquatic Ecosystems in Streams

Irmak, A.

Performance Evaluation of Soil Heat Flux Models in Great Plains

Irmak, S.

Recursive and Explicit Combination Methods for Calculating Reference Evapotranspiration

J

Return to top

Jacobi, Sarah K.

A Bayesian Framework for Cost Effective Management of Sediment Reduction in the Minnesota River Basin

Jacobs, Tom A.

Analyzing the Impacts of a Retrofit Detention Basin Flow Control Strategy on Biodiversity in an Urban Stream System

Innovative Design at Lake Lenexa

Brentwood Stream Restoration Project – Lenexa, Kansas

The Impact of Smaller Detention Basins on Flood Hazard Areas in Lenexa, Kansas

Jacobs, Tom

10,000 Rain Gardens, One Green Region

Kansas City—Balancing Green Infrastructure with Traditional Approaches for CSO Control

Jacobsen, Laura

An Integrated Approach for Distribution System Hydraulic Criticality and Emergency Response

Jacobson, Gary

Implementing a Contamination Warning System at a Department of Defense Facility: Case Study—Port Hueneme, California

Jadlocki, S. J.

Field Evaluation of Indicator Bacteria Removal by Stormwater BMPs in North Carolina

Jalali, M. R.

Deriving Rule Curve for Hydropower Reservoirs: Seymareh Experience

Jamka, Leslie

Beyond Compliance and toward Sustainability: Advantages of Systems Environmental Engineering

Jang, S.

Statistical Characteristics of Land Surface Properties for the Regional Hydroclimate Model

Jang, Wonyong

Modeling of Chlorinated VOCs Transport under Dual Bioreactions

Janke, R.

Simple Model of Attachment and Detachment of Pathogens in Water Distribution System Biofilms

Janke, Robert

Sensor Network Design and Performance in Water Systems Dominated by Multi-Story Buildings

Preliminary Spatial-Temporal Statistical Analysis of Hourly Water Demand at Household Level

Jarchow, Pete

Kansas River Bank Stabilization and Post-Project Conditions

Protecting Infrastructure: Emergency Streambank Stabilization

Jensen, D. G.

Water Supply and Energy Generation

Jensen, James H.

Concentrate Management and Disposal Practices in Australia

Jensen, Mark R.

New Floodplain Delineation Capabilities in HEC-RAS

Jensen, Marvin E.

Adjusting Wind Speed Measured over Variable Height Alfalfa for Use in the ASCE Standardized Penman-Monteith Equation

Jeong, Sangman

Use of Hydraulic Modeling to Develop a Small Dam for the Geum River Reach in Sejong City

Ji, Min

Research and Application of Activated Sludge Models

Ji, Un

Sedimentation Characteristics of the Lower Nakdong River Upstream of the Nakdong River Estuary Barrage

Jia, S.

Runoffs of the Xiangride and Qaidum Rivers in the Arid Qaidum Basin, Northwest China

Jia, Xinhua

Comparison of Sensible Heat Flux Measurements by a Large Aperture Scintillometer and Eddy Correlation Methods

Jia, Yafei

Numerical Modeling of Ozonation of Organic Chemicals in Surface Water

Numerical Simulation of Chemical Spills Using CCHE2D Model and Chemical Property Database

Numerical Simulation of Sediment Transport and Morphological Change of JiJi Weir Reservoir

Jiang, Hua

Innovative Strategies Alleviate Water Stress in South East Queensland, Australia

Jiang, Yan

Research and Application of Activated Sludge Models

Jin, Yongliang

A Direct Method for Determining Riprap Size for Erosion Protection in Rivers

Johnson, Benjamin W.

Application of a Mass Balance-Based Subsurface Contaminant Transport Model

Johnson, Esther M.

Treatment Performance of Wastewater Lagoons in South Yungas Province of Bolivia

Johnson, Jeff

Rehabilitation of Mine Impaired Creek in Idaho

Johnson, Ronald S.

Considerations, Opportunities, and Strategies for Infiltration Stormwater BMPs

Johnston, Charlene

Data Reporting Guidelines for Certification of Manufactured Stormwater BMPs: Part II

Johnstone, Ralph

Developing Green Streets Prototypes to Reduce Combined Sewer Overflows for Cincinnati, Ohio

Jokerst, A. W.

An Evaluation of Graywater Reuse Utilizing a Constructed Wetland Treatment System

Jones, G. D.

Redesigning Constructed Stormwater Wetlands: An Integrated Modeling Approach to Optimize Form and Function

Jones, Gerrad

Developing a Water Budget for a Constructed Stormwater Wetland

An Investigation of Infiltration in a Constructed Stormwater Wetland and Implications for Groundwater Quality

Jones, Jonathan

Challenges in Attaining Recreational Stream Standards for Bacteria: Setting Realistic Expectations for Management Policies and BMPs

Integration of Low Impact Development Studies into the International Stormwater BMP Database

Jones, Matthew

Effect of Bioretention on Runoff Temperature in Trout Sensitive Regions

Rainwater Harvesting Experiences in the Humid Southeast USA

Jones, Norman

A Heuristic Algorithm for Optimal Alignment and Matching of Borehole Stratigraphy

Jones, R. Gavin

Deployable Decentralized Biofilm System to Degrade Organic Carbon, Nutrients and Benzene from Wastewater

Jothiprakash, V.

Reservoir Sedimentation Estimation Using Genetic Programming Technique

Jung, B. S.

Comparison of Pressures Simulated Using Transient Analysis with Field Data from a Full-Scale Distribution System

Jung, Bong Seog

Multi-Objective Design of Transient Network Models

Jung, Younghun

Asymptotic Variance of Regional Growth Curve for Generalized Logistic Distribution

Jurado, César M.

Calibration of Water Distribution Network Models as a Tool for Detecting Missing and Erroneous Cadastral and Hydraulic Information

Just, Craig

Upper Mississippi River Basin Envirohydrologic Observatory

K

Return to top

Kaatz, Laurna

Looking for a Solution—Joint Front Range Climate Change Vulnerability Study

Kabala, Zbigniew

Vadose Zone Transport of Nitrate in the Sierra Pelona Groundwater Basin, Agua Dulce, California

Kadavy, K. C.

The Effect of Step Height on Energy Dissipation in Stepped Spillways

Kadir, Tariq N.

Water Resources Planning under Non-Stationary Hydroclimate in a Snow Dominant Watershed

Kadiyala, Raja

Advances in Data Validation, Event Detection, and Communications Structures for a CWS: Case Study—Glendale, Arizona

Implementing a Contamination Warning System at a Department of Defense Facility: Case Study—Port Hueneme, California

Kaini, P.

Generating Different Scenarios of BMP Designs in a Watershed Scale by Combining NSGA-II with SWAT

Kakuturu, S. P.

Engineered Waste Materials as Amendments to Prevent Erosion and to Stabilize Contaminated Sites

Kalin, Latif

Studying the Impact of Land Use/Cover Changes on the Water Quality of Weeks Bay, AL: Model vs. Regression

Kaluvakolanu, Preethi

The Lawrence Technological University Greenroof Performance Evaluation Project

Kamojjala, Sri

An Integrated Approach for Distribution System Hydraulic Criticality and Emergency Response

Kang, D. S.

Design of Dual Water Supply Systems

Kang, Doo Sun

New Concepts for Meter Placement in Water Distribution Systems for Demand Estimation

Real-Time Valve Operation for Water Quality Improvement in Water Distribution Systems

Kang, Joo-Hyon

Maintenance of Stormwater BMPs

Kansal, Mitthan Lal

Threat Perceptions and Risk Management in Urban Water Supply Schemes

Kanta, Lufthansa

A Multi-Objective Evolutionary Computation Approach to Hazards Mitigation Design for Water Distribution Systems

Kao, C. M.

Application of Biopile System for the Remediation of Petroleum-Hydrocarbon Contaminated Soils

Kao, Shih-Chieh

A Spatio-Temporal Drought Analysis for the Midwestern US

Kapelan, Z.

Operational Perspective of the Impact of Failures in Water Distribution Systems

Karamouz, M.

Development of Sustainable Water Supply Scheme in Reservoir Operation: Case Study

Evaluation of Uncertainties in the Simulation of Watershed Nutrient Load: A Case Study

Karamouz, Mohammad

Optimal Design of Water Diversion System: A Case Study

Economic Sustainability Evaluation of an Inter-Basin Water Transfer Project Using GWP Statement

Long-Lead Forecasting of Monthly Rainfall Using Large Scale Climate Signals and Statistical Disaggregation Models

Karimipour, Shohreh

Laboratory Testing Guidelines for Certification of Manufactured Stormwater BMPs

Karney, B. W.

Comparison of Pressures Simulated Using Transient Analysis with Field Data from a Full-Scale Distribution System

Karuppasamy, Elangovan

Analyzing the Impacts of a Retrofit Detention Basin Flow Control Strategy on Biodiversity in an Urban Stream System

The Impact of Smaller Detention Basins on Flood Hazard Areas in Lenexa, Kansas

Kato, T.

A Study on Spatial Distribution of Water Quality and the Behavior of Do Concentration in Tidal Area of Urban Rivers

Kaur, Jagjit

Managing Salinity in the Upper Santa Clara River System of California

Kavcar, Pinar Cakir

Effects of Gas Ebullition on Cohesive Sediment Resuspension and Cap Stability

Experimental Results on the Stability of Non-Cohesive Sediment Beds Subject to Vertical Pore Water Flux

Kavvas, M. L.

Statistical Characteristics of Land Surface Properties for the Regional Hydroclimate Model

Kavvas, M. Levent

Historical Reconstruction of Hydroclimatic Data Based on the Control Runs of GCMs over Sabah and Sarawak, Malaysia

Kawamura, M.

A Study on Spatial Distribution of Water Quality and the Behavior of Do Concentration in Tidal Area of Urban Rivers

Kayhanian, Masoud

Field Testing Guidelines for Certification of Manufactured Stormwater BMPs: Part II

Laboratory Testing Guidelines for Certification of Manufactured Stormwater BMPs

Potential Data Analysis Methodology to Evaluate the Performance of Manufactured BMPs

Kealy, M.

Ecosystem Services Approach to Public Facility Planning

Kebede, Y. K.

Environmental Impact of Coffee Processing Effluent on the Ecological Integrity of Rivers Found in Gomma Woreda of Jimma Zone, Ethiopia

Keedwell, E.

Application of Optimization Technology to Water Distribution System Master Planning

Keefer, Laura

Modeling the Hydrology and Hydraulics of the Cache River System

Keener, M.

The Value of Protecting Ozark Streams: An Economic Evaluation of Stream Bank Stability for Phosphorus Reduction

Keller, Andy

Comparison of Evapotranspiration Estimates from Remote Sensing (SEBAL), Water Balance, and Crop Coefficient Approaches

Kenny, John

A Student-Led Effort to Assess the Effect of Urban Runoff on Potter Lake

Khai, Rysbekov Yusup

How to Save the Second Aral Sea?

Khambhammettu, Uday

Field Testing Guidelines for Certification of Manufactured Stormwater BMPs: Part II

Khanal, Nabin

Integrated Planning for Dual Distribution Systems

Khatri, K. B.

Water Demand Forecasting for the City of the Future against the Uncertainties and the Global Change Pressures: Case of Birmingham

Khedun, Prakash

Improving Hydrologic Sustainability of Texas A&M University Campus

Khosronejad, Ali

Numerical Modeling of Flushing Process in Dez Dam Reservoir by HR Wallingford Method

Kiang, J. E.

Quantifying Uncertainty in Discharge Measurements: A New Approach

Kieffer, Janna M.

A Tool for the Performance Assessment of Hydrodynamic Separators

Killgore, Mark W.

Recent Developments in Water Policy in the Americas

Kim, Byungdal

Sedimentation Characteristics of the Lower Nakdong River Upstream of the Nakdong River Estuary Barrage

Kim, Chulyun

Evaluation of Alternative Geospatial Models Using Image Ranking and Machine Learning: An Application in Shallow Groundwater Recharge and Discharge

Kim, Dohoon

Sedimentation Characteristics of the Lower Nakdong River Upstream of the Nakdong River Estuary Barrage

Kim, H. S.

Nonlinear Dependence in Hydrologic Time Series

Kim, Leehyung

Use of Hydraulic Modeling to Develop a Small Dam for the Geum River Reach in Sejong City

Kim, Taesoon

Inflow Forecasting for Real-Time Reservoir Operation Using Artificial Neural Network

Kim, W.

Measurement of Velocity and Discharge of a Stream Using a New Floating Rod Equipped with a GPS Receiver

Kimes, Tom

Framing the Design Process in an Undergraduate Environmental Engineering Class

Kindscher, Kelly

Long-Term Effectiveness of a Bioretention System Treating Road Runoff in Northeastern Kansas

Kinser, Palmer

How to Build a Broadly Useable GIS Toolset for Estuary Analysis

Kirchhoff, Christine J.

Characteristics of Integrated Water Resource Management in the Zambezi River and Great Lakes Basins: A Comparison of Two Approaches

The Memorandum of Understanding (MOU) between the University of Zambia and the University of Michigan: Conception and Subsequent Implementation Goals

Kirshen, Paul

Generalized Storage-Reliability-Yield Equations for Rainwater Harvesting Systems

Kitzmiller, David

High Resolution Radar Precipitation Evaluation

Gauge-Based Adjustment of Historical Multi-Sensor Quantitative Precipitation Fields and Resulting Effects on Hydrologic Simulations

Kjaersgaard, J. H.

Independent Comparisons among Calibration and Output of Energy Balance Components Estimated by the METRIC Procedure

Automated Selection of Anchor Pixels for Landsat Based Evapotranspiration Estimation

Kleczyk, Ewa

Case Study: Homeowner's Preference Trade-Offs toward Plumbing Systems in Pipe Failure Prone Area

Klein, Ross

Improving Hydrologic Sustainability of Texas A&M University Campus

Kleiner, Yehuda

Drinking Water Infrastructure Assessment: The National Research Council of Canada Perspective

Klenzendorf, Brandon

Water Quality and Hydraulic Properties of the Permeable Friction Course

Klenzendorf, J. Brandon

Current Water Management Practices and the Effects of Climate Change on the Colorado River Basin

Kliem, John A.

Framework for Improving Water Security in the Middle East

Planning for Climate Change

Water Treatment Industry Course Correction

Klimetz, Lauren

Developing Linkages between Biological Impairment and Stream Siltation: A Case Study in the Northern Great Plains Ecoregion

Klingel, Philipp

Integrated Hydraulic Analysis and Data Management Tool for Water Supply Systems in Developing Countries

Klinger, R. E.

Habitat Restoration on the Middle Fork John Day River

Klocke, Norman L.

Irrigation Scheduling for Deficit Irrigation

Klosterman, Stephen

Comparing Single- and Multi-Species Water Quality Modeling Approaches for Assessing Contamination Exposure in Drinking Water Distribution Systems

Klumpp, Cassie

Two Dimensional Hydraulic Modeling of the Lower Skokomish River

Knight, Scott

Hardening a Great and Growing City's Water Supply

Koci, Don

Hutchinson, KS—4th and Carey Groundwater Remediation and Reverse Osmosis Water Treatment Facility Project

Hutchinson, KS—4th and Carey Site Groundwater and Source Control Measures at Two Grain Elevators

Koehler, Jennifer A.

A Tool for the Performance Assessment of Hydrodynamic Separators

Koelliker, James K.

Historical Changes in the Streamflow in Kansas Streams: Variation, Causes, and Implications

Kokorian, Vahe

“Let It Rain”—Gage-Adjusted Radar Rainfall (GARR) Data for Peachtree Creek Sewer Basin Modeling

Koren, Victor

Distributed Hydrologic Modeling: From Research to Operational Forecasting

Kose, Omer

Mathematical Modeling of Bed—Topography Changes at Bridge Abutments

Koseff, J. R.

Simulations of Aquaculture Dissolved Waste Transport and Mixing in Near-Coastal Waters

Kouchakzadeh, Mahdi

Estimation of Regional Reference Evapotranspiration from Land Surface Temperature and Co-Kriging Method at Tehran Province, Iran

Kramber, W.

Automated Selection of Anchor Pixels for Landsat Based Evapotranspiration Estimation

Krambis, C. Jr.

Projecting Future Groundwater Availability for Power Generation Plant Licensing

Kramer, Casey M.

One-Dimensional Modeling of Sedimentation Processes on the Puyallup River

Krause, Andreas

Robust Sensor Placement for Detecting Adversarial Contaminations in Water Distribution Systems

Krishnan, E. Radha

Development of a Community Water Security Filtration System Using Composite Cartridges

Evaluation of a UV/Ozone Treatment Process for Removal of MTBE in Groundwater Supplies in New Mexico

Krishnan, R.

Removal of Waterborne Particles by Electrofiltration

Kroll, Dan

Getting More from Your Investment Using Water Security Monitoring Technology for Everyday Operations

Krom, Thomas D.

A Novel Approach to Groundwater Model Development

Kropp, I.

Evaluating Risk of Multi-Segment Pipes for Prioritizing Pipe Rehabilitation

Krug, Claudia T.

Vadose Zone Transport of Nitrate in the Sierra Pelona Groundwater Basin, Agua Dulce, California

Krug, Claudia

A Tale of Two Cities—Source Water Protection Case Studies for Systems in Rural Settings

Kuai, Ken Z.

Stochastic Non-Equilibrium Bedload Transport Model

Kuiry, S. N.

A Process-Based Unsteady Model for Wave-Current-Morphodynamic Changes in Two-Dimensions

Kulp, Matt A.

Understanding Water Quality Responses to Long-Term Acidic Deposition in a High-Elevation Southern Appalachian Watershed: A Focus on Soil Watershed Processes

Kulp, Matt

The Effect of Natural Hydrological Disturbances (Defined from HSPF Simulated Hydrographs) on Trout Populations in Ungaged Streams of the Great Smoky Mountains National Park

Kumar, Jitendra

Characterizing Reactive Contaminant Sources in a Water Distribution System

Kumar, K. Santhosh

Agent Based Models for Simulation of Watersharing in a River Basin

Kumar, Pradeep

Risk Assessment to the Environment Due to Anionic Surfactants in Treated Sewages and Dried Sludges

Riverbank Filtration for Water Supply: Indian Experience

Kumar, Remya G.

A Digital Floc Camera for Nonintrusive Measurement of Floc Parameters

Kumar, Vivek

Water Retention and Hydraulic Conductivity of Different Media Used for Containerized Agriculture Systems

Kupferle, Margaret J.

Field-Scale Assessment of a Multispecies Water Quality System: A Chloramination Study

Kure, S.

Statistical Characteristics of Land Surface Properties for the Regional Hydroclimate Model

L

Return to top

Lackey, Laura W.

Bench-Scale Ozonation of Raw Industrial and Municipal Wastewater

Lai, Fu-hsiung

Multiple Watershed Scales Approach for Placement of Best Management Practices in *SUSTAIN*

Lai, Yong G.

Predicting Rock Scour in an Alluvial River with a One-Dimensional Model

Predicting Rock Scour in an Alluvial River with a Two-Dimensional Model

On a Two-Dimensional Temperature Model: Development and Verification

Lal, Chhedi

Sustainable Development of Agriculture: Urban Waste Water a Viable Mean for Irrigation

Lamb, Jessica

Drive for Zero Net Carbon Impact

Lambert, Martin F.

Damage Detection of Operating Transmission Mains with Measured Boundary Conditions

Lambert, Martin Francis

The Impact of Biofilm Development on Pipe Roughness and Velocity Profile

Lamers, John P. A.

Investigating Aquatic Ecosystems of Small Lakes in Khorezm , Uzbekistan

Lampe, L. K.

Water Supply and Energy Generation

Lampe, Les

Future Water Supply Desalination Technology: Forward Osmosis Co-Located with Power Generation

Landa, Guillermo Cardoso

Vulnerability of the Hydraulic Resources of the River Basin of the San Juan-Brave River with the Global Climatic Change

Lane, Richard

A Novel Approach to Groundwater Model Development

Lane, W.

Developments on Stochastic Analysis, Modeling, and Simulation (SAMS 2009)

Langman, Jeff

Geochemistry of Yukon and Copper River Tributaries, Alaska

Langsdale, S.

Developing Best Practices for Computer Aided Dispute Resolution

Does Collaborative Modeling Lead to Better Management of Our Water Resources?

Langseth, David E.

Solute Flux Rate Uncertainty Evaluation at a Monitored Boundary

Lansey, K.

Optimal Pump Scheduling by Linear Programming

Multi-Objective Sensor Placements with Improved Water Quality Models in a Network with Multiple Junctions

WDS Water Quality Parameter Estimation and Uncertainty

Design of Dual Water Supply Systems

Lansey, Kevin

New Concepts for Meter Placement in Water Distribution Systems for Demand Estimation

Real-Time Valve Operation for Water Quality Improvement in Water Distribution Systems

Lanyon, Richard

Flow Augmentation for Dissolved Oxygen Improvement in Chicago Waterways

Larson, C. J.

Fish Passage and Abundance around Grade Control Structures on Incised Streams

Lasorso, Daniel

Protocol Considerations to Improve the Reliability of Data Collection in a Radio Telemetry System

Lauth, T. J.

Application of Radio Frequency Tracers to Individual and Group Particle Displacement within a Laboratory

Lavoie, J.

Comparison of Pressures Simulated Using Transient Analysis with Field Data from a Full-Scale Distribution System

Lawrence, Bryce

From Grey to Green: Strategies and Concepts for Implementing Green CSO and Wet Weather Solutions

Kansas City's Stream Setback Ordinance: A Case Study on the Benefits of Stream Buffers in Urban Areas

le Roux, A. S.

Modeling Domestic Water Demand on a Suburb Level

Lecina, Sergio

Increasing Field Work Productivity in Irrigation Evaluation Processes through the Use of Combined Irrigation Models

Lee, C.

Measurement of Velocity and Discharge of a Stream Using a New Floating Rod Equipped with a GPS Receiver

Lee, E. T.

Nonlinear Dependence in Hydrologic Time Series

Lee, Jae-Young

Estimating Groundwater Seepages to St. Lucie Estuary

Lee, Jonah-Jong M.

A War for Water

Lee, Joo-Heon

Use of Hydraulic Modeling to Develop a Small Dam for the Geum River Reach in Sejong City

Lee, Joong Gwang

Evaluation and Optimization of Distributed Stormwater Controls in Spreadsheet

Lee, Juneseok

Case Study: Homeowner's Preference Trade-Offs toward Plumbing Systems in Pipe Failure Prone Area

Low Pressure Propagation at Service Lines

Lee, Ming-Kuo

Environmental Impacts on Surface Water and Groundwater for Expanding Urban Water Supply Capacity Using Stone Quarries

Lee, Seung Uk

Uncertainty and Sensitivity Analysis for Models with Calibrated Parameters

Lee, T. S.

Developments on Stochastic Analysis, Modeling, and Simulation (SAMS 2009)

Lee, Yeongho

Preliminary Spatial-Temporal Statistical Analysis of Hourly Water Demand at Household Level

Leeds, Terry

Kansas City, Missouri Overflow Control Plan Summary

Lefkowitz, Jamie

The Economic and Environmental Significance of Nonpoint Source Abatement in Large Watersheds

Leisenring, Marc

Combining GIS, BMP Performance, and Strategic Planning to Support Water Quality Implementation Planning

Integration of Low Impact Development Studies into the International Stormwater BMP Database

Lemke, D.

Drainage Main Rehabilitation in Iowa

Lenhart, James H.

Design Optimization of Hydrodynamic Separators

Potential Data Analysis Methodology to Evaluate the Performance of Manufactured BMPs

León, Arturo S.

A Robust and Fast Model for Simulating Street Flooding

Boundary Conditions for Simulating Complex Storm-Sewer Systems in Free Surface, Pressurized, and Mixed Flow Conditions

Leonard, Kathleen M.

Integrating Design Heuristics in an Environmental Engineering Course

Leven, Blase

Beyond Compliance and toward Sustainability: Advantages of Systems Environmental Engineering

Lewis, Cathie

Hydraulic Modeling and Engineering Evaluation of Fort Myers Beach's Water Distribution System

Lewis, James W.

Physical Processes Resulting in Geyser Formation in Rapidly Filling Stormwater Tunnels

Ley, Thomas W.

ASCE Standardized Penman-Monteith Alfalfa Reference ET and Crop ET Estimates for Arkansas River Compact Compliance in Colorado

Adjusting Wind Speed Measured over Variable Height Alfalfa for Use in the ASCE Standardized Penman-Monteith Equation

Ley, Thomas

Alfalfa Reference ET from a Weighing Lysimeter and Estimates from the ASCE Standardized Reference ET Equation in the Arkansas Valley of Colorado

Li, Cui-Mei

Water Price Forecasting Method Based on Marginal-Cost Theory: A Case Study in China

Li, Guohua

Air/Vacuum Valve Breakage Caused by Pressure Surges – Analysis and Solution

Li, Ping

Identification of the Hydraulic Model from Operational Measurements for Supervisory Pressure Control

Li, R.

Runoffs of the Xiangride and Qaidum Rivers in the Arid Qaidum Basin, Northwest China

Li, Y.

Removal of Waterborne Particles by Electrofiltration

Li, Yingkui

GIS-Based Landscape Parameters for Wetland Evaluation Related to Amphibian Health

A GIS-Based Decision-Making Methodology for Evaluation of Environmental Justice Impacts of Community Infrastructure Projects

Li, Z.

Axial Dispersion Coefficients for Laminar Flows in Water Distribution Systems

Li, Zhiwei

Assessing the Impact of Climate Change on Drinking Water Treatment Plant Design and Operation

Needs and Trends of the Nation's Water Infrastructure—The Utility Perspective

Lian, Yanqing

Modeling the Hydrology and Hydraulics of the Cache River System

Liang, Zhihua

Biological Nutrient Removal from On-Site Wastewater Treatment Systems Using a Membrane Aerated Bioreactor

Liao, Chung-Ta

Numerical Simulation of Sediment Transport and Morphological Change of JiJi Weir Reservoir

Lin, Che-Jen

Deployable Decentralized Biofilm System to Degrade Organic Carbon, Nutrients and Benzene from Wastewater

Lin, Hsin-Chi (Jerry)

Integrated Watershed Modeling

Lin, S.

Runoffs of the Xiangride and Qaidum Rivers in the Arid Qaidum Basin, Northwest China

Lin, Yu-Feng

Smart Pipe—Nanosensors for Monitoring Water Quantity and Quality in Public Water Systems

Evaluation of Alternative Geospatial Models Using Image Ranking and Machine Learning: An Application in Shallow Groundwater Recharge and Discharge

Linder, Greg

Competing Risks and the Development of Adaptive Management Plans for Water Resources: Field Reconnaissance Investigation of Risks to Fishes and Other Aquatic Biota Exposed to Endocrine Disrupting Chemicals (EDCs) in Lake Mead, Nevada, USA

Little, Edward E.

Competing Risks and the Development of Adaptive Management Plans for Water Resources: Field Reconnaissance Investigation of Risks to Fishes and Other Aquatic Biota Exposed to Endocrine Disrupting Chemicals (EDCs) in Lake Mead, Nevada, USA

Litvan, M. E.

Fish Passage and Abundance around Grade Control Structures on Incised Streams

Liu, Chang

Smart Pipe—Nanosensors for Monitoring Water Quantity and Quality in Public Water Systems

Liu, D.

Runoffs of the Xiangride and Qaidum Rivers in the Arid Qaidum Basin, Northwest China

Liu, H.

A Lattice Boltzmann Model for Dam Break Flows

Liu, Li

A Hybrid Heuristic Search Approach for Contaminant Source Characterization

Liu, Mingfa

One- and Two-Dimensional Modeling of Deep Gravel Mining in the Rio Salado

Liu, Sui-qing

Water Price Forecasting Method Based on Marginal-Cost Theory: A Case Study in China

Liu, Xiaofeng

Upstream Intrusion Effect of CSO Event in Bubbly Creek, IL

Two-Dimensional BOD and DO Water Quality Model for Engineering Applications: The Case of Bubbly Creek in Chicago, Illinois

Boundary Conditions for Simulating Complex Storm-Sewer Systems in Free Surface, Pressurized, and Mixed Flow Conditions

Liu, Yi

Analytical-Numerical Solution for Seepage along an Earth Canal Disconnected from the Shallow Aquifer

Lockaby, Graeme

Studying the Impact of Land Use/Cover Changes on the Water Quality of Weeks Bay, AL: Model vs. Regression

Loechle, John

Neighborhood Channel is Redefined with Boulder Armoring

Loganathan, G. V.

Low Pressure Propagation at Service Lines

Lohani, Vinod K.

Case Study: Homeowner's Preference Trade-Offs toward Plumbing Systems in Pipe Failure Prone Area

Low Pressure Propagation at Service Lines

Long, Brett V.

Rainwater Harvesting for Non-Potable Use in Gardens: A Comparison of Runoff Water Quality from Green vs. Traditional Roofs

Loperfido, J. V.

Upper Mississippi River Basin Envirohydrologic Observatory

Lopes, João E. G.

Climate Flow Forecast Model for the Brazilian Hydropower System

Lopes, João E.

Multireservoir Simulation Using Multipurpose Constraints and Object-Oriented Software Design

Lopes, João Eduardo G.

Impacts of the Upstream Storage Reservoirs on Itaipu Hydropower Plant Operation

López-Fuster, P.

Some Results of Evapotranspiration Measured by Three Weighing Lysimeters in La Mancha, Spain

López-Urrea, R.

Some Results of Evapotranspiration Measured by Three Weighing Lysimeters in La Mancha, Spain

Lopitz, Janice

Breaking Down the Barriers to Low Impact Development in Colorado

Loucks, Daniel P.

Experiences Teaching a Multi-Disciplinary Course

How Reliable is New York City's Water Supply?

Loucks, Eric D.

Selection of Overflow Control Strategies for the Austin Clean Water Program

Louie, Brian

Managing Salinity in the Upper Santa Clara River System of California

Love, Ashleigh D.

pH Variation and Its Effect on Metal Concentration during Electrokinetics

Lu, Qingguang

Application of NEXRAD for Freshwater Inflow Estimates to Texas Bays and Estuaries

Lucas, William C.

Design of Integrated Bioinfiltration-Detention Urban Retrofits with Continuous Simulation Methods

Lund, Jay R.

Challenges of Managing California's Sacramento—San Joaquin Delta

Luong, Thuy

Water Subdivision for Modeling

Luster-Teasley, S.

Water Resources in Sudan: Enhancing Rainfall Harvesting Methods for Water Supply

Luster-Teasley, Stephanie

Development of Slow-Release Chemical Oxidation Methods for Environmental Remediation

Lynch, Scott

Removal of Selenium and Nitrate from Surface Waters Using a Subsurface Microbial Filter

Lyon, Stephen

Removal of Selenium and Nitrate from Surface Waters Using a Subsurface Microbial Filter

M

Return to top

Ma, Rui

Sorption and Desorption of Testosterone in Agricultural Soils

Machusick, M. D.

The Observed Effects of Stormwater Infiltration on Groundwater

Mahajan, Rishab

A Simplified Model of Combined Sewer Overflows to Estimate Event Driven Enteric Pathogen Concentrations in Drinking Water Sources

Mahanta, C.

Quantifying the Spread of Arsenic Contamination in Groundwater of the Brahmaputra Floodplains, Assam, India: A Threat to Public Health of the Region

Mahinthakumar, G. (Kumar)

A Hybrid Heuristic Search Approach for Contaminant Source Characterization

Mahinthakumar, G.

Characterizing Reactive Contaminant Sources in a Water Distribution System

Maidment, David R.

FEMA Flood Map Accuracy

Mailloux, Jim

Data Reporting Guidelines for Certification of Manufactured Stormwater BMPs: Part II

Laboratory Testing Guidelines for Certification of Manufactured Stormwater BMPs

Maloney, Shawn

Addressing Contaminated Groundwater and Promoting Environmental Stewardship in Wichita, Kansas—The Gilbert and Mosley Project Story

Marengo, Brian

Developing Green Streets Prototypes to Reduce Combined Sewer Overflows for Cincinnati, Ohio

Mariño, M. A.

MOPSO in Multipurpose Operation of Single-Reservoir System

Reliability Based Design of Water Distribution Network (WDN) Considering the Reliability of Nodal Pressures

Markwell, Ken

Protecting Infrastructure: Emergency Streambank Stabilization

Marm, Courtney

Developing Green Streets Prototypes to Reduce Combined Sewer Overflows for Cincinnati, Ohio

Martin, D.

Investigation of Land-Use Change and Hydrologic Forcing upon Streambank Erosion and In-Stream Sediment Processes Using a Watershed Model and Sediment Tracers

Martinez, F. Javier

Statistical Analysis of Water Distribution Networks Design Using Harmony Search

Maslia, Morris L.

A Methodology to Reconstruct Groundwater Contamination History with Limited Field Data

Mason, R. R. Jr.

Quantifying Uncertainty in Discharge Measurements: A New Approach

Matasovic, Neven

Considerations, Opportunities, and Strategies for Infiltration Stormwater BMPs

Mateos, L.

Integrated Water Management in an Ancestral Water Scheme in a Mountainous Area of Southern Spain

Matondo, J. I.

A Decision Support System for Beneficial Use of National Dam Water Resources in Swaziland

Mays, D. C.

Groundwater Mixing Using Pulsed Dipole Injection/Extraction Wells

Mazzola, M. R.

Sampling of Residential Water Use for Leak Control via Water Budgets

McArthur, Karl

HCFCD M3 System: Maximizing and Maintaining Local Investments in Floodplain Modeling

McBean, Edward

Comparative Evaluation of Two Algorithms for Locating Contaminant Ingress Points

McCoy, E. R.

Implementation and Performance of Stormwater Best Management Practice Retrofits in Wilmington, NC

McCready, Mary

Evaluation of Irrigation Scheduling Efficiency and Adequacy by Various Control Technologies Compared to Theoretical Irrigation Requirement

McCurry, Gordon

Implementing Source Water Protection Programs in Texas

A Tale of Two Cities—Source Water Protection Case Studies for Systems in Rural Settings

Selection and Prioritization of Best Management Practices for Potential Sources of Contamination in a Wellhead Protection Area

McCutcheon, Matthew

Needs and Trends of the Nation's Water Infrastructure—The Utility Perspective

McDonald, Jon

Laboratory Testing Guidelines for Certification of Manufactured Stormwater BMPs

McEachern, Preston

Spatial Variation of Sediment Oxygen Demand in Athabasca River: Influence of Water Column Pollutants

McEnroe, B. M.

Are Rational C Values Too Low?

Regional Regression Analysis and the Rational Method

McEnroe, B.

Bankfull Discharge for Kansas Natural Alluvial Channel Design

McEnroe, Bruce M.

A Simple Analytical Design Method for Small Alluvial Channels

McGrath, Marcus

Representation of Linear Terrain Features in a 2D Flood Model with Regular Cartesian Mesh

McKenna, Sean A.

Trajectory Clustering Approach for Reducing Water Quality Event False Alarms

McKinney, Daene C.

Hydrologic Modeling for Assessing Climate Change Impacts on the Water Resources of the Rio Conchos Basin

Hydrological Feasibility of Environmental Flows in the Rio Grande/Bravo Basin

McLane, G. A.

Assessing Postulated Accidental Releases of Radioactive Liquid Effluents from Nuclear Power Plants

McNett, J. K.

Water Quality Assessed by Benthic Macro-Invertebrates: Proposing the WQABI Method

McPhillips, Munsell

A Monitoring and Assessment Framework to Evaluate Stream Restoration Needs in Urbanizing Watersheds

Meaks, L.

Irrigation Rain Sensors Accuracy

Mecikalski, John R.

Design of Solar Radiation Sensor Network Using Geo-Statistical Methods

Meckley, Monika N.

Modeling Water Quality Impacts in Delaware's Coastal Bays with AGNPS

Medina, Dan

Modeling Impacts of Conventional and Low Impact Stormwater Controls on Receiving Streams

Medina, Sebastian

Drive for Zero Net Carbon Impact

Mefford, Brent

Physical Modeling of River Spanning Rock Structures: Evaluating Interstitial Flow, Local Hydraulics, Downstream Scour Development, and Structure Stability

Mehrotra, Indu

Riverbank Filtration for Water Supply: Indian Experience

Meier, Matthew

Statistical Seasonal Streamflow Forecasting: An Intercomparison and Evaluation of Current Forecasting Procedures

Melching, Charles S.

Evaluation of Methods to Reduce Backflows from the Chicago Waterway System to Lake Michigan

Flow Augmentation for Dissolved Oxygen Improvement in Chicago Waterways

Melton, Marjorie

City of St. Louis Permeable Pavement Alley Pilot Study

Melvin, S.

Drainage Main Rehabilitation in Iowa

Mendi, S. Engin

An Efficient Solution for Water Supply Networks

Mengel, D.

Post Project Appraisal of Riparian, Wetland, and Aquatic Habitat Restoration at Best Slough, Beale Air Force Base, Marysville, CA

Mengel, Denny

Integrating Fluvial Geomorphology and Two-Dimensional Hydraulic and Sediment Transport Modeling to Support Sustainable Design of Large River and Floodplain Improvements: The Trinity River Corridor Project, Dallas, Texas, USA

Meniconi, S.

In-Line Partially Closed Valves: How to Detect by Transient Tests

Mensing, D. M.

Zona Rosa and Rush Creek Conservation Area—Applied Ecology in a Mixed-Use Development

Merayyan, S.

The Effect of Municipal Landfill Leachate on the Characterization of Fluid Flow through Clay

Water Resources in Jordan: Challenges and Accomplishments

Mercer, Gary

The Economic and Environmental Significance of Nonpoint Source Abatement in Large Watersheds

Merino, Mercedes

Groundwater Baseflow Sourced from Miocene Rocks and Residuals Carries Elevated Selenium into Southern California

Merkley, Gary P.

Increasing Field Work Productivity in Irrigation Evaluation Processes through the Use of Combined Irrigation Models

Meskele, Tadesse

Impacts of Different Rainfall Estimates on Hydrological Simulation and Satellite Rainfall Retrieval Error Propagation

Mhaske, S. Y.

Environmental and Water Resources in Developing Countries: Development of Micro Irrigation Facility at Parsoda Village

Michael, Y.

On the Local-Scale Spatial Variability of Daily Rainfall in the Highlands of the Blue Nile: Observational Evidence

Michaud, W.

Does Collaborative Modeling Lead to Better Management of Our Water Resources?

Miglio, Edie

Representation of Linear Terrain Features in a 2D Flood Model with Regular Cartesian Mesh

Mihelcic, J. R.

Non-Traditional University Research Partners That Facilitate Service Learning and Graduate Research for Sustainable Development

Mihelcic, James R.

Treatment Performance of Wastewater Lagoons in South Yungas Province of Bolivia

Mihyar, M.

Water Resources in Jordan: Challenges and Accomplishments

Mikula, J. Bradley

Pollutant Transport within the Vadose Zone: Interactions of Soil Horizon Chemistry on Water Quality

Miller, Dennis

High Resolution Radar Precipitation Evaluation

Miller, Julianne

The Role of the Clast Layer of Desert Pavement in Rainfall-Runoff Processes

Miller, Mark

Laboratory Testing Guidelines for Certification of Manufactured Stormwater BMPs

Mills, Aaron

Prediction of Nitrate Concentration in Stream Water Based on Watershed Land Use and Stream Flow Rate

Mines, Richard O. Jr.

Bench-Scale Ozonation of Raw Industrial and Municipal Wastewater

Minsker, B. S.

Analysis of Model Sensitivity and Uncertainty for Chlorine Transport and Decay in a Water Distribution System

Minsker, B.

Predicting CSOs for Real Time Decision Support

Minsker, Barbara

Evolutionary Optimization of Combined Sewer Overflow Control

Mirbagheri, Seyed Ahmad

Application of Enhanced Methods of Phosphorous and Nitrogen Removal from Wastewater

Mirzaei, Farhad

Controlled Drainage Effects on Crop Yield and Water Use Efficiency under Semi-Arid Conditions of Iran

Moffitt, Jim

“Let It Rain”—Gage-Adjusted Radar Rainfall (GARR) Data for Peachtree Creek Sewer Basin Modeling

Mogavero, K. A.

Redesigning Constructed Stormwater Wetlands: An Integrated Modeling Approach to Optimize Form and Function

Mogavero, Kristen

Developing a Water Budget for a Constructed Stormwater Wetland

An Investigation of Infiltration in a Constructed Stormwater Wetland and Implications for Groundwater Quality

Moghaddam, M. Naseri

Probable Maximum Precipitation for 24 Hour Duration over Four Central Provinces in Iran

Mohamed-Ali, S.

Water Resources in Sudan: Enhancing Rainfall Harvesting Methods for Water Supply

Mohammadi, S.

Development of Sustainable Water Supply Scheme in Reservoir Operation: Case Study

Mohan, S.

Agent Based Models for Simulation of Watersharing in a River Basin

Application of Genetic Algorithms for Estimation of Flood Routing Model Parameters

Mohseni, Omid

A Tool for the Performance Assessment of Hydrodynamic Separators

Accurate Sampling of Suspended Solids

Assessing Hydrodynamic Separators under High Water Flow Conditions

Assessment of Standard Sumps for Stormwater Treatment

Laboratory Testing Guidelines for Certification of Manufactured Stormwater BMPs

Moin, Syed M. A.

Determining the Causes of Declining Upper Great Lakes Levels—Phase I of the International Upper Great Lakes Study by the St. Clair River Task Team

Mojahedi, S. A.

Water Sustainability Index: Application of CWSI for Ahwaz County

Mojahedi, S. Ali

A Comparative Study of Water Quality Indices for Karun River

Economic Sustainability Evaluation of an Inter-Basin Water Transfer Project Using GWP Statement

Monk, Suzanne K.

Fish Passage Can Be Improved by Introducing Hydraulic Refuge: Can the Effects Be Quantified?

Montoro, A.

Some Results of Evapotranspiration Measured by Three Weighing Lysimeters in La Mancha, Spain

Mood, Negar Sharifi

Controlled Drainage Effects on Crop Yield and Water Use Efficiency under Semi-Arid Conditions of Iran

Mooney, D.

San Joaquin River Restoration Program Monitoring and Management Plans

Mooney, David

On a Two-Dimensional Temperature Model: Development and Verification

Moore, Georgianne

Improving Hydrologic Sustainability of Texas A&M University Campus

Moore, Ginny

Kansas City—Balancing Green Infrastructure with Traditional Approaches for CSO Control

Moore, Steve E.

Understanding Water Quality Responses to Long-Term Acidic Deposition in a High-Elevation Southern Appalachian Watershed: A Focus on Soil Watershed Processes

Moore, Steve

The Effect of Natural Hydrological Disturbances (Defined from HSPF Simulated Hydrographs) on Trout Populations in Ungaged Streams of the Great Smoky Mountains National Park

Moore, T. L.

Impacts of Biota on Bioretention Cell Performance during Establishment in the Midwest

Mora, Daniel

Statistical Analysis of Water Distribution Networks Design Using Harmony Search

Moradkhani, Hamid

Impacts of Different Rainfall Estimates on Hydrological Simulation and Satellite Rainfall Retrieval Error Propagation

Parameter Uncertainty Estimation of Hydrologic Models Using Bootstrap Resampling

Statistical Seasonal Streamflow Forecasting: An Intercomparison and Evaluation of Current Forecasting Procedures

Morales, C. A.

Use of Lightning and Storms Life Cycle Information in Radar Rainfall Estimation

Morales, Santiago

Treatment Performance of Wastewater Lagoons in South Yungas Province of Bolivia

Moreda, Fekadu

Transitioning NWS Operational Hydraulics Models from FLDWAV to HEC-RAS

Moridi, Ali

Optimal Design of Water Diversion System: A Case Study

Motamarri, Srinivas

The Development of a Neural-Based Biomarker Forecasting Tool for Classifying Recreational Water Quality

Motta, Davide

Upstream Intrusion Effect of CSO Event in Bubbly Creek, IL

Two-Dimensional BOD and DO Water Quality Model for Engineering Applications: The Case of Bubbly Creek in Chicago, Illinois

Mount, Jeffrey F.

Challenges of Managing California's Sacramento—San Joaquin Delta

Mountz, Thomas W.

Comparison of HEC-RAS and InfoWorks RS: A Case Study in Grand Prairie, Texas

Moyle, Peter B.

Challenges of Managing California's Sacramento—San Joaquin Delta

Mrayyan, S.

Water Resources in Jordan: Challenges and Accomplishments

Mroz, M.

Application of Northeast Regional Climate Center Research Results for the Purpose of Evaluating and Updating Intensity-Duration-Frequency (IDF) Curves –Case Study: Rochester, New York

Mryyan, Sam

Characterization of a Perchlorate Contaminated Site

Msibi, K. M.

A Decision Support System for Beneficial Use of National Dam Water Resources in Swaziland

Mueller, David S.

Measuring Discharge with ADCPs: Inferences from Synthetic Velocity Profiles

Muga, H. E.

Non-Traditional University Research Partners That Facilitate Service Learning and Graduate Research for Sustainable Development

Muga, Helen E.

Treatment Performance of Wastewater Lagoons in South Yungas Province of Bolivia

Muhammad, Nur

Development of a Community Water Security Filtration System Using Composite Cartridges

Muleta, Misgana

Multi-Objective Design of Transient Network Models

Munevar, Armin

Assessing Potential Implications of Climate Change for Long-Term Water Resources Planning in the Lower Colorado River Basin

Mungray, Arvind Kumar

Risk Assessment to the Environment Due to Anionic Surfactants in Treated Sewages and Dried Sludges

Murphy, Brian

Rehabilitation of Mine Impaired Creek in Idaho

Murphy, J.

Removal of Waterborne Particles by Electrofiltration

Murray, Daniel J. Jr.

EPA Aging Water Infrastructure Research Program: State of the Technology for the Condition Assessment and Rehabilitation of Wastewater Collection Systems

Murray, R.

Simple Model of Attachment and Detachment of Pathogens in Water Distribution System Biofilms

Murray, Regan

Sensor Network Design and Performance in Water Systems Dominated by Multi-Story Buildings

Effects of Redesign of Water Systems for Security and Water Quality Factors

Comparing Single- and Multi-Species Water Quality Modeling Approaches for Assessing Contamination Exposure in Drinking Water Distribution Systems

Murukannappa

Effective Management of Natural Resources under Dry Land Farming through Watershed Basis

N

Return to top

Nabavi, M. B.

The Effect of Sewage Pollutant of Bandar Imam Petrochemical Company on Benthic Macofauna Community Using Biodiversity Indices and Bioindicators

Najjar, Yacoub

Characterization of a Perchlorate Contaminated Site

Nam, Woosung

Asymptotic Variance of Regional Growth Curve for Generalized Logistic Distribution

Nanía, Leonardo S.

A Robust and Fast Model for Simulating Street Flooding

Naylor, R. L.

Simulations of Aquaculture Dissolved Waste Transport and Mixing in Near-Coastal Waters

Nazariha, Mehrdad

Prediction of Thermal Stratification in Proposed Bakhtyari Reservoir with CE-QUAL-W2

Nazif, S.

Development of Sustainable Water Supply Scheme in Reservoir Operation: Case Study

Nazif, Sara

Long-Lead Forecasting of Monthly Rainfall Using Large Scale Climate Signals and Statistical Disaggregation Models

Neale, Christopher M. U.

Increasing Field Work Productivity in Irrigation Evaluation Processes through the Use of Combined Irrigation Models

Neff, Keil J.

The Effect of Natural Hydrological Disturbances (Defined from HSPF Simulated Hydrographs) on Trout Populations in Ungaged Streams of the Great Smoky Mountains National Park

Nelson, E. James

Assessment of Lumped, Quasi-Distributed and Distributed Hydrologic Models of the US Army Corps of Engineers

Neupauer, R. M.

Conditioned Backward Probability Modeling to Identify Contamination Sources in a Water Distribution System

Groundwater Mixing Using Pulsed Dipole Injection/Extraction Wells

Wavelet Analysis of Characteristic Length Scales of Permeability in Stationary and Non-Stationary Porous Media

Nevulis, Richard

Selecting Optimal Water Supply Options—A Regional Water Supply Case Study in the Upper Kissimmee Basin, FL

Ng, T. L.

Water Quality Effects of Varying Crop, Fertilizer, and Carbon Prices

Ngo-Kidd, Dzung Kim

Evaluation of a UV/Ozone Treatment Process for Removal of MTBE in Groundwater Supplies in New Mexico

Ni, Hongzhen

Study on the Water Value Conversion between Economy and Ecology and Countermeasures of Water Resources Distribution for Coordinated Development of Economy and Ecology

Nicholas, Brent W.

A Comparison of Formed Suction Inlets for Flood Control Applications

Nicholson, Natasha

Rainwater Harvesting for Non-Potable Use in Gardens: A Comparison of Runoff Water Quality from

Green vs. Traditional Roofs

Nicklow, J. W.

Generating Different Scenarios of BMP Designs in a Watershed Scale by Combining NSGA-II with SWAT

Niemann, Ted

Neighborhood Channel is Redefined with Boulder Armoring

Niezgoda, Sue L.

Using Watershed Scale Geomorphic Assessment to Improve Urban Stream Restoration Design

Developing Probability of Failure Estimates for Stream Restoration Design Components

A Monitoring and Assessment Framework to Evaluate Stream Restoration Needs in Urbanizing Watersheds

Niño, César A.

Water Distribution Systems Corrective Maintenance Supported by Real-Time Use of Hydraulic Models

Nishonov, Bakhriddin

Investigating Aquatic Ecosystems of Small Lakes in Khorezm , Uzbekistan

Niyogi, Dev

A Spatio-Temporal Drought Analysis for the Midwestern US

Nnadi, Fidelia (Ola)

Non-Point Source Nutrient Loading in an Urban Watershed

Noori, Navideh

Long-Lead Forecasting of Monthly Rainfall Using Large Scale Climate Signals and Statistical Disaggregation Models

Nourzad, S. H. H.

Industrial Distribution System Simulation for Optimal Water Resource Assignment Using Probabilistic Tabu Search

Nyambe, Imasiku A.

Impacts of Mining in the Upper Zambezi River Basin: An Overview of the Zambian Copperbelt

Nyambe, Imasiku

Characteristics of Integrated Water Resource Management in the Zambezi River and Great Lakes Basins: A Comparison of Two Approaches

The Memorandum of Understanding (MOU) between the University of Zambia and the University of Michigan: Conception and Subsequent Implementation Goals

Nzewi, E.

Water Resources in Sudan: Enhancing Rainfall Harvesting Methods for Water Supply

Nzewi, Emmanuel U.

Designing Effective Rainfall Harvesting Systems in Developing Areas of Sub-Saharan Africa

O

Return to top

O'Bannon, Deb

Hypothesis-Based Flow Monitoring for Green Solutions

Framing the Design Process in an Undergraduate Environmental Engineering Class

O'Bannon, Deborah

Kansas City—Balancing Green Infrastructure with Traditional Approaches for CSO Control

O'Connor, Thomas P.

Enhancing Rain Garden Design to Promote Nitrate Removal

Pervious Pavement System Evaluation

O'Neill, Sean W.

Analysis of Bioretention Media Specifications and Relationships to Overall Performance

Oberg, Kevin A.

Measuring Discharge with ADCPs: Inferences from Synthetic Velocity Profiles

Ochoa, Susana

Water Distribution Systems Corrective Maintenance Supported by Real-Time Use of Hydraulic Models

Calibration of Water Distribution Network Models as a Tool for Detecting Missing and Erroneous Cadastral and Hydraulic Information

Ogintz, Joanna B.

Design Optimization of Hydrodynamic Separators

Oglesby, Cary M.

Bench-Scale Ozonation of Raw Industrial and Municipal Wastewater

Oh, Jungsun

Modeling of Sediment Particle Deposition and Resuspension Processes Using a Stochastic Jump Diffusion Particle Tracking Model

Ohara, N.

Statistical Characteristics of Land Surface Properties for the Regional Hydroclimate Model

Ohara, Noriaki

Historical Reconstruction of Hydroclimatic Data Based on the Control Runs of GCMs over Sabah and Sarawak, Malaysia

Okabe, M.

A Study on Spatial Distribution of Water Quality and the Behavior of Do Concentration in Tidal Area of Urban Rivers

Okalebo, Jane

Visualizing Hydrologic Drought Information on the Web Using State-of-the-Art Geospatial Mapping Technology

Ollig, Erin

Kansas City, Missouri Wet Weather Solutions Program: A Twelve Step Program

Olsen, Roger

Addressing Contaminated Groundwater and Promoting Environmental Stewardship in Wichita, Kansas—The Gilbert and Mosley Project Story

Olson, C. C.

A Tool for Determining Effectiveness and Whole Life Costs of BMPs

Olson, Mira

Prediction of Nitrate Concentration in Stream Water Based on Watershed Land Use and Stream Flow Rate

Olszewski, J. M.

Bioretention/Bioinfiltration Performance in the Mid-Atlantic

Onderlinde, Matthew

Use of NEXRAD Rainfall Data to Develop Climatologically Homogenous Rain Areas for Central and South Florida

Onochie, Patrick

Development of Slow-Release Chemical Oxidation Methods for Environmental Remediation

Orloff, S. B.

Mid-Summer Deficit Irrigation of Alfalfa as a Strategy for Saving Water

Ormsbee, L.

Peracetic Acid as an Alternative Disinfection Technology for Wet Weather Sewer Overflows

Osei, Kwabena

Laboratory Testing Guidelines for Certification of Manufactured Stormwater BMPs

Ostfeld, A.

Multi-Objective Sensor Placements with Improved Water Quality Models in a Network with Multiple Junctions

Analysis of Model Sensitivity and Uncertainty for Chlorine Transport and Decay in a Water Distribution System

Ostfeld, Avi

Online Hydraulic State Prediction for Water Distribution Systems

Evolutionary Optimization of Combined Sewer Overflow Control

Osting, Tim D.

Expanded Method for Filtering Submerged Objects in Echosounder Data

Oswald, Jared K.

On-Line Irrigation Scheduling within the Belle Fourche Irrigation District

Otieno, Fred

Application of Multi-Objective Differential Evolution Algorithm (MDEA) to Irrigation Planning

Otis, Stephanie C.

Diversion of S-4 Basin Drainage from Lake Okeechobee: Hydraulic Modeling of Alternatives Using HEC-RAS

Ozeren, Yavuz

Representation of Linear Terrain Features in a 2D Flood Model with Regular Cartesian Mesh

P

Return to top

Palomo, Mónica

Peroxidase-Mediated Stabilization of 2,4-Dichlorophenol in a Model Humin-Mineral Geomaterial

Panday, Sorab

Managing Salinity in the Upper Santa Clara River System of California

Pandey, J.

Air-Borne Heavy Metal Contamination to River Ganga (India)

Pandey, Richa

Air-Borne Heavy Metal Contamination to River Ganga (India)

Papanicolaou, A. N. (Thanos)

Using Tracers to Derive Sediment Provenance after the Occurrence of a 500-Year Flood in a Midwestern Stream

Effects of Rainfall-Runoff on Soil Surface Roughness and Erosion Processes

Effects of Freezing and Thawing Processes on Bank Stability

Papanicolaou, A. N.

Application of Radio Frequency Tracers to Individual and Group Particle Displacement within a Laboratory

Fish Passage and Abundance around Grade Control Structures on Incised Streams

Papanicolaou, Athanasios (Thanos) N.

The Connectivity of Upland and Instream Processes

Park, Daeryong

Modeling Performances of Detention Basins with Uncertainty Analysis

Park, Sang-Kil

Sedimentation Characteristics of the Lower Nakdong River Upstream of the Nakdong River Estuary Barrage

Park, Y. S.

Seoul (Korea) Online Water Quality Monitoring of Drinking Water

Parker, Gary

Sediment Load Based Single Thread Alluvial Channel Classification

Parker, Joseph

The Effect of Natural Hydrological Disturbances (Defined from HSPF Simulated Hydrographs) on Trout

Populations in Ungaged Streams of the Great Smoky Mountains National Park

Parr, A. David

Using HEC-RAS Hydraulic Design Functions for Geomorphic Channel Design and Analysis

Parsinejad, Masoud

Controlled Drainage Effects on Crop Yield and Water Use Efficiency under Semi-Arid Conditions of Iran

Pasha, M. F. K.

Optimal Pump Scheduling by Linear Programming

WDS Water Quality Parameter Estimation and Uncertainty

Passantino, Laurel

Integrated Planning for Dual Distribution Systems

Patel, R.

Combined Energy and Pressure Management in Water Distribution Systems

Patel, Ridwan

Identification of the Hydraulic Model from Operational Measurements for Supervisory Pressure Control

Patel, Sehul

Deployable Decentralized Biofilm System to Degrade Organic Carbon, Nutrients and Benzene from Wastewater

Pathak, Chandra S.

Design of Solar Radiation Sensor Network Using Geo-Statistical Methods

Adjustment of the Z-R Relationship in Real-Time for Use in South Florida

Use of Lightning and Storms Life Cycle Information in Radar Rainfall Estimation

Use of NEXRAD Rainfall Data to Develop Climatologically Homogenous Rain Areas for Central and South Florida

Understanding Uncertainties in Water Budget for Large Constructed Wetlands

Pathak, Chandra

Evaluation of Improvised Spatial Interpolation Methods for Infilling Missing Precipitation Records

Pathak, Dhundi R.

Combining Rule-Based Fuzzy Model with GIS to Predict Groundwater Vulnerability to Contamination

Pathak, N.

Quantifying the Spread of Arsenic Contamination in Groundwater of the Brahmaputra Floodplains, Assam, India: A Threat to Public Health of the Region

Patterson, C.

Removal of Waterborne Particles by Electrofiltration

Patterson, Craig L.

Development of a Community Water Security Filtration System Using Composite Cartridges

Protocol Considerations to Improve the Reliability of Data Collection in a Radio Telemetry System

Patterson, Craig

Production of Drinking Water from Lake Water Sources with a Nanofilter Membrane to Prevent the Formation of Disinfection Byproducts

Evaluation of a UV/Ozone Treatment Process for Removal of MTBE in Groundwater Supplies in New Mexico

Paudel, Murari

Assessment of Lumped, Quasi-Distributed and Distributed Hydrologic Models of the US Army Corps of Engineers

Payne, J.

San Joaquin River Restoration Program Monitoring and Management Plans

Pearson, David

Production of Drinking Water from Lake Water Sources with a Nanofilter Membrane to Prevent the Formation of Disinfection Byproducts

Pedeux, Xavier

An Approach for Integrated Optimization of Wastewater, Recycled, and Potable Water Networks

Peltier, Edward

A Student-Led Effort to Assess the Effect of Urban Runoff on Potter Lake

Long-Term Effectiveness of a Bioretention System Treating Road Runoff in Northeastern Kansas

Peng, Y.

A Lattice Boltzmann Model for Dam Break Flows

Pereira, Luis S.

Estimating Crop Coefficients from Fraction of Ground Cover and Height

Perrin, C. A.

Implementation and Performance of Stormwater Best Management Practice Retrofits in Wilmington, NC

Perry, Scott

Laboratory Testing Guidelines for Certification of Manufactured Stormwater BMPs

Perry, Seth

Development of a National GIS Database for Municipal Water and Wastewater Pipe Infrastructure System

Petersen, Christina

Implementing Source Water Protection Programs in Texas

Petersen, Tina

A Tale of Two Cities—Source Water Protection Case Studies for Systems in Rural Settings

Selection and Prioritization of Best Management Practices for Potential Sources of Contamination in a Wellhead Protection Area

Phillips, Heather

Wastewater Utilities: Are You Ready for Kansas' Nutrient Removal Policy?

Phillips, L. D.

Non-Traditional University Research Partners That Facilitate Service Learning and Graduate Research for Sustainable Development

Pickrell, John

Beyond Compliance and toward Sustainability: Advantages of Systems Environmental Engineering

Pierce, C. L.

Fish Passage and Abundance around Grade Control Structures on Incised Streams

Piety, L.

Habitat Restoration on the Middle Fork John Day River

Pitt, Robert E.

Land Use and Runoff Uncertainty

Pitt, Robert

Kansas City—Balancing Green Infrastructure with Traditional Approaches for CSO Control

Association of PAHs with Size Fractionated Sediment Particles

Physical Experimentation and CFD Modeling to Evaluate Sediment Scour in Catchbasin Sumps

Controlled Full-Scale Field Testing of an Up-Flow Filtration Device

Polak, Jonathan L.

Lake Winnebago Dam Relocation Project

Pomeroy, Christine A.

Analyzing the Impacts of a Retrofit Detention Basin Flow Control Strategy on Biodiversity in an Urban Stream System

Cost Estimating Tools for Low-Impact Development Best Management Practices

The Impact of Smaller Detention Basins on Flood Hazard Areas in Lenexa, Kansas

Pomeroy, Christine

A Monitoring and Assessment Framework to Evaluate Stream Restoration Needs in Urbanizing Watersheds

Poole, Ethan

The Dubai Palms: Construction and Environmental Consequences

Porter, England

A Student-Led Effort to Assess the Effect of Urban Runoff on Potter Lake

Ports, Michael A.

Source Control: The Solution to Stormwater Pollution

Kansas City—Balancing Green Infrastructure with Traditional Approaches for CSO Control

Ports, Michael

How the Heart of America is *Goin' Green* to Solve Water and Sewer Issues

Postel, Natalie A.

Analyzing the Impacts of a Retrofit Detention Basin Flow Control Strategy on Biodiversity in an Urban Stream System

Postel, Natalie

The Impact of Smaller Detention Basins on Flood Hazard Areas in Lenexa, Kansas

Postlethwaite, Ian

Identification of the Hydraulic Model from Operational Measurements for Supervisory Pressure Control

Poulton, M.

Evaluating Risk of Multi-Segment Pipes for Prioritizing Pipe Rehabilitation

Powell, David N.

Watershed Models for Storm Water Management: Comparing Hydrologic and Hydraulic Procedures

Preis, A.

Multi-Objective Sensor Placements with Improved Water Quality Models in a Network with Multiple Junctions

Preis, Ami

Online Hydraulic State Prediction for Water Distribution Systems

Prempain, Emmanuel

Identification of the Hydraulic Model from Operational Measurements for Supervisory Pressure Control

Prévost, M.

Comparison of Pressures Simulated Using Transient Analysis with Field Data from a Full-Scale Distribution System

Putnam, D.

Mid-Summer Deficit Irrigation of Alfalfa as a Strategy for Saving Water

Q

Return to top

Qi, X.

Wavelet Analysis of Characteristic Length Scales of Permeability in Stationary and Non-Stationary Porous Media

Qiu, Jinwei

Challenges on Three-Dimensional Simulations of Free Surface Flow

Quigley, Marcus

Integration of Low Impact Development Studies into the International Stormwater BMP Database

Quimpo, M. S.

General Hydraulic Characteristics of an Open Channel with Narrow Path

Quinn, Shane Pearse

The Impact of Biofilm Development on Pipe Roughness and Velocity Profile

R

Return to top

Radabaugh, C. R.

Groundwater Mixing Using Pulsed Dipole Injection/Extraction Wells

Rader, Russell

Fish Passage Can Be Improved by Introducing Hydraulic Refuge: Can the Effects Be Quantified?

Radhakrishnan, Venkatraman

Integrated Planning for Dual Distribution Systems

Radi, Micheal

Deployable Decentralized Biofilm System to Degrade Organic Carbon, Nutrients and Benzene from Wastewater

Radwan, Hany G.

Specific Problems Related to Partially Penetrating Wells in Confined Aquifers

Tool for Estimation of Additional Drawdown Due to Partially Penetrating Wells in Confined and Semi-Confined Aquifers

Rahman, Shikha

Simulation of Subsurface Water Flow by Galerkin Finite Element Method in Dhaka City Aquifer

Rajani, Balvant

Drinking Water Infrastructure Assessment: The National Research Council of Canada Perspective

Raju, K. Srinivasa

Multiobjective Differential Evolution and Differential Evolution for Irrigation Planning

Ramamurthy, A.

Modeling the Evolution of Incised Streams in Hammar Mesopotamian Marsh with Emphasis on the Contribution of Tidal Flow in the Filling Requirements

Ramsburg, C. Andrew

Exploring the Potential of Nonlinear and Non-Equilibrium Alcohol Partitioning for Assessment of DNAPL Source Zone Architecture

Rana, Samagra

Watershed Management in the Indian Himalayan Region: Issues and Challenges

Randall-Smith, M.

Application of Optimization Technology to Water Distribution System Master Planning

Ranjithan, Ranji

Characterizing Reactive Contaminant Sources in a Water Distribution System

Ranjithan, S. Ranji

A Hybrid Heuristic Search Approach for Contaminant Source Characterization

Rapp, Derek

Breaking Down the Barriers to Low Impact Development in Colorado

Rasmussen, T. J.

Water Quality of Streams in Johnson County, Kansas, 2002-07

Rasouli, Kabir

Simulation of Tehran Air Pollution Using Artificial Neural Networks

Rast, Brian

Nexus Projects in Kansas City's Suburban Watersheds

Ravikumar, Neetha

Improving Hydrologic Sustainability of Texas A&M University Campus

Ray, Maya R.

Simulation Study for Minimizing Diurnal Variation of Flow in a Hydroelectric Project to Reduce Downstream Impact

Ray, T.

Assessment of Flood Risk Due to Storm Surge in Coastal Bayous Using Dynamic Hydraulic Modeling

Razzaghi, Mehemed A.

Evaluation of Atriplx Shrubs Growth in Semi Arid Area

Records, M. K.

Conditioned Backward Probability Modeling to Identify Contamination Sources in a Water Distribution System

Reddi, L. N.

Engineered Waste Materials as Amendments to Prevent Erosion and to Stabilize Contaminated Sites

Reed, Seann

Transitioning NWS Operational Hydraulics Models from FLDWAV to HEC-RAS

Inundation Mapping Using Hydraulic Models and GIS: Case Studies of Steady and Unsteady Models on the Tar River, NC

Flash Flood Forecasting for Ungauged Locations with NEXRAD Precipitation Data, Threshold Frequencies, and a Distributed Hydrologic Model

Gauge-Based Adjustment of Historical Multi-Sensor Quantitative Precipitation Fields and Resulting Effects on Hydrologic Simulations

Reents, Nathan W.

Treatment Performance of Wastewater Lagoons in South Yungas Province of Bolivia

Rees, Paula Sturdevant

The Importance of In-Stream Hydraulics in River Water Quality Models: Lessons from the Blackstone River

Rehmann, Chris R.

Measuring Discharge with ADCPs: Inferences from Synthetic Velocity Profiles

Renetzky, David W.

Importance of Levees in the Kansas City Area

Richardson, Jerry R.

Redesign and Rehabilitation of Railroad Bridges with Advanced Adverse Lateral Migration

Richardson, Jerry

The Rush Creek Detention Facility: Planning a Permanent BMP in the Real World

Richarson, Jerry R.

Adverse Effects of Flood Flow at Skewed Railroad Crossings

Ripl, Klaus

Simulation of Particle Transport in Drinking Water Distribution Systems

Rippole, Joseph

Assessing Potential Implications of Climate Change for Long-Term Water Resources Planning in the Lower Colorado River Basin

Ritter, William F.

Permitting of Confined Animal Feeding Operations: Issues and Challenges

Manure Application to Soybeans in the Chesapeake Bay Watershed

Modeling Water Quality Impacts in Delaware's Coastal Bays with AGNPS

Rivas, Ivan

Design and Implementation of Optimized Hydrologic Unit Watersheds for Rainfall-Runoff Modeling

Riverson, John

Multiple Watershed Scales Approach for Placement of Best Management Practices in *SUSTAIN*

Robinson, H. J.

Distributed Hydrologic Model for Flood Prevention in the Yuna River Water shed, Dominican Republic

Robinson, H.

Analysis of Water Quality Trends and Pollutant Loading for Cypress Creek Watershed

Robinson, P. M.

The Next Generation of Irrigation Management Programs

Robinson, R. Bruce

Understanding Water Quality Responses to Long-Term Acidic Deposition in a High-Elevation Southern Appalachian Watershed: A Focus on Soil Watershed Processes

Rodgers, K.

The Value of Protecting Ozark Streams: An Economic Evaluation of Stream Bank Stability for Phosphorus Reduction

Rodriguez, Alfredo

Looking for a Solution—Joint Front Range Climate Change Vulnerability Study

Whatever It Takes: From Water Availability Model to Cost of Water

Rodríguez, Daniel

Calibration of Water Distribution Network Models as a Tool for Detecting Missing and Erroneous Cadastral and Hydraulic Information

Rodríguez García, José Luis

Vulnerability of the Hydraulic Resources of the River Basin of the San Juan-Brave River with the Global Climatic Change

Roehl, Edwin A. Jr.

Using “Big Data” to Optimally Model Hydrology and Water Quality across Expansive Regions

Roesner, L. A.

A Tool for Determining Effectiveness and Whole Life Costs of BMPs

An Evaluation of Graywater Reuse Utilizing a Constructed Wetland Treatment System

Roesner, Larry A.

Modeling Performances of Detention Basins with Uncertainty Analysis

Design and Implementation of Optimized Hydrologic Unit Watersheds for Rainfall-Runoff Modeling

Roesner, Larry

Graywater Irrigation as a Means to Meet Water Demands in Arid Regions

Gray Water and Treated Effluent Reuse

Roetsch, Dietmar

Reliability Analysis of Water Distribution Systems Using Graph Decomposition

Rogers, C. K.

Application of Optimization Technology to Water Distribution System Master Planning

Rome, A. C.

Are Rational C Values Too Low?

Regional Regression Analysis and the Rational Method

Romero-Gomez, P.

Axial Dispersion Coefficients for Laminar Flows in Water Distribution Systems

Romero, Miriam

GIS-Based Landscape Parameters for Wetland Evaluation Related to Amphibian Health

Rosario, Roberto A.

Air/Vacuum Valve Breakage Caused by Pressure Surges – Analysis and Solution

Roseen, Robert M.

Data Reporting Guidelines for Certification of Manufactured Stormwater BMPs: Part II

Examination of Pervious Concrete and Porous Asphalt Pavements Performance for Stormwater Management in Northern Climates

Field Testing Guidelines for Certification of Manufactured Stormwater BMPs: Part II

LID-SWM Practices as a Means of Resilience to Climate Change and Its Effects on Groundwater Recharge

Potential Data Analysis Methodology to Evaluate the Performance of Manufactured BMPs

Sediment Monitoring Bias by Autosampler in Comparison with Whole Volume Sampling for Parking Lot Runoff

Rosen, Michael

Investigating Aquatic Ecosystems of Small Lakes in Khorezm , Uzbekistan

Rowe, Amy A.

Enhancing Rain Garden Design to Promote Nitrate Removal

Pervious Pavement System Evaluation

Rowley, Brian

Clark County Regional Flood Control District Arc Hydro (CCRFCD Arc Hydro): Toward Ongoing Stormwater Master Planning

Roznowski, Steven

Gray Water and Treated Effluent Reuse

Ruan, Ben-qing

Analysis on Effect to EVW from Policy Intervention

Rubio, Christabel Jane

Use of Hydraulic Modeling to Develop a Small Dam for the Geum River Reach in Sejong City

Ruiz, Ariel

A Digital Floc Camera for Nonintrusive Measurement of Floc Parameters

Rukovets, R. Boris

Impact of Wet-Weather Peak Flow Blending on Disinfection Performance

Rushton, Betty

Field Testing Guidelines for Certification of Manufactured Stormwater BMPs: Part II

Russell, Kendra

Field Evaluation of Engineered Large Woody Debris for Structure Performance and Habitat Value

Quantitative Evaluation of Rock Weir Field Performance

Russo, J. P.

Investigation of Land-Use Change and Hydrologic Forcing upon Streambank Erosion and In-Stream Sediment Processes Using a Watershed Model and Sediment Tracers

Ryan, Andrea

Improving Hydrologic Sustainability of Texas A&M University Campus

Ryan, Jean M.

Does Polymer Have an Effect on Bacterial Regrowth in Anaerobically Digested Biosolids?

Ryu, Jae

Visualizing Hydrologic Drought Information on the Web Using State-of-the-Art Geospatial Mapping Technology

S

Return to top

Sadana, Ajit

Numerical Modeling of Ozonation of Organic Chemicals in Surface Water

Saddoris, David

Assessing Hydrodynamic Separators under High Water Flow Conditions

Sadiq, Rehan

Drinking Water Infrastructure Assessment: The National Research Council of Canada Perspective

Saito, Laurel

Coordinating and Implementing a Graduate Course on Interdisciplinary Modeling for Water-Related Issues

Investigating Aquatic Ecosystems of Small Lakes in Khorezm , Uzbekistan

Salas, J. D.

Developments on Stochastic Analysis, Modeling, and Simulation (SAMS 2009)

Saldarriaga, Juan G.

Water Distribution Systems Corrective Maintenance Supported by Real-Time Use of Hydraulic Models

Calibration of Water Distribution Network Models as a Tool for Detecting Missing and Erroneous Cadastral and Hydraulic Information

Salehi, M.

Suspended Sediment Concentration Measurements of Muddy Sediments with an ADV

Samuels, William

Sensor Network Design and Performance in Water Systems Dominated by Multi-Story Buildings

Sanden, B. L.

Mid-Summer Deficit Irrigation of Alfalfa as a Strategy for Saving Water

Sandoval-Solis, Samuel

Hydrological Feasibility of Environmental Flows in the Rio Grande/Bravo Basin

Sansalone, John J.

Proposed Scaling Relations for Manufactured Stormwater BMPs

Urban Stormwater Management in 2050

Sansalone, John

Field Testing Guidelines for Certification of Manufactured Stormwater BMPs: Part II

Saour, William

Improving Hydrologic Sustainability of Texas A&M University Campus

Sarma, Arup Kr.

Simulation Study for Minimizing Diurnal Variation of Flow in a Hydroelectric Project to Reduce

Downstream Impact

Saulters, Oral

Beyond Compliance and toward Sustainability: Advantages of Systems Environmental Engineering

Savabi, M. Reza

Water Retention and Hydraulic Conductivity of Different Media Used for Containerized Agriculture Systems

Savi•, D. A.

Operational Perspective of the Impact of Failures in Water Distribution Systems

Savic, D.

An Operative Approach to Water Distribution System Rehabilitation

Savic, Dragan A.

Effects of Redesign of Water Systems for Security and Water Quality Factors

Sayde, Chadi

A Web-Based Advisory Service for Optimum Irrigation Management

Measuring Soil Moisture in a Heterogeneous Field

Schlaman, James C.

From Grey to Green: Strategies and Concepts for Implementing Green CSO and Wet Weather Solutions

Schlebusch, Marc

Potable Water from a Superfund Site?

Schmalz, Richard A. Jr.

Comparison of the Princeton Ocean Model and the Regional Ocean Modeling System Hindcasts in the Delaware River and Bay

Schmidt, A. R.

An Innovative Approach for Modeling Large Urban Hydrologic Systems

Schmidt, A.

Predicting CSOs for Real Time Decision Support

Schmidt, Arthur R.

Monitoring the Hydrologic Effects of an Extensive Green Roof

Boundary Conditions for Simulating Complex Storm-Sewer Systems in Free Surface, Pressurized, and Mixed Flow Conditions

Schmidt, Arthur

Evolutionary Optimization of Combined Sewer Overflow Control

A Robust and Fast Model for Simulating Street Flooding

Schmitz, Erich

Hypothesis-Based Flow Monitoring for Green Solutions

Kansas City—Balancing Green Infrastructure with Traditional Approaches for CSO Control

Schnabel, William E.

A Decision Support System for Water Resources Planning and Management for the North Slope of Alaska

Schoen, Mary

Bayesian Load Duration Curves for Bacterial Total Maximum Daily Loads: Urban Case Study

Schöpfer, C.

Implementation of the Sustainable Development Concept in the Field of Groundwater Management

Schrempp, T.

Hydrogeologic Investigation for New Water Supply for Water District No. 1 of Johnson County, Kansas

Schrottenbaum, I.

Simple Model of Attachment and Detachment of Pathogens in Water Distribution System Biofilms

Schueler, Tom

The Runoff Reduction Method

Schulte, Scott

From Grey to Green: Strategies and Concepts for Implementing Green CSO and Wet Weather Solutions

Kansas City's Stream Setback Ordinance: A Case Study on the Benefits of Stream Buffers in Urban Areas

Schulze, Roland

A Framework for Determining the Possible Impacts of a Changing Climate on Water Supply

Schwar, Michael

Considering River-Scale Ecological Improvements within Flood Management Planning: The Lower Menomonee River Watercourse Status Report

USACE River Ecosystem Restoration Planning: Lessons Learned from the Illinois River Study

Schwartz, John S.

Developing Linkages between Biological Impairment and Stream Siltation: A Case Study in the Northern Great Plains Ecoregion

Bedload Composition and Development of 2D Stream Sediment Model for Stream Restoration Design Applications in Urbanizing Watersheds

A Monitoring and Assessment Framework to Evaluate Stream Restoration Needs in Urbanizing Watersheds

Understanding Water Quality Responses to Long-Term Acidic Deposition in a High-Elevation Southern Appalachian Watershed: A Focus on Soil Watershed Processes

Schwartz, John

The Effect of Natural Hydrological Disturbances (Defined from HSPF Simulated Hydrographs) on Trout Populations in Ungaged Streams of the Great Smoky Mountains National Park

Scott, Julian

Investigating Aquatic Ecosystems of Small Lakes in Khorezm , Uzbekistan

Scott, Rick

Advances in Data Validation, Event Detection, and Communications Structures for a CWS: Case Study—Glendale, Arizona

Seleshi, Y.

On the Local-Scale Spatial Variability of Daily Rainfall in the Highlands of the Blue Nile: Observational Evidence

Selker, John

Measuring Soil Moisture in a Heterogeneous Field

Semlitsch, R. D.

Development of an Amphibian Biotic Index to Evaluate Wetland Health in Northern Missouri

Semlitsch, Raymond

GIS-Based Landscape Parameters for Wetland Evaluation Related to Amphibian Health

Seneviratne, Sanjaya A.

Developing Artificial Neural Networks to Represent Salinity Intrusions in the Delta

Sethi, Sandeep

Synopsis of National Research Council's Report on Desalination

Sever, V. Firat

Adding Value to Sanitary Sewers—An Important Asset of Municipalities

Seville, Rick

Development of a Community Water Security Filtration System Using Composite Cartridges

Seyedabadi, M.

Evaluation of Uncertainties in the Simulation of Watershed Nutrient Load: A Case Study

Shafii, M.

Multi-Criteria Decision Making under Uncertainty in Rainfall-Runoff Calibration: A Fuzzy Compromise Programming Approach Based on Alpha Level Sets

Shahabifar, Mahdi

Estimation of Regional Reference Evapotranspiration from Land Surface Temperature and Co-Kriging Method at Tehran Province, Iran

Shanafield , Margaret

Investigating Aquatic Ecosystems of Small Lakes in Khorezm , Uzbekistan

Shanahan, Peter

Generalized Storage-Reliability-Yield Equations for Rainwater Harvesting Systems

Shang, Feng

Real-Time Implementation of Contamination Source Identification Method for Water Distribution Systems

Preliminary Spatial-Temporal Statistical Analysis of Hourly Water Demand at Household Level

Sharifi, F.

Deriving Rule Curve for Hydropower Reservoirs: Seymareh Experience

Sharma, Kusumakar

Spatial Variation of Sediment Oxygen Demand in Athabasca River: Influence of Water Column Pollutants

Sharvelle, S. E.

An Evaluation of Graywater Reuse Utilizing a Constructed Wetland Treatment System

Sharvelle, S.

Decentralized Anaerobic Treatment of Blackwater: A Sustainable Development Technology Concept for Urban Water Management

Sharvelle, Sybil

Graywater Irrigation as a Means to Meet Water Demands in Arid Regions

Shaw, Andrew R.

Recycling of Multiple Waste Streams for Transportation Fuel Production via Algae Cultivation at Wastewater Treatment Plants

Sheehan, Emily

Use of In-Planta Solid Phase Sampling Devices to Delineate VOC Plumes

Shelley, J.

Bankfull Discharge for Kansas Natural Alluvial Channel Design

Shelley, John E.

A Simple Analytical Design Method for Small Alluvial Channels

Shelley, John

Using HEC-RAS Hydraulic Design Functions for Geomorphic Channel Design and Analysis

Shen, Hailiang

Comparative Evaluation of Two Algorithms for Locating Contaminant Ingress Points

Sheng, Z.

Runoffs of the Xiangride and Qaidum Rivers in the Arid Qaidum Basin, Northwest China

Sheng, Zhuping

Analytical-Numerical Solution for Seepage along an Earth Canal Disconnected from the Shallow Aquifer

Sherman, Kevin M.

Using Media Filters in a Distributed Wastewater System Serving an Ecotourism-Oriented Development

Shields, F. Douglas Jr.

River Bed Sediment Classification Using ADCP

Shih, Hui-Ming

Alternatives Study of Willwood Diversion Dam Siltation Removal in Wyoming, USA

Shin, Hongjoon

Asymptotic Variance of Regional Growth Curve for Generalized Logistic Distribution

Shin, Kwangseob

Use of Hydraulic Modeling to Develop a Small Dam for the Geum River Reach in Sejong City

Shin, P. S.

Seoul (Korea) Online Water Quality Monitoring of Drinking Water

Shin, Yee-Sook

Modeling Framework for Establishing Water Quality Trading Units near Pacific, Missouri

Shitta, Kazeem Akorede

Lithostratigraphy of Nigeria—An Overview

Shockey, Sheila

Kansas City, Missouri Wet Weather Solutions Program: A Twelve Step Program

Shoemaker, Christine A.

A Comparison of a SWAT Model for the Cannonsville Watershed with and without Variable Source Area Hydrology

Shoemaker, Leslie

Multiple Watershed Scales Approach for Placement of Best Management Practices in *SUSTAIN*

Shubhashish, K.

Air-Borne Heavy Metal Contamination to River Ganga (India)

Shulse, C. D.

Development of an Amphibian Biotic Index to Evaluate Wetland Health in Northern Missouri

Shulse, Christopher D.

GIS-Based Landscape Parameters for Wetland Evaluation Related to Amphibian Health

Shultz, Steve

Integrated Management of a Finite Water Supply in the Desert

Siew, Calvin

Augmented Gradient Method for Head Dependent Modelling of Water Distribution Networks

Sim, Youn

Development of Watershed Management Modeling System: The Los Angeles County Flood Control District's Watershed Based Approach for Urban Runoff and Stormwater Quality

Simon, Andrew

Developing Linkages between Biological Impairment and Stream Siltation: A Case Study in the Northern Great Plains Ecoregion

Simpson, Angus R.

Damage Detection of Operating Transmission Mains with Measured Boundary Conditions

Reliability Analysis of Water Distribution Systems Using Graph Decomposition

A Framework for Alternative Formulations of the Pipe Network Equations

Singh, Harsh Vardhan

Studying the Impact of Land Use/Cover Changes on the Water Quality of Weeks Bay, AL: Model vs. Regression

Singh, R. K.

Performance Evaluation of Soil Heat Flux Models in Great Plains

Singh, Shashank

Application of Remote Sensing Based Tillage Mapping Technique to Evaluate Water Quality Impacts of Tillage Management Decisions in Upper White River Basin

Singh, Vijay P.

Copula Approach for Reducing Uncertainty in Design Flood Estimates in Insufficient Data Situations

Singleton, Thomas L.

A Pragmatic Cycle for Ongoing Water Resources Research and Management

Sinha, R.

Removal of Waterborne Particles by Electrofiltration

Sinha, Rajib

Production of Drinking Water from Lake Water Sources with a Nanofilter Membrane to Prevent the Formation of Disinfection Byproducts

Development of a Community Water Security Filtration System Using Composite Cartridges

Evaluation of a UV/Ozone Treatment Process for Removal of MTBE in Groundwater Supplies in New Mexico

Sinha, Sumit

Upstream Intrusion Effect of CSO Event in Bubbly Creek, IL

Sinha, Sunil

Development of a National GIS Database for Municipal Water and Wastewater Pipe Infrastructure System

Sitler, Ruth A.

Looking Upstream and into the Watershed for the Big Picture of Stream Health

Siu, Christina Y. S.

Codorus Creek Restoration—A Case Study for the Chesapeake Bay

Looking Upstream and into the Watershed for the Big Picture of Stream Health

Sivakumar, B.

Nonlinear Dependence in Hydrologic Time Series

Sizirici, Banu

Time Series Analysis of Performance Data from Closed Landfills to Forecast Post Closure Monitoring Needs

Skworcow, P.

Bursts Identification in Water Distribution Systems

Combined Energy and Pressure Management in Water Distribution Systems

Slate, Louise O.

A Monitoring and Assessment Framework to Evaluate Stream Restoration Needs in Urbanizing Watersheds

Sliwinski, Timothy M.

Developing Probability of Failure Estimates for Stream Restoration Design Components

Small, Mitchell J.

Decision Making under Information Constraints

Small, Mitchell

Bayesian Load Duration Curves for Bacterial Total Maximum Daily Loads: Urban Case Study

Smith, D. P.

A New Methodology to Evaluate Pollutant Removal of Gross Solids Separation Devices

Smith, Joseph D.

Selection of Overflow Control Strategies for the Austin Clean Water Program

Smith, Michael

Distributed Hydrologic Modeling: From Research to Operational Forecasting

Smith, Rachelle

Deployable Decentralized Biofilm System to Degrade Organic Carbon, Nutrients and Benzene from Wastewater

Smith, Tony L.

Parameterization of Seasonal Freshets for the Study of Effects of Freshwater Inflows on Galveston Bay

Smolen, M. D.

Construction and Performance of Bioretention Cells

Sofranko, Anna

Prediction of Nitrate Concentration in Stream Water Based on Watershed Land Use and Stream Flow Rate

Solis, Ruben S.

Application of NEXRAD for Freshwater Inflow Estimates to Texas Bays and Estuaries

Song, Y. R.

Seoul (Korea) Online Water Quality Monitoring of Drinking Water

Soppe, Richard

Comparison of Evapotranspiration Estimates from Remote Sensing (SEBAL), Water Balance, and Crop Coefficient Approaches

Sosnikhina, Irina

Cost Comparison of Membrane Treatment and Concentrate Management Practices at Drinking Water Treatment Plants in Florida

Sowells, Camille W.

Implementing Source Water Protection Programs in Texas

A Tale of Two Cities—Source Water Protection Case Studies for Systems in Rural Settings

Selection and Prioritization of Best Management Practices for Potential Sources of Contamination in a Wellhead Protection Area

Spafford, Mark

Spatial Variation of Sediment Oxygen Demand in Athabasca River: Influence of Water Column Pollutants

Speight, Vanessa

Integrated Planning for Dual Distribution Systems

Spencer, A.

Change in Surface Hydrology Due to Land Use Change in a Midwestern Watershed

Spenn, Jacob

HCFCD M3 System: Maximizing and Maintaining Local Investments in Floodplain Modeling

Spicher, Julia

Rainwater Harvesting for Non-Potable Use in Gardens: A Comparison of Runoff Water Quality from Green vs. Traditional Roofs

Srikishen, Jayanthi

Design of Solar Radiation Sensor Network Using Geo-Statistical Methods

St. Clair, Martin

Denitrifying Bioreactors for Treatment of Tile Drainage

Stander, Emilie K.

Enhancing Rain Garden Design to Promote Nitrate Removal

Pervious Pavement System Evaluation

Stansbury, John

Multi-Criteria Assessment of Pallid Sturgeon Habitat Restoration for the Missouri River

Starks, Patrick J.

Do Upland Soil Conservation Measures Reduce Watershed Sediment Yield?

Stedinger, Jery R.

Uncertainty and Sensitivity Analysis for Models with Calibrated Parameters

Steele, Dean D.

Comparison of Sensible Heat Flux Measurements by a Large Aperture Scintillometer and Eddy Correlation Methods

Steele, Kelly A.

Rainwater Harvesting for Non-Potable Use in Gardens: A Comparison of Runoff Water Quality from Green vs. Traditional Roofs

Stefan, Heinz

Assessment of Standard Sumps for Stormwater Treatment

Stein, Stuart

Communicating Drought Severity and Re-Evaluating Firm Yield—Cumberland County, Tennessee As a Case Study

Stein, Walt

Data Reporting Guidelines for Certification of Manufactured Stormwater BMPs: Part II

Stewart, Ken

South Florida Water Control System Tracker: Real-Time Water Budgeting for Pragmatic Water Control Operations

Stinson, Mary K.

Impact of Wet-Weather Peak Flow Blending on Disinfection Performance

Stipanovi•, Dušan M.

A Decentralized Optimization Algorithm for Multi-Agent System Based Watershed Management

Stockstill, Richard L.

3D Numerical Modeling of John Day Lock Tainter Valves

A Three-Dimensional Numerical Model for Flow in a Lock Filling System

Stoleru, Radu

Improving Hydrologic Sustainability of Texas A&M University Campus

Stolinski, Ted

Case Study: Impact of Varying Mitered Suction Elbows on Large Wastewater Pumps

Stone, Loyd R.

Irrigation Scheduling for Deficit Irrigation

Storm, D. E.

Construction and Performance of Bioretention Cells

Straw, Dale E.

ASCE Standardized Penman-Monteith Alfalfa Reference ET and Crop ET Estimates for Arkansas River Compact Compliance in Colorado

Straw, Dale

Alfalfa Reference ET from a Weighing Lysimeter and Estimates from the ASCE Standardized Reference ET Equation in the Arkansas Valley of Colorado

Strecker, Eric

Combining GIS, BMP Performance, and Strategic Planning to Support Water Quality Implementation Planning

Integration of Low Impact Development Studies into the International Stormwater BMP Database

Engineering Natural Filtration Systems to Remove Selenium, Nitrate, and Bacteria from Impaired Surface Waters—Foundational Studies

Strom, K. B.

Suspended Sediment Concentration Measurements of Muddy Sediments with an ADV

Strom, Kyle B.

A Digital Floc Camera for Nonintrusive Measurement of Floc Parameters

Stromberger, Mary

Graywater Irrigation as a Means to Meet Water Demands in Arid Regions

Struck, Scott D.

Kansas City—Balancing Green Infrastructure with Traditional Approaches for CSO Control

Struck, Scott

Evaluation and Optimization of Distributed Stormwater Controls in Spreadsheet

Kansas City, Missouri Overflow Control Plan Summary

Stuart, A.

Non-Traditional University Research Partners That Facilitate Service Learning and Graduate Research for Sustainable Development

Stutzman, Lynn C.

Alternatives Study of Willwood Diversion Dam Siltation Removal in Wyoming, USA

Styles, Stuart W.

Evaluation of Magnetic Meters for Irrigation Pipeline Measurement

Su, Yu-Chun

HCFCD M3 System: Maximizing and Maintaining Local Investments in Floodplain Modeling

The Geneva Dam, IL, Hydraulic Roller Problem: Design of a Temporary Steep Riprap Ramp

Suen, Jian-Ping

Use of Artificial Neural Networks for Habitat Unit Composition Modeling

Examining the Flow Regime Alteration and Its Potential Impacts to Freshwater Ecosystems under Changing Climate Conditions

Sullivan, Michael

Agricultural Drainage Management Systems Task Force (ADMSTF)

Summerton, Mark

A Framework for Determining the Possible Impacts of a Changing Climate on Water Supply

Sun, Detong

Estimating Groundwater Seepages to St. Lucie Estuary

Sundberg, Randy

Engineering Natural Filtration Systems to Remove Selenium, Nitrate, and Bacteria from Impaired Surface Waters—Foundational Studies

Removal of Selenium and Nitrate from Surface Waters Using a Subsurface Microbial Filter

Sunder, Shiva

Use of the Basin Development Factor to Evaluate Urban Watershed Response

Sung, W. P.

Application of Biopile System for the Remediation of Petroleum-Hydrocarbon Contaminated Soils

Surampalli, Rao Y.

Application of Biopile System for the Remediation of Petroleum-Hydrocarbon Contaminated Soils

Susilo, Ken

Combining GIS, BMP Performance, and Strategic Planning to Support Water Quality Implementation Planning

Considerations, Opportunities, and Strategies for Infiltration Stormwater BMPs

Engineering Natural Filtration Systems to Remove Selenium, Nitrate, and Bacteria from Impaired Surface Waters—Foundational Studies

Sveinsson, O.

Developments on Stochastic Analysis, Modeling, and Simulation (SAMS 2009)

Svoboda, Mark

Visualizing Hydrologic Drought Information on the Web Using State-of-the-Art Geospatial Mapping Technology

Swanson, James

Integrated Planning for Dual Distribution Systems

Sweazy, Chris

Selecting Optimal Water Supply Options—A Regional Water Supply Case Study in the Upper Kissimmee Basin, FL

Szabo, J.

Simple Model of Attachment and Detachment of Pathogens in Water Distribution System Biofilms

T

Return to top

Tabatabaie, T.

EPM Approach for Erosion Modeling by Using RS and GIS

Tabatabaie, Taybeh

The Effect of Sewage Pollutant of Bandar Imam Petrochemical Company on Benthic Macofauna Community Using Biodiversity Indices and Bioindicators

Tacker, Phil

The Arkansas Irrigation Scheduler

Taheriyoun, M.

Evaluation of Uncertainties in the Simulation of Watershed Nutrient Load: A Case Study

Takbiri, Zeinab

Optimal Design and Operation of Fuse-Gates Considering Water Loss Due to Gates Tilting

Tanellari, Eftila

Case Study: Homeowner's Preference Trade-Offs toward Plumbing Systems in Pipe Failure Prone Area

Tansel, Berrin

Time Series Analysis of Performance Data from Closed Landfills to Forecast Post Closure Monitoring Needs

Water Retention and Hydraulic Conductivity of Different Media Used for Containerized Agriculture Systems

Cost Comparison of Membrane Treatment and Concentrate Management Practices at Drinking Water Treatment Plants in Florida

Tanyimboh, Tiku T.

Augmented Gradient Method for Head Dependent Modelling of Water Distribution Networks

Tarquin, Anthony J.

Membrane Treatment of Rio Grande Water for Municipal Water Production during the Non-Irrigation Season

Taxon, Tom

Sensor Network Design and Performance in Water Systems Dominated by Multi-Story Buildings

Taylor, S. W.

Assessing Postulated Accidental Releases of Radioactive Liquid Effluents from Nuclear Power Plants

Teague, A.

Analysis of Water Quality Trends and Pollutant Loading for Cypress Creek Watershed

Teegavarapu, Ramesh S. V.

Evaluation of Improvised Spatial Interpolation Methods for Infilling Missing Precipitation Records

Optimization of Regional Stormwater Quality Control Systems Using Genetic Algorithms

Teegavarapu, Ramesh S.

Design of Solar Radiation Sensor Network Using Geo-Statistical Methods

Understanding Uncertainties in Water Budget for Large Constructed Wetlands

Teng, Jingjie

Prediction of Nitrate Concentration in Stream Water Based on Watershed Land Use and Stream Flow Rate

Teng, Zheng

pH Variation and Its Effect on Metal Concentration during Electrokinetics

Thapa, Bir

The Use of Soil-Water Sensors in Turf Irrigation Control—How Effective Are They?

Thoman, Robert W.

Construction of a Low-Flow Channel in Barber Creek: Case Study in the Powder River Basin, Wyoming

Thoman., Robert W.

Sustainable Design and Construction of Earthen-Dam Reservoirs for Water Produced in Association with

Coalbed Natural Gas in the Powder River Basin, Wyoming

Thomas, J. T.

Fish Passage and Abundance around Grade Control Structures on Incised Streams

Hungry Canyons Alliance: Streambed Stabilization in Western Iowa

Thompson, David B.

Use of the Basin Development Factor to Evaluate Urban Watershed Response

Water Subdivision for Modeling

Thompson, Kenneth A.

Advances in Data Validation, Event Detection, and Communications Structures for a CWS: Case Study—Glendale, Arizona

Implementing a Contamination Warning System at a Department of Defense Facility: Case Study—Port Hueneme, California

Thompson, Stacia L.

Novel, Rapid Molecular-Based Technique for Detecting Contamination in Drinking Water Distribution Systems

Thoreson, Bryan

Comparison of Evapotranspiration Estimates from Remote Sensing (SEBAL), Water Balance, and Crop Coefficient Approaches

Thornton, Christopher I.

Physical Modeling of River Spanning Rock Structures: Evaluating Interstitial Flow, Local Hydraulics, Downstream Scour Development, and Structure Stability

Tidwell, Amy C.

A Decision Support System for Water Resources Planning and Management for the North Slope of Alaska

Todini, E.

Enhanced Global Gradient Algorithm: A General Formulation

Togawa, Noboru

Controlled Full-Scale Field Testing of an Up-Flow Filtration Device

Tomasko, David

An Analytical Solute Transport Model for In Situ Estimation of Retardation

Tompkins, M. R.

Post Project Appraisal of Riparian, Wetland, and Aquatic Habitat Restoration at Best Slough, Beale Air Force Base, Marysville, CA

Tompkins, Mark R.

Integrating Fluvial Geomorphology and Two-Dimensional Hydraulic and Sediment Transport Modeling to Support Sustainable Design of Large River and Floodplain Improvements: The Trinity River Corridor Project, Dallas, Texas, USA

Tootle, Glenn A.

Paleo Pacific Ocean Sea Surface Temperature Variability and Upper Colorado River Basin Streamflow

Trauth, K. M.

Development of an Amphibian Biotic Index to Evaluate Wetland Health in Northern Missouri

Trauth, Kathleen M.

GIS-Based Landscape Parameters for Wetland Evaluation Related to Amphibian Health

A GIS-Based Decision-Making Methodology for Evaluation of Environmental Justice Impacts of Community Infrastructure Projects

Modeling Framework for Establishing Water Quality Trading Units near Pacific, Missouri

Traver, R. G.

Bioretention/Bioinfiltration Performance in the Mid-Atlantic

Stormwater Infiltration Retrofits: Experience Gained through Long Term Monitoring

The Observed Effects of Stormwater Infiltration on Groundwater

Treanor, Patrick

Desalination Concentrate: Bay vs. Ocean

Treese, Daniel P.

Pollutant Transport within the Vadose Zone: Interactions of Soil Horizon Chemistry on Water Quality

Trezza, R.

Automated Selection of Anchor Pixels for Landsat Based Evapotranspiration Estimation

Trinkaus, Steven D.

The Application of Environmental Site Design Processes to Design a Residential Subdivision

Assessing Pollutant Loads and Evaluation of Treatment Systems to Achieve Water Quality Goals for Land Development Projects

Tripathi, Shivam

On the Use of Data Uncertainty in Hydro-Climatic Modeling: A Bayesian Approach

Trotz, M. A.

Non-Traditional University Research Partners That Facilitate Service Learning and Graduate Research for Sustainable Development

Trout, Thomas

Water Production Functions for High Plains Crops

Tsai, Christina W.

Modeling of Sediment Particle Deposition and Resuspension Processes Using a Stochastic Jump Diffusion Particle Tracking Model

Stochastic Non-Equilibrium Bedload Transport Model

Tsai, F. T.-C.

Simulation of Multilayer Shallow Water Fluid Flow Using Lattice Boltzmann Modeling and High Performance Computing

Tubbs, K. R.

Simulation of Multilayer Shallow Water Fluid Flow Using Lattice Boltzmann Modeling and High Performance Computing

Tune, Jenna

Drinking Water Field Analyses for the Detection and Enumeration of Coliform Bacteria in Rural Guatemalan Highlands

Turner, T.

Habitat Restoration on the Middle Fork John Day River

Tustison, Ben

Reining in Log-Pearson Type III Flow-Frequency Estimates—Applying a Reasonable Bound through the Skew Parameter

Tyagi, Aditya

Threat Perceptions and Risk Management in Urban Water Supply Schemes

Selecting Optimal Water Supply Options—A Regional Water Supply Case Study in the Upper Kissimmee Basin, FL

Integrated Management of a Finite Water Supply in the Desert

Tye, I. J.

Retrofitting Stormwater BMPs in a Supercritical Flow Regime: A Hydraulic Perspective

Tyree, Shannon W.

Lake Winnebago Dam Relocation Project

Tzatchkov, V. G.

Inexpensive Modeling of Intermittent Service Water Distribution Networks

U

Return to top

Uber, J.

Simple Model of Attachment and Detachment of Pathogens in Water Distribution System Biofilms

Uber, James G.

Real-Time Implementation of Contamination Source Identification Method for Water Distribution Systems

Preliminary Spatial-Temporal Statistical Analysis of Hourly Water Demand at Household Level

Uber, James

Comparing Single- and Multi-Species Water Quality Modeling Approaches for Assessing Contamination Exposure in Drinking Water Distribution Systems

A Simplified Model of Combined Sewer Overflows to Estimate Event Driven Enteric Pathogen Concentrations in Drinking Water Sources

Uhl, Wolfgang

Simulation of Particle Transport in Drinking Water Distribution Systems

Ulanicki, B.

Bursts Identification in Water Distribution Systems

Combined Energy and Pressure Management in Water Distribution Systems

Ulanicki, Bogumil

Identification of the Hydraulic Model from Operational Measurements for Supervisory Pressure Control

Urbonas, B. R.

A Tool for Determining Effectiveness and Whole Life Costs of BMPs

Urbonas, Ben

Challenges in Attaining Recreational Stream Standards for Bacteria: Setting Realistic Expectations for Management Policies and BMPs

V

Return to top

Vairavamoorthy, K.

Water Demand Forecasting for the City of the Future against the Uncertainties and the Global Change Pressures: Case of Birmingham

Vairavamoorthy, Kala

Development of a Fuzzy Based Pipe Condition Assessment Model Using PROMETHEE

Valocchi, Albert J.

Spatial Evolutionary Algorithms for Characterizing Large-Scale Spatial Groundwater-Vegetation Dynamics in Arid Region

van den Broeke, Joep

Advances in Data Validation, Event Detection, and Communications Structures for a CWS: Case Study—Glendale, Arizona

van Zyl, J. E.

Modeling Domestic Water Demand on a Suburb Level

VanBriesen, J. M.

Propagation of Chlorine Demand Signals Induced by Microbial Contaminants in a Drinking Water Distribution System

VanBriesen, Jeanne M.

Decision Making under Information Constraints

Novel, Rapid Molecular-Based Technique for Detecting Contamination in Drinking Water Distribution Systems

VanBriesen, Jeanne

Bayesian Load Duration Curves for Bacterial Total Maximum Daily Loads: Urban Case Study

Vanrenterghem-Raven, A.

Evaluating Risk of Multi-Segment Pipes for Prioritizing Pipe Rehabilitation

Varyu, David R.

Numerical Model of Channel Meandering in the Middle Sacramento River

Varyu, David

Quantitative Evaluation of Rock Weir Field Performance

Vasan, A.

Multiobjective Differential Evolution and Differential Evolution for Irrigation Planning

Vasconcelos, Jose G.

Physical Processes Resulting in Geyser Formation in Rapidly Filling Stormwater Tunnels

Vazifedoust, Majid

Numerical Modeling of Flushing Process in Dez Dam Reservoir by HR Wallingford Method

Vazquez, Oscar

Effect of Acid Mine Drainage on Aluminum Release from Clay Minerals

Veerapaneni, Srinivas

New Strategies for Managing Desalination Concentrate with Zero Liquid Discharge from Two WRF Research Projects

Velez, Rafael

Controlling Saltwater Intrusion to Environmental Sensitive Areas Due to the Construction of the Rio Anton Ruiz Flood Control Project

Vemulapally, Rahul

Development of a National GIS Database for Municipal Water and Wastewater Pipe Infrastructure System

Venayagamoorthy, S. K.

Simulations of Aquaculture Dissolved Waste Transport and Mixing in Near-Coastal Waters

Verma, S. B.

Performance Evaluation of Soil Heat Flux Models in Great Plains

Viswanadh, G. K.

Evaluation of Land Use Land Cover Changes in Palleru (K-11) Sub Basin of River Krishna Using GIS and NDVI

Vitello, Matthew

A Mobile Emergency Drinking Water System Powered by Renewable Energy

Vivas, G.

Integrated Water Management in an Ancestral Water Scheme in a Mountainous Area of Southern Spain

Vogel, Richard M.

Generalized Storage-Reliability-Yield Equations for Rainwater Harvesting Systems

The Implications of Discretizing Continuous Random Variables: An Example Using the U.S. Geological Survey Reporting Standards for Streamflow Data

Vories, Earl

The Arkansas Irrigation Scheduler

Vugrin, Eric

Trajectory Clustering Approach for Reducing Water Quality Event False Alarms

W

Return to top

Wadzuk, B. M.

Redesigning Constructed Stormwater Wetlands: An Integrated Modeling Approach to Optimize Form and Function

Wadzuk, Bridget M.

An Investigation of Infiltration in a Constructed Stormwater Wetland and Implications for Groundwater Quality

Wadzuk, Bridget

Developing a Water Budget for a Constructed Stormwater Wetland

Wagdy, Ahmad

Specific Problems Related to Partially Penetrating Wells in Confined Aquifers

Tool for Estimation of Additional Drawdown Due to Partially Penetrating Wells in Confined and Semi-Confined Aquifers

Wagener, T.

Reducing Uncertainty of Continuous Streamflow Predictions in Ungauged Basins (PUB) Using Regional Constraints: Using Regional Constraints for PUB

Waisner, Scott A.

Deployable Decentralized Biofilm System to Degrade Organic Carbon, Nutrients and Benzene from Wastewater

Walker, B.

Change in Surface Hydrology Due to Land Use Change in a Midwestern Watershed

Walker, Jeffrey D.

The Importance of In-Stream Hydraulics in River Water Quality Models: Lessons from the Blackstone River

Walker, Jeffrey

The Economic and Environmental Significance of Nonpoint Source Abatement in Large Watersheds

Walker, Jennifer J.

Modeling Techniques to Incorporate Low Impact Development Features into Detention Analyses

Walker, Wynn

Application of SIRMOD to Evaluate Potential Tailwater Reduction from Improved Irrigation Management

Wall, Jack D.

Watershed Models for Storm Water Management: Comparing Hydrologic and Hydraulic Procedures

Walsh, Thomas K.

The Importance of In-Stream Hydraulics in River Water Quality Models: Lessons from the Blackstone River

Walski, Thomas M.

Modeling a Hydraulic Response to a Contamination Event

Walski, Thomas

Pressure vs. Flow Relationship for Pipe Leaks

Walter-Shea, E. A.

Performance Evaluation of Soil Heat Flux Models in Great Plains

Waltermire, Kendra

Use of In-Planta Solid Phase Sampling Devices to Delineate VOC Plumes

Wang, Cheng-li

Analysis on Effect to EVW from Policy Intervention

Wang, Dangxian

Study on the Water Value Conversion between Economy and Ecology and Countermeasures of Water Resources Distribution for Coordinated Development of Economy and Ecology

Wang, Dingbao

Estimating Groundwater Pumping and Return Flow Based on Hydrologic Recession Analysis

Wang, Hao

Study on the Water Value Conversion between Economy and Ecology and Countermeasures of Water Resources Distribution for Coordinated Development of Economy and Ecology

Wang, Hui

A Markov Chain Monte Carlo Implementation of Bayesian Contaminant Source Characterization in Water Distribution Systems under Stochastic Demands

Wang, J.

A Critical Realization Identification Method Based on Pareto Dominance Analysis

Wang, Jihua

Spatial Evolutionary Algorithms for Characterizing Large-Scale Spatial Groundwater-Vegetation Dynamics in Arid Region

Wang, Sam S. Y.

Numerical Modeling of Ozonation of Organic Chemicals in Surface Water

A Process-Based Unsteady Model for Wave-Current-Morphodynamic Changes in Two-Dimensions

Numerical Simulations of Coastal Floods and Morphological Changes Due to Sea Level Rise and Hazardous Storm

One-Dimensional Modeling of Water Quality and Aquatic Ecosystems in Streams

A Depth-Averaged 2-D Model of Non-Cohesive Dam/Levee Breach Processes

Numerical Simulation of Sediment Transport and Morphological Change of JiJi Weir Reservoir

Prediction of Changes in Soil Moisture Due to Rainfall, Infiltration, and Evapotranspiration Using a Physically-Based Model

Wang, Wei

ARC Population and Employment Allocation Disaggregator—A Simple GIS-Based Tool for Parcel-Scale Population Projection

Wanielista, Marty

Comparative Study of Two Standard Septic Tank Drain Fields Using Different Sand with Recirculation for Nutrient Removal

Investigating the Temperature Effects on Nutrient Removal in Green Sorption Media

Nutrient and Pathogen Removal with an Innovative Passive Underground Drainfield for On-Site Wastewater Treatment

Wankhede, N. N.

Environmental and Water Resources in Developing Countries: Development of Micro Irrigation Facility at Parsoda Village

Waratuke, Andy

Hydraulic Model Study of Canoe Chute and Fish Passage for the Chicago River North Branch Dam

Ward, George H. Jr.

Parameterization of Seasonal Freshets for the Study of Effects of Freshwater Inflows on Galveston Bay

Wardman, Brian G.

One-Dimensional Modeling of Sedimentation Processes on the Puyallup River

Warren, Courtney

Drive for Zero Net Carbon Impact

Watkins, David W. Jr.

Probabilistic Streamflow Forecasts Based on Hydrologic Persistence in Central Texas

Weaver, W. J.

McCormick Place West Hall Conference Center Stormwater Reclamation Tunnel and “Green Roof” Helps Advance Chicago’s Clean Water Agenda

Webb, Joseph R.

Fish Passage Can Be Improved by Introducing Hydraulic Refuge: Can the Effects Be Quantified?

Culvert Retrofit and Fish Passage: An Update

Weber, Chuck

Water Distribution Optimization: Taking SCADA One Step Forward

Wei, Wenge

Probabilistic Streamflow Forecasts Based on Hydrologic Persistence in Central Texas

Weingartner, Andreas

Advances in Data Validation, Event Detection, and Communications Structures for a CWS: Case Study—Glendale, Arizona

Weiss, Peter T.

Maintenance of Stormwater BMPs

Weist, Jamie H.

Watershed Models for Storm Water Management: Comparing Hydrologic and Hydraulic Procedures

Welch, Gregory

Integrating Fluvial Geomorphology and Two-Dimensional Hydraulic and Sediment Transport Modeling to Support Sustainable Design of Large River and Floodplain Improvements: The Trinity River Corridor Project, Dallas, Texas, USA

Wendell, Daniel

Integrated Management of a Finite Water Supply in the Desert

Werner, Hal D.

On-Line Irrigation Scheduling within the Belle Fourche Irrigation District

Werth, Charles J.

Monitoring the Hydrologic Effects of an Extensive Green Roof

Werth, David

A Comparison of Formed Suction Inlets for Flood Control Applications

Case Study: Impact of Varying Mitered Suction Elbows on Large Wastewater Pumps

Weston, David

Controlling Saltwater Intrusion to Environmental Sensitive Areas Due to the Construction of the Rio Anton Ruiz Flood Control Project

Westphal, Kirk

The Economic and Environmental Significance of Nonpoint Source Abatement in Large Watersheds

Whisler, Jordan

Smart Pipe—Nanosensors for Monitoring Water Quantity and Quality in Public Water Systems

White, Kristin

Modeling Techniques to Incorporate Low Impact Development Features into Detention Analyses

Whitman, Brian

Pressure vs. Flow Relationship for Pipe Leaks

Whittle, Andrew

Online Hydraulic State Prediction for Water Distribution Systems

Wible, Daniel

Developing Green Streets Prototypes to Reduce Combined Sewer Overflows for Cincinnati, Ohio

Wilcock, Peter R.

A Bayesian Framework for Cost Effective Management of Sediment Reduction in the Minnesota River

Basin

Wilkerson, Gregory

Sediment Load Based Single Thread Alluvial Channel Classification

Wilkison, Donald H.

Water-Quality Assessment of the Largely Urban Blue River Basin, Metropolitan Kansas City, USA, 1998 to 2007

Williams, David T.

The Geneva Dam, IL, Hydraulic Roller Problem: Design of a Temporary Steep Riprap Ramp

Uncertainty Analysis: You Need to Know What You Don't Know

Williams, Greg

Potential Data Analysis Methodology to Evaluate the Performance of Manufactured BMPs

Williams, Gregory

Proposed Scaling Relations for Manufactured Stormwater BMPs

Williams, Gustavious P.

A Heuristic Algorithm for Optimal Alignment and Matching of Borehole Stratigraphy

Williams, Gustavious Paul

An Analytical Solute Transport Model for In Situ Estimation of Retardation

Williams, Tim

Data Reporting Guidelines for Certification of Manufactured Stormwater BMPs: Part II

Field Testing Guidelines for Certification of Manufactured Stormwater BMPs: Part II

Wilson, C. Bruce

Maintenance of Stormwater BMPs

Wilson, Christopher G.

Using Tracers to Derive Sediment Provenance after the Occurrence of a 500-Year Flood in a Midwestern Stream

Wilson, G. V.

Predicting Streambank Seepage Flows: Sensitivity to Soil Properties and Layering

A Seepage Erosion Sediment Transport Function and Geometric Headcut Relationships for Predicting Seepage Erosion Undercutting

Wilson, Joel

An Approach for Integrated Optimization of Wastewater, Recycled, and Potable Water Networks

Winslow, Kyle

Integrating Fluvial Geomorphology and Two-Dimensional Hydraulic and Sediment Transport Modeling to Support Sustainable Design of Large River and Floodplain Improvements: The Trinity River Corridor Project, Dallas, Texas, USA

Winston, Ryan J.

A Level Spreader—Vegetated Buffer System for Urban Stormwater Management

Winters, Brad

The Geneva Dam, IL, Hydraulic Roller Problem: Design of a Temporary Steep Riprap Ramp

Wobig, Loren

The Geneva Dam, IL, Hydraulic Roller Problem: Design of a Temporary Steep Riprap Ramp

Wolcott, S. B.

Application of Northeast Regional Climate Center Research Results for the Purpose of Evaluating and Updating Intensity-Duration-Frequency (IDF) Curves –Case Study: Rochester, New York

Wolf, Lorraine

Environmental Impacts on Surface Water and Groundwater for Expanding Urban Water Supply Capacity Using Stone Quarries

Wolters, Andreas

Reliability Analysis of Water Distribution Systems Using Graph Decomposition

Woo, Michael H.

Evaluating the Mixing Mechanism of Outfall Discharges from Municipal Separate Storm Sewer Systems

Woodbury, Josh

A Comparison of a SWAT Model for the Cannonsville Watershed with and without Variable Source Area Hydrology

Wright, J. D.

Field Evaluation of Indicator Bacteria Removal by Stormwater BMPs in North Carolina

Research of Hydrologic and Water Quality Performance of Four Linear Wetlands in Eastern North Carolina

Implementation and Performance of Stormwater Best Management Practice Retrofits in Wilmington, NC

Wright, James L.

Estimation of Evaporation and Evapotranspiration during Nongrowing Seasons Using a Dual Crop Coefficient

Wright, Jason

Rainwater Harvesting Experiences in the Humid Southeast USA

Wright, Jeff R.

Environment and Water Resources in 2050: The Challenge for Engineering Education

Wright, Steven J.

Effects of Gas Ebullition on Cohesive Sediment Resuspension and Cap Stability

Experimental Results on the Stability of Non-Cohesive Sediment Beds Subject to Vertical Pore Water Flux

Physical Processes Resulting in Geyser Formation in Rapidly Filling Stormwater Tunnels

Wu, J. S.

Proposed Scaling Relations for Manufactured Stormwater BMPs

Wu, Kuowei

Predicting Rock Scour in an Alluvial River with a One-Dimensional Model

Predicting Rock Scour in an Alluvial River with a Two-Dimensional Model

Wu, Shaorong

High Resolution Radar Precipitation Evaluation

Wu, Weiming

One-Dimensional Modeling of Water Quality and Aquatic Ecosystems in Streams

A Depth-Averaged 2-D Model of Non-Cohesive Dam/Levee Breach Processes

Prediction of Changes in Soil Moisture Due to Rainfall, Infiltration, and Evapotranspiration Using a Physically-Based Model

Wu, Zheng Yi

Scalable Parallel Computing Framework for Pump Scheduling Optimization

Wynn, Tess M.

A Monitoring and Assessment Framework to Evaluate Stream Restoration Needs in Urbanizing Watersheds

Wyrick, J. R.

Modeling Stormwater Basins for Potential Retrofit Designs

X

Return to top

Xia, Renjie

Using Computational Model ADH to Evaluate Relationship of Water Surface Elevation to Wing Dikes

Xiao, M.

Engineered Waste Materials as Amendments to Prevent Erosion and to Stabilize Contaminated Sites

Xiao, Ming

pH Variation and Its Effect on Metal Concentration during Electrokinetics

Xu, Feng-ran

Analysis on Effect to EVW from Policy Intervention

Xu, Jianhua

Decision Making under Information Constraints

Xu, Shiguo

The Nitrogen Budget of DRW in Northeastern China

Xuan, Zhemin

Comparative Study of Two Standard Septic Tank Drain Fields Using Different Sand with Recirculation for Nutrient Removal

Nutrient and Pathogen Removal with an Innovative Passive Underground Drainfield for On-Site Wastewater Treatment

Y

Return to top

Yahja, Alex

Evaluation of Alternative Geospatial Models Using Image Ranking and Machine Learning: An Application in Shallow Groundwater Recharge and Discharge

Yamada, T.

A Study on Spatial Distribution of Water Quality and the Behavior of Do Concentration in Tidal Area of Urban Rivers

General Hydraulic Characteristics of an Open Channel with Narrow Path

Yan, H.

Runoffs of the Xiangride and Qaidum Rivers in the Arid Qaidum Basin, Northwest China

Yang, Chih Ted

Alternatives Study of Willwood Diversion Dam Siltation Removal in Wyoming, USA

Yang, Jeff

Needs and Trends of the Nation's Water Infrastructure—The Utility Perspective

Yang, Xueyao

The Impacts of Demand Variability on Distribution System Hydraulics and Transport

Yang, Y. Jeffrey

Assessing the Impact of Climate Change on Drinking Water Treatment Plant Design and Operation

Yang, Yi-Chen E.

A Decentralized Optimization Algorithm for Multi-Agent System Based Watershed Management

Yanmaz, A. Melih

Mathematical Modeling of Bed—Topography Changes at Bridge Abutments

Yap, A.

Ecosystem Services Approach to Public Facility Planning

Yates, Dave

City of St. Louis Permeable Pavement Alley Pilot Study

Yazdanpanahrostami, Ali

Simulation of Tehran Air Pollution Using Artificial Neural Networks

Yeh, D.

Non-Traditional University Research Partners That Facilitate Service Learning and Graduate Research for Sustainable Development

Yeh, Gour-Tsyh (George)

Reaction Rates in a Transport System with Both Kinetic and Equilibrium Reactions

Integrated Watershed Modeling

Yeh, Gour-Tsyh

Estimating Groundwater Seepages to St. Lucie Estuary

Yeh, Hund-Der

Composite Analysis of Test-Well and Observation-Well Data during Constant-Head Test

Yeh, Keh-Chia

Numerical Simulation of Sediment Transport and Morphological Change of JiJi Weir Reservoir

Yeh, William W.-G.

Impacts of the Upstream Storage Reservoirs on Itaipu Hydropower Plant Operation

Yin, Jun

The Role of the Clast Layer of Desert Pavement in Rainfall-Runoff Processes

Yord, William

The Rush Creek Detention Facility: Planning a Permanent BMP in the Real World

Adverse Effects of Flood Flow at Skewed Railroad Crossings

Redesign and Rehabilitation of Railroad Bridges with Advanced Adverse Lateral Migration

Young, C. B.

Are Rational C Values Too Low?

Young, C. B.

Bankfull Discharge for Kansas Natural Alluvial Channel Design

Regional Regression Analysis and the Rational Method

Young, C. Bryan

A Student-Led Effort to Assess the Effect of Urban Runoff on Potter Lake

Long-Term Effectiveness of a Bioretention System Treating Road Runoff in Northeastern Kansas

A Simple Analytical Design Method for Small Alluvial Channels

Young, L. E.

Assessing Postulated Accidental Releases of Radioactive Liquid Effluents from Nuclear Power Plants

Young, Michael

The Role of the Clast Layer of Desert Pavement in Rainfall-Runoff Processes

Young, Nathan

Upper Mississippi River Basin Envirohydrologic Observatory

Yu, Tong

Spatial Variation of Sediment Oxygen Demand in Athabasca River: Influence of Water Column Pollutants

Yue, Feng

Modeling the Hydrology and Hydraulics of the Cache River System

Z

Return to top

Zambon, Renato C.

Climate Flow Forecast Model for the Brazilian Hydropower System

Impacts of the Upstream Storage Reservoirs on Itaipu Hydropower Plant Operation

Zanfelice, Fabio R.

Climate Flow Forecast Model for the Brazilian Hydropower System

Zavislak, Matthew

Adaptive Long-Term Monitoring at BP Environmental Restoration Sites

Zecchin, Aaron C.

Damage Detection of Operating Transmission Mains with Measured Boundary Conditions

Zechman, E. M.

Hydrologic Footprint Residence: A New Metric to Assess Hydrological Alterations Due to Urbanization

Zechman, Emily

A Multi-Objective Evolutionary Computation Approach to Hazards Mitigation Design for Water Distribution Systems

Improving Hydrologic Sustainability of Texas A&M University Campus

Zeinivand, H.

Spatially Distributed Modeling of Soil Erosion and Sediment Transport at Watershed Scale

Zhang, Chun-ling

Analysis on Effect to EVW from Policy Intervention

Zhang, Hui

Optimal Distribution of Pressure Measurement Points in Water Distribution Networks

Zhang, Tian C.

Sorption and Desorption of Testosterone in Agricultural Soils

Zhang, Xiaodong

Comparison of Sensible Heat Flux Measurements by a Large Aperture Scintillometer and Eddy Correlation Methods

Zhang, Yaoxin

Numerical Simulation of Sediment Transport and Morphological Change of JiJi Weir Reservoir

Zhang, Yu

Flash Flood Forecasting for Ungauged Locations with NEXRAD Precipitation Data, Threshold Frequencies, and a Distributed Hydrologic Model

Gauge-Based Adjustment of Historical Multi-Sensor Quantitative Precipitation Fields and Resulting Effects on Hydrologic Simulations

Zhang, Ziya

Distributed Hydrologic Modeling: From Research to Operational Forecasting

Flash Flood Forecasting for Ungauged Locations with NEXRAD Precipitation Data, Threshold Frequencies, and a Distributed Hydrologic Model

Zhao, Bo

Study on the Water Value Conversion between Economy and Ecology and Countermeasures of Water Resources Distribution for Coordinated Development of Economy and Ecology

Zhen, Jenny

Multiple Watershed Scales Approach for Placement of Best Management Practices in *SUSTAIN*

Zheng, Pearl

A Bayesian Framework for Cost Effective Management of Sediment Reduction in the Minnesota River Basin

Zhou, J. G.

A Lattice Boltzmann Model for Dam Break Flows

Zhou, Yi

Development of a Fuzzy Based Pipe Condition Assessment Model Using PROMETHEE

Zhu, David

Spatial Variation of Sediment Oxygen Demand in Athabasca River: Influence of Water Column Pollutants

Zhu, Qi

Scalable Parallel Computing Framework for Pump Scheduling Optimization

Zhu, Tingting

Numerical Modeling of Ozonation of Organic Chemicals in Surface Water

Numerical Simulation of Chemical Spills Using CCHE2D Model and Chemical Property Database

Zimmer, Andrea

Evolutionary Optimization of Combined Sewer Overflow Control

Zink, Vincent J.

Adverse Effects of Flood Flow at Skewed Railroad Crossings

Redesign and Rehabilitation of Railroad Bridges with Advanced Adverse Lateral Migration

Zomorodi, Kaveh

Simplified Solution for Groundwater Mounding under Round Stormwater Infiltration Facilities

Zotarelli, Lincoln

Physiological and Yield Response of Green Bell Pepper to Soil Moisture Sensor Controlled Drip Irrigation